

# Contents

---

<b>U</b>	UL5	1	<b>G</b>	G02	159	<b>H</b>	HS01	265
	U5	1		G03	163		HS02	273
	UL6	2		G04	172		HS03	322
	U6	2		G07	179		HS04	328
	U7	3	<b>A</b>	GAI.08	185		HW01	331
	U8	4		GAI.10	188		HW02	345
<b>IA</b>	JSG01	5		GAII.04	193		HW03	347
	JSG02	16		GAII.05	197		HW04	350
	JSG03	19		GAII.06	200	HW05	353	
	JSA01	25		GAII.07	208	HW06	357	
	JSA07	27		GAI.07	208	HW07	361	
	JSA08	38		GAI.05	210	HW08	374	
	JSA09	41		GAI.06	217	<b>M</b>	MI03	381
	JSH01	42		GAI.07	222		MI05	384
	JWH01	48		GAI.08	225		MI06	393
	JSM03	54	GAI.09	227	MI07		394	
	JSM04	57	GAI.10	229	MI08		398	
	JSM10	62	GAI.11	236	MI09		400	
	JSM11	69	GAI.14	241	MC02		403	
	JSM14	72	GAI.02	244	MC03		410	
	JSM15	83	GAI.03	246	MC04		420	
	JSP04	86	GAI.04	249	MC05		425	
	JSP06	92	GAI.05	249	MC08		439	
	JSP07	97	GAI.06	252	MC11		442	
	JSP08	99	GAI.07	256	MC12		448	
JSP09	103	GAI.07	261	MC17	452			
JSP10	109	<b>S</b>		SS03	459			
JSP11	121			SS04	487			
JSS06	127			SS05	513			
JSS07	143			SW03	515			
				SW04	519			
		SW05	522					
		<b>INDEX</b>		Alphabetical listing				
				of authors	527			

# Key to Abstract Book

---

1. Symposium and Workshop are listed according to organizing or leading Association, where:

- U** = UNION
- IA** = INTER-ASSOCIATION (IAG, IAGA, IAHS, IAMAS, IAPSO, IASPEI and IAVCEI)
- G** = IAG
- A** = IAGA
- H** = IAHS
- M** = IAMAS
- P** = IAPSO
- S** = IASPEI
- V** = IAVCEI

2. Poster Session

Posters are displayed all day at Site D (Sapporo Media Park, SPICA) according to the poster session schedule. All poster sessions are assigned a core time for a morning or afternoon. During this time poster presenters are expected to be present at your poster for at least one hour. Some conveners have given specific times when they would like presenters to be at their posters. For other sessions, presenters can choose the time when they will be present at the poster. There will be a note on the poster where presenters can write when they will be present at their poster.

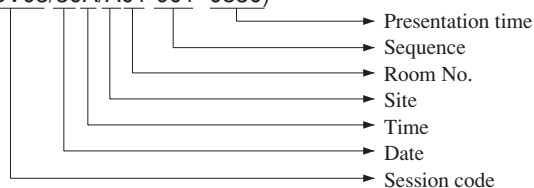
# Key to Index

---

Authors are listed alphabetically, followed by the code of their abstract and indication of date, time and location of presentation, where:

## Oral Presentation

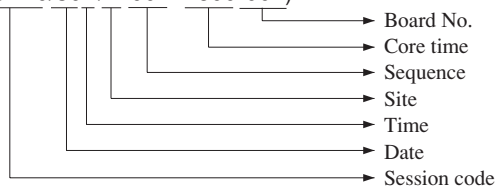
SMITH, John Y. (JSV03/30A/A01-001 0830)



Example: JSV03/30A/A01-001 0830 = JSV03, June 30, presentation in the morning (AM), Site A, Room 1, first paper in that session, Presentation begins at 8:30)

## Poster Presentation

SMITH, John Y. (JSA10/30P/D-001 1600-001)



Example: JSA10/30P/D-001 1600-001 = JSA10, June 30, presentation in the afternoon (PM), Site D, first paper in that session, core time begins at 16:00, Poster Board No.: 001)

N.B: IUGG cannot accept any responsibility for textual errors to the content of the submissions. Due to regional differences in software, some specific symbols may have been automatically substituted by the publishers native version.

IUGG apologise for any confusion that these errors may cause.

## UNION LECTURE FOR U5

Monday, July 7

## MODELING OF THE EARTH'S DYNAMO

Location: Site D, Room 32

U5/07A/D32-001

0800

## MODELING OF THE EARTH'S DYNAMO

Gary A. GLATZMAIER (University of California)

It has been nearly a decade since the first three-dimensional (3D) magnetohydrodynamic computer models produced simulations of convection and magnetic field generation in the Earth's core. Since then several research groups around the world have developed similar models of the geodynamo. All of these produce dipole-dominated magnetic fields outside the core that resemble the geomagnetic field. The non-dipolar part of these simulated magnetic fields drifts westward, like the Earth's, and in some models the axial dipole part occasionally and spontaneously reverses. Some models also predicted the eastward super-rotation of the solid inner core that was subsequently inferred from seismic analyses, although early estimates of the amplitude of this rotation rate may have been too large. These highly nonlinear simulations have confirmed the basic concepts of geodynamo theory, i.e., that a magnetic field like the Earth's can be generated by convection in the Earth's core. They have also provided much greater insight into the details of how the geodynamo may be operating. However, our understanding of the geodynamo is far from complete. No global geodynamo simulation has yet been able to computationally afford the spatial resolution required to simulate turbulent convection, which surely must exist in the Earth's low-viscosity fluid outer core. They all employ greatly enhanced "eddy" diffusivities to stabilize the low resolution numerical solutions and crudely account for the transport and mixing by the unresolved (subgrid scale) turbulence. Consequently the simulated convection in current models is very laminar, having only large spatial scales instead of a broad spectrum of turbulence. So, how robust are the results of the current geodynamo models? We will not know until the next generation of geodynamo models are able to run at much higher spatial resolution and much lower viscosity, which will require better numerical methods and computers. In the meantime we can get some insight by testing two-dimensional (2D) magnetoconvection models, which, although lacking the correct geometry, can simulate strong turbulence. Current 2D tests reveal new important sources of vorticity and Alfvén waves that are suppressed in current 3D geodynamo simulations. This new vorticity will play an important role in the generation of magnetic field; the high frequency Alfvén waves will require more sophisticated numerical methods. Movies of both 3D and 2D simulations are presented that illustrate these issues.

## U5

Monday, July 7

## STRUCTURE AND DYNAMICS OF THE EARTH'S INTERIOR

Location: Site D, Room 32

Monday, July 7 AM

U5/07A/D32-001

0900

## THE EARTH'S CORE: AN APPROACH FROM FIRST PRINCIPLES

G. David PRICE, L. VOCADLO, D. ALFE, M.J. GILLAN (UCL)

The Earth's core is largely composed of iron (Fe). The phase relations and physical properties of both solid and liquid Fe are therefore of great geophysical importance. As a result, the properties of Fe have been extensively studied experimentally over the past fifty years. However, achieving the extreme pressures (~350 GPa) and temperatures (~6000K) found in the core provide a major experimental challenge, and it is not surprising that there are still considerable discrepancies in the results obtained by different experimental techniques. In the past fifteen years quantum mechanical techniques have been applied to predict the properties of Fe. Here we review the progress that has been made in the use of first principle methods in the study of Fe, and focus upon (i) the structure of Fe under core conditions, (ii) the high-P melting behaviour of Fe, (iii) the thermodynamic properties of hexagonal close packed (hcp) Fe, (iv) the rheological and thermodynamic properties of high-P liquid Fe, and (v) the composition and thermal structure of the inner and outer core.

U5/07A/D32-002

0930

## CORE-MANTLE BOUNDARY INTERACTIONS

Bruce BUFFETT (Department of Geophysical Sciences, The University of Chicago)

The interface between the core and the mantle defines a dramatic change in physical and chemical properties. The mantle side is composed of a crystalline silicate that slowly creeps under stress, whereas the core side is comprised of a liquid iron alloy with a viscosity comparable to that of water. Convection in each region creates two giant heat engines, which power plate tectonics in the mantle and generate the magnetic field in the core. These two heat engines can interact at the core-mantle boundary in a variety of ways. Current speculations can be divided into mechanical, thermal and chemical interactions. Mechanical interactions permit an exchange of angular momentum between the core and the mantle, which is detectable as a fluctuation in the rotation of the Earth's surface and may offer clues about the dynamics of the core. Thermal interactions arise mainly from non-uniform heat flow across the core-mantle boundary, profoundly affecting convection in the core and possibly influencing the rate of magnetic reversals. Chemical interactions can result from chemical reactions between the silicate and iron, or may simply reflect the ongoing differentiation of the Earth. An enrichment of Os isotopes in some mantle plumes is often cited as evidence for an exchange of mass between the core and the mantle. Efforts to unraveling the nature and consequences of these interactions are guided by parallel efforts to interpret the structural complexity of the boundary region. Seismic tomography models of the mantle provide evidence of large-scale chemical heterogeneity in the lowermost mantle. More extreme variations in seismic-wave speed have been detected in thin layers at the base of the mantle, called ultra-low-velocity zones (ULVZ). A survey of recent advances in our understanding of structural complexity at the core-mantle boundary is used to motivate discussion of the possible causes and consequences of core-mantle interactions. Suggestions for future work is presented.

U5/07A/D32-003

1030

## CORE-MANTLE BOUNDARY STRUCTURES AND PROCESSES

Thorne LAY<sup>1</sup>, Edward J. GARNERO<sup>2</sup> (<sup>1</sup>Earth Sciences Department, University of California, Santa Cruz, <sup>2</sup>Department of Geological Sciences, Arizona State University)

The lowermost mantle is now recognized as one of the most heterogeneous regions within the Earth. The presence of a large temperature increase across a thermal boundary layer at the base of the mantle has long been inferred based on estimates of the geotherm. The recent seismological observations of intermittent 10 to 30 percent reductions of shear and compressional velocities near the base of the mantle, often found beneath extensive regions of 2-3 percent low velocities and negative velocity gradients, raise the possibility that partial melting takes place in the lowermost mantle, possibly in an (Mg,Fe)O phase. Observations of shear wave anisotropy in the lowermost mantle are also being mapped out, and the strength of anisotropy tends to correlate with increasing shear velocity anomaly on both regional and global scales. Experimental efforts suggest that it is again the (Mg,Fe)O component of the lower mantle that is the likely cause of these observations, as suitable slip systems develop in that mineral at high pressures that can be reconciled with the predominantly transverse isotropy observed in the boundary layer. The possible presence of partial melting, with resultant viscosity reductions, coupled with the interpretation of dislocation glide mechanisms for producing anisotropy in relatively cool, high velocity areas, provide new perspectives and constraints on boundary layer dynamics at the core-mantle boundary. Continued mapping of lower mantle stratification in the form of P and S wave velocity discontinuities several hundred kilometers above the core-mantle boundary suggests very widespread occurrence of this complexity, which is not uniquely associated with regions of possible mantle downwellings inferred from mantle seismic tomography. Small scale undulations in the reflectors, which appear to involve as much as 100 km of topography over length scales of 250 km laterally appear to preclude explanation of these features as phase changes, and tend to favor interpretations in terms of chemical heterogeneity. Regions with stronger S velocity reductions than P velocity reductions than can be attributed solely to temperature or even partial melting also favor the notion of strong chemical heterogeneity in the core-mantle boundary transition zone. Whether this region serves as a reservoir for volatiles and or slowly recycled slab components continues to be a hot debate.

U5/07A/D32-004

1100

## SEISMIC MANTLE STRUCTURE: TRAJECTORY OF MANTLE FLOW

Yoshio FUKAO (Earthquake Research Institute, University of Tokyo (also at IFREE/IAMSTEC))

The three-dimensional structure of the mantle has been revealed by global seismic tomography, and used as a basis for extensive discussion of the mantle flow field. Mantle down flow manifests itself as plate subduction, whereas plate accretion is a shallow process that is different in nature from large-scale mantle upwelling. We review the seismic imaging of plate subduction, and discuss its implications for mantle down flow. The review results can be summarized as follows. 1) Subducted slabs generally extend further than the leading edge of the deep seismic zone. 2) This aseismic portion tends to flatten in the upper and lower mantle transition region, either above, across or below the 660-km discontinuity. 3) There is little indication for direct slab continuation down to the deep lower mantle far beyond the transition region. 4) The subducted slabs imaged in the deep lower mantle are e.g. those of the Farallon and Indian plates, which are separate entities from the presently active surface plates. The slab images summarized above indicate a stagnant nature of mantle down flow in the transition region and its possible role in plate tectonic history, particularly in the global change of plate motions e.g. in the Eocene. Recognizing that the slabs imaged in the transition region post-date the Eocene plate reorganization, slab subduction has a role of mass injection into the mantle transition region, which must induce a counter flow to carry transition region material upward. This counter flow may need to be taken into account in order to understand magmatic processes in island arcs. We report clear evidence of a hot anomaly (negative P-velocity anomaly with a depression of the 400-km discontinuity) on the oceanic side of the subducted slab that may be associated with this counter flow. We also report evidence of oceanic crust residing near the bottom of the slab image at depths below the 660-km discontinuity, suggesting a density reversal in the slab between its crustal part and mantle part upon phase transformations at the 660-km discontinuity, and their subsequent overturn within the softened slab body."

U5/07A/D32-005

1130

## MANTLE CONVECTION AND GEOCHEMICAL CONSTRAINTS

Yanicck RICARD (Laboratoire de Sciences de la Terre, Ecole Normale Supérieure de Lyon)

Although more and more robust evidence of whole mantle convection comes from seismic tomography and geoid modelling, the rare gases and other isotopic or trace element signatures of MORB and OIB indicate the presence of various isolated geochemical reservoirs in the mantle. We discuss this discrepancy between the fluid dynamic views of mantle convection and the chemical observations. It has often been argued that an increase of viscosity with depth could be responsible for some stratification of the mixing properties of the mantle. We test this assumption by means of 2D and 3D models of convection and conclude that a viscosity layering does not induce any vertical stratification of the mixing properties of the mantle (at least for a viscosity increase with depth lower than by a factor 200). We discuss the possibility to hide geochemical heterogeneities into the deep mantle in the form of an isolated primitive or enriched reservoir. To be stable and not to be advected by convection, this reservoir has to be denser and with a low thermal expansivity. These two conditions are present in D'' and seem difficult to hold in the mid lower mantle. We use mineralogical data to constrain the density of the oceanic crust and lithosphere in the lower mantle. We suggest that a significant part of the subducted oceanic crust transformed into dense eclogitic assemblages, partially segregates to form a D'' layer growing in time. This D'' layer would trap a significant amount (1/3) of the Earth's radioactive and incompatible elements. A complementary cold and depleted harzburgitic lithosphere remains above. The hotspots would tap in variable proportions material from both the residual deep mantle and D''. The difference between HIMU and awaiian basalts is attributed to HIMU being mostly from the strongly degassed oceanic crust, though enriched in incompatibles (D''), while Hawaii is mostly from MORB-source residuals variably degassed and depleted. We will discuss quantitatively the geochemical implications of this models by means of both box-models and fluid dynamic simulations.

**UNION LECTURE FOR U6** **Wednesday, July 9****THE GRAVITY FIELD OF THE EARTH DETERMINED BY NEW SATELLITE MISSIONS**

Location: Site D, Room 32

**U6/09A/D32-001****0810****THE GRAVITY FIELD OF THE EARTH DETERMINED BY NEW SATELLITE MISSIONS**Christoph REIGBER (GeoForschungsZentrum Potsdam, Department 1 Geodesy & Remote Sensing<sup>1</sup>)

The Earth is a highly dynamic planet, undergoing perpetual change, driven by internal and external forces, and shaped by interactions between its geosphere, hydrosphere, atmosphere and biosphere on diverse spatial and temporal scales. Variations of the land topography, sea level, ice sheets, the water table and changes of the atmosphere can be observed all the times. Phenomena such as core dynamics, mantle convection and plate tectonics characterize changes taking place in the Earth's interior. All these phenomena are associated with mass movements and lateral density variations, manifested in spatial and temporal variations of the Earth's gravitational field. After remarkable achievements in static gravity field modeling over the last four decades, the new millennium with its just started sequence of dedicated gravity satellite missions shows great promise for order of magnitude improvements of the global mean gravity field modeling and for unravelling the temporal variability of the field. The recently launched German mission CHAMP (2000), the American/German mission GRACE (2002) and the European Space Agency future mission GOCE (2006) provide a progressive increase in gravity field resolution and accuracy. This will allow for the first time- in combination with other geophysical data- comprehensive experiments for imaging and modeling complex Earth structures and processes and to carry out detailed studies of gravitational signals associated with mass exchange between the solid Earth and the hydrological, oceanic and atmospheric components of the Earth system. The striking results obtained from the CHAMP mission data and the very promising initial results from the GRACE twin satellite observations prove that with advanced satellite and sensor technology a permanent high precision monitoring of the global gravity field from space is feasible. Such a permanent monitoring with improved spatial as well as temporal resolution is urgently needed within various fields of environmental and global change monitoring and prognostics. The lecture will highlight the space gravity results obtained so far from the two successfully operating new missions CHAMP and GRACE, will demonstrate on the basis of a few examples the impact gravity modeling improvements can have on our improved understanding of geo-processes and will give an outlook on plans and prospects for further gravity improvements from space.

**U6****Wednesday, July 9****NEW SENSORS OF OUR PLANET. WHAT IS POSSIBLE**

Location: Site D, Room 32

**Wednesday, July 9 AM****U6/09A/D32-001**

Invited

**0910****HIGH-RESOLUTION GRAVITY MAPPING: THE NEXT GENERATION OF SENSORS**

Christopher JEKELI (Geodetic Science, Ohio State University)

Gravity sensors have long been used to infer Earth's mass density variations at all spatial scales. Instruments on airborne platforms are now commonly employed for oil exploration and geoid modeling. Satellite systems (GHAMP and GRACE) have recently been launched and new missions are in development (GOCE) to map the gravity field globally up to resolutions better than 100 km. In addition, the precision of these space-borne sensors is sufficient to discern the monthly (and longer-term) temporal variations of the field, thus enabling improved modeling of the time variations in continental hydrology, sea level, polar ice mass, and ocean bottom pressure. Improvements in terrestrial instrumentation, primarily in gravity gradiometry, portend similar capabilities at much finer spatial scales. Regional temporal variations in the continental water storage, and the crust's vertical motion associated with earthquakes, volcanic eruptions, and extractions of water and oil deposits, can all potentially be detected with new gradiometers currently under development. One of the leading technologies is based on the cold-atom interferometer that uses the wave-like properties of laser-cooled atoms to infer their acceleration in a gravitational field. In all cases of sensors deployed on a moving platform, Einstein's Principle of Equivalence (of inertial and gravitational mass) confounds the separation of gravitational quantities from kinematic accelerations (linear and/or angular). This paper gives a statistical analysis of gravitational signals and errors of current and future moving-base sensors and provides an outline of capabilities, limitations, and requirements for applications in geodesy and geophysics.

**U6/09A/D32-002**

Invited

**0935****STUDIES OF EARTH'S CORE AND MANTLE USING SATELLITE MAGNETIC FIELD MEASUREMENTS**

Catherine G. CONSTABLE (Scripps Institution of Oceanography)

Satellite magnetic field measurements provide a global view of the geomagnetic field. Vector field missions typically consist of a fluxgate magnetometer combined with a star camera to determine attitude of the spacecraft, GPS for positioning, and a scalar magnetometer for calibration of the vector field instrument. From late 1979 the Magsat mission provided vector magnetic field measurements for a period of about six months: prior to that several satellites had carried scalar magnetometers. Following a 20 years hiatus, there are recurrently several magnetometry satellites in near-Earth orbit. The measured magnetic field is an admixture of all field sources: external, ionosphere, crust, mantle, and core. It remains a significant challenge to separate the relevant contributions to study aspects of interest here: these are (1) the field generated in Earth's core and associated secular variations that provide a view of the workings of the geodynamo, and (2) fields induced in Earth's mantle by external magnetic variations; these are used in studies of electrical conductivity. Crustal magnetization, itself a major topic of geophysical interest, contributes significantly to the measured field, and must be considered in attempts to isolate the fields in both core and mantle. Modeling the core field and its variations relies on identifying quiet measurements that are minimally perturbed by external field variations, and solving Laplace's equation in a field-free region. Under the assumption that Earth's mantle is source free with zero electrical conductivity, such models are downward continued to the core surface. Additional assumptions are invoked to estimate

the fluid flow at the core surface. Newsatellite measurements provide an unprecedented view of changes in the core over the past 20 years; further measurements will allow identification of the temporal spectrum of these secular variations. Secular changes are coupled to changes in length of day, and recent modeling of torsional oscillations in the core can provide an explanation for the abrupt changes in the field known as geomagnetic jerks. Mantle induction studies require a comprehensive approach to magnetic field modeling. Unwanted internal field contributions must be removed yielding time series of external variations and their induced counterparts: improved modeling, combined with the increased accuracy measurements, and longer term magnetic measurements make conductivity studies feasible with modern satellites. The one-dimensional global conductivity response has been estimated under strong assumptions about the structure of the source field. Ongoing improvements to this work will take account of more complicated source-field structure, three-dimensional Earth structure, and spatio-temporal aliasing due to satellite motion. Modeling of three-dimensional near surface conductivity structure, and the use of time-domain rather than frequency-domain techniques to estimate the 3-D Earth response are needed. Progress in this area is likely to be furthered by future magnetometer missions that involve multiple satellite configurations.

**U6/09A/D32-003**

Invited

**1000****DENSE GPS ARRAY: NEW VERSATILE SENSOR OF THE EARTH**

Kosuke HEKI (Div. Earth Rotation, National Astronomical Observatory)

Dense GPS arrays (average distances of a few tens of kilometers) in regional/local scales would be one of the most versatile tools to sense our planet. Densification of the GPS stations enhances the chance of detecting co- and post-seismic crustal deformation from short distances, and provides important information on plate dynamics near boundaries. As for seismology, GPS detected earthquakes too slow to be detected by seismometers, and rapid sampling was found useful to record ground displacements when seismic waves pass by. GPS is also useful to monitor volcanic activities, but recent experiences suggest it necessary to deploy even denser networks temporarily to detect useful signals. Delays of GPS signals in propagating media are rich in information on atmospheric water vapor, which has been found to improve numerical forecast of strong rainfalls. Ionospheric delays are important to study upper atmospheric dynamics, and GPS-derived ionospheric models offer a convenient way to remove ionospheric effects from radio tracking data of spacecraft. By analyzing periodic components in GPS station coordinates, we can study seasonal hydrological cycles in soil, accumulation of snow loads on the surface, etc. in a scale too small to be detected by current accuracy of satellite gravity missions such as GRACE. In this study I review examples of multi-disciplinary applications of the Japanese dense GPS array, GEONET, and addresses its future prospects in various fields such as seismology, volcanology, meteorology, hydrology, tectonics, etc..

**U6/09A/D32-004**

Invited

**1050****4-D IMAGING OF THE EARTH'S SUBSURFACE USING INSAR: MOVING BEYOND THE SINGLE INTERFEROGRAM**

Howard A. ZEBKER (Department of Geophysics, Stanford University)

Interferometric synthetic aperture radar (InSAR) techniques are perhaps the most exciting advance in geodesy in the past decade. The ability to map surface deformation at fine resolution over wide areas has led to many new insights into geophysical processes. Most studies to date have resulted from analysis of a single radar interferogram, and permit identification of subsurface phenomena such as fault slip, magma chamber inflation, or dynamics of the polar ice sheets. The ready availability of multiple data sets, as afforded by ERS or other spaceborne sensors, coupled with the decrease in computational and data storage costs, now allows analysis of time series data: the examination of how deformation patterns change with time. These 4-D images present much more information about how processes at depth evolve and are more predictive about future events, an important capability for observing natural hazards such as earthquakes and volcanic activity. Special filters may be devised to discriminate steadily changing deformation patterns from those that are more episodic in nature. We review here results from several techniques based on temporal analysis of interferograms, including faulting on active volcanoes, pore fluid migration due to changes in seismic stress, hydrologic aquifer analysis, and permanent scatterer analysis of tectonic deformation.

**U6/09A/D32-005**

Invited

**1115****REMOTE SENSING OF SOIL MOISTURE AND SOIL WATER STORAGE**

James S. FAMIGLIETTI (Department of Earth System Science, University of California, Irvine)

Mass movements in the global water cycle are fundamental Earth system phenomena. In particular, changes in the amount of water stored on land are critical indicators of global change, and have important feedbacks to the climate system. Recent advances in space observations of terrestrial hydrology now make satellite observations of terrestrial water storage variations possible. In particular, microwave radiometers such as AMSR, AMSR-E, TMI and SSM/I can provide information on soil moisture storage in the surface few centimeters of the soil, while GRACE can provide information on variations in total terrestrial water storage variations. The two types of information play complementary roles in understanding the distribution of water on land, both laterally and vertically. This presentation will review the state-of-the-art in water storage monitoring using both microwave and gravity-based sensors. Potential new missions and additional sensors required for comprehensive monitoring of terrestrial water storage will also be discussed, as will novel applications of satellite-based water storage observations in an Earth system context.

**U6/09A/D32-006**

Invited

**1140****WIDE-SWATH ALTIMETRIC MEASUREMENT OF OCEAN SURFACE TOPOGRAPHY**

Lee-Lueng FU, Ernesto RODRIGUEZ (MS 300-323 Jet Propulsion Laboratory)

This paper describes a new approach to making altimeter measurements from off-nadir radar signal returns and its scientific and operational applications. The approach is based on the technique of radar interferometry and the new instrument is called the Wide-Swath Ocean Altimeter (WSOA). WSOA is designed to be flown with a Jason-1 class conventional dual-frequency altimeter system, including a multi-frequency radiometer for the correction of the effects of water vapor in the troposphere. WSOA will extend the measurement from a line along the nadir to a swath of 200 km centered on the nadir track. The most important application of WSOA is to provide the first synoptic maps of the global oceanic eddy field. The strong currents and water property anomalies (in temperature, salinity, oxygen, etc.) associated with ocean eddies are a major factor affecting the oceanic general circulation and maritime operations such as offshore oil drilling, ship routing, fisheries, marine debris dispersion, etc. WSOA is expected to be an essential part of the future ocean observing

system for addressing these applications. WSOA will also provide measurements that allow the monitoring and study of coastal currents and tides that affect the lives of half of the world's population.

**U6/09A/D32-007** Invited **1205**

**GLOBAL NAVIGATION SATELLITE SOUNDING (GNSS) OF THE ATMOSPHERE AND GNSS ALTIMETRY: PROSPECTS FOR GEOSCIENCES**

Thomas P. YUNCK (Jet Propulsion Laboratory)

With the emergence of large-scale geodetic ground networks, both regional and global, and affordable spaceborne GNSS scientific receivers, space geodetic techniques are finding diverse and unexpected new applications in many areas of Earth remote sensing. Basic GNSS navigation receivers are now all but indispensable to low earth orbiting missions of all kinds. Science applications of spaceborne GNSS today include centimeter-level precise orbit determination for gravity mapping, ocean altimetry, geocenter detection, and enhanced global geodesy; high resolution 3D imaging of the global ionosphere; occultation limb sounding to recover precise profiles of atmospheric refractivity, density, pressure, temperature, water vapor, and geopotential heights; and the experimental detection of GNSS ocean reflections for direct ocean altimetry and scatterometry. In the past five years there has been an explosion in the use of both ground and spaceborne geodetic receivers for direct sensing of the atmosphere to provide data for weather prediction and research in global climate change. Atmospheric applications of space geodesy are generating increasing scientific interest. Dense GPS networks in Japan, North America, Scandinavia, Europe, and elsewhere are now routinely providing data for assimilation into daily weather forecasts. A constellation of six orbiting occultation receivers, such as the COSMIC mission to be launched in 2005, can measure atmospheric refractivity with a precision equivalent to 0.1 K in temperature within a climate region corresponding to 1/30 the earth's surface, with just a few weeks of data. Vertical resolution can reach below a hundred meters. This offers perhaps the most promising approach yet to detecting and discriminating among subtle forced climatic signals, which may amount to only a few tenths of a Kelvin average temperature change per decade. More speculative, but having equally great potential, is the detection of GNSS reflections from the surface, primarily oceans and ice. This bi-static radar technique can be used, for example, to determine sea surface topography, significant wave height, surface winds, and possibly sea surface temperature and salinity, and could become valuable for monitoring the evolution of ice sheets. The technique is already practical from airborne platforms. With the prospect of substantially increased signal strength in the next decade from both GPS and Galileo, it may soon become a reality from space as well. This presentation will survey the techniques and Earth science applications of GNSS atmospheric sounding and bi-static radar, and will describe promising developments for the future.

**U7** **Friday, July 11**

**HISTORY OF IUGG**

Location: Site D, Room 32

**Friday, July 11 AM**  
Presiding Chair: A.A. Ashour

**U7/11A/D32-001** **0900**

**THE INTERNATIONAL ASSOCIATION OF GEODESY 1862 - 1916: FROM A REGIONAL PROJECT TO AN INTERNATIONAL ORGANIZATION**

Wolfgang TORGE (Institut fuer Erdmessung, Universitaet Hannover)

Modern geodesy started in the 18th century with the French arc measurements, which proved the spheroidal shape of the Earth postulated for an equilibrium figure. These large-scale operations naturally required international collaboration, and continued in many parts of the world until the 20th century, mostly within the frame of national geodetic surveys. Around 1850, extended latitude arc measurements existed in western Europe, in Russia, in India and elsewhere. Central Europe, on the other hand, was characterized by a number of astronomical observatories and local triangulations, but due to the political splitting up these surveys were not connected to a large-scale network, and could not be used for the investigation of the Earth's curvature. It was at this point, where the geodesist and retired Prussian General Johann Jacob Baeyer started in 1861, by submitting a memorandum on the establishment of a Central European arc measurement. The aim of this proposal was to connect the astronomical observatories by existing and planned triangulation networks in order to determine the regional and local curvature anomalies produced by the gravity field. The King of Prussia approved this plan, and by the end of 1862 already fifteen European states had affirmed their participation in the "Central European Arc Measurement". A first General Conference of this organization took place in Berlin in 1864, and fixed both the organisational structure and the research programme, which included the systematic investigation of the deflections of the vertical at all principal triangulation points, the determination of the intensity of gravity and the standardisation of the measurement units. It is notable that this organisation had a governmental character, but was composed by well-known geodesists and astronomers. With Baeyer as its first President, the organisation soon expanded into the "European Arc Measurement", and the Prussian Geodetic Institute established in 1870 was entrusted with the operation of a Central Bureau. After Baeyer's death, Friedrich Robert Helmert became in 1886 Director of the Geodetic Institute and of the Central Bureau, and with the extension to the "Internationale Erdmessung" (Association Internationale de Géodésie), the scientific programme was essentially broadened and extended over the whole Earth. Among the major achievements of this Association are the International Meter Convention and the adoption of the Greenwich Meridian as initial meridian for longitude and time, the establishment of the International Polar Motion Service and of the Potsdam Gravity System, the determination of gravity values and deflections of the vertical in many regions of the world, investigations on mean sea level, on the geoid and on isostasy, as well as observations of the Earth tides. In 1916, the last intergovernmental agreement for the "Internationale Erdmessung" lapsed and was not renewed, which ended the first fruitful period of international cooperation in geodesy, although several neutral states continued some of the programmes, especially the polar motion observations. When the International Union of Geodesy and Geophysics was established in 1919, geodesy became one of its sections, which started the second period of the International Association of Geodesy.

**U7/11A/D32-002** Invited **0930**

**GRAVITY MEASURING INSTRUMENTS AND GRAVITY REFERENCE SYSTEMS**

James E. FALLER (JILA, National Institute of Standards and Technology and University of

Colorado)

This paper will describe, in a historical context, gravity measuring instruments and gravity reference systems. The use of pendulum (for relative and absolute measurements), spring-type gravity meters (for measurements on land and at sea) and the development of free fall gravimeters (for absolute measurements) will be discussed. Historic and present-day gravity reference systems, based on measurements made with these various types of instruments, will also be discussed. The development of these instruments and the creation of these reference systems made possible by evolving instrumental and calculating capabilities as well as the active support and encouragement of the IAG.

**U7/11A/D32-003** Invited **1000**

**HISTORY AND FUTURE OF THE SERVICES OF THE INTERNATIONAL ASSOCIATION OF GEODESY (IAG)**

Gerhard BEUTLER<sup>1</sup>, Hermann DREWES<sup>2</sup>, Andreas VERDUN<sup>1</sup> (Astronomical Institute, University of Bern<sup>1</sup>, Deutsches Geodätisches Forschungsinstitut<sup>2</sup>)

Towards the end of the 19th century astrometric observations could be made with an accuracy of a few tenths of an arcsecond. The accuracy stayed roughly on this level, till the space age opened the door for milliarcsecond (mas) astrometry. Astrometric observations allowed it at the end of the 19th century to prove the existence of polar motion. The insight that polar motion is almost unpredictable led to the establishment of the International Latitude Service in 1899. Similar observation techniques allowed it to create geodetic networks of continental size. The ILS is but one example for a service working under the auspices of the International Association of Geodesy (IAG). It was actually succeeded in 1989 by the International Earth Rotation Service (IERS). The example shows that new technologies (like distance measurements with Lasers, observations of artificial satellites using microwave signals, observation of Quasars with radio-telescopes) have significant impact on the development of IAG's service structure. The word "service" implies that products of interest to a broad scientific and other professional communities are generated, documented, and made available. The services of the IAG are based on the three pillars of modern geodesy, namely geometry, gravity, and Earth rotation. The rapid evolution of measurement techniques (e.g., Laser distance measurements, microwave observations, etc.) led to the creation of new and abolishment of "old" IAG services in the twentieth century. We give an overview of the development of the IAG services in the previous century and conclude with an outlook on the establishment of IGGOS, the Integrated Global Geodetic Observation System, which shall be established as IAG's key project of the decade. The IGGOS is based on the currently active IAG services. IGGOS intends to make available geometric and gravimetric products on a relative consistency level of one ppb (part per billion). These products are, among other, the scientific backbone for global change research.

**U7/11A/D32-004** Invited **1100**

**HISTORY OF IASPEI**

Eric Robert ENGDAHL (University of Colorado)

When it became evident in the latter part of the 19th century that seismic signals propagate through the Earth over large distances, the need arose for an international organization to coordinate, collect and distribute the data, and promote earthquake research. During two "International Conferences on Seismology", in 1901 and 1903 in Strasbourg, the establishment of an "International Association of Seismology" (IAS) was proposed. The Association was inaugurated in 1904 and joined by 18 nations. In 1919, the International Union of Geodesy and Geophysics (IUGG) was created with the "Seismological Section" as one of its founding components. In 1933, the name was changed to "International Association of Seismology" of the IUGG. In 1951, with the expansion of its scope to include material properties of the Earth's interior, it was renamed the "International Association of Seismology and Physics of the Earth's Interior" (IASPEI), as it is known today. The 1960's brought major changes, and much growth, both to seismology and to IASPEI. In this presentation IASPEI's history and those trends that can be seen retrospectively, to be important and that have evolved into many of the ongoing activities within IASPEI during the modern era will be reviewed.

**U7/11A/D32-005** Invited **1130**

**THE INTERNATIONAL SEISMOLOGICAL ASSOCIATION (ISA) - FORERUNNER OF IASPEI**

Johannes SCHWEITZER (NORSAR)

In the 1890s, shortly after the first teleseismic signals could be identified it became evident that for better results in seismology and earthquake research an international and even transcontinental cooperation was needed. In 1895, such global cooperation was proposed by John Milne in England and Ernst von Rebeur-Paschwitz in Germany. After Rebeur-Paschwitz's death in 1895, Prof. Georg Gerland from Strasbourg in particular promoted the idea of an international organization for earthquake research. He invited all seismologists to the 1st International Seismological Conference in 1901 in Strasbourg. In 1903, a second conference followed and then in 1904, the International Seismological Association (ISA) was founded. Until the beginning of World War I in 1914, 23 states joined the ISA as members. The Central Bureau of the ISA was located in Strasbourg, where Gerland was its director until his retirement in 1910. After World War I, the ISA ceased to be operational, and was officially dissolved in April 1922, and in May 1922 at the First General Assembly of the IUGG in Rome, the new Seismology Section of IUGG was founded, which later became IASPEI. During the few years of ISA's existence, its staff in Strasbourg mainly worked on earthquake catalogues based on instrumental and macroseismical observations, development and testing of new instruments, installation of seismic stations, research on distinguished earthquakes, and organizing of international meetings.

**U7/11A/D32-006** **1150**

**THE INTRODUCTION AND EVOLUTION OF INSTRUMENTAL SEISMOLOGY IN THE PHILIPPINE ISLANDS (1865 - 1902)**

Josep BATLLO (Dept. Matemàtica Aplicada I, Universitat Politècnica de Catalunya)

Instrumental seismology in the Philippine Islands started at the Manila Observatory after 1865. Its early development shows some characteristic features: It developed faster than in Spain (the dominating power at that time) and it is the unique example of development of the Italian seismological tradition in the Far East. Otherwise, seismological studies on the colonial Philippine Islands were not reduced to the research done at the Manila Observatory. Other interesting developments (mainly related to the seismological engineering) took place at that time. An introductory study, discussion and evaluation of the initial moments of instrumental seismology in Philippines and related seismological research is presented.

Friday, July 11 PM  
Presiding Chair: A.A. Ashour

U7/11P/D32-001

1400

**SHORT HISTORICAL REVIEW ON COOPERATION IN GEOMAGNETISM**

Youry P. SIZOV<sup>1</sup>, Thoa Thi Kim NGUEN<sup>2</sup>, Hao Quang TRUONG<sup>2</sup>, Chau Ha DUYEN<sup>2</sup>, Victor N. BOBROV<sup>3</sup>, Youry P. TSVETKOV<sup>3</sup>, Vladislav N. LUGOVENCO<sup>3</sup> (<sup>1</sup>Geoelectromagnetic Research Institute of RAS, <sup>2</sup>Hanoi Institute of Geophysics, <sup>3</sup>Institute of terrestrial magnetism, ionosphere and radio wave propagation of RAS)

The talk presents the main historical milestones of cooperation in Geomagnetism between academic institutes of Russia, and Vietnam, Mongolia, Cuba, Mozambique, FSU and other countries of the World (Geoelectromagnetic Research Institute of Russian Academy of Sciences (RAS), Institute of terrestrial magnetism, ionosphere and radio wave propagation of RAS and Hanoi Institute of Geophysics of NCNS etc.). To enumeration of milestones it should be included: Installation and adjustment of 3-component Magnetic Variation Stations (MVS) at the geomagnetic Observatories (GMO) of Mongolia, Cuba, Vietnam, and all other above mentioned countries (Ulanbator, Habana, Maputo, Sapa, Dalat, Bac-lieu, Ashgabad, Almaty, Dusheti, Odessa, Lviv, Kiev GMO, etc). Installation and adjustment of the MVS near Hanoi-city; Construction the new GMO in Dalat city (~200 km to North from Hochiminh city), Installation and adjustment quartz magnetic D, H and Z sensors and registration device with control at GMO mentioned, absolute magnetometers in Dalat GMO; Construction the new GMO near the geomagnetic Equator in Bac-lieu, Installation and adjustment the quartz D, H and Z magnetic sensors and registration device with control in Bac-lieu GMO; Experimental field missions to collect rock samples for paleomagnetic investigations, to carry out absolute magnetic measurements of module and components for the magnetic anomalies investigation. The Main Magnetic Field and Secular variations study; special missions to investigate the Equatorial Ionospheric Electrojets by means of the temporal magnetic stations meridian chain (additionally to the Vietnam all GMO net) on the base of MVS and proton magnetometers. This permitted to determine daily and secular movement, dynamics and features of the Equatorial Ionospheric Electrojets and its coupling with high latitude geophysical phenomena etc.

U7/11P/D32-002

1450

**NIKOLAY PUSHKOV, SCIENTIST AND ORGANIZER (1903-1981)**

Viktor N. ORAEVSKY, Vadim P. GOLOVKOV (IZMIRAN)

History of a man, who created a powerful infrastructure of Institutes and organized the geomagnetism and aeronomy study in the former USSR, a man who was one of organizers of the International Geophysical Year and joined in this way Soviet Unions scientists to the world scientific community and made the Association of Geomagnetism and Aeronomy to be really the International one.

U7/11P/D32-003

Invited

1505

**A BRIEF HISTORY OF IAVCEI**

Stephen R. MCNUTT (Geophysical Institute UAF)

IAVCEI, the International Association of Volcanology and Chemistry of the Earth's Interior, has been in existence for 81 years. The organization is committed to understanding volcanic processes and mitigating their impact on society. IAVCEI was initially formed as the Section de Volcanologie, a section of IUGG at its first General Assembly in Rome, May 1922. The name was changed to Association Internationale de Volcanologie in 1930 in Stockholm, then to its present name in 1971 at the Moscow IUGG General Assembly. IAVCEI is one of the seven associations of IUGG. IAVCEI's initial main tasks were to 1) inform by telegraph the national committees of the onset of important eruptions, 2) establish a central international volcanological library, and 3) publish a Bulletin Volcanologique and a bibliography of all aspects of volcanoes, from their activity to description of their products. Over the years various communications technologies have changed considerably, however, the basic functions have remained intact. Alfred Lacroix (France) was the first of 15 formally appointed IAVCEI presidents, following A. Ricco (Italy). From 1922 until 1963 the presidents were all from Europe, followed by H. Kuno (Japan) from 1963-1967. There were then 16 years of alternating presidents from the USA and USSR (1967-1983). Since 1983 presidents have been from many different countries, reflecting a global approach to volcanology and studies of the earth's interior. The current President is Steve Sparks (UK). IAVCEI has had eight Secretaries General, by tradition serving at least two terms. The first six were from Europe (1922-1991), followed by Australia (1991-1999) and the USA (1999-present). The current Secretary General is Steve McNutt (USA). IAVCEI changed its statutes and by-laws to introduce personal memberships in 1995, and the organization now has over 700 members. IAVCEI produces 3 newsletters each year, continues to sponsor the Bulletin of Volcanology, hosts a web site [www.iavcei.org](http://www.iavcei.org), and coordinates the activities of 13 commissions. General Assemblies or workshops are held almost yearly, with an emphasis to assist young scientists and scientists from developing countries. The field of volcanology is so broad that earth scientists from many disciplines must cooperate in studying and understanding volcanoes, and studies of volcanic systems and processes therefore overlap with the fields of interest of many IUGG Associations. This broad interdisciplinary aspect is characteristic of many IAVCEI endeavours and is the primary reason why IAVCEI belongs to IUGG and seeks cross-links with the other six Associations.

U7/11P/D32-004

1535

**THE HISTORY OF OCEANOGRAPHY AND IAPSO**

Fred E. CAMFIELD (Inter. Assoc. for the Physical Sciences of the Oceans)

The formal study of oceanography owes its origins to scientific voyages in the late 17th and the 18th centuries. While these early voyages made general scientific observations, there was recognition by the late 19th century of a desire for voyages specifically for oceanography. These voyages were carried out by a number of Western European nations. At the same time, formal experimental and theoretical studies were carried out from the 1830's onward, particularly on waves and tides, but eventually extending to wind driven currents and to the deeper ocean. Prince Albert I of Monaco was trained as a naval officer and became interested in oceanography after seeing reports of French voyages. He financed several ships and carried out observations in the Atlantic and the Mediterranean in the late 19th and early 20th centuries. He recognized the need for an international organization and, when IUGG was organized in 1919, he organized the oceanographic section and served as its first president. Most of the early oceanographic work was carried out by Western European nations, and that is recognized by the membership of IAPSO's early executive committee which was dominated by Western European representative with one from the U.S.A. After 1930, there was strong representation from Denmark, Finland, and Norway, indicative of the oceanographic contributions of those countries, particularly

Norway. While some representatives began to appear from the rest of the world, it was not until after 1957 that IAPSO's executive committee began to acquire a more global character. Oceanography began to expand after 1946, with an apparent rapid expansion starting in the 1960's. Many new programs were established. IAPSO's activities have reflected this expansion of the science. There has also been a recognition since its founding of the need to interact with other sciences, both within and outside IUGG, and discussions of whether IAPSO should reside within an oceanographic union (with biological oceanographers) or a geophysical union (with atmospheric scientists, etc.). There has been a recognition of the fact that the oceanography is international, and the science crosses over the boundaries of the oceans into the atmosphere and the solid earth. References: Wooster, W.S., *Sciences of the Oceans, Physical and Otherwise, Oceanography*, 15:1, pages 128-134. Munk, W., *The Evolution of Physical Oceanography in the Last Hundred Years, Oceanography*, 15:1, pages 135-141.

U8

Friday, July 11

**GEOSCIENCES: THE FUTURE (GTF)**

Location: Site A, Room 2

Friday, July 11 AM

This symposium will be a panel discussion among a group of young scientists nominated by the seven Associations. They have been charged with the task of presenting their views on the future of the geosciences in the years to come including issues, challenges, and opportunities. What are the most pressing scientific and societal problems that can be productively addressed by the geoscience community? For example, the past few decades have seen an explosion in quantitative geoscience. Our observational systems now produce data streams at temporal and spatial resolution unprecedented in human history. The computational tools available for interpretation and prediction dwarf the state-of-the-art of merely 10 years ago. Where can we go from here?

JSG01

Monday, July 7 - Tuesday, July 8

**SECULAR, TRANSIENT AND PERIODIC CRUSTAL MOVEMENTS AND THEIR GEOPHYSICAL IMPLICATIONS (IAG, IASPEI)**

Location: Site A, Room 1

Monday, July 7 AM

Presiding Chair: P. Segal

JSG01/07A/A01-001

0900

**THE VERTICAL DISPLACEMENTS OF JAPAN REVEALED BY MULTIPLE GEODETIC TECHNIQUES**

Makoto MURAKAMI<sup>1</sup>, Tetsuro IMAKIIRE<sup>1</sup>, Tadashi SAITO<sup>2</sup>, Tsugunori NARITA<sup>3</sup>, Seiji OKAMURA<sup>4</sup>, Toshio KUNIMI<sup>5</sup>, Eiichi HAKOIWA<sup>6</sup>, Hiroyuki NAKAGAWA<sup>7</sup>, Kazuo KOMAKI<sup>8</sup> (<sup>1</sup>Geography and Geodynamics Research Center, The Geographical Survey Institute, <sup>2</sup>The Geodetic Department, The Geographical Survey Institute, <sup>3</sup>The Tohoku District Office, The Geographical Survey Institute)

Japan is situated in one of the most tectonically active region on the earth. Even in the premodern era people noticed vertical deformations associated with destructive earthquakes and volcanic eruptions and documented them. Since the introduction of sophisticated geodetic techniques about 100 years ago the nation has been repeatedly surveyed by precise leveling. Using those data the general trend of the vertical deformation of Japan was illustrated. In addition remarkable deformations associated with seismic and volcanic episodes were detected. A network of tidal gauges was also established and has been in operation for about 100 years, providing precious data to trace the evolution of vertical crustal deformations of Japan. In the last decade, GPS and InSAR are introduced to monitor the deformation of the land. The construction of the nationwide permanent network (GEONET) was initiated in 1994 and the number of sites now counts 1200. Daily positions of all the stations are computed on a daily basis. Although the precision of the vertical component of GPS is less than the horizontal ones, even the crustal deformations as small as a few mm/year become detectable by continuing the measurement for several years waiting the signal sums up. Using the accumulated GPS data since 1994 we computed the secular component of the vertical displacements. They basically agree well with leveling and tidal data but some new findings are obtained. We list them below: 1) Subsidence is revealed in the area far apart from the subducting plate boundary and it infers that the plates couples in the deeper portion of the boundary, 2) Subsidence is revealed along Itoizawa-Shizuoka Tectonic Belt where uplift is expected due to collision of two tectonic blocks, 3) Similar subsidence is revealed along a belt running from Niigata to Kobe where uplift is inferred by the dominating horizontal contraction along the belt, 4) Uplift is revealed widely in the north of Usu volcano in Hokkaido before its eruption in March 2000. Those are interesting findings, which may lead us to modifications of existing theories about tectonics of related regions of Japan. In the presentation we will show more the details of vertical displacements revealed by continuous GPS. We also will compare them with other geodetic data from the past and discuss tectonic implications of those new findings.

JSG01/07A/A01-002

0915

**ESTIMATE OF COUPLING ALONG THE SUBDUCTING PLATE BOUNDARY AROUND THE JAPANESE ISLANDS BASED ON A NEW INVERSION METHOD**

Honglin JIN, Teruyuki KATO, Shin'ichi MIYAZAKI, Muneo HORI (Earthquake Research Institute, University of Tokyo)

The Japanese Islands are located at the boundaries among Eurasia, Pacific, North America and Philippine Sea plates. Collision and subduction of these plates cause overall crustal deformation in the Japanese islands. Recent studies of geodetic inversion of dense GPS array data have shown that the distribution of inter-plate coupling is not homogeneous along the subducting plate boundaries. It is important to elucidate the distribution of coupling rates along the boundaries for understanding subduction process and nature of slow slip episodes as well as for earthquake prediction studies. In the previous inversion scheme, all physical processes involved (surface measurements due to fault dislocation, in this case) are represented by Green's function, and directly computed slip distribution from measurement data using singular value decomposition. This scheme can not determine accurate inverse operator because of the ill-posedness of inverse problem. In order to solve this problem, Hori (2001) introduced a new inverse approach in which inversion operator (Green function as an operator) is determined without considering the method of measurement by introducing the spectral decomposition of Green function. Since inverse operator is obtained through numerical spectral decomposition of Green's function, it clarifies the mathematical reason of the ill-posedness of the inverse problem. Moreover, the new approach can manifest the limit of measurement accuracy, and pick up only measurable modes. Measured data is only used to determine deformation function by least square method, and then the deformation function is used for solving the inverse problem to predict slip function at the plate boundary using inverse operator. We have applied this new inversion method to the Japanese GPS data and estimated the distribution of back-slip (or coupling) on a subducting Philippine Sea plate. Before applying the method, we considered that the vertical component of GPS data is important in estimating distribution of coupling along the plate boundary. For this purpose, first, we reduced the noise in the vertical components of GPS time series by removing correlated scatter among neighboring stations. The calculated slip distribution on the Philippine Sea plate indicates that the slip generally directs to the northwest with the maximum speed of about 8 cm/yr, consistent with motion of Philippine Sea plate. The present is harmonious with the result conventional inversion method (e.g. Yabuki and Mutsuura, 1992). It is interesting to point out estimated and observed vectors are consistent in Shikoku and Chugoku areas, but are significantly different in Kinki area. This might suggest that surface deformation near Kinki might be affected by other tectonic disturbance.

JSG01/07A/A01-003

0930

**SECULAR CRUSTAL DEFORMATION IN CENTRAL HONSHU ARC, JAPAN, DEDUCED FROM WAVELETANALYSIS OF GPS TIME-SERIES DATA, AND ITS SEISMOTECTONIC IMPLICATIONS**

Kaoru MIYASHITA<sup>1</sup>, Jianxin LI<sup>2</sup>, Vijay Kumar KATHAMANA<sup>3</sup>, Takahiko SUZUKI<sup>1</sup> (<sup>1</sup>Department of Environmental Sciences, Ibaraki University, <sup>2</sup>School of Marine Science and Technology, Tokai University, <sup>3</sup>GNSS Technologies Inc.)

Secular crustal deformation in the central part of Honshu Arc, Japan was deduced by applying the wavelet decomposition analysis to the GPS time-series data from GSI/GEONET (Geographical Survey Institute/GPS Earth Observation NETWORK). The time-series data during the period from April 1996 to March 2002, which have been re-analyzed to be

improved (Hatanaka et al., 2001), were considered to be composed of secular (a linear trend), seasonal, discontinuous (co-seismic or artificial jumps), and noisy (white noises) components. The NS (north-south), EW (east-west), and UD (up-down) components of the time-series data were also assumed to be mutually independent. After removing data-jumps in the time-series, we decomposed each of the NS, EW, and UD time-series to the 8th level by using Daubechies wavelets. We could find out a seasonal variation clearly in the detail part of the 8th decomposition component, and could estimate a secular velocity from the approximation part at the same level. We estimated secular velocities at about 450 GPS sites in the study region on the basis of the wavelet decomposition analysis, and then evaluated secular velocities at 7 km x 7 km grid points covering the study region by applying the least-square collocation method. We also estimated distributions of several kinds of secular strain rates, i.e., dilatational, maximum shear, and principal strain rates in the study region. From these distributions of secular strain rates, we could find out several kinds of characteristics concerning the secular crustal deformation in the central part of Honshu Arc. Firstly, we could recognize that (1) the entire region is generally under a compressive regime. Next salient features were as follows: (2) there exist remarkable concentrations of maximum-shear and compressive strains near Tokyo Bay and Boso Peninsula in the Kanto region; (3) there is a dilatational area in and around Mt. Fuji and Mt. Hakone in the Tokai region. We tried to explain the observed characteristics of the secular crustal deformation on the basis of the back-slip model, which has multiple faults along the plate boundaries, i.e., Sagami and Suruga-Nankai Troughs, and Japan Trench. However, there was a need to consider other mechanisms in order to explain the characteristics stated above. It might be a possibility that near Tokyo Bay and Boso Peninsula there locates a relatively weak zone such as a potentially faulting zone. It might be also suggested that near Mt. Fuji and Mt. Hakone there is a compressive source, associated with a volcanic flow.

JSG01/07A/A01-004

0945

**ACTIVE FAULT SEGMENTS AND BLOCK MOVEMENT IN NORTH CHINA**

Caijun XU<sup>1</sup>, Zhicai LI<sup>1</sup>, Yanxing LI<sup>2</sup> (<sup>1</sup>School of Geodesy and Geomatics, Wuhan University, <sup>2</sup>First Crustal Deformation Monitoring Center, China Seismological Bureau, Tianjin, 300180, P.R.China)

Research on interseismic fault movements is of considerable importance, not only for academic interest but also for the estimation of hazard zones and earthquake prediction, since any slip deficit at shallow or intermediate depths at a fault could be filled by a future earthquake. North China as a lithospheric dynamics sub-plate is located in the middle part of eastern China. It is characterized by more intense neotectonism and seismic activities in comparison with northeast China and south China. North China block could be divided into 5 blocks from geology information and seismic distribution. The Repeated GPS surveys, had been carried out in the region in 1992, 1995, 1996, 1999, 2001 respectively by the First Crustal Deformation Monitoring Center (FCDMC) of the China Seismological Bureau (CSB), provide a direct measurement of current crustal motions to study the tectonic activity and earthquake hazards in this area. There are more than 70 reoccupied stations after 1995 campaign. At each station, observation was made continuously for at least 72 hours in each campaign. These GPS data were firstly processed together with Global IGS stations using the GAMIT software to get the baseline solutions, then GPS velocity fields in ITRF2000 frame and with respect to Eurasia were obtained based on these baseline solutions and their variance-covariance matrix using the GPS network adjustment software PowerADJ developed by Wuhan University. Methods for the determination of active fault segments and block movements by inversion of GPS velocity and seismic moment tensor are presented. The geophysical implications of the active fault segments and block movements are discussed in this paper.

JSG01/07A/A01-005

1000

**JOINT INVERSION OF GPS VELOCITY AND OBSERVED GRAVITY FOR ACTIVE FAULT SEGMENTS IN SICHUAN-YUNNAN RHOMBUS BLOCK**

Zhicai LI, Caijun XU (School of Geodesy and Geomatics, Wuhan University)

The rhombus block in Sichuan and Yunnan province, lying northeast margin of the Tibet subplate and adjacent to Southchina subplate and southeast Asia plate, is one of the most active block in China. More than 200 earthquakes (ML>5.0) have occurred in this area since 1970, especially including 14 great earthquakes (ML>7.0). So the block is the key area to do investigations by geophysicists. Since the early 1990s, several regional GPS networks for active tectonic studies were established in continental China (Lai et al., 1992; Abdakmatov et al., 1996; Bilham et al., 1997; King et al., 1997; Larson et al., 1999; Li et al., 1995; Shen et al., 2000; Bendick et al., 2000; Wang et al., 2000) We obtain the station velocity in Sichuan-Yunnan block and find that the movement trend of the block is southeast to south. In this paper, We study movement of the Xianshuihe fault in Sichuan province, Honghe fault and Xiaojiang fault in Yunnan province by using GPS and gravity data. We have inverted the fault parameters by using GPS data and gravity data (from 1985 to 1999 in west of Yunnan province) separately and jointly with multi-faults dislocation model. The methodology used here is random cost method, which is one of the Monte Carlo (MA) algorithms. The results from the joint inversion indicate that these faults are presently active. The displacement field and strain-stress field in this block are also discussed in the paper.

JSG01/07A/A01-006

1015

**AN IMPROVED APPROACH FOR CALCULATING THE SURFACE STRAIN RATES FROM GEODETIC NETWORKS WITH APPLICATION TO TAIWAN**

Ya Ju HSU<sup>1</sup>, Mark SIMONS<sup>2</sup>, Shui-Beih YU<sup>3</sup> (<sup>1</sup>Institute of Geophysics, National Central University, <sup>2</sup>Seismological Laboratory, Division of Geological and Planetary Sciences, California Institute of Technology, <sup>3</sup>Institute of Earth Sciences, Academia Sinica)

We use the Taiwan GPS velocity field for the time period 1993 to 1999 to estimate spatially varying strain and rotation rates for the entire island. We use a modified version of Ward (1998) for calculating strain rates in spherical geometries. Our particular method considers three different types of weights: observational errors ( $W_o$ ), distance between the observation and the location of estimation ( $W_d$ ), and an additional weight to account for variable station density ( $W_s$ ). Each weight contributes equally to the inversion. The construction of  $W_o$  and  $W_s$  has been described in Ward (1998). Given the difficulty in interpreting strain rates calculated at using variable length scales at different positions, we choose to make separate strain maps, each with a fixed length scale used in the estimation procedure. This fixed scale approach results in variable numbers of observations used in our strain estimates as a function of space. This variability is reflected in companion error maps. We estimate  $W_s$  using the distribution of Voronoi cells associated with the geodetic network. The actual value  $W_s$  corresponds to the cell area associated with a given GPS station. We find that our approach provides more stable and interpretable strain estimates than previous studies, especially when stations are irregularly distributed or when we use larger spatial length scale of estimation. In either case, dense pockets of observations would dominate the strain estimates.

JSG01/07A/A01-007

1050

**INTERSEISMIC CRUSTAL DEFORMATION IN THE TAIWAN PLATE BOUNDARY ZONE (1993-1999)**

Shui-Beih YU, Long-Chen KUO, Ya-Ju HSU, Horng-Yue CHEN (Institute of Earth Sciences, Academia Sinica)

The island of Taiwan is situated in the plate boundary zone between the Eurasian and the Philippine Sea plates. As a consequence of plate interaction, there are highly active seismicity, rapid crustal deformation, and numerous active faults in and around Taiwan. The disastrous Chi-Chi earthquake (Mw 7.6) occurred on 21 September 1999. This event caused very large coseismic movements and significant transient postseismic deformation. Continuous and annually surveyed GPS data collected before the Chi-Chi earthquake from 1993 to 1999 are utilized to study the interseismic deformation in the Taiwan area. The horizontal and vertical velocity fields with respect to the Chinese continental margin are firstly estimated from temporal changes of station coordinates. Then the strain rates are calculated from velocity gradients taking into account the observational errors, distance between the observation and the location of estimation, and variable station density. The convergence across the Taiwan arc-continent collision zone is as high as 80 mm/yr and about 40% of the shortening is accommodated in the Longitudinal Valley area of eastern Taiwan, the suture zone of two plates. The western Taiwan is undergoing compressive tectonic stress with contraction rates of 10-40 mm/yr in the E-W to NWW-SEE directions. The Ilan Plain in northeastern Taiwan shows remarkable NW-SE extension associated with the opening of Okinawa Trough, while the significant NEE-SWW extension in the southern Central Range may be related to crustal exhumation. The lateral extrusion in the Kao-Ping area of southern Taiwan is also prominent. An uplift rate of up to 10 mm/yr is observed in the Central Range and the maximum subsidence of 70 mm/yr due to underground water withdrawal is found in the coastal area of southwestern Taiwan.

JSG01/07A/A01-008

1105

**CRUSTAL DEFORMATION IN EASTERN TURKEY CONSTRAINED BY GLOBAL POSITIONING SYSTEM MEASUREMENTS BETWEEN 1992 AND 2002**Mehmet Emin AYHAN<sup>1</sup>, Bahadır AKTUG<sup>1</sup>, Mustafa OCAK<sup>1</sup>, Coskun DEMIR<sup>1</sup>, Onur LENK<sup>1</sup>, Robert REILINGER<sup>2</sup> (<sup>1</sup>General Command of Mapping, <sup>2</sup>Massachusetts Institute of Technology)

To investigate crustal deformation in Eastern Turkey in the east of 35° E, we compute velocity field in a frame fixed to Eurasia from Global Positioning System (GPS) measurements between the years 1992 and 2002. The resulting velocity field reveals the decoupling of Anatolian plate from Eurasia and Arabia along dextral North Anatolian Fault (NAF) and sinistral East Anatolian Fault (EAF). Velocities indicate a westward motion of Anatolia and diffused deformation in Eastern Turkey between the Bitlis suture and the Caucasus. We derive a best fitting Euler vector of Arabia-Anatolia motion 35.18° ± 0.09°N, 38.14° ± 0.11°E, 1.40° ± 0.02°/Myr. The Euler vector gives about 7 mm/yr for an upper bound on left lateral slip on the EAF. We also compute the strain rate components. Dextral shear strain rates accumulating along the NAF indicate plate boundary deformation zone having a width of about 100 km. We obtain dextral shear strain accumulation extending from Karliova triple junction area to the east with a rate of 90 nstrain/yr around Karliova. We compute sinistral shear strain rates along the EAF between Türkoglu and east of Bingöl, reaching maximum of 70 nstrain/yr around Pötürge, within a relatively narrow plate boundary deformation zone. We reckon anticlockwise solid body rotation rates in Anatolia and plate boundary deformation zone along the EAF, and clockwise rotation along the NAF. Rotation rate is about -6°/Myr and 4°/Myr around Karliova and Pötürge respectively. Finally, dilatation rates reveal a general compressional regime in Eastern Turkey although we observe regional extensional areas.

JSG01/07A/A01-009

1120

**MEDITERRANEAN SEA LEVEL VARIATIONS, 1985-2002: ALTIMETRY VERSUS TIDE GAUGE DATA**Isabel VIGO<sup>1</sup>, David GARCIA<sup>1</sup>, Benjamin Fong CHAO<sup>2</sup> (<sup>1</sup>Dpt. Applied Mathematics, University of Alicante, Alicante, Spain, <sup>2</sup>Space Geodesy Branch, NASA Goddard Space Flight Center, Greenbelt, Maryland, 20771, USA.)

We study the sea level variabilities in the Mediterranean Sea, both in space and time, and focus on the complementarity of the two available data sources for sea level: tide gauge data and altimetry data. We will use the sea-surface height (SSH) data from TOPEX/Poseidon (T/P) for the periods 1992-2002 and Geosat data for 1985-1988, and examine selected tide gauge data along the Mediterranean coast and compare them with the closest T/P data point. Also included is a study on Mediterranean-specific oceanic general circulation models that are under development in terms of their applicability. Preliminary results indicate that the SSH rate of change in Mediterranean is about 3 times the global average during the past 10 years. The differences between long-term trends (or linear slopes) of the altimetry data and the tide gauge data are indications of vertical ground motion of the tide gauge location. Apart from possible systematic errors in both data sets (especially in tide gauges depending on the history of data collection) these differences potentially contain information about local deformation and, more importantly, tectonic motions in the region. We will also present a survey of available GPS measurements co-located with tide gauges, but in general the GPS time series are too short to be useful at the present time.

JSG01/07A/A01-010

1135

**GUADALUPE ISLAND GPS PRELIMINARY RESULT: IS THE PACIFIC PLATE RIGID?**Jose Javier GONZALEZ-GARCIA<sup>1</sup>, Joachim GENRICH<sup>2</sup>, Linette PRAWIRODIRDJO<sup>3</sup>, Duncan AGNEW<sup>4</sup>, Yehuda BOCK<sup>5</sup>, Ken HUDNUT<sup>6</sup> (<sup>1</sup>Seismology Dept., Centro de Investigacion Cientifica y de Educacion Superior de Ensenada, Baja California, <sup>2</sup>Scripps Institution of Oceanography, University of California, San Diego, <sup>3</sup>United States Geological Survey, Pasadena, California)

We present results from survey mode GPS data collected in northern Baja California and Guadalupe Island in the Pacific Ocean. This data were combined with data from continuous stations from Southern California Integrated GPS Network (www.scign.org, http://sopac.ucsd.edu); that includes CIC1, SPMX, CORX (Coronados Island) and recently GUAX (Guadalupe Island) in México. Altogether we have 4 sites on Guadalupe Island: GUAD and GAIR (1991-2002), RMGU (1999-2002), and GUAX (2001-2003). Solutions were derived in the International Terrestrial Reference Frame 2000 (ITRF2000) and computed with GAMIT software using global fiducial data from the International GPS Service. Station velocities were computed using a linear regression on the position time series. The motion obtained for sites on Guadalupe Island agree to within 1 mm/yr with a mean of 23.8 ± 1.0 mm/yr for the north component and -44.6 ± 1.1 mm/yr for the east. This result is very close to that of the NNIRNuvel 1-A model (23.1, -44.7) and is slightly lower than that predicted by Beavan et al. [2002] (25.2, -48.6), for a Guadalupe Island traveling on a rigid Pacific Plate. We compute a pole of rotation for the Pacific Plate using our results for CHAT, KOKB, KWJL,

MKEA, THTI and Guadalupe Island with the mean result: Lat.= 63.71° S, Long. = 109.25° E and angular velocity = 0.668°/Myr. The  $\chi^2$  for fitting a Pacific Plate pole with and without Guadalupe does not differ significantly. If the Guadalupe Island GPS preliminary result obtained here represents its secular motion, the Pacific Plate is rigid (<3 mm/yr), considering the uncertainties of plate tectonics on a spherical Earth (NNR 1-A) and that of the ITRF realization. This confirms the basic assumption made for Plate Tectonics by Morgan [1968]: "If the distances between Guadalupe Island, Wake Island and Tahiti, all within the Pacific block, were measured to the nearest centimeter and then measured again several years later, we suppose these distances would not change". Finally, when our ITRF2000 GPS result is rotated into a North America reference frame we obtain a "full" velocity field of 49.6 ± 1.0 mm/yr between Puerto Peñasco on the northeastern shoreline of the Gulf of California and Guadalupe Island. For the presentation we will include data for the first quarter of 2003.

JSG01/07A/A01-011

1150

**VISCOELASTIC DEFORMATIONS DURING A SEISMIC CYCLE AND OVER CYCLES AROUND A SUBDUCTION ZONE - SIMULATION FOR A REALISTIC SNRVEI EARTH**Shuheiki OKUBO<sup>1</sup>, Jun'ichi OKUNO<sup>1</sup>, Yoshiyuki TANAKA<sup>2</sup> (<sup>1</sup>Earthquake Research Institute, University of Tokyo, <sup>2</sup>Geographical Survey Institute, Japan)

Although there are many previous works to estimate crustal deformations around a subduction zone during one or over many repeated seismic cycles, they are not free from unrealistic assumptions to avoid intrinsic numerical difficulties; some ignore the earth's self-gravitation, some compressibility, and others radial stratification. We develop here a new recipe to compute post-seismic deformation in a realistic, spherically symmetric, non-rotating, visco-elastic, and isotropic (SNRVEI) earth. The calculation is done without the forementioned unrealistic approximations. The essential point of the new algorithm is to perform the Laplace inversion integration without evaluating contribution from the innumerable poles. Using this method, we present a complete set of the Green function, i.e. time variations of displacement, gravity, geoid height on the surface for 4 independent types of point dislocation: strike-slip on a vertical plane, dip-slip on a vertical plane, tensile faulting on a horizontal plane and tensile faulting on a vertical plane. As an earth model, we employ the 1066A together with the standard viscosity profiles. The result shows a diverse spatial pattern due to a viscous structure or a source depth. In particular, ratio of the source depth to the lithosphere thickness governs the evolution of the post-seismic deformation. Of particular interest is that the far-field deformation (epicentral distance > a few hundreds km) clearly reveals transient behavior. This makes a contrast to the near field deformation where coseismic change dominates. It follows that post-seismic gravity change might be detected with satellite missions because the wavelength exceeds 100 km, if a sufficiently large earthquake occurs. If the back-slip hypothesis holds at a subduction zone, integration of the Green functions over a finite fault plane allows us to compute both transient and secular displacement and gravity change. We shall compare the theoretical result with the observed secular uplift and gravity change at the Tokai region where a large earthquake is anticipated to occur in a near future.

JSG01/07A/A01-012

1205

**POSTSEISMIC DEFORMATION MODELING OF THE 1992 LANDERS, CALIFORNIA, EARTHQUAKE**Yuehua ZENG<sup>1</sup>, Yongge WAN<sup>2</sup>, Zhengkang SHEN<sup>3</sup> (<sup>1</sup>Seismological Lab, UNR and Institute of Earth Sciences, Academia Sinica, <sup>2</sup>College of Hazard Prevention, China Seismological Bureau, <sup>3</sup>Dept of Earth and Space Sciences, UCLA and Institute of Geology, China Seismological Bureau)

We model the postseismic deformation of the June 28, 1992 Mw 7.3 Landers earthquake to understand the fault zone rheology and the crust and upper mantle structure. GPS data have been collected periodically from a network of about 2-dozen stations located in the rupture zone and its vicinity since the earthquake. The data were processed to derive the deformation time series at the sites. To model the postseismic deformation we need to account for both secular and the earthquake induced deformation. A regional secular deformation model is developed based on the GPS data collected before the Landers earthquake and EDM data collected in 1970s-1980s. These data are inverted to fit a block-fault model and solve for fault slip rates along block boundaries beneath the locking depth. After removal of the secular effect, the observed deformation shows a "butterfly" pattern in general, mimicking the coseismic deformation but with much smaller amplitude and with less gradient from the epicenter to far field. The temporal pattern shows a relatively fast acceleration for the first couple of months, and a much longer secular trend afterwards. We model the postseismic deformation as a result of rheological response to the coseismic stress change in a layered crust and upper mantle. The coseismic stress change is produced using the coseismic slip model of the 1992 Landers earthquake by Wald and Heaton (1994). Our preliminary result suggests that two mechanisms operate simultaneously to produce the observed spatial and temporal patterns of the postseismic deformation: visco-elastic relaxation in the lower crust and rheological after-slip at the downdip of the coseismic rupture zone. We find that a model consisting of a 13-km thick lower crust with a viscosity of 10<sup>19</sup> pas, an upper mantle with a viscosity of 10<sup>20</sup> pas, and an after-slip at the downdip of the coseismic rupture equivalent to 5% of the coseismic moment release provides the best fit to the observation.

Monday, July 7 PM

Presiding Chair: T. Kato

JSG01/07P/A01-001

1400

**VARIATION OF STRAIN PROMOTED BY THE SLOW SLIP EVENT IN THE TOKAI REGION REVEALED BY THE CONVERTED STRAIN FROM GPS DATA**

Sumio YOSHIKAWA, Takeyasu YAMAMOTO (The Seismology and Volcanology Research Department, Meteorological Research Institute)

The slow slip event (SSE) detected by the GPS network (GEONET) of the Geographical Survey Institute has been growing up steadily in the southern coastal area of the central Japan, that is the Tokai region, since 2001. Appreciable changes corresponding to SSE are not yet observed by the borehole strainmeters of the Japan Meteorological Agency in the area. We evaluated space and time variation of the strain caused by SSE before we can detect it by the strainmeters. Use of strain has merits on evaluation of a localized event. That is, i) strain does not reflect a common displacement observed in a wide area, ii) strain is comparable directly with outputs of borehole strainmeters, and iii) the elastic strain caused by a source diminishes rapidly as compared with displacement, say, in inverse proportion to the cube of distance from it, which means easiness in estimating the source location. We used the GEONET data from 1997 to 2002 for strain analysis. Variation of the horizontal principal strains was calculated from daily changes in lengths and azimuths of three base lines in each triangle elements of GPS network. Spatial distribution of horizontal strain components was calculated from grid-data of displacement vectors transformed from the

original data using the GMT function (e.g. Wessel & Smith, 1998). Annual- and semi-annual variations estimated for the period from 1998 to 1999 were subtracted from the original data, and linear trends for the same period were also subtracted from them when it was necessary. According to the analysis, we could detect strain changes associating with SSE clearly. Expansion appeared in and around Hamanako region of the central part of the Shizuoka prefecture, and at the same time contraction was caused around Omaezaki and Atsumi regions in the east and west of Hamanako region, respectively. The peak of expansion is now moving northeastward and steadily growing up and the contraction is gathering intensity. The maximum principal contraction rates increase three or four times after the commencement of SSE in 2001. The total moment release estimated from the distribution of dilatation in the late 2002 becomes  $(1.3\sim 1.5) \times 10^{19}$ [Nm] and the moment magnitude becomes around 6.75. High concentration of the Coulomb fracture stress is seen in the eastern Tokai region.

#### JSG01/07P/A01-002 1415

##### MIGRATION OF ANOMALOUS CRUSTAL DEFORMATION IN TOKAI AREA, JAPAN

Masaru KAITZU, Shinzaburo OZAWA (Geography and Crustal Dynamics Research Center, Geographical Survey Institute)

Since early 2001, anomalous crustal deformation is being observed in Tokai area, central Japan. The deformation is supposed to be related to aseismic slow slip on plate interface. The event lasts already more than 2 years. The center of deformation seems to migrate as is the case in normal earthquake, though the deformation in Tokai area is quasi static. Temporal variation of horizontal deformation and upheaval suggests that the center of slip on the plate interface migrated from under Hamamatsu to northeast direction along the western edge of estimated source region of coming Tokai earthquake. The slip started at the northeast slope of ridge like feature of the plate boundary. As the direction of subduction of Philippine sea plate is toward north-north-west in this area, it is likely that the slip started here. After migration of center of slip, GPS station at Hamamatsu started to move in normal direction. Observational study of the process of this slow slip event will provide image of quasi-static analogue of seismic rupture process. Migration of deformation on the surface will be examined using time series of GPS station coordinates.

#### JSG01/07P/A01-003 1430

##### POSTSEISMIC DEFORMATION FOLLOWING THE 1997 UMBRIA-MARCHE (ITALY) MODERATE NORMAL FAULTING EARTHQUAKES

Abdelkrim Aoudia<sup>1</sup>, Alessandra BORGHI<sup>2</sup>, Riccardo RIVA<sup>3</sup>, Riccardo BARZAGHI<sup>2</sup>, Boudewijn AMBROSIOUS<sup>4</sup>, Roberto SABADINI<sup>1</sup>, Bert VERMEERSEN<sup>5</sup>, Giuliano PANZA<sup>1</sup> (SAND Group, Abdus Salam International Centre for Theoretical Physics & Dept. of Earth Sciences, University of Trieste, Trieste - Italy, <sup>2</sup>DIAR, Politecnico di Milano, Milan, Italy, <sup>3</sup>DEOS, Faculty of Aerospace Engineering, Delft University of Technology, Delft, Netherlands, <sup>4</sup>Dept. of Earth Sciences, University of Milan, Milan, Italy)

We combine aftershock strain mapping, GPS measurements and leveling profiles with forward modeling of viscoelastic relaxation to study the postseismic deformation of the 1997 Umbria-Marche (Central Apennines) earthquake sequence. We explore the feasibility of GPS monitoring of postseismic transients, for the first time in Italy, generated by shallow and moderate sources. Our data allow us to distinguish a preferred coseismic faulting model as well as insight into the rheology of the Central Apennines Earth's crust. The faulting model requires a listric geometry with most of the energy released in the lower half part of the elastic crust. The rheological model consists of an elastic thin upper crust, a transition zone of about  $10^{18}$  Pa s underlain by a low-viscosity lower crust, ranging from  $10^{17}$  to  $10^{18}$  Pa s. The postseismic deformation is, both distributed in the transition zone - lower crust and confined to the fault zone.

#### JSG01/07P/A01-004 1445

##### THE PRESENT-DAY TRANSIENT AND SECULAR DEFORMATION FIELD OF THE ANDEAN SUBDUCTION ZONE

Juergen KLOTZ<sup>1</sup>, Amir ABOLGHASEMI<sup>2</sup>, Klaus BATAILLE<sup>3</sup>, Rodrigo MATORANA<sup>4</sup>, Raul PERDOMO<sup>5</sup> (<sup>1</sup>GeoForschungsZentrum Potsdam, <sup>2</sup>Univ. de Concepcion, Chile, <sup>3</sup>IGM Chile, Santiago, Chile, <sup>4</sup>Univ. Nac. La Plata, Argentina)

GPS-observed crustal movements in the Southern and Southern-Central Andes are governed by different phases of the earthquake deformation cycle. Most of the transient deformation can be explained by inter-seismic, co-seismic, and post-seismic phases of interplate thrust earthquakes. The area of the great 1960 Mw 9.5 Chile earthquakes shows a pronounced post-seismic deformation 40 years after the event and a significant change in the displacement field with time. Secular crustal movements are derived by subtracting model velocities from observations. Along the Andes, the most obvious secular deformation signal is visible in the back-arc of the subduction where the Brazilian Shield underthrusts beneath the Subandean zone. Here, GPS observations suggest a slower back-arc convergence than geological rates. The analysis of the residual velocity field and strain rates within the fore-arc of the subduction indicates the presence of trench-perpendicular and trench parallel extension in accordance with geologic findings. Also, part of the transient elastic deformation might be transferred into permanent plastic deformation. Further insight into the plate boundary system comes from 3D FE-Models that we used to explain the present-day deformation.

#### JSG01/07P/A01-005 1500

##### THE NATURE OF EPISODIC SLIP ALONG THE NORTHERN CASCADIA MARGIN: REGULAR AND NOT-SO-SILENT

Herb DRAGERT (Geological Survey of Canada)

Data from continuous GPS stations across the northern Cascadia Margin have been re-analyzed and they reveal an intriguing regularity of transient movements on the deeper subduction interface underlying southern Vancouver Is. and the eastern Olympic Mountains. Surface motions at GPS sites in this region are characterized by a pronounced "sawtooth" displacement pattern reflecting elevated stress increase for a period of about 60 to 70 weeks followed by a two-week period of stress reduction during which motions are reversed. These reversals have been modelled by gradual slips of 2 to 4 cm on the deep subduction interface, down dip from the seismogenic zone. At a given GPS site in the region of detection, the transient surface displacements observed for successive slip events are strikingly similar in amplitude, direction, and duration, indicating a repetitive process within a confined location. The rates of strain accumulation between slip events also appear uniform, again suggesting a recurring process that is spatially confined. To date, this behaviour has not been observed in other subduction zones or even to the north or south of this geographic region. Examination of digital seismic records from the same area has revealed unique, non-earthquake-like, seismic signatures accompanying the slip events. These seismic signals,

similar in nature to those identified in the Nankai subduction zone, appear to have no spatial correlation with earthquake patterns in the region, but the source appears to correlate with the zone of repeating slip. Episodic generation of fluids from pulses of metamorphic dehydration may be responsible for both the slip and the seismic chatter, although details of the process are yet to be understood. The fact that similar slip events have not been observed elsewhere may be due to smaller slip signals combined with a lack of GPS coverage.

#### JSG01/07P/A01-006 1515

##### THE SEISMIC SIGNATURE OF TRANSIENT SLIPS ON THE CASCADIA SUBDUCTION ZONE

Garry ROGERS, Herb DRAGERT, Honn KAO, John CASSIDY (Geological Survey of Canada)

Repeated slip events have been detected on the deep interface of the northern Cascadia subduction zone by observing surface deformation on a network of continuous Global Positioning System sites. These slip events, originally characterized through their temporal and spatial surface displacement patterns, have now been found to have unique, non-earthquake, seismic signatures which have been detected by the digital seismic network monitoring the same subduction zone region. The observed tremor-like seismic signatures correlate temporally and spatially with the slip events over the past six years. The sources of these tremors appear to be coincident with, or overlie, the region of the subducting slab interface where transient slip is occurring, migrating with the progression of the slip. During the time-period between slips, this seismic tremor activity is very minor or non-existent. At the time of the slip events, the seismic activity is marked by pulsating bursts of activity lasting from a few minutes to a few hours for the duration of the slip event, usually about 10 to 15 days. The frequency content of the seismic signature, predominantly 1 to 4 Hz, is lower than the frequency content of nearby earthquakes, and most of the energy is in the horizontal components. These seismic signatures have a similar appearance to the deep tremor identified by Obara in the Nankai subduction Zone. However, the frequency of occurrence is different and accompanying slip events have not been identified in Nankai. These slip related seismic signals appear to have no correlation with the deep or shallow earthquake patterns in the Cascadia region. If the one-to-one correlation between transient slip and seismic signatures proves to be robust, then the tremor-like seismic signals can provide real-time indicators of the occurrence of slip. Since slip events on the deep slab interface increment the stress across the seismogenic zone, it is conceivable a slip event would trigger a larger earthquake on the locked subduction thrust. Consequently, the onset of tremor activity could lead to recognized times of higher probability for the occurrence of megathrust earthquakes in the Cascadia subduction zone.

#### JSG01/07P/A01-007 1530

##### INTERPLATE COUPLING DERIVED FROM THE GPS TRAVERSE ACROSS THE HINGE-LINE IN KII PENINSULA AND ITS IMPLICATION TO PRESEISMIC CHANGES IN GROUNDWATER LEVEL BEFORE THE 1946 NANKAI EARTHQUAKE

Manabu HASHIMOTO, Yasuhiro UMEMA, Kensuke ONOUE, Fumio OHYA, Yoshinobu HOSO, Kazutoshi SATO (Disaster Prevention Research Institute, Kyoto University)

The hinge-line in the south Kii peninsula, which is the boundary between uplift and subsidence due to the 1946 Nankai earthquake, can be related to the lower margin of the coupling zone. We established 10 GPS observation sites, which fill the gaps in the GEONET operated by GSI, along two lines nearly parallel to the relative motion between the Philippine Sea and Amurian plates. Resultant average spacing is 5~10km. We have repeated the campaign survey of this traverse across the hinge-line in the Kii peninsula using dual-frequency receivers since March 2001. The obtained velocities of observation sites are about 3cm/yr in the middle part of Kii peninsula and 4.5cm/yr at its southern tip, respectively, relative to the Amurian plate. Their directions are WNW. The gradient is almost linear, which suggests that the coupling zone is rather wide. We apply a dislocation model with a uniform slip to this observed velocity field in order to estimate interplate coupling beneath the Kii peninsula. Changing the width of the Ando's(1975) fault model, we compare the fitness of the theoretical displacement with the observed one. The calculation indicates that the original Ando's model is too narrow to represent the observed velocities. In order to explain the observed velocities in the middle Kii peninsula, we must double the width of the model fault. This implies the coupling zone between the subducting Philippine Sea and Amurian plates might be extended much deeper than the depth previously suggested from the thermal model and others. Groundwater level drops before the 1946 Nankai earthquake were reported in middle and south Kii peninsula and southern coastal region of Shikoku. We assume this change in Kii peninsula is caused by a preseismic slip on the fault plane or its deep extension, and perform forward calculation of dilatation. The deepest segments of the model faults by Sagiya and Thatcher (1999) produce dilation south of the hinge-line, which does not coincide with the distribution of wells of reported anomalous changes. This result suggests that preseismic slip must occur on the deeper extension beneath the middle Kii peninsula. The coupling zone derived from our GPS observation might be the source region of such preseismic slip.

#### JSG01/07P/A01-008 1605

##### TRANSIENT DEFORMATION BEFORE THE 2002 DENALI FAULT EARTHQUAKE, CENTRAL ALASKA

Jeffrey Todd FREYMUELLER, Hilary J. FLETCHER, Sigrún HREINSDÓTTIR, Hisashi SUITO (Geophysical Institute, University of Alaska Fairbanks)

Repeated GPS surveys in central Alaska document two sources of transient deformation prior to the 2002 Denali Fault earthquake. The first and most obvious is a large transient interpreted as a creep event on the Pacific-North America plate interface down dip of the seismogenic zone. This event began in 1998 and lasted for 2-2.5 years. The creep event produced large displacements at the surface, as large as ~10 cm total displacement. Based on dislocation and finite-element models, we interpret the source of the event to be accelerated creep on a patch of the plate interface roughly 100x150 km in size, with 15-20 cm of creep above the normal rate of plate motion (5.5 cm/yr). The large displacements caused by this event were centered well to the south of the Denali fault, but it caused measurable extensional strain normal to the Denali fault, which would have the effect of unclamping the fault and bringing it closer to failure. A second, more subtle transient event appears to have occurred near the epicentral region of the 2002 Denali fault earthquake between mid-2000 and mid-2002. Summer 2002 GPS surveys of sites near the Denali fault are systematically offset from the trend of the previous surveys, which were done from 1997-2000. West of the 2002 epicenter, the anomalous motion appears as an eastward displacement of 1-2 cm for sites south of and very close to the Denali fault. Out of all sites in central Alaska that were surveyed in 2002, only sites very close to the Denali fault deviate from their priortrends. If these displacements result from precursory slip, they do not appear to result from slip on the Denali fault, but might be related to slip on thrust faults such as the fault that initiated the Denali earthquake rupture.

**JSG01/07P/A01-009****1620****POSTSEISMIC DEFORMATION FOLLOWING THE 2002 DENALI FAULT EARTHQUAKE**

Jeffrey Todd FREYMUELLER<sup>1</sup>, Roland BURGMANN<sup>2</sup>, Eric CALAIS<sup>3</sup>, Andy FREED<sup>3</sup>, Evelyn PRICE<sup>1</sup>, Hilary J. FLETCHER<sup>1</sup>, Sigrún HREINSDÓTTIR<sup>1</sup>, Christopher F. LARSEN<sup>1</sup> (<sup>1</sup>Geophysical Institute, University of Alaska Fairbanks, <sup>2</sup>Department of Earth and Planetary Science, University of California, Berkeley, <sup>3</sup>Department of Earth and Atmospheric Sciences, Purdue University)

The November 3, 2002, Mw=7.9, Denali fault earthquake was the largest on-landstrike-slip rupture in the US since 1857. Geodetic measurements of the postseismic response triggered by this event are providing significant insight into postseismic deformation processes and lithospheric rheology. Data from campaign GPS sites show postseismic displacements up to 60 mm of horizontal motion over the first 11 days after the earthquake at near-field sites. These rates of motion are ~200 times the interseismic rates. Significant vertical displacements are also observed, and most sites everywhere within 50-75 km show significant postseismic motion within the first few weeks. Within two weeks after the earthquake, we installed 10 continuous GPS sites in the region of the rupture. Displacements of these sites over the next six weeks are as large as ~45 mm. The data show evidence for a very rapid pulse of deformation within the first few days to two weeks, followed by a slower rate, although this slower rate is still ~50 times the interseismic rate. We will report on the latest results and models to explain the rapid postseismic deformation we have observed.

**JSG01/07P/A01-010****1635****POST-EARTHQUAKE DEFORMATION FROM INSAR AND STRAINMETERS CORRELATED TO PORE-PRESSURE TRANSIENTS**

Paul SEGALL<sup>1</sup>, Sigurjón JÓNSSON<sup>2</sup>, Rikke PEDERSEN<sup>3</sup>, Kristján AGUSTSSON<sup>4</sup>, Grimur BJORNSSON<sup>5</sup> (<sup>1</sup>Geophysics Stanford University, <sup>2</sup>Earth and Planetary Sci, Harvard University, <sup>3</sup>Nordic Volcanological Institute, Reykjavik, Iceland, <sup>4</sup>Iceland Meteorological Office, Reykjavik, Iceland, <sup>5</sup>National Energy Authority, Reykjavik, Iceland)

Despite considerable effort, it has proven difficult to distinguish between competing models of postseismic deformation based on direct field observations. Here we present unique measurements consisting of satellite radar interferograms, borehole strainmeters, and water level changes in geothermal wells following two magnitude 6.4 earthquakes in the South Iceland Seismic Zone. The deformation recorded in the interferograms cannot be explained by either afterslip or visco-elastic relaxation but are consistent with pore-elastic rebound in the first one to two months following the earthquakes. This interpretation is confirmed by direct measurements which show rapid (1-2 month) recovery of the earthquake induced water level changes. In contrast, the duration of the aftershock sequence is projected to be ~3.5 years, suggesting that pore-fluid flow does not control aftershock duration. However, because the surface strains are dominated by pore-pressure changes in the shallow crust, we cannot rule out a longer pore-pressure transient at the depth of the aftershocks. The aftershock duration is consistent with models of seismicity rate variations based on rate and state dependent friction. A borehole dilatometer located ~3 km from the June 17, 2000 rupture recorded a large (~10 microstrain) compression followed by a roughly one month strain relaxation (dilation). For an instantaneously introduced fault in a poroelastic medium the postseismic volume strain is predicted to increase as the induced pore pressure gradients relax, that is the strain increases with the same sign as the instantaneous coseismic response. However, because there is no fluid exchange with the dilatometer, the strain measured by the strainmeter is not in general the same as the strain in the surrounding rock. More generally, the instrumental strain is related to the strain within the rock far from the borehole and the change in fluid pressure. If the rock strain is held constant, the dilatometer response relaxes from the undrained to the fully drained states. Two dimensional poroelastic solutions demonstrate that the observed strainmeter response is qualitatively consistent with theory.

**JSG01/07P/A01-011****1650****STRESS-INDUCED MIGRATION OF SEISMIC SCATTERERS ASSOCIATED WITH THE 1993 PARKFIELD ASEISMIC TRANSIENT**

Fenglin NIU<sup>1</sup>, Paul G. SILVER<sup>2</sup>, Robert M. NADEAU<sup>3</sup> (<sup>1</sup>Department of Earth Science, Rice University, <sup>2</sup>Department of Terrestrial Magnetism, Carnegie Institution of Washington, <sup>3</sup>Berkeley Seismological Lab., Univ. of California, Berkeley)

A major goal of seismologists is to identify temporal variations in the seismic structure of the crust in response to stress changes near a fault zone. One of the approaches to this problem is to compare waveforms generated by repeat earthquakes, which have nearly the same location and mechanism and produce nearly identical seismograms when recorded at the same station. We have chosen to measure the difference in waveforms of several tight clusters of repeat events that occurred on the Parkfield segment of the San Andreas Faultland recorded by a network of borehole strainmeters in the same area (HRSN). An exceptionally well-documented aseismic transient took place on this segment around the beginning of 1993, and we wanted to determine whether it produced observable structural changes in the medium as well. We used two parameters: the lag time,  $\tau(t)$ , and the decorrelation index,  $D(t)$ , to characterize the difference between two seismograms at elapsed time,  $t$ . The lag time  $\tau(t)$  is evaluated at the maximum of the cross correlation,  $C_{\text{corr}}$ , and the decorrelation index  $D(t)$  is defined as  $1 - C_{\text{corr}}$ . We have found a significant change in a particular section of the S-wave coda between two sets of events (1988-1992 and 1993-1997), which appears as a spike in both  $\tau(t)$  and  $D(t)$ . We have run a series of tests which strongly suggests that the observed changes in waveforms are not due to variations in earthquake location (verified by relocating the events from the observed S-P times at different stations) nor due to a uniform change of the background medium. Instead, the likeliest explanation is that there has been a change in the location of distinct scatterer(s) by a few meters. We utilize a simple procedure for locating spatially those scatterers whose properties have changed in time. For each station, we first construct a differential seismogram  $\delta s(t)$  by taking the difference of the average of the pre- and post-1993 seismograms. For noise-free seismograms,  $\delta s(t)$  will consist only of energy from any scatterers whose propagation characteristics (travel time or amplitude) have changed, while an unchanged scatterer will be removed by this procedure. We then performed an nth-root ( $n=1$ ) stack of the amplitude,  $A(x)$ , of  $\delta s(t)$  from each station, stacking on the predicted arrival time of a candidate scatterer originating from location  $x$ . This function reaches a maximum about 2 kilometers to the southeast of the cluster and at about 3 km depth. The migration of the scatterer(s) occurred at seismogenic depth and therefore is less likely due to the environmental effects. As the difference is almost absent in the P-wave coda, we infer that the scatterer(s) is probably related to the redistribution of fluid-filled fractures which are more efficient in scattering S-wave energy compared to P. The location and timing of this change in the medium strongly suggests that it is a manifestation of the 1993 Parkfield aseismic transient. As such, it likely represents the stress-induced redistribution of fluids in the crust at seismogenic depths.

**JSG01/07P/A01-012****1705****INSAR-BASED SEISMISITY STUDY OF SOUTH-WESTERN AUSTRALIA EARTHQUAKE PRONE ZONE**

Diana POLONSKA<sup>1</sup>, Clive COLLINS<sup>2</sup>, Phil CUMMINS<sup>3</sup>, Craig J.H. SMITH<sup>4</sup>, Linlin GE<sup>1</sup>, Chris RIZOS<sup>1</sup> (<sup>1</sup>Satellite Navigation & Positioning Group, School of Surveying and Spatial Information Systems, The University of New South Wales, Sydney NSW 2052 Australia, <sup>2</sup>Geoscience Australia GPO Box 378 Canberra ACT 2601 Australia)

An analysis of intraplate seismicity within a seismically active area of Western Australia using spaceborne Synthetic Aperture Radar Interferometry (InSAR) was made. Despite the limitations imposed by availability and timing of satellite passes, ground relief and instabilities influencing the radar signal, the demonstrated resolution and accuracy of InSAR make this technique feasible as a tool for exploring regional tectonics. The manifestations of regional tectonics in earthquake prone areas are highly site-dependent so SAR images at fine spatial and temporal scales and information on low intensity earthquake events were incorporated within the analyses. High precision georeferencing of the input layers was assisted by GIS technology. Preliminary findings of this study suggest that there is correlation between crustal deformations and local patterns of geological origin. In particular, the concentration of hypocentres of the earthquakes along the direction of interferometric fringes, corresponding to the chosen time interval, can clearly be identified. This indicates that clustering in time and space of shallow seismic events can be traced using InSAR-based analysis, and that the method can be used to improve our understanding of intraplate earthquakes. Combined with the precise positioning of ground reference points using GPS for InSAR data processing, new insights into transient crustal deformations studies can be expected. Using this approach, the determination of the magnitude of strain rates and orientation of crustal stress associated with earthquake generation is possible.

**JSG01/07P/A01-013****1720****SEASONAL VARIATION OF SCALE OF GEONET NETWORK AND ZTD BIASES**

Yuki HATANAKA (Geographical Survey Institute, Japan)

The seasonal signals in the time series of the site coordinates were evaluated based on the new solutions of GPS Earth Observation Network (GEONET) of GSI, Japan, which were obtained by the reanalysis with an improved and uniform analysis strategy by Hatanaka et al. (2003). There are spatially systematic features in the seasonal motion of the solutions. A dominant part of them is the seasonal change of the network scale of 6.4 ppb, which accounts about 70 % of the whole power of the seasonal signals for the horizontal components. The comparison of the tropospheric zenith total delays (ZTD) estimated in the GEONET analysis with those derived from radiosonde data of Japan Meteorological Agency also shows the seasonal variation of the bias in the ZTD estimates. The sense and magnitude of the scale variation roughly agree with those expected from the variation of ZTD bias. The residuals of the seasonal signals, after removing the systematic components, do not show correlations with the direction of plate motions around Japan, although they still show spatially coherent signals, parts of which are explained by the snow loading effect proposed by Heki (2001) and by the neglect of tropospheric gradient (Hatanaka, 2003, presented in this assembly).

**JSG01/07P/A01-014****1735****SEASONAL CRUSTAL DEFORMATION IN JAPAN: FINAL SYNTHESIS**

Kosuke HEKI (Div. Earth Rotation, National Astronomical Observatory)

Strong annual signatures found in the Japanese dense GPS array were partly caused by seasonal scale changes of possibly non-crustal origin, but significant part is caused by real seasonal crustal deformation caused by change of various surface loads. Recently, Heki (2001) studied the northeastern Honshu area and found snow load the most important source to drive seasonal crustal deformation there. In the present study, I extend the investigation to the whole country and evaluate every potential contributor including snow, atmospheric pressure, soil moisture, water storage in dams, and non-tidal ocean loads. Most of these effects can be calculated a-priori using various meteorological and geophysical data and models, although their reliabilities vary among items. I compare synthesized annual GPS site displacement curves with the observed ones and discuss their differences, to be attributed to factors yet to be modeled, such as dependence of snow depth on ground elevations (meteorological sensors do not necessarily represent the whole country), water storage changes related to agricultural activities, etc..

**Tuesday, July 8 AM**

Presiding Chair: K. Heki

**JSG01/08A/A01-001****0900****THE KINEMATICS OF ANATOLIA: SPECTRAL ANALYSIS OF CONTINUOUS GPS DATA**

Ali TURKEZER, Onur LENK, Ali Ihsan KURT, Semih ERGINTAV (Geodesy Department, General Command of Mapping)

Three-dimensional geodetic networks supported by continuous GPS data are capable of yielding valuable tools in order to account for regional realization of International Terrestrial Reference Frame (ITRF) and monitoring deformations of the solid earth in the area of interest. Turkish Permanent GPS Network (TPGN) stations consisting of 16 stations, played an utmost role in the analyses and the surveying stage of Turkish National Fundamental GPS Network (TNFGN), which was completed in 2000, by providing 24-hour continuous data in connection with International GPS Service (IGS) global stations. Being in Alpine-Himalayan collision zone, Turkey and its surrounding have very active tectonic nature characterized by the collision of African, Arabian and Eurasian tectonic plates. Such a phenomena made use of TPGN data with a great extent in the evaluation of both secular variations of the positions of the stations and the abrupt changes of the positions associated with the earthquakes. At the preliminary stage of TURPEGN analyses, the horizontal velocity values have been obtained in ITRF96 and they have been used in order to constrain the inter-seismic velocity field of the area. Also, the acute displacements during 17 August 1999 Izmit (Mw=7.5) earthquake yielded the information for co-seismic velocity field as well as post-seismic process utilizing the data from more dense stations. The analysis of five stations operating before the earthquake showed the actual co-seismic displacements with a magnitude of 53 cm and -33 cm in east and north components respectively near the epicenter of the earthquake and the post-seismic behavior of the region which has an exponential function delay time of about 70 days and 50 days in East and North components respectively. The analysis includes 900 days beginning from 1999 day 185 till the end of year 2001. Also, the periodical components of the time series have been investigated using power spectrums. Finding the index coefficient of about 1 revealed that there is significant periodicity on the obtained series. The periodicity analysis of time series

indicates the meaningful annual periodicity in height components and about 300 days in north and east components. It is anticipated that time series evolution and the signal analyses of TPGN stations in the long-term period excluding abrupt events will help to monitor the kinematics of the region as well as the stability of the stations.

**JSG01/08A/A01-002****0915**

#### DEFORMATION IN YELLOWSTONE'S UPPER GEYSER BASIN: ARE DEEP PRESSURE FLUCTUATIONS DRIVING FLUID FLOW AT OLD FAITHFUL GEYSER?

Anahita A. TIKKU<sup>1</sup>, David C. MCADOO<sup>2</sup>, Mark S. SCHENEWERK<sup>3</sup>, Ralph C. TAYLOR<sup>4</sup> (<sup>1</sup>Lamont-Doherty Earth Observatory of Columbia University, <sup>2</sup>NOAA Laboratory for Satellite Altimetry, <sup>3</sup>Give 'em an Inch Inc., <sup>4</sup>National Park Service volunteer)

We present the first absolute gravity and global positioning system (GPS) time-series analysis from a geyser basin. Observations were made in 2000, 2001, and 2002 over periods of 2 to 10 days within 200-800 meters from the Old Faithful geyser in the Upper Geyser Basin of Yellowstone caldera located in Wyoming, USA. Over the course of three campaigns we observed consistent large vertical motions of up to 10 cm over a large areal extent (up to 600 m) and corroborative gravity anomalies of up to 15 microGals occurring on the timescale of hours to days. Deformation on this timescale has been previously undetected in active magmatic or hydrothermal systems. We postulate that the vertical motions are due to fluctuations in pressure at depth in the hydrothermal-magmatic system. We also find that the gradient of the large vertical motions are correlated with deviations in the time between eruptions at Old Faithful geyser and postulate that this is caused by lateral fluid flow into and out of the geyser conduit. The correlation is significant because Old Faithful's eruptions are periodic and predictable. Changes in the vertical load will either eject or inject water into the geyser conduit if the conduit is treated as a permeable zone of intensely fractured rock with high compressibility surrounded by a less permeable rock matrix with a lower compressibility. Changing the volume of water in the geyser conduit changes the interval between eruptions assuming this time is controlled by the volume of water available for an eruption. Our new work is important as it reveals the processes of fluid movement both in the larger scale geyser basin hydrothermal-magmatic system and at the scale of individual geysers.

**JSG01/08A/A01-003****0930**

#### SIGNAL OF ATMOSPHERIC PRESSURE LOADING IN LASER RANGING DATA

Toshimichi OTSUBO, Toshihiro KUBO-OKA, Tadahiro GOTOH, Ryuichi ICHIKAWA (Communications Research Laboratory)

Ranging precision of satellite laser ranging technology has improved to 5-7 mm in a single shot basis and 1 mm or even better in a normal point (compressed data) basis. Compared to other microwave-based geodetic techniques, laser observation has an advantage in accurate model of propagation delay, which must result in accurate determination of a vertical component of station coordinates. Variation of a vertical component due to atmospheric loading effect has been researched throughout the last decades, and is typically 1 cm peak-to-peak or less. The effect was already seen in GPS and VLBI data, and we found it also possible to detect the vertical variation as a function of atmospheric pressure from recent LAGEOS laser ranging data. In our orbit analysis software "concerto", a new adjusting parameter, height per pressure, was implemented. The parameter was estimated simultaneously with other parameters such as orbits and station coordinates, and we obtained -0.1 to -0.5 mm/hPa for major 12 laser ranging stations in the world.

**JSG01/08A/A01-004****0945**

#### RESPONSE OF WELL WATER LEVEL TO HEIGHT CHANGE IN HAMAOKA, SHIZUOKA PREFECTURE, JAPAN

Norio MATSUMOTO, Makoto TAKAHASHI, Ryu OHTANI, Naoji KOIZUMI (Geological Survey of Japan, AIST)

Height change of BM 2595 in Hamaoka town, Shizuoka prefecture, Japan as referenced to BM 140-1 in Kakegawa city has been observed to detect an uplift prior to the anticipated Tokai earthquake since 1962 by the Geographical Survey Institute. The height of BM 2595 has subsided persistently about 5 mm/year accompanied with about 1 cm of seasonal fluctuation. Our three observation wells and subsidence meter are located around BM 2595. In order to evaluate response of well water level to the height of BM 2595 quantitatively, we compare well water levels and subsidence meter data with the height data. Depths of the observation wells are 55 m, 210 m and 270 m, respectively. The subsidence meter was installed the 210 m well. This instrument can measure the vertical length between the bottom of the 210 well and the ground surface. During the period from 1985 to 2002, well water level in the 55 m well decreased 3.5 m accompanied with 1.2 m of seasonal change, and well water level in the 270 m well changed one third of that in the 55 m well. On the other hand, 4 mm subsidence together with 0.5 mm of seasonal change was observed by the subsidence meter in the same period. The subsidence observed by the subsidence meter is obviously caused by the decrease in well water level at the 55 m well, because the data of subsidence meter changes several days after the changes in the well water level. A seasonal adjustment analysis is applied to the observed height and corrected height eliminating the subsidence change, respectively. Persistent subsidence rate and amplitude of seasonal change in the corrected height are reduced by 10% and 5% in the observed height, respectively.

**JSG01/08A/A01-005****1000**

#### A STUDY ON SEASONAL VARIATION OF LEVELING DATA IN OMAEZAKI REGION

Tetsuro IMAKIIRE<sup>1</sup>, Minoru TAJIMA<sup>2</sup> (<sup>1</sup>Geography and Crustal Dynamics Research Center, Geographical Survey Institute(GSI), <sup>2</sup>Chuo College of Technology)

Geographical Survey Institute(GSI) has been carrying out leveling survey in Omaezaki region, four times per year, since 1981. This leveling survey revealed that Hamaoka(BM2595) is subsiding about 5mm/yr referred to Kakegawa(BM140-1). Though the rate of subsidence is steady for long term, it is pointed out that seasonal variation is laying over the trend. The amplitude of seasonal variation is as much as 1cm(peak to peak). Various hypothesis has been proposed for the origin of this variation. As GPS data does not show such significant seasonal variation, it is suspected that the origin of this variation would be a factor which is uniquely related to leveling observation itself. One of such doubtful sources is atmospheric refraction. This study deals the statistic parameters of this seasonal variation for 13 unit sections, which is the leveling route from one bench mark to another neighboring bench mark. If the atmospheric refraction is the cause of seasonal variation, two characteristics would be expected. 1)The amplitude of variation is proportional to the height difference of two bench marks. 2)The phase of variation is reverse between ascending sections and descending sections. We examine 13 sections of the leveling route from Kakegawa to Sagara(SF1354) to estimate the long term trend and seasonal variation using least square method. We compared AIC(Akaike Information Criterion) values

calculated from two different types of the models to examine which model is preferable. One is a linear model, which means the subsidence rate is constant and seasonal variation is random. Another model is linear function plus sine function with one year cycle, which means seasonal variation can be modeled by sine curve. We found the latter model is better than linear model in nine of the thirteen sections. However we also found linear model is preferable for other four sections. The phase of variation in the most sections agree with each other. The residual from linear trend is positive in summer and negative in winter. This means the phase does not relate whether the section is ascending or descending. The amplitude of seasonal variation seems to have no relation between the height difference in each section. Therefore the current result is negative for concluding that seasonal variation is related to atmospheric refraction.

**JSG01/08A/A01-006****1015**

#### ENVIRONMENTAL EFFECTS AND OCEAN TIDAL LOADING IN TILT DATA OF NOKOGIRIYAMA OBSERVATORY

Steffen GRAUPNER<sup>1</sup>, Hiroshi ISHII<sup>2</sup>, Gerhard JENTZSCH<sup>1</sup>, Shigeru NAKAO<sup>3</sup>, Adelheid WEISE<sup>1</sup> (<sup>1</sup>Institute for Geosciences, University of Jena, Germany, <sup>2</sup>Tono Research Institute for Earthquake Science, Japan, <sup>3</sup>Earthquake Research Institute, University of Tokyo, Japan)

Nokogiriyama Observatory of Tokyo University, Earthquake Research Institute (ERI), established in summer 1993, is situated on Boso peninsula at the eastern side of the entrance to Tokyo Bay, located at the foot of a hill at about 600 m distance east from the coastline. It comprises underground galleries and a building for data acquisition. In connection with several neighbouring observatories the purpose is the monitoring of seismicity and crustal deformation in the earthquake area around Tokyo, as well as the testing of new sensors. We compare the results of the ERI water tube tiltmeters and the borehole tiltmeter No. 106 of the Askania type, in April 1997 installed in a 10 m deep borehole inside the gallery close to the ERI tiltmeters. It operated with only a small drift until June 1999. The analyses show a good correspondence between the signals of the two instruments, not only regarding the tides but also concerning meteorological effects like air pressure changes and precipitation, predominant in E-W direction. Due to the short distance to the sea we observe strong ocean loading signals disturbing the body tide parameters. Amplitude factors are amplified up to values of 10 and phases are shifted between 150° and 360° (N-S) and 40° and 120° (E-W), respectively. Loading computations were carried out using the ocean tidal model of the National Astronomical Observatory NAO99b and NAOJb (global and for the Japanese area, resp.), and the software GOTIC2 based on GOTIC. The loading signals in E-W are bigger than in N-S by a factor of about 2 to 3. In N-S the observed loading is explained by the models by about 60% to 90%, whereas in E-W the fit is between 40% and 50%. We do not assume that the existing discrepancy between computed and observed loading tides are due to a misfit of the models; we rather suggest another explanation: The short distance to the sea is a great drawback, esp. for tilt, because the loading of such small scale loading is not possible. Further, we must take into account strain-tilt coupling due to the strong ocean loading and the rough topography, which may be the cause for the slight differences in the tidal parameters.

**JSG01/08A/A01-007****1050**

#### ON THE SEASONAL VARIATIONS OBSERVED IN THE GSI SOUTH PACIFIC GPS NETWORK SOLUTIONS

Hiroshi MUNEKANE, Shigeru MATSUZAKA (Space Geodesy Research Division, Geographical Survey Institute, Japan)

A significant seasonal variability was found in the coordinate solutions from the Geographical Survey Institute (GSI) South Pacific GPS Network, which covers a wide range of the Pacific Ocean. The ocean mass loading is a very plausible cause for this variability since the ocean surrounds every site. In this presentation, the characteristics of the variations are shown, and the effect of the ocean mass loading is evaluated. The seasonal variability is seen in almost all sites. It is found that dominant frequencies are annual and semi-annual from the spectrum analysis, though the amplitudes vary from year to year. The amplitudes are strongest in the vertical components, and annual amplitudes reach 1cm at the maximum. The annual amplitudes and phases are changing systematically from site to site, though there is no clear latitude dependence. As for the IGS stations, Dong et al. (2001) already presented the amplitudes and phases of the annual variations. Those are consistent with our results. As a preliminary estimate for the effect of the ocean mass loading on the coordinate variability, the admittance between amplitudes of annual signals in coordinates and tide-gauge data nearby is estimated. First, the amplitudes of annual signals in the nearest tide-gauges are estimated. The tide-gauge data archived by Univ. Hawaii Sea Level Center are used for this purpose. After correction for atmospheric loading effect using IB model, steric-height correction is done assuming the linearity between SST and steric height. Then linearity between annual amplitudes of tide level change and annual variability of the vertical coordinates is examined. It is found that there exists a linearity between them, and the admittance factor is estimated to be 0.1mm/(annual vertical displacement)/1mm/(annual sea level change). However, to evaluate the ocean mass effect more quantitatively, it is necessary to employ the green-function method with altimetry data. In the presentation, the synthetic variability calculated with the green function method will be presented, and its ability to explain the spatio-temporal variations observed in the coordinates is discussed.

**JSG01/08A/A01-008****1105**

#### STABILITY OF GEODETIC REFERENCE POINTS IN PERMAFROST REGION - A CASE STUDY

Hans-J. KUEMPEL<sup>1</sup>, Marcus FABIAN<sup>2</sup> (<sup>1</sup>Leibniz Institute for Applied Geosciences (GGA), <sup>2</sup>Section of Geophysics, Geological Institute, University of Bonn)

Comparison of station velocities of VLBI and GPS reference points at the Ny-Ålesund Space Geodetic Observatory, Spitsbergen has questioned the stability of the basements of the antennas over time spans of several years. Due to its high latitude of almost 79° N, the site is of crucial importance for the world geodetic reference frame. The two antennas which became operational some ten years ago are roughly 100 m apart from each other. They have been fixed to concrete basements, erected in the permafrost ground, at 40 m above sea level. At the test site, the subsoil is melting down to 3 or 4 meters during the arctic summer. The basement of the VLBI antenna which has a diameter of 20 m is more massive than that of the GPS antenna. Both the basements are in contact with the bedrock, consisting of a folded sedimentary hard rock at several meters depth. In near distance from the basements, the terrain falls steeply to the Kongsfjord. From August 2001 up to October 2002 we have operated three continuously recording tiltmeters of resolution 0.1 microrad on the tops of the basements. The purpose of this campaign was to monitor micro-movements over a period where relevant changes in ground frost conditions take place which might affect the stability of the antenna basements. By using tiltmeters we are unable to see any translational movements e.g., in vertical direction; rather we can infer from the presence of significant tilt movements that the stability of the basement is reduced. Several tests with various configurations of instrumental set-ups were conducted in the initial phase of the

## INTER-ASSOCIATION

campaign. Analysis of these tests has revealed that the magnitude of tilt induced through repositioning of the VLBI antenna is of order 10 microrad. The dominant part of this tilting appears to be internal deformation (bending) of the concrete basement. Inspection of the 13 months long recordings suggests stable conditions for the basement of the GPS antenna at Ny-Ålesund, on the 50 microrad level. For the basement of the VLBI antenna, the situation is less clear. There is evidence for permafrost-driven instability in May - July 2002 at this place, however, with some doubts remaining due to partial malfunctioning of the single tiltmeter that was operated here. The instrument was exposed to large temperature variations and presents questionable temperature sensitivity in one of its components. Still, adopting conservative estimates, the total observed tilt signal reflects rotational movements of the entire basement, which do not exceed 1 millimetre (per length of the basement).

### JSG01/08A/A01-009 1120

#### ON THE VERTICAL CRUSTAL MOTION AND GRAVITY AT METSÄHOVI, FINLAND

Heikki J. VIRTANEN, Joel J. AHOLA (Finnish Geodetic Institute)

Metsähovi is a geodetic laboratory with a large number of observations program: permanent GPS, satellite laser ranging, DORIS beacon, absolute gravity and superconducting gravimeter. We present results on vertical crustal motion as seen in the gravity data of the superconducting gravimeter GWR T020 at Metsähovi station for years 1994 - 2002. The refined tide free gravity have corrected by known seasonal hydrological effect, such as groundwater level changes. We have associated temporal height variations with the loading effects of the atmosphere and of the nearby Baltic Sea at the distance of 15 km. Theoretical loading calculations using Green's functions formalism are performed for both vertical motion and gravity and the modelled gravity is compared with a large amount of observational data. For Baltic Sea loading effects we have used data of the nearest tide gauge in Helsinki at the distance of 30 km as well as data of several tide gauges around the Baltic. The loading by atmosphere has been computed using a detailed surface pressure field from HIRLAM (High Resolution Limited Area Model) for North Europe. The gravity data are congruent with loading calculations. The loading effect of the Baltic Sea can exceed 10 mm and the deformation by atmosphere 25 mm. However, the effects partly oppose each other. Though the sensitivity of superconducting gravimeter is far of other co-located instruments, the loading effects of air pressure and Baltic Sea level can be large enough affect the observations with other techniques. We show comparisons between variation in GPS height and in gravity observations for some shorter periods. We discuss the results of the loading calculations and achieved improvements in gravity residuals.

### JSG01/08A/A01-010 1135

#### THE SOLID EARTH RESPONSE ON CHANGING ICE LOADS IN WEST GREENLAND INFERRED FROM REPEATED GPS OBSERVATIONS

Reinhard DIETRICH, Axel RUELKE, Mirko SCHEINERT (TU Dresden, Germany)

Bedrock areas in the marginal regions of ice sheets are especially suited to study vertical crustal deformations caused by the viscoelastic response of the Earth on changing ice loads. Our research concentrates on the ice-free part of West Greenland. In this region, a GPS network consisting of 14 stations was established and observed in 1995. A complete reobservation was carried out in 2002. We will describe the design of the network as well as the observation strategy, which aims especially at a control of systematic effects and at a high accuracy of the height determination. The data analysis has been carried out using the Bernese Software v4.2. Since we were looking for height changes the analysis was concentrated on single baselines. The achieved accuracies will be discussed. Finally, the obtained results will be compared with the present knowledge and model predictions of recent crustal uplift rates in West Greenland.

### JSG01/08A/A01-011 1150

#### DERIVING NEW CONSTRAINTS ON GLACIAL LOAD HISTORY BY GEODETIC OBSERVATIONS IN DRONNING MAUD LAND, ANTARCTICA

Mirko SCHEINERT<sup>1</sup>, Erik IVINS<sup>2</sup>, Reinhard DIETRICH<sup>1</sup>, Axel RUELKE<sup>1</sup> (<sup>1</sup>TU Dresden, Germany, <sup>2</sup>Jet Propulsion Laboratory, USA)

A variety of geodetic and glaciological observations in central Dronning Maud Land (DML), East Antarctica provide information that may constrain both the recent isostatic crustal uplift pattern and the recent and past ice sheet configuration and flow character. Using GPS observation campaigns in 1996 and 2001, it is possible to bound regional postglacial uplift rates. These geodetic data, when coupled with additional constraints on recent and past ice mass changes, allow a self-consistent glacial load history to be investigated. We examine a spectrum of viable load histories and compute the associated isostatic deformation signatures. Our limited goal is to reconcile the modelled signals and the observations and to define what further observational strategies might be undertaken to simultaneously constrain combinations of DML load history and the deep solid earth rheological response.

### JSG01/08A/A01-012 1205

#### VERTICAL MOTION AND GLACIAL ISOSTATIC ADJUSTMENT IN THE GREAT LAKES REGION

Alexander BRAUN<sup>1</sup>, C.K. SHUM<sup>2</sup>, Laramie V. POTTS<sup>2</sup>, Chung-Yen KUO<sup>2</sup>, Andrew TRUPIN<sup>1</sup> (<sup>1</sup>Byrd Polar Research Center, The Ohio State University, <sup>2</sup>Department of Civil and Environmental Engineering and Geodetic Sciences, <sup>3</sup>Oregon Institute of Technology)

The deglaciation cycles of the Laurentide ice sheets have dominated the Glacial Isostatic Adjustment (GIA) in the Great Lakes region in the Northern United States/Canada. However, beside the GIA induced deformation, it has been shown that tectonic processes and mantle flow have a significant contribution on the deformation of the lithosphere. A separation of these two signals is necessary before assimilating deformation data to constrain Earth parameters, like the viscosity, or the ice loading history. The Great Lakes region is covered by a suite of different geodetic sensors allowing to quantify the vertical motion at particular sites. A combination of GPS, absolute gravity, satellite altimetry and water-level gauges provide independent means to measure present-day crustal motion. Absolute gravity measurements have been carried out for almost a decade at some sites west of the Great Lakes. The technique to use satellite altimetry data and water-level gauges to measure vertical motion has been validated by comparison with vertical motions from the BIFROST project in Fennoscandia. The derived results are highly accurate and can also be obtained in regions, where permanent GPS is not available. In general, the vertical motion in the Great Lakes region shows uplift in the Northern part, while the Southern part, namely Lake Erie and Lake Michigan, is subsiding. Since the maximum Southern extend of the Laurentide ice sheet was located in that particular area, analyzing the present-day deformation can deliver valuable constraints on Earth parameters. The visco-elastic response at the former ice margin due to deglaciation shows a significantly different sensitivity to viscosity compared to the former center of the ice sheet or the far field. Here, the visco-elastic response is

especially sensitive to the uppermost mantle viscosity. The Great Lakes area is therefore an excellent opportunity to study these specific parameters, which are difficult to constrain in the central uplift regions, where the signal is largest, but spatially uniform. Vertical motions in the Great Lakes region from multiple observations (GPS, GIA models, altimetry-water level gauges) are presented together with results of the separation of the tectonic and GIA induced signals. Multi-resolution analysis of gravity data using wavelets has been employed to find spatial and spectral characteristics. These characteristics help to identify regions, where tectonic or GIA influence dominates the vertical motion signal. GIA modeling with assimilation of vertical motion observations has been carried out in order to get improved constraints of GIA parameters. The model results obtained so far are presented together with results of geodetic observations to estimate spatial distribution of vertical motion in the Great Lakes region.

## JSG01-Posters

Tuesday, July 8

### SECULAR, TRANSIENT AND PERIODIC CRUSTAL MOVEMENTS AND THEIR GEOPHYSICAL IMPLICATIONS (IAG, IASPEI)

Location: Site D

Tuesday, July 8 PM

### JSG01/08P/D-001 Poster 1400-001

#### STRAIN DISTRIBUTION AROUND THE HANAORI FAULT IN KINKI DISTRICT OF JAPAN BY DENSE GPS NETWORK

Fumio OHYA, Kunihiro SHIGETOMI, Yoshinobu HOSO, Kajuro NAKAMURA (Disaster Prevention Research Institute, Kyoto University)

We have constructed a dense GPS network around the southwest half of the Hanaori fault in Kinki district, Southwest Japan since 1997. This fault is one of the major active faults in Japan. The surface trace of the fault is about 45km long and the slip direction is right lateral inferred from some geological evidences, but ongoing creep on the fault surface is not recognized on the outcrop. On geological point of view, central Kinki area forms a triangular shape named as "Kinki Triangle" by Huzita (1962). The Hanaori fault is a part of northwest border of the Triangle. On seismological point of view, the northwest side of this fault is Tamba highlands, where the seismic activity has increased after the Hyogo-ken Nanbu Earthquake (Jan.17,1995, M7.2). And the result of the triangulation surveys over a century revealed the strain contrast around the fault. Surveys in our dense GPS network were started motivated by two interesting points, one is the cause of the contrast in various data, such as geological, seismological and geodetic. The second point is earthquake prediction on this fault. The analysis of the coordinates of the permanent stations in GEONET, which is national GPS array in Japan operated by GSI, proved high strain rate zone from Awaji Island, located at southwest of Kobe, to Niigata at the Japan Sea coast. The northwest border of "Kinki Triangle" is located in this zone and also the Hanaori fault is. The mechanism causing this zone is not obvious and the information on strain distribution in this zone is necessary to reveal the mechanism. Our network consists of 17 newly constructed observation points and the data are analyzed including those at neighboring GEONET stations and some existing stations of Kyoto University. We operate continuously single or dual frequency receiver at four stations of new stations and have made epoch observations twice a year in the other stations. A GEONET station whose seasonal variation in their coordinates is smallest in the surrounding area is decided as a reference point in the analysis. The displacement field referred to the reference point reveals the clockwise rotation. We will finally present the strain distribution in this network. The strain distribution in space is mainly contractive and the dominant direction of the strain is NW-SW direction. But obvious discontinuity in strain cannot be found.

### JSG01/08P/D-002 Poster 1400-002

#### INTER-PLATE COUPLING BENEATH THE NE JAPAN ARC INFERRED FROM 3 DIMENSIONAL CRUSTAL DEFORMATION

Yoko SUWA, Satoshi MIURA, Akira HASEGAWA, Toshiya SATO, Kenji TACHIBANA (Tohoku University)

NE Japan is located at a typical subduction zone, and is a seismically very active region where large interplate earthquakes have occurred repeatedly. The nation-wide network of GPS observation (GEONET) recently constructed enables us to investigate the crustal deformation in detail. Based on data obtained by this network, interplate coupling has been studied by inverse methods (e.g. Nishimura et al., 2000). Because of relatively poor accuracy in the vertical component of displacements, however, they estimated model parameters by weighting the horizontal components largely, and sometimes encountered the inconsistency between calculated vertical displacements and observed ones. In this study, we devise a new model for interplate coupling by means of 3D displacement field to explain not only horizontal components but vertical ones. We used data of continuous GPS stations operated by GSI and Tohoku University from 1997 to 2001, and the data was analyzed using the Precise Point Positioning (PPP) technique of GIPSY/OASIS-II in order to derive vertical displacements more reliably. We assumed each displacement component as a linear function of time to estimate the velocity. Obtained result shows that vertical displacements near the Japan Sea coast show uplift, while those near the Pacific Ocean coast show subsidence. This characteristic pattern of vertical deformation is in good agreement with the result of leveling survey operated by GSI, which indicates that vertical components of the velocity derived by GPS are reliable and can be used as the data of the inverse method. In this study, we used a geodetic inversion method, GDBYS, developed by Yabuki and Mitsuura (1992). Obtained result shows that strong coupling is estimated in two areas, off Tokachi and off Miyagi, which correspond to the northern asperity of the 1968 M7.9 Tokachi-Oki earthquake, and to the asperity of the 1978 M7.4 Miyagi-Ken-Oki earthquake, respectively. The depth of the aseismic front is seismologically estimated to be 50-60km, and the region shallower than this depth is regarded as the coupled zone of the plate boundary (e.g. Igarashi et al., 2001). The back-slip distribution derived from 3D displacement field in this study, however, extends down to about 100-120km depth. One possible cause for this may be the existence of a transition zone, where the coupling rate decreases from about one at about 60 km depth to zero at around 100km depth, due to the subduction of old and cold oceanic slab.

JSG01/08P/D-003 Poster 1400-003

**TECTONICS IN THE KINKI DISTRICT, JAPAN**

Kunio FUJIMORI (Graduate School of Science, Kyoto University)

A GPS array with about 1,000 stations (GEONET) is operating in Japan. The GPS data obviously show secular crustal deformation in the Japan island. When homogeneous strain was removed from observed strain field, spatial distribution of local crustal deformations can be found. Based on daily coordinate data of the GPS stations in the center part of the Kinki district, the E-W and N-S components of GPS horizontal displacements were reduced by 0.04 mm/km/year and 0.02, respectively. As a result, a fine boundary appeared in displacement vector distribution. On the northwest side of the boundary the vectors are small, and on the southeast side the vectors to the west are large. The vectors show a right lateral movement of about 3 mm/year on the boundary. A vertical movement of about 3 mm/year is seen too. Therefore, it is thought that the boundary is a creep fault with a share zone of about 20km in width. The fault will extend from the Akashi strait to the north part of the Chubu district through the north Biwa lake. In addition, it is recognized that historical large earthquakes ( $M \geq 7$ ) occurred in the fault neighborhood and that the fault crosses a lot of active faults. The existence of this creep fault will mean that a giant shear fracture is progressing slowly in the center part of the Japan island, the Kinki and Chubu districts, under the E-W compression. It is said also that the large earthquakes in Western Japan were generated before and after the great earthquakes on the Nankai trough. When the great earthquake are compared with the historical large earthquake along the creep fault at occurrence time, it seems that the cycles of the large earthquake occurrences along the creep fault were reset by every other great earthquake on the Nankai trough. It is thought that earthquakes of M7 class can be predicted if continuous observation stations for crustal deformation are arranged along the creep fault because strain changes before earthquakes were observed at the stations which were located on this creep fault.

JSG01/08P/D-004 Poster 1400-004

**SPATIO-TEMPORAL DISTRIBUTION OF INTERPLATE COUPLING IN SOUTHWEST JAPAN DEDUCED FROM INVERSION ANALYSIS**

Takeo ITO, Manabu HASHIMOTO (RCEP, DPRI, Kyoto University)

From the viewpoint of long-term forecasts of great earthquakes, it is important to clarify the accumulation process. In order to clarify the accumulation process of tectonic stress, one strategy is to perform an inversion analysis using the available crustal deformation data. The crustal deformation data contain useful information about the spatio-temporal distribution of slip on the plate interface. We try to obtain the spatio-temporal distribution of the strength of interplate coupling from geodetic data such as leveling, triangulation and trilateration, and GPS surveys during recent 100 years in SW Japan. To evaluate this spatio-temporal distribution on the plate interface, we develop a new inversion method. This inversion method can treat the long-term crustal deformation data, the earthquake cycle and the stress relaxation of the viscoelastic asthenosphere. In our inversion method, the spatio-temporal slip rate distribution is expressed by the superposition of basis functions (B-spline functions of one degree in time domain and bi-cubic B-spline functions in space). Therefore, we can deduce the amount and direction of slip rate, and their temporal change by determining the coefficients of each basis function. We used the dislocation theory in viscoelastic body to calculate displacement rates at each observation points from slip rates on the plate interface. We also apply prior information about the smoothness of spatio-temporal distribution of slip rates. We construct a highly flexible model in which relative importance between observed and prior data is controlled by hyperparameters. To determine the most optimal hyperparameters, we used ABC. Therefore, we can uniquely determine the spatio-temporal distribution of slip rates. From this analysis, we obtain afterslips in the deeper part of the plate interface following the 1946 Nankaido earthquake at postseismic stage. The maximum afterslip is found beneath central Shikoku, and the total afterslip is about 1.0m. The slip deficit rate at interseismic stage is 5-6 cm/year in the N45W-N70W direction, which is almost consistent with the relative plate motion between the Philippine Sea and the Amurian plates. A strongly coupled region is found in the shallower portion than 30 km, and the slip deficit rate takes its maximum at the depth of about 20 km. The interplate coupling is very weak on the plate interface deeper than 30 km. If we assume recurrence time of interplate earthquakes to 92 years, the predicted amount of coseismic slip may reach about 6m off Shikoku and about 3m off Kii peninsula.

JSG01/08P/D-005 Poster 1400-005

**A MODEL WITH RIGID ROTATIONS AND SLIP DEFICITS FOR THE GPS DERIVED VELOCITY FIELD IN SOUTHWEST JAPAN**

Sou NISHIMURA, Manabu HASHIMOTO (Research Center for Earthquake Prediction, Disaster Prevention Research Institute, Kyoto University)

In order to know kinematic tectonics of southwest Japan, GPS derived velocity field is analyzed. It consists of two factors; the one is the elastic deformation caused by slip deficits on the locked portion along the block boundary, and the other is rigid motion of regional tectonic blocks (or plates). Therefore rigid motions cause significant errors to the estimation for slip deficits. For example, the velocity field in southwest Japan cannot be fully explained only by a model with slip deficits. Residuals in such model imply the influence of E-W collision between southwest Japan and northeast Japan and the backarc spreading along the northern extension of the Okinawa trough. We interpret the velocity field in southwest Japan by a superposition of the elastic deformation caused by slip deficits and rigid motions. Based on strain rate field and crustal seismicity, we apply a model with 3 blocks (Inner Arc, Outer Arc, and the northern Ryukyu) and slip deficits along the block boundaries. Some interesting features of southwest Japan are revealed: (1) westward motion of the outer arc relative to the Amurian plate and the inner arc, (2) southward motion of the northern Ryukyu block relative to the Amurian plate, (3) small right lateral slip deficits along the boundary at the latitude 32°N in southern Kyushu, (4) small left lateral slip deficits along the Median Tectonic Line and the Beppu-Shimabara Graben, (5) slip deficit rates on the plate interface smaller than in the case that rigid rotations are not considered, (6) clockwise deflection of the direction of slip deficits from that estimated in the case that rigid rotations are not considered.

JSG01/08P/D-006 Poster 1400-006

**CRUSTAL DEFORMATION OF THE NE JAPAN ARC AS DERIVED BY CONTINUOUS GPS OBSERVATIONS**

Toshiya SATO, Satoshi MIURA, Yoko SUWA, Akira HASEGAWA, Kenji TACHIBANA (Research Center for Prediction of Earthquakes and Volcanic Eruptions, Graduate School of Science, Tohoku University)

A dense GPS network was established in 1997 around Ou Backbone Range (OBR), northeastern Japan, by deploying 9 new continuous GPS stations so as to complement

sparse portions of GPS Earth Observation Network (GEONET) operated by Geographical Survey Institute of Japan (GSI). This observation network is aimed to investigate the present surface deformation and to understand the relationship between the occurrence of intraplate earthquakes and the deformation process of the island-arc crust. Our GPS data are analyzed using a precise point positioning technique of GIPSY/OASIS-II. Coordinates of the GEONET stations have been supplied in daily SINEX files by GSI. Obtained results of vertical displacements show slight upheaval near the Japan Sea coast, while subsidence near the Pacific Ocean coast. This overall pattern is in good agreement with the result obtained from the leveling surveys operated by GSI. In addition, the subsiding rates in the region between 39.0N and 39.6N are slightly larger than the surrounding regions. This may be related to the strain accumulation in OBR. Producing grid data of horizontal displacement velocities and taking spatial derivatives, we can draw a map of strain velocity distribution. The result shows that a region between 38.8N and 39.8N in OBR demonstrates notable concentration of EW contraction. The region coincides with the area of active seismicity and includes the focal areas of 1896 (M7.2), 1962 (M6.5), and 1970 (M6.2) events. Observed strain is too large to explain by a total moment release of earthquakes that occurred in the same period as the GPS observations. There must be some possible sources of the strain concentration: viscoelastic deformation due to the large earthquakes, or aseismic slip along the deeper extension of active faults.

JSG01/08P/D-007 Poster 1400-007

**TECTONIC CREEP OF THE ATOTSUGAWA FAULT SYSTEM, INFERRED FROM GPS OBSERVATION**

Yuki MATSUURA, Akira TAKEUCHI (Department of Earth Sciences, Toyama University)

The Atotsugawa fault system (AFS) consisting of a series of NE or ENE striking right-lateral strike-slip faults, such as the Atotsugawa fault, Ushikubi fault, and Mozumi-Sukenobe fault, is the most active structure in the northern Hida region of central Japan. Previous studies had been conducted on the fault system, and revealed high seismicity of micro earthquakes along the fault trace, for example. Recent geodetic studies have suggested the creep movement of Atotsugawa fault, the main fault of the AFS, probably. But, so far, laser ranging across the fault only shows the creep movement near surface on the central portion of the Atotsugawa fault. It is not clear whether creep movement on the other fault of AFS is possible, and depth of creeping. In this study, in order to reveal nature of creep movement of area inserted into the fault system, we analyzed the GPS data around the AFS, from both Geographical Survey Institute of Japan, and the Atotsugawa GPS array observation points of Nagoya University. In a data of period from April 24 1997 to August 31 2002, the solution results in creep movement of the AFS: (1) the results show right-lateral creep movements occurring on both the Atotsugawa fault and the Ushikubi fault. (2) All observation points in central and eastern areas between the Atotsugawa and Ushikubi faults show clockwise rotation, suggesting one rigid block of between the two faults. (3) Furthermore, for a rate ingredient of the perpendicular displacement to the fault trace of the AFS, it shows that the Atotsugawa fault is possessed of bigger distortion than the Ushikubi fault. Lastly, (4) it is possible that Atotsugawa fault system might extend northeastwards, based on the displacement of eastern end region of the AFS. This study shows an interesting result of rotational displacement of area between the Atotsugawa fault and Ushikubi fault. But to reveal the detailed feature of this area, we will install additional observation points.

JSG01/08P/D-008 Poster 1400-008

**CURRENT DEFORMATION AT THE ITOIGAWA-SHIZUOKA TECTONIC LINE IN CENTRAL JAPAN DETECTED BY GPS**

S. Jason ZHAO, Y. KANEDA (Japan Marine Science &amp; Technology Center)

The Itoigawa-Shizuoka Tectonic Line (ISTL) represents the boundary between the Amurian and North American plates in central Japan. Geological investigation reveals that it is a left-lateral strike-slip fault with a motion rate of 3-10 mm/yr. Results from Paleo-seismological study show that at least three events occurred in 224-186 A.D., 150-334 A.D., and 839-189 B.C., respectively, and the left-lateral coseismic slip during the last earthquake is about 6-9 m (Okumura and Imura, EOS, 76, No. 46, F363, 1995). Although there are more than 40 permanent GPS stations near or around ISTL, there is no direct assessment available for the current motion of ISTL. Crustal deformation in the region is dominated by subducting Pacific (43-50 mm/yr) and Philippine Sea plates (73-79 mm/yr), so that the deformation of small magnitude (<10 mm/yr) associated with active faults has been masked. In this study, using GPS observations and geometry of subducted slabs as constraints, we first construct a three-dimensional kinematic model to simulate the subduction of the Philippine Sea plate at the Suruga and Sagami troughs and the Pacific plate at the Japan trench. Then, we determine local deformation by removing the regional deformation associated with plate subduction from the GPS observations. As a result, relative motion between two flanks of ISTL is clearly exposed. In northern Kanto, the west-southwestward motion of GPS stations indicates the motion of the North American plate relative to the Amurian plate. The distinct boundary between two different types of motion trend revealed by GPS clearly demonstrates the current motion of ISTL. An inversion analysis of observed surface deformation for active segments on the ISTL indicates that the motion of ISTL in the north has been mostly accommodated by its NE branch with a right-lateral strike-slip, which could be connected to the Nagano fault system. The upper part (depth < 15 km) of the central segment of ISTL is locked, whereas slip at the lower part of the crust accommodates the relative motion between the Amurian and North American plates in the region. Deformation in the south is compounded with interplate deformation and displays a complex pattern. Since the horizontal width of locked middle segment of ISTL is large (~100 km), its capability of generating large earthquakes is relatively low comparing with a narrow locked fault zone. However, inland earthquakes could occur in the surrounding area of the ISTL due to stress localization at the margin of locked zone. <http://www.geocities.com/subduction99/index.html>

JSG01/08P/D-009 Poster 1400-009

**CURRENT PLATE KINEMATICS IN NORTHEASTERN ASIA BY GPS DATA: INTERACTION OF AMURIAN OKHOTSK, EURASIA AND NORTH AMERICAN PLATES**Hiroaki TAKAHASHI<sup>1</sup>, Evgenii I. GORDEEV<sup>2</sup>, Vilory F. BAKHTIAROV<sup>3</sup>, Vasily E. LEVIN<sup>1</sup>, Nikolay F. VASILENKO<sup>4</sup>, Alexei IVASHCHENKO<sup>5</sup>, Mikhail D. GERASIMENKO<sup>6</sup>, Nikolay SHESTAKOV<sup>7</sup>, Vladimir A. BORMOTOV<sup>8</sup>, Minoru KASAHARA<sup>1</sup> (1Institute of Seismology and Volcanology, Hokkaido University, 2Kamchatka Experimental and Methodical Seismological Department, Russian Academy of Sciences, 3Institute of Marine Geology and Geophysics, Russian Academy of Sciences, 4Institute of Applied Mathematics, Russian Academy of Sciences, 5Institute of Tectonics and Geophysics, Russian Academy of Sciences)

A continuous GPS network has been established in far eastern Russia with more than 15 new stations to investigate the current plate kinematics in northeastern Asia. We succeeded to install new sites in Kamchatka, Komandorski Island, Sakhalin, Khabarovsk and Primorskiy regions. These data have helped to illustrate the crustal deformation associated with the plate interactions in this region. We recognized the independent eastward motion of the Amurian plate relative to the Eurasian plate, which generates the plate convergence along

## INTER-ASSOCIATION

the eastern margin of Sea of Japan with 2-3cm/yr and gives new framework of plate kinematics around Japan. The station at Komandorskiy island clearly indicates full coupling of the transform boundary between the North American and Pacific plates. Stations at Kamchatka have been secularly affected by the subducting Pacific plate and both coseismic and post-seismic rebound have been recorded. Our data so far does not yet indicate whether the Okhotsk plate exists or not because the Kamchatka region is very complex and the data observation period has been too short to separate the effects of the plate subduction along the Kamchatka trench. Combined with the IGS network, our GPS data will give geodetic constraints needed to establish plate kinematics in northeastern Asia, Bering and Alaska regions.

**JSG01/08P/D-010** Poster **1400-010**

### ON THE CRUSTAL DEFORMATION STUDY FROM PERMANENT GPS STATIONS IN KOREA

Hong-Sic YUN, Jae-Myoung CHO (Department of Civil & Environmental Engineering, Sungkyunkwan University)

The Korean peninsula is 200~300km wide and 1000 km long from north to the south, protruding from the eastern part of the Eurasian continent. The Korean peninsula extends southward from northeast Asia and has a close affinity with the Asian continent, especially with the Northeast China paraplatform, in geological and tectonic setting. In historical documents many destructive earthquakes were recorded, especially in 6th~7th, 13th and 16th~18th centuries. They remarked that steady accumulation of crustal strain and its sudden release by earthquakes occurred repeatedly in the Korean peninsula during those times. In Korea, National Geography Institute (NGI) has established fourteen permanent GPS sites in a continuously operating reference station network since 1995 for the purpose of cadastral surveying, geodynamic application and atmospheric research. The purpose of this study the characteristics of strain pattern by using permanent GPS stations in Korea in terms of seismic activity and tectonics. In this study the GPS network is composed of fourteen permanent GPS stations. Each of the analyzed fourteen stations has at least 3 years of continuous data during 1999 and 2002. The data were analyzed using the GIPSY-OASIS II. For the solution of baseline vectors we designed the triangulation network which consist of fourteen stations. One baseline was allocated to each ten day and ten daily solutions were computed for each baseline. Allocation of one baseline per ten days ensured that separate baseline solutions were independent. We could calculate horizontal strains from the difference of the mean baseline vectors of ten daily solutions between the time span of three years, if they had enough accuracy for the present strain calculation. The main characteristics of the strain change during the three years in Korea obtained from the present study are revealed that the mean rate of the maximum shear strain change is 0.122 $\mu$ /yr and the direction of the principal axis is about 85°. The mean rate of dilatation is also -0.004 $\mu$ /yr. The GPS network composed of fourteen stations in Korea shows localized deformation with maximum shear oriented NNE-SSW and compression deformation from negative dilatation. This mean rate of maximum shear strain is nearly one third of the mean rate of Japan deduced from the data of the revision survey of the first order triangulation net. Considering the relationship with the results of present research, there is a clear difference in the direction of the axis between the Korean peninsula and the East sea side of Chugoku district of Japan, notwithstanding the similarity in the seismicity and the strain rate in the both areas. This gives a strong likelihood of the existence of a certain tectonic line between the southern part of the Korean peninsula and the Chugoku district, Japan.

**JSG01/08P/D-011** Poster **1400-011**

### CRUSTAL DEFORMATION ALONG PLATE BOUNDARY OF TAIWAN

Chi-Ching LIU (Institute of Earth Sciences, Academia Sinica)

Geodetic monitoring, including precise leveling, trilateration, tidal gauge station, and GPS, have been conducted for two decades along the eastern coast of Taiwan. These geodetic networks covers several significant tectonic regimes such as the Ryukyu trench-arc system, the Okinawa Trough north of the arc, and the collision boundary between the Philippine Sea Plate and the Eurasian plate. The Ilan Plain which located at the southwest continuation of the Okinawa Trough, show that the whole basin tilted to the east at a rate of 0.44  $\mu$ radian/yr. The subsiding rate is faster at the center axes of the trough with rate of 20 mm/yr. At south bound of the basin, the subsidence was episodic, and was controlled by the local seismicities. Both precise leveling and GPS results show that the southern edge of the plain has been opening clockwise with rate of about 1  $\mu$ radian/yr, and the process is still going on. The Hualien area right above the subduction zone experienced several episodic uplift during the period of study. Uplifts of several decimeters were observed as coseismic or postseismic events. Evidences from both sea level observation and precise leveling also indicated fast uplifting of 20cm during the six month period between two major earthquakes in this area. For the hundred km long coast along the collision boundary show a consistent overall northward tilting rate of about 0.2  $\mu$ rad/yr. There are several events occurred during the last two decades which caused some significant elevation changes in the local area, but the overall tilting rate is still kept constant. Uplift rate derived from the morphology of the marine terraces and their dates also shows similar tilt pattern with rate of about 0.1  $\mu$ rad/yr. However the rates derived from the marine terraces, which indicate the average uplift rate for the past thousands of years, are only about half of the rate derived from precise leveling in the past two decades. Borehole strainmeters and dense continuous GPS network are deployed in this area, and an integrated geodetic network will cover this plate boundary as part of the Plate Boundary Observatory of Taiwan in the next few years.

**JSG01/08P/D-012** Poster **1400-012**

### NICOYA, COSTA RICA, TRANS-PENINSULA GPS EXPERIMENT AND INTER-PLATE COUPLING

Takeshi IINUMA<sup>1</sup>, Marino PROTTF<sup>2</sup>, Koichiro OBANA<sup>3</sup>, Shin'ichi MIYAZAKI<sup>1</sup>, Victor GONZALEZ<sup>2</sup>, Rodolfo VAN DER LAAT<sup>2</sup>, Teruyuki KATO<sup>3</sup>, Yoshiyuki KANEDA<sup>1</sup>, Enrique HERNANDEZ<sup>2</sup> (<sup>1</sup>Earthquake Research Institute, University of Tokyo, <sup>2</sup>Observatorio Vulcanológico y Sismológico de Costa Rica, Universidad Nacional, <sup>3</sup>Institute for Frontier Research on Earth Evolution, Japan Marine Science and Technology Center)

We have been carrying out a GPS (Global Positioning System) observation project in Nicoya peninsula, Costa Rica, since 2001. Costa Rica is located in the western margin of the Caribbean plate, and the Cocos plate is subducting beneath the Caribbean plate from the Middle American Trench. The convergent rate between these two plates is about 90mm/yr in this area. Because of this rapid convergence, large earthquakes often occur at the western coast of Costa Rica. The Nicoya subduction segment in northwestern Costa Rica has ruptured with large earthquakes in 1853, 1900 and 1950. Recently, two large earthquakes occurred around this peninsula (Mw 7.0 in 1990 to the southeast and the 1992 Mw 7.6 off Nicaragua to the northwest). There is a clear seismic gap, the "Nicoya seismic gap" between the rupture areas of these two earthquakes. In the Nicoya seismic gap, a strong coupling of the two plates is manifested by low background seismicity, the sharp edge of aftershock zone of the 1990 and 1992 earthquakes (Protti *et al.*, 1995), and the northeastward

movement of the Nicoya peninsula recorded with GPS observations (Lundgren *et al.*, 1999). Protti *et al.* (2001) estimates that a Mw=7.5 earthquake is likely to occur in the Nicoya seismic gap. Since Nicoya peninsula lies above this gap, GPS observations in this peninsula provide invaluable data for various studies about the seismic coupling, the up dip and down dip extends of the seismogenic zone and the potential earthquake. Thus we started a new GPS survey program in Nicoya peninsula in 2001 by Observatorio Vulcanológico y Sismológico de Costa Rica, Universidad Nacional (OVVICORI-UNA) and Japan Marine Science and Technology Center (JAMSTEC) with support of the Japan International Cooperation Agency (JICA). Seven new benchmarks for GPS campaign observations were installed completing a 10 sites transect across Nicoya peninsula (Obana *et al.*, 2002). In 2002, the project was progressed by OVVICORI-UNA, JAMSTEC and Earthquake Research Institute, University of Tokyo (ERI) as a cooperative operation of JICA. The second campaign observation was held during the period from September 23, to October 12, 2002, and we obtained displacement vectors from the data. We will be presenting the results of GPS campaign observations and results from one-dimensional inversion analysis about inter-plate coupling using obtained displacement data.

**JSG01/08P/D-013** Poster **1400-013**

### DETECTION OF RECENT TECTONIC MOVEMENTS AT THE WESTERN PART OF NORTH ANATOLIAN FAULT ZONE (NAFZ) BY GEODETIC TECHNIQUES

Haluk OZENER, Asli Garagon DOGRU, Onur YILMAZ, Bulent TURGUT, Onur GURKAN (Department of Geodesy, KOERI, Bogazici University)

Turkey, having a long history of destructive earthquakes, is located in the Alpine-Himalayan seismic belt. In the past years, many researchers have focused on the activity in the North Anatolian Fault Zone (NAFZ) which is one of the most active fault zones in the world. Since 1972 geodetic studies have been concentrated at the Western Part of NAFZ. The region that has a high risk of earthquakes is about 150 km east of Istanbul with a high density of population and industrial infrastructure. The aim of these geodetic studies is to detect crustal deformations in this area. Three microgeodetic networks that are at Izmit with 10 points, Sapanca with 7 points, and Akyazi with 10 points on NAFZ have been established in order to monitor crustal displacements by Geodesy Department of Kandilli Observatory and Earthquake Research Institute (KOERI) of Bogazici University. These microgeodetic networks were constructed to control the Izmit-Mekece fault zone, the Izmit-Sapanca fault zone and their intersection area, the Mudurnu fault zone. The first period observations were performed by using terrestrial methods in 1990 and these observations were repeated annually until 1993 by using total-station and electromagnetic distance-meter instruments. Since 1994 GPS measurements have been carried out at the temporary and permanent points in the area and the crustal movements are being monitored. Horizontal deformations which have not been detected by terrestrial methods were determined from the results of GPS measurements. During the recent 3 years after the August 17, 1999, M=7.4, Izmit Earthquake that caused extreme damage in the region, many investigations have been pursued. One of them is an international project performed with the collaboration of MIT, Turkish General Command of Mapping, Istanbul Technical University, TUBITAK Marmara Research Center and Geodesy Department of KOERI. In this project, GPS campaigns have been performed at least twice a year at distributed 49 points that spread over Marmara region. During these surveys, another network with 6 points has been formed by using 2 points from each 3 microgeodetic networks on NAFZ with appropriate coverage and geometry. These points have been connected by GPS observations to monitor the deformations. This expanded microgeodetic network has been occupied with Istanbul-Kandilli continuous GPS point (KANT). This study reports the evaluation of data from expanded microgeodetic network observations.

**JSG01/08P/D-014** Poster **1400-014**

### 3-D VISCOELASTIC FEM MODELING OF POSTSEISMIC DEFORMATION CAUSED BY THE 1964 ALASKA EARTHQUAKE, SOUTHERN ALASKA

Hisashi SUITO<sup>1</sup>, Jeffrey T. FREYMUELLER<sup>1</sup>, Steven C. COHEN<sup>2</sup> (<sup>1</sup>Geophysical Institute, University of Alaska, Fairbanks, <sup>2</sup>Geodynamics Branch, NASA's Goddard Space Flight Center)

To complement previous modeling efforts to understand the postseismic deformation following the 1964 Alaska earthquake, we are implementing a three-dimensional viscoelastic model using the Finite Element Method. Rapid postseismic uplift reached as large as 125 cm, was observed on the central part of the Kenai Peninsula over the 35 years following the earthquake. Recent precise GPS observations show heterogeneous plate coupling, and a vigorous ongoing postseismic response to the 1964 earthquake. Past models of the postseismic deformation have focused on afterslip models because earlier viscoelastic-only models did a poor job at predicting the cumulative uplift observations, but this might be due to unrealistic assumptions for the model geometry. We are working toward a realistic 3D viscoelastic model that, in concert with afterslip models, can be used to understand how much each component contributes to the total postseismic deformation. We must develop a model with a realistic three-dimensional structure, viscoelastic response, and coseismic slip distribution. The rupture distribution was highly non-uniform, with most of the moment being released by two separate asperities. The largest moment release occurred offshore and beneath the Prince William Sound and the eastern Kenai Peninsula. The other moment release occurred beneath Kodiak Island, and much less slip occurred in the area between these two asperities. We will report the results of two-dimensional models with layered structure, with a dipping subducting slab and very low dip fault. We will generalize these models to three dimensions, and evaluate which aspects of the model are most important for predictions of total uplift and present deformation rates. We compare these simpler models with the results of realistic three-dimensional model.

**JSG01/08P/D-015** Poster **1400-015**

### SECLAR AND TRANSIENT CRUSTAL MOVEMENTS IN THE 1964 ALASKA EARTHQUAKE SUBDUCTION ZONE

Steven Charles COHEN<sup>1</sup>, Jeffrey FREYMUELLER<sup>2</sup>, Chris LARSEN<sup>3</sup>, Hisashi SUITO<sup>3</sup>, Chris ZWECK<sup>3</sup> (<sup>1</sup>Geodynamics Branch, Goddard Space Flight Center, <sup>2</sup>Geophysical Laboratory, University of Alaska Fairbanks, <sup>3</sup>Alfred-Wegener-Institut)

Precision leveling surveys, tide gauge measurements, and GPS observations conducted over the four decades since the 1964 Great Alaska earthquake have revealed a temporally and spatially complex pattern of crustal deformation. In the years immediately following the earthquake, rapid uplift occurred in the region that subsided coseismically. Initially the uplift rate exceeded 150 mm/yr, in some locals, but the rate of uplift decreased rapidly after a few years. The mechanism most likely to have been responsible for the uplift is aseismic slip occurring down-dip of the earthquake rupture. The cumulative postseismic uplift since the earthquake is 1 m or more where the postseismic uplift was most rapid. In other locales, postseismic uplift rates have changed with time, but the initial rates were smaller and the transient relaxation times are longer than those just mentioned. At yet other locales, there has been no apparent change in the rate of uplift since the earthquake, but a variety of arguments suggest that the uplift rates will not be sustained over the entire recurrence time

until the next major event. It is likely that some of the longer lived transient deformations are associated with viscoelastic rebound. There are other forms of transient deformations that have been observed including deep aseismic creep events on the plate interface (silent earthquakes), whose signal at the surface is a reversal in the direction of horizontal crustal movement from that seen when strain is accumulating. Taken as a whole the observations suggest that there are temporal and spatial variations in the coupling at the plate interface. Some of the spatial variations appear to correlate with the complex asperity rupture pattern of the earthquake.

**JSG01/08P/D-016** Poster **1400-016**

**POSTSEISMIC DEFORMATION FOLLOWING THE 2000 WESTERN TOTTORI EARTHQUAKE, SOUTHWEST JAPAN, USING GEONET AND URGENT CAMPAIGN GPS DATA**

Manabu HASHIMOTO<sup>1</sup>, Takeo ITO<sup>1</sup>, Takao Tabei<sup>2</sup>, Takeshi SAGIYA<sup>3</sup> (<sup>1</sup>Disaster Prevention Research Institute, Kyoto University, <sup>2</sup>Kochi University, <sup>3</sup>Geographical Survey Institute)

The 2000 Western Tottori earthquake of Oct. 6, 2000 is a typical inland earthquake in Japan with left-lateral strike-slip faulting on a NNW-SSE trending vertical fault plane. The Geographical Survey Institute have been operating continuous GPS observation network (GEONET). Since the average spacing of observation sites are too sparse to observe postseismic deformation, GSI and The Japanese University Consortium for GPS Research (JUNCO) deployed temporal observation sites. JUNCO deployed a dense GPS network with 16 dual frequency receivers surrounding the source region immediately after the main shock. Most observations were carried out continuously until the end of October 2000, and some sites equipped with dual frequency receivers were reoccupied in March 2001. GSI established two temporal sites with dual frequency receivers in October 2000 and continued the observation till the end of 2001. We observed a slowly decaying movement at every site. The spatial pattern shows left lateral motion across the source fault, similar to the coseismic displacements. We derived the amount of afterslip on a shallow part of the source fault from this spatial pattern. We also estimate the distribution of afterslip using a multi-segment fault model and obtain the largest slip of about 4cm near the epicenter of the main shock, while the northernmost segment appears to have the smallest slip of about 2cm. If we fit exponentially decaying functions to the data from the JUNCO sites occupied in March 2001, we obtain time constants of 20 to 40 days. However, this may be inconsistent with the idea of afterslip on the source fault or its extension, since an exponential decay function is closely related to the relaxation of stress in a viscoelastic layer. Here we fit the temporal variation of coordinates of JUNCO sites with the following logarithmic decay function proposed by Marone et al. (1991). In this nonlinear fitting, we assume a non-negative constraint on the parameter related to coseismic velocity. We obtained positive coefficient of friction at 6 of 12 sites. They give a value of (a-b) consistent with laboratory data for a velocity-strengthening layer at a shallow depth. Mainly because of the lack of data between October 2000 and March 2001, appropriate values could not be obtained at other sites. We will present results of the analysis using both GSI and JUNCO's data.

**JSG01/08P/D-017** Poster **1400-017**

**SYSTEMATIC DETECTION OF TRANSIENT AND PERMANENT CRUSTAL DEFORMATION USING HIGH-DENSITY GPS NETWORK DATA**

Yuzo TOYA, Minoru KASAHARA (Institute of Seismology and Volcanology, Hokkaido University, Japan)

A scheme is being developed for systematic detection of transient and permanent crustal deformations using large-scale GPS network data. Network operated by the Geographical Survey Institute of Japan covers the Japanese Islands with approx. a thousand observation stations, 25 km apart. Their recordings of station position changes that we used here have accumulated length of about 5-6 years. To systematically measure transient and permanent deformations, we started by evaluating the validity of our linear approximation to each time-series dataset. For example, how 'transient' an event is depends on the reference-duration of observation, or sampling time-interval. First, we (1) removed most obvious high-frequency noise, with five-point median filtering, and (2) removed additive seasonal variations (annual and semi-annual components) from observation time-series, hypothetically to isolate geodynamic signals besides other noises. Before subtracting the seasonal components, the drift (approximated by 2nd-order polynomial) and a major step were temporarily eliminated from each time-series. (3) Datasets containing significant irregularities in their time-series were isolated and later classified according to source types of those transient events or noises. Mean absolute error [MAE] was used to measure the deviation of observation data from our linear approximations. At the onset of a transient event, say a step of given positive height and slope, absolute (apparent) velocity would become much higher than the background rate for a duration [Tp] that of a fixed sampling time-interval plus the transient event length. Maximum absolute velocity and its corresponding MAE are, in general, positively correlated with step height and slope, while the parameters also depend on the duration of observation. The longer the observation period is, the less significant a transient event appears. (4) Datasets that have good fits to linear approximations (the goodness of fit with 95% conf.) were then applied to map horizontal distribution of strain rates. Before calculating strain rates, velocity vectors were interpolated and filtered with a median averaging window (e.g., R=50km; grid spacing=0.15deg). This technique helps reduce noises and outliers; besides it upholds robust trends in data. Spatial resolution in the original high-density station arrangement was well-maintained in result. Resultant maps effectively highlighted many known tectonic features. Bands of high maximum shear-strain and shortening rates characterize active transient and/or permanent geodynamic processes. Recently discovered distribution of low-frequency tremors along Sanbagawa Metamorphic Belt, western Japan, matches well with one of the bands of high strain rates. Furthermore, a sequence of strain-rate maps markedly suggests intermediate-term transitions in the regional stressing environment. It is partly supported by the observable shifts in orderly strain-rate distribution patterns from one period to another. Moreover, strain rates in southern Kanto and along Itoigawa-Shizuoka Tectonic Line to Suruga-Bay are noticeably increasing.

**JSG01/08P/D-018** Poster **1400-018**

**PRECISE MEASUREMENT OF SOUND VELOCITY AND ATTENUATION IN SITU FOR AN ESTIMATION OF SMALL STRESS CHANGE**

Osam SANO<sup>1</sup>, Keiko YAMAMURA<sup>2</sup>, Yasuko TAKEI<sup>1</sup>, Shigeru NAKAO<sup>1</sup>, Hisashi UTADA<sup>1</sup>, Yoshio FUKAO<sup>1</sup> (<sup>1</sup>Earthquake Research Institute, University of Tokyo, <sup>2</sup>Osaka University)

It is often difficult to get high reliability in the observation of small change for long period, e.g., 0.01 micro-strain even for a month, by using extensometers, tilt meters and borehole strain meters, although it is easy to get high resolution for short period. Environmental disturbances and possible time-dependent deformation within the stress concentrated region could be responsible for such a low reliability. Drifts in the DC-offset and gain of the amplification are also responsible. A measurement of the sound velocity is one of the candidates to overcome such a problem, because the reliability of the temporal change in the sound velocity is fundamentally determined by the base clock of the system and the

clock is one of the most stable transducers. Timing error in the triggering the waveform recorder can easily be reduced by an averaging method. A phase drift can also be reduced by employing an amplification system with sufficiently wide frequency range. Precise and continuous measurements of in situ sound velocity and attenuation have been carried out for the past 8 years, 4 years and 2 years in the vaults at Kamaishi (Iwate, northeastern Japan), Aburatsubo (Kanagawa, central Japan) and Mizunami (Gifu, central Japan), respectively. The overburden depth at Kamaishi was 450 m, and those of Aburatsubo and Mizunami were 10 m and 50 m, respectively. In order to get high stability and resolution, piezoelectric transducers were used as ultrasonic wave sources. The resolution of the temporal change in the sound velocity was about 1 ppm at Kamaishi, 10 ppm at Mizunami and 100 ppm at Aburatsubo. At Kamaishi test site, a clear dependence of the sound velocity on the barometric pressure was found. The stress sensitivity of the sound velocity at Kamaishi was estimated as 1.4 ppm/hPa, based on the effect of barometric pressure. At Kamaishi, an increasing trend of the sound velocity has been observed for the past 8 years. The estimated increasing rate of the compressive stress was about 600 hPa/yr, corresponding to the strain rate of 0.7 micro-strain/yr. This rate is several times higher than the strain rate of the northeastern Japan estimated by GPS measurement. At Aburatsubo, near the coast of Miura bay, relatively large periodic variations in both velocity and attenuation, corresponding to the diurnal and semi-diurnal lunar and solar tides, were found. These variations correlate well with the in situ areal strain change due to tidal ocean loading. The highest peak of the velocity and the lowest peak of the attenuation occurred at every time of the minimum peak in the areal strain. The opening/closure of pores or cracks due to stress change was responsible for these periodic variations. The velocity variation showed a remarkable 14-day-periodicity corresponding to the spring and neap tides. This periodicity in the sound velocity was explained in terms of a nonlinear response of the velocity change, brought from the strain rate dependence of the closure process of the cracks and pores.

**JSG01/08P/D-019** Poster **1400-019**

**CRUSTAL DEFORMATION IN THE KANTO-CHUBU DISTRICT AT AND AFTER THE 2000 SEISMO-VOLCANIC EVENT IN THE NORTHERN IZU ISLANDS**

Akio KOBAYASHI<sup>1</sup>, Hiromi TAKAYAMA<sup>1</sup>, Takeyasu YAMAMOTO<sup>1</sup>, Akio YOSHIDA<sup>2</sup> (<sup>1</sup>Seismology and Volcanology Research Department, Meteorological Research Institute, Japan Meteorological Agency, <sup>2</sup>Kakioka Magnetic Observatory, Japan Meteorological Agency)

The GPS observation network of the Geographical Survey Institute has revealed that the 2000 seismo-volcanic event in the northern Izu islands produced a remarkable crustal deformation in the Kanto-Chubu region, central part of Honshu Island, Japan (Nishimura et al., 2001). By subtracting average movements during the period from May 1997 through May 2000 as well as seasonal variations, we investigated detailed time evolution of the crustal deformation since the outbreak of the 2000 seismo-volcanic event. We found that three kinds of crustal deformation of different spatial pattern occurred successively in the Kanto-Chubu region. The first and most prominent one was the deformation produced by the activity in the sea region between Miyake and Kozu islands, where a large earthquake swarm occurred. The source can be modeled as a combination of a dike intrusion, fault motion of major earthquakes and a creeping slip. A creeping source is needed to explain eastward movements. The second kind of deformation appeared after the peak of the first one, and is characterized by a southward displacement of the crustal block in the Chubu district. A notable feature of the deformation is that it showed a diffusive pattern. The third kind of deformation is the ongoing southeastward displacements in the Tokai region that became noticeable in early 2001. Ozawa et al. (2002) explained the displacements by an occurrence of an aseismic slip on the plate boundary in the western Tokai region centered on Lake Hamana, adjacent to the anticipated Tokai earthquake source area. We think it is very probable that physical and/or mechanical condition on the boundaries between the Philippine Sea plate, Izu microplate and Eurasian plate was affected by the unusually large 2000 seismo-volcanic event in the northern Izu islands, and that change in the coupling condition between the plates has produced three kinds of the crustal deformations in the Kanto-Chubu district successively. We are grateful to the Geographical Survey Institute for providing the GPS data.

**JSG01/08P/D-020** Poster **1400-020**

**HORIZONTAL STRAIN CHANGES IN SOUTHWEST JAPAN USING PARTITIONING MODEL AND GPS DATA (1997-2000)**

Sayyed Keivan HOSSEINI<sup>1</sup>, Takeshi MATSUSHIMA<sup>2</sup>, Sadaomi SUZUKI<sup>1</sup> (<sup>1</sup>Department of Earth and Planetary Sciences, University of Kyushu, <sup>2</sup>Institute of Seismology and Volcanology, University of Kyushu)

Southwest Japan is located at the east-central margin of the Eurasian plate, and is underthrust beneath the Nankai Trough by the Philippine Sea plate, converging with the margin suborthogonally along a general northwesterly trend. In order to estimate the horizontal strain of southwest Japan for the period of Nov.1997 to Nov.2000, using GPS data of Geographical Survey Institute of Japan, after making an unbiased data, we derived two empirical covariance functions by applying least-square prediction method. During a repeated calculation, we compared the effect of correlation distances with the measurement vectors of different points and partitioned whole Japan in to two main regions, where the correlation distances for two E-W and N-S components could be equal. The partitioning boundary has a good coincidence with the Fossa Magna where assume to be a plate boundary between Okhotsk and Eurasian plates. We estimated the correlation distance of southwest Japan as 270 km and derived two new covariance functions to compute the horizontal strain of this region. During Nov.1997-Nov.1998, from central Kyushu toward east, there is a widespread shear anomaly,  $\sim 0.24 \times 10^{-9}/\text{yr}$ , that could refer to the Hyuganada earthquake (Mw 6.7) effect. Also this anomaly is extended into Shikoku Island and could be related to some slow slip displacements because of lacking any large events. Most of the Shikoku Island is under shear strain that extended to the south part of the Kinki area too. The strain state in Southwest Japan is NW-SE contractional in most of place that may be attributed to the convergence of Eurasian, Philippine Sea and Pacific plates. In central Kyushu Island, N-S extension could be due to the mantle pluming under western off the Kyushu. Also the NW-SE and E-W extension in southwest of Kyushu and west off Yakushima Islands could be consider for the expansion of Okinawa trough.

**JSG01/08P/D-021** Poster **1400-021**

**CHARACTERISTIC SILENT EARTHQUAKES IN THE EASTERN PART OF THE BOSO PENINSULA, CENTRAL JAPAN**

Shinzauro OZAWA<sup>1</sup>, Shin'ichi MIYAZAKI<sup>1</sup>, Yuki HATANAKA<sup>1</sup>, Tetsuo IMAKIHI<sup>2</sup>, Masaru KAIJZU<sup>1</sup>, Makoto MURAKAMI<sup>1</sup> (<sup>1</sup>Geographical Survey Institute of Jpana, <sup>2</sup>Earthquake Research Institute, University of Tokyo)

The Philippine Sea plate is subducting beneath the Boso peninsula, central Japan, with the Pacific plate underlying the Philippine Sea plate. Because of this complicated tectonic setting, seismic events are numerous off the coast of the Boso peninsula. Permanent GPS observation sites set up by the Geographical Survey Institute of Japan (GSI) detected

## INTER-ASSOCIATION

southeastward ground motion deviating from the steady northwestward deformation in 1996. From the detected abnormal crustal deformation, an aseismic slip was estimated off the east coast of the Boso peninsula with its rupture propagating to the south with time duration of about 7 days [Sagiya, 2003]. Six years after the 1996 event, quite similar abnormal crust movements started from around October 4 2002 for about fifty days, indicating occurrence of another interplate aseismic slip in this region. By employing a Kalman filter, we estimated the time evolution of the 2002 Boso aseismic slip and compared the 2002 event with the 1996 silent earthquake to investigate the nature of silent earthquakes. Our result shows an area of aseismic slip with moment magnitude (Mw) 6.6 centered off the Boso peninsula, adjacent to associated seismic activity. Slip evolution of the 2002 aseismic slip migrated from north to south with temporary subsidence and restart of slipping in a southerner area. Southward aseismic slip migration which occurred both in 1996 and 2002 events suggests a tendency of aseismic slip nucleation in a weakly coupled northern area and propagation to a more tightly coupled southern area. Similarities in focal area and slip process between the 1996 event and the 2002 aseismic slip suggest the Boso aseismic slips share characteristic features as is observed for characteristic radiative earthquakes. In addition to similarities between the past two Boso events, repetitive swarm seismicity of six to seven years interval supports the hypothesis that Boso silent earthquakes are characteristic silent earthquakes with recurrence interval of about six years. A more tightly coupled southern area that did not release enough energy in the 1996 event may have caused differences in magnitude and central slip area between the 1996 and the 2002 events despite having similar duration for strain accumulation, if characteristic earthquake hypothesis holds.

**JSG01/08P/D-022** Poster **1400-022**

### APPLICATION OF KALMAN FILTERING TECHNIQUES TO POST-SEISMIC SLIP PREDICTION OF THE 1999 TAIWAN CHI-CHI EARTHQUAKE

Din-Yao JENG, Wei-Cheng HUANG (Department of Earth Science, National Cheng Kung University)

From the 1999 Chi-Chi earthquake (Mw = 7.6; 1999/9/20, 17:47:15.9 GMT; at 23.853N, 120.816E, depth of 7.5km), The Ministry of Interior, ROC, started the work of verification and survey of first-order GPS control point and re-announced related resulting data to meet the requirement of re-construction work. This study focus on the point if there still exist apparent affect of GPS network displacement, especially the Post-seismic Slip of the Chi-Chi EQ, for the verification work has been done over three years. The Kalman Filtering Techniques can be applied to problems that can be described or approximated by linear time-varying equations, with non-stationary system and measurement input noise statistics. And, the Kalman Filter formulation can then be readily designed for estimation, smoothing, and prediction of the physical parameter of interest. An advantage of a Kalman Filter is that it allows one to use "state noise" to compensate for errors in the mathematical model. This study use the received data of GPS from 1999 to 2002, and combined the received data from the GPS tracking stations set by The Ministry of The Interior to acquire the coordinates of each GPS control point. Then, we use kalman filtering techniques to predict the Post-seismic Slip of the Chi-Chi EQ. We propose a high resolution prediction results. We also compare the results with re-announced coordinates. There is 5-30cm displacement of points around the earthquake stripe of the central part of Taiwan, 5-10cm of displacement for the points at the northern part of Hsin-Chu which are not verified and surveyed, 10-20cm displacement for the points at the southern part of Chai-Yi which are not verified and surveyed from the result of analysis.

**JSG01/08P/D-023** Poster **1400-023**

### THE SILENT EARTHQUAKE OF 2002 (MW=7.3) IN THE GUERRERO SEISMIC GAP, MEXICO: MAPPING OF SLIP ON THE PLATE INTERFACE AND THE ASSOCIATED STRESS CHANGE

Shri Krishna SINGH<sup>1</sup>, Vladimir KOSTOGLODOV<sup>1</sup>, Kristine M. LARSON<sup>2</sup>, Anthony R. LOWRY<sup>3</sup>, Roger BILHAM<sup>4</sup>, Takeshi MIKUMO<sup>5</sup>, Miguel SANTOYO<sup>6</sup>, Arturo IGLESIAS<sup>1</sup> (<sup>1</sup>Instituto de Geofisica, UNAM, Mexico, <sup>2</sup>Department of Aerospace Engineering Science, University of Colorado, Boulder, CO, USA, <sup>3</sup>Department of Physics, University of Colorado, Boulder, CO, USA, <sup>4</sup>Department of Geological Sciences, University of Colorado, Boulder, CO, USA)

Guerrero seismic gap is a 200 km-long segment along the Mexican subduction zone that may rupture in an earthquake of Mw 8.4. An aseismic, slow slip event began in the gap in January 2002 and lasted for 4 months. The slow slip was detected by 7 continuous GPS receivers located over an area of ~550x250 km<sup>2</sup>. We inverted the GPS displacement data for slip on the plate interface. The result shows that during the steady-state phase, the plate interface, lying ~50 to 170 km from the trench, was almost completely locked. The slow slip, however, occurred mostly down dip from the seismogenic, locked plate interface, presumably on the transition zone, in the depth range of ~35 to 40 km and the distance range of 100 to 170 km from the trench. The average slip was about 16 cm. The event released a seismic moment of ~1.2 x 10<sup>27</sup> dyne-cm (equivalent Mw=7.3). The strain release due to slow slip over the plate interface in the distance range of ~100 to 170 km from the trench essentially cancelled the strain accumulated during the previous 3 years of steady-state loading. The slow-slip phase resulted in an increase of ~0.1 bar of Coulomb failure stress, favoring reverse faulting on the shallow part of the completely locked interface, thus enhancing the probability of rupture of the Guerrero seismic gap in the near future. Some features of two important earthquakes, which occurred in the region before and during the slow-slip phase, may also be explained by the change in the Coulomb failure stress.

**JSG01/08P/D-024** Poster **1400-024**

### PRINCIPAL COMPONENT ANALYSIS FOR THE DISPLACEMENTS OF GPS STATIONS IN THE KANTO AND TOKAI DISTRICTS IN JAPAN

Masashi KAWAMURA<sup>1</sup>, Koshun YAMAOKA<sup>2</sup> (<sup>1</sup>Division of Earth and Environmental Sciences, Graduate School of Environmental Studies, Nagoya University, <sup>2</sup>Research Center for Seismology and Volcanology, Graduate School of Environmental Studies, Nagoya University)

Principal component analysis (PCA) is applied to the displacements recorded by more than 100 GPS stations in the Kanto and Tokai Districts in Japan for the period including the following three major events. (1) The Miyake-Kozu event in 2000, which includes large-scale dyke intrusion between Miyake and Kozu volcano to the south of Japanese main island. This event was accompanied by fivephreatic eruptions in Miyake Volcano, and intensive earthquake swarm near Kozu volcano. (2) The Tokai slow slip event, which started and is still continuing at a plate boundary between the Eurasian plate and the Philippine Sea plate in the Tokai District in 2000. (3) The Boso slow slip event, which lasted for less than a month in October 2002 at a plate boundary between the North American plate and the Pacific plate near the Boso Peninsula. Such events have been detected as displacements of GPS stations around their sources. Using PCA, we attempt to decompose the data into representative spatial modes and their temporal modes. We apply PCA to the following four data sets to check the reliability of the analysis; (A) Horizontal and vertical components from January 2000 to December 2002 (2) Horizontal and vertical components from January 2001 to December 2002 (3) Only horizontal components from January 2000 to December 2002 (4) Only

horizontal components from January 2001 to December 2002. We successfully decomposed the data into the modes corresponding to the Miyake-Kozu event, the Tokai slow slip event and the Boso slow slip event, as a major contribution to the total displacement field. Some prominent characteristic areas follow. In the temporal mode corresponding to the Miyake-Kozu event, the ramp-like step is followed by a prolonged tail which asymptotically approaches a constant level up to now. The development of the Tokai slow slip event is revealed to be initiated soon after the Miyake-Kozu event from its temporal mode. Eastward motion in the Kanto District also synchronizes with the Tokai slow slip event. The Boso slow slip event is more clearly observed in the datasets for only horizontal components than that for both horizontal and vertical components. This may be due to larger variance and smaller amplitude of the signal on the vertical components than on the horizontal ones. The total contribution of the above three modes to the data is more than 70 percent.

**JSG01/08P/D-025** Poster **1400-025**

### POSTSEISMIC CHANGES OBSERVED IN JAPAN NATIONWIDE TILTMETER ARRAY

Hitoshi HIROSE, Fumio YAMAMIZU, Kazushige OBARA (National Research Institute for Earth Science and Disaster Prevention)

National Research Institute for Earth Science and Disaster Prevention (NIED) has installed over 500 tiltmeter stations that cover most parts of Japan. The tiltmeter can detect smaller crustal deformations than those which can be done by GPS, so that this is expected to be a powerful tool for exploring the crustal deformations due to fault motions during earthquakes. We report the postseismic deformations detected by this tiltmeter array during its observation period. One example is the records following the October 6, 2000 West Tottori earthquake (Mw 6.7). It is shown that the GPS sites near the source area detect the postseismic surface displacements following the earthquake (Hashimoto et al., 2001). On the other hand, the tiltmeters which are relocated at least 60 km away from the epicenter detect tilt changes which obey logarithmic decay. Second example is the March 24, 2001 Geiyoe earthquake (Mw 6.8, 47 km in depth). The tiltmeter at KURH station, which is located about 20 km from the epicenter, clearly detects the postseismic decay, whereas there is no report for postseismic deformation which observed by GPS due to this earthquake. Postseismic tilt changes following the smaller earthquakes are also detected. On January 4, 2001, a moderate earthquake (Mw 5.3) occurred at Central Niigata. At the YZWH station, 15 km away from the hypocenter, logarithmic decay with time constant of about 1 hour is recorded following the large step caused by the main shock. We attempt to explain these postseismic deformations by afterslips on the source faults. Some studies point out that the time constant of the postseismic deformation correlates with the magnitude of the main shock (Yamauchi, 1975; Takai et al., 2000). This correlation possibly shows an aspect of the physical process of the earthquake source. We show the tiltmeters can detect smaller postseismic crustal deformation than GPS. This demonstrates that the tiltmeters have potential to constrain the earthquake source process by constructing a statistical property of the afterslips.

**JSG01/08P/D-026** Poster **1400-026**

### SPATIAL AND TEMPORAL DISTRIBUTION OF AFTERSLIP FOR THE 1995 HYOGO-KEN NANBU EARTHQUAKE INFERRED FROM SURFACE DISPLACEMENT DATA OBTAINED WITH GPS OBSERVATIONS

Takehide NAKANO, Kazuro HIRAHARA (Graduate School of Environmental Studies, Nagoya University)

Global Positioning System (GPS) observations indicate that significant postseismic deformation occurred following the January 17 1995 Hyogo-ken Nanbu earthquake (M=7.2). The postseismic deformations reached 2.0 cm at some stations. In order to estimate the spatial and temporal distribution of the afterslip on the fault and on its possible extension, we use an inversion method. We seek the best explained slip distribution that minimizes the discrepancy between the observed displacements by GPS and the predicted ones in a least squares sense with some smoothness constraints of slip distribution, starting from the search for the fault size and the location. It is concluded that the afterslip of about 40 cm occurred in the deeper portion under the fault at 15 to 25 km from the middle of the north segment. Though the GPS stations are distributed mainly along the fault strike but not in the fault normal direction, which makes it rather difficult to obtain good spatial resolution of estimated afterslip distribution, some resolution tests require the existence of the obtained afterslip including that at depths. The time dependent analysis indicates that afterslip started at different time at a few points on the fault surface and continued for different durations.

**JSG01/08P/D-027** Poster **1400-027**

### IS THE MOTION OF THE SOUTH HEMISPHERE SLOWING DOWN?

Shuanggen JIN, Wenyao ZHU (Shanghai Observatory, Chinese Academy of Sciences)

The Earth is a rotating planet in the universe, but the variation of rotating attitudes with time will cause the change of the inertial force, which leads to its interior motion, especially the relative glide or extrusion along the rotation axis of the Earth. In addition, the variations of the inertial and centrifugal force of the Earth, and the interactions of the atmosphere, Ocean and other celestial bodies perhaps bring on changes of the Earth motion state. Now the higher-accuracy space techniques, such as VLBI, SLR and GPS, with a longer observation time span, a much wider and more average distributions of observation sites, can detect the current slight variation of the Earth hemisphere state. In this note, we measure the contemporary relative motion rates of adjacent plates in the South hemisphere using space geodetic data in recent 20 years. Comparing them with results from the NUVEL1A model in three millions years and geological data in 25 millions years displays that the motion of the South hemisphere is slowing down. In order to know about the stability and continuity of the South hemisphere motion, we calculate divergent and convergent rates of adjacent plates in the South hemisphere at year 25, 35, 45, 55, and 70 million using hotspot data and geomagnetic data. Comparing the results in 80 millions years shows the South hemisphere is stable in 80 millions years. Accordingly the motion of the South hemisphere is slowing down in 25 millions years and yet is quite stable in whole 80 millions years.

**JSG01/08P/D-028** Poster **1400-028**

### THE STRAIN FIELD AROUND THE NORTHERN PART OF THE NASSER LAKE, EGYPT, DERIVED FROM GPS MEASUREMENTS AND ITS TECTONIC IMPLICATIONS

Gamal EL-FIKRY<sup>1</sup>, Divakar REDDY<sup>2</sup>, Ali TEALEB<sup>3</sup> (<sup>1</sup>National Research Institute of Astronomy and Geophysics, Helwan, Cairo, Egypt, <sup>2</sup>Indian Institute of Geomagnetism, Mumbai 400005, India)

GPS measurements collected in campaign mode during 1997 - 2002 have been analyzed to derive velocity vectors around northern part of the Nasser Lake, Egypt. Estimated horizontal velocity vectors in ITRF2000 are found to be in the range of 28.8 - 32.2 mm/yr with an average of 30.4 ± 2.1 mm/yr in N31 ± 3W. The horizontal velocity field further used for quantitative estimation of crustal deformation parameters. The Least-Squares

prediction(LSP) technique was employed to segregate the signal and noise from the velocity vectors. Estimated signals (displacement vectors) were used to reconstruct the strains; dilatations, maximum shear strains, and principal axes of strains. The distribution of the dilatational strains indicates that the region around the northern part of Nasser Lake is mainly divided into two areas: the northern part with predominant compressive strain and the southern part exhibiting extensive strain of about 0.6 ppm/yr. In addition to this, there are some of the areas with low compressional and extensional strains in the medial of the studied region. Maximum shear strains show some patches of high values of strains over northern, northwestern, and southwestern parts of the studied region. The paper also presents the relationship among the crustal strains, the hydrological situation in the lake, and the seismic activity in the area.

**JSG01/08P/D-029** Poster **1400-029**

#### RELATIVE DISPLACEMENT ACROSS THE FRACTURE ZONE

Keisuke TANIGUCHI<sup>1</sup>, Kazuo OIKE<sup>2</sup> (<sup>1</sup>Department of Education, Kyoto University of Education, <sup>2</sup>Faculty of science, Kyoto University)

Geodetic survey and continuous observation of crustal deformation across faults or fracture zones have led to many evidences that crust was consisted of loosely coupled blocks mostly bounded by faults or fracture zones. In order to study the relative movement of two crustal blocks bounded by the fracture zone in the tunnel of Hokuriku observatory of Kyoto University in Japan, three-dimensional relative displacement meters were designed and have been set up across that fracture zone since 1986. They have measured tidal and seismic relative displacements between two fixed points in three orthogonal directions. Results are 1) Tidal strain across the fracture zone was about four times as large as the theoretical, whereas that near the fracture zone was only half of the theoretical. Strain seismograms across the fracture zone are from 5 to 15 times as large as that in the neighborhood and larger than the calculated strain seismograms with seismographs set up in the same tunnel. 2) Deformation by earth-tide and seismic waves mainly take place at fracture zone. 3) Amplification factor of earthquakes is related to propagation azimuth of them. This result indicates that the amplification of seismic waves is caused by the change of the width of fracture zone, in other words, compress-extension motion at the fracture zone. 4) The vector of each tidal and seismic relative displacement across the fracture zone is almost fixed. This may be caused by the existence of plane-like fracture zone. 5) It was confirmed that block bounded by that fracture zone spreads in vertical. The calculation with FEM suggests that fracture zone extends to several km in dip direction.

**JSG01/08P/D-030** Poster **1400-030**

#### QUANTITATIVE EVALUATION OF LOADING EFFECTS ON SEASONAL VARIATION IN GEONET GPS DATA

Hiroshi TAKIGUCHI, Yoichi FUKUDA (Graduate School of Science, Kyoto University)

Murakami and Miyazaki [1999] reported that seasonal variation could be seen in the daily solutions of GEONET (the GPS Earth Observation NETWORK) GPS site coordinates. Since then, several scientists tried to interpret the seasonal variation (e.g. Hayashi et al. [2000], Heki [2001, 2002] and Hatanaka [2001, 2002]). We also investigated seasonal variation in the baseline length changes and reported most of the baselines expand in summer and contract in winter (Takiguchi and Fukuda [2000, 2001]). From these studies, we could summarize that the seasonal variation does not depend on the strength of plate coupling nor analysis software/strategy, and it is mainly caused by the systematic scale changes suggested by Hatanaka (2001) and the loading effects due to local or broad mass changes, i.e., snowfall, ocean tide, non-tidal ocean load and atmospheric pressure. Using the globally network data, D. Dong [2002] showed that 40% of the observed annual vertical variations can be explained by the joint contribution of pole tide, ocean tide, atmospheric pressure, non-tidal ocean, and groundwater loading. Other contributions were some modeling errors (wet troposphere effect and orbit etc) and bedrock thermal expansion. In this study, we investigate the seasonal variation in GEONET GPS sites to confirm whether the above estimations are valid for the GEONET data. For this purpose, we employed surface vertical variation and area strain which calculated from annual baseline changes of three baselines shaping a triangle. And then we compared the vertical variation and area strain with seasonal variation of snowfall load calculated from 1997 to 1999 AMeDAS data sets and atmospheric load calculated from atmospheric pressure data at the Japan Local Metrological Observatory. We found that the seasonal variation of GPS data could not be explained by snowfall load nor atmospheric load. We will search for other load sources and discuss the joint contribution of them.

**JSG01/08P/D-031** Poster **1400-031**

#### THE SEA LEVEL VARIATION IN THE RANGE OF PERIODS FROM 1 HOUR TO 2 DAYS IS THE NEW SOURCE OF INFORMATION ABOUT TO UNDERWATER EARTHQUAKE

Vladimir V. IVANOV (Institute of Marine Geology & Geophysics Eastern Branch of Russian Academy of Science)

1. The sea level variations, which were recorded by tidal stations, which were smoothed by time interval 2 hours, are the new source of information about development of the earthquake process with characteristic time several hours. The amplitude of variations -1 - 5 cm, the duration of variations 10 - 30 hours for the great earthquakes in Pacific ocean. 2. The signal of the low frequency variations of sea level is the recording of changing of the Earth's volume if the earthquake occurs in closed basin. 3. The basin is the closed basin if the duration of the wave propagation is less than the time of the level conservation. 4. For Japan sea the time of wave propagation is 2 hours, time of sea level conservation is 30 hours. The Japan Sea is the closed basin if duration of variations is less than 1 day. 5. The regarded signal for earthquake July 12, 1993 at Japan Sea did not depend from point of observation inside the Japan Sea, had the amplitude 3-4 cm, frontal time 4 hours, duration 20 hours. 6. The physical parameters of the full process of the earthquake July 12, 1993 are the next: volume variations - 10 16 cm<sup>3</sup>, energy- 6 10 24 erg, ZZ component of seismic moment 2 10 28 dn cm.

**JSG01/08P/D-032** Poster **1400-032**

#### GEODETIC INFRASTRUCTURE IN INDIA, WHAT IS WRONG AND WHAT NEEDS TO BE DONE

Nand Kishore AGRAWAL (Director, Retd., Survey of India, National Correspondent, IAG, MD, Geodesy and GPS Services)

Geodetic Infrastructure in India is inadequate. It needs a fresh look and complete revision. Indian Geodetic Datum, Reference Surface, Horizontal Control, Vertical Datum, Height Control, Indian Geoid and Mean Sea Level, Gravity datum, Projection System for Maps, and Indian Grid, are all inadequate or inappropriate. Indian Geodetic Datum is based on Everest Spheroid as Reference Surface. Center of this reference surface is estimated to be about 1

km away from the center of gravity of the Earth. The datum is a local datum and in error. Scientific and Defense studies of vital cannot be based on such a system. It is necessary that the datum should be redefined at the earliest. Horizontal Control resulted from The Great Trigonometrical Survey. Different triangulation series are inconsistent between each other and not adjusted properly. Stations are burdened with varying degrees of error. It is necessary that fresh observations be carried out to get a set of vectors by GPS and least square adjustment is done for the whole country at one go to get control points. Vertical Datum for Heights was chosen as Mean Sea Level at a group of nine tidal observatories at Indian ports. Level network in India is of moderate to high precision at different places. No gravity observations were carried out. Network has not been properly adjusted. It is required that a fresh datum for heights based on MSL at one tidal observatory is adopted. High Precision Leveling should be carried out afresh to get a network along with gravity observations and adjusted. It is necessary to have a Gravity Datum. Presently there is no absolute gravity station in India. Gravity values in India are based on relative observations based on gravity datum in another country. It is necessary to establish some absolute gravity stations, adopt a gravity datum and carry out relative observations to get a 1st order gravity network. No satisfactory Indian Geoid is available. To get heights above MSL by GPS observations we need a geoid that can give geoidal undulation of accuracy of 25 cm or better. A project should be taken up to obtain such geoid. Projection for topographical maps in India is Polyconic. Each individual sheet is projected assuming no distortion along parallels and neglecting distortion along meridians. Meridians and parallels are assumed as straight lines. We can say that The Earth/Ellipsoid has been assumed to be flat for individual sheets. This creates problems in digitization, integration and compilation of maps. It is necessary to abandon polyconic projection and adopt either Lambert Conformal Conic or Transverse Mercator Projection. Indian Grid on Lambert Conformal Conic Projection for superimposition on topographical maps has 9 zones with scale factors at central parallel as 649/650 and 823/824. The design is unsatisfactory as scale error at central parallel should be 1 in 2000 or better. It is necessary to design grids on Transverse Mercator or LCC similar to SPCS in USA.

**JSG01/08P/D-033** Poster **1400-033**

#### STRAINMETER UNITS IN A TERRESTRIAL REFERENCE FRAME SERVING

Ludmila A. LATYNINA<sup>1</sup>, Mstislav N. DUBROV<sup>2</sup> (<sup>1</sup>Institute of Physics of the Earth, RAS, <sup>2</sup>Institute of Radio-engineering and Electronics of RAS, Fryazino, Russia)

Recent developments of the Global Positioning System (GPS) and its wide spreading to the Earth's crustal motion measurements have advanced the problem of a terrestrial reference significantly. Nevertheless the concept of modern reference frame service still needs the close networks of high accuracy geodetic and geophysical instrumentation. Whenever geophysical aspects of global change are concerned the quality assessment of the network data has to be carried out. Actually, after the past decade of geodynamic phenomena monitoring by such global networks as Very Long Baseline radio Interferometry (VLBI), GPS, etc. the necessity of anchoring them to the limited number of the fundamental stations has been evidently shown. This circumstance can be explained by two main reasons. (1) When the local crust motions are taken into account the accuracies of such global systems as VLBI or GPS lose 1-2 orders in comparison with the precision of such modern geophysical instruments as gravimeters, tiltmeters and strainmeters. (2) The temporal resolution of the global systems is restricted by the principals of measurements and rates of data processing, while the modern wide-band geophysical instruments allow the continuous real time observations to be made. In comparison with gravimeters and tiltmeters the Earth's strain measuring instruments allow to detect simultaneously the number of spatial component of the geological medium deformations. High sensitivity of strainmeters is ensured by their constructions and technology of fabrication. The top instrument resolutions of the rod strainmeters d/L = 10(-10) and the laser strainmeters d/L = 10(-12) have been proved on the great variety of geophysical experiments. We present our experience in the achievements of these parameters and their verification. The results of observations of the aseismic fault movement and the earth surface strains due to meteorological and hydrological effects at the observatories Protvino and Fryazino will be discussed. The information on local tectonic strains and plate motions would be very important for every GPS or VLBI user to reduce undesirable antennas or receivers mechanical displacements. One should be able to eliminate another anthropogenic or atmospheric effects. We guess the terrestrial reference based on the space radio nets is to be added by the multi-component deformation measuring systems. The gathering of the local, regional, and global measuring tools should give both more accurate positioning frame and more intelligent geodynamic data source.

**JSG01/08P/D-034** Poster **1400-034**

#### AN INVERSION METHOD OF CRUSTAL DEFORMATION ON THE BASIS OF DISCONTINUOUS DEFORMATION ANALYSIS (DDA) AND BOUNDARY ELEMENT METHOD (BEM)

Yun WU, Chong-yang SHEN, Shao-qun JING, Hui WANG (Department of Geodesy and Crustal Deformation, Institute of seismology, CSB, P. R. China)

In this paper, an inversion method on the basis of Discontinuous Deformation Analysis (DDA) and Boundary Element Method (BEM), is presented for determining boundary relative movements, displacements and stresses of blocks in a multi-block system, in which the kinematic constraints required for reasonable movement between blocks in the system is discussed, and the judgment for contact between blocks, that indicates where a kinematic constraint is necessary, is also investigated in detail. This method, simply called as «DDA and BEM» has characteristics of linearity, uniqueness and stability of the solution, that is, the linearization foundation is the dispersion of integral equations. This is reasonable logically in the mathematics, the uniqueness condition that the simultaneous equations for each block is dependent on the number of the points measured in any block, which must be greater than the number of the boundary elements, and not collinear, and for the unstable called as «ill condition» the Damping Least Square Method can be used to obtain damping solution. So that, it seems theoretically that the method of «An Inversion Method of Crustal Deformation on the Basis of Discontinuous Deformation Analysis and Boundary Element Method» would be more suitable for the problems in which the relative movements on the block boundaries and the deformation inside the blocks need investigating and analyzing.

**JSG01/08P/D-035** Poster **1400-035**

#### MODERNIZATION OF THE NATIONAL GEODETIC NETWORK

Maturana Alejandro Maturana (Geodetic Department, Military Geographic Institute)

Rodrigo Maturana, Hector Parra Military Geographic Institute (IGM), Nueva Santa Isabel 1640, Santiago, Chile, owing to its special geographic location and resulting from its long and very extensive territory, has had to adopt several geodesic reference systems. These, as a whole, make up the National Geodesic Network (RGN) upon which the cartographic structure of the country can be based. Current requirements for precision in horizontal measurements, which are growing ever greater, and the need for homogeneity in

## INTER-ASSOCIATION

this data among related sectors of territory, have made it necessary to modernize the current framework for geodesic measurements and checks. The efficient incorporation of satellite systems (GPS) into the implementation of extensive networks for horizontal control and the adoption in the South American region of the "Geocentric Reference System for the Americas" (SIRGAS), has established a basis for structuring a modern Geodesic Network for Chile, a single and homogenous network for the whole country and the rest of the continent. This text has as its objective the presentation of the structure, the measurement campaigns and the final results of the processing and adjustments for the new National Geodesic Network, which will be the new official reference framework for all cadastral, cartographic and geodesic activities to be carried out in Chilean territory. Also, the transformation parameter between local and new datum will be presented.

**JSG01/08P/D-036** Poster **1400-036**

### SEISMIC GROUND MOTION OBSERVED BY THE TAIWAN CONTINUOUS GPS ARRAY - IN THE CASE OF 31 MARCH 2002 HUALIEN EARTHQUAKE

Hong-Yue CHEN<sup>1</sup>, Long-Chen KUO<sup>1</sup>, Wang-Shung CHUNG<sup>1</sup>, Shui-Bei YU<sup>2</sup> (<sup>1</sup>Research Assistant, <sup>2</sup>Research Fellow)

A  $M_L=6.8$  earthquake occurred on 31 March 2002 off northeastern Hualien. The instantaneous relative displacements have been tracked by newly established continuous GPS stations, which are part of the TCGN. There are seven stations of the TCGN with 1 Hz data sample rate, which recorded the instantaneous ground motion of the 331 earthquake. Applying the post-processing QIF algorithm to study the 331 earthquake, the displacements with respect to station TSHO are computed. Based on the relative positioning, the displacement of the computing station with respect to the fixed station can be obtained at the arrival time, and the displacement of the fixed station can be acquired at the time of the second maximum ground motion. Hence the first arrival times are different at each of subplots and the time of the second maximum ground motion is at the same location. It is obvious that the seismic ground motion can be observed by 1 Hz sampling rate continuous GPS stations.

**JSG01/08P/D-037** Poster **1400-037**

### DISTORTIONS IN DENSITY DUE TO INACCURATE AVERAGE DEPTH OF A LAYER IN THE LOWER HALF-SPACE

Ateya Ismail LUKANDU, Shuzo TAKEMOTO (Department of Geophysics, Kyoto University)

The position of an intermediate horizontal layer in the lower half-space can be given inaccurately without any change in the thickness of the effective layer either by a slight layer shift upwards or downwards. Even though the layer shifts might be minimal, it could significantly alter the density variations of the disturbing masses in the effective layer. Here we investigate and demonstrate the effect of the variations in the position of the horizontal layer to the determined density variations. Subsequently due to the direct relationship between disturbing masses and the positions of the contact surfaces in an intermediate horizontal layer, the later are also determined. We finally demonstrate the efficacy by applying to actual geophysical data i.e. gravity data, for a micro-gravimetry site and/or localized structures in the Central Ranges of the Chubu District in Japan.

**JSG01/08P/D-038** Poster **1400-038**

### EFFECTS OF A HORIZONTAL SURFACE LAYER ON STATIC AND DYNAMIC DISPLACEMENTS

Ryou HONDA<sup>1</sup>, Kiyoshi YOMOGIDA<sup>2</sup> (<sup>1</sup>Institute of Seismology and Volcanology, Hokkaido University, <sup>2</sup>Graduate school of science, Hokkaido University)

Recent development of geophysical observation instruments such as GPS have allowed us to obtain precise broad band data in wide dynamic and wide frequency range, including static displacements in a large area. While detailed crustal structure around a damaged area is surveyed for source parameters obtained by seismic waveform inversions, the effects of a layered medium are often not considered in practical analyses of geodetic data. In this study, we calculate static as well as dynamic displacements with the discrete wavenumber method and compare them with analytical as well as numerical solutions for a half-space. The existence of a soft surface layer is found to affect both amplitude and spatial distribution of static displacement near a fault, which is not in a similar manner to those of dynamic displacement. In a horizontal surface layer case, the largest effect of a surface layer is shown in the case of a vertical strike-slip fault. While dynamic motions are amplified monotonically with the thickness of the surface layer, the amplification of static displacement is limited if the surface layer reaches the top of the fault because the moment release there is then reduced. Errors in the estimation of the fault depth and the amount of slip reaches as large as 30 % of the true values in the worst case. If we introduce a non horizontal layer (e.g., a basin), the spatial distributions of static displacement should be affected strongly. The effects are important not only for inland earthquakes but also inter-plate earthquakes which causing a large tsunami. Our results strongly suggest that strong bias may be introduced to the conventional estimation of fault parameters, assuming a medium to be a half space, from static displacement or geodetic data by the existence of a low-velocity or low-rigidity surface layer.

**JSG02-Posters** **Wednesday, July 9**

### INTERDISCIPLINARY EARTH SCIENCE FROM IMPROVED GRAVITY FIELD MODELING (IAG, IAHS, IAPSO, IASPEI)

Location: Site D

**Wednesday, July 9 AM**

**JSG02/09A/D-001** Poster **0830-001**

### A DIGITAL METHOD FOR AUTOMATIC 3-D GRAVITY INVERSION OF DENSITY INTERFACES USING VARIABLE DENSITY

Chakravarthi VISHNUHOTLA, Harinarayana TIRUMALACHETTY (National Geophysical Research Institute, Uppal Road, Hyderabad, India.)

A new 3-D inversion technique to interpret the gravity anomalies of density interfaces above which the density contrast shows a systematic variation with space coordinates is presented. The technique involves both a robust methodology and the associated software to achieve the task. Initial depth estimates of a density interface below the said grid nodes of a

rectangular/ square mesh are computed automatically from the measured gravity anomalies and are improved iteratively until the theoretical gravity anomalies fit the observed ones. The quantum of misfit function is allowed to vary in the downhill direction in the parameter space, thus paving a way for obtaining more accurate results. An automated computer program AUTOG3DIN is developed based on the suggested algorithm. Two gravity anomaly maps are interpreted and the results are compared with borehole information.

**JSG02/09A/D-002** Poster **0830-002**

### OVERVIEW OF THE GRAVITY FIELD OF ANTARCTICA

Muriel LLUBES, Nicolas FLORSCH, Benoit LEGRESY, Jean-Michel LEMOINE, Frederique REMY (LEGOS-OMP)

CHAMP, flying at an altitude of about 400 km, is the first of a new generation of satellites dedicated to Earth gravity field observation. The high quality data has generated new gravity field models: EIGEN-1S in 2001, and EIGEN-2S more recently. The gravitational potential is decomposed into spherical harmonic coefficients and used, in this study, the free-air gravity anomalies reconstituted up to degree 60, at a zero altitude. The anomalies for the Antarctic continent range from -57 to 65 mGal. We have modeled the gravity effect from the ice, the ocean and the bedrock, using a 666 km cut-off filter to simulate the resolution obtained by CHAMP. Computing the differences between this terrain effect and CHAMP map provides a map of the Bouguer anomalies. Because of the dominant influence of the crust, we first used a crustal thickness model from seismology. This gives a map of the mantle Bouguer anomalies, the range of which is still large (between -255 and 216 mGal) indicating imperfections in the crust model. By appealing to isostasy we then imposed the condition that this mantle Bouguer anomaly should vanish and therefore solve for a new resulting crustal thickness. This gravity-based crust model gives thicknesses from 8.5 to 42.6 km in the zone of interest. There is a good general agreement with seismological models, but our models show more detail, particularly in the western part of the continent. These details are in agreement with geological studies.

**JSG02/09A/D-003** Poster **0830-003**

### GEOID AND OCEAN CIRCULATION IN THE NORTH ATLANTIC (GOCINA)

Per KNUDSEN<sup>1</sup>, Rene FORSBERG<sup>2</sup>, Ole B. ANDERSEN<sup>1</sup>, Dag SOLHEIM<sup>3</sup>, Roger HIPKIN<sup>4</sup>, Keith HAINES<sup>5</sup>, Johnny JOHANNESSEN<sup>6</sup>, Fabrice HERNANDEZ<sup>7</sup> (<sup>1</sup>National Survey and Cadastre - Denmark, Geodesy, <sup>2</sup>National Survey and Cadastre - Denmark, Geodynamics, <sup>3</sup>Statens Kartverk, Norway, <sup>4</sup>University of Edinburgh, UK, <sup>5</sup>University of Reading, UK, <sup>6</sup>Nansen Environmental and Remote Sensing Center, Norway, <sup>7</sup>Collecte Localisation Satellites, France)

The investment in Earth observing satellites has been significant. It is therefore of great importance that the value and utilization of space borne data can be properly demonstrated in the context of ocean monitoring. The aim of the EU supported project GOCINA is to enhance European capacity in Earth observation technologies by promoting and developing methods for the joint exploitation of the approved European Space Agency ENVISAT (Radar Altimeter) and GOCE missions for ocean circulation studies and associated climate modelling and operational data assimilation. The central quantity bridging the geoid and the ocean circulation is the mean dynamic topography, which is the difference between the mean sea surface and the geoid. The initial studies will focus on the assessment of the initially available models of the geoid, the mean sea surface and the mean dynamic topography to obtain the current state of these geoid models and to identify areas of problems from their discrepancies. In some areas the residual will be small enough to be within the error bounds of the other fields. In other regions the residuals are larger than expected on the basis of the individual calculations. This mismatch will indicate areas where one or more of the error analyses are inaccurate.

**JSG02/09A/D-004** Poster **0830-004**

### GRAVITY MODEL DEVELOPMENT FOR ICESAT PRECISION ORBIT DETERMINATION

Hyung-Jin RIM, John C. RIES, Sungpil YOON, Charles E. WEBB, Srinivas BETTADPUR, Bob E. SCHUTZ (Center for Space Research, University of Texas at Austin)

The main scientific objective of the EOS ICESat mission is to measure long-term changes in the volumes (and mass) of the Greenland and Antarctic ice sheets with sufficient accuracy to assess their impact on global sea level, and to measure seasonal and interannual variability of the surface elevation. To monitor the ice sheet topography, ICESat features the Geoscience Laser Altimeter System (GLAS) to determine the height of the GLAS instrument above the ice sheet by measuring a laser pulse round-trip time of flight, emitted by the GLAS and reflected by the ice sheet. This laser altimeter measurement combined with the satellite height information from the Precision Orbit Determination (POD) will result in the geocentric height of the ice surface. To achieve the main scientific objective, the position of the GLAS instrument should be known with an accuracy of 5 cm and 20 cm in radial and horizontal components, respectively. This knowledge will be acquired from data collected by the on-board GPS receiver and ground GPS receivers. Following the successful launch of ICESat on Jan. 13, 2003, 00:45 UTC, the GPS receiver was turned on successfully on Jan. 17, 2003, tracking up to 9 GPS satellites. It has been shown from pre-launch POD studies that the gravity model error is the dominant source of ICESat orbit errors. Pre-launch gravity models, such as TEG-4 and EGM-96, predict about 7 cm and 15 cm radial orbit errors for ICESat, respectively. To meet the 5 cm radial orbit determination requirement using these models, it is necessary to either 1) estimate many empirical parameters to reduce the effect of the gravity model errors, or 2) tune the gravity model with ICESat tracking data. Recent gravity models from the GRACE mission also show promising results on ICESat POD. This paper summarizes the gravity model development efforts for ICESat POD.

**JSG02/09A/D-005** Poster **0830-005**

### ON THE COMBINATION OF ALTIMETRY AND SATELLITE DERIVED GRAVITY FIELD MODELS

Wolfgang BOSCH (Deutsches Geodätisches Forschungsinstitut (DGFI))

The gravity missions CHAMP, GRACE and GOCE will considerably improve the spatial and temporal resolution of the Earth gravity field. Nevertheless, satellite altimetry will be further needed to derive very small-scale features of the gravity field. The potential of altimetry is indicated by the 2'x2'-resolution of most recent mean sea surface models (a 5'x5' grid corresponds to aharmonic series above degree and order 2000). Up to now, altimetric derived gravity anomalies were used for the combination with satellite derived gravity field solutions. The anomalies are either derived by solving the inverse Stokes equation or by a "synthetic geoid", obtained by reducing the mean sea surface by an independent (e.g. oceanographic) model of the sea surface topography. The first approach is rather indirect and numerically instable. In the latter case errors of the sea surface topography are directly projected into the high resolution gravity field model. Here, a more direct approach is considered to combine altimetry and satellite derived gravity field solutions. The large-scale

structure is assumed to be sufficiently accurate determined by the satellite based gravity solution. Slope and even more the curvature of the mean sea surface are little or not at all affected by the (unknown) dynamic topography. Therefore, slope and curvature are used to set up observation equations that are accumulated to the normal equation system of a satellite derived gravity field solution. It is then investigated how much the combined solution becomes more stable and to what extent the resolution of the gravity field can be improved by adding satellite altimeter data.

**JSG02/09A/D-006** Poster **0830-006**

### 3D ASPHERICAL EARTH'S MODEL AND 3D ATMOSPHERIC LOADING FOR THE NEW GRAVITY MISSIONS

Pascal GEGOUT, Hilaire LEGROS, Jacques HINDERER (IPGS UMR 7516)

High precision modelling of temporal variation of the gravity field generated by atmospheric masses redistributions and Earth's masses redistributions are nowadays needed to separate accurately atmospheric contributions from oceanic and hydrologic contributions. We therefore developed a deformation model of an aspherical Earth with lateral heterogeneities. The corresponding pressure, tidal and loading Love numbers characterize these deformations. Boundary conditions on this Earth's model imposed by the atmosphere are revisited: we distinguish surface stress induced by the pressure and winds/currents at the solid Earth's topography from the gravitational force generated by the three dimensional structure of the atmosphere. Taking into account the 3D structure of the atmosphere to calculate direct gravitational attraction on low orbiting artificial satellites is required. A static response of the ocean to solid earth deformations and barometric forcing is included. A model of a non-global ocean overlying an elastic deformable earth and forced by ECMWF atmospheric pressure surface fields is used to predict and interpret these global masses redistributions. These processes lead to a wide range of gravity variations, from global to local spatial scales, and from diurnal to interannual variations. From these model results we identify the significant processes and their corresponding signatures in geodetic observations (Earth's surface deformation, global gravity changes and surface gravity measurements). We focus on high frequency gravity perturbations, which may be aliasing during the recovery of the global gravity field from the new generation of gravity satellites. Possible comparisons between spatial and ground gravimetric measurements are also investigated.

**JSG02/09A/D-007** Poster **0830-007**

### TEMPORAL GRAVITY FIELD RECOVERY FROM CHAMP AND GRACE

Shin-Chan HAN, C.K. SHUM, C. JEKELI (Department of Civil and Environmental Engineering and Geodetic Science, The Ohio State University)

The CHALLENGING Minisatellite Payload (CHAMP) and Gravity Recovery and Climate Experiment (GRACE) satellite missions are mapping Earth mean and temporal gravity fields with unprecedented accuracy and resolution. Measurements from these gravity mapping satellite missions have demonstrated and are expected to provide significant improvement in our knowledge of the Earth's gravity field whose temporal components are climate-sensitive signals. CHAMP and GRACE are expected to monitor these signals for a time period of 5 years or longer. New models and observations of Earth's mean and time-variable gravity fields will be available with a temporal resolution of one month (primarily by GRACE). For the successful recovery of time-variable gravity fields, geophysical effects such as ocean tides, atmospheric mass redistribution, and high-frequency barotropic ocean signals should be removed from the GRACE measurements to observe climate-sensitive signals such as hydrology, ice sheet mass balance, and oceanic mass redistribution. Imperfect modeling of these corrections, resonant orbit errors, and effect of temporal aliasing will contaminate GRACE monthly solutions. In this study, we quantify the effects due to the inherent modeling error and temporal aliasing caused by ocean tides, atmosphere, and ground surface water mass on monthly mean GRACE gravity estimates. By simulating GRACE range-rate perturbations due to modeling error along the orbit, we analyze their effects on the estimated gravitational coefficients, as well as the temporal aliasing, by fully inverting monthly GRACE data. Finally, we discuss the feasibility of the CHAMP mission to recover the long wavelength temporal gravity fields by analyzing one year of CHAMP data.

**JSG02/09A/D-008** Poster **0830-008**

### REPEATED HIGH-PRECISION GRAVITY AND GPS MEASUREMENT TECHNIQUES

Paul GETTINGS<sup>1</sup>, Robert N. HARRIS<sup>1</sup>, Rick ALLIS<sup>2</sup>, David S. CHAPMAN<sup>1</sup> (<sup>1</sup>Department of Geology & Geophysics, University of Utah, <sup>2</sup>Utah Geological Survey)

Repeated high-precision gravity and GPS measurements are becoming a common tool for tracking changes in subsurface reservoirs. Despite this, there is little literature which discusses measurement techniques and the expected errors. Our research has focused on improving measurement techniques to be applied to ground water and geothermal steam reservoirs, including quantifying the minimum error levels with modern equipment. We applied these methods in two studies: ground water monitoring of the southern Salt Lake valley, Utah, USA, and steam monitoring of the Geysers geothermal field, California, USA. Gravity measurements using modern relative high-precision meters, such as Scintrex CG-3Ms or L&R E series, can now be routinely made to an accuracy of 5  $\mu$ Gal. Such accuracy requires the use of time series analysis at each station, and non-linear instrument drift functions. Modern computerized meters are capable of internally storing a time series of measurements for each station; older meters can often be fitted to such data to a field computer. This time series, typically of 10-15 minute duration in our work, can then be analyzed in several ways to produce stable estimates of the gravity reading. In particular, our research has emphasized using a weighted arithmetic average (for long occupations), or a Thiele extrapolation scheme (for shorter station occupations). Instrument drift is removed through a superposition of a linear long-term drift function, and an empirical staircase function formed from differences between repeated station occupations. To achieve high-accuracy GPS measurements while maximizing the number of field stations in a survey, rapid-static measurements are necessary. We have tested the effect of occupation time and processing schemes on the absolute accuracy of the resulting GPS position. Using a post-processing differential method with a fixed (but not necessarily continuous) base station within 15 km, positioning error of < 4 cm vertical is achievable with 30 minute occupations and broadcast orbital parameters. There is a definite correlation between baseline length and positioning accuracy. Using precision orbital parameters removes this correlation. Occupations of 60 minutes or more also improve accuracy; combining 1 hour occupations with precise orbital data yields a vertical error of < 3 cm for all stations within 20-30 km of the fixed reference. In both case studies, gravity measurements tracked known mass changes in the reservoir. In the southern Salt Lake valley study, mass changes measured along the line of gravity stations qualitatively tracked water well level changes, but very complicated local hydrology precluded more detailed quantitative comparisons. At the Geysers, the station grid shows coherent spatial signals, with gravity changes that are within measurement error of theoretical predictions.

JSG02

Wednesday, July 9

## INTERDISCIPLINARY EARTH SCIENCE FROM IMPROVED GRAVITY FIELD MODELING (IAG, IAHS, IAPSO, IASPEI)

Location: Site A, Room 5

Wednesday, July 9 PM

Presiding Chairs: G. Balmino, R. Rummel

**SG02/09P/A05-001** Invited **1400**

### THE EFFECT OF THE GENERATION OF NEW GRAVITY MODELS FROM CHAMP, GRACE AND GOCE ON GEODESY

Reiner RUMMEL, Jakob FLURY, Thomas GRUBER (Institute for Astronomical and Physical Geodesy, Technical University Munich)

It is our expectation that after completion of the missions CHAMP, GRACE and GOCE the static and the time variable part of the earth's gravity field are known with high precision and resolution. For the stationary part a geoid and gravity anomaly precision of 1 cm and 0.1 mGal, respectively, are envisaged with a spatial resolution of somewhere between 70 km or 100 km half wavelength. In combination with geodetic positioning techniques such as VLBI, SLR and GPS height systems could be unified at cm-level, if local short wavelength gravity information is available, too. Thus, once the new generation of global gravity models becomes available, the remaining key question will be, whether systematic distortions in nowadays gravimetry (land and sea), deflections of the vertical and topographic data bases can be identified and eliminated. This would imply, that along with the long and medium wavelength improvements also the short wavelength gravity field material would be significantly improved from these missions.

**JSG02/09P/A05-002** Invited **1425**

### IMPACT OF AIRBORNE GRAVIMETRY ON GEODESY AND OCEANOGRAPHY

Rene FORSBERG (Department of Geodynamics, KMS)

Airborne gravimetry has developed rapidly in recent years, primarily thanks to the development of kinematic GPS. With typical best accuracies at the 1-2 mgal r.m.s. level, with near bias- and drift-free performance, airborne gravimetry is an ideal tool for geoid determination and regional gravity field mapping, allowing vast and inaccessible areas to be quickly and economically covered. In continental areas geoid models from airborne, surface and satellite data, combined with detailed elevation data (e.g., from the SRTM mission) could readily meet most needs of height determination by GPS, reducing or eliminating the need for levelling. In the marine areas, the possibility for seam-less coverage of near-coastal regions, and the ability to detect systematic errors in existing marine gravimetry, would enable the generation of improved geoid models, giving improved direct measurement of dynamic sea-surface topography from satellite (or airborne) altimetry. In the paper a brief overview is given of the current status of airborne gravimetry and some future trends. The applications for land and marine geoid determination are illustrated by a number of KMS cooperative survey projects, spanning from major surveys in the Arctic, over European sea areas, to some experiences in tropical jungle regions.

**JSG02/09P/A05-003** Invited **1450**

### GEOID HEIGHT TIME DEPENDENCE DUE TO GLOBAL GLACIAL ISOSTASY: A FILTER FOR GRACE DATA ANALYSIS

Richard W. PELTIER (Dept. of Physics, University of Toronto, Toronto, Ontario, Canada)

The Gravity Recovery And Climate Experiment (GRACE) will, within the next several years, deliver an observation of the time dependence of geoid height that will resolve not only the annual cycle of this field with high spatial accuracy, but also its secular component. Although the annual cycle and its interannual variability will be dominated by atmospheric and surface hydrology effects, the secular component will provide important information concerning the origins of global sea level rise. However the secular signal will also be significantly influenced by the ongoing impact of the glacial isostatic adjustment process due to the most recent polar deglaciation event which ended approximately 10,000 years ago. If it were possible to construct a sufficiently accurate a-priori model of this contribution to the global secular change signal that GRACE will observe, then this component could be removed so as to more clearly reveal the modern climate change related influences more clearly. I will discuss the considerable further progress that has been made in the construction of a GIA filter for GRACE, emphasizing the extent to which Holocene relative sea level observations have made it possible to calibrate the model. These data have recently led to an improvement in the model of net glacial forcing and to confirmation of the important role that rotational feedback plays in determining the largest spatial scale characteristics of the expected GIA contribution to the GRACE observations.

**JSG02/09P/A05-004** Invited **1515**

### TIME-VARIABLE GRAVITY: CASE STUDIES OF GEOPHYSICAL AND CLIMATIC MONITORING AND MODELING

Benjamin Fong CHAO (Space Geodesy Branch, NASA Goddard Space Flight Center)

Precise time-variable gravity data from dedicated space missions enable us to study the mass transport processes that occur in the Earth system, from high atmosphere to deep in the Earth interior. This can be done in much higher spatial resolutions than provided by the satellite-laser-ranging (SLR) technique. We will review the quarter-century of SLR observation of low-degree time-variable gravity, which have already led to important discoveries in terms of large-scale geophysical and climatic mass movements. We will then discuss new quantitative aspects accentuated by the high precision of the space missions such as GRACE. For example, the atmosphere pressure field will have to be considered not in 2-D thing-layer approximation but in its full 3-D structure. Certain cases will be raised, where interesting geophysical and climatic mass variations can either serve as ground validations for the space mission observations, or benefit from independent quantitative constraints afforded by the time-variable gravity data, depending on their temporal and spatial resolutions.

**JSG02/09P/A05-005** Invited **1555**

**CAN CONTINENTAL WATER MASS VARIABILITY DERIVED FROM SATELLITE GRAVITY MISSIONS BE USED TO CORRECT FOR THE LONG-WAVELENGTH HYDROLOGICAL LOADING SIGNAL IN GEODETIC TIMESERIES?**

Tonie M. VAN DAM<sup>1</sup>, John M. WAHR<sup>2</sup> (<sup>1</sup>European Center for Geodynamics and Seismology, <sup>2</sup>Department of Physics, University of Colorado, Boulder)

Model estimates of the annual variations in continental water storage are of sufficient magnitude to induce peak-to-peak changes in the vertical position of geodetic stations of up to 3 cm. Signals of this magnitude need to be removed from the geodetic data if the geodetic trend is to be interpreted in terms of geodynamic processes. Unfortunately, considerable errors are probably present in the model-derived water storage estimates due to errors in the model forcing, parameters and model formulation. If these models are used to correct the geodetic data, it is likely that the continental water storage signal is being improperly removed from the geodetic data sets. A large number of satellite gravity missions have been recently launched, or will come online in the near future, that will measure changes in Earth's surface hydrology with unprecedented accuracy. Gravity missions such as CHAMP, GRACE and GOCE, and other satellite missions have the potential to significantly improve our understanding of many hydrologic processes, as well as improving our ability to monitor and predict the partitioning of continental water mass into snow, precipitation, soil moisture and ground water. In this paper, we investigate the possibility that estimates of water storage variations derived from satellite gravity missions can be used to correct geodetic data for the long wavelength component of the water storage signal.

**JSG02/09P/A05-006** Invited **1620**

**GRACE - UTILITY AND VALIDATION: MAPPING THE TIME-MEAN CIRCULATION OF THE NORTH ATLANTIC OCEAN**

Steven Robert JAYNE (Dept. of Physical Oceanography, Woods Hole Oceanographic Inst.)

The precise measurement of the geoid by the Gravity Recovery and Climate Experiment (GRACE) mission permits the estimation of the ocean's time-mean, three-dimensional, geostrophic circulation. The time-mean sea surface height measured by satellite altimetry includes the ocean's dynamic topography (order 1 meter), however this signal is obscured by the much larger signal of the Earth's geoid (order 100 meters). Traditional estimates of the Earth's gravity field (*i.e.* EGM96 by Lemoine *et al.* 1998) incorporated the time-mean sea surface height, heretofore preventing the estimation of permanent ocean currents such as the Gulf Stream, the Kuroshio, and the Antarctic Circumpolar Current. The GRACE geoid, measured independently of altimeter data, allows for more accurate estimation of the ocean's dynamic topography. The three-dimensional structure of geostrophic ocean currents is estimated from the combination of dynamic height, computed from altimetry of temperature and salinity, and the mean sea surface height. This circulation estimate can be independently tested against the dynamic pressure estimated from deep float displacements. The preliminary results indicate that the GRACE estimate is a substantial improvement over the EGM96 geoid for calculating the general circulation of the North Atlantic Ocean at large spatial scales.

**JSG02/09P/A05-007** **1645**

**THE GRAVITY RECOVERY AND CLIMATE EXPERIMENT: STATUS AND EARLY RESULTS**

Byron TAPLEY<sup>1</sup>, Christoph Reigber<sup>2</sup> (<sup>1</sup>University of Texas Center for Space research, <sup>2</sup>GeoForschung Zentrum Potsdam)

The Gravity Recovery and Climate Experiment (GRACE) is a dedicated satellite mission whose objective is to map the global gravity field with unprecedented accuracy over a spatial range from 400 km to 40,000 km every thirty days. The measurement precision will provide a mean gravity field whose accuracy in this frequency range is between 10 and 1000 times better than our current knowledge. The gravity measurements are applicable to studies of the general ocean circulation and ocean-atmosphere heat and mass exchange. Measurements of continental aquifer mass change, polar ice mass change and ocean bottom currents are examples of a completely new remote sensing capability whereby we can use satellite measurements to look into the earth's interior. The GRACE mission involves two identical satellites orbiting one behind the other at an approximate distance of 200 km. The primary measurement is provided by the High Accuracy Inter-satellite Ranging System (HAIRS), which measures range change between the two satellites. The range change will be measured with a precision better than 10 microns. A highly accurate three-axis accelerometer, located at the satellite mass center, will be used to measure the non-gravitational accelerations. Satellite GPS receivers will position the satellites over the earth with sub-centimeter level accuracy. With this set of measurements, the two GRACE satellites will provide highly accurate measurements of the global gravity field once every thirty days. The two satellites were launched on March 17, 2002, and are designed to operate for a period of five years. This presentation will summarize the mission status, the satellite and instrument performance, and will describe some of the early results and the impact of these results on global climate change investigations.

**JSG02/09P/A05-008** **1700**

**SCIENTIFIC ACHIEVEMENTS FROM THE FIRST PERIOD (1997-2003) OF THE GLOBAL GEODYNAMICS PROJECT USING A WORLDWIDE NETWORK OF SUPERCONDUCTING GRAVIMETERS**

Jacques HINDERER<sup>1</sup>, David CROSSLEY<sup>2</sup> (<sup>1</sup>EOST/PGS (UMR 7516 CNRS-ULP) Strasbourg France, <sup>2</sup>Department of Earth and Atmospheric Science Saint-Louis University)

The first term of the GGP (Global Geodynamics Project) of a worldwide network of superconducting gravimeters (SGs) started in July 1997 for a duration of 6 years. A special effort was made by all the SG groups to record pressure and gravity to uniform standards of precision and sampling, with standard data acquisition filters. We also agreed to prepare one minute data in an homogeneous way with identical exchange formats before uploading the files to the database hosted at ICET (Brussels, Belgium). This effort has allowed us to collect high quality records of time-varying gravity from about 15 stations with a cluster in Europe and Japan, and individual stations in Canada, United States, Australia, South Africa, Indonesia, Antarctica and in the Arctic (Spitsbergen). We paper is devoted to here review the main scientific results obtained from this set of gravity records. We first emphasize the seismic frequency band (periods below 54 min) where SGs have shown to be better than broadband seismometers for the observations of long-period fundamental normal modes after large earthquakes. A noise comparison from all the stations also shows that these instruments are uniquely suited to study in the best available conditions the sub-seismic band (periods above 54 min and below the tides) where it is predicted there should be the core modes and the Slichter triplet of the inner core. Second, we discuss significant new results that have been obtained concerning the tides: zonal long-period components, ocean

loading, detection of non-linear tides, and Free Core Nutation resonance effects. Third, we deal with the long-term gravity changes and show that SGs, thanks to their extremely low instrumental drift, are also a useful tool for detecting seasonal changes due to various loading effects (hydrological, non-tidal oceanic, atmospheric), as well as the contribution from the pole motion at the Chandler period. Finally we will demonstrate the possibility that a regional network of SGs, such as currently operated in Europe, can validate/calibrate time-varying satellite gravity data from the new space missions, e.g. CHAMP and GRACE.

**JSG02/09P/A05-009** **1715**

**MODELLING OCEAN MASS REDISTRIBUTIONS IN THE HADLEY CENTRE CLIMATE MODEL**

Keith HAINES, Rory BINGHAM (Environmental Systems Science Centre, Reading Univ.)

Oceanic mass redistribution leads to temporal changes in the Earth's gravitational field. The GRACE satellite mission launched in March 2002 promises the opportunity to observe these changes with unprecedented accuracy. This study is an attempt to characterise the spatial and temporal scales of mass redistribution in the ocean. We further consider gravitational effects of this redistribution. We derive bottom pressure anomaly fields from the output of the one hundred year control run of the Hadley Centre coupled ocean-atmosphere model HadCM3. From the bottom pressure time-series we derive time varying geoid displacements to degree and order 100. Together these two data sets form the basis of our study. We use a variety of mathematical and statistical techniques to separate the time-series into frequency bands. The mean power spectrum reveals that, as expected, the annual harmonic is the dominant bottom pressure signal. Significant power was also found at the semi-annual and third-annual harmonics. Each of the bottom pressure annual and higher harmonics was isolated and its effect on the geoid calculated. A comparison of the annual geocenter motion was made between this study and the limited number of other studies for which such a calculation has been performed. Relatively good agreement was found for the x component with much poorer agreement between the models in the two other directions. The oceanic processes leading to the geocenter motion are considered. Empirical Orthogonal Function (EOF) analysis confirmed the dominance of the annual signal. The second mode had a decadal frequency and a spatial pattern suggestive of basin wide transport between the Pacific and Atlantic oceans. We consider the relationship between this mode and observed modes of climate variability. A composite method was also used to characterise the mass redistribution associated with the model ENSO events. Impact on variability of large scale quantities such as J2 are considered.

**JSG02/09P/A05-010** **1730**

**IMPACT OF NEW GRAVITY MISSIONS FOR SATELLITE ALTIMETRY APPLICATIONS**

Thomas GRUBER, Jakob FLURY, Thomas PETERS, Drazen SVEHLA (Institute for Astronomical and Physical Geodesy, Technical University Munich)

The new gravity field missions CHAMP, GRACE and GOCE promise to provide significantly improved global gravity field models of the Earth. Satellite altimetry, which closely links the geoid and oceanographic areas of research, immediately benefits from improved gravity field information in two ways. Apart from possible improvements in the radial accuracy of altimeter satellite orbits by using better gravity field information, the oceanic geoid and its variations is the quantity of main interest, because it enters into the determination of dynamic ocean topography and into bottom pressure variations. The paper investigates both aspects based on the most recent CHAMP (and if available GRACE) gravity field solutions. (1) Orbits for altimeter satellites based on the new gravity field models are analysed in order to identify the impact of the new gravity field models on their radial accuracy. (2) The ocean geoid, derived from these models is analysed in the spatial and spectral domains in order to identify its impact on newly computed sea surface topography solutions. For this purpose several sea surface topography solutions are computed by subtracting the oceanic geoid from altimetry derived mean sea surfaces and subsequent filtering. Comparisons to oceanographically derived sea surface topography solutions are used to assess the quality of the new gravity field solutions over the oceans.

**JSG02/09P/A05-011** **1745**

**CO-SEISMIC GEOID AND GRAVITY CHANGES DETECTABLE BY GRAVITY SATELLITE MISSIONS**

Wenke SUN, Shuhei OKUBO (Earthquake Research Institute, University of Tokyo)

Recently, a number of dedicated satellite missions is and will be available for gravity field determination from space, such as, CHAMP, GRACE and GOCE. Especially, the primary objective of GRACE is to provide an unprecedented accuracy, global and high-resolution estimates of the constant and time-variable part of the earth's gravity field for every 30 days in 5 years. It can be expected that almost all time change problems in geosciences can be detected and well studied in the near future. The temporal gravity variations causing a global signature is usually considered to result from atmospheric mass redistribution, ocean circulation, sea level changes due to polar ice melting or aggregation, and the visco-elastic response of the Earth's lithosphere to past and present loads. However, another potential application of the gravity missions is that they provide us with powerful means to detect gravity and geoid changes caused by earthquake, which have never been detected up to the present. A case study of 1964 Alaska earthquake (Sun and Okubo, 1998) indicated that the gravity change could be detected on the earth surface by super-conducting gravimeter even as far as 5,000 km away. A geoid height change due to the earthquake could reach at 1.5 cm. Such gravity and geoid height changes are expected to be detectable by modern space techniques, like Altimetry and gravity missions. However, due to the limit spatial resolution of the gravity satellite missions, co-seismic deformations must calculated with a truncation of the harmonic degrees, i.e., the contribution of higher degree part than the resolution of the space missions should be removed out. This requires a corresponding investigation for individual or group wavelength, i.e., a theoretical work and simulation on truncated co-seismic deformation is necessary. This purpose can be approached by the dislocation theory (Sun and Okubo, 1993) for a spherical model since it is expressed in spherical harmonics. For this purpose, in this research, a concept of truncated co-seismic geoid and gravity changes is proposed and corresponding expressions are presented to compute co-seismic geoid and gravity changes for spherical harmonic degree within the spatial resolution of the gravity satellite missions. So that numerical results of any individual harmonic degree or summation to an interested degree can be used to compare with the precession of the gravity missions, to investigate whether the co-seismic gravity and geoid changes are detectable. A numerical computation of truncated co-seismic gravity and geoid changes is performed for a source equivalent to the fault size of the Alaska earthquake (1964,  $m_w=9.2$ ). Results indicate that both gravity and geoid changes are about two orders larger than the precession of the gravity missions. It implies that co-seismic deformations caused by a smaller earthquake (e.g.,  $m < 8$ ) are still detectable.

JSG03 Wednesday, July 9 - Thursday, July 10

**INTERDISCIPLINARY SCIENCE FROM REMOTE SENSING -  
RADAR ALTIMETRY, ATSR, SAR, OCEAN COLOR AND OTHER  
SENSORS (IAG, IAHS, IAPSO, IASPEI, ISPRS)**

Location: Site A, Room 12

Wednesday, July 9 PM

JSG03/09P/A12-001

1400

**METHOD OF RESERVOIR STORAGE MONITORING BY SATELLITES**Jun MAGOME<sup>1</sup>, Hiroshi ISHIDAIRA<sup>2</sup>, Kuniyoshi TAKEUCHI<sup>2</sup> (<sup>1</sup>Graduate Student, University of Yamaguchi, <sup>2</sup>Graduate School of Engineering, University of Yamaguchi)

More than 41,413 dams over the height of 15m are now in operation in the world serving for various important purposes in their region. Their efficient use is the most important subject in water resources management. Therefore it necessitates the regional monitoring of water storage in reservoirs, especially its seasonal variation. Since the ground observations of reservoir storages are often not available to the users due to lack of proper information transmission network as well as, in some cases, administrative barriers, it is desirable to develop technology to monitor water storage by the use of satellite remote sensing technique. In this study, we propose new methods for estimating water storage in reservoirs based on satellite observations and digitized topographical data. First method is the combination of area of water surface (A) extracted from satellite image and change in water level (dH) measured by satellite altimeter. Second one is the combination of satellite data and relationship between water level (H), area of water surface (A), and reservoir storage (V), i.e. A-V curve, H-V curve, and H-A curve. If these relations are available, satellite measured A or H can be translated into the V. These methods are applied to the Yagisawa-reservoir in Japan and Volta Lake of Akosombo dam in Ghana to verify the possibility of estimating the water storage in reservoir. In order to identify the area of water surface of reservoirs (A), the satellites and sensors used are : JERS-1/SAR, SPOT/HRV, ADEOS/AVNIR and TERRA/MODIS. The radar altimeter system mounted on TOPEX/POSEIDON was used for deriving water level. For Yagisawa - reservoir, the derived average accuracy based on satellite images and A-V curve estimated from DEM was , in terms of percentage error, 8.3% (SPOT/HRV and ADEOS/AVNIR : semi-automated), 8.2% (JERS-1/SAR : image reading) and 19.7 % (JERS-1/SAR : semi-automated) as against observations at dam site. As for Volta Lake, all proposed methods can provide seasonal to inter-annual variability of reservoir. In comparison with Volta River Authority report, in which the change in water storage from 1999/1/1 to 1999/12/31 was reported as 27.89 km<sup>3</sup>, the error of estimated results are the less than 10 %. Each method has its advantages and limitations depending upon the availability of data, scale and location of reservoir, and so on. However, these methods have high potential to be used for monitoring the reservoir storage without in-situ observations. Because new satellites and geographic information are being prepared on a global scale, proposed methods are considered to be able to monitor regional water storage in reservoirs more precisely by using these data.

JSG03/09P/A12-002

1420

**REMOTE SENSING OF LAKE ICE: LAKE BAIKAL, SPRING PHYTOPLANKTON BLOOM STUDIES**Sergei V. SEMOVSKI<sup>1</sup>, Nikolay Yu. MOGILEV<sup>2</sup>, Petr Yu. PUSHISTOV<sup>3</sup> (<sup>1</sup>Limnological Institute SB RAS, Irkutsk, Russia, <sup>2</sup>Institute of Solar-Terrestrial Physics SB RAS, Irkutsk, Russia, <sup>3</sup>Yugra Institute of Information Technologies, Khanty-Mansijsk, Russia)

The state of the ice cover, and the freeze-up and breakup dynamics of lakes are influenced by a climate variability and are good indicators of large-scale climate changes. The spatial distribution and the state of the ice cover of lakes determine in a multitude of ways the occurrence of many processes in lake ecosystems, and the formation of hydrophysical fields. The algal bloom intensity in lakes depends in many respects on the optical properties of ice. Routine observations of the conditions of the snow and ice cover at a stationary hydrometeorological network are usually poorly representative, and the main part of the water surface remains unexplored by researchers. The generation and sample applications of a set of multispectral remotely sensed products for investigations of Lake Baikal's ice cover variability are described. During the period from mid-January to the end of April, the lake is completely covered with ice, and by analyzing satellite information it is possible to investigate in detail the distribution and dynamics of the main types of ice cover. Different ice cover classes and unfrozen water distributions are estimated from calibrated and navigated NOAA AVHRR 1.1-km imagery of Lake Baikal for January 1994 through May 2002. The processing strategy and characteristics of the products are reviewed. The utility of this type of multiparameter dataset for modeling applications and process studies is discussed. High-resolution Resurs, ERS SAR, ASTER and MODIS images are used for detailed representation of different ice classes distributions. *Aulacoseira baicalensis* diatom is a dominant pelagic endemic species of Lake Baikal during spring. The diatom begins to multiply in February-March under the ice and its concentration reaches a maximum in April-May. The under-ice bloom intensity of diatoms shows a strong interannual variability. The causes of these changes are unclear yet; however, the photosynthetic active irradiance transmission through the ice during the springtime depends largely on ice optical properties. The heat-driven convection intensity, turbulence and stratification structure are also associated with changes in persistence of the ice cover. Both optical and hydrodynamic factors form conditions for diatoms growth. The known spatial and temporal distribution of ice for the whole lake is used in bio-optical model of water ecosystem dynamics for spring bloom simulation. Optical properties of ice classes derived using remote sensing data and available downward irradiance on the water surface are estimated using field observational data. This information is used as external fluxes in the large eddies model of the under-ice convective boundary layer. Bio-optical model of two-component phytoplankton dynamics (heavy diatoms and light picoplankton) coupled with heat-driven hydrodynamics is developed. Equations of the ecodynamics model are based on general principles of population dynamics. The impact in optically active ecosystem components in the underwater spectral irradiance field is simulated.

JSG03/09P/A12-003

1440

**SURFACE SKIN TEMPERATURE DIURNAL CYCLE OVER LAND FROM COMBINED PASSIVE MICROAVE AND INFRARED SATELLITE OBSERVATIONS - APPLICATION TO SOIL MOISTURE RETRIEVAL**Filipe AIRES<sup>1</sup>, Catherine PRIGENT<sup>2</sup>, William B. ROSSOW<sup>3</sup> (<sup>1</sup>GISS/NASA - Columbia University and LMD/IPSL/CNRS - Ecole Polytechnique, <sup>2</sup>CNRS, LERMA, Observatoire de Paris, Paris, France, <sup>3</sup>NASA/Goddard Institute for Space Studies, New York, USA)

Land surface temperature (Ts) diurnal cycle and its difference with the temperature of the overlying air mass (Tair) govern the exchange of energy fluxes at the land-atmosphere interface. Adequate measurements of Ts over land over the whole diurnal cycle would not only enable model evaluation of coupled land-atmosphere climate model, it would also provide an additional constraint on latent and sensible heat flux calculations. However accurate measurements of Ts over continents are not yet available for the whole globe, for clear and cloudy skies, with a time sampling adequate to resolve the diurnal cycle. Unlike Tair, Ts is not conventionally observed by the meteorological weather stations. Ts are estimated from satellite infrared radiance observations, but are limited to clear conditions because of the inability of infrared to penetrate clouds. A neural network inversion scheme has been developed to retrieve the surface skin temperature along with atmospheric water vapor, cloud liquid water, and surface emissivities over land from passive microwave from the Special Sensor Microwave / Imager [Aires et al., JGR, 2001; Prigent et al., JAM, 2003]. The results of the neural network inversion are very encouraging, with r.m.s. theoretical error of 1.3K in clear sky conditions and 1.6K in cloudy scenes for Ts over the globe. In the absence of routine in situ surface skin measurements, retrieved Ts values are evaluated by comparison to Tair measured by the meteorological station. The Ts/Tair difference shows all the expected variations with solar flux, soil characteristics, and cloudiness. Microwave Ts retrieval presents a very attractive complement to the infrared estimates in cloudy areas and time record of land surface temperature can be produced. However, the SSMI microwave observations on board the Defense Meteorological Satellite Program (DMSP) polar orbiters do not provide the adequate time sampling for a full description of the surface skin temperature cycle under cloudy condition. A study is underway to reconstruct the complete daily surface skin temperature diurnal cycle over the globe from a limited number of observations for both clear and cloudy conditions, based on a statistical analysis of the observations datasets and excluding model calculations. In a second phase, soil moisture retrieval is examined from combined passive microwave and infrared observations. Surface soil moisture information can be derived from passive microwave observations, even at SSM/I above 15 GHz. In addition, analysis of the amplitude of the surface skin temperature cycle can also provide indirect information on the soil moisture content. Soil moisture from NCEP are systematically compared to passive microwave satellite information and to retrieved surface skin diurnal cycle, in order to analyze their sensitivity to spatial and temporal variations of the soil moisture, on a global basis and for a year. This sensitivity analysis will lead to the development of a soil moisture retrieval scheme from combined microwave and infrared observations. It will make use of satellite observations that have been available for more than a decade and will thus enable global scale studies of the intra and inter annual variability of soil moisture.

JSG03/09P/A12-004

1500

**CLUSTER ANALYSIS OF REMOTELY SENSED DATA FOR DISCRIMINATING SINKS AND SOURCES OF NATURAL ADMIXTURES IN CASE II WATERS**Lioudmila Y. AMETISTOVA<sup>1</sup>, Genrikh S. KARABASHEV<sup>2</sup> (<sup>1</sup>Ocean Technology Group, University of Sydney, Australia, <sup>2</sup>PP Shirshov Institute of Oceanology, Moscow, Russia)

Remote sensing is unique in its capabilities for monitoring ocean colour and subsequent assessment of biogeochemical properties of the waters. Sea-viewing Wide Field-of-view Sensor (SeaWiFS) is the most popular sensor for interpreting remotely sensed data from aquatic environments. The basic assumption for chlorophyll retrievals from water-leaving radiances is that there exists a more or less universal relationship between ocean colour and phytoplankton pigment concentration (case I waters). Unrealistically high chlorophyll values obtained with the standard OC4 algorithm in coastal waters of high latitudes (case II waters) is the result of the failure of such an assumption. In turbid waters photosynthetic pigments, coloured dissolved organic matter, organic as well as inorganic solids colour the water. Due to significant river runoff and shallowness of the White Sea (Russian Arctic), it represents typical optically complex case II waters. Cluster analysis was applied to the White Sea L2 SeaWiFS water-leaving radiances in 6 visible wavelengths ( $\lambda = 412, 443, 490, 510, 550$  and  $675$  nm) for all dates available from August 1997 (SeaWiFS launch) till October 2001. For total 712 days 10 clusters were identified. Negative values were encountered in over 60% of the cases in the 412 nm band, which indicates atmospheric correction failure in the coastal zone due to particulate matter presence and thus inability to use SeaWiFS standard chlorophyll algorithm. The most abundant pattern has a slightly negative 412 nm band and a radiance peak at 550 nm ranging between 0.3-0.5 mW/cm<sup>2</sup>/um/sr. Almost parallel is a cluster with more pronounced negative part of the spectra (first three bands have negative radiances). Mentioned spectra are found in the outer parts of the major bays. Due to pronounced 550 nm peak and taking into consideration typical values of particulate matter, chlorophyll and yellow substance concentrations encountered in the White Sea, spectra in the regions of river discharge reflect very high yellow substance concentrations as well as particulate matter presence. Found closer to the shore (but not in the river discharge basins) are the spectra with unrealistically high values in all visible bands - presumably caused by strong bottom reflection in optically pure shallow waters. In these areas Barents sea waters intrusion into the White Sea is observed. In case II waters yellow substance absorption and particulate matter backscatter determine water optical properties. Therefore, only strong chlorophyll blooms can be detected in such waters using SeaWiFS data. The study was supported by the Russian Foundation for Basic Research, project no. 02-05-64680.

JSG03/09P/A12-005

1520

**ESTIMATION OF SEASONAL PARTIAL PRESSURE CO2 IN NORTH WEST PACIFIC OCEAN BY SHIP AND SATELLITE DATA**Takahiro OHSAWA<sup>1</sup>, Keiko HANAWA<sup>1</sup>, Chaofang ZHAO<sup>2</sup>, Yasuhiro SUGIMORI<sup>1</sup> (<sup>1</sup>Department of Information Science, Chiba University, <sup>2</sup>National Laboratory of Ocean Remote Sensing of MOE)

Determination of seasonal and high-resolution partial pressure CO<sub>2</sub> (pCO<sub>2</sub>) in surface seawater is one of the most challenging problems in order to estimate CO<sub>2</sub> flux between air-sea interfaces. The new empirical relation among pCO<sub>2</sub>, different physical and geochemical parameters has been established in the surface ocean using recent WOCE and JGOFS data. This data has been tested in the Northwest Pacific Ocean. Compared with pCO<sub>2</sub> investigations, the results show a good agreement in the tropical ocean and subtropical gyres throughout the year, as well as temperate waters in the summer season. The mean value of pCO<sub>2</sub> is well-simulated using Levitus climatological dataset. The temporal and spatial variations of pCO<sub>2</sub> are dominantly controlled by sea surface temperature, which implies a combination of operational AVHRR dataset. This datasets may produce high resolution of pCO<sub>2</sub> and its seasonal variation in the study area. In winter season, when intense upwelling occurs in the subarctic region, a systematic underestimation of about 74  $\mu$ atm is found for the proposed parameterization method, mainly attributed to the rich nutrients from the deep water and TCO<sub>2</sub> accumulated through biological pump. After correcting this bias, the calculated pCO<sub>2</sub> coincides well with the historical investigations. Further effort is necessary for modeling the study area where upwelling is active in winter season, especially using remote sensing data (e.g., SeaWiFS, MODIS and GLI).

**JSG03/09P/A12-006** **1540**

**MAPPING SEA SURFACE SALINITY IN COASTAL WATERS WITH AN AIRBORNE MICROWAVE RADIOMETER**

Malcolm Lewis HERON<sup>1</sup>, Derek M. BURRAGE<sup>2</sup>, Thomas C. STIEGLITZ<sup>3</sup>, Arnstein PRYTZ<sup>1</sup> (MARINE GEOPHYSICAL LABORATORY, <sup>2</sup>The University of Southern Mississippi, MS, USA)

A prototype scanning low frequency microwave radiometer (SLFMR), developed by NOAA and NRL and constructed by ProSensing Ltd has been calibrated and validated in deployments on river plumes in the Great Barrier Reef Lagoon in North Queensland, Australia. The spatial resolution, when the aircraft is flying at 3,000 m, is about 1 km and a 6 km swath is mapped across the heading direction of the aircraft. The salinity resolution is about 1 psu. The SLFMR is a null measurement system with a Dicke switch between the antenna and a noise diode which is controlled by a feedback voltage. The compartment is thermally controlled at about 40 OC with thermistors placed at key locations. The calibration of the instrument is sensitive to small differences in the temperatures within the compartment. Also, there is an aging influence on the calibration. We established a calibration procedure which uses the cosmic background and room temperature as two calibration points, and we assume that the correction effects are linear in between. The calibration procedure is performed before and after each campaign (usually for a duration of about two weeks). With careful attention to the calibration, we have successfully mapped river plumes and groundwater runoff from the wet tropics of the North Australian continent, demonstrating that the SLFMR is a valuable tool for coastal oceanography studies. Examples are shown of river plumes from the Herbert River in North Queensland. When the wind speed is low, well formed plumes can be seen being swept alongshore by the prevailing coastal current. Under these conditions there is a strong stratification and the surface layer is highly mobile. When the wind rises to above about 6 m s<sup>-1</sup> the plume is rapidly vertically mixed. One of the most pressing problems for the Great Barrier Reef Marine Park Authority (which is a regulatory authority set up by the Federal Government to ensure the sustainable use of the Marine Park) is to determine and manage the effect of river runoff into the main lagoon region. The rivers carry sediments and nutrients into the Lagoon. It has been shown that the sediments predominantly form a coastal wedge and affect only the coastal fringing reefs. The destination and effect of nutrients is less certain and the SLFMR is proving to be a uniquely useful instrument in providing a measure of advective and diffusive mixing of the fresh water into the Lagoon.

**JSG03/09P/A12-007** **1620**

**REMOTE SENSING & DECISION SUPPORT FOR ENVIRONMENTAL SUSTAINABILITY**

Gilbert L. ROCHON<sup>1</sup>, Chris JOHANSEN<sup>2</sup>, Steve MAYO<sup>3</sup>, Mohamed MOHAMED<sup>4</sup>, Marseyas FERNANDEZ<sup>5</sup>, Sarada MAJUMDER<sup>6</sup>, Larry BIEHL<sup>7</sup> (<sup>1</sup>Purdue University, Information Technology/Earth & Atmospheric Sciences, <sup>2</sup>Purdue University, Agronomy Dept./Lab. for Applications of Remote Sensing (LARS), <sup>3</sup>Purdue University, Information Technology (ITaP), <sup>4</sup>Pioneer Geomatics, Inc., <sup>5</sup>Imagine Software, Inc.)

It has been observed that some decisions which have significant impact on inter-generationally prudent management of terrestrial resources are made without awareness of the regional historical context (e.g. landcover, landuse, hydrology, biodiversity, human impact, natural geomorphology) and/or with either innocence or insouciance with respect to the future collateral damage associated with such decisions. It has further been observed that the volume and complexity of data derived from multi-temporal, multi-satellite remote sensing, particularly when combined with in situ data sources, can be overwhelming for even well-intentioned highly trained and inter-generationally ethical decision makers. Accordingly, it was determined that a prototype decision support system that was able to incorporate region-specific legacy data, contemporary input and the capacity to generate evocative representations of "what if" scenarios, could be a useful adjunct to both rule-based and quantitative decision support systems. In developing prototypical tools for enabling and monitoring region-specific environmental sustainability, the focus advanced herein is the potential benefit of providing the decision maker with virtual hindsight, through real-time rapid exploration of the archival satellite data with on-the-fly change detection, and associated in situ data, as well as virtual foresight, through visualization of alternative future scenarios. The limitations and contributory roles of remote sensing, GIS, GPS and visualization technologies in such prototyping are examined within the context of regions within Africa. The complexity of sustainable agri-cultural ecosystems in support of regional food security and the potential regional impact of climate change provide challenges to effective tool development. Moreover, the need to establish practical dissemination of the appropriate technologies and associated infrastructure in a manner so as to benefit the nutritionally vulnerable segment of the population is of paramount importance. Case studies are presented to illustrate the potential contribution of remote sensing enabled decision support for sustainable development and food security within African contexts and to assess alternative implementation strategies.

**JSG03-Posters** **Wednesday, July 9**

**INTERDISCIPLINARY SCIENCE FROM REMOTE SENSING - RADAR ALTIMETRY, ATSR, SAR, OCEAN COLOR AND OTHER SENSORS (IAG, IAHS, IAPSO, IASPEI, ISPRS)**

Location: Site D

**Wednesday, July 9 PM**

**JSG03/09P/D-001** **Poster** **1640-009**

**INSAR OBSERVATION OF THE AMUNDSEN BAY, ANTARCTICA**

Makoto OMURA<sup>1</sup>, Katsuki KOIKE<sup>2</sup>, Koichiro DOI<sup>3</sup>, Kazuo SHIBUYA<sup>1</sup>, Shigeru AOKI<sup>1</sup> (<sup>1</sup>Dept. of Environmental Science, Kochi Women's Univ., <sup>2</sup>Faculty of Engineering, Kumamoto University, <sup>3</sup>National Institute of Polar Research)

InSAR technique is useful method to observe the surface topography and to monitor the ice sheet and glaciers in the Antarctic region. We selected the Amundsen Bay, Enderby Land, Antarctica as a test site for the InSAR observation. There are some preliminary InSAR researches on the movements of ice sheet (Ozawa, et al., 1998), Glacier (Omura et al., 2000) and topography (Omura et al., 2001). SAR data from JERS-1, ERS-1 and ERS-2 were received at the Showa Station. Some good InSAR pair including the tandem mission of ERS-1/2 data and JERS-1 SAR L-band data were analyzed by three kind of processing system. We will show the characteristics of topography and its changes around the Amundsen Bay and the system dependent difference in interferograms. This study is carried out as a joint scientific research program of National Institute of Polar Research, Tokyo, Japan.

**JSG03/09P/D-002** **Poster** **1640-010**

**RESPONSE OF LAKE VOSTOK TO ATMOSPHERIC PRESSURE CHANGE**

Koichiro DOI<sup>1</sup>, Kazuo SHIBUYA<sup>1</sup>, Shigeru AOKI<sup>1</sup>, Tsutomu YAMANOKUCHI<sup>2</sup>, Reinhard DIETRICH<sup>3</sup>, Anja POTZSCH<sup>3</sup> (<sup>1</sup>National Institute of Polar Research, <sup>2</sup>. Remote Sensing Technology Center/The Graduate University for Advanced Studies, <sup>3</sup>. Institut für Planetare Geodäsie, Technische Universität Dresden)

More than 70 subglacial lakes were discovered with airborne radio-echo sounding in Antarctica (Oswald & Robin, 1973). The Lake Vostok is the largest one, which locates in east Antarctica around 77°S, 105°E. Ice thickness over the subglacial lake is more than 3km and dynamics of the lake is very interesting. Some geodetical observations like as GPS, SAR interferometry, and gravity measurements will be effective to detect surface displacements over the lake. Schneider and Simon (1976) observed solid earth tides for about 5 month in 1969 with a gravimeter Gs 11 No. 140 at Vostok station, which is on an ice sheet over the Lake Vostok. We reanalyzed the gravity data using a tidal analysis program BAYTAP-G (Tamura et al. 1991) and obtained gravimetric factors for diurnal and semidiurnal tides as well as phase differences of each constituent from theoretical solid tides. The obtained results are consistent with those by Schneider and Simon (1976). We also estimated the response in gravity to atmospheric pressure changes by the program and the obtained value is -3.7 micro-gal/hPa (1 micro-gal = 10<sup>-8</sup>ms<sup>-2</sup>). Since the response value takes around -0.3 micro-gal/hPa in ordinal observation on the ground, this value is remarkably large. The obtained response value means upward displacement of ice surface under the condition of pressure increment. We suspect that some movements of fresh water beneath the ice sheet affect the surface response to atmospheric pressure changes. We can examine the vertical displacements of ice surface due to atmospheric pressure change by the combination of SAR interferometry and atmospheric pressure data estimated from the NCEP/NCAR reanalysis data. We will detect surface displacements from some interferometric scene pairs observed by ERS-1 and ERS-2 over the lake and discuss the response of the subglacial lake.

**JSG03/09P/D-003** **Poster** **1640-011**

**LAKE LEVEL MONITORING FROM ALTIMETRY MEASUREMENTS**

Jean-Francois CRÉTAUX<sup>1</sup>, Anny CAZENAVE<sup>1</sup>, Franck MERCIER<sup>2</sup>, Alexey KOURAEV<sup>2</sup>, Benoit LEGRESY<sup>2</sup>, Frederique REMY<sup>2</sup>, Gaetan VINAY<sup>3</sup>, Fabrice PAPA<sup>1</sup> (<sup>1</sup>CNES/LEGOS-GRGS, <sup>2</sup>LEGOS)

With the recent missions of satellite altimetry (Topex-Poseidon, Jason-1, Envisat, ERS-1 and ERS-2) it is possible to measure with a great precision inland sea level variations that can be interpreted as water mass balance. The Legos laboratory is involved in this field of analysis since many years. In the frame of an INTAS project we have calculated the Aral Sea level variations with the Topex / Poseidon measurements from 1993 to 2002, ERS1&2 from 1991 to 2002, and Jason measurements in 2002. It has been shown that the so called big and small Aral have separate water level variations. Big Aral is continuously drying out with a slope of around 80 cm/year, while in the north, the level of the small Aral fluctuates at an annual time scale (due to climatic seasonal variations) and present also a lower decrease (less than 10 cm/yr). Traditionally lake level variations (that are usually in continental areas) have been measured with Topex / Poseidon mission, but the use of data from ERS satellites is also of a big interest due to their higher spatial resolution than the Topex / Poseidon or Jason satellites. Moreover, sea level variations that result from variation of hydrological parameters such as river discharge, precipitation and evaporation, are very sensitive indicators of regional climate variations. Based on an high spatial resolution bathymetry map which has been digitalized in 2002 we have preferred to compute variations of volume of the small and big Aral seas, which is a parameter more interesting in term of water mass balance than water level.

**JSG03/09P/D-004** **Poster** **1640-012**

**MICROWAVE REMOTE SENSING OF SOIL MOISTURE IN FIFE FROM 1987 TO 1988**

Hiroshi MATSUYAMA<sup>1</sup>, Sachiko ICHIKAWA<sup>1</sup>, Tosiuyuki NAKAEGAWA<sup>2</sup> (<sup>1</sup>Department of Geography, Tokyo Metropolitan University, <sup>2</sup>Meteorological Research Institute)

This study evaluates the possibility of estimating surface soil moisture through passive microwave remote sensing of 19 GHz. Spatial average of the surface 5 cm soil moisture in the grassland of FIFE study area (15 km by 15 km, First ISLSCP Field Experiment, International Satellite Land Surface Climatology Project) from July 1987 to October 1988 are compared with the observation from SSM/I (Special Sensor Microwave / Imager) on board DMSP (Defense Meteorological Satellite Program). Also, LAI (Leaf Area Index) calculated from NDVI (Normalized Difference Vegetation Index) of NOAA/NASA (National Oceanic and Atmospheric Administration / National Aeronautics and Space Administration) Pathfinder AVHRR (Advanced Very High Resolution Radiometer) 8-km land data set, is used to investigate the effect of phenology on the soil moisture estimation. The relationship among soil moisture, LAI and the polarization index (PI) is investigated. PI is defined as the brightness temperature of the vertical polarization minus that of the horizontal polarization, which is normalized by the average of these temperatures. By using PI, it is not necessary to consider the variation of surface skin temperature or effective temperature in the ground. The multiple regression analysis is applied to estimate the surface soil moisture by using LAI and PI. The incorporation of LAI into the multiple regression analysis reveals the higher accuracy of the estimation of soil moisture (r = 0.53 in 1987 and r = 0.76 in 1988) in comparison with the single regression analysis between soil moisture and PI (r = 0.42 in 1987 and r = 0.73 in 1988). Also, AIC (Akaike's Information Criteria) of the multiple regression analysis is smaller than that of the single regression analysis. Namely, the importance of phenology on the estimation of surface soil moisture is statistically confirmed. The standard error of the multiple regression analysis (ca. 20-30 % of volumetric soil moisture) is as large as the coefficient of spatial variation of the observed soil moisture in the FIFE study area. Concerning the transferability of this method, LAI and PI of 1988 (1987) are substituted into the multiple regression equation obtained in 1987 (1988). The estimations are evaluated by the observed soil moisture in 1988 and 1987, respectively. In the United States, it was relatively wet in summer 1987 while it was very dry in summer 1988. Nonetheless, about 50 % of the total variance is explained by this method in both years, which is as accurate as or more accurate than previous studies. From these results, it is possible to estimate surface soil moisture to some extent with the use of SSM/I and NOAA/AVHRR data alone, when the regression equation is once established. Since the method adopted in this study has fairly large generosity, it is possible to transfer this method to other grasslands in the world where soil moisture data are available at least for one year.

**JSG03/09P/D-005** **Poster** **1640-013**

**GLOBAL SCALE LAND HYDROLOGY MONITORING USING SATELLITE ALTIMETRY**

Philippa Anne BERRY<sup>1</sup>, Ralph Allen PINNOCK (Earth And Planetary Remote Sensing Lab, De Montfort University)

The new generation of altimeter-bearing satellites, Envisat and Jason-1, bring enhanced monitoring capability, with currently increased temporal sampling when combined with existing missions, and increased spatial sampling from the three tracking modes on Envisat, which allows data to be retrieved over widely varying topographic surfaces. Combined with the multi-satellite historical record, this provides a unique time-series of water flow over the earth's land surface. This paper combines data from Envisat, Jason-1, ERS-1, ERS-2 and Topex to investigate the historical record, demonstrate the current abilities of altimeters to monitor the global land surface water flow, and illustrate the future potential of this technique.

**JSG03/09P/D-006** Poster **1640-014**

**THE CLASSIFICATION OF VEGETATION OF WETLAND BASED ON REMOTE SENSING DATA, OVER KUSHIRO MARSH HOKKAIDO JAPAN**

Aosier BUHE<sup>1</sup>, K. TSUCHIYA<sup>2</sup>, M. KANEKO<sup>3</sup>, S.J. SUNG<sup>4</sup> (<sup>1</sup>Hokkaido Institute of Environmental Sciences, <sup>2</sup>Hiroshima Earth Environmental Information Center, <sup>3</sup>Faculty of Environment Systems, Rakuno Gakuen University, <sup>4</sup>Agriculture Department, Hokkaido University)

In this research, we proposed the method of the wetland vegetation classification using the Landsat/Enhanced Thematic Mapper (ETM+) multi-band data. A land cover classification map of wetland vegetation in Kushiro Marsh, Hokkaido, Japan was produced from the calculated results of the Normalized Difference Vegetation Index (NDVI), Normalized Difference Soil Index (NDSI) and Normalized Difference Water Index (NDWI), based on the data from Landsat ETM+. The composition of NDVI, NDSI and NDWI value with different proportion in each pixel, the area can be distinctively separated into forest, grassland and water body which exactly match the results of the land cover types from the field research. A comparison of DN value for both ETM+ and Advanced Space-borne Thermal Emission and Reflection Radiometer (Terra/ASTER) in broad-leaved forest, grass (*Phragmites australis*), soil (riverbank) and clean water shows that RED band reflection of wetland derived from ASTER is significantly higher than Theoretically, others than water body, all the NDVI of woody plants and wetland are larger than zero no matter which sensor is used. With the comparison of the four sensors, Advanced Very High Resolution Radiometer (NOAA/AVHRR), Moderate Resolution Imaging Spectrometer (Terra/MODIS), ETM+ and Terra/ASTER, it is found that the NDVI of MODIS, ETM+ and ASTER have the similar trend except AVHRR due to it relatively large pixel size in comparison to the study site. The statistical analysis of the NDVI computed from the data acquired with the four multi-spectral sensors show that the value computed from the AVHRR data has the largest mean with the smallest standard deviation and the range while that computed from the ASTER data has the smallest mean and the largest standard deviation and the range respectively. The result well reflects the effect of spatial resolutions of the sensors with 1 km for AVHRR and 15 m for ASTER. In one pixel of AVHRR there are nearly 4356 pixels of ASTER. Although the study area is a wet land, there is no negative value in the NDVI computed from the AVHRR data while there are negative values in those computed from other data with the largest absolute value in that computed from the ASTER data.

**JSG03/09P/D-007** Poster **1640-015**

**REMOTE SENSING OF CHLOROPHYLL A DISTRIBUTIONS AND WATER CONDITIONS IN THE GULF OF TONKIN, SOUTH CHINA SEA**

DanLing (Lingzis) TANG, Hiroshi KAWAMURA, Ming-An LEE (Tohoku University)

The Gulf of Tonkin is a semi-closed gulf northwest of the South China Sea, experiencing reversal seasonal monsoon. Previous studies of water conditions have been conducted in the western waters of the gulf, but very few studies of the Chlorophyll-a (Chl-a) distribution have been carried out for the entire gulf. The present study investigates seasonal and spatial distributions of Chl-a and water conditions in the Gulf of Tonkin by analyzing Sea-viewing Wide Field-of-View Scanner (SeaWiFS) derived Chlorophyll-a (Chl-a), in situ measurements, sea surface temperatures (SST), and other oceanographic data obtained in 1999 and 2000. The results show seasonality of Chl-a and SST in the Gulf of Tonkin, and reveal phytoplankton blooms in the center part of the gulf during the northeast monsoon season. In summer, Chl-a concentrations were relatively low ( $< 0.3$  mg m<sup>-3</sup>) and distributed uniformly throughout most of the area, with a belt of higher Chl-a concentrations along the coast, particularly the coast of Qiongzhou Peninsula; in winter, Chl-a concentration increased (0.5 mg m<sup>-3</sup>) in the entire gulf, and phytoplankton blooms offshore-ward from the northeast coast to the center of the gulf, while Chl-a concentrations reached high levels (0.8-1 mg m<sup>-3</sup>) in the center of the blooms. One peak of Chl-a concentrations was observed during the northeast monsoon season in the year. SST were high (27-29 oC) and distributed uniformly in summer, but lower with a large gradient from northeast (17 oC) to southwest (25 oC) in winter, while strong northeast winds (8-10 meters/second) were parallel to the east coast of the gulf. Comparison of Chl-a values shows that SeaWiFS derived Chl-a concentrations match well with in situ measurements most parts of the gulf in May 1999, but SeaWiFS derived Chl-a are higher than in situ data in river mouth waters. The seasonal variation of Chl-a concentrations and SST distribution were associated with the seasonally reversing monsoon; the winter phytoplankton blooms were related to vertical mixing and upwelling nutrients drawn by the northeast wind.

**JSG03/09P/D-008** Poster **1640-016**

**INFLUENCE OF WATERS OF DIFFERENT OPTICAL DOMAINS ON THE PHOTOSYNTHETICALLY ACTIVE RADIATIONS**

Harilal Bhaskara MENON (Department of Marine Science and Biotechnology, University of Goa)

Results from both field measurements and Laboratory simulations are used to assess the effects of turbidity on the optical properties of water column. For this two regions of differing optical domains have been considered. The coastal and estuarine regions. The Lambertian reflectance (remote sensing reflectance - R<sub>rs</sub>), optical properties such as absorption and diffuse attenuation coefficients of different water constituents at wavelengths 400 - 700 nm are examined in relation to turbidity. In addition the specular reflectance at the sea surface have also been examined in the wavelength range. The optical properties have been generated spectrophotometrically while remote sensing reflectance has been derived through measurement of Eu λ (Upwelling irradiance) and (Downwelling irradiance) Ed λ. As the remote sensing reflectance has been computed for every 1 nm, it differentiate the effect of individual constituent, such as chlorophyll, sediment and yellow substances (Dissolved organic matter DOM), on R<sub>rs</sub>. From the data it's clear that DOM decreases reflectance in the blue part of the spectrum (450 nm). Moreover the decrease of reflectance is a non-linear function of wavelength λ within the 400 - 580 nm range while in the range 580 - 700 nm, the reflectance is linear. This is due to the overlapping of reflectance due to DOM, chlorophyll and sediment in the shorter part of the wavelength. The computed values of R<sub>rs</sub> agrees with the measured values within rms error of  $\pm 10\%$ ,  $\pm 14\%$ ,  $\pm 23\%$ ,  $\pm 15\%$ ,  $\pm 14\%$ , and  $\pm 10.2\%$  at wavelengths 412 nm, 443 nm, 490 nm, 510 nm, 555 nm, 670 nm and 683 nm respectively.

**JSG03/09P/D-009** Poster **1640-017**

**EFFECTS OF THE TROPOSPHERIC DUST ON THE SEA SURFACE TEMPERATURE DERIVATION FROM SATELLITE OBSERVATION**

Myoung-Hwan AHN, Ja-Min GU, Ju-Yong CHUNG, Jae-Chul NAM (Remote Sensing Research Lab/METRI)

The effect of the tropospheric dust on the derived sea surface temperature (SST) from the satellite observation is investigated. To analyze the effects, we use a set of simulated radiance using the vertical profiles of temperature and humidity with and without the aerosol presence as an input of a radiative transfer model. The simulation results show that the presence of dust aerosol reduces the upwelling radiances at the top of atmosphere at the infrared window channel, as much as 15 K of brightness temperature at high dust loading. The presence of dust aerosol also reduces the dual channel difference in the split window channels, which also introduces error in the derived SST, mainly toward cold bias. The overall effect of dust aerosol on the derived SST is determined mainly by the single channel deficit of radiance due to the dust loading. The simulation results are further validated by using the actual observation of the GMS-5 data for two cases, for a very heavy and a moderate dust loading. When the dust amount is very high, the cloud screening and quality control procedures used for the operational derivation of SST could detect and remove the dust-loaded data. However, when the dust loading is moderate or weak, the dust-affected data pass through the two procedures and remains as the final products. The dust effect is clearly shown by the comparison between the SST value derived from satellite data and measured by buoy. Most of cases, the error due to the dust loading is only about 3 K in the hourly SST value and is further reduced in the weekly averaged SST. However, this is only true for when the dust does not occur for a long time period during the week and sufficiently large number of clear sky SST values is available at a given position.

**JSG03/09P/D-010** Poster **1640-018**

**REGIONAL ACE ANALYSIS OF SEA LEVEL, SEA SURFACE TEMPERATURE, AND SEAWIFS OCEAN COLOR DATA IN THE NORTH SEA**

Per KNUDSEN<sup>1</sup>, Klaus B. HILGER<sup>2</sup>, Allan A. NIELSEN<sup>2</sup>, Ole B. ANDERSEN<sup>1</sup>, Thomas KNUDSEN<sup>1</sup> (<sup>1</sup>National Survey and Cadastre, Geodesy, <sup>2</sup>Informatics and Mathematical Modelling)

Alternating Conditional Expectations Algorithm (ACE) is used to estimate canonical variates (CV) that describes the highest correlation between altimetric sea level height, ocean surface temperature and ocean colour data from SeaWiFS during 1999. ACE can handle arbitrary mixtures of continuous and categorical variables. The method is data-driven and non-parametric with minimal assumptions concerning the data distribution and the form of the optimal transformations. In this investigation, the ACE analysis has been set up to create the best fitting additive model to model the relationship between altimetric sea level height, ocean surface temperature and ocean colour data from SeaWiFS during 1999. Time series of SeaWiFS ocean colour, AVHRR sea surface temperature and TOPEX/POSEIDON and ERS sea surface height have been used for the present investigation. The SeaWiFS data are level 3 processed sets of CHLO, CP1G, K490, and L555. Tidal and meteorological contributions to the altimetric sea surface height is modeled and removed by the Mike 21 hydrodynamic model. The residual heights used for the simulations are applied in a multiple regression setting using the SeaWiFS and AVHRR measurements as predictors. When predicting the sea surface height in the Skagerrak region in the easternmost part of the North Sea from the SeaWiFS and the SST data a reduction in the residual variance of 39% is obtained by means of linear ACE based CV. If (noninvertible) nonlinear transformation of the SSH residual is introduced the residual variance reduction amounts to 51%, demonstrating that a non-linear relationship between changes in sea level height, sea surface temperature and amount of biological substance can be established empirically.

**JSG03/09P/D-011** Poster **1640-019**

**A MESOSCALE FEATURES OF THE SOUTH PACIFIC CURRENT OBSERVED FROM SATELLITE ALTIMETRY AND IN SITU OBSERVATIONS**

Alexander M. SIROTA<sup>1</sup>, Sergey A. LEBEDEV<sup>2</sup> (<sup>1</sup>Department of Fisheries Oceanography, Atlantic Research Institute of Fisheries and Oceanography, <sup>2</sup>Geophysical Center, Russian Academy of Sciences)

In September 2002 oceanographic expedition had been sent by the Atlantic Research Institute of Fisheries and Oceanography to the region of the Southeastern Pacific. The main purpose of the expedition is investigation of oceanographic conditions in the region. These investigations were supported with data of satellite observations. Processing of satellite data and mapping were carried out in the AtlantNIRO. To improve the spatial coverage beyond that available from in situ data from CTD survey, satellite SST and surface dynamic topography data were being prepared and transmitted to the vessel. Data source for SST, derived from AVHRR, was the NOAA Satellite Active Archive. Surface dynamic topography derived from the TOPEX/POSEIDON Quick-Look GDR v.1 data. Preliminary results of analysis of mesoscale variability of that region as well as comparison of in situ observation with satellite data are presented. Efficiency of use altimetry products for support of exploratory researches is estimated.

**JSG03/09P/D-012** Poster **1640-020**

**OCEAN TIDE MODELING IN THE SOUTHERN OCEAN**

Yuchan YI<sup>1</sup>, C.K. SHUM<sup>1</sup>, Sangho BAEK<sup>1</sup>, Yu WANG<sup>1</sup>, Ole ANDERSEN<sup>2</sup> (<sup>1</sup>Dept. of Civil/Env. Engineering & Geod. Sci., Ohio State Univ., USA, <sup>2</sup>National Survey and Cadastre, Denmark)

Ocean tides play a significant role in the complex interactions between the atmosphere, ocean, sea ice and floating glacial ice shelves. Tidal currents create turbulent mixing at the bottom of the ice shelf contributing to the creation of rifts for the possible detachment of part of the icebergs and can influence heat transport between the ice shelf and seawater. Tides near and, in particular, under floating ice shelves and sea ice influence grounding line locations. And, depending on surface and basal slopes, grounding line migrates with time within a grounding zone. Improved knowledge of the grounding line is inherently necessary to study ice mass balance and its contribution to the global sea level change. Even with the availability of most recent suite of global tide models based primarily on TOPEX/POSEIDON data, e.g., GOT00, NAO99, FES99 models, extreme southern ocean tides (below 60S) are limited both in accuracy and resolutions, especially in regions near Antarctica, seasonally or permanently sea-ice-covered oceans. In SAR tidal deformation analysis using ERS-1/2 tandem missions over Ross Sea and in a test region over the Sulzberger Ice Shelf (77.5S, 210E), Ross Sea, will be presented. In our initial study with the objectives to improve tides in Antarctica oceans for accurate prediction of grounding line locations to enhance ice mass balance studies, we provide an assessment of accuracy of tide models in the region. In addition to global models, finer resolution regional models in the Antarctica Ocean such as the Padman model are available. Coarse resolution tidal models using available over-ocean and over sea-ice/ ice-shelf data from T/P, JASON, ERS-1, ERS-2, GFO, and ENVISAT in

IA

## INTER-ASSOCIATION

the Southern Ocean below 50S will be presented. In particular, retracked altimeter data over ice-shelf (IGDR) from GSFC's Ice Pathfinder Data Center, and altimeter data from GFO and ENVISAT are used. Analysis of tidal aliasing will be discussed. Finally, initial results for a fine-resolution test ocean tide model using combined radar altimeter and ERS tandem mission InSAR data over the Sulzberger Ice Shelf will be described.

**JSG03/09P/D-013** Poster **1640-021**

### CROSS-CALIBRATION OF ENVISAT RANGE USING MULTI-SATELLITE ALTIMETRY AND TIDE GAUGE DATA

Luciana FENOGLIO-MARC (Darmstadt University of Technology, Institute of Physical Geodesy)

Envisat altimeter data are compared during the calibration phase against data from other satellites (ERS-2, T/P, Jason-1) using crossover and collinear track techniques in order to identify systematic, time variant and geographically correlated differences between the data from the various satellites and to cross-calibrate the Envisat range. The Mediterranean Sea is selected for the regional analysis, where tide gauge data from selected stations are used to cross-calibrate the various altimeters over the same short calibration period. The long-term monitoring of the Envisat altimeter range stability using the identified stations is discussed based on the preliminary three months results and on the long-term monitoring of the Topex/Poseidon mission. The differences between the sea level heights observed by the altimeter and by the tide gauge are analysed over the ten years at a few locations taking into account effects due to instruments, corrections, coast and circulation.

**JSG03/09P/D-014** Poster **1640-022**

### OCEANIC FRONTS AND EDDIES ON THE SYNTHETIC APERTURE RADAR IMAGES

Andrei Yu. IVANOV (Department of ocean remote sensing, P.P.Shirshov Institute of Oceanology, Russian Academy of Sciences)

Oceanic fronts are boundaries between water masses with different physical-chemical properties, while eddies are vortical dynamic ocean structures including fronts at their peripheries. Typical oceanic fronts and eddies includes large-, meso-, and small-scale ones of different origin. Synthetic aperture radar (SAR) signatures of oceanic fronts, as well as eddies, are mainly action result of 3 mechanisms affecting the sea surface roughness. The most important are: (1) surface wave-current interaction modulating spectrum of surface waves, (2) damping short wave due to oil film accumulations in convergent zones, and (3) difference in atmospheric boundary layer stability due to air-sea temperature differences across front. Eddies are usually visible in the SAR imagery as a result of wave/current interaction or indirectly due to the presence of natural films trapped within spiraling lines, associated with spiral motion; they outline the shape of eddy. However the role of these mechanisms is still poor known and there're no general models describing observed SAR signatures. The paper gives a review of frontal and vortical ocean dynamic features on the basis of analysis of the SAR images collected by Almaz-1, ERS-1/2 and Radar sat satellites over the ocean. As recently shown by Ivanov & Ginzburg (2002) ocean frontal/vortical features can be easily classified (by type of surface manifestations and generation mechanisms) on the basis of SAR imagery analysis. Having classified, the expected behavior of phenomenon can be predicted. Author's classification of oceanic fronts, detected in the SAR imagery, includes large-scale fronts of climatic origin, mesoscale fronts reflecting synoptic processes, and small-scale fronts of local origin. Current fronts and coastal fronts of different scales usually represent them in the ocean. Author's classification of oceanic eddies includes the ocean rings (generated by meandering currents), associated vortices, open ocean eddies, eddies due to coastal line or bottom topography heterogeneity (so-called wakes and von Karman vortex streets), mushroom-like eddies (dipoles) etc. The analyzed SAR images also represent combination of the above mentioned types forming both frontal meanders and wakes or chains of eddies. Examples of SAR images showing the fronts/eddy of different types are presented and discussed. It is concluded that the spaceborne SAR gives valuable information on ocean dynamical features, such as fronts and eddies, allowing to extract temporal and spatial characteristics. Moreover, an accurate analysis allows to retrieve both kinematic parameters and responsible generation mechanism. However, further progress in their studying will be associated with regular access to multi-sensor satellite imagery combined with contact measurements.

**JSG03/09P/D-015** Poster **1640-023**

### INVESTIGATIONS OF SPACE-TIME VARIABILITY OF THE SEA LEVEL IN THE BARENTS SEA AND THE WHITE SEA BY SATELLITE ALTIMETRY DATA AND RESULTS OF HYDRODYNAMIC MODELLING

Sergey A. LEBEDEV<sup>1</sup>, Oleg I. ZILBERSTEIN<sup>2</sup>, Sergey K. POPOV<sup>3</sup>, Olga V. TIKHONOVA<sup>3</sup> (<sup>1</sup>Geophysical Center, Russian Academy of Sciences, <sup>2</sup>Hydrometeorological Center Research, Russian Federation)

The problem of retrieving of the sea level anomalies in the Barents and White Seas from satellite can be considered as two different problems. The first one is to calculate the anomalies of sea level along the trek taking into account all amendments including tidal heights. The second one is to obtain of fields of the sea level anomalies on the grid over one cycle of the exact repeat altimetry mission. Experience results show that there is preferable to use the regional tidal model for calculating tidal heights. To construct of the anomalies fields of the sea level during the exact repeat mission (cycle 35 days for ERS-1 and ERS-2), when a density of the coverage of the area of water of the Barents and White Seas by satellite measurements achieves maximum. It is necessary to solve the problem of the error minimum. This error is based by the temporal difference of the measurements over one cycle and by the specific of the hydrodynamic regime of the both seas (tidal, storm surge variations, tidal currents). To solve this problem it is assumed to use the results of the hydrodynamic modeling. The error minimum is performed by the regression of the model results and satellite measurements. As a version it is considered the possibility of the utilizing of the neuronet obtained by the model results to construct maps of the sea level anomalies. The comparison of the model results and the calculation of the satellite altimetry variability of the sea level of Barents and White Seas shows a good coincidence between them. The satellite altimetry data of ERS-1/2 and TOPEX/POSEIDON of Ocean Altimeter Pathfinder Project (NASA/GSFC) has been used in this study. Results of the regional tidal model computations and three dimensional baroclinic model created in the Hydrometeocenter have been used as well. This study also exploited the atmosphere date of the Project REANALYSIS. The research was undertaken with partial support from the Russian Basic Research Foundation (Project No. 01-07-90106).

**JSG03/09P/D-016** Poster **1640-024**

### CURRENT SHEAR MEASUREMENT BY USING SYNTHETIC APERTURE RADAR

Akitsuugu NADAI (Advanced Research and Standards Division, Communications Research Laboratory)

The synthetic aperture radar (SAR) is one of the powerful tools to measure ocean features. It can detect oceanic fronts, eddies, waves, and so on. Many spaceborne SAR systems and airborne SAR systems have observed the ocean and their data have been analyzed. The spatial resolution of these systems is not enough to measure the spatial change of ocean wave spectra in about 10km separation. The Communications Research Laboratory and the National Space Development Agency of Japan has developed and operated an airborne high-resolution SAR systems called Pi-SAR. The Pi-SAR is a dual-frequency polarimetric radar operating L-band and X-band frequency. The X-band radar, moreover, has interferometry function to measure terrain elevation with accuracy of 2m. The resolution of L-band and X-band radar is 3m and 1.5m, respectively. Based on this hi-resolution, the Pi-SAR can measure the ocean wave spectra from its data of about 10 square kilometers. This paper presents the spatial change of ocean wave spectra observed by the Pi-SAR and the technique for current shear measurement based on wave-current interaction. The Pi-SAR observed southern ocean off Kii peninsula, Japan. The observation path extended about 200km length from Kii peninsula toward south. The Kuroshio ran just south of the Kii peninsula at the observation time, so the path crossed the Kuroshio current. On the intensity images, there were ocean waves with wavelength of about 80m propagating to/from northwest-southeast direction. Because the low-pressure system existed southeast of the observation area, the swell was estimated to propagate from southeast to northwest. The peaks of swell on ocean wave spectra rotate clockwise with approaching to the Kii peninsula (south to north). This rotation agrees with the effect of Kuroshio based on the wave-current interaction. The clockwise rotation component of Kuroshio changed the swell component. The wave-current interaction model suggests that the swell component parallel to current affected by current shear though that perpendicular to current is conserved. Also the magnitude of spectrum change is proportional to the magnitude of current shear. Based on the wave-current interaction model, the current shear by the Kuroshio was estimated. The result presents that the Kuroshio shear is almost east-west direction and that the Kuroshio becomes faster with approaching to Kii peninsula. These results agree with the real situation at the observation. The result shows the ability of current shear measurement by using the high-resolution SAR system. In these days, there are many plans of the spaceborne high-resolution SAR system. The current shear measurement by using SAR systems will give us more important information about global current system.

**JSG03/09P/D-017** Poster **1640-025**

### DOES OCEAN SURFACE RADAR WORK IN THE SURF BREAK ZONE?

Malcolm Lewis HERON, Thomas C. STIEGLITZ, Arnstein PRYTZ (MARINE GEOPHYSICAL LABORATORY)

Ocean surface radars are being used routinely to map surface currents over tens of kilometres at resolutions typically around 3 km. At higher radar frequencies, in the VHF band, the Bragg wavelength for backscatter is reduced so that at 152 MHz the dominant scatterer is from a wave with wavelength 1 m compared to 5 m at 30 MHz. This is about the lower limit of the gravity wave spectrum for wind waves on the sea. At this frequency the Bragg lines still dominate the spectrum but the side-band structure in the spectrum indicates deeper modulation (in the radio communications sense) by the longer waves in the wind wave and swell spectra. The spectral feature which enables surface current mapping is the Doppler shift of the Bragg lines. It is shown that the position of the peak can be identified in VHF backscatter spectra, even in the breaker zone. The COSRAD VHF ocean surface radar has been developed at James Cook University in North Queensland and has been deployed on many occasions to map features in the surface current on a resolution (grid) scale of 100 m and over a spatial range of up to 1.3km. This is useful for evaluating the effects of coastal engineering projects, and identifying rip currents and small scale eddies around obstacles like headlands. A deployment at Coffs Harbour on the North Coast of New South Wales in Australia was carried out in 2000 to assist in the design and location of a new sewerage outfall. An upward-looking acoustic Doppler current profiler was deployed within the area that was mapped by the radar for comparison. The depth at the study site was about 14 m and at times the surface was white with breaking waves. A self-consistency analysis of the ADCP data indicate that the current profiles are of acceptable quality from the bottom of the water column up to about 7-8 m. After that the current values become increasingly scattered. The VHF radar values compare favourably with the ADCP current values 7.8 m above the floor. During the deployment, the wind varied over a wide range and included a southerly storm which drove the whole near-coast body of water towards the north. During the storm the whole bay was white. Data indicate that the deep ADCP current measurements and the surface VHF radar measurements retained their integrity. Our conclusion is that the VHF COSRAD radar can successfully map surface currents even in the presence of breakers and white water. It has clear potential to monitor rip currents and coastal vortices under these conditions when conventional techniques become strained.

**JSG03/09P/D-018** Poster **1640-026**

### MEASUREMENT OF OCEANIC VARIABLES FROM DUO-FREQUENCY ALONG-TRACK INTERFEROMETRIC SAR DATA

Duk-jin KIM, Woolil M. MOON (Seoul National University)

Microwave remote sensing of the ocean surface using Synthetic Aperture Radar (SAR) is effective and of great interest because of the high spatial resolution and the almost instantaneous observation potential of large ocean areas. But it is difficult to retrieve significant ocean wave heights and surface current from conventional SAR data, because the imaging mechanism of ocean waves by a conventional SAR is determined by the three basic modulation processes arise through the tilt modulation, hydrodynamic modulation and velocity bunching, which are poorly known functions. Recently, airborne Along-Track Interferometric (ATI) SAR has been widely investigated, which has the potential of measuring ocean surface currents and wave heights. The ATI SAR employs two antennas that are separated physically along the platform flight path (along track) direction. The phase difference between two ATI SAR antennas is a measure of the Doppler shift of the backscattered signal and thus of the line-of-sight velocity of the scatterers. This interferometric velocity is sum of the orbital motion due to ocean surface waves, phase velocity of the Bragg wave, and ocean surface current. In this paper, we developed a new method for extracting ocean surface currents utilizing duo-frequency ATI SAR measurements. The method is applied to C- and L-band ATI SAR measurements acquired at the Ulsan coast from Korea. In addition, the surface gravity wave information (e.g. wave direction, wave velocity, wave height) is estimated using the ATI SAR velocity measurements.

**JSG03/09P/D-019** Poster **1640-027**

### OCEAN WAVE SPECTRUM MEASUREMENT BY USING AN AIRBORNE INTERFEROMETRIC SAR

Chieko KAMESHIMA<sup>1</sup>, Noboru SUDO<sup>2</sup>, Haruhisa SHIMODA<sup>3</sup>, Yoshiaki MATSUMAE<sup>2</sup>, Toshibumi SAKATA<sup>2</sup>, Akitsuugu NADAI<sup>1</sup>, Seiho URATSUKA<sup>1</sup> (<sup>1</sup>Electro Photo Optics, The Graduate School of Engineering, Tokai University, <sup>2</sup>Tokai University, <sup>3</sup>Communications Research Laboratory)

The ocean waves take an important role on the global climate. For example, it affects the gas transfer and momentum exchange between atmosphere and ocean. So, the global measurement of ocean waves is needed to monitoring the global climate. Because the global monitoring of ocean waves by direct measurement is difficult, the remote sensing technique is important. By using the synthetic aperture radar (SAR), the ocean waves can be measure under any meteorological condition. The wave spectrum measurement by using SAR is usually based on the intensity spectra of backscattered radar wave. The interferometric SAR, on the other hand, is able to measure the topography of ocean surface directly and the influence of the geometry of observation is decreased. The Pi-SAR is the high resolution airborne Synthetic Aperture Radar developed by the Communications Research Laboratory and National Space Developing Agency of Japan. The Pi-SAR is a dual frequency radar operating at L-band (frequency: 1.27GHz) and X-band (frequency: 9.55GHz) frequencies with polarimetric functions and can observe high resolution (X-band: 1.5m, L-band: 3m) to a target. Moreover, the X-band system has a cross-track interferometric function that can measure a terrain elevation with accuracy of 2m. The cross-track interferometry technique used in this experiment measures the surface elevation by phase difference of between received signals by two antennas installed at right angles to the flight direction. Two SAR observation were done at the northwest sea off Okinawa (9 November 2001) and southern sea off Hokkaido (13 June 2002). In each observation, the Pi-SAR observed same ocean area from different directions. From the collected data, the intensity image and topography map is produced. The wave spectrum is able to be analyzed by the 2-dimensional spectrum of ocean surface elevation as same as by the 2-dimensional spectrum of intensity image. In the spectrum analysis result of the Okinawa observation experiment, a strong peak on the intensity depended not only to the dominant wave component but to the flight direction, and interferometry spectra had a peak only to the dominant wave component regardless of the flight direction. This result shows that the strength of ocean wave component on the surface elevation spectrum is independent to the geometry of observation, though that on the intensity spectrum depends on the geometry. It is because the intensity image contains tilt-modulation effect and hydrodynamic-modulation effect, and the interferometry image indicates change of surface elevation. Therefore, it was shown that the measurement of ocean wave by interferometric SAR is effective. When the interferometry image compared with the intensity image, however, interferometry images are not clear than the intensity images. Also the topographic spectra are not clear than intensity spectra. Since the interferometric function of Pi-SAR was developed in order to observe terrain elevation, the sensitivity of radar and the accuracy of topographic measurement are nearly critical for ocean wave measurement. As solution, in order to measure the phase difference and spectrum clearly development of interferometric function which improved topographic accuracy is required.

**JSG03/09P/D-020** Poster **1640-028**

**SEISMIC AND SATELLITE IMAGE ANALYSIS IN THE VICINITY OF LAKE PUMA YUMCO LOCATED IN SOUTHERN TIBETAN PLATEAU, SW CHINA**

Atsushi IWASHITA<sup>1</sup>, Tomohiro KAMOSHITA<sup>2</sup>, Yoshifumi MISAWA<sup>3</sup>, Liping ZHU<sup>4</sup> (<sup>1</sup>Department of Space and Earth Information Technology, Kyushu Tokai University, <sup>2</sup>Ocean Engineering Co., Ltd., JAPAN, <sup>3</sup>School of Marine Science and Technology, TOKAI University, JAPAN, <sup>4</sup>Institute of Geographical Sciences and Natural Resources, Chinese Academy of Sciences, CHINA)

In April 2001, TOKAI University and Chinese Academy of Sciences carried out scientific exploration at Lake Puma Yumco located in the southern Tibetan plateau in southwestern CHINA. We had acquired the data of geologic and topographic field exploration, remote sensing image analysis by using Landsat ETM+ and ASTER VNIR, and topographic and seismic exploration in lake bottom and sub bottom area by using Bubble Pulser and Echo Sounder in the vicinity of the Lake. Purposes of this study are to confirm, 1) existence of structural relation among lake bottom and neighbor land area, 2) relation among topography and lineaments and its lengths by using distribution of extracted lineaments, 3) relation between the number and the length of lineaments. Seismic sections were interpreted and classified the bottom materials into three acoustic layers. Layer A is the top layer with thickness of approx. 10 m, layer B is the second layer with thickness of around 30 m, and the layer C is the third layer as basic rock. The top depth of layer C is approx. 70 m in the center of the channel. We had found the several structural anomalous zones in the seismic sections along northeastern offshore. They are running through north to south along the shoreline. Faults are also found clearly in the survey lines A and 29 corresponding to above structural zones. We have found that the lake bottom acoustic anomalous zones are suggested to continue to land structures. As for remote sensing image interpretation, we had extracted the structural anomalies and lineaments from different types of images. Landsat ETM+ with 30 m ground resolution that can be interpret wide area. ASTER VNIR can be seen detailed surface interpretation with 15 m resolution. ETM+ images indicate clear structural features around the Lake. These are essential information for geologic interpretation of Earth's surface and subsurface. We had extracted lineaments from both ETM+ and VNIR images and analyzed the characters of those lineaments reflecting distribution of the fractures. We can recognized several structural patterns running almost WNW to ESE. The "m" values in each area are calculated, and may reflect some geological and structural characters of the earth's surface.

**JSG03/09P/D-021** Poster **1640-029**

**LARGE-SCALE DISPLACEMENT CORRESPONDING TO THE 1999 CHICHI EARTHQUAKE, INSIGHTS FROM SPACE GEODETIC OBSERVATIONS**

Chung-Pai CHANG<sup>1</sup>, Chi-Tien WANG<sup>2</sup>, Tsui-Yu CHANG<sup>3</sup>, Kun-Shan CHEN<sup>1</sup>, Long-Shin LIANG<sup>1</sup>, Yuan-Hsi LEE<sup>1</sup> (<sup>1</sup>Center for Space and Remote Sensing Research, <sup>2</sup>Institute of Geophysics, <sup>3</sup>Central Geological Survey, MOEA)

The Chichi earthquake (Mw 7.6), struck central Taiwan on 20th September 1999 (UTC), has caused heavy casualties and widespread damage in Taiwan. During this earthquake, an approximately 80 km long upthrust unit underwent displacement of several meters upward and westward along the range-bounding Chelungpu thrust fault. By means of the SAR interferometric method, ERS2 radar image pairs adopted from the periods before and after the 1999 Chichi earthquake have been used to determine the co-seismic surface displacement of the flat region. In the near field, our interferometric results reveal a relative shortening in the round trip distance between the radar antenna and the ground of the footwall side of Chelungpu fault, during the earthquake. This shortening progressively increases from the west coast to the east and reaches the maximum amount of about 26 cm near the central segment of the Chelungpu fault. Further to the south of the Chelungpu fault, the co-seismic deformation is much slight, whereas a right-lateral movement in EW-trending has been observed to dominate the coseismic deformation of this area during the Chi-Chi earthquake. Furthermore, we projected the GPS coseismic measures to the radar slant range direction and implemented a forward simulation from the ground truth displacement to SAR interferogram, so as to evaluate our phase unwrapping performance. This analysis has confirmed our interferometric result and clarified its relationship with the ground truth displacement.

**JSG03/09P/D-022** Poster **1640-030**

**JERS-1 SAR AND ASTER VNIR INTERPRETATION IN THE VICINITY OF HUA-TUNG LONGITUDINAL VALLEY, EAST COAST TAIWAN**

Atsushi IWASHITA<sup>1</sup>, Hisatoshi BABA<sup>2</sup>, Susumu IIZUKA<sup>3</sup>, Yu-Feng LIN<sup>2</sup>, Yi-Sheng YANG<sup>2</sup>, Hwa-Chu SHEU<sup>4</sup>, Toshikazu MOROHOSHI<sup>1</sup>, Masanao HARA<sup>5</sup> (<sup>1</sup>Department of Space and Earth Information Technology, Kyushu Tokai University, <sup>2</sup>Research Institute of Science and Technology, TOKAI University, JAPAN, <sup>3</sup>Faculty of Marine Science and Technology, TOKAI University, JAPAN, <sup>4</sup>DAHAN Institute of Technology, TAIWAN, <sup>5</sup>National Research Institute for Earth Science and Disaster Prevention, JAPAN, <sup>6</sup>Vision Tech Inc., JAPAN)

Southwestern Ryukyu Arc and Eastern Taiwan region are characterized by subduction or collision of the Philippine Sea plate and Eurasian plate. The Hua-Tung Longitudinal Valley (HTLV) is huge valley running from the cities of Hua-Lien to Tai-Tung about the length of 130 km. This valley is located between Central Mountain Range and Coastal Mountain Range. Since 1990, DAHAN Institute of technology of Taiwan started to measure GPS and EDM (Electro Optical Distance Meter) data to monitor the crustal deformation in the northern part of HTLV. In 2001, Kyushu TOKAI University, Research Institute for Earth Science and Disaster Prevention (NIED) and Vision Tech Inc. had generated the first interferometric fringe pattern in the northern part of HTLV by using JERS-1 SAR dual data acquired 45 days apart in between Central and Coastal Mountain Ranges. Satellite image analysis had carried out by using ASTER VNIR and field excursion data were also acquired conducted by Kyushu TOKAI University. Some specific active faults existing in this area have been studied in the past several decades by international researchers. Image interpretation is one of the most adequate methods to acquire wide distributed geologic information to understand the target area. We have processed and interpreted Terra ASTER VNIR data to clarify the existence of active faults in the northern part of HTLV in East Coast Taiwan and detected several geologic information as well as lineaments. We have confirmed clearly some of these active faults existing in Coastal Range. We were able to confirm boundaries of specific geology, but some of boundaries were not confirmed. As for distribution of lineaments, we have manually extracted lineaments in the entire area of HTLV and found many lineaments existing especially in some part of Coastal Range. As the results, we had confirmed the typical features in HTLV showing colored fringe patterns that means the possibility of the movement. We have also confirmed specific active faults along HTLV. For the future study, we continue to measure Long Term period GPS data corresponding to the fringe pattern.

**JSG03/09P/D-023** Poster **1640-031**

**REFINEMENT OF JERS-1'S STATE VECTORS AND CORRECTION OF SAR INTERFEROGRAM FOR THE ATMOSPHERIC DELAY EFFECT USING THE METEOROLOGICAL SIMULATION**

Shigeki KOBAYASHI<sup>1</sup>, Akira OTSUKA<sup>2</sup> (<sup>1</sup>Department of Space and Earth Information Technology, Kyushu Tokai University, <sup>2</sup>National Agricultural Research Center)

JERS-1 L-band SAR interferograms are easily obtained over the wide range of height despite vegetation or slope. In general, however, remarkable phase patterns due to the atmospheric excess path delay remains near the summit of mountains on differential interferograms, even if errors in the satellite's state vector are precisely corrected. Therefore, it is inevitable to identify and correct for the atmospheric effects to detect surface deformations around high active volcanoes. Atmospheric effect contains two components. **Pattern 1)** Residual topographic phase pattern correlated with height in the first order, which is due to the difference in the static structure of water vapor at two SAR observation times: This pattern can be verified by calculating the relationships between height and the atmospheric delay using data from a radiozonde launched within the SAR scene extent. However, even if this effect is corrected in the first order, there remain complicate and irregular phase patterns in some cases [e.g. Iwate volcano in April, 1998 - July, 1998]. **Pattern 2)** Complicate phase pattern (e.g. mountain wave, foehn phenomenon) which not correlated with topography: For example, strong atmospheric noises, which appeared as phase undulation with about 15 km in wavelength, were observed by using data acquired just passing or approaching of developing cold front [e.g. Izu Peninsula on June 15, 1998; Mt. Fuji on August 20, 1993]. Such wavelike patterns of phase noises may be caused by mountain wave flowing high mountain. We developed a meteorological method to quantify the water vapor effect by 3-dimensional numerical simulation of atmospheric dynamics. Our model has 82x82 grids of 1.5 km square in the x-y plane and 32 layers in the z direction. The model also includes the topography of the same x-y resolution. The initial atmospheric condition was given using the radiozonde data of the nearest weather station. The result shows that a mountain wave, a standing wind, appeared on the lee of the mountain. Also it revealed that the downward (upward) winds in the mountain wave corresponded well to the relatively dry (wet) area of the differential phase pattern. Upward wind increase wet delay, downward decreases. Therefore, the atmospheric correction with the meteorological method is essentially required to prove the subtle crustal movements in particular near the summit of high volcano in the SAR interferometry.

**JSG03/09P/D-024** Poster **1640-032**

**AIRBORNE LASER SCANNING - FOR MAPPING OF SLOPE FAILURE POTENTIAL SPOTS**

Hiroshi P. SATO<sup>1</sup>, Tatsuo SEKIGUCHI<sup>2</sup> (<sup>1</sup>Geography and Crustal Dynamics Research Center, Geographical Survey Institute, <sup>2</sup>Geographic Department, Geographical Survey Institute)

In order to take effective measures against landslide, it is important to know spatial distribution of stable and unstable slopes in detail. Purpose of this study is to map unstable spots at the foot of landslides by using Digital Elevation Model (DEM). Here, unstable slope means high-potential slope failure spot. Study area is Kuchisakamoto area in Shizuoka City. The area, where landslide moved at maximum rate of 400 mm per day in July 1993, is one of the many landslide areas in Japan. In April 5 and 6, 2003 this area was measured by airborne laser scanner (ALS). ALS is the new technology by which DEM was obtained. An ALS is an active sensor that measures the distance from the sensor to the ground on which the laser beam is reflected. In this study Optech ALTM1225 was used as an ALS. Considering a safety factor, actual measurement specifications were as follows; pulse rate 25,000 Hz; flying altitude: nominally 600 m above the ground; flight speed 180 km/h. DEM measurement accuracy was checked at several checking areas. Discrepancy between the twice measurement was 0.05 m in X, -0.04 m in Y and 0.06 m in Z directions on average. Unstable spots mapping method is as follows. First, contour map was depicted using the DEM. Then, the past slope failure spots, which are as training data, were manually delineated on the contour map. In the delineation aerial photos were interpreted. Next, the past slope failure spots were identified on the grids on the DEM. By using DEM slope  $\theta$  and drainage area  $A$  were calculated on each grid of past slope failure. And liner regression was obtained,  $\log_{10}(\tan\theta) = -a \log_{10}A + \log_{10}F$  where,  $a$  and  $F$  are constant. Correlation coefficient was about 0.3. Slope  $\theta$  and drainage area  $A$  were calculated on each DEM grid of the past non-failure spots. These values were substituted for the above formula when  $F$  in the formula was treated as parameter, and  $F$  was calculated. Finally, when calculated value was more than the constant value  $F$ , the grid was mapped as unstable spots. Correct ratio

## INTER-ASSOCIATION

was about 55 %, which was calculated by mapped grid counts divided by whole grid counts on the training data. The mapping result shows conformity with on-site condition. In this paper, method and result will be explained and discussed in detail.

**JSG03/09P/D-025** Poster **1640-033**

### FIRST DIGISONDE 256 MEASUREMENTS AND TEC AT TUCUMAN AND COMPARISON WITH IRI PREDICTIONS

Victor Hugo RIOS, Cesar Francisco MEDINA, Blas DE HARO, Francisco SORIA, Enzo GOMEZ, Pascual PADILLA, Antonio Perez GOMEZ, Isabel LOMAS (Department of Physics, University of Tucumán)

The Digisonde first results from Tucuman (26.9 S, 65.4 W) and TEC obtained by Global Positioning System (GPS) are used to compare the observations with IRI predictions. The data were registered during November-December 2002 day to day. The comparison is made for the F region parameters NmF2, hmF2 and TEC and for true height profiles as well. The analysis, based on quietest days during the data period, shows that while IRI provides realistic profiles during daytime hours, it seems to underestimate the bottomside electron density during the early morning and late afternoon hours. The F-layer peak density obtained are underestimated for most of the nighttime hours during summer months. Comparative study of TEC indicates that the IRI underestimate significantly measured TEC during daytime on this period. This discrepancy between the IRI and observations has been reported at other low latitude stations even for low solar activity. When we look to ionospheric slab thickness, discrepancy between the IRI and observations due to the discrepancy in the topside profile is minus serious than TEC.

**JSG03/09P/D-026** Poster **1640-034**

### PLASMA DENSITY ENHANCEMENTS ASSOCIATED WITH EQUATORIAL SPREAD F (ESF)

Guan LE<sup>1</sup>, C.-S. HUANG<sup>2</sup>, R.F. PFAFF<sup>3</sup>, S.-Y. SU<sup>4</sup>, H.-C. YEH<sup>5</sup>, R. A. HEELIS<sup>6</sup>, F.J. RICH<sup>7</sup>, M. HAIRSTON<sup>8</sup> (NASA/GSFC, Greenbelt, MD, USA, <sup>2</sup>MIT Haystack Observatory, Westford, MA, USA, <sup>3</sup>Institute of Space Science, National Central University, Chung-Li, Taiwan, <sup>4</sup>William B. Hanson Center for Space Sciences, The University of Texas at Dallas, Richardson, TX, USA, <sup>5</sup>Space Vehicles Directorate, Air Force Research Laboratory, Hanscom Air Force Base, MA, USA)

Large-scale plasma density depletions are typically associated with equatorial spread F (ESF) plasma irregularities in the nightside F region, especially in the post-sunset sector. Data from the Ionospheric Plasma and Electrodynamic Instrument (IPEI) onboard the ROCSAT-1 spacecraft reveal numerous cases of localized, discrete plasma density enhancements associated with regions of regular ESF plasma density depletion structures at 600 km altitude. Within these discrete regions, the plasma density may be enhanced by ~ 2-3 times above the background density. The density enhancement regions have sharp, distinct edges and appear to have similar scale sizes as plasma density depletions. They generally occur at edges of the regular plasma depletion region, poleward in latitudes and either earlier or later in local times. In all of the cases we examined so far, they occur in local times at least three-hours after the sunset. The ion velocity data within the density enhancement regions show upward plasma drifts perpendicular to the magnetic field, similar to those within adjacent plasma depletion regions. The magnetic field-aligned plasma flows are generally poleward within the density enhancement regions. In some cases with nearly simultaneous DMSP observations at 800 km available, similar density enhancements are also seen in the same local time sector. We present observational characteristics of the density enhancements and discuss possible mechanisms in this paper.

**JSG03** Wednesday, July 9 - Thursday, July 10

### INTERDISCIPLINARY SCIENCE FROM REMOTE SENSING - RADAR ALTIMETRY, ATSR, SAR, OCEAN COLOR AND OTHER SENSORS (IAG, IAHS, IAPSO, IASPEI, ISPRS)

Location: Site A, Room 12

Thursday, July 10 AM  
Presiding Chair: P. Kundsen

**JSG03/10A/A12-001** **0830**

### APPLICATION OF THE SATELLITE ALTIMETRY AND RADIOMETRY FOR ANALYSIS OF ANTHROPOGENIC POLLUTANTS OF A MARINE ENVIRONMENT

Sergey A. LEBEDEV (Geophysical Center, Russian Academy of Sciences)

Ecological monitoring of a marine environment of last years has shown that alongside with processes of a destruction and deposition of pollutants not last role is played by dynamics of a marine surface, as the basic mass transfer. The models, existing on the present time, of calculation of currents usually use oceanographic and meteorological data obtained by the contact measurement methods. The apparent successes in development of ocean remote sensing methods open a path to creation of operating systems of ecological monitoring of a marine environment. The sea surface or dynamic topography calculated by satellite altimetry data, allows to analyze dynamics of the surface currents, which are not having brightly expressed thermal nature, as for instance, strong jet streams. In turn sea surface temperature, obtained by the satellite radiometry data, was used for more precise count of destruction processes of pollutants. Time-space scale of the satellite data from a ocean surface allow actively to use them in different models, that enables with a split-hair accuracy to make the physically reasonable forecast. Surface temperature and dynamic topography data sharing realized in the automated system "Regional Ecological Monitoring of a Marine Environment — Black Sea", which basis by model of pollutant propagation. The research was undertaken with partial support from the Russian Basic Research Foundation

**JSG03/10A/A12-002** **0850**

### SYNERGISTIC USE OF NEAR-REAL TIME RADAR ALTIMETRY AND ATSR-2 DATA FOR OCEAN CIRCULATION STUDIES AROUND CAPE VERDE

C. LAZARO, M.J. FERNANDES (Faculdade de Ciências, Universidade do Porto)

The Cape Verde Archipelago lies under the influence of the south-eastern North Atlantic subtropical gyre. Cold and nutrient-rich waters upwelled at the Northwest African coast, one of the major coastal upwelling areas in the world, are transported south-westward by the Canary and the North Equatorial currents. Due to its seasonal migration, the eastward North

Equatorial Counter-Current can affect the region around the archipelago and, being responsible for a northward transport of warm water along the African coast, suppress the coastal upwelling. Seasonal changes also occur with respect to extension and position of the Guinea Dome, a cyclonic circulation feature south of the archipelago. The subject of this work is the synergistic use of satellite remote sensing data for the characterisation of the seasonal cycle and variability of the flow field and oceanographic phenomena in the Cape Verde region. Synoptic maps of absolute dynamic topography (ADT) and sea surface temperature (SST) from near real time ERS-2 data were created in order to study the seasonal cycle associated with the flow field and the coastal upwelling for the period from June 2001 to May 2002. Based upon the ADT maps, intensity and direction of surface geostrophic currents were calculated. The methodologies adopted for the automation of the near real time data processing are described and particular emphasis is given to the evaluation of near real time altimetric data, by comparison with the information available with a delay of several months (OPR products). The purpose of this analysis, covering the period from January 2001 to December 2002, is to investigate the confidence level of the oceanographic information extracted from near real time data.

**JSG03/10A/A12-003** **0910**

### OCEAN CIRCULATION AND TRANSPORT BETWEEN THE NORTH ATLANTIC AND THE ARCTIC SEA, (OCTAS)

Hans-Peter PLAG<sup>1</sup>, Helge DRANGE<sup>2</sup>, Arne GIDSKEHAUG<sup>3</sup>, Johnny A. JOHANNESSEN<sup>4</sup>, Hossein NAHAVANDCHP<sup>5</sup>, Ove Christian Dahl OMANG<sup>6</sup>, Dag SOLHEIM<sup>7</sup> (Geodetic Division, Statens kartverk, Kartverksveien 21, N-3511 Honefoss, Norway and Mathematical Institute, University of Oslo, Postboks 1053 Blindern, 0316 Oslo, Norway, <sup>2</sup>Geodetic Division, Statens kartverk, Kartverksveien 21, N-3511 Honefoss, Norway, <sup>3</sup>Department of Mapping Sciences, The Agricultural University of Norway, Postbox 5034, N-1432 AAs, Norway, <sup>4</sup>Nansen Environmental and Remote Sensing Center (NERSC), Edvard Griegsvei 3a, N-5059 Bergen, Norway, <sup>5</sup>Department of Geomatics, Hogskoleringen 7G, N-7491 Trondheim, Norway, <sup>6</sup>University of Bergen, Institute of Solid Earth Physics, Allegt. 41, N-5007 Bergen, Norway)

The Norwegian OCTAS Project running from 2003 to 2006 focuses on the ocean circulation in the Fram Strait and adjacent sea with the main objective to improve sea surface topography determination and to study the impact on ocean modelling. Up to the expected launch of GOCE in 2005 the gravimetric geoid is not known with sufficient accuracy to allow full use of the massive sea surface height information, which several satellite altimetry missions have regularly provided since the early 90-ies, in global analysis of the ocean circulation. However, in a few marine regions in the world sufficient in-situ information about the Earth's gravity field exists to compute a more accurate geoid. The region covering the Northern North Atlantic and the Nordic seas between Greenland, Iceland, Norway and the UK, including the Fram Strait is one of those regions. One goal of the OCTAS Project is therefore to determine an accurate geoid in the Fram Strait and the adjacent seas. Together with the results from the on-going EU-funded project GOCINA, where in a similar approach an accurate geoid is determined for the region between Greenland and the UK, this will create a platform for validation of future GOCE Level 2 data and higher order scientific products. The new and accurate geoid is used together with an accurate Mean Sea Surface (MSS) to determine the Mean Dynamic Topography (MDT). Another major goal of OCTAS is to use this new and accurate MDT for improved analysis of the ocean circulation. The ocean transport through the Fram Strait is known to play an important role in the global circulation. Gulf Stream water flows into the Nordic seas and feeds the formation of heavy bottom water that returns back into the Atlantic Ocean. Recent results have shown that changes in this bottom water transport may cause the inflow of Gulf Stream water to slow down or change into another stable circulation mode over a few decades. Such a change of the Gulf Stream with even a possible shut down of the heat transport towards high latitudes would have a huge impact on the North European climate. The OCTAS project, in coordination with the GOCINA project, attempts to elucidate the role of the water exchange between the Arctic and Greenland Seas in this process.

**JSG03/10A/A12-004** **0930**

### COMBINED REMOTE SENSING OF OCEAN COLOR, RADIATION TEMPERATURE AND RADAR ALTIMETRY IN THE TRANSITION ZONE BETWEEN THE NORTH SEA AND THE BALTIC SEA

Niels Kristian HOEJERSLEV (Niels Bohr Institut for Astronomy, Physics and Geophysics, University of Copenhagen)

In the transition zone between the North Sea and the Baltic Sea hydrographic measurements of both temperature and salinity extending from the surface down to bottom have been performed routinely since 1886 from light vessels together with sea level measurements from the land bordering the sea. In addition optical in-situ measurements of daylight penetration and ocean color have been physically measured since 1922. From all these data the steric effect, the light penetration depth and the heat diffusion in the sea can be modeled. Consequently, from known surface temperatures the bottom temperature can be calculated quite accurately. This implies that remote sensing of the radiation temperature, SST provide useful information about the bottom temperature being important with respect to both steric effects and oxygen depletion in water layers near the bottom. Modeled bottom temperatures deviate typically by less than 1 degree Kelvin compared to the measured ones. During the last 12 years combined remote sensing measurements of ocean color, radiation temperature and altimetry have been daily business. In the transition zone the modeled light penetration depth is of the order of a few meters in accordance with the in-situ measurements and the difference between SST and in-situ surface temperature are typically below 1 degree Kelvin. The annual amplitude of the sea level is around 5 cm on average and the steric effect due to heating and cooling of the water column attains half the value. Radar altimetry in the transition zone demonstrates that the sea level during warm summers systematically is about 1 cm higher than during cold ones due to changes in the steric effect. The measuring accuracy of the radar altimetry is obviously better than 1 cm. During the winter the steric effect can be either positive and negative (and therefore also negligible) because the salinities varies around 24.65 in the surface waters. Radar altimetry as well as water level measurements since 1886 show clearly no steric effects especially at the end of the winter for this reason. Analysis of the radar altimetry data suggest that the measuring precision must be of the order of 1 mm. Remote sensing measurements of ocean color, SST and altimetry in combination are therefore a powerful tool in environmental and climatic studies since even small changes in the water level can be safely detected.

**JSG03/10A/A12-005** **0950**

### ICESAT LASER ALTIMETRY GEODETIC RESULTS

Bob Ewald SCHUTZ (Center for Space Research, University of Texas)

The Ice, Cloud and land Elevation Satellite (ICESat) was launched 2003 January 13 00:45 UTC from Vandenberg on a Delta-II into a near circular, 94° inclination orbit with an altitude of 590 km. The primary instrument carried by ICESat is the Geoscience Laser Altimeter System (GLAS), a new space geodetic tool. The GLAS instrument has been developed by NASA

Goddard and was mated to the spacecraft bus, built by Ball Aerospace, in June 2002. The GLAS altitude measurements collected by GLAS will produce elevation time series of the Greenland and Antarctic ice sheets, which will enable determination of present-day elevation change and mass balance. Additional applications of the altimetry channel include precise measurements of land topography and vegetation canopy heights, sea ice roughness and ocean elevations. Spacecraft commissioning was conducted during the first 30 days after launch. The spacecraft systems have performed as expected and the spacecraft is being phased into the required 8-day repeat track to support calibration/validation activities. Preliminary analysis using data collected by the BlackJack GPS receiver shows that some minor tuning of the gravity field, provided by GRACE, will be required to meet the better than 5 cm radial orbit accuracy requirement. The GLAS laser is scheduled to be powered up in mid-February and an intense period of GLAS commissioning and calibration/validation will follow. This paper will provide an overview of the geodetic results to date for precision orbit determination, precision attitude determination, verification of the instrument performance and validation of the data products.

**JSG03/10A/A12-006****1040****ADVANCE TECHNOLOGY OF REMOTE SENSING, GIS AND GPS FOR SEISMIC HAZARD ASSESSMENT**

Trinh Trong PHAN, Hoang Quang VINH, Trinh Hai DOAN (Institute of Geological Sciences)

Satellite image is origin of progress in earth observation and geological mapping. It gives us also a very powerful tool for the prediction and warning of natural hazards. We focus in three applications in Vietnam: seismic hazard assessment, landslide hazard and coastal zone erosion. The most important application is the estimation of seismic risk. We use TM, SPOT, ASTER, RADAR imagery and airborne images to determine active fault length, their characteristics (normal, reverse or strike-slip, slip rate) and measure horizontal displacement accumulated in Holocene. Directional filter of SPOT and TM images in combining with DEM from topographic data and RADA image could make in evidence active fault segment. The parameters are used to estimate maximum credible earthquake magnitude. The result of satellite analysis is combined with other data of geomorphology, topographic DEM, earthquake epicenter, radon distribution, stress field by the Geographical Information System. Some examples in application of spatial technology and GIS for seismic evaluation are presented. Radar interferometry help to create the DEM. Spot Panchromatic and multispectral image allows precise mapping of fault traces and estimate of fault displacement. The offset of landforms such as river and drainage patterns, alluvial fans, terraces can be observed and measured from Spot and Saious images. If the age of landforms is estimated reasonably, a fault slip rate can be estimated. The satellite analysis is combined with field study and other measurement such classic geodesy, Global Positioning System and analysis of earthquake focal mechanism. Our study in Vietnam will illustrate for the application of thematic study of remote sensing. We that if remote sensing technique is associated with other studies of Geology, geophysics and geomorphology, it will be a powerful tool to study active faulting and seismic hazard assessment. From this, if one relate with other results deduced from other works of intermediate prediction of earthquake, this technique will be useful for assessment of seismic hazards.

**JSG03/10A/A12-007****1100****HYPERSPECTRAL REMOTE SENSING APPROACH FOR ROCK SURFACE MINERALOGY MAPPING IN ARID ENVIRONMENT**

Patrick C. PINET<sup>1</sup>, Esther HARRIS<sup>2</sup>, Marie PYTHON<sup>3</sup>, Georges CEULENEER<sup>1</sup>, Yves DAYDOU<sup>1</sup>, Aurélien CORD<sup>1</sup>, Patrick LAUNEAU<sup>2</sup>, Hilal AL AZRI<sup>3</sup>, Sabine CHABRILLAT<sup>4</sup>, Xavier LÉNOT<sup>5</sup>, Stéphane CHEVRELS<sup>6</sup> (UMR5562/CNRS/GRGS/Toulouse University, <sup>2</sup>. UMR-CNRS 6112, Faculté des Sciences et Techniques, Nantes University, Nantes, France, <sup>3</sup>. Directorate General of minerals, Ministry of Commerce and Industry, Muscat, Oman, <sup>4</sup>. Remote Sensing section, GeoForschungsZentrum, D-14475, Potsdam, Germany, <sup>5</sup>. Optics Department, ONERA, BP 4025, Toulouse, France, <sup>6</sup>. B.R.G.M.-ARN, F45-060, Orléans, France, <sup>7</sup>. UPRES-A 8013/CNRS/ Côte d'Opale University, Wimereux, France)

The massif of Maqsd lies in a desertic region of Oman and is a large exposure of mantle rocks, bordered by a sedimentary massif of limestone rocks. Spaceborne, airborne and in situ hyperspectral sensors deliver measurements produced by spectro-imagery and field spectrometry. These data, analyzed by means of advanced processing tools and methodologies relying on multidimensional statistics and unmixing techniques, explore quantitatively the geological surface heterogeneity at different spatial scales, ranging from the centimetric rock-scale to the integrated landscape and remote sensing scale of the observation (10 to 50m). The results demonstrate that for arid environments in all cases where an extensive groundtruth has been acquired with the objective of encompassing all the local vegetal and geological variability at 50-100 m scale, it is impossible to explain the subpixel variability in the images by simple combinations of 3 to 5 key components, generally involving 2-3 mineralogy-driven ones, 1-2 types of vegetation, and/or 1 environmental shade component accounting for the different illumination conditions. From this analysis, one can select the key components present on the field and use them as endmembers in an iterative multiple mixture approach. With the support of field spectrometer and laboratory data, these endmembers can be interpreted in terms of first-order petrology information. It reveals that spatially organized variations do occur within the field of peridotites that can be used to produce a new type of lithology / mineralogy maps and it gives potentially access to the synoptic mapping of subtle petrologic variations. With the dramatic improvement of the spatial resolution of the present and soon-to-come observations, optical heterogeneities related to the physical properties of the surface have to be taken into account at the subpixel scale and this requires experimental laboratory studies on natural rocky surfaces. Efforts are currently underway for producing quantitative compositional estimates with many applications to terrestrial land surfaces and planetary environments such as the lunar and martian surfaces.

**JSG03/10A/A12-008****1120****GLOBAL IONOSPHERIC MODELS BEHAVIOR AT DIFFERENT GEOMAGNETIC REGIONS AND AT DIFFERENT LOCAL TIME**

Amalia Margarita MEZA<sup>1</sup>, Alejandro Raul DIAZ<sup>2</sup>, Claudio Antonio BRUNINI<sup>1</sup> (Facultad de Cs. Astronomicas y Geofisicas, Universidad Nacional de La Plata, <sup>2</sup>Instituto Tecnológico de Buenos Aires)

The dual frequency altimeter on board TOPEX/Poseidon satellite allows to measure the vertical total electron content (VTEC) of the ionosphere. Due to the dispersive properties of the ionosphere, subtracting the range measurements in the C-band (5.30 GHz) and in the Ku-band (13.65 GHz), the VTEC is obtained. In this work, we compare the climatologies predicted by a global GPS-derived empirical ionospheric model and the International Reference Ionosphere model IRI95 with TOPEX VTEC measurements. These climatological comparisons are performed in periods of various geomagnetic conditions. The periods taken in this analysis are equinoxes and solstices. The comparisons are binned in geomagnetic latitude stripes and in local time stripes, where the mean VTEC differences, weighted by the

cosine of the geomagnetic latitude are computed, as well as the standard deviations. We show a quantitative analysis of the VTEC differences between TOPEX measurements and ionospheric models. From this results we conclude that the GPS-based model gives a better description of the ionosphere than IRI95, in almost all local times. We also show that the equatorial anomaly is one of the main source of discrepancy. At sunset, both models have a worse relative representation at middle latitude wherever it is summertime.

**JSG03/10A/A12-009****1140****MEASURING STRATOSPHERIC AEROSOLS, POLAR MESOSPHERIC CLOUDS AND POLAR STRATOSPHERIC CLOUDS USING THE GOMOS EXPERIMENT ONBOARD ENVISAT**

Filip VANHELLEMONT, Didier FUSSEN, Christine BINGEN, GOMOS Cal-Val team (Belgian Institute for Space Aeronomy)

GOMOS (Global Ozone Monitoring by Occultation of Stars), one of the atmospheric experiments onboard the European ENVISAT satellite, uses the technique of stellar occultation to measure the transmittance of starlight through the atmosphere. From these measurements, altitude density profiles for gases such as O<sub>3</sub>, NO<sub>2</sub>, H<sub>2</sub>O, OClO, air, and stratospheric aerosol extinction profiles are derived. In addition, the experiment has been able to detect the presence of noctilucent clouds (polar mesospheric clouds, or PMCs) and polar stratospheric clouds (PSCs). First observational results are presented and discussed for the aerosols and clouds.

**JSA01****Tuesday, July 8****LONG-TERM TRENDS IN THE MESOSPHERE, THERMOSPHERE AND IONOSPHERE (IAGA, IAMAS)**

Location: Site A, Room 12

**Tuesday, July 8 AM**

Presiding Chairs: J. Lastovicka, A. Danilov

**JSA01/08A/A12-001****0905****REVIEW OF TRENDS IN MESOSPHERIC TEMPERATURES**

Gufran BEIG (Indian Institute of Tropical Meteorology, PUNE-411008 INDIA)

In recent time, it has become increasingly clear that releases of trace gases from human activity have a potential for causing a change in the upper atmosphere. During the past decade, several attempts have been made to analyze different series of long-term observations and to deduce mesospheric temperature trends. The comparison of the results obtained by different observations separated by several decades is complicated. These are related to maintenance of the same equipment sensitivity, noise level, and the method of data processing. Nevertheless, there are a number of occasions where a majority of the temperature trend results indicate consistency and some of the differences are even understandable. In this talk, a review of the long-term trend in temperature of the region from 50-100 km has been made based on available up-to-date understanding of measurements and model calculations. An objective evaluation of the data sets is attempted and important factors of uncertainties are discussed. There are a growing number of experimental results centered on, or consistent with zero temperature trends in the mesopause region. The most reliable data sets show no significant trend, but with an uncertainty of at least 2K/decade. Most studies recognize negative trends in the lower and mid-mesosphere with amplitude of few degrees (2-3K) per decade.

**JSA01/08A/A12-002****0935****IMPACT OF NATURAL VARIABILITY IN THE 11-YEAR MESOPAUSE REGION TEMPERATURE OBSERVATION OVER FORT COLLINS, CO (41N, 105W)**

Chiao-Yao SHE, David A. KRUEGER (Physics Department, Colorado State University)

The Colorado State University Sodium Lidar has measured temperatures in the mesopause region (80-105km) since 1991. Based on 7 years' observation, an episodic change with a warming of 11.8K in 1993 at the mean mesopause altitude of 98km, attributable to Mt. Pinatubo eruptions, was reported. With 11 years of data to the end of 2001, we observed a maximum solar response of 0.06K/SFU at 99km, which decreases at lower and higher altitudes to nearly zero and appears to change sign at ~82km and ~104km. The phase changes are consistent with earlier mid-latitude observation with incoherent scatter radar above and Rayleigh lidar below the altitudes we observed, providing clear experimental evidence of dynamical influences throughout different layers of Earth's atmosphere. Along with the reporting of these natural variability, we determine, and discuss their impact on the long-term mesopause temperature trends by re-analysis with one more year of data to the end of 2002.

**JSA01/08A/A12-003****0955****AN UPDATE ON GREEHOUSE COOLING IN THE MESOSPHERE AND THERMOSPHERE**

Rashid A. AKMAEV (CIRES, University of Colorado)

Infrared radiation in the 15- $\mu$ m band of carbon dioxide is the major cooling mechanism of the middle and upper atmosphere. Increasing amounts of atmospheric CO<sub>2</sub> impose strong anthropogenic influence ("greenhouse cooling") all the way through the mesosphere and thermosphere. Collisions with atomic oxygen are the primary excitation mechanism of CO<sub>2</sub> molecules in the thermosphere. Negative radiative forcing due to the CO<sub>2</sub> increase is roughly proportional to the rate of collisional excitation which in turn is proportional to the rate constant of collisional deactivation. The rate constant is still somewhat uncertain at present with various measurements and estimates varying within about a factor of 4. In light of recent laboratory measurements, two sets of numerical simulations have been performed to estimate the thermospheric response to doubling and a 15% increase of CO<sub>2</sub> for two values of the rate constant that differ by a factor of 2. Surprisingly, the temperature and density changes due to the CO<sub>2</sub> increases are practically independent of the rate constant. Simple diagnostics show that two physical mechanisms are primarily responsible: the strong temperature dependence of the radiative forcing itself in a combination with a strong temperature dependence of molecular heat conduction. Since the scenarios considered for the higher rate constant generally operate at colder temperatures, the two physical mechanisms combined provide sufficiently strong negative feedbacks to entirely offset the

**IA**

## INTER-ASSOCIATION

initially stronger radiative forcing. Possible effects of solar heating in the CO<sub>2</sub> near-infrared bands will also be discussed.

**JSA01/08A/A12-004**

**1025**

### TRENDS IN CHEMICAL COMPOSITION OF THE MESOSPHERE INDUCED BY LONG-TERM CHANGES OF ATMOSPHERIC BASIC PARAMETERS (MIDDLE LATITUDES)

Alexei A. KRIVOLUTSKY, Tatyana Yu. VYUSHKOVA, Vladimir N. GLAZKOV (Department of Chemistry and Dynamics of the Atmosphere, Central Aerological Observatory)

The results of temperature and pressure (rocket data at Russian station Volgograd, 50 N, 1970 -1990) regression analysis were used to calculate corresponding changes in chemical composition (first of all concentration of ozone). The data sets based on long-term rocket sounding revealed negative trends in both parameters with increased amplitude in the mesosphere. Corresponding magnitudes of these trends have been used in 1-D photochemical model. This 1-D time-dependent photochemical model used for this study describes photochemical interaction between more than 50 minor compounds in the range 0-90 km. Long-term changes in atmospheric parameters such as the temperature and pressure influence on gas-phase chemistry determining the velocity of ozone production in three molecular reactions and changing the photolysis rates. So, only temperature and pressure (which determine the concentration of the air) had trends in model runs, and there were no any other kind of long term forcing. The annual cycle in the basic parameters have been introduced in the model also. The results of photochemical calculations gave corresponding trends (negative) in vertical ozone model distribution. Vertical structure of such trend is very similar to observed trends revealed from SAGE-II observations. Calculated magnitudes of trends in ozone and other minor species content in the stratosphere and mesosphere depends on season. Such annual dependence in the results of photochemical model runs determined by annual variability of air density and by solar UV radiation intensity.

**JSA01/08A/A12-005**

**1115**

### THE INFLUENCE OF INCREASING GREENHOUSE GASES ON THE STRUCTURE AND COMPOSITION OF THE MESOSPHERE AND LOWER THERMOSPHERE

Daniel R. MARSH, Douglas KINNISON, Fabrizio SASSI, Rolando R. GARCIA, Byron A. BOVILLE (National Center for Atmospheric Research)

While it is accepted that concentrations of radiatively active (or greenhouse) gases are increasing in the troposphere, the impact of these changes on the upper atmosphere has yet to be fully assessed. Increases in carbon dioxide are expected to cool the mesosphere and lower atmosphere (MLT), but certain observational evidence suggests there is no cooling trend near the high-latitude mesopause. Large increases in water vapor, brought about in part by changes in methane, are also observed. These changes significantly impact mesospheric ozone, and may affect the formation of polar mesospheric clouds. Using the Whole Atmosphere Community Climate Model (WACCM), a General Circulation Model that extends from the surface to 140 km, we quantify their response of the MLT to recent increases in carbon dioxide, methane, nitrous oxide and chlorofluorocarbons. In particular, trends in both temperature and composition between 1980 and 2000 are analyzed and compared with the observational record.

**JSA01/08A/A12-006**

**1145**

### TRENDS IN NOCTILUCENT CLOUDS - NEW RESULTS

Sheila Catherine KIRKWOOD (Atmospheric Research Programme, Swedish Institute of Space Physics)

For a number of years many scientists have believed that there is strong evidence for a secular increase in noctilucent cloud (NLC) occurrence and explanations have been proposed in terms of decreased temperature from increased carbon-dioxide cooling or increased water vapour from increased methane, or even from space-vehicle emissions. A recent reassessment of the observational NLC record from NW Europe, however, shows that there is no significant trend in the occurrence of NLC during the last 40 years. This is confirmed by the observational record from Moscow. Even the reported absence of NLC observations in Europe before 1885 has been questioned, with the illustration of what appear to be NLC included in a painting from 1837. In this talk the evidence for trends and shorter-term variability in the NLC observations will be first reviewed. The role of variable upper-atmosphere dynamics in secular and shorter-term longitudinal shifts of the regions where NLC can be observed will be discussed. Finally, possible explanations for a zero secular trend in NLC occurrence despite increasing carbon-dioxide, methane and water vapour, will be presented.

**JSA01/08A/A12-007**

**1215**

### LONG-TERM TREND OF MESOPAUSE SCENERIO

Dipak K. CAKRABARTY (Centre for Environment Survey)

Information about long-term changes of several parameters in the mesopause region is gradually coming out. It is now almost established that in this region the temperature has been going down, the density of major neutral constituents has been decreasing, carbon dioxide content has been increasing and water vapor content has been increasing. The trend of change in nitric oxide density is controversial and the trend of change in electron density is also controversial. There is no information on the changes of atomic oxygen and ozone. Using an ion chemical scheme, in which both positive and negative ions have been considered, we have examined the effect of all these changes on the ionization of this region to arrive at a picture which conform to all these changes. It is evident from this analysis that electron density has been decreasing, percentage of both positive and negative clustered ions has been increasing and both  $f^+$  (ratio of positive molecular ions to clustered ions) = 1 and  $\lambda$  (ratio of negative ions to electrons) = 1 levels have been going up over the years.

Tuesday, July 8 PM

Presiding Chairs: G. Beig, M. Jarvis

**JSA01/08P/A12-001**

**1400**

### TRENDS IN THE MLTI FROM A POLAR PERSPECTIVE

Martin J. JARVIS (British Antarctic Survey)

The middle and upper atmosphere may provide a sensitive indicator that anthropogenic influences are changing Earth's environment. However, such signatures occur against a background variability driven largely by external forcing on a range of time scales. It is

essential therefore to be able to differentiate between externally and anthropogenically forced changes. To understand the attribution of trends in the MLTI we need to take a global perspective. In this respect, comparing observations in the polar regions both with those observed at lower latitudes and with those observed at the opposite pole should provide pointers to the causative mechanisms. This presentation will discuss some comparisons using Antarctic and Arctic data and suggest areas to investigate further.

**JSA01/08P/A12-002**

**1430**

### LONG-TERM TRENDS IN THE LOWER IONOSPHERE BELOW 120 KM

Jan LASTOVICKA<sup>1</sup>, Juergen BREMER<sup>2</sup> (<sup>1</sup>Institute of Atmospheric Physics, Bocni II, 14131 Prague, Czech Republic, <sup>2</sup>Institute of Atmospheric Physics, Schloss-str. 6, Kuehlsburg, Germany)

The increasing concentration of greenhouse gases in the atmosphere is expected to modify also the mesosphere and lower thermosphere (MLT region). However, the greenhouse cooling instead of heating at these heights is expected by models and generally confirmed by observations. This should more or less affect various ionospheric parameters at these heights. Observations show that in spite of general cooling, at some altitudes and some latitudes during some seasons we observe no trend (e.g. high latitudes, summer, NLC heights of 82-83 km) or even slight heating, whereas under the majority of conditions the cooling is observed, which is sometimes somewhere quite strong. The spatial and temporal structure of temperature trends in the MLT region is quite complex and, therefore, such structure occurs for trends in the lower ionosphere, as well. In the lower part of the ionosphere below about 90 km, the rocket measurements of electron density and the indirect phase reflection height measurements reveal positive trends in electron density, which correspond to cooling and shrinking of the mesosphere. Above 90 km, the nighttime LF reflection height measurements and the E-region ionosonde data provide trends corresponding to the overall cooling and shrinking of the atmosphere, while sparse rocket data display an opposite trend of decrease of electron density. Ionosonde data show that there is a model-expected trend in the maximum electron concentration of the E region ionosphere. foE is slightly increasing. On the other hand, the height of the normal E layer, h'E, is slightly decreasing. The radio wave absorption and rocket electron density measurements clearly display a substantial dependence of trends on height. The role of the solar cycle and other longer-term variability of natural origin in the observational trends must not be neglected. In spite of a general qualitative agreement with model expectations, there is still some controversy between various observational trend results (hopefully rather apparent than real), which needs to be clarified.

**JSA01/08P/A12-003**

**1500**

### TRENDS IN THE NEUTRAL AND IONIZED PARTS OF THE MLT REGION

Bremer JUERGEN (Leibniz-Institute of Atmospheric Physics)

From long-term phase height observations in the LF range a continuous decrease of ionospheric reflection heights has been detected if the solar and geomagnetically induced variations have carefully been removed. Results of other reflection height observations confirm the lowering of the meso- and lower thermosphere (MLT) region. This shrinking can mainly be interpreted by a general cooling of the strato- and mesosphere caused by an increasing atmospheric greenhouse effect. Beside this cooling due to an increasing infrared radiation to space also long-term changes of the nitric oxide density and/or the effective recombination coefficient may play an important role for the explanation of the observed trends of ionospheric reflection heights. Observation of long-term trends of ionospheric absorption at different frequencies may help to decide if trends of the nitric oxide density and of the effective recombination coefficient have to be taken into account. From the combined analysis of different reflection height, absorption and ionosonde data series mesospheric temperature trend profiles have been derived for summer and winter conditions. Maximum cooling is observed during summer up to about -0.45 K/year and up to about -0.35 K/year in winter. These trends agree reasonable with other experimental trends derived from lidar and rocket experiments. The experimental trends are however stronger than the model results derived from the global circulation model COMMA-IAP if the known trends of carbon dioxide and ozone have been used in these calculations.

**JSA01/08P/A12-004**

**1520**

### SOLAR-CYCLE VARIATION OF BACKGROUND COSMIC RADIO NOISE OBSERVED BY THE IMAGING RIOMETER IN THE POLAR CAP

Masanori NISHINO<sup>1</sup>, Hisao YAMAGISHI<sup>2</sup>, Jan HOLTET<sup>3</sup> (<sup>1</sup>Solar-Terrestrial Environment Laboratory, Nagoya University, JAPAN, <sup>2</sup>Upper Atmosphere Division, National Institute of Polar Research, JAPAN, <sup>3</sup>Department of Physics, University of Oslo, Norway)

The 30 MHz imaging riometer (IRIS) was installed at Ny Ålesund, Svalbard (76.1° MLAT) in September 1991 in order to study dynamics of auroral particle precipitation in the polar cusp/cap. The IRIS has two-dimensional 8 x 8 multiple-beams and thus can obtain ionospheric absorption image due to precipitation of auroral particles. The IRIS observation has been carried out since September 1991. For the ionospheric absorption measurement, quiet-day-curves (QDC) have been determined from background cosmic radio noise (CRN) in each month. The long-term reduction of the monthly QDC is important for evaluation of its availability. We examined the long-term variation from the monthly QDC data during ten years (1991-2001) in the solar-cycles 22 and 23. As the result, the variation showed seasonal changes during years depending on sunlit condition in the polar cap ionosphere. It was also found that the long-term variation (trend) showed an amplitude change of 0.6 - 1.0 dB during the solar-cycles. This indicates that the specific monthly-QDC could be unavailable in different months in the same year and also unavailable on the same month in different years during ten years. Here it should be remarked that the long-term variation of the background CRN showed a good correlation with the annual variation of galactic cosmic ray fluxes (GCR) measured by neutron counter at Oulu in Finland, which is generally modulated inversely by solar activity. This gives us a conclusion that the long-term variation of the background CRN is governed by precipitation of high-energetic protons due to GCR into the lower ionosphere and the mesosphere in polar region, not by ionization in the ionosphere due to solar radiation. Further discussions are needed for the problem that the observed amplitude change is larger than that calculated change theoretically from the electron density profiles and the collision frequencies.

**JSA01/08P/A12-005**

**1610**

### LONG-TERM TRENDS OF F2-LAYER PARAMETERS INDEPENDENT OF GEOMAGNETIC ACTIVITY

Alexei D. DANILOV (Institute of Applied Geophysics)

A detailed analysis of the foF2 data at the series of ionospheric stations is performed to reveal long-term trends independent of the long-term changes of geomagnetic activity during the recent decades (nongeomagnetic trends). It is found that there is a relative

nongeomagnetic trend of  $-0.0012$  per year (or an absolute nongeomagnetic trend of about  $-0.012$  MHz per year) for the period between 1958 and the mid-nineties. The consideration of the earlier period (1948-1985) for a few stations for which the corresponding data are available provides significantly lower foF2 trends, the difference between the later and earlier periods being by a factor of 1.6. This is a strong argument in favor of an anthropogenic nature of the trends derived. The situation with the hmF2 trends is more complicated, but for the majority of the stations considered positive nongeomagnetic trends of hmF2 are obtained. Presumably these trends are a manifestation of the changes occurring during the recent decades in the upper thermosphere (thermosphere) due to its pollution in the process of space exploration. A possible relation of the ionospheric and thermospheric trends is discussed.

**JSA01/08P/A12-006****1640****THE MLTI IMPACTS OF SOLAR ACTIVITY TRENDS IN THE 20TH AND 21ST CENTURIES**

Mark Andrew CLILVERD<sup>1</sup>, Ellen CLARKE<sup>2</sup>, Henry RISHBETH<sup>3</sup>, Thomas ULICH<sup>4</sup> (<sup>1</sup>British Antarctic Survey, <sup>2</sup>British Geological Survey, <sup>3</sup>University of Southampton, <sup>4</sup>Sodankylä Geophysical Observatory)

The aa index provides the longest geomagnetic data set that can be used in the analysis of magnetospheric and ionospheric phenomena. All phases of the solar cycle show increases in storm activity since the end of cycle 14 in 1915. The activity increase does not appear to be strongly associated with any instrumental, ionospheric or magnetospheric effects. Small effects have been confirmed in the long-term change in ionospheric Pedersen and Hall conductivities due the changing dipole moment of the Earth, but not due to increasing greenhouse gases. Three instrumental effects have been identified where significant changes in quiet-time conditions can be seen i.e. 1938, 1980, and 1997. These do not account for the majority of the increase in aa. Noise levels for the aa index are now close to those seen at the beginning of the dataset. The prime cause of the increase in storm activity is an increase in solar activity. The average aa in cycle 23 should be about  $1\text{--}n\text{T}$  less than predicted from previous cycles due to the reduction in baseline noise levels at the start of the cycle (1997). We consider the likely levels of solar activity in 2100 AD by analysing the previous history of these long-term solar and geomagnetic activity indexes. In particular, we make use of super-posed periods of similar variations in the DELTA C-14 record that have occurred during the last 11,000 years. This leads us to conclude that we could expect solar activity conditions in 2100 AD to be equivalent to those of about 1900 AD when a small minimum in solar activity took place, rather than increase at the relatively high rates of the last 100 years.

**JSA01/08P/A12-007****1700****REGIONAL VARIABILITY OF LONG-TERM VARIATIONS OF MIDLATITUDE E SPORADIC LAYER**

Oleg Nikolaevich SHERSTYUKOV, Sergey Vladimirovich MAKSYUTIN (Department of Physics, University of Kazan)

Accumulation of long rows of experimental ionospheric data during last several decades has allowed a number of researchers to conduct a study of long-term variations of various parameters of ionosphere. Thus and so consideration of global climatic variations of E sporadic layer parameters is interesting. These studies were already conducted earlier for number station of South hemisphere, but further consideration of long-term variations of E sporadic layer parameters is necessary for more amount of stations during a long periods. At work presented long-term variations of critical frequency E sporadic layer (foEs) were analyzed for 20 mid-latitude stations of north hemisphere (16 from them is situated within latitude band 45-65N, one-43N and last three stations - within latitude band 65-75N) during a period 1957-1990. For analysis hour values of foEs were averaged for the whole day (00-23 LT), as well as for light (9-15 LT) and dark (21-03 LT) time of a day separately. Before the segregating of trends, values of foEs were averaged for the current year by reason of eliminating an influence of seasonal variability of foEs. Analysis of long-term variation season-averaged values of foEs was conducted also. Linear regression dependencies of year-averaged and season-averaged values of foEs from a time are segregated by way of foEs =  $A \cdot t + B$ , where  $t$  is a time. The values of linear regression slope parameter (A) were used as quantitative characteristic of segregated trends (it has dimensionality MHz / year). A significance of segregated trends were estimated for confidential probability 90%. As a result of conducted analysis were discovered significant trends of year-averaged and season-averaged values of foEs, observed during light (09-15 LT) and dark (21-03 LT) time of day and during whole day (00-23 LT). A magnitude of segregated trends of foEs for considered stations is about  $0,01$  MHz per year. However, the sign of segregated trends is not same for all considered stations. Thus as result year-averaged values of foEs analysis negative trend is observed for 13 stations (and for 7 stations it is significant) but positive trend is observed for the rest 7 station (and it is significant for 6 stations). Difference of segregated trends sign for considered stations conceivably caused by the different geographical situation of stations on continent. Thus for stations situated in the central Europe dominate a positive trend but for stations situated in north region of Europe and at heart of continent dominate a negative trend. The work was conducted under the support of grant RFBR 01-05-65251.

**JSA07****Thursday, July 10****REGIONAL CRUSTAL MODELS BASED ON SEISMIC, ELECTROMAGNETIC, POTENTIAL FIELD, AND GEOTHERMAL STUDIES (IAGA, IASPEI)**

Location: Site A, Room 5

**Thursday, July 10 AM**

Presiding Chairs: J.V. Korhonen, W.D. Mooney

**JSA07/10A/A05-001**

Invited

**0830****DENSITY STRUCTURE OF THE UPPER MANTLE UNDER NORTH AMERICA**

Walter D. MOONEY<sup>1</sup>, Mikhail K. KABAN<sup>2</sup> (<sup>1</sup>USGS, <sup>2</sup>Institute of Physics of the Earth, Moscow)

We present a new high-resolution density model for the lithosphere and upper mantle of North America and analyse its geodynamic and tectonic implications. This model is based on an integrated analysis of gravity, seismic refraction, seismic tomography, drill-hole, and geological data. The thickness of sedimentary cover was determined from geological maps, and the average density-depth relationship was estimated for each specific basin from published data. The density model of the consolidated crust (including Moho variations) is

derived from seismic determinations. By removing the effect of the crust we calculate the residual 'mantle' gravity anomalies and the residual topography which are due to density inhomogeneities in the upper mantle. A joint analysis of these results with seismic tomography data (Van der Lee et al., 2000) leads to a construction of a 3D density model of the upper mantle under North America that is consistent with the residual gravity and produces the dynamic topography which is close to the residual one. The obtained density variations in the upper mantle under North America change significantly with depth. We conclude that they can not be explained solely by variations in temperature (Goes and Van der Lee, 2001) but a substantial part of them should be due to compositional differences. Under the Canadian Shield this difference is negative and is equal on the average to  $-40 \pm 5$  kg/m<sup>3</sup> which corresponds to 1.2% depletion. The opposite 'compositional' anomaly is found in the southern part of North America adjoining to Gulf of Mexico, it exceeds 30 kg/m<sup>3</sup>. The origin of this anomaly is disputable.

**JSA07/10A/A05-002****0900****THE ELECTRICAL LITHOSPHERE OF NORTHWESTERN CANADA**

Alan G. JONES<sup>1</sup>, Juanjo LEDO<sup>2</sup>, Ian J. FERGUSON<sup>3</sup> (<sup>1</sup>Geological Survey of Canada, Ottawa, Canada, <sup>2</sup>Universitat de Barcelona, Spain, <sup>3</sup>University of Manitoba, Winnipeg, Canada)

Lithoprobe's SNORCLE transect traverses over 1200 linear km from the Archean Slave craton hosting the oldest rocks in the world, across Proterozoic orogenic terranes then Phanerozoic accretionary terranes of the Northern Cordillera of Canada, to end at the Pacific coast within sight of a currently-active transform fault. Electromagnetic surveys, using the natural-source magnetotelluric (MT) technique, have been an integral component of SNORCLE activities from the outset, and MT data have been acquired along all three SNORCLE reflection transects, plus a supplementary profile connecting two of the Corridors (2 and 3). Additional MT data acquisition, funded by Lithoprobe, industry, Canada's Dept. of Indian and Northern Affairs, the U.S. National Science Foundation and the GSC, extended observations across the whole of the Slave craton. Taken together, these MT data, from over 300 locations, facilitate construction of maps of electrical parameters (resistivity, strike direction, anisotropy) for various depths as well as a 1500-km-long lithospheric-scale, electrical cross-section from Contwoyto Lake, in the northern part of the Slave craton (NWT), to Stewart, on the Pacific coast of B.C. The maps of apparent resistivity display strong lateral variation at all lithospheric depths, with the most resistive lithospheric mantle beneath the Anton complex of the Slave craton, and the most conductive beneath Stikinia. There is a remarkable difference in lithospheric electrical parameters between Corridors 2 and 3 in the Cordillera, attesting to different physical conditions of the mantle beneath those locations. The model displays local features known previously from more detailed study. In addition, it shows regional features that pertain to the protracted tectonic history of the region, including a northeast dipping mantle conductor likely a remnant of the recent Kula plate subduction.

**JSA07/10A/A05-003****0920****3-D ELECTRICAL CONDUCTIVITY MODEL OF THE SLAVE CRATON LITHOSPHERE**

Pamela LEZAETA<sup>1</sup>, Alan CHAVE<sup>2</sup>, Alan G. JONES<sup>3</sup>, Rob EVANS<sup>1</sup> (<sup>1</sup>Woods Hole Oceanographic Institution, MA 02543, USA, <sup>2</sup>Geological Survey of Canada, Ottawa, Ontario, K1A 0E9, Canada)

The Archean Slave Craton, northwestern Canada, exposed outcrop of the oldest known rocks on Earth over an area of about  $600 \times 400$  km<sup>2</sup>. The discovery of economic diamondiferous kimberlite pipes during the early 1990s motivated extensive research in the region. During the years 1998 to 2000, two magnetotelluric (MT) surveys to determine the regional-scale three-dimensional (3-D) electrical structure were carried out in lakes of the Slave Craton using ocean-bottom instrumentation deployed from float airplanes. Each set of surveys occupied one year since field operations could occur only in the summertime when the lakes were not frozen. During the first month of each survey the data were recorded at a higher sample rate for imaging crustal features. The instruments then switched to the standard lower sample rate (30 s) in the following ten months for the purpose of obtaining long period MT data, permitting deep penetration into the lithospheric mantle. The time series were processed into MT responses using a bounded influence algorithm. An unexpected noise source was found in the magnetic field data, from instrument motion induced by surface gravity waves when the lakes were not frozen. The noise was removed using an adaptive correlation canceler filtering method prior to computing MT responses. A regional 3-D conductivity model was constructed to fit the long period MT data, revealing a NW-SE dipping mantle conductor, which together with other geophysical and geochemical results allowed to build an hypothesis for the evolution of the Slave craton's mantle lithosphere. We extend the 3-D model to utilize all of the MT and induction vector data. We test the major features of the model for uniqueness and resolution, and discuss the implications for the evolution of the Slave craton.

**JSA07/10A/A05-004****0940****HIGH-RESOLUTION GEOPHYSICAL IMAGING OF A VOLCANIC MARGIN: ISLE OF SKYE (SCOTLAND)**

Sophie HAUTOT<sup>1</sup>, Pascal TARITS<sup>2</sup>, the SIMBA Team<sup>3</sup> (<sup>1</sup>School of Earth, Environmental and Geographical Sciences, University of Edinburgh, UK, <sup>2</sup>UMR CNRS 6538, <sup>3</sup>SIMBA Project)

The characterization of the deep structure of volcanic margins is a problem in conventional seismic imaging because of the thick extruded basalt flows that act as high impedance screens, thus masking the underlying structures. The SIMBA Project is an integrated geoscience approaches to sub-basalt imaging. In the framework of this project, the Isle of Skye Volcanic Province (North Atlantic Margin) is studied with different techniques (gravity, geology, seismics, magnetotellurics). The results obtained with these techniques will be integrated in order to obtain a high-resolution 3-D model of a typical example of a volcanic margin. Here, we focus on the magnetotelluric experiment. The magnetotelluric method is well suited to sub-basalt imaging: in contrast to seismic methods, MT soundings are insensitive to the highly electrically resistive volcanic structures, and are sensitive to the more conductive underlying formations. 21 MT soundings have been collected on Skye in order to obtain a full three-dimensional model of the sedimentary basins beneath the lava flows. The MT modeling results and the preliminary integration with the others geophysical results are presented. In the MT model, a high resistivity contrast between the different geological formations allow to constrain the geometry of the sedimentary structures beneath the basaltic layers.

**JSA07/10A/A05-005****1000****EVOLUTION AND COLLISION RELATED STRUCTURE OF THE EARLY PRECAMBRIAN LITHOSPHERE IN THE EASTERN FENNOSCANDIAN SHIELD: SYNTHESIS OF DEEP REFLECTION PROFILING, GEOLOGICAL AND GEOTHERMOLOGICAL DATA**

Michael V. MINTS<sup>1</sup>, Robert G. BERZIN<sup>2</sup>, Alexander N. KONILOV<sup>1</sup>, Vladimir M. STUPAK<sup>3</sup>, Arsen K. SULEIMANOV<sup>2</sup>, Nadezhda G. ZAMOZHNIYA<sup>2</sup>, Valery L. ZLOBIN<sup>1</sup> (<sup>1</sup>Laboratory of the Early Precambrian Tectonics, Geological Institute RAS, <sup>2</sup>SPETSGEOPHIZIKA, Povarovka)

## INTER-ASSOCIATION

Recently recorded 1-EU and 4B CDP profiles crossed the main tectonic units of the eastern Fennoscandian Shield (EFS) and together with earlier completed KOLA-SUPERDEEP and EGGI profiles provided image of seismic reflections in the crust and in some cases upper mantle from the surface to about 80 km depth (25 s). The reflectivity of the crust varies significantly, however there is no clear difference between reflectivity of upper, mid and lower crust. The mantle is generally transparent although 4B profile displays two levels of slight subhorizontal events, near 17 and 20 s. The base of crustal reflectivity at 36-40 km depth (Moho discontinuity) is clear obvious. The crustal structure is dominated by low- and moderate-angle surfaces, mostly 20-30° dip. Main tectonic units known from geological mapping can be traced to the depth using reflection image geometry and cross-section (down to 15 km depth) formed by calculated values of the effective acoustic impedance. The Neoproterozoic Karelian granite-greenstone terrain (KGGT) and Central-Kola granulite belt, the Palaeoproterozoic Pechenga and East-Karelian suture zones and Lapland granulite belt and Neoproterozoic Palaeoproterozoic Belomorian gneiss belt are formed by the systems of tectonic crustal slices some of which can be traced down to the lower crust and in some cases reach Moho discontinuity. Usually their boundaries flatten to lower crustal level, however in the 4B profile eastern flank one of the crustal slices cuts Moho discontinuity. The Moho discontinuity is to be treated as mechanical and tectonic boundary. The system of the Palaeoproterozoic sedimentary-volcanic belts in the eastern flank of the Karelia craton has been interpreted as imbricated thrust and nappe belt that is formed by alternating tectonic slices of the Neoproterozoic Palaeoproterozoic Palaeoproterozoic volcano-sedimentary complexes deformed with creation of the tectonic duplexes. Geological, geochemical and geochronological data evidence that the EFS Archaean lithosphere has been completely formed to the end of the Neoproterozoic and then rifted, disrupted and finally transected by a number of the Palaeoproterozoic volcano-sedimentary suture belts. Geochronological data demonstrate that Neoproterozoic KGGT spread out mainly in westward direction resulting from 2.94-2.86, 2.84-2.8 and 2.7-2.6 Ga accretion-collision events. Initial ages of some crustal fragments reach 3.2-3.1 Ga, ancient inclusions were dated at 3.6-3.4 Ga. The Palaeoproterozoic evolution of the EFS included four main stages: 2.51 - 2.44 Ga Superplume Event and Initial Rifting of the Archaean Supercontinent, 2.44 - 2.0 (2.11) Ga Quiescent Within-plate Development, (2.11) 2.0 - 1.95 Ga Superplume Event, 1.95 - 1.75 (1.71) Ga Combined Plume- and Plate Tectonic-related Evolution. They were followed by the late-collisional and anorogenic magmatism. During Palaeoproterozoic final collision volcano-sedimentary successions of riftogenic basins and intracontinental oceans were transformed in suture zones. Combined interpretation of seismic and geological data allow to consider the structure of the Early Precambrian lithosphere of the EFS as a combination of folded thrust and nappe and upthrust-underthrust structural ensembles.

**JSA07/10A/A05-006**

**1050**

### LITHOSPHERIC SOURCES OF MAGNETIC AND GRAVITY ANOMALIES OF THE FENNOSCANDIAN SHIELD

Juha Ville KORHONEN, Heikki SÄÄVUORI, Tapio KOISTINEN (Espoo Unit, Geological Survey of Finland)

The Precambrian geological formations of the Fennoscandian Shield have been divided in 12 major groups on the Geological map of the Fennoscandian Shield 1:2, 000,000, representing evolution from Neoproterozoic to Neoproterozoic. Corresponding petrophysical properties, measured from hand specimens and drill cores, have been averaged for the groups, and provide an idea of evolution of bulk density, and induced and remanent magnetisation of the shield in time. Neoproterozoic and late Palaeoproterozoic formations exhibit lowest average densities, ranging from 2670 to 2700 kg/m<sup>3</sup>. These include re-melted Palaeoproterozoic crust, the Rapakivi granites that are visible on Bouguer anomaly map as wide rounded minima. Densities of rocks of the Palaeoproterozoic Svecofennian orogeny, and evolution leading to it, range 2760-2700 kg/m<sup>3</sup>. Average density of formations on the Archaean craton is 2790 kg/m<sup>3</sup> and on Proterozoic craton 2760-2910 kg/m<sup>3</sup>. Induced magnetisation varies from 0.3 A/m of Archaean to 0.6 A/m of Palaeoproterozoic and to 1.5 A/m of Mesoproterozoic formations. The Q-value of formation averages ranges from 2 to 6 for Archaean and Palaeoproterozoic and from 0.4 to 1.7 for Mesoproterozoic. Q-value changes by stabilisation of the crust after the Svecofennian orogeny. In addition to the upper crustal petrophysical samples some mafic granulite xenoliths of the lower crustal levels of the Archaean Domain have been available. Xenoliths represent three density populations of average grain density 3090, 3240 and 3380 kg/m<sup>3</sup>, corresponding to total magnetisation of 2.0, 1.9 and 3.6 A/m. Heat flow studies reveal that the Curie isotherm of magnetite is deeper than Moho in the area. Hence these three populations may represent deep crustal sources of both magnetic and gravity anomalies of the shield.

**JSA07/10A/A05-007**

**1110**

### GIS BASED SATELLITE MAGNETIC FIELD MODELLING RESULTS FOR THE EUROPEAN PLATFORM

Kumar HEMANT, Stefan MAUS (GeoForschungsZentrum, Potsdam)

Satellite missions for last three decades have been a rich source of magnetic data which are used to generate the total field anomaly maps of the lithosphere. The CHAMP satellite in a low-earth orbit is particularly suited for the study of crustal magnetic anomalies. Our aim here is to interpret these maps in terms of known geology and to infer properties of the lower crust. A GIS based modelling technique has been developed to generate a vertically integrated susceptibility (VIS) model at every point on a map by assigning a standard susceptibility value to the known rock types for a particular region and multiplying it with the 3SMAC seismic crustal structure. The Total field anomaly is computed at an altitude of 400 km using this initial VIS model and is compared with the observed CHAMP total field anomaly map. The modelling result in the Baltic shield region and around Kiruna agrees very well with the observed anomaly map for the same region. The high associated with Kursk-Voronezh uplift fits well with the observed map. The extent of the anomaly in the Southern Urals follows the observed map, however, a part of the anomaly further inside the platform region is yet unaccounted for. The NW-SE anomaly following the Tornquist Teisseyre Zone (TTZ) is not directly related to some high magnetic geological body but is a result of the bulk susceptibility increase from the thin crust in the west of TTZ to the thick crust in the east. The basement below the Phanerozoic cover of the East European platform is clearly visible in the magnetic field but it does not cover the entire platform. We show that the basement of the East European platform extends from the southern boundary of the Baltic shield down to the centre of the platform, extending upto the northern edge of the Ukrainian Shield in the west and the middle Urals in the east. The results suggest that the platform basement behaves as a single large unit below the Phanerozoic crust.

**JSA07/10A/A05-008**

**1130**

### MAGNETIC MODELS FOR THE DIFFERENT GEOLOGICAL STRUCTURES OF THE SOUTH-WESTERN PART OF THE EAST EUROPEAN CRATON

Mikhail I. ORLYUK<sup>1</sup>, Inna K. PASHKEVICH<sup>2</sup>, Svetlana V. ELISEEVA<sup>3</sup> (<sup>1</sup>Department of geomagnetism, Institute of Geophysics, <sup>2</sup>Department of geomagnetism, Institute of Geophysics, <sup>3</sup>Department of geomagnetism, Institute of Geophysics)

The comprehensive of the interpretation nearsurface magnetic field, its regional component and MAGSAT anomalies were used for modelling. Petro-magnetic data for the upper crust, the depths to the basement and to the Moho discontinuity and other geodata were used also as a priori information. 3D magnetic models of the crust have been compiled for the East European Craton (EEC) (1 : 5 000 000) and its SW part (1 : 2 500 000). A regional 4D magnetic model of the consolidated crust of Ukraine is constructed on the base of geomagnetic and geochronology data. According to 4D magnetic model of the Ukraine the high-magnetic bodies are formed cyclically during the time intervals: 2.90-3.20; 2.25-2.55; 1.90-2.00; 1.60-1.70; 0.90-0.95; 0.35-0.44 Ga. The high-magnetic blocks are related mainly to epochs of extension answering to the tectonic situations as rifts, basic granulite nuclei, subduction zones, while low-magnetic ones are associated with periods of constriction of the crust (collisional orogens and compression structures). The nature of the deep magnetic sources reflects two mechanisms of their formation: riftogenic and subductional. The first mechanism consists in saturating of the crust by basic magmatic rocks (in oxidation-reduction condition favourable for the realization of iron as ferimagnetic minerals). Such sources form at the early stages of the evolution of major tectono-magmatic cycles in rift zones and the magmatic activation. The subductional type of the magnetic inhomogeneities is considered on an example of the palaeoisland and present island arcs. The mechanism of its formation is dual: on the one part it is underthrusting of the magnetic crust of oceanic type (and possible "doubling" in some zones of the lower crust) by subduction and, on the other part, the melting of the subducted crust with the saturation of the upper part of the section by respective rocks according to the first mechanism.

**JSA07/10A/A05-009**

**1150**

### CRUSTAL MODELS AND EVOLUTION OF THE MARGINS OF EAST-EUROPEAN CRATON IN RUSSIA BASED ON SEISMIC AND POTENTIAL FIELD STUDIES

Sergey Leonidovich KOSTYUCHENKO, Anatoly Vasilievich EGORKIN, Leonid Nikolaevich SOLODILOV (Center GEON)

The Mezen basin and the Timan Range, in the north-east, the Urals, in the east, and the Pre-Caspian basin and the Karpinsky Swell, in the south, are the tectonic units, which are astride or adjacent to the margins of East-European craton in Russia. The architecture of the crust and upper mantle and evolution of the area of study are imaged by seismic data (DSS, Passive observation and CMP) and by results of interpretation of gravity and magnetic fields. Within the Mezen basin, the rifts developed from Mesoproterozoic to Neoproterozoic 1 and 2 and the post-rift sedimentary cover accumulated since the Neoproterozoic III time. The thickness of the consolidated crust under the basin decreases from 42 km to 36 km and it is about 30-32 km within the rifts. The Timan Range stretches from NW to SE along in the eastern boundary of the Mezen basin. The deep refraction and wide-angle reflection observations give evidences that the crystalline crust of East-European craton underlies the up to 10 km thick Riphean successions constituting the Range. Based on deep geophysical data, the Timan Range overthrusts from east to west onto the East-European craton margin. There are crustal roots under the Urals mounting. The roots are about 50 km under the Northern and Southern Urals and about 45 km under the Middle Urals. Combine study of DSS, CMP and potential field data as well as result of teleseismic tomography experiment give evidences that West-Siberian lithosphere overthrusts onto the eastern margin of the East-European craton. Within the Pre-Caspian basin, the basement dips to 20-22 km while the Moho varies between 42 km and 34 km of depth. Plume tectonics is suggested to explain the evolution of the basin within the area, which is just in the south from East-European craton. The signatures of shortening and overthrusting of the Palaeozoic sedimentary successions which constitute the Karpinsky Swell onto the southern margin of East-European craton occur in the crust of the Swell. The crust-mantle mixture, which is imaged by the velocity of 7.6-7.8 km/s, exist between 37 km and 50 km of depth under the southern portion of the Karpinsky Swell.

**JSA07/10A/A05-010**

**1210**

### 3-D LITHOSPHERE DENSITY MODEL FOR NORTHEASTERN RUSSIA AND ITS GEOLOGIC, PETROLOGIC AND DYNAMIC-KINEMATIC INTERPRETATIONS (GRAVITY AND OTHER GEOPHYSICAL METHODS)

Yury Ya. VASHCHILLOV, Olga V. SAKHNO, Viktor V. LYUBOMUDROV, Larissa I. GUTOROVA (North-East Interdisciplinary Scientific Research Institute FEB RAS)

Mass quantitative interpretation of gravity anomalies for 3-D source block models underlie 3-D lithosphere density model for northeastern Russia. Gravity anomalies were interpreted by of independent and self-sufficient methods of a "new interpretative gravity", which has certain advantages even in comparison with seismic prospecting of deep structures of Earth's upper layers. In addition to this, results of seismic and electromagnetic studies, and magnetic prospecting were also used. This 3-D density model for northeastern Russia consists of a set of intersecting and interrelated vertical density sections of lithosphere at depths greater than 100 km and density horizontal sections at depths 10, 20, 30, 40 and 60 km (density gravity tomography). Absolute density values were established at different levels using methods of lithosphere density "probing" developed by the authors of this paper. Density inhomogeneities and their petrologic analogs change at diverse depth. Areas of well-expressed and reduced (or initially absent) "granite" layer are well-defined at 20 km horizontal section. A well-developed "granite" layer may have thickness of 15-20 km and more ("mesozoids"). A reduced "granite" layer is present in Anadyr-Koryak area featured by Mesozoic-Cenozoic tectonics. In Earth's crust, having thickness 30-40 km and less, basite-hyperbasite rocks become mainly spread. Vertical faults of Okhotsk-Chukchi Volcanic Belt (OCVB) are separating structures between areas of Mesozoic tectonics and pre-Riphean crystal rock masses (continental zone) and Anadyr-Koryak area featured by Mesozoic-Cenozoic tectonics (near-oceanic zone). According to interpreted gravity anomaly data obtained for Near-Magadan part of OCVB, its faults root usually occur at average depth of about 100 km. The top of asthenosphere occurs at this depth, which is supported, both directly and indirectly, by results of electromagnetic, gravity and seismology studies. The top of asthenosphere throughout northeastern Russia plunges to 160-180 km depth toward eastern edge of Siberian Platform. According to geophysical data, some "weak" parts of it are found throughout this area of our consideration at depth less than 100 km (polyasthenosphere). Within near-oceanic zone featured by a "reduced" granite layer, core of some anticlinal uplifts are marked by local positive anomalies and consist of basite-hyperbasite sequences of Late Mesozoic. In continental zone they are marked by local negative anomalies and consist of Late Mesozoic granitoids. It was just upward movement of magma that resulted in anticlinal structures genesis. Some anticlinal uplifts occurring within near-oceanic zone (Talovsko-Mainsky, Murgalsky and Vostochno-Taigonosky) are continuous, as the local linear positive gravity anomalies, within northern area of Sea of Okhotsk.

Thursday, July 10 PM  
Presiding Chairs: F.T. Freund, A.G. Jones

JSA07/10P/A05-001

1400

**COMPOSITION OF THE LOWER CRUST BENEATH SOUTHEASTERN MARGIN OF NORTH CHINA CRATON: CONSTRAINTS FROM SEISMIC, THERMAL AND GEOCHEMICAL STUDIES**

Yang WANG (School of Earth Sciences and Resources, China University of Geosciences, Beijing 100083, China)

Based on the one by one longitude-latitude grid P-wave velocity structure of southeastern margin of North China Craton (NCC), which was derived from the seismic refraction profiles, we infer crustal composition as a function of depth by comparing the velocities with the results from high-pressure laboratory measurements of P-wave velocity for crustal lithologies. The velocities were corrected to the standard P-T condition (25 degree C and 600 MPa) according to the geotherms constructed by downward continuation calculation of heat flux data under steady state conductive assumption and the relationship between elevation and thermal state. The average velocities are calculated for each position at 5-km depth intervals to Moho depth. Then, the model for crustal composition of southeastern margin of NCC was developed. For the lower crust, the corrected P-wave velocity is 6.7 ~ 7.0 km/s with a gentle tendency of increasingly value with depth. According to geothermobarometric calculation and geochemical study, the granulite xenoliths in the Neogene basalt occurred in Jiashan, Anhui Province, the SE corner of NCC, was considered as a representative of the lithology of lower portion of the crust beneath the region, with the depth range of 20 to 30 km. The estimates on P-wave velocity of these granulites, which are derived from the weighted average of minerals' velocities, were compared with the seismic velocity model. The estimates are consistent with the seismic observation well. The average chemical composition of the granulites is mafic with ~ 51% SiO<sub>2</sub> and 0.74% K<sub>2</sub>O as well as heat production of 0.16E-6W/m<sup>3</sup>. This result means a mafic lower crust beneath SE margin of NCC, rather than the intermediate estimate by Gao et al (1998, *Geochimica et Cosmochimica Acta*, v62, 1959), which obtains ~58% SiO<sub>2</sub>, 1.86% K<sub>2</sub>O and heat production of 1.08E-6W/m<sup>3</sup>.

JSA07/10P/A05-002

1420

**ESTIMATION OF WATER CONTENT IN THE CRUST FROM RESISTIVITY STRUCTURE – A CASE STUDY IN BACK-ARC AREA OF THE TOHOKU DISTRICT, NE JAPAN –**

Makoto UYESHIMA<sup>1</sup>, Yasuo OGAWA<sup>2</sup> (<sup>1</sup>Earthquake Research Institute, the University of Tokyo, <sup>2</sup>Volcanic Fluid Research Center, Tokyo Institute of Technology)

In order to estimate crustal rheology and to synthesize tectonic process such as seismic and volcanic activities beneath the island arc, crustal water content and its connectivity is one of the most important parameters. Owing to significant improvements in instruments, data processing methods and inversion schemes, we are now coming to obtain detailed crustal resistivity structures. On the other hand, dependence of whole rock resistivity versus temperature and water content can be estimated by referring resistivity-temperature dependence for dry rocks and water from laboratory experiments, and by assuming a connection rule of the interstitial water. Then, if we can estimate temperature structure successfully, spatial distribution of crustal water content can be estimated for the connection rule directly from the resistivity cross section. In this presentation, as a case study, we try to estimate spatial distribution of water content from a 2-D resistivity structure beneath back-arc area of the Tohoku district, NE Japan (Ogawa, et al., 2001), and compare the results with a seismic structure (Matsubara et al., 2003). Temperature structure was first determined from thermal parameters such as surface heat flow, thermal conductivity and crustal heat generation compiled by Furukawa, 1995 and Tanaka et al., 2000. Based on this temperature structure, we estimated whole rock resistivity versus depth dependences for various water contents, by referring laboratory experiment results compiled by Kariya & Shankland (1983) (for dry rocks) and Nesbitt (1993) (for crustal fluids). Here, we assumed that upper and lower crust is respectively granitic and gabbroic, and we estimated whole rock resistivities for Hashin & Strikman (1962)'s perfectly connected (HSc) and isolated (HSi) models. For the HSi model, whole rock resistivity takes almost the same value as that of dry rocks unless water content becomes more than 10 %, and more than 90 % water content is necessary almost throughout the crust to explain the observationally determined resistivity range: from 0.1 to 10k Ohm.m. On the other hand, for the HSc model, water content range from 0.01% to several % can explain the 2-D resistivity cross section. Ogawa et al., 2000's 2-D resistivity cross section contains three remarkable low resistivity portions in the upper crust beneath three tectonic faults in the area (Kita-Yuri thrust fault, Senya fault and Kitakami Lowland West Boundary fault). Depths of these low resistivity portions range 10-20 km and resistivity is as low as 1-10 Ohm.m. In order to explain this low resistivity, interstitial water should be connected and its content is estimated as 0.5-5 %. This estimation is not inconsistent with the water content estimation only from tomographic results for P and S seismic wave velocity perturbations (Matsubara et al., 2003). But joint analysis using both electric and seismic information will reveal more detailed features of the interstitial water and enhance persuasiveness of the estimation.

JSA07/10P/A05-003

1440

**A STUDY ON THE CONDUCTIVITY STRUCTURE OF THE KOREAN PENINSULA BY GEOMAGNETIC DEPTH SOUNDING**

Seokhoon OH<sup>1</sup>, Jun-Mo YANG<sup>1</sup>, Duk Kee LEE<sup>1</sup>, Yong-Hoon YOUN<sup>1</sup>, Byung-Doo KWON<sup>2</sup>, Seung-Hwan CHUNG<sup>3</sup>, Yoonho SONG<sup>3</sup>, Kyung Duk MIN<sup>2</sup>, Toru MOGI<sup>4</sup>, Masao NAKADA<sup>5</sup> (<sup>1</sup>Marine Meteorology & Earthquake Research Lab., METRI/KMA, Seoul, Korea, <sup>2</sup>Dept. Earth Science Education, Seoul National University, Seoul, Korea, <sup>3</sup>Korea Institute of Geoscience and Mineral Resources, Daejeon, Korea, <sup>4</sup>Dept. Earth System Sciences, Yonsei University, Seoul, Korea, <sup>5</sup>Inst. Seismology and Volcanology, Hokkaido University, Japan, <sup>6</sup>Dept. Earth and Planetary Sciences, Kyushu University, Fukuoka, Japan)

We have performed a geomagnetic depth sounding (GDS) and analyzed the data in terms of induction arrows to investigate the deep electrical structure in and around the Korean Peninsula between Japan, the tectonic boundary of Pacific Ocean, and China, where intraplate earthquakes have been frequently occurring. The GDS results strongly suggest evidence to elucidate relations between the tectonic tension and the deep electrical structure in this area. The inland anomalous pattern of induction arrows appears to indicate the direction of NE-SW, which is similar to that of the axis of tectonic compression of this area. Especially, the results of observations in the middle of the peninsula imply an anomalous pattern on the tectonic area near the Imjin River Belt, thought of as an extension of the Qinling-Dabie-Shandong continent collision belt of Eastern China. Induction arrows in the mid-southern area appear to be related with the thick sediment layer, called the Ogcheon Belt, that is another tectonic boundary in the Korean Peninsula. The overall pattern of arrows observed in coastal area and islands was affected by the surrounding sea. Nevertheless, the pattern adjacent to the southern coastline of the peninsula and Jeju Island near Kyushu, Japan showed southward highly conductive anomalies for the long period band, similar to

the previous study. This result might suggest geoelectrical anomalies in the East China Sea. A three-dimensional (3-D) magnetotelluric (MT) modeling technique was adopted to calculate the sea effect and infer the deep structure.

JSA07/10P/A05-004

1500

**PASSIVE HIGH-RESOLUTION SEISMIC ARRAY STUDY OF THE CRUSTAL AND UPPER MANTLE STRUCTURE BENEATH THE DABIE SHAN REGION**

Qiyuan LIU<sup>1</sup>, Rainer KIND<sup>2</sup>, Jihui CHEN<sup>1</sup>, Xiaohui YUAN<sup>1</sup>, Shuncheng LI<sup>1</sup>, Biao GUO<sup>1</sup>, Wylegalla KURT<sup>2</sup>, Yuangen LAI<sup>2</sup> (<sup>1</sup>Institute of Geology, China Seismological Bureau, <sup>2</sup>Geoforschungszentrum Potsdam, Telegrafenberg A17, Potsdam, D-14473, GERMANY)

The Qinling-Dabei orogenic belt through the central China was formed about 240Ma ago due to the collision between the Yangtze and North China plates. In 1980's the investigation of its orogenic evolution and the ultra-high pressure metamorphism was promoted greatly by the discovery of coesite and microdiamond within eclogites in the Dabie Shan mountain. Since that, many results from geological study have been published. But the geophysical investigations are only limited to some of low-resolution observations. Up to now, the structure and deformation of the collision margin in the crust is still unclear. A high-resolution exploration of the crust and upper mantle structure beneath the Dabie Shan region is necessary for a better understanding of its dynamic evolution. For this purpose, in April of 2001, we deployed a passive seismic profile across the Dabie Shan region and north China platform. This profile consisted of 34 broadband seismic stations is about 400 km long. The space between stations in the Dabie Shan region is about 3-8 km and about 20 km in other part. During one year field observation, several hundreds events were recorded. In this presentation we give the 2-D receiver function profile as well as the crustal and upper mantle structure along our profile, which are obtained by using the receiver function migration and nonlinear inversion methods, respectively. Our results illustrate that the crust structures beneath the Dabie Shan region and North China plate are completely different. Their demarcation is near 32°03'. The crust below the Dabie Shan mountain becomes thick. The largest depth of the Moho discontinuity reaches 48 km, and the crust thickness in both sides of the mountain area is only 30-32 km. The crust structure beneath the Dabie Shan mountain is asymmetric. The Moho discontinuity below the mountain on the side to the Yangtze plate has the schuppen structure and there is a clear offset of the Moho discontinuity near 31°24'. The result from the receiver function inversion reveals a low-velocity body in the middle crust beneath the Dabie Shan mountain. The lowest S wave velocity is only 2.5 km/sec. Our observations illustrate that the Yangtze plate was an active as a part of its crust-mantle boundary was smashed in the Dabie Shan collision orogeny. The low S-wave velocity body in the middle crust indicates that the brittle crust has become fragmental after the collision. The further investigation of the subcrustal mantle is still necessary to confirm the deep continental subduction.

JSA07/10P/A05-005

1520

**STRUCTURE AND GEODYNAMICS OF THE CRUST AND UPPER MANTLE ALONG THE PROFILE OBLUCHIE - DATTA CAPE ACCORDING TO THE COMPLEX OF GEOLOGICAL AND GEOPHYSICAL DATA**

Lev Aleksandrovich MASLOV<sup>1</sup>, Valery KUZNETSOV (<sup>1</sup>Laboratory for Mathematical Modeling in Geology and Geophysics, Computing Center of the Russian Academy of Sciences, <sup>2</sup>State Control Department, Ministry of Natural Resources, Khabarovsk, RUSSIA)

The profile Obluchie - Datta Cape crosses the juncture area of the Bureya massif with the Sikhote-Alin fold system and the superposed structures of the Middle-Amur depression. It is a 700 km long profile. Deep structure of the crust and upper mantle was studied using seismological (MECW - method of converted waves from distant earthquakes) and geoelectric (MTS) methods. Seismological and geoelectric models of the section were constructed. Seismological and geoelectric data were added by the gravity and magnetic anomalies along the profile. The density model of the section was constructed as the solution of the inverse gravimetric problem with restrictions due to seismological data. The density inhomogeneities of the crust were considered as the source of volumetric force and, consequently, mechanical stress in the medium. The solution of the corresponding mechanical problem allows us to obtain mechanical stress distribution in the crust and upper mantle of the profile under consideration. The geophysical observations data, as well as results of geodynamic modeling were combined in a model of the deep section to be analyzed and interpreted. It has been shown that the density and topographic inhomogeneities of the crust are capable of generating stresses sufficient enough to start up different geodynamic processes occurring not only in the crust but also in the upper mantle. It has been shown also that the gravity and magnetic anomalies, the compositional, density and stress inhomogeneities combined with electric conductivity of the section constitute the single structural unity. All the elements of the unity are interrelated and their interaction is feasible in the single conceptual system. The central element of this system is the Earth's crust whose density and topography inhomogeneities, reflected in the gravity and magnetic fields, are capable of generating stresses inducing different geodynamic processes in the upper mantle. The quantitative characteristics of the results of geophysical observations and those of the geodynamic modeling are presented.

JSA07/10P/A05-006

1610

**LITHOSPHERIC STRUCTURE AT CONTINENTAL BREAK-UP REVEALED BY MAGNETOTELLURICS ACROSS THE NORTHERN ETHIOPIAN RIFT**

Kathryn A. WHALER<sup>1</sup>, Sophie HAUTOT<sup>1</sup>, Laike ASFAW<sup>2</sup> (<sup>1</sup>School of GeoSciences, University of Edinburgh, <sup>2</sup>Geophysical Observatory, Addis Ababa University, Addis Ababa, Ethiopia)

The transition from fault-controlled continental rifting to magma supply-controlled seafloor spreading is not understood. The Ethiopian rift is one of the few places to study this. Seismic experiments undertaken include a refraction/wide angle reflection line across the rift traversing a magmatic segment, but the melt body has low velocity and its top will give high amplitude reflections. Hence broadband magnetotelluric data will be collected in January/February 2003 along the line to image the crust and upper mantle, specifically to investigate the volume of melt present, how it has modified crustal structure, whether border faults are accommodating extensional strain, and whether there is asthenospheric upwelling beneath the magmatic segment. Preliminary results and interpretation from this experiment will be presented, linking to any results available from the seismic experiments.

JSA07/10P/A05-007

1630

**CRUSTAL MODELLING ACROSS THE RENNICK GLACIER AREA (EAST ANTARCTICA)**

Fausto FERRACCIOLI<sup>1</sup>, Emanuele BOZZO<sup>2</sup>, Egidio ARMADILLO<sup>2</sup>, Detlef DAMASKE<sup>3</sup>, Gernot REITMAYR<sup>1</sup>, Nicola AGOSTINETTI<sup>4</sup>, Giovanni TABELLARIO<sup>2</sup> (<sup>1</sup>British Antarctic Survey, High Cross, Madingley Road, Cambridge, CB3 0ET UK, <sup>2</sup>Dipartimento per lo Studio del Territorio e delle sue Risorse, Univ. Genova, Viale Benedetto XV, 5, 16132 Genova ITALY, <sup>3</sup>BGR, Stillweg 2, 30655 Hannover Germany, <sup>4</sup>Istituto Nazionale di Geofisica e Vulcanologia, Via di Vigna Murata 605, 00143

## INTER-ASSOCIATION

Roma, Italy)

During the joint German-Italian campaign 1999-2000 a variety of geophysical investigations were performed over northern Victoria Land, Oates Land and George V Land (East Antarctica). These included aeromagnetics, ground gravity surveys, geomagnetic depth soundings and seismological investigations. As part of these regional studies we shall present the first results derived from crustal modelling across the Rennick Glacier area in northern Victoria Land. Geological evidence suggests that this glacier may conceal a major tectonic feature, namely the Rennick Graben structure. Geodynamic models predict that this graben relates to Cretaceous or alternatively to Cenozoic sea floor spreading between the Australian and Antarctic plates. Just to the east of the Rennick structure, a fossil suture zone between the allochthonous Bowers Terrane and the autochthonous Wilson Terrane has been identified. However, recent brittle-fault studies suggest that this is not a fossil Early Paleozoic structure. Rather, Cenozoic reactivation of the inherited fault zone may have occurred and induced strike-slip faulting along the margins of the Rennick Graben. Prior to our study, no integrated geophysical investigations had been performed neither to test these geologic models nor to assess deeper crustal structure in the Rennick area. Modelling of longer wavelength aeromagnetic anomalies now shows that magmatic arc basement flooring the Rennick Graben is indeed faulted. Modelling of higher-frequency anomalies indicates that Jurassic sills and basalts are also faulted. The down-faulted Rennick Graben is also marked by a prominent Bouguer gravity low. In contrast, the adjacent uplifted Bowers Mountains block features a 100 mGal high. Modelling reveals that this anomaly is caused by a buried high-density body. This body may be a remnant of Early Paleozoic oceanic crust. Whether uplift of this block is due to Early Paleozoic obduction, or to the presence of a Cenozoic(?) horst along the eastern flank of the Rennick structure is unclear. However, apatite fission track data seem to support the latter hypothesis. Deep electrical conductivity models show that the Rennick Graben is a resistive feature, formed by two sub-basins, separated by a structural high. Therefore, there is no clear indication for a prominent thermal anomaly, which should show up as a major conductor beneath the Rennick structure. Finally, seismologic models image the crust beneath the Rennick Graben as being only 26 km thick. Typically, the crust beneath the Transantarctic Mountains is about 35 km thick. Hence, the Rennick structure may represent a major continental rift structure, rather than a mere graben. We speculate that the Rennick rift is a passive rift, which may have formed in response to regional Cenozoic transtension between East and West Antarctica.

**JSA07/10P/A05-008**

**1650**

### INTEGRATED GEOPHYSICAL STUDY OF THE SEISMICALLY ACTIVE BHUJ REGION, INDIA

Anand P. SASHIDHARAN, Mita RAJARAM, Vinit ERRAM (Indian Institute of Geomagnetism)

The catastrophic Bhuj earthquake of 26th January 2001 with magnitude Mw 7.7 (Ms 8) was the most damaging in the last 50 years and was felt in nearly all parts of India. The Kutch rift basin is considered to be a major seismogenic domain (zone V) due to occurrence of four earthquake of high intensity and forms a crucial geodynamic part of the Western Continental Margin of Indian sub-continent. Number of geophysical investigations including Ground Magnetic, Geomagnetic Deep Sounding, Long Period Magnetotellurics, GPS etc were conducted to study the seismotectonics of the Bhuj earthquakes at the Indian Institute of Geomagnetism. The F and Z maps were generated from the collected ground data and the magnetic sources were mainly associated with the exposed and subsurface trap flows and were controlled by Vigodi fault and Katrol hill fault. The magnetic sources, derived by analytical signal method, form four independent structural units related to the neo-tectonic activity of the region and appear to be controlled by faults in the area. The four tectonic blocks delineated, match rather well with the blocks defined by the displacement vectors of Pollitz's visco-elastic model over Bhuj. The induction vectors derived from the thin sheet model (Arora, 2002) of conductance based on surface geology did not reproduce the observed short period GDS. However when the thin sheet model was based on the block structures derived from magnetization (high conductivity for low magnetizations assuming it due to fluids in the sedimentary column) the match between the observed and calculated induction vector for 12min period was remarkable. GPS results (Reddy et al, 2002) showed changes in East-West, North-south and vertical components of the baselines during 21-28 February, 2001 that indicated no displacements. N-S compression of about 0.1 micro-strain/year is seen in the region between Ratanpar and Dhamadkapir. The long period magnetotelluric measurements in the period range of 105-16000s have shown evidence of a crustal conductor in the depth range of 10-17 km. Depth sections of the aftershocks of 800 events indicate that the events are mostly generated at a shallow depth of up to 8km and 15-38 km depth (Kayal et al, 2002, JGSJ, 395-417). The depth range from 8-15 km produced no after shocks and this aseismic layer coincides well with the crustal conductor. The gravity data are also analysed and the common magnetic and gravity sources appear to coincide with the block east of Anjar. A tectonic model has been constructed integrating the geophysical data sets. The deformation has been calculated for the fault parameters of the Bhuj earthquake considering a viscoelastic layer between 17km (from LMT) and 30km (crustal depth derived from MAGSAT) and compared with the GPS results.

**JSA07/10P/A05-009**

**1710**

### APPARENT DENSITY MAPPING FROM GRAVITY DATA OF CHINA

Hualin ZENG<sup>1</sup>, Deshu XU<sup>2</sup>, Tianfeng WAN<sup>3</sup> (<sup>1</sup>Deptment of Applied Geophysics, China University of Geosciences(Beijing), <sup>2</sup>Institute of Geophysical and Geochemical Exploration, Ministry of Land and Resources, <sup>3</sup>School of Earth Science and Resources, China University of Geosciences (Beijing))

We present an apparent density mapping of China from Bouguer gravity anomaly and a comparison of the mapping with the tectonic outline and geography data of China. Transformation of gravity anomaly into apparent density is carried out by the following methods: (1) A subtraction of upward continuation of gravity anomaly to a height from the anomaly at observation level enhance the gravity anomaly due to an upper layer of the crust with a thickness equal to the height, and attenuate the anomaly due to lower layer. In other words, the upward continuation height can approximate the thickness of the layer, of which an apparent density is evaluated, and it is possible to enhance gravity anomaly caused by the upper crust with a thickness that equals to the magnitude of the upward continuation distance. (2) A preferential upward continuation operator, which is derived from Wiener filter and Green's equivalent layer principles and can attenuate short-wavelength anomaly due to shallow-source while minimally attenuating long wavelength signals due to deep source, is used to separate the anomaly caused by the shallow layer from the regional anomaly due to the deeper layer. (3) An inversion using a series of right rectangular prisms and from computation of the first vertical derivative of the gravity anomaly is applied to transform the anomaly due to the shallow layer yielded by the subtraction and the preferential upward continuation into an apparent density map. By means of the above methods the gravity anomaly due to a layer with a thickness of 10 km within the upper crust is separated from the Bouguer gravity map of China, which was digitalized with a sampling distance of 10 km, and an apparent density mapping of a layer in upper crust with a thickness of 10 km of China is derived. A comparison of the mapping with the tectonic outline map and geography data of China shows that characteristics such as closed maxima or closed minima of apparent density correspond well with the known tectonic units such as boundaries or collisional

suture between plates, tectono-magma belts, basins, stable blocks, granites and mountains. For example, modern mountains correspond to low density areas; the plates and basins to high density areas; and the large magmatic belts to low apparent density. The method is an effective one for the calculation of apparent density of the upper crust with a given thickness from gravity anomaly in an area, and a careful comparison of the apparent density map with tectonic geomorphology must provide interesting new geological inferences. The key of the method is to separate the anomaly due to the layer of which the apparent density is calculated. Depending on the method for calculating the apparent density the calculated density is an average ones of an area, which indicates regional structures. Gravity interpretation is of nonuniqueness so it is important that the interpretation of the apparent density map should be based on the known geological data.

**JSA07/10P/A05-010**

**1730**

### RESULTS OF DENSITY MODELING OF THE LITHOSPHERE IN THE PHILIPPINE-TO-ASIAN PLATE TRANSITION ZONE, AS EXEMPLIFIED FROM THE RYUKYU ISLAND ARC

Gulya Zabirowna GILMANOVA<sup>1</sup>, Vladimir Yakovlevich PODGORNYY<sup>2</sup> (<sup>1</sup>Pacific Oceanological Institute, FEB RAS, <sup>2</sup>Institute of Tectonics and Geophysics, FEB RAS)

The lithosphere modeling has been carried out along the geophysical profile by R/V "Professor Gagarinsky" in 1993 through 1994. The study area is located east of Taiwan and is considered to be an area of the Eurasian and Philippine plate interaction. Profile crosses the Okinawa Trough, the Ryukyu island arc, the Ryukyu trench, passing out to the West Philippine Basin water area. Three computation models have been constructed: the lithosphere, divided into the water layer and the solid part, the lithosphere, whose solid part is subdivide into the crust and subcrustal part and that with account of the seismic crustal layering. It has been shown, that the lithosphere is clearly divided into three parts: that of low density (2.955 g/cm<sup>3</sup>), with significantly continental crust, the density one (3.3 g/cm<sup>3</sup>), with significantly oceanic crust, and that of intermediate density, 3.09 g/cm<sup>3</sup>. The latter covers a part of the section starting from the northern framing of the Okinawa Trough to the Ryukyu Trench. The analogous density subdivision of the crust by types is not seen. A decrease in the density of about 0.10 g/cm<sup>3</sup> is established in the subcrustal part of the lithosphere beneath the northern part of the Okinawa Trough. The asymmetric cone-like unconsolidation area, that of the truncated top, is discerned in the northern part of the section to which the location of the Sinji-Taiwan fold belt corresponds. Being expanded downward, the unconsolidated area makes continuation down to the asthenosphere. The southern part of the unconsolidation area is more moderate as compared to the northern one and testifies to a clearly expressed tendency of superimposition of the material layers with higher density from the south as in the crust so in the subcrustal mantle. The inclined boundaries of the density heterogeneities are distinguished also beneath the middle part of the Okinawa Trough and in the zone of juncture of the oceanic crust of the West-Philippine Basin with the island arc one. In the density section the Ryukyu trench is not clearly discerned. This is related to the fact that the profile under consideration crosses the island arc and the Ryukyu trench in the area of their degradation as the morphological structures. Low density is observed for the southern slope of the Ryukyu arc Aeyama Ridge. South of the Ryukyu arc there exists the asymmetrical negative anomaly of the geoid surface as its submerging of the order of 10 m. The area of the maximum subsidence is located between the axes of the Nanao depression and the Ryukyu trench, that is, it corresponds completely to location of the Aeyama Ridge. The lack of compensation masses as in the subcrustal part of the lithosphere, so beneath it, testifies that the gravity instability is mainly related here to the crust and its aqueous loading, and it is not compensated by the subcrustal mantle.

**JSA07-Posters**

**Friday, July 11**

### REGIONAL CRUSTAL MODELS BASED ON SEISMIC, ELECTROMAGNETIC, POTENTIAL FIELD, AND GEOTHERMAL STUDIES (IAGA, IASPEI)

Location: Site D

**Friday, July 11 AM**

Presiding Chair: J.V. Korhonen

**JSA07/11A/D-001**

**Poster**

**0830-001**

### STRUCTURE AND GEODYNAMICS OF THE EARTH'S CRUST AND UPPER MANTLE OF JAPAN AND PHILIPPINE MARGINAL SEAS ACCORDING TO THE COMPLEX OF GEOLOGICAL AND GEOPHYSICAL DATA

Gulya GILMANOVA<sup>1</sup>, Ruslan KULINICH<sup>2</sup>, Lev MASLOV<sup>3</sup> (<sup>1</sup>Pacific Oceanological Institute Russian Academy of Sciences, Vladivostok, RUSSIA, <sup>2</sup>Computing Center of the Russian Academy of Science, 65, Kim Yu Chen Str.,)

The gravity modeling as well as mechanical stress simulation has been carried out along two profiles: the latitudinal profile (~N21.5°) stretching from the West Philippine Basin to South China Sea and the profile across the Sea of Japan stretching from the Siberia Seamount (NW part of the Sea of Japan) to the Yamato Rise. Density models of deep sections were constructed as the solution of the inverse gravimetric problem with restrictions due to seismological data. The density inhomogeneities of the crust were considered as the source of volumetric force and, consequently, mechanical stress in the medium. The stress distribution in the crust and upper mantle of profiles was obtained as solution of the corresponding mechanical problem. Geoid's height anomalies and magnetic data have been used for a comprehensive study of the area under consideration. Gravity modeling results, as well as results of geodynamic simulations, has been interpreted on the basis of tectonic, morphostructural, compositional and seismological characteristics of profiles. The results obtained allow us to conclude that numerous peculiarities of recent geodynamics, tectonic structure and geophysical fields are determined mainly by density heterogeneities of the crust and upper mantle in these active areas. It is shown that geodynamics of the Philippine Sea profile is determined by a relaxation process of the mantle bulge of the West Philippine Basin and smoothing out of the deep density and topography inhomogeneities in the gravity field of our planet. In the Sea of Japan the Earth's crust zoning for genetic types is specified. Areas with different modes of mechanical stress and movements of the crust-mantle matter flow are determined. Downward matter flow takes place on the continental shelf edge and slope of the Primorye region. Deep-see Japan Basin is characterized by a descending movement of the crust-mantle masses. Ascending movements of the mantle material prevail in the Yamato Rise area. The lateral component of the vector flow field in the same area speaks in favor of unilateral closure of the Sea of Japan.

JSA07/11A/D-002 Poster 0830-002

**LATERAL VARIATION OF THE LOWER CRUST COMPOSITION BENEATH NORTHERN MARGIN OF SOUTH CHINA SEA**

Yang WANG (School of Earth Sciences and Resources, China University of Geosciences, Beijing, 100083, China)

The lower crust composition of northern margin of South China Sea (SCS) was inferred from the P-T corrected seismic velocity structure, which is based on the seismic refraction profiles and the geotherms derived from downward continuation of heat flux as well as the cooling plate non-steady heat transfer model. The result shows a significant lateral variation of lower crust velocity beneath the northern margin of SCS. The thick high velocity ( $>7.0$  km/s) lower crust exists in the eastern and middle portions of the margin. Meanwhile, the velocity of lower crust in western portion is in range of 6.5-6.8 km/s. The lithology of lower crust in eastern and middle portions was inferred as mafic garnet granulite, or the mixture of mafic granulite and upper mantle rocks. The composition of lower crust in western portion is the mixture of felsic lithologies and mafic granulite, with a tendency of increasingly mafic component with depth. Since the variation of crustal properties are believed to result primarily from contrasting, pre-rift crustal structure across the margin (Nissen et al, 1995, JGR, v100, 22407), we proposed that the composition-related rheological heterogeneity of lower crust had influenced the basin evolution in northern margin of SCS. The ability of crustal rock to flow affects the style and kinematics of rifted region (Bertotti et al, Tectonophysics, 2000, v320, 195). No flow occurred in the relative rigid eastern portion of the margin, and subsidence affected the extending areas to form the Pearl River Mouth basin. However, the felsic lower crust beneath Xisha Trough of western portion could not prevent the flow to take place. The lower crustal rocks move towards the rifted zone causing isostatically driven upward movements. These may explain why Xisha Trough has thin post-rifting sediment, and failed to develop into the stage of sea-floor spreading.

JSA07/11A/D-003 Poster 0830-003

**A STUDY ON THE CHARACTERISTICS OF DIFFERENCE ARROW BY THREE-DIMENSIONAL MT(MAGNETO-TELLURIC) MODELING**Junmo YANG<sup>1</sup>, Seokhoon OH<sup>1</sup>, Duk Kee LEE<sup>1</sup>, Heuisoon LEE<sup>2</sup>, Yong-Hoon YOUN<sup>1</sup> (<sup>1</sup>Meteorological Research Institute, Korea Meteorological Administration, <sup>2</sup>Department of Science Education, Incheon National University of Education)

We perform the three-dimensional MT (Magnetotelluric) modeling to examine the validity of difference arrow of GDS (Geomagnetic Depth Sounding) survey. In this study, we investigate the validity of the difference arrow in three configurations of conductors; which are located 1) at a surface, 2) at a deep part and 3) vertically extended from surface to the deep part, respectively. For conductors located at the surface, the validity of difference arrows is certified by our numerical model when long periods over 40 min are used or the distance between conductor and sea is over 150 km. However, for conductors located at the deep part, mutual coupling between conductor and sea decreases comparing with that of conductor located at surface. And the increase of the buried conductor size reinforces the mutual coupling. Moreover, the conductor vertically extended from surface to the deep part enhances the mutual coupling for all periods, so that this case makes the validity of difference arrow considerably in doubt even for long periods. Therefore, the mutual coupling between conductor and sea must be examined to remove the known conductor effect such as the sea effect from the observed induction arrow. And the difference arrow that certifies the validity in this way can only provide meaningful support for subsurface information.

JSA07/11A/D-004 Poster 0830-004

**3-D CRUSTAL VELOCITY TOMOGRAPHY IN SOUTHERN KOREAN PENINSULA**Qinghe LI<sup>1</sup>, Su Gu KIM, Yuansheng ZHANG (<sup>1</sup>Seismological Bureau of Jiangsu Province, China Seismological Bureau, <sup>2</sup>Seismological Institute of Korean, Hanyang University, Korea, <sup>3</sup>Lanzhou Institute of Seismology)

A new technique of simultaneous inversion for 3-D seismic velocity structure by using direct, reflected, refracted waves and the genetic algorithm for optimization applied to the southern Korea Peninsula. The 1223 of Pg, Sg, Pm, Sm, Pn, Sn arrival times of 197 events are inverted for locations and crustal structure.  $10^{\circ}10$  blocks with about  $0.5^{\circ}$  and 7 layer (4km each layer) model was inverted. 3-D seismic crustal velocity tomography including 7 sections from surface to Moho, 18 profiles along latitude and longitude. Moho depth distribution were got. The results demonstrate: (1). The average velocities of sediment is 5.04km/s, thickness of are 3-4km, the velocity of basement is 6.11km/s;(2). The velocities fluctuate strongly in the upper crust. The velocity distribution of lower crust under Conrad appears basically horizontal; (3). The average depth of Moho is 30.4km and velocity is 8.01km/s;(4). From the sedimentary depth, velocity of sediment, basement thickness and velocity, form of upper crust, Moho depth and form we can find the obvious difference among different geological province. (5). The difference of crust structure between continent and ocean is obvious.. (6). The dynamic process and evolution for eastern Asia was analysed.

JSA07/11A/D-005 Poster 0830-005

**SPECIALIZED HARDWARE-SOFTWARE COMPLEX OF GEOPHYSICAL OBSERVATORY**

Sergey Eduardovich SMIRNOV, Alexandr Vladimirovich BUZEVICH (Institute of Cosmophysical Researches and Radio Wave Propagation Far Eastern Branch Russian Academy of Sciences)

Specialized hardware-software complex (SHSC) is intended to solve a wide range of tasks, in particular: to study the influence of solar activity on the processes in the upper and lower atmosphere and their connection with the geodynamics of the earth's crust in the Kamchatka region; to solve the problem of allocation and distinction of short-term and operative electromagnetic earthquakes' precursors. The kinds of observations were chosen so as to reveal the whole chain of cause and effect connections from the source of disturbance to the lithospheric response of the earth. These are the H, D, Z components of the magnetic field of the earth, which allow to reveal the effect, connected with the active sun formations and their reflection in the Earth's ionosphere. It is the level of space absorption of radio noise at the frequency of 32 MHz, which reflects the reaction of the D-stratum of the ionosphere in connection with the galactic influence and solar cosmic rays. These are the low-frequency barovariations in the atmosphere, which allow to judge about the character and the level of turbulence in the lower atmosphere. It is the vertical component of the electric field in the near-ground stratum of the atmosphere and the electrical conductivity of the near-ground stratum of the atmosphere. These are the measurements of the emanium level of Radon, which allow to reveal geodeformational processes in the possible earthquakes centers. It is the registration of meteoroparameters. SHSC can solve the following tasks: Data gathering and processing from 16-channel GSP with the interval from 1 second and more. The removed monitoring of DSP data in real time received from other computers of local computer network (LCN). The organization of the all the received data for the further processing and

archiving. Automatic generation of samples on the given interval of averaging and transformation of the data by E-mail. Automated data processing received by E-mail. The complex includes a set of service programs: 1. The program of the operative exchange of messages. 2. The program of the notification in case of malfunctions of operation of any kind of measurements. 3. The program of the measurements correctness for each kind of measurements. 4. The program of data sampling for each kind of measurements. 5. The program of data's visual presentation. 6. The program of the measured data correction. 7. The program of time shifts correction. 8. The program of SMS-message sending to the GSM-phone in case of observations stops. The system has functioned since November, 1996, registering geophysical fields with the interval of 2 seconds on 12 information channels, and it has proved to be reliable and stable. The complex is easily scaled. On the basis of this complex the method of the earthquakes' forecast "The method of the phase picture" was worked off. According to this method 6 earthquakes of the energy class more than 13.0 were officially predicted.

JSA07/11A/D-006 Poster 0830-006

**3-DIMENSIONAL DETAILED MODEL OF THE STRUCTURE OF THE COASTAL SHELF IN THE SOUTH-EAST AQUATORY OF THE EAST-SIBERIAN SEA AND THE ROLE OF PROCESSES OF BASIFICATION IN THEIR FORMATION ( INTERPRETATION OF THE GRAVITY DATA)**

Yury Ya. VASHCHILLOV, Vladimir Ye. GLOTOV, Tamara P. ZIMNIKOVA, Victor V. LYUBOMUDROV, Olga V. SAKHNO, Irina P. TSYGANKOVA (North-East Interdisciplinary Scientific Research Institute FEB RAS)

The work has been done by the financial support of RFFI (project 02-05-64010). 3-D density and structural-substantial models of lithosphere of the coastal shelf were created by the methods of new gravity interpretation. Maps of gravity anomalies in the Bouguer reduction with the net of observations points on sea ice approximately 2x2 km were used for quantitative interpretation.. The geological and petrological interpretation was given for the 3-dimensional density model. It is represented by the scheme of block tectonics, system of horizontal sections at depths of 1, 6, 10, 20, 30, 40, and 60 km (gravity tomography) and by the three vertical section. On the scheme of faults and blocks (density heterogeneity) calculated depth of roots of most faults and blocks change from 8-10 km down to 65-70 km. Meridional North-Aionsky fault, which is stretched along meridian  $168^{\circ} 35' e.l.$ , has calculated depth of root not less than 65 km. Density horizontal section at the depth of 1 km is transformed into the geological map-scheme with the age classification of rocks. Diapason of density change on 6-km horizontal section change from 2680 up to 2930 kg/m<sup>3</sup>. Both weakly metamorphosed sedimentary rocks with the density about 2680 kg/m<sup>3</sup> and dense basites are represented within this diapason. To the east of the North-Aionsky fault, roof of basite layer is situated on depth 6 km and more. The thickness of the Earth's crust is 38-40 km here. Rocks of basite type prevail at horizontal section of 10 km; basites and basite-hyperbasites - 20 km; rocks of basite-hyperbasite type of the lower parts of the Earth's crust with the calculated density of 3000-3160 kg/m<sup>3</sup> prevail at horizontal section 30 km. Undercrust substance with the density more than 3200 kg/m<sup>3</sup>, that is characteristic for the deep ultramafites, occurs lower than 40 km. The crust with great thickness of basite and basite-hyperbasite layers occurred as a result of the Late Mesozoic basification of continental crust. During the cooling, very density solidified lithosphere undergone lowering as a result of the thermoisostasy. To west of North-Aionsky fault, crust and lithosphere for the depths down to 65 km have less density. The crust has the typical continental character of composition with the developed "granitic" layer. The lowering of the Earth's surface took place here because of lower lithosphere parts density increasing.

JSA07/11A/D-007 Poster 0830-007

**GEOTHERMAL STRUCTURE OF PRECAMBRIAN CRUST**

Svet Yurievich MILANOVSKY (Institute of Physics of the Earth RAS)

In this work we present some results obtained during years of case geothermal study of Precambrian continental crust based on superdeep drilling, DSS and gravity field in Russia. The main objects discussed below are: 1) Results of heat flow study in Superdeep Kola Hole; 2) Investigations of hydro-geothermal regime in the upper crust; 3) Radiogenic heat generation data for Kola Hole; 4) Heat generation model for Precambrian crust based on deep drilling; 5) Geothermal, DSS, petrological and gravity study of the exposed high metamorphic terrains. Presented results are a part of the program to investigate geothermal field in Precambrian crystalline crust. The reason for such study was the possibility to do hydro-geothermal observations in the deepest hole in the world - Kola SG-3 and in many prospecting boreholes surrounding it (in relatively small area 6-7 km<sup>2</sup> - on nickel deposit «Verhnee»). It was established: 1) Increasing with depth thermal gradient and heat flow density; 2) Negative-correlation between filtration coefficient and geothermal gradient; 3) Existence of exogenous zone in the upper crust containing free meteoric water; up to 2000m; 4) Space heterogeneity of geothermal and filtration parameters for the upper crust reflecting anisotropy of transport and hydraulic properties of the rocks in the upper crust; 5) Relationship between hydro-geothermal field heterogeneity and stress field in the crust. From the analysis of U, Th and K distribution in the Kola borehole section, the radiogenic heat generation value has been estimated to a depth of 12064 m and, using the calculated composition of deeper zones. The total crustal radiogenic contribution to a depth of 12064 m is estimated at 9.7 mW·m<sup>-2</sup>. Detailed studies of U, Th and K in Achaean sections from other deep boreholes on Russian Plate as well as data for the Earth's oldest rocks from the published literature have been incorporated into a heat generation model for the granite - gneiss (12 - 20 km), gneiss-granulite (20 - 30 km) and the lower-most primary crustal or autochthonous restite (30 - 40 km) layers of the Precambrian crust. For the area of Anabar Shield we investigated geology, seismic, gravity and thermal fields. The Earth crust of Anabar presents a relict of most ancient sialic cover of the Earth. Our interest for the study granulitic terrains is caused by the possibility to see the inner structure of the deep eroded crust from the surface geology and in the same time to study it with geophysical technology. Gravity field of the crust within Anabar is characterized by linear maxima, which are oriented in NW-SE direction and coincide with zones of granulites. 3D analysis of gravity field gives the same direction of inclination of high density blocks in the crust that was found from surface geology and seismic model along DSS profile "Sapat". Thermal field of the Anabar Shield is characterized by very low heat flow. The average crustal heat generation was estimated to be 0.36 mW·m<sup>-3</sup>. The present-day crust being a possible model for the consideration of the lower crust.

JSA07/11A/D-008 Poster 0830-008

**GEOELECTRICAL DEEP STRUCTURE OF PRIMORYE REGION REVEALED BY MAGNETOVARIAIONAL INVESTIGATION**

Sergey Stanislavovich STARJINSKY (V. I. Il'ichev Pacific Oceanological Institute Far Eastern Branch Russian Academy of Science, 43 Baltiyskaya Str., Vladivostok 690041, Russia.)

The magnetovariational studies were carried out in Primorye territory at 10 sites. On the basis of this investigation the geomagnetic coast effect at this region was studied and

## INTER-ASSOCIATION

geomagnetic transfer functions, real and imaginary induction arrows were estimated. The orientation of the real induction arrows in a short period range reveals a linear conducting zone in upper crust extended from Khanka lake to the Amurskiy bay. All sites are characterized by strong geomagnetic effect. In order to find the reason of geomagnetic effect we have used the forward digital 2D electromagnetic TE mode modeling for two dimensional data and found that this effect can not be explained only by the conductivity of the sea water layer. Then we test a different models of the deep geoelectrical structure (GS) in the vicinity of the site in order to minimize the misfit between calculated and observed geomagnetic transfer functions. The model with minimum misfit was accepted as a final result. Using a such approach we have taken a three models of deep GS: two for coastal sites and one for shore-inland profile, including a third shore site located near Vladivostok city. The last model is characterized by a presence of conductive layer under sea at 15 to 140 km depth relative a sea level with resistivity  $\rho = 5 \text{ Ohm.m}$ , dipping in inland direction. At a depth greater than 140 km under sea it was necessary to allow a block with  $\rho = 1000 \text{ Ohm.m}$  to minimize a misfit at long periods. In north-east direction from this profile on a shore site Kiyevka bay model includes a conductive layer under sea at 47 to 140 km depth with  $\rho = 1 \text{ Ohm.m}$  vertically bounded by land layer with  $\rho = 1000 \text{ Ohm.m}$ . Deeper than 140 km under land resistivity is 10 Ohm.m and at the same depth under sea 1000 Ohm.m. The last site section was modeled near the Olga bay has infinitely deep layer under sea floor with  $\rho = 10 \text{ Ohm.m}$  and a roof at 7 km depth. In shelf field this layer has a vertical border with two land layers having resistivities 1000 Ohm.m and 10 Ohm.m, from up to down. The thickness of the first layer is 140 km. The general property of all models is a powerful conductive layer beneath the sea bottom near the coast of Primorye territory. It is in accordance with the anomalously high heat flow at a sea floor this region while at the continent it is normal.

**JSA07/11A/D-009** Poster **0830-009**

### 3-D SHALLOW CRUSTAL SHEAR VELOCITY STRUCTURE AROUND THE SOURCE REGION OF THE 1999 CHI-CHI (TAIWAN) EARTHQUAKE DERIVED FROM SHORT-PERIOD SURFACE WAVE DISPERSION DATA

Guey-Kuen YU<sup>1</sup>, Guey-Kuen YU<sup>1</sup>, Ruey-Der HWANG<sup>2</sup>, Wen-Yen CHANG<sup>3</sup> (<sup>1</sup>Department of Civil Engineering, Van-Nung Institute of Technology, Chungli, Taiwan, <sup>2</sup>Center of General Education, Hsing-Kuo University, Tainan, Taiwan, <sup>3</sup>Department of Natural Science and Mathematics, National Science Council, Taipei, Taiwan)

A detailed 3-D shallow crustal shear velocity structure around the source region of the 1999 Chi-Chi earthquake is derived in this study by inversion of short-period Rayleigh-wave dispersion data. The result shows that the Chelungpu and Shuilikeng faults are two main boundaries to clearly divide the source region into three different geological provinces. Shear velocities increase systematically from west to east, reflecting the geological features around the source area. Velocity heterogeneity on the eastern side of the source region is stronger and more complicated than that on the western side. This result agrees fairly with the thin-skinned thrust model interpretation. Furthermore, this study may also imply that the Chi-Chi earthquake is probably initiated not only near the border on which large velocity gradient varies, but at the position where the dip-angle of the fault is changed from sharp to gradual.

**JSA07/11A/D-010** Poster **0830-010**

### VELOCITY STRUCTURE OF NORTHERN PART OF ATERA FAULT SYSTEM, CENTRAL JAPAN

Makoto OKUBO<sup>1</sup>, Harumi AOKI<sup>1</sup>, Masazumi ONISHI<sup>2</sup> (<sup>1</sup>Tono Research Institute of Earthquake Science, Association for the Development of Earthquake Prediction, JGI, Inc.)

The Atera fault system, extending more than 70km northwesterly in central Japan is known as a prominent active fault with left-lateral offset of 7km, a vertical of 700m and crush zone width of 300m at maximum. According to the strip map of Atera fault system (GSJ, 1973), the northern part of the fault system consists of three parallel active faults, Kowachi, Yugamine and Gero fault. However the southern extensions of Yugamine and Gero are not clear. Therefore, TRIES (Tono research institute of Earthquake Science) directed the reflection/refraction survey across these faults in 2000. Along with the general reflection survey with vibrator, a new technique, named "ground-level tomography", was tried along two parallel observation lines, across the faults. The velocity distribution near the surface between two observation lines can be analyzed using a *cross-well tomography* technique. In same experiment, clear side-reflections from the fault plane were frequently observed on field records. The inclination of fault plane could be suggested from the appearance and disappearance of side reflections. A refraction survey was also executed with explosive sources for the survey of deep structure. Some of field records were used for the simultaneous determination of time-terms and basement velocities. A new graphic method was successfully adapted in this case. The velocity distribution deduced from ground-level tomography, the distribution of time-terms / shallow reflectors and the faults location provided us with a model of faulting. A sharp velocity contrast between fault zone and outside of it suggests a pull-apart structure in the northern part of Atera fault system.

**JSA07/11A/D-011** Poster **0830-011**

### 3D CRUSTAL DENSITY STRUCTURE AND ITS GRAVITY ANOMALY OF CENTRAL TAIWAN

Jian ZHANG<sup>1</sup> (<sup>1</sup>The Graduate School of the Chinese Academy of Sciences, <sup>2</sup>Department of Earth and Planetary Science University of California, Berkeley, <sup>3</sup>The Graduate School of the Chinese Academy of Sciences, <sup>4</sup>Department of Geophysics Peking University, <sup>5</sup>Department of Earth and Planetary Science University of California, Berkeley)

Taiwan is a mountainous island that rises locally to ~4 kilometers. It was formed since the late Cenozoic, with the oblique collision between the Luzon volcanic arc on the Philippine Sea plate and the China continental margin. The prevailing structural trend in Taiwan is that of an elongated arc convex to the west. Northeast of Taiwan, the Philippine Sea plate subducts northward beneath the Ryukyu arc-trench system. South of Taiwan, the oceanic crust of the South China Sea is subducting eastward beneath the Philippine Sea plate at the Luzon arc. Our study focuses on the central section of Taiwan because it is away from the subduction zones and thus offers a simpler picture on the collisional mountain-forming tectonics. We construct a 3D crustal density model in central Taiwan from the available seismic velocity. Since density and seismic velocity of crustal rocks are closely related (e.g., Birch, 1961; Christensen and Mooney, 1995), it is reasonable to construct the 3D model for the crustal density in central Taiwan on the basis of the available seismic velocity and an empirical velocity-density relation. 3D tomographic P-wave velocity structures for Taiwan have been published by Rau and Wu (1995) and Cheng (2000). Our study uses Cheng's tomographic velocity model because it was specifically designed for central Taiwan. The model was based on a simultaneous inversion of 24,230 P-wave travel times from 2,582 events, as recorded by the Central Weather Bureau seismic network. This velocity model is converted to a density model by using an empirical relationship between velocity and density. The empirical relationship is obtained by fitting the experimental data presented by Ludwig et al. (1970) for both crystalline and sedimentary rocks at  $V_p > 2 \text{ km/s}$ . Next, we calculated the gravity anomaly of the 3D density model. The contribution of the 3D-density

model to the gravity anomaly is calculated with the finite element method. In this study we represent the crustal block in central Taiwan by a finite-element mesh of 76,500 elements, each 2x2x2 km<sup>3</sup> in size. Since the average density does not contribute to gravity anomaly, we subtract the average density of each horizontal layer from the initial density model, leaving only the density difference. The result shows that the calculated gravity anomaly for the density model are negative values on the western side of the island, reflecting the relatively low density of the sedimentary rocks, and positive values on the eastern side, reflecting the relatively higher density of the metamorphic rocks and the crystalline basement. Besides, there is a crustal root beneath the Central Range. Southern of Taiwan, the crustal root trends NNE and lies directly beneath the Western Central Range. At higher latitudes, however, the crustal root turns clockwise towards NE to lie beneath the Eastern Central Range. Acknowledgement: This work was supported by NSFC (No.40074022, 40174027) and NSF (No.EAR-01-06802).

**JSA07/11A/D-012** Poster **0830-012**

### CORRELATION BETWEEN STRONG EARTHQUAKE ACTIVITY AND ACTIVE CRUSTAL-BLOCK IN CHINA MAINLAND AND ITS ADJACENT REGIONS

Hongsheng MA, Guomin ZHANG, Jie LIU, Li LI (Center for Analysis and Prediction, China Seismological Bureau, Beijing 100036, China)

By the hypothesis of the active crustal-block and based on the research of the active crustal-block, the correlation between strong earthquake activity and active crustal-block, in China mainland and its adjacent regions, has been discussed in this paper. The results show that large tectonization and strong earthquakes mainly occur on the active crustal-block boundaries. All the huge earthquakes over Ms 8 and 86% strong earthquakes over Ms 7 cluster on the active crustal-block boundaries which only occupy 17% space of the whole area. The active crustal-block boundaries have controlled almost all the strong earthquakes in China mainland and its adjacent regions. In general, not only strong earthquake activity shows notable rhythm, but also the active and low phases are similar to those of China mainland. Sometimes, the active periods of strong earthquake in some cycles are longer than those of China mainland. The main areas of strong earthquake activity for each seismic cycle show that active crustal-block moves differently in different seismic cycle. Based on present crustal movement, the potential correlation between active crustal-block movement velocity and strong earthquake activity has been discussed in this paper. Key words: hypothesis of the active crustal blocks active crustal-block boundaries strong earthquake activity active crustal-block movement velocity.

**JSA07/11A/D-013** Poster **0830-013**

### LITHOSPHERE ELECTROMAGNETIC WINDOWS: SPATIAL DISTRIBUTION, CONSTRUCTION, PROPERTY

Yuri Buddich BASHKUEV, Valery Bazhevich KHAPTANOV, Darima Garnaevna BUYANOVA, Mikhail Georgievich DEMBELOV (Buryat Scientific Center SB RAS)

The report is devoted to the detail study of electrical properties, construction and spatial distribution of lithosphere electromagnetic windows on the Earth. We call the electromagnetic windows as areas of the upper part of the earth crust with very low electric conductivities ( $10^{-4} \div 10^{-6} \text{ Sm/m}$ ) that have sizeable squares. As a rule, they correspond to crystal massifs of the rocks on the earth surface. The crystal massifs as prominences on daytime surface of the high-resistance fundament are studied very insufficiently because of difficult soundings on direct current and limited frequency range for MTZ method. In this time regions that have low electric conductivities ( $10^{-4} \div 10^{-6} \text{ Sm/m}$ ) occupy sizeable territories (on our estimations - up to hundreds kilometers in length and width). These spots with low electric conductivities are commensurable with ionosphere conductivity and can play an important role in the global electric chain, in particular, when we consider mechanisms of the lithosphere-atmosphere-ionosphere interaction. Our investigations and fund materials on electric exploring in the East part of the Russia (Zabaikalie, Aldan and Anabar shields and etc.) show that crystal massifs with very low electric conductivity are least studied objects as a white spot. In the report an approach based on registration in calculating models of an essential inhomogeneity of electrical properties of the earth crust in the depth direction and on square (3-dimensional geoelectrical model) is developed. We decided the problem of research of electric properties of crystal massifs by means of methods using artificial and natural fields in more high frequency range from ULF-ELF to LF-HF. A possibility to study of electric conductivity and dielectric permeability of the medium and higher precision of its measurements when radiostation fields and other artificial sources are used is as an advantage of such approach. It is necessary to note that methodology of magnetic telluric and radio impedance soundings are common. Thus, a big volume of experimental and fund materials is obtained, summarized and analyzed. An elaboration of models that describe electric condition of the upper high resistance part of the earth crust (maps and sections) is made. The main results: 1) a method of search of earth crust areas with assigned electric characteristics is developed to discover territories with high resistance of upper part of the earth crust; 2) a spatial disposition of the lithosphere electromagnetic windows on the globe is defined; 3) electromagnetic sounding and profiling of crystal massifs of the east part of Russia in ELF-VLF-LF ranges is made; 4) geoelectric models of upper high resistance part of the consolidate earth crust for some regions of Zabaikalie, Aldan shield and Bureya massif are created; 5) a method of definition of dielectric permeability of the crystal rocks in conditions its natural dispositions is created; 6) geoelectric maps with different scales are created for studied crystal massifs.

**JSA07/11A/D-014** Poster **0830-014**

### DEEP GEOPHYSICAL MODEL FOR THE AREA OF THE KURILE-KAMCHATKA AND ALEUTIAN ISLAND ARCS JUNCTION

Yuri F. MOROZ, Larisa I. GONTOVAYA (Institute of Volcanic Geology and Geochemistry, FEB RAS)

The results of magnetotelluric sounding (MTS), seismic tomography and their complex interpretation are described. The MTS interpretation has been made by application of the present-day approaches taking into consideration the effect of local and regional near-surface geoelectrical heterogeneities. Using 3-D numerical modeling of the magnetotelluric field, the inversion of the MTS curves was carried out. As a result, a 3-D model of deep electrical conductivity of the region has been obtained. Based on the DSS and seismological data and using seismic tomography method, a 3-D velocity model for lithosphere has been created. Based on the complex analysis of geoelectric and seismic models and other geologic-geophysical information, the following peculiar features have been revealed in the deep structure of the junction area of the arcs. At depths of 100-200 km, the upper mantle hosts the asthenospheric layer associated with partial melting of the ultrabasic rocks. The roof of this layer forms a riseup to the depth of 80 km beneath the zone of the present-day volcanism of the Kurile-Kamchatka island arc including the Klyuchevskay group of volcanoes and the Shiveluch volcano. The rise is located above the seismofocal zone. It is connected with a mantle source feeding present-day volcanoes. The lithosphere contains transverse conducting zones of the Aleutian direction. Conducting zones are suggested to represent

deep faults with hydrotherms. The faults are the result of the arcs' interaction. They may serve as channels for the fluids supply from the Major Kamchatkan deep fault and from the Pacific Ocean. One of such zones is distinguished within the earth crust at the depths of 10-30 km. It goes through the Klyuchevskaya group of volcanoes. In this region this zone forms a projection with anomalously low electrical resistivity. The low velocity anomaly of the seismic waves continuing down to the asthenospheric rise is confined to it. The anomalies are connected with the crust magmatic source that is approximately  $50 \times 50 \times 25 \text{ km}^3$  in size. The occurrence of this source is a consequence of the magmatic melts supply from the asthenospheric rise and the result of the additional rock melting within the crust fault. By rough estimates, the melt content in the crust source attains about 2%. The total volume of melt ranges from 20 to 60  $\text{m}^3$ . Another lithosphere transverse zone of low electrical resistance is found at the extension of the Aleutian island arc. It is probably more than 100 km long. Low electrical resistance may be due to the hydrothermal solutions filling rock fissures. The low velocity anomaly within the low parts of the earth crust is confined to the western area of the zone. This anomaly is associated with the crust magmatic chamber feeding the Shiveluch volcano.

**JSA07/11A/D-015** Poster **0830-015**

#### THE RELATION BETWEEN MOVEMENTS AND DEFORMATIONS OF ACTIVE CRUSTAL-BLOCKS AND SEISMOLOGY IN EAST ASIA

Hui WANG<sup>1</sup>, Guomin ZHANG<sup>1</sup>, Yun WU<sup>2</sup> (<sup>1</sup>Center of Analysis and Predict, China Seismology Bureau, <sup>2</sup>Seismology Institute, China Seismology Bureau)

Based on the hypothesis of active crustal-blocks in China and its adjacent region, used GPS (Global Position System) survey results and the method of DDA (discontinuity deformation analysis) on spherical surface, the present-day movements and deformations of each active crustal-blocks were calculated. The results show that although the movement and deformation of each active crustal-block in east region and in west region were different, the blocks in the same region were coherent. For the boundary zones of active crustal-blocks were consisted of rupture zones, the relative velocities of boundary zones can be looked as rupture zones' velocities. The model results were coherent with geological results. From the kinetic character of boundary zones, the rupture zones can be classed to three type: creep rupture zones, locked rupture zones and mixed rupture zones. When the strong earthquakes in last ten year in this region were considered, the conclusion can be drawn that the most strong earthquakes occupied in rupture zones and although the velocity of mixed rupture zones were not the biggest, the strain energy can concentrated easily in that region, the strong earthquake occupied more oftenly.

**JSA07/11A/D-016** Poster **0830-016**

#### GRAVITY ANOMALIES OF THE HOKKAIDO ISLAND, NORTH JAPAN

Masao KOMAZAWA<sup>1</sup>, Hiroshima TOSHIO<sup>1</sup>, Yasuaki MURATA<sup>1</sup>, Masahiko MAKINO<sup>2</sup>, Rie MORIJIRI<sup>3</sup>, Kazunari NAWA<sup>1</sup> (<sup>1</sup>Institute of Geoscience, Geological Survey of Japan, AIST, <sup>2</sup>Research Center for Deep Geological Environments, Geological Survey of Japan, AIST)

Bouguer gravity anomaly map of the Hokkaido Island that has been compiled from about 84,000 land gravity measurement data and a lot of shipborne gravity data of surrounding area. All measured gravity data were referred to the International Gravity Standardization Net 1971 (IGSN71), and the normal gravity values were estimated according to Gravity Formula 1980. Terrain corrections were conducted with respect to the distance range up to 60 km by approximating the real topography to an assemblage of annular prisms interpolated by mesh terrain data and random terrain data of gravity points. The effect due to the earth's curvature was taken into consideration. Bouguer corrections within the range of 60 km in arc-distances were made using a spherical cap crust formula. The features of gravity anomalies, Bouguer anomalies, are as follows. In the central part of Hokkaido, a remarkable high gravity anomaly runs north to south along a line that extends from the Hidaka Mountains through the district of Asahikawa and east of the Teshio Mountains to Hamatonbetsu. This gravity anomaly coincides with the collision zone between the Kurile Arc and the Northeast Japan Arc and is associated with exposures of high-density mafic igneous and metamorphic rocks derived from the deep crust. The gravity high is paralleled on the west by a north-south-trending gravity low that extends from the Hidaka Basin through the Ishikari Lowland, Yubari Mountains, Takikawa Lowland and Teshio Mountains to the Teshio Plain. This low gravity anomaly is associated with deep basins that are filled with Neogene to Quaternary age sediments. The Hidaka basin occurs in a large-scale crustal downwarp that formed in advance of a thick sheet of deeper crustal rocks which were thrust over the surface by the westward movement of the Kurile Arc. The negative gravity anomaly associated with this basin reaches -100mGal, which value is similar to the gravity low associated with a large depression on the backside of the uplifted crust along the coast of Tokachi. Another distinctive gravity high is observed over the Kabato Mountains and the west side of the Ishikari Lowland. This high anomaly is associated with widely distributed high density Late Oligocene to Quaternary volcanics. The complicated patterns observed in this gravity anomaly are associated with uplifted and downthrown areas within the underlying basement. Northeast-southwest-trending oval-shaped gravity lows are observed around Obihiro and along the Daisetsu Range in central Hokkaido. The gravity low around Obihiro is interpreted to be result from a 2-km-thick sequence of relatively low-density sediments. However, Mts. Daisetsu, Tomuraushi and Tokachi-dake, which constitute the Daisetsu Range, are volcanoes composed largely of andesite. Thus, the low gravity anomaly is interpreted to result from subsidence of the basement beneath these volcanoes. A positive gravity anomaly that reaches 200mGal in value extends from the district of Kushiro to the Habomai Islands. The region coincides with Cretaceous sedimentary rocks distributed along a fore-arc highland. However, the region is also associated with a high magnetic anomaly, which implies that high-density mafic igneous rocks probably underlie the Cretaceous sediments.

**JSA07/11A/D-017** Poster **0830-017**

#### HIGH BOUGUER ANOMALY MEASURED NEAR AND AROUND THE YAMASAKI FAULT, SOUTHWEST JAPAN

Fumiaki TAKEUCHI, Kazuo MATSUMURA, Kajuro NAKAMURA, Kunihiko WATANABE (Disas. Prev. Res. Inst., Kyoto Univ.)

We measure gravity values near and around the Yamasaki fault, Hyogo, Okayama and Tottori, southwest Japan, from 1984 to 1999, to develop the regional structure. The total length of this fault is about 90 km, some of the longest ones in Japan. However, it is divided into some sub-faults, Ohara, Hijima, Yasutomi and Kuresaka-toge from west to east. The regions of these faults are some 10 km northwest of Kobe Earthquake in 1995 (Mj7.2) and about a hundred km southeast from the Western Tottori Earthquake 2000 (Mj7.3). It is also said that Harima-Yamashiro Earthquake 868 (M > 7) near the faults. So many microearthquakes are occurring nowadays along the strike (WNW - ESE), especially a M5.6 earthquake with many aftershocks occurred in 1984 very near the Kuresaka-Toge fault. Almost all microearthquakes occur in depth from 0 to 20 km. The Yamasaki fault is left lateral, and the horizontal displacement is totally 50 - 400 m depending upon the region. Our

first aim is to decide the structure of the fault by gravity measurement data. We mainly use G615 LaCoste-Romberg gravimeter (G615) for observation. The measuring point intervals are usually set as 500-2000 m, and in many cases they make traverse lines to the fault. The observation points are usually selected from the points where the latitude, longitude and height values are shown in the 1/25,000 maps (Geographical Survey Institute). However, if such kind of data is unable to obtain, we use maps from local governments. Then we obtain data from 968 points, and other 987 data from Metal Mining Agency of Japan. Then our data cover almost 20 km width through the fault. Using these data, we calculate the Bouguer anomaly by setting density to be 2.67 g/cm<sup>3</sup>. The result shows that the Bouguer anomaly is somehow bigger near the fault than other regions, which is anomalous to other faults. In order to make this fact clear, we collect 35 stones from points around the fault, mainly from the stream beds or slopes of mountains. After carrying back them to our laboratory, we saturate them with water to measure the density. The values show 2.44 - 3.04 g/cm<sup>3</sup>. By using these values, we calculate the upper crustal structure by 2-dimensional Talvani method. It shows a similar results as the upper one (density 2.67 g/cm<sup>3</sup>), however, this makes much clear the depth and width of high density areas. The widths of high density areas are a few km and their depths distributes 500 - 5,000 m depending on the fault location.

**JSA07/11A/D-018** Poster **0830-018**

#### LOWER-CRUSTAL REFLECTOR BENEATH THE TAMBA PLATEAU, CENTRAL JAPAN

Hiroshi KATAO (Disaster Prevention Research Institute, Kyoto University)

Distinct later phases following direct S wave are observed in the Tamba Plateau, which is an active microearthquake swarm area in northern Kinki District, Japan. These phases are interpreted as reflected S wave from the reflector in the lower crust. The amplitude ratios of reflected S waves to direct S waves are estimated to be 0.1-0.4. Even though the radiation pattern is considered on the focal mechanisms, this amplitude ratio is very high. In order to explain such high amplitude of the reflection phase, S wave velocity contrast across the reflector surface must be large, suggesting that the reflector is a surface of fluid layer. The locations of reflectors are derived from more than 200 reflection phases. Depth of the inclined reflector is about 20-25 km in the lower crust. The reflector is not parallel to the horizontal cut-off boundary of shallow seismicity, and is dipping toward the north. The shape of the reflector is related strongly to the deep structure and tectonic movement of the large active fault: Arima-Takatsuki Tectonic Line. Since no Quaternary volcanic activities exist around this region, these features of the reflector beneath the Tamba Plateau are different from that of other mid-crustal reflectors found at volcanic regions in Japanese Islands.

**JSA07/11A/D-019** Poster **0830-019**

#### COMPLEX MODEL OF THE ONEGA REGIONAL MAGNETIC ANOMALY (RMA) IN THE FENNO-SCANDIAN SHIELD

Victor A. ZEMTSOV (Institute of Geology, Karelian Research Centre, RAS, Petrozavodsk, RUSSIA)

Continental RMA are caused, as a rule, by unknown magnetic field sources located at various depths and are interpreted in different ways. Deep-seated rocks are known to have high magnetization values in the extension zones of the Precambrian earth crust (to 5 A/m on the Canadian Shield). On the contrary, RMA in fold belts, which are younger (for example, in the Urals), are explained by subsurface magnetic sources, and the magnetization of the lower crust approaches zero. The Onega RMA was filtered by means of transformation of the total vector of the anomalous magnetic field at an altitude of 25 km. Its center is located in the southeastern Fennoscandian Shield on the Zaonezhsky Peninsula of Lake Onega. It has a round shape, slightly extended in a northwestern direction, and a diameter of about 200 km. There is a local maximum at the altitude of transformation, and the total RMA value can be as high as +400 nT. This anomaly is presumably caused by several magnetic sources distributed in two plutonic levels. One of them plunges to a depth of 10 km and the other is deeper and more spacious. If the Curie boundary of magnetite here coincides with the crust base (35 km), the magnetization of the upper column of the crust would be 8.8 A/m. For the lower layer it would be 4.4 A/m, which seems unlikely. The Onega RMA spatially overlaps the minimum heat flow anomaly (less than 20 mW per square metre), which is unique in Europe. In this case, the Curie surface will always be deep in the mantle. Available DSS data show a considerable rise in seismic velocity (to 8.4 km/s), which begins here at a depth of 60 km. Also occurring in this area are the largest mafic rock intrusions, breccia pipes and the Suisari plutonic volcanogenic complex. The complexity of the crust-mantle boundary here is due to a special structure (SS) between the apparent crust and the real mantle surface. Based on geological and geophysical data, a magnetic model of the Onega RMA was developed. If we assume that the average magnetization of the lower layer of the crust and (SS) rocks to a depth of 50 km is identical and homogeneous here, then the magnetization of this block would be 0.7 A/m, provided the concentration of magnetite in the rocks is about 0.05%. The model developed is, of course, an approximation to real conditions.

**JSA07/11A/D-020** Poster **0830-020**

#### AN ATTEMPT OF INTERPRETATION IN PETROLOGICAL TERMS OF THE P- AND S-WAVE MODELS ON THE SEISMIC REFRACTION LINE VRANCEA 99, ROMANIA

Victor RAILEANU<sup>1</sup>, Franz HAUSER<sup>2</sup>, Andrei BALA<sup>1</sup>, Claus PRODEHL<sup>2</sup>, Werner FIELITZ<sup>1</sup> (<sup>1</sup>National Institute for Earth Physics, Bucharest, Romania, <sup>2</sup>Geophysical Institute, University of Karlsruhe, Germany, <sup>3</sup>Geological Institute, University of Karlsruhe, Germany)

A seismic-refraction line was recorded in 1999, in the southeastern part Romania, to study the crustal and uppermost mantle structure underneath the Vrancea epicentral region. It is a contribution to the joint German-Romanian research programme "Strong Earthquakes - A Challenge for Geosciences and Civil Engineering" installed by the Co-operative Research Center 461 at the University of Karlsruhe, Germany, in collaboration with various research institutions in Romania. Data quality is very variable along the seismic line: it is better on the southern half with signal-to-noise ratios decreasing towards north. In a first step of data processing and interpretation, a P-wave velocity model was developed. It shows a multi-layered crust with velocities increasing with depth. The upper part of the model delineates the velocity structure of the sedimentary cover composed of the Carpathian Nappes, the Neogene sediments of the Foredeep and the autochthonous cover of the Moesian Platform. The upper and lower crustal layers are marked by constant velocities along their interfaces and by a variable thickness. The model displays a thickened upper crust in the central part of the seismic line, decreasing towards both ends. In a second stage a S-wave velocity model is achieved. It displays about the same crustal structure as the P wave model as it keeps the same depths of the crustal interfaces. Based on the Vp/Vs ratio a Poisson's ratio model is computed. It shows a larger variation of this parameter for the sedimentary cover (0.22-0.35) and a narrow range (0.22-0.25) for the crystalline crust. An interpretation in petrological terms of the Poisson ratio model indicates the most probable rock types that could make up the crustal section. Clay, marl, sand, sandstone, limestone for the sedimentary cover, granite-gneiss and granodiorite for the upper crust and gneiss, greenschist facies basalt and amphibolite for the lower crust. In the upper mantle Poisson ratio's is 0.28. This value is well

matched for the rocks in eclogite facies.

**JSA07/11A/D-021** Poster **0830-021**  
**NEW TRANSECT ACROSS MOSCOW SEDIMENTARY BASIN: DEEP STRUCTURE AND HISTORY OF FORMATION REVEALED BY JOINT ANALYSIS OF GEOPHYSICAL DATA AND SUBSIDENCE CURVES**

Robert G. BERZIN<sup>1</sup>, Arsen K. SULEIMANOV<sup>1</sup>, Yury N. ANDRYUSCHENKO<sup>1</sup>, Nadejda G. ZAMOJNAYA<sup>1</sup>, Elena A. KISELEVA<sup>2</sup>, Valentin O. MIKHAILOV<sup>2</sup>, Ekaterina A. PSHECHENKOVA<sup>2</sup>, Sergei A. TIKHOTSKI<sup>1</sup>, Dina Yu. SHUR<sup>2</sup>, Mikhail V. MINTZ<sup>2</sup>, Tatyana N. KHERASKOVA<sup>3</sup> (<sup>1</sup>Spestgeofizika enterprise, Moscow, Russia, <sup>2</sup>United Institute of Physics of the Earth, RAS, Moscow, Russia, <sup>3</sup>Geological Institute RAS, Moscow, Russia)

Joint analysis of CDP reflection seismic data and data of gravity, magnetic and telluric measurements has been performed for the new transect 1EV running across the Moscow sedimentary basin. Obtained structure of sedimentary cross-section and crystalline basement as well as new information on position and structure of Riphean grabens were compared to the subsidence history from the Late Riphean to Carboniferous. Dense net of seismic refraction and reflection profiles, numerous boreholes and other data have been collected for the East European platform to perform a correction of the Bouguer anomalies for known inhomogeneities, including corrections for the gravity effect of sedimentary layers (taking into account laterally variable and depth-dependent density of sediments), gravity effects of the Moho discontinuity and Riphean grabens. As a result a set of gravity maps has been constructed. These maps demonstrated fairly good correlation with crustal structures revealed by 1EV transect. The density model of the deep crustal structure was constructed, taking into account magnetic anomalies and telluric data. Joint analysis of this data set results in tectonic and compositional interpretation of the crustal structure. In particular, seismic data imaged a synform (syncline type) structure in the central part of the Moscow basin. An outer layer of this synform has lower density and composed of very low resistivity and weakly magnetized rocks, while its core is composed of dense and strong magnetized rocks. We interpret this as a result of high fluid and (or) carbon content in the outer layer. For the analysis of the subsidence history we used the data from 23 boreholes situated in the vicinity of the transect. The study of regional and local components of tectonic subsidence and their comparison to the model of crustal structure demonstrated that the Moscow sedimentary basin has been formed in result of two main tectonic events. The first tectonic event took place in the period from Late Riphean to Early Vendian. The style of extension had been strongly controlled by crustal structure formed before Late Riphean. During the second tectonic event, which took place from Middle Devonian to Late Carboniferous, crustal control was not so strong. Amplitude of uplift and subsidence were almost the same all over the basin. The second tectonic event was probably result of uplift of a mantle plume (e.g. Wilson, Lyashkevich, 1996). This plume supposed to be formed in deep mantle and later separated into several smaller plumes when it moved through the upper mantle. This plume initiated strong tectonic activation of all East European Platform resulted in opening of 2500 km-long system of rift basins at its periphery and differential, mainly downward movements in its central part.

**JSA07/11A/D-022** Poster **0830-022**  
**HEAT FLUX FROM LUNAR CORE AND CONTINENTAL MASCONS ON THE MOON**

Alexander GUSEV, Natasha PETROVA (Geophysics, Kazan University)

The question of lunar core existence is still an open question. Nevertheless, many modern observational data, such as the noticeable free librations in the presence of great dissipation, involve the appropriate consideration of active lunar internal stratigraphy, including elliptical liquid core and rigid or viscous mantle. According to calculation of Konrad and Spohn (1997), the lunar core composed of Fe, FeS and Fe-FeS has a melting temperature from 1950K (for pure Fe) to 1250-K (for eutectic proportion). By this means the presence of a fluid core with a turbulent or convective layer at the CMB (Yoder, 1981) appears to be the plausible source not only for great dissipations, but also for exciting and maintaining of free librations. The differential rotation of the rigid mantle and liquid core in the Moon, the interaction between them is responsible for the formation of specific transition zone - core-mantle boundary that plays an important role in the lunar dynamics (Petrova & Gusev, 2001). Extensive discussion of seismic, magnetometric and librational data were performed by Dickey et. al. (1994) for the parameters (sizes, shape, rheological properties etc.) of the lunar core and CMB. From additional LLR data and an improved gravity field from Lunar Prospector have found four dissipation terms, that can be explained with the combined effects of tide plus core: 2/3 of the 0.26" term comes from a tidal friction and 1/3 comes from the CMB friction without considering the CMB ellipticity. As result Q~37±5 at a one month period and Q=60(-15,+40) at one year (Williams, 1999). Dissipative effects arising from the core-mantle interaction are responsible for additional heating of the planet's interior, causing convective motion in the mantle and grows of the early lunar lithosphere; for the exciting and maintaining of free librations in the Moon; for arising of plumes that are responsible for the formation of ancient hot spots and "mascons" in the crust (Gusev & Petrova, 1999). With the Yoder's boundary layer theory, approximate estimation of the heat flow from lunar CMB was made. For a liquid iron core with a radius of 350 km and kinematical viscosity  $\eta=3300\text{St}$  and differential velocity  $\Delta\omega=1.37\cdot 10^{-4}\text{rad/sec}$  the estimation of the heat flux from the core to the mantle is  $1.5\cdot 10^{10}\text{W}$ . In this connection many new cosmic experiments - Lunar-A, SELENE, SMART, ILOM - will give a possibility to determine the size and composition of a lunar core, the magnetic and heat characteristics of the Moon.

**JSA07/11A/D-023** Poster **0830-023**  
**GRAVITY AND MAGNETIC MEASUREMENTS ON THE BLACK SEA ROMANIAN CONTINENTAL SHELF AND THE SIGNIFICANCE OF THEIR RESULTS**

Constantin Stefan SAVA (National Institute of Marine Geology and Geoecology - GeoEcoMar, Bucharest - Constanta, Romania)

In the past years, Romanian offshore has attracted much attention because of the oil and gas discovery. The major regional study required an important effort for the seismic acquisition. Interpretation of seismic data had provided a good image of stratigraphy and tectonics, but many explanations are still necessary. In view of improved knowledge on the geological structure at depth under the Black Sea Romanian Shelf as well as to gather more data about the continuation of land geological structures into the sea, gravity and magnetic measurements have been made in addition to seismic. Gravimetric research was done by the use of underwater and onboard marine gravity meters produced in Russia. At the same time magnetic research was carried out. An original method, which made possible the use of land magnetometers at sea, was first applied. Later, marine proton magnetometers were used. All the magnetic equipment used at sea was made in Romania. We have also drawn up all the programs for the marine gravity and magnetic data processing as well as the 2D and 3D geophysical modelling. The first results of marine and magnetic surveys were presented in maps on scale 1:500,000. Then the territory was mapped systematically on the scale 1:200,000. At this scale, the gravity map could be interpolated at intervals of 2.5 mGals and the magnetic map at the intervals of 50 nT. Further, we started detailed work on several

maps on the scale 1:50,000, particularly in the coastal zone, in order to clarify the detailed relations between the land and the marine geological structures. These maps were interpolated at intervals of 1.0 mGal for the gravity one and 10 nT for the magnetic one. Initially, the geological data obtained onshore was correlated to offshore geophysical surveys and drillings in order to obtain a better understanding of the offshore geological structure. Later, offshore geological data was used for establishing a more detailed model of the onshore Dobrogea geological structure. This idea is clearly illustrated by the evolution of the conceptions regarding the geological structure of the on- and offshore areas of the Constanta sector of the Moesian Platform. We have to emphasize the necessity of drawing up the gravity and magnetic maps of the entire Black Sea in a unitary system, through international cooperation, in order to improve the contribution of these geophysical methods to the geological knowledge of the area. To conclude, we could say that the completed magnetic and gravity surveys bring an important contribution to the worldwide knowledge of the Earth magnetic and gravity fields.

**JSA07/11A/D-024** Poster **0830-024**  
**SEISMIC ANISOTROPY AND MANTLE CREEP IN YOUNG OROGENS**

Rolf MEISSNER<sup>1</sup>, Irina M. ARTEMIEVA<sup>2</sup>, Walter D. MOONEY<sup>3</sup> (<sup>1</sup>Kiel University, <sup>2</sup>EOST, <sup>3</sup>USGS)

We discuss the origin of anisotropy in the crust and uppermost mantle in terms of processes that are controlled by temperature, rheology, and deformation. We disregard anisotropy within sedimentary basins and instead concentrate on anisotropy owing to the lattice preferred orientation (LPO) of anisotropic minerals. We focus on young mountain belts that have thick crustal roots and high geothermal gradients. We compare the orientation of this Pn anisotropy with the direction of compressive stress, which nearly always shows a mountain-perpendicular component in the upper crust. From the discrepancy of directions between the fast axis of mantle anisotropy and compressive crustal stresses, we therefore postulate the existence of a decoupling layer. This layer is generally found in the middle or lower crust in all areas with high geothermal gradients and especially in young and warm mountain belts. A decoupling layer corresponds to a low-viscosity layer capable of creep owing to tectonic stress. Tectonic escape or "lateral extrusion" was first suggested for southern China by Molnar & Tapponier (1975). It is today considered to be a lithospheric process and not limited to the crust.

**JSA07/11A/D-025** Poster **0830-025**  
**SHEAR WAVE VELOCITY, SEISMIC ATTENUATION, AND THERMAL STRUCTURE OF THE CONTINENTAL LITHOSPHERE**

Irina M. ARTEMIEVA<sup>1</sup>, Magali BILLIEN<sup>1</sup>, Jean-Jacques LEVEQUE<sup>1</sup>, Walter D. MOONEY<sup>2</sup> (<sup>1</sup>EOST, <sup>2</sup>USGS)

Theoretical models based on laboratory studies of dissipation of energy in the crystalline rocks typical for the Earth's mantle suggest a temperature dependence of attenuation through the activation energy. We therefore compare global maps of the thermal structure of the continental lithosphere with the inverse attenuation of seismic shear waves Qs and seismic velocity Vs as determined from surface wave dispersion and amplitudes. Our study is based on recently available global databases. We compare the values of Qs, Vs, and temperature T at the depths of 50, 100, and 150 km in the continental lithosphere. We find that qualitatively (by the sign of the anomaly) the maps of Qs closely correlate with lithospheric temperatures. The best correlation is observed for the depth of 100 km, where the resolution of the attenuation model is the highest. At this depth, the contour of zero attenuation anomaly approximately corresponds to the 1000°C contour of lithospheric temperature, in agreement with laboratory data on a sharp change in seismic attenuation and shear velocities in upper mantle rocks at 900-1000°C. The correlation between Vs and two other parameters (T and Qs), though present, is less distinct. We find that most cratonic regions (the Siberian Craton, the East European Platform and the Baltic Shield, the North American Craton, West Africa, western Australia) show high lithospheric Vs, Qs and low T. In contrast, the South African craton has neither high Qs, nor low temperatures. Several prominent low Qs regions correlate with high lithospheric temperatures; this includes the Paleozoic West Siberian Basin, the Cenozoic-Paleozoic structures of the Western Europe, and western North America. We calculate correlation coefficients between Vs, Qs and T and find that at any depth, for any pair of the parameters the correlation is less than 0.42. It implies that even if temperature variations in the lithosphere are the main cause of seismic velocity and attenuation variations, the relation between temperature and seismic properties is non-linear and the concept of the compositionally homogeneous lithospheric roots is not true.

**JSA07/11A/D-026** Poster **0830-026**  
**HOW THICK IS THE EARTH'S CRUST?**

Walter D. MOONEY<sup>1</sup>, Gary S. CHULICK<sup>2</sup>, Shane T. DETWEILER<sup>1</sup> (<sup>1</sup>US Geological Survey, <sup>2</sup>St. Xavier University)

Thorough knowledge of the Earth's crustal structure is necessary for understanding continental evolution and other geological processes. We present a recently updated contour map of the thickness of the Earth's crust using a 10-km contour interval, and the 45-km contour. This contour map was created from over 5000 individual crustal data points that have been acquired during the past 60 years. The contour map honors all available seismic refraction measurements for features with a dimension greater than 2 degrees. Crustal thickness in Eurasia, North America, and Australia is well constrained by seismic refraction data, while Antarctica, South America, Africa, and Greenland are less well constrained. To a first approximation, the continents and their margins are outlined by the 30-km contour. The part of the continental interior enclosed by the 40-km contour and regions with crustal thickness of 45 to 50 km are found on all well-surveyed continents. Continental crust with thickness in excess of 50 km is exceedingly rare and accounts for less than 10% of surveyed continental crust. These observations, now available on a global basis, provide important information to be used for numerous scientific studies.

**JSA07/11A/D-027** Poster **0830-027**  
**ARE THE CRATONIC MARGINS VERTICAL? THE CASE STUDY FROM THE TESZ FROM THERMAL AND SEISMIC DATA**

Irina M. ARTEMIEVA<sup>1</sup>, Walter D. MOONEY<sup>2</sup>, Maria A. KRASNOVA<sup>3</sup> (<sup>1</sup>EOST, <sup>2</sup>USGS, <sup>3</sup>Institute of Physics of the Earth, Moscow)

We use joint interpretation of seismic and thermal data for the transition region from the Precambrian to the Paleozoic Europe (the Trans-European Suture Zone) to refine some new insights into the evolution of the sub-continental upper-most mantle beneath the western margin of the East-European Platform (EEP) and to examine how the tectonic boundaries expressed in surface geology continue in the upper mantle and either the cratonic boundary is vertical or the structure, composition and the age of the uppermost mantle in the transition

region do not correlate with the properties (age) of the overlying crust. In the absence of reliable data on the age of the upper mantle of the region, this question can be addressed by analyzing seismic data and distinguishing the effects of temperature and composition on seismic velocities. We compiled available seismic data on the structure of the upper mantle down to the depth of 100-150 km in the transition region. Data on the thermal regime of the lithosphere of the region (Artemieva and Mooney, 2001) were used to correct observed seismic velocities for the temperature effect. At the cratonic margin (i.e. across the TESZ) Moho temperature can change by 300 °C at a distance of less than 500 km, while the lithosphere thickness varies by more than a hundred km. We find that at the top of the mantle the sharp NW-SE boundary between low and high temperature-corrected Pn velocities approximately coincides with the surface manifestation of the TESZ. However, at the depth of 100-150 km the transition zone shifts eastwards both in N and S parts of the TESZ. Precambrian crust of the SW EEP overlies the mantle with the properties similar to the mantle of the Paleozoic Europe, while the subcrustal lithosphere of the SW Baltic Shield was thermally modified during Proterozoic tectonic activity of the region when the marginal part of the cratonic lithosphere was either detached or metasomatised.

**JSA07/11A/D-028** Poster **0830-028**

#### CORRELATION OF POTENTIAL FIELD ANOMALIES, PETROPHYSICAL PROPERTIES AND EVOLUTION OF THE FENNOSCANDIAN SHIELD

Juha Ville KORHONEN<sup>1</sup>, Sven AARO<sup>2</sup>, Tarmo ALL<sup>3</sup>, Seppo ELO<sup>4</sup>, Tapio KOISTINEN<sup>1</sup>, Anatali KULINICH<sup>5</sup>, Jussi KÄÄRIÄINEN<sup>6</sup>, Jan Reidar SKILBREF<sup>7</sup>, Dag SOLHEIM<sup>8</sup>, Rein VAHER<sup>10</sup>, Ludmila ZHDANOVA<sup>9</sup> (\*Espoo Unit, Geological Survey of Finland, <sup>2</sup>Geological Survey of Norway, <sup>3</sup>Geological Survey of Sweden, <sup>4</sup>State Company Mineral, <sup>5</sup>Finnish Geodetic Institute, <sup>6</sup>Norwegian Mapping Authority, <sup>7</sup>National Land Survey of Sweden, <sup>8</sup>Virg-Rudgeofizika, <sup>9</sup>Geological Survey of Estonia, <sup>10</sup>Institute of Geology, Tallinn Technical University)

Grids of magnetic DGRF-65 and Bouguer IGSN-71 anomalies of the Fennoscandian Shield and nearby area have been compiled as a joint venture between Finland, Norway, Sweden and Russia. Information from Denmark, Estonia, Latvia and Lithuania has been included. Anomaly maps derived from grids have been printed on a scale of 1:2 million. The aim was to provide an overall view of the anomaly structure of the Shield and its margins, and especially assist in correlating Precambrian geological formations across seas, state borders and areas covered by younger formations. Insert maps on a scale of 1:15 million are aimed to correlate anomaly components in different source scales: pseudogravitimetric anomaly with Bouguer anomaly, DGRF-65 anomaly with pseudomagnetic anomaly, magnetic vertical derivative with second derivative of Bouguer anomaly. Sample level data on bulk density, induced magnetisation, total magnetisation, Q-value and lithology has been presented as scatter diagrams and averages on maps to delineate variation and evolution trends of properties in space and time. The lithospheric anomaly sources are illustrated in interpreted 2.5-D sections across the western lobe of the Fennoscandian land uplift area and across a rapakivi area of age 1550. Apparent susceptibility and depth-integrated magnetisation have been compared with averaged bulk density and total magnetisation. Major source areas, shallower than 5 km include granites of Central Finnish Lapland and Central Finland, and Estonian high-grade rocks. Depth extent class of 5 - 10 km includes rapakivi granites of 1650 Ma and 1550 Ma groups, and the northern Fennoscandian magnetic high. Unexposed long wavelength sources locate below central part of the Gulf of Bothnia and Caledonian front. Both exposed and unexposed anomaly sources continue across the present Shield Boundary, with exceptions of Oslo and Kandalaksha rifts and NE coast of Kola Peninsula.

**JSA07/11A/D-029** Poster **0830-029**

#### CRUSTAL MODEL FOR SOUTHERN AND CENTRAL FINLAND (FENNOSCANDIAN SHIELD)

Koslovskaya ELENA<sup>1</sup>, Juha Ville KORHONEN<sup>2</sup>, Seppo ELO<sup>3</sup>, Sven-Erik HJELT<sup>4</sup>, Jukka YLINIEMI<sup>5</sup>, Markku PIRTTIJÄRVI<sup>6</sup> (\*Finnish Academy, C/o Oulu University, <sup>2</sup>Espoo Unit, Geological Survey of Finland, <sup>3</sup>Oulu University, <sup>4</sup>Oulu Unit, Sodankyl Geophysical Observatory)

The paper presents the first version of a crustal and upper lithospheric 3-D distribution model of P- and S-wave velocity, bulk density and magnetisation for the southern and central Finland. The model is intended for reduction of teleseismic travel times prior to the tomographic inversion of the SVEKALAPKO seismic array data and correction for regional magnetic and Bouguer anomalies in upper crustal studies, plus as a background for crustal - lithospheric evolution studies. The main part of the geological evolution of the area took place from Mesoproterozoic to Palaeoproterozoic. The bedrock stabilised after the Svecofennian orogeny, rapidly developing to a peneplane where later sedimentary rocks accumulated. Anorogenic magmatic activity, like rapakivi events, intrusion of mafic dykes, alkaline rocks and kimberlite pipes continued until Mesozoic. Erosion of sedimentary cover since Cambrian exposed the present Fennoscandian Shield. The model will be based on joint interpretation of Bouguer anomalies and seismic P- and S-wave velocities from previous DSS-studies, combined with interpretation of magnetic total field anomalies and reflection seismic profiles. The boundary values of density and magnetisation at the upper surface of the Shield will be adapted from the petrophysical data base of Finland. The co-ordinate system is national KJ that can be transferred to ETRS89, when eventually extending the model to nearby areas. In this case the difference of anomalies in the planar model to an ellipsoidal model is to be estimated. As a preliminary stage we present a stepwise, planar model of P-wave velocity and density on a 2 km x 2 km x 2 km grid. The P-wave velocity model, compiled from previous DSS profiles in the area, consists of upper, middle, lower, and lowermost crust plus upper mantle with P-wave velocities of 5.9 - 6.4, 6.4 - 6.8, 6.8 - 7.0, 7.0 - 7.9, and 7.9 - 8.2 km/s. Depths to velocity boundaries vary between limits of 10 - 20, 27 - 30, 34 - 39, and 38 - 64 km (Moho). The densities for the P-wave velocity layers were found by inverting the Bouguer anomaly in IGSN 71 gravity system. The inversion algorithm is based on stochastic quasi-linear relationship between P-wave velocity and density. The interpreted densities are correspondingly: 2620 - 2900, 2800 - 3000, 2800 - 3000, 3050 - 3250 and 3250 - 3450 kg/m<sup>3</sup>. The model demonstrates that the high velocity lower crust does not completely compensate the gravity effect of the Moho depressions. Mass compensation may be achieved by adding mafic rock densities in the upper and middle crustal model.

**JSA07/11A/D-030** Poster **0830-030**

#### MAGNETIC PETROLOGY DATABASE FOR INTERPRETATION SATELLITE MAGNETIC ANOMALIES. STATUS OF DEVELOPMENT

Katherine A. NAZAROVA (NASA/GSFC Raytheon ITSS)

A Magnetic Petrology Database (MPDB) is now being developed at NASA/Goddard Space Flight Center in cooperation with Russian and Ukrainian Institutions. The purpose of this database is to provide the geomagnetic community with a comprehensive and user-friendly method of accessing magnetic petrology data via Internet for more realistic interpretation of magnetic anomalies. Recently MPDB has been redesigned and now it can be found on the Geodynamics Branch web server of Goddard Space Flight Center at [http://core2.gsfc.nasa.gov/research/terr\\_mag/php/MPDB/frames.html](http://core2.gsfc.nasa.gov/research/terr_mag/php/MPDB/frames.html). User submission forms have been developed. To submit new data one can use Data Entry Forms in EXCEL

format at [http://core2.gsfc.nasa.gov/research/terr\\_mag/php/MPDB/doc.html](http://core2.gsfc.nasa.gov/research/terr_mag/php/MPDB/doc.html) Data on Iron Quartzites (10000 samples) from the area of Kursk Magnetic Anomaly, serpentinized rocks from all around the world (670 samples), volcanic sedimentary rocks recovered by Kola and Krivoy Rog Deer BoreHoles (703 samples) are included into database. More data on xenoliths, granulites and Archean Proterozoic sequences are coming. The database searchable engine was utilized to perform a magnetic study of rocks recovered by Kola and Krivoy Rog deep boreholes. A fully working database is expecting in July 2003.

**JSA07/11A/D-031** Poster **0830-031**

#### MAGNETIC STUDY OF ROCKS IN THE KOLA AND KRIVOY ROG DEEP BOREHOLES

Katherine A. NAZAROVA (NASA/GSFC RAYTHEON ITSS)

Magnetic properties of rocks from Kola superdeep borehole and Krivoy Rog deep borehole have been compared. These data can be found on the Magnetic Petrology Database which is now being compiled at the Geodynamics Branch of NASA/Goddard Space Flight Center and published on the web at [http://core2.gsfc.nasa.gov/research/terr\\_mag/php/MPDB/frames.html](http://core2.gsfc.nasa.gov/research/terr_mag/php/MPDB/frames.html) Extremely high values of remanent magnetization (NRM), magnetic susceptibility (K) and Königsberger ratio (Qn) are found at approximately the same depths of about 2000 m for both boreholes. Highly magnetic serpentinized peridotites and sedimentary rocks affected by sulfide mineralization were recovered at the Kola borehole for a depth interval of 1540-1940 m. The Krivoy Rog borehole recovered highly magnetic iron quartzites of Band Iron Formations at depths of 1853-2040 m. There is no obvious reason why high magnetizations should occur in two boreholes with different lithologies at the same depth. Magnetic surveys and surface sampling in the nearby Krivoy Rog and Kursk Magnetic Anomaly areas have revealed iron quartzites with high magnetization, similar to values given here. AF demagnetization tests suggest that hard and stable NRM component which is caused by hematite occurred in iron quartzites in different forms and grain sizes ranges. Hematite deposits recently discovered on Mars in western equatorial areas of Aram Chaos crater and Sinus Meridiani layered topography formation could be of hydrothermal origin and can cause magnetic anomalies registered by Mars Global Surveyor.

**JSA07/11A/D-032** Poster **0830-032**

#### GRAVITY AND MAGNETIC STUDIES IN THE PORCUPINE BASIN, OFFSHORE IRELAND: INSIGHTS INTO BASIN FORMATION

Brian M. O'REILLY, Peter W. READMAN (Dublin Institute for Advanced Studies, 5 Merrion Square, Dublin 2, IRELAND)

The Porcupine Basin lies west of Ireland on the edge of the west European continental margin. It developed in response to multiple late Palaeozoic and Mesozoic continental rifting episodes. The gross crustal structure can be derived using potential field techniques after removing the effects of the sediment fill using the shallow seismic velocity structure. The resultant structure is integrated with deep seismic profiles to constrain the depth to the Moho and the crustal structure of the surrounding region. The results from gravity and magnetic modelling of five transects along seismic reflection profiles are presented. These cross the entire Porcupine Basin between 50°-53° N. The results indicate that sedimentary basin and crustal structure change abruptly along the axis of the basin at around 51.6° N. In the north a dense and reversely magnetized body extends from acoustic basement to the Moho(?). The basin broadens to the south where an axial gravity low is flanked by highs similar to the anomaly pattern in the neighbouring Rockall Trough where it is due to a seismically imaged thickening of the crust towards the basin centre. This change in crustal geometry is marked by a set of NW-trending gravity lineaments which are interpreted as a cross-basin transfer fault system that control large-scale segmentation of the extensional deformation. Currently published models for the opening of the Porcupine Basin involve a clockwise rotation of the adjacent crustal block leading to a southward broadening of the basin. The results of our gravity studies suggests that the sense of rotational deformation was different on either side of the interpreted transfer fault system. Correlations with the deep seismic structure in the region suggest that this fault system was important in controlling fluid flow in the sub-crustal lithosphere during syn-rift deformation. The modelling results used in this presentation were undertaken on behalf of the Irish Petroleum Infrastructure Programme.

**JSA07/11A/D-033** Poster **0830-033**

#### AN APPRAISAL OF GRAVITY SIGNATURES IN THE SOUTHERN PART OF BOMBAY OFFSHORE BASIN, WESTERN INDIA

Subba Raju Venkata LAKAMRAJU, Krishna Sri KOLLURU, Anil K. CHAUBEY, Subrahmanyam VANDRAPU, Gopal Chandra BHATTACHARYA (National Institute of Oceanography, Dona Paula, Goa 403 004, INDIA)

A 2-mGal Bouguer gravity contour map is prepared from ship-borne gravity data of the southern part of Bombay offshore Basin, located on shelf and upper slope region between 10 and 1000 m water depths. The Bouguer gravity map reveals four prominent zones related to tectonically controlled igneous bodies emplaced during northward motion of Indian plate over the Reunion hotspot during Early Tertiary. The upper slopes in 1000-400 m water depths show relatively high gradient indicating fault-controlled structures. A significant gravity closure of +34 mGals on the outer shelf reveals the presence of igneous rock, which may represent one of the vents of Reunion hotspot. In the mid shelf region, the gravity reduces smoothly from +34 to -20 mGal indicating i) absence of basaltic formations and ii) the gravity effect due to the Archaeans and the overlying Tertiaries. The inner shelf is significantly characterised by several gravity closures ranging from -8 to -62 mGals. These low gravity closures are interpreted as several depot centers of Tertiary period. In the southern portion of the study area, a spur-like formation running from the coast toward shelf edge is observed. The structure is terminated due to the existence of NNW-SSE trending basaltic formation related to Reunion hotspot. The seismic profiles over the region from shelf edge to the deeper waters and along the shelf edge show the dissection of the Archaeans formations with horst and graben structures indicating the block faulting and igneous intrusions covered with Tertiary sediments. The prominent structures observed in seismic profiles are well reflected in the Bouguer gravity map. A density model of the southern part of Bombay offshore basin is generated using the forward gravity modeling under available seismic constraints. The limits of the basaltic formations with the help of density model in the study area is interpreted and spur-like structure as well as the vent of the hotspot are discussed.

**JSA07/11A/D-034** Poster **0830-034**

#### 2-D CRUSTAL THERMAL STRUCTURE OF THE NARMADA- SON LINEAMENT IN CENTRAL INDIA ALONG UJJAIN-MAHAN DEEP SEISMIC SOUNDING PROFILE

S. N. RAI, S.O. THIAGARAJAN, D. V. RAMANA (National Geophysical Research Institute, Uppal Road, Hyderabad 500 007, India)

The ENE-WSW trending Narmada- Son Lineament (NSL) in the central India extends

## INTER-ASSOCIATION

eastward for about 1600 km from the west coast of India and lies approximately between 72-88E longitudes and 21.5-24N latitudes. It is characterized by the presence of numerous hot springs, feeder dykes from Deccan traps, and seismicity all along its length. In order to understand the crustal structure of this region Deep Seismic Sounding (DSS) surveys were carried out along five profiles. Interpretation of seismic data along these profiles indicate that the NSL is divided into two parts by Baswani-Sukta Fault (BSF). To the west of this fault a graben exists while to the east basement uplift is found in the form of horst. The horst structure is bounded by Narmada North Fault (NNF) and Narmada South Fault (NSF). The present work deals with the two-dimensional thermal modeling for the delineation of crustal thermal structure along a 220 km segment of the Ujjain-Mahan DSS profile which is located just east of BSF fault traversing the horst structure. P-wave velocity distribution obtained from DSS studies has been used to estimate the heat generation values in the middle and lower crust. For the upper part of the crust we use exponential heat generation model to estimate the distribution of radiogenic sources. Numerical results indicate that the Moho temperature varies between 500 to 550°C which more or less coincides with the Curie isotherm. The estimated surface heat flow varies between 46.3 to 47.1 mW/m<sup>2</sup>, with the maximum between Ujjain to Dorwa and the minimum over the Tapti basin. Although measured heat flow values in the study area along the profile are not available for comparison, these values are found to be in close agreement with the measured surface heat flow values at Mohpani (49 mW/m<sup>2</sup>) in the NSL zone east of this profile and Lonar and Yavatmal area (47 mW/m<sup>2</sup>) south of NSL in the Deccan traps. The present study reveals that the upper mantle in this part of NSL is relatively cooler than the north Cambay region on the western margin of India. The low value of the mantle heat flow in this region can be used to infer the brittle nature of the lower crust which is supported by the occurrence of deep crustal Satpura (1938) and Jabalpur (1997) earthquakes of NSL region.

### JSA07/11A/D-035 Poster 0830-035 ANCIENT COLLISIONAL CONTINENTAL MARGINS IN THE SOUTHERN INDIAN SHIELD: GRAVITY SIGNATURES AND DERIVED CRUSTAL TRANSECTS

Anand P. SINGH, D. C. MISHRA (National Geophysical Research Institute, Hyderabad)

The southern Indian shield is one of the areas of the world, which had preserved the earliest formed crust. Litho-tectonic diversity, missing threads of Precambrian record and for the most part obliterated by imprints of later tectonic events have made it unique in the study of the early evolutionary history of the earth crust. Earlier it was widely believed that the southern Indian shield forms a singular crustal domain. In contrast, a mosaic of smaller litho-tectonic domains, which were once separate but brought and welded together during their evolutionary history, is another notion. Demarcation of these original crustal domains that welded together during the geological past is first and foremost important task in order to understand the evolutionary processes operative at that point of time it has been suggested that the paired (positive and negative) gravity signature characterizes deep crustal breaks along the boundaries between ancient crustal domains. This gravity signature for Late Archaean to Late Proterozoic plate tectonics is analysed/reviewed and a case is presented for the role of plate tectonics in developing reactivated Precambrian terranes with discussion centring on the Dharwar craton of the southern Indian shield. Further support is provided by geologically analogous terranes of the Canadian shield.

### JSA07/11A/D-036 Poster 0830-036 INVESTIGATION OF EFFECTS OF EXPLOSIONS ON THE OIL PIPES AT MARVAK DAM SITE IN LORESTAN REGION (IRAN)

Shayesteh MEHRABIAN, Ahmad SADIDKHOI (Department of Earth Sciences, University of Tehran)

In this study the effects of vibrations due to 25 performed explosions on the oil pipes by using the delay time are investigated. Vibrations are recorded by four seismographs (PDAS, L4-3D seismometer). The obtained data are analysed and processed by using suitable methods and available soft wares. According to the obtained relationships between the particle velocity and scaled distance, a criterion for reduction the effects of vibrations on the oil pipes is proposed. Finally these geophysical data are used to describe a regional crustal model which can lead to robust geophysical interpretations.

### JSA07/11A/D-037 Poster 0830-037 ESTIMATION OF LITHOSPHERIC THICKNESS BENEATH SEISMICALLY ACTIVE REGIONS OF THE DECCAN VOLCANIC PROVINCE OF INDIA

Venkata Ramana DRONAMRAJU (National Geophysical Research Institute)

Thermal evolution of the lithosphere is primarily governed by heat conduction and plays a key role in deforming the lithosphere and controlling its structure. Surface heat flow is major observation for estimating the temperature field of the lithosphere. It consists of two parts (i) contribution from the mantle, and (ii) heat generation within the lithosphere due to radiogenic heat sources. In continental lithosphere, radiogenic sources account for about 40 percent of the total surface heat flow. Previous models for the estimation of thermal structure of the Indian continental lithosphere used exponential/step model of radiogenic heat sources distribution. Since continental crust consists of rocks having very different concentration of these radiogenic sources, it is important to consider the vertical heterogeneity in the thermal parameters to construct the thermal structure. The vertical distribution of the radiogenic heat sources is obtained by direct measurements of the heat generation in different rock types or by estimating it from the observed seismic velocities using an empirical relationship between the heat generation and P-wave velocities. In the present work the radiogenic sources in the mid – and lower crust for Killari and Koyna locations of the Deccan Volcanic Province have been estimated by using deep crustal seismic velocity information and the thermal structure is obtained by treating the lithosphere as an n-layered model. The results reveal a relatively thick thermal lithosphere for these locations.

### JSA07/11A/D-038 Poster 0830-038 SEISMOLOGICAL CONSTRAINTS ON CRUSTAL EVOLUTION IN SOUTH INDIA

S. S. RAI, Sandeep GUPTA (National Geophysical Research Institute, Hyderabad, INDIA)

Receiver function analysis of teleseismic waveforms from 32 broadband seismic stations in South India suggest significant difference in the crustal structure. The eastern Dharwar Craton, Deccan Volcanic and Cuddapah basin show very similar crustal thickness 33-39 km. The western Dharwar Craton (WDC), however, has thicker crust (42-51 km). The crustal thickening in WDC occurs in step fashion, Moho offsets coinciding with surface expression of N-S elongated shear zones. The thickest crust (~60 km) is observed beneath the Nilgiri hills. Elsewhere, in the Southern Granulite Terrain (SGT), crust is 40-53 km thick. Considering 20-30 km crustal exhumation in the southern part of WDC and SGT, we speculate possibly 70-90 km thick crust across WDC-SGT during Archean. This suggests of a Himalaya type geodynamic frame work for the evolution of granulite terrain.

### JSA07/11A/D-039 Poster 0830-039

#### CRUSTAL STRUCTURE IN THE SIKKIM HIMALAYA FROM NEW GRAVITY AND MAGNETIC DATA

Virendra Mani TIWARI, M.B.S. VYAGRESWARA RAO, R. S. RAJESH, D. C. MISHRA (National Geophysical Research Institute)

Recently, we have recorded gravity and magnetic data in the Sikkim Himalayas to elucidate the subsurface structure in this part of Himalayas. The recorded profile starts from Gangetic plain and runs across main tectonic features like MBT and MCT. Data are recorded at 1 km spacing and location and elevation of the stations are determined using differential GPS. All the main tectonic features are reflected in the gravity and magnetic data. The gravity and magnetic anomalies are modelled for subsurface structures.

### JSA07/11A/D-040 Poster 0830-040

#### SOME PROPERTIES OF THE MAGNETOTELLURIC ROTATION INVARIANT TENSORS

Suman DEY<sup>1</sup>, Shashi Prakash SHARMA<sup>1</sup>, Kalyan Kumar ROY<sup>2</sup>, Someshwar SRIVASTAVA<sup>3</sup> (Department of geology and geophysics, IIT(Kharagpur), India., <sup>2</sup>Department of Geological Sciences, Jadavpur University, Calcutta-700032, India, <sup>3</sup>AFPRO, IC/262, Ashoke Nagar, Ranchi-834002, Jharkhand, India)

Rotation Invariant Tensors (RITs) can be used for interpretation of magnetotelluric field data. Three RIT apparent resistivities and their phases, viz, rho-determinant, rho-average and rho-central generate much more closer apparent resistivities than the conventional Cagniard TE and TM mode Swift rotated apparent resistivities and their phases near prominent geological lateral heterogeneities. RITs generate perfect rotation invariance with noisy field data with larger error bar. RITs generate stable apparent resistivities and phases for longer period signals where TE and TM mode values may show instability and fluctuations. Field data from Archean and Proterozoic terrain may generate best 2D model with 1D inverted data using RITs. Even 2D Rapid Relaxation Inversion algorithm using RITs generates much more stable models than those obtained using TE and TM mode data. Two eigen values of the impedance tensors are also rotationally invariant and generates respectively higher and lower apparent resistivities in comparison to rotated and unrotated apparent resistivities. In a complex domain the tensor elements Zxx, Zyy, Zxy and Zyx generates ellipses of widely variable ellipticities where as RITs describe just one point. The diagonal elements of the impedance tensor are nonzero and nontrivial even after optimum rotation for a 3D structure. Therefore RITs will have a role in the interpretation of MT data because through determinant and central RITs, information from diagonal elements enter into interpretation.

### JSA07/11A/D-041 Poster 0830-041

#### MAGNETIZATION MODELING OF THE MAUD RISE CRUST IN THE SOUTHWEST INDIAN OCEAN

Hyung Rae KIM<sup>1</sup>, Ralph R.B. VON FRESE<sup>1</sup>, Alexander V. GOLYNSKY<sup>2</sup>, Patrick T. TAYLOR<sup>3</sup>, Jeong Woo KIM<sup>4</sup> (<sup>1</sup>Dept. of Geological Sciences, The Ohio State Univ., <sup>2</sup>VNII Okeangeologia, 1, St. Petersburg, Russia, <sup>3</sup>Code 921 Geodynamics branch, GSFC, NASA, Maryland, USA, <sup>4</sup>Dept. of Earth Science, Sejong Univ., Republic of Korea)

We produced a crustal magnetization model for the Maud Rise in the southwest Indian Ocean off the coast of East Antarctica using magnetic observations from the Ørsted satellite and near-surface surveys compiled by the Antarctic Digital Magnetic Anomaly Project (ADMAR). New inversion modeling of the two anomaly fields suggests that the magnetic effects due to crustal thickness variations and remanence involving the normal polarity Cretaceous Quiet Zone (KQZ) dominate at satellite altitude (≥700 km). The crustal thickness effects were modeled in the Ørsted data using crustal thickness variations derived from satellite altitude gravity data. Modeling of the residual Ørsted and near-surface magnetic anomalies supports extending the KQZ eastwards to the Astrid Ridge. The remaining near-surface anomalies involve crustal features with relatively high frequency effects that are strongly attenuated at satellite altitudes. The crustal modeling can be extended by the satellite magnetic anomalies across the Indian Ocean Ridge for insight on the crustal properties of the conjugate Agulhas Plateau. The modeling supports the Jurassic reconstruction of Gondwana when the African Limpopo-Zambezi and East Antarctic Princess Astrid coasts were connected as part of a relatively demagnetized crustal block.

### JSA07/11A/D-042 Poster 0830-042

#### GRAVITY ANOMALIES AND ASSOCIATED TECTONIC FEATURES OVER THE INDIAN PENINSULAR SHIELD AND ADJOINING OCEAN BASINS

Dinesh Chandra MISHRA, K. ARORA, V. M. TIWARI (National Geophysical Research Institute, Hyderabad, India)

A combined gravity map over the Indian Peninsular Shield (IPS) and adjoining oceans brings out well the inter-relationships between the older tectonic features of the continent and the adjoining younger oceanic features. The NW-SE, NE-SW and N-S Precambrian trends of the IPS are reflected in the structural trends of the Arabian Sea and the Bay of Bengal suggesting their probable reactivation. The Simple Bouguer anomaly map shows consistent increase in gravity value from the continent to the deep ocean basins, which is attributed to isostatic compensation due to variations in the crustal thickness. A crustal density model computed along a profile across this region suggests a thick crust of 35-40 km under the continent, which reduces to 22-24 km under the Bay of Bengal. Large crustal thickness and trends in the gravity anomalies similar to the structural trends of the southern part of IPS suggest a transitional crust in the Bay of Bengal. The crustal thickness under the Laxmi Ridge and east of it in the Arabian Sea is 20 and 14 km respectively. The crustal density model in this part of the Arabian Sea (east of Laxmi ridge) and the structural trends similar to the Indian Peninsular Shield suggest a continent-ocean transitional crust (COTC). The COTC may represent down dropped and submerged parts of the Indian crust evolved at the time of break-up along the west coast of India and passage of Reunion hotspot over India during late Cretaceous.

### JSA07/11A/D-043 Poster 0830-043

#### UPPER MANTLE HETEROGENEITY BENEATH THE CAMBAY RIFT BASIN, INDIA: INSIGHT FROM GRAVITY MODELLING

Bijendra SINGH, D. C. MISHRA (National Geophysical Research Institute)

The Cambay rift basin, which is one of the major petroliferous basins of India indicates anomalous gravity signatures. The Bouguer anomaly map of basin and the adjoining regions depicts number of large amplitude circular gravity 'high's related to high density intrusive/extrusive igneous plugs resulting from Deccan Volcanism. The small wavelength gravity 'low's are caused by Tertiary and Mesozoic sediments and are superimposed on a

large wavelength small amplitude gravity 'low' suggesting source at deeper level. Modeling of gravity anomalies across the basin incorporating constraints from seismic and borehole information requires a low-density (3.04 g/cm<sup>3</sup>) upper mantle and a high-density (3.10 g/cm<sup>3</sup>) underplated lower crust with Moho at a shallow depth (32 km) beneath the basin. This low-density upper mantle extends over hundreds of kilometres on either side of the basin. These features are typical of continental rift evolved from a thermal source. Presence of high heat flow, extremely thin thermal lithosphere, Deccan volcanism and low velocity zone associated with low-density body probably indicate region of elevated temperature suggesting partial melting condition in the upper mantle. This might have resulted due to interaction of Reunion plume with the Indian lithosphere during the northward migration of the Indian plate in late Cretaceous after the break up of the Gondwana land.

**JSA07/11A/D-044** Poster **0830-044**

#### LITHOSPHERIC STRUCTURING OF THE TUNISIAN NORTHEASTERN AFRICAN PLATE MARGIN

Mourad BÉDIR<sup>1</sup>, Fouad ZARGOUNI, Chokri JALLOULI, Badiia CHULLI-ZENATI (<sup>1</sup>Department of Georesources, Institute of scientific and technic research of Tunisia, <sup>2</sup>Facult des Sciences de Tunis, Campus Universitaire, 1060 Tunis, Tunisia., <sup>3</sup>Facult des Sciences de Bizertes, Tunisia.)

**Key Word :** Tunisia, Geophysics, CrustGeological and geophysical data from the different regions of the Tunisian Atlantic and Mediterranean zones permit the reconstruction of the structuring and the evolution of the crustal margin and its tectonic and sedimentary cover mechanisms. Reflection and refraction seismic investigations, geothermal studies and gravimetric Bouguer and residual anomalies had highlighted the deep tectonic framework of the Eastern Tunisian margin. This domain is characterized by a deep structural discontinuities trending North-South, East-West, Northeast-Southwest and Northwest-Southeast corresponding to a deep-seated flower fault corridors. These discontinuities bound the main tectonic blocks of the margin. The Mohoroviitchi discontinuity depth evolves from the South to the North-East from forty to twenty kilometres. The upper levels are respectively to the North at the Galite granitic Island latitude and to the North-East along the Tunisian- Sicilian Pantellaria and Linosa volcanic islands straight. This rising of the Moho corresponds to the important magmatic activity in these zones since the Triassic until the Neogene times and the high geothermal rates encountered in the petroleum wells of these areas. From the South to the North the margin is subdivided in three main geotectonic blocks. The Eastern-Northeastern Sahel-Pelagian block. From the Triassic to Cenozoic times these blocks evolves progressively across a mosaic of tilted platforms and grabens. This area is affected by an important tectonic activity of transtensional and transpressional deep-seated faults that create a mosaic of Mesozoic and Cenozoic Grabens, Horsts, Platforms and folds. During the Mesozoic times, took place marine to deep marine carbonate basin and platform deposits intruded by magmatic volcanic basaltic rocks. Triassic halokinetic movements are also active. A great subsidence occurs in the Tertiary where the horizons are composed by thick deposits of Paleocene marls, Eocene platform carbonates, deep-marine marls and black shales. The Oligocene consists on deltaic and fluvial sandstones deposits. Paleocene to Eocene series are intercalated by volcanic alkaline explosive rocks. Miocene deposits comprise deep-marine to thick deltaic series marked by an alternations of marls, platform carbonates and clay packages with sandstone turbidites. Burdigalian to Langhian series are interbedded in some offshore wells by basaltic rocks. To the offshore basins Pliocene deposits are formed by a thick deep marine marls and sandstone turbidites. These Neogene deposits are engaged in a claykinesis and clay intrusives along the strike-slip fault corridors. The treatment of these data had permitted to propose a geodynamic model for this particular margin.

**JSA07/11A/D-045** Poster **0830-045**

#### GRAVITY CONSTRAINTS ON THE CRUSTAL THICKNESS OF NORTHERN AFRICA, WESTERN MEDITERRANEAN

Chokri JALLOULI<sup>1</sup>, Kevin L. MICKUS<sup>2</sup> (<sup>1</sup>Department of Geology, FST, Univ. Tunis El Manar, <sup>2</sup>Department of Geosciences, southwest Missouri State Univ., Springfield, MO 65804, USA)

The evolution of western Mediterranean region of northern Africa involves several complex tectonic environments controlled by the interaction between the Eurasian and African plates. As a result of this interaction, two orogenic belts (Atlas and Tell Mountains) were formed in northern Africa. Most workers are in general agreement on the tectonic events affecting northern Africa however, the general crustal and upper mantle structure of this region remains relatively unknown due to the lack of deep seismic data and regional geophysical analyzes. To provide insights on the deep crustal structures under the Atlas and Tell Mountains and the African northern margin, gravity data were analyzed in conjunction with available drill hole, geologic and deep seismic data. Bouguer, free-air, isostatic residual gravity anomaly maps and two 2D gravity models across the Tell and Atlas mountains in Algeria and Tunisia were constructed. The gravity models provide estimates of the crustal thickness (37 km in Algeria and 30 km in Tunisia) and the amount of crustal shortening caused by the collision of the African and Eurasian plates. The isostatic residual gravity anomaly maps and the gravity models provide evidence of a thick crustal root under the Atlas Mountains in Algeria, while a thin crustal root is suggested under the Atlas Mountains in Tunisia. The Atlas Mountains are partially to fully compensated implying crustal shortening. However, based on the gravity models, and the amplitude and width of the Bouguer gravity anomalies over the Saharian Atlas in Algeria and the Tunisian Atlas Mountains, the amount of crustal shortening was greater in Algeria than in Tunisia.

**JSA07/11A/D-046** Poster **0830-046**

#### MAGNETIC INTERPRETATION OF THE ONSHORE GEBEL EL-ZEIT AREA, GULF OF SUEZ, IN EGYPT USING INTERPRETATION TECHNIQUES

Essam About ABoud, Keisuke USHJIMA, Ahmed SALEM (Essam About)

This paper documents the result of an integrated interpretation technique of magnetic data carried out on the onshore of Gebel EL-Zeit area, Gulf of Suez, in Egypt of magnetic data carried out on the onshore of Gebel EL-Zeit area, Gulf of Suez. The objective of this study is to identify the possible subsurface structure framework that may assist in delineation of promising areas for hydrocarbon reservoir. Gradient techniques including Euler Deconvolution and analytic signal have been applied to the observed magnetic data by National Research Institute of Astronomy and Geophysics, Egypt. Then the result of this study geological trends and depths of subsurface geologic structures are defined. The central portion of the area is characterized by basin block forming a graben bounded by major uplifting faults striking in the NW-SE direction. Depth to the basement of basin structure ranges about 1.5 km in the eastern and western parts of the study area and gets deeper toward the central part up to 4.5 km. Moreover, gradient interpretation techniques supplied by geologic and drill hole information enabled delineation of promising areas which are highly recommended for further hydrocarbon exploration in the area.

**JSA07/11A/D-047** Poster **0830-047**

#### MAGNETIC AND GRAVITY MODELLING ON FUEGUINIAN FOLD-AND-THRUST BELT, ARGENTINE

Alejandro Alberto TASSONE<sup>1</sup>, Juan Francisco VILAS<sup>2</sup>, Maria Alejandra COMBA<sup>3</sup>, Horacio Francisco LIPPAI<sup>4</sup>, Emanuele LODOLO<sup>5</sup>, Marco MENICETTI<sup>6</sup>, Jose Luis HORMAECHEA<sup>7</sup> (<sup>1</sup>18270, <sup>2</sup>9848, <sup>3</sup>18277, <sup>4</sup>18273, <sup>5</sup>19228, <sup>6</sup>19233, <sup>7</sup>19220)

The studied area is located in the central northern side of the Fuegian Andes, where the structures of the external thrust front propagate through to the Magallanes thin-skinned foreland fold-and-thrust belt. A system of Oligocene-Quaternary E-W (the Magallanes-Fagnano Fault System, MFS) left-lateral strike-slip faults with an extensional component overprints the contractional structures and is responsible for the main depression of the Lago Fagnano. A Quaternary system of N-S faults with right-lateral strike-slip attitude crosses all the previous structures and probably constitutes the present day deformation strain field in the eastern part of the Island. Geophysical field surveys allowed to acquire 440 DGPS-fixed data points where gravity, magnetic and magnetic susceptibility measurements were performed. In the surveyed area, the MFS segments have clear morphological expression, and are associated with localized gravity minima in correspondence of their unconnected ends. At the ESE tip of Lago Fagnano, the magnetic data suggest the existence of several intrusive bodies in the subsurface. The magnetic anomaly for each of these bodies indicates a rotation in relation to the N-S direction. The geophysical modeling of an outcropping monzonioritic body revealed a piston shape. A 2D numeric modeling was performed (employing the IGMAS software) with the data of total Bouguer anomaly. The model displays a N-S section of about 40 km through the upper 10 km. A 2D numeric modeling was performed with the data of total magnetic anomaly using the Geomodel software. The model N-S cross-section through the area combines the acquired gravity data with the field geological information and the geometry of the deep structures derived from industrial seismic reflection lines. A very good fitting was observed between the measured and computed values for the basement depth whose modeled geometry indicates a southward deepening from 5 km to 7 km. The model geometry of the deep duplex with buried leading edge is geometrically similar to the structures exposed in the western part of the Island. The model geometry of passive roof thrusts and back-thrust that develop the triangle zone north of the Lago Fagnano area is well constrained with the geological field data and well marked by the seismic reflectors of the shear zones. The lower detachment levels have up to 40% of shortening, while the upper structures display less than 20% of contraction. In the modeled section the MFS is related to a -49 mGal minimum. The offset of the strike-slip faults toward the plane of the section constitutes one of the main uncertainties for lack of geometrical tags. Field geological data and regional considerations indicate that the offset could be about few tens of km.

**JSA07/11A/D-048** Poster **0830-048**

#### RELATION BETWEEN TECTONIC FEATURES AND EPICENTER SEISMIC DISTRIBUTION PATTERN (ARGENTINE CENTRAL ANDES)

Guillermo Hector RE<sup>1</sup>, Maria Silvia JAPAS<sup>2</sup>, Silvia Patricia BARREDO<sup>1</sup> (<sup>1</sup>Dpto. Geologia - Universidad de Buenos Aires, <sup>2</sup>CONICET - Argentina)

The Cordillera de los Andes system lies parallel to the Peruvian-Chilean trench, which delineates the meet zone between the subducted oceanic plate (Nazca Plate) and the continental plate (South American Plate). This active margin shows numerous and important tectonic changes along its entire strike. One of the most conspicuous characteristics is the significant change in the subduction angle along the South American Coast. It is thus that two sub-horizontal subduction segments are observed (between 2° S and 15° S and between 27° S and 33° S). Anomalies located in the convergence process along the west margin of the South American plate would be caused by the subduction of aseismic ridges and chains of submarine foothills dragged by the Nazca Plate during its descent. Another effect caused by the change in the subduction angle is the displacement of the different tectonic fronts several hundred kilometers towards the East, and the subsequent rise of numerous mountain systems in the West sector of Argentina since Miocene up to the present times (Precordillera, Western Sierras Pampeanas, Sierra de Famatina, Eastern Sierras Pampeanas). These rises have conditioned the development of important continental sedimentary basins. Where the epicentres of South America margin are plotted two types of distribution patterns can be noticed: between 17° S and 23° S the fabric shows a bending design parallel the continental margin; from 24° S onwards there is an earthquake alignment tendency with depth following NNE, NNW and ENE-WSW directions. Taking into account only those of shallower depths a persistence of the alignments previously defined can be observed. In addition, it is outstanding the good correspondence between the northern NNE lineament observed with respect to the present volcanism boundary. Another striking point, is the correspondence (localization and orientation) between the NNE and NNW lineaments and those which, for this particular zone, can be defined from the localization of the seismic epicenters. This latter would not only certify the kinematic importance of the major lineament already described but would also provide the scale thereof as a direct consequence of the involvement of the continental lithosphere deeper portions. In the case of the ENE - WNW seismic epicenters alignment the orientation permits to suspect the incidence of the subduction of the Juan Fernández ridge. Another significant characteristic is the correspondence between those lineaments defined in surface on the basis of the above mentioned elements and the deep earthquake alignments in the subducted plate. This apparent correspondence is major for the flat-slab subduction zone, probably due to the interplate coupling.

**JSA07/11A/D-049** Poster **0830-049**

#### MEASUREMENT OF COMPARATIVE TERRESTRIAL STRESS AT XIAN AND NEARBY AREAS AND EARTHQUAKE FATALNESS STUDY

Wen-xiang WANG, Wu-yang YANG (China Coal Research Institute, Xi'an Branch)

Through studying the distribution-configuration and variation-characteristics of deep underground depth terrestrial stress, the on the ground location of where the earthquake will occur can be determined, the magnitude of the future earthquake can be calculated, and the timing of the earthquake occurrence could be held. With the DYL Type Terrestrial Stress Measurement Instrument, installed on a vehicle or on a train, using a natural electromagnetic wave field source, can directly and rapidly measure the comparative terrestrial stress magnitude of which geological bodies are subjected to at deep underground depths of 5km, 7km and 10km. Through the study method of terrestrial stress isoline analysis, can determine the configuration and size of future earthquake source zones, explain locations of deep and major faults and terrestrial heat abnormal zones. In accordance with the background data, detected and measured by the MDCB Instrument, indicating that damaging earthquake underlies dormant in areas nearby Xian, as well as the Xian Seismology Bureau's consultation and study opinion on situation of earthquakes nearby Xian for the year 2001, the Xian Municipal Government and the Xian Municipal Science Committee approved to establish the project for studying the conditions of terrestrial stress at deep underground depths at Xian and nearby areas. This paper is the resulting report of the

## INTER-ASSOCIATION

completion study on this project. Upon review and examination by concerned specialists from the State Seismology Bureau of China, it was concluded that this report provides important seismological and geological basis for determining the on the ground location for where damaging earthquake(s) could occur nearby Xian in the future, and for the Xian area to establish earthquake resistance, earthquake prevention measures and earthquake precursor monitoring and measurement measures.

**JSA08**

**Wednesday, July 9**

### **EFFECTS OF SOLAR VARIABILITY ON CLIMATE CHANGE (IAGA, IAMAS)**

Location: Site A, Room 8

**Wednesday, July 9 AM**

Presiding Chairs: K. Labitzke, L. Gray

**JSA08/09A/A08-001**

**0900**

#### **THE ROLE OF EXTRATROPICAL WAVE FORCING DRIVING POSSIBLE SOLAR CYCLE VARIATIONS IN THE TROPICAL LOWER STRATOSPHERE**

Lon L. HOOD<sup>1</sup>, Boris E. SOUKHAREV<sup>2</sup> (<sup>1</sup>Lunar and Planetary Laboratory, University of Arizona, <sup>2</sup>Dept. of Climatology, University of St. Petersburg)

Records of column ozone, temperature, and geopotential height with lengths greater than 20 years are consistent with the existence of a long-term, quasi-decadal oscillation (QDO) of the tropical and subtropical lower stratosphere. This long-term variation has been approximately in phase with the 11-year solar cycle during the period for which accurately calibrated data are available. Two-dimensional models demonstrate that direct solar UV photochemical and radiative forcing in the lower stratosphere is unlikely to produce a QDO of the observed amplitude. We have therefore investigated whether solar UV variations in the upper stratosphere may modulate extratropical wave forcing. The latter is an important driver of the Brewer-Dobson circulation, which influences the tropical lower stratosphere by changing the rate of vertical transport. For this purpose, daily and monthly mean meridional eddy heat fluxes have been calculated at a series of lower stratospheric pressure levels over a 23-year period using National Centers for Environmental Prediction (NCEP) Reanalysis data. A decadal variation of the low-pass filtered extratropical eddy heat flux is present in both hemispheres with an amplitude that increases with increasing altitude. A simplified model of the contribution of extratropical wave forcing to long-term variations in tropical lower stratospheric ozone and temperature is then formulated based on the ozone chemical continuity and thermodynamic energy equations. Using this model together with empirically derived regression relationships between short-term changes in extratropical eddy heat flux and tendencies in both tropical column ozone and lower stratospheric temperature, it is found that decadal variations of extratropical wave forcing in both hemispheres are sufficient to explain approximately both the amplitude and the phase of the observed QDO of the tropical lower stratosphere.

**JSA08/09A/A08-002**

**Invited**

**0915**

#### **EVIDENCE OF THE SOLAR CYCLE IN THE GENERAL CIRCULATION**

Murry L. SALBY<sup>1</sup>, Patrick F. CALLAGHAN<sup>2</sup> (<sup>1</sup>The University of Colorado, <sup>2</sup>Atmospheric Systems and Analysis)

NCEP reanalyses are used to isolate systematic variations in the stratosphere that operated coherently over the last 4 decades with the 11-yr variation of UV irradiance. A systematic variation is scarcely visible at low frequency, which would reflect a simple linear response that drifts with solar flux,  $F_x$ . However, a systematic variation manifests itself clearly at high frequency, which involves changes between neighboring years. Corresponding to interannual variability, the systematic variation at high frequency reflects a more complex, nonlinear response to the 11-yr variation of UV irradiance. It is analogous to a similar variation found earlier in the QBO of equatorial wind,  $u_{eq}$ . Interannual variability undergoes a frequency modulation that systematically alters its phase during winter, when planetary waves couple the polar and equatorial stratosphere. The polar-night vortex is then sensitive to equatorial wind, which itself varies systematically with  $F_x$ . Monte Carlo simulations indicate that the systematic variation of wintertime phase is highly significant. The systematic variation appears prominently in the wintertime tendency of temperature, which is coupled directly to the residual mean circulation. In fact, the anomalous wintertime tendency operating coherently with  $F_x$  has the same basic structure as that operating coherently with anomalous forcing of the residual circulation. Each reflects anomalous downwelling over the Arctic that is compensated at lower latitude by anomalous upwelling. The structural similarity of these anomalies suggests that the systematic variation at high frequency enters through changes of the residual circulation. Accompanying the variation of zonal-mean structure is a systematic amplification and decay of wave-number 1 at high latitude. It represents a poleward advance and retreat of the critical region, or surf zone, where planetary waves experience strong absorption that forces residual motion. This variation of wave structure, along with anomalous residual motion it forces, parallels the systematic variation of equatorial wind. Wintertime-mean  $u_{eq}$  suggests a reversal in anomalous downwelling between solar min and solar max, one broadly consistent with the observed reversal in anomalous temperature.

**JSA08/09A/A08-003**

**0945**

#### **SOLAR ACTIVITY AND GLOBAL/REGIONAL WARMING AND COOLING**

Hengyi WENG (LASG, Institute of Atmospheric Physics, Chinese Academy of Sciences)

The coherence between the solar activity and global and North Pacific winter sea surface temperature (SST) variation on centennial timescales such as the Gleissberg cycle (~80-90 yrs) and the Suess wiggles (~200 yrs), may be a manifestation of solar impacts on global and regional warming trend since the beginning of the 20th century. The additional harmonics of the Gleissberg cycle (~40-45 yrs and 27-30 yrs) and the subharmonics of the 11-yr solar cycle (33 yrs and 44 yrs) may be related to the SST variability on interdecadal timescale with two warm periods in the 1940s-50s and 1980s-90s, and the cool period in the 1960s-70s. The sunspot number may be a rather good predictor for global and North Pacific SST variation on interdecadal timescale. If the predicted sunspot number published by NOAA/NGDC is reliable, then the global and the North Pacific winter SST may undergo a cooling decade at the beginning of the 21st century based on the reduced solar activity up to 2007, compared with the last decade in the 20th century.

**JSA08/09A/A08-004**

**1000**

#### **WINTER NAO VERTICAL STRUCTURE PROFILE CHANGES IN ASSOCIATION WITH THE SOLAR ACTIVITY, GEOMAGNETIC ACTIVITY AND THE QBO**

Pavel HEJDA, Josef BOCHNICEK (Geophysical Institute, Academy of Sciences, 141 31 Prague, Czech Republic)

The aim of the paper is to analyse the association between the solar activity, geomagnetic activity and the QBO phase on one side and the changes of NAO vertical structure profiles going through eastern part of North America continent, eastern Atlantic, middle Europe, western part of Asia continent and eastern Pacific on the other. For this purpose, corresponding NAO meridional cross-sections were created on the series of pressure, temperature and prevailing wind distribution in the levels between sea level and 100 mb level. Changes in the meridional cross-sections observed in winter (January+February) periods 1952-2001 were investigated by the composite method. The occurred changes seem to be associated with both the activities as well as the QBO phases. Statistical significance of the composite maps were tested using Student's t-test. Meteorological data in the winter periods 1952-2001 for pressure and temperature, and in winter periods 1964, 1967-1969, 1971-2001 for prevailing winds were taken from the NCAR Research Data Sets.

**JSA08/09A/A08-005**

**1015**

#### **THE IMPORTANCE OF STRATOSPHERIC DYNAMICS IN DETERMINING THE RESPONSE OF THE TROPOSPHERE TO SOLAR FORCING**

Michael Anthony PALMER<sup>1</sup>, Lesley GRAY<sup>1</sup>, Myles ALLEN<sup>2</sup> (<sup>1</sup>Rutherford Appleton Laboratory, <sup>2</sup>University of Oxford)

In order to quantify the potential impact of anthropogenically induced climate change, it is vital to understand the natural variability of the climate system. A crucial, unresolved question involves the climatic effect of changes in total solar irradiance (TSI), and in particular the role that the stratospheric circulation plays in inducing anomalous flow at lower tropospheric levels. Using the Unified Model, in a configuration with an mixed-layer ocean and a well resolved stratosphere, we investigate the role of stratosphere/troposphere coupling in governing the response to solar forcing. The importance of realistically simulating the natural variability of the stratosphere is studied, by comparing model runs both with and without a scheme to account for the vertical propagation of gravity waves. The implications of our results for climate change detection studies, which have tended to use models without a well resolved stratosphere, is discussed.

**JSA08/09A/A08-006**

**1030**

#### **STUDY OF LONG TERM CHANGES IN THE GEOMAGNETIC FIELD, CUTOFF RIGIDITIES, COSMIC RAYS, AND POSSIBLE RELATION TO CLIMATE CHANGES**

Don Frederick SMART, Margaret Ann SHEA (CSPAR, University of Alabama in Huntsville)

The possibility of a connection between cosmic radiation and climate has intrigued scientists for the past several decades. The studies of Friis- Christensen and Svensmark have reported a variation of 3-4% in the global cloud cover between 1980 and 1995 that appeared to correlate with the change in galactic cosmic radiation flux over a solar cycle. We present results of a study of geomagnetic cutoff rigidity changes over a 400-year interval. These results show that the change in cutoff rigidity over the last 400 years results in a change of the cosmic radiation flux impacting the earth that is approximately equal to the relative change in flux over a solar cycle. These changes in cutoff rigidity are non-uniform over the globe with both significant increases and decreases at mid-latitude locations. We suggest that in long term studies of possible cosmic ray correlations with climate, not only the solar cycle modulation of cosmic radiation be considered, but also the changes in the cosmic radiation impinging at the top of the atmosphere as a result of the long term evolution of the geomagnetic field.

**JSA08/09A/A08-007**

**1045**

#### **THE POSSIBLE CONNECTION BETWEEN IONIZATION IN THE ATMOSPHERE BY COSMIC RAYS AND LOW LEVEL CLOUDS**

Enric PALLE<sup>1</sup>, John C. BUTLER<sup>2</sup>, Keran O'BRIEN<sup>3</sup> (<sup>1</sup>Big Bear Solar Observatory, <sup>2</sup>Armagh Observatory, <sup>3</sup>Northern Arizona University)

Recent analysis of monthly mean cloud data from the International Satellite Cloud Climatology Project (ISCCP) have uncovered a strong correlation between low cloud and the cosmic ray flux for extensive regions of the Earth. New data has been recently released up to September 2001. With it, we have made a new study of the geographical variation of the correlation between low cloud and predicted ionization level from cosmic rays at 2 km altitude. We find a latitude dependence of the correlation that does not correspond to that expected from the geographical variation in cosmic ray flux. In addition, we find that there is an unexplained longitude dependence. Moreover, the fact that satellite monitoring of low cloud must frequently be made through intermediate higher level cloud gave rise to a concern that the result may have been influenced by the presence of higher clouds. Here, by excluding days when mid-level and higher clouds are present, we provide evidence that the low cloud variation over the period 1983-1994 is real and not due to overlapping higher clouds. Thus, some evidence supports the connection between cosmic rays and low cloud whilst other evidence mitigates against. We use a toy model to calculate the climatic impact should the correlation be confirmed. We show that, under the most favorable conditions, a reduction in low cloud factors since the late 19th century, combined with the direct forcing by solar irradiance can explain most of the global warming over the past century but not all. However, this computation assumes that there is no feedback or changes in cloud at other levels.

**JSA08/09A/A08-008**

**Invited**

**1130**

#### **A LIKELY DECADEAL SOLAR-CYCLE EFFECT IN THE TROPICS**

Harry VANLOON (Colorado Research Associates)

The availability of global precipitation data after 1978 enables an examination of the influence of the 11-years solar cycle on the rainfall associated meteorological elements in the tropics during three solar maxima and two minima. In July-August the mean rainfall in solar maxima was higher than in the minima from India southeastward to the Pacific warm pool in the ocean and in the Intertropical Convergence Zones of the North Pacific and Atlantic Oceans. The mean difference between solar maxima and minima in tropospheric vertical motion and in the mean outgoing long-wavelength radiation was consistent with the difference in the rainfall: the vertical motion was more upward / less downward and the OLR was from higher cloudtops in the areas higher rainfall in the solar maxima than in the minima. The signal is found in the tropical centers of action. The difference in vertical motion

between maxima and minima of the solar cycle suggests a solar influence on the Hadley and Walker cells. Similar signals are found between extremes in the Southern Oscillation in July-August of the year<sup>2</sup> in the extremes; but the signals is larger by the factor of two to four.

**JSA08/09A/A08-009****1200****THE GLOBAL SIGNAL OF THE 11-YEAR SUNSPOT CYCLE IN THE ATMOSPHERE: WHEN DO WE NEED THE QBO?**

Karin LABITZKE (Institut fuer Meteorologie, FU Berlin)

The global structure and the size of the signal of the 11-year sunspot cycle (SSC) in the stratosphere and troposphere was examined in earlier studies. The correlations between the solar cycle and heights and temperatures at different pressure levels were mainly carried out with the whole data set and only during the northern winters the Quasi-Biennial Oscillation (QBO) was introduced. Here, this work is expanded and it is shown that the QBO must be introduced especially during the northern summers, because the solar signal is very different in the respective phases of the QBO, particularly over the tropics and subtropics. The structure of the solar signal in (northern) summer appears to indicate that the mean meridional circulations (Hadley and Brewer-Dobson Circulations) are influenced by the SSC especially during the east phase of the QBO. This result may help to find the mechanism through which the solar cycle (and the connected variation of the UV radiation) can influence the atmosphere.

**JSA08/09A/A08-010****1215****OSCILLATIONS IN THE SUN-EARTH SYSTEM AS MANIFESTATION OF FORCES OF ASTRONOMICAL ORIGIN**

Tamara V. KUZNETSOVA, Lev B. TSIRULNIK (IZMIRAN, Russian Academy of Sciences)

Spectra of interplanetary magnetic field (IMF) modulus and solar wind velocity  $V$  used measurements in space during 1963-1998 years at 1 AU near the ecliptic plane has been calculated by a method of a non-linear spectral analysis (MGM). The most power (in short-periodic part of the spectra) non-stationary (with varying phase and amplitude) oscillations at periods  $T=1.3$  years detected both in spectrum of  $B$  and  $V$  are discussed, their parameters are described (time intervals of damping, building up, and regime change of oscillations, time changes of amplitude and phase etc.). It is shown that time changes of the non-stationary oscillations does not depend on 11-year solar cycle that allows placing the source of the oscillations under the convection zone of the Sun. Additional arguments are presented (such periodicity was detected in the spectrum of neutrino flux, in variations in the rate of the Sun near the base of the convection zone with the same period etc). Remarkable feature of the cycle at  $T=1.3$  yr. is that the regime change (from damping to building up) of the oscillations (marked by phase shifts called by phase catastrophes) took place simultaneously both in solar and interplanetary data. Besides, time intervals marked by extreme points of the second derivatives of phase with respect to time of the cycle at  $T=1.3$  yr. coincide with the time intervals of well-known geomagnetic jerk events (secular variation impulse). Periodicity 1.3 yr. was extracted from different geophysical data. Possible sources of the Sun-Earth oscillations are discussed. Thorough analysis of the spectra shows that its periods can be interpreted as periods (and overtones) of astronomical periods reflecting dynamics of the external planets of the solar system (starting from the Earth). In particular, oscillations at  $T=1.3$  yr. are forced by perturbed tide forces (this component of the tide force is connected with motion of the Sun relative to the mass center of the solar system) of Mars, Jupiter, Saturn and Uranus. Amplitude of oscillations at  $T=1.3$  yr. is increasing for now. Long-periodic changes in the IMF and  $V$  have essentially different character. It is shown determining contribution of the long-periodic parts of the spectra to the changes of velocity and IMF at the Earth's orbit.

**Wednesday, July 9 PM**  
Presiding Chairs: M. Salby, K. Kodera

**JSA08/09P/A08-001****1400****TREND DISCOVERED IN TOTAL SOLAR IRRADIANCE DURING SOLAR CYCLES 21-23**

Richard Clayton WILLSON (CCSR Columbia University)

Results from a series of satellite total solar irradiance (TSI) observations covering the period 1978 - 2003 can be combined in a precise composite TSI database by determining the relationship between two non-overlapping components: SMM/ACRIM1 and UARS/ACRIM2. An ACRIM composite TSI time series using Nimbus7/ERB results to relate ACRIM1 and ACRIM2 demonstrates a significant secular upward trend of 0.05 percent-per-decade between consecutive solar activity minima. The PMOD TSI composite of Frohlich and Lean uses ERB results to relate ACRIM1 and ACRIM2 and differs from the ACRIM composite in two significant respects: a negligible trend between solar minima and lower TSI during solar maxima. These differences are shown to be artifacts of ERB degradation and modifications of Nimbus7/ERB and ACRIM1 published results that produce better agreement with the predictions of TSI/solar proxy models.

**JSA08/09P/A08-002**

Invited

**1420****DYNAMICAL RESPONSE TO THE SOLAR CYCLE**

Kunihiko KODERA (Meteorological Research Institute)

The dynamical impact of the 11-year solar cycle is investigated with the focus on the stratosphere region where solar ultraviolet heating is greatest. The results of the analysis suggest that in a climatological mean state, the stratosphere circulation evolves from a radiatively controlled state to one dynamically controlled during winter in both hemispheres. The transition period is characterized by a poleward shift of the westerly jet. The solar cycle effect appears as a change in the balance between the radiatively and dynamically controlled states. The radiatively controlled state lasts longer during the solar maximum phase and the stratosphere subtropical jet reaches a higher speed. The large dynamical response to relatively weak radiative forcing may be understood by the bi-modal nature of the winter atmosphere due to interaction with meridionally propagating planetary waves and zonal-mean zonal winds. It is suggested that the solar influence produced in the upper stratosphere and stratosphere region is transmitted to the lower stratosphere through (i) modulation of the internal mode of variation in the polar night jet and (ii) a change in the Brewer-Dobson circulation. The first process is significant in the middle and high latitudes, whereas the latter is prominent in the equatorial region.

**JSA08/09P/A08-003****1450****A MODEL OF SOLAR SPECTRAL IRRADIANCE NEAR MG II**Jeff Stanley MORRILL<sup>1</sup>, Kenneth P. DERE<sup>1</sup>, Clarence M. KORENDYKE<sup>1</sup>, Linton E. FLOYD<sup>2</sup>, JudithL. LEAN<sup>1</sup> (E. O. Hulburt Center for Space Research, Naval Research Laboratory, <sup>1</sup>Interferometrics Inc., Chantilly, Virginia, USA)

We are currently developing an empirical model of solar spectral irradiance variability near Mg II that combines areas and locations of plage and sunspots with wavelength dependent contrast factors in order to estimate the solar spectrum. These areas are derived from full disk solar images of Ca II K. At UV wavelengths, earlier models have relied on estimated or calculated contrast factors that are often at low resolution. Using quiet sun, plage, and sunspot spectra near 280 nm measured by the NRL HRTS instrument, we have recently derived the wavelength dependent contrast factors for plage and sunspots. We have also examined wavelength dependent limb darkening. In this presentation we will discuss the details of the current model including the use of measured high resolution contrast factors and limb darkening in the 276.5 - 288.5nm region. A preliminary comparison of model results with SUSIM observations will be presented. These comparisons will examine spectral irradiance variations on solar rotational and solar cycle timescales.

**JSA08/09P/A08-004****1510****WAVELET TRACING OF SOLAR, GEOMAGNETIC AND CLIMATE CHANGES**

Dmitri I. PONYAVIN (Institute of Physics, University of St.Petersburg, 198504, Russia)

Wavelet technique was applied to the sunspot, geomagnetic and air surface temperature records in the Northern hemisphere. Patterns of reconstructed wavelet coefficients were compared to find their similarities and coherence at different time and time-scale. We found a quasi 11-year oscillation in the regional temperature time series established since 1930. It was also found a quasi three-cycle periodicity in all studied data. Predictions of the current and future solar cycles, geomagnetic activity and climatic regional changes were made using trends discovered.

**JSA08/09P/A08-005**

Invited

**1550****MODELLING THE INTERACTION OF THE SOLAR AND QUASI BIENNIAL INFLUENCE ON THE STRATOSPHERIC WINTERTIME CIRCULATION**Lesley J. GRAY<sup>1</sup>, Simon CROOKS<sup>2</sup> (<sup>1</sup>Meteorology Dept., Reading University, <sup>2</sup>Oxford University, U.K.)

The equatorial quasi biennial oscillation of wind direction in the lower stratosphere is known to influence the propagation of planetary waves in the Northern Hemisphere winter-time. Recent model and data studies have suggested that the equatorial wind direction in the upper stratosphere is also influential on the frequency of sudden stratospheric warmings. The equatorial upper stratosphere is a region that is highly influenced by solar variability and current estimates of the zonal wind anomalies associated with the 11-year solar cycle are of the same order of magnitude as the QBO anomaly in this region. It is possible that these two upper equatorial influences may explain the observed interaction of the solar and QBO signals in northern high latitudes. The recent model and data studies will be summarised. New experiments using both a stratosphere-mesosphere model and a full GCM will then be described. In all studies a zonal wind anomaly at the equator is imposed and the response of the northern polar vortex variability is analysed. Experiments range from a simple comparison of the influence of the upper versus the lower equatorial stratosphere through to simulations that have an imposed QBO throughout the stratosphere and also an imposed 11-year solar cycle.

**JSA08/09P/A08-006**

Invited

**1620****REALISTIC SOLAR SIGNAL IN THE FUB-CMAM**

Katja MATTHES, Ulrike LANGEMATZ (Institut fuer Meteorologie, Freie Universität Berlin)

So far, GCM studies have not been able to capture the magnitude and characteristics of the observed 11-year solar signal in the stratosphere satisfactorily. Here, results from model experiments with the "Freie Universität Berlin Climate Middle Atmosphere Model (FUB-CMAM)" are presented which are for the first time comparable with observations. The experiments used realistic spectral solar irradiance changes, ozone changes from a 2D chemical model, and a relaxation towards observed equatorial wind profiles throughout the stratosphere. The results suggest that irradiance and ozone changes alone are not sufficient to reproduce the observed solar signal in a GCM. They emphasize the important role of equatorial winds in achieving a more realistic wind climatology and therefore a more realistic solar signal. Interestingly, only the magnitude of the anomalies during the dynamically active season improves, whereas the summer signal as well as the signal at low latitudes is still too weak. It will be shown that not only the solar signal is reproduced in the model experiments but also the interaction with the QBO. Similar to observations, major stratospheric warmings occur preferentially in the west phase of the QBO during solar maximum years.

**JSA08/09P/A08-007****1650****A MECHANISM FOR SOLAR VARIABILITY EFFECTS ON SURFACE CLIMATE**

Mark P. BALDWIN (Northwest Research Associates)

Despite the observational, theoretical, and modeling evidence in favor of a solar cycle influence on climate, a coherent mechanism (that amplifies the solar signal in the upper stratosphere and brings it to the surface) is not well understood. I will discuss one possible mechanism that involves wave, mean-flow interaction and would be capable of transmitting circulation anomalies in the upper stratosphere to Earth's surface. In observational data zonal wind anomalies in the stratosphere tend to progress northward and downward through the stratosphere on a timescale of a few weeks. The process of wave, mean-flow interaction in effect amplifies the anomalies as the progress downward from ~1 hPa to below the 100 hPa surface. This mechanism does not appear to be capable of propagating the anomalies from just above the tropopause to Earth's surface, but in observations the anomalies do descend. Once annular mode anomalies are just above the tropopause, they are observed to bias the tropospheric annular mode to be, on average, the same sign as that in the lowermost stratosphere. To date, specific mechanism to couple the stratosphere and troposphere has not been identified. Although several mechanisms could be at work, I will show that most of the evidence points toward an interaction between anomalies in the lowermost stratosphere and synoptic-scale waves in the upper troposphere. Once the waves (specifically, the wave momentum fluxes) are affected, the tropospheric response is a combination of zonal-mean flow adjustment and zonal-mean surface pressure changes. These surface pressure changes are seen as shifts in the surface annular mode, or Arctic Oscillation. The mechanism described above operates on an intraseasonal timescale, but would presumably operate consistently with interannual (or long-term) changes to forcing in the upper stratosphere. Observationally, a considerable difficulty is that the 11-year solar cycle is not the only forcing, and its effects seem to be dwarfed by the QBO and other natural interannual variability. Since the observational data record is less than 50 years,

**IA**

## INTER-ASSOCIATION

other effects (the QBO, ozone loss, greenhouse gas increases, etc.) make the signal difficult to see. This mechanism is not specific to the solar cycle, and would also allow for the downward propagation of any other signals from the stratosphere. This mechanism may help explain why the climate system is sensitive to circulation anomalies in the upper stratosphere, regardless of their origin.

**JSA08/09P/A08-008**

**1710**

### THE MANIFESTATION OF SOLAR ACTIVITY IN CLIMATE CHARACTERISTICS OF THE BAIKAL REGION

Gelii A. ZHEREBTSOV, Vladimir A. KOVALENKO (Institute of Solar-terrestrial Physics)

Long-term ground air temperature (GAT) variations have been analyzed. It is shown that the main meaningful GAT variations in the Baikal region for the period 1881-1960 were caused by solar variability, and the amplitude of these variations was 1 degree. Since the 1960s, with the persisting solar variability influence, the effect of another factor has been observed, the role of which was steadily increasing, and in the last decade it has already exceeded the contribution from solar variability. During the period from 1960 to 1997, the temperature rise, not associated with solar variability, was 1.5 degree. Analysis of the seasonal GAT variations showed that the ongoing variations are most clearly pronounced in the winter-spring period and are associated with the reduction of the stationing time of the Siberian anticyclone. This indicates that the mechanism of realization of the regional climate variability is the global atmospheric circulation rather than a local change in the atmospheric energy balance. It is most likely that this new factor are the global changes in the thermal regime of the atmosphere caused by the anthropogenic effect. An analysis of the data characterizing the forms of atmospheric circulation confirms the assumption made about the determining role of the influence of the global circulation on the Siberian anticyclone's stationing time and characteristics. Since solar cycle 20 (end of the 1960s) there has been a substantial change of the correlation between the zonal and meridional circulation in favor of the latter. Thus the region's ground air temperature is very sensitive to global variations of the atmosphere because of the enhancer: in the form of atmospheric global atmospheric circulation influence on the Siberian anticyclone characteristics. An analysis is made of the atmospheric radiation balance elements from stations located in the Baikal region of east Siberia, and from the network of other stations. It is established that in the overwhelming part of the territory, the last 50 years have seen a statistically significant decrease in direct and total solar radiation making up, respectively, 6.3% and 2.5% for 10 years. It is established that the scattered radiation distribution spanning the period 1939-1986 reveals a clear 11-year periodicity. Scattered radiation maxima that are clearly pronounced in the spring-summer period correspond to the minima of solar activity and to maximum intensities of galactic cosmic rays. Since the 1960s-1970s, this correlation has been disturbed. A possible physical mechanism of solar-tropospheric couplings is discussed.

**JSA08/09P/A08-009**

**1730**

### ABSORPTION PHENOMENA OF SOLAR XUV-RADIATION BY UPPER EARTH ATMOSPHERE IN THE NUMERICAL MODEL OF THE NEUTRAL ATMOSPHERE WMA01

Kirill A. BOYARCHUK<sup>1</sup>, I.A. ZHITNIK<sup>2</sup>, G.S. IVANOV-KHOLODNY<sup>1</sup>, A.V. KARELIN<sup>1</sup>, O.P. KOLOMIITSEV<sup>1</sup>, A.S. TRUSHIN<sup>2</sup> (Institute of Terrestrial Magnetism, Ionosphere and Radiowave Propagation, Lebedev Physical Institute)

The numerical model of a neutral Earth's atmosphere - working model of atmosphere 2001 (WMA01), designed in Institute of the Terrestrial Magnetism, Ionosphere and Radiowave Propagation, was corrected on the basis of the data of atmospheric sounding in X-ray range. The absorption phenomena by a Earth's atmosphere of solar XUV-radiation observed in the Sun's images obtained by a telescope TEREK-K (Space Vehicle "Koronas-1") in May-June 1994 at low activity of the Sun and instrumentation SPIRIT (Space Vehicle "Koronas-F") in October - November 2001 in a maximum of activity are studied in this research. The images of the Sun were registered on orbit segments when satellites moving in a shadow of the Earth and en satellites moving out of a shadow. So the upper Earth's atmosphere was sounded at altitudes 100 - 500 kms. The telescope TEREK-K was tuning on spectrum range 175 A and 304 A. The scientific equipment SPIRIT were tuning on spectrum range 175, 304 and 8.42 A. Integral value of absorption, direction of a density gradient of atmosphere, the local variations of absorption on an altitude to scale 1 km can be obtained by using of this technique. This method can essential supplement traditional techniques of research of the upper atmosphere and ionospheres.

**JSA08-Posters**

**Thursday, July 10**

### EFFECTS OF SOLAR VARIABILITY ON CLIMATE CHANGE (IAGA, IAMAS)

Location: Site D

**Thursday, July 10 PM**

Presiding Chair: K. Labitzke

**JSA08/10P/D-001**

Poster

**1400-001**

### THE PHYSICAL MECHANISM OF FAST CHANGES OF SOLAR IRRADIANCE AND CLIMATE

Alexey I. LAPYUKHOV (IZMIRAN, Russian Academy of Sciences)

As known from theoretical hydrodynamics and observations, the rotation of the Sun, stars, atmospheres and liquid nucleuses of planets is differential and unstable. Therefore the Sun fluctuations of angular rotation speed and magnetic field are always observed. It means, that some types of own fluctuations of the Sun (connected to its rotation and internal magnetic field) are unstable. In the established condition amplitudes of fluctuations are such, at which the surplus of energy of fluctuations (generated in unstable types with frequency Fun) is equal to dissipation of energy in all steady modes with frequencies Fsi, i, n=1,2,3, ΔEif, for example, 2Fu1-Fs2=0 (or in more general case in view of a magnetic field: Fun +Fum +-Fsi +-Fsj=0), then the interaction of modes of fluctuations has resonant character and consequently one is very strong. Let's speak in this case, that the Sun is in a resonant condition. It is important to understand, that in a resonant condition the amplitude of unstable own (but not forced (!)) oscillations is established minimal (but not maximal). Really, at condition of an almost strict resonance because of strong interaction oscillations modes the surplus of energy (generated in unstable modes) transfers to steady already at SMALL amplitudes of oscillations. Than the condition of a resonance is more precisely executed, the less amplitude established oscillations, the less activity of the Sun and speed of reorganization (change) of his structure, the more time Sun life in such condition. At an exit

from a resonant condition (for example, due to slow change of chemical composition as a result of nuclear reactions) the amplitude of fluctuations of unstable modes grows. Activity of the Sun and speed of change of its structure too are increased. Because of it the own frequencies of oscillations change, and the former resonant condition is carried out worse and worse, and the new resonant condition (with other set of own frequencies) is carried out at first poorly, and then it is better and better. In result the Sun passes from one almost stationary and resonant condition in another. The time of such transition is much smaller than Sun life-time in a resonant condition. More in detail about this mechanism it is possible to read in the published in Russian work: [Laptyukhov A.I. A role of nonlinear resonant interactions in fluctuations of the Sun and his evolution // Solar plasma and geomagnetic disturbances. M.1989. p.5-12]. We see, that the evolution of the Sun occurs not to constant speed, but numerous (and already therefore small), short-term jumps. It is quite possible, that now on the Sun begins to occur or already actively there is one of such next jumps. Such transition is accompanied by small changes of all basic characteristics of the Sun, including it energy output. Probably, it explains observable changes of the Earth climate.

**JSA08/10P/D-002**

Poster

**1400-002**

### SHARP CHANGES AND OSCILLATIONS OF CLIMATE IN SOLAR-TERRESTRIAL DATA IN THE PAST, PRESENT AS BASIS FOR FORECASTING THE FUTURE CLIMATE CHANGES

Tamara V. KUZNETSOVA, Lev B. TSIRULNIK (IZMIRAN, Russian Academy of Sciences)

It is generally recognized that climate regime shifts are connected with sudden changes of other geophysical systems although these systems are controlled by different physical mechanisms. However, this speed and the global synchronicity of climate changes are the major problems in understanding links between the Milankovich forcing of astronomical origin and climate data. Time series of different solar-terrestrial data (on solar activity, geomagnetic field variations, Be-10, C-14, anomaly of global surface temperature, etc) are analysed by a method of non-linear spectral analysis (MGM method) to detect time intervals of appearance of non-stationary oscillations of large amplitude and times of abrupt changes of their oscillation regime. The most power non-stationary (with varying phase and amplitude) sinusoid at mean period T-2230 yr. (and its overtones), reflecting oscillations of non-dipole part of the geomagnetic field in C14 data and variations of long-term solar activity), is connected with climate variability and its abrupt changes. Amplitude of the cycle is increasing for present. It is well-known high correlation between changes of the geomagnetic and gravitational fields. Elements of geomagnetic field are the most sensitive to global changes. In particular, our spectral analysis of the longest data set of the inclination variations on the Earth in Hartland showed: trend described by a polynomial has two extreme points: at t-1815 yr. and at t-1993 yr.; t-1815 yr. is marked by violation of Gnevishhev-Ohl rule for solar cycles; t-1993 yr. is marked by the violation of the same rule (1989-1994 yrs is a time interval of deceleration in the Earth's rotation too). Besides, warm phase of SOI lasted during maximal time interval (1990-1995) for all period of observations (140 yr.). Our careful comparative analysis of all results clearly shows that beginning of global changes at present will be marked by global warming, decreasing of the value of the magnetic moment of the Earth, reaching maximum of over-long cycle in sunspot formation and etc; all these features are favourable for abrupt climate changes for the decades after 2012 yr. Analysis shows that the most power cycles of the calculated spectra can be interpreted by periods (and overtones) of astronomical origin. It is possible to separate in orbital motion of each celestial body non-perturbed (Kepler's) part and perturbed one. The non-perturbed part of tide force characterizes non-evolving orbital motion (analogous to normal part of geophysical fields, for instance, gravitational and geomagnetic); respectively, perturbed part of tide force characterizes evolving orbital motion (analogous of anomalous part that can be extracted from observation). A possible physical mechanism is presented showing a possibility of transformation of signals of perturbed tide forces of astronomical origin (arising during orbital motion of the Earth) to geophysical systems through small variations of dissipative parameters of a dynamo system.

**JSA08/10P/D-003**

Poster

**1400-003**

### SOLAR AND CLIMATE VARIATION RELATIONSHIP SEARCHED BY STUDYING TREE RING INDEX TIME SERIES FROM CHILE (1588 - 1994 A.D.)

Nivaor Rodolfo RIGOZO<sup>1</sup>, Daniel Jean Roger NORDEMANN<sup>2</sup>, Heloisa Helena FARIA<sup>3</sup>, Ezequiel ECHER<sup>4</sup>, Luiz Eduardo Antunes VIEIRA<sup>5</sup>, Alan PRESTES<sup>6</sup> (Faculdade de Educação e Tecnologia Thereza Porto Marques (FAETEC) and Instituto Nacional de Pesquisas Espaciais (INPE), Instituto Nacional de Pesquisas Espaciais (INPE))

This work presents a study of the relations between solar and climate variations during the last four centuries by spectral analysis of tree ring index, sunspot number, rainfall and temperature anomalies time series. Trees used for this study were cupressaceous *Pilgerodendron* from Glaciar Pio XI, in Chile. Rainfall and temperature time series from Punta Arenas, in Chile were used. The spectral analysis of tree ring index shows that 11, 22 and 80 year periodicities of the solar cycle were present in tree ring data with 0.95 confidence level. This result suggests a solar modulation of climate variations, as recorded by the tree ring growth. Short-term variations, between 2-5 years, are also present in tree ring data. This spectral analysis shows that both, solar and climate factors, are recorded in the tree ring data.

**JSA08/10P/D-004**

Poster

**1400-004**

### SOLAR MAGNETIC FIELD AND MASS EJECTIONS DURING CYCLE 23

Ahmed Abdel HADY (Cairo University)

The solar cycle 23 started in 1996 and its maximum was in May 2001. More than ten high energetic flares (Proton flares) occurred from solar active region's of large and complex magnetic fields of strength 2500 to 3000 gauss. The mass ejection measured by artificial satellites for proton of energies more than 10 Mev. The increased of the solar wind in velocity and density, which occurred after the releasing of the solar eruptive flares was measured by artificial satellites. The geomagnetic storms and the sudden ionospheric disturbance measured by ground stations. The used data will be world-wide solar-geophysical data as that of NOAA, USA and Beijing observatory, China. The results lead to important role of the local magnetic field of the solar active region in production of high-energetic solar flares and its effect on the electromagnetic component and dynamic component of the flare. The effect of the magnetic field on the three different phase of the eruptive flare were given (thermal phase, impulsive phase, and recovery phase). Our results in this study, may be help in flare prediction and mass ejection estimation before its reach to the earth and produce geomagnetic storms.

JSA08/10P/D-005 Poster 1400-005

**ON THE INFLUENCE OF HELIO-GEOPHYSICAL PARAMETERS ON GLOBAL CIRCULATION PATTERNS**

Tomas HALENKA (Dept. of Meteorology and Environment Protection, Fac. of Mathem. and Physics, Charles University)

To represent an objective characteristics of circulation patterns the spectral structure of both stratospheric and tropospheric fields is analysed in terms of spherical harmonics coefficients. The aim of this study is to compare the long-term behaviour of global circulation structures and their connections to some helio-geophysical influence, especially solar activity, solar magnetic field and geomagnetic activity. NCEP/NCAR database of reanalyses is used with appropriate spectral coefficients available for period 1948-2002 four times per day in 28 levels for vorticity, divergence, temperature, etc. Temporal analysis of significant spherical harmonics is introduced as well as the comparison of their changes with respect to the changes of different sets of solar, geomagnetic and global circulation indices. Quite strong connections to a set of extraterrestrial parameters appear for some distinctive shapes of polar vortex. The natural variability connected to the extraterrestrial influence is studied as well as interannual variability with the emphasis to the QBO and ENSO. The systematic review of the appropriate correlations is presented and decadal variability and long-term trends are pointed out for some of wave numbers. The connections between stratospheric and tropospheric circulation is also discussed in terms of coefficients of spherical harmonics affected by extraterrestrial influence. Long-term changes in the variability of the circulation patterns are analysed by means of wavelet analysis as well.

JSA09 Thursday, July 10

**CHALLENGES OF GLOBAL CHANGE IN FORCING FROM BELOW AND ABOVE (IAGA, IAMAS)**

Location: Site A, Room 8

Thursday, July 10 AM  
Presiding Chair: J. Lastovicka

JSA09/10A/A08-001 Invited 0830

**NONLINEARITIES, THRESHOLDS AND SURPRISES: WILL THE FUTURE SURPRISE US?**

Michael C. MACCRACKEN (International Commission on Climate)

Climate change can result from external changes in climate forcing and from internal fluctuations that move energy among elements of the climate system. Although changes in forcing can be unexpected and relatively abrupt, it is generally assumed that the large thermal capacities of the oceans and cryosphere are likely to moderate all but the very largest changes (e.g., from asteroid impacts). However, paleoclimatic records suggest that large and relatively rapid shifts in climatic conditions have occurred, at least on scales from regional to semi-hemispheric. As context for this symposium on the potential for large or sudden changes in forcing, this paper will summarize the results of IUGG symposium MC10, which is focused on understanding past and potential future changes in climate that were in the past, or could be in the future, larger, more rapid, or more unexpected than straightforward climate sensitivity analyses would indicate.

JSA09/10A/A08-002 Invited 0900

**LONG-TERM VARIATIONS OF THE MIDDLE ATMOSPHERE SEMI ANNUAL OSCILLATION (SAO)**Dirk OFFERMANN<sup>1</sup>, Matthias DONNER<sup>1</sup>, Peter KNIELING<sup>1</sup>, Annette MENZEL<sup>2</sup>, Barbara NAUJOKAT<sup>3</sup> (<sup>1</sup>Department of Physics, Wuppertal University, <sup>2</sup>Department of Ecology, Technical University, Munich, <sup>3</sup>Institute of Meteorology, Free University of Berlin)

Long-term temperature data are available in the upper mesosphere from hydroxyl emission measurements at Wuppertal (5° N, 7° E), in the stratosphere from SSU data, and in the lower stratosphere from the Berlin analysis. Temperatures are influenced by solar forcing from above and by dynamical forcing from below. They are corrected for these effects. The strong seasonal temperature variations in the middle atmosphere allow to define a summer duration by means of a threshold temperature, or by the circulation turn-around. This summer length has changed by a few weeks in the last two decades: it has increased in the mesosphere and decreased in the stratosphere. This will be compared to vegetation data on the ground, where the length of the growing season has increased in a comparable way. The middle atmosphere summer changes are related to considerable changes of the SAO. These changes are found to be anticorrelated in the mesosphere and the stratosphere. Latitude and longitude dependence of the phase changes will be analyzed by means of CRISTA and SSU data. Circulation reversal data in the lower stratosphere go back by more than four decades. They are used to discuss a possible anthropogenic influence on the trends presented, and to give a respective prognosis.

JSA09/10A/A08-003 0930

**THE EARTHSHINE PROJECT: MEASURING THE EARTH'S ALBEDO. LATEST RESULTS**Enric PALLE<sup>1</sup>, Pilar MONTANES RODRIGUEZ<sup>1</sup>, Phillip R. GOODE<sup>1</sup>, Steve E. KOONIN<sup>2</sup>, Jiong QIU<sup>1</sup>, Jeff HICKEY<sup>2</sup> (<sup>1</sup>Big Bear Solar Observatory, <sup>2</sup>California Institute of Technology)

Since December 1998, photometric observations of the bright and dark side of the Moon have been regularly carried out at Big Bear Solar Observatory, with the aim of determining a precise and absolutely calibrated global albedo of the Earth. The up-to-date synoptic, seasonal and long term variation in the Earth's albedo are reported in this paper, together with comparison with modelled albedo using modern cloud satellite data and Earth Radiation Budget Experiment (ERBE) scene models. The Earth's albedo has a major role in determining the Earth's climate. During the past 4 years, a significant increasing trend in the averaged Earth's reflectance has been detected in the observational data. More scarce data from 1994 and 1995 allow us to take a longer-term look at the Earth's albedo variability and the possibility of a response of this parameter to solar activity is discussed. Simultaneously, spectroscopic observations of the earthshine have been carried out at Palomar Observatory. First results and comparison between the spectral and photometric observations are also being presented.

JSA09/10A/A08-004 0945

**VARIABILITY IN SOME NEGLECTED ATMOSPHERIC PARAMETERS**

Gufran BEIG (Indian Institute of Tropical Meteorology, PUNE, INDIA)

This talk will briefly touch upon some silent features related to the 'changing atmosphere' and set the platform for further deliberations. There may be several reasons for such variability some may have long lasting and another may have sporadic impacts. Impact of such effects (natural or anthropogenic) on some of the atmospheric parameters are seldom discussed because they have such slow effects that even their additive results are difficult to perceive. One such example is the ion chemistry of troposphere and stratosphere which gets highly influenced by volcanic eruptions as well as growing level of Human induced greenhouse gases and pollutants led by carbon-dioxide. Emphasis will be placed to such parameters.

JSA09/10A/A08-005 Invited 1030

**STRATOSPHERIC AND TROPOSPHERIC FORCING OF THE ARCTIC OSCILLATION BY THE 1991 MT. PINATUBO ERUPTION**Georgiy L. STENCHIKOV<sup>1</sup>, Alan ROBOCK<sup>1</sup>, Kevin HAMILTON<sup>2</sup>, V. RAMASWAMY<sup>3</sup>, M. Daniel SCHWARZKOPF<sup>3</sup> (<sup>1</sup>Department of Environmental Sciences, Rutgers University, New Brunswick, New Jersey, <sup>2</sup>International Pacific Research Center, University of Hawaii, Honolulu, <sup>3</sup>NOAA Geophysical Fluid Dynamics Laboratory, Princeton University, Princeton, New Jersey)

Observations show that strong equatorial volcanic eruptions have been followed by a pronounced positive phase of the Arctic Oscillation (AO) for one or two Northern Hemisphere winters. To understand the atmospheric processes that cause the AO response, we studied stratosphere-troposphere interaction forced by the explosive volcanic eruption of Mt. Pinatubo on June 15, 1991, which caused the strongest volcanic effect on the atmosphere and climate in the 20th century. Following large volcanic eruptions, the radiative perturbation from stratospheric aerosols exerts a strong influence on the climate system. Volcanic aerosols cool the Earth's surface because of reflection of solar radiation, and heat the lower stratosphere because of absorption of thermal IR and solar near-IR radiation. The ozone depletion that results from the presence of the stratospheric aerosols also perturbs the radiation. In addition, radiative effects of aerosols and ozone interact with the quasi-biennial oscillation (QBO) that dominates a tropical stratospheric circulation. We implemented volcanic aerosols, observed ozone anomalies, and the QBO in the GFDL SKYHI GCM and conducted a series of control and perturbation experiments to examine the evolution of the circulation in the two years following the Pinatubo eruption. We were able to simulate fairly realistically the observed temporal and spatial structure of stratospheric temperature variations when QBO and aerosol forcings are included. The phase of the QBO appears to modulate climate system sensitivity to a volcanic forcing. The QBO in its westerly phase strengthens the AO response. Because of nonlinear interactions, aerosols and the QBO together produce a stronger response than linear superposition of responses to each of these forcings. Aerosol radiative heating in the tropical lower stratosphere strengthens the equator-to-pole temperature gradient in the lower stratosphere and produces a stronger polar night jet that in turn affects the propagation of planetary waves and tends to cause a positive phase of the AO in winter. Ozone depletion causes a positive phase of the AO in late winter and early spring by cooling the lower stratosphere in high latitudes, strengthening the polar night jet, and delaying the final warming. Aerosol-induced tropospheric cooling in the subtropics decreases the meridional temperature gradient in the winter troposphere between 30N and 60N. The corresponding reduction of mean zonal energy and reduction of amplitudes of planetary waves in the troposphere decrease wave activity flux into the lower stratosphere. The resulting strengthening of the polar vortex forces a positive phase of the AO. We suggest that this mechanism can also contribute to the observed long-term AO trend being caused by greenhouse gas increases, because they also weaken the tropospheric meridional temperature gradient due to polar amplification of warming.

JSA09/10A/A08-006 1100

**THE GLOBAL CHANGES OF WATER LEVELS IN SOME EARTH SYSTEMS**

Nikolay V. SOKOLOV (Water Problems Institute of Russian Academy of Sciences)

There are global changes in Earth Systems that connect with the water intakes for agricultural and industry. The global changes may be seen on regional levels too. Four mathematical models have been created for simulating these global changes of water levels in earth Systems and it influences on regional levels. The first is a model of simulating to change water's layers in Dead Sea under influence of men intake water from Jordan River. The creation of this model has been connected with the following. Evolution of water column and the density, salinity and temperature profiles that influenced it were traced from 1960 to 1980. In 1960, as for many years before, a large density difference (caused by a large change in salinity) separated the variable upper layers from the deep fossil waters. By the 1976 the interface between the surface and fossil waters had descended. The upper layers' salinity and density had increased, but in summer warming decreased the surface density. These trends continued in 1977, but there was a new reverse salinity gradient in the summer. In 1978 the salinity was uniform throughout the column; a small temperature difference (arrow) maintained the stability of the fossil water body. In 1979, after the overturn, the fossil water body had been dissipated and the entire column was more saline and somewhat warmer. In 1980 after a rainy winter, there was a new but shallow salinity gradient. These phenomena are study with the aid of a created mathematical model of Dead Sea now. The second environmental model is a model of changes of Aral Sea under influence of men intake waters from rivers that discharge into this Sea. It is well known that the square of this Sea is decreasing now. Salt is moved from squares of former sea bottom to the villages and fields. A socio-economic danger connects with it. The third environmental mathematical model connects with the changes of salinity of Azov Sea. They study process water and salts moving to Azov Sea from Black Sea and rivers of Don and Kuban under influence of increasing of water intakes. They will take into account the change of numbers of fishes in the Azov Sea with the aid of this model. The fourth model is a model of water level decreasing in mountain Sevan Lake. The using of lake's waters for hydroelectric power stations have led to a decreasing of evaporation and volume of rain's waters go return to the Sevan Lake. One former island of this lake has been a peninsula under decreased water level. Thus, the changes of water level and some bio-physic characteristics are study in the seas and lakes with the aid of these mathematical models. The socio-economic perspectives are analyzed with the aid of this simulating too.

JSA09/10A/A08-007 1115

**HORIZONTAL T-S MIXING AND FRONTOGENESIS IN THE WESTERN PACIFIC WARM POOL AREA**Alexander V. SOLOVIEV<sup>1</sup>, Roger LUKAS<sup>2</sup> (<sup>1</sup>Oceanographic Center, NOVA Southeastern University, <sup>2</sup>Department of Oceanography, University of Hawaii)

## INTER-ASSOCIATION

In the western Pacific warm pool, convective rains produce surface "puddles" containing salinity and density anomalies. These puddles store significant potential energy, which release plays an important role in the dynamics and thermodynamics of the warm pool area. This effect -- largely ignored by the existing bulk ML parameterizations -- is analyzed here with a nonlinear advection-diffusion one-layer model of Ferrari and Young (1997). Analysis of the nonlinear problem allows us to hypothesize the existence of an equilibrium wavenumber range, in which the 1-D spectrum of horizontal T, S, and density inhomogeneity follows a  $k^{-\alpha}$  law. A numerical experiment illustrates how nonlinear diffusion transforms initial horizontal density anomalies into the structures with increased buoyancy curvature and leads to a  $k^{-\alpha}$  wavenumber spectrum. These structures represent an equilibrium state. The data collected during TOGA COARE demonstrate agreement with the theoretical  $k^{-\alpha}$  law, for horizontal wavelengths less than 16 km. The increased buoyancy curvature drives frontogenesis, which requires non-hydrostatic modeling. Incorporation of these results into high-resolution ocean models with bulk ML may improve the simulation of the ENSO cycle.

**JSA09/10A/A08-008**

**1130**

### A PRELIMINARY STUDY OF THE SOFIA FREE TROPOSPHERE/LOW STRATOSPHERE PARAMETERS IN AN ASSOCIATION WITH GLOBAL CHANGES

Staytcho KOLEV (National Institute of Meteorology and Hydrology-BAS.)

Reports in 2001 from the Intergovernmental Panel of Climate Change (IPCC), said unequivocally that human induced climate change was happening and that it was likely to get a whole lot worse. The reports claimed that the carbon dioxide produced from burning fossil fuels was already warming up the world and that if nothing was done it would have all sorts of disastrous consequences. There had been a slight increase in the temperature on the ground. But satellite measurements showed, that higher up in the so-called "free troposphere", things didn't seem to be getting much warmer. Anyway, the status of the free troposphere became a very big deal. A regionally study of the locally trends of the free troposphere experimental measured parameters will be of great profits to clear up the variability of meteorological conditions controlling the local air pollution dispersion and chemical processes in the atmosphere. The most of the warming predicted in the models came from a feedback involving main meteorological parameters. The aims of the present work are to investigate magnitude changes of the temperatures, dew point temperatures and wind directions at the main isobar standard levels in the free troposphere over Sofia and their tendency. The behavior of these parameters at different altitudes up to 20 km, influenced by the global atmosphere change has been analyzed.

**JSA09/10A/A08-009**

**1145**

### ATMOSPHERIC ELECTRICITY MEASUREMENTS AT MAITRI, ANTARCTICA DURING ANTARCTIC SUMMER

Panneerselvam CHITHIRAIVEL<sup>1</sup>, S. GURUBARAN<sup>1</sup>, K. JEEVA<sup>1</sup>, B.N. RAINA<sup>1</sup>, R. RAJARAM<sup>2</sup>, A.K. KAMRA<sup>3</sup>, C.G. DESHPANDE<sup>3</sup> (<sup>1</sup>Equatorial Geophysical Research Laboratory, Indian Institute of Geomagnetism, <sup>2</sup>Indian Institute of Geomagnetism, Colaba, <sup>3</sup>Indian Institute of Tropical Meteorology)

Simultaneous surface measurements of the atmospheric electrical parameters viz ionosphere to ground currents, electric field and conductivity have been carried out at an Indian station, Maitri (70.75° S, 11.75° E, 117 m above mean sea level), Antarctica, during austral summer for the year of 2001 and 2002. The response of the quality of data to changes in background conditions such as winds, drifting or falling snow; cloudiness, fog effects etc. have been examined and presented in a consolidated form. The measurement shows that atmospheric conductivity is more or less stable during fair weather days at this station. The averaged pattern of diurnal variations in the electric field and vertical conduction current density averaged over fair weather days follow nearly the Carnegie curve, with a minimum at about 03 UT and a maximum near 19 UT. However during magnetically disturbed days, there is a departure from universal diurnal variation in both the electric field and vertical conduction current indicating the influence of solar activity. Day-to-day variation in the diurnal curves of electric conduction current and field, probably due to day-to-day variation in global thunderstorm activity, are clearly evident.

**JSA09/10A/A08-010**

**1200**

### SOLAR AND VOLCANIC EFFECTS ON THE EARTH CLIMATE OVER THE LAST 300 YEARS

Elena A. KASATKINA<sup>1</sup>, Oleg I. SHUMILOV<sup>1</sup>, Oleg M. RASPOPOV<sup>2</sup>, Nils A. MORNER<sup>3</sup> (<sup>1</sup>Polar Geophysical Institute of Kola Science Center RAS, <sup>2</sup>St.-Petersburg Filial of IZMIRAN, St.-Petersburg, Russia, <sup>3</sup>Department of Paleogeophysics and Geodynamics, Stockholm University, Stockholm, Sweden)

The influence of cosmic rays modulated by solar variability and volcanic activity on the aerosol layer is considered. The acidity index obtained from the Greenland ice cores has been used for an analysis. It has been shown that the sunspot numbers correlate with the background value of acidity in Greenland ice, characterizing the variation in the atmospheric aerosol component. This supports the mechanism of the influence of solar and galactic cosmic rays on the aerosol concentration and cloudiness in the atmosphere. The results of the analysis have indicated that acidity records in ice cores can be used to characterize the influence of cosmic rays on climate in the past, after excluding the peaks associated with volcanic activity.

**JSA09/10A/A08-011**

**1215**

### IMPACTS OF THE 11-YR SOLAR MODULATION OF THE SEASONAL CYCLE ON THE GENERIC QBO IN CLIMATE SYSTEM

Hengyi WENG (LASG, Institute of Atmospheric Physics, Chinese Academy of Sciences)

The generic QBO (quasi-biennial oscillation) in climate system, with a cycle-length slightly above or below 2 years, is studied in a simple forced dynamical system. The fundamental cause of the quasi-biennial periodicity of the QBO is the nonlinear subharmonic resonance of the system to the seasonal forcing that is modulated by the 11-yr solar cycle. For a given nonlinearity, the cycle-length and the amplitude of the QBO depend on the intensity of both the seasonal forcing and the 11-yr solar modulation, which may be one of the reasons why the QBO properties in climate vary with time and space.

**JSA09-Posters**

**Friday, July 11**

### CHALLENGES OF GLOBAL CHANGE IN FORCING FROM BELOW AND ABOVE (IAGA, IAMAS)

Location: Site D

**Friday, July 11 PM**

**JSA09/11P/D-001**

**Poster**

**1400-050**

### ENSO - A QUASIPERIODIC FORCED DYNAMICAL SYSTEM

Nadejda Nazarovna IVACHTCHENKO (Hydrometeorological Research Center of Russia)

Several years ago a scenario of the ENSO timing has been proposed connected with an ENSO phase-locking to the annual period. The respective bifurcation sequence from an invariant two-torus, via a resonant limit cycle on this torus, and then either the cycle doubling, tripling, or quadrupling that finishes in chaos is well-known in the mathematical dynamical systems theory for this scenario. Accordingly this scenario, the shape of the ENSO power spectra must consist of a continuous background with a finite number of power density peaks superimposed on this background at combinatory harmonics of the annual period. But, the really observed shape of the ENSO spectra is quite different from that. The real ENSO spectra reveal very many peaks within a wide band of frequencies. Many of these peaks cannot be attributed to any sub- and superharmonic of the annual period for certain. Therefore, the proposed phase-locking scenario must be improved. Mention that similar shapes of spectra are inherent to NAO, AO, and NPO too. Thus, it seems there is a common external driver of all of these phenomena that is more complex than a simple annual periodic forcing. The aim of this report is to show that the shape of the real spectra of ENSO and other above phenomena can be better reproduced if the existence of a second forcing periodicity at a frequency that is essentially incommensurate to the annual frequency is taken into consideration. In the case of a quasiperiodic forcing, the dynamical systems theory indicates another scenario connected with the arising of an invariant three-torus, and the subsequent bifurcation of the loss of the three-torus smoothness, and then the arising of the so-called strange nonchaotic attractor (SNA). Typically, the SNA power spectrum consists of innumerable peaks and spikes re-distributed along the frequency axis by a self-similar manner. It is just the shape of the power spectrum that is seen in the real ENSO etc. power spectra. One can suppose that the pole tide excited by the well-known Chandler wobble in the Earth's pole motion (of the about 14-month-long period) may be considered as the second external driver of the ENSO etc. dynamics. A parametric excitation seems to be a reason for an enhancement of the ENSO etc. responses to the pole tide force. Because of the "worst" incommensurability of the annual and pole tide periods not only interannual but even interdecadal ENSO, AO, NAO and NPO variability can be excited. Thus, the mystery of the interdecadal variability of these phenomena may be explained.

**JSA09/11P/D-002**

**Poster**

**1400-051**

### OBSERVATIONS OF IONOSPHERE TO EARTH CURRENT DENSITY FROM A LOW LATITUDE CONTINENTAL STATION TIRUNELVELI (8.7°N, 77.8°E)

Panneerselvam CHITHIRAIVEL<sup>1</sup>, K. JEEVA<sup>1</sup>, K.U. NAIR<sup>1</sup>, C. SELVARAJ<sup>1</sup>, S. GURUBARAN<sup>1</sup>, B.N. RAINA<sup>1</sup>, R. RAJARAM<sup>1</sup> (<sup>1</sup>Equatorial Geophysical Research Laboratory, Indian Institute of Geomagnetism, <sup>2</sup>Indian Institute of Geomagnetism, Colaba)

The observations of ionosphere to ground current from the low latitude continental station close to the dip equator, Tirunelveli (8.7°N, 77.8°E), India, are presented in this study. The horizontal long-wire antenna with an effective collecting area of around 140 Sq. Meters is used as a sensor. Results of a comprehensive systematic study of the influence of background winds on the current measurements are presented. It is found that during the summer months no reliable measurements of the air-earth currents can be carried out at the station. On fair weather days during winter and equinox, the mean variations follow the Carnegie pattern except for a clear and persistent sunrise effect. The sunrise effect is observed during fair weather days in both winter and equinox conditions. The measured current starts increase about 30 minute before sunrise and last for nearly an hour and a half. The possibility of the sunrise effect being associated with the sunrise at upper boundary of the global electric circuit in the ionosphere is discussed.

**JSA09/11P/D-003**

**Poster**

**1400-052**

### MONITORING OF SCHUMANN RESONANCE AT EQUATORIAL ELECTROJET LATITUDE

C. PANNEERSELVAM<sup>1</sup>, C. SELVARAJ<sup>1</sup>, K. JEEVA<sup>1</sup>, K.U. NAIR<sup>1</sup>, S. GURUBARAN<sup>1</sup>, B.N. RAINA<sup>1</sup>, R. RAJARAM<sup>1</sup> (<sup>1</sup>Equatorial Geophysical Research Laboratory, Indian Institute of Geomagnetism, <sup>2</sup>Indian Institute of Geomagnetism, Colaba)

Using a pair of induction coils, the north-south and east-west components of geomagnetic field have been continuously monitored for more than six months at Tirunelveli (7.8°N, 77.8°E), a station under the equatorial electrojet. The data offers the unique possibility of studying the influence of the equatorial ionospheric conductivity profile on the phenomenon of Schumann resonance. The resonant frequencies were obtained the application of Fast Fourier Transforms on the individual time series. The analysis reveals that the first resonant mode is between 7.75 and 8.0 Hz and the second mode between 14.0 and 14.25 Hz. The strength of individual resonant oscillations averaged over a large number of days reproduces the Carnegie type universal time variations. For further validation the results measured power in the resonances is compared with data of worldwide distribution of the lightning flashes available from the space based observatory (TRMM Observatory). On fairly large number of the days the diurnal variations of strength of the resonance and lightning flashes have a fairly good agreement. The lack of universal agreement is discussed in terms of contamination due to local oscillations not linked with Schumann resonance.

**JSH01**

**Monday, July 7 - Tuesday, July 8**

### THE REMOTE SENSING OF THE CRYOSPHERE (IAHS [ICSI, ICRS], IAMAS, IAPSO)

Location: Site C, Room 27

Monday, July 7 AM  
Presiding Chair: J. Dowdeswell

## GLACIERS AND SEA ICE

JSH01/07A/C27-001

0940

### FORM AND FLOW OF ARCTIC ICE CAPS: REMOTE-SENSING INVESTIGATIONS FROM AIRCRAFT AND SATELLITES

Julian A. DOWDESWELL (Scott Polar Research Institute, University of Cambridge)

The ice caps and glaciers of the Arctic islands make up about 45% of the 540,000 km<sup>2</sup> or so of ice outside Antarctica and Greenland. If the small glaciers and ice caps on Greenland and Antarctica are included, there is a global total of 680,000 km<sup>2</sup> and about 180,000 km<sup>3</sup> of ice, excluding the great ice sheets. In either case, the glaciers and ice caps of the Arctic islands form a significant area and volume of the World's ice. In addition, atmospheric General Circulation Models (GCMs) predict that the Arctic will warm preferentially over the next hundred years or so, relative to lower latitudes, thus making the mass balance of Arctic glaciers and ice caps critical to future projections of global sea level in a warming World. However, the form and flow of many of the larger Arctic ice caps (104 km<sup>2</sup>) are relatively little known. Satellite investigations of these ice caps, using Landsat and ASTER high-resolution visible-band imagery, yield information on ice-cap area, drainage-basin configuration and, in the case of ASTER, elevation. The drainage basins of Austfonna, Svalbard (8,200 km<sup>2</sup>) and Academy of Sciences Ice Cap in Severnaya Zemlya (5,500 km<sup>2</sup>), for example, have been defined in this way. Synthetic aperture radar (SAR) methods have also been used to calculate the ice-surface velocity structure, using phase data, and the distribution of snow and ice on the surface, using backscatter data. The next generation of polar orbiting satellites, IceSat and Cryosat, will provide further opportunities to measure ice-surface elevation to an accuracy of a few tens of centimetres, allowing calculations of change through time. Airborne radio-echo sounding at MHz frequencies remains the only method of acquiring ice-thickness data over large areas, and this method has been used to derive the thickness and ice volume of a number of large ice caps in the Arctic islands of Canada, Svalbard and Russia. Combining data on marginal ice thickness and velocity allows calculation of the mass loss through iceberg production from these ice masses. In some cases, iceberg calving may account for about 40% of total mass loss from marine-terminating Arctic ice caps.

JSH01/07A/C27-002

1000

### APPLICATION OF ASTER IMAGES TO ESTIMATE GLACIER SYSTEM CHANGES IN THE CENTRAL TIEN SHAN DURING THE SECOND HALF OF THE 20TH CENTURY

Tatiana Y. KHROMOVA<sup>1</sup>, Mark B. DYURGEROV<sup>2</sup>, Roger G. BARRY<sup>3</sup> (<sup>1</sup>Department of Glaciology, Institute of Geography Russian Academy of Sciences, <sup>2</sup>Institute for Arctic and Alpine Research (INSTAAR), University of Colorado, Boulder, US, <sup>3</sup>National Snow and Ice Data Center (NSIDC), University of Colorado, Boulder, US)

The optical satellite sensor ASTER (Advanced Spaceborne Thermal Emission and Reflection Radiometer) on board Terra offers new possibilities for worldwide glacier monitoring. We present the results of comparisons of glacier-extent and volume determined by comparison of ASTER-imagery taken in September 2001 with two repeated-mapping surveys by aerial photography in 1943 and 1977 over the Akshirak Glacier system, central Tien Shan. The Akshirak Range reaches 5,100 m asl, or about 1500 m above the central Tien Shan plateau (43°N, 75°E). The range is heavily glacierized with a total ice area of about 400 km<sup>2</sup>. The ENVI, ERDAS, ARC/GIS, and ARC/View software packages were used to manipulate, transform and overlay the ASTER image and historical data for the Akshirak Range. A substantial change in glacier area is observed to have taken place since the 1977 survey. The changes involve: a decrease in average size of glaciers, an increase in the area of outcrops and in the perimeters of water divides between individual glaciers, the appearance of new glaciers and disappearance of former small ones. The number of glaciers has not changed greatly. A significant loss of glacier area locally has been caused by the direct impact of the exploitation of mineral resources. BRThe changes in climate, based on data from a meteorological station located on the high plateau at 3614 m a.s.l., close to glacier termini of the Akshirak Range, show increases in summer and annual air temperature and decrease in annual precipitation. Moreover, the ratio between summer (June-August) and winter (October-May) precipitation has decreased especially since the mid-1970s accompanied by increased summer air temperature. This presents the most unfavorable climatic conditions for glaciers in Central Asia where summer precipitation plays the crucial role in the annual mass balance. Our findings confirm the results of earlier studies of the regime of Tien Shan glaciers and their sensitivity to summer conditions. BROur study illustrates the value of combining remotely sensed data and historical observations to monitor ongoing changes in glaciers. The disintegration of the compact high-altitude Akshirak glacier system in Central Asia has been identified and the increased glacier wastage quantified.

JSH01/07A/C27-003

1020

### DISTRIBUTION OF CRYOCONITE ON THE SURFACE OF A GLACIER DERIVED FROM A LANDSAT TM IMAGE

Nozomu TAKEUCHI<sup>1</sup>, Reginald R. MUSKETT<sup>2</sup> (<sup>1</sup>Research Institute for Humanity and Nature, <sup>2</sup>International Arctic Research Center, University of Alaska Fairbanks)

Cryoconite, biogenic surface dust on the glacial surface, can affect the surface albedo of snow and ice thereby accelerating ablation. Distribution of cryoconite on the surface of an Alaska glacier (Gulkana Glacier in the Alaska Range) has been analyzed using Landsat TM band 2 and 5 ratio. The band ratio was relatively lower in the area near terminus and snow line in the ice area, suggesting higher cryoconite concentration in this area. In situ measurement of cryoconite on the glacier agreed with the cryoconite distribution derived from the band ratio. The biological analysis of the cryoconite collected from the glacier revealed that the cryoconite distributed in the area near the terminus mainly consisted of mineral particles, and that the cryoconite near the snow line, on the contrary, contained large amounts of snow algae and dark-colored organic matter. Results suggest that the albedo reduction by biological activity is significant in the area near snow line on the glacier. Depending on the percentage area distribution of the biological activity, the albedo reduction could affect glacier mass balance during the ablation season. A positive feedback may exist between biological activity and abnormally high melt rate years as a consequence of global warming in the northern hemisphere. Research is continuing to investigate the biological activity - albedo reduction with satellite imagery and in-situ field measurements on other glaciers with wide geographic distribution in Alaska and Central Asia.

JSH01/07A/C27-004

1140

### ANALYSIS OF ASTER AND PANCHROMATIC IMAGES FOR SURFACIAL CHARACTERISTICS OF THE GANGOTRI GLACIER, GARHWAL HIMALAYA, INDIA

Syed Iqbal HASNAIN, Sarfaraz AHMAD, Meenakshi YADAV (School of Environmental Science, Jawaharlal Nehru University)

Quantitative and qualitative analysis of the Gangotri glacier surface and various geomorphological features have been carried out by using ASTER (Advance Spaceborne Thermal Emission and Reflection Radiometer) and Panchromatic IRS 1D image and field studies. The area of the main Gangotri glacier is about 77 km<sup>2</sup> in 2001 Panchromatic image, while this area is 87 km<sup>2</sup> in the toposheet surveyed in 1985. This implies that glacier has vacated about 12% area in last 17 years. The entire glacier area between snout and accumulation has been divided into three zone on the basis of tonal and textural characteristics. Zone 1 ranging between 3975 and 4507 masl is characterised by non-uniform thick debris-cover with highly fractured ice, whereas Zone 2 is less fractured and characterised by uniform thin debris-cover. At junction of Zone 1 and Zone 2 between elevation 4507 and 4663 masl, there are about six ice-dammed lakes varying in size between 25 - 200 m<sup>2</sup>. Moraine are better identified by ASTER as compared to Panchromatic IRS 1D image, as it provide different spectral signature for dry and ice covered debris.

JSH01/07A/C27-005

1200

### APPLICATIONS OF SEA-ICE MOTION AND DEFORMATION DERIVED FROM SATELLITE DATA

Antony K. LIU, Yunhe ZHAO (Oceans and Ice Branch, NASA Goddard Space Flight Center)

QuikSCAT backscatter and DMSP SSM/I radiance data have been used to derive sea ice motion for both the Arctic and Antarctic region using the wavelet analysis tracking method. Both results from QuikSCAT and SSM/I are compatible with buoys and can then be merged by data fusion method to generate composite sea ice motion maps for more complete coverage. Furthermore, based on this merged data set daily sea-ice deformation (shear, and convergence) maps have been produced and show consistent spatial and temporal patterns. Temporal correlation maps between ice deformation and SSM/I ice concentration show interesting results in the Arctic, especially in the coast area. In this study, principal component analysis to both the merged ice tracking result from satellite data and pressure field from buoy has also been examined for the relationship between the principal components and eigenvectors from these two data sets. While the result shows that principal components of modes 1 and 2 from two data sets are highly correlated which confirms that wind forcing is a major factor driving the ice drift, it also reveals that other high-energy modes are not highly correlated which maybe caused by coastal effects. Principal component analysis of sea-ice motion during fall/winter period in different years has also been used to correlate with the results of Arctic Oscillation study.

JSH01/07A/C27-006

1220

### IMPROVING THE NEAR-REAL TIME QUIKSCAT/SEAWINDS SEA-ICE EDGE

Joerg HAARPAINTNER<sup>1</sup>, David G. LONG<sup>2</sup>, Mike L. VAN WOERT<sup>3</sup> (<sup>1</sup>Polar Science Team, National Ice Center, <sup>2</sup>MERS Laboratory, Brigham Young University)

The current QuikScat/SeaWinds sea ice edge is a daily product and part of the operational data set at the National Ice Center in Washington DC. The sea ice edge is extracted from the near-real time resolution-enhanced SIR data that are 36-hour composites of the Polar Regions. Given the highly dynamic nature of the marginal ice zone and the importance of the daily standard deviation in the algorithm to separate ocean from sea ice, the extracted ice edge corresponds to high ice concentration above 50%. The main reason for not detecting low concentrations is that the temporal variability of the location of the ice edge exceeds the effective resolution of the composite by up to an order of magnitude. By reducing the integration time for the composites, we can therefore improve locally the determination of the ice edge to lower ice concentration and new ice. In this paper we study the optimal balance between maximum resolution and minimum integration time to detect the lowest possible ice concentration.

Monday, July 7 PM  
Presiding Chairs: M. Tranter, E. Brun

## PERMAFROST

JSH01/07P/C27-001

1400

### GEOPHYSICAL MONITORING OF HYDROTECHNICAL OBJECTS IN PERMAFROST ZONE

Vyatcheslav Aleksandrovich ISTRATOV<sup>1</sup>, Svet Yurievich MILANOVSKY<sup>2</sup>, Sergei Aleksandrovich VELIKIN<sup>3</sup> (<sup>1</sup>Radiation Ltd, Moscow, <sup>2</sup>Institute Physics of the Earth RAS, Moscow, <sup>3</sup>Vilui Permafrost Research Station of Permafrost Institute RAS, Chernishevskii)

Frozen rocks in permafrost zone are very sensitive to natural and man-caused influences because of possibility of phase transition from frozen state to thawed and back. Together with temperature field, fluid mineralization and hydrogeological conditions determine durability of the rock massive and its mechanical properties. We discuss peculiarities of temporal and spatial changes in frozen soils that are primarily conditioned by constitutional ice - pore solution transformations. During these transformations all physical properties of frozen medium change, the most sensitive of which are electrical and mechanical. The hydro technical engineering objects which are carried up in permafrost zone like Western Sakha Yakutia, are exposed to action of a different sort of the negative factors step-by-step resulting some of them in a labile state, down to catastrophic. Owing to these circumstances for last 5-8 years on a number of hydro technical objects of Western Sakha Yakutia are observed thawing-filtration processes, are found out local filtration zones posing under threat their secure exploitation. Due to a difficult and hardly predictable geocryological situation in this area, the geophysical methods were included into the system of local monitoring. Authors present original results of long-term geophysical study on hydrotechnical objects (constructing and exploiting reservoirs) analyzing problems associated with use of geophysical methods for the study of rocks and soils in permafrost area. We present results of complex experimental control observation of the development of filtration process. More and more relevant role in these studies is gained with a georadar study. The georadar observations were carried out on Mirnii region in a complex with electric-prospecting observations and temperature logging. The georadar SIR 2000 (production of the company GSSI, USA) with antennas 40, 200 MHz was applied. The data were processed with software packages RADAN (GSSI, USA) and RadExPro + (GSD Production, Russia). The purpose of inter-well radiowave investigations was, first, to control the frozen rock thawing (talk) within the coastal zone of the reservoir and to assess the dynamics of the process, and second, to identify and to locate places of the most intensive thawing and filtration of

## INTER-ASSOCIATION

water from the reservoir. Thawing process leads to a decrease of electrical resistivity. Besides, the high saturation of the filtering layer must be reflected in an increase of relative dielectric permittivity within the same interval. As a result of these observations the quite good correlation between applied geophysical methods was established. The most interesting results of observations documented by excavation and visual observations will be presented in the report. On the base of detailed surface and boreholes geophysical observations the 2D-numerical model of the part of right-bank contiguity was done. The model shows temperature evolution of thawing zone as a function of air and water temperature, lithology, thermal properties of the section. Observed geophysical data compared with numerical modeling.

**JSH01/07P/C27-002**

**1420**

### PERMAFROST MAPPING AND DEFORMATION MONITORING USING SAR INTERFEROMETRY

Zhen LI, Xinwu LI, Xin REN, Qing DONG (Institute of Remote Sensing Applications, Chinese Academy of Sciences)

The interferometric SAR technique has demonstrated its capability to measure ground deformation in wide range of application. For the purposes of some applications, especially those that involve engineering projects, a quantitative use of the InSAR results must be required. The seasonal transition of the land surface between frozen and non-frozen condition affect a number of ecological and hydrological processes the cycle between wintertime dormant and summertime active states. At the same time, the freeze/thaw transition will cause the deformation of ground surface, which is the main factor for engineering construction in permafrost region. At microwave frequencies, freezing results in a dramatic decrease of the dielectric constant of soil, which significantly decreases their radar back-scattering properties. The obvious difference on soil moisture between frozen and unfrozen area can be detected by SAR images. Usually, soil and vegetation are considered as a single medium when single-polarization, single-frequency SAR data is employed. But the vegetation covered on the permafrost will influence the permafrost detection, because of the volume scattering effect of vegetation. The permafrost and the seasonal frozen ground cover respectively 1,272,709 km<sup>2</sup> and 1,146,399km<sup>2</sup> in the Tibetan Plateau. China begins construction of Qinghai-Tibet railway in 2002. The first handicap will be the permanent frozen earth. About 550km of the railway will pass through such areas. Continuous permafrost and some island permafrost underlie the entire region, and the maximum active-layer depth at the site reached approximately 0.4-1.5m. Extensive areas of frozen ground hold large quantities of moisture in wintertime conditions. Thawing and temperature rising has a great influence on railway stability. In order to study the process of railway building deformation for different permafrost types and geophysical environments, deformation monitoring is very important. In this study, 6 scenes SAR SLC images, including Tandem data, are used to produce multiple interferograms. The techniques to classify permafrost using SAR data, conference analysis, and two typical methods for deformation detection are discussed. One method is the InSAR measure with the high accurate DEM used to reduce the terrain effect, the other is differential InSAR. The results be validated and compared quantitatively base on precise and accurate geodetic data derived from field measurement. We analyzed the precision and reliability of two methods. The suitable technique is chosen for deformation monitoring using ERS-1/2 SAR data in Qinghai-Tibet Plateau. Then, an InSAR monitoring system of frozen ground deformation is proposed for the Qinghai-Tibet railway building. The results showed that multi-temporal SAR data could be used to discriminating permafrost from other targets with high accuracy, and interferometrical SAR are fairly good use to permafrost deformation monitoring.

**JSH01/07P/C27-003**

**1440**

### REMOTE SENSING DETERMINATION OF THE PERMAFROST THICKNESS

Vil S. YAKUPOV, Sergey V. YAKUPOV (Institute of Space Physic Research and Aeronomy)

The possibility of increasing by factors power potential (PP) of pulsed-type radar sounding station (RSS) based on super-conductivity technology magnetic moment generators and SQUID-magnetometers allow to use it for frozen strata thickness determination. For this purpose the remote sensing survey becomes possible both from the ground and the air. Let us estimate the depth to which it might be possible to determine frozen strata thickness at different assumptions about electrical properties of frozen and underlying it thawed rocks considering them homogenous. Let resistivity of frozen rocks  $\rho$  be equal 300, 1 000, 3 000 and 10 000  $\Omega$  m and resistivity of frozen unconsolidated deposits with massive cryogenic texture — 1 000, 3 000 and 10 000  $\Omega$  m. Relative permittivity  $\epsilon$  for them be equal 9 and 4 in frozen condition and 15 for thawed ones. Then limits of possible values of Frenel coefficient will be 0,1 (for rocks) and 0,3 (for unconsolidated deposits), with specific absorption 0,18 — 0,05 dB/m ( $\epsilon = 9$ ) and 0,8 — 0,1 dB/m ( $\epsilon = 4$ ) accordingly. The possible depth of investigation for lower boundary of permafrost when PP = 560 dB and  $\epsilon = 4$  (unconsolidated deposits) will be for  $\rho = 1 000 \Omega$  m 410 m, for  $\rho = 3 000 \Omega$  m — 1 230 m, for  $\rho = 10 000 \Omega$  m — 3 900 m. When it is possible to accumulate reflected signals to increase PP up to 600 dB these depth estimations will be 450, 1 340 and 4 300 m. For frozen rocks ( $\epsilon = 9$ ) these values will be 125 ( $\rho = 300 \Omega$  m), 400, 1 200 and 3 800 m when PP = 560 dB and 135, 440, 1 300 and 4 200 m when PP = 600 dB. Remote sensing from air (PP = 560 dB) decreases these estimates to 370, 1 150 and 3 500 m for unconsolidated deposits and to 120, 380, 1 150 and 3 500 m for rocks due to losses on double passing the air-ground boundary. Simultaneously another important task can be solved: determination of frozen unconsolidated deposits thickness if the resolution of their lower boundary in relation to the ground surface and to the lower boundary of frozen rocks can be achieved. Identification of found interface nature could be made by comparing its depth with drilling and direct current sounding data. Thus, the possibility of remote sensing determination of the frozen strata and, as well, of frozen unconsolidated deposits thickness seems to be real using radar sounding by mighty magnetic pulses both from the ground and the air everywhere when  $\rho \geq 1 000 \Omega$  m if the resolution of their lower boundaries is possible.

**JSH01/07P/C27-004**

**1500**

### DETECTING THE NEAR-SURFACE SOIL FREEZE-THAW CYCLE USING A COMBINED FROZEN SOIL ALGORITHM

Tingjun ZHANG, Richard L. ARMSTRONG, Jeff SMITH (National Snow and Ice Data Center, University of Colorado at Boulder)

Better knowledge and understanding of the near-surface freeze/thaw cycle of soils are prerequisite for evaluating the impact of cold season/cold region processes on surface and subsurface hydrology, regional and global climate, carbon exchange between the atmosphere and the land, and the terrestrial ecosystem as a whole. The challenge is to develop new techniques and methodologies to obtain data and information of the near-surface soil freeze/thaw cycle. A combined frozen soil algorithm was developed and validated to detect the near-surface soil freeze-thaw cycle over snow-free and snow-covered land areas. The combined frozen soil algorithm consists of two parts: (i) over snow-free land areas, passive microwave satellite remote sensing algorithm was used to detect the near-

surface soil freeze-thaw cycle; (ii) over snow-covered land areas, a one-dimensional numerical heat transfer model with phase change was used to detect soil freeze-thaw status under snow cover. Using the Defense Meteorological Satellite Program's Special Sensor Microwave Imager (SSM/I) data, the passive microwave satellite remote sensing algorithm utilizes a negative spectral gradient between 19 GHz and 37 GHz, vertically polarized brightness temperatures and a cut-off brightness temperature at 37 GHz with vertical polarization (TB(37V)). A cut-off brightness temperature of 258.2K was obtained based on a linear correlation ( $r^2=0.84$ ) between the soil temperature at 5 cm depth and the TB(37V). Soil temperatures used in the correlation were measured from 26 stations over the contiguous United States for the period from July 1, 1997 through June 30, 1998. Using soil temperature data measured from the same stations for the period from July 1, 1998 through June 30, 1999, the combined frozen soil algorithm provides the accuracy of frozen soil detection of about 76% and the correct classification of both frozen and unfrozen soils of approximately 83% with the percent error of about 17%. The combined frozen soil algorithm was used to investigate the timing, duration and number of days, and daily area extent of the near-surface frozen soils from July 1, 1997 through June 30, 1999 over the contiguous United States. The primary results indicate that the maximum area extent of frozen ground during the winter of 1997/98 was about 4.4 x 106 km<sup>2</sup> or 63% of the total land area of the contiguous United States, while during the winter of 1998/99, the maximum extent was about 5.2 x 106 km<sup>2</sup> or 74%. The duration of the seasonally frozen ground ranges from less than one month in the south to over eight months in the Rocky Mountains. The actual number of days of soil freezing varies from a few weeks to more than several months. Further validation is needed to improve the accuracy of frozen ground detection and to estimate thickness of the seasonally frozen ground using the combined frozen soil algorithm.

**JSH01/07P/C27-005**

**1520**

### ELECTROMAGNETIC DIAGNOSTICS OF PERMAFROST OF THE NORTHEAST PART OF THE RUSSIA BY MEANS OF GROUND AND REMOTE METHODS OF RADIOIMPEDANCE SOUNDING AND PROFILING

Mikhail Georgievich DEMBELOV<sup>1</sup>, Yuri Buddich BASHKUEV<sup>1</sup>, Viktor Petrovich MELCHINOV<sup>2</sup>, Ludmila Khanharaevna ANGARKHAeva<sup>1</sup> (<sup>1</sup>Buryat Scientific Center SB RAS, <sup>2</sup>Yakut State University)

The report is devoted to detail research of electrical properties of the permafrost of the northeast part of the Russia. Regions of the Aldan plateau, the central Yakutia and tundra areas that are near the Arctic Ocean coast are objects of investigations. The aim of the research is to define of its electric characteristics and to create geoelectric models of different types of the permafrost. The main results: 1. Detail physical description and classification of electric properties, construction and structure of the permafrost on the depth of skin-layer in the VLF range is offered. 2. According to measurements on typical cryogen rocks systems the season variations of geoelectric sections (GES) parameters, surface impedance and electromagnetic field are discovered. The geoelectric model for a permafrost stratified section that takes into account main climate generating factors and season processes for freezing and thaw of grounds is developed. The model of stratified medium with structure and properties that are changed depending on climate conditions describes season impedance variations of the border surface and ground electromagnetic field. The model allows to predict propagation of VLF-MF electromagnetic waves over permafrost paths in different year seasons with the precision that is enough for practice. 3. It is established that frequency dispersion of the electric resistance of the frozen friable sediments layer between direct current and high frequency currents of VLF-MF ranges is a feature of electric properties of the permafrost. A good conformity between calculated values obtained from data of vertical electromagnetic sounding (VES) and measured values of surface impedance of the horizontally stratified cryogen medium for areas of "high temperature" frozen layers disposition and for cases of small contrast of GES layers is received. This fact confirms absence of the frequency dispersion of electric properties of frozen layers that are in position close to melted condition. A difference of electric resistivity (ER) on direct and alternating currents for GES that have frozen friable sediments is established. ER values that are reconstructed after the inverse problem solution on data obtained from radioimpedance sounding are less in 3-10 times than on data obtained from VES method. A physical interpretation of obtained results for frozen layers that takes into account the influence of conductive engaging in multi-phase heterogenic medium is offered. 4. A method of physical-statistical prediction of the geoelectric section for main types of permafrost is developed. The predicted map of geoelectric sections of the Yakutia and geoelectric maps of the Aldan plateau with different scales are created. 5. A method of radioimpedance sounding and profiling in VLF-MF ranges for ground electric cartography of Arctic lakes and coastal zone of the Arctic Ocean area of water on resistivity in the framework of multi-sectional model of the ground with high and low conducting foundation is developed. 6. An estimation of efficiency of the vertical electric transmitter in LF-MF ranges of electromagnetic waves is made. It is shown that the efficiency for emitted antennas situated on the permafrost does not exceed 28 per cents.

**SNOW HYDROLOGY**

**JSH01/07P/C27-006**

**1600**

### COMBINING REMOTE SENSING ADVANCES, DATA RELAY, AND INTERLINKED HYDROLOGIC MODELS TO IMPROVE SNOWMELT RUNOFF FORECASTING IN THE RIO GRANDE BASIN

Albert RANGO<sup>1</sup>, Enrique GOMEZ-LANDESA<sup>1</sup>, Max BLEIWEISS<sup>2</sup>, David DEWALLE<sup>3</sup>, Geoff KITE<sup>4</sup>, Jaroslav MARTINEC<sup>5</sup>, Kris HAVSTAD<sup>6</sup> (<sup>1</sup>USDA/ARS/Jornada Experimental Range, New Mexico State University, 2995 Knox St., Las Cruces, NM 88003, USA, <sup>2</sup>Department of Entomology, Plant Pathology, and Weed Science, New Mexico State University, Las Cruces, NM 88003, USA, <sup>3</sup>Pennsylvania State University, 107 Land and Water Building, University Park, PA 16802, USA, <sup>4</sup>Hydrologic Solutions, Bryn Erthin, Cefn Bychan Road, Pantymwyn, Flintshire, WA CH7 5EN, UK, <sup>5</sup>7270 Davos-Platz, Switzerland)

Remotely-sensed data can be used with modern hydrological models to provide effective snowmelt-runoff forecasts and to evaluate water resource management options. MODIS, on both TERRA and AQUA satellites, is likely the optimum sensor for snow mapping because it has a best resolution of 250m (two bands), it passes over daily, it is free from downloading, and it provides a logical transition from 1 km NOAA-AVHRR data. Its worth for snow mapping has been proven both in the Rocky Mountains of the United States and the Pyrenees of Spain. Still, research to solve automated and operational problems is ongoing including correction of the "Bow Tie" effect, mapping in shaded and heavily vegetated areas, and using bidirectional reflectance distribution functions to retrieve snow albedo. As the remote sensing improvements are made, the data are used in the Upper Rio Grande Basin for improvement of the snowmelt forecasting system. Remote snow water equivalent site data is acquired through the Natural Resources Conservation Service SNOTEL system employing meteor-burst relay. These data can be used for early season (November-December) volumetric forecasts which increase water management flexibility. The MODIS-derived snow cover data are input to the Snowmelt Runoff Model (SRM) for generating daily streamflow forecasts over the entire melt season. Because snowmelt runoff is not significant throughout the entire basin, SRM outflow from snowmelt basins is linked to the Semi-

distributed Land Use-based Runoff Process (SLURP) model as an input. SLURP is a comprehensive distributed model now operating on the entire Rio Grande basin to assist in water management decision-making today and to evaluate future scenarios for improving long range planning. SLURP also uses remote sensing inputs to establish current land cover throughout the basin. Examples of forecasts made from 2001-2003 in the Upper Rio Grande basin are presented.

JSH01/07P/C27-007

1620

#### THE SNOW WATER EQUIVALENT SCALING EXPERIMENT: OVERVIEW AND INITIAL RESULTS

Chris P. DERKSEN, Chris P. DERKSEN, Anne E. WALKER, Barry E. GOODISON (Climate Research Branch, Meteorological Service of Canada)

Passive microwave snow water equivalent (SWE) retrieval algorithms are influenced by a range of land cover and snowpack state variables that are present at a range of scales. Because of the relatively low levels of naturally emitted microwave energy, pixel dimensions of spaceborne passive microwave brightness temperatures are large (10 to 25 km). A single passive microwave derived SWE estimate, therefore, integrates multiple land and snow cover conditions into a single measurement. Multi-scale brightness temperature datasets with coincident ground sampling are required to quantify the impact of spatially heterogeneous land cover and snowpack properties on passive microwave SWE retrievals. New multi-scale research datasets will be acquired through the Snow Water Equivalent Scaling Experiment, conducted near Prince Albert, Saskatchewan, Canada in February 2003. Passive microwave brightness temperature datasets will be acquired from tower-based sensors, airborne radiometers (100 m resolution), and spaceborne sensors (Advanced Multichannel Spaceborne Radiometer — AMSR ~ 10 km resolution; Special Sensor Microwave/Imager — SSM/I ~ 25 km resolution) for a 25 by 25 km study area centred at the Old Jack Pine Boreal Ecosystem Research and Monitoring Site (BERMS). A coincident ground sampling program will characterize in situ SWE, depth, and density using a land cover sensitive sampling scheme. A suite of micrometeorological variables from seven distributed tower sites will complement the passive microwave brightness temperature and in situ snow datasets, while land and forest cover datasets including land cover type, canopy closure, and forest stem volume have already been obtained. This presentation will provide an overview of the field experiment, and results of initial dataset analysis. A preliminary investigation of pre-campaign airborne microwave data indicates that a high degree of brightness temperature variability is evident along individual flight lines, with strong associations to forest cover properties. Following full airborne dataset acquisition in February, various scaling techniques will be used to link the variability in small footprint airborne brightness temperatures with the coarse scale spaceborne AMSR and SSM/I data. The degree to which brightness temperature variability is captured by the 10 km AMSR data relative to the 25 km SSM/I data will be determined. The in situ snow measurements will illustrate the variability in SWE, depth, and density that can be found on spatial scales ranging from individual trees and clearings to inter-species stand-to-stand variability. The distributed micrometeorological data will be used to identify physical influences on brightness temperature variability. For instance, species specific relationships between tree temperature and air temperature have clear impacts on measured brightness temperature in forested environments. Ongoing analyses of these datasets will advance our understanding of important scale and process issues related to the remote estimation of SWE.

JSH01/07P/C27-008

1640

#### ESTIMATION OF SNOW WATER EQUIVALENT AND SNOWMELT WATER USING THE SNOW INDEX - A CASE STUDY IN THE KUROBE BASIN, JAPAN-

Yuichi SHIMAMURA, Takeki IZUMI, Daichi NAKAYAMA, Hiroshi MATSUYAMA (Department of Geography, Graduate School of Science, Tokyo Metropolitan University)

The snow index 'S3' (Saito and Yamazaki, 1999) is applied to Landsat-5/TM images, to estimate the snow water equivalent and the snowmelt water. This index considers the mix of snow and plants using reflectance of one visible (Band 3 of TM) and two infrared (Bands 4 and 5), so the index should obtain the distribution of the snow-covered area under the plants more exactly than other indices using only visible band(s).  $S3 = B4 \cdot (B3 - B5) / ((B4 - B3) \cdot (B4 + B5))$ . 'S3' was developed for ADEOS-II/GLI, but the satellite has just been launched on 8th December, 2002. This research is, therefore, the first case to apply 'S3' for satellite data. In the Kurobe basin (Toyama prefecture, Japan) in the spring of 1986, the snow-covered area is clustered from 'S3' with threshold value of 0.0 which is proposed by Saito and Yamazaki (1999). Then, the gross volume of the snow water equivalent is estimated with the relationship that snow water equivalent increases linearly with altitude. When Landsat-5 passed over the study area, the snow water equivalent can be calculated from the altitudinal distribution of the snow-covered area and the increasing ratio of the snow water equivalent; the ratio is called 'altitudinal distribution factor' and the value in the basin was surveyed by KEPCO (the Kansai Electric Power Co., Inc.) in 1959. The amount of the snowmelt water is calculated as the difference of the snow water equivalent estimated by two scenes (14th and 30th April, 1986). In this study, there are no ground truth data, so results are validated indirectly by the estimation error of snowmelt water. The relative error is based on the difference between the estimated amount of the snowmelt and the observed runoff which flowed into the Kurobe-daiyon-dam (Kuroyon dam) from 14th to 30th April, 1986. When 'S3' is used for extracting the snow-covered area, the estimation error is -8.2 percent. Even if the effect of rainfall and time lag of snowmelt-runoff are taken into account, the error ranged with  $\pm 10$  percent. While the snow-covered area is extracted by the other method which does not consider the disturbance by vegetation, the error is as large as -23.8 percent. Since 'S3' can capture the ground snow under the plant canopy, the index has higher precision. Namely, this guarantees the snow index 'S3' as the better method for extracting the snow-covered area.

JSH01/07P/C27-009

1700

#### STREAMFLOW RESPONSE TO SNOWCOVER EXTENT CHANGE IN LARGE SIBERIAN RIVERS

Daqing YANG<sup>1</sup>, David ROBINSON<sup>2</sup>, Yuanyuan ZHAU<sup>1</sup>, Thomas ESTILOW<sup>3</sup>, Baisheng YE<sup>1</sup> (<sup>1</sup>University of Alaska Fairbanks, <sup>2</sup>Rutgers University, <sup>3</sup>Chinese Academy of Sciences)

The Lena, Yenisei and Ob rivers are the three largest rivers in the Arctic regions. They contribute more than 45% of total freshwater inflow to the Arctic Ocean and have great impacts to the regional/global ocean and climate systems. Snowcover melt and associated floods are the most important hydrologic event of the year in the northern river basins. To better understand the streamflow regime and variation in the high latitude regions, this research uses the weekly NOAA snowcover extent data to study the streamflow hydrology in Siberia. The focus of this research is to examine the streamflow response to snowcover extent change on a weekly basis particularly during the spring melt period. In this analysis, we calculated the basin-mean snowcover extent over the watersheds for the entire NOAA records (1966-present) and generated a weekly snowcover time-series. We used these weekly data to examine the seasonal changes of snowcover extent, such as defining the

weekly snowcover climatology, determining the dates of snowcover formation/disappearance and duration of snowcover, and quantifying the rates of snowcover change during the accumulation and melt seasons. We examined the weekly correlation of streamflow with basin-mean snowcover extent, and determined the consistency between snowcover and runoff changes during the snowmelt period. We also investigated the associations between snowcover and runoff anomalies, identified extreme snowmelt runoff cases, and examined their correspondence with snowcover and climate conditions. Based on these analyses, we defined the weekly relation between snowmelt runoff and snowcover changes for the watersheds. This study explores the potential of using remotely sensed snowcover information to improve our capability of snowmelt runoff modeling and forecasting over large northern river basins. The results demonstrate that the NOAA weekly snowcover extent data are useful for understanding and predicting streamflow changes in the arctic regions. Snowcover water equivalent data obtained from ground and via remote sensing will be examined in further studies.

JSH01/07P/C27-010

1720

#### STUDY ON SNOWMELT RUNOFF SIMULATION AND FORECAST USING GIS AND REMOTE SENSING DATA IN THE MOUNTAINOUS REGION OF WESTERN CHINA

Jian WANG<sup>1</sup>, Yongchao LAN<sup>2</sup> (<sup>1</sup>Cold and Arid Regions Environmental and Engineering Research Institute (CAREER), Chinese Academy of Sciences (CAS), <sup>2</sup>The State Key Laboratory of Frozen Soil Engineering Chinese Academy of Sciences)

In this paper, the progresses of studying on monitoring the water resource derived from snow cover melting in western of China are introduced. Commonly, the Remote Sensing data and Geographic Information System (GIS) techniques are the important methods and tools. The key parameter—snow cover area can be computed through satellite images from Multi-platform, multi-temporal and multi-spectral. Supervised classification filter has chosen to yield clusters of snow cover. Meanwhile, GIS will provide abundant information in order to obtain the remaining parameters of simulating model. The simulated models and predicting results about snowmelt runoff serving for the water resource management office and reservoirs will also be mentioned in detail. The samples about successful simulations and predicting snowmelt runoff extracted from two typical mountainous regional covered by snow-cover will be presented.

JSH01/07P/C27-011

1740

#### IMAGERY OF SNOW WATER EQUIVALENT FROM SSM/I AND MODIS DATASETS IN QINGHAI-TIBETAN PLATEAU

Tao CHE<sup>1</sup>, Xin LI<sup>1</sup>, Richard L. ARMSTRONG<sup>2</sup>, Rui JIN<sup>1</sup> (<sup>1</sup>Remote Sensing and GIS Lab, Cold and Arid Regions Environmental and Engineering Research Institut, CAS, <sup>2</sup>National Snow and Ice Data Center, University of Colorado)

Snow water equivalent is a key factor in the variable study of snow storage and water resources management. Passive microwave remote sensing data (SSM/I) have a faculty to penetrate clouds and snow cover and to provide dual polarization information at different frequencies. In fact, due to its low spatial resolution and complex topographic condition of the Qinghai-Tibetan plateau region, the estimation of snow water equivalent cannot be obtained a result of satisfaction yet. MODIS data as an important complement has a high spatial resolution. Using the MODIS data to decompose mixed-pixels of passive microwave bright temperature data is an available method to advance the spatial resolution of SSM/I data. After fusion of the two datasets, the snow cover, frozen ground and desert-soils regions are distinguished in the SSM/I sub-pixel scale. Three separate algorithms were developed based on the surface environments (snow cove, frozen ground, and desert-soils). A final snow water equivalent value represents the area-weighted average based on the proportional land cover within each SSM/I pixel. In this study, one day, 5 day, and 10 day averaged passive microwave derived SWE imagery for the winter season (December-February) are compared to in situ data from the Bureau of Meteorology in Qinghai and Tibet, in order to assess algorithms performance. The results have shown that retrieved SWE remains within  $\pm 10$ -20mm of surface observations, independent of fractional within-pixel land cover.

Tuesday, July 8 AM

Presiding Chair: R. Armstrong

### SNOW PROPERTIES

JSH01/08A/C27-001

0910

#### CRYOSPHERIC REMOTE SENSING AND THE NASA COLD LAND PROCESSES FIELD EXPERIMENT

Edward KIM<sup>1</sup>, Don CLINE<sup>2</sup>, Robert DAVIS<sup>3</sup>, Cold Land Processes Working Group (<sup>1</sup>NASA Goddard Space Flight Center, <sup>2</sup>NOAA National Operational Hydrologic Remote Sensing Center, <sup>3</sup>US Army Cold Regions Research and Engineering Laboratory)

The Cold Land Processes Field Experiment (CLPX) has been designed to advance our understanding of the terrestrial cryosphere. Developing a more complete understanding of fluxes, storage, and transformations of water and energy in cold land areas is a critical focus of the NASA Earth Science Enterprise Research Strategy, the NASA Global Water and Energy Cycle (GWEC) Initiative, the Global Energy and Water Cycle Experiment (GEWEX), and many other programs. Quantitative understanding of cold land processes over large areas will require synergistic advancements in (1) understanding the spatial scaling behavior of cold land processes, (2) improved representation of cold land processes in coupled and uncoupled land-surface models, and (3) a breakthrough in large-scale observation of hydrologic properties, including snow characteristics, soil moisture, the extent of frozen soils, and the transition between frozen and thawed soil conditions. Major scientific questions to be addressed through CLPX research, strategies, and expected outcomes will be discussed. The CLPX Plan has been developed through the efforts of over 60 interested scientists that have participated in the NASA Cold Land Processes Working Group (CLPWG). A major product of the experiment will be a legacy data set including satellite, airborne, and ground-based remote sensing as well as comprehensive ground truth. Field observations were conducted by in February and March, 2002 and 2003 within a 25,000 km<sup>2</sup> domain in Colorado, USA. Participants included researchers from several countries. A detailed description of the field campaigns will be presented along with some preliminary examples of field data.

**JSH01/08A/C27-002 0930**

**PRELIMINARY RESULTS FROM THE VALIDATION OF SNOW COVER PRODUCTS DERIVED FROM AMSR-E**

Richard L. ARMSTRONG, Mary Jo BRODZIK, Matt SAVOIE, Ken KNOWLES (CIRES/NSIDC)

The National Space Development Agency of Japan (NASDA) has developed two Advanced Microwave Scanning Radiometers: AMSR-E, built for NASA's Earth Observing System (EOS) launched on 4 May 2002 on the Aqua platform and AMSR which was launched by Japan on December 14, 2002 on "Midori-II" the Advanced Earth Observing Satellite-II (ADEOS-II). The AMSRs provide improved spatial resolution, varying with frequency from 6 km x 4 km at 89.0 GHz to 75 km x 43 km at 6.9 GHz, compared to earlier generations of space-borne passive microwave instruments (e.g., SMMR and SSM/I) and they include more frequencies than their predecessors (horizontally and vertically polarized brightness temperatures at 6.9, 10.7, 18.7, 23.8, 36.5 and 89.0 GHz). Given the large footprint of passive microwave sensors, snow cover within a footprint is seldom uniformly distributed and large differences between station or gauge measurements (a point) and satellite estimates (an area integration) can be expected. Therefore it is necessary to develop schemes to compare areal snow cover with satellite derived snow cover and our present study relies on several such validation data sources. These include comparisons of AMSR-E derived SWE with snowmelt runoff models and stream gauge data for selected large river basins such as the Lena River Basin in Russia, comparisons with SSM/I algorithm output and comparisons of snow extent with Moderate Resolution Imaging Spectroradiometer (MODIS) data. In addition, using data obtained during the NASA Cold Land Processes Field Experiment (CLPX) during February and March of 2003 in northwestern Colorado, we validate the AMSR snow products based on a wide range of measurements from the ground-based and airborne components of this field experiment. Aircraft data will be available from the NASA P3 (radiometers:10-220 GHz), the NASA DC-8 (AIRSAR) and the NOAA AC690 (gamma measurements) combined with ground measurements coming from the University of Tokyo GBMR-7 ground-based AMSR simulator and University of Michigan ground radars (L, C, X, Ku) as well as intensive manual ground sampling. These manual measurements will provide a sampling density that is unprecedented and will include 9,000 snow depth measurements and 288 snow pit profiles (snow water equivalent, snow density, grain size type and size and temperature) to characterize the snow cover over three 25 x 25 km Meso-cell Study Areas (MSAs) providing data at a spatial scale appropriate to the analysis of AMSR-E retrievals. We also present results from our development of enhanced snow cover mapping through blending of microwave (SSM/I and AMSR) and optical (MODIS) satellite data.

**JSH01/08A/C27-003 0950**

**MULTISENSOR REMOTE SENSING OF SNOW COVER**

Sverre Thune DOKKEN, Rune SOLBERG, Jostein AMLIEN, Rune ØDEGÅRD, Per-Ove HUSØY, Hans KOREN (Department of Statistical Analysis, Image Analysis and Pattern Recognition, Norwegian Computing Center)

Snow cover has a substantial impact on interaction processes between atmosphere and surface. Our goal is to improve methodologies for remote sensing of snow parameters and the use of snow parameters in hydrological models in order to achieve better water management practices related to snow. This should result in improved climatologic data collection, as well as better flood prediction, management of rivers and dams, and hydropower production planning. Present snow algorithms are developed using a number of satellite sensors, data formats, programming languages as well as being of variable quality. In view of new satellite sensors recently launched, we endeavour to improve the understanding of how satellite-measured microwaves and light interact with snow cover in mountainous areas, and thereby develop new and improved algorithms for snow parameter retrieval. A multisensor and multitemporal approach is applied in order to utilise the complementary sensor characteristics of optical and radar data. The methods are particular suitable for Envisat's Medium Resolution Imaging Spectrometer, Advanced Along Track Scanning Radiometer and Advance Synthetic Aperture Radar as well as the EOS AM-1's Moderate Resolution Imaging Spectroradiometer and Multi-angle Imaging SpectroRadiometer. We have developed a snow retrieval algorithm laboratory environment including both single and multisensor algorithms under the Environment for Visualizing Images. The main parameters are snow water equivalent, snow cover area, snow wetness, albedo and snow surface temperature. The presentation will focus on the applicability and the quality of the different selected methods and how they can be used to make seasonal and decadal snow trend analyses.

**JSH01/08A/C27-004 1030**

**USE OF THE TOPEX-POSEIDON ALTIMETER OVER LAND SURFACES AN APPLICATION TO ESTIMATE TERRESTRIAL SNOW DEPTH**

Fabrice PAPA, Benoit LEGRESY, Frederique REMY (legos/OMP)

The capability of Topex-Poseidon radar altimeter data for land surface studies at regional or global scale has been investigated. The analyzed data, available since mid-1992 consist of dual-frequency backscattering coefficients values (Ku and C band) estimated at the nadir pointing angle along the satellite tracks between 66 S and 66N. Over the snow covered areas of the Northern Hemisphere, backscatters particularly exhibit a strong seasonal variability and in that context, the use of T-P is investigated to recover snow depth evolution through winter. Snow pack thickness and extent, and the duration of the snow period are important parameters to characterize and to understand climate changes. Global average surface temperature has increased by approximately 0.5°C since the last half of the nineteenth century and climate models suggest that an anthropogenic global warming should manifest itself most strongly over the land in high latitudes. In that context, changes in snow cover characteristics take a special significance. Active and passive microwave measurements obtained from the Northern Great Plains of the United States are used to develop a snow pack radar backscatter model, based on the decreased of the mean value of the backscattering coefficient as the snow cover thickened through the winter. The model results are compared to daily time series of surface snow observations made by the U.S. National Weather Service, especially during the extreme winter 1996-97. First the beginning and the end of the winter snow pack are accurately determined with in the repeat cycle of the satellite. Then, the model results show that Ku band provides more accurate snow depth determinations than does C band. Comparing the snow depth determinations derived from the Topex-Poseidon nadir looking passive microwave radiometers with the oblique looking SSM/I passive microwave observations and surface observations shows that both instruments accurately portray the temporal characteristics of the snow depth time. While both retrievals consistently underestimate the actual snow depths, the Topex-Poseidon results are more accurate. We will also enlarge study area from local to global scale, presenting mean global backscatter images of the entire land surfaces in Ku, C band and the difference C-Ku, which exhibit a strong dependence with classical global vegetation and surface slopes maps. Statistics and major temporal signals over nine entire years are presented. First results of the use of T-P data over continents at global or regional scale look very promising and indicate the high capabilities of Topex-Poseidon radar altimeter data for

land surfaces monitoring and its complementarities for future synergy with passive microwave radiometer data over continents or other active sensors such as wind-scatterometer.

**JSH01/08A/C27-005 1050**

**INTERANNUAL VARIABILITY OF BRIGHTNESS TEMPERATURE OVER SNOW COVERED REGION**

Ramesh P. SINGH<sup>1</sup>, V.D. MISHRA<sup>2</sup>, P. MATHUR<sup>3</sup>, Netramani HARIJAN<sup>3</sup>, Sagnik DEY<sup>1</sup>, Nitin KATIYAR<sup>1</sup>, S.P. SINGH<sup>1</sup>, Y.P. SINGH<sup>1</sup> (<sup>1</sup>Professor, Department of Civil Engineering, Indian Institute of Technology, Kanpur, <sup>2</sup>SASE, Chandigarh, India, <sup>3</sup>Department of Civil Engineering, IIT Kanpur)

The snow cover in the northern part of India controls the climatic conditions of Indian continent and also snow is considered as one of the important natural resources. The northern part of Indian region where immense snow resources lie is often covered by clouds and in winter the sun is not seen. The knowledge of the snow cover and the thickness of the snow is very important in understanding the radiation budget and also useful in estimating the surface runoff in the Indo-gangetic plains, flood conditions and recharge of ground water. The visible remote sensing data has limitations due to the cloud cover and it also fails to provide any quantification estimate of snow cover. In high altitude and cloud cover regions, the microwave remote sensing data have been proved to be one of the important tools in quantification of snow cover and also studying the snow covered characteristics. We have carried out detailed analysis of SSM/I data over northern part of India covered with snow for various frequencies and polarizations for the year 1989-1998. The brightness temperature variations show cyclic nature with minimum value in winter season and maximum value in summer season. The brightness temperature shows a linear trend with small variations during 1989-1998. From the brightness temperature data emissivity of the snow covered region for seven locations have been extracted. At these seven locations, ground parameters have been routinely recorded by the scientists from SASE, Chandigarh. In the present paper, the characteristics of the brightness temperature, emissivity for the period 1989-1998 will be presented. The interannual variability of brightness temperature and emissivity in view of the nature of the snow cover. The use of SSM/I data in monitoring of snow avalanches will be presented.

**JSH01/08A/C27-006 1110**

**IMPROVING THE SNOW DEPTH ESTIMATION OF SMM/I IMAGES IN TIBET PLATEAU BY USING THE AVHRR DATA**

Mingguo MA, Xin LI (CAREERI,CAS)

Normally the SMM/I images are used to estimate the snow depth. But the snow depth is always over-estimated in Tibet Plateau of China by using the SMM/I images. This paper uses the AVHRR images to improve the snow depth estimation.

**JSH01-Posters Tuesday, July 8**

**THE REMOTE SENSING OF THE CRYOSPHERE (IAHS [ICSI, ICRS], IAMAS, IAPSO) Location: Site D**

**Tuesday, July 8 PM**  
Presiding Chair: R. Armstrong

**JSH01/08P/D-001 Poster 1400-039**

**MONITORING OF IMJA GLACIER LAKE IN THE EAST NEPAL USING THE SATELLITE IMAGE**

Hironori YABUKI (Frontier Observational Research System for Global Change)

The research of the glacial lake in the Nepal Himalaya region is carried out since 1990's (Ex. Yamada, 1998). The glacial lake has been stopped in the unstable moraine. The size of the lake expanded by the melting of the glacier ice in mountain region by the global warming. GLOF (Glacier Lake Over Flood) occurred by the moraine can not sustaining and collapsing quantity of water of glacial lake. However, unclear points such as glacial lake forming condition and process of the glacial lake extension have been left. In this study, the quantitative evaluation was carried out using satellite image in respect of the extension of glacial lake of Imja glacial lake in East Nepal of which a risk of a glacial lake collapse is high. The analysis was carried out on climate change and glacial lake formation using global temperature data. The analysis period was from 1962 to 2000, 10 scenes (1962, 1964, 1968, 1975, 1977, 1987,1991, 1993, 1995, 2000) in this period were analyzed. Used satellite image was used in 4 types. One is high-resoluble military affairs reconnaissance satellite CORONA image that the U.S.A. of which the resolution is 7.6m photographed was used in 60's. And LandsatMss of which the resolution was 83m was used in 70's. And SPOT of which the resolution was 10m was used in 80's and 90's. And Landsat ETM+ of which the resolution was 15m was used in 2000. Each image carried out the geometric correction using the map. Climatological data used Global Historical Climate network Ver.2 of National Climate Data Center (NCDC). The glacial lake was formed around 1960, and that the area expanded after it at the almost fixed speed clarified. Glacial lakes were four small ponds at the initial stage in 60's. Next, glacial lakes spread during around 70's to the downstream direction by the expansion of those ponds. Those ponds expanded, and it became one lake. The end in the glacial lake did the extension by 1991, and it was stabilized after it. The glacial lake expanded to the upstream direction from the middle of 70's. ICIMOD (2000) is said that many glacial lakes of Himalayas would rapidly develop in here 1960's. The Imja glacial lake is also similar. The global warming is being caused from before formation of glacial lake with the mean deviation of annual mean temperature of the Northern Hemisphere. The shrinkage of the glacier by the global warming occurred before formation of glacial lake. The glacial lake might be formed by the glacier shrinkage process.

**JSH01/08P/D-002 Poster 1400-040**

**GIS-BASED GLACIER INVENTORY OF CHINA**

Zong Li WU, Xin LI (Cold and Arid Regions Environmental and Engineering Research Institute)

The project of the Glacier Inventory of China initialized in 1979 was just accomplished in 2000. This inventory was compiled based on numerous LandSat TM images, aerial photographs, and topographic maps. More than 40 Chinese glaciologists made their great

efforts in this work. With the newest statistics from the inventory, there are total 46388 glaciers in China; the total area is 60050 km<sup>2</sup> and the ice volume is 5591 km<sup>3</sup>. The largest glacier locate in Tianshan Mts. (length: 63.5m, area: 392.84km<sup>2</sup>, code: 5Y673K1). The highest latitude of moraine is 6560 meter and the lowest latitude of moraine is 2240meter. Comprehensive statistics of glaciers in China are followed as:

Unit	Area(km <sup>2</sup> )	number	Ice Volume (km <sup>3</sup> )	source
Qilian Mts.	1931	2751	94	1981
Altai Mts.	293	416	16.5	1983
Tianshan Mts.	9196	8908	1011	1986,1987
Pamirs	2448	1147	232	2001
Karakorum Mts.	5925	3059	684.5	1989
Kunlun Mts.	8737	5947	848	1992,1994
Changjiang River	1895	1332	147	1994
Huanghe River	213	176	12	1981,1992
Tibetan Plateau	7814	5213	698	1988
Langcangjiang River	316	380	18	2001
Nujiang River	1730	2021	115	2001
Ganga River	18101	13005	1620	2002
Indus River	1451	2033	94	2002

We launched a new project to digitize the 11 volumes of published glacier data and all the distribution maps of glaciers in China. Large-scale topographic maps were also used as reference to reconstruct a more accurate geographic coordinate system of the inventory. We paid particularly attention to the data quality control. The properties of both the spatial and attribute data were carefully examined with a few operations by manual and computerized checks. We will discuss the comparison of the areas between the books and digital data in this paper. Since the digital inventory lays a baseline for the monitoring of glacier change, we are going to release the database on the Internet and with CD-ROMs. In additions, the second glacier inventory in Pumqu River drainages (Tibet) was carried out. New generation remote sensors such as ASTER and LandSat ETM+ were used to identify glacier change in many areas. Preliminary results showed that the change is significant.

**JSH01/08P/D-003** Poster **1400-041**

#### INVENTORY OF GLACIAL LAKES AND IDENTIFICATION OF GLACIAL LAKE OUTBURST FLOODS IN THE PUMQU BASIN, TIBET

Tao CHE, Xin LI, Rui JIN, Zong Li WU (Remote Sensing and GIS Lab, Cold and Arid Regions Environmental and Engineering Research Institut, CAS)

There are 999 glaciers in the Pumqu basin in total, covering a large area of 1,556 square kilometers. However, these glaciers are retreating in the face of accelerating global warming. They are particularly vulnerable to climate change, and the resultant long-term loss of natural fresh water storage will have as yet uncalculated effects on communities downstream. More immediately, as glaciers retreat, glacial lakes form behind some of the now exposed terminal moraines. Rapid accumulation of water in glacial lakes, particularly in those adjacent to receding glaciers, can lead to a sudden breaching of the unstable dam behind which they have formed. The resultant discharges of huge amounts of water and debris, namely a glacial lake outburst flood (GLOF), often have catastrophic effects downstream. These GLOFs have resulted in many deaths, as well as the destruction of houses, bridges, fields, forests and roads. The lakes at risk, however, are situated in remote and inaccessible areas. The study's major objective was to identify areas where GLOF events had occurred and lakes that could pose a potential threat of a GLOF in the near future. First, we digitalized glaciers and glacial lakes based on the topographic maps published three decades ago, and remote sensing images (ASTER) acquired in 2001/2002. Secondly, the inventory of glaciers and glacial lakes was obtained according to the spatial and attribution data. Thirdly, we analyzed the change of glacial lakes in the two periods. Finally, on the basis of actively retreating glaciers and other criteria, the potentially dangerous glacial lakes were identified using the spatial and attribute database complemented by multi-temporal remote-sensing data sets. The final results have shown that there are 225 glacial lakes with a total area of 1,062 square kilometers, and there are 24 glacial lakes were identified as the potentially dangerous lakes in Pumqu basin. However, due to the influence of the acquisition seasons of remote sensing images, the field survey is necessary to more soundly identify the potentially dangerous glacial lakes.

**JSH01/08P/D-004** Poster **1400-042**

#### SEQUENTIAL ESTIMATION OF MESO-SCALE SEA ICE MOTION FROM SATELLITE IMAGES OF MULTIPLE RESOLUTIONS

Tsuyoshi WAKAMATSU<sup>1</sup>, Motoyoshi IKEDA<sup>2</sup> (<sup>1</sup>Institute of Ocean Sciences, DFO, Canada, <sup>2</sup>Graduate School of Environmental Earth Science, Hokkaido University, JAPAN)

We will propose new approach to extract meso-scale sea-ice motion from satellite images with multiple spatial resolutions. In order to merge data from different sources, we construct simple sea-ice model consist of Lagrangian equations, which forecast locations of sea-ice particles, and interpolation kernel, which simulate the gridded value of signal intensity corresponding to observed data. The estimation system is designed to correct forecasted ice particle positions using sea-ice images as input data based on optimal interpolation technique. Then sea-ice motion is reconstructed from the estimated ice particle positions. Preliminary result from simple numerical experiments shows that merging several data with different resolution helps to correct ice positions when error distributions of each data and forecasted positions are given.

**JSH01/08P/D-005** Poster **1400-043**

#### SEA ICE CLASSIFICATION USING QUIKSCAT SEAWINDS SCATTEROMETER DATA

Rasmus T. TONBOE<sup>1</sup>, Joerg HAARPAINTNER<sup>2</sup> (<sup>1</sup>Danish Meteorological Institute, <sup>2</sup>Polar Science Team, National Ice Center)

The Ocean and Sea Ice Satellite Application Facility project (O&SI SAF) from the European Organisation for the Exploitation of Meteorological Satellites (EUMETSAT) is now entering the operational phase. A data fusion sea ice product (O&SI SAF ice product) is issued daily. The supervised Bayesian classification method is used to combine microwave radiometer data, visual/infrared and microwave scatterometer data. The derived sea ice parameters are: ice cover concentration, ice type and ice edge. The aim of this study is to establish statistical values for selected ice classes in order to implement SeaWinds scatterometer data in the operational and automated O&SI SAF sea ice product. These ice class signatures are produced by co-location of two years (2000-2002) SeaWinds data and ice charts around Greenland from the Danish Meteorological Institute (DMI). Our results show that SeaWinds data are useful for sea ice classification during the cold season (September-May). Four SeaWinds parameters are used in the classification: 1) horizontally and 2) vertically polarised backscatter, 3) the polarisation ratio, and 4) the daily standard deviation of the backscatter. The backscatter separation between first year ice and multi year ice is most effective for high ice concentrations (>70%), but SeaWinds ice class parameters are also separated for intermediate ice concentrations (30-70%). Ice types can not be separated for

low ice concentrations (<30%) and these classes also overlap ocean backscatter parameters at high wind speeds (>15m/s). In summer (June-August) it is impossible to discriminate ice types because of ice surface melt. However separation between ice and water is still possible. Initial results will be presented at the conference.

**JSH01/08P/D-006** Poster **1400-044**

#### ASSESSMENT OF AMSR-E SEA ICE PRODUCTS USING IN-SITU OBSERVATIONS AND MODELING

James Andrew MASLANIK<sup>1</sup>, Julienne STROEVE<sup>1</sup>, Matthew STURM<sup>2</sup>, Thorsten MARKUS<sup>3</sup>, John HEINRICH<sup>4</sup>, Don CAVALIERI<sup>1</sup> (<sup>1</sup>University of Colorado, <sup>2</sup>USA CRREL, <sup>3</sup>NASA GSFC, <sup>4</sup>Fort Hays State University)

As part of the validation effort for AMSR-E onboard the EOS Aqua platform, in-situ measurements of a variety of sea ice and snow cover parameters were collected on shore-fast ice areas near Barrow, Alaska, USA in March 2003. These measurements were carried out in conjunction with NASA P-3 aircraft flights over the in-situ locations as well as P-3 flights over portions of the Beaufort and Chukchi sea ice pack. Coincident atmospheric data were obtained using flights of Aerosonde unpiloted aerial vehicles. The in-situ measurements and P-3 observations are used to assess the performance of AMSR-E sea ice product algorithms through direct comparisons of data sets and via forward modeling of microwave radiances using MWMOD and MEMLS. Results to be presented will highlight the performance of the AMSR snow depth and ice temperature algorithms, and will address the effects of snow properties on AMSR-E retrievals of snow and sea ice information.

**JSH01/08P/D-007** Poster **1400-045**

#### SATELLITE INVESTIGATIONS OF FAST ICE BREAKUP IN EAST GREENLAND FJORDS

Evelyn K. DOWDESWELL (The Scott Polar Research Institute, University of Cambridge)

Landsat satellite imagery is used to provide a record of the breakup of fast ice in several major fjord systems in East Greenland (68-74 deg N). The areas considered are Kangerdlugssuaq Fjord, Scoresby Sund, Kong Oscars Fjord and Kejser Franz Josephs Fjord. Thematic Mapper and Multispectral Scanner QuickLook images from 1979 indicate that the breakup of fast ice generally occurs by a regular pattern of thinning and polynya development prior to the breakup and disappearance of landfast ice. Interannual variability in timing of breakup is compared with climate records for these years. The spatial and temporal pattern of fast-ice breakup places constraints on iceberg calving and the potential sediment flux into these fjord systems.

**JSH01/08P/D-008** Poster **1400-046**

#### SATELLITE OBSERVATIONS OF SEA ICE TRANSPORT IN THE SEA OF OKHOTSK

Hiroyuki ENOMOTO<sup>1</sup>, Kazutaka TATEYAMA<sup>2</sup>, Takashi KUMANO<sup>3</sup> (<sup>1</sup>Department of Civil Engineering, Kitami Institute of Technology / FORSGC, <sup>2</sup>Institute of Low Temperature Science, Hokkaido University, <sup>3</sup>Kitami Institute of Technology)

The dominant pattern of sea ice drift was analyzed in the Sea of Okhotsk using DMSPP SSM/I data. Dominant ice drift along the Sakhalin Island was apparent in the satellite derived ice drift map in the Sea of Okhotsk. The flow pattern was indicated by the trace lines adopted on the vector field of ice drift. The flow pattern shows a dominant stream along the east coast of Sakhalin. Many flow path of sea ice were converged in the coastal zone of Sakhalin. Recurring polynya area in the northeast of Sakhalin was indicated as absence of steady flow lines. In the southern part of Okhotsk Sea, ice flow was highly variable due to mesoscale eddies. Ice group of almost same path can follow different paths due to affecting different eddies. Seasonal and local variations of ice drift were analyzed along the Sakhalin and Hokkaido. The alternative patterns of convergence and divergence along the ice drift zone affect ice deformation and thickness change. There are convergence zone along the Sakhalin Island. The convergence in this zone can cause significant compacting, rafting and deformation of sea ice. Interannual variations of ice mass transport in this stream were estimated by applying an algorithm of ice thickness estimation by satellite. Large amount of freshwater and latent heat can be transported as a form of sea ice by the dominant ice stream. Sea ice coverage decreased between 1989 to 1996. The ice area was minimum in 1996 during the last 20 years. The mean ice thickness in the ice stream zone was also estimated to be minimum, and then recovered in the recent years. However, the ice transport was not increased since the ice drift speed was remained in the lower range. For the evaluating sea ice change concerning energy and mass, combinations of ice coverage, thickness and drift are required. This study introduced available approach of estimation and recent fluctuation of sea ice in the Okhotsk Sea.

**JSH01/08P/D-009** Poster **1400-047**

#### REMOTE SENSING OF SNOW GRAIN SIZE AND SNOW IMPURITY CONCENTRATIONS AND THEIR IMPACT ON THE RADIATION BUDGET

Teruo AOKI<sup>1</sup>, Masahiro HORI<sup>2</sup>, Knut STAMNES<sup>3</sup>, Hiroki MOTOYOSHI<sup>4</sup>, Tomonori TANIKAWA<sup>5</sup>, Akihiro HACHIKUBO<sup>6</sup> (<sup>1</sup>Meteorological Research Institute, <sup>2</sup>National Space Development Agency of Japan, <sup>3</sup>Stevens Institute of Technology, <sup>4</sup>Space Service Inc., <sup>5</sup>University of Tsukuba, <sup>6</sup>Kitami Institute of Technology)

Snow grain size and concentration of snow impurities are vitally important snow physical parameters required to determine the spectral snow albedo. According to radiative transfer simulations of spectral snow albedo, it depends sensitively on the concentration of snow impurities in the visible, and on snow grain size in the near infrared. The remote sensing of these snow physical parameter will be operationally made with ADEOS-II/GLI data since 2003 by National Space Development Agency of Japan. We conducted preliminary performance tests of the algorithm using global data set of TERRA/MODIS in 2001-2002. The algorithm worked well except for melting areas in sea ice. We also made a validation experiment in northern Hokkaido, Japan in February, 2002. The snow physical parameters retrieved from TERRA/MODIS data agreed with the ground truth data within operational uncertainties. In addition, we have made continuous radiation budget observations and semi-continuous measurements of snow pit work on the snowfields in northern Japan. The effects of snow physical parameters on the visible and the near infrared albedos are calculated using a radiative transfer model for the atmosphere-snow system and compared with the measured ones. The measured broadband albedos were close to the theoretically calculated ones as functions of these snow physical parameters. These results suggest the possibility to develop a physically based snow albedo scheme for describing land-surface processes in climate models. Furthermore, the snow albedo scheme could be validated with the satellite remote sensing data mentioned above.

**JSH01/08P/D-010** Poster **1400-048****SNOW ACCUMULATION STUDIES IN ANTARCTICA WITH GROUND PENETRATING RADAR USING 50, 100 AND 800 MHZ ANTENNA FREQUENCIES**

Anna Katarina SINISALO<sup>1</sup>, Aslak GRINSTED<sup>1</sup>, John MOORE<sup>1</sup>, Eija Kärkäs<sup>2</sup>, Rickard PETTERSON<sup>3</sup> (<sup>1</sup>Arctic Centre, University of Lapland, <sup>2</sup>Division of Geophysics, Department of Physical Sciences, University of Helsinki, Finland, <sup>3</sup>Department of Physical Geography, Stockholm University)

Snow radar profiles were measured in Dronning Maud Land in the vicinity of the Finnish research station Aboa during the austral summer 1999-2000. The aim was to study the annual layering in the upper 50 meters of the snow pack and to compare the results obtained by three radar antenna frequencies. The radar profiles measured by three antenna frequencies (50, 100, and 800 MHz) are compared with each other, and some internal layers shown to be visible with different antennas. Sparse accumulation rate data from stake measurements and snow pits are compared with layer depths and exhibits a great deal of scatter due to the larger inter-annual variability in accumulation patterns. Using the radar layers as isochrones together with a model of depth-density-radar wave velocity allows the individual accumulation data to be integrated and a better estimate of accumulation patterns obtained. Using the radar layering seems to be a much better method of estimating accumulation rate than short series of stake measurements in this region, even in the absence of deep ice cores to directly date the radar layering.

**JSH01/08P/D-011** Poster **1400-049****A PROCEDURE FOR CLASSIFYING DRY SNOW, WET SNOW AND FROZEN SOIL BY USING MICROWAVE REMOTE SENSING**

Xin LI<sup>1</sup>, Tao CHE<sup>1</sup>, Richard L. ARMSTRONG<sup>2</sup>, Lizong WU<sup>1</sup> (<sup>1</sup>Cold and Arid Regions Environmental and Engineering Research Institute, CAS, <sup>2</sup>National Snow and Ice Data Center, University of Colorado)

The purpose of land classification by using microwave remote sensing is not only to discriminate different landcover types such as snow, soil, and vegetation but also to identify surface status such as melting or dry snow, frozen or unfrozen soil, precipitation or cloud liquid water. This kind of classification, with the help of other ancillary information as DEM, can be used to improve the accuracy of retrieval models. We developed a decision-tree classification procedure for classifying a wide range of surface and atmospheric features by using the (Defense Meteorological Satellite Program) DMSP Special Sensor Microwave/Imager (SSM/I). Main foci were put on those features have similar scattering/absorbing properties since it significantly affects the quantitative retrieval of geophysical parameters. For example, snow water equivalent is overestimated in some areas because snow and frozen soil are not discriminated. The first step of the procedure is to classify the absorbing and scattering materials using the combination of 85 GHz and 22 GHz vertical polarization channels. Then, using some rules between 22 GHz and 85 GHz, precipitation can be discriminated from other scattering materials. Sand is identified when  $Tv19 Th 19 > 20$ . For dry snow and frozen soil, their scattering properties are very similar. We use the equation given by Robinson and other a priori information to classify them. After the classification, different models can be used to retrieve different geophysical parameters according to the different surface features.

**JSH01/08P/D-012** Poster **1400-050****SPECTRAL CHARACTERISTIC-BASED VEGETATION AND SNOW INDICES ON VARIOUS SURFACES IN THE AIRBORNE MULTI-SPECTRAL SCANNER (AMSS) TWO-ALTITUDE OBSERVATION IN 2001**

Ken MOTOYA (Frontier Reserch System for Global Change)

Spectral characteristics and spectrum-based snow and vegetation indices from one visible and two near-infrared bands, on various surface categories were evaluated, using an Airborne Multi-Spectrum Scanner (AMSS) in 2001. The AMSS was improved in sensitivities of near-infrared channels compared with those in 1998. Interrelations between the indices (or visible-to-near-infrared albedo) and vegetation density were also discussed with field observations of forest density in a high spatial resolution. In addition, differences of atmospheric effects on both the AMSS data and the snow and vegetation indices were estimated with observations at two altitudes and compared with the result of a radiative transfer model. From observation at the higher altitude (13200ft), radiances at bands less than 490 nm in wavelength were strongly affected by the Rayleigh scattering. However, the visible (625 nm) and short (865 nm) near-infrared channels of the snow and vegetation indices, were not affected so much by the atmospheric effects and long (1650nm) near-infrared also has only a small effect of the water vapor absorption. The indices were little affected by the atmosphere in general. Moreover, viewing-angle dependencies of detectors on near-ultraviolet (380 nm), visible (625nm), and short and long (865 nm and 1650 nm) near-infrared channels were investigated. As a result, fore-scattering was representative on snow surface in its viewing-angle dependency and forest has a Lambert-like dependency. The dependency at wavelengths of more than 1000nm was approximately half of that in the AMSS of 1998 because the IFOV of those channels was expanded from 2.5 mrad to 5 mrad.

**JSH01/08P/D-013** Poster **1400-051****MICROWAVE AND MICROMETEOROLOGICAL OBSERVATIONS OF WINTER SNOW IN ROCKY MOUNTAIN**

Haoyu GU, A. W. ENGLAND, R. DEROO, H. PHAM, D. BOPRIE (Department of Atmospheric, Oceanic and Space Sciences, University of Michigan)

Snow plays an important role on earth's hydrology cycle, and significantly interacts with global weather and climate. However, snow melt processes and their interaction with soil, vegetation and atmosphere are still not well understood. Microwave radiometry is a technology which promises to enable space-based remote sensing of snow pack wetness. To understand the radiometric signature of a wet snow pack, we are participating in the NASA Cold Land Processes Field Experiment (CLPX) in the Rocky Mountains of Colorado during winter and spring of 2003. We are using our Truck Mounted Microwave Radiometer System (TMRS3) and our Micrometeorological Station (MMS). TMRS3 includes dual-polarized 1.4, 6.7, 19 and 37 GHz radiometers. The MMS measures air temperature, relative humidity, soil heat flux, two soil temperature and moisture profiles and a snow temperature profile. These MMS data complement the meteorological data collected as part of CLPX. This presentation will cover both radiometric and meteorological observations made during the experiment. These data will be used to test and improve a Soil Vegetation Atmosphere Transfer (SVAT)/Radiobrightness Model coupled with SNThERM, a one-dimensional snow energy budget model. The coupling of the two models is underway. The observational data will be archived in National Snow and Ice Data Center for access by other researchers.

**JWH01** **Wednesday, July 9 - Thursday, July 10****SNOW PROCESSES: REPRESENTATION IN ATMOSPHERIC AND HYDROLOGICAL MODELS (IAHS/ICSI, IAMAS)**

Location: Site C, Room 30

**Wednesday, July 9 AM**

Presiding Chair: T. Ohta

**JWH01/09A/C30-001** **0900****EXPERIENCE OF APPLICATION OF PHYSICALLY-BASED MODELS OF SNOWMELT RUNOFF GENERATION AND ASSIGNING OF MODEL PARAMETERS**

Lev S. KUCHMENT (Water Problems Institute, Russian Academy of Sciences)

Experience of application of physically based models of snowmelt runoff generation for different physiographic conditions is analyzed. Case studies have carried out for three river basins in the central part of the European Russia and for two basins in the Far East part of Russia. The models are based on the finite-element schematization of river basins and include a detailed description of snow processes, soil freezing and thawing, infiltration into the frozen and thawed soil, overland and subsurface flow, water movement in the river channel system. It is assumed that the snow water equivalent, the saturated hydraulic conductivity and the depth of frozen soil have subgrid stochastic variability and the ways of taking into account this variability have suggested. The structure of the models is chosen on the basis of results of sensitivity analysis and analysis of runoff generation mechanisms in given river basins. The part of parameters are the measured basin characteristics, several parameters are determined on the basis of empirical dependencies including the measured characteristics, and the rest of parameters are calibrated against runoff or other water balance component measurements. Comparisons of measured and calibrated model parameters as well as the empirical formulas obtained for determination of parameters for different river basins are given. Possibilities of using different empirical dependencies and transferability of these dependences and model parameters between basins are considered. Numerical experiments have been carried out to test ability to apply the suggested physically based models of snowmelt runoff generation for the poorly gauged river basins. It has been showed that only 2-4 of most important parameters should be calibrated using comparatively short series of runoff measurements, whereas the values of the rest 10- 12 parameters can be regionalized.

**JWH01/09A/C30-002** **0920****WATER AND ENERGY TRANSFER IN SNOW AND FREEZING SOIL IN EASTERN HOKKAIDO, JAPAN**

Tomoyoshi HIROTA, Yukiyoishi IWATA (National Agricultural Research Center for Hokkaido Region)

Eastern Hokkaido is one of the largest agricultural regions in Japan. Low air temperature (annual minimum air temperature is  $-30^{\circ}\text{C}$ ) and relatively thin snow covers on the ground cause the topsoil to freeze over the winter in this region. But recently, trends in maximum frozen soil depth in a year tend to decrease due to timing of snow covers earlier. Despite the importance of frozen soil and snow for agriculture, very few comprehensive meteorological and hydrological studies were conducted in this region until recent years. The study objectives are to 1) conduct a detailed and long-term field study under snow and soil freezing condition, 2) identify key parameters affecting the water and energy transfer at the ground surface and in the soil, and 3) develop predictive tools for assessing the impacts of farming practices and climate change on the frozen soil. The field study has been conducted in agricultural experimental field located Memuro, Tokachi, Hokkaido since October 2001. We have observed atmospheric factors (temperature, humidity, wind speed, precipitation, short and long wave radiation (upward and downward)), soils factors (vertical temperature profiles, vertical water content profiles by TDRs, water potentials beneath frozen layer by tensiometers, surface soil heat flux, frozen depth by frost tube filled with 0.03% methylene blue solution), snow factors (snow depth, snow water equivalent (SWE) by pressure sensor measurement, snow temperature vertical profiles) and a weighing lysimeter for measuring evaporation and snowmelt. Almost sensors have measured automatically and continuously every 10 to 60 minutes. In 2001-2002 years winter observation period, maximum frozen soil depth was 20 cm however maximum snow depth was relatively thick; 80 cm, maximum SWE was 225 mm. Seasonal variations of the soil water status was characterized into four stages; 1) beginning of winter (December); Due to thin snow layer (less than 20 cm), frozen soil depth was increased, surface soil liquid water content was decreased rapidly, direction of soil water flux was upward from deeper soil layer to surface layer, 2) mid of winter (January to February). After thick snow layer covered (over 40 cm depth), developing of frozen soil depth stopped, soil liquid water content was almost constant, direction of soil water flux was changed from upward to downward, 3) beginning of snow melt season (from begging to mid of March), occurring following phenomena simultaneously; starting snowmelt, snow temperature raised rapidly near  $0^{\circ}\text{C}$ , frozen soil was partially thawed. 4) End of snowmelt season (end of March), snowmelt water moved into subsoil by gravitational flow though frozen soil depth was still 10 cm. We also discuss new snow and soil temperature model developed by Hirota et al., 2002 in JGR called the extended force-restore method using detailed our field datasets.

**JWH01/09A/C30-003** **0940****A MODEL OF ANNUAL HYDROLOGICAL CYCLE FOR ARCTIC TUNDRA**

Hiroyuki HIRASHIMA<sup>1</sup>, Tetsuo OHATA<sup>1</sup>, Yuji KODAMA<sup>1</sup>, Hironori YABUKI<sup>2</sup> (<sup>1</sup>Institute of Low Temperature Science, Hokkaido University, Kita 19, Nishi 8, Kita-ku, Sapporo 060-0819, Japan., <sup>2</sup>Frontier Observational Research System for Global Change, Tokyo 105-0013, Japan.)

In arctic region, it is remarked that rising of temperature by the effect of global warming is most serious. The influence of global warming to annual hydrological condition can be usually estimated by one-dimensional model. However, in arctic tundra region, snow is distributed non-uniformly due to low vegetation and strong wind. Thus, discussion on hydrological condition distribution must be considered for simulation to such a place. Distributed hydrological model for warm period and snow distribution model for cold period have been developed in recent years. In the present study, distributed annual hydrological cycle model was developed to simulate thermal condition and hydrological term for such a non-uniform snow distributed region. This model consists of snow and subsurface multi-layer model, snow distribution model and distributed hydrological model and simulates energy and hydrological processes in cold and warm period. The model is spatially distributed model and simulates using meteorological and topographical input data. In cold period, this model simulates snow redistribution by calculating blowing and drifting snow amount. Snow depth and profiles of snow temperature, density and water content are simulated simultaneously

using one dimensional snow multi-layer model for each grid. In warm period, this model estimates snowmelt amount by energy balance method. The snowmelt water contributes to the hydrological process (e.g. soil moisture, evaporation and river runoff) with liquid precipitation. Vertical water movement and horizontal water movement by subsurface flow and surface flow are calculated by multi-layer diffusion model, Darcy's law and Manning's equation, respectively. Permafrost is assumed to be impermeable layer. Since hydrological process in permafrost region depends on thermal condition, ground temperature profile and thaw depth was calculated simultaneously. In this study, numerical simulation with this hydrological model was carried out in Siberia tundra region, Tiksi. The simulated result was validated using observational data obtained under the GAME-Siberia project. Simulated soil temperature was compared with observed one obtained at the meteorological station and agreed well. The snow distribution observed by helicopter, suggested that the snowdrift was mainly formed at the hollow region such as river, and the model reproduced this characteristic. However, simulated river runoff was too much in melt period and too little in the latter half of warm period than observed river runoff. This result suggests the infiltration of melt water to frozen soil is important process here. The simulation results of hydrological cycle model considering this process are going to be discussed as well.

**JWH01/09A/C30-004****1000****A COMPLETE MODEL FOR SNOW DRIFT PROCESSES IN STEEP ALPINE TERRAIN**

Michael LEHNING, Judith DOORSCHOT, Norbert RADERSCHALL (Swiss Federal Institute for Snow and Avalanche Research SLF)

Since blowing and drifting snow is a major factor influencing avalanche danger and the local micro climate, a high resolution, objective and quantitative assessment and forecast of snow transport by wind is of great practical value. Wind transport of snow is governed by three components: the erodability of the snow pack, the current snowfall and the wind field. A snowdrift model has been developed that combines an atmospheric model analysis of the high resolution wind field over steep topography, a novel formulation for snow drift and a snow cover model. For modeling snow drift, the transport modes saltation and suspension are distinguished. The flow field over steep topography is modeled using the meteorological model system ARPS (Advanced Regional Prediction System). It is shown that important features of the wind field such as speed-up over the crest and flow separation in the lee can be reproduced by the flow model using a high resolution computational mesh. Also discussed are the turbulence fields, which are important for the simulation of the drift modes saltation and suspension. A novel model for snow saltation is presented, which is suitable for steep terrain. Based on a computationally efficient equilibrium approach, the description of saltation uses explicit trajectory calculations to estimate mass fluxes on steep slopes. The snow cover is represented by the model SNOWPACK. SNOWPACK is a detailed model of the snow cover development and simulates the erodability of deposited snow as well as metamorphic changes, heat and mass fluxes and phase changes. Emphasis of the presentation is further on the coupling between the snow cover, the drifting and blowing snow and the wind field. For a correct description of the erosion and deposition pattern, the formulation of the coupling functions is of major importance. The full model system is applied to predict snow loading in avalanche slopes. Results for the avalanche winter 1998 / 1999 are presented. The evaluation of the results show that major characteristics of snow redistribution are captured by the model. In steep terrain, saltation appears to contribute less to snow redistribution than previously assumed. Preferential deposition during snow fall events appears to be a major factor influencing snow distribution in small scale steep terrain. Preferential deposition is the process that during snow fall events the snow is already inhomogeneously distributed, even when the wind velocities are too small for saltation and thus erosion of deposited snow to happen. This process is not represented in other snow drift models. Remaining uncertainties of the model system concern the formulation of suspension and the accuracy of the flow simulation. Suggestions for improvements are made. Finally, the importance of an adequate representation of snow processes for improvements in meteorological prediction models and climate models is pointed out.

**JWH01/09A/C30-005****1020****MODELLED AND OBSERVED REDISTRIBUTION OF SNOW ACROSS AN ANTARCTIC ICE RISE**

John C. KING<sup>1</sup>, Phil S. ANDERSON<sup>1</sup>, David G. VAUGHAN<sup>1</sup>, Graham W. MANN<sup>2</sup>, Stephen D. MOBBS<sup>3</sup> (<sup>1</sup>British Antarctic Survey, <sup>2</sup>School of the Environment, University of Leeds)

The ice sheets of Antarctica provide ideal, simple environments for testing models of the redistribution of snow by the wind. Between January 2000 and January 2002 we carried out a detailed campaign of measurements along a transect of Lyddan Ice Rise (LIR), Antarctica (74°S, 22°W). LIR is an approximately two-dimensional ridge about 15 km wide which rises 125 m above the surrounding ice shelves. The local prevailing winds blow approximately perpendicular to the axis of the ridge. Snow accumulation variability along the transect was determined from a ground penetrating radar survey and snow stake measurements. The survey revealed variations in accumulation of up to 50% of the area mean, both on the scale of the LIR itself and on scales of a few hundred metres. The broad-scale pattern of redistribution is consistent with estimates of snow transport made using wind measurements from 3 automatic weather stations installed along the transect line. In order to test whether the small-scale variability in accumulation was also due to redistribution, the surface wind field over the LIR was modelled using a simple airflow model. The model was forced using radiosonde observations from nearby Halley station and the computed surface stress field was used to calculate snow transport using a simple parametrisation. The modelled snow redistribution matches the observed spatial variations in accumulation extremely well. This confirms that the observed spatial variability in accumulation is driven by variations in snow transport which are, in turn, caused by rather small topographic variations on a variety of scales.

Presiding Chair: E. Martin

**JWH01/09A/C30-006****1110****DISTRIBUTED SNOW ACCUMULATION AND MELT MODELING - ROLE OF SNOW DRIFT, VALIDATION AND UNCERTAINTY OF THE SIMULATIONS**

Juraj PARAJKA, Ladislav HOLKO, Zdeno KOSTKA (Institute of Hydrology, Slovak Academy of Sciences)

Distributed snow modelling in seasonally snow covered areas is potentially very important for proper assessment of the amount of water contained in snow and its release into river network during the snowmelt. However, many uncertainties may appear in practical applications of distributed snow models. How to obtain true distributed input data and model parameters? Can the spatial predictions be validated and how? What is the value of a distributed snow model compared to the lumped one? We have tested modified distributed version of the energy based Utah Snow Accumulation and Melt Model (UEB-EHZ) in small mountain catchment of the Jalovecky creek, Slovakia (area 22.2 km<sup>2</sup>, mean elevation 1500 m a.s.l.). Special attention was paid to distributed parameterization of snow drift. Values of snow drift based on snow survey measurements performed in winters 1989-2001 were

combined with theoretical distribution of wind speed and topographic features of the catchment. Produced snow drift map was used to simulate the spatial distribution of snow water equivalent in two winters - the snow rich winter of 2000 and the snow poor winter of 2001. The results were validated against snow surveys and ground photographs of the catchment. Synchronisation between modelled snowmelt and measured catchment runoff and comparison of snowpack development in the forest and at open areas served as additional qualitative validation measures of the model. The simulations confirmed that there is essential difference in model parameters for forested and open areas. Consideration of spatially distributed drift factor resulted in prolonged snowmelt. However, there is high uncertainty in the estimation of snow drift. While spatial patterns of snow erosion and deposition areas can be easily estimated from DEM and other analyses, the concrete values of drift in mountains can only be estimated from field measurements.

**JWH01/09A/C30-007****1130****MODELING REGIONAL AND GLOBAL SCALE SUBGRID HETEROGENEOUS SNOW COVER**

Glen E. LISTON (Department of Atmospheric Science, Colorado State University)

To improve the depiction of autumn through spring land-atmosphere interactions and feedbacks within regional and global weather, climate, and hydrologic models, a Subgrid SNOW Distribution (SSNOWD) submodel that explicitly includes subgrid snow-depth and snow-cover variability has been developed. From both atmospheric and hydrologic perspectives, the subgrid snow-depth distribution is an important quantity to account for within large-scale models. In the natural system, these subgrid snow-depth distributions are largely responsible for the mosaic of snow-covered and snow-free areas that develop as the snow melts, and the impacts of these fractional areas must be quantified in order to realistically simulate grid-averaged surface fluxes. SSNOWD's formulation incorporates observational studies showing that snow distributions can be described by a log-normal distribution and the snow-depth coefficient of variation. Using an understanding of the physical processes that lead to these observed snow-depth variations, a global distribution of nine subgrid snow-depth-variability categories was developed, and coefficient-of-variation values were assigned to each category based on published measurements. In addition, SSNOWD adopts the physically realistic approach of performing separate surface energy balance calculations over the snow-covered and snow-free portions of each model grid cell and weighting the resulting fluxes according to these fractional areas. Using a regional atmospheric model (ClimRAMS) over a North American domain, SSNOWD was compared with a snow-cover formulation similar to those currently used in most general circulation models. The simulations indicated that accounting for snow-distribution variability has a significant impact on snow-cover evolution and associated energy and moisture fluxes.

**JWH01/09A/C30-008****1150****FEATURES OF SPATIAL DISTRIBUTION DYNAMICS OF SNOW COVER DURING SNOW MELTING PERIOD IN SUBARCTIC TUNDRA OF EASTERN SIBERIA**

Georgiadi GEORGIADI, Vladislav MALYSHEV, Alexander ZOLOTKRYLIN, Nikolai OZEROV (Institute of Geography, RAS)

Low mountains (up to 300 m above sea-level) and piedmont plains with big enough number of lakes are the main features of subarctic tundra relief of Eastern Siberia in the vicinity of Tiksi polygon of GAME/Siberia program. Mentioned features as well as strong wind during winter period redistribute of snow and as a result non-homogeneous snow cover is formed. Main part of territory is characterized by relatively thin snow depth. Much snow is accumulated in river valleys, depressions etc. These features of snow spatial distribution determine character of snow clearing of territory. Snow disappears during several days of active snow melting in main part of territory while snow is melting rather long time in the places of accumulation of much snow. In 1999-2001 a complex remote sounding of the Suonannakh river basin (in vicinity of Tiksi) was fulfilled. It was aimed to investigate of spatial-temporal distribution features of areas covered by snow, their spectral brightness, surface temperature, albedo before and during snow melting period. Remote sensing measurements were conducted by a complex of equipment from board MI-8 helicopter from a height of 400-2000 m along special routes. The equipment complex included: spectrometer recording reflecting characteristics of underlying surface in absolute values of spectral density of energy brightness within 0.4-0.85 micrometers of electromagnetic wave band with 450 spectral channels; digital video camera working in RGB channels; radiometer working over 8-14 micrometers for recording of surface temperature as well as piranometer. Results of analysis of spatial distribution dynamics of snow cover during snow melting period based on remote sensing data are presented.

**JWH01/09A/C30-009****1210****SNOWMIP, AN INTERCOMPARISON OF SNOW MODELS: COMPARISON OF SIMULATED AND OBSERVED INTERNAL STATE**

Charles G. FIERZ<sup>1</sup>, Pierre ETCHEVERS<sup>2</sup>, Ross BROWN<sup>3</sup>, Michael LEHNING<sup>4</sup>, Yves LEJEUNE<sup>5</sup>, A. BOONE<sup>6</sup>, Y. GUSEV<sup>7</sup>, Rachel JORDAN<sup>8</sup>, E. KOWALCZYK<sup>9</sup>, R.D. PYLES<sup>10</sup>, T. YAMAZAKI<sup>11</sup> (<sup>1</sup>Swiss Federal Institute for Snow and Avalanche Research SLE/WSL, <sup>2</sup>Centre d'Etudes de la Neige, CNRM Météo-France, Grenoble, France, <sup>3</sup>Canadian Meteorological Service, Dorval, Qc, Canada, <sup>4</sup>Météo-France, Toulouse, France, <sup>5</sup>Laboratory of Soil Water Physics, Institute of Water Problems, Russian Academy of Sciences, Moscow, Russia, <sup>6</sup>CRREL, Cold Regions Research and Engineering Laboratory, Hanover, U.S.A., <sup>7</sup>CSIRO Atmospheric Research, Aspendale, Australia, <sup>8</sup>Cooperative Institute for Research in the Environmental Sciences, Boulder, U.S.A., <sup>9</sup>Frontier Observational Research System for Global Change, Tohoku University, Sendai, Japan)

Snow-cover models are now widely used for various applications such as hydrology, snow ecology, global circulation models, snow monitoring, snow physics research and avalanche forecasting. The degree of complexity of these models is highly variable, ranging from simple index methods to multi-layer models simulating the snow-cover stratigraphy and texture. The main objective of the project SnowMIP (Snow Model Intercomparison Project) is to identify key processes for each application. Four sites have been selected as representative of typical snowpacks and because of the availability of both input and verification data. 26 models have participated in SnowMIP by simulating the snow-cover with the observed meteorological parameters. However, comparison should not only deal with bulk energy and mass budgets but also with the internal state of the snow-cover. Indeed, both the structure (layering) and the microstructure (shape and size of both grains and bonds) of the snow-cover are relevant to many important processes and properties of the snow-cover such as albedo, liquid water content or microwave emissivity. With varying degree of complexity, 8 of the 26 models participating in SnowMIP simulated the internal state of the snow-cover too. This paper focuses on the comparison of observed snow pit profiles to model profiles according to a simple and standardised evaluation procedure. The method provides a quantitative statistical similarity measure between either snow pit and modelled profiles or numerical results from different models. In particular, special care is given to the varying degree of complexity shown by the different models. Finally, in light of this comparison of internal state simulation, sensitivity of selected key processes to input parameters such as either albedo or new snow density are presented.

Wednesday, July 9 PM  
Presiding Chair: J. King

**JWH01/09P/C30-001**

**1400**

**SNOWMIP (SNOW MODELS INTERCOMPARISON) : MAIN RESULTS OF THE MASS AND ENERGY BUDGETS SIMULATIONS**

Pierre ETCHEVERES<sup>1</sup>, Eric MARTIN<sup>1</sup>, Ross BROWN<sup>2</sup>, Charles FIERZ<sup>3</sup>, Yves LEJEUNE<sup>1</sup>, E. BAZILE<sup>4</sup>, A. BOONE<sup>5</sup>, Y.-J. DAF<sup>6</sup>, R. ESSERY<sup>7</sup>, A. FERNANDEZ<sup>8</sup>, Y. GUSEV<sup>9</sup>, R. JORDAN<sup>9</sup>, V. KOREN<sup>10</sup>, E. KOWALCZYK<sup>11</sup>, N.O. NASONOVA<sup>12</sup>, R.D. PYLES<sup>13</sup>, A. SCHLOSSER<sup>14</sup>, A.B. SHMAKIN<sup>15</sup>, T.G. SMIRNOVA<sup>16</sup>, U. STRASSER<sup>17</sup>, D. VERSEGHY<sup>18</sup>, T. YAMAZAKI<sup>19</sup>, Z.-L. YANG<sup>20</sup> (\*Centre d'Etudes de la Neige, Météo-France, <sup>2</sup>Canadian Meteorological Service, <sup>3</sup>Swiss Federal Institute for Snow and Avalanche Research (SLF), <sup>4</sup>Météo-France, CNRM, Toulouse, France, <sup>5</sup>Institute of Atmospheric Physics; Chinese Academy of Sciences, Beijing, China, <sup>6</sup>Met Office, Bracknell, Berks. U.K., <sup>7</sup>Instituto Nacional de Meteorología, Madrid, Spain, <sup>8</sup>Laboratory of Soil Water Physics, Institute of Water Problems, Russian Academy of Sciences, Moscow, Russia, <sup>9</sup>CRREL, Cold Regions Research and Engineering Laboratory, Hanover, U.S.A., <sup>10</sup>NOAA/NWS/OH1/HRL, Silver Spring, MD 20910 U.S.A., <sup>11</sup>CSIRO Atmospheric Research, Aspendale, Australia, <sup>12</sup>Cooperative Institute for Research in the Environmental Sciences, Boulder, U.S.A., <sup>13</sup>COLA/GES, Calverton, U.S.A., <sup>14</sup>Laboratory of Climatology, Institute of Geography, Russian Academy of Sciences, Moscow, Russia, <sup>15</sup>Forecast Systems Laboratory, Boulder, USA, <sup>16</sup>Dept. of Earth and Environmental Sciences, University of Munich, Munich, Germany, <sup>17</sup>Frontier Observational Research System for Global Change, Yokohama, Japan, <sup>18</sup>Dept of Hydrology and Water Resources, The University of Arizona, Tucson, U.S.A.)

Many snow models have been developed for various applications such as hydrology, global circulation models, snow monitoring, snow physics research and avalanche forecasting. The degree of complexity of these models is highly variable, from simple index methods to multi-layer models simulating the snow cover stratigraphy and texture. The main objective of the intercomparison project SnowMIP (Snow Model Intercomparison Project) is to identify key processes for each application. Four sites have been selected for the representativeness of their snowpack and the quality of the collected data. Two of them are situated in the European Alps, the two others in North America. 26 models have participated in intercomparison by simulating the snowpack using the observed meteorological parameters. A precise analysis of the models results has been done. The paper focuses on the variability of the results quality for the mass and energy budgets, which can be explained by the sites specificities and the models features. A particular attention is paid to the model complexity impact. The mass balance simulations are validated by comparison with local observations (snow depth, snow pits, snow bottom runoff). The models performances are interpreted using the results of the energy budget simulation. The paper also presents the sensitivity of the models results to physical processes parametrization like the snow albedo or the fresh snow density. Lastly, a general classification of the models is proposed, based on the application field and the required complexity level.

**JWH01/09P/C30-002**

**1420**

**DEVELOPMENT OF MRI/JMA-SIB AND ITS IMPACT ON GLOBAL FORECAST BY GSM**

Mitsuo OHIZUMI<sup>1</sup>, Masahiro HOSAKA<sup>1</sup>, Masayuki HIRAI<sup>2</sup>, Park BYOUNG-KWON<sup>3</sup> (\*Meteorological Research Institute, <sup>2</sup>Japan Meteorological Agency, <sup>3</sup>Korea Meteorological Administration)

New land-surface model (MRI/JMA-SIB) has been developed under a cooperative project between MRI (Meteorological Research Institute), JMA (Japan Meteorological Agency) and KMA (Korea Meteorological Administration). Its aim is to improve a performance of GSM (JMA operational global weather forecasting model) and MRI/JMA98 (MRI climate community model) in mid and/or high latitudes. MRI/JMA-SIB consists of three sub-models, Canopy, Snow and Soil. Canopy sub-model treats momentum, heat and moisture transfer between a surface boundary layer and ground vegetation/bare soil. It is basically the same as the operational SIB implemented in GSM (Sato, 1989), except dependency of stomatal resistance on soil water. Snow sub-model is newly designed, and Soil sub-model is extended from three layers SIB implemented in MRI/JMA98. They are incorporated into MRI/JMA-SIB to simulate precisely cryosphere. Snow sub-model deals with snow mass evolution from snow accumulation to melting, with taking account of the following; initial fallen snow density, compactive viscous flow, low heat conduction, albedo change due to aging, and water holding of snow. Snow cover is classified into two categories, partial snow cover or full snow cover. Partial snow cover (snow patch) coexists with ground grass/bare soil, and has only one snow layer in constant depth with changing a grid fraction of occupation. Full snow cover is discretized into some snow layers, with changing from one to three according to snow water equivalent. Uppermost snow layer is intended to reproduce diurnal change. Lowermost is provided for snowmelt at the bottom. Mid snow layer is expected as a buffer of heat and mass. Soil sub-model consists of three layers, where heat conduction, soil water diffusion due to unsaturated Darcy's flow and soil ice freeze/thaw are formulated. Heat conductivity of a frozen (or an unfrozen) soil layer of dry soil, soil water, (soil ice,) and air, is assumed to be that of a mixture by Farouki(1981). Soil ice is presumed to decrease the effective porosity of the soil layer, so that coexistence of soil water and soil ice in the soil layer increases both the effective soil water degree of saturation and the soil matrix potential, but on the other hand decreases the soil water permeability. Offline sensitivity experiments on snow depth, forced by surface meteorological data in Hokkaido, show that, 1) snow albedo affects weekly on snow depth, 2) snow compactive viscosity has an effect during all winter season, and 3) snow heat conductivity is a dominant factor in melting season. Online preliminary forecast experiments in April 2002 with GSM indicate that snow cover evolution in Tibetan Plateau is better simulated by MRI/JMA-SIB than by the operational SIB which gives too early snowmelt compared with SSM/I. However, too fast retreat of the southern edge of snow cover in Siberia and negative bias in 850 hPa temperature in mid latitudes are generally not improved by MRI/JMA-SIB. This implies that further improvement and tunings of Snow/Soil sub-model are required.

**JWH01/09P/C30-003**

**1440**

**UNDERSTANDING SNOWMELT MECHANISMS OVER THE SIERRA NEVADA REGION USING THE NCAR/PSU MESOSCALE MODEL (MM5)**

Jiming JIN, Norman L. MILLER (Lawrence Berkeley National Laboratory)

Snowmelt is essential to climate and water resource variabilities in the Sierra Nevada region. The Penn State-National Center for Atmospheric Research fifth generation Mesoscale Model (MM5) has been used to investigate snowmelt mechanisms in this region. The model with a one-way nested 48km-12km domains was driven by a 6-hourly reanalysis dataset from the National Centers for Environment Prediction during the 1998 snowmelt season (April-June). The results showed that the snowpack was substantially underestimated due to the lower initial snowdepth and the faster snowmelt, which resulted in higher surface temperature and stronger convective precipitation because of the unstable atmospheric structure. Although the assimilation of observed daily snowpacks in the model collected from the automated Snowpack Telemetry system dramatically alleviated the warm bias and the exaggerated

precipitation, the simulated snowmelt was still not significantly improved. Further investigations indicated that the faster snowmelt resulted from intensified solar radiation absorption on the snow surface, which is caused by a lack of simulation of the effects of vegetation fraction in MM5's land-surface scheme, the Oregon State University canopy-atmosphere-plant-soil model. The lower simulated albedo also had contributions to the stronger snowmelt. The results from a sophisticated land-surface model driven by the MM5 output over the region emphasized that the realistic descriptions of the vegetation fraction and surface albedo gave rise to an accurate simulation of snowmelt, which implies that a physically-based land-surface model is critical to the mesoscale model's predictability. In the meantime, the variations of snowmelt in the region are also strongly correlated with atmospheric patterns because of their influences on the incoming radiation and the air temperature above the snow surface.

**JWH01/09P/C30-004**

**1500**

**UNCERTAINTY IN MEASUREMENT AND MODELLING OF LONGWAVE RADIATION AND IMPLICATIONS FOR SNOWMELT**

John W. POMEROY<sup>1</sup>, Alexander N. GELFAN<sup>2</sup>, Richard L.H. ESSERY<sup>1</sup>, Jean E. SICART<sup>1</sup>, Raoul J. GRANGER<sup>3</sup>, Janet P. HARDY<sup>4</sup> (\*Institute of Geography & Earth Science, University of Wales, Aberystwyth, <sup>2</sup>Water Problems Institute, Russian Academy of Sciences, Moscow, Russia, <sup>3</sup>National Water Research Institute, Environment Canada, Saskatoon, Canada, <sup>4</sup>US Army Cold Regions Research and Engineering Laboratory, Hanover, NH, USA)

Net longwave radiation fluxes can have an extremely important role in providing the energy to melt snow, however their observation remains particularly difficult and models often have a high degree of uncertainty. Longwave radiation measurements over snow from standard and experimental sensors were examined from sites in Russia, Canada, USA and Bolivia. The uncertainty in some standard radiation measurements is large and can result in longwave flux estimates in error by over 100%. Where a vegetation canopy is present, there is a substantial spatial variability to the downward longwave flux, which depends upon the energetics of the canopy as well as atmospheric conditions. There are several methods used in hydrological modelling to estimate incoming longwave to snow from the atmosphere (Kuz'min, Satterlund, Gray), the transferability of these regionally-derived relationships is examined. Standard methods for modelling sub-canopy downward longwave radiation are assessed in light of recent measurements of the spatial variability of longwave. Net longwave flux is discussed with respect to the difficulty in diagnosing the radiant temperature of snow from its internal energetics. Finally, the sensitivity of snowmelt to the uncertainty in longwave radiation in various environments is demonstrated from a combination of observations and modelling.

**JWH01/09P/C30-005**

**1520**

**WATER AND ENERGY BUDGET IN THE SOUTHERN MOUNTAINOUS REGION OF WETERN SIBERIA**

Junpei KUBOTA<sup>1</sup>, Kazuyoshi SUZUKI<sup>2</sup>, Tetso OHATA<sup>3</sup>, Vasily VUGLINSKY<sup>4</sup> (\*Research Institute for Humanity and Nature, <sup>2</sup>Frontier Observational Research System for Global Change, <sup>3</sup>Institute for Low-Temperature Sciences of Hokkaido University, <sup>4</sup>State Hydrological Institute, St Petersburg, Russian Federation)

Siberia, which is located in the northern part of the Eurasia continent, has the widest permafrost area on earth. The runoff provided big rivers in Siberia, like Lena River, plays an important role as fresh water supply to the Arctic Sea, affecting not only the hydrological and thermal conditions of the Arctic Sea, but also the polar region climate. In order to understand water and energy cycle in Siberia, An intensive field campaign was carried out at a small forested watershed in the southern mountainous region, which is the main source of the Lena River. The Mogot watershed is located at 55.5N, 124.7E and its basin area is 30.2km<sup>2</sup>. The elevation ranges from 550m to 1150m. The dominant species are larch, birch and pine. Both the catchment scale hydrological study, including time and spatial distribution of thawing depth and soil moisture, and the observation of water, heat and CO<sub>2</sub> fluxes between land surface and atmosphere using a tower were carried out in the Mogot watershed. The amounts of precipitation, discharge, evapotranspiration by flux measurement and interception loss, in the warm period from April 19 to October 13, 2001 (178 days) were 434.5mm, 204.1mm, 127.5mm, and 82.6mm, respectively. According to measurements of transpiration by the sap flow method and the evaporation from forest floor by the pan method, the contribution of the evaporation from forest floor was significant, around 80% of the total. The Bowen ration after the snowmelt, in the middle of April, was around 2.0. Just after the opening leaves at the beginning of June, it decreased due to transpiration, then began to increase at the end of August with falling leaves.

**JWH01/09P/C30-006**

**1540**

**SPATIAL ENERGY BALANCE SNOWMELT MODELING OF THE ECHAUREN AND TOKOPAH WATERSHEDS**

Constance M. BROWN-MITIC, Noah MOLOTCH, Roger BALES (SAHRA, Department of Hydrology and Water Resources, University of Arizona)

Describing the spatial distribution of snow water equivalent (SWE) as well as the space-time characteristics of snowmelt in alpine/subalpine basins is important for water resources management. Distributed SWE is critical for forecasting seasonal runoff and provides the initial condition for forecasting the timing of runoff. A spatial energy balance snowmelt model was used in two alpine watersheds: the 4.7 km<sup>2</sup> Echauren basin of the Chilean Andes (33.58° S, 70.13° W) and the 19.1 km<sup>2</sup> Tokopah basin of the Sierra Nevada, California, U.S.A. (36.60° N, 118.66° W), to melt snow from peak SWE accumulation to the end of the melt season. The model utilizes peak SWE accumulation maps generated from remotely sensed snow covered area and ground observations of snow depth and density, digital elevation models, gridded meteorological data generated from meteorological stations within the watersheds, and incident solar radiation images. Binary regression trees were employed to distribute point observations of snow water equivalent (SWE) and snow depth across the study areas. Four annual peak-SWE accumulation snow surveys consisting of an average of 77 depth measurements and two density measurements from snow pits were used to estimate SWE in the Echauren basin. An average of 319 depth measurements and 53 density measurements were collected in the Tokopah basin in April, May and June 1997. The snowmelt analysis was conducted on an hourly time step from peak-accumulation. Unrouted meltwater generated by the model were then used to create simple hydrographs for the watersheds, which were then compared to the observed basin hydrograph. The model run for the Tokopah basin was also evaluated at several stages during the snowmelt season. Modeled snow ablation was compared to observed SWE during the May and June snow surveys. The modeling approach applied in this research calculates the energy flux occurring at the snow/ atmosphere interface and therefore has low input requirements and computational expense relative to more complex models.

JWH01/09P/C30-007

1630

## COMPOSITE MODELLING OF SNOWMELT AND WATER EQUIVALENT OF SNOW

Shigeo SUIZU (Geosystems Inc.)

The state of deposited snow and snowmelt is deeply related to human life and it would be useful to grasp its conditions quantitatively. The purpose of this study is to develop a practical snowmelt and water equivalent snow model for water resource management. A simplified heat balance method has been developed and daily snowmelt can be calculated based on heat balance method with a few meteorological elements. The model has been further developed and it can provide the distribution and time series of snowmelt and water equivalent of snow in an extensive area. Daily amounts of solid precipitation are predicted with the data of precipitation and air temperature. Daily amounts of snowmelt are predicted with only the data of precipitation, sunshine duration, air temperature and  $K_{sc}$  by calculating all heat balance components over snow cover.  $K_{sc}$  is the coefficient of sensible and latent heat transfer and its value can be decided with the data of precipitation, sunshine duration, air temperature and snow depth. Daily amounts of solid precipitation and snowmelt lead to a calculation of water equivalent of deposited snow. All meteorological data that are used for the calculation are collected by Automatic Meteorological Data Acquisition System (AMeDAS), operated by Japan Meteorological Agency. AMeDAS is the most densely meteorological network in Japan. The calculation has been further developed to be capable of being applied to everywhere in an extensive area. The model uses a digital elevation model (DEM), meteorological data and vegetation. Precipitation, sunshine duration and air temperature are related with topography so these values at any site are estimated with observed AMeDAS data and topographic factors of the site. The topographic factors express topographic features such as elevation, the distance from the sea, slope and so on. All topographic factors are calculated by the use of DEM. The analysis of  $K_{sc}$  has shown its dependency on topographic features and its value also can be estimated with the topographic factors. Topographic shading, slope and aspect angles influence snowmelt because they change short and long-wave radiation on snow surface. These influences are estimated with DEM. Trees also influence snowmelt because they reduce wind speed and short-wave radiation and change long-wave radiation. Trees—covered influence is estimated with those reduction ratios that depend on the type of vegetation. The model was applied to northern and central parts of Japan. The estimates of snowmelt and water equivalent of snow are compared with observed data and the model is successfully verified.

JWH01/09P/C30-008

1650

## THE ANALYSIS OF THE SNOW WATER EQUIVALENT DISTRIBUTION USING SNOW MODEL AND SATELLITE INFORMATION OF SNOW IN TOHOKU DISTRICT IN JAPAN

Takehiro TOTSUKA, Yoshihiro ASAOKA, So KAZAMA, Masaki SAWAMOTO (department of civil engineering, school of engineering, Tohoku University)

Spatial and temporal SWE (Snow Water Equivalent) distribution in the Tohoku district in Japan was estimated using elevation, meteorological and satellite data. The estimation terms were from December 1998 to April 1999 and from December 1999 to April 2000. Digital elevation data was made by Geographical Survey Institute Japan (GSLJ), and its mesh size was restructured from 250m to 1100m resolutions. As meteorological data, Daily mean temperature and daily total precipitation from AMeDAS (Automated Meteorological Data Acquisition System) provided by Japan Meteorological Agency (JMA) were prepared. Observation points of AMeDAS are about 250 points in the Tohoku district. As the satellite data, eastern Japan images of JAIDAS (Japan Image DAtabaSe) were compiled from NOAA (National Oceanic and Atmospheric Administration) Satellite data. The time variation of snow water equivalent was simulated from snowfall and snowmelt models. Explanation on estimation method of the amount of snowfall is as follows. Snowfall model is based on temperature discriminating between snowfall and rainfall. Then, the temperature at each mesh was interpolated with observed data using weighted average distance method. The temperature at each mesh was corrected by temperature lapse rate,  $0.6^{\circ}\text{C}/100\text{m}$ , with digital elevation data. The amount of snowfall was interpolated with observed data using weighted average distance method with consideration for altitude dependency data of snowfall. Secondly, snowmelt distribution was estimated. The amount of the snowmelt on each mesh was calculated by degree-day method. Snow melt rate factor was decided comparing snow covered area by snow model involving the certain snow melt rate factor with the snow area map composed with the JAIDAS images. After some snowmelt rate factors were tried, the highest correlation coefficient in degree-day method was selected to estimate snow water equivalent variation. Snowmelt factor was determined using snow area maps in every month. The snowmelt rate factors were about  $4(\text{mm}/\text{day})$  in most months during estimation terms. As the results, this algorithm could show as better SWE distribution than previous models. As the most interesting results, almost uniform snowmelt rate factor were obtained during winter.

JWH01/09P/C30-009

1710

## A NEW SNOW COVER PARAMETERIZATION FOR USE IN GCMS

Andreas ROESCH (Institute for Atmospheric and Climate Science)

Snow cover fraction (SCF) has a significant influence on the surface albedo and thus on the radiation balance and surface climate. Long-term three dimensional simulations with General Circulation Models (GCMs) show that the SCF greatly affects the climate in the Northern Hemisphere. By means of both ground observations and remotely sensed data, several deficiencies in the SCF simulated by the current ECHAM4 GCM were identified: over mountainous areas a substantial overestimation in the SCF was found whereas flat areas showed a distinctly underestimated SCF. This paper proposes a new parameterization of the SCF for use in GCMs. Evaluations illustrate that it is beneficial to distinguish between the following three terrains: (i) flat, non-forested areas, (ii) mountainous regions and (iii) forests. The modified SCF parameterization for flat, non-forested areas was derived by using global datasets of ground-based snow depth and remote sensing observations of snow cover data. A 3-dimensional ECHAM4 simulation showed that this modification raises the SCF by up to approximately 20%, mainly in areas with a relatively thin snow cover. The comparison between remotely sensed and simulated mean monthly surface albedo revealed a significant overestimation of the surface albedo in snow-covered mountainous areas. An extension of the current SCF parameterization in ECHAM4 to take into account mountain effects, based on the French climate model Arpège, yielded a close agreement with satellite-derived surface albedo. The adoption of the submodel for snow albedo, as used in the Canadian Land Surface Scheme (CLASS), combined with a newly-developed simple snow interception model, demonstrated the ability to capture the main physical processes of snow-covered canopies, including the albedo. The validation of the new parameterization with Boreal Ecosystem-Atmosphere Study (BOREAS) field data showed that the modification is appropriate to capture the main features of the albedo over snow-covered forests during and after heavy snowfall events.

JWH01/10A/C30-001

0830

## TESTING THE IMPACT OF PARAMETERIZATIONS IN INTERNAL SNOW PHYSICS AND INTERFACE PROCESSES ON THE SIMULATION OF SNOW COVER AND RUNOFF AT VEGETATED AREAS

Yongkang XUE<sup>1</sup>, Shufen SUN<sup>2</sup>, Daniel S. KAHAN<sup>3</sup>, Yanjun JIAO<sup>4</sup> (<sup>1</sup>Department of Geography, Department of Atmospheric Sciences, University of California, Los Angeles, <sup>2</sup>Institute of Atmospheric Physics, Chinese Academy of Sciences, China, <sup>3</sup>Department of geography, University of California, Los Angeles (UCLA), USA)

To improve the prediction potential in snow cover regime in vegetated environment, a biophysical model, SSiB, has been coupled with a comprehensive snow model, SAST, which includes important physical processes for simulation of seasonal snow cover change. Based on analyses of diurnal and seasonal variations of snow temperature, SAST includes an efficient snow cover layering system for better prediction. The volumetric specific enthalpy is used as the prognostic variable instead of temperature, which simplifies the formulations in phase change processes. The coupled SSiB/SAST model includes the vegetation regime, snow cover regime and ground surface regime. Snow cover interacts with both vegetation cover above and ground surface below. In the coupled model, the snow surface temperature and canopy temperature are solved simultaneously to ensure the energy and water conservation in the vegetation-snow interface, which is crucial in the study of snow effects in global as well as regional climate models. A series of numerical experiments have been designed to understand the physics at the soil-vegetation-snow-atmosphere interface and to find the major parameterizations/parameters, which are crucial to simulate cold season processes. Observational data sets from Col de Porte de France, Övre Långsjö of Sweden, and Gander of Canada were used to help interpret the results. This study shows that snow layering and compaction are important to properly simulate snow depth, snow water equivalent, surface temperature, and surface runoff. The fixed snow density could produce as high as 100 percent error in estimating the snow depth and cause significant biases in SWE simulation mainly during the melting period. Furthermore, with a bulk snow/soil layer, the simulated surface temperature would persistently be close to the freezing point and its variability is substantially hampered, and the variability and the amplitude of the runoff during the snow-melting season could be severely underestimated. The experiments also show that the proper snow albedo is crucial during the ablation period and affects the magnitude and timing in both SWE and runoff simulations. Furthermore, this study indicates that the parameterizations in the surface aerodynamic resistance in the stable regime play an important role in determining the sensible and latent heat fluxes during the winter season, and then affect the snow depth simulations and prediction of snow melting as well as runoff timing. Although the snow may fully cover the ground in cold regions during the winter, numerical experiments in this study show the vegetation still exerts a substantial influence in the snow depth and runoff simulations. Numerical experimentation shows that with two ground conditions: bare soil and forests, less downward sensible heat flux on the bare ground condition produces thick snow cover and extremely high peak runoff, which leads to a typical deforestation scenario in cold regions.

JWH01/10A/C30-002

0850

## PARAMETERIZATION OF SNOW PROCESSES WITHIN BOREAL ECOSYSTEMS

Yeugeniy M. GUSEV, Olga N. NASONOVA (Institute of Water Problems, Russian Academy of Sciences)

The boreal zone determines significantly the rate of climatic processes on the planet, plays an important role in the formation of hydrological cycle and influences the stability of the Earth as a global ecological system. For these reasons, problems related to studying and modelling heat and water exchange within boreal ecosystems are of a great interest and importance. The goals of the present work are to develop parameterizations of snow processes occurring within boreal ecosystems (especially evergreen coniferous forests), to include new parameterizations into one of the land surface models, namely SWAP (Soil Water - Atmosphere - Plants) model, previously developed by the authors, and to validate the new version of SWAP. Evergreen coniferous forest represents tall vegetation intercepting significant part of precipitation (both liquid and solid). That is why two active surfaces were used to schematise heat and water exchange within the forest during the cold season: the surface of forest crowns and the surface of forest floor. Modelling of heat exchange between these two surfaces and the atmosphere is based on the Monin-Obukhov similarity theory with accounting for the specific features of energy exchange within a forest. Thus, it was taken into account that trees extinguish incoming solar radiation and produce longwave emission in all directions, in particular, toward the forest floor, and that turbulent heat exchange between the forest floor and the forest crowns exists. When the water balance of the boreal forest was calculated, interception of solid and liquid precipitation by vegetation, as well as snowmelt and water freezing on the forest crowns were taken into account. Snowpack formation at the forest floor was modelled with considering phase changes of water within snow cover as well as water yield of snow on the forest crowns during melting. The developed blocks of snowpack formation on the forest crowns and on the forest floor were added to the main module of SWAP. The developed new version of SWAP was validated against a vast set of intensive observations obtained by the Valdai Scientific-Research Hydrological Laboratory during 18 years (1966-1983) at forested and grass experimental catchments located in the central part of the Valdai Hills (the boreal zone, Russia). The validation data included, in particular, intercepted solid and liquid precipitation, snow density, snow depth, snow water equivalent, snow sublimation, soil water storage, and runoff. In addition, the validation of simulation of snow processes by SWAP was performed using the observed data on snow depth (1986-1989) for 24 sites located in the French Alps. The results of validation allow us to conclude that the land surface model SWAP parameterizes heat and water exchange processes (including snow processes) which occur in the boreal zone quite reasonably.

JWH01/10A/C30-003

0910

## A STUDY ON HYDRO-METEOROLOGICAL EFFECT OF INTERCEPTED SNOW USING A ONE-DIMENSIONAL LAND SURFACE MODEL

Takeshi YAMAZAKI<sup>1</sup>, Hironori YABUKI<sup>2</sup>, Reiko OKUBO<sup>3</sup>, Tetsuo OHATA<sup>4</sup> (<sup>1</sup>Frontier Observational Research System for Global Change /Tohoku Univ., <sup>2</sup>Frontier Observational Research System for Global Change, <sup>3</sup>NEC Soft, Ltd., <sup>4</sup>Frontier Observational Research System for Global Change /Hokkaido Univ.)

In order to simulate full-year water and energy exchange between the atmosphere and land surface, snow interception is one of the least known processes. Hydro-meteorological effect of intercepted snow has been studied using a one-dimensional land surface model with a snow-interception model recently proposed by Okubo and Yamazaki (2000). The land surface model includes three submodels; vegetation, snow cover, and soil. It can calculate water and energy fluxes above and within forest, if meteorological data over the forest are

given as input. The interception model has been developed to consider both liquid and solid water on forest, melting and freezing, changing transfer coefficient of sensible and latent heat fluxes, and albedo changing. Since vegetation submodel has two layers of crown space, difference of evaporation timing between top and lower branches can be simulated. Preliminary study shows that the model can simulate intercepted snow mass and snow depth on forest floor observed previously at Morioka and Sapporo in Japan. When snow-interception is considered, we can find large differences on energy and water budgets compared with the cases of no interception or same treatment with rain. For example, the forest works as a heat source for no interception, however, latent heat is dominant and sensible heat is almost transferred from the atmosphere to vegetation when the intercepted snow is considered. Moreover, the snow cover on the forest floor strongly depends on the treatment of interception. On the other hand, the effect of albedo increasing is transient; it does not produce obvious differences of energy and water budgets in winter average. As a result, we find that it is important to heat and water budgets that snow interception is more in quantity and cooler than rain interception, and it is essential to need much energy for melting and evaporating the intercepted snow. The model is also applied to a taiga forest in eastern Siberia, Russia. Meteorological and hydrological observations were carried out there as part of GAME (GEWEX Asian Monsoon Experiment). The effect of snowfall interception is discussed quantitatively in intensively cold region such as Siberia. Since the dominant species is larch, which is deciduous, in the taiga in eastern Siberia, branch/stem area density is important especially in winter. Frost or condensation is also considered in this model, although sometimes remarkable frost is observed in the site in winter.

**JWH01/10A/C30-004** **0930**

**DEGREE-HOUR MODEL OF MOUNTAIN SNOW WATER EQUIVALENT AND EVALUATION USING SNOW LYSIMETERS BENEATH THE FOREST CANOPY**

Andrew C. WHITAKER, Hironobu SUGIYAMA (Graduate School of Science and Technology, Niigata University)

Snow modeling issues are examined through the application of a degree-hour model in the Asahi Mountains of Niigata Prefecture on the Japan Sea coast. In the study basin, average annual precipitation is >2900mm with snowfall December to March and seasonal snow cover December to May in elevations up to 950m. Vegetation is mainly natural mixed beech and planted cedar and larch. Model evaluation is achieved by using three lysimeter plots of which two are located beneath the forest canopy: (a) large opening, (b) cedar stand, and (c) larch stand. Air temperature, relative humidity, snow depth and albedo, snow surveys, and snowmelt discharge are measured at each lysimeter plot. Snow surveys and air temperature are also measured at high elevations of 550m and 750m. Remaining uncertainties in modeling snow water equivalent in mountain areas include; under-catch of snowfall by precipitation gauges, variable threshold temperature to distinguish rain/snow, variability in air temperature and lapse rates, and orographic enhancement and spatial variability of precipitation. In forested areas there is additional uncertainty regarding interception and sublimation losses in the forest canopy, and the influence of the forest canopy on the energy balance and snowmelt process. This study addresses the critical lack of data on snow water equivalents and snowmelt dynamics beneath the forest canopy within a simple modeling framework.

**JWH01/10A/C30-005** **0950**

**SNOW PROCESSES IN THE SOUTHERN MOUNTAINOUS TAIGA OF EASTERN SIBERIA. I. SNOW ABLATION PROCESS UNDER A LARCH FOREST CANOPY**

Kazuyoshi SUZUKI<sup>1</sup>, Jumpei KUBOTA<sup>2</sup>, Yinsheng ZHANG<sup>3</sup>, Tsutomu KADOTA<sup>4</sup>, Tetsuo OHATA<sup>5</sup>, Vasily VUGLINSKY<sup>6</sup> (<sup>1</sup>Frontier Observational Research System for Global Change, <sup>2</sup>Research Institute for Humanity and Nature/ Frontier Observational Research System for Global Change, <sup>3</sup>Institute for Low-Temperature Sciences of Hokkaido University/ Frontier Observational Research System for Global Change, <sup>4</sup>State Hydrological Institute)

An intensive field campaign in the spring of 2002 was carried out at southern mountain taiga region of Siberia where it is the headwater of the Lena River and Baikal basins, in order to clarify the water and energy balance of snow and soil under larch forest canopy. More than 90% percentages of these regions are covered by forest, which is composed mainly of larch tree. There are many study of snow ablation under forest canopy (e.g. Suzuki et al. 1999). In this study, we focused on the snow ablation process beneath a sparse larch forest canopy, which included the effect of snowmelt water on the forest floor evaporation. Three sites with different topographic and surface conditions were selected to observe meteorological elements, snow water equivalent and snow surface energy balance. A sparse larch forest covers Site LF at the bottom of valley (610m asl.), and Site OP was covered by grassland (608m asl.). Site ES contains a sparse larch forest of east slope (635m asl.). We applied the snow and soil model (SNThERM, Jordan 1991) to evaluate the water and energy balance within a snowpack and soil layers at the three sites and directly observed water and energy balance above snow surface by eddy covariance method at Site LF. Our study obtained the following results, 1) According to eddy covariance method, the contribution of snow surface evaporation to the snow ablation at Site LF was about 8.7% during a thaw of 2002. Whereas the large portions of snowpack melted, river discharge was insignificant during a thaw period because the river water still had frozen. 2) The most effective energy to snowmelt was net radiation because the most of turbulent fluxes were negative value to the snowmelt energy. 3) When snowcover disappeared on 7 May 2002 at Site LF, sensible and latent heat fluxes increased quickly and both values were mostly equivalent. The daily mean evaporation on forest floor with free snow in May 2002 was 0.94 mm/day. This value was similar with a value of evapotranspiration above forest canopy during a summer season in this region. This result showed the melt water contributed to the large evaporation from forest floor because our previous study showed a roughly half of melt water infiltrated into the frozen ground.

**JWH01/10A/C30-006** **1040**

**DYNAMIC CHARACTERISTICS OF SNOW COVER IN THE LENA RIVER BASIN, SIBERIA**

Tetsuo OHATA<sup>1</sup> (<sup>1</sup>Institute of Low Temperature Science, Hokkaido University, <sup>2</sup>Frontier Observational Research System for Global Change)

Snow cover is the important component in climate system determining the winter water storage and thermal response of the earth surface. Many studies has been made to characterize their structure, find process related to their accumulation and ablation. In the present paper, summary of characteristics of seasonal variation, structure and further issues will be discussed in relation to the behavior of snow cover in the northern continental region of Siberia studied during the GAME-Siberia Project phase 1 (1996-2002). Additional information will be added from past studies. The local research sites in GAME-Siberia were Tiksi (71N, 129E), Yakutsk (62N, 130E) and Tynda(55N, 125E), expanding in the range of 16 degrees north-south. Tiksi is tundra facing the Arctic Sea, Yakutsk is in a region of forest called taiga and Tynda is also taiga area but the topography is hilly with higher summer precipitation. The discussions will made on the (1) Seasonal variation of snow cover depth and SWE.(2) Process related to accumulation and ablation of snow cover.(3) Snow-cover vegetation interrelation.(4) Satellite derivation of snow cover using microwave sensors.(5)

Future issues on the snow studies in this regions related to modeling.

**JWH01/10A/C30-007** **1100**

**THE REPRESENTATION OF SNOW IN THE UPPER DANUBE CATCHMENT AREA - A MODELLING APPROACH**

Heidi ESCHER-VETTER<sup>1</sup>, Michael KUHN<sup>2</sup>, Wolfram MAUSER<sup>3</sup>, Stefan NIEMEYER<sup>1</sup> (<sup>1</sup>Commission for Glaciology, Bavarian Academy of Sciences, <sup>2</sup>Institute of Meteorology and Geophysics, University of Innsbruck, AUSTRIA, <sup>3</sup>Department of Earth and Environmental Sciences, University of Munich, GERMANY)

In 2001, the research programme GLOWA-Danube was started with the aim to investigate water-related issues in the catchment area of the upper Danube including alpine tributaries. GLOWA incorporates DANUBIA, a decision support system for a widerange of ecologic as well as socio-economic problems. DANUBIA is a network-based, distributed system, designed in UML (Unified Modelling Language) and implemented as a cluster of Java-programmes. Within DANUBIA, the spatial resolution is 1 km<sup>2</sup>, the time step varies from fifteen minutes to one year. The watershed of the upper Danube is distributed over five countries and comprises a multitude of terrains: lowland agricultural regions, pastures in the lowerland meadows in the upper pre-alpine part, rocks and glaciers in the highermountains. The whole area covers nearly 77000 km<sup>2</sup>, the altitudes range from 288 m to 3770 m a.s.l.. Snowfall occurs in the whole basin with a highlyvariable space and time spectrum. For the representation of snow within DANUBIA, different surface types had to be combined with different modelling approaches. While generally a 1 km grid was used, sub-grid calculation was required in areas of strong relief. The presentation starts with a short overview of the whole GLOWA-Danube programme and concentrates on the first results of two modelling approaches, one with an energy balance concept and one with a hydro-meteorological model.

**JWH01/10A/C30-008** **1120**

**ANALYZING THE EFFECT OF SNOW STORAGE ON BASIN-WIDE RUNOFF**

Makoto NAKATSUGAWA<sup>1</sup>, Kiyoshi HOSHIF<sup>2</sup> (<sup>1</sup>Civil Engineering Research Institute of Hokkaido, <sup>2</sup>Foundation of Hokkaido River Disaster Prevention Research Center)

To secure water for irrigation, hydroelectric power and drinking, the dam reservoirs in cold, snowy regions need to be maintained at high water levels in spring, because snowmelt is the predominant water resource in these regions. For this reason, heavy rainfall combined with snowmelt, an event that has become increasingly likely with the acceleration of global warming, is problematic to flood regulation of dam reservoirs in early spring. The Hoheiky Dam basin in southern Sapporo, Hokkaido Prefecture has been threatened twice by unseasonably heavy spring rainfall. In mid-May of 2000, heavy rain combined with snowmelt to cause a particularly large and unexpected inflow, and flood regulation of the dam became temporarily impossible. In late April of 2000, about 1.7 times as much rain fell as during a similar number of days in mid-May of the same year. However, the peak inflow in the mid-May event was 300 m<sup>3</sup>/s, versus 210 m<sup>3</sup>/s for that in late April. This means that outflow in late April was 0.7 times that in mid-May. To properly quantify the above situation, the storage effect of soil and snow cover on runoff should be considered, which requires the modeling of long-term hydrologic processes. These processes must be clarified not only for flood prediction under heavy rain combined with snowmelt but also for adaptive water management throughout the watershed. Hydrologic processes related to snow play a particularly important role in cold, snowy regions such as Hokkaido, northern Japan, so the snow accumulation condition and the snowmelt amount need to be properly estimated, as does evapotranspiration according to the conditions of ground surface and vegetation, in order to clarify the basin-wide water budget. The Two-layer model proposed by Kondo et al. that considers the heat balance in the atmosphere, in the vegetation layer and at the ground surface was applied to estimate hydrologic processes, and the long-term runoff was calculated by the Tank model. The model evaluates hydrologic processes in relation to the conditions of snow pack and snowmelt amount. Based on the calculated snow accumulation condition and snowmelt amount, the snow storage amount was provided as the initial condition of a flood runoff model to reproduce the relationship between rainfall and runoff. In this way, the storage routing relating to snow processes was evaluated and its modeling was found to have promise toward rational and practical estimation of the hydrologic processes in cold, snowy regions.

**JWH01/10A/C30-009** **1140**

**SNOW COVERED AREA AND VEGETATION DATA CONSIDERATIONS IN MODELING SNOWMELT STREAMFLOW FOR TWO SOUTHWESTERN US HEADWATER BASINS**

Kevin Andrew DRESSLER<sup>1</sup>, Steven Richard FASSNACHT<sup>2</sup>, Roger C. BALES<sup>1</sup> (<sup>1</sup>Department of Hydrology and Water Resources, University of Arizona, <sup>2</sup>Department of Forest, Rangeland, and Watershed Stewardship, Colorado State University)

Seasonal, snowpacks in mountains of the Southwestern USA contribute the major source of water for streamflow, typically over 85% in the Colorado River basin, and groundwater recharge. Modeling of streamflow for forecasts depends on accuracy of snow condition inputs and on parameters, particularly vegetation. To examine implementation of improved inputs for modeling snowmelt streamflow, sub-pixel Advanced Very High Resolution Radiometer (AVHRR) satellite-derived snow-covered area (SCA), interpolated snow water equivalent (SWE), and several vegetation cover types are used as input and parameterization data for the USGS Precipitation Runoff Modeling System (PRMS). The spatial distribution of modeled (1989-1999) and AVHRR-derived SCA is significantly different both in the White River (Arizona) and Upper Rio Grande (Colorado) basins. The SCA data are fractional representations of snow-covered extent within a 1-km<sup>2</sup> pixel, and are illustrated to provide a significant improvement over the snow versus no snow representation (binary SCA). The SWE data are derived from snow telemetry (SNOTEL) point data and also compare differently to modeled results. Several vegetation/land cover data sources are compared for the two basins and indicate differences in the amount and distribution of cover types. Since the majority of the spatially extensive datasets are derived from composite AVHRR imagery, the datasets and simulated streamflows are also compared to Landsat Thematic Mapper (TM) land cover maps. Several simulations are run using the various vegetation sources, including TM, and results are compared in relation to cumulative observed streamflow over a 10-year (1989-1999) simulation.

**JWH01/10A/C30-010** **1200**

**ESTIMATION OF SNOW WATER EQUIVALENT IN THE MOUNTAINOUS REGION OF JAPAN**

Hiroshi ISHIDAIRA<sup>1</sup>, Kuniyoshi TAKEUCHI<sup>1</sup>, Zongxue XU<sup>1</sup>, Naoki YAMAMOTO<sup>2</sup>, Tomomi ISHIHARA<sup>2</sup> (<sup>1</sup>University of Yamanashi, <sup>2</sup>Graduate School, University of Yamanashi)

Japan is a country enriched with abundant snow resources. Although a heavy snow can be a

cause of the disaster such as avalanches, a large quantity of freshwater resulted from the snowmelt in the mountainous regions is a valuable resource, which can be provided to satisfy the water demands in the agriculture, industry, municipal water supply and power generation. In order to effective use this kind of resources, it is important to ascertain the spatial and temporal distribution of snow. However, it is very difficult to measure and observe snows because of geographic conditions. Fortunately, it is possible to obtain various meteorological information through the network of weather stations, and the progress of data processing technology in recent years has also provided useful means to obtain some basic data in this respect. With the meteorological data and the snowmelt model, the distribution of the snows and its equivalent water quantities can be estimated. In this paper, a method to estimate the spatial and temporal distribution of snows and its equivalent over a basin is presented. The extent of snow-covered area is detected from satellite images, and the snow water equivalent over snow-covered area is estimated by using a snowmelt model with the meteorological data. The proposed method is applied to the upper Tone-River basin, which is the second longest main river (322km) with the largest catchment area (16,840km<sup>2</sup>) in Japan. The spatial distribution of snow-covered area, snow water equivalent, and the amount of snowmelt water are estimated for past 10 years, and the correctness of the estimation by the model was confirmed by the test at observational snow water equivalent (SWE) station. The result of application shows that snowmelt water occupies about 40% of total discharge from April to June, and it shows the importance of snowmelt for water resources in the basin.

Thursday, July 10 PM  
Presiding Chair: R. Essery

**JWH01/10P/C30-001** **1400**

**BREAKUP OF INVERSION LAYER OVER SNOWY FORESTED BASIN**

Toru IWAKURA<sup>1</sup>, Yuji KODAMA<sup>2</sup>, Nobuyoshi ISHIKAWA<sup>2</sup> (<sup>1</sup>Hokkaido Gijutsu Consultants Inc., <sup>2</sup>Institute of Low Temperature Science, Hokkaido University)

Breakup of inversion layer over snowy forested basin was observed using tethered balloon and its seasonal characteristics was obtained by analyzing the surface and volumetric heat balances. In summer season (no snow), the inversion layer was destroyed by the development of mixing layer. In winter (dry snow) the inversion layer of the basin was diminished by lowering the top of the inversion layer and no mixing layer was observed. In the snowmelt season, both the lowering of the inversion layer top and the development of mixing layer was observed. The analysis of volumetric heat balance suggested that the heat source of the breakup is the sensible heat flux from the basin bottom in summer, in winter the sum of sensible heat flux at the basin bottom and radiative flux divergence was negative, suggesting some heat flux from other than the basin bottom, and in snowmelt season the same sum was positive but small. In snowmelt season the strong contrast of albedo of snow at the flat basin bottom to the forest at the surrounding slopes would cause the differential heating between the basin bottom and the surrounding slopes and the anabatic situation on the surrounding slopes. These conditions of the basin could form a local circulation, which might be responsible for the breakup of the inversion layer in snowmelt season.

**JWH01/10P/C30-002** **1420**

**PHYSICALLY-BASED HYDROLOGICAL MODEL OF SNOW ACCUMULATION, SUBLIMATION AND MELT EVALUATION IN NORTHERN RUSSIA**

Alexander GELFAN<sup>1</sup>, John W. POMEROY<sup>2</sup>, Lev S. KUCHMENT<sup>1</sup> (<sup>1</sup>Water Problems Institute, Russian Academy of Sciences, <sup>2</sup>University of Wales, Aberystwyth)

A comprehensive, physically based model of snow accumulation, redistribution, sublimation and melt for open and forested catchments was assembled, based on algorithms derived from hydrological process research in Russia and Canada. The model includes full radiation and multiphase mass balance, blowing and intercepted snow redistribution and sublimation algorithms. The model calculates radiation terms explicitly and includes the canopy effect on long and shortwave radiation and on turbulent transfer. Model parameters were derived from the results of snow process experiments in both Russia and Canada. The model was used to evaluate the long-term snow mass balance of a forested and an agricultural catchment in north-western Russia using a 17 year dataset. The model was used to provide an uncalibrated simulation of snow water equivalent during both accumulation and melt periods in both forest and agricultural catchments. Mean errors in snow water equivalent were less than 5 mm over the 17 years. Blowing snow redistribution was minimal due to low wind speeds. Intercepted snow storage in the forested catchment ranged up to 18.6 mm; some of this snow sublimated resulting in a cumulative loss of 30 mm per season on average. Surface sublimation losses were small ranging from 10 mm per season in the forest to 20 mm in the open. Mid-winter melting was greater in the agricultural catchment than in the forested. Because of typically cold winter conditions, losses due to intercepted snow sublimation from the forest overcame greater surface snow sublimation and mid winter melting in the agricultural catchment in 14 seasons out of 17, resulting in an average 15% greater maximum snow water equivalent in the agricultural catchment. Because this model does not require calibration, it has potential to help estimate the water resources of poorly-gauged cold regions catchments.

**JWH01/10P/C30-003** **1440**

**SOLAR VARIABILITY BENEATH OPEN AND DENSE CONIFER CANOPIES**

Janet P. HARDY<sup>1</sup>, Rae A. MELLOH<sup>1</sup>, Geoff G. KOENIG<sup>1</sup>, John W. POMEROY<sup>2</sup> (<sup>1</sup>Cold Regions Research and Engineering Laboratory, <sup>2</sup>University of Wales, Aberystwyth)

Snow dynamics under forest canopies are strongly influenced by the large spatial variability of energy transfers in this environment. Incoming solar radiation is an important transfer that has a particularly high degree of spatial variability. Transmission of solar radiation through a canopy varies with the size and location of the canopy gaps and with canopy leaf area. Modeling this transmission has proven challenging due to the highly variable structure of forest canopies. This study aims to describe and simulate the solar variability incident on the snow surface beneath an open, discontinuous canopy and a relatively uniform, dense conifer canopy. The objectives are 1) to evaluate the variability of incoming solar radiation data with respect to canopy structure and cloudiness, and 2) to correlate measured solar radiation data with measured canopy gap fractions and predicted solar transmission based on analysis of hemispherical photographs. Observations were made during winters of 2002 and 2003 in predominately lodgepole pine (*Pinus contorta*) stands, one open and one dense, at the Local Scale Observation Site (LSOS) in Fraser, Colorado USA as part of the Cold Land Processes Mission. The canopy structure of all trees in a 100 x 100-m<sup>2</sup> plot was measured in detail (species, tree location, height, crown height, diameter at breast height). Incoming global solar radiation at the snow surface beneath the open and the dense canopies was measured using arrays of upward looking radiometers (10 pyranometers, 2 pyrgeometers at each site). Incoming global solar radiation was also measured above the canopy. Hemispherical photographs were taken with a Nikkor 8mm/f2 lens at each radiometer

location in both canopies, and were analyzed with Gap Light Analyzer (GLA) software. Measured mean transmissivity for the dense pine canopy was 0.27, while the mean transmissivity in the open canopy was 0.46, with large spatial variations. The point transmissivities determined at each individual radiometer location, using above and below canopy solar incidence data, compared well with predicted transmissivities using hemispherical photographic analysis.

**JWH01/10P/C30-004** **1500**

**A SENSITIVITY STUDY OF SNOWMELT TO THE DENSITY OF THE FOREST CANOPY**

Jean E. SICART<sup>1</sup>, John W. POMEROY<sup>2</sup>, Raoul J. GRANGER<sup>2</sup>, Richard E. ESSERY<sup>1</sup>, Alexander N. GELFAN<sup>3</sup> (<sup>1</sup>Institute of Geography and Earth Sciences, University of Wales, Aberystwyth, UK, <sup>2</sup>National Water Research Institute, Canada, <sup>3</sup>Water Problems Institute, Russian Academy of Sciences, Russia)

This study deals with the relations between the snowmelt in forested environments and the radiative properties of the canopy. Due to low wind speeds, turbulent fluxes under the canopy are generally of secondary importance and snowmelt strongly depends on the radiative fluxes. As the canopy density increases, two competitive processes affect the snowmelt rate: the solar irradiance decreases and the long-wave irradiance is enhanced compared to an open environment. The decrease in solar transmissivity of the canopy is generally the dominant effect and melting is reduced. Here, we used a simplified one-dimensional radiative model to describe the dependence of the surface net radiation to the canopy characteristics in terms of solar transmissivity and sky view factor. The model results are compared with measurements taken from Canada and Russia.

Presiding Chair: J. Pomeroy

**JWH01/1JWH01/10P/C30-005** **1600**

**REPRESENTING SNOW-COVERED SURFACES IN ATMOSPHERIC MODELS : WHICH PROCESSES AND PARAMETERS MATTER ?**

Richard ESSERY<sup>1</sup>, Pierre ETCHEVERS<sup>2</sup>, Eric MARTIN<sup>2</sup> (<sup>1</sup>Centre for Glaciology, University of Wales, <sup>2</sup>Centre d'Etudes de la Neige, CNRM Météo-France)

Among other applications, snow models are required for calculating surface heat and moisture fluxes as boundary conditions for atmospheric models over snow-covered surfaces. The computational demands of large-scale models, however, mean that the complexity with which snow processes are represented may be limited and snow parameters may be poorly defined. In this study, an adjustable snow model is used to investigate the influence of common snow process representations and parameter ranges on simulations of snow depth, surface temperature and fluxes. Features examined include albedo, thermal conductivity, snow hydrology and discontinuous snow cover. Results are compared with the range of results produced by 26 different models in the Snow Model Intercomparison Project (SnowMIP).

**JWH01/10P/C30-006** **1630**

**COMPARISON OF SNOW COVER ENERGETICS DURING SPRING AT OPEN AND FORESTED SITES**

Danny G. MARKS, Adam WINSTRAL (Northwest Watershed Research Center, USDA-ARS)

A forest canopy modulates precipitation, meteorological conditions and energy available for warming and melting the seasonal snowcover. A detailed evaluation of meteorological conditions and snow cover energy balance at a site on an exposed ridge, in a protected grove of trees, and below a dense fir canopy is presented. In general the ridge site accumulates the least snow with meltout in early spring, while the grove site accumulates nearly twice as much snow and melts nearly a month later. At the fir site snow accumulation is restricted by interception so the site accumulates only a little more snow than the ridge site, and meltout occurs only a week later than the ridge site. At the ridge site energy for snowmelt is primarily from sensible heat exchange, because net solar radiation is not large enough to overcome longwave heat losses at night so net allwave radiation is generally negative. At the grove and fir site energy for snowmelt is primarily from net radiation because wind speeds are low, and turbulent fluxes are small. At the forested sites thermal radiation is enhanced by the canopy, and net solar radiation increases with higher sun angles in spring. As melt begins, debris on the snow surface decreases snow albedo, enhancing net solar radiation. Though net thermal radiation is small or slightly negative, net all-wave radiation is positive because of input from net solar radiation. This research will improve our understanding of the effect forest cover has on snow surface energy balance.

**JWH01-Posters** **Thursday, July 10**

**SNOW PROCESSES: REPRESENTATION IN ATMOSPHERIC AND HYDROLOGICAL MODELS (IAHS/ICSI, IAMAS)**

Location: Site D

Thursday, July 10 PM

**JWH01/10P/D-001** **Poster** **1400-006**

**THE SNOW COVER MODEL SNOWPACK-ECO: RADIATION AND SOIL MODULES TO STUDY PLANT GROWTH AND PERMAFROST**

Michael LEHNING, Martina L. SCHG, Ingo Meirold-MAUTNER, Charles FIERZ, Perry BARTELT (Swiss Federal Institute for Snow and Avalanche Research SLF)

The snow cover model SNOWPACK represents many physical processes within the snow cover, at the interface snow atmosphere and at the interface snow soil. It is therefore suitable to give a detailed description of the snow cover development for avalanche warning, which is its original purpose. However, because the snow cover is an important part of the land surface ecosystem, many additional problems can be addressed. One aspect of growing importance is the interface between the snow cover and the soil, from the point of view of both plant ecology and permafrost development. In this context, this presentation discusses two innovations implemented in SNOWPACK: First, a new radiation transfer scheme and its application to plant ecology and second, a model module describing underlying soil layers for permafrost studies. The very sensitive and spectrally selective response of plants to radiation requires an adequate description of radiation transfer into the snow cover. This is achieved by a novel radiation transfer scheme based on Mie theory and the ?-Edgington model, which treats multiple scattering. It predicts the flux densities for

wavelength intervals. The new scheme is evaluated against laboratory measurements and data collected on summit in Greenland. As an application, the response of snow covered plants to radiation via photosynthesis or photoperiodism is modeled. In addition, plants that reach into the snow cover are an effective trap for radiation and can create their local microclimate. These three mechanisms influence the survival and growth of plants under harsh alpine conditions. The soil snow interface has a major influence on the development of permafrost. Changes in permafrost in Alpine areas can lead to slope instability and melt water release. SNOWPACK has been extended to simulate a variable number of soil layers and its physical processes heat conduction, phase change and water transport. The new model module is tested against laboratory behavior of different soils. The model is applied to predict permafrost behavior under climate change scenarios.

**JWH01/10P/D-002** Poster **1400-007**

**CHEMICAL PROPERTY OF SNOW IN THE JAPAN ALPS**

Keisuke SUZUKI, Katsutaka YOKOYAMA (Department of Environmental Sciences, Shinshu University)

A chemical study of the new snow was conducted in the Japan Alps during 2000-2003 winter seasons. The samples were filtered, and conductivity and pH were measured with a conductivity meter and pH meter, respectively. Anions and cations were determined by an ion chromatography (DIONEX: DX-500). A relationship was observed between ion concentration of the new snow and the height of sampling site.

**JWH01/10P/D-003** Poster **1400-008**

**SNOW PACK IN THE SWISS ALPS UNDERCHANGING CLIMATIC CONDITIONS: AN EMPIRICAL APPROACH FOR CLIMATE IMPACTS STUDIES**

Martin BENISTON, Franziska KELLER, Stephane GOYETTE (Department of Geosciences, University of Fribourg)

In many instances, snow cover and duration are a major controlling factor on a range of environmental systems in mountain regions. When assessing the impacts of climatic change on mountain ecosystems and river basins whose origin lie in the Alps, one of the key controls on such systems will reside in changes in snow amount and duration. At present, regional climate models or statistical downscaling techniques, which are the principal methods applied to the derivation of climatic variables in a future, changing climate, do not provide adequate information at the scales required for investigations in which snow is playing a major role. A study has thus been undertaken on the behavior of snow in the Swiss Alps, in particular the duration of the seasonal snow-pack, on the basis of observational data from a number of Swiss climatological stations. It is seen that there is a distinct link between snow-cover duration and height (i.e., temperature), and that this link has a specific "signature" according to the type of winter. Milder winters are associated with higher precipitation levels than colder winters, but with more solid precipitation at elevations exceeding 1,700 - 2,000 m above sea-level, and more liquid precipitation below. These results can be combined within a single diagram, linking winter minimum temperature, winter precipitation, and snow-cover duration. The resulting contour surfaces can then be used to assess the manner in which the length of the snow-season may change according to specified shifts in temperature and precipitation. While the technique is clearly empirical, it can be combined with regional climate model information to provide a useful estimate of the length of the snow season with snow cover, for various climate-impacts studies.

**JWH01/10P/D-004** Poster **1400-009**

**SECOND PEAK OF THE SOLUTE CONCENTRATION IN SNOW MELT WATER**

Gaku YAMAZAKI, Yoshiyuki ISHII (Institute of Low Temperature Science, Hokkaido)

A hydrochemical study of the meltwater from the base of the snowpack was carried out using snow lysimeter during the snowmelt seasons at Moshiri, northern Hokkaido, which is known for severe cold and deep snow depth. Two snow lysimeters (13 square meters) were installed at 290m (Site A) and 535m (Site B) above mean sea level. Discharge of the meltwater was measured by a tipping bucket gauge with a pulse counter. Specific electrical conductivity of meltwater was monitored automatically. Samples of meltwater were collected by automatic water samplers. Snow stratigraphies beside the snow lysimeters were observed just prior to the snowmelt season in 2002, and snow samples were collected from each snow layer. Many studies reported that solute concentrations were highest in the initial meltwater flux and decreased in subsequent days. This pattern was also observed at our stage sites in 2000 and 2001. However, in 2002, the solute concentrations in the middle of snowmelt season increased again after they had decreased from high concentrations in the early snowmelt season. The onset of this increase at Site A was 4 days earlier than Site B. If dry or wet deposition to the surface of snowpack had caused this increase, both sites would start to increase simultaneously. On the other hand, the solute concentrations of the meltwater in each site increased when the snow depths decreased to the thick granular snow layers at each site. These layers were formed when the daily average temperature exceeded zero degree-Celsius in the middle of January. Anion concentration in snow layer samples and meltwater samples were compared. The anion concentration of an upper snow layer sample was different from a lower sample, because atmospheric deposition of northeast Asia occurred intermittently in March and April. Before the increase, the anion concentration in meltwater samples were close to the concentration in an upper snow layer sample. And then the concentration in meltwater samples changed remarkably as the solute concentration started to increase. After the increase, the concentration in meltwater samples were close to the anion concentration of a lower snow layer sample. These results indicated that the chemical substances in lower snow layers were retained until the snow depths decreased to the thick granular snow layers in each site. As the chemical substances are generally released from melting snow, we postulated that the meltwater from the near surface snow flowed through preferential channels in deeper snow layers and the meltwater didn't flow in the part of deeper snow layers outside of the preferential channels. The part of deeper snow layers outside of preferential channels retained the chemical substances until the snow depths decreased to the thick granular snow layers.

**JSM03/08A/A13-001** **0900**

**LAND - OCEAN INTERACTION FOR INTEGRATED COASTAL ZONES MANAGEMENT**

Lalitkumar Pandit CHAUDHARI (Institute for sustainable development and research)

Water is the key to development of the agricultural as well as social and economic development of the world. Considering the shortage of water, cost involved in water storage and conveyance to the users end, it is necessary to adopt the innovative methods of conjunctive use of water for agricultural production using water effectively and efficiently. Aquaculture is such an innovative tool in the urban and also in rural agriculture to use and reuse the water as well as waste water. Aquaculture has emerged as one of more promising industries in the world with considerable growth potential and excepted to contribute around a quarter a global fishery harvest of year 2000. Availabilities of water is a constraint in nonirrigated agriculture system. The Aquafarming has a multidimensional context in perspective agricultural growth. It is tool for utilizing land and water more economically and optimally for increasing productivity, of both, land and water, through sustainable agriculture. The countries in the Asia-Pacific region have vast and varied Aquafarming resources. Oftenly these are the main source of irrigation, coastlines, marshy land along coast lines reservoirs etc in this region. The overuse of water, the saline water intrusion from the coast line causes salinity problems in many countries reducing the cultivable area resulting reduction in agricultural production. An attempt has been made in this poster to develop the plan for water management for the agriculture, aquaculture and horticulture using innovative technologies from Indian experience. The poster also evaluates the waste water quality criteria for increasing the aquacultural productivity along the coastal zones of the Maharashtra state. The poster also explain the innovative small scale methods and technologies for food production using non conventional source of water in the coastal zones for increasing the productivity.

**JSM03/08A/A13-002** **0920**

**FRESHENING OF COASTAL GROUNDWATER SYSTEMS DURING SEA REGRESSIONS: EXAMINING THE TRANSITION ZONE THROUGH NUMERICAL EXPERIMENTS**

Michele R. MINIHANE<sup>1</sup>, Henk KOOP<sup>2</sup> (<sup>1</sup>Environmental Fluid Mechanics & Hydrology, Stanford University, <sup>2</sup>Faculty of Earth and Life Sciences, Vrije Universiteit, the Netherlands)

The salinity distribution in coastal aquifer systems plays a key role in water resource development and land use issues. Groundwater salinity patterns are often very complex due to sea-level changes and the associated shifts in coastlines on time scales of many tens of thousands of years and the more recent impact of human activities on coastal groundwater systems. Most research focuses on the latter influences; notably that of sea-water intrusion. The influence of sea transgressions and regressions has received very little attention, but is of prime importance to understand and predict offshore occurrences of fresh and brackish groundwater that are known to extend up to 100 km from the coast. This study uses numerical modeling experiments to gain insight into the way in which freshening of groundwater systems occurred during sea regressions and determine critical factors impacting the shape and salt distribution of the saltwater-freshwater transition zone. A finite-element, variable-density flow and transport code (Metropol3) is used that incorporates advection, diffusion and dispersion. It is found that for slow but steady regression of the sea, the transition initially becomes wider, and then reaches a stable width. The observed stability in transition zone width and salt distribution suggests that, for these scenarios, the transport processes reach a dynamic balance causing the transition zone to maintain a stable shape and follow the withdrawing sea. The steady width of the transition zone increases with increasing regression rate and decreases with increasing topographic (subaerial and seafloor) gradient. It is anticipated that at higher regression rates (beyond a certain threshold value), the dynamic balance cannot be attained, causing the transition zone to become ever wider. These results can be used as a starting point for analysis of the extent to which offshore sediments on continental shelves and other shallow seas were freshened during periods of sea-level fall during glacials.

**JSM03/08A/A13-003** **0940**

**SALINIZATION ALONG PARTS OF THE EAST COAST OF INDIA IN THE CONTEXT OF CLIMATE CHANGE**

U. ASWATHANARAYANA (MAHADEVAN INTERNATIONAL CENTRE FOR WATER RESOURCES MANAGEMENT)

The biophysical and socioeconomic fluxes in the coastal zones along parts of the east coast of India are studied in order to evaluate the extent of perturbation of coastal systems by human activities. Saline incursions may arise from natural causes (such as, tides, floods, cyclones, storm surges, etc., as has happened due to the supercyclone in Oct. 1999 along the Orissa coast) or may be anthropogenic (such as, excessive drawdown of freshwater for use in drinking, irrigation and industry, as has happened in the Krishna river delta). An attempt is made to delineate how rising sea levels as a consequence of global warming would affect the interlinked geomorphic, pedogenic and hydrologic elements in the evolution of the lowlands of the east coast of India. Saline incursions would not only salinize the soils, but would also degrade the groundwater resources. There is little doubt that sea level rise and possible increase in the frequency of extreme weather events will undoubtedly exacerbate the coastal salinization. The structure of the saline / fresh water interfaces is studied on the basis of the geomorphic evolution of the coastal zones, geophysical methods (e.g. self-potential and resistivity logs), geochemical (contents of Ca<sup>2+</sup>, Mg<sup>2+</sup>, Na<sup>+</sup>, K<sup>+</sup>, Cl<sup>-</sup>, SO<sub>4</sub><sup>2-</sup>, HCO<sub>3</sub><sup>-</sup>, etc.) and isotopic methods (tritium profiles, isotopes of H, O, C and S), etc. Infiltration of excess quantities of freshwater (river water or rain water) to flush the salt water backwards, and the construction of artificial recharge structures, are some of the ways employed to roll back the coastal salinization. It is now widely realized that mitigation methodologies for climate change developed on the basis of the biophysical studies alone have very little chance of success, unless they have been drawn up in consultation with stakeholders right from the beginning. We need to find out how the socioeconomic factors in the developing countries such as India, are contributing to the global change, and how the global change is feeding back into the system and affecting the communities. Studies are needed for the economic valuation of ecosystem services, integration of biophysical and socioeconomic approaches, and developing adaptation scenarios (e.g. saline agriculture) to mitigate the consequences of the salinization. A case history is presented in regard to the adaptation measures (hydraulic methods, biological methods, and engineering structures) through stakeholder participation to keep in check the salt water intrusion in the Krishna River delta (Dr. I. Radhakrishna, person. commun.).

**JSM03** **Tuesday, July 8**

**LAND-OCEAN-ATMOSPHERE INTERACTIONS IN THE COASTAL ZONE (IAMAS, IAPSO, IAHS)**

Location: Site A, Room 13

JSM03/08A/A13-004

1000

**VERTICAL AND HORIZONTAL STRUCTURE OF THE ATMOSPHERIC BOUNDARY LAYER OBSERVED BY A MOBILE AIRPLANE (AEROSONDE) OVER SUB-TROPICAL OCEAN UNDER THE SUPPRESSED CONDITION**

Atsushi HIGUCHI, Tetsuya HIYAMA, Taro SHINODA, Hiroki TANAKA, Hiroshi UYEDA, Kenji NAKAMURA (Hydropheric Atmospheric Research Center (HyARC), Nagoya University, Japan)

For the better understanding of internal structure within the atmospheric boundary layer (ABL) over the ocean, a mobile airplane measurement was carried out near the Shimoji Island, located East China Sea, Japan. A mobile airplane (Aerosonde, operated by Aerosonde Inc., Australia) can measure air temperature, relative humidity, air pressure, and wind speed and its direction with the flight. This overall ABL field campaign was conducted as a part of Lower Atmosphere and Precipitation Study (LAPS) project, supported by Core Research for Environmental Science and Technology (CREST), Japan Science and Technology Corporation (JST). The mobile airplane flight was designed to achieve dataset for both horizontal and vertical profiles internal and above the ABL, thus we set the "flight pass" with approximately 4 km length (from 24.80 N to 24.85 N in latitude, and parallel to the line of 125.08 E in longitude) over the ocean near the Shimoji Island. Flight pass was fixed as the seven-height (100m, 200m, 400m, 600m, 800m and 900m) a.s.l. A mobile airplane measurement was carried out in five days (21, 22, 24, 25 and 26 August, 2002). Measurement period was characterized synoptically as; northern wind phase (phase I) from 21 to 23 with dry-air suppression above ABL, and southern wind phase (phase II) from 24 to 26 with relatively wet within ABL, obtained from radiosonde profiles in the same period (once per 3 hours). We focus on the phase I, the mobile airplane observed the many plumes (corresponding to same phase change both potential temperature and specific humidity, usually, opposite sense) at the height of 100 m flight pass, however, significant upward transfer of the plume could not confirmed within the ABL (200m, 400m, sometimes 600m). Since entrainment and detrainment between the top of ABL and lowest free atmosphere were observed frequently at the height of 600m, 700m and 800m. We found the shallow convective type clouds in phase I, from the aerosonde path measurements, cloud (low potential temperature & high specific humidity) and downward suppression (high potential temperature & low specific humidity) with the horizontal scale of around two kilometers.

JSM03/08A/A13-005

1040

**SIMULATIONS OF THE SUBTROPICAL SEA BREEZE**

Kevin WALTER, John W. NIELSEN-GAMMON, Craig EPIFANIO (Texas A&amp;M University, College Station, Texas USA)

Theoretical and numerical studies of the sea breeze have progressed from idealized linear, two-dimensional models to fully realistic simulations of actual events with few intervening studies of intermediate complexity. As a result, there are significant gaps in our understanding of the sea breeze, despite the common view that the sea breeze is a solved problem. In this study, we use a sophisticated two-dimensional model to examine fundamental aspects of the subtropical sea breeze that are not explained by conventional theory. These aspects include: the behavior of the sea breeze near the critical latitude on a beta-plane; the observed upward phase propagation over land; the dependence of the critical latitude and the inertia-gravity wave response on the background flow; and the interaction of the sea breeze and a coastal nocturnal low-level jet.

JSM03/08A/A13-006

1100

**GAP WIND-INDUCED SUMMER UPWELLING IN THE SOUTH CHINA SEA AND ITS INTERANNUAL VARIATIONS**Qiang XIE<sup>1</sup>, Shang-Ping XIE<sup>1</sup>, Haiming XU<sup>1</sup>, Dongxiao WANG<sup>2</sup>, W. Timothy LIU<sup>3</sup> (<sup>1</sup>International Pacific Research Center, University of Hawaii at Manoa, Honolulu, Hawaii, 96822, USA, <sup>2</sup>LED, South China Sea Institute of Oceanology, Chinese Academy of Sciences, 510301, China, <sup>3</sup>Department of Meteorology, School of Ocean and Earth Science and Technology, University of Hawaii at Manoa, Honolulu, Hawaii, 96822, USA, <sup>4</sup>Department of Atmospheric Sciences, Nanjing Institute of Meteorology, Nanjing, China, <sup>5</sup>Jet Propulsion Laboratory, California Institute of Technology, Pasadena, CA, 91109, USA)

Seasonal and interannual variations of the summer upwelling off the Vietnamese coast and the eastward spread of the cold water are investigated using high-resolution satellite measurements. The development of this cold jet disrupts the summer warming of the South China Sea (SCS) and causes a pronounced semi-annual cycle in SST. In summer, as the southwesterly winds approaches a north-south running mountain range, a strong wind jet occurs at its southern tip along the 10°-11°N. The strong curl of this wind jet appears to be the dominant mechanism for upwelling on the Vietnam coast. In July and August an ocean anticyclonic eddy develops to the southeast and advects the cold jet toward into the open ocean. The maximum wind speed is located consistently south of the maximum surface cooling, indicating that the open-ocean upwelling also helps to cool the SST. Further evidence for the cold jet can also be found in chlorophyll data as the upwelled water has higher nutrients for the growth of phytoplankton. Furthermore, the cold jet is a key element to interannual variability in summer SCS. In 1998, this mid-summer cooling never took place because of the decreased wind speed, which led to the strongest surface warming on records in SCS. Interannual SST variance has a local maximum over the cold jet, and is much greater than the variance over the adjacent Indian and western Pacific Oceans. A cold jet index is constructed, which displays significant correlation with SST in the East Pacific and Indian Oceans at a lag of 5-6 months, suggesting a teleconnection from ENSO.

JSM03/08A/A13-007

1120

**THE APPEARANCE OF PROUDMAN RESONANCE AND HARBOUR SEICHES IN THE AREA OF SPLIT (ADRIATIC SEA)**

Ivica VILIBIC, Hrvoje MIHANOVIC (Hydrographic Institute)

The paper examines the occurrence of Proudman resonance in front of Split harbour (Adriatic Sea) and harbour seiches, including the possibility of their coupling. The dataset comprises air and sea pressure (sea level) data collected in August-December 2000, characterized by rather strong synoptic disturbances that took place over the harbour. The analyses encompass empirical tools such as time-series analysis, high- and band-pass filtering, spectral and wavelet analyses, whereas the theoretical approach includes the conceptual model of the resonance and barotropic 2D numerical model of the harbour seiches. The resonance seems to be generated in front of the harbour and then propagates inside, covering the periods between 7.7 and 28.5 min as a result of a complex atmospheric gravity wave structure and having a gain between air pressure and sea level equalling 5-40 cm/hPa. The seiches were documented to occur at the periods of 6.5, 3.0, 1.6 and 1.15 min, and were verified by the barotropic 2D numerical model. In addition, two model runs were executed: the first one with present topography and the second one with the nautical marina removed (built in 1972). The comparison quantify the influence of the marina on the seiche

characteristics. Namely, the leading seiche modes of 7.1-min and 5.0-min periods, calculated for the present topography, were probably joined in the 6.2-min mode before 1972. On the other hand, the numerical model showed that the 3.0-min seiche mode keeps its period, having the maximum amplitude at the north end of the harbour calculated for both runs. Finally, the seiches and resonance may endanger the navigation near the entrance and within the marina during the enhanced seiche episodes.

JSM03/08A/A13-008

1140

**MECHANISMS OF NIGHT-MORNING RAINS OFF A MOUNTAINOUS TROPICAL COAST**Brian E. MAPES<sup>1</sup>, Thomas T. WARNER<sup>2</sup>, Mei XU<sup>2</sup>, Andrew NEGRI<sup>1</sup> (<sup>1</sup>Climate Diagnostics Center, <sup>2</sup>National Center for Atmospheric Research, <sup>3</sup>NASA Goddard Space Flight Center)

The rainiest place in the Americas, and arguably the rainiest Earth, is in western Colombia. Here the western slopes of the Andes mountains face the Pacific ocean across a ~100 km coastal plain, just north of the Equator. The rainfall climatology in this region exhibits a complex geographical pattern and an interesting diurnal cycle. We explored diurnal rainfall processes in this region using the MM5 mesoscale model with nested domains, with a finest resolution of 2 km to resolve convection explicitly. Many modeling issues arose in this exercise, especially regarding cumulus parameterization. In the end, the model simulated the diurnal cycle well enough to permit a detailed investigation of physical processes. The sea breeze is the most familiar aspect of diurnal variation in coastal regions. An analogous "land breeze" has been invoked to explain nocturnal events, but is unsatisfying in this setting for two reasons: 1. Nocturnal cooling of land is much weaker than daytime heating. 2. Cooling a fluid from below is inefficient at driving circulations. We show that the eruption of convection offshore after midnight is caused not by a land breeze, but rather by gravity waves radiated from the diurnally varying heat source of the mixed layer over land, which is raised up into the stratified layers of the adjacent marine atmosphere by the mountains.

Tuesday, July 8 PM

Presiding Chair: G.L. Geernaert

JSM03/08P/A13-001

1400

**STUDY OF AIR TEMPERATURE MULTI-YEAR VARIATION AND ITS RELATION TO SEA ICE IN THE BOHAI SEA USING EMD METHOD**Jie SU<sup>1</sup>, Jinping ZHAO<sup>2</sup> (<sup>1</sup>Oceanography Department, Ocean University of China, <sup>2</sup>First Institute of Oceanography, State Oceanic Administration)

In this paper, Empirical Mode Decomposition (EMD) method was adopted to analyze air temperature multi-year variation and its relation to sea ice. The data was obtained from marine stations along the seashore of the Bohai Sea. EMD method can give new information of data's multi-year variation which other data statistics method can't present. This will provide some ideas of acquiring information that implied in data's frequency. The analysis result shows that the first mode of EMD presents seasonal variation. And air temperature shows obvious regional difference among the stations. The last mode presents long-term variation. Winter contributes to warm trend mainly. The other modes present multi-year variation. Intrinsic relation exists between air temperature and sea ice feature in the Bohai Sea.

JSM03/08P/A13-002

1420

**EFFECTS OF STABILITY WITHIN SPARSE CANOPIES ON AERODYNAMIC RESISTANCE IN ROUGHNESS SUBLAYER OBTAINED BY WIND TUNNEL EXPERIMENT**

Susumu KURITA (Atmospheric Environment and Applied Meteorology Research Department, Meteorological Research Institute)

Under neutral and weakly stable conditions, effects of stability within sparse canopies on aerodynamic resistance in roughness sublayer above it were studied systematically by wind tunnel experiment using Laser Doppler anemometer and cold-wire thermometer. Two types of canopy were utilized. One is block canopy and the other is pole canopy. The frontal indexes of them are 0.36 and 0.12, respectively. They belong to sparse canopies. The heights of the elements were 95mm for block, and 100mm for pole, respectively. Fetch was 13.9 m. Stable stratification was established by cooling the floor of the wind tunnel. Including neutral condition, five stabilities were utilized. The stability indexes of the canopies defined by H/L0 ranged from 0 to 0.15. The H is the height of the canopy and L0 is the Obukhov's stability length just above it. One of the purposes of this experiment is to obtain stability dependent feature of horizontal area average in the roughness sublayer above the canopy. The horizontal average of the results were compared with the conventional log-linear treatment, which assumes fixed (neutral) values of roughness length (z0) and zero-plane displacement (d). Following results were found. (1) The aerodynamic resistances obtained show a considerable difference from the conventional treatment for both canopies. (2) Introduction of stability dependencies of the roughness length and zero-plane displacement can compensate the differences. (3) Horizontal average of wind speed and temperature profiles can also be fit by the conventional treatment using the stability dependent parameters in the roughness sublayer. (4) For example, using the conventional log-linear form and the constants recommended by Hogstrom (1996), the zero-plane displacement increased and the roughness length decreased under the stable stratifications. To realize the stable conditions in the wind tunnel of MRI, wind speeds were required to be weak (from 0.85 m/s to 1.5 m/s in inflow). This means that the Reynolds number of the canopies in wind tunnel becomes small compared with that of canopy under atmospheric boundary layer. So there is a possibility that effects of the Reynolds number change caused the results, because the stability change was accompanied by wind speed change at canopy height. To estimate contributions of Reynolds number dependence, wind speed dependencies of the resistances were also obtained under neutral condition. It was found that the effect of wind speed change is very small compared with stability effects. So far effects of a canopy have been parameterized by its geometry only in an atmospheric surface layer. Stability effects within a canopy have not been paid much attention independently. But this is not a *priori* thing as pointed out early. The results of this experiment suggest a possibility that thermal stratification within a canopy may affect on the canopy-atmosphere interaction independently.

JSM03/08P/A13-003

1440

**THE COASTAL OCEAN DRAG COEFFICIENT**

Gerald L. GEERNAERT (Los Alamos National Laboratory)

During the past four decades, the air-sea interaction community has reached a general consensus that the drag coefficient is larger for steep wave conditions and smaller for older wave states. The predictability of the drag coefficient for swell conditions is less certain.

## INTER-ASSOCIATION

These tentative conclusions, in most part, are based on wave and wind stress data measured from stable platforms, most which are located in coastal zones. Recent data from the open ocean, and theoretical analysis of flux divergence for coastal offshore flow, suggest the opposite, i.e., that the wave dependent drag coefficient might, at times, be a misinterpretation of flux computations when there is strong flux divergence in the surface layer. Our analysis suggests that if one correctly treats the surface layer as a layer of weak to moderate flux divergence, drag coefficient measurements will become nearly constant with fetch and will only insignificantly depend on wave state. This presentation will review the data and theory, as it applies to coastal zones, and recommendations on how to go forward will be presented.

**JSM03/08P/A13-004**

**1500**

### COUPLED RADIATIVE AND THERMAL TRANSFER REGIMES OVER SHALLOW-WATER BENTHIC ENVIRONMENTS

Enrico C. PARINGIT, Kazuo NADAOKA (Department of Civil Engineering, Graduate School of science and Engineering, Tokyo Institute of Technology)

Knowledge on the regimes and dynamics of thermal and light climate is essential for proper understanding of biological responses from shallow-water benthic flora and fauna. A method to compute combined heat conduction and radiative transfer in a transparent water medium is proposed. The heat equation is solved by an implicit finite-difference scheme and the radiation is simulated using a ray-tracing method for different types of benthic structures such as seagrasses, corals, macroalgae and sand. Stability and convergence for the coupling of both methods is shown together with its performance relative to field measurements of temperature and irradiance. The model is extended to predict light requirements and heat tolerance, potential distributions and densities of benthic habitats in turbid, light-limited environments as a function of flow, degree of nutrient enrichment, sediment abundance and effect of inland outflows. The implications of modeling for monitoring and remote sensing temperature and irradiance retrievals, particularly of coral reef areas are discussed.

**JSM03/08P/A13-005**

**1540**

### LAND OCEAN INTERACTIONS IN THE COASTAL ZONE: ON THE ROLE OF COASTAL FLORA IN STABILIZING TERRESTRIAL GAINS

Balchand N. ALUNGAL (IAPSO)

The tropical shoreline of State of Kerala exhibits features of dynamic equilibrium acting under varying forces of land - ocean interactions. Erosion/deposition is common along the coastal plain, particularly during the southwest monsoon season when wind - wave - precipitation is predominant to alter beach stability. However, in recent years, conspicuously, coastal flora is playing a significant role in stabilizing those areas which have been won over from the sea. Social forestry coupled with active beach protection measures ensures the upkeep and stability of many a number of sites along the vulnerable beaches. The integration of new plant species and continued vegetation practices have aided acceleration to beach nourishment programs apart from implementing concrete steps to take advantage of land - ocean interactions. The coastal processes are described in light of changes in ocean dynamics during different seasons and the appropriate approaches on a regional to local scale are elaborated in order to achieve better results. These include use and regulation of beaches and material therein, promotion of eco-friendly coastal flora growth, restricted human interferences, wave damping - cum - regulated beach sediment movements, conducive eco-tourism and all the more, a through perspective of the prevailing coastal climate and its responses to land - ocean interactions. Examples from Azhikkal, Vypeen, Thankkasherry and other locations of Kerala state exemplify the ongoing practices and the resultant achievements.

**JSM03/08P/A13-006**

**1600**

### CHANGE IN CHLOROPHYLL CONCENTRATION AFTER EARTHQUAKES AND ASSOCIATED LAND-OCEAN-ATMOSPHERIC PROCESSES

Ramesh P. SINGH<sup>1</sup>, Sagnik DEY<sup>2</sup> (<sup>1</sup>Professor, Department of Civil Engineering, Indian Institute of Technology, Kanpur, <sup>2</sup>Department of Civil Engineering, Indian Institute of Technology, Kanpur)

Earthquake is a complex phenomenon, which induces change in land, ocean and atmospheric parameters. Detailed analysis of multisensor data has been carried out to study the changes in ocean and atmospheric parameters. Significant changes in chlorophyll concentrations in ocean have been found along the Gujarat coast after the earthquake. In the present paper, we present the analysis of IRS P4 OCM (Ocean Color Monitor) data. Prior and after the Andaman earthquake (13.087 N, 93.112 E) of September 14, 2002. IRS P4 OCM data have better ground resolution (236 m along track and 360 m across track) compared to SeaWiFS data. The data are mostly covered by clouds, however the chlorophyll concentrations from the cloud free regions have been deduced which show changes in chlorophyll concentration after the Andaman earthquake of September 14, 2002. The significant changes in chlorophyll-a concentrations in the ocean are also found to be associated with other earthquakes around the globe. The detailed analysis of OCM and SeaWiFS data from the earthquake affected region show that the chlorophyll concentration is associated with the shallow earthquakes (focal depth < 30 km). The associated land-ocean-atmosphere processes will be discussed in view of the changes observed after the earthquake.

**JSM03/08P/A13-007**

**1620**

### TRANSFERTS DE FLUX ET STABILIT - DE LA FACADE MARITIME DU DELTA DU FLEUVE SÉNÉGAL

Alioune KANE (department of geography/ Faculty of Arts and Human Sciences/ University Cheikh Anta Diop)

La bordure maritime du delta du fleuve Sénégal entre dans la catégorie des littoraux où l'équilibre des côtes sableuses est le résultat d'un bilan qui concerne la plage, mais aussi tout le profil actif, du sommet du cordon dunaire aux fonds de 10 à 20 m environ. C'est un système complexe et instable sous l'effet de la conjugaison de phénomènes naturels et de phénomènes anthropiques liés à l'édification du barrage de Diama. Le delta du Sénégal a été classé parmi le type extrême à prédominance très nette des effets de houle, qui a pour résultat une dérive littorale édifiant des cordons littoraux parallèles à la côte. Les contours de la côte du delta du Sénégal sont le résultat d'un état d'équilibre entre l'action du fleuve et des courants de houle. Au niveau et en aval de Saint-Louis, le fleuve n'est séparé de l'océan que par un cordon sableux. La Langue de Barbarie, résultat d'un long processus alternatif d'engraissement et de démaigrissement de la plage par la dérive littorale. L'embouchure du Sénégal, depuis son origine, s'est acheminée régulièrement vers le sud, avec des replis de 4 - 5 km vers le nord. L'évolution du bief estuarien est sous la dépendance des apports sédimentaires transportés par les flots de la crue, et par les actions de remontée des eaux

océaniques dans l'estuaire. Les observations à Gandiole montrent une variation moyenne en volume se traduit par un déficit de l'ordre de 400 m<sup>3</sup> par mètre linéaire de rive, soit un approfondissement de 30 cm. Le transport solide du fleuve Sénégal reste relativement faible. C'est un fleuve de faible compétence dans l'estuaire, qui ne joue pas un rôle essentiel dans l'édification de la flèche littorale, mais peut contribuer à l'érosion des cordons. L'embouchure jusqu'à Gandiole demeure largement sous influence marine avec des courants de marée qui semblent s'intensifier, empêchant l'envasement du chenal qu'on note plus au nord. L'évolution sédimentologique montre vers l'embouchure, un lit du fleuve chargé en sables à grains moyens et homogènes. Plus en amont, les formations sont des dépôts fluvio-deltaïques sableux fins silto - argileux, le lit du fleuve se charge en sables fins à très fins et plus hétérogènes. La fraction fine négligeable dans les sédiments de l'embouchure devient importante dès qu'on remonte le bief estuarien. Les sables sont grossiers en fin de crue du fait de la prépondérance des apports marins et de l'érosion des berges. Par contre là où le chenal est limité par des dépôts fluvio - deltaïques et où les actions marines sont réduites, les lutites deviennent très importantes dans les sédiments. L'instabilité de l'embouchure du fleuve demeure limitée depuis l'avènement des barrages. En vue des aménagements portuaires, les profondeurs relevées sont insuffisantes pour permettre une navigation de gros bateaux pour assurer le désenclavement du Mali. La sédimentation marine dominante constitue un obstacle majeur pour la navigation.

**JSM03/08P/A13-008**

**1640**

### RESERVOIR INTERCEPTION OF GLOBAL SEDIMENT FLUX TO THE COASTAL ZONE

Charles J. VOROSMARTY<sup>1</sup>, Michel MEYBECK<sup>2</sup>, Balazs M. FEKETE<sup>3</sup>, Keshav SHARMA<sup>4</sup>, Pamela GREEN<sup>1</sup>, James SYVITSKI<sup>1</sup> (<sup>1</sup>Water Systems Analysis Group, University of New Hampshire, <sup>2</sup>Earth Sciences Department, University of New Hampshire, <sup>3</sup>UMR Sisyphe, Université de Paris IV, <sup>4</sup>Dept of Hydrology and Meteorology, Babar Mahal, <sup>5</sup>INSTAAR, University of Colorado at Boulder)

A framework for estimating global-scale impacts from reservoir construction on riverine sediment transport to the ocean is presented. Study results depict a large, global-scale, and growing impact from anthropogenic impoundment. This study analyzes data on 633 of the world's largest reservoirs (LRs) ( $\geq 0.5$  km<sup>3</sup> maximum storage) and uses statistical inference to assess the impact of the remaining >44,000 smaller reservoirs (SRs). Information on the LRs was linked to a digitized river network at 30ÅE(latitude x longitude) resolution. A residence time change (Dtr) for otherwise free-flowing river water is determined locally at each reservoir and used with a sediment retention function to predict the proportion of incident sediment flux trapped within each impoundment. More than 40% of global river discharge is intercepted locally by the LRs analyzed and a significant proportion (= 70%) of this discharge maintains a sediment trapping efficiency in excess of 50%. Half of all discharge entering LRs shows a local trapping efficiency of 80% or more. Several large basins such as the Colorado and Nile show nearly complete trapping due to large reservoir construction and flow diversion. From the standpoint of sediment retention rates, the most heavily regulated drainage basins reside in Europe. North America, Africa, Australia/Oceania are also strongly affected by LRs. Globally, greater than 50% of basin-scale sediment flux in regulated basins is potentially trapped in artificial impoundments, with a discharge-weighted sediment trapping due to LRs of 30%, and an additional contribution of 23% from SRs. If we consider both regulated and unregulated basins, the interception of global sediment flux by all registered reservoirs (n = 45,000) is conservatively placed at 4 to 5 Gt yr<sup>-1</sup> or 25-30% of the total. There is an additional but unknown impact due to still smaller unregistered impoundments (n = 800,000). From a global change perspective, the long-term impact of such hydraulic engineering works on the world's coastal zone appears to be significant but has yet to be fully elucidated.

**JSM03/08P/A13-009**

**1700**

### APPLICATION OF LASER STRAINMETERS IN GEOPHYSICAL STUDIES OF TRANSITIONAL ZONES

Grigoriy I. DOLGIKH (Dep. of Seismoacoustics)

Laser strainmeters have been applied in geophysical studies for a long time. Laser strainmeters of IPIO FED RAN are applied to the study of generation and dynamics of infrasonic waves in the hydrosphere and their transformation at the atmosphere-hydrosphere-lithosphere interface. Using laser strainmeters of the equal-and unequal-arm types in one-coordinate, two-coordinate, and spaced variants, the following results were obtained: the loading effect of the diurnal and semi-diurnal ocean tides on the microstrain level of the crust was estimated; some ultralow-frequency oscillations of the Earth can be produced by seiche of adjacent water areas; the energy of internal sea waves is not transformed into the energy of small-scale turbulence, as was previously believed, but is converted into the energy of elastic vibrations of the seafloor (lithosphere); and general regular patterns of the origination of microseisms of first and second kind due to the interaction of standing and traveling waves with the seafloor in the shelf zone have been established and their main spectral characteristics have been studied. During the interaction of internal and surface sea waves with the seafloor, the energy is withdrawn into the lithosphere, mostly in the form of Rayleigh waves, and the major semiaxis of the polarization ellipse of the latter contributes most to vertical displacements of the crust. In order to obtain accurate numerical estimates of the energy withdrawn into the lithosphere, not only horizontal components of displacements but also vertical ones should be measured. For this purpose, a laser strainmeter with a vertically oriented measuring arm should be developed and mounted in a hole of a suitable size. The joint use of vertical and two horizontal (oriented N-S and E-W) laser strainmeters is promising for the environmental monitoring in a wide frequency range with energy estimation of wave processes and study of main parameters of waves and vibrations, as well as the medium of their propagation. In 2000, a laser strainmeter with a vertically oriented measuring 3.5-m arm was created and tested at a distance of 50 m from a horizontal laser strainmeter with a measuring 52.5-m arm at the marine expedition station of IPIO FED RAN (the Shultz Promontory). Both laser strainmeters are located on the Sea of Japan coast 30 m above the sea level. Their optical schemes are based on a modified Michelson interferometer using as a light source a frequency-stabilized He-Ne laser with a long-term stability of . The main parameters of the setup are as follows: a sensitivity , a microdisplacement measurement accuracy of 0.3 nm, the working frequency range from (conventionally) 0 to 1000 Hz, and a virtually unlimited dynamic range. The possibility of joint application of vertically and horizontally oriented laser strainmeters in geophysical studies of transitional zones is analyzed in a case study of recording elastic vibrations and waves from a seismoacoustic frequency-tuned radiator and earthquakes, as well as surface sea waves.

**JSM03-Posters**

**Wednesday, July 9**

**LAND-OCEAN-ATMOSPHERE INTERACTIONS IN THE COASTAL ZONE (IAMAS, IAPSO, IAHS)**

Location: Site D

Wednesday, July 9 AM

JSM03/09A/D-001 Poster 0830-035

**NUMERICAL SIMULATION OF STRONG WIND SITUATIONS NEAR THE MEDITERRANEAN FRENCH COAST: COMPARISON WITH FETCH DATA**Alessandro PEZZOLI<sup>1</sup>, Gilles TEDESCHF, François RESCH<sup>2</sup> (<sup>1</sup>DITIC - Turin Polytechnic (ITALY), <sup>2</sup>LEPI - University of Toulon and Var (FRANCE))

A detailed analysis of typical strong wind situations near the Mediterranean French coast is presented. Special attention is focused on the NNW wind in the Gulf of Lions that is commonly called Mistral. The analysis is made from both the synoptic and mesoscale point of view, with the aid of numerical simulations based on the RAMS model (Regional Atmospheric Modelling System). The main atmospheric, climatic and meteorological characteristics are discussed. The simulations were carried out using this model from 20 to 22 March 1998 and from 24 to 26 March 1998. Afterwards a comparison was made with meteorological measurements collected during the international FETCH campaign in the Gulf of Lions in March and April 1998. The comparison between simulated wind fields and values measured by coastal meteorological stations and oceanographic buoys at sea help to fully understand the complicated physical processes that characterize strong wind situations in coastal zones. Indeed, the results of the model show that, on the one hand it is possible to observe a representation of the wind direction by the model that can be considered close to the reality, while, on the other hand, the calculated wind speed values are, in most cases, underestimated compared with the measured values. It is noted, however, that this is a discrepancy commonly observed in the study and analysis of strong winds coming from the land in an unstable atmosphere and complex orography. In such cases, models are able to simulate the phenomena but often underestimate the wind speed. It is for this reason that it becomes essential, during the final now-casting phase, to compare the measured values with the calculated results. This consideration helps to understand how important it is to have reliable measurements distributed over the entire field using remote measuring methodologies for capturing the meteorological parameters. Furthermore, the comparison between the wind fields at sea obtained by the RAMS model and the wind direction and intensity values measured by the ASIS buoy confirms the effective variability of the Mistral. The study also shows how, under unstable atmospheric conditions, the wind rapidly changes direction and intensity from the coast towards the open sea. Consequently, the wave fetch cannot be considered as constant in space when the wind is coming from the land. This latter consideration is particularly important since the parametric equations that give the significant wave height and the wave period are based on the hypothesis of a constant fetch and completely ignore the atmospheric stratification of the boundary layer. It is therefore possible to conclude that it could be interesting to analyse, in a future research, the possibility of introducing correction factors into these equations. These equations could be based on the thermal characteristic parameters of the boundary layer deduced from in-situ measurements or, possibly more promising, from data obtained from simulations using atmospheric models with limited scale.

JSM03/09A/D-002 Poster 0830-036

**PROFILE MEASUREMENT OF THREE-DIMENSIONAL WIND SPEED OVER A COASTAL ZONE OF SHIMOJI ISLAND, JAPAN**

Tetsuya HIYAMA, Hiroki TANAKA, Atsushi HIGUCHI, Taro SHINODA, Kenji NAKAMURA (Hydropheric Atmospheric Research Center, Nagoya University)

For better understanding the development of lower atmospheric boundary layer (ABL) over the ocean, a profile measurement of three-dimensional wind speed has been carried out on Shimoji Island, Japan. The observation period was from 21 to 27 August 2002. This observation has been conducted as a part of the Lower Atmosphere and Precipitation Study (LAPS), Core Research for Evolutional Science and Technology (CREST), Japan Science and Technology Corporation (JST). A Doppler Sodar (Acoustic Wind Profiler; XFAS, Scintec, Germany) was used for the measurement. It measures Doppler shift of acoustic waves backscattered due to atmospheric turbulence for a vertical beam and four oblique beams. Using 10 frequencies of acoustic waves, vertical profiles of three-dimensional wind speed and those variances due to turbulent fluctuation were obtained up to the inversion height of the ABL. From the flux measurement deployed on the Cape Nishi-Henna-saki, Miyako Island, the observation period was divided into two short periods according to the dominant wind direction. These were northern wind from 21 to 23 August (P-N period), and southern wind with fluctuation from 24 to 27 (P-S period). Although the Doppler Sodar was located less than 500 m inland from the coast during P-N period, large values of vertical wind speed and its variances were observed from 100 up to 700 m (inversion height) above the ground surface. The maximum values of vertical wind speed and its variances were around 0.5 ms<sup>-1</sup> which observed in the middle of the ABL. A mobile research aircraft observation using a model aircraft (Aerosonde, Australia), equipped with temperature and humidity sensors, revealed occurrences of turbulent plumes over the sea surface. Thus it seemed that the Doppler Sodar has also detected the turbulent plumes developed on the sub-tropical sea surface. Because the sensible and latent heat fluxes over the sea surface were from -2 to 32 Wm<sup>-2</sup> and from 0 to 145 Wm<sup>-2</sup>, respectively, it seemed that the turbulent plumes were developed due to a wet convection system. Turbulent plumes occurred over the sub-tropical sea surface have rarely been observed in previous studies. This study suggests importance of shallow convection system within humid ABL over the sub-tropical sea surface.

JSM03/09A/D-003 Poster 0830-037

**FLUX OBSERVATION ON THE CAPE NISHI-HENNA-SAKI, SOUTHWESTERN ISLAND, JAPAN**

Hiroki TANAKA, Tetsuya HIYAMA, Kenji NAKAMURA (Nagoya University)

In order to understand the lower boundary condition for development of atmospheric boundary layer over the ocean, a flux observation has been carried out on the tip of the Cape Nishi-Henna-saki, Hirara city, Japan, at 24.91N and 125.26E, from 15th to 27th August 2002. The observation has been conducted as part of the Lower Atmosphere and Precipitation Study (LAPS), Core Research for Evolutional Science and Technology (CREST), Japan Science and Technology Corporation (JST). The measured items on a 10-meter mast were the solar radiation, reflective radiation, atmospheric radiation, sensible heat flux, latent heat flux, momentum flux, carbon dioxide flux, sea surface temperature, ground surface temperature, air temperature profile, relative humidity profile, and the wind velocity profile. The seawater temperature also measured at 5 points under the sea surface. The sea surfaces were expanded from north or southwest from the observation mast, while land surfaces covered with bush were distributed southeast, and a rock pinnacle was mounted on the northwest edge of the cape. Observed solar radiation exceeded 1000Wm<sup>-2</sup> on clear days, and the averaged value was 298Wm<sup>-2</sup>. The reflective radiation, which might mainly come from the land surface around the mast, was observed as 20% of the solar radiation. The atmospheric radiation varied from 380-420Wm<sup>-2</sup> at nighttime to 450-500Wm<sup>-2</sup> in daytime, accompanied with the change in the air temperature. The mean atmospheric radiation was 428Wm<sup>-2</sup>. The sea surface temperature obtained by an infrared radiometer agreed well with seawater temperature sensors, when it was computed using the emissivity

of 0.97. The seawater temperature varied 28.9-30.9 degree during the first half of the observation period and 29.4-32.7degree during the second when the wind velocity was smaller. The wind velocity suddenly decreased at 21:00 on 22nd August, then the wind direction suddenly changed at 20:00 on 23rd August from north to south. The observation period was divided into three short periods according to the dominant wind direction. The wind direction was southeast during the period P-SE from 15th to 17th, north during the P-N from 18th to 23rd, and mainly south but fluctuated during the P-S from 24th to 27th. The latent heat and carbon dioxide fluxes during the P-SE and part of the P-S showed the effect of the plant's activities such as transpiration, respiration, and photosynthesis, while the fluxes might be come from the northern sea surface during the P-N. The sensible heat flux during the P-N varied -2-32Wm<sup>-2</sup> and the latent heat flux 0-145Wm<sup>-2</sup>. The average values were 9Wm<sup>-2</sup> for the sensible heat flux and 58Wm<sup>-2</sup> for the latent heat flux.

JSM04

Wednesday, July 9

**TERRESTRIAL ECOSYSTEMS, ATMOSPHERIC COMPOSITION, CLIMATE (IAMAS, IAGA)**

Location: Site B, Room 23

Wednesday, July 9 AM

Presiding Chair: H. Akimoto

JSM04/09A/B23-001

0900

**THE IMPACT OF LAND-USE CHANGE ON GREENHOUSE GAS EMISSIONS IN TROPICAL ASIA**

Haru TSURUTA<sup>1</sup>, Shigehiro ISHIZUKA<sup>2</sup>, Yasuhiro NAKAJIMA<sup>3</sup>, Seiichiro YONEMURA<sup>3</sup>, Shigetō SUDO<sup>4</sup>, Kazuyuki INUBUSHI<sup>5</sup>, Shingo UEDA<sup>6</sup>, Daniel MURDIYARSO<sup>7</sup>, Iswandi ANAS<sup>8</sup>, Abdul HADI<sup>9</sup>, Mochamad ALP<sup>10</sup> (<sup>1</sup>Faculty of Agriculture, Tokyo University of Agriculture and Technology, <sup>2</sup>Forestry and Forest Product Research Institute, JAPAN, <sup>3</sup>National Institute for Agro-Environmental Sciences, JAPAN, <sup>4</sup>Department of Horticulture, Chiba University, JAPAN, <sup>5</sup>College of Bioresource Sciences, Nihon University, JAPAN, <sup>6</sup>Bogor Agricultural University, INDONESIA, <sup>7</sup>Lambung Mangkurat University, INDONESIA, <sup>8</sup>Jambi University, INDONESIA)

Land-use change in the Asia-Pacific region has been rapidly progressing since the 1970s, and part of tropical forests has been converted to agricultural fields, rubber and oil-palm plantations, which is different from that in tropical America and Africa. The impact of land-use change on the greenhouse gas (GHG) emissions, however, was not studied in southeast Asia. An intensive field program on the influence of land-use change in terrestrial ecosystems on GHG emissions and soil dynamics was carried out during 1997-2002, in Sumatra and Kalimantan, Indonesia, where humid tropical forests and peat wetlands are typical terrestrial ecosystems. The following sub-programme were included: (1) Field measurements of GHG emissions (CO<sub>2</sub>, CH<sub>4</sub>, N<sub>2</sub>O) from soils under different land-use and on a regional scale in humid tropical forests in Jambi province, Sumatra, and in peat wetlands in south Kalimantan and east Jambi; (2) Studies on controlling factors of greenhouse gas emissions from soils in humid tropical forests in Jambi; (3) Meteorological and biological influences on carbon dioxide(CO<sub>2</sub>) flux and carbon budget in the tropical secondary forests in Bukit Soeharto, Samalinda, east Kalimantan, and (4) Development of database for ecosystem changes and of methodology for scaling-up the estimate of GHG emission on a regional scale. The major findings of (1) and (2) are summarized as follows: (1) N<sub>2</sub>O emission rate from humid tropical forests in Jambi was less than 10 ugN m<sup>-2</sup> h<sup>-1</sup> much lower than in other tropical regions, and was affected by soil and land-use types. N<sub>2</sub>O emission was greatly enhanced after the forest was cut and burned, while it decreased to the same level as that before deforestation within two and half years. Nitrification is the major process for N<sub>2</sub>O production by incubation experiment. The uptake rate of CH<sub>4</sub> was about 20 ug m<sup>-2</sup> h<sup>-1</sup>, and CH<sub>4</sub> flux frequently was positive, which was strongly affected by termite. It was very low after the forest was cut and burned, and was gradually increased to the same level as that before deforestation. The emission of CO<sub>2</sub> from the forest soils was lower than in other tropical regions. (2) In peat wetlands in South Kalimantan, N<sub>2</sub>O emission rate was in a range of 0.06-0.14 mgN m<sup>-2</sup> h<sup>-1</sup>, higher than in the humid tropical forests in Jambi. CH<sub>4</sub> emission rate was less than 3 mg m<sup>-2</sup> h<sup>-1</sup> much lower than in Amazonia, and rice paddy fields. The land-use change in peat wetlands to agricultural fields also enhanced the GHG emissions.

JSM04/09A/B23-002

0930

**ATMOSPHERIC TRACE GAS EMISSIONS FROM LIVESTOCK IN SOUTH, SOUTHEAST, AND EAST ASIA**

Kazuyo YAMAJI, Hajime AKIMOTO, Toshimasa OHARA (Frontier Research System for Global Change)

Our group has been developing an original emission database of atmospheric trace compositions to provide input data for models predicting future atmospheric and climate change. We focus on the spatial distribution of trace gas emissions with high resolution of a 0.5 degree x 0.5 degree latitude-longitude. The target area of this study is South, Southeast, East Asia, that is one of the most important sources of various trace gases and is also an area worthy of attention in the light of the atmospheric composition change which may be brought about by the changes of industrial structure, life style, and land use due to economic growth here. In this presentation, we focus on atmospheric trace gas emissions from livestock which is one of important anthropogenic sources of atmospheric compositions, CH<sub>4</sub>, NH<sub>3</sub>, and N<sub>2</sub>O. The increase of human population and the changes of land use due to recent rapid economic growth have expanded livestock breeding and changed its forms, especially in South, Southeast, and East Asia, so it is worthwhile to construct more accurate the emission database incorporating emission factors and activity data with enough regional specifics and detailed geographical information in this area. Hence, this presentation shows the spatial distribution of CH<sub>4</sub>, NH<sub>3</sub>, and N<sub>2</sub>O from livestock in South, Southeast, and East Asia in 2000 with a 0.5 degree x 0.5 degree. The basic methodologies to obtain the emissions were quoted from the IPCC guidelines and the EMPE / CORINAIR guidebooks. These emissions were estimated using livestock populations in each country and in divided regions of some countries (India, China and Japan) and the emission factors with considering regional specificity. Our primary source of the livestock population was the FAO database. In addition, livestock populations at province (state, prefecture etc.) level were available from other countries' statistical databases. As country specific emission factors for some countries were used, CH<sub>4</sub> emissions from livestock which summed up emissions from their manure management systems and enteric fermentation were about 30 TgCH<sub>4</sub> comparatively agreed with emissions calculated from the default IPCC emission factors. NH<sub>3</sub> and N<sub>2</sub>O from manure management systems were estimated at about 13.0 TgNH<sub>3</sub>-N and 0.3 TgN<sub>2</sub>O-N using the default emission factors, respectively. These emissions were allocated into a 0.5 degree grid indicating vegetations and land covers that domestic animals seem to

## INTER-ASSOCIATION

be bred on using grided datasets; area grid database (GPW area estimates on a 2.5' grid); land cover database (AARS Asia 30-second Land Cover Data Set); 1km mesh dataset in geographical information for Japan. With expanded livestock populations in this area, on the other hand, these emissions have been increasing recently, for example, CH<sub>4</sub> emissions from livestock increased at a rate of 2% a year during 1965-2000 in average. In particular, recent upward tendency was remarkable in China.

**JSM04/09A/B23-003**

**1000**

### **CARBON ISOTOPE EXCHANGE BETWEEN THE ATMOSPHERE AND BIOSPHERE: IMPACT OF LAND-USE**

Marko SCHOLZE (Max-Planck-Institut für Meteorology)

One of the fundamental challenges in carbon cycle studies concern the identification of the different sources and sinks of atmospheric CO<sub>2</sub>. Changes in the concentration and stable isotope ratio of atmospheric CO<sub>2</sub> can be used to constrain the global carbon budget and imply location and magnitude of carbon sources and sinks. During the last years the global average rate of CO<sub>2</sub> increase and also the isotopic ratio of carbon dioxide has varied widely and somewhat irregularly, and it is believed that the terrestrial biosphere contributes significantly to these signals. A common top-down method to infer the ocean and land contributions to these variations is the double-deconvolution of the atmospheric CO<sub>2</sub> and <sup>13</sup>C records. This partitioning calculation is sensitive to various quantities, one of them the assumed isotopic disequilibrium between uptake and release of terrestrial carbon. However, the isotopic signature of the terrestrial biosphere is highly variable in space and time due to vegetation composition but also to inter-annual climatic variability. Here, the isotope LPJ framework, which includes isotopic fractionation of <sup>13</sup>C during assimilation and a full isotopic terrestrial carbon cycle, is used to calculate the atmosphere-biosphere exchange flux of CO<sub>2</sub> and its  $\delta^{13}C$  for the years 1901 to 1998. The model thus allows a quantitative analysis of both, the net ecosystem exchange of CO<sub>2</sub> and <sup>13</sup>C with the atmosphere as a function of present and past equilibrium and transient observed forcing factors: changes in atmospheric CO<sub>2</sub> and its isotope ratio, climate and changes in land use over the industrial era (approx. last 100 years). In addition, the impact of C<sub>4</sub> land use (e.g., corn and sugarcane but also tropical C<sub>4</sub> pastures) on the isotopic disequilibrium will be analyzed.

**JSM04/09A/B23-004**

**1030**

### **STABLE CARBON ISOTOPES IN SEDIMENTS OF THE EAST-SIBERIAN SEA**

Igor P. SEMILETOV<sup>1</sup>, Oleg DUDAREV<sup>2</sup>, Kyung-Hoon SHIN<sup>1</sup>, Nori TANAKA<sup>1</sup> (<sup>1</sup>International Arctic Research Center/University Alaska Fairbanks, <sup>2</sup>Pacific Oceanological Institute)

The Arctic Ocean accounts for 20% of the world's continental shelves. The amount of terrestrial organic carbon stored in the wide circum-Arctic shelf and slope areas is certainly of importance for calculation of organic carbon budgets on a global scale [Aagaard et al., 1999; Codispoti et al., 1990; Gobeil et al., 2001; Macdonald et al., 1998]. Greater than 90% of all organic carbon burial occurs in sediment deposition on deltas, continental shelves, and upper continental slopes [Hedges et al., 1999], and the significant portion of organic carbon withdraw occurs over the Siberian shelf [Bauch et al., 2000, Fahl and Stein, 1999]. The Arctic coastal zone plays a significant role in the regional budget of carbon transport, accumulation, transformation, and seaward export. Hydro-chemical anomalies obtained over the shallow Siberian shelves demonstrate significant role of coastal erosion in the formation of the biogeochemical regime in the Arctic seas [Semiletov, 1999; Dudarev et al., 2001] that could affect a hydro-chemical regime of the surface and halocline waters over the Arctic Basin. Determining the magnitude of particulate and dissolved fluxes of old organic carbon and other terrestrial material from land is critical to constraining a range of issues in the Arctic shelf-basin system, including carbon cycling, the health of the ecosystem, and interpretation of sediment records. Most of the eroded terrestrial organic matter accumulates in coastal zones; however, significant amounts of this material are transported further offshore by different processes, such as sea-ice, ocean currents, and turbidity currents. The role of the coastal zone in transport and fate of terrestrial organic carbon has not been discussed sufficiently. In this report we present a new data about the distribution of the organic carbon (C-13) and nitrogen (N-15) isotope ratios, OC/N, mineralogy and size distribution of the surface sediment in the most unexplored area of the Arctic Ocean: the East-Siberian Sea.

**JSM04/09A/B23-005**

**1115**

### **BIOSPHERIC CONTROL OF ATMOSPHERIC COMPOSITION IN AMAZONIA**

Paulo ARTAXO<sup>1</sup>, Meinrat O. ANDREAE<sup>2</sup>, Alex B. GUENTHER<sup>3</sup>, Daniel ROSENFELD<sup>4</sup>, Luciana V. GATTI<sup>5</sup>, Jose V. MARTINS<sup>6</sup> (<sup>1</sup>Instituto de Física, Universidade de São Paulo, Rua do Matao, Travessa R, 187, São Paulo, SP, CEP 05508-900, Brazil, <sup>2</sup>Biogeochemistry Department, Max Planck Institute for Chemistry, P.O. Box 3060, D-55020 Mainz, Germany, <sup>3</sup>Atmospheric Chemistry Division, National Center for Atmospheric Research, PO Box 3000, Boulder CO USA 80307-3000, United States, <sup>4</sup>Institute of Earth Sciences, The Hebrew University of Jerusalem, Jerusalem 91904, Israel, <sup>5</sup>Laboratório de Química Atmosférica, IPEN, Av. Lineu Pretes, 2242; Cidade Universitária, São Paulo, CEP 05508-900, Brazil.)

There is growing evidence that the Amazonian forest has some mechanisms that controls the composition of the atmosphere above it, in terms of trace gases and aerosols. The majority of the cloud condensation nuclei population (CCN) under natural conditions is biogenic in origin. The CCN population consists of small particles from gas-to-particle conversion of some biogenic VOCs, and in the large particle fraction there is a significant number of primary biogenic aerosol particles that are efficient as CCN. Under pristine conditions, PM10 aerosol concentrations are in the range of 10-15 ug/m<sup>3</sup>, of which 70-80% consists of organic matter. Natural sulfate and nitrate concentrations are very low compared to other sites influenced by anthropogenic emissions. Due to the high precipitation rate, the basin-wide influence of marine aerosols is small. Concentrations of soil dust particles are also low, because the forest litter and low wind speeds under the forest canopy makes soil resuspension difficult for most of the forested area of Amazonia. The cloud field is of shallow clouds, mostly with warm precipitation, making a quite efficient precipitation mechanism. The emission of VOCs from the vegetation varies significantly both seasonally and geographically, and the control mechanisms are not fully understood. Ozone concentrations in undisturbed forest are low (peaks at 10-14 ppb), and CO background concentrations are on the range of 50-100 ppb. The forest CO<sub>2</sub> flux have strong seasonal dependence, from the dry to the wet season, and also varies from site to site, but in general consists of a small sink of CO<sub>2</sub>. The radiative forcing of aerosol particles in the dry season is very strong, peaking at up to 300 watts/m<sup>2</sup>. The complex biospheric control of the atmospheric composition possibly has some important climate feedbacks.

**JSM04/09A/B23-006**

**1145**

### **A COMPARISON OF MODIS AEROSOL OPTICAL THICKNESS TO HANDHELD SUN PHOTOMETER AND AERONET SUN PHOTOMETER MEASUREMENTS DURING THE DRY SEASON IN WESTERN AMAZON BASIN, BRAZIL, 2002**

Wei Min HAO<sup>1</sup>, R.E. BABBITT<sup>1</sup>, B.L. NORDGREN<sup>1</sup>, E.N. LINCOLN<sup>1</sup>, S.P. BAKER<sup>1</sup>, R.A. SUSOTT<sup>1</sup>, M. YAMASOE<sup>2</sup>, P. ARTAXO<sup>3</sup>, B.N. HOLBEN<sup>4</sup> (<sup>1</sup>USDA Forest Service Fire Sciences Laboratory, Missoula MT, <sup>2</sup>Instituto de Astronomia, Geofísica e Ciências Atmosféricas, Universidade de São Paulo, SP, Brazil, <sup>3</sup>Instituto de Física, Universidade de São Paulo, SP, Brazil, <sup>4</sup>NASA/Goddard Space Flight Center, Laboratory for Terrestrial Physics, Greenbelt, MD)

The MODIS instrument on the NASA Terra and Aqua satellites provides global measurements of aerosol optical thickness (AOT). Our previous work during the fire season in Zambia, 2000 has shown that the MODIS AOT was lower by 40%-50% compared to ground-based measurements of Forest Service handheld sunphotometers and AERONET sun photometers. Part of the algorithm used to derive the MODIS aerosol optical thickness was based on the results of field experiments during the SCAR-B Campaign in Brazil, 1995. Therefore, it is essential that we compare the MODIS AOT with the AOT values from ground-based measurements in Brazil. Thirty-five handheld sun photometers were deployed in the Western Amazon Basin, Brazil from early September to late October 2002, coinciding with the LBA-SMOCC Campaign. The sites were distributed over a wide variety of land cover types. Eight of the 35 handheld sun photometers were co-located with AERONET sun photometers in the study area. We also retrieved more than 260 MODIS AOT images from the Terra satellite and 180 AOT images from the Aqua satellite over the study area. We will present the results of the comparison in aerosol optical thickness at spectral bands of about 660, 550 and 470 nm measured by the MODIS instruments, handheld sun photometers, and AERONET sun photometers. We will discuss the effects of land cover properties, look angles, and the homogeneity of atmosphere on the derivation of aerosol optical thickness from the MODIS instruments.

**JSM04/09A/B23-007**

**1215**

### **A DETAILED MICROCLIMATE MODEL TO PREDICT BVOC EMISSION FLUXES ABOVE THE CANOPY**

Sabine A. WALLENS<sup>1</sup>, Jean-Francois J. MULLER<sup>1</sup>, Alex B. GUENTHER<sup>2</sup> (<sup>1</sup>BIRA-IASB (Belgian Institute for Space Aeronomy), <sup>2</sup>NCAR-ACD)

Natural emissions of volatile compounds are an important component of the Earth system responsible for determining the composition of the atmosphere. The biogenic volatile organic compounds (BVOC) are produced by vegetation and emitted into the atmosphere. In addition, the emissions of BVOC depend on the leaf level microclimate, in particular on leaf temperature and Photosynthetically Active Radiation (PAR) (Guenther et al., 1993, 1995). For these reasons, the need for accurate estimates of BVOC emissions as input to global chemistry and transport model led us to 1) the development of a detailed canopy environment model and 2) the validation of the BVOC emission algorithms used in Guenther et al., 1995. Among the large Earth ecosystems, tropical rainforests are estimated to be a major source of BVOC, mainly isoprene and monoterpenes. Here, we present comparisons between the emission fluxes estimated using a detailed canopy model and measurements obtained in a typical forest, Tapajós in Amazonia.

**Wednesday, July 9 PM**

Presiding Chair: H. Akimoto

**JSM04/09P/B23-001**

**1400**

### **CARBON AND NITROGEN WET DEPOSITION IN AMAZON BASIN: CONSEQUENCES OF LAND-USE CHANGES**

Luciene Lorandi LARA<sup>1</sup>, Paulo ARTAXO<sup>2</sup>, Theotônio PAULIQUEVIS<sup>3</sup> (<sup>1</sup>Lab of Isotopic Ecology, University of São Paulo, <sup>2</sup>Instituto de Física, Universidade de São Paulo Brazil)

In tropical regions convective clouds produce abundant rainfalls which are the main sink of water-soluble gases and aerosols emitted into the atmosphere through wet deposition processes. Wet deposition plays an essential role in controlling the biogeochemical cycles of carbon and nitrogen and as a source of nutrients to ecosystems. In the LBA experiment (Large Scale Biosphere Atmosphere Experiment in Amazonia), rainwater chemistry composition has been studied in three different sites: Rondonia, Balbina and Santarem, with different degrees of anthropogenic activities. Rondonia site is located in the western part of Amazonia, and is a heavily disturbed site with significant land use changes. Balbina is located in Central Amazonia, about 150 Km North of Manaus and represents a pristine area and Santarem is the closest site to the sea. During one year samples of rain water were sampled and analyzed for ion chromatography (inorganic and organic ion), DOC (dissolved organic carbon) and DIC (dissolved inorganic carbon). For the three sampling sites H<sup>+</sup> was the most abundant ion. However, the sequence of the other most abundant ions was not the same for the sites, indicating that there are differences in the composition of the rainwater in these sites. In fact, due to the anthropogenic activities, N deposition was significantly higher in Rondonia while DOC deposition was significantly lower in this site. By the other hand, in Balbina the VWM concentration of organic anions (acetate, formate, oxalate) was significantly higher than the other sites, which is probably associated with biogenic emissions. Principal component analysis results showed that there are different sources of rain acidity in each site, which are associated with land cover. The main source of compounds in the rainwater composition are also different in these three sites. Biomass burning appears to be the main source in Rondonia, biogenic emissions in Balbina and in Santarem a mixing of sea-salt and biogenic emissions. If the deforestation process continues at the present rate, in a few years, significant regional biogeochemical cycles changes can be expected and, also alterations in the regional climate with possible global impacts.

**JSM04/09P/B23-002**

**1430**

### **VARIABILITY IN GLOBAL AND DIFFUSE PAR AT A TROPICAL SOUTHEAST ASIAN SITE AND ITS SIGNIFICANCE FOR TERRESTRIAL PHOTOSYNTHESIS**

Dennis G. DYE<sup>1</sup>, Yoshifumi YASUOKA<sup>2</sup>, Akkaneeewut CHABANGBORN<sup>3</sup>, Boossarasiri THANA<sup>4</sup> (<sup>1</sup>Ecosystem Change Research Program, Frontier Research System for Global Change, Japan, <sup>2</sup>Ecosystem Change Research Program, FRSGC, and IIS, Univ. of Tokyo, Japan, <sup>3</sup>Dept. of Geology, Chulalongkorn Univ., Thailand)

Recent research indicates that the radiation-use efficiency and CO<sub>2</sub> assimilation rate of an unstressed vegetation canopy tends to increase as the diffuse fraction of incident (global) photosynthetically active radiation (PAR, 400-700 nm) increases. Because measurement data on diffuse PAR are rare, much of this research has relied upon model estimates of diffuse PAR. Such estimates typically ignore the 3-dimensional cloud effects on the surface irradiance, and thus may include biases or uncertainties that hinder a more exact

determination of radiation-canopy-photosynthesis relations. As part of a broad effort aimed at an improved ability to monitor PAR by satellite remote sensing and to model the role of PAR dynamics in the terrestrial carbon cycle, we have initiated a project to measure diffuse and global PAR at multiple sites representing diverse ecosystems and climate regimes. In this paper, we examine variability in global, diffuse, and direct PAR at a seasonally moist tropical site in north-central Thailand (Sri Samrong, 17.1 deg. N, 99.9 deg. E), and discuss its significance for modeling of vegetation canopy light absorption, primary production and ecosystem-atmosphere carbon exchange.

JSM04/09P/B23-003

1500

#### METHANE EMISSION FROM RICE FIELDS IN MAINLAND CHINA: AMOUNT, SEASONAL AND SPATIAL DISTRIBUTION

Xiaoyuan Yan YAN<sup>1</sup>, Zucong CAF, Toshimasa OHARA<sup>1</sup>, Hajime AKIMOTO<sup>1</sup> (Frontier Research System for Global Change, <sup>1</sup>Institute of Soil Science, Chinese Academy of Sciences)

China is the largest rice producer in the world. Methane (CH<sub>4</sub>) emission from its rice fields has been widely measured since the late 1980s. In this study, we collected results of most of the field studies available so far, which constitutes 207 season-treatment measurements conducted on 23 sites. Analysis of these data shows that input of organic materials such as green manure, animal waste, and crop straw increases CH<sub>4</sub> emission by a factor of 2; average CH<sub>4</sub> flux from intermittently irrigated rice fields is 53% of that from continuously flooded rice field; and average CH<sub>4</sub> emission flux from late rice fields is 1.6 and 2.3 times those from early and single rice fields. There is regional difference in emission factors, with a decreasing trend from south to north. We assume half of the rice fields in China received organic input and two-thirds of the irrigated rice fields were intermittently flooded by taking into account of expert judgments and the frequencies of these managements in field studies. Based on these assumptions and the region-specific emission factors and statistical data on rice area of 1995, we estimated CH<sub>4</sub> emission from rice fields during rice-growing season (from transplanting to harvest) in Mainland China to be 7.67 Tg yr<sup>-1</sup>, with a range of 5.82 to 9.57 Tg CH<sub>4</sub> yr<sup>-1</sup> due to the uncertainties in the assumption on rice area receiving organic input and under intermittent irrigation. This estimate is significantly lower than many earlier ones. A generalized seasonal flux pattern was developed separately for early, late and single rice. Monthly distribution of the annual emission was estimated from rice calendar and these flux patterns, showed that highest emission occurs in August. Geographically, the emission mainly occurs in the middle and lower reaches of Yangtze River, around 30°N.

JSM04/09P/B23-004

1600

#### ANNUAL VARIATION AND LONG-TERM OF GREENHOUSE GASES CONCENTRATION AND IT'S CAUSES IN THE BACKGROUND AREA OF THE KOREAN PENINSULA

Jae-Cheon CHOI<sup>1</sup>, Hyo-Sang CHUNG<sup>2</sup>, Sung-Nam OH<sup>1</sup>, So-Young BANG<sup>1</sup>, sang-Soon PARK<sup>1</sup> (<sup>1</sup>Korea Global Atmosphere Watch Observatory of KMA, <sup>2</sup>Meteorological Research Institute, KMA)

The greenhouse gas is one of the major parameters of climate change which makes a role of positive radiative forcing, and Korea Meteorological Research Institute (METRI) has started systematic monitoring on the greenhouse gases recently, in Korea Global Atmospheric Watch Observatory (KGAWO) in Anmyeon-do, which is a regional station measuring the background concentration in East-Asian region. In this study, the fluctuation tendency of greenhouse gases is analyzed by using 3-year measurement (January 1999–December 2001) of KGAWO. The measured CO<sub>2</sub> concentration data is validated by the method of World Data Center for Greenhouse Gases (WDCGG), and compared with the flask sampling data operated by NOAA/CMDL, to assess the level of greenhouse gases in Korea. The variation of the concentration by wind direction and other meteorological parameters is also investigated from the measured data. By using statistical method, the relationships among each greenhouse gas and trace gases are analysed to explain the effect on the background concentration. The results of this study is expected to be an essential information for the prediction of climate change in Korean peninsula, and to establish a tool for prediction of climate change by learning the advanced application technology of climate data in participating the round robin. The measurement of greenhouse gases which is used in this study will be operated systematically based on the standard of WMO, so that it will be used as a basic information to work out a counter measure for the united nations framework convention on climate change.

JSM04/09P/B23-005

1630

#### INFLUENCES OF THE WARMING ON PLANT PHENOLOGY IN EAST ASIA

Futoshi MATSUMOTO, Yoshitaka FUKUOKA (Rissshou University)

Recent changes of plant phenology such as budding, flowering and change in color and falling of leaves are related to global warming. For example flowering dates of cherry blossoms (*Prunus yedoensis*) have been getting earlier annually in Japan. Because many weather stations which observe the plant phenology are located in urban area. So it is considered that these phenomena are caused by climatic changes such as urban warming including global warming. In this study the authors examined the effects of urban warming on flowering dates of *Prunus yedoensis* in Kumagaya City, Saitama Prefecture, Japan. This study consists of observing both the distribution of flowering dates of *Prunus yedoensis* and the spatial urban climate at the same time in spring in urban area. The objects of this study are firstly to evaluate how urban climate influences the flowering dates of *Prunus yedoensis*, and secondly to search whether the flowering dates of *Prunus yedoensis* are possible indicators that show climatic changes such as urban warming including global warming. The results of this study are follows: 1. Flowering dates of *Prunus yedoensis* in the center are 2 days earlier than those in the suburbs in urban area. 2. Heat island phenomena, which are known as high temperature occurrences in central part of a city, are observed. Therefore it is concluded that heat island influences the flowering dates of *Prunus yedoensis*. Heat island or the distribution of urban temperatures at observation time is calibrated to the mean monthly temperatures in March, which has a close relation to the flowering dates of *Prunus yedoensis*. As a result, the mean difference between mean monthly temperatures in urban area (at the earliest flowering dates points) and that in suburban area (at the latest flowering dates points) is evaluated as 0.64 degrees. So it is estimated that the influences of urban warming on the spatial quickening of the flowering dates of *Prunus yedoensis* are at a rate of 1 day per about 0.3 degrees. 3. On the other hand, the influences of warming on the year-to-year quickening of flowering dates of *Prunus yedoensis* at Kumagaya Meteorological Observatory are also at a rate of 1 day per about 0.3 degrees. And it is possible to evaluate the effects of urban warming by substituting the spatial variation in Kumagaya City for the year-to-year variation of flowering dates of *Prunus yedoensis* at Kumagaya Meteorological Observatory. 4. It is clarified that the flowering dates of *Prunus yedoensis* are possible indicators that show climatic changes and urban warming.

JSM04/09P/B23-006

1700

#### VARIABILITY OF AEROSOL PARAMETERS IN NORTHERN INDIA

Sagnik DEY<sup>1</sup>, Ramesh P. SINGH<sup>1</sup>, Brent HOLBERN<sup>2</sup> (<sup>1</sup>Department of Civil Engineering, Indian Institute of Technology, Kanpur, India, <sup>2</sup>NASA Goddard Space Flight Center, Greenbelt, Maryland 20771, USA)

**ABSTRACT** Due to the urbanization and industrialization in the Ganga basin the pollution level is increasing, which has been mapped by ADEOS Polder 1 data. The air pollution in this region has also been detected by satellite data. The observations are supported by the measurements by CIMEL SUNPHOTOMETER, deployed in Kanpur in collaboration with NASA AERONET on January 2001. In the present paper, the seasonal variations of the spectral aerosol optical depth (AOD), size distribution of the aerosols, the radiative forcing of the aerosols which affect the climatic condition of the region and single scattering albedo (SSA) have been studied using CIMEL SUNPHOTOMETER. The aerosol over the Kanpur shows strong seasonal influence. Seasonal variability of the AOD shows highest values (> 0.7) during the month of August. Another peak in the AOD values has been observed during the month of November, but only at the wavelengths less than 500 nm. The size distributions of the aerosols indicate considerable amount of anthropogenic input over the last few years. The air monitoring data measured by Central Pollution Control Board supports the increasing air pollution. The SSA, a climatically unique parameter retrieved by AERONET and its significance in the climate of the north India has also been studied. The spectral and temporal variability of the aerosol parameters over northern India will be discussed in view of the meteorological parameters and the increasing human activities as a part of the monitoring the air pollution in the northern India.

JSM04/09P/B23-007

1730

#### WEATHER DROUGHT INDEX AND FIRE IN BERBAK PARK, SUMATRA

Asril Asril ASRIL<sup>1</sup>, Daniel MURDIYARSO<sup>2</sup>, Bambang Hero SAHARJO<sup>2</sup> (<sup>1</sup>Agency for the Assessment and Application of Technology, <sup>2</sup>Post Graduate Program, Bogor Agricultural University)

The fires in Sumatra and Kalimantan in 1997 have caused extensive environmental damage including transboundary haze that blanketed the region and the neighbouring countries. Around 10.5 million hectares land and forest have burnt (Saharjo, 1999) with total cost (caused by fire and haze) of more than US\$ 9 billion (ADB, 2001). Climate and weather, together but in different way, affect forest fire (Chandler, *et al.*, 1983). This study is conducted at Berbak National Park, Sumatra and aimed at evaluating fire opportunity based on weather dryness index, fuel characteristics and burning practices conducted by the local people. Weather dryness index (named Keetch-Byram Dryness Index, KBDI) is determined by Keetch-Byram method that employs daily maximum air temperature and 24-hour rainfall as inputs (Keetch and Byram, 1968). Biomass measurements to estimate fuel load follow Hairiah, *et al.* (1999). Fire intensity to identify the intensity of a fire was calculated using Byram's equation (Chandler, *et al.*, 1983). Fuel load was observed at two areas, representing the protected area inside the Berbak National Park (including the area that burnt in 1997 fire) and the buffer zone of the park. The results show that the peaks of drought occur between May and October. The drought intensity varies throughout the years and extreme drought when the KBDI was higher than 1,950 occurred in 1991, 1993, 1994 and 1997. The longest and most extreme drought occurred in 1997 from August 1st through November 9th. The fire in Berbak Park began at least early September (Dennis, 1999), after extreme drought occurred for a month. The similar drought pattern occurred in 1994 but there was no fire in Berbak Park. Surface fuel load at protected zone was 647.4 ton/ha and at buffer zone was 139.4 ton/ha. Dead-fuel moisture at protected zone (40 %) was relatively higher than at buffer zone (17 %). Fuels at both study area were able to burn (flammable) since their moisture content lower than the moisture of extinction, the maximum moisture content that a fuel can have and still support flaming combustion (Chandler, *et al.*, 1983). Fuels at protected zone were more burnable since they had silica content (4.75 %) lower than at buffer area (6.63 %). Based on these fuel characteristics, the protected zone was at higher danger to catch fire. Fire intensity at several burning practices varied between 90 kW/m at small fire flame and 1,994 kW/m at big fire flame. Fire from several burning practices may escape and ignite unexpected fires. It is seemed that the combine of extreme drought and burning practice have caused the fire in Berbak Park.

JSM04-Posters

Wednesday, July 9

#### TERRESTRIAL ECOSYSTEMS, ATMOSPHERIC COMPOSITION, CLIMATE (IAMAS, IAGA)

Location: Site D

Wednesday, July 9 PM

JSM04/09P/D-001

Poster

1400-038

#### THE CLIMATIC SIGNIFICANCE OF δ<sup>13</sup>C IN TREE-RING ON TIBET AND THE IMPLICATIONS FOR CLIMATIC RECONSTRUCTIONS

Xiaohong LIU<sup>1</sup>, Dahe QIN<sup>1</sup>, Xuemei SHAO<sup>2</sup>, Tuo CHEN<sup>1</sup>, Jiawen REN<sup>1</sup> (<sup>1</sup>Cold and Arid regions environment and engineering research institute, Chinese academy of sciences, <sup>2</sup>Institute of Geographic Sciences and Nature Resources Research, CAS)

Based on cross-dating tree-ring age, stable carbon isotope ratios in tree rings were measured on the α-cellulose of Linzhi region on Tibetan plateau. The global-descending of delta-<sup>13</sup>C in CO<sub>2</sub> which induced by the increasing concentration of atmosphere carbon dioxide, were recorded in delta-<sup>13</sup>C series of fir and spruce. There are different response to concentration change of CO<sub>2</sub> between two species. Through the standardization of delta-<sup>13</sup>C series (Δ<sup>13</sup>C), there were common climatic information in two delta-<sup>13</sup>C series. Using meteorological data from Nyingchi observatory, the responds of standardization series of delta-<sup>13</sup>C to climatic factors were analyzed. The results suggest that the Δ<sup>13</sup>C time series is in good correlation with precipitation and relative humidity of 9-11 months in local instrumental data, and with strong "lag effect". Compared with other results in China and other countries, the Δ<sup>13</sup>C series with good relationship to the climatic factors of 9-11 month (November) are different with the climatic information in delta-<sup>13</sup>C of trees in arid region and Semi-arid region. This difference may be a results of distinct climate on Tibetan plateau.

**JSM04/09P/D-002** Poster **1400-039****STABLE CARBON ISOTOPE EXCHANGE BETWEEN THE TERRESTRIAL BIOSPHERE AND ATMOSPHERE SIMULATED BY AN ECOSYSTEM MODEL**

Akihiko ITO (Ecosystem Change Research Program, Frontier Research System for Global Change)

There remain substantial uncertainties in stable carbon isotope ( $^{12}\text{C}$  and  $^{13}\text{C}$ ) dynamics of terrestrial ecosystems, leading to an uncertainty in our quantification of the global carbon cycle. The uncertainties include the followings. (1) How strong is the discrimination effect of photosynthetic  $\text{CO}_2$  assimilation on stable carbon isotope ratio (i.e.  $\delta^{13}\text{C}$ )? (2) How much carbon is assimilated by  $\text{C}_4$  plants, which have disparate isotopic discrimination effect from  $\text{C}_3$  plants? (3) How much of  $\text{CO}_2$  released from plant and soil is re-cycled within canopy, leading to apparently larger isotopic discrimination effect? (4) How large isotopic disequilibrium does take place, due to human emission of  $\text{CO}_2$  with lower  $\delta^{13}\text{C}$  to the atmosphere? In this study, we address these uncertainties with a process-based model of terrestrial carbon cycle (Sim-CYCLE), in which terrestrial carbon dynamics from photosynthesis to decomposition is simulated in an ecophysiological manner. Sim-CYCLE considers the isotopic discrimination effect at three levels: (I) leaf-level gas exchange and enzymatic  $\text{CO}_2$  assimilation, (II) canopy-level recycling of  $\text{CO}_2$  respired from plants and microbes, and (III) continental-level distribution of  $\text{C}_3$  and  $\text{C}_4$  plants in grassland ecosystems. Based on the NCEP/NCAR reanalysis climate data and observed concentration and  $\delta^{13}\text{C}$  of the atmospheric  $\text{CO}_2$ , carbon budget of the terrestrial biosphere was estimated for the period from 1953 to 1999. Sim-CYCLE estimated that the average annual gross photosynthesis is  $121 \text{ Pg C}$ , and average isotopic discrimination (compared with  $\delta^{13}\text{C}$  of atmospheric  $\text{CO}_2$ ) is  $-18.2$  per mil. The recycling of  $\text{CO}_2$  within canopy resulted in a larger discrimination effect by on average  $2.1$  per mil; this effect was especially larger in closed forests with higher leaf area index. Because of the predominance of  $\text{C}_4$  plants, tropical savannas and temperate grasslands have smaller isotopic discrimination than forest ecosystems. Interannual variability in the magnitude of discrimination effect seems small, compared with latitudinal and seasonal variability. During the 47-year experimental period, average  $\delta^{13}\text{C}$  value of the biospheric carbon storage decreased by  $0.3$  per mil, while  $\delta^{13}\text{C}$  of atmospheric  $\text{CO}_2$  dropped by  $0.7$  per mil. The long residence time of biospheric carbon, especially in woody stem and soil humus, is responsible for the isotopic disequilibrium. These results are verified by comparing with observations at different site, with respect to seasonal phase and amplitude of atmospheric  $\text{CO}_2$  concentration and isotopic composition. Based on the simulation result, finally, I will discuss how to improve our understanding of the global carbon cycle by means of stable isotopes and model experiments.

**JSM04/09P/D-003** Poster **1400-040****THERMAL HISTORY RECONSTRUCTION AND THERMAL MATURATION OF HYDROCARBON-BEARING FORMATION IN EAST CHINA SEA BASIN**Shengbiao HU<sup>1</sup>, Shuchun YANG<sup>1</sup>, Dongsheng CAI<sup>2</sup>, Xiaojie FENG<sup>2</sup> (<sup>1</sup>Institute of Geology & Geophysics, Chinese Academy of Sciences, <sup>2</sup>Research Center, China National Offshore Oil Corporation)

Based upon the available vitrinite reflectance and fission track data as well as present-day temperature logs from borehole in the East China Sea Basin, thermal history are reconstructed and applied to the maturation of source rocks. The pre-Tertiary formation, distributed in the western Taibei Depression reached their maximum paleotemperature at the Paleocene, with a average paleo-heat flow value of  $81 \text{ mW/m}^2$ , and the Tertiary formation in the eastern Xihu Depression experienced their maximum temperature at the end of the Oligocene, with a mean of paleo-heat flow of  $83 \text{ mW/m}^2$ , corresponding the end of rifting as indicated by the subsidence history. Incorporated with the thickness of the removed section on the unconformity, the hydrocarbon generation period and maturation for both the pre-Tertiary and Tertiary formations have been evaluated.

**JSM04/09P/D-004** Poster **1400-041****INFLUENCE OF WATER SOLUBLE SALTS ON THE ICE NUCLEATING ABILITY OF AGI-AGCL-CUI WATER**

Sivanesan SUBRAMANIAN, Balasubramaniam NALLATHAMBI, Ramamurthy VEERAPPAN (Chemical Engineering)

Salt content is an inescapable factor which will have bearing upon the heterogeneous freezing nucleation of cloud droplets in the atmosphere. Moreover, the generator effluent that contains appreciable amount of soluble salts largely affects the ice nucleating properties of the seeding materials. More relevant to natural or induced precipitation process in clouds are possibly the studies made with specific nucleants along with soluble salts. From the survey of literature, it has been found that the heterogeneous freezing nucleation can be appreciably influenced by the soluble salts and the effects were found to be specific to each nucleant tested. In the earlier studies the author has reported that the 50:25:25 mole percent composition of AgI, AgCl and CuI has the lowest misfit with ice and hence the highest nucleation temperature. In order to evaluate the solute effects on this specific AgI-AgCl-CuI ice nucleant, the present study has been undertaken. This will help to draw a conclusion of the influence of soluble salts on the ice nucleability of AgI-AgCl-CuI. Salts such as NaCl, MgCl<sub>2</sub> and Na<sub>2</sub>SO<sub>4</sub> were chosen. Since they include a number of components of sea salt, which is one of the main sources of hygroscopic aerosols. In addition, the halides of NH<sub>4</sub> and Li, the sulphates of K, Na, NH<sub>4</sub> and Mg were also considered. In the present study, the various salt solutions at different concentrations with the nucleant have shown an appreciable influence on nucleation temperature. Also, the activity is found to decrease with the increase in concentration of the salts, due to the production of water disruption and breaking of bonds by the salts. Among the soluble salts examined, the sulphates have better performance with nucleant at  $0.01 \text{ M}$  concentration. As a matter of fact, (NH<sub>4</sub>)<sub>2</sub>SO<sub>4</sub> at  $0.01 \text{ M}$  concentration has significantly improved the nucleation activity of the nucleant and the nucleation temperature is as high as  $-0.60 \text{ }^\circ\text{C}$ . The possible reason for the enhanced nucleation activity has been discussed.

**JSM04/09P/D-005** Poster **1400-042****A NUMERICAL STUDY OF GLOBAL CO<sub>2</sub> INTERACTIONS USING SIM-CYCLES BIOSPHERE MODEL**Takao IGUCHI<sup>1</sup>, Hideji KIDA<sup>2</sup> (<sup>1</sup>Disaster Prevention Research Institute, Kyoto University, <sup>2</sup>Department of Geophysics, Graduate School of Science, Kyoto University)

To investigate the role of terrestrial ecosystems to play in the global budget of atmospheric  $\text{CO}_2$ , numerical simulations were performed using a global transport model and a biosphere model (Sim-CYCLE). The transport model developed by Iguchi and Kida calculates three-dimensional  $\text{CO}_2$  distribution. The Sim-CYCLE model of Ito and Oikawa (1998) predicts the amount change of carbons in plant and soil. Both models are driven by given wind, temperature, pressure, humidity, solar radiation, and so on. In this study, ECMWF/TOGA and NCEP/NCAR re-analysis data sets were employed. The first stage of  $\text{CO}_2$  increasing

experiment was run with Sim-CYCLE only.  $\text{CO}_2$  increase since the industrial revolution was decided by the data of ice core collected at Antarctica and  $\text{CO}_2$  monitoring at Mauna Loa, Hawaii. As input climate data, NCEP/NCAR reanalysis data set for 50 years (1951-2000) was repeatedly used for the 250 years experiment. Our result showed that the carbon reservoir of terrestrial ecosystems increased as atmospheric  $\text{CO}_2$  concentration did. 10 years average of increase of carbon reservoir in 1990s was  $1.57 \text{ GtC/yr}$ . Inter-annual variation of flux was approximately  $1.0 \text{ GtC/yr}$  in maximum amplitude. Next, atmospheric  $\text{CO}_2$  distribution of 1990 was simulated together with the transport model and Sim-CYCLE. The two models are combined through  $\text{CO}_2$  concentrations; the change of carbon reservoir of terrestrial ecosystems calculated by Sim-CYCLE was treated as  $\text{CO}_2$  flux in the lowest layer of transport model, and the  $\text{CO}_2$  concentrations calculated by the transport model were input to Sim-CYCLE. Time step is 20 minutes for the transport model and 1 day for Sim-CYCLE. There is no diurnal variance of  $\text{CO}_2$  flux from vegetation. As  $\text{CO}_2$  flux from fossil fuel combustion, ocean, and land use change, NASA/GISS  $\text{CO}_2$  flux data was used. The result at beginning day of the 1990 in the former  $\text{CO}_2$  increasing examination was given as the initial condition of the simulation. The present result was compared with the observation and also the result of our past simulation using the transport model including  $\text{CO}_2$  flux data from vegetation. For observed  $\text{CO}_2$  distribution, WMO/WDCGG observation data set was employed and the  $\text{CO}_2$  concentrations at the grid points were interpolated from the observed data. Our past simulation without the Sim-CYCLE model showed some unsatisfied discrepancies of seasonal change of zonal mean of  $\text{CO}_2$  concentrations, but the present simulation with the ecosystem model greatly improved such past shortcoming. In concluding, the need of a  $\text{CO}_2$  ecosystem is stressed in this study and the estimated carbon absorption by terrestrial ecosystems in 1990 was  $1.24 \text{ GtC}$ .

**JSM04/09P/D-006** Poster **1400-043****TRACE ELEMENTS IN ANDEAN BACKGROUND AEROSOL FROM A NEVADO ILLIMANI ICE CORE, BOLIVIA, FROM 1919 TO 1999**Alexandre L. CORREIA<sup>1</sup>, Robert J. DELMAS<sup>2</sup>, Remi FREYDIERE<sup>3</sup>, Jefferson C. SIMOES<sup>4</sup>, Jean-Denis TAUPIN<sup>5</sup>, Bernard DUPRE<sup>6</sup>, Paulo ARTAXO<sup>6</sup> (<sup>1</sup>Institute of Physics, University of Sao Paulo, Rua do Matao, Tr R. 187, 05508-900 Sao Paulo, Brazil; <sup>2</sup>LGGE, CNRS and Universite Joseph Fourier, <sup>3</sup>LGGE, CNRS and Universite Joseph Fourier, <sup>4</sup>UMR5563, LMTG, CNRS and Universite Paul Sabatier, <sup>5</sup>Institute of Geosciences, University of Rio Grande do Sul, <sup>6</sup>LGGE and IRD, <sup>7</sup>Institute of Physics, University of Sao Paulo)

Atmospheric aerosols play an important role in climate, with physico-chemical characteristics highly variable in temporal and spatial scales. In South America only a limited number of studies have documented these characteristics over the Andes Cordillera. This work addresses this issue, by studying the trace elemental composition of aerosol deposited in an ice core along 20<sup>th</sup> century over Eastern Andes, which receive a strong impact from easterly air masses coming from Amazon Basin. In 1999 a 137 m ice core was drilled from Eastern Bolivian Andes (Cordillera Real) at the summit of Nevado Illimani ( $16^\circ 37' \text{ S}$ ,  $67^\circ 46' \text{ W}$ , 6350 m asl). The upper 50 m of this ice core were dated by multi-proxy analysis. This 50-m ice core section corresponds to a record of environmental variations of about 80 years from 1919 to 1999. It was sub-sampled under laminar flow in a clean bench in 744 aliquots. These aliquots were analyzed by several techniques, among which Inductively Coupled Plasma Mass Spectrometry (ICP-MS) for the concentration of 45 chemical species from Li to U. The high number of samples produced translates into high temporal resolution along the record, allowing classification of samples as belonging to dry or wet seasons. Average Li concentration along 20<sup>th</sup> century is  $0.035$  and  $0.90 \text{ ng g}^{-1}$  for wet and dry seasons, respectively. Main Li sources in the region are ubiquitous salt lakes, like Salar de Uyuni for instance. Regional crustal dust load in the aerosol deposits is overwhelming during dry season, obfuscating the contribution of other possible sources like plumes of biomass burning from Amazon Basin. As a result of that, dry season aerosol has low crustal enrichment factors and typically high elemental concentration values, while wet season samples are more enriched and show lower elemental concentration values. Heavy metals typically associated with anthropic origins show high average crustal enrichment factors, indicating a contribution of these sources to the aerosol deposits at Illimani. During wet season, average Cu crustal enrichment is above  $10^3$ , while As, Sb, Zn, Cd, Mo, Co, Ni and Cr are between  $10^2$  and  $5 \times 10^2$ . P and K have average wet season enrichment factors above  $10$ . Zn, together with P and K are important elements participating of biogeochemical cycles in Amazon Basin, and their crustal enrichment factors during wet season suggest they may originate from multiple sources. Allying the large number of samples analyzed from Illimani ice core with a simple tool like the assessment of crustal enrichment factors, it was possible to derive an effective chemical characterization of the deposited background Andean soil dust aerosol, based on the 45 elemental concentrations measured, during 20<sup>th</sup> century.

**JSM04/09P/D-007** Poster **1400-044****THE IMPACT OF BIOMASS BURNING SOOT OVER TAIWAN**

Hsiao-Wen LIN, Jen-Ping CHEN (Department of Atmospheric Science, National Taiwan University)

Biomass burning, the burning of vegetation, occurs in developing countries quite frequently. It is one of the sources of greenhouse gases, and also of aerosols. What made it different from other anthropogenic sources is that biomass burning is highly 'episodic' it varies with locations and seasons. Among all the emitted aerosols, soot entered the center stage recently. First, this is because soot not only cools the surface but also heats the atmosphere by absorbing solar radiation. Its warming effect could be compared in the magnitude with greenhouse gases like  $\text{CO}_2$ , CFC, or methane. Furthermore, local air quality is severely influenced by soot. There are several major sources of biomass burning emissions in East Asia. Southeastern Asia is a previously well-known hot spot. But our data showed that Mainland China is also a large source that cannot be ignored. Most intensive emissions occur in springtime, but events in pre-spring wintertime are reported. Since the geographical location of Taiwan is somewhat between two of the heavy emission sources of biomass burning mentioned above, long-range transport of soot from biomass burning over Taiwan is of great concern. However, biomass burning can not be avoided in Taiwan either. To know the impact of soot over Taiwan, we must know the ratio of soot from long-range transport and local emission. To access this, we adopted FLEXPART 3-D Lagrangian trajectory tracer model developed by Andreae Stohl(1996) to see the transport route of biomass burning over East Asia. Then we use the soot emission data in Taiwan Air Quality Module (TAQM) to look at the details of soot transformation during transportation, and to estimate the ratio between long-range transported and locally generated soot. The results will be verified with NASA's MODIS L3 Aerosol Index and Fire product.

**JSM04/09P/D-008** Poster **1400-045****CHEMICAL AND PHYSICAL PROPERTIES OF ASIAN DUST IN KOREA PENINSULAR**Ki-Jun PARK<sup>1</sup>, Jae-Cheon CHOI<sup>1</sup>, So-Young BANG<sup>1</sup>, Sung-Nam OH<sup>2</sup>, Byoung-Cheol CHOI<sup>1</sup>, Kyoung-Sook CHO<sup>1</sup> (<sup>1</sup>Korea Global Atmosphere Watch Observatory of KMA, <sup>2</sup>Meteorological Research Institute, KMA)

Atmospheric particles are emitted from natural sources such as sea spray, volcanic

emissions and yellow sand(or Asian dusts) and from anthropogenic processes such as fossil fuel combustion and industrial emissions. In this study, airborne particle matter(0.3~25µm) and particulate smaller than 10m were collected in Anmyeon-do Korea Atmosphere Watch Observatory (KGAWO). Through the chemical and statistical analysis of particulate composition, an attempt was made to elucidate the chemical characteristics and contributing sources of atmospheric aerosols in Anmyeon-do KGAWO during spring when Asian dust event occurred. The aerosol samples were collected by Optical Particle Counter(OPC), PM<sub>10</sub> High Volume Air Sampler(HVAS) and β-ray PM10 sampler. The sampling of PM<sub>10</sub> has been basically carried out three times a week. The measurement items were mass concentration and chemical composition by PM<sub>10</sub> sampler and particle number concentration by OPC. The aerosol number concentration was also analyzed with the 8 channels(0.30µm-25µm) measurement. In general, the variation of total particle number concentration was well agreed with that of mass concentration by β-ray PM<sub>10</sub> sampler. The major ion components in PM<sub>10</sub> were SO<sub>4</sub><sup>2-</sup> and Ca<sup>2+</sup> with the concentration of severe yellow sand was 8.459µg/m<sup>3</sup> and 10.891µg/m<sup>3</sup>, respectively.

**JSM04/09P/D-009** Poster **1400-046**

**VARIABILITY OF TRACE GAS CONCENTRATIONS DURING THE LBA/SMOCC 2002 BIOMASS BURNING EXPERIMENT IN THE AMAZON BASIN**

Luciana Vanni GATTI<sup>1</sup>, Amelia YAMAZAKI<sup>1</sup>, Carlos A. Bauer AQUINO<sup>2</sup>, Lizia MURBACH<sup>3</sup>, Paulo ARTAXO<sup>3</sup>, Duli CHAND<sup>3</sup>, Meinrat ANDREA<sup>3</sup> (<sup>1</sup>Atmospheric Chemistry Laboratory, Travessa R. 400, CEP 05508-900, Sao Paulo, Brazil - lvgatti@net.ipen.br, <sup>2</sup>Univ. Luterana do Brasil - Ji-Paraná(ULBRA), <sup>3</sup>Instituto de Física, Universidade de Sao Paulo, Brazil, <sup>4</sup>Biogeochemistry Department, Max Planck Institute for Chemistry, Mainz, Germany)

The LBA/SMOCC 2002 experiment (Smoke Aerosols, Clouds, Rainfall and Climate) was aimed at understanding the connection between the composition and abundance of biomass burning aerosol, and its climatic effects, in particular on cloud structure and physics. This experiment was performed in Rondônia, a region in Amazonia that is severally perturbed by biomass burning emissions, with a ground based sampling station located in Ji-Paraná (10°46.42'S, 62°20.22'W). The experiment was run during September to November 2002. The concentrations of O<sub>3</sub>, CO and NO<sub>x</sub> were measured simultaneously with aerosol mass, light scattering and absorption. Several meteorological parameters such as solar radiation, PAR, temperature, humidity, wind speed and direction were also monitored. In the dry season, it was observed three different atmospheric regimes: the peak of burning season (1), the transition where the biomass burning happens at lower scale (2) and the initial part of the wet season (3). During the regime 1, the trace gases concentrations were up to 5 times higher than in the step 3, emphasizing the critical importance of biomass burning in determining atmospheric concentrations in Amazonia. During nighttime, the average for the three regimes for CO concentration were 1,100 ppb, 400 ppb during the step 2 and less than 200 ppb during the step 3. During daytime similar values were around 600, 300 and 150 ppb respectively. The average ozone concentration during the regimes 1 and 2 were the same during daytime, at around 50 ppb, and during nighttime O<sub>3</sub> values were around 13 ppb. The average for the wet season regime was 22 ppb for daytime and 10 ppb for nighttime O<sub>3</sub>. The atmospheric oxidant capacity is so high that the NO concentrations were less than 50 ppt during 95% of the sampling time. A very high correlation for the dry season between CO, NO<sub>x</sub>, and black carbon and aerosol mass was observed, but a rather different variability patterns for NO<sub>x</sub> was observed, probably due to chemical transformations during regional transport. Research project financed by CNPq.

**JSM04/09P/D-010** Poster **1400-047**

**OZONE PROFILES AND AEROSOL MEASUREMENTS OVER THE WESTERN AMAZON DURING THE DRY SEASON**

Ana Maria CORDOVA<sup>1</sup>, L.V. GATTI<sup>1</sup>, P. ARTAXO<sup>2</sup>, K.M. LONGO<sup>3</sup>, A. SILVA DIAS<sup>3</sup>, M.O. ANDREA<sup>3</sup>, G. NISHIOKA<sup>3</sup> (<sup>1</sup>Departament of Environmental Chemistry - IPEN, <sup>2</sup>Instituto de Física, Universidade de São Paulo, Brazil, <sup>3</sup>Instituto de Astronomia, Geofísica e Ciências Atmosféricas, Universidade de São Paulo, Brazil, <sup>4</sup>Centro de Previsão de Tempo e Estudos Climáticos, Brazil, <sup>5</sup>Biogeochemistry Department, Max Planck Institute for Chemistry, Mainz, Germany)

Land use changes in Amazonia cause large changes in atmospheric composition, especially because of the biomass burning emissions during the dry season. Trace gases and aerosol concentrations were measured at ground sites as well as in large scale using an instrumented aircraft, as part of the Smoke Aerosols, Clouds, Rainfall and Climate (SMOCC) experiment in the dry season 2002. Horizontal and vertical distributions of carbon monoxide (CO), ozone (O<sub>3</sub>), carbon dioxide (CO<sub>2</sub>) and aerosol were measured over the Western Amazon. Thirty one flights were performed from 25 September to 19 October 2002 of which twenty-four vertical profiles were performed from 400 to 4500 m in Rondonia and Acre States, Brazil. CO, CO<sub>2</sub> and aerosol concentrations present a good correlation, with general concentrations decreasing with altitude. On the contrary, ozone concentrations present a distinct behavior from the other gases, were in the majority of the cases the O<sub>3</sub> concentrations increases with altitude. The vertical profiles over Rebio Jaru Tower (10° 05,15'S 61° 56,04'W) show concentrations next to surface (500-1500m) of 350-1500 ppb for CO, 4000-6000 particles/cm<sup>3</sup> for aerosol number and 395 ppm for CO<sub>2</sub>. Peaks of CO, CO<sub>2</sub> and aerosol concentrations were observed between 3000 and 4000 m, but the concentrations were lower than near the ground. Ozone presented concentrations of 70 ppb at 3000m, in general, but with strong biomass burning impacts O<sub>3</sub> can present a similar behavior to other gases, with concentrations of 150 ppb near the surface. The higher O<sub>3</sub> concentrations at larger altitudes suggest the influence of long range transport for this gas. Horizontal flights at 990 m from Ji Paraná to Rolim de Moura towns show ozone concentrations of 60 ppb. CO and CO<sub>2</sub> concentrations were 350 ppb and 374 ppm respectively. Aerosol concentrations were on the order of 3,000 particles/cm<sup>3</sup>. Large trace gas and aerosols gradients were observed from regions heavily impacted by biomass burning, to relatively pristine regions, indicating the large atmospheric impact of land use change in Amazonia, with possible regional climatic impacts.

**JSM04/09P/D-011** Poster **1400-048**

**ASSESSMENT OF DAILY EVAPOTRANSPIRATION USING REMOTE SENSING DATA**

Gouldaria Karimovna NOURBAEVA, So KAZAMA, Masaki SAWAMOTO (Department of Civil Engineering, School of Engineering, Tohoku University)

Estimation of daily evapotranspiration is one of the key points in hydrological problems. For practical use the daily value of evapotranspiration (ET) is meaningful. Operational technique to derive daily ET estimates from instantaneous value is based on assumption that diurnal curve of solar radiation can be approximated by sine function. The instantaneous estimation of ET is obtained from the modified Priestly-Taylor equation, which relies primarily on remotely sensed inputs. To derive the ET estimates the coefficient α of Priestly-Taylor equation is ranged using two step linear interpolation based on the correlation between surface temperature and Normalized Difference Vegetation Index (NDVI) value. The parameterization of ET comes from two assumptions, based on physical relationship between land surface parameters. First step was to classify the image pixels by NDVI

values, which were associated with land uses. Within each NDVI class the upper and lower boundaries of parameter α were determined by ranging proportionally to NDVI values, assuming that high ET value can be found on the pixel with maximum NDVI and vice versa. The global minima of parameter α equals to zero and the global maxima can be found on the pixel with the maximum NDVI for whole catchment. At the second step within each NDVI class, the parameter α was corresponded to each pixel using the value of land surface temperature (LST). The classification based on idea that the highest ET value can be obtained from the pixel corresponding to the lowest temperature within NDVI class and the highest temperature pixel gives the lowest NDVI values. Consequently, the ET values for each of the pixels can be determined using the spatial context of remotely sensed parameters LST and NDVI. To assess the land surface temperature value and NDVI within a catchment, the remote sensed data from 1km NOAA-14 AVHRR sensor is utilized. Proposed scheme allows obtaining the time series of daily evapotranspiration map over the Natori River basin in 1992. Results of modeling have reasonable agreement with estimates from general water balance equation and Thornthwaite equation. Taking into account that the data from NOAA-14 AVHRR sensor are available once a day, proposed scheme can be useful for operational assessment of water resources redistribution over a large area at temporal and spatial scale.

**JSM04/09P/D-012** Poster **1400-049**

**MEASUREMENTS OF ISOPRENE FLUXES BY A GRADIENT TECHNIQUE IN DIFFERENT REGIONS IN THE AMAZON FOREST**

Carla R. TROSTDORF<sup>1</sup>, Luciana V. GATTI<sup>1</sup>, Amelia YAMAZAKI<sup>1</sup>, Carlos A.B. AQUINO<sup>2</sup>, Williams C. MARTINS<sup>3</sup>, Lizia L. MURBACH<sup>3</sup> (<sup>1</sup>Department of Environmental Chemistry - IPEN, <sup>2</sup>ULBRA, <sup>3</sup>Universidade Federal do Para)

Volatile organic compounds (VOCs) emissions from vegetation have been estimated to be several times higher than anthropogenic emissions. On a global scale, the largest biogenic VOC emissions occur in the tropics with isoprene being the dominant compound emitted, and tropical rainforests are estimated to be the major source of VOCs into the atmosphere, due to combination of high temperatures and large biomass densities. Measurements of vertical fluxes of isoprene above a west and east Amazon forest by the gradient technique are reported in this paper. The sampling was performed as part of the Large-scale Biosphere atmosphere experiment in Amazonia (LBA) from December, 2001 through October, 2002 at four sites in Amazonian. The first two sites near Santarém, Para State, Brazil in the National Forest of Tapajós, one at a primary forest and another at a forest were selective logging is taking place. The measurements were made at 65 and 55 m heights simultaneously in an LBA Tower. The other two sites are located in the Rondônia state, at a primary forest (Biological Reserve of Jaru) and also at a pasture site (grass vegetation). The forest site is with the gradient measurements taking place at 65 and 55 m above the ground and in the pasture site the gradient measurements are taking place at 8 and 5 m above the ground. The mean daytime isoprene fluxes were 1.5 mg m<sup>-2</sup>h<sup>-1</sup> and 0.9 mg m<sup>-2</sup>h<sup>-1</sup> at the primary forest and selectively logged sites, respectively, and the peak fluxes were 3.0 mg m<sup>-2</sup>h<sup>-1</sup> and 1.0 mg m<sup>-2</sup>h<sup>-1</sup> in the Para State. In the Rondônia state, the mean daytime isoprene fluxes were 1.2 mg m<sup>-2</sup>h<sup>-1</sup> and 0.2 mg m<sup>-2</sup>h<sup>-1</sup> at the primary forest and pasture site, respectively, and the peak fluxes were 3.2 mg m<sup>-2</sup>h<sup>-1</sup> and 0.4 mg m<sup>-2</sup>h<sup>-1</sup>, respectively. The expected seasonality of VOC fluxes and emissions are being captured. The results are being used to evaluate emission models.

**JSM04/09P/D-013** Poster **1400-050**

**GLOBAL CHANGE AND CHANGING CHEMISTRY OF THE ATMOSPHERE: A STUDY WITH REFERENCE TO IMPACT OF HUMAN ACTIVITIES ON AIR POLLUTION IN MAJOR METROPOLITAN CITIES OF INDIA: IDENTIFICATION OF MAJOR DIMENSIONS**

Shanmuganandan SAMARAJALINGAM (Madurai Kamaraj University)

The changing chemistry of the atmosphere has already caused environmental and economic damage to the resource industries (forests, fisheries, agriculture, ecotourism, hydroelectric generation) in tropical countries including India. Some of the atmospheric changes are local but continental- and global scale processes are also at work. The purpose of the present study is to analyze the extent of anthropogenic activities has caused a change in the atmospheric chemistry of major selected metropolitan cities (Delhi, Mumbai (Bombay) and Chennai (Madras)). The study probes into the man made activities responsible for an increase in the concentration of major pollutants (carbon monoxide, nitrous oxide, carbon dioxide etc.) in the selected major metropolitan cities in India and also attempted to identify the major dimensions with reference to selected variables drawn from urbanization, industrialization, socioeconomic and sociocultural activities as initiated by human activities. The study was based on the secondary data collected from published sources and the data were analyzed with the help of multivariate statistical analysis factor analysis to identify the major dimensions. The study has also made an attempt to conduct a perception study of the city dwellers on the impacts of pollution and also possible causes for changing local atmospheric conditions and chemistry. The study identified the major dimensions such Volume of Traffic and atmospheric pollution, Atmospheric pollution and Industrialization, Changing atmospheric chemistry and historic land use changes, Urban growth and Impact of anthropogenic activities and Increasing air pollutants etc. determined local atmospheric conditions of the selected major metropolitan activities. Although the human activities and their extent may differ from region to region, the concentration of air pollutants in various composition ultimately determined the atmospheric chemistry within the Earth system.

**JSM04/09P/D-014** Poster **1400-051**

**WEST SIBERIA REGION AND LARGE URBAN AREA IN NORTHERN EUROPE (ST.-PETERSBURG) AS ATMOSPHERIC METHANE SOURCES**

Svetlana V. JAGOVKINA<sup>1</sup>, Igor L. KAROL<sup>1</sup>, Alexander I. RESHETNIKOV<sup>2</sup>, Nina N. PARAMONOVA<sup>2</sup>, Victor E. LAGUN<sup>3</sup> (<sup>1</sup>Main Geophysical Observatory, <sup>2</sup>Research Center for Atmospheric Remote Sensing, <sup>3</sup>Arctic and Antarctic Research Institute)

Methane plays an important role in atmospheric warming being one of the strongest greenhouse gases. Also methane is among of the main sinks for hydroxyl therefore it influences the life times of active atmospheric species and it is one of the ozone precursors forming the background ozone levels. The atmospheric methane content increases since the middle of XIX century due to anthropogenic impact mainly. Due to the long life time of methane this atmospheric compound is spread almost evenly over the globe, nevertheless there are enclosing strong and permanent methane sources regions with higher methane concentrations, such as West Siberia and some industrial areas. Present investigation is devoted to the assessment and inventory of methane sources from such regions as West Siberia with intensive methane fluxes from gas deposits and wetlands and large urban area (Saint-Petersburg) located in the Northern part of Europe. The estimations of methane emission scenarios, proposed in this study is based on combination of specially organized measurement campaigns with 3D transport modeling of methane distribution which allowed to correct the estimate of methane flux intensity in these regions. The comparison of two regions is presented and main paths of air masses are traced. Statistical analysis of multiyear surface methane measurements near Saint-Petersburg is presented. Seasonal

## INTER-ASSOCIATION

and interannual variations of methane concentration are discussed. Natural and anthropogenic methane fluxes are calculated for studied areas for numerical input estimation into regional and global budget of greenhouse gases.

**JSM04/09P/D-015** Poster **1400-052**

### ATMOSPHERIC TRACE GAS AND AEROSOLS MEASUREMENTS DURING WINTERS OF 1999 TO 2002 IN THE URBAN AREA OF SAO PAULO, BRAZIL

Angelica PRETTO<sup>1</sup>, Luciana Vanni GATTI<sup>1</sup>, Luiz Augusto DE PAULA REINO<sup>1</sup>, Jose Roberto ROGERO<sup>1</sup>, Amelia YAMAZAKI<sup>1</sup>, Paulo ARTAXO<sup>2</sup> (<sup>1</sup>Department of Environmental Chemistry - IPEN, <sup>2</sup>Instituto de Física, Universidade de Sao Paulo, Brazil)

The Sao Paulo city area is located in the south eastern part of Sao Paulo state (23o32'S and 46o38'W). The urban area comprises 8000 km<sup>2</sup> ranging in elevation from 650 to 1200 m. The population is about 18 millions people and 5.5 millions vehicles. Nowadays the main pollutants are NO<sub>2</sub>, NO, CO, PM and Ozone. The vehicular air pollution represents 95% of the total air pollution emission with the remaining 5% mainly generated by industries. A study integrating measurements of ozone (O<sub>3</sub>), nitrogen oxide (NO), nitrogen dioxide (NO<sub>2</sub>), carbon monoxide (CO) and sulphur dioxide (SO<sub>2</sub>) with aerosol mass concentration, organic and elemental carbon concentration and black carbon concentration particle measurements was performed in Sao Paulo at the winters of 1999 to 2002. Meteorological variables such solar radiation, temperature, relative humidity, wind speed and direction were also measured. The objective is to study the associations between trace gas and aerosol particle concentrations with meteorological conditions. The variation of NO<sub>2</sub>, NO, CO, SO<sub>2</sub> and aerosols for favorable dispersion days and unfavorable dispersion days show that the common concentrations of gases related to direct emissions depends of behavior of traffic and of meteorological conditions, such as wind speed and direction for dispersion, boundary layer height, temperature, relative humidity and other factors. The cloudy day has the highest wind speed and the trace gases and aerosols for this days is the smallest concentration because this day good dispersion conditions. The daily variability of O<sub>3</sub>, NO<sub>2</sub>, NO, CO, SO<sub>2</sub> and aerosols with meteorological conditions are discussed and the interrelationship between the trace gas concentrations can be easily observed in the plots. The SO<sub>2</sub> concentrations were very low, because of the reduced emissions in the urban area of Sao Paulo. (Research project financed by FAPESP and CNPq)

**JSM04/09P/D-016** Poster **1400-053**

### SOLAS ACTIVITIES IN CHINA

Guangyu SHI<sup>1</sup>, Hui WANG<sup>2</sup>, Xiu-Lin WANG<sup>3</sup>, Hui-Wang GAO<sup>3</sup>, Xin LI<sup>1</sup> (<sup>1</sup>The Institute of Atmospheric Physics, Chinese Academy of Sciences, China, <sup>2</sup>Division of Marine Science, National Science Foundation of China, Beijing, China, <sup>3</sup>Ocean University of China, Qingdao, China)

During the past two years, Chinese scientist from the oceanic and atmospheric sciences made great efforts to participate in the International Surface Ocean and Lower Atmosphere Study (SOLAS). A Chinese Working Group for SOLAS (CWG-SOLAS) has been established in September, 2001. And a preliminary China – SOLAS Program was reported in the SOLAS Amsterdam Meeting which was held in June, 2002, by Dr. SHI as a national contact person. China SOLAS is intent to focus on biogeochemical interactions between upper ocean and low atmosphere in the regime of China Seas, and is attempting to answer how these biogeochemical interactions will affect the global and regional environmental variability. It reflects overall the initiative for the international SOLAS programs while China SOLAS will be focusing on processes that are critically important in order for tackling China Seas' regional environment issues that have broader global impact. An example is given to Asian dust: its transport, input and its impact on the surface ocean productivity. It emphasized the China Seas in the context of regional and global environmental/climate change since the China Seas are located at a significantly sensitive region in the Earth Climate System modulated by Tibet Plateau and Equatorial Pacific Warm Pool and by significant land-sea interactions driven by large Chinese river systems such as Changjiang, Huanghe and Zhujiang. Considering both of the international SOLAS science plan and actual condition in China Seas, the presentation reflects the six FOCI from the international SOLAS science plan as follows: (1) Exchange processes at the air-sea interface; (2) Air-sea CO<sub>2</sub> flux in China Seas; (3) The impacts of sulfur emission from China Seas on the processes of clouds and radiation; (4) Contribution of Atmospheric Nitrogen Deposition to Nutrients in the China Seas; (5) The impacts of Asian dust on marine primary productivity in China Seas; and (6) Radiation transmission in the atmosphere-ocean system and primary productivity in the coastal waters of China. Each focus is divided in several activities. Recently Chinese National Committee for IGBP (CNC-IGBP) has approved formally to establish a Working Group for SOLAS and the National Science Foundation of China (NSFC) has decided to set up a Key Project for supporting the SOLAS Activities in China. This paper will introduce the China – SOLAS Program, the structure of the CWG-SOLAS and the activities related to the SOLAS in China in some details.

**JSM04/09P/D-017** Poster **1400-054**

### CHARACTERISTICS, TREND AND CHEMICAL COMPOSITION OF ATMOSPHERIC PRECIPITATION AT SHAHROOD, NORTHEAST IRAN

Gholam Abbas KAZEMI, Hossein MEHDIZADEH (Department of Geology, University of Shahrood)

The trend, characteristics and chemical composition of atmospheric precipitation at Shahrood, a medium size city in the northeast Iran, are largely affected by the role of Alborz Mountain Ranges acting as the barrier for the rain bearing clouds originating from the Caspian Sea. While the long term average annual precipitation of the city in the form of snow and rain is 153 mm, a major drought has severely hit the region over the past 9 years causing extensive pressure on existing water resources. Statistical analysis indicate that the present drought is similar to early 1970's drought and is thus expected to last for another 3-4 years. Large temporal variations (daily, monthly and annual) are of the characteristics features of the precipitation in the region. Year 1972, for example, had a rainfall of 286 mm while the total rainfall in year 1961 was only 65 mm, i.e. less than a forth. Similarly, the maximum recorded monthly precipitation is 103 mm, 25 folds higher than 40% of the months which have a rainfall of less than 5 mm. Daily precipitation show the highest variations. In 1996, for instance, 42 mm of rain fell in one day which accounted for 23% of the whole year rain. Chemical analysis of precipitation samples show that while the pH of the precipitation is about 7, its total dissolved solids (TDS) is higher than the world average and reaches 400 mg/l in some events. The dominant cation is calcium with an average concentration of 11.5 mg/l and the average concentration of nitrate and sulfate is 2.4 and 7 mg/l, respectively. There is a good correlation between the depth of precipitation, the number of precedent dry days and the TDS of precipitation at any event. The enrichment factor (the ratio of Ion/Cl sample to the Ion/Cl seawater) for most ions indicates that the precipitation salts are of continental origin. The high TDS of the precipitation is believed to be due to low average rainfall, mountainous landscape, wind and weather pattern, anthropogenic impacts and less likely analytical errors.

**JSM10**

**Monday, July 7 - Tuesday, July 8**

### CRYOSPHERE-CLIMATE INTERACTIONS (IAMAS [ICCL, ICPM], IAPSO, IAHS)

Location: Site B, Room 23

**Monday, July 7 AM**

Presiding Chair: J. Ukita

### THE CRYOSPHERE, SNOW, ICE SHEET MASS BALANCE AND ICE CORES

**JSM10/07A/B23-001**

**0900**

### THE WORLD CLIMATE RESEARCH PROGRAMME (WCRP) CLIMATE AND CRYOSPHERE PROJECT (CLIC): A GLOBAL INITIATIVE

Barry E. GOODISON<sup>1</sup>, Ian ALLISON<sup>2</sup>, Roger G. BARRY<sup>3</sup>, Chad DICK<sup>4</sup>, Vladimir RYABININ<sup>5</sup> (<sup>1</sup>Climate Research Branch, Meteorological Service of Canada, Environment Canada, Downsview, Ontario, Canada M3H 5T4, <sup>2</sup>Australian Antarctic Division and Antarctic CRC, Private Bag 80, Hobart, Tasmania, 7001, Australia, <sup>3</sup>National Snow and Ice Data Center, U. Colorado, Boulder, CO, 80309-0449, U.S.A., <sup>4</sup>International ACSYS/CLIC Project Office, Norwegian Polar Institute, NO-9296, Tromsø Norway, <sup>5</sup>Joint Planning Staff for WCRP, WMO Secretariat, Geneva 2, CH-1211, Switzerland)

The objectives of the World Climate Programme (WCRP) are to understand the physical climate system, develop a predictive capability and understand the extent of human influence on climate. Through its projects – CLIVAR, GEWEX, SPARC and ACSYS/CLIC – WCRP provides a coordinating mechanism for research on the climate system. ACSYS (the Arctic Climate System Study), whose scientific goal is to ascertain the role of the Arctic in global climate, will sunset at the end of 2003. The new core WCRP project "Climate and Cryosphere" (CLIC), established by WCRP in March 2000, is global in scope. CLIC aims to improve understanding of the cryosphere (snow cover, sea-, lake- and river- ice, glaciers and ice caps, ice sheets and shelves, and frozen ground including permafrost) and its interactions with the global climate system, and to enhance the ability to use parts of the cryosphere for detection of climate change. The principal goal of CLIC is to: 'Assess and quantify the impacts of climatic variability and change on components of the cryosphere and their consequences for the climate system, and determine the stability of the global cryosphere. In order to achieve this goal, CLIC has the supporting objectives to: 'Enhance the observation and monitoring of the cryosphere -Improve understanding of the physical processes through which the cryosphere interacts within the climate system -Improve the representation of cryospheric processes in models. CLIC seeks to develop activities and facilitate international co-ordination of research aimed at increasing the understanding of four main scientific themes involving: interactions between the atmosphere and snow and ice on the land surface; interactions between glaciers and ice sheets and sea level; interactions between sea ice, oceans, and the atmosphere; and, cryosphere-climate interactions on a global scale. The scientific strategy is similar in each of the areas of interaction: a combination of measurement, observation, monitoring and analysis, field process studies and modelling over a range of time and space scales. A CLIC modelling strategy must address improved model parameterization of the direct interactions between all components of the cryosphere, the atmosphere, and the ocean at scales from regional to global, and with a hierarchy of models. It is essential to provide improved in-situ and remote sensing data sets needed for validation of models and parameterization schemes and the development of cryospheric indicators of climate change. This paper will provide an overview of the planned approach of CLIC to address cryosphere and its role in the climate system. It will introduce some of the scientific issues considered to be important, summarize planned activities and discuss the critical importance of co-ordination with national and international initiatives and scientific bodies. Open discussion and feedback on the project is welcomed.

**JSM10/07A/B23-002**

**0940**

### HISTORICAL TRENDS IN LAKE ICE COVER IN CANADA

Claude R. DUGUAY (Geophysical Institute, University of Alaska Fairbanks)

Long series of lake ice observations can serve as a proxy climate record, and the monitoring of freeze-up and break-up trends provide a convenient integrated and seasonally specific index of climatic perturbations. The most recent study on historical freeze-up and break-up records of ice on lakes (Magnuson et al., Science, 2000) indicates that later freezing and earlier break-up dates are observable around the Northern Hemisphere from 1846 to 1995. However, some lake sites may deviate from this general trend depending on the hydroclimatic region in which they are located. In a country as large as Canada, lakes are likely to respond differently from east to west and north to south. Given this and the fact that global climate models predict that high latitude regions will be the most strongly affected by climate warming, a study was undertaken to test for temporal trends in freeze-up and break-up dates across Canada. A set of 91 lakes, with time series of 20 years or longer, was analyzed using the Mann-Kendall test for monotonic trend. Trends towards earlier break-up dates are observed for most lakes during the period of study (1940s to 1990s). Freeze-up dates, on the other hand, show few significant trends as well as a low temporal coherence when compared to break-up dates. These results suggest that freeze-up dates are influenced by local factors more than break-up dates.

**JSM10/07A/B23-003**

**1000**

### RELATIONS BETWEEN SPATIAL PATTERNS OF SNOW WATER EQUIVALENT AND SYNOPTIC SCALE TROPOSPHERIC CIRCULATION FOR CENTRAL NORTH AMERICA 1978 - 2001

Chris P. DERKSEN<sup>1</sup>, Chris P. DERKSEN<sup>2</sup>, Ellsworth F. LEDREW<sup>3</sup>, Anne E. WALKER<sup>1</sup>, Barry E. GOODISON<sup>4</sup> (<sup>1</sup>Climate Research Branch, Meteorological Service of Canada, <sup>2</sup>Department of Geography, University of Waterloo, Canada)

Characterizing regional snow cover patterns and identifying the atmospheric triggers to their accumulation and ablation is significant given the important role that snow cover plays in global energy and water cycles. Satellite passive microwave data are a useful source of snow cover information for synoptic scale studies of this nature because of all-weather imaging capabilities, rapid scene revisit, and the ability to derive quantitative estimates of snow water equivalent (SWE). When Special Sensor Microwave/Imager (SSM/I; in operation 1987 to present) and Scanning Multichannel Microwave Radiometer (SMMR; 1978 - 1987) data are combined, the time series of dual polarized, multichannel, spaceborne passive microwave brightness temperatures extends from 1978 to the present. In this study, 23 winter seasons (December, January, February 1978/79 to 2000/01) of five day averaged

(pentad) passive-microwave derived SWE data are derived for a ground-validated western North American study area using a land cover sensitive algorithm suite developed at the Meteorological Service of Canada. When no brightness temperature adjustments are employed, SWE estimates derived during SMMR winter seasons are systematically and significantly lower than retrievals during SSM/I seasons. The SMMR brightness temperatures were subsequently adjusted to an SSM/I F-8 baseline using regression relationships from the August 1987 SMMR and SSM/I overlap period. The resulting adjusted SWE dataset produces a time series of acceptable cross-platform homogeneity when assessed with in situ SWE measurements and remotely sensed snow extent data. Rotated principal components analysis (RPCA) was used to identify the dominant spatial patterns for a cross-platform (SMMR and SSM/I) pentad-to-pentad change-in-SWE ( $\Delta$ SWE) dataset. Eight dominant patterns are identified within the time series: the positive and negative phases of the first four rotated  $\Delta$ SWE components. A composite analysis of 500 mb geopotential height fields produced from National Center for Environmental Prediction (NCEP) data illustrate that regional SWE increases occur when there is a deep 500 mb Arctic low over eastern North America, which displaces a ridge westward over the eastern Pacific resulting in strong north-south advection of cold Arctic air through the continental interior. Alternatively, regional patterns of decreasing SWE are associated with an eastward migration of the 500 mb ridge, allowing advection of warm air into central North America from the south-west. Difference-of-means tests illustrate that significant differences in tropospheric circulation between increasing and decreasing SWE events are expressed in a tripole pattern with centers of action over Alaska, the continental interior, and the Eastern Canadian Arctic. Geopotential height data alone are insufficient to explain tropospheric links with specific  $\Delta$ SWE component patterns; however, model produced isentropic potential vorticity (IPV) fields show potential for identifying linkages between regions of synoptic development and the dominant patterns of  $\Delta$ SWE.

**JSM10/07A/B23-004****1020****INFLUENCE OF SNOW PROCESSES ON SURFACE EXCHANGE OF MASS AND ENERGY**

Michael LEHNING, Perry BARTELT, Thomas EXNER, Charles FIERZ, Ingo Meirold MAUTNER, Norbert RADERSCHALL, Sergey SOKRATOV (Swiss Federal Institute for Snow and Avalanche Research SLF)

There are many influences of snow on the surface exchanges of mass, energy and momentum. The most important ones are: a) Change of surface albedo through snow on the ground; b) Change of surface roughness through snow on the ground; c) Change of surface roughness through drifting snow; d) Change of latent heat transfer (sublimation) through drifting snow; e) Insulation of soil layers and vegetation through snow on the ground. When analyzing the processes in more detail, it becomes clear that all exchange processes are highly interdependent and cannot be separated from the processes that take place within the snow cover. For example, metamorphic changes of surface snow such as the formation of a wind slab or a melt-freeze crust will prevent subsequent erosion of the snow. Or erosion of snow will create surface ripples and sastrugis with the effect of changing surface momentum and heat fluxes. Another example is the dependence of the surface latent heat flux on ventilation and vapor flux in the upper snow layers. Thus, the correct representation of snow processes is a crucial part in assessing the snow atmosphere interaction. This presentation gives an overview of the relevant processes at the snow atmosphere interface. It shows how these processes are represented in the detailed snow cover model SNOWPACK. Focus is on the interaction between latent heat and thus moisture fluxes, surface roughness, vapor transport within the snow and snow ventilation effects as well as radiation transfer in snow. The energy balance over and in the snow cover is discussed using field data from summit at Greenland, from the Weissfluhjoch experimental site at Davos Switzerland and laboratory data from the cold wind tunnel in Davos Switzerland. It is shown that the correct representation of the snow processes is necessary to close the energy balance. At the same time, snow development itself depends crucially on these processes. Applications of such a detailed model are discussed, which include avalanche warning, ice core interpretation and ecological research.

**JSM10/07A/B23-005****1100****SURFACE PROCESSES AND ICE SHEET MASS BALANCE**

Elizabeth M. MORRIS (Scott Polar Research Institute, University of Cambridge)

This talk will review the surface processes involved in snow ablation, accumulation rates over glaciers and ice sheets. It will also review relevant processes in the surface boundary layer. The role these different processes play in the large scale dynamical response of ice sheets to climate change will be discussed using both models and observations. Detailed observations of snow stratigraphy from cores will be presented using a new sensor that detects annual variations in snow density. The review will also include recent remotely sensed data of ice sheets and ice shelves and will discuss their implication for terms in the overall mass balance of ice sheets.

**JSM10/07A/B23-006****1140****CHARACTERISTICS OF PRESENT CLIMATIC CHANGE RECORDED BY MALAN ICE CORE CENTRAL QINGHAI-TIBETAN PLATEAU**

You-Qing WANG, Tandong YAO, Ninglian WANG, Jianchen PU, Keqin DUAN, Weizhen SUN (Key Laboratory of Ice Core and Cold Regions Environment, CAREERI, CAS)

The climatic change during 1920~1998a was reconstructed based on annual  $\delta$ 18-O from a 102.07 m ice core recovered from the Malan Ice Cap in Kekexili region in central Tibet in May 1999. Malan ice core shows that the warming trend of present climate in central Qinghai-Tibetan Plateau is similar to the warming of the Northern Hemisphere and records around the Qinghai-Tibetan Plateau. The warmest period recorded by Malan ice core is during the earlier 1980s, oppositely, the climate during the 1990s was colder. The record suggests that the global warming is evident global, and short term cooling fluctuation might be happening in some regions.

**JSM10/07A/B23-007****1200****SEASONAL DIFFERENCES OF FRESH SNOW CHEMISTRY FROM MT. EVEREST: IMPLICATIONS FOR ICE CORE DATING**

Shichang KANG<sup>1</sup>, Paul A. MAYEWSKI<sup>1</sup>, Dahe QIN<sup>2</sup>, Junying SUN<sup>2</sup>, Sharon A. SNEED<sup>1</sup> (Institute for Quaternary and Climate Studies, University of Maine, Orono, ME 04469, USA, <sup>1</sup>Key Laboratory of Ice Core and Cold Regions Environment, Cold and Arid Regions Environment and Engineering Research Institute, CAS, Lanzhou 730000, P. R. China)

Essential to the reconstruction of ice core records is dating accuracy. One ice core dating method is to measure the seasonal variation of chemical species and use these to count annual layers. This requires investigating the modern timing of precipitation chemistry in the

region from which the ice core has been extracted. Presently, chemical data of fresh snow are available only for two climbing seasons on the northern slope of Mt. Everest: spring (April to May) and late summer (August to September). Here we present chemistry data from fresh snow sampled during the late 1998 summer from Mt. Everest and compare our data with earlier results from Jenkins and others (1987) to investigate seasonal differences of snow chemistry and their significance for ice core dating on Mt. Everest. The glaciochemistry from snowpits are also presented to verify our results. The mean value of ion balance  $\Delta$ C (sum of anions - sum of cations) for the summer fresh snow samples is 1.08  $\mu$ eq/L, indicating that there is an excess of anions. Average relative ion composition (%) shows that Cl and Ca<sup>2+</sup> are the dominate species. The crustal species Ca<sup>2+</sup> and Mg<sup>2+</sup> correlate with SO<sub>4</sub><sup>2-</sup> and NO<sub>3</sub><sup>-</sup> indicating potentially associated sources for these species (e.g. local crustal aerosols). NH<sub>4</sub><sup>+</sup> doesn't correlate with the others suggesting it has unique sources in summer (e.g. biogenic sources). From our data set, there is no significant effect of elevation on snow composition. Compared with earlier results from Jenkins and others (1987), the ion concentrations of fresh snow in 1998 summer are much lower than those in 1986 spring. The most dramatic difference of chemical composition between the two seasons is crustal Ca<sup>2+</sup> concentration in which the spring value is about 22-fold higher than summer value. Differences of SO<sub>4</sub><sup>2-</sup> and Na<sup>+</sup> concentrations between seasons are also striking. Due to the absence of NH<sub>4</sub><sup>+</sup>, K<sup>+</sup> and Mg<sup>2+</sup> measurements in 1986 snow (Jenkins and others, 1987) we cannot compare these species. The marked seasonal differences for crustal species (e.g. Ca<sup>2+</sup> and SO<sub>4</sub><sup>2-</sup>) are much more distinct than others (e.g. NO<sub>3</sub><sup>-</sup>). Thus, these crustal species may present the most definitive indicators for ice core dating in the Mt. Everest region. To examine the possibility of ice core dating through variations of crustal species, the chemical compositions of the snow pit from 1998 summer on Mt. Everest is investigated. Generally, the chemical differences between summer and spring snow from the snow pit agree with those from fresh snow. Notably, the spring Ca<sup>2+</sup> peak in the snow pit is more dramatic than for other species and is consistent with fresh snow results. This study verifies the assumption that the maximum of Ca<sup>2+</sup> concentration in spring snow is a significant horizon for dating ice cores on the northern slope of Mt. Everest. High spring concentrations of other species (e.g. Na<sup>+</sup> and Mg<sup>2+</sup>) may also provide additional references layers for ice core dating.

**Monday, July 7 PM**

Presiding Chair: S. O'Farrell

**MARINE CRYOSPHERE: SEA ICE AND ICE SHELVES****JSM10/07P/B23-001****1400****CLIMATE INTERACTIONS IN THE MARINE CRYOSPHERE**

Ian ALLISON (Antarctic CRC and Australian Antarctic Division)

Sea ice forms a boundary between the atmosphere and the ocean over about 10% of the surface area of the global ocean, considerably influences atmosphere-ocean interaction, and thus plays a key role in the global heat balance and the global thermohaline circulation. A retreat of sea ice may therefore have global consequences and contribute, through various feedback processes, to enhanced climate change. To facilitate credible prediction of the state of the polar pack ice, both theoretical and observational knowledge of the processes of interaction among the ice, the ocean, and the atmosphere must continue to be improved. This paper reviews what we know about the mean state and natural variability of sea ice characteristics in both polar regions (although with an emphasis on the Antarctic) and the physical processes that determine these. A special focus is made on ice formation and water mass modification in Antarctic coastal polynyas, regions of intense heat loss from the ocean to the atmosphere, and significant as "ice factories" for the total sea-ice zone. In some cases processes in polynyas play a role in control of the vertical overturning that regulates the thermohaline circulation. Evidence of trends in sea ice volume and distribution in both hemispheres is discussed as is the possible impacts of projected global warming.

**JSM10/07P/B23-002****1440****AIR-ICE INTERACTIONS DURING THE SHEBA DEPLOYMENT IN A 2-DIMENSIONAL COUPLED MODEL**

Xiangdong ZHANG<sup>1</sup>, Bin CHENG<sup>2</sup>, Timo VIHMA<sup>3</sup>, John E. WALSH<sup>1</sup> (Frontier Research System for Global Change, International Arctic Research Center, University of Alaska Fairbanks, <sup>1</sup>Finnish Institute of Marine Research, P. O. Box 33, FIN-00931, Helsinki, Finland, <sup>2</sup>International Arctic Research Center, University of Alaska Fairbanks, Fairbanks, AK99775, USA)

It has been demonstrated that synoptic activities, such as cyclones, has increased during recent decades in the Arctic Ocean (Serreze et al. 2001). The effects of cyclones on the sea-ice export through Fram Strait (Brummer et al., 2000) and on the local ocean hydrography in the Beaufort Sea (Yang et al. 2001) were detected. However, such effects on the sea-ice pack and their feedback have not been documented well. From a large-scale point of view, cyclones may also leave a lasting imprint on sea-ice states and, in turn, affect climate variability. One important feature of a cyclonic system is its accompanying advection of warm air, which originates from low latitudes. The SHEBA deployment was carried out for an entire year from October 1997 to October 1998 and captured an outstanding warm air advection event in the middle of May 1998, when a well-developed cyclonic system moved slowly northward from the Bering Sea and the Gulf of Alaska. The Beaufort Sea was covered by the advection of warm air mass from east to west during a period from 10th through 12th May. We employed a 2-dimensional coupled atmospheric boundary layer (ABL) and sea-ice thermodynamics model (Cheng and Vihma, 2003) to investigate the air-ice interactions during this period. The model domain was configured in the dominant direction of the prevailing winds and extended 420km downwind from the SHEBA Camp with a horizontal resolution of 5 km. The ABL had 50 levels from surface up to 3 km, while the snow and the sea-ice had 10 vertical layers, respectively, in the model. The ABL inflow boundary condition was updated every hour based on the SHEBA rawinsonde data. The ABL and the sea-ice models were spun up to a quasi-equilibrium in which the modeled surface temperature was close to the AVHRR retrieval skin temperature. During the three-day simulation, the model apparently captured the warm air advection well. The modeled spatial distribution of surface temperatures were close to the AVHRR derived values. An increase of temperature occurred in the snow and upper sea-ice layer, in response to the penetration of solar radiation and invasion of warm air mass into the model domain. The former factor predominates, while the latter amplifies the effects of the former. Heat accumulates in the snow layer, a response in part to the increasing solar radiation during this transition season. Due to the increases of air moisture carried by the advection, condensation occurs. The diurnal amplitude of the low-level air temperature and the snow/ice temperature is damped in the simulation. Parallel simulation in an uncoupled model provided insight into the feedback produced by the coupling.

**JSM10/07P/B23-003****1500****SURFACE ENERGY BUDGETS AND CLOUD FORCING ON THE ARCTIC ICE CAP: ONE YEAR OF DATA FROM THE SHEBA EXPERIMENT**Chris W. FAIRALL<sup>1</sup>, Janet INTRIERI<sup>1</sup>, Taneil UTTAL<sup>1</sup>, Ola PERSON<sup>2</sup> (<sup>1</sup>NOAA Environmental Technology Laboratory, <sup>2</sup>University of Colorado Cooperative Institute for Research in Environmental Sciences)

From November 1997 to October 1998 the Surface Heat Budget of the Arctic (SHEBA) engaged in a variety of atmospheric, ice, and oceanic measurements on the Arctic icecap as part of ice station SHEBA. The ice station was launched at 143 W and 75 N and ended at 166 W and 80 N. The measurements included eddy-correlation measurements of sensible and latent heat flux, upward and downward solar and IR fluxes, and snow/ice temperatures. Profiles of cloud information were obtained with an 8-mm-wavelength Doppler cloud radar and a 0.523 micron wavelength depolarization and backscatter lidar (dabul). This is the first set of eddy-correlation heat flux, radiative fluxes, and comprehensive cloud data obtained over an entire annual cycle on the ice cap. In this paper we will present simple statistics on the annual cycle of the components of the surface heat budget and cloud properties (fraction, thickness, ice vs water, etc). We will also provide a detailed analysis of the annual cycle of cloud forcing of the surface heat budget of the icecap. Comparisons with several climate models will be presented.

**JSM10/07P/B23-004****1520****MOMENTUM CONSERVING ICE-OCEAN COUPLING FOR INERTIAL AND TIDAL SEA ICE VARIABILITY**William HIBLER III<sup>1</sup>, Petra HEIL<sup>2</sup>, Harper SIMMONS<sup>1</sup>, Jennifer K. HUTCHINGS<sup>1</sup> (<sup>1</sup>University of Alaska Fairbanks, <sup>2</sup>University of Tasmania)

Most ice ocean circulation models utilize separate ice and ocean models with the stress transfer between the ice and ocean treated by the stress between the ocean and ice. While such a stress transfer is quite useful for the study of boundary layer dynamics, in a full three dimension ocean circulation model this procedure distorts the overall stress transfer into the coupled ice ocean model. It can be shown, for example, to introduce artificial discontinuities into the ice margin ocean dynamics even if the wind stress over ice and water are identical. Such a coupling differs substantially from the coupling utilized by Hibler and Bryan (1987) for three dimensional ocean circulation models whereby the stress transfer into the upper layer of the ocean is taken to be the wind stress less the ice interaction. This latter coupling is however, difficult to implement in a manner that preserves high frequency variability in the ocean if separate ice and ocean models are employed. Recently, Heil and Hibler (2002) have employed an ice model utilizing an embedding procedure whereby the ice is embedded in the oceanic boundary layer following a procedure proposed by McPhee ( ) and modified the ice drift equation so one equation is solved for the ice momentum balance, ice interaction and boundary layer motion. Utilizing this procedure they obtained greatly improved high frequency inertial variability in the predicted ice drift as well as low frequency predicted drift of ice motion compared to the classic passive drag formulation. Interestingly, the high frequency variability in the ice motion, which for both drift and deformation was found to be coherent with detailed hourly buoy drift and deformation results, was found to be generated by a non linear cascade of energy induced by ice mechanics forced by low frequency wind forcing. Insignificant linear correlation between wind forcing and the essential linear boundary layer formulation was found. In this paper we extend the coupling procedure to a full multilevel zco-ordinate ocean model and investigate the response of this coupled model for the Arctic Basin with fixed baroclinic forcing, but 6 hourly varying wind forcing. A free surface ocean model is utilized so the effect of tidal forcing is also examined by non coupled tidal results from a barotropic tidal model (Kowalik and Proshutinsky). Using this framework this model is integrated over a multi year period for the Arctic basin with a variable thickness sea ice model and compared to models using more conventional 'stress' coupling. The comparisons include detailed comparisons to buoy motion and deformation but also include analysis of the increased tidal response and its effects on the ice mass budget as well as the modifications to the ice mass balance in the central Arctic due to inertial and tidal effects in the full three dimension ice ocean model.

**JSM10/07P/B23-005****1600****MODELLING OF THE THICKNESS DISTRIBUTION OF THE ARCTIC SEA ICE**Jari Juhan HAAPALA<sup>1</sup> (<sup>1</sup>Department of Physical Sciences, University of Helsinki, <sup>2</sup>Finnish Institute of Marine Research, Helsinki, Finland)

In the framework of the Finnish global change research program (FIGARE) a new advanced sea ice model applicable for climate research has been developed. The model resolves sea ice thickness distribution for arbitrary numbers of undeformed and deformed sea ice thickness categories. The sea ice model has been implemented in the ocean circulation model, MPI-OM-1, developed in the Max-Planck Institute of Meteorology. The MPI-OM-1 model is global, however it employs curvilinear coordinates which allows to model coastal regions and adjacent seas of the Arctic Ocean with a high horizontal resolution, which are known to be vital regions for a sea-ice production. Ten-years simulations have been made with the global model and the evolution of the sea ice thickness distribution in the Arctic has been analysed. The temporal behaviour and horizontal extension of the deformation regions was largely dependent on the synoptic scale wind field. Deformed ice production regions were concentrated in coastal regions, particular important regions were found to be the Lincoln Sea, the Beaufort Sea and the Northern regions of the Spitsbergen, Franz Josef Land and the Severnaya Zemlya.

**JSM10/07P/B23-006****1620****THE RELATIONSHIP BETWEEN ANTARCTIC COASTAL TEMPERATURES AND SEA ICE EXTENT**Steven Richard COLWELL<sup>1</sup>, John TURNER (British Antarctic Survey)

Passive microwave satellite imagery has shown that the total extent of Antarctic sea ice has increased by about one percent per decade since the late 1970s. However, there is a high degree of spatial variability in the trend in the sea ice around the continent, with there having been a marked decrease of ten percent per decade in sea ice over the Bellingshausen Sea since the satellite record began. In this region there is a high correlation between the winter season extent of the sea ice and the temperatures at the coastal stations on the western side of the Antarctic Peninsula. Since the late 1970s winter temperatures have risen as the sea ice has decreased. The warming is much less in the other seasons. The Peninsula is unique in the Antarctic in that it is the only significant northward extension of the continent that projects into the circumpolar trough the belt of low pressure that rings the continent over 60-70 S. Low pressure systems become slow-moving over the Bellingshausen Sea and the western side of the Peninsula is under a prevailing north to north-westerly flow. This area is the only region of the Antarctic where the prevailing wind is orthogonal to the ice edge, giving

a close linkage between surface pressure over the Bellingshausen Sea and the meridional extent of the sea ice. For the rest of the Antarctic, the relationship between coastal temperatures and sea ice extent is less clear. Earlier studies, covering a 15 year period up to 1987, suggested a correlation between temperature and sea ice trends, but this was much less than on the western side of the Peninsula. In this talk we will present a new analysis of temperature and sea ice trends for the Antarctic. The temperature data have been taken from the READER project (<http://www.antarctica.ac.uk/met/READER/>), where monthly mean temperatures were re-derived from the 6 hourly synoptic reports. Sea ice data were from the Ocean Modelling Branch of NOAA/NESDIS.

**JSM10/07P/B23-007****1640****EFFECTS OF SURFACE FRESHWATER FLUX INDUCED BY SOUTHERN HEMISPHERE SEA ICE TRANSPORT ON THE GLOBAL THERMOHALINE CIRCULATION**

Yoshiki KOMURO, Hiroyasu HASUMI (Center for Climate System Research, University of Tokyo)

Effects of surface freshwater flux induced by sea ice formation and melting on the thermohaline circulation are investigated by numerical experiments. A sea ice-ocean coupled general circulation model is used. The model domain is global, and the model is forced by monthly climatology derived from the NCEP reanalysis data. Restoring to the observed sea surface salinity is not employed in order to precisely evaluate the sea ice effects. We perform three cases, that is, a control case, a case in which sea ice motion is turned off, and a case in which salt and freshwater flux between sea ice and the ocean is turned off. All the cases are integrated for 3100 years. In the control case, mass transport associated with thermohaline overturning circulation is realistically represented, and the amount of northward sea ice transport in the southern hemisphere is reasonable compared with observations. Deep water formation around Antarctica occurs under compact sea ice cover. Precipitation exceeds evaporation in this region, but positive annual-mean sea ice production and resultant salt input into the sea surface are responsible to salinify the underlying water and maintain the deep water formation. When sea ice motion is turned off, annual-mean sea ice production is almost zero everywhere, and the deep water formation as in the control case is no longer maintained. Instead, it is driven primarily by thermal destabilization of water columns. Consequently, the deep ocean around Antarctica is warmer and less saline compared with that for the control case, and the Atlantic bottom circulation is weakened by 16%. We analyze salt transport in the deep ocean in both the cases, and show that northward salt transport from the Southern Ocean in the bottom layer also decreases in the case without sea ice motion. The amount of the decrease is greater by one order of magnitude than that of the surface salt input associated with sea ice in the control case. In the case where the freshwater flux at the ice-ocean interface is turned off, results are similar to the case without sea ice transport, although surface heat and momentum fluxes significantly differ between them. This suggests that the influence of sea ice on surface freshwater/salt flux is more important than on surface heat and momentum fluxes in affecting the global thermohaline circulation.

**JSM10/07P/B23-008****1700****ICE SHELVES SHAPING THE SOUTHERN OCEAN ENVIRONMENT**

Hartmut H. HELLMER (Alfred Wegener Institute for Polar and Marine Research)

The importance of ice shelves and the processes at their base for the Southern Ocean and beyond was recognized late during Antarctic exploration. Modification of dense shelf waters due to melting and freezing at glacial bases can be directly linked to the formation of bottom waters at the continental shelf break and the ventilation of the world ocean abyss. To study the impact of ice shelf/ocean interaction on the southern environment the results of two numerical realizations were compared using the regional coupled ice-ocean model BRIOS2.2 with and without most of Antarctica's ice shelf cavities. The dominant effect of closing the cavities is the missing freshwater outflow destabilizing a weakly stratified shelf water column. As a result, deep convection enhances, increasing shelf water salinities and thinning the sea ice cover on and beyond the continental shelf, and the northward transport of dense bottom water intensifies. This study therefore indicates the effects of decreasing sub-ice freshwater fluxes on the Southern Ocean not only due to present ice shelf decay but also past ice shelf advances which closed or reduced the cavity size beneath.

**JSM10/07P/B23-009****1720****THE AMISOR PROJECT: AMERY ICE SHELF DYNAMICS AND ICE-OCEAN INTERACTION**Ian ALLISON<sup>1</sup>, Helen FRICKER<sup>2</sup>, Mike CRAVEN<sup>1</sup>, Neal YOUNG<sup>3</sup> (<sup>1</sup>Antarctic CRC and Australian Antarctic Division, <sup>2</sup>Institute of Geophysics & Planetary Physics, Scripps Institution of Oceanography, University of California, San Diego, USA)

The Amery Ice Shelf (70oS, 70oE) is the third largest embayed shelf in Antarctica, and the largest entirely within East Antarctica. This ice shelf has been studied by the Australian Antarctic program for more than 50 years, although only in the past decade has the importance of ice-ocean interaction beneath the shelf become fully apparent. This has led to the establishment of a project of ' Amery Ice Shelf Ocean Research (AMISOR) This multidisciplinary project has overall aims of quantifying the interaction between the ocean and the Amery Ice Shelf (AIS); and determining the implications of this interaction for the discharge of grounded ice and to water mass modification. The project includes components of hot-water drilling through the AIS to make measurements in the underlying cavity; glaciological measurements of the ice shelf velocity, strain and thickness; oceanographic measurements in Prydz Bay; investigation of sub ice shelf sediments and sediment dynamics; remote sensing; and numerical modelling of ice shelf-ocean interaction and ice shelf dynamics. This paper provides an overview of the AMISOR project and the preliminary results from it.

Tuesday, July 8 AM

Presiding Chair: H. Hellmer

**CLIMATE VARIABILITY AND CLIMATE CHANGE****JSM10/08A/B23-001****0830****HIGH-LATITUDE CLIMATIC RESPONSE TO ENHANCED GREENHOUSE FORCING**

John E. WALSH (University of Illinois, Urbana, IL USA)

A challenging feature of recent global climate model simulations is that the response to external forcing is greater in polar regions than elsewhere, while at the same time the simulated climates show the largest cross-model variance in the polar regions. The well-known polar amplification of greenhouse warming is actually stronger in the Arctic than in the Antarctic in most models because of the land-sea configuration and the role of sea ice.

Feedbacks involving water vapor and the atmospheric circulation also play roles in the polar response to greenhouse forcing. The amplification's strong seasonality in most models is potentially useful for the detection and attribution of future climate changes. A comparison of the current generation of global climate model simulations shows that ocean-ice-atmosphere coupling leads to widely varying greenhouse scenarios in the Antarctic and in the subpolar North Atlantic, where changes in oceanic convection represent a "wild card" in the climatic response. Oceanic mixing reduces, and sometimes eliminates, the warming locally in some models, while in others a freshening of the upper ocean serves to cap the convection, with broader consequences for much of the ocean thermohaline circulation. The rate of retreat of sea ice is generally proportional to the rate of warming in the models, although the rate of retreat is also related to the amount of sea ice in the control simulation. Physical processes related to the distribution of sea ice in the model scenarios include changes in the atmospheric circulation and cloudiness, in addition to radiatively driven warming and changes in the upper ocean hydrography of the polar seas. Nearly all models project an acceleration of the hydrologic cycle in the polar regions, where enhanced precipitation and evapotranspiration accompany the higher temperatures and the reduced coverage of sea ice and snow cover. The hydrologic consequences include an earlier and stronger springtime discharge pulse, a longer (and warmer) melt period that hastens the degradation of permafrost, and a negative mass balance of small glaciers. The glacier wastage, in turn, contributes to a freshening of coastal waters. The response of the larger ice sheets is further complicated by increases in snowfall. A potentially noteworthy caveat concerning projected rates of change is that many global climate models show less sensitivity to variations of external forcing than is indicated by paleoclimatic evidence from the actual climate system.

**JSM10/08A/B23-002****0910****RESPONSE OF THE PAN ARCTIC AND NORTH ATLANTIC OCEAN CLIMATE TO THE ARCTIC OSCILLATION**

Jia WANG<sup>1</sup>, Bingyi WU<sup>2</sup>, Moto IKEDA<sup>3</sup>, John E. WALSH<sup>4</sup> (<sup>1</sup>IARC-FRSGC, University of Alaska Fairbanks, <sup>2</sup>Institute of Marine Science, University of Alaska Fairbanks, USA, <sup>3</sup>Graduate School of Environmental Science, Hokkaido University, Japan, <sup>4</sup>IARC, University of Alaska Fairbanks, USA)

Using a coupled ice-ocean model developed by Wang et al. (2002), we investigate the responses of the Arctic Ocean climate (or ice-ocean system) to the Arctic Oscillation (AO). Seven high AO index winters and six low AO index winters were simulated by the coupled ice-ocean model under forcing provided by the NCEP/NCAR reanalysis. Statistical analyses and tests were applied to the composite differences between the high and low AO indices. For the high AO index phase that predominated during the 1990s, the results showed a reduction of sea ice in the Arctic Basin accompanied by an increase of sea ice in the Labrador Sea. This pattern resembles the North Atlantic Oscillation seesaw pattern (Roger and van Loon 1979; Wang et al. 1994). During the high AO phase, the Arctic surface salinity increases and the surface temperature decreases, implying that more new ice was produced. The enhanced ice production is a consequence of greater ice export from the Arctic Ocean in response to anomalous cyclonic wind stress. From the subsurface layer to the Atlantic water layer, there is also a seesaw pattern in ocean temperature between the Barents and the Labrador Seas. During the high AO phase, the model reproduces the anomalous temperature intrusion of the Atlantic Water. While both the anomalous surface wind stress and the thermodynamical forcing contribute to sea ice and ocean variability, statistical analyses (EOF, regression, etc.) and significance tests (T-test and F-test) show that the wind stress accounts for a greater portion of these changes during the high AO phase than the thermodynamical forcing.

**JSM10/08A/B23-003****0930****NORTHERN HEMISPHERE SEA ICE VARIABILITY AND ITS LINKAGE TO THE NAO AND ENSO**

Jinro UKITA<sup>1</sup>, Meiji HONDA<sup>2</sup>, Hisashi NAKAMURA<sup>3</sup>, Yoshihiro TACHIBANA<sup>4</sup>, Hiroshi KOIDE<sup>5</sup>, Donald J. CAVALIERI<sup>6</sup>, Claire L. PARKINSON<sup>7</sup> (<sup>1</sup>GEST, UMBC/NASA-GSFC, <sup>2</sup>Frontier Research System for Global Change, <sup>3</sup>University of Tokyo, <sup>4</sup>Tokai University, <sup>5</sup>Meteorological Research Institute, <sup>6</sup>NASA Goddard Space Flight Center)

Evidence is presented that Northern Hemisphere (NH) wintertime sea-ice variability on interannual time scales has a distinct modal structure characterized by a set of two orthogonal modes. One mode is spatially dominant and composed of synchronous seesaws in the North Atlantic and the North Pacific. This mode is closely linked to the North Atlantic Oscillation (NAO) with an extended domain of influence over the North Pacific. The other mode is the residual of the first mode with respect to the NH total SIE and closely related to the influence of the El Niño-Southern Oscillation (ENSO) phenomenon. This set of modes explains a significant part of the temporal and spatial variations in NH wintertime sea-ice and provides a clue as to how sea-ice extent responds to the NAO and ENSO on the hemispheric scale.

**JSM10/08A/B23-004****0950****NORTHERN HEMISPHERE CLIMATIC COVARIABILITY BETWEEN CRYO-, HYDRO- AND ATMOSPHERE ON SEASONAL TO SUB-DECADAL TIME SCALE**

Kazuyuki SAITO<sup>1</sup>, Judah COHEN<sup>2</sup> (Hydrological Cycle Research Program, Frontier Research System for Global Change, <sup>2</sup>Atmospheric and Environmental Research, Inc.)

By use of visible-derived satellite observations and NCEP/NCAR reanalysis data for 1971-2000, correlation analysis of monthly timeseries has recently shown that the continental-scale snow cover extent (SCE) in the warm (May - August) as well as fall (October - November) season has significant association with the dominant mode of atmospheric variability (annular mode or AO/North Atlantic Oscillations or NAO) in the wintertime Northern Hemisphere, and suggested that the former may play an important role in keeping persistency of the latter. Greater than normal SCE in either season is associated with the negative phase of the winter AO/NAO. On the longer time scale, according to cross-spectral analysis of the monthly normalized and low-passed timeseries, the two climatic variables have common preferred time scales, quasi-biennial and sub-decadal, and their coherency at low frequency (sub-decadal) is statistically significant with the snow cover leading the atmosphere by several months. These results suggest potential roles of the continental-scale snow cover on a range of time scales. Linkage between the fall SCE variability (mostly in eastern Eurasia) and the winter AO/NAO has been considered as dynamical through troposphere-stratosphere coupling and/or middle atmosphere wave-meanflow interaction. It is more adequate to infer, however, that the warm season snow cover is a reflector, rather than an activator or a modifier, of the mechanism at work, for the geographical extent of its fluctuation is limited mostly in the high latitude coastal areas. In order to search for the factors bridging variabilities between the warm season SCE and the atmosphere, we look at fluctuations in the hydrological variables (river discharge for Obi and Yenisei for 1971-1999, and Lena for 1971-1994; 'Global Runoff Data Centre' (GRDC)), permafrost conditions (soil temperature for most stations until 1995; Russian Historical Soil Temperature Data by National Snow and Ice Data Center), and the sea ice

concentration (sic) for 1971-2000 ('HadISST 1.1dataset'). On the seasonal time scales larger discharge in Lena for August - September, which implies larger snow melt, is associated with positive phase of the AO/NAO for the next winter. In the Arctic Ocean April to June sic in the region of [140-80W, 80-90N] also show significant correlation. On longer time scale significant coherency is found between the Lena river discharge show and the AO/NAO around six-year period with no lead or lag, while the SIC of the above region shows significant covariability in the lower frequency (almost decadal). Connection of these signals with the SCE and atmospheric fluctuation and possible mechanisms are discussed.

**JSM10/08A/B23-005****1010****THE POTENTIAL ROLE OF SNOW COVER IN FORCING SEASONAL-TO-INTERANNUAL VARIABILITY OF THE MAJOR NORTHERN HEMISPHERE MODE**

Judah L. COHEN<sup>1</sup>, Kazuyuki SAITO<sup>2</sup> (<sup>1</sup>AER, Inc., <sup>2</sup>Frontier Research System for Global Change)

Decadal trends have been noted in the leading mode of boreal winter variability. Given that this mode is thought to be an internal mode of the atmosphere it remains unclear as to what is responsible for seasonal to interannual oscillations of this mode. We demonstrate that continental-scale snow cover varies at the same multi-year time periods as the atmosphere but leads the atmosphere by several months through their mutual oscillations. Therefore we propose snow cover as a potential contributor to the seasonal-to-interannual variability of the leading boreal winter mode of the atmosphere.

**JSM10/08A/B23-006****1050****CLOUD EFFECTS ON THE DECAYING TREND IN THE ARCTIC ICE COVER**

Motoyoshi IKEDA<sup>1</sup>, Jia WANG<sup>2</sup>, Alexander MAKSHATAS<sup>2</sup> (<sup>1</sup>Graduate School of Environmental Earth Science, Hokkaido University, <sup>2</sup>International Arctic Research Center, University of Alaska)

The sea ice cover in the Arctic Ocean has declined in the last 40 years, while its decadal variability has increased. One might imagine that the ice reduction is an indication of global warming as a consequence of positive feedback between a sea ice reduction and an albedo decrease. In this study, however, the trend is clearly influenced by the radiation balance over all seasons. A cloudiness increase in the fall, winter and spring has been detected with North Pole (drifting) Station data and contributes to a reduction in the absolute amount of net long wave radiation at the sea surface. In the summer, the reduced cloud cover has led to an increase in shortwave radiation, permitting more net outgoing radiation, and yielding a small increase in the total incoming radiation. All of these trends promote ice reduction. The effects of clouds and radiation are comparable with the albedo reduction associated with more open water, which absorbs more solar radiation in the summer. Analyses of the decadal variabilities reveal qualitatively the same effects as those of the radiation on the ice cover. Although some of doubled CO<sub>2</sub> experiments seem to reproduce the current global warming, the further analysis is recommended to verify these models by identifying the mechanisms of the ice reduction.

**JSM10/08A/B23-007****1110****IMPACTS OF CLIMATE CHANGE IN THE ARCTIC**

Gunter E. WELLER (University of Alaska Fairbanks)

Regional assessments of climate change and its impacts are a high priority in the international programs on global change research. In the Arctic, climate models indicate an amplification of the global greenhouse warming, but the observed high-latitude climate trends over the last few decades are much more regional and patchy than predicted by the models. While considerable uncertainties remain in the long-term prediction of change there is some agreement between model results and observed trends by season on shorter time scales. The warming observed over the landmasses of the Arctic over the last few decades is matched by corresponding observed decreases in snow cover and glacier mass balances, by thawing of the permafrost, and by reductions in sea ice extent and thickness. The available evidence strongly suggests that the observed changes are in part due to anthropogenic global warming. While uncertainties exist about the future, climate change in the Arctic during the past few decades can be shown to have had major impacts already on the arctic environment. If these trends continue, as they are expected to do, the natural resource-dependent economies of many regions in the Arctic, as well as the polar ecosystems with their distinct fauna and flora, will be affected. Socio-economic consequences to populations, industry, and lifestyles will be inevitable. Not all of these changes are necessarily negative as will be discussed in this paper.

**JSM10/08A/B23-008****1130****CLIMATE CHANGE IN THE POLAR REGIONS MODELLED BY THE CSIRO MK3 COUPLED MODEL**

Siobhan OFARRELL, Hal GORDON (CSIRO Atmospheric Research, PMB 1, Aspendale, Victoria, 3195, AUSTRALIA)

Two transient climate change experiments have been performed with the CSIRO Mk3 climate model. The model has been forced with the observed changes in radiative forcing for the 20th Century and the A2 scenario for changes in greenhouse gases and sulphate aerosols for the 21st Century. The talk will focus on changes in the climate in the polar regions, the changes to sea ice and changes in both the atmospheric and ocean components. The talk will compare these results with the previous results from the CSIRO Mk2 model. A particular focus will be on understanding changes in the Southern Ocean thermohaline circulation. Progress on plans to incorporate additional cryospheric components into the coupled model will be discussed.

**JSM10/08A/B23-009****1150****THE IMPACT OF THE VARIABILITY IN SEA ICE ON THE CLIMATE OF THE ANTARCTIC PENINSULA IN A GLOBAL CLIMATE MODEL**

Tom LACHLAN-COPE (British Antarctic Survey)

The variability of the surface temperature on the western side of the Antarctic Peninsula is the highest in southern hemisphere. Also surface air temperature observations in the same area have shown a warming during the last 50 years. This study investigates the role of sea ice in the variability of the climate and as a possible cause of the observed warming. The atmosphere only version of the Hadley centre global climate model (HadAM3) is forced with a range of observed sea ice fields for the last 25 years and also with possible scenarios for future sea ice extents. It is found that model surface warming over the last 25 years agrees well with the surface observations of temperature. We have also looked at climate produced in the coupled atmosphere/ocean version of the Hadley centre global climate model (HadCM3) that include the observed anthropogenic forcing for the last 100 years. These

IA

## INTER-ASSOCIATION

runs do not reproduce a realistic sea ice for the Antarctic Peninsula region; the sea concentrations in the Bellinghousen Sea in the model are much lower than those observed. However by looking at areas around Antarctica where the sea ice decreases over the last 50 years we can investigate the cause of these decreases and speculate on the role of ice-ocean-atmosphere feedback in these areas.

**JSM10/08A/B23-010**

**1210**

### MODELING THE ENSO MODULATION OF ANTARCTIC CLIMATE IN THE LATE 1990S WITH POLAR MM5

David H. BROMWICH, Andrew J. MONAGHAN, Zhichang GUO (Byrd Polar Research Center, Ohio State University)

The Polar MM5 is employed to examine the strong El Niño-Southern Oscillation (ENSO) modulation of Antarctic climate for July 1996-June 1999. This provides a more comprehensive assessment than can be achieved with observational datasets by using a regional atmospheric model adapted for high-latitude applications (Polar MM5). The most pronounced ENSO response is observed over the Ross Ice Shelf-Marie Byrd Land and over the Weddell Sea-Ronne/Filchner Ice Shelf. In addition to having the largest climate variability associated with ENSO, these two regions exhibit anomalies of opposite sign throughout the study period, which supports and extends similar findings by other investigators. The dipole structure is observed in surface temperature, meridional winds, cloud fraction and precipitation. The ENSO-related variability is primarily controlled by the large-scale circulation anomalies surrounding the continent, which are consistent throughout the troposphere. When comparing the El Niño / La Niña phases of this late 1990s ENSO cycle, the circulation anomalies are nearly mirror images over the entire Antarctic, indicating their significant modulation by ENSO. Large temperature anomalies, especially in autumn, are prominent over the major ice shelves. This is most likely due to their relatively low elevation with respect to the continental interior making them more sensitive to shifts in synoptic forcing offshore of Antarctica, especially during months with considerable open water. The Polar MM5 simulations are in broad agreement with observational data, and the simulated precipitation closely follows the European Centre for Medium-Range Weather Forecasts Tropical Ocean - Global Atmosphere precipitation trends over the study period. The collective findings of this work suggest the Polar MM5 is capturing ENSO-related atmospheric variability with good skill and may be a useful tool for future climate studies.

**Tuesday, July 8 PM**  
Presiding Chair: T. Lachlan-Cope

## GLACIERS AND PERMAFROST

**JSM10/08P/B23-001**

**1400**

### RESPONSE OF MOUNTAIN GLACIERS AND PERMAFROST TO CLIMATE CHANGE

Andreas KAEAEB (Department of Geography, University of Zurich)

Snow, glaciers and permafrost in cold mountain areas are especially sensitive to changes in atmospheric conditions, because of their proximity to melting conditions. In addition, mass wasting is most intense in high mountain areas with steep slopes. As a consequence, environmental variations most strongly affect high mountain regions. Changes in ice occurrences and corresponding impacts on physical high-mountain systems could, in fact, be among the most directly visible signals of global warming and seriously affect human activities. Glacier mass-balance depicts a direct climate signal. Recent world-wide mass-balance series, as collected by the World Glacier Monitoring Service (WGMS), underline a continuous trend of accelerated loss of mountain glacier mass in most regions of the world. Such trend can be best illustrated from glacier area changes. Within the Glacier Measurements from Space project (GLIMS) glaciers are globally monitored using satellite remote sensing. For the Swiss Alps, for instance, a loss of more than 10% per decade since 1985 was observed compared to a loss of less than 5% per decade since the Little Ice Age. Especially small glaciers turned out to be affected. For regions such as the Himalayas many mountain glaciers are not any more capable to dynamically adjust for the accelerated warming by retreat, but rather react by down-wasting and decoupling of glacier parts. Compared to glaciers, the influence of climate change on permafrost in high mountains is much less visible, more complex, and, thus, less known. On the other hand, mountain permafrost covers significantly larger areas than glaciers do. Primarily, changes in climate conditions affect the permafrost ground thermal regime. Borehole monitoring in high mountain regions shows indeed a trend of ground warming. Also, changes in the stability of frozen slopes become more and more evident. An upward shift of the permafrost belt in high mountains is, therefore, expected to take place presently and in the near future. The ongoing changes in the cryospheric systems have (already today) severe impacts on the environment. Water runoff is affected with consequences for drinking water supply and hydropower generation. Well visible landscape changes such as glacier retreat have a considerable effect on the awareness of the environmental consequences of climate change, and they influence tourism industry. Here, we especially focus on glacier- and permafrost-related hazards, and their potential development under atmospheric warming. Accelerated glacier retreat is responsible for the evolution of gigantic glacier lakes, which outburst floods endanger entire valleys. An increasing number of rock/ice avalanches and debris flows is expected from the lower boundary of the permafrost zone. Related devastating consequences are illustrated by recent disasters such as the 20 September 2002 rock/ice avalanche in the Caucasus that killed over 120 people.

**JSM10/08P/B23-002**

**1440**

### EVALUATION OF SNOW COVER AND PERMAFROST FEATURES IN NORTHERN EURASIA FOR SOME CLIMATE CHANGE SCENARIOS

Andrey B. SHMAKIN (Laboratory of Climatology, Institute of Geography)

Several series of experiments has been carried out using SVAT model involved in PILPS and alike projects, and a simplified (or intermediate complexity) model of heat/water exchange. Input meteorological variables were specified for some possible scenarios of future climate change in Northern Eurasia. SVAT model allowed us to evaluate changes in snow cover features and permafrost thawing depth under climate change conditions at several locations tested for the study. The simplified model made it possible to study main features of continental-scale snow distribution. Qualitative estimates of snow period length and snow water equivalent variations under changing climate are made. Typical interannual variations of snow characteristics under climate change scenarios are evaluated too. With limited warming, the snow parameters don't change considerably, except for the territories with unstable snow cover. Under considerable warming scenario, seasonal snow cover in Eurasia shrinks substantially, especially in the western regions. Average depth of permafrost seasonal thawing for tested sites is examined. Under limited warming, the depth of thawing doesn't change significantly to take this into account. As the climate warming becomes stronger, thin permafrost layers disappear completely in several decades - first centuries

time scale, while the depth of seasonal thawing increases significantly much faster. The study was supported by the Russian Foundation for Basic Research (grant 01-05-64707).

**JSM10/08P/B23-003**

**1500**

### SEASONAL CHANGES IN RUNOFF CHARACTERISTICS AT A SMALL WATERSHED IN THE SOUTHERN MOUNTAINOUS REGION, EASTERN SIBERIA

Yusuke YAMAZAKI<sup>1</sup>, Jumpei KUBOTA<sup>2</sup>, Kazuyoshi SUZUKI<sup>1</sup>, Tetsuo OHATA<sup>4</sup>, Valery S. VUGLINSKY<sup>3</sup> (<sup>1</sup>Graduate School of Agriculture, Kyoto University, <sup>2</sup>Research Institute for Humanity and Nature, <sup>3</sup>Frontier Observational Research System for Global Change, <sup>4</sup>Institute of Low Temperature Science, Hokkaido University, <sup>5</sup>State Hydrological Institute)

Water and energy cycle in Siberia is characterized by permafrost. Climate changes by the global warming in high latitude. Siberia is expected to be greater than for many other places on earth. The objective of this study is to clarify the effects of seasonal changes in active layer thickness on runoff characteristics using the hydrological and meteorological data obtained by the observations carried out by State Hydrological Institute, Russia (SHI). The Mogot experimental watershed is located in the southern mountainous region in eastern Siberia. The watershed area is 30.8km<sup>2</sup>. The elevation ranges from 550m to 1130m. The average annual precipitation and discharge from 1976 to 1985 were 572mm and 303mm, respectively. The average annual air temperature was -7.7 degrees centigrade in the same time. Larch is dominant at the lower part of slopes and birch and red pine are dominant in other areas. Hydrological and meteorological observations were carried out from 1976 to 1985 by SHI. Active layer thickness increased with temperature. Although temperature began to decrease at the middle of July, active layer thickness still kept increasing till the end of September, exceeding 150cm. The increasing rate was small at the beginning. It became large till the middle of July, then it became small again. In order to analyze effects of active layer thickness on runoff characteristics, we focused on seasonal changes in direct runoff ratio and recession gradient with time. Usually, there are few breaks in a recession period of storm hydrograph. We defined an amount of direct runoff as a volume of the upper part above a straight line between the rising point and the first break point. Also we analyzed the second recession gradient between first break point and the second one, also the third recession gradient. There was weak tendency that direct runoff ratio was high in spring and decreased with time. Both gradients of second and third components were the highest in spring and decreased at the same rate with time. The observation results suggest that frozen soil plays the same role as impermeable layer and the water holding capacity in the active layer, which thickness changes with time, controls runoff characteristics, such as direct runoff ratio and recession gradient. Seasonal change in active layer thickness is one of the key factors that controls runoff characteristics in permafrost regions.

**JSM10/08P/B23-004**

**1520**

### ON THE USE OF A DISTRIBUTED ENERGY BALANCE MODEL TO SIMULATE THE MELTING OF A TROPICAL GLACIER

Jean E. SICART<sup>1</sup>, Regine HOCK<sup>2</sup>, Pierre RIBSTEIN<sup>3</sup> (<sup>1</sup>Department of Geography and Earth Sciences, University of Wales, Aberystwyth, UK, <sup>2</sup>Department of Physical Geography and Quaternary Geology, Sweden, <sup>3</sup>IRD, Maison des Sciences de l'Eau, Montpellier, France)

This study deals with the melt discharge of an Andean tropical glacier: the Zongo glacier, Bolivia (16°S). The year is marked by a dry season in austral winter (May-August) and a wet season in summer (December-March). One important peculiarity of tropical glaciers is that both accumulation and ablation are maximum in wet season. Melting is derived from energy fluxes measured on the glacier by meteorological stations. The fluctuations of net radiation, the main source of energy, are controlled by cloud cover and surface albedo. This latter depends on sporadic snowfalls covering a permanent melting surface. The tropical glaciers are characterized by a marked seasonality of net long-wave radiation: almost zero in wet season, in dry season it represents an important sink of energy during the day. The turbulent fluxes are small in wet season; in dry season the energy lost by latent heat (sublimation) exceeds the gain by sensible heat. The simulation of melt discharge with the distributed energy balance model of Hock [1998] allows for a better understanding of the melting processes. The discharge remains high in wet season because of the alternation of ice melting by solar radiation during cloudless periods with snow melting by thermal radiation during cloudy periods which cause precipitation. The reduction of melting in dry season is mainly due to long-wave radiative losses during the day and cooling of the glacier during the night, but also to the energy lost by sublimation. The study of the energy exchanges at the surface of the glacier allows the inter-annual variability of the glacier mass balance to be related to climate. We show that 'El Niño' events are associated with a marked mass balance deficit because of a delay in the set-up of the wet season, in turn causing a peak of melting around the austral summer solstice.

**JSM10/08P/B23-005**

**1600**

### MODELLING THE DEGREE OF CONTINENTALITY OF GLACIER REGIMES AS A TOOL FOR CLIMATE HISTORY RECONSTRUCTION

Georg KASER (Institut fuer Geographie, Universitaet Innsbruck)

Various climatic proxy data for the Younger Dryas in the European Alps and the circumalpine region show that subarctic climatic conditions prevailed in central Europe during this period, which lasted from ca. 12,700 - 11,500 cal BP. The reconstruction and interpretation of Younger Dryas glaciers and derived equilibrium line altitudes (ELAs), combined with biological and geological proxy data, show not only lower temperatures compared to present day climate but also remarkable changes in the degree of continentality and its spatial gradients. Different combinations of processes related to the advection of atmospheric moisture allow to explain the reconstructed distribution of Younger Dryas ELAs. The obtained general picture clearly indicates a pronounced westerly to northwesterly atmospheric circulation patterns under generally cooler conditions responsible for the observed spatial ELA variability. This example shows how observed and/or reconstructed glacier fluctuations in any climatic scale can be useful indicators for changing atmospheric circulation patterns. A glacier mass balance model which provides the implementation of humidity related variables as a measure for continentality is presented. The model is based on the analytical reconstruction of vertical mass balance gradients, which are highly sensitive to continentality related climatic variables. A sensitivity analysis quantifies how glacier behaviour can be different due to different air humidity and moisture conditions under given thermal conditions. Under different humidity conditions a given change in temperature leads to varying responses of glacier behaviour. This concept of climate reconstruction from carefully documented glacier history shows the importance of changes in climatic variables other than air temperature. The model-based interpretation of observed ELA patterns may serve as a check for the validity of the results from Atmospheric General Circulation Models.

JSM10/08P/B23-006

1620

**RETREAT OF SUNTAR-KHAYATA GLACIERS AS A CONSEQUENCE OF THE REGIONAL CLIMATE CHANGE**Maria D. ANANICHEVA<sup>1</sup>, Jean Luc MERCIER<sup>2</sup> (<sup>1</sup>Institute of geography RAS, <sup>2</sup>Faculty of geography, Louis Pasteur University, Strasbourg, France)

Comparison of data obtained in the end of 1950-s and 2001 about the Suntar-Khayata glaciers (North-East of Asia, Okhotsk Sea basin) positions and their regime shows that they have undergone appreciable changes. The fixed changes require a substantiation of the reasons for the dynamics specified, and first of all within external factors. Internal properties of the given glaciers (low energy of glaciation, low temperatures of the ice thickness, etc.) do not encourage fast changes in their position and regime due to high inertia. Since temperature regime of Suntar-Khayata region in the 20th century is suggested to be the most essential factor of glacier size changes, in the paper the long-term records of temperature and precipitation for 13 meteo-stations within 62-72 N and 121-152 E, have been analyzed. The analysis of trends was carried out by non parametric test of Kendall-Mann-Snayers with preliminary transformation of the series due to their extraordinary amplitude. We revealed two phases of temperature fluctuations from 1940-s: cooling and subsequent warming taking place up to now. For these phases the annual, winter and summer trends were calculated, spatial schemes of their distributions were obtained. In the mountains during cooling temperature drop is reached at the account of autumn and spring that makes period with negative temperatures longer; however during warming phase the growth is mostly in summer that enhances ablation. Trends of total precipitation until 1992 were slightly negative for the majority of met stations, solid precipitation, calculated by special technique, have been growing insignificantly since 1970-s. The comparison of schematic distributions of seasonal trends and directions of these values increasing in particular, specifies different "sources of intensification" for the winter and summer trend. The former grows from northeast to southwest, under the influence of warming, coming from the central part of Asia, the latter enhances from NW to SE, under the influence of warming of the Okhotsk sea south part. We can also hypothesize that the impact of "continental" winter trend and "marine" of summer trend sources exhibit themselves in the factor analysis performed on a matrix of the 12\*473 monthly values from 1953 to 1992. The two first factors described respectively 61.45 % and 23.89 % of the whole variance encompasses more than 85.3 % of the relation between the annual temperature within the extended region under consideration. The two first factors are described by the same three variables, the warming duration, the maximum thermal amplitude and the standard deviation of temperature. Using temperature trend rates and received earlier empirical relationship ablation and mean summer temperature for the region we obtained fluctuation of ablation at the ELA of representative for the Suntar-Khayata Glacier 31. Ablation turned to increase since 1958 (start of warming in the region) totally at 500 mm with gradient of 250 mm per 1 degree C. Under the same trend in 10 years it will reach 120 cm at the ELA area. Similar tendency is anticipated for the other glaciers of the Northern Massif of Suntar-Khayata Ridge.

JSM10/08P/B23-007

1640

**THE STUDY OF GLACIER FLUCTUATIONS USING REMOTE SENSING IN PURUOGANGRIMOUNTAINS OF TIBET**

Anxin LU, Tandong YAO, Shiyin LIU, Liangfu DING (Cold and Arid Regions Environmental and Engineering Research Institute)

In this paper, supported by GIS, the aerial photos, satellite images, topographical maps and the digital elevation model (DEM) were applied to analyze glacier variations during the Little Ice Age (LIA) maximum, 1974 and 2000. Puruogangri Mountains, with more than 420 km<sup>2</sup> area of glacier in Tibet of China, was selected as the test area. The aerial photographs of 1974 and The Landsat TM data in 2000 were used for interpretation on the computer screen and the glacier database (1:100000) were set up combined with DEM. Then towards the main problems of glacier variation, the special statistical analysis and dynamic comparisons were carried out using the database. The main results from this work: (1) The results of interpretation from aerial of 1974 and from TM data for 2000; (2) The dynamic monitoring results of LGM, LIA, 1974 and 2000 show that the area of glacier were decreased. The conclusions are: 1. By the combination of using aerial photographs and Landsat TM remote sensing data and rich un-remote sensed data, the trend of climate variation during the Little Ice Age (LIA) maximum, 1974 and 2000. 2. For the past years, the area of glacier was decreased remarkable in the Puruogangri Mountains, which meets with the air temperature increasing.

JSM10/08P/B23-008

1700

**GLACIER CHANGE AND ITS FORCING CAUSE IN THE SOURCE REGIONS OF THE YANGTZE AND YELLOW RIVERS ON THE TIBETAN PLATEAU**

Yongjian DING, Yang JIANPING, Chen RENSHENG, Liu SHIYIN, Lu ANXIN (Cold and Arid Regions Environmental and Engineering Research Institute, Chinese Academy of Sciences)

Glacier is an important component of eco-environment in the source regions of the Yangtze and Yellow Rivers. The effects of glacier change on eco-environment attract researcher's attentions for a long time in the source regions. GIS provides an efficient tool to analyze the status and change of glaciers. In the paper, the Geladandong area in the source region of the Yangtze River and A'nyëmaqên Mountains in the source region of the Yellow River are selected as the test areas. Based on RS data in the two periods-one in 1969a and the other in 2000a in Geladandong area of the source region of the Yangtze River, one in 1966a and the other in 2000a in A'nyëmaqên Mountains of the source region of the Yellow River, glacier variation during the Little Ice Age(LIA) maximum, in 1969(1966) and 2000 are analyzed by means of aerial photos, satellite image, topographical map and the derived digital elevation model(DEM). Glacier changes in the whole source regions of the Yangtze and Yellow Rivers are inferred from study of the above two test areas. The results indicate that the glacier area had decreased about 1.7% from 1969 to 2000 in Geladandong area of the source region of the Yangtze River, while about 17% from 1966 to 2000 in A'nyëmaqên Mountains of the source region of the Yellow River, and that the largest retreat rate of glacier terminus is 41.5m per year in Geladandong area, while 57.4m per year in A'nyëmaqên Mountains. Compared with glaciers in the source region of the Yellow River, withdrawal rate of glaciers is smaller and glaciers seem almost steady in the source region of the Yangtze River. Glaciers advance markedly from 1969 to 1995 in the source region of the Yangtze River and from 1966 to 1981 in the source region of the Yellow River. At this period the majority of glaciers is in advance or stable. The changing time from advance into retreat in glacier in the source region of the Yangtze River is later about 10 than that in the source region of the Yellow River. Glaciers retreat to a great extent since the 1980s. Significant increasing air temperature in summer and decreasing precipitation are the basic cause of glacier retreat. Glacier retreat results in 7 million cubic meter losses in glacier water resources every year in the source regions of the Yangtze and Yellow Rivers, respectively. **Key words:** the source region of the Yangtze River; the source region of the Yellow River; glacier change; forcing cause

JSM10-Posters

Wednesday, July 9

**CRYOSPHERE-CLIMATE INTERACTIONS (IAMAS [ICCL, ICPM], IAPSO, IAHS)**

Location: Site D

Wednesday, July 9 PM

JSM10/09P/D-001

Poster

1400-055

**SEASONAL VARIATION OF SURFACE FLUXES OBSERVED OVER TUNDRA IN EASTERN SIBERIA**Yuji KODAMA<sup>1</sup>, Norifumi SATO<sup>1</sup>, Hironori YABUKI<sup>1</sup>, Yoshiyuki ISHII<sup>1</sup>, Mutsumi NOMURA<sup>3</sup>, Tetsuo OHATA<sup>2</sup> (<sup>1</sup>Institute of Low Temperature Science, Hokkaido University, <sup>2</sup>Frontier Observation Research System for Global Change, <sup>3</sup>Field Science Center for Northern Biosphere, Hokkaido University)

Tundra area has a unique water cycle due to the existence of frozen ground, drifting snow and tundra vegetation. In order to better understand the water cycle over tundra, micro-meteorological and hydrological observations have been carried out near Tiksi, Eastern Siberia. A 10m meteorological mast was erected and air temperature, humidity, wind speed and direction were measured at the different height from the ground. Concurrently carried out was the observations of 4 radiation components, soil temperatures and moistures, barometric pressure and precipitation. The heat budget equation at the tundra surface was solved approximating the surface temperature by iteration. In the equation, sensible and latent heat fluxes were expressed by a bulk method and the soil heat flux by the gradient method. The bulk coefficient was a function of the bulk Richardson number and the evaporation efficiency and the thermal conductivity of the surface soil was a function of surface soil moisture. The result was obtained for 1998 and 1999, and well compared with result of Bowen ratio method, but not with the eddy correlation method. The seasonal change of heat balance components was also dependent on the atmospheric conditions. In this watershed, where locates 7 km from the Laptev Sea of the Arctic Ocean, the southwesterly wind was warm and dry, gave the sensible heat flux towards the ground surface and the northeasterly wind was cold and damp, gave the large sensible heat flux to the atmosphere from the tundra surface. The energy fluxes as well as the water fluxes were strongly dependent on the wind direction.

JSM10/09P/D-002

Poster

1400-056

**THE SURFACE MASS BALANCE OF MD364, ANTARCTICA ESTIMATED FROM THE ICE CORE ANALYSE**

Makoto IGARASHI, Hideaki MOTOYAMA, Teruo FURUKAWA, Yoko TOYAMA, Fumihiko NISHIWO, Kazuhide SATOW, Takawo KAMEDA (National Institute of Polar Research)

Japanese Antarctic Research Expedition (JARE) has collected shallow ice cores in East Queen Maud Land during the last two decades. The object of retrieving the ice cores is to obtain records of climate, atmospheric chemistry and surface mass balance through the ice core analyses. The ice core study is a part of the ITASE (International Trans-Antarctic Scientific Expedition) program, which is an international effort to obtain paleoclimatic records and clarify past environmental changes during the last few hundreds years in the Antarctic. We have been analyzing a shallow ice core drilled at MD364 (74°00'29"S, 42°59'48"E, 3353 m a.s.l.). The drilling site is located on the way from Syowa station to Dome Fuji. To determine the annual accumulation rate, we employed snow stake data from 1992 to 2000, tritium content, solid ECM and concentration of chemical constituents. The average annual surface mass balance at MD364 is 16 mm a<sup>-1</sup> in water equivalent (w. e.) during the last 9 years from continuous accumulation data, 24 mm a<sup>-1</sup> in w. e. between 1966 and 1993 by tritium content and 20 mm a<sup>-1</sup> in w. e. by solid ECM and concentration of chemical constituents which detected the eruption of Mt. Tambora (AD 1815). These results, which are obtained from three methods, suggest that the annual surface mass balance at MD364 was not stable for last 200 years. The age of Tambora eruption corresponds with the 11.2 m depth and it is only top part of the ice core. We will continue to analysis of the more deep part (until 80 m depth) and estimate the annual accumulation rate of the whole core.

JSM10/09P/D-003

Poster

1400-057

**ONE-DIMENSIONAL NONSTATIONARY MODEL OF SEA ICE**

Boris Viacheslavovich IVANOV, Oleg Mikhailovich ANDREEV (Arctic&amp;Antarctic Research Institute, 38-Bering str., 199397, Saint-Petersburg, Russia)

ONE-DIMENSIONAL NONSTATIONARY MODEL OF SEA ICE. B.V. Ivanov (1), O.M. Andreev (1). (1) State Research Center of the Russian Federation - Arctic and Antarctic Research Institute b\_ivanov@aar.i.nw.ru/Fax: (812) 3522685, (812) 3522688 The heat exchange provided by radiation of the atmosphere and the underlying sea ice is an important component of the Arctic climate system. In the Earth's polar regions the change of the radiation characteristics of the atmosphere and the underlying surface makes influence on the climatic conditions more than in any other place of the globe. It occurs primarily due to significant seasonal albedo changes of the aforementioned surfaces. The development of large-scale motions in atmosphere also depends on the energy exchange intensity including the radiation exchange with the underlying surface. The short-wave solar radiation, unlike the incoming long-wave radiation, is not fully absorbed by the surface penetrating to the lowerlying snow and ice layers. The penetration determines the change in thermal physical, radiation and physical-mechanical properties of these media. Data of the radiation-thermal physical properties of snow are necessary to improve parameterization of the snow-ice cover melting processes in modern thermodynamic models of sea ice. Based on the numerous experimental data obtained in the Arctic areas, a mathematical model of the sea ice cover was developed at AARI. The model allows us to calculate the temperature profile in the snow and ice cover given the actual variability of the ambient meteorological parameters and the radiation-thermal physical characteristics of the snow and sea ice. Additionally, the vertical turbulent heat and moisture fluxes are calculated by this model using integral aerodynamic formulas with heat and moisture exchange coefficients depending on atmospheric stratification in the surface air layer. The long-wave radiation balance is calculated by the method specifically developed for the Arctic conditions. The short-wave radiation balance is determined by actual incoming global radiation data and moderate estimations of snow and ice albedo. One of the main peculiarities of our model is a correct account of solar radiation, which penetrates into the snow or sea ice active layer. Relationship between the transmission and extinction coefficients and thermophysical features of snow and ice and parameters of model numerical chart (grid vertical interval) has been proposed. The obtained results make it possible to define more correctly the amount of short-wave solar radiation penetrating to snow and ice cover and also simulate more adequately the processes of sea ice cover melting from the physical aspect. The described snow cover model is an integral

## INTER-ASSOCIATION

part of a one-dimensional thermodynamic model of the snow-ice cover developed at AARI. Our model, based on good agreement of experimental and calculated data, can be used both for estimation of the state and variation of drifting ice in Central part of Arctic Basin and for land fast ice of near of shore areas.

**JSM10/09P/D-004** Poster **1400-058**  
**IMPACT OF SEA ICE DYNAMICS ON THE SEA ICE DISTRIBUTION**

Tomoo OGURA, Ayako ABE-OUCHI, Hiroyasu HASUMI (Center for Climate System Research, The University of Tokyo)

Sea ice has a substantial influence on the atmosphere and the ocean on a global scale as an interactive component of the climate system. Among many factors controlling the sea ice distribution, we focus on the sea ice dynamics (advection) and assess their effect on the present-day sea ice climatology. Previous studies using numerical models have shown that summer sea ice area in the Southern Ocean decreases due to the sea ice dynamics. In winter, on the other hand, sea ice dynamics cause little difference in the simulated sea ice area. However, one of the reasons for this less sensitivity in winter may be that dynamic response of the ocean, such as convection, has not been incorporated in the sea ice models used in the experiments. In the present study, therefore, we employ a coupled ocean-atmosphere GCM (OAGCM) to verify whether sea ice dynamics can affect sea ice distribution by controlling the ocean convection process. The model used in the experiments is the low resolution version of the OAGCM being developed at CCSR. It consists of the CCSR/NIES AGCM5.6 at T21 resolution (11 vertical levels), the CCSR OGCM (COCO2.1) with 2.8 x 2.8 resolution (20 vertical levels), and a dynamic-thermodynamic sea ice model. Two kinds of numerical experiments are conducted to evaluate the impact of sea ice dynamics: 1. 'CONTROL', in which a dynamic-thermodynamic sea ice model is used, and 2. 'NO-DRIFT', in which a thermodynamic sea ice model (without dynamics) is used. Significant difference between the two numerical experiments appears in the time evolution of winter sea ice area in the Southern Ocean. Sea ice area fluctuates in a decadal scale in the NO-DRIFT run, while it is kept more stable in the CONTROL run, suggesting that sea ice dynamics suppress one mode of decadal variation in the Southern Ocean. The fluctuation of sea ice area in the NO-DRIFT run mainly occurs around the Weddell Sea, accompanied by variation in the ocean convection intensity. Smaller ice extent corresponds to more intense ocean convection. More detailed comparison between the CONTROL and the NO-DRIFT reveals that two factors contribute to the greater stability of sea ice distribution in the CONTROL run: (a) sea ice dynamics increase the static stability of the ocean by enhancing freshwater release near the ice edge, and (b) sea ice dynamics increase the static stability by decreasing the sea ice concentration and thickness, which enhances the deep water cooling in winter (especially near the Antarctic continent). In the Northern Hemisphere, on the other hand, sea ice dynamics made little impact on the sea ice extent, although significant effect on sea ice thickness was found. The reason for this different behavior of sea ice distribution between the Arctic and the Antarctic will be discussed at the symposium.

**JSM10/09P/D-005** Poster **1400-059**  
**LONG-TERM AND INTER-ANNUAL VARIABILITY OF ICE CONDITION IN THE OKHOTSK - BERING-CHUKCHI SEAS**

Larisa S. MUKTEPAVEL<sup>1</sup>, Roger COLONY<sup>2</sup>, Vladimir PLOTNIKOV<sup>3</sup> (<sup>1</sup>Pacific Research Fisheries Center (TINRO), <sup>2</sup>International Arctic Research Center/UAF, <sup>3</sup>Pacific Oceanological Institute)

The intermediate time-scales of sea ice allows it to be a good indicator of large scale variability of ocean/ice/atmosphere system. The annual cycle of sea ice extent in each of the three seas is shown with statistics for both intra-annual variability and inter-annual variability. Coverage studies indicate that ice extent in the Okhotsk and Bering seas are out of phase-reduced ice extent in the Okhotsk is usually associated with increased ice in the Bering while ice extent in the Bering is positively correlated with ice extent in the Chukchi Sea. A trend analyses (1960-2000) reveal that all seas and all months have decreasing ice cover. However, only mid-winter ice for the Sea of Okhotsk passed the 95% confidence test. Ice pack has considerable time lag that results in its being optimal indicator of large scale variability of ocean/ice cover/atmosphere system. The nature of large-scale variability of ice pack in some areas of water of the Northern hemisphere is similar, and is determined by evolutionary processes of climatic system. Being located at the turn of the Arctic and Pacific basins, Chukchi/Bering Seas system to some extent conducts the processes going on in those basins. The mechanism of halocline formation in Arctic basin confirms it. Halocline is formed by means of the transfer of salted waters of the northern part of the Bering sea through the Bering Strait. Those salted waters are formed during the winter period as the result of the process of ice formation.

**JSM10/09P/D-006** Poster **1400-060**  
**SENSITIVITY OF A COUPLED ICE SHELF - OCEAN SYSTEM TO CHANGES IN CLIMATIC BOUNDARY CONDITIONS**

Henner SANDHAEGGER<sup>1</sup>, Klaus GROSFELD<sup>2</sup>, Manfred A. LANGE<sup>1</sup>, Hartmut H. HELLMER<sup>1</sup> (<sup>1</sup>Alfred Wegener Institute for Polar and Marine Research, Bremerhaven, Germany, <sup>2</sup>Department of Geoscience Modeling, University of Bremen, Germany, <sup>3</sup>Institute of Geophysics, University of Muenster, Germany)

The largest interface between the Antarctic Ice Sheet and the Southern Ocean corresponds to the bases of floating ice shelves which constitute about one half of Antarctica's coast line. Heat and mass (melting and freezing) fluxes across this interface directly affect ice shelf geometry, dynamics, mass balance, and steady state configuration. Since changes in ice shelf geometry influence adjacent regions of grounded ice, ice shelf - ocean interaction seems also to be important in the context of the stability of the West Antarctic Ice Sheet. Furthermore, basal melting and freezing significantly contribute to water mass formation and modification. The export of Ice Shelf Water from huge ice shelf cavities to the open ocean leads to a preconditioning of shelf waters and the formation of deep water at the continental shelf break. In order to quantify the impact of melting and freezing on the combined ice shelf - ocean system, we performed a series of basic model studies with a dynamic ice shelf model coupled to an OGCM. The results obtained for idealised configurations (comparable in size to the Filchner-Ronne Ice Shelf) indicate high sensitivity of system geometry and dynamics especially in regions, where high ablation or accretion rates occur. Model runs with different boundary conditions (surface accumulation rate, ocean temperature) reveal a strong dependence of system evolution on climatic forcing within decadal time scales.

**JSM10/09P/D-007** Poster **1400-061**

**RELATIONSHIPS BETWEEN SEA ICE AND PRESSURE DISTRIBUTION IN SEA ICE DECREASING PERIOD AROUND THE SEA OF OKHOTSK**

Takashige KAWAI (Department of Earth Information Mathematical Sciences, Graduate school of Integrated Basic Sciences, Nihon University)

The sea of Okhotsk is one of seasonal sea ice area. Its variability is presumed to be larger than annual sea ice area. Seasonal differences of interactions between sea ice and atmosphere are considered. Interactions of sea ice increasing period are presumed mainly atmosphere to sea ice. In sea ice decreasing period, they are presumed reverse. In this study, focusing sea ice decreasing period, variability of sea ice area and its effect to the atmospheric circulation in and around the Sea of Okhotsk are investigated. Significant correlations are found between sea ice decreasing area in the Sea of Okhotsk and 1000hPa, 850hPa and 500hPa monthly mean geopotential heights in the northern part of the Sea of Okhotsk in June. Thereupon, differences of pressure distribution pattern between large sea ice decreasing (SID) years and small SID years are explored. In large SID years, Mongolian cyclones are extended to eastward at 1000hPa. North part of the Sea of Okhotsk is included a cyclonic anomaly area. Troughs are found in the Sea of Okhotsk to west Bering Sea at 850hPa. These results suggest in large SID years, cooling water mass from sea ice melting is stronger cooling of lower atmosphere than normal years. Reversely, small SID years, the North Pacific anticyclones are extended to northwestward at 1000hPa. North part of the Sea of Okhotsk is included an anticyclonic anomaly area. Ridges are found in the Sea of Okhotsk to west Bering Sea at 850hPa. In monthly mean weather charts, this anticyclonic anomaly is shown a part of the North Pacific anticyclone. But from individual weather chart, the Okhotsk anticyclone as separated from the North Pacific anticyclone is found. A development of the Okhotsk anticyclone in June is presumed to be related sea ice phenomena. However, small SID years and large anticyclonic anomaly years in the sea of Okhotsk is not corresponded all cases. Former researchers found some characters of Okhotsk anticyclone. Sea ice phenomena are presumed to affect in limited cases of Okhotsk anticyclones.

**JSM10/09P/D-008** Poster **1400-062**

**ANNUAL VARIATION OF ACTIVE LAYER IN ALASKA**

Takeshi SATO<sup>1</sup>, Kenji YOSHIKAWA<sup>2</sup>, Atsushi SATO<sup>3</sup> (<sup>1</sup>Snow and Ice Research Group, National Research Inst. for Earth Science and Disaster Prevention, <sup>2</sup>Water and Environment Research Center, University of Alaska Fairbanks, <sup>3</sup>Snow and Ice Research Group, National Research Institute for Earth Science and Disaster Prevention)

The temperature rise due to the recent global warming is remarkable in Alaska, Canada and Eurasia. This leads to the melting of permafrost in the polar region, which will enhance the emission of greenhouse effect gas such as methane. In this paper, the annual variation of the active layer, a part of permafrost which melts in summer, is investigated focusing on its relationship to the air temperature and snow cover which vary year by year. Meteorological and snow cover observations have been conducted at Caribou Poker Creek (CPC), located in the suburb of Fairbanks, since Aug, 1997. Meteorological elements, snow depth, soil temperature etc. have been measured continuously. By comparing the temporal variations of snow depth and soil temperature profile, it was found that the cooling of soil in winter is small in the year with much snow due to the thermal insulation effect of snow cover and the heating of soil in the subsequent summer is large, which suggests that the active layer develops. And the converse is clear in the year with little snow. The database of the active layer thickness in the Arctic region after 1990 is opened on the web of the CALM project. Analysis of the data of active layer thickness in Alaska showed the difference in its annual variations between the 3 sites around Fairbanks and the 3 sites around Barrow. The relationship between the active layer thickness and the mean air temperatures, in summer (Jun-Aug) and in winter (preceding Dec-Jan) were analyzed. The correlation between the active layer thickness and summer air temperature is positive around Barrow, and there is no such correlation around Fairbanks. There is a site around Fairbanks which has positive correlation between the active layer thickness and winter air temperature. Next, the correlation between the active layer thickness and the maximum snow depth from the preceding Nov to Jan was examined. There is a good correspondence around Fairbanks, that is, the active layer thickness tends to increase as the snow depth increases up to about 60cm, which agrees with the observations at CPC. And beyond 60cm, the active layer thickness does not depend on snow depth or slightly decreases with the increase in snow depth, which may be ascribed to the additional effects of snow cover such as the increase of melt water and/or the delay in the snowmelt season. On the other hand, snow depth dependence is not clear around Barrow. Since the snow cover is thin around Barrow, the active layer thickness is controlled mainly by the temperature in summer. However, snow depth greatly influences the active layer thickness around Fairbanks where snow cover is thick.

**JSM10/09P/D-009** Poster **1400-063**

**SPATIAL DISTRIBUTION OF ABLATION ON KORYTO GLACIER, KAMCHATKA, RUSSIA**

Keiko KONYA, Takane MATSUMOTO, Renji NARUSE (Institute of Low Temperature Science, Hokkaido University)

To estimate a glacier's discharge and mass balance, it is necessary to investigate the spatial distribution of the glacier's ablation rate. However it is difficult to observe the hourly ablation rate continuously over the whole glacial area. Using ablation models with published meteorological data, it is easily accomplished to investigate inaccessible glaciers. Empirical models have been used for a long time, but they cannot be used for many glaciers because they are not sufficiently accurate. On the other hand, physically based models require a lot of observation data for the calculations. In this study, we constructed a model for a maritime glacier with fewer parameters than previous models and used it to estimate the ablation rate of Koryto Glacier on the Kamchatka Peninsula. For this glacier, we measured the daily melt rate using snow stakes and recorded hourly meteorological data on the glacier. As a result of our heat balance calculations for the accumulation area, we obtained the mean contribution rates to ablation for 50 days in mid-summer 2000 as follows: net radiation 33%, sensible heat flux 44%, and latent heat flux 23%. In the model, continuous meteorological and established geographical data are used as parameters to estimate the distributed ablation rate on snow and ice surfaces. The difference in ablation rate along the crossing line is caused by the distribution of global radiation, which is affected by the surrounding ridges and slope of the glacier surface. To estimate hourly surface melt rates, we solved the equations for each snow and ice surface using multi-regression from the calculated hourly heat balance and our meteorological data. Calculations were done using GIS (Geographical Information System, ArcView version 3.2) with 50-m spatial resolutions. We obtained an asymmetric pattern for the hourly ablation rate over the glacier, which flows from east to west.

JSM10/09P/D-010 Poster 1400-064

## PRECIPITATION CHANGE IN CENTRAL HIMALAYAS OVER THE PAST 300-YEAR

Ke Qin DUAN (China)

The melt water from glaciers in Himalayas form the headwaters of such important rivers as the Indus and the Ganges. Precipitation in Himalayas is responsible for the glacier development and hydrology circulation in Himalayas region. In the global warming condition, what precipitation and glaciers in Himalayas change will influence directly on the water level of the important rivers. However, there exists only limited knowledge concerning precipitation variations in Himalayas in secular time scale due to its high altitude, which limits our ability to predict variability of glacier. This data gap can be addressed with high-fidelity paleoclimate records from ice core in Himalayas. As snow deposits and metamorphoses into ice, ice sheets continuously record the chemical and physical nature of the Earth's atmosphere. The water amount of an annual ice layer in the glacier accumulation area is almost equal to that of the snow deposited on the glacier surface in one year. This means we can reconstruct the precipitation history in Himalayas by recovering the annual ice layer of a glacier. Here, we present a 300 years precipitation record reconstructed from Dasuopu glacier in central Himalayas, Tibet, which allows us to examine the long-term precipitation variability in Himalayas under the condition of the Global warming. The result shows that the central Himalayas has suffered a dry period in early 1800-1820, thereafter a wet condition between 1820-1930, and again a dry period since 1930 to present. Moreover, there exists a strong negative correlation between the precipitation in central Himalayas and the northern global temperature. According to IPCC reports, a global temperature will increase of 0.1-0.2°C/10a. If this is the case, the glaciers on Himalayas, including our studying site, have been continual retreating, decreasing precipitation and accumulation and negative mass balance. Just as science online report, if the Himalayan glaciers continue to dissolve at their current pace over the next 25 years, the Ganges will swell and then, with the most vulnerable portions of the glaciers gone, get perilously low in summer.

JSM11 Thursday, July 10

## GLOBAL SEA LEVEL RISE, GLOBAL CLIMATE CHANGE AND POLAR ICE SHEET STABILITY (IAMAS [ICDM, ICCL, ICPM], IAPSO, IAG, IAHS)

Location: Site B, Room 18

Thursday, July 10 AM

Presiding Chair: R. Peltier

JSM11/10A/B18-001 0900

## ANTARCTIC ICE-SHEET MASS BALANCE FROM SATELLITE ALTIMETRY 1992 TO 2001

H. Jay ZWALLY<sup>1</sup>, Anita C. BRENNER<sup>2</sup>, Helen CORNEJO<sup>2</sup>, Mario GIOVINETTO<sup>2</sup>, Jack L. SABA<sup>2</sup>, Donghui YF<sup>1</sup> (NASA Goddard SFC, <sup>2</sup>Raytheon ITSS)

A major uncertainty in understanding the causes of the current rate of sea level rise is the potential contributions from mass imbalances of the Greenland and Antarctic ice sheets. Estimates of the current mass balance of the Antarctic ice sheet are derived from surface-elevation changes obtained from 9 years of ERS-1&2 radar altimeter data. Elevation time-series are created from altimeter crossovers among 90-day data periods on a 50 km grid to 81.5 S. The time series are fit with a multivariate linear/sinusoidal function to give the average rate of elevation change (dh/dt). On the major Ronne-Filchner, Ross, and Amery ice shelves, the dh/dt are small or near zero. In contrast, the ice shelves of the Antarctic Peninsula and along the West Antarctic coast appear to be thinning significantly, with a 23 +/- 3 cm per year surface elevation decrease on the Larsen ice shelf and a 65 +/- 4 cm per year decrease on the Dotson ice shelf. On the grounded ice, significant elevation decreases are obtained over most of the drainage basins of the Pine Island and Thwaites glaciers in West Antarctica and inland of Law Dome in East Antarctica. Significant elevation increases are observed within about 200 km of the coast around much of the rest of the ice sheet. Farther inland, the changes are a mixed pattern of increases and decreases with increases of a few centimeters per year at the highest elevations of the East Antarctic plateau. The derived elevation changes are combined with estimates of the bedrock uplift from several models to provide maps of ice thickness change. The ice thickness changes enable estimates of the ice mass balances for the major drainage basins, the overall mass balance, and the current contribution of the ice sheet to global sea level change.

JSM11/10A/B18-002 0920

## GREENLAND CLIMATE CHARACTERISTICS IN HADCM3

Jeff RIDLEY<sup>1</sup>, Philippe HUYBRECHTS<sup>2</sup>, Jonathan GREGORY<sup>1</sup>, Jason LOWE<sup>1</sup> (Met Office, <sup>2</sup>Free University of Bruxelles)

The HadCM3 AOGCM has been coupled to a 3D dynamic model of the Greenland ice sheet, which includes a visco-elastic solid Earth model. Once every year the AOGCM provides the ice sheet model with precipitation and temperature anomalies which it uses in order to calculate ablation, ice dynamics and basal rebound. A new orography and fresh water fluxes are passed back to the AOGCM to be utilised over the subsequent year. The water from the melting of calved icebergs is applied evenly to the sea region adjacent to Greenland whilst runoff enters the ocean through 'river' outlets. A multiple century experiment starting from the present day ice sheet with an atmospheric CO<sub>2</sub> concentration of four times pre-industrial levels is being undertaken to determine the rate of ice ablation and the impact of ice sheet changes on simulated sea level, and oceanic and atmospheric circulation. The effect of orographic changes in the ice sheet on its own mass balance is also of interest. The results from the first 180 years of the simulation indicate that the modelled surface air temperature over Greenland in the 4xCO<sub>2</sub> climate is around 8 degrees warmer than in the pre-industrial control, compared with a global mean difference of 5 degrees. Precipitation is increased by 33% in the 4xCO<sub>2</sub> experiment but the rate of ablation rises by 640%, causing a direct sea-level rise of 5mm per year. To understand the mechanisms of change we will examine the spatial patterns of temperature and precipitation anomalies for the model control and 4xCO<sub>2</sub> experiments and compare them with data from anomalously warm years determined from in situ (ice core) data.

JSM11/10A/B18-003 0940

## COMBINING TIME VARIABLE GRAVITY AND OTHER GEODETIC MEASUREMENTS TO UNDERSTAND THE POLAR ICE SHEETS

Isabella VELICOGNA, John WAHR (CIRES and Dept of Physics, Univ. of Colorado)

Predictions of the future evolution of the Antarctic and Greenland ice sheets require knowledge of the present state of ice sheet mass imbalance. Ice flows to achieve equilibrium, redistributing the mass and changing surface elevations. In principle, these changes are observable using geodetic observations of various types: GPS measurements of crustal motion, measurements of changes in the Earth's gravity field from space and from the Earth's surface, and radar and laser altimeter measurements of changes in ice sheet elevations. Each of these data types is sensitive to the mass imbalance and post glacial rebound in a different way, and each is subject to ambiguities in interpretation. It is not trivial to separate effects of present-day mass imbalance from the effects of the Earth's continuing viscous response to mass imbalance in the past. This talk will describe the characteristics of present-day mass imbalance and viscous rebound signals that are likely to be present in geodetic observations with particular focus on Antarctica. We will examine how different observation types can be combined to better understand the evolution of the ice sheets, and we will discuss the strengths and limitations of combining different data sets.

JSM11/10A/B18-004 1000

## RECENT THICKENING OF GLACIER PERITO MORENO, SOUTHERN PATAGONIA

Renji NARUSE<sup>1</sup>, Pedro SKVARCA<sup>2</sup> (<sup>1</sup>Institute of Low Temperature Science, Hokkaido University, <sup>2</sup>Instituto Antartico Argentino, Cerrito 1248, Buenos Aires 1010, Argentina)

Most of 70 outlet glaciers from two Patagonia Icefields (total area: 17,200 km<sup>2</sup>) calve into lakes on the east side and into fjords on the west side. Analyses of various kinds of data since 1945 revealed that the most calving glaciers have significantly been retreating: e.g. 5 km during the last 20 years at Glacier Upsala. Thickening rates of ice were also measured as -3.5 m/a (1983-98) at Glacier Soler, -3.7 m/a (1985-93) at Glacier Tyndal, and -11 m/a (1990-93) at Glacier Upsala: all indicated large thinning. Based on these ground and satellite data, Anya (1999) roughly estimated the contribution of the shrinkage of Patagonian glaciers to the global sea-level change as about 2 mm in 51 years, which corresponds to about 3.6% of the sea-level rise since 1945. Among major glaciers in Patagonia, the behavior of an eastward outlet Glacier Perito Moreno is rather unusual because of its near-steady terminus position during the last half century. The glacier, 30 km long and 258 km<sup>2</sup> in area, flows northeastward from the ice divide on the Southern Patagonia Icefield. The ablation area forms a valley-type glacier about 4 km wide, and calves into the southwestern arm of Lago Argentino. The glacier front reaches currently the opposite bank with an ice tunnel which drains water in the lake. Small-scale but frequent oscillations of the terminus are known at the glacier during the 20th century, and ruptures of ice-dams were recorded about ten times. However, it is regarded that the glacier has been almost stable since 1970. As to ice flow velocity, seasonal fluctuations were not recognized significantly, but daily variations were markedly. Surface elevations of the ablation area of Glacier Perito Moreno were measured five times in 1990, 1993, 1996, 1999 and 2002, with the conventional survey method using an electronic distance meter. As the results, average thickening rates of seven points in the mid-reaches were obtained as +0.2 m/a in 1990-93, -0.2 m/a in 1993-96, +0.5 m/a in 1996-99, and +1.5 m/a in 1999-2002. Thus, while the glacier has been almost in the equilibrium profile in the early half of the 1990s, it has recently been thickening with accelerating rates. Judging from other features of the glacier behaviors, this thickening trend is not likely to relate to a surge, but may be attributed to the dynamic causes of the glacier.

JSM11/10A/B18-005 1020

## RANDOM FLUCTUATIONS OF THE ICE SHEETS BOUNDARY CONDITIONS AND THEIR RELATION WITH SEA LEVEL

Frederique REMY, Benoit LEGRESY (Legos-OMP)

Ice sheet mass balance changes are mostly controlled by atmospheric, dynamics and sea level changes. However, due to the large inertia of the ice sheet dynamics and to the non-linear effects of some changes in the boundary conditions, the short-scale fluctuations of the ice sheets environment or boundary may induce a large-scale signal on ice sheet mass balance and then on sea level. We will focus the presentation on the effect of random change in accumulation rate and in the outlet glaciers conditions. First, the large relaxation time of an ice sheet induces a low-frequency response to random fluctuations of snow accumulation. However, the time scale of the response is big compared to the average human lifetime and the effect of these random fluctuations on sea level change may be important even if they are not linked to climatic change. Short-term changes in the volume of ice sheets as analyzed by radar altimetry may not be related to long-term climatic change. We express the relaxation time of an ice sheet with respect to the ice thickness, surface slope and ice velocity. These parameters are deduced from the precise topography derived from the geodetic cycle of the ERS1 radar altimeter. Then we apply a stochastic process to model the accumulation rate random fluctuations. The variance of the induced effect on ice elevation is found to be around 3 m over a 30-yr scale and with a maximum of 10 m in Wilkes Land and in the western part of the West Antarctic ice sheet. Near the coast, this effect can mask a climatic signal and thus be critical for altimetric mass balance surveys. The estimated changes in Antarctica's elevation between Seasat (1978) and ERS (1993) epochs could be explained at least partially by such processes. In terms of sea level change over the 30-yr scale, the standard deviation of the induced effect is 8 ± 2.8 cm. Finally, we show that the probability of a present day, induced sea level rise of between 0.5 and 1 mm/yr over a 30-yr time scale is estimated at 10% ± 10%, with coastal areas accounting for half of this signal. Second, the boundary conditions of the outlet glaciers are controlled by ice dynamics and sea level. Any changes affect the grounding line position or on the ice thickness near the coast that in turn affect the flow ice volume in the upslope direction. The propagation is very long so that the actual state does not correspond to actual boundary conditions. The effect of the past fluctuation in outlet glaciers conditions will be investigated in term of ice sheet mass balance change and of sea level change.

JSM11/10A/B18-006 1040

## SYOWA STATION, ANTARCTICA, FOR GLOBAL GEODYNAMICS NETWORK STATION (A REVIEW REVISITED)

Kazuo SHIBUYA, Koichiro DOI, Shigeru AOKI (Center for Antarctic Environment Monitoring, National Institute of Polar Research)

Shibuya (1993) made a review of the solid-earth geophysics programme by the Japanese Antarctic Research Expedition (JARE) at Syowa Station, Antarctica, and summarized the status of each component at the year of 1993. VLBI was in the planning stage yet, AG team just arrived for the first measurement, SG observation also just started. GPS was yet in a campaign mode. After 10 years, with continuing support from the geodetic society, Syowa

IA

## INTER-ASSOCIATION

Station has now become one of the key stations for global geodynamics in the southern hemisphere, and the JARE program will maintain all components including VLBI, GPS (IGS and regional), DORIS, SG and AG, sea level variation by BPG, together with monitoring by broadband seismometer, magnetic variographs, etc. Syowa 11-m antenna also acquired many SAR scenes of JERS-1 and ERS-1/2 tandem orbits, covering approximately 3/4 of the East Antarctic ice sheet. In this symposium many results in relation to Syowa observations are presented. We will make brief review of current status of each component and present near-future plans. Detection of time variable gravity fields by GRACE is a challenging topic in relation to the mass balance of the Shirase Glacier region and the ground truth surveys which are tied to the Syowa reference marks will also be introduced.

Thursday, July 10 PM

Presiding Chair: J. Zwally

**JSM11/10P/B18-001**

**1400**

### LOW-FREQUENCY OCEAN VARIABILITY AND THE GLOBAL MEAN SEA LEVEL RISE PROBLEM

Rui M. PONTE<sup>1</sup>, Detlef STAMMER<sup>2</sup>, Carl WUNSCH<sup>3</sup> (<sup>1</sup>Atmospheric and Environmental Research, Inc., <sup>2</sup>Scripps Institution of Oceanography, <sup>3</sup>Massachusetts Institute of Technology)

Sea level records contain much variability at seasonal to decadal scales, which can make the determination of long term trends difficult and erroneous. The correct estimation of the seasonal to decadal signals over the global oceans is thus very important for understanding mean sea level rise, both regionally and globally. Here we use in situ tide gauge and hydrographic data, satellite altimeter measurements, and multidecadal numerical model simulations to quantify the low-frequency signals in sea level, and how they relate to variability in the ocean circulation and atmospheric forcing, as a function of region and time scale. Particular attention is given to analyzing mismatches between data and model simulations, determining the impact of the seasonal to decadal variability on the long term trend estimates, and providing ways to improve those estimates.

**JSM11/10P/B18-002**

**1420**

### DETECTING THE FINGER-PRINT OF FORCING FACTORS CONTRIBUTING TO DECADAL AND SECULAR SEA LEVEL VARIATIONS

Hans-Peter PLAG (Geodetic Institute, Norwegian Mapping Authority, Kartverksveien 21, N-3511 Honefoss, Norway)

The main forcing factors contributing to coastal relative sea level variations at decadal to century time scales are (1) steric changes, i.e. changes in the volume of the sea water, (2) mass exchange with the continental cryosphere and hydrosphere, (3) post-glacial rebound, (4) local vertical movement of the crust, and (5) variations in the atmospheric circulation. Utilising the large and global database of local monthly mean sea level values available at the Permanent Service for Mean Sea Level, a search is carried out for the "finger-prints" of the different forcing factors in the sea level. A complex regression model is used to weight the "finger-prints" of the different factors. The forcing factors are represented by model predictions (General Circulation Models for steric effects, geophysical model for post-glacial rebound), theoretical finger-print functions (for mass exchange with the cryosphere, where the static sea-level equation is used to compute the finger-print functions for the sea-level signal due to linear trends in the Antarctic and Greenland ice sheets), and observational data (atmospheric circulation). For each forcing factor, a parameterised contribution is included in the regression. In an inversion, these parameters are determined for large sets of models and/or assumptions. Particular emphasis is on the correlation between the different forcing factors, which is found to be as high as 0.4 in some cases. As a particular result, the secular changes for the Antarctic and Greenland ice sheets will be discussed.

**JSM11/10P/B18-003**

**1440**

### SECULAR SEA LEVEL RISE IN THE RUSSIAN SECTOR OF THE ARCTIC OCEAN

Richard W. PELTIER<sup>1</sup>, Andrey PROSHUTINSKY<sup>2</sup> (<sup>1</sup>Department of Physics, University of Toronto, <sup>2</sup>Woods-Hole Oceanographic Institution)

Tide gauge observations of secular sea level change continue to provide the only means whereby one may estimate the global rate of sea level rise that has been characteristic of the most recent 50-100 years of Earth history. Until recently, the only such estimates that have been available were based upon the analysis of data from sites contributing to the Permanent Service for Mean Sea Level and which were included in the archive prior to 2003. One characteristic of this data is that it included very little information from either high northern or southern latitudes. Very recently, however, the data base has been expanded by the addition of measurements from a large number of sites in the Russian sector of the Arctic Ocean. A total of approximately 60 such time series, each of 50 years or greater duration, are now included in the archive. Given the duration of each of these records they are expected to enable one to average out the influence of interannual variability upon estimates of the secular rates of change. The availability of such Arctic records is especially important as the thermal expansivity of ocean water near the poles is substantially less than that which is characteristic of lower latitudes. For a given increase in surface temperature the contribution of the thermal expansion of the oceans to the rise of sea level is therefore expected to be significantly less at high latitude than at mid- or equatorial latitudes. We have analysed the secular rates of sea level rise recorded on this dense set of Russian gauges by employing a detailed model of the process of global glacial isostatic adjustment to filter the influence of the last deglaciation event of the current ice age from the data. When we average over the filtered results we obtain an estimate for the rate at which the influence of modern climate change may be causing sea level to rise in the Arctic Ocean of approximately 2.3 mm per year. This rate is very close to that inferred on the basis of analysis of data from the East Coast of the US, for which region a value of approximately 2 mm per year was determined. It is also close to but somewhat greater than the most recent estimate of approximately 1.85 mm per year for the globally averaged rate of sea level rise. These numbers all significantly exceed the IPCC best estimate of the global rate of relative sea level rise. Possible reasons for this discrepancy will be discussed.

**JSM11/10P/B18-004**

**1500**

### WHAT IS THE MAIN CAUSE OF SEA LEVEL CHANGE AROUND JAPAN DURING 1969-1998

Sin-Iti IWASAKI, Tomonori MATSUURA, Wataru SASAKI, Isao WATABE (National Research Institute for Earth Science and Disaster Prevention)

A trend of the oceanic origin sea level change was deduced from the tide gauge records for the last 30 years around Honshu Is. of Japan. The Height Difference Data (results of the ground leveling from 1969 to 1998 made by Geographical Survey Institute of Japan) was

used to extract the effect of the crustal movements from the tide gauge records. It was assumed that the Japan Datum of Leveling had been stable. The trend of the oceanic origin sea level change can be divided into two parts by the 137°E longitude line. Average rate of the oceanic origin sea level change for the West Japan was +2.4 mm/year, while it was -3.1 mm/year for the East Japan. The relation between the trend of the oceanic origin sea level and the sea surface temperature was also investigated. We found that the trend of the oceanic origin sea level had good correlation to the trend of the sea surface temperature. Separately from our work, Cabanes et al. (2001) stated that the sea level rise observed by the satellite and tide gauges was well explained by the thermal expansion of the seawater. Our results agree well with their conclusions. Reference: Cecile Cabanes, Anny Cazenave and Christian Le Provost, Sea Level Rise During Past 40 Years Determined from Satellite and In Situ Observations, Science, 294, 840-842, 2001

**JSM11/10P/B18-005**

**1600**

### LONG TERM VARIABILITIES OF TIDES AND MEAN SEA LEVEL IN BRAZIL

Joseph HARARI<sup>1</sup>, Carlos Augusto De Sampaio FRANÇA<sup>1</sup>, Ricardo DE CAMARGO<sup>2</sup>, Afranio Rubens DE MESQUITA<sup>1</sup> (<sup>1</sup>Instituto Oceanográfico da Universidade de São Paulo, <sup>2</sup>Instituto Astronômico, Geofísico e Ciências Atmosféricas da Universidade de São Paulo)

Sea surface level measurements have been regularly performed along the Brazilian coast and have provided relevant information about long-term variabilities of BR tides and mean sea level (computed by filtering out the tidal oscillations BR in the observations). Results of analyses are relative to two parts of the BR North / Northeastern coast (Belém, 1° 26.2' S 048° 29.6' W, with observations from 1948 to 1987, and Recife, 8° 3.3' S 034° 51.9' W, 1946 - 1987) and two BR of the Southeastern region (Santos, 23° 57' S 048° 19' W, 1944 - 1989, and BR Cananéia, 25° 01' S 047° 55' W, 1954 - 1990). There is special interest on BR monthly, seasonal and annual mean levels, which indicate seasonal BR hydrodynamical variations and long term trends. The following rates were BR computed: mean sea level variations of 3.500 (Belém), 5.432 (Recife), BR 1.132 (Santos) and 4.046 cm/decade (Cananéia); M2 amplitude trends are, BR respectively, -1.100, 0.070, -0.162 and 0.470 cm/decade; M2 phase rates are BR 0.600, 2.200, 0.191 and 70.370 degrees/decade; S2 amplitudes vary with BR -0.290, 0.090, 0.130, 0.531 cm/decade; and S2 phases present trends of BR 1.000, 2.600, 0.425 and 0.160 degrees/decade. These trends must be carefully interpreted since they are superimposed to several long period oscillations BR and the ports are subject to many human activities, such as periodic BR dredges in the Port of Santos. Efforts have been made in order to insert BR recent observations in the study and correlate the results to other BR long-term analyses, especially atmospheric temperatures at the surface and BR precipitation rates. These correlations will indicate the importance of the BG greenhouse effect and its possible consequences melting of polar caps, BR increase of mean sea level in tropical and sub-tropical areas, and BR modifications in the tidal propagation regimes.

**JSM11/10P/B18-006**

**1620**

### SEA LEVEL CHANGE IN INDONESIAN ARCHIPELAGO DERIVED FROM A DECADE TIDE GAUGE DATA

Parluhan MANURUNG, Bambang S. PRATOMOSUNU, Rudolf W. MATINDAS, Cecep SUBARYA, Joko ANANTO (National Coordinating Agency for Survey and Mapping (BAKOSURTANAL), Jl. Raya Jakarta-Bogor Km 46 Cibinong, INDONESIA)

Data derived from tide gauge stations operated by the National Coordinating Agency for Survey and Mapping (BAKOSURTANAL) since 1986 was used to determine mean sea level series. The stations were selected with criteria namely, (i) continuously observing from more than ten years, (ii) connected to well established benchmarks, (iii) the locations could represent water level condition of the main and several small islands of Indonesian archipelago. The trend of mean sea level series derived from both monthly and annual data suggest that there is an indication of sea level change in the Indonesian archipelago. The initial result shows that the trend is larger than that of Intergovernmental Panel and Climate Change. This suggests that efforts should be made for precise monitoring of the tide gauge benchmarks, allowing separation of tectonic and local effects from the sea level signal. It is expected that participation of BAKOSURTANAL in the ongoing international program for performing continuous GPS observations at tide gauges would make a significant contribution to the sea level monitoring of Indonesia.

**JSM11-Posters**

Thursday, July 10

### GLOBAL SEA LEVEL RISE, GLOBAL CLIMATE CHANGE AND POLAR ICE SHEET STABILITY (IAMAS [ICDM, ICCL, ICPM], IAPSO, IAG, IAHS)

Location: Site D

Thursday, July 10 PM

Presiding Chair: F. Remy

**JSM11/10P/D-001**

Poster

**1700-010**

### RECENT EXAMPLES FOR THE CONSEQUENCES OF CLIMATE CHANGE ON THE FLOODS

Hamza OZGULER (General Directorate of State Hydraulic Works)

Leading serious damages and harms both on people and land, flooding events are very common in Turkey. Especially in the recent years, a number of devastating flood events have occurred in the various river basins of Turkey. Considering the climatic characteristics of the country whose social and economical structure is changing and developing rapidly, the information on flood events that frequently hits urban areas, infrastructures, industrial facilities, agricultural land and recreational sites is getting more important. Climate change is among the trigger agents of unusual floods. It causes changes in timing, regional patterns and intensity of precipitation events, and in particular, in the number of days with heavy and intense precipitation occurrences. Floods are now being experienced in areas where there were no floods in the past. This implies the regional impacts of the global climate change. In this paper, it is intended to give some local examples to be able to indicate for the regional consequences of the climate change.

**JSM11/10P/D-002** Poster **1700-011**

**FORECASTING THE CASPIAN SEA LEVEL**

Sadegh YARI, Nahid KHODAYARI (Author)

During two last decades significant fluctuations in Caspian Sea level have resulted and continued to result in ecological and economic damage that estimated at 1500 billion Rials (less than 200million \$) in Iranian coastal areas. It is evident that the availability of reliable calendar forecasts of sea level fluctuations would help reduce such damage, but it would not eliminate them entirely. The principal solution for these fluctuation problems would be management of Caspian Sea level where the level would be fixed at some optimal mark. This management approach would need to use forecast of sea level fluctuation. Long-term fluctuations in the level of Caspian Sea vary over a wide range. As an analysis of information available over several decades shows, the water level of Caspian Sea is formed by: fluctuations in river inflow, evaporation from and precipitation into reservoir, and outflow into the Kara-Bogaz-Gol Bay and climatological changes like greenhouse effect and men's effect. In order to decrease the economic and ecological losses caused by Caspian Sea level fluctuations, it is necessary to use sea level forecasting and undertake measures that decrease sea level variation. Adequate information about interannual changes in sea level is available only for the last 150 years. When regular measurements of the level were carried out, using several measuring devices. The amplitude of sea level fluctuations for the period of instrumental observations (1830 to present) was 3.8m, with the highest recording in 1882 at -26.2m and the lowest in 1977 at -29.0m. In 1995, the mean annual level was -26.51m. Conditionally, tree time periods, having sharply distinct sea level regimes can be distinguished:1. Up to the beginning of the 1930s2. From 1931 to 1977, and3. From 1978 to present. The first of these periods had a stable level, a mean annual level of about -26.2m and maximum amplitude of fluctuations that did not exceed 1.5m. In the second period, the level declined annually and, by 1941, the mean annual reduction in level was 16cm. The total decline in Caspian Sea level for the second period was 2.8m. In the third period, a continuous rise in level over 18 years averaged about 14cm per year. The total rise in sea level in this period was 2.5m. The studies executed have shown that the forecast based on the dynamic-stochastic model of the Caspian Sea level fluctuations has come true. In Iranian coast of Caspian Sea, there are some observatory stations (in Anzali, Astara, Noushahr, Babolsar, Amirabad, Bandar-Torkman) that report sea level fluctuations daily. The oldest station is in Anzali, since 1927. Now there is a projects that its goal is forecasting Caspian Sea level and so reducing the damages caused by Caspian Sea level fluctuations.

**JSM11/10P/D-003** Poster **1700-012**

**GLOBAL ATMOSPHERE WATCH AND CLIMATE CHANGE MONITORING IN KOREA**

Sung-Nam OH (Meteorological Research Institute, Korea Meteorology Administration)

The earth's climate has increased 0.7C for the past 100 years. However by the increase in greenhouse gases, the increase of temperature in the troposphere appears more strongly in the high latitude region, and so in the Korean peninsula, the atmospheric temperature has almost risen 1°C since 1880. This phenomenon is interpreted to be a result of global warming. However, this is related to the economical and industrial development of the countries in North East Asia, centered on the Korean area and is also related the entrainment of aerosol due to the desertification of China regions. Since the year of 1996 when the Korean Global Watch Observatory(KGAWO) was established, the techniques in measuring and collecting data have continuously been developed in this country, and so some of the techniques in measuring greenhouse gases are ranked to be the level of the world standard. In particular, the monitoring of climate change in the Korean peninsula includes the measurement technique that observes the background atmospheric constituents such as greenhouse gases, aerosols, and radiation together with the various other factors affecting climate change, the modeling technique for estimating the budget and transfer process of the atmospheric radiation, and the radiative forcing technique due to greenhouse gases and aerosols in the regional climate change. The objectives and study include as : (1) Measurement of background concentration of greenhouse gases atmospheric and the trend analysis on their variation. (2) Establishment of monitoring system for the effect of Asian particles by continental desertification and climate environments. (3) Measurement of atmospheric radiation and development of its data analysis technique. The results of our study are as follow : (1) The concentration of CO2, analyzed by using the flask-sampling method during the period 1990-2000 at Kosan in Cheju, maintains larger seasonal fluctuations as an amplitude of about 16 to 17 ppm every year.(2) The background concentrations of atmospheric CFC-11 and CFC-12 have been monitored to assess their effect on stratospheric ozone depletion and global warming during the period of 5 yrs from September 1995 to March 1999 atKosan, Korea. (3) The size-separated number concentrations of aerosols ranging from 0.3 to 25 µm were observed by using the Optical Particle Counter (OPC) in Seoul and Anmyon Island in the west coast of Korea during Asian dust period in spring 1998. (4) The aerosol optical properties of the background atmosphere in the Korean peninsula were measured at both of Jeju Kosan super-site and Anmyondo GAW station during the intensive observation period (IOP) of ACE-Asia campaign.

**JSM11/10P/D-004** Poster **1700-013**

**GLOBAL AND REGIONAL SEA LEVEL CHANGES FROM ALTIMETRY - RELATION WITH SEA SURFACE TEMPERATURE AND CLIMATE INDICES**

Ole B. ANDERSEN<sup>1</sup>, Per KNUDSEN<sup>1</sup>, Brian BECKLEY<sup>2</sup> (<sup>1</sup>National survey and Cadastre - KMS, <sup>2</sup>Raytheon ITSS, Goddard Space Flight Center)

TOPEX/POSEIDON (T/P) and JASON-1 sea level observations and Reynolds AVHRR sea surface temperature observations for the last decade have been used to study regional changes and regional correlations between long-term changes in sea level and sea surface temperature taking into account sea level changes due to ice mass fluctuations. The effect of the recent recalculated sea state bias correction for the T/P Alt B observations has been taken into account, as well as the effect of the bias between T/P and JASON-1 observations. Consistent increases in both sea level and sea surface temperatures are found in most parts of the Atlantic Ocean over this period. In the Indian Ocean and particularly the Pacific Ocean, the trends in both sea level and temperature are dominated by the large changes associated with the El Niño/Southern Oscillation (ENSO), and the Pacific Decadal oscillation (PDO). Spatial correlation between sea level changes and pressure indices like NAO, SOI, PDO and ENSO are carried out to investigate these in more detail. Sea level changes over the most recent decade detected by T/P sea level observations are correlated with changes in the Reynolds AVHRR sea surface temperature observations with a global averaged correlation of more than 0.65. On regional scales this number becomes higher. Specifically, in the tropical part of the Pacific and Atlantic Ocean where the correlation computed over 10 and 20° latitude bands increases to more than 0.9.

**JSM11/10P/D-005** Poster **1700-014**

**CHANGES IN THE ANTARCTIC AND GREENLAND ICE SHEETS MASS AND THE INSTABILITY OF THE EARTH ROTATION OVER THE LAST 110 YEARS**

Nikolai S. SIDORENKOV (Hydrometeceer of Russian Federation)

The redistribution of water masses on the Earth entails changes in the components of the Earth's inertia tensor and causes the motion of poles and changes of the Earth's rotation speed. N.S.Sidorenkov (1982) has deduced equations which connect the fluctuations of the World Ocean water mass  $\zeta_o$  or the ice mass of Antarctica  $\zeta_a$ , Greenland  $\zeta_g$  and "the rest part of land"  $\zeta_c$  with the parameters of the Earth's rotation (coordinates of the North Pole  $v_x, v_y$  and velocity of rotation  $v_z$ ). Presently, parameters  $v_x, v_y$  and  $v_z$  of the Earth's rotation are measured with a very high accuracy and can be used for the calculation of water exchange (values  $\zeta_o, \zeta_a, \zeta_g$  and  $\zeta_c$ ). According to this idea, we have calculated the unknown increments of the specific amount of water in the World Ocean  $\zeta_o$  and the accumulation of ice in Antarctica  $\zeta_a$ , Greenland  $\zeta_g$  and "the rest part of land"  $\zeta_c$  for 1891-2000 with a one-year step. The computed (theoretical) series  $\zeta_o, \zeta_a, \zeta_g$  are compared with the empirical values  $\zeta_o, \zeta_a, \zeta_g$ . A close correlation between theoretical and empirical series  $\zeta_a$  for Antarctica and  $\zeta_g$  for Greenland is revealed.

**JSM11/10P/D-006** Poster **1700-015**

**INVESTIGATION OF VERTICAL LAND MOVEMENT AND CURRENT EUSTASY BY MEAN SEA LEVEL TWO-FRAGMENT SERIES**

George S. METREVELI (IAG)

BR The global climate warming, wich started in the 1880's, has provoked the BR current eustasy- a level permanent rise in the oceans and seas because BR of water thermal expansion and a shift in the continental water budget BR toward the World ocean.BR Therefore every MSL series contents two trends. The first trend is result BR of Vertical land movement (VLM), wich represents high-inertial, long-term BR process (geological or epeirogenic trend, C mm/year). The second trend BR is result of the global climatic warming (eustasy trend, ΔH mm/year). BR So long as the eustasy started about 15-45 years late than modern climate cycle,BR some of MSL series, contents SL data of eustasy period and before it. BR Consequently, such series may be divided into two fragments. MSL series,BR wich are consist two fragments has a form:BR H1,H2,...Hk,Hk+1,...Hn = (Hij)ixcl;=1,K ,(Hij) ixcl;=K+1,n l=1,2,...,k,...n.BR Trend of the first fragment {Hij} ixcl;=1,K, V1 represents geological trend - BR VLM rate (C), but with the opposite sign: BR V1= -C. BR Trend of the second fragment {Hij} ixcl;=K+1,n, V2 is algebraic sum of both trends: BR V2= ΔH + C. BR For calculation of numerical meanings of ΔH and C may be use regression BR analysis methods (such as method of the least squares). Finally, MSL climatic BR trend can be calculated as:BR ΔH = V2 - C.BR It's really, that the numerical meanings of ΔH and C are rates of MSL BR climatic rise and VLM. Clearly, that successful fulfillment of such operations BR represent some difficulties. The initial operation for its is selection BR of MSL long series into two fragments, statistical duration of wich is enough BR for determination ΔH and C to within 0,1 mm/year. The following steps BR are separation of fragments and implementation some mathematical operation BR for their preparation for computation. The final operations are oceanography BR generalization of local magnitude of the eustasy (ΔH) and determinationBR of regional and global climatic influences on SL.BR By this method eustatic level rise was started in 1896-1900 at Aberdeen II,BR in 1906-1908 at Brest and later at the Cascais and in the Mediterranean and BR Black sea basin in 1914-1926. The average rates of level rise at BR the Aberdeen II, Brest, Cascais, Sevastopol, Batumi and Sidney Fort Denis BR amounted to 2,9; 2,6; 2,0; 2,0; 2,6 and 1,5 mm/year. The average rates BR of the VLM at that towns are accordingly: 1,7; -0,3; 0,8; 0,2; 0,4 and BR 0,7 mm/year. BR These investigation was made by information till 1990's.BR One of the merits of methods is using statistically enough duration fragments, BR on wich have effect all SL accuracy determined factors; BR The methods accuracy is increased as far as of fragment's lengthening;BR The method's accuracy was estimated by results of the Repeated Geodesy Survey BR RGS), wich was realized in 1902 and 1952 along railway on the Caucasus coasts.

**JSM11/10P/D-007** Poster **1700-016**

**GLOBAL MEAN SEA LEVEL RISE DURING THE 1990S AND THE PREVIOUS DECADES**

Anny CAZENAVE<sup>1</sup>, R.Steven NEREM<sup>2</sup>, Alix LOMBARD<sup>1</sup> (<sup>1</sup>LEGOS-GRGS/CNES, <sup>2</sup>CCAR, University of Colorado, Boulder, CO, USA)

For now 10 years, global mean sea level variations are routinely measured by the Topex/Poseidon altimeter satellite. Sea level rise measured by Topex/Poseidon during the 1990s amounts to 3 mm/yr. Based on in situ ocean temperature data, we show that thermal expansion is the dominant contribution to the observed rate of rise. We quantify thermal expansion and water mass exchange with continental reservoirs not only during the Topex/Poseidon lifetime but also for the previous few decades. Regional analyses as well as EOF decomposition of the thermal component over the last five decades allow us to give some insight into the spatio-temporal behavior of thermal expansion. We show that the steric sea level has experienced two periods of accelerated rate of rise, in the early 1970s and early 1990s. We also show that the Atlantic ocean is the main contributor to this behavior. Recently published estimates of continental glaciers melting, ice sheets melting and land water mass change suggest that the latter sources have contributed to about 1 mm/yr eustatic (i.e., non steric) sea level rise during the 1990s. This observation raises the following question: since Topex-derived sea level rise is well explained by thermal expansion, this additional 1 mm/yr water mass contribution has to be counterbalanced by a similar contribution of opposite sign. Possible sources of sea level drop are water vapor stored in the atmosphere, ocean waters salinity increase and water mass stored in continental reservoirs as a result of human activities. Among these, the anthropogenic contribution is the most likely cause of sea level drop, albeit still very poorly known.

**JSM11/10P/D-008** Poster **1700-017**

**BASAL SLIDING OF ICE SHEET OBTAINED FROM BALANCE VELOCITY AND SURFACE TOPOGRAPHY IN THE EAST DRONNING MAUD LAND, EAST ANTARCTICA**

Shuhei TAKAHASHI<sup>1</sup>, Okitsugu WATANABE<sup>2</sup> (<sup>1</sup>Department of Civil Engineering, Kitami Institute of Technology, <sup>2</sup>National Institute of Polar Research)

The Japanese Antarctic Research Expeditions (JAREs) have made glaciological studies on ice sheet dynamics and surface mass balance in the East Dronning Maud Land, mainly around Shirase Glacier drainage basin, during 30 years or more. The ice flow velocity was observed along a route transversal to the Shirase Glacier flow by the optical survey method in 1969 to 1974, along two routes of a longitudinal route to Shirase Glacier and a transversal route from Mizuho Station to the Sor Rondane mountains by the satellite doppler positioning system of NNSS (Navy Navigation Satellite System) in 1982 to 1987, and along a route from coastal region to Dome Fuji Station by GPS (Global Positioning System) In 1992 to 1995. In



## INTER-ASSOCIATION

these observations the thinning of ice sheet was observed in the middle part of Shirase drainage basin, which was suggested to be caused from basal slip of ice sheet. On the same observation period, surface mass balance was extensively obtained in the East Queen Maud Land mainly by snow stake method. From the surface mass balance and ice sheet thickness, balance velocities were obtained on the assumption of steady flow, which were well correlated with observed surface velocities. Assuming no-basal slip flow, the balance velocity has some relation with surface gradient that derives from flow law. In inland region the obtained balance velocity were well correlated with surface gradient in this relation, but in coastal region and in the middle part of Shirase drainage basin the balance velocity was larger than the one predicted from this relation, which means the basal slip occurred at the bottom of ice sheet. Along ice streamlines the existence of basal slip was examined and a distribution of basal slip was obtained. Relating to this basal slip, the instability of ice sheet flow and the difference of observed and estimated mass balance of Shirase glacier are discussed.

**JSM11/10P/D-009** Poster **1700-018**

### SEA LEVEL CHANGE IN THE LAST DECADE-WHAT DO WE UNDERSTAND

Jens SCHROETER, Joanna STANEVA, Manfred WENZEL (Alfred-Wegener-Institut for Polar and Marine Research)

Global and regional sea level change is studied by assimilating satellite altimetry, sea surface temperature and hydrographic data into an ocean general circulation model. The free sea surface of the model changes due to steric expansion, mass exchange through the surface and local redistribution by internal dynamic processes. These processes are analyzed separately in order to interpret the measurements correctly and understand the underlying reasons, which are prerequisite for predicting sea level change. The global mean sea level of the model is most sensitive to the global ocean mass budget, i.e. inflow by rivers, melting ice, precipitation and evaporation. This budget is poorly known in comparison to the evolution of the volume of the ocean as determined from altimetry. It seems more reasonable to use the assimilation results to improve the estimates of freshwater fluxes than to use measured fluxes to determine the ocean's mass change.

**JSM11/10P/D-010** Poster **1700-019**

### MODELLING GLOBAL CYCLE OF CARBON DIOXIDE IN SYSTEM OF "ATMOSPHERE-OCEAN" AND GLOBAL WARMING EFFECT

Alexander GLUSHKOV<sup>1</sup>, Valery KHOKHLOV<sup>1</sup>, Elena PONOMARENKO<sup>2</sup> (<sup>1</sup>Innovative Geosciences Researchs Centre, <sup>2</sup>. Department of environment monitoring, Odessa Environmental University)

A studying the global warming phenomenon, global cycle of the carbon dioxide etc attract a great interest. The purpose of this paper is carrying out the detailed model of the CO<sub>2</sub> global turnover in system of 'atmosphere-ocean'. Practically all carried out models are functioning in the average annual regime and accounting for the carbon distribution in biosphere in most general form (c.f. Nefedov-Narko, 1995; Glushkov et al, 1999). We construct a modified model for cycle of the carbon dioxide, which allows to reproduce a season dynamics of carbon turnover in ocean with account of zone ocean structure (up quasi-homogeneous layer, thermocline and deepest layer). It is taken into account dependence of the CO<sub>2</sub> transfer through the boundary between atmosphere and ocean upon temperature of water and air, wind velocity, buffer mechanism of the CO<sub>2</sub> dissolution. It is obtained a temporal and space distribution for concentration of non-organic carbon in ocean, partial pressure of dissolved CO<sub>2</sub> and value of exchange on the border between atmosphere and ocean. It is estimated a role of the wind intermixing of the upper ocean layer. The increasing of this effect leads to increasing the plankton mass and further particles, which are transferred by wind, contribute to more quick immersion of microscopic shells and organic material. It is fulfilled investigation of sensibility of the master differential equations system solutions from the model parameters. The master differential equations system, describing a dynamics of the CO<sub>2</sub> cycle, is numerically integrated by the four order Runge-Cutt method under given initial values of variables till output of solution on periodic regime. At first it is indicated on possible realization of the chaos scenario in system. On our data, the difference of the average annual values for the non-organic carbon concentration in the upper quasi-homogeneous layer between equator and extreme southern zone is 0.15 mol/m<sup>3</sup>, between the equator and extreme northern zone is 0.12 mol/m<sup>3</sup>, the maximum amplitude of season oscillations (40°-50°n.l.) is 0.07 mol/M<sup>3</sup>.

**JSM14** Monday, July 7 - Wednesday, July 9

### DYNAMICS AND PREDICTABILITY OF SEVERE WEATHER EVENTS (IAMAS [ICDM, ICCP], IAHS)

Location: Site A, Room 5

Monday, July 7 AM

Presiding Chairs: Y. Asuma, Z. Kawasaki

**JSM14/07A/A05-001** Invited **0915**

### OVERVIEW OF THORPEX: A GLOBAL ATMOSPHERIC RESEARCH PROGRAM

Melvyn Allen SHAPIRO<sup>1</sup>, Alan J. THORPE<sup>2</sup> (<sup>1</sup>Noaa Office of Weather and Air Quality, <sup>2</sup>University of Reading)

Despite steady increases in forecast skill over the past three decades, there continue to be significant limitations in our ability to predict high-impact weather and to fully utilize forecast information for the benefit of society. High-impact weather is defined by its effect on society and the economy and is often associated with: cyclones of arctic, extratropical and tropical origin; flooding precipitation events; zones of very high surface wind-speeds; dust-storms; heat stress and droughts. Overcoming current limitations in forecasting such weather events and the associated hazards is one of the great scientific and societal challenges of the 21st century. High-impact weather forecasts are strongly influenced by the evolving global-to-regional context within which the subsequent local hazardous weather develops. Emerging advances in atmospheric science and technology provide the means to respond to this challenge. These developments include: (i) advances in knowledge of atmospheric predictability, including the dependence of forecast skill on inter-annual, and intra-seasonal climate variability; (ii) new satellite, aircraft, and earth-based observing technologies, including advanced methods for assimilating their observations into operational numerical weather prediction systems; (iii) improved forecast models aided by exponential increases in computational technology; (iv) innovative approaches to maximize the societal and economic benefits of weather forecasts. The expertise to develop and exploit these advances resides across many nations. Accelerating improvements in forecast skill therefore requires an

organised international effort of the scope of THORPEX. THORPEX is a ten-year international programme designed to accelerate improvements in short-range (up to 3 days), medium-range (3 to 7 days) and extended-range (week two) weather predictions and advanced forecast products. The programme builds upon ongoing advances within the basic-research and operational-forecasting communities.

**JSM14/07A/A05-002** Invited **0950**

### CANADIAN WEATHER RESEARCH PROGRAM: TRANSFER FROM RESEARCH TO OPERATIONS

James David ABRAHAM (Meteorological Service of Canada)

In response to a decline in available resources and a measurable deterioration in performance, the Meteorological Service of Canada (MSC) recently initiated the Canadian Weather Research Program (CWRP). The CWRP is currently the highest priority activity within the Environment Canada's meteorological research program. Furthermore, the CWRP is developing significant collaborations with the United States Weather Research Program (USWRP) and the World Weather Research Program (WWRP). Within this strategy of collaboration, government and university scientists are partnering on a variety of weather research initiatives. Universities are using these collaborations to obtain funds through opportunities like the CFCAS (Canadian Foundation for Climate and Atmospheric Science) and the CFI (Canadian Foundation for Innovation). The general objective of CWRP is to improve our forecast ability at all scales, and in particular the forecast of extreme weather. Given the important impact of precipitation, and in particular snow and freezing rain, precipitation is being emphasized within CWRP. Furthermore, CWRP will emphasize the transfer of science to operational forecast offices, and improve the links between prediction of extreme weather and reduced socio-economic impacts. The CWRP initiative led to the MSC becoming partners with the U.S. National Weather Service (NWS) and the University Corporation in Atmospheric Research (UCAR) in the COMET program (Cooperative Program for Operational Meteorology Education and Training) to facilitate the research infrastructure being used for professional development of meteorologists. Government scientists are working in collaboration with universities on a number of important research programs within CWRP. Some of these include: understanding the behavior of hurricanes affecting Eastern Canada; improved prediction of precipitation in the short-term (nowcasting) using our new Doppler Radar Network; better forecasts of precipitation amounts using numerical weather prediction models and assimilation of data; better forecasts of heavy snow near the Great Lakes; improved detection and prediction of hazardous aircraft icing; understanding the formation of severe thunderstorms and heavy rain induced by lake breezes; development of new ways to observe weather over the data sparse Pacific Ocean. In the spirit of collaboration within CWRP, the MSC along with McGill and Laval Universities have partnered to obtain Canadian Foundation for Innovation support for the installation of a world class remote sensing observatory and high density observing network in the Montreal area. Furthermore, the research and development and operational weather forecast communities in the Montreal area are forming a special consortium (Extreme-Weather Academic Research Network: E-WARN) to effectively transfer science to applications using the research infrastructure in Montreal. This presentation will provide the rationale for developing the CWRP, along with a number of examples of progress and achievements, as well as future plans.

**JSM14/07A/A05-003** **1025**

### ON STEADY-STATE PROPERTIES AND STATISTICAL DISTRIBUTION OF TORNADO-LIKE VORTICES IN THE ATMOSPHERE

Michael V. KURGANSKY<sup>1</sup> (<sup>1</sup>Department of Atmospheric and Ocean Physics, Faculty of Physical and Mathematical Sciences, University of Concepcion, Chile, <sup>2</sup>A.M. Obukhov Institute of Atmospheric Physics, Russian Academy of Sciences, Moscow, Russia)

Both thermodynamical and fluid dynamical arguments are given to construct a simple version of the similarity theory for the mature, quasi-steady stage of a helical moist-convective vortex. On this basis, a steady equilibrium negative-exponential distribution of tornado-like vortices with respect to their size is introduced, which corresponds to a two-dimensional Maxwell distribution on maximum wind intensity. This reference distribution is critically compared to some statistical data on tornadoes distribution with respect to the Fujita scale wind speed, over territory of USA and Russia. A question of estimating the probability of a tornado occurrence at a given location is shortly addressed, using the above reference statistical distribution. Finally, some peculiarities in inter-decadal variations of the tornadoes statistics, possibly related to overall climate changes, are discussed briefly.

**JSM14/07A/A05-004** **1040**

### SIMULATION EXPERIMENT OF TORNADO ASSOCIATED WITH SUPERCELL USING THE CLOUD RESOLVING STORM SIMULATOR

Kazuhiisa TSUBOKI<sup>1</sup>, Atsushi SAKAKIBARA<sup>2</sup> (<sup>1</sup>Hydrospheric Atmospheric Research Center, Nagoya University, <sup>2</sup>Research Organization for Information Science and Technology)

We have developed a cloud-resolving numerical model which was named the Cloud Resolving Storm Simulator (CReSS). In this paper, characteristics of CReSS will be introduced and results of simulation experiment of tornado which occurred within a supercell will be presented. CReSS is formulated based on the non-hydrostatic and compressible equation system with terrain-following coordinates. Prognostic variables are three-dimensional velocity components, perturbations of pressure and potential temperature, subgrid-scale turbulent kinetic energy (TKE), and cloud physical variables. A finite difference method is used for the spatial discretization and the mode-splitting technique is adapted for time integration. Cloud physics is formulated by a bulk method of cold rain with variables of mixing ratios and number densities of water substance. The turbulence is parameterized by the 1.5 order closure with TKE. Parallel processing is performed by the Message Passing Interface (MPI). Three severe tornadoes occurred in the Tokai District, the central part of Japan, on 24 September 1999. Observation showed that their width was several hundred meters and their rotation was cyclonic. The Doppler radar of Nagoya University observed the parent mesoscale convective systems (MCSs) of the tornadoes and found characteristics of supercell in the MCSs: a hook-shaped echo and a bounded weak-echo region. Vorticity of the meso-cyclones within the MCSs estimated from the Doppler velocity was an order of 0.01/s. The simulation was aiming at resolving the vortex of the tornado within the supercell. The computation domain was about 45 km in horizontal with grid size of 75 m and 12.5 km in vertical with the smallest grid size of 25 m. The basic field was given by a sounding at 00 UTC, 24 September 1999. After about one hour from the initial time, a quasi-stationary supercell was simulated. An intense updraft occurred along the surface flanking line. At the central part of the updraft, a tornadic vortex was formed after 90 minutes from the initial time. This simulated tornado was successively developed and maintained at the central part of the strong updraft. The diameter of the vortex was about 500 m and the maximum of vorticity was about 0.5 /s. These characteristics correspond to the observed tornado. The central pressure perturbation of -12 hPa was in the cyclostrophic balance with the rotating flow of the tornado. In this simulation experiment, both the supercell and the tornado were simulated in the common uniform grids. The tornado was produced purely by the dynamic process

formulated in CReSS. Detailed analyses of the simulated data showed the mechanism of the tornado genesis within the supercell.

**JSM14/07A/A05-005****1115****RECENT STUDIES ON THE DYNAMICS OF LINE SQUALLS IN WEST AFRICA USING SATELLITE DATA**

Simon Oyediran OJO (Department of Geography, University of Lagos)

With recently available satellite data in Nigeria, there arises a big challenge to use the data to critically examine the characteristics and patterns of line squalls and their consequences on climate and environmental dynamics in West Africa. This paper therefore uses some of the available satellite data to examine the variability characteristics and consequences of line squalls as a weather event in the study region during the 1996-98 rainy seasons with particular reference to (a) the beginning of the rainy season (b) the middle of the rainy season (c) the little dry season and (d) the end of the rainy season. The paper first examines the significance of line squalls as an element and factor of climate in the region relative to other factors (including the intertropical discontinuity (ITD) and the ocean factor, winds, topography and land and sea contrasts, which are especially significant for local scale weather systems. The paper also examines the variability characteristics of the weather event with particular reference to wind speeds, frequency of occurrence and impacts on aspects of rainfall, which in the region may be equated to climate. The results of the study show that in general (a) the source regions of most of the line squalls include the highland areas around (i) Congo (Brazzaville) at the beginning of the rainy season (ii) Central African Republic in the middle of the rainy season and (iii) the Ethiopian Highlands at the end of the rainy season (b) wind speeds accompanying line squalls are generally stronger in the south than in the north by about 30-50 per cent (c) while wind speeds in the south vary from between 25-40 knots, those of the north vary from between about 35-50 knots sometimes reaching extremes of more than 60 knots (d) the frequency of occurrence are generally more at the beginning and end of the rainy season than in the middle of the rains (e) the frequencies of occurrence are more in the northern areas than in the south (f) the relative contributions to rainfall at the beginning and end of the rainy season are more than at the middle of the rainy season and (g) the relative contributions to rainfall in the north are more than the contributions in the south. More detailed illustrations of the variations and variability of the characteristics of the climatic event are discussed using monthly and daily values for some representative stations in the region. The paper finally discusses the problems of predictability of the climatic event in the study region especially with respect to problems of data availability on the weather event and discusses the need to improve data acquisition especially through the continued acquiring of satellite data in the region.

**JSM14/07A/A05-006****1130****CONVECTIVE ACTIVITY AND LOCAL CIRCULATION OBSERVED AT SERPONG, WEST JAVA, INDONESIA**Ryuzo ARAKI<sup>1</sup>, Manabu D. YAMANAKA<sup>1</sup>, Fumie MURATA<sup>1</sup>, Hiroyuki HASHIGUCHI<sup>1</sup>, Tien SRIBIMAWATI<sup>1</sup>, Mahally KUDSY<sup>2</sup>, Findy RENGGONO<sup>3</sup> (<sup>1</sup>Graduate School of Science and Technology, Kobe University, <sup>2</sup>Radio Science Center for Space and Atmosphere, Kyoto University, <sup>3</sup>Agency for the Assessment and Application of Technology (BPPT), Indonesia)

Wind variations with daytime rainfalls in November 1994 at Serpong near Jakarta, Indonesia (6.4 S, 106.7 E) were investigated by utilizing a UHF-band wind profiler, Geostationary Meteorological Satellite and a tipping-bucket type rain gauge data. Serpong is situated at the south of Java Sea coastline which roughly extends to east-west direction. Distance from the coastline to Serpong is about 40 km. There are no mountains between the coastline and Serpong. Serpong is located in a plain area. Sea-land breeze circulation is dominant in meridional wind in the dry season at Serpong. Sea-breeze (northerly) and return flow (southerly) were observed at a height range of 0.5 - 1.2 km and 1.2 - 2.0 km, respectively, during 12 - 19 LST (LST = UTC + 7). Land-breeze (southerly) and return flow (northerly) were observed at 0.5 - 1.0 km and 1.6 - 2.0 km, respectively, during 06 - 11 LST. November 1994 corresponded to the end of dry season. The peak time of sea-breeze (13 - 15 LST) corresponded to the time of strong precipitations, which 5 minutes mean rain intensity was more than 50 mm/hr, at Serpong. The number of days in which strong precipitation occurred (Strong precipitation days) were 5 days in this period. Sea-breeze (northerly) velocities from 0.3 to 1.0 km height on the strong precipitation days were stronger than those on the non-precipitation days. In November 1994, diurnal variation of the convective activity became strong in the mountainous range in the south of Serpong. However, strong precipitations at Serpong were not due to clouds developed in the mountainous range. They occurred when Serpong was covered with clouds developed in the plain area. It was thought that convective activity with daytime strong precipitations at Serpong interacted with sea breeze in this period.

**JSM14/07A/A05-007****1145****A COMPREHENSIVE STUDY ON TROPICAL MESOSCALE CONVECTIVE SYSTEMS USING VHF AND UHF RADARS OVER A TROPICAL STATION**

Kishore Kumar KARANAM, Atma Ram JAIN (National MST radar Facility, India)

A large number of recent observational studies of mesoscale systems have been signifying a renewed interest in tropical mesoscale convective systems (TMCS) and their impact on general atmospheric circulation and hence the global climate. There is a need to thoroughly understand each and every physical process associated with these systems, so that one can exactly parameterize them for improved numerical weather models. Thus, a need of global climatology of the convective systems has been driving many research groups across the globe to carry out various experiments to explore such systems. In this regard, several campaigns have been carried out to study the convective systems over Gadanki (13.50N, 79.20E), a tropical station in India, using VHF and UHF radars. Structure and Dynamics of the convective systems are among the central objectives of these campaigns. The height-time sections of several convective systems are studied to explore their reflectivity, turbulence and vertical velocity structure. The observed systems are classified into single, multi and super cell systems and height-time sections of the same are presented. It has been observed that most of the convective systems at this latitude are multi cell systems. It has been noted that the vertical velocity cores play a significant role in providing heavy rainfall observed at the surface. Simultaneous VHF and UHF radar data are used to classify the observed precipitating systems as convective, transition and stratiform regions. Composite height profiles of vertical velocities in these regions were obtained and the same were compared with the profiles obtained at other geographical locations. These composite profiles of vertical velocity in the convective region of TMCS have shown their peak in the mid troposphere indicating that the maximum latent heat being released at those height regions. These profiles are very important for numerical simulations of the convective systems, which vary significantly from one geographical location to the other.

**JSM14/07A/A05-008****1200****NUMERICAL SIMULATION OF KANGNUNG HEAVY RAINFALL EVENT OCCURRED BY 'LUSA' DURING AUG. 30-31, 2002 WITH CRESS**

Jai ho OH, Jeong-Hui KIM, Tae-Hun KIM, Kazuhisa TUSBOKI (Department of Env. &amp; Atmos. Sci., Pukyong National University)

In summer season, because topography is very complex in Korea and moistures are supplied from south-western ocean, heavy rainfall case around a northern area of Jiri mountain are often occurred (Kim and Chun 2000). During 30-31 August 2002, when typhoon 'Rusa' passed Korea, a heavy rainfall about 890 mm within one day occurred around Kangnung area. This heavy rainfall might be related to the fact that huge amount of moisture was supplied to the mountainous regional by typhoon 'Rusa'. In this study, we try to reproduce this heavy rainfall event occurred at Kangnung during Aug. 30-31, 2002 with cloud resolving model 'CReSS'. To simulate the 15th typhoon 'RUSA' case for the period of Aug. 30 to 31, 2002, we provided the initial and boundary data from the JMA (Japan Meteorological agency) RSM (regional spectral model) output. As results the typhoon's eye-wall and cloud and rain bands were clearly reproduced with CReSS model simulates the location of typhoon's eye-wall and cloud and rain band clearly. As 'Rusa' moved northward to Korean peninsula, heavy rainfall started at Jeju island and Jiri mountain area, and then at the east coastal mountainous region including Kangnung by strong easterly associated with 'Lusa'.

**JSM14/07A/A05-009****1215****SIMULATION OF A RECENT TROPICAL CYCLONE IN BAY OF BENGAL USING MM5 MODEL AND A COMPARITIVE STUDY OF DIFFERENT CUMULUS AND PBL SCHEMES**Venu G. NAIR<sup>1</sup>, Sijikumar S<sup>1</sup>, Mohankumar K<sup>2</sup> (<sup>1</sup>Research Fellow, <sup>2</sup>Professor)

Tropical cyclones are frequent in Bay of Bengal during the Pre-monsoon (Apr-May), Southwest monsoon (Jun-Sep) and Northeast monsoon (Oct-Nov) periods. The climatological study of the Occurrence of the storms indicates that an average of five nos. of cyclones develops in a year in Bay of Bengal. A detailed study of the cyclogenesis and the movements of these tropical revolving storms is one of the major challenges in front of the Meteorologists. With the advent of the latest Meso-Scale models like MM5, the scientists could have made a remarkable attempt to predict the track of the system. In the present study an attempt has been made to simulate the cyclone which formed in the Southeast Bay of Bengal on 10-11-2002 and moved north-northeast direction and finally made a land fall on 14-11-2002. The model simulated the cyclone well with varying accuracy of different combinations of the parameterization schemes. Present study simulated the cyclone with eight different combinations of cumulus and PBL schemes. The study has been carried out for the two cases. In the first case PBL scheme is fixed with MRF and the four cumulus schemes (Grell, Anthes-Kuo, Kain-Fritsch and Betts-Miller) have been used. The second case is tested with Blackadar in the PBL with same four Cumulus schemes. The best physics options which produces this tropical cyclone are Grell-Blackadar, Kane-Fritsch-MRF and Kane - Fritsch - Blackadar. Grell-Blackadar combination well produces the central pressure of the system and matches with the direction of the system as observed. It even catches the formation of the system and the others are lacking in it.

Monday, July 7 PM

Presiding Chairs: M.V. Kurgansky, M. Yoshizaki

**JSM14/07P/A05-001**

Invited

**1400****ENVIRONMENTAL CONTROL OF TROPICAL CYCLONE INTENSITY**

Kerry EMANUEL (Program in Atmospheres, Oceans and Climate, MIT)

The influence on tropical cyclone intensity of various environmental factors is explored using a simple coupled ocean-atmosphere model. It is first demonstrated that this model is capable of accurately replicating the intensity evolution of storms which move over oceans whose upper thermal structure is not far from monthly mean climatology and which are relatively unaffected by environmental wind shear. A parameterization of the effects of environmental wind shear is then developed and shown to work well in several cases for which the magnitude of the shear is relatively well known. When used for real-time forecasting guidance, the model is shown to perform better than other existing numerical models while being competitive with statistical methods. In the context of a limited number of case studies, the model is then used to explore the sensitivity of storm intensity to its initialization and to a number of environmental factors, including potential intensity, storm track, wind shear, upper ocean thermal structure, bathymetry and land surface characteristics. All of these factors are shown to influence storm intensity, with their relative contributions varying greatly in space and time. It is argued that in most cases, the greatest source of uncertainty in forecasts of storm intensity is uncertainty in forecast values of the environmental wind shear.

**JSM14/07P/A05-002****1435****SIMULATION EXPERIMENT OF TYPHOON SPIRAL BANDS BY THE CLOUD RESOLVING STORM SIMULATOR**Mitsuharu NOMURA<sup>1</sup>, Kazuhisa TUSBOKI<sup>1</sup>, Atsushi SAKAKIBARA<sup>2</sup>, Taro SHINODA<sup>1</sup> (<sup>1</sup>Hydrospheric Atmospheric Research Center, Nagoya University, <sup>2</sup>Research Organization for Information Science and)

Spiral bands are mesoscale characteristics of a developing typhoon. Observational study showed that spiral bands cause strong rainfall. It is still unknown what dynamic and microphysical processes work to produce the strong rainfall within spiral bands, because it is difficult to perform an in-situ observation of a typhoon in its mature stage. Previous numerical studies have been reported the typhoon-scale distribution and structure of spiral cloud bands. Detailed three-dimensional mesoscale structure and physical processes of the typhoon spiral band, however, are little known. In order to simulate detailed structure of a spiral band within a typhoon and to reveal its dynamic and microphysical processes, we used the Cloud Resolving Storm Simulator (CReSS) (Tsuboki and Sakakibara, 2002) in this study. CReSS is a three-dimensional cloud resolving numerical model which is formulated in the non-hydrostatic and compressible equation system with the cold rain parameterization of the microphysics. In order to understand the mesoscale structures and physical processes of the spiral band, a numerical experiment was conducted with a fine mesh. Horizontal and minimum vertical resolutions are 1km and 100m, respectively. In the present study, Typhoon 0216 in mature stage was simulated. The result showed that the mesoscale structures of spiral bands, an eyewall and the eye were successfully simulated. We focus on the three-dimensional structure of the spiral band and its developing and maintenance processes. The maximum mixing ratio of precipitation particles was present on the outer side of the maximum of cloud mixing ratio in the radial direction and on the lee side in the tangential direction. It is shown that the structure and intensity of the spiral band were related to

## INTER-ASSOCIATION

distributions of cloud and precipitation particles of spiral bands. For understanding developing and maintenance of the spiral band, cloud microphysical processes were examined. This showed that cold rain processes are important to intensify the rainfall. In particular, generation and growing of graupel are the most effective processes to produce the intense spiral band.

**JSM14/07P/A05-003**

**1450**

### DETECTION AND TRACKING OF TYPHOON 0115 CENTER FROM DUAL DOPPLER RADAR MEASUREMENTS

Masayuki MAKI<sup>1</sup>, Koyuru IWANAMI<sup>1</sup>, Ryohei MISUMI<sup>1</sup>, Sang-Goon PARK<sup>1</sup>, Mihoko STO<sup>1</sup>, Takeshi MAESAKA<sup>2</sup>, Masaki KATSUMATA<sup>3</sup>, Daisuke HASHIMOTO<sup>4</sup> (<sup>1</sup>National Research Institute for Earth Science and Disaster Prevention, <sup>2</sup>Hokkaido University, <sup>3</sup>Japan Marine Science and Technology Center, <sup>4</sup>Tsukuba University)

To improve nowcasting of heavy rainfalls and strong winds, experimental observations with two X-band radars were carried out in 2001 in the Kanto plain, Japan. This paper demonstrates usefulness and possibilities of real time monitoring of severe storms by dual Doppler radar measurements. Two research radars MP-X and X-DOP of NIED were set up in Tsuchiura (N36°04'09.7", E140°14'39.1") and Kitakawabe (N36°12'28.4", E139°39'54.0"), respectively. Reflectivity data and Doppler velocity data dealiased by the dual pulse repetition frequency technique were sent to the National Research Institute for Earth Science and Disaster Prevention (NIED) via 128kbps telephone lines. Doppler velocity data from two radar sites were analyzed on real time and retrieved wind fields were opened to public on a web site. The example shown in this paper is the Typhoon 0115 which landfall near Kamakura City September 11, 2001. Dual Doppler radar measurements started at 1017LST, 11 Sep. when the center of T-0115 approached the dual Doppler radar analysis area. Two research radars were able to track the typhoon center in the dual Doppler analysis area until 1306LST when the wind speed exceeded the critical value for MP-X radar operation. Detailed wind field near the typhoon center is retrieved every 90 seconds during about three hours from the volume scan data with three tilt angles. A simple algorithm to find and track the typhoon center using wind filed is developed and applied to the retrieved wind field. The obtained trajectory of typhoon center shows trochoidal movement. The speed of the typhoon center is variable ranging from 3.5 ms<sup>-1</sup> to 10 ms<sup>-1</sup>. A sudden decrease in moving speed is observed at the turning point of the trochoidal motion. Analysis of kinematic properties around the typhoon center show clear change in deformation: stretching begins to decrease and shearing begins to increase at the turning point of trochoidal motion.

**JSM14/07P/A05-004**

**1505**

### LABORATORY AND NUMERICAL MODELING OF TYPHOON-LIKE VORTEX

Gennadiy BOGATYRYOV<sup>1</sup>, Gennadiy BOGATYRYOV<sup>1</sup>, Ilya KOLESNICHENKO<sup>2</sup>, Galina LEVINA<sup>2</sup>, Mikhail POVARNITSYN<sup>3</sup>, Andrey SUKHANOVSKY<sup>2</sup> (<sup>1</sup>Perm State University, Perm, <sup>2</sup>Institute for Continuous Media Mechanics, Ural Branch of the Russian Academy, Perm, <sup>3</sup>Space Research Institute, Russian Academy of Sciences, Moscow, <sup>4</sup>Institute for Thermophysics of Extreme States.)

Results of laboratory and numerical experiments carried out to confirm a fundamental theoretical hypothesis on hydrodynamic alpha-effect are presented. This phenomenon is based on special generating properties of small-scale helical turbulence favoring the large-scale structure formation in turbulent media. Conditions for excitation of the large-scale helical vortex under thermal turbulent convection in rotating fluid and ways for controlling this vortical instability are investigated. Laboratory experiments to generate a typhoonic vortex, which rotates in a rotating frame, were carried out in a fluid layer with a large aspect ratio of horizontal to vertical dimension and local heating from below in the central zone. Such a scheme of experiment is assigned to simulate a mechanism of typhoonic vortex generation based on the interaction between an intensive updraft formed in the central zone by small heat carriers rising from a temperature boundary layer near the heater, large-scale advective flow and the Coriolis force. Two different experimental apparatuses were used: with a cylindrical and square in a plane cuvette filled with a fluid. Various liquids were tested so that the corresponding Prandtl numbers could differ in two times and greater. To study the influence of spatial temperature distribution in the heated area on initiation of the vortex, different heaters were used. It has been found that there exists a threshold for the vortex excitation that strongly depends on how uniform is a temperature distribution along the heater. Neutral curves in terms of rotation - intensity of convection have been obtained for different liquids and heaters of divers constructions. They showed no dependence for vortex generation on the Prandtl number and favorable influence of slow rotation for all the experiments. An increase in the angular velocity of apparatus leads to a decrease in the angular velocity of vortex rotation, and finally, to the vortex break. Numerical modeling by DNS has been performed for flows generated in the laboratory apparatus with square cuvette and showed a good agreement between DNS results and experimental observations. A way proposed to influence the rotating vortex is connected with introducing of an external small-scale helicity into the fluid layer. To this purpose small propellers were used in the square cuvette. This allowed us to suppress the initiation of the vortex as well as to change the rotation intensity of developed vortex. This work is supported by the RFBR, Grants No. 01-05-64232, MAC 02-05-06209, 02-05-06210.

**JSM14**

**Monday, July 7 - Wednesday, July 9**

### DYNAMICS AND PREDICTABILITY OF SEVERE WEATHER EVENTS (IAMAS [ICDM, ICCP], IAHS)

Location: Site A, Room 5

**Monday, July 7 PM**

Presiding Chairs: M.V. Kurgansky, M. Yoshizaki

**JSM14/07P/A05-005**

**Invited**

**1620**

### CHARACTERISTICS OF CLOUD CLUSTERS AROUND THE MEIYU/BAIU FRONT

Hiroshi UYEDA, Kohei SAKAMOTO (Hydrospheric Atmospheric Research Center, Nagoya University)

To understand the formation and maintenance mechanism of Mesoscale Convective Systems (MCSs) around the Meiyu/Baiu front, characteristics of Cloud Clusters (CCs) which appeared around the front over China continent and East China Sea during June and July of five years (1998-2002) were investigated by using infrared TBB data of Geostationary Meteorological Satellite (GMS). Diurnal variation of convective activity is predominant over land during warm season in East Asia. The magnitude of the diurnal variation is known to be

different over different geography like a plain, mountains, ocean, etc. However few researchers have investigated the relationship between the appearance characteristics of CC and the geography. In this study, analysis areas containing the eastern part of China and East China Sea, where CC appears frequently along the Meiyu/Baiu front, were classified into four domains: Yangtze River basin, Southeast Mountains, northern part of East China Sea, southern part of East China Sea. Characteristics of CC were investigated for each of the four domains and surrounding areas. An algorithm to detect and identify CC objectively was developed and 2044 CCs were tracked. Following characteristics of CC around the Meiyu/Baiu front in the four domains were clarified. Over land, diurnal appearance of CC having an afternoon peak was predominant in Yangtze River basin in July, and Southeast Mountains in both June and July. However, it was not predominant in Yangtze River basin in June. CCs in Southeast Mountains had shorter lifetime and smaller maximum area than those in Yangtze River basin on average. Over East China Sea, a lot of CCs appeared around 6 o'clock (local time) in the northern part in both June and July. They had longer lifetime and larger maximum area than those over land. Though CCs in the southern part were smaller and lived shorter, some of them appeared simultaneously nearby each other and developed to a huge cluster. Diurnal variation of surface temperature calculated from objective analysis data provided by Japan Meteorological Agency was consistent with the diurnal appearance of CC in each domain. These findings would contribute for the improvement of forecasting CCs and associated heavy rainfalls. By tracking CCs objectively, a generation area of CCs, which develop to meso-alpha low and produce heavy rainfalls, was recognized around the downstream of Yangtze river and the west part of East China Sea. The relation between characteristics of CC in the Meiyu/Baiu front and structure of rainfall systems is discussed in comparison with Doppler radar analyses on a few intensive field experiments.

**JSM14/07P/A05-006**

**Invited**

**1655**

### RADAR OBSERVATIONS OF MESOSCALE CONVECTIVE SYSTEMS IN THE TAIWAN MEIYU SEASON

Jong-Dao Ben JOU (Professor, Department of Atmospheric Sciences, National Taiwan University)

Individual thunderstorms developed into organized thunderstorm lines or complex mesoscale convective storms are commonly observed in the Taiwan Meiyu season. The spatial scale of these storms is about hundred kilometers in long axis and the time scale spans from a few hours to about a day. Significant precipitation and rapid change of wind causes severe damages to the society frequently. Meiyu period in Taiwan, i.e., May and June, is a season of transition. In this season, the cold air mass from Siberia is weakening and the warm air mass from Tropics is strengthening. The boundary of these two air masses forms a stationary front in the subtropical area, extending from south of Japan to Taiwan and southern China. Accompany with the stationary front, a wide cloud band with embedded organized convective systems are commonly observed from satellite images. Strong interaction between Taiwan topography and the frontal system induced many interesting weather phenomena along the coast and over the island. The Weather Bureau of Taiwan has just completed an around-the-island NEXRAD-type Doppler radar network by 2002. This data set provides an unprecedented opportunity for meteorological scientists in Taiwan to study the severe local storms in great depth. In this paper, four kinds of mesoscale convective systems with different organization characteristics observed by the Doppler radar network in Taiwan are summarized. Cases of prefrontal squall lines, frontal rainbands, mountain convections, and tropical convections will be presented and the effort on prediction of these storms will be also described.

**JSM14/07P/A05-007**

**1730**

### NUMERICAL STUDIES OF THE MESOSCALE PRECIPITATION SYSTEMS OVER TAIWAN

Pay-Liam LIN (National Central University)

The particular shape of the Central Mountain Range (CMR) over Taiwan is oriented in NNE-SSW direction with the maximum height over 3000m. Over this complicated topography, there are not only the passage of environment flow will be modified by CMR tremendously, but also severe local storm associated with local circulations will be initiated resulted from the differential heating and the terrain blocking effects. It is also found that the rainfall distribution is concentrated on some special region and location in Taiwan. When northeastern monsoon prevailed, precipitation in the windward side of northeastern Taiwan was very significant. For example, the maximum of long-term monthly mean precipitation at I-Lan occurred in Autumn season. The percentage of monthly precipitation to annual precipitation ranged from 11% to 17% during Autumn season. The maximum daily rainfall amount during this season can be over 300 mm at some station in northeastern Taiwan. The Mei-Yu is a climatic phenomenon found over southeaster China, Taiwan and Japan. It occurs during the transition period between the northeasterly monsoon in the winter and the southwesterly monsoon in summer. During this period, a number of flash floods occurred in the island of Taiwan. In this study, the PSU/NCAR MM5 was used to simulate the mesoscale weather and precipitation systems over Taiwan to investigate the orographic effects on the distribution and characteristics of precipitation in Taiwan and the surrounding area. A Mei-Yu front passed over Taiwan during 7-8 June 1987. There were two types of precipitation system found during this passage. One of them is the prefrontal local convection, and the other is the frontal precipitation. Modeling studies showed that prefrontal convection is at first triggered on the slope of CMR by the local convergence formed by the environmental flow with the thermal induced circulation. The sensitivity tests also indicate that the land-sea breeze, latent heat release and the surface fluxes have influence effects on the generation on the mesoscale convection systems. As the shallow front penetrated to Taiwan, the local convergence was intensified due to the interaction between Mei-Yu front and the CMR. Deep convection associated with front passage made heavy rainfall in the inland area of Taiwan. For the northeasterly monsoon precipitation, the heavy rain event occurred on 10-12 December, 1998 will be presented in this studies. It is found that the northeasterly flow was retarded by the CMR and the local convergence was generated in the windward slope. The upstream influence results from the flow blocking and splitting with the supplying moisture and the surface fluxes triggered the local convective systems.

**JSM14/07P/A05-008**

**1745**

### REGIONAL VARIABILITY OF WARM-SEASON CLOUD/PRECIPITATION EPISODES OVER EAST ASIA BASED ON GMS INFRARED OBSERVATIONS

Chung-Chieh WANG<sup>1</sup>, George Tai-Jen CHEN<sup>2</sup>, Richard E. CARBONE<sup>3</sup> (<sup>1</sup>Department of Environmental Management, Jin-Wen Institute of Technology, <sup>2</sup>Department of Atmospheric Sciences, National Taiwan University, ROC, <sup>3</sup>MMM, National Centers for Atmospheric Research, USA)

Based on radar data, Carbone et al. (2002) have recently reported that heavy precipitation episodes in distance/time space over the continental United States during the warm season (May-August) exhibit coherent patterns and propagating characteristics. The longevity of these episodes, up to 60 h, suggests an intrinsic predictability with a lead-time significantly longer than the lifetime of individual convective systems, and thus the potential for

improvements in precipitation forecasts at the range of 6-48 h. Using GMS Infrared brightness temperature, Wang and Chen (2002) have also compiled a similar climatology of cloud episodes for East Asia (20-40 N, 95-145 E). Results suggest that statistics for events that exhibit stronger propagating characteristics are comparable to those found in the North America, while regional differences are also evident due to a more complicated atmospheric environment as well as variations in the underlying surface inside the calculation domain. The present study extends the work of Wang and Chen (2002) and examines regional variations in characteristics of warm-season cloud episodes in East Asia. The domain is further divided into western and eastern halves using the 120 E meridian, as well as the northern and southern halves using 30 N. Preliminary results suggest that longer cloud streaks (> 2000 km and 30 h) occur more frequently over the ocean, and also more frequently in the Meiyu season (May-June) than in mid-summer. When the calculation domain is limited to the northern half, passages of synoptic-scale baroclinic waves show stronger influence and nearly all cloud streaks propagate eastward even in mid-summer. Over the southern half of domain, on the other hand, cloud streaks are considerably less organized and less propagating, and diurnal forcing show a relatively strong control. Under the influence of subtropical high, westward propagating events originating at lower latitudes are also common during most part of the warm season, from middle of June through August. Other aspects of statistics and periodicity of events in the four quadrants are also examined, compared, and discussed.

Tuesday, July 8 AM

Presiding Chairs: J. Abraham, H. Uyeda

JSM14/08A/A05-001

Invited

0835

#### CHINA HEAVY RAINFALL EXPERIMENT AND STUDY (CHERES)

Yunqi NI (Chinese Academy of Meteorological Sciences)

Heavy rain is one of major disastrous in China. To understand detailed structure of mesoscale heavy rains within Meiyu front and its formation and evolution, experimental observation in the area has been designed reasonably according to intensive observing approaches available for the field observational experiment rather than just based on routine observation networks. The design of observational system for CHERES is divided into three parts: One is a large-scale background field observation. Another is two mesoscale intensive observation areas (meso-alpha scale) for the middle and lower reaches of the Yangtze River. Still another is three meso-beta intensive observation areas for the same region. The background field, which is presented by routine upper air sounding of meteorological operational system and ground-based air observations within the large-scale region, provides environmental condition for heavy rain system. The intensive observation in middle reaches of Yangtze River constructed by Doppler and digital weather radar located in Yichang, Wuhan, Nanchang and Jinzhou, while the radar system located in Shanghai, Hefei, Fuyang, Nanjing, Huangshang and Hangzhou for lower reaches of Yangtze River area and other remote sensor platforms as well as with the advantage of time-intensive routine meteorological data both for surface and upper-air observation, are expected to address the 3D structure of the meso-alpha scale convective system within the Meiyu front. Three meso-beta intensive observation areas, one in middle reaches of Yangtze River, another two in lower reaches of Yangtze River, use dual or three Doppler Weather Radar array, wind profiler, and boundary-layer observation for further providing observational fact on study of precision structure and triggering mechanism of heavy rainfall. The experimental periods are respectively from 10th June to 20th July in 2001 and 2002. The studies of this project based on the above field experiments have made distinct progresses, indicating that to advance the ability of heavy rain prediction is possibly. Firstly, a formation mechanism and physical pattern of the persistence heavy Rain systems in Yangtze River Basin was shown properly. Secondly, large amount of work has been done on the retrieving of satellite remote sensing data concerning the heavy rain systems. Thirdly, significant improvements have been made on the retrieval of the three dimensional structure of heavy rains with single and multiple Doppler radars. Fourthly, the three dimensional variation analysis system has been set up and a new four-dimensional variation data assimilation system is being developed on the basis of AREM. Fifthly, the meso-scale heavy rainfall numerical model AREM has been developed and experimentally predicted with real time. At same time, the new generation non-static and higher-resolution meso-scale model has been developing now.

JSM14/08A/A05-002

0910

#### A CASE STUDY ON THE EVOLUTION OF A MESO- $\alpha$ -LOW IN ASSOCIATION WITH THE MEIYU FRONTAL ACTIVITY OVER CHINA AROUND 28 JUNE 1999

Kuranoshin KATO<sup>1</sup>, Yafei WANG<sup>2</sup> (<sup>1</sup>Faculty of Education, Okayama University, <sup>2</sup>Chinese Academy of Meteorological Sciences)

Meso- $\alpha$ -scale lows sometimes appear on the Meiyu/Baiu front and play important roles in the multi-scale interaction processes between the large-scale and the meso- $\beta$ - and  $\gamma$ -scale convective systems. However, the processes on initiation of a meso- $\alpha$ -scale low and its interaction with the rainfall systems show great variety dependently upon the features of the basic fields around the Meiyu/Baiu front. The previous studies pointed out the important role of the so-called SW vortex initiated around the eastern foot of the Tibetan Plateau. On the other hand, our group presented that a meso- $\alpha$ -low is sometimes initiated after activation of the Meiyu frontal activity. In such cases, the heat-low over the arid region in China played an important role in the temporal activation of the Meiyu front, together with the moisture transport by the subtropical high. Meso- $\alpha$ -low initiated over China also affects the frontal-scale water cycle around the Japan Islands, as illustrated in a case around 29 June 1999 by our group. In the last case, meso- $\alpha$ -scale low was initiated in Central China (the lower reach of the Changjiang River Basin). Thus the present study will examine the evolution process of the meso- $\alpha$ -low over China around 28 June 1999, based on the operational observational data together with the GAME/HUBEX data. The Meiyu cloud zone was once weakened after the eastward passage of a meso- $\alpha$ -low in Central China around 00 UTC 26 June. The GMS IR data shows that the area with low TBB on the Meiyu front enhanced and expanded from 12 UTC 26 to 06 UTC 27 June (around 30N/115-120E) (referred to as Convection Developing Stage). After that, meso- $\alpha$ -low in the lower layer was generated there around 18 UTC 27 June (Low Formation Stage). Then the meso- $\alpha$ -low began to move eastward toward the western part if the Japan Islands with its center pressure decreasing (from 18 UTC 26 to 12 UTC 26) (Low Propagation Stage). Interestingly, the trough was not extended to the upper layer (e.g., 500 hPa level) from the surface-level low until the Low Propagation Stage. In this case, activation of the Meiyu front in the Convection Developing Stage seems to be associated with approach of a low-level cyclonic circulation from the southeastern edge of the Tibetan Plateau (maybe, the so-called SW vortex). However, the vortex itself did not propagated to the Central China directly and it might contribute to the generation of a new meso- $\alpha$ -low by activating the Meiyu frontal rainfall in its eastern area.

JSM14/08A/A05-003

0925

#### A NUMERICAL EXPERIMENT OF A MESOSCALE DISTURBANCE ALONG THE MEI-YU FRONT OBSERVED DURING GAME/HUBEX 98

Kozo NAKAMURA<sup>1</sup>, Yasushi FUJIYOSHI<sup>1</sup>, Kazui SAITO<sup>2</sup>, Masanori YOSHIZAKI<sup>1</sup> (<sup>1</sup>Frontier Research System for Global Change, Yokohama, Japan, <sup>2</sup>Numerical Prediction Division, Japan Meteorological Agency, Tokyo, Japan, <sup>3</sup>Meteorological Research Institute, Tsukuba, Japan)

One of the research subjects of the Hydrological Cycle Research Program (HCRP) of FRSGC is to understand and to model the mesoscale organization processes of the cloud and precipitation system. In order to improve our understanding of the processes, we performed a numerical experiment of the system observed near Fuyuang radar site (115.83 E, 32.93 N) on July 2nd, 1998. The model used in this study is Non Hydrostatic Model (NHM) developed by the Meteorological Research Institute. We used two datasets, i.e., the GAME-Reanalysis and ECMWF data to make initial and boundary conditions, and we investigate the organizing process by comparing the two results. The land surface temperature is predicted by the heat balance equation with wetness parameter denoted by  $w$  ( $w=0.1$  for land,  $w=1.0$  for sea in the control runs). We used the data at 06UTC (14 BST, Beijing Standard Time) July 1 for the initial condition. In both data, a subtropical high was analyzed to the south of Japan, strong southerly wind in the southern part of China, which went to the large shear zone at the Meiyu front. The difference between the two data sets, such as the intensity of the vorticity, does not seem so large, except the surface air temperature in the southern part of China, which is much warmer in the GAME Reanalysis data than in the ECMWF data. It can produce active convection that might enhance the moisture transport to the front area. In both runs, the model successfully reproduced the development of the large-scale horizontal shear, convergence, and the precipitation along the Meiyu front. However, the disturbance of the GAME-Reanalysis run was too strong and moved too fast to the northeastward, and after its movement there is no intense convection. On the other hand, in the ECMWF run, there occurred many convection systems along the front region and properly reproduced the persistent heavy rainfall area. We performed several experiments ( $w=0.1$ ,  $w=1.0$ ) to investigate the effect of the surface conditions. It is shown that although the effect of the wetness parameter on the boundary layer structure is large, its effect on the convective activity appears to be small. When the surface wetness is large, the moisture becomes large in the boundary layer, while the surface temperature becomes lower because of the evaporation. Because the effects of these two processes on the convective activity are opposite with each other, the convection does not becomes so active. The reason why the effect of the wetness parameter is small may be because the runs are started at 06UTC, when the surface temperature becomes highest.

JSM14/08A/A05-004

0940

#### THE STRUCTURE AND EVOLUTION OF A RAINBAND INDUCING HEAVY RAINFALL IN THE DOWNSTREAM OF YANGTZE RIVER

Biao GENG, Hiroyuki YAMADA, Krishna REDDY, Hiroshi UYEDA (Frontier Observational Research System for Global Change)

This paper investigates the structure and evolution of a rainband observed in the downstream of Yangtze River during the Meiyu season in 2001. The rainband, which developed over a Meiyu front in the early morning of June 24, brought more than 110 mm rainfall in a narrow region within only two hours. The rainband was stationary and oriented from southwest to northeast. The length of the rainband was more than 200 km, while the width of the rainband was only about 50 km. A low-level southerly jet was observed in the south side of the rainband. Meanwhile, a medium-scale low-pressure system existed under the rainband. The southerly flow was lifted over the rainband, with the stronger ascent area corresponding to the stronger radar echo area. It is interesting to find that the whole rainband and related rainfall intensified with about 40-min periodicity. The development of the rainband was associated with the periodical development of updrafts within the rainband and surface pressure and wind under the rainband. Meanwhile, downdrafts within the rainband were weak and no distinct gust evolved under the rainband. The in-phase covariance between the surface pressure, wind and rainfall under the rainband suggests that the evolution of the rainband was associated with a kind of mesoscale gravity wave. The interaction between gravity wave, low-level jet and Meiyu front would be important for the development of the strong rainband and the heavy rainfall.

JSM14/08A/A05-005

0955

#### SYNOPTIC-SCALE DYNAMICS OF 18-DAY LONG CONSECUTIVE MESOSCALE CONVECTIVE SYSTEMS DURING THE HEAVY RAIN PERIOD OF 1998

Dong-Kyou LEE, Jeong-Gyun PARK, Jo-Han LEE (Atmospheric Sciences Program, School of Earth and Environmental Science, Seoul National University)

The 18-day long lasting heavy rainfall events occurred over the Korean Peninsula from 31 July to 17 August in 1998. These consecutive heavy rainfall events were a climatologically exceptional heavy rain period with record-breaking cases over South Korea from 1980 to 1999. The 18-day mean synoptic fields well revealed synoptic environments of the successive occurrence of mesoscale convective systems responsible for heavy rain. The continental polar lows north of Korea and the westward extended, strong western Pacific high south of Japan maintained an elongated monsoon front which were supported by baroclinic forcings for about 20 days. The strong southwesterly flows that were sustained by the increased pressure gradient between the continental low and the western Pacific high played an important role in accumulated sufficient moisture over Korea, establishing a widespread baroclinically unstable region over the Korean Peninsula. The synoptic-scale upward motions over Korea was concentrated on the mid- and lower-level attributing to diabatic heating and shearing deformation forcings. Primary pattern of vertical motion was produced by the diabatic heating forcing. Synoptic-scale vertical motion was relatively weak and confined in the lower troposphere because the shearing and stretching deformation forcing contributed mainly to horizontal ageostrophic motion in the upper levels. The vertical structure of the apparent heat source and moisture sink indicated that rainfall over central China was frontal precipitation with upper tropospheric stratiform cloud, while that over Korea and Japan had deep convective characteristics. For the 18-day period, the heavy rainfall occurred with periods of 1 day and 2-3 days and with meridional variation in the South Korean Peninsula. The variation of the heavy rainfall events was highly related with the variation of the upper level wind, lower level temperature and moisture, and middle level geopotential height. The synoptic variables were interacted with each other by secondary circulations and diabatic processes, producing the periodic feature of heavy rainfall occurrence.

IA

**JSM14/08A/A05-006****1010****SEVERE EAST-ASIAN MONSOON STORM SYSTEMS AND CLOUD PRECIPITATION PARTICLES**

Tsumotu TAKAHASHI (Core Education Center, Obirin University)

Monsoons often produce torrential rainfall. During the past 15 years, 208 videasondes have been launched into monsoon clouds from 13 different locations in east Asia. The camera in the sonde captures particle images and transmits them to a ground station and associated Doppler radars record the systems through which the videasondes flew. The storm systems differ in different areas. When intense, low-level southerlies blew over Shanghai, rainbands developed within a meso-rain system. A cloud cell within a meso-rain system moving over southern Kyushu during Baiu suddenly ceased its forward motion. As small cells from the front and side merged into it, the stationary cell grew larger and produced heavy rainfall. A vortex, having formed over the sea off Vietnam, entered a monsoon through over Chiangrai. A meso-rain system developed, composed of a thick upper layer and low-level stratocumulus and produced heavy rain for about three hours. At Songkhala, a typhoon and a northeasterly monsoon formed low-level convergence from which multi-cellular clouds formed, one after the other, producing heavy rain. At Ubou, thunderstorms, formed over the mountains, merged, producing an extremely large, anticyclonic echo. Outflow from this area produced a new rainband in the northeast. Over Melville Island, near Darwin, a cloud cluster developing along an east-west line within a sea-breeze convergence, suddenly changed direction, forming a north-south squall line, producing torrential rain and frequent lightning. Heavy rain over Ponape was produced from a rainband. Data from videasondes revealed three regions in which precipitation processes differed: Cool rain over interior China; mixed rain over the maritime continent; and a frozen drop mechanism over the western Pacific. Although the distribution of precipitation particles differed greatly in different storm systems, one common feature during torrential rain was the explosive growth of graupel, hail, and frozen drops in a narrow area just above the freezing level. The physical processes of rain accumulation through such explosive particle growth has been examined using a three dimensional cloud model containing detailed microphysics.

**JSM14/08A/A05-007**

Invited

**1040****REVIEWS OF FIELD OBSERVATIONS ON MESOSCALE CONVECTIVE SYSTEMS OVER EAST CHINA SEA AND KYUSHU IN THE BAIU SEASON AND OVER THE JAPAN SEA IN WINTER**

Masanori YOSHIZAKI, Teruyuki KATO, Chiashi MUROI, Hisaki EITO, Shugo HAYASHI (Meteorological Research Institute, Japan Meteorological Agency)

Several field observations on mesoscale convective systems (MCSs) and associated disturbances were conducted over East China Sea and Kyushu in the Baiu season and over the Japan Sea in winter. Some observed cases were studied by using the non-hydrostatic numerical model with fine horizontal resolutions. Various types of MCSs were observed: propagating rainbands, orographic stationary lines, meso-beta-scale vortices, longitudinal modes, transverse modes, and so on. Analytical works were done with data of upper-air sounding, Doppler radars, boundary-layer radars, GPS instruments and aircrafts. We review these MCSs and associated disturbances briefly.

**JSM14/08A/A05-008****1115****STRUCTURE OF A COLD FRONT INDUCING A HEAVY RAINFALL DURING X-BAIU-99**

Teruyuki KATO (Meteorological Research Institute)

The band-shaped heavy rainfall observed in northern Kyushu on 29 June 1999 during the special observation of X-BAIU-99 was brought by the passage of a cold front that had been rapidly enhanced for a few hours. Radar observations show that when the cold front passed over northern Kyushu, convective cells in the front moved eastward at a speed of 15 m/s and northward at a speed of 20 m/s. The cells organized several meso-beta-scale convective systems (MbCSs). Each MbCS moved eastward at a speed of 10 m/s and northward at a speed of 5 m/s. Its speed was slow and the direction of its movement has a southward component in comparison with those of the cells. New convective cells repeatedly generated at the upstream edge of each MbCS. This buck-building formation maintained the present precipitation system. The present heavy rainfall was successfully reproduced by a nonhydrostatic model with a horizontal grid of 2 km. The structure with three horizontal scales of the cold front, MbCSs and convective cells was also simulated well. Developing height of simulated cells can divide into two levels. Most simulated cells developed to middle level of a height of 5-7 km in the western part of the simulated rainband, while developed heights of simulated cells in the eastern part of it have two peaks at the middle level and the tropopause (about 14 km). These peaks are not resulted from the release of latent heat of solidification because almost the same result can be gotten even in a sensitive experiment without the ice-phase processes. Since drier and colder air flowed from the west into the middle level of the eastern part of the simulated rainband, the convective instability was enhanced there. The convective cells reaching the middle level could develop to the tropopause.

**JSM14/08A/A05-009****1130****STRUCTURE AND FORMATION PROCESS OF AN OROGRAPHIC LINE-SHAPED SYSTEM DURING BAIU SEASON IN WESTERN KYUSHU, JAPAN**Ayako NAKAMURA<sup>1</sup>, Hiroshi UYEDA<sup>1</sup>, Osamu MORITA<sup>2</sup>, Yasufumi KITAZAKI<sup>1</sup>, Hideki BEPPU<sup>1</sup> (<sup>1</sup>Hydrospheric Atmospheric Research Center, Nagoya University, <sup>2</sup>Graduate School of Sciences, Kyushu University, <sup>3</sup>Fukuoka District Meteorological Observatory, Japan Meteorological Agency)

During Baiu season, orographic line-shaped rainfall systems often appear in the west of Kyushu Island. They extend northeastward from an isolated island or a peninsula. One of them is the Goto line: the line-shaped rainfall system extending from the Goto Islands locating to the west-northernmost coast of Kyushu Island. The line forms along the northwestern coast of Kyushu Island. This system has about 150 km length, although its appearance is not much. The northeastern end of the line brings heavy rainfall over Fukuoka, which is a major city about 130 km far from the Goto Islands. For an accurate prediction of the heavy rainfall, case studies on formation mechanisms of the Goto line are necessary. As few researchers have studied the Goto line, the purpose of my study is to clarify the structure and formation process of the Goto line with the maximum length of 200 km on 19 June 2001. According to surface weather charts, the Goto Islands are located in the warm sector on the southern side of the Baiu front before the formation of this system. Upper-air sounding data in Fukuoka shows that the lower atmosphere has much moisture and nearly convectively stable stratification. There is a strong wind shear in the lower layer, with southerly winds around the surface and southeasterly on the low-middle level. The JMA Fukuoka operational radar data at 2.0 km height indicates that rainfall region extends northeastward from the northeastern side of the Goto Islands and forms a line-shaped rainfall system about 150 km in length with many convective cells. The axis of this line-shaped system rotates

counterclockwise gradually with the shift of middle-level wind direction. In terms of a generation of individual cell that makes up the line, there are not only convective cells generating near the northeast side of the Goto Islands but also convective cells generating on the coast and mountain peaks of northern Kyushu in the downstream of the Goto Islands. On the former, it was found that the upslope forcing due to isolated obstacles triggered convection from high Froude number ( $Fr=3.2$ ). They are advected by middle-level winds. Some convective cells can re-develop or generate on the coast and mountain peaks of northern Kyushu. In this way, the Goto line keeps having about 150 km length and brings heavy rainfall at its northeastern end. We will discuss factors for the appearance of such orographic line-shaped rainfall systems.

**JSM14/08A/A05-010****1145****CASE STUDY OF A DISSIPATING CLOUD CLUSTER: A TRMM-AIRCRAFT SIMULTANEOUS OBSERVATION**Sento NAKAI<sup>1</sup>, Kenji NAKAMURA<sup>2</sup>, Haruya MINDA<sup>3</sup>, Hiromu SEKO<sup>1</sup> (<sup>1</sup>Snow and Ice Research Group, NIED, JAPAN, <sup>2</sup>Hydrospheric Atmospheric Research Center (HyARC), Nagoya University, JAPAN, <sup>3</sup>Forecast Research Department, Meteorological Research Institute, JAPAN)

A simultaneous observation of a dissipating cloud cluster (CC) was made over the East China Sea by Tropical Rainfall Measuring Mission (TRMM) and a dropsonde-equipped aircraft. Hourly GMS equivalent blackbody temperature (TBB) showed that the CC was in the dissipating stage. SSM/I precipitable water (PW) data showed that the CC developed in the area where  $PW > 60$ mm. The structure of the CC was analyzed using TRMM, dropsonde and rawinsonde data. The precipitation within the CC cloud area was mostly stratiform, and corresponded to dense anvil of the CC. The CC had multi-layer structure and thin anvil extended out of apparent CC cloud area. Shallow convection was developed below the thin anvil. The shallow convection generated the outflow from its upper part, resulting in a wet southerly flow directed toward the stratiform precipitation area. A minimum of potential temperature and a maximum of relative humidity were seen below thin cirrus of the CC. They were accompanied by increase of the wind speed. A positive potential temperature anomaly in the upper troposphere induced the negative pressure anomaly at the lower levels. The negative pressure anomaly could contribute to the acceleration of the southerly wind generated by the shallow convection in the lower troposphere. Meanwhile, southeasterly dry wind blew into the stratiform precipitation area of the CC. The dry inflow was cooled by evaporation within the precipitation of the CC, then mixed with the southerly flow, resulting in the formation of the negative potential temperature anomaly. Evaporation cooling occurred in the stratiform precipitation region, however, the negative temperature anomaly did not reach to the surface. The development of the shallow convection was not by convergence between ambient air and a cold pool, and can be attributed to the very humid environment of the lower troposphere favorable to the development of a convection.

**JSM14/08A/A05-011****1200****A HIGH-RESOLUTION WIDE-RANGE NUMERICAL SIMULATION OF CLOUD BANDS ASSOCIATED WITH THE JAPAN SEA POLAR-AIR MASS CONVERGENCE ZONE (JPCZ) IN WINTER USING A NON-HYDROSTATIC MODEL ON THE EARTH SIMULATOR**Hisaki EITO<sup>1</sup>, Chiashi MUROI<sup>1</sup>, Syugo HAYASHI<sup>1</sup>, Jun-ichi ISHIDA<sup>2</sup>, Kouhei ARANAMI<sup>1</sup>, Teruyuki KATO<sup>1</sup>, Masanori YOSHIZAKI<sup>1</sup>, Takayo MATSUO<sup>1</sup> (Meteorological Research Institute, Japan Meteorological Agency, <sup>2</sup>Numerical Prediction Division, Japan Meteorological Agency)

A high-resolution wide-range simulation of cloud bands associated with the Japan Sea Polar-air mass convergence zone (JPCZ) in winter is performed using a non-hydrostatic model (NHM) with a 1-km horizontal resolution and a 1000 x 1000 km calculation domain (1km-NHM) on the Earth Simulator (ES). During winter monsoon season, broad cloud bands extending southeastward from the base of the Korean Peninsula sometimes bring heavy snowfalls to the Japan-Sea-side coastal regions of the Japan Islands. These cloud bands form over the JPCZ to which two cold airflows with different property converge. In this study, typical broad cloud bands that developed over the Sea of Japan on 14 January 2001 are examined. The NHM developed by Japan Meteorological Agency (JMA) is used in this study. The fully compressible equations with the conformal mapping are employed as the basic equations of NHM. Primary physical processes such as cloud physics, atmospheric radiation and mixing in the planetary boundary layer are also included in NHM. The NHM has been transferred to the ES, which is the fastest supercomputer in the world. The optimization of NHM to the ES is underway. In the present study, the vertical grid with a terrain-following coordinate contains 38 levels with a variable grid interval of 40 m near the surface and 1090 m at the top of the domain. The model top is 20.36 km. The time step interval is 5 seconds. The 1km-NHM is one-way nested within the forecast of the NHM with a 5-km grid (5km-NHM). The initial and boundary conditions for the 5km-NHM are provided from output produced by Regional Spectral Model (RSM). The RSM with a horizontal grid size of about 20km is a hydrostatic model used operationally in JMA. The 1km-NHM successfully reproduced cloud bands associated with the JPCZ, extending southeastward from the base of the Korean Peninsula to the San-in and Hokuriku districts over the Sea of Japan. Several cloud streets were also simulated around cloud bands. The JPCZ formed due to the convergence between warmer west-northwesterly flow from Korea Peninsula and colder north-northwesterly flow from Primorskii. A strong horizontal convergence line and an updraft line were found at the southwestern edge of the JPCZ. Deep convective clouds with a height of about 4 km formed along this line. Ice and snow particles from the convective clouds were transported by the southwesterly flow and organized anvil-like stratiform clouds extending northeastward. These two types of clouds formed the cloud bands over the JPCZ. The simulated features almost agree with those of the observations using by meteorological satellites, meteorological radars and an instrumented aircraft.

**JSM14/08A/A05-012****1215****DIABATICALLY FORCED CIRCULATIONS AS TRIGGER FOR THE RELEASE OF STRONG CONVECTION**

Manfred KURZ (Institute of Meteorology, University of Karlsruhe)

One prerequisite for the formation of mesoscale convective systems is the existence of moist potentially unstable air masses in the lower troposphere. For the release of the instability, however, often an ascending motion is necessary in order to destroy stable layers on top of the moist air which would prevent convection, and to bring the air to saturation. In this respect the macroscale ascent ahead of an approaching upper trough or the mesoscale circulation across active fronts may function as trigger for the release of convection. During summer real fronts are often ill defined over the continent. There is, however, a mechanism which may lead to the formation of a very strong temperature contrast near surface within short time. That happens at the edge of larger cloud and precipitation areas during day time due to the different heat fluxes at both sides of the edge: Whereas the temperature below the cloud masses remains constant or is even reduced by the evaporation of falling rain, it rapidly increases due to heating from the ground in the area with no or only few clouds. As consequence of this diabatically forced frontogenesis a solenoidally direct circulation across

the newly established frontal zone is released with ascent of the heated air, descent of the cooler air and an ageostrophic motion from the cold to the warmer air near surface. If the warm air is potentially unstable, the ascent may lead to the release of the instability and the formation of convective clouds ahead of the cloud edge and parallel to it. Due to the production of cold air in the downdraft of these clouds the temperature contrast to the warm air is further enhanced which in turn leads to an intensification of the circulation. Altogether the new front may be transformed into a squall-line. As example for such a process a weather situation from July 2001 is presented. On two consecutive days marked surface fronts originated during the forenoon at the edge of cloud and precipitation areas produced by macroscale ascent ahead of short wave troughs over western and central Europe becoming vigorous squall-lines later and causing a lot of damage and even loss of life. It is important to note that the operationally used high-resolution model of Deutscher Wetterdienst provided clear signals for the described development of the surface fronts and also for the transformation into mesoscale convective systems.

**Tuesday, July 8 PM**

Presiding Chairs: M. Shapiro, J. Turner

**JSM14/08P/A05-001** Invited **1400**

**THE AUGUST 2002 FLOOD IN CENTRAL EUROPE - LESSONS LEARNED**

Gerd TETZLAFF, Manfred MUDELSEE, Michael BOERNGEN (Institut f?E Meteorologie Universitat Leipzig)

Large parts of eastern Central Europe were affected by catastrophic floods in August 2002, caused by widely spread large precipitations. The damage was extraordinary high in particular in the catchment area of the river Elbe and its tributaries. The damage in Elbe region amounted to altogether over 5 Billion?. In the discussion following the flood many reasons were suggested to be responsible for the enormous height of the damage ranging from local land use to global climate changes. The return periods of the rains and the floods exhibited a wide interval between about 100 to 200 years for the Elbe Flood and the areal precipitation, while on the slope of the Erzgebirge some of the smaller catchment areas return periods of up to about 1000 years were observed. The maximum measured 24 hour precipitation was 312 mm on the ridge of the Erzgebirge, a hitherto unreached magnitude. These rains were going with a weather situation all to well known to cause heavy rains on the mountain ranges of eastern Central Europe. The actual rain bearing low followed the so called Vb path, part of an otherwise outdated classification of paths of low pressure systems. This path starts south of the Alpine Mountain range and curves northwards just east of the Alps. In August 2002 it brought warm and humid air to the north in a rather slow moving cyclone. The region of the Elbe catchment is characterised by several horizontally long mountain chains with different orientations, forcing the air to rise. No matter what exact orientation the air flow shows, there is always a mountain ridge there to enhance the upward air flow and the precipitation. In August 2002 it was the Erzgebirge that was located in the air flow and which was doubly effective, first in the southern flow and then with the propagation of the cyclone centre with the northern flow. The main rains were observed on the 12th of August. The main part of the rains, that is more than 100 mm, fell within one day, mainly on the northward slope of the Erzgebirge and its immediate northern surroundings. In some parts the major part of the rains fell within a time period of less than 12 hours. This caused two different of flood types. The small river and streams in or close to the mountain ranges experienced flash flood waves with often devastating effects, enormous damage and short warning periods. The Elbe flood wave had the character of an inundation. The weather forecast showed a rather good quality about 72 hours before the strong downpour started it was clear that unusually high amounts of precipitation were to be expected. The forecasts were substantiated until about 24 hours before the event. However, although the warnings were distributed timely it often proved difficult to transmit this information right through all levels down to the later victims.

**JSM14/08P/A05-002** Invited **1435**

**DYNAMICS OF HEAVY PRECIPITATION EVENTS ON THE SOUTH-SIDE OF THE EUROPEAN ALPS**

Huw C. DAVIES, Francois GHEUSI, Alexia MASSACAND, Heini WERNLI (Atmospheric and Climate Science, ETH Zurich)

During autumn there are frequent events of heavy precipitation on the south-side of the European Alps. Diagnoses are undertaken of (a) realized events using ECMWF analysis fields and (b) simulated events using an NWP model. The diagnoses are geared to examining :- (i) the significance and origin of the upper-level precursor flow signature that takes the form of a potential vorticity (PV) streamer, (ii) the sensitivity of an event to the internal structure of the streamer, (iii) the dependence of the near Alpine precipitating flow to the strength and direction of the incident low-level flow field, and (iv) the role of sub-Alpine topographic features in determining the location of geographically-preferred regions of heavy precipitation.

**JSM14/08P/A05-003** **1510**

**SPECTRAL CHARACTERISTICS OF THE BORA WIND**

Mirko ORLIC, Miroslava PASARIC, Zoran PASARIC (Department of Geophysics, Faculty of Science, University of Zagreb)

Bora is a cold, dry wind that blows above the Adriatic from the northeast quadrant, most often during winter season. Its average speed is usually not high, but - due to the gustiness - the bora speed maxima may surpass 60 m/s. Thus, bora is one of the severest local winds in the world. Previous measurements of the bora speed and direction were performed either with the large sampling intervals (greater than 1 min) over a day or more or with the small sampling intervals (1-16 s) over an hour at most, thus tending to emphasize low- or high-frequency part of the spectrum, respectively. Measurements carried out recently at Senj, east Adriatic station which is notorious for its strong bora outbreaks, with a 1 s sampling interval over two months (December 2001 - January 2002), enabled for the first time broad characteristics of the wind spectrum to be determined. Micro-m-asta TM anemometer was positioned at the coast, 15 m above sea level. During the two-month measurement interval it recorded more than 20 bora episodes, the longest lasting over 82 hours. The maximum wind speeds surpassed 40 m/s, and they were - as expected - related to gusts, the low-pass filtered speeds being smaller than 20 m/s. Spectral analysis revealed (1) an increase of energy from the smallest resolved period (2 s) to about 1 min, (2) further increase of energy between 1 and 10 min with frequently occurring spectral maxima, (3) a spectral gap between about 10 min and 1 h, and (4) renewed increase of energy from 1 h to the largest periods as determined by the length of bora episodes. The last two are well-known characteristics of wind spectra observed worldwide. What makes the bora wind special is the energy continuum extending from 2 s to 1 min and accounting for more than 50% of the total wind variance - an obvious sign of strongly turbulent wind regime, and significant spectral peaks observed at periods from 3 to 8 min during most bora episodes. The position and intensity of

the peaks vary from one bora episode to the other, and even within an episode, but no regularity could be noticed in their occurrence. This seems to agree with the prevailing wisdom, according to which the bora gustiness is related to unstable gravity waves that develop at the upper boundary of the bora layer.

**JSM14**

**Monday, July 7 - Wednesday, July 9**

**DYNAMICS AND PREDICTABILITY OF SEVERE WEATHER EVENTS (IAMAS [ICDM, ICCP], IAHS)**

Location: Site A, Room 5

**Tuesday, July 8 PM**

Presiding Chairs: M. Shapiro, J. Turner

**JSM14/08P/A05-004** Invited **1625**

**MOIST SINGULAR VECTORS AND DAMAGING EUROPEAN CYCLONES**

Brian HOSKINS, Mariane COUTINHO (Department of Meteorology, University of Reading)

Singular vectors (SVs) are the structures that give optimal growth in a specified time. An investigation has been made of the extratropical impact of the inclusion in the ECMWF SV calculations of a linearised version of the full physics parametrization package. It has been found that it is in general the addition of a representation of large-scale condensation that is important. This leads to somewhat smaller-scale structures and larger growth. Both dry and moist SVs occur in regions of large baroclinicity but the location of the moist SVs is also determined by the availability of significant atmospheric water vapour. A number of damaging European cyclone cases has been studied. In each of these the addition of moist processes led to more focus on the area of actual development. The importance of a tongue of very humid air on the warm side of an extended region of high baroclinicity is apparent.

**JSM14/08P/A05-005** **1700**

**MOIST BAROCLINIC LIFE CYCLES ON A ZERO-PVE JET**

Maurizio FANTINI (ISAC - CNR)

A family of mean atmospheric states in which the release of latent heat has its maximum possible effect on large scale flows is designed starting from the condition of zero equivalent potential vorticity. The above hypothesis is discussed and the growth of baroclinic waves on such mean states is studied, comparing the dry with the saturated behaviour, both in linear and nonlinear phases of evolution. Specifically, we show growth rates, equilibration amplitudes, eddy fluxes and their feedback on the mean state, and overall structure of the meteorological fields, and discuss the impact that the release of latent heat has on idealized simulations of baroclinic cyclones, leading to severe weather events.

**JSM14/08P/A05-006** **1715**

**HAILSTORM MODELING USING DOWNSCALING TECHNIQUE**

Ernest N'Dri KOFFI, Stephane GOYETTE, Marc WUEST, Marjorie PERROUD (Department of Geosciences, University of Fribourg)

Global warming of about 0.6°C has been observed during the last century with a marked increase of the mean temperature of the lower atmosphere during the last 10 years. If anthropogenic emissions would not be reduced, current global climate models (GCM) predict a global warming of about 2°C between 1990 and 2100. Such warming may increase the frequency and the intensity of extreme climatic events (i.e., windstorms, heavy rain, tornadoes, thunderstorm days, and hail). The increase of severe weather events may have important impacts on societies, such as loss of life and property damage. However, due to the limited resolutions of GCMs that resolve only large and synoptic atmospheric features, they cannot predict how. To compensate for the limited resolutions of the GCMs, regional climate models (RCM) have been developed during the last decade for downscaling GCM simulations at regional scales. Such technique may be used to simulate severe local weather events, such as tornadoes, thunderstorm and hailstorm events. The purpose of this study is to assess the ability of the Canadian regional climate model (CRCM-2) to help predicting hailstorm events. The CRCM-2, which is a limited-area grid-point non-hydrostatic model that uses a three-time-level semi-Lagrangian semi-implicit time marching scheme, has been applied to the simulation of a hailstorm event observed in Switzerland in 1993. Sensitivity experiments of the model's results to the nested domain and to two moist convection schemes are also presented.

**JSM14/08P/A05-007** **1730**

**PREDICTABILITY OF HAILSTORM DEVELOPMENT IN VICINITY OF DEEP VALLEY**

Mladjen M. CURIC, Dejan JANC, Vladan VUCKOVIC, Dragana VUJOVIC (Institute of Meteorology, University of Belgrade, 11000 Belgrade, YUGOSLAVIA)

The area of central Serbia is mountainous and intersected by numerous valleys. Strong hailstorms formed in such region produce extensive damage to property. Therefore, better knowledge of hailstorm dynamics as well as the predictability of their behavior in vicinity of deep valley are of essential importance. In this paper we analyze two characteristic cases. The first one relates to the hail cloud which moves down into the valley if the mid-tropospheric wind is parallel to the valley axes orientation. Initially, such cloud can be with or without precipitation and its base is lower compared to the top heights of valley sides. Observations clearly show that such cloud moves fastly along the valley due to the cell regeneration in front of the mother cloud. Due to the relationship between surface friction and pressure gradient force, the leading edge of the cold air outflow can lie close the front boundary of the mother cloud, which in turn, lead to the forced warm moist air updraft and cell regeneration. Such formed cell merges by the mother cloud. This process will prolong the cloud life and increase its propagation speed. Some other cloud moving in the same direction outside the valley, under same other environmental conditions, would have quite different behavior. The other case considers the hail cloud which generates and develops outside valley if the mid-tropospheric wind is not parallel to the valley. The such cloud then changes direction of movement and continues its development along the valley. Its development is controlled by cold air outflow and forced warm air updrafts over its leading edge. Further, the cloud regeneration during its motion along the valley is the same as in the first case. The prediction of behavior of such hail clouds in both cases is very difficult. Because of that, we simulate such cloud characteristics by help of the three-dimensional, fully-compressible cloud model (ARPS) with detailed treatment of hail spectrum. We

**IA**

## INTER-ASSOCIATION

performed two experiments with initial soundings. In the first case, the mid-tropospheric wind is parallel to the valley axes and in the second case it is with an angle of in counter clockwise direction relative to the valley axes. Our simulations show that observed characteristics of considered clouds are well reproduced. This gives us the hope that the direction and duration of cloud life in complex terrain conditions could be predicted successfully by using the numerical models.

**JSM14/08P/A05-008**

**1745**

### ANALYSIS AND SIMULATION OF THE 4TH NOVEMBER 1966 STORMOVER ITALY

Piero LIONELLO<sup>1</sup>, Andi NUHU<sup>2</sup>, Simona DE ZOLT<sup>3</sup> (<sup>1</sup>Univ. of Lecce, Italy, <sup>2</sup>Univ. of Padua)

The 4th November 1966 storm was a very intense cyclone that developed in the western Mediterranean Sea, produced by the orographic cyclogenesis associated with a large low pressure system passing over Northern Europe. The 4th November cyclone, blocked by a large high pressure system over Eastern Europe, moved slowly across the Gulf of Genoa and Northern Italy, before being absorbed by a new large low pressure that arrived over Northern Europe from the Atlantic Ocean. During the passage of the cyclone across Italy, a huge amount of precipitation fell over the central and northern regions and the Italian coasts were hit by severe winds and waves. In the center of Florence, flooded by the Arno river, the water level reached the first floor of the houses. The storm surge in Venice reached almost two meters, by far the highest ever recorded level. Damages to the artistic heritage and property were huge. In this study, a regional coupled atmosphere-wave-ocean model is used for the simulation of the event, using both NCEP and ECMWF re-analysis, testing coupled and uncoupled model setup, and different initial conditions. The simulations reproduce correctly the event and are very close to the observations, also for the atmospheric precipitation and the surge level, showing that the present model and computer capabilities would be able to predict the event.

**Wednesday, July 9 AM**

Presiding Chairs: K. Moore, D. Hudak

**JSM14/09A/A05-001**

Invited

**0905**

### THE 1998 ICE STORM: PLANETARY AND MESOSCALE ASPECTS

John Richard GYAKUM, Paul J. ROEBBER (Department of Atmospheric and Oceanic Sciences, McGill University)

The Ice Storm of 5-9 January 1998, affecting the northeastern United States and the eastern Canadian provinces, was characterized by freezing rain amounts greater than 100 mm in some areas. Economic damage exceeded five billion dollars. We study the thermodynamic impact of this unprecedented event with the use of a four-dimensional data assimilation spanning an 18-day period ending at 0000 UTC 9 January 1998. The Ice Storm consisted of two primary synoptic-scale cyclonic events. The first event was characterized by trajectories arriving in the precipitation zone that had been warmed and moistened by fluxes over the Gulf Stream Current and the Gulf of Mexico. The second and more significant event was associated with air parcels arriving in the precipitation zone that had been warmed and moistened for a period of several days in the planetary boundary layer of the subtropical Atlantic Ocean. These parcels had equivalent potential temperatures of approximately 330 K at 800 hPa as they traveled into the Ice Storm's precipitation zone. We also examine mesoscale processes to understand their role in regulating the persistence, phase and intensity of the event. The region of maximum precipitation occurred in a deformation zone between an anomalously-cold surface anticyclone to the north and a surface trough axis extending from the Gulf of Mexico into the Great Lakes. The persistently cold near-surface air in the precipitating region was linked to orographic channeling of winds from the cold anticyclone to the north. Our model-based results show that, in the absence of the orographic channeling, little or no freezing precipitation would have occurred at Burlington, VT (BTV) during the Ice Storm. A frontogenetical focus within the St. Lawrence, Ottawa and Lake Champlain valleys was provided by orographic channeling of the cold air in combination with geostrophic southerlies in the warm air. The frontogenesis was an important contributor to the higher precipitation amounts during the Ice Storm, with model sensitivity estimates indicating that in the absence of the valleys, total freezing rain volumes would have been reduced by 12.1% and 16.5% in the first and second episodes, respectively. A discussion of the expected predictability of such an event is provided.

**JSM14/09A/A05-002**

**0940**

### PROGRESS IN THE PREDICTION OF HAZARDOUS WEATHER IN THE UK

Brian William GOLDING (Met Office)

Recent severe weather episodes in Europe and the UK have coincided with the 50th anniversary of three major weather disasters: the East Coast storm surge, the Lynmouth flash flood, and the last London smog to highlight the importance of accurate warnings in enabling action to be taken to protect life and property. As well as issuing its own weather warnings, the Met Office provides forecasts at a range of lead times to enable partner organisations to generate warnings and initiate protective action. Considerable effort has recently been put into developing closer relationships with these partners, particularly through tailoring the forecasts to the expected impact of the hazard, in addition to its occurrence. Early warnings of major hazards are provided up to about 5 days in advance using information from the ECMWF Ensemble Prediction System (EPS). An automated processing system, PREVIN, has been developed that calibrates EPS output and identifies occasions when probability thresholds are reached for specific hazardous events. A first guess warning message is prepared for the forecaster on duty, which he may modify before issue. Results from the last winter season will be presented which indicate that successful probabilistic warnings are now being issued significantly earlier than without this guidance. Work is at an early stage to extend these capabilities to shorter ranges. Some good results have been achieved with an international experiment to create a Poor Man's Ensemble, and this is now being built upon with plans for a Europe-wide super-ensemble. Development of a Met Office short range ensemble as a contribution to this, has just started and plans will be presented. Work is also focussed on impacts at this range, with a particular emphasis on health. At very short range the Nimrod nowcast scheme has been extended to the whole of Europe at 5km resolution and upgraded over the UK to include soil moisture and run-off, with river flow under development. A 2km grid version includes the Gandolf thunderstorm lifecycle models and is specifically focussed on improving the predictability of flash floods in the UK. Current work is focussed both on predicting the impact of severe weather, and on the potential of very fine resolution Numerical Weather Prediction to provide improved nowcasts.

**JSM14/09A/A05-003**

**0955**

### SPECTRAL AND WAVELET ANALYSIS OF PRECIPITATION FROM MODELS AND RADAR

Charles A. LIN<sup>1</sup>, Slavko VASIC<sup>2</sup>, Isztar ZAWADZKI<sup>1</sup>, Diane CHAUMONT<sup>3</sup>, Lei WEN<sup>2</sup> (<sup>1</sup>Dept. of Atmospheric and Oceanic Sciences, McGill University, <sup>2</sup>Centre de Recherche en Calcul Applique (CERCA))

We perform a scale decomposition of precipitation fields from weather prediction models and compare with radar-retrieved precipitation fields. Two models are examined: GEM (Global Environmental Multiscale) model of the Meteorological Service of Canada, and the ETA model of NCEP (National Centers for Environmental Prediction) in the U.S. Precipitation values from the U.S. radar network are used to evaluate the model precipitation. A 6-day rain event from May 24-30, 2001 over a domain of extent 3,000 km in the continental US is examined. Spectral and wavelet methodologies are used for the scale decomposition of 3-hour precipitation accumulation in wavenumber space. The radar precipitation is aggregated to the model resolution, which is 24 km for both GEM and ETA models. The model results show less power than the radar at high wavenumbers. Cross spectral analyses of GEM/radar, ETA/radar and GEM/ETA are also performed, which reveal model bias and model uncertainty.

**JSM14/09A/A05-004**

**1010**

### STRUCTURES AND ENVIRONMENT OF EXPLOSIVE DEVELOPING EXTRATROPICAL CYCLONES IN THE NORTHWESTERN PACIFIC REGION

Akira YOSHIDA, Yoshio ASUMA (Division of Earth and Planetary Sciences, Graduate School of Science, Hokkaido University)

The characteristics for explosive developing extratropical cyclones in the northwestern Pacific region were analyzed using a global objectively analyzed data set (GANAL) provided by the Japan Meteorological Agency (JMA). We classified these cyclones into three types by the positions of formation and by the positions of most deepening. The first type originated over the eastern Asian Continent and developed over the Sea of Japan or Sea of Okhotsk (OJ type). The second one also originated over the Asian Continent and developed over the northwestern Pacific Ocean (PO-L type). The last one originated and developed over the northwestern Pacific Ocean (PO-O type). Statistical analyses suggest that: OJ type cyclones frequently appeared in late fall and their deepening rates were the smallest among the three types; PO-L type cyclones had medium deepening rates and mostly occurred in early and late winter; and PO-O type cyclones had the largest deepening rates and mostly occurred in mid-winter. Two kinds of composite analyses were conducted to understand their structures and mechanisms of development. The first composite analysis was the geographically fixed composite analysis. The results suggest that the atmospheric favorable condition for each type cyclone is highly connected to the formation of the cold air mass over the Asian Continent. These conditions are largely related to the seasonal variation over the area. The other analysis was a composite for the cyclone structure at maximum deepening. The analyses suggest that: the OJ type cyclone had a short wave upper-level trough accompanied with jet streak and a stronger shallow cold front; the PO-L type cyclone, associated with a zonally stretched strong narrow jet stream, had a remarkable front system in the mid-level and the warm front was clearly defined than the cold front at the surface; and the PO-O type had a short and wide strong jet streak, also a distinct front system in the mid-level, and strong precipitation around the cyclone center. The analyses using the Zwack-Okossi development equation suggest that the crucial mechanism for the development was vorticity advection for OJ type cyclones, temperature advection for PO-L type, and latent heat release for PO-O type, respectively. We concluded that the difference of cyclone structures between the three types affected the distribution of the vorticity, temperature advections, and latent heat release within the cyclone systems and caused their characteristic deepening rates.

**JSM14/09A/A05-005**

**1025**

### SIMULATION OF AN EXTREME STORM EVENT: THE DECEMBER 1999 LOTHAR EVENT

Martin BENISTON, Stephane GOYETTE (Department of Geosciences, University of Fribourg)

Winter storms have been seen to be on the increase in recent decades in the North Atlantic; while many of these affect northern Europe, some track further south and tend to generate very severe loss of life and damage to trees, agriculture, ecosystems, and infrastructure in regions that are not adapted to storminess (and hence are far more sensitive). In Switzerland, two very severe storms with wind velocities exceeding 175 km/hour (i.e., hurricane-force winds in the mid-latitudes) have been recorded in 1990 and 1999. This paper will present the dynamics leading to the mature phase of the Lothar wind storm that affected France and the alpine region on December 25-26, 1999. Use of the Canadian Regional Climate Model successfully tracked the storm as it entered Europe from the Atlantic sector, and then swept across France into Switzerland, generating a vigorous secondary system that exerted most of the damage in Switzerland. An animated sequence of the storm development will be shown, to enhance the details of the storm's evolution, e.g., precipitation, enhancement of wind velocities, interactions with the surface, etc.

**JSM14/09A/A05-006**

Invited

**1100**

### HAZARDOUS WINTER PRECIPITATION: ITS FORMATION AND STORM ENVIRONMENT

Ronald Earl STEWART<sup>1</sup>, Kit K. SZETO<sup>2</sup> (<sup>1</sup>Department of Atmospheric and Oceanic Sciences, McGill University, <sup>2</sup>Meteorological Service of Canada)

Precipitation often leads to the the greatest impact of winter storms. Within extra-tropical cyclonic storm systems, this precipitation can occur in various forms including snow, rain, freezing rain and ice pellets as well as combinations of these. The precipitation is typically initiated through ice-phase processes although, before reaching the surface, it often undergoes phase changes as it falls, for example, through inversions having temperatures above 0C. These phase changes affect the surrounding thermodynamic environment and, consequently, its dynamics. The nature of the precipitation reaching the surface is closely coupled with such responses in its interacting and surrounding environment. In this presentation, a review will be given of our knowledge of precipitation formation within extra-tropical cyclonic storms and the interactions with its environment. This will be followed by an examination of key outstanding scientific issues associated with this topic.

**JSM14/09A/A05-007**

**1135**

### LEE CYCLOGENESIS IN THE WESTERN CANADIAN ARCTIC REGION

Masaya KATO, Yoshio ASUMA (Division of Earth and Planetary Sciences, Graduate School of

Science, Hokkaido University)

Lee cyclogenesis frequently occurs in the mountainous west coast region of the North American continent. Several cases were observed in the western Canadian Arctic region during the BASE (Beaufort and Arctic Storms Experiment) in 1994. A strong, almost stationary, parent low was over the Gulf of Alaska. There was a quasi-stationary Arctic front over the western Canadian Arctic region on the lee side of the mountainous west coast regions. A positive potential vorticity anomaly in the upper level separated over the Gulf of Alaska and moved across the mountains over the Arctic front. Stability decreased and relative vorticity increased in the lower frontal zone due to potential vorticity conservation, and secondary depression occurred in the lee region. To investigate these mechanisms and structures, we analyzed the 16 September 1994 case, focussing on structures of a potential vorticity, a potential temperature, and moisture using a global objectively analyzed data set (GANAL) provided by Japan Meteorological Agency (JMA) and PSU/NCAR MM5 numerical model. Horizontal temperature gradient associated with an Arctic front intensified due to warm air advection from the parent low. As a result, baroclinicity increased in the lee region. A positive potential vorticity anomaly moved over the region and generated cyclonic circulation. The moisture from the Pacific Ocean advected into the region and the secondary cyclone was depressed. We found that the moisture advection was also an important mechanism for lee cyclogenesis.

**JSM14/09A/A05-008** 1150**HIGH-RESOLUTION MODELING OF A POLAR LOW OVER THE LABRADOR SEA**

Rebekah E. MARTIN, G.W.K. MOORE (Department of Physics, University of Toronto)

Polar lows are short-lived, intense mesoscale storm systems that develop over oceans in polar regions. The interaction of the very cold atmosphere with the relatively warm ocean below is what provides these storm systems with their intense energies. As a result of their small spatial and temporal scales, and their development in regions where observational coverage is minimal, models and observations can easily miss the genesis and lifetime of a polar low. A polar low that was imaged by the RADARSAT-1 satellite on December 29, 1997 is simulated with the Penn State/NCAR fifth-generation Mesoscale Model (MM5). Model results of the near surface wind fields are compared to the SAR imagery from the satellite and are found to possess strikingly similar features. Specifically, the low wind speed eye of the storm and high wind speed fronts are apparent in both the SAR image and the model output. The high-resolution output of the model provides a particularly detailed view of the structure and dynamics of this polar low.

**JSM14/09A/A05-009** 1205**IN-SITU MEASUREMENTS AND THE SYNOPTIC CONDITION OF A POLAR LOW OVER THE NORWEGIAN SEA DURING THE AAMP98 CAMPAIGN**Yoshio ASUMA<sup>1</sup>, Masataka SHIOBARA<sup>2</sup>, Makoto WADA<sup>3</sup>, G.W.K. MOORE<sup>3</sup> (<sup>1</sup>Division of Earth and Planetary Sciences, Graduate School of Science, Hokkaido University, <sup>2</sup>National Institute of Polar Research, <sup>3</sup>Department of Physics, University of Toronto)

Airborne measurements were made within a polar low over the Norwegian Sea on March 9, 1998, during the AAMP98 (Arctic Airborne Measurement Program in 1998). In this presentation, we will report the synoptic scale and meso-scale structures of the polar low using the PSU-NCAR mm5 meso-scale model. A comma-shaped meso-alpha scale low appeared in the NOAA satellite images and the cloud head of the low turned around and became less organized. A well defined polar low formed at the end of the cloud head with a distinct secluded core ("eye") and convective cloud lines. The meso-scale model results show a cold-core vortex over the Scandinavian Peninsula and the meso-alpha scale low was formed over the wedge of relatively warm SST extended toward the west coast of the Svalbard Islands. Although the polar low needs further investigation in the model, an upper level short wave which was deepened by the warm air advection of a strong synoptic scale low over the Iceland approached over the area and a polar low was formed in the actual case.

**JSM14-Posters** Wednesday, July 9**DYNAMICS AND PREDICTABILITY OF SEVERE WEATHER EVENTS (IAMAS [ICDM, ICCP], IAHS)**

Location: Site D

Wednesday, July 9 PM

**JSM14/09P/D-001** Poster 1400-065**STRUCTURE OF RAINDROP SIZE DISTRIBUTIONS FROM POLARIMETRIC RADAR VARIABLES IN A TROPICAL SQUALL LINE**S.-G. PARK<sup>1</sup>, K. IWANAMI<sup>1</sup>, M. MAKI<sup>1</sup>, R. MISUMI<sup>1</sup>, T.D. KEENAN<sup>2</sup>, H. MORIWAKI<sup>1</sup> (<sup>1</sup>National Research Institute for Earth Science and Disaster Prevention, <sup>2</sup>Bureau of Meteorology Research Centre, Melbourne, Australia)

Spatial structure of raindrop size distributions (DSDs) within a tropical squall line is analyzed based on estimates by an improved DSD estimation method using polarimetric radar variables. The improved method is similar to the algorithm of Seliga and Bringi (1976) and Zhang et al. (2001). The key of the improved method is to estimate modified gamma DSD parameters through minimizing a cost function that consists of differences between three polarimetric variables (radar reflectivity ZHH, differential reflectivity ZDR, and specific differential phase KDP) observed by radar and theoretical reference data calculated by T-matrix scattering simulations. In addition, the cost function is constrained by three relationships among the gamma DSD parameters, i.e.,  $N_0$ - $\mu$ ,  $N_0$ - $\Lambda$ , and  $\mu$ - $\Lambda$ , with different weights. According to experiments using simulated radar data based on ground-based disdrometer data, it was found that the improved method can estimate  $\Lambda$ ,  $D_0$ ,  $\text{Log}(N_0)$ , and  $\mu$  with fractional standard errors of 13.4%, 11.5%, 4.0%, and 47.9%, respectively, when the  $N_0$ - $\mu$  and  $N_0$ - $\Lambda$  relationships are considered as weak constraints with weight of 0.01, while the  $\mu$ - $\Lambda$  relationship is considered as a weaker constraint with weight of 0.001. The improved DSD estimation method was applied to a tropical squall line of oceanic type observed in Darwin at 0920 UTC 15 January 1999 by C-band polarimetric radar (C-POL) of Bureau of Meteorology Research Centre (BMRC), Australia. The squall line exhibited a deep convective cell in leading area and stratiform region embedding bright bands in trailing area. In particular, the bright bands were collocated with the generating cells aloft that characterized by large positive KDP indicating the presence of ice crystals with their major axes oriented horizontally, such as dendritic crystals. According to the analyses of the

estimated DSDs, the convective region was characterized by large-drop spectra (median volume diameter  $D_0=2.2$  mm) due to strong convective motions. In the stratiform region, DSDs below bright band collocated with the generating cell aloft were characterized by relatively large-drop spectra ( $D_0=1.7$  mm), while the stratiform DSDs without bright band are characterized by relatively small-drop spectra containing numerous small drops ( $D_0=1.4$  mm). This result in stratiform region suggests that ice crystals in generating cell aloft play an important role controlling production of large raindrops by the seeder-feeder mechanism. On the vertical variations of DSDs, the stratiform DSDs were close to the exponential DSD and were characterized by little variations, while the convective DSDs exhibited large variations.

**JSM14/09P/D-002** Poster 1400-066**EXTRATROPICAL TRANSITION OF TROPICAL CYCLONES: CANADIAN FORECAST CHALLENGE AND RESEARCH EFFORTS**

James David ABRAHAM, Walter STRAPP, Chris FOGARTY (Meteorological Service of Canada)

Extratropical transition (ET) has been raised as a forecast challenge by meteorologists from all ocean basins affected by tropical cyclones. ET is associated with the poleward movement of a tropical cyclone (TC) into the middle latitudes, and is normally associated with the weakening or decaying stage of the TC as it enters a highly sheared baroclinic environment, moving over a cooler sea surface or over land. However, this transition from tropical to extratropical can result in an increase in the storm intensity and the associated hazardous weather elements. The objective of this presentation is to examine this threat. Typical problems for weather forecasters in all regions that experience ET include accurately predicting their track, intensity, and impacts. The most challenging issues are associated with the potential large amounts of precipitation, continued high wind speeds, and the generation of large ocean surface waves and swell. Furthermore, the forward speed of these storms often accelerates from a typical 5 m/s in the tropics to in excess of 25 m/s in the midlatitudes. This requires that warnings are issued with adequate lead-time for mariners or others to take action in order to prevent loss of life or economic damage. Given the ET forecast challenges in Canada, the Meteorological Research Branch and the Canadian Hurricane Centre of the Meteorological Service of Canada (MSC) agreed to consider modest ET field studies. One aspect of this program would be the use of the National Research Council's (NRC) Convair 580 to conduct meteorological and microphysical investigations of ETs passing offshore Atlantic Canada. As it turns out, there had never been an aircraft field investigation of ET behaviour before this initiative. During the period 17-20 October 2000, Hurricane Michael provided this opportunity, and a flight was conducted on the afternoon of the 19th. A follow-up flight was conducted nearly one year later on 15 October 2001 into Tropical Storm Karen. In this presentation, we describe an overview of the ET forecast challenge in the Western Atlantic Basin. As well, we provide a brief overview of the details of research flights into two distinct tropical cyclones undergoing extratropical transition near Nova Scotia. This preliminary data set shows substantial asymmetries in moisture and winds associated with these ET systems. Their capacity to maintain large moisture contents while interacting with midlatitude baroclinicity poses a threat of intense rainfall while their rapid translational speeds can create very high winds east of their tracks, endangering the lives of mariners. Furthermore, very strong winds and wind shears in the low-levels reveal the potential danger these storms pose in particular to aviation and marine interests. Further analyses of this data, including comparisons with model simulations and inclusion of additional oceanographic data are planned. These results are also being used to justify a collaborative atmospheric-oceanographic ET field experiment being considered for the 2003 and 2004 hurricane seasons.

**JSM14/09P/D-003** Poster 1400-067**A DIAGNOSTIC CASE STUDY OF EXTRATROPICAL TRANSITION OVER EAST ASIA**Chih-Shin LIU<sup>1</sup>, George Tai-Jen CHEN<sup>1</sup> (<sup>1</sup>Department of Atmospheric Sciences, National Taiwan University, <sup>2</sup>Weather Forecast Center, Central Weather Bureau)

As tropical cyclones recurve poleward and move into midlatitudes, they often interact with baroclinic systems and transform into extratropical cyclones. During and after extratropical transition (ET), these cyclones can at times develop rapidly, produce extremely heavy precipitation and strong winds, and cause damage of properties and loss of lives. Unfortunately, such processes are often not well predicted by operational models, and still challenge weather forecasters. Recently, the ET process has attracted considerable attention in various regions of the world. But over East Asia, the topic is rarely studied. The present study diagnoses the ET process of Typhoon Winnie (1997) over mainland China. Results suggest that the ET of Typhoon Winnie is different from many prior ET processes, which are similar to Petterssen Type-B scenario. After making landfall over mainland China on 18 August 1997, Winnie weakened rapidly, recurved, and transformed into an extratropical cyclone possessing both cold and warm fronts in the lower troposphere. The cyclone subsequently interacted with midlatitude system and reintensified with a maximum deepening rate of 10 hPa in 12 hours. The mechanism responsible for the cold frontogenesis associated with the transforming cyclone at low levels was evaporative cooling, which strengthened the cold tongue at the western section of the cyclone. Such a frontogenic process is very different from that of a midlatitude cold front associated with an ordinary extratropical cyclone. Preliminary results of diagnosis through the use of piecewise PV inversion indicate that PV anomalies associated with the cyclone in the lower to middle levels induced evident warm-air and cold-air advectations at mid-levels when the cyclone migrated into a mid-level baroclinic zone. Through hydrostatic relationship, the dipole structure of temperature advectations caused an amplification of the initially weak upper level waves, which, with a proper phase and strong vertical coupling, caused the cyclone to develop rapidly. Through an analysis on the dynamic topopause (defined by the 2.5 PVU surface where  $1 \text{ PVU} = 10^6 \text{ K m}^2 \text{ kg}^{-1} \text{ s}^{-1}$ ), it was found that the PV anomalies associated with the cyclone contributed to an unusual summer tropopause folding, which in turn contributed directly to the surface cyclogenesis as the cyclone was most intense after ET. As a result, the interaction between the cyclone and the baroclinic systems led to the development of upper level waves, which in turn contributed to surface cyclogenesis first by vertical coupling and then by superposition processes. Thus, it is suggested that the cyclones' re-intensification was a manifestation of the self-amplification process.

**JSM14/09P/D-004** Poster 1400-068**REGIONAL NUMERICAL SIMULATIONS AND VALIDATION OF A RAINFALL EXTREME EVENT USING TWO DIFFERENT CUMULUS PARAMETRIZATION**

Giovanni DOLIF NETO, Tercio AMBRIZZI (Department of Atmospheric Sciences, University of Sao Paulo)

This work presents numerical simulations of a rainfall extreme event that occurred in October 1st, 2001 in the State of São Paulo, Brazil. The amount of precipitation during this event was around 103 mm in 24 hours, being one of the biggest of the year. The Emergency State Agency registered 15 flooding points and 2 deaths. The rainfall was associated with a squall line propagating parallel to a cold front. The PSU/NCAR MMS regional model was run with two schemes of cumulus parametrization: Anthes-Kuo and Grell. There were three nested

## INTER-ASSOCIATION

grids, with 90, 30 and 10 Km of resolution. Based on the literature (Dudhia et al., 2001), the Grell scheme was fixed for the nests 2 and 3 and, for the mother domain the Grell and Anthes-Kuo schemes were used. The validation was qualitative and it was done by analyzing the three grids. Accumulated precipitation fields every 3 hours were compared with satellite images and with 3 Km CAPP1. The qualitative comparison showed that the Anthes-Kuo scheme used in mother domain had the precipitation spatial field much closer to the observed than the Grell scheme. This result was also found for the nests 2 and 3 because of the "two-way interaction" for the three nests. Therefore the Anthes-Kuo scheme seems better than Grell for a 90 km grid resolution. On the other hand, both schemes underestimated the precipitation over the great Grande São Paulo region.

**JSM14/09P/D-005** Poster **1400-069**

### BAIU HUNTER 2003 IN KYUSHU BY AEROSONDE

Tetsuo NAKAZAWA (Meteorological Research Institute)

Special Observation on heavy rainfall system along the Baiu Front over Kyushu by using Aerosonde, Baiu Hunter 2003, is now performed in this June/July 2003. The main objective of the observation is to improve and verify Non-Hydrostatic Model by assimilating the detailed observation data of the Baiu Front over the west of Kyushu and heavy rainfall systems associated with the Front. Under the Global Warming Mission of Japanese Model of "Project on Harmonious Coexistence of Human, Nature and Earth" funded by the Ministry of Education, Culture, Sports, Science and Technology, JMA and MRI will take charge of a program named "Development of high accuracy and resolution climate model". This program includes the observation component to verify and improve the high-resolution model. The observation is for the heavy rainfall systems in the Baiu Frontal Zone. The main observational platform for the observation is an unmanned aircraft, Aerosonde. The observation by Aerosonde is different from the previous passive one, but plunge into the disturbed atmospheric phenomena directly and actively to measure temperature, moisture and wind.

**JSM14/09P/D-006** Poster **1400-070**

### SHORT-RANGE RAINFALL FORECAST WITH QUANTITATIVE PRECIPITATION MODEL

Jai Ho OH<sup>1</sup>, Ok-Yeon KIM<sup>1</sup>, Hanse HANSE YI<sup>1</sup>, Tae-Kuk KIM<sup>1</sup>, Ryohei MISUMI<sup>2</sup> (Dept. of Env. Atmo. Sci., Pukyong National Univ., Busan, Korea, <sup>2</sup>National Institute for Earth Science and Disaster Prevention, Tsukuba, Ibaraki, Japan)

Recently, many people have suffered from the unusual severe weather phenomena such as heavy rains and very wild typhoons. However, it is not easy task to provide reasonable information on these severe weather events. Accordingly it has been eager to find a suitable methodology to provide an early warning against these severe weather events. Quantitative precipitation forecasts and probabilistic quantitative precipitation forecasts (QPFs and PQPFs, respectively) might be one of the most promising methodologies for reasonable warning on the flash floods. QPFs and PQPFs must be on time because severe weather phenomena have a tendency to be developed very quickly and locally. By these reasons, they may not allow to be announced in a reasonable advanced time. Accordingly it is desired to develop a methodology to provide detail information locally and quickly. A fine-mesh non-hydrostatic mesoscale model can be hired, however, it requires a significant computational resources as well as integration time so that it may not meet the time restriction to be forecasted in operational sense. An alternative way to provide necessary information on fine-mesh rainfall is utilizing a diagnostic rainfall model to avoid heavy computational requirement fine-mesh full-dynamic non-hydrostatic mesoscale model. In this study we examine the capability of diagnostic rainfall model in terms of how well represented the observed several rainfall events and which is the most optimistic resolution of the mesoscale model in which diagnostic rainfall model is nested. Also, we examine the integration time to provide reasonable fine-mesh rainfall information. The diagnostic rainfall model used in this study is the named QPM (Quantitative Precipitation Model), which calculates the rainfall by considering the effect of small-scale topography which is not treated in the mesoscale model. As a result, QPM has a capability to provide fine-mesh rainfall information in terms of time and accuracy compared to full dynamical fine-mesh mesoscale model.

**JSM14/09P/D-007** Poster **1400-071**

### STRUCTURE OF CUMULONIMBUS CLOUDS DEVELOPED OVER THE SLOPE OF MOUNTAIN IN SUMMER

Tetsuya SANO<sup>1</sup>, Kazuhisa TSUBOKI<sup>1</sup>, Ichiro TAMAGAWA<sup>2</sup> (<sup>1</sup>Hydrosheric Atmospheric Research Center, Nagoya University, <sup>2</sup>River Basin Research Center, Gifu University)

In moist atmosphere, the severe precipitation phenomenon often occurs by a forcing of topography over a mountain region. Especially, in summer, many cumulonimbus clouds in the mountain region develop greatly and cause severe precipitation. In this study, the structure of the cumulonimbus clouds which developed over the south slope of the Ibuki mountains in the afternoon of July 5, 2000, was investigated by Doppler radar observation. The Ibuki mountains are located in the southwest area of Gifu prefecture in Japan (136.6°E, 35.6°N) and have the strike from southwest to northeast. A cold air trough moved over Japan and the atmosphere was convectively unstable. Many cumulonimbus clouds therefore developed in the mountain regions. The direction of vertical wind shear of the environment was from northwest to southeast which was almost parallel to the direction of the south slope of the Ibuki mountains. The cumulonimbus clouds were observed by Doppler radars for about 2 hours over the south slope of the Ibuki mountains. It had about 20 cellular echos with successive generation and disappearance. It was aimed to the behavior of the cellular echos. First cellular echo, named Primary cell, weakening with tilting to downshear side moved down the slope. Thereafter some new cellular echos, named Secondary cells, occurred and developed with tilting to downshear side or standing upright on the upstream side of Primary cell, around the occurrence point of Primary cell. There were 6 systems in the convective echo and they occurred with lining in parallel to the strike of the Ibuki mountains. The systems of cellular echos, especially the development of Secondary cells, contributed to the development of the cumulonimbus clouds. When Secondary cells were developing, the warm wind from the mountain side to the convective echo was observed for about 1 hour at an AMEDAS point, Tarumi, in the Ibuki mountains. It is considered that the existence of the warm air over the top side of the mountains has influenced to the development of Secondary cells.

**JSM14/09P/D-008** Poster **1400-072**

### A MESOSCALE SIMULATION STUDY OF A HEAVY RAIN EVENT OVER SOUTHERN TAIWAN IN MEIYU SEASON

Lisa T.C. CHANG, George T.J. CHEN (Department of Atmospheric Sciences, National Taiwan University)

There are about 4-5 frontal systems affecting Taiwan during Meiyu season each year. The

Meiyu front is usually accompanied by a nearly continuous cloud band, which produces stratiform and/or convective precipitation. During the period of 28-30 May 2001, a series of mesoscale convective systems (MCSs) developed in a weakly synoptic-scale control environment near Taiwan along a retrograde moving Meiyu front. The development and northeastward propagation of the MCSs produced heavy rainfall over southern Taiwan, with a maximum 24-h accumulation rainfall of 300 mm. This study presents the results of a numerical simulation of this heavy rain event using the atmospheric part of the Coupled Ocean/Atmospheric Mesoscale Prediction Systems (COAMPS) developed by Naval Research Laboratory (Hodur 1997). Part of the difficulty in simulating MCSs is the lack of mesoscale details in the initial state. The mesoscale features may play a more important role in initiating a deep convection especially when the synoptic-scale forcing is weak. In this case, the initial convection developed over the ocean where observational data were sparse. One of the practical approaches to include mesoscale features in the model initial condition is to blend satellite scatterometer QuikSCAT surface wind measurements into the COAMPS analysis procedure where the NOGAPS 1°x1° global analysis data were used as the first guess. The COAMPS control run was conducted with full physics and with the improved initial condition. The ability of the model to reproduce the structure and evolution of these MCSs will be evaluated. Some of the preliminary results from the sensitivity tests, as an effort to investigate effects of different mechanisms in initiating and maintaining of the convective precipitation, will be discussed as well. References: Hodur, R.M., 1997: The Naval Research Laboratory's Coupled Ocean/Atmosphere Mesoscale Prediction System (COAMPS). Mon. Wea. Rev., 125, 1414-1430.

**JSM14/09P/D-009** Poster **1400-073**

### BAIU-FRONTAL MESOSCALE CONVECTIVE SYSTEMS IN THE LEEWARD SIDE OF SMALL ISLANDS (KOSHIKIJIMA LINES) OBSERVED WITH A BOUNDARY LAYER RADAR AND RAWINSONDES

Yasuko UMEMOTO<sup>1</sup>, Michihiro TESHIBA<sup>2</sup>, Yoshiaki SHIBAGAKI<sup>1</sup>, Hiroyuki HASHIGUCHI<sup>1</sup>, Yoshinobu TANAKA<sup>4</sup>, Manabu D. YAMANAKA<sup>3</sup> (<sup>1</sup>Graduate School of Science and Technology, Kobe University, <sup>2</sup>Radio Science Center for Space and Atmosphere, Kyoto University, Japan, <sup>3</sup>Osaka Electro-Communication University, Japan, <sup>4</sup>Meteorological Research Institute, Japan Meteorological Agency, <sup>5</sup>Frontier Observational Research System for Global Change, Japan)

In order to understand the structures and mechanisms of mesoscale convective systems (MCSs) associated with the Baiu front, a special observational campaigns called X-BAIU have been conducted in East China sea and Kyushu Island, located in the western part of Japan, from 1999 to 2002. We installed a boundary layer radar (BLR) at the western side of Kyushu Island to observe the inner structures of MCSs seen frequently in the observational area. In this study, we notice line-shaped MCSs generated by some mountains of Koshiki Island, called "Koshikijima line", and reveal vertical profiles of wind and stability by using the BLR and GPS-sonde soundings. While the Koshikijima line is observed, Kyushu Island is located in the warm sector of a cyclone, and covered by southwesterly winds and a moist convectively unstable atmosphere associated with the cyclone. The direction of the line extends to the leeward of the mountains (Koshiki Islands), and the line lasts for about half a day with the development and weakening. From the results observed by the BLR, we find that the vertical shear of horizontal wind, especially of the component normal to the line, is about 3 m/s/km or larger without depending upon whether the Koshikijima line exists or not. We have observed Koshikijima lines also in 1999, of which the development is much larger than that in 2002. Differences between the cases in 1999 and in 2002 are found in relative humidity and horizontal wind speed. In 2002, relative humidity and horizontal wind speed in the lower troposphere below about 3km altitude are about 80 percent and 20 m/s, respectively, which are both smaller than those in 1999. We consider that the lower humidity and the smaller horizontal wind speed contribute to the shorter lifetime and the suppressed development in 2002.

**JSM14/09P/D-010** Poster **1400-074**

### OBSERVATIONAL STUDY OF THE OROGRAPHIC EFFECT ON THE PROPAGATION OF CONVECTIVE SYSTEMS IN NARA-OSAKA AREA

Ken-ichiro ARAI<sup>1</sup>, Masayuki KAWASHIMA<sup>1</sup>, Yasushi FUJIYOSHI<sup>1</sup>, Masahito ISHIHARA<sup>2</sup> (<sup>1</sup>Institute of Low Temperature Science, Hokkaido University, <sup>2</sup>Japan Meteorological Agency, Tokyo, JAPAN)

The evolution of convective systems that developed in Nara-Osaka area, central region of Japan, is described using data from dual-Doppler radar system and surface meteorological instruments. At first, convective cells developed in the Nara Basin, which locates on the lee side of the Mountain Range of Ikoma. Then they were reorganized into a stationary rainband. Convective radar echoes began to move to the Osaka Plain when cold air generated by thunderstorms flowed into the windward side through the col of the mountains. It is suggested that cold outflows from the decaying convective system over the Nara Basin triggered the new convective cells over the Osaka Plain by forcing-lifting mechanism. The analysis suggests the important and interesting role of the Mountain Range of Ikoma. First, it may contribute to the development and formation of stationary rainband in the lee side of the mountain. Second, it seems to block the outflow of evaporationally-induced cold air into the Osaka Plain until the cold air becomes deep enough. However, once the deep cold air flow out of the Nara Basin, it would be accelerated on the slope of Ikoma and then triggered strong convections and heavy rainfall at the front. The cold air also causes the hazardous strong gust for aviation.

**JSM14/09P/D-011** Poster **1400-075**

### STRUCTURE OF MESOSCALE CONVECTIVE SYSTEMS OBSERVED WITH UHF RADAR INTEGRATED SOUNDING SYSTEM DURING THE SOUTH CHINA SEA MONSOON EXPERIMENT (SCSMEX) AND THE GREEN ISLAND MESOSCALE EXPERIMENT (GIMEX)

Pay-Liam LIN, Hsin-Hon LIN (National Central University)

The NCU (National Central University) ISS (Integrated Sounding System) was deployed in Dongsha island during May 5 to June 25, 1998 for the SCSMEX and deployed in the southeastern coast of Taiwan (Cheng-Kung station) during May 5 to June 30, 2001 for the GIMEX. The primary goal of these deployments were to measure the mesoscale structure of convective weather system associated with the onset, maintenance and variability of the monsoon over the South China Sea area and the southeastern coast area of Taiwan. A wide variety of convective systems were observed during SCSMEX and GIMEX. The ISS observations provide a detail kinematic and thermodynamic structure change of the monsoon flow and the local circulations. The UHF profiler radar that operates at 915 MHz in ISS are useful for precipitation structure measurement because of its sensitivity to hydrometers. The identification and classification of the falling particles associated with precipitation is very helpful for the understanding of the stratiform and the convective characteristics, and the cloud physics and dynamics of the convective systems. The three moments of the Doppler Spectrum provide us with information about the hydrometers in the mesoscale convective systems. Correlations between vertical radial velocity and range corrected signal power of 915 MHz radar wind profiler can be used to determine weather or

not precipitation is present and what type of precipitation it is. Several major convective events occurred in SCSMEX and GIMEX will be discussed and compared in this investigation.

**JSM14/09P/D-012** Poster **1400-076**

#### HEAVY RAINFALL PRODUCED BY A LONG-LIVED LINE-SHAPED PRECIPITATING CONVECTIVE-CLOUD SYSTEM

Sachie KANADA<sup>1</sup>, Kazuhisa TSUBOKI<sup>2</sup>, Haruya MINDA<sup>2</sup> (<sup>1</sup>Advanced Earth Science & Technology Organization (AESTO), <sup>2</sup>Institute for Hydrospheric-Atmospheric Sciences, Nagoya University)

Heavy rainfall is very often caused in subtropical humid-climate region by a meso-scale precipitating convective cloud system, which are subject to orographic effect. In 1997 dual-Doppler radars of Nagoya University were installed in the Nagasaki Peninsula and Amakusa in the Kyushu District, respectively, in order to study the relationship between an orographically modified convective-cloud system and heavy rainfall. During the observation period, line-shaped precipitating systems were often seen in the observation area. Especially line-shaped precipitating systems around the base of the Nagasaki peninsula lasted longer period than other ones and brought a huge rainfall amount at the same place. The main purpose of this study is to reveal the structure and maintenance processes of the long-lived line-shaped system that produce heavy rainfall. On July 11 in 1997 an extremely heavy rainfall was concentrated around the base of the Nagasaki Peninsula in the Kyushu District. The horizontal distribution of total rainfall amount from 0900 LST on July 11 to 0300 LST on July 12 showed highly concentrated rainfall amount of 176 mm as maximum value. It is noted that total rainfall amounts larger than 10 mm were observed only in the limited area around the base of the peninsula. Radar-data analysis revealed that this highly concentrated rainfall was produced by a long-lived line-shaped convective cloud system that was maintained for about 18 hours almost in the same place and which extended in the direction of low-level ambient winds. The length and width of its radar-echo band were over 60 km and about 10 km, respectively. Interestingly its length extended with period of 2 to 3 hours. The radar-echo band was composed of many convective cells whose radar-echo tops were about 6 km. Most of them formed successively in the upwind side of the band and moved along its direction at a speed of 17 m/s. Totally 72 cellular-echoes were observed in Line-1 and they had a tendency to be intensified, moving in the downwind direction in the area fixed geographically. The intensification of radar-echo was seen in three areas between two mountains, named 'the Bay of Isahaya'. The three-dimensional distributions of airflows were observed by the dual-Doppler radars. The convergence and divergence zone extend widely along the radar-echo band in the northwestern side and the southeastern side, respectively. This feature is evident during the developing stage. The convergence zones distribute all over the half side of the line-system not among each cellular-echo. This feature indicates that this convergence zone comes from not individual convective activity of cellular-echoes but effected by orography. 3-dimensional structure of this line-shaped system including airflow field were analyzed in detail and the characteristic pattern of wind fields affected by orography was revealed. The results of more detailed analysis will be presented together with the results of numerical simulation on airflows and precipitating convective clouds around the Nagasaki Peninsula.

**JSM14/09P/D-013** Poster **1400-077**

#### CHARACTERISTICS OF ENVIRONMENT DETERMINING LIFETIME OF CONVECTIVE CELLS WITHIN MESOSCALE CONVECTIVE SYSTEM IN HUMID SUBTROPICAL REGION

Shingo SHIMIZU<sup>1</sup>, Hiroshi UYEDA<sup>1</sup>, Kazuhisa TSUBOKI<sup>1</sup>, Taro SHINODA<sup>1</sup>, Yoshimasa TAKAYA<sup>2</sup>, Teruyuki KATO<sup>3</sup>, Masanori YOSHIZAKI<sup>1</sup>, Hiroyuki YAMADA<sup>3</sup>, Biao GENG<sup>2</sup> (<sup>1</sup>Hydrospheric Atmospheric Research Center, Nagoya University, <sup>2</sup>Meteorological Research Institute, Japan Meteorological Agency, <sup>3</sup>Frontier Observational Research System for Global Change)

In order to reveal the maintenance mechanism of severe Mesoscale Convective System (MCS), we need to investigate what mechanism determines lifetime of convective cells within MCS in a humid subtropical region. Because MCSs in a humid subtropical region have convective cells with different lifetime from that in a dry region as the Great Plains in the U.S. The aim of this study is to clarify characteristics of environment determining features of convective cell within MCS in the humid subtropical region such as East Asia. An isolated MCS, observed over the Kanto Plain on 24 May 2000, and three line-shaped MCSs, observed during heavy rainfall experiment in the downstream region of Yangtze River from June to July 2001, were selected as examples of MCS developing in the humid subtropical region. These four MCSs were investigated with dual Doppler radar analysis, Meteorological Research Institute Non-Hydrostatic Model (MRI-NHM), and Japan Meteorological Agency Regional objective ANALYSIS (RANAL). Dual Doppler radar analysis revealed that the four MCSs had following features. The isolated MCS was supercell type with a short-lived convective cell. Three line-shaped MCSs were back-building rainband type with long-lived convective cells (BBL), back-building rainband type with short-lived convective cells (BBS), and broken rainband type with short-lived convective cells (BRS). By using MRI-NHM and RANAL, it was revealed that each MCS was formed in environments possessing different buoyancy, vertical wind shear, and vapor distribution. This study compared the differences among environments in which four MCSs were formed. Mid-level humidity mainly determined the lifetime of convective cell. In a moist mid-level environment, a convective cell within BBL maintained for 78 minutes. On the contrary, in a dry mid-level environment, convective cells within the supercell, BBS, and BRS maintained for only 30 minutes. The strength of evaporatively-cooled downdraft corresponded to the lifetime. This paper explained maintenance mechanism of the supercell with short-lived convective cell, and back-building rainband with long-lived convective cell in the humid subtropical region by focusing mid-level humidity. The quantitative, observational or numerical verification of these qualitative understandings obtained in this study would lead us to acquire comprehensive understanding of maintenance mechanism of MCS.

**JSM14/09P/D-014** Poster **1400-078**

#### THE APPLICATIONS OF NONLINEAR OPTIMIZATION TO THE PREDICTABILITY OF NUMERICAL WEATHER PREDICTION

Mu MU, Wansuo DUAN, Jiacheng WANG (LASG, Institute of Atmospheric Physics, Chinese Academy of Sciences)

The uncertainties caused by the errors of the initial states and the parameters in the numerical model are investigated. Three problems of predictability in numerical weather prediction are proposed, which are related to the maximum predictable time, the maximum prediction error, and the maximum admissible errors of the initial values and the parameters in the model respectively. The three problems are then formulated into nonlinear optimization problems. Effective approaches to deal with these nonlinear optimization problems are provided. The results of numerical experiments are also provided.

**JSM14/09P/D-015** Poster **1400-079**

#### STATISTICAL ANALYSIS OF DUST STORMS IN THE ARAL SEA REGION

Lyudmila Yur'evna SHARDAKOVA (Central Asian Research Hydrometeorological Institute (SANIGMI))

STATISTICAL ANALYSIS OF DUST STORMS IN THE ARAL SEA REGION. SHARDAKOVA LYUMILA.YU., Usmanova Lyumila.V. Central Asian Research Hydrometeorological Institute, 72, K.Makhsuov st., Tashkent, 700052, Uzbekistan. The Aral Sea coast is a large center of dust storms springing up over the territory of Central Asia. Last ten years the Aral Sea region is a zone of ecological crisis caused by the recession of the Aral Sea level. To analyze the phenomenon of dust storms in this region the database has been developed (MS ACCESS), informative basis of which were the data from 14 meteorological stations for the period 1990-2002. Data-base contains information about 2000 registered occurrences such as dust storms, dust drifts, dust hazes which were observed over considered territory. Input information: date and time of observations; geo-graphical information about meteorological stations; information about speed, direction of wind and maximal gust at the time of occurrence; characteristics of dust storm intensity and cloudiness. Output information is result of database queries at temporal, spatial and other categories. Statistical analysis of more than 1400 dust storms events was carried out. Next characteristics were obtained: duration of dust storms; daily, annual variations and inter-annual change of dust storms for each meteorological station in this region; geographic distribution of intensity and duration of dust storms events; wind speed spectrum. The characteristics obtained were compared with ones of previous years.

**JSM14/09P/D-016** Poster **1400-080**

#### APPLICATION OF A NEW WIND GUST PARAMETERISATION. MULTI-SCALE CASE STUDIES PERFORMED WITH THE CANADIAN RCM

Stéphane GOYETTE<sup>1</sup>, Olivier BRASSEUR<sup>2</sup>, Martin BENISTON<sup>1</sup> (<sup>1</sup>Dept of Geosciences, University of Fribourg, Switzerland, <sup>2</sup>Laboratoire d'étude des Transferts en Hydrologie et Environnement, Domaine Universitaire, Grenoble, France.)

The implementation of a physically-based parameterisation used for diagnostic computations of wind gust is described. Based on an innovative off-line method proposed by Brasseur (2001) to compute wind gusts, it is reasonable to implement a similar subgrid-scale parameterisation in a numerical model to simulate them on-line, i.e., during the course of a simulation. The method assumes that gusts occurring at the surface result from the deflection of air parcels flowing higher in the boundary layer. The trigger mechanism for this deflection is attributed to turbulent eddies. This parameterisation is tested against real documented events. Consequently, to illustrate the performances, two severe mid-latitude windstorms are simulated with the Canadian RCM at various resolutions combined with the gust parameterisation using NCEP-NCAR reanalysis as driving data. The study is carried out for these two severe wind cases over the complex terrain of Switzerland and over the smoother topography of Belgium. A preliminary analysis indicates that this parameterisation performs as well over flat as over mountainous regions and it responds properly in the strengthening as well as the weakening phases of wind storms. However, the storm-dependent results are also a function of the model configuration during the self-nesting procedure. Consequently, the spatial and temporal distributions of the simulated gusts depend on the accuracy of the simulated flow fields. Furthermore, the gust speeds are highly resolution-dependent: when compared with observations, the simulated gusts are generally more realistic at higher resolution over the complex topography of Switzerland but less sensitive over the relative flat terrain of Belgium. The model response is also dependent upon the resolved topography distribution and height, and on the types of lower boundary conditions which affect the stability of the boundary layer. The latter also modulate the mean anemometer-level winds, which serve as a lower bound of the gust speed. This study also shows that simple scaling coefficients relating gust speeds with resolutions can not be easily determined over these two countries regarding these two storms.

**JSM14/09P/D-017** Poster **1400-081**

#### HINDCAST SIMULATIONS OF SEVERE WEATHER EVENTS BY A HIGH-RESOLUTION ATMOSPHERIC GENERAL CIRCULATION MODEL ON THE EARTH SIMULATOR CASE 1: THE AUGUST 2002 STORMS

Wataru OHFUCHI<sup>1</sup>, Takeshi ENOMOTO<sup>2</sup> (<sup>1</sup>Earth Simulator Center, Japan Marine Science and Technology Center, <sup>2</sup>Institute for Global Change Research, Frontier Research System for Global Change)

Numerical weather forecasts sometimes fail in predicting severe weather events associated with downstream development. Improvement of their predictabilities is one of the main goals of THORPEX. In association with this project, hindcast simulations of high-impact weather are conducted with a high-resolution global atmospheric model on the Earth Simulator. Hindcast simulations of the August 2002 storms, that caused flood in Europe, with various horizontal resolution and lead times will be presented in CASE 1.

**JSM14/09P/D-018** Poster **1400-082**

#### HINDCAST SIMULATIONS OF SEVERE WEATHER EVENTS BY A HIGH-RESOLUTION ATMOSPHERIC GENERAL CIRCULATION MODEL ON THE EARTH SIMULATOR. CASE 2: THE NOVEMBER 2002 STORMS

Takeshi ENOMOTO<sup>1</sup>, Wataru OHFUCHI<sup>2</sup> (<sup>1</sup>Institute for Global Change Research, Frontier Research System for Global Change, <sup>2</sup>Earth Simulator Center, Japan Marine Science and Technology Center)

As in CASE 1, high-resolution global atmospheric hindcast simulations of a severe weather event are performed on the Earth Simulator with various horizontal resolution and leadtimes. In CASE 2, another example of downstream development in November 2002 is examined. This event seems to be initiated by bursts of convection in the tropics, and the associated downstream development resulted in severe weather events around the globe.

**JSM14/09P/D-019** Poster **1400-083**

#### SUMMER SEVERE WEATHER PREDICTABILITY IN SOUTHERN ONTARIO - A DOPPLER RADAR PERSPECTIVE

David Ronald HUDAK, Norman DONALDSON, Sudesh BOODOO, Paul JOE, Robert PATERSON (Meteorological Service of Canada)

A methodology has been developed for creating a summer severe weather climatology from Doppler radar related products. Advanced software (URP) is used to process the King City radar 15 year data archive that extends back to 1988. URP is the operational radar software for the Canadian weather service. Its modular structure that permits the modification of existing modules and the saving of intermediate results for separate analysis makes it well

## INTER-ASSOCIATION

sited to research applications. Radar parameters of particular interest are areas where Ze > 40 dBZ and extend above 5.5 km, mesocyclone occurrence, vertically integrated liquid, maximum reflectivity in a vertical column, and the bounded weak echo region. These parameters were examined to determine their ability to identify severe weather. Observations of severe weather events from surface reports compiled at the regional weather centre were used to tune the severe weather algorithm thresholds. URP's Cell Identification, Cell Tracker, and Storm Assessment modules were then applied to the derived radar parameters. The result is a ranking of storm severity and the temporal and spatial distributions of the severe weather events. Conceptual models of severe weather occurrence and evolution are emerging from this analysis that highlight the importance of the Great Lakes in triggering convective instability. Additionally, the year-to-year variation in severe weather occurrence is being examined and related to larger scale weather patterns in an attempt to determine some planetary precursors to severe weather. The identification of radar artifacts and range biases were a major consideration in the analysis. A comparison of results from two adjacent radars (King City and Exeter) for three summers is showing important benefits in making composite depictions of severe weather events. Many of the patterns of severe weather over this area are on the 100 km scale - too large for effective single radar coverage. However, two radars allow almost complete coverage of southern Ontario. In addition, the continuity of patterns through the area covered by two radars increases confidence in the validity of results.

**JSM14/09P/D-020** Poster **1400-084**

### USING ISENTROPIC AND PV TECHNIQUES TO ANTICIPATE THE EFFECTS OF A STRONG UPPER COLD FRONT

Chris DOYLE (Environment Canada, Meteorological Service of Canada)

On the afternoon of May 2nd 2002, a strong cold front moving swiftly southward along the British Columbia coast helped foster gale-force northwesterly winds over the waters of the inner south coast of BC and gusty surface winds that exceeded warning criteria over southern Vancouver Island. In addition, several strong and unexpected thunderstorms also occurred with the frontal passage. Traditional forms of NWP guidance were not indicative of the severity of the event. Isentropic NWP guidance is a valuable tool an operational meteorologist can use to forecast these highly dynamic and mesoscale events; especially forecasts of IPV - Isentropic Potential Vorticity. IPV forecasts and trajectory data were examined *post-facto* and found to be very useful in evaluating the dynamics of the frontal feature. In addition, ground level ozone measurements can be used, in part, to assist in the verification of strong fronts with tropospheric folds.

**JSM14/09P/D-021** Poster **1400-085**

### AN AUTOMATED SYNOPTIC CLIMATOLOGICAL PROCEDURE TO PREDICT FREEZING RAIN: APPLICATION FOR OTTAWA, ONTARIO

Chad Shouquan CHENG, Heather AULD, Guilong LI, Joan KLAASSEN, Bryan TUGWOOD (Meteorological Service of Canada-Ontario Region, Environment Canada)

Freezing rain is a major weather hazard, which can compromise human safety, significantly disrupt transportation, and damage and disrupt built infrastructure such as telecommunication towers and transmission wires. In this study, an automated synoptic climatological procedure used principal components analysis, average linkage clustering procedure and discriminant function analysis to classify the weather types which were most likely to be associated with freezing rain events at the city of Ottawa, Ontario. Meteorological data that was used in the analysis included hourly surface observations from the Ottawa International Airport and 6 atmospheric levels of 6-hourly NCEP-NCAR upper-air reanalysis weather variables for the winter months (Nov.-Apr.) of 1958/59-2000/01. The data were divided into two parts: a developmental dataset (1958/59-1990/91) for construction (development) of the model and an independent dataset (1990/91-2000/01) for validation of the model. The procedure was able to successfully identify weather types that are most highly correlated with freezing rain events at Ottawa. Stepwise logistic regression was performed on all days within the freezing rain weather categories to analytically determine the meteorological variables that can be used as forecast predictors for the likelihood of freezing rain occurrence at Ottawa. The results show that the model is best able to identify freezing rain events occurring several hours during a day. For example, in the independent or validation dataset, for likelihood values 0.6, the procedure was able to identify 74% of all freezing rain events occurring 6 hrs or more during a day. Similarly, the procedure was able to identify 91% of all freezing rain events occurring 8 hrs or more during a day. The statistical procedure is being extended to other locations in Ontario, as well as to U.S. cities near the Canada-U.S. boundary. A trends analysis of freezing rain events and their associated weather type frequencies will allow the authors to assess the risks of Ontario communities to severe ice storms. This study has further potential to be adapted to an operational forecast mode to assist in the prediction of major ice storms.

**JSM14/09P/D-022** Poster **1400-086**

### SYNOPTIC TYPING AND ITS APPLICATION TO ANALYSIS OF FREEZING RAIN EVENTS IN ONTARIO, CANADA AND THE NORTHEASTERN UNITED STATES

Chad Shouquan CHENG, Joan KLAASSEN, Heather AULD, Guilong LI, Qian LI (Meteorological Service of Canada-Ontario Region, Environment Canada)

Freezing rain is a major weather hazard which affects many parts of Canada and the United States; however, in Canada, it is especially common in a corridor from Ontario to Newfoundland; and in the U.S., it frequently occurs in the Northeastern U.S. and the Appalachian region. In this study, principal components analysis and average linkage clustering procedure were used to automatically classify distinctive synoptic categories based on the differentiations and similarities of weather types characteristics. Meteorological data that was used in the analysis included hourly surface observations of air temperature, dew point temperature, sea-level air pressure, total cloud cover, wind speed/direction and occurrence of freezing rain as well as 6 atmospheric levels of 6-hourly NCEP-NCAR upper-air reanalysis weather variables of air temperature, dew point temperature, wind speed and direction for the winter months (Nov. - Apr.) of 1958/59-2000/01 for Canadian stations and 1973/74-1999/2000 for the U.S. stations. The study area consists of 14 weather stations in Ontario, 1 station in Montreal, Quebec and 12 stations bordering the Great Lakes. Hourly surface meteorological data were retrieved from Environment Canada's Digital Archive of Canadian Climatological Data for Canadian stations and from the U.S. National Climatic Data Center for the U.S. stations. The statistical procedure was able to successfully identify weather types that were most highly correlated with freezing rain events in the study area. Four weather types were most highly related to freezing rain events in the entire study area, while up to 2 additional weather types were identified at some of the stations. The freezing rain-related weather types that were identified account for 70% to 100% of the freezing rain events over the entire study period for occurrences greater than or equal to 1, 4 and 6 hours during a day. In addition, the relationships among monthly total freezing rain events, monthly total frequencies of freezing rain-related weather types and monthly mean temperature were investigated. In general, monthly total occurrences of freezing rain events

increase/decrease with monthly total frequencies of the freezing rain-related weather types. Trend analyses of the occurrences of freezing rain and the related weather type frequencies were also assessed.

**JSM14/09P/D-023** Poster **1400-087**

### SNOWFALL AROUND NAGAOKA CLASSIFIED BY SNOW-ECHO MODES

Sento NAKAI<sup>1</sup>, Koyuru IWANAMI<sup>1</sup>, Ryohei MISUMI<sup>1</sup>, Sang-Goon PARK<sup>2</sup>, Masujiro SHIMIZU<sup>1</sup>, Toshiichi KOBAYASHI<sup>1</sup> (Snow and Ice Research Group, NIED, <sup>2</sup>Advanced Technology Research Group, NIED, Tsukuba, JAPAN)

Snow clouds develop over the Japan Sea with sensible and latent heat supply from the sea surface. The snow clouds cause many disastrous phenomena such as avalanche and blizzard after landing on the Japan Islands. We made Doppler-radar observations of the snow clouds and analyzed the relation between the "snow-echo mode" and the precipitation distribution. Equivalent radar reflectivity factor (Ze) and Radial velocity (Vr) was observed by an X-band Doppler radar (X-POL) settled on the roof of Nagaoka Institute of Snow and Ice Studies located in the central area of Niigata Prefecture (Chuu-Etsu). Ze and Vr obtained on a polar coordinate were interpolated on a Cartesian coordinate whose resolution was 1 km in horizontal direction and 500 m in vertical direction. The analysis period was 10-19 February 2000. The period contained a latter half of a cold-air outbreak and whole of another cold-air outbreak. To classify the snow-echo mode, we made an animation of horizontal sections of Ze and Vr at a height of 1.1 km. The analysis period was divided into 14 cases by examining the animation. Mean Ze was derived for each of the identified cases. Observed snow-echoes were classified into four snow-echo modes, that is, L-, T-, S-, and M-modes. L- and T- modes are well-known longitudinal and transversal snow bands. S-mode was characterized by the precipitation that continued to cover most of the observation area. M-mode means that stationary precipitation was observed around the windward slope of the mountains. L-mode was often seen when the wind direction was west-northwest. T- and M-modes were accompanied by more northerly winds. Mean Ze of L-mode cases showed that the precipitation was strong over the sea as well as over the land. On the contrary, mean Ze of T-mode cases showed that strong precipitation was only over the land. Mean Ze of S-mode cases showed no specific distribution. Mean Ze of M-mode cases showed that the precipitation was mainly over the mountain slope, especially over the slope facing against the prevailing wind. To understand the snowfall processes of snow clouds over the land, it is necessary to solve the problems such as Z-R relation, low-level wind and orographically forced updraft. Comparison between mean Ze and surface data showed that the mean Ze distribution and surface precipitation distribution was qualitatively consistent in many cases. Similar comparison without snow-echo mode classification showed bad relation between Ze and surface data. It suggests that classifying snow-echo mode is important to know the characteristic precipitation distribution and that each snow-echo mode has its characteristic snowfall processes.

**JSM14/09P/D-024** Poster **1400-088**

### OBSERVATIONAL AND NUMERICAL STUDIES OF A POLAR LOW FORMED OVER THE JAPAN SEA ON 27 JANUARY 2001

Syugo HAYASHI, Masanori YOSHIZAKI, Teruyuki KATO, Hisaki EITO (Meteorological Research Institute, Japan Meteorological Agency)

In January 2001, "Winter MCSs Observations over the Japan Sea 2001" (WMO-01) was conducted (Yoshizaki et al. 2001). On 27 January in WMO-01 IOP, a synoptic-scale low passed on southern side of Japan. At the same time a meso- $\alpha$ -scale low formed over the Japan Sea in the northwestern side of the synoptic-scale-low, and is called a polar low in this study. This polar low was observed by observation ships and an instrumented aircraft (Gulfstream-2). Murakami et al. (2001) flew this polar low and observed inner structure of organized snow cloud systems. The echo areas were circular/spiral in shape and quasi-stationary, although they were weak in intensity. Characteristic wind fields were detected below the height of 1.5 km. Remarkable cyclonic wind patterns were found at the height of 0.3 km, in which the easterly winds with a speed greater than 10m/s were on the northern side and westerly winds on the southern side. The warm core was found in the central/southern part of the polar low, where equivalent potential temperature at the height of 1.5 km is higher by 2-3 degrees than its surroundings. The purpose of this study is to clarify the structures and the developing processes of the polar low numerically. First, we try to (1) reproduce the polar low using a cloud-resolving non-hydrostatic model, (2) investigate its structures in detail and (3) examine the developing processes with sensitivity experiments. The model used in this study is the Meteorological Research Institute / Numerical Prediction Division unified Nonhydrostatic Model (MRI/NPD-NHM: Saito et al. 2001). It is 5 km horizontal resolution, containing 300 x 300 grids (1500 km square) in horizontal and 38 layers in vertical. The cold rain scheme is used as the cloud microphysics. The MRI/NPD-NHM is nested in the Regional Spectral Model (RSM) of Japan Meteorological Agency (JMA). The RSM is a hydrostatic model with 20 km horizontal resolution, and is used operationally in JMA. The initial and boundary conditions for the MRI/NPD-NHM are produced by the forecasts of the RSM. The structures of the polar low were studied by using MRI/NPD-NHM. The observed features such as the horizontal distributions of the wind and movement of the polar low were well reproduced. The vertical extent of the polar low is about 3 km and its horizontal scale is about 300 km. The center of the polar low and the horizontal wind shear line were occupied by high  $\theta_e$ . To investigate the development processes of the polar low, sensitivity experiments were conducted. The condensational heating plays a primary role for developing of the polar lows.

**JSM14/09P/D-025** Poster **1400-089**

### DEVELOPMENT PROCESSES OF COASTAL SNOWBANDS OBSERVED DURING WMO-01

Tetsuya KAWANO<sup>1</sup>, Tatsuya TANAKA<sup>2</sup>, Masanori YOSHIZAKI<sup>1</sup>, Teruyuki KATO<sup>3</sup>, Hisaki EITO<sup>3</sup>, Yoshinobu TANAKA<sup>4</sup>, Ken-ichi KUSUNOKI<sup>1</sup>, Koyuru IWANAMI<sup>1</sup> (<sup>1</sup>Department of Earth and Planetary Sciences, Faculty of Sciences, Kyushu University, <sup>2</sup>NEC Soft, Ltd., <sup>3</sup>Meteorological Research Institute, Japan Meteorological Agency, <sup>4</sup>National Research Institute for Earth Science and Disaster Prevention)

The authors investigated the development processes of two convective snowbands which formed on the coastal area of the Joetsu district, the western part of Niigata Prefecture, Japan during WMO-01 (Winter Mesoscale convective systems Observations over the Japan Sea - January 2001). One of the snowbands developed on 17 and the other on 18 January 2001, which corresponded to the period when the winter monsoon cold air outflow from Siberia weakened. The snowbands were observed by two three-dimensional scanning Doppler radars located at Joetsu and Ohmi, respectively. The dual Doppler radar analysis revealed that both snowbands have common features. The bands were about 100km in length and about 10km in width and aligned from the east-northeast to west-southwest. The orientation was approximately parallel to the coastline. The successive development of convective echoes occurred in the snowbands. The echoes (the horizontal scale is about 10km and the vertical scale about 4km) moved approximately eastward and the systems

slowly south-southeastward. The low-level convergence region was located along the northern flank of the bands. The convergence layer was about 1 km in depth. Furthermore, in order to investigate the formation processes of the snowbands, numerical simulations with the horizontal resolution of 2 km were performed using a full compressible, non-hydrostatic numerical model, MRI/NPD-NHM (Meteorological Research Institute / Numerical Prediction Division Unified Nonhydrostatic Model), which is one-way nested within the MRI/NPD-NHM with the horizontal resolution of 5 km. The initial and boundary conditions for the 5 km-MRI/NPD-NHM are provided from the forecasts of RSM (Regional Spectral Model), which is the operational forecast model of the Japan Meteorological Agency. The simulated snowfall areas corresponded to the observations. The convectively unstable layers with 1.5-2 km in depth were found over the Japan Sea north of the systems in both cases. Also, the convergence regions were located in the northern flank of both of the simulated snowbands. The convective cells developed in the convergence region and then the snowbands formed in the region. In the two simulated cases, however, the processes producing the low-level convergence region were different from each other. In the 18 January case, the cold air pool on the coast intensified the low-level convergence. On the other hand, the remarkable cold pool was not found in the area around the snowband in the 17 January case. The convergence region in the case was produced between the winter monsoon flow and the lowest-level offshore flow.

**JSM14/09P/D-026** Poster **1400-090**

**VORTEX CLOUD STREET AND ITS EVOLUTION OVER THE WESTERN OFFSHORE OF HOKKAIDO, JAPAN**

Yoshio ASUMA, Atsuo TSUBOTA (Division of Earth and Planetary Sciences, Graduate School of Science, Hokkaido University)

Snow cloud bands are one of the causes for the heavy snow precipitation in Hokkaido and sometimes disturb human activities during winter seasons. The cloud band usually organized in the parallel (L-mode) or perpendicular (T-mode) direction to the prevailing wind. It sometimes observed to be organized as a vortex cloud street. An example was observed by weather radar between 12th and 13th January 1998 over the western offshore of Hokkaido Island. Weather radar and satellite images showed that it appeared at the southwestern offshore of Hokkaido around 18UTC (03JST) 12th January 1998, gradually moved toward the north over the Sea of Japan and finally formed a meso-alpha scale vortex over the northern offshore of Hokkaido around 12UTC (21JST) 13th. The surface wind data showed a strong wind shear between the vortex cloud street. A regional objectively analyzed data set (RANAL) provided by JMA (Japan Meteorological Agency) showed a weak cold air outbreak from the Asian Continent was prevailed over the northern Sea of Japan. A cold air outbreak also occurred from Hokkaido Island and converged in the lower atmosphere at the western offshore of Hokkaido. A vortex cloud street appeared in this convergence zone. The vorticity analysis showed a strong vorticity concentration in this area. The lower level convergence zone gradually moved toward north over the Sea of Japan along the west coast of Hokkaido. An upper level short wave trough, which was associated with cold vortex over the Asian Continent, approached from the continent. The vortex cloud street was finally organized as a meso-alpha scale vortex under the upper level short wave trough. We simulated these conditions with the PSU-NCAR mm5 meso-scale model.

**JSM14/09P/D-027** Poster **1400-091**

**EXPLOSIVELY DEVELOPED CYCLONES AND WATER TRANSPORTATION OVER THE NORTHWESTERN PACIFIC REGION**

Yoshio ASUMA, Akira YOSHIDA, Masaya KATO (Division of Earth and Planetary Sciences, Graduate School of Science, Hokkaido University)

The extratropical cyclone is one of the important driving forces of the heat and water vapor transportation from the lower latitude to the higher latitude. As it brings a large amount of solid precipitation over the area during cold seasons, its activity would affect the growth and decay of the cryosphere. We analyzed explosively developed cyclones over the Northwestern Pacific area during cold seasons between 1994 and 1999 using a global objectively analyzed data set (GANAL) provided by Japan Meteorological Agency (JMA). Explosive cyclones were classified into three types by the places of formation and maximum deepening positions. They are Okhotsk and Japan Sea type cyclones, Pacific Ocean - Land type cyclones, and Pacific Ocean - Ocean type cyclones. These types of cyclones have characteristics for their seasonal appearance frequencies and maximum deepening rates. By the composite analysis, it was found that these characteristics are reflected by the interior structures of the cyclone. Water vapor acts as a driving force for the development of the cyclone through the latent heat release and the water vapor is carried into the cyclone center at its maximum deepening. The cyclone reaches its center sea level pressure minimum after explosive development and achieves large horizontal vapor transportation. Vertically integrated horizontal vapor flux and cyclone tracks were analyzed by month and the following tendencies were found: water vapor transports into the Arctic circle over the Kamchatka Peninsula during the Okhotsk and Japan Sea type cyclones predominant month; it zonally transports toward the Gulf of Alaska during the Pacific Ocean - Land type cyclones predominant month; and it transports into the Arctic circle through the Bering Strait during the Pacific Ocean - Ocean type cyclones predominant month.

**JSM14/09P/D-028** Poster **1400-092**

**A VERIFICATION OF ICEBERG DRIFT OFF CANADA'S EASTERN COAST**

Thomas CARRIERES<sup>1</sup>, Mohamed SAYED<sup>2</sup>, Stuart SAVAGE<sup>1</sup>, Greg CROCKER<sup>1</sup> (<sup>1</sup>Canadian Ice Service, <sup>2</sup>Canadian Hydraulics Centre, <sup>3</sup>McGill University, <sup>4</sup>Ballicater Consulting)

Icebergs pose the greatest hazard to marine operations off Canada's east coast. In our ongoing effort to improve ice products and services, the Canadian Ice Service has developed a new iceberg drift and deterioration model. The model drift is compared to more than 50 iceberg drift tracks monitored in 2002 for drilling platforms in the Grand Banks area. The model drift corresponds quite well to observations and errors are generally reduced compared to our older operational model. Iceberg drift direction is better predicted than speed and the latter has a negative bias for larger icebergs. Geographic patterns to the drift error vectors imply that predicted ocean currents are the largest error source. Other significant error sources include underwater shape and the effect of wave radiation stress.

**JSM14/09P/D-029** Poster **1400-093**

**CLIMATE CHANGE AND ITS IMPACT ON MOUNTAINOUS REGION: A STUDY OF SNOW AND ICE IN HIMALAYAN MOUNTAIN ECOSYSTEM AND ITS IMPACT**

Shanmuganandan SAMARAJALINGAM (Madurai Kamaraj University)

Global climate change is expected to bring severe impacts in Alpine regions particularly with reference to snow hydrology of mountainous regions of the world. The Alpine regions are particularly vulnerable to the impacts of global climatic change both from an economic and

environmental perspective with climate dependent economies and a vulnerable environment. Usual environmental risk like torrents floods and avalanches are supposed to increase. The Himalayas is amongst one of the youngest folded mountainous formations of the world, and the youngest in India. By comparison the Himalayas date back to only 40-45 million years. They traverse an arc for about 2500 km between the Indus and the Brahmaputra. The average width of this mountain range along the entire longitudinal extension ranges from 100 to 400 km. Being the world's highest mountain chain, the Himalayas is characterized by a complex geologic structure, snowcapped peaks, large valley glaciers, deep river gorges and rich vegetation. A complex interplay of climatic and geological processes, patterns of resource use and economic conditions have led to resource degradation and associated environmental consequences in the Himalayan ecosystem. The present study is an attempt to analyse the extent of global change and its impact on snow and ice in the last several decades and also to observe the major ecological concerns and the underlying driving factors (both human and natural processes), socio-economic impacts and the responses. This is followed by an overview of the state of the environment in the region and a detailed analysis of key environmental issues: water resources and their sharing, biodiversity loss, glacier recession, deforestation, land degradation and agriculture systems, natural disasters. This is followed by an overview of the state of the environment in the region and a detailed analysis of key environmental issues. The current employment pattern might be disrupted by climate change. In particular local Alpine communities and districts will feel the effects. An attempt is done to quantify the expected losses due to climate change on a local level. As the pace of warming is still unknown the scenarios of warming are provided. Local decision makers should be enabled to judge the economic magnitude of the problem and to develop counter strategies against climate change. The study was based on the secondary data collected extensively from case studies and also from published reports available for Himalayan region on various aspects of snow and ice and also about the Himalayan ecosystem. The study also used the hydro meteorological data to observe the variation in water resources potential due to the impact of climate change in the last several decades. The data on selected variables of climate change and ecosystem were analyzed with the help of factor analysis to identify the major dimensions and spatial pattern of variation is observed. The analysis of findings revealed that there is a need to work out a strategy for sustainable mountain ecosystem in view of the changes introduced by man made changes on mountain ecosystem and also the changes effected by climate change.

**JSM15**

**Monday, July 7**

**SPECIAL NAKAYA-MAGONO CELEBRATION: THE GROWTH OF ICE CRYSTALS AND SNOW (IAMAS [ICCP, ICPM], IAHS)**

Location: Site B, Room 18

**Monday, July 7 AM**

Presiding Chairs: C. Knight, M. Kuhn, N. Maeno, Y. Fujiyoshi

**JSM15/07A/B18-001** Invited **0900**

**MOLECULAR DYNAMICS SIMULATIONS OF ICE SURFACES AND ICE/WATER INTERFACES**

Hiroki NADA<sup>1</sup>, Yoshinori FURUKAWA<sup>2</sup> (<sup>1</sup>Institute for Environmental Management Technology, National Institute of, <sup>2</sup>Institute of Low Temperature Science, Hokkaido University)

Molecular-scale structures of the surfaces of an ice crystal and the ice/water interfaces are investigated using a molecular dynamics simulation. For the ice surfaces, simulations are carried out for both an ice(0001) and an ice(0001) faces (basal and prismatic faces, respectively) over a temperature range from 170 to 250K. The simulation results clearly indicate that structural transitions occur on both faces as the temperature increases to the melting point, and that the temperatures of the transitions are completely different between in the case of basal and prismatic faces. Especially, we emphasize that the anisotropy in surface melting between the faces obtained by the present simulation study agrees with the experimental results obtained by ellipsometric measurements. The anisotropic surface melting will be discussed on the basis of the interface structures between the quasi-liquid layer and the underlying ice crystal. Moreover, molecular dynamics simulations of ice/water interface at the supercooling state are also performed to elucidate the anisotropic growth kinetics of ice. The simulations are carried out for two kinds of interfacial orientations, namely, an ice(0001)/water and an ice(1010)/water interfaces. It should be emphasized that not only the interface structures but also the growth kinetics are completely different between the interfaces. The simulation results indicate that the growth kinetics are the layer-by-layer process for the ice(0001)/water interface and the collected molecules process for the ice(1010)/water interface. The results will be also discussed in relation to the experimental results of ice growth.

**JSM15/07A/B18-002**

**0930**

**CAPACITANCE OF SOLID AND HOLLOW ICE CRYSTALS**

Mihai CHIRUTA, Pao K. WANG (Department of Atmospheric and Oceanic Sciences, University of Wisconsin-Madison)

It is increasingly clear that cirrus clouds have important impact on the global climate process because the ice crystals in them interact strongly with both solar and terrestrial radiations. Using a two-dimensional explicit microphysical cirrus model coupled with radiation, we have demonstrated recently that the heating rate in a cirrus strongly depends on the habit of its constituent ice crystals. The model results indicate that the difference of peak heating and cooling rates between a cirrus of rosette ice crystals and a cirrus of ice spheres can be as much as 600%! Much of this difference is due to the different growth rates of these crystals. To assess the impact of cirrus on climate, therefore, it is important to estimate more precisely the growth rates of ice crystals. Although the growth rates of crystals of simpler shapes, such as columns and plates, are known, many important crystals that are commonly observed in cirrus clouds are not. The latter include spatial crystals such as solid and hollow bullet rosettes and hollow columns. The present paper is to report our recent calculations of the capacitance of these crystals. The electrostatic analogy is currently the main theory used to calculate the ice crystal growth rates and the central quantity in this theory is the capacitance. Due to the complicated shapes and difficulties in experimental techniques, their capacitances are not known. We have recently calculated the capacitances of a number of solid rosette crystals using finite element techniques. This paper will report on our more recent progress in computing the capacitances of hollow columns and hollow rosettes. We will compare the capacitances of solid and hollow crystals and the implications of the different capacitances in the climatic impacts of cirrus clouds.

**JSM15/07A/B18-003****0945****MASS FLUX AND RECRYSTALLIZATION OF SNOW CRYSTALS AGGREGATES AT THE MICROSTRUCTURAL LEVEL**

Sergey A. SOKRATOV, Martin SCHNEEBELI (Swiss Federal Institute for Snow and Avalanche Research)

Most modern practical applications require not only the understanding of the crystal growth phenomena at the single-crystal scale, but also knowledge of the interactions of growing crystals in multi-element systems. Up to now, there is no accepted theory fully describing these processes. Snow is the material corresponding to a multi-element system naturally being at the temperature very close to the melting point. The physical conditions for the formation of different shapes for single ice crystals are well known. However, very few data are available on the corresponding processes in snow as a multi-elements system. Collecting data on how different the shapes and the activity of recrystallization are in snow is of great interest not only to snow physics, but to material science in general. Laboratory experiments and mathematical modeling are done concurrently to understand the mechanism of crystal growth in snow under regulated thermophysical conditions. Experiments are made in a cold laboratory on samples of natural snow. The time-variation of the shape, size and specific surface area, and the corresponding change in the thermophysical properties of the snow samples are observed undisturbed using X-ray computed micro-tomography simultaneously with heat-flux and temperature measurements. The results of this study are presented.

**JSM15/07A/B18-004****1000****MONTE CARLO SIMULATION OF SNOWFLAKES**Ken-ichi MARUYAMA<sup>1</sup>, Yasushi FUJIYOSHIF<sup>2</sup> (<sup>1</sup>National Research Institute for Earth Science and Disaster Prevention, <sup>2</sup>Institute of Low Temperature Science, Hokkaido University, <sup>3</sup>Frontier Research System for Global Change)

A stochastic aggregation model for snowflake was developed, in which the time evolution of the size distribution and the shape of snowflakes are calculated simultaneously and explicitly by combining the Monte Carlo method of Gillespie (1975) with a simple aggregation model. Simulations were performed to study the effect of complexity of shape on the evolution of snowflake size distribution. (1) The size distribution of generated snowflakes is broader than those of the sphere model. The mean radius ( $R_m$ ) and mass of generated snowflakes are also larger than those of the sphere model. (2) The relationships between the maximum diameter and mass of generated aggregates are fitted with the equation  $D \sim m^b$ . The larger the initial variation of size distribution is, the larger the value of  $b$ . Besides, the larger constituent particles' density is, the smaller the value of  $b$ . These relationships are consistent with observational results, although the relationships strongly dependent on the parameters of the initial distribution. (3) On average, the density in a snowflake decreases from the center of mass to the edge, because generated aggregates have many branches near the edge. Sensitivity experiments show that small density of constituent particles leads to concentration of mass near the center, and relative variation of the initial size distribution of ice crystals does not cause any significant change in the structure of generated snowflakes.

**JSM15/07A/B18-005****1015****THE CLASSIFICATION OF ATMOSPHERIC ICE PARTICLES, A CRITICAL REVUE**

Roland LIST (UNIVERSITY OF TORONTO)

In 1949 the International Commission of Snow and Ice agreed on the "classical" schematic display of ice particles normally shown in textbooks. It lists 10 categories, with additional special letters to specify size and other characteristics. Its weakness is that 6 code numbers out of 10 are devoted to pristine ice crystal shapes, while only four remain to deal with the meteorologically important particles. While beautiful to look at, these definitions are rather useless. This is supported by the observation that there are no consistent climatological investigations or any scientific papers which make use of this classification. Thus, a revision is indicated which aims at the real world and not the aesthetics. A product is needed which can be applied and is scientifically useful. While there is no attempt made to come up with a completely new classification, suggestions will be made and a procedure will be described on how to arrive at a better product. At the same time the "standard" definitions of the different types of ice crystals will be critically reviewed and proposals will be made about possible improvements and replacements.

**JSM15/07A/B18-006****1045****PATTERN FORMATION OF ICE CRYSTAL GROWN IN SUPERCOOLED WATER AND PERIODIC FOR SPACE EXPERENTS**Etsuro YOKOYAMA<sup>1</sup>, Yoshinori FURUKAWA<sup>2</sup>, Wataru SHIMADA<sup>3</sup> (<sup>1</sup>Computer Center, Gakushuin University, <sup>2</sup>Institute of Low Temperature Science, Hokkaido University)

Development of the interfacial pattern during the growth of a crystal from its melt is a typical example of pattern formation under nonlinear and non-equilibrium conditions. It is well known that the growth form of an ice crystal freely growing in supercooled bulk water changes from a circular disk, to a perturbed disk, and finally to a well-developed dendrite with hexagonal symmetry. It means that the pattern formation of ice crystal displays unusually strong anisotropy in interfacial kinetics. We are now embarking on space experiments involving solidification of ice. We present our experimental results and a new model to understand the unstable ice disk morphologies. First of all, the experimental results for the ice disk growth under the condition of normal gravity are summarized. (1) Two different modes of ice disk growth were observed, depending on the growth kinetics of basal plane. (2) The transition from stable to unstable growth occurs when the disk thickness reaches a critical value,  $h_c$ .  $h_c$  was proportional to the reciprocal of supercooling. (3) The asymmetric morphological instability was always observed at the periphery of ice disk. Furthermore, an experiment on ice crystal growth under the microgravity condition of the period of 6 minutes was carried out using a NASA sounding rocket, TR1A#7. We observed the asymmetric pattern formation in the microgravity condition again. This result means the asymmetric pattern formation at the edge of ice disk is essentially related to the mechanism of morphological instability. These experimental results are explained by a theoretical model recently developed by Yokoyama, Sekerka and Furukawa, (J. Phys. Chem., 2000, B104, 65). In the case of disk growth, the growth of the edge plane is dominantly controlled by the thermal diffusion efficiency of the latent heat but the growth of basal planes is dominated by the interfacial kinetics. We mention that this anisotropic growth characteristic is essential for understanding these growth features of ice disks. On the other hand, we also carried out in-situ observations of thermal diffusion field around a growing ice dendrite under the short-time microgravity condition. The interference fringes obtained by this experiment were analyzed by the newly developed image-processing methods. As a result, clear images of thermal diffusion field were first obtained. In conclusion, we

emphasize that the ice disk growth gives a challengeable aspect of space experiment.

**JSM15/07A/B18-007****1100****OBSERVATIONS OF SNOW AND ICE CRYSTALS USING LOW-TEMPERATURE SCANNING ELECTRON MICROSCOPY**Albert RANGO<sup>1</sup>, William WERGIN<sup>2</sup>, Richard ARMSTRONG<sup>3</sup>, Edward JOSBERGER<sup>4</sup>, James FOSTER<sup>5</sup>, Eric ERBE<sup>6</sup>, Christopher POOLEY<sup>7</sup> (<sup>1</sup>USDA/ARS/Jornada Experimental Range, New Mexico State University, 2995 Knox St., Las Cruces, NM 88003, USA, <sup>2</sup>USDA-ARS-Electron Microscopy Unit, Beltsville Agricultural Research Center, Beltsville, MD 20705, USA, <sup>3</sup>University of Colorado, National Snow and Ice Data Center, Boulder, CO 80309, USA, <sup>4</sup>U.S. Geological Survey, 1201 Pacific Ave., Suite 600, Tacoma, WA 98416, USA, <sup>5</sup>Laboratory for Hydrological Sciences, NASA Goddard Space Flight Center, Greenbelt, MD 20771, USA)

The use of low-temperature scanning electron microscopy (LTSEM) to observe snow and ice crystals has been developed in recent years to provide a viable, alternative method to light microscopy (LM). Since 1994, the methods to collect, preserve, transport, and store snow and ice crystals have been perfected so that samples can be obtained in remote snow and ice regions anywhere in the world and then viewed and photographed with the LTSEM. The LTSEM technique increases the resolution and ease with which samples of snow and ice can be observed, studied, and photographed. The use of conventional LM for observing snow crystals has required cooling of the laboratory and instrumentation to temperatures below freezing. Furthermore, the samples must be analyzed and photographed near the place and time of collection. These disadvantages have been rectified using LTSEM. Additional advantages of LTSEM include the ability to image at high magnifications (up to 150,000x), improved depth of focus and resolution, three-dimensional (stereo) viewing, and the capability to store samples for long periods of time (at least five years). We have compared LM and LTSEM images of the identical crystals (as well as of similar crystals collected under the same environmental conditions in a large field experiment) to document this LTSEM capability. The greater resolution of LTSEM was evident when examining and resolving the small frozen cloud droplets associated with rime and graupel, whereas the greater depth of focus provided clear photographs of these crystals as well as other large crystals such as depth hoar. In addition, LTSEM images specifically illustrate the structural features of the crystal surface that is being imaged, whereas with LM, the surface features are sometimes masked and confused by internal structures and their effect on reflected, refracted, and transmitted light. In comparison to the crystals imaged or described by the Japanese scientists Nakaya and Magono, the LTSEM can also be used to provide higher resolution to characterize the irregular crystals that Nakaya (1954) termed "a lump of frozen droplets". For the 80 different types of snow crystals specified by Magono and Lee (1966), our LTSEM images from field work cover over 70 of their snow crystals plus we have encountered at least 20 types of crystals not included in their classification scheme. Future studies will interface the LTSEMs with energy dispersive x-ray microanalysis systems so that the elemental constituents of contaminants in a snow crystal can be identified. It is hoped that the LTSEM capabilities will be useful in furthering the original studies of Nakaya and Magono.

**JSM15/07A/B18-008****1115****ICE PARTICLE HABITS IN STRATIFORM CLOUDS**Alexei KOROLEV<sup>1</sup>, George A. ISAAC<sup>2</sup>, John HALLETT<sup>3</sup> (<sup>1</sup>Sky Tech Research Inc., <sup>2</sup>Meteorological Service of Canada, <sup>3</sup>Desert Research Institute)

In calculations for climate change predictions, weather forecasting of precipitation, and remote sensing retrievals, idealized crystal shapes such as columns, needles, plates and dendrites are assumed. The existence of such crystals were supported by numerous laboratory studies. The current work presents results of aircraft studies of cloud particle habits in natural clouds. The images of cloud particles were measured by two instruments: PMS Optical Array Probe-2DC (OAP-2DC) at 25 mm resolution, and a newly developed SPEC Cloud Particle Imager (CPI) at 2.3 mm resolution, installed on NRC Conqair-580. The processing of OAP-2DC images was conducted with the help of an originally developed algorithm for pattern recognition. Approximately 4.6 10<sup>6</sup> images of cloud particles having a size larger 125 μm were analyzed from data collected during four field campaigns from 1994 to 1998 in stratiform clouds mainly associated with frontal systems. The cloud particles were classified into four categories: spheres, irregulars, needles and dendrites. The frequency of occurrence of different habits was found for each 50C temperature interval in the range -450C < T < 00C. One important conclusion of this study is that the majority of ice particles in natural clouds have an irregular shape for all temperature intervals. On average, the frequency of occurrence of irregular shaped particles is about 84%. High-resolution CPI images showed that pristine monocrySTALLINE ice particles such as plates and columns occur only in 3% of all cases. Some unusual shapes of ice particles were found in the CPI imagery. Since the data were collected in different climatic zones and covered a significant cloud path length (3.7 10<sup>4</sup> km), the conclusions from this work should apply to clouds in other regions.

**JSM15/07A/B18-009****1130****THE ROLE OF ICE IN TROPICAL LIGHTNING**

Tsumomu TAKAHASHI (Core Education Center, Obirin University)

Data from TRMM-LIS show strong differences between tropical lightning activity over the open ocean and over continents. Even in east-Asia, flash rates are two orders of magnitude smaller over the western Pacific than over the maritime continent (Christian et al. 2002). Laboratory wind tunnel experiments and field works in Hokuriku and southern Kyushu indicate that the main charging process in these thunderstorms is the riming electrification mechanism. According to the thunderstorm model given in Takahashi, 1984, the number concentration of ice crystals and graupel required to accumulate sufficient electric charge to initiate lightning must exceed 50/1 and 1.5/1. During the past 15 years, this concept has been examined using data from 208 videosondes launched into Asian monsoon clouds from 13 different areas (Ponape, Manus Is., Brunei, Melville Is., Songkhala, Surat Thani, Phuket, Ubon, Chaingrai, Pingliang, Shanghai, Tanegashima, and Kagoshima). Data acquired from these videosondes show that the number concentrations of ice crystals and graupel differ greatly between the open ocean and the maritime continent. As lightning activity over the open ocean is two orders of magnitude less than that over the maritime continent, the number concentrations of ice crystal and graupel over the ocean are also lower by the same magnitude. Smaller concentrations of snow over the open ocean lead to different precipitation mechanism: a frozen drop mechanism over the ocean in comparison to a mixed rain process over the maritime continent. Results from a three dimensional microphysics cloud model illustrate the different rain patterns and organizations between the two areas.

JSM15/07A/B18-010

1145

## SURFACE INSTABILITY OF ICICLES

Naohisa OGAWA, Yoshinori FURUKAWA (Institute of Low Temperature Science, Hokkaido University)

Quantitatively unexplained stationary waves or ridges often encircle icicles. Such waves form when roughly 0.1-mm-thick layers of water flow down an icicle. These waves typically have a wavelength of about 1 cm, which is independent of external temperature, icicle thickness, and the volumetric rate of water flow. In this paper, we show that these waves cannot be obtained by a naive Mullins-Sekerka instability but are caused by a quite different type of surface instability related to thermal diffusion and the hydrodynamic effect of a thin water flow. References: Physical Review E 66, 041202 (2002)

JSM15-Posters

Monday, July 7

## SPECIAL NAKAYA-MAGONO CELEBRATION: THE GROWTH OF ICE CRYSTALS AND SNOW (IAMAS [ICCP, ICPM], IAHS)

Location: Site D

Monday, July 7 PM

Presiding Chairs: G. Isaac, E. Yokoyama

JSM15/07P/D-001

Poster

1400-001

## EFFECT OF ANTIFREEZE GLYCOPROTEIN FOR ICE CRYSTAL GROWTH KINETICS

Yoshinori FURUKAWA<sup>1</sup>, Yoshihiro NISHIMURA<sup>1</sup>, Etsuro YOKOYAMA<sup>2</sup>, Naomi INOHARA<sup>1</sup>, Takanori TERASAWA<sup>1</sup> (<sup>1</sup>Institute of Low Temperature Science, Hokkaido University, <sup>2</sup>Computer Center, Gakushuin University)

Freezing of organisms in cold weather can cause death of life. Many organisms have developed a tolerance to both freezing and recrystallization. In particular, it is well known that certain polar and near polar fishes survives by the work of Antifreeze Glycoprotein (AFGP, their molecular weights are ranged in 2000-30000). These proteins suppress the freezing temperature of water. Namely, fish bodies are kept in the supercooling state, but they never freeze. The mechanism of freezing prohibition is considered that AFGP molecules adsorb at the interface between ice and water, and restricts the step migration at the interface. This is the static effect for the ice growth prohibition by AFGP molecules. However, the details of the kinetic mechanism by which these proteins function (so-called dynamic effect) have not been clarified up to now. We have carried out in detail the in-situ observations of the growing interfaces and pattern developments. In this paper, we present the results of one-directional growth experiments of ice from the aqueous solution of AFGP, and discuss the interfacial pattern formation. Based on the experimental results, we determine the interfacial kinetic supercooling of growing interfaces. One-directional growth experiments of ice crystals were carried out by a very thin growth cell, and the interfacial pattern developments were observed in situ using an interferometer. Initial concentration of AFGP was less than 0.1wt%. An interface, which was flat before the beginning of growth, changed to a randomly perturbed one after the beginning of growth, and finally to a periodically jagged pattern that composed of flat prismatic faces. This kind of pattern formation is completely different from that driven by the so-called constitutional supercooling. Interfacial supercooling temperatures,  $\delta T$ , were directly determined from the analysis of zigzag patterns. We clarified that distance between the top and bottom of zigzag patterns relates to the degree of  $\delta T$ . We found that  $\delta T$  increases with increasing growth rate when the growth rate is lower, but this relation is reversed when the growth rate increases. Assuming that  $\delta T$  proportionally depends on the adsorption density of AFGP molecules at the growing interfaces; we will discuss the relationship between the AFGP adsorption and the growth rate. Furthermore, the self-oscillatory growth was also observed during the ice crystal growth in the AFGP solution. The mechanism is discussed based on the nucleation of new interface and the adsorption of AFGP on the ice/water interface.

JSM15/07P/D-002

Poster

1400-002

## GROWTH PATTERN DIAGRAM OF SNOW CRYSTALS

Norikazu MAENO<sup>1</sup>, Yoshinori FURUKAWA<sup>1</sup>, Keiji HIGUCHI<sup>2</sup> (<sup>1</sup>Institute of Low Temperature Science, Hokkaido University, <sup>2</sup>Nagoya City Science Museum)

A growth pattern diagram of snow crystals was first constructed by Nakaya (1954), who tried to show by the diagram that the variety of growth forms of snow crystals can be classified as functions of air temperature and degree of super-saturation of water vapor with respect to ice. Large numbers of laboratory and theoretical results by Nakaya (1954), Shaw and Mason (1955), Kobayashi (1957), Hallett and Mason (1958), and others, were consolidated and summarized by Kobayashi (1961) in a growth pattern diagram of snow crystals. At present, however, it is often noted that the correct form of the diagram is not always introduced in literatures and textbooks in the world, leading to unnecessary misunderstanding and confusions. The present paper aims at making clear the situation and trying to renew the important implication of the diagram by discussing other factors affecting growth patterns of a snow crystal than temperature and super-saturation of water vapor.

JSM15/07P/D-003

Poster

1400-003

## MORPHOLOGY OF SNOW CRYSTALS GROWN AT LOW TEMPERATURES IN FREE FALL

Chuji TAKAHASHI (Department of Earth Science, Faculty of Education, Saitama University)

It is well-known that the habit of snow crystals changes with the temperature and the supersaturation since the experiments of artificial snow crystals by Nakaya. However these experiments were carried out for limited conditions of temperatures above about -25°C. Recently snow crystals, which are observed at polar regions(1) or in cirrus clouds(2), has been attracted interest in relation to the study of climatic change. Such snow crystals grow mostly at temperatures below -25°C. The author investigated the growth of snow crystals at low temperatures by using a diffusion cloud chamber(3). He showed that combination of bullet type snow crystals grew at temperatures below -40°C. This study was carried out to investigate the morphology of snow crystals which grow at low temperatures in free fall by using a large cloud chamber of 6.5 m in height. Supercooled cloud was produced in the large cloud chamber and were seeded with kaolinite(clay mineral), silver iodide smoke or frozen water droplets(less than 20µm in diameter). Frozen water droplets were produced by spraying distilled water and allowed the water droplets to fall in the small cooling chamber

attached at the top of the large cloud chamber. They are considered to be nucleated by homogeneous nucleation. Experiments were made also on the condition that no ice nucleus was seeded. In this condition snow crystals grew from natural ice nuclei. Snow crystals were collected at the bottom of the chamber and were classified into six types, single-crystalline plates, single-crystalline columns, assemblages of plates, assemblages of plates and columns, combinations of columns and unusual crystals. The percentages of each crystal types were derived. (1)Single-crystalline columns were observed frequently when supercooled cloud were seeded with silver iodide smoke or no ice nucleus seeded. It is considered that about 30% of snow crystals are single-crystalline column when they grow from natural nuclei. (2)Assemblages of plates or assemblages of plates and columns were observed frequently when kaolinite or frozen water droplets were seeded. The percentages of assemblages of plates decreased and those of assemblages of plates and columns increased with the decrease of temperatures. (3)The percentage of combinations of columns was small when a supercooled cloud was seeded with kaolinite or silver iodide smoke, or when no ice nucleus was seeded. But it was 16% when frozen droplets were seeded at a temperature -33°C. References (1)Iwai,K. Memo.Natl.Inst.Polar Res.Spec.Issue, 45(1979), 38-46 (2)Miloshevich, L.M. and A.Heymsfield, J.Atmos.Oceanic Technol., 14(1997), 753-768 (3)Takahashi C., Proceeding of 11th intr. conf. on clouds and precipitation, Montreal (1992), 42-43

JSM15/07P/D-004

Poster

1400-004

## GROWTH PATTERNS OF SNOW CRYSTALS

Etsuro YOKOYAMA<sup>1</sup>, Toshiharu IRISAWA<sup>1</sup>, Yoshinori FURUKAWA<sup>2</sup> (<sup>1</sup>Computer Center, Gakushuin University, <sup>2</sup>Institute of Low Temperature Science, Hokkaido University)

A spherical single crystal of ice grown from supersaturated vapor in clouds first becomes a hexagonal prism bounded by two basal and six prism faces. At low supersaturation, such a hexagonal prism can grow in a stable manner and retains its form. For higher supersaturations, it changes form by means of preferred growth of edges and corners. A model of formation of two-dimensional patterns during the growth of snow crystals was developed [1]. The model takes into account the following elementary processes relevant to the growth: (1) A surface kinetic process for incorporating molecules into a crystal lattice, and (2) a process for diffusing molecules through air toward the crystal surface. We develop the model and show the effect of aspect ratio on morphological instability during growth of hexagonal prisms. Furthermore, we discuss the conditions for the formation of side branch patterns. Reference [1] E. Yokoyama and T. Kuroda, Phys. Rev. A 41(1990)2038.

JSM15/07P/D-005

Poster

1400-005

## PATTERN FORMATION AT INTERFACE BETWEEN ICE AND SALT SOLUTION DURING ONE-DIRECTIONAL GROWTH

Kazushige NAGASHIMA<sup>1</sup>, Yoshinori FURUKAWA<sup>2</sup> (<sup>1</sup>Department of Physics, Meiji University, <sup>2</sup>Institute of Low Temperature Science, Hokkaido University)

Development of the interfacial pattern during the one-directional growth of ice crystal from the water containing impurities was observed in-situ using an interferometer. Generally, these kinds of growth experiment are very useful in a discussion of pattern formation and have carried out for many kinds of materials. This methodology was applied to the ice crystal growth from the KCl solution. The solute distribution in front of directionally growing ice crystals was observed in situ as well as the three-dimensional interfacial patterns, using a Mach-Zehnder interferometer. We were able to observe the occurrence of morphological instability at the interface and the development of cellular patterns. We gave a direct evidence for the constitutional supercooling and discussed the wavelength selection of perturbation through the analysis of interference fringes. We also found that the interfacial patterns were developed in three-dimensions, and the instabilities in the direction of cell thickness occurred first and then wavy perturbation appeared in the direction of growth cell width. The relationship between the development of constitutional supercooling and the subsequent instabilities was discussed. The three dimensional patterns were also strongly unsymmetrical in the thickness direction. The precise analysis of interference fringes indicated that this asymmetry was originated from the effect of gravity. These experimental results can be applied to the crystal growth of sea ice.

JSM15/07P/D-006

Poster

1400-006

## DYNAMIC VISUALIZATION OF SNOW METAMORPHISM USING COMPUTED TOMOGRAPHY

Martin SCHNEEBELI, Sergey A. SOKRATOV (Swiss Federal Institute for Snow and Avalanche Research)

Changes in the shape of snow during metamorphism are observed until now at discrete time-steps, without the possibility to follow the changes of the microstructure within the multi-element crystals. We used x-ray computed tomography at a high spatial resolution (40 µm) and time steps of 8 hours to visualize the changes in crystal morphology. The insulated measurement chamber contains a snow sample of 50 mm diameter and variable height from 20-60 mm. Because a controlled temperature gradient can be produced in the measurement chamber we are able to determine at the same time the effective thermal conductivity. We developed a method to visualize and calculate the changes in the surface, and by that the effective sublimation and re-sublimation at the level of single microstructural units can be measured. Our preliminary results show that the rate of sublimation and re-sublimation is higher than estimated on classical grain size measurement, because the crystals growth seems not to be a steady process, but the grains undergo within a relatively short time span several sublimation-resublimation phases.

JSM15/07P/D-007

Poster

1400-007

## GROWTH OF LARGE FROST CRYSTALS IN COLD CHAMBER

Keiji HIGUCHI<sup>1</sup>, Hiroji FUSHIMI<sup>2</sup>, Yukari NISHIMURA<sup>3</sup>, Eri SANDA<sup>4</sup>, Sakie SUMIKAWA<sup>5</sup>, Sakae SHIMABAYASHI<sup>6</sup>, Kenzo KANDA<sup>3</sup> (<sup>1</sup>Nagoya City Science Museum, <sup>2</sup>Explorer Museum Nishibori Eizaburo Memorial, <sup>3</sup>Nakaya Ukichiro Museum of Snow and Ice, <sup>4</sup>School of Environmental Science, Univ of Shiga Prefecture)

Formation of large crystals of frost was found on the wall and ceiling of cold chamber of the Explorer Museum Nishibori Eizaburo Memorial. Size of frost crystals are in order of cm, and largest one was over 10 cm. These frost crystals can be classified into three types; (1) cup, (2) needle, and (3) plate. During the period when air temperature in the cold chamber was warm, the wall of chamber was covered by frost crystals of plate, needle and cup, from the top to the bottom of the wall. During the period when air temperature was cold, the wall was covered only by cup crystals. On the basis of results obtained by observations of types of frost crystals on the wall and measurement of air temperature near the wall, it can be concluded by the transition of types from plate to needle was nearly -1°C, and that for transition from needle to cup was nearly -4 to -7°C. Forms of cup

## INTER-ASSOCIATION

crystal are quite characteristic, and many of them have one side opening inward and continued in hexagonal scroll. Such cup crystals in scroll form were observed in Greenland by Wegener (1935), and in the Antarctic by Knight and De Vries (1985). Detailed observations of scroll form of cup crystals developed in the cold chamber were possible after making plastic replica of them, which will be exhibited at the presentation. In the investigation on artificial snow crystals by Nakaya (1954), it was shown that formation of cup crystal in scroll form occurred at air temperature of -8°C. In the case of the experiments by Kobayashi (1957), scroll development occurred at air temperature of -6°C. These experimental results are in good agreement with air temperature conditions as mentioned above. On the other hand, cup crystal grew at air temperature in the range from -6°C to -10°C, but also -20°C, in the case of experiments by Nakaya. Similarly, sheath or cup crystals grew at air temperature in the range from -7°C to -10°C, and also at air temperature in the range lower than -22°C, in the case of experiments by Kobayashi. Therefore, it would be reasonable to consider that formation of cup crystal in the cold chamber occurred in the warmer temperature range in their experiments, and formation of cup crystals in Greenland and the Antarctic occurred in the cold temperature range.

**JSP04** **Wednesday, July 9 - Thursday, July 10**  
**ARCTIC ENVIRONMENT CHANGE (IAPSO, IAMAS, IAHS)**  
Location: Site A, Room 6

**Wednesday, July 9 AM**  
Presiding Chairs: M. Steele, M. Lange

**JSP04/09A/A06-001** **0900**  
**NORTH POLE ENVIRONMENTAL OBSERVATORY AND THE SEARCH PROGRAM**

James Howe MORISON<sup>1</sup>, James OVERLAND<sup>2</sup>, Toshi TAKAZAWA<sup>3</sup> (<sup>1</sup>Polar Science Center, Univ of Wash, <sup>2</sup>NOAA Pacific Marine Environmental Laboratory, <sup>3</sup>Japan Marine Science and Technology Center)

The Arctic has undergone a complex of significant, interrelated, atmospheric, oceanic, and terrestrial changes in recent decades. These changes are affecting every part of the Arctic environment and are having repercussions on society. There is evidence that these changes are connected with the positive trend in the strength of the circumpolar vortex as often characterized by the Arctic Oscillation (AO) index. It is unclear what feedback processes on climate or ecosystems may be involved in the recent changes, but modeling and retrospective studies indicate they could be characteristic of global warming. In any event, observations suggest that the impact at high latitudes is substantial. The North Pole Environmental Observatory (NPEO) is an international effort to maintain a distributed observatory centered on the North Pole. It includes annual establishment of an automated drifting station and deep ocean mooring as well as repeated hydrographic surveys. NPEO observations in this critical region have shown that the ocean and ice are to a large extent still in the changed condition characteristic of the 1990s. In many ways NPEO is an example of the measurement philosophy and approach that can be used to implement the Study of Environmental Arctic Change (SEARCH). SEARCH has been conceived as an interdisciplinary, interagency program with international ties and a core aim of understanding the complex of recent changes.

**JSP04/09A/A06-002** **0920**  
**ARCTIC-CHAMP: THE NSF PAN-ARCTIC COMMUNITY-WIDE HYDROLOGICAL ANALYSIS AND MONITORING PROGRAM**

Charles J. VOROSMARTY<sup>1</sup>, Larry HINZMAN<sup>2</sup> (<sup>1</sup>University of New Hampshire, <sup>2</sup>University of Alaska Fairbanks)

There is extensive and mounting evidence that the contemporary environment of the high north is changing and doing so over a broad, pan-Arctic domain. Water is central to the functioning of the climate, hydrology, heat balance, biology and biogeochemistry of the Arctic and is thus of critical importance to human society. Thus, Arctic environmental change must necessarily encompass changes to the hydrology of the region. Productivity, carbon balance, energy balance - in particular evapotranspiration - and hence runoff are all coupled closely and will be affected by the combined changes in temperature and precipitation. Over decadal time scales the stature and relative abundance of plants may be changing as well, producing new patterns of feedback to the climate system by altering regional-to-global scale energy and carbon balances. Increases in freshwater transport to the Arctic Ocean are now clearly documented and may at some point reduce the formation of North Atlantic Deep Water, resulting in a cooling in the North Atlantic region. These changes have enormous biogeophysical consequences that in turn make them critical to society and sound policy-making. The Arctic CHAMP is a new program supported by the National Science Foundation that seeks a better understanding of arctic hydrology and the natural linkages of hydrology with closely related atmospheric, terrestrial, and oceanic processes and cycles. A review of the status of this program and how it will contribute toward a better articulation of these important issues will be presented.

**JSP04/09A/A06-003** **0940**  
**AN INTEGRATED ASSESSMENT OF CLIMATE CHANGE IN THE BARENTS REGION**

Manfred A. LANGE (Institute for Geophysics, University of Muenster)

Global and climate changes will be amplified in the Arctic due to a number of complex feedback processes between marine-, terrestrial- and the climate system. Thus, assessing the impacts of such changes for nature and people in the circumpolar North attains a high priority. Because of the regional manifestation of climate changes and as a result of the inter-linkages between natural and societal systems, integrated regional impact studies (IRISs) have been identified as suitable tools to address this challenge. In the framework of an IRIS, two tasks become central: (i) an assessment of major impacts of climate change to key environmental and economic sectors and their various interlinkages and feedbacks and (ii) the development of an integrated assessment model (IAM). The first issue has been pursued within the Barents Sea Impact Study (BASIS), a former Priority Project of the International Arctic Science Committee which was funded by the European Commission (ENV4-CT97-0637). We considered marine and terrestrial ecosystems as well as the hydrological cycle and fishery, forestry and reindeer herding as important economic sectors. With regard to the Barents Sea, years with enhanced inflow of Atlantic water (so-called 'warm' years) result in a reduced sea ice cover, a 30% increase in primary production and an enhanced CO<sub>2</sub>-uptake by 8% relative to years with a reduced inflow of Atlantic waters ('cold years'). Findings related to terrestrial ecosystems indicate a significant diversity of responses patterns of individual species to climate change, similarly differentiated impacts on population dynamics of present

pests and invaders under varying climate conditions and slightly inconsistent climate signals for the last 100 years between the Kola Peninsula and rest of study region. Our results, while indicating a number of important consequences of climate change also demonstrate the importance of non-climatic drivers in the future development of the Barents Sea Region. In order to more thoroughly explore vulnerabilities of the region to climate change, a follow-on project has been funded by the EU and is currently being implemented (BALANCE; Global Change Vulnerabilities in the Barents Region: Linking Arctic Natural Resources, Climate Change and Economics; EVK2-CT2002-00169). A central goal of BALANCE is the development and application of an IAM, which consists of modules describing processes in marine and terrestrial ecosystems and their consequences for key economic sectors. The models are driven by results from a dedicated regional climate model for the Barents Region. The involvement of stakeholders in the project, similarly to BASIS, will be of considerable importance.

**JSP04/09A/A06-004** **1000**  
**VARIATIONS OF ATMOSPHERIC CONSTITUENTS AND THEIR CLIMATIC IMPACT IN THE ARCTIC**

Takashi YAMANOUCHI<sup>1</sup>, Makoto WADA<sup>1</sup>, OTHERS<sup>2</sup> (<sup>1</sup>National Institute of Polar research, <sup>2</sup>Alfred-Wegener Institute for Polar and Marine Research, Nagoya University, Tohoku University, Hokkaido University and NIPR)

The research project *Variations of atmospheric constituents and their climatic impact in the Arctic (1999-2004)* has been conducted to clarify the variation of greenhouse gases, aerosols, and clouds in the Arctic troposphere and stratosphere; to explain the transport and transformation processes, source and sink; to compare with the Antarctic and evaluate the radiative effect and then the climate impact. The following specific research has been carried out during the current year based on support by Norwegian Polar Institute. (1) Long term observations of greenhouse gases: At the Rabben observatory in Ny-Ålesund scientific station, Svalbard, we continued our long term air sampling for greenhouse gases, and continuous measurements of surface ozone and meteorology. Through these observations, and stable isotope analysis, we hoped to clarify the variation in concentrations of greenhouse gases and the causes of variability. We also planned to analyze data accumulated concerning exchange of carbon dioxide between ocean and atmosphere, and to continue relevant operations in collaboration with the oceanographic group (eg. EU project CONVECTION). (2) Aerosol and cloud observations: Measurements of aerosol number concentrations, optical depth, vertical distributions, composition and precursor gases; and observations of precipitable water, cloud liquid water, ice water amount and precipitated snow particles, have been continued at Ny-Ålesund to determine the relationship between aerosols, clouds and precipitation. Doppler radar observation at Bear Island is also coordinated. (3) ASTAR 2000 (Arctic Study of Tropospheric Aerosols and Radiation): In collaboration with the Alfred-Wegener Institute of Polar and Marine Research together with support by other institutions, coordinated airborne and ground-based observations of aerosols (Arctic haze) and radiation were carried out in the Svalbard area through March and April, 2000. A German aircraft Polar 4 (Dornier 228) was used to measure vertical distributions of aerosols and radiation, while remote sensing, sound observations and sampling were conducted on ground. Trajectory analysis was made using objective analysis data for the same period to estimate the transportation process and the relation to atmospheric circulation in the Arctic. In addition, SAGE-II satellite observations were compared, and the radiative forcing of aerosols over a wide area was evaluated by incorporating into an Arctic regional climate model (HIRHAM). (4) AAMP 98 and 02 (Arctic Airborne Measurement Program): Two similar campaigns of airborne observation using jet plane (Gulfstream-II) were carried out in March 1998 and 2002 with long range stratosphere flights over the Arctic Ocean and local profiling flights in the vicinity of Svalbard. Research objectives were to elucidate spatial distribution, long-range transport and transformation of greenhouse gases and aerosols, related to stratosphere-troposphere exchange and polar vortex; optical properties of aerosols and their radiative forcing; the structure of atmospheric disturbance, especially of polar low, and its microphysical process.

**JSP04/09A/A06-005** **1050**  
**DATA MANAGEMENT SUPPORT FOR NSF ARCTIC FIELD PROJECTS**

James A. MOORE, Greg STOSSMEISTER, Scot M. LOEHRER (Joint Office for Science Support, University Corporation for Atmospheric Research)

Access to and integration of multidisciplinary data from field projects in the Arctic Basin recently completed or underway is particularly critical to the timely and accurate understanding of the rapid changes that are now underway in the Arctic. The NSF Arctic System Science (ARCSS) Program is committed to facilitating data archival and provide easy mechanisms for data exchange among researchers interested in the Arctic system. JOSS offers some specific capabilities that address these two important ARCSS objectives. The University Corporation for Atmospheric Research (UCAR) Joint Office for Science Support (JOSS) has been involved in the data management support for a number of ARCSS field projects, both domestic and international, including the Surface Heat Budget of the Arctic Ocean (SHEBA), Arctic Transitions in Land, Atmosphere System (ATLAS), International Tundra Experiment (ITEX), Western Arctic Shelf Basin Interactions Project (SB) and Arctic Regional Climate Modeling Intercomparison Project (ARCMIP). JOSS also participates on committees to further improve the collection, archival and dissemination of all manner of Arctic datasets. JOSS has developed and maintains a state-of-the-art data archive and dissemination system that provides single source access to complete project datasets. Most data are accessible for browsing and orderable on-line with connectivity to distributed archives. If the project includes single or multi-year field phases, JOSS can provide a web-based, on-line field catalog or project web pages to support near real-time documentation of activities and selected data displays. This presentation will discuss data management strategies that have been successfully implemented in ARCSS projects, provide some examples of specific support to projects, including specialized products and datasets, and discuss some of what the future holds for data management support to ARCSS field research.

**JSP04/09A/A06-006** **1110**  
**ICE-DRIFTING BUOY OBSERVATIONS OVER THE ARCTIC MID OCEAN RIDGE**

Takashi KIKUCHI<sup>1</sup>, Hirokatsu UNO<sup>2</sup>, Kiyoshi HATAKEYAMA<sup>1</sup>, James H. MORISON<sup>3</sup> (<sup>1</sup>Japan Marine Science and Technology Center, <sup>2</sup>Polar Science Center, Applied Physics Laboratory, University of Washington)

We have been conducting temperature, salinity and ocean current observations by ice-drifting buoy, named J-CAD (JAMSTEC Compact Arctic Drifter), in the Arctic Ocean since 2000, in collaboration with North Pole Environmental Observatory (NPEO) Project. J-CAD 4, which was installed on the ice of the Amundsen Basin (88.5N, 76.9E) on April 26 2002, has crossed over the Arctic Mid Ocean Ridge to the Nansen Basin of the Arctic Ocean. J-CAD 4 is equipped with 6 CT/CTD sensors that measure water mass properties at the maximum depth of 250m and an ADCP measuring current data up to 120m. Observational results

show that water mass characteristics in the Amundsen Basin, over the Arctic Mid Ocean Ridge, and in the Nansen Basin are clearly different and the frontal structures exist on the either side of the Arctic Mid Ocean Ridge. Especially, surface salinity of the Arctic Mid Ocean Ridge is higher than that of the two Basins. In other words, there is a weak stratified structure over the Arctic Mid Ocean Ridge. Current data measured by ADCP indicates that there is a steady current with an averaged speed of 1.0-2.0 cm/s flowing toward the Atlantic Ocean along the Arctic Mid Ocean Ridge. This observational data mostly corresponds to the results from J-CAD 1 which was installed in April 2000 and drifted over the Arctic Mid Ocean Ridge. Moreover, the geostrophic velocities calculated from the CTD observation by Oden91 cruise (August to October, 1991) indicate a current with the speed of several cm/sec to the Atlantic Ocean along the Arctic Mid Ocean Ridge. Therefore, it is presumed that over the Arctic Mid Ocean Ridge, there is a weak, average current flowing toward the Atlantic Ocean along the bottom topography.

JSP04/09A/A06-007

1130

#### SENSITIVITY EXPERIMENTS OF SEA-ICE PROCESSES ON WORLD OCEAN CIRCULATION BY USING A GLOBAL COUPLED OCEAN AND SEA-ICE MODEL

Kenji KOMINE<sup>1</sup>, Tatsuo MOTOI<sup>2</sup>, Keiko TAKAHASHI<sup>1</sup>, Xiangdong ZHANG<sup>3</sup>, Nobumasa KOMORI<sup>1</sup>, Hirofumi SAKUMA<sup>1</sup>, Motoyoshi IKEDA<sup>4</sup>, Tetsuya SATO<sup>5</sup> (Earth Simulator Center, <sup>1</sup>Frontier Research System for Global Change, <sup>2</sup>International Arctic Research Center University of Alaska Fairbanks, <sup>3</sup>Graduate School of Environmental Earth Science Hokkaido University)

Recent dramatic change of the cryosphere including sea-ice is considered as a silent precursor of the effect of the global warming to be maximized in the polar region and the development of a reliable sea-ice model is one of the urgent issues for climate variability studies and the global warming assessment. As a branch project of the Earth Simulator initiative, we are collaborating with FRSGC to try to implement the IARC sea-ice model into our OGCM code optimized for the Earth Simulator. The basic design of the IARC sea-ice model is that of Hibler (1979) dynamics and Parkinson and Washington (1979) thermodynamics with some modifications in treating such physical processes as snow and open water as well as in coupling schemes and with a recent contribution on sea-ice and ocean interaction process by Zhang and Zhang (2001). As a first step towards such a goal, we have implemented the IARC model into the OFES (MOM3-based OGCM for the Earth Simulator). In this presentation, we will give a brief description of the current status of our coupled model development and will show some basic physical performances of our model manifested in a test validation of fifty years of time integration. In the validation, it takes five or six years for the sea-ice to reach a quasi-equilibrium state. Sea-ice distribution pattern and the seasonal cycle of thickness and concentration both in the Arctic and Antarctic Oceans turn out to be close to the observational ones. Sea-ice thickness piles up from the Beaufort Sea to the Canadian Archipelago and the northern coast of Greenland. We also performed experiments to explore sensitivity of sea-ice to some physical parameters like ice strength as an example and sensitivity to model resolution. The results show sea-ice motion and thickness changed subject to changes of these physical parameters and model resolution, which finally affect global temperature and salinity through sea-ice/ocean interactions in the polar regions.

JSP04/09A/A06-008

1150

#### SIMULATING SEASONAL CYCLES OF THE ICE-OCEAN SYSTEM IN THE PAN ARCTIC AND NORTH ATLANTIC OCEAN

Jia WANG, Meibing JIN, Moto IKEDA (IARC-FRSGC, University of Alaska Fairbanks)

A coupled ice-ocean model (CIOM) is configured for the pan Arctic and North Atlantic Ocean (PANAOC) with a 27.5km resolution. The model is driven by the monthly atmospheric climatology averaged from the 40-year NCEP reanalysis (1958-1997). The ocean model is the Princeton Ocean Model (POM), while the sea ice model is based on a full thermodynamic and dynamical model with plastic-viscous rheology. A sea ice model with multiple categories of sea ice thickness is utilized. We first focus on seasonal cycles of sea ice and ocean circulation. This model reasonably reproduces seasonal cycles of both the sea ice and the ocean. Climatological sea ice areas derived from historical data are used to validate the ice model performance. The simulated sea ice cover reaches a maximum of  $14 \times 10^6 \text{ km}^2$  in winter and a minimum of  $6.7 \times 10^6 \text{ km}^2$  in summer, which are close to the 95-year climatology with a maximum of  $13.3 \times 10^6 \text{ km}^2$  in winter and a minimum of  $7 \times 10^6 \text{ km}^2$  in summer. The simulated general circulation in the Arctic Ocean, the GIN seas, and northern North Atlantic Ocean are qualitatively consistent with historical mapping. We found that the winter low salinity or freshwater content in the Canada Basin tends to converge due to the strong anticyclonic atmospheric circulation that drives the anticyclonic ocean surface current, while summer low salinity or freshwater tends to spread inside the Arctic and exports out of the Arctic, due to the relaxing wind field. We also found that the warm, saline Atlantic Water intrudes farther into the Arctic in winter than summer due to prevailing winter wind stress over the northern North Atlantic that is controlled by the Icelandic Low. Seasonal cycles of temperature and salinity at several selected representative locations reveals regional features that characterize different water mass properties.

JSP04/09A/A06-009

1210

#### CIRCULATION AND VOLUMEN, ICE AND FRESHWATER TRANSPORTS OF BAFFIN BAY

C.L. TANG, E. DUNLAP, T. YAO (Bedford Institute of Oceanography)

Baffin Bay is connected to the Arctic Ocean through the Canadian Arctic Archipelago and to the Labrador Sea through Davis Strait. The variability of its mass and freshwater transports is closely related to oceanographic conditions in the Arctic Ocean and Labrador Sea. Freshening of the Arctic Ocean can promote ice growth in Baffin Bay, which may lead to a strong stratification and weak winter convection in the Labrador Sea and a weak thermohaline circulation in the North Atlantic. To investigate the role of Baffin Bay in Arctic-Atlantic interaction, a modelling study in conjunction with data analysis is carried out to quantify the circulation and transports of Baffin Bay. The model used is a coupled ice model and Princeton Ocean Model encompassing the entire Labrador Sea and Baffin Bay with open boundaries along  $42^\circ \text{ W}$ ,  $40^\circ \text{ N}$  and  $55^\circ \text{ W}$ . Volume transports are prescribed on the open boundaries and at three northern channels according to data and largescale models. Objectively analyzed high-resolution monthly temperature and salinity fields are used to initialize the model. The model results show that the circulation of Baffin Bay is cyclonic. A branch of the Western Greenland Current flows into the bay through the eastern side of Davis Strait. This northward current spreads over the eastern shelf and converges at the shelf edge at  $75^\circ \text{ N}$ . In the western part of Baffin Bay, the water flows in the southeast direction parallel to the coast except an excursion into Lancaster Sound. The strongest current occurs over the shelf edge between  $70^\circ \text{ N}$  and  $72^\circ \text{ N}$ . The model currents are compared to current meter measurements across Davis Strait and at several sites around the shelf edge taken by C. Ross. There is a general agreement between the model and the data. The current meter data show bottom intensification at the western shelf edge, which is reproduced in the model. The net volume transport through Davis Strait from the model is

2.2 Sv, which compares favourably with the transport calculated from the current meter data, 2.5 Sv. The estimated freshwater and ice transports through Davis Strait based on available data are  $3120 \text{ km}^3 \text{ yr}^{-1}$  and  $870 \text{ km}^3 \text{ yr}^{-1}$ , respectively. Sensitivity of the model transports to boundary conditions and meteorological forcing is discussed.

Wednesday, July 9 PM

Presiding Chairs: J. Wang, M. Ikeda

JSP04/09P/A06-001

1400

#### A COUPLED SEA ICE-OCEAN MODEL OF BAFFIN BAY AND THE NORTH WATER POLYNYA

Todd E. ARBETTER<sup>1</sup>, Lawrence A. MYSAK<sup>2</sup>, Blandine L'HEVEDER<sup>3</sup> (<sup>1</sup>Cooperative Institute for Research in Environmental Sciences, University of Colorado, <sup>2</sup>Department of Atmospheric and Oceanic Sciences, McGill University, <sup>3</sup>Rennes, France)

The North Water polynya, located in Smith Sound in the northern reaches of Baffin Bay, represents a geophysically interesting area of the Arctic. Despite its high latitude, the polynya is characterized by very thin or absent ice cover throughout winter and spring. Recent field work has greatly increased the amount of information available in the northern Baffin Bay region, but the oceanic processes associated with the polynya are not fully understood. The physical setting of the Baffin Bay region is not well-reproduced in typical general circulation climate models, which have too few grid points to accurately resolve the region. Here, we present a regional coupled ice-ocean model (with granular sea ice rheology) which is specifically developed to model the Baffin Bay region and the North Water polynya. An initial series of sensitivity tests examines the effects of lateral ocean boundary conditions; it is found that the manner in which they are applied has dramatic effects on the solution over the entire model domain, particularly on the simulated stratification of ocean salinity. We believe that active restoring of salinity and potential temperature along the lateral open ocean boundaries provides the most realistic simulation; however, there remain other issues such as surface (atmospheric) forcing which need to be explored.

JSP04/09P/A06-002

1415

#### ANNUAL VARIATION OF SEA-ICE DRAFT DISTRIBUTION AT THE NORTH POLE ENVIRONMENTAL OBSERVATORY

Richard E. MORITZ, Rebecca WOODGATE, Knut AAGAARD, Jamie MORISON (Polar Science Center, University of Washington)

A time series of sea-ice draft  $D(t)$  was estimated from measurements made by an Upward Looking Sonar (ULS) from 10 April, 2001 to 21 April, 2002. Themoooring was located at the North Pole Environmental Observatory (NPEO), Latitude  $89.56 \text{ N}$ , Longitude  $66.65 \text{ E}$ . Sample statistics and probability density distributions (PDFs) of  $D(t)$  have been estimated by grouping the data in nonoverlapping, two-week intervals with equal weight given to each observation. The sample mean draft varied from 3.7 meters in early April to 2.3 meters in late August, with an overall annual mean of 3.0 meters. The sample mean draft estimated for 15 September, 2001 is 2.3 meters, a value near the middle of the seasonally adjusted estimates derived from submarine sonar profiles near the North Pole in the 1990's (Rothrock, et al., GRL, 26, 1999, 3469-3472). The modal draft of the sample PDF lags behind the sample mean, with extrema of 2.3 meters in late June, 2001 and 1.6 meters in early January, 2002. The open water fraction (OWF) is defined by integrating the sample PDFs over ice drafts less than .05 meters. OWF exceeded 1 percent from mid-June to early October, and for a brief period in late December. The maximum OWF of 13 percent occurred in mid-July. The evolution of the ice draft PDF on time scales of a few days to one year is discussed with reference to physical processes and to the problem of estimating trends in the climatology of  $D$ .

JSP04/09P/A06-003

1430

#### BASAL HEAT FLUX NEAR THE NORTH POLE DURING THE SUMMER OF 2002

Miles G. MCPHEE<sup>1</sup>, Takashi KIKUCHI<sup>2</sup>, James H. MORISON<sup>3</sup>, Timothy STANTON<sup>4</sup> (<sup>1</sup>McPhee Research Inc., <sup>2</sup>Japan Marine Science and Technology Center, <sup>3</sup>Polar Science Center, University of Washington, <sup>4</sup>U.S. naval Postgraduate School)

Basal heat flux is a major factor in the heat and mass balance of Arctic sea ice. In summer, insolation through open leads, thin ice, and melt ponds is sufficient to heat the mixed layer to well above freezing, despite continual loss of heat at the interface as ice melts. We use data from the North Pole Environmental Buoy Project to estimate basal heat flux during 2002 in a region bounded by  $83\text{--}86 \text{ deg N}$  latitude and  $17\text{--}34 \text{ deg E}$  longitude. Ocean-to-ice heat flux is parameterized as proportional to the product of interface friction velocity (square root of kinematic stress) and the elevation of mixed layer temperature above freezing. Reliable values for the heat and momentum exchange coefficients have been derived from several manned drift stations, most notably the SHEBA drift in 1997-98. Our results are compared with data from two previous manned drift projects: AIDJEX (1975) and SHEBA (1998). We find a surprisingly uniform temporal distribution of mixed layer temperature elevations during summer, despite wide geographic distribution (latitude) in the Arctic, and very different mixed layer salinities. We review the methods used for estimating heat flux, then estimate total basal heat transfer and the amount of solar radiation entering the mixed layer during summer.

JSP04/09P/A06-004

1445

#### DENSE WATER TRANSPORT ON BOTTOM SLOPE IN HIGH LATITUDE

Jun TAKAHASHI, Jia WANG, Motoyoshi IKEDA (Frontier Research System for Global Change)

Oceanographic observations have revealed importance of dense water formation and its spreading in the Arctic shelf and slope. The dense water is believed as one of the source of cold halocline, and is thought to be carried from coastal region toward basin through mainly bottom boundary layer. Bottom boundary plays an important role in ocean circulation. Bottom boundary layer carries dense water to one's neutral depth on formation process of intermediate and deep water. Fine grid interval is needed to simulate bottom boundary layer, but now computational resources are not sufficient to simulate bottom boundary layer exactly, especially in global ocean circulation experiment with coarse grid. Several bottom boundary layer models therefore have been developed. But transport by bottom boundary layer is not simulated well as observed, and tends to underestimate the transport. It is important to improve bottom boundary layer model with coarse grid. So we carry out sensitivity experiments with bottom boundary layer model on its parameterization, especially on bottom friction and height of bottom boundary layer. Numerical experiments of descending of dense water with and without bottom boundary layer is done. The primitive equation model with z-coordinate (MOM) is used for rectangular idealized model ocean. The model ocean assumes the shelf region in the Arctic Ocean, with zonal lateral boundary condition

## INTER-ASSOCIATION

being cyclic. Bottom is inclined meridionally as northern side is deeper. Forcing of surface salt flux is added from southern boundary to  $y=30$  km. The forcing assumes brine rejection in coastal polynya in the Arctic. The flux gradually decreases from  $y=30$  km, and becomes zero at 50 km, and is homogeneous zonally. Only salt flux is used, and surface wind and heat flux are not used. Bottom boundary layer following Gnanadesikan's model is used. The layer depth is constant. Numerical experiments with coarse grid are carried out to simulate descending of the dense water. The surface salt flux makes surface water denser at southern boundary. The water descends to bottom, and starts to flow along bottom slope. In case of experiments without bottom boundary layer model, dense water flows almost along coast. On the other hand, in case of experiments with bottom boundary layer model, dense water starts to descend toward ocean basin, and descending of dense water on inclined bottom is reproduced. Transport of dense water of coarse grid experiment is well simulated even in case of coarse grid experiment.

**JSP04/09P/A06-005** **1500**

### DEVELOPMENT OF A QUADRILATERAL SPECTRAL/HP ELEMENT OCEAN MODEL

Hideaki KITAUCHI (Frontier Research System for Global Change)

An accurate and fast, vertical two-dimensional non-hydrostatic ocean model is being developed by using a quadrilateral spectral/hp element method. In this approach a computational domain is partitioned into quadrilateral elements like a finite element method; within each of these elements every dependent variable is approximated as a truncated polynomial expansion like a spectral method. The Galerkin formulation is employed to derive a set of semi-discrete, ordinary differential equations for the expansion coefficients of the dependent variable in each element. Temporal integration is performed by the use of the second-order explicit-implicit stiffly stable scheme; the diffusion term is treated implicitly; the others explicitly. A system of the obtained discrete equations is solved numerically under continuity conditions on the variable between the adjoining elements, appropriate boundary and initial conditions. The advantage in the spectral/hp element method is to achieve a high numerical accuracy in a complex geometry. We will present a progress report on the quadrilateral spectral/hp element ocean model.

**JSP04/09P/A06-006** **1545**

### EVALUATION OF BE AS A TRACER OF RIVER WATER IN ARCTIC FAST ICE ZONE, CHUKCHI AND BEAUFORT SEAS

Noriyuki TANAKA<sup>1</sup>, Hisashi NARITA<sup>2</sup> (IARC, UAF, FORSG, <sup>3</sup>GRADUATE SCHOOL OF ENV. EARTH SCI. HOKKAIDO UNIV.)

Ba concentration in Arctic seawater has been recommended to use as a chemical tracer to identify river water influences in fresh water burden in Arctic surface water, especially for American river waters with significantly high Ba contents. Since Ba is biologically active elements in the ocean, biogeochemical effects on the Ba concentration should be closely examined for its more quantitative use in the Arctic Ocean. In 2000 and 2002, surface water samples have been collected during cruises of R/V "MIRAI" Arctic expeditions in northern Bering Sea shelf, Chukchi and Beaufort Seas in late summer. Stable isotope composition, silicate and Ba concentration of collected seawater were analyzed. Assuming that summer surface water consists of three water components; upper halocline water, sea ice meltwater and river water, fractions of those components of each water sample are estimated based on stable isotope composition and salinity. Applying typical silicate and Ba concentrations of McKenzie river and upper halocline water, preformed silicate and Ba concentrations for each sample are estimated. Preformed concentration is defined by the concentration, which is determined only by physical mixing of water masses. By subtracting observed values from the preformed values, we could obtain how much portions of silicate and Ba have been removed from the surface water presumably by biological uptake. The results show 1) up to 100% of silicate removal, 2) about 50% of removal of Ba and 3) The constant removal ratios of Ba/Si about 1.04 to 1.17 (95% of confidence level) but slight large pronounced sea ice melt water, which may imply abiological removal of Ba associated with sea ice. Constancy of the removal ratios give us warrant for further investigation to improve trace ability of Ba as American river water sources.

**JSP04/09P/A06-007** **1600**

### CHARACTERIZATION OF CHROMOPHORIC DISSOLVED ORGANIC MATTER IN THE BEAUFORT SEA: IMPLICATIONS FOR RIVER WATER INFLUENCE

Celine GUEGUEN, Laodong GUO, Noriyuki TANAKA (IARC/Frontier, University of Alaska Fairbanks)

Arctic climate and environmental changes may have a profound impact not only on the global heat budget and ocean circulation but also on biogeochemical cycles of organic carbon. Dissolved organic matter (DOM) is an important component in global carbon budgets. A fraction of the DOM pool, which absorbs visible and near-ultra-violet radiation, is referred to chromophoric DOM (CDOM). It is proposed that CDOM can be used as a potential tracer in oceanic water mixing, especially in the Arctic Ocean where there is a large share of global river discharge and higher concentration of terrigenous DOM. During September-October 2002, seawater samples were collected from the Beaufort Sea onboard the R/V Mirai and characterized for their optical properties and dissolved organic carbon (DOC) concentrations. The terrestrial CDOM was characterized by a higher emission maximum than its marine counterpart, with a difference as large as 50 nm. Higher concentrations of DOC and abundance of CDOM were related to inputs from the Mackenzie River. In general, the fluorescence intensity was correlated to the DOC concentration, suggesting a possible high resolution DOC measurement using optical properties. In addition, fluorescence intensity decreased with increasing salinity from the Mackenzie River plume to the Beaufort Sea and increased from the west channel to the east channel. Freshwater inflow from the Mackenzie River to the Beaufort Sea was found mostly through the east channel during our sampling season, consistent with results derived from other hydrographic data.

**JSP04/09P/A06-008** **1615**

### DETECTION OF THE CARBON DIOXIDE FLUX IN THE AIR-SEA ICE-WATER SYSTEM: THE AMERASIAN ARCTIC

Igor P. SEMILETOV, Alexander P. MAKSHAS, Edgar ANDREAS (CRREL) (International Arctic Research Center/University Alaska Fairbanks)

Atmospheric carbon dioxide levels monitored in Barrow, Alaska, show the largest winter-to-summer variations in the world as well the highest levels of concentration (www.noaa.gov). Measurements along the coast of the Arctic Ocean show that the concentration of carbon dioxide has increased substantially over the past several decades, that tends to coincide with the general shrinking of the sea ice cover in the Arctic Ocean. To our knowledge, over the last decade, most Arctic CO<sub>2</sub> research has been focused on terrestrial ecosystems

(Laurila et al., 2001; Oechel et al., 2002, 1998), whereas the Arctic Ocean had been generally ignored in the global CO<sub>2</sub> budget (Anderson et al., 1999). During the last five years, only a few expeditions have performed studies of carbonate chemistry in the free-ice Arctic seas. The role of CO<sub>2</sub> transport across the sea ice in the regional carbon budget has not been evaluated because of the lack of experimental data, except for the pioneering measurements of Gosink et al. (1976) and Kelly and Gosink (1979) in the 1960-70s. They found that numerous tiny brine channels cross the young sea ice allow gases to penetrate through the ice. During the summer, the sea ice and underlying water and numerous leads can be a sink for atmospheric CO<sub>2</sub> because of photosynthesis, especially in the coastal zone and over the shelf, whereas in winter the sea ice can become a source (Kelley and Gosink, 1988) for atmospheric CO<sub>2</sub>. In this report, we present results of the first measurements of CO<sub>2</sub> fluxes above and through fast sea ice. We made these measurements in the coastal zone near the Barrow over the Chukchi Sea in June 2002. Our technique was eddy-correlation using a LI-COR 7500 open-path CO<sub>2</sub>/H<sub>2</sub>O analyzer and a three-axis sonic anemometer/thermometer installed on a tower 3.8 m high. Additionally, to evaluate the CO<sub>2</sub> concentration and to obtain rough estimates of CO<sub>2</sub> fluxes through different types of ice cover (melt ponds, dry snow, bare ice), we used a chamber technique and a closed cell LI-COR 820 gas analyzer. We used the static headspace technique for measuring CO<sub>2</sub> partial pressure (pCO<sub>2</sub>) in ice brine and in sub-ice water samples taken just beneath the ice and at depths below the sharp shallow halocline just beneath the sea ice bottom. We found that the magnitude of the CO<sub>2</sub> flux (generally directed from air to the sea ice) is typically 0.01-0.02 mg m<sup>-2</sup> s. This is close to values measured in late June by Oechel et al. (1998) over tundra on the North Slope of Alaska. Our preliminary results demonstrate that the ice-covered Arctic ocean cannot be ignored in the regional carbon budget of the Arctic. Additional research is required, however.

**JSP04/09P/A06-009** **1700**

### DISSOLVED AND PARTICULATE ORGANIC MATTER IN THE SOUTHEASTERN BERING SEA SHELF

Laodong GUO<sup>1</sup>, Tomoyuki TANAKA<sup>1</sup>, Deli WANG<sup>1</sup>, Noriyuki TANAKA<sup>1</sup>, Akihiko MURATA<sup>2</sup> (International Arctic Research Center, University of Alaska Fairbanks, <sup>3</sup>Japan Marine Science and Technology Center, Yokohama, 237-0064, Japan)

The Arctic region has witnessed dramatic environmental and climate changes. How these changes alter the biogeochemical cycling of organic matter in the Arctic region is still poorly understood. Seawater samples were collected along a transect at ~166°W across the continental shelf in the southeastern Bering Sea during September 2001 onboard the R/V Mirai, and measured for dissolved (DOC), colloidal (COC) and particulate organic carbon (POC), dissolved organic nitrogen (DON), and particulate nitrogen (PN), as well as stable isotopic composition (δ<sup>13</sup>C and δ<sup>15</sup>N) of suspended particulate organic matter. The phase partitioning of organic carbon between dissolved (<1 kDa), colloidal (1 kDa-0.7 μm) and particulate (>0.7 μm) phases was examined based on filtration and ultrafiltration. Concentrations of DOC ranged from 61 to 92 μM (averaging 76±9 μM) with a decreasing trend from the south (outer shelf) to the north (inner shelf) along the 166°W, and were negatively correlated with salinity. DON concentrations varied from ~5 to 10 μM, with a more dynamic distribution feature. On average, POC comprised 14±6% of the total organic carbon pool in the water column, and colloidal organic carbon (COC) made up of 36±8% of the TOC, leaving 50±5% of the TOC present in the <1 kDa dissolved phase. Suspended particulate organic matter seems mostly marine in origin, with an average C/N ratio of 7.4±1.1 and a significant correlation between POC and chlorophyll-a concentrations in the water column. Values of stable isotopes in the suspended particles varied from 2.86 to 9.98 per mil (with an average of 6.01±1.92 per mil) for δ<sup>15</sup>N and from -27.17 to -23.41 per mil (averaging -24.57±0.91 per mil) for δ<sup>13</sup>C. Interestingly, particulate δ<sup>15</sup>N values were negatively correlated with NO<sub>3</sub> at lower NO<sub>3</sub> concentrations (<5 μM) but positively correlated with NO<sub>3</sub> when NO<sub>3</sub> concentrations were higher (>5 μM), indicating distinct isotopic fractionation mechanisms under different nutrient regimes.

**JSP04/09P/A06-010** **1715**

### ICE ALGAE PRODUCTION PROCESSES IN THE COASTAL FAST ICE IN THE WESTERN ARCTIC OCEAN

Kyung-Hoon SHIN<sup>1</sup>, Noriyuki TANAKA<sup>1</sup>, Tomoyuki TANAKA<sup>1</sup>, Terry WHITLEDGE<sup>2</sup> (Frontier Observational Research System for Global Change / International Arctic Research Center, Univ. of Alaska Fairbanks, <sup>3</sup>Institute of Marine Science, University of Alaska Fairbanks)

To investigate ice algae production processes and its related carbon flux, is important and urgent research subject in the Arctic Ocean. Because there is very little understanding regarding to the effect of recent Arctic climate changes on the sea-ice algae production and its contribution to the ecosystem and carbon cycle in the Arctic Ocean. During the last two spring seasons in 2001-2002, time series sea-ice observations and in situ ice algae incubation experiments were conducted off Pt Barrow in the northern Alaska. There are three objectives in this study as follows: 1) to clarify ice algal production processes in the coastal fast ice, 2) to evaluate ice algal contribution to carbon cycle in the Arctic, 3) to provide the data for the Arctic biogeochemical model related to climate change. Chl. a and POC concentrations were extremely high in the bottom layer of sea-ice with the development of brown coloration depending on light availability. The Chl. a concentration in the bottom ice algal layer (bottom 10 cm) was the highest in early May in 2001-2002, showing the large annual variation which might be attributed to the development of ice thickness. The stable isotope ratio (δ<sup>13</sup>C) of POC indicates that terrestrial organic matter may be the main source of POC in the entire ice core except bottom 10cm, exhibiting comparatively lighter isotopic values. The δ<sup>13</sup>C ratios of POC were heavier in the bottom 10 cm (reflecting ice algal origin) in June. POC production rate was larger in May rather than in June 2001, indicating faster POC turnover rate in May. In particular, particulate fatty acids turnover rate was remarkably faster, resulting from their large production and consumption rates. Additionally, as an indicator for ecophysiological state of marine diatoms population, C16-PUFA index (a measure of the percentage of C16 fatty acids that are polyunsaturated) suggests ice algae population was in a nutrient-limited condition. Comparing Chl. a concentrations in the bottom 10cm of ice algal biomass between 2001 and 2002, Chl. a concentration on April 3, 2002 was approximately 2 fold higher than on April 5, 2001, and the maximum Chl. a concentration was around 2 fold larger on May 1, 2002 than on May 5, 2001. This observational result reveals that ice algal biomass have a large annual variation between 2001 and 2002. However, the variability of ice algal biomass may be affected by the environmental conditions such as ice thickness, cloudiness and nutrients supply and physical events. Therefore, more thorough investigation should be necessary to understand the ice algal biomass variability.

**JSP04/09P/A06-011** **1730**

### ONE-DIMENSIONAL BIOGEOCHEMICAL MODEL FOR THE SOUTHEASTERN BERING SEA

Clara Jodwalis DEAL<sup>1</sup>, Meibing JIN<sup>2</sup>, Jia WANG<sup>3</sup>, Zhenwen WAN<sup>4</sup>, Noriyuki TANAKA<sup>1</sup> (Frontier Observational Research System for Global Change/International Arctic Research Center, University

of Alaska Fairbanks, <sup>2</sup>Institute of Marine Sciences, University of Alaska Fairbanks, USA, <sup>3</sup>Frontier Research System for Global Change/International Arctic Research Center, University of Alaska Fairbanks, USA, <sup>4</sup>Marine Biological Laboratories, Woods Hole, Massachusetts, USA)

To improve our understanding of how physical factors (such as retreating sea ice and local climate change) and biogeochemical changes (such as nutrient concentrations) may influence phytoplankton and zooplankton dynamics and thus dimethylsulfide (DMS) dynamics in the Bering Sea, we are developing a physical-ecosystem model (PhECoM). As a first step in this modeling process, we have developed a one-dimensional physical model coupled with a one-dimensional biogeochemical model that is nitrogen-based (i.e. all biomasses and uptakes are converted into units of nitrogen concentration). This model may provide insights into how environmental changes affect the initiation and maintenance of the coccolithophore bloom in the Bering Shelf. The first recorded bloom of the coccolithophore [*Emiliania huxleyi*] in the Bering Sea was coincident with unusual climatic conditions in 1997 and 1998. Two types of phytoplankton (diatoms and flagellates), three nutrients (nitrate + nitrite, ammonium, and silicon), three size-classes of zooplankton, detritus and DMS are included in the model. The model is driven by meteorological data: wind velocity, air temperature, sea surface temperature, specific humidity, cloud cover and light. A unique combination of convective, mechanical and turbulent mixing parameterizations, and high vertical resolution allow more realistic interactions of biological processes in the model. Simulations for the southeastern Bering Sea middle-shelf domain in relatively high and low sea surface temperature years, 2000 and 1999 respectively, have been performed. Sensitivity analysis results will be used to help select parameter values for the upcoming three-dimensional version of the model, which will include sea ice and may have applications elsewhere in the Arctic.

JSP04/09P/A06-012

1745

#### LATEST ESTIMATION OF PRIMARY PRODUCTIVITY IN THE ARCTIC OCEAN UNDER THE CONSIDERATIONS OF SEA-ICE CONDITIONS AND ITS YEAR TO YEAR CHANGE

Tohru IKEYA, Masayuki Mac TAKAHASHI (Graduate School of Arts & Sciences, The University of Tokyo)

The reported values of primary productivity in the Arctic Ocean thus far indicates that spatial and seasonal change is large due to latitudinal variations of seasonal changes of solar irradiance, distribution of sea ice and stability of water column, in addition to the spatial structure of sea ice itself. However, the estimations of primary productivity in water column and sea ice in the Arctic Ocean have been made for algal habitats independently categorized into coastal and offshore water, and seasonal and multi-year ice (cf. Legendre *et al.* 1992). The primary production at ice concentration higher than 50% is offset in the satellite radiometer data for the global primary production (Antoine *et al.* 1996). However, the recent confirmation of statistically significant decreasing trend of annual means of the entire arctic sea ice at a rate of 2.7% per decade by satellite observation (Parkinson and Cavalieri 2002) urges establishment of the methodology to estimate primary productivity in the Arctic Ocean in relation to the possible influence of the recent changes of sea ice extent. The estimation of primary productivity not only in the sea ice but in the water column should be made under the dynamic changes of sea ice extent. Thus, in the present study, the examination of geographical structure of the primary production in the Arctic Ocean was based on the latitudinal distributions of multi-year and seasonal ice instead of conventional categories of coastal and offshore water. For the estimation of annual productivity, growing period was assumed to be 120 in seasonal ice regions north of 65°N and 90 in multi-year ice regions most of which locate at higher latitudes north of 70°N. The estimation was made using the values reported by Gosselin *et al.* (1997) who measured algal production in the water column and sea ice in multi-year and seasonal ice regions along a transect across the central Arctic Ocean. The estimated annual production in the water column plus sea ice in multi-year regions was 5.9 g C m<sup>-2</sup> y<sup>-1</sup> and lower than the previous estimation. Nevertheless, the annual total primary production in the Arctic Ocean was estimated to be 0.79 Gt C y<sup>-1</sup> and nearly three times higher than the previous value. The high value was due to previously unmeasured contribution of dissolved organic carbon release which amounts to around 30% of particulate production and the high productivity in water column in seasonal ice regions (90 g C m<sup>-2</sup> y<sup>-1</sup>). The primary productivity within sea ice was 1.3 and 9.1 g C m<sup>-2</sup> y<sup>-1</sup> in multi-year ice and seasonal ice regions, respectively, and the total annual production within sea ice was 9% of the total primary production in the Arctic Ocean. The primary productivity in seasonal ice regions was around 1.6 times as high as that in open water regions and suggests that potentially high productivity occurs around these regions.

JSP04a-Posters

Wednesday, July 9

#### ARCTIC ENVIRONMENT CHANGE (IAPSO, IAMAS, IAHS)

Location: Site D

Wednesday, July 9 PM

JSP04a/09P/D-001

Poster

1400-094

#### TRENDS IN PHYTOPLANKTON AND NUTRIENTS OF LAKE BAIKAL DUE TO GLOBAL WARMING

Mikhail N. SHIMARAEV, Sergei V. SEMOVSKI, Valentina N. DOMYSHEVA, Olga I. BELYH (Limnological Institute SB RAS, P.O.Box 4199, Irkutsk, 664033, Russia)

Changes in global climate are reflected in high latitude ecosystems, which are critically sensitive to temperature variations, season duration *et al.* Ecosystems of northern lakes are good indicators of climate variations due to low anthropogenic impact. Global warming as a result of human activity can threaten the ecosystems of ancient lakes that require conditions to be within narrow ranges. Lake Baikal – the deepest and the most voluminous lake in the World is a natural laboratory for climate change studies because of the long history of its studies (more than 150 years), still stable industrial activity in its basin and peculiar hydrological conditions preventing endemic biota from exchange with surrounding ecosystems. Baikal's ecosystem formation was a long evolutionary development with a stable low temperature regime. Under such specific conditions this ecosystem evolved with 2500 species, 80% of which are endemics, narrowly adapted to the special environmental conditions. Therefore, it is a very important to investigate the possible change in structure of the hydrobiotic populations, which would occur from any changes in the Baikal temperature regime. During last decade of 20<sup>th</sup> century factors of global warming have been reflected in such regional indicators as local air temperature, date of complete freezing and break-up. In the same period significant decreasing of some nutrients in the whole water column was noted using regular field measurements. For instance, dissolved silicon is assimilated by diatoms mainly during under-ice spring bloom. In condition of relatively stable silicon influx from tributaries, silicon vertical structure is strongly correlated with biological activity and processes of vertical mixing. Inverse box model of silicon dynamics have been used to

estimate intensity of its assimilation by diatoms, rate of vertical turbulent mixing and rate of occasional events of deep penetrative convection, which is able to transport surface waters to the deepest layers of the Lake Baikal. During 90° dissolved silicon concentration in the Baikal water column demonstrates significant decreasing. Picoplankton, green-blue of *Synechococcus* and *Synechococcus* taxa, is one of the main primary producers of Lake Baikal. Regular observations of picoplankton using electronic microscopy show increasing trend in its annual biomass. Numerical bio-optical model of two-component phytoplankton community dynamics in the pelagic ecosystem of the Lake Baikal can serve as a tool to study, in which way climatic factors control productivity of water ecosystem. It is shown that the main factor leading to changes in productivity and therefore to nutrient concentration maybe changes in warm season duration and influence of changes in the temperature is not so significant.

JSP04a/09P/D-002

Poster

1400-095

#### INTERANNUAL VARIATIONS OF CO<sub>2</sub>, CH<sub>4</sub> AND N<sub>2</sub>O FLUXES IN BOREAL FOREST SOILS SINCE FROSTFIRE BURNING EXPERIMENT, CENTRAL ALASKA

Yongwon KIM, Noriyuki TANAKA (INTERNATIONAL ARCTIC RESEARCH CENTER /UNIVERSITY OF ALASKA FAIRBANKS)

Flux measurements at black spruce stand soils from an area of Long-Term Ecological Research (LTER) interior Alaska during the growing seasons of 1998 to 2002 are used to estimate the fluxes of CO<sub>2</sub>, CH<sub>4</sub>, and N<sub>2</sub>O since 1998. The fluxes of CO<sub>2</sub> and N<sub>2</sub>O measured in burned black spruce stand showed the increasing tendency with time after the fire, suggesting that the burned forest soils enhance the microbial activity and the soil temperature. Relationships between the fluxes of CO<sub>2</sub> and N<sub>2</sub>O and the soil temperature before and after the fire showed good exponential correlations, indicating that soil temperature was one of the factors determining the fluxes of CO<sub>2</sub> and N<sub>2</sub>O in burned boreal forest soils. However, CH<sub>4</sub> flux did not depend on the temperature throughout the observation period. Q<sub>10</sub> values between the fluxes of CO<sub>2</sub>, CH<sub>4</sub>, and N<sub>2</sub>O and the temperature at 5 cm below the surface were 2.84±0.22, 1.09±0.02, and 3.32±0.26 for light chamber and 2.79±0.31, 2.28±0.12, and 2.38±0.18 for dark chamber in unburned soils, respectively. Q<sub>10</sub> values in burned soils since 1998 between the fluxes of CO<sub>2</sub>, CH<sub>4</sub>, and N<sub>2</sub>O and the temperature at 5 cm were 2.75±0.25, 3.27±0.28, and 2.96±0.18 for light chamber and 1.79±0.34, 2.86±0.19, and 3.90±0.19 for dark chamber, respectively. Therefore, the higher soil temperature after the fire may be led to the enhanced diffusion of CO<sub>2</sub> and N<sub>2</sub>O by microbial activity between the atmosphere and the forest soils, and to the enhanced flux of trace gases in burned black spruce stand soils. Average net respiration rates by aboveground vegetations in soil surface correspond to 56% and 38% of total soil respiration rate in unburned and burned black spruce soils, respectively. This demonstrates that net respiration by the vegetations (mainly moss and lichen) was one of the sources of atmospheric CO<sub>2</sub> in boreal forests.

JSP04a/09P/D-003

Poster

1400-096

#### ORIGIN AND CONTENT OF METHANE IN SIBERIAN PERMAFROST DEPOSITS

Anatoli BROUCHKOV, Masami FUKUDA (Research Center for North Eurasia and North Pacific Regions of Hokkaido University)

Methane contribution to greenhouse effect and global warming is considerable; permafrost will be melting due to increased temperatures, however, its distribution in permafrost is almost unknown. Frozen alluvial deposits and ice complex were studied for methane and carbon dioxide content from the depths of up to 5 m and more in Eastern Siberia. Methane concentration of pore air is high, up to 60000 ppmv, though ice inclusions do not contain as much methane as frozen soils. Average methane content in permafrost could be estimated minimally as 0.05–10 ml/kg. The anti-proportional relationship between values of concentration of methane and carbon dioxide performed in permafrost indicates possible occurrence of methane oxidizing process in deposits. On the whole, methane and carbon dioxide content in frozen soils rise in accordance to water content increase. Type of landscape determinates methane distribution in upper permafrost. It was found that thermokarst depressions contain less concentration of methane than undisturbed areas; thus, the older the permafrost the more methane it contains. Established relationship between volumetric air content and both values of methane and carbon dioxide concentration in permafrost also suggests thawing-freezing history. Based on published data and the research an estimation of additional emission of methane from permafrost areas was made. It shows that a considerable additional emission of methane could be expected in case of permafrost melting of 0.5 m depth, but probably not as a release of trapped gas, and an additional producing in the active layer. Microorganisms might be also responsible for microbial methane formation in permafrost. Long-term soil incubation experiments in flasks have shown a slow production of methane in different frozen soils at -5°C. Effect of decrease of methane concentration in the pore air during freezing was established. Colonies of microorganisms survived the incubation lasting more than 1 year at -8°C were found.

JSP04a/09P/D-004

Poster

1400-097

#### MASS, HEAT AND SALT BALANCES IN THE EASTERN BARENTS SEA OBTAINED BY INVERSION OF A HYDROGRAPHIC SECTION

Gleb PANTELEEV<sup>1</sup>, Motoyoshi IKEDA<sup>1</sup>, Dmitri NECHAEV<sup>2</sup>, Max YAREMCHUK<sup>3</sup> (<sup>1</sup>Frontier Research System for Global Change, <sup>2</sup>University of Southern Mississippi, USA, <sup>3</sup>International Pacific Research Center, University of Hawaii, USA)

Standard hydrological section data, collected in the eastern Barents Sea in September of 1997, have been analyzed using the variational data assimilation technique. This method enables us to obtain the temperature, salinity and velocity fields which are balanced within the framework of steady state dynamical constraints under the assumption of large scale geostrophic circulation. Errorbars which are statistically and dynamically consistent with the optimized fields are obtained by explicit inversion of the Hessian matrix. The optimized velocity field is in agreement with independent velocity measurements from surface drifter trajectories in the southwestern part of the Barents Sea. Optimized fields provide the following estimates of integral circulation features: 1. The North Cape current transport is 2.12±0.25 Sv; 2. The Karskie Vorota Strait throughflow is 0.7±0.06 Sv; 3. Heat flux with Atlantic water is 4.7±0.16 10<sup>11</sup> W; 4. Salt import from the Atlantic ocean is 7.41±0.46 10<sup>9</sup> kg/s.

JSP04a/09P/D-005

Poster

1400-098

#### RELATIONSHIP BETWEEN SIBERIAN SPRING SURFACE AIR TEMPERATURE AND SUMMER ATMOSPHERIC CIRCULATION

Shinji MATSUMURA<sup>1</sup>, Koji YAMAZAKI<sup>2</sup> (<sup>1</sup>Frontier Research System for Global Change, <sup>2</sup>Graduate School of Environmental Earth Science, Hokkaido University)

Surface air temperature over Siberia of northern Eurasia rapidly rises in the snow-melting season and reaches the maximum temperature in July. The interannual variability of the

IA

## INTER-ASSOCIATION

temperature rise in the snow-melting season is also large, resulting snow cover condition. On the other hand, there are still sea ice on the Arctic in the snow-melting season, and the contrast of temperature between land and sea also reach the maximum. It is thought that these boundary conditions in summer, in which jet stream is weak, affect the mid-high latitude atmospheric circulation in the position of external forcing. In the point of sight, seasonal simulation has been conducted with the CCSR/NIES atmospheric GCM (AGCM) to investigate the predictability of early summer climate in 1993 which is the typical year. An ensemble experiment consisting of 10 independent integrations from April 21, 22, ..., 30 to the end of August of 1993 was conducted giving observed global monthly SSTs as the lower boundary condition. The initial atmospheric conditions are prepared using the NCEP/NCAR reanalysis data. The initial conditions for snow amount and soil wetness are taken from the model climatology. The ensemble mean reproduces reasonably well the observed patterns of geopotential height anomalies in July. Surface warming over northern Siberia found in the snow-melting season 1993 also appears. These relation can be found by observational data with interannual variability and some year in the CTL run.

**JSP04a/09P/D-006** Poster **1400-099**

### PRODUCTION AND FATE OF DIMETHYLSULFONIOPROPIONATE (DMSP) IN ARCTIC FAST ICE

Naoaki UZUKA (International Arctic Research Center, Frontier Observational Research System for Global Change)

Dimethylsulfide (DMS) is the most abundant biogenic sulfur compound emitted from the ocean to the atmosphere. Subsequently, DMS is oxidized in the atmosphere and forms aerosols, which affect the radiative balance of the Earth both directly and indirectly. DMS is formed from its precursor dimethylsulfoniopropionate (DMSP), which is produced by marine phytoplankton. Ice algae are known to accumulate high amounts of intracellular DMSP for the purpose of cryoprotection in addition to osmoregulation. Thereby, substantial amounts of DMSP may be released to the water column resulting in high DMS emissions to the atmosphere during the spring ice-melt season. However, studies of DMSP production by Arctic ice algae are scarce. Observations were conducted six times between March and June, 2002 at a fixed station in the land fast sea-ice zone in Barrow, Alaska. Vertical distributions of DMSP and chlorophyll *a* concentrations in ice cores were obtained. Concentrations of DMSP showed remarkable temporal variation. High amounts of DMSP, together with high chlorophyll *a* concentrations were observed at the lowermost part of the ice cores, where ice algae actively developed. Especially high amounts of DMSP (15  $\mu\text{mol/l}$ , 150 times higher than in seawater) and chlorophyll *a* (0.6  $\text{mg/l}$ ) were obtained in early-May, 2002 from the bottom 2 cm layer. The highest DMSP concentration in seawater (130  $\text{nmol/l}$ ) was observed in late-May, when sea ice was melting and DMSP in the sea-ice decreased to 5.5  $\mu\text{mol/l}$ , suggesting mass release of DMSP from detached ice algae to the water column under the sea-ice. This confirms that ice algae in the fast sea ice produce DMSP efficiently and may contribute to the subsequent DMS sea-to-air flux in the Arctic.

**JSP04** Wednesday, July 9 - Thursday, July 10

### ARCTIC ENVIRONMENT CHANGE (IAPSO, IAMAS, IAHS)

Location: Site A, Room 6

Thursday, July 10 AM

Presiding Chair: S. Minobe

**JSP04/10A/A06-001** **0900**

### SIMULATED ARCTIC FRESH WATER EXPORT VARIABILITY 1900-2000

Cornelia KOEBERLE, Ruediger GERDES, Frank KAUKER, Michael KARCHER (Alfred Wegener Institute for Polar and Marine Research)

The fresh water export from the Arctic exhibits decadal to multi-decadal variability that is made possible by the reservoir of fresh water in the Arctic halocline and sea ice. We will present ocean-sea ice model results from hindcasts forced by NCEP reanalysis data that indicate a decline of the Arctic fresh water reservoir from the mid-1960s until today. This is achieved by an imbalance in the fresh water supply and export through Fram Strait, the Barents Sea opening and the Canadian Archipelago. A long term trend is superimposed by several fresh water export events. Hindcast simulations are constrained by the availability of consistent and comprehensive atmospheric forcing data sets like the 55-years NCEP reanalysis data set. The presence of multidecadal variability in the northern North Atlantic and the Arctic, however, requires longer simulation periods. The most comprehensive single component available for about the last century is that of sea level pressure. From that, wind can be derived and 2m-air temperature can be reconstructed with some confidence. So additional model results will be presented for the years 1900-2000. We will discuss the origin of variability in the fresh water reservoir and the export. The pathways and travel times of the Arctic fresh water into the Arctic and subarctic North Atlantic will be presented. The impact of the fresh water on the horizontal and overturning motion in the North Atlantic will be discussed in comparison to the effects of other forcing components.

**JSP04/10A/A06-002** **0920**

### RECENT AND HISTORICAL CHANGE OF SEA ICE EXTENT IN THE ARCTIC

Roger L. COLONY (IARC/Frontier, U of Alaska)

"Northern Hemisphere spring and summer sea-ice extent has decreased by about 10 to 15% since the 1950s", is a quote from the *Summary for Policymakers* in IPCC report (2001), *Climate Change 2001: The Scientific Basis*. There is general consensus on estimates of the recent reduction of ice extent, which are based on a combination of aircraft reconnaissance and satellite remote sensing. However, the statement takes on real meaning when examined in terms of other geophysical variables and/or the historical perspective of ice extent variability. Using the ACSYS Historical Ice Chart Database, recent changes in ice extent can be placed in historical context. In 1596, Willem Barentsz maintained a log of ice conditions during his exploration of the waters around Svalbard. Barentsz also reported a large whale population in the north Greenland and northeast Barents seas; within a few years, highly organized commercial whaling was established with bases on Spitzbergen. These whalers provided additional information on ice edge position during the early 17th century and throughout the 18th century. In the middle of the 19th century, Norway began systematic seal hunting along the ice edge from Iceland to Novaya Zemlya. Ice edge information from many of the whaling and sealing activities were archived by the Norwegian Polar Research Institute. An analysis of the historical record shows general ice edge retreat since the first decade of the 19th century. Recent changes of the April ice extent in the Barents Sea are slightly less than the 200-year trend, while recent changes in the August ice extent appear

slightly larger than the long-term trend. Covariance studies suggest that the ice edge position responds more directly to the mean temperature of the Northern Hemisphere than to the arctic mean. What about the future? Although physically based models are unable to accurately simulate the present ice-edge boundary, there is significant agreement in change. Most models simulate a 40% reduction in sea ice area by the year 2080. This feature of future climate change has gone unreported by the IPCC Summary for Policymakers.

**JSP04/10A/A06-003**

**0940**

### THE BERING STRAIT'S GRIP ON THE WORLD CLIMATE

Agatha M. DE BOER, Doron NOF (Florida State University)

The Holocene interglacial period of the last 10,000 years and the penultimate interglacial approx. 125,000 years ago have been characterized by distinctly stable climates. An analytical-dynamical model, which includes both wind and thermohaline processes, is used here to show that, during interglacial periods, variability in North Atlantic Deep Water (NADW) formation are damped out because of an Arctic freshwater feedback. During glacial periods, the stabilizing feedback is prevented by the closure of the Bering Strait (BS). The open-strait thermohaline circulation recovers exponentially from an internal perturbation with a rapid e-folding time of 32 years. However, a prolonged external forcing anomaly, such as the suggested increase in precipitation due to global warming, may shut down NADW formation entirely.

**JSP04/10A/A06-004**

**1030**

### SENSITIVITY OF THE ARCTIC HIGH TO SEA ICE DYNAMICS IN A PALAEOCLIMATE MODEL

Jennifer K. HUTCHINGS<sup>1</sup>, Steve VAVRUS<sup>2</sup>, William HIBLER III<sup>1</sup> (IARC, University of Alaska Fairbanks, <sup>2</sup>University of Wisconsin)

We investigate the influence of sea ice dynamics on the atmospheric pressure pattern over the Arctic Ocean. The Genesis palaeoclimate models run with and without ice dynamics, and two dynamical models, with and without shear stress are considered. The influence of ice dynamics on the current climate is discussed. It is found that the atmospheric pressure field is improved with the inclusion of ice dynamics. A future climatic warming scenario is run, and the influence of ice dynamics on the evolving atmospheric-ocean coupling is investigated.

Thursday, July 10 PM

Presiding Chair: L. Mysak

**JSP04/10P/A06-001**

**1400**

### UNAAMI - RECENT LARGE BASIN-WIDE CHANGES IN THE ARCTIC

James E. OVERLAND<sup>1</sup>, James H. MORISON<sup>2</sup> (NOAA Pacific Marine Environmental Laboratory, <sup>2</sup>Polar Science Center, University of Washington)

Unaami, the Yup'ik word for tomorrow, has been chosen by the Study of Environmental Arctic Change (SEARCH) program to represent the broad interrelated changes occurring in the Arctic. These changes are documented through examination of 86 regionally-distributed time series for 1965-1995 representing seven data types: climate indices, atmosphere, ocean, terrestrial, sea ice, fisheries, and other biological data. These changes are compared with 19th and 20th century temperature records. Although visual inspection of the data collection indicates that Arctic change is complex, two patterns are evident. The pattern based upon the first Principal Component (PC1), representing 23% of the variance, shows an upward trend and has a single regime-like shift near 1989 based on a large number of time series, including projections from a strong stratospheric vortex in spring, the Arctic Oscillation, sea ice declines in several regions, and changes in selected mammal, bird, and fish populations. Most land processes such as snow cover, greenness, Siberian runoff, and permafrost temperatures and certain subarctic sea-ice records show a more linear trend over the 30-year interval that also contributes to PC1; these variables are from lower latitudes and often integrate the atmospheric or oceanographic influence over several seasons or years including summer. The pattern based on the second Principal Component (PC2) shows interdecadal variability over the Arctic Ocean Basin north of 70N; this variability is observed in surface wind fields, sea ice, and ocean circulation. Historical surface temperature data support these two patterns with an interdecadal high-latitude/NAO type pattern, and a long-term, pan-Arctic change since the end of the little ice age. That more than half of the data collection projects strongly onto the two patterns, suggests that the Arctic is responding as a coherent system over at least the previous three decades.

**JSP04/10P/A06-002**

**1420**

### SPACE/TIME CHANGES IN ARCTIC ICE AGE DISTRIBUTION

William J. EMERY, Charles FOWLER, James A. MASLANIK (Univ of Colorado)

With the use of information from satellite instruments, fairly dramatic changes in the Arctic have been observed in recent years in atmospheric patterns, ice extent and ice velocities, which should also result in changes in the distribution of the ages of multi-year ice. Using ice extent determined from passive microwave instruments and advecting the ice using velocities from merged buoy, AVHRR, and passive microwave imagery, it is possible to track the progression of the ice pack as it moves around the Arctic basin until it is lost from melt, either during the summer or as the ice drifts to lower latitudes. Each year, the ice contained within the minimum ice extent is aged one year. This time series of progressively "aged" sea ice demonstrates a dramatic shift of multi-year ice cover with substantial overall decrease of the oldest ice and a shift of location of this oldest ice to just north of the Canadian Archipelago and directly across the central Arctic to the Siberian Shelf. A separation of the Arctic basin into eastern and western halves shows that the greatest overall loss of the oldest ice is from the eastern Arctic, which is primarily through the Fram Strait. The total reduction in Arctic sea ice coverage is consistent with earlier studies while our unique approach demonstrates the changing nature in the spatial distribution of ice ages through the 24-year time series from 1978 to 2002.

**JSP04/10P/A06-003**

**1440**

### SENSITIVITY OF MODELED SEA ICE TO PARAMETERIZATIONS OF HEAT EXCHANGE PROCESSES

Alexander P. MAKSHAS<sup>1</sup>, Sergey V. SHOUTILIN<sup>2</sup> (International Arctic Research Center, University of Alaska Fairbanks, <sup>2</sup>Arctic and Antarctic Research Institute, Russia)

A dynamic-thermodynamic sea ice model with 50-km spatial and 24-hour temporal

resolution and zero-dimensional thermodynamic sea ice models are applied to investigate long-term spatial and temporal variability of the sea ice cover and surface energy exchange in the Arctic Basin. The models satisfactorily reproduce the averaged main characteristics of the sea ice, the sea ice extent, and the surface heat exchange for different parts of the Arctic Basin. In particular, estimates of the year-to-year difference between mean sea ice thickness in September show reasonable agreement with the essential thinning of sea ice in the Canadian Basin that Rothrock et al. (1999) found. Model shows that the main reason for sea ice thinning is the changes in the atmospheric circulation. It time the evaluation of atmospheric forcing data, namely air surface level temperature and surface wind velocity from NCEP, and cloudiness amount from Gershkov Atlas show large disagreement with data obtained on the drifting stations "North Pole". The numerical experiments with zero-dimensional sea ice model reveal that some negative feedbacks existing in nature and reproducing in the models artificially reduce the influence of inaccuracy of forcing parameters on the results of modeling. Additionally the dependence of model results to description of heat processes in leads, prescribed geometry and melting rate of ridges, and parameterization of short-wave radiation is investigated.

JSP04/10P/A06-004

1500

#### QUASI-PERIODIC WARMINGS OF THE ATLANTIC LAYER OF THE ARCTIC IN A HINDCAST SIMULATION 1948-2002

Ruediger GERDES, Michael KARCHER, Ursula SCHAUER, Cornelia KOEBERLE (Alfred Wegener Institute for Polar and Marine Research)

The observed 1990s warming of the Atlantic layer in the Arctic has been interpreted in various ways. A major uncertainty is due to possible multidecadal variability of the high latitude climate system. Observations in the West Spitzbergen Current (WSC), the source of the Fram Strait Branch of Atlantic water in the Arctic, show previous warm events. Here, we use a model hindcast for the 1948-2002 period to identify several such warm events in the WSC and their propagation through the Arctic. While decadal time scale warmings are clearly present at many locations in the Eurasian Arctic, an upward temperature trend can be discerned over the period investigated. The relation to large scale atmospheric and oceanic forcing functions will be discussed. The Barents Sea Branch of Atlantic water plays an important role in modifying some of the warm events.

JSP04/10P/A06-005

1520

#### A NEW VIEW OF PACIFIC WATER CIRCULATION IN THE ARCTIC OCEAN

Michael STEELE<sup>1</sup>, James H. MORISON<sup>1</sup>, Wendy ERMOLD<sup>1</sup>, Ignatius RIGOR<sup>1</sup>, Mark ORTMEYER<sup>1</sup>, Koji SHIMADA<sup>2</sup> (<sup>1</sup>Applied Physics Laboratory, University of Washington, <sup>2</sup>Japan Marine Science and Technology Center)

What is the fate of summer Pacific water in the Arctic Ocean? Our focus here is on the circulation and variability of the layer containing the slightly warm (usually less than 1 degree above freezing) temperature maximum that resides just below the mixed layer in the western Arctic Ocean. Following recent and much older studies, we separate this layer into 2 salinity ranges which may each contain a temperature maximum. The fresher (shallower) layer is Arctic Coastal Water (ACW), which contains a significant runoff fraction (especially from the Yukon river). The saltier (deeper) layer is Bering Sea Water (BSW), which occupies much of the central Chukchi Sea. A data base of cruise data from the 1990's is used to trace the extent and variability of these water masses. We also include recent data obtained in 2000 and 2001 as part of the North Pole Environmental Observatory. We find that when the Arctic Oscillation (AO) index is low, the Beaufort Gyre contains both ACW and BSW, and the Transpolar Drift Stream (TDS) has a low Pacific water contribution. On the other hand, when the AO index is high, ACW dominates the Beaufort Gyre, while BSW dominates the TDS. This result is used to explain time series data from the Lincoln, Beaufort, and East Siberian Seas. We also speculate on downstream implications for the flow through Fram Strait and the Canadian Archipelago.

JSP04/10P/A06-006

1600

#### DECADAL VARIABILITY IN THE ARCTIC OCEAN SHOWN BY HYDROCHEMISTRY AND OTHER ENVIRONMENTAL DATA

Motoyoshi IKEDA, Hiroyasu YAMAGUCHI, Takayoshi IKEDA (Graduate School of Environmental Earth Science, Hokkaido University)

Sea ice distribution and atmospheric conditions have shown significant decadal variabilities: i.e., the ice area reduced (increased) along Russian coast, responding to the more intense (weaker) Polar Vortex and higher (lower) air temperature. In contrary, it has been difficult to find a corresponding signal in the ocean interior due to unavailable data. The recent distribution of Russian data set collected from the Arctic Basin has opened up a new source for exploring ocean interior variability. Among various ocean data, silicate can be used as an indicator of the boundary between the silicate-rich Pacific Water and the opposite Atlantic Water, although it is influenced by seasonal biological productivity and outflow from Siberian rivers. The silicate distribution shows a clear maximum around 100-m depth in the Canada Basin. The vertical gradient below 100 m provides information on a vertical motion of the upper boundary of the Atlantic Water. The boundary shifted upward (downward) corresponding to the more intense (weaker) Polar Vortex or positive (negative) Arctic Oscillation, even though the data give significant signals only for two decades (1965-85). The further study is suggested to compare this new data set and a coupled ice-ocean model with atmospheric forcing so that deeper understanding may be achieved on decadal and longer-term variabilities in the Arctic Ocean.

JSP04/10P/A06-007

1620

#### DETECTING ARCTIC CLIMATE CHANGE USING KÖPPEN CLIMATE CLASSIFICATION

Muyin WANG<sup>1</sup>, James E. OVERLAND<sup>2</sup> (<sup>1</sup>JISAQ, University of Washington, <sup>2</sup>PMEL/NOAA)

Ecological impacts of the recent warming trend in the Arctic are already noted as a decrease in tundra area with replacement by shrubs, and changes in the tree line. The potential impact of vegetation changes to feedbacks on the atmospheric climate system is enormous because of their large land surface area and the multiyear memory of the vegetation cover. While much of the vegetation information is anecdotal, and satellite NDVI (Normalized Difference Vegetation Index) estimates, which began in 1981, are good source and are rather accurate information. The Köppen climate classification can be used to relate surface types to monthly mean air temperature from the NCEP/NCAR reanalysis and station data, and thus serves as proxy data for earlier period. In Köppen classification, tundra area is defined as the warmest summer monthly mean temperature being less than 10°C. We found a decrease in tundra area from the mid 1970s to the present, similar to the trend of the NDVI data. The decreases are largest in NW Canada, and eastern and coastal Siberia. Köppen proxies show an increase in tundra area from the late 1950s to the 1970s. The calculated tundra area minimum in the 1950s was similar to present conditions, and occurred about 10

years after the previous 20th century temperature maximum.

JSP04/10P/A06-008

1640

#### SEARCHING FOR EVIDENCE OF CLIMATIC CHANGE IN THE LENA RIVER BASIN TOWARD FEEDBACK TO THE LAPTEV SEA HYDROGRAPHY

Svetlana BEREZOVSKAYA<sup>1</sup>, Igor DMITRENKO<sup>2</sup> (<sup>1</sup>Russian State Hydrometeorological University, St. Petersburg, Russia, <sup>2</sup>International Arctic Research Center, University of Alaska Fairbanks, Fairbanks, USA)

The Lena river, major source of fresh water into the Laptev Sea, tends to integrate the hydrological and meteorological response of broad territories. Within the frame of this study the river runoff into the Laptev Sea has been considered not only as a freshwater flux but also as an effective indicator of spatially distributed changes. The study is based upon the spatially distributed hydrological, meteorological information for the period 1936-1990 (1995) and hydrographical CTD data from 1965 until 2000. The variability of river discharge, air temperature, and precipitation time series has been analysed by application of the statistical methods. The study shows statistically significant increase of air temperature since 1975 and arising of precipitation since mid-sixties. Furthermore, the annual water balance calculation has been provided for the three catchments within the Lena basin to detect the spatial and temporal scale of alteration. The evaluation of a link to climatic factors demonstrates a weak feedback of the water balance components to air temperature increase. Analysis of the runoff variability for the different hydrological seasons (excluding the winter season) indicates that the variance and means have been stable at least till 1990. It has been also shown, that the 30 % increase of the Lena River winter runoff (since 1970) is merely caused by human activity along the Vilui river. However, even a 30 % increase of winter riverine discharge has a weak influence on marine hydrography. The role summer river runoff plays with the Laptev Sea shelf thermohaline structure has greater order than any other factors. The physical mechanisms that transport riverine waters off the delta region are primarily related to the atmospheric circulation over the Arctic Ocean. The cyclonic (CCR) and anticyclonic (ACCR) atmospheric circulation regimes essentially affect the propagation and redistribution of the Lena river runoff as well as different mechanisms of river and marine water interaction. River discharge itself controls the freshening of the surface water layer under cyclonic circulation: onshore winds prevailing under CCR conditions prevent the northward propagation of the river plume (downwelling); the river plume becomes thicker and stably stratified with limited vertical entrainment, which provides minimum convection through pycnocline. During ACCR periods river runoff via the entrainment of the ambient salty waters favour the salinization of the upper layer: offshore winds persisting under ACCR result in considerable plume northward redistribution and weakening of the vertical density gradient.

JSP04/10P/A06-009

1700

#### INFLUENCE OF DECADAL ARCTIC OSCILLATION ON JAPAN (EAST) SEA AND OKHOTSK SEA

Shoshiro MINOBE (Graduate School of Science Hokkaido University/ Frontier Research System for Global Change)

The subsurface water temperatures in the Japan Sea and the southern part of the Okhotsk Sea are studied by using newly produced gridded temperature anomaly datasets for the late 20th century. These datasets are the first gridded temperature datasets suitable for studies of interannual to decadal variations of those marginal seas. The EOF and CEOF analyses showed that the both marginal seas are strongly influenced by the quasi-decadal component of the Arctic Oscillation via the changes of Siberian Highs. The strong influence of the Arctic Oscillation on the mid-latitude east Asian marginal seas is consistent with the fact that the maximal temperature anomaly associated with the Arctic Oscillation is located far eastern Asia as shown by Thompson and Wallace (1998). The oceanic response of the Japan Sea is more complicated than that of the Okhotsk Sea, involving substantial phase difference between the northeastern and southwestern Japan Sea, with the northeastern temperatures varying in phase with the changes of the Siberian High as well as the Okhotsk Sea. The stronger Siberian high associated with stronger east-Asian winter monsoon corresponds to cold temperatures in the northeastern Japan Sea and the Okhotsk Sea.

JSP04/10P/A06-010

1720

#### INFLUENCE OF INCREASED ATMOSPHERIC MOISTURE IN THE PROJECTED FUTURE CLIMATE ON THE ARCTIC OCEAN

Xiangdong ZHANG<sup>1</sup>, Moto IKEDA<sup>2</sup>, John E. WALSH<sup>3</sup> (<sup>1</sup>Frontier Research System for Global Change, International Arctic Research Center, University of Alaska Fairbanks, <sup>2</sup>Graduate School of Environmental Earth Science, Hokkaido University, <sup>3</sup>International Arctic Research Center, University of Alaska Fairbanks)

Changes of the Arctic ocean and sea-ice due to surface air temperature increase and its amplification over the polar cap has been documented and paid much attention. Accompanying the green house gases and surface air temperature increasing, atmospheric moisture and precipitation may rise noticeably in the projected future climate changes over the Arctic region, which has not been well investigated. We employed an Arctic coupled ocean/sea-ice model to examine the changes of Arctic ocean forced by the projected atmospheric moisture increase in future. Our forcing data come from the output of three ensembling experiments of the CCCMA (Canadian Climate Center for Modeling and Analysis) coupled climate model (refer to [www.ccmma.bc.ca/data/cgcm1/cgcm1.html](http://www.ccmma.bc.ca/data/cgcm1/cgcm1.html)), in which the atmospheric concentration of green house gases (GHG) corresponds to that observed from 1900 to present and is increasing at a rate 1% per year thereafter until year 2100 and the direct effect of sulphate aerosols (A) is included. In order to solely investigate the effects of increasing atmospheric moisture, all other forcing parameters keep the same as their climatology except 2m air specific humidity and the parameters for latent heat flux calculation. The projected moisture increase is represented by the difference of specific humidity between 2040-60 and 1975-95. The modeling results indicate that evaporation decreases in the Norwegian Sea, the Barents Sea and the marginal area along the Eurasian coast due to the atmospheric moisture increase. Accordingly, the latent heat flux in the Norwegian Sea and the Barents Sea is much decreased, which consequently results in a considerable ocean surface temperature increase, with a maximum occurring in the Barents Sea. The Atlantic layer on the Eurasian side also becomes warmer. A warmer tongue starts from the St. Anna Trough towards the southeastern Nansen Basin and, then, goes towards east along the break of Arctic basin and towards north along the Lomonosov Ridge. Ocean surface and salinity decreases over a large part of the model domain, except a local area near the St. Anna trough, in the Barents Sea, and near the Novosibirskiy Island. Moreover, the Atlantic layer becomes fresher too. Further studies are continuing with the output from the B2 scenario of green house gas increase.

JSP04b-Posters

Thursday, July 10

ARCTIC ENVIRONMENT CHANGE (IAPSO, IAMAS, IAHS)

Location: Site D

Thursday, July 10 PM

JSP04b/10P/D-001

Poster

1400-020

**INTENSE WARMING OF ARCTIC GLACIERS SUBJECTED TO SUB-SURFACE MELTING**

Oleg V. NAGORNOV, Yurii V. KONOVALOV (Department of Environmental Modeling, Moscow Engineering Physics Institute (State University))

Many Arctic glaciers are subjected to melting due to high air temperatures during summer. It results to the warming of glaciers that is much greater than average increase of regional temperature. Melt water percolates into the snow-firn sequences. Melting intensity during summer months is proportional to the third power of the mean air temperature. Hence, small changes of summer air temperatures induce big changes of the active layer temperatures. The refreezing of melt water results in the sub-surface accumulation of heat. Quantitative estimates of warming in the Eurasian Arctic are obtained by solution of inverse problems for the past temperature retrievals by two new methods. The first one is based on measured temperature profiles and determination of parameters of the oxygen-isotopic paleothermometer with accounting for the "melting-freezing" processes, and this allows for reconstructing both the past surface temperature and power of the sub-surface heat source in the past. The second method retrieves the past temperatures at the low boundary of active layer. It is based on the regularization of the ill-posed problem. The borehole temperatures have been measured in the biggest ice caps in Eurasian Arctic: Austfonna (Svalbard), Windy Dome (Franz Josef Land) and Akademii Nauk (Severnaya Zemlya). These ice caps are located in Western, Central and Eastern parts of the Eurasian Arctic. The calculated surface temperatures of the glaciers exhibit weak dependence on the variations of the accumulation rate at the surface and the geothermal flow in the last 200 years. The bottom parts of the Akademii Nauk Ice Cap and Windy Dome are in a steady state while Austfonna Ice Cap is in non-steady state as a result of the bottom melting. The estimated rate of melting of the Austfonna bottom ice is in the range from 2 to 7 mm/y. The lowest surface temperatures of the Austfonna Ice Cap occurred during the Little Ice Age, started five hundred years ago. Drastic warming recorded in the borehole temperatures started approximately 150 years ago. One hundred and fifty years ago the ice temperatures here were colder by 10-11 C than those that were six hundred years ago. Present ice temperatures are the highest for the last 2000 years. The lowest surface temperatures at the Windy Dome were 300-320 years ago in the middle of the Little Ice Age. They were 13 C colder than the warmest temperatures of approximately 30-40 years ago. The most interesting feature of the recent climate change here is almost 3 C cooling that takes place for the last 30-40 years. With the exception of recent warming the most eastward Academia Nauk Ice Cap had temperature changes similar to the Windy Dome. The Medieval Warming is noticeable only in the Western Arctic. The scale of warming we have calculated for the Arctic glaciers for the last 150 years (about 8 C) turned out to be essentially greater than that averaged over the Arctic region (about 2 C).

JSP04b/10P/D-002

Poster

1400-021

**A DATA-MODEL COMPARISON STUDY OF ARCTIC SEA-ICE VARIABILITY, 1958-1997**Anne ARMSTRONG<sup>1</sup>, Bruno TREMBLAY<sup>2</sup>, Lawrence A. MYSAK<sup>1</sup> (<sup>1</sup>Department of Atmospheric and Oceanic Sciences, McGill University, <sup>2</sup>Columbia University, Lamont-Doherty Earth Observatory)

The granular rheology sea-ice model of Tremblay and Mysak is validated against 40 years of observed sea ice concentration (SIC) data. Subsequently, the mechanisms responsible for producing SIC anomalies in the model are evaluated by studying the coupled variance (using the Singular Value Decomposition (SVD) method) between the simulated SIC anomalies and the ice speed and air temperature anomalies. To execute this validation, a 49-year (1949-97) simulation (including a 9-year spin-up) of the Arctic and peripheral sea-ice cover using daily varying winds and monthly mean air temperatures is produced. In general, the simulated SIC variations for 1958-97 in the East Siberian, Chukchi and Beaufort seas are in agreement with observations, while large discrepancies occur in the Laptev and Kara seas. Moreover, the sensitivity of the model to southerly wind anomalies in creating summer SIC anomalies compares well with the observed sensitivity; however, the model's sensitivity to summer air temperature anomalies is weaker than observed. Results from the SVD analysis show that the main source of variability in the peripheral seas is associated with the variation in the strength of the Arctic High; in the East Siberian and Laptev seas, the strengthening and weakening of the Transpolar Drift Stream also plays an important role. The SVD analysis also shows that over the entire Arctic domain, surface air temperature anomalies are negatively correlated with sea-ice anomalies. Finally, the observed downward trend in total sea-ice cover in the last two decades as well as record minima in the East Siberian Sea are reproduced in the simulation.

JSP04b/10P/D-003

Poster

1400-022

**RECENT VARIABILITY ON THE WATER MASS CHARACTERISTICS IN THE CENTRAL ARCTIC OCEAN**Takashi KIKUCHI<sup>1</sup>, Kiyoshi HATAKEYAMA<sup>1</sup>, James H. MORISON<sup>2</sup> (<sup>1</sup>Japan Marine Science and Technology Center, <sup>2</sup>Polar Science Center, Applied Physics Laboratory, University of Washington)

Hydrographic observational data since 1990s is investigated to understand recent variability on the water mass characteristics in the central Arctic Ocean. The data have been obtained by icebreaker cruises, air-borne CTD surveys, submarine cruises, ice-drifting buoy observations, and so on. Especially in the early 2000s, surface salinization and Atlantic Water warming in the Amundsen basin of the Arctic Ocean are clearly found from CTD and buoy observational data from North Pole Environmental Observatory (NPEO) Project. The surface salinization in the Amundsen Basin was observed at the Siberian side in late 1993, extended to the Atlantic side in the mid 90s, and is now still observed in the Amundsen Basin. However, the higher anomalies of the surface salinity are weakening especially over the Lomonosov ridge in the early 2000s. As for the horizontal distribution of the surface salinization, there is no significant salinization of the surface mixed layer on the Makarov Basin side of the Lomonosov ridge since 1990s. The surface salinization in the Amundsen Basin may be related with retreat of the cold halocline layer which have been reported in the previous researches. Atlantic Water warming is also observed in the Siberian side of the Amundsen Basin since early 90's, and extended toward the Atlantic side. Advection speed of the Atlantic Water warming is slower than that of the surface salinization in the Amundsen Basin and the area of the Atlantic Water warming extends to the Makarov basin side of the Lomonosov ridge. In the early 2000s, the anomaly of the Atlantic Water temperature is still high in the Amundsen Basin and over the Lomonosov Ridge.

JSP04b/10P/D-004

Poster

1400-023

**SEA ICE VARIABILITY AND FUTURE ARCTIC MARINE OPERATIONS**Lawson W. BRIGHAM<sup>1</sup>, Michael S. TIMLIN<sup>2</sup>, John E. WALSH<sup>1</sup> (<sup>1</sup>Arctic Research Commission, Arlington, VA, <sup>2</sup>University of Illinois, Urbana, IL)

One of the principal challenges for Arctic sea ice modeling is to provide planners with more reliable and useful projections of changes in access to the Arctic for marine operations. There is already substantial observational evidence that the Arctic sea ice cover is undergoing significant changes, which include larger areas of open water (especially during summer), a diminished presence of multiyear sea ice, and a thinning of sea ice in the central Arctic Ocean. Any continuation of these changes will have important implications for future Arctic marine transport and offshore development systems. As part of the Arctic Climate Impact Assessment, projected changes of Arctic sea ice coverage through the 21st century have been evaluated in the context of potential enhancements of marine access to the Arctic. The evaluation is based on monthly fields of sea ice from simulations by five different global climate models, forced by the conservative B2 scenario of increasing greenhouse gas concentrations. Regionally and seasonally varying bias-corrections based on the models' simulations of present-day ice coverage were applied to the projected sea ice coverage, although these corrections do not remove the differences between the interannual variability of the models and that of observational data for recent decades. The greenhouse warming reduces sea ice coverage in all models, especially during summer. However, there is considerable range among the retreats projected by the different models. The five-model mean decrease of sea ice coverage projected for 2100 is approximately 60% in September (ranging among models from 9% to 100%) and approximately 15% in March (ranging among models from 11% to 18%). One model projects an ice-free Arctic during summer in the 2070-2090 time slice, while three other models lose most of their summer ice by that time. The seasonality of the retreat (largest in summer) is consistent with trends in observed sea ice coverage over the past few decades. The Northern Sea Route offers the potential for a major reduction of transit times between the Far East and Europe. The region is a good candidate for study because the Russian Arctic coastal waters, except several narrow straits, are open to the Arctic Ocean and therefore reasonably well represented despite the coarse resolutions of all of today's models. By the 2070-2090 time slice, the models project a lengthening of the navigation season in the Laptev and East Siberian Seas by an average (over the five models) of 60-90 days, although the lengthening ranges among models from as few as 10 to as many as 100 days. In most of the model simulations, the retreating ice continues to interact with the northern tip of Severnaya Zemlya, implying a reliance on a transit route through Vilkitski Strait between the Kara and Laptev Seas.

JSP04b/10P/D-005

Poster

1400-024

**THE RESULTS OF THE COMPLEX ANALYSIS OF SEISMOACTIVITY, TREE-RINGS AND CLIMATIC CHARACTERISTICS FOR THE AREA OF THE WHITE SEA**Taisya Yakovlevna BELENOVICH<sup>1</sup>, Svetlana Vladimirovna VIDYAKINA<sup>2</sup> (<sup>1</sup>Laboratory of a deep geological structure and dynamics lithosphere, Institute of the Ecological Problems of the North UD of RAS, <sup>2</sup>Center for ecological research, Pomor State University)

In this work the complex analysis of the results of the researches of the changes of seismoactivity, tree-ring chronologies and climatic characteristics for the area of the White sea is carried out. The statistic analysis of 15 tree-ring chronologies (year indices) on a pine shows, that distinctions in meanings of a standard deviation, received for trees in different types of the forest, between chronologies is not observed, and chronologies have a high variability. The results of calculation of coefficients of linear correlation between chronologies have distinguished two groups of chronologies, general period from 1902 to 1971. Inside the groups the coefficient of linear correlation is from 0.7 up to 0.8. The areas on coefficient of linear correlation are well coordinated with contemporary stretch of seismic zones limiting megablocks (Belenovich et al., 1997). The following stage of the work was carrying out the spectral-temporary analysis of the long-term characteristics, including the meteorological data. Meteorological series of annual and seasonal characteristics on atmospheric pressure, air temperature nearest to tree-ring chronologies of meteorological stations (Kandalaksha, Kem, Onega, Arkhangelsk, Mezen, Solovki, the data of the archives of Hydrometeorological center of Murmansk and Arkhangelsk) and the index of circulation of the atmosphere above the Northern Atlantic (index Jonsa) were processed. The made analysis has distinguished the dominant periods close by 30 years. The cycle close to 30-year's, is revealed in the work of V.V. Klimenko (1997), where is shown that the 26 years period is characteristic time of rotation of carbon of a long-lived biota. Taking into account physiological peculiarities of growth of trees, the examination of the 30-year's period excludes from the analysis the smaller periods and is justified for the characteristic of the climate. The results of a low-frequency filtration of the data on average summer pressure and chronologies reveal 30-years period on an examined interval of time, with minimal meanings 1905 - 1907 and 1943 - 1946, showing, that maximum of atmospheric pressure correspond to the minima of ring-widths of trees growing in seismic zones. The results of low-frequency filtrations of air temperatures, the index of North Atlantic Oscillation have shown a positive coordination with the atmospheric factors of ring-widths of trees growing in relatively calm seismoactive areas. Thus, for the period from 1902 to 1971, for the area of the White sea, the factor of circulation of the atmosphere and temperatures dominates for trees located within megablocks (relatively calm in seismoactivity), positively coordinating in time, and the factor of pressure dominates for trees located in seismic zones, (seismoactive areas), negatively coordinating in time.

JSP06

Monday, July 7 - Tuesday, July 8

**THE GLOBAL OCEAN OBSERVING SYSTEM (IAPSO, IAG, IOC)**

Location: Site B, Room 21

Monday, July 7 AM

Presiding Chair: P.-Y.L. Traon

JSP06/07A/B21-001

0900

**IMPROVING SATELLITE OCEAN COLOR DATA PROCESSING BY THE USE OF NEURAL NETWORKS - THE NAOCC PROGRAM.**Michel R. CREPON<sup>1</sup>, Sylvie THIRIA<sup>1</sup>, Annick BRICAUD<sup>2</sup>, Antoine MANGIN<sup>3</sup>, Roland DOERFFER<sup>4</sup>, Frank FELL<sup>5</sup>, Jesus MORALES<sup>6</sup>, Dan CORNFORD<sup>7</sup> (<sup>1</sup>LODYC, BC 100, University P. et M. Curie, <sup>2</sup>LOV, CNRS, 06230, Villefranche/mer, France, <sup>3</sup>ACRI, 06560, Sophia-Antipolis, France, <sup>4</sup>GKSS, D21502, Geesthaacht, Germany, <sup>5</sup>FUB, D12165, Berlin, Germany, <sup>6</sup>CICEM, 21071, Huelva, Spain, <sup>7</sup>ASTON University, B47ET, Birmingham, England)

Spaceborne ocean color sensors which are now operational or under preparation, have a

large number of spectral band. NAOC, which is an EC supported programme, proposes to use advanced neural methodology which are well suited to deal with this multi-spectral information for retrieving ocean constituents. NAOC is divided into for major tasks : First NAOC intends to perform classification of the satellite signal at the Top of the Atmosphere according to specific criteria (energy, pattern of the spectrum) by using Topological Neural network Algorithm. This allows us to extract information on aerosol and on water type which will be used for atmospheric correction and ocean constituent retrieval. Second NAOC is determining improved algorithms for atmospheric correction which is crucial for obtaining accurate ocean product. As atmospheric correction is sensitive to ocean parameter for case 2 waters, NAOC intends to determine specific Multi-Layer-Perceptron (MLPs) for case 1 and case 2 water atmospheric correction. NAOC will then determine specific Neural Network algorithms for ocean constituent retrieval. At last NAOC is developing an advanced inversion algorithm based on the Spectral matching method of Gordon (1997). This algorithm inverts the radiative transfer equations both in the atmosphere and the ocean by using a combination of variational and Neural method. As it takes into account both atmospheric and oceanic parameters, it is well suited to deal with absorbing aerosols.

**JSP06/07A/B21-002****0920****HIGH RESOLUTION OCEAN SURFACE VECTOR WINDS**

W.Timothy LIU, Wenqing TANG (Jet Propulsion Laboratory, MS 300-323)

Spacebased scatterometers, at present, provide ocean surface wind vector at 25 km spatial resolution covering approximately ninety percent of the global ocean under clear and cloudy conditions, night and day. The spatial resolution is not sufficient to study small weather systems, such as tropical cyclones, nor processes in coastal oceans. The spatial resolution of the vector winds can be improved to approximately 12.5 km resolution by using range-compressed backscatter. These high-resolution scatterometer winds can be supplemented by observations of the synthetic aperture radar or assimilated into meso-scale numerical models to cover the last 10 km towards the coastline. Monitoring and predicting weather systems requires wind field at 6-12 hourly frequencies. For oceanographers, the highest frequency requirements are set by the inertial period timescales in mid-latitude and the diurnal timescale near the equator. Such temporal requirements cannot be achieved with a scatterometer flying on a single polar orbiting platform. At present, we have two identical scatterometers flying on QuikSCAT and ADEOS-2, and another scatterometer will be launch on the European operational spacecraft at the end of 2005. The scientific opportunities offered by flying more than one scatterometer in tandem, and producing vector winds at higher spatial and temporal resolutions will be discussed.

**JSP06/07A/B21-003****0940****AN OPERATIONAL BUOY NETWORK FOR CLIMATE SST**

Huai-Min ZHANG, Richard W. REYNOLDS, Thomas M. SMITH (NOAA/NESDIS/National Climatic Data Center)

Over the last decade, international groups have been actively pursuing strategies to accurately monitor global climate change. Part of the planning calls for the design and implementation of a Global Ocean Observing System (GOOS). Our effort under GOOS is to design a system to produce global SST with sufficient accuracy for climate studies. Specifically, we use SST observations from satellite and in situ instruments (including ships and drifting and moored buoys) and statistical tools, such as Optimal Interpolation and Optimal Averaging, to generate SST error for specified spatial and temporal resolutions. We then add simulated buoys, where needed, to reduce the SST error to acceptable levels. These simulated buoys are the buoys needed, henceforth "Buoy Need," to reduce the SST error to the required accuracy. Buoys are needed for two purposes: bias correction of satellite data and to supplement SST data in regions without adequate satellite and/or in situ data. Thus, we need to consider bias error as well as sampling and random errors. The Buoy Need is designed to reduce both type of errors. The Buoy Need is first computed as a nowcast, and then by a simulation scheme, including advection of drifting buoys, climatological seasonal adjustments, and current large scale climate events to produce a forecast for the next season. We will show variations of the Buoy Need for seasonal and interannual variations (e.g., El Nino).

**JSP06/07A/B21-004****1000****NEW GENERATION SEA SURFACE TEMPERATURE FOR GODAE**

Kawamura HIROSHI (Center for Atmospheric and Oceanic Studies, Graduate School of Science, Tohoku University)

Early in 2000, the GODAE project sent "Prospectus for a GODAE SST Project" to world SST researchers to encourage developments of high-resolution satellite-based sea surface temperature (<http://www.bom.gov.au/bmrc/mlr/nrs/oopc/godae/HiResSST/>). Our group has been developed, in the middle of 2001, the new generation SST (NGSST), which is daily, high-spatial resolution, quality-controlled cloud-free SST products merging AVHRR, GMS and TRMM SSTs. Since each of the satellite products are tuned against SSTs of the drifting buoys, they have a common observational basis for data merging. Using the hourly GMS solar radiation and the surface winds from SeaWinds, SSMI and TRMM, diurnal effects are eliminated to adjust all SSTs acquired at different times in a day to the daily minimum SSTs at around 1m depth. Then, all SSTs are merged using an objective analysis for one year, October 1999 to September 2000. The diurnal variation is not treated explicitly, but implicitly involved in the product generation process. The generated data and information are opened through <http://www.ocean.caos.tohoku.ac.jp/~adeos/sst/>. The second version NGSST has been developed after the release of first version products. The strong signal of diurnal variation at 1m-depth appears in the western equatorial Pacific, where the TAO/TRITON buoys are densely deployed. Examination of the signals shows a common feature of SST increase in the morning to noon, which is parameterized by the diurnal SST amplitude. In contrast, the SST decrease pattern from its peak in the afternoon is rather variable. Introduction of the diurnal pattern enables us to produce the SST at any time in a day. The Version 1.0 products were examined by comparing against moored buoy SSTs at 1m depth. Wavelet analysis shows that the decorrelation scales of SST field are seasonally/regionally dependent. They are obtained for the sea south of Japan, and used in the production of second version of NGSST (NGSST-2.0). The processing procedure of NGSST2.0 is modified largely from the first version to the second version. Validation of the NGSST-2.0 using the buoy observations shows that the accuracy of NGSST does not change, but the SST patterns are improved. The global microwave SSTs are now available from the AMSR-E/Aqua and AMSR/DEOS-II. The NGSST-2.0 is now tested using the AMSR SSTs, which will be released through the NASDA GODAE SST server for the GODAE research community in a day after their global observations. Real-time generation system of the NGSST-2.0 is now under development, and planned to be functioning early in 2003.

**JSP06/07A/B21-005****1030****THE GODAE HIGH-RESOLUTION SEA SURFACE TEMPERATURE PILOT PROJECT**Craig J. DONLON<sup>1</sup>, Chelle L. GENTEMANN<sup>2</sup> (<sup>1</sup>EC Joint Research Centre - Institute for Environmental and Sustainability, <sup>2</sup>RSMAS - University of Miami)

The Global Ocean Data Assimilation Experiment (GODAE) High-Resolution Sea Surface Temperature Pilot Project (GHRSSST-PP) has been established to provide international focus and coordination for the development of a new generation of global, multi-sensor, high-resolution, sea surface temperature products provided in near real time. Its primary aim is to oversee the development, assembly and processing of high-quality, global scale, SST products at a fine spatial and temporal resolution, and timely delivery for the diverse needs of GODAE. Regional Data Assembly Centers (to be located in Japan, Europe, and the US) will provide collated, quality controlled, individual satellite retrievals. These data streams are to be integrated together at a Global Data Analysis Center, responsible for providing the global merged analysis in near real time. A Diagnostic Data Set, with sites distributed throughout the global ocean, will provide an easily assessable sub-sample of all data sets for validation purposes. Cool-skin effects, diurnal warming, multi-sensor data fusion methodologies, and validation studies are under deliberation by the Science Team. Status of these analyses and progress of the GHRSSST-PP will be presented.

**JSP06/07A/B21-006****1120****SEA SURFACE SALINITY IN THE TROPICAL PACIFIC AND THE ENSO OBSERVING SYSTEM**Thierry DELCROIX<sup>1</sup>, Michael MCPHADEN<sup>2</sup>, Kentaro ANDO<sup>3</sup> (<sup>1</sup>IRD / LEGOS, <sup>2</sup>NOAA / PMEL, <sup>3</sup>JAMSTEC)

Sea Surface salinity (SSS) in the tropical Pacific, despite the relative paucity of the observations, has proven to be valuable for describing and understanding climate variability, for assessing and improving numerical model performance, and for improving ENSO prediction lead times in statistical models. The importance of SSS in the climate system has also motivated the development by European and US space agencies of dedicated satellite missions to enhance global SSS observations. This presentation will aim at : a) reviewing the scientific rationale which justify the value and utility of SSS observations as part of the ENSO observing system, b) describing the present SSS measurements collected from thermosalinograph instruments installed onboard merchant and research ships and on the TAO/TRITON mooring arrays, and c) discussing possible evolution of the time/space sampling strategy based on computed SSS time and space scales.

**JSP06/07A/B21-007****1140****AQUARIUS/SAC-D AND SMOS: FUTURE ADDITIONS TO THE SATELLITE OCEAN OBSERVING SYSTEM TO MEASURE GLOBAL SEA SURFACE SALINITY AND STUDY THE COUPLING BETWEEN THE WATER CYCLE, OCEAN CIRCULATION AND CLIMATE**Gary S.E. LAGERLOEF<sup>1</sup>, Jordi FONT<sup>2</sup>, Chester KOBILINSKY<sup>3</sup>, Raul COLOMB<sup>4</sup> (<sup>1</sup>Earth and Space Research, Seattle, USA, <sup>2</sup>Institut de Ciències del Mar, Barcelona, Spain, <sup>3</sup>NASA Goddard Space Flight Center, USA, <sup>4</sup>Comision Nacional de Actividades Espaciales, Argentina)

Two new satellite missions to map sea surface salinity (SSS) are now being developed for launch in 2007. Systematic global SSS observations are required to study processes that link climatologic changes in the water cycle to the dynamics of ocean currents and air-sea interactions. These include how SSS variations influence the ocean's overturning thermohaline circulation, ENSO dynamics, and closure of the net air-sea water and heat flux budgets. Present day SSS observations are very sparse, with large ocean areas (>24%) devoid of measurements. The satellite data will provide the first synoptic global coverage on weekly to monthly time scales to measure the global mean field, the seasonal to interannual variability and to test climate models. The European Space Agency Soil Moisture Ocean Salinity (SMOS) mission is a dual land/ocean science mission using the 1.4 GHz passive microwave channel suitable to measuring both parameters. The sensor is a technically complex two-dimensional phased-array system designed principally for soil moisture retrievals. The SMOS program includes a focused effort to retrieve salinity data over the ocean. The observatory will provide global coverage every 3 days and ~50 km resolution for a 3-5 year mission. The salinity data will be averaged over broader scales to reduce measurement error. Aquarius/SAC-D is a dedicated salinity mapping mission being developed by the US and Argentina for a three-year baseline mission. The principal salinity sensor will be a high-precision 1.4 GHz radiometer system plus radar backscatter measurements to correct the large effects of surface wind roughness. The focus of the Aquarius/SAC-D design is to optimize the salinity retrieval accuracy for global climate studies. Aquarius/SAC-D will provide global maps every 8 days at 100 km resolution with a three-beam push-broom configuration of 60-90 km single-beam footprint. Measurement errors will meet the mission's key science objectives with an rms uncertainty <0.2 psu on monthly time scales globally and closer to 0.1 psu in the tropics. A strong collaboration exists between the Aquarius/SAC-D and SMOS projects for both science and calibration. The latter will rely heavily on SSS measurements provided by the Global Ocean Observing System (GOOS).

**Monday, July 7 PM**

Presiding Chair: G.J. Goni

**JSP06/07P/B21-001****1400****RECENT ADVANCES IN THE TRITON PROJECT: SURFACE MOORING ARRAY IN THE WESTERN TROPICAL PACIFIC AND EASTERN INDIAN OCEANS**

Yoshifumi KURODA (JAMSTEC)

JAMSTEC has developed a surface moored-buoy system named TRITON (TRIangle Trans-Ocean buoy Network) for the better understanding of ENSO and the Asian monsoon. The TRITON buoy can measure wind vector, air temperature, relative humidity, shortwave radiation, atmospheric pressure, precipitation, current vector, subsurface temperature and salinity. It enables us to measure surface heat and fresh water flux, and also subsurface salinity changes to elucidate the heating and water mass mixing process. The four TRITON buoys along 156E were deployed in 1998 in the western tropical Pacific Ocean. TAO buoys west of 156E were replaced with TRITON buoys, and the TAO/TRITON array for monitoring ENSO was officially started in January 2000 harmonized with TAO array. The TRITON array was extended in the western most Pacific along 130E and two TRITON buoys were deployed in the eastern Indian Ocean in October 2001. At present in January 2002, eighteen TRITON buoys are working. The following topics will be presented, (1) development of TRITON array, (2) data quality of surface meteorological and subsurface temperature and salinity sensors, (3) data distribution, (4) scientific applications focusing on TRITON salinity

## INTER-ASSOCIATION

data: e.g., water mass mixing process off the New Guinea coast; and water mass variations in the eastern Indian Ocean.

### JSP06/07P/B21-002

1420

#### THE ARGO PROJECT: OBSERVING THE GLOBAL OCEAN IN REAL-TIME

Dean H. ROEMMICH (Scripps Institution of Oceanography)

The Argo profiling float project (<http://argo.jcommops.org>) is a key global element in the ocean observing system, measuring large-scale temperature and salinity (T/S) variability in the upper ocean for climate research and other applications. As of January 2003 there were 620 active Argo floats, drifting at 1-2 km depth and collecting a T/S profile and a measurement of mid-depth current every 10 days. When fully implemented in 2006, Argo will include 3000 profiling floats covering all of the world's ice-free, deep oceans. Data are made publicly available through the GTS and internet (<http://www.usgodae.org> or <http://www.ifremer.fr/coriolis/cdc/argo.htm>), usually within 24 hours of collection. Argo is an international effort endorsed by the IOC and WMO, and is a part of WCRP/CLIVAR and GODAE. Floats are being contributed by many nations, including Australia, Canada, China, Denmark, the European Union, France, Germany, India, Japan, Korea, New Zealand, Norway, the Russian Federation, the U.K. and the U.S., with coordination by the international Argo Science Team. Scientific studies with Argo float data have begun, based on the extensive float arrays in the North Atlantic and North Pacific and the developing arrays in the tropics and Southern Ocean. Recent and ongoing studies by a number of international investigators are reviewed to illustrate the wide uses of the Argo array: - Subtropical Mode Water Formation in the northwest and the southeast Pacific - Detection of mid-depth T/S variability in the southern Indian Ocean - Local and regional heat balances in the North Atlantic and North Pacific - Combination of Argo data with satellite altimetry - ENSO variability in the salinity of the tropical Pacific and eastern Indian Ocean Argo has many applications in basic oceanographic research and operational oceanography through its measurements of the physical state of the upper ocean on large spatial scales. Argo by itself will describe patterns of broadscale variability in upper-ocean temperature and salinity globally, and will enable interpretation of the subsurface expression of sea surface height variability observed by the Jason satellite altimeter. Argo together with other elements of the observing system will better reveal the role of the ocean in the climate system and will provide the necessary data for powerful new data assimilation and forecast models, to satisfy a broad range of applications.

### JSP06/07P/B21-003

1450

#### QUALITY OF ARGO SALINITY DATA MAINTAINED BY DELAYED-MODE QUALITY CONTROL

Taiyo KOBAYASHI<sup>1</sup>, Shinnya MINATO<sup>2</sup>, Toshio SUGA<sup>1</sup> (<sup>1</sup>Frontier Observational Research System for Global Change, Japan Marine Science and Technology Center, <sup>2</sup>Ocean Observation and Research Department, Japan Marine Science and Technology Center)

Argo, one of the key components of the global ocean observing system, consists of a global array of autonomous temperature/salinity profiling floats. How to calibrate the sensors, especially salinity sensors, of these floats is a major concern because direct comparison between the float data and any standardized data is not usually available. It has been agreed to use the "PMEL\_QC method" (Wong et al., 2003) as the standard delayed-mode quality control procedure for Argo salinity data. This method evaluates and corrects the Argo salinity data by comparing the float data with the local climatology at float locations estimated from nearby historical data by an objective mapping technique. This method will perform well when the float data are compared in the deep where natural variability of temperature-salinity relation is relatively small. Although the Argo Programme recommends that temperature-salinity profiles should be measured down to 2000dbar, quit a few floats with their deepest profiling depths are shallower than 2000dbar have been deployed mainly for technical reasons including the limitation in buoyancy control capacity. It is thus important to examine how the precision of salinity data by corrected by the PMEL\_QC method depends on the maximum depths of the observed profiles. We perform the PMEL\_QC method to several sets of the real profiling data reaching to 2000dbar and compare the results with another results for the same data when the profiles become artificially shallower to 1500dbar or 1000dbar. As the profiling depths become shallower in the subtropical region, estimation errors of the salinity correction increase; they are lower than  $\pm 0.01$ psu, about  $\pm 0.01$ - $0.015$ psu, and about  $\pm 0.02$ - $0.04$ psu for the profiling depths of 2000dbar, 1500dbar and 1000dbar, respectively. Estimation errors in the subarctic region are generally larger than those in the subtropical and tropical regions; about  $\pm 0.01$ - $0.015$ psu, about  $\pm 0.015$ - $0.03$ psu, and about  $\pm 0.02$ - $0.05$ psu when profile depth is 2000dbar, 1500dbar, and 1000dbar, respectively. It is because the temperature range effectively used for the salinity correction becomes narrower in the subarctic regions. Therefore, in order to maintain the data quality which almost satisfies the goal of the Argo Programme (accuracy of salinity  $\pm 0.01$ psu) with PMEL\_QC method, the profiles measured by Argo floats should reach as deep as 1500dbar at least constantly in the subtropical and tropical region, but have to reach as deep as 2000dbar constantly in the subarctic region.

### JSP06/07P/B21-004

1510

#### GLOBAL ARGO DATA REPOSITORY: A GATEWAY TO ARGO DATA, INFORMATION, AND SERVICE

Charles SUN (U.S. National Oceanographic Data Center/NOAA)

A long-term archive for Argo data, developed at the U.S. National Oceanographic Data Center (NODC), is presented in this paper. Argo data include real-time and delayed-mode profiles of ocean temperature and salinity (and conductivity, if any) measured by the Argo profiling floats. The purpose of this paper is to describe the development of a system for acquiring, preserving, and disseminating Argo data and information to the public. In the year 2000, a global array of approximately 3,000 free-drifting profiling floats, known as the Argo Ocean Profiling Network, was planned as a major component of the ocean observing system. Argo originated from the need to make climate predictions on both short and long time scales and has led to international participation and collaboration to ensure global coverage. Centers to handle the data collected by profiling floats have been established in a number of countries. All Argo data are publicly available in near real-time via the GTS (Global Telecommunications System) and in scientifically quality-controlled form with a few months delay. Two Argo Global Data Assembly Centers (GDACs), the US GODAE (Global Ocean Data Assimilation Experiment) Argo server and the French IFREMER (Institute for Research and Exploitation of the Sea) Argo server, are established to assemble the near real-time Argo data and provide them to the Argo users in a timely manner. The U.S. National Oceanographic Data Center (NODC) operates the long-term archive, also known as the Global Argo Data Repository (GADR), for Argo data. The GADR has the responsibilities for (1) preserving the data passed to the US NODC, (2) managing updates to Argo data that are re-analyzed some time later and for which corrections may be applied and (3) providing high quality Argo data to a wide variety of users in a timely and useful manner. Argo data are available both online to clients with high speed Internet access and on CD-ROM discs to

those who have poor Internet connections. The data served by the GADR are in the NODC netCDF format (fully compatible with ncBrowse) and the tab-delimited spreadsheet text format (compatible with Java OceanAtlas and Ocean Data View). The clients will use a "Web browser" to browse the Argo CD-ROM discs and "Acrobat Reader" to view, navigate, and print documents in the Adobe Portable Document Format (PDF) within a web browser. The CDs will be platform and operating system independent and inter-operable among browsers as well. It will provide assertive technology accommodations and services to persons with disabilities and ensure people with disabilities have equal access to Argo data and information.

### JSP06/07P/B21-005

1600

#### THE PACIFIC HIGH RESOLUTION XBT/XCTD NETWORK: MEAN AND TIME-VARYING MASS AND HEAT BALANCE OF THE TASMAN BOX

Dean H. ROEMMICH<sup>1</sup>, John GILSON<sup>1</sup>, Josh WILLIS<sup>1</sup>, Ken RIDGWAY<sup>2</sup>, Richard BAILEY<sup>3</sup>, Philip SUTTON<sup>3</sup> (<sup>1</sup>Scripps Institution of Oceanography, <sup>2</sup>CSIRO Marine Research, <sup>3</sup>National Institute of Water and Atmospheric Research - New Zealand)

Since the late 1980's, a network of zonal and meridional High Resolution XBT/XCTD (HRX) transects has been occupied through a multi-national collaborative effort, spanning the Pacific basin on a quarterly basis (<http://www-hrx.ucsd.edu>). With a scientist or technician on board, tight probe spacing resolves boundary currents and eddies in order to measure seasonal to interannual variability in temperature, salinity and geostrophic circulation from the mesoscale to the basin-scale. The Pacific HRX dataset covers up to 17 years along some transects, and is a valuable resource for climate-relevant research. As an example of HRX research, the seasonal-to-interannual balance of mass, heat, and salt in the southwestern Pacific is described. There, an 11-year HRX time-series has been collected along the perimeter of a region we call the Tasman Box. The region contains the South Pacific's subtropical western boundary current system. The East Australian Current carries about 15.6 Sv southward in the upper 800 m (referenced to 2000 m) near Brisbane, separating from the coast to form recirculations plus eastward flowing filaments in a region of strong mesoscale variability. Net geostrophic plus Ekman transport of waters warmer than 20.5-degrees C is about 6.3 Sv southward into the box across the Brisbane-Fiji line, with about 4.4 Sv warmer than 15.5-degrees C flowing eastward out of the box across Auckland-Fiji. Net water mass conversions in the upper ocean - inflow waters averaging about 26-degrees C and 35.4 psu, balanced by outflow averaging 18-degrees C and 35.7 psu - reflect the net evaporation and heat loss in the formation of Subtropical Mode Water. Transports are seasonally varying with a range of about 4 Sv in each transect, and maxima about March in both the southward inflow and eastward outflow. Interannual variability is also substantial. The 11-year mean heat balance shows good agreement between ocean heat transport into the box (averaging 40 w/m\*\*2) and heat loss to the atmosphere (35 w/m\*\*2). The seasonal balance is between air-sea flux and storage, with a smaller contribution from transport. The interannual balance shows substantial anomalies in all three terms of the heat budget, with largest interannual variability (30 w/m\*\*2) in ocean transport and interior storage. Maxima in the heat transport into the box occurred in 1993, 1997 and 2001.

### JSP06/07P/B21-006

1620

#### MERIDIONAL TRANSPORT OF NORTH PACIFIC INTERMEDIATE WATER ACROSS 37N BASED ON THE OBJECTIVE ANALYSIS OF LOWERED ACOUSTIC DOPPLER CURRENT PROFILER DATA

Hiroshi YOSHINARI<sup>1</sup>, Ichiro YASUDA<sup>2</sup>, Motoyoshi IKEDA<sup>3</sup> (<sup>1</sup>Graduate School of Environmental Earth Science, Hokkaido University, <sup>2</sup>Department of Earth and Planetary Science, Graduate School of Science, University of Tokyo)

The Meridional transport and the origin of North Pacific Intermediate Water (NPIW) in the Kuroshio-Oyashio interfrontal zone (K/O zone) were examined using hydrographic and directly-measured velocity data with LADCP (Lowered Acoustic Doppler Current Profiler) along 37°N in the observation performed in July 1998. The optimal interpolation method was applied to objectively derive transports and their spatial-interpolation errors. A statistically significant northward transport of 12.0±4.6 Sv was observed in the density of 26.6–27.5σθ from coast (141°E) to the Shatsky Rise (157°E). In the upper part of NPIW (26.6–27.0σθ), total transport was 4.1±1.2 Sv, of which Kuroshio component was 3.0±0.7 Sv and Oyashio 1.1±0.5 Sv. In the lower NPIW (27.0–27.5σθ), the total transport was 7.9±3.4 Sv, of which Kuroshio was 4.7±1.9 Sv and Oyashio 3.2±1.5 Sv. A southward transport of 4.4±3.6 Sv was observed from the Shatsky Rise to 179.5°E in the density of 26.6–27.5σθ. In the region west to the Shatsky Rise, the Oyashio mixing ratio derived from temperature and salinity in the K/O zone is larger than the ratio in the Oyashio and the Kuroshio transports, implying the southward transport of 1 Sv Oyashio water across the Oyashio Front in the upper NPIW. On the other hand, both kind of ratios is almost same in the lower NPIW, suggesting that the lower NPIW in the same region is maintained only by the northward transport of the NPIW formed near the Kuroshio Extension.

### JSP06/07P/B21-007

1640

#### BASIN-SCALE OCEANOGRAPHIC PROBLEMS OF THE ARCTIC OCEAN AND A MONITORING SYSTEM FOR THEIR SOLUTION

Andrey PROSHUTINSKY, John TOOLE, Richard KRISHFIELD (Woods Hole Oceanographic Institution)

It is common perception now that the recent history of the Arctic is characterized by a significant change in circulation, sea ice thickness and extent, heat and salt content. But these changes could be erroneous because observations in the Arctic Ocean are scarce and there are huge gaps in the data in space and time. In order to fill these gaps in future studies, we propose an observational Arctic Ocean Monitoring System (AOMS) that can serve for sustained, long-term efforts to document and understand variability in the ocean and sea ice. Building on the successful Moored Profiler technology, we propose to initiate development of an automated, long-lived, ice-tethered buoys capable of returning high-vertical-resolution profiles of upper ocean temperature and salinity in the Arctic Ocean during all seasons.

### JSP06/07P/B21-008

1700

#### NEAR-GOOS DATA SYSTEM

Takashi YOSHIDA (Japan Meteorological Agency)

The North-East Asian Regional - Global Ocean Observing System (NEAR-GOOS) is a regional pilot project of GOOS in the Western Pacific region, presently with the participation of China, Japan, the Republic of Korea and the Russian Federation, with a view to demonstrating the usefulness of a regional ocean observing system within the framework of GOOS. The essence of NEAR-GOOS in its initial phase is to promote free oceanographic data exchange in real-time through Internet in support of daily mapping of sea conditions in

marginal seas bordered by NEAR-GOOS participating countries, benefiting a wide range of marine users. In order to promote the data exchange, a data exchange system called NEAR-GOOS data system has been established by the four participating countries. The system started its operation in 1996 and oceanographic data not only in the NEAR-GOOS region but also in the global ocean have been distributed through the system. It consists of Regional Real Time and Delayed Mode Data Bases (RRTDB and RDMDDB) and national real time and delayed mode data bases. RRTDB and RDMDDB are in charge of distributing all oceanographic data in the region. National data bases are in charge of distributing oceanographic data obtained in each country. One of the major data sources of RRTDB is the Global Telecommunication System (GTS), which interconnect meteorological telecommunication centers in order to exchange meteorological and oceanographic data in real time. Marine weather observations from voluntary observing ships and buoys, subsurface temperature and salinity profiles observed by ships of opportunity, research vessels, buoys and profiling floats are exchanged through GTS. RRTDB, which is operated by the Japan Meteorological Agency, retrieves those oceanographic data from GTS and provides them to registered users. RDMDDB, which is operated by the Japan Oceanographic Data Center (JODC), serves to provide secondhand RRTDB data and other oceanographic data gathered by JODC and archive them. Even though the data system has been successfully operated, the data exchanged through it are still limited. Extension of the types and volume of the exchanged data should be given high priority in the future NEAR-GOOS activity.

## JSP06-Posters

Monday, July 7

## THE GLOBAL OCEAN OBSERVING SYSTEM (IAPSO, IAG, IOC)

Location: Site D

Monday, July 7 PM

JSP06/07P/D-001 Poster 1400-008

## GLOBAL MEAN SEA SURFACE HEIGHT MODE BASED ON SATELLITE ALTIMETRY DATA

Jianguo HU<sup>1</sup>, Jiancheng LI<sup>2</sup>, Weiping JIANG<sup>2</sup> (<sup>1</sup>Chinese Academy of Surveying and Mapping, <sup>2</sup>Wuhan University)

Nowadays, global environment change is one of the most important questions we mankind pay attention to. There are many factors which have influence on environment, for example, weather change, sea level change, gravity field change, volcano activity, El Niño and so on. As a focus of geo-science and environment science, mean sea surface height (MSSH) is one of these questions. In the paper, the overall editing criteria for altimetric data are considered and the geophysical correction model is improved. The datum for various altimetric data is also unified, and the method of a full-combined crossover adjustment for different altimetric tracks is used to improve the radial orbits of Geosat, ERS-1 and ERS-2 data. The data used to compute MSS include 8 years of Topex/Poseidon data (cycle 11 to 284), 2 years of Geosat ERM data (cycle 1 to 44), 5 years of ERS2 data (cycle 1 to 52) and all ERS-1 168-day data. The MSS is determined with a grid resolution of 2° × 2° within the ±82° latitude and its precision is better than 0.05m. Moreover, 3.75° × 3.75° CLS\_SHOM98.2 MSS, 3° × 3° GFZ MSS95A and 3.75° × 3.75° OSU MSS95 are compared with the computed MSS to test the model in this paper.

JSP06/07P/D-002 Poster 1400-009

## A NEW FALL-RATE EQUATION FOR THE JAPANESE T-5 XBT PROBES

Shoichi KIZU, Kimio HANAWA (Department of Geophysics, Graduate School of Science, Tohoku University, Aramaki Aza Aoba, Aoba-ku, Sendai 980-8578 JAPAN)

The expendable bathythermograph (XBT) is a free-fall instrument, which is dropped from air into water and measures temperature at a fixed sampling rate as it falls through the water column. Due to its simple, could be automatic, operation, XBT has become very popular throughout the world for the temperature measurement of the upper ocean. However, since it carries no pressure sensor, we always need to infer the depth of measurement from the time elapsed, using the time-depth conversion equation (fall-rate equation). The manufacturer supplied different equations for different models of XBT probe to take account of their different shapes and weights in water, but the reliability of the supplied equations has been a matter of debate for a long time. T-5 XBT can reach the greatest depth (nominally 1850 meters) among all XBT models in the market. Here we investigated the accuracy of the manufacturer's fall-rate equation for the model, about which the past studies showed inconsistent results. More than 200 pairs of XBT-CTD (Conductivity-Temperature-Depth profiler) temperature measurement were collected from various oceans on the earth, and the depth error is estimated by the method of Hanawa *et al.* (1995) with modifications. We found that the manufacturer's fall-rate equation does not seem to have bias when applied to the T-5 XBT by Sippican, Inc., in USA, the largest supplier of the instrument, while it overestimates depth when applied to T-5 by TSK, Co. Ltd., in Japan, the second largest and the dominant supplier to the Asian countries. It is found that the depth error increases approximately linearly with depth and approaches one hundred meters at the deepest part of measurement. Based on these results, we propose a new fall-rate equation for T-5 XBT by TSK, which is  $D(t) = 6.4751 T - 0.00175 T^2$ , where  $D$  is the depth in meters at time  $T$ , in seconds.

JSP06/07P/D-003 Poster 1400-010

## OCEAN OBSERVATIONS IN CLIVAR

Michael SPARROW, Katy L. HILL, Howard CATTLE, Roberta BOSCOLO, Zhongwei YAN (International CLIVAR Project Office)

CLIVAR, the Climate Variability and Predictability study of WCRP started in 1995 with an ambitious plan to explore coupled climate variability and predictability at global scales from seasons to centuries. The structure of CLIVAR is based around different principal research areas. These range from the study of ENSO, Asian-Australian and American Monsoon and African climate variability on seasonal to interannual timescales to Atlantic, Pacific, Indian and Southern Ocean climate variability on decadal to centennial time scales, and anthropogenic climate change. Each principal research area is distinct, in its aims, phenomenological base, geographical region of interest and, in some respects, scientific approach required. Ocean observations are a key element of the CLIVAR programme. CLIVAR aims to establish the appropriate mix of measurement platforms and synthesis techniques to determine the full suite of ocean variables, including air-sea fluxes, required for CLIVAR research, taking into account existing and new technologies. To achieve this CLIVAR is working, amongst others, with the emerging operational observing systems of the Global Ocean Observing System, the implementation activities of the Joint Commission on

Oceanography and Marine Meteorology and its panels, the Ocean Observations Panel for Climate and the Partnership for Observation of the Global Ocean. The planning of CLIVAR ocean observations is mainly coordinated through the CLIVAR Ocean Observation Panel and the regional basin panels: The Atlantic, Pacific, Southern Ocean Panels and the Asian-Australian Monsoon Panel (which currently has responsibility for the Indian Ocean). CLIVAR's needs for sustained ocean observations to enable implementation and development of its programme are described in this poster, with illustration of their application to ongoing and planned activities in the ocean basins.

JSP06/07P/D-004 Poster 1400-011

## FERHRI PRESENT ACTIVITY WITHIN NEAR-GOOS AND RELATED PROJECTS

Evgeniy Viktorovich KARASEV<sup>1</sup>, Aleksander Nikolaevich MAN'KO<sup>2</sup>, Evgeniy Petrovich URAEVSKIY<sup>3</sup>, Nikolay Afanasievich RYKOV<sup>4</sup> (<sup>1</sup>Vice-director, Far Eastern Regional Hydrometeorological Research Institute, <sup>2</sup>Department of Oceanography and Marine Ecology, Far Eastern Regional Hydrometeorological Research Institute < RUSSIA, <sup>3</sup>Department of Mathematical Analysis, Far Eastern Regional Hydrometeorological Research Institute, RUSSIA, <sup>4</sup>Department of Oceanography and Marine Ecology, Far Eastern Regional Hydrometeorological Research Institute, Russia)

EVGENIY KARASEV, Aleksander Man'ko, Evgeniy Uraevskiy, Nikolay Rykov Far Eastern Regional Hydrometeorological Research Institute, Vladivostok, Russia The Russian Hydrometeorological Service carries problems of operative information management on ocean to the paramount questions demanding constant attention. On the Russian Far East the given problem, alongside with other divisions of Hydrometeorological Service, Far Eastern Regional Hydrometeorological Research Institute (FERHRI) is engaged in the decision. The decision of a problem of operative maintenance is carried out by the information on ocean in two ways. The first way is the decision of a problem within the framework of the national program of creation of uniform system of the information in the World Ocean (USIWO). The main goals of the system are directed to engineering such modules as operative supervision, transfer, gathering and distribution of the information to users on uniform principles for all Russian Federation, with use of technical decisions and development of normative documents. Creation of the special centers is stipulated, one of which is planned to organize in FERHRI for realization of system of accumulation and distribution of the information. The second way is direct participation in the international projects, which objective includes operative reception of the information on ocean. FERHRI is one of participants from the Russian side of project NEAR-GOOS, which is regional component of GOOS. Within of this project FERHRI conducts the national operative database being a part of system of operative maintenance by the information on ocean in area of NEAR-GOOS responsibility. Web-site regarding NEAR-GOOS project is created in FERHRI both in English and Russian versions. While development of the ARGO project FERHRI makes the big efforts for connection of Russia to this program. Decision on Russian membership in ARGO project will be defined this year. Last October, FERHRI as the representative of the Russian side has carried out start of two floats in the NW Pacific, it is created Web-site "Russian-ARGO", researches in a direction of active mastering the information received during performance of the program are carried out. Realization of the specified programs will allow Russia to play more active role in operative maintenance with the information on ocean in the North Pacific.

JSP06/07P/D-005 Poster 1400-012

## THE TROPICAL ATLANTIC OBSERVING SYSTEM

Silvia Lucia GARZOLI<sup>1</sup>, Jacques SERVAIN<sup>2</sup>, Gustavo Jorge GONI<sup>1</sup> (<sup>1</sup>National Oceanic and Atmospheric Administration, Atlantic Oceanographic and Meteorological Laboratory, <sup>2</sup>Center IRD de Bretagne)

The oceanic in-situ data base in the Atlantic has been derived primarily during the last decades from volunteer observing ship (VOS) programs, coastal and island tide gauge stations, and a small number of drifting buoys. However, VOS measurements of surface meteorology and subsurface temperatures are concentrated mainly along well-traveled shipping routes, among which there are large data gaps. Satellite estimates of some key variables are available over the whole Atlantic basin with more uniform spatial and temporal resolution. However, satellites do not deliver direct measurements of the subsurface thermal structure in the ocean, which is essential for understanding processes affecting the evolution of SST and the thermocline depth. Since 1997 a program, called PIRATA, of moored measurements has been under development in the Atlantic provide high-resolution measurements of surface heat, moisture fluxes, temperature and salinity. Simultaneously to the start of the PIRATA moorings, and to the global Drifter Array, a program was started at NOAA/AOIML to significantly increase the deployment of surface drifters in the tropical Atlantic. The purpose of the program is to observe the basin-wide scale tropical Atlantic current and SST fields on seasonal to inter-annual time scales. Currently, 80 drifters per year are deployed from ships of opportunity and research vessels providing an accurate picture of the surface current field and filling up gaps for needed observations of SST. Together with the existing observations provided by the ships of opportunity, the PIRATA array and the surface drifters constituted the initial tropical Atlantic Observing System. In the year 2000, two new and important components were added: a new high density XBT line (AX08) that runs between Cape Town, South Africa and the north-east coast of the US and the ARGO program. The main objective of AX08 is to measure the upper ocean thermal structure and to characterize both the mean and the time-dependent upper ocean properties of the tropical portion of the MOC and of the shallow subtropical cell in the Tropical Atlantic. The resolution along the line is 30 km between 10S and 10N and 40 km between 20S and 10S and 10N and 20N. This line is occupied four times per year, in four different seasons. ARGO is an international program whose goal is to deploy an array of 3,000 free-drifting profiling floats in a period of five years. Approximately 700 floats will be operating in 2003 in the Atlantic, of which about one third will be in the tropical basin. These profiling floats measure the temperature and salinity of the upper 1000 to 2000 m of the ocean.

JSP06/07P/D-006 Poster 1400-013

## ON THE MEAN AND FLUCTUATING TEMPERATURE FIELD IN THE SUBTROPICAL NORTH ATLANTIC OCEAN

Molly O'Neil BARINGER, Dennis MAYER, Gustavo GONI (NOAA/AOIML)

High density XBT sections along tracklines from the Gibraltar Straits to the Straits of Florida (AX7) and from New York to Puerto Rico (AX10) starting in 1995 and 1997 respectively with average spatial sampling of 30-40 km show representative features seen on many previous hydrographic surveys in the area. The improved resolution along these sections provides a new look at the spatial scales of variability and improves estimates of heat transport. The spatial variability is diagnosed by examining an ensemble of Fourier transformed temperature data as a function of depth and examining the amount of variance contained in the mean versus the perturbation (mesoscale) fields. This resulted in scales of about 600 km that distinguish the large scales from the mesoscale in both the meridional and horizontal directions. At the depth of the main thermocline along AX7, the scales increase rapidly,

## INTER-ASSOCIATION

reaching gyre scale (on the order of 6000 km) by 800 m and characterize an intrinsic anisotropy consistent with the gyre structure, implying that mesoscale features are increasingly important with depth. Decorrelation scales, computed by a structure function analysis, showed that the perturbation temperatures have much smaller scales (less than 100 km). Implicit in these findings is that the large scales require XBT sampling of 200-600 km and perturbation scales require sampling of order 30-50 km (2-3 XBTs per length scale). To assess how this increased spatial sampling has improved estimates of heat transport, we examined errors in baroclinic heat transport for reduced sampling. We found that the average baroclinic heat transport was  $-0.87 \pm 0.21$  PW southward, consistent with earlier hydrographic estimates near this latitude. The errors incurred by reducing the station spacing rapidly increase with increased station spacing. Errors of about  $\pm 0.2$  PW occur for spacing between 150-600 km (i.e. sampling of the synoptic and mesoscale structure), including a  $-0.05$  PW mean bias. Errors reduced dramatically for spacing less than 150 km, where the mesoscale field is resolved (as determined by the decorrelation analysis).

**JSP06/07P/D-007** Poster **1400-014**

### NEAR-GOOS RDMDB AND THE RELATED JODC ACTIVITIES

Satoshi SATO (Japan Oceanographic Data Center)

The first phase of NEAR-GOOS (North-East Asian Regional GOOS) was intended to provide a regional framework for gathering and distributing oceanographic data. Based on the recommendation of the NEAR-GOOS Coordinating Committee, the Japan Oceanographic Data Center (JODC) has operated the NEAR-GOOS Regional Delayed Mode DataBase (RDMDB: <http://near-goos1.jodc.go.jp/>) since 1996. RDMDB is an on-line data retrieval system. It receives and archives the oceanographic and marine meteorological data from the Regional Real Time DataBase (RRTDB) operated by the Japan Meteorological Agency 30 days after they are collected. RDMDB also receives oceanographic data and products from other sources, e.g., the National Delayed Mode DataBases of the member countries. Such data are provided through Internet without charge. JODC has operated another on-line database, J-DOSS (JODC Data On-line Service System: <http://www.jodc.go.jp/service.htm>). JODC has fulfilling the role of the synthetic marine data bank of Japan in acquisition of various oceanographic data obtained by research institutes and organizations in Japan. Those who need the oceanographic data in the world can search and download the data by using J-DOSS. At the present time, J-DOSS provides 12 kinds of data and information, serial station data, ocean current data, tide data (hourly value), marine biological data (plankton), 500m mesh depth-sounding data around Japan, 3 statistical data (temperature, salinity, and ocean current), NOPs (National Oceanographic Programs), CSRs (Cruise Summary Reports), IOC publications, and Oceanographic Abbreviation/Acronym Dictionary.

**JSP06/07P/D-008** Poster **1400-015**

### COMPARISON OF HYDROGRAPHIC AND ALTIMETER BASED ESTIMATES OF SEA LEVEL HEIGHT VARIABILITY IN THE ATLANTIC OCEAN

Dennis MAYER, Molly O'Neil BARINGER, Gustavo GONI (NOAA/AOML)

Our ability to understand the means by which mass and heat are exchanged between the tropics and subtropics is seriously compromised when using only sea level data because the exchange processes span a wide range of variability across the different dynamical regimes in our domain. Expendable bathythermograph XBT profiles and TOPEX/Poseidon T/P altimeter data are compared to temperature anomalies TA and to dynamic height anomalies DHA for the period 1993 through 1997 to determine how much can be inferred about the internal field of mass from sea level changes. Our focus is on the annual cycle along two well-sampled XBT sections on the western and eastern sides of the Atlantic Ocean from 10°S to 40°N. XBT profiles were matched time/location to Sea height anomalies SHA derived from T/P data, converted into DHA using TS relationships and then binned monthly into 2° of latitude by 4° of longitude boxes. The vertical mass distribution cannot always be inferred from SHA alone, unless there is a strong relationship between SHA and DHA and an understanding of the details of how temperature variability affects DHA. These relationships can be problematic if SHA are small. This occurs in zones of transition in the vicinity of troughs where small fluctuations in SHA belie the true nature of water column variability. These areas separate the mid-latitudes where surface buoyancy fluxes dominate from those in the equatorial region where ocean dynamics cause thermocline effects that dominate the forcing of sea level. Thus, the variability of SHA in transition regions tends to be small because both surface and thermocline variability may be significant but compensating in nature. This emphasizes how important direct observations in situ data can be in interpreting SHA correctly. Strong relationships between SHA and DHA are suggested where more than half of the SHA variance in the annual cycle can be accounted for by DHA approximately 30% of the positions along the two XBT sections. These relationships between SHA and DHA for residual variability obtained by removing the annual cycle are weak. The exceptions are in two areas of large sea height variability in the western basin where there is significant interannual variability. The first is in the tropics in the vicinity of the tropical gyre trough near 50°W 8°N. The second is in the Gulf Stream near 70°W 38°N. An analysis of Panulirus data at 32.2°N, 64.5°W suggests that in situ data may be needed down to at least 1000m where interannual variability accounts for about 40% of the SHA variance.

**JSP06/07P/D-009** Poster **1400-016**

### PATHWAYS OF NORTH PACIFIC INTERMEDIATE WATERS

Yuzhu YOU (The University of Sydney Institute of Marine Science (USIMS), University of Sydney, Australia)

Updated hydrographic data are used in a water mixing scheme to identify the spreading paths of North Pacific Intermediate Waters (NPIWs) in the subtropical gyre. The mixing scheme comprises two NPIW formation sources from the subpolar regions, Okhotsk Intermediate Water (OIW) and Gulf of Alaska Intermediate Water (GAIW), and a transformed aged NPIW (aNPIW) in the northwestern subtropical gyre southeast of Japan. Three conservative variables, potential temperature, salinity and potential vorticity are used as model input signals. The NPIW layer is spanned by four neutral density surfaces,  $\sigma_{\theta N} = 26.5, 26.9, 27.2$  and  $27.4$ . Mixing fractions as model outputs on neutral density surfaces imply spreading paths of NPIW. Results show that NPIW source waters enter the subtropical gyre mainly from the northeastern subtropical gyre. The shift of the axes of NPIW salinity minimum, changed from dominantly westward in the southern rim of the subtropical gyre on  $\sigma_{\theta N} = 26.5$  to northeast-southwestward crossing the gyre on  $\sigma_{\theta N} = 26.9$ , is the cause of forming the subtropical NPIW.

JSP06

Monday, July 7 - Tuesday, July 8

THE GLOBAL OCEAN OBSERVING SYSTEM (IAPSO, IAG, IOC)

Location: Site B, Room 21

Tuesday, July 8 AM

Presiding Chair: H. Kawamura

JSP06/08A/B21-001

0900

### ANNUAL TO INTERANNUAL VARIABILITY IN THE GLOBAL INTEGRAL OF UPPER OCEAN HEAT CONTENT

Josh K. WILLIS, Dean ROEMMICH, Bruce CORNUELLE (Scripps Institution of Oceanography, University of California, San Diego)

Because of its large heat capacity and organized circulations, the ocean plays important roles in the Earth's climate system through the storage and transport of heat. As globally averaged atmospheric temperature rises, it becomes increasingly important to quantify the ocean's ability to absorb and sequester excess heat, as well as to understand how a heated ocean affects the atmosphere and cryosphere. Describing variability in globally averaged, upper-ocean heat content is therefore an important step toward understanding the ocean's role in the global heat budget. A time series of upper-ocean heat content from 1993 to the present is calculated using a combination of *in situ* temperature profiles and satellite altimetry data. The time series is calculated using a new technique to combine *in situ* and satellite data (Willis et al., *JGR*, submitted Dec., 2002) that results in substantially less error than estimates made from either data set alone. The time series shows annual to interannual variability of heat content in the upper 800 m of the water column, averaged over the globe, including inland and marginal seas. Maps of the yearly heat content anomaly will also be presented. The merged TOPEX/Poseidon - ERS product from AVISO was used to provide altimetry data for the estimate. By compiling data from several different sources, approximately 950,000 temperature profiles were found for the time-period from 1992 to the present. This includes a large number of profiles taken by subsurface floats as part of the Argo program. In recent years, subsurface floats have begun to contribute a substantial fraction of the globally available profiles as well as to provide data in historically data-sparse regions such as the Southern and Indian Oceans. In addition to quantifying interannual variability on a global scale, this work also illustrates the importance of maintaining continuously updated monitoring systems that provide global coverage of the world's oceans. Such ongoing projects, like the TOPEX/Jason satellite altimetry program and the Argo float program provide a critical foundation for characterizing variability on regional, basin, and global scales and quantifying the ocean's role as part of the climate system.

JSP06/08A/B21-002

0920

### COMBINED USE OF ALTIMETRY AND IN-SITU DATA FOR OCEAN CLIMATE MONITORING

Shiro IMAWAKI<sup>1</sup>, Hiroshi UCHIDA<sup>2</sup>, Daisuke AMBE<sup>3</sup> (<sup>1</sup>Research Institute for Applied Mechanics, Kyushu University, Kasuga, Fukuoka 816-8580, JAPAN, <sup>2</sup>Japan Marine Science and Technology Center, Natsushima, Yokosuka 237-0061, JAPAN, <sup>3</sup>Interdisciplinary Graduate School of Engineering Sciences, Kyushu University, Kasuga, Fukuoka 816-8580, JAPAN)

Satellite altimeters can measure the sea-surface dynamic topography down to the oceanic mesoscale and provide irreplaceable information for ocean climate monitoring. The altimeter data can be utilized much more efficiently by being combined with *in situ* oceanographic data. Here are shown two examples; one is the surface flow field of the North Pacific derived by combined use of altimeter and surface drifter data, and the other is the Kuroshio transport estimated from altimeter data by using empirical relationship between the transport and sea-surface height difference, which has been obtained from *in situ* intensive observations. Example 1: The surface flow field. In the altimeter data processing, the information on the temporal mean topography is lost. Here, the mean surface flow field is estimated by combining anomalies of sea-surface dynamic topography obtained from altimeter data with *in situ* surface velocities estimated from trajectories of surface drifters, as follows. Sea-surface velocity may be divided into the temporal mean and anomaly. The velocity anomalies are derived from satellite altimeter data with geostrophic approximation. Where a drifter measured the surface velocity, the temporal mean velocity can be estimated by subtracting the altimeter-derived velocity anomaly at that time from the drifter-measured surface velocity. The method is applied to the surface flow field of the North Pacific, using TOPEX/POSEIDON and ERS-1/2 altimeter data (CLS gridded data), and WOCE-TOGA surface drifter data obtained from October 1992 through August 2001. The temporal mean velocity field is estimated with a resolution of quarter degrees in both latitude and longitude. The instantaneous velocity field is estimated by summing up the temporal mean velocity field and velocity anomalies, every ten days during the nine-year period of 1993-2001. The instantaneous flow field shows energetic variability of the Kuroshio Extension vividly. Example 2: The Kuroshio transport. In 1993-1995, the ASUKA (Affiliated Surveys of the Kuroshio off Cape Ashizuri) Group carried out intensive observations of the Kuroshio south of Japan, including direct current measurements and frequently repeated hydrographic surveys along a subsatellite track of TOPEX/POSEIDON. Velocity sections are obtained by geostrophic calculation using the hydrographic survey data, referenced to velocities observed at mid and abyssal depths. Estimated transports of the Kuroshio have a high correlation with sea-surface height differences across the Kuroshio. Having this relationship and using the altimeter data, we obtained a time series of Kuroshio transport over nine years (1993-2001) at ten-day intervals. The Kuroshio transport, excluding contributions by local recirculations, is estimated to be 43 Sv on average. The range of annual fluctuation is found to be much smaller than that of transport expected from the interior wind stress curl.

JSP06/08A/B21-003

0950

### UPPER OCEAN DYNAMICS IN THE TROPICAL AND SOUTH ATLANTIC FROM HIGH DENSITY XBT LINES AX08 AND AX18

Gustavo Jorge GONI<sup>1</sup>, Molly O'Neil BARINGER<sup>1</sup>, Silvia Lucia GARZOLI<sup>1</sup>, Qi YAO<sup>2</sup>, Claudia SCHMID<sup>3</sup> (<sup>1</sup>National Oceanic and Atmospheric Administration, Atlantic Oceanographic and Meteorological Laboratory, <sup>2</sup>University of Miami, Rosenstiel School of Marine and Atmospheric Science, CIMAS)

We present results obtained from two high density XBT lines that run across the Atlantic Ocean, from Cape Town to New York City (AX08) and from Cape Town to Buenos Aires (AX18). A total of six and two realizations were carried in lines AX08 and AX18, respectively, by January 2003. XBTs are deployed in high density mode (every 30-40 km), except along AX08 north of 20N where they are deployed in low density (every 100-150 km) mode. Additionally, profiling floats are also deployed to obtain salinity profiles in some transects. The temperature sections reveal the major ocean currents in the upper 800 m. The

Tuesday, July 8 AM

Presiding Chair: C. Jago

five AX08 transects are used to compute the water mass transport of the major currents in the tropical Atlantic and to investigate their spatial and temporal variability. The two temperature sections across the South Atlantic (AX18) are used to estimate the upper ocean contribution to the Meridional Overturning Circulation by integrating the geostrophic transport across the subtropical gyre. In both lines, dynamic heights are computed using the XBT temperature profiles with salinity derived from historical T-S relationships. The dynamic heights estimated by combining altimeter data with climatological dynamic height fields are compared with the XBT-derived values. The error in XBT-derived dynamic height introduced by using historical T-S relationships instead of synoptic salinity data from profiling floats are of the order of 1.5 cm in the tropical Atlantic. The structure exhibited in the dynamic height and in the altimeter-derived sea height fields do not reveal all the components of the upper ocean current system, making the temperature sections presented here critical for computing transports and investigating the temporal and spatial variability of the upper ocean dynamics. Four and two transects are expected to be carried out each year in lines AX08 and AX18, respectively. Data and preliminary results from these and other AOML-maintained high density XBT lines can be found in: <http://www.aoml.noaa.gov/phod/hdenxbt/>

**JSP06/08A/B21-004****1040****OPERATIONAL ALTIMETRY : SSALTO/DUACS READY FOR GODAE**

Pierre-Yves LE TRAON (CLS Space Oceanography Division)

The near real time (NRT) processing of altimeter data was developed by CLS as part of DUACS (Developing Use of Altimetry for Climate Studies), a European Commission 3-year project which started in February 1997. DUACS was coordinated by CLS, and gathered four of the major climate research teams in Europe. Since the end of DUACS, the system has continued to provide NRT altimeter data for operational oceanography applications. During that time period, a new version of the system was also developed and has been operational since early 2002. The new system called SSALTO/DUACS is part of the CNES SSALTO multi-mission ground segment and is funded by CNES and the Midi-Pyrénées regional Council. It incorporates several improvements in the processing algorithms and is able to process TOPEX/POSEIDON (TP), ERS-2, GEOSAT Follow On (GFO), Jason-1 and ENVISAT data. The most recent geophysical corrections are applied and improved orbit error and long wavelength error reduction schemes are used. SSALTO/DUACS now provides MERCATOR, GODAE and climate forecasting centers with directly useable, high quality NRT altimeter data. Delayed mode high quality data are also produced for reanalysis activities. An overview of the SSALTO/DUACS system will be given and its main applications and users will be described.

**JSP06/08A/B21-005****1100****GODAE: THE GLOBAL OCEAN DATA ASSIMILATION EXPERIMENT**

Neville Ross SMITH (BMRC, Bureau of Meteorology)

The Global Ocean Data Assimilation Experiment (GODAE) was conceived in 1997 as a path-finding initiative for operational oceanography. While several agencies already had operational models and services, in general the community lacked the observational power and sophisticated model and data assimilation systems to fully exploit the accrued knowledge and recognized potential. The vision behind GODAE is that new societal and economic advantages can be provided through a global system of observations, communications, modelling and assimilation, that will deliver regular, comprehensive information on the state of the oceans in a way that will promote and engender wide utility and availability of this resource for maximum benefit to society. GODAE is a practical demonstration of feasibility and utility and of near-real-time, routine global ocean data assimilation. Through 2002, individuals and groups have formed a partnership to develop both regional and global prototype systems and have worked with relevant agencies to develop the infrastructure needed for GODAE. This year marks the beginning of the Demonstration Phase (2003-2005) and already many groups are routinely producing ocean analysis and forecasting products, ranging from short-range marine environmental predictions to sophisticated estimates of the ocean climate circulation. This presentation will review the strategy, discuss different aspects of the implementation of GODAE, and provide a context for GODAE within the general context of ocean and climate research. GODAE has a sound technical and scientific basis. Comprehensive integrated, global measurement networks provide the observational foundation, with satellites and Argo playing crucial roles. Full functionality depends on improvements in data management and data and product serving technology and GODAE is fostering innovative solutions to meet these needs. Ocean models and data assimilation provide the power to interpret and extrapolate complex observations into ocean products of broad utility. Several applications will be described, with the focus on value-adding and user products.

**JSP06/08A/B21-006****1130****THE ECCO ROUTINE GLOBAL OCEAN DATA ASSIMILATION SYSTEM**

Ichiro FUKUMORI, Tong LEE, Dimitris MENEMENLIS (Jet Propulsion Laboratory, California Institute of Technology)

An ocean data assimilation system producing regular analyses is established so as to monitor global ocean circulation and to better understand processes underlying the ocean's seasonal-to-interannual changes. The data assimilation system is a product of the consortium "Estimating the Circulation and Climate of the Ocean (ECCO)" and its contribution to GODAE. The system is based on a near-global primitive equation model of high resolution (1-deg telescoping to 0.3-deg with 10m near surface layers). Measurements from satellite altimetry (TOPEX/POSEIDON, Jason-1) and in situ hydrography (XBTs, moorings, floats, and climatology) are assimilated. The assimilation is based on a hierarchical approach that consists of 1) a Green's function method to adjust gross characteristics of the model, 2) a partitioned Kalman filter and smoother for routine assimilation and analysis, and 3) an adjoint method for periodic rigorous optimization. Analyses are regularly updated and are available via a Live Access Server at <http://www.ecco-group.org/las>. The data assimilation system will be reviewed and examples of its applications will be described.

**JSP07****Tuesday, July 8****THE COASTAL OCEAN OBSERVING SYSTEM (IAPSO, IAG, IOC)**

Location: Site B, Room 17

**JSP07/08A/B17-001**

Invited

**0900****STUDYING BIOGEOCHEMICAL PROCESS ON THE MID-ATLANTIC CONTINENTAL SHELF USING AN OCEAN OBSERVATORY**

Oscar SCHOFIELD, Scott GLENN, Robert CHANT (COOL, Rutgers University)

The Ocean Sciences Decadal Committee in laying out oceanography's future suggested "The very few existing time-series stations paint a compelling picture of important oceanic changes in physics, chemistry and biology. Yet these stations capture the time domain at only a single point. New strategies for observing the appropriate spatial correlation are required." The question confronting the community is how do we get there? Key enabling technologies are opening the door. These include: (1) long-duration moorings or cabled observatories for subsurface time, (2) high-frequency RADARs providing real-time surface current maps over shelf scales, (3) a growing international constellation of high-resolution ocean color satellites, and (4) an emerging class of long-duration remotely-controlled Autonomous Underwater Vehicles (AUVs). These technologies, operated in an integrated manner, form the backbone of the New Jersey Shelf Observing System (NJ-SOS). This observationally rich environment changes the relationship between models and observation. In the well-sampled ocean, forecast errors are dominated by uncertainties in the model formulations or boundary conditions, and ensemble forecasts with differing parameterizations can be compared to observations so as to improve our understanding of errors associated with various model assumptions. The new paradigm of an observationally rich environment will in the near future feed ensemble biogeochemical models allowing us to assess many critical assumptions in elemental cycling on continental shelves. These approaches will fundamentally alter how biologists and chemists study the ocean processes.

**JSP07/08A/B17-002****0930****THE CAROLINA COASTAL OCEAN OBSERVATION AND PREDICTION PROJECT**

Lian XIE, Leonard J. PIETRAFESA, John M. MORRISON (Department of Marine, Earth and Atmospheric Sciences, North Carolina State University)

This presentation will introduce the Carolinas Coastal Ocean Observing and Prediction System (Caro-COOPS) and preliminary results from the 2001-2002 activity. This project is founded upon a partnership -- led by the University of South Carolina's Belle W. Baruch Institute (USC), with North Carolina State University (NCSSU), and the University of North Carolina at Wilmington (UNCW) -- and establishes the capacity to monitor and model estuarine and coastal ocean conditions in the Carolinas, USA. It will provide a capability for real-time predictions and ultimately forecasts to mitigate natural hazards, support management of living resources and marine ecosystems, and facilitate safe and efficient marine operations and support national security efforts. The central goal of Caro-COOPS is prediction of coastal ocean processes. The overall objectives are to: a) integrate information on the causal biological, chemical, and physical processes in the Carolinas coastal ocean to provide a thorough understanding of how physical forcing and biological responses are coupled on regional spatial scales and seasonal and inter-annual time scales; b) assess the predictability of specific coastal processes and events; c) develop accurate forecasting models; and d) create tools for applying and evaluating these predictions in the context of "end-to-end" early warning systems. Caro-COOPS will represent a wholly integrated system for coastal observations and their application to user-driven research, societal, and economic needs. Moreover, it will provide three major advances in observing system capacities and capabilities: 1) It will establish an extensive array of instrumented moorings in the South Atlantic Bight, which currently receives extremely sparse coverage compared with other significant coastal regions, such as the Gulf of Mexico, New England coast, and the Chesapeake Bay. 2) It includes the development of a comprehensive data management system, essential for access to, and integration of, high quality, real-time data; the system will be designed to maximize flexibility and utility, with a view towards serving as a model and/or support for other coastal ocean observing systems; 3) It incorporates an advanced suite of integrated models that will markedly improve the predictive capacities of real-time physical data from coastal ocean instrumentation.

**JSP07/08A/B17-003****0950****THE EUROPEAN SEA LEVEL SERVICE (ESEAS): A CONTRIBUTION TO THE COASTAL OCEAN OBSERVING SYSTEM**

Hans-Peter PLAG (Geodetic Institute, Norwegian Mapping Authority, Kartverkveien 21, N-3511 Honefoss, Norway)

This abstract describes work carried out by the ESEAS and the ESEAS Research Infrastructure project (ESEAS-RI) teams (to be found at <http://www.eseas.org>). The ESEAS started its work in June 2001 and has the major objective to provide sea-level and sea-level related information for the European waters to scientific and non-scientific users both from inside and outside Europe. The ESEAS aims to achieve this goal in cooperation with other relevant organisations such as the PSMSL, EuroGOOS, GLOSS, EUREF and IGS. The ESEAS strives to guarantee and co-ordinate the long-term monitoring activities and data exchange along the entire European coastline. This includes but is not limited to tasks like setting up standards for observations and data processing, quality control of the large European database of hourly sea level data, upgrading of the ESEAS Observing Sites, collocation of tide gauges with CGPS, and provision of derived products such as secular trends and estimates of extremes. The EU-funded ESEAS-RI project started on 1 November 2002 with 25 institutions from 17 countries included. The project will run over three years and provides substantial resources for improving the observational network as well as the tools for exploitation of the data. In particular, Work Package (WP) 1 (Quality Control of Sea Level Observations) will make available a quality-controlled data set of hourly tide gauge data from most ESEAS Observing sites. WP2 (Absolute sea level variations) will concentrate on the determination of vertical crustal motion at the ESEAS Observing sites. WP3 (Decadal to inter-decadal sea level variations) will produce as main result an empirical model of the sea level variations in the European Seas for the last hundred years and give coherent estimates of long-term trends along the European Coasts. Finally, in the frame of WP4 (Improving the sea level observing system), a number of ESEAS Observing Sites will be upgraded and/or augmented with CGPS.

**JSP07/08A/B17-004****1010****AN INTEGRATED OBSERVING AND MODELING SYSTEM FOR TAMPA BAY, FLORIDA**

Mark E. LUTHER, Steven D. MEYERS, Sherry A. GILBERT, Vembu SUBRAMANIAN (College of Marine Science, Univ. of South Florida)

The USF College of Marine Science has developed an integrated observing system and circulation, wave, sediment transport, and water quality model. The model system ingests

## INTER-ASSOCIATION

real-time observations of the physical forcing functions for Tampa Bay to produce three-dimensional fields of circulation, temperature, salinity, wave spectra, sediment resuspension, sediment transport, and turbidity. A water quality module is under development. The hydrodynamic model is fully operational in either a nowcast-forecast mode or a hindcast mode and is described on our web site (<http://ompl.marine.usf.edu/TBmodel>). The integrated observing and modeling provides a decision support tool that is used to enhance safety and efficiency of maritime transportation, to guide search and rescue efforts, and to evaluate the bay ecosystem response to environmental stressors. Such stressors include severe storms, seasonal and interannual changes in fresh water input, as well as human impacts, such as hazardous material spills, river withdrawals, nutrient loading, changing land use patterns, and alterations in bay bathymetry. In addition to its routine use by the Tampa Bay Pilots and the US Coast Guard, the model system has been used to support management decisions in several environmental issues affecting the bay. For example, the model was used to investigate the effects of concentrate discharge from a seawater desalination facility recently built on Tampa Bay for the regional water supply authority; to simulate the trajectory of partially treated process water discharged from the Piney Point phosphate plant for the Florida Department of Environmental Protection; to predict trajectories of raw sewage spills into the bay for the Pinellas County Health Department; and to evaluate changes in salinity and estuarine residence time in the Palm River and McKay Bay for the Southwest Florida Water Management District. The Tampa Bay integrated observing and modeling system is being coupled to a similar integrated ocean observing system for the West Florida Shelf coastal ocean (see <http://comps.marine.usf.edu>).

### JSP07/08A/B17-005

1100

#### A NEW TECHNOLOGY FOR THE COASTAL-SEA ENVIRONMENT MONITORING-COASTAL ACOUSTIC TOMOGRAPHY (CAT)-

Arata KANEKO<sup>1</sup>, Noriaki GOHDA<sup>1</sup>, Hong ZHENG<sup>2</sup>, Keisuke YAMAGUCHI<sup>1</sup>, Ju LIN<sup>3</sup>, Fadli SYAMSUDIN<sup>1</sup>, Hidetaka TAKEOKA<sup>1</sup>, Masaji MATSUYAMA<sup>4</sup>, Yoshio TAKASUGI<sup>5</sup> (Graduate School of Engineering, Hiroshima University, 1-4-1 Kagamiyama, Higashi-Hiroshima, Hiroshima 739-8527, Japan, <sup>1</sup>SEA Corporation, IU Bldg 4F, 2-23 Shiohama, Ichikawa, Chiba 272-0127, Japan, <sup>2</sup>Center for Marine Environmental Studies, Ehime University, Bunkyo-machi, Matsuyama, Ehime 790-8577, Japan, <sup>3</sup>Tokyo University of Fisheries, 4-5-7 Konan, Minato-ku, Tokyo 108-8477, Japan, <sup>4</sup>National Institute of Advanced Industrial Science and Technology, 2-2-2 Hiro-Suehiro, Kure, Hiroshima 737-0197, Japan)

The deep-sea acoustic tomography has a two-decade history as a three-dimensional mapping tool of mesoscale sound speed (temperature) and current velocity structures. The acoustic tomography is recently applied to the semi-enclosed coastal sea as has been seen with continuous effort of Hiroshima University group since 1994. The first 5 km-scale experiment using five sets of self-contained type coastal acoustic tomography (CAT) systems was successfully carried out on March 1999 in the Neko-Seto Channel of the Seto Inland Sea, Japan where a strong tidal jet induces a pair of vortices. A rapid process of initiation, growth, translation and decay of the vortices was well mapped every five minutes through the reciprocal sound transmission and receiving of 5.5-kHz sound among five stations equipped with a transmitter and a hydrophone. This CAT system is extended to an advanced system with a two/four-hydrophone array to catch baroclinic structures of current, and the number of the system is increased up to eight. Seven two-hydrophone systems were deployed to Uwajima Bay of the Seto Inland Sea, Japan with a horizontal scale of about 10 km in late summer of 2002 where most active fish and pearl aquacultures exist. The CAT surface buoy is floated up inside the raft of fish aquaculture or beside the surface buoy of pearl aquaculture. In early winter of 2002 the four-hydrophone systems were used in Tokyo Bay for measuring the winter circulation in the 20-km scale bay. Major part of the CAT system was put on the land near the vertical wall of wharfs and piers at eight sites surrounding Tokyo Bay, and the transmitter and hydrophone array were suspended down into water along the vertical wall. An overview of the advanced CAT system and the recent observational results will be presented in the symposium.

### JSP07/08A/B17-006

1120

#### WAVEFORM RETRACKING OF T/P ALTIMETER IN CHINA SEAS AND ITS VICINITY

Lifeng BAO, Yang LU, Hou-Tse HSU (Institute of Geodesy and Geophysics of Chinese Academy of Sciences)

Just as in the open ocean, the altimeter data in the coastal zone can provide valuable information on wave heights, structure of the geoid and the associated gravity field, and dynamic sea surface topography. Because of this wealth of information, many scientists are seeking to extend the use of altimeter data to the shoreline. There are many different methods described in the literature that are available for retracking altimeter waveform data. All the various retracking algorithms have their own unique advantages and disadvantages, and it is generally accepted that no single algorithm can meet the diverse needs of all altimetry data users. To obtain accurate altimeter data in offshore of China Sea and its vicinity, we have reprocessed the raw Topex/Poseidon altimeter waveform data using more sophisticated algorithms, based on a fit of the waveform to a 5 or 9 parameter function, than those implemented in the altimeter hardware. Retracking altimetry data is done by computing the departure of the waveform's leading edge from the tracking gate of altimeter and correcting the satellite range measurement accordingly. On the base of colleagues' experience, reprocessed Topex/Poseidon altimeter waveform data is used to generate a time series of sea surface height. The post-processed altimeter waveform data is compared with the data from several tide gauge stations in China Sea, which close to the ground tracks of satellite, and Topex/Poseidon GDR data. The comparison shows that the post-processing data based on a nonlinear 5 parameters function is more accurate than post-processing data based on a nonlinear 9 parameters function in China Seas and its vicinity. With post-processing data, shallow water areas can be investigated with much more data and closer to the coastal line than the official products. It is shown that waveform retracking can extend the altimeter derived sea surface topography several kilometers shoreward in China seas and its vicinity.

### JSP07/08A/B17-007

1140

#### MONITORING OF OIL POLLUTION WITH MOBIL AUTONOMOUS LANDER PLATFORMS AS A PART OF THE COASTAL OCEAN OBSERVING SYSTEM

Alexei Evgenievich KONTAR, Leopold Isaevich LOBKOVSKY (Laboratory of Seismology and Geodynamics, P.P. Shirshov Institute of Oceanology, Russian Academy of Sciences)

The present generation of submarine oceanographic hydrocarbon discharge field programs are fundamentally limited by too few measurements, taken too slowly, at too great a cost. One approach to provide more extensive access to oil pollution on the sea floor is to use robotic mobile lander platforms to characterize hydrocarbon seepage and the distribution of pollution on the seabed at different spatial and temporal resolutions. The term "lander" in sub-sea technology refers to vehicles that descend to the sea floor, carry out a series of tasks autonomously for a period of days to years storing data on board, and then ascend to the surface at the end of the mission for recovery by a surface ship. A typical lander

comprises a chassis, buoyancy module, recovery module and ballast with release mechanism. One or more scientific payloads can be attached, depending on the size of the lander, for monitoring processes in the surface layers of the sediment and the bottom water. Landers have evolved from conventional oceanographic instrument moorings such as current meters or sediment trap arrays but are characterized by an instrument package standing or suspended close to the sea floor such as seismographs and geophones. Environmental monitoring systems like those described above have applications beyond oceanographic science. A range of mobile lander platforms is under development, from a relatively fast survey vehicle, to a much slower but longer endurance buoyancy driven system. However, the design of sampling strategies to make the best use of mobile lander platforms is an unsolved problem for all but the simplest circumstances. Such strategies are necessary because even with the increase in sensing capability provided by many small lander platforms, most processes will still be under sampled. Thus the emerging challenge is to determine the most effective use of available observational assets to obtain the desired information, given the physics of the phenomena under study and the constraints of the lander platforms and sensors available for detecting of oil pollution on the sea floor. This presentation will review some emerging paradigms for employing the lander platforms for seabed environmental monitoring as a part of the coastal ocean observing system and will present results from field experiments in the Black Sea.

### JSP07/08A/B17-008

1200

#### MORPHODYNAMIC CHARACTERIZATION OF THE FORESHORE USING PERIODIC DGPS OBSERVATIONS: THE AVEIRO LAGOON BEACH CASE

Paulo BAPTISTA<sup>1</sup>, Luisa BASTOS<sup>1</sup>, Cristina BERNARDES<sup>2</sup>, Oscar FERREIRA<sup>1</sup>, Alveirinho DIAS<sup>3</sup> (Astronomical Observatory, University of Porto, <sup>2</sup>Department of Geosciences, University of Aveiro, <sup>3</sup>Marine Geosciences, UCTRA, University of Algarve)

The Aveiro Lagoon Littoral sandy beach that extends along 50 Km from Ovar to Mira, in central coast of Portugal, is exposed to the highly energetic North Atlantic Ocean. The coastal erosion usually associated to the action of storm events has strong impacts in the anthropic activities creating some difficulties in coastal management. The mean annual significant offshore wave height is about 2.2m, with an average peak period of 11.3s. As the foredune erosion and consequent destruction by overwashes are related with the foreshore and backshore morphology, the study of the morphodynamic evolution of these areas of the beach is of special interest. In the scope of the RIMAR project (Natural Hazards related with sea level changes), the changes that have taken place in the foredunes, backshore and foreshore areas are being monitored since 1998. The survey method presently used is based on a prototype system developed at the Astronomical Observatory. It consists of a two GPS antenna system installed on a four-wheel motor quad. The observation methodology consists in the establishment of grids along long stretches of the coast that are surveyed in DGPS kinematic mode. The accuracy of this system is under centimetre level, which makes it adequate for morphodynamic studies. One stretch with about 10 kilometres extension has been monitored since November 2001, with near monthly re-observations. The computed volumetric and slope changes along the study area were used for a macroscale morphodynamic characterisation using the most common morphodynamic parameters namely the *surf scalling parameter* and the *surf similarity parameter*. The establishment of correlations between the morphological data and wave data provides new insights on the volumetric recovery period of the beach along the year and after storm events. For the prediction of the erosion and coastal retreat associated with storms, the *Kriebel and Dean* convolution model was used, which has been tested previously with good results for the Portuguese coast. By applying the convolution model to wave data, obtained offshore, and to information from the monitored beach profiles, it is possible to establish a relation effect between storm and beach erosion. The results obtained show that the implemented methodology can be very useful for the characterisation of the beach behaviour and the prediction of beach erosion.

Tuesday, July 8 PM

Presiding Chair: O. Schofield

### JSP07/08P/B17-001

Invited

1400

#### MODELLING: MORE QUESTIONS THAN ANSWERS?

Paul TETT (School of Life Sciences, Napier University)

Most models of marine ecosystems can be seen in terms of a set of equations of standard form:  $\{\partial Y/\partial t = -\nabla \Phi + \beta, \}$  and their numerical solutions. In the equation, Y is a state variable belonging to a set that could include, for examples, temperature, velocity, energy, and concentrations of nutrients and organisms. The first right-hand term is the divergence of physical transport flux vectors at a given spatial location and time; this term conserves the quantities totalled over a simulation domain except for boundary fluxes. The second right-hand term summarises the sources and sinks of each variable at a given location and time. It is not required to be conservative for any single variable, although conservation laws (e.g. for total energy, total nitrogen) may be introduced to constrain conversions between variables. Instances of this equation range from the simple first dynamical plankton model of Riley (1946) to modern, complicated, models such as ERSEM and COHERENS-PROWQM. This paper will consider two fundamental questions: 1) Is marine modelling largely an engineering problem - i.e. taking established scientific truths and using them to build models that can be used for system diagnosis and prognosis - or part of the scientific process - using models as tools for testing hypotheses? We know less than we think about marine ecosystem dynamics, and so need to continue making and testing hypotheses. Nevertheless, there is a pressing practical need for models that can be diagnostically and prognostically. 2) What are the entities which are quantified by the Y variables? The paper will explore how the idea of microplankton (comprising all pelagic bacteria and protists, both autotrophic and heterotrophic) can be used to develop efficient parameterisations of marine pelagic ecosystems at several levels of model complexity. These complicated simplifications can be further simplified to make a model that looks much like the original model of Riley, and can in turn be developed into a steady state solution embodying the precautionary principle that is practically useful in diagnosing or predicting the trophic status of water bodies. Examples will draw on modelling work carried out in several EC supported projects: CANIGO, COHERENS, OAEERRE and PROVESS.

### JSP07/08P/B17-002

1430

#### VARIABILITY OF SOLAR TRANSMISSION AND RADIANT HEATING RATE IN THE COASTAL OCEAN: OPTICAL IMPACTS

Grace C. CHANG, Tommy D. DICKEY (Ocean Physics Laboratory, University of California Santa Barbara)

Understanding of solar energy transmission is important for quantification and modeling of ocean radiant heating and primary productivity. Solar transmission and ocean radiant heating affect the intensity and depth of upper water column stratification. Stratification can

impact upper ocean ecology by limiting or facilitating vertical motion of phytoplankton; nutrient entrainment and availability; and movement of riverine inputs, suspended matter, and pollutants. The variability of solar transmission is dependent on the in-water spectral solar attenuation coefficient and the sea surface albedo, which are both influenced by meteorological and upper ocean physical processes, and bio-optical parameters. Past experimental and modeling studies of ocean radiant heating and solar transmission have primarily been executed for the open ocean. Studies regarding the impacts of coastal ocean processes on solar transmission have been limited until recently. An extensive physical and bio-optical time series data set, coupled with radiative transfer simulations, is used to characterize the processes and parameters that contribute to the variability of spectral solar transmission, sea surface albedo, and upper ocean radiant heating rates (RHR) in coastal waters. The data were collected from a mooring off the east coast of the United States in 24 m water depth in summer 2001. Three different analyses are utilized: (1) time series statistical analyses; (2) examination of processes and parameters affecting solar transmission, sea surface albedo, and RHR using radiative transfer simulations; and (3) investigation of bio-optical effects on RHR and heat content. (1) Quantitative coherence analyses suggest that cloud cover, chlorophyll concentration, and colored dissolved organic matter (CDOM) have the greatest impacts on solar transmission in the upper ocean in the visible wavelengths. All of these parameters are significantly coherent (negative phase) with solar transmission on a scale of about 1 week. Empirical orthogonal function (EOF) analyses show that the mixed layer depth (MLD) exhibits the strongest inverse correlation with solar transmission and RHR. (2) Radiative transfer simulations indicate that chlorophyll concentration, followed by absorption and attenuation coefficients, have the most significant impact on solar transmission variability. Solar angle and cloud cover greatly influence sea surface albedo. (3) Our data demonstrate that solar transmission is 14% lower and albedo is 1% higher for waters with higher concentrations of chlorophyll ( $\sim 5 \mu\text{g l}^{-1}$ ) as compared with lower chlorophyll concentration ( $\sim 1 \mu\text{g l}^{-1}$ ). In addition, the heat content of the upper mixed layer can increase by orders of magnitude during periods of deep mixing. For a shallow mixed layer (2 m), the mean hourly heat content is  $90 \text{ W m}^{-2}$  as compared to  $280 \text{ W m}^{-2}$  for a deeper mixed layer (6 m).

JSP07/08P/B17-003

1450

#### SPATIAL GRADIENTS IN BIOGEOCHEMICAL FLUX TO THE SEABED IN TIDE-STIRRED SHELF SEAS

Colin F. JAGO, Sarah E. JONES (School of Ocean Sciences, University of Wales Bangor)

A hypothesis is presented that the combined impact of dynamics, nutrients, and suspended matter produces enhanced biogeochemical fluxes to the seabed on the stratified side of tidal mixing fronts in tide-stirred shelf seas. In summer much of the algal production in the euphotic zone takes place in the thermocline and the greatest production occurs near tidal mixing fronts. This probably results from in situ growth of plankton due to optimal combination of light and nutrients: nutrient renewal during the summer, due to mixing by tide and wind, and surface stabilisation and reduction of the mixed layer optical thickness during fairweather and neap tides. A chlorophyll maximum is observed at the thermocline and at fronts. The optimal conditions for rapid algal growth are at fronts since lateral mixing across a front is greater than vertical mixing across the thermocline. Organic matter generated by algae is incorporated in suspended particulate matter (SPM) with most of the mass in large aggregates which settle to the seabed. Aggregation is facilitated by carbohydrates produced by the algae. In mixed waters, aggregated matter is frequently resuspended by tides so that significant remineralisation takes place in the water column. In stratified waters, low turbulence at the base of the thermocline provides conditions for aggregation and export of organic matter to the seabed where there is only limited resuspension; but remineralisation takes place as SPM sinks through the extended water column. Remineralisation therefore limits biogeochemical supply to the seabed in both mixed and stratified waters. In frontal zones, the potential for remineralisation is reduced due to rapid settling and limited resuspension. Combination of enhanced algal production, rapid settling of aggregates, and limited resuspension means that fluxes of aggregated biogeochemical components per unit area of seabed are greatest under fronts. However, resuspension in combination with cross-frontal mixing in summer and storms in winter should disperse benthic SPM away from fronts. Net deposition of this material is most likely on the stratified side of the frontal regions. The end result is that there should be spatial gradients in the supply of biogeochemical components to the seabed across mixed, frontal, and stratified zones. This is important because deposition of aggregates as benthic fluff controls redox conditions at the seabed and determines whether biogeochemical exchanges are oxic or anoxic. Temporary anoxia occurs even in mixed regions but it is particularly marked on the stratified side of frontal zones. High benthic oxygen demand occurs near the Frisian frontal, compared with the mixed, zone of the southern North Sea. Biogeochemical gradients also impact on the biota. Spatial gradients in dinoflagellate cysts and foraminifera in sediments occur across the Celtic Sea front. It is likely that the proposed biogeochemical gradient has significant impacts on benthic and pelagic biota and exchanges in tide-stirred shelf seas.

JSP07/08P/B17-004

1510

#### EXAMINATION OF SILICATE LIMITATION OF PRIMARY PRODUCTION IN JIAOZHOU BAY, NORTH CHINA IV TRANSECT OFFSHORE FROM THE COAST WITH THE ESTUARIES

Dongfang YANG (college of Fishery Science, Shanghai Fisheries University)

Jiaozhou Bay data collected from May 1991 to February 1994, 12 seasonal investigations, and provided the authors by the Ecological Station of Jiaozhou Bay, were analyzed to determine the characteristics, dynamic cycles and trends of silicate. The results indicated that the rivers around the Jiaozhou Bay supplied the rich silicate to the whole Bay so that the silicate concentration varied with the flow varying. The horizontal variation of silicate concentration transect offshore from the coast with estuaries showed that after the flow's carrying plentiful silicate into the Bay, the longer the distance was from the coast with estuaries, the lower the silicate concentration is in the waters. The vertical variation of silicate concentration transect offshore from the coast with estuaries showed that silicate sank and deposited to the marine bottom by the action of phytoplankton take-up and death, and zooplankton excretions. In this way, silicon would endlessly be transferred from terrestrial sources to marine bottom. The characteristics and transferences of diatoms and the ingestions and excretions of zooplankton elucidated the biogeochemical process of silicon, which showed the reason of phytoplankton's being lack of silicon. These results further proved that nutrient silicon is a limiting factor of phytoplankton growth.

JSP07/08P/B17-005

1530

#### A REVIEW TO DISTRIBUTION OF MACRO-MEIOFAUNA AND SUBSTRATE CHARACTERISTICS IN IRANIAN CASPIAN SEA SHORES OFF GUILAN PROVINCE

Alireza MIRZAJANI (Department of Ecology, Caspian Sea Bony Fishers, Research Center)

The Caspian sea is a limited and brackish water that 724 species and 566 species microbenthos distributed in Caspian sea. In Iranian water of Caspian sea, the Hydrology and

hydrobiology studies was started from late decade 1980. The study area was Caspian Sea at Guilan province on the 30 transect and 4 depths. Distribution of macrobenthic biomass had not a large changes for many years. During study of autumn 1995 to summer 1996 on 9 transect and 4 depths (10, 20, 50, 100 meter) the biomass was various from 1.69 to 65.45 gr/m<sup>2</sup>. The groups of Pseudocumidae, Amphipoda, Tubificidae, Chironomidae, Amphatridae, Nereidae, Cardidae and Scrobiculidae were studied. Generally the highest biomass was shown in a small region with biomass of higher than 18 gr/m<sup>2</sup>. The biomass was larger in 10 meter than another depths and the biomass had not the significant difference in all season. The study of meiofauna showed that Bivalva, Foraminifera, Nematoda, Ostracoda, Copopoda were dominate from 12 identified groups. The Foraminifera and Bivalva were the most abundant groups. There was a significant difference between average abundance of meiofauna at 4 depths, That 20 meter had the most average that it decreased in 50 and 100 meter depths. The average abundance of meiofauna varied from 825 to 29315 ind./cm<sup>2</sup> in 100 and 20 meter respectively while the frequency of meiofauna was various from 80 to 133382 ind./10cm<sup>2</sup>. The most frequency was shown in small part of the west study area with higher than 3000 ind./10cm<sup>2</sup> however the most frequency percentage had been seen with frequency of lower than 150 ind./cm<sup>2</sup>. Results of substrate characteristics studies showed that the organic matter was the most in 50 meter and it was the lowest at 10 meter depth. Fig. 4 shows the distribution of T.O.M. in study area that the most surface belong to 4-8 % organic matter, however a large surface of study area have belong to organic matter percentage of higher than 12 > % .The silt percentage was the most than other grain size (1, 0.5, 0.25, 0.076 mm) in all of depths and percentage of grain size for different depths for 0.076 mm size was more in 10 meter than other depths. The comparison of macrobenthic biomass distribution maps with fish catch data showed a positive relation. Also the overlapping of meiofauna abundant map on organic matter and grain size maps showed that the most abundant of meiofauna was in 4-8 % organic matter and there was a negative relation between meiofauna and silt values.

IA

JSP07-Posters

Tuesday, July 8

#### THE COASTAL OCEAN OBSERVING SYSTEM (IAPSO, IAG, IOC)

Location: Site D

Tuesday, July 8 PM

JSP07/08P/D-001

Poster

1400-052

#### PECHORA SEA'S MICROPHYTOBENTHOS AT LATE AUTUMN AND ITS RELATIONS WITH TIDAL CYCLE

Filipp Vjacheslavovich SAPOZHNIKOV (P.P.Shirshov Institute of Oceanology)

Extremely high biomass rates benthic diatom algae had been occurred at summer and autumn 1998 in Pechora sea. Material was collected during the cruises of the RV "Academic Sergey Vavilov" and hydrographic vessel in the south-east part of Barents sea – the Pechora sea. The biomass of microphytobenthos was ranged from some tens to several hundreds grams per square meter on the depths 6-15 m. Usually, the biomass of microalgae in subtidal sediments of Arctic seas is about several grams. Extremely high biomass of microalgae – over 1 kg/m<sup>2</sup> – was found on a single shallow-water. Samples were consist mainly of plankton species (63,36 %). The most abundant was *Coscinodiscus cf. stellaris*. But mean density of plankton assemblage was about thousands cells per liter and some hundreds milligrams per liter. Sedimentation of cells from high light reach horizon makes considerable influence on formation of bottom community in before winter period. However, number of phytoplanktonic organisms was not reach enough to support a high density of bottom diatoms. It could be suggested, that near the bottom exist some specific density populated sestonic assemblages. This communities in particular consist of plankton diatoms, which actively utilize organic sediments. Most of cells of *Coscinodiscus* and *Thalassiosira* had viable chromatofores in the moment of fixing. Some of them were in process of cell division. Its important that during the collecting a material in this region penetration of light was not very deep. It was because of plentiful suspension. That's why we think that benthos microalgae use in general heterotrophic type of nourishment. Its possible, that sedimentation on bottom of alive plankton diatoms of high-performance seston assemblages accounts lashings of this creature in benthic communities. The most high density of alive diatoms was on depths 13-15 m. Biomass of cells approximately was more then 0.5 kilogram per square meter. At that time the number of cells was ranged from 20 to 40 millions per square centimeter of surface of bottom. Benthic diatoms were largely represent to. That all demonstrate the high concentration of organic substance on this depths. This substance is used by diatoms. We think, this phenomenon - high density of microphyts - can be supported by termoclines' and picnoclines' passing on researching depths. Perhaps, high density of diatoms in that conditions is connected with fluctuation of termoclines' level during the process of tidal cycle. With a tidal the termocline is getting up. Cold waters with high salinity come to bottom layer. That waters are rich with organic substance and biogenic elements. This time, diatoms, which live in high horizon of sediments and, perhaps, in seston actively use organic substance which are necessary for grow. Then starts a low tide. And termoclines level falls down. The same time, thickness of water layer is reducing above the communities. On account of that the light impenetrate deeper. That makes the cells of diatoms to reproduce oneself.

JSP08

Wednesday, July 9

#### COASTAL PROCESSES AND STORM SURGES (IAPSO, IAMAS, LOICZ/[IGBP])

Location: Site B, Room 19

Wednesday, July 9 AM

Presiding Chair: T. Yanagi

JSP08/09A/B19-001

Invited

0900

#### MESOSCALE FEATURES IN A MEDITERRANEAN COASTAL AREA REVEALED BY A HF RADAR

Giorgio BUDILLON, Marco TRAMONTIN (Istituto di Meteorologia e Oceanografia, Universita' di Napoli PARTHENOPE)

## INTER-ASSOCIATION

A HF Coastal Dynamics Application Radar (CODAR) has been used to study the seasurface circulation in the coastal area between Ancona and Senigallia (Northern Adriatic Sea) throughout one year of measurement (July 07th 1997 - July 06th 1998) over a 30 x 30 km area including 401 grid points having a spatial resolution of 1.5 Km. Preliminary results show the well-known southeastward (i.e. alongshore) coastal jet that extends its influence as far as 10-15 Km from the coast; farther offshore a cyclonic eddy, with a diameter of 10-20 km typically occurs. This circulation can be occasionally reversed showing an anticyclonic eddy that forces a northward coastal current with a far less energetic signature. The spectral analysis reveals a propagation of the semidiurnal frequencies from NW to SE according to the propagation of a Kelvin wave theory; conversely an exponential increase from the coast to offshore has been identified for the near-inertial frequencies. An analysis of the mean kinetic energy during both 'Bora' and 'Scirocco' wind episodes, from north-east and from south-east respectively, describes the typical dynamic of a surface layer driven by an impulsive atmospheric forcing. In this work the CODAR velocity data have been used to perform also an Empirical Orthogonal Function (EOF) analysis and principal modes and variance are reported.

**JSP08/09A/B19-002**

**0930**

### STUDYING THE WATER CIRCULATION ALONG THE EGYPTIAN MEDITERRANEAN COAST USING THREE DIMENSIONAL NUMERICAL MODEL

Sayed H. SHARAF EL-DIN, Khaled A. ALAM EL-DIN, Omneya M. IBRAHIM (Department of Oceanography, University of Alexandria)

The water circulation along the Egyptian Mediterranean Coast was studied using three dimensional numerical model. Numerical simulation was achieved using the Princeton Ocean Model (POM) with horizontal resolution of 2' grid interval and 14 vertical sigma levels. The bathymetric map of the Egyptian coast was digitized with high resolution from the Admiralty charts which is updated by the Egyptian Government Survey Authority and Egyptian Navy. The initial fields of temperature, salinity and current used to run the model were taken from MODB dataset. The surface momentum, heat and fresh water fluxes were taken from ECMWF monthly data for the period 1986-1992. The simulation results showed that the surface circulation of the Egyptian Mediterranean waters is dominated by the easterly flow along the coast. Mersa-Matruh anticyclone occupies the area between 27°E to 28°E longitude. Also a cyclonic gyre takes place between 28°E and 30°E longitude. In the central region, a weak anticyclone persists in front of Nile Delta. In the Eastern part, El-Arish cyclonic gyre exists intensively.

**JSP08/09A/B19-003**

**0950**

### THE RESPONSES OF THE WEST FLORIDA CONTINENTAL SHELF TO THE WINTER STORMS

Ruoying HE, Robert WEISBERG (College of Marine Science, University of South Florida)

Two large extra-tropic storm systems produced significant coastal ocean responses on the West Florida continental shelf in March 2001. Taking the month of March 01 as the study window, we describe the shelf circulation responses to the evolution of these two storms with in-situ measurements of winds, sea levels and currents. The responses of the west Florida shelf circulation are found to be sensitive to the wind direction primarily due to the variations of the coastal line orientation facing the ocean. Driven by NCEP EDAS winds and surface pressure only, a three-dimensional coastal ocean circulation model is used to simulate the west Florida shelf circulation in March 01 by assuming the remote forcing of deep ocean boundary current (i.e., Loop Current) is secondary. Model/Data comparisons indicate that the coastal ocean model is highly skillful and that the shelf circulation during this period indeed responds primarily to the local wind forcing.

**JSP08/09A/B19-004**

**1010**

### CURRENT STRUCTURE AND BEHAVIOR OF THE RIVER PLUME IN SUO-NADA, JAPAN

Shinya MAGOME, Atsuhiko ISOBE (Department of Earth System Science and Technology, Kyushu University)

The behavior of the river plume in Suo-Nada is studied using a primitive equation numerical model, Princeton Ocean Model. Special attention is given to the current structure and behavior of the anticyclonic eddy (bulge) induced by high freshwater inflow changing in a timescale of one week. First, in order to investigate the fundamental process on the bulge, the freshwater is supplied from a river to a rectangular basin with a simple topography. An anticyclonic bulge near the river mouth and a coastal current in the direction of the Kelvin wave propagation are revealed after the river discharge increases. The anticyclonic bulge has the upwelling (downwelling) inside (along the fringe of) the bulge. When the river discharge subsides after reaching its peak value, the bulge propagates upstream (i.e., opposite to the direction of the Kelvin wave propagation). Next, in order to investigate the behavior of the bulge in Suo-Nada, the freshwater is supplied from major eight rivers to the basin with the realistic topography. The less saline water mass in the southern part of Suo-Nada propagates to the west (i.e., upstream direction) after the river discharge increases. It is consistent with an observational fact that the less saline water mass appears in the western part of Suo-Nada, suggesting that the upstream propagation of the bulge is possible in the real ocean. On the basis of the results of the model with the simple topography, a cause of the upstream propagation is considered. Onshore currents appear in the bottom layer beneath the bulge, propagating upstream. They produce an anticyclonic barotropic eddy due to the conservation of the potential vorticity. The current component associated with the eddy crosses normally to the isohaline in the upper layer, and therefore transports the bulge upstream. Other current component (surface current velocity minus vertically-averaged value) is not responsible for the upstream propagation of the bulge.

**JSP08/09A/B19-005**

**1030**

### QUANTIFICATION OF CONTAMINANT FLUX IN AN IMPACTED ESTUARY, WINYAH BAY, SOUTHEASTERN USA

Yong Hoon KIM, Mary CATHEY, George VOULGARIS, Miguel GONI, Richard STYLES (Department of Geological Sciences and Marine Science Program, University of South Carolina)

A multidisciplinary approach was used to examine the dynamics of flow-particles-contaminants in an impacted estuarine environment. An intensive suite of field measurements was acquired along the upper region of Winyah Bay estuary, southeastern USA during October 2001 (low river discharge condition). Our work was focused on examining the relative importance of advection versus remobilization of contaminants within the estuarine turbidity maximum (ETM) as processes controlling their overall fate. Concurrent measurements of hydrographic properties, currents, sediment concentration and particle size distribution were combined with the geochemical analyses of water samples. Water samples were filtered to measure the concentrations of total suspended sediments

(TSS), particulate and dissolved organic carbon (POC and DOC), and particular nitrogen (PN), as well as stable carbon isotopes, and polycyclic aromatic hydrocarbons (PAHs). The tidal and residual circulation pattern and its influence on suspended sediment distribution are established for the prevailing conditions using the physical data. Residual current along the main channel axis shows typical estuarine circulation, outward flow near the surface and inflow near the bottom. The magnitude of landward-directed flow is much higher than seaward flow. Analysis of suspended sediment concentration exhibits a tidal asymmetry with higher concentrations during the flood (up to 0.94 g/l). Geochemical analyses of water samples show that POC concentrations were significantly lower (1-4 mg/L) than DOC (5-9 mg/L). At all stations POC concentrations increase with depth, showing a strong positive relationship with current. In contrast, the highest DOC concentrations precede peak flow by several hours. The trends in the POC/PN and stable carbon isotope ratios measured in POC indicate differential transport of organic materials during distinct periods of the tide. In addition, during flood tide, resuspension of vascular plant derived OM appears to occur, as evident by shifts towards typical terrestrial POC/PN (>20) and  $\delta^{13}C_{org}$  (-28 ‰) values. The results show that net landward fluxes of suspended sediments and POC over a tidal cycle, indicating that Winyah Bay is flood dominated during low discharge. The overall consequence of this behavior is a significant input of organic material from the lower reaches of the bay towards the ETM.

**JSP08/09A/B19-006**

**1100**

### CURRENTS AND TURBULENT EXCHANGE PROCESSES IN LAKE ONTARIO

Ram Rao YERUBANDI (Environment Canada-NWRJ)

The coastal circulation and turbulent exchange processes during spring and summer stratification in Lake Ontario has been examined using concurrent measurements of velocity profiles from moored broadband ADCPs, and ship based transects. Temperature profiles at two thermistor moorings provided data on the thermal structure during the summer period. During May ship based ADCP transect data clearly shows the circulation associated with the thermal bar. During the summer period energy spectra of currents and temperature shows a primary peak located at 10-12 day period due to large scale circulation and a secondary peak at near-inertial frequency-band. The horizontal turbulent exchange parameters during summer stratification shows non-isotropic conditions in the surface layers and isotropic conditions in the bottom layers at the offshore location. The alongshore exchange coefficients are generally higher than cross-shore components. Upwelling and downwelling of isotherms are a common feature during the summer stratification. It is observed that during upwelling horizontal exchange coefficients are reduced in the surface layers while they are increased in the bottom layers. Near bottom layers are affected by intense turbulence associated with increased vertical current shear. During downwelling events with migration and intersection of the thermocline with the bottom, the vertical exchange coefficients are relatively small due to strong static stability.

**JSP08/09A/B19-007**

**1120**

### TEMPORAL AND SPATIAL ASYMMETRIES IN THE TIDAL RESPONSE OF SHALLOW INLETS AND BACK-BARRIER BASSINS

Emil V. STANEV, Joerg-Olaf WOLFF (ICBM, University of Oldenburg)

In this paper we study water exchange between tidal basins and open ocean using data from observations and numerical simulations. The study area covers the East Frisian Wadden Sea, which consists of seven tidal basins. The major interest is focused on the tidal basins in the vicinity of the islands Spiekeroog and Langeoog and the inlets connecting them with the open ocean. We analyze the contribution of hypsometric control and Stokes transport to the overall dynamics of well-mixed tidal basins. The theoretical concepts are compared against results of direct observations and simulations with a numerical model. The data have been collected during the period 1995-2000 and consist of cross-channel ADCP transects. The numerical simulations are based on the 3-D primitive equation General Estuarine Transport Model (GETM) with a horizontal resolution of 200 m and terrain following vertical coordinates. The results of the observations and simulations reveal a distinct difference between transports in the upper layer, which is dominated by the Stokes drift and the deep layer being dominated by the hypsometric properties of the intertidal basin. The difference between these two transports gives rise to the existence of avertical overturning cell: net inward motion in the upper layer and net outward motion in the deeper parts of the tidal channels. This vertical circulation is also well documented in our numerical simulations, and shows a clear dependency of transport patterns on the local depth. The interplay between transports and turbulence explains the major trends in the transport of sediment.

**JSP08/09A/B19-008**

**1140**

### SEASONAL VARIABILITY OF NUTRIENTS SUPPLY TO THE PULICAT LAKE, EAST COAST OF INDIA

Jaya Raju NADIMIKERI (sri venkateswara university)

SEASONAL VARIABILITY OF NUTRIENTS SUPPLY TO THE PULICAT LAKE, EAST COAST OF INDIA Detailed studies of the nutrients of the pulicat lake have shown that the Northern and Channel parts differ considerably in the way that nutrients are supplied and regenerated. The Channel part is very much under the influence of the Bay current, and is affected both by upwelling at the shelf-break, and by the advection of warm, nutrient-poor surface water from perturbations along the landward edge of the current. This leads to the establishment of a two layer system for much of the year, with the thermoclines intensifying during the summer. The Northern part, in contrast, is more away from the upwelling region of the Bay. Here, deep mixing during monsoons favoured by the fresh water inflow, wind stress and thermocline formation during the summer is less intense. Bottom water supply appears to be from the Bay rather than the fresh water inflow from the land and localised patches of oxygen-depleted water are formed as a result of lowered advection. The variability in source waters and the forcing fields over the two regions of the lake leads to differences in the nutrient concentrations in the surface waters. These, in turn, affect the productivity of the region and the attendant biodiversity in general and fish stocks in specific.

**JSP08/09A/B19-009**

**1200**

### DEVELOPMENT OF A SEMI-SPECTRAL COASTAL OCEAN MODEL AND ITS APPLICATION TO THE NEKO SETO SEA IN THE SETO INLAND SEA

Masazumi ARAI (Graduate School of Engineering, Hiroshima University)

For studying coastal ocean processes such as tidal vortices, frontal instability of the Kuroshio and Kyucho, a new ocean model is developed based on the semi-spectral method using the primitive equations with hydrostatic balance on a sigma-coordinate system. The feature of the present model is that the vertical mode is used as a basis, which is different from the previous work of Haidvogel et al. (1991). As a first step of the development of the model, the Fourier cosine series is used as a basis by assuming that the reference density is

homogeneous or linearly stratified. To test the performance of the model with homogeneous density, the model is applied to the regional model of the Neko Seto Sea in the Seto Inland Sea. In the Neko Seto Sea, a tidal vortex is generated due to the barotropic instability of a strong tidal jet, so this is a suitable region to test a homogeneous model. Here the model tidal current is driven by the tide imposed at the boundaries of the model domain. The model result is intensively compared with the observational result of ADCP by the research group of Hiroshima University (Yamaoka et al. 2002). For the barotropic component of velocity, the correlation between the model result and ADCP result is quite high. The correlation coefficient is 0.84 (0.65) for the eastward (northward) component. Since the position and magnitude of the tidal jet is well simulated in the model, the correlation coefficient of the eastward component is higher. The vertical structure of the horizontal component of velocity is also compared with ADCP. The core structure of the tidal current passing through the narrow strait is well realized in the model. To test the accuracy of the baroclinic pressure gradient term, the linearized model with density stratification is applied to the seamount problem proposed by Beckmann and Haidvogel (1993). The maximum velocity associated with the pressure gradient error in a sigma-coordinate system is comparable to those of the previous models. The above results demonstrate the good performance of the present model. The model will be applied to the model of the Bungo Channel for studying the mechanism of Kyucho.

**JSP08/09A/B19-010****1220****WEAK WIND-WAVE/LOW-FREQUENCY CURRENT INTERACTION WITH DUE REGARD FOR BOTTOM MOBILITY**

Boris KAGAN<sup>1</sup>, Oscar ALVAREZ<sup>2</sup>, Alfredo IZQUIERDO<sup>3</sup>, Rafael MANANES<sup>2</sup>, Begonia TEJEDOR<sup>2</sup>, Luis TEJEDOR<sup>2</sup> (<sup>1</sup>Shirshov Institute of Oceanology, Russian Academy of Sciences, St.Petersburg Branch, 30 Pervaya Liniya, 190053 St.Petersburg, Russia, <sup>2</sup>Departamento de Física Aplicada, Universidad de Cadiz, Apdo. 40., <sup>3</sup>Departamento de Física Aplicada, Universidad de Cadiz. Unidad Asociada Oceanografía Interdisciplinaria UCA-CSIC. Apdo. 40.)

The formulation of weak wind-wave/low-frequency current interaction is extended to the moveable rough bottom case using the bottom roughness predictors of Nielsen (1983) and Tolman (1994). This 'extended' formulation is then implemented in a 2D depth-averaged, non-linear, high-resolution hydrodynamic model and the modified model is applied to study the changes in the tidal dynamics of Cadiz Bay due to wind-wave/tide interaction and bottom mobility. The inclusion of the second of these factors leads to nonqualitative changes in the fields of tidal characteristics compared to those obtained with allowance for the first one alone. Certain quantitative changes, however, occur. These are such that an agreement between the predicted and observed tidal elevation amplitudes and phases tends to be improved if both of the above factors are accounted for. It is shown that quantitative distinctions between the solutions derived when employing Nielsen's (1983) and Tolman's (1994) bottom roughness predictors are not so much as might be expected from comparison of the appropriate values of the mobility parameter. That is because the mobility parameter defined as the ratio of the wave-induced change in the bottom roughness length to the wave reference bottom roughness length appears in the expression for the drag coefficient not by itself, but in combination with the ratio between the wave and tidal reference bottom roughness lengths (bottom roughness lengths in the immobile rough bottom case). It is for this reason that these lengths cannot be set equal to each other. Otherwise, the solution becomes unreasonable: the drag coefficient increases to an extent that the tidal elevation and velocity in the region of interest either degenerate in part when using Nielsen's (1983) bottom roughness predictor or are too reduced to be realistic when using Tolman's (1994) bottom roughness predictor. The fields of other tidal characteristics are also transformed beyond recognition.

**JSP08/09A/B19-011****1240****SEA-BREEZE-MODULATED SEASONAL VARIABILITY IN THE K1 TIDAL DYNAMICS IN NEARSHORE REGIONS**

Oscar ALVAREZ<sup>1</sup>, Begonia TEJEDOR<sup>1</sup>, Luis TEJEDOR<sup>1</sup>, Boris KAGAN<sup>2</sup> (<sup>1</sup>Department of Física Aplicada, University of Cadiz. Unidad Asociada Oceanografía Interdisciplinaria UCA-CSIC, <sup>2</sup>Shirshov Institute of Oceanology, Russian Academy of Sciences., <sup>3</sup> Department of Física Aplicada, Universidad de Cadiz, Apdo.40, Puerto Real, Spain)

The role of sea breezes in the development of nearshore wave climate, diurnal current velocity and sea surface elevation, and beach topography has been extensively studied (see, e.g., O'Brien et al., 1977; Rosenfeld, 1988; Craig, 1989; Chen and Xie, 1997; Pattiaratchi et al., 1997; Militello and Kraus, 2001; Hyder et al., 2002). The same cannot be said in respect to the influence of seabreezes on tidal dynamics in coastal waters. All we know is that sea breezes are responsible for the formation of the S1 solar diurnal tide. This viewpoint was held by a number of tidalists, including Shureman (1941), Munk and Cartwright (1966) and Zetler (1971). There were, however, dissenters. So, Godin (1990) speculated that the S1 tide, even though its gravitational potential is weak, is of gravitational origin and determined by a diurnal inequality in the tide-generating force due to a slight asymmetry in the shape of geoid. We show that sea breezes may be considered as a major source of the seasonal variability in the K1 tidal dynamics in near-coastal shallow regions. This fact is explained as follows: if the K1 tidal response to boundary forcing is subjected to the sea-breeze impact, the superposition of the K1 signal and the S1 signal, independent of what is its origin, will produce a seasonal modulation of the K1 tidal dynamics and, hence, seasonal variations in the K1 tidal characteristics. This finding results from the well-known expression for an amplitude- and phase-modulated oscillation. It is also supported by simulating the response of Cadiz Bay to sea-breeze wind stress and tidal boundary forcing - individually and in combination - through a 2D depth-averaged, non-linear, high-resolution hydrodynamic model.

**Wednesday, July 9 PM**

Presiding Chair: T. Yanagi

**JSP08/09P/B19-001**

Invited

**1400****NET SAND TRANSPORT BY TIDAL PUMPING IN A MACROTIDAL ESTUARY**

Colin F. JAGO (School of Ocean Sciences, University of Wales Bangor)

Data are presented which provide sand fluxes and sedimentation rates in a macrotidal estuary on tidal to decadal time scales. The dynamics of the Taf Estuary in Wales (UK) are established by a macrotidal regime with a tidal range up to 10 m. The tidal wave is asymmetric with a short flood tide of <3 h and fast spring tide currents exceeding 2 m s<sup>-1</sup>. The estuary is sandy and characterised, at low water, by intertidal sandflats and shallow channels and, at high water, by a well mixed, or partially stratified, water column. Freshwater input is small (mean discharge 7 m<sup>3</sup> s<sup>-1</sup>) in comparison with saltwater input (mean tidal prism 10<sup>7</sup> m<sup>3</sup>). The estuary is exposed to large waves from the North Atlantic but much of the wave energy is dissipated across a wide shoreline before waves reach the estuary mouth. The fast tidal currents generate intense sand transport and rapid morphological change. A unique 30 year time series of sedimentation rate has been obtained. The sand budget has been

determined by periodic surveys of the sand flats at low water. Levelling of fixed transects across the estuary over a 30 year period shows that the estuary has been infilling with sand at a mean annual sedimentation rate of 0.02 m. Mineralogical analysis of the sand proves that it is sourced from offshore rather than via river input. A testable hypothesis is that the landward transport of marine sand is due to tidal pumping associated with the time-velocity asymmetry of the tidal currents rather than to storm events. The very fine sand of the sandflats is entrained into suspension for most of every tidal cycle. Bed load transport is minimal, and total sand transport can be quantified by measurement of the suspended sediment load. The suspended sand flux has been determined by measurements of current velocity and suspended sand concentration (SSC) along 2 transects across the estuary. Measurements were made through the water column over several tidal cycles, during fair-weather conditions, using profiling transmissometers for SSC. Flood sand flux exceeded ebb sand flux on all tides; hence there was a net landward flux on all tides. Relationships between sand flux and tidal height were determined and used to extrapolate the annual flux and annual sedimentation rate. The annual sedimentation rate is 0.014 ± 0.036 m. This ignores any forcing other than tidal. The long term budget and short term flux measurements provide very similar estimates of the sedimentation rate in the estuary. This provides compelling evidence that the high sand fluxes and sedimentation rates of the estuary are determined predominantly by the tidal regime. It is concluded that the hypothesis that tidal pumping, rather than storms, controls net sediment transport is correct.

**JSP08/09P/B19-002****1430****COASTAL ESTUARINE-LAGOON SYSTEM BEHAVIOUR IN RESPONSE TO TYPHOON EVENTS, EASTERN HAINAN ISLAND, CHINA**

Shu GAO (Department of Geo-Ocean Sciences, Nanjing University)

A series of estuary-lagoon systems are distributed along the eastern Hainan Island coastlines. Here, coastal development for tourism has become progressively intense, because of the clean air and water. However, this section of coastlines is also subjected to typhoons, which often result in sequential disasters. During a typhoon event, strong winds damage forests and houses, large storm waves erode the shoreline, typhoon induced heavy rain causes flood in the drainage basins, and combined action of storm surge and increased river flow leads to flooding in lagoonal areas. Boao Harbour, now being developed into a middle-sized coastal city, provides a good example. The sand spit that semi-encloses the lagoon to form an estuarine / tidal inlet system was breached at its northern section three times during storms in the past sixty years; these resulted from the storm waves, together with strong river flow inside the lagoon. The timing of the large river water discharge into the lagoon tends to match the storm-induced high water (because the rivers are relatively short); hence flooding in the low-lying lagoonal areas occurs once every two to five years. Human activities add further risks to flooding. For instance, at the Xiaohai inlet, the entrance channel was artificially narrowed for navigation purposes. This engineering work has hampered the river discharge into the open sea, causing an extremely severe flooding in 2000. Recently, artificial modification to the entrance channel to Boao Harbour has been proposed. For such an engineering scheme, however, additional flooding risk assessment must be carried out. Based upon analyses of the regional patterns of typhoon-induced sequential disasters and the related processes and mechanisms, the risk of flooding will be enhanced by inappropriate modifications to the entrance channel. Numerical studies indicate that the shape of the designed entrance channel for navigation is an important factor for the modified flood water levels.

**JSP08/09P/B19-003****1450****ESTIMATION OF LONGSHORE SEDIMENT TRANSPORT RATE OFF DAMIETTA HARBOR, EGYPT**

Sayed H. SHARAF EL-DIN, Fahmy Mohamed EID, Farid AbdelRahman ABDALLA (Departement of Oceanography, University of Alexandria)

Using the wave and longshore current data which collected by the coastal Research Institute during the period from Aug. 1997 to Dec. 1998 along Damietta area, the sediment transport rate is estimated at three places, east, west of Damietta harbor and west of Damietta mouth using two common models and field measurements. The results revealed that: The predominant direction of sediment transport takes place eastward. The gross transport is very large during winter, while it is low during spring and summer seasons. The average sediment transport rate is about 543 x 10<sup>6</sup> m<sup>3</sup>/year. The results of streamer sediment traps showed that, the sediment flux and sediment transport rate density have their maximum value at the east of study area than the western side. Using the fluorescent tracer grains, the result showed that, the amount of sediment transport moving on the eastern side is more than at western side of study area. Also, the percentage of occurrence of sediment transport from onshore to offshore during spring is more than that occurs in the autumn. In addition, the comparison between the different methods of estimation of sediment transport rate was done.

**JSP08/09P/B19-004****1510****UNSTEADY DYNAMICS OF EDGE WAVES**Efim PELINOVSKY<sup>1</sup>, Andrey KURKIN<sup>2</sup> (<sup>1</sup>Laboratory of Hydrophysics, Institute of Applied Physics, <sup>2</sup>Department of Applied Mathematics, Nizhny Novgorod State Technical University, 24 Minin Street, Nizhny Novgorod, RUSSIA)

Wave propagation in the coastal zone can induce both scattering and capturing of wave energy. The latter phenomenon is of great interest due to the weak attenuation of waves over long distances. Trapped waves are an important component of sea disturbances produced by cyclones moving along coastlines and their existence explains the non-uniform character of tsunami height along the coastline. Edge waves may be generated from normally incident wind waves due to the strong nonlinearity of wind waves and many field observations demonstrate the occurrence of these edge waves in coastal environments. Edge waves are often considered as the major factor in the long-term evolution of irregular coastal morphology, forming rhythmical crescentic bars. There is good agreement between the characteristic scales of these morphological features when measured in laboratory experiments and the natural environment. However, the energetics of the wave processes is poorly understood and the sediment transport rates associated with the edge wave field has neither been estimated nor measured. The main goal of this paper is to study the unsteady dynamics of the progressive and standing edge wave propagation above a sloping beach. In particular, the mechanism of the spatial-temporal focusing (dispersion enhancement) of multi-modal edge waves in the shelf zone is investigated in the framework of shallow water theory both analytically and numerically. The asymptotic solution is derived for the wave evolution above a sloping beach smoothly varied in along-shore direction. The unusual appearance of the coastal flood tongue is demonstrated in the framework of developed theory.

## INTER-ASSOCIATION

**JSP08/09P/B19-005**

**1600**

### STATISTICS OF EXTREME WINDS; STORM SURGES AND OCEAN WAVES ALONG THE NORTH SEA COASTLINE, 1960 UNTIL TODAY

Hans VON STORCH<sup>1</sup>, Ralf WEISSE<sup>1</sup>, Arnt PFIZENMAYER<sup>1</sup>, Frauke FESER<sup>1</sup>, Saskia ESSELBORN<sup>2</sup>, Trygve ASPELIEN<sup>1</sup> (<sup>1</sup>Institute for Coastal Research, GKSS Research Center, Geesthacht, Germany, <sup>2</sup>Geoforschungszentrum Potsdam, Germany)

The evolution of storm surge statistics along the North Sea coasts during the past 50 to 100 years is reconstructed using statistical and dynamical models with and without data assimilation. It turns out that the mean water level has increased since the 1960s by a few centimeters along the southern and eastern coast lines, but that the variations relative to the annual mean have undergone hardly any changes. This sea level rise is reflecting the tendency of the last decades for more frequent westerly wind conditions, which is not only associated with higher water levels in the southeast of the North Sea, but also with increased wave energy reaching the eastern shoreline as well as higher waves in the German Bight.

**JSP08/09P/B19-006**

**1620**

### CLIMATOLOGY OF STORM SURGES IN THE ARCTIC OCEAN

Andrey PROSHUTINSKY<sup>1</sup>, Igor ASHIK<sup>2</sup>, Tatiana PROSHUTINSKY<sup>3</sup> (<sup>1</sup>Woods Hole Oceanographic Institution, <sup>2</sup>Arctic and Antarctic Research Institute, <sup>3</sup>University of Alaska Fairbanks)

The shore of the arctic seas are generally of low relief and the combination of waves and high water levels during late summer and fall storms before the development of significant sea-ice cover can be particularly damaging to shorelines. Gravel barrier beaches can be overwashed and eroded while bluffs consisting of un lithified ice-bonded sediment and segregated ice can fail and retreat. Storm surge climatology of the arctic marginal seas is investigated based on observational data and a 2-Dcoupled ice-ocean barotropic model results. Meteorological forcing is calculated based on NCAR/NCEP reanalysis data for 1948-present period. The spatial resolution of the model is 13.89 km. The sea ice conditions (concentration and thickness) are prescribed on the mean monthly basis. The model was calibrated based on the most strong storm surges observed in the Kara, Laptev, East-Siberian, Chukchi and Beaufort Seas. Simulation results are in relatively good agreement with observations of sea level heights and ice drift. Detailed studies showed that the spatial and temporal resolution of the NCEP/NCAR sea level pressure data (2.5x2.5 degree, 6 hours) are too low and can not reproduce well extreme conditions in the relatively small polar cyclones but storm surge event frequency is reproduced very well. The results of this study can be used to aid current and future scenario risk assessments of coastal flooding and coastal erosion rates.

**JSP08/09P/B19-007**

**1640**

### THE DEVELOPMENT OF A STORM SURGE MODEL INCLUDING EFFECT OF WAVE SET UP FOR OPERATIONAL FORECASTING

Nadao KOHNO<sup>1</sup>, Masakazu HIGAKI<sup>2</sup>, Tatsuo KONISHI<sup>3</sup> (<sup>1</sup>Typhoon Research Department, Meteorological Research Institute, JMA, <sup>2</sup>Climate and Marine Department, Japan Meteorological Agency)

Storm surges often lead to enormous disasters in coastal areas, and accurate predictions are crucial for disaster prevention. Recently storm surge predictions using numerical models have advanced and been operationally used in several countries. JMA operates a 2-dimensional linear storm surge model with horizontal grid resolution of 1 minute in each direction, which is much finer than those of weather models. Accuracy of this model is reasonable for inland bay areas, since the topographies of coasts and water depth mainly determine storm surges in inland bay. On the other hand, it is difficult to estimate storm surges accurately along coasts and islands shores where high waves tend to hit, even using a 3-dimensional storm surge model. This reason could be due to effects of ocean waves like wave set-up, which is not included in conventional storm surge models. A development of a storm surge model, which includes effects of ocean waves, is necessary. We have developed such a storm surge model for operational predictions. It consists of a storm surge model based on Princeton Ocean Model (POM) and the third generation wave model MRI-3 originally developed at MRI. Radiation stresses are calculated in the wave model and used in storm surge calculation. The expression of stress to storm surge is parameterized, since grid resolution is coarser than the scale of wave set-up phenomena. In August 2000, TY KIROGI (0003) passed by Hachijo Island located in the Pacific Ocean and a large storm surge of almost 250cm is observed at the Yaene tidal station located on the western coast of Hachijo Island. We simulated this case by this new model. The maximum storm surge at Yaene tidal station simulated by a conventional storm surge model was much lower (about 50cm) than the observation. This calculated value is explained just by static pressure balance. The effect of wind set-up is not crucial since Yaene Port is quite small bay with rather deep water depth. From our wave calculation, quite high waves (wave height of 7 m) hit Yaene Port when the storm surge occurred. As a result, wave set-up must play a significant role in the storm surge. Our new model estimated maximum storm surge of about 170cm, and the value of about 120cm is improved by considering wave set-up. This value still indicates underestimation and it seems to result from some factors like grid resolution or wind estimation. We simulated other cases and the results of the simulations indicate that improvements are quite well. We have a plan to put this model into operation in near future.

**JSP08/09P/B19-008**

**1700**

### LOICZ-RELATED STUDY IN THE CHINESE ACADEMY OF SCIENCES

Fan WANG, Dunxin HU (Laboratory of Ocean Circulation and Wave Study, Institute of Oceanology, Chinese Academy of Sciences)

Supported by the Chinese Academy of Sciences (CAS), the research into the Land-Ocean Interactions in the Coastal Zone (LOICZ) was initiated in China in 1997. Two CAS projects, "Land-Ocean Interactions in the China Seas and Their Environmental Impacts" (1997-2000) and "Study on Land-Ocean Interactions in the Chinese Main Estuaries and Adjacent Continental Shelf" (2000-2003), were successively carried out and led by the Institute of Oceanology, the CAS. The projects focused on some important issues in the Chinese coastal seas involved with the LOICZ, such as the variability of materials discharged from the Yangtze and Yellow Rivers, the processes of circulation and transportation of water, fine material and nutrients on the East China Sea (ECS) and Yellow Sea (YS) continental shelves, the distribution and variation of primary production limiting factors in the ECS, the contributions and their evolutions of the Yangtze River diluted water and Taiwan Warm Current to the nutrient supply of the Zhoushan Fishery Ground, and the sand transport dynamics in the Yellow River Estuary. Many progresses have been made and are reviewed in this paper.

**JSP08/09P/B19-009**

**1720**

### TODOS OS SANTOS BAY: AN OCEANOGRAPHIC CHARACTERIZATION BASED ON IN SITU DATA AND NUMERICAL SIMULATIONS

Mauro CIRANO, Guilherme Camargo LESSA (Centro de Pesquisa em Geologia e Geofísica)

The Todos os Santos Bay (TSB) is the second largest coastal bay in Brazil, with an area of approximately 1270 km<sup>2</sup>. The tides in the bay are semi-diurnal, with a mean range of 2 m, and a slight distortion that favors stronger ebb-tidal currents. The bay average depth, volume and tidal prism are 5.2 m, 12.5 x 109 m<sup>3</sup>, 3.36 x 109 m<sup>3</sup>, respectively, and average fresh water input from all catchments is calculated as 111.10 m<sup>3</sup>/s. Fresh water discharge is three orders of magnitude smaller than the estimated average spring-tidal discharge at the bay mouth (1.30 x 105 m<sup>3</sup>/s). Under these circumstances, mixing of the water column appears to be effective throughout the year. Based on a massive data collection campaigns during two different seasons (summer and winter), a characterization of the circulation of TSB and its interaction with the associated continental shelf is provided. The hydrographic data collected during each season includes 17 current-meter stations (involving the deployment of 27 mechanical and electromagnetic current meters, as well as 2 ADCPs), 8 tide-gauging stations, 3 wind-gauging stations and 12 water-column profiling stations (CTD samplings during 1 spring and 1 neap tidal cycle). Currents inside the TSB are tidal driven, with average values between 10-30 cm/s, and residual velocities varying from 1-4 cm/s. The residual currents directed landward in the low water column may help to explain an extensive deposition of a several meters thick layer of mud in the shallower, inner half of the bay, where a turbidity maximum zone might exist. Outside the TSB, the inner shelf stations show higher values of residual velocities (4-14 cm/s) as well as a change in direction depending on the season, which indicates the influence of other forcing mechanisms in the area. Temperature and salinity gradients between the adjacent shelf and the innermost region of TSB can be as high as 2.7°C and 3.6 psu respectively and according to the season. Based on all the data available, the Princeton Ocean Model was run in its three-dimensional model, and a comparison of the results from the in situ data and the numerical simulations is presented as part of this oceanographic characterization.

**JSP08/09P/B19-010**

**1740**

### EFFECTS OF WINDS, TIDES, AND STORM SURGES ON OCEAN SURFACE WAVES IN THE JAPAN/EAST SEA

Wei ZHAO<sup>1</sup>, Shuyi S. CHEN<sup>1</sup>, Cheryl Ann BLAIN<sup>2</sup>, Jiwei TIAN<sup>3</sup> (<sup>1</sup>Division of Meteorology and Physical Oceanography, University of Miami, Miami, Florida, USA, <sup>2</sup>Oceanography Division, Naval Research Laboratory, Stennis Space Center, MS, USA, <sup>3</sup>Laboratory of Physical Oceanography, The Ocean University of China, Qingdao, P. R. China)

Ocean surface waves are strongly forced by high wind conditions associated with winter storms the Japan/East Sea (JES). They are also modulated by tides and storm surges, especially near the coasts. The effects of the variability in surface wind forcing, tides, and storm surges on the waves are investigated using a wave model, a high-resolution atmospheric mesoscale model, and a hydrodynamic ocean circulation model. We conduct three month-long wave model simulations to examine the sensitivity of ocean waves to various wind forcing fields, tides, and storm surges during January 1997. Comparing with observed mean wave parameters (i.e., significant wave heights and wave periods), our results indicate that the variation in the wave fields is mainly caused by the variability of wind forcing. Tides and storm surges seem to have a significant impact on the waves near shores when mean water depth decreases sharply from a few hundreds of meters to less than 10 m along the west coast of Japan. Improving surface wind forecasts will be crucial for the prediction of surface waves and storm surges in JES, especially near the coastal regions.

**JSP08-Posters**

**Wednesday, July 9**

### COASTAL PROCESSES AND STORM SURGES (IAPSO, IAMAS, LOICZ[IGBP])

Location: Site D

**Wednesday, July 9 PM**

Presiding Chair: T. Yanagi

**JSP08/09P/D-001**

Poster

**1400-100**

### ECOLOGICALLY SUSTAINABLE INTEGRATED COASTAL DEVELOPMENT IN BANGLADESH: PRESENT PRACTICES, ITS CONSEQUENCES AND A POLICY FRAMEWORK

Md. SALEQUZZAMAN (Ph.D. Candidate and Researcher, Institute for Sustainability and Technology Policy (ISTP), Murdoch University, Australia, and Associate Professor, Environmental Science Discipline, Khulna University, Bangladesh)

Coastal environment is highly valued and greatly attractive on its richness of various resources. Presently these coastal resources are critical to global sustainable development, particularly in developing countries like Bangladesh. Evidence suggests that activities in a variety of different sectors like energy, agriculture, industry, health and overall other coastal resources work better when these resources are ecologically integrated across disciplines and boundaries upon a strongly participatory and decision-making approaches and processes. Community can create authentic choices to achieve sustainable development by adopting integrative frameworks that could balance social, economic, and ecological concerns. Bangladesh belongs to a vast coastal area with a long coastal belt, most of which are protected by embankments and sluice gates. This coastal area possesses many resources and regarded as productive zone. But presently most of these resources are managed in an unplanned and unsustainable way. Although coastal environment of Bangladesh has had a good history of ecologically sustainable development practiced in the past. The main causes of present unplanned and unsustainable development are the lack of integration and lack of vision of future development. Among integration, electricity is an important indicator of modernisation, industrialisation and sustainable development. Presently this electricity is completely absent in coastal Bangladesh. The research identified tidal ranges in some areas of coastal Bangladesh are an important resource for the production of small-scale tidal energy. Thus the paper will briefly describes the various components necessary to integrating tidal energy in coastal Bangladesh. However, the core aim of integrated coastal development is to guide coastal area development in an ecologically sustainable fashion. Therefore the paper also identify factors responsible for ecologically sustainable integrated development through the examination of past environmental, socio-cultural and economical history of coastal Bangladesh. On the other hand, integrated coastal development is holistic and interdisciplinary in nature, especially with regard to science and policy. Therefore finally the paper will give a policy

recommendation that 'how coastal Bangladesh could be developed on ecologically sustainable manner'.

**JSP08/09P/D-002** Poster **1400-101**

**BLACK SAND CONCENTRATIONS AND COASTAL PROCESSES OF AZEMMOUR BEACH AND OUM ER RBIA ESTUARY, MOROCCAN ATLANTIC COAST**

Nadia MHAMMDI<sup>1</sup>, Addi AZZA<sup>2</sup> (Département Physique du Globe, Université EMohammed V, ministère de l'Energie et des Mines, PB 6208, rabat Instituts, Maroc)

Heavy-mineral sand-deposits are the main sources for the world supply of rare metals as zirconium and titanium. Concentrations of these minerals are known to occur in beach and dune sands. The economic importance of the Black Sands is attributed to their contents of industrial minerals such as ilmenite, hematite, magnetite, zircon, garnet and monazite. These deposits usually may visually be recognized by a darker colouring of the sands. Since heavy-mineral concentrations are often found in beach ridges it is generally accepted that the concentration took place by the selective removal of the lighter minerals such as quartz during erosion along a sandy coast. The presence of heavy minerals in beaches and dunes can therefore be used as an indicator for coastal development processes (erosion). The studied sector is situated on the Atlantic coast of Morocco about twenty km to the Northeast of El Jadida, near of Azemmour town. It belongs to the Moroccan Meseta crossed by the Oum Er-Rbia river. Climate, geomorphology, hydrology and geology of the Oum Er Rbia basin control the morphology and the sedimentation on this area. The climatically regime of this basin is under the influence of a Mediterranean climate of semi-arid type. Sand samples (thirty) were collected along of perpendicular beach profiles to the shore (river and sea) spaced of 50m to left of the river and 200m along of the beaches in order to examine the sorting patterns of heavy minerals that develop during cross-shore and alongshore sediment transport. Grain-size analysis, quartz morphology, heavy mineral and CaCO<sub>3</sub> content analyses were performed on all the samples. The heavy fraction was separated from the light fraction by the gravity separation method. Selected samples for the analysis include the polished thin-sections prepared for modal analysis and isomagnetic separated fractions were investigated.

**JSP09** Thursday, July 10 - Friday, July 11

**PHYSICAL ASPECTS OF AIR-SEA INTERACTION (IAPSO, IAMAS)**

Location: Site B, Room 20

Thursday, July 10 AM

Presiding Chairs: C. Fairall, S. Josey

**JSP09/10A/B20-001** Invited **0900**

**MEASUREMENT AND PARAMETERIZATION OF AIR-SEA FLUXES: RECENT DEVELOPMENTS IN BULK FLUX ALGORITHMS**

Chris W. FAIRALL (Clouds, Radiation and Surface Processes Division)

Direct measurement of air-sea fluxes remains a technological challenge that is practiced by only a few research groups around the globe. Accurate measurements of fluxes from ships and buoys in a routine, unattended mode are still not practical. Thus, virtually all estimates of global or regional fluxes are obtained from bulk flux models, which use more easily obtained near surface meteorological data. Ultimately, bulk model coefficients must be traced to direct measurements obtained in very demanding intensive field programs. In the last decade great progress has been made on several technological fronts to improve the quality of the direct flux data. Similarly, several theoretical advances in representations of interfacial and boundary-layer processes has removed earlier pathological problems and linked the parameterizations more closely to the underlying physics. In 1996 version 2.5 of the COARE bulk algorithm was published and has become one of the most frequently used in the air-sea interaction community. In this talk we describe steps taken to improve the algorithm and a comparison with new data. This new version of the algorithm (COARE 3.0) was based on published results and 2777 one-hour covariance flux measurements in the ETL inventory. To test it, we added 4439 new values from field experiments between 1997 and 1999, which now dominate the database, especially in the wind speed regime beyond 10 m/s where the number of observations increased from 67 to about 800. In the paper we will discuss measurement issues, how these results compare with classic results from other field programs and models, and prospects for extending beyond 20 m/s.

**JSP09/10A/B20-002** **0930**

**REAL-TIME ON-BOARD AIR-SEA FLUX MEASUREMENT SYSTEM WITH EDDY COVARIANCE METHOD**

Osamu TSUKAMOTO<sup>1</sup>, Satoshi TAKAHASHI<sup>1</sup>, Ken'ichi OKADA<sup>1</sup>, Hiroshi ISHIDA<sup>2</sup> (Okayama University, Department of Earth Sciences, <sup>2</sup>Maritime University of Kobe/ Frontier Observational Research System for Global Change)

Air-sea fluxes of momentum, energy or trace gases are key parameter to understand the air-sea interaction. A lot of approaches are carried out including satellite remote sensing. However most of the sea surface flux estimates are based on bulk aerodynamic formulas. While, the bulk algorithm includes bulk transfer coefficients, which are experimentally determined and some uncertainty remains in the transfer coefficients. Eddy correlation method or eddy covariance method are rather direct method for surface flux measurement without any assumptions or experimental coefficients. Now it is widely applied over land surface flux measurements (e.g. GEWEX, FLUXNET...). The application of the eddy covariance method over open sea is rather complex as the platform (ships or buoys) sways with surface waves. Some research groups have already succeeded in the ship motion correction and on-board flux measurements are reported. Our group is one of them and unique in Japan. Present authors have installed the eddy flux system on R/V MIRAI, JAMSTEC and operating throughout a year as her all cruises in the Pacific since June, 2000. Her cruise extended from the Arctic to the tropics and encounters a lot of atmospheric and sea state conditions. A large amount of the dataset was analyzed and air-sea fluxes of sensible and latent heat were evaluated until the end of 2001. However, the data needs detailed quality control to remove noises and unfavorable conditions due to ship operations. The selected results are reported and compared with bulk fluxes. Now our measurement system evolved into a second generation since 2002. A open-path CO<sub>2</sub> gas flux sensor was introduced and air-sea CO<sub>2</sub> flux are now available as eddy covariance values. The sensor (LI-7500) also measures water vapor flux and humidity sensor was replaced as more long-life instrument. It can be used more than a year without special maintenance. Another development is the automated data processing system as real-time in-situ display system.

Our previous system requires off-line data processing job after the cruise. Now our on-line system can show you air-sea flux time series as real-time operating system. The present flux system can be applied to many cruising ships and more accurate air-sea fluxes are available in global scale. It should be helpful for the sea truth of satellite remote sensing or numerical model outputs.

**JSP09/10A/B20-003** **0945**

**CONSTRAINING THE INERTIAL DISSIPATION METHOD USING THE VERTICAL VELOCITY VARIANCE**

Genevieve M. DARDIER<sup>1</sup>, Alain WEILL<sup>2</sup>, Helene DUPUIS<sup>3</sup>, Christine GUERIN<sup>2</sup>, William M. DRENNAN<sup>4</sup>, Sidonie BRACHET<sup>5</sup>, Fabienne LOHOU<sup>3</sup>, Rodrigo PEDREROS<sup>2</sup> (Stevens Institute of Technology, 711 Hudson Street, Hoboken, NJ 07030, <sup>2</sup>CETP, 10-12 av. de l'Europe, 78140 Velizy, France, <sup>3</sup>DGO, Université Bordeaux I, UMR58, av. des Facultés, 33405 Talence, France, <sup>4</sup>RSMA, University of Miami, 4600 Rickenbacker Causeway, Miami, FL, 33149, USA)

The Inertial Dissipation Method (IDM) is commonly used to measure turbulent fluxes over the ocean. It has the advantage over more direct methods in that it depends on the turbulent fluctuations only in the high frequencies of the so-called inertial subrange. These frequencies are above those of typical ship motions, and are considered to be relatively unaffected by flow distortion. However, a drawback in applying the method is that the problem is underdetermined: estimation of the fluxes requires knowledge of the Obukhov length  $L$ , which is itself a function of the fluxes. The problem is typically solved by iteration, using an initial  $L$  estimated from bulk formulae. This introduces a possible dependency on the initial bulk estimate and problems of convergence. To avoid this problem, IDM algorithms use an iterative approach, using an estimate of  $L$  as a 'first guess'. This initial estimate is typically derived from bulk relations or using the bulk Richardson number. The latter approach has been found to improve convergence but there remains the problem that for a significant number of cases the method does not converge. Also, the solution can be dependent on the initial estimate. We explore an alternative approach to the problem. In order to constrain the equations resulting from the IDM, we use the vertical velocity variance,  $\sigma_w$ , measured from the research vessel, l'Atalante and an ASIS buoy, both deployed during the 1998 FETCH experiment. These data are compared to several parameterisations of  $\sigma_w$  on stability derived in experiments over land. For unstable cases, the data are found to be well described by the Panofsky and Dutton [1984] parameterisation, although the scatter of the data is higher for swell conditions than for pure wind sea, indicating a likely sea state effect. Using measured values of  $\sigma_w$  and this parameterisation, the inertial dissipation problem is fully specified. The convergence of the method is satisfactory, and it offers  $u^*$  estimates independent of bulk formulae.

**JSP09/10A/B20-004** **1000**

**SEA STATE AND SURFACE CURRENT MEASUREMENTS WITH X-BAND MARINE RADAR ABOARD THE EXPLORER OF THE SEAS**

Hans C. GRABER<sup>1</sup>, Katrin HESSNER<sup>2</sup> (University of Miami, <sup>2</sup>OceanWaves, GMBH)

The Wave Monitoring System **WaMoS II**, a real time ocean wave and surface current monitoring system designed for operational measurements under harsh environmental conditions, has been installed aboard the Royal Caribbean International cruise ship *Explorer of the Seas*. Standard methods are applied to derive directional wave spectra from a sequence of nautical radar images and then compute standard wave parameter like significant wave height, peak wave period, peak wave direction and peak wavelength. The measurement and data analysis takes about 2 minutes for standard, commercial nautical radars and sea state parameters are available in real time. A minimum wind speed of 3 m/s is required to obtain good wave measurements. The ship sails weekly on a seven-night Eastern Caribbean itinerary from Miami and cross the Gulf Stream to the major passages between the Atlantic Ocean and Caribbean Sea and the tradewind region. This ship's repetitive cruise track allows scientists to collect wave and surface current information continuously during weekly cruises. These observations will eventually provide improved descriptions of seasonal to interannual variability of the sea state and surface currents in this tropical regime. Results will show sea state information such as directional wave spectra, significant wave height, wave period and wave direction along the cruise track. The data is used to study wave-current interaction in the Florida Current and the effect of sheltering and diffraction around islands.

**JSP09/10A/B20-005** **1015**

**INFRARED INTERFEROMETRIC MEASUREMENTS OF THE AIR-SEA TEMPERATURE DIFFERENCE**

Peter J. MINNETT<sup>1</sup>, Kevin A. MAILLET<sup>1</sup>, Brian J. OSBORNE<sup>2</sup> (University of Miami, <sup>2</sup>University of Wisconsin-Madison)

The use of a well-calibrated, high-accuracy Fourier-Transform Infrared (FTIR) Interferometric Spectroradiometer on ships permits the derivation of many atmospheric parameters. Included amongst these is the air-sea temperature difference. Downward-looking measurements in transmissive parts of the infrared atmospheric absorption spectrum provide measurements of the surface skin temperature of the ocean, and upward-looking measurements in the less transmissive parts give air-temperature. Thus the air-sea temperature difference can be measured accurately with a single instrument. The Marine-Atmospheric Emitted Radiance Interferometer (M-AERI) has been deployed on several ships in a wide range of environmental conditions. The characteristics of the air-sea temperature difference revealed by radiometric measurements are different to those derived from conventional data, especially in the tropics. The larger variability in the conventional measurements is not surprising, but the presence of spurious mean signals in the conventional measurements may have significant and misleading consequences on our understanding of air-sea coupling. The interferometric measurement technique is presented with examples of at-sea measurements; the differences between these and conventional measurements are discussed along with some of their consequences.

**JSP09/10A/B20-006** Invited **1045**

**SHIP-BASED MEASUREMENTS OF AIR-SEA FLUXES**

Sergey K. GULEV (P.P. Shirshov Institute of Oceanology, RAS)

We discuss the major problems of the development of the global and regional climatologies of sea-air surface fluxes on the basis of Voluntary Observing Ship (VOS) data. Uncertainties inherent in the individual variables and flux components are quantified using the COADS (Comprehensive Ocean-Atmosphere DataSet) collection of VOS observations for a couple of decades. The main sources of uncertainties are the use of different parameterizations of fluxes, the accuracy of the meteorological variables used for the flux computations, and insufficient sampling. These uncertainties have different impacts on the closure of the surface ocean heat balance and on the adequate representation of the climatic variability of surface

## INTER-ASSOCIATION

fluxes. In particular, sampling problems may have a time-dependent nature and, thus, can seriously affect variability patterns on regional scales. Intercomparison of VOS-based flux products with those available from numerical weather prediction (NWP) systems and remote sensing is presented in order to identify strengths and weaknesses of VOS with respect to the other flux data sources. Approaches to minimize different uncertainties are overviewed. These approaches are based on the application of the advanced objective analysis methods (to overcome the sampling problems) and the usage of the alternative information about the regional energy balances. Some perspectives in the use of VOS data for the computations of advanced sea-air flux parameters (e.g., sea-state-based wind stress and albedo) are discussed.

**JSP09/10A/B20-007**

**1115**

### AIR-SEA HEAT AND FRESHWATER FLUXES: A NEW APPROACH FOR VALIDATION AND ESTIMATION BASED ON THE TIME-DEPENDENT ENERGY AND BUOYANCY BUDGETS OF NATURAL VOLUMES

Huai-Min ZHANG<sup>1</sup>, John M. TOOLE<sup>2</sup>, Michael J. CARUSO<sup>2</sup> (<sup>1</sup>NOAA/NESDIS/National Climatic Data Center, <sup>2</sup>Woods Hole Oceanographic Institution)

Accurate knowledge of air sea fluxes is central to advancing climate study and improving weather prediction, but currently available products have large uncertainties. Error is manifested by intercomparisons of various flux products, but such cross checks cannot determine which product is superior. And while validation against direct flux measurements is of great value, such estimates are rare and of limited temporal span; resultant flux adjustments based on these data are possibly location dependent. Here we propose application of oceanic heat and buoyancy conservation to evaluate air sea heat and freshwater fluxes, demonstrated with the heat flux into the tropical warm water pools. If the average oceanic vertical mixing is known at the base of such a control volume (physically the mixing must be down gradient), the method can be used to reduce air-sea flux errors/offsets. The method will be of greater value for freshwater flux when the satellite mission for SSS (Aquarius) is launched in the near future. The heat flux technique builds on the work of Niiler and Stevenson (1982) and Walin (1982) by examining the heat budget for natural control volumes defined by an isotherm. We applied the method to the tropical warm water pools of the Indo-Pacific and Atlantic Oceans, sites of intense convection in the atmosphere and thus key areas of air sea interaction. The dominant terms in the energy budget include time rate of change in pool heat content, net air pool heat flux over the whole pool surface, and turbulent and penetrating radiative heat fluxes integrated over the pool base. We find that the SOC and unconstrained COADS annual climatologies are most consistent with the mean annual march of ocean heat content in that consistently down gradient turbulent ocean heat fluxes are inferred, with relatively constant dia-thermal diffusivity of 2.8 cm<sup>2</sup>/s for the 28°C Indo Pacific pool and 1.5 cm<sup>2</sup>/s for the 27°C Atlantic pool. In contrast, other air sea flux climatologies (constrained COADS, NCEP and ECMWF) show inconsistencies with oceanic energy change in some seasons. On the mean annual cycle we find a dominant two term balance between seasonal changes in air pool heat exchange and change in pool energy content. On interannual time scales, all terms in the pool energy budget contribute, but high correlation is obtained between the air pool heat flux (estimated from the unconstrained COADS climatology) and the inferred turbulent ocean flux (as well as with the inferred diffusivity). We hope to explore this further in the context of coupled ocean atmosphere models where the turbulent fluxes can be estimated directly from model quantities.

**JSP09/10A/B20-008**

**1130**

### BALANCING THE HEAT BUDGET OF THE SOC AIR-SEA FLUX CLIMATOLOGY THROUGH AN INVERSE ANALYSIS WITH OCEAN HEAT TRANSPORT CONSTRAINTS

Simon A. JOSEY, Jeremy P. GRIST (James Rennell Division, Southampton Oceanography Centre)

The Southampton Oceanography Centre (SOC) air-sea flux climatology, in common with other ship-based climatologies, exhibits an imbalance of 30Wm<sup>-2</sup> in the global ocean heat budget. We have attempted to balance the climatology using linear inverse analysis. Up to ten hydrographic measurements of ocean heat transport from the Atlantic and North Pacific Oceans have been used as constraints. An additional constraint that the global mean net heat flux lies in the range 0±2 Wm<sup>-2</sup> was also utilized. A solution is obtained with all ten transport constraints but without the requirement of global closure in which the global net heat bias is reduced to -5Wm<sup>-2</sup>. This change is largely due to a 15% increase in the latent heat flux and a 9% reduction to the shortwave flux. When the global constraint is included with the hydrographic constraints the solution requires increases in the latent heat flux, the longwave flux and the sensible heat flux of 19%, 9% and 7% respectively and a decrease in the shortwave flux of 6%. This solution results in an adjusted climatology with a global net heat flux of -2 Wm<sup>-2</sup>. It also provides good agreement with recent estimates of the global ocean heat transport obtained using residual techniques and from atmospheric model reanalyses. However, additional comparisons of the adjusted fluxes with measurements made by various Woods Hole Oceanographic Institute research buoys indicate that significant regional biases still exist. Results of ongoing research, aimed at identifying the causes of these biases, will be presented.

**JSP09/10A/B20-009**

**1145**

### DIURNAL VARIATIONS OVER TROPICAL OCEANS AND THEIR IMPLICATIONS FOR AIR-SEA INTERACTIONS

Aiguo DAI, Kevin E. TRENBERTH (National Center for Atmospheric Research (NCAR))

We have analyzed high-resolution surface meteorological and oceanic data from TOGA COARE, Tropical Atmosphere-Ocean (TAO) buoys, WHOI buoys, and Nauru99 R/V Mirai to quantify the diurnal cycle at tropical ocean surfaces and determine the factors controlling the oceanic diurnal cycle. We have found that the diurnal (mean-to-peak) amplitude of sea surface skin temperature (T<sub>skin</sub>) can be over 4 deg.C under calm (< 2 m/s winds) and clear-sky conditions in the Tropics. Under windy (> 4 m/s) conditions, the amplitude is less than 2 deg.C. T<sub>skin</sub> peaks around 1-2 pm. Sea surface temperatures (SSTs) within the top 2m depth have a diurnal amplitude of 0.2-2.5 deg.C, with the maximum around 3-4pm. Surface air temperatures (T<sub>a</sub>) have a diurnal amplitude of 0.4-5.0 deg.C with high values in the afternoon (2-4pm). The T<sub>a</sub> amplitude increases with diurnal amplitudes of surface specific humidity, wind stress, sensible and latent heat fluxes, but is not correlated with daily mean wind speeds and maximum solar radiation. Time-averaged diurnal amplitudes are much smaller than those of individual days. Amplitudes of monthly SSTs are about 0.3-0.6 deg.C on the Equator and 0.1-0.3 deg.C off the Equator in the Pacific. Using daily mean wind speed or SSTs results in large errors in surface latent (up to 60 W/s) and sensible (up to 12 W/s) fluxes on hourly time scales.

**JSP09/10A/B20-010**

**1200**

### AN ASSESSMENT OF THE SURFACE TURBULENT HEAT FLUXES FROM THE NCEP REANALYSIS OVER THE WESTERN BOUNDARY CURRENTS

Kent MOORE<sup>1</sup>, Ian RENFREW<sup>2</sup> (<sup>1</sup>Department of Physics, University of Toronto, <sup>2</sup>British Antarctic Survey)

With the completion of the NCEP and ECMWF reanalyses there are now global representations of air-sea surface heat fluxes with sufficient spatial and temporal resolution to be useful in characterizing the air-sea interaction associated with individual weather systems, as well as in developing global-scale oceanic heat and moisture budgets. However these fluxes are strongly dependent on the numerical models used, and as a result, there is a clear need to validate them against observations. Accurate air-sea heat flux estimates require a realistic representation of the atmospheric boundary layer, and the implementation of an appropriate surface flux parameterization. Previous work at high latitudes has highlighted the shortcomings of the surface turbulent heat flux parameterization used in the NCEP reanalysis during high wind speed conditions; especially when these are combined with large air-sea temperature differences. Here we extend this result through an examination of the air-sea heat fluxes over the western boundary currents of the North Atlantic and North Pacific Oceans. These are also regions where large transfers of heat and moisture from the ocean to the atmosphere take place. A comparison with in-situ data shows that the surface-layer meteorological fields are reasonably well represented in the NCEP reanalysis, but the turbulent heat flux fields contain significant systematic errors. It is argued that these errors are associated with shortcomings in the bulk flux algorithm employed in the reanalysis. Using the NCEP reanalysis surface-layer meteorological fields and a more appropriate bulk flux algorithm, adjusted fields for the sensible and latent heat fluxes are presented that more accurately represent the air-sea exchange of heat and moisture over the western boundary currents.

**JSP09/10A/B20-011**

**1215**

### FRESH WATER FLUXES AND SEA SURFACE SALINITY

S.Daniel JACOB<sup>1</sup>, Chester J. KOBLINSKY<sup>2</sup> (<sup>1</sup>GEST, NASA GSFC/ UMBC, <sup>2</sup>NASA GSFC, Greenbelt, MD 20771, USA.)

Oceanic fresh water transport has been shown to play an important role in the global hydrological cycle. With more than 70% of global evaporation and precipitation occurring over world's oceans, it has also been pointed out that small changes in these will cause major changes in the terrestrial water budget. Sea Surface Salinity (SSS) is representative of the surface fresh water fluxes and the upcoming NASA Aquarius mission will provide excellent spatial and temporal SSS coverage to better estimate the net transfer. However, SSS is also controlled by advection and mixing processes, therefore the main objective of this study is to understand and quantify various mechanisms controlling SSS in relation to surface fresh water fluxes over interannual time scales. Using a near-global HYbrid Coordinate Ocean Model (HYCOM) configured with different mixing schemes SSS variability and controlling mechanisms are investigated in this paper for different forcing data sets. Results suggest significant variability in the tropical and subtropical ocean regions due to differences in forcing climatologies.

Thursday, July 10 PM

Presiding Chair: S. Gulev

**JSP09/10P/B20-001**

Invited

**1400**

### THE WHOI DAILY FLUX PRODUCT AND ITS COMPARISON WITH IN SITU FLUX MEASUREMENTS AND THE SOC CLIMATOLOGY

Lisan YU<sup>1</sup>, Robert A. WELLER<sup>1</sup>, Simon A. JOSEY<sup>2</sup> (<sup>1</sup>Department of Physical Oceanography, Woods Hole Oceanographic Institution, <sup>2</sup>James Rennell Division, Southampton Oceanography Centre, UK)

Efforts have been taken at the Woods Hole Oceanographic Institution (WHOI) to develop high-quality, gridded, time-dependent surface turbulent and radiative fluxes to support studies of climate variability and predictability under the auspices of the NOAA CLIVAR Atlantic program. The emphasis of this presentation will be on the newly constructed latent and sensible fluxes product and its comparison with in situ flux buoy measurements and the SOC climatology. The product has daily, 1° by 1° resolution and covers the period from 1988 to 1999. It is developed by using a weighted objective analysis approach to improve the estimates of flux-related basic surface meteorological variables (e.g., wind speed, air humidity, air temperature, and sea surface temperature) through synthesizing data from satellite retrievals and outputs from NCEP and ECMWF global analysis/forecast models. The state-of-the-art COARE bulk flux algorithm 2.6a is then applied to compute the flux fields. Two types of errors can affect the representativeness of a flux product, i.e., the systematic error that influences the mean and the random error that influences the variance. Therefore, the two aspects at the heart of the comparison study are the mean and variability of flux fields. The primary reference data used in the comparison are high accuracy in situ buoy measurements. Comparisons are also made with the analysis of the Southampton Oceanography Centre (SOC) flux climatology. The latter provides high-quality depiction of global air-sea heat exchanges on climatological mean basis, while the former, though available for only limited locations and short spanning periods, provide the benchmark time series to identify regional biases. Good agreement is found between the new WHOI flux product and the independent research buoy measurements. The analysis also shows that the mean field structure and year-to-year variations of the WHOI latent and sensible fluxes are very similar to those obtained from the SOC fluxes, despite the different methods used to produce the two datasets. The buoy and SOC comparisons show that the WHOI synthesis is a considerable improvement over those of the ECMWF and NCEP2 outputs and the improvement comes not only from the use of a better flux algorithm but more importantly from the use of improved estimates of bulk variables.

**JSP09/10P/B20-002**

**1430**

### AIR-SEA INTERACTION ASSOCIATED WITH GREENLAND TIP JETS

Rebekah E. MARTIN<sup>1</sup>, G.W.K. MOORE<sup>1</sup>, Ian A. RENFREW<sup>2</sup> (<sup>1</sup>Department of Physics, University of Toronto, <sup>2</sup>British Antarctic Survey, Cambridge U.K.)

High wind speed events are a frequent occurrence downstream of Cape Farewell, Greenland in synoptic situations characterized by low-level westerly/northwesterly flow. It has been suggested that the dynamics of these so-called tip jets are governed by the conservation of the Bernoulli function, which leads to an acceleration as air parcels undergo orographic descent on the eastern (leeward) side of Greenland. In addition, it has been proposed that the air-sea interaction associated with tip jets plays a role in triggering deep oceanic convection in the lee of Greenland. Recent work has however shown that the surface layer parameterization in many numerical models have roughness length

formulations for heat and moisture that are biased high in conditions such as those associated with tip jets. In this presentation, we will show results of one such event from a numerical model whose surface layer parameterization has been validated against observations in conditions similar to those observed during tip jet events.

**JSP09/10P/B20-003****1445****SST FORCING TO SURFACE WIND SPEED OVER THE MALVINAS/BRAZIL CONFLUENCE AND NORWEGIAN SEA**

Hiroki TOKINAGA, Youichi TANIMOTO (Graduate School of Environmental Earth Science, Hokkaido University)

Over most of the mid-high latitudes, sea surface temperature (SST) is cold (warm) under the strong (weak) surface wind on basinwide scales. This negative correlation between SST and surface wind speed anomalies indicates that SST changes over the mid-high latitudes are mainly dominated by an atmosphere-to-ocean forcing. However, the positive SST-wind correlation is detected over the Malvinas/Brazil Confluence and Norwegian Sea in the South and the North Atlantic, respectively. The cold northward-flowing Malvinas Current encounters the warm southward-flowing Brazil Current east of Argentina. The confluence of these currents forms a sharp SST gradient all through the year, leading to a remarkable cold (warm) tongue west (east) of the SST gradient, where the annual mean surface winds are westerlies under the influence of the subtropical jet. High-resolution satellite datasets clearly depict that surface wind speeds are weak over the colder flank of the SST gradient while strong over the warmer flank all through the year. This relationship between SST and surface wind speed is indicative of an ocean-to-atmosphere forcing. In addition, we detect that such a positive SST-wind correlation is explained by the vertical mixing mechanism, using difference between SST and surface air temperature from high-resolution in-situ datasets. The same relationship between SST, surface wind speed and surface air temperature is identified in the Norwegian Sea.

**JSP09/10P/B20-004****1500****INTERCOMPARISON OF HEAT FLUXES IN THE SOUTH ATLANTIC: PART II: INTERANNUAL VARIABILITY**

Fabrice M. VAUCLAIR, Ilana WAINER (Dept. of Physical Oceanography, University of São Paulo)

Inter-comparison of the interannual variability of sea surface temperature, net heat and latent heat flux, for 2 observation based products (DaSilva, SOC), output of the two major atmospheric model reanalysis (NCEP, ECMWF) and the results for the NCAR CCSM coupled model are examined in order to gain an improved understanding of the South Atlantic characteristic spatial patterns. Their spatial structure and associated temporal variability, related ocean dynamics evolution are also discussed. The key regions of the Brazil-Malvinas confluence, Agulhas retroflection and Benguela upwelling region off Africa were chosen for a closer examination of the fluxes. These key regions were identified as being the regions with the highest variance in the South Atlantic. Preliminary results show significant interannual variability from each data product, but large differences among them. The merchant ship based interannual patterns are highly dependent of the spatio-temporal data distribution. Interannual patterns of the CCSM are coherent with the reanalysis products.

**JSP09/10P/B20-005****1515****AN EXTENDED ASSOCIATE PATTERN ANALYSIS OF ENSO**

Maochang CUI<sup>1</sup>, Jun MO<sup>2</sup>, Yongqiang YU<sup>2</sup> (<sup>1</sup>Institute of Oceanology, Chinese Academy of Sciences, <sup>2</sup>LASG, Institute of Atmospheric Physics, Chinese Academy of Sciences)

To further study the causes of El Niño events Extended Associate Pattern Analysis (EAPA) is adopted again with monthly sea surface wind stress and precipitation besides sea level pressure (SLP) and sea surface temperature (SST) in or over the Pacific and related seas in present paper since 1979 in present paper. The results show that El Niño events mean a SST redistribution covering almost the whole Pacific that needs a huge amount of energy provided by air-sea interaction in the most Pacific regions; It is the west burst and wind convergence, coming from middle latitudes directly, instead of Kelewin waves that produce the strong SST warm signal in Niño regions; Two negative SLP anomalies in middle of the North and South Pacific, most likely produced by the average air pressure decreasing effect of explosive cyclones through precipitation, and the positive SLP anomaly over the Asia-Australia land bridge, coming mainly from the south hemisphere with a little influence from the Asian continent, are the three major causes for El Niño onset, they work together to produce the west bursts, wind convergence in Niño regions and anomalous westerly in the middle Pacific that results in a warm tongue and cold pinners gearing together; Basically, during its early stage the ocean is forced by the atmosphere, while during its late stage the atmosphere is forced by the ocean.

**JSP09/10P/B20-006****1530****INFLUENCE OF TRANSIENT ATMOSPHERIC CIRCULATION ON THE SURFACE HEATING AND TEMPERATURE OF THE PACIFIC WARM POOL**

Ming-Dah CHOU<sup>1</sup>, Shu-Hsien CHOU<sup>1</sup>, Pui-King CHAN<sup>2</sup> (NASA Goddard Space Flight Center, <sup>2</sup>Science Systems & Applications, Inc.)

Analyses of data on clouds, winds, and surface heat fluxes show that the transient behavior of basin-wide large-scale circulation has a significant influence on the warm pool sea surface temperature (SST). Trade winds converge to regions of the highest SST in the equatorial western Pacific. These regions have the largest cloud cover and smallest wind speed. Both surface solar heating and evaporative cooling are weak. The reduced evaporative cooling due to weakened winds exceeds the reduced solar heating due to enhanced cloudiness. The result is a maximum surface heating in the strong convective and high SST regions. Data also show that the maximum surface heating in strong convective regions is interrupted by transient atmospheric and oceanic circulation. Due to the seasonal variation of the insolation at the top of the atmosphere, trade winds and clouds also experience seasonal variations. Regions of high SST and low-level convergence follow the Sun, where the surface heating is a maximum. As the Sun moves away from a convective region, the strong trade winds set in, and the evaporative cooling enhances, resulting in a net cooling of the surface. During an El Niño, the maximum SST and convective region shifts eastward from the maritime continent to the equatorial central Pacific. Following the eastward shift of the maximum SST, the region of maximum cloudiness and surface heating also shift eastward. As the atmospheric and oceanic circulation returns to normal situations, the trade winds increase and the surface heating decreases. We conclude that the evaporative cooling associated with the seasonal and interannual variations of trade winds is one of the major factors that modulate the SST distribution of the Pacific warm pool.

**JSP09/10P/B20-007****1545****DENSE WATER GENERATION IN THE NORTH ADRIATIC: THE ROLE OF SURFACE FLUXES AND RIVER DISCHARGES**

Ivica VILIBIC<sup>1</sup>, Nastjenka SUPIC<sup>2</sup> (<sup>1</sup>Hydrographic Institute, <sup>2</sup>Centre for Marine Research)

The analyses of winter thermohaline properties of the North Adriatic were performed at the transect Po-Rovinj in the 1967-2000 interval, based on the data of temperature and salinity collected primarily at two stations: the first positioned near the Po River mouth (station 5) and the second located close to the eastern shore (station 2). The analyses comprised single and double correlation analyses between temperature, salinity and sigma-t values in February as outputs to the surface fluxes (temperature versus heat flux, salinity versus water flux, density versus buoyancy flux) calculated for the North Adriatic and Po River discharge values as inputs. The February was chosen as the minimum in temperature and maximum in density have been measured then. Winter thermohaline properties are predominantly influenced both by Po River discharge and advection of warmer and saline waters from the southeast; therefore, bottom temperature is always lower near the western shore whereas the salinity is higher close to the eastern flank in general, but such distribution can be reversed during the years when the Po River plume is detached from the shore. Correlation analyses indicate that bottom water properties in February are driven dominantly by fluxes in September (salinity versus water flux) and in June, October and December/January (temperature versus heat flux) at the station 2, and in February/March (salinity versus water flux and Po River discharge) and October (density versus buoyancy flux) at the station 5. The strongest influence on the west side has the pycnocline destruction that usually occurs in October, bringing warmer and less saline waters to the bottom. Correlation for sigma-t values is calculated to be significant at 99.99 % level, but correlation vanishes at station 2, due to the impact of the advective processes there. Correlation with February/March Po River discharges is a consequence of deepening of the waters influenced by Po River, which can be brought to the bottom during the period of vertical instability (February/March), then spreading in the bottom layer and reaching eastern side after a month (April). Finally, it should be pointed out that thermohaline properties at the bottom of the North Adriatic are not correlated to the dynamics that occurs at the zero phase lag (February) as one should expect, due to temporal characteristics of the fluxes and strong vertical stratification in January/February near the Po River delta.

**JSP09/10P/B20-008****1615****SIGNATURES OF AIR-SEA INTERACTIONS IN A COUPLED ATMOSPHERE-OCEAN GCM**

Jin-Song VON STORCH (Institute of Meteorology, University Hamburg, Germany)

Various types of air-sea interactions are studied based on the general properties of cross covariance function and the well-defined shapes of these functions obtained from conceptual models. The analysis is applied to sea surface temperature and surface fluxes obtained from along integration with the coupled ECHAM3/LSG model. The results suggest that the atmosphere plays a dominant role in generating the coupled variability. Covariances between SST and wind stress in the extratropics are close to zero when SST leads, suggesting that SST anomalies, once being generated, do not feed back to the atmosphere. The interactions between SST and tropical wind stress involve various types of feedbacks. For heat flux, the antisymmetric shape of cross covariance functions indicates that heat flux anomalies generate SST variations and the interaction tends to reverse the sign of the earlier SST anomalies. The atmosphere plays also an important role in generating coupled variations of SST and evaporation, and of SST and extratropical precipitation. The most dominant role of the ocean is found in the tropics. The results can be used to verify simple atmospheric models, which are used in ocean-only modelling studies. Cross covariance functions found in such simple coupled models should be similar to those found in a fully coupled atmosphere-ocean GCM, if the simple models produce the same interactions found in fully coupled GCMs.

**JSP09/10P/B20-009****1630****AN ACTIVE ROLE OF EXTRATROPICAL SEA SURFACE TEMPERATURE ANOMALIES IN DETERMINING ANOMALOUS TURBULENT HEAT FLUX**

Youichi TANIMOTO<sup>1</sup>, Hisashi NAKAMURA<sup>2</sup>, Takashi KAGIMOTO<sup>3</sup>, Shozo YAMANE<sup>3</sup> (<sup>1</sup>Frontier Research System for Global Change and Graduate School of Environmental Earth Science, Hokkaido University, <sup>2</sup>Frontier Research System for Global Change and Department of Earth and Planetary Science, University of Tokyo, <sup>3</sup>Frontier Research System for Global Change)

Relative importance among observed anomalies in sea surface temperature (SST), surface air temperature and wind speed in determining the anomalous turbulent heat fluxes is assessed through linearizing flux anomalies calculated from individual ship reports contained in Comprehensive Ocean-Atmosphere Data Set (COADS). Over the central basin of the North Pacific, changes in the atmospheric variable associated with basin-scale changes in mid-latitude westerlies, including air temperature and wind speed, are primarily responsible for the generation of local SST variations by changing turbulent heat flux, which supports a conventional view of extratropical air-sea interaction. In the western North Pacific along Kuroshio and its extension where ocean dynamics is much important in forming SSTAs, in contrast, SSTAs that have been formed in early winter play the primary role in determining mid- and late-winter turbulent heat flux anomalies, indicative of the SST forcing upon the overlying atmosphere. Specifically, both decadal scale SSTAs in the western Pacific subarctic frontal zone and El Niño related SSTAs south of Japan are found to be engaged actively in such forcing on the atmosphere. The atmospheric response to this forcing appears to include the anomalous storm track activity in the northwestern portion of the North Pacific. Fidelity of these observational results is discussed with NCEP/NCAR reanalysis data.

**JSP09/10P/B20-010****1645****AIRCRAFT OBSERVATIONS OF AIR MASS MODIFICATION OVER ADVANCING ICE COVER IN THE SEA OF OKHOTSK**

Jun INOUE, Masayuki KAWASHIMA, Yasushi FUJIYOSHI, Masaaki WAKATSUCHI (Institute of Low Temperature Science, Hokkaido University, Japan)

In order to investigate a role of leads in advancing of ice cover, turbulent heat transport processes over the ice-covered Sea of Okhotsk was studied by use of aircraft observations during two cold-air outbreaks. One case is characterized by a heterogeneous ice concentration containing numerous wide open leads, and the other one occurred over relatively narrow leads. By using the technique of joint frequency distribution, it is found that the buoyancy flux is mainly generated by the rising thermals over the upwind leads for each case. The sensible heat flux by these thermals abruptly decreases from 600 W/m<sup>2</sup> to 100 W/m<sup>2</sup> with increase of accumulated fetch-width of upwind leads up to 5 km within the ice cover. These results suggest that the role of the accumulated open water is as important

## INTER-ASSOCIATION

as that of coastal polynyas for the new-ice formation and resultant advance of sea-ice extent in theseasonal ice zone during cold-air outbreaks.

**JSP09/10P/B20-011**

**1700**

### THE MODIFIED CLOUD PHYSICAL ASPECTS OF A COLD AIRMASS CROSSING OVER THE JAPAN SEA AND ITS COASTAL REGION

Xueliang GUO<sup>1</sup>, Ronghui HUANG<sup>1</sup>, Hiroshi NIINO<sup>2</sup> (<sup>1</sup>Institute of Atmospheric Physics, Chinese Academy of Sciences, <sup>2</sup>Ocean Research Institute, University of Tokyo, Tokyo, Japan)

The modification process of a cold airmass crossing over the Japan Sea and its coastal region on 29 January 1993 was simulated using a three-dimensional compressible non-hydrostatic cloud model with detailed microphysics coupling with a simple first-order boundary layer parameterized model. The microphysics characteristics of the shallow convective snow clouds formed in association with the cold airmass as well as the heat and moisture transfer processes between air and sea were investigated. The simulation of the cold airmass was initiated based on the rawinsonde soundings taken from middle of Japan Sea (42N, 135E) at 00Z on 29 Jan 1993. The domain size for the simulation was 36 x 36 km in the horizontal and 19 km in the vertical. The grid intervals were  $\Delta x = \Delta y = 1$  km,  $\Delta z = 0.5$  km. A cold pool placed in the center of model domain with size of 8 x 8 km in the horizontal and 2 km in the vertical was used to initiate convection in the cold airmass (Tao et al., 1990). The peak temperature perturbation in the center of thermal bubble was 0.5 K. is assumed to be homogeneous in the horizontal and keep constant during the simulation time. The maximum lifting velocity of is taken as 0.1 ms<sup>-1</sup>. The 10°C and 0°C of temperatures are used in the simulation for the sea and land surface, respectively. The simulation results show that the simulated clouds experience three pronounced phases while crossing the Japan Sea and its coastal region, which is the same as that observed. The first stage is shown as a rapid intensification of the simulated radar echo due to the formation of a considerable number of snow aggregate particles in the clouds over the warm sea. In the second stage the snow clouds appear as a rapid decrease of radar echo due to the heavy snowfall along the coastal region. The third stage shows that the snow clouds become gradually intensive again due to the production of a limited number of graupel particles after landing the Japan Islands. The echo structure is changed from the isolated type to the diffused type during landing process.

**JSP09/10P/B20-012**

**1715**

### IDENTIFICATION FOR INTERACTION BETWEEN ATMOSPHERE AND SEA SURFACE DEVELOPMENT CONDITIONS ABOVE INDOONESIAN REGION DURING THE RAINY SEASON 2002 (FROM JANUARY TO MARCH 2002)

Edison KURNIAWAN (Meteorological and Geophysical Agency)

The weather-pattern above the Indonesian region has been vary and fluctuation for physico-dynamic atmosphere related to the interaction between atmosphere and sea surface conditions. From those conditions, some regions in Indonesia received the big impact which is caused from natural disaster such as floods and landslides. Based from the unstable-weather which is occurred for the months before, some descriptions about the analysis including its impact will be summarized by observing the atmosphere and sea surface development conditions above the Indonesian region from January to March 2002. All of the weather parameters which is analysed such as air-pressure, relative humidity, sea surface temperature, cloud activity and wind circulation-pattern from surface and beyond. Besides that, the developing of water vapour above sea surface has been counted related to the warming of sea surface on the Indonesian ocean. In this case, the formation of cloud could become the rainy day in the earlier 2002. The identification for interaction between atmosphere and sea surface development conditions above the Indonesian region during the rainy season 2002 from January to March 2002 has been done using the daily-weather parameters i.e. air-pressure above the northern hemisphere and southern hemisphere, the analysis of cloud activity from GMS satellite, wind circulation from surface and beyond, sounding-data, sea-surface temperature and SOI Index. Those parameters will give the illustration about the conditions of atmosphere on the Indonesian region. The yields from this research has shown the fluctuation of dynamic-physic atmosphere and sea surface condition along those periods. It caused the extreme-weather which is being impact such as floods and landslides in all of Indonesian provinces. The results obtained from this reserch will be presented in this papper.

**JSP09/10P/B20-013**

**1730**

### WIND ENERGY INPUT TO SURFACE WAVES

Wei WANG<sup>1</sup>, Rui Xin HUANG<sup>2</sup> (<sup>1</sup>Physical Oceanography Lab, Ocean University of China, <sup>2</sup>Department of Physical Oceanography, Woods Hole Oceanographic Institution, Woods Hole, MA 02543)

Wind energy input into the ocean is primarily produced through the surface waves. The total rate of this energy source, integrated over the world oceans, is estimated at 60TW, based on empirical formula and results from a numerical model of surface waves. Thus, surface wave energy input is about 46 times larger than the energy input into the surface geostrophic current (1.3TW) and 17 times larger than the total tidal dissipation rate (3.5TW). Most of the surface wave energy input is concentrated within the Antarctic Circumpolar Currents. The total energy input through surface waves is transferred into other forms and locations by three mechanisms: wave-current interaction, wave-wave interaction, and dissipation. The amount of energy going through wave-current interaction is unclear. The wave-wave interaction transfers energy from short waves into longwaves. All the input energy is either transferred into other form of energy, such as currents, internal waves and turbulence, or eventually dissipated. The dissipation is primarily through two channels: wave breaking in the open ocean dissipates about 36TW of energy and waves breaking and dissipation along the beaches take up about 20TW of energy.

**JSP09/10P/B20-014**

**1745**

### STATISTICAL CHARACTERISTICS OF WAVES AND CURRENTS IN FRONT OF THE COASTAL WATER OF DAMIETTA, EGYPT

Fahmy M. EID, Sayed H. SHARAF EL-DIN, Farid A. ABDALLA (Department of Oceanography, University of Alexandria)

The data of waves and currents which are measured off Damietta area throughout the period from Aug. 1997 to Dec. 1998 are analyzed in details to give a clear picture on sediment transport along the coast or in the on/offshore direction. The results of this analysis showed that: The main wave direction is mainly from NNW for all months with the highest maximum wave height of about 4.3 m during winter. The average significant wave height and period were approximately 0.46 m and 6.4 second respectively. The current speed in winter were greater than that at the other seasons with a maximum values of about 69.9 cm/sec. The current direction off Damietta area lies between NE and ENE direction. The current direction beyond breaker zone in front of Damietta Nile branch mostly tending westward and

accompanied with a rip current on the western side which is responsible to remove sediment from onshore to offshore direction and thus excrete coastal erosion in this area. The predominant direction of long shore current is from west to east. Littoral Current velocity are higher during the winter than in other seasons due to the stormy waves prevailing during winter and swells in summer.

Friday, July 11 AM  
Presiding Chairs: T. Liu, N. Ebuchi

**JSP09/11A/B20-001**

Invited

**0830**

### OCEAN-ATMOSPHERE COUPLING OBSERVED FROM SPACE

W. Timothy LIU<sup>1</sup>, Xie XIAOSU<sup>1</sup>, Shang-Ping XIE<sup>2</sup> (Jet Propulsion Laboratory, MS 300-323, JPRC, Univ. of Hawaii)

The ocean is forced at the surface largely through the exchanges of water, heat, and momentum. The exchanges drive the transport and change the storage of heat, water, and greenhouse gases, and thus moderate the world's climate. The ocean feedback to climate changes must be manifested through these exchanges, without which the Earth would be a more hostile habitat. Adequate observations at significant temporal and spatial scales can only be achieved from the vantage point of space. An overview of present spacebased sensors that contribute to the estimation of these exchanges will be presented. The manifestation of ocean-atmosphere coupling, as the correlation between two well-established spacebased measurements - sea surface temperature and surface wind, has long been studied. Two perspectives on the correlation will be presented - atmosphere or the ocean as the driving force. Negative lag correlations are found between seasonal changes of curl of wind stress and sea surface temperature caused by monsoons, and at the wake of tropical cyclones, largely because of wind-driven Ekman pumping and vertical mixing in the ocean. Negative lag correlations are also observed between wind-driven evaporative cooling and sea surface temperature in both annual and interannual time scales over global oceans. In these cases, the atmosphere drives the ocean. The case of ocean driving the atmosphere is best demonstrated in the two mechanisms that sustain the double intertropical convergence zones (ITCZ). The stronger ITCZ occurs when the northerly trade winds meet the southerly trade winds over water with sea surface temperature above threshold for deep convection. The weaker ITCZ occurs over cooler water and is caused by the deceleration of the surface winds as they approach the cold upwelling water near the equator. Decreases in vertical mixing and increases in vertical wind shear in the atmospheric boundary layer are suggested to be the causes of the deceleration of the trade winds as they move from warmer to colder water. This boundary instability mechanism is ubiquitous and may be the dominant mechanism for air-sea coupling when SST is below deep-convection threshold. The resultant positive contemporary correlation has been observed in tropical instability waves, in the cold wake of tropical cyclones, and in bathymetry induced and warm-current induced SST fronts.

**JSP09/11A/B20-002**

**0900**

### THE SECOND VERSION OF THE HAMBURG OCEAN ATMOSPHERE PARAMETERS AND FLUXES FROM SATELLITE DATA (HOAPS-II): IMPROVEMENTS AND NEW ANALYSIS CAPABILITIES

Stephan BAKAN<sup>1</sup>, Karsten FENNIG<sup>2</sup>, Christian KLEPP<sup>2</sup>, Joerg SCHULZ<sup>2</sup> (<sup>1</sup>Max-Planck-Institut f. Meteorologie, <sup>2</sup>Meteorologisches Institut, Universität Hamburg, <sup>3</sup>Meteorologisches Institut, Universität Bonn)

This paper presents the new version of the Hamburg Ocean Atmosphere Parameters and Fluxes from Satellite Data set (HOAPS), its improvements, and new analysis capabilities. HOAPS-II contains global fields of turbulent heat fluxes, precipitation, evaporation minus precipitation, and all basic state variables needed for the derivation of the fluxes. The climatology is enhanced by new atmospheric parameters like the total precipitable water and the cloud liquid water content that are also derived from SSM/I data using standard retrieval schemes. All variables are derived over the ice free ocean and delivered in a variety of temporal and spatial resolutions. The HOAPS-II time series is now extended to December 2001. Through the use of earlier HOAPS data in various climate studies and comparison activities a few accuracy issues and data problems emerged and are fixed now. HOAPS-II utilizes all SSM/I data available at the same time in a multi-satellite average, which required an inter-calibration of the SSM/I measurements from different platforms. This has been achieved by using 10 day mean values of brightness temperatures during overlapping periods. The mean correction factors turned out to be only about 1K in each channel, indicating a stable on-board calibration of the radiometric measurements. The resulting sampling frequency is not the same for each year as the number of SSM/Is in space was increasing from one in the beginning to four at the end of the nineties. In Remarkable biases in the precipitation and longwave net radiation products mainly over mid-latitude oceans have been experienced in the earlier HOAPS version due to the failure of the 85GHz channel on the DMSP F08 platform during 1989 and 1990. This has been corrected by adjusting the replacement retrieval regression coefficients during periods with available 85 GHz channel and applying these new values to the years in question. This correction reduces precipitation estimates over mid-latitude oceans considerably, making them far more realistic. HOAPS-II is provided as two different data sets serving different application areas. HOAPS-S is a scan-wise oriented data set containing instantaneous estimates of the parameters. This data set should be most useful for case studies and nowcasting applications. HOAPS-G is a gridded data set with temporal resolutions ranging from daily to monthly and spatial resolutions compatible with major global circulation models. This part of HOAPS-II is ideally suitable for climate studies and the evaluation of re-analysis data sets.

**JSP09/11A/B20-003**

**0915**

### THE SURFACE ENERGY BUDGET FOR TROPICAL OCEANS FROM TRMM

Bing LIN, Alice FAN (Langley NASA)

Tropical Rainfall Measuring Mission (TRMM) is a joint project between the US National Aeronautics and Space Administration (NASA) and National Space Development Agency of Japan to measure the tropical rainfall distribution. Data collected from CERES, VIRS, and TMI instruments onboard the TRMM satellite can be used to retrieve the major heat fluxes at sea surface, top of atmosphere, and within atmosphere simultaneously. The major heat energy values include shortwave (SW) and longwave (LW) radiation fluxes, and turbulent latent heat and sensible heat, and rain induced sensible heat fluxes in air-sea interface. This study investigates the major flux components over tropical oceans (30N to 30S). The LW and SW net fluxes are estimated by CERES project (Weilicki et al. 1996) with an accuracy of  $\sim 2$  and  $\sim 3$  W/m<sup>2</sup> at the top of atmosphere and  $\sim 8$  and  $\sim 15$  W/m<sup>2</sup> at sea surfaces, respectively. The turbulent latent and sensible heat fluxes are calculated from TRMM Microwave Imager (TMI) retrievals of near sea surface wind speeds, air humidity, and temperature using bulk formulae derived from TOGA COARE experiment. The turbulent fluxes are compared to those of Goddard Satellite-Based Surface Turbulent Fluxes (GSSTF)

version 2 products derived from SSM/I data collected by Defense Meteorological Satellite Program (DMSP) satellites with a difference of less than  $7 \text{ W/m}^2$  from monthly mean values. The rain induced sensible heat fluxes are estimated from the level 2 TMI Profiling rainfall data assuming that raindrops are in thermal equilibrium with the environments, and have the wet bulb temperatures of surface air when they hit ocean surfaces. Depending on the season and region, the monthly 1 by 1 degree grid mean values vary from 0 to  $300 \text{ W/m}^2$  for SW net flux, from 0 to  $100 \text{ W/m}^2$  for LW net flux, from 0 to  $300 \text{ W/m}^2$  for latent heat flux, and from 0 to  $30 \text{ W/m}^2$  for turbulent sensible heat, and 0 to  $3 \text{ W/m}^2$  for rain induced sensible heat. The positive tropical total surface net fluxes is generally balanced by the loss of fluxes in higher latitudes. This study provides instantaneous, hourly, daily, monthly, and seasonal gridded and zonal means for the major components of the ocean surface heat fluxes. The monthly and seasonal variations will be examined. Although TRMM is designed for precipitation sciences, this study expands it to a new research area.

**JSP09/11A/B20-004****0930****IMPACT OF IMPROVED FLUX ESTIMATES DERIVED FROM SCATTEROMETER WINDS ON THE TROPICAL PACIFIC HEAT BUDGET**LuAnne THOMPSON<sup>1</sup>, Kathryn A. KELLY<sup>2</sup>, Chuanli JIANG<sup>1</sup> (School of Oceanography, University of Washington, <sup>2</sup>Applied Physics Laboratory, University of Washington)

In addition to improving ocean circulation, scatterometer winds can be used to improve the upper ocean heat budget. Three distinct effects of the winds have been identified: changes in the latent and sensible heat fluxes from wind speed, ocean heat flux divergence associated with changes in the currents, and changes in mixed layer depth which in turn affect SST. Comparisons with NCEP (National Center for Environmental Prediction) wind stress and NCEP-derived fluxes show substantial differences with the scatterometer-derived heat and momentum fluxes, particularly in the equatorial Pacific near the Intertropical Convergence Zone. To test the impact of the scatterometer winds on a modeled tropical Pacific Ocean, we run a three-dimensional isopycnal general circulation model with a domain from  $30\text{S}$  to  $30\text{N}$  at  $0.5$  degree resolution. The model has 16 layers in the vertical and includes an active mixed layer. The model is forced with NCEP stress for spinup, and then parallel runs are done using the NCEP and QuikSCAT stress fields. The surface thermal boundary condition is calculated from the COARE bulk formulae, using the model SST with NCEP atmospheric variables and either NCEP stress or QuikSCAT stress. There are significant differences between the two model runs, with QuikSCAT winds generally giving better performance relative to observations both in the mean model oceans and in the variability. Along the equator, the QuikSCAT runs show a smaller SST gradient and a lower maximum SST, both of which match the observations better. The mixed-layer temperature budget on intraseasonal time scales also compares well with a previous observational analysis. Both of these results can mostly be explained by significant differences in the mixed-layer depth in the eastern equatorial Pacific. Additional model experiments are performed to test whether the differences come about from changes in dynamics or from thermodynamics. To do this, we perform one model run where we use NCEP for all model fields except for the momentum flux (wind stress); one model run with all NCEP fields except for latent and sensible heat flux; and finally, one model run with all NCEP fields except for wind mixing ( $u^*$ ). The QuikSCAT winds show promise in improving our understanding of tropical ocean circulation and the upper ocean heat budget during the ENSO cycle.

**JSP09/11A/B20-005****0945****DIURNAL SEA SURFACE TEMPERATURE MODELING WITH SATELLITE DATA**Chelle Leigh GENTEMANN<sup>1</sup>, Peter J. MINNETT<sup>1</sup>, Craig J. DONLON<sup>2</sup>, Gary A. WICK<sup>3</sup> (<sup>1</sup>RSMAS, University of Miami, <sup>2</sup>EC Joint Research Centre, Institute for Environmental Studies, <sup>3</sup>NOAA/ETL)

The formation of a near-surface diurnal warm layer, particularly in regions with low wind speeds, is clearly present in daytime satellite sea surface temperature (SST) measurements. This has consequences for ocean-atmosphere heat flux calculations. The satellite retrievals reveal significant diurnal amplitudes covering large oceanic regions, with regional distribution and amplitude of warming varying significantly within annual cycles. Additionally, the diurnal amplitudes are shown to have inter-annual variability correlated to ENSO events. Analysis of TMI, AMSR-E, AVHRR satellite SSTs reveal that the onset of warming sometimes begins as early as 8 AM and generally peaks near 3 PM, with a magnitude of  $2.8 \text{ C}$  during favorable conditions. After this peak, the signal decays, but sometimes extends until 11 PM. A simple empirical model was calculated from satellite SSTs, satellite wind speeds, and modeled insolation. Diurnal warming is measurable for wind speeds less than  $10 \text{ m/s}$ , with daily-average insolation values greater than  $96 \text{ Wm}^{-2}$ . The character and magnitude of diurnal variability witnessed by ship-based observations are compared with both the empirical model and physical warm layer models.

**JSP09/11A/B20-006****1000****THE DIFFERENCE BETWEEN INFRARED SEA SURFACE TEMPERATURE AND PASSIVE MICROWAVE SEA SURFACE TEMPERATURE AND ITS RELATIONSHIP TO LATENT HEAT FLUX**

William J. EMERY, Sandra CASTRO, Gary A. WICK (Univ of Colorado)

Global differences between thermal infrared sea surface temperatures (SST's) and passive microwave SST's are found to have similar spatial patterns as do climatological estimates of latent heat flux computed from historical averages of bulk formulae observations. A comparison with global patterns of passive microwave estimates of atmospheric water vapor demonstrate that this is not the cause of the observed SST differences. Comparisons between these same SST differences and in situ measurements of accurate eddy correlation fluxes also show a good correspondence between latent heat flux and the SST differences. This correspondence also occurs between these SST differences and latent heat fluxes computed from TAO moored buoy bulk aerodynamic observations. These correspondences are found to hold throughout the seasonal cycle with equivalent changes in spatial distributions occurring in both the SST differences and in the latent heat flux distributions. Earlier comparisons between bulk and skin SSTs exhibited similar spatial patterns. Statistical and numerical physical models of the upper ocean skin and mixed-layer stratification are used to explain these correspondences between latent heat flux and satellite SST differences. In addition, other skin-bulk comparisons will be used to evaluate the satellite SST differences.

**JSP09/11A/B20-007****1015****ESTIMATION OF WIND-DRIVEN OCEANIC TRANSPORT IN THE SUBTROPICAL GYRE BY SCATTEROMETER WIND PRODUCT**

Kunihiro AOKI (School of Marine Science and Technology, Tokai University)

Product of gridded surface wind-stress constructed by satellite scatterometer (ERS-1/2) data is used to estimate wind-driven transport in the subtropical gyre of the North Pacific and

Atlantic Oceans and to verify the Sverdrup balance in the interior region. Zonally-integrated Sverdrup transport at  $30^{\circ}\text{N}$  in the North Pacific, corresponding to the transport of the western boundary current, calculated from 8-year (1992-99) mean field by ERS-1/2 is about  $32 \times 106 \text{ m}^3 \text{ s}^{-1} (\text{Sv})$ . The value is larger than that ( $27 \text{ Sv}$ ) by the ECMWF product and smaller than the NCEP's ( $42 \text{ Sv}$ ), meaning that the estimated wind-driven transport is sensitive to the selection of wind product. Using dynamic height field (referred to 1000db) calculated from the World Ocean Atlas (WOA) 98 database, we also estimate the meridional component of geostrophic transports in the interior region of the subtropical gyre and compare them with the wind-driven ones. Wind-driven transport by the ERS wind product at  $30^{\circ}\text{N}$  in the North Pacific is  $0.3\text{-}0.4 \text{ Sv}$  between  $165^{\circ}\text{E}$  and  $150^{\circ}\text{W}$ , close to that by the WOA98, which suggests the validity of the Sverdrup balance in this region. On the other hand, the estimate ( $0.45\text{-}0.5 \text{ Sv}$ ) by NCEP winds is larger than those, suggesting overestimation of wind-driven transport using the NCEP field. A similar approach for the zone of  $25^{\circ}\text{N}$  in the North Atlantic reveals that the values by the ERS and NCEP winds are not only closer to each other ( $0.3\text{-}0.45 \text{ Sv}$ ) but also similar to that by WOA98 database.

**JSP09/11A/B20-008**

Invited

**1045****INTERCOMPARISON AND VALIDATION OF LATENT HEAT FLUX OVER THE GLOBAL OCEAN**

Masahisa KUBOTA, Hiroyuki TOMITA (School of Marine Science and Technology, Tokai University)

Latent heat flux plays an important role in the global climate system. Though it was difficult to globally monitor latent heat flux over the ocean for many years, the situation is rapidly changing by the use of satellite data. Since a bulk formula is used to estimate turbulent heat flux using satellite data, we need wind speed, sea surface temperature and specific humidity data. Various satellite sensors can accurately observe wind speed and sea surface temperature. On the other hand, it is not easy to accurately estimate specific humidity using satellite data. Now several algorithms for estimating specific humidity have been proposed and applied to construct latent heat flux data sets. Latent heat flux data sets derived from satellite data such as J-OFURO, HOAPS and GSSTF are available at present. Since the algorithm and used satellite data are not the same between them, the characteristics of each data set may be different. Therefore, it is important to clarify the difference between each data set and investigate the cause of the difference in latent heat flux estimates. In this paper we summarize the present state of the art with regard to the turbulent heat flux estimation by using satellite data. Also we present the comparison results of latent heat flux fields including not only satellite-derived flux fields but also analysis fields. Moreover, we investigate the accuracy of the various data sets by comparison with buoy observation data.

**JSP09/11A/B20-009****1115****INTERCOMPARISON OF LATENT HEAT FLUXES OVER GLOBAL OCEANS**Shu-Hsien CHOU<sup>1</sup>, Eric NELKIN<sup>2</sup>, Joe ARDIZZONE<sup>3</sup>, Robert M. ATLAS<sup>4</sup>, Ming-Dah CHOU<sup>1</sup> (<sup>1</sup>NASA Goddard Space Flight Center, <sup>2</sup>Science Systems and Applications, Inc., <sup>3</sup>Science Applications International Corporation)

Turbulent fluxes of momentum, moisture, and heat at the air-sea interface are essential for climate studies. Version 2 Goddard Satellite-based Surface Turbulent Fluxes (GSSTF2) has been derived from the Special Sensor Microwave/Imager (SSM/I) radiance measurements. This dataset, covering the period July 1987-December 2000 over global oceans, has a spatial resolution of  $1$  degree  $\times$   $1$  degree lat-long and a temporal resolution of 1 day. Turbulent fluxes are derived from the SSM/I surface winds and surface air humidity, as well as the 2-m air and sea surface temperatures (SST) of the NCEP/NCAR reanalysis, using a bulk aerodynamic algorithm based on the surface layer similarity theory. The GSSTF2 bulk flux model, and retrieved daily wind stress, latent heat flux, wind speed, and surface air humidity validate well with ship observations of ten field experiments over the tropical and mid-latitude oceans during 1991-99. The global distributions of 1988-2000 annual- and seasonal-mean turbulent fluxes show reasonable patterns related to the atmospheric general circulation and seasonal variations. Latent heat fluxes and related input parameters over global oceans during 1992-93 have been compared among GSSTF1 (version 1), GSSTF2, HOAPS (Hamburg Ocean Atmosphere Parameters and Fluxes from Satellite Data), NCEP/NCAR reanalysis, and one based on COADS (Comprehensive Ocean-Atmosphere Data Set). Our analyses suggest that the GSSTF2 latent heat flux, surface air humidity, surface wind, and SST are quite realistic compared to the other four flux datasets examined. However, significant differences are found among these five flux datasets. The GSSTF2, available at [http://daac.gsfc.nasa.gov/CAMPAIGN\\_DOCS/hydrology/hd\\_gsstf2.0.html](http://daac.gsfc.nasa.gov/CAMPAIGN_DOCS/hydrology/hd_gsstf2.0.html), is useful for climate studies

**JSP09/11A/B20-010****1130****UNCERTAINTIES IN MEAN AND SEASONAL STRESSES OVER THE OCEAN CAUSED BY ERRORS IN SUB-WEEKLY WINDS**

Rui M. PONTE, Richard D. ROSEN (Atmospheric and Environmental Research, Inc.)

Variability in surface winds on synoptic time scales can have an effect on the mean and seasonal stress on the ocean, owing to the nonlinear dependence of stress on wind speed. We use multi-year satellite-derived and operational wind products to show that the impact of these rapid wind signals is indeed important and most pronounced at mid and high latitudes, in regions of strong synoptical activity. Using differences in various wind products as a proxy for error, we find that uncertainties at sub-weekly periods can lead to substantial errors in the mean and seasonal ocean stresses. Results point to the importance of accurately determining wind variability at sub-weekly periods, thereby placing constraints on sampling strategies for observing winds over the ocean.

**JSP09/11A/B20-011****1145****ESTIMATION OF SAMPLING ERRORS IN ALTIMETER WAVE MEASUREMENTS**Gavrikov Alexander VLADIMIROVICH<sup>1</sup>, Sergey Konstantinovich GULEV<sup>1</sup>, David WOOLF<sup>2</sup>, Andreas STERL<sup>3</sup> (<sup>1</sup>P.P. Shirshov Institute of Oceanology, RAS, <sup>2</sup>Southampton Oceanography Centre, Southampton, United Kingdom, <sup>3</sup>Royal Netherlands Meteorological Institute, De Bilt, The Netherlands)

Remotely sensed observations from space now provide measurements of the basic wind wave variables for the period of about 15 years. These data are influenced by sampling uncertainty, resulting from the relatively sparse separation of satellite tracks and some irregularity of these tracks in space and in time. Sampling uncertainty may have an influence on the reliability of climatological characteristics derived from the space-based observations. In order to estimate sampling uncertainty in altimeter wave measurements we used Ku-band altimeter wave data from GEOSAT, TOPEX/POSEIDON and ERS-1/2 crafts for the period overlapping with the ERA-WAM wave hindcast. Despite possible biases inherent into the model wave data, they provide regularly high sampling over the globe. Model data were sub-

IA

## INTER-ASSOCIATION

sampled in accordance to the locations and time of individual satellite tracks. Then these "undersampled" wave fields intercompared with (i) original model data to assess the effect of sampling and (ii) with altimeter data in order to obtain reliable estimates of the differences in wave parameters between satellite measurements and model hindcast. The derived sampling uncertainties were compared with sampling errors in visual wave observations derived from Voluntary Observing Ship (VOS) data.

**JSP09/11A/B20-012** **1200**

### VARIDATION OF QUIKSCAT OCEAN SURFACE DATA BY A SMALL ISLAND DATA

Tetsuo NAKAZAWA, Shunsuke HOSHINO (Meteorological Research Institute)

The ocean surface wind by QuikSCAT is compared with the in-situ data. It is really difficult to find a validation wind dataset for speeds greater than 25 m/s. We chose a small island in the western Pacific, Okinotorishima (20°25'N, 136°04'E), to check the QuikSCAT high-wind data. There are two datasets at the Observatory, operated by the Japan Marine Science and Technology Center: one is 30 min. averaged wind, and the second is the 4-sec averaged maximum wind during each 30 min. The QuikSCAT data we used in this study were obtained from the Remote Sensing Systems (RSS), <http://www.ssmi.com>. The data period is from July 1999 through December 2000. The study shows that the difference between the QuikSCAT data and the in-situ observation has a small bias with large scattering. It may be due to the time averaging. The QuikSCAT data is instantaneous and the in-situ data is the averaged one in 30 min. The strongest wind at the site was about 31 m/s. Thus we need more data in high-wind regime to verify the accuracy of the QuikSCAT data.

**JSP09/11A/B20-013** **1215**

### OCEAN CURRENTS INFERRED FROM DIFFERENCES BETWEEN QUIKSCAT AND TAO WINDS

Kathryn A. KELLY<sup>1</sup>, Suzanne DICKINSON<sup>1</sup>, Gregory C. JOHNSON<sup>2</sup> (<sup>1</sup>Applied Physics Laboratory, University of Washington, <sup>2</sup>Pacific Marine Environmental Laboratory, NOAA)

Differences between the winds from the Tropical Atmosphere-Ocean (TAO) buoys and from the QuikScat scatterometer are used to estimate time-varying ocean surface currents. The scatterometer measures backscatter from centimeter waves caused by the wind blowing over the ocean; when ocean and atmosphere move together, no waves are generated. Thus, the scatterometer measures the motion of the air relative to the moving ocean surface, the quantity needed to estimate surface stress. On the other hand, an anemometer measures the motion of the air relative to a fixed platform. Therefore, the difference between an anemometer wind and a scatterometer "wind" is primarily the ocean surface current. Estimates of currents from TAO anemometer winds minus NSCAT or QuikSCAT scatterometer winds show good agreement with carefully collocated current measurements from moored current meters on the equator and from acoustic Doppler current profilers (ADCP) mounted on ships servicing the TAO array. For this comparison currents in the South Equatorial Current (SEC) are about 1.2 m/s westward and currents in the North Equatorial Countercurrent (NECC) are about 0.6 m/s eastward. Neglect of these strong tropical currents in this region of relatively weak winds (5-7 m/s) leads to errors in stress of 25-50% and to even larger errors in wind stress curl. In addition we estimate time-varying surface currents over 3 years and compare with the current estimates derived from drifters, ADCP, and the altimeter. The seasonal cycle of the estimate of zonal winds is in excellent agreement with the other measurements, particularly the altimeter, which also gives a surface current. The meridional winds are much noisier, as is the case for all the other current measurements, but show reasonably good agreement with an estimate of the Ekman current component off the equator. On the equator, current estimates show surprisingly good agreement with a simple model of forced motion.

Friday, July 11 PM  
Presiding Chairs: L. Shay, P. Black

**JSP09/11P/B20-001** **1400**

### STUDY FOR ESTIMATION OF AIR-SEA CO<sub>2</sub> GAS TRANSFER BY WAVE BREAKING MODEL USING SATELLITE DATA

Naoya SUZUKI<sup>1</sup>, Naoto EBUCHI<sup>2</sup>, Takahiro OSAWA<sup>3</sup>, Yasuhiro SUGIMORI<sup>4</sup> (<sup>1</sup>Center for Air Sea Interaction, Rosenstiel School of Marine and Atmospheric Science, Division of Applied Marine Physics, University of Miami, <sup>2</sup>Institute of Low Temperature Science, Hokkaido University, <sup>3</sup>Center for Environmental Remote Sensing, Chiba University)

CO<sub>2</sub> transfer velocity at air-sea interface associated with different mechanisms such as turbulence and wave breaking, which are closely related with wind speed, has been studied from satellite data in this work. The determination of wind friction velocity from satellite-derived wind data will take an important role in computation of CO<sub>2</sub> flux transfer. It is necessary for relation between wind speed and wind friction velocity to determine that of relation between non-dimensional roughness length and wave age, included with all parameters (wind, wave). Because of the large variation of the non-dimensional roughness length, it is difficult to describe wave influence by the single wave age. In this study we observed directional wave spectra at the Hiratsuka Tower of National Research Institute for Earth Science and Disaster Prevention (NIED) in Sagami Bay, Japan. As the result, the data set was separated into two kinds of directional spectrum types. Case 1 contains only swell and wind waves, but Case 2 consists of a lot of component waves due to several different wind fetch in the bay. The results show that Case 2 is associated with the large variation in the relation between non-dimensional roughness length and wave age. As wave age is associated with fetch, and a new relationship between non-dimensional roughness length and wave age was proposed, based on in situ wind and wave data after considering wind fetch effect. A new method was proposed to estimate  $u^*$ , which is based on the new relationship between non-dimensional roughness and wave age, after considering fetch and wave directionality. We estimated the wave frequency from two methods: 3/2 powers law (Toba, 1972) and WAM model (WAMDI, 1988). The results are compared with the results estimated from Charnock formula (1955), and the influence of wave effects on the wind stress is also discussed. A new relationship was established to determine CO<sub>2</sub> exchange coefficient based on whitecap model (Monahan and Spillane 1984), using U10-u\* relationship in the North Pacific Ocean, satellite data of NOAA/AVHRR (SST) and DMSP/SSM/I (wind speed) in Oct., Nov., and Dec. 1991. The CO<sub>2</sub> exchange coefficient estimated by other models (Wanninkhof, 1992; Liss and Merlivat, 1986; Tans et al., 1990) is also compared with these results. Also, we investigated wave effect for CO<sub>2</sub> exchange coefficient in numerical simulation using Whitecap model (Monahan and Spillane, 1984) and the new relationship between non-dimensional roughness length and wave age. These results show the importance of wave breaking effect.

**JSP09/11P/B20-002** **1415**

### SENSITIVITY OF THE EQUATORIAL PACIFIC OCEAN CIRCULATION TO CHLOROPHYLL MODULATION OF PENETRATIVE SOLAR IRRADIANCE IN AN OGCM

Kyozo UEYOSHI<sup>1</sup>, Detlef STAMMER<sup>1</sup>, Shoichiro NAKAMOTO<sup>2</sup>, Bulusu SUBRAHAMANYAM<sup>3</sup>, Prasanna KUMAR<sup>4</sup>, Kei MUNEYAMA<sup>5</sup> (<sup>1</sup>SCRIPPS INSTITUTION OF OCEANOGRAPHY, UNIV. OF CALIFORNIA, SAN DIEGO, <sup>2</sup>Advanced Earth Science and Technology Organization, Bussan Bldg. Annex, 1-1-15 Nishi-shinbashi, Minato-ku, Tokyo 105-0003, Japan, <sup>3</sup>Center for Ocean Atmospheric Prediction Studies, Florida State University, Tallahassee, FL 32306-2840, USA, <sup>4</sup>Physical Oceanography Division, National Institute of Oceanography, Dona Paula, Goa 403 004, India, <sup>5</sup>Japan Marine Science and Technology Center, 2-15 Natsushima-cho, Yokosuka, 237, Japan)

The sensitivity of the dynamics and thermodynamics to details in the vertical profile of short-wave radiative heating rate is investigated in the MIT z-coordinate ocean general circulation model with initial focus to the tropical Pacific. In this study we examine the hypothesis that surface chlorophyll pigment induces geostrophic current at subsurface level in the equatorial Pacific ocean, proposed by Nakamoto et al.(2001). For this purpose the biological vertical heating rate parameterization of Morel and Anotine(1994) is used to simulate the effects of space-time varying phytoplankton content in the upper ocean in conjunction with monthly mean SeaWiFS chlorophyll pigment concentrations. The results from this simulation are compared to those from a control run in which a clear water body is mimicked by assigning a minimum constant pigment concentration value in the same parameterization scheme. The difference between these two simulations is regarded as the effects of phytoplankton on the penetration of solar radiation in the model ocean. A year-round, higher concentration of chlorophyll pigment in the equatorial Pacific leads to a decrease of the mixed layer depth due to heat accumulation in the mixed layer accompanied by equatorward shoaling of mixed layer base. In the central equatorial Pacific between 5N and 5S, anomalous geostrophic currents are generated which balance with the slope of the mixed layer shoaling toward the equator. Anomalous eastward currents are seen along the isopycnal surface of  $\sigma_t = 26$ , extending from the  $\sim 200$  m depth in the western equatorial Pacific (160E) to the surface level in the eastern equatorial Pacific at 90W. The divergence of anomalous surface currents in the eastern equatorial Pacific is accompanied by meridional convergence in the level below, consistent with the enhanced water mass in the equatorial undercurrents in SeaWiFS chlorophyll pigment ocean. Anomalous vertical velocity induced by modulated penetration of solar radiation by phytoplankton leads to upwelling of cold water along the equator extending from the eastern equatorial Pacific towards the dateline. This upwelling is associated with surface divergence and subsurface convergence due to heat localization and subsequent geostrophic balance in the equatorial Pacific. Our results with SeaWiFS chlorophyll pigment data generally support the hypothesis of Nakamoto et al. (2001) that phytoplankton in the equatorial Pacific induces subsurface currents that merges into the equatorial undercurrents, resulting in biomass-induced upwelling in the eastern equatorial Pacific. The results from several different absorption models for the shortwave solar radiation are currently being examined and will also be presented.

**JSP09/11P/B20-003** **1430**

### AIR-SEA FLUX ESTIMATION IN HIGH WIND BOUNDARY LAYERS: PLANS AND INITIAL RESULTS FROM THE HURRICANE COUPLED BOUNDARY LAYER AIR-SEA TRANSFER (H-CBLAST) EXPERIMENT

Peter Gerard BLACK (Hurricane Research Division, NOAA)

The USA Office of Naval Research (ONR) in collaboration with the National Oceanic and Atmospheric Administration's Hurricane Research Division (NOAA/HRD) is conducting a 5-year Coupled Boundary Layer Air-Sea Transfer (CBLAST) experiment designed to improve the accuracy of typhoon and hurricane intensity prediction through an improved understanding of the air-sea flux processes at high winds. The specific objective of this experiment is to develop a new surface wave-dependent flux parameterization for the high wind hurricane boundary layer containing secondary (roll-vortex) circulations over fetch limited seas in the presence of sea spray and one or more swell components from an airborne platform. We will test the following hypotheses: 1) that surface momentum exchange coefficients increase with wind speed for moderate winds ( $>30$  m/s), are enhanced by fetch-limited waves or opposing swell, but level off or decrease above a high wind threshold ( $>45$  m/s), especially in quadrants where swell has a significant downwind component, 2) that compensating mechanisms for enhanced surface air-sea enthalpy fluxes over and above current parameterizations must exist for storm maintenance and growth above some high-wind speed threshold, and 3) that candidate mechanisms are separable and can be estimated, such as a) enhanced turbulent fluxes due to wave interactions, b) spray evaporation and c) secondary flow circulations (roll-vortex type). To begin the process of examining these hypothesis, instrument testing and calibration as well as aircraft flight plan experimentation were conducted in 2002. Observations on both sides of the air-sea interface were made concurrent with surface wave spectra. Intensive experimental work is planned for the Atlantic hurricane seasons of 2003 and 2004. The airborne in-situ and remote sensing instrumentation suite used for this purpose is briefly described along with the planned array of air-deployed drifting buoys and subsurface floats. Recent tropical cyclone flux estimates are described, and new studies on the variation of air-sea exchange coefficients with wind speed are summarized.

**JSP09/11P/B20-004** **1500**

### ATMOSPHERE-WAVE-OCEAN COUPLING IN TROPICAL CYCLONES

Shuyi S. CHEN, Wei ZHAO, Joseph E. TENERELLI, Mark A. DONELAN (RSMAS, University of Miami)

Over the last a few decades tropical cyclone (TC) track forecasts have improved significantly, whereas very little progress made in TC intensity forecasts. The lack of the skill in the intensity forecasts may be attributed to deficiencies in the current prediction models: insufficient horizontal resolution, inadequate surface and boundary layer formulations, and no full coupling to the ocean. The extreme high winds, intense rainfall, large ocean waves, and copious sea spray push the surface-exchange parameters for temperature, water vapor, and momentum into untested new regimes. To resolve the TC eyewall structure, crucial in intensity forecasting, the horizontal resolution need to be at  $\sim 1-2$  km. The air-sea interaction in the eyewall region is largely unknown with very little observations. While TCs draw energy from the ocean surface, they cool the ocean by wind-induced surface fluxes and vertical mixing. The enthalpy and momentum exchange coefficients under the high-wind conditions are difficult to determine. The stress is supported mainly by waves in the wavelength range of 0.1-10 m, which are unresolved by wave models. Rapid increase in computer power and recent advance in technology in observations have made it possible for us to develop a strategy for the next generation of high-resolution TC prediction models. We begin by examining key parameterizations including effects of the wave spectral tail on drag coefficients, the source term for sea spray, and subgrid-scale turbulence property at 1-2 km resolution. The components of the coupled model system are the PSU/NCAR MM5, WAVEWATCHIII, and the University of Miami HYCOM. Model simulation of the Hurricane Floyd (1999) is compared observations of surface wave spectra, surface fluxes, and vertical

profiles of atmospheric boundary layer hurricane field programs. Remotely sensed SST, surface winds, and rainfall are used to evaluate and validate model simulations, develop parameterizations of the air-sea interface, and initialize the models over the open ocean. Model simulated TC intensity change is very sensitive to various parameterizations of the air-sea interface. For example, maximum surface wind speeds differ by 10-30 m/s using different wind-wave coupling parameters.

**JSP09/11P/B20-005****1515****EFFECTS OF OCEANIC MIXED LAYER ENTRAINMENT CLOSURE ON THE AIR-SEA FLUXES DURING A TROPICAL CYCLONE PASSAGE**

S. Daniel JACOB<sup>1</sup>, Chester J. KOBLINSKY<sup>2</sup>, Lynn Keith SHAY<sup>3</sup>, George R. HALLIWELL<sup>3</sup> (<sup>1</sup>GEST, NASA GSFC/ UMBC, <sup>2</sup>NASA GSFC, Greenbelt, MD 20771, USA, <sup>3</sup>RSMAS, University of Miami, Miami, FL 33149, USA)

Upper ocean heat content is an important factor in the rapid intensification of tropical cyclones. During storm passage, a large fraction of upper ocean cooling and reduction in heat content is due to entrainment of cooler less turbulent water from below the oceanic mixed layer. Analysis of high-resolution measurements acquired during the passage of hurricane Gilbert (1988) in the western Gulf of Mexico revealed that the heat and mass budgets strongly depended upon the entrainment scheme used. In this paper, the time evolution of mixed layer quantities for different entrainment closure schemes during Gilbert is investigated using a high resolution numerical model with realistic forcing fields and the results are compared to observations. The main objective is to understand the upper ocean heat and mass budget variability due to the various entrainment closure schemes. The HYbrid Coordinate Ocean Model (HYCOM) initialized with observational data and realistic forcing is used in this study. This model is configured with four entrainment mixing schemes. Results indicate a qualitatively similar pattern of oceanic mixed layer temperature and depth changes, but the entrainment rates differ for these schemes confirming observational findings. Simulated fields are compared to observations to identify a scheme that performs well. This is crucial for the upper ocean and coupled response studies and the resulting air-sea fluxes during storm passage.

**JSP09/11P/B20-006****1545****OCEANIC AND ATMOSPHERIC MEASUREMENTS ACQUIRED IN TROPICAL CYCLONES ISIDORE AND LILI**

Lynn K. SHAY<sup>1</sup>, Thomas M. COOK<sup>1</sup>, Scott A. GUHIN<sup>1</sup>, Peter G. BLACK<sup>2</sup>, Eric W. UHLHORN<sup>2</sup>, Joseph J. CIONE<sup>1</sup>, Sean R. WHITE<sup>1</sup>, Michael L. BLACK (<sup>1</sup>Division of Meteorology and Physical Oceanography, RSMAS, University of Miami, <sup>2</sup>National Oceanic and Atmospheric Administration, Hurricane Research Division, Miami)

As part of a National Science Foundation and NOAA sponsored research project, coupled ocean and atmosphere measurements were acquired during the passage of Tropical Cyclones (TC) Isidore (18-25 Sept 2002) and Lili (28 Sept- 4 Oct) from the NOAA WP-3Ds in the Caribbean Sea and Gulf of Mexico. For both TCs, the aircraft-based strategy sampled pre-storm, storm and post-storm current, temperature and salinity conditions in the Caribbean Sea and the Gulf of Mexico in and north of the Yucatan straits using airborne expendable ocean profilers. Profiles of temperature, wind and humidity were acquired simultaneously during the storm flights to examine the atmospheric boundary layer structure as well as remotely sensed surface conditions of waves and winds. As Isidore moved along the periphery of pre-storm ocean grids across the Yucatan Straits, he intensified to a Category 3 storm. Preliminary results suggest that upwelling and vertical mixing processes were balanced by the horizontal advection of thermal gradients by the Loop Current. Thus, no significant cooling was observed in the straits. By contrast, the water over the Yucatan shelf significantly cooled as the storm made landfall on the Yucatan Peninsula as the TC was downgraded to a tropical storm. The storm subsequently moved northward and created an area of broad cooling with ~28°C SSTs prior to landfall in Louisiana on 25 Sept. Lili (28 Sept) formed in the northwest Caribbean Sea and followed Isidore's track. Due to deep, warm layers in this oceanic regime, no significant SST cooling was observed from the ocean profilers. Lili then moved over the western tip of Cuba and into the Gulf of Mexico directly over the pre- and post-Isidore ocean grids. During this period, she intensified to a Category 4 hurricane just north of the Loop Current boundary. As in the Isidore case, no significant cooling was observed in the Loop Current, however, north of this boundary, SSTs decreased by an additional ~2°C due to shear-induced ocean mixing processes. As Lili interacted with the cooler wake induced by Isidore a few days prior in the northern Gulf of Mexico, she suddenly weakened in strength prior to landfall on 4 Oct. In this context, the 3-dimensional upper ocean heat budgets were important in documenting processes that affected air-sea fluxes and hence TC intensity changes in these two storms.

**JSP09/11P/B20-007****1600****OCEAN EFFECTS ON TROPICAL CYCLONE INTENSIFICATION IN A MINIMAL THREE-DIMENSIONAL COUPLED MODEL**

Hongyan ZHU, Wolfgang ULRICH, Roger K. SMITH (Meteorological Institute, University of Munich)

The interaction between a tropical cyclone and the ocean is investigated using a minimal three-dimensional tropical-cyclone model coupled with a two-layer ocean model. Two representations for entrainment into the ocean mixed layer are compared: one based on the assumption that the velocity scale for entrainment is the surface friction velocity, the other on the assumption that this scale is the magnitude of the mean velocity difference across the base of the mixed layer. On a beta-plane with no background flow, the model cyclone moves towards the northwest. With ocean coupling, it leaves a cold wake behind it, mostly to the right of its track. The cooling reduces the heat flux from the ocean and thereby the moist static energy in the boundary layer. As a result, the cyclone is less intense in the mature stage than in the case without cooling. The magnitude and distribution of the cooling depends strongly on the method for representing entrainment. The method based on the surface friction velocity is more effective in reducing the heat flux from the ocean to the storm under the eyewall region and leads to a greater reduction of the tropical cyclone intensity. With ocean coupling, the surface heat flux and moist static energy in the boundary layer are reduced mainly in the rear-right quadrant of the cyclone core. The region of convergence in the lower troposphere in the coupled experiments rotates counterclockwise from the rear quadrant of inner core to the east of the core, presumably in response to the change in the distribution of moist static energy in the boundary layer. In addition, the region of maximum upward motion in the core region shifts from the rear-right quadrant to the front-right quadrant. These changes are associated mainly with changes in the divergence pattern in the lower troposphere rather than in the boundary layer.

**JSP09/11P/B20-008**

Invited

**1615****AIR-SEA INTERACTIONS DURING PASSAGE OF A WINTER STORM OVER THE GULFSTREAM: A 3-DIMENSIONAL, COUPLED, ATMOSPHERE-OCEAN MODEL STUDY**

Huijie XUE<sup>1</sup>, Yongping LI<sup>1</sup>, John M. BANE<sup>2</sup> (<sup>1</sup>School of Marine Sciences, University of Maine, <sup>2</sup>Shanghai Typhoon Institute, <sup>3</sup>Dept. of Marine Sciences, University of North Carolina)

A three-dimensional, regional, coupled atmosphere-ocean model with full physics is developed. The model performs well in simulating the cyclone that developed off the Carolina coast and traveled over the northwestern Atlantic Ocean on 19-20 January 1998. Model diagnosis is used to examine the air-sea heat and momentum exchanges and the responses in the upper ocean. Maximum heat flux appears over the Gulf Stream in the South Atlantic Bight (SAB), which results in rapid deepening of the cyclone off the Carolina coast. After the cyclone leaves the SAB, the heat flux maximum moves to over the Gulf Stream off Cape Hatteras and later northeast of Hatteras, which in turn enhances the wind locally. Oceanic response is closely related to the wind direction. Southerly and southwesterly winds tend to strengthen the Gulf Stream at the surface, whereas the northeasterly winds reduce the Gulf Stream and also generate the southwestward flows on the shelf. Running the atmospheric model alone with unchanged SST overestimates the oceanic effect on the cyclone, with the surface wind being about 5 to 10 per cent stronger. Large differences in the surface heat flux appear near the Gulf Stream meander troughs due to wind-driven lateral shifts of the stream, which in turn enhance the local northeasterly winds.

**JSP09/11P/B20-009****1645****SYNOPTIC VARIABILITY OF OCEAN-ATMOSPHERE TURBULENT FLUXES ASSOCIATED WITH ATMOSPHERIC CYCLONES**

Olga ZOLINA<sup>1</sup>, Sergey GULEV<sup>2</sup> (<sup>1</sup>Meteorologisches Institut, Universität Bonn, <sup>2</sup>P.P. Shirshov Institute of Oceanology, RAS)

We analyse synoptic scale variability in the air-sea turbulent fluxes in the areas of mid-latitude western boundary currents. In the Gulf Stream area ocean-atmosphere fluxes on synoptic space-time scales are clearly coordinated with the propagating synoptic scale atmospheric transients. Statistical analysis of 6-hourly resolution sea level pressure and surface turbulent fluxes from the NCEP/NCAR Reanalysis for the period from 1948 to 2000 in the area of strong sea surface temperature gradients in the Gulf Stream give a strong proof for the association between the propagating cyclones and synoptic patterns of surface turbulent fluxes. We show that sea-air interaction in this area is controlled by the sharpness of surface temperature gradients in the ocean and by the intensity of the advection of the air masses in different parts of cyclones during the cold-air and warm-air outbreaks. A simple parameter based on the joint consideration of the characteristics of sea surface temperature and sea level pressure fields is used to characterize synoptic variability of air-sea turbulent fluxes. Effectiveness of the relationship between surface temperature and surface pressure on one side and air-sea flux anomalies on the other vary from year to year in phase with variability in the frequencies of deep atmospheric cyclones in the Gulf Stream area. The limits of applicability of the approach, its sensitivity to higher resolution sea surface temperature data, and the possibility of its further applications are discussed.

**JSP09/11P/B20-010****1700****A STUDY OF HIGH-FREQUENCY AIR-SEA INTERACTION PROCESSES**

Chung-Hsiung SUI<sup>1</sup>, June CHANG<sup>2</sup> (<sup>1</sup>Institute of Hydrological Sciences, National Central University, <sup>2</sup>National Center for Ocean Research, Taiwan)

The focus of this study is air-sea exchange processes of momentum, heat and fresh water from the diurnal to intraseasonal time scales in various regions including western Pacific, Kuroshio current, and S. China Sea. In particular, a systematic investigation on the effects of such air-sea exchanges on typhoon and intraseasonal oscillations (ISOs) at both regional and local scales is being performed. The regional-scale study concerns region-wide effects of surface winds, warm SSTs, air-sea exchanges, and upper-ocean thermal/dynamic structures on typhoons and ISOs. The local-scale study concerns air-sea exchange processes in general, and particularly in high wind speed (>35 ms<sup>-1</sup>) and ocean surface wave conditions. The research tasks basically consist of three steps. First, oceanic mixing processes in response to observed surface forcing will be carried out using mixed layer ocean models and 3-D ocean models. Second, the atmospheric response to the same observed surface forcing will be performed using an atmospheric model. Then the atmospheric model will be coupled with the ocean models for fully coupled study. In this meeting, I will report a preliminary analysis of observed surface fluxes based on ECMWF operational assimilation data and TRMM data for the summer of 2000 and 2001, and the upper-ocean response to the observed forcing. The latter is based on two 1D-ocean mixed layer models: a Kraus-Turner type mixed layer model and a Mellor-Yamada type model. For typhoons in the South China Sea and Western Pacific, the effect of shear-induced turbulent mixing and Ekman upwelling on the upper ocean is being evaluated carefully. For tropical intraseasonal oscillations, the relative role of heat fluxes to wind stresses in affecting upper ocean heat content is being analyzed.

**JSP10****Tuesday, July 8 - Friday, July 11****ROTATING AND STRATIFIED FLUIDS (IAPSO, IAGA, IAMAS, SEDI)**

Location: Site B, Room 21

**Tuesday, July 8 PM****JSP10/08P/B21-001**

Invited

**1400****LARGE-SCALE EXPERIMENTAL STUDY OF THE FORMATION OF ZONAL JETS IN CONVECTIVELY-DRIVEN GEOSTROPHIC TURBULENCE ON A TOPOGRAPHIC BETA-PLANE**

Peter Leonard READ<sup>1</sup>, Stephen LEWIS<sup>1</sup>, Paul WILLIAMS<sup>1</sup>, Yasuhiro YAMAZAKI<sup>1</sup>, Kuniko YAMAZAKI<sup>1</sup>, Joel SOMMERIA<sup>2</sup>, Adam FINCHAM<sup>2</sup>, Henri DIDELLE<sup>2</sup> (<sup>1</sup>Department of Physics, University of Oxford, <sup>2</sup>LEGI-Coriolis, Grenoble, France)

One of the most striking aspects of the appearance of the gas giant planets in the outer solar system is the persistent and stable organisation of their upper cloud decks into zonal-

## INTER-ASSOCIATION

oriented belts and zones, in association with a pattern of strong latitudinally-alternating zonal winds. Since the early numerical model simulations of Williams (1978), it has been suggested that this zonal organisation of the atmospheric circulation on these planets arises from highly nonlinear interactions between convectively-driven eddies in the background potential vorticity gradient produced by the rotation and spherical curvature of the planet (the so-called 'Rhines effect'). More recent numerical studies have qualitatively confirmed this effect under various circumstances, and shown to lead under some circumstances to strongly anisotropic spectra and transfers of energy and enstrophy. Until recently, however, experimental confirmation of this effect in the laboratory has been sparse, owing mainly to the extreme conditions needed to access the relevant flow regimes. In a new set of experiments, carried out on the 13m diameter Coriolis Platform in Grenoble, convective geostrophic turbulence was driven by a uniform buoyancy flux introduced at the free surface of the rapidly-rotating tank by a continuous spray of dense, salty water. The resulting flow was allowed to develop in the presence of a conical lower boundary, and was visualised and measured over periods of up to 5-6 hours. In this talk, we describe the experimental setup and report on new results which demonstrate the formation of up to 5 alternating zonal jets across the domain, depending on the strength of background rotation, topographic slope and the intensity of buoyancy forcing.

**JSP10/08P/B21-002**

**1430**

### RECONSIDERATION OF EQUATORIAL INERTIAL INSTABILITY

Hiroshi TANIGUCHI, Masaki ISHIWATARI (Graduate School of Environmental Earth Science, Hokkaido University)

Planetary-scale zonally non-symmetric temperature disturbances (called as "pancake structures") appear near the equatorial stratopause in winter hemisphere. The disturbances are usually interpreted as inertial instability (Hitchman *et al.*, 1987 and Hayashi *et al.*, 1998, Hayashi *et al.*, 2002). However, so-called "inertial instability" is a symmetric instability in rotating system (Boyd and Christidis, 1982, Dunkerton, 1981, 1983, and Stevens, 1983). It has not been discussed neatly whether non-symmetric pancake structures correspond to symmetric inertial instability. The purpose of this study is to examine the physical mechanism of unstable non-symmetric modes and unstable symmetric modes in equatorial atmosphere. The linearized non-dimensional primitive equations on the equatorial beta plane are solved for investigating the linear stability problem on latitudinal shear flows. Values of Lamb's parameter,  $E$ , are from 0.0031622 to 31622777. The results show that non-symmetric unstable modes appear for  $E > 0.1$  and that symmetric unstable modes appear for  $E > 1.204$ . Symmetric modes are most unstable for  $E$  greater than 16, otherwise non-symmetric modes are most unstable. In order to consider the physical difference of calculated unstable modes, dispersion relations of modes are examined from the viewpoint of resonance between neutral waves, that is, the discussion that instabilities are caused by resonance between modes with positive pseudomomentum and modes with negative pseudomomentum (Cairns, 1979; Iga, 1993, 1999). For small values of  $E$  in which only non-symmetric modes are unstable, resonance between equatorial Kelvin-wave mode and continuous modes occurs. This result suggests that non-symmetric instabilities are caused by unstable equatorial Kelvin waves, and is consistent with the discussions of Boyd and Christidis (1982) and Natarov and Boyd (2001). Unfortunately, for larger values of  $E$  in which both of symmetric and non-symmetric unstable modes appear, it is difficult to identify modes which are resonant since their dispersion curves are hidden by superimposed dispersion curves of continuous modes. However, the changes of dispersion curves of most unstable mode with changing the values of  $E$  can be observed. This suggests that the combination of neutral modes which are resonant are different for different values of  $E$ . The future problem is to identify neutral modes hidden by continuous modes and to give physical interpretation on the difference between symmetric modes and non-symmetric modes.

**JSP10/08P/B21-003**

**1450**

### SUPPRESSION OF THE RHINES-EFFECT BY STRONG HORIZONTAL DIVERGENCE IN A SYSTEM GOVERNED BY THE CHM EQUATION ON A BETA-PLANE

Akira OKUNO, Akira MASUDA (Dynamics Simulation Research Center, Research Institute for Applied Mechanics, Kyushu University)

An investigation is made on the effect of strong stratification, or horizontal divergence, on almost freely decaying geostrophic turbulence on a  $\beta$ -plane. In the periodic domain of a model ocean, the surface layer is assumed to be active above the quiet deep layer, so that barotropification was prohibited *a priori* to purify the effect of horizontal divergence. In other words the Charney-Hasegawa-Mima equation is adopted as the governing equation. Spectral evolution is accelerated numerically by an adjustment to keep kinetic energy constant against the retarding effect of horizontal divergence. First, numerical experiment is carried out for small or moderate horizontal divergence as control runs for comparison;  $UF/\beta < O(1)$ , where  $U$  is the characteristic velocity of turbulence and  $F$  the squared inverse of the radius of deformation. As has been reported repeatedly, the  $\beta$ -effect induces a highly anisotropic field characterized by a band of zonal currents, which phenomenon is known as the Rhines effect. It is confirmed also that kinetic energy has a one-dimensional spectrum approximately proportional to  $k^2$  at high wavenumbers  $k$ . A moderate value of  $UF/\beta$  slightly increases the preferred meridional scale of the zonal currents. Then, horizontal divergence is enlarged enough so that  $UF/\beta \gg 1$ , for which geostrophic turbulence turns out to behave just as on an  $f$ -plane: (1) the field becomes isotropic with no significant zonal currents; (2) the inverse cascade of energy is not hindered by the  $\beta$ -effect though it takes a longer time for turbulence to transfer energy to longer scales; and (3) the one-dimensional spectrum of kinetic energy (not total energy) is proportional to  $k^2$  at high wavenumbers. An argument based on the physics of long baroclinic Rossby waves is presented to explain why strong horizontal divergence suppresses the  $\beta$ -effect. Furthermore a transform of variables leads to a modified governing equation, which clearly shows that the  $\beta$ -effect should disappear for large horizontal divergence. This argument is confirmed by additional experiments based on those different forms of governing equations; the resulting spectra cannot be distinguished one from another, indicating the total suppression of the  $\beta$ -effect for strong horizontal divergence.

**JSP10/08P/B21-004**

**1510**

### SHEAR INSTABILITY IN SPHERICAL SHALLOW WATER SYSTEM

Shin-ichi IGA, Yoshihisa MATSUDA (Dept. of Earth and Planetary Science, Univ. of Tokyo)

Shear instability in spherical linear shallow water system is investigated using wind profiles observed near Venus cloud top. Results from two different wind profiles are presented. The first profile has a uniform zonal wind velocity between 60N and 60S with wind decreasing poleward of these latitudes; it is barotropically and inertially stable. The other has a zonal wind velocity of  $100\text{ms}^{-1}$  at the equator and high-latitude jets of  $160\text{ms}^{-1}$  at around 60N and 60S; it satisfies sufficient condition for both barotropic and inertial instability. For the former profile, the most preferred growing mode appears at a zonal number of  $m=2$  and  $(gH)^2(2a\Omega)^{-1} = 0.11$ . It has an e-folding time of about 100 days and an equivalent depth corresponding to a vertical wavelength of  $\sim 1\text{km}$  near the cloud top. In a frequency - Lamb-parameter diagram,

this mode corresponds to an intersection of the Kelvin mode curve and the continuous modes region, which ranges from the frequency corresponding to minimum basic angular velocity to that of maximum basic angular velocity. The intersections of eastward propagating gravity mode curves and continuous mode region sometimes generate another growing mode, whereas the intersections of westward propagating gravity mode curves and continuous mode region do not generate growing mode. For the latter profile, the most preferred growing mode appears at a zonal number of  $m=1$  and  $(gH)^2(2a\Omega)^{-1} > 0.1$ . It has an e-folding time of about 2 days and an equivalent depth corresponding to a vertical wavelength of below  $\sim 2\text{km}$  near the cloud top. This mode corresponds to an intersection of modified Rossby mode curve and continuous modes region. In these growing modes, angular momentum is conveyed equatorward. This particular feature is expected for explaining the superrotation of Venus atmosphere. Using the concept of resonance between different neutral modes, the cause of these growing modes is discussed. For the former profile, for example, the eastward propagating gravity modes and Kelvin mode having positive pseudo angular momentum resonate with continuous modes, which originally have negative (i.e. opposite sign) pseudo angular momentum. On the other hand, the westward propagating gravity modes, which originally have negative pseudo angular momentum cannot resonate with continuous modes with negative (i.e. same sign) pseudo angular momentum.

**JSP10/08P/B21-005**

**1530**

### INSTABILITIES OF INTERNAL SHEAR LAYERS IN ROTATING FLUIDS

Nathanael SCHAEFFER, Philippe CARDIN (LGIT, Observatoire de Grenoble)

Many free shear layers can be found in rotating systems, like atmosphere motion, oceanic currents, core dynamics or gaseous planets. We study the shear layer produced by differential rotation in cylindrical or spherical shells, numerically and experimentally. The quasi-geostrophic model we developed is not limited to small-slope containers, accounts for global mass conservation, and fully includes the Ekman pumping effects. It has been developed to simulate as well as possible our experiments in spherical shells, involving water, sodium or gallium; thermal convection or mechanical forcing; magnetic field or not. When the depth is constant, the destabilization follows a local Reynolds number criteria, and is well understood. However, when the depth is not constant, the instability has to break the Proudman-Taylor constraint, and thus the slope plays a major role in determining the threshold. Furthermore we show that in the latter case, the instability is a Rossby wave. A first experiment consists of two corotating disks in a spherical shell, which drive a shear layer. We study the stability threshold, and the instabilities that take place. We obtain asymptotical laws, supported by simple theoretical considerations, as well as numerical results. A second experiment uses an "inner core" that is differentially rotating to generate the shear layer. Again, the stability threshold is studied and asymptotical laws are exhibited. Recently, we found that such quasi-geostrophic flows are able to produce magnetic fields. Taking advantage of the quasi-geostrophic nature of the flow, we are writing a numerical code that could be able to lower both Ekman and Prandtl number significantly compared to regular geodynamo simulations.

**JSP10-Posters**

**Tuesday, July 8**

### ROTATING AND STRATIFIED FLUIDS (IAPSO, IAGA, IAMAS, SEDI)

Location: Site D

**Tuesday, July 8 PM**

**JSP10/08P/D-001**

Poster

**1610-053**

### ON THE FORM DRAG CAUSED BY TOPOGRAPHICALLY FORCED ROSSBY WAVES IN A BAROTROPIC BETA CHANNEL

Keisuke UCHIMOTO, Atsushi KUBOKAWA (Graduate School of Environmental Earth Science, Hokkaido University)

It is well known that form stress is exerted on fluid when fluid flows over the uneven topography. It is thought that the form drag is important in the Antarctic Circumpolar Current. When the primary sink of the momentum is the form drag, how is the mean steady velocity of a  $\beta$  channel flow driven by a surface-wind stress determined? This study addresses this question using a nondimensional barotropic quasi-geostrophic  $\beta$ -channel model, which consists of the zonal momentum equation and the vorticity equation. The applied wind stress is spatially uniform eastward one. The momentum equation includes only the wind stress term and the form stress term, and the mean zonal velocity,  $U$ , is determined by the two terms. The potential vorticity equation includes horizontal diffusion. Both the length and the width of the channel are  $\pi$ . The bottom topography  $\eta$  is one of the simplest forms:  $\eta = \eta_0 \sin 2x \sin y$ . First, we perform numerical experiments applying a constant wind stress. The initial conditions are quiescent. The solution behavior depends on the magnitude of the wind stress. When the wind stress is weak, the final  $U$  is determined well by the viscous linear solution. When the wind stress is too strong,  $U$  is infinitely accelerated. When the wind stress is between some values,  $U$  approaches a certain value almost independent of the magnitude of the wind stress. The solution driven by a weak wind stress has a similar structure as that of the linear viscous solution or nonlinear inviscid solution in which a cyclonic circulation exists over the elevation of  $\eta$  and an anticyclonic one over the trough. In the solution in which  $U$  is almost independent of the wind stress, the circulations reverse. In order to interpret the experimental results, we numerically obtain steady solutions for given values of the mean zonal current speed,  $U$ , by the revised Marquardt method. From these computations, it is found that there are two types of steady solution; one of them is similar to the linear solution which gives a small form drag, and the other is strongly nonlinear, giving a large form drag. The structures of the solutions are similar to those obtained by the numerical experiments. The transition between the two types of the solution occurs at a certain  $U$ . This certain velocity corresponds to a speed of a Rossby mode. Although the wave number is not the same as that of the topography, we refer to this velocity as a "resonant velocity". When the amplitude of the bottom topography is higher, the transition occurs at the resonant velocity of a higher mode. Around the "resonant velocity", the nonlinear interaction between the modes becomes active, and transition to the solution with large form drag occurs. The present result suggests that the mean zonal current speed is not necessarily proportional to the magnitude of the wind stress.

**JSP10/08P/D-002** Poster **1610-054**

**TOPOGRAPHIC EFFECTS ON WIND DRIVEN OCEANIC CIRCULATION**

Sebastien BIGORRE, William K. DEWAR (Florida State University)

A large scale oceanic anticyclone has been recently observed above the Zapiola Drift in the Argentine Basin. Its transports are comparable to those of the Gulf Stream. Its proximity to the Malvinas-Brazil current confluence renders it potentially important to several aspects of the South Atlantic oceanic climate. A conceptual multilayer turbulent quasigeostrophic model simulated a comparable anticyclonic circulation in the presence of an isolated topography. The model is able to generate an upslope eddy mass flux, in agreement with downgradient eddy potential vorticity diffusion. Maps of EKE are consistent with the eddy kinetic energy minimum observed by TOPEX above the Zapiola Drift. This paper investigates the time dependent dynamics of the flow, from a 150 years long simulation. Compared to the flat bottom case, the spectrum over the bump is redder, a multi-year (7 years) band is energized, and a decadal or multi-decadal oscillation created. The presence of the decadal oscillation is variable and connected to an apparent tendency for the flow regime to switch between "stable" and "unstable" states. During unstable periods, the phenomenology of the oscillation consists of the slow development of a large potential vorticity anomaly above the seamount driven by surface Ekman pumping. This is followed by a rapid ejection phase. In stable regimes, the potential vorticity anomaly can persist for longer periods and is accompanied by a stronger eddy variability. Eddy potential vorticity fluxes show that relative vorticity flux, caused by vortex tube stretching along the slope of the seamount is dominant. A low order relaxation oscillator model has successfully reproduced the results of the turbulent numerical model.

**JSP10/08P/D-003** Poster **1610-055**

**NONHYDROSTATIC SIMULATIONS OF THE IMPACT OF PLANETARY ROTATION ON CROSS-SLOPE FLOWS**

Patrick Charles GALLACHER, Steve PIACSEK (Oceanography Division, Naval Research Laboratory)

Barotropic tides can generate internal waves that propagate up the continental slope and force deep water onto the continental shelf. Also dense water formed by winter cooling on the shelf flows down the continental slope to the deep ocean. Canyons are preferred locations for these cross-slope flows because the slopes are steeper than the average, thus accelerating the flows. Since cross-slope flows have an inherent vertical acceleration, they are nonhydrostatic. Hence these flows should be poorly simulated in hydrostatic models. We used a nonhydrostatic model to study the effects of slope, canyon width and planetary rotation on these cross-slope flows and their mixing and entrainment of ambient water. We will compare and contrast the results to those obtained with hydrostatic and quasihydrostatic models. Previous simulations of internal bores over flat topography have demonstrated that nonhydrostatic models are required to obtain the correct dynamics of the head, the mixing region and the large amplitude internal waves of the bore.

**JSP10/08P/D-004** Poster **1610-056**

**CHAOTIZATION OF A PULSATING BAROTROPIC FLOW OVER AN ELLIPTIC SEAMOUNT**

Yuri G. IZRAILSKY (IACP FEB RAS)

A study of the chaotic advection in the barotropic inviscid unidirectional pulsating flow over a seamount of elliptic form is presented. The process of passive markers carry out from vortical region into the flow-through region is studied and in particular the evolution of the corresponding Poincaré sections with the change of frequency and amplitude of oscillations is presented. An approach to study the mechanism and parameters of chaotic advection in the open systems with finite life-time trajectories, based on study of the distribution of time necessary to carry out markers into the flow-through region, is presented.

**JSP10/08P/D-005** Poster **1610-057**

**CHAOTIC ADVECTION IN BACKGROUND CURRENTS MODELS OF GEOPHYSICAL HYDRODYNAMICS**

Konstantin V. KOSHEL, Vadim Fedorovich KOZLOV (Laboratory of geophysical hydrodynamics, Pacific Oceanological institute)

The concept of background currents is offered in the example of barotropic quasigeostrophic model. The background currents are characterized by constant value of potential vorticity, which minimize a kinetic energy of a system. The proposed approach allows to unambiguously defining background currents in areas with known boundary conditions as the sum of stationary vortical planetary-topographical and non-steady nonvortical flow components. Hamiltonian character of fluid particles motion equations allows to apply such models to study of chaotic advection. Instances of problems for a half-disk with linear bottom relief and a system of a source - sink in angular points of boundary line, about developing chaotic advection in unidirectional pulsating flow above a seamount of the Gaussian form, about effect of an anisotropy the localized submarine elevation on evolution of process, about roles of rectilinear boundary line in a neighborhood of point vortices are considered. Mainly with the help of numerical experiments and developed in the theory of dynamic systems technique of quantitative characteristics construction the processes of passive tracers carry out from a vortex region to flowing region are studied as functions of frequency, phase and relative amplitude of the background current flowing component oscillations. The geophysical interpretation of proposed models is presented.

**JSP10/08P/D-006** Poster **1610-058**

**OCEANIC FLOWS DRIVEN BY AN EKMAN PUMPING DIPOLE IN A QUASI-GEOSTROPHIC MODEL**

Atsushi KUBOKAWA, Atsushi MOTOKI, Keisuke UCHIMOTO (Graduate School of Environmental Earth Science, Hokkaido University)

Recent observations by satellite boarded micro-wave scatterometers have revealed that the surface wind field contains small scale shears. If the small scale wind shear is persistent, it will affect ocean current. For example, Xie et al. (2001, Science 292, p.2057-) showed that the dipole-shaped wind-stress curl produced by interaction between the easterlies and the Hawaiian Islands can drive an eastward current similar to the Hawaiian Lee Counter Current (HLCC). Although wind-driven currents are usually explained by the Sverdrup theory, the nonlinearity of such a current might be too strong for the Sverdrup theory to be applied, because of the small horizontal length scale and strong wind shear. On the other hand, the subpolar/subtropical gyre system might be able to be regarded as a current system driven by a large scale dipole-shaped wind stress curl. It is not very clear, however, how the current

structure in the west of the forcing region depends on the horizontal length scale and strength of the forcing. Motivated by this issue, we investigate the structure of the ocean current driven by a dipole-shaped Ekman pumping velocity in which the Ekman pumping velocity is positive in the north and negative in the south, using a 3-layer quasigeostrophic model. The parameters considered here are the strength of the Ekman pumping (nonlinearity) and the ratio of the lateral length scale of the forcing region to the baroclinic deformation radius. A series of numerical experiments in a wide range of parameters suggests that the parameter space can be classified into several domains. For example, in a domain with  $O(10)$  nonlinearity and  $O(1)$  horizontal scale, a mode type vortex pair appears, and in a domain with  $O(1)$  nonlinearity and  $O(1)$  horizontal scale, active eddies appear in the west of the forcing region and eastward flow in the far west is significantly weakened in comparison with that expected from the Sverdrup theory. For large scale forcing, a domain in which the eastward current is separated into two jets is also found. A theoretical argument is given based on the instability criteria and wave mode propagation, and it is shown that the domain where the double jets occur corresponds to the parameters for which the second baroclinic mode cannot propagate westward along the central latitude of the model after the lower mode adjustments are completed.

**JSP10/08P/D-007** Poster **1610-059**

**AN ASSESSMENT OF BOUNDARY LAYER PUMPING IN THE INVISCIDLY BALANCED APPROXIMATION EQUATION SYSTEM: LINEAR TRANSIENT PROBLEM**

Shin-Ichi ISHIDA, Takahiro IWAYAMA (Graduate School of Science and Technology, University of Kobe)

It is well known that a boundary layer pumping is one of the important decaying mechanisms of vortices in the free atmosphere. After the pioneering work by Ekman (1905), many formulae for the boundary layer pumping have been proposed. In this study, the boundary layer pumping in the inviscidly balanced (IB) approximation equation system that is recently proposed by Kanehisa (2000) is examined following the linear transient study of Bannon (1998). The IB system is compared with four approximation equation systems derived from the primitive equation on the  $f$  plane. Bannon (1998) concluded that in the case of the decaying vortex these are the geostrophic (SG) approximation equation system is the most accurate approximation of the primitive equation system, and in the case of the developing vortex SG and Ekman momentum (EM) approximation equation systems are the best. However, the geostrophic momentum (GM) approximation system is not better than the SG and EM systems. In this study, it is shown by the concept of an equilibrium flow that the IB system is equivalent to the GM system. Therefore, the pumping in the IB system is not good approximation. It is also pointed out that the energy equation in the IB system contains unphysical contribution from Coriolis force. This is a major failure of the IB system.

**JSP10/08P/D-008** Poster **1610-060**

**A NEW TYPE OF ISLAND RULE FOR THE ABYSSAL CIRCULATION BASED ON THE VOLUME TRANSPORTS IN BOUNDARY LAYERS AND ITS APPLICATION TO THE WIND-DRIVEN CIRCULATION IN AN OCEAN WITH MULTIPLE ISLANDS**

Akira MASUDA, Akira OKUNO (Dynamics Simulation Research Center, Research Institute for Applied Mechanics, Kyushu University)

A new type of island rule is developed for the abyssal circulation of the Stommel-Arons scheme. The island rule is formulated so as to determine two unknowns of volume transports in the boundary layers west of the northern and southern tips of an island, using two conditions of mass conservation and the circulation law. No stream functions need to be assumed in this island rule. These features are to be contrasted with those of previous island rules, which are concerned with the one unknown of the stream function around an island, based on the circulation law. The derivation and the resulting formulas are compared with those of previous ones. In comparison with Pedlosky's island rule, the present derivation does not go into details of boundary layers, though their presence was assumed as in the classical theory of the abyssal circulation by Stommel and Arons. Furthermore the present formulas apply to equatorial regions, where the approximation of the quasi-geostrophic stream function is inadequate. Two kinds of island rules are presented in different forms, but they turn out to be equivalent with each other. Also either Godfrey's or Pedlosky's island rule is shown to agree with the present island rule when there exists a stream function. To confirm the validity of the present island rule, numerical experiments were carried out with a diffusive reduced-gravity model, in which the upwelling velocity from the abyssal layer is determined autonomously through diffusive stretching. The experiment confirmed the prediction of the present island rule in particular for the equatorial abyssal circulation. Further the island rule is applied to the wind-driven circulation in an ocean with multiple islands. This problem was once studied numerically by Nakajima, who pointed out that the circulation depends not only on the wind stress curl, but also on the wind stress itself. The circulation in the interior region is determined easily from the Sverdrup relation, but the boundary currents must be calculated using the island rule. A recursive formula is obtained to relate the volume transports in the boundary layers one another. The equation is solved to yield an analytical formula, which clearly shows that the volume transports in the boundary layers surely depend on the wind stress itself. Finally the total circulation of the ocean is represented as the superposition of the interior flow and the boundary layer current. The latter is expressed by the structure function of the boundary layer (which depends on the properties of the boundary layer, in particular on the principal dissipative process there) multiplied by the amplitude or the volume transports in the boundary layers. These arguments were confirmed as well by numerical experiment based on the diffusive reduced-gravity model.

**JSP10/08P/D-009** Poster **1610-061**

**EXPERIMENTAL AND NUMERICAL INVESTIGATION OF LABORATORY VORTICES WITH DATA ASSIMILATION**

Martin Paul GALMICHE<sup>1</sup>, Joel SOMMERIA<sup>1</sup>, Emmanuelle THIVOLLE-CAZAT<sup>1</sup>, Jacques VERRON<sup>2</sup> (<sup>1</sup>Coriolis, Laboratoire des Ecoulements Géophysiques et Industriels, <sup>2</sup>MEOM, Laboratoire des Ecoulements Géophysiques et Industriels)

Meso-scale vortices play a crucial role in the transport of heat, mass and momentum in the ocean. The behaviour of an unstable, two-layer vortex in a rotating fluid is here investigated at the laboratory scale using experimental measurements, numerical simulations and data assimilation. The experiments are performed on the Coriolis turntable (Grenoble, France). The large dimensions (13m diameter) enable oceanic processes to be reproduced with a good level of similarity. To generate the vortex, a cylinder is introduced across the interface of the two-layer fluid, the interface is displaced inside the cylinder and the cylinder is removed at  $t=0$ . After a short adjustment period, a vortex is formed which, when unstable, undergoes baroclinic instability and splits into two or more new vortices. The velocity field is measured with high precision and resolution in both layers using Particle Image Velocimetry but the interface elevation is not measured and, therefore, no potential vorticity measurement is available. In order to obtain more information on the flow evolution, numerical simulations are thus performed using a two-layer, shallow-water model and data assimilation of the

IA

## INTER-ASSOCIATION

experimental velocity data is used to drive the model close to reality. The assimilation scheme is a Kalman filter similar to the sequential filters used in real-scale simulations of the ocean. The use of data assimilation for experimental purposes is a novel technique and has many applications. First, the combined experimental and numerical data provide a complete and realistic description of the flow. In particular, the potential vorticity anomaly can be computed, a quantity that is generally impossible to measure but which is crucial to a better understanding of the baroclinic instability (behaviour of fronts, propagation of patches, ...). The obtained flow field can also be used as an initial condition to test the numerical model. This makes it possible to quantify the systematic forecast errors. In the present study, the forecast errors are mainly due to the hydrostatic approximation. Lastly, the properties of the assimilation scheme can be analysed in details, in particular when only a reduced set of velocity data is assimilated. For instance, it is possible to test the accuracy of the assimilation scheme when only surface velocity data are available. This is clearly of practical interest because vertical extrapolation of the measured surface quantities is a great challenge in oceanography.

**JSP10/08P/D-010** Poster **1610-062**

### INSTABILITY OF A COLUMNAR VORTEX IN A STRATIFIED FLUID

Benjamin CARITEAU, Jan-Bert FLOR (LEGI-CNRS)

We investigate a columnar vortex generated by a rotating flap around a vertical axis in a linearly stratified fluid. This flap was accelerated and subsequently decelerated to create an intense Gaussian vortex with Reynolds number  $Re = UR/\nu \sim 1000$ , with  $U$  its maximum azimuthal velocity and  $R$  the corresponding radius. The vortex instability was explored as a function of the Froude number  $Fr = U/(RN)$ , with  $N$  the buoyancy frequency, which was varied between 0.5 and 5. Experimental observations reveal a slow developing elliptical instability of the core as well as the centrifugal instability at the rim of the vortex. In addition, for approximately  $1 < Fr < 2$  a helical wave was observed to develop near the radius of maximum azimuthal velocity, which leads to quasi-horizontal co-rotating vortices unlike the mushroom-shaped vortices observed for centrifugal instability. The wavelength of this instability increases with the Froude number. The sinusoidal oscillation of the core has a wavelength  $2R$  which grows exponentially until the core breaks down into vortex lenses. We discuss the different instabilities that occur.

**JSP10/08P/D-011** Poster **1610-063**

### SPONTANEOUS FORMATION OF STEP-LIKE STRATIFICATION DUE TO DIFFUSIVE INSTABILITY

Takashi NOGUCHI, Hiroshi NIINO (Ocean Research Institute, The University of Tokyo)

A mechanism of spontaneous formation of multi-layered convection due to double-diffusive convection in an unbounded uniformly stratified fluid was investigated. The fluid is unbounded and initially at rest and is stratified in "diffusive" sense (i.e., both temperature and salinity decrease linearly with height). A linear stability analysis predicts that there are growing modes when the ratio of the density gradient due to temperature to that due to salinity,  $\gamma$ , is larger than 0.876. The fastest growing mode (FGM) has a thin columnar shape which extends infinitely in the vertical direction and exhibits oscillation with increasing amplitude with time. A direct nonlinear numerical simulation in two-dimensional ( $x$ - $z$ ) plane was performed for  $\gamma = 0.88$ . In this numerical simulation, the perturbations from the basic state are assumed to be periodic both in horizontal and vertical directions. A white noise with random phase was introduced to velocity field to initiate the calculation. The initial growth of disturbances were consistent with the linear theory, but eventually overturning motions commenced and a series of well-mixed region was formed. These well-mixed regions gradually started to organize into multi-layered convection. The convective motions which resemble Rayleigh-Benard convection cells at a high Rayleigh number and the well-mixed layers were sandwiched by thin diffusive interfaces which have very sharp density gradient. Based on the results of the direct simulation, we analysed the detailed nonlinear evolution of the disturbances that led to the layer formation. First, the disturbances were decomposed into Fourier modes and nonlinear energy transfer among modes were examined. During the period right before the layer formation, it is found that the interactions among four modes play an essential role for the layer formation. These four modes include: (A) FGM of the linear stability analysis ( $k, m = (k_x, 0)$ ), (B) a growing mode ( $k_x, m_x$ ), (C) a layer mode ( $0, m_x$ ), and (D) a mode which corresponds to the resulting layer ( $0, 2m_x$ ), where  $k$  and  $m$  are horizontal and vertical wavenumber, respectively. Note that modes C and D are decaying modes according to the linear analysis. A truncated model which considers only the nonlinear interactions among the four modes turned out to reproduce successfully the growth of layer modes C and D. Layer modes C and D are shown to gain energy from the growing modes A and B through nonlinear interactions, grow and finally catch up with FGM (mode A). Once the amplitude of mode C or D becomes as large as that of A, it is found that vertical diffusion acting on the disturbed stratification, starts to enhance the layered stratification, thus leading to the layer formation.

**JSP10/08P/D-012** Poster **1610-064**

### INERTIA-GRAVITY WAVE GENERATION FROM UNSTABLE CURRENTS

Marie-Pascale G. LELONG, Timothy J. DUNKERTON (NorthWest Research Associates)

Inertia-gravity wave generation resulting from the instability of an energetic ocean current is investigated by means of high-resolution numerical simulations. We consider the efficiency of the generation mechanism as a function of current intensity, structure, position relative to lateral and bottom boundaries and atmospheric forcing. We identify preferred regions of wave generation on the evolving instability wave. The structure of the resulting wave field, its dependence on the characteristics of the unstable current and its tendency to radiate away from the source region is investigated. We also compare our results to those of Ford (1995) and Ford et al (2000).

**JSP10/08P/D-013** Poster **1610-065**

### EXTENDED JETS PRODUCED BY A FREE OSCILLATING BODY ON A NEUTRAL BUOYANCY HORIZON IN A CONTINUOUSLY STRATIFIED LIQUID

Yuli D. CHASHECHKIN, Vladimir V. LEVITSKIY, Yuri V. PRIKHODKO (Laboratory of Fluid Mechanics, Institute for Problems in Mechanics of the Russian Academy of Sciences)

We study experimentally a flow pattern around a free falling and then oscillating body on a neutral buoyancy horizon in a continuously stratified brine in a laboratory tanks with sizes 50 (length) x 15 (width) x 50 (height) cm and 70 x 25 x 70 cm filled with a linearly stratified salt brine (buoyancy period is  $T = 5.7; 9.8; 13.4$  s). The spheres with diameter 3.1; 4.5; 6.7 cm and vertical circular cylinder with flat tips (with diameter 3.2 cm and length of 5.5 cm) are used in the experiments. The flow pattern is visualized by the different method (conventional "vertical slit-Foucault knife", Maksoutov's "slit-thread", "natural rainbow" colour schlieren and schlieren interferometric) by the schlieren instrument IAB 458. A conductivity probe

measures particle displacements in the emitted internal waves. We have measured the body displacements, time series of its variable velocity, length scales of structural elements, wave amplitudes. We have compared experimental data with conventional theory and found rather large discrepancies. We have found that the pattern of flow around the body besides of the downstream wake with immersed vortices, boundary layer on the body surface, emitting transient internal waves contains elongated regular jets, forming in vicinity of trajectory turning point in the space regions where the body did not come. These mushrooms like jets firstly with convex and then with concave head are formed in result of interaction of the upstream blocked fluid with emitting internal waves. They are bounded by a high gradient envelope. The narrow jets move directly to the body supporting its oscillatory motion. It is precisely inside this area that we can observe the maximum values of the velocities and displacement amplitudes of the fluid particles. The jets appearance and disintegration correlate with body oscillations. The length of these secondary jets increases with their number. They are placed in the region of the body first diving even if the body is not symmetric and displaces from its initial position. Time series of the body displacements shows that firstly amplitude of oscillations relaxes rather fast and then the rate of oscillations damping dramatically decreases. The tips of the jets act as instantaneous source of transient internal waves, which do not contact with the body surface directly. Usually the upper set of jets is shadowed by the downstream wake and become visible only if the initial body displacement from the neutral buoyancy level is small and the wake is characterized by a simple structure. As a whole, the simplicity of the sphere trajectory does not reflect the complexity of observed non-stationary flow pattern. Similar effects can affect on accuracy of the ocean parameter measurements from submerged buoys that is from neutral buoyancy tracers.

**JSP10/08P/D-014** Poster **1610-066**

### A FINE STRUCTURE OF A STRATIFIED FLOW AROUND A HORIZONTAL STRIP UNIFORMLY MOVING IN A CONTINUOUSLY STRATIFIED FLUID

Vladimir Y. MITKIN, Yuli D. CHASHECHKIN, Roman N. BARDAKOV (Laboratory of Fluid Mechanics, Institute for Problems in Mechanics of the RAS)

We study theoretically and experimentally 2D problem of generation of macro- and micro disturbances by a plane horizontal strip uniformly moving in a viscous exponentially stratified fluid. We have neglected by diffusion effects and constructed an exact solution of the completely linearized problem with right boundary conditions that are no-slip for velocity and decay of all disturbances on infinity. We have applied an integral transforms method taking into account all set of roots of a dispersion relation. The solution describes upstream transient and downstream stationary (lee) internal waves as well as a set of boundary layers on the moving strip and on the rigid surface beneath it. We have visualized the fields of vector (velocity, vorticity, density gradients) as well as scalar parameters (density, pressure) numerically and calculated the same parameters asymptotically in an approximation of weak stratification and small viscosity. We have compared different solutions between themselves and have drawn fields of differences between exact and asymptotic data. We have visualised side view of flow pattern in stratified brine by different schlieren methods ('slit and knife', 'slit and thread', 'colour rainbow method') and have measured wave displacements by a conductivity probe. Profiles of upstream velocity are visualised by long density markers that are produced by wakes past vertically ascending small gas bubbles or descending sugar crystals. Asymptotic methods give qualitatively compatible data with exact solution and the laboratory study results only in limited areas past the obstacle. Ahead of the body both the exact solution and laboratory data describe transient waves with sloping rays and asymptotic solutions shows stationary horizontal wave columns. Pattern of attached internal waves past the obstacle is displaced in asymptotic representation. Patterns of exact solutions and laboratory observations correspond between themselves rather good. With increasing of towing velocity the horizontal boundary layer split on sub-layers and motion of sloping streaky structures is observed. In supercritical regimes downstream vortices are formed and density wake become wavy. Extrapolation on an environmental condition is discussed.

**JSP10/08P/D-015** Poster **1610-067**

### GENERATION OF 3D PERIODIC INTERNAL WAVE BEAMS BY A COMPACT SOURCE IN AN EXPONENTIALLY STRATIFIED FLUID

Aleksey Yu. VASILIEV, Yuli D. CHASHECHKIN (Laboratory of Fluid Mechanics, Institute for Problems in Mechanics of the RAS)

We study generation of 2D and 3D periodic internal wave beams in continuously stratified viscous liquid basing on a complete set of governing equations and exact boundary conditions that is no-slip for velocity and attenuation of all disturbances at infinite distance from the source. The linearized governing equations are solved by an integral transform method. A total set of dispersion equation roots contains terms corresponding to internal waves and additional roots describing two kinds of periodic boundary layers. The first one is a viscous boundary layer and has an analogue in a homogeneous fluid that is a periodic or Stokes' flow. Its thickness is defined by a kinematic viscosity coefficient and a buoyancy frequency. The second one, an internal boundary layer, is a specific feature of stratified flows. Its thickness besides the Stokes' scale contains additional factor depending on relative wave frequency and geometry of the problem. The thickness depends on the local slope of emitting surface and a direction of the wave propagation. We have constructed exact solutions of linear problems describing generation of 2D and 3D periodic waves by a strip and a rectangular with an arbitrary ratio of sides moving along or normally to a plane, which are placed on the sloping plane. We also calculated the wave pattern generated by a part of a vertical cylinder surface with different ratios of intrinsic scales that is of cylinder radius, thickness of the boundary layer and internal viscous scale. All solutions are regularly matched between themselves in limiting cases. The spatial decay of the waves depends on the dimension and geometry of the problem. Non-linear generation of internal waves by interacting boundary layers on an arbitrary moving vertical strip is investigated too. We found conditions of generation of the main frequency and its harmonics. In experiments periodic wave beams from different described above sources are visualised by the schlieren instrument and measured by conductivity probes. The probes are dynamically calibrated before each set of experiments. Calculated parameters of periodic internal wave beam are able to fit the best recent experimental data exquisitely well. Extrapolation on the environment is discussed.

**JSP10/08P/D-016** Poster **1610-068**

### NUMERICAL SIMULATION OF THE CIRCULATION PATTERN OF THE LEVANTINE BASIN

Khaled A. ALAM EL-DIN, Sayed H. SHARAF EL-DIN, Omneya M. IBRAHIM (Department of Oceanography, University of Alexandria)

Numerical modeling was used to study the circulation pattern under climatological conditions and the understanding of the relative importance of the forcing functions of the Levantine basin. The model domain extends from 25° E to 36° E longitudes and from 30° N to 37° N latitudes. The numerical simulation was performed using 3D hydrodynamical Princeton

Ocean Model (POM). The horizontal resolution was about 5° grid interval with 14 vertical sigma levels and a number of grid points of about 121x 85. The model bathymetry was obtained from the MODB data bathymetry. The initial fields of temperature, salinity and current used to spin up the model were taken from MODB Med4 dataset. The surface momentum, heat and fresh water fluxes were taken from ECMWF monthly data for the period 1986-1992. The model results can successfully show the well-known flow phenomena of the Levantine basin (North African current, Rhodes cyclonic gyre, Mersa-Matruh anticyclonic gyre, El-Arish cyclonic gyre and Shikmona anticyclonic gyre).

**JSP10/08P/D-017** Poster **1610-069**

**ULTRASOUND SCATTERING FROM STRATIFIED WAKES PAST A 2D BODY AND SINGULAR CIRCULAR VORTEX**

Viktor E. PROHOROV, Yuli D. CHASHECHKIN (Laboratory of Fluid Mechanics, Institute for Problems in Mechanics of the RAS)

We study experimentally scattering of the ultrasound pulses (operating frequency 1 MHz, ping duration 40 microseconds, repetition period 0.16 s, acoustic pattern angle 2 degree) from the downstream wakes past different 2D bodies and horizontally moving singular vortex rings. The experiments have been performed in the laboratory tank with dimensions 240 (length)x40 (width)x60(height) cm filled with continuously stratified brine. Pattern of the flow is visualized by schlieren instrument. Different optical techniques (conventional, Maksutov's slit thread, natural rainbow colour methods) are used. The experiments with the horizontally moving cylinder of different diameters (0.8, 1.5, 2.5, 5.0 and 7.6 cm) are conducted over a range of the flow parameters corresponding to laminar wake bounded with two sharp envelopes, with central sharp interface surrounded with microstructure region, also wake with vortex bubbles periodically dispensed along the trajectory. As has been shown from the backscattering experiments, the intensity scattered by sharp high gradient envelopes exceeds by several orders the entire scattering created by volume microstructures. Scattering indicatrix measured by bistatic configuration is subdivided into three parts. The middle one is a narrow resonance region of sound wave numbers corresponding to the specular scattering, and is a direct consequence of the reflection by the sharp interface. This region is adjacent by the ranges of volume scattering. Intensity of the reflection is larger by two orders of magnitude than that of volume scattering. To extend laboratory data to marine environment, a production of scattering volume cross section by the sound wavelength is employed. According to the estimation, the scattering of the pure microstructural inhomogeneities is comparable with that created by biota in the ocean. Pattern of the flow around horizontally moving vortex ring is similar to flow around a solid body, and includes upstream disturbances, set of internal waves and downstream wake with the finest elongated laminas. Microstructural components, which are responsible for volume scattering from the wake past the vortex, are characterized by internal boundary scale, which is analogous to the Stokes scale and defined by square root from kinematic viscosity over the buoyancy frequency. Experimentally the scale of the microstructural components is obtained from acoustic measurements of the buoyancy frequency extracted from the energetic spectra of the scattered signals. Additionally, the scales of the small-scale components are obtained from the schlieren images of the vortex wakes. The scales measured both acoustically and optically are very close. This testifies that the singular interfaces produced by internal boundary currents are the main contributors to the sound scattering. The internal boundary currents can separate from the rigid boundaries and can be formed directly inside the continuously stratified liquid without any solid bodies.

**JSP10** Tuesday, July 8 - Friday, July 11

**ROTATING AND STRATIFIED FLUIDS (IAPSO, IAGA, IAMAS, SEDI)**

Location: Site B, Room 21

Wednesday, July 9 AM

**JSP10/09A/B21-001** Invited **0900**

**THE DISPERSION RELATION FOR MID-LATITUDE OCEANIC PLANETARY WAVES IN THE PRESENCE OF MEAN FLOW AND TOPOGRAPHY**

Peter Douglas KILLWORTH, Jeffrey Ralph BLUNDELL (Southampton Oceanography Centre)

A great deal of research concerning phase and group speeds of oceanic planetary waves has taken place since the discovery from satellite altimeter data that such waves are ubiquitous, but travel somewhat faster than predicted by linear theory. Almost all of this research has concentrated on long, i.e. geostrophic, waves for simplicity. In this work we consider the dispersion relation for planetary waves of any wavelength, subject only to the requirement that the wave frequency be small compared with the Coriolis parameter, when the wave is propagating through a mean background flow, varying stratification, and with a sloping bottom. In most cases, a new wave mode appears for short waves which is essentially non-dispersive, concentrated around some mid-depth value, and is evanescent towards surface and floor. This mode is approximately Doppler-shifted with the local mean flow component along the wavevector.

**JSP10/09A/B21-002** **0930**

**WAVE-PACKET RESONANCE : ATMOSPHERIC STORM TRACKS DYNAMICS**

Mankin MAK, Yi DENG (Department of Atmospheric Sciences, University of Illinois at Urbana-Champaign)

Localized and persistent jets are ubiquitous in the atmosphere and oceans. The instability of a three-dimensional localized jet over western North Pacific Ocean in winter gives rise to the so-called Pacific storm-track. The disturbances associated with such a storm track are three-dimensional propagating wave-packets. It is hypothesized that the intensification mechanism can be succinctly interpreted as resonant interactions among the constituent potential vorticity anomalies associated with a representative unstable wave packet in the presence of such a jet. Those interactions give rise to mutual influences among the PV anomalies due to their individual advection of the background potential vorticity field. Supporting evidence from a model analysis for this hypothesis will be presented. It is also instructive to distinguish barotropic resonant interactions from baroclinic resonant interactions. A complementary diagnosis of the local energetics of an unstable disturbance will be reported, further delineating how such general instability takes place. Furthermore, the maintenance of a storm track will be discussed on the basis of an analysis of the nonlinear simulation. The intensity of the Pacific storm track is also known to be distinctly weaker in mid-winter, when the jet is strongest, than in early- or late- winter. If time permits,

a dynamical account for this counter-intuitive phenomenon known as 'mid-winter suppression' will be proposed.

**JSP10/09A/B21-003** **0950**

**LIMITATION OF THE BALANCED DYNAMICS IN THE F-PLANE SHALLOW WATER SYSTEM**

Norihiko SUGIMOTO, Shigeo YODEN (Department of Geophysics, Kyoto University)

The limitation of balanced dynamics which contain the coupling of slow Rossby mode and fast gravity mode are investigated in the *f*-plane shallow water system. First, we investigate the linear stability of zonal jets in this system, and compare the stability characteristics with those obtained in the quasi-geostrophic system for a wide range of Rossby *Ro*, and Froude *Fr*, numbers. As for the maximum growth rate, quasi-geostrophic approximation is good for a wide parameter range of  $Fr/Ro^2 > 1$  and  $Fr < 1$ , even for high *Ro*. However, unstable modes in this parameter range are different between high *Ro* and low *Ro*. In low *Ro* ( $Ro < O(1)$ ), there is a regime in which geostrophic balance is dominant. In this regime, the ratio of the amplitude of divergent component  $\psi$  to that of rotational one  $\phi$ ,  $|\psi|/|\phi|$  is proportional to  $Ro/Fr^2$ , and  $\phi$  is symmetric to the center of jet. On the other hand, in high *Ro* ( $Ro > O(1)$ ), another regime does exist. Here dominant balance is related to the basic flow.  $|\psi|/|\phi|$  is proportional to  $1/Fr$ , and antisymmetric component in  $\phi$  is dominant. In addition, for high *Ro* and  $Fr (Ro > O(1), Fr > O(1))$ , there is a regime of gravity-wave instability. These all results can be explained by order estimate of the linearized equations. Second, gravity wave radiations from balanced Rossby flow are investigated in the full nonlinear *f*-plane forced-dissipative shallow water system. We use two types of basic flow; zonal jets and hurricane-like vortices. Unlike the well known linear Rossby adjustment problem, gravity waves are continuously and intermittently radiated from these basic flows. Furthermore, these radiations are occurred for small *Ro* and *Fr*. Therefore, it is fundamentally different from gravity-wave instability which is found in the linear stability analysis for the case of high *Ro* and *Fr*. We analyze these radiations in detail for a wide range of parameters.

**JSP10/09A/B21-004** **1010**

**EFFECT OF THERMAL FORCING ON THE GENERAL CIRCULATION AND MEAN FLOW EDDY INTERACTIONS**

Oliver STENZEL, Jin-Song VON STORCH (Institute of Meteorology, University Hamburg, Germany)

The classical laboratory simulations suggest that the general circulation of a rotating fluid is determined both by the rotation rate and by the differential diabatic heating. As these laboratory experiments only crudely represent the atmosphere, it is worthwhile to further quantify the effect of the two external forcings using numerical models. So far numerical experiments have been mainly focused on the role of the earth's rotation rate. As a complementation, this paper studies the impact of the latitudinal heating from the sun on the general circulation. A 'dry' atmospheric GCM is used for this purpose. The diabatic forcing is parameterized by a Newtonian forcing. With this parameterization, the strength of the net latitudinal differential heating is controlled by the pole-to-equator difference in the restoring temperature,  $\Delta T$ . To study the effect of differential thermal forcing on the general circulation, the model is integrated using different  $\Delta T$ . It is found that an increase in the differential heating leads to strengthen the general circulation. The strengthening is characterized by regimes with different types of mean-flow eddy interactions. For extremely weak differential heating, the general circulation is described by a Hadley circulation with no eddy activity. As the differential heating increases, an indirect circulation in conjunction with large-scale waves emerges at the mid-latitudes and a weak polar cell appears in the polar region. The most pronounced waves are synoptic ones, and have wave number 6 and 7. As the differential heating further increases, the indirect circulation increases both in strength and size and covers the entire mid-latitude and polar region. This change is accompanied by a change in waves. The waves have now larger spatial scales with the dominant wave number being 3. The changes in the general circulation and the mean-flow eddy regimes can be summarized from an energetic point of view. The increase in differential heating leads to an increase in available potential energy, which is then transferred into the mean kinetic energy (i.e. the energy of the mean circulation). As long as the mean circulation is weak and stable, as generated by a weak differential thermal forcing, the available potential energy generated by the differential forcing will be entirely used to generate and maintain the mean circulation. Once the mean circulation becomes unstable, the available potential energy will also be used to 'feed' the eddies. In this sense, the different mean-flow eddy regimes represent different ways of a fluid to adapt to an increase in available potential energy.

**JSP10/09A/B21-005** **1040**

**BAROCLINIC GEOSTROPHIC ADJUSTMENT IN A ROTATING CIRCULAR BASIN**

Geoffrey W. WAKE<sup>1</sup>, Gregory N. IVEY<sup>1</sup>, Jörg IMBERGER<sup>1</sup>, N. Robb MCDONALD<sup>2</sup> (<sup>1</sup>Centre for Water Research, University of Western Australia, <sup>2</sup>Department of Mathematics, University College London)

A weakly nonlinear baroclinic geostrophic adjustment in a rotating basin is investigated in a laboratory study. The adjustment process is separable into a linear phase followed by a nonlinear phase on the basis of scaling arguments. This work describes in detail the hydrodynamics and energetics of the linear phase of the adjustment process from an initial step height discontinuity in the density interface  $\Delta H$  to a final response consisting of geostrophic and periodic components. For a forcing length scale  $r_f$  equal to the basin radius  $R_b$ , the geostrophic component consists of a double gyre while the periodic component is composed of baroclinic Kelvin and Poincaré waves. The Burger number  $S = R_b / r_f$  ( $R_b$  is the baroclinic Rossby radius of deformation) and the scaled depth  $\epsilon = \Delta H / H_1$  ( $H_1$  is the upper layer depth) characterise the response of the adjustment process. In particular, an excellent agreement between an analytical solution and the laboratory measurements is observed for times  $\tau < 1/2 \epsilon^{-1}$ , indicating this is the duration of the linear phase of the adjustment process. Over this timescale, the analytical solution can thus be used to calculate the energetics of the baroclinic geostrophic adjustment in a rotating basin. The results of this energetics study are found to compare favourably with previous studies with partitioning of energy between the geostrophic and periodic components exhibiting a strong dependence on  $S$ .

**JSP10/09A/B21-006** **1100**

**SIMPLE FRONTAL MODELS OF BAROCLINIC INSTABILITY**

Mateusz K. RESZKA<sup>1</sup>, Gordon E. SWATERS<sup>2</sup> (<sup>1</sup>Department of Physics, University of Toronto, <sup>2</sup>Department of Mathematical and Statistical Sciences, University of Alberta)

A class of layered mesoscale models is presented, relevant for oceanographic studies of baroclinic frontal instabilities and propagation of coherent structures. The models allow for finite thickness variations in the frontal layer and continuous stratification in the ambient

## INTER-ASSOCIATION

layer(s). The governing equations are derived in a formal asymptotic reduction of the primitive equations, assuming subinertial dynamics and leading-order geostrophy. The resulting systems are not quasigeostrophic (QG), however, since they allow for vanishing thickness of the frontal layer. The linear stability problem is solved for idealized and realistic steady basic states, in the presence of linearly sloping topography. Linear stability criteria suggest that introduction of ambient stratification reduces the size of the stable region of parameter space. Indeed, perturbation growth rates associated with the linearized equations are shown to increase with the stratification number, in agreement with previous laboratory experiments. For monotonic frontal profiles, the bottom topography tends to be a stabilizing influence when the interfacial and bottom slopes are of the same sign. This trend is consistent with traditional QG stability results, however, the present models are better suited than QG theory to the description of true fronts, which intersect the topography or fluid surface. Dependence of the instability characteristics on the width and relative thickness of the associated current is also investigated. Oceanographic and experimental applications of the frontal models are discussed, with particular emphasis on instability of the Denmark Strait Overflow and laboratory investigations of axisymmetric buoyancy fronts. Long-term numerical integration of the models demonstrates plume formation and ejection of coherent vortex features, in agreement with similar primitive-equation studies of coastal processes. In contrast to some previous studies, however, irregularities in the coastline or topography are not necessary for the onset of instability.

**JSP10/09A/B21-007**

**1120**

### NONLINEAR GEOSTROPHIC ADJUSTMENT OF DENSITY FRONT

Alexandre STEGNER<sup>1</sup>, Pascale BOURUET-AUBERTOT<sup>2</sup>, Thierry PICHON<sup>3</sup> (LMD, IPSL, Ecole Normale Supérieure, <sup>2</sup>LODYC, IPSL, Université Paris 6 Jussieu, <sup>3</sup>UME, ENSTA Palaiseau)

This study deals with the non-linear cyclo-geostrophic adjustment of a circular density front in a two-layer fluid. Laboratory experiments have been performed to investigate the dynamical evolution of a fixed volume of buoyant water, initially confined within a bottomless cylinder, which is quickly released in a dense rotating fluid. This configuration corresponds to a rapid input of potential energy in a geostrophic fluid layer and reproduces some dynamical processes which occur during oceanic upwelling or stratospheric warming events. We focus our efforts on the visualisation techniques in order to have simultaneous and independent measurements of both the horizontal velocity field and the vertical density field. We thus obtained, for the first time, quantitative measurements of the potential vorticity and the flow balance after a geostrophic adjustment process. The density profile of the mean adjusted state observed in the experiment is in good agreement with the prediction of the standard adjustment theory based on Lagrangian conservation of potential vorticity except in the frontal region. There, strong three-dimensional motions (plume structures, shocks and rapid transient instabilities) take place during the early stage of adjustment. These transient three-dimensional motions could dissipate up to 50% of the initial energy of the system, especially when the size of the initial density anomaly is close or larger than the deformation radius. Therefore, it significantly changes the velocity and the energy budget predicted by the standard Rossby adjustment. Both the kinetic energy of the mean adjusted state and the energy transferred to inertia-gravity waves modes are reduced by these transient dissipative processes. During the adjustment, an important part of the initial potential energy is released to inertia-gravity waves modes. These modes exhibit a non-trivial structure where the kinetic energy fluctuations are concentrated in the frontal region while significant potential energy fluctuations may occur in the central region. For all the cases studied, the first deviation of the density interface oscillate at the inertial frequency. Hence, the energy released to the wave modes during the adjustment is mainly concentrated at the inertial frequency. Afterwards, frequency doubling could occur for large amplitude wave.

**JSP10/09A/B21-008**

**1140**

### THE STABILITY OF ALONG ISOBATH CURRENTS FOR A SHELF-CONTINENTAL SLOPE OROGRAPHY

Don L. BOYER<sup>1</sup>, Andjelka N. SRDIC-MITROVIC<sup>1</sup>, Sergey A. SMIRNOV<sup>1</sup>, Peter G. BAINES<sup>2</sup>, Joel SOMMERIA<sup>3</sup> (Environmental Fluid Dynamics Program, Dept. of Mechanical and Aerospace Engineering, <sup>2</sup>CSIRO Atmospheric Research, Aspendale VIC 3141, Australia, <sup>3</sup>LEGI Equipe Coriolis, Université Joseph Fourier-CNRS-INPG Grenoble, France)

Mesoscale numerical models have difficulty in representing oceanic flows past steep topography. Here we describe laboratory experiments for comparison with numerical models and to explore the character of instabilities that occur. The experiments were conducted for geometrically identical systems, on both a large turntable (13 m in diameter) and a smaller one (1.8 m in diameter) with the flow in the former being transitional or turbulent and laminar in the latter. The topography, which is placed in the center of the test cell, includes a vertical coastline, a horizontal shelf, a continental slope and a deep ocean. Experiments were conducted for both homogeneous and linearly stratified fluids that were initially in a state of solid body rotation. The motion relative to the topography was established by impulsively increasing (or decreasing) the rotation rate, to provide along-isobath, downwelling (upwelling) favorable currents. The flow properties depend on the Rossby, the Burger and to a lesser extent, the Ekman number. Spin-up or spin-down first develops on the spin-up timescale, and then possible instabilities develop. This baroclinic flow was either stable as evidenced by circular, along-isobath streamlines, or unstable, in the sense that the azimuthal motions began to develop small scale disturbances which eventually developed into basin-scale eddies which encompassed the entire test facility. These observations have been compared with theoretical model of the extended Eady type, and quantitative agreement between the two is highly satisfactory. These results show that baroclinic eddy formation occurs naturally as part of stratified spin-up/down, and may be a significant factor in producing eddies in coastal currents.

**JSP10/09A/B21-009**

**1200**

### THE SPLITTING OF EDDIES BY ISLANDS

Harper L. SIMMONS<sup>1</sup>, Doron NOF<sup>2</sup> (International Arctic Research Center and Geophysical Fluid Dynamics Laboratory, <sup>2</sup>Florida State University)

Previous theoretical work has shown that, in an unbounded domain, anticyclones are prohibited from splitting on their own due to limitations imposed by the conservation of angular momentum. By explicitly considering the role of angular momentum exchange between eddies and boundaries (neglected by previous theories), splitting criteria for an anticyclonic lens colliding with a long and thin island are established analytically. The inviscid analytical model consists of an isolated patch of fluid in a reduced gravity regime. Nonlinear analytical solutions are constructed by connecting the initial and final states using conserved quantities. For the conceptual case of a lens pierced by a thin moving wall, the result is that, in order for a zero potential vorticity lens to split into two equal offspring, the wall length must be at least 1.19 of the lens' radius. Even for infinitesimal splitting, which arises from weak collisions (where the wall merely "brushes" the lens), the wall must be the order of the radius. This is because the "parent" lens can split into two offspring only when the wall allows sufficient spreading of the lens, which increases its relative angular momentum, and

thereby enables the lens to form two distinct "offspring." Numerical experiments employing Lagrangian floats reveal that the splitting is accomplished by a jet that leaks fluid along the wall, forming a second lens. The fluid initially found along the rim of the parent lens occupies both the core and the rim of the second lens; the fluid found at an intermediate radius in the second lens is derived from fluid situated at an intermediate radius in the parent lens. In general, a very good agreement between the numerics and the analytical theory is found. The numerical simulations demonstrate that the integrated angular momentum is a far stronger constraint than energy conservation. Using the numerics, we extend the moving wall theory to the splitting of finite vorticity lenses and lenses on a  $\beta$ -plane. We find that the basic requirement of mass redistribution by a wall is relevant in all the regimes that we examined, and, therefore, is likely to also be relevant to collisions of eddies with actual islands. This supports our application of the theory to Meddy splitting by seamounts, where we find that the seamounts can provide the necessary torque for recently observed Meddy splitting and destruction.

**JSP10/09A/B21-010**

**1220**

### EDDIES GENERATED BY A HUGE MOUNTAIN IN A ROTATING STRATIFIED FLUID

Yu HOZUMI<sup>1</sup>, Hiromasa UEDA<sup>1</sup>, Weiming SHA<sup>2</sup> (Section of severe storms, Division of atmospheric disasters, Disaster Prevention Research Institute of Kyoto University, <sup>2</sup>Department of Science, University of Tohoku)

The numerical simulations of flows on a huge-scale are performed supposing a rotating stratified fluid so as to understand the effects of the interaction between flows and very large-scale obstacle. These include coloris forcing and a huge-scale obstacle in order that Rossby number is less than a unity, and the buoyancy frequency of the flow and mountain's height are kept large in order Froude number with definition using mountain height keeps less than a unity. This situation includes the remarkable effects of stratification and rotation of the fluid, so the phenomena cause of interactions between flows and obstacle, concretely speaking a comparison the flow around mountain with over mountain and Taylor cap phenomenon, keep difficulties of understanding. A numerical model including primitive equations and no-slip boundary condition on bottom helps getting insights of a lot of effects, for example, the dynamical mechanism of a jet around a mountain and formation of an advecting cyclonic eddy near from mountain's top. To make clear these mechanisms and relation between the phenomenon and non-dimensional numbers of this fluid, further simulation are carried out with some values of the buoyancy frequency and wind speed. Results of these simulations clarify that (a) the jet flows separated to left and right on looking downward are kept by different reasons each other, one of the cause is concerned with the quasi-geostrophic flow pattern and another is concerned with the downdraft from higher level flow releasing the potential energy, (b) the maximum value of advecting cyclonic eddy depends on the upward flow speed and the buoyancy frequency, and shows that eddy is made of the tilting effect with quasi-geostrophic theory and the horizontal shear by the confluent jets at leeward. These results have the applicability to the understanding of the flow pattern near an actual huge mountain and of the phenomena in the mid latitude.

Wednesday, July 9 PM

**JSP10/09P/B21-001**

Invited

**1400**

### GRAVITY CURRENTS AND LENSES IN A ROTATING STRATIFIED AMBIENT - NUMERICAL SIMULATIONS

Marius UNGARISH<sup>1</sup>, Herbert E. HUPPERT<sup>2</sup> (Computer Science, Technion, <sup>2</sup>Institute of Theoretical Geophysics, DAMTP, University of Cambridge, Wilberforce Rd., Cambridge CB3 0WA, UK)

The behaviour of an axisymmetric high-Reynolds-number gravity current in a rotating frame which is released from a lock and then propagates over a horizontal boundary at the base of a stratified ambient fluid is considered. A finite-difference numerical code for the Navier-Stokes formulation is developed. The typical grid has 300 radial and 200 axial intervals (refined near the bottom to resolve the Ekman layer). The numerical results are compared with novel shallow-water approximations (also presented at this conference in a separate lecture) and with previous computations for non-stratified cases. The dependency on the dimensionless parameters predicted by the shallow-water formulation is confirmed. However, the numerical results of the stratified case display density waves that are not incorporated in the shallow-water formulation.

**JSP10/09P/B21-002**

**1420**

### GRAVITY CURRENTS AND LENSES IN A ROTATING STRATIFIED AMBIENT - SHALLOW-WATER THEORY

Herbert E. HUPPERT<sup>1</sup>, Marius UNGARISH<sup>2</sup> (Institute of Theoretical Geophysics, DAMTP, University of Cambridge, Wilberforce Rd., Cambridge CB3 0WA, UK, <sup>2</sup>Department of Computer Science, Technion, Haifa 32000, Israel)

The behaviour of an axisymmetric inviscid gravity current in a rotating frame which is released from a lock and then propagates over a horizontal boundary at the base of a stratified ambient fluid is considered. The one-layer shallow-water formulation is developed. This is an extension of recent theoretical investigations by the present authors of a gravity current in a non-rotating rectangular geometry which showed good agreement with corresponding experiments by Maxworthy et al (2002). The theory indicates that the inviscid flow is governed by (1) two dimensionless parameters, a stratification number  $S$  (which varies from 0 for the homogeneous ambient to 1 for a density at base equal to that of the dense fluid) and the initial height ratio  $H$  of the ambient to the dense fluid (which varies from 1 up to large values) and (2) a nose Froude number correlation between velocity and pressure head (which is, apparently, not influenced by the value of  $S$ ). In the rotating case an additional parameter, the ratio of Coriolis to inertia forces,  $C$ , appears. We assume that  $C$  is small. The time-dependent propagation is solved by a Lax-Wendroff scheme and compared with non-stratified and non-rotating cases. The results provide insights into the influence of the combined effects of stratification and rotations on the motion of the gravity current. In general, the stratification reduces the velocity of propagation and enhances the Coriolis effects in a rotating system. The shallow-water equations admit a steady-state lens solution, which is also investigated by numerical and asymptotical means. The problem of a lens in a stratified rotating fluid has been studied somewhat in the past, but the considered generating process was a slow injection of fluid from a point source, not a true gravity current. There is, however, good agreement between our results and previous predictions concerning the aspect ratio of the lens. The present shallow-water formulations filters out the stratification waves, whose effect can be captured by numerical solutions of the Navier-Stokes equations (also presented at this conference in a separate lecture).

JSP10/09P/B21-003

1440

**STABILITY AND EVOLUTION OF DENSE CURRENTS ON SLOPING TOPOGRAPHY**

Bruce R. SUTHERLAND, Kerianne YEWCHUCK, Joshua NAULT, Gordon E. SWATERS (Department of Mathematical and Statistical Sciences)

Driven by a need to understand the propagation and stability of abyssal ocean currents, there have been numerous idealised studies examining the dynamics in a rotating frame of reference of dense fluid on a slope underlying a less dense ambient fluid. This circumstance is characteristic, for example, of the Denmark Strait Overflow and the Western Boundary Undercurrent. A starting point of many theoretical and numerical studies is to assume the ambient is stationary and the current moves initially at a constant speed set by geostrophic balance. However, recent laboratory experiments (e.g. Lane-Serff and Baines (1998)) have shown that the continuous injection of a dense current from a localised source can significantly accelerate the ambient fluid and the consequent interaction between the two moving fluids cannot be neglected. We have performed a series of laboratory experiments designed to examine the temporal as well as spatial stability characteristics of the current. In these experiments a 90 centimetre diameter cylindrical tank on a rotating table is filled with fresh water. Dyed salt-water is injected uniformly through an annular slit on the conical-shaped bottom of the tank thus creating a uniform circular current. When instability occurs we observe a sinusoidal mode with phase speed approximately equal to that of the induced surface flow. The results are shown to be consistent with barotropic instability of the ambient rather than baroclinic instability of the dense current.

JSP10/09P/B21-004

1500

**BAROCLINIC INSTABILITY OF COASTAL CURRENTS AND VORTICES IN LABORATORY EXPERIMENTS**

Emmanuelle THIVOLLE-CAZAT, Joel SOMMERIA, Martin GALMICHE (LEGI/Coriolis)

Laboratory experiments are performed in the large Coriolis rotating tank in Grenoble (France) in order to study the development of coastal currents. The large dimensions of the turntable (13m diameter) provides large Reynolds and small Rossby numbers, allowing a good dynamical similarity with oceanic flows. A boundary current is produced by introducing light water over a heavier (more salty) fluid layer near a straight vertical wall. The fluid injector is shaped to produce a geostrophically balanced current. Measurements of horizontal and vertical velocity fields have been realized at different distances of the injector. The horizontal velocity field is measured by PIV (Particle Image Velocimetry) at two depths in the homogeneous water and in the current in a 2,5m x 2,5m domain. The vertical velocity field is also measured by PIV using a vertical laser sheet. The position of the density interface is controlled by ultrasonic probes downstream of the PIV domain. The unstable behavior of the current in the upper layer and in the lower one and the subsequent generation of meander and vortices or dipoles is analyzed. A comparison with the theory of baroclinic instability is performed, using the experimental analysis of perturbation phase and growth rate. Comparison with the baroclinic instability of a circular vortex is also discussed. A numerical model of the system is performed, using a two layer shallow water model (MICOM). Data assimilation (with the Singular Extended Kalman Filter) of the measured fields allows to capture the initial perturbations at the origin of the instability. Then a precise comparison between model and experiments can be performed.

JSP10/09P/B21-005

1520

**WAVE GENERATION BY INTRUSIONS IN TWO-LAYER AND CONTINUOUSLY STRATIFIED FLUIDS**

Morris R. FLYNN, Patrick KYBA, Bruce R. SUTHERLAND (University of Alberta)

Substantial mixing occurs near the margins of the ocean basin at the continental shelf. However, the dynamics by which this mixed fluid collapses and intrudes in the stratified ambient is not well understood, nor is the process of internal wave generation from such intrusions. As a starting point in examining these dynamics, in particular of an intrusion propagating along an interface such as the thermocline, we have performed a series of experiments in which a fluid intrusion is released along the interface of a two-layer fluid and also between a uniformly stratified fluid and a uniform fluid. In the former case, dye-tracking is used to measure transport and interfacial wave characteristics. In the latter case "synthetic schlieren" is used to measure the amplitude of vertically propagating internal waves generated from the intrusion. We compare the intrusion speed with predictions by Holzer and Huppert (1980). They agree well with two-layer fluid experiments in which the density of the lock fluid is established by uniformly mixing the ambient fluid. However, when the lock fluid is made more dense by adding salt to the mixture, the resulting evolution of the intrusion, which generates large amplitude interfacial waves, is quite complex and is not captured by theory. In experiments with a stratified lower layer, schlieren reveals that internal waves are generated within a narrow frequency band.

JSP10/09P/B21-006

1540

**A NUMERICAL STUDY ON MEDDY FORMATION**

Hidenori AIKI, Toshio YAMAGATA (Frontier Research System for Global Change, The University of Tokyo)

We have conducted a series of three-dimensional numerical experiments on a density current over a sloping bottom to study how Meddies (Mediterranean Water eddies) are generated off the Portuguese coast. It is demonstrated that the presence of a pointed cape can lead to periodic formation of anticyclonic lenses as part of baroclinic dipolar vortices. The size and rotation of the anticyclonic lens simulated in the model are in good agreement with the Meddies in the Iberian Basin. Noteworthy is the formation interval of about 30 days, which confirms the estimate that ten Meddies are shed per year near Cape St. Vincent (Bower et al., 1997). The transport of the density current is 0.5 Sv at the source region and 1.0 Sv past the cape. This downstream increase is associated with the entrainment of the ambient fluid; thereby the dense water on the bottom slope is converted into low potential vorticity water. The relative vorticity at the core of the dense water changes its sign from positive (cyclonic) to negative (anticyclonic), corresponding to the offshore ejection of the water parcels past the cape. We also discuss whether the surface cyclones are generated by the diapycnal volume flux due to the bottom water mixing. Additional experiments with reducing the mixing show no separated eddies from the density currents. To clarify some aspects regarding the generation of surface currents established in the above z-coordinate experiments, we simplify the problem of water intrusion and introduce a 5-layer model forced by a source/sink distribution of water mass. For an injection rate of 1.0 Sv, we observe the shedding of dipolar vortices which is remarkably similar to that observed previously. We find that the surface cyclones are generated as a result of the interaction between the coastal boundary current and the cape, rather than the density mixing near the bottom slope. It is demonstrated that the background current is induced by the passage of barotropic topographic waves associated with the subsurface water intrusion. We suggest that the background current is

essential for the subsurface lenses to drift far away from the source region (cf. Hogg and Stommel, 1990), thereby the eddy shedding event is repeated (cf. Nof and Pichevin, 1996). The overall results in this study suggest three necessary elements required for eddy shedding: a localized variation in the coastline as a trigger of cyclonic vortices, mixing of Mediterranean Water with the surrounding fluids leading to anticyclonic rotation of Meddies, and background currents which advect the detached vortices out of the source region.

JSP10/09P/B21-007

1620

**ROTATIONAL SUPPRESSION OF RAYLEIGH-BENARD AND RAYLEIGH-TAYLOR INSTABILITY**

Paolo ORLANDI (Dipartimento di Meccanica ed Aeronautica)

The retarding effect of rotation on the Rayleigh-Taylor instability is examined from the point of view of the vortex structures that develop during the instability. In numerical simulations, we found that it is possible to completely suppress RTI by the application of sufficiently strong rotation. To understand the role of viscosity and thermal diffusivity in this suppression, we turned to the more tractable Rayleigh-Benard problem. The linear dynamics of rotating RB convection has been investigated by Chandrasekhar [1] who numerically determined the marginal stability boundary for the onset of convection and overstability. Using a different approach, we are able to present remarkably simple analytical expressions for these boundaries. Finally, we find that if the fluid has either zero viscosity or zero diffusivity, the system is always unstable suggesting that both viscosity and diffusivity, as well as rotation, are necessary for the observed complete suppression. [1] S. Chandrasekhar *Hydrodynamic and hydromagnetic stability*. Oxford University Press. (1961)

JSP10/09P/B21-008

1640

**CONVECTION IN SMALL BASINS**

William K. DEWAR (Dept. of Oceanography, Florida State University)

Convection in the world's oceans often occurs in small, semi-enclosed basins where bottom slopes and nearby continental shelf breaks are commonplace. The evolution of convectively generated heat anomalies in such settings studied using quasi-geostrophic finite difference and point vortex models. The displayed behaviors divide essentially into two categories: whole fluid column convection, in which bottom slope effects are felt immediately by the convective patch, and partial fluid column convection, in which topographic effects can be delayed. In the latter, the sequence of events is somewhat richer and leads to differing scenarios involving bottom and lateral topography. In both cases, topography significantly modifies the evolution of convectively formed heat anomalies from that recently articulated for open ocean convection. It is suggested that topographic interactions are important to the preconditioning and dispersal phases of convection noted in water mass formation areas. Applications to the Labrador Sea and Mediterranean Seas are discussed.

JSP10/09P/B21-009

1700

**TWO-DIMENSIONAL NONLINEAR HORIZONTAL CONVECTION IN A ROTATING STRATIFIED FLUID**

Atsushi MORI, Hiroshi NIINO (Department of Astronomy and Earth Science, Tokyo Gakugei University, Department of Physical Oceanography, Ocean Research Institute, The University of Tokyo)

Horizontal convection due to differential heating is one of the most basic problems in geophysical fluid dynamics. Typical examples in the atmosphere are heat/cool island circulations (hereafter referred to as HCIC) and land-and-sea breeze circulations. There have been extensive observational, numerical and theoretical studies on HCIC. However, they are mostly confined themselves to the steady-state circulations, and surprisingly small number of studies have been made on the formation processes of the HCIC. Recently, we have made a theoretical study on the time evolution of a non-linear HCIC in a non-rotating linearly stratified Boussinesq fluid (Mori and Niino, J. Atmos. Sci., 2002), where the temperature of a half of the infinite bottom is suddenly lowered by a certain amount and maintained thereafter. We have found that the time evolution of the resulting horizontal convection is clearly categorized into three distinct flow regimes: Diffusion Regime (DR), Gravity Current Regime (GCR) and Gravity Wave Regime (GWR). We have also found that there exists a self-similar solution in each regime, i.e., the flow pattern and the temperature field remain similar with time if they are suitably scaled by prescribed functions of the elapsed time; the scaling functions for the horizontal length scales in the three regimes are shown to be given by diffusivity spread (DR), propagation distance of a gravity current (GCR) and propagation distance of a hydrostatic gravity wave (GWR), respectively. In the present study, we extended the above study to a rotating system. The results are summarized as follows: When the elapsed time is shorter than the inertial period, the time evolution of the flow field is similar to the non-rotating case. When the elapsed time becomes comparable to the inertial period, however, the horizontal length scale of the circulation ceases to increase and the flow fields become to be horizontally confined to a suitably defined 'radius of deformation'. As in the non-rotating system, there exist three regimes: DR, GCR and GWR. Accordingly, the radii of deformation for DR, GCR and GWR are scaled by diffusivity spread, propagation distance of gravity current and propagation distance of gravity wave within one inertial period, respectively. Once the flow fields start to be confined to the radius of deformation, they start to expand upward and eventually approach a steady state. For the steady state in each regime, dominant dynamical balances above the Ekman layer found to be the thermal wind balance. We have also examined the momentum budget and the three-dimensional linear stability.

JSP10/09P/B21-010

1720

**FLOW REGIMES OF NON-LINEAR HEAT ISLAND CIRCULATION**

Hiroshi NIINO, Atsushi MORI, Takehiko SATOMURA, Kiyoka AKIBA (Ocean Research Institute, The University of Tokyo, Tokyo Gakugei University, Geophysical and Planetary Sciences, Kyoto University, Suntory Ltd.)

Heat island circulation is one of the typical examples of horizontal convections in geophysical fluids. The most fundamental configuration for the heat island circulation is such that a finite area of the lower boundary of a stably-stratified Boussinesq fluid with constant kinematic viscosity and thermal diffusivity is maintained at a constant temperature slightly higher than that of the rest of the boundary. It is known from laboratory and numerical experiments (e.g. Kimura, 1975) that the non-linear heat island circulation generated for such a configuration has two different flow regimes: The first regime (hereafter referred to as Regime E) is characterized by two maximums of updraft at both coastlines of the heat island, while the second regime referred to as Regime C by a single maximum of updraft at the center of the island. In the present study, a theoretical consideration is made to suggest that the flow for such a configuration is governed mainly by two non-dimensional parameters: a newly defined non-linear parameter  $N$  and a Prandtl number. Thus, when the fluid is specified, the

IA

## INTER-ASSOCIATION

flow regime is principally determined by the non-linear parameter. A numerical experiment is performed to confirm the theoretical prediction. The steady-state flow regimes obtained from the numerical experiment in fact belong to either Regime E or Regime C. In accordance with the theoretical prediction, the transition between two regimes occurs at a constant value of  $N$ . When  $N$  is larger (smaller) than this value, Regime C (E) is realized. The physical meaning of  $N$  has been interpreted based on our recent theoretical study (Mori and Niino, J. Atmos. Sci., 2002) on the initial value problem of a non-linear horizontal convection. It is shown that when the non-linear parameter  $N$  is large, the gravity current initiated at the coastline reaches the center of the island before it experiences a transition to the gravity wave regime, so that Regime C is realized. The numerical experiments reveal that, however, there is a parameter range in which the flow never attains a steady-state but experiences a time-dependent state. The shape of the boundary curve that separates the steady-state and time-dependent state on the parameter space is shown to be well explained by an initiation of Rayleigh-Benard convections near the bottom boundary due to the boundary heating.

**JSP10/09P/B21-011**

**1740**

### TRANSVERSE ROLL CONVECTION FORMED IN A ROTATING HORIZONTAL SHEAR FLOW

Yutaka YOSHIKAWA<sup>1</sup>, Kazunori AKITOMO<sup>2</sup> (<sup>1</sup>Research Institute for Applied Mechanics, Kyushu University, <sup>2</sup>Graduate School of Science, Kyoto University)

The previous linear study by Davies-Jones (1971) showed that the horizontal velocity shear of background flow prefers parallel roll convection. However, our recent numerical experiment (Yoshikawa et al. 2001) suggests that the horizontal shear can organize convection into the roll whose axis is transverse to the background flow (transverse roll). This study is intended to make clear the effect of horizontal velocity shear on convection in detail. Numerical experiments are first carried out to examine whether transverse roll convection is actually formed in a horizontal velocity shear flow. We observe that the transformation of convection structure takes place in the linear stage of perturbation growth; in the nonrotating or slowly rotating case, the transformation from cellular to parallel roll convection occurs. In the rapidly rotating case, on the other hand, the transformation from cellular to parallel roll via transverse roll convection occurs. As a consequence, the transverse roll convection of finite amplitude is allowed to be formed in the rapidly rotating frame, if it becomes finite in amplitude when it is transformed into transverse roll. This transverse roll convection appears only for a short period of time just after its onset. This is the reason why the transverse roll convection was not found by Davies-Jones (1971), in which convection after a infinitely long time has passed is examined. The mechanism of the transformation is investigated by linear analysis. We formulated the problem so that the horizontal structure of the perturbation is sheared by the background flow as observed in numerical experiments. This formulation can significantly illuminate the underlying dynamics of the perturbation growth in the case where the advection speed of the perturbation is equal to the background flow. By this formulation, the perturbation is separated into the transverse mode (that is sheared by the background flow) and the parallel mode, and the governing equations change from partial ordinary differential equations for perturbation amplitude with respect to time. Integration of the ordinary differential equations and complementary eigen analysis make it clear that in the rapidly rotating case where the Coriolis acceleration greatly changes the direction of the horizontal velocity vector to the right, the shearing of the perturbation by the background flow results in enhancing potential energy conversion of the transverse mode. As a consequence, the transverse mode dominates over the parallel mode. The present result might explain some aspects of transverse roll convection observed in the atmosphere of planets such as in the Jupiter.

Thursday, July 10 AM

**JSP10/10A/B21-001**

**0830**

### ON ESTIMATING THE DIAPYCNAL DIFFUSIVITY IN THE PRESENCE OF DENSITY STRATIFICATION

Gregory N. IVEY (Centre for Water Research, University of Western Australia)

The future development of atmospheric and oceanic models requires improved description both of many fundamental flow processes and of the internal mixing. Recent laboratory and numerical studies have examined one aspect of this problem, the estimation of the diapycnal diffusivity in the presence of a stable background density stratification. The laboratory experiments were conducted in a closed system filled with a high Pr fluid with turbulent stirring by a horizontally oscillating vertical grid. Estimates were made of the rate of turbulent dissipation, turbulent length scales and diapycnal diffusivities over a very wide range of the turbulence intensities. In the energetic regime, for example, diffusivities were found to have both a different parameter dependence and to be smaller than predicted by traditional models. Some recent Direct Numerical Simulations in a density stratified shear flow at a  $Pr=0.7$  provide an independent means of examining some of the predictions from these laboratory experiments. What emerges from the laboratory and numerical studies is a picture of how the diapycnal diffusivity smoothly makes the transition from the molecular value at very low turbulent intensities to very high diffusivities at the highest turbulent intensities attainable.

**JSP10/10A/B21-002**

**0900**

### NUMERICAL EXPERIMENTS OF CONVECTION UNDER POLYNIA

Naosuke OKADA<sup>1</sup>, Motoyoshi IKEDA<sup>1</sup>, Shoshiro MINOBE<sup>2</sup> (<sup>1</sup>Division of Ocean and Atmospheric Sciences, Graduate School of Environmental Earth Science, Hokkaido University, <sup>2</sup>Division of Earth and Planetary Sciences, Graduate School of Science, Hokkaido University)

In the ocean partially covered by sea ice, nearly uniform atmospheric cooling can induce much more intense cooling through an open water area (polynya or lead), and hence, more rapid brine rejection from ice formation than the ice-covered portion. This non-uniform negative buoyancy flux produces a unique situation of convection: an area of convection is comparable with a convective plume. To investigate the relationship between effects on the dense water formation of convection and external parameters (the horizontal length scale of the buoyancy forcing, the strength of the cooling, or rotation) in this situation, numerical experiments of convection driven by horizontally restricted forcing (isolated convection) are carried out. A three-dimensional ocean model is developed without a hydrostatic assumption. The model domain is a doubly periodic box 2560m square by 200m deep. The spatial resolution is 10m in both the horizontal and vertical direction. The buoyancy forcing region has a disc shape and is set at the center of the model domain. In this region, buoyancy loss is introduced by subtracting a decrement of density from top grid throughout the model integration. The initial density profile is neutral. Many experiments were conducted for the different sets of external parameters. From results of these experiments, the two dynamical regimes described in Jacobs and Ivey (1999): the baroclinically unstable convection and the

baroclinically stable convection is confirmed. These two regimes are distinguished by the Rossby number  $R_{\text{rot}}=(B_0/fR^2)^{1/4}$ . Here  $B_0$  is the buoyancy flux,  $f$  is the Coriolis parameter,  $R$  is the radius of the forcing disc and  $H$  is the total ocean depth. In the baroclinically stable convection, it is found that the shift of the chimney is important, and the density scale of newly formed water has stronger dependency against the radius of the forcing disc than the previous studies. In the case where  $R_{\text{rot}}$  is high and  $R/H$  is low, multiple convective plume does not fully developed. And, the density scale has nearly no dependency against the radius of the forcing disc. That is considered as a new regime. The change of dependency of density scale is explained by scaling analysis. The term balance in the vertical plain vorticity equation is crucial to this change. The information about the density of newly formed water is useful for parameterizing dense water formation under the ice cover in a numerical model with a large (a few tens of km or larger) grid size.

**JSP10/10A/B21-003**

**0920**

### EFFECTS OF UNSTEADINESS, INITIAL CONDITIONS AND MOLECULAR DIFFUSION ON THE SCALAR FLUXES IN STRATIFIED TURBULENCE

Hideshi HANAZAKI (Institute of Fluid Science, Tohoku University)

Turbulent fluxes of passive and active scalar in unsteady strongly stratified homogeneous turbulence are analyzed using the rapid distortion theory (RDT) [1]-[2]. Analytical solutions of the RDT equations demonstrate that the initial conditions, i.e., the initial cross correlation between passive scalar and active scalar (density), and the initial potential energy, make difference between the passive and active scalar flux in the vertical direction, giving difference between the turbulent diffusion coefficients for passive and active scalars. This is in contrast to the previous literature which usually assumed the same diffusion coefficient for the passive and active scalars. On the other hand, our results show that the zero initial correlation between passive and active scalars leads to complete correlation between the passive and active (density) scalar in a long time, in contrast again to the previous discussions in the literature that initial strong correlation is necessary for the final strong correlation. The difference between the passive scalar flux and active scalar (density) flux appears in the passive scalar flux in its components slowly oscillating at frequency  $N$  ( $N$ : Brunt-Vaisala frequency), while the active scalar flux has only the twice as rapidly oscillating components with frequency  $2N$ . It is also found that the correlation coefficient between passive and active scalars is not a good measure of identifying the agreement or disagreement of the turbulent diffusion coefficients for these scalars, since if the passive scalar variance is initially large, final correlation coefficient becomes small even when the turbulent diffusion coefficients are equal for the active and passive scalars. The above results suggest the importance of the 'unsteady' analysis and the 'initial conditions' in the diffusion problem in stratified turbulence, which has been largely ignored in the previous studies. Effects of molecular diffusion of passive scalar (Schmidt number  $Sc$ ) and density (Prandtl number  $Pr$ ) show that if  $Sc > 2/(1+1/Pr)$ , the slowly oscillating mode with half frequency  $N$  decays more slowly than the fast mode with frequency  $2N$ . Then the difference between the passive and active scalar fluxes will become even more significant in a long time. This would be important in practical applications since in most practical conditions in the atmosphere/ocean  $Pr > 0.7$  and  $Sc > 1$  hold so that the condition  $Sc > 2/(1+1/Pr)$  is usually satisfied. [1] H. Hanazaki, "Linear processes in stably and unstably stratified rotating turbulence," J. Fluid Mech. 465, 157--190 (2002). [2] H. Hanazaki, "Effects of initial conditions on the passive and active scalar fluxes in unsteady stably stratified turbulence," Phys. Fluids (2003, in press).

**JSP10/10A/B21-004**

**0950**

### INTERNAL STRUCTURE OF PERIODIC BOUNDARY LAYERS IN A VISCOUS STRATIFIED FLUID WITH DIFFUSION

Anatolii V. KISTOVICH, Yuli D. CHASHECHKIN, Marina A. DAVYDOVA (Laboratory of Fluid Mechanics, Institute for Problems in Mechanics of the RAS)

We have applied two supplementary methods to solve the linearized problem of 3D disturbances generation in a viscous exponentially stratified liquid by an oscillating surface taking into account diffusivity effects. The source of disturbances is a part of vertical circular cylinder performing infinitesimal vertical or torsion periodic oscillations. We study the problem with both large and small Schmidt numbers. To calculate the fluid motion in the body vicinity we have applied the well-known method of singular boundary layers functions. The 3D spectral expansion technique is also used to calculate set of boundary layers on the solid surface and wave beams far from the source. We have found that in the general case produced set motions consist of emitting internal wave beams and three types of boundary layers even if the Schmidt number is equal to unity. The first one is a periodic Stokes boundary layer existing even in a homogeneous fluid. Its thickness is defined by kinematic viscosity and the frequency of the source oscillation. Two other layers, which are named internal viscous and diffusion boundary layers, are characterized by a more complex structure. Their thickness is defined besides intrinsic (Stokes) length scales by a similar scale including diffusivity coefficient, some derivative length scales and geometrical factors. In a limiting case of a weak viscosity and even more weak diffusivity the set of singular components of motion includes two types of split boundary layers. The ratio of their transverse sizes is proportional to the square root from the Schmidt number. The wave part of the solution describes internal gravity waves propagating along a wave cone as in an ideal fluid. To calculate wave fields far from the source, which satisfy right boundary conditions, we have used the spectral expansion method taking into account all set of regular and singular roots of the dispersion relation. The constructed exact solutions also describe the set of the same boundary layers and emitting 3D periodic internal wave beams. The transverse structure of the beam is defined by the ratio of the source size to intrinsic combined internal length scale. If the characteristic size of the generator is smaller than the combined internal length scale the beam is unimodal. In opposite case near the source the wave beam is bimodal. We have calculated the distance from the source where the bimodal beam transforms into the unimodal one. Constructed solutions present in the form adopted for comparison with the laboratory data. Given schlieren images demonstrate sections of wave cones and flows produced separating boundary currents from the periodically oscillating disks and rectangular in a continuously stratified fluid. Results of laboratory experiments a reasonable agreement with the calculations.

**JSP10/10A/B21-005**

**1030**

### TWO-DIMENSIONAL TURBULENCE ON A BOUNDED DOMAIN

Gert-Jan F. VAN HEIJST, Herman J.H. CLERCX (Department of Physics, Eindhoven University of Technology)

In contrast to its counterpart in the 3D world, turbulence in 2D is characterized by an inverse energy cascade. The presence of this inverse cascade in 2D turbulence is visible in the so-called self-organization of such flows: larger vortices and structures are observed to emerge from initially random flow fields. The lecture will address the evolution of 2D turbulent flows on a finite domain with no-slip walls. Results of both laboratory experiments and numerical simulations reveal the crucial role played by the unsteady boundary layers: the domain

boundaries act as important sources of large-amplitude vorticity filaments. In addition, spectral characteristics and some aspects of (chaotic) tracer transport will be highlighted.

**JSP10/10A/B21-006****1100****WHY DOES A TURBULENT CHANNEL FLOW TEND TO HAVE A SHEAR ZONE OF ZERO ABSOLUTE VORTICITY IN A ROTATING SYSTEM?**

Akira MASUDA, Yutaka YOSHIKAWA (Dynamics Simulation Research Center, Research Institute for Applied Mechanics, Kyushu University)

It has long been known that turbulent channel flows tend to have a zone of mean shear with nearly zero absolute vorticity in homogeneous rotating fluids. This feature was observed either in a numerical experiment for the Couette flow or in a tank experiment for the Poiseuille flow. This paper is intended to give a plausible account of how this curious property of turbulent channel flows is maintained in a rotating system, on the basis of an analogy between rotating and stratified fluids. The analogy itself has been well-known since Veronis. In reality, some arguments along this line have already been attempted for the presence of the shear zone of nearly zero absolute vorticity by such as Bradshaw and Tanaka et al. Nevertheless convincing explanation does not seem to have been proposed so far. Here the argument is improved first by showing that the zonally averaged flow in the rotating fluids is governed by the same equations as those for the zonally averaged flow in stratified fluids, even though the second moment may differ in the two systems. Then, as is usual, the shear zone of zero absolute vorticity in the rotating fluids is identified with nearly homogeneous layers in stratified fluids. The Couette flow in the rotating system corresponds to the thermal convection driven by cooling at the top and heating at the bottom. Likewise and remarkably the Poiseuille flow in the rotating system can be compared to the stratified fluid that suffers from steady body cooling along with the stabilizing heating from above. In order to confirm the validity of this analogy numerical experiments were carried out for the zonally averaged field in the stratified system to model the turbulent channel flows of Couette and Poiseuille types in the rotating system. In both cases, thermal convection yielded nearly homogeneous layers. The profile of the mean density profile in stratified fluids is translated to the mean zonal flow in rotating fluids including the linear shear due to the Coriolis parameter. The results showed a good agreement between the picture based on the analogy with stratified fluids and previous numerical or tank experiments in rotating fluids. Additional experiments were carried out, where fluctuating forms of body cooling were superposed to the inherent regular one in the stratified system corresponding either to the Couette or the Poiseuille flow in the rotating system. Even under the fluctuating body forcing, we observed the robust formation of nearly homogeneous layers that corresponds to the shear zone of zero absolute vorticity. The results suggest that the basic mechanism for maintaining the shear zone of nearly zero absolute vorticity is the inertial instability analogous to the gravitational instability in stratified fluids and that the maintenance of the shear zone of zero absolute vorticity does not depend on the details of turbulent motion.

**JSP10/10A/B21-007****1120****INTERACTION OF DECAYING 2D TURBULENCE WITH RIGID BOUNDARIES: LABORATORY EXPERIMENTS**

Yakov D. AFANASYEV, Jennifer WELLS (Department of Physics and Physical Oceanography, Memorial University of Newfoundland)

Results from a new series of experiments on quasi-two-dimensional turbulence decaying in a rectangular container are presented. The flows are generated electromagnetically in a thin layer of conducting fluid when different configurations of permanent magnets are used to specify the initial characteristics of the flow. The Particle Image Velocimetry method is used to determine the velocity and vorticity fields. These fields are further used to determine the global characteristics of the flow such as the energy, enstrophy and the net angular momentum with respect to the centre of the container. The experimental results demonstrate that variations of net angular momentum occur due to the interactions of coherent vortex dipoles/jets with the walls of the container. The variation of the angular momentum of the system which occurs due to the action of stresses at the solid boundary can be obtained quantitatively if the initial linear impulse exerted by the magnets on the fluid is known. The analysis of external forces and torques allows one to predict that during the intermediate state of the flow evolution a pattern of the flow will be a rotating quadrupole.

**JSP10/10A/B21-008****1140****SELF-SIMILARITY OF VORTICITY DYNAMICS IN DECAYING CHM TURBULENCE**Takahiro IWAYAMA<sup>1</sup>, Theodore G. SHEPHERD<sup>2</sup>, Takeshi WATANABE<sup>3</sup> (<sup>1</sup>Graduate School of Science and Technology, Kobe University, <sup>2</sup>Department of Physics, University of Toronto, <sup>3</sup>Department of System Engineering, Nagoya Institute of Technology)

In decaying 2D Navier-Stokes turbulence, Batchelor's similarity hypothesis fails due to the existence of coherent vortices. However, it is shown that decaying 2D turbulence governed by the Charney-Hasegawa-Mima (CHM) equation is well described by Batchelor's similarity hypothesis for length scales much greater than the Rossby deformation radius, suggesting that vortices in this regime are not really coherent. A theory for the self-similarity of energy and enstrophy spectral fluxes is also presented. It is argued that the possibility of complete self-similarity depends on the choice of dissipation operators.

**JSP10/10A/B21-009****1200****STRONG TURBULENCE OF INTERNAL NONLINEAR KELVIN WAVES**

Vadim V. NOVOTRAYSOV (V.I.II'ichev Pacific Oceanological Institute, FAR-EASTERN BRANCH OF RUSSIAN ACADEMY OF SCIENCES)

Turbulence at boundaries in rotating stratified fluids is supposed to be considered as a random field of weak nonlinear internal Kelvin waves (IKW). Theory of this turbulence is considered on the base of Burger's equation. It is shown that the energy spectrum of this turbulence has a universal structure: on the young-age stage the energy spectrum is proportional to the third power of the frequency, on the old-age stage the energy spectrum is proportional to the second power of the frequency at small frequencies and decreases exponentially at high frequencies. The coefficient of the proportionality is determined by the nonlinear effects on the initial stage of the propagation. We presented observations of the IKW in the coastal zone of Japan sea. Data collected from moored instrument and repeated profile measurements during the September 1999 show an energetic, large amplitude semi-diurnal IKW. Spectrums of temperature, current variations and IKW are constructed. Comparison of IKW spectrum with model random nonlinear IKW spectrum has revealed their good agreement. Work supported by RFBR grants 02-05-64277.

**JSP10/10P/B21-001****1400****NONLINEAR DYNAMICS OF A STRAINED VORTEX**

Richard R. KERSWELL (Department of Mathematics, University of Bristol)

It is now well known that elliptically-distorted vortices are linearly unstable to pairs of inertial waves if the fluid viscosity is small enough. These growing inertial waves themselves become unstable beyond a threshold amplitude so that the resulting flow quickly grows in both spatial and temporal complexity. At this point, direct numerical simulation offers the only practical tool for probing the breakdown further. We will present the results of such an exploration for the closely related flow of a precessing vortex (Mason & Kerswell 2002). (The precessing vortex is a strained vortex in which the strain takes the form of a  $\exp(i\phi)$  perturbation as opposed to a  $\exp(2i\phi)$  perturbation in an elliptical vortex.) This flow is more naturally simulated in a numerically-accessible plane layer model and is interesting in its own right having application to the Earth's precessing outer core. The exact basic flow can be written simply as  $u_{\text{basic}} = (-y, x, 2\epsilon \sin^2 z, 0)$  in cartesian velocity components where  $\epsilon$  measures the straining of the vortex in a frame rotating at an angular velocity of  $\epsilon$  in the  $x$ -direction. The flow solution consists of 'sheared' circular streamlines where the line joining their centres is no longer perpendicular to their plane (the strain is out of the plane of motion). Numerical results confirm that the initial instability occurs through a pairwise inertial wave instability at  $\epsilon_{\text{crit}} = O(E^{1/2})$  where  $E$  is the Ekman number, and that a weakly nonlinear regime only exists for  $\epsilon_{\text{crit}} - \epsilon$ . Beyond this, secondary instabilities occur which lead to a multitude of co-existing solution branches, some of which are chaotic. Interestingly, all the nonlinear flow solutions found remain within  $O(\epsilon_{\text{crit}})$  (in an energy norm) of  $u_{\text{basic}}$ . This indicates that the precessional instability is not able to remove energy from the underlying rotation of the vortex but instead merely feeds off the strain perturbation. Why this conclusion appears at variance with experimental realisations of precessing flows (Malkus 1968) and elliptical vortices (Malkus 1989, Eloy et al. 2000) will be discussed. Eloy, C., Le Gal, P. & Le Dizès, S. 2000 'Experimental study of the multipolar vortex instability' *Phys. Rev. Lett.* **78**, 1900-1903. Malkus, W.V.R. 1968 'Precession of the Earth as a cause of geomagnetism' *Science* **169**, 259-264. Malkus, W.V.R. 1989 'An experimental study of the global instabilities due to the tidal (elliptical) distortion of a rotating elastic cylinder' *Geophys. Astro. Fluid Dynam.* **48**, 123-134. Mason, R.M. & Kerswell, R.R. 2002 'Chaotic dynamics in a strained rotating flow: a precessing plane fluid layer' *J. Fluid Mech.* **471**, 71-106.

**JSP10/10P/B21-002****1430****THREE-DIMENSIONAL LINEAR INSTABILITY OF AN ELLIPTICALLY STRAINED VORTEX TUBE**

Yasuhide FUKUMOTO (Graduate School of Mathematics, Kyushu University)

The global linear stability analysis for a straight vortex tube embedded in a pure shear flow is revisited. This problem was originally addressed by Moore and Saffman (1975) and Tsai and Widnall (1976), and the three-dimensional instability of an elliptically strained vortex tube is now well known as the Moore-Saffman-Tsai-Widnall instability. We restrict our attention to the case of uniform vorticity. Without shear, the basic flow is the Rankine vortex. The Rankine vortex supports neutrally stable three-dimensional waves called the Kelvin waves. A pure shear deforms the core into an ellipse and thus breaks the circular symmetry, causing a parametric resonance between right- and left-handed helical (bending) waves. Resonance instability is possible between any combination of the Kelvin waves with their azimuthal wavenumber difference being 2. Eloy and Le Dizès (2001) showed that this is indeed the case and that the resonances other than bending-bending wave interaction are equally dangerous. The results of Tsai and Widnall (1976) are simplified by providing an explicit expression for disturbance flow field, whereby an improvement in numerical accuracy is achieved. Given the wavenumber and the frequency of the intersection points of dispersion curves of Kelvin waves with azimuthal wavenumber difference 2, the growth rate is expressible solely in terms of the modified Bessel functions, and so is the unstable wavenumber range. The parametric resonance instability occurs at every intersection point. For bending-bending waves resonances, the amplification rate of non-rotating waves is by far larger than that of rotating waves. Direct relations of this static instability are established with the two-dimensional displacement instability in the long-wave limit (Moore and Saffman 1971) and with the elliptical instability in the short-wave limit (Bayly 1986; Waleffe 1990). For other resonances of higher azimuthal wavenumbers, amplification rate is larger at a particular sequence of intersection points of dispersion curves, which are the only surviving modes in the short-wavelength limit. Its growth rate approaches that of the elliptical instability. An account for this instability is given from the viewpoint of Hamiltonian spectra. The energy of the Kelvin waves is calculated by invoking Cairns' formula. The instability result is compatible with Krein's theory for parametric resonance in Hamiltonian systems; for instance, the non-rotating instability mode emerges as a result of collision of eigenvalues of zero-energy waves.

**JSP10/10P/B21-003****1450****INTERACTION BETWEEN A Q-VORTEX AND EXTERNAL TURBULENCE**

Naoya TAKAHASHI, Takeshi MIYAZAKI (Department of Mechanical Engineering and Control Systems)

Interactions between intense columnar vortices and surrounding turbulent motions are often produced in engineering and environmental flows, and they occur naturally in most sheared turbulent flows, such as circular jet, plane jet, and mixing layer. These interactions are thought to play an important role in the three-dimensionalization of the flow fields. It is, also, of practical interest to estimate the lifetime of trailing vortices under the influence of atmospheric turbulence. We investigate the instability of the columnar vortex with axial flow, embedded in ambient turbulence, using direct numerical simulation (DNS). We consider the columnar vortex of various values of swirling parameter  $q[1]$  ( $q \rightarrow \infty, -3.0, -1.5$  and  $-0.45$ ). We produced an external turbulence numerically by the Fourier-spectral method ( $Re$  is about 120). In the case of  $q = -0.45$ , twist structures are formed inside the vortex core. Its growth rate agrees with that of the linear instability analysis [2]. After two revolutions, the secondary instability is excited. Then the columnar  $q$ -vortex collapses, and many fine scale vortices appear abruptly. The mean energy density decreases, and the disturbance energy density increases outstandingly after the vortex break down. The cases of  $q = -1.5$  and  $-3.0$  are less unstable. From Stewartson and Leibovich [3], we expect modes with  $lm$  much larger than 1 are stabilized for  $|q| > \text{square root of } 2$ , then our simulations are well resolved. In these cases, we find that generation of thin spiral structures. These structures, generated around the surface of the core, are wound up by the columnar vortex, and they are stretched to be very thin spirals. In the case of  $q = \infty$  (a.k.a. Lamb-Oseen vortex), we find that the columnar vortex, which itself expands slightly, winds up the worms, which enhance energy dissipation considerably. Using the two-point energy spectrum tensors, we capture such phenomena as the 'Blocking Effect' (fluid particles cannot invade the core of the ordered vortex) and the excitation of bending and axisymmetric vortex waves. During these processes, we can also observe suppression of the scalar diffusion by the core and

## INTER-ASSOCIATION

enhancement of the diffusion by fine scale structures. [1] Lessen, M. and Paillet, F.: J. Fluid Mech. **65** (1974). [2] Mayer, E.W. and Powell, K. G.: J. Fluid Mech. **245** (1992) 91. [3] Leibovich, S. and Stewartson, K.: J. Fluid Mech. **126** (1983) 335.

**JSP10/10P/B21-004**

**1510**

### QUASIGEOSTROPHIC ELLIPSOIDAL VORTICES: INSTABILITY, INTERACTION AND SCALAR MIXING

Takeshi MIYAZAKI, Wei QIN, Kensei SAKAMOTO (Department of Mech. Eng. Control Systems, University of Electro-Communications)

In geophysical flows, coherent vortex structures persist for long time and their interactions dominate the dynamics of geophysical turbulence. Miyazaki *et al.* have derived a Hamiltonian dynamical system of  $3N$  degrees of freedom, describing the interactions of  $N$  ellipsoidal vortices, where each coherent vortex was modeled by an ellipsoid of uniform potential vorticity (Meacham *et al.*). Chaotic motions are observed even in a two-body system. In this paper, direct numerical simulations based on a Contour Advection Semi-Lagrangian algorithm (CASL) are performed in order to investigate the instability and the interaction of ellipsoidal vortices. First, the instability of a tilted spheroidal vortex is investigated. A prolate spheroid becomes unstable against the third Legendre mode when the aspect ratio is less than  $0.44$  and the inclination angle is larger than  $0.48$ . An oblate spheroid may become unstable if the aspect ratio is larger than  $1.62$ , even if the inclination angle is very small. Weakly unstable prolate spheroidal vortices emit thin filaments from their top and bottom, whereas strongly unstable slender prolate spheroidal vortices are broken up into two pieces. Unstable oblate spheroids emit thin sheets of vorticity to become stable oblate (or prolate) spheroid. Secondly, the interaction of two co-rotating spheroidal vortices on slightly different vertical levels, which plays a key role in the turbulence dynamics, is studied. The Hamiltonian model can predict the critical distance of symmetric and asymmetric mergers well, although in asymmetric interactions vorticity exchange occurs (not "two to one merger") along the threshold determined by the Hamiltonian model. The smaller vortex loses some of its original volume, and the larger vortex expands slightly absorbing the filaments ejected from the smaller vortex. This is a new dynamical process linked with the energy and enstrophy cascades. Thirdly, the interaction of two counter-rotating spheroidal vortices on slightly different vertical levels. These vortices are quite robust, i.e., they keep the dipole structure by emitting filaments, even if they are placed within the model threshold initially. Finally, scalar transport around an ellipsoidal vortex (almost a tilted spheroid) is investigated analytically and numerically. When a spheroidal vortex is embedded in an otherwise quiescent fluid, it rotates rigidly with a constant angular velocity. A fluid particle moves along a streamline in the coordinate system rotating with the spheroid. There are two saddles and heteroclinic orbits connecting them on the horizontal plane through the vortex center. The heteroclinic orbits change into homoclinic orbits on the horizontal plane slightly off center ( $z > 0$ ). The Melnikov functions computed along the heteroclinic and homoclinic orbits intersect zero transversely, suggesting the occurrence of chaotic mixing of fluid particles. In fact, numerically computed stroboscopic Poincaré plots scatter along the heteroclinic and homoclinic orbits even when the perturbations are very weak.

**JSP10/10P/B21-005**

**1530**

### A LAGRANGIAN VIEW OF VORTEX MERGER

Oscar U. VELASCO FUENTES (Departamento de Oceanografía Física, CICESE)

Two circular vortices of equal size and strength in an otherwise quiescent fluid may exhibit three types of behaviour depending on their relative position. When the intercentroid distance  $d$  is much larger than the vortex radius  $R$  ( $d/R > 3.45$ ), the vortices rotate about one another quasi-steadily while undergoing some deformation. When the distance is in the range  $3.3 < d/R < 3.45$  the vortices still rotate about one another, but they also approach and exchange mass. Finally, when the distance is smaller than the critical value  $d/R = 3.3$  the vortices merge into a single vortex. These regimes are reviewed here using ideas and methods from the theory of transport in dynamical systems. The Lagrangian flow geometry (i.e., the hyperbolic trajectories and their associated stable and unstable manifolds) is computed and analysed for initial conditions in the range  $3.2 < d/R < 3.5$ . It is observed that the regime transitions are associated with changes in the relative position of the stable manifolds with respect to each other and with respect to the vortices' edges. Finally, the results are contrasted with the conventional explanation for the regime transitions (namely, the vortex location with respect to a co-rotating streamfunction) which uses an Eulerian point of view.

**JSP10/10P/B21-006**

**1610**

### ON THE VERTICAL ALIGNMENT OF GEOPHYSICAL VORTICES IN STABLY STRATIFIED INVISCID LIQUID

Michael Thomas MONTGOMERY<sup>1</sup>, David A. SCHECTER<sup>2</sup>, Paul D. REASOR<sup>1</sup> (Dept. of Atmospheric Science, Colorado State University, <sup>2</sup>Dept. of Earth and Planetary Sciences, Harvard University)

Observations and numerical models demonstrate that a broad class of geophysical vortices freely evolve toward vertically aligned states. This intrinsic drive toward symmetry opposes destructive shearing by the environment and is believed an essential element in the robustness and emergence of coherent vortex structures. This talk presents new results on the vertical alignment and axisymmetrization of both weak (Rossby number much less than unity) and intense (Rossby number greater than unity) centrifugally-stable vortices in stably stratified inviscid fluid. For potential vorticity (PV) towers whose upper- and lower-layer PV cores overlap, the alignment dynamics can be represented accurately as the excitation and evolution of a three-dimensional "vortex Rossby wave" that evolves within the "slow-manifold" (balanced) subspace of the three-dimensional primitive equations. The wave, that is, the tilt, decays by two distinct pathways depending on the core Rossby number and the ratio of the horizontal vortex scale to the ambient Rossby deformation radius. Given these two parameters, the tilt decays either via sheared vortex Rossby waves, or an exponentially decaying vortex Rossby wave mode. Alignment in the latter case is controlled by the sign and magnitude of the radial PV gradient at a critical radius, where the fluid rotation is resonant with the mode. The decay rate of the tilt is shown to be sensitive to the form of the vortex. For the case of a "Rankine-with-skirt" vortex, the magnitude of the decay rate decreases (initially) with decreasing deformation radius. On the other hand, for the case of a "Gaussian" vortex, the magnitude of the decay rate increases with decreasing deformation radius. A discrete vortex Rossby wave can also resonate with an outward propagating inertia-buoyancy wave (Lighthill radiation), inducing BOTH to grow. At large Rossby numbers, this growth mechanism can be dynamically relevant. All balance models neglect inertia-buoyancy waves, and therefore ignore the possibility of a Rossby-inertia-buoyancy (RIB) instability. We show that a large radial potential vorticity gradient (of the proper sign) at the critical radius can suppress the RIB instability, and thereby preserve balanced flow, even at large Rossby number. The relationship of these results to the problem of robustness of tornado and hurricane vortices will be discussed.

**JSP10/10P/B21-007**

**1640**

### RESONANT ROSSBY WAVE TRIADS AND THE SWINGING SPRING

Peter LYNCH (Assistant Director, Met Eireann)

The wave solutions discovered by Rossby are of fundamental importance for atmospheric dynamics. The nonlinear interactions between these waves determine the primary characteristics of the energy spectrum. These interactions take place between triplets of waves known as resonant triads and, for small amplitude, they are described by the three-wave equations. These same equations also govern the dynamics of a simple mechanical system, the elastic pendulum or *swinging spring*. This equivalence allows us to deduce properties, not otherwise evident, of resonant triads from the behavior of the mechanical system. In particular, the characteristic stepwise precession of the swing-plane, so obvious from observation of the physical spring pendulum, is also found for the Rossby triads. This phenomenon has not been previously noted and is an example of the insight coming from the mathematical equivalence of the two systems. The implications of the precession on predictability of atmospheric motions are considered. The pattern of breakdown of unstable Rossby waves is very sensitive to unobservable details of the perturbations, making accurate prediction very difficult.

**JSP10/10P/B21-008**

**1700**

### SPIN-UP FROM REST IN A STRATIFIED FLUID

Jan-Bert FLOR<sup>1</sup>, John W.M. BUSH<sup>2</sup>, Marius UNGARISH<sup>3</sup> (<sup>1</sup>LEGI-CNRS, <sup>2</sup>Department of Mathematics, MIT, Cambridge MA 01239, USA, <sup>3</sup>Department of Computer Science, Technion, Haifa, Israel)

We present the results of an examination of spin-up from rest of a stratified fluid. A vertical cylindrical container of radius  $R$  and height  $2H$  containing fluid of viscosity  $\nu$  and characterized by a constant buoyancy frequency  $N$  is set impulsively to rotate about its symmetry axis with angular speed  $\Omega = f/2$ . The characteristic Ekman number  $E = \nu/\Omega R^2$  is small and the Schmidt number  $S = \nu/D_s$  (where  $D_s$  is the diffusivity of salt) is large. The initial stage of the spin-up is characterized by an axisymmetric circulation driven by nonlinear Ekman layers adjoining the horizontal boundaries. Fluid is drawn by the boundary layers from the stationary, stratified interior and transported into corner regions. It is shown that the corner regions are restricted to a height of approximately  $0.3R/f/N$  from the horizontal boundaries, beyond which the fluid remains unperturbed apart from that spun up by diffusion of momentum from the side-wall boundary. Two distinct regions thus emerge: rotating corner regions, and a quiescent stratified core. After a time  $1.3/(E^{1/2}N)$ , the corner regions cover the bulk of the horizontal boundaries and the boundary layer suction is suppressed. Our study provides a framework for understanding the subsequent evolution of the spin-up process, which may be characterized by axisymmetry-breaking instabilities of the stratified core (Flor, Ungarish and Bush, 2002, J. Fluid Mech. **472**). The subsequent evolution of the central vortex depends critically on  $N_f/f$ , with  $N_f$  the stratification in the core region. For  $N_f/f > 1$  and  $R > 1$ , the axisymmetry of the system is retained throughout the spin-up process: the central vortex attains a state of near solid body rotation by the diffusion of vorticity from the sidewalls. For  $N_f/f > 1$  and  $H/R \ll 1$ , the central vortex breaks up into a series of vertical vortices that enhance transfer of angular momentum from the boundaries and so expedite the spin-up process. For  $N_f/f < 1$ , the interface between the core and corner region is (mode two) unstable, leading to a simple tipping of the central stratified vortex. In a tall tank, the centerline of the central vortex is twisted from its vertical position, and the resulting instability gives rise to a stack of vortices.

**JSP10/10P/B21-009**

**1720**

### INVARIANT PROPERTIES OF BASIC SETS OF GOVERNING EQUATIONS OF ENVIRONMENTAL FLUID MECHANICS

Vasily G. BAYDULOV, Yuli D. CHASHECHKIN (Laboratory of Fluid Mechanics, Institute for Problems in Mechanics of the RAS)

A main goal of given study is to test a level of compatibility of different mathematical models that are widely used in investigations of environmental flows. As the basis the Navier-Stokes equations supplemented by the heat and mass transport together with an empirical equation of state are chosen. We compare sets of local symmetries of the basic and derivatives models using the continuous (Lie) groups theory and methods of symbolic calculations. To perform extended algebraic calculations symbolic system Maple has been adopted. We have investigated symmetry properties of a general set of multi-component stratified fluid governing equations and different well-known models: stationary ones, the Boussinesq approximation, 1D and 2D flows, elimination of diffusion, temperature transport and viscosity effects, the boundary layer model and different well-known models of turbulence. In general case we have performed detail investigation of the effects of algebraic equation of state on the symmetry properties of the set of governing equations. We found that the general set of governing equations is characterized by a set of symmetries, containing ten-parametric Galilean group of symmetry and infinite-dimensional sub-algebra of pressure shifts. Additional expansion groups can be found if the state equation is taken in a specific form. Diffusion impacts on invariant properties more essentially than viscosity. 1D transient and stationary problems are characterized by irreducible set of symmetries. One of specific generators corresponding to the expansion group of the heat conduction equation describes set of diffusion induced internal boundary currents producing sets of boundary layers on a moving body and singular interfaces inside the liquid. Analysis of symmetries in the expanded space of jets including all known non-dimensional parameters reveal the number of non-dimensional parameters completely describing stratified flows. Model of isotropic turbulence does not satisfy the Galilean principle of relativity. Some more sophisticated energy-dissipation models of turbulence have no the rotational symmetries. We also have applied given methods for solutions some concrete problems. We have analyzed formation for the flow past abrupt begin-ning of motion of a horizontal cylinder in a stratified liquid. We have constructed complete set of eigen-functions of 3D periodic motion including a regular part (internal waves) and a singular part (boundary layers on bounding surfaces and internal boundary layers in a fluid interior. We have defined conditions of superposing of non-linear periodic and lee (attached) waves from several independent sources and presented recommendation for introducing of generalizes variables and specific potentials to increase the stability of solutions with respect to errors and incompleteness of an initial data set. Results of laboratory experiments are used to illustrate main theoretical conclusions concerning structures of regular and singular components of motion in-side a stratified fluid.

**JSP10/10P/B21-010**

**1740**

### MEAN-FIELD HYDRODYNAMICS FOR TURBULENT FLOWS SUBJECTED ROTATION

Arakel S. PETROSYAN, Denis TSYGANKOV (Space Research Institute, Russian Academy of Sciences)

Many turbulent flows that must be understood are subjected to a rotation. The present study is concerned with Reynolds Averaged Navier-Stokes equations for rotating system with and without convection. There are two basic observations: limited application of the turbulent viscosity hypothesis and possibility for turbulent viscosity to become negative in rotating systems. Our prime interest here is to find nontrivial parameterizations of Reynolds stresses describing contribution of turbulence to the large-scale momentum flux. For this purpose we use statistical perturbation methods to analyze the way the basic flow is modified by a weak large-scale perturbation. It is apparent that Reynolds stresses, expanded in the gradient Taylor series, contain term directly proportional to the large-scale velocity as well as that proportional to the large-scale velocity gradient. First mentioned term is precisely that term which can lead to nontrivial large-scale dynamics, while the second one describes eddy-diffusive modification of molecular transport of momentum. Our main concern here is to derive analytic expressions for nontrivial terms as well as turbulent viscosity terms. The global breaking of mirror symmetry in turbulence is often considered as probable cause of nontrivial dynamics. We consider model homogeneous helical turbulence as an initial basic state in Reynolds stresses computations. It is well known, that any large-scale perturbation of the velocity field in homogeneous helical turbulent flow will only dissipate in non-rotating system since non-zero helicity density implies low energy cascade from large wave numbers to smaller one. Nevertheless, nontrivial dynamics of large-scale flows exists when turbulence in rotating system has been treated. There are quite a lot of ways of closing the equations. Using the first-order smoothing approximation we have investigated the large-scale flow interaction with small-scale turbulence in linear approximation for two cases: with and without convection. It has been found that non-helical component of the turbulent field and the presence of the rotation leads to the additional terms in the Reynolds stress tensor. These terms are proportional to the first spatial derivatives and may cause an additional wave-like transport of momentum. Helical component of basic turbulence leads to the phase velocity difference of such wave-like motions in direct and backward propagating directions. In the presence of convection, described in Boussinesque approximation, we found the possibility for decreasing turbulent viscosity value in comparison with the rotating system without convection.

Friday, July 11 AM

JSP10/11A/B21-001

0830

**DECAYING GRID TURBULENCE IN A ROTATING STRATIFIED FLUID**

Joel SOMMERIA, Olivier PRAUD (LEGI/Coriolis)

Rotating grid turbulence experiments have been carried out in stably stratified fluid at large Reynolds number (10000), using the "Coriolis" turntable in Grenoble. Under effects of rotation and stratification the flow degenerates into quasi horizontal motions. This regime is investigated using a scanning imaging velocimetry which provides time resolved velocity in a volume. The most obvious effect of rotation is the inhibition of the kinetic energy decay which is in agreement with the quasi geostrophic model which predicts an absence of direct energy cascade, like in two dimensional turbulence. In the regime of small Froude and Rossby numbers, the results show that the dynamics are non-dissipative and associated with a  $K_0^{-3}$  energy spectra and highly intermittent vertical vorticity field, involving intense vortices of both signs. For higher Rossby number, the results show fundamental differences with the quasi geostrophic model. A significant decay of kinetic energy which does not depend on stratification is indeed observed. Moreover, although both cyclones and anticyclones are initially produced, cyclones tend to dominate the flow.

JSP10/11A/B21-002

0900

**ENERGY DISSIPATION IN LARGE WAVENUMBER REGION OF QUASI-GEOSTROPHIC TURBULENCE**

Keita IGA (Research Institute for Applied Mechanics, Kyushu University)

Large scale motions in the atmosphere and in the oceans are well expressed using quasi-geostrophic systems. Simple one-layer quasi-geostrophic potential vorticity equation (also called Charney-Hasegawa-Mima equation as an equivalent) often describes the essential dynamics of such large scale motions. In turbulent motions governed by this quasi-geostrophic equation, the energy is transported upward to the small wavenumber region and thus coherent patterns are formed. The energy upward cascade is also observed in two-dimensional turbulence, but there are some quantitative differences such as the speed of the upward cascade. Dynamic scaling laws for quasi-geostrophic turbulence, which describes quantitatively this energy upward cascade, is developed by Watanabe et al. (1998) theoretically and by numerical simulations. However, in their theory, they evaluated a parameter necessary for the dynamic scaling law from the result of numerical calculation: a parameter which shows the total energy dissipation rate. In the quasi-geostrophic turbulence, most of the energy is transported to the small wavenumber region, but a small amount of energy is transported to the large wavenumber region owing to the small but finite dissipation. We estimated the energy dissipation rate based on the assumption that the total energy dissipation in this system is equal to the energy transported to the large wavenumber region. The shift of the energy spectrum to the small wavenumber region must be balanced with the energy transport to the large wavenumber region, and this relation enables us to evaluate the energy transported to the large wavenumber region from the wavenumber of the energy spectrum peak. This theoretical estimation complements the dynamic scaling laws of Watanabe et al. (1998): the parameter expressing the total energy dissipation which is left unknown and empirically determined in their study is theoretically derived. In numerical calculations with finite cut-off wavenumber, we use artificial hyperviscosity coefficients in order to avoid the pile-up of the cascaded energy near the cut-off wavenumber region. This estimation also suggests the means to determine the appropriate hyperviscosity coefficient used in numerical simulations. Considering that the artificial dissipation near the cut-off wavenumber region is a substitute of the energy which should have been transported beyond the cut-off wavenumber, we can determine the appropriate value of the hyperviscosity from the condition that the energy dissipated by the hyperviscosity should be the same as the energy cascaded to the large wavenumber region. In the numerical calculation by Watanabe et al. (1998), the energy spectrum has a too steep gradient in the large wavenumber region. The numerical calculation using the value suggested by the consideration here successfully derived the theoretically expected energy spectrum.

JSP10/11A/B21-003

0920

**KINETIC ENERGY SPECTRUM IN STRATIFIED TURBULENCE AND ITS APPLICATION TO THE ATMOSPHERIC MESOSCALES**

Yuji KITAMURA, Yoshihisa MATSUDA (Graduate School of Science, The University of Tokyo)

It is known from observations that the horizontal kinetic energy spectrum follows a  $k^{-5/3}$  power law in the mesoscale phenomena in the upper troposphere. Nastrom et al. (1984) found the  $k^{-5/3}$  power law in the scales less than about 500 km from the observation in the upper troposphere. From the aircraft observation, Cho et al. (1999) showed that this spectral slope

can be applied to atmospheric motion with the horizontal scales less than 100 km in the troposphere except the boundary layer. Lilly (1984) attempted to understand the energy spectrum in the mesoscales from inverse energy cascades in stratified turbulence. However the results from numerical simulations of stratified turbulence indicate that inverse energy cascades does not occur unless the Coriolis parameter  $f$  is extremely large (Herring and Metais; 1989, Metais et al., 1994). On the other hand, Vallis et al. (1997) reproduced the above spectral slope in the mesoscales with the regional model including water vapor and Koshykand Hamilton (1999) did with GFDL SKYHI GCM. These models include many physical processes so that it is difficult to understand their results as energy cascades in stratified turbulence. We conduct numerical experiments with a three dimensional nonhydrostatic model assuming the Boussinesq approximation in order to consider upscale and/or downscale energy cascades in stratified turbulence. The results obtained in these experiments are as follows. When the dynamical forcing function has a peak at the horizontal scale of 20 km, inverse energy cascading due to interactions between horizontal vortices is too weak to explain the spectral slope in the mesoscales, even if the amplitude of the forcing function and the stratification are strong. When the forcing is given at the domain size (400–800 km), the  $k^{-5/3}$  spectral slope are formed as the result of downscale energy cascades only if the forcing amplitude is sufficiently large. However, in this case the spectral amplitude is about two order larger than that obtained by the observational studies. For the weak forcing, the spectral slope tends to be steeper and this result is not improved by the smaller eddy viscosity. We also examine the Smagorinsky-Lilly parameterization and the 1.5 order TKE parameterization, which are well known as subgrid-scale turbulent parameterization. In both parameterizations, the kinetic energy at the grid scale is not sufficiently removed because of too weak eddy viscosity at this scale, while the energy spectrum in the scales larger than 20–30 km is close to that of the observations. We will also discuss details of energy cascade processes and better subgrid-scale parameterization.

JSP10/11A/B21-004

0940

**DYNAMICS OF THE SELF-SIMILAR SPECTRAL EVOLUTION OF QUASI-GEOSTROPHIC TURBULENCE ON AN F-PLANE AFFECTED BY HORIZONTAL DIVERGENCE**

Akira MASUDA (Dynamics Simulation Research Center, Research Institute for Applied Mechanics, Kyushu University)

An investigation is made on the self-similar spectral evolution of quasi-geostrophic (QG) turbulence on an  $f$ -plane affected by horizontal divergence, which is proportional to the squared inverse of the radius of deformation. To purify the effect of horizontal divergence we adopt the Charney-Hasegawa-Mima equation as the governing equation. First, freely decaying turbulence is examined as a first step. In case of vanishing horizontal divergence, Batchelor provided a well-known theory for self-similar spectral evolution of two-dimensional turbulence. One more parameter of horizontal divergence invalidates such a purely dimensional argument as by Batchelor. A similarity form is proposed here including the effect of horizontal divergence. The formula is reduced to that of Batchelor when there is no horizontal divergence. On the other hand it turns out to agree with the spectral evolution discussed later for strong horizontal divergence. Next, spectral forms in inertial ranges are studied based on the balance of terms in the vorticity equation. In this argument the power of the stream function or kinetic energy is preferred to that of total energy. In reality the kinetic energy spectrum in the inertial subrange is shown to be the same irrespective of the strength of horizontal divergence:  $k^{-5/3}$  for energy cascade and  $k^{-2}$  for enstrophy cascade with  $k$  being the wavenumber, just as in the ordinary two-dimensional turbulence without horizontal divergence. Finally self-similar spectral evolution is discussed in terms of the ordinary differential equations (ODEs) for the three variables of peak wavenumber, total energy and total enstrophy. The dynamics based on the ODEs gives quite a comprehensive and systematic explanation to the self-similar evolution of QG turbulence on an  $f$ -plane with and without horizontal divergence in various situations including the classical case of Batchelor. The method can be applied to both freely decaying and forced turbulence, which may suffer finite dissipation near the truncation wavenumber in numerical experiment. In order to examine the validity of the argument a numerical experiment was carried out, where the kinetic energy (not total energy) was kept constant by a rather artificial numerical adjustment for the case of strong horizontal divergence. Numerical experiment showed a good agreement with the prediction based on the dynamics that the spectral peak scale increases as a third power of time.

JSP10/11A/B21-005

1000

**NUMERICAL STUDY OF STRUCTURES AND SPECTRA FOR STABLY STRATIFIED TURBULENCE**Yoshi KIMURA<sup>1</sup>, Jackson R. HERRING<sup>2</sup> (<sup>1</sup>Graduate School of Mathematics, Nagoya University, <sup>2</sup>National Center for Atmospheric Research)

The structural and statistical aspects of stably stratified turbulence is studied by way of Direct Numerical Simulations (DNS) of the Navier-Stokes equations under the Boussinesq approximation. It is well-known that the structures generic to homogeneous isotropic turbulence are "vortex tubes" while "vortex pancakes" which are randomly scattered throughout the flow, are often observed for stably stratified turbulence. An issue here is whether vortex tubes are somehow part of the stably stratified flow or not. This problem is concerned with the universality of the production mechanism of small-scales in turbulence which is an essential assumption of most Large Eddy Simulations (LES) in meteorology. We shall report the results of DNS with  $512^3$  grid points for both decaying and randomly forced stratified turbulence. For the decaying case, it is observed that stratified turbulence leads to a near self-similar decay. It is also noticed that the decay rate of energy in large scales differ from the unstratified turbulence. For the forced case, two issues which are related with the aspect of energy transfer for stratified turbulence will be discussed; (1) a spectrum close to  $k^{-2}$ , steeper than  $k^{-5/3}$  for homogeneous isotropic turbulence, is observed, and (2) large scale horizontal layers are formed rather suddenly at a later stage of the flow development.

JSP10/11A/B21-006

Invited

1040

**UNBOUNDED ROTATING FLOWS WITH AND WITHOUT STABLE STRATIFICATION**

Claude J. CAMBON (LMFA, Ecole Centrale de Lyon)

A statistically homogeneous three-dimensional (3D) turbulent flow is considered in a rotating frame and possibly in a stably stratified medium. Both angular velocity and mean density gradient are in the vertical direction, with constant system vorticity and Brunt Väisälä frequency. In addition to various DNS in periodic boxes, a recent experimental study (Praud and Fincham) has been performed in a very large rotating tank, giving access to much larger Reynolds numbers. The structure of isotropic turbulence is deeply altered by dominant rotation, with emergence of columnar structures ('cigar' type), and with polarized sheets ('pancake' type) if stratification is dominant. The mechanisms responsible for this structuring are briefly reviewed here, and statistical theory/modelling is used, ranging from wave-turbulence theory to EDQNM (Eddy Damped Quasi Normal Markovian). In the presence of rapid rotation, without stratification, the flow consists of superimposed inertial

## INTER-ASSOCIATION

waves, which are weakly coupled through nonlinearity. Wave-turbulence theory is really relevant to explore a transition from 3D to 2D structure with the Rossby number being the small control parameter. By contrast, the well-known Proudman theorem only says that the slow motion is the 2D one, but cannot explain the 'nonlinear' 3D to 2D transition. Using the slow amplitudes of the eigenmodes of the linear operator as new dependent variables, an EDQNM technique is shown to be equivalent to an Eulerian wave-turbulence theory, at least in the limit of vanishing eddy damping. The energy transfer in Fourier space reduces to surface integrals along the surfaces of resonant triads. The spectral density of kinetic energy appears to be governed by a strongly anisotropic energy flux, with evolution (in term of a 'slow' time) tending to concentrate this energy towards horizontal wavevectors. A complete two-dimensionalisation, however, cannot be achieved, but the trend is quantified in a reliable way. In the presence of stable stratification, things are different. The wave-turbulence theory is not valid in general, since the eigenmodes decomposition includes a non-wavy mode: this is the part of the toroidal velocity field which corresponds to the quasi-geostrophic mode in geophysics. Except for pure poloidal turbulence, nonlinearity does not vanish with the Froude number, and resonant inertia-gravity waves are only marginally involved. Without rotation, the initially 3D flow is shown to evolve towards the slow mode (zero frequency) of gravity waves, but this slow mode (Fourier mode related to vertical wavevector) has nothing to do with the 2D mode, and may be considered as 1D instead. If the flow is initially quasi-2D or forced in a quasi-2D manner, a good candidate for explaining a partial transition 2D-1D is the zig-zag instability, evidenced at length by Billand and Chomaz. An alternative scenario for the transition 3D-1D is proposed here, based on consistent EDQNM/DNS results, with no need for organized vertical vortices in the initial data.

**JSP10/11A/B21-007**

**1110**

### ON INSTABILITIES AND TURBULENCE IN STRONGLY STRATIFIED FLOWS

James J. RILEY<sup>1</sup>, Kraig B. WINTERS<sup>2</sup>, Stephen M. DEBRUYNKOPS<sup>3</sup> (<sup>1</sup>University of Washington, <sup>2</sup>Scripps Institution of Oceanography, <sup>3</sup>University of Massachusetts)

Recent laboratory experiments have suggested that turbulent mixing events in a stably-stratified fluid, unless provided with some external forcing mechanism, inevitably decay to a low Froude number regime in which the stratification effects dominate. For example, turbulent wakes evolve into remarkably stable, quasi-horizontal vortex patches of alternating sign in this regime. The Reynolds number in the low Froude number regime in the experiments is rather low, however, raising the question of whether the results scale up to geophysical scales. In this presentation we will report on high resolution direct numerical simulations and analytical scaling arguments which have been used to understand the dynamics of turbulence in the low Froude number regime, and to estimate the Reynolds number above which laboratory experiments must be conducted in order for the results to scale up to geophysical scales. It is found that the simulated quasi-horizontal flows evolve to a state with high vertical shearing of the horizontal velocity, leading to locally low Richardson numbers and susceptibility to shear instabilities. This occurs even though the nominal Richardson number is greater than order one. Kelvin-Helmholtz instabilities were observed to be one pathway to turbulence in the simulated flows. It is estimated that instabilities and turbulence in these flows will occur if the product of the local Reynolds number times the local Froude number squared is greater than order 1, where the local Reynolds and Froude numbers are based upon the horizontal motions.

**JSP10/11A/B21-008**

**1130**

### A SPECTRAL MODEL FOR PROCESS STUDIES OF DENSITY-STRATIFIED, ROTATING FLOWS

Kraig B. WINTERS, Jen A. MACKINNON, Bren MILLS (Scripps Institution of Oceanography, University of California, San Diego)

The features and use of a spectrally based numerical model designed to provide approximate solutions to the Navier-Stokes equations for density-stratified fluids in a rotating reference frame will be presented. The code is freely available and is intended for use as a tool for process oriented simulations of stratified fluid flow, in particular for nonlinear interactions between internal gravity waves and transitional processes and instabilities resulting in disordered, three-dimensional motions. For our purposes here, we refer to this latter class of flows as turbulent. The algorithm is designed to be run on distributed memory multiprocessor computers using a data-parallel programming paradigm. Within the practical limits of memory and speed on the various platforms, the model can be run on machines ranging from Macintosh laptop computers, to workstation clusters, to large-scale community resources such as the Cray T3E. The code itself is portable and easy to configure for real problems via simple user-defined functions for initial conditions and time dependent forcing. Sub-models include a spectrally based Lagrangian particle tracker and auxiliary passive tracers. In this talk I will present some of the numerical techniques underlying the model, show results illustrating the types of problems that can be addressed using the model and demonstrate the ease of configuration for a study of stability of quasi-horizontal vortex motions.

**JSP10/11A/B21-009**

**1150**

### WAKES IN STRATIFIED FLUIDS: PROGRESS DURING THE LAST TWENTY YEARS

Alan BRANDT (Johns Hopkins University Applied Physics Laboratory)

Oceanic turbulent wakes can arise in the lee of seamounts and other topographic discontinuities, at the shelf-break, and from the motion of ships, submarines and mobile ocean creatures, the latter ranging in size from plankton to whales. As such, stratified wakes can contribute to ocean mixing affecting local stratification, the distribution of nutrients, dissolved oxygen, and CO<sub>2</sub>, thus affecting bio-feeding patterns, primary productivity, and global ocean balances. Wakes in stratified fluids embody many of the fundamental processes inherent to stratified flow dynamics that are of interest to this symposium, including: stratified mixing and collapse, internal wave generation, and the appearance of coherent, late-wake vertical vorticity. While all of these fundamental processes were known over twenty years ago, the review by Lin and Pao (Ann. Rev. Fluid Mech. 1979, 11: 317-38), focused on wake turbulence and collapse, giving only passing reference to late-wake eddies. The presence of the wake-generated internal wavefield was not mentioned. Since that time, laboratory and numerical studies have considerably furthered our understanding of these processes. The processes governing the evolution of stratified wakes have been found to be a function of the evolution time scale, which is related to the inherent period of oscillation of the ambient water column, the Brunt-Väisälä frequency. At early times the wake does not 'feel' the stratification and thus the wake behaves as though stratification were not present. At intermediate times there exists a 'non-equilibrium regime' where the wake collapses and potential energy is converted into kinetic energy. At late times the stratification causes a cessation of vertical motion and a quasi-two dimensional, horizontal motion persists. While wake turbulence results from the turbulent boundary layer on the body, the sources of the internal wavefield are more diverse. Internal waves are generated by displacement of the ambient fluid by the body itself, the overall collapse of the wake, and small-scale turbulent fluctuations within the wake. This review will discuss the processes extant in each of these wake flow regimes,

covering advances during the past twenty years, including some recent, hitherto unpublished findings. Recent results include studies on the coupling of the wake flows to the internal wave field at low Froude numbers, where this coupling is quite substantial, and on the nature of the three-dimensional density distributions in the early wake, which pose the initial conditions that drive the intermediate and late wake dynamics (and provide appropriate initial conditions for numerical simulations). Outstanding issues regarding our understanding of the evolution of stratified wakes will also be discussed.

**JSP10/11A/B21-010**

**1210**

### CYCLONE-ANTICYCLONE ASYMMETRY OF GEOPHYSICAL VON KARMAN STREET

Alexandre STEGNER<sup>1</sup>, Gaele PERRET<sup>1</sup>, Marie FARGE<sup>1</sup>, Thierry PICHON<sup>2</sup> (<sup>1</sup>LMD, IPSL Ecole Normale Supérieure, Paris., <sup>2</sup>UME, ENSTA, Palaiseau, France.)

Unlike the classical bi-dimensional Von-Karman street, geophysical vortex streets are affected by the earth rotation and the vertical stratification. We performed laboratory experiments and numerical simulations to study the specific dynamics of Von-Karman street in a rotating shallow-water layer from small (150) to intermediate (1000) Reynolds number. It is shown that ageostrophic effects (finite Rossby number) or large-scale effects (small Burger number) both induce an asymmetric vortex street. These effects occur in an oceanic context especially when the island size becomes larger than the local deformation radius. On one hand, ageostrophic effects lead to elliptical cyclones which could enhance the mixing in the near wake behind the island. On the other hand, large-scale effects, induce a long tail behind the obstacle where no vortices emerge. The vortex shedding occurs far away from the island, leading to an asymmetric vortex street with triangular cyclones.

Friday, July 11 PM

**JSP10/11P/B21-001**

**1420**

### VARIABILITY OF MIXING EFFICIENCY IN STRATIFIED SHEAR FLOWS

Colm-cille P. CAULFIELD<sup>1</sup>, W. Richard PELTIER<sup>2</sup> (<sup>1</sup>Department of Mechanical and Aerospace Engineering, University of California, San Diego, <sup>2</sup>Department of Physics, University of Toronto)

Flows where both the velocity and density vary with height (i.e. stably stratified shear flows) are ubiquitous in nature. Of crucial interest to appropriate description of the redistribution of heat, momentum and chemical species within such flows is a detailed understanding both of the fundamental processes that trigger transition to turbulence and also the mixing characteristics of the ensuing turbulence. Significant progress towards addressing this problem has been made through the relatively recent advent of adequately resolved three-dimensional simulations. When combined with innovative theoretical, experimental, and observational results, a detailed picture is beginning to emerge of the qualitative and quantitative aspects of the time-dependent irreversible mixing associated with small-scale disordered motion within such flows. Of particular importance is the efficiency of the mixing, i.e. the proportion of the kinetic energy that is lost by the underlying shear flow that leads to irreversible increases in the potential energy of the system. In this talk, we will review the characteristics of mixing within a range of stratified shear flows. We will focus on two important aspects. Firstly, we will analyze the time-dependence of the mixing, drawing a clear distinction between mixing associated with the coherent instabilities that develop within the flow and the (more important) later mixing associated with small-scale disorder after flow transition. Secondly, we will discuss the dependence of mixing on the bulk flow parameters in the parameterization of stratified mixing events. As we demonstrate, controlling parameters include flow Reynolds number, bulk Richardson number, and the particular structure of the velocity and density profiles. Since we show evidence for the non-monotonic dependence of the mixing efficiency on overall stratification, it appears that the generic end-state for a stratified shear flow has a layered density profile, with relatively thin regions of strong density gradient separating deeper well-mixed layers with weak density gradient.

**JSP10/11P/B21-002**

**1450**

### HIGH REYNOLDS NUMBER LABORATORY MOUNTAIN-WAVE BREAKING

Olivier EIFF, Frederic HUTEAU (IMFT / Météo-France)

Mountain-wave breaking was studied in the large linear salt-stratified towing tank of Météo-France with a Gaussian-shaped quasi-two-dimensional obstacle, attaining Reynolds numbers of about 10<sup>4</sup>. To investigate the large-scale dynamics and turbulence generated by the wave-breaking, simultaneous velocity measurements were performed in two orthogonal planes via digital particle image velocimetry. The results have been compared to previous laboratory and direct numerical simulations obtained at low Reynolds numbers (10<sup>2</sup>) but otherwise similar conditions. The comparison reveals a dynamically similar development leading to wave-breaking for a flow started from rest. In particular, a two-dimensional roll-up of the steeping wave is observed which is rapidly followed by a three-dimensional Rayleigh Taylor-like convective instability. This instability results in large-scale ring-like vortical structures encompassing the wave-breaking zone, as has been found at low Reynolds numbers. Preliminary estimates of the turbulence statistics in the wave-breaking region have also been evaluated.

**JSP10/11P/B21-003**

**1510**

### WAVE-VORTEX INTERACTIONS IN A ROTATING STRATIFIED FLUID AND TRANSPORT THROUGH A DYNAMICAL BARRIER

Frédéric Y. MOULIN<sup>1</sup>, Jan-Bert FLOR<sup>2</sup> (<sup>1</sup>Dynamic Marine Meteorology, Department of Physical Oceanography, Ocean Research Institute, Tokyo University, JAPAN, <sup>2</sup>THEO team, Laboratory for Geophysical and Industrial Flows (L.E.G.I.-CNRS), BP 53, 38041 Grenoble Cedex 09, FRANCE)

Eddies of vortices are examples of dynamical barriers, and prevent fluid captured inside the vortex from mixing with the ambient. The existence of a cross-barrier transport material is relevant to large-scale geophysical flows, in which vortices are redundantly present. Breaking internal waves at the vortex edge can enhance such a transport. We have experimentally investigated wave-vortex interactions in a rotating stratified fluid, and address questions about wave induced mixing in the vortex and possible wave-vortex energy transfer. We consider the interaction of planar waves with baroclinic vortices, continuously forced by a small rotating disk, and with freely evolving barotropic vortices initially generated by an elongated sink. Only cyclonic vortices are considered. The wave pattern observed in the experiments is well captured by numerical simulations of ray tracing, based on WKBJ theory. Waves interacting with a baroclinic vortex are trapped along inclined critical layers, where their wavelength decreases towards zero due to vertical shear without triggering wave breaking. Trapped waves are wrapped around the vortex centre and lead in some cases to a spiral-like pattern in the velocity field. Waves propagating against a barotropic vortex are trapped along almost vertical critical layers, leading to wave breaking in case the viscous damping time-scale is long compared to the typical time-scale over which the wavelength

decreases. A critical Reynolds number for wave breaking is introduced, based on these two competing time-scales. In the experiments with barotropic vortices, the wave breaking is due to a local inversion of the density field, which drives a buoyancy induced instability, and leads eventually to a deposit of negative azimuthal momentum in the outer part of the vortex. Meanwhile, mixing is driven by two distinct processes: vortex streamlines are perturbed by periodic waves leading to bands where chaotic mixing occurs on a large time scale; wave breaking leads to turbulent patches of which the impact depends on the amount of energy provided by the breaking waves.

JSP10/11P/B21-004

1530

#### A LABORATORY STUDY OF VORTEX-INDUCED MIXING IN THE FRONTAL REGION OF BUOYANT SURFACE PLUMES USING PARTICLE-TRACKING METHODS

Thomas A. MCCLIMANS<sup>1</sup>, Walman HUTAHAEAN<sup>2</sup>, Oivind A. ARNTSEN<sup>3</sup> (<sup>1</sup>SINTEF Fisheries and Aquaculture, Trondheim, Norway, <sup>2</sup>(1) Indonesian Institute of Sciences, Research and Development Centre for Oceanology (LIPI-P3O), Ancol, Jakarta, Indonesia, <sup>3</sup>(2) Norwegian University of Science and Technology, Department of Civil and Transport Engineering, Trondheim, Norway)

Examples of buoyant plumes entering a large basin include the Indonesian throughflow in the Banda Sea, rivers flowing into bays and fjords and fjord water flowing into a coastal current. Mixing between the inflowing and ambient waters occurs along fronts between the masses. Elsewhere, energy from wind and tides often dominate the mixing and homogenizing of water masses. In larger quiescent regions, double-diffusion can also be important. Near the fronts, both buoyancy and rotation govern the type of processes that contribute to diapycnal mixing. The processes include Kelvin-Helmholtz instabilities and frontal instabilities that form eddies and sometimes intense frontal tornadoes. These latter processes have been studied in the 5-m diameter Coriolis basin at SINTEF/NTNU in Trondheim. Inflow of buoyant water from a strait to a wide basin was simulated at a Froude number near 1 and Rossby numbers from 1 to infinity. Particle tracking methods used to measure the flow fields are photogrammetry to obtain three-dimensional Lagrangian trajectories and particle image velocimetry (PIV) to obtain horizontal divergence and vertical vorticity. This combination allows us to answer questions of the nature of the plume circulation and mixing processes. Internal wave motions in the plume are seen in the photogrammetry and frontal tornadoes penetrating in the lower layer are revealed by the PIV. The analysis of these results for computing the dependency of entrainment and mixing on vortices is attempted.

JSP10/11P/B21-005

1610

#### LATERAL STIRRING BY THE RELAXATION OF DIAPYCNAL MIXING EVENTS

Marie-Pascale G. LELONG<sup>1</sup>, Miles A. SUNDERMEYER<sup>2</sup> (<sup>1</sup>NorthWest Research Associates, <sup>2</sup>School for Marine Science and Technology, University of Massachusetts Dartmouth)

Analysis of a series of tracer-release experiments conducted during the late summer stratification over the New England continental shelf has shown that the observed isopycnal dispersion cannot be explained by existing models of lateral dispersion (Sundermeyer, 1998; Sundermeyer and Ledwell, 2001). Similar dispersion behavior was also found during the North Atlantic Tracer Release Experiment in the pycnocline of the open ocean (Sundermeyer and Price, 1998). Using a 3d numerical model (developed by K. Winters) for the Boussinesq equations coupled with an advection/diffusion equation for a passive dye tracer, we performed numerical simulations of lateral dispersion. The objective of our study was to test the conjecture that observed rates of lateral dispersion can be explained by the presence of vortical motions created through the relaxation of diapycnal mixing events. The rates of vertical and lateral dispersion and their dependence on ambient stratification, and vertical and horizontal scales of diapycnal mixing events were investigated. Our results indicate that lateral dispersion caused by vortical modes is more than an order of magnitude larger than predicted theoretically by Sundermeyer and Ledwell (2003), can readily account for the dispersion on scales of 1-10 km observed during the Coastal Mixing and Optics (CMO) experiment and may be significant in other regions of the ocean as well.

JSP10/11P/B21-006

1640

#### INTERACTION OF INERTIA-GRAVITY WAVES WITH A BAROCLINIC SHEAR FLOW

Chantal STAQUET<sup>1</sup>, Neil R. EDWARDS<sup>2</sup> (<sup>1</sup>LEGI, University of Grenoble, France, <sup>2</sup>Climate and Environmental Physics, University of Bern, Switzerland)

The interaction of inertia-gravity waves (which are internal gravity waves modified by rotation) with a horizontal mean flow in a stably stratified fluid has received much attention when the mean flow is vertically sheared ( $U(z)$ ). When the mean flow is horizontally sheared ( $U(y)$ ), thus modelling the edge of an atmospheric vortex or an oceanic current, the problem amounts to the interaction with a dynamical barrier. The interaction process is addressed here when the horizontal mean flow also displays a vertical dependence ( $U(y,z)$ ). WKB theory has been used as a preliminary step to analyse the problem, for a simple flow configuration: an inertia-gravity packet confined along the  $y$  and  $z$  directions propagates into a horizontal shear layer with a vertical dependence. Linear and fully nonlinear direct numerical simulations of the three-dimensional Boussinesq equations have also been conducted. Results concerning the wave-mean flow interactions will be presented for this hierarchy of models, along with the resulting transport properties across the barrier, if any.

JSP10/11P/B21-007

1700

#### PERIODIC MOTIONS PRODUCED BY CIRCULAR DISK PERFORMING TORSION OSCILLATIONS AND SUPERPOSED UNIFORM ROTATION IN A CONTINUOUSLY STRATIFIED LIQUID

Yuli Dmitrievich CHASHECHKIN (Laboratory of Fluid Mechanics, Institute for Problems in Mechanics of the RAS)

Pattern of flow around a horizontal or sloping circular disc performing periodic torsion oscillations with or without superposed uniform rotation with a permanent angular velocity in exponentially stratified brine is visualised by a schlieren instrument. Parameters of internal waves are measured by a 'single electrode' conductivity probe. The probes are statically and dynamically calibrated before each experiment. A set of boundary layers forming on upper and lower sides of a horizontal disk performing harmonic oscillations is observed. Outer edges of boundary layers contact with two monotonically growing circular rotating rings. When direction of the disc rotation is changed the rings are displaced by the new growing pair of rings and are separated from the disc. Separated rings are collapsed symmetrically under the action of a buoyancy forces. They lose their symmetry and tend to go uniformly to the central plane of the source. Their lower parts arise and upper parts sink producing set of long-loving closed structures. Both horizontal and sloping discs performing pure torsion oscillations generate periodic internal waves propagating along the wave cone. The angle the wave cone depends on frequency of periodic torsion oscillations. Experiments are performed in a wide range of the problem parameters (buoyancy period, diameter and the

angle of the disc slope to horizontal, circular velocities of permanent and periodic components of rotation) corresponding to laminar, transient and non-regular regimes. The system consisting from the disc and surrounding disturbances generates regular internal waves even if the complex irregular fluid motion is observed near the disc. The frequency of waves is larger in two times exactly than the frequency of periodic torsion oscillations. With increasing of angular velocity of superposed permanent rotation the waves with the main frequency of the disc torsion oscillations become more pronounced. For interpretation of experiments the non-linear problem of internal wave generation by the periodic boundary layer on the oscillating horizontal disc is solved analytically. Received expressions describe dependence of the internal wave beams shapes, value of the waves amplitude and their spatial attenuation as a function of the buoyancy frequency, the fluid viscosity, size of the disc and parameters of its motion. In a wide range of parameters calculations are in a good agreement with experimental data without any fitting factor. Diverges between theory and experiment with a large value of angular velocity is presented and discussed. The data can be used for testing of analytical and numerical models of boundary layers, vortices and 3D internal waves including problems of their generation and non-linear interaction.

JSP10/11P/B21-008

1720

#### TAYLOR-COUETTE FLOW IN A TWO-FLUID SYSTEM: INSTABILITIES AND MIXING

Evgueni V. ERMANYUK<sup>1</sup>, Jan-Bert FLOR<sup>2</sup>, Beatrice JANIAUD<sup>3</sup> (<sup>1</sup>Lavrentyev Institute of Hydrodynamics, Novosibirsk, Russia, <sup>2</sup>Laboratoire des Ecoulements Geophysiques et Industriels, Grenoble)

Mixing in a density stratified fluid plays important role in numerous geophysical and engineering applications, being responsible for the transport of heat, nutrients and pollutants in ocean and atmosphere, as well as in various technical devices. In many cases the fluid flow may have a large vorticity component aligned with the main direction of the flow (a natural example of such a flow in the Ocean is known as Langmuir circulation). This report presents the experimental results on entrainment, mixing and instabilities in a particular case of non-isotropic turbulent flow, namely, a stratified Taylor-Couette flow in a two-fluid system, with the upper layer of pure water and the lower layer of salt solution in water. The fluid flow is driven by the rotation of the inner cylinder, with the outer cylinder held fixed. As the rotation rate of the inner cylinder increases, the flow in the smooth pycnocline between the upper and lower fluid layers undergoes the transition from wave regime (with waves propagating in vertical direction from the middle of the pycnocline toward its upper and lower boundaries) to the regime of stratified Taylor vortices. This transition is accompanied by the abrupt increase of the characteristic frequency of the time-dependent flow parameters measured at fixed locations. Vortical motion leads to the formation of fine multi-layer structure (with multiple clearly visible interfaces) inside the pycnocline. Experiments on mixing in the two-fluid Taylor-Couette flow were focussed on the case of large Reynolds numbers. At sufficiently high velocity of rotation the erosion of the initial density profile is extremely effective, leading to formation of a single sharp interface between the fluid layers. The resulting two-fluid system is ultimately destroyed by entrainment of salt across the density interface at the time-scale of several hours. Since the initial (two-fluid system) and final (homogeneous fluid) stages of the mixing process are well-defined, it is possible to estimate the overall mixing efficiency characterized by the flux Richardson number. The estimated values of the flux Richardson number are quite low (of order 0.01). Experimental data suggests that in the studied range of parameters the flux Richardson number is proportional to the Reynolds number.

JSP10/11P/B21-009

1740

#### INTERNAL WAVE GENERATION FROM A TURBULENT LAYER

Kathleen B. DOHAN, Bruce R. SUTHERLAND (Department of Mathematical and Statistical Sciences, University of Alberta)

High turbulent dissipation rates are observed in the ocean interior over mid-ocean ridges and are most likely attributed to breaking internal waves generated by tidal flows over the topography. The turbulence created by the rubbing of tidal currents over the rough topography may be an additional internal wave source, and may contribute to the high dissipation rates. We report on laboratory experiments that examine the properties of the internal wave field excited from an overlying oscillating grid-generated turbulent region. In the first of two non-intrusive visualization methods, dye lines are used to mark the vertical motions of isopycnal layers. The dye lines highlight large tank-scale wave modes which are generated from a large-scale circulation that develops in the turbulent region. The amplitudes of the isopycnal lines,  $A$ , vary with buoyancy frequency,  $N$ , as  $A \sim N^{-1.5}$ . The second visualization method, "synthetic schlieren," measures the entire wave field and allows us to isolate the properties of the strongest eddy-scale waves that propagate from the base of the turbulent layer. These waves have a narrow range of frequencies and vertical wavenumbers. The angles of wave propagation from the vertical for the eddy-scale waves lie in the range  $\Theta = 42-55$  degrees. These waves are of large amplitude with vertical displacements from 2%-4% of their horizontal wavelength and follow a relation  $A \sim N^{-1.8}$ . We discuss a continuation of this investigation into wave-turbulence interaction through numerical simulations.

JSP11

Monday, July 7 - Tuesday, July 8

#### GEOPHYSICAL RISK AND VULNERABILITY: THE POPULATION-HAZARD INTERACTION (IAPSO, IAGA, IAHS, IAMAS, IASPEI, IAVCEI)

Location: Site A, Room 10

Monday, July 7 AM

Presiding Chair: R. Singh

JSP11/07A/A10-001

Invited

0900

#### GEOPHYSICAL HAZARD AND HUMAN VULNERABILITY

Tom BEER (CSIRO Environmental Risk Network)

Earthquakes, volcanic eruptions, landslides, floods, droughts, tsunamis, storm surges, wildfires, tropical cyclones, tornadoes and extreme space weather events become major societal risks when they impinge on vulnerable populations. The growth in world population, its urbanization, and the possibility of climate change and global climate change exacerbate the vulnerability. Three factors that influence vulnerability are examined. Connectivity, susceptibility and resilience. We examine the role of these three factors for episodic disasters, such as those listed above, as well as for chronic hazards, such as air

## INTER-ASSOCIATION

pollution. The IUGG Commission on Geophysical Risk and Sustainability intends to establish a web encyclopedia of geophysical risks and hazards to document the population-hazard interaction.

**JSP11/07A/A10-002**

**0930**

### **DRASTIC; A SYSTEMATIC APPROACH FOR GROUNDWATER VULNERABILITY MAPPING**

Sanjeev KUMAR<sup>1</sup>, Shakeel AHMED<sup>1</sup>, Shikha RAJPUT<sup>1</sup> (I.F.C.G.R., NATIONAL GEOPHYSICAL RESEARCH INSTITUTE, KURUKSHETRA UNIVERSITY, INDIA)

The aim of this paper is to present a study on DRASTIC groundwater pollution vulnerability assessment. Aquifer vulnerability mapping is the acquisition and accumulation of aquifer attribute spatial data, placing the spatial data into a database, and using the database in a Geographic Information System (GIS) to show where an aquifer is at risk to pollution. GIS is the dynamic tool for study hydrologic setting and various parameters, which influence the groundwater vulnerability i.e., drastic parameters. The study area is located in Haridwar district, Uttaranchal, India. DRASTIC is a methodology for identifying vulnerability to groundwater pollution. It uses seven parameters, which are a combination of geologic, hydrologic, geomorphologic and meteorological factors, to relate an aquifer to the sources of its water and the constituents within that water. The parameters (Depth to water, annual Recharge, Aquifer media, Soil media, Topography, vadose zone Impact, and hydraulic Conductivity) are weighted according to their relative importance in determining the ability of a pollutant to reach an aquifer. The parameters are used to produce DRASTIC index numbers from which maps are constructed. The relative ranking scheme uses a combination of weights and rating to produce a numeric value called the DRASTIC index, which helps to prioritize areas with respect to pollution potential. GIS, due to its capabilities in terms of management, analysis, and manipulation of spatial data can be efficiently be used for generation of vulnerability maps for the study area. The vulnerability map of study area indicates that different parts of the area are susceptible to ground water pollution to different degrees i.e. highly susceptible and least susceptible. The pollution risk to the study area drinking water system will increase as a result of urban sprawl. Thus, it is prudent to protect the drinking water system by determining aquifer pollution risk through mapping aquifer vulnerability prior to urban sprawl. The Drastic ranking scheme can then be applied to enlighten layman for valid comparative evaluation with acceptable results.

**JSP11/07A/A10-003**

**1000**

### **NONLINEAR GROWTH OF CUMULATIVE LOSSES FROM DISASTERS IS COMPATIBLE WITH THE CONCEPTION OF SUSTAINABLE DEVELOPMENT OF SOCIETY**

Mikhail V. RODKIN, Vladilen F. PISARENKO (Geophysical Centre of the Russian Academy of Sci.)

It was noticed that the numbers of victims from natural disasters (earthquakes, floods, hurricanes etc.) as well as losses from disasters have a tendency to a non-linear increase with time. This effect is commonly related to the rate of population growth, to spreading of potentially dangerous technologies and to environment degradation. Thus, the process is assumed to be non-stationary which evidently interferes with the idea of the sustainable development of society. However, the alternative model of this effect can be suggested. We have shown that the non-linear growth of cumulative losses from earthquakes and floods is connected with the "heavy tail" in the loss distribution rather than with a change in distribution or occurrence rate of disasters, the latter being of minor importance. This effect occurs in the cases when distribution function  $F(x)$  of losses has a "heavy tail". In such cases it can be described satisfactorily by the Pareto distribution:  $F(x) = 1 - (a/x)^b$ , where  $b > 1$ . This distribution law is often used for modelling both natural and man-made disaster data. For the Pareto law the cumulative sum of losses increases with time as  $a$ , where  $a = 1/b > 1$ . In this case, the process is fully stationary, and the tendency to the non-linear growth is caused by an increase of probability of realisation of a huge disaster with time. The regime of non-linear increase of losses should saturate at some time moment because of practical limitation of possible loss size. Methods of evaluation of saturation parameters are presented and obtained results are discussed in connection with the social and economic situation in different regions. Besides, it was shown that after proper normalisation by size of the population and by per capita income the losses have a tendency to decrease with the level of social and economic development. Thus, in contrast with the wide-spread opinion, the regime of losses from natural disasters is compatible with conception of the sustainable development of society, moreover, it can be considered as an example of realisation of this conception.

**JSP11/07A/A10-005**

**1050**

### **IMPACT OF TRAFFIC ON THE AIR QUALITY OF THE CITY OF BANGKOK AND ITS APPLICATION TO CLIMATE CHANGE IMPACT ASSESSMENT IN THAILAND**

Suwannee ADSAVAKULCHAI (King Mongkut's University of Technology Thonburi)

The main atmospheric pollutants in Bangkok are total suspended particles (TSP), particle matter smaller than 10 microns (PM-10), carbon monoxide (CO), ground-level ozone (O<sub>3</sub>), nitrogen oxides (NO<sub>x</sub>) and sulphur oxides (SO<sub>x</sub>)-which contribute as greenhouse gases to global warming. Air pollution in Bangkok results from a combination of transport (diesel fuel) and industrial sources. SO<sub>2</sub> originates primarily from industrial processes. NO<sub>x</sub> and CO originate primarily from vehicles. TSP pollution is caused in large part by street dust blown from unpaved roads, open lands and eroded hillsides surrounding the city. Diesel buses and industrial sources also contribute significantly to PM-10 emissions. Conventional urban air pollutants are considered the most important problem. In addition, there is atmospheric pollution with toxic substances, such as hydrocarbons. This study contains the application of simple method for estimation of urban background pollution and the Street Pollution. Furthermore, a GIS-based is a model for automatic mapping of street pollution levels in an entire urban area. This method of city mapping is a powerful tool to investigate possible effects of street configuration on pollution concentrations in a city.

**JSP11/07A/A10-006**

**1110**

### **CERES-WHEAT MODEL APPLICATION UNDER CLIMATE CHANGE CONDITIONS OVER I. R. OF IRAN**

Sohailla JAVANMARD, Ali KIANI, Javad BODAGHJAMALI (Climatological Research Institute (CRI), I. R. of Iran Meteorological Organization (IRIMO), P. O. Box 91735-491, Mashhad, Iran)

About 64 percent of the warming effect due to greenhouse gas increase during the last 200 years, is caused by carbon dioxide. The global climate change will affect all economic sectors to some degree, but the agricultural sector is perhaps the most sensitive and vulnerable. The impact of climate variability on agricultural production is important at local and regional, as well as global scales. In this research, the CERES-Wheat v.3.5 model after

calibration was used to determine the vulnerability of current agricultural management in Mashhad city climatic conditions. In order to predict of climate change due to doubling carbon dioxide concentration on two wheat cultivars, Alamout and Alvand, NASA-GIS model was used. The results of the modeling showed that grain yield are increased by 7.5 and 11.7 percent, respectively for Alamout and Alvand cultivars.

**JSP11/07A/A10-007**

**Invited**

**1130**

### **GEOMAGNETIC HAZARD RESEARCH IN CANADA**

Lawrence Richard NEWITT, Larisa TRICHTCHENKO, David H. BOTELER (Natural Resources Canada, Geomagnetic Laboratory)

Features of the Earth's natural electromagnetic environment have many practical applications, from navigation to HF radio communication. However, the same electromagnetic environment can also have negative consequences. Activities in near-Earth space, such as satellite broadcasting, Earth observation, GPS, and the International Space Station are vulnerable to sudden changes in the geomagnetic field and in the radiation environment caused by space weather events. Building long conducting networks such as power lines, pipelines, or telephone cables on the surface of the Earth changes the electromagnetic environment. Because of significant inductive coupling to the geomagnetic field, these networks became vulnerable to variations of magnetic field such as those that occur during geomagnetic storms. In extreme cases the disruptions in distribution of the electric energy, communications or unexpected degrading of the pipeline can lead to conditions hazardous to people. Effects on these systems are greater at higher latitudes where geomagnetic disturbances are especially severe. Canada, which is bisected by the auroral zone, is particularly vulnerable, which prompted Natural Resources Canada to begin research on geomagnetic hazards more than 25 years ago. Research has been directed into three areas: forecasting of geomagnetic activity; determining the geomagnetic climate in different regions of the country; and mitigating the effects of geomagnetic activity on power lines and pipelines by understanding the underlying physical processes.

**JSP11/07A/A10-008**

**1200**

### **DEGRADATION OF QUIET MAGNETIC ACTIVITY AND ITS IMPACT ON HUMAN CONDUCTIVITY**

Tamara GULYAEVA (Institute of Terrestrial Magnetism, Ionosphere and Radio Wave Propagation)

Studies of the long-term trend of the geomagnetic aa-indices has revealed that occurrence probability of quiet magnetic conditions ( $aa < 7$  nT) has been gradually reduced during the 20th century from 50% to 10%. Similar trend of local magnetic k indices at Moscow during 2002 at the declining phase of the 23rd solar cycle has been compared with electrocupunctural (EAP) measurements of human electrical conductivity carried out at Institute of Terrestrial Magnetism, Ionosphere and Radio Wave Propagation (IZMIRAN) since 1998 (<http://helios.izmiran.rssi.ru/helioecology/index.html>). Method of electrocupunctural diagnostics of health condition by R.Voll is used (M.V. Ragoulskaya, V.V. Lyubimov, Investigation of natural magnetic fields' influence on human biological active points: methods, equipment, results. El. J. of Biomedical Electronics, Nov. 2000). Accumulation of k-index for 27 days (corresponding to rotation of the Sun) preceding day of EAP measurements is used for estimate the percentage occurrence probability of k-index ( $k < 2$  for quiet magnetic conditions and  $k > 2$  for disturbed magnetic conditions). It is shown that average daily human conductivity EAP index has been gradually reduced during 2002 correlated with the same trend of occurrence of quiet local k-index at Moscow and several other local and planetary estimated k indices. Our EAP results confirm that human conductivity is sensitive to reduced quiet (grown disturbed) magnetic activity. Technological developments may be required for human adapting to reduced quietness of magnetic field.

**JSP11/07A/A10-009**

**1220**

### **DIURNAL DYNAMICS OF RATS RESISTANCE TO HYPOXIA DURING VARIOUS GEOMAGNETIC ACTIVITY**

Youry P. SIZOV<sup>1</sup>, Maryam L. KHACHATURYAN<sup>2</sup>, Mikhail M. TEJBLUM<sup>3</sup> (<sup>1</sup>Geelectromagnetic Research Institute of RAS, <sup>2</sup>Russian State medical university, <sup>3</sup>Institute of rentgenoradiology)

The objective was to find the influence of geomagnetic activity (GMA) on diurnal dynamics of rats resistance to acute hypoxia. METHODS. The resistance to acute hypoxia of rats male Wistar (mass 150-180 g) was estimated by life time (LT) in sec after "rise" to "altitude" 11.5 km above sea level in different seasons of the year. The  $C=0,34$  and  $C=0,66$  quantiles of LT values distribution served as boundaries for LT of low (LR), middle (MR), high resistant to hypoxia rats (HR). The GMA for an hours of LT determination was assessed by K-indices: less than 3 - quiet (QGMA), from 3 to 5 - disturbed (DGMA). Time rows of LT values were studied by spectral analysis and cosinor-analysis. Nonparametric methods of statistics were used too: analysis of variance, correlation analysis, Dunn's method and X<sup>2</sup>. RESULTS. Diurnal dynamics was determined by circadian and ultradian rhythms. The influence of GMA and day time on LT was found ( $p < 0,05-0,01$ ), GMA alteration being accompanied by LT rhythms alteration. The basic rhythms during QGMA were chiefly circadian rhythms, more rarely ultradian ones. The part of ultradian rhythms increased (2.5 times), the part of circadian rhythms decreased (3.5 times) among LT basic rhythms during DGMA in winter and spring, the rats rhythms periods (except those of HR and MR in spring) being shorter than those during QGMA (1.2-4.0 times). About 70 % of the number of the circadian and ultradian LT rhythms revealed during QGMA changed during DGMA for the year as a whole. At different day periods of all seasons of the year LT decreased 2-3 times more often than increased. LT altered almost 2 times more often in the middle and at the end of the day than at its beginning. Stages of LT alteration were found as GMA disturbed during a day and a year and as well as after passing different time after its disturbance. CONCLUSION. GMA disturbance is accompanied by alteration of circadian and ultradian LT rhythms number and their parameters, that stipulated increase of fluctuating LT alterations during a day. During GMA disturbance life time of low Resistant more often decreases particularly in autumn.

**Monday, July 7 PM**  
Presiding Chair: A. Ismail-Zadeh

**JSP11/07P/A10-001**

**1400**

### **SUSTAINABILITY OF WATER RESOURCES IN A COASTAL CITY IN A CHANGING ENVIRONMENT**

Shadananan K. NAIR (Department of Physical Oceanography, Cochin University of Science & Technology)

Rapid urbanization is a complicated issue in many parts of the World, the effect more felt in developing counties with poor economies. Providing basic necessities, essentially safe water has become a difficult task. Coastal cities face additional problems like the saltwater

intrusion and pollution that deteriorates the water resources. The metropolitan city of Kochi situated in the southwest coast of India is a good example for this. It lies just one metre above mean level of the adjoining Arabian Sea. Western part of the city is separated from the mainland by the backwater lying within few kilometres and almost parallel to the Seashore. Monsoons and thunderstorms produce more than 300cm of annual rainfall. But, proximity to the backwater and sea, and pollution from industrial and domestic sources makes the surface and groundwater not usable, especially in the western parts of the city. Water has to be brought from the river from the point several kilometres upstream. Improper public water supply system and unexpected power failure always affect availability of water. Though the city has so many inter connected canals, high intensity of rainfall and unscientific design of sewage system block the water, resulting flooding and blocking the roads. Deposition of mud in the canals and careless disposal of solid wastes worsen the situation. Earth filling of paddy fields, ponds and wetlands has also affected the freshwater availability and wastewater outflow. Water-borne diseases have become a common hygienic issue. Increasing migration and worsening environmental conditions pose a serious threat to the life in the city. Present population density of the city is 6250/km<sup>2</sup> with a decadal growth rate of 10.3%, excluding migration. In this study, a comprehensive investigation on the problems related to water in Kochi – its availability, effect of environmental degradation, water logging and flooding – have been made. Extremes of weather and water conditions here during the last 100 years have been computed to provide guidelines for the overall development of the city.

#### JSP11/07P/A10-002 1430

##### GENPATSU-SHINSAI: CATASTROPHIC MULTIPLE DISASTER OF EARTHQUAKE AND QUAKE-INDUCED NUCLEAR ACCIDENT ANTICIPATED IN THE JAPANESE ISLANDS

Katsuhiko ISHIBASHI (Department of Earth and Planetary Sciences, Kobe University)

The most serious factor of civilized infrastructure that has maximized vulnerability to earthquakes in Japan is a cluster of nuclear power plants distributed all along the coastlines of the world's most earthquake-prone archipelago. At present, 16 commercial nuclear power stations with 52 large-scale reactors are being operated in tiny and densely-populated islands. The most dangerous nuclear power station is Hama'oka located just above the hypothesized huge fault plane of the impending M8-class Tokai earthquake on the Pacific coast of central Japan. If this earthquake, a nationwide concern and the subject of a special countermeasures act, happens, the seismic disaster will definitely be devastating in a broad area between Tokyo and Nagoya with officially estimated collapsed buildings of more than 200 thousands and huge tsunami. If this earthquake causes a severe accident to the Hama'oka station with massive leakage of radioactivities outside, then the rescue and restoration works in the earthquake disaster area becomes impossible, and at the same time, management of the nuclear accident and evacuation of inhabitants from radioactivity are extremely difficult due to the earthquake damages. Therefore, the nuclear accident would be left to expand to the maximum scale and victims of radiation exposure and ordinary earthquake disaster would become numerous. Even a few tens of million inhabitants around Tokyo, nearly 200 km away from Hama'oka, would be forced to evacuate. I call this disaster of earthquake-nuclear complex as "Genpatsu (nuclear power plant)-Shinsai (earthquake disaster)," which is a totally new type of natural-manmade disaster that the human beings have never encountered. Its final effect will be global as well as a fatal blow to Japan, and affect deeply future generations. The authorities concerned claim that the seismic measures of Japanese nuclear power plants are perfect and all plants and related atomic facilities are safe against any kind of earthquake. But, construction of nuclear power plants in Japan was started around the early 1960's, just on the eve of the birth and spread of two basic theory of modern earthquake science, fault model of earthquakes and plate tectonics. Therefore, the official standards of seismic design of nuclear facilities are oldish and insufficient in view of modern earthquake sciences. Not only Hama'oka but also most other nuclear power stations in Japan seem accident-prone due to large earthquake, because many are located in seismic gaps with clear active faults or just above subducted oceanic plate where large slab earthquakes may occur. These kinds of scientific matters were not taken into account during planning and construction of plants. In order to avoid Genpatsu-shinsai we should first face this problem squarely and assess its risk as objectively as possible. I think this serious vulnerability of modern society is not restricted in Japan but should also be a global concern.

#### JSP11/07P/A10-003 1500

##### THE FINAL STAGE OF PLATE DETACHMENT - THE CARPATHIAN MODEL

Victor I. MOCANU (University of Bucharest)

The Carpathian area is a key zone for understanding the post-collisional fate of subducted lithosphere which can only be observed and monitored on a very few spots on the Earth. The slab detachment (?) and the following sinking of the detached lithosphere slab into the deeper mantle is strictly restricted to a few million years. The detachment process itself is rarely observable and not really understood. It is not clear whether the detachment takes place in form of brittle failure suddenly removing the slab or whether visco-elastic processes play a relevant role, so that the detachment is not a real "break", but more likely a long-winded elongation and thinning of parts of the subducted lithosphere. The Vrancea region in the SE-Carpathians (Romania) is one of the regions where to study this geodynamic process. There, a nearly vertical hanging slab segment is probably breaking nowadays. Seismicity beneath Vrancea is characterized by the occurrence of intermediate depth earthquakes in very epicentral and hypocentral regions, with occurrence times of 10 years for  $M_w > 6.5$  and 50 years for  $M_w > 7.4$ . A very complex approach is clearly necessary in order to shed light on the processes associated with this very active area. Seismic investigations of the Carpathian Orogen area form one component of a few multidisciplinary initiatives. The main objectives are: (1) the architecture of the Tertiary/Quaternary; (2) the presence and geometry of structural detachments; (3) the relationship between crustal structures related to basin evolution, especially neotectonic structures, with deeper (mantle) structure and seismicity; and (4) integration with complementary studies in the Carpathian region, the evaluation and validation of competing geodynamic models. A complex tomography experiment from 1999 shows a good resolution down to 350 km depth. As a preliminary result, the high velocity body extends between 70 km and more than 350 km, deeper than the deepest event (220 km). The 350 km are key for ocean closure reconstruction as it represents the entire lithosphere subducted in the area of SE-Carpathians. The earthquake hypocenters are concentrated at the eastern outer part of the high velocity body. The subduction of a foreland slab is associated to surface deformation as indicated by the crustal seismicity and by leveling comparison data. Repeated GPS measurements gives two basic kinds of information: the precise location of the present deformation, and the direction of velocities of block movements. The precise location of deformations has important implications for determination/confirmation of the main risked areas and therefore on the future development of the area. The measurement of the present-day deformation can permit to propose an estimation of the locked surface and then an estimation of the importance of the next crustal earthquake. In particular, we try to answer if the subducted slab has detached from the foreland plate or not. We also have information on the origin of the convergence (eastern or western plate) and about the (de)coupling of the Carpathians with the foreland plate.

#### JSP11/07P/A10-004 Invited 1550

##### POPULATION DYNAMICS AND RISK VULNERABILITY IN INDIA

Ramesh P. SINGH, Anup K. PRASAD, Nilima BHOI (Indian Institute of Technology, Kanpur, India)

Population of India is presently more than one billion and it is expected that it will increase by 60 per cent by 2050. The Indian regions suffer with numerous natural hazards (earthquake, cyclone, floods, landslides, forest fire, subsidence, droughts, lightning, cloud bursts) from which loss of lives and properties occur from time to time. A review of various types of natural hazards in India will be presented. Efforts have been made to carry out GIS modelling to study the vulnerability of the Indian region based on the various types of hazards and their interactions with the Indian population. The present analysis show that the northern part of Indian region is one of the risk prone Indian regions.

#### JSP11/07P/A10-005 1620

##### SEISMIC MICROZONATION OF DELHI, INDIA: AN APPROACH USING SITE SPECIFIC RESPONSE

KAMAL ..., Sriram. V., Mundepi A. K. ( Wadia Institute of Himalayan Geology, Dehradun, INDIA)

Seismic microzonation of mega cities in India is the need of the hour in wake of increasing seismicity in the region. In last decade, India has seen many damaging earthquakes. The capital city, New Delhi and its surroundings are one of the most densely populated regions of the world. It is also located in one of the most seismically active area on the globe. This combination makes the city of New Delhi, India as the most seismically vulnerable place. A systematic survey using short period velocity transducers was carried out in the city, in order to designate areas of vulnerability during a future earthquake in Himalaya. Half of the city is located on the alluvial planes of the river Yamuna, which is susceptible to produce large accelerations during a mega event in Himalaya, thus exposing a large population to the damage. A brief account of the results obtained during the survey is presented. An attempt to delineate zones of vulnerability is also made in the paper.

#### JSP11/07P/A10-006 1640

##### AN INTEGRATED FRAMEWORK FOR EARTHQUAKE DAMAGE ASSESSMENT OF REINFORCED CONCRETE BUILDING

Zengqing WEN, Hongshan LU (Institute of Geophysics, China Seismological Bureau)

Structural damage during recent earthquakes, such as Northridge, USA; Kobe, Japan; Taiwan, China demonstrates that it is necessary to develop a comprehensive model to estimate building damage as a kernel part of a seismic risk management system. Local site effects have enormous influence on the intensity and character of earthquake motion. The amplitude and frequency content of the ground motions from an earthquake can be greatly affected by properties and configuration of the near surface materials via mechanisms such as selective filtering (including resonance), damping and focusing. Building damage in earthquakes is frequently a direct result of the local site geological conditions affecting the incident ground motion. Consequently, any attempt of seismic damage assessment should take into account the local site conditions. This study is devoted to establish the procedure for seismic damage assessment of reinforced concrete building in seismic regions, which is integrated seismic environment and site condition into the framework of seismic response analysis and earthquake damage assessment. The model developed for earthquake damage assessment has four stages: i) probabilistic seismic hazard assessment at rock site, ii) site response analysis, iii) the seismic response estimation for reinforced concrete building, and iv) structural damage assessment. In this paper, a 24-story shear wall-structure in Beijing is selected as an example to demonstrate the procedure. The multi-degree-of-freedom lump mass systems are used to represent a high-rise reinforced concrete building. The one-dimension site response models using the equivalent linear analysis method for site seismic response analysis and the equivalent lateral force method for structure seismic analysis are incorporated to investigate the site effects on seismic response of building and building damage distribution among various damage states. By comparing the damage distribution under the acceleration response spectra with 63%, 10% and 2% probability of exceedance in 50 years at rock site and specific site, it can be observed that the site effect is very important and seismic environment and site condition should be considered at same time.

#### JSP11/07P/A10-007 1700

##### NEW APPROACH TO PARAMETERIZATION OF THE DISTRIBUTION OF STRONG EARTHQUAKES: EVALUATION OF THE CROSSOVER POINT AND ITS CONNECTION WITH TECTONIC CHARACTERISTICS

Mikhail V. RODKIN, Vladilen F. PISARENKO (Geophysical Centre of the Russian Academy of Sci.)

Main losses from the earthquakes are caused by rare major events. Thus, the problem of risk assessment is connected essentially with the evaluation of probability of rare strong events. It was shown that for some seismic regions with a larger number of strong events (as well as for global catalogue too) the distribution law of major earthquakes differs from that of typical events. An important characteristic of distribution of moderate and major events is so-called crossover point, determining the passage of distribution tail to a more rapid decreasing rate. Several approaches to the evaluation of the crossover point are discussed and compared. First method is based on the use of the so-called Generalized Pareto Distribution (GPD) describing the limiting Peak Over Threshold (POT) distribution. The second approach is based on the Maximum Likelihood Estimation of the crossover parameter for a particular parametric model of distribution function possessing necessary smoothness. The third approach is connected with the change of the regime of growth of cumulative effects from the non-linear law typical of the moderate earthquakes to the linear one typical of major disasters. The statistical uncertainty of suggested estimates of the crossover parameter is derived. The obtained values of the crossover point and the tendencies in their change are discussed. It is shown that the crossover values depend on the tectonic characteristics in particular region. The revealed correlation of the tectonic parameters (velocity of subduction, plate age, etc) with the seismic regime is discussed in connection with the hypothesis of universality of the seismic moment-frequency law. The obtained results give possibility to characterize the specific character of distribution of major earthquakes in more details. Using this result the new method of parameterisation of the distribution of strong events was suggested. This method of parameterisation can be used in the seismic zoning problem.

JSP11/07P/A10-008

1720

## GLOBAL HAZARD MAPS BASED ON UNIFIED SCALING LAW FOR EARTHQUAKES

Anastassia K. NEKRASOVA, Vladimir G. KOSSOBOKOV (IIEPT&amp;MG, Russian Acad. Sci.)

The evident heterogeneity of patterns of seismic distribution and dynamics are apparently scalable according to the generalized Gutenberg-Richter recurrence law that accounts for the fractal nature of faulting. The results of our global and regional analyses imply that (i) the recurrence of earthquakes in a seismic region, for a wide range of magnitudes and sizes, can be characterized with the following law:  $\log N(M,L) = A - B(M - 5) + C \log L$ , where  $N(M,L)$  is the expected annual number of earthquakes of magnitude  $M$  within an area of linear size  $L$  (recently Bak et al. (2002) came independently to a reformulation of essentially the same "Unified Scaling Law for earthquakes"); (ii) for a wide range of seismic activity,  $A$ , the balance between magnitude ranges,  $B$ , varies from 0.6 to 1.4, while the fractal dimension,  $C$ , changes from under 1 to 1.6; (iii) an estimate of earthquake recurrence rate depends on the size of the territory that is used for averaging and may differ dramatically when rescaled in traditional way to the area of interest. The confirmed multiplicative scaling of earthquakes changes the traditional view on the recurrence of earthquakes, the catastrophic ones in particular, and has serious implications for estimation of seismic hazard, for the Global Seismic Risk Assessment, as well as for earthquake prediction. We demonstrate the Global Seismic Hazard maps that display at resolution of one by one degree the  $A$ ,  $B$ , and  $C$  for the recurrence of earthquakes.

JSP11/07P/A10-009

1740

## HIGH-FREQUENCY HYDRO ACOUSTIC SIGNALS (40 - 110 HZ) DETECTED BEFORE THE EARTHQUAKES ON THE PACIFIC SHELF OF THE KAMCHATKA PENINSULA

Victor E. MOROZOV (Tsunami laboratory, Shirshov Institute of Oceanology RAS)

Kuril-Kamchatka arc is a well-known tsunami risk region. Almost all earthquakes in the region occur in the coastal zone. Many of such events can produce landslides and tsunamis. Early prediction of earthquakes is very important. The objective of this study is to make an attempt to forecast earthquakes using hydro acoustic signals, which can be recorded before the main shock. A joint analysis of the local Kamchatka earthquake catalogue data and hydro-acoustic measurements obtained during the Acoustic Thermometry of Ocean Climate (ATOC) experiment was carried out. Records were obtained from a horizontal cluster of hydrophones located on the shelf of the Kamchatka Peninsula in the Pacific Ocean. The 160 records available are about 22 minutes long each. They contain information from 14 smaller hydrophone clusters, which form the main cluster. The location of the source of acoustic signal can be found from the cross analysis of the data collected by different clusters of hydrophones. Acoustic noise was recorded from July 1998 to March 1999, thus the records contain seasonal variations in the noise. Spectral analysis of the main signal was carried out. In addition, the acoustic signals were analyzed by usual listening. The time series of acoustic records coincident with the earthquakes or measured immediately before the beginning of earthquakes were analyzed. The total period of the time series was divided into smaller parts and spectra were calculated for each of the small intervals. Changes in the form of the spectra with intensive peaks in the frequency range within 40-110 Hz were observed in many records preceding an earthquake. These changes could be also distinguished in the audio record of the signal as clearly recognized cracks. Two types of signals were distinguished from the hydro acoustic records: the micro-earthquakes, whose focuses were located in the same area as the seismic focus of main earthquake and the seismic noise, which appears before the main shock. The duration of micro-earthquakes was about several seconds. If the time interval between the hydro acoustic record and earthquake exceeded 4 hours no micro-earthquakes were observed. This hydrophone cluster was located in the region of high seismic activity; therefore we can evaluate the structure of micro-earthquakes and distinguish them from other non-seismic signals. We conclude that hydrophone records of the ocean noise can supply information about the processes, which occurred at the ocean bottom several hours before the beginning of an earthquake, and can make it is possible to forecast the area of the further main shock of the earthquake. A theoretical model of this process has been contrived to compare field data with the model.

Tuesday, July 8 AM

Presiding Chair: P. Dunbar

JSP11/08A/A10-001

Invited

0900

## ASSESSMENT OF TSUNAMI HAZARD FOR DIFFERENT COASTAL AREAS IN THE PACIFIC

Viatcheslav K. GUSIAKOV (Department of Geophysics, Institute of Computational Mathematics and Mathematical Geophysics)

The paper describes a potential application of the Expert Tsunami Database (ETDB) for estimation of the long-term tsunami hazard. The ETDB has been developed and is being maintained at the Novosibirsk Tsunami Laboratory under the joint project of the IUGG Tsunami Commission (IUGG/TC) and the International Coordination Group for the Tsunami Warning System in the Pacific (ICG/ITSU). The concept of the ETDB is based on the integration of historical data, numerical models, processing and analyzing tools along with supporting mapping software. These components are embedded inside a specifically developed GIS-type graphic shell providing fast and efficient manipulation of maps, models and data. The ETDB is intended to be a comprehensive source of historical data on tsunami occurrence and coastal manifestation along with additional reference information related to the tsunami problem in the Pacific. Three main parts of the ETDB data storage subsystem are TSUNAMI database, EARTHQUAKE database and GEOGRAPHY database. The TSUNAMI database consists of the catalog of tsunamigenic events in the Pacific (Level I data) and the catalog of historical observations of tsunami run-up heights (Level II data). The collected data can be easily retrieved from the database by a number of criteria and are readily available for further display and analysis. Availability of this large amount of digital data on tsunami run-up heights enables us to develop a special application tailored to specific needs of coastal communities for having long-term estimates of tsunami risk. The approach to the long-term tsunami hazard assessment, implemented in the ETDB software, is based on the statistical analysis of historical run-up observations near a particular site and involves the following four basic steps: (1) selection of a particular coastal area within which available historical run-up observations can be considered as spatially correlated; (2) retrieval of historical run-up measurements from the database, displaying them along the time axis and analyzing their time-spatial relation; (3) plotting the data against the "wave height - frequency occurrence" diagram and obtaining the "height - frequency" relation by linear regression; (4) calculation of the so-called "hazard curves" for the estimation of probability that a particular wave height of  $H$  (m) will not be exceeded for the given time interval of  $T$  (years). For a particular coastal area, this type of analysis can be interactively made using a special pop-up menu and dialog windows. The results can be immediately displayed on the screen in the form of hazard curves and evaluated by an expert. This analysis can be easily repeated for different subsets of data in order to evaluate its

variability depending on the data quality and completeness. Some examples of the ETDB application for the tsunami hazard assessment in the different tsunamigenic areas in the Pacific are presented.

JSP11/08A/A10-002

0930

## STRENGTHENING THE MAPPING SYSTEM OF JAKARTA (INDONESIA) FOR FLOOD HAZARD MITIGATION MANAGEMENT

Hasanuddin Zainal ABIDIN<sup>1</sup>, Samsul HADFI<sup>2</sup>, Joenil KAHAR<sup>3</sup>, Rudolf MATINDAS<sup>4</sup> (Department of Geodetic Engineering, Institut Teknologi Bandung (ITB), Jl. Ganesha 10, Bandung 40132, INDONESIA, <sup>2</sup>Land and Mapping Office of DKI Jakarta, Jakarta, INDONESIA, <sup>3</sup>National Coordinating Agency for Survey and Mapping, Cibinong, Bogor, INDONESIA)

Jakarta is the capital city of Indonesia with a population of about 10 million people, inhabiting an area of about 25-km by 25-km. Due to several natural and man-made factors, Jakarta is yearly affected by flood. It causes a lot of damages and creates physical, social and economic impacts. Several approaches have been implemented for flood hazard mitigation in the area. One aspect that limits the effectiveness of the approaches so far is the lack of detail, comprehensive and up-to-date spatial information of Jakarta and its surrounding areas, both in forms of maps or GIS databases. This paper will review the status and development of mapping system in Jakarta. Strengthening analysis will be performed in order to make the system also useful for flood hazard mitigation management. Preliminary analysis concluded that for flood management at least there are five maps (databases) that their making have to be added to the system, namely height contour, watershed, drainage, water penetration, and land subsidence maps (databases). Social mapping should also be performed in order to map and identify the social and economic conditions of the peoples living in the flood prone areas. Strategic issues and problems related to this mapping system strengthening will be presented and discussed. Paper will be sum up with conclusions and recommendation along with plans for future activities.

JSP11/08A/A10-003

0950

## LANDSLIDE HAZARD MONITORING AND SURVEY OF THE VITAL AREAS IN INDONESIA

Surono (Directorate of Volcanology and Geological Hazard Mitigation)

Landslide hazard in Indonesia has caused many victims of people killed and number of casualties. This was created by such geologic condition, climate and human factors. Especially for the areas, in which economic and transportation is vital, monitoring of landslide by using GPS has been done episodically. The result of monitoring for Bandung - Jakarta and Bandung - Jogjakarta main roads within 2 months period in rainy season, showed 5 cm road sliding was detected. Two dimensional resistivity imaging survey was done in understanding the degree of sliding slope and thickness of the upper layer. Usually for the upper layer of 3-5 m in thickness with slope of 20 degrees, causing the damage of building, roads and many other public facilities. The areas of those fulfill the above criteria was stated to be unlikely for human living, limited farmer activities and needs road maintenance with a special engineering technique.

JSP11/08A/A10-004

1010

## SUSTAINABLE COASTAL DEVELOPMENT: PERSPECTIVES OF LOCAL KNOWLEDGE AND COMMUNITY-BASED CO-MANAGEMENT IN SOUTHEAST ASIAN COASTAL COMMUNITY

Md. SALEQUZZAMAN (Ph. D. Candidate and Researcher, Institute for Sustainability and Technology Policy (ISTP), Murdoch University, Perth, WA-6150, Australia & Associate Professor, Environmental Science, Khulna University, Bangladesh)

Coastal environment is the most resourceful and productive zone in the world. On the other hand, most Southeast Asian coastal communities are in great risk due to climate change and other anthropogenic disturbance. Therefore the coastal environment needs to become sustainable, because rest of the world human population depends on the sustainability of the coastal environment. Local knowledge about the environment and natural resources is being shown to be an important asset in coastal communities. Such knowledge provides the basis for traditional community-based management systems, and its acquisition, use and transmission are extremely relevant to livelihoods in subsistence fishing over most of the world, especially in Southeast Asian Coastal Community. Presently community-based coastal resource management, particularly fisheries management is an alternative of sustainable development in coastal communities of Southeast Asia, especially in Bangladesh. In Bangladesh, traditional local knowledge and community-based participatory management are extremely successful for sustainable development in some localised area of coastal community. This management with scientific input is now expanding to other coastal communities of Bangladesh. The paper will analyse the successful of sustainable development in coastal communities of Bangladesh and identify the different factors behind this successful history. The key sustainable development planning and management issues are formal and informal education, awareness, community consultation, community participation and implementation of local community-based rules and legislation, which cover the nature conservancy as well. On the other hand, financial support and technical help including need-based education are the important factors to achieve the sustainability of the Southeast Asian coastal communities. Strong decision-making processes from local, national and international community will strengthen to the achievement of the coastal sustainable development. Institutional and research involvement is another factor to implement this process. Therefore, finally the paper will recommend a policy framework on how overall coastal Bangladesh and other Southeast Asian coastal community will enjoy the opportunity of sustainable development.

JSP11/08A/A10-005

1050

## MONITORING DROUGHT OVER NORTH-EAST OF I. R. OF IRAN USING STANDARDIZED PRECIPITATION INDEX (SPI)

Javad BODAGHJAMALI<sup>1</sup>, AliMohammad NOORIAN<sup>2</sup>, Sohaila JAVANMARD<sup>3</sup>, Abdolhosein MOGHADAM<sup>4</sup>, Reza SHIRMOHAMADI<sup>5</sup> (Climatological Research Institute (CRI), I. R. of Iran Meteorological Organization (IRIMO), P. O. Box 91735-491, Mashhad, I. R. of Iran, <sup>2</sup>President of IRIMO, I. R. of Iran Meteorological Organization, Meraj Ave., Tehran, I. R. of Iran)

Drought is the most complex of all natural hazards, that is so difficult to define, detect, and measure, and researchers have been striving to develop indices to accomplish these tasks. In 1993, researchers at Colorado State University developed a new drought index, the Standardized Precipitation Index (SPI), which is based on precipitation alone. The SPI was designed to be a relatively simple, year-round index applicable to all water supply conditions. Its fundamental strength is that it can be calculated for a variety of time scales from one month out to several years. This versatility allows the SPI to monitor short-term water supplies, such as soil moisture important for agricultural production, and longer-term water

resources such as groundwater supplies. Drought impacts are usually first apparent in agriculture, but gradually move to other water-dependent sectors. Recovery time for water stored in surface and subsurface systems can be quite long under severe drought conditions. Risk of drought is still a major concern in parts of I. R. of Iran, where precipitation amounts are low extremely variable. The SPI is a relatively new index, and it has not been widely applied or tested. In this research, we tested the SPI for different climatic regions and investigated its potential use as a tool for monitoring drought in I. R. of Iran. SPI values have been computed for 100 synoptic stations of IRIMO network for 3-, 6-, 12-, and 24-month scales, covering 1960-2002. The results of the research shows that at the 3-month scale drought frequency increases but its duration decreases. On the other hand, as the time scale increases, the index responds more slowly.

**JSP11/08A/A10-006** Invited **1110**

#### ECOLOGICAL POLICY AND RISK ASSESSMENT OF RADIOACTIVE CONTAMINATION IN THE BLACK SEA

Alexei Evgenievich KONTAR (Laboratory of Seismology and Geodynamics, P.P. Shirshov Institute of Oceanology, Russian Academy of Sciences)

Environmental problems in the Black Sea continue to be serious, even though governments have initiated a regional approach to the management and protection of the marine environment. Following the Chernobyl accident in 1986, the Black Sea riparian countries (viz., Bulgaria, Georgia, Romania, Russia, Turkey, and Ukraine) identified radioactive pollution as a serious problem. This paper presents some results of the project which is part of the fundamental research carried out by the P.P. Shirshov Institute of Oceanology of the Russian Academy of Sciences. The aim of the project is to develop the policy and methods for assessing the risk and fate of the Chernobyl radionuclides in the Black Sea. The risk assessment mathematical model has been designed to investigate the fate and distribution of the Chernobyl radionuclides in sediments of the Black Sea. One of the regions of intensive radioactive precipitation during the Chernobyl disaster was the northwestern Black Sea region. There are some canyon systems in this region, where bottom sediments of the shelf zone are removed to the continental slope region and finally to the abyssal part of the sea. Occasionally there are dramatic velocity increases in the near-bottom current, the so-called "bottom or benthic storms". Different eddies above the area studied are supposed to be the cause of the observed events. In the following it is suggested that additional mechanisms are needed to explain some observations of bottom storms and mixing processes in the Black Sea. The importance of periodic bottom storms springs from the fact that they stir up bottom sediments with radionuclides incorporated, which are then captured and transported over large distances by weaker but stable currents. Some so-called "warm" bottom storms are connected with lutite flows, forming in the upper horizon of the slopes. This is due to bottom erosion, resulting from landslides and creeps of sediment, frequently shaken by local submarine earthquakes. As a result of this work scientifically provided recommendations have been elaborated for assessing risk of pollutants in the Black Sea and near-bottom dynamics interaction with the environment in natural and man-induced hazards and also suggestions for monitoring the near-bottom environment, aimed at minimizing negative ecological effects. The results of this work have confirmed once again by research that the Black Sea crisis calls for a concerted international approach and that it is critical for the future of the Black Sea that various programs addressing the Black Sea's environmental problems be coordinated to work together. It will promote sustainable development of efforts towards improved environmental management and risk assessment in the Black Sea region. The results obtained for the Black Sea can be used in comparable regions of Russia for elaborating a policy, strategy and methodology of predicting the fate of pollution in the sea. Solution of these problems is particularly acute for the new social and economic conditions in Russia.

**JSP11/08A/A10-007** **1140**

#### GUIDELINES FOR SUSTAINABLE PROVISION OF ARSENIC FREE WATER SUPPLY IN BANGLADESH

Md. SALEQUZZAMAN<sup>1</sup>, Mostafa Md. KHALEQUZZAMAN<sup>2</sup> (Associate Professor, Environmental Science Discipline, Khulna University, Bangladesh; and Ph.D. Candidate and Researcher, Institute for Sustainability and Technology Policy (ISTP), Murdoch University, Western Australia, Perth, WA 6150, Australia, email: salek@central.murdoch.edu.au / msalequzzaman@hotmail.com, <sup>2</sup>Paediatrics Consultant, General Hospital, Magura, Bangladesh.)

Ground water arsenic pollution becomes a serious environmental health issue of the people of Bangladesh. The issue has been taken a priority agenda by the government and many local, national and international organisations, but very few successes have been made for its remediation and sustainable management. A lot of recommendations have been suggested from many national and international seminars, symposia and conferences; and in the national and international journal as well. In a real sense, very few workable efforts have reached to the victims, most of whom are very poor people. The reasons include a lack of coordination among different organizations and selection of locally available, low-cost alternative solutions and treatment technologies. This paper will discuss the real barriers to solutions of this arsenic calamity. Finally, the paper will recommend sustainability guidelines for the management of arsenic calamity of Bangladesh.

**JSP11/08A/A10-008** **1200**

#### MONITORING OF LANDSLIDE PHENOMENA BY USE OF INTEGRATED SURVEY SYSTEM

Paolo RUTIGLIANO<sup>1</sup>, Francesco SDAO<sup>2</sup>, Francesco VESPE<sup>3</sup> (<sup>1</sup>Telespazio Spa, <sup>2</sup>Universita della Basilicata, <sup>3</sup>Agenzia Spaziale Italiana)

This paper summarises the geological and geomorphologic studies and the main results of the monitoring survey carried out on some landslides in some areas in Basilicata region (southern Italy). The landslide monitoring was done using an integrated approach: traditional survey systems and applications based on the GPS technique. The adoption of a "mixed" approach, with the contemporary use of classical techniques and GPS, has been introduced since the space geodesy tools become very effective for the monitoring of landslide movements. The success of GPS for landslide monitoring is due to its characteristics such as a relative easiness in the acquisition of data and a very high precision and accuracy in the measurements. In addition, the GPS allows an easy reconstruction of the velocity field of a landslide, which adds a really helpful information for the modelling of the phenomena. However the surface velocity obtained by GPS could be not representative of the deep movements of gravitational phenomena. This means that in the monitoring of landslides GPS can not be used in stand-alone mode: the use of classical methods is necessary to really understand the evolution of a landslide. One test site was at Lauria locality, an urbanised area interested by large and active landslides; the last is subject to frequent reactivation causing severe damage to the urban structures. Results of GPS survey, in good agreement with the information's coming from geomorphologic studies, show that large part of the investigated area are affected by slow but continue deformations. Other results came from the survey (in progress) about slope instability processes observed in two areas of the Parco

*Archeologico Storico Naturale delle Chiese Rupestri del Materano*. In the investigated areas, the lithological defects and intense fracturing state of carbonate rocks cause it's the cause of mass movements of blocks (rock falls, topples and rockslides) that could seriously damage some fine rupestrian heritages present in the area. The potentially unstable carbonate blocks have been defined by geological and geomorphologic studies and actually this sites are under monitoring with a survey system, made up by a traditional topographic survey, GPS measures and a deformation measurement system.

**JSP11/08A/A10-009**

**1220**

#### EFFECTS OF EARTHQUAKES AND VOLCANIC ACTIVITIES ON CITIES AROUND THE LAKE KIVU BASIN, WESTERN RIFT VALLEY OF AFRICA

Mifundu WAFULA<sup>1</sup>, Kasereka MAHINDA<sup>1</sup>, Mavonga TULUKA<sup>1</sup>, Munyololowa YEMBA<sup>2</sup>, Hiroyuki HAMAGUCHI<sup>3</sup> (<sup>1</sup>Department of Geophysics, C.R.S.N./Lwiro D.S. Bukavu, D.R.Congo, <sup>2</sup>Lwiro station of C.R.G.M./Kinshasa, D.R.Congo, <sup>3</sup>Graduate School of Sciences, Tohoku University, Sendai 980-8578, Japan)

The Western Rift Valley is the west branch of the East African Rift System. This rift valley is one of the most seismically and volcanically active region in the African Continent. The Western rift valley is characterized by the shallow seismic activities with normal faulting type. Volcanoes Nyiragongo and Nyamuragira standing at the north of Lake Kivu are characterized by frequent basaltic eruptions in the recent history. The most catastrophic disastrous eruption occurred on Jan. 17, 2002 and the thick lava flows covered over about 13 percent of Goma city, 80 percent of its commercial district and killed 100 people. The Bukavu and Goma (D.R.C.), and Gisenyi (Rwanda) are the main cities located around the lake Kivu margin. The whole population in these cities is more than one million. From the seismic and volcanic studies, field observations and testimonies of inhabitants in the basin, it is revealed that, since 1997 the lake Kivu basin had become more active than before. Several moderate earthquakes with local magnitude more than 4.0 accompanied with foreshocks and aftershocks have been recorded in basin every year. This seismic activity is supposed to be related partly to the reactivation of faults in the basin area and partly to volcano-magmatic activity. The last earthquake of Mw 6.2 occurred recently at the western escarpment of the Rift system near the lake Kivu on October 24, 2002. The damages caused by this event were recorded on houses in Bukavu, Lwiro, Kalehe, Nyabibwe, Kirosho, Gisenyi and even in farther city like Kigali in Rwanda. The most heavily damaged zone was the territory of Kalehe where 90% of masonry D were destroyed and masonry C affected. In total 8 persons were killed and 1700 houses damaged. Very slight damages were observed in Goma and Bukavu. Landslides phenomenon, which has been already observed in Bukavu area since 1997, was accelerated by the occurrence of this earthquake. In addition to the seismic activity prevailing, some factors such as: the regressive erosion, the presence of aquifer nape, the deforestation, and parcelling on the steep slopes are contributing to the landslides phenomenon and inundation in Bukavu, where big catastrophic event may be expected in the future. Except some seismological and geological results available, no serious studies have been done on soil engineering; foundation soil, special treatment of slope instability and subsidence, modification of strong-motion parameters. Every year several people are killed directly by earthquake or by landslides and inundations. The earthquakes associated to the Nyiragongo eruption on January 17, 2002 killed 4 people, injured 18 and damaged more than 400 houses, most of masonry D in Gisenyi. Therefore, geophysical monitoring must be reinforced quickly around Lake Kivu region in order not only to understand what are occurring beneath the basin and volcanic regions but also to reduce the geophysical risk in future.

IA

**JSP11-Posters**

**Tuesday, July 8**

#### GEOPHYSICAL RISK AND VULNERABILITY: THE POPULATION-HAZARD INTERACTION (IAPSO, IAGA, IAHS, IAMAS, IASPEI, IAVCEI)

Location: Site D

**Tuesday, July 8 PM**

**JSP11/08P/D-001**

Poster

**1400-070**

#### THE EFFECT OF SMAZE ON PRECIPITATION PROCESS OVER TEHRAN

Seyed Alireza SADEGHI HOSSEINI, Javad RAHELI SALIMI (Department of Meteorology, Space Group, Institute of Geophysics, Tehran University)

In recent decades, the problem of air pollution, specially particulate type in large cities as Tehran has created health problems to people. Here, from different perspective, the relationship between the precipitation process and the air pollution in Tehran have been investigated. The climatic changes in Tehran from 1950 to 2000 is considered to be mainly due to urbanization, as well as topographic setting of this city. This study shows that the annual mean maximum and minimum temperatures in Tehran are large than those of Karaj, a smaller city in west of Tehran. The same is true for the mean annual minimum temperature for Varamin, a city just east of Tehran. Although the annual maximum temperature in Varamin is larger than that of Tehran which is mainly due to topographic effect. The records indicate that the visibility in Tehran has a gradual decrease around 1975s, which is considered as the start of an accelerating city expansion, hence increase of air pollution. The frequency of smaze events has increased substantially since 1975s. The precipitation records also indicate that the mean annual precipitation has relatively increased over Tehran more than Karaj and Varamin, although local precipitation (based on sudden increase in local relative humidity) has been reduced that could be due to over seeding of the clouds by pollutant aerosols.

**JSP11/08P/D-002**

Poster

**1400-071**

#### RHYTHMS OF RATS RESISTANCE TO HYPOXIA DEPEND ON GEOMAGNETIC ACTIVITY

Youry P. SIZOV<sup>1</sup>, Maryam L. KHACHATURYAN<sup>2</sup> (<sup>1</sup>Geoelectromagnetic Research Institute of RAS, <sup>2</sup>Russian State medical University)

The objective was to find the influence of geomagnetic activity (GMA) on rhythms of rats resistance to acute hypoxia. METHODS. The resistance to acute hypoxia of rats-male Wistar was assessed by life time (LT) in sec after "raise" during 1 minute up to the "altitude" 11.5 km above sea level in the different seasons of one year from 13.00 to 21.00 h. GMA for an hour of LT determination was estimated by K-index for Moscow. Time rows of LT and K-indexes values were studied by spectral analysis. The differences among periods (in percents of the value of the nearest largest period) of LT and GMA rhythms were determined. The periods of

## INTER-ASSOCIATION

one type of rhythms were compared. GMA rhythms number coincided with one LT rhythm (GMAC) for each type of rhythm was determined. Nonparametric methods of statistics were used: analysis of variance, correlation analysis, Dunn's method and X<sup>2</sup>. RESULTS. The same types of GMA and LT rhythms: circaseptal, circasemisepthal, infradian, circadian, ultradian were found. The majority of circa- and ultradian rats LT rhythms periods coincided with GMA rhythms periods. The basic rhythms of GMA and LT appeared to be either circadian ones, or multiple to them. Frequency of corresponding GMA and LT rhythms was practically equal and rose as periods decreased, i.e. it was the largest for ultradian rhythms (68 and 63% for the whole year) particularly at the first half of the year: max in spring and min in autumn (GMA), in summer (LT). At the same time the absolute number of GMA rhythms exceeded that of LT rhythms of corresponding rhythms types. The relative differences between periods of both GMA and LT rhythms diminished as the size of the periods decreased, i.e. were min for ultradian rhythms. The relative differences between periods of GMA and LT rhythms were more evident at the first half of the year. In rhythms with periods more than those of the basic rhythms amplitude increased as periods decreased. In rhythms with periods less than those of the basic rhythms amplitude also diminished as periods decreased. Apparently similarity of GMA and LT rhythms was stipulated by influence of GMA rhythms on LT ones by means of synchronization of rhythms.

**JSP11/08P/D-003** Poster **1400-072**  
**DROUGHT MONITORING USING NORMALIZED DIFFERENCES VEGETATION INDEX (NDVI) OVER I. R. OF IRAN**

Javad BODAGHJAMALI<sup>1</sup>, Sohaila JAVANMARD<sup>1</sup>, Mehdi RAHNEMA<sup>2</sup>, Sara ATTARCHI<sup>1</sup> (Climatological Research Institute (CRI), I. R. of Iran Meteorological Organization (IRIMO), P. O. Box 91735-491, Mashhad, I. R. of Iran, <sup>2</sup>GIS and RS Department, Shahid Beheshti University, Tehran, I. R. of Iran)

Sever drought has been occurred in most regions of I. R. of Iran in recent years. In order to the drought risk management, monitoring of drought using drought indices, such as Standardized Precipitation Index (SPI), Palmer Drought Severity Index (PDSI), Percent of Normal (PN), and Normalized Difference Vegetation Index (NDVI), should be applied for interested regions. Drought monitoring could be carried out using the remote sensing of vegetation status. During the periods of drought conditions, physiological changes within vegetation may become apparent. Satellite sensors are capable of discerning many such changes through spectral radiance measurements and manipulation of this information into vegetation indices which are sensitive to the rate of plant growth as well as to the amount of growth. Such indices are also sensitive to the changes in vegetation affected by moisture stress. The National Remote Sensing agency in India has developed NDVI to determine vigour of vegetation. In this research, the NDVI spatial distribution has been derived over I. R. of Iran, from AVHRR sensor of NOAA satellite images. In order to estimate the amount of rainfall using the satellite images, Kerr model has been applied. To test the model, the data of 115 synoptic stations of I. R. of Iran Meteorological Organization (IRIMO) have been used. The correlation shows good agreement between the estimated rainfall and NDVI value in most part of Iran. Based on the results of this research, it is going to use NDVI as an operational drought index in most regions of Iran.

**JSP11/08P/D-004** Poster **1400-073**  
**NORTH ARMENIAN SEISMIC RISK ASSESSMENT**

Edvard Grigori GEDAKYAN, Mkrtchyan MARIAM (Header Researcher, Institute of Geophysics and Engineering Seismology NAS of Armenia)

Availability of a great number of mass inhabited and industrial objects, growth of population and its dense setting on a comparatively limited territory increase the earthquake destructive effect. Lessons of the Spitak earthquake in 1988 (M=6.9) showed that absence of the complex of antiseismic programmes on the basis of seismic risk assessment considerably increased the material and social damage. For the seismic risk assessment of the North Armenian territory the modified approach to creation of the following models was applied: a) the model of investigating of seismicity territory; b) the model of spatial distribution of intensity of ground shaking; c) the model of the effect, which the given object experiences from the shaking. On the basis of the above mentioned models and their combinations seismic risk parameters were calculated according to the discrete main points of the North Armenian territory map. When constructing the territory seismicity model the following task was set: to describe all the main seismicity parameters (the repetition law, average annual number of earthquakes according to calculated and quantitative descriptions of the strained-deformed state. For construction of the model of shaking intensity distribution over the earth surface and determination of the intensity macroseismic damping coefficients, maps of assists of the North Armenian strongest earthquakes were used. Among these maps one of the spatial importance due to its detailed and exact character the map of the Spitak earthquake macroseismic display. When creating the intensity distribution model some important factors were taken into account, such as earthquake focal mechanisms, types of rupture-formation in the earthquake focus. This part of the work aims at determination of the isoseist parameters (such as area, ratio of semi-axes  $1 = a/b$  and azimuth  $A$  of the long axes) dependence on the magnitude, focal depth  $H$ , focal mechanism type and the type of rupture-formation. The model of solitary earthquake effect was constructed according to the data about destructions and damages during the Spitak earthquake main shock and its strongest aftershocks. On the basis of the above mentioned models and their combinations seismic risk parameters were calculated according to the discrete main points of the North Armenian territory map. They include: 1 - average of earthquakes threatening to the object of research,  $A$  - average effect,  $B/P = 0,9$  - the appear threshold of the effect,  $P_0$  - probability of the fact that the effect is equal to zero. Availability of these values of the seismic risk parameters serve as a basis for working out of a system of activities aiming at prevention and reduction of earthquake destructive consequences.

**JSP11/08P/D-005** Poster **1400-074**  
**DETERMINATION OF SUBSURFACE STRUCTURE OF TOTTORI PLAIN USING SEISMIC METHOD AND GRAVITY EXPLORATION**

Tatsuya NOGUCHI, Ryohei NISHIDA, Takuo OKAMOTO (Department of Civil Engineering, Tottori University)

Microtremor observations and a gravity survey were made to determine the subsurface structures of the Tottori Plain. This area was severely damaged during the 1943 Tottori earthquake (M7.2), damage being concentrated in the plain. Microtremors were recorded by seismic arrays (8 sites) and 3-component single-site observation (417 points). Gravity data were obtained at about 400 points. The microtremor data were analyzed by the spatial auto correlation (SPAC) method and the horizontal-to-vertical spectral ratio. The subsurface structures were determined by 1) S-wave velocity structure models obtained at the array observation sites, 2) a 3D bedrock configuration based on the horizontal-to-vertical spectral ratio and the residual gravity anomaly, 3) 2D density structures for three cross sections obtained using the gravity anomaly based on a depths of S-wave velocity structures. A shallow bedrock area extends over a belt-like zone along the coast. This bedrock suddenly

deepens from the eastern mountainous area to the plain.

**JSP11/08P/D-006** Poster **1400-075**  
**PROBABILISTIC SEISMIC HAZARD ASSESSMENT IN ALBANIA**

Betim MUCCI<sup>1</sup>, Anastasia KIRATZIF, Shyqyri ALIAJ<sup>1</sup>, Eduard SULSTAROVA<sup>1</sup>, Siasi KOCIU<sup>1</sup>, Veronika PECE<sup>1</sup>, Emmanuel SCORDILIS<sup>2</sup> (<sup>1</sup>Seismological Institute, Tirana, Albania, <sup>2</sup>Geophysical Department of Aristotle University of Thessaloniki, Greece)

Albania is situated in the Alpine-Mediterranean seismic belt and accommodates part of the deformation due to collision of the Adriatic micro-plate with the Eurasian plate. Albania has repeatedly been the site of historical earthquakes with considerable losses and as evidenced from the instrumental era the country suffers a lot of damage even from moderate size events. The fact is attributed mainly to the poor quality of the construction in rural areas. During Albania's passing from an isolated and communist dictatorship to an open and democratic society in the beginning of 90's, a boom in the construction sector commenced which made imperative a modern seismic hazard assessment. In this work an evaluation of probabilistic seismic hazard in Albania is presented based on an updated seismicity catalogue. For this reason Albania has been subdivided in 8 seismogenic zones on the basis of seismotectonic criteria as well as on the spatial and temporal distribution of earthquake epicenters. The earthquake catalogue adopted contains 553 earthquakes with M<sup>4.5</sup> for the time period 58 AD - 2000. Ground Acceleration (PGA) for different probability levels of exceedance are obtained for a grid (each element having dimensioned 10 km x 10 km) over the territory of Albania. Respective maps are also presented.

**JSP11/08P/D-007** Poster **1400-076**  
**CRUSTAL UNDULATIONS IN RELATION TO COASTAL HAZARDS**

Shigehisa NAKAMURA (Kyoto University (Ret'ed))

There are several factors affecting to the human activities in the coastal zones. In this work, some typical cases of the interested natural processes are introduced with some geophysical consideration. One of the typical cases is sea level rising caused by the global warming of climate. In fact, some report informs us that several countries of the islands in the Pacific and in the Indian Ocean are threat to disappear under the sea surface by the increase of the sea level rising, especially when the every season of the annual local high tides. If the global warming process is surely affecting to the human activities on the coast, we should be active to clarify what effects could be expected for us in a scope of geophysical sciences. This sea level rising must be realized as a result of the climate change induced by the global warming as a trigger of the increased melting of the ice covers developed on the Antarctic and on the Green Land. Now, it is hard to give any direct answer how to predict and control the climatological processes. The author here would introduce a conceptual model in order to raise to start an urgent research project, even though there might be many of the projects running in the world. Now, it is noticed that an increase of the sea level rise could be a loading to the crust under the sea water. Then, we have to be careful to consider about some possible problems at set back of the coast line especially in the coastal zone facing an ocean. This notice could be reduced as a result of an equivalent thin plate model for considering an undulation of the earth's crust around the coastal zone. This undulation could possibly give an understanding about an expected set back of the coast line. Adding to the above, it could be noted there might be a relation at considering a local co-seismic crustal upheaval with some assumptions in the scope of geophysical dynamics.

**JSP11/08P/D-008** Poster **1400-077**  
**ASSESSMENT OF LANDSLIDE HAZARDS USING GEOPHYSICAL TOMOGRAPHY**

Simeon G. KOSTIANEV, P. STEFANOV, P. STOEVA (Dept. of Mathematical Geophysics, University of Mining & Geology)

Landslides and unstable slopes are among the major natural and man-made hazards affecting mankind and yet their causes, their consequences for human life and property, and possible strategies for mitigating their effect are not very well understood. We will note, that only in Bulgaria there are over thousand active landslides on populated and health resort areas. The material and social losses have not been calculated yet. But in preliminary data they are enormous. Numerous and dangerous are the landslides and unstable slopes in open cast coal-mines too. In this paper we offer methods for combined application of high resolution electrical (resistivity) tomography and seismic ray tomography for characteristic of landslide hazards and unstable ones. The major aim here is to predict where and when landsliding will occur, establishing their variability in space and time, and appraising their impact on the natural and socio-economical environment. The above methods are applied for studying of concrete landslide in Bulgarian Black Sea and on some unstable slopes in an open cast coal-mine of Maritza-Iztok area. This combined application of electrical and seismic tomography for assessment of landslide hazard is very useful.

**JSP11/08P/D-009** Poster **1400-078**  
**DROUGHT MONITORING USING PALMER INDEX OVER NORTH-EAST OF I. R. IRAN**

Sohaila JAVANMARD<sup>1</sup>, Javad BODAGHJAMALI<sup>1</sup>, GholamAli KAMALI<sup>1</sup>, Mohamad Javad AHMADIAN<sup>1</sup> (Climatological Research Institute (CRI), I. R. of Iran Meteorological Organization (IRIMO), P. O. Box 91735-491, Mashhad, I. R. of Iran, <sup>2</sup>Atmospheric Science and Meteorological Research Center (ASMERC), IRIMO, P. O. Box 14965-114, Tehran, I. R. of Iran)

Sever drought has been occurred in most regions of Iran in recent years. In order to drought risk management, monitoring of drought using drought indices such as Standardized Precipitation Index (SPI), Palmer Drought Severity Index (PDSI), Percent of Normal (PN), Normalized Difference Vegetation Index (NDVI) should be applied. A drought index calculated from known values of selected parameters enables us to evaluate the drought hazard over an area and assess the current extent and severity of drought over region. PDSI was specifically designed to treat the drought problem in semiarid and dry sub humid climates. The Palmer drought index is widely used by a variety of people, such as hydrologist, foresters, field meteorologists, economists, policy decision makers, new media, private consultants, and researchers, as a tool to monitor and assess long-term meteorological drought and wet spell conditions. As pointed out by National Drought Mitigation Center (NDMC), it is most effective measuring impacts sensitive to soil moisture conditions, such as in agriculture, and it has been used to start or end drought response actions. In this research, drought monitoring using PDSI has been carried out in CRI over Khorasan province (Northeast of Iran), from 2000 to 2003 for 3 years as well as field measurement of soil moisture in 10 Agricultural Meteorological stations over there. There was a good agreement between the soil moisture situation and derived PDSI over the mentioned stations.

JSS06

Monday, July 7 - Thursday, July 10

EARTH STRUCTURE AND GEODYNAMICS (IASPEI, IAVCEI, IAG, IAGA)

Location: Site A, Room 4

Monday, July 7 PM

Presiding Chair: P. Tackley

JSS06/07P/A04-001

1400

**SEISMIC TOMOGRAPHY AND THE BOUNDARY BETWEEN UPPER AND LOWER MANTLE**

Adam Marian DZIEWONSKI, Yu Jeffrey GU (Earth and Planetary Sciences, Harvard University)

It is difficult to think of a more controversial geophysical problem than the flow of the mantle material across the boundary between the upper and lower mantle. There is, however, strong evidence for strong impedance to flow across this boundary. It is based, in part, on the estimates of the patterns of large-scale velocity anomalies above and below the 660 km discontinuity. Gu et al. (2001) show that it is possible to satisfy a large and diverse set of traveltimes data with a model that has distinctly different spectral characteristics above and below the discontinuity. Even when the continuity is imposed, the velocity anomalies 100 km below and above the 660 km discontinuity are fully de-correlated, indicating a very steep change in the pattern of heterogeneity. Additional information comes from studies of the topography of the 400 and 660 km discontinuities, using SS - SdS differential precursor times (Shearer and Masters, 1992). Simultaneous inversion for mantle shear velocity and topography of the transition zone discontinuities shows very little large wavelength topography on the 400 km discontinuity and much larger relief on the 660 km; the shape of the two surfaces is de-correlated (Gu et al., 1998). However, the 660 km topography is highly correlated with the velocity anomalies in the transition zone. A simple, although not unique, interpretation is that the negatively buoyant slabs pond in the transition zone. A shortcoming of the seismic tomography is that it provides only a snapshot of the heterogeneity. Attempts to extrapolate it in time are uncertain. But the ponding of slabs does indicate the possibility that this material could be, at least in part, recirculated in the upper mantle. At the same time, it is impossible to ignore the correlation between the distribution of subduction zones and the circum-Pacific ring of high velocities in the lowermost mantle, which might indicate communication, perhaps episodic, between upper and lower mantle.

JSS06/07P/A04-002

1420

**AVALANCHES REVISITED: EFFECTS OF THE PYROXENE-GARNET SYSTEM ON THE EXTENT OF MANTLE LAYERING AT 660 KM**

Paul J. TACKLEY (Dept. Earth and Space Sciences and Inst. of Geophysics and Planetary Physics, University of California Los Angeles)

Much research in the early-to-mid 1990s was directed towards understanding the extent of mantle layering caused by the endothermic garnet-spinel to perovskite+magnesiowüstite phase transition at around 660 km depth, and the consensus that emerged was that of basically whole mantle convection with some temporary inhibition and avalanching of downwelling slabs today, with a potentially much greater effect in the past. However, published models assumed that the mantle is made of 100% olivine and its high pressure phases, whereas it is well known that the garnet-pyroxene system accounts for at least 40% of the mantle. Phase changes in the latter system occur over a wider depth range, and the equivalent 660 transition was thought to have a neutral or even positive Clapeyron slope, leading to the expectation that it would dilute or even act against the dynamical effect of the endothermic olivine-spinel transition (Weidner and Wang, 1998). However, recent measurements by Chudinovskikh and Boehler indicate a strongly negative Clapeyron slope (-6 MPa/K) for the ilmenite to perovskite transition, which is likely to be the relevant one at temperatures near the 660. Furthermore, when compositional effects are considered, subducted oceanic crust is likely to be buoyant in the depth range 660-740 km [Ringwood, 1994; Ono et al., 1991]. Thus, the situation warrants careful investigation. Here these matters are examined using high-resolution numerical convection calculations that incorporate both the olivine and pyroxene-garnet systems, and comparing to calculations with only the olivine system. The Clapeyron slopes of each phase transition are varied within the current range of uncertainty. Both isochemical models, and models that incorporate chemical differentiation, are considered. Preliminary results that include chemical differentiation indicate a substantial chemical stratification induced by the combined phase system even with a neutral Clapeyron slope in the Pyroxene-Garnet system. With a strongly negative slope, layering is enhanced compared to a purely olivine system.

JSS06/07P/A04-003

1440

**SYSTEMATIC STUDIES OF THE MANTLE DISCONTINUITIES**

Arwen DEUSS, John H. WOODHOUSE (Department of Earth Sciences, University of Oxford)

We report a systematic search for reflectors in the upper and lower mantle using a global data set of SS-precursors. A bootstrap resampling algorithm is employed to determine robust reflectors (at the 95% confidence level). The results demonstrate that reflectors can be found from a large variety of depths, and having substantial lateral variations. Such observations can be used as a probe for local mantle composition and temperature. To investigate the regional existence and lateral variations of discontinuities, we search for robust reflectors within spherical caps of 10 degree radius, and make comparisons with the corresponding stacks for synthetic seismograms. The 410 and 660 km reflectors are global features and the results can be used to map their variation in depth. The 520 km discontinuity is confirmed in many regions but is absent in others. There are a number of regions in which we observe two discontinuities at approximately 500 and 560 km depth, an effect that can be interpreted as 'splitting' of the 520 km discontinuity. Stacks for particular tectonic regions, for example North America or Indonesia, show additional reflectors in both upper and lower mantle at depths of 220 km and 1000-1200 km. The locations in which discontinuities are found are correlated with features in the shear velocity distributions in tomographic models. In addition to the transition zone discontinuities, the largest number of robust reflections comes from a depth of 220 km, showing that the Lehmann discontinuity is a major feature in the upper mantle. This discontinuity is observed beneath both continental and oceanic areas, though the largest amplitudes occur beneath the continents. There is also evidence for weak discontinuities at approximately 260 and 310 km depth, for example in the region of the South Pacific Superswell which could be related to processes in the upwelling plume. There are also suggestions of lower mantle reflectors with a weak peak for 800 km depth; deeper in the lower mantle there are reflections from a continuous range of depths. Clear reflections from 1000-1200 km depth are found beneath North America and in the Indonesian subduction zone area, where other studies have also found reflections. The locations

correlate with fast features in tomographic models. As we find discontinuities from a range of depths in different types of tectonic regions, we do not expect that only one mechanism is responsible for all reflections. We discuss different possible explanations for these seismic discontinuities in terms of phase transitions and compositional and rheological changes.

JSS06/07P/A04-004

1500

**OBSERVATIONS AND IMPLICATIONS OF MID-MANTLE SEISMIC REFLECTORS BENEATH THE MARIANA SUBDUCTION ZONE**Fenglin NIU<sup>1</sup>, Hitoshi KAWAKATSU<sup>2</sup>, Yoshio FUKAO<sup>2</sup> (<sup>1</sup>Department of Earth Science, Rice University, <sup>2</sup>Earthquake Research Institute, University of Tokyo)

A clear later phase approximately 80 s after the direct P-wave is observed in most of individual seismograms recorded by a short-period seismometer network in Japan (J-array) from a cluster of deep earthquakes that occurred at the northern Mariana subduction zone. This phase (1) shows a P-wave particle motion; (2) arrives later from earthquakes with shallower focal depths; (3) has a steeper incident angle than that of P wave; and (4) shows a deviation of a few degrees in the arrival azimuth from that of P wave. We interpret it as an S to P converted wave which takes off downward from the source and is reflected at a velocity discontinuity (reflector) below the earthquakes. Applying an inversion technique to the data set shows that the seismic reflector dips toward southwest by about 20° at 24.25° N 144.75° E 1115 km with a lateral extension at least 100 x 100 km. The location corresponds to the lower edge of a high-velocity anomaly in global tomographic models. Amplitude and waveform analyses suggest a decrease of S-wave velocity by 2-6% and an increase of density by 2-9% within the reflector. There is almost no difference in P-wave velocity (<1%) between the reflector and the surrounding mantle. The estimated thickness of the reflector is about 12 km. These observations indicate that the observed seismic structure is more likely to be a chemical reservoir rather than a purely thermal anomaly. The seismic reflector might be a piece of subducted oceanic crust, as suggested by a previous study. It also could be related to the break down of the D-phase of dense hydrous magnesium silicates (DHMS) at mid-mantle pressure condition reported by recent mineral physics studies. Both scenarios imply that either mechanical or chemical segregation might occur within the subducted slab at mid-mantle condition.

JSS06/07P/A04-005

1540

**THICK MANTLE TRANSITION ZONE BENEATH THE PHILIPPINE SEA AS INFERRED USING THE RECEIVER FUNCTION METHOD FOR DATA FROM THE LONG TERM BROADBAND OCEAN BOTTOM SEISMOGRAPH ARRAY**Daisuke SUETSUGU<sup>1</sup>, Hajime SHIOBARA<sup>2</sup>, Hiroko SUGIOKA<sup>1</sup>, Shunichi KODAIRA<sup>1</sup>, Yoshio FUKAO<sup>1</sup>, Kimihiro MOCHIZUKI<sup>1</sup>, Toshihiko KANAZAWA<sup>3</sup>, Ryota HINO<sup>4</sup>, Tomoharu SAITA<sup>4</sup> (<sup>1</sup>IFREE/JAMSTEC, <sup>2</sup>ERI/Univ. Tokyo, <sup>3</sup>RCEP/Tohoku Univ., <sup>4</sup>RCSV/Nagoya Univ.)

We analyzed broadband waveforms recorded by the broadband ocean bottom seismograph network in the Philippine Sea to investigate the mantle transition zone structure beneath the Philippine Sea. This is the first attempt to study the mantle discontinuities beneath the Philippine Sea using broadband ocean bottom seismographs. As a part of the Ocean Hemisphere network Project (OHP), fifteen Long-term Broadband Ocean Bottom Seismographs were deployed from November 1999 to July 2000 along a profile from the Saipan Island to the Amami Island across the mid Philippine Sea. All of the stations were equipped with semi-broadband sensor (WB2023LP, PMD and 24-bit data loggers). The sensor has a flat velocity response from 0.03 Hz to 30 Hz, which provides high fidelity for the long-period P wave trains analyzed in the present study. We analyzed seismograms from recovered and selected 7 stations with low S/N ratios. We determined the depths of the 410 km and 660 km discontinuities and thickness of the mantle transition zone under the Philippine Sea region by the Velocity Spectrum Stacking Method, where we can take into consideration the three-dimensional velocity variation in determining the discontinuity depths. The 410 discontinuity is shallower than the global average by 17 km and the 660 discontinuity is deeper than the average by 37 km, resulting in the transition zone thicker than the average by 54 km. The western part of the Philippine Sea has the 660 km discontinuity at a depth of 703 km, which is deepest in the studied area. Existing tomographic models have high velocity anomalies there, which is interpreted as the cold stagnant Izu-Bonin slab, suggesting that the deep 660 km discontinuity is related to temperature anomalies associated with the stagnant Izu-Bonin slab. The Mariana trough has also the deep 660 km discontinuity at a depth of 691 km in spite that the Mariana slab seems to be subducted vertically into the lower mantle and no high-velocity anomalies are present in the tomographic models. This cannot be explained only by the cold temperature and compositional factors, e.g., influence of water dehydrated from the Mariana slab may contribute to the transition zone thickness.

JSS06/07P/A04-006

1600

**MANTLE STRUCTURE AND COMPOSITION TO 800 KM DEPTH BENEATH SOUTHERN AFRICA AND SURROUNDING OCEANS FROM BROADBAND BODY WAVES**Rapelang E. SIMON<sup>1</sup>, Cedric WRIGHT<sup>2</sup>, M. Tarzan O. KWADIBA<sup>3</sup>, Eldridge M. KGASWANE<sup>1</sup> (<sup>1</sup>Present address: Department of Physics, University of Botswana, Private Bag UB704, Gaborone, Botswana., <sup>2</sup>Bernard Price Institute of Geophysical Research, University of the Witwatersrand, Johannesburg, Private Bag 3, Wits 2050, South Africa., <sup>3</sup>Also: Department of Geological Survey, Private Bag 14, Lobatse, Botswana., <sup>4</sup>Present address: Council for Geoscience, Private Bag X112, Pretoria 0001, South Africa.)

Average one-dimensional P and S wavespeed models from the surface to depths of 800 km were derived for the southern African region using travel times and waveforms from earthquakes recorded at stations of the Kaapvaal and South African seismic networks. The Herglotz-Wiechert method combined with ray tracing was used to derive a preliminary wavespeed model, followed by refinements using phase-weighted stacking and synthetic seismograms to yield the final model. Travel times combined with ray tracing were used to derive the S wavespeed model, which was also refined using phase-weighted stacking and synthetic seismograms. The presence of a high wavespeed upper mantle lid in the S model overlying a low wavespeed zone between depths of 210 km and about 345 km that is not observed in the P wavespeed model was inferred. The 410 km discontinuity shows similar characteristics to that in other continental regions, but occurs slightly deeper at 420 km. Depletion of iron and/or enrichment in aluminium relative to other regions is the preferred explanation, since the P wavespeeds throughout the transition zone are slightly higher than average. The average S wavespeed structure beneath southern Africa within and below the transition zone is similar to that of the IASP91 model. There is no evidence for a discontinuity at 520 km depth. The 660 km discontinuity also appears to be slightly deeper than average (668 km), although the estimated thickness of the transition zone is 248 km, similar to the global average of 241 km. The small size of the 660 km discontinuity for P waves, compared with many other regions, suggests that interpretation of the discontinuity as the transformation of spinel to perovskite and magnesiowüstite may require modification. Alternative explanations include the presence of garnet-rich material or ilmenite-forming phase transformations above the 660 km discontinuity, and the garnet-perovskite

IA

transformations as the discontinuity.

**JSS06/07P/A04-007 1620**

**IMAGING THE MANTLE DISCONTINUITY STRUCTURE BENEATH THE SOUTH INDIA**

K. SURIYAPRAKASAM<sup>1</sup>, B.K. BANSAL<sup>2</sup>, T.J. OWENS<sup>3</sup>, S.S. RAI<sup>1</sup> (<sup>1</sup>National Geophysical Research Institute, Hyderabad, INDIA, <sup>2</sup>Department of Science & Technology, New Delhi, INDIA, <sup>3</sup>Department of Geological Science, University of South Carolina, Columbia, USA)

We investigate the nature of seismic strain markers in the mantle beneath South India, analyzing the waveforms from teleseismic events recorded over a 32 station broadband temporary network operated during 1999-2002. The network encompasses largely Archean and Proterozoic terrains of South India. We apply a three-dimensional stacking method to the receiver function to determine the location of mantle discontinuities using the IASPI91 velocity model as the reference. The 410 and 660 km discontinuity are well defined at their respective depths except the depression in 660 km discontinuity by about 30 km in the Proterozoic Granulite terrain. The other transition zone discontinuity at 520 km is also observed at a few places. The images also reveal the presence of 8° and 220 km discontinuity in South India.

**JSS06/07P/A04-008 1640**

**SEISMIC EVIDENCE FOR A THICKER-THAN-NORMAL TRANSITION ZONE AND SUBDUCTED OCEANIC CRUST BENEATH SOUTHERN AFRICA**

John Anthony BLUM<sup>1</sup>, Yang SHEN<sup>2</sup> (<sup>1</sup>Department of Physics, University of Michigan, <sup>2</sup>University of Rhode Island, Graduate School of Oceanography)

Observations of P-to-S conversions reveal the shoaling of the 410-km discontinuity and the deepening of the 660-km discontinuity beneath the oldest parts of the Archean cratons in southern Africa; consequently, the mantle transition zone is 20 km thicker than beneath post-Archean regions and the global average. The thicker-than-normal transition zone correlates strongly with surface geology and does not follow the track of plate motion as numerical simulations of small-scale convection beneath the cratons predict. Thus, the thicker-than-normal transition zone suggests that the cold and mechanically strong cratonic keels penetrate into the transition zone. A negative-polarity P-to-S conversion is also found within the transition zone beneath southern Africa. The negative polarity of the converted phase indicates a  $-2.2 \pm 0.2\%$  S-velocity decrease with depth at a seismic discontinuity near 570-600 km depth. The normal to low velocity contrast at the 660-km discontinuity beneath the study area requires an anomalously high velocity gradient near the base of the upper mantle. The exsolution of Ca-perovskite in former oceanic crust at depth greater than 600 km provides a plausible explanation for the apparent paradox between the significant negative velocity discontinuity and the normal to low velocity contrast at the 660-km discontinuity.

**JSS06/07P/A04-009 1700**

**VP/Vs AND MINERALOGY OF THE TRANSITION LAYER OF THE EARTH'S MANTLE**

Hideyuki FUJISAWA (ABIKO Geoscience Laboratory)

Constituents of the mantle transition layer is discussed based on comparison between the seismic Vp/Vs and those of mantle minerals. Vp/Vs means the ratio between a longitudinal wave velocity and a transverse wave velocity. At present two different hypotheses are proposed on mineralogical composition of transition layer. An isochemical, olivine-phase change hypothesis has long been a standard model for the earth's mantle. High pressure experiment on phase changes in mantle minerals has shown validity of this hypothesis. Until recently, however, elastic wave velocity measurements was technically difficult, and the data was not enough. In recent years the velocity measurement has been made extensively, and it brought controversy in mineralogy of the earth's transition. The author measured the elastic wave velocity of forsterite and its beta-form, and found discrepancy between the seismic velocity jump at 410 km discontinuity and that observed in the forsterite-beta spinel phase change. To explain this discrepancy the author introduced "eclogite" hypothesis on mineralogical composition of the transition layer in the earth's mantle. The "eclogite" model means that major constituents of the transition layer are high pressure versions of eclogite minerals. To judge these two hypotheses we need essentially new method of discussion of the problem. In this presentation the author discuss new aspect of elastic properties of olivine, spinels and eclogite minerals. Elastic properties of crystalline solid is mainly determined by its crystal structure, if elements which constitute the solid are similar. Garnet type structure is more rigid compared to that of silicate spinels. Rigidity of crystalline solid is directly related to a transverse velocity (Vs) of the solid. So the ratio Vp/Vs would reflect essential difference of elastic property among olivine-spinel group minerals and garnet-type minerals effectively, and could be a judgment standard for the problem. First of all, the author discuss the Vp/Vs ratio of the upper mantle. To estimate the ratio of the mantle, data of Vp and Vs must be chosen very carefully, because, in most case, Vp and Vs distribution are determined independently using different observational data. At present the author used the Vp and Vs distributions, which were determined by the same author or the same group of authors using similar data. Values of this mantle ratio show steep increase in the depth range between moho and the 410 km discontinuity, and in the transition layer the ratio does not change with depth. Temperature and pressure dependence of the Vp/Vs ratio of peridotite and olivine-spinel group minerals is highly positive, and peridotite upper most mantle might be verified. The seismically determined Vp/Vs ratio in the transition layer, on the contrary, suggest a garnet type material in the layer.

**JSS06/07P/A04-010 1720**

**THE ROLE OF A SLAB AVALANCHE IN THE RECENT EVOLUTION OF THE NEW HEBRIDES SUBDUCTION ZONE**

Miaki ISHII<sup>1</sup>, Russell N. PYSKLYWEC<sup>2</sup>, Jerry X. MITROVICA<sup>3</sup> (<sup>1</sup>Department of Earth and Planetary Sciences, Harvard University, <sup>2</sup>Department of Geology, University of Toronto, <sup>3</sup>Department of Physics, University of Toronto)

The recent evolution of the New Hebrides subduction boundary exhibits a more complex deformation history than would be expected from simple plate-tectonic theory. In the late Miocene, highly oblique southward consumption of the Pacific plate along the Vitiāz trench ceased as subduction jumped across the New Hebrides arc and north-dipping subduction of the Australian plate commenced. Subsequent, rapid rotation of the New Hebrides arc away from the extinct Vitiāz trench was accompanied by substantial back-arc opening and the development of the North Fiji Basin. The mechanism responsible for this dramatic reorganization has remained elusive. We propose that an ongoing avalanche of cold slab material into the lower mantle, recently imaged by seismic tomographic methods, provides a unifying geodynamic framework for reconciling the recent evolution of the region. We present numerical models which satisfy disparate observational constraints, including the change in polarity of plate subduction, the rapid migration of the New Hebrides arc, opening of the North Fiji Basin, and the present-day geometry of slabs associated with both active and

extinct subduction zones.

**JSS06/07P/A04-011 1740**

**CHEMICAL STRATIFICATION IN A NUMERICALLY MODELED TWO-DIMENSIONAL MANTLE WITH MAGMATISM AND MOVING PLATES**

Masaki OGAWA (Department of Earth Sciences & Astronomy, University of Tokyo at Komaba)

A self-consistent numerical model is presented for magmatism in a convecting mantle with moving plates. Mantle convection is modeled as a thermal-chemical convection of binary eutectic material with Newtonian rheology in a two-dimensional rectangular box internally heated by incompatible radioactive elements. Viscosity is assumed to depend on stress-history as well as temperature and pressure to self-consistently reproduce moving plates. The effects of solid-solid phase transitions at depths around 660 km on the convection is also taken into account. Magmatism is modeled as a permeable flow of basaltic melt produced upon decompression melting of the binary eutectic material through the coexisting matrix. Magmatism makes mantle chemically stratified with the shallower part occupied by chemically buoyant residue of magma depleted in radioactive elements and the deeper part occupied by hot but chemically dense materials enriched in basaltic component and radioactive elements. The magmatism is mostly induced by mantle overturn when internal heating is sufficiently strong or weak but is induced by moving plates (ridge volcanism) and hot plumes uprising from the 660 km phase boundary or the hot region enriched in basaltic component at depth in the lower mantle when the internal heating is moderate; plate motion is significant only when the internal heating is moderate. When plates move, subducting slabs penetrate deep into the lower mantle and induce broad thermal and chemical heterogeneity at depth in the lower mantle. The mantle with moderate internal heating is compared to the earth's mantle.

Tuesday, July 8 AM  
Presiding Chair: U. Christensen

**JSS06/08A/A04-001 0830**

**WHAT DETERMINES ISOTOPIC AGE? CLUES FROM NUMERICAL MODELS OF MANTLE CONVECTION WITH EVOLVING GEOCHEMICAL HETEROGENEITY**

Paul J. TACKLEY, Shunxing XIE (ESS and IGPP, UCLA)

Isotopic measurements on Mid Ocean Ridge Basalts and Ocean Island Basalts indicate effective "ages" (from e.g., Pb-Pb or Sm-Nd systems) in the range 1-2 billion years - much less than the age of the Earth, even though melting should have been much more vigorous early on, skewing the mean time since melting to older values. This relatively young "age" has generally been explained in terms of stretching of heterogeneities by mantle convection, which might reduce them to dimensions too small to be individually distinguishable in short timescales of less than 1 Gyr. On the other hand, published numerical models that use tracers to track differentiated material (Christensen and Hofmann, 1994; Davies, 2002) suggest that Earth-like "ages" can be obtained without taking stretching-induced erasure of tracer signatures into account, although this might effectively happen if the lengthscale for sampling the isotope systems was large enough. In those models, the only explicit mechanism for resetting isotope systems was re-melting, but for this to explain the isotopic ages observed for basalts, the global rate of melting in the recent past would have had to be very much higher than present-day values. To investigate stretching vs. re-melting we have conducted numerical experiments of a cooling mantle with plate tectonics, differentiation and evolution of important isotopic systems, as is fully described in another presentation at this meeting. The time of last melting and the total strain is tracked on each tracer (in addition to isotopic information). The results confirm that a model matching todays crustal production rate and with a reasonable secular cooling history generates "ages" that are substantially larger than those observed, with the extent of crustal settling above the CMB making some difference but not enough. The effect of sampling lengthscale on observed "age" is also tested and found to be insufficient to explain the data. Thus, these results reaffirm the importance of stretching as a key mechanism for effectively deleting older heterogeneities. From analysis of strain vs. age and matching of the observed ages, it is estimated that erasure of heterogeneities occurs at strains of  $10^3$ - $10^4$ , somewhat larger than has often been assumed.

**JSS06/08A/A04-002 0850**

**HOTSPOT MOTION INFERRED FROM LARGE-SCALE MANTLE FLOW MODELS: IMPLICATIONS ON GLOBAL PLATE RECONSTRUCTIONS**

Bernhard Maximilian STEINBERGER<sup>1</sup>, Richard J. O'CONNELL<sup>2</sup> (<sup>1</sup>IFREE, JAMSTEC, <sup>2</sup>Dept. of Earth and Planetary Sciences, Harvard University)

The Hawaiian hotspot track predicted from a plate circuit, assuming that the Hawaiian hotspot is fixed relative to African hotspots, does not fit the observed track: The divergence is steadily increasing back to 43 Ma, and the predicted track does not show a bend. Here we use a model of plumes distorted by global mantle flow to compute hotspot motion, and test whether this motion can explain the misfit. Computations consistently predict a south-to-southeastward motion of the Hawaiian hotspot, and a motion of about 1000 km southward during the past 80 Ma is within the range of model results. Thus, we find that our model of hotspot motion can account for the divergence from 0 to 43 Ma, but can not account for the bend and the track prior to 43 Ma. For this, both a rather sharp change in hotspot motion at 43 Ma, and a westward component of hotspot motion prior to 43 Ma would be required, and neither is predicted in the model. However, a combination of modelled hotspot motion and a relatively modest motion between W and E Antarctica - about 15 degrees clockwise rotation of W vs. E Antarctica - would permit a fit to the Hawaiian track from 80 to 43 My. The required deformation on the Antarctic plate could have been accomplished entirely within continental crust, with rates similar to e.g. present extension in the western U.S., and is not in conflict with, but actually supported by geologic evidence.

**JSS06/08A/A04-003 0910**

**MANTLE DYNAMIC AND TRUE POLAR WANDER**

Marianne GREFF-LEFFTZ (Departement de Geomagnetisme, Institut de Physique du Globe de Paris)

True polar wander (TPW), the coherent motion of Earth's surface with respect to its rotation axis, is most likely controlled by internal mass redistribution within mantle. Recent paleomagnetic study find that true polar wander appears to be episodic in nature, with periods of quasi-stationary alternating with periods of faster TPW. The typical duration of these periods is on the order of a few tens of millions of years with wander rates during fast tracks on the order of 30 to 50 km/Ma. Here, we investigate mechanisms able to produce abrupt changes in the TPW. We first present some results about the influence of a plume crossing the mantle on the polar motion in order to explain fast excursion of TPW. In a

simple example where the upwelling plume is simply modeled by a sphere -with a radius variable as a function of the heatflux within the conduit- crossing the mantle at the Stokes velocity, we have investigated the influence of the phase change (physical or chemical) and of the viscosity contrast at the 670 km depth discontinuity. In some cases, fast changes may occur in the principal inertia direction but the weak amplitude of the inertia tensor perturbations involves that the rotation axis is not significantly affected by this upwelling plume. We extend these results to the study of the effects of two superswells, located one beneath Africa and the other one beneath Polynesia, on TPW. These superswells are modelled by two domes oscillating vertically within the mantle with periodicity of about 100 Ma. We find that such mantle mass anomalies can significantly perturb the TPW (with wander of about  $0.5^\circ/\text{Ma}$ ) and involve polar motion with periods of slow velocity alternating with periods of faster TPW.

JSS06/08A/A04-004

0930

#### WHAT DRIVES PLATE TECTONICS? SLAB PULL, RIDGE PUSH OR GEOMAGNETIC TORQUE FROM THE CMB? A NEW LOOK AT THE OLD PLAYERS VIS-A-VIS AN EXCITING NEW ONE

Miles F. OSMASTON (The White Cottage, Sendmarsh, Ripley, Woking, Surrey GU23 6JT, UK; miles@osmaston.demon.co.uk)

Fundamental reappraisal of the mechanisms that drive plate tectonics suggests the remarkable conclusion that, for at least the past 130Ma, a major agent has been a CW-directed torque (probably of electromagnetic origin at the CMB) reaching the deep ( $>600\text{km}$ , e.g. Gu et al 1998 EPSL) tectospheric keel of the Antarctic craton, via the high-viscosity lower mantle. Major changes in spreading direction marked both ends of the 122-85Ma Cretaceous Superchron and started by forming the Ontong Java Plateau. Action of MORs as gearlike linkages has driven Africa and India CCW since Gondwana breakup and continues to drive the Pacific plate CCW. In the Arctic there is now no cratonic keel to pick up any corresponding polar torque, so northern hemisphere plate tectonics is far less active. My multifaceted study (over 25 years) of the subduction process has indicated that the rapid development of 'flat-slab' interface profiles involves the physical removal of hanging wall material (be it lower crust or mantle) in front of the downbend by basal subduction tectonic erosion (STE). Historically this, and its active seismological manifestation known as seismic coupling, only occurs where the subducting plate was/is  $<70\text{Ma}$  old. Hence the requisite subducting plate buoyancy must be thermal and slab-pull an unlikely agent for such subduction - a conclusion reinforced by the abundant development of progressive foreland-directed thrusting during the STE process, which intermittently couples ridge push to the upper plate. Lots of ridge push is needed to drive that thrusting and the subduction of such buoyant plates. Accordingly, a redesign of the MOR process has incorporated the suboceanic LVZ as a physically integral part of the plate (Osmaston 2000 IGC Rio). This model not only generates much more (but still being quantified) ridge push, as required, but has turned out to be very successful in relation to MOR structures. The heat content takes the form of a superadiabatic gradient in the now-stiff LVZ, and is partially trapped (until subduction) by the much ( $>30\%$ ) lower thermal conductivity resulting from its (say 3%) interstitial melt. Perhaps surprisingly, this incorporated ocean-plate-heat is indeed evident as slab reheating during active subduction. Examples from among numerous circum-Pacific tomographic transects, kindly provided to me, all show that the 'slab' high-Vp signature peters out at between 175 and 350km (plate age-dependent and even at 130Ma) and a second high-Vp signature then begins close to the top of the TZ and goes on into the lower mantle. This latter signature must be mineralogical, not thermal, and arguably is not mantle but is only a stream of dense stishovitic lumps residual from partial melting of subducted oceanic crust at TZ pressures. Where now is the slab pull beloved of modellers? A different cause exists for 'roll-back'. I conclude that CMB torque initiated the Atlantic and is probably the primary driver of plate tectonics, that ridge push comes second and slab pull a doubtful third. To generate such torque may require the presence of semiconductor properties in the CMB region.

JSS06/08A/A04-005

0950

#### IS TRUE POLAR WANDER IN THE LAST 200 MILLION YEARS A SIGNATURE OF EPISODIC INTER-HEMISPHERIC MOTION OF PRIMARY HOTSPOTS AND LOWER MANTLE CONVECTION?

Vincent E. COURTILOT, Jean BESSE, Anne DAVAILLE (Institut de Physique du Globe)

Apart from a surge in true polar wander (TPW) in the last 5-10Ma, which could be related to the recent history of ice loading, there has essentially been no TPW back to 50 Ma ago. This standstill was preceded by a period of moderate, rather uniform TPW at a mean rate of 3 km/Ma. Although earlier data become more uncertain, a standstill prior to 130 Ma seems possible (though given uncertainties, some amount of rather jerky TPW is possible). These observations suggest that TPW is an episodic process (its second derivative can be approximated by a series of Dirac distributions separated by irregular intervals on the order of 50 Ma or more). There is however no convincing evidence for the episodes of super-fast TPW which have been proposed recently by a number of authors, though much additional paleomagnetic data is still desirable to analyze specific periods. One problem is that the TPW curve is derived from hotspot data restricted to the Indo-Atlantic hemisphere and is therefore not truly global. An independent (and methodologically distinct) determination using the far more limited Pacific plate database shows that, to first order, episodic and rather slow TPW with moderate amplitudes is a real feature of Earth dynamics. All current geodynamic models fail to account for the observed features. On closer inspection, the Pacific and Indo-Atlantic determinations of TPW fail to agree in the 50-100 Ma time window. Based on a set of five (geophysical, geochemical and geological) criteria, we have recently proposed that 7 out of 49 hotspots, 3 in the Pacific hemisphere, 4 in the Indo-Atlantic, which we have called primary, may have a very deep origin (this number might be somewhat higher but available data and the criteria we use do not allow to ascertain this yet). Hotspots in each hemisphere move at less than 5mm/a, whereas there has been significant (up to 50mm/a) episodic motion between the two hemispheres. These episodes coincide with those in TPW (over the limited range of the last 100 Ma when they are sufficiently well constrained). The primary hotspots passively trace the motions of quadrupolar lower mantle convection. The episode of TPW which may have started some 130Ma ago and stopped some 45-50Ma ago may have been triggered by an avalanche in the lower mantle (?) or by major change in plate boundaries. Another change at the time of generalized collision of India/Arabia/Africa with Eurasia and disappearance of huge subduction zones between these plates may be responsible for the 50 Ma halt in TPW and hotspot motion. In the last 50 Ma, Earth has mostly been in a quiescent stage.

JSS06/08A/A04-006

1010

#### MODELLING OF DYNAMICS OF DESCENDING SLAB AND TECTONIC STRESS IN THE EARTHQUAKE-PRONE VRANCEA REGION, SE-CARPATHIANS

Alik T. ISMAIL-ZADEH<sup>1</sup>, Birgit MUELLER<sup>2</sup>, Friedemann WENZEL<sup>3</sup> (<sup>1</sup>IEPT, Russian Academy of Sciences, Moscow, and Geophysical Institute, University of Karlsruhe, Germany, <sup>2</sup>Geophysical Institute, University of Karlsruhe, Germany)

Repeated intermediate-depth large earthquakes of the SE-Carpathians (Vrancea) attract an attention of geoscientists to the region. Recent regional P-wave seismic tomographic images of the mantle revealed a high-velocity body in a nearly vertical position. The body is interpreted as a lithospheric slab descending into the mantle, and Vrancea seismicity is associated with the slab. To understand processes of stress generation in and around the descending slab, mantle flow and tectonic stress beneath the region are analysed by means of analytical and numerical modelling and on the basis of available geophysical data. An analytical model of corner flow predicts that the maximum shear stress migrates from the upper surface of the slab to its lower surface in the course of changes in slab dynamics from its active subduction through roll-back movements to sinking solely due to gravity. The changes in stress distribution can explain the location of hypocentres of Vrancea events at the side of the slab adjacent to the Eastern European craton. A 2D thermomechanical FE model of a sinking slab predicts lateral compression in the slab as inferred from the stress axes of earthquakes and its thinning and necking. The maximum stress occurs in the depth range of 80 km to 200 km, and the minimum stress falls into the depth range of 40 km to 80 km. The area of maximum shear stress coincides with the region of high seismicity, and minimum shear stress in the model is associated with the lower viscosity zone. Uplift of the crust starts before the slab detachment. Just after the detachment the tectonic stress in the slab is still high enough to lead to a seismic activity, and the stress decreases significantly in several Ma. Using recent experimental data on elastic parameters and anelasticity, we obtain a model of temperature at 50 to 350 km depth beneath the SE-Carpathians from the seismic tomography model of P-wave velocity anomalies. The modeled thermal structure beneath the SE-Carpathians predicts a cold area associated with the descending Vrancea slab and relatively hot mantle regions surrounding the slab. We analyse a mantle flow and tectonic stress induced by the sinking slab by means of 3D numerical modelling. Input model data are the geometry of the crust and slab, temperature-dependent density and viscosity. The crustal movements predicted by the numerical models are consistent with GPS data on the regional vertical motions. Modeled tectonic stress predicts a horizontal compression beneath the Vrancea region, and it coincides with the stress regime defined from fault-plane solutions for intermediate-depth earthquakes. The stress reaches maximum at depths of 70 to 110 km and 130 to 180 km and decays below being in a good agreement with the observed seismicity.

JSS06/08A/A04-007

1050

#### WAVEFORM MODELING OF MANTLE ANISOTROPIC ELASTIC STRUCTURE

Mark P. PANNING, Barbara ROMANOWICZ (Berkeley Seismological Laboratory, University of California, Berkeley)

Seismic tomography is a useful tool in determining structure and dynamics of the Earth's mantle. While early models depended primarily on short period travel times and surface wave phase velocities, using full seismic waveforms of both surface waves and body waves provides opportunities for improved resolution, especially in the lower mantle, when appropriate sensitivity kernels are used (e.g. Li and Romanowicz, 1996). Our previous work in waveform modelling has focussed on isotropic shear velocity structure of the mantle, but we have recently extended our waveform modelling method to a transversely isotropic model, anisotropic medium with hexagonal symmetry and vertical symmetry axis, and applied it to the upper mantle (Gung et al., 2003), where the anisotropic structure is well documented both in terms of radially symmetric structure, as in PREM (Dziewonski and Anderson, 1981), and lateral variations (Montagner and Tanimoto, 1991; Ekström and Dziewonski, 1998). However, there is also strong evidence for significant anisotropy in  $D'$  and, more recently, several studies have suggested the presence of anisotropy near the transition zone between the upper and lower mantle. Although transverse isotropy is often described by the five elastic parameters,  $A, C, F, L$ , and  $N$ , we reparameterize in terms of isotropic  $P$  and  $S$  velocity, and three terms related to anisotropy. We further apply scaling relationships to invert only for our best-resolved quantities, isotropic  $S$  velocity and  $\xi$ , an anisotropic parameter related to SH velocity over SV velocity. For the uppermost mantle, our results are quite consistent with our earlier work (Gung et al., 2003), as well as regional studies. We see a positive  $\xi$  anomaly ( $SH > SV$ ) under the oceanic basins in the depth range 80-200 km, as well as deeper positive  $\xi$  anomalies beneath most continental cratons from 200 to 400 km depth. We also see negative  $\xi$  anomalies ( $SV < SH$ ) in the transition zone that correlate well with the locations of fast isotropic velocity anomalies associated with downwelling slabs.  $D'$  in our model is characterized by a predominantly positive  $\xi$  signature, extending to the entire globe results of regional studies based on the splitting of diffracted S waves. This  $SH > SV$  signature may be related to dominant horizontal deformation in a mechanical boundary layer for mantle convection, although the mineral physics behind  $D'$  anisotropy is still an area of active research (e.g. Karato, 1998). However, the low velocity areas corresponding to "superplumes" are a notable exception to the positive  $\xi$  dominance. These regions appear to be more variable, and contain large regions with either very small positive or negative  $\xi$  anomalies, also generalizing some regional results.

JSS06/08A/A04-008

1110

#### GLOBAL UPPER MANTLE SHEAR VELOCITY AND ANISOTROPY FROM WAVEFORM ANALYSIS OF FUNDAMENTAL AND HIGHER MODE RAYLEIGH WAVES

Eric DEBAYLE<sup>1</sup>, Alessia MAGGI<sup>1</sup>, Anne SIEMINSKI<sup>1</sup>, Sylvana PILIDOU<sup>2</sup>, Maggy HEINTZ<sup>2</sup>, Keith PRIESTKEY<sup>2</sup>, Brian KENNETT<sup>3</sup>, Jean-Jacques LEVEQUE<sup>1</sup>, Michel CARA<sup>1</sup> (<sup>1</sup>CNRS and EOST, Université Louis Pasteur, Strasbourg, France, <sup>2</sup>Bullard Laboratories, University of Cambridge, United Kingdom, <sup>3</sup>Laboratoire de Tectonophysique, CNRS and Université de Montpellier II, France, <sup>4</sup>RSES, Australian National University, Canberra, Australia.)

A collaboration between researchers from the University of Cambridge, the Australian National University in Canberra, the University of Montpellier and the Ecole et Observatoire des Sciences de la Terre in Strasbourg has allowed us to successfully match the waveforms of more than 40 000 fundamental and higher mode Rayleigh waves, using multi-mode synthetic seismograms computed for a path-average upper mantle elastic model. The selected waveforms are associated with relatively short epicenter-station paths ( $< 10000$  km) typical of regional surface wave tomography at the scale of a tectonic plate. They provide a quasi-global coverage of the Earth with an original dataset, less likely to be affected by spurious effects such as multipathing or focusing/defocusing, compared to the longer R1 and R2 paths classically used in global tomography. The resulting tomographic model has a horizontal resolution smaller than 1000 km for the uppermost 500 km of the Earth and allows us to put new constraints on the upper mantle structure. In particular, our preliminary results show that well-resolved deep low velocities extending down to at least the transition zone are observed beneath some major hotspots, but also in other regions where they are not directly associated with hotspot volcanism at the surface. This would support in some oceanic regions a model of plume-fed asthenosphere. In addition, our model also suggests that the high velocity lid associated with cratonic roots is relatively thin and rarely exceeds 250 km depth.

**JSS06/08A/A04-009 1130**

**MAPPING 3D SEISMIC ANISOTROPY FOR UNDERSTANDING STRUCTURE AND THICKNESS OF THE MANTLE LITHOSPHERE**

Jaroslava PLOMEROVA, Vladislav BABUSKA (Institute of Geophysics, Czech Academy of Sciences, Bocni II, 141 31 Prague 4, Czech Republic)

The alignment of olivine crystals is the dominant source of seismic anisotropy in the sub-crustal lithosphere and asthenosphere. Three-dimensional modelling of seismic anisotropy of the upper mantle, based on joint inversion and interpretation of body waves, revealed large anisotropic domains in the continental mantle lithosphere. The domains are often sharply bounded by sutures cutting the whole lithosphere. Different components of large-scale anisotropy can be traced in depth distributions of the radial and azimuthal anisotropy of surface waves. We proposed a global model of the lithosphere-asthenosphere boundary (LAB) as a transition between a 'frozen-in' anisotropy in the lithosphere to anisotropy in the sub-lithospheric mantle related to the present-day flow. Base of the lithosphere, in this sense understood as the Lehmann discontinuity, plunges not deeper than down to 200 and 250 km even beneath the stable Precambrian shields and platforms. Due to different prevailing orientations of velocity maxima in the anisotropic subcrustal lithosphere and the asthenosphere, the velocity contrast related to the LAB can increase in particular directions. We model fabric of the anisotropic lithospheric domains by peridotite aggregates with hexagonal symmetry exhibiting dipping (a,c) foliation planes, or orthorhombic symmetry with dipping lineations (a-axes). The large-scale fabric, consistent on a scale of hundreds of kilometres, occurs due to preferred orientation of olivine - the most abundant mineral of peridotites - as a result of stress field acting during the formation, or later deformations of the mantle lithosphere. Subsequent continental break-ups and re-arrangement of micro-plates resulted in observed complicated structure of continental mantle lithosphere mostly retaining 'frozen-in' anisotropy of mantle domains. Thus we observe, e.g., European Variscan Massifs formed by several microplates of different origin and development, large-scale structures in the stable lithosphere of northern Proterozoic/Archean Baltic Shield, and/or a shift/rotation between crust and mantle parts of the Phanerozoic and Proterozoic lithospheres around the Trans-Europen Suture Zone. Mapping the anisotropic structures of individual mantle domains contributes to our understanding how the present-day continents were formed and evolved.

**JSS06/08A/A04-010 1150**

**ANISOTROPY UNDER CONTINENTS AND OCEANS: EVIDENCE FOR LATERAL VARIATIONS IN THE DEPTH OF THE ASTHENOSPHERE**

Yuancheng GUNG, Barbara ROMANOWICZ (UC BERKELEY)

We show that the lack of correlation between different global tomographic models of S velocity, in the depth range 200-400 km, can be explained by the presence of anisotropy, with a strong  $V_{sh} > V_{sv}$  component, under most continental cratons. To confirm the presence of this anisotropy, already pointed out by Montagner (1995), we have developed an inversion procedure for transverse isotropy using three component surface and bodywaveform data, in the framework of normal mode asymptotic coupling theory (NACT, Li and Romanowicz, 1995), which in particular, involves the use of 2D broadband anisotropic sensitivity kernels appropriate for higher modes and body waves. This method allows the inclusion of higher mode surface wave and body waveforms, which provide better depth resolution in the upper mantle than standard inversions based on fundamental mode surface waves. Our resulting degree 16 anisotropic model (SAW16AN) confirms the global  $(-N/L)$  distribution found in previous studies in the depth range 100-200km, which is dominated by the striking positive  $dn_{xi}$  anomaly in the central Pacific and a similar one in the Indian Ocean. However, at depths greater than 250 km, the character of the distribution changes: positive  $dn_{xi}$  emerges under the Canadian Shield, Siberian Platform, Baltic Shield, southern Africa, Amazonian and Australian cratons. At 300 km depth, the roots of most cratons are characterized by positive  $dn_{xi}$  which extend down to about 400 km. Interestingly, the East Pacific Rise has a signature with  $dn_{xi} < 0$  down to 300km, indicative of a significant component of vertical flow. At 400km depth, we also note the negative  $dn_{xi}$  around the Pacific ring, consistent with quasi-vertical flow in the subduction zone regions in the western Pacific and south America. We propose that the  $V_{sh} > V_{sv}$  anisotropy, in the depth range 200-400km under cratons, and 80-200km under ocean basins are both related to shear in the asthenospheric channel, located at different depths under continents and oceans. The seismically defined tectosphere is then at most 200-250 km thick under old continents, in agreement with other geophysical observations. The Lehmann discontinuity, observed under stable continents in the depth range 200-240 km, would then correspond to the top of the asthenosphere, and would mark a transition from the weakly anisotropic bottom of the mechanical lithosphere to the strongly anisotropic asthenosphere, in agreement with early interpretations (Leven, 1984). One would not expect to observe this discontinuity at these depths under oceans, where the lithosphere/asthenosphere transition is much shallower.

**JSS06/08A/A04-011 1210**

**HIGH RESOLUTION P-WAVE TOMOGRAPHY IN A GLOBAL MANTLE MODEL**

Christian WEIDLE<sup>1</sup>, Sri WIDIYANTORO<sup>2</sup>, CALIXTO Group (<sup>1</sup>Geophysical Institute, Karlsruhe University, Hertzstr. 16, 76187 Karlsruhe, GERMANY, <sup>2</sup>Institut Teknologi Bandung, INDONESIA)

Many seismological tomography experiments with mobile stations and a local or regional focus have been carried out over the past 20 years. These experiments provided data sets which allow for a regional inversion of the seismic velocities in the upper mantle. Usually this inversion was done using a linearized inversion scheme where the resulting velocity model was linearized around a 1-D input model. This method proved to show reliable results, but only to a certain depth depending on the dimensions of the station network. To improve the resolution in depth we integrate regional data sets from experiments with mobile station networks into a global data basis and invert for the entire earth's mantle using a non-linear, iterative inversion scheme and a parameterization adjusted to the data density and the region of interest. In this way we can use the advantages of both global and teleseismic tomography: - by using a 3-D Ray tracing algorithm and an iterative, non-linear inversion scheme on the entire earth's mantle, heterogeneities in the velocity structure of the mantle can be localized and are therefore not mapped into the region of interest. In combination with the fact that the global data set has no frame dueto its global distribution of stations, we can expect a better resolution with depth as for teleseismic tomography alone, which is especially important in regions of deep structures, like subduction zones or mantle plumes. - On the other hand, the dense station coverage in the region of interest allows for a regional finer parameterization and therefore a regional higher resolution of the velocity structure comparable to the resolution of teleseismic tomography. Additionally our result is not isolated but in the context of the larger scale velocity structure and can be interpreted in a greater frame than just the region of interest. We apply this approach to south-eastern Europe, where a high quality teleseismic data set of first arrival times from the 1999 CALIXTO-Experiment (Carpathian ArcLithosphere X-Tomography) is integrated into an updated version of the widely used global data set by Engdahl et al. with recordings from 1964-1998. The CALIXTO data set includes 60 azimuthal equally distributed events which

were recorded between May and November 1999 at around 120 stations in the Carpathians (Romania). One critical geodynamic problem of the area refers to the depth extend of a remnant slab (Vrancea slab) that is currently detached and hosts strong intermediate-depth earthquakes. The inversion results provide an improved resolution in depth compared to results of an inversion using the linearized ACH-method. The velocity models also show some amplitude exaggeration in the shallower parts of the model which can be ascribed to missing correction terms for station- and crustal effects (e.g. Moho topography). These results are supported by several synthetic resolution tests.

**JSS06a-Posters**

**Tuesday, July 8**

**EARTH STRUCTURE AND GEODYNAMICS (IASPEI, IAVCEI, IAG, IAGA)**

Location: Site D

**Tuesday, July 8 PM**

Presiding Chair: T. Irifune

**JSS06a/08P/D-001 Poster 1400-079**

**SLAB PENETRATION INTO THE DEEP MANTLE LAYERING: 2D VS. 3D**

Takashi NAKAGAWA<sup>1</sup>, Paul J. TACKLEY<sup>2</sup> (<sup>1</sup>Department of Earth and Space Sciences, University of California, Los Angeles, <sup>2</sup>Department of Earth and Space Sciences and Institute of Geophysics and Planetary Physics, University of California, Los Angeles)

Our previous study [Nakagawa and Tackley, 2003] focused on the possible thermo-chemical structure in the mantle that satisfies both seismological and geochemical constraints in two dimensional geometry. However, the model used in that study did not include three-dimensionality or tectonic plates, which may be generated by semi-brittle, semi-ductile yielding in the lithosphere, and are important for understanding seismic structure in the shallow mantle. In this presentation the interaction between subducting slabs and deep mantle layering, and its influence to the seismic structure in the whole mantle, are focused on using two- and three-dimensional models of mantle convection. The model assumes thermo-chemical convection of an anelastic and infinite Prandtl number fluid with temperature-, depth- and yield stress-dependent viscosity in a two- and three-dimensional rectangular box of dimensions 4x1 and 4x4x1. Cases that include either a thick chemical layer (30% of convective domain) or thin layer (10% of convective domain) will be presented in both 2D and 3D. We will show the fields of temperature, viscosity, chemical and seismic velocity anomaly, and compare spectral heterogeneity maps of seismic anomalies with those of actual tomographic models, in order to constrain the possible thermo-chemical structure in the mantle.

**JSS06a/08P/D-002 Poster 1400-080**

**PHYSICAL DISPERSION WITH A REFERENCE FREQUENCY OF 2 HZ: BRIDGING BETWEEN SHORT- AND LONG-PERIOD S TRAVEL TIMES**

Satoko OKI<sup>1</sup>, Yoshio FUKAO<sup>2</sup>, Masayuki OBAYASHI<sup>1</sup> (<sup>1</sup>Earthquake Research Institute, Univ. of Tokyo, <sup>2</sup>Institute for Frontier Research on Earth Evolution, JAMSTEC)

The P to S velocity ratio carries important information about the composition and state of the mantle. Comparison of the existing P and S tomography models, however, may not be always justified because of large differences in their accuracy and resolution. Our plan is to start from short-period S wave tomography consistent with P travel time tomography. At the present stage, we confirmed the validity of our method to measure S travel time with an unexpected finding about the reference frequency of the physical dispersion. Picking an arrival time of S wave is in general difficult, and waveform correlation is a method to solve this problem. With an assumption of a point source model, P and S waveforms at the source are identical, and so S waveform can be synthesized from observed P waveform by correcting attenuation effect. We take into account the physical dispersion which is characterized by two parameters  $t^*$  and  $f_0$ . The reference frequency  $f_0$  is conventionally set to 1 Hz. A search is made for the value of  $t^*$  that gives the maximum cross-correlation for the first half cycle of waveform. Then S-P differential travel time is measured by cross-correlating synthetic and observed S wave. The measured S-P times have an advantage of being little affected by the uncertainty of origin time. Our method is justified for the consistency of measured travel times and those of AK135. To examine more detail, our cross-correlation method was checked against about 100 hand-picked S-P times. If the onset frequency were 1 Hz as conventionally regarded, the measured S-P with a reference frequency of 1 Hz and the hand-picked S-P should be close. We, however, found a systematic discrepancy of about 0.5 s between these two S-P times. This indicates a higher value for the reference frequency to be consistent with the onset frequency of short-period body waves. The 0.5 s discrepancy disappears when the reference frequency is taken to be 2 Hz. This result should be of great significance in bridging between long- and short-period S travel times. The body wave models and associated travel time curves such as JB, IASP91 and AK135 should be those at a reference frequency of 2 Hz, not 1 Hz. If one wishes to combine these body wave models to those derived from normal mode data by taking physical dispersion into account, some correction is required for the Q model.

**JSS06a/08P/D-003 Poster 1400-081**

**ESTIMATE OF ISOTROPIC AND ANISOTROPIC STRUCTURES OF THE EARTH BY SPECTRAL INVERSION INCORPORATING TOROIDAL-SPHEROIDAL COUPLING**

Hitoshi ODA (Department of Earth Sciences, Okayama University)

The effect of isotropic and anisotropic velocity perturbations of seismic body waves on low-frequency multiplets of the earth's free oscillation was investigated using synthetic spectra calculated for an aspherical earth model, in which the velocity perturbations regionally vary. Hexagonal anisotropy of which the c-axes lie horizontally is assumed in the upper mantle. The influence of the velocity perturbations on the vertical component spectrum appears as amplitude anomaly, "quasi-toroidal" mode resulting from toroidal-spheroidal coupling. Azimuthal dependence of the spectral amplitude of the quasi-toroidal mode excited by a vertical strike-slip fault is similar to the Love wave radiation pattern. In addition the free oscillation spectrum, especially the quasi-toroidal mode spectrum, is more sensitive to anisotropic velocity perturbation than to isotropic velocity perturbation. This means that the free oscillation spectrum may provide not only constraints on isotropic lateral structure but also those on anisotropic lateral structure. In order to retrieve the isotropic and anisotropic velocity perturbations from free oscillation spectra incorporating the quasi-toroidal mode, we presented an inversion method, "mixed-coupling spectral inversion" where three kinds of splitting functions were defined for toroidal, spheroidal and mixed-coupling modes,

respectively. We confirmed that the isotropic and anisotropic lateral structures were correctly estimated from the free oscillation spectra and that mixed-coupling spectral inversion made it possible to estimate the odd order interior structure of the earth, which has been unable to be determined by the conventional spectral inversion with taking no account of the mixed-coupling. It was demonstrated that the mixed-coupling biases the estimate of higher order structure when the conventional spectral inversion is applied to the amplitude spectra incorporating the mixed-coupling.

**JSS06a/08P/D-004** Poster **1400-082**

**INTERNAL STRUCTURES OF THE TERRESTRIAL PLANETS FROM GRAVITY AND TOPOGRAPHY CORRELATIONS: A STUDY OF OBSERVATIONAL CONSTRAINTS ON EVOLUTION MODELS OF PLANETS**

Laramie Vance POTTS, C.K. SHUM (Laboratory for Space Geodesy and Remote Sensing Research, The Ohio State University)

The internal structures of terrestrial planets are commonly constrained by seismic data and geochronological considerations. Analysis of satellite-measured gravity and topography can provide crust-to-core mass variation models for considering the geologic evolution of terrestrial planets. These mass differentiated models facilitate developing new perspectives on the poorly understood crustal and subcrustal features of the terrestrial planets. We suggest that these constraints may be augmented by gravity drilling that focuses on interpreting satellite altitude free-air gravity observations for boundary undulations of the internal density layers related to mass flow. This approach involves separating the free-air gravity anomalies into terrain-correlated and -decorrelated components based on the correlation spectrum between the anomalies and the gravity effects of the terrain. The terrain-decorrelated gravity anomalies are largely devoid of the long wavelength interfering effects of the terrain gravity and hence provide enhanced constraints for modeling mass variations of the mantle and core. For the Earth, subcrustal interpretations of the terrain-decorrelated anomalies are constrained by radially stratified densities inferred from seismic observations. For other differentiated bodies like the Moon, Mars and Venus, seismic soundings are largely lacking so that geochemical and moments-of-inertia considerations must be invoked to constrain the radial density structures in interpreting the terrain-decorrelated free-air anomalies. These anomalies, with frequencies that clearly decrease as the density contrasts deepen, facilitate mapping mass flow patterns related to the thermodynamic state and evolution of the interior. Results for the moon obtained from inversions of the lunar subcrustal anomalies inferred boundary undulations of the lunar core-mantle boundary, asthenosphere-lithosphere, and middle-upper mantle during bombardment time. The elevated core beneath the Procellum basin is consistent with the uplifting effects of the Imbrium impacts and the development of the great lunar hotspot. Topographic undulations inferred for the lower and middle mantle reflect a dichotomized thermal evolution of the lunar near-and farside. Our results further suggests that on the nearside, a relatively thinner and hotter lithosphere developed by mantle convection which facilitated the diapiric rise of magma and mare flooding of basins. Viscous entrainment of lower density material into the lower mantle on the farside developed a thicker and cooler lithosphere that may also have restricted basin flooding. We are currently extending our procedure for comparison of global gravity analysis for the Earth, Mars and Venus.

**JSS06a/08P/D-005** Poster **1400-083**

**NUMERICAL STUDY OF EFFECTS OF CONTINENTAL PLATES ON MANTLE DYNAMICS**

Yasuyuki IWASE<sup>1</sup>, Satoru HONDA<sup>2</sup> (Department of Earth and Ocean Sciences, National Defense Academy, <sup>2</sup>Earthquake Research Institute)

Numerical simulation of mantle convection with continental plates is carried out to investigate the dynamic interaction between them. Three-dimensional spherical shell mantle convection model is used, in which mantle is assumed an incompressible and infinite Prandtl number fluid and Boussinesq approximation is adopted. The continental plates are modeled by high viscosity region of the mantle and are assumed to be moved by the horizontal averaged mantle flow velocity within the region. Numerical experiments are conducted for three cases, in which number of the continental plates are one, two and four, respectively. In each case, the total areas of the continental plates are almost equal. Mantle temperature beneath the continents increases for all the cases due to the blanket effect of the continents. Although the volume averaged mantle temperatures show small increases and decreases with time, which is related to the locations of hotplumes and continents, the time averaged temperatures are almost the same for all the cases. However, the amplitude of temperature difference between mantle beneath continents and other part is larger, if the number of continents is smaller, i.e., area of a continent is larger. For the single continental plate case, huge rising plume is generated beneath the continent and the continent is drifted away from the plume by the horizontal flow accompanying with the plume generation. Then, the huge plume weakens and a new plume grows beneath the continent. As a result, spectrum of temperature field show that spherical harmonic degree  $l=1$  is dominant for almost all the time. In cases of two and four continents, when the continents are located closely each other, plumes assemble beneath the continents and merge into a large plume. Flow associated with plume disperses the continents but they can be assembled again at the antipode due to the sphericity of the mantle surface. Thus, the dominant wave length of the thermal structure alternates between  $l=1$  and  $l=2$  or 4 with time. The results of this study suggest that the thermal evolution of the whole mantle is controlled by the total size of the continental area but the magnitude of the super plume may be affected by the size of each continent. The generation of the super plume and the aggregation, breakup and separation of continents may be explained by the dynamic thermal interaction between mantle and continental plates.

**JSS06a/08P/D-006** Poster **1400-084**

**THERMAL EVOLUTION OF THE EARTH WITH CONVECTION MODEL BASED ON MIXING LENGTH THEORY**

Yasuko YAMAGISHI, Takatoshi YANAGISAWA (Institute for Frontier Research on Earth Evolution, JAMSTEC)

The thermal history of the Earth is supposed to have been essentially a cooling process. Convection is main mechanism for the process and plays a substantial role in the Earth's structural evolution. Most of the thermal history models for the Earth take the convective heat transport into account by adopting the method of the parameterized convection. The convection occurring in the Earth's interior, however, has some complicated aspects, including a large variation of the viscosity, internal heating and phase boundaries. Especially, the temperature dependency of the viscosity affects strongly on the efficiency of the convective heat transport and in the mantle, the viscosity should have strong dependency on the temperature and then have a large contrast. The parameterized convection needs to know the Rayleigh number of the convective region for the calculation of the efficiency of the heat transport. If the viscosity depends on the temperature, it inevitably differs with the position and the representative Rayleigh number of the convective layer should be decided arbitrarily. Therefore, the parameterized convection must treat the viscosity variation

artificially. There is an alternative method to calculate the efficiency of the convective heat transport, which we have developed based on the concept of 'mixing length theory'. This method needs only the local value of the various physical properties to calculate the efficiency of the convective heat transport. When using this method, the influence of the temperature dependency of the viscosity on the convective heat transport can be taken into account very easily, and the temporal change of the horizontally averaged temperature profile in the convective layer can be investigated by solving a mere thermal conduction problem. In this study, we firstly demonstrate that this method can calculate the efficiency of the convective heat transport correctly by comparison with the experimental results and 2D computational calculations. Next we actually calculate the one dimensional thermal history of the Earth by using this new method, taking account of the temperature dependency of the viscosity in the mantle and heat generation by the decay of the radiogenic isotopes and by the solidification of the inner core, and compare our models with the previous studies by using the parameterized convection.

**JSS06a/08P/D-007** Poster **1400-085**

**DYNAMIC EVOLUTION OF PASSIVE FLOWS DUE TO LARGE-SCALE THERMAL ANOMALIES INSERTED INSTANTANEOUSLY WITHIN THE STATIC LAYERED MANTLE**

Takao EGUCHI<sup>1</sup>, Kiyoshi MATSUBARA<sup>2</sup>, Mizuho ISHIDA<sup>3</sup> (<sup>1</sup>Dept. Earth and Ocean Sci., National Defense Academy, Yokosuka, JAPAN, <sup>2</sup>Fuji Research Institute, Tokyo, JAPAN, <sup>3</sup>N.I.E.D, Tsukuba, JAPAN)

To study three-dimensional unsteady mantle convection, we carried out numerical simulation on passive flows due to simplified local hot sources just above the CMB and/or large-scale cool masses beneath smoothed subduction zones. We utilized our individual numerical simulation code developed with the finite difference method. The basic three equations are for the continuity, the motion with the Boussinesq (incompressible) approximation, and the (thermal) energy conservation. The mantle viscosity in our model is sensitive to temperature. To obtain time integration with high precision, we followed the Newton method. The mantle velocity was initially set to zero throughout the layer. The temperature is 300K at the surface, ~ 2000K at the top of the lower mantle, 4,000K at the CMB. In the first model, the mantle viscosity has the temperature dependence which increases gradually from the CMB to the surface. The maximum and minimum values of the viscosity are  $3.8E+24$  (Pa s) at the surface and  $1.6E+22$  near the CMB, respectively. The second model has depth-fixed viscosity profile in which the averaged viscosity of the lower mantle is higher than that of the upper mantle. The maximum viscosity in the second model is  $5E+22$  (Pa s) at ~ 1,900 to 2,000 km depth and the minimum is  $1E+21$  at both regions of ~ 100 to 400 km and ~ 2,800 to 2,900 km depth. We in this study neglected the effect of surface plate motions, mineral phase changes and internal heating, etc. The Rayleigh number (Ra) is initially ~  $1E+7$ . To demonstrate numerically the viscosity dependence in the passive mantle flows, we input instantaneously a local cool mass (hereafter, case A) and great-circle cooling ring (case B) as a finite negative buoyancy source near the top of the lower mantle, ~ 670 km depth. Also, as a finite positive buoyant source in the lowermost mantle layer, initial input of a local warm mass (case C) and great-circle warm ring (case D) were incorporated in the simulation. We describe the simulation result of cases A to D for the two viscosity models: In both the viscosity models, due to the negative or positive buoyancy of the thermal anomaly inserted initially at ~ 670 km depth or at the CMB, respectively, the mantle exerts gradually itself a large-scale viscous flow system. The passively excited flows in the second viscosity model show relatively higher velocities especially at distant regions from the buoyant source than those in the first model. For cases A and B, the angle distances for sites of major upwelling measured from the locus of the initial thermal anomaly input are ~ 30 deg. in the first model and ~ 35 deg. in the second model. For cases C and D, the angle distances measured from the site of the initial thermal anomaly to the place of the major down-welling are ~ 25 deg. in the first model and ~ 35 deg. in the second model.

**JSS06a/08P/D-008** Poster **1400-086**

**THREE-DIMENSIONAL ELECTRICAL CONDUCTIVITY STRUCTURE BENEATH NORTH PACIFIC**

Takao KOYAMA<sup>1</sup>, Hisayoshi SHIMIZU<sup>2</sup>, Hisashi UTADA<sup>2</sup> (<sup>1</sup>IFREE, Japan Marine Science and Technology Center, <sup>2</sup>Earthquake Research Institute, University of Tokyo)

In this paper, we present a model of three-dimensional electrical conductivity structure in the mid-mantle beneath the North Pacific by a semi-global three-dimensional inversion of EM data. We used data of voltage variations obtained by eight submarine cables and magnetic field variations at eight geomagnetic observatories/stations as well as C responses published Fujii and Schultz [2002]. We assumed that 3-D heterogeneous conductivity distribution can be separated into radially symmetric (1-D) structure and 3-D perturbation, in which the 1-D reference model beneath the North Pacific by Utada et al. [2003] is used. 3-D perturbation was inversely estimated so that the observation-calculation misfit is minimized with an additional mathematical constraint such that perturbation is smooth in space. For this analysis, a new three-dimensional inversion algorithm was developed by combining the steepest descent and the quasi-Newton methods. An integral equation solver using the modified IDM (e.g. Singer, 1995) was used as a forward solver. The 1-D reference model consists of 17 layers with 50 km thickness. Perturbation is assumed to exist in the depth range from 350 km to 850 km in a quarter of the Earth centered by the North Pacific, that is, in the horizontal range from 90 to 270 degrees of longitude and from 0 to 90 degrees of colatitude. This region of perturbation is divided into  $12 \times 6 \times 5$  grids, i.e., total 360 grids of 15 degrees laterally and 100 km radially with unknown conductivity parameters, while the grid size for calculation is 3 degrees horizontally and 50 km in the depth. In the oceanic region, the ocean-land contrast makes a significant effect on EM responses, so we took into consideration the oceanic effect by including a priori ocean distribution with 3 S/m conductivity in the inversion. Total number of data parameters which are complex MT and GDS responses are 330. We have made a checkerboard test and found the spatial resolution depends on the distribution of observation sites (cables and magnetic stations). Considering this, following features can be pointed out that can be comparable to results of seismic tomography (e.g. Fukao et al., 2001; Megnin and Romanowicz, 2000): 1) There is a conducting zone in the transition zone beneath Hawaii with a conductivity perturbation of factor of three. 2) The uppermost lower mantle beneath Philippines is less conductive by a half. 3) The transition zone beneath Mariana is more conductive by three times. Assuming the heterogeneities purely of thermal origin, we found that they correspond to temperature anomalies of 200 - 300 degrees.

**JSS06a/08P/D-009** Poster **1400-087**

**ISOTOPIC EVOLUTION OF THE MANTLE IN NUMERICAL CONVECTION MODELS**

Shunxing XIE, Paul TACKLEY (Department of Earth and Space Sci., University of California, Los Angeles, USA)

To investigate dynamical mechanisms that have been proposed to explain geochemical observations, a model of mantle convection that combines a treatment of major and trace element geochemical evolution with a dynamically-consistent mantle convection-plate

## INTER-ASSOCIATION

tectonics is presented. Melting is simulated using a realistic solidus and is responsible for the generation of heterogeneity including the partitioning of trace elements between oceanic crust and residue; the subsequent hydrothermal alteration of element concentrations in the crust is also included. Trace elements studied are the U-Th-Pb and Sm-Nd isotope systems, helium and argon. Both olivine and pyroxene-garnet system phase transformations are included, with the relative density profiles of basalt, pyrolyte, and harzburgite following those of Ringwood (1990) and Ono et al. (2001) up to 800km depth, but varied in the deeper mantle to reflect present uncertainties. A suite of numerical experiments has been run to systematically investigate the sensitivity of the results to uncertain physical properties such as the density of subducted crust in the deepest mantle and elemental partition coefficients. In order to test whether the volumetric heterogeneities (associated with crustal differentiation and lower mantle segregation) obtained in our thermochemical models exist in Earth, we establish their observational signatures and compare to seismic observations. Statistical diagnostics such as field filtering, radial correlation functions and spectral heterogeneity map are used to characterize the observational signature of the thermochemical structures. Results indicate that the system can self-consistently evolve regions that have a HIMU-like signature (by segregation of subducted crust at the CMB) and regions with high He3/He4. Low He3/He4 ratios evolve in crustal material even though He may be more incompatible than U, due to outgassing of He to the atmosphere. Some parameter combinations simultaneously lead to Earth-like distributions of He3/He4 ratios, Pb-Pb and Sm-Nd ratio plots for erupted material, and ~50% outgassing of radiogenic Ar40 consistent with geochemical constraints. In the preferred model, helium is highly incompatible and crust is dense near the CMB. The Sm-Nd age is 1-2 billion years. Earth-like He3/He4 histograms are produced (in erupted material) when sufficient subducted crust mixes back into the shallow mantle to bring its Helium ratio down to the MORB-like range. Our results confirm that strong heterogeneities caused by crustal differentiation and subduction are in agreement with seismic tomographic models.

**JSS06a/08P/D-010** Poster **1400-088**

### 3D MANTLE P-VELOCITY MODEL BASED ON UNIFORM TETRAHEDRONIZATION OF THE EARTH AND THE NATURAL NEIGHBOUR INTERPOLATION METHOD

Jianfeng PAN, Adam M. DZIEWONSKI (Harvard University)

Traditional parameterization of three dimensional (3D) Earth models consists of radial, and horizontal basis functions on a constant lateral grid size independent of depth. As a result, the horizontal basis functions become more densely distributed with increasing depth. The nominal resolution thus becomes finer. For example, in the lower mantle and D'' region, current whole-mantle models appear to be characterized by particularly short-wavelength structures and high gradients, which might not be real features. In this study, we use instead a 3D parameterization generated by an "advancing front method" (NETGEN), given an initial triangulation on the surface of the Earth. The result is a number of tetrahedrons with optimal and, more or less, similar size making up of the Earth's volume. We then utilize the natural neighbour interpolation technique to set up the whole mantle 3D inverse problem. The functional value (in our case, perturbation to the P-velocity) in any point within the Earth can be interpolated by the values of its natural neighbours (on the order of 10). The number of nodes decreases with depth as the volume decreases. The basis function at each node is smooth, and dependent on the distances of other nodes around it. No separation of radial and horizontal basis functions is needed. Synthetic test with a 3D S-model S362 shows that most of the significant structures of S362 are recovered. The major differences exist: (1) at depth 2,500km and 2,800km, the recovered model is smoother and has less short-wavelength signal than S362; (2) at the surface and CMB, the recovered S-velocity perturbation tends to be larger. Currently we are deriving a whole mantle P-model. The preliminary result is promising. Compared to the traditional approach to employ both radial and horizontal basis functions in other studies, this parameterization allow a true 3D representation of the Earth's seismic velocity perturbations. It is also straight-forward to build norm and roughness damping matrices and apply them to the target model. Because of the ease of the grid generation and the grid-dependent basis function, it is also possible to introduce multigrid (denser grid points for some part but coarser for the rest) into the 3D seismic tomography to achieve multi-scale resolution.

**JSS06a/08P/D-011** Poster **1400-089**

### 3-D WAVEFORM SENSITIVITY KERNELS FOR SURFACE WAVES

Kazunori YOSHIKAWA (Division of Earth and Planetary Sciences, Hokkaido University)

With the assumption of scalar wave propagation in laterally heterogeneous structure, two-dimensional sensitivity kernels for surface-wave phase speeds for a single frequency can be efficiently constructed using the Born approximation linked to asymptotic ray theory [Yoshizawa and Kennett, 2002]. The combination of the two-dimensional sensitivity kernels for phase-speed structures and one-dimensional sensitivity kernels for the reference Earth model yields a representation of the three-dimensional sensitivity of travelling surface waves to shear wave speed structures. Using these time-dependent 3-D sensitivity kernels, suitably filtered seismograms can be inverted directly for 3-D shear wave speed structure without intermediary measurements of the phase and amplitude of surface waves as a function of frequency. The three-dimensional kernels generally exhibit sensitivity to wide areas around a geometrical ray path, which corresponds to a few orders of the Fresnel zones, with the maximum sensitivity near source and receiver locations. Source radiation patterns have significant influence on the sensitivity kernels, which suggests that the sensitivity kernels can be contaminated by errors in source parameters. Introducing differential waveforms between two nearby stations, we can construct 3-D sensitivity kernels for the differential waveforms by working with appropriate transfer functions with corrections for slight differences in both propagation distances and azimuths between two stations. Such differential 3-D kernels have nearly zero sensitivity to the source region, leaving high sensitivity to relatively small areas around the receivers. The use of the differential waveforms of two nearby stations as a secondary observable will enable us to investigate shear wave speed structures in and around regional seismic arrays taking the effects of finite frequency into account, and will be of great help in improving the reliability of regional surface wave tomography.

**JSS06a/08P/D-012** Poster **1400-090**

### REFERENCE 3-D P-VELOCITY MODEL OF THE MANTLE BENEATH EURASIA AND FLANKED OCEANIC MARGINS: THE NEW TECTONIC AND GEODINAMIC VIEW

Valentin GEYKO, T. TSVETKOVA, L. LIVANOVA, K. GEYKO, L. SHUMLANSKAYA, I. BUGAYENKO, L. ZAYETS (Institute of Geophysics of NAS Ukraine)

An analysis of the model yields the following observations: The mantle of the explored subcontinent together with the flanked margins of the Pacific, Atlantic and Arctic falls into the two shells by the global boundary situated at 550-680 km depth. The upper shell (tectonosphere) is notably inhomogeneous laterally, while the lower one is more near to radial-symmetry (deeper than 750-780 km). The boundary of the upper and lower tectonosphere situated at depths 390-450 km - the asthenosphere - is not global. The former

is peculiar to the ancient and formed tectonic structures and later to those actively living at the present. The velocity anomalies correspond to known plate tectonic elements, but also reveal the presence of ancient tectonic features. Orogens seem to coincide with gently sloping subducted slabs. In some cases low velocity anomalies extend from the surface to large depths, perhaps relating spreading with rising asthenospheric material. The thickness of the tectonosphere is related to its age and genesis. The tectonic structures of the first order (plates) have 'roots' piercing full the tectonosphere, while those of higher order are clear-cut in the upper and unclear in the lower tectonosphere. Sutures and structural discontinuities are reflected in the mantle by large velocity contrasts. Thus, not only are major structural regions at the surface associated with velocity anomalies at depth, but the boundaries between them show anomalous velocities, perhaps reflecting the structural history of the region. Large tectonic structures have opposite velocity anomalies in the upper and lower tectonosphere. Seismic belts and regions of high seismicity are strongly connected with certain velocity anomalies.

**JSS06a/08P/D-013** Poster **1400-091**

### MULTIMODE SURFACE WAVEFORM TOMOGRAPHY OF THE UPPER MANTLE UNDER THE SOUTH PACIFIC SUPERSWELL

Alessia MAGGI<sup>1</sup>, Eric DEBAYLE<sup>1</sup>, Keith PRIESTLEY<sup>2</sup>, Guilhem BARRUOL<sup>3</sup>, Fabrice FONTAINE<sup>4</sup>, Dominique REYMOND<sup>5</sup> (EOST, CNRS and Université Louis Pasteur, Strasbourg, France, <sup>2</sup>Bullard Laboratories, University of Cambridge, United Kingdom, <sup>3</sup>Jeune équipe Terre Ocean, CNRS and université de la Polynésie Française, Faaa, French Polynesia, <sup>4</sup>Laboratoire de Tectonophysique, CNRS and Université de Montpellier II, France, <sup>5</sup>Laboratoire de Géophysique, CEA, Faa, French Polynesia)

The expanse of the South Pacific is punctuated by a swarm of volcanic island chains -- the Society Islands, Austral Islands, and Marquesas -- superimposed on a broad topographic high known as the South Pacific super swell (McNutt, 1998). The region is also characterised by a large-scale, low velocity anomaly in the lower mantle (e.g. Su et al., 1994) and anomalous converted phases from the 660 km discontinuity (Vinnik et al., 1997). We present preliminary results of a multimode surface wave tomographic study of the region. Except in its southernmost part, the Pacific plate is surrounded by subduction zones that provide an excellent azimuthal distribution of deep events with well excited overtones. The station distribution around the margins of the Pacific is also relatively dense, due to the high seismic risk of these regions. The resulting dense ray coverage, however, thins out in the South Pacific, and is insufficient for high-resolution imaging of an eventual Pacific super plume. As part of PLUME (Polynesian Lithosphere and Upper Mantle Experiment, funded by the French Ministry of Research), ten broadband stations have been deployed in French Polynesia, as far as -27 degrees South. The stations provide the necessary data to the south of the main location of the super swell to facilitate high-resolution imaging of its upper mantle expression. We initially analyse only Rayleigh wave seismograms, which constrain the isotropic SV structure of the upper mantle. Our preliminary results, obtained using the automated (Debayle, 1999) version of the Cara and Leveque (1987) method, will help answer questions about the possible existence and/or morphology of upper mantle upwelling (plume?) connecting with the Pacific super swell.

**JSS06a/08P/D-014** Poster **1400-092**

### THERMO-CHEMICAL EVOLUTION OF THE CONVECTING MANTLE AND CORE: IMPORTANCE OF COMPOSITIONAL ANOMALIES IN THE CMB REGION

Takashi NAKAGAWA<sup>1</sup>, Paul J. TACKLEY<sup>2</sup> (<sup>1</sup>Department of Earth and Space Sciences, University of California, Los Angeles, <sup>2</sup>Department of Earth and Space Sciences and Institute of Geophysics and Planetary Physics, University of California, Los Angeles)

The heat flow through the core-mantle boundary is the most important quantity for understanding the thermal evolution of the coupled core-mantle system, and it is strongly influenced by the presence and distribution of compositional anomalies above the core-mantle boundary. In a previous study [Nakagawa and Tackley, 2002 on AGU Fall Meeting] we showed how the thermal history of the convecting mantle-core system is affected by the presence of primordial compositional layering above the CMB. However, another proposed origin for the compositional anomalies in the CMB region is the build-up of recycled oceanic crust from subducted slabs. Here the thermal evolution of the coupled, convecting mantle-core system is studied using a two-dimensional cylindrical shell mantle convection model with self-consistently generated tectonic plates and material recycling. Thermal evolution histories are compared to previous models with primordial layering and to compositionally homogeneous models, and considered in the context of various constraints on heat budget. In order to understand how heat transfer through the CMB scales in the presence of dense compositional anomalies, an improved parameterized model, analogous to an upside-down version of a parameterized model used to treat the effects of continents [Grigne and Labrosse, 2001], will be considered and calibrated using the dynamical models.

**JSS06a/08P/D-015** Poster **1400-093**

### DEEP STRUCTURE OF THE EURASIA-PACIFIC TRANSITION ZONE

Ludmila P. ZABARINSKAYA, Alexander G. RODNIKOV, Natalia A. SERGEYEVA (Russian Academy of Sciences, Geophysical Center)

The deep structure of the Eurasia-Pacific transition zone was investigated under the Geotraverse International Project along the deep sections of the tectonosphere, including the lithosphere and the asthenosphere, based on the complex interpretation of geological and geophysical data. The first geotraverse, investigated in cooperation with Japanese geoscientists, crossed the region of the Japan Sea. The second geotraverse, investigated in cooperation with Japanese and Chinese geoscientists, crossed the region of the Philippine Sea and the North China Plain. The third geotraverse crossed the region of the Okhotsk Sea. The total length of the geotraverses amounted to a few thousand kilometers with a depth of 100 km. The structure of the study region is distinguished by the fact that its upper mantle includes an asthenospheric layer with its diapirs of hot anomalous mantle, responsible for the formation of a transitional zone. The asthenosphere has a depth of 50-80 km under the old Paleogene basins, such as the West Philippine Basin, a roughly 30-km depth under the Neogene basins, such as the Parece Vela Basin of the Philippine Sea or the Kuril Basin of the Okhotsk Sea, and a merely 20-10-km depth under the Pliocene-Quaternary inter-arc basins, where it caused the break-up of the lithosphere, the formation of rifts, basalt magma flow, and hydrothermal activity. The sedimentary basins of the marginal seas are distinguished by an abnormal deep structure characterized by the localization of asthenospheric diapirs under these basins, the development of rifts and spreading centers at their bases, volcanic activity during the early phase of their formation, associated with hydrothermal processes and sulfidic formation, and the high heatflow caused by the rise of the asthenosphere toward the surface. It appears that the asthenospheric diapirs with the partial melting of rocks represent channels by which hot mantle fluids from the asthenosphere penetrate to the sedimentary basins. Based on these geotraverses, researchers from the Geophysical Center of the Russian Academy of Sciences created a database including the deep geological and geophysical sections of the lithosphere under the

transition zone from Eurasia to the Pacific and the related primary geological and geophysical data, the results of the bathymetric, magnetic, and gravity surveys, heat flow measurements, deep seismic sounding, tomography, seismology, the results of studying the fine structure of the Bcnioff zone, some data on the chemistry and age of the rocks, and the results of deep-sea drilling and dredging. This work was supported by the Russian Foundation for Basic Research, projects 01-05-64400 and 01-07- 90233.

**JSS06a/08P/D-016** Poster **1400-094**

#### HIGH-RESOLUTION RECEIVER FUNCTION IMAGING OF THE CRUST AND THE MANTLE BENEATH THE JAPAN ISLANDS

Kazuro HIRAHARA<sup>1</sup>, Makiko YAMAUCHI<sup>1</sup>, Takashi TONEGAWA<sup>1</sup>, Takuo SHIBUTANI<sup>2</sup> (<sup>1</sup>Graduate School of Environmental Studies, Nagoya University, <sup>2</sup>DPRI, Kyoto University)

In recent 5 years, we have obtained the detailed images of receiver function (RF) in the crust and the upper mantle beneath the Japan Islands. In this paper, we show our strategy and some of interesting results. Though the number of stations is still increasing now, we have so far processed data observed at 203 J-array (operated by universities and JMA) and 634 Hi-net (NIED) short-period stations and at 63 J-array and 64 F-net (NIED) broadband ones. We use data during a period from 1996 to 2000 for J-array and F-net, and from 2000 to 2002 for Hi-net. At present, for the crust and the uppermost mantle, we use both short-period and broadband data, retaining high-frequencies up to 1 Hz, while only broadband data are used with low-pass filtering of 0.3 Hz for the deeper upper mantle. We employ Singular Value Decomposition (SVD) filtering to enhance the coherent phases. With a reference velocity model of iasp91, we transform the time domain RFs to the depth domain ones, assuming that phases in radial RFs are P to S converted ones at depths. We stack the depth domain RFs to project onto 2-D cross-sections along several profiles. In the crust, we find the remarkable positive Moho Ps phases in RFs, whose amplitudes vary locally, and we obtain the distribution of the depth and converted amplitudes. Generally, the clearer Moho Ps phases are seen in southwest Japan than in northeast Japan. The Conrad Ps phases are not clearly seen all over the Japan, but locally seen in the Kinki and the Chugoku regions of southwest Japan. For Hi-net data, we try to execute the analyses retaining the higher frequencies up to 3 Hz. In southwest Japan, such higher frequency RFs observed at some stations show the prominent wave-packets between the Conrad Ps phases and the Moho ones, which are possible Ps phases converted at the lower crustal reflective layers. Beneath southwest Japan, the short-period RFs clearly delineate the 3-D configuration of the subducting Philippine Sea plate (PHS) from Kii Peninsula to the Shikoku regions, which is consistent with the hypocentral distribution and the previous tomographic results. Further down to depths of 60 to 80 km, we can trace positive RFs in the deeper extended regions which is the aseismic PHS. The Pacific plate (PAC) subducts westwards from the Japan trench to a depth of 600 km, which are estimated from the earthquake distribution and the tomographic studies. Correspondingly, we see the positive RF amplitudes down to a depth of 150 km or more. Almost all over the Japan Islands, we can trace the 410 and the 660 km Ps phases, which are undulated due to the cold PAC. The 410 km discontinuity is locally elevated in the cold PAC by 80 km, and the 660 km one is downwarped in a larger scale toward the PAC. For these upper mantle discontinuities, also see the detailed discussion by Tonegawa et al. in this symposium.

**JSS06a/08P/D-017** Poster **1400-095**

#### RECEIVER FUNCTION IMAGE OF THE 410 AND 660KM SEISMIC VELOCITY DISCONTINUITIES BENEATH THE JAPAN ISLANDS

Takashi TONEGAWA<sup>1</sup>, Kazuro HIRAHARA<sup>1</sup>, Takuo SHIBUTANI<sup>2</sup> (<sup>1</sup>Graduate School of Environmental Sciences, Nagoya University, <sup>2</sup>)Disaster Prevention Research Institute, Kyoto University)

In the Japan Islands, several short-period and broadband seismic networks have recently been installed or are still under construction at present, which realize one of the highest densities of station spacing in the world. Among these networks, we apply Receiver Function (RF) analyses to teleseismic P-wave coda portions observed at 63 J-array and 64 F-net broadband stations and investigate the detailed structure of the upper mantle velocity discontinuities. We examine the observed waveforms from the teleseismic events with the magnitudes greater than 5.5, which occur during a period from 1996 to 2000. We discard almost 30,000 RFs with low signal-to-noise ratios, and finally keep a total of 5555 RFs from 153 events. Since such numbers of data and stations used in this study are largely augmented comparing with those in the previous RF analyses around the Japan Islands such as Li et al. (2000), we can reveal the far more detailed upper mantle structure. RFs are conventionally constructed through frequency domain division of radial components by vertical ones with a water level of 0.01. The low-pass Gaussian-filter of 0.3Hz is also applied. Assuming the phases in RFs are produced by Ps converted ones at depths, we transform the time domain RFs to the depth domain ones using a reference velocity model of iasp91. This process may be called migration. Then, SVD-filtering is applied to the depth domain RFs. We keep largest 6 eigenimages to construct filtered RFs. Finally, we construct 2-D stacked RF image projected on cross-sections along several profiles to see the detailed velocity discontinuity structure. Beneath the Japan Islands, the Pacific plate (PAC) is subducting westwards from the Japan trench to a depth of 600km, while the Philippine Sea plate (PHS) is subducting from the Nankai trough to a depth of 60-80km in southwest Japan. Beneath the whole Japan Islands, the dipping positive RF amplitude traces can be recognized to a depth of 150km or more, which coincide with the distribution of deep earthquakes occurring within PAC. In southwest Japan, however, we cannot clearly see the RF image of the descending PHS. In the deeper upper mantle, the remarkable positive RF traces corresponding to the 410 and 660km velocity discontinuities are recognized clearly all over the Japan Islands, while the 510km discontinuity can not be seen. The 410 and 660km discontinuities are undulated due to the subducting cold PAC slab. Beneath central to southwest Japan with the highest density of conversion points of these phases, RF images remarkably delineate that the 410 km velocity discontinuity is locally elevated by about 80 km within the subducting PAC. The 660km discontinuity is gradually downwarped westwards toward the PAC in a larger scale, whose deepest depth is about 690km.

**JSS06a/08P/D-018** Poster **1400-096**

#### LATERAL VARIATIONS OF THE D'' DISCONTINUITY BENEATH THE CENTRAL PACIFIC

Megan Sue AVANTS<sup>1</sup>, Thorne LAY<sup>1</sup>, Sara RUSSELL<sup>2</sup> (<sup>1</sup>Department of Earth Sciences, University of California, Santa Cruz, <sup>2</sup>Weston Geophysical Corporation)

The lowermost ~ 250 km of the mantle is characterized by a laterally heterogeneous thermal and chemical boundary layer, the D'' Region. In many areas a strong velocity gradient or velocity discontinuity is found near the top of D'', which is variously interpreted as being the result of a phase change, a chemical contrast, a transition in fabric to an anisotropic layer, or a relic subducted slab thermal/chemical anomaly. Seismic waves from events in the Tonga-Fiji region encounter the D'' zone beneath the Central Pacific and are recorded by dense broadband seismic networks in western North America. Recent waveform stacking

efforts suggest the presence of coincident P and S velocity discontinuities at about 230 km above the core-mantle boundary under the Central Pacific. The velocity contrasts at the discontinuities are weaker (0.75% and 1.7%, respectively) than found in circum-Pacific regions. It is also found that the S wave velocity decrease below the D'' discontinuity is abnormally strong with respect to the P velocity decrease in this region. Being far removed from present subduction zones, the existence of D'' discontinuities in the low velocity mantle under the Central Pacific is particularly intriguing. Lateral heterogeneities within this zone, combined with complex crustal structure at the receivers, make the depth and magnitude of the velocity discontinuities difficult to resolve. We extend analysis of shear wave data from Tonga-Fiji earthquakes recorded by broadband networks in western North America to better resolve small scale features in D'' under the Central Pacific. Our approach includes deconvolving reference source wavelets, binning and stacking localized subsets of data, and modeling features in the stacks to provide improved resolution of the nature of the D'' discontinuity beneath the Central Pacific. Preliminary binning of data into subsets has shown that the depth and strength of this discontinuity vary widely across the region sampled by the events in our data set. The results of more refined binning as well as waveform modeling of observed features will better resolve the character of the D'' discontinuity beneath the Central Pacific, allowing us to compare these results to D'' structure in circum-Pacific regions, ultimately providing insight as to the cause of D'' discontinuities.

**JSS06a/08P/D-019** Poster **1400-097**

#### WAVEFORM MODELING OF 3D STRUCTURE AT THE BASE OF THE MANTLE USING A COUPLED SEM/NORMAL MODE APPROACH

Akiko TO, Yann CAPDEVILLE, Barbara ROMANOWICZ (UC Berkeley)

The presence of strong lateral heterogeneity in D'' is now well documented, and represents a problem for seismic modeling, when using standard ray or mode approaches, because of the theoretical limits of validity of these methods. Consequently, present tomographic models are only able to represent the large scale, smooth features of the structure. They may also not reflect the amplitudes of lateral variations accurately. We use a coupled normal mode/Spectral Element Method (SEM) to compute synthetic seismograms of Sdiff in the D'' part of a 3D tomographic model (SAW24B16, Mégnin and Romanowicz, 2000) down to a corner frequency of 1/12s. This coupled method is much faster than standard SEM, as the numerical part of the computation is restricted to the D'' region. The rest of the mantle is assumed 1D, and there the wavefield is computed using efficient normal mode summation. We compare the synthetics thus obtained with observed waveforms for a collection of deep earthquakes in the Western Pacific and stations in North America. For deep earthquakes, the effect of strong heterogeneity in the crust and upper mantle is avoided. Observed and synthetic travel time trends are very consistent, although in most cases the observed residuals are significantly larger. Waveform amplitudes are less consistent. We also compare the predictions using SEM with those obtained by more approximate methods: ray theory on the one hand, NACT (Non-linear asymptotic coupling theory, a normal mode perturbation approach) on the other. The comparison with ray theory demonstrates that it generally over estimates travel times; the fit is somewhat better with NACT, but erratic discrepancies in amplitudes remain. Starting with the tomographic model, and correcting for mantle structure outside of D'' using approximate NACT predictions, we next invert for perturbations to the tomographic model, using the coupled SEM/mode computation for the forward part of the modeling, in several regions of the D'' under the Pacific which are well sampled by available Sdiff data. We present and discuss the inversion technique and the resulting models, and in particular explore whether the Pacific "superplume" structure requires sharp borders, as has been suggested for the African one.

**JSS06a/08P/D-020** Poster **1400-098**

#### TO THE QUESTION OF NEW INTERPRETATIONS OF MECHANISMS OF EVOLUTION OF THE TERRESTRIAL STRUCTURE AND SOME CONSEQUENCES THEREFROM

Eugeni Yakovlevich SMIRNOV (author)

The project 'Creation of a Computing Complex for the Study of Evolution of the Terrestrial Structure on the Account of Sciences of the Earth' (see [http://tspm.icape.ru/geya/eng/lab\\_e.htm](http://tspm.icape.ru/geya/eng/lab_e.htm)) is described. In the project some non-traditional models of the terrestrial magnetic field generation mechanism are proposed that do not conflict with the available metrical information; of the mechanisms of tectonic forces action, earthquakes, dislocations of Earth's crust, underground waters and magma; of the process of generation of ores of the volcanic and hydrothermal types.

See also [http://www.physical-congress.spb.ru/english/SmirnovEA/smironov\\_EA\\_Eng.asp](http://www.physical-congress.spb.ru/english/SmirnovEA/smironov_EA_Eng.asp)

**JSS06a/08P/D-021** Poster **1400-099**

#### PRINCIPLE OF THE EARTH GRAVITATIONAL ENERGY MINIMIZATION AND THE MECHANISMS OF ITS EMBODIMENT

Vladimir V. KUZNETSOV (JSS06)

The self-gravitational ball (star, planet, the major satellite) is treated as a self-regulating, self-organizing system in terms of the theory of self-organizing and optimum processes. The effect of the gravitational potential's minimization principle results in the Earth, as well as the other planets, to aspire to minimize its surface area. It means, that at the Earth there is a force, which aspires as to bring it to a state of a standing balance, and as to reduce the shape of the Earth into the equilibrium shape of sphere by minimization of the geoid height. This force initiates the shift tensions which involve the matter flow at the surface layer of the earth crust. This force is similar to force of the surface tension of liquid. The surface forces cause the motion of continents, the formation of mountains, seismicity and volcanicity through embodying of the Principle.

**JSS06a/08P/D-022** Poster **1400-100**

#### ANALYSIS OF BROADBAND SEISMIC ARRAY FOR THE INVESTIGATION OF THE TOP OF THE EARTH'S OUTER CORE BENEATH THE INDIAN OCEAN

Satoru TANAKA (Research Center for Prediction of Earthquakes and Volcanic Eruptions, Graduate School of Science, Tohoku University)

The issues of stable stratification and possible heterogeneity at the top of Earth's outer core are important to understand not only the core-mantle interaction but also the dynamics of the outer core. Previously some seismological studies had revealed vague features of the region using the seismological networks of the former generations, but their results were not consistent each other. The recent data accumulation under the modern seismic networks or arrays consisted of broadband seismographs makes it possible to try a further study. Here we show the examples of the analysis using the Kaapvaal broadband seismic array that was temporarily deployed in the South Africa since 1997 to 1999. The target of analysis is SmKS (m=1,2,3,4) seismic phases. Seismograms were deconvoluted using the instrumental response to displacement, and rotated the horizontal components into the radial ones. The

## INTER-ASSOCIATION

relative times were corrected to align on the peak locations of S2KS or S3KS. We applied the phase-weighted stack to separate the SmKS phases in the time-slowness space. The peak location of SKS and S3KS were picked on the vespagrams from the original seismograms while the Hilbert transformed seismograms were used for picking S2KS and S4KS because of the phase shift of the SmKS. Until now, we have analyzed the array records of one intermediate-depth earthquake (1997/04/23 in Mariana, distance from 116 to 127 degrees), and two deep earthquakes (1997/09/04 in South Fiji, distance from 117 to 126 degrees; 1998/03/29 in Fiji, distance from 130 to 135 degrees). The ray paths are distributed under the Indian Ocean. Differential travel times and relative slowness were obtained for the combination of  $S(m+1)KS$  and SmKS. PREM was used for the calculation of the ray theoretical travel times and slowness as a reference. The residuals of differential travel times for  $T(S3KS-S2KS)$  and  $T(S2KS-SKS)$  were scattered from -1.6 to 1.6 s indicating no systematic geographic pattern. Since only small parts of the Fresnel zones of S2KS and S3KS coincide for the predominant period of 5-10 s, it is difficult to separate the effects of the D' and the outermost core. Only the deep Fiji event shows clear S4KS seismic phases, and the residual of  $T(S4KS-S3KS)$  was 0.0 s while the residual slowness was 0.14 s/deg. Main parts of the Fresnel zones of S3KS and S4KS coincide and the ray paths cross the CMB regions with the small velocity perturbation. If this measurement is confirmed by the other combination of an event and array, the velocity gradient in the outermost about 50 km of the core should be slightly modified without the change of the average velocity.

**JSS06a/08P/D-023** Poster **1400-101**

### SEISMIC OBSERVATION OF NARROW PLUMES IN THE OCEANIC UPPER MANTLE

X. LI<sup>1</sup>, R. KIND<sup>1</sup>, X. YUAN<sup>1</sup>, S.V. SOBOLEV<sup>1</sup>, W. HANKA<sup>1</sup>, D.S. RAMESH<sup>2</sup>, Y. GU<sup>3</sup>, A.M. DZIEWONSKI<sup>1</sup> (GFZ Potsdam, Germany, <sup>2</sup>NGRI, Hyderabad, India, <sup>3</sup>Harvard University, USA)

We have found seismic evidence for the existence of narrow (about 200 km diameter) and hot plumes in the upper mantle above the 410 km discontinuity. They are located mainly under ocean islands, not however, under the central parts of major continents. These results are obtained from comparing globally the observed travel time differences between Ps conversions and SS precursors from the discontinuity at 410 km depth, using published data and new observations from ocean island stations. Comparison of SS precursors and Ps conversions, however, leads also to indications of significantly fewer narrow plumes in the upper mantle transition zone between 410 and 660 km depth, than in the upper mantle above 410 km depth.

**JSS06a/08P/D-024** Poster **1400-102**

### SEISMIC WAVE SPEEDS AND ATTENUATION IN THE UPPER MANTLE INTERPRETED THROUGH LABORATORY MEASUREMENTS

Ulrich FAUL, John D. FITZ GERALD, Ian JACKSON (Earth Materials Department, Australian National University)

The influence of a small basaltic melt fraction (0.004-0.037) on the seismic properties of fine-grained synthetic polycrystals of Fo90 olivine has been explored at seismic frequencies with torsional forced oscillation/microcreep methods. The presence of a broad dissipation peak superimposed on the monotonically frequency and temperature dependent background clearly distinguishes materials containing as little as ~ 0.5 % melt from their melt-free equivalents. In both types of material the observed dissipation is attributed to grain-boundary sliding involving a mixture of elastic and diffusional accommodation. The difference in mechanical behaviour is ascribed to the rounding of olivine grain edges at melt-bearing grain-edge tubules? allowing sufficient localisation of dissipation in frequency-temperature space to produce a resolvable peak attributable to elastic accommodation. Empirical models have been developed that adequately describe the dependence of  $1/Q$  upon period, temperature, average grain size and, for the melt-bearing materials, maximum melt fraction. These models have been extrapolated to the larger grain sizes and P-T conditions representative of the upper mantle. The inferred levels of attenuation for melt-free material are broadly consistent with those observed seismologically suggesting that the same grain-boundary diffusional processes thought to dominate the behaviour of the fine-grained materials tested in the laboratory might also account for much of the wave speed variability and attenuation in the mantle. For melt-bearing olivine, the extrapolated attenuation is generally somewhat higher than the highest seismologically measured attenuation, but the low spatial resolution of seismological studies means that the latter may average the properties of melt-free and partially molten parts of the upper mantle. The superposition of the melt-related dissipation peak upon the monotonic background is such that, for appropriate combinations of grain size, melt fraction and temperature, nearly frequency-independent attenuation is to be expected. Progress will be reported in the development of a procedure for the simultaneous inversion of laboratory dissipation and associated shear modulus dispersion data for the creep function that provides a complete description of the viscoelastic behaviour. Knowledge of the respective creep functions for melt-free and melt-bearing olivine-based materials will allow an interpretation of specific seismological velocity-attenuation models more closely guided than hitherto by laboratory studies.

**JSS06a/08P/D-025** Poster **1400-103**

### STRUCTURE OF THE DISCONTINUITIES BENEATH TONGA SUBDUCTING ZONE AND ITS IMPLICATION

Yuan Ze ZHOU, Shao Xian ZANG (Department of Geophysics, Peking University)

Tonga subduction zone has caused a big attention from the geoscientists because there are the deepest Wadati-Benioff zone, a lot of big intermediate and deep earthquakes and complicated geodynamics processes. Some authors have utilized the abundant data to study mantle discontinuities in this region. In this study the discontinuities beneath the Tonga region are investigated with SdP converted phases near source. Short period vertical component data for the 58 events from 1988 to 2000 beneath Tonga region recorded by hundreds stations of PNSN and NCSN in the western USA are retrieved from IRIS and NCEDC. The data are processed with the N-th root slant stack method (Zang and Zhou, 2002) to pick out faint secondary phases from mantle discontinuities where the n is 4. Based on the differential slowness, differential travel time and relative amplitude of each possible phase, SdP phases are picked out and the corresponding position and depths of the converted points are calculated with the successive integration along ray paths with PREM. Those converted points are counted in the depth range. The results show that there are several depths where the converted points are concerted which appear before the pP. There are discontinuities possibly existed though the scale of discontinuity may vary. The discontinuity near the 660 km depth seems a multiple. There are 2 obvious peaks between the depths of 630 and 760km when the constraint of slowness difference ( $\Delta p$ ) between the observed and theoretical differential slowness is less than 0.1 or 0.2 s/deg. The converted points existed between the depths of 630 and 760km whose related  $\Delta p$  is less than 0.1 s/deg are projected to three profiles which are determined based on the configuration of Wadati-Benioff zone. There are clear double parallel layers at 640 and 680 km at the north part of Tonga and each layer depresses nearly 60 km; the middle part of Tonga shows a

complicated structure near 660 km and just a little depression near the subducted slab; the south part of Tonga also has double parallel layers near 660 and 720 km and each has 20 km depression. From the analysis above, the "660 km discontinuity" varies from region to region and is affected by the Tonga subducted slab. The complicated structure near 660 km is discussed.

**JSS06a/08P/D-026** Poster **1400-104**

### SYNTHETIC SEISMOGRAM ASSOCIATED WITH AN EARTHQUAKE AT A SUBDUCTION ZONE

Arabinda ROY (Dept Of Applied Mathematics, Calcutta University)

The distributions of epicenter locations and focal depths of intermediate and deep Earthquake gives important and deep earthquakes give important evidences of the seismic processes active at a subduction zone. Comparison of the theoretical synthetic seismogram with actual seismogram for an earthquake in the subduction zone can provide a suitable model of the structure of the Lithosphere near the subduction zone as well as the seismic process. In our model we choose the region near the subduction zone as a two layered Wedge shaped media with an inclined surface separating the media. The Earthquake is simulated by a source acting inside one of the media or at the interface i.e. on the plunging plate. We have computed theoretically the synthetic seismo0gram associated with the model considered. Presently even for SH wave such solutions are not known for a two layered wedged shaped medium. For a lateral inhomogeneous medium, such solutions are not known for SH wave in case of two quarter spaces in contact. We have successfully developed an integral equation method to solve the problem in the general case. Iterative solutions of the integral equations give the ray picture in the two layered Wedge shaped media. Our method is equally applicable for both SH as well as P,SV cases. The synthetic seismogram can be generated by piecing together the iterative solution of the integral equations. Comparing the synthetic seismogram so constructed with the actual seismogram of an Earthquake will help in better modeling of the structure near the Lithosphere.

**JSS06a/08P/D-027** Poster **1400-105**

### THE MOBILITY OF THE EARTH'S INNER CORE AND PROCESS OF LATITUDE VARIATIONS

Yuri N. AVSYUK (Institute of Physics of the Earth of Academy of Sciences Of Russian Federation)

The Earth's orbital motion around the Sun is the sum of the movements: the one-year motion of the center of the Earth-Moon system (barycenter) around the Sun and the Earth's monthly motion around the barycenter. The lunar inequality  $L=6''.4356$  is the parallax of the Earth's orbit with respect to the barycenter. The solar attraction is dynamically balanced at the Earth-Moon center of mass (barycenter) rather than at the Earth's center. The Earth motion around the barycenter is the exact motion of the Moon whose perturbation moduli are 81.3 times smaller than the modulus perturbations in the motion of the Moon. The tidal force from the real motion contains the Kepler term (the Laplace formula) plus perturbations of the Earth's orbital motion around the barycenter; their modulus and periodicity depend on the Earth orientation relative to the direction to the Sun, i.e., on the difference between the longitudes of the Earth  $\lambda_{\oplus}$  and Sun  $\lambda_{\odot}$  (Avsyuk, 1996). The Earth longitude  $\lambda_{\oplus}$  is, in turn, related to the direction angles of the node  $\Omega$ , perigee  $\Gamma$ , and anomaly  $W$ , as well as to their temporal variations having periods of 18.6 years, 8.85 years, and 27.5 days, respectively; i.e., we have  $\lambda_{\oplus} - \lambda_{\odot} = \Omega + \Gamma + W - \lambda_{\odot} = (\Omega + \Gamma - \lambda_{\odot}) + W$ . Consequently, the analysis of the perturbations should resolve fortnightly and monthly (27.5 days) periodicities if a one-day sampling interval is used and a periodicity of 412-437 days ( $\Omega + \Gamma - \lambda_{\odot}$ ) if a one-month sampling interval is used. This can be confirmed by resolving the tidal force acting on the IC into three components:  $F_x$  along the rotation axis and  $F_y$  and  $F_z$  in the equatorial plane along the Greenwich meridian and  $90^\circ W$ , respectively. The resulting harmonics have periods of 13.6, 27.5, 365, and 412-437 days and 6 years (Avsyuk, 1980). The comparison between the periodicities of the forces and those of the rotation axis motion within the Earth suggests that the IC experiences forced movements changing the coordinates of the origin ( $X(T)$ ,  $Y(T)$ ,  $Z(T)$ ) and displacing the rotation axis within the Earth. With a modulus of the solar tide effect of about  $50 \times 10^8$  cm/s<sup>2</sup> and a density difference between the inner core and outer core of 0.2-0.3 g/cm<sup>3</sup>, the IC displacements in the static approximation are estimated at about 10 m. The power associated with the IC motion in its surrounding melt is characterized by a value of  $10^{18}$  erg/s. Based on the complete frequency correspondence between the force and response (axis variations observed at the surface), we state that the IC moves within the Earth.

**JSS06a/08P/D-028** Poster **1400-106**

### MANTLE LATERAL VARIATIONS AND ELASTIC DEFORMATIONS

Laurent METIVIER, Marianne GREFF-LEFFTZ, Michel DIAMENT (Institut de Physique du Globe de Paris)

Earth strain and gravity responses to phenomenon such as tides or atmospheric loads, are generally calculated assuming earth models radially stratified, and at hydrostatic equilibrium. However, some local observations show unexplained perturbations on the tidal gravity signal. A possible cause for those perturbations may be the neglect of rheology and density lateral variations as well as the non hydrostaticity of the Earth. We have investigated a non radially symmetrical earth numerical model with the intent to study the earth response to low frequency forcings. This model has used a finite element method (spectral element) developed on the "cubed sphere" mesh (Ronchi et al., 1996), and has resolved gravito-elasticity equations. As a validation of our model, we have computed the effect of the hydrostatic ellipticity of the Earth and have compared, for simple model (homogeneous planet), our numerical results with the analytical solutions obtained using Maple computation. As a first application, we have investigated the influence of the lateral variations induced by the oceanic-continental crust distribution. Finally, the non hydrostaticity of the Earth has been taken into consideration by a first order perturbation theory, and we have investigated the possible influence of a mega-plume on gravity tide.

**JSS06a/08P/D-029** Poster **1400-107**

### PRELIMINARY INVESTIGATION OF INHOMOGENEOUS VISCOUS STRUCTURE OF UPPERMOST MANTLE BENEATH JAPANESE ISLANDS: ITS IMPLICATION TO QUASI-STATIC DEFORMATION OF SUBDUCTION ZONE

Satoru FUJIHARA (Earth Simulator Center, Japan Marine Science and Technology Center)

Based on its known inhomogeneous-inelastic properties, it may be more suitable to assume the (regional scale) subduction zone as visco-elastic, at least for simulating (the cyclic property of) quasi-static earthquake generation [For example, Yoshioka and Suzuki, 1999; Hirahara, 1999]. In addition, a priori knowledge of rheological state of subduction zone is essential for visco-elastic modeling in that quasi-static response depends on whether the

region surrounding around the assumed seismic fault region is elastic or visco-elastic. Based on the better understanding of the spatial pattern of brittle-ductile transition, the realistic and complex boundary of elastic-visco-elastic media can be assigned more realistically in the visco-elastic modeling. Along with those effects of inhomogeneity within volume, it is also important to physically interpret the empirically-determined frictional parameters of Rate and state dependent frictional law (For example, [Tue and Rice, 1986]), and to understand the spatial variation of frictional parameters in horizontal and vertical direction. Hirahara and Earth Simulator Research Group for Earthquake Generation Process (2002) and Hirahara (1999) introduced the very realistic scheme that assumes 3-D visco-elastic model and Rate and state dependent frictional law along the faults, numerically simulating the cyclic, quasi-static large earthquake generation. These studies emphasized the very importance of realistic, three-dimensional visco-elastic medium, instead of the homogeneous, half space-elastic model. Many efforts have been made for estimating a reasonable viscosity distribution for a various scale (For example, [Peltier 1998; Suito and Hirahara, 1999]). However, significant discrepancy in viscosity value can be often seen probably based on technical differences, nature of dataset, amount of noise, and rather many assumptions. Here, a preliminary model of uppermost mantle viscous structure of was discussed beneath the Japanese Islands, based on the empirical relationship (Sato, 1991) between viscosity and seismic attenuation factor that was derived by combining homologous temperature dependence of viscosity (Borch and Green, 1987) and attenuation factor of seismic wave (Sato, 1989), of high pressure and temperature conditions. Solidus temperature was referred to Takahashi (1986). The dominant rock type of upper mantle is assumed as peridotite. Based on assumption of thermal activation process and homologous temperature dependence of seismic attenuation factor (Sato, 1989), viscosity is expected to be largely dependent on temperature, as a first order estimation. The seismic attenuation structure beneath the Japanese Islands of (Fujihara .et al, 2001) was used, which was obtained by using many broadband waveform data of Freesia network of Japan. Scattering effect was assumed to be less dominant on attenuation of seismic wave amplitude than absorption effect.

**JSS06** Monday, July 7 - Thursday, July 10

**EARTH STRUCTURE AND GEODYNAMICS (IASPEI, IAVCEI, IAG, IAGA)**

Location: Site A, Room 4

Wednesday, July 9 AM

Presiding Chair: F. Niu

**JSS06/09A/A04-001** 0900

**EAST-WEST HEMISPHERICAL DICHOTOMY OF SEISMIC STRUCTURE AT THE TOP OF THE INNER CORE AND ITS IMPLICATIONS**

Fenglin NIU<sup>1</sup>, Lianxing WEN<sup>2</sup> (<sup>1</sup>Department of Earth Science, Rice University,, <sup>2</sup>Department of Geosciences, State University of New York at Stony Brook)

We collect a global data set of PKiKP and PKiKP phases recorded by the Global Seismic Network and many regional seismic arrays to study seismic structure in the top of the Earth's inner core. The PKiKP and PKiKP observations show different characteristics between those sampling the "eastern" hemisphere (40°E-180°E) of the inner core and those sampling the "western" hemisphere (180°W-40°E). PKiKP phases (1) arrive about 0.4 s earlier than the theoretical arrivals based on Preliminary Reference Earth Model (PREM) for those sampling the eastern hemisphere of the inner core and about 0.3 s later for those sampling the western hemisphere (131°-141°); (2) bifurcate at smaller epicentral distances for those sampling the eastern hemisphere, compared to those sampling the western hemisphere; and (3) have smaller amplitudes for those sampling the eastern hemisphere. Waveform modeling of these observations suggests two different types of models for the two "hemispheres" of the top of the inner core, with a model in the eastern hemisphere having a P velocity increase of 0.765 km/s across the inner core boundary, a small radial velocity gradient of 0.00055 (km/s)/km, and an average Q value of 250, and a model in the western hemisphere with a P velocity increase of 0.633 km/s across the inner core boundary, a radial velocity gradient of 0.000533 (km/s)/km and an average Q value of 600. The hemispherical difference of seismic structures may be explained by different geometric inclusions of melt and/or different alignments of iron crystals with anisotropic properties in both velocity and attenuation. We speculate that this large-scale pattern of seismic heterogeneities may be caused by a large-scale heat flow anomaly at the bottom of the outer core and/or different vigorosity of convection in the top of the inner core between the two hemispheres.

**JSS06/09A/A04-002** 0920

**INNER-MOST INNER CORE: A DISTINCT REGION AT THE CENTER OF THE EARTH**

Miaki ISHII, Adam M. DZIEWONSKI (Department of Earth and Planetary Sciences, Harvard University)

Although the presence of anisotropy in the inner core is widely accepted, inferences of its strength and depth dependence vary considerably from model to model. We have recently shown that a significant fraction of inner-core sensitive data is reconciled by a model in which anisotropy does not vary with radius. This simple anisotropy model fits the absolute travel-time data well at all distance ranges except between 173° and 180°. This distance range corresponds to the inner-most 300 km of the Earth, where normal-mode constraints are weak, and where constraints from differential travel times (AB-DF) are likely contaminated by strong heterogeneity near the core-mantle boundary. When the travel times are inverted for anisotropic parameters of the inner-most inner core, we obtain a model with a slow direction oriented ~45° from the equator, in contrast to the bulk inner core where the slowest wave propagation occurs when the rays are parallel to the equatorial plane. The existence of the inner-most inner core has significant consequences in our understanding of the Earth's evolution. This region may represent fossil evidence of two episodes of inner core development, changes in chemistry, or changes in the pattern of convection in the outer core. Furthermore, if the inner-most inner core represents a preserved region of the early Earth, then the development of subsequent anisotropy is limited to mechanisms acting close to the inner-outer core boundary.

**JSS06/09A/A04-003** 0940

**PKP TRAVEL TIME DATA: COMPLEXITY IN INNER CORE ANISOTROPY STRUCTURE?**

Barbara A. ROMANOWICZ, Aimin CAO (Univ. of California at Berkeley)

Twenty years ago now, Poupinet et al. (1983, Nature) observed that PKP waves travelling on

polar paths arrived earlier, by a few seconds, than those travelling on equatorial paths. Several years later, it was proposed that this was due to inner core anisotropy, as was anomalous splitting of core sensitive free oscillations (Morelli et al., 1986; Woodhouse et al., 1986). The originally proposed model was simple: constant transverse isotropy with axis parallel to the axis of rotation of the earth, and could conceivably be related to the alignment of iron crystals within the inner core. Since then, much data has been accumulated, in the International Seismological Center (ISC) bulletins as well as high quality broadband waveform data, and the models have become increasingly complex. When interpreted solely in terms of structure in the inner core, broadband data seem to require significant hemispherical differences in the strength of anisotropy, a layer of isotropic structure at the top of the inner core, with strongly varying thickness, which is hard to reconcile with free oscillation data. Most recently, Ishii and Dziewonski (2002) proposed the existence of a distinct innermost inner core. On the other hand, some authors have suggested that the data may be biased by the uneven sampling of available paths through the inner core, and that a significant portion of the observed trends should be sought outside of the inner core, in the deep mantle as well as, perhaps the outer core (e.g. Romanowicz et al., 2002). We have assembled a comprehensive dataset of absolute PKP(DF) travel times measured on high quality broadband and short period digital seismograms, including data at antipodal distances. This complements our previous collection of differential PKP(AB-DF) and PKP(BC-DF) data (Tkalcic et al., 2002). We discuss the trends in these data, in particular to verify the plausibility of the existence of the innermost inner core and consider possible alternative interpretations.

**JSS06/09A/A04-004** 1000

**LONG-TIME ANGULAR MOMENTUM AND MASS TRANSPORTS IN THE CORE**

Sergei V. STARICHENKO (Geoph. Observ. Borok of Russian Academy of Sciences)

Averaged (on a time-scale about million years) mass and angular momentum transports are investigated in the almost rigidly and rapidly rotating Earth's core, which inner rigid part is growing in expense of the outer liquid part. This results in an original 'momentum' torque with value between 1,000 and 10,000 TN m accelerating the rigid core's rotation relative to the mantle. Balancing this 'momentum' torque with viscous torques I get the rigid core's super-rotation of order one degree per year for the molecular viscosity, while sufficiently smaller super-rotation value appears for more realistic 'turbulent' viscosity in accordance with the modern seismic investigations and 3D MHD numerical models. The power connected with my 'momentum' torque is between 0.1 and 1 TW, that is enough to support all the convection and valuable geomagnetic field in the core, if one prescribe this torque only without any other driving force in the core.

**JSS06/09A/A04-005** 1040

**PRODUCT SPECTRAL DENSITY OF THE TIDAL GRAVITY DATA OBSERVED WITH GLOBAL SUPERCONDUCTING GRAVIMETERS AT GGP STATIONS: A SEARCH FOR THE INNER CORE TRANSLATION TRIPLET**

Jian-Qiao XU<sup>1</sup>, He-Ping SUN<sup>1</sup>, Bernard DUCARME<sup>2</sup> (<sup>1</sup>Institute of Geodesy and Geophysics, Chinese Academy of Sciences (CAS), <sup>2</sup>Belgium National Fund for Scientific Research, Royal Observatory of Belgium)

In recent years, a special attention was paid to the translational oscillations of the Earth's solid inner core. They are Earth's fundamental free modes (Slichter, 1961) which are usually called Slichter triplet or Slichter modes, as they include three modes: the equatorial prograde, the axial and the equatorial retrograde translational oscillations. In 1993, four long-term high-quality tidal gravity data, recorded with superconducting gravimeters (SG) in central Europe, have been used to form a product spectrum (Smylie et al 1993). Three weak resonance signals with central periods of 3.5820h, 3.7665h and 4.0148h were found, corresponding to the periods theoretically computed under the subsismic approximation (Smylie et al 1992). Similar results were obtained using six globally distributed SG observations (Courtier et al, 2000). However, Hinderer et al (1995) and Jensen et al (1995) are contradicting these results using the SG data from Strasbourg/France and Cantley/Canada. In our study, the 21 long SG series of the Global Geodynamics Project (GGP) network are used to investigate Slichter triplet. The original observations are pre-processed with identical technique in order to remove anomalous signals, instrumental drift, tidal gravity signal and barometric influence. The product spectral density of the tidal gravity residuals and station barometric pressure are estimated respectively. Three significant spectral peaks are found with central periods of 4.93438h, 4.42734h and 4.09269h, in close agreement with the eigenperiods of Slichter triplet theoretically computed by Smith (1976).

**JSS06/09A/A04-006** 1100

**THE ELECTRICAL CONDUCTIVITY STRUCTURE OF THE EUROPEAN LOWER MANTLE**

Pascal TARITS<sup>1</sup>, Mioara MANDEA<sup>2</sup> (<sup>1</sup>UMR CNRS Domaines Oceaniques, IUEM/UBO, <sup>2</sup>Institut de Physique du Globe de Paris)

Monthly mean values of the geomagnetic field from about 120 observatories have been analyzed. We selected time windows of 30-35 years which was appropriate for most of the available observatory data. Transfer functions in the period range 2.5-24 months have been obtained at 24 European observatories that sample the mantle in the depth range 700-2000 km. Conductivity profiles obtained from the inversion of the transfer functions show that conductivity increases rapidly from less than 1 S/m to about 3-5 S/m from 700-1300 km and is about constant at greater depth. In the uppermost lower mantle, the conductivity would agree with Al-free perovskite while deeper, a conductive phase should be added. Possible petrological models include Al-bearing perovskite or connected magnesowüstite. The conductivity beneath Europe seems to vary laterally as much as radially. Anomalous conductivity profiles - defined as the log-difference with respect to a one dimensional global conductivity model obtained from the analysis of all available observatories - are compared to velocity anomaly profiles and reveals a complex combination of correlation and anticorrelation with the seismic parameters. The results are discussed in terms of temperature and compositional variation in the lower mantle.

**JSS06/09A/A04-007** 1120

**TOMOGRAPHIC EVIDENCE FOR SUBDUCTION INDUCED RIFTING OF THE NAZCA PLATE**

Tom HILDE<sup>1</sup>, Sri WIDIYANTORO<sup>2</sup>, Yoshio FUKAO<sup>3</sup> (<sup>1</sup>Department of Geology & Geophysics, Texas A&M University, <sup>2</sup>Department of Geophysics and Meteorology, Bandung Institute of Technology, <sup>3</sup>Earthquake Research Institute, University of Tokyo)

Mendana FZ (MFZ), a NE striking structure within the eastern Nazca Plate, intersects the Peru Trench at 10 deg 20'S. Previous bathymetric, magnetic and seismic reflection mapping and sonar imaging reveal that MFZ: 1) is 100km wide at the Peru Trench and narrows SW

IA

## INTER-ASSOCIATION

to 25km at 83 deg 30'W, 12 deg 00'S,2) consists of 5-10km spaced, FZ parallel, ridges and troughs. 3) has exposed igneous basement along the ridges, and 4) displays an associated set of NE striking magnetic lineations. The linear magnetic anomalies have been modeled and interpreted as seafloor spreading/magnetic field reversals. An axial Brunhes anomaly correlates with rift axis structure, and anomaly 2A (~3Ma) is observed near the MFZ margins from the Peru Trench seaward ~200km. These data suggest that MFZ is a seafloor spreading center, active for the last 3+Ma, that has propagated ~400km seaward at a rate of 115-130km/Ma which will divide the Nazca Plate into separate plates in 30-35Ma. Subsequent heat flow measurements across MFZ are anomalously low which appears inconsistent with the above observations and interpretation. We have employed seismic tomography to examine subducted Nazca Plate velocity structure beneath Peru. Our results show a generally complex upper mantle velocity structure. Included is an ~400km wide 2% low velocity gap, relative to subducted Nazca Plate velocities beneath Peru, which is located across the subduction projection of MFZ. Our results support the conclusion that the Nazca Plate is being rifted apart along MFZ by subduction related extensional stresses.

**JSS06/09A/A04-008**

**1140**

### DISCONTINUITIES IN THE LOWER-MANTLE BENEATH WESTERN PACIFIC REGION

Shao Xian ZANG, Yuan Ze ZHOU (Department of Geophysics, Peking University)

Lower mantle discontinuities draw more attention nowadays because they challenge the traditional ideas on Earth's interior structure. Abundant inter-mediate and deep earthquakes occurred in Western Pacific subduction zone, which can be used to study the deep velocity structure beneath the region. Faint converted phases from the mantle discontinuities or heterogeneities can be observed from stacked data for single event recorded by arrays or networks or from stacked data for multiple events recorded by one permanent high quality broadband station. Beside the discontinuities at the depth of 410, 520 and 660 km, discontinuities or regional heterogeneities near the depths of 900, 1070 and 1170 km are also reported to be observed in certain places. In this paper, the interfaces in lower mantle are studied. Through carefully selection of the records for each event, short period vertical component data of 27 events beneath Okhotsk Sea from 1982 to 2001 and 10 events beneath Japan Sea from 1982 to 2000 recorded by hundreds of stations at western USA, United Kingdom and Germany and the data for the 58 events beneath Tonga from 1988 to 2000 recorded by hundreds of stations located at western USA were retrieved. All the data are processed by the N-th root slant stack method (Zang and Zhou 2002) and SdP phases are picked out. The depths of conversion points are inverted with the successive integration along ray paths with PREM. From analysis, it can be found that there are interfaces at 730, 810, 880, 950, 1020, 1090, 1130, 1370, 1450, 1610 and 1770 km beneath Tonga subduction zone, 900 km beneath Okhotsk Sea region and 760 and 1120 km beneath Japan Sea region. Compared the result obtained in this study with the others, there are two interfaces coincident with each other. They exist near the depths of 900 and 1170 km. The scale or horizontal extension of the interfaces is not able to constrain at the moment. More work should be done to make sure whether other interfaces are discontinuities or regional heterogeneities related to stagnant materials of subducted slab.

**JSS06/09A/A04-009**

**1200**

### ESTIMATING THE PLAUSIBLE TEMPORAL CHANGE IN THE THERMAL STATE OF D' LAYER DUE TO SUPERPLUME EPISODES

Uppendra RAVAL (National Geophysical Research Institute)

The D'' layer in the lowermost part of the mantle and within few hundred km from the core mantle boundary is the modulator of the heat received from the outer core. The seismically deduced ultra low velocity zone (ULVZ) in D'' layer, with reduction up to 10% in P-wave and 30% in S-wave velocities, provides strong evidence for the thermal (or magmatic pumping) of this thermal boundary layer. Since these thermal inputs generate instabilities in form of mantle plumes it is apparent that the outward flow of heat from core acts as a major source for the development of these instabilities (or plumes). It is also noted in this context that the plumes (or more correctly the super-plume) events are episodic in nature which in turn indicates that during the interval a major instability originates, the thermal state of the D'' would significantly change. Using the various parameters available from high pressure temperature studies and long period geomagnetic variation this study tries to model the diffusion of electromagnetic field through the D'' during (1) Superplume formation and (2) inter Superplume period. The simulation also takes into account the laterally heterogeneous nature of the D''. The theoretical experiment tries to estimate whether significant difference exists between the electrical and thermal characteristics of the two states and if it could be observed through temporal (or secular) geomagnetic variations.

Wednesday, July 9 PM

Presiding Chair: B. Kennett

**JSS06/09P/A04-001**

**1400**

### ONSET OF SUBLITHOSPHERIC SMALL-SCALE CONVECTION AND ITS IMPLICATIONS FOR UPPER MANTLE STRUCTURE

Jinshui HUANG, Shijie ZHONG, Jeroen VAN HUNEN (Dept of Physics, University of Colorado)

The rich structures in the Pacific upper mantle suggested from recent seismic studies with the body-wave and surface-wave techniques prompt us to re-examine the dynamics of small-scale convection by formulating numerical models with realistic mantle rheology. Our study is focused on the onset and consequences of sublithospheric small-scale convection. In our models, small-scale convection is mainly controlled by two parameters: activation energy E and the upper mantle viscosity, the latter can be recast as Rayleigh number Ra. Our numerical studies suggest that the onset time for small-scale convection for flows cooling from above scales as  $E^{0.742}Ra^{0.679}$  when the large-scale plate motion is absent. The E-dependence of onset time is significantly weaker than that predicted from Davaille and Jaupart [1994]. We found that our results of onset time are rather insensitive to large-scale plate motion and initial perturbation whose effects are generally less than 20%. Sublithospheric small-scale convection eventually causes surface heat flux Q to deviate from the predicted from a simple half-space cooling model. The elapsed time from the onset of small-scale convection to when Q significantly deviates from the half-space cooling scales as  $E^{1.516}Ra^{-0.648}$ , and this is controlled by thermal diffusion through the stable portion of lithosphere (i.e., stagnant lid), as evident from  $E^{0.794}Ra^{-0.393}$  scaling for the thickness of stagnant lid. Q during the period of a few onset times immediately after the onset scales as  $E^{-0.529}Ra^{0.323}$ . We found that thermal anomalies associated with fracture zones significantly reduce the onset times, implying that small-scale convection always first starts near fracture zones. We also found that a thin asthenosphere can significantly delay the onset.

**JSS06/09P/A04-002**

**1420**

### LITHOSPHERIC STRUCTURE IN THE AUSTRALIAN REGION- A SYNTHESIS OF SURFACE WAVE AND BODY WAVE STUDIES

Brian L.N. KENNETT, Stewart FISHWICK (Research School of Earth Sciences, Australian National University)

The configuration of earthquake belts around Australia provides a wealth of events at suitable distances to be used as probes into the seismic structure of the upper mantle. The limited number of permanent high-fidelity seismic stations on the continent have been supplemented with extensive deployments of portable broadband stations for periods of a few months at each site. The combination of long term recording at the permanent stations and the broad spatial coverage of the portable stations have been exploited in a range of studies of the three-dimensional structure in the mantle. The large amplitude surface waves in the later part of the seismogram travel nearly horizontally and can be used in a tomographic inversion to determine the 3-D variations in shear wavespeed. This approach relies on matching the waveforms on individual paths and then mapping the path-specific constraints on shear structure into a 3-D model. In contrast, the higher frequency body wave arrivals are refracted back from the variations in structure in the mantle and are particularly sensitive to discontinuities in structure. Observations out to 3000 km provide coverage of the structures down through the transition zone and for the region below northern Australia, the combination of short-period and broadband observations provides detailed information on both P and S wavespeeds and attenuation structure. The combination of the different classes of results reveal a complex pattern of 3-D structure beneath the Australian region. The cratonic region in the centre and west of Australia is underlain by a thick mantle lithosphere extending to around 210 km depth with fast wavespeeds (especially for S waves). In the asthenosphere below the S wavespeeds diminish and there is significant attenuation and also some level of seismic anisotropy. Beneath the eastern zone with Phanerozoic outcrop the lithosphere is generally thinner (less than 140 km) and the asthenosphere has a pronounced low velocity zone for S again with high attenuation. The variations in seismic wavespeeds extend through the upper mantle with noticeable differences in the transition zone. There is also evidence for pervasive small scale heterogeneity (scale lengths of 100-200 km) superimposed on the broader scale variations that can be imaged using tomographic methods.

**JSS06/09P/A04-003**

**1440**

### ON NATURE OF SEISMIC FOCAL ZONE AND RELATED TO IT PROCESSES WITH REFERENCE TO THE KURIL-JAPAN REGION

Roman Z. TARAKANOV (Institute of Marine Geology and Geophysics, Russian Academy of Sciences)

The paper deals with simple interpretation of the seismic focal zone nature. From the theory of dislocations it has been known that if near-horizontal forces of compression or extension affect the pattern, then maximum tangential stresses and the zone of disturbances are oriented at the angle 45 degree to the acting forces. Let us take the entire continent-ocean transition zone, which is constantly affected by near-horizontal compression forces caused by the interaction between continental and oceanic structures as a large-scale "pattern". In this case maximum tangential stresses will be also oriented at the angle 45 degree to the acting forces. The seismic focal zone as a system of deep faults will coincide with the zone of maximum tangential stresses and will be one of the nodal planes defined by the theory of dislocations. Seismic focal zone crossing the layers of higher and lower strength-velocity characteristics is continuously fed up with maximum tangential stresses and irregular rotational mode of the Earth. In the area of intersection with the layers of higher velocity this energy will be constantly accumulated and can reach extra values which will lead to the movement of separate blocks, i.e. to the earthquake. In asthenospheric layers of lower velocity (lower viscosity) this energy will be relaxed increasing the layer temperature and finally can lead its separate parts to the partial melting state, which can be the feeding medium for volcanoes. It is remarkable that the Kuril-Kamchatka island arc and volcanic chains are located above the area, where the asthenospheric layer (120-150 km) is intersected with the seismic focal zone. Let us give some seismological data, which are not agreed with the plate tectonics concept: 1. We should expect an increase in seismicity manifestations as the plate would go deeper into the upper mantle. But in fact the deepest seismic events are typical for relatively young island arcs (Kuril-Kamchatka, Izu-Bonin etc.). 2. A correlation of vulcanite compositions with depths of occurrence of Benioff zones testifies to the fact that magma emerges to the surface from different levels of upper mantle, but is not the result of melting down from the lithospheric plate. 3. From the plate tectonics positions it is difficult to explain the reasons of the successive pushing forward of Benioff zones with the oceanic trenches towards the Ocean. By general movement of the lithospheric conveyor from the ocean to the continent it would be natural to expect that these structures will move in the same direction (Vlasov, 1994). Geological objections against global tectonics have been expounded in some G.M. Vlasov's papers (1981; 1994 etc.) and in papers of other geologists. Results of works on mathematical (Demir, Zharinov, 1986, 1988) and physical modeling (Guterman, 1987) showed plausibility of the stated viewpoints on the nature of seismic focal zones.

**JSS06/09P/A04-004**

**1500**

### COMPARISONS OF MODELLING RESULTS FROM TELESEISMIC P-WAVE TOMOGRAPHY IN PROJECT TOR

Soren GREGERSEN<sup>1</sup>, Hossein SHOMALI<sup>1</sup>, Peter VOSS<sup>1</sup>, Tor Working Group<sup>1</sup> (<sup>1</sup>National Survey and Cadastre - Denmark, <sup>2</sup>Swedish Geological Survey)

Within Project Tor, which is about Telesismic Tomography across the Tornquist Zone in Germany-Denmark-Sweden, we have detected very significant deep lithosphere differences and are able to compare results of various interpretations. In 1996-1997 our 120 seismographs constituted the largest seismic antenna ever in Europe. The Tor area was chosen along a well studied crustal profile of an earlier project, and the inversion efforts were concentrated on the deep lithosphere and asthenosphere differences to depths around 300 km. The Tor investigation can be called two-and-a-half dimensional, as it has a 900 km profile length with 100 km width plus a few seismographs off the profile. The Tor data have been subjected to P-wave travel time tomography, surface wave and receiver function analysis as well as anisotropy and scattering measurements. It was always considered an important goal of the project to make several independent inversions of the tomography data, and compare the results in an attempt to evaluate accuracy, resolution and uniqueness of these inversions. The present paper reports on these comparisons. The outcome is a substantiation of earlier statements like: "The transition is interpreted to be sharp and steep and abrupt in three places. It goes all the way through the lithosphere at the Tornquist Zone near the border between Sweden and Denmark, and here the lithosphere difference is large. Another less significant lithosphere difference is found near the border between Denmark and Germany. Also this transition is sharp and steep, and goes all through the lithosphere. These two sharp transitions divide the Tor region into 3 different lithosphere structures distinguishable in P-wave travel time tomography, surface wave dispersion, P- and S-wave

anisotropy and partly in P-wave scattering". In addition we have found a sharp and steep transition region 100 km into the shield in Sweden. Unfortunately a detail like the slope of the lower lithosphere transition right under the Tornquist Zone cannot be constrained even if this is where the resolution is best, and the curiosity largest.

JSS06/09P/A04-005

1520

### STRUCTURE OF THE LITHOSPHERE-ASTHENOSPHERE AND VOLCANISM IN ITALY AND SURROUNDINGS

Giuliano PANZA<sup>1</sup>, Antonella PONTEVIVO<sup>2</sup>, Angela SARAO<sup>3</sup>, Abdelkrim AOUDIA<sup>1</sup>, Angelo PECCERILLO<sup>4</sup> (<sup>1</sup>SAND Group, Abdus Salam International Centre for Theoretical Physics & Dept. of Earth Sciences, University of Trieste, Trieste - Italy, <sup>2</sup>Dept. of Earth Sciences, University of Trieste, Trieste - Italy, <sup>3</sup>Dept. of Earth Sciences, University of Perugia, Perugia - Italy)

The Italian peninsula and the Tyrrhenian Sea are some of the geologically most complex regions on Earth. Such a complexity is expressed by large lateral and vertical variations of the physical properties as inferred from the lithosphere-asthenosphere structure and by the wide varieties of Plio-Quaternary magmatic rocks ranging from tholeiitic to calcalkaline to sodium- and potassium-alkaline and ultra-alkaline compositions. The integration of geophysical, petrological and geochemical data allows us to recognise various sectors in the Tyrrhenian Sea and surrounding areas and compare different volcanic complexes in order to better constrain the regional geodynamics. A thin crust overlying a soft mantle (10% of partial melting) is typical of the back arc volcanism of the central Tyrrhenian Sea (Magnaghi, Vavilov and Marsili) where tholeiitic rocks dominate. Similar lithosphere-asthenosphere structure is observed for Ustica, Vulturno and Etna volcanoes where the geochemical signatures could be related to the contamination of the side intraplate mantle by material coming from the either ancient or active roll-back. The lithosphere-asthenosphere structure and geochemical-isotopic composition do not change significantly when we move to the Stromboli-Campanian volcanoes, where we identify a well developed low-velocity layer, about 10 km thick, below a thin lid, overlain by a thin continental crust. The geochemical signature of the nearby Ischia volcano is characteristic of the Campanian sector and the relative lithosphere-asthenosphere structure may likely represent a transition to the back arc volcanism sector acting in the central Tyrrhenian. The difference in terms of structure beneath Stromboli and the nearby Vulcano and Lipari is confirmed by different geochemical signatures. The affinity between Vulcano, Lipari and Etna could be explained by their common position along the Tindari-Letojanni-Malta fault zone. A low velocity mantle wedge, just below the Moho, is present in all the regions related to the inactive recent volcanoes (Amiata, Vulturno, and Cimino, Vico, Sabatini, Albani Hills) in the Tuscany and Roman regions. A very thick rigid body is found in the upper mantle beneath the Ernici-Roccamonfina province that exhibits very distinct geochemical and isotopic compositions when compared with the Roman province.

JSS06/09P/A04-006

1600

### 3D P-WAVE VELOCITY IMAGING OF THE TORNIQUET SUTURE ZONE USING MARKOV CHAIN MONTE CARLO INVERSION AND TELESEISMIC P-PHASE ARRIVALS

Peter VOSS<sup>1</sup>, Klaus Teddy MOSEGAARD<sup>2</sup>, Soren GREGERSEN<sup>1</sup> (<sup>1</sup>National Survey and Cadastre - Denmark, <sup>2</sup>Niels Bohr Institute, University of Copenhagen)

In this study we have applied the Markov Chain Monte Carlo inversion algorithm to the teleseismic tomographic problem, using teleseismic P-phase arrivals measured during the TOR-project. TOR was a 1000km long and 100km wide antenna of mobile broadband and shortperiod seismographs, that continuously collected data in Sweden, Denmark and Germany, for half a year from 1996 to 1997. Inversion is performed using the relative arrival time of 3510 P, PKiKP and Pdiff phases, from 51 earthquakes, in an area 1350km long and 750km wide and from 50km to 350km depth. The travel time data are corrected for the relatively well-known crustal and upper mantle structure to depth 50km. Synthetic travel time calculations for 3D forward modeling of teleseismic wavefronts are performed by a finite difference algorithm. Wavefront arrival times at 350km depth are computed using the IASP91 model. The transition between the Baltic Shield and the geologically younger lithosphere to the south west is found to be narrow, near vertical and more than 300km deep.

JSS06/09P/A04-007

1620

### THE LITHOSPHERE AND ASTHENOSPHERE OF THE ICELAND HOT SPOT

Ingi Thorleifur BJARNASON (Science Institute, University of Iceland)

High resolution Love and Rayleigh waves [period 5-85 s] recorded on the ICEMELT broadband network resolve a structural landscape of the Icelandic lithosphere. It has large lateral variation in velocity, anisotropy and thickness. The main characteristic variation in the asthenosphere is anisotropy. A large asymmetry is in the thickness of the lithosphere from east to west. The mantle lid part of the lithosphere under the Eastfjords is at least 40 km thicker than the Westfjords lid, adding up to over 100 km thick lithosphere in the east. The thick east lithosphere deflects the mantle plume head to the west. The highest observed S lid velocities (4.5 pm 0.1 km/s) are also under these oldest (10-15 Ma) parts of Iceland. The asymmetry in thickness can not be explained by age (cooling) as the age is assumed by surface geology to be similar on both sites of the ridge. Starting at ~12 km depth the Eastfjords have 4-6% lower velocity than the standard gabbroic Icelandic lower crust down to the 30 km depth of the mantle lid there. The seismic structure of the Eastfjords from 12km depth down is thus very similar to a continental structure inviting the hypothesis of a buried continental fragment under the basaltic lava pile. The surface waves show a maximum of 5-7% lateral variation in the SH and SV velocities in the crust, excluding the top 2-km, where it can be higher. The lateral variation in the mantle lid velocity is less, generally under 5% in SH and SV. The anisotropic variation seen by the surface waves is larger. Up to 5-10% in the crust and up to 5-8% in the mantle lid. Some parts of the lithosphere seem isotropic, especially the top half the Eastfjords lithosphere. All observations show anisotropic asthenosphere with between 3-7% anisotropy. Under central Iceland at 30-60 km depth the anisotropy can be so large (8%) that it is not straight forward to determine what is lid and what is asthenosphere. There is some evidence that this zone may be transverse isotropic and that these observations of SH > SV can be explained by a horizontal layer cake structure of partially molten soft layers and stiffer layers between in the mantle. Similar anisotropy feature in character and magnitude is observed with onset at 5 km depth in the crust and at least 7 km thick in both rift zones of Iceland. There the SV velocity is at least 6% lower than in normal Icelandic lower crust. Partial melt may be required to explain such a large anomaly. At the same depth MT measurements find a good conductor. The observed surface wave anisotropy in the asthenosphere below 90 km depth agrees qualitatively with SKS derived azimuthal anisotropy with NNW fast direction under central Iceland and NNE fast direction under west Iceland and the Westfjords.

JSS06/09P/A04-008

1640

### IMAGING THE RESULTS OF ARCHEAN TECTONIC PROCESSES: EM AND TELESEISMIC STUDIES OF THE SLAVE CRATON, CANADA

Alan G. JONES<sup>1</sup>, David SNYDER<sup>1</sup>, Bill DAVIS<sup>1</sup>, Wouter BLEEKER<sup>1</sup>, Herman GRUTTER<sup>2</sup>, Pamela LEZETA<sup>3</sup>, Alan D. CHAVE<sup>3</sup>, Rob L. EVANS<sup>3</sup>, Ian J. FERGUSON<sup>4</sup> (<sup>1</sup>Geological Survey of Canada, Ottawa, Canada, <sup>2</sup>Mineral Services Canada, Vancouver, Canada, <sup>3</sup>Woods Hole Oceanographic Institution, Woods Hole, U.S.A., <sup>4</sup>University of Manitoba, Winnipeg, Canada)

Geophysical (magnetotelluric and teleseismic) data from the sub-continental lithospheric mantle (SCLM) of the central Archean Slave craton, northern Canada, have imaged collocated electrical conductivity and seismic impedance interfaces that correlate spatially with a unique two-layer SCLM geochemical stratigraphy and with the distribution of low-Cr (G10) garnets in xenoliths. The ultra-depleted harzburgitic layer at 80-140 km is both highly conducting and lower impedance than the underlying Iherzolitic lower lithosphere layer. Taken together, these geophysical and geochemical observations imply a three-part NE-SW to E-W zonation of the Slave's SCLM that is at a high angle to the north-south trending isotope boundaries between Mesoarchean and Neoproterozoic crustal domains. This NE-SW mantle zonation parallels the orientation of late geological structures, including an F1 fold belt and distribution of ca. 2.63-2.62 Ga plutonic rocks. Extensive Neoproterozoic plutonism, crustal melting and associated HT-LP metamorphism argue for widespread elevated mantle heat input to the crust, a feature most consistent with thin (<100 km) lithosphere. We propose that the present-day mantle lithosphere developed by tectonic imbrication of one or more slabs subducted beneath the craton at 2.63-2.60 Ga. Subsequent collision, possibly accompanied by partial delamination of some of the underthrust lithosphere, produced widespread deformation and granite plutonism throughout the province at 2.6-2.58 Ga. The consequence of this model is that the Slave's mantle lithosphere, model-dated to be, in part, Mesoarchean in age, is exotic to its crust, and that the existing tectosphere grew from about 2.6 Ga onwards by subcretion (early) and thermal cooling (later).

JSS06/09P/A04-009

1700

### RAYLEIGH WAVE PHASE VELOCITIES BENEATH THE NORTHERN PHILIPPINE SEA DETERMINED BY DATA FROM LONG TERM BROADBAND OCEAN BOTTOM SEISMOGRAPHS

Takehi ISSE<sup>1</sup>, Daisuke SUETSUGU<sup>1</sup>, Hajime SHIOBARA<sup>2</sup>, Yoshio FUKAO<sup>3</sup>, Kimihiro MOCHIZUKI<sup>4</sup>, Toshihiro KANAZAWA<sup>2</sup>, Hiroko SUGIOKA<sup>1</sup>, Shuichi KODAIRA<sup>1</sup>, Ryota HI NO<sup>1</sup> (<sup>1</sup>Institute for Frontier Research on Earth Evolution, Japan Marine Science and Technology Center, <sup>2</sup>Earthquake Research Institute, University of Tokyo, <sup>3</sup>Research Center for Prediction of Earthquakes and Volcanic Eruptions Graduate School of Science, Tohoku University)

This study is the first attempt in the world to measure the dispersion curves of surface waves using long term broadband ocean bottom seismographs. The Philippine Sea, a marginal basin of the Pacific Ocean, has a complex tectonic history, which should be reflected in its upper mantle structure. In previous surface wave dispersion studies, events and seismic stations were restricted to the periphery of the Philippine Sea because there are no earthquakes and seismic stations in the Philippine Sea. This situation has limited the resolution in elucidating lateral heterogeneities of the relevant upper mantle structure. As a part of the Ocean Hemisphere network Project (OHP) a sea floor broadband seismic observation was conducted across the Philippine Sea in a period from November, 1999 to July, 2000 with eight Long Term Broadband Seismometers LT-BBOBS. We measured phase velocities of the fundamental Rayleigh waves over the northern Philippine Sea region sandwiched by the Japanese broadband network (FREESIA) to the north and the LT-BBOBS array to the south, using a two-station method in a frequency range from 0.01 to 0.05 Hz. Owing to the deployment of a broadband OBS array we were able to determine pure path Rayleigh wave dispersion curves across the old Pacific Sea floor, the young Shikoku Basin, the Parece-Vela Basin and the actively spreading Mariana Trough, respectively. The pure path phase velocities obtained by the present study for the Pacific Sea floor with ages older than 110 Ma are consistent to the result by Nishimura & Forsyth (1988). The average phase velocity across the young Shikoku Basin is slow as compared with the model velocity of the Pacific Sea floor of the same age, which may be related to the anomalously deep sea floor depth in the Shikoku Basin. The average phase velocity across the actively spreading Marian Trough is lowest in the analyzed area. The dispersion curves of the phase velocity across the Mariana Trough are consistent to the model velocity of the Pacific Sea floor of the same age. The observation by LT-BBOBS array enabled us to measure the pure path phase velocity even in a small marginal basin and determine the structural difference of the Philippine Sea precisely. The observed deviation of the dispersion from the age-dependant velocity model may indicate the presence of a compositional anomaly beneath the Shikoku Basin, which is an important subject in the future study.

JSS06/09P/A04-010

1720

### SV-WAVESPEED HETEROGENEITY BENEATH ASIA

Keith F. PRIESTLEY<sup>1</sup>, Eric DEBAYLE<sup>2</sup>, Sylvana PILIDOU<sup>1</sup> (<sup>1</sup>Bullard Laboratories, <sup>2</sup>Ecole et Observatoire des Sciences de la Terre, <sup>3</sup>Bullard Laboratories)

We have inverted almost 17,000 fundamental and higher mode regional Rayleigh surface waveforms to build a high resolution Sv-wavespeed tomographic model for the upper mantle beneath eastern Asia and the surrounding regions. We construct the 3D upper mantle model by first determining the 1D path-average upper mantle velocity models compatible with the observed waveforms, and then combining the 1D velocity models in a continuous tomographic inversion to obtain the local Sv-wavespeed and azimuthal anisotropy at each depth. Depending on the signal-to-noise ratio, fundamental mode are analyzed in the period range between 50 and 160 s and up to the fourth higher modes are analyzed in the period range between 60 and 90 s. We evaluate the horizontal and depth reliability of our model using a series of synthetic experiments that reproduce both steps of the analysis procedure. These synthetic tests confirm that the dense path coverage and rich higher mode content allow us to achieve a horizontal resolution of a few hundred kilometers down to at least 400 km depth. The well resolved features of the model include: (1) a high velocity lid with respect to PREM extending to about 200 km depth beneath most of the Siberian platform and the west Siberian basin, (2) a high velocity lid beneath the western Sino-Korean Craton but low upper mantle velocities beneath the eastern Sino-Korean Craton, (3) high velocities at depths below about 120 km beneath the Hangai Dome of north-central Mongolia, and (4) high upper mantle velocities beneath southern Tibet. There is a complex pattern of azimuthal anisotropy at shallow depths (< 175 km) but the amplitude of azimuthal anisotropy decreases and the pattern becomes more uniform at deeper depths (> 225 km).

JSS06/09P/A04-011

1740

## UPPER MANTLE ANISOTROPY BENEATH JAPAN FROM SHEAR WAVE SPLITTING

Maureen D. LONG<sup>1</sup>, Rob D. VAN DER HILST<sup>2</sup> (<sup>1</sup>Department of Earth, Atmospheric, and Planetary Sciences, Massachusetts Institute of Technology, <sup>2</sup>Faculty of Earth Sciences, Universiteit Utrecht)

Shear wave birefringence is a consequence of seismic anisotropy and is often used to characterize the upper mantle. Together with constraints from mineral physics, shear wave splitting can yield information on the pattern of upper mantle deformation. In the context of a subduction zone, however, the relationship between measured shear wave splitting parameters ( $\Phi$ ,  $\Delta t$ ) and geodynamical processes is not straightforward. The three-dimensional pattern of anisotropy in a subduction zone should reflect processes such as subduction itself, back-arc extension, corner flow in the mantle wedge, flow around the slab edge, and motion of the overriding plate. This relationship can be further complicated by complex slab morphology, by the presence of anisotropy in the slab itself, and by the presence of volatiles such as water, which can dramatically change the relationships between strain geometry and resulting anisotropy. Because a single shear wave splitting measurement represents a path-integrated picture of anisotropy, and because most splitting studies use phases with near-vertical incidence angles, the complexities of anisotropic structure associated with subduction zones are difficult to detect. In this study, we take advantage of dense station coverage in Japan and use phases covering a wide range of incidence angles, incoming polarization angles, and back azimuths. We avoid making the simplifying assumption of a single, horizontal anisotropic layer, and take advantage of the good data coverage needed to consider complexities in structure such as multiple anisotropic layers, dipping symmetry axes, and small-scale lateral variations in anisotropic properties. We utilize data from the Japanese F-net network, which comprises 65 broadband seismic stations. We analyze shear wave splitting parameters at each station using methods due to Silver & Chan [1991], Levin et al. [1999], and Chevrot [2000]. We use recordings of local and teleseismic direct S phases as well as core-refracted SKS and SKKS phases. Because the purpose of this study is to investigate three-dimensional anisotropic structure, we search for variations in measured splitting parameters ( $\Phi$ ,  $\Delta t$ ) with incidence angle and incoming polarization angle at each station. As well as examining complexities in anisotropic structure beneath individual stations, we map the large-scale spatial variations of shear wave splitting parameters over the area of the network. These spatial variations of shear wave splitting presumably reflect the pattern of mantle flow associated with subduction beneath the Japanese islands.

Thursday, July 10 AM

Presiding Chair: D. Sandwell

JSS06/10A/A04-001

0830

## ENHANCEMENT OF DECOMPRESSION MELTING IN THE PRESENCE OF CONTINENTAL ROOT IN PLUME- LITHOSPHERE INTERACTION MODELS

A. MANGLIK<sup>1</sup>, U.R. CHRISTENSEN<sup>2</sup> (<sup>1</sup>National Geophysical Research Institute, Uppal Road, Hyderabad 500007, India., <sup>2</sup>Institut fuer Geophysik, Herzberger Landstrasse 180, 37075 Goettingen, Germany.)

Global distribution of Large Igneous Provinces (LIPs) shows that in many of these provinces massive volcanic events associated with starting plume heads occurred at the margins of continental lithosphere. The contrast between the thick lithospheric root and adjacent thinner lithosphere affects the spreading of the plume head below the plate. In the present study, we analyse the effect of lithospheric roots on the pattern of plume flow and decompression melting in three-dimensional numerical models. We also incorporate horizontal shear due to plate motion. We assume the viscosity to be temperature- and depth-dependent and define the lithosphere as mechanically strong, high viscosity lid. Decompression melting is computed by using the batch melting model of McKenzie and Bickle. Presence of a root inhibits uniform lateral spreading of the plume. The plume material rising beneath the lithospheric root deflects away from the root and rises to comparatively shallow depth at its margin. Our results show that the deflection of plume material towards one side can facilitate a more than three fold enhancement in the total melt production rate in comparison to models without root. The model reproduces the characteristics of melting rates and melt volumes seen in flood basalt provinces without invoking an excessively high plume thermal anomaly. Our results also support juxtaposition of late-stage and main phase of volcanism in a flood basalt province.

JSS06/10A/A04-002

0850

## GLOBAL DEVIATORIC STRESS IN THE LITHOSPHERE FROM GEOID HEIGHT, TOPOGRAPHY, AND STYLE OF FAULTING

David T. SANDWELL, Bridget SMITH (Scripps Inst. of Oceanography)

Stress in the Earth's lithosphere is due to three forces: slab pull, swell-push, and asthenospheric drag. While the swell-push force can be measured from geoid height variations across seafloor spreading ridges, the global stress field of the Earth is still poorly determined because the dominant slab-pull force is largely unknown. Here we attempt to develop a 3-D global stress model of the lithosphere that is consistent with three key observations; geoid height, topography, and style of faulting. Our method follows: 1) Part of long-wavelength (> 400 km) 2-D global stress field can be estimated from geoid height. The geoid is decomposed into a "lithosphere" contribution and a "deep mantle" contribution by making plausible assumptions about the compensation mechanisms of the continents and the seafloor spreading ridges (i.e., ridges are weak). This "lithospheric" contribution is used to construct a partial global stress model. 2) The topography of the Earth is high-pass filtered to isolate wavelengths shorter than 400 km. We use a (3-D) semi-analytic solution for the loading of an elastic half-space from both surface topography and compensating Moho topography to calculate the stress in the crust and lithosphere. This short-wavelength stress field is added to the long-wavelength field to construct the trial global 3-D stress model. 3) Finally, we test the style of faulting predicted by this model (normal, strike-slip, or thrust) with the known active faults along plate boundaries. For example, the model predicts 12 MPa of extension, at 6 km depth, in the Transverse Ranges of the Big Bend area. Because the method of faulting through the Big Bend area is primarily strike-slip, there must be a 12 MPa tectonically-induced compressional stress that is not predicted by the model. We will explore the possibility of correcting the model by applying the appropriate tractions along the plate boundaries.

JSS06/10A/A04-003

0910

## THE ROLE OF DEEP LITHOSPHERIC STRUCTURES IN THE GENESIS OF LARGE AND SUPERLARGE ORE DEPOSITS IN UZBEKISTAN

I. Kh. KHAMRABAEV, I.P. SIDOROVA, A.A. KUSTARNIKOVA (Institute of Geology &amp; Geophysics)

The present thesis reviews the main results of studies carried out in Uzbekistan in the years of 1996-2000 under the project "interrelations between Deep Lithospheric Structures and Metals Concentrations". The investigations have been carried out in two regions of Uzbekistan: in the Almalyk-Angren region, and in Central Kyzylkums. These regions provide nearly 100% of ore output of the Republic (gold, silver, copper, fluorite, uranium) and ensure the 7-8<sup>th</sup> place in world production. The main conclusions are: 1. The upper part (10-20 km) of the earth's crust in the Almalyk-Angren and Central Kyzylkum ore regions has a stratified-block structure. The upper sedimentary stratum of Mesozoic-Cenozoic age, with a thickness of 0 to 2 km, is not developed in all places. The other part is composed of Paleozoic and pre-Paleozoic sedimentary and magmatic rocks of various composition. They were metamorphosed from greenschist to amphibolite facies. In addition, the Central Kyzylkum rocks were dynamo-metamorphosed as a result of elastic-viscous tectonic deformations. 2. Both the above regions are, at the present level, characterised by weak anomalies regional gravity and magnetic fields. The both regions are areas of present uplift (2-8 mm/year), where endokinetic energy is produced. At the same time, large ore deposits are characterized by a reduced gravity field and lower velocities of seismic waves, indicative of high jointing (uncondensivity) of ore-bearing blocks. 3. The anomalies of heat flow and electrical conductivity are connected with zones of deep-seated faults. The latter are, in places, marked by emissions of underground gases (hydrogen, methane, etc.). 4. Both regions are characterized with multiply prolonged (40-60 million years) development of tectonic and magmatic processes, with formation of large granitoid plutons and various (differing in form and composition) rocks of volcano-tectonic structures, differing in composition, in age, as well as in character and scale of mineralization. 5. On the base of revealed and formulated geological and geophysical parameters of local possibilities of origin of large and superlarge endogenic deposits. Purposeful carrying out of prospecting can be allowed to reveal some new deposits and increase resources of precious, base and rare metals, that will provide for a long time working of mines and establishing the new ones. On the other hand established and described new kinds of connections between deep structures and peculiarities of magmatism and metallogeny are of planetary character and general theoretical significance.

JSS06/10A/A04-004

0930

## A PLUME BENEATH THE NORTHEASTERN AFRO-ARABIAN CONTINENT?

Michel J. CARA<sup>1</sup>, Eric DEBAYLE<sup>2</sup>, Georges HERQUEL<sup>1</sup>, Jean Jacques LEVEQUE<sup>1</sup>, Anne SIEMINSKI<sup>1</sup>, Deborah SICILIA<sup>2</sup>, Jean Paul MONTAGNER<sup>2</sup>, Atalay AYELE<sup>3</sup>, Jamal M. SHALAN<sup>4</sup> (<sup>1</sup>EOST, University of Strasbourg, <sup>2</sup>Institut de Physique du Globe de Paris, <sup>3</sup>Geophysical Observatory, University of Addis-Ababa, <sup>4</sup>National Seismological Observatory Center, Dhamar)

A cooperation program linking the University of Addis Ababa, the National Seismological center of Dhamar and "Institut National des Sciences de l'Univers" - France, led us to install 5 broad-band STS2 seismometers in Ethiopia and Yemen during the years 1999-2002. Thanks to the records available at other permanent and temporary stations (GEOSCOPE, IRIS and PASSCAL), a large set of broad-band teleseismic data have been collected and processed in the northeastern Afro-Arabian region. In this presentation, we review the results obtained by the different groups participating in the cooperation program, and we discuss in particular the question of the origin at depth of the Afar hot spot. Surface-wave tomographic models based on two different waveform inversion techniques have been constructed, constraining the location of a low shear-wave speed anomaly in the upper 250 km beneath the Ethiopian Plateau, Afar, the Red Sea, the Gulf of Aden and southwestern Arabia. The waveform inversion technique of Cara an L v que (1987) allows us to get reasonable resolution down to the upper mantle transition zone. The result of this tomographic model suggests the presence of a deeply rooted low velocity material beneath the South of the Red Sea and the Arabian plate (Debayle et al., 2001). This result is discussed in the light of observation of receiver function peaks related to the 410 and 670 km depth discontinuities in the region. Other constraints on the shallower asthenospheric flow is provided by azimuthal anisotropy coming from the inversion of fundamental mode Rayleigh-waves. The directions of fast SV-waves inferred from the Rayleigh-wave data is compared with the directions of polarization of the fast SKS waves in the region, allowing us to put some constraints on the upper-mantle flow beneath the region.

JSS06/10A/A04-005

0950

## 3-D RHEOLOGICAL STRUCTURE OF THE LITHOSPHERE FOR THE ORDOS BLOCK AND ITS ADJACENT AREA

Shao Xian ZANG, Rong Qiang WEI, Yong Gang LIU (Department of Geophysics, Peking University)

Ordos block is in the northern-central China. It connects with Tibet plateau, but it is an inactive block surrounded by active deformed zones so it causes a big attention from geoscientists. In this paper, we study the rheological structure of Ordos block and its surrounding area to study the reason for the special behavior and provide the necessary parameters for geodynamic study. It needs the velocity structure, composition and the thermal structure of the lithosphere for studying the rheological structure. The velocity structure of the crust was obtained from exploration seismology and seismic tomography. The lower boundary of the thermal structure is taken as the lower lithosphere boundary because there is no constraint from seismic exploration study. The thermal structure was obtained using the surface heat flow data. The composition are taken as granite in the upper crust, Anorthosite in the middle crust, felsic granulite in the lower crust, wet peridotite in the upper mantle part of the lithosphere. According to the results in the laboratory, three main rheological deformation mechanisms in the lithosphere, namely frictional sliding, brittle fracture and creep are considered. The state of stress deduced from earthquake mechanism in the Ordos area is that the maximum and minimum principle stresses are horizontal and the medium principal is vertical, so Byerlee's law in Anderson faulting system is used for strength of frictional sliding. The brittle fracture mechanism is usually ignored in some rheological studies because the strength of the brittle fracture obtained from small samples is too big when comparing it with other two mechanisms. We obtained the strength of the brittle fracture deduced from results on small-scale specimen and subjected to the constraint of a few existing data on large-scale specimen. The Dorn equation is used for the strength of creep. The rheological structure of the lithosphere is obtained by different constraint: constant strain rate, constant tectonic force, strain rate-dependent force and realistic strain rate constraint. The results show that the rheological structure changes with the different constraint and is vertical layering and horizontal variation. The influence factors and applications are discussed.

JSS06/10A/A04-006

1010

## THE VRANCEA NATURAL LABORATORY OF GEODYNAMICS

Dorel ZUGRAVESCU, Vladimir Nicolaevich STRAKHOV, Alexander Olegovich GLIKO, Constantin Stefan SAVA, Vladimir Georgievich BOUDANOV (Institute of Geodynamics)

In the Romanian Carpathians bending zone the geotectonic conditions assured the constitution of a true natural geodynamics laboratory, which allows the survey of an ensemble of physical parameters causally linked with the complex phenomena that lead to

the cumulating/triggering of seismic energy. Its characteristic geodynamic features and its geographical position make this laboratory unique in the world, a laboratory offered by nature to researchers in particularly favorable conditions, allowing optimal circumstances for research, from the point of view of its structure (perfectly spatially delimited) and from the point of view of the socio-economic interests implied and its accessibility. Among the features that confer the seismogenic zone of Vrancea as a geodynamics laboratory its uniqueness, the following must be emphasized: the small, strictly delimited area of the epicentral zone, corresponding to an ellipse-shaped area having the large axis oriented North-East to South-West of about 70 km and the small axis of about 35 km; the situation of the hypocenters till depths that, exceptionally, may exceed 180 km, with a practically aseismic zone situated between 40 and 60 km; the high frequency of earthquake occurrence corresponding to the same epicentral area (small magnitude earthquakes occur, practically, daily); the fact that, several times per century, earthquakes with a magnitude significantly higher than 7.0 on the Richter scale are triggered; the extended area, situated in Romania, the Republic of Moldova, Bulgaria, Hungary, Yugoslavia, and even in Ukraine and Russia, affected by the strong earthquakes triggered in that zone, the area being intensely populated (the city of Bucharest has approximately 3 million inhabitants) and comprising edifices of highest socio-economic importance, including nuclear power stations; the presence of an ensemble of geodynamics observatories and observation points, grouped in a Polygon of Geodynamics, which benefit both from historical observations extending over more than a millennium, and from instrumental observations initiated approximately a century ago and improved continuously by the addition of new instrumentation; its accessibility: the Polygon of Geodynamics Căldărușani - Tulnici includes the international airport Otopeni, the city of Bucharest - Romania's capital, and a dense network of roads and railways crisscrosses it. In order to give to the interested scientists the possibility to work together for enhancing the knowledge on this natural polygon, using all available modern means, in the frame of an international form of cooperation, the Institute of Geodynamics "Sabba S. Stefanescu" of the Romanian Academy and the United Institute of Earth Physics "O.Yu. Schmidt" of the Russian Academy of Sciences, founded the "International Virtual Laboratory of Geodynamics" in the year 2001. Other research units from Romania, France, Germany, Belgium and Republic of Moldova have already expressed their intention to participate in the activities of this Virtual Laboratory.

JSS06/10A/A04-007

1050

#### LITHOSPHERIC THERMAL AND MECHANICAL STRUCTURE OF EASTERN TIBETAN PLATEAU WITH TECTONIC IMPLICATION

Yong ZHENG<sup>1</sup>, Xiong XIONG<sup>2</sup>, Rongshan FU<sup>1</sup> (<sup>1</sup>Department of Earth and Space Sciences, University of Science and Technology of China, <sup>2</sup>Institute of Geodesy and Geophysics, Chinese Academy of Sciences)

The mass eastward flow of Tibetan Plateau is one of the most prominent tectonic features of the plateau. The mass move eastwards, and tend to run nearly southeastwards in front of the Sichuan Basin. On the other hand, the results from both the numerical simulation and subcrustal stress field induced by mantle flow suggest that the crustal deformation is strongly decoupled from that of the mantle in the eastern Tibetan Plateau. So, the questions are addressed: why the mass moving direction changes from the east to the nearly southeast, and what is the mechanical background of the decoupling between the deformation of the crust and the mantle. To clarify the questions, a two-dimensional algorithm is designed to determine the steady state lithospheric thermal and strength structure along two profiles crossing the main tectonic units of the eastern Tibetan Plateau. The temperature distribution within the lithosphere and at any material boundary is calculated by a finite element technique with the surface heat flow, heat generation and the thermal conductivity as the input data. With the given rheological parameters of crustal and mantle medium, the strength distribution and the total lithospheric strength is determined in the selected columns. The numerical results show significant variation of the lithospheric temperature and strength distribution of different tectonic units. The temperature is very high in the active tectonic regions, such as Kunming, Lijiang and Tengchong, while is low in the Sichuan Basin, a stable tectonic unit titled "cold basin" in China continent. The zone with the strongest lithosphere is the Sichuan Basin, while those with weakest lithosphere are Tengchong, Lijiang and Kunming. The brittle deformation zone is confined within the first 20km in most study areas except the Sichuan Basin. The result agrees with that obtained from studies on gravity and lithospheric flexure, which shows that the lithosphere is very weak in Tibetan Plateau, especially in the eastern plateau. In addition, our result shows very weak strength distribution within the lower crust, which is suggested to be one of the most important factors for the decoupling of deformation between the crust and mantle. As usual, the mass movement usually takes the weak zone as the preferential flowing direction. Since the Sichuan Basin, with a strong lithosphere, is a very stable tectonic unit in China continent, it may be a barrier for the mass eastwards flowing. When the mass flowing encounters the Sichuan Basin, it tends to take the zones with weak lithospheric strength as the preferential direction and move along them. So, the mass moving direction changes from east to nearly southeast in front of the Sichuan Basin. It is suggested that the lithospheric thermal and strength distribution in various tectonic units may play an important role for the crustal movement in the eastern Tibetan Plateau.

JSS06/10A/A04-008

1110

#### PN TOMOGRAPHIC IMAGING OF MANTLE LID VELOCITY AND ANISOTROPY AT THE JUNCTION OF THE ARABIAN, EURASIAN, AND AFRICAN PLATES

Ali I. AL-LAZKI<sup>1</sup>, Eric SANDVOL<sup>2</sup>, Dogan SEBER<sup>3</sup>, Muawia BARAZANGI<sup>4</sup>, Niyazi TURKELLI<sup>5</sup>, Randa MOHAMAD<sup>6</sup> (<sup>1</sup>Department of Earth Sciences, Sultan Qaboos University, <sup>2</sup>Department of Geological Sciences, University of Missouri, <sup>3</sup>Institute for the Study of the Continents, Snee Hall, Cornell University, <sup>4</sup>Department of Geophysics, Kandilli Observatory and Earthquake Research Institute, <sup>5</sup>Syrian National Seismological Center, General Establishment of Geology and Mineral Resources)

The Arabian plate's interaction with the Eurasian plate has played a major role in building the young mountain belts along the Zagros-Bitlis continent-continent collision zone. Arabia's northward motion is considered to be the primary driving force behind the present-day westerly escape of the Anatolian plate along the North and East Anatolian fault zones as well as the formation of the Turkish and the Iranian plateaus. In this study we mapped Pn wave velocity and anisotropy structures at the junction of the Arabian, Eurasian, and African plates in order to elucidate the upper mantle dynamics in this region. Pn is a wave that propagates within the mantle lid of the lithosphere and is often used to infer the rheology and fabric of the mantle lithosphere. Using a strict selection criterion we used arrival times of 166,000 Pn phases to invert for velocity and anisotropy in the region. Using a least squares tomographic code, these data were analyzed to simultaneously solve for both velocity and azimuthal anisotropy in the mantle lithosphere. We found that most of the continental regions in our study area are underlain by low Pn velocity structures. Broad scale (~500 km) zones of low (< 8 km/s) Pn velocity anomalies underlie the Anatolian plate, the Anatolian plateau, the Caucasus region, northwestern Iran, and northwestern Arabia and smaller scale (~200 km), very low (< 7.8 km/s) Pn velocity zones underlie southern Syria, the Lesser Caucasus, the Sparta Angle, central Turkey, and the northern Aegean Sea. The broad scale low velocity regions are interpreted to be hot and unstable mantle lid zones, whereas very low Pn

velocity zones are interpreted to be regions of no mantle lid. The low and very low Pn velocity zones in eastern Turkey, northwestern Iran, and the Caucasus region may be associated with the latest stage of intense volcanism that has been active since the Late Miocene. The low Pn velocity zones beneath the Anatolian plate, eastern Turkey, and northwestern Iran may in part be a result of the subducted Tethyan oceanic lithosphere beneath Eurasia. We also found a major low velocity zone beneath northwestern Arabia and the Dead Sea fault system. We interpret this anomaly to be a possible extension of the hot and anomalous upper mantle of the Red Sea and East Africa rift system. High Pn velocities (8.1 - 8.4 km/s) are observed to underlie the Mediterranean Sea, the Black Sea, the Caspian Sea, and central and the eastern Arabian plate. Observed Pn anisotropy showed a higher degree of lateral variations in comparison to the Pn velocity structure. Though the Pn anisotropy varies even in a given tectonic region, in eastern Anatolia very low Pn velocity and Pn anisotropy structures appear to be coherent.

JSS06/10A/A04-009

1130

#### SIGNIFICANCE OF MANTLE DYNAMICS IN INTERACTION BETWEEN THE SUBMARINE INTERFACES

Xianglong JIN, Gao JINYAO (Second Institute of Oceanography and Key Lab of Submarine Geosciences, SOA)

The significance of mantle dynamics in interaction between the subseafloor interfaces is elaborated from the mantle dynamic features reflected by hotspots, mantle low-velocity zones and mantle-convection stress fields, the secular processes of submarine mineralization for hydrothermal mineral, polymetallic nodule and cobalt crust, and possible the short-term phenomena changing the Earth hydrology and climate system. Mid-Ocean ridges around the Earth are important channels for the substance and energy from mantle in interaction between the submarine interfaces. Hydrothermal vents with abundant polymetallic elements transported into oceanic basins by ocean currents are mineralization resources for polymetallic nodules. The hotspots have good correspondence to seamount chains distributed on low, middle latitudes, also being mineralization resources for seamount cobalt crusts. Now that mid-ocean ridge spreading, hotspot and hydrothermal activities of geological scale possess a long-term accumulation of mantle energy, and may cause the abrupt nonlinear events in a short time, such as earthquake, volcanism and tsunami, even oceanic and climate process. El Nino could be related with mantle dynamics. The El Nino occurs at the warm pool with high temperature and sea level in the western Pacific Equator, and migrates from western Pacific to eastern Pacific along the equatorial zone. The western Pacific warm pool is near by the highest uplift of the global geoid surface (New Guinea: 5°20.4'S, 142°40.2'E), beneath which there are a broad magma province, a huge convergence of mantle substance and stress. The warm pool could be due to the mantle energy conveyed by magmatic process. Under the Equator and low latitude Pacific, there exists a low-velocity zone in mantle, which shrinks towards the Equator down to lower mantle. This indicates that upper mantle is highly melted and releases enormous energy along the Equator. Much thinner than continental crust, oceanic crust is relatively easy to release mantle energy through hydrothermal activities along various scales of fractures. Twenty-five main hotspots are all distributed in the seafloor of southern Hemisphere. Of them, eight hotspots between 0°-30° S in the middle and eastern Pacific, eleven hotspots in south of 30° S around Antarctica, with the tectonic and hydrothermal activities along the eastern Pacific ridge, are all probably provide enough substance and energy transported through the middle and deep oceanic currents for mineralizing process. Nowadays observation techniques and accumulated data are not enough to prove the processes impacting the transportation of mantle substance and energy, and the submarine mineralization. One of the most difficult problems is severe shortage of seafloor heat flow data along the Equator and low latitude Pacific. For this reason it is needed to establish a global or regional observatory network in the context of international cooperation, including middle and deep oceanic current observations.

JSS06/10A/A04-010

1150

#### MUTUAL INTERACTION BETWEEN MAGMATISM AND GEODYNAMICS IN THE CARPATHIAN-PANNONIAN REGION, EASTERN EUROPE

Ioan SEGHEDI<sup>1</sup>, Hilary DOWNES<sup>2</sup>, Alexandru SZAKÁCS<sup>1</sup>, Zoltán PÉCSKAY<sup>1</sup> (<sup>1</sup>Institute of Geodynamics, Birkbeck/UCL Research School of Geological and Geophysical Sciences, Birkbeck College, Malet St., London WC1E 7HX, UK, <sup>2</sup>Institute of Nuclear Research of the Hungarian Academy of Sciences, P.O. Box 51, Bem ter 18/c, H-4001 Debrecen, Hungary)

The Carpathian-Pannonian Region is a result of convergence between Africa and Europe and a good example of the link between magmatism and geodynamics. A complex spectrum of microplate motion and related geologic processes (subduction, collision and extension) are inferred. Kinematics of the Intracarpinian blocks (Alcapa, Tisia) up to the collision with European Plate were responsible for the generation of various kinds of magmas (calc-alkaline, alkaline). Relevant examples suggest that mantle dynamics is deduced from petrological features of the magmas, refining the existing geodynamic models: (1) In the Western Carpathians and Pannonian Basin felsic explosive volcanic activity occurred (21-18 Ma), then felsic and intermediate calc-alkaline volcanic activity was generated across a large area (18-12 Ma, sporadically between 12-8 Ma). In several small areas between 10-0.1 Ma alkali-mafic volcanism was generated. The age relationships and geochemical features suggest south toward north youngness and admit sediment and fluid decrease, initially a crustal source, then a mixing between crustal and mantle source and finally a mantle source. This magmatism at its inception was subduction-related. Extrusion and counter-clockwise rotations of Alcapa, rollback and collision triggered partial melting either by delamination or straight asthenosphere upwelling. Finger-like asthenosphere upwelling likely generated younger alkali-mafic magmatism. (2) In the westernmost East Carpathians simultaneous (15-9 Ma) calc-alkaline volcanism is spread across ca. 100km in several parallel lineaments. The geochemical features reveal significant mantle-source variation in back-arc setting and larger fluid induced metasomatism, source-enrichment and assimilation toward the trench. This magmatism suggests subduction-related rollback triggered melting, since its generation was probably related to the rollback of a subducted slab and collision, followed by back-arc extension, asthenosphere rise and presumably breakout processes. (3) In the Apuseni Mountains typical calc-alkaline and adakite-like magmas (15-9 Ma) do not show relationships with contemporaneous rollback processes in front of the orogen. OIB-like alkali-basaltic magmatism (2.5 Ma) and shoshonitic magmatism (1.6 Ma) ends the magmatic activity. The mechanism of magma genesis is lithosphere breakup during rotations (~60 degree) between 14-12 Ma, which generated decompressional melting of the lithospheric (early) and asthenospheric (later) sources. Transension and rotation triggered melting processes are inferred. Alkali-basalts suggest decompressional melting of OIB-like rising asthenosphere. Such asthenospheric melts mixed with lithospheric melts to generate alkaline-shoshonitic rocks during the transension and attenuation of the lithosphere along an east-west reactivated fault-system. (4) At the southeastern part of the Eastern Carpathians contemporaneous eruption (2-0.3 Ma) of adakite-like calc-alkaline, shoshonitic and alkali-basaltic magmas occurred following normal calc-alkaline magmas. Decompressional melting of an OIB-like asthenospheric mantle (producing alkali-basaltic magmas) coupled with fluid-dominated melting of the subducted slab (generating adakite-like magmas) and mixing between slab-derived melts and asthenospheric melts (generating shoshonites) is supposed.

## INTER-ASSOCIATION

Breakoff and tearing of the subducted slab at shallow levels in the extreme southern part of the arc can explain this situation, as heat from the asthenosphere plume produced melting of the hydrated torn slab, as well as generating melt via decompression. This magmatism can be characterized as related to rollback, breakoff and tearing triggered melting processes.

**JSS06/10A/A04-011**

**1210**

### SEISMIC ANISOTROPY AND PLATE-MANTLE INTERACTION

Götz BOKELMANN (Stanford University)

Seismic anisotropy is a powerful tool which allows us to constrain the degree of plate-mantle interaction. Some questions we are interested in are: How strong is the mechanical coupling between continental plates and underlying mantle? Is there an asthenosphere under continental plates, i.e. under shield regions? How important are the forces acting at the base of the plate for driving the plates? Are individual plates driven by ridge push and slab pull or rather by mantle convection? Are lithospheric deformation and surface tectonics do some degree caused by deeper motions? The answer to those questions may lie in observing the deformation state of the deep lithosphere, using seismic anisotropy. We may determine the direction of relative motion between plate and deeper mantle if finite grain rotation at the base of the lithosphere is incomplete and the fast anisotropic axes show a plunge angle different from horizontal. We have examined plunge angles for a large number of seismological stations on Earth, e.g. the Canadian Shield. For the latter we have found that fast axes under the shield dip to the west, roughly in the direction of absolute plate motion, and that the anisotropy is consistent with a simple-shear deformation of the deep lithosphere. This is consistent with basal tractions under the shield aiding the motion of the continent rather than resisting it (e.g., Bokelmann 2002, GJI 248, 2, 278-287; Geology 30, 11, 1027-1030). A similar result has been obtained recently by Lui and Bird (2002, GRL 29(24), 2164, doi:10.1029/2002GL016002) based on tectonic modeling. Clearly, seismic anisotropy may play an important role in the integration of seismology and geodynamics. A rheological continent model based on observed seismic anisotropy suggests that the level of stress is on the order of a few MPa (Bokelmann and Silver, 2002, GJI, 29(23), 2091, doi:10.1029/2002GL015925) which indicates that the coupling of continental plates to the deeper mantle can not be ignored. It also suggests that there is probably no well-developed zone of localized deformation (asthenosphere) under the central parts of stable continental areas. For pdf-files see my homepage <http://pangea.stanford.edu/~goetz/home.html>.

**JSS06b-Posters**

**Thursday, July 10**

**EARTH STRUCTURE AND GEODYNAMICS (IASPEI, IAVCEI, IAG, IAGA)**

Location: Site D

**Thursday, July 10 PM**

Presiding Chair: J. Plomerova

**JSS06b/10P/D-001**

Poster

**1400-025**

### SEISMOTECTONICS OF THE LITHOSPHERE OF ACTIVE OCEANIC MARGINS

Serguey A. BOLDYREV (Institute of Physics of the Earth, Russian Academy of Sciences, B.Gruzinskaya 10 Moscow 123995 RUSSIA)

In the present work, using the Kamchatka sector of the Pacific Mobile Belt as an example, we discuss the results of a structural analysis of the earthquake focus distribution and a mechanism of elastic stress realization at the active oceanic margins. To describe the seismic field of the lithosphere in the studied region, we used data of the Kamchatka seismological survey (KAM) on shallow-focus ( $H < 60$  km) seismicity for the period from 1962 through 1998. The principal peculiarities of the shallow-focus seismicity in the Kamchatka region are the local, selective character of the origination of earthquakes and the spatial stability of areas with elevated seismic activity throughout the observation period. These stable areas are clustered into linear systems. The sites of intersections of such systems are distinguished for their high seismic activity. They are commonly associated with instrumental epicenters of the strongest ( $M > 6.5$ ) earthquakes. As was mentioned above, the character of seismotectonic processes and physical properties of the lithosphere within the study area are fundamentally dissimilar in segments situated north and south of the main lineament at 55° N. This lineament is traced from the central Kamchatka rift zone to the Bering Sea coast of the Komandorskie Islands. The volcanic ridge is displaced along this lineament by almost 70 km; however, the lineament is practically not expressed in the topography and principal geophysical fields. The near-surface seismicity ( $H < 30$  km) dominating northward of 55° N, is caused by nearly horizontal compressive stresses with azimuth of 170-100°. It is represented by sublatitudinal lineaments spaced with a periodicity of 35-40 km. In the southern segment, the seismicity is governed by nearly horizontal compressive stresses (azimuth 123-70°). The majority of the foci appear in the subcrustal lithosphere, and the block dimension governed by the seismotectonic processes is 120 x 80 km. The lineaments oriented along the SFZ are dominated by upthrow-type displacements, which results in thrusting of lithospheric blocks from the west and east over the central segment of the SFZ. As a result, the central part subsides, affecting the configuration of the crust-mantle interface. On the whole, a direct relation between the seismotectonics and geomorphology of active ocean margins is not observed. In transition zones, the shallow seismicity is likely to reflect the structural features of the crust-mantle interface.

**JSS06b/10P/D-002**

Poster

**1400-026**

### SPATIAL VARIATION IN ISOSTATIC PARAMETERS REVEALED THROUGH THE CONTINUOUS WAVELET TRANSFORM

Jonathan KIRBY<sup>1</sup>, Christopher SWAIN<sup>2</sup> (<sup>1</sup>WA Centre for Geodesy, Curtin University of Technology, <sup>2</sup>20 Bedwell Crescent, Booragoon, WA, Australia)

A new technique based on anisotropic admittance and coherence functions and the two-dimensional continuous wavelet transform (2D-CWT) will be presented in this paper. This approach is considered necessary because existing isostatic analyses tend to use the approximation of isotropic responses and the Fourier transform technique. It is argued here that the wavelet transform allows for amore regional analysis that preserves spatial structure and relationships. Some preliminary results of the new technique will be presented from a case study over central Australia, where there is a reasonably homogeneous coverage of gravity and terrain data. These results indicate that the technique does offer an advance upon existing methods. Comparisons of variations in effective elastic thickness estimated using the new technique, with those derived from teleseismic experiments, show good agreements, indicating that the new technique is effective.

**JSS06b/10P/D-003**

Poster

**1400-027**

### THE EFFECT OF NOISE ON ESTIMATES OF THE ELASTIC THICKNESS OF THE CONTINENTAL LITHOSPHERE BY THE COHERENCE METHOD

Christopher SWAIN<sup>1</sup>, Jonathan KIRBY<sup>2</sup> (<sup>1</sup>20 Bedwell Crescent, Booragoon, WA, Australia, <sup>2</sup>WA Centre for Geodesy, Curtin University of Technology, Perth, Australia)

We model the lithosphere as a uniform elastic plate overlying a fluid and loaded with both surface and subsurface fractal loads to generate synthetic topography and gravity data. We simulate data having low (topographic) signal to (gravity) noise ratio by using an algebraically larger exponent for the subsurface load in the spectral synthesis fractal algorithm. The gravity powerspectrum then decays less rapidly than that of topography, the spectra resembling those for central Australia. We then apply the coherence method to the synthetic data, using periodogram spectral estimation, and find that it correctly estimates the plate thickness. Using multitapers for either coherence or admittance spectra always yields significant underestimates unless the data window is larger than several times the flexural wavelength. We quantify this bias for the parameters used here for both low and normal signal-to-noise ratio data. We then apply the bias as a correction to an effective elastic thickness estimate, made using the multitaper coherence method, for central Australia: it yields 120 +/- 25 km.

**JSS06b/10P/D-004**

Poster

**1400-028**

### ON THE INSTANTANEOUS MOTION OF THE SOUTH TASMAN SEA AND ITS EFFECT ON THE ANTARCTIC PLATE

Atsuki KUBO<sup>1</sup>, Yoshifumi NOGI<sup>2</sup>, Tetsuzo SENO<sup>3</sup> (<sup>1</sup>Natl. Res. Inst. for Earth Sci. and Disas. Prev., <sup>2</sup>National Institute of Polar Research, <sup>3</sup>Earthquake Research Institute, University of Tokyo)

Earthquake slip vectors deviate from the NUVEL-1 relative motions for both Pacific (PAC)-Australia (AUS) and AUS-Antarctic (ANT) plate boundaries near the Macquarie triple junction (Frohlich et al., 1997; DeMets et al., 1988). The South Tasman Sea, nominally part of AUS, plate might be a microplate or a diffuse deformation zone. However this idea has been denied based on one focal mechanism at its northern possible boundary by DeMets et al. (1988). A large earthquake (Mw 8.1) occurred within ANT southwest of the triple junction on March 25, 1998. The microplate hypothesis including part of ANT did not explain the deviation of the slip vector of the 1998 earthquake (Condor and Forsyth, 2000). The stress-strain fields produced by the relative plate motions and/or topography forces did not explain the stress axes of the earthquake either (Kreemer and Holt, 2000). We propose the possibility of a rigid microplate in the South Tasman Sea based on the slip vector deviations, and examine its dynamical effect on the occurrence of the large earthquake. We estimate the WSW motion (~5 mm/yr) of the South Tasman Sea microplate with respect to AUS to satisfy the slip vector deviations. This motion is nearly normal to the AUS-ANT transform faults, and would produce the compression normal to the faults. This is similar to the fault-normal compression seen in the San Andreas fault (Zoback et al., 1991). This compressional stress field is consistent with the P-axis direction of the focal mechanism of the large 1998 earthquake, and we suppose that the collision of the South Tasman Sea to the Antarctica plate probably induced the large 1998 earthquake. *References* DeMets et al. (1988) JGR, 93, 11877; Frohlich et al. (1997) JGR, 102, 5029; Condor and Forsyth (2000) Geophys. Res. Lett., 27, 2309; Zoback, M. D. (1991) Phil. Trans Roy astr Soc. Lond. A., 337, 141; Kreemer and Holt (2000) Geophys. Res. Lett., 27, 2297

**JSS06b/10P/D-005**

Poster

**1400-029**

### HOW THICK IS THE LITHOSPHERE?

Irina M. ARTEMIEVA<sup>1</sup>, Walter D. MOONEY<sup>2</sup> (<sup>1</sup>EOST, <sup>2</sup>USGS)

Seismic and thermal estimates suggest a highly variable thickness of Precambrian lithosphere (140-350 km), with a bimodal distribution for Archean cratons (~220 km and ~350 km). We discuss the origin of such large variations in lithospheric thickness and examine mechanisms of lithospheric erosion. Our analysis shows that the horizontal and vertical dimensions of Archean cratons are strongly correlated: larger cratons have thicker lithosphere. The basal drag model of lithosphere erosion (Sleep, 2001) is tested as a means of explaining the present-day bimodal distribution of lithospheric thicknesses of the Archean cratons. In agreement with theoretical predictions, we find that lithospheric thickness in Archean keels is proportional to the square root of the ratio of the craton length (along the direction of plate motion) to the plate velocity. These results show that the basal drag model provides a viable explanation for the variation in thickness of Archean cratonic roots. Basal drag may have varied in magnitude over the past 4 Ga. Higher mantle temperatures in the Archean would have resulted in lower mantle viscosity. This in turn would have reduced basal drag and basal erosion, and promoted the preservation of thick (>300 km) Archean keels, even if plate velocities were high during the Archean.

**JSS06b/10P/D-006**

Poster

**1400-030**

### CONTINENT-CONTINENT COLLISION TECTONICS, REGIONAL UNDERPLATING AND ASSOCIATED KCR VOLCANISM IN CENTRAL INDIA

Saurabh Kumar VERMA (National Geophysical Research Institute, Hyderabad)

The central Indian region, comprising Son-Narmada-Tapti lineament and the Central Indian Mobile Belt (CIMB), represents a major geological setting that holds key to the evolution of Indian sub-continent. The CIMB separates the Bundelkhand-Aravalli cratonic block in the north from the southerly cratonic blocks of Dharwar and Bastar. It possibly represents the suturing of various cratonic blocks resulting from continent-continent collision tectonics during the Mesoproterozoic time. Recent studies considering Bouguer gravity, DSS and MT data reveal the presence of regional underplating all along the central Indian tectonic zone. High heat flow values and seismic tomography results further suggest the presence of a thin lithosphere which has interesting implications on the occurrence of diamondiferous kimberlite clan rocks in the region. It is now well established by geochronological studies that the volcanism associated with various kimberlite fields mentioned above was confined to a narrow window in time. Spatially widespread and coeval nature of these K/L's suggests a major thermo-magmatic activity of regional nature around 1.1 Ga. In order to understand their origin, it is imperative to study the paleo-geographic distribution of various proto-cratonic blocks that evolved into present day Bundelkhand, Dharwar, Bastar, and Singhbhum Cratons. Based on available geochronological and paleomagnetic data, a reconstruction in time reveals that most of the proto-cratonic blocks were formed proximally around Paleoproterozoic time. Suturing of northern proto-cratonic (Bundelkhand) block with the southern (Dharwar, Bastar, and Singhbhum) blocks was completed along the central Indian tectonic zone (CITZ) by Late Archean/Paleoproterozoic time. Lithosphere(s) below these blocks grew steadily with time and by Mesoproterozoic time thickness of lithosphere below various cratonic blocks was sufficient to have P-T conditions suitable for the preservation of diamonds. Around 1.1 Ga, various Indian cratons; as well those from west Australia, central and southeast Africa, and Sao Francisco Craton in South America; were contiguous and formed part of the Rodinia supercontinent. It is interesting to note that most of the

Proterozoic kimberlites in the world are located in these regions and show an age around 1.1 Ga. Thus a common causative factor like a superplume seems to be able to explain the origin of such a large number of Proterozoic kimberlites in regions that are presently separated by thousands of miles. The proposed model also explains some of the deeper characteristics of the sub-cratonic lithosphere below CITZ deciphered by seismic sounding and tomography, heat flow, gravity, and MAGSAT studies.

**JSS06b/10P/D-007** Poster **1400-031**

#### HIGH RESOLUTION SURFACE WAVE TOMOGRAPHY IN EAST ASIA AND WEST PACIFIC MARGINAL SEA

Jieshou ZHU, Jia Min CAO, Xue Lin CAI, Zhong Qun YAN (Dept. Geophysics, Chengdu University of Technology)

According to approximately 12,000 long-period digital seismic waveforms from 704 events ( $7.0 \geq M \geq 5.0$ ) recorded by 58 digital seismic stations from CDSN, GSN, GDSN, and GEOSCOPE network in Eurasia and west Pacific regions, 5,007 accurate surface wave dispersion curves with periods ranging from 8 to 250 seconds were selected and employed for inversion. The high resolution 3-D shear wave velocity images in this area were constructed by inversion of both dispersion and waveform showing a notable lateral variation in lithosphere and asthenosphere. The images of shear wave velocity indicate that from upper crust to the depth of 70 km, high velocities are displayed in the region of eastern part of East Asia and West Pacific marginal sea, in contrast, extremely low velocities illustrated in the Qinghai-Tibet Plateau and its surrounding areas. The low velocity anomaly chain is located along the convergence belt of Tethys from Mediterranean Sea, through Turkey, Iran, Himalayan orogens, Burma to Indonesian islands. In the depth of 85 km to 250 km a giant low velocity belt, which extends from north to south, about 2 500-4 000 km in width, 8 000 km in length, is strikingly located at the east part of East Asia and West Pacific marginal sea. In general it is divided by a boundary at  $110^\circ\text{E}$  in lateral direction, and divided by depth of 70-85 km in vertical direction, the velocity images show striking differences. The western part mainly features an accumulated and thickened lithosphere caused by collision between India and Eurasia, and the eastern part displays mainly the extending and thinning lithosphere caused by asthenosphere upwelling. The lithosphere in the west part is 100 km thicker than in east part. The shear wave velocity of lithosphere in west is 0.2 km/s to 0.25 km/s higher than in east, the temperature in the bottom of lithosphere in eastern parts is  $300^\circ\text{C}$ - $400^\circ\text{C}$  higher than western parts. In Paleocene Indian lithospheric slab subducted beneath the Eurasian continent with low angle. A thick lithosphere root (140-180 km) is formed in Qinghai-Tibet Plateau. The lithospheric mantle has the characteristics of craton. In contrast it shows low velocity in crust because of the partial melt and flow motion of crustal material. The giant low velocity belt in East Asia and West Pacific marginal sea is similar with East Pacific ridge, Atlantic ridge and Indian ridge. The tectonic evolution may undergo the following stages. The lithosphere of east edge of Asia was broken up and the asthenosphere upwelling forming the giant rifts system in mid and late Mesozoic. The present trench-islands arc-basin system in West Pacific marginal sea is the results of interaction with Pacific plate, Australian plate and Eurasian plate in Cenozoic.

**JSS06b/10P/D-008** Poster **1400-032**

#### UPPER MANTLE HETEROGENEITIES BENEATH ANTARCTICA FROM MULTIMODE RAYLEIGH WAVEFORMS

Anne SIEMINSKI, Eric DEBAYLE, Jean-Jacques LEVEQUE (Institut de Physique du Globe de Strasbourg, CNRS and Université Louis Pasteur)

We applied a waveform inversion method to about 3300 regional Rayleigh-wave seismograms to construct a 3D model of the shear velocity structure in the upper mantle beneath Antarctica. The fundamental mode and the first four overtones are modelled in the waveform analysis. The resulting model shows a good agreement with surface tectonics and the previous surface wave tomographic studies in the region for the uppermost 200 km. It also reveals broad, low-velocity anomalies at 200 km depth beneath the South Pacific Ocean extending in some locations down to at least 400 km depth. At these depths, the structure is mostly constrained by the overtones. We thus expect a resolution for depths beyond 200 km better than in the previous studies which were all based on inversion of the fundamental mode dispersion curves only. Synthetic experiments confirm that our dense coverage in fundamental mode and overtones allows to properly retrieve velocity anomalies in the uppermost 400 km of the mantle, so that the deep low-velocity anomalies we found should not be artefacts. We interpret them as the effects of upwelling material. This kind of structures support a model of a plume-fed asthenosphere as proposed by Phipps Morgan et al. (1999) although their locations do not directly correspond to any reported hotspot in the region.

**JSS06b/10P/D-009** Poster **1400-033**

#### CONTINENTAL SURFACE AREA AND THE ASSEMBLY TIME FOR SUPERCONTINENTS

Gary T. JARVIS (Department of Earth and Atmospheric Science, York University)

We employ a kinematic numerical model of circular continental blocks moving about randomly on a two-dimensional periodic model of the Earth's surface and monitor the time required for all of the blocks to assemble into a single model supercontinent. We examine the sensitivity of the assembly times of our modelsupercontinents to the size of individual continental blocks, the fraction of the model Earth's surface covered by the continents, the degree of continental deformation upon collision and the initial spatial distribution of the continents. Assembly times are found to be most sensitive to the total continental surface area. We show that in the absence of any dynamic effects due to deep mantle flow, continents of present-day scale moving randomly about the Earth's surface would naturally aggregate into a single mass in approximately 0.4 Gy. Although this is a purely geometrically imposed time scale, which would be modulated by the dynamic effects of convection in the mantle, it is comparable to the time scales of both mantle fluctuations and the time intervals between successive supercontinent formations. Consequently, continental surface area will be an important factor to include in future dynamic models of supercontinent formation.

**JSS06b/10P/D-010** Poster **1400-034**

#### CHAOTIC TOPOGRAPHY AND 'GODZILLA MULLION' IN THE PARECE VELA BASIN, IMPLICATIONS FOR COLD MANTLE AND DOMINANT AMAGMATIC EXTENSION

Kyoko OKINO<sup>1</sup>, Yasuhiko OHARA<sup>2</sup>, KR03-01 Shipboard Scientific party<sup>(1)</sup>Ocean Research Institute, University of Tokyo, <sup>(2)</sup>Hydrographic and Oceanographic Department of Japan)

The seafloor formed over the Miocene in the Parece Vela Basin (PVB) is characterized by chaotic topography and the well-developed mullion structures, indicating a weak magma supply and mantle exposure at the intermediate spreading rate (full rate = 8.8 to 7.0 cm/yr)

system due to an unusual cold underlying mantle. The recent studies by Ohara and others reported a large, 55\*125 km giant megamullion and petrological characteristics of peridotite from the Parece Vela Rift (PVR), the extinct spreading center of the basin. During KR03-01 cruise in January 2003 (R/V Kairei), we conducted 18 dredge hauls and geophysical mapping in order to understand the amagmatic tectonics in the region. This poster presents the preliminary results of the geophysical mapping, in which we show the anomalous seafloor fabrics formed under the amagmatic backarc spreading. The mapped area consists of two parts, 1) chaotic terrain in the western PVB and 2) ridge-transform intersections of PVR including giant megamullion. Although the chaotic terrain is surrounded by «normal» well-organized north-south abyssal hills area, it is characterized by very deep depth, rugged bathymetry with isolated highs, and high Bouguer gravity anomaly, indicating thin crust. We found at least four new mullion structures, each consisting of domed highs with continuous corrugations. The most prominent mullion has two clear, large corrugations, which continue from the 1500 m domed high to the smaller, 600 m high to the west. The corrugated pattern stops at the N-S trending minor ridge at its west and also N-S trending, but gently eastward convex lineament at its east. These features can be interpreted as the breakaway zone and the termination, corresponding to the start and end of the amagmatic phase with mantle exposure. The giant megamullion structure in the central PVR is quite large, so we propose to name it «Godzilla Mullion». It has the following unique characteristics compared with other seafloor megamullions; 1) its exceptional magnitude, 2) development over an entire segment (not only the inside corner), 3) «high» intermediate spreading rate (7.0 cm/yr), and 4) moderate gravity anomalies. Peridotites were recovered over the whole mullion structure in the cruise. The ridge-transform intersections of the Godzilla Mullion area and northern PVR also show the anomalously deep rift, mullions, remnant inside corner highs and peculiar abyssal ridge bends. These features are compatible with the existence of cold mantle and dominant amagmatic extension.

**JSS06b/10P/D-011** Poster **1400-035**

#### TELESEISMIC BODY- AND SURFACE-WAVE STUDIES IN THE LITHOPROBEWESTERN SUPERIOR TRANSECT: GLIMPSES INTO THE DEEPER ARCHITECTURE OF AN ARCHEAN CRATON

Stephane SOL, Colin J. THOMSON, Michael KENDALL, Don WHITE, Isa ASUDEH (IASPEI)

The Archean Western Superior Province in northern Ontario, Canada, is internally divided into a number of east-west trendingmetasedimentary, metaplutonic and granite-greenstone subprovinces which getprogressively younger from north to south. Recognition of this geologicalarchitecture played an importantrole in the formation of ideas about Archean tectonics, specificallythat modern-day accretionary processes could have operated in a broadly-similar manner in theearly Earth. In order to characterize the underlying upper mantle, broadband teleseismic data were recordedduring a 5-month deployment of 17 instrumentsin an array cross-cutting the subprovince boundaries, with two more stationsextending coverage further north into the trans-Hudson orogen (THO). SKS splitting results within the W. Superior are broadly consistent with those of earlier nearby experiments. Large (up to 2.1 s) splitting times can be seen and we believe that an evolution in fast shear-wave polarization direction can be discerned as the subprovinces are traversed. One station is anomalous and we attribute that to lateral variations (see below). The two trans-Hudson stations show virtually no SKS splitting, in stark contrast with the largest splitting seen in the closest (and oldest) part of the W. Superior just to the south. Travel-time tomography shows significant lateral variations deep into the upper-mantle, perhaps extending to 670 km. While the best-resolved structures are reminiscent of subduction with an appropriate orientation, we cannot be sure if this represents a paleo-slab, possibly recently delaminated from the continental root, or the signature of small-scale convection. Indeed, a break in the pattern of the tomography images at around 300 km may represent the bottom of the lithosphere. Results from a collinear refraction/wide-angle-reflection (R/WAR) survey also suggest dipping structures just below the Moho. Rayleigh and Love dispersion across the array indicates that (i) the NS profile is best treated in three segments and (ii) there is a Rayleigh/Love discrepancy suggesting anisotropy is important. Analysis along an orthogonal EW path from permanent station ULM supports the latter idea, as does a close inspection of the Rayleigh/Love particle motions in various frequency bands for surface-waves arriving from all azimuths. Several thought-provoking observations arise from jointly considering all these observations. In the younger terranes, SKS fast orientation seems to coincide with apparent subduction direction imaged in the tomography, an exception being anomalous station 5070. The divergent observations at this station are consistent with the presence of «shallow» lateral variations nearby. Similarities are also observed between the R/WAR velocity model and the one inferred from surface-wavedispersion. Both indicate crustal thinning moving northward and faster upper-mantle velocity in the E-W direction. Lastly, although SKS indicates null splitting at the THO station BPW, surface-wave polarizations provide evidence of significant anisotropy.

**JSS06b/10P/D-012** Poster **1400-036**

#### LATERAL VARIATIONS OF SHEAR-WAVE SPLITTING BENEATH THE BOHEMIAN MASSIF - FIRST RESULTS OF PASSIVE SEISMIC EXPERIMENT BOHEMA

Jaroslava PLOMEROVA<sup>1</sup>, Ludek VECSEY<sup>2</sup>, Vladislav BABUSKA<sup>1</sup>, Ulrich ACHAUER<sup>3</sup>, Michel GRANET<sup>3</sup>, BOHEMA Working Group (<sup>1</sup>Institute of Geophysics, Czech Academy of Sciences, Bocni II, 141 31 Prague 4, Czech Republic, <sup>2</sup>EOST- Institut de Physique du Globe Strasbourg, 5, rue R. Descartes, 67084 France)

A dense network of stations, consisting of 61 permanent and 84 temporary stations, has been deployed to operate during 2001-2003. The array is centered in the geodynamically active part of the Variscan Bohemian Massif (BM, central Europe) around the crossing of the Eger Graben (EG) with the Mariánské Lázně Fault (MLF). The BOHEMA (BOHEMIAN MASSIF Anisotropy and Heterogeneity) research team is formed by scientists from 10 institutions of the Czech Republic, Germany and France. The team will develop geodynamic model of the lithosphere-asthenosphere system beneath the western part of the BM, which will be based on all available geophysical, geological and petrological data. A three-dimensional anisotropic tomographic model will be one of major results of the experiment. A joint inversion of the shear-wave splitting parameters and P-residual spheres aims at finding a general 3D orientation of anisotropic structures. We present first results of the shear-wave splitting analysis which show lateral variations of anisotropy across and along the EG, and compare them with the near-surface tectonics. Mapping changes in anisotropic parameters delimits large-scale domains of mantle lithosphere - Saxothuringian to the north-west and Moldanubian and Tepla-Barrandian to the south-east - with divergent orientation of dipping anisotropic structures on both sides of the rift structure of the EG. The research will further concentrate on distinguishing between thermal anomalies and anisotropic structures and try to answer the question about a possible existence of a thermal plume in the mantle beneath the western EG. The resulting geodynamic model will shed light on possible causes of earthquake swarms, which periodically occur in the region.

<b>JSS06b/10P/D-013</b>	<b>Poster</b>	<b>1400-037</b>
-------------------------	---------------	-----------------

**CONSTRAINTS ON PALEOBOUNDARIES OF MICROCONTINENTS FROM LATERAL VARIATIONS OF SEISMIC ANISOTROPY IN THE MANTLE LITHOSPHERE**

Vladislav BABUSKA, Jaroslava PLOMEROVA (Institute of Geophysics, Czech Academy of Sciences, Bocni II, 141 31 Prague 4, Czech Republic)

Systematic preferred orientation of olivine crystals is the dominant source of large-scale seismic anisotropy in the subcrustal lithosphere and asthenosphere. Both the surface waves and body waves indicate "frozen-in" dipping anisotropic structures in the mantle lithosphere and a mostly sub-horizontal anisotropy due to the present-day flow in the asthenosphere. From lateral variations and magnitude of the observed seismic anisotropy we deduce a "frozen-in" origin of the continental mantle fabric created most probably in a stress field acting during the formation of individual lithosphere domains. The dipping structures may represent remnants of accreted pieces of ancient oceanic lithosphere and paleosubductions inferred also from dipping seismic reflectors extending into the mantle. Joint analysis of shear-wave splitting parameters and patterns of teleseismic P- residual spheres provide a good resolution for identification of boundaries of lithospheric domains with different fabric orientations, e.g., in the Variscan massifs of central and western Europe and in the Baltic Shield. The domains characterised by consistent orientation of anisotropy may represent individual cycles of "accretion" process. Boundaries of these domains are zones of potential weakness for later processes like rifting, volcanism and intraplate earthquakes. While most methods of continental reconstructions study the uppermost crust, seismic anisotropy allows us to contribute to modelling of the structure and development of the mantle lithosphere, which plays in many aspects decisive role in crustal tectonics.

<b>JSS06b/10P/D-014</b>	<b>Poster</b>	<b>1400-038</b>
-------------------------	---------------	-----------------

**THE STRUCTURE OF LITHOSPHERE AND ASTHENOSPHERE IN EAST ASIA AND WEST PACIFIC MARGINAL SEA**

Jiieshou ZHU, Jia Min CAO, Xue Lin CAI, Zhong Qun YAN (Dept. Geophysics, Chengdu University of Technology)

The continent of East Asia and West Pacific marginal sea was formed by convergence of a series of micro-plates and blocks in the late Paleozoic (about 250-220 Ma). Since Mesozoic (about 150 Ma) the asthenospheric material upwelling caused the lithosphere extension and thinning, and with strong activities of volcano and magma. In Cenozoic the continental margin continued to develop large scale rifts and marginal sea, a series of extending oceanic ridges and basins appeared. In Paleocene epoch the Indian sub-continent collided with the Eurasian continent causing the crust to be shortened and rapidly uplifted, forming the highest of Qinghai-Tibet plateau and the largest convergent region on the Earth. Consequently, reconstruction the 3-D structure of lithosphere and asthenosphere is significant to understand the relationships between the surface tectonics and the deep earth's structures and dynamics in this region. We employed about 55,000 km high precision explosion deep seismic profiles and high resolution seismic tomographic images in the studied area (60°E-150°E, 0°S-60°N) to make 2°×2° grid point model. For each point the layered parameters of depth, density, velocities Vp and Vs in the crust, lithospheric mantle, asthenosphere to 410 transition zone are given. The thickness of lithosphere in East Asia and West Pacific marginal sea varies from 50 km to 200 km. The thinning lithosphere with thickness of 50-80 km is located in West Pacific marginal sea, eastern part of North China, and southeastern part of South China. The thickness of 80-100 km is located in transition region of eastern part of East Asia. The thickness of 100-130 km is located in transition region of middle part of East Asia. In the continental craton and accumulated thicken lithosphere regions, such as India, Tarim, Yangtze, Qinghai-Tibet, Siberia, Kazakhstan, the thickness of lithosphere can reach 130-200 km. There is tremendously thick lithosphere of 180-200 km in the eastern part of Qinghai-Tibet Plateau and in Pamir and northern India. The Pacific and Philippine plate show highest velocity that indicates the characteristics of lithosphere of these oceanic plates are remarkably different with the continent. There exists a giant low velocity belt in the asthenosphere with length of about 8,000 km, width of about 2,500-4,000 km from Sea of Okhotsk, Kuril basin, Sea of Japan, North China and South China, South China Sea to Philippine Sea. The characteristics of the low velocity belt is not same with subduction zone in East Pacific, however, it is the same with the Pacific Ocean rise, Atlantic Ocean ridge and Indian Ocean ridge. The tectonic evolution may undergo the following stages. The lithosphere of east edge of Asia was broken up and the asthenosphere upwelling forming the giant rifts in Mesozoic. The present trench-islands arc-basin system in West Pacific marginal sea is the results of interaction with Pacific plate, Australian plate and Eurasian plate in Cenozoic.

<b>JSS06b/10P/D-015</b>	<b>Poster</b>	<b>1400-039</b>
-------------------------	---------------	-----------------

**THE 3D STRUCTURE OF LITHOSPHERE AND AND ITS DYNAMIC IMPLICATIONS IN QINGHAI-TIBET PLATEAU**

Jiieshou ZHU, Zhong Qun YAN, Shen QU (Dept. Geophysics, Chengdu University of Technology)

The Qinghai-Tibet plateau and its surrounding areas including Indian subcontinent, Xinjiang, Mongolia, is a largest lithosphere convergence place in the world, which characterized by continent-continent collision with a thick lithosphere. The high resolution seismic surface wave tomographic inversion has been conducted for studying the 3D velocity structure of lithosphere and asthenosphere in those areas. About 1400 long period surface waveform recordings are available for both dispersion and waveform tomographic inversion. The block inversion by grid 1°×1° in Qinghai-Tibet plateau show the high resolution 3D shear wave velocity variation from earth's surface to 400km depth. The images of S-wave velocity at different depths show significant characteristics of lithosphere and asthenosphere structure in Qinghai-Tibet plateau and its surrounding areas. In depth of 16-32 km the Qiangtang terrane indicates extremely low velocity, in opposed, the surrounding areas show relative high velocity such as in Indian peninsula, Pamir and Hindu Kush region, Tarim basin. In depth of 40-70 km the low velocity areas are extended to the surrounding terranes. In depth of the 85-130 km the still shows low velocity, however, the Laha terrane has a relatively high velocity. It clearly shows the correlation between the S-wave velocity in the top of upper mantle and the Pn wave velocity (based on earthquake Pn phase tomographic image) with characteristics of low velocity in Qiangtang terrane. It is identified, for the first time, by seismic tomography that the high velocity blocks of both Indian and Eurasian plates occur in the lower part of lithosphere in plateau. The velocities of the Vs in the blocks are between 4.60 and 4.70km/s, and the two blocks were collided against each other. The bottom of lithosphere generally ranges 140 to 160 km and up to 185km in region of the southeast plateau where continent lithosphere roots existed. The asthenosphere thickness is generally range 140 to 180km, and the Vs velocities from 4.35 to 4.45km/s within the asthenosphere. Since the collided of India and Eurasia in the beginning of Cenozoic (about 55 Ma), a continental root with the thickened lithosphere of 140 km-180 km thick was formed in Qinghai-Tibet Plateau and central Asia. The Indian lithospheric slabs subducted beneath the Qinghai-Tibet Plateau and the lithosphere shortened about 2,500 km. The manner of lithosphere shortening is delamination and accumulation. The lithospheric mantle of Qinghai-Tibet Plateau has the characteristics of craton (lower temperature and small deformation)

that shows high velocity. In contrast the crust in plateau shows low velocity that may be related with the higher temperature and strong deformation causing the crust partial melt and flow. The velocity profiles of surface wave tomography in Qinghai-Tibet plateau indicate the subducted detached Indian lithospheric slab beneath the plateau. The location of collision of Indian lithospheric slab with Eurasian is along the Jinsaijiang suture zone.

<b>JSS06b/10P/D-016</b>	<b>Poster</b>	<b>1400-040</b>
-------------------------	---------------	-----------------

**SUBDUCTION ZONE STRUCTURE BENEATH INDONESIA (REVISITED)**

Sri WIDIYANTORO<sup>1</sup>, Gede SUANTIKA<sup>2</sup>, Wahyu TRIYOSO<sup>1</sup> (<sup>1</sup>Department of Geophysics and Meteorology, Institut Teknologi Bandung, <sup>2</sup>Volcanological Survey of Indonesia)

Seismic tomographic images of the Earth's mantle beneath the Indonesian island arcs presented in earlier publications depict the complex morphology of subducted oceanic lithospheric slabs. Slab penetration into the lower mantle with and without deflection, slab lying flat on the 660-km discontinuity, slabs subducted in two-opposing directions and slab detachment represent co-existence of slab styles within the study region. Recently, we have revisited the Indonesian subduction zone structure by means of a non-linear tomographic imaging technique in which 3-D ray tracing has been carefully implemented. We have used P- as well as S-wave arrival times from an updated version of the reprocessed global data set by Engdahl et al. The results provide some improvements in the positioning of heterogeneity. Intriguing slab morphologies are observed, for instance: (i) penetration into the lower mantle of the westward dipping slab of the two opposing subducted slabs of the Molucca Sea plate by taking the form of folded slab; (ii) southward subducted back-arc oceanic crust below Bali; and (iii) possible slab detachment below central Sumatra. The first two observations represent new features revealed by this revisit and the detachment below part of Sumatra to some extent supports our previous result. The inversion of travel-time residuals of direct S phases generally confirms the inferences from the P-wave information with comparable detail resolved. We present the new tomographic models for the Indonesian subduction zone in detail. Inspired by the nature of subduction processes that is closely related to volcanism, we have also applied the non-linear seismic tomographic imaging approach to a volcano tomographic investigation. This has been conducted in part under the encouragement of the IASPEI-IAVCEI Working Group on Subduction Zones Located in Developing Countries. Here, a preliminary result from tomographic investigation of Mount Guntur in West Java is also presented.

<b>JSS06b/10P/D-017</b>	<b>Poster</b>	<b>1400-041</b>
-------------------------	---------------	-----------------

**INTERMEDIATE DEPTH EARTHQUAKES DISTRIBUTION AND THEIR FOCAL MECHANISM IN VRANCEA SEISMOGENIC ZONE, ROMANIA**

Andrei BALA, Mircea RADULIAN, Emilia POPESCU (NATIONAL INSTITUTE FOR EARTH PHYSICS, Bucharest, Romania)

The Carpathian Orogen is of Alpine age, composed of many Mesozoic and Cenozoic terranes. Back-arc volcanism, and back-arc extension in the Pannonian area, accompanied the Neogene subduction. A bent paleosubduction zone was recognized in the Eastern Carpathians, along which the original oceanic basement of flysch and the Subcarpathians nappes were consumed. A small portion of this zone is still seismically active in the Vrancea area. This prominent south-eastern zone of the Carpathian Orogen lies above a nest of strong recent earthquakes (1940, MW = 7.7; 1977, MW = 7.5; 1986, MW = 7.2; 1990, MW = 6.9) situated between 60 and 200 km depth. This is the only place in the entire Carpathians where folding and thrusting occurred during Pleistocene in the outermost zones between two deep faults in the Moesian Platform. These recent crustal movements recorded in the area are accompanied by moderate crustal seismic activity (between 10 - 50 km depth and Mmax = 5.5), which together with intermediate depth seismicity produce high seismic risk in a densely populated area. In Vrancea area, the original oceanic lithosphere descended to more than 200 km depth, as indicated by the intense intermediate depth seismic activity. Recent works in seismic tomography indicate that regional scale anomalies of the seismic velocities are appearing down to 350 km depth. The tectonic plate evolution of the whole Carpathian Arc and Pannonian back-arc Basin indicates that at least three tectonic units have been in contact and, at the same time, in relative motion: the East European Plate, the Moesian plate and the Intra-Alpine plate. There were represented 526 hypocenters of earthquakes from the period 1929 - 2000 which have computed focal mechanism. Most of the epicenters are situated in an area which includes Vrancea zone (25° - 28.5° E, 44.5° - 47° N). Because of the great number, they were found to describe well the limits of the tectonic plate (plate fragment?) which is supposed to be subducted in this region. These limits were put in direct relations with the known geology and tectonics of the area. A conclusion to these observations is that at least one seismogenic zone is present in the crust and 2 zones are present in the domain of the intermediate earthquakes: the first from 60 - 100 km and the second from 100-110 km to 200 km depth. These 3 zones have clearly different characteristics both in the number of earthquakes occurred and also as the total released energy of the earthquakes occurred in each zone. They are also different in respect with the orientation angle of the blocks, which is changing at about the same depth. The "transition zone" (around 100 - 110 km depth) appears as a relatively low activity seismic zone. Available fault plane solutions for the intermediate depth earthquakes are analyzed in several depth intervals indicated by the seismic activity. Correlation of the focal parameters in connection with the depth of the hypocenters is discussed.

<b>JSS06b/10P/D-018</b>	<b>Poster</b>	<b>1400-042</b>
-------------------------	---------------	-----------------

**ANISOTROPIC VELOCITY STRUCTURE OF THE JAPAN ISLANDS**

Motoko ISHISE<sup>1</sup>, Hitoshi ODA<sup>2</sup> (<sup>1</sup>Graduate School of Natural Science and Technology, Okayama University, <sup>2</sup>Department of Earth Science, Okayama University)

Assuming that seismic anisotropy is attributable to hexagonal anisotropy of which the c-axes lie horizontally, we investigated the lateral variations of isotropic and anisotropic P-wave velocity beneath the Japan Islands composed of two island arcs, the southwest and northwest Japan arcs, under which the Philippine Sea plate and Pacific plate subduct, respectively. The P-wave velocity anisotropy is described by direction of the hexagonal c-axis and intensity of anisotropy at grid points that are spaced out 0.5° in the N-S and E-W directions and 10-30 km in depth under the study area. In the Tohoku district, northeast Japan, the tomographic image of the isotropic P-wave velocity reveals a high velocity slab corresponding to the descending Pacific plate and a low velocity region upwelling above the plate. The anisotropic velocity structure is found to be different between the eastern and western regions of the Tohoku district. The seismic anisotropy of the western region is characterized by the c-axes which are orientated in the east-west direction that is nearly parallel to the descending direction of the Pacific plate, whereas the c-axes in the eastern region are in the north-south direction that is nearly perpendicular to the geomagnetic lineation observed near the Japan trench. Comparison between the anisotropic and isotropic lateral structures shows that the east-west direction of the c-axes are dominant in the pronounced low velocity zone of the upper mantle and the north-south direction is conspicuous in the high velocity Pacific plate. In the Chugoku and Shikoku districts, southwest Japan, a clear difference is found in the P-wave anisotropy of the crust and upper

mantle. The crust exhibits the seismic anisotropy characterized by the c-axes orientated in the east-west direction. A systematic change of the axis distribution is found in the upper mantle, where the c-axes are in the north-south direction within the south side region of a boundary line located at 34° N and in the east-west direction within the north side region. The location of the boundary is coincident with that of leading edge of the seismic belt of the upper mantle earthquakes occurring in the Chugoku and Shikoku districts. The mantle anisotropy in the south side region of the boundary is attributed subduction of the Philippine Sea plate, while the regional stress field due to interaction between the Eurasia and Pacific plates arises the mantle anisotropy of the north side region and crustal anisotropy.

**JSS06b/10P/D-019** Poster **1400-043**

**SELF-CONSISTENT DYNAMICAL MODELS OF THE SUBDUCTION IN THE MANTLE CONVECTION SYSTEM: ON THE DRIVING FORCE AND THE ROBUSTNESS OF GENERATION OF THE PLATE TECTONICS**

Tomoeiki NAKAKUKI, Chiho HAMADA (Department of Earth and Planetary Systems Science, Hiroshima University)

We have developed self-consistent dynamical models of the plate-mantle convection system to understand dynamics of initiation of the subduction. We utilize rheology depending on the hysteresis of the stress to realize the subduction-like descending flow of a cold thermal boundary layer with high viscosity (Honda et al., 2000). No external forces are applied to the surface boundary and the plate in the model. We introduce heterogeneity of the surface region, i.e., "oceanic" and "continental" region, which is treated as a horizontal heterogeneity of the yield stress and/or the composition at the surface. We here use realistic rheology including Arrhenius-type temperature and pressure dependence and maximum yield strength whose values are in the range of 200 to 600 MPa (400 to 1200 MPa in a differential stress) as large as those reported by the experimental studies for the rheology of the lithosphere. We also examine effects of a preexisting weak zone at the oceanic-continental plate boundary. Our results show that the subducted slab is formed when the strength of a fault zone at the plate boundary is small enough. This does not strongly depend on the maximum strength of the lithosphere, namely, the subduction successfully occurs even at the highest value in the model (600 MPa). We also analyze forces working on the plate and the slab. At the initial condition, motion of the plate begins with compressive force induced by the shape of the plate (ridge push force) and plume (mantle-drag force). A negative buoyancy by the slab balanced with resistance by the overriding plate until the slab penetrates into the depth of 150 to 200 kilometers. This implies that the force continuously pushing the plate such as mantle-drag force to initiate the subduction until the slab reaches the depth at which the slab-pull force overcomes the resistance. When the weak zone is not set in the initial condition, the subducted plate is generated under the condition with the yield strength less than 200 MPa. This suggest that the other mechanism fracturing the plate may be required to generate the initial weak zone which develops the plate boundary.

**JSS06b/10P/D-020** Poster **1400-044**

**FLUID DISTRIBUTION IN THE MANTLE WEDGE OF NE JAPAN INFERRED FROM SEISMIC VELOCITY AND ATTENUATION STRUCTURES**

Junichi NAKAJIMA, Akira HASEGAWA (Tohoku University)

Our recent tomographic work [Nakajima et al., 2001] revealed detailed P- and S-wave velocity structures beneath the northeastern (NE) Japan arc. The results show that inclined seismic low-velocity zones are continuously distributed in the mantle wedge of the NE Japan arc in parallel to the down-dip direction of the subducting slab. They corresponded to the seismic high attenuation zones estimated by Tsumura et al. [2000]. These zones have been interpreted as the ascending flow from deeper portion of the back-arc side, which perhaps contains large amount of fluids. In order to know the shape of fluid-filled pores and volume fraction of fluid in these low-velocity zones, we first estimated temperature distribution in the mantle wedge by applying experimental results of high-temperature and low-frequency internal friction in Peridotite [Kampfmann and Berckhemer, 1985] to the P-wave attenuation structure [Tsumura et al., 2000]. Estimated temperature in the mantle wedge ranges from 1000°C to 1200°C. We calculated values of  $d\ln V_s/d\ln V_p$  by using the results of Nakajima et al. [2001] after correcting P- and S-wave velocity variations caused by temperature heterogeneities, which enables us to know whether or not melt or aqueous fluid in the low-velocity zones is in the state of textural equilibrium [Takei, 2002]. As a result, it is found that fluid phase exists in the low-velocity zones of the mantle wedge in NE Japan. We infer that the fluid phase in the low velocity zones is not H<sub>2</sub>O but melt, since the estimated temperature in the low velocity zones exceeds wet solidus of Peridotite [Kushiro et al., 1968]. Aspect ratios of melt-filled cracks and their volume fractions are approximately 0.01-0.1 and 0.1-1 %, respectively, which suggests that melt pockets are distributed in the low velocity zones. Aspect ratio of melt-filled cracks varies with depth. It is approximately 0.1 at a depth of 90 km or so and less than 0.1 at shallower depths. This shows that the melt existing in rocks is far from textural equilibrium at shallower depths (at least shallower than 65 km), which would suggests that melt migration through interconnected cracks is dominantly occurring in the shallow part of the ascending flow in the mantle wedge of NE Japan.

**JSS06b/10P/D-021** Poster **1400-045**

**ON THE RELATIONSHIP BETWEEN ISOTOPE HETEROGENEITY AND CONVECTION IN THE EARTH'S MANTLE**

Yury V. MIRONOV<sup>1</sup>, Vladimir M. RYAKHOVSKY<sup>1</sup>, Alexander A. PUSTOVOY<sup>2</sup> (<sup>1</sup>Department of Geoinformation Systems, Vernadsky State Geological Museum of RAS, Moscow, Russia, <sup>2</sup>L'antinc branch, Shirshov Institute of Oceanology of RAS, Kaliningrad, RUSSIA)

One of the topical questions of modern global geodynamics - how to coordinate chemical heterogeneity and convection in the Earth's mantle? We have tried to answer this question by comparison of the isotope and tomographic data on the Atlantic and Indian oceans, and also on adjacent continents. The Arctic (the spreading ridges of Northern Atlantic, Norwegian-Greenland sea and Arctic ocean, islands Iceland and Jan-Mayen, Iceland-Faroe Rise, traps of Norway, Britain, and Greenland), Northern-Central (Mid-Atlantic Ridge from Reykjanes ridge up to 24ES, numerous islands and rises, located at the same latitudes, Cameroon Line, African and European rifts, Aden and Red sea spreading centers, and also Comores in Indian ocean), Southern (Gough, Tristan-da-Kunha, Walvis ridge, Rio Grande Plateau, Discovery, traps of Southern America and Africa, islands and mid-ocean ridges in Indian ocean), and Bouvet-Antarctic (the rises Spiss and Shona, the most southern part of Mid-Atlantic ridge, island Bouvet, an adjacent part of Southwest-Indian Ridge, and also traps and rifts on northern coast of Antarctic Continent) Sr-Nd-Pb isotope sublattitudinal provinces are chosen in this region. They include mid-ocean ridges, oceanic rises and islands, as well as Late Mesozoic-Cenozoic continental rifts and traps. The specificity of these provinces determine either end-members of Zindler-Hart's "mantle tetrahedron" HIMU (Northern-Central and Bouvet-Antarctic provinces) and EM1 (Southern province), or component ARCTIC. The latter locates outside "tetrahedron" and is widespread in the Arctic province. The common component in magmatic rocks from all provinces and types of structures is certain component F ("focal"). It represents average characteristic of all known

intratetrahedron components (FOZO, C, PREMA etc.), updated by methods of multidimensional statistics. In withinplate structures component F forms quasi-binary mixtures with specific component (for given province). Mid-ocean ridge basalts (MORB) from different provinces vary in stable admixture of the same specific components, but as a whole represent admixture between F and DM, DM+HIMU is less abundant. Basing on the newest Becker-Boschi's tomographic model two types of low velocity mantle area, which are considered as a place of superplum generating, was separated. Both low-mantle and mid-mantle plums are discordant to the isotopic provinces, but differ on depth, size and relation to riftogeneous structures and areas of modern magmatism. Probably, all mantle plums are originated in relatively homogeneous reservoir F and later reacted with heterogeneous the most upper part of mantle. The main components of the latter are DM, HIMU, EM, ARCTIC. As against the majority of researchers we count, that top border of F reservoir is on rather small depths as the component F is widely distributed in products of the least deep magmatism out of the plums (MORB). The offered model can remove the fundamental contradiction between the fact of mantle heterogeneity and necessity of convection in its basic volume. The work is supported by RFBR, and federal program "World Ocean".

**JSS06b/10P/D-022** Poster **1400-046**

**LONG-TERM EVOLUTION OF THE GLOBAL WATER AND CARBON CYCLES**

Siegfried A. FRANCK, Christine BOUNAMA, Werner VON BLOH (Potsdam Institute for Climate Impact Research)

We investigate the thermal and degassing history and future of the Earth with the help of a parameterised mantle convection model including the exchange of water and carbon between the mantle and the surface reservoirs. Both volatiles are of specific importance because they exert a major influence on a wide range of geological, biogeochemical and biological processes. Water and carbon dioxide provide the necessary conditions for the emergence and maintenance of photosynthetic-based life. Water is the most abundant volatile and is drawn from the surface reservoirs to the mantle by subduction of the ocean floor. Outgassing of water from the mantle occurs at mid-ocean ridges. The water content of the mantle is directly coupled with the thermal and degassing history via a water-dependent rheology of mantle material. Carbon dioxide is much less abundant than water but believed to have a main influence on the Earth's climate. Our model for the global carbon cycle contains the reservoirs mantle, ocean floor, continental crust, biosphere, kerogen, as well as the aggregated reservoir ocean and atmosphere. Both global cycles (water and carbon) are mainly coupled via the process of volatile exchange between mantle and surface reservoirs (i.e. subduction and spreading). We calculate the evolution of all water and carbon reservoirs over Earth's history and into the long-term future under a maturing Sun. We obtain reasonable values for the present distribution of carbon in the surface reservoirs. The water content in the surface reservoirs shows an outgassing event at the beginning of planetary evolution followed by a subsiding process to end up in the recent situation of one ocean at the Earth's surface. In the long-term future only about 1/4 of the modern ocean will be subducted into the mantle. The life span of the photosynthesis-based biosphere will end up about 1.2 billion years. This results from too low atmospheric carbon content and not from a lack of water in the surface reservoirs or from too high surface temperatures. At this time mean global surface temperatures will be in the order of about 40°C.

IA

**JSS07** Wednesday, July 9 - Thursday, July 10

**TSUNAMIS: THEIR SCIENCE, ENGINEERING AND HAZARD MITIGATION (IASPEI, IAVCEI, IAPSO)**

Location: Site A, Room 2

Wednesday, July 9 AM  
Presiding Chairs: S. Tinti, Y. Tsuji

**JSS07/09A/A02-001** **0900**

**THE NATIONAL TSUNAMI HAZARD MITIGATION PROGRAM**

Eddie N. BERNARD (NOAA/PMEL)

The National Tsunami Hazard Mitigation Program is a state/Federal partnership that was created to reduce the impacts of tsunamis to U.S. Coastal areas. It is a coordinated effort between the states of Alaska, California, Hawaii, Oregon, and Washington and three Federal agencies: the National Oceanic and Atmospheric Administration (NOAA), the Federal Emergency Management Agency, and U.S. Geological Survey. Because of NOAA's responsibility to provide tsunami warning services to the nation, NOAA has led the effort to forge a solid partnership between the states and the Federal government. The partnership has established a mitigation program in each state that is preparing coastal communities for the next tsunami. Inundation maps are now available for many of the coastal communities of Alaska, California, Hawaii, Oregon, and Washington. These maps are used to develop evacuation plans and, in the case of Oregon, for land use management. The partnership has successfully upgraded the warning capability in NOAA so that earthquakes can be detected within 5 minutes and tsunamis can be detected in the open ocean in real time, paving the way for improved tsunami forecasts. An overview of the program will be given along with the results of a review of the program's accomplishments.

**JSS07/09A/A02-002** **0915**

**SEISMIC ACTIVITY AND TSUNAMI ACTIVITY OF THE MAIN TSUNAMIGENIC REGIONS IN THE PACIFIC: A COMPARATIVE STUDY**

Viatcheslav K. GUSIAKOV (Department of Geophysics, Institute of Computational Mathematics and Mathematical Geophysics)

The historical tsunami catalog collected within the HTDB/PAC (Historical Tsunami Database for the Pacific) Project contains the most complete parametric tsunami data covering the whole Pacific and the full historical period of available observations (from 47 BC to present). As a supplementary part, the database contains the parametric earthquake catalog having more than 230 000 historical earthquakes occurred in the Pacific region. The collected data give us a possibility to study the variability of the tsunami potential of submarine earthquakes over the main tsunamigenic regions in the Pacific. For each region, the tsunamigenic potential is evaluated on the basis of the tsunami efficiency (TE) coefficient which is calculated as ratio between the number of tsunamis of tectonic, landslide and unknown origin and the total number of the coastal and the submarine earthquakes with magnitude  $M_s = 7.0$  and depth  $h < 100$  km. In this study, only the instrumental part of both catalogs (from 1901 to present) has been used. In the Pacific, the tsunami efficiency, calculated in the above manner, varies from 84% for the South America region to 36% for the New Zealand -

## INTER-ASSOCIATION

Tonga region. The comparison of the variation of the TE ratio with the position of the main sedimentation zones in the Pacific (Lisitsyn, 1974) shows that the regions located within the equatorial humid zone (New Guinea - Solomon, Indonesia, Philippines) have the increased number of tsunamigenic events as compared to the regions located in other zones. The circum-continental zonation in the sedimentation rate resulted in the highest TE ratio for the South America region where the tsunamigenic sources are located closest to land. The higher sedimentation rate results in a higher potential for the submarine slumping thus considerably increasing the efficiency of the tsunami generation mechanism. The earthquakes in the marginal seas (the Japan Sea, the Okhotsk Sea, the Bering Sea) have a higher tsunami efficiency as compared to the earthquakes in the Pacific ocean. For Hawaii, the TE ratio exceeds 100%, which shows that some events were generated by the earthquakes with magnitudes less than 7 or even had a non-seismic origin.

### JSS07/09A/A02-003 0930

#### SOURCE MODELING OF HOLOCENE TSUNAMIS ALONG THE KURIL TRENCH

Kenji SATAKE<sup>1</sup>, Futoshi NANAYAMA<sup>2</sup>, Shigeru YAMAKI<sup>3</sup> (<sup>1</sup>Active Fault Research Center, GSI/AIST, <sup>2</sup>Institute for Marine Resources and Environment, GSI/AIST, <sup>3</sup>Seamus Corporation)

Numerical tsunami modeling along the Kuril trench indicate that unusual tsunami deposits in eastern Hokkaido were brought by large earthquakes with longer ruptures than those recorded in the region's 200 years of written history. Eastern Hokkaido's historical tsunamis are typically from interplate earthquakes, with rupture length of 100 - 200 km. Such events, occurred in 1952 (Mw 8.1) and 1973 (Mw 7.8) as well as 1843 (M 8.0) and 1894 (M 7.9), rarely produced tsunami heights more than 4 m. These earthquakes have been considered characteristic of the southern Kuril trench. Extensive tsunami deposits, recently found and mapped in eastern Hokkaido, indicate larger prehistoric tsunamis. At Kiritappu, for instance, sand sheets extend as much as 3 km inland, whereas the historic tsunami inundated no more than 1 km. Ten sheets of tsunami deposits indicate recurrence of such unusual tsunami with an average recurrence interval of about 500 years. The most recent event occurred in the 17th century. Geologic evidence of coastal uplift was also found for the 17th century, while historic documents in Honshu rules out unusual tsunamis that would cause damage along the Sanriku coast. We made numerical modeling of tsunamis by using finite-difference computations of the non-linear long-wave equation, to calculate coastal tsunami heights for the Hokkaido and Honshu coasts and inundation for selected sites where the tsunami deposits were mapped. For the inundation, moving boundary condition with the minimum grid interval of 25 m is adopted. We modeled various fault parameters. The fault widths are 50 km (tsunami earthquake), 100 and 150 km (typical interplate events), 200 and 250 km (wide faults that would uplift the coast). We also varied fault length along the trench axis as 100 - 200 km (single segment) and 300 km (multi-segment). On the Hokkaido coast, the largest tsunami heights are computed from multi-segment fault or tsunami earthquake. The wide faults produce smaller heights, because the coast is also uplifted. The computed heights from tsunami earthquake locally vary because of the shorter wavelength. The tsunami inundation is largest from the multi-segment fault, reproducing the extent of tsunami deposits. The wide faults produce less inundation, whereas the single-segment fault or tsunami earthquake does very little inundation. On the Sanriku coast, the tsunami heights from the wide faults are large enough to have caused damage. Other models produce smaller tsunamis that can be escaped from historic documents. In summary, only multi-segment fault can explain the tsunami deposits and lack of documented damage on Sanriku coast. Geologic evidence of uplift can be explained by aseismic slip on deeper part of plate interface.

### JSS07/09A/A02-004 0945

#### TSUNAMI WAVES GENERATED BY 1883 KRAKATAU ERUPTION: ANALYSIS, SOURCE DEFINITION AND NUMERICAL SIMULATION

Efim PELINOVSKEY<sup>1</sup>, Alexander STROMKOV<sup>1</sup>, Irina DIDENKULOVA<sup>1</sup>, ByungHo CHOI<sup>2</sup> (<sup>1</sup>Laboratory of Hydrophysics, Institute of Applied Physics, <sup>2</sup>Department of Civil and Environmental Engineering, Sungkyunkwan University, Suwon, 440-746, KOREA)

The 1883 Krakatau volcanic eruption has generated a destructive tsunami higher than 40 m on the Indonesian Coast where more than 36,000 lives were lost. Sea level oscillations related with this event have been reported on significant distances from the source in the Indian, Atlantic and Pacific Oceans. Evidence of many manifestations of the Krakatau tsunami was a subject of the intense discussion. Thirty-five tide-gauge records are collected by the Royal Society and published in the special report in 1886. All records are digitized with time sep 30 s and processed. First of all, the tide components are calculated and eliminated from the records. Then the Fourier spectra of the residual records are calculated and analyzed. The spectral analysis is applied to determine the generated wave in the tsunami source. It has the pulse form with characteristic duration about 30 min. The form of generated wave is in agreement with tsunami records in near-epicentral zone (Sunda Strait) and generation mechanism by Nomanbhoy and Satake (1995). The results of given analysis are compared with the results of the direct numerical simulation of the tsunami wave propagation in the framework of the linear shallow-water theory using the ETOPE2 bathymetry. Data of witness reports are also used for comparison of the numerical results.

### JSS07/09A/A02-005 1000

#### DISTRIBUTION OF CUMULATIVE TSUNAMI ENERGY FROM ALEUTIAN-ALASKA TO WEST CANADA

Tokutaro HATORI (Member of the Seism. Soc. Japan)

Large Aleutian-Alaska tsunamis have been recorded since 1788. The 1946 Aleutian tsunami associated with a moderate earthquake (Ms 7.4) hit the Hawaiian Islands. The 1964 Alaska tsunami was observed in the whole of the Pacific regions. Tsunami magnitude was the largest (Imamura-Iida scale:  $m=4$ ). The source areas of large tsunamis in 1957, 1964 and 1965 extend 600-900 km along the trench. In the present paper, the distribution of cumulative energy (square value of tsunami height,  $H^2$ , where H: the mean height in segment unit) for each 200 km segment along the Aleutian-Alaska trench is investigated for the recent 103-year (1900-2002) and historical (1788-1899) periods. For the total tsunamigenic energy,  $\Sigma H^2$ , during 215-year period, percentages of the received energy in the 1,000 km range were 39% in Central Alaska, 32% in the Alaska Peninsula and 11% in Central Aleutian Islands. During the recent 103-year, the energy value in Central Alaska is nearly comparable with those of the Kamchatka and South Chilean regions. If the tsunami energy is accumulated with the mean rate since 1788, the expected value in Central Alaska is small comparing with the observed value of the recent 103-year, because of the 1964 event. On the contrary, the expected value in the ranges of the Central Alaska Peninsula (400 km length) and Yakutat regions is about twice larger than the observed value, suggesting high tsunami risk.

### JSS07/09A/A02-006 1015

#### DAMAGES TO HOUSES BY THE 1964 TSUNAMI IN CRESCENT CITY, CALIFORNIA

Nobuo SHUTO (Faculty of Policy Studies, Iwate Prefectural University)

To remind the 1964 tsunami in Crescent City, California, on March 28, a book "Dark Disaster 64/84" was published by W.H. Griffin in 1984. Articles in this book are analyzed to give threshold of damage to houses, by locating the houses and buildings and estimating the tsunami in the city area. The 1964 tsunami hit Crescent City, as a far-field tsunami after travelling over 3,000 km. It began with rather gentle and small inundation of the first and second waves that inundated only small, shoreline parts of the city. Before the biggest fourth wave came, the seawater receded to show the bottom of Crescent bay, and most of ships and boats got aground. Then the fourth wave came and showed the spilling breaking near the shoreline. The seawater, however, entered the city area as a gentle current, except the area of I and J streets where the wave front formed a wall of water 5 feet high. The largest water depth was about 8 feet above ground. This inundation height was lower than the ceiling of the first story of houses and shops. Many wooden houses were floated, moved and damaged. The major cause of the damage was not impact of water flow near the wave front nor floated materials such as cars, ladders and debris, but buoyancy due to seawater. Typical examples are as follows. In case of a one-story house, "Hearing a strange noise, I got out of bed and throwing a light weight bedspread over my shoulders, went to investigate. As I did my house was torn loose from its foundation and floated for about 50 feet". The water depth was estimated as deep as 4 to 7 feet. In case of a two-storied building with a large attic, built of redwood, it was lifted completely from its foundation and moved some 30 feet or more. The estimated water depth was about 4 feet. Fourteen examples of wooden houses showed that a wooden house not connected with foundation would be lifted by seawater of 4 feet high. Other nineteen examples showed that non-wooden buildings were not moved by seawater less than 8 feet deep, even though windows and doors were completely broken by seawater or floated materials. The tsunami-related fire in Crescent City should not be forgotten in the coastal development in any country. An extremely small possibility to ignite brought a big fire because of oil tanks.

### JSS07/09A/A02-007 1030

#### THE SEARCH FOR TSUNAMI SOURCE DISCRIMINANTS IN THE NEAR AND FAR FIELDS

Emile OKAL<sup>1</sup>, Costas E. SYNAOLAKIS<sup>2</sup> (<sup>1</sup>Department of Geological Sciences, Northwestern University, <sup>2</sup>Department of Civil Engineering, University of Southern California)

We seek to identify observables of tsunami waves, both in the near and farfield, which could be used to discriminate between dislocation and landslidesources. In the far field, we derive asymptotic expressions for the energy, spectral amplitude and directivity of tsunami waves generated by double-couples obeying universal scaling laws, and by landslides modeled as single forces. We discuss the influence of Dahlen's [1993] quadrupole corrections for the latter, which we find crucially important in the case of tsunami waves. We show that the spectrum of landslide tsunami waves is significantly offset to high frequencies (10 mHz), where dispersion becomes important thus diminishing far-field amplitudes. We reproduce the result of Kajiura [1981] on the growth of the energy of earthquake tsunamis as the power 4/3 of the seismic moment. We show that the total energy generated into a tsunami wave by a landslide of acceptable size remains dwarfed by that generated by a mega-thrust dislocation. We discuss the far-field directivity pattern due to source finiteness for both dislocation and landslide models, and conclude that strong directivity, i.e., a narrow azimuthal lobe of maximal amplitudes, requires generation by a dislocation source in the case of tsunami waves, and can thus be used as source discriminant. In the near field, we use numerical simulations to explore the influence of earthquake source parameters on observable properties of tsunami run-up amplitudes. These include earthquake geometry (source depth, strike, dip, slip angles), size (seismic moment), location (distance from shore and centroid depth), as well as beach geometry (water depth and beach slope). We focus both on maximum run-up and on the distribution of computed run-up along the beach, which leads to two dimensionless parameters, namely (i) the ratio of maximum run-up to the amount of slip on the fault; and (ii) the aspect ratio of abell curve fitted to the lateral distribution of run-up. We find that the first parameter remains of order 1, while the second one remains smaller than the maximum strain released during the earthquake, itself an invariant. By contrast, in the case of landslidesources, the aspect ratio of the lateral distribution of run-up along the beach can be 1 to 2 orders of magnitude greater, suggesting its use as a potential discriminant in the near field. We apply these discriminants to the case of the 1946 Aleutian tsunami, and suggest that its source must have involved both a large slow earthquake (to explain the far field tsunami) and a coeval landslide (responsible for the near field tsunami).

### JSS07/09A/A02-008 1100

#### INTEGRATED WEB-BASED ORACLE AND GIS ACCESS TO TSUNAMI AND EARTHQUAKE DATA FOR QUALITY CONTROL AND ANALYSIS

Paula Kay DUNBAR<sup>1</sup>, John C. CARTWRIGHT<sup>2</sup>, Daniel KOWAL<sup>2</sup>, Thomas GAINES<sup>2</sup> (<sup>1</sup>National Geophysical Data Center, <sup>2</sup>Cooperative Institute for Research in Environmental Sciences)

The National Geophysical Data Center (NGDC) catalogs information on tsunamis and significant earthquakes, including effects such as fatalities and damage. NGDC also maintains a large collection of geologic hazards photos. All of these databases are now stored in an Oracle relational database management system (RDBMS) and accessible over the Web as tables, reports, and interactive maps. Storing the data in a RDBMS facilitates the search for earthquake and tsunami data related to a specific event. For example, a user might be interested in all of the tsunami events near Japan. The user could then directly access related information from the tsunami tables such as tsunami runups, additional comments, and references. If the event is in the significant earthquake database, the user could access related information from the earthquake tables without having to run a separate search of the significant earthquake database. Users could also first access the significant earthquake database and then obtain related tsunami information. The ArcIMS-based interactive maps provide integrated Web-based GIS access to these databases as well as additional auxiliary geospatial data. The first interactive map provides access to individual GIS layers of tsunami sources, tsunami effects, significant earthquakes, volcano locations, and various spatial reference layers including topography, population density, and political boundaries. The map service also provides tip links and hyperlinks to additional hazards information such as NGDC's extensive collection of geologic hazards photos. For example, a user could display all of the tsunamis that have caused damage in Alaska and then by using a hyperlinks tool, display images showing damage from a specific event such as the 1946 Aleutian Islands event. The second interactive map allows users to display related natural hazards GIS layers. For example, a user might first display tsunami source locations and select tsunami effects as the related feature. Using a tool developed at NGDC, the user could then select a specific tsunami event and automatically display the tsunami effect locations related to that event. The user could also select significant earthquake events and display tsunami events related to specific quakes. These tools improve data access and are being used to quality control the data. These capabilities also help coastal communities

assess their risks, identify hazards, and promote public awareness of tsunamis and earthquakes.

**JSS07/09A/A02-009**

**1115**

**VULNERABILITY ASSESSMENT AND PREVENTION MEASURES FOR TSUNAMI FLOODING OF URBAN AREAS AND INDUSTRIAL PORTS OF MEXICO**

Salvador F. FARRERAS, Modesto F. ORTIZ (Oceanology Division, CICESE Research Center of Mexico)

The Middle-America Trench subduction zone adjacent to the southwestern coast of Mexico accounts for a consistent and regular history of locally destructive tsunamis generated by large earthquakes. The 19 September 1985, 9 October 1995 and 22 January 2003 are the most recent events, with maximum wave heights from 2.5 to 5.0 meters. This coast is the site of two major industrial ports and an approximately 1000 km corridor of tourist resorts and urban communities. Among them, the heavy industrialized port of Lázaro Cárdenas with two steel mill plants, a fertilizer factory, a container port, metal and mineral docks, grain storage silos, and a fuel oil terminal, located on the sand shoals of a river delta. An important element for the vulnerability assessment is the determination of probable tsunami wave elevations and expected inundation limits at each location. The best alternative to determine these parameters is through numerical simulation of wave generation and propagation from the source to the shoreline and inland areas. Three and five meters are the maximum wave heights representative of the low and middle risk tsunamis most frequently arriving to this coast. These two cases were simulated in a computer. An ocean water disturbance produced by a sea-floor earthquake was assumed. Earthquake fault parameters were derived from the Harvard centroid moment tensor of two past events. Deep-water linear wave theory for the far ocean, and shallow water non-linear one for the near shore and interaction with the coast, were considered. Non-fixed boundaries with discharges conditioned to the state of the water level at the borders, were used to model the flooding and recession at the coast. The equations were solved through an explicit central finite-difference "leap-frog" algorithm for interconnected grids of different sizes. The model was validated comparing the results with recorded sea level data and run-up and flooding extension measurements from the two past tsunamis. Results of the numerical simulations show the maximum computed water levels and the boundaries of the inundation areas under threat. Inundation maps showing this information were produced. The tsunami vulnerability assessment for two cases, an urban settlement and an industrial port, is described in detail. For the industrial port: a low risk event will produce slight damage, railroad tracks destroyed, access bridges washed out, and ledges of sand removed or deposited on the beaches; and a middle risk event will produce major and extensive property damage to the installations and danger to life. With the exception of the steel factory which is located adjacent to the hills, escape routes through the single access bridge and road to other facilities will be useless. Recommendations include the relocation of urban settlements, installations and services, and the establishment of evacuation routes and emergency shelters.

**JSS07/09A/A02-010**

**1130**

**PROGRESSES IN THE ASSESSMENT OF TSUNAMI GENESIS AND IMPACTS AROUND THE PORTUGUESE COASTS**

Luis MENDES-VICTOR<sup>1</sup>, Antonio RIBEIRO<sup>2</sup>, Luis MATIAS<sup>3</sup>, Maria Ana BAPTISTA<sup>3</sup>, J.Miguel MIRANDA<sup>4</sup>, Pedro MIRANDA<sup>4</sup>, Nevio ZITELLINI<sup>4</sup>, Eulalia GARCIA<sup>5</sup>, Carlos CORELA<sup>6</sup>, Pedro TERRINHA<sup>7</sup> (Instituto Geofísico da Universidade de Lisboa, <sup>1</sup>LATTEX, Portugal, <sup>2</sup>CGUL, Portugal, <sup>3</sup>IGM, Italy, <sup>4</sup>UTM-CSIC, Spain)

The tsunami generated by the 1755.11.01 earthquake was probably the major event of this kind felt all over the North Atlantic well reported by coeval sources. The coasts of the Iberian Peninsula, Northwest Morocco were deeply affected by that phenomenon which tremendous impacts on the city of Lisbon and several other ones have been well documented. The last 20 years, the scientific European community, thanks to the support received from EU (Projects DETWS, IAM, GITEC, GITEC-TWO and BIGSETS) and from FCT (Projects MATESPRO and RIMAR) was able to develop successive steps improving considerable knowledge on the parameters and functions of sources and tsunami propagation. In order to evaluate the tsunami hazard, comprehensive studies were developed recognizing the importance of the inter-disciplinary approach for this kind of phenomena. Tsunami propagation models were designed being the simulations controlled by real data deduced from historical report or instrumental data. In order to assess the considerable impacts along the Portuguese coasts different run-up models have been used and tested. The location of the 1755.11.01 source has been a key question, motivating intensive marine research in the southern area of Portugal looking for unquestionable morphological or geological evidence of fault rupture and local source area present-day seismic activity.

**JSS07/09A/A02-011**

**1145**

**SOUTH AMERICAN TSUNAMI IMPACT IN NEW ZEALAND**

Gaye L. DOWNES (Institute of Geological & Nuclear Sciences)

Documenting the effects of historical events is crucial for understanding tsunami hazards and risks and for use in persuading public authorities and the public that tsunami are a real threat. The data are also useful for identifying, for paleotsunami studies, sites suitable for preserving in the geological record a known event and possibly a succession of previous events. Further, good run-up data are essential for the calibration and validation of numerical tsunami propagation and inundation modelling. Historically, New Zealand has been particularly vulnerable to tsunami from South America. The 1868, 1877 and 1960 tsunami had significant impact along the east coast of the North and South Islands, and at outlying islands. The damage was limited by the sparseness of coastal settlement and by the near coincidence of the largest waves with low tide at several of the most affected locations in all three events. Nevertheless, houses, bridges, boats, and harbour facilities were damaged with wave heights of up to 4 m (peak to trough, over 7 m) on the two main islands. On the outlying Chatham Islands, 800 km to the east of the main islands, the 1868 tsunami was devastating, causing one death, and destroying an entire Maori village and several European houses with run-up of 6-6.3 m. This height is documented in a recently-found inundation map and reconnaissance report produced within a month or so of the tsunami. This and other recently found data as well as re-evaluation of previously known information on the 1868 and 1877 tsunami now provide an excellent picture of inundation at more than thirty New Zealand sites, and at several other Pacific island sites. Of the hundred or so observations of these two tsunamis in the 'Tsunamis in the Pacific 47BC 2000AD database, over one third come from New Zealand. These observations and that of other tsunami that have affected New Zealand should prove invaluable in future numerical modelling of tsunami from sources around the Pacific Rim, the results of which will benefit many island nations of the South Pacific as well as New Zealand.

**JSS07/09A/A02-012**

**1200**

**TSUNAMI SIMULATION FOR THE SOUTHWESTERN COAST OF ANATOLIA**

Ahmet Cevdet YALCINER<sup>1</sup>, Baris HABOGLU<sup>1</sup>, Efim PELINOVSKY<sup>2</sup>, Fumihiko IMAMURA<sup>4</sup>, Costas SYNOLAKIS<sup>3</sup> (<sup>1</sup>Dept. of Civil Engineering, Ocean Engineering Research Center, Middle East Technical University, <sup>2</sup>Department of Applied Mathematics, Nizhny Novgorod State Technical University, Nizhny Novgorod, Russia, <sup>3</sup>Dept. of Civil Engineering, University of Southern California, Los Angeles, CA, USA, <sup>4</sup>Disaster Control Research Center, Graduate School of Eng., Tohoku University, Aoba 06, Sendai, Japan)

The deepest region of the Mediterranean sea lies as a trench more than 4000m depth, at the coordinates 28.7°E, 35.7°N, with the size of 80km in E-W direction and 60 km in S-N direction. This trench expands towards North to Dalaman coast at South of Anatolia in Turkey. The coastal environment around this trench at southwestern Anatolia is very attractive and densely used by all kinds of tourist affairs. There are numerous earthquakes and tsunamis that occurred in this region are documented in historical records. The paleotsunami studies could provide valuable information and detected the traces of historical tsunamis at the Dalaman and Fethiye coasts. The well know fault zone Hellenic Arc lies from South of island Crete in W-E direction, bends towards NE at East of Rhodes and enters Anatolia near Dalaman town. This fault zone is directly dependant on the subduction zone in the region and have significant normal component which is one of the important mechanism to cause tsunamis. The slopes of this deep trench are steep enough to cause probable slope failures or submarine landslides which are another important sources of tsunami generation mechanism. There have not been made the detailed marine surveys to identify the sediment characteristics and slope stability in the region. But the importance of tsunami generation and coastal amplification still remain an unanswered question. There are 293 significant earthquakes and 13 tsunamis in the region have been documented in between the years 0-1900. There are 403 earthquakes with magnitude greater than 5, and 5 tsunamis in the region occurred in between 1900-2002. As seen from this simple information, the reliability of the databecomes higher with the years coming to present time. Using this data 28 different tsunami scenarios related to the generation by fault break is selected. 12 different tsunami scenarios related to the generation by submarine landslides are determined for the tsunami effect on the coastal environment in the region. The model applications to understand the tsunami behavior and coastal amplification related to various source mechanisms in the region are performed for this problem. The two different models using shallow water equations for solving the tsunami generation, propagation and coastal amplification are used. These models are TUNAMI-N2 (for fault generated tsunamis) and TWO LAYER (for underwater landslide generated tsunamis) written in Tohoku University, Japan. The distribution of maximum positive tsunami amplitudes at 50 different coastal stations are determined for totally 40 different tsunami scenarios and the results are discussed.

**JSS07/09A/A02-013**

**1215**

**DB DRIVEN QUICK TSUNAMI FORECASTING IN KOREA**

Ho Jun LEE<sup>1</sup>, Yong Sik CHO<sup>2</sup> (<sup>1</sup>Senior Researcher, National Institute for Disaster Prevention, Seoul 121-719, Korea, <sup>2</sup>Associate Professor, Department of Civil Engineering, Hanyang University, Seoul 133-791, Korea)

Theoretical and numerical researches including survey of past tsunamis have been studied in Korea. These include tsunami generation, propagation and run-up in the East Sea. The results show complicated characteristics in the East Sea. Especially, in case of Korean Eastern Coast, it is convinced that energy divergence from the Yamato Rise which located at the center of sea causes unusual tsunami height in specific region. Therefore, we should compute tsunami accurately using fine spatial grid size in numerical model. To use a numerical model covering entire region of Korean eastern coast with finer grid meshes, it needed high performance computer and large time computation. However we have about two hours from its generation to arrival in Korea, maintenance of an effective forecasting system is important for tsunami disasters countermeasure. This research presents a way to predict tsunami in a few minutes with high accuracy on PC. To solve linear long wave equation which explains tsunami propagation, superposition of its sub-solution as Eq. (1) could be used.  $F(x,y,z,t) = \sum f_i(x,y,z,t)$  (1) Where, F is a solution of linear long wave equation,  $f_i$  is the sub-solution of equation when we divide initial sea surface profile of tsunami into number of elements, and  $i$  is the number of partitions. Generally, in tsunami computation, we simplify the fault plane as a single or number of rectangle as its shapes. If the fault is simplified as two planes, summation of independently computed result for each fault would be equal to the real tsunami event in linear computation. Then the function is equivalent to a solution of independent tsunami event, and the F is to the solution of real tsunami. In advance, we can compute using unit event having 5 X 5 km area and 1m height unit event located along the entire active faults in the East Sea. Through the tsunami computation for every unit event, time series of sea water levels at certain locations along the Korean Eastern Coast are gathered for each computation. Finally, these are multiplied by real initial sea surface displacement at every location of unit event in real tsunami event. Then, summations of the each value on time axis will gives sea water levels in real tsunami computation. Consequently, only simple computation of the initial tsunami waves and manipulation of pre-computed data set, makes it possible to deduce tsunami heights and arrival time along the coast in a few minutes on PC. Using this method, the 1983 tsunamis are deduced and compared with the results which computed from the tsunami numerical model, and it shows good agreement each other. This study has accomplished for the quick estimation of detail tsunami heights along the Korean Eastern Coast. We are now computing the unit events using SX-5 super computer of KMA. After the establishment of DB, quick estimation of tsunami will be used for its forecasting and diminishing its damages. This research was financially supported by the Korea Meteorological Administration.

**Wednesday, July 9 PM**

Presiding Chairs: E. Bernard, N. Shuto, L. Kong, Y. Nishimura

**JSS07/09P/A02-001**

**1400**

**STUDY ON THE TSUNAMI BEHAVIORS NEAR THE ULCHIN NUCLEAR POWER PLANT SITE**

Sobeom JIN<sup>1</sup>, Fumihiko IMAMURA<sup>2</sup> (<sup>1</sup>Structural systems and site evaluation Dept. KINS, <sup>2</sup>Disaster Control Research Center, Graduate School of Engineering, Tohoku University)

When a nuclear power plant is to be located at an area which is subjected to tsunamis, a comprehensive analysis to estimate the potential effects of tsunamis should be carried out and the design code based on historical as well as probable maximum tsunami should be obtained to protect all potentials of tsunamis. We have three main issues in this subject; (1) what kind of damage caused by a tsunami can be expected, (2) what code or numerical model can be applied to estimate such damage, (3) how we can evaluate the probable maximum tsunami to ensure that the plant will be adequately protected against all potential tsunami effects. All nuclear power plants in Korea are located along the coastline for taking

cooling water. As typical example, the nuclear power plant site at Ulchin is located along the eastern coast of the Korean Peninsula, which has been effected by tsunami historically (1741, 1964, 1983 and 1993 events). Recently, it is reported that many undersea earthquakes have occurred around the Korean Peninsula, and its occurrences would increase. And seismic gaps that could affect huge tsunami attacks at the Ulchin site have been pointed out. Numerical analyses at Ulchin were performed for three recent tsunami events (1964, 1983 and 1993 tsunami events) and a virtual/possible tsunami event along the eastern coastline of the Korean Peninsula. The maximum run-up and draw-down heights are numerically estimated by using a combined numerical model based on the shallow-water theory. On the historical tsunamis, calculated run-up and draw-down heights are compared with field measurements. Although a slight discrepancy is observed, we obtain the overall agreement reasonably. The maximum run-up and draw-down heights at Ulchin site should be predicted to evaluate the safety of plants. Those of 1983 tsunami event; 3.30m and (-)3.10m on the still water level are selected as maximum value. As the result, it is concluded that the plants of Ulchin site might be safe against the four tsunami events. Hereafter, as the other effects of tsunamis, the integrity assessment of cooling water structure against tsunami attacks should be reviewed. And the sand sediment by tsunami could affect the safety features of the plant should be taken into account. Furthermore, for more conservative condition as the probable maximum tsunami, the parameter study on the seismic gaps should be carried out.

**JSS07/09P/A02-002** **1415**  
**ESTIMATION OF AN EFFECT OF HETEROGENEOUS TSUNAMI SOURCES IN A SEISMIC GAP OFF SAKATA COAST FOR A TSUNAMI HEIGHT DISTRIBUTION**

Tomoyuki TAKAHASHI (Faculty of Engineering and Resource Science, Akita University)

The 1983 Japan Sea Earthquake Tsunami and the 1993 Hokkaido Nansei-Okai Earthquake Tsunami (Okushiri Tsunami) occurred along the Eastern Margin of the Japan Sea. In a plate boundary along the margin, there are other seismic gaps. A seismic gap off Sakata coast is one of them, and it locates on the south of the Japan Sea Earthquake. If an earthquake will occur there, a huge tsunami will be generated. A damage of the tsunami would happen along the Japan Sea coastal zone not only in Japan but also in the Korea Peninsula and Russia. Especially, Yamagata Prefecture and Akita Prefecture in the Tohoku district in Japan face to the tsunami source, so the tsunami will attack there directly. Furthermore, because distances between the tsunami source and these prefectures are very short, the damage due to the tsunami depends on a heterogeneous dislocation of tsunami source. In this study, an effect of the heterogeneity of tsunami source in the seismic gap off Sakata coast for a distribution of tsunami height along shore is estimated with the tsunami numerical simulation. The heterogeneity of tsunami source, however, has not been studied well as compared with the asperity of fault. We can find one example in a study on the Nankai Trough. Many earthquakes as large as magnitude 8 class had occurred along the Trough at an interval of 100 to 150 years. The giant tsunamis generated by these earthquakes gave huge damages to Japan and they propagated toward some countries along the Pacific Rim. Many studies on the earthquakes and the tsunamis along the Nankai Trough has been conducted and Japanese government released the assumed models for the disasters and their estimated damages based on those research results. Because the earthquake model has taken in the asperity of fault, it is improved as compared with past models. The tsunami model, however, reproduces the 1707 Housai event which was largest tsunami along the Trough, and the heterogeneity of tsunami source has not been discussed. The tsunami sources in the seismic gap off Sakata coast are close to land, therefore tsunami heights along coasts would be affected by the heterogeneity of tsunami source strongly. If an estimation of tsunami damage is carried out without the heterogeneity source, it is possible that there are underestimated areas. In this study, as a first step of research about the effect of the heterogeneous tsunami source, I have estimated a variance of tsunami height distribution along shore due to some parameters which are a magnitude of heterogeneity, distance between tsunami source and coast, strike of fault, depth of fault, water depth where tsunami generated and bathymetry.

**JSS07/09P/A02-003** **1430**  
**ON THE REFLECTION OF AN OBLIQUELY INCIDENT BORE FROM AN INCLINED WALL**

Hideo MATSUTOMI, Kentaro IMAI (Department of Civil and Environmental Engineering, Akita University)

Edge bores were witnessed, photographed and videotaped on the north Akita coast in Japan at the time of the 1983 Nihonkai-Chubu earthquake tsunami, and the necessity of studying them from a viewpoint of tsunami disaster prevention was pointed out. In relation to the edge bores, physical experiments are carried out to examine a few fundamental characteristics of the reflection of an obliquely incident bore from an inclined plain wall. The experimental flume is 100 cm wide, 10 cm high and 350 cm long with a horizontal bed. Incident bores are generated by rapidly pulling up a gate, installed 1 m from one end of the flume. The experimental conditions are that the initial water depth  $h_1$  in the upstream region of the gate is three cases of 7, 8 and 9 cm, the constant water depth  $h_0$  in the downstream region of the gate is 2 cm, the inclined angle  $\theta$  of the wall is three cases of  $10^\circ$ ,  $20^\circ$  and  $90^\circ$  (vertical), and the incident angle  $\alpha$  of the bore is three cases of  $60^\circ$ ,  $70^\circ$  and  $80^\circ$  (nearly parallel to the wall). Wave gauges are arranged at about 30 locations to measure time histories of the incident and reflected bore surface elevations. In addition, the state of the incident and reflected bores are videotaped to grasp their features and to model the reflected bore. A simplified model is presented for the case of the vertical wall, which can estimate the bore heights  $\Delta H$  and  $\Delta H_3$  of the reflected bores propagating upstream and downstream respectively, the propagation velocities  $\omega$  and  $\omega_3$  of the reflected bores propagating in the respective directions, and the angle  $\beta$  between the reflected bore front line in the upstream region of the incident bore and the installed direction of the vertical wall. Through examinations and comparisons of the experimental results and the solutions of the model, it is concluded that the developed model is useful, the propagation velocity  $\omega$  is not zero, the angle  $\beta$  is not so affected by the intensity of the incident bore and so on.

**JSS07/09P/A02-004** **1445**  
**A STUDY OF THE GENERATION MODEL OF TSUNAMI CAUSED BY A COLLAPSE OF VOLCANIC ISLAND- A CASE OF THE 1741 OSHIMA-OSHIMA TSUNAMI -**

Kei KAWAMATA<sup>1</sup>, Kazuaki TAKAOKA<sup>1</sup>, Kazuhiko BAN<sup>1</sup>, Fumihiko IMAMURA<sup>2</sup>, Shigeru YAMAKI<sup>1</sup>, Eiji KOBAYASHI<sup>1</sup> (<sup>1</sup>Nuclear Power Dept., Electric Power Development Co., Ltd., <sup>2</sup>Disaster Control Research Center, Tohoku University, <sup>3</sup>Seamus Ltd., <sup>4</sup>Kaihatsu Computing Service Center, Ltd.)

Although the frequency of tsunamis generated by a volcanic eruption including debris, lava flow, failure, and collapse is less than those generated by an earthquake under the sea, the former tsunamis are reported to cause more damage than the latter. Because the wave height is locally amplified and attacked the surrounding area. The 1741 Oshima-Oshima tsunami is a representative tsunami documented in the Japan Sea, which would be caused

by the sector collapse of the Oshima-Oshima. So far it is not exactly clear about the detailed mechanism of the sector collapse and the tsunami generation. A landslide induced tsunami can be modeled in several ways. The first is to model the water disturbance caused by landslide, which is calculated by the motion of fault with horizontal and vertical movement (Satake, 2001). The second is to model motion of landslide as a fluid flow and solve the equations for multi-phase fluid flow. The authors selected the second and introduced a two-layers model (Imamura & Imteaz, 1999). A calculation in the whole Japan Sea including the Korean Peninsula was performed to reproduce the 1741 Oshima-Oshima tsunami. The main features of tsunami caused by the volcanic eruption with major collapse could be clarified by the observation in the hydraulic experimental study. The 1st is that the wave height of forward-wash and back-wash nearby wave source is higher. The 2nd is that the period of tsunami is short, suggesting the importance of wave frequency dispersion. Based on the hydraulic study, the authors improved the two-layers model which was developed by Matsumoto et al.(1998) through estimating proper coefficients and introduce the interface stress model, and applied the improved two-layers model to the 1741 Oshima-Oshima tsunami in order to reproduce the tsunami heights from the Hokkaido coast to the Korean Peninsula in the Japan Sea. The topographic data before and after the sector collapse was given by Satake (2001). A propagation of tsunami was based on the linear Boussinesq equation considering the wave transformation in addition to the nonlinear long wave equation. It was found from the calculation results that the computed tsunami was much not decayed in spite of short-period wave about five minutes, the computed tsunami heights well reproduced the observed tsunami heights in distant places such as Noto, Shimane, the Korean Peninsula. But a question of reproducibility remains unsettled that is related to a directivity of tsunami energy in the north and south flank of the Oshima-Oshima.

**JSS07/09P/A02-005** **1500**  
**TSUNAMI SIMULATION CONSIDERING DYNAMIC OCEAN-BOTTOM DISPLACEMENT DUE TO SEISMIC FAULTING**

Hiroyuki MATSUMOTO<sup>1</sup>, Tatsuo OHMACHI<sup>2</sup>, Hiroshi TSUKIYAMA<sup>3</sup> (<sup>1</sup>Deep Sea Research Department, Japan Marine Science and Technology Center, <sup>2</sup>Department of Built Environment, Tokyo Institute of Technology, <sup>3</sup>Tsukiyama Research Inc.)

A new technique of tsunami numerical computation that includes the dynamic motion of ocean-bottom is conducted. The traditional tsunami computations assume long-wave (or shallow water) approximation, i.e., the initial water surface displacement is the same as the static displacement of ocean-bottom. In this study, the dynamic motion of ocean-bottom is used as the boundary condition and 3-D numerical computations are carried out. Dynamic displacements of the ocean-bottom caused by the seismic faulting are simulated first by a 3-D boundary element method (BEM). Then, by applying velocity associated with the displacement at the ocean-bottom, water waves are simulated by a 3-D finite difference method (FDM) taking into account acoustic effects. As a result, the acoustic (or Rayleigh) waves that propagate through water could be reproduced in addition to tsunamis. It should be noted that the simulated tsunami is found to be remarkably larger in the wave height especially in the near-field where the acoustic effects are significantly appeared. In the far-field, however, as compared with the traditional computation, there is a little difference in the wave height. Finally, the present technique is applied to actual tsunami caused by the 1983 Nihonkai-Chubu earthquake and the 1993 Hokkaido-Nansei-Okai earthquake. These simulated tsunamis are found to agree well with the observations.

**JSS07/09P/A02-006** **1515**  
**HYDRODYNAMIC INVERSION OF THE SOURCE PARAMETERS OF TSUNAMIGENIC EARTHQUAKES**

Pedro M. MIRANDA, Carlos A. PIRES (Dep Physics, Centro de Geofisica, University of Lisbon)

Tsunamis produced by large submarine earthquakes contain information on the location and geometry of the earthquake source that may, in some cases, be successfully inverted providing an independent contribution to the general problem of earthquake inversion. Tide gauge series from near-shore tsunamis are potentially richer in information content, as their signals are less distorted by propagation effects. Even in those cases, it is not easy to deal with a number of difficulties, arising from observational errors at the tide gauges, from insufficient knowledge of the small scale bathymetry and from many model uncertainties. In this study we use the adjoint method as an inversion tool for tsunami data, incorporating both the hydrodynamic propagation and the earthquake source parameterization. The method is designed to perform the direct optimization of the tsunami fault parameters, from tide-gauge data, imposing strong geophysical constraints to the inverted solutions, leading to a substantial enhancement of the signal-to-noise ratio, when compared with the classical technique based on Green's functions of the linear long-wave model. A 4-step inversion procedure, which can be fully automated, consists (i) in the source area delimitation by adjoint backward ray-tracing, (ii) adjoint optimization of the initial sea state, from a vanishing first-guess, (iii) non-linear adjustment of the fault model and (iv) final adjoint optimization in the parameter space. Results with a set of idealized and real bathymetries, show that the method works well in the present of reasonable amounts of error and it provides, as a by-product, a resolution matrix that contains information on the inversion error, identifying the combinations of source parameters that are best and worst resolved by the inversion.

**JSS07/09P/A02-007** **1530**  
**A PROPERTIES OF THE CARRIER-GREENSPAN MAPPING APPLICATED TO WAVE RUN-UP ON A SLOPING BEACH**

Victor M. KAISTRENKO (Institute of Marine Geology and Geophysics, Russian Academy of Sciences)

Carrier and Greenspan (1958) found a representation for variables of the non-linear shallow water system on a sloping beach by the scalar potential satisfying the linear wave equation. This approach is used for wave run-up description. It is important that the exact solutions received in frames of this approach can be used for testing of the numerical models. There is a simple modification of this mapping which transforms non-linear shallow water system into similar linear shallow water system. This mapping has several interesting properties: 1. Each equation of the initial non-linear system after multiplication by Jacobian of transformation  $(x,t) \rightarrow (x',t')$  gives the corresponding equation of the linear system. The new parameters  $(x',t')$  of the linear system are likewise to space and time variables of the initial system. There are an integral equalities tying the non-linear and corresponding linear expressions. 2. Jacobian of transformation  $(x,t) \rightarrow (x',t')$  written using new variables is a product of two linear expressions. This fact simplifies investigation of zeroes of Jacobian corresponding to wave breaking. 3. Considered mapping is asymptotically equal because it is an initial part of the Taylor expansion. 4. The non-linear and corresponding linear shallow water systems have its own simple invariant group of scale transformations. Basing on it's a non-trivial two-parameter invariant group of transformations of non-linear system was created. These transformations allow to get a set of solutions from the one solution of the non-linear shallow water system. 5. Under several conditions a wave field described by the non-linear shallow water system on sloping beach in the full domain can be gotten from the run-up height

depending from the time. 6. Several examples are considered. The work was supported by the Russian Foundation for Basic Research. References. Carrier G.F., Greenspan H.P. Water waves of finite amplitude on a sloping beach. *J.Fluid Mech.*, 1958, v.4, N 1, pp.97-109

**JSS07/09P/A02-008****1600****CONSTRUCTING LANDSLIDE TSUNAMI SOURCES**

Philip WATTS<sup>1</sup>, Stephan T. GRILLF<sup>2</sup>, Francois ENET<sup>2</sup>, Joseph S. WALDER<sup>1</sup>, Andrea PANIZZO<sup>1</sup>, Christopher F. WAYTHOMAS<sup>3</sup> (<sup>1</sup>Applied Fluids Engineering, Inc., <sup>2</sup>University of Rhode Island, <sup>3</sup>USGS, Cascade Volcano Observatory, <sup>4</sup>Universite degli Studi dell' Aquila, <sup>5</sup>USGS, Alaska Volcano Observatory)

A considerable amount of experimental work has been performed in order to characterize the mechanics of tsunami generation by landslides of both subaerial- and subaqueous origin. This work has proceeded along with significant advances in numerical simulations of landslide tsunamis, using complete and accurate fluid dynamic models. These efforts, carried out in tandem, have provided considerable insight into the mechanics of landslide tsunamis. However, both laboratory experiments and numerical simulations are often costly, time-consuming activities that many tsunami researchers do not have the means to access or perform. Fortunately, because many of the tsunami features documented in the experimental and numerical work are coherent structures of predictable scale, much of the experimental and numerical results can be generalized. While further experimental and numerical work will certainly refine our understanding of tsunami generation, sufficient information currently exists with which to construct reliable initial conditions, or tsunami sources, as inputs to a tsunami propagation and inundation model. A tsunami source comprises a statement of the initial free surface shape and velocity distribution. We demonstrate in detail a general technique of constructing tsunami sources for underwater landslides, subaerial landslides, and pyroclastic flows. We evaluate the time scale of tsunami generation and perform scaling analyses for each type of mass failure, following the same procedure yet finding different results. With these different time, amplitude, and wavelength scales in hand, we interpret the available experimental and numerical results with accurate curve fits using dimensionless quantities. These curve fits allow us to construct tsunami sources. We compare the resulting tsunami sources with the original experimental and numerical results on which they are based, in order to test the accuracy of the complicated fitting techniques. However, tsunami sources can also be constructed, through interpolation, away from the original tsunami data. We find that underwater landslides are most sensitive to landslide volume and depth, that subaerial landslides are most sensitive to volume flux and duration of motion in the water, and that pyroclastic flows behave effectively as a subaerial landslide with respect to tsunami generation. We finish our presentation with demonstrations of tsunami source calculations, performed in real time, and we summarize the numerous successful case studies already carried out to date with such tsunami sources.

**JSS07/09P/A02-009****1615****WAVES AND RUN-UP GENERATED BY A THREE-DIMENSIONAL SLIDING MASS**

Costas Emmanuel SYNOLAKIS<sup>1</sup>, Fred RAICHLN<sup>2</sup>, Jose BORRERO<sup>3</sup>, Burak USLU<sup>4</sup> (<sup>1</sup>department of civil engineering, university of southern california, <sup>2</sup>department of civil engineering, california institute of technology)

We report results from small and large scale laboratory experiments with the objective to understand the basic fluid mechanics of water waves generated by partially aerial and submarine landslides. We use two both wedge and hemispherical shaped bodies. We have conducted small-scale three-dimensional experiments in a wave tank 38cm wide with a slope (1:2.08) constructed at one end to represent the near-shore region. A triangular shaped lead block with a horizontal length of 18 cm, a 9 cm high front-face and a width of 5 cm was used to represent a landslide. The block was released from rest abruptly moving down-slope by gravity. Water surface-time histories were obtained in front of and to the side of the at-rest position of the wedge. While the data were useful, it is only with an investigation conducted at a large enough size so as to reduce scale effects that reliable data can be obtained to confirm numerical models as used to establish coastal inundation limits and to define the run-up. Large scale experiments were conducted in a wave tank with a length 104 m, width 3.7 m, and depth 4.6 m and with a plane slope (1:2) located at one end. A freely sliding wedge with a horizontal length of 91 cm, a vertical face 46 cm high and a width of 61 cm was used to represent the landslide. A hemisphere of 46cm radius was also used. Both bodies were instrumented with an accelerometer and a position indicator, and their initial position (with varied mass and two different orientations) ranged from totally aerial to fully submerged. The surrounding water surface variation and the run-up time histories were measured electronically. The results provide a carefully obtained set of data conducted at a scale which minimizes viscous and capillary effects. These experimental data are compared to numerical models which define the run-up.

**JSS07/09P/A02-010****1630****TSUNAMI GENERATION BY NON-LINEAR PHENOMENA IN SOURCE**

Mikhail A. NOSOV, Sergey V. KOLESOV, Sergey N. SKACHKO (Physics Faculty, M.V.Lomonosov Moscow State University)

This study is focused on tsunami generation mechanism due to non-linear energy transfer from high-frequency oscillations of water layer to low-frequency gravitational surface waves. The non-linear tsunami generation mechanism is related to seismic bottom motions; however the mechanism differs from a simple water displacement by bottom deformations. During bottom earthquake water layer can be considered as incompressible or as compressible fluid. These two cases can be distinguished taking into account the position of the bottom displacement frequency spectrum relatively the lowest normal acoustic frequency  $4H/c$ , where  $H$  is ocean depth,  $c$  is sound velocity in water. Thus in case of "shallow water", the incompressible fluid theory can be applied, whereas "deep ocean" ought to be considered as a compressible fluid. The main response of a compressible water layer from bottom deformation is elastic oscillations, which are caused by repeated reflections of an acoustic impulse from bottom and top surfaces. In case of incompressible fluid a periodic bottom motions are assumed. Mathematical description of the non-linear tsunami generation mechanism is based on the non-linear Euler equations. It is assumed that fluid velocity, density and pressure can be expressed as a sum of variable (fast) and time averaged (slow) terms. The fast components are calculated as a linear response of water layer (compressible or incompressible) to bottom motions. Averaging the Euler equations in time we obtain equations to describe the time-averaged flow (surface gravitational waves). The non-linearity of the Euler equations introduces additional terms in the time-averaged flow equations which can be interpreted as external mass force and distributed mass source. The time-averaged flow equations are solved within framework of the linear shallow water theory. The amplitude of the surface gravitational wave generated by the non-linear mechanism is estimated as a function of ocean depth and of duration and velocity of bottom displacement. It is shown that this mechanism can provide a noticeable contribution to tsunami amplitude.

**JSS07/09P/A02-011****1645****A SHARED-USE, LARGE-SCALE, MULTIDIRECTIONAL WAVE BASIN FOR TSUNAMI RESEARCH**

Solomon YIM, Daniel COX, Charles SOLLITT, Cherri PANCAKE, Harry YEH

Under the Network for Earthquake Engineering Simulation (NEES) program, the US National Science Foundation is funding the expansion of Oregon State University's multidirectional wave basin to create a shared-use next-generation experimental facility for tsunami research and engineering practice. The new facility addresses the unique requirements posed by tsunami research, with basin dimensions and wave generation capabilities closely matching the community's vision of the ideal basin. When completed in 2004, the basin will support high resolution, unprecedented-scale experiments with very dense instrumentation. Researchers will be able to test and validate advanced analytical and numerical models of tsunami phenomena induced by sub-sea earthquakes, spanning a full range of ocean, coastal, and harbor studies. An integral part of the project is the exploitation of advanced network technologies to allow researchers located at distant sites to play active roles in experiments at the facility, viewing data and images in real time and participating in decision-making. The broader research community will benefit from this large tsunami experiment facility, a comprehensive experiment databank, with specialized interfaces for experiment replay, searching and browsing archives of past experiments, extraction of experimental data for use in validating numerical models, and a community repository for numerical simulation codes.

**JSS07a-Posters****Wednesday, July 9****TSUNAMIS: THEIR SCIENCE, ENGINEERING AND HAZARD MITIGATION (IASPEI, IAVCEI, IAPSO)**

Location: Site D

**Wednesday, July 9 PM**

Presiding Chairs: L. Kong, Y. Nishimura

**JSS07a/09P/D-001**

Poster

**1700-102****MODELING THE 1741 TSUNAMI FROM OSHIMA-OSHIMA ERUPTION IN JAPAN SEA**

Kenji SATAKE<sup>1</sup>, Stefano TINTI<sup>2</sup> (<sup>1</sup>Active Fault Research Center, GSJ/AIST, <sup>2</sup>Dipartimento di Fisica, Universit di Bologna)

The 1741 Oshima-Oshima tsunami, the most destructive historical tsunami in Japan Sea, was generated by submarine landslide associated with the eruption of Oshima-Oshima volcano. The small island is located between the source regions of the 1983 Japan Sea (M 7.7) and 1993 Southwest Hokkaido (M 7.8) earthquakes, both caused extensive tsunami damage. The 1741 tsunami caused 2,000 casualties along the Hokkaido coast and damage as far as along the Korean Peninsula. The estimated tsunami heights are 3-13 m on Hokkaido coast, 3-6 m on Tsugaru peninsula, 1-5 m on other coasts of Honshu, and 3-4 m on the Korean peninsula. There was no record documenting ground shaking from an earthquake in 1741. In contrast, a large-scale sector collapse occurred on Oshima-Oshima volcano, but the volume change associated with the subaerial landslide was too small to explain the observed tsunami heights. Recent swath bathymetry surveys indicate that the landslide extended to ocean bottom with the volume change of about 2.5 km<sup>3</sup>, nearly an order of magnitude larger than the subaerial slide. We computed the tsunami generation from landslide, both subaerial and submarine, by using two different models: a block model and a simple kinematic landslide model. The mapped bathymetry change is used as initial conditions. The tsunami propagation is computed in two different grids, 6° around the source and 1° grid for the entire Japan Sea. The computed heights from the block model well reproduced the estimated tsunami heights. For the kinematic landslide model, we searched parameters that best match the observed and computed tsunami heights. They are the horizontal slide velocity of 40 m/s and rise time of 2 min.

**JSS07a/09P/D-002**

Poster

**1700-103****Holocene Tsunami Deposits from Large Earthquakes along the Kuril Subduction Zone, Eastern Hokkaido**

Futoshi NANAYAMA<sup>1</sup>, Kenji SATAKE<sup>2</sup>, Ryuta FURUKAWA<sup>3</sup>, Koichi SHIMOKAWA<sup>2</sup>, Kiyoyuki SHIGENO<sup>4</sup> (<sup>1</sup>Institute for Marine Resources and Environment, Geological Survey of Japan, <sup>2</sup>Active Fault Research Center, Geological Survey of Japan, <sup>3</sup>Institute of Geoscience, Geological Survey of Japan, <sup>4</sup>Meiji Consultant Co. Ltd.)

Holocene tsunami deposits in eastern Hokkaido between Nemuro and Hiroo show that the Kuril subduction zone repeatedly produced earthquakes and tsunamis larger than those recorded since AD 1804. Twenty-two postulated tsunami sand layers from the past 9500 years are preserved in lake bottom near Kushiro City, and almost ten postulated tsunami sand layers from the past 3000 years are preserved in peat layers on the coastal marsh of eastern Hokkaido. We dated these ten tsunami deposits (named Ts1 to Ts10 from shallower to deeper) in peat layers by radiocarbon and tephrochronology, correlated them with historical earthquakes/tsunamis, and surveyed their spatial distribution to estimate the tsunamis inland inundation limits. Ts1 is inferred 20th century and may correspond to the tsunami from the AD 1960 Chilean earthquake (M 9.5) or the AD 1952 Tokachi-oki earthquake (Mt 8.2). Ts2 is inferred 19th century (Edo era) and is correlated with the AD 1843 Tempo Tokachi-oki earthquake (Mt 8.0) recorded in a regional document Nikkanki of Kokutai-ji temple at Akkeshi. Ts3 is located just below 17th century tephra, Us-b and Ta-b (AD 1667-1663), so it is also dated as 17th century (Edo era). Ts4 is dated around 13th century (Kamakura era). Ts5 to Ts8 are between two regional tephra layers, B-Tm (Ca 9th century) and Ta-c2 (ca 2.5 ka). In particular, Ts5 is found just below B-Tm tephra, so it is dated 9th century (Heian era). Ts9 and Ts10 are under the regional tephra Ta-c2 (ca. 2.5 ka) and represent prehistorical events. Our detailed surveys indicate that Ts3 and Ts4 can be traced more than 3 km from the present coast line in Kirittapu marsh, much longer than the limits (< 1 km) of recent deposits Ts1 and Ts2 or documented inundation of the 20th century tsunami events. The recurrence intervals of great tsunami inundation are about 100 to 500 years, longer than that of typical interplate earthquakes along the Kuril subduction zone. The longer interval and the apparent large tsunami inundation indicate unusual origin of these tsunamis.

**JSS07a/09P/D-003** Poster **1700-104**

**Tsunami Fluid Force on Vegetation**

Kentaro IMAI, Hideo MATSUTOMI (Department of Civil and Environmental Engineering, Aikita University)

One of the features of the 1998 Papua New Guinea tsunami is that the maximum tsunami height of 14.8 m was observed on the sand spit with vegetation of Sissano lagoon faced the tsunami source, which caused a large number and high rate of human casualties. In countries of the western Pacific Ocean area, the coastal vegetation attracts their attention as a means of tsunami countermeasures from the economical and environmental reasons. In the light of these situations, physical experiments are carried out to examine a few fundamental characteristics of the tsunami fluid force acting on vegetation. The experimental flume is 0.3 m wide, 0.5 m high and 11.0 m long with a horizontal bed. Tsunamis are modeled by bores and generated by rapidly pulling up a gate, installed 5 m from one end of the flume. The bores propagate, in order, in the regions of the constant water depth, a uniformly sloping beach, the sand spit with vegetation, and a lagoon with a constant water depth. Model tree consists of the trunk with the diameter  $d$  of 0.24 cm and the foliage with the void ratio of 0.7. The model trees are arranged in both the staggered and grid patterns on the sand spit. The vegetation density  $\kappa$  (= total cross section area of trunks/vegetation area =  $\pi(d/L) \cdot dn/4$ ) is four cases of 0, 0.5, 1.0, 1.5%, where  $L$  is the depth length of the vegetation area and  $n$  is the number of trees per unit width along the shore. These conditions make Shuto's 'vegetation thickness  $dn'$  0 ~ 400 and are realistic. Through analyses of the experimental data using Morison's equation added a linear wave making resistance term (caused by the trembling of the foliage), it is clarified that (1) the drag coefficient  $CD$  is 0.5 ~ 1.4, the added mass coefficient  $CM$  1.1 ~ 1.4 and the coefficient  $\theta'$  of the linear wave making resistance 0.2 ~ 0.6, (2) these coefficients decrease as  $\kappa$  increases, (3)  $CD$  and  $CM$  change with the same tendency as those of group of piles in open channel flows, (4) the inertia force  $FI$  reaches 20 % of the maximum drag force  $FD_{max}$  at the early stage, and after that the drag force  $FD$  and the linear wave making resistance force  $FA$  become dominant, (5) as the ratio of  $FA$  to  $FD_{max}$  is about 0.2,  $FA$  can not be ignored.

**JSS07a/09P/D-004** Poster **1700-105**

**Timing and Scale of Tsunamis Caused by the 1994 Rabaul Eruption, East New Britain, Papua New Guinea**

Yuichi NISHIMURA<sup>1</sup>, Mitsuhiro NAKAGAWA<sup>2</sup>, Jonathan KUDUON<sup>3</sup>, Joseph WUKAWA<sup>4</sup> (Institute of Seismology and Volcanology, Hokkaido University, JAPAN, <sup>2</sup>Graduate School of Science, Hokkaido University, JAPAN, <sup>3</sup>Rabaul Volcanological Observatory, Geological Survey of Papua New Guinea, PNG)

The 1994 Rabaul eruption series is one of the most recent eruptive events which accompanied significant tsunamis. On September 19, 1994, Vulcan and Tavuvur Volcanoes erupted almost at the same time. These volcanoes are located at the eastern and western side of Simpson Harbour, respectively. During the main stage of the Vulcan eruption, small tsunamis were recorded on tide gage installed at the township of Rabaul. According to the eyewitness accounts and reported damages, tsunamis occurred several times at Matupit Island, south of Rabaul (with the largest wave invading 100-200 m inland) and also on the southern part of Rabaul. In order to investigate the timing and scale of the 1994 Rabaul tsunamis, we conducted reconnaissance geological mapping of the 1994 tsunami deposits. Around Rabaul, the tsunami deposits are identified as sand layers or characteristic pumiceous sand (mixes pumice and sand) layers sandwiched by tephra from both Vulcan and Tavuvur Volcanoes. The tephra might play an important role to preserve the original structures of the tsunami deposits. According to the chronological studies of both tephra and tsunami deposits, we infer that the tsunami was not generated by the first small eruption from Vulcan Volcano although this eruption occurred close to the coast. The tsunamis were excited several times or continuously by larger pyroclastic flows and base surges during the climactic stage of the volcano. Tsunami run-up heights estimated from distribution of the tsunami deposits are ca. 5 meter around western to southern shore of Matupit Island.

**JSS07a/09P/D-005** Poster **1700-106**

**Characteristics of Historical Tsunami Events of Eastern Hokkaido, Japan, Revealed by Sedimentary Facies of the Tsunami Deposits**

Yuichi NISHIMURA<sup>1</sup>, Kazuomi HIRAKAWA<sup>2</sup>, Yugo NAKAMURA<sup>2</sup>, Naomichi MIYAJI<sup>1</sup>, Masayoshi KOMATSU<sup>3</sup> (Institute of Seismology and Volcanology, Hokkaido University, JAPAN, <sup>2</sup>Graduate School of Environmental Earth Science, Hokkaido University, JAPAN, <sup>3</sup>Department of Geosystem Sciences, Nihon University, JAPAN)

Based on recent works on tsunami deposits, eastern Hokkaido was known to be affected by large tsunamis more than 10 times during the last 5000 years (Hirakawa et al. 2002, Nanayama et al., 2002). Most these tsunamis are thought to be caused by large earthquakes along the Kuril Trench. Earthquake recurrence along the trench has been estimated by dating these tsunami deposits. The sizes of the events were also estimated for the case if their invaded areas are well traced. Here, we investigated sedimentary characteristics of these tsunami deposits to consider whether these historical tsunamis are all similar or not. This consideration is necessary to re-evaluate the earthquake and tsunami recurrence along the Kuril trench. We found some fields where plural tsunami deposits lie between peat deposits and are traced inland by hand excavation. For example, near the mouth of Tokachi River, eastern Hokkaido, we could identify six tsunami layers in a ca. 1 meter thick peat deposit. We traced them along a small channel in a glass field up to 1500 meter inland from the beach. The tsunami deposits were identified as continuous sand layers that consist of very coarse to fine sand. The sand layers show the typical characteristics of reported tsunami deposits: thickness and mean grain size of the deposits decrease with the distance from the sea (Nishimura and Miyaji, 1995). However, grain size analyses of the sand deposits indicate that the size-decreasing patterns are significantly different among the tsunami deposits. We speculate that these sedimentary facies of the tsunami deposits are mostly linked to the wave height, wavelength and invaded direction of each tsunami, because there are no evidence for critical environmental change in the peat deposit.

**JSS07a/09P/D-006** Poster **1700-107**

**Run-up Calculation of Hokkaido Southwest Earthquake Tsunami with Dispersion Effect**

Masafumi YOSHINO<sup>1</sup>, Toshifumi MIKAMI<sup>1</sup>, Takahiro AKITA<sup>1</sup>, Hiroyuki IWASE<sup>2</sup> (Engineering Department, Alpha Hydraulic Engineering Consultants Co., Ltd., <sup>2</sup>Ecoh Co., Ltd.)

1. Introduction Hokkaido Southwest earthquake tsunami occurred on July 12th 1993 (M 7.8). During this tsunami disaster, Okushiri Island suffered serious damages (casualties: 230 dead and missing persons), and run-up height of more than 30m was recorded at Monai coast, face to tsunami source. In the recent years computation model becomes an important and decisive tool for planning tsunami counter-measures. Shallow water theory models were

used in many cases, but for this particular event some improvement was needed. In order to reproduce accurately the tsunami propagation, it is not possible to ignore dispersion effect in shallow sea. Consideration of soliton fission of tsunami, wave profile curvature effect and breaking are necessary. In this study, we reproduced the 1993 tsunami by the use of non-linear dispersive long wave theory model with two-step mixed finite difference scheme, and compared results accuracy versus non-linear long wave theory model and observed run-up height. 2. Numerical model We used depth-integrated Madsen-Sørensen equations which includes dispersive terms. The computation model is based on two-step mixed finite difference scheme, alternating implicit and explicit scheme. Initial surface elevation was calculated by the use of Mansinha and Smylie method from fault model of DCRC. Computation area consists in a set of nested grids. Maximum grid size is 1800m, and minimum is 12.5m. Time step is 0.2sec. Calculation period is 60 minutes. 3. Conclusion As a key result of this study, tsunami height was amplified in the shallow sea by soliton fission effect, and accuracy of wave height distribution was improved versus non-linear long wave model. Maximum run-up height and flooding area was similar to observed value.

**JSS07a/09P/D-007** Poster **1700-108**

**Evaluation for Tsunami Source Area Based on a Precise Analysis of Crustal Deformation--Verification on Tsunami Run-up Heights by the 1993 Hokkaido-Nansei-oki Earthquake --**

Masafumi MATSUYAMA, Yasuhira AOYAGI, Hiroyoshi TANAKA, Shintaro ABE (Central Research Institute of Electric Power Industry)

The purpose of this study is to confirm that a new tsunami source model, constructed by Aoyagi et al. (another presentation), can give an evaluation of tsunami run-up heights on the safe side. Targeted area is a source of Hokkaido-nansei-oki Earthquake tsunami. The model is intended to be applied to safe design basis against tsunami for important coastal facilities. In the source model, crustal deformation, that is tsunami initial condition, is calculated by a 3D finite element model with fault parameters re-examined by the distribution of aftershock hypocenters etc. The calculation is carried out on the assumption that only hanging side of reverse faults is displaced. As a result of numerical simulation based on shallow water theory with dynamic fault parameters, the model gives reasonable results around Okushiri Island. Especially, along the southwest coast of Okushiri Island, where the run-up heights over 20m were recorded, tsunami heights obtained by the model, can envelop measured run-up heights, while previous models caused underestimation along southwest coast. Consequently, these results demonstrate that the new source model can evaluate the tsunami run-up heights on the safe side.

**JSS07a/09P/D-008** Poster **1700-109**

**Cause of the Tsunami of the Aitape Earthquake of 17th July, 1998, Papua New Guinea**

Yoshinobu TSUJI (Earthquake Research Institute, University of Tokyo)

The Aitape Earthquake (Mw 7.1) occurred in the sea area off the north coast of Sissano Lagoon at 8h49min, 17th July, 1998 (UT). After the earthquake a huge tsunami hit the several villages near the mouth of Sissano Lagoon, and about 2000 people were killed. We made a field survey on the damaged coast and gathered eyewitnesses' accounts of survivors living in the villages around the lagoon. Survivors of Warapu and Arop, villages on the western and the eastern sandspits of the lagoon testified that they felt eminent shakings three times, the second one was the strongest, and that the huge tsunami came just after (or at the same time of) the third shaking. The board band seismograph at Jayapura, about 155km west of the hypocenter of the main shock, recorded the main shock (M7.1) at 8h 49min and the maximum aftershock at 20.3 minutes after it (9h 09min). No another eminent shock was recorded, but a shock of not a seismic origin was recorded between 8.6 and 9.5 minutes after the main shock (around 8h 57min). We also made an aftershock observation at three points (Aitape, Vanimo, and Lumi) on the coastal region from the beginning of August to the end of September, 1998. Locations of hypocenters of 49 aftershocks were decided. The distribution of those aftershocks shows that the location of the main shock is distributed in the sea area just in front of Sissano Lagoon between the coastline to the trench axis (depth: about 4000m) which runs about 50 km apart from the coastline in parallel to it. Running time of a long water wave (tsunami) is estimated to be 12 minutes from trench area to the coast. JAMSTEC made marine survey researches for four times by the vessels Natsushima and Kairei from December 1998 to February 2001, and detailed sea bottom topography was clarified, sea bottom observations, and echo-sounding profiling were made. We found out a round shaped crater, called 'mpitheater' with diameter 7-8km in the sea area just the front of the lagoon, 25km apart from the shoreline. We found out several fresh cracks on the south slope of the crater, and folding on the foot of the slope, and a trace of a slumping with debris. Many traces of surface layer sliding were found out on the sound profiling charts generally at almost all slopes including those in the Amphitheater. Considering all those results, together with eyewitnesses' accounts, the following scenario could be assumed; 1. The tsunami, which hit the coastal villages was not caused by the main shock. 2. The tsunami was supposed to be formed by a sliding of surface sediment layer on a slope in or near the Amphitheater. It occurred at 9 minutes after the main shock.

**JSS07a/09P/D-009** Poster **1700-110**

**Bay on Troubled Waters: Modelling Tsunami Heights along the Coasts of Southwestern Luzon and Manila Bay from Earthquakes along the Manila Trench and Manila Bay Area**

Ishmael C. NARAGI<sup>1</sup>, Erlinton B. OLAVERE<sup>1</sup>, Bartolome C. BAUTISTA<sup>1</sup>, Ma. Leonila P. BAUTISTA<sup>1</sup>, Yuichiro TANIOKA<sup>2</sup> (Seismological Observation and Earthquake Prediction Division, Philippine Institute of Volcanology and Seismology, <sup>2</sup>Hokkaido University, Hokkaido, JAPAN)

Tsunami hazard along the Manila Bay is one of the least studied earthquake-related hazards. The tsunami threat comes from earthquakes originating from the Manila Trench located west of the bay as well as from a source region in the bay area. Meanwhile, a previous study on earthquake hazards in Metro Manila had suggested that the metropolis has a low vulnerability to tsunami hazards due to the narrow configuration of the mouth of Manila Bay, the presence of Corregidor Island near the mouth of the bay which has an abating effect on any tsunami wave and the relatively deep slab of the Manila Trench beneath the bay. However, historical records show that there were accounts of at least two earthquakes that mentioned occurrence of unusual sea waves after a felt earthquake that affected Manila shores and its nearby vicinity. For the past ten years, the coastline population and industries along Manila Bay has significantly increased which warrants the need to verify whether the tsunami hazard in the study area is indeed low. In order to do this, a modelling study was conducted in order to determine possible tsunami heights that may result from an earthquake along the Manila Trench and a source zone in Manila Bay. The present modelling effort uses bathymetric grids generally interpolated from available digital bathymetry data and corrected from available bathymetric maps. Source parameters for representative earthquakes were inferred from available seismic data and estimated magnitudes of historical events occurring in the study region. Tsunami waveforms were

numerically computed by a finite-difference computation of the linear long-wave equations. Model runs were made for earthquakes with various magnitude sizes for the Manila Trench as well as for the 1863 Manila Bay Earthquake. Risks and vulnerability analyses could be done effectively if we could consider effects of variations of tsunami heights for different earthquakes especially in areas with existing communities and industries in the bay. In order to determine whether the configuration of the Manila Bay will have an effect on the ensuing tsunami, finer bathymetric data will be gathered and further modelling will be done to determine better tsunami heights.

**JSS07a/09P/D-010** Poster **1700-111**

**STUDY OF DIATOM FLORA FOR PALEO-TSUNAMI EVENTS IDENTIFICATION**

Nadezhda G. RAZJIGAEVA<sup>1</sup>, Tatiana A. GREBENNIKOVA<sup>1</sup>, Larissa A. GANZEI<sup>1</sup>, Alexander Ya. ILYEV<sup>2</sup> (<sup>1</sup>Pacific Institute of Geography, Russian Academy of Sciences, <sup>2</sup>Institute of Marine Geology and Geophysics, Russian Academy of Science)

The presence of marine diatoms in the deposits show marine influence, that may resulted by different causes: marine transgression, strong storm surges and tsunami. Diatoms was studied in 16 key sections of Kunashir island from sand layers of peat bogs and barrier palaeo-lake deposits and from overlying and underlying deposits. The studied sections are located on different distance from coastal line (up to 2.5 km). Diatoms analysis can provide valuable evidence for the validity of proposed tsunami deposits. Presence of marine and brackish species in sandy layers suggest a seaward source for the sand, as opposed to a downriver flood deposits and reflect configuration of ancient coastal line. Diatom analysis suggests that the tsunami may have deposited finer-grained sediments and diatoms at last distance farther upland where sand layers have not been observed. Content of marine species and their diversity depend as by distance from sea coast as sand layer thickness that possibly is connected with tsunami intensity. Content of neritic and oceanic species is higher in tsunami layers compare to marine deposits of Holocene transgressive phases. Appearance and high percent content of deep-sea species is connected to strong marine water flow, penetrated far landward and brought large amount these forms as compared with storm-induced surge. Possibly this fact can serve as informative sign of palaeo-tsunami. It should be noted that some of the marine taxa found under the sand layers may be due to infiltration of marine water into peat. The rarely and poor preservation of diatom valves indicate long-distance transport during a high-energy event. The most palaeo-tsunami deposits are late Holocene that explains predominance of south- and north-boreal diatoms, typical for modern sublittoral environment of this region. Warm-water species were found in middle-Holocene palaeo-tsunami deposits that was connected with Kuroshio current system shift northward. The results of this study show the usefulness of diatom palaeoecology as a tool for reconstructing the ecological effect of tsunami on swamp geosystems. Freshwater diatom assemblage from tsunami layers and overlying deposits indicates that palaeo-tsunami had an influence on environment pH. After tsunami diatom assemblage common for acid swamp environments (acidophilous and acidobiontic) changed by diatom flora of neutral and alkaline environments. Thus, palaeo-tsunami influence to environment results in changes of development tendency of swamp system, that could have effect to landscape development. The work was supported by the Russian Foundation for Basic Research, grants 01-05-79184, 01-05-79024, 02-05-65409 and Far Eastern Division of the Russian Academy of Sciences.

**JSS07a/09P/D-011** Poster **1700-112**

**REGIONAL AND LOCAL TRIGGERING OF THE AUGUST 17, 1999 TSUNAMI IN THE IZMIT BAY (TURKEY)**

Stefano TINTI<sup>1</sup>, Anna MANUCCI<sup>1</sup>, Gianluca PAGNONI<sup>1</sup>, Filippo ZANIBONI<sup>1</sup>, Alberto ARMIGLIATO<sup>1</sup> (Department of Physics, Sector of Geophysics, University of Bologna, Italy)

We present the main results of a set of numerical simulations of the tsunami occurred on August 17, 1999 along the coasts of north-western Turkey, and in particular of the Gulf of Izmit. The tsunami followed a devastating  $M_w = 7.4$  earthquake which affected mainly the easternmost part of the Sea of Marmara. The earthquake supposedly broke at least five long right-lateral strike-slip segments of the North Anatolian Fault: a very relevant part of theseismic energy was released along fault segments placed partly or completely offshore. The rupture scenario is further complicated by the slipping of dip-slip ancillary faults connecting the main strike-slip segments, and by liquefaction and subsidence phenomena, reported to have occurred in a large number of coastal places. Concerning the dip-slip faults, they are mainly found in the central and eastern basins of the Izmit bay and were identified on the basis of both bathymetric and geological data analysis. Numerous field surveys, performed soon after the event, allowed to identify and measure the effects of the tsunami in the Gulf of Izmit. The run-up measurements range typically in the interval 1-3.5 m along the entire coastline of the Izmit Bay. A significant exception is represented by the small town of Degirmendere, where a local slump was accompanied by the collapse of some buildings along the shoreline: here, some eye-witnesses reported water waves exceeding 10 m. In the present study, we investigate numerically the August 17, 1999 tsunami trying to reproduce the water wave heights both along the entire Izmit Bay coastline and locally in Degirmendere. For this purpose, our analysis is carried out through two main experiments. In the first, we utilize the most recent hypotheses on the ruptured faults and simulate the tsunami propagation in the Izmit Bay and its impact along the coast, comparing the numerical results with the experimental measurements. In the second experiment, we study the triggering and the evolution of the local slump occurred in Degirmendere, and the consequent water movement generation. The main result of our approach is that, on the scale of the entire Izmit Bay, it is possible to reproduce the observed tsunami effect only by considering the rupture occurred on the secondary dip-slip faults; moreover, the local effects seen in Degirmendere must be considered the consequence of the local slump alone and not of the earthquake-induced tsunami that affected the Izmit Gulf.

**JSS07a/09P/D-012** Poster **1700-113**

**RESTORATION OF A TSUNAMI SOURCE BY INVERSION OF THE COASTAL TIDE-GAUGE RECORDS**

Tatjana A. VORONINA<sup>1</sup>, Viacheslav K. GUSIAKOV<sup>1</sup>, Vladimir A. TCHEVERDA<sup>2</sup> (<sup>1</sup>Institute of Computational Mathematics and Mathematical Geophysics, SD RAS, <sup>2</sup>Institute of Geophysics, SD RAS)

The inversion of the tsunami wave records obtained on the coastal tide-gauges is widely used to determine the initial water displacement in a tsunami source area. Mathematically, this problem is formulated as an inverse problem of mathematical physics for restoration of the initial water displacement in the source area by the water level oscillations observed on the number of points distributed along the coastline. As it was shown by Kaisrenko (1972), in a general case of an arbitrary source, this inverse problem does not have a unique solution. Its solvability depends on a number of a priori assumptions, one of which is that the source function can be presented as a product of space- and time-dependent functions, where the time-dependent function is supposed to be known. Even under this assumption, the problem remains to be an ill-posed problem whose solvability depends on the number and length of

waveforms used in the inversion, their spatial distribution and the signal-to-noise ratio. As a mathematical model of the problem, we use the linear shallow water equations numerically solved (by finite difference method) on the model bottom relief having some basic morphological features typical for the island arc regions. The inverse problem is solved by least square inversion using a truncated SVD approach. The quality of the solution obtained is evaluated as relative errors (in L2-norm) in restoration of the source function. As a model of the initial water displacement we used a dipolar displacement representing the surface deformation due to the typical tsunamigenic earthquakes with the reverse dip-slip or the low-angle thrust mechanisms. On the basis of a series of numerical experiments made we conclude that (1) the quality of the source restoration strongly depends on the number of waveforms used and their azimuthal coverage; (2) to obtain a reasonable quality of source restoration we need to use at least 5 records smoothly distributed over the space domain that is comparative in size to the projection of the source area onto the coast line; (3) complexity of a source function and the presence of the background noise imply serious limitations on the accuracy of the restoration procedure, more complex sources require larger number of wave records and finer computational grid used for the calculation of synthetic waveforms.

**JSS07a/09P/D-013** Poster **1700-114**

**POST-EVENT SURVEY OF THE DISASTROUS TSUNAMI OF 30 DECEMBER 2002 HITTING STROMBOLI ISLAND, ITALY**

Stefano TINTI<sup>1</sup>, Alberto ARMIGLIATO<sup>1</sup>, Laura GRAZIANI<sup>2</sup>, Alessandra MARAMAF<sup>1</sup>, Anna MANUCCI<sup>1</sup>, Gianluca PAGNONI<sup>1</sup>, Filippo ZANIBONI<sup>1</sup> (<sup>1</sup>Department of Physics-Geophysics, University of Bologna, Italy, <sup>2</sup>Istituto Nazionale di Geofisica e Vulcanologia, INGV, Rome, Italy)

Stromboli volcano is located in south Tyrrhenian sea, Italy and is known to have been affected by several tsunamis during its recent eruption history. Following a period of intense volcanic activity, on December 30, 2002 a series of landslides occurred in the NW flank of the volcano, called Sciarra del Fuoco. The two largest ones took place with a time separation of about 7 minutes according to the seismic signals, and involved tens of cubic meters of material. The total mass failure affected the subaerial as well as the submarine flank of the volcano. Both slides produced a tsunami, but the first one was by far the most violent. The post-event survey was conducted in a number of campaigns under the control of the civil protection authorities that were limiting the access to the island owing to the persistent danger of tsunamigenic collapses and explosions. The tsunami was observed in the whole south Tyrrhenian sea. It was disastrous in Stromboli and hit severely the neighbouring island of Panarea. Waves as high as 7-10 m attacked especially the northern coast of Stromboli and destroyed most of the houses on the water front. Severe damage was also caused to houses and structures on the north-eastern coast of Stromboli. The physical effects of the waves were spectacular: erosion channels, deposition of large sheets of sediments, transport of large breakwaters blocks, of boats and trailers, uprooting of trees, destruction of brick and stone walls, production of local coastal slumps, etc. The tsunami caused no fatalities and injured only a small number of people since it occurred in winter: all the houses destroyed were uninhabited, but are usually full of tourists in peak season. The occurrence of the tsunami has shown the inadequacy of the recording system of long sea waves in Italy and has posed dramatically the issue of the implementation of an early alert and warning system for tsunamis.

**JSS07a/09P/D-014** Poster **1700-115**

**MODELLING OF THE HOLOCENE MEGATSONAMI INDUCED BY THE SECTOR COLLAPSE OF STROMBOLI IN THE TYRRHENIAN SEA, ITALY**

Stefano TINTI<sup>1</sup>, Kenji SATAKE<sup>2</sup>, Gianluca PAGNONI<sup>1</sup>, Filippo ZANIBONI<sup>1</sup> (<sup>1</sup>Department of Physics-Geophysics, University of Bologna, Italy, <sup>2</sup>Active Fault Research Center, AIST, Japan)

Stromboli is one of the most active volcanoes in the Aeolian Islands arc in south Tyrrhenian sea, Italy. Flank collapses have occurred frequently in the history of the volcano. In the last 13 ka at least four such episodes have taken place, involving volumes in the order of 1 cubic kilometer. The last collapse occurred presumably less than 5 ky BP. It was responsible of the formation of the Sciarra del Fuoco (SdF), a huge scar in the NW flank of the volcano that is now almost completely refilled by the eruption products of the volcano which is characterised by persistent activity. The SdF extends underwater down to 800 m bsl and deposits associated with the collapse have been probably identified in the Stromboli channel at depths larger than 2000 m. The collapse generated likely a megatsunami that hit Stromboli with powerful waves and that radiated in the whole Tyrrhenian sea. Following previous studies that were centered on the tsunami evolution in the generation region and in the near-field, here the propagation of the waves in the Tyrrhenian sea is studied in order to identify the coastal segments of the Tyrrhenian coasts that were most affected by the tsunami. The collapse is simulated by means of a block model that subdivides the sliding volume into 2D matrix of adjacent blocks and computes their motion under a Lagrangian approach. The tsunami is modelled by means of a shallow water finite-difference technique over a grid covering the Tyrrhenian sea.

**JSS07a/09P/D-015** Poster **1700-116**

**SEISMICITY OFFSHORE IBERIA: THE 1761 IBERIAN EARTHQUAKE AND TSUNAMI**

Maria Ana BAPTISTA<sup>1</sup> (<sup>1</sup>ISEL, CGUL, <sup>2</sup>CGUL, FCUL, Portugal, <sup>3</sup>CIMA, UA, Portugal)

Earthquake catalogues for the Iberian Peninsula report several moderate to strong magnitude events. In the 18th Century three major earthquakes, of magnitude greater than 7, are reported: 27.12.1722, 1.11.1755, 31.03.1761. Their source area is controversial due to the lack of detailed and coherent descriptions. Any attempt to shed new light on the source location contributes to the evaluation of seismic and tsunami risk in Iberia. The 31 March 1761 earthquake was felt in Lisbon at noon, alarming the inhabitants and throwing down ruins of the past 1st November 1755 earthquake. According to coeval sources the earthquake was followed by a tsunami that was observed in Cornwall (United Kingdom), Cork (Ireland). The Portuguese catalogues locate this event on the Horse Shoe Abyssal Plain, south of Gorringe Bank and 7.5 magnitude, while the Caribbean tsunami catalogue (Lander et al., 2002), locates the event further north 37N 10W and the estimate of the epicentral intensity MMI is IX. In this study we present: a reappraisal of the available historical reports, concerning the 1761 event, a revision of the macroseismic intensities along Iberia and the tsunami observations along the western Portuguese and Galicia coasts, England, Ireland and West Indies. With this dataset we use backward ray tracing techniques to discuss the location of the event and its integration with one of the major tsunami generation areas in the western Portuguese margin.

**JSS07a/09P/D-016** Poster **1700-117**

**HUGE TSUNAMIS BASED ON TSUNAMI DEPOSITS ALONG THE PACIFIC COAST OF EAST HOKKAIDO, NORTHERN JAPAN**

Kazuomi HIRAKAWA<sup>1</sup>, Yugo NAKAMURA<sup>1</sup>, Yuichi NISHIMURA<sup>2</sup> (<sup>1</sup>Graduate School of Env.

It is well known that large earthquakes have occurred every several tens of years along the Kuril Trench off the coast of East Hokkaido, Japan. This study aims at first to examine huge tsunamis and their recurrence interval since last 6,500 years, based on the tsunami deposits along the Pacific coast of Tokachi to Nemuro region, secondly to show the significance of some types of landforms for such discussion and thirdly to consider the earthquakes which have generated those tsunamis. Major results are as follows: 1. We have so far identified 6 sand (gravel) layers with tsunami deposits along the Tokachi coast since last 2.5 ~3.0 ka. They are distributed not only in the alluvial lowland (at least 2.5 km inlandward from the present coast), but also on the terrace with sea cliff up to ca. 15 m in height. 2. On the basis of dated marker tephra and C-14 dates, occurrence age of the tsunami should be AD 16/17th Century, 13th C., 6~7th C., 3rd C., BC3rd rd ~4th C. in descending order respectively. Thus the recurrence interval of these tsunamis must be 400~600 years. 3. Another 9 marine sand layers are intercalated in the peat and muddy sediments filling the former lagoon. They might show the tsunami occurrence ca 3.2, 3.7, 3.9, 4.2, 4.6, 4.9, 5.0, 5.6 and 6.0 ka BP, referring to the C-14 dates. 4. Although large earthquakes (Magnitude 8.0 +), ex. 1843-, 1894-, and 1952-earthquakes had occurred with the recurrence interval less than 100 years also since the last huge tsunami of AD 16/17 C., they are not recorded as the tsunami sand layer indicated above. Sand bar landform closing lagoons from the Pacific Ocean, 5~6 m above sea level is wholly covered with a volcanic ash Ta-b erupted in AD 1667. This fact means that the tsunami higher than 5 m in wave height had not occurred since then. The landforms such as the sand bar and coastal terraces with adequate height of cliff might be significant for the evaluation of magnitude of tsunami. 5. Thus we should expect that tsunami sand layers on the sea cliff had been supplied by extraordinarily huge tsunamis which had attacked the coastal area of Pacific Ocean in Hokkaido every 400 to 600 years. 6. Source areas of such huge tsunamis off the coast of Tokachi region and Nemuro region seems to have been mostly same. The earthquake which had caused such huge tsunamis might have occurred in the intraplate relatively near the coast.

**JSS07a/09P/D-017** Poster **1700-118**

**AN FEM MODELING FOR THE TSUNAMI SOURCE AREA OF THE 1993 HOKKAIDO NANSEI-OKI EARTHQUAKE, JAPAN**

Yasuhiro AOYAGI<sup>1</sup>, Shintaro ABE<sup>1</sup>, Masafumi MATSUYAMA<sup>2</sup>, Hiroyoshi TANAKA<sup>3</sup> (<sup>1</sup>Geosphere Environmental Science Department, Central Research Institute of Electric Power Industry, <sup>2</sup>Fluid Science Department, Central Research Institute of Electric Power Industry)

We propose a modeling method of tsunami source area to evaluate tsunami run-up height on the safe side. This method should be applied to the design of important coastal structures, which combines safety and economical efficiency against tsunami. We choose the 1993 Hokkaido Nansei-oki earthquake tsunami as a case study, because large tsunami run-up heights were measured at the coasts of the Okushiri Island close to the source area and further we can acquire good geophysical datasets for model parameters. First, to decide the fault dimension, we relocated the first 1-day aftershock hypocenters determined by JMA (Japan Meteorological Agency), by referring to the hypocenters determined by an OBS-network later installed at the source area. The relocated hypocenters are concentrated onto some clusters correlating well with the en-echelon oceanic ridges with N-S strike over 100km long. We classified them to six fault segments. Secondly, we constructed a 3-D FEM crustal model including the shape of the faults and displaced those hanging wall sides upward as reverse faults in order of the source process for about 70 seconds. The amount of displacement on each fault was estimated from fault area, seismic moment and rigidity. The calculated vertical deformation of seafloor finally shows subsidence in northwest, uplift in northeast, very large uplift in southwest and subtle subsidence in southeast of the source area. As a result of following numerical simulation based on shallow water theory using the dynamic tsunami source model, the calculated tsunami run-up heights became equal or more than observed ones all around the Okushiri Island. Since we didn't revise the source model with trial and error to fit the observed tsunami run-up heights, the method can be an advantage to evaluate tsunami run-up height on the safe side. See Matsuyama's abstract to know tsunami calculation in detail.

**JSS07a/09P/D-018** Poster **1700-119**

**FIELD SURVEY AND PRELIMINARY MODELING OF THE SEPTEMBER 9, 2002 WEWAK, PNG EARTHQUAKE AND TSUNAMI**

Jose C. BORRERO<sup>1</sup>, Jose BORRERO<sup>1</sup>, James BU<sup>2</sup>, Christine SAIANG<sup>2</sup>, Burak USLU<sup>3</sup>, John FRECKMAN<sup>4</sup>, Brandon GOMER<sup>3</sup>, Hugh DAVIES<sup>2</sup>, Emile OKAL<sup>3</sup>, Costas SYNOLAKIS<sup>1</sup> (<sup>1</sup>Department of Civil Engineering, University of Southern California, <sup>2</sup>Department of Geology, University of Papua New Guinea, <sup>3</sup>(4) Department of Geological Sciences, Northwestern University, <sup>3</sup>(3) Marine Facilities Division, California State Lands Commission)

We report the results of field surveys and tsunami modeling efforts conducted in the aftermath of the Papua New Guinea earthquake and tsunami of September 9, 2002. The 2002 earthquake generated a moderate tsunami and occurred only 120 km ESE of the infamous 1998 event, which caused a catastrophic tsunami that killed over 2000 people. The 2002 earthquake had a larger seismic source and contributed more destruction (reaching MMI intensity IX and causing 5 fatalities) than the 1998 seismic event. On the other hand, its tsunami was relatively benign, with maximum runup heights of 5 m in the offshore islands, and 2.5 m on the mainland. The distribution of runup along the coast from the 2002 tsunami also features an aspect ratio representative of standard dislocation sources. The disparity between the 1998 and 2002 tsunamis is a direct consequence of the generation of the former by a massive underwater landslide, which was not the case in 2002. Detailed modeling results from the two events represented which highlight the differences in the runup signatures of the two tsunami generation sources.

**JSS07** Wednesday, July 9 - Thursday, July 10

**TSUNAMIS: THEIR SCIENCE, ENGINEERING AND HAZARD MITIGATION (IASPEI, IAVCEI, IAPSO)**

Location: Site A, Room 2

**SS07/10A/A02-001**

**0830**

**TSUNAMI DEPOSITS AND THEIR SEDIMENTARY PROCESS OF THE 1993 HOKKAIDO-NANSEI-OKI EARTHQUAKE AND 1741 OSHIMA-OSHIMA ERUPTION, SOUTHWESTERN HOKKAIDO**

Futoshi NANAYAMA<sup>1</sup>, Kenji SATAKE<sup>2</sup>, Koichi SHIMOKAWA<sup>3</sup>, Kiyoyuki SHIGENO<sup>4</sup> (<sup>1</sup>Institute for Marine Resources and Environment, Geological Survey of Japan, <sup>2</sup>Active Fault Research Center, Geological Survey of Japan, <sup>3</sup>Meiji Consultant Co. Ltd.)

We examined sedimentary facies, structure and grain size distribution of tsunami deposits from the 1993 Hokkaido-Nansei-oki earthquake and the 1741 Oshima-Oshima eruption along the western coast of Oshima Peninsula, southwestern Hokkaido. The 1993 tsunami of July 12th, 1993, left continuous onshore sand deposits along the west coast of the peninsula. Tsunami deposits along the estuary of Usubetsu River at Taisei consist of mainly medium to fine grained marine sands with gravels. The thickness decreases with landward distance from the shoreline, and finally they pinch out like a lenticular shape at the most upper limit of tsunami run-up. The deposits can be grouped into four sedimentary units. Each of these units is bounded by erosional bases, and interpreted as deposited by up flow of first run-up (Unit 1), return flow of first run-up (Unit 2), up flow of second run-up (Unit 3) and return flow of second run-up (Unit 4), respectively, by current directions. The upper unit (Unit 4) is more widely distributed and associated with coarser grains than the lower units (Units 1-3), because the second run-up was larger than the first run-up. Grain size distributions of up flow and return flow deposits are clearly different. Namely, Unit 4 deposits have a peak at 2.5 phi (Pu-1). In contrast, Unit 3 deposits have bimodal peaks at -0.5 to 1.5 phi (Pu-2) and 2.5phi (Pu-1). While the Pu-1 population is constant regardless of distance from the shoreline, the P-2 population clearly varies with the distance. The different sources account for the difference; the Pu-1 population was originated from the sea bottom and Pu-2 was provided from river bottom during the tsunami run-up process. On Oshima-Oshima, a small volcanic island southwest off Hokkaido, a violent eruption and sector collapse occurred on August 29th, 1741, and very destructive tsunami was also documented in this region. The 1741 tsunami deposits were found by Nishimura et al. (2000) along the Ayukawa Coast in Kumaishi. We tried new trench survey on a sand dune and studied sedimentary structures in detail. The deposits can be grouped into two sedimentary units, Unit I (lower unit) and Unit II (upper units). Each unit shows sedimentary features, such as grain size or thickness variation, very similar to those of the 1993 tsunami. Grain size distributions of up flow (Unit I) deposits have bimodal peaks at -1 to 0.5 phi (Pa-2) and 2.0 phi (Pa-1), while the return flow deposits (Unit II) have a peak at 2.0 phi (Pa-1). Again, the different sources account for the difference: the Pa-1 population was originated from the sea bottom and Pa-2 was provided from gravel coat during the tsunami run-up process.

**JSS07/10A/A02-002**

**0845**

**TRACES OF TSUNAMIS OF MAJOR NANKAI EARTHQUAKES IN THE BOTTOM SEDIMENTARY LAYERS OF TADASUGA-IKE AND KIRIMA-IKE LAGOONS, SUSAKI CITY, KOCHI PREFECTURE, SHIKOKU ISLAND**

Yoshinobu TSUJII<sup>1</sup>, Makoto OKAMURA<sup>2</sup>, Yumi MATSUOKA<sup>2</sup>, Yuichi NAMEGAYA<sup>1</sup> (<sup>1</sup>Earthquake Research Institute, University of Tokyo, <sup>2</sup>Kochi University)

A series of gigantic earthquakes accompanied with huge tsunamis occurred in the sea region off Nankai District, the Pacific side of Shikoku Island and the western part of Honshu Island periodically in the intervals of about one hundred years. Lagoons Tadasuga-Ike and Kirima-Ike are located on the south-east coast of Shikoku, separated from the Pacific ocean by sand dunes. Whenever a gigantic earthquake occurred in the open ocean area, sea water rushed into these lagoons by tsunami waves, and thin sand layers were formed. We gathered piston core sampling at several points for the bottom sedimentary layers of both of the lagoons, and found out more than ten thin sand layers formed by historical and pre-historical tsunamis. We made dating for several layers by the carbon 14 method. We found out three historical tsunami traces of the 684 Hakuho, the 887 Nin-na, and 1099 Kowa Nankai Earthquakes, and in addition that, we obtained more than ten pre-historical tsunami traces. The oldest trace of Tadasuga-Ike lagoon shows the year of about 20-th century BC.

**JSS07/10A/A02-003**

**0900**

**PALEOTSUNAMI DEPOSITS INVESTIGATIONS ON THE KUNASHIR ISLAND**

Alexander Ya. ILYEV<sup>1</sup>, Nadezhda G. RAZJIGAEVA<sup>2</sup>, Victor M. KAISTRENKO<sup>1</sup>, Elena V. GRETSKAYA<sup>1</sup>, Larisa A. GANZEY<sup>2</sup>, Elena A. TIKHONCHUK<sup>1</sup>, Andrey A. KHARLAMOV<sup>3</sup> (<sup>1</sup>Institute of Marine Geology and Geophysics, Russian Academy of Sciences, <sup>2</sup>Pacific Institute of Geography, Russian Academy of Sciences, <sup>3</sup>P.P. Shirshov Institute of Oceanology, Russian Academy of Sciences)

During the 2001-2002 years many tsunami traces were found on the Pacific coast of the Kunashir Island which is located in the region with very high tsunami activity. Upper tsunami traces were related to October 4, 1994 event and many others were related to old events having Holocene age. As main the tsunami traces are the layers of well sorted sand between peat and lacustrine silt-pelitic sediments and diatom oozes on the terraces near the sandy coast. Several tsunami traces are pumice layers. To evaluate the paleotsunami height the geomorphologic profiles were created for all examples of the tsunami traces. More than 150 sections (excavated trenches or outcrops) in the peat areas and paleo-lakes along the Kunashir Island coast were investigated, and the found examples were used for the following analysis (radiocarbon dating, chemical analysis of tephra, grain-size and mineralogical analysis of tsunami sands, biostatigraphy). At times inside these layers we found a wood scraps which were analysed by radiocarbon method to evaluate the layer age. Many tephra examples were used to estimate the tsunami layers age too. The time period related to the found tsunami deposits is about 6000-7000 years. The reconstructions of tsunami heights and inundation were based on the present configuration of the coastal line because in the late Holocene it was similar to the modern one. Most of the studied sections are located on the coastal plain and low marine terrace sequences. Tsunami deposits are represented by very thin sandy sheets (thickness 1-5 mm, rare up to 3 cm) found beyond storm-wave influence with penetration in land up to 2.5 km. This sand from such sheets is well sorted (So = 2-3) and distribution of the size of particles generally is two-modal whose peaks are locating in the range 0.07-0.12 mm. This testifies to a single deposition of found sandy layers. Good age correlation of such sandy layers from the sites located in different places of the coasts is one of the criteria for tsunami origin of the deposits. These events can be correlated with historical and prehistorical tsunamis of the Eastern Hokkaido and Iturup Island. One of the partial problems of the field investigation was the looking for tsunami traces on the Okhotsk sea coast related to the possible tsunami generated by explosion of the underwater volcanoes locating in the Okhotsk sea. Possibly, one sandy layer of 10 cm thick found at the height about 10 m near Tretyakovo settlement and having marine origin is related to volcanogenic tsunami because Pacific tsunamis penetrating into Okhotsk sea have no such amplitudes. The work was supported by the Russian Foundation for Basic

Research, grants01-05-79184, 01-05-79024, 02-05-65409 and Far Eastern Division of the Russian Academy of Sciences.

**JSS07/10A/A02-004**

**0915**

**ESTIMATES OF TSUNAMI RUN-UP HEIGHTS FROM TSUNAMI DATA FOR THE COAST OF PERU**

Eygueni A. KULIKOV, Alexander B. RABINOVICH (Shirshov Institute of Oceanology, Russian Academy of Sciences)

We have used data from the World Data Center-A (Boulder, Colorado) to estimate tsunami statistics and heights for the coasts of Peru and northern Chile. Two types of database search were conducted: "Tsunami Event" and "Tsunami Run-up." For each search, we selected all data for the Pacific coast from 0°S to 35°S, including Peru, northern Chile, and Ecuador. From the "Tsunami Event" search, we selected 180 events for the period 1562 to 1996. From the "Tsunami Run-up" search, we found more than 400 run-up values for different coastal sites. Instrumental recording of sea level variations began systematically only in the 20th century, so that the quality of the recently acquired historical data is markedly different. Basically, we have statistics for "small" tsunami events (wave heights less than 1-2 m) for the last 80-90 years. Despite the irregular spatial distribution of historically reported tsunami run-up for the coasts of Peru and northern Chile, the tsunami risk for the whole coast seems to be quasi-uniform in that it does not appear to depend on latitude. This can be explained by the almost uniform spatial distribution of tsunami sources (earthquake epicenters) and the relatively uniform structure of seafloor topography along the coast. Run-up heights cannot be expected to be uniformly distributed along the coast for a single tsunami source. Maximum run-up heights are normally observed near the source. Statistically, tsunami heights decrease away from the source region according to  $\sqrt{R}$ , where R is the distance from the source. However, for purposes of this analysis, the statistical distribution of tsunami run-up heights is treated as uniform from 5° to 35° latitude. The spatial distribution of tsunami heights along the coast may be significantly modified by local topography, shoreline irregularities, shelf resonance effects, and other topographic factors. Thus, to correctly estimate tsunami heights for a selected coastal site, the above effects need to be examined over a broad neighboring segment of the coast. Due to differences in data quality for the recent and historical periods, we provide separately: (1) A statistical analysis of all data from 1562 to 1996; and (2) a statistical analysis of recent data from 1906 to 1996. According to these analyses, the historical data from 1562 to 1900 are devoid of small tsunamis with run-up heights less than 1 m. In the 20th century, coinciding with the beginning of sea level surveys and instrumental recording, the number of observed small tsunamis increases dramatically, similar to the numbers of earthquakes. For this reason, the distribution for the full data set falls below the distribution for recent data for small heights (less than 2-3 m). However, for large run-up (greater than 3-4 m), both graphs merge. We find that for large tsunami run-up, the tsunami run-up height h is given by the function  $h \sim T^p$ , where T is the return period is typical of lognormal distributions (Gumbel, 1962). This approximation has been used to estimate tsunami run-up heights for the basic return periods of 5, 10, 20, 50, and 100 years.

**JSS07/10A/A02-005**

**0930**

**THE COMPARISON BETWEEN THE 1936 AND 1978 MIYAGI-OKI EARTHQUAKES**

Yuichiro TANIOKA (Hokkaido University)

On June 12, 1978, a large earthquake ( $M=7.4$ ) occurred off the Pacific coast of Miyagi prefecture, northeastern Japan. The earthquake killed 28 persons and caused extensive damage in Miyagi prefecture. The previous large earthquake occurred in this region was the 1936 Miyagi-oki earthquake which also caused extensive damage. Therefore, a next large earthquake is expected in this region in near future. It is important to estimate the slip distribution of both the 1978 and 1936 events in order to discuss a possible rupture area of the next event. We estimate the slip distribution of the 1978 Miyagi-oki event using the tsunami waveforms observed at 14 tide gauge stations along the Pacific coast of northeastern Japan. We also analyze a tsunami waveform generated by the 1936 earthquake. Previously, the rupture process of the 1978 Miyagi-oki earthquake was estimated using the seismological data (ex. Seno (1980)). Seno (1980) show that the focal mechanism of the earthquake is a thrust type and the seismic moment is  $3.1 \times 10^{20}$  Nm. The event was separated into two subevents, one ruptured the eastern (trench-ward) part and the other ruptured the western (landward) part of the aftershock area. We numerically compute the tsunami waveforms using the finite-difference computation. The grid size is basically 20 sec of arc (about 600m), but finer grids (4 sec of arc) are nested near the tide gauge stations. Tsunami waveforms at 14 stations are computed for 6 subfaults with a unit amount of slip, and use as the Green's function for the inversion. The subfault size is 30km X 30km. The result of the inversion shows that the largest slip of 1.3 m was found in the western (landward) part of the fault area. The total seismic moment is calculated as  $1.7 \times 10^{20}$  Nm ( $M_w=7.5$ ) assuming that the rigidity is  $5 \times 10^{10}$  N/m<sup>2</sup>. The slip pattern of our study is consistent with the previous study by Seno (1980). Next, an original tsunami waveform observed at Hachinohe for the 1936 Miyagi-oki earthquake was found in Hachinohe observatory of JMA. A detail bathymetry map of Hachinohe port in 1936 was also found. Using those data, we compute the tsunami waveforms at Hachinohe from the fault model estimated for the 1978 earthquake. The result shows that the computed tsunami amplitude was about three times larger than the observed amplitude but the computed waveform pattern is consistent with the observed one. This suggests that the moment magnitude ( $M_w$ ) of the 1936 earthquake is about 7.1. More data are necessary to estimate a slip distribution of the 1936 earthquake.

**JSS07/10A/A02-006**

**0945**

**THE LATER PHASE OF THE TSUNAMI OF THE NEMURO-HANTO-OKI EARTHQUAKE OF JULY 17, 1973**

Yuichi NAMEGAYA, Yoshinobu TSUJI (Earthquake Research Institute, University of Tokyo)

A large earthquake ( $M=7.4$ ) occurred in the sea region eastern off Nemuro peninsula, Hokkaido on 17 June 1973 and was accompanied with a small tsunami. Tidal stations on the Pacific coasts in east of the Japanese Islands recorded the tsunami. The tsunami height of more than 150 [cm] was recorded at Hanasaki, Nemuro city. On the tsunami records at the several stations on the Pacific coasts of Hokkaido and the north part of Honshu, an obvious later phase waves were recorded independently at 2 to 2.5 hours after the arrival of the initial wave. The later phase waves appeared in such way that after the initial wave train was once attenuated, suddenly another eminent train of the later phase waves appeared. At several stations the wave height of the later phase exceeded the initial one. In order to clarify the reason why such an eminent phase waves appear about 2 hours later than the arrival of the initial wave, we made a numerical calculation of the propagation of the tsunami. We assumed the length, width of the fault to be 100 [km] and 100 [km]. The dip angle and the amount of dislocation were assumed to be 27 [deg] and 0.96 [m]. In addition, we use the calculation grid of the spherical coordinate system with the intervals of 1 [min] both in EW and NS directions. The influence of the rotation of the earth and the fluid viscosity were

neglected. We introduced bottom friction of the amount to be 0.05 to 0.1, for giving the equivalent energy dissipation to the effect of the reflection of the waves at the coastline. The calculated time length was 6 hours with using the leap frog method, and time interval of one step was 1.5 [second]. We found out that a large reflective wave was generated on the southern coast line of Kunashiri Island and it reached the Pacific coasts of Hokkaido and North Honshu about 2.5 hours later after the arrival of the initial wave train, and it is supposed to be the later phase wave train.

**JSS07/10A/A02-007**

**1000**

**SOURCE AREA AND RUPTURE PARAMETERS OF THE 31 DEC. 1881  $M_w=7.9$  CAR NICOBAR EARTHQUAKE ESTIMATED FROM TSUNAMIS RECORDED IN THE BAY OF BENGAL**

Modesto ORTIZ<sup>1</sup>, Roger BILHAM<sup>2</sup> (<sup>1</sup>Department of Oceanography, CICESE, <sup>2</sup>CIRES and Geological Sciences, University of Colorado)

On the morning of 31 December 1881 a submarine earthquake beneath the Andaman Islands generated a tsunami with a maximum crest height of 0.8 m that was recorded by eight tide gauges surrounding the Bay of Bengal. Since the earthquake occurred 8 years before the construction of the world's first teleseismic-recording seismometer, little has been known about its rupture parameters or location. Waveform and amplitude modeling of the tsunami indicated that it was generated by a  $M_w=7.9-0.1$  rupture on the India/Andaman plate boundary resulting in 10-60 cm of uplift of the island of Car Nicobar. The rupture consisted of two segments: the northern 40-km-long segment is separated from the southern 150-km-long segment by a 100 km region corresponding to the westward projection of the West Andaman spreading center. The main rupture occurred between 8.5°N and 10°N with a total area of 150 km x 60 km dipping 20°E with a mean slip of 2.7 m. The recurrence time for 1881-type events is estimated to be 114-200 years based on inferred GPS convergence rates and inferred plate closure vectors, although slip partitioning in the region may extend this estimate by as much as 30%.

**JSS07/10A/A02-008**

**1015**

**TSUNAMI RESONANCE CURVE OF BAYS BASED ON THE OBSERVED NATURAL PERIODS**

Kuniaki ABE (Niigata Junior College, Nippon Dental University)

Sea level oscillations were observed using a portable pressure gauge at heads of 36 bays in Sanriku district, Japan and the natural periods were obtained from the most predominant periods in the spectra. The natural periods obtained vary from 7 to 60 minutes and the average was 25 minutes. On the other hand amplification factors of tsunami as the ratio of the maximum inundation level observed at the head to one observed at the mouth were calculated at each bay for large tsunamis of 1896 Sanriku, 1933 Sanriku, 1960 Chile and 1968 Tokachi-oki. The maximum inundation levels were taken from survey data after the tsunami invasions. The ones at the mouth were taken to be half of the maximum inundation levels averaged at open coast. They are 5 m (north coast), 2.0 m (south coast) for the 1896 tsunami, 2.5 m for the 1933 tsunami, 1.3 m for the 1960 tsunami and 1.5 m (north coast), 0.75 m (south coast) for the 1968 tsunami, respectively. Plotting the factors as a function of the natural period for each tsunami we obtained a tsunami resonance curve of bays. Assuming the representative period of tsunamis as 10 minutes for 1896 tsunami, 9.4 minutes for the 1933 tsunami, 49 minutes for 1960 tsunami and 22 minutes for 1968 tsunami, we summarized the result as a resonance curve of tsunami using the natural period normalized by the tsunami periods. The assumed periods were determined from the most predominant periods of the tsunamis observed at Ayukawa tide station except for the 1960 tsunami, in which it was determined as average of the most predominant periods in many tide stations. All the data fit the resonance curve having maximums at unit value of the normalized natural period. Thus, it is clarified that a bay has a role of resonator to tsunami. At the same time it is emphasized that most predominant periods in a usual sea level oscillation and tsunami are important factors to understand the amplification.

**JSS07/10A/A02-009**

**1030**

**STUDY ON THE EFFECT OF TSUNAMI REDUCING BY COASTAL CONTROL FOREST**

Kenji HARADA, Fumihiko IMAMURA (Graduate School of Engineering, Tohoku University)

The artificial coastal barrier such as seawalls and break waters have been constructed in Japan and have played an important role in protecting the city and coastal area from natural hazards such as tsunamis, tidal waves, high waves. However, these barriers need high cost of construction and maintenance, and change the present environment and have forced inconvenient in ordinal life along coastal area. Therefore, new countermeasures considering combination with artificial and natural functions such as coastal forest and strengthen such natural one are necessary for reducing natural disaster and keeping good environment. However, concrete functions of coastal forest to reduce tsunamis are not established and formulated. It is time to provide with technical information and guideline for coastal barrier by using natural and artificial functions for more appropriate management. In order to use a coastal control forest positively and effectively as countermeasures against tsunamis, evaluation of the hydrodynamic effect by a tsunami control forest and clarification of a disaster prevention function are further required. Therefore, the present paper aims to find and compile functions of tsunami disaster prevention by a control forest from old tsunami reports and other studies, and to obtain results on tsunami reduction effect estimated by the numerical simulation including the resistance of tsunami control forest. From old tsunami reports and other studies, the function of control forest for tsunami disaster prevention can be summarized as follows; 1) to stop driftwoods and other drifts moved by tsunamis, and to prevent the secondary disaster of house damage by attack of drifts. 2) to reduce tsunami energy, inundation depth, inundation area, tsunami current and hydraulic force at behind of a forest by reflection and resistance of trees. 3) to provide a life-saving means by catching persons carried by tsunamis. 4) to form dunes which act as barrier against tsunamis, and to reduce inflow of tsunamis toward inland. In order to evaluate these reduction effects quantitatively, the tsunami numerical simulation with the resistance of forest were carried out. The forest conditions selected from general coastal forests are 10,30,50 trees per 100 square meters in forest density and 50,100,200,400m in forest width. The drag coefficient of the coastal forest is estimated by the hydraulic experiment with the model of branches and leaves by changes of inundation depth. The inertia coefficient is determined to be 1.7. From the calculated results, the spatial distribution of the maximum inundation depth, current and hydraulic forces can be shown and compared. It is found that increasing of forest width at behind of coastal forest can reduce not only inundation depth but also current and hydraulic force. A strong current in coastal forest can be possible to scour roots. And effects of tsunami reducing become more effective by increasing of forest density. By use these results, effects of reducing tsunamis can be evaluated quantitatively related to the tsunami and forest conditions.

JSS07/10A/A02-010

1100

## NUMERICAL SIMULATIONS OF THE 2002 STROMBOLI ISLAND TSUNAMI, ITALY

Stefano TINTI, Alberto ARMIGLIATO, Gianluca PAGNONI, Filippo ZANIBONI (Department of Physics-Geophysics, University of Bologna, Italy)

Stromboli is a volcanic island in southern Tyrrhenian sea, Italy, that is known to have unstable flanks. The Sciarola del Fuoco (SdF) on its NW flank is a deep scar produced by a huge sector collapse in the order of 1 Km cubic meters that very likely originated a large tsunami in Holocene time. Since that collapse, the SdF was progressively refilled by eruption products, and is nowadays a steep sector mostly formed by poorly consolidated heterogeneous rocks. On 30 December 2002 two large slides with a total volume of tens of millions cubic meters detached from the SdF slope. Probably both slides generated a tsunami, but the first was much larger. It caused severe destruction in Stromboli, produced some damage in the archipelago, and was seen in several coastal places in the south-Tyrrhenian sea. Here the numerical simulations of the event are shown. The mass failure is simulated by means of a block model, implying that the mass is subdivided into a number of interacting blocks sliding down the volcanic flank. In the simulation the block gain soon very high velocities, owing to the large steepness of the slope. The tsunami is simulated through a finite-element model in the near-field over a domain covering Stromboli and Panarea. The results of the simulations are in satisfactory agreement with the observations collected after the event. Within a few minutes time, the entire coast of Stromboli is attacked by the tsunami, and it takes only 5 minutes to the tsunami to attack the neighbour island of Panarea. The wave train travels around the island radiating from the source. The computed wave height decreases in moving away from the source (SdF), but in many places of the northern coasts it exceeds 7-9 m in agreement with the data.

JSS07/10A/A02-011

1115

## DEVELOPMENT OF A TSUNAMI CATALOGUE FOR THE PACIFIC COAST OF CANADA

Fred E. STEPHENSON<sup>1</sup>, Olga N. SOLOVIEVA<sup>2</sup>, Sydney O. WIGEN<sup>1</sup>, Boris W. LEVIN<sup>2</sup>, Alexander B. RABINOVICH<sup>1</sup>, Evgenii A. KULIKOV<sup>1</sup>, Olga I. YAKOVENKO<sup>2</sup> (Institute of Ocean Sciences, <sup>1</sup>Tsunami Laboratory, P.P. Shirshov Institute of Oceanology, 36 Nakhimovsky Prosp., Moscow, 117851, RUSSIA)

The Canadian coast is the only segment on the west coast of North America for which no comprehensive tsunami catalogue exists. The "Catalogue of Tsunamis on the Eastern Shore of the Pacific Ocean" (Soloviev and Go, 1975) lists 61 tsunamis that have affected the region of "The United States, Canada, and Southeast Alaska", with cited Canadian observations or measurements for only 5 of these events. The "Historical Tsunami Database for the Pacific Region" (Gusiakov, 2001) contains 9 tsunamis (events or runups) observed on the Pacific coast of Canada, including the recent Queen Charlotte tsunami of October 12, 2001. These catalogues do not include any Canadian information on many other tsunami events, in particular the Alaska tsunami of March 28, 1964 (several million dollars damage in Port Alberni, British Columbia) and the Chile tsunami of May 22, 1960, both of which were well documented in Canada. Sydney Wigen inspected the analogue records of tide stations on the west coast of Canada looking for possible wave action associated with 1451 events occurring over a 75 year period (1906-1980) and collected other data on tsunami manifestation for the Canadian coast. But he summarized and published the results of his work only for one station - Tofino, a long-term station on the west coast of Vancouver Island with 43 recorded tsunamis of 6 cm or more (Wigen, 1983). The results of the searches carried out by Wigen at the other tide stations existed only in the form of hand-written tabulations. Several measurable tsunamis have been recorded on the Canadian coast in the last twenty years, but no attempt has been made until now to continue to the work of Wigen and to incorporate this information with the earlier work to produce a comprehensive catalogue of tsunami observations and measurements. The development of a tsunami catalogue was undertaken as a joint project between the Institute of Ocean Sciences and the Tsunami Laboratory of the P.P. Shirshov Institute of Oceanology. The preparation of this catalogue provides an opportunity to review and update the Canadian information included in the "Tsunami Database" and to capture through scanning or other means data sets not previously available to tsunami researchers. The prepared list of tsunamis includes 57 events from 1891 to 2001 observed on the Pacific coast of Canada.

JSS07/10A/A02-012

1130

## TSUNAMIS AND METEOROLOGICAL TSUNAMIS NEAR THE KURIL ISLANDS: INFLUENCE OF SOURCE AND TOPOGRAPHY

Alexander B. RABINOVICH (P.P. Shirshov Institute of Oceanology, Moscow, Russia)

The Kuril Islands are a region of high seismic and atmospheric activity. The Pacific coast of these islands is highly exposed to the threat of tsunami waves that arrive from the open ocean and amplified due to resonance on the shelf and/or in the local bays, inlets and harbors. Pronounced long-wave oscillations in the region are also generated by atmospheric disturbances, in particular by typhoons and atmospheric fronts. These "meteorological tsunamis" significantly affect coastal areas and may be of high danger for coastal population. Despite the different origin of tsunamis and meteotsunamis, both are modified and amplified by topography in a similar way, so it is often difficult to distinguish between these two phenomena without knowing the exact source characteristics. Recognition and separation of these phenomena are important for the revision/improvement of existing tsunami catalogues but also to better understand the generation mechanisms for destructive waves and to mitigate their catastrophic effects. To investigate this problem and to compare seismic and meteorological tsunamis, we used historical tsunami records from coastal tide gauges collected for the coast of the South Kuril Islands, in particular those associated with tsunamis in 1960, 1963, 1975, 1991, and 1994. We also used long-term series of 1-min data from a number of bottom pressure stations deployed in 1990-1992 in various bays and inlets of Shikotan Island and three precise microbarographs working simultaneously on the coast. Our analysis was based on the assumption that both tsunamis and meteotsunamis are formed by the combined effects of external forcing and topography. So, for different events recorded at the same site, similarities are because of the topography while differences arise from the forcing. In contrast, for the same event recorded at different stations, similarities are mainly associated with the forcing while differences are related to local topographic features. Analysis of the spectral distributions and comparison with background noise enabled us to reconstruct the topographic transfer functions for all sites on the Kuril Islands and to estimate the sources. The estimated source functions for long waves associated with seismic events were found to have typical periods of approximately 8 to 40 min, while those generated by a storm had shorter periods and energy pumping from high-frequencies due to non-linear interaction of wind waves and swell.

JSS07/10A/A02-013

1145

## POST-DISASTER TECHNICAL CLEARINGHOUSES: AN OPERATIONAL MODEL FOR TSUNAMIS AND EARTHQUAKES IN HAWAII

Laura S. L. KONG<sup>1</sup>, Brian YANAGI<sup>2</sup>, Stan GOOSBY<sup>3</sup>, Ray ISAWA<sup>4</sup> (<sup>1</sup>International Tsunami Information Center, and Hawaii State Tsunami Advisor, <sup>2</sup>Hawaii State Civil Defense, <sup>3</sup>Pacific Disaster Center)

A disaster, whether a damaging tsunami or earthquake, can attract a large number of local, national, and international professionals interested in investigating its scientific, economic, and social impact on affected communities. At the same time, scientists, structural engineers, and social scientists are wanting to document the phenomenological data and obtain eyewitness observations from those directly affected, emergency responders and government officials must focus their highest priorities on public safety, field damage reconnaissance, and integrity evaluation of critical support lifelines and infrastructure. Without a data management system that is integrated into government emergency operations, perishable data collection may be logistically difficult to acquire before erosion or bulldozers eliminate the evidence, and in all likelihood, could interfere with emergency responder activities. The establishment of an electronic Post-Disaster Technical Clearinghouse (PDTCC) can provide a modern framework for the coordination of activities, and integration of scientific and engineering investigations with emergency operations. The Hawaii Post-Disaster Technical Clearinghouse is an initiative of the Hawaii State Civil Defense Tsunami Technical Review Committee (TTRC) and Hawaii State Earthquake Advisory Committee, and the Pacific Disaster Center, to develop a web-based, electronic technical clearinghouse for archiving and displaying information in a Geographical Information System (GIS) database. The PDTCC is envisioned as a multi-hazard system for disaster intelligence gathering to collect, report and store information following a disaster. The PDTCC web site, activated immediately following a damaging earthquake or tsunami, will provide users with a central shared repository for efficiently accessing, managing, and viewing all data, surveys, and reports, and provide a single resource point for widespread information exchange among researchers, emergency managers, and practitioners, and for sharing with the media and public. Trusted users may post and access data or damage reports, or may utilize the web-based GIS tools to select map layers to plot for use in emergency operations or as reports to the media or other interested parties. The PDTCC implementation strategy highlights a four-phase approach in which user requirements are identified, system design architecture developed, system implementation and maintenance resources and costs identified, and finally a prototype PDTCC created for user evaluation. Data to be archived at the PDTCC includes the following: seismological information, including seismicity, shaking intensity, and earthquake source characteristics; tsunami information, including maregrams, runup and inundation, tsunami damage, and eyewitness accounts; geotechnical information, including ground deformation and failure; structural and non-structural impacts to building, structures, lifelines, and critical facilities; and social and economic impacts. In Hawaii, the tsunami PDTCC coordinators will be the State and County Tsunami Advisors. The International Tsunami Information Center can provide coordination assistance for national and international tsunami scientists seeking participation. In order to collect perishable tsunami data, TTRC scientists have written the Hawaii Post-Tsunami Scientific Survey Plan, which upon activation will deploy trained local volunteers to record tsunami arrivals and impacts on significant coastlines; the tsunami observers will be pre-cleared to allow them access into restricted, but safe areas.

JSS07/10A/A02-014

1200

## THE PUERTO RICO TSUNAMI WARNING AND MITIGATION PROGRAM AND RELATED TSUNAMI RESEARCH IN THE CARIBBEAN

Aurelio MERCADO<sup>1</sup>, Ms. Christa VON HILLEBRANDT<sup>2</sup>, Victor HUERFANO<sup>3</sup>, Harry JUSTINIANO<sup>4</sup> (<sup>1</sup>Department of Marine Sciences, University of Puerto Rico, <sup>2</sup>Puerto Rico Seismic Network, University of Puerto Rico)

The Caribbean Sea region is well known for the hurricane hazard. But recent history has shown that in its northeast region, where the islands of Hispaniola, Puerto Rico, and the US Virgin Islands are located, the tsunami threat is another natural hazard that must be considered. Since 1867 three big, destructive, and local tsunamis have occurred in this region: the 1867 Virgin Islands tsunami, the 1918 Puerto Rico tsunami, and the 1946 Dominican Republic tsunami. Because of this "forgotten hazard", local and federal agencies have funded a series of applied research studies, and public outreach programs, with the purpose of quantifying the threat, and of public education. In addition, it is in NOAA's plans to have a local tsunami warning system in Puerto Rico involving both the San Juan National Weather Office and the Puerto Rico Seismic Network. Here we will present the work involved in the several tasks of the Puerto Rico Tsunami Warning and Mitigation Program, including coastal flood mapping and development of algorithms for local and regional near real time characterization of seismic fault characteristics.

JSS07/10A/A02-015

1215

## REDUCING TSUNAMI CASUALTIES: MITIGATION LESSONS FROM RECENT TSUNAMIS

Lori A. DENGLER (Humboldt State University)

Since 1990, 56 tsunamis have been observed or recorded, 22 of which were damaging. 13 events caused deaths contributing to at least 4000 tsunami fatalities in this time period. Only 3 of these events were recorded in the far field and produced no damage or casualties outside of the source region. At present, the primary focus of international tsunami mitigation efforts is the Tsunami Warning System in the Pacific. This system is designed to issue warnings for distant-source events and warnings played no direct role in reducing the impact of the tsunamis of the past 12 years. While recognizing that distant-source tsunamis pose a credible threat and the Warning System must be maintained and improved, significant reduction of tsunami casualties will only come by addressing the near-field vulnerability. During the past 12 years, International Tsunami Survey Teams (ITST) have studied 15 tsunami events. While the primary focus of these teams has been inundation, they have also gathered information on the human response to tsunamis and identifying factors that exacerbate or reduce impact. This paper summarizes the mitigation lessons from ITST reconnaissance studies. - The major cause of life loss is exposed populations coupled with a lack of awareness of the tsunami hazard. - Tsunami awareness can significantly reduce casualties. However, past experience in some cases can lead to increased vulnerability - The media can play a major role in education and awareness. - Lack of 24 hour emergency communications significantly slows response and increases morbidity. - ITST can play an important role in encouraging local tsunami mitigation efforts. The scientific tsunami community needs to bolster tsunami awareness by - Identifying and working with curriculum providers such as Non-Governmental Organizations - Supporting 24 hour emergency contact points in developing countries - Developing inexpensive, easily reproducible tsunami information materials available on-line in many languages - Improving and maintaining media contacts to provide consistent information when tsunami events occur.

Thursday, July 10 PM

Presiding Chairs: V. Gusiakov, A. Yalciner, A. Rabinovich, F. Imamura

**JSS07/10P/A02-001****1400****CHANGES TO PACIFIC TSUNAMI WARNING CENTER PROCEDURES AND CRITERIA**

Charles S. MCCREERY (Pacific Tsunami Warning Center)

The Richard H. Hagemeyer Pacific Tsunami Warning Center (PTWC) in Ewa Beach, Hawaii, is the operational center for the Tsunami Warning System in the Pacific, alerting most countries in the Pacific Basin to the threat of destructive tsunamis. It will soon implement new procedures and criteria for issuing its tsunami warnings. Magnitude criteria will be based on moment magnitude,  $M_w$ , rather than the Richter surface-wave magnitude,  $M_s$ . While correlations of tsunami magnitude with  $M_w$  are not necessarily better than with  $M_s$ ,  $M_w$  more accurately measures the very largest earthquakes that have the most potential to generate widespread destructive tsunamis.  $M_w$ , in combination with  $M_s$  or other more high-frequency measures of earthquake size, should also provide a better measure of the tsunami potential of anomalous "slow" or "tsunami" earthquakes, or events such as the April 1, 1946 Aleutians earthquake, with an  $M_w$  greater than 8 but an  $M_s$  of only around 7, that produced one of the most destructive tsunamis of the last century. Lastly,  $M_w$  can be estimated from broadband P-wave energy using Mwp, providing a quicker magnitude than  $M_s$  that requires much later surface wave arrivals. Consequently, PTWC should be able to disseminate initial warnings based on  $M_w$  in about 20 minutes on average in comparison to the current 30-40 minutes. PTWC will simultaneously raise its magnitude threshold for an expanding regional tsunami warning and watch from  $M_s$  greater than 7.5 to  $M_w$  greater than 7.8. A non-expanding regional warning will be issued for  $M_w$  greater than 7.5 but less than or equal to 7.8. These changes should help reduce the number of unnecessary warnings while still affording sufficient protection for all major destructive tsunamis.

**JSS07/10P/A02-002****1415****U.S. NTHMP EFFORTS TO DEVELOP FAR-FIELD TSUNAMI FORECAST GUIDANCE TOOLS**

Frank I. GONZALEZ<sup>1</sup>, Paul M. WHITMORE<sup>2</sup>, Charles S. MCCREERY<sup>3</sup>, David C. BURWELL<sup>1</sup>, Vasily V. TITOV<sup>4</sup>, Kwok Fai CHEUNG<sup>5</sup>, Harold O. MOFJELD<sup>1</sup>, Stanley GOOSBY<sup>3</sup> (<sup>1</sup>NOAA/Pacific Marine Environmental Laboratory, <sup>2</sup>NOAA/West Coast and Alaska Tsunami Warning Center, <sup>3</sup>NOAA/Pacific Tsunami Warning Center, <sup>4</sup>University of Hawaii at Manoa, Department of Ocean Resources and Engineering, <sup>5</sup>Pacific Disaster Center, Applications Development Division)

The U.S. National Tsunami Hazard Mitigation Program (NTHMP) is led by the National Oceanic and Atmospheric Agency (NOAA), in partnership with the U.S. Geological Survey (USGS), the Federal Emergency Management Agency (FEMA) and State agencies of Alaska, California, Hawaii, Oregon and Washington. A primary goal of the NTHMP is improvement in the speed, reliability and utility of tsunami warnings. NOAA's Pacific Marine Environmental Laboratory (PMEL) conducts R&D in support of this goal, in collaboration with NOAA's Tsunami Warning Centers (TWCs), emergency managers in the five partner states, academic researchers, and national and international institutions focused on disaster mitigation and management. Tools to provide operational forecasts of shoreline tsunami height and inland inundation are currently under development, as are methodologies for interpreting this information into the impact of the tsunami on humans and structures. The overall strategy is to combine tsunami model simulations with real-time seismic data and tsunami observations acquired by NOAA's coastal tide gages and DART (Deep-ocean Assessment and Reporting of Tsunamis) network through data assimilation and inversion methodologies. Predicted tsunami wave height and currents can then be used as input to methodologies to estimate the impact. We will discuss the issues and challenges in meeting TWC operational requirements -- speed, accuracy, and user interfaces that provide guidance that is easy to interpret -- and the current status and plans of this effort.

**JSS07/10P/A02-003****1430****TSUNAMI AMPLITUDE PREDICTION DURING EVENTS: A TEST BASED ON PREVIOUS TSUNAMIS**

Paul Michael WHITMORE (NOAA/NWS/West Coast-Alaska Tsunami Warning Center)

The U.S. West Coast/Alaska Tsunami Warning Center's far-field tsunami amplitude prediction method is tested by applying the technique to nine previous, well-recorded tsunamigenic events. The technique bases far-field amplitude predictions on pre-computed tsunami models and observed tsunami amplitudes (Whitmore and Sokolowski, 1996). Maximum modeled tsunami amplitudes are saved at 99 different locations along the Pacific coast of North America, Hawaii, and at the NOAA DART tsunami buoys for each of 204 hypothetical earthquakes. The earthquake locations range throughout the main ocean-wide tsunami generating zones of the Pacific basin; that is, Japan, Kuril Is., Kamchatka, Aleutian Is., Alaska, Cascadia, and Chile. Earthquakes of several different magnitudes are modeled at each location. Earthquake hypocentral parameters are based on previous earthquakes in the region and tectonic considerations. Vertical sea floor deformation is computed from the hypocentral parameters using static dislocation formulae (Okada, 1985). This deformation is the initial condition to a non-linear, shallow-water tsunami model. The equations of motion and continuity are solved using a finite difference technique (Kowalik and Whitmore, 1991) employing nested grids to accommodate areas which require higher spatial resolution. During an event, the most appropriate model, based on earthquake location and moment magnitude, is chosen from the 204 previously computed models. The pre-computed amplitudes outside the source zone are scaled based on the observed tsunami amplitude at nearby tide gages or DART buoys versus modeled tsunami amplitude. As the tsunami propagates further, the scaling factor is averaged with each new recording. Using this technique, predicted tsunami amplitudes outside the source area are shown to be sufficiently accurate to guide warning cancellation/restriction/expansion decisions. The technique is tested on the 1946, 1952, 1957, 1960, 1964, 1965, 1986, 1994, and 2001 tsunamis. Average error per event ranged from 0.04m to 0.29m with error defined as the absolute value of the difference between the recorded amplitude and the predicted amplitude. Had this technique been available during the 1986 Aleutian Is. and the 1994 Kuril Is. tsunami warnings, the warned areas likely would not have been expanded to include the U.S. West Coast, Canada, and Alaska east of Kodiak Island.

**JSS07/10P/A02-004****1445****ASSESSING TSUNAMI MAGNITUDE FOR INUNDATION FORECAST**

VASILY V. TITOV<sup>1</sup>, Frank I. GONZALEZ<sup>2</sup>, Mikhail LAVRENTIEV<sup>2</sup>, Anatolii BEJAEV<sup>3</sup>, Andrey MARCHUK<sup>4</sup>, Alexander AVDEEV<sup>4</sup> (<sup>1</sup>NOAA/PMEL, <sup>2</sup>Institute of Mathematics, Novosibirsk, Russia, <sup>3</sup>Institute of Computational Mathematics and Mathematical Geophysics, Novosibirsk, Russia)

Forecast of tsunami inundation is one of the main goals of applied tsunami research. As part of the U.S. National Tsunami Hazard Mitigation Program (NTHMP), an effort is underway to

develop practical tsunami modeling tools for real-time inundation forecast guidance. Quality of the model-based tsunami inundation estimates directly depends on the accuracy of the tsunami source evaluation. Tsunami sources are rarely available for direct observation. Instead, the source mechanism is usually inferred from various indirect measurements, mostly seismic and water-level data. Studies have shown that good inundation predictions are possible when comprehensive set of data is used for tsunami source estimates. However, very few of the measurements are routinely available in real-time (i.e. before a tsunami hit the forecasted shoreline): preliminary epicenter and magnitude of the earthquake are inferred from the seismic data (for earthquake-induced tsunamis); some of the water-level data from real-time reporting gages become available during tsunami propagation. Many modeling studies have demonstrated that the seismic data alone are often insufficient for estimating magnitude of tsunamis. Models provide adequate inundation estimates only when constrained by direct tsunami measurement (water-level data, runup measurement). The water level data can be inverted to determine source of the wave. At the same time, traditional tsunami inversion techniques may not be effective in real-time, when very limited data are available. The present study evaluates feasibility of determining tsunami magnitude (as oppose to earthquake magnitude) from real-time measurements and its use for practical inundation forecast. In particular, the potential of the Deep-ocean Assessment and Reporting of Tsunamis (DART) system is evaluated for real-time tsunami source evaluation. Tsunami scenarios are examined using available deep-ocean and coastal water-level data of historical events.

**JSS07/10P/A02-005****1500****THE CHILEAN TSUNAMI WARNING SYSTEM AND APPLICATION OF THE TIME PROJECT TO THE CHILEAN COAST**

Dante Gutierrez BESA (SERVICIO HIDROGRAFICO Y OCEANOGRAFICO DE LA ARMADA DE CHILE)

The Chilean coast is frequently exposed to the effects of near and far field tsunamis generated in the Pacific Ocean. For instance, the catastrophic events of 1868 and 1877 overwhelmed the coast of the northern region of the country. During this century, the most important disaster was the 1960 earthquake and tsunami of Valdivia. It is well known that this event had a great impact on the coasts of most of the coastal states in the Pacific Ocean, mostly in Hawaii and Japan. The most recent event (Camana, Peru) recorded in the Chilean coast was the tsunami occurred at June 23, 2001. This historic situation has contributed to an awareness of the tsunami threat and therefore to the development of the research on several aspects of this phenomenon in Chile. In the last few years, new developments in technology have made it possible to improve the quality of the information to assess the potential risk of a tsunami event off Chilean coast. Starting from the year 2003, shoas will have operating a bouy system DART (Deep-ocean Assessment and Reporting of Tsunami), that will be installed in the north coast of Chile, in the proximities of Arica. The DART Project was conceived as part of the National Tsunami Hazard Mitigation Program of the United States (NTHMP), a continuous effort to develop and to implement the capacity of early detection and report in real time of tsunamis in the deep ocean. As a very important complement to the operative work, inundation maps by tsunamis for the Chilean coast, following the techniques of the TIME project have been developed. The first maps for the four largest port cities in the northern part of Chile, namely Arica, Iquique, Antofagasta and Mejillones have been completed during 1997 and 1998. Arica and Iquique are located in a "seismic gap" zone. These inundation maps are being used for tsunami hazard planning by the national civil protection agency (ONEMI) and other government institutions. During the last years have been elaborated 20 maps for the rest of the ports and bays of the central area and south of the country. This paper provides information on the Chilean Tsunami Warning System and also reproduces the log of all actions taken in relation to the last event of Peru, June 23, 2001, considering both, internal and external information. On the light of the flow of information gathered, the System was ready to generate a warning message on a "real tsunami". Fortunately, at the very last moment this message was not sent to the national authorities in charge of the evacuation plan, as new information collected, recommended not to do so. On the contrary, a message of "no tsunami threat" was issued, providing relief to the mentioned authorities.

**JSS07/10P/A02-006****1515****TSUNAMI OBSERVATION FROM SATELITE BY DATA TOPEX\_POSEIDON MISSION**

Vladimir V. IVANOV (Institute of Marine Geology and Geophysics Far Eastern Branch of Russian Academy of Science)

1. The Topex-Poseidon mission provides the information, which can be used for tsunami wave observation. It is possible to observe the wave with delay several hours (from the main shock of the Earthquake) on the distance several hundreds of kilometers (from the epicenter). In the case of tsunami July 12, 1993 at Japan Sea we have the records with delay 2 hours 40 minutes on the distance 400 kilometers. The data are recorded reliable on the depth more 200 m. 2. In the case of tsunami July 12, 1993 the records has the next parameters. The amplitude of wave was 1 - 3 cm, the characteristic distance was 100 - 200 km. Its corresponded to the low frequency component of the wave recorded by the tidal stations. 3. The high frequency component of the wave, which was observed on the tidal stations as a sequence of the intensive peaks, was observed on the satellite data as a small variations which contained several digital points with amplitude less than cm. 4. It is necessary to refine satellite data by using the special software for separating the tsunami wave. This separation is possible due to the next peculiarities of the background signal. The first peculiarity is that the main part of observed variations were not changed from one cycle to another. The second peculiarity is that the main part of the variable part of signal caused by the variations of the satellite orbit from cycle to cycle. After refining the level variations can be observed with random noise with amplitude less than cm.

**JSS07/10P/A02-007****1530****OPTIMAL PLACING OF THE TWS SEA LEVEL STATIONS FROM POINT OF VIEW OF TIMELY TSUNAMI WARNING**

Alexander A. POPLAVSKY (Institute of Marine Geology and Geophysics, Russian Academy of Sciences)

The real water basins have very complicated, contrasting bottom relief. This circumstance allows us to find near the coasts a few points possessed the next property. Tsunami wave from arbitrary source will arrive in these points earlier than the rest coastal spots in the most of cases. So, these points are the best points for placing of the TWS sea level stations near the coast, because they have the minimal tsunami expected time. These points are the end-points of the main-high speed tracks for tsunami propagation. The open sea level stations placing near such tracks will detect the tsunami earlier than near-coastal stations. Known extreme properties of the differences of the tsunami expected times in two points allow us to find the optimal placing of the TWS sea level stations. We have found such placing for regions: to the East from Kamchatka and Kurile Islands and Japan Sea.

JSS07/10P/A02-008

1600

**LOCAL TSUNAMI WARNING PROBLEM AND HYDRO-ACOUSTICAL SIGNAL DETECTION FOR EARLY LOCATION OF THE SEISMIC SOURCE PREPARATION**

Boris W. LEVIN, Elena V. SASSOROVA, Victor E. MOROZOV (Tsunami laboratory, Shirshov Institute of Oceanology of RAS)

The problem of local tsunami warning remains up to now unsolved problem. The local tsunamis are generated within waterside no far than 100 km from coastal line and their propagation time from a source to coast is less than 1 hour. It makes these tsunamis extremely dangerous. The locations of tsunamigenic earthquake epicenters (earthquakes with magnitudes  $M_S > 6.0$ ) near the Kamchatka Peninsula over a period of 50 years (from 1950 to 2000) was analyzed. All earthquake epicenters are located in the near-shore zone. Mean distance between EQ source and coastal line for all selected events is less than 18 km. It makes impossible to prepare the warning message both theoretically and practically for near-shore seismic events. We have the same situation for the Pacific coast of the Kuril Islands. A possible way to solve this problem is to pick up the acoustic signals preceding underwater near-shore earthquakes, which appear in the critical state of the earthquake preparation. It is well known that the natural seismic noise pulses in the form of the acoustic signals with the frequency 0.01-1 kHz may forego large earthquake occurrence. In case of an oceanic earthquake, an acoustic and seismic emission radiation from the crust quake source must generate an acoustic signal in a water layer where this signal may propagate far because of a weak attenuation of the signal in the incompressible water. Now we have received the possibility to analyze the observation data from the long-term records of high-quality hydro-acoustic receiving array. A joint analysis of the local Kamchatka earthquake catalogue data and hydro-acoustic measurements was carried out. Two types of signals were detected from the zones of a bottom earthquake preparation: the micro-earthquakes (MEQ) whose focuses were located in the same area as the seismic focus of main earthquake and the seismic noise, which appears just before the main shock. The duration of MEQs was about 3-4 seconds, frequency - 40-75 Hz. If the time interval between the hydro-acoustic record and earthquake exceeded 4 hours no micro-earthquakes were observed. We conclude that the hydro-acoustic monitoring of the ocean noise opens the possibility to receive new information about the peculiarities of the earthquake preparation process and may be used for local tsunami warning system development.

JSS07/10P/A02-009

1615

**CAN MICRO-TSUNAMI ANALYSIS BE USED A NEW ADDITIONAL TOOL FOR EARTHQUAKE LOCATION AND SOURCE PARAMETER STUDY?**Kenji HIRATA<sup>1</sup>, Eric L. GEIST<sup>2</sup>, Kenji SATAKE<sup>3</sup>, Yuichiro TANIOKA<sup>4</sup>, Hiroaki TAKAHASHI<sup>5</sup> (Japan Marine Science and Technology Center, <sup>2</sup>U.S.Geological Survey, <sup>3</sup>Active Fault Research Center, National Institute of Advanced Industrial Science and Technology, <sup>4</sup>Institute of Seismology and Volcanology, Hokkaido University)

The sensitivity of micro-tsunami waveforms on hypocenter location, fault size, and amount of slip as well as the high accuracy of ocean-bottom pressure gauges to detect micro-tsunamis makes it possible to locate hypocenter and source parameters for moderate-sized subduction earthquakes. We demonstrate this through analysis of micro-tsunami data from the January 28, 2000 earthquake (Mw 6.8) off Nemuro Peninsula, Hokkaido, Japan. The data was recorded on a cabled seafloor observatory south of Hokkaido that was deployed by JAMSTEC (Japan Marine Science and Technology Center) in 1999. Regional seismic networks provide the best estimates of hypocenter location of small to moderate earthquakes. Regional networks are, however, usually distributed on land and have a narrow station coverage for subduction zone earthquakes, resulting in a systematic location errors. Ocean-bottom seismographic (OBS) studies have suggested that the epicenters located by land-based regional seismic data alone tend to shift hypocenters a few tens of kilometers toward the trench. The focal-depth determination for subduction zone earthquakes is also less accurate if only land-based seismic network data are used. The cause of this systematic deviation is (1) narrow source-to-station coverage and (2) insufficient knowledge on the crustal and uppermost mantle structures in subduction zones. Tsunami generation depends upon earthquake source parameters such as source depth, fault size, and amount of slip along the fault. In other words, earthquake source information is retained by the tsunami waveform. Furthermore, tsunami propagation is controlled by bathymetry only and the first arrival times of tsunamis are closely related to their epicenter location. Therefore, analysis of small tsunamis from moderate-sized subduction zone earthquakes may constrain the hypocenter, as well as other source parameters. Standard tide gauges on the coast, however, cannot usually record small tsunamis because of ambient noise from wind waves and harbor resonance. Ocean-bottom pressure measurements, which are free from the complicated non-linear effects of the nearshore bathymetry on the tsunami wavefield, provide precise tsunami data with a high signal-to-noise ratio. To locate the earthquake hypocenter and to investigate source parameters from the micro-tsunami of the January 28, 2000 earthquake, we compare observed and theoretical micro-tsunami waveforms calculated assuming rectangular faults. The best-fit solution is obtained at (N43.0593°, E146.6407°, h=45 km), as the center of the fault, using a least-squares, grid-searching algorithm. This location is approximately 20 km to the WNW (toward the Kuril Islands) from a previous estimate of the fault center defined by regional seismic networks. The best-fit fault length and width are estimated to be 15 km and 30 km, respectively. The average amount of slip on the fault is estimated to be 0.80 m. The seismic moment is estimated at  $2.42 \times 10^{19}$  Nm. This estimate is only 20% larger than  $1.98 \times 10^{19}$  Nm obtained from the Harvard CMT inversion, and therefore micro-tsunami analysis can give a good estimation for scalar seismic moment. As demonstrated by these results, micro-tsunami waveform analysis provides improved accuracy of source parameters for studying small tsunamigenic earthquakes occurring along subduction zones.

JSS07/10P/A02-010

1630

**DETECTING AND STUDYING TSUNAMI FROM IONOSPHERIC MONITORING**Juliette ARTRU<sup>1</sup>, Vesna DUCIC<sup>2</sup>, Victor TSAI<sup>3</sup>, Hiroo KANAMORI<sup>1</sup>, Philippe LOGNONNE<sup>2</sup>, Makoto MURAKAMI<sup>3</sup> (<sup>1</sup>California Institute of Technology, <sup>2</sup>Institut de Physique du Globe de Paris, <sup>3</sup>Geographical Survey Institute)

GPS ionospheric monitoring performed with high-resolution data from dense networks allowed detection of ionospheric signals induced by tsunamian seismic waves, through dynamic coupling between the Earth and the atmosphere. In both cases, what we observe is the ionosphere response to an atmospheric acoustic-gravity wave induced by the vertical displacement of the surface. Observation of tsunami waves using this technique presents a very good signal-to-noise ratio, as signal from ocean surface waves is filtered out through the atmosphere. This type of measurements could open a new era for tsunami studies, as it can be performed above the open ocean, and possibly in real-time. We will present here a study of the signal observed on GEONET data for a tsunami wave triggered by a Mw 7.6 earthquake in the Volcano Island region in March 2000, with an emphasis of the possible interpretation in terms of wave height at the surface. Both propagation properties of atmospheric waves and geometry of measurement have to be taken into account. We use

for that purpose TriNet seismic network data and from SCIGN network GPS ionospheric monitoring to compare the wavefield at the surface to the corresponding ionospheric perturbation. We present results from a study of (1) Rayleigh-acoustic waves after the Mw 8.2 Alaska earthquake in Nov 2002, (2) Atmospheric solitary gravity waves detected at the ground level on TriNet seismic records and barographs. In a second part we will address how GPS measurements could be used to perform systematic studies of tsunamis, in terms of sampling, spatial resolution and sensitivity.

JSS07/10P/A02-011

1645

**FORECASTS OF TSUNAMIS FROM THE ALASKA-ALEUTIAN AND JAPAN-KURIL-KAMCHATKA SOURCE REGIONS**

Kwok Fai CHEUNG, Yong WEI, Yoshiki YAMAZAKI (Dept. of Ocean and Resources Engineering, University of Hawaii at Manoa)

A methodology is developed to assess the severity of a tsunami in progress based on real-time water-level data near the source. The inverse method, which uses tsunami signals in water-level data to infer seismic source parameters, is extended to predict the tsunami waveforms away from the source. This study focuses on the Alaska-Aleutian and Japan-Kuril-Kamchatka source regions and their potential threats to Hawaii. The algorithm divides each source region into a number of subfaults based on analyses of major historical tsunamigenic earthquakes. For unit slip of the subfaults, a linear long-wave model generates a database of synthetic mareograms at selected water-level stations near the source and at locations where the tsunami waveforms need to be predicted. When a tsunami occurs, regression of recorded tsunami signals near the source using the mareograms provides the slip distribution as well as the expected waveforms near Hawaii and at strategic locations in the Pacific basin. A jackknife resampling scheme provides the confidence interval bounds of the predictions. The algorithm along with the database has been tested and verified using numerically simulated and actual water-level data of past tsunami events.

JSS07b-Posters

Thursday, July 10

**TSUNAMIS: THEIR SCIENCE, ENGINEERING AND HAZARD MITIGATION (IASPEI, IAVCEI, IAPSO)**

Location: Site D

Thursday, July 10 PM

Presiding Chairs: A. Rabinovich, F. Imamura

JSS07b/10P/D-001

Poster

1700-047

**ESTABLISHMENT OF A TSUNAMI ASSESSMENT MANUAL FOR NUCLEAR POWER FACILITIES**Hiroyoshi TANAKA<sup>1</sup>, Makoto TAKAO<sup>2</sup>, Tadashi ANNAKA<sup>3</sup> (<sup>1</sup>Fluid Science Department, Abiko Research Laboratory, Central Research Institute of Electric Power Industry, <sup>2</sup>Nuclear Power Engineering Department, Tokyo Electric Power Company, 1-3, Uchisaiwai-cho 1-chome Chiyoda-ku, Tokyo 100-8560 JAPAN, <sup>3</sup>Advanced Engineering Operation Center, Tokyo Electric Power Services Company, 3-3, Higashiueno 3-chome, Taito-ku, Tokyo 110-0015 JAPAN)

Since studies on tsunamis are developing with recent occurrence phenomena as turning points, it would be essential to improve further the safety and reliability of coastal power facilities by reflecting findings newly obtained from these phenomena to the technique setting design tsunami. From the above-mentioned viewpoint, the present study summarized a manual related to the setting of design tsunami for nuclear power facilities in consideration of the results of technological progress. Characteristics of the tsunami assessment method are as follows. 1) Our principle is to assess the maximum water ascent and descent levels on the basis of the tsunamis resulting from the estimated earthquakes that would occur at neighboring plate boundaries, Japan Sea eastern margin, marine active faults and according to circumstances at overseas plate boundaries. 2) Various uncertainties and errors intervene in the processes of tsunami assessment but it is difficult to decompose and indicate them one by one quantitatively. Consequently, we focus only on uncertainty of tsunami source which has major influence on tsunami assessment and contains many factors having no assured value. First, we select the greatest influence condition on calculated tsunami height at the assessment spot by varying the most dominant factor such as fault position within a reasonable range. Secondly, after fixing the extracted first factor condition we select the greatest influence condition by varying the second factor such as fault strike direction within a reasonable range. Thirdly, after fixing the extracted first and second factor conditions we select the greatest influence condition by varying the third factor such as fault dip angle. Finally, after going through such processes called parameter study we can determine conditions of all the factors. Tsunami height obtained by applying the determined conditions is expected to considerably exceed tsunami height considering the original uncertainty of tsunami source and to absorb the assessment risk generated by errors in numerical calculations and data errors of submarine and coastal configurations. Validity of this way of thinking was confirmed by the result that the tsunami heights finally obtained by the above-mentioned parameter study exceed the run-up trace heights at 185 spots on the Japanese coast. 3) Adequacy of the tsunami applied to design is verified by confirming that the tsunami height exceeds all the run-up trace heights of the historical tsunamis at a planned nuclear power plant site. In the case of no run-up trace of utility value at the site, the adequacy is verified by satisfying the following two items. a) At the site, the design tsunami height exceeds the reproduction calculation heights of the historical tsunamis. b) In the vicinity of the site, the envelop of the numerous tsunami heights obtained in the processes of the parameter study exceeds all the run-up trace heights of the historical tsunamis.

JSS07b/10P/D-002

Poster

1700-048

**CREATION OF THE GRIDDED BATHYMETRY FOR REGIONAL TSUNAMI MODELING**

Andrei G. MARCHUK, Anatoly Yu. BEZHAEV (Institute of Computational Mathematics and Mathematical Geophysics)

For the numerical modeling of tsunami waves propagation, the gridded digital bathymetry is needed. At present such a bathymetry of the required resolution is available only for a few regions. In this study, the method of creating the detailed bathymetry on rectangular grids is proposed. The information about the ocean depths can be found as soundings and bathymetric charts. A great number of depth soundings are contained in the digital databases "Marine Trackline Data" and "Hydrographic Survey Data". In the areas tightly filled with data points, it is possible to create the digital bathymetry of a good quality. In the areas with an insufficient amount of sounding data, the information from bathymetric charts can be used for creating the digital arrays of depths. In this case, the scanned maps should

be digitized using a specially developed digitizing interface. At the final stage, the algorithm, developed by the authors, recalculates arbitrarily distributed values of depths into a detailed gridded bathymetry. For the calculation at each grid point, where depth is to be found, the algorithm uses up to 9 points from a data source. They are chosen using two criteria: the first - the points must be located in various sectors (N, NE, E, SE, S, SW, W, NW) from a grid-point being calculated. And the second - they must be the nearest ones to this point in each sector. Then the spline interpolation is used for defining the value of depth at the grid-point. Another algorithm uses the linear interpolation for obtaining depth value at the grid-point. Several new digital bathymetry datasets on the rectangular grid with 30 arc seconds resolution have been created for the numerical modeling of tsunami propagation. These data include four rectangular arrays of depths, which cover a 200 km zone around the Kuril Islands and Kamchatka from 41.00° N up to 61.00° N. Tsunami propagation from real and model sources was numerically simulated. Using the proposed method it is possible to create detailed arrays of depths for different tsunami-prone regions.

**JSS07b/10P/D-003** Poster **1700-049**

#### THEORY OF EM MONITORING OF TSUNAMI WAVES FAR FROM A SHORE

Oleg Bencionovith NOVIK, Sergey Valentinovitch ERSHOV, Irina Borisovna MIKHAYLOVSKAYA (Inst. Terrestrial Magnetism, Ionosphere and Radio Wave Propagation Russian Acad. Sci., 117246, POB 51, Moscow, Russia, onovik@online.ru)

Tsunamis and earthquakes in near sea regions are manifestations of powerful geodynamic processes beneath the World Ocean's floor covering about 75% of the earth surface. Electromagnetic (EM) signals associated by researches with seismic activity of ocean lithosphere have been detected, especially in Pacific regions (the most tectonically active segment of the Earth), more then once but their physical mechanism is not well understood. Basing on the theory of elasticity, electrodynamics, fluid dynamics and thermodynamics, we formulate a nonlinear mathematical model of seismo-hydro-EM field interaction and calculate generation and propagation of seismic disturbances of these fields (with a proper visualization) in the basin of a model marginal sea (2D schematization of the central part of the Sea of Japan), including transfer of seismic and EM energy from focal depths in lithosphere into a sea and EM emission from its surface into atmosphere, up to the low boundary of ionosphere. Mathematical investigations of algorithms and physical interpretation of numerical results were performed. Amplitude of the computed magnetic signals (500, 300, 200, 50, and 30 pT at the top of the sea bottom sedimentary layer, ocean-atmosphere interface and at the height of 10, 30 and 50 km resp.,  $t = 10$  s after the beginning of seismic excitation in the ocean lithosphere), their main frequency (0.25 Hz), delay of the seismic wave in regard to the magnetic signal (20 s for receivers at the shore) and other parameters of computed seismic signals are of orders observed. In particular, the computed long (150 km) seismo-hydrodynamic wave of a small amplitude (up to 20 cm by the velocity of order of a few hundreds of km/h at different points far from the shore) corresponds to observations as well. So, to discover a seismic activation in ocean lithosphere and a tsunami wave far from a shore, the magnetic recordings at the sea surface and above (buoys, balloons, proton magnetometers, and, may be, satellite instrumentation) should be combined with seismic, magnetic and temperature (0.001 K to 1 K, quartz thermosensors should be applied; the magnetic signal parameters see above) recordings at the sea bottom.

**JSS07b/10P/D-004** Poster **1700-050**

#### DEVELOPING A COMPREHENSIVE TSUNAMI SIMULATOR FOR POSSIBLE TSUNAMI DISASTER PREPAREDNESS IN A COASTAL COMMUNITY

Shunichi KOSHIMURA<sup>1</sup>, Toshitaka KATADA<sup>2</sup>, Noriyuki KUWASAWA<sup>3</sup>, Akichika ISHIBASHI<sup>1</sup>, Kimiro MEGURO<sup>1</sup> (<sup>1</sup>Disaster Reduction and Human Renovation Institution, <sup>2</sup>Gunma University, <sup>3</sup>Nippon Koei Co., Ltd, <sup>4</sup>University of Tokyo)

Coastal communities along the Pacific coast in Japan are under the threat of gigantic tsunamis accompanied with possible megathrust earthquakes along the Nankai Trough within 30 to 40 years. To protect the coastal residents from the tsunami, it is evident that each coastal community should have its own disaster reduction strategy and tools to evaluate if it works. The aim of the present study is to develop a comprehensive tsunami simulator to evaluate each community's tsunami disaster preparedness and mitigation strategy, that consists of constructing tsunami hazard scenario, issuing warning guidance for evacuation, communication between residents, evacuation planning, and estimation of human casualties. Tsunami hazard scenario is provided by the result of tsunami propagation and inundation modeling based on the non-linear shallow water theory, assuming possible great earthquake of Mw 8.6 along the Nankai Trough. Resident communication and evacuation analysis is based on network model theory by using one of the functions of GIS. Human casualty estimation model takes account of hydrodynamic force of tsunami inundation flow as it affects the human body to decide the possibility of evacuation. The present simulator is applied to Owase City that has a population of 24000 and is one of the most vulnerable coastal communities against the tsunami due to great earthquakes along the Nankai Trough.

**JSS07b/10P/D-005** Poster **1700-051**

#### TOWARDS THE OPTIMIZATION OF REGIONAL TSUNAMI WARNING SYSTEMS VIA EARLY DETECTION AND MODELING

Atilio A. ASTE<sup>1</sup>, Modesto ORTIZ<sup>2</sup>, Salvador F. FARRERAS<sup>3</sup> (<sup>1</sup>Oceanology Division, DHN of Peru and Cicece of Mexico, <sup>2</sup>Oceanology Division, CICESE Research Center of Mexico)

Early tsunami warning delivery is fundamental for inundation risk evaluation and preventive countermeasure implementation. The possibility to develop a real-time methodology to minimize flooding risk estimations uncertainly from regional tsunamis, based in the analysis of early sea level observations and modeling, is explored. Local tsunamis, like the recent Nicaragua 1992, Flores 1992, Shikotan 1994, Mexico 1995 and Peru 2001, occur more frequently than the remote trans-Pacific ones and cause severe localized damage and casualties mostly near the generation area. However, for this type of tsunamis the evaluation of expected wave heights at the arrival to nearby or remote locations is uncertain, and there is a lack of adequate criteria to decide if a widespread tsunami warning message should be issued or not. A methodology to evaluate with enough certainty and as early as possible the regional and pacific wide threat to minimize the damage and loss of lives or avoid costly and unnecessary evacuations, is needed. The propagation of tsunamis generated by synthetic earthquakes, as Impulse functions, with sources in several areas of the eastern Pacific Subduction zones, are computer simulated. This ensemble of synthetic tsunamis define a universe of Green functions. The optimum location and number of real-time sea level observing stations along the coast to minimize the uncertainty in the evaluation of source area size and location, are determined. These sea level observations determine in real-time the number and magnitude of impulse functions needed to reproduce the initial conditions. Shallow water non-linear theory for the synthetic tsunami propagation in the near shore and interaction with the coast, is considered. Non-fixed boundaries with discharges conditioned to the state of the water level at the borders, were used to model the flooding

and recession at the coast. The equations were solved through an explicit central finite-difference algorithm for interconnected grids of different sizes. The expected wave heights at each location are so determined in real time from their corresponding Green functions, and are already available for a more confident and less uncertain issue of tsunami warning messages to nearby and remote locations.

**JSS07b/10P/D-006** Poster **1700-052**

#### A TSUNAMI DETECTION SYSTEM USING RTK-GPS IN OFUNATO CITY, NORTHEASTERN JAPAN

Teruyuki KATO<sup>1</sup>, Yukihiro TERADA<sup>2</sup>, Shun'ichi KOSHIMURA<sup>3</sup>, Takenori ABE<sup>2</sup> (<sup>1</sup>Earthquake Research Institute, University of Tokyo, <sup>2</sup>Technical Research Institute, Hitachi Zosen Corporation, <sup>3</sup>Disaster Reduction and Human Renovation Institution)

More than two years have passed since we deployed a new experimental tsunami detection system using RTK-GPS offshore Ofunato city, northeastern Japan. The system has been operated without any significant failure except occasional short term failures of PC or transmission system. During the experiment so far, the system was able to observe a small tsunami due to Peru earthquake of June 24, 2001, with peak-to-peak amplitude of less than 20cm. The similarity of wave form with tide gauge record at nearby tidal station of Ofunato confirmed that the present system is capable of detecting tsunami of a few centimeters, if appropriate real-time low-pass filtering is applied to the raw data. The system is broadcast to the City Hall and Fire Station of Ofunato city in real-time manner. In addition, the processed data are transferred to the web server placed at the Hitachi Zosen Corporation to disseminate the data every 30min through webpage (<http://tsunami.ekankyo21.com/>). Therefore, anyone can observe the sea-surface at any time at any place as far as internet is reachable. The internet system is soon be upgraded for real-time monitoring. In order to improve the system for more practical tsunami-detection and disaster mitigation system, some problems are to be solved. The hardest problem is longer-distance RTK because early warning system may be more effective if the GPS buoy is deployed farther offshore. Currently commercially available RTK software ensures only 10km at most for estimating a few centimeters in positioning accuracy. To tackle this problem, we made a short term experiment in which long-distance observation setting GPS sites farther away from the Ofunato city. The present study shows the results obtained for this experiment.

**JSS07b/10P/D-007** Poster **1700-053**

#### A NEW TSUNAMI DETECTION SYSTEM USING RTK-GPS FOR LONG-DISTANCE OBSERVATION

Yukihiro TERADA<sup>1</sup>, Teruyuki KATO<sup>2</sup>, Keiji ITOH<sup>1</sup>, Shuichi NAGATA<sup>1</sup>, Takashi FUJITA<sup>1</sup>, Takenori ABE<sup>3</sup>, Toshihide MIYAKE<sup>1</sup>, Toshihiko NAGAI<sup>1</sup>, Shun'ichi KOSHIMURA<sup>4</sup>, Shin'ichi MIYAZAKI<sup>1</sup> (<sup>1</sup>Technical Research Institute, Hitachi Zosen Corporation, <sup>2</sup>Earthquake Research Institute, The University of Tokyo, <sup>3</sup>Independent Administrative Institution, Port and Airport Research Institute, <sup>4</sup>Disaster Reduction and Human Renovation Institution)

We propose a new tsunami detection system using RTK-GPS for observing the sea-surface at long-distance from the coast. Detection of tsunami as early as possible before its arrival to the coast is a keen inquiry for mitigating tsunami disaster along the coast. We have developed tsunami-detection systems for more than five years and a system is now in operation about 2km offshore of Ofunato city, northeastern part of Japan, for more than two years. In order to deploy a RTK-GPS tsunami buoy in farther location from the coast, however, several difficult problems need to be solved. The hardest problem is the accuracy in estimating ocean height in a few centimeters or better, because RTK-GPS allows only less than 10km to ensure its accuracy of a few centimeters. To tackle this problem, we have proposed two new algorithms in estimating ocean surface heights; PVD (Point precise Variance Detection) method and KVD (Kinematics for precise Variance Detection) method. To make the methods applicable for practical real-time operation, we have developed a new algorithm applying a Kalman filter. The technique will be tested in our new tsunami-detection system which will be deployed 10-15 km off Muroto Promontory, Shikoku, southwestern part of Japan. The area is now highlighted in terms of special monitoring region for earthquake disaster mitigation project by the Japanese government. We plan to display a new monitoring system of ocean surface using hybrid data transmission using radio and broadband so that anyone can observe offshore GPS-buoy at any location as far as internet is available in real-time manner.

**JSS07b/10P/D-008** Poster **1700-054**

#### MARINE EMERGENCY RESPONSE TO A CASCADIA MEGATHRUST EARTHQUAKE AND TSUNAMI

Fred E. STEPHENSON, Josef Y. CHERNIAWSKY (Institute of Ocean Sciences)

The Cascadia Subduction Zone extends 1000 km from southern British Columbia to Northern California, and at its northern end the deformation front is less than 100 km from the coast of Vancouver Island. A megathrust earthquake in this area will have a catastrophic effect on the communities along the adjacent coast. The coastline of the west coast of Vancouver Island is very complex with many channels and inlets. Much of the island is rugged and access to many communities along the west coast is by a single road. In the event of a major earthquake slides, slumping, and bridge failures etc. will likely cut off road access to many of these communities. In the days immediately following the earthquake most of the emergency response will have to come by sea. Emergency response and mitigation studies often focus on the land-based response to a tsunami, but in this instance the marine component is of equal importance. Are search and rescue (SAR) facilities and SAR vessels in these communities likely to survive a destructive tsunami, and if they do, how are local conditions going to limit their effectiveness for marine search and rescue? In response to the disaster, the Navy and Coast Guard will both dispatch vessels to the most severely effected areas. Will the tsunami and its aftermath effect the ability of vessels to navigate safely in these areas, and will it effect their ability to provide both water and land based support? A three year modelling study, funded by the Canadian Coast Guard's SAR program, is being carried out to predict coastal sea level changes and currents in southern British Columbia harbours due to a tsunami that may result from a megathrust earthquake in the Cascadia Subduction Zone. The present modelling effort uses bathymetric grids up to two orders of magnitude finer than previous studies. The finer resolution gives more accurate results and allows us to see water level and current variations within harbours that were not possible with previous models. This will assist Coast Guard SAR in preparing emergency response plans for their facilities and for the local marine communities they serve.

**JSS07b/10P/D-009** Poster **1700-055**

#### ANALYSIS AND NUMERICAL MODELING OF THE NOVEMBER 18, 1929 GRAND BANKS LANDSLIDE-GENERATED TSUNAMI

Alexander B. RABINOVICH<sup>1</sup>, Isaak V. FINE<sup>2</sup>, Brian D. BORNHOLD<sup>3</sup>, Richard E. THOMSON<sup>3</sup>, Evgueni A. KULIKOV<sup>2</sup> (<sup>1</sup>P.P. Shirshov Institute of Oceanology, Moscow, Russia, <sup>2</sup>Institute of Ocean

## INTER-ASSOCIATION

Sciences, Sidney, BC, Canada, <sup>3</sup>Heat and Mass Transfer Institute, Minsk, Belarus, <sup>4</sup>International Tsunami Research, Sidney, BC, Canada, <sup>5</sup>University of Victoria, Victoria, BC, Canada)

The landslide-generated tsunami of November 18, 1929 that occurred at the southern edge of the Grand Banks, 250 km offshore from Newfoundland, was probably the most catastrophic tsunami in Canadian history (27 people killed). This tsunami was associated with a huge submarine slump (200 km<sup>3</sup>), triggered by a  $M = 7.2$  earthquake. This slump transformed into a turbid flow of clay, silt, and sand that moved eastward up to 1,500 km at speeds of up to 100 km/hr, breaking many telegraph cables. The generated tsunami was observed along the Atlantic coast of Canada and the U.S., as well as on the coasts of Portugal and the Azores Islands. Tsunami waves had amplitudes of 2 to 7 m and runup up to 13 m along the coast of the Burin Peninsula (Newfoundland). To examine this tsunami we used all available historical observational data, including actual tide gauge records, and formulated a finite difference numerical model for tsunami simulation. The slide was assumed to be a thin, viscous, incompressible fluid layer; water was inviscid and incompressible. The shallow-water approximation was assumed for both the slide and water waves. The parameters of the slide were the following: slide area = 25,000 km<sup>2</sup>, thickness = 5 m, volume = 125 km<sup>3</sup>, density = 2.0 g cm<sup>-3</sup>, kinematic viscosity = 0.01, and drag coefficient = 0.0025, slide motion time = 1000 s. The preliminary results of our numerical modeling are encouraging in that the computed and observed tsunami heights and arrival times are in reasonable agreement. Further progress would be achieved if we were able to determine more precisely the slide parameters (slide thickness, volume, shape, density) and able to find additional tide gauge records of the 1929 tsunami for comparison with simulated records.

**JSS07b/10P/D-010** Poster **1700-056**

### NUMERICAL SIMULATION OF TSUNAMI IN LINEAR AND NONLINEAR PROBLEMS BY IMAGINARY VARIABLE GRID SYSTEM METHOD USING NUMERICAL DISPERSION

Yoshinori SHIGIHARA, Fumihiko IMAMURA (Disaster Control Research Center, Graduate School of Engineering, Tohoku University)

Most of numerical simulations for tsunami propagation in practical problems are carried out with long wave approximation excluding a wave frequency dispersion. However, in the following cases the dispersion effect can not be ignored: (1) linear dispersion in a tsunami propagation with long distance in a deep-sea region for the Chilean tsunami of 1960 as example, and (2) nonlinear dispersion in propagation of a tsunami containing higher frequency components in a shallow region in the case such as the 1983 Japan sea earthquake tsunami. For such cases, the dispersive wave theory such as Boussinesq and KdV should be solved by implicit scheme method requiring more computing time. Imamura and Shuto (1989) proposed a unique method to use numerical error in the scheme replacing the physical dispersion. If the spatial grid size in the numerical model with the linear long wave equation can be properly selected, the numerical results show the same accuracy as the linear Boussinesq equation, saving computational time. However, this method has remained the problems in the application to complicated bathymetry with non-uniform sea bottom because it is rather difficult to change the grid size depending on the water depth. In this study, a new idea of imaginary Variable Grid System (VGS) method is proposed to improve the applicability of Imamura & Shuto (1989) method. In this method, the spatial size in the numerical scheme at each grid can be imaginarily changed to be satisfied with the condition of Imamura & Shuto (1989) in the Leap-Frog difference method for the each water depth. The variables of discharge and water level at the imaginary grid can be obtained by the interpolation from original variables by using third approximation spline function. First of all, the numerical results of the linear long wave theory using imaginary VGS method agree with theoretical solution on the flat bottom. Furthermore, the numerical results on a slope changing water depth with different spatial grids are the almost same. Secondly, we applied the method in the shallow water where non-linearity is not neglected. Since the numerical error of the dissipation induced by the up-wind scheme in the convection term reduce the higher frequency components, we need to introduce a method to reduce the damping effect. In this study, we select Iwase et al. (1998) method to introduce an artificial dissipation with the opposite sign canceling the numerical one. Numerical model of the shallow-water theory with imaginary VGS method and Iwase et al. (1998) method can simulate well wave profiles on a slope of shallow water obtained by the numerical solution of the nonlinear dispersive wave theory, showing that imaginary VGS method enables to simulate wave frequency dispersion such as a tsunami and flood tide. Moreover, we found imaginary VGS method can reduce into about 1/2 CPU time of the simulation of implicit scheme.

**JSS07b/10P/D-011** Poster **1700-057**

### A HYDRAULIC EXPERIMENT AND NUMERICAL SIMULATION FOR THE WAVE BREAKING TRANSFORMATION OF SOLITON FISSION WAVES

Hiroyuki IWASE<sup>1</sup>, Fumihiko IMAMURA<sup>2</sup> (<sup>1</sup>ECOH Co., Ltd., <sup>2</sup>Tohoku University)

In the 1983 Nihonkai-Chubu earthquake tsunami, soliton fission waves causing powerful wave force and damage on blocks and ships were observed in shallow water on a mild and long slope. In order to reproduce these waves including the wavemform curvature effect, we have to use the Boussinesq equations as the governing equation with wave frequency dispersion and breaking. Although, the effect of dispersion is going to be included into the tsunami model, problem on the model of breaking still remains. Consequently, the numerical model with Boussinesq equations mostly overestimate wave height and the runup on land. Furthermore, it is reported that the depth integrated Boussinesq-type models underestimate the wave height in front of breaking point. So it is important to develop the numerical model with the proper dispersion as well as breaking effects in the coastal. In this study, a wave breaking model for soliton fission waves in shallow water is examined through the comparison of the hydraulic experiment and numerical simulations with various types of the models. At the first, the relation between wave height and still water depth of the wave breaking point for several solitary waves was discussed by the hydraulic experiment. At the second, we examined the model of artificial amplification of a water height, dissipation, at front of breaking point and the wave breaking model. We use the previous research work (Iwase & Goto, 2000) on the breaking models and carry out the simulation to be compared with the hydraulic experiments in order to calibrate the coefficient of these models. The models with the calibrated one is applied in the wave crest of breaking point at front and rear wave trough. The calculation result agrees with the experiment result well on the average of wave heights before and after the breaking.

**JSS07b/10P/D-012** Poster **1700-058**

### TWO- AND THREE-DIMENSIONAL NUMERICAL MODELS FOR A TSUNAMI PROPAGATION PASSING AN OBSTACLE

Sung Jin HONG, Fumihiko IMAMURA (Disaster Control Research Center, Tohoku University)

Some numerical models are tried to be developed for analyzing the resistance force interacted between wave and structures and applied with sufficient accuracy to practical problems. In the computation, however, it is normally assumed either that there are no solid

structures capable of withstanding tsunami, or that the effect of a solid structure can be expressed in terms of a roughness coefficient, such as Manning's  $n$ . Since the effect of obstacles are important for disaster prevention due to tsunami in shallow water and on land, it is necessary to analyze the interacted resistance force. However, so far two-dimensional numerical model with Manning's  $n$  which is selected without consideration of the hydraulic characteristics could not represent the interaction between wave and structures because that model could not analyze exactly the effect of structures for tsunami. In the present study, we have proposed two kinds of numerical model. One of those models is the two-dimensional tsunami model with equivalent roughness based on shallow water theory, which can be utilized to obtain appropriate friction coefficient at the bottom using percentage of the structures. The quantitative verification about the model has been clarified through comparing with the results of upper model and experiment data that is measured by hydraulic experiment at the open-channel. In front of the obstacles, the comparison of calculated and measured data has a good agreement because reflected wave doesn't reach this region. In middle around obstacles, though physical modeling error might be predominant because tsunami is affected and reflected by structures; reflection, diffraction and refraction, which phenomena can not be included fully in the two-dimensional model, the comparison has a general agreement in specific numerical conditions. Finally, in back of obstacles, the effect of obstacle would not appear in propagation of tsunami wave after passing through obstacles, due to small physical error. In addition, we can estimate that the physical error is taken the component of linearly increasing error in the function of distance. The other is three-dimensional numerical tsunami model which can analyze the nonlinear behavior of flow around obstacles based on Navier-Stokes equations. We employed the method of MAC (Marker and Cell) method and improved it to be fitted with the experiment result.

**JSS07b/10P/D-013** Poster **1700-059**

### ANALYTICAL STUDY ON SEABED DISPLACEMENT RESULTING FROM SEISMIC FAULTING

Shusaku INOUE, Tatsuo OHMACHI (. Department of Built Environment, Interdisciplinary Graduate School of Science and Engineering, Tokyo Institute of Technology)

In late years, serious damages are caused by near field tsunamis that reach the seashore within a few minutes from the occurrence of the tsunami-genic earthquake. The 1999 Hokkaido-nansei Oki, Japan tsunami still remains vividly in our memory. More than 200 persons were killed mostly by this near-field tsunami. Reportedly, the first wave of this tsunami reached the Okushiri Island within 5 minutes after the occurrence of the earthquake. In current tsunami warning systems, it usually take at least a few minutes to announce the tsunami warning, because seismic faults are estimated after collecting seismic data observed at several points. Hence, the current warning system seems to be almost helpless for near field tsunamis that will attack us within a few minutes. On this basis, we are trying to develop a new tsunami warning system whose final target is to detect tsunamis from real-time data observed at a single point. In the first step of our development of quick and accurate tsunami warning system, we have focused our attention on the seabed displacement which will induce sea surface disturbance such as tsunamis and acoustic waves in the seawater. The sea surface disturbance associated with the acoustic waves is characterized by its large velocity and short-period components in comparison with tsunamis. Because of the large velocity, the short-period disturbance is observed before seismic tsunamis. The sea surface disturbance of the short-period components has rarely been discussed in detail. From our previous study on the dynamic displacement of seabed due to seismic faulting, it has been found that the sea surface disturbance is mainly excited by Rayleigh waves propagated along the seabed. Thus, if we can find good correlation between static uplift of the seabed and characteristics of the Rayleigh waves, we can make use of the Rayleigh waves for our tsunami-warning system. For this purpose, we have calculated the seabed displacement resulting from seismic faulting by using the boundary element method. The seabed displacement includes many items such as uplift volume, uplift width and maximum displacement in several cases with different fault parameters. As a result, it was found that the maximum displacement of the seabed is mainly governed by depth of the seismic focus and dip angle of the fault plane.

**JSS07b/10P/D-014** Poster **1700-060**

### NUMERICAL SIMULATION OF LANDSLIDE TSUNAMI

Yasuyuki IWASE, Hiroshi IGARASHI, Hiroyuki FUJITA (Department of Earth and Ocean Sciences, National Defense Academy)

Submarine landslide is one of the origins of the tsunami and it may cause larger tsunami as is expected by seismic fault. We conduct numerical study of tsunami propagation generated by landslide. In order to study the detail flow in the ocean, we develop three-dimensional numerical simulation code for tsunami propagation. In which, the hydrostatic pressure is assumed, since the wave length of the tsunami is much larger than the ocean depth. Finite volume method is used and vertical length is normalized by the thickness of the fluid, i.e., distance between sea floor and sea surface, to treat vertical boundary condition easily. The landslide is modeled as the movement of a doom-like shaped mass on the sea floor, whose height is not changed during sliding. We investigate the relationship between wave height of tsunami and velocity of the landmass on a flat sea floor. If the speed of the landmass is slower than the tsunami wave, several small waves appear and if the speed is larger, a few waves that have the height equivalent to that of the landmass are observed. However, when the landmass speed is nearly the tsunami wave propagation speed, a few large waves are generated, especially in front of moving landmass. These results suggest that if the landslide with the velocity about  $(gh)^{1/2}$  ( $h$  is ocean depth) occur, large tsunami can be generated independently by the magnitude of the earthquake and the size of the landslide mass. The landslide generated tsunami is simulated at Tokai area, Japan, where the earth and sand transported by large rivers is accumulated and the potential occurrence of landslide is suggested. We assume that the earth and sand of 10 km diameter and 10 m height on the sea bottom near Omaezaki, where the depth of sea floor is about 1000 m, is slumped toward south-east direction for 28 km where the ocean depth is about 2500 m. Velocity of the landslide is 120 m/s, which is equivalent to the tsunami wave velocity in the 1500 m depth ocean. A pair of large positive and negative waves (about 10 m height) have progressed to both south-east and north-west directions from around the landslide area, while the waves in north-east and south-west directions are very small. In this case, the tsunami propagation is also affected by the topography of ocean bed. Diffraction of tsunami for peninsula is observed. As a result, tsunami wave higher than 1 meter hits on the south-east area of the Izu Peninsula and west side of the Omaezaki Cape.

**JSS07b/10P/D-015** Poster **1700-061**

### THE USING OF INFORMATION ABOUT SEA LEVEL IN TSUNAMI WARNING CENTER

Tatyana N. IVELSKAYA<sup>1</sup>, TATYANA N. IVELSKAYA<sup>1</sup>, Peter V. DUSHENKO<sup>1</sup>, George V. SHEVSHENKO<sup>2</sup>, Peter D. KOVALEV<sup>3</sup> (<sup>1</sup>Sakhalin Tsunami Warning Center, <sup>2</sup>Marine Geology and Geophysics Institute)

For increasing of efficiency acting of Tsunami Warning System for Sakhalin area there was developed an equipment and software, which allows to solve operative and scientific problems. Though for the Sakhalin island the tsunami do not present so awesome danger, as on Pacific seaside of Kuril island, however, port of Korsakov occurred flooding repeatedly, particularly powerfully under tsunami of Kamchatka, 1952 and Chilean, 1960. And 6 events of tsunami were registered on tide gauge in a port of Kholmsk (Kamchatka 1952, Chile 1960, Urup 1963, Niigata 1964, Moneron, 1971, Akita 1983). The Specialists of Tsunami Center in Yuzhno-Sakhalinsk and laboratory of tsunami of Institute of marine geology was executed installing of the equipment. This complex consists of bottom sensor and coastal center. The duty-engineer in the Tsunami Center has a possibility be connected to coastal center and get information on sea level for necessary period. The complex allows to produce counting out since period before 1 seconds. Due to this possible solve not only operative, but also different scientific problems. There were analysed records of all long wave processes, registered in port Korsakov. The tidal fluctuations dominated in records. The level of the natural long wave noise increases in highfrequency part of spectrum at passing deep cyclone that is associated with phenomena of harbor oscillation. Increasing the amplitudes of the long waves is fixed for period about 8 mines and within the range of 10-30 mines. The comparison spectrum of records with spectrum Chilean tsunami has shown the coincidence a peaks in lowfrequency of a part of spectrum. In particular, there is powerful peak in all spectrum for period around 4.8 hour, connected with resonance fluctuations between island Sakhalin and Hokkaido. The Comparative spectral analysis of the got record in Kholmsk during passing of the cyclone and in usual weather has revealed growth the energy of the fluctuations within the range of period from 2 before 25 mines that usually at tsunami, as well as presence two maximum for period beside 8 and 3 mines. There were digitized records of all tsunami, registered in port of Kholmsk. If the sources of tsunami were found in Japanese sea, caused significant increasing the energy within the range of period 5 - 25 mines, but waves, coming from the Pacific ocean, were shown in more lowfrequency part of the spectrum. The executed analysis has allowed to define the structure of frequency of the dangerous sea phenomenas, which can exist in Korsakov and Kholmsk and take into account, connected with them reinforcement of negative consequence of tsunami, which arose in this moment.

**JSS07b/10P/D-016** Poster **1700-062**

#### MOMENTUM AS A USEFUL QUANTITY IN TSUNAMI SCIENCE

Harold G. LOOMIS (retired)

At the time of the generation of a tsunami, horizontal forces might apply a significant impulse to the body of water producing a horizontal momentum. This would be so in the cases of pyroclastic flows into the ocean, landslides into or within the ocean, and, in some cases, horizontal motions of earthquakes. Whatever the confused water motions at the time of generation, when viscous friction has dissipated the rotational component of the motions, the resultant irrotational, long-waves will still contain all of the original momentum delivered to the water by the initial impulses, diminished only slightly by bottom friction. This momentum can be reflected and refracted by shorelines and by varying water depths as waves are. One reason why momentum might be a valuable quantity to consider is that the momentum delivered by a horizontal impulse is very directional as compared to the momentum that results from the waves spreading out from a generalized surface displacement. Therefore, tsunamis generated with a significant horizontal impulse could be more directional than tsunamis resulting only from vertical surface displacements.

**JSS07b/10P/D-017** Poster **1700-063**

#### TSUNAMI RUN-UP SIMULATION TAKING INTO ACCOUNT DYNAMIC SEABED DISPLACEMENT DUE TO SEISMIC FAULTING

Atsushi MURAKAMI, Tatsuo OHMACHI, Shusaku INOUE (Department of Built Environment Interdisciplinary Graduate School of Science and Engineering, Tokyo Institute of Technology)

Recently authors have developed a numerical technique for tsunami simulation taking into account dynamic seabed displacement resulting from fracturing of a seismic fault, which is referred to as a tsunami dynamic simulation technique. The development of the method aims to simulate processes of tsunamis as precisely as possible by using the state of the art of numerical technology and knowledge on seismic faulting. Among the processes from generation to run-up of tsunamis, the tsunami dynamic simulation method has demonstrated to reproduce the processes of generation and propagation. Thus, the objective of the present study is to extend the ability of the method in order to make it possible to simulate the tsunami run-up process. In conventional tsunami-simulation techniques, simplifications have been employed by neglecting the dynamic seabed displacement and considering only the static contribution. The water layer is also assumed to be incompressible, regardless of its acoustic effects. In the dynamic simulation technique, however, the tsunami simulation is conducted without using these kinds of simplification and takes into account effects of both dynamic seabed displacement and acoustic waves of the seawater. In this technique, weak-coupling is assumed between the seabed and the seawater, from which the motion of the seawater is influenced by that of the seabed, but the motion of the seabed is not influenced by that of the seawater. Based on this assumption, the present technique consists of a two-step simulation. The first step is to simulate the dynamic seabed displacement resulting from a seismic faulting using the boundary element method (BEM), and the second is the generation of the seawater disturbance followed by its propagation and run-up. The seawater disturbance which includes tsunamis, is simulated by solving the Navier-Stokes equation, using the finite difference method (FDM), and imposing the velocity of the dynamic seabed displacement as an input to fluid domain at the seabed. To simulate tsunami run-up onto a coastal area, in general, we had better make the grid size as small as possible because of three-dimensional complexity in geography in and around the area. For this reason, we have introduced the so-called VOF (Volume of Fluid) based method and nesting technique into the second step simulation. The VOF method can handle the complex free surface flow like tsunami run-up, and the nesting technique enables us to conduct the simulation of a large area from the ocean to the seashore with efficiency. The present study focuses on the introduction of the VOF method and the nesting technique into the dynamic analysis simulation, and verify the validity of the introduction. In the nesting, to minimize interpolation error, the Hermite interpolation has been applied because of its higher order accuracy. To check the algorithm, several models such as dam breakage and tsunami run-up have been simulated to demonstrate its validity. Nesting gives higher resolution in the coastal area and higher resolution and VOF enables run-up simulation. The extended dynamic simulation technique will especially help us to predict the behavior of near-field tsunamis with high accuracy.

**JSS07b/10P/D-018** Poster **1700-064**

#### EFFECTS OF DYNAMIC FAULT PARAMETERS ON TSUNAMI CHARACTERISTICS

Masahiro TOBATA, Shusaku INOUE, Tatsuo OHMACHI (Department of Built Environment, Interdisciplinary Graduate School of Science and Engineering, Tokyo Institute of Technology)

In the conventional tsunami analysis, dynamic seabed displacement resulting from seismic

fault rupturing has been neglected and only static contribution has been considered. The initial waveform of tsunami is decided as a static displacement of the seabed and using of long wave approximation simulates tsunami propagation. Moreover, when estimating the fault model that is the cause of generating of tsunami, the fault model estimated by tsunami data often differs from seismic fault model estimated by seismic data. It is thought that the cause of these problems is derived from above approximation. In order to solve these problems, actual tsunami analysis is important and effective in terms of predicting tsunami in high accuracy. In recent years, it has an interest in 'tsunami earthquake'. Tsunami earthquake generates larger tsunamis than expected from its magnitude. Seismological studies showed that the duration time is longer than that of usual earthquake, but the mechanism of tsunami earthquake is not understood yet. In Japan, the 1896 Sanriku earthquake was classified into 'tsunami earthquake' and the damage of 22000 victims occurred. As an example of other tsunami earthquakes, there are the 1946 Aleutian earthquake, the 1992 Nicaragua earthquake, etc. The mechanism of 'tsunami earthquake' is not understood yet and the tsunami warning system of Japan is said to be powerless to 'tsunami earthquake'. Our actual simulation considering the dynamic displacement of seabed and Navier-Stokes equation seems to be effective to find out the mechanism of tsunami generation due to 'tsunami earthquake'. In conclusion, findings from the present study follow. 1. A main feature of tsunami earthquakes lies in slowness of seismic fault rupturing, for which rise time and rupture velocity of the seismic faulting are governing factors. 2. Another important feature of the earthquakes is their large magnitude such as 8 or 9 in terms of the moment magnitude. From this feature, the tsunami wave height tends to grow higher than the usual ones. 3. From the above two features, we had better try to observe Rayleigh waves of longer period up to 50 sec in order to detect the tsunamis from the earthquakes.

**JSS07b/10P/D-019** Poster **1700-065**

#### THE 1946 EVENT: A TRANSOCEANIC TSUNAMI GENERATED BY AN UNDERWATER LANDSLIDE

Philip WATTS<sup>1</sup>, Gerard J. FRYER<sup>2</sup>, Stephan T. GRILLI<sup>3</sup>, James T. KIRBY<sup>4</sup>, Fumihiko IMAMURA<sup>1</sup> (<sup>1</sup>Applied Fluids Engineering, Inc., <sup>2</sup>University of Hawaii, <sup>3</sup>University of Rhode Island, <sup>4</sup>University of Delaware, <sup>5</sup>Tohoku University)

The 1946 Aleutian tsunami inflicted significant far-field damage and fatalities from a narrow beam of wave energy that passed just east of Hawaii, struck the Marquesas and Pitcairn head on, and spent itself against the Antarctic Peninsula. The aftershock zone was too narrow, by a factor of five, for the main rupture to have produced such a transoceanic beam. Large near-field runup on Unimak and Sanak Islands was too large to have been generated by coseismic slip and too restricted (and too early) to have come from an earthquake's trench axis or lower slope deformation. In the far field, the emergent and dispersive nature of the wave train on tide gauge records -- consistent with a landslide source -- contrasted markedly with the minimum-delay character of earthquake-generated tsunamis. The source region of the tsunami, determined by back-projecting travel times, cannot exist without a delay on the order of ten minutes in tsunami generation. The source region, some considerable distance from the epicenter of the main shock, is the upper slope of the Aleutian Trench, a region mantled by thick glacial deposits interleaved with thin, weak, high-stand clays. A massive slope failure is apparent in the USGS GLORIA image of the source location, with a headwall at a depth of about 100 m on the continental shelf and a scar length of at least 60 km. The failure appears to have been triggered 30 km down from the headwall at the back of a 4-km-deep mid-slope terrace. The exposed failure surface appears to have blow-outs and other signs of over-pressuring or gas hydrate eruption. An analysis of landslide motion indicates speeds approaching 200 m/s, a speed entirely consistent with other submarine landslides if the square-root-of-slide-length scaling is applied. We confirm the speed using the viscoelastic model BING, which predicts that all but the trailing tail of the landslide approached the long wave celerity. With landslide speed and tsunami speed nearly equal (but only in the direction of slide motion), slide energy is efficiently fed into the tsunami, and the far-field observations of a narrow beam and large waves are explained. We reproduce all near-field observations by coupling a 3D Boundary Element Method model of tsunami generation to the Boussinesq tsunami propagation and inundation code Geowave. For far-field simulation, we couple our tsunami source to the spherical coordinate model TUNAMI-F2 and propagate the tsunami across the Pacific Basin. We obtain a narrow beam of wave energy that matches the far-field observations. The tsunami of 1946 shows that even continental slope failures off remote shorelines can generate transoceanic tsunamis.



G02

Monday, July 7

**ADVANCED SPACE TECHNOLOGY. MEETING OF IAG SECTION II**

Location: Site C, Room 25

Monday, July 7 AM

Presiding Chairs: K.-H. Ilk, Y. Fukuda

**GRAVITY FIELD / PLANETARY INSTRUMENTS**

G02/07A/C25-001

0900

**CHAMP GLOBAL GRAVITY FIELD RECOVERY - STATUS IN SATELLITE - ONLY AND COMBINED MEAN FIELD SOLUTION**

Christoph REIGBER<sup>1</sup>, Peter SCHWINTZER<sup>1</sup>, Richard STUBENVOLL<sup>1</sup>, Rolf KOENIG<sup>1</sup>, Karl-Hans NEUMAYER<sup>1</sup>, Franz BARTHELMES<sup>1</sup>, Georges BALMINO<sup>2</sup>, Richard BIANCALE<sup>1</sup>, Jean-Michel LEMOINE<sup>1</sup>, Sylvain LOYER<sup>2</sup>, Felix PEROSANZ<sup>1</sup> (GeoForschungsZentrum Potsdam, Department 1, Centre National d'Etudes Spatiales, GRGS - 18, Av. Edouard Belin, 31401 Toulouse Cedex 4, France)

After being three years in orbit and delivering continuously GPS high-low satellite-to-satellite tracking and accelerometer data, the CHAMP mission has succeeded in opening a new era in global gravity field modelling. The first gravity field models, EIGEN-1S and EIGEN-2, derived from several months of CHAMP data, have already demonstrated that an accuracy improvement by almost a factor 10 could be achieved in long-wavelength gravity field recovery. In the meantime new CHAMP model versions of the mean geoid and gravity field were generated based upon a longer CHAMP data series. The CHAMP-only field was combined with other laser satellite tracking data, and normal equation systems from surface gravity and altimetry to get a higher spatial resolution. The achievements and problems of the various gravity field solution are discussed.

G02/07A/C25-002

0920

**GRAVITY FIELD RECOVERY FROM GRACE DATA AT GFZ POTSDAM**

Christoph REIGBER, Roland SCHMIDT, Frank FLECHTNER, Rolf KOENIG, Ulrich MEYER, Karl-Hans NEUMAYER, Peter SCHWINTZER, Sheng Yuan ZHU (GeoForschungsZentrum Potsdam, Department 1)

The US-German twin-satellite mission GRACE (Gravity Recovery And Climate Experiment), in orbit since March 2002, has delivered highly valuable data during the commissioning phase for assessing its gravity recovery capabilities. In addition to GPS high/low satellite-to-satellite tracking (SST), accelerometry and space-craft attitude from star sensors measured on both satellites, the GRACE mission features a micrometer precise low/low SST link between the GRACE satellites. Based on multi-months of high quality data sets estimates of the static gravity field of the Earth and its temporal variability are derived. The capability of the low/low SST data for precise gravity recovery is revealed in the determination of the static gravity field with unprecedented accuracy which is validated through comparisons to external satellite data (CHAMP) and terrestrial gravity-related quantities. Recovery of temporal variations of the Earth's gravity field from GRACE data is in reach but still needs intensive examination. This contribution presents results and experiences from GRACE data analysis of the GFZ GRACE team.

G02/07A/C25-003

0940

**GRAVITY FIELD TEMPORAL VARIATIONS FROM TWO YEARS OF CHAMP MISSION**

Richard BIANCALE, Jean-Michel LEMOINE, Felix PEROSANZ, Sylvain LOYER (CNES / GRGS)

The new satellite missions like CHAMP and GRACE bring considerable improvements in modelling the Earth gravity field, its static part and its temporal variable part. The global approach using GPS tracking data is very CPU time consuming when computing the partials of the spherical harmonic expansion coefficients. This is why an alternative faster method in two steps has been tested and evaluated from CHAMP satellite dynamic orbit computation. The first step consists in computing reduced dynamic orbits of CHAMP using GPS SST data. These orbits are then used in a second step as pseudo-observations in order to compute gravity field model coefficients. About two years of data have been processed in both methods and results intercompared in terms of geoid, long wavelength temporal variations and calibration parameters of the accelerometer as well.

G02/07A/C25-004

0955

**ABSOLUTE GRAVIMETRY IN THE FENNO-SCANDIAN LAND UPLIFT AREA: MONITORING OF TEMPORAL GRAVITY CHANGES FOR GRACE**

Juergen MUELLER, Ludger TIMMEN, Heiner DENKER (Institute of Geodesy, University of Hannover)

During the mission duration of GRACE (about five years), a temporal geoid change of about 3.0 mm can be expected in the centre of the Fennoscandian land uplift area, corresponding to a gravity change of about 10  $\mu\text{Gal}$ . This gravity change over five years (linear trend) can be observed with an accuracy of  $\pm 1 \mu\text{Gal}$  by absolute gravimetry. As the geoid derived from GRACE data can be determined with an accuracy of  $\pm 0.1 \text{ mm}$  (at spherical harmonic degrees between 2 and 50), the land uplift causes a measurable signal in the observations. Therefore absolute gravimetry can be used very well to validate GRACE results, i.e. it can provide ground truth for the satellite measurements. But it contributes also to the separation of the various time-variable parts in the GRACE data. It is planned to perform absolute gravity measurements yearly to improve the knowledge about the Fennoscandian uplift with respect to accuracy and reliability, where also the tide gauges have to be connected and monitored, and the combination with GPS data is striven for. The main result of the project will be an improved model of the land uplift (gravity and geoid changes), which can be used for the validation of the GRACE measurements. In a next step, the gravity variations and the models of temporal phenomena obtained from GRACE data analysis can further be processed and may serve as additional input for the determination of a better spatial model of the total land uplift process (synergy effect).

G02/07A/C25-005

1010

**GRAVITY FIELD RECOVERY AND VALIDATION BY ANALYSIS OF SHORT ARCS OF A SATELLITE-TO-SATELLITE TRACKING EXPERIMENT AS CHAMP AND GRACE**

Karl Heinz ILK, Martin FEUCHTINGER, Torsten MAYER-GUERR (Institute of Theoretical Geodesy, University of Bonn)

A procedure for regional gravity field determination is presented based on the analysis of short arcs of a low flying satellite as CHAMP and GRACE. The use of short arcs might have some advantages over longer ones because they are less sensitive to disturbing forces and reference system parameters. Furthermore the short arcs can be adapted to the undisturbed orbit segments between thruster events of the low satellite. The mathematical setup is based on a semi-analytic method by transferring the original intersatellite observations in a time series of short arcs. The time series coefficients can be expressed by integrals of the unknown gravity field, modeled by parameters tailored to the special task. In case of a regional refinement of the gravity field space-localizing gravity field parameters defined on a discrete grid can be selected, as e.g. spline base functions on a triangular grid, while for global applications a spherical harmonics expansion might be the proper choice. Basically, this procedure can be applied to high-low intersatellite observations as well as to low-low SST-measurements. In case of the high-low mode it is preferable to process the orbits of the low satellite directly instead of the high-low intersatellite links. The reason is that the orbits, derived from a precise kinematic orbit determination procedure based on GPS observables might be more precise than the high-low intersatellite links, provided the a-posteriori correlations of the orbit positions have been taken into account in a proper way. The method is tailored especially to regional gravity field refinements in those cases where residual gravity field effects are recognizable in the short arcs. To detect these effects, a preprocessing step based on the energy balances along the short arcs is applied. To minimize instabilities caused by the high frequent parts in the residuals a tailored regularization can be applied to stabilize the downward continuation process. Furthermore, residual oscillations in the solution caused by the intrinsic improper posedness of the problem can be removed by a posteriori filtering procedure of the space localizing gravity field parameters. A critical aspect is a proper balance between the regularization parameter and the filtering method. A validation step, again based on an energy balance check along the short arcs, concludes the analysis procedure. First results are presented by using kinematic orbits of CHAMP derived from real observations over selected regions with rough gravity field features. A mission as CHAMP is certainly not a proper candidate for a regional gravity field recovery. Therefore, to demonstrate the applicability to a tailored low-low experiment the procedure is applied to a GRACE simulation scenario.

G02/07A/C25-006

1030

**APPLICATION OF SPACE GRAVITY SPECTROSCOPY TO CHAMP, GRACE AND GOCE**

Erik W. GRAFAREND, Gerrit AUSTEN, Petar MARINKOVIC, Tilo REUBELT (Department of Geodetic Science, Stuttgart University)

This contribution introduces the latest achievements of the research done at the Department of Geodetic Science, Stuttgart University, on three major LEO satellite global gravity field recovery missions, namely CHAMP, GRACE, GOCE. Solution strategies by means of the spectral analysis of the Earth's gravitational field are outlined. Specifically, in the case of CHAMP space gravity spectroscopy is performed by means of the analysis of kinematic satellite orbits while in the case of GRACE and GOCE spectroscopy is based on models comprised of satellite orbits and mission specific measurements, e.g. ranges, range-rates and range-accelerations (GRACE) or gravity-gradients (GOCE). For purposes of data validation and error analysis of LEO satellites directly measured values a stochastic model for the homogeneous and isotropic analysis is studied. An isotropic analysis is represented by the homogeneous distribution of measured values and statistical properties of the model are calculated. In particular, correlation structure functions are defined by n-th order tensors (Taylor-Karman tensors) for the ensemble average of a set of incremental differences in measured components. All aspects of the operability and applicability of the Space Gravity Spectroscopy approach are documented by numerical studies.

G02/07A/C25-007

1100

**CALIBRATION/VALIDATION OF GOCE DATA BY TERRESTRIAL TORSION BALANCE OBSERVATIONS**

Gyula TOTH<sup>1</sup>, J. ÁDÁM<sup>1</sup>, L. F&Ouml;LDVÁRY<sup>1</sup>, I.N. TZIAVOS<sup>2</sup>, H. DENKER<sup>3</sup> (Department of Geodesy and Surveying, Budapest University of Technology and Economics, P.O.B. 61, H-1521 Budapest, Hungary, <sup>2</sup>Department of Geodesy and Surveying, Aristotle University of Thessaloniki, Univ. Box 440, 54124 Thessaloniki, Greece, <sup>3</sup>Institute fuer Erdmessung, Universitaet Hannover, Schneiderberg 50, D-30167 Hannover, Germany, <sup>4</sup>Institute for Astronomy and Physical Geodesy, Technical University of Munich, D-80290 Germany)

One promising method for the external validation and calibration of the upcoming GOCE satellite mission data is the use of ground gravity field data continued upward to satellite altitude. There is a unique situation for Hungary in this respect since surface gravity gradients are available at 20143 points over an approximately 350 by 350 km<sup>2</sup> area, measured by the classical Eötvös torsion balance. The concept of this contribution is to use these point gravity gradient observations for upward continuation to the GOCE satellite orbit in combination with different geopotential models and other gravity field information. The computations are based on the least squares collocation method and the direct numerical integration of the torsion balance data. For the latter method, the spectral combination technique and the classical integration kernels are considered. Furthermore, various other data sources, such as the  $T_{21}$  gravity gradients based on the gravity and terrain data collected within the frame of the European Geoid Project, are utilized for comparisons. Besides the comparisons between the different satellite gravity gradient computations, the results are also evaluated using simulated GOCE gravity gradient data over Hungary. Moreover, an error analysis of the results and the effect of using different geopotential models is presented.

G02/07A/C25-008

1115

**KINEMATIC PRECISE ORBIT DETERMINATION FOR GRAVITY FIELD DETERMINATION**

Drazen SVEHLA, Markus ROTHACHER (FESG, TU Munich)

The main outcome of the kinematic and reduced-dynamic precise orbit determination (POD) we performed for CHAMP over a period of one year showed that kinematic orbits for the LEO satellite can be determined with an accuracy of 1-3 cm, and that, therefore, kinematic LEO positions can be used as pseudo-observations for gravity field determination. Using these kinematic orbits several gravity field models were already computed and temporal variations of the gravity field are presently studied. Among all space geodetic techniques (SLR, DORIS, VLBI, etc.) only GPS allows purely kinematic precise orbit determination where kinematic satellite positions are estimated independently of orbit altitude and force

modeling like, e.g., gravity field, air-drag, solar radiation, etc. The use of kinematic positions together with variance-covariance information as an interface to gravity field determination avoids the simultaneous adjustment of gravity field coefficient together with a huge amount of global GPS parameters, like GPS satellite clocks, GPS orbits, zero- or double-difference ambiguities, station coordinates, troposphere parameters, Earth rotation parameters, etc. External validation with SLR and comparison with reduced-dynamic orbits show that, due to the nature of the phase observable connecting epochs, kinematic positions are very smooth from epoch to epoch. This is also visible in the variance-covariance information between epochs. As a consequence high frequency gravity signals may be extracted from these positions. In this paper we describe kinematic orbit determination as a method that can be used for High-Low SST gravity field determination. Our focus is to show the advantages and disadvantages of kinematic orbits compared to classical reduced-dynamic orbits. When kinematic positions with higher sampling are provided, numerical differentiation is more accurate and high accurate kinematic velocities and accelerations can be obtained. On the other hand, increasing the sampling of kinematic positions requires that the global IGS network has to be processed with the same sampling rate, either to compute GPS satellite clocks or to form baselines with the LEO satellite. Over the last two years we developed several approaches in kinematic and reduced-dynamic orbit determination ranging from pure zero-difference to double-difference methods with ambiguity resolution. Accuracy assessment of kinematic LEO orbits will be given using SLR data and the influence of GPS orbit and satellite clock errors will be studied. The impact of ambiguity resolution on double-difference kinematic orbits will be analyzed from the point of view of efficiency and accuracy.

**G02/07A/C25-009 1130**  
**EFFICIENT STOCHASTIC ORBIT MODELING TECHNIQUES USING LEAST SQUARES ESTIMATORS**

Adrian JAEGGI, Gerhard BEUTLER, Urs HUGENTOBLE (Astronomical Institute, University of Berne)

Present and future satellite missions for gravity field recovery and atmosphere sounding like CHAMP, GRACE and GOCE pose very high requirements on precise orbit determination for low earth orbiters (LEO's). The approach followed so far at the Astronomical Institute of the University of Berne (AIUB) was mainly kinematic point positioning using data of the GPS receivers on board of the LEO's. On the other hand there exist a wide range of different dynamic (or reduced dynamic) orbit modeling techniques making the attempt to completely parametrize a LEO orbit. We will focus on new orbit parametrization procedures, especially on (pseudo) stochastic modeling techniques which are well suited to deal with model deficiencies. We will analyze different stochastic orbit parametrization methods (e.g., the use of instantaneous velocity changes, piecewise constant accelerations, etc.) regarding their mutual benefits using simulated measurements as well as real GPS-data stemming from spaceborne receivers. In an operational environment it is extremely important to have not only precise but also efficient orbit determination procedures available. Kalman filtering is one way of achieving this goal. We will study the efficiency of alternatives based on least squares estimators and compare them to the performance of Kalman estimators.

**G02/07A/C25-010 1145**  
**SATELLITE GRAVITY FOR OFFSHORE OIL AND GAS EXPLORATION**

Minghua ZHANG<sup>1</sup>, Jiaqiang ZHANG<sup>1</sup>, Gang CAI<sup>1</sup>, Lin WU<sup>2</sup> (<sup>1</sup>Research Center, China Geological Survey, <sup>2</sup>China Geological Survey)

Satellite derived gravity data can be used to delineate offshore sediment basin structures today in integration interpretation. A test area in Yellow Sea, China has proved that satellite gravity data of 10Km wave-length resolution can be used to outline not only basin boundaries, but main structures within large basins. Comparisons between satellite gravity data and ship-boarded gravity data along 20 ship survey lines, totally some 1000Km, shows that almost all the anomalies identified by ship-board gravity data can be found the similar size and features in satellite gravity data. Total absolute average difference of point-to-point comparison is less than 3mgl. Root-mean-square is 7.3mgl. The satellite gravity data is thus then adopted in interpretation as a main data source, especially for the region where ship can not go. Detail studies of what satellite gravity can reveal shows, that it can delineate all the secondary structures in Yellow Sea China. Main features clearly defined by satellite gravity are the south boundary of Yangzi platform in northeast direction from Shanghai, China to Kwangju, South Korea, the northwest directional fault belts of Huangnan Basin near the coast, boundary of Huangbei Basin and its inner structures in different directions, and boundary of North Yellow Sea basin and its inner doming areas. These features are coincided with seismic reflection data interpretation. Although there were many ship-boarded gravity surveys in the past in Yellow Sea, resolution of a whole map of it is still not satisfied for detail interpretation to the scale of 1:1,000,000 due those surveys were of different time, different instrument and of different resolution. Satellite gravity data is now then a good replacement to this scale, and some area may be used to scale of bigger than this. And economically say, satellite gravity is much more fast and cheaper to get a general look on marine basins and structures for oil and gas exploration. It is thus adaptable as one data source in marine geological survey at least at scale of 1:1,000,000. It is of high significance in geological survey, basin structure studies, and in the first stage of off shore oil and gas exploration.

**G02/07A/C25-011 1200**  
**ANTICIPATED ACCURACY OF LUNAR GRAVITY FIELD MODEL FROM RSAT/VRAD MISSION**

Koji MATSUMOTO<sup>1</sup>, Kosuke HEKI<sup>1</sup>, Hideo HANADA<sup>1</sup>, Seiitsu TSURUTA<sup>1</sup>, Yusuke KONO<sup>2</sup>, Nobuyuki KAWANO<sup>3</sup>, Takahiro IWATA<sup>3</sup>, Noriyuki NAMIKI<sup>4</sup>, David D. ROWLANDS<sup>5</sup> (<sup>1</sup>Earth Rotation Division, National Astronomical Observatory, <sup>2</sup>National Space Development Agency of Japan, <sup>3</sup>Kyushu University, <sup>4</sup>NASA Goddard Space Flight Center, <sup>5</sup>Radio Astronomy Division, National Astronomical Observatory)

We will report the result of feasibility study for lunar gravity field recovery mission in SELENE to be launched in 2005. Many lunar gravity field model have been developed so far, but they are based on 2-way Doppler measurement in the near-side only. We propose two new satellite tracking methods in SELENE to improve lunar gravity field model; (1) 4-way Doppler measurement by relaying Doppler signal to/from the main orbiter by means of a relay satellite (RSAT mission), and (2) differential VLBI measurement between artificial radio source on board the relay satellite and a VLBI satellite (VRAD mission). The former enables direct measurement of lunar gravity field in the far-side, and the latter contributes to more complete understanding of structure of lunar gravity field by adding sensitivity normal to the line-of-site direction. It is almost impossible to carry out feasibility study by analytical method because the problem is so complicated involving multi tracking methods of multi target satellites by multi tracking stations. We numerically estimated anticipated accuracy of lunar gravity field model from SELENE by using GEODYN II and SOLVE software. Limitations on tracking data acquisition become clear as the mission goes into the detailed design phase. They include operation condition of tracking stations, duration of sunshine on satellites,

satellite visibility, antenna beam pattern, and so on. The latest analysis counting in such limitation on data acquisition shows that accuracy of lunar gravity coefficients of degrees 2-30 will be improved by one order of magnitude compared to LP100J.

**G02/07A/C25-012 1215**  
**NEIGE: A GEODETIC NETWORK ON MARS, TO STUDY THE INTERNAL STRUCTURE OF THE PLANET, AND THE BALANCE OF VOLATILES**

Jean-Pierre BARRIOT<sup>1</sup>, Julien VIENNE<sup>1</sup>, Veronique DEHANT<sup>2</sup>, Marie YSEBOODT<sup>3</sup>, Pascal ROSENBLATT<sup>3</sup>, Julien DURON<sup>3</sup>, William FOLKNER<sup>4</sup> (<sup>1</sup>UMR5562/CNES, <sup>2</sup>Obs. Royal de Belgique, <sup>3</sup>Jet Propulsion Lab.)

The Netlander Geodesy and Ionosphere Experiment is part of the Netlander mission to Mars, that will land on the red planet in 2009 or 2011. Four microstations of 20kg each will materialize a reference frame on the surface of the planet. The orientation of this frame with respect to inertial space will be monitored by Doppler tracking from the microstations to a Mars orbiter, and from the Mars orbiter to the Earth. The Doppler signal will be affected by the Mars nutations, length of day, and polar motion. The presence of a Mars liquid core will affect slightly the nutations, and the CO2 mass exchanges along the martian year will affect the length of day and polar motion. We show that we will be able to extract these geophysical signatures after an observation time of half a martian year.

**G02/07A/C25-013 1230**  
**RESULTS OF THE CRITICAL DESIGN OF RSAT/VRAD MISSION INSTRUMENTS ON SELENE SUB-SATELLITES RSTAR/VSTAR FOR SELENODES**

Takahiro IWATA<sup>1</sup>, Takeshi SASAKI<sup>1</sup>, Tatsushi IZUMI<sup>1</sup>, Yusuke KONO<sup>2</sup>, Hideo HANADA<sup>2</sup>, Nobuyuki KAWANO<sup>3</sup>, Fuyuhiko KIKUCHI<sup>4</sup> (<sup>1</sup>National Space Development Agency of Japan, <sup>2</sup>National Astronomical Observatory, <sup>3</sup>Tohoku University)

We will report results of the critical design for the selenodetic observation system conducted by two micro sub-satellites of SELENE; Relay Satellite (Rstar) and VLBI Radio Satellite (Vstar). Global mapping of the lunar gravity field will be conducted with higher accuracies using these sub-satellites. Four-way Doppler measurements toward SELENE Main Orbiter above the lunar far side will be conducted by the Relay Satellite Transponder (RSAT) on Rstar. Differential VLBI observations will be conducted for three pairs of S-band and a pair of X-band carriers emitted from "the Differential VLBI Radio Sources (VRAD)" on Rstar and Vstar. These sub-satellites aim to detect so small lunar gravity turbulence that they have not any orbital and attitude control equipments except a nutation dumper for spin stabilization. We have designed a simple structured and light weighted release mechanism, and confirmed the release properties by ground and on-orbit tests. Attitude and spin motions of the satellites will be settled by the release properties. Mission analysis shows that these properties affect the selenodetic observation, which has been confirmed to be analytically estimated and calibrated in data processes.

**G02/07A/C25-014 1245**  
**APPLICATION OF PZT TELESCOPE TO INSITU LUNAR ORIENTATION MEASUREMENT (ILOM)**

Hideo HANADA<sup>1</sup>, Kosuke HEKI<sup>1</sup>, Hiroshi ARAKI<sup>1</sup>, Seiitsu TSURUTA<sup>2</sup>, Seiichi TAZAWA<sup>2</sup>, Kazuyoshi ASARI<sup>1</sup>, Tsuneya TSUBOKAWA<sup>3</sup>, Koji MATUMOTO<sup>4</sup>, Nobuyuki KAWANO<sup>5</sup>, Yusuke KONO<sup>6</sup>, Taihei YANO<sup>6</sup> (<sup>1</sup>Earth Rotation Division, National Astronomical Observatory, <sup>2</sup>Mizusawa Astrodynamics Observatory, National Astronomical Observatory, <sup>3</sup>Radio Astronomy Division, National Astronomical Observatory, <sup>4</sup>The Institute of Physical and Chemical Research)

We are proposing a selenodetic mission, In situ Lunar Orientation Measurement (ILOM) to study lunar rotational dynamics by direct observations of the lunar physical libration and the free librations from the lunar surface with an accuracy of 1 milli-arc-second as the post-SELENE project. Year-long trajectories of the stars provide information on various components of the physical librations and we will also try to detect the lunar free librations in order to investigate the lunar mantle and the liquid core. The PZT on the moon is similar to that used for the international latitude observations of the Earth except for the half mirror above the objective, a CCD with high well capacity, and the heater beneath the mercury pool. Although a star position on the focal plane does not change even if the telescope inclines in principle, the tilt of the telescope affects the star position due to aberrations of the objective in actual case. We obtained the relation between the deviation of the star position in CCD and the tilt of the telescope by ray tracing method and found that tilt of less than 100 arc seconds did not affect the star position by larger than 1 mas. Thermal test of a tube made of CFRP showed that the tube did not incline by more than 100 arc seconds even in condition of the lunar surface. Positioning accuracy of star images on a CCD surface is approaching to 1/500 of a pixel size in laboratory experiments using a CCD.

**G02-Posters Thursday, July 10**

**ADVANCED SPACE TECHNOLOGY. MEETING OF IAIG SECTION II**

Location: Site D

**Thursday, July 10 PM**  
 Presiding Chairs: G. Appleby, H. Tsuji

**G02/10P/D-001 Poster 1400-066**

**THE IMPACT OF GPS SATELLITE CONFIGURATION ON POSITIONING**

Jenn-Taur LEE (Dept. of Information Management, Chung Yun Institute of Technology, Chung Li, Taoyuan 320 Taiwan)

GPS provides the capability of global, weather-independent as well as continuous navigation and positioning, so GPS technique has been extensively applied and rapidly developed for decades. However, just like any other surveying tasks, the precision of GPS positioning is limited by the systematic and random errors that is dependent on two major factors. One is precision of observation, which is determined by various error resources such as space satellite, signal propagation, and receivers. The other is the configuration of the observed satellites. Owing to the orbit inclination of GPS satellite constellation, the satellite geometry is significantly important for the outcomes of positioning and also is closely related to the observer's site (latitude), i.e., the configuration of the observed satellites are completely different at the equator, middle, and high latitude, respectively. The visibility of GPS satellite,

which is described with azimuth and zenith angle, is introduced in this paper. With the influences of various errors based on the similar condition, a set of the observed GPS raw data is used to simulate different satellite configuration. The aim is to understand the magnitude of the positioning precision caused by GPS satellite configuration. The baseline vector processing and network adjustment was done. In addition, the preliminary analysis and conclusion is indicated in the paper.

**G02/10P/D-002** Poster **1400-067**

**IMPROVED DETERMINATION OF GRAVITY FIELDS FROM GRACE RANGE RATES USING A REFINED ORBITAL PERTURBATION THEORY**

Chenway HWANG, Cheng-Gi WANG (Department of Civil Engineering, National Chiao Tung University)

An improved theory of linear orbital perturbation theory is developed for range rate type of observations. This theory maps the Keplerian perturbations onto perturbations in range rate between two low earth-orbiting satellites such GRACE. The mapping functions are derived and tested using simulated range rates. Compared to existing simplified theories, the new theory yields a better fit to the range rates from numerical integrations. In the practical application, range rates based on a priori geopotential model must be first determined. Residual range rates obtained by differencing the observed and the computed range rates are used to establish observation equations for least-squares estimation of corrections of geopotential coefficients with respect to the a priori coefficients. This paper will report the improvement of gravity determination using simulated range rates of the GRACE mission.

**G02/10P/D-003** Poster **1400-068**

**CENTRE-OF-MASS CORRECTION OF SPHERICAL GEODETIC SATELLITES FOR MILLIMETRE LASER RANGING**

Toshimichi OTSUBO<sup>1</sup>, Graham M. APPLEBY<sup>2</sup> (<sup>1</sup>Communications Research Laboratory, <sup>2</sup>NERC Space Geodesy Facility)

The temporal spread of optical pulse signals due to reflection from multiple onboard reflectors is now a critical problem in satellite laser ranging. The full-rate residual profile of single-photon laser ranging can be used to model the response function of geodetic satellites, resolving the uncertainty of far-field diffraction. We constructed the response function model for three types of laser ranging targets already in Earth orbit, the LAGEOS, AJISAI, and ETALON satellites. The centre-of-mass correction depends on the ranging system and observation policy at terrestrial stations, such as a single-photon system, a C-SPAD system, and a photomultiplier system. Our numerical simulation gives the centre-of-mass correction systematically variable about 1 cm for LAGEOS and 4-5 cm for AJISAI and ETALON. This study would help the satellite laser ranging technology to make full use of its potential accuracy in the determination of geodetic parameters, especially the orbits, the terrestrial reference frame and the gravitational scale *GM*.

**G02/10P/D-004** Poster **1400-069**

**PHOTOMETRIC OBSERVATION OF LAGEOS-2 FOR DETERMINING ITS SPIN BEHAVIOUR**

Toshimichi OTSUBO<sup>1</sup>, Robert A. SHERWOOD<sup>2</sup>, Philip GIBBS<sup>3</sup>, Roger WOOD<sup>2</sup> (<sup>1</sup>Communications Research Laboratory, <sup>2</sup>NERC Space Geodesy Facility)

The spin rate and spin axis orientation of the LAGEOS-2 satellite were determined by analysis of photometric observation data. A photometer system developed at the Space Geodesy Facility at Herstmonceux, East Sussex, UK, was used to time solar glints from the rotating satellite at 1 ms time resolution. It was found that the spin period of LAGEOS-2 got longer from 21 sec in March 2000 to 80 sec in December 2002; and that over this period the direction of the spin axis orientation had a complicated but smooth precession with respect to the Earth's spin axis, the inclination varying from nearly zero to 50 degrees. Moreover, the precise photometric data revealed that the direction of the spin was the reverse of that of the Earth's rotation, and that the optical alignment of a reflector surface on LAGEOS-2 can deviate from its position vector by up to 15 arcminutes. Detailed knowledge of the evolution of the spin motion will help analysts construct precise acceleration models for use in precise orbit determination of the satellite. It should be noted that the opportunities for photometric observations are time-limited because, as the spin slows over the coming years, we will gradually observe fewer and fewer glints until (as for LAGEOS-1 today) glints become very rare events.

**G02/10P/D-005** Poster **1400-070**

**PHYSICAL GEODESY WITH GPS**

Fei LI, Wu CHEN (Wuhan university)

In the first place, the problems as following are analysed: the effect caused by GPS on the theory and methods of the physical geodesy, the change in the function of some objects investigated in physical geodesy. Secondly, the discussions on the application of Neumann boundary value problem and the determination of height system are made. Then, a new geodetic boundary value problem is researched, which includes: the definition and an corresponding integral equation, an approach solution and its application in determining the quasi-geoid and deflections of vertical and external gravity field. Finally, the advantages and problems of GPS boundary value problem in physical geodesy are discussed.

**G02/10P/D-006** Poster **1400-071**

**A NEW PROJECT OF GRAVITY MISSION STUDIES IN JAPAN**

Yoichi FUKUDA<sup>1</sup>, Toshimichi OTSUBO<sup>2</sup>, Taizoh YOSHINO<sup>3</sup>, Shuhei OKUBO<sup>3</sup> (<sup>1</sup>Department of Geophysics, Kyoto University, <sup>2</sup>Kashima Space Research Center, Communications Research Laboratory, <sup>3</sup>Earthquake Research Institute, University of Tokyo)

We have started a new project of GPS occultation and satellite gravity mission studies in Japan. This project, which is funded by MEXT (Ministry of Education, Culture, Sports, Science and Technology) for a 3 years project (FY2002-2004), primarily aims at developing a calibration free satellite observation system for monitoring the Earth's environmental changes related to global warming. For this purpose, we try to employ two different but closely related techniques of GPS occultation and Satellite Gravity Mission, and we organized two study groups accordingly. The first group led by Toshitaka Tsuda of Kyoto University, who is also the leader of the project, devotes the GPS occultation, and the second group led by Yoichi Fukuda devotes the gravity mission studies. In this paper, we briefly introduce the project plan of the gravity mission studies in particular. It is quite a new technique to monitor the Earth's environment, for instance, global water cycling, by measuring very small gravity fluctuation using satellites. The idea is successfully coming

true by the GRACE mission. However, GRACE employs a microwave link for SST (satellite to satellite tracking) and its sensitivities and spatial resolution are still unsatisfactory for the monitoring of regional scale phenomena. Thus we aim future application of a SSI (Satellite to Satellite Interferometer) mission to improve the sensitivities and spatial and temporal resolutions consequently. In this project, as feasibility studies, we carry out some basic experiments/developments; (1) development of new precise orbit determination software, (2) studies of laser interferometer techniques by a newly developed ground simulator, (3) development of a newly designed 3-axis accelerometer and its performance test on ground. We also carry out some simulations for the further application of these techniques, and aim to propose a basic design of a future gravity mission.

**G02/10P/D-007** Poster **1400-072**

**MODELLING OF GPS SATELLITE CLOCKS**

Veronika BROEDERBAUER, Robert WEBER (Department of Advanced Geodesy, Technical University of Vienna)

Since November 2000 the IGS (International GPS Service) provides so-called Ultra-Rapid products comprising precise GPS satellite orbits and satellite clocks. This solution, issued twice daily, contains both an observed and a predicted part. The predicted part covers a period of 24 hours. While the orbits are output to an integration of the well-known force field the clocks have to be extrapolated by means of an experienced prediction model. We present clock-prediction models for all GPS satellites currently active. In a first step all observed and predicted Ultra Rapid clock values of the IGS Analysis Centres are compared to the IGS Rapid solutions. IGS Rapid solutions are usually available at 17 UTC the next day and serve in our calculations as the reference. After a linear fit the clock-rms, is calculated both for the observed (about 0.1 – 0.4 ns) and the predicted part, which in fact is just a very coarse control of the quality of the clock values. The results are displayed in diagrams at the homepage of the Department of Advanced Geodesy at the TU Vienna (<http://luna.tuwien.ac.at/>). In a second step the available IGS Rapid solutions and the observed part of the IGS Ultra Raps of the past 48 hours are used as input data to a least squares adjustment to determine the coefficients of a polynomial of second order. Depending on the clock behaviour (caesium or rubidium) we add cyclic terms to predict the satellite clock values over the upcoming 24 hours. Finally our predictions can be compared with the IGS Rapid solutions and to the solutions of the individual IGS Analysis Centres. The quality of our clock predictions is usually at the sub-nanosecond level over the upcoming 6 hours and at the 3 ns level over a 24 hours period.

**G02/10P/D-008** Poster **1400-073**

**ORBIT DETERMINATION OF THE NOZOMI SPACECRAFT USING DIFFERENTIAL VLBI TECHNIQUE**

Ryuichi ICHIKAWA<sup>1</sup>, Mamoru SEKIDO<sup>2</sup>, Tetsuro KONDO<sup>3</sup>, Yasuhiro KOYAMA<sup>4</sup>, Hiroo OHSAKI<sup>1</sup>, NOZOMI DVLBI group<sup>2</sup> (<sup>1</sup>Kashima Space Research Center, Communications Research Laboratory, <sup>2</sup>ISAS, NAO, NASDA, Gifu University, Hokkaido University, and Yamaguchi University)

We performed a preliminary differential VLBI (DVLBI) observation with National Astronomical Observatory (NAO) and the Institute of Space and Astronautical Science (ISAS) to determine precise orbit of the GEOTAIL spacecraft on June 4, 2002. The purpose of this observation is to establish the positioning technology for the interplanetary spacecraft using differential VLBI in realtime. Our main concern is to determine the PLANET-B (NOZOMI) orbit just before the second swing-by on next June [Yoshikawa et al., 2001]. It is significantly important to get the timing to maneuver the spacecraft before the swing-by. However, the usual range and range rate orbit determination will not be available because it will be difficult to point the high-gain antenna mounted the spacecraft toward the earth at that time. So we need a new technique to determine the precise orbit of the NOZOMI. We performed several DVLBI observations for the NOZOMI spacecraft since September 2002 using the "IP-VLBI system" which is under development at Communications Research Laboratory [Kondo et al., 2002]. We are developing a orbit determination software package to analyze the DVLBI observables. The VLBI delay model for finite distance radio source is already implemented in the package [Sekido et al., 2003]. The package will include the DVLBI observation scheduling to take account of the passage of the spacecraft near the quasar line of sight and the propagation delay estimating for the ionosphere and the neutral atmosphere. We will present the orbit determination accuracy of our package and an evaluation of the propagation delay models in the meeting.

**G02/10P/D-009** Poster **1400-074**

**AN EVALUATION OF POSITIONING ERROR ESTIMATED BY THE MESOSCALE NON-HYDROSTATIC MODEL**

Ryuichi ICHIKAWA<sup>1</sup>, Hiromu SEKO<sup>2</sup>, Michael BEVIS<sup>3</sup> (<sup>1</sup>Kashima Space Research Center, Communications Research Laboratory, <sup>2</sup>Meteorological Research Institute, Japan Meteorological Agency, <sup>3</sup>Pacific GPS Facility, University of Hawaii)

We evaluate atmospheric parameters (equivalent zenith wet delay and linear horizontal delay gradients) derived from slant path delays obtained by ray-tracing through the non-hydrostatic numerical weather prediction model (NHM) with 1.5 km horizontal resolution. Our ultimate purpose is to establish a new method for reducing atmospheric effects on geodetic positioning. We first seek to establish the level of positioning error due to intense mesoscale phenomena such as the passing of cold fronts, heavy rainfall events, and severe storms. The NHM provides temperature, humidity and pressure values at the surface and at 38 height levels (which vary between several tens meters and about 35 km), for each node in a 1.5 km by 1.5 km grid that covers Izu peninsula of the central Japan and surrounding ocean. We performed ray tracing experiments for the entire grid of the NHM at one epoch of the 1200 UT 3/7/1997. For each station we invert the simulated data set, consisting of 52 slant delays, using an isotropic and an anisotropic delay model. The isotropic model has only one parameter - the zenith wet delay (ZWD). The anisotropic delay model of Chen and Herring (1997) has two additional lateral gradient parameters. We compare the "true" ZWD, computed by directly integrating the wet refractivity field of NHM, with the ZWD estimated by least squares inversion of the "observed" slant delays obtained by ray tracing. We did this using the isotropic and the anisotropic delay models [e.g. MacMillan, 1995; Chen and Herring, 1997]. A characteristic GMS cloud pattern caused by the mountain lee waves is presented in the study area. At the east of the Izu peninsula ZWDs are lying in a north-south band about 10 km in width and about 50 km in length. This ZWD pattern is consistent with that of cloud image. Large gradient vectors are shown nearby the north-south ZWD band. In addition the biggest gradients occur at the northern part of the peninsula where topographic variations produce a much more complex distribution of water vapor. We are numerically examining positioning errors calculated from the slant delays through the NHM, assuming single point positioning and relative positioning. The behavior of the positioning errors under the atmospheric disturbance in local scale, the relation between the slant delay errors and the vertical positioning errors, and the efficiency of the reduction of the azimuthal anisotropy of the atmosphere using the anisotropic mapping function will be represented.

**G02/10P/D-010** Poster **1400-075**  
**GROUND SIMULATOR DEVELOPMENT FOR INTER-SATELLITE LASER INTERFEROMETER**

Taizoh YOSHINO<sup>1</sup>, Hiroo KUNIMORI<sup>2</sup>, Mizuhiko HOSOKAWA<sup>3</sup>, Seiji KAWAMURA<sup>4</sup>, Shigeo NAGANO<sup>5</sup>, Isao NAITO<sup>6</sup>, Takashi SATO<sup>7</sup>, Masashi OHKAWA<sup>8</sup> (<sup>1</sup>Kashima Space Research Center, Communications Research Laboratory, <sup>2</sup>Communications Research Laboratory, <sup>3</sup>National Astronomical Observatory, <sup>4</sup>Niigata University)

Japan is one of the most active area in geophysical aspects. Hence, we have interests in the time varying gravity field observation from the space. As a feasibility study of future gravity field mapping from the space, laser interferometric technique is studied by developing the Ground Simulator to improve the sensitivity of the current inter-satellite system, GRACE, which is based on radio technique. The design of the Ground Simulator system is Mach-Zender optical interferometer type. It is composed of stabilized laser, gravity field simulator and its retrieval system. The simulator will be developed in three years. As a first step, we are going to develop a stabilized laser. Firstly, semiconductor laser (780nm) locked to Rb absorption line is developed. Expected stability is  $10^{-13}$ . A prototype system and its performance including the stability data will be shown. Next year, we will improve its performance and assemble the rest of the system. Using the existing satellite laser system, GRACE satellites are observed. The observation results will be also reported. We exchange the technical information with the related technology group in Japan: a) Gravity wave detection system(TAMA300), b) NeLS (Inter-satellite optical link for communication) under R&D, c) OICETS (Optical Inter-orbit Communications Engineering Test Satellite) to be launched in 2005. Our study is supported by the fund of Ministry of Education, Culture, Sports, Science and Technology.

**G02/10P/D-011** Poster **1400-076**  
**RELATIVISTIC VLBI DELAY MODEL FOR FINITE DISTANCE RADIO SOURCE**

Mamoru SEKIDO, Toshio FUKUSHIMA (Communications Research Laboratory)

Precise VLBI delay model including general relativity is required for analyzing VLBI data of finite distance radio source in the Solarsystem. One of the example of VLBI target is spacecraft "NOZOMI", which was launched for investigation of Mars by the Institute of Space and Astronautical Science (ISAS). However, such VLBI delay model has not been reported so far. We derived a VLBI delay model for finite distance radio source based on linearized Parameterized Post Newtonian (PPN) metric. The derivation procedure is as follows: Making a form of relation between VLBI delay and baseline vector in the barycentric frame of the solar system, where the motion of photon is expressed simpler than geocentric frame. Introducing a transformation of time scale and spatial coordinates between barycentric frame and geocentric frame with based on PPN metric. Here we used local Minkowskian laboratory coordinates approximation by following the procedure of Hellings (1986). Deriving a form of relation between VLBI delay measured by a clock on the geoid and baseline vector measured by scale on the geoid by using the relations introduced in (1) and (2). The accuracy of the model is in an order of picoseconds. This model was implemented in a VLBI delay model computation software realized by modification of CALC, which is widely used VLBI delay model calculation software developed by NASA/GSFC. The spacecraft "NOZOMI" is going to swing-by with the Earth in June 2003, then it will depart for the Mars. It is required to measure the position of "NOZOMI" by VLBI in the period between February and May of 2003 for accurate swing-by in June. Our VLBI delay model is used for VLBI data analysis for "NOZOMI".

**G02/10P/D-012** Poster **1400-077**  
**STUDYING ERUPTION COLUMN OF THE AUGUST 18, 2000 MIYAKEJIMA ERUPTION, JAPAN, BY CONTINUOUS GPS MEASUREMENT**

Dudy DARMAWAN<sup>1</sup>, Bambang SETYADJF, Fumiaki KIMATA<sup>2</sup>, Kazuro HIRAHARA<sup>3</sup> (<sup>1</sup>Graduate School of Environmental Studies, Nagoya University, <sup>2</sup>Departement of Geodetic Engineering, Institute of Technology Bandung, <sup>3</sup>Graduate School of Science, Nagoya University)

Miyakejima Volcano is an active basaltic andesite stratovolcano located about 200 km south of Tokyo, Japan. The recent intense activity of the volcano occurred during the period from June 26 to September 4, 2000, which was noticed by several earthquakes and summit eruptions. The largest eruption occurred on August 18, 2000, lofting up the volcanic materials more than 8 km. In this research, we attempt to study such eruption by using GPS technique. Since the eruption was not certainly associated with a large volcanic earthquake, we therefore are interested in analyzing the ejected volcanic materials distribution during the eruption. At first, we inspect the effect of the volcanic materials to GPS signal travel and eventually to the estimated GPS baseline. As will be shown, the signal travel is delayed by the volcanic materials and the baseline is extended to some centimeters. Second, we estimate the GPS excess path delay by modeling it using an integration expression derived from ray theory. The estimated excess path delay is generally about 10 cm, except for the site located in the western part of the volcano (more than 10 cm). Lastly, we estimate the distribution of the volcanic materials during the eruption by using GPS tomography technique. The result shows that the eruption was firstly detected around 17.20 JST and declined around 18.00 JST by GPS measurements. Wet delay corrections for GPS stations located near western part of the volcano are higher than other sites. The estimated tropospheric refractive index derived from the tomography technique show clearly that the high refractive value appear near western and south-western part of the island. We therefore expect that the eruption column were to be heaviest near such area. These results are consistent with information released by Japan Metrological Agency (JMA).

**G02/10P/D-013** Poster **1400-078**  
**GROUND-BASE VERIFICATION OF FOUR-WAY DOPPLER MEASUREMENT FOR THE SELENE MISSION**

Hiroto NODA<sup>1</sup>, Kazuyoshi ASARI<sup>1</sup>, Yusuke KONO<sup>2</sup>, Takahiro IWATA<sup>3</sup>, Noriyuki NAMIKI<sup>4</sup>, Hideo HANADA<sup>5</sup>, Nobuyuki KAWANO<sup>6</sup>, Zen'ichi YAMAMOTO<sup>7</sup> (<sup>1</sup>Division of Earth Rotation, National Astronomical Observatory, <sup>2</sup>National Space Development Agency, <sup>3</sup>Kyushu University, <sup>4</sup>The Institute of Space and Astronautical Science)

In Japan's lunar mission called SELENE, detailed measurements of the lunar gravity field will be carried out by using two methods. The first is the differential VLBI measurement with two sub-satellites, and the second is the four-way Doppler measurement by using a sub-satellite which relays radio waves from the main lunar orbiter. Especially the lunar far-side gravity field will be directly measured for the first time by using the relay satellite, which will give us new information about the inner structure of the Moon. The instruments are now under development, and various tests of Usuda Deep Space Center (UDSC) and of instruments onboard SELENE have been conducted in order to confirm the expected function of the four-way Doppler measurement. Through these tests, it has been confirmed that our four-way measurement system has potential to determine the position and line-of-

sight velocity of the sub-satellite within the error of 1m and 0.2mm/s~0.3mm/s respectively. The test of the proto-flight-model(PFM) is also scheduled at UDSC in Feb. 2003. In our paper, the results of these ground-base tests will be reported.

**G02/10P/D-014** Poster **1400-079**  
**QUASI REAL-TIME POSITIONING OF SPACECRAFTS USING THE INTERNET VLBI SYSTEM**

Tetsuro KONDO, Yasuhiro KOYAMA, Ryuichi ICHIKAWA, Mamoru SEKIDO, Hiro OSAKI (Kashima Space Research Center, Communications Research Laboratory)

Communications Research Laboratory is developing new real-time VLBI system using Internet protocol (IP) technology to reduce network-cost and to expand connection sites of VLBI network. We call this system IP-VLBI or Internet VLBI. We are developing the system consisting of a personal computer (PC)-based sampler equipped with a PCI-bus Versatile Scientific Sampling Processor (VSSP) board and FreeBSD (and/or Linux) software to carry out an automated observation, real-time data transmission, reception and correlation. The IP-VLBI system developed at CRL is dedicated to taking over current geodetic VLBI system which usually receives 14 to 16 frequency channels at S and X bands. A VSSP board can sample 4 channel data simultaneously, hence 4 sets of boards (i.e., 4 PCs) can cover the current geodetic VLBI system and the system assembled this way is called K5. In parallel with the development of the real-time system, we are also developing a quasi-real time (QRT) VLBI system. In the QRT system data are stored in a hard disk at first, then transmitted to a correlation site with the available transmission speed of network. Off-line operation is also possible. In this case, data are transmitted after observations are made using an FTP or equivalent file transmission protocol. We started the development of technique to determine spacecraft's position in quasi real-time using the IP-VLBI system in collaboration with the Institute of Space and Astronautical Science (ISAS). A number of VLBI observations receiving Japanese spacecraft GEOTAIL and NOZOMI have been carried out since June 2002 to establish an observation method and to evaluate the measurement accuracy, and found that it is possible to measure group delay without ambiguities for telemetry signals. Phase delay measurements are also tried to increase the measurement accuracy and results will be reported in the meeting.

**G02/10P/D-015** Poster **1400-080**  
**THE QUALITY OF GNSS ORBITAL SOLUTIONS DETERMINED FROM SATELLITE LASER RANGING**

Graham Michael APPLEBY<sup>1</sup>, Toshimichi OTSUBO<sup>2</sup> (<sup>1</sup>NERC Space Geodesy Facility, <sup>2</sup>Communications Research Laboratory)

In this investigation we consider the use of precise laser range observations to perform independent checks on the accuracy of published orbits of a subset of the GPS and GLONASS navigational satellites. Laser range measurements to two GPS satellites and several of the GLONASS satellites obtained by the tracking network of the International Laser Ranging Service are compared in two ways with precise orbits computed by the International GPS and GLONASS Services; by direct comparison of SLR measurements to ranges computed from the microwave orbits, and by comparison of SLR-based orbits to the microwave orbits. Our previous work, which is also outlined here, has shown that in such comparisons it is vital to understand both the potential for systematic range ambiguity induced by the laser reflector arrays and the need for accurate on-satellite positions of the array phase centres. For the GLONASS and GPS satellites these parameters are now accurately known for the several different types of array currently in orbit, and the SLR results provide an accurate assessment of the radial quality of the IGS orbits.

**G02/10P/D-016** Poster **1400-081**  
**PRESENT-DAY DIFORMATION IN THE ZAGROS MOUNTAINS INFERRED FROM GPS MEASUREMENTS**

Faramarz NILFOROUSHAN<sup>1</sup>, Khaled HESSAMI<sup>2</sup>, Christopher J. TALBOT<sup>3</sup> (<sup>1</sup>Geodynamics Department, <sup>2</sup>International Institute of earthquake Engineering and Seismology, <sup>3</sup>Hans Ramberg Tectonic Laboratory, Department of Earth Sciences, Uppsala University)

Continental convergence between Arabia and Eurasia is taken up by distributed deformation in Iran. The relative motion between these plates and hence the overall deformation across Iran is known from global plate models such as NUVEL-1 (DeMets et al., 1990). The Arabia-Eurasia rotation pole at 24.6° N, 13.7° E, predicts a N-S convergence of about 32 mm/yr at the longitude of central Iran. For the study of recent crustal movements, geological methods need to be complemented by geodetic methods. GPS has clear potential and advantage as compared to any other techniques (e.g. classical methods) so that it has been widely used to measure recent local/regional crustal deformation with higher accuracy. It was utilized to reflect the velocity field (i.e., orientation and rate of movements) and the strain field associated with convergence movements between Arabian and Eurasian plates (Nilforoushan F. et al 2002). The main convergence is occurred in Zagros and Makran in South-West and Alborz and Kopet-Dag in the North. We present results of Global Positioning System (GPS) measurements at 36 stations across and within the Zagros Mountains, SW Iran, for 3 epochs February 1998, December 1999 and June 2001. Preliminary motion estimates show that deformation is distributed differently on either side of the Kazerun Fault Zone. To the east shortening is up to 10 mm/yr to SW relative to the Stable Eurasia. However, to the west stations move slower (up to 6 mm/yr) due to west. These rates are much slower than the relative convergence rates between Arabia and Eurasia of about 31 mm/yr, predicted by NUVEL-1A and 6 to 8 times than the rate calculated from summing of seismic moments. The apparent discrepancy between the rates of shortening of sedimentary cover within the Zagros and plate convergence rates suggests that the vast majority of the motion of Arabia is transferred northeastward across the Main Zagros Thrust.

**G02/10P/D-017** Poster **1400-082**  
**A SIMULATION STUDY OF GRAVITY FIELD RECOVERY BY MULTIPLE GRAVITY SATELLITES**

Keiko YAMAMOTO, Yoichi FUKUDA (Department of Geophysics, Graduate School of Science, Kyoto University)

The dedicated gravity satellite GRACE, which has been successfully launched in 2002, will provide spherical harmonic coefficients of the earth gravity field for every one month. Those extreme high precision gravity field data are expected to determine the temporal variations of the gravity fields due to time varying geophysical phenomena such as global water cycling. Although there is no doubt that even only one GRACE satellite should greatly contribute to those studies, one interesting question is how the spatial and/or temporal resolution of gravity field recovery will be improved if more than one gravity satellites will be operated simultaneously. As a matter of fact, both CHAMP and GRACE are under operating, and this means the situation of multiple satellites is real even at the present day. In future,

there may be a chance that more than one GRACE /GRACE-FO type missions could be realized simultaneously. In this study, we thus carry out simulation studies of gravity field recovery by assuming multiple-satellite observation of GRACE and/or GRACE-FO. The simulation procedure is as follows; 1) synthesize time varying gravity fields using surface pressure data of ECMWF reanalysis data sets, 2) calculate multiple satellite positions and observe the synthesized gravity field data, 3) calculate spherical harmonic coefficients using the observed data and compare with the true synthesized gravity fields. We tested several combinations of multiple satellites, for instance, same orbit heights with same sensitivities, different orbit heights with different sensitivities, and so on, and we finally discussed effective combination of the satellites for the gravity field recovery.

**G02/10P/D-018** Poster **1400-083**

**THE CONTRIBUTION OF OPERATIONAL RESEARCH TO EFFECTIVE GRAVITY MODEL IMPROVEMENT**

Hussain A. SALEH (Institut de Recherches Interdisciplinaires et de Développements en Intelligence Artificielle, University Libre de Bruxelles)

With the coming of the space age, technologies have been developed that enabled a systematic observation of the entire Earth. It is being realized that in order to be able to understand the complex nature of the dynamic Earth, a multidisciplinary procedure is necessary in which the mapping of the Earth's gravity and magnetic fields with high resolution and accuracy is a prerequisite. High-resolution models of the gravity and magnetic fields of the Earth will help in modelling and understanding the structure of the Earth and the driving forces behind plate tectonics, motion associated with earthquakes, lithospheric motions, etc. In addition, a high-resolution gravity field model will help to establish a physically meaningful reference surface for oceans (within this context, the geoid). With the extensive collected (meteorological and geometrical) data sets of past, current and future geoscientific missions, ocean variations with respect of this surface can be efficiently studied on different geometrical and temporal scales. In addition, by combining these huge of collected data sets (altimetry and gravity), ocean currents can be deduced and possibly long-term effects like global sea level change can be thoroughly investigated. The developments of computationally computerised techniques that can provide a complementary procedure to combine and model gravity field information are lagging behind the general developments in the geoscience's research. Therefore, this advanced area of research using Artificial Intelligence (AI) is a promising direction to determine a global high-accuracy gravity field model with a higher resolution. In the last two decades model-based on ideas of the AI has been an important research area where new methodologies have been proposed, studied and experimented. Today AI is entering its maturity and this is witnessed by the number of applications which have been implemented and deployed, and by those which are currently under investigation. Within the Global Navigation Satellite Systems (GNSS) technology, metaheuristic techniques, which are often based upon ideas from AI have been researched, implemented, investigated and achieved good results in GNSS surveying. In this paper, these ideas are dynamically expanded to efficiently provide flexible and computerized procedures for determining a global high-accuracy gravity field model with a higher resolution. To successfully achieve this model, metaheuristic techniques, from the field of Operational Research (OR), have been proposed and implemented. These techniques are applicable to a wide range of important problems that occur in a variety of disciplines, such as statistics and engineering. OR attempts to provide a systematic and rational approach to the fundamental elements involved in the control of a problem by making decisions which, in some sense, achieves the best results in light of all the information that is available. Metaheuristic techniques play an effective role in OR applications by reducing the huge number of evaluations.

**G02/10P/D-019** Poster **1400-084**

Adriaan Z.A. COMBRINK (Space geodesy Programme, Hartebeesthoek Radio Astronomy Observatory)

**G03-Posters**

**Monday, July 7**

**DETERMINATION OF THE GRAVITY FIELD. MEETING OF IAG SECTION III**

Location: Site D

**Monday, July 7 PM**

**G03/07P/D-001** Poster **1400-023**

**DETERMINATION OF ABSOLUTE GRAVITY VALUES USING A FG5#210 IN BANDUNG AND YOGYAKARTA, INDONESIA**

Toshihiro HIGASHI<sup>1</sup>, Yoichi FUKUDA<sup>1</sup>, Maiko ABE<sup>1</sup>, Shuzo TAKEMOTO<sup>1</sup>, Sjafra DWIPA<sup>2</sup>, Dendi Surya KUSUMA<sup>3</sup>, Achmad ANDAN<sup>2</sup>, Koichiro DOI<sup>4</sup>, Yuichi IMANISHI<sup>1</sup>, Giuseppe ARDUINO<sup>5</sup> (<sup>1</sup>Department of Geophysics, Graduate School of Science, Kyoto University, <sup>2</sup>Geothermal Division, Directorate of Mineral Resources Inventory, Indonesia, <sup>3</sup>National Institute of Polar Research, <sup>4</sup>Ocean Research Institute, University of Tokyo, <sup>5</sup>UNESCO Office, Jakarta)

In November 2002 we carried out absolute gravity measurements for the first time in Bandung and Yogyakarta, Indonesia. Hitherto there was no absolute gravity station in Indonesia, therefore the absolute gravity measurements had been strongly desired. At first, we installed the absolute gravimeter FG5#210 at the Geological Museum in Bandung. Absolute gravity measurement was performed from November 15 to 20 in 2002. Measurements are repeated at intervals of 15 seconds and one set consists of 160 drops in 40 minutes. Number of total drops was about 20,000. The data are corrected for the solid earth tides (tidal gravity factor 1.164), the ocean tides, the pole tide (using IERS Bulletin A), the atmospheric pressure (admittance of 0.30µgal/hPa), and the instrumental height. For the vertical transfer correction, we measured by two LaCoste and Romberg gravimeters and obtained the gravity gradient of  $-2.743\mu\text{gal}/\text{cm}$ . We determined the absolute gravity value at metal mark on the floor of the Geological Museum using a gravity vertical gradient. Obtained preliminary absolute value is 977976.7019 mgal. The primary base station of gravity for Indonesia (DG-0) is established in the same Museum. We carried out the relative gravity measurements at absolute gravity point (metal mark) and DG-0 using the LaCoste and Romberg gravimeters. The obtained result is consistent with about 20µgal. On November 22-26, we also carried out the absolute gravity measurements in Yogyakarta near Merapi volcano. Number of total drops was about 15,000 and the gravity gradient is  $-2.873\mu\text{gal}/\text{cm}$ . The tentative gravity value obtained after the same corrections is 978203.0919 mgal. Determined absolute gravity values will contribute not only for the establishment of a precise gravity network in Indonesia but also for the detecting of gravity changes caused by seismic and volcanic activities.

**G03/07P/D-002** Poster **1400-024**

**THE NEW GRID OF GRAVIMETRIC TERRAIN CORRECTIONS OVER TURKEY COMPUTED FROM HIGH-RESOLUTION DIGITAL TERRAIN MODEL**

Ali KILICOGLU, Mehmet Emin AYHAN, Coskun DEMIR, Orhan FIRAT, Ersin AKIZ (Department of Geodesy, General Command of Mapping)

Terrain correction, which represents the gravitational attraction of topography deviating from the Bouguer plate, generates a gravity signal that must be removed from any modelling process. The digital terrain model (DTM) including the bathymetry for Turkey on a 450 x 450 meter grid has enabled the computation of gravimetric terrain corrections. DTM was the result of the combination of a number of regional and global sources of topography, and was checked against systematic errors and isolated error points. The rectangular prism of constant density (2.67g/cm<sup>3</sup>) is used for numerical integration of the terrain effect. The effect of the far topography up to 50 km from the computation point was taken into account. A pre-tested technique with standardized inputs -such as appropriate algorithm, DTM resolution and quality, innermost area computation, effect of near/far topography- was used in this study. GRAVSOF gravity field software package, in which the terrain correction computation with many features is fully implemented, was used in order to compute terrain corrections on a regular grid of 450 x 450 meter. Then, the total topographic effect including the effect of the Bouguer plate and plus terrain correction at the same grid was computed for further use in Bouguer anomaly computation. These products can be used in practice by interpolating at any desired station. The maximum, mean and standard deviation of the computed terrain corrections on land points were found to be 99.9 mGal, 1.79 mGal and 4.23 mGal respectively. The relation between terrain corrections and the topography was investigated using spectral techniques.

**G03/07P/D-003** Poster **1400-025**

**CALIBRATION OF THE SUPERCONDUCTING GRAVIMETER WITH AN ABSOLUTE GRAVIMETER FG-5 IN BANDUNG, INDONESIA**

Maiko ABE<sup>1</sup>, Toshihiro HIGASHI<sup>1</sup>, Yoichi FUKUDA<sup>1</sup>, Shuzo TAKEMOTO<sup>1</sup>, Sjafra DWIPA<sup>2</sup>, Dendi Surya KUSUMA<sup>3</sup>, Achmad ANDAN<sup>2</sup>, Yuichi IMANISHI<sup>1</sup>, Koichiro DOI<sup>4</sup> (<sup>1</sup>Department of Geophysics, Graduate school of Science, Kyoto University, <sup>2</sup>Geothermal Division, Directorate of Mineral Resources Inventory, Indonesia, <sup>3</sup>Ocean Research Institute, University of Tokyo, <sup>4</sup>National Institute of Polar Research)

Since December 1997, gravity observations using a superconducting gravimeter (SG TT-70 #008) have been carried out in Bandung in cooperation between the Graduate School of Science, Kyoto University and the Volcanological Survey of Indonesia (VSI). In order to obtain reliable gravity data by means of SG observation, it is necessary to calibrate the SG system by comparing results with absolute gravimeter (AG). We carried out AG measurements by employing the FG-5 (#210) during the period November 10-19<sup>th</sup> 2002 at the Geological Museum near the Bandung SG station. We carried out 227 sets each of which has 160 drops of measurements at 15 seconds intervals. The total number of drops was 36,320, and we used 29,000 drops for the SG calibration. The calibration factor preliminary obtained is  $-52.281\pm 0.10\mu\text{Gal}/\text{V}$ . This value is in good agreement with the currently adopted values of  $-52.23\mu\text{Gal}/\text{V}$ . The precision of the newly obtained factor is about 0.2%. Although the precision may be slightly worse than those required for the studies of Earth tides and dynamics in the Earth's deep interior, there are still some blunders in the AG data sets and the precision could be improved by removing those data.

**G03/07P/D-004** Poster **1400-026**

**NEW GRAVITY ANOMALY MAPS FOR ARGENTINA: MAGARG 2003**

Eduardo Andres LAURIA<sup>1</sup>, Maria Cristina PACINO<sup>2</sup>, John Derek FAIRHEAD<sup>3</sup>, Denizar BLITZKOW<sup>4</sup> (<sup>1</sup>Instituto Geográfico Militar, <sup>2</sup>Universidad Nacional de Rosario, <sup>3</sup>GETECH, <sup>4</sup>Universidade de Sao paulo)

Gravity surveys have been carried out in Argentina over the last century by Instituto Geográfico Militar, academic institutions and oil and mining companies. Part of these data was already used to produce several gravity maps on the national territory. However, the large number of new height and gravity data acquired during the past few years demands the reprocessing of the updated gravity data to enhance and maximise its use. Furthermore, recent developments in geodetic and geophysics applications require precise geoid models, which demand good quality gravity grids. In this sense, new gravity maps (Bouguer and free air anomaly) were produced. This contribution describes the reprocessing of existing gravity data as well as the improvements reached from this process. All the activities are developed under the umbrella of the National Committee of the International Union of Geodesy and Geophysics (Subcommittee of Geodesy).

**G03/07P/D-005** Poster **1400-027**

**A PRACTICAL COMPARISON OF HELMERT'S FIRST AND SECOND METHOD OF CONDENSATION IN THE PRECISE GEOID DETERMINATION**

Szabolcs ROZSA, Bernhard HECK (Geodetic Institute, University of Karlsruhe)

According to the widely applied Helmert's second method of condensation, the topographic masses are condensed to a surface layer, which is situated on the geoid. In this case the downward continued free-air anomalies are equal to the Faye-anomalies supposing the vertical gravity gradient to be equal to the normal vertical gravity gradient. Heck proposed to use a generalized method of condensation involving a deeper compensation level, because of the roughness of the residual anomaly field in the previous case. This procedure extends Helmert's first method of condensation, where the topographic masses are shifted to a layer situated 21 km below the geoid. In this paper the gravimetric geoid solutions are computed for Hungary in order to compare the two methods. For the calculations altogether 58800 gridded terrestrial mean free-air anomalies are used, with the spatial resolution of 1.5' and 1' in the E-W and N-S directions respectively. Moreover a DEM with the resolution of 500m is used for calculating the effect of the topographic masses. However in order to investigate the effect of the depth of the condensation layer, the calculations have been made using different condensation depths. In order to compare the results to GPS/levelling data, altogether 308 GPS/levelling points are also included in the investigations, which are distributed equally over the study area. Out of these stations altogether 95 have a levelled elevation which stems from measurements after the GPS campaigns.

**G03/07P/D-006** Poster **1400-028**

**PREDICTION OF VERTICAL GRAVITY GRADIENTS USING GRAVITY AND ELEVATION DATA**

Gyula TÓTH<sup>1</sup>, Szabolcs ROZSA<sup>2</sup> (<sup>1</sup>Budapest University of Technology and Economics, Department of Geodesy and Surveying, H-1521, Budapest, Muegyetem rkp. 1-3., <sup>2</sup>University of Karlsruhe,

The vertical gravity gradients play an important role in the reduction of absolute gravity measurements and in the geoid determination, too. In order to enhance the precision of the gravity reductions and the geoid computations the difference between the vertical gravity gradient of the real and normal gravity fields should be taken into account. In this paper the vertical gravity gradients are computed by prism integration using constant and variable densities for the crustal masses and a high resolution (10m) digital elevation model to represent the topography in the Sósokút test area. On the other hand gravity gradients are predicted from 1610 point gravity data using the least-squares collocation method, too. The calculated gradient values are compared to each other, and they are validated using terrestrial measurements in 6 points in the Sósokút test area. The measurements of the vertical gravity gradients were carried out by the Lorád Eötvös Geophysical Institute and have the accuracy better than 80E, and are within the interval of 3189-3805E. The vertical gradient values calculated from the DEM are in the interval of 3123-4171 E, and the values fitted to the measured values with the root-mean-square of 290E, and the maximal residual of 400E. Moreover the application of the predicted gravity gradients in the precise gravimetric geoid determination is investigated, and the effect of variable gravity gradients is also computed for the study area.

**G03/07P/D-007** Poster **1400-029**  
**GRAVITY-BASED FAULT MAPPING: THE ISHIKARI LOWLAND OF HOKKAIDO, JAPAN**

Akihiko YAMAMOTO (Institute of Seismology and Volcanology, Hokkaido University)

The Ishikari Plain is characterized by the largest alluvial lowland (the Ishikari Lowland) in Hokkaido, Japan. In the eastern margin of this plain lies the Ishikari Teichi Touden Fault Zone (ITTFZ) which borders on the Miocene hill belts (Iwamizawa, Kurisawa and Umaoi hills). In the central part near Sapporo City of this plain, the Nopporo Hill is bordered by largely WNW-ESE striking faults, the Nopporo Hill Fault Zone (NHFZ). Past gravity studies in the Ishikari Lowland showed that low anomalies corresponding to Quaternary sediments are dominant over the plain, whereas detailed gravity structures particularly across the ITTFZ and the NHFZ have not been reported so far. This research examines gravity structures of the Ishikari Lowland by focusing relief-shaded Bouguer gravity, specifically to relocate the faults (the ITTFZ and the NHFZ), and to present a gravity-based active fault mapping in the plain for correct determination of fault segmentation. Gravity analyses are based on dense gravity data measured by various institutes. Bouguer anomaly relief is produced by illuminating the light from eight directions to effectively display the detailed gravity features varying laterally along the azimuth direction. The active fault distribution in the region is mapped through the relief-shaded Bouguer anomaly. A striking linearity of the relief-shaded Bouguer gravity along the ITTFZ is found on most of the relief maps, particularly on the maps for the azimuth of the due east and west. This lineament shows a good agreement with distributions of both the old and new active faults in the northern and southern parts of the ITTFZ. In the central part of the ITTFZ, however, the lineament in the relief-shaded Bouguer map does not bear a good correlation with the active fault distributions. It is also shown that the ITTFZ largely consists of N-S oriented two parallel fault zones and their gravity anomalies associated with two high anomaly belts reflect the complicated subsurface structure. In addition, the gravity relief for the azimuth of the due north (or south) exhibits a remarkable lineament, extending southward from near Bibai, whose southward continuation can be traced to the south-east until south of Atsuma along the westernmost boundaries of pre-Neogene volcanics. This implies that the geometry of the southern end of the known fault system (the ITTFZ) provides continuity along the relief-shaded Bouguer lineament roughly to the south-east. While gravity anomalies around the Nopporo Hill are small in amplitude and are associated with no abrupt gravity changes compared to its topography and surrounding fault distributions. Any of relief-shaded Bouguer gravity maps does not show a sharp lineament around the NHFZ. This implies that no sharp density contrast is appreciable around the NHFZ at depths.

**G03/07P/D-008** Poster **1400-030**  
**OPTIMISATION OF DENSITY PARAMETER IN GRAVITY PREDICTION FROM BATHYMETRY**

David Michael SPROULE<sup>1</sup>, A.H.W. KEARSLEY<sup>1</sup>, R. FORSBERG<sup>2</sup> (<sup>1</sup>School of Surveying and Spatial Information Systems, University of New South Wales, <sup>2</sup>KMS, National Survey and Cadastre, Denmark)

This paper describes experiments conducted to examine the combination of gravity values predicted from bathymetric data with observed gravity data to increase the resolution of offshore gravity data. The density parameter in the prediction is optimised empirically. The gravity effect resulting from bathymetric features can provide short wavelength features of the gravity field, but at longer wavelengths subsurface features begin to influence the gravity signal. By using a combination of observed gravity and gravity predicted from bathymetry, the long wavelength features present in the direct observations can be preserved while using the bathymetric data to fill-in the short wavelength features. The computation scheme is described, and some numerical results are presented. The effect of increasing the distance between the observed gravity data is examined. For the calculation of the gravity signal arising from the bathymetry, a single density value is chosen for the entire area. Due to density variations this density may not be optimal. Different density values are tested to examine the effect this choice has on the resulting predicted gravity.

**G03/07P/D-009** Poster **1400-031**  
**A VERSATILE GRAVIMETRY/GADIOMETRY SIMULATION SOFTWARE**

Olivier JAMET<sup>1</sup>, Yassine AZZOUT<sup>2</sup> (<sup>1</sup>Laboratoire LAREG, Ecole Nationale des Sciences Géographiques, <sup>2</sup>Ecole Supérieure d'Ingénierie Leonard de Vinci)

**Context:** With the forthcoming GOCE mission, that will provide gradiometric measurements from space, it will be possible to study geophysical phenomena at horizontal resolutions from 50km to 100km. Besides, the improvement of the accuracy of the ground measurements let us foresee the possibility to compute regional geoids at one centimeter accuracy. For both reasons, we need to better understand the relation between the crustal structure and the gravity field computation, and are developing a new software for simulating the potential field and its derivatives from a given geology at the local to regional scale. **Theory:** On areas wider than 50km, the approximation of a flat Earth does not hold, and the formulas for the prism, as published by Nagy et al. (2000) are not sufficient. We use the approach of Petrovič (1996), which allows to express the potential of any homogeneous polyhedral body, as well as its derivatives. These expressions are suitable to compute the gravity potential, acceleration and gradiometry from a 3D model of the crustal structure through a simple scan of its edges. Though, their accuracy drops down when the point of interest is located far away from the edges of the 3D model. This is in particular the case when simulating satellite measurements. To cope with this issue, we propose an approximate expression, whose accuracy is assessed, and which allows to compute the potential (and its first and second derivatives) at a given accuracy at any point of the 3D space. **Software specifications:** The

software computes the potential and its derivatives at given locations (from ground to satellite orbit altitudes) of the gravity generated by polyhedral structures supplied in cartographic coordinates and formatted to VRML 2.0. The output can be formatted to scattered measurement points, acquisition lines, or regular grids. **Application:** We present the results of such a computation for the granitic basement on a 100km wide area of the west of France. This example allows to evaluate the effect of the uncertainty of the rock density on the geoid computation. **Further work:** Further developments will include the contribution of the long wavelengths of the potential through a mixing of the results with existing spherical harmonic models of the geopotential. **Acknowledgement:** We thank the French Bureau de Recherches Géologiques et Minières for supplying us with the geological data presented in this study. **References:** (Petrovič 1996) S. Petrovič: Determination of the potential of homogeneous polyhedral bodies using line integrals, *Journal of Geodesy*, vol.71 n. 1, pp. 44-52 (Nagy et al. 2000) D. Nagy, G. Papp and J. Benedek: The gravitational potential and its derivatives for the prism, *Journal of Geodesy*, vol.74 n. 7-8, pp. 552-560

**G03/07P/D-010** Poster **1400-032**  
**A GRAVITY DATABASE OF SOUTHWEST JAPAN: APPLICATION TO BOUGUER GRAVITY IMAGING IN KYUSHU DISTRICT, SOUTHWEST JAPAN**

Ryuichi SHICHI<sup>1</sup>, Akihiko YAMAMOTO<sup>2</sup>, Takeshi KUDO<sup>3</sup>, GRG SWJ<sup>1</sup> (<sup>1</sup>Chubu Univ., <sup>2</sup>Hokkaido Univ., <sup>3</sup>Tono Geoscience Center, <sup>4</sup>Gravity Research Group in Southwest Japan)

Two large gravity databases in Japan have been issued for public use in 2000 and 2001. One is the "Gravity CD-ROM of Japan" published by the Geological Survey of Japan (GSJ) (GSJ, 2000). The other is the "Gravity Database of Southwest Japan" published by the Gravity Research Group in Southwest Japan (GRGSJWJ) (2001). Both databases were formed mutually complementary in their distributions of gravity data. Consequently, by combining these two databases, gravity data of southwestern area of the Japanese Islands lose their non-closely-spaced character and spread evenly over the area. Although both databases have been compiled with a higher precision of about 1 mgal, they still contain gravity data with a precision no better than a few milligals or more which are not accurate enough for a detailed mapping. We are now executing further revisions to remove those poorly-calibrated data by careful scrutiny. We have accomplished this revision in the area of Kyushu District, southwest Japan, and it becomes possible to draw very precise gravity anomaly atlas which fully guarantees a precision of 1 mgal in the whole area. Characteristic features of a new precise gravity anomaly in Kyushu District are tersely summarized as follows: (1) The Aso Caldera, central Kyushu, is characterized by a prominent low gravity anomaly accompanying several closed minima inside the caldera. This gravity depression is nearly circular shaped, with a steep rim and a flat bottom. Gravity changes along the rim have the amplitude of more than 10 mgal/km. This implies that the Aso Caldera has a piston-shaped cylinder (not funnel-shaped) structure. (2) The Oita-Kumamoto Tectonic Line (OKTL), running nearly along the Tertiary-Pre-Tertiary geologic boundary in central Kyushu, is considered to be a westward extension of the Median Tectonic Line from Shikoku District. By forming a belt-like structure of 5-10 km width, a dominant steep gravity gradient zone which is running through the Aso Caldera is observed along the ENE-WSW trending OKTL. Southwestward continuation of this gradient zone is passing through the northern coast of the Uto Peninsula and can be traced to Hondo (central Amakusa, southern part of the Inner Zone of Kyushu). Adjacent to the north of this steep gradient zone lies a huge and strong low anomaly belt. (3) A strong negative Bouguer anomaly is observed over the Hyuganada Basin, southeastern Kyushu, and characterized by a sharp inlandward increase of Bouguer gravity. This gravity low constitutes arcuate-shaped depression whose northwesternmost boundary is sharply cut by Pre-Tertiary volcanics. This implies that subsurface structure beneath the basin may be correlated to the tectonic drag caused by subduction of the Philippine-Sea Plate. (4) Trend-reduced Bouguer gravity shows a large positive anomaly over the Pre-Tertiary formations in the northern part of Kyushu. In contrast, negative anomalies are dominant over the Pre-Tertiary formations in the southern part of Kyushu, particularly around the Kyushu Mountains. While the Amakusa Islands are characterized by a strong gravity high in detrended Bouguer map, which is well corresponded with Paleogene formations.

**G03/07P/D-011** Poster **1400-033**  
**REPEATED MEASUREMENTS OF GRAVITY WITH THE ABSOLUTE GRAVIMETER FG5 #210 AT MATSUHISHI, JAPAN AND COMPARISON WITH THE SUPERCONDUCTING GRAVIMETER T011**

Yuichi IMANISHI<sup>1</sup>, Toshihiro HIGASHI<sup>2</sup>, Yoichi FUKUDA<sup>3</sup>, Mitsuyuki HOSHIBA<sup>3</sup>, Kazuya KOKUBO<sup>4</sup> (<sup>1</sup>Ocean Research Institute, The University of Tokyo, <sup>2</sup>Department of Geophysics, Graduate School of Science, Kyoto University, <sup>3</sup>Matsushiro Seismological Observatory, Japan Meteorological Agency)

We have been conducting absolute gravity measurements at Matsushiro Seismological Observatory, Japan Meteorological Agency. The measurement site is a gravity station called the Fundamental Gravity Station (FGS) built by Geographical Survey Institute. This station is located in the gravimeter room inside the major tunnel of the observatory, about 2 m apart from the superconducting gravimeter (SG) T011. The main purpose of the measurements is to monitor the long term gravity changes by combining absolute gravity data with continuous gravity data from the SG. This should help also in calibrating the instrumental drift of the SG. In addition, comparison of the two gravimeters provides an opportunity for calibration of the instrumental sensitivity of the SG. Since this station is in a very good condition in terms of ground noise level and environment, it is expected that long term changes in gravity (if any) could be observed with high accuracy. The absolute gravity measurements took place in April 2000, December 2000, December 2001 and August 2002. The same instrument (FG5 #210) and procedure were used throughout these four experiments. The experiments spanned from one to four weeks. In each experiment, the measured gravity values followed a normal distribution, and the determination of the local gravity acceleration appeared to be successful. The gravity estimates (referred to the top of the FGS metal plate) from these experiments are, in the MKS unit,  $9.797729815 \pm 0.000000072$  (April 2000),  $9.797729769 \pm 0.000000090$  (December 2000),  $9.797729948 \pm 0.000000099$  (December 2001) and  $9.797729845 \pm 0.000000070$  (August 2002). Among these, the December 2001 result may be regarded as an outlier, which could be attributed to instability of the rubidium clock used for our FG5. Evidences show that, in the December 2001 experiment, the frequency may have been lower than the prescribed value by some parts in  $10^5$ . This should have resulted in an estimate of gravity acceleration larger than the true value by  $(5-10) \cdot 10^{-9} \text{ ms}^{-2}$ . This fact points to the necessity of precise calibration of the rubidium clock against other frequency standards, such as a well-calibrated rubidium clock or a cesium clock, which we have already included in our routine. On the other hand, the SG at Matsushiro has been very stable and had no large steps in these years. The instrumental drift of the SG T011 is almost linear in time, and the residual gravity indicates small changes probably associated with hydrological effects. Aside from the December 2001 result, the absolute gravity data are in agreement with the SG data within  $(2-4) \cdot 10^{-9} \text{ ms}^{-2}$ . No clear evidences for secular changes in gravity have been observed.

G03/07P/D-012 Poster 1400-034

**ABSOLUTE GRAVITY MEASUREMENTS IN IRAN RESULTS OF BASE GRAVITY NETWORK & ALBORZ PROJECT**

Morteza SEDIGHI<sup>1</sup>, Jacques HINDERER<sup>2</sup>, Kourosh GHAZAVI<sup>1</sup>, Roger BAYER<sup>3</sup>, Faramarz NILFORUSHAN<sup>3</sup>, Brenard LUCK<sup>2</sup>, Farokh TAVAKOLI<sup>1</sup>, Martine AMALVICET<sup>1</sup>, Hamid Reza NANKALI<sup>1</sup> (<sup>1</sup>National Cartographic Center, <sup>2</sup>CNRS France)

National Cartographic Center (NCC) of Iran, IPGS\_CNRS/ University of Strasbourg and LGTS-CNRS/ University of Montpellier II from France in a common project, measured the absolute gravity of Gravity Base Network of Iran. The measurements at seven stations of Network were done during 2000 and 2002. The absolute gravimeter was FG5(#206) from Strasbourg university. The computations was done by new version of Absolute Gravity Data Acquisition and Processing Software. During the computation we tested all possibility for tidal and ocean loading corrections. The results show the precision from 1.40 - 4.04  $\mu$ Gal. The Berger tidal model + FES ocean loading corrections give better results in computations. We hope to finish the network in 2003.

G03/07P/D-013 Poster 1400-035

**ESTABLISHMENT OF NEW GRAVITY CALIBRATION LINE FOR IRAN**

Kourosh GHAZAVI, Farokh TAVAKOLI (Gravity and geoid, National cartographic center)

In recent years, 2000-2002, most important gravimetry activities in Iran were involved with absolute gravity measurements on stations of Gravity Base Network of Iran (GBNI). In collaboration with French scientist from university of Strasbourg 9 absolute stations of this network were measured by FG5 absolute gravimeter with accuracy about 3 mGal. For establishment of new Iranian National Gravity calibration line (INGCL) we used 5 stations of GBNI that are located along north west to south east direction of Iran. All old stations were inspected and those were located near the roads or damaged were reconstructed. In north - west part old line were changed in order to connect new line to absolute station at Tabriz and then extend it to Bazargan at near the boundary of Turkey. New line divided into 2 main parts. North part which begins from Bazargan, continues to absolute station of Tabriz next to Rasht (one of the relative station of GBNI) and finally reaches to absolute station at Tehran, capital of Iran. This part contains 38 stations along about 800 km where mostly located in rough area. South part begins from Tehran to absolute station of Qom then from there connected to absolute station at Esfehan and finally continues to absolute point in Shiraz. This part contains 25 stations along about 1000 km. All stations were measured simultaneously with 3 relative gravimeter (Scintrex CG-3M) that 2 of them manufactured last year and the other one 6 years ago. Each part of this line occupied 2 times, i.e. from Tehran to Bazargan (in north) or Shiraz (in south) and vice versa. In addition observations carried out using A-B-C-B-A method and in each station we measured at least 5 measurements to reach 5 mGal accuracy for repeatability of readings. Then all readings were checked and bad observations removed from survey files, after that readings corrected for drift and tide by OASIS MONTAJ software. Between each two absolute stations, relative differences of 2 new gravimeters were controlled with absolute difference values and errors were adjusted. We computed the absolute value of each station with accuracy better than 10 mGal by combination of corrected results that obtained from observations of 2 new gravimeters. Comparing difference of these values with which were measured by old gravimeter, using Least Square Adjustment method, old gravimeter was calibrated with accuracy about 100 ppm which is in order of best accuracy for calibrating of relative gravimeters on calibration lines.

G03/07P/D-014 Poster 1400-036

**IDENTIFICATION OF LONG-WAVELENGTH ERRORS IN AUSTRALIAN GRAVITY ANOMALIES AND GEOID HEIGHTS USING CHAMP DATA**

Will FEATHERSTONE (Western Australian Centre for Geodesy, Curtin University of Technology)

This study quantifies long-wavelength differences (from ~850 km to ~5,000 km) between terrestrial free-air gravity anomalies in the Australian region and gravity anomalies implied by the EIGEN2 global geopotential model, which is derived purely from the CHAMP dedicated satellite gravimetry mission. An 850 km low-pass cosine filter is used to remove the high-frequency components from the terrestrial gravity anomalies. Given the homogeneous and accurate long-wavelength CHAMP data, the differences are attributed to long-wavelength errors in the Australian gravity anomalies, due to a combination of observation and reduction errors. These long-wavelength differences are then used to quantify the effect on the regional gravimetric geoid model, using the unmodified Stokes kernel and no limit on the cap radius (i.e., all terrestrial gravity anomalies in the region). The unmodified Stokes kernel is used with no cap radius because, unlike some modified kernels with limited cap radii, it does not high-pass filter terrestrial gravity data errors during the transformation to the geoid. As such, this represents a somewhat worst-case scenario of how the long-wavelength terrestrial gravity anomaly errors could affect the Australian gravimetric geoid model.

G03/07P/D-015 Poster 1400-037

**COMPILATION AND EVALUATION OF A CONSISTENT MARINE GRAVITY DATA SET SURROUNDING EUROPE**

Heiner DENKER, Markus ROLAND (Institut fuer Erdmessung, Universitaet Hannover)

Various institutions have collected shipborne gravimetric measurements during the last decades. Due to different standards used for the processing of the observations and the necessary corrections, significant inconsistencies exist between different cruises. This contribution aims at producing a consistent marine gravity data set surrounding Europe, which can then be used for high precision geoid modelling, dynamic sea surface topography estimation, and other applications. Besides our own marine gravity data holdings, data were collected from the Bureau Gravimetricque International (BGI), the National Imagery and Mapping Agency (NIMA, formerly DMA), and the National Geophysical Data Center (NGDC). The area of investigation is spanning the latitudes from 20°N to 80°N and the longitudes from 40°W to 40°E. The quality of the data varies between the individual cruises, as they originate from many different projects over a long period of time. Hence, systematic errors are likely to exist. Such errors can be significantly reduced by a crossover adjustment of the individual ship tracks. As the track information is not available for all cruises, this information was regenerated by different procedures. Furthermore, duplicate sources were removed before the crossover adjustment. The crossover adjustment is based on a bias per track error model. The adjustment of about 2 million observations in more than 20000 tracks lead to a consistent high quality marine gravity data set. The RMS of the about 60000 crossover differences reduced by a factor of 2 to 3 through the adjustment process. The final RMS crossover difference is about 3 mgal. The second part of this contribution deals with the evaluation of the marine gravity data set using altimeter derived gravity anomalies from different sources. These comparisons also prove the effectiveness of the crossover adjustment.

G03/07P/D-016 Poster 1400-038

**GRAVITY CHANGES IN CHINA CONTINENT**

Hui LI, Guangyu FU, Shaoran SUN, Dongzhi LIU, Xiaoquan WANG, Aiming XIANG, Canfei XING (Institute of seismology, CSB)

Since 1988, three times gravimetry in China Continent had been carried out in 1998, 2000 and 2002 by employing absolute and relative gravimeters. The gravity network comprised of about 400 gravity stations. This paper firstly analyses the repetition of the measurements, and then the gravity changes are calculated, at last the precision of gravity changes and their relationship to the strong earthquake is discussed. According to the results, we get following points: 1) the repeated measurement stations is about 340, 2) precision of gravity changes about 30 microGal is reliable, 3) the gravity changes are among the +150 to -120 microgal, 4) the gravity changes is strongly related to the strong earthquake, the common feature is about the gravity decrease before the quake, and increase after quake, especially for the Kunlun quake (Ms8.1) occurred in November 11, 2001. Before the quake, the gravity change around the epicenter is decrease, which spread out over than 1000KMx1000KM, the maximum changes reach to 120 microGal. Compared gravity before and after quake, we found the gravity changes is recovering individually, and typical four-quadrant distribution is displayed covering whole western half China Continent. This will benefit to our geodynamics study.

G03/07P/D-017 Poster 1400-039

**THE ESTIMATION OF WATER MASS REDISTRIBUTION ON GRAVITY EFFECT**

Xuhua ZHOU, Houze HSU, Bin WU (Institute of Geodesy and Geophysics, Chinese Academy of Sciences)

Using monthly mean precipitation and temperature data over 7000 land meteorological station, TOPEX/Poseidon Satellite Altimeter data, WOA98 temperature and salinity model in multi-layers seawater, the gravity variation for some superconducting stations are estimated by the change of continental water and oceanic mass redistribution. Synthesizing the predicted gravity variation caused by change of continental water and oceanic mass redistribution, the result indicate that the effect on gravity observation caused by water mass redistribution has exceeded the accuracy of gravity observation, and it can achieve 5 microgals in some stations. In addition, we also discuss the effect of using different load Love numbers and continental water storage models on the estimation result. Key Words: Gravity, Water mass redistribution

G03/07P/D-018 Poster 1400-040

**TERRAIN CORRECTION ON THE MOVING EQUAL AREA CYLINDRICAL MAP PROJECTION OF THE SURFACE OF A REFERENCE ELLIPSOID**

Alireza A. ARDALAN<sup>1</sup>, Abdolreza SAFARI<sup>1</sup>, Erik W. GRAFAREND<sup>2</sup> (<sup>1</sup>Department of Surveying and Geomatics Engineering, University of Tehran, <sup>2</sup>Department of Geodesy and GeoInformatics, Stuttgart University)

An operational algorithm for computing the ellipsoidal terrain correction based on the application of closed form solution of the Newton integral in terms of Cartesian coordinates in the cylindrical equal area map projected surface of the reference ellipsoid has been developed. As the first step, the mapping of the points on the surface of a reference ellipsoid onto a cylinder passing through the parallel of a point on the surface of reference ellipsoid, i.e. the cylindrical equal area map projection, has been closely studied and the corresponding map projection formulas are derived. Ellipsoidal mass elements with various sizes on the surface of the reference ellipsoid are selected and the gravitational potential and the vector of gravitational intensity of those mass elements have been computed via the solution of Newton integral in terms of ellipsoidal coordinates. The four edge points of base area of the selected ellipsoidal mass elements on the surface of reference ellipsoid are transferred into cylindrical equal area map projection and using the transformed area elements, Cartesian mass elements with the same height as that of the ellipsoidal mass elements are constructed. Using the closed form solution of the Newton integral in terms of Cartesian coordinates the potential of the Cartesian mass elements are computed and compared with the same results based on the application of the ellipsoidal Newton integral for the ellipsoidal mass elements. The results of the numerical computations show that difference between computed gravitational potential of the ellipsoidal mass elements and Cartesian mass elements in the cylindrical equal area map projection is less than  $1.6 \cdot 10^{-8} \text{ m}^2/\text{s}^2$  for a mass element with the cross section area of  $10 \text{ m} \times 10 \text{ m}$  and the height of 10000m. For a mass element with cross section area of  $1 \text{ km} \times 1 \text{ km}$  with the height 10000m the difference between computed gravitational potential based on the two aforementioned methods is less than  $1.5 \cdot 10^{-4} \text{ m}^2/\text{s}^2$ . The results of the numerical computations indicate that a new method for computing the terrain correction based on the closed form solution of the Newton integral in terms of Cartesian coordinates and with accuracy of ellipsoidal terrain correction has been achieved! In this way one can enjoy the simplicity of the solution of the Newton integral in terms of Cartesian coordinates and at the same time the accuracy of the ellipsoidal terrain correction, which is needed for the modern theory of geoid computations!

G03/07P/D-019 Poster 1400-041

**UNIFIED EUROPEAN GRAVITY REFERENCE NETWORK 2002 (UEGN2002)**

Gerd BOEDECKER<sup>1</sup>, Olivier FRANCIS<sup>2</sup>, Ambrus KENYERES<sup>3</sup> (<sup>1</sup>Bavarian Academy of Sciences / BEK, Munich, Germany, <sup>2</sup>European Centre for Geodynamics and Seismology / Institut Supérieur de Technologie, Luxembourg, <sup>3</sup>FOMI Satellite Geodetic Observatory, Péc, Hungary)

The latest realisation of the Unified European Gravity Reference Network has been prepared in 1994 (UEGN94), covering 11 West European countries. Since that time significant work has been done (e.g. in the frame of the UNIGRACE project) that focused on the establishment of absolute gravity stations in Central and East European countries. The European Subcommittee of the IGGC (International Gravity and Geoid Commission of the IAG) promoted to complete the unification of the gravity networks on the continental level. During the IAG2001 Scientific Assembly held in Budapest in September 2001, the decision was taken that a new continental gravimetric reference network (so-called UEGN2002) has to be realised. The UEGN2002 network covers 25 countries, the expected number of stations exceeds 1000. The data processing is done using raw absolute and relative gravity observations. The tidal corrections are computed on a uniform manner and based on the most advanced standards. The common adjustment of all observations provides a homogeneous reference stations set throughout Europe and hence contribute to the common European infrastructure. The presentation will provide a status report including the countries and stations involved, the models used and preliminary results.

**G03/07P/D-020** Poster **1400-042**

**COMPARATIVE ANALYSIS OF DIFFERENT ADJUSTMENT METHODS FOR THE HUNGARIAN PART OF THE UNIFIED EUROPEAN GRAVITY NETWORK (UEGN)**

Geza CSAPO<sup>1</sup>, Marta KIS<sup>2</sup>, Lajos VOLGYESI<sup>3</sup> (<sup>1</sup>EOTVOS LORAND GEOPHYSICAL INSTITUTE, <sup>2</sup>BUDAPEST UNIVERSITY OF TECHNOLOGY AND ECONOMICS)

The first version of the Unified European Gravity Net (UEGN) was set up in 1993, based on the participation of 11 countries. The aim was basically the generation of the unified European geodetic basement for global geologic and geodynamic purposes. The unified scale of the network is ensured by numerous absolute gravimetric stations. Since 1995 further countries (inter alia Hungary) have been joined to the unified network. In this paper the adjustment of the Hungarian net part consist of 39 points is presented by the authors. The observed data were also adjusted by the help of robust procedures besides the least squares method, as both a free and a constrained network. A comparative analysis of the results achieved by the different methods is also presented in this paper.

**G03/07P/D-021** Poster **1400-043**

**VALIDITY CONTROL OF THE SEA GRAVITY DATA; CASE STUDIES**

Abdolreza SAFARI, Alireza A. ARDALAN (Department of Surveying and Geomatics Engineering, University of Tehran)

The sea gravity data, which are collected via shipborne techniques, due to the measuring environment at sea, are usually with low accuracy and contaminated with various systematic errors. One of the current problems of the international gravity centers like BGI is how to control the validity of the sea gravity data. In this paper we are offering a new method for validity control of sea gravity data based on satellite altimetry and the modern high-resolution geopotential models. The main steps of this method are as follows: First, the accuracy of the selected geopotential model at the test area is determined. Having assured of the accuracy of the geopotential model at the test area the instantaneous sea level height from satellite altimetry is used to compute the gravity data at the sea surface. The computed gravity data is then used to test the validity of an existing sea gravity data set. The details of the theory and the results of the case studies will be presented.

**G03/07P/D-022** Poster **1400-044**

**APPLICATION OF ALTIMETRY DATA FOR GRAVITY RESEARCH IN THE BLACK SEA**

Ivan Vladimirovich LYGUINE<sup>1</sup>, Vjacheslav Romanovich MELIKHOV<sup>1</sup>, Andrey Aleksandrovich BULYCHEV<sup>1</sup>, Vladimir Alexseevich LYGIN<sup>2</sup> (<sup>1</sup>Geophysical Department, Geological faculty, Moscow Lomonosov M.V. State University, <sup>2</sup>Marine Gravity and Magnetometry Department, NIPOceangeophysics, Krymskaya 18, Gelendjik, Krasnodar region, RUSSIA)

From ideology of altimetry measurements follow that optimal regions for altimetry are open zones of the World Ocean, where depths' measurements have minimal deviations. But there is a necessity for clearing up a question about possibility of application altimeter data not only for open regular abyssal parts of seas, but for investigations of dynamic active sea areas with sharply cross-bottom (e.g. mid-ocean ridges), offshore and enclosed seas, continental shelf and transit zones with strong effect of shore relief. It is very important for Russia because of insufficient studying its north coasts. We studied amplitude and phase characteristics of altimeter data (Predict-relief, Topex-relief, Sandwell-gravity-2, Topex-gravity) in comparison with results of high-accuracy square marine gravity surveys and detailed bathymetry for some areas of the Black Sea. We found out, that contemporary processing system of satellite altimeter tracks is the same both for open marine areas and for transit zones. In the future such defects can be eliminating, but "dead" zone along-shore will be exist. Taking into account bias marine gravity data and Topex-Gravity calculated anomalous gravity field of the Black Sea is not worse than data of average-scaled gravity surveys of 197x years. Determined that altimeter data may be used only for areas far from continental shelf (~100 km) for 1: 500 000 scale and only under the control of marine surveys.

**G03/07P/D-023** Poster **1400-045**

**COMPUTATION OF A GEOPOTENTIAL MODEL FROM GOCE DATA USING FAST SPHERICAL COLLOCATION - A SIMULATION STUDY**

C.C. TSCHERNING<sup>1</sup>, Dimitrios N. ARABELOS<sup>2</sup> (<sup>1</sup>Department of Geophysics, University of Copenhagen, Juliane Maries Vej 30, 2100 Copenhagen, Denmark, <sup>2</sup>Department of Geodesy and Surveying, Aristotle University of Thessaloniki, 54124 Thessaloniki, Greece)

Realistic orbit for GOCE from IAG SC7 was used to create a 0.5 T<sub>g</sub> grid of simulated data at mean satellite altitude. To this purpose, the SC7 positions along the orbit were converted from the inertial frame to geodetic coordinates in an earth-fixed frame. From these values the contribution of EGM96 to degree 24 was subtracted and the resulted data set was used to predict the 0.50 T<sub>g</sub> grid, covering the area of the Earth from -83° to +83° latitude using local Least-Squares Collocation. Noise was added to the simulated data using an optimistic and a pessimistic model of the noise. The simulated data sets were used to generate geopotential coefficients using Fast Spherical Collocation (FSC), with a global covariance function. Different experiments were carried out: (a) using a grid obtained from noise-free data and (b) using grids obtained from the data with noise. In all cases, the results of the computations are assessed by comparing the simulated input data with corresponding data from the predicted geopotential coefficients.

**G03/07P/D-024** Poster **1400-046**

**CALIBRATION AND VALIDATION OF GOCE GRAVITY GRADIENTS**

Johannes BOUMAN<sup>1</sup>, Radboud KOOP<sup>1</sup>, Roger HAAGMANS<sup>2</sup>, Juergen MUELLER<sup>3</sup>, Nico SNEEUW<sup>4</sup>, Christian TSCHERNING<sup>5</sup>, Pieter VISSER<sup>6</sup> (<sup>1</sup>SRON National Institute for Space Research, The Netherlands, <sup>2</sup>European Space Agency, ESTEC, <sup>3</sup>Institut fuer Erdmessung, University of Hannover, <sup>4</sup>Department of Geomatics Engineering, University of Calgary, <sup>5</sup>Department of Geophysics, University of Copenhagen, <sup>6</sup>Delft Institute for Earth-Oriented Space Research, Delft University of Technology)

GOCE will be the first satellite ever to measure the second derivatives of the Earth's gravitational potential in space. With these measurements it is possible to derive a high accuracy and resolution gravitational field if systematic errors have been removed to the extent possible from the data and the accuracy of the gravity gradients has been assessed. It is therefore necessary to understand the instrument characteristics to setup a validation model. The calibration parameters of this model could be determined by using GOCE data themselves or by using independent gravity field information. Also the accuracy or error assessment relies on either GOCE data or independent data. We will demonstrate how state-of-the-art global gravity field models, terrestrial gravity data and observations at satellite track

crossovers can be used for calibration/validation. In addition we will show how GOCE data or high quality terrestrial data could play a prominent role in error assessment.

**G03/07P/D-025** Poster **1400-047**

**THE EGYPTIAN GEOID EGGG2003**

Hussein A. ABD-ELMOTAAL (Civil Engineering Department, Minia University)

An optimum combination of all currently available free-air gravity anomalies in Egypt and neighbouring countries (both point values and gridded points on land and sea) is considered in this investigation. The best data combination is used to compute the gravimetric geoid for Egypt in the framework of the well-known remove-restore technique using a set of 30" x 30" and 3' x 3' Digital Height Models for computing the effect of the topography and its compensation on the gravity anomalies and on the geoid undulations (the indirect effect). The so-called window technique has been used to avoid the double consideration of some of the topographic-isostatic masses in the neighbourhood of the computational point. The commonly used Airy-Heiskanen isostatic hypothesis is applied (with and without window technique). The EGM96 global geopotential model and its adapted version according to the window technique are used till different upper degrees N<sub>max</sub> (to get a better fitting to the Egyptian gravity field) for computing the effect of the reference field. The gravimetric geoids are computed for Egypt using Stokes' integral in the frequency domain by 1-D FFT technique. The computed geoids are scaled/fitted to the GPS/levelling derived geoid. A wide comparison between the geoids computed in this investigation is carried out.

**G03/07P/D-026** Poster **1400-048**

**THE NEW GRAVIMETRIC GEOID MODEL FOR TURKEY (TG03)**

Ali KILICOGLU, Mehmet Emin AYHAN, Coskun DEMIR, Orhan FIRAT, Ersin AKIZ (Department of Geodesy, General Command of Mapping)

The geoid model referring to a global geocentric datum is essential in the determination of orthometric heights by GPS/levelling. The new Turkish Geoid-2003 (TG03) was computed as new and more data were available. Heterogeneous data (gravity, topography and geoid heights) were used by Least Squares Collocation (LSC) in a remove-restore procedure. EGM96 was used as the reference model of the earth's geopotential. The data used consist of surface gravity anomalies, gravity anomalies derived from ERS1, ERS2 and TOPEX/POSEIDON altimetry data, GPS/levelling geoid heights, and topographic heights. Surface gravity values are in Modified Potsdam Datum, and the free air anomalies were computed in GRS80. No surface gravity data were used outside the Turkish border while topographic heights were obtained from GTOPO30 global topography. The RTM effect of the topography was computed using a high-resolution Digital Terrain Model (450x450 m). The DTM used consist of high-resolution topographic heights within the borders, and dense bathymetry near the shoreline. Evenly distributed GPS/levelling geoid heights were introduced so as to compute the final geoid in agreement with GPS ellipsoidal heights. Ellipsoidal heights of the GPS/levelling points refer to well-established Turkish National GPS Network (aligned to ITRF96), while orthometric heights refer to Turkish National Vertical Datum (fixed to mean sea level). The gravity and geoid prediction at the observation points gave an internal precision below 3 mGal and 10 cm respectively. The geoid heights at 3'x3' grid points within Turkey (25E-46E, 35N-43N) were computed to be further interpolated in practical use. The final geoid was tested at GPS/levelling stations, which were not used in the computations, and the external accuracy was found to be within a decimeter as varying with respect to the data distribution and density.

**G03/07P/D-027** Poster **1400-049**

**ACCURACY ASSESSMENT OF THE AVAILABLE GEOID MODELS IN ALGERIA**

Sid Ahmed BEN AHMED DAHO<sup>1</sup>, J.D. FAIRHEAD<sup>2</sup>, S. KAHLOUCHE<sup>1</sup>, A. ZEGGAI<sup>1</sup> (<sup>1</sup>Geodetic Laboratory, National Centre of Spatial Techniques, <sup>2</sup>GETECH-University of Leeds - Department of Earth Sciences - Leeds LS2 9JT - United Kingdom)

The determination of orthometric heights by traditional techniques, such as spirit levelling, is known to be a difficult and expensive task, especially in big countries like Algeria where the establishment of a levelling network covering all parts of the country would be impractical and furthermore may not be possible principally in the mountainous areas and in the south of the country. On the other hand, the combined use of GPS heights and geoid heights provides an efficient alternative to derive orthometric heights and therefore, to avoid the arduous task of precise spirit levelling. In this paper we want to determine, the best combination possible among the available geoid models in Algeria with GPS/levelling that gives sufficiently accurate results in order to check the possibility to substitute the classical spirit levelling. For this study, we have used two national gravimetric geoid models, all have been computed by Geodetic Laboratory of the National Centre of Spatial Techniques from two sets of gravity data supplied respectively by BGI in 1997 and by the Geophysical Exploration Technology Ltd (GETECH) in 2002, and three global geopotential models namely OSU91A, EGM96 and GPM98b. The GPS data are collected from the international TYRGEONET project and the local GPS/levelling surveys with baseline length ranging from about 3 to 800 km. However, and in order to minimise all possible datum inconsistencies and others systematic effects between geoid and GPS/levelling undulations, we have tested various kinds of functions. The number of stations GPS used in this investigation was 246; the most of these points are located in the north of Algeria, which 16 are benchmarks of the first order levelling network. Only ten well distributed GPS levelling points are used as benchmark points. The remaining points were used to check the quality of the fitting the different gravimetric geoid solutions to a set of GPS levelling points. The data used in framework of this work and their distribution, the adopted methodology, the computation procedure, and the obtained results will be presented and widely discussed. Key words: GPS/levelling, Geoid undulations, Geopotential model.

**G03/07P/D-028** Poster **1400-050**

**ON THE DETERMINATION OF MARINE GEOID MODELS BY LEAST-SQUARES COLLOCATION AND SPECTRAL METHODS USING HETEROGENEOUS DATA**

Georgios S. VERGOS, Ilias N. TZIAVOS, Vassilios D. ANDRITSANOS (Department of Geodesy and Surveying, Aristotle University of Thessaloniki)

In the frame of the EU-sponsored GAVDOS project the need of a new high-resolution and high-accuracy geoid model for the calibration of the satellite altimeters (e.g., JASON-1, ENVISAT and EURO-GLOSS) and for sea level monitoring purposes has become apparent. This is mainly due to the fact that the already available solutions have been determined using outdated datasets and fail to meet the wanted, cm-level, accuracy requirements. To determine the new geoid models multi-satellite (ERS1, GEOSAT, TOPEX/POSEIDON (T/P)) altimetry and land and marine gravity data have been used. Furthermore, two global geopotential models, namely EGM96 and GPM98b, have been employed to describe the long wavelengths of the gravity field spectrum, while the effect of the bathymetry has been

taken into account using recently developed local Digital Depth Models (DDMs). Several solutions have been estimated, based on the different data and methods used, presenting a resolution of 5 and 3 arcmin. The estimation of the purely altimetric, gravimetric and combined geoid models has been performed using the Fast Fourier Transform (FFT) based Input Output System Theory (IOST) and Least Squares Collocation (LSC). The accuracy of the new models has been determined through comparisons with T/P data and other geoid solutions for the area under study. Finally, the consistency between the solutions has been assessed by comparing the geoid height value they provide for the Gavdos Tide Gauge (TG) station on the isle of Gavdos. From the results it is shown that the precision of the new geoid models is close to 1 cm, their accuracy ranges between 5 and 10 cm level and their differences at the TG station between 0.2 - 10 cm.

**G03/07P/D-029** Poster **1400-051**

#### OPTIMAL MARINE GEIOD DETERMINATION IN THE ATLANTIC COASTAL REGION OF ARGENTINA

Claudia TOCHO<sup>1</sup>, Georgios S. VERGOS<sup>2</sup>, Michael G. SIDERIS<sup>3</sup> (<sup>1</sup>Facultad de Ciencias Astronomicas y Geofisicas, Observatorio Astronomico, <sup>2</sup>Department of Geodesy and Surveying, Aristotle University of Thessaloniki, <sup>3</sup>Department of Geomatics Engineering, University of Calgary)

The determination of an optimal high-accuracy and high-resolution marine geoid model for the Atlantic coastal region of Argentina is investigated using satellite altimetry and shipborne gravity data. Altimetric data from the latest releases of the mapping phases of the ERS1 and GEOSAT satellite missions are used together with marine gravity data to estimate altimetric, gravimetric and combined marine geoid models for the area. The effect of the Quasi-Stationary Sea Surface Topography (QSST) is taken into account in correcting the altimetric Sea Surface Heights (SSHs) to derive geoid undulations. Special emphasis is placed on reducing the effects of the Sea Surface Variability (SSV) on the densely spaced altimetric SSHs with low - pass filtering and through a regional crossover adjustment scheme. The satellite and shipborne data are combined in the spectral domain, in an effort to improve the overall accuracy of the purely gravimetric and altimetric solutions close to the coastline. The accuracy of the final models is assessed through comparisons with stacked year-three TOPEX/POSEIDON (T/P) SSHs, known for their high precision. The results show that a purely altimetric geoid accurate at the 5 to 7 cm level, in terms of the standard deviation of the differences with T/P SSHs, is feasible while the pure gravimetric solution gives poorer results by about 10 - 15 cm. By combining the satellite and shipborne data with the proposed algorithms the accuracy of the gravimetric geoid model is improved by about 30 - 40%.

**G03/07P/D-030** Poster **1400-052**

#### IMPROVED FITTING BETWEEN GRAVIMETRIC AND GPS/LEVELLING GEOIDS USING AN EXTENDED SIMILARITY TRANSFORMATION MODEL: A CASE STUDY IN JOHOR, MALAYSIA

Christopher KOTSAKIS<sup>1</sup>, Muhammad N.J.P. VELLA<sup>2</sup> (<sup>1</sup>Department of Geomatics Engineering, University of Calgary, Calgary, Alberta, Canada, <sup>2</sup>Center of Geodetic and Geodynamic Studies (CGGS), Faculty of Engineering and Geoinformation Science, University of Technology Malaysia, Johor, Malaysia)

The comparison between gravimetrically-derived and GPS-derived geoid undulations, over a network of spirit levelled benchmarks (BMs), is a standard procedure in geodetic practice. The differences obtained from such comparisons provide useful information for studies involving: (i) the optimal fitting of gravimetric geoids to local vertical datums through ties to GPS/levelling BMs, (ii) the unification of different vertical datums by satellite positioning methods, and (iii) the external accuracy evaluation of gravimetrically computed geoids with GPS and levelling data. To facilitate these types of applications which depend, one way or another, on the combination of ellipsoidal, orthometric and geoid heights, various "low-order" parametric models are implemented to describe the general trend of the discrepancies between gravimetric geoid surfaces and local vertical datums. Additional modelling procedures, based on the use of least-squares collocation and other interpolatory-type schemes, are often applied to the remaining residuals to capture the finer details of these differences and to further improve the transition between geometric and orthometric heights. In this paper we study the performance of a general 8-parameter transformation model for low-order fitting of gravimetric geoid surfaces to GPS/levelling data. The model is based on a differential similarity transformation concept and it provides a straightforward generalization of the classic 4-parameter trend corrector surface that is usually applied in GPS-geoid tailoring applications. A case study for a control test network located in the state of Johor in Malaysia is presented, using both global and regional gravimetric geoid solutions along with national GPS and levelling databases. The results show an improvement in the fitting performance of almost 50% when the extended 8-parameter model is applied for trend removal, as opposed to the use of the simpler 4-parameter version. Additional numerical comparisons with other low-order parametric models of polynomial type (up to fourth degree) have also been performed, which further demonstrate the effectiveness of the extended similarity-based transformation to describe the long-wavelength differences between gravimetric geoids and local vertical datums.

**G03/07P/D-031** Poster **1400-053**

#### GRAVIMETRIC GEIOD COMPUTATION IN THE ANDES

Claudia Noemi TOCHO<sup>1</sup>, Michael G. SIDERIS<sup>2</sup>, Graciela FONT<sup>1</sup> (<sup>1</sup>Facultad de Ciencias Astronomicas y Geofisicas, Universidad Nacional de La Plata, <sup>2</sup>Department of Geomatics Engineering, University of Calgary)

As a preliminary analysis for the development and evaluation of a precise gravimetric geoid for Argentina, different gravimetric geoid solutions were computed using different gravity reduction techniques in the roughest area of the country. The rugged area bounded by latitude 20° S to 42° S and longitude 72° W to 68° W was chosen to compute the geoids using the following terrain reductions methods: Helmert's second condensation method, Rudzki's inversion method, the Airy-Heiskanen topographic-isostatic reduction, and the residual terrain model (RTM) method. The remove-restore method was employed using the most homogenised gravity database (with data blunders were removed) referenced to a unified datum, the EGM96 global geopotential model and different digital elevation models, to take into account the short-wavelength component of the gravity signal. Different values of the maximum degree of the geopotential model were used to compute residual gravity anomalies. For these reduced gravity anomalies, geoid undulations were estimated using Stokes's integral with different cap sizes in order to investigate the effect of truncating the geopotential model in favour of local gravity. Stokes's formula was evaluated using the rigorous spherical kernel by the one-dimensional fast Fourier transform algorithm. The external accuracy of the gravimetric geoid models was evaluated by comparing them with undulations derived from GPS/levelling data. A four-parameter transformation and a seven-parameter transformation model were used to remove the systematic datum differences between the gravimetric geoid and the GPS/levelling undulations, and the possible long wavelength errors of the geoid.

**G03/07P/D-032** Poster **1400-054**

#### TOWARDS A PRECISE GEIOD MODEL FOR ARGENTINA

Maria Cristina PACINO<sup>1</sup>, Eduardo Andres LAURIA<sup>2</sup>, Denizar BLITZKOW<sup>3</sup> (<sup>1</sup>Department of Geotopocartografia, Universidad Nacional de Rosario, <sup>2</sup>Instituto Geografico Militar, <sup>3</sup>Universidade de Sao Paulo)

Several improvements as regards gravity and height data have been done since the calculation of previous geoid models for Argentina. Thus, thousands of new gravity stations had been measured, new DTMs had been calculated and hundreds of GPS/levelling points had been acquired. The reprocessing of preexisting and new data in the framework of the remove-restore technique yielded to GeoArg2003, a new geoid model for Argentina. This paper describes the procedure for geoid computation, statistical evaluations of the model and some improvements from previous geoid charts. All the activities are developed under the umbrella of the National Committee of the International Union of Geodesy and Geophysics (Subcommittee of Geodesy).

**G03/07P/D-033** Poster **1400-055**

#### ADVANCES IN THE CENTIMETER GEIODAL DETERMINATION OF MEXICO

Antonio HERNANDEZ-NAVARRO<sup>1</sup>, Mario Alberto REYES-IBARRA<sup>2</sup> (<sup>1</sup>Coordinador de Geodesia, Direccion General de Geografia, Instituto Nacional de Estadística, Geografía e Informática, <sup>2</sup>Director General, Direccion General de Geografía, Instituto Nacional de Estadística, Geografía e Informática)

This contribution shows the works made in Mexico by the *National Institute of Statistics, Geography and Informatics (INEGI)* to obtain a centimeter geoidal solution for the interest region. The solution adopted use the Stokes-Helmert scheme, developed at University of New Brunswick under leadership of Prof Petr Vanicek.

**G03/07P/D-034** Poster **1400-056**

#### WAVELET EVALUATION OF SOME SINGULAR GEODETIC INTEGRALS

Michael G. SIDERIS<sup>1</sup>, Quanwei LIU<sup>2</sup> (<sup>1</sup>Department of Geomatics Engineering, University of Calgary, <sup>2</sup>Applanix Corporation, Richmond Hill, ON, Canada)

The wavelet transform is a powerful tool in evaluating singular geodetic integrals. Due to its localization properties in both of the time (space) and frequency (scale) domains, and because the kernels of some geodetic integrals have singular points and decay smoothly and quickly away from the singularities, a large number of wavelet transform coefficients of the kernels become zero or negligible, and only a small number of wavelet transform coefficients are significant. It is thus possible to significantly compress the kernels of these integrals in a wavelet basis by neglecting the zero coefficients and the small coefficients below a certain threshold. Therefore, wavelets provide a convenient way for evaluating these integrals efficiently, in terms of fast computational speed and savings of computer memory. In this contribution, a modified algorithm for the wavelet evaluation of Stokes's integral is presented. The same modified algorithm is also applied to the evaluation of the Vening Meinesz and terrain correction integrals, whose kernels have stronger singularities than that of Stokes's kernel. Numerical examples illustrate the efficiency and accuracy of the wavelet methods.

**G03/07P/D-035** Poster **1400-057**

#### KMS2002 GLOBAL MARINE GRAVITY FIELD, BATHYMETRY AND MEAN SEA SURFACE

Ole B. ANDERSEN<sup>1</sup>, Per KNUDSEN<sup>1</sup>, Steve KENYON<sup>2</sup>, Ron TRIMMER<sup>2</sup> (<sup>1</sup>National survey and Cadastre - KMS, <sup>2</sup>National Imagery and Mapping Agency, St Louis, USA)

During the last three years the KMS global marine gravity field has been improved in corporation with National Imaginary and Mapping Agency (NIMA). These improvements have resulted in a release of KMS99 and KMS2001 gravity fields. Especially, the KMS99 gravity field presented a significant improvement in comparisons with marine observations, as well as global coverage within the 82 degree parallels by adding the ERS-ERM data. The subsequent, KMS2001 only resulted in minor improved gravity field modelling. A new revised global high resolution marine gravity field KMS2002 is presented in this Combining this fine-tuning with careful edition of data are expected to improve the KMS2002 gravity field, in particularly coastal regions. Improved resolution and data coverage in particularly ice-covered regions are other improvements which is currently under investigation. The KMS gravity field modelling approach uses the observed sea surface height anomalies relative to EGM96 and converts these into gravity using FFT techniques. For the KMS2002 focus has been on improved mapping of the intermediate wavelength (100-250 km) of the gravity field using the exact repeat mission data from the TOPEX/POSEIDON and ERS-2 satellite missions. The KMS2002 gravity field is accompanied with a high-resolution bathymetry model and a high resolution mean sea surface.

**G03/07P/D-036** Poster **1400-058**

#### ARCTIC ALTIMETRIC GEIOD AND GRAVITY FIELD

Ole B. ANDERSEN, Per KNUDSEN (National survey and Cadastre - KMS)

The new global high resolution marine gravity field KMS2002 has been improved in several ways. One of this is improved modelling of the intermediate to long wavelength (100-1000 km) of the gravity field using the exact repeat mission data from the ERS-1 and 2 altimetry in the Arctic Ocean, and modelling of intermediate wavelength (100-250 km) in other regions of the world. Satellite altimetry from the TOPEX/POSEIDON and ERS-2 Exact repeat missions was used for the study. Altimetry indicate large offsets between the altimetric mean sea surface and the EGM96 geoid errors in the Arctic Ocean, the Caspian Sea, the Pacific Trench regions and several other regions, i.e. the Canary Islands in the Atlantic Ocean. GEOSAT altimetry shows a consistent mean sea surface slope of more than 10 meters relatively to EGM96 crossing the Caspian Sea. Assuming that the mean dynamic topography (MDT) is small/neglectable in the Arctic Ocean and the Caspian Sea the observed "mean sea surface" can be turned directly into residual geoid signal and associated gravity field anomalies. In other regions of the world where MDT is known to be present, the MDT can be removed using spherical harmonic function before computing residual geoid signal. Preliminary long wavelength gravity field model from the GRACE satellite mission, will hopefully be available to validate the findings from satellite altimetry.

**G03/07P/D-037** Poster **1400-059**

**A MODEL OF GRAVITY FIELD OF THE EARTH COMPILED ON THE BASIS OF ABSOLUTE VALUES OF GRAVIT**

Simeon G. KOSTIANEV, Stoyan AVDEV (Dept. of Mathematical Geophysics, University of Mining & Geology)

An optimal point model of the global gravity field has been compiled on the basis of data for absolute values of gravity. It has been composed of point masses. Optimum parameters of the masses have been determined by the least squares method. This model is univalent and stable for the set of data used and provides the best description of the field with the least number of parameters of its sources. It approximates the used absolute values of the gravity with a mean squared error about 40 mGal, and only for data in the USA territory - 30 mGal. The field of the optimum point model is similar to the field of the rotary ellipsoid (the normal gravity field), and the other anomalies - to the free air anomalies. An advantage of the point model of the global field of the Earth in comparison to the ellipsoidal one is its flexibility and higher precision for information processing and its application in geophysics and geodesy.

**G03/07P/D-038** Poster **1400-060**

**EVALUATION OF NEWTON'S INTEGRAL IN SPACE AND FREQUENCY DOMAIN**

Michael KUHN<sup>1</sup>, Kurt SEITZ<sup>2</sup> (<sup>1</sup>The Western Australian Centre for Geodesy, Curtin University of Technology, <sup>2</sup>Geodetic Institute, University of Karlsruhe, Germany)

Newton's integral can be evaluated either in space domain by a direct integration approach or in frequency domain by a spherical harmonic approach. In the first approach Newton's integral is evaluated by a discretised numerical integration using the gravitational potential (or its derivatives) caused by regularly shaped bodies such as prisms or tesseroids (i.e. spherical volume elements). In the second approach Newton's integral is expressed by spherical harmonic expansions of height or density functions, which can be interpreted as the gravitational effect of different mass layers. This paper studies the theoretical and practical differences between these two approaches. Therefore the gravitational effect of the global topographic masses described by a digital elevation model (DEM) is evaluated using both approaches and subsequently compare the results. Hereby the direct integration approach is realized by using the gravitational effect induced by tesseroids. Numerical examples are given for evaluation points located directly on the Earth's surface and at different heights (e.g. flight levels) above it.

**G03/07P/D-039** Poster **1400-061**

**CONCEPTS OF A REGIONAL GEOID DETERMINATION OUT OF MASS MODELS**

Urs MARTI (Swiss Federal Office of Topography)

The Swiss geoid CHGEO98 is in use now for several years. It is a combined solution of astro-geodetic, gravimetric and GPS/leveling measurements. Its accuracy of about 3 cm could be verified in most regions by many new measurements (mainly GPS/leveling) after the calculation of CHGEO98. But despite of this high accuracy there remain some systematic differences between gravimetry and the deflections of the vertical on one side and GPS/leveling on the other side that reach maximal amounts of about 7 cm. These differences generally show a north-south trend but also some local effects. They are supposed to be a consequence of weaknesses in the geoid solution rather than of systematic errors in leveling or GPS. Therefore new efforts aim to improve the national geoid model. One part is the introduction of new measurements (gravimetric, astro-geodetic and GPS/leveling) in poorly covered regions or in areas where local discrepancies appear. Another part is the improvement and introduction of new mass models into the geoid determination. In the solution CHGEO98 the principal models, besides of a few local density models, were a 25 meter DEM and a model of the crust-mantle boundary (Moho). Both models only were available for a limited area of about 50 to 100 km around the country. This limitation most probably leads to long wavelength errors of the geoid. Our new models practically cover the whole earth. This should reduce the global trends in the error of our solution and together with improved local 3D density models should bring us a step forward in the determination of a 'Newtonian' geoid out of mass models only. The poster shows the concept of the new geoid (CHGEO2003) and the first results which are mainly the effects of the newly introduced mass models such as global DEM, density models and Moho, but also the atmospheric effect and the influence of local density anomalies.

**G03/07P/D-040** Poster **1400-062**

**ON THE NUMERICAL SOLUTION OF PARAMETERS OF THE LEAST SQUARES MODIFICATION OF STOKES' FORMULA**

Artu ELLMANN (Geodesy Group, Department of Infrastructure, Royal Institute of Technology)

In regional gravimetric geoid determination, it has become customary to utilize the modified Stokes' formula, which combines regional terrestrial data with a global geopotential model (GGM). The modification of Stokes' formula, originating with M.S. Molodensky, aims to reduce the truncation error that occurs when the area of Stokesian integration is limited to a spherical cap. Over recent decades several modifications of Stokes' formula have been presented, but many of them aim at reducing the truncation error only. With access to a recent high-degree GGM, the truncation error loses some of its significance, and the errors of the geopotential coefficients become more important. One should also consider the erroneous terrestrial data within the integration area. A modification method, proposed by L.E. Sjöberg in 1984 (with later developments), allows least squares minimization the influence of any known or estimated, random or systematic errors in geoid modelling. In this approach, depending on the local gravity data quality, the chosen radius of integration, and the characteristics of the used GGM, the modification parameters  $s_i$  vary. This study concerns the numerical computation of the parameters  $s_i$ . New satellite gravity missions (i.e. CHAMP, GRACE and GOCE) are expected to improve significantly the accuracy of geopotential models. Of particular interest is the evaluation of the impact of future (i.e. post-GOCE) geopotential coefficients. For this purpose simulated error degree variances are utilized. A set of least squares modification parameters is determined from the system of linear equations, aiming at minimizing of the global mean square error of geoid estimator. Some difficulties may be encountered when practically computing the least squares modification parameters. In particular, for certain parameters the design matrix suffers from numerical ill-conditioning. Therefore, a special regularization procedure must be undertaken to stabilize the numerical solution. In particular, the Philips-Tikhonov regularization method seems to be satisfactory in providing a solution for the modification parameters. Numerical results are presented to illustrate the applicability of the obtained least squares modification parameters in geoid modelling by comparing with GPS-leveling data.

**G03/07P/D-041** Poster **1400-063**

**A NUMERICAL COMPARISON OF DIFFERENT ELLIPSOIDAL CORRECTIONS TO STOKES' FORMULA**

Artu ELLMANN (Geodesy Group, Department of Infrastructure, Royal Institute of Technology)

Stokes' formula for the gravimetric geoid modelling holds only on a spherical boundary. However, gravity anomalies are observed on the Earth's surface, which can be approximated by an ellipsoid. This suggests that the observed anomaly must be upward or downward continued to a sphere, before Stokes' integral can be applied. This procedure, however, is often neglected in practical computations. The systematic error caused from neglecting the flattening of the ellipsoid may reach several decimetres. Hence, for an accurate geoid model it is important to estimate the effect of the Earth's flattening. Different authors have studied the ellipsoidal correction for the original Stokes' formula. A new solution for computing the ellipsoidal correction for Stokes' formula was recently derived by L.E. Sjöberg. Here the two cases - the original and the modified Stokes' formulas are considered. The new ellipsoidal corrections can also be expressed by means of the spherical harmonics of a GGM, and the new method allows the estimation of the ellipsoidal corrections directly on the geoidal height, which is a computational advantage. In order to assess the applicability of the new approach, this paper describes various methods for computing the ellipsoidal corrections, and compares them numerically. It is notable that the approaches disagree either in their appearance or numerical results. Furthermore, the solutions are given in different coordinate systems (geocentric, geodetic and ellipsoidal) and they are related to various boundaries. Consequently, different approaches are not directly comparable, and some scaling factors need to be introduced. Compared to other approaches the new formulas are much simpler and easier to implement in practical computations. In contrary to the original Stokes formula, the ellipsoidal corrections for the modified Stokes' formula, which combines regional terrestrial gravity data with a global geopotential model (GGM), have received less attention in the geodetic literature. This is caused by the misleading assumption that this correction is negligible. However, the results of numerical investigations demonstrate that the ellipsoidal correction for the modified Stokes' formula may be significant in areas with large gravity anomalies and in higher latitudes.

**G03/07P/D-042** Poster **1400-064**

**FAST LEAST SQUARES COLLOCATION WITH FILTERED HETEROGENEOUS DATA IN GEOID DETERMINATION**

Kosasih PRIJATNA<sup>1</sup>, Roger HAAGMANS<sup>2</sup> (<sup>1</sup>DEOS, Physical, Geometrical, & Space Geodesy, Delft University of Technology, <sup>2</sup>European Space Agency, ESTEC)

The method of least squares collocation has been utilized successfully in gravity field modelling, especially in geoid determination. A disadvantage in using the method can occur when dealing with large number of data due to the correlation between them. In such situation we have to invert a nearly full matrix of large dimension. It needs much space in terms of computer memory and is very time consuming. The matrix is largely shaped by the signal covariance describing the signal correlation among data, and assuming limited or no correlation among the errors. The covariance functions usually used in physical geodesy decay approximately exponentially with distance. By choosing spectral weights (bandpass filters), applying these to the covariance function, and subsequently truncating the function at a certain maximum spatial distance, a sparse covariance matrix can be constructed. Having such a sparse structure, the matrix inversion can be handled more easily. In this paper, the application of the above mentioned algorithm on local geoid determination for Indonesian region will be described and investigated. The geoid determination is based upon combination of heterogeneous data types for a kind of multi-resolution solution. The data are global geopotential model, GOCE's vertical gravity gradients, and terrestrial or airborne gravity data.

**G03/07P/D-043** Poster **1400-065**

**THE DETERMINATION OF A PRECISE GEOID FOR PARANA STATE, BRAZIL**

Marcia C.L. QUINTAS, Vivian FERNANDES (Department of Geomatics, Federal University of Parana)

Geoid determination is one of the most fundamental problems in geodesy. The precise model of the geoid not only enable us to transform satellite-derived heights to physically meaningful heights based on The Earth's gravity field, but also plays an important role in geophysics and oceanography. The intention of this paper is to construct a regional geoid on the basis of gravity anomalies in Parana State, Brazil. In order to achieve this goal, a database was designed to integrate gravity and topographic data, as well as their attributes. Those data have been collected in Parana State and surroundings by different organizations, such as Federal University of Parana (UFPR), Sao Paulo University (USP) and Energy Company of Parana State (COPEL) since 1985. This study comprises: the preparation of terrestrial gravity and terrain data; the use of appropriate geodetic datum during gravity data reduction; the selection of the best fitting global geopotential model; the application of the gravimetric terrain corrections; the gridding of the gravity anomalies prior to geoid computation; and comparisons of a preliminary Parana State gravimetric geoid solution with geometrical control, provided by Global Positioning System (GPS) measurements in conjunction with leveling data. This study also uses a geographic information system (GIS) to overlay different kind of maps. The GIS database constructed for this work includes graphic and nongraphic data. They are stored in conventional alphanumeric formats and linked with GIS technology.

**G03/07P/D-044** Poster **1400-066**

**DETERMINATION AND EVALUATION OF SHENZHEN GEOID, P.R.CHINA**

Zhicai LUO<sup>1</sup>, Jinsheng NING<sup>1</sup>, Zhanji YANG<sup>2</sup>, Yongqi CHEN<sup>3</sup> (<sup>1</sup>School of Geodesy and Geomatics, Wuhan university, <sup>2</sup>Land Planning Department of Shenzhen, Shenzhen 518028, P.R.China, <sup>3</sup>Department of Land Surveying and Geo-Informatics, The Hong Kong Polytechnic University)

The geoid of Shenzhen with one-kilometer resolution, has been constructed with remove-restore technique using the following data: (1) 65 GPS/leveling data with the accuracy better than 2 cm and about 10 kilometers average station interval, (2) 3608 gravity data on land with the accuracy better than 0.1mGal and one-kilometer resolution, (3) 1262 gravity data on sea with the accuracy of 1.6mGal and one-kilometer resolution, (4) 343 gravity data in Hong Kong with 2-4 kilometers resolutions, (5) digital terrain model with 100m resolutions covering the whole territory of Shenzhen, and (6) earth's gravity field model WDM94 as reference model. Then the modeled geoid heights were compared with the observed ones derived from 29 GPS/leveling data with the accuracy better than 2cm that not applied to the construction of Shenzhen geoid. The test results show that the standard deviation of the differences is  $\pm 1.4$  cm, and that the overall relative accuracy is better than 10-6.

G03/07P/D-045 Poster 1400-067

**USE OF STOCHASTICALLY MODIFIED KERNELS IN AUSTRALIAN GRAVIMETRIC GEOID COMPUTATION**Will FEATHERSTONE<sup>1</sup>, Lars SJOBERG<sup>2</sup> (<sup>1</sup>Western Australian Centre for Geodesy, Curtin University of Technology, <sup>2</sup>Department of Infrastructure, Royal Institute of Technology)

Gravimetric geoid models of Australia have been computed using a combination of the EIGEN2 and EGM96 global geopotential models, the 2001 release of the Australian land gravity database, the version 2 GEODATA 9 arc-second digital elevation model, and GMGA02 satellite altimeter-derived marine gravity anomalies. Residual geoid undulations were computed using the 1D-FFT technique with the spherical Stokes kernel and two stochastically modified kernels: Wenzel's spectral combination and Sjöber's biased least squares modification. Attempts were also made to optimise the integration radius using a nation-wide set of 1013 GPS-leveling data. This paper will present a summary of the theory used, and the results of comparisons of the various gravimetric geoid models, for different kernel modifications and cap radii, with GPS-leveling data on the Australian Height Datum.

G03/07P/D-046 Poster 1400-068

**THE CHAMP DATA FOR GEOID STUDY IN INDONESIAN REGION**Adolfientje KASENDA<sup>1</sup>, Bill KEARSLEY<sup>1</sup>, Av OLESEN<sup>2</sup> (<sup>1</sup>SCHOOL OF SURVEYING, UNSW, <sup>2</sup>National Survey and Cadastre - Denmark)

To date, every Indonesian gravimetric geoid has suffered from the inaccuracy and poor coverage of the gravity information within the region. The 1981 geoid model which was based on the global Marsh and Chang geoid model was reported to have  $\pm 5$  m accuracy. The INDGED96 computed from the available terrestrial data in combination with the potential model OSU91A improved the accuracy to  $\pm 1.5$  m or better, at least in the western parts of the country. With the advent of new global geopotential models based upon satellites launched specifically for gravity field studies, our understanding of the regional gravity field in this region should improve significantly, especially in the long to medium wavelengths. In order to test these expected improvements, we analyse the results from the newly released global coefficient potential - Eigen2, derived from the orbit analysis of the gravimetric satellite CHAMP. These parameters (gravity anomalies, geoid heights) are evaluated and compared to those derived from the existing terrestrial data, and from EGM96. We find that Eigen2 model still has severe deficiencies in this area, in some regions showing a bias of more than 200 mGal over an area of 5 degrees. The associated geoid heights are also compared to EGM96 geoid model and to GPS/Leveling results at control points, and show similar large discrepancies.

G03/07P/D-047 Poster 1400-069

**DEVELOPMENT OF A HIGH RESOLUTION HEIGHT REFERENCE SURFACE FOR GERMANY USING GRAVITY AND GPS/LEVELLING DATA**Heiner DENKER<sup>1</sup>, Johannes IHDE<sup>2</sup>, Juergen MUELLER<sup>1</sup>, Uwe SCHIRMER<sup>2</sup> (<sup>1</sup>Institut fuer Erdmessung, Universitaet Hannover, <sup>2</sup>Bundesamt fuer Kartographie und Geodaesie)

Two methods are investigated for the computation of a high resolution height reference surface (quasigeoid) for Germany using gravity and GPS/levelling data. Both methods are based on the remove-restore technique and use the global geopotential model EGM96, point gravity data with a spacing of a few km, a digital terrain model and GPS/levelling control points. The first method uses a two-step procedure. First, the gravity and terrain data are combined with the global geopotential model using the least squares spectral combination technique with integral formulas. Then a smooth corrector surface is developed from the GPS/levelling data by least squares collocation, including a signal and a trend component. The corrector surface is added to the gravimetric quasigeoid, giving the final height reference surface that is consistent with the GPS and levelling data in Germany. The second method is based on a common adjustment of the EGM96 reduced gravity and height anomaly observations using point masses and appropriate weight relations. The point masses are arranged at depths of 5 km, 30 km and 200 km. Both computation techniques are studied from the methodological and numerical point of view. The results are intercompared and discussed. The agreement of both techniques is at the cm level. The final result from this project shall serve as a standard for the transformation of GPS heights into levelling heights in Germany.

G03/07P/D-048 Poster 1400-070

**STRATEGIES FOR A NEW EUROPEAN GEOID COMPUTATION**Heiner DENKER<sup>1</sup>, Riccardo BARZAGHI<sup>2</sup>, Rene FORSBERG<sup>3</sup>, Ambrus KENYERES<sup>4</sup> (<sup>1</sup>Institut fuer Erdmessung, Universitaet Hannover, <sup>2</sup>Politecnico di Milano, Istituto di Topografia, <sup>3</sup>National Survey and Cadastre, Geodetic Division, Copenhagen, <sup>4</sup>Inst. of Geod., Cart. and Remote Sensing, Satellite Geodetic Observatory, Budapest)

Continental-scale (quasi)geoid models are nowadays required with an accuracy at the 1 cm level in order to meet the demands of geodesy (especially GPS heighting), geophysics, oceanography and engineering. Since 1990, the development of a high resolution (quasi)geoid model for Europe is supported through the International Association of Geodesy (IAG), Gravity and Geoid Commission, Subcommission Europe, with the Institut für Erdmessung (IfE) serving as a computing center in this project. Within the new structure of the IAG, it is planned to setup a working group within the framework of the International Gravity Field Service (IGFS) in order to continue this work and to support the derivation of an improved (quasi)geoid model for Europe. The most recent European geoid and quasigeoid model EGG97 was published in 1997. The model has an accuracy at the cm level over distances up to a few 100 km in areas with a good data coverage and accuracy, while long wavelength errors of about 0.1 to 1 ppm exist in many regions. These long wavelength errors are coming from the inaccuracies of the underlying global gravity field model and systematic errors in the terrestrial data. Furthermore, high resolution gravity field data is lacking in the EGG97 model for many countries in East Europe and in some marine areas. Hence, the accuracy of the EGG97 model is not homogeneous. Several improvements of the European geoid and quasigeoid model EGG97 appear to be possible now or in the near future. Such improvements comprise the use of better global gravity field models from the new satellite gravity field missions, new terrain data sources (e.g., GTOPO30, SRTM), updated or new terrestrial and airborne gravity data sets (e.g., Arctic Gravity Project, regional geoid projects in the Nordic and Mediterranean areas), the optimal merging of ship and altimetric gravity anomalies, the inclusion of GPS/levelling data, and improved gravity field modelling techniques. In order to make an update of the existing European (quasi)geoid model possible, international cooperation with persons and institutions all over Europe is essential. The poster outlines the status and possible improvements of the European (quasi)geoid, and shall serve as a basis for discussions with interested people.

G03/07P/D-049 Poster 1400-071

**IMPROVING LOCAL GEOID MODEL OF TAIWAN USING TWVD2001 GPS/LEVELING DATA**

Kwo-Hwa CHEN, Ming YANG, Kun-Shu CHANG (Department of Surveying Engineering National Cheng Kung University)

From 2000 to 2003, a new national vertical datum, Taiwan Vertical Datum 2001 (TWVD2001) has been established. The datum was built by combining the observations of geodetic leveling; Global Positioning System (GPS) and surface gravity collected at 2065 newly established benchmarks within a network of 4500-km first-order leveling lines. The existing local geoid model of Taiwan was calculated using observations of sea surface gradients derived from satellite altimetry, land gravity anomalies, ship gravity anomalies, and the EGM96 model. The accuracy of this model was approximately  $\pm 20$ -30 cm. In this study, the GPS/leveling data within the TWVD2001 network was used to improve the accuracy of the local geoid model of Taiwan using the least-squares collocation (LSC) technique. The results were then compared with independent, near-fault GPS/leveling data obtained from 223 GPS monitoring points and leveling benchmarks in 232-km leveling lines. Comparison results show that the accuracy of the improved model has reached  $\pm 10$  cm.

G03/07P/D-050 Poster 1400-072

**COMBINING TERRESTRIAL AND MARINE GRAVITY FOR GEOID MODELLING IN VENEZUELA**Gustavo A. ACUNA<sup>1</sup>, Wolfgang BOSCH<sup>2</sup> (<sup>1</sup>Laboratorio de Geodesia Fisica y Satelital, La Universidad del Zulia, <sup>2</sup>Deutsches Geodätisches Forschungsinstitut (DGFI))

For the region 285°E-305°E and 0°N-20°N, covering the territory of Venezuela, a new geoid model with a resolution of 1'x1' has been derived through the combination of terrestrial and marine gravity anomalies. The EGM96 geopotential model was used as reference for the large-scale structure of the regional gravity field. High resolution digital elevation models were taken to compute the topographic corrections. The marine gravity anomalies were obtained from multi-mission satellite altimetry, combining data of Seasat, Geosat, ERS-1, ERS-2, TOPEX/Poseidon and GFO. The mean water level of the POCM model was used to correct the marine geoid for ocean dynamic heights. Overall, more than 6 million data points were used. Least Squares Collocation was used for the gridding of residual gravity anomalies. In order to solve the Stokes integral Fast Fourier Transform in spherical approximation was applied. Comparison to previous geoid models suggest that the new model provides an essential improvement. Independent evaluation with precise GPS positioning and leveling indicate that the precision of the new geoid model is better than three decimeter.

G03/07P/D-051 Poster 1400-073

**COMPARISON OF NEW GEOID MODELS AND EIGEN-2S IN THE NORTH ATLANTIC REGION**Ove Christian Dahl OMANG<sup>1</sup>, Rene FORSBERG<sup>2</sup>, Gabriel STRYKOWSKI<sup>3</sup> (<sup>1</sup>Department of Mapping Sciences, Agricultural University of Norway, N-1432 AAs, Norway, <sup>2</sup>Geodynamic Dept., National Survey and Cadastre (KMS), Rentemestervej 8, DK-2400 Copenhagen NV, Denmark)

As a result of the dedicated gravity satellite missions CHAMP, GRACE and GOCE new geopotential models will arrive. These models are expected to give a better representation of the long wavelength part of the Earth's gravity field than previous geopotential models. A two step test procedure was executed to verify the quality of the EIGEN-2S geopotential model compared to the EGM96 model. Our test area covered the North Atlantic Sea region, including the Greenland Sea and the Norwegian Sea. The verification of the geopotential models and the creations of the new geoid models were split into a two step procedure. In the first step, a set of geoids, based on the geopotential models only, were created by varying the spherical harmonic degree,  $n_{max}$ . In the second step, a gravimetric geoid was produced by combining the best geopotential model and available gravity data. A set of these geoids were created by varying the truncation degree in the Stokes function. The resulting geoids were compared to GPS networks in the Nordic countries and to mean sea surface height (MSSH) data from ERS-2, TOPEX/POSEIDON and GFO missions over the ocean. Results from the first step show that the EIGEN-2S geopotential model give better fit to GPS and MSSH than EGM96 up to degree 50. Results from the second step show similar features as in step 1 but not that evident. Gravimetric geoids using EIGEN-2S as a reference model give better fit to the GPS and GFO MSSH data up to degree 20 and for ERS-2 up to degree 60.

G03/07P/D-052 Poster 1400-074

**RGQG-2003: THE NEW GEOID AND GRAVITY FIELD MODEL FOR TERRITORY OF RUSSIA AND SEA AREAS AROUND RUSSIA**Petr P. MEDVEDEV<sup>1</sup>, V. NEPOKLONOV<sup>2</sup> (<sup>1</sup>Geophysical Center of Russian Academy of Sciences, <sup>2</sup>29 Research Institute of the Defence Ministry RF, Moscow, Russia)

The remove-restore procedure with the newly created geopotential model as reference field complete up to degree and order 360 was used for computation of the detailed quasigeoid for land territory and sea areas around Russia. The numeric model of the Russian Gravimetric Quasigeoid - 2003 (RGQG-2003) obtained in 2003 is the grid of quasigeoid height values over common reference ellipsoid calculated with latitude (B) and longitude (L) spacing of 5' for  $40^{\circ} \leq B \leq 90^{\circ}$ ,  $26^{\circ} \leq L \leq 192^{\circ}$ . The computations were based on a data set consisting of 5'x5' mean gravity anomalies and topography information of updated geodesy, satellite altimetry and gravity data base. The topography data were represented by detailed digital terrain model. The structure of the data base and processing system presented. The gravimetric geoid heights was compared with heights obtained by GPS-leveling and European geoid EGG97 for western region of Russia. The comparison with geoid heights derived from recent geopotential models and satellite altimetry data was made as well. The Russian Gravimetric Quasigeoid - 2003 (RGQG-2003) will be accessible via Geophysical center RAS web-server. The present state and future opportunities are considered. The research is supported by RFBR (Project 01-07-90106).

G03/07P/D-053 Poster 1400-075

**ON THE PRECISE CONVERSION BETWEEN GEOID AND QUASI-GEOID**Shaofeng BIAN<sup>1</sup>, Jianhua XU<sup>2</sup> (<sup>1</sup>Department of Engineering, Navy University of Engineering, <sup>2</sup>Bei Sanhuanzhonglu 69, Beijing 100088)

Geoid and Quasi-geoid are two important reference surfaces in physical geodesy. The conventional conversion was discussed in the book of Physical Geodesy written by Haskanen and Moritz. This conversion is not adequately accurate. We follow the idea presented by Sjöberg and presented a more accurate conversion.

**G03/07P/D-054** Poster **1400-076****REFINED COMPUTATION OF THE (QUASI)GEOID MODEL FOR COLOMBIA USING THE NEW GRAVITY SATELLITE MISSIONS**

Laura SANCHEZ (Instituto Geografico Agustin Codazzi, Bogota, Colombia. Presently at the Dresden University of Technology, Germany)

In Colombia, the comparison of GPS-derived geoid undulations with gravimetric geoid models presents still discrepancies in the decimetre-level. To find the origin of these discrepancies a new gravimetric (quasi)geoid model is computed. The available local (terrestrial, aerial) gravity observations were re-processed in order to avoid possible inconsistencies in the short wave components. The result is a homogeneous set with approximately 80 000 gravity points. The long wavelength component is calculated using a global gravity model derived from the new satellite missions. Since the topographic and geological features in Colombia are very complicated, the formulation of mass distribution hypothesis to geoid and orthometric height computation is too difficult. In the same way a quasigeoid model is estimated. The gravimetric geoid undulations (and height anomalies) are compared with those obtained from combining ellipsoidal heights from GPS and orthometric (or normal) heights from spirit levelling.

**G03/07P/D-055** Poster **1400-077****NRG-2003 GEOID MODEL OF THE NORDIC AND BALTIC AREA**

Rene FORSBERG<sup>1</sup>, Gabriel STRYKOWSKI<sup>2</sup>, Dag SOLHEIM<sup>2</sup>, Harli JURGENSON<sup>3</sup> (<sup>1</sup>Kort & Matrikelstyrelsen, Rentemestervej 8, DK-2400 Copenhagen NW, Denmark, <sup>2</sup>Geodetic Division, Statens kartverk, Kartverksveien 21, N-3511 Honefoss, Norway, <sup>3</sup>Estonian Agricultural University, 51014 Tartu, Kreutzwaldi 64, Estonia)

A new geoid model of the Nordic/Baltic area have been made, using spherical FFT methods and terrain reductions, similar to the earlier geoid model NKG96. A number of new data sources have been incorporated, especially in Norway, Sweden, around the Baltic Sea, and in the interior Danish waters and northern Germany. The model incorporates the NKG airborne gravity survey of the Baltic Sea 1999, and large geoid changes are evident due to this survey, especially in the marine regions. The geoid is compared to GPS-levelling data, and a local geoid is fitted to GPS in Denmark as an illustration of an operational regional cm-level GPS geoid.

**G03/07P/D-056** Poster **1400-078****NEW GEOID COMPUTATIONS IN TAIWAN**

Gwo-Chyang TSUEI (Department of Civil Engineering, National I-LAN Institute of Technology, Taiwan)

With the rapid expansion applications of GPS positioning and the improvement of positioning accuracy. There is a demanding need for a unified gravimetric geoid of high accuracy. It can be used together with the GPS-derived heights to provide orthometric heights. A new, high-resolution and high-precision geoid has been computed for the Taiwan area, ranging from 21.55° N to 25.50° N in latitude and 119.50° E to 122.45° E in longitude. Using EGM96 geopotential model, 3' \* 3' mean gravity anomaly grid and digital terrain model carried out the computations. The remove-restore technique was adopted for the computation of terrain effect by Helmert's condensation reduction. The contribution of the local gravity data to the geoid was computed strictly by the ID-FFT technique, which allows for the evaluation of the discrete spherical Stokes' integral without any approximations. In this study, we compared the difference of the geoid undulations computed by 2D spherical FFT and ID spherical FFT method. We also tested the adapt ability of using EGM96 to calculate the gravitational quantities in the region of Taiwan. The terrain effects on the geoid computation were also studied. The comparison of the gravimetric geoid with GPS/levelling-derived undulations shows the RMS is less than 10cm.

**G03/07P/D-057** Poster **1400-079****SATELLITE-TO-SATELLITE TRACKING IN HIGH-LOW MODE: RELATIONSHIPS AND FEATURES**

Rafael A. KASCHEEV (Department of Astronomy, University of Kazan)

Future prospects for developing comprehensive planetary gravity models will depend on the new satellite techniques. Several satellite gravity field mapping missions, such as CHAMP, GRACE, GOCE, SELENE are on the way in order to improve the terrestrial and lunar gravity fields with high resolution. The satellite-to-satellite tracking (SST) which measure the effect of the potential difference on a satellite pair is expected to be able to determine the gravity to a greater accuracy than is feasible by the classical approach of satellite geodesy. At this takes place, not only the static part of the gravity field can be determined with unattained accuracy also some temporal effects can be detected. The concept of SST is possible either in the low-low (GRACE) or in the high-low (CHAMP, SELENE) modes. In the later case only one satellite is placed into a low orbit while the other satellite describe orbits with high altitudes. Intersatellite range-rate data measure the difference between the velocity perturbations along the direction of the intersatellite range in the process. This study is concerned with gravity field recovery from high-low satellite-to-satellite relative line-of-sight (LOS) velocity measurements transformed into LOS accelerations through numerical differentiation procedure. This allows to construct an observation equation of HL SST LOS velocities in terms of observation equation of LOS acceleration. A brief description of the solution used here is the following. Based on reported observation equation of LOS acceleration a transformation into the local reference frame is performed. This frame whose principal plane contains both satellites is rotating with respect to the planetary center of mass. Appropriate harmonic coefficients related to each local orbital configuration at each point in time are lumped coefficients. These lumped coefficients would constitute linear combinations of the harmonic coefficients of the gravity potential model compatible with inertial reference frame. To search for an orbital configuration provides most accurate gravity parameters a number of plausible orbits are considered. Using the proposed model least squares error analysis is performed by computer simulation. The results of this analysis indicate that a significant improvement in the errors of gravity parameters are obtained when the satellite orbital planes are considerably separated. Namely, it is desirable to pick the difference in inclination of two orbital planes between 30°-50°. It also shown that the positions of both satellites must be known with sufficient accuracy, for that purpose appropriate measurements (using GPS, for example) remain to be made. Furthermore, it was found that the uncertainty in a reference gravity model is the main error source using SST method. The work was supported by Ministry of Education of Russian Federation, Grant E00-7.0-4.

**G03/07P/D-058** Poster **1400-080****GOCE GRAVITY FIELD RECOVERY**

Hans SUENKEL<sup>1</sup>, Roland PAIL<sup>2</sup>, Peter PESEK<sup>1</sup> (<sup>1</sup>Space Research Institute, Austrian Academy of Sciences, <sup>2</sup>Graz University of Technology, Dept. Theoretical Geodesy)

The European Space Agency is preparing for its first dedicated gravity field mission GOCE (Gravity Field and Steady-state Ocean Circulation Explorer) with a proposed launch in 2006. The mission's goal is the mapping of the Earth's static gravity field with a very high resolution and utmost accuracy on a global scale. GOCE is a drag-free mission, flown in a circulate and sun-synchronous orbit at an altitude between 240 and 250 km. Each of the two operational phases will last for 6 months. GOCE is based on a sensor fusion concept combining high-low satellite-to-satellite tracking (SST) and satellit gradiometry (SGG). The transformation of the GOCE sensor data into a scientific product of utmost quality and reliability requires a well-coordinated effort of experts in satellite geodesy, applied mathematics and computer science. The central issue of GOCE data processing is the determination of the global gravity field model using three independent mathematical-numerical techniques which had been designed and pre-developed in the course of several scientific preparatory studies of ESA: 1. The direct solution which is a least squares adjustment technique based on a pre-conditioned conjugated gradient method (PCGM). The method is capable of efficiently transforming the calibrated and validated SST and SGG observations directly or via lumped coefficients into harmonic coefficients of the gravitational potential. 2. The time-wise approach considers both SST and SGG data as a time series. For an idealized repeat mission such a time series can be very efficiently transformed into lumped coefficients using fast Fourier techniques. For a realistic mission scenario this transformation has to be extended by an iteration process. 3. The space-wise approach which, after having transformed the original observations onto a spatial geographical grid, transforms the pseudo-observations into harmonic coefficients using a fast collocation technique. A successful mission presupposed, GOCE will finally deliver the Earth's gravity field with a resolution of about 70 km half-wavelength and a global geoid with an accuracy of about 1 cm.

**G03/07P/D-059** Poster **1400-081****EVALUATION OF GRAVITY DATA BY EIGEN-1S MODEL IN CHINA**

Yang LU, Hongling SHI (Key Laboratory of Dynamic Geodesy, Institute of Geodesy and Geophysics, Chinese Academy of Sciences)

Plan along with the satellite gravity field missions of puts into practice and provided the powerful research tool for the research of the Earth gravity field, the high accuracy global gravity field models derived from the satellite gravity missions CHAMP, GRACE and GOCE are expected to significantly improve the gravity field in terms of a homogeneous and high accuracy and resolution. To date the CHAMP mission has led to a new global long wavelength gravity field model called EIGEN-1S, which firstly adopted the satellite to satellite tracking techniques. The model has the ability to study long wavelength errors of the terrestrial gravity data. First the long wavelength gravity field components will be studied based on the EGM96 model and the EIGEN-1S model. Second we utilize the 2D Gaussian low-pass filter to distill the long wavelength components of the terrestrial gravity data, including mainland gravity anomalies, marine gravity anomalies and gravity anomalies derived from satellite altimetry, for China and its vicinity. The gravity data will be devoted to study the long wavelength agreement between the terrestrial data and the global models. The results shown that the global gravity field models EIGEN-1S and EGM96 are consistent up to about degree 36, while above this degree the EIGEN-1S may have inferior estimates. The evaluation of the terrestrial gravity data for China by comparison with the EIGEN-1S model has confirmed the existence of larger errors and systemic discrepancy. The majority of larger errors appear in the Northwestern and the Tibet plateau of China, the maximal long wavelength error achieves 28mGal. It was found apparent inconsistencies between the EIGEN-1S model and altimeter data on the Northwestern Pacific, which a mean discrepancy on long wavelength component is about 2.5mGal and increase about 4.0mGal in offshore. The reasons for the revealed errors may be traced back to lacking or poor quality gravity data, especially in the Western mainland of China, while in offshore we suspect datum inconsistencies or errors in the ship surveying data and satellite altimeter data.

**G03/07P/D-060** Poster **1400-082****CHAMP GRAVITY FIELD MODEL UCPH2003\_01**

Carl Christian TSCHERNING, Eva HOWE, Lars STENSENG (IAG)

The German CHALLENGING Minisatellite Payload (CHAMP) was launched in July 2000. It carries a GPS receiver and a three-axes accelerometer. From GPS measurements a precise orbit of the satellite in August 2001 has been determined by DEOS at TU Delft. With these orbits and pre-processed accelerometer data it has been possible to determine a global gravity field model to degree and order 90. The gravity field model has been determined using least squares collocation and by considering energy conservation. The satellite loses kinetic energy due to external forces. The tidal potential from the sun and the moon, energy dissipation and the explicit time variation of the gravitational potential in inertial space are taken into account.

**G03/07P/D-061** Poster **1400-083****THE IMPACT OF THE NEW MISSIONS DATA IN THE DEVELOPMENT OF FUTURE GRAVITY MODELS**

Enricos C. PAVLIS (JcET/UMBC - NASA/GSFC)

JcET is contributing to NIMA's current effort to enhance the geopotential model underlying the World Geodetic System 84 (WGS 84), and in particular, with the incorporation of data from new missions such as CHAMP and GRACE at present, and GOCE in the future. One of the many enhancements that the new development incorporates is the modeling of temporal variations for the long wavelength components of the field, in order to avoid aliasing of these signals and a consequent degradation in the quality of the new model. The Terrestrial Reference Frame (TRF) plays an important role in the multi-technique monitoring of temporal variations in the gravitational field and its very low degree and order components, as well as changes in the inertia tensor as a result of angular momentum exchanges in the Earth system. Currently, and until we accumulate several years of GRACE data, the best data source for determining these variations are satellite laser ranging geodetic targets (such as the LAGEOS, ETALON, AJISAI, STARLETTE, STELLA, etc.). We are now routinely analyzing Satellite Laser Ranging (SLR) data from ETALON 1 and 2, along with our nominal data set from LAGEOS and LAGEOS 2 for this effort. While the data from these satellites provide the definition of the underlying TRF, its crust-fixed orientation, and the temporal variations in the long wavelength, the detailed components of the gravitational model will be primarily determined from the data of dedicated missions such as CHAMP, GRACE, and GOCE in the future. We present here preliminary results of a new analysis of our expanded data set for the definition of the long wavelength harmonics of the geopotential. The data

were reduced using NASA Goddard's GEODYN/SOLVE II software. We will discuss our solution and compare with other solutions based on data from new missions alone, or in combination with other satellite and surface gravimetric data.

**G03/07P/D-062** Poster **1400-084**

#### AGMAF-03: AN ARCHIVING FORMAT FOR ABSOLUTE GRAVITY MEASUREMENTS

Jean-Pierre BARRIOT<sup>1</sup>, Michel SARRAILH<sup>1</sup>, Jacques LIARD<sup>2</sup>, Gerd BOEDECKER<sup>1</sup> (UMR5562/CNES/BGI, <sup>2</sup>Geodetic Survey Division - Ottawa, Canada, <sup>3</sup>Bayer. Akademie der Wissenschaften, Munich, Germany)

We present in full details the AGMAF-03 (Absolute Gravimetry Measurements Archiving Format - 2003), developed at the Bureau Gravimétrique International (BGI) in Toulouse (France), to store absolute gravity measurements. This format is oriented toward FG-5 absolute gravity meters, and has been written in close connection with users and the International Gravity and Geoid Commission (IGGC) of the International Association of Geodesy (IAG). The format is available on line at <http://bgi.cnes.fr>

**G03/07P/D-063** Poster **1400-085**

#### COMPARISON OF DIFFERENT DOWNWARD CONTINUATION METHODS OF AIRBORNE GRAVIMETRY DATA

Felix MUELLER (Institut of Theoretical Geodesy, University of Bonn)

The determination of the precise gravity field and the geoid represents a central task in geodesy. Despite the fact that spaceborne gravity field missions such as CHAMP, GRACE and GOCE will improve our knowledge of the Earth's gravity field in the short, medium and long wavelength parts in the near future, it is necessary to supplement this gravity field information with available terrestrial data and additional measurements in those areas where no gravity field information is available or where its precision is not sufficient. In this matter airborne gravimetry provides a fast and reliable method especially for those regions which are difficult to access. With respect to the spectral representation of the gravity field airborne gravimetry is capable to fill the gap in the range of wavelength between 1 and 50km. With current airborne gravity systems an accuracy of 2 to 3 mGal (rms) with a resolution of 6 to 15km can be achieved and has been proven by experiments. Data processing becomes more significant to meet the demands for a geoid with centimeter-accuracy. Besides the task of preprocessing which results in band-limited gravity disturbances at flight level, the choice of a proper downward continuation method gains in importance. In general the downward continuation is an improperly posed problem and requires regularization, which in principle results in filtering the noise. Regularization is indispensable in satellite geodesy and some effective techniques have been proposed. Nevertheless, various questions are still open and no satisfying procedure exists how to scale the regularization parameter which rules the balance between noise and signal. In case of airborne gravimetry especially in those cases where the airplane cruises at relatively high altitudes even more questions are still open. In this investigation different downward continuation methods are compared and the impact of regularization of airborne gravimetry data is shown. It is investigated whether it is useful to apply a filtering technique in a subsequent post processing step. The investigations are based on simulated data sets to control the results and applied to a real test area.

**G03/07P/D-064** Poster **1400-086**

#### EFFICIENT CALCULATION OF TOPOGRAPHIC REDUCTIONS BY THE USE OF TESSEROIDS

Kurt SEITZ, Bernhard HECK (Geodetic Institute, University of Karlsruhe)

The calculation of topographic reductions is one of the most time-consuming operations in geoid and quasi-geoid calculation as well as in geophysical interpretation of the gravity field. A new procedure, based on so-called tesseroids (volumetric mass elements bounded by geographical grid lines and surfaces of constant heights), has been further developed. The formulae describing the potential and the attraction of spherical tesseroids is shortly reviewed; the respective volume integrals are solved by Taylor expansions of 3<sup>rd</sup> order. Testcomputations show the high numerical efficiency of this method in comparison with the generally used prism formulae. Exploiting the properties of this approach provides further refinements, e.g. in considering ellipsoidal tesseroids.

**G03/07P/D-065** Poster **1400-087**

#### NATIONAL REPORT ON THE STATUS OF THE RECOMPUTATION OF PRECISE LEVELLING OF IRAN

Rohallah KARIMI, Aïreza A. ARDALAN, Farrokh TAVAKOLI (Department of Surveying and Geomatics Engineering, University of Tehran)

Iran has the heritage of 23 years of precise leveling observations. These data comprises of 11500 first order leveling stations with length of 31000km. In this paper we are presenting the current status of the precise leveling observations and the results of the latest recomputations of the geopotential numbers at the first order leveling stations.

**G03/07P/D-066** Poster **1400-088**

#### DISCUSSION OF BOUGUER ANOMALY

Petr VANICEK<sup>1</sup>, Robert TENZER<sup>1</sup>, Lars E. SJOBERG<sup>2</sup>, Zdenek MARTINEC<sup>3</sup> (<sup>1</sup>Department of Geodesy and Geomatics Engineering, University of New Brunswick, <sup>2</sup>Division of Geodesy, Department of Geodesy and Photogrammetry, Royal Institute of Technology, <sup>3</sup>Department of Geophysics, Faculty of Mathematics and Physics, Charles University in Prague)

In this paper we attempt to answer some of the questions that people started to ask recently. These were: Is the spherical version of the complete Bouguer anomaly the same as the standard planar version? How can the complete Bouguer anomaly be continued downward to the geoid from the surface of the earth? Is the complete Bouguer anomaly harmonic above the geoid? In order to answer these, and other questions, we have had to go back to the very basic principles and definitions of the theory of gravity field. We had to introduce the distinction between solid" (defined in the 3-D sense) and "surface"(defined in the 2-D sense) gravity anomalies, and show how these two are related. Then we showed that the spherical complete Bouguer anomaly is quite different from the standard variety. While the spherical kind is indeed harmonic above the geoid, the standard kind is not. While the spherical kind can be continued from the surface of the earth down to the geoid using the Poisson approach, the standard kind cannot.

**G03/07P/D-067** Poster **1400-089**

#### RIGOROUS ORTHOMETRIC HEIGHT

Petr VANICEK<sup>1</sup>, Robert TENZER<sup>1</sup>, Marcelo SANTOS (University of New Brunswick, Department of Geodesy and Geomatics Engineering)

In this paper, a rigorous definition of the mean value of gravity along the plumbline is formulated. The mean gravity along the plumbline is evaluated as a sum of the mean value of gravity generated by earth's masses within the geoid and the mean value of the gravitational attraction generated by topographical masses. By removing the gravitational attraction of topographical masses from the gravity generated by the whole earth, the gravitational field above the geoid becomes harmonic. Approximating the geoid by the geocentric reference ellipsoid, the geoid-generated gravity, i.e., the "No Topography gravity" (Vaniček et al., 2003), is split into the normal gravity and the "No Topography gravity disturbance" (Tenzer and Vaniček, 2003). The mean "No Topography (NT) gravity" is then evaluated as a sum of the mean values of the normal gravity and the NT-gravity disturbance along the plumbline. The mean value of the NT-gravity disturbance along the plumbline is evaluated through upward continuation of the NT-gravity disturbances referred to the geoid in the "No Topography space". Applying the Poisson theory, we solve Dirichlet's boundary value problem for each point between the earth surface and the geoid along the plumbline to obtain individual point values. Then we perform the integral averaging of all these values to get the desired average. Alternatively, when the NT-gravity disturbances are known on the earth surface, Dirichlet's inverse problem is solved to obtain the mean NT-gravity disturbance. To the average of geoid-generated gravity we add the average of gravitational attraction generated by topography. The gravitational attraction of topographical masses is computed for each point along the plumbline by means of Newton's integral over the topographical masses around the world and averaged in the integral sense between the earth surface and the geoid. Based on the rigorous definition of mean gravity, the rigorous relation between the orthometric and normal heights is also formulated. Not surprisingly, this relation turns out to be just a function of the mean values of the gravitational attraction of topographical masses and the NT-gravity disturbance along the plumbline.

**G03/07P/D-068** Poster **1400-090**

#### GRACE LEVEL-1 DATA PROCESSING

Gerhard L. KRUIZINGA, William I. BERTIGER, Kelley E. CASE, Christopher J. FINCH, Larry J. ROMANS, Michael M. WATKINS, Sien C. WU (California Institute of Technology, Jet Propulsion Laboratory)

The beginning of the science processing for the GRACE mission, called Level-1 processing, consists of data reformatting, data compression, editing, and precise time tag alignment based on GPS precise orbit determination for the formation of the dual one way range. This task is performed at the Jet Propulsion Laboratory, California Institute of Technology (JPL) GRACE Science Data System team working in cooperation with the Physical Oceanography Data Active Archive Center (PO-DAAC). In this poster an overview will be given of the data flow from raw telemetry (Level-0) to Level-1 data which is used to estimate gravity fields by the Level-2 processing centers at the Center for Space Research, University of Texas at Austin, Geo Forschungs Zentrum, Potsdam and JPL. Furthermore, the quality control assessment for all dataproducts will be discussed as well as experience gained by processing the GRACE data set. Finally an overview will be given of all science data products to be distributed to the science community and the method of distribution.

**G03/07P/D-069** Poster **1400-091**

#### THE QUASI-GEOID OF SOUTH AMERICA AFTER ONE DECADE OF IMPROVEMENT ON THE DATA

Denizar BLITZKOW<sup>1</sup>, Ana Cristina Cancorro MATOS<sup>1</sup>, Maria Cristina LOBIANCO<sup>2</sup>, Carlos Alberto Correia CASTRO JR.<sup>3</sup> (<sup>1</sup>Department of Engineering Transportation, University of Sao Paulo, <sup>2</sup>Instituto Brasileiro de Geografia e Estatística - DEGED)

A very strong and international effort has been made in the last ten years to improve the distribution and quality of the gravity and topography data in order to determine the quasi-geoid of South America. The study has improved the gravity data, digital terrain model (DTM) and GPS observations on the leveling network. Most countries in South America have participated to this challenging study which resulted in an important contribution for the establishment of an altimetric reference for South America that is linked to the quasi-geoid model. In this paper, the activities that have been coordinated by EPUSP and IBGE are described. The work has involved many organizations in Argentina, Brazil, Chile, Colombia, Ecuador, Paraguay, Uruguay and Venezuela. The list of organizations involved in each country are too many to reference, but, include the Military Institutes in most of the countries, Universities and government agencies. Contribution of GETECH - University of Leeds and NIMA are also acknowledged. The study has paid particular attention to the different computation softwares used used to generate the quasi-geoid in order to guarantee a reliably and accurate solution. As a consequence, this presentation compares the different computations. The results of the new computations using the improved coverage data, DTM and softwares are presented and discussed.

**G03/07P/D-070** Poster **1400-092**

#### GEOIDAL MODEL OBTAINED BY MULTILAYER PERCEPTION NEURAL NETWORK

Paulo Cesar Lima SEGANTINE<sup>1</sup>, Tule Cesar Barcelos MAIA<sup>2</sup> (<sup>1</sup>Department of Transportation, University of São Paulo-EESC/USP, <sup>2</sup>Department of Civil Engineering at University Catholic of Goiás)

This paper has the goal to show the artificial neural networks as a tool in the geoidal undulation model. In the first part of the project, was developed a neural network applying Multilayer Perception (MLP) technique to estimate the geoidal undulation gave by geopotential model EGM96. It was chosen an area between the -17° and -27° parallels and -43° and -53° meridians. It was determined different geopotential undulation with grade and order equal 50, 70, and 360 of EGM96 to verify the approximation of surface gave by the neural network in relation to the gave by EGM96. For neural network training it was organized a 5x5AEgrid of undulations related with EGM96 and another one 1x1 Egrid for each surface created to verify the network learning. For each file, containing the input signal and neural network output, it was done four different types of data normalization. It was changed the activation functions types, the numbers of layers and neuron of the artificial network with the intent to get the best result. All the preliminaries results for the geoidal undulations represented by the MLP neural network type has been shown the average differences of 5mm for geopotential models with short grade and order (50 and 70) and extremes errors around 9mm and -7mm in the grid edge. The amplitude of geoidal undulations was from the 6.270m to -12.653m. For the grade and order equal to 360 the mean differences were around 20mm with extreme errors of 17cm and -6cm in the grid edge too. The MLP network used in the surface representation has 747 coefficients. The result

obtained in this research has shown that the artificial neural networks are efficient tools to determine surfaces that do not have a defined mathematical form.

**G03/07P/D-071** Poster **1400-093**

**ANALYTIC FORMULAS FOR THE GRAVITATIONAL GRADIENTS GENERATED BY TRIANGULAR VERTICAL PRISMS WITH SLOPED TOPS**

Christopher JEKELI, Putipol DUMRONGCHAI (Geodetic Science, Ohio State University)

Analytic formulas for the gravitational gradients generated by rectangular blocks are well known and routinely used to generate the gradient field from finite element models of the near-field terrestrial masses. We have developed closed analytic formulas for triangular vertical prisms with sloped tops. These can be used to generate the gradients of finite element models produced by a triangulation of a surface. Such finite element models have a continuous bounding surface and thus are smoother than the rectangular block models. It is shown that higher-order smoothness in the model surface yields elliptic integrals for the gradients that, therefore, are not amenable to further reduction to closed analytic expressions. Numerical examples derived from a digital elevation model with constant density are used to compare the generation of gradients due to the triangular-prism and rectangular-block finite element models.

**G03/07P/D-072** Poster **1400-094**

**VECTOR AIRBORNE GRAVIMETRY FOR IMPROVED GEOID DETERMINATION**

Juan Gilberto SERPAS, Christopher JEKELI (Geodetic Science, Ohio State University)

Airborne gravimetry is now a proven technique to obtain high-resolution geoid undulations with accuracies approaching a few cm, in relative precision. The usual approach relies on the standard solution to a boundary-value problem where the boundary values are the vertical gravity disturbances measured with an airborne gravimeter or accelerometer. We have shown that measuring the horizontal disturbances with an airborne three-dimensional GPS/INS configuration yields the relative geoid using simple line integrals with comparable precision. Combining the vertical and horizontal gravity disturbances naturally improves the solution, especially near the edges of a survey area, where the solution to the standard boundary-value problem is subject to the largest model errors. Both least-squares collocation and Hotine's integral combined with line integrations can be used to obtain the geoid from all disturbance vector components. We apply both methods to derived data as well as observed disturbances collected in the Canadian Rockies (supplied by the University of Calgary).

**G03/07P/D-073** Poster **1400-095**

**DETERMINATION OF INDONESIAN GRAVITY FIELD FROM COMBINATION OF SATELLITE ALTIMETER, SURFACE GRAVITY AND DIGITAL TERRAIN MODEL DATA**

Leni S. HELIANI, Yoichi FUKUDA, Shuzo TAKEMOTO (Graduate School of Science, Kyoto University)

The Indonesian gravity field has been computed from combination of satellite altimeter, surface gravity, digital terrain model and EGM96 geopotential model data by means of Least Square Collocation (LSC). This is adopted to solve the variability of utilized data. Two spectral methods were also used in sub-area for investigation purposes, and demonstrate that three methods have almost similar results. Comparison with GPS-levelling shows substantial improvement over INDGED96, the previous geoid model, and depicts the application of local coordinate in leveling data. However, large differences show in comparison with tide gauge data, which mainly due to differences in reference system among the compared data. From connection between the comparison with GPS-levelling and with tide gauge data, suggests the possibility of the present Indonesian height system is higher than the actual by about 1.2 m.

**G03/07P/D-074** Poster **1400-096**

**CHALLENGING THE LIMIT IN THE DEVELOPMENT OF A SUPER HIGH RESOLUTION EARTH GRAVITY FIELD MODEL**

Kefei ZHANG<sup>1</sup>, Yang LU<sup>2</sup>, Rod DEAKIN<sup>1</sup>, Norm EDWARDS<sup>1</sup> (<sup>1</sup>Department of Geospatial Science, RMIT University, <sup>2</sup>Wuhan Institute of Geodesy and Geophysics, Chinese Academy of Science)

A new Australian regional geopotential model (AGM\_RMIT5400) with spherical harmonic coefficients to degree and order 5400 has been developed using the "tailoring" method. The new model incorporates state of the art development in extra-terrestrial gravity field recovery techniques (EIGEN-1S model from the dedicated satellite gravity missions, CHAMP), state of the art satellite information (satellite altimetry, GPS) and other heterogeneous data (land and marine gravity, air-borne gravimetry, local gravimetric geoid and digital terrain model etc.). High-powered computing facilities are necessary in order to perform the intensive computations with the huge amount and variety of data involved and the numerical stability problem. The Victorian Partnership for Advanced Computing (VPAC) high performance computing facility (a 128 processor Compaq Alphaserver SC, with 64 Gbyte of memory and 1.4 Tbyte of disk) is used. The numerical stability of the Legendre function has been investigated using both double and quad precision arithmetic over different areas of the earth. It is demonstrated that the highest degree and order model that can be developed is limited to about 2200 when double-precision arithmetic is used. It is also found that the numerical stability problem occurs around latitude of  $\pm 40^\circ$ . It is demonstrated that a much higher degree and order gravity field model can be developed when quad-precision arithmetic is used. This paper presents the new development of the model (AGM\_RMIT5400) including its methodology, new data sources, numerical stability, special computation requirements, limitations and detailed evaluation against "the ground truth data". It is shown that the RMS differences between AGM\_RMIT5400 and the mean land gravities and the latest Australian gravimetric geoid (AUSgeoid98) are  $\pm 2.62\text{mGal}$  and  $\pm 0.14\text{m}$  respectively. It is concluded that the new model offers significant improvements when it is compared with any existing high degree and order models. Further comments regarding a number of challenging issues in the development of a super-high geopotential model are presented.

**G03/07P/D-075** Poster **1400-097**

**THE AUSTRIAN GEODRECENT STEPS TO A NEW SOLUTION**

Norbert KUEHTREIBER<sup>1</sup>, Bernhard HOFMANN-WELLENHOF<sup>1</sup>, Erhard ERKER<sup>2</sup>, Norbert HÖGGERL<sup>3</sup>, Erich IMREK<sup>2</sup> (<sup>1</sup>Institute of Geodesy, Graz University of Technology, <sup>2</sup>Federal Office of Metrology and Surveying (BEV), Vienna)

A recomputation of the new Austrian geoid denoted as GEOID2000<sup>®</sup> has been finished and the results will be released soon. GEOID 2000 is a common project of the BEV in Vienna

and the Graz University of Technology, Institute of Geodesy under the umbrella of the Austrian Geodetic Commission. In a first step, all data sets had to be improved. The BEV established a high precision height model with a resolution of 45 x 49 m. Furthermore, the data sets including gravity anomalies, deflections of the vertical, density and satellite data have been updated and checked. The territory of Austria serves as ideal test area for applying different computational methods. At the Institute of Geodesy in Graz, existing methods for the geoid determination were tested with respect to their usability and achievable precision. As a result of the investigations, the remove-restore technique and least squares collocation was used for the computation. Finally, the optimal combination of the geoid solution with geoid heights resulting from GPS-levelling has been investigated. An overview of the computation process and the main results are discussed in the paper.

**G03/07P/D-076** Poster **1400-098**

**TOPEX ALTIMETRIC MEAN SEA LEVEL AND GRAVIMETRIC GEOID ON THE NORTH OF ALGERIA**

Salem KAHLLOUCHE, Ali RAMI, Sid Ahmed BENAHEM DAHO (Laboratory of Geodesy - National Center of Space Techniques)

The mean sea level is processed from Topex altimetric measurements collected on the Algerian coasts (on the South West of the Mediterranean Sea) during a three months period (April 20 to July 28, 2000). The model used, based on the Barrick-85 model, permits the determination of the instantaneous sea surface heights for 80 cycles distributed on 8 orbital arcs. The pre-processing of the raw data (electromagnetic bias, low reflected power,...) permit the selection about 75 % of the measurements. The processing of the fitted data, by polynomial adjustment, is done after the correction of the main disturbed effects (instrumental correction, ionospheric and tropospheric propagation,...) and the reduction of the radial component of the orbital error. The analysis of the mean arcs in the crossing points by the least squares adjustment allows a centimetric accuracy of the mean sea level. The surface obtained was extrapolated to the North of Algeria (surroundings the coasts) and compared to a gravimetric geoid calculated with a set of BGI free air gravity anomalies and GETECH data using the FFT techniques implemented in the Geofour program [Tscherning, 1994]. The metric difference obtained is due to the insufficient altimetric and gravimetric data distribution, and to the extrapolation method used. The availability of an exhaustive gravity measurement, particularly the gravity cruise data (sea data), and a long period altimetric measurement, will allow a strong comparison between the surfaces.

**G04** Monday, July 7 - Tuesday, July 8

**GENERAL THEORY AND METHODOLOGY. MEETING OF IAG SECTION IV**

Location: Site C, Room 25

Monday, July 7 PM  
Presiding Chairs: B. Heck, P. Xu

**G04/07P/C25-001** **1430**

**ON TOTAL LEAST-SQUARES ADJUSTMENT WITH CONSTRAINTS**

Burkhard SCHAFFRIN<sup>1</sup>, Yaron FELUS<sup>2</sup> (<sup>1</sup>Department of Civil and Environmental Engineering and Geodetic Science, The Ohio State University, Columbus, Ohio 43210-1275, U.S.A., <sup>2</sup>Department of Surveying Engineering, Ferris State University, Big Rapids, Michigan 49307 - 2291, U.S.A.)

For calibration purposes, oftentimes various datasets are compared in such a way that observations enter the coefficient matrix of a Linear Model ("errors-in-variables"). In such a case, the Total Least-Squares approach would be appropriate that was pioneered by G. Golub and Ch. Van Loan in the early eighties. In essence, rather than solving the usual normal equations system for the estimated parameters, the smallest singular values of a slightly extended system is set to be zero, and its eigenvector is re-scaled to provide the estimated parameter vector. The authors have recently presented their studies that show the potential of this technique to provide improved variograms for geostatistical Kriging applications. Sometimes, however, stability or slow convergence problems may occur with the algorithm as designed so far. In order to increase the stability, additional parameters have been introduced to represent the functional model under investigation, but with a number of constraints that keep the original redundancy unchanged. In the end, the same Total Least-Squares Fit is supposed to result after fewer iterations from the newly developed scheme that, for the first time, allows the integration of constraints between the parameters. A few simple, but typical examples will show the performance of this powerful approach to solving a case that was long considered "untreatable" by the original TLS algorithm.

**G04/07P/C25-002** **1450**

**NONLINEAR FILTERING OF CONTINUOUS SYSTEMS: FOUNDATIONAL PROBLEMS AND NEW RESULTS**

Peiliang XU (Disaster Prevention Research Institute, Kyoto University, Gokasho, Uji, Kyoto 611-0011, Japan)

This paper is to extend the work of Xu (1999) on discrete nonlinear filtering to the continuous systems. The new results are summarized as follows: (i) we work out a second order unbiased prediction of the true state governed by a vector stochastic differential equation; (ii) we derive a set of coupled differential equations for a new truncated second order nonlinear filter and its variance-covariance matrix from the frequentist point of view. The new filter is proved to be unbiased to the second order approximation; and most importantly, (iii) comparing our new filtering and accuracy results with the literature on nonlinear filtering has indicated that more than forty years of nonlinear filtering of continuous systems may have had fundamental defect in the foundation.

**G04/07P/C25-003** **1510**

**GNSS BEST INTEGER EQUIVARIANT ESTIMATION**

Peter J.G. TEUNISSEN (Department of Mathematical Geodesy and Positioning, Delft University of Technology)

Carrier phase ambiguity resolution is the key to high precision Global Navigation Satellite System (GNSS) positioning and navigation. It applies to a great variety of current and future models of GPS, modernized GPS and Galileo. The so-called "fixed" baseline estimator is known to be superior to its "float" counterpart in the sense that its probability of being close to

the unknown but true baseline is larger than that of the 'float' baseline, provided that the ambiguity success rate is sufficiently close to its maximum value of one. Although this is a strong result, the necessary condition on the success rate does not make it hold for all measurement scenarios. In this contribution we will answer the question whether or not it is possible to take advantage of the integer nature of the ambiguities so as to come up with a baseline estimator that is always superior to both its 'float' and 'fixed' counterparts. We will show that this is indeed possible, be it that the result comes at the price of having to use a weaker performance criterion.

G04/07P/C25-004

1530

#### SENSITIVITY ANALYSIS FOR GNSS INTEGER CARRIER PHASE AMBIGUITY VALIDATION TEST

Jinling WANG, Hung-Kyu LEE, Steve HEWITSON, Chris RIZOS, Joel BARNES (School of Surveying and Spatial Information Systems, University of New South Wales, Sydney, NSW 2052, Australia)

Global navigation satellite systems have been widely used for many precise positioning and navigation applications. In satellite-based precise positioning, the determination of correct integer carrier phase ambiguities is the key. Therefore much effort has been invested in developing a robust quality control procedure which can validate the ambiguity resolution results. Such a quality control procedure has been traditionally based on the so-called F-ratio Test. A major shortcoming of the F-ratio measure is that its probability distribution is still unknown, which precludes the possibility of defining the confidence level for the ambiguity validation test. To overcome such a shortcoming, a new ambiguity validation test based on the so-called W-ratio Test has been proposed (Wang J. et al., 1998: A discrimination test procedure for ambiguity resolution on-the-fly, *Journal of Geodesy*, 72:644-653). This paper presents a sensitivity analysis for the new ambiguity validation test based on the W-ratio. The analysis is concerned with the sensitivities of the W-ratio measure to undetected gross errors, unmodelled (remaining) systematic errors, and various specifications in the stochastic models, as well as geometric strength due to a variety of satellite constellations (such as GPS, GPS/pseudolite and GPS/Galileo combinations).

G04/07P/C25-005

1620

#### GPS ON-THE-FLY AMBIGUITY SEARCH BY FUZZY-LOGIC MULTI-CRITERIA DECISION MAKING TECHNIQUE

Stefan LEINEN (Institute of Physical Geodesy, Darmstadt University of Technology)

On-the-fly (OTF) ambiguity search is the most challenging task in kinematic GPS positioning with high accuracy (few centimetres level). Starting with an approximate position all combinations of integer values lying in a specified search volume have to be considered as potentially correct ambiguity values. From these the solely correct integer set has to be selected based on certain criteria. In terms of decision theory this task is a multi-criteria decision making (MCDM) problem. The candidate integer sets form the alternatives whose plausibilities are assessed by means of various attributes, i.e. the selection criteria in this application. Based on this assessment the decision is made if the correct ambiguity values can be identified or not. Usually the criteria or attributes in OTF ambiguity search are formulated as tests of values derived from the data evaluation using the candidate integers against thresholds which might be based on statistics, experience, or other assumptions. Results of such tests are crisp in the sense that only two statements are possible: test is passed or not. High-precision OTF GPS positioning is affected by a number of uncertainties: cycle-slips and signal reacquisition, multipath, vegetation, tropospheric and ionospheric refraction etc. lead to varying noise and systematic effects of unknown size in the data. Its impossible to account for all such effects in the data evaluation. This means that one has to deal with a more or less un-quantifiable amount of uncertainty. Doing MCDM in the crisp way as described above means to ignore these uncertainties. Depending on the measurement conditions the risk of false solutions might be high and the reliability respectively low. Clearly the use of such a method is limited to optimal conditions only. In this presentation a fuzzy-logic MCDM technique is introduced for application to the OTF ambiguity search problem. This approach is motivated by the fact that the theory of fuzzy sets and systems might facilitate the proper handling of the above described uncertainties in data and mathematical model. The mathematical formulation of the fuzzy-logic MCDM is presented and its key features and characteristics are investigated in comparison with the traditional crisp MCDM procedure. In addition the performance of both kinds of MCDM methods when applied to exemplary data sets is compared in terms of success rate, reliability and working range (distance of rover to base station under different conditions).

G04/07P/C25-006

1640

#### PARAMETRIC VERSUS NON-PARAMETRIC METHODS FOR OPTIMAL WEIGHTED AVERAGING OF NOISY DATA SETS

Christopher KOTSAKIS<sup>1</sup>, Ilias N. TZIAVOS<sup>2</sup> (<sup>1</sup>Department of Geomatics Engineering, University of Calgary, Calgary, Alberta, Canada, <sup>2</sup>Department of Geodesy and Surveying, Aristotle University of Thessaloniki, Thessaloniki, Greece)

The problem of optimal weighted averaging of multiple data sets that correspond to noisy recordings of a given signal is studied. Identified as one of the most primitive applications of least squares methods, data averaging can be employed either at the pre-processing stage of geodetic data analysis (e.g., for noise reduction in repeat-track altimetric data profiles), or as a stand-alone tool in cases where an unknown signal needs to be estimated by a linear combination of its ensembles. In view of the continuously increasing load of gravity field and altimetry data coming from current and future satellite missions, data fusion procedures which utilize signal averaging techniques provide an efficient tool for many areas of geodetic research. Generalizing the classic averaging problem in statistics where the mean of a single random variable is approximated by the sample mean of a set of its values, signal averaging offers interesting hidden challenges from a theoretical as well as an applied viewpoint. For instance, the noise correlation in the individual data sets is not taken into account if a single scalar weighting factor is assigned to each signal ensemble. In order to overcome this limitation, more general averaging schemes must be introduced that allow for: (i) the auto-correlation of data noise within each signal ensemble, and (ii) the noise cross-correlation among the different ensembles, to be properly considered. In any case, the determination of the optimal ensemble weights according to a mean-square-error (MSE) criterion requires the knowledge of the noise covariance (CV) function for each data set, which is often not available in practice. An alternative weighted averaging method will be presented herein which is free of any a-priori assumptions about the statistical characteristics of the noise and/or the underlying signal. Our approach is based on the minimization of an empirical signal-to-noise ratio and it results in optimal ensemble weights than can be directly computed from the available data values. Hence, it essentially provides a non-parametric technique for weight determination since any hypothesis regarding the second-order statistics of the data noise is avoided. Various numerical tests are presented using simulated gravity anomaly profiles with both white and coloured Gaussian random noise. The experiments include comparisons between simple (uniform) and weighted averaging

schemes for noise reduction in the observed gravity anomaly signal, and reveal the significance of proper weighting, especially for cases with very high noise level in the input data sets. Our empirical non-parametric approach for weight determination also shows satisfactory results which justify its use in practice, when a-priori statistical information for the data noise is not available.

G04/07P/C25-007

1700

#### THE STATISTICAL INFERENCE OF EIGENSPACE COMPONENTS OF A SYMMETRIC RANDOM DEFORMATION TENSOR

Jianqing CAI, Erik W. GRAFAREND (Department of Geodesy and Geoinformatics, University of Stuttgart)

The *eigenspace components* (principal components, principal directions) of random deformation tensors, for instance strain and stress, are of focal interest in geodesy, geophysics and geology. They play an important role in interpreting the geodetic phenomena like earthquakes (seismic deformation), plate motions and plate deformations among others. Let us assume that the strain or stress tensor has been directly observed or indirectly determined by other measurements. According to the *Measurement Axiom* such a symmetric tensor is *random*. For its *statistical inference*, we assume that the random tensor is *tensor-valued Gauss-Laplace normal distributed*. The *eigenspace synthesis* relates the eigenspace elements to the observations by means of a nonlinear vector-valued function establishing a *special nonlinear multivariate Gauss-Markov model*. For its linearized form we have succeeded to construct *BLUUE* of the eigenspace elements and *BIQUUE* of its variance-covariance matrix. The related *linear hypothesis test* has documented large confidence regions for the eigenspace components, namely *eigenvalues and eigendirections*, based upon real measurement configurations. They lead to the statement *to be cautious* with data of type extension and contraction as well as the orientation of principal stretches. In lieu of a case study, *statistical inference* is applied to the observations of geodetic surface strain rate tensor in two-dimensions and the seismic strain rate in three-dimensions.

G04/07P/C25-008

1720

#### SAMPLING-BASED STATISTICAL INFERENCE FOR HIGH-RESOLUTION GRAVITY MODELS

Juergen KÜSCHE<sup>1</sup>, Karl-Rudolf KOCH<sup>2</sup>, Brigitte GUNDLICH<sup>1</sup> (<sup>1</sup>PHYSICAL GEOMETRICAL AND SPACE GEODESY, TU DELFT, <sup>2</sup>THEORETICAL GEODESY, BONN UNIVERSITY, <sup>3</sup>MATHEMATICAL GEODESY AND POSITIONING, TU DELFT)

For a spherical harmonic (SH) model of the Earth's gravity field, it is desirable to have a stochastic quality description. The idea is to propagate this stochastic model into a quality description for various derived quantities such as geoid heights or height differences, gravitanomalies, or satellite orbits. The common approach is to compute the variance-covariance matrix of the SH model by inverting the normal equations in the first place. There are some problems related to this approach: (1) For high-resolution models, a large matrix of normal equations has to be assembled and explicitly inverted. (2) Error propagation to gridded linear functionals like geoid heights requires intensive computations. (3) For quantities that do not exhibit a simple linear relation to the harmonic coefficients, error propagation is only possible if a linearization is appropriate. In contrast, statistical inference for gravity models and derived quantities can be based on Monte Carlo integration. A sampling method will then provide random realizations of the SH model. By exploiting the Gibbs sampler, we can avoid an explicit inversion of the matrix of normal equations. We have generated error samples for the EGM96 model and for a projection of a GOCE-derived model. Using improved Monte Carlo estimation, only very few samples are necessary for linear and nonlinear error propagations.

G04/07P/C25-009

1740

#### SYNTHETICALLY ADAPTIVE ROBUST FILTERING FOR SATELLITE ORBIT DETERMINATION

Yuanxi YANG<sup>1</sup>, Yuanlan WEN<sup>2</sup> (<sup>1</sup>Xian Research Institute of Surveying and Mapping, <sup>2</sup>College of Aerospace and Material Engineering, National University of Defense Technology, Changsha)

The quality of the satellite orbit determination is rested on the knowledge of perturbing forces acting on the satellite and stochastic properties of the observations, and ability of controlling various kind of errors. After a brief discussion on the dynamic and geometric orbit determinations, a Sage adaptive filtering and robust filtering are reviewed. A new synthetically adaptive robust filtering based on a combination of robust filtering and Sage filtering is developed; It is shown, by derivations and calculations, that the synthetically adaptive robust filtering for orbit determination is not only robust but also simple in calculation. It controls the effects of the outliers of tracking observations and the satellite dynamical disturbance on the parameter estimates of the satellite orbit.

Tuesday, July 8 AM

Presiding Chairs: C. Jekeli, P. Holota

G04/08A/C25-001

0840

#### EQUIVALENT-SOURCE MODELING TO IMPROVE PRECISE GEOID DETERMINATION

Gabriel STRYKOWSKI (National Survey and Cadastre, Rentemestervej 8, DK-2400 Copenhagen NV, Denmark, E-mail:gs@kms.dk)

Present day methods of precise geoid determination involve gravity reductions [e.g. residual terrain model (RTM), Helmert's second method of condensation or different topographic-isostatic reduction methods]. These methods use the gravity and terrain information as is. Only very large inconsistencies between the two data types can be detected. Clearly, the quality of the final geoid is limited by the quality of input data. This limitation cannot be bridged by any conventional method unless it includes a detailed cross-validation between the above data types. Such cross-validation is justifiable on physical grounds; any gravitational signal must be generated by a physical source (Newton's law). Furthermore, geophysical bounds on the possible intensity of mass density contrasts combined with the high quality of present day digital elevation models (DEM) constrain the local sources and the local gravitational field. A special problem with respect to the original definition of the geoid by Gauss and Listing is that in standard methods a simplified mass density contrast for the topography is traditionally used, e.g. 2670 kg/m<sup>3</sup>. It means, that even if a gravitational signal is generated by an intra-topographic source, it is implicitly associated with a source below the geoid. Consequently, in standard geodetic methods (and except for the topography) the local source of the residual gravitational signal should be perceived as a gravi-equivalent source below the geoid. In my presentation I will discuss and demonstrate how to model reasonable local sources and quantify in what way they will constrain the

geoid. The main idea is to model sub-centimeter geoidal height differences for small horizontal separation distances (1 km -10 km) by imposing the existence of a local geophysical source. One can safely claim that a change of geoid over small horizontal distances, if real, must be related to such local source. Distant or large sources cannot produce such effect. In fact, the more elevated the terrain the better the modeled geoidal height differences. The content of this contribution coincides with the work of IAG's Special Study Group 4.188.

**G04/08A/C25-002** **0900**

**A MINIMUM ENERGY CONDITION FOR THE INVERSE GRAVIMETRIC PROBLEM**

Olivier JAMET<sup>1</sup>, Michel DIAMENT<sup>2</sup> (<sup>1</sup>Laboratoire LAREG, Ecole Nationale des Sciences Géographiques, <sup>2</sup>Laboratoire de Gravimétrie et de Géodynamique, Dept. Géophysique Spatiale et Planétaire (UMR 7096), Institut de Physique du Globe de Paris)

The problem of finding the density distribution of the Earth from gravity data is called the inverse gravimetric problem. It is well known that this problem has no unique solution. A possible approach to force the uniqueness of the solution is to impose the solution to realize a minimum of energy, that is to be the equilibrium distribution. Several authors have considered this possibility by setting the energy to the sole energy of the potential field, called the potential energy. It is then necessary to impose constraints on the density distribution, so as to avoid that the material collapse towards the center of the Earth. H. Moritz (1990), for instance, considers that a given density interval occupies a fixed volume, and computes, under this condition, the figure of the equilibrium ellipsoid. We consider the more general case of the real Earth, and assume we know the potential outside of it. The density distribution is modeled as a function of the 3D space member of a Hilbert space. We suppose its second derivatives exist inside the earth (but of course not at its boundary). We show that searching the minimum potential energy density distribution under constraints such as Moritz's is equivalent to maximizing a norm within a convex set. As a consequence, the solution is necessarily located at the boundary of this convex set. It is thus highly dependent from the imposed constraints. In order to formulate an equilibrium condition leading to a better solution, we propose to introduce a compression energy in the formulation of the energy to be minimized. We choose the state equation of Murnaghan to express this compression energy, and show that, under widely admitted hypothesis (in particular on the choice of the value of the first derivative  $K_0$  of the bulk modulus), the minimum of the total energy exists. We discuss then, with  $K_0=4$  (which is a reasonable value for the upper mantle), several properties of the minimum energy density distribution. All the density distributions  $\rho$  of minimum energy have the same potential energy and obey to a differential equation of the form :  $\rho(k_1 + k_2 \nabla \cdot (\rho^2 \nabla \rho)) = 0$  (where  $k_1$  and  $k_2$  are constant,  $\nabla \cdot$  and  $\nabla$  are respectively the divergence and gradient operators). We are still far from a general demonstration of the uniqueness of the solution, but our work is a first step towards such a result. In future works, we plan first to tackle the uniqueness problem for the equilibrium figure of the ellipsoid. References: H. Moritz (1990) *The figure of the Earth : Theoretical geodesy and the Earth's interior*, Ed. Wichmann

**G04/08A/C25-003** **0920**

**SUCCESSIVE APPROXIMATIONS IN THE SOLUTION OF A WEAKLY FORMULATED GEODETIC BOUNDARY-VALUE PROBLEM**

Petr HOLOTA (Research Institute of Geodesy, Topography and Cartography)

Though for many purposes a sphere or an ellipsoid approximate the figure of the Earth fairly well, the real shape of the Earth's topography causes effects that continuously stimulate a considerable research effort. In contrast to the concept of the so-called shrinking parameter in a classical setting, successive approximations are applied in the treatment of the effect within a variational or a weak formulation of the problem. In this connection the role of the analytical continuation and of its interpretation in approximating the solution by means of linear combinations of basis functions is discussed. Related functional estimates are investigated in the process of iteration steps. Some problems associated with a particular choice of basis functions and their construction through spherical and ellipsoidal harmonics are also treated. Various singularity functions and also reproducing kernels are in the focus. Finally, as a part of the process of successive approximations, problems are approached that are associated with an oblique derivative of the solution (i.e. the disturbing potential) in the boundary condition.

**G04/08A/C25-004** **0940**

**ELLIPSOIDAL SPECTRAL PROPERTIES OF THE EARTH'S GRAVITATIONAL POTENTIAL AND ITS FIRST AND SECOND DERIVATIVES**

Karla BÖLLING, Erik W. GRAFAREND (Department of Geodetic Science, Stuttgart University)

The spectral analysis of the Earth's gravitational potential, its first and second derivatives is performed in spherical / ellipsoidal harmonics relative to the *International Reference Sphere / International Reference Ellipsoid*. The highlights of the diagrammatic approach are: (i) Up- and downward continuation of *gravity gradients*, (ii) Downward continuation of *gravity gradients* (four tensor-valued harmonic functions) to the *gravitational potential* on the *International Reference Figure*, (iii) *Direct Conversion of external gravity gradients to geoidal undulation* by means of the spherical / ellipsoidal *Brunns Formula*. The *International Reference Ellipsoid* has been chosen as an equipotential surface in the SOMGLIANA-PIZZETTI reference potential field.

**G04/08A/C25-005** **1000**

**ELLIPSOIDAL CORRECTIONS TO GRAVITY ANOMALIES OBTAINED FROM SATELLITE ALTIMETRY DATA**

Bernhard HECK, Kurt SEITZ (Geodetic Institute, University of Karlsruhe)

Gravity anomalies over oceanic regions can be derived from satellite altimetry data, assuming that the (corrected) altimeter heights can be identified with geoidal heights. Generally the practical solutions of this problem are based on a simplified relationship between gravity anomalies  $\Delta g$  and geoidal heights  $N=T-\gamma$ , involving spherical and constant radius approximation. In the space domain these simplifications result in a spherical integral, the inverse Stokes integral. A more accurate solution of the respective inverse Stokes problem is achieved by retaining the first order "ellipsoidal effects" in the boundary condition relating  $\Delta g$  and  $T$ , neglecting terms of order  $f^2$  ( $f$ = flattening of the reference ellipsoid). These ellipsoidal effects are recomposed of three constituents, depending on the geometrical flattening  $f$ , the dynamical flattening  $J_2$ , and the angular velocity  $\omega$  of the Earth's rotation. In the paper, two first-order solutions of the extended, ellipsoidal problems are considered, both keeping the general structure of the inverse Stokes integral. In the first procedure, a correction term is added to the gravity anomalies calculated from the spherical integral, while in the second one the geoidal heights - entering the spherical integral - are corrected. A numerical evaluation of the ellipsoidal corrections for both approaches is provided on the basis of the EGM96 geopotential model, showing a dominant low-frequency behaviour of

the correction terms.

**G04/08A/C25-006** **1050**

**GRAVITY RESPONSE OVER A FRACTAL SUBSURFACE REPRESENTED BY VORONOI TESSELLATION**

Vijay P. DIMRI, Ravi Prakash, SRIVASTAVA (National Geophysical Research Institute, Hyderabad, India)

Inversion of geophysical data is carried out in two steps: in first step geophysical response is computed for a pre-assigned geometry and in second step this response is compared and corrected till there is satisfactory match between computed and observed values. In gravity method the first step is performed by assuming the geometry of interfaces, which could be planar and near parallel or nearly planar so that they can be represented with splines. Alternatively the space is assumed to be filled up by polygons or polyhedra, which in turn are represented by their vertices. If the vertices are perturbed, in second step i.e. inversion, there would be no guarantee that the space is still filled up or that the polyhedra do not overlap or the regions do not become reentrant. In this work the interfaces or tessellating domains are represented by a set of geometric points and a small number of additional parameters. These geometrical points and parameters can be perturbed by any amount without getting into representational problems faced by the conventional techniques. To accomplish such representation Voronoi tessellation is used, which in two-dimensional space consists of enclosing every center by a Voronoi polygon such that a common edge of adjacent polygons is a perpendicular bisector of the line joining the centers on the two sides of that edge. Here, the notion of the Voronoi tessellation is generalized by using  $L^p$  distances, instead of the Euclidian distances so that Voronoi domains are not necessarily polygonal or polyhedral, where  $p$  can hold any value. This approach is used here to generate the fractal subsurface representation, which is quite close to the realistic geometry than the conventional planar or polygonal representation. The technique is illustrated here to obtain synthetic gravity response over a fractal subsurface generated by Voronoi tessellation using  $L^p$  norm distance.

**G04/08A/C25-007** **1120**

**ASYMPTOTIC DISLOCATION THEORY OF A SPHERICAL EARTH FOR CALCULATING CO-SEISMIC DISPLACEMENTS**

Wenke SUN, Shuhei OKUBO (Earthquake Research Institute, University of Tokyo)

To study response of the Earth to seismic dislocation, the Earth is often simplified into simple geometric models, such as a half-space, a homogeneous sphere and a stratified sphere, and corresponding dislocation theories are presented. The theory for a half-space is usually expressed in analytical form (Okada, 1985; Okubo, 1991) and is easily applied to study or inverse seismic faults due to its mathematical simplicity. However, validity of these theories is limited to a near field because the Earth's curvature and radial heterogeneity are not included. Sun and Okubo's (2002) recent study indicates that both curvature and vertical layering have significant effect on co-seismic deformation field. On the other hand, since modern geodesy is able to detect far-field deformation, even a global co-seismic deformation, dislocation theory for a more realistic earth model is demanded to interpret the deformation. Sun and Okubo (1993, 1998) and Sun et al. (1996) presented theories to calculate global displacement and gravity change caused by arbitrary dislocations in spherically symmetric earth models. These theories, however, are hard to be applied due to their mathematical complexity. To overcome the disadvantages exist in the above dislocation theories, therefore, this study presents a new theory for calculating asymptotic displacements excited by a point dislocation in a spherically symmetric earth model as an approximation of the dislocation theory for a spherical earth model (Sun et al., 1996). This theory is derived in an analytical form by employing the reciprocity theorem (Okubo, 1993) and the asymptotic solutions of an elastic earth to tidal, press and shear forces (Okubo, 1988). This theory is mathematically simple and physically reasonable since it includes earth sphericity and radial structure. Both theoretical and numerical investigations indicate that the theory is valid for all types of seismic sources and for an epicentral distance of at least  $20^\circ$  with a relative error less than 1% compared to results calculated by the dislocation theory for a spherical earth model (Sun et al., 1996). For a vertical strike-slip source, the asymptotic theory is valid for the entire earth surface. The numerical results given in this research are calculated for a homogeneous earth model. Comparison of the asymptotic results with both the exact results and the corresponding flat-earth results shows that for any distances the exact results are approximated better by the asymptotic results than by the flat-earth earth results. Especially, the asymptotic theory is obviously superior to the flat-earth theory due to a big sphericity effect for the tensile opening on a vertical fault. Owing to its mathematical simplicity, this theory can be applied easily to calculate co-seismic displacement, just as the theory for a half space earth model like Okada (1985).

**G04/08A/C25-008** **1140**

**TOPOLOGICAL VECTOR SPACE OF HARMONIC FUNCTIONS AND THE TRACE OPERATOR**

Fernando SANSONO, Giovanna VENUTI (DIAR - Politecnico di Milano)

In physical geodesy there is an approach to model the problem of determining the earth gravity field, which heavily relies on the theory of boundary value problems (BVP); since the "solution" in the end is the earth anomalous potential,  $T$ , which is harmonic outside the earth surface, these problems are naturally formalized as BVPs in spaces of harmonic functions. So, given a harmonic  $T$  belonging to some Hilbert or, more generally, to some topological vector space of harmonic functions, one has an operator  $B$  transforming  $T$  into some function which for simplicity is here considered as defined on the bounding sphere,  $S$ . Solving the BVP is then inverting  $B$ . To study this problem one has first to understand the characteristics of the boundary operator  $B$  in its direct action. When  $T$  belongs to classical Sobolev spaces, there are well known trace theorems defining the regularity of  $(BT)_s$ . This has been generalized, several decades ago, by Cimmino when  $(BT)_s$  is assumed to belong to  $L^2_s$ . The paper considers the full scale of Hilbert spaces which include Sobolev spaces of any order and their duals, giving a theorem on the generality of the  $-1/2$  rule. The most general case of functions harmonic in the open domain outside the sphere is considered too.

**G04/08A/C25-009** **1200**

**THE USE OF ENERGY BALANCE RELATIONS FOR VALIDATION OF GRAVITY FIELD AND ORBIT DETERMINATION RESULTS**

Karl Heinz ILK, Anno LOECHER (Institute of Theoretical Geodesy, University of Bonn)

The measurement of the gravity field of the Earth is based on the field and balance equations of all physical systems, which are involved in the measurement process. The balance equations describe the exchange of dynamical quantities, as for example energy, momentum or moment of momentum. Future satellite borne measurement techniques, as

SST and SGG are based on local measurement principles while the classical techniques exploit accumulated disturbing effects of the inhomogeneous gravity field onto the satellite's motion. Energy exchange relations of the satellites' motion with the gravity field of the Earth seem to be useful for the validation and the consistency check of gravity field models and orbit determination results when applied in the sense of a forward computation process. Integrations techniques as well as downward continuation procedures, frequently applied for this validation task, are avoided in this procedure. It is well-known that both procedures are susceptible for numerical errors and regularisation effects, respectively. In this paper the balance equations for the energy exchange as well as motion and energy integrals are derived for satellite orbits as well as for the satellite-to-satellite motion within the gravity field of the Earth. The formulation is based in principle on the Hamiltonian formulation of classical mechanics. It is well-known that the classical energy balance which describes the exchange of kinetic and potential energy is valid only in case of conservative forces. Therefore, in case of a constantly rotating Earth the Jacobi-Integral has to be applied instead of the simple energy balance relation along the orbits. The Jacobi integral has to be extended if the rotation of the Earth is considered not uniform and time variable disturbing forces as tidal forces exerted by the Moon and the Sun, Earth tides etc. and surface forces as e.g. air drag and solar radiation pressure have to be included into the balance relation. The same holds if the sum of all surface forces are measured in-situ by accelerometers. With these extensions energy balance relations represent an independent tool for validation of gravity field solutions and dynamic or reduced dynamic orbit determinations based on these fields. Applied to a pure kinematic orbit determination result, the energy balances are able to detect deficiencies of gravity field recovery results over certain regions. The procedure is applied to various simulation scenarios and to orbits derived from a pure kinematic orbit determination of CHAMP as well as to GPS satellites. The application of the procedure to relative orbits as in case of satellite-to-satellite tracking is demonstrated as well.

**Tuesday, July 8 PM**  
Presiding Chair: B. Heck

**G04/08P/C25-001**

**1410**

**BIHARMONIC SPLINE WAVELETS VERSUS GENERALIZED MULTI-QUADRICS FOR CONTINUOUS SURFACE REPRESENTATIONS**

Rainer E. MAUTZ<sup>1</sup>, Burkhard SCHAFFRIN<sup>2</sup>, Julia KASCHENZ<sup>3</sup> (<sup>1</sup>Department of Civil and Environmental Engineering and Geodetic Science, The Ohio State University, Columbus, Ohio 43210-1275, U.S.A. <sup>2</sup>Department of Astronomical, Physical and Mathematical Geodesy, Technical University of Berlin, Germany, <sup>3</sup>Department of Civil and Environmental Engineering and Geodetic Science, The Ohio State University, Columbus, Ohio 43210-1275, U.S.A., <sup>4</sup>GeoForschungsZentrum Potsdam, Department 1: Geodesy and remote sensing, Telegrafenberg C3, D-14473 Potsdam, Germany)

In some respect, the continuous representation of surfaces such as the geoid, the topography, or other spatial phenomena, is superior to discrete forms like the TIN (Triangular Irregular Network) or a raster DEM (Digital Elevation Model) as long as these surfaces exhibit a certain degree of local smoothness. One of the well-established methods is based on Universal Kriging which, under certain conditions, can be shown to give equivalent results to interpolations with splines or Hardy's multi-quadrics, respectively. In this contribution, we shall concentrate on the special study of biharmonic spline wavelets and of generalized multi-quadrics (which may or may not form a wavelet basis by themselves), with the emphasis on increased efficiency - which is oftentimes a problem with Kriging (also known as "least-squares collocation") - while maintaining the local approximation quality up to the desired resolution. As a third interpolation technique a newly developed global search algorithm will be adapted to this environment. It is based on heuristic methods that would allow the user to handle gridded as well as arbitrarily scattered data. The number of coefficients for data representation using the global optimization will be extremely small and the magnitude of deviations still acceptable. On the other hand, long computation times have to be taken into account. Concerning the functional model one may face fewer restrictions for its structure when using global methods because no derivatives have to be computed and no approximate values need to be provided. Some geodetic examples will show the potential of the new techniques, particularly in view of the more classical Fourier analysis.

**G04/08P/C25-002**

**1430**

**APPLICATION OF WAVELET TRANSFORMATION FOR INTELLIGENT STRUCTURAL HEALTH MONITORING USING MEMS-BASED INERTIAL SENSORS**

Naser M. EL-SHEIMY<sup>1</sup>, Aboelmagd NOURELDIN<sup>2</sup>, Mahmoud R. TAHA<sup>3</sup> (<sup>1</sup>Department of Geomatics Engineering, <sup>2</sup>Department of Electrical and Computer Engineering, Royal Military College, Kingston, Ontario, Canada, <sup>3</sup>Stantec Consulting Ltd., Calgary, Alberta, Canada)

The premise in using principles of vibration-based damage identification in structural health monitoring (SHM) is that when damage occurs, the mechanical properties of the structure stiffness will be altered and thus the vibration response of the structure to externally applied loads and environmental conditions will be changed. Although, the concept looks simple, system development for SHM of civil infrastructure is challengeable. This is because of the low frequency of the excited structures and the limited effect of local damage on vibration characteristics of these structures which are attributed to their relatively large mass. A new intelligent SHM system that measures (senses) multiple responses of the structure under unknown set of loads is currently being developed and examined. The small size and low cost of force-balanced Microelectromechanical systems (MEMS) based inertial sensors make them a preferable alternative in the new system. This article describes the use of MEMS based inertial sensors in SHM systems of civil infrastructures. The paper examines some of the challenges in utilizing low-cost MEMS sensors including the need to enhance its stability, repeatability, to control its drift and to limit/filter its noise. The paper also introduces the Wavelet multi-resolution analysis as a promising technique for damage identification. Analytical analysis of simulated as well as genuine sensor signals significantly corrupted by other noise signals showed that the wavelet multi-resolution analysis was able to separate the different frequency components and to identify the original simulated structural response. The input signal to the wavelet algorithm will be basically decomposed into two parts: first called "the approximation" of the input signal includes the normal structural frequencies and some highly attenuated disturbances. Second, called "the details" of the input signal contains the noise component of the sensor signal and other disturbances. Automation of the systems necessitates the utilization of intelligent algorithms. Thus, the Wavelet analysis output is supplied to artificial intelligence algorithms (here neural-fuzzy inference system) to convert the problem of damage identification into a systematic pattern recognition problem

**G04/08P/C25-003**

**1450**

**REMOVE-RESTORE DATA COMPRESSION FOR SATELLITE GRAVITY GRADIOMETRY**

Wolfgang KELLER (Geodetic Institute, University Stuttgart)

The dominating method for gravity field recovery from satellite gradiometry data is the so-called time-wise approach. This approach leads to huge normal equations with an almost

block-diagonal form. On the other hand, in the so called space wise approach only 2\*N\*N observation, placed on a special regular grid, would be sufficient to recover the gravity field up to the resolution limit N. The paper aims at an approach to condense the huge amount of observation data into representative normal data, prescribed to the nodes of the integration grid. For this purpose a remove-restore technique is applied. The gravity field solution of the CHAMP mission is subtracted from the observations which leads to synthetic gravity gradient observations of the residual gravity field. The residual gravity field is much smoother than the original one. From the data of the smoothed residual field the residual data in the nodes of the integration grid can be easily interpolated. After interpolation the effect of the CHAMP gravity field has to be restored again, leading to the so called normal data. It can be shown that the error of this remove-restore compression technique is below 0.001 E.U. From the normal data in the nodes of the integration grid the spherical harmonics coefficients can be recovered by a combination of FFT along the parallels and Gaussian quadrature along the meridians.

**G04/08P/C25-004**

**1510**

**ON THE USE OF 1D-FFT TO INVERT GEODETIC INTEGRALS**

Ramon V. GARCIA, Castulo A. ALEJO, Anibal I. ARANA, Carlos R. MORAILA (UNIVERSITY AUTONOMOUS OF SINALOA)

The use of the 1D-FFT technique to evaluate geodetic integrals has the capability of being more efficient than direct numerical integration and more precise than 2D-FFT methods. A similar situation exists for the inversion case. Nevertheless, the errors associated for instance to the deconvolution involved may make the 1D-FFT method less precise than the direct numerical integration method. An inversion method based on 1D-FFT deconvolution is presented. In order to handle larger data set, the method is implemented using the iterative projected Landweber method, which is used for solving constrained least square problems and allows to reduce deconvolution associated errors. The method is almost as precise as the direct matrix inversion approach but still computationally more efficient. Two cases are studied using synthetic data. One is the downward continuation of gravity anomalies from the Earth's surface to the geoid employing Poisson's integral and the other is the inversion of Hotine's integral to obtain gravity disturbances from geoid undulations. For the case of downward continuation the stabilization is made using the Tikhonov regularization technique. Convergence is also analyzed and comparisons with respect to the direct matrix inversion method using simple Jacobi's iteration are presented.

**G04/08P/C25-005**

**1530**

**APPLICATION OF CLEBSCH-GORDAN COEFFICIENTS AND ISOMORPHIC FRAME TRANSFORMATIONS TO INVERT EARTH'S CHANGING GEOMETRICAL SHAPE FOR CONTINENTAL HYDROLOGICAL LOADING AND SEA LEVEL'S PASSIVE RESPONSE**

Geoffrey BLEWITT<sup>1</sup>, Peter J. CLARKE<sup>2</sup>, David LAVALLÉE<sup>3</sup>, Konstantin NURUTDINOV<sup>3</sup> (<sup>1</sup>Nevada Bureau of Mines and Geology, and Seismological Laboratory, University of Nevada, Reno, <sup>2</sup>School of Civil Engineering and Geosciences, University of Newcastle upon Tyne)

The hydrological cycle induces mass exchange between the oceans and continents, and redistribution of water within the continents. In turn, relative sea level passively responds to the change in shape of both the geoid and the ocean bottom. The time variation in these two surfaces must self-consistently relate to the total mass redistribution. Here we show formally how, if given a time series of station coordinates from a global network of geodetic stations, we can invert for the separate contributions to the total mass redistribution due to water on the continents and water in the oceans. If we characterize the deformation of the solid Earth in terms of a truncated vector spherical harmonic expansion, the solution to this problem can be formulated in terms of Clebsch-Gordan coefficients, which are familiar for the calculation of branching ratios in elementary particle physics. As part of a rigorous solution to this problem, we formally address the definition of reference frame by applying the concept of an "isomorphic frame transformation," which conserves the formal theoretical relationship between surface deformation and load distribution by a simultaneous translation of origin and change of degree-one load Love numbers. We show explicitly how the solution to the inversion problem is derived and implemented, and we present examples of this procedure in practice using real GPS data from the IGS network.

**G04-Posters**

**Tuesday, July 8**

**GENERAL THEORY AND METHODOLOGY. MEETING OF IAG SECTION IV**

Location: Site D

**Tuesday, July 8 PM**

**G04/08P/D-001**

Poster

**1400-108**

**PHYSICAL CORRELATION? IT MAY BE DANGEROUS!**

Mikhail D. GERASIMENKO<sup>1</sup>, Nikolay V. SHESTAKOV<sup>2</sup>, Minoru KASAHARA<sup>3</sup> (<sup>1</sup>Laboratory of Geodesy and Geodynamics, Institute of Applied Mathematics FEBRAS, <sup>2</sup>Institute Seismology and Volcanology, Hokkaido University)

Unknown and inestimable systematic errors that influence on different observations give a reason for introducing the physical correlations and not just algebraic ones. Especially it is important in case of GPS measurements. For example different researchers have obtained values of correlation coefficients regarding these reasons of up to 0.85 for identical satellite configuration. They attempt to introduce these correlations or some correlation functions into post-processing of GPS measurements. As illustrated in our report, it may be very problematic in practice and could lead to extraordinarily wrong results. One of these unexpected effects may be artificial increasing of the weight P of the final results. In limit we could obtain  $P \rightarrow \infty$  as a result if weight even of one observation  $p \rightarrow 0$ . This is a clearly absurd result and it has no physical sense. That is why the formal estimates of accuracy do not reflect the real situation in case of physically correlated observations. Such artificial accuracy improving has no physical sense. We have met this phenomenon when we developed the software for optimal GPS geodetic network design for fault-mechanics studies. Considering this undesirable phenomenon we do not exclude the necessity for revision of some methods used for improving of GPS results, especially methods are using a different non-diagonal covariance matrices of observations.

**G04/08P/D-002** Poster **1400-109**

**EXPERIMENTS OF ADAPTIVE FILTERS FOR KINEMATIC GPS POSITIONING APPLIED IN ROAD INFORMATION UPDATING IN GIS**

Yuanxi YANG, Yingze TANG, Qingtian LI, Yijiang ZOU (Xian Research Institute of Surveying and Mapping)

The experiments for the road information updating in the geographical information system by using GPS receiver mounted on a vehicle have been performed in Xian area of China. The navigation software accompanied with the GPS receiver, Sage filtering method and a new developed adaptively robust Kalman filtering method are employed and compared in the experiments. It is shown by experiments that the new adaptively robust filtering is not only simple in calculation but also robust in controlling the influences of the outliers of the GPS pseudoranges and kinematic state disturbing of the vehicle.

**G04/08P/D-003** Poster **1400-110**

**THE ANALYTICAL COLLOCATION OF THE ERROR DISTRIBUTION**

Shi-Jian ZHOU, Yunlan GUAN, Tieding LU, Deyan ZANG (Dept. of Surveying Engineering, East China Institute of Technology)

It is well known that the error for the observational data be exist always, the error be eliminated is one of the main task for the survey data processing. To obtain the best estimated results, the error processing should be obey the optimal principle, such as the Least Square(LS) principle, but the optimal principle be determined should based on the property and the distribution type of the observational error, so that the distribution type of the observational error must first be established before the observational error processing. In the traditionally, the distribution type of the error has been determined using the distribution collocation test method or figure method by magnitude of errors, but it is difficult to obtain the specific distribution of the error, and there exist cockamamie for implement and complex for computation, therefore, the suitable method to determined the error distribution must be found. To obtain the reasonable method that more than the traditional method, the authors have proposed that the error distribution be collocated using the exponential distribution. The exponential distribution is a general distribution that can describe the arbitrary sequential distribution while the distribution parameter  $p$  is different, the property and the characteristic for the exponential distribution have been discussed in this paper. The analytical collocation method that determine the specific distribution of error has been proposed first by the authors, the main idea for the analytical collocation is that the known parameter  $A, C$  of the exponential distribution and the distribution parameter  $p$  are determined using the error interval value and the frequency for the special error interval, the computational formulae have been derived in detail, so that the explicit expression for the error distribution can be described by the parameter  $A, C$  of the exponential distribution and the distribution parameter  $p$ . Finally, the two numerical examples have been calculated and analyzed, the experiment results show that the analytical collocation method of the error distribution is very convenient and feasible, the computational results are identical with conventional methods obtained by the references.

**G04/08P/D-004** Poster **1400-111**

**ESTIMATION OF VARIANCE COMPONENTS THROUGH A COMBINED ADJUSTMENT OF GPS, GEOID AND LEVELLING DATA**

Georgia FOTOPOULOS, Christopher KOTSAKIS, Michael G. SIDERIS (Department of Geomatics Engineering, University of Calgary)

The method of GPS-levelling for obtaining orthometric heights is not a new concept. In fact, as a result of case studies that have been conducted in different regions all over the Earth, the question of whether GPS-levelling can provide a viable alternative to traditional techniques is no longer an issue. The important question that should be asked and has yet to be satisfactorily solved is, 'What accuracy level can be achieved using this approach?' Over the past decade, numerous advances have been made which have placed us in a position where we can begin to address the issue with more confidence, namely (i) improved mathematical models/techniques for dealing with GPS and geoid data, (ii) increased data availability for gravimetric geoid models, and (iii) improved data processing capabilities. In this paper a statistical approach for estimating the variance components of heterogeneous groups of observations is used in the combined adjustment of GPS, geoid and levelling data. Specifically, the minimum norm quadratic unbiased estimation (MINQUE) algorithm is employed to determine the individual variance components for each of the three height types. The challenges encountered when implementing this well-known algorithm in practice with real data sets from Canada and Switzerland are discussed. The analysis provides some indication into the practicality and usefulness of estimating variance components in mixed vertical networks. Notably, the estimation of realistic variance components provides us with important insight with regards to the GPS-levelling problem in addition to other uses of combined GPS, geoid and levelling data, such as assessing the accuracy of a gravimetric geoid model.

**G04/08P/D-005** Poster **1400-112**

**STOCHASTIC MODELLING ISSUES FOR NETWORK-BASED GPS POSITIONING**

Tajul MUSA, Jinling WANG, Chris RIZOS (School of Surveying and Spatial Information Systems, The University of New South Wales, Sydney NSW 2052, Australia)

The development of network-based GPS techniques has enabled the performance of conventional single reference station, carrier phase-based techniques to be also extended over longer baselines. Using a network-based approach, real-time kinematic (RTK) positioning is carried out using concepts such as the Virtual Reference Station (VRS). However, the key to precise positioning using VRS-RTK techniques is the resolution of the carrier phase ambiguities between the reference receivers in the network. Advances in functional models and stochastic modelling of observations have been made during the last half decade or so. This paper focusses on the challenge of stochastic modelling, because most GPS data processing algorithms still assume that raw measurements are independent and have the same accuracy. Such an assumption is clearly not realistic. An investigation of the stochastic properties of VRS observations is being conducted with a view to constructing appropriate VCV matrices that optimise the ambiguity resolution process within VRS network. A better understanding of the stochastic properties of VRS networks will lead to an increase in the ambiguity success rate, hence permitting fast ambiguity resolution to support VRS-RTK positioning. This paper describes the challenges of stochastic modelling, and presents results of investigations by the authors.

**G04/08P/D-006** Poster **1400-113**

**PERFORMANCE COMPARISON OF THE BIEU ESTIMATOR WITH THE FLOAT AND FIXED GNSS AMBIGUITY ESTIMATORS**

Sandra VERHAGEN, Peter J.G. TEUNISSEN (Departement of Mathematical Geodesy and Positioning, Delft University of Technology)

The goal of ambiguity resolution is to make optimal use of the available information, and it is the key to high precision GNSS positioning and navigation. However, it should only be applied in case the probability of correct integer ambiguity resolution, i.e. the success rate, is very close to one. In that case, the probability that the fixed baseline will be closer to the true but unknown baseline is larger than that of the float baseline. Clearly, this condition will not be fulfilled for each measurement scenario, and that means that for low success rates a user will prefer the float solution. However, there exists a baseline estimator that will always be superior to its float and fixed counterparts, albeit that this superiority is measured using a weaker condition. This baseline estimator is the Best Integer Equivariant Unbiased (BIEU) estimator. In this contribution, the three different estimators are compared. For that purpose, we will focus on the geometry-free GNSS models, either single frequency or dual frequency. The performance of the estimators is compared based on their probability density functions, the mean squared errors of the different estimators, and the probabilities that the baseline estimators are within a certain convex region symmetric with respect to the true baseline. This will provide information on whether or not the BIEU estimator could be useful in positioning applications.

**G04/08P/D-007** Poster **1400-114**

**GPS BASELINE PROCESSING ASSISTED WITH DAUBECHIES AND SPLINE FUNCTIONS**

Jenn-Taur LEE (Dept. of Information Management, Chung Yun Institute of Technology, Chung Li, Taoyuan 320 Taiwan)

To reach the highly accurate GPS positioning and navigation, the cycle slip detection and fixing of GPS phase observations in the pre-processing stage is necessary and important, because few cycle slips can break down the precision of GPS positioning and navigation to meter level or worse. The conventional approaches to handle the cycle slips are generated from the linear combination of GPS phase observations, which can normally resolve the cycle slip problem, but not perfect. The wavelet technique is a new tool for digital signal processing and GPS observations are also the digital signal, so the wavelet technique applied to control the cycle slips of GPS phase observations is the major subject in this study. Since the Daubechies function has the multi-resolution and de-noising capability to overcome the drawbacks of the conventional approaches, a new algorithm was developed to do the wavelet transformation and the simulated experiments were used to investigate the feasibility and reliability of the wavelet technique after reviewing the conventional approaches. It finds that the proposed approach can detect the tiny slips and then the cycle slips can be repaired by spline function for the real GPS observations. Finally, the baseline vector solution is more precise than that obtained from the conventional processing.

**G04/08P/D-008** Poster **1400-115**

**USING SECOND-GENERATION WAVELETS ON A SPHERE TO GENERATE A MULTIREOLUTION OF GRAVITY ANOMALIES**

Christopher JEKELI, Xiaopeng LI (Geodetic Science, Ohio State University)

We define wavelets on the sphere according to the theory of Sweldens and Schröder using an icosahedral triangulation as the coarsest subdivision level. Finer subdivisions are obtained by successively dividing each triangle into four equal triangles. The seventh-level subdivision is approximately similar to a 0.5 deg x 0.5 deg spherical coordinate grid. With basis functions defined according to the butterfly scheme, we use a wavelet transform to decompose the gravity anomaly on the sphere as implied by the EGM96 model. This signal is re-constructed using lossy inverse wavelet transforms at various levels and compared to the original in order to assess the utility of using such representations, with different data compression ratios, for further processing in the geodetic boundary-value problem.

**G04/08P/D-009** Poster **1400-116**

**PATCHING LOCAL EMPIRICAL COVARIANCE FUNCTION - A PROBLEM IN ALTIMETER DATA PROCESSING**

Per KNUDSEN (National Survey and Cadastre, Geodesy)

In least squares collocation a covariance function model that agrees with the empirical covariance function should be used in order to obtain optimal estimates. When estimations are carried out in a local area it is advised to use a covariance function that reflects the local statistical characteristics. When gravity field modelling is carried out in larger regions a subdivision of the region into smaller areas is carried out in order to handle the data. Such a procedure may create problems in the estimation since the use of the optimal local covariance function may give different results at borders since the statistical characteristics change from one area to the next area. In the processing of altimetry for the KMS marine gravity fields such problems exist. In this study the variability of statistical parameters in the North Atlantic Ocean is analysed. Furthermore, some ways of describing and modeling spatially varying (non-homogeneous) covariance functions are presented.

**G04/08P/D-010** Poster **1400-117**

**COMPUTATION OF GEOPOTENTIAL COEFFICIENTS FROM GRAVITY ANOMALIES ON THE ELLIPSOID**

Sten CLAESSENS, Will FEATHERSTONE (Western Australian Centre for Geodesy, Curtin University of Technology)

The computation of spherical harmonic geopotential coefficients from gravity anomalies is a fundamental stage in all modern geoid computation. For the evaluation of low-degree coefficients, a numerical least-squares adjustment is usually applied, but because of the large computational burden of this numerical method, analytical formulas are normally used for higher degrees. The standard approach is to compute the coefficients on a bounding sphere from upward-continued surface data, and this approach was used for the construction of early geopotential models such as OSU86. This approach also forms the basis for an iterative solution that has been developed by Petrovskaya (J.Geod., 2001). The OSU91 and EGM96 models were based on an alternative procedure developed by Jekeli (Manu.Geod., 1988) (the 'etalon' solution), based on an expansion of the geopotential in the form of an ellipsoidal harmonic series, which is then transformed into a spherical harmonic series. Recently, Sjöberg (J.Geod., in press) has formulated an approach in which the coefficients can be determined from the disturbing potential on the ellipsoid using Green's

second identity. However, his formulation makes use of series that are limited to terms of the order of the first numerical eccentricity-squared, which is not sufficient for the computation of geopotential coefficients of medium and high degrees due to slow convergence. It is shown in this paper that the influence of the individual terms in the series even increases over the first few terms, but then decreases always leading to convergence. Therefore, more terms need to be taken into account in the case of high degrees, and for this reason Sjöberg's theory is expanded to include an arbitrary number of higher order terms. For this purpose, a general expression for the complete series has been derived in this paper, which depends on a newly derived relation between associated Legendre functions. This new relation makes it possible to transform a Legendre function multiplied by the sine of latitude to an arbitrary power into a sum of Legendre functions of equal order. Finally, ellipsoidal corrections to coefficients of odd or even degree terms respectively are given as a summation over weighted odd or even coefficients of the same order. The weighting functions depend only on the shape of the ellipsoid (semi-major axis and first numerical eccentricity) and the degree and order of the coefficient to be evaluated, and they can easily be computed. This new method will be compared numerically to Jekeli's 'etalon' solution and Petrovskaya's iterative solution. In these comparisons the accuracy and efficiency of the approach will be determined and this will reveal whether it is a viable alternative for earlier solutions.

**G04/08P/D-011** Poster **1400-118**

**ADVANCED HARMONIC DEVELOPMENT OF THE EARTH TIDE GENERATING POTENTIAL**

Sergey M. KUDRYAVTSEV (Department of Celestial Mechanics, Sternberg Astronomical Institute, Moscow State University)

First we present a new technique for spectral analysis of a function tabulated over a long period of time. Expansion of the function directly to Poisson series can be made where both the amplitudes and arguments of the series' terms are high-degree polynomials of an independent variable (e.g. of time) as opposed to the classical Fourier analysis where the terms' amplitudes are constants, and the arguments are linear functions of time. This leads to an improvement in accuracy of the spectral analysis of the function over long-term intervals and allows one to better separate terms of close frequencies. The technique is applied to make a new harmonic development of the Earth tide generating potential (TGP) over two thousand years centered at epoch J2000.0. The adopted model of the TGP accounts for the Moon, Sun, Venus, Mars, Jupiter, Saturn, and Mercury gravity attraction as well as for the Earth flattening effects. The latest NASA/JPL long-term ephemeris DE/LE-406 has been used as the source of the Moon and planets coordinates. The final development of the TGP made with use of the new technique includes some 27,000 terms of amplitudes down to the level of  $1 \cdot 10^{-8}$  m<sup>2</sup>/sec<sup>2</sup> and is valid over 1000AD–3000AD. Calculation of gravity tides at a mid-latitude station (BFO Schiltach, Germany) by using the new TGP development is made in order to check the quality of the latter. The obtained accuracy in calculation of gravity tides at the station is better than 0.025/0.4 ngal (the r.m.s./maximal error, respectively) when comparing with a benchmark gravity tide series numerically computed with use of the most accurate ephemeris DE/LE-405 at every hour within 1600-2200 (the complete period of time covered by the ephemeris). It exceeds the accuracy of the best previously made harmonic development of the TGP (Hartmann and Wenzel, 1995; Roosbeek, 1996) by a factor of at least 3 and is stable over a much longer interval of time. The work is supported in part by grant 02-02-16887 from the Russian Foundation for Basic Research.

**G04/08P/D-012** Poster **1400-119**

**GENERALIZED BOUGUER ANOMALY (1): BOUGUER ANOMALY FREE FROM THE BOUGUER REDUCTION DENSITY AND THE FUNDAMENTAL EQUATION OF PHYSICAL GEODESY**

Kyozo NOZAKI (5428)

In this study, we present a new concept of the generalized Bouguer anomaly, which is defined upon the datum level of gravity reduction of an arbitrary equi-potential surface with a non-zero elevation. Discussions are particularly focused on how to realize the  $\rho_a$ -free Bouguer anomaly, namely, the generalized Bouguer anomaly that is free from the assumption of the Bouguer reduction density, and what is meant by the  $\rho_a$ -free Bouguer anomaly in relation to the fundamental equation of physical geodesy. First, we define and formulate the generalized Bouguer anomaly by taking into account the four distinct quantities: the elevation (orthometric height) of the datum level of gravity reduction, geoid height, vertical gradient of gravity anomaly, and the truncation angle in a spherical scheme of gravity corrections. Secondly, we introduce a concept of the specific datum levels such that the generalized Bouguer anomaly is not affected by the topographic gravitational effects. Upon the specific datum levels, the equations of the generalized Bouguer anomaly become free from the Bouguer reduction density and/or the terrain correction. Thirdly, by utilizing these equations, an approximate equation for estimating the Bouguer reduction density is derived from the gradient of free-air anomaly with respect to the specific datum levels. Finally, in a simple case of neglecting the vertical gradient of gravity anomaly, a formula to compute a Bouguer anomaly on the geoid is shown by level transformation of the generalized Bouguer anomaly from the specific datum level to the level of geoid. These procedures give a new approach to obtain a Bouguer anomaly distribution, which is free from the assumption of the Bouguer reduction density. Also, it is pointed out that the generalized Bouguer anomaly upon the specific datum level is the gravity disturbance that defines the fundamental equation of physical geodesy. The author expresses sincere thanks to Dr. Shozaburo Nagumo, Professor Emeritus of the University of Tokyo, the chief technical adviser of OYO Corporation, for his enthusiastic encouragement and frequent discussions throughout the research. Also the author wishes to express his grateful thanks to Professor Shuhei Okubo of the University of Tokyo for his hearty guidance and critical comments, and to Professor Yoshio Fukao of the University of Tokyo for his stimulating discussions and continuous encouragement during the research. The author's thanks are also extended to Drs. Masaru Kaidzu and Yuki Kuroishi of the Geographical Survey Institute for their helpful discussions on the basic concepts of the modern physical geodesy.

**G04/08P/D-013** Poster **1400-120**

**GENERALIZED BOUGUER ANOMALY (2): ON THE SIMULTANEOUS ESTIMATION OF THE BOUGUER REDUCTION DENSITY, GEOID HEIGHT AND BOUGUER ANOMALY UPON THE NORMAL ELLIPSOID SURFACE**

Kyozo NOZAKI, Koji IWAMOTO, Kenichi OSHITA

In the present study, we present a new method on the simultaneous estimation of the Bouguer reduction density, geoid height and Bouguer anomaly upon the normal ellipsoid surface. This new method is based on the free-air anomaly  $FA$ , which is equivalent to the gravity anomaly in the modern physical geodesy, and the specific datum levels of gravity reduction, which is introduced in the theory of the generalized Bouguer anomaly proposed by Nozaki (2003, another presentation of IUGG 2003). The specific datum levels  $h_{sp}$ ,  $h_{st}$ , and  $h_{ze}$

are so defined as that the generalized Bouguer anomaly ( $\Delta g_{i,red}$ ), which is defined upon the datum level of an arbitrary equi-potential surface at  $h_p$ , is not affected by the topographic gravitational effects. On the other hand, the free-air anomaly  $FA$  is represented as a function of each specific datum level  $h_{sp}$ ,  $h_{st}$ , and  $h_{ze}$ , respectively. Then, we plot the free-air anomaly ( $FA$ ) as a longitudinal axis against the identical axis of abscissa as  $h_p = h_{sp}$ ,  $h_{st}$ , or  $h_{ze}$  for every gravity station. In this paper, we call the diagram of these plots  $FA$  vs.  $h_p$  diagram. The characteristics found in the  $FA$  vs.  $h_p$  diagram are summarized as follows: 1) One can observe the gradients  $dFA/dh_{sp}$ ,  $dFA/dh_{st}$ , and  $dFA/dh_{ze}$  of regression lines  $h_{sp}$ -line for  $FA$  vs.  $h_p$  plot,  $h_{st}$ -line for  $FA$  vs.  $h_p$  plot, and  $h_{ze}$ -line for  $FA$  vs.  $h_p$  plot, respectively. 2) There exists, in general, an intersection  $C(\Delta h_p, \Delta \gamma_p)$  of regression lines  $h_{sp}$ -line and  $h_{ze}$ -line. The intersection  $C$  does not generally coincide with the origin (0,0). Note that the intersection  $C$  is definite because the  $h_{sp}$ -line and  $h_{ze}$ -line are computable from the known quantities. and 3) One can draw a specified regression line for  $FA$  vs.  $h_p$  plot ( $h_p$ -line) such that it passes through the intersection  $C$ . Note that  $h_p$ -line originally has a degree of freedom for parallel translation along the abscissa because the defining equation of  $h_p$  contains an unknown quantity of the elevation of the normal ellipsoid  $h_e$ . For 1), it is shown that one can estimate the Bouguer reduction density from the gradients  $dFA/dh_{sp}$  of  $h_{sp}$ -line and  $dFA/dh_{st}$  of  $h_{st}$ -line. For 2) and 3), it is shown that the value of the abscissa  $\Delta h_p$  must be  $h_p$  when we adjust the specific datum level  $h_p$  to  $\Delta h_p$ . Namely, the geoid height ( $N$ ) is given as  $N = -\Delta h_p$ . Also, it is demonstrated that the intersection  $C(\Delta h_p, \Delta \gamma_p)$  must satisfy the equation  $\Delta g_p \Delta h_d = \Delta \gamma_p + \beta \Delta h_p$  ( $\beta$  is the vertical gradient of the normal gravity field), which is equivalent to the fundamental equation of physical geodesy. This equation implies the generalized Bouguer anomaly at  $\Delta h_p$  ( $\Delta g_p \Delta h_d$ ), which is equivalent to the gravity disturbance upon the normal ellipsoid whose elevation is  $h_p = \Delta h_p$ , can be computed from the known quantities  $\Delta h_p$  and  $\Delta \gamma_p$  at the intersection point  $C$ .

**G04/08P/D-014** Poster **1400-121**

**GLOBAL ISOTROPIC ISOSTATIC RESPONSE FUNCTION IN TERMS OF ZONAL SPHERICAL HARMONICS**

Hussein A. ABD-ELMOTAAL (Civil Engineering Department, Minia University)

Geophysical evidences prove that the density anomaly is proportional to the earth's radius vector (the depths). Hence, one may assume that the density anomaly is linearly related to the topography by a convolution of the topography and an isotropic kernel function. Accordingly, one can derive that the vertical derivative of the isostatic potential (the attraction of the compensating masses) is also a convolution of the topography and an isotropic isostatic response function. Such an isostatic response function can be determined by deconvolution. The paper gives the necessary derivation of such a deconvolution by means of spherical harmonics. A practical determination of the isotropic isostatic response function needs the harmonic analysis of both the topography and the attraction of the compensating masses. Creating compensating masses by means of an isostatic hypothesis already implies an assumption of the earth's isostatic response. Instead, one may wish to compute the isostatic response of the earth without postulating an isostatic hypothesis. This may be achieved by the principle of inverse isostasy, by which we aim to have zero isostatic anomalies. Thus, the attraction of the compensating masses equals the Bouguer anomalies with a negative sign. The harmonic analysis of the Bouguer anomalies is thus a combination of the harmonic analysis of the topographic potential and the already existed global (free-air) reference models. Two global reference models have been used. They are: EGM96 model (complete to degree and order 360) and GPM98CR (complete to degree and order 540). The needed harmonic analysis of the topography has been carried out using TUG87 and TBASE digital height models after smoothing to 20' and 30' resolutions. The results show that the isotropic isostatic response functions derived by inverse isostasy behave in the same sense as those postulated by flexure models (Vening Meinesz isostatic model).

**G04/08P/D-015** Poster **1400-122**

**PARANA BASIN: AN ISOSTATIC MODELING USING A GEOGRAPHIC INFORMATION SYSTEM TO DELINEATE THE MAIN BASEMENT STRUCTURES**

Marcia C.L. QUINTAS (Department of Geomatics, Federal University of Parana)

This paper presents a contribution to the localization of the main basement structures of the Parana Basin. This Ordovician-Cretaceous sedimentary basin is intracratonic and located in the S-SE portion of Brazilian territory. In order to achieve this goal, a quantitative method of determining the state of isostasy at a geological feature was used in this study. This method assumes that free air gravity anomalies are caused by topography and its compensation, and attempts to determine a function which, when convolved with topography, reproduces the gravity anomaly. The advantage of this method is that this function may be derived from observational data, independent of a particular isostatic model. Approximately 7,100 gravity stations took part in this study and those data were collected by different organizations, such as Federal University of Parana (UFPR), Sao Paulo University (USP), National Observatory (ON) and Mining Company (CPRM). With the modeling was possible to identify variations in the basement gravimetric signature, revealing different compositions. The main result of this study using isostatic modeling was to compute the gravimetric anomaly caused by sediments and igneous rocks that fulfill the basin, and the "root" created by the isostatic adjustment. This study uses Kriging methods with a geographic information system (GIS), to overlay and delineate the main basement structures of the Parana Basin. The results are not discussed with a geological insight.

**G04/08P/D-016** Poster **1400-123**

**STOCHASTIC BOUNDARY VALUE SOLUTIONS TO SATELLITE GRAVITY GRADIOMETRY**

Zhicai LUO<sup>1</sup>, Xueguang CHENG<sup>2</sup>, Jinsheng NING<sup>2</sup> (<sup>1</sup>School of Geodesy and Geomatics, Wuhan university, <sup>2</sup>School of Mathematics and Statistics, Wuhan University)

Satellite gravity gradiometry (SGG) is known as one of the most promising techniques for the future progress in the determination of global gravity field. The gradiometry data is given at satellite altitude, but the solution of gravitational potential is needed at the surface of the Earth. Hence, the solution of satellite gravity gradiometry problems somehow includes the harmonic downward continuation. This process is known to be unstable. Therefore, additional ground gravity data has to be included to improve the solution. Considering the stochastic properties of gradiometry data, the stochastic satellite gradiometry boundary value problem is formulated as the functional model and the stochastic model in the paper. Then the practical solution model is derived using pseudodifferential operator theory (PDOT) and general function in Sobolev spaces, and stochastic harmonic field theory in Hilbert spaces.

**G04/08P/D-017** Poster **1400-124**

**COLLOCATION VERSUS NUMERICAL INTEGRATION IN GOCE DATA ANALYSIS**

Federica MIGLIACCIO<sup>1</sup>, Mirko REGUZZONI<sup>1</sup>, Fernando SANSO<sup>1</sup>, CarlChristian TSCHERNING<sup>2</sup>

The spacewise approach to the analysis of satellite borne data, e.g. from a gradiometric mission like GOCE, amounts to analyse such data in a way similar to the solution of a boundary value problem. This can be done indeed in several ways, for instance by applying numerical integration formulas, when the boundary functionals have a relatively simple forms like  $T_r$  or  $T_{\lambda}$ , by some least-squares approach or by collocation. In particular this technique can be applied to extensive grids of data, e.g.  $1^\circ \times 1^\circ$  grids, thanks to the recent implementation of a procedure called Fast Spherical Collocation. It is believed that the collocation approach, through the damping of high degrees corresponding to some prior information on the degree variances, can control better than the other techniques the aliasing between degrees which are not modeled and those that enter into the final solution. This problem is analysed by applying two techniques, namely the numerical integration and the collocation, to the same simulated data sets, with or without measurement noise. This provides as well a comparison of the noise propagation through different gridding procedures. The effect of spherical gaps on the two solutions is investigated too.

**G04/08P/D-018** Poster **1400-125**

**SERIES EXPRESSION FOR NORMAL GRAVITY ABOVE THE REFERENCE ELLIPSOID**

Ziqing WEI (Xian Research Institute of Surveying and Mapping)

A Taylor series expression for normal gravity above the reference ellipsoid, if it could produce results with desired accuracy, would be preferable to the exact expression in closed form in terms of numerical manipulation. A series expression yielding normal gravity with sub-microgal precision for high geodetic heights has been developed on the basis of the exact formulas expressed in terms of ellipsoidal coordinates  $\mu, \beta, \lambda$ . The series expression for total normal gravity at geodetic height  $h$  at geodetic latitude  $\phi$  assumes the form  $\gamma = \gamma_0 + (\zeta_0 + \zeta_1 \cos^2 \phi + \zeta_2 \cos^4 \phi) h + (\eta_0 + \eta_1 \cos^2 \phi + \eta_2 \cos^4 \phi + \eta_3 \cos^6 \phi + \eta_4 \cos^8 \phi) h^2 + (\rho_0 + \rho_1 \cos^2 \phi + \rho_2 \cos^4 \phi + \rho_3 \cos^6 \phi) h^3 + (\sigma_0 + \sigma_1 \cos^2 \phi) h^4$  where  $\gamma_0$  is the normal gravity at the ellipsoidal surface;  $\zeta_0, \zeta_1, \dots, \sigma_0, \sigma_1$  are constant coefficients. Also, series expansions have been developed for components  $\gamma_r$  and  $\gamma_\theta$  of the total normal gravity vector as well,  $\gamma_r$  being collinear with the geodetic normal line and  $\gamma_\theta$  orthogonal to it and in the meridian plane. As examples, numerical constants for the series expansions for the 1980 ellipsoid and WGS84 ellipsoid are given in the presentation. Results show that the accuracy of computed total normal gravity as well as its component in geodetic height is better than 0.1  $\mu$ Gal for height up to 20km and than 0.3  $\mu$ Gal and 1  $\mu$ Gal for up to 50km and 70km respectively, proofing its superiority to existing formulas.

**G04/08P/D-019** Poster **1400-126**

**FAR-ZONE CONTRIBUTION IN ELLIPSOIDAL STOKES BOUNDARY-VALUE PROBLEM**

Vahid Ebrahimzadeh ARDESTANI (Institute of geophysics, Tehran university)

In the first attempt to solve the Stokes boundary-value problem in ellipsoidal coordinates numerically (Ardestani and Martinec, 2000), we focused on the near-zone contribution since the effect of the ellipsoidal Stokes function in the far-zone contribution has not been considered. We present a method for solving the ellipsoidal Stokes integral in far-zone contribution. The numerical results of computing the magnitude of this term for an area in north of Canada are presented.

**G04/08P/D-020** Poster **1400-127**

**GRAVITY EARTH TIDE OBSERVATION IN CHINA SEISMOLOGICAL BUREAU**

Hui LI, Xiaoquan WANG, Jieli YU, Canfei XING (Institute of Seismology, CSB)

Since 60s of last century, China seismological Bureau start to set up the stations for gravity earth tide observation. Until now the gravity earth tide observation have been carried out at more than 30 stations. In next five years, CSB will build 22 station including 4 revision station and 18 new stations. It will form a new After the new gravity earth tide observation network. This paper will firstly introduce the new network and its goal, and the show the observation results of the gravity earth tide including the precision, spacial distribution of the parameters using the long time observation data.

**G04/08P/D-021** Poster **1400-128**

**MEAN ORBITAL MOTION OF A CONSTELLATION OF GEODETIC SATELLITES: NEW RESULTS FOR GEODYNAMICS**

Florent DELEFLIE, Pierre EXERTIER, Gilles MÉTRIS, Philippe BERIO, Olivier LAURAIN (Department CERGA of OCA / GRGS Grasse)

New developments have been achieved since a few years to improve the theory of mean orbital motion of artificial satellites : in particular, singularities with eccentricity have been removed from the averaged equations of dynamics, which are integrated in a numerical way. It is now therefore possible to compute mean orbits of geodetic satellites over large time scales (typically : from 10 to 20 years). By linking geodynamical phenomena to corresponding effects on the orbits, this long period approach enables to study the changes of the gravity field of the Earth over large spatial scales. For these studies, we use « observed » mean elements which have been carefully computed from Satellite Laser Ranging (SLR) measurements, and which have been first reduced by classical orbit fits on short arcs. The results are one single long arc per considered satellite : over 22 years for LAGEOS-1, 10 years for LAGEOS-2, 18 years for STARLETTE, 15 years for AJISAI, 9 years for STELLA. In this context, the adjustment of geodynamical parameters is now based on the combination of observation equations deduced from these long arcs. In this paper, we investigate the long term evolution of the first zonal terms of the Earth gravity field (typically : from J2 to J6). In particular, we adjust the static and the secular parts, and we give time series of these coefficients which enlightens small but cumulative effects. We observe also how redistribution of oceanic mass around the equator can affect the value of the dynamical flattening of the Earth (J2dot). As a consequence, we show that specific geodynamical parameters are all the more well decoupled one from another as the orbits have a long period of time, this taking advantage of our method.

**G04/08P/D-022** Poster **1400-129**

**MULTISCALE STABILISATION PROCEDURE FOR THE INVERSE DIRICHLET PROBLEM**

Juraj JANAK<sup>1</sup>, Karol MIKULA<sup>2</sup>, Vladimír MINARECH<sup>3</sup> (<sup>1</sup>Department of Theoretical Geodesy, Slovak University of Technology, <sup>2</sup>Department of Mathematics and Descriptive Geometry, Slovak University of Technology, <sup>3</sup>student, Slovak University of Technology)

In geodesy the inverse Dirichlet problem can be encountered in geoiddetermination process

and it is known as downward continuation of the gravity data. The aim is to obtain the gravity data on the boundary surface, i.e. on the geoid. If the gravity data is a harmonic function above the geoid, the problem can be solved and the solution is theoretically unique. From numerical point of view the solution is inherently unstable, meaning that even a small fluctuation in the input function can result in a large response after the downward continuation. Short wavelength fluctuations are enlarged more than the long wavelength disturbances. Therefore a standard stabilising procedure is to create mean values of the input function with the sufficiently large discretization step. Such a procedure has some disadvantages, e.g. it is not possible to continue downward a function in a detailed resolution because the original discretization step is enlarged. In this contribution we suggest to use a multiscale stabilisation procedure based on a successive decreasing of the input data smoothing. In this procedure the original discretization step is preserved. Both stabilisation procedures are compared and tested.

**G04/08P/D-023** Poster **1400-130**

**ON DISCRETE SCHEMES IN DOWNWARD CONTINUATION OF GRAVITY**

Wenke SUN (Earthquake Research Institute, University of Tokyo)

According to geodetic boundary value theory, gravity is required to be known on geoid, i.e., observed gravity on a terrain surface must be transformed onto geoid. This transformation is called downward continuation of gravity. For this purpose, discretization of the Poisson integral is necessary (Bjerhammar, 1962; Heiskanen and Moritz, 1967), so that the gravity field on geoid can be obtained by solving the discretized linear system. Bjerhammar (1962) studied this problem for the first time using a point scheme; i.e., he discretizes the Poisson integral by simply taking a point value of Poisson kernel at an observed point. This point scheme was also adopted by other scientists up to the present. Vanicek et al. (1996) and Sun and Vanicek (1998) studied downward continuation of a 5'x5' mean Helmert gravity anomaly. They discretized the Poisson integral using a double mean scheme. They proved that a discretized system of Poisson integral equations can always be solved (Bjerhammar, 1962; 1987) for 5'x5' discretization. However, numerical investigation indicated that the double mean scheme engendered tedious numerical work, greatly constraining its application potential. On the other hand, although the above two systems of linear equations are mathematically tractable, they produce different gravity on geoid for the same input (Martinec, 1996; Sun and Vanicek, 1998). The main reason for the discrepancy is considered to arise from discretization of the Poisson kernel; while this problem has not received much attention up to the present. Actually, mathematical solvability does not mean that its solution is correct. The key point is whether the system is well structured, or, whether discretization is reasonable. Therefore, this research investigates some discretizations of the Poisson integral. A single mean scheme is proposed to overcome the disadvantage of the double mean scheme. Basically the single mean scheme is the same as the double one, but it is numerically simple since it greatly reduces numerical work. Comparison between the point and mean schemes shows that, for a limit topographical grid size, the point discrete scheme presents a serious theoretical problem, i.e., it greatly devalues gravity on geoid, and even gives suspicious result for an extreme case. It is found that difficulty of dealing with the Poisson integral is due to behaviors of the Poisson kernel. Numerical analysis indicates that the diagonal values for the point scheme on a 5' by 5' division are much larger than those of the mean scheme. Therefore, a careful consideration of constructing matrix coefficient of the discrete system of the Poisson integral is much more important. A basic principle of a valid discretization for any integration is that the discrete kernel function value should well approximate the true value on each grid; otherwise discretization will bring a serious error to result.

**G04/08P/D-024** Poster **1400-131**

**GLOBAL OPTIMUM SEARCH REGARDING THE PERIODOGRAM BASED ON INTERVAL NEWTON METHOD**

Rainer E. MAUTZ<sup>1</sup>, Svetozar PETROVIC<sup>2</sup> (<sup>1</sup>Department of Civil and Environmental Engineering and Geodetic Science, The Ohio State University, Columbus, Ohio 43210-1275, U.S.A., <sup>2</sup>Department of Astronomical, Physical and Mathematical Geodesy, Technical University of Berlin, Germany, <sup>3</sup>Geoforschungszentrum Potsdam, Department 1: Geodesy and remote sensing, Telegrafenberg A 17, D-14473 Potsdam, Germany)

When fitting a physical model to a given set of observations, the estimation of the model parameters becomes a minimization problem. Is the model nonlinear, this optimization problem may have many local minima. In case that the approximate values for the parameters cannot be provided with sufficient precision, a global search is required. Recently, heuristic point methods like Simulated Annealing or related random-based strategies have been applied to geodetic parameter estimation problems. Although they seem to work in general, the user has to accept the large computational burden and the lack of reliability. In this contribution an Interval Newton Method is proposed as a bounding method. It consists of a gradient method for attaining local solutions and a global strategy by a so-called feasible point finder, which identifies all roots (zeros) of a function. The feasible point finder becomes a global optimization technique when applied to the objective function minus the value of the previous lowest local minimum. A unique root will indicate that the global solution is found. The feasible point finder guarantees the identification of the root (if unique) or roots by systematically excluding all areas without feasible root. An application of the feasible point finder requires the continuity of functions and the existence of the first derivative. Geodetic L2-Norm based target functions fulfill this condition. Finding the best fitting sine function for an observational dataset is a global optimization problem for the frequency variable. Plotting the estimate of the power spectral density (PSD) of a signal using the "periodogram" function, the large number of local minima becomes obvious. Fourier techniques oftentimes fail - in particular when the data are not equidistant. Point methods do not make use of the function's derivative and cannot guarantee a global solution since there is no information between sampled points. Applying the proposed interval method to the "frequency" problem, it now becomes possible to guarantee the global solution within finite time. An upgrading toward time-dependent frequencies and multi-dimensional problems looks promising.

**G04/08P/D-025** Poster **1400-132**

**ON COSMOLOGICAL ORIGIN OF CERTAIN GEODETIC FEATURES OF THE EARTH (I)**

Akindele Oluwole ADEKUGBE-JOSEPH (-)

The slight westward deflection in the north and eastward deflection in the south of continental plates; the observed ratio of polar diameter to equatorial diameter of the earth of about 0.997 and the inclination to ecliptic of the earth's rotational axis at angle 66.5°, have been explained as local consequences of a new cosmological model. An instantaneous rate of increase of earth's radius of 0.108cm/yr, as well as instantaneous relative drift rate of 0.108  $\Delta\phi$  cm/yr of two points with longitudinal separation  $\Delta\phi$  along the equator, have also been calculated within the new model, as consequences of the expansion of the earth with the universe. These numbers as well as the westward deflection in the north and eastward deflection in the south of continental plates are slowly increasing. This first part of this article

is devoted to the summaries of a new two-theory approach to relativistic gravitation and the new cosmological model based on it.

**G04/08P/D-026** Poster **1400-133**

#### ON COSMOLOGICAL ORIGIN OF CERTAIN GEODETIC FEATURES OF THE EARTH (II)

Akindele Oluwole ADEKUGBE-JOSEPH (-)

This second part of this article is devoted to the local consequences on the earth of the new cosmological model summarized in the first part. The rotational slanting of the earth of  $66.5^\circ$  is linked to the calculated rate of expansion,  $dR/dt = 0.92c$ , of the edge of the universe at present, where  $c$  is the speed of light. The rotational slanting of the earth is therefore epoch dependent and slowly increasing. The oblateness of the earth of  $0.997$  is recalculated as 'length contraction' of the earth of the new epoch dependent cosmological metric, as an alternative approach to the existing Newton's approach to the calculation. Continental drift, polar wandering and slight westward deflection in the north and eastward deflection in the south of continental plates are explained as consequences of the expansion of the earth with the universe. An excellent agreement of the rotational slanting of  $66.5^\circ$  and oblateness of  $0.997$  of the earth, as well as calculated continental drift rate of  $0.108\Delta\phi$  cm/yr of two positions with longitudinal separation  $\Delta\phi$  along the equator and polar wandering rate of  $0.108$  cm/yr, with derived cosmological data of the rate of expansion of the edge of the universe of  $0.92c$ , Schwarzschild radius  $D_s$  of the universe of  $10^{19}$  light years and half-period of the cycle of expansion and contraction of the universe of 13 billion years has been found.

**G04/08P/D-027** Poster **1400-134**

#### DATUM TRANSFORMATION SOFTWARE TKY2JGD FROM TOKYO DATUM TO A GEOCENTRIC REFERENCE SYSTEM

Mikio TOBITA (Geographical Survey Institute)

Coordinate transformation software "TKY2JGD", which supports the revision of Japanese national geodetic Datum from Tokyo Datum (with Bessel ellipsoid) to Japanese Geodetic Datum 2000 (JGD2000=ITRF94, with GRS80 ellipsoid), was developed. The software includes a GUI program "TKY2JGD for Windows" and a transformation parameter file. The program reads the parameter file and conduct bilinear-interpolation with read parameters at four corners to transform a coordinate inside the four corners. The parameter file contains about 380,000 sets of regional transformation parameters at each grid, which spacing is 30 and 45 sec second in latitude and longitude, which are about 1km, respectively. The transformation parameters are expressed as dB, latitude difference in arc second, and dL, longitude difference in arc second. The differences are due to differences in coordinate system and ellipsoid, and distortion of the national geodetic network (i.e., Tokyo Datum). By estimating only the difference due to the network distortion, the precision of the transformation has improved, because the difference in coordinate system and ellipsoid is known and systematic. The transformation parameters depend on the ellipsoidal height of the position, because surfaces of the two ellipsoids are slightly inclined ( $\sim 17$  arc sec). For example, 3,800m ellipsoidal height (e.g., Mt. Fuji) introduces 32 cm of horizontal positional error. To reduce this error, ellipsoidal height at each grid is required. Very fortunately, "Japanese Geoid 96" and 50m-spacing Digital Elevation Model (DEM) were just released in 1997 and 2000, which means we could calculate ellipsoidal height at each grid by adding the geoidal height and the orthometric height harmonizing their reference systems and reference ellipsoids. A user does not need to input any height. The position on the ground surface will be automatically transformed by TKY2JGD. "Kriging" method was adopted for filling grids using dB and dL of about 38,000 precise geodetic network stations, i.e., first-order, second-order, and third order triangulation points. Though the Kriging method is computationally intensive, recent high-powered CPU could make the grid interval small. The above new algorithms and the small grid interval provided transformation precision of 1.4 cm. The parameters also cover 58 island areas, which are in independent geodetic reference systems. To indicate regions that may have large transformation errors mainly due to crustal deformation, an error index (square root of summation of squared gradient of dB or dL) was developed and the distribution of the index was mapped in color. The high precision and the wide coverage of TKY2JGD software will reduce the total cost of transition to the new national datum, reducing the need of re-survey or re-adjustment.

**G04/08P/D-028** Poster **1400-135**

#### THE ROLE OF ALGEBRA IN MODERN DAY GEODESY

Joseph AWANGE<sup>1</sup>, Erik GRAFAREND<sup>2</sup> (<sup>1</sup>Department of Geophysics, Kyoto University, <sup>2</sup>Department of Geodesy and Geoinformatics, University of Stuttgart)

Algebra, in particular the "Abelian Group" and the "Semi Group" (also known as "Monoid") axioms which form a "ring with identity" are employed to define the "polynomial ring". The polynomial ring theory enables the solution of geodetic observations that can be converted into (algebraic) polynomial rings via the "Multipolynomial resultant" or "Groebner basis" approach. It is shown that the adoption of algebraic approach alleviates the need for iteration and approximation procedures common in numerical methods. Several geodetic examples are presented to validate the proposed role of Algebra in Geodesy. These examples include; the GPS atmospheric sounding, the transformation of Geocentric Cartesian coordinates into Ellipsoidal (Baltic Sea Level Project), the P4P positioning problem and the Conformal  $C_7$  parameter transformation problem among others. The overriding advantage of the algebraic approach is the removal of the requirement of approximate starting values, they are non iterative and enable the detection of outliers.

**G07** Thursday, July 10

#### GLOBAL GEODETIC OBSERVING SYSTEM. IAG SYMPOSIUM

Location: Site A, Room 3

Thursday, July 10 AM

Presiding Chairs: G. Beutler, S. Zerbin, R. Rummel, M. Rothacher

**G07/10A/A03-001** **0900**

#### IGGOS RUMMEL RATIONALE

Reiner RUMMEL<sup>1</sup>, Gerhard BEUTLER<sup>2</sup> (<sup>1</sup>Institute for Astronomical and Physical Geodesy, Technical University Munich, <sup>2</sup>Astronomical Institute, University Bern)

The Integrated Global Geodetic Observing System (IGGOS) will provide the scientific and infrastructure basis for all geodetic global change research. The objective of IGGOS is to

integrate in a well-defined global terrestrial reference frame (1) the orientation and rotation of our planet, (2) the geometric shape of the earth's surface (solid earth, ice and ocean) and its temporal variations and (3) the stationary and time variable gravity field. In order to meet its objectives these three components have to be combined with a relative precision of 1 p.p.b. or better and with a spatial and temporal consistency and stability over decades. This will allow - as a unique and novel contribution to earth system research to monitor and investigate global deformation processes, global mass balance/imbalance and mass exchange among system components. IGGOS will, therefore, become the central geodetic research focus related to earth sciences. It shall represent the official contribution of IAG to United Nations Integrated Global Observing Strategy and to all relevant international research pro-grams related to global change.

**G07/10A/A03-002** **0920**

#### TERRESTRIAL REFERENCE FRAME REQUIREMENTS WITHIN THE IGGOS PERSPECTIVE

Claude BOUCHER, Zuheir ALTAMIMI (IGN France)

One of the main objectives of the promising and challenging IAG project IGGOS (Integrated Global Geodetic Observing System) is the availability of the Global Terrestrial Reference Frame Earth Science applications, particularly Earth Rotation, Gravity Field and geophysics. With the experience gained within the ITRF activities (IERS, IGS), the combination method proved its efficiency to establish a global frame benefiting from the strength of the various techniques and, in the same time, underline their bias and weaknesses. In this paper we focus on the limitation factors inherent to each technique and to the combination, such as the current status of the observing networks, distribution of the collocation sites and their quality and accuracy of the combined frame parameters. Results of some TRF and EOP simultaneous combinations will be used to illustrate the current achievement and to help drawing up future goals and improvements in the IGGOS framework. Beyond these technical aspects, the overall visibility and acceptance of ITRS/ITRF as international standard for science and applications is discussed.

**G07/10A/A03-003** **0940**

#### THE IGGOS VIEWED FROM THE SPACE GEODETIC SERVICES

John M. DOW<sup>1</sup>, Werner GURTNER<sup>2</sup>, Wolfgang SCHLUETER<sup>3</sup> (<sup>1</sup>ESA/ESOC, <sup>2</sup>University of Bern, Switzerland, <sup>3</sup>BKG-Fundamentalstation, Wetzell, Germany)

The Space Geodetic (Technique) Services of the International Association of Geodesy, viz. the International VLBI Service for Geodesy and Astrometry (IVS), the International Laser Ranging Service (ILRS) and the International GPS Service (IGS) will make major contributions to the proposed Integrated Global Geodetic Observing System (IGGOS) through the provision of time series of parameters which describe the fundamental components of global reference frames, in particular the International Celestial Reference Frame (ICRF) and the International Terrestrial Reference Frame (ITRF), and parameters of the transformation between them (EOPs, nutation, origin, scale). The three techniques VLBI, SLR and GPS are represented by services which in the last years have taken over the coordination of the supporting components including observation sites, data routing and management, and analysis facilities, and finally the responsibility for consolidated product delivery by timely provision of high quality time series, with temporal latency in some cases approaching near real time. The results of the different services reflect the distinct characteristics of the technique observables, which are partly similar and partly complementary. Due to the independence and different sensitivity of the techniques, systematic errors between the three techniques can be detected by appropriate combination of the results and to some extent at the level of the observables. Such a procedure will increase the reliability and the consistency of the products in satisfying the requirements of IGGOS. This paper reviews the different techniques with regard to their advantages and indicates sources of systematic errors. It will focus on requirements which have to be fulfilled for the combination of the service-dependant time series and might provide a basis for discussion on future plans in order to evolve the services themselves towards fulfilling the objectives of IGGOS.

**G07/10A/A03-004** **1000**

#### THE IERS - A SERVICE FOR A GLOBAL EARTH OBSERVING SYSTEM

Bernd RICHTER<sup>1</sup>, Markus ROTHACHER<sup>2</sup>, Jan VONDRAK<sup>3</sup> (<sup>1</sup>BKG, Frankfurt am Main, Germany, richter@iers.org, <sup>2</sup>FESG, TU Munich, Germany, rothacher@bv.tum.de, <sup>3</sup>Astronomical Institute, Prague, Czech Republic, vondrak@ig.cas.cz)

The International Earth Rotation Service (IERS) was established in 1987 by the International Astronomical Union (IAU) and the International Union of Geodesy and Geophysics (IUGG). Over the last years the availability of and the easy access to highly accurate and consistent products of the IERS has become of vital importance for geodetic, geodynamic and geophysical projects. Future research and in particular the new satellite missions will require an accurate global reference frame as a crucial basis to accomplish their scientific goals, be it for precise orbit determination, monitoring of sea level change or other geodynamic and geophysical purposes. The IERS is responsible for the appropriate combination of the IGS, IVS, ILRS technique centre (TC) products into official IERS products as well as for the long-term and internal consistency of these official products. The responsibilities of the IERS to establish and maintain the celestial and terrestrial reference frames and supply the earth orientation parameter series are taken over by the corresponding IERS product centres ICRS Centre, ITRS Centre and EOP Centre. The Rapid Service/Prediction Centre with its publication of twice weekly bulletins of preliminary and predicted earth orientation parameters completes the wide range of products. The Global Geophysical Fluids Centre with its 8 special bureaus provides relevant geophysical data sets and related computational results to the scientific community which are the base for, e.g., appropriate correction models for atmospheric, oceanic and hydrological influences on IERS products. Under the guidance of the IERS Conventions Editorial Board the Convection Centre continues the IERS conventional models, constants and standards. The Rapid Service/Prediction Centre monitors the TC and PC activities to ensure the quality and timeliness of the products, whereas the methods of integrating the different observation techniques into a consistent global observing system of the Earth will be developed by the Combination Research Centres.

**G07/10A/A03-005** **1100**

#### THE GRAVITY FIELD AND IGGOS

Rene FORSBERG<sup>1</sup>, M.G. SIDERIS<sup>2</sup>, C.K. SHUM<sup>3</sup> (<sup>1</sup>Department of Geodynamics, <sup>2</sup>Department of Geomatics Engineering, University of Calgary, Canada, <sup>3</sup>Dept. of Civil and Environmental Engineering and Geodetic Science, Ohio State University, USA)

The gravity field of the earth is a natural element of IGGOS. Gravity field quantities are special in the way that measurements at the ppb-accuracies, matching the earth geometrical

parameter determination, is either a function of wavelength (e.g., the long-wavelength mm-geoid from satellite gravity field missions), or based on point sampling (absolute gravimetry), from which anomalous quantities of much lower accuracy are derived by normal gravity field models. From an IGGOS global perspective, one of the main challenges is to ensure the consistency of the global and regional geopotential and geoid models, and the temporal changes of the gravity field at large scales. The International Gravity Field Service, an umbrella "level-2" IAG service under preparation (incorporating the International Gravity Bureau, International Geoid Service, International Center for Earth Tides, and new services on satellite measurements and digital terrain models), would be a natural key element contributing to IGGOS. Major parts of the work of the services would, however, remain separate from the IGGOS contributions, which should focus on the long-wavelength issues and the procedures for local data handling and reductions etc., ensuring validity of long-wavelength gravity field spatial and temporal variations.

**G07/10A/A03-006 1120**  
**ALTIMETRY AS A NEW SERVICE IN IGGOS**

Wolfgang BOSCH<sup>1</sup>, C.K. SHUM<sup>2</sup> (<sup>1</sup>Deutsches Geodätisches Forschungsinstitut (DGFI), <sup>2</sup>Ohio State University (OSU))

Today, research and applications in geodesy and other geosciences are based on space techniques with internationally coordinated services, that take care of data collection, analysis, generation and distribution of products, recommendations of scientific standards, and research for innovative use of the particular geodetic technology. IERS, IGS, IVS and ILRS are examples of such services for Earth rotation, GPS applications, Very Long Baseline Interferometry, and Laser tracking respectively. These services - most of them operating under the umbrella of the Federation of Astronomical and Geophysical Data Analysis Services, FAGS, - will become elements of the new Integrated Global Geodetic Observing System, IGGOS. Satellite altimetry is another space technique, proven to be extremely important for geosciences, in particular geodesy, oceanography and geophysics: Over the oceans the figure of the Earth is today far better known than over most parts of the continents. Altimetry contributed essentially to an improved knowledge of the Earth gravity field and will continue its impact on high resolution gravity field determination - even in the context with the new dedicated gravity missions CHAMP, GRACE and GOCE. Altimetry is also critical for research in climate change signals such as sea level rise, ice sheet mass balance, El Niño/La Niña, decadal oscillations (PDO, NAO), general ocean circulation including quantifying total heat transport across ocean basins. Satellite altimetry, with currently six missions (ERS-2/T/P, GFO, JASON, ENVISAT, ICESAT) operating simultaneously, is poised to be an operational instrument in future plans such as U.S. NPOESS. In spite of its impact, there is up to now no internationally coordinated service for altimetry. Up to a certain level product generation and distribution is mostly performed by the agencies that operate altimeter missions. However, altimeter data bases are definitely non-uniform and partially not up-to-date. Therefore, a few centres or small groups outside these agencies harmonized the data and generate "value-added" products. Many scientific users with exceptionally results did rely on such "value-added" products. The paper considers conditions and requirements for the establishment of an altimeter service as a core element of IGGOS. Technical, scientific, operational as well as political aspects are discussed.

**G07/10A/A03-007 1140**  
**GEOPHYSICAL NUTATION AND POLAR MOTION MODELS AS CONTRIBUTION TO IGGOS**

Véronique DEHANT (Royal Observatory of Belgium)

Nutation and polar motion are motions of a conceptual axis in space and in a frame tied to the Earth. Most of the geophysical contributions to these motions can be computed from modeling the Earth interior and the forcing acting on it. This is the case for the gravitational forcing of the Moon, the Sun and the planets on Earth. This paper presents the computed aspects of these contributions to nutation and polar motion and show how well integrated geodetic observing system such as Very Long Baseline Interferometry, may help to understand the physics of the Earth interior. Additionally, the Earth gravity field coefficients need to be known to compute other contributions than the classical long-term contributions, showing the importance of the gravity field for Earth rotation studies as well. Additional contributions from the external geophysical fluids such as the atmosphere and ocean forcing at the same frequencies as nutations, can be computed. Their contributions to polar motion at long timescale are computed from general circulation models. We shall examine the short term contribution to polar motion as well, and show how important it is to have global observation in these field too. Considering the necessary interdisciplinary approach of nutation and polar motion modeling, and the increasing needs for precision of the future models, this paper shows the advantages that could be obtained from converging researches and emphasises the importance of an Integrated Global Geodetic Observing System.

**G07/10A/A03-008 1200**  
**A UNIFIED GLOBAL HEIGHT REFERENCE SYSTEM AS A BASIS FOR IGGOS**

Johannes IHDE<sup>1</sup>, Hermann DREWES<sup>2</sup>, Laura SANCHEZ<sup>3</sup> (<sup>1</sup>Federal Agency for Cartography and Geodesy, <sup>2</sup>Deutsche Geodätische Kommission, <sup>3</sup>Instituto Geografico Agustin Codazzi)

A global height reference system is based on gravity field parameters, sea surface and a three-dimensional geometric reference frame. Gravity measurements, tide gauge records, ITRF coordinates, and spirit levelling are combined for the realization of a reference frame in collocation points. Satellite gravity missions, airborne gravimetry, satellite altimetry over oceans and land, and radar interferometry contribute to an integrated surface model. Observations and parameters have to be consistent with respect to the used standards, conventions and models. They have to provide unified reference surfaces (geoid and sea surface). The continental reference systems of Europe (EUREF, ECGN) and South America (SIRGAS) are considering these requirements in their strategies. Slightly different definitions and realizations will be discussed.

Thursday, July 10 PM  
 Presiding Chairs: H. Drewes, G. Sideris

**G07/10P/A03-001 1400**  
**THE INTEGRATED GLOBAL GEODETIC OBSERVING SYSTEM (IGGOS) VIEWED FROM THE PERSPECTIVE OF HISTORY**

Gerhard BEUTLER<sup>1</sup>, Hermann DREWES<sup>2</sup>, Andreas VERDUN<sup>1</sup> (<sup>1</sup>Astronomical Institute, University of Bern, <sup>2</sup>Deutsches Geodätisches Forschungsinstitut)

Towards the end of the 19th century astrometric observations could be made with an

accuracy of a few tenths of an arcsecond. The accuracy stayed roughly on this level, till the space age opened the door for milliarcsecond (mas) astrometry. Astrometric observations allowed it at the end of the 19th century to prove the existence of polar motion. The insight that polar motion is almost unpredictable led to the establishment of the International Latitude Service in 1899. Similar observation techniques allowed it to create geodetic networks of continental size. The insight that big networks can only be set up through international collaboration led to the establishment of an international collaboration called "Central European Arc Measurement", the predecessor of the International Association of Geodesy (IAG). The scope of IAG activities was extended already in the 19th century to include gravity. The IAG and the ILS were the tools (a) to establish and maintain the terrestrial and celestial reference systems, including the transformation parameters between the two systems, and (b) to determine the Earth's gravity field. Satellite techniques and astrometric radio-interferometry techniques revolutionized geodesy. Satellite Laser Ranging (SLR) and methods based on the interferometric exploitation of microwave signals (stemming from Quasars and/or from satellites) allow it to realize the celestial reference frame with (sub-)mas accuracy, the global terrestrial reference frame with (sub-)cm accuracy, and to monitor the transformation between the systems with a high time resolution and (sub-)mas accuracy. This development led to the replacement of the ILS through the IERS, the International Earth Rotation Service in 1989. In the pre-space era the Earth's gravity field "could" only be established by terrestrial methods. The determination of the Earth's gravitational field was truly revolutionized twice in the space era, namely first by observing geodetic satellites using optical, Laser, and Doppler techniques, secondly by implementing a continuous tracking using spaceborne GPS receivers in connection with satellite gradiometry. The sequence of the satellite gravity missions CHAMP, GRACE, and GOCE allow it to name the first decade of the 21st century the "decade of gravity field determination". The techniques to establish and monitor the geometric and gravimetric reference frames are about to reach a mature state and will most likely be the prevailing tools of the following decades. It is our duty to work in the spirit of our forefathers by creating similarly stable organizations within IAG with the declared goal to produce the geometric and gravimetric reference frames (including their time evolution) with the best available techniques and to make accurate and consistent products available to wider Earth sciences community as a basis for meaningful research in global change. IGGOS, the Integrated Global Geodetic Observing System is IAG's attempt to achieve these goals. It is based on the well-functioning and well-established network of IAG services.

**G07/10P/A03-002 1420**  
**THE IGGOS AS A PARTNER IN THE IGS AND OTHER GLOBAL PROJECTS**

Philip Leslie WOODWORTH<sup>1</sup>, Thorkild AARUP<sup>2</sup> (<sup>1</sup>Proudman Oceanographic Laboratory, <sup>2</sup>Intergovernmental Oceanographic Commission)

Research into global change has long been recognised as requiring global networks based on space and in-situ systems, together with programmes of scientific investigation to exploit the data sets. IGGOS has the potential for providing many of the necessary geodetic tools needed for global change research. This presentation will discuss the relationship of the proposed IGGOS activity to the existing G3OS (Global Ocean/Terrestrial/Climate Observing Systems) and to its place within the Integrated Global Observing Strategy (IGOS).

**G07/10P/A03-003 1440**  
**MESI - A POSSIBLE GFZ CONTRIBUTION TO IGGOS**

Christoph REIGBER (GeoForschungsZentrum Potsdam, Department 1 Geodesy & Remote Sensing)

In the context of the restructuring process of the Hellmoltz association research centers, GFZ and some other geoscience oriented HGF centers are presently developing a program entitled "Geosystem: The Changing Earth". This program aims to understand and quantify global processes in the solid Earth, and its interaction with the atmosphere and hydrosphere as a prerequisite to provide society with appropriate strategies to safeguard future life on our dynamic planet. The tasks will be to continuously measure and model key geoprocesses, to monitor the status and trends of the system Earth, to understand and assess the impact and risk of these processes for the human habitat, and to develop geotechnologies for the use of the Earth's subsurface. For this purpose, a large-scale Modular Earth Science Infrastructure (MESI) will be established and operated in national and international collaboration. This modular infrastructure integrates near-Earth satellites, air-borne sensing systems, a global network of permanent geophysical and geodetic stations, observatories, mobile instrument arrays, as well as drilling devices and integrated analytical and experimental facilities. Components of MESI could be designed and developed as integral part of the International Global Geodetic Observing System (IGGOS). The presentation will explain the MESI architecture, its functions and schedules and will develop ideas for integration steps into international over-arching structures, such as the planned IGGOS.

**G07/10P/A03-004 1500**  
**INTEGRATION OF SPACE GEODESY: A US NATIONAL GEODETIC OBSERVATORY**

Thomas P. YUNCK, Ruth E. NEILAN (Jet Propulsion Laboratory)

In the interest of improving both the performance and efficiency of space geodesy a diverse group in the US, in collaboration with IGGOS, has begun to establish a unified National Geodetic Observatory (NGO). To help launch this effort an international team will conduct a 3-year program of joint research into the technical issues of integrating SLR, VLBI, and GPS geodesy to produce a unified set of global geodetic products. The goal is to improve measurement accuracy by up to an order of magnitude while lowering the cost to current sponsors. Principal benefits will be to open new vistas of research within both the Geodynamics and Surface Change themes while freeing funds for scientific studies. The NGO campaign will be conducted in full partnership with, and under the auspices of, the International Association of Geodesy (IAG) as a central element of the IGGOS (Integrated Global Geodetic Observing System) project. The international collaboration will be conducted within, and will make full use of, the IAG's existing international services (IGS, IVS, ILRS, and IERS). A principal secondary goal is to expand and diversify international sponsorship of space geodesy. Under NGO the space geodetic techniques in the US will operate within an independent, self-governing federation to create a unified system architecture and establish joint goals, priorities, and proposals, guided by a shared strategic vision. The aim is to bring stability and continuity to providers and users alike while pushing the limits of geodetic accuracy, improving efficiency, nurturing emerging techniques, responding quickly to changing needs, and reducing the financial burden to current sponsors. Specific objectives are to: -- Review the current state of space geodesy; -- Develop the analytical underpinnings of integrated space geodesy; -- Unify the planning and operations for space geodesy within NASA and internationally; -- Broaden sponsorship by enlisting the many institutions and agencies that use and benefit from space geodetic products. Initial seed funding for NGO, to support organizational activities and assist the technical analysis, will come from the Solid Earth and Natural Hazards Program within NASA's Earth Science Enterprise. The NASA contribution will be amplified many-fold by the efforts and contributions of our US and international partners through the broader IGGOS. Other

essential proposals are under review, including one for an integrated geodetic data system known as INDIGO (Interservice Data Integration for Geodetic Operations), also submitted to NASA. INDIGO will offer improved efficiency in geodetic science by providing uniform access to heterogeneous space geodetic data systems and will extend the GPS Seamless Archive (GSAC) philosophy to all geodetic data types. This presentation will review the status and prospects for NGO and INDIGO, and describe their roles as elements of the greater IGGOS campaign.

## G07-Posters

Thursday, July 10

## GLOBAL GEODETIC OBSERVING SYSTEM. IAG SYMPOSIUM

Location: Site D

Thursday, July 10 PM

G07/10P/D-001

Poster

1400-085

## DORIS AS A POTENTIAL PART OF A GLOBAL GEODETIC OBSERVING SYSTEM

Pascal WILLIS<sup>1</sup>, Yoaz E. BAR-SEVER<sup>2</sup>, Gilles TAVERNIER<sup>3</sup> (<sup>1</sup>Institut Geographique National, <sup>2</sup>Jet Propulsion Laboratory, <sup>3</sup>Centre National d'Etudes Spatiales)

In 1990, the first DORIS receiver has been launched around the Earth on the SPOT-2 satellite. Since the end of 1992, there has been always more than 2 DORIS satellites continuously and 6 in 2002 after the successful launches of JASON, SPOT-5 and ENVISAT. Since 1990, the DORIS tracking network has been very stable and possesses a lot of collocation with other fundamental geodetic techniques. With newly improved DORIS on-board receivers and the increase in the number of DORIS measurements, it is now possible to obtain more precise ground stations coordinates using only a week of observations. The goal of this paper is to present the current accuracy currently achieved at JPL using the Gipsy/Oasis software in a free network approach for different types of geodetic results : ground stations time series of coordinates for weekly and monthly solutions, ground stations positions and velocities, geocenter variations, global scale factor monitoring, earth orientation parameters. In particular, emphasis will be put on new results obtained in 2002 with the new type of DORIS receivers and the availability of 6 satellites simultaneously. Finally, we will discuss the opportunity of bringing DORIS as a new participant of a Global Geodetic Observing System, as the DORIS analysis community is now almost ready to begin operation as an IAG geodetic scientific service.

G07/10P/D-002

Poster

1400-086

## THE IGGOS AS THE BACKBONE FOR GLOBAL OBSERVING AND LOCAL MONITORING: A USER-DRIVEN PERSPECTIVE

Hans-Peter PLAG (Geodetic Institute, Norwegian Mapping Authority, Kartverksveien 21, N-3511 Honefoss, Norway, e)

The Integrate Global Observing Strategy (IGOS) emphasises the necessary transition from scientific to operational observing systems serving both scientific and non-scientific users. Another focus of IGOS is the accessibility of data, products and information for user. A key geodetic contribution for both the three Global Observing Systems (G3OS) and initiatives like the European Global Monitoring for Environment and Security (GMES) is an accurate, long-term stable, and easily accessible reference frame as the backbone. Many emerging scientific as well as non-scientific high-accuracy applications require access to an unique, technique-independent reference frame decontaminated for short-term fluctuations due to global Earth system processes. Such a reference frame can only be maintained and made available through an integrated global geodetic observing system providing sufficient information on changes in the Earth figure and gravity field. A likely candidate for this future unique global reference frame, in fact, is the ITRF. In designing the IGGOS, it may be worthwhile to take, at least for a moment, a user-driven top-down approach. Based on a number of examples from monitoring of infrastructure, point positioning, maintenance of national reference frames to global changes studies, likely future accuracy requirements for a global terrestrial reference frame can be set up as function of time scales. Briefly, expected accuracy requirements for a large range of high-accuracy applications are less than 5 mm for diurnal and sub-diurnal time scales, 2-3 mm on monthly to seasonal time scales, better than 1 mm/yr on decadal to 50 years time scales. Using these requirements, specifications of a geodetic observing system meeting the requirements will be ventilated. Focus will be on selected topics of the complete chain from observations to high-accuracy end-users, including the observation network, quality assurance and user access. For the latter, specifications leading to easy access will be proposed. With respect to quality assurance based on system monitoring and performance assessment, principal considerations for the observational network will be discussed.

G07/10P/D-003

Poster

1400-087

## IMPROVEMENTS TO THE NEW MONGOLIAN REFERENCE FRAME MONREF 97 AND PLANS FOR IMPROVEMENTS TO THE MONGOLIAN GEOID

Mijiddorj SAANDARI (Director Monmap LLC)

The Mongolian GPS network consists of 38 stations and one GPS station serving approximately 49000-sq. km. The GPS network survey was executed on the existing second order triangulation points to approximately estimate seven parameter datum conversion coefficient between WGS-84 and local system Krassovsky end to establish a primary high accuracy GPS network with ITRF connection in Mongolia. MONREF 97 is now realized at 38 points at 34 different locations (at three locations there are 2 or three points - Ulaanbaatar, Sukhbaatar and Hovd). To perform geodetic surveying in an efficient way the GPS network need to be further densified. It is also important to determine the permanent reference station at SAcAc, ULB01, in MONREF 97. As mentioned above the orthometric height system will not be replaced. To meet the requirement of today and the future this leveling network need to be renovated and improved by GPS leveling. Furthermore a geoid model is needed for the link between the three dimensional system MONREF 97 and the orthometric height system based on the Baltic Sea Level. A geoid modeling will make height determination with GPS leveling and results of SRTM possible for very large areas. For establishing a geoid model, more densified ground gravity measurements and airborne gravity survey have to be considered. To maintain the high accuracy the MONREF 97 reference system has to be monitored, by repeated campaigns, permanent GPS reference stations and also tracking stations, to keep track on the tectonic movements within the country.

G07/10P/D-004

Poster

1400-088

## COMBINATION OF VLBI, GPS, AND SLR OBSERVATIONS AT THE OBSERVATION LEVEL

Per Helge ANDERSEN (Div. E, Forsvarets forskningsinstitutt)

Forsvarets forskningsinstitutt (FFI, the Norwegian Defence Research Establishment) has during the last 18 years developed a software system called GEOSAT (Andersen, 1995) for the analysis of any type of high precision space geodetic observations. A unique feature of GEOSAT is the possibility of combining any combination of different space geodetic data at the observation level with one consistent model and one consistent strategy. This is a much better strategy than the strategy in use today where different types of observations are processed separately using analysis software developed specifically for each technique. The results from each technique are finally combined a posteriori. In practice the models implemented in the software packages differ at the 1-cm level which is almost one order of magnitude larger than the internal precision of the most precise techniques. Another advantage of the presented method is that for example VLBI and GPS can use the same tropospheric model with common parameterization. The same is the case for the Earth orientation parameters, the geocenter coordinates and other geodetic or geophysical parameters. The analysis with GEOSAT is automated for the combination of VLBI, SLR and GPS observations. The data are analyzed in batches of one day where the result from each daily arc is a SRIF array (Square Root Information Filter). A large number of SRIF arrays can be combined into a multi-year solution using the CSRIFS program (Combination Square Root Information Filter and Smoother, Andersen 2000). Four parameter levels are available and any parameter can, at each level, either be represented as a constant or a stochastic parameter (white noise, colored noise, or random walk). The batch length (i.e. the time interval between the addition of noise to the SRIF array) can be made time- and parameter dependent. GEOSAT and CSRIFS have been applied in the analysis of VLBI and SLR data (LAGEOS I & II) from the period January 1993 to Dec 2002. A few hundred arcs also include GPS data. Earth orientation parameters, geocenter motion, station coordinates and velocities, and GPS transmitter antenna phase center offset and nadir variation were estimated simultaneously with the coordinates of the radio sources and satellite orbital parameters. Recent software improvements and results of analyses will be presented at the meeting.

G07/10P/D-005

Poster

1400-089

## DEVELOPMENT OF THE GPS ISRAELI ACTIVE NETWORK

Yosef MELZER, Moshe ROSENBLUM (Survey of Israel)

The Survey of Israel is planning to develop and progress the GPS Israeli Active Network (GIAN) during 2003. In 1996, the first 3 stations were established during the national GPS geodetic campaign. Today, 11 permanent GPS stations are in continuous operation. In 2002 we realized that great progress should be made in order to serve present and future needs. It motivated us to plan the various aspects of the GPS active network development, and to make arrangements to carry it out. Our plan is to develop the following components of GIAN: Technology: Servers, Software, Communication, Internet. Professional: Geodetic regulation, Geoid model, Geodetic software, Datum upgrade. Products: Files, Archive, Software, Knowledge. Technical Support: Basically to the geodetic community. Research and Science: Geodynamics, Reference frame. The poster describes our plans and strategy in this matter.

G07/10P/D-006

Poster

1400-090

## AN ONLINE SATELLITE ALTIMETRY DATA PROCESSING SYSTEM: ADS CENTRAL

Tilo SCHOENE<sup>1</sup>, Achim HELM<sup>2</sup>, Alexander BRAUN<sup>2</sup>, Hanjiang WEN<sup>3</sup>, Christoph REIGBER<sup>1</sup> (<sup>1</sup>GeoForschungsZentrum Potsdam (GFZ), Germany, <sup>2</sup>now at Byrd Polar Research Center, Ohio, USA)

Answering the emerging questions about human-driven climate changes and, more specifically, the sea level change, an interdisciplinary interpretation of various data sets is needed. Several groups on the national and international level are recently active in building up services to facilitate the access to geoscientific data to a broader community, especially the access to higher level products. GFZ Potsdam is currently developing the Modular Earth Science Infrastructure (MESI) into which the German Earth Science and Information System (GESIS) is integrated. In the frame of GESIS the Altimeter Database System (ADS) has been already developed and implemented. The ADS module provides high quality altimetry data for a variety of different altimetry missions and, moreover, processing capabilities for radar altimetry data to a wide range of users. ADS is an attempt to offer easy access to the daily growing satellite altimetry database and numerous geophysical correction models and orbits. Due to the effectiveness of the underlying data structure and software system, new missions and models can be added to the system at any time. The system has undergone several tests by external and internal users successfully and has been proven to be very useful. Especially to those users not having convenient access to a satellite altimetry data processing system and database, ADS offers new possibilities for research activities. ADS can be accessed worldwide via the internet based user-interface "ADS Central" with a standard browser at <http://gesis.gfz-potsdam.de/ads>. After a registration process the system offers higher level standard products, calculated routinely from the harmonized and inter-calibrated satellite database. Additionally, ADS allows to generate individual user specific products. The user is able to perform several processing and analyzing steps, e.g. to generate mean sea surface height grids, to extract altimetry data time series around a given location, to analyze parameter variability, or to perform a crossover analysis. Furthermore, the user can specify general parameters like the time interval or regional subsets and may select different correction models (e.g. tidal models). It is further possible to enter several quality parameters to optimize the data for individual applications. These individual user defined products are automatically processed by ADS at GFZ Potsdam and are subsequently distributed to the user.

G07/10P/D-007

Poster

1400-091

## THE ORIGIN OF THE TRF FROM SATELLITE LASER RANGING

Erricos C. PAVLIS (JcET/UMBC - NASA/GSFC)

The origin of the Terrestrial Reference System (TRS) is realized through the adopted coordinates of its defining set of positions and velocities at epoch, constituting the conventional Terrestrial Reference Frame (TRF). Since over two decades now, these coordinates are determined through space geodetic techniques, in terms of absolute or relative positions of the sites and their linear motions. The continuous redistribution of mass within the Earth system causes concomitant changes in the Stokes A coefficients describing the terrestrial gravity field. Seasonal changes in these coefficients have been closely correlated with mass transfer in the atmosphere, hydrosphere and the oceans. The new gravity-mapping missions, CHAMP and GRACE, and to a lesser extent the future mission

GOCE, address these temporal changes from the gravimetric point of view. For the very low degree and order terms, there is also a geometric effect that manifests itself in ways that affect the origin and orientation relationship between the instantaneous and the mean reference frame. Satellite laser ranging (SLR) data to LAGEOS 1 and 2 contributed in this effort the most accurate results yet, demonstrating millimeter level accuracy for weekly averages. Other techniques, like GPS and DORIS, have also contributed and continue to improve their results with better modeling and more uniformly distributed (spatially and temporally) tracking data. We will present the results from our latest analysis of several years of LAGEOS 1 and 2 SLR data, assess their accuracy and compare them to results from the various other techniques. Finally, we will look into potential improvements in the future, which will likely lead us to even finer resolution and higher accuracy through the constructive combination of the individual time series.

<b>G07/10P/D-008</b>	<b>Poster</b>	<b>1400-092</b>
----------------------	---------------	-----------------

**GLOBAL COMPARISON OF SLR, DORIS, AND GPS POSITION TIME SERIES FOR COLLOCATED SITES**

Joelle NICOLAS<sup>1</sup>, Laurent SOUDARIN<sup>2</sup>, Jean-Mathieu NOCQUET<sup>3</sup>, Zuheir ALTAMIMI<sup>4</sup>, David COULOT<sup>5</sup> (<sup>1</sup>Observatoire de la Côte d'Azur / CERGA, <sup>2</sup>Collecte Localisation Satellites, <sup>3</sup>Department of Earth Sciences / Oxford University, <sup>4</sup>IGN/ENSG/LAREG, <sup>5</sup>IGN/ENSG/LAREG OCA/CERGA)

In space geodesy, and in all its scientific applications, the accuracy of the terrestrial reference frame plays a crucial role in the expression of the results. The current accuracy reached by space geodetic techniques allow the estimation of quasi-periodic station displacements at a few or even a sub-centimeter level mainly due to the loading effects induced by mass redistribution in the oceans, the atmosphere and continental water. The magnitude of such signals requires an optimal definition of the underlying terrestrial reference frame and its time evolution. In this study, we focus on the comparison of position time series obtained for the 1997-2002 period provided by three independent geodetic techniques: Satellite Laser Ranging (SLR), Doppler Orbitography and Radiopositioning Integrated by Satellite (DORIS), and Global Positioning System (GPS) for geodetic sites where these techniques are collocated. Since these sites are used to tie the different solutions from different techniques for the International Terrestrial Reference Frame (ITRF) computation, it is crucial to study their time behavior and the level of agreement between techniques at these locations. Our SLR time series is based on monthly LAGEOS -1 and -2 combined solutions. The DORIS time series is based on monthly solutions with a combination of the data of the SPOT-2, -3, -4, and TOPEX/POSEIDON satellites. The GPS time series is derived from weekly combined global solutions. Time-dependent displacements of stations usually have magnitude close to the accuracy of each individual geodetic technique, and it still remains difficult to extract the geophysical signal from possible artifacts inherent to each space geodetic technique. We use the comparison of our three independent solutions to re-assess uncertainties and determine possible bias associated with each individual technique or processing strategy. The possible origin of the discrepancy noticed between the 3 techniques is also discussed. Special attention is paid to the vertical component for which the geophysical signal is stronger and for which the microwave techniques DORIS and GPS have a less accurate determination than the SLR technique. The comparison allows us to distinguish the common signal observed by the three techniques and to extract the geophysical signal from the noise inherent to each individual geodetic technique. We finally propose a discussion on the possible geophysical meaning of the extracted signal.

<b>G07/10P/D-009</b>	<b>Poster</b>	<b>1400-093</b>
----------------------	---------------	-----------------

**THE IERS INFORMATION AND DATABASE SYSTEM**

Bernd RICHTER, Wolfgang SCHWEGMANN, Wolfgang R. DICK (Department of Geodesy, Bundesamt fuer Kartographie und Geodaesie)

The IERS information system includes information about the structure, the organisation and the publications of the IERS as well as products from the various Product Centres. General information related to the fields of Earth rotation and reference frames will complement the system. All products within the IERS are generated by an enormous investigation of human and financial resources. Typically they are applied by professional users operating standard procedures of information technologies to receive the data from the various IERS product centres. To make the products also available to a broader scientific and non-scientific community a strategy is going to be developed how the diversity of information within the IERS can be presented in a customer friendly way. Presently facts about all IERS products (e.g. ITRF, ICRF, EOPs, etc.) including links to the product centres and the related data are listed in the IERS Information System. In the future, the IERS Central Bureau will operate a Data Centre to store and archive all data which are necessary for the IERS products and also those which are necessary to re-compute the products. As IERS database input, meta information will be extracted from the archived IERS products and data. The individual database tables will reflect the structure of the represented data and the dependencies between them. Special requests can then be generated to browse all available data with respect to a specific concern. The Central Bureau will utilize the latest technology in Internet-based information exchange with open access to data files and employing security features as required today. Thus, the information system will be run on an Apache Web Server, while the open source relational database management system PostgreSQL is used to model and store the meta information of the products. The Web interface to access and browse this information is realized in PHP, a widely-used general-purpose scripting language that is especially suited for Web development and can be embedded into HTML. Examples will be given how the information about the main IERS products is obtained and stored in the database and how it can be browsed to perform specific requests on the data.

<b>G07/10P/D-010</b>	<b>Poster</b>	<b>1400-094</b>
----------------------	---------------	-----------------

**THE CONTRIBUTION OF THE IERS TO THE IGGOS CONCEPT**

Bernd RICHTER<sup>1</sup>, Markus ROTHACHER<sup>2</sup>, Jan VONDRAK<sup>3</sup> (<sup>1</sup>Department of Geodesy, Bundesamt fuer Kartographie und Geodaesie, <sup>2</sup>Technical University Munich, Munich, Germany, <sup>3</sup>Astronomical Institute, Prague, Czech Republic)

The International Earth Rotation Service (IERS) established in 1987 as an inter-union service by the International Astronomical Union (IAU) and the International Union of Geodesy and Geophysics (IUGG), accepted as member of FAGS, understands itself as a substantial part of the future IGGOS. Over the last years the availability of and the easy access to highly accurate and consistent products of the IERS has become of vital importance for geodetic, geodynamic and geophysical projects. Future research and in particular new satellite missions will require the most accurate, reliable and consistent global reference frame as a crucial basis to accomplish their scientific goals, e.g., precise orbit determination, monitoring of sea level change or other geodynamic and geophysical challenges. The IERS is making use of the advantages and strengths of the individual space techniques by appropriately combining the IGS, IVS, ILRS technique centre (TC) products and supplementary information into official IERS products, striving for the long-term and internal consistency of these official products. The concept of IGGOS is based on the

integration of the three pillars of geodesy, namely the geometry and kinematics, Earth orientation and rotation, and gravity field and dynamics. The IERS already provides important combined products to the first two pillars, i.e., the celestial and terrestrial reference frames and Earth orientation, with its ICRS, ITRS and EOP Centres complemented by the Rapid Service/Prediction Centre. With the guidance of the Analysis Coordinator the Combination Research Centres started the development of methods and software to integrate the different observation techniques into a consistent set of products as a contribution to a future global integrated observing system. The PC and Combination Centre activities will ensure the realisation, reliability and timeliness of these new products. The Convention Centre continues to develop and promote the IERS conventional models, constants and standards to generate consistent and rigorous combined products. Concerning the third pillar it should be mentioned that the IERS functions already include significant non-geometric components, e.g., monitoring of the geocentre and other contributions from the Global Geophysical Fluids Centre. These are the basis of appropriate correction models for atmospheric, oceanic and hydrological influences on all three IGGOS pillars and for the study of geodynamic processes of the Earth system. The IERS sees its participation in the IGGOS project as an organisational and scientific challenge.

<b>G07/10P/D-011</b>	<b>Poster</b>	<b>1400-095</b>
----------------------	---------------	-----------------

**QUINS - GRADIOMETRIC MISSION WITH FIVE MICROSATELLITES**

Erik W. GRAFAREND<sup>1</sup>, Gerrit AUSTEN<sup>1</sup>, Oliver BAUR<sup>1</sup>, Petar MARINKOVIC<sup>1</sup>, Mohammad A. SHARIFI<sup>1</sup>, Hans P. ROESER<sup>2</sup>, Maria V. SCHOENERMARK<sup>2</sup> (<sup>1</sup>Department of Geodetic Science, Stuttgart University, <sup>2</sup>Institute of Space Systems, Stuttgart University)

"QUINS" is a proposed satellite mission beyond the new satellite missions CHAMP, GRACE and GOCE. A cluster of four nearby microsatellite track each other relative to a fifth *master micro satellite by Nano Distance Measurements*. All microsatellites are equipped with small but efficient electrical propulsion systems enabling formation flights with different satellite constellations, e.g. line, cross, triangles, tetrahedron. The *master micro satellite* is packed with the required and essential technology, serves a main computer system and will provide the downlink to the ground stations. The additional four smaller microsatellites are identical and carry a minimum technology package to fulfil the performance. The GRACE observation principle is applied. The four nearby satellites form a high resolution gradiometer of low costs. The satellite system "QUINS" is simulated and first gradiometric results of the *Eötvoös tensor* are presented with respect to the barycentre of the satellite cluster. They document a very high resolution of the Earth's gravity field, one order better than possible today. According to the optimal life time of "QUINS" the long term time variations of the terrestrial gravity field can be detected.

<b>G07/10P/D-012</b>	<b>Poster</b>	<b>1400-096</b>
----------------------	---------------	-----------------

**THE INTERNATIONAL LASER RANGING SERVICE AND ITS SUPPORT FOR IGGOS**

Michael R. PEARLMAN<sup>1</sup>, Carey E. NOLL<sup>2</sup>, Van S. HUSSON<sup>3</sup> (<sup>1</sup>Harvard-Smithsonian Center for Astrophysics, <sup>2</sup>NASA Goddard Space Flight Center, <sup>3</sup>Honeywell Technical Solutions Inc)

The International Laser Ranging Service (ILRS) was established in September 1998 as a service within the IAG to support programs in geodetic, geophysical, and lunar research activities and to provide data products to the International Earth Rotation Service (IERS) in support of its prime objectives. Now in operation for more than four years, the ILRS develops (1) the standards and specifications necessary for product consistency and (2) the priorities and tracking strategies required to maximize network efficiency. The Service collects, merges, analyzes, archives and distributes satellite and lunar laser ranging data to satisfy a variety of scientific, engineering, and operational needs and encourages the application of new technologies to enhance the quality, quantity, and cost effectiveness of its data products. The ILRS works with (1) the global network to improve station performance, (2) new satellite missions in the design and building of retroreflector targets to maximize data quality and quantity and (3) science programs to optimize scientific data yield. The ILRS Central Bureau maintains a comprehensive web site as the primary vehicle for the distribution of information within the ILRS community. The site, which can be accessed at: <http://ilrs.gsfc.nasa.gov> is also available at mirrored sites at the Communications Research Laboratory (CRL) in Tokyo and the European Data Center (EDC) in Munich. The ILRS currently includes more than 40 SLR stations, routinely tracking more than 20 retroreflector-equipped satellites and the Moon in support of user needs. Through international partnerships, the global distribution of SLR stations continues to improve, especially in the Southern Hemisphere, where coverage has been historically weak. The recently established stations in Tahiti (MOBLAS-8) and Hartebeesthoek, South Africa (MOBLAS-6) are already very important contributors to the network. The Totally Integrated Geodetic Observatory (TIGO), the multi-technique facility developed by the BKG, is now also fully established the site at Concepcion, Chile. New missions added to the ILRS tracking roster over the past two years include CHAMP, GRACE-A and -B, Jason (in tandem with TOPEX), ENVISAT (in tandem with ERS-2), REFLECTOR, Meteor-3M, and ADEOS-II. An intensive tracking activity has also been undertaken on the Etalon satellites to support EOP and gravity field studies. During the last two years, the ILRS has addressed very important challenges: (1) Data from the field stations are now submitted hourly and made available immediately through the data centers for access by the user community, (2) Tracking on low satellites has been significantly improved through the subdaily issue of predictions, drag functions, and the real-time exchange of time biases, (3) Analysis products are now submitted in SINEX format for compatibility with the other space geodesy techniques, (4) The Analysis Working Group is heavily engaged in Pilot Projects as it works toward an ILRS "standard" global solution, and (5) SLR has significantly increased its participation in the International Terrestrial Reference Frame (ITRF) activity.

<b>G07/10P/D-013</b>	<b>Poster</b>	<b>1400-097</b>
----------------------	---------------	-----------------

**DEVELOPMENT OF TWO COLOR INTERFEROMETER FOR DISTANCE MEASUREMENT WITH AN AUTOMATIC CORRECTION OF AIR REFRACTIVE INDEX**

Souchi TELADA, Ichiro FUJIMA, Hirokazu MATSUMOTO (Length Standard Section, National Metrology Institute of JAPAN AIST)

A two color heterodyne interferometer has been developed as a reference standard for a laser interferometer and an electronic distance meter. An accuracy of a distance measurement with a light wave in air is mainly caused by a refractive index of air. In order to obtain the refractive index of air along the light path, it is necessary to measure the environment of the air, such as temperature, pressure, humidity and carbon dioxide. But it is hard to measure the parameters over a long optical path. So, we have made a two color interferometer which can correct the refractive index of the air without measuring the environmental parameters. The refractive indices for two wavelengths are different in the same air. The refractive index of the air can be corrected based on the difference. The two color interferometer consists of two independent heterodyne interferometers. One uses the fundamental wavelength of a Nd:YAG laser (1064nm). The other uses the second harmonic wavelength of the laser (532nm). Both beams travel along the same path and interfere with each other. After the interference, these are separated and each beam goes to each photo

detector. For the two color interferometer, the accuracy becomes about 65 times worse than that of each interferometer. The '65' depends on both wavelengths. In order to obtain the difference between two optical lengths measured by each interferometer in the air with high accuracy, common noises for the interferometers are reduced by changing reference arm lengths with a feed back servo technology. In this way, it is successful to measure the distance with an accuracy of  $10^8$  relatively with 100 m linear stage in the NMIJ optical tunnel. The accuracy depends on an accuracy of the constant of '65' which is calculated from an equation for refractive index of air called Ciddor's Equation.

**G07/10P/D-014** Poster **1400-098**

**THE INTERNATIONAL VLBI SERVICE FOR GEODESY AND ASTROMETRY (IVS) AND ITS PROSPECTIVE**

Wolfgang SCHLUETER<sup>1</sup>, Nancy VANDENBERG<sup>2</sup> (<sup>1</sup>Bundesamt fuer Kartographie und Geodäsie, Fundamentalstation Wettzell, <sup>2</sup>NVI, Inc. / Goddard Space Flight Center)

The VLBI technique has been employed in geodesy for nearly 40 years. Covering intercontinental baselines with highest accuracy, monitoring Earth rotation at the state of the art and providing the quasar positions as the best approach to an inertial reference frame, VLBI significantly contributed to the tremendous progress made in geodesy over the last decades. VLBI was a primary tool for understanding the global phenomena changing the "Solid Earth". Today VLBI continuously monitors Earth rotation and its variations and also crustal movements in order to maintain global reference frames, coordinated within the International VLBI Service for Geodesy and Astrometry (IVS) – a service of the IAG and IAU. Science and applications set the requirements for the realization and maintenance of global reference frames at VLBI's technical limitations. VLBI as the unique technique for providing a celestial reference frame and for deriving the full set of Earth rotation parameters, plays the fundamental role of generating the basis for many applications and research in the geosciences. IVS coordinates the international collaboration of organizations which operate or support VLBI components in order to provide the support for geodetic, geophysical and astrometric research and operational activities, to promote research and development activities and to interact with the community of users of VLBI products. As service of the IAG and IAU the IVS has taken over responsibility for the provision of the VLBI products, their quality and timeliness. Since 2002 the IVS observing program has been set up promoting the quality and availability of products towards the requirement of the coming up IGGOS. This paper describes the operations of IVS, summarizes and qualifies its products generated continuously. Prospective developments and wishes for the products and the related observing programs are given.

**G07/10P/D-015** Poster **1400-099**

**FROM NETWORKS OF STATIONS TO SPATIALLY CONTINUOUS LAND SURFACE DISPLACEMENTS: INTEGRATION OF TECHNIQUES AT REGIONAL SCALE**

Susanna ZERBINI<sup>1</sup>, Johannes IHDE<sup>2</sup>, Alessandro FERRETTI<sup>3</sup>, Luciano LAGO<sup>4</sup>, Bernd RICHTER<sup>5</sup>, Fabio ROCCA<sup>6</sup>, Claudia ROMAGNOLI<sup>7</sup>, Dietrich SIMON<sup>8</sup> (<sup>1</sup>Department of Physics, University of Bologna, <sup>2</sup>Bundesamt fuer Kartographie und Geodäsie, Frankfurt am Main, Germany, <sup>3</sup>Terlevamento Europa, Milano, Italy, <sup>4</sup>Dipartimento di Elettronica ed Informazione, Politecnico di Milano, Italy, <sup>5</sup>Dipartimento di Scienze della Terra e Geologico Ambientali, Università di Bologna, Italy)

Space geodetic techniques provide the means to monitor in a global reference system horizontal as well as vertical velocities of stations on the Earth's surface. Space observations also allow tying together ensembles of terrestrial measurements performed at different spatial scales and temporal resolution. However, fine-tuning in the knowledge of these motions has not yet been reached and it constitutes an important step for the next decade or so. Land surface variations or changes are taking place continuously at very different spatial and temporal scales ranging from very local to global, and from seconds to millions of years. Among the space techniques, SLR, VLBI and CGPS (continuous GPS) provide information which is continuous in time, however in space the information is limited to the station location. On the other hand, techniques such as InSAR and Lidar have proven capability to provide spatially continuous information, which, however, is limited in temporal coverage. There are many challenges that we are faced with in the attempt to understand the processes responsible for land surface changes/variations and to acquire a predictive capability in order to mitigate the relevant risks and to define the implementation of practical societal applications. Among them, there is a primary need for defining and establishing an appropriate observational methodology characterized by the capability to measure, with high accuracy, spatially and time continuous deformations of the land surface. Space, airborne and terrestrial techniques can be adopted and used together by taking advantage of the complementary strengths of the different techniques. A contribution towards the realization of such an observational capability is provided. We describe the ensemble of space and terrestrial techniques, which were co-located in southeastern Po Plain and along the Adriatic coast, in Italy, to study, in particular, land subsidence. One example is the Medicina station, near Bologna, where CGPS, VLBI, a superconducting gravimeter and a multitude of terrestrial in formation is available. For the Adriatic coast a first comparison between CGPS and InSAR is presented.

**G07/10P/D-016** Poster **1400-100**

**DEVELOPMENT OF AN EUROPEAN COMBINED GEODETIC NETWORK (ECGN)**

Johannes IHDE<sup>1</sup>, Trevor BAKER<sup>2</sup>, Carine BRUYNINX<sup>3</sup>, Oliver FRANCIS<sup>4</sup>, Jacques HINDERER<sup>5</sup>, Ambrus KENYERES<sup>6</sup>, Jaakko MAKINEN<sup>7</sup>, Hans ROHDE<sup>8</sup>, Jaroslav SIMEK<sup>9</sup>, Herbert WILMES<sup>1</sup> (<sup>1</sup>Federal Agency for Cartography and Geodesy, <sup>2</sup>Proudman Oceanographic Laboratory, <sup>3</sup>Royal Observatory of Belgium, <sup>4</sup>European Center for Geodynamics and Seismology, <sup>5</sup>Ecole et Observatoire des Sciences de la Terre, Institut de Physique du Globe de Strasbourg, <sup>6</sup>FOMI Satellite Geodetic Observatory, <sup>7</sup>Finnish Geodetic Institute, <sup>8</sup>International Hydrographic Bureau, <sup>9</sup>Research Institute of Geodesy, Topography and Cartography)

In order to ensure the long-time stability of the terrestrial reference system with an accuracy of  $10^8$  in the global scale and for Europe the interaction between different time dependent influences of the system Earth to the terrestrial reference system and the related observation has to be considered in the evaluation models. The proposal is to establish a kinematic EUROPEAN COMBINED GEODETIC NETWORK (ECGN) to combine the spatial and height reference system with earth gravity field parameter estimation. It is in agreement with the planned IAG project of an Integrated Global Geodetic Observation System (IGGOS). ECGN is an European network for the integration of time series of spatial/geometric observations (GNSS - GPS/GLONASS and in the future GALILEO), gravity field related observations and parameters (gravity, tides, ocean tides), and supplementary information (meteorological parameters, surrounding information of the stations e.g. eccentricities and ground water level). The call for participation is from the point of view of time structured in two stages. The first call is directed to the implementation of the ECGN stations following the concept of the project. The ECGN stations have the standard observation techniques GNSS (GPS/GLONASS, GALILEO), gravity (super conducting gravimeter and/or absolute gravimeter), levelling connections to nodal points of UELN/EVRS and meteorological

parameters. Standard for the ECGN stations is a local network for the derivation of eccentricities in a 1 mm accuracy level in all three spatial components. All ECGN stations are part of the EPN. For the observation techniques guidelines has to be fulfilled. In parallel to the first call the ECGN working group has to prepare the second step for the call of analysis and investigations. The main action of the ECGN working group in the first step is a pilot study of combination of different observations with available stations to get experiences in combination of spatial information with gravity field related data. For super conducting gravimeter data the GGP data centre could be used for data collection. Levelling data of ECGN will be collected at the UELN/EVRS data center. Local data centers for absolute gravity data and super conducting gravimeter data should be installed in the first stage by the ECGN working group.

**G07/10P/D-017** Poster **1400-101**

**THE INTERNATIONAL GEIOD SERVICE: ACTIVITIES AND FUTURE PLANS**

Riccardo BARZAGHI, Fernando SANSONO, Ludovico BIAGI, Alessandra BORGHI (DIAR-Politecnico di Milano)

The International Geoid Service (IGeS) promoted in the last four years several activities centred on geoid computation. One of the main tasks of IGeS was to promote and organise schools on geoid determination, focussed on theoretical and practical aspects. Four international schools have been organised by IGeS in the last years. The general purpose of these schools was to prepare new graduate students, young scientists and employees of national agencies and services or industry staff to use and compute gravimetric geoids for the main scientific and technical applications. Furthermore, IGeS has actively participated in a relevant project for geoid determination in South America, which was carried out in strict co-operation with NIMA and the Escola Politecnica Universidade de Sao Paulo. Future plans will involve IGeS in geoid estimation activities in Antarctica and in South Africa and in the estimate of the new European geoid. IGeS web has also been updated during these last four years and contains at present regional geoid estimates, global geopotential models and software for geoid computation. Another important activity, which has been continued and improved, was the publication of the IGeS Bulletin that became a reviewed scientific journal. Finally, IGeS proposed, together with BGI, NIMA, ICET and GFZ, the creation of a new IAG service, the International Gravity Field Service (IGFS). This new structure aims at collecting, validating and distributing data and software with the purpose of determining the gravity potential of the Earth, or any of its functional, and the surface of the Earth.

**G07/10P/D-018** Poster **1400-102**

**THE INTERNATIONAL GPS SERVICE TRACKING NETWORK: ENABLING DIVERSE STUDIES AND PROJECTS THROUGH INTERNATIONAL COOPERATION**

Angelyn W. MOORE, Ruth E. NEILAN (Jet Propulsion Laboratory, California Institute of Technology)

The International GPS Service (IGS), formulated beginning in 1989 and formalized in 1994, was founded on the collaborative operation of approximately 30 permanent GPS stations to benefit global geodynamics. The same cooperative principles, today applied to a network of over 300 stations, still serve to maximize global benefit without unnecessary duplication of investment in global infrastructure. The scope of applications of the dataset has grown to include atmospheric, oceanographic, subdaily, and low-earth orbiter activities through working groups and pilot projects fostered within the IGS in the now traditional IGS spirit of collaboration. These activities and the IGS infrastructure are viewed as critical elements to the Integrated Global Geodetic Observing System. This presentation will review the present nature of the IGS tracking network and its ability to support new applications.

**G07/10P/D-019** Poster **1400-103**

**FROM CLEARINGHOUSE SYSTEMS FOR SATELLITE PRODUCTS TO INTEGRATED DATAWAREHOUSE SERVICES FOR SCIENTISTS, DECISION MAKER AND THE INTERESTED PUBLIC**

Bernd RITSCHEL, Knut BEHRENDTS, Stephan BRAUNE, Sebastian FREIBERG, Ronny KOPISCHKE, Hartmut PALM, Andrea SCHMIDT (GFZ Potsdam, Data Center)

The scientific products based on the GFZ satellite mission CHAMP and the JPL, CSR and GFZ collocated GRACE mission are managed by the related CHAMP-ISDC respectively GRACE-ISDC. Every Information System and Data Center (ISDC) consists of six main components. The operational system is responsible for the product input and output. The clearinghouse, the heart of the ISDC has been designed as a powerful catalog system based on mandatory product metadata. All products are stored and archived in the product archive system consisting of an online RAID harddisc part and a quasi online tape part, designed for backup reasons. The product ordering system controls the access to the products depending on the different user requests. Spatial retrieval and presentation as well as product visualization are features of the datawarehouse component. The access to requested information and products are realized by a customer-friendly WWW based graphical user interface. Whereas the ISDCs are developed and operated as solitary project dependent systems, the scheduled GESIS (German Earth Science Information System) will network and integrate unique information and products. One main component of GESIS will be a powerful datawarehouse. Clearly, this system will base on a harmonized portfolio of most different products of different projects or missions managed by the different ISDCs. In the foreground of GESIS stands the processing and solution of sophisticated geo-scientific problems which require a variety of information and products. Diverse scientific services from spatial product retrieval to complete scientific processing workflows will be provided by GESIS. Furthermore, services for decision maker, e.g. in the area of disaster and risk management or specific services for the interested public will be integrated.

**G07/10P/D-020** Poster **1400-104**

**A CONTRIBUTION OF THE GEODETIC OBSERVATORY PECNY, CZECH REPUBLIC, TO INTERNATIONAL GEOSCIENTIFIC SERVICES AND PROJECTS**

Jaroslav SIMEK, Jan DOUSA, Jakub KOSTELECKY, Vojtech PALINKAS (Geodetic Observatory Pecny, RIGTC)

The Geodetic Observatory Pecny has been operating since 1957. Since the beginning its activities have been oriented to astrometric and satellite positioning, to continuous gravimetric observations and to analysis and interpretation. In 1995 the GOP became an IGS operational station. Nowadays it regularly provides a variety of observation files of GPS and GLONASS satellites ranging from 1 second/15 minute to 30 second/1 day files. The EUREF Local Analysis Center GOP has been operating at the Observatory since the beginning of 1997 and at present it is processing 35 stations of the European Permanent Network. The EUREF LAC GOP is also involved in the EUREF special project "Troposphere" and in the action COST716 (applications of ground-based GPS for meteorology) by continuous evaluation of ZTDs from observations of 39 permanent GPS stations for the

numerical weather predictions. In support of near-real time applications a special data center was established in 2000/2001. The activities of the analysis center GOP were extended by a regular production of hourly orbits of the GPS satellites. The gravimetric earth tides have been regularly observed at the GOP since 1970 and the results have been provided to the International Center on Earth Tides (ICET). Thanks to significant instrumental upgrades achieved at the end of nineties the records of classical gravimeters (Gs15 No.228 and LCR 137) have been processed at the ICET along with the results of superconducting gravimeters. Parallel to gravimetric tidal observations the environmental effects (meteorological parameters , ground water level) have been recorded. After 14 absolute gravity measurements carried out in the period 1978 - 2001 systematic absolute measurements have been carried out by the absolute meter FG5 No.215 since August 2001. The time series includes up to the end of Jan 2003 35 absolute gravity campaigns. A complex approach aimed to a combination of space geodetic observations with terrestrial relative and absolute gravity measurements and environmental information results in joining the newly launched project of the European Combined Geodetic Network (ECGN). The activities of the GOP are described in detail and illustrated by examples of results coming from individual activities.

GAI.08

**CONDUCTIVITY OF CRUST AND MANTLE: RELATION TO GEODYNAMICS (SEDI)**

Location: Site A, Room 14

Tuesday, July 8 AM

Presiding Chairs: A.G. Jones, Y. Ogawa

GAI.08/08A/A14-001

0830

**THE ELECTRICAL STRUCTURE OF THE CRUST AND UPPER MANTLE ALONG PROFILE CROSS CONJUNCTION AREA BETWEEN TIBET PLATE AND NORTH CHINA PLATE**

Guoze ZHAO, Yan ZHAN, Ji TANG, Xiaobin CHEN, Qianhui DENG, Jijun WANG, Junmeng ZHAO (Institute of Geology, China Seismological Bureau)

MT data has been recently obtained along 5 profiles in conjunction area of Tibet Plate (TB) and North China plate (NC). The longest profile of about 950km started from Dari in north-eastern margin of TB at southwest end of the profile, then crossed North-South Seismotectonic Belt (NSSB) and ended at Jingbian in Ordos plate of NC in NE direction. The RRI 2-D inversion method was used in the profile and 2-D electrical structure was obtained. The electrical structure of the profile shows that four sub-blocks appeared. They are, from southwest to northeast, Bayankela block (Bb), Qinling-Qilian block (QQb), Haiyuan block (Hb) and Ordos block (Ob). The boundaries between each two adjacent blocks from southwest to northeast correspond to Maqin fault belt (F1), Lanzhou fault belt (F2) and Majiatan-Dashuikeng fault belt (F3) respectively. Different characteristic images of resistivity existed in four blocks. Low resistivity zones in the crust appeared in three blocks Bb, QQb and Ob at depth of about 25km, 15km and 27km respectively. But in the Hb block no large area with low resistivity occurred. Resistivity distribution of Hb is just representative of margin area of 4 plates (about 200km width): TB including Bb and QQb is to southwest side of F2. NC is to northeast side of F3. Alashan plate is in NW side and South China plate is in SE side. This area (Hb) is also called as Conjunction Area (CA). The CA is a part of the NSSB where quite a lot big earthquakes occurred according to the history record especially in the surrounding boundary area of the CA. Lanzhou earthquake (M=7, 1125), Tianshui earthquake (M=8, 1654) and Haiyuan earthquake (M=8.5, 1920) located respectively near west, south and east boundary of CA. F1 is eastern section of a big fault belt (Kunlun fault). Kunlun earthquake (M=8.1, 2001) occurred in the western section of this fault. The electrical structure shows that F1 is a bigger electrical boundary. Some other faults were also detected along profile. Except for Haiyuan fault being the bigger the others are the smaller. Seismic reflection/refraction data along same profile indicates that the Moho discontinuity becomes shallower from southwest to northeast, (from around 60 km to around 40 km). The low velocity zones in middle crust appeared in Bb, QQb and Hb, but not in the Ob. The agreement and disagreement between low resistivity zones and low velocity zones in the mid-lower crust was discussed. It is postulated that low resistivity zones in Bb, QQb and Ob blocks are caused by the fluids in the crust. Due to the deformation of the crust was weak in these blocks, porous water in layers of mid-lower crust was preserved well and shown bigger zones of low resistivity. Due to deformation of the crust in CA area (Hb block) was serious, the layer with porous water may be suffered from strong deformation. Therefore no bigger zone with low resistivity appeared.

GAI.08/08A/A14-002

0850

**LONG PERIOD MAGNETOTELLURIC MEASUREMENTS IN NW- HIMALAYA: IMPLICATIONS FOR MANTLE CONDUCTIVITY**

Baldev Raj ARORA, Gautam RAWAT, Vipul NAGAR (Indian Institute of Geomagnetism)

Long period magnetotelluric (10-10,000s) measurements are undertaken along a profile extending across Indus Tsangpo Suture (ITS) in Northwest Himalaya. The data supplements the information on the electrical state of the deeper parts of the upper mantle than that was probed earlier by the broadband MT data (300Hz-1000s). The dimensionality analysis shows period dependence strike. In period range below ~700s, the strike is dominantly directed along N 40°W and shows good correspondence with the regional tectonic fabric. However for periods greater than ~700 s, the strike direction is N-S or 10°W, when the phases of single column are same but show significant phase split for two principle polarizations. The uniformity of the strike and near constant phase split around 4000 s at all stations could be a pointer of anisotropic layer at the base of the lithosphere. The nature of vertical fields along the profile is used to constrain the anisotropy or lateral variations in the conductive layer at depth. The varying strike directions in the upper mantle and crust are discussed in terms of the past trajectory of the Indian plate motion and post-collision rotation.

GAI.08/08A/A14-003

0910

**ELECTROMAGNETIC IMAGING OF THE INDIA-ASIA COLLISION ZONE**Alan G. JONES<sup>1</sup>, Jessica E. SPRATT<sup>2</sup>, K. Doug NELSON<sup>3</sup>, Martyn J. UNSWORTH<sup>1</sup>, The INDEPTHMT Team (<sup>1</sup>Geological Survey of Canada, Ottawa, Canada, <sup>2</sup>Syracuse University, Syracuse, U.S.A., <sup>3</sup>University of Alberta, Edmonton, Canada)

Project INDEPTH was initiated in 1992 to develop a better understanding of the deep structure and mechanics of the Himalaya-Tibet region, and magnetotelluric surveying was added during INDEPTH Phase II in 1995. Broadband and long period data were acquired in 1995 along a N-S transect crossing the India-Asia collision zone, the Yarlung-Zangbo suture, at 90E longitude. However, these data failed to penetrate to the deep crustal and mantle depths due to low solar activity, and the thick and conducting crust. Deep crustal and mantle information is key for this region to provide a test of the model of subcretion to southern Tibet by the stiff Indian mantle lid. In order to obtain such information, and to provide a second image of the Yarlung-Zangbo suture zone to test along-strike variability, a magnetotelluric experiment was performed in 2001 along longitude 92E, containing an ultra-long period component. MT data were acquired at 28 locations along the new profile, with long period data at 15 of these. Modelling of these data allows a comparison of possible along-strike variation of the Indus-Zangbo suture by comparing the results from this survey with those obtained in 1995. Initial comparisons indicate a similar along-strike electrical conductivity structure even in fine details, suggesting that the dynamic processes are similar.

GAI.08/08A/A14-004

0930

**DEEP GEOELECTRIC MODEL OF THE TIEN SHAN LITHOSPHERE AND SOME GEODYNAMIC IMPLICATIONS**

Anatoly K. RYBIN, Vlad BATALEV, Gennady TCHELOCHKOV, Elena BATALEVA, Ilya

SAFRONOV (Scientific Station of Institute for High Temperatures-Association, RAS, Bishkek-49, 720049, Kyrgyz Republic)

The Tien Shan orogen area in Central Asia is an ideal, but not simple natural laboratory for investigating processes of lithospheric-mantle formation and evolution. Six dense submeridional profiles of magnetotelluric and magnetovariation soundings in active Central Tien Shan region and the relatively stable neighboring Kazakh Shield and Tarim Plate are integrated to provide a view of large scale structure, tectonic activity, fluid state, thermal regime and strength of the crust and upper mantle. Regional 2-D electrical structure with latitudinal EM-strike was revealed. Basic element of this model is the conductive layer in the middle-lower crust which resistivity varies from north to south from 50-100 Ohm.m to 7-15 Ohm.m. Top surface of layer is risen beneath Tien Shan orogen. Total longitudinal conductivity of this layer is equal about 300-400Sm beneath northern parts of profiles, and the maximal value of 2000Sm is reached beneath Middle Tien Shan. Major active fault zones of Tien Shan are imaged as different geoelectric structures, in first order, with low resistivity blocks (faults: Nikolaev Line, Central-Terskey, Atbashi-Inilchek) and high resistivity blocks (Talas-Fergana Fault). Comparison magnetotelluric and seismic tomographic results gives the basis to consider that simultaneous decrease of both electrical conductivity and seismic wave velocity could be explained by the small fluid content. The coincidence of water content estimated for independent geoelectric and seismic data serve as the strongest argument for the fluid nature of the conductive zone. Porosity and permeability of the upper and lower crust were estimated using the combined analysis of MT and seismic data. Three different-scale factors which are principal candidates for creating of mechanically weakened condition of rocks with high conductivity are considered. The found spatial correlation between surface deformation field, distribution of weak seismicity and geometry of the conductive layer in the Earth's crust beneath Central Tien Shan indicates that the deformation field constructed on GPS data and seismic distribution is uniform tectonic process response which is connected to deep structure of the Earth's crust obtained with the help of MT-study. Weak seismicity of researched territory occurs above a conductive layer horizon, apparently, because it's viscous nature cannot serve for accumulation of elastic stress. As continuation of geoelectric results interpretation, the regional Tien Shan geodynamical schematic model based on combined geophysical data was constructed. Crustal conductive layer, according MT, geology, seismotomography data, takes place in basement of Tarim's underthrusts at the depth 35-45 km and uplifts to the surface beneath Tien Shan. To the east from Talas-Fergana Fault this conductive layer takes place at the depths from 20 km in the southern margin to 30-35 km in the northern part, it has some inclination and loss of electrical activity beneath Kazakh platform. Conductive layer bounds earthquake hypocenters distribution. Assumption that zone of Tien Shan lower crust's conductive layer is plastic-viscous zone, which was formed, mainly, as result of pressure indentation of Tarim plate to middle-lower Tien Shan crust was done. More complicated interplay of Northern Tien Shan crust's blocks and southern edge of Kazakh plate could be noted.

GAI.08/08A/A14-005

0950

**MANTLE UPWELLING IN THE WEST OF KYUSHU ISLAND AND ANOMALIES OF TEMPORAL GEOMAGNETIC VARIATIONS**Hiroaki TOH<sup>1</sup>, Sawako HOMMA<sup>2</sup> (<sup>1</sup>Dept Earth Sciences, Toyama University, <sup>2</sup>Graduate School of Science and Technology, Toyama University)

A nation-wide dataset of induction vectors has been obtained so far (Fujiwara and Toh, 1994). The dataset consists of more than 100 land sites and around 20 seafloor sites. If the coast effect, arising from the complicated land-sea distribution and the deep seas in the vicinity of Japan, is subtracted out using non-uniform thin sheet approximation (McKirdy et al., 1985), it is clear that there exist three major induction anomalies in terms of large residual vectors. They are those around the Hokkaido Island, Central Japan and in the west of the Kyushu Island. The former two are those strongly influenced by conduction effects of Tsugaru Strait and Ishikari Sedimentary Basin (Nishida, 1976), and the well-known Central Japan Anomaly (Rikitake, 1970). The anomaly in the west of Kyushu Island has already been pointed out by previous workers (Handa et al., 1992; Shimoizumi et al., 1997) to show residual vectors with intense westward components. In this study, the possible existence of a mantle upwelling western off Kyushu Island was examined by a newly developed Genetic Algorithm (GA) inversion using the non-uniform thin-sheet approximation as a forward engine. GA inversion yielded a model that has a large conductance anomaly in East China Sea, western off Kyushu, and it successfully reproduced the westward components. The conductance anomaly ranged from southwestern edge of the Korean Peninsula to Goto Islands, Nagasaki, Japan and was found to require additional conductances of the order to 10<sup>4</sup> S.

GAI.08/08A/A14-006

1010

**MAPPING PLATE BOUNDARIES USING MT METHOD ALONG THE LONGITUDINAL VALLEY, EASTERN TAIWAN**

Chow-Son CHEN, Chien-Chih CHEN (Institute of Geophysics)

Taiwan is located on the convergent boundary between the Eurasian plate on the west and the Philippine Sea plate on the east. The Longitudinal Valley (LV) of eastern Taiwan is believed to be the suture zone between these two plates. In order to detect the subsurface structure and locate the LV fault, magnetotelluric (MT) surveys were carried out. Two units of five component wide-band MT system (Phoenix MTU5) and 2 units of two component telluric system (Phoenix MTU2E) were used to map geoelectric structures beneath the LV. All of these equipments were synchronized using GPS. More than 40 soundings were uniformly covering this valley during 2002. The 2-D apparent resistivity and phase response has been obtained from the observed data. The inversion process by using smoothness constraint obtained the resistivity structure. Both qualitative and quantitative interpretations indicate that the resistivities variations observed to be closely correlated to the change of the surface geology of the LV down, at best, to a depth of the upper 20 km. The resistivity pattern in the western part of the LV is apparently higher, in contrast with an average lower resistivity in eastern LV. This feature correlates well with the surface geology of continental crust on the west to oceanic crust on the east. Moreover, the organized 3-D plots also suggested one predominant electrical discontinuity in the LV, which agrees well with the known suture trace on the surface between the Philippine Sea and the Eurasian plates. The present 3-D configuration of the resistivity patterns also supports the geologic viewpoint that the LV is undergoing severe compression-closure action; the northern part of the valley seems to have been already closed; while the southern part remains opened.

GAI.08/08A/A14-007

1050

**RESISTIVITY STRUCTURE OF THE WESTERN PART OF THE NORTH ANATOLIAN FAULT ZONE BY MAGNETOTELLURICS METHOD**S.Bulent TANK<sup>1</sup>, Yoshimori HONKURA<sup>1</sup>, Yasuo OGAWA<sup>1</sup>, Naoto OSHIMAN<sup>2</sup>, Mustafa Kemal TUNCER<sup>3</sup>, Masaki MATSUSHIMA<sup>4</sup>, Cengiz CELIK<sup>1</sup>, Elif TOLAK<sup>1</sup> (<sup>1</sup>Tokyo Institute of Technology, <sup>2</sup>Kyoto University, <sup>3</sup>Bogazici University)

The deep crustal resistivity structure of the western part of the North Anatolian Fault (NAF) Zone has been investigated by using Magnetotelluric (MT) method, since the area is considered as one of the most seismically active zones in the Earth. Several MT profiles were set up in a region where the strike-slip fault separates into two branches. In this study, we introduce two-dimensional models of these profiles. The inversion code used in the creation of the models was developed by Ogawa and Uchida (1996). Both transverse magnetic (TM) and transverse electric (TE) modes were used for the apparent resistivity and phase data that were inverted. A remarkable similarity has been detected between the models and the surface geology. Particularly, the sediments of Izmit Bay basin and an anticline that is cut by the southern branch of the NAF, were clearly seen. Another striking result of the models was that the resistivity is low in general between the two branches of the NAF. The aftershocks of the 17th August 1999 Izmit earthquake clusters on the edge of resistive regions neighbouring the conductor regions supporting the idea of fluid involvement in the earthquake generation process.

**GAI.08/08A/A14-008 1110**  
**TRANS-EUROPEAN SUTURE ZONE (TESZ) AND ITS GEODYNAMIC INTERRELATION WITH THE VRANCEA SEISMOGENIC SLAB, ROMANIA**

Dumitru I. STANICA, Maria STANICA (Institute of Geodynamics of the Romanian Academy, 19-21, J.L.Calderon Str, R-70201, Bucharest, Romania)

Despite the vast number of previous TESZ studies, many questions about its extent and distribution in the crust and upper mantle persist. While the seismic techniques are well suited to identifying structural boundaries, they have a more difficult time quantifying physical properties, thus other complementary methods are needed. Here we present results obtained from another technique, the magnetotelluric (MT) method, which is sensitive to the bulk electrical resistivity in the lithosphere, to explain both the TESZ's interrelation with seismogenic volume and the effect of the geodynamic torsion process of the relic slab, as a possible mechanism for triggering the seismic events in the Vrancea zone. In this respect, the results based on the deep MT soundings carried out along five profiles, placed on seismic active areas and its surroundings, electromagnetic tomographic images accomplished at different levels in depth (20km, 40km, 60km, 100km, 150km and 200km), including a map drawn up at the brittle/ductile transition zone in the lower crust, as well as the MT specific parameters obtained by using the tensor impedance decomposition technique, permitted us to get the following information: (1) the TESZ on the Romanian territory is well marked by a deep lithospheric scar, delineated by a very high electrical conductivity anomaly, along the Eastern Carpathians and plays a main role in the confining clearly enough both the seismogenic relic slab and the European Platform, thus emphasizing the continental origin of the first one; (2) the progressive counterclockwise changes of the slab strike direction within the intermediate-depth interval (70-150 km), suggesting the continuous torsion process of the relic slab. We consider that this geodynamic process, mainly generated by asthenospheric currents, may be associated with the appearance of cracks inside of the slab, and, together with the dehydration-induced faulting, may represent a realistic mechanism for triggering the intermediate-depth earthquakes occurred in the Vrancea region.

**GAI.08/08A/A14-009 1130**  
**CONDUCTING LOWER CRUST BELOW EASTERN GHAT MOBILE BELT EASTERN INDIA**

Kalyan Kumar ROY<sup>1</sup>, S. DEY<sup>2</sup>, S. SRIVASTAVA<sup>3</sup>, T. DUTTA<sup>4</sup> (<sup>1</sup>Department of Geological Sciences, Jadavpur University, <sup>2</sup>Department of Geology and Geophysics, Indian Institute of Technology, <sup>3</sup>APPRO, Schlumberger Bombay Oil Field)

Magnetotelluric survey from Khorda to Jiral across rivers Mahanadi and Brahmani in Proterozoic Eastern Ghat Mobile Belt (EGMB) within the MT signal time period range of 0.25 seconds to 4096 seconds was carried out using Metronix MMS 02E. From Khorda to Athgarh the data were first inverted using 2D RRI in TE and TM mode. RRI models were chosen as the initial guesses for REBOCC (Reduced Base Occam) inversion. TE, TM, TP (Tipper mode) and TE+TM+TP (Joint inversion) mode inversions were done with improved convergence level. Joint inversion mode reveals that high grade granulite facies rocks like khondalites, charnockites and granulites do not exit in their present high resistive form below 7/8 km depth. Beyond that depth the crust is highly conducting. Information from deep seismic sounding reveals that the crust is transparent up to 7/8 km. Beyond that depth, the crust is highly reflective and ductile. High conductivity and high ductility are complementary information. Earth's crust is horizontal below EGMB for a stretch of about 100 km. Several major faults exit along the profile. Therefore collision of the EGMB with the Archaean Singhbhum craton is a possibility. Graben type of structures below Mahanadi river and presence of major faults near Brahmani river are responsible for percolation of meteoric water. That might have generated an upper crustal conductor of about 10 km thick. Khondalites, granulites and charnockites contain plenty of biotites, graphites, banded iron formations (BIFs) and magnetite quartzites. These highly conducting metallic and nonmetallic minerals getting mixed with meteoric water in this rifted terrain generated highly conducting lower crust. TE, TM and TP mode MT models show the signatures of Moho and Lithosphere-Asthenosphere boundary at depths 38km and about 100km respectively. Signature of Moho came out in this terrain because of high conductivity of the lower crust. Electrical conductivity of olivine at moHo temperature may be considerably less than those of granulite facies rocks in the lower crust. Theoretical one dimensional modeling revealed that detectibility of Moho enhances when the crust mantle structures are more or less horizontal. Estimation of the depth of the lithosphere-asthenosphere boundary by TE, TM and TP mode are more or less the same. Since vertical component of the magnetic field Hz originates in the presence of lateral heterogeneities in plane wave Electromagnetics, Hz component should be included in interpretation. Induction of tipper mode is just one of the ways to include Hz.

**GAI.08/08A/A14-010 1150**  
**LITHOSPHERIC ELECTRICAL CONDUCTIVITY STRUCTURE FROM MAGNETOTELLURIC STUDIES IN SOUTH INDIAN SHIELD REGION**

Naganjaneyulu K., Harinarayana T. (National Geophysical Research Institute, India)

Deep geoelectric structure of Eastern Dharwar Craton and Southern Granulite Terrain were accomplished with 106 magnetotelluric (MT) stations. MT stations were acquired along 6 different profiles with a total length of over 600 km. An east-west trending 200 km long profile across the Proterozoic Cuddapah basin was occupied with 21 MT stations. Towards the south, north-south trending profiles cross the major shear zones viz., Palghat Cauvery shear zone and Moyar Bhavani shear zone. The terrain boundary of the Dharwar craton towards north and Southern Granulite Terrain towards south has shown marked variation in electrical resistivity. The data were subjected to both 1-D and 2-D modeling. The Cuddapah basin boundaries towards the east and western parts of the profile were clearly demarcated in the present study with a sharp change in electrical resistivity. The basement resistivity structure also showed significant variation below the basin as compared to adjacent region.

The upper crust is high resistive (> 10000 ohm-m) on either side of the basin, while it is less resistive (1000 ohm-m) within the basin. The mid-lower crust is less resistive (500 - 2000 ohm-m) all along the profile. In Southern Granulite Terrain, Moyar Bhavani shear zone has exhibited anomalous high conductivity. The derived models are correlated with other geophysical methods viz. gravity and deep seismic sounding. For example, conductive layer at mid-lower crust showed good correlation with low velocity layer at many locations. The correlation of the anomalous geophysical properties of conductivity, density and velocity revealed the juxtaposition of crustal blocks controlled by major faults/shear zones. Lithospheric electrical conductivity structure in the south Indian shield region is compared with the other shields viz. Canadian shield, Baltic shield and discussed.

**GAI.08/08A/A14-011 1210**  
**PRECAMBRIAN INDIAN SHIELD REGION – THERMALLY UNDERESTIMATED DUE TO FLUIDS –**

Vijay K. RAO, S.N. PRASAD (National Geophysical Research Institute, CSIR)

A detailed study of seismic and electromagnetic models and features detected thereof at various depths, in the Indian shield region around Hyderabad has been carried out in conjunction with thermal characteristics, delamination process, underplating and Poisson's ratio. Studies reveal that the nature of Hyderabad crust at the crustal / sub-crustal level is either of constant composition or anisotropic medium connected with amphibolites and the velocities are close to Paleozoic crust. The nature of the crust of the Indian shield is yet to be fully explored in the backdrop of Paleozoic tectonothermal processes. Pan-African orogeny and associated tectonothermal processes have been experienced by whole of the Indian sub-continent. In order to get some tentative estimate, an attempt has been made following an empirical relationship, to deduce the age of the crust based on the modeled thickness of the crust. Poisson's ratio suggests that hornblende is the possible mineral in amphibolite rocks or amphibolite facies for the existence of mid-crustal conductor. An excess of this mineral has been found to be an indicator of lower Paleozoic crust; and is connected by differentiation process around Moho. It has also been inferred that possibly Hyderabad region was reactivated during early Paleozoic that initiated the formation of Gondwana rifts. Existing heat-flow values seem to have been underestimated because of fluid pockets in the crust due to amphibolite's dewatering in the mid-crust, restricting the migration of heat to the surface. We suggest delaminated differentiation in the lithosphere in the region has possibly resulted in crustal thinning and formation of Hale's discontinuity. This discontinuity existing in the range of 90 – 110 km matches global pattern and brings the association of fluids in sheared zones of upper mantle.

**GAI.08-Posters**  
**CONDUCTIVITY OF CRUST AND MANTLE: RELATION TO GEODYNAMICS (SEDI)**  
 Location: Site D

Tuesday, July 8 PM  
 Presiding Chairs: A.G. Jones, Y. Ogawa

**GAI.08/08P/D-001 Poster 1400-136**  
**ELECTRICAL CONDUCTIVITY STRUCTURE BENEATH EUROPE ESTIMATED BY GDS METHODS**

Takao KOYAMA<sup>1</sup>, Hisayoshi SHIMIZU<sup>2</sup>, Hisashi UTADA<sup>2</sup> (<sup>1</sup>IFREE, Japan Marine Science and Technology Center, <sup>2</sup>Earthquake Research Institute, University of Tokyo)

We had estimated a 1-D reference model of the electrical conductivity beneath the Pacific by inverting MT and GDS responses calculated from long submarine cable voltage data as well as geomagnetic data from several observatories/stations, taking into account the effect of conductivity contrast of the ocean and land in the inversion (Utada et al., 2003). This structure indicates jumps at 400 km and 650 km depths by two and a half orders of magnitude, respectively. The profile is very similar to the result of the laboratory measurement of electrical conductivity of mantle materials (Xu et al., 1998). Next question is whether this radially symmetric model can be used as a global reference. In this study we tried to examine whether the present model obtained from Pacific data is consistent with data from Europe. Hourly mean values for 1960 - 1999 at 7 geomagnetic observatories in Europe were used. The GDS responses were estimated in the periods from 5 to 100 days, in which the external source of geomagnetic field variations can be well approximated by P<sub>1</sub>-10 distribution in the geomagnetic coordinate. As the result of D+ and Occam's inversions, these responses indicate that the electrical conductivity at the lower mantle is higher by two orders of magnitude than one at the upper mantle. Sharp boundaries of the electrical conductivity in the transition zone were not detected because we used GDS responses at only long periods and they are not sensitive to jumps of the electrical conductivity around this zone. These responses are consistent with the model response from the 1-D reference model beneath the Pacific. On the other hand, the joint D+ analysis by using all the magnetic field data showed that the observed responses are inconsistent with a 1-D model. This means significant 3-D heterogeneity may exist beneath Europe.

**GAI.08/08P/D-002 Poster 1400-137**  
**CONDUCTIVITY AT CRUSTAL AND UPPER MANTLE DEPTHS: GLOBAL, CONTINENTS, EUROPE**

Oldrich PRAUS, Vaclav CERV, Svetlana KOVACKOVA, Josef PEK, Jana PECOVA (Geoelectricity, Geophysical Institute, Acad. Aci.)

To obtain resistivity estimates at global and continental scales, specifically for the European region, we have started new analysis of geomagnetic long period variation data obtained from NGDC in Boulder. Analysis that is being performed recently, involves three large blocks of data: (i) Hourly means of XYZ components in individual months of minimum solar activity year 1965 with no gaps in data were at our disposal for 24 observatories distributed mainly in Europe and North America. On interpolating data with only isolated missing hourly means, we increased the number of observatories to the total of 43. Removing five D-days for each month, we calculated monthly mean Sq and estimated subsequently 6 Fourier harmonic components. (ii) As the monthly completeness of the data reduces the number of stations and global coverage, we used special individual Q-days selected and recommended by Schmucker (GJL, 1999). Estimates of 6 time harmonic components were obtained at a number of observatories increased to about 80 - 85. This analysis has been completed for blocks of Q-days in October and May 1965. (iii) The time series of three-year 1096 daily means of the XYZ geomagnetic components for interval of 1958, 59, 60 (maximum activity)

and 1963,64,65 (minimum activity) at 41-43 world observatories were processed by FFT and power spectral analysis. Among spectral peaks for certain bands of periods between 8 and about 50 days, the dominating were those corresponding to 27-day variation and its harmonics at 13 and 9 days. Using the results of analyses in form of the real or complex vectors as input for the spherical harmonic analysis, we obtained complex coefficients  $X_{jm}$  and  $Z_{jm}$ , separated the internal/external fields and transformed them to the substitute perfect conductor with its corresponding depth. The estimates are summed up in a graph. Magnetotelluric sounding data recorded at the observatory of Budkov (49.08° N; 14.02° E) provided us with estimates of the apparent resistivity distribution in the crust and uppermost mantle of the Bohemian Massif (BM) representing a resistive consolidated block of the Variscan branch of the European Hercynides. Independent estimates of electrical resistivity at mid-mantle depths were provided by Schultz & Larsen's (1987) complex inductive scale lengths (ISL) for previous observatory Pruhonice (49.99° N; 14.55° E) (closed in 1972 for industrial noise conditions). We present estimate of both observatories in a joint curve representing the resistivity distribution at the mid-mantle depths of the BM. The results for long periods suggest resistivities approaching the lower limit of the deep geomagnetic sounding estimates and they also fit with reasonable scatter to resistivity ranges at several other European observatories. Acknowledgement: The results were obtained within the project No. 205/03/1001 supported by the Grant Agency of the Czech Republic.

**GAI.08/08P/D-003** Poster **1400-138**

**EMTESZ - ELECTROMAGNETIC PROBING OF THE TRANS EUROPEAN SUTURE ZONE**

Vaclav CERV<sup>1</sup>, Josef PEK<sup>1</sup>, Maxim SMIRNOV<sup>2</sup>, Tomasz ERNST<sup>3</sup>, Vladimír SEMENOV<sup>4</sup> (Geophysical Institute AS CR, <sup>2</sup>Uppsala University, <sup>3</sup>Institute of Geophysics PAS)

The Trans European Suture Zone (TESZ) marks the division of the European continent in a Phanerozoic part to the west and a Proterozoic part to the East. The project EMTESZ is directed towards a magnetotelluric study of this zone along several profiles preferentially coinciding with recent refraction seismic lines in Poland. The studies aim at inferring the main features of the resistivity structure of the lithosphere-asthenosphere system by using modern broad band magnetotelluric array measurements. We present the results of pilot measurements in 2001 and 2002 from the northwestern part of the TESZ in Pomerania. We will focus on the quality of earth response functions with respect to man/made noise known to create considerable problems for MT soundings in Poland. Several long period magnetotelluric measurements together with magnetovariational responses from near observatory Belsk give us possibility to estimate the regional geoelectrical structure of the upper part of the mantle. A preliminary model of the geoelectric structure of the crust across the TESZ will be presented.

**GAI.08/08P/D-004** Poster **1400-139**

**INVERSION MODELS OF THE CONDUCTANCE IN THE THIN SHEET ON THE EASTERN MARGIN OF THE EUROPEAN HERCYNIDES**

Svetlana KOVACIKOVA, Vaclav CERV, Oldrich PRAUS (Geophysical Institute, Academy of Science, Czech Rep.)

The results of inversion modeling of conductance distribution on the contact of the Bohemian Massif with the West Carpathians are presented. The region of interest represents a contact zone of the Paleozoic Hercynian and Tertiary Carpathian orogenic systems. Their marginal zones are characterized by significant contrasts of the electrical conductivity in the middle and lower crust indicated by the induction vectors distribution. With respect to the period range of the recorded data (1000 - 6000) approximation with the unimodal thin sheet at a specified depth both in free space and in the medium with defined conductivity is used. Our inversion algorithm is based on minimization of a parametric functional, that sums the squared norm of the data residuals and stabilizing functional, and employs conjugate gradient optimization. The minimum gradient support focusing is used for generation of focused conductance images with respect to specific character of the geomagnetic induction anomalies, which are connected with sharp tectonic boundaries. Model transfer functions are calculated in original profile points.

**GAI.08/08P/D-005** Poster **1400-140**

**MAGNETOTELLURIC SOUNDING IN THE NAIPEER COMPLEX, EAST ANTARCTICA**

Akira YAMAZAKI<sup>1</sup>, Peter DOLINSKY<sup>2</sup>, Minoru FUNAKI<sup>1</sup>, Naoto ISHIKAWA<sup>4</sup>, Yasuo OGAWA<sup>4</sup> (<sup>1</sup>Seismology and Volcanology Research Department, Meteorological Research Institute, <sup>2</sup>Hurbanovo Magnetic Observatory, Geophysical Institute of Slovak Academy of Sciences, <sup>3</sup>National Institute of Polar Research, <sup>4</sup>Graduate School of Human and Environmental Studies, Kyoto University, <sup>5</sup>Volcanic Fluid Research Center, Tokyo Institute of Technology)

The Napier Complex in Enderby Land, East Antarctica, is one of the oldest complexes in the world, as reported 3930 Ma. The 42nd Japanese Antarctic Research Expedition (JARE42, 2000-2001) carried out a magnetotelluric (MT) survey in the Mt. Riiser-Larsen Area, located on the eastern coastline of Amundsen Bay, East Antarctica, in order to investigate the resistivity structure of the Napier Complex. It was a first trial as JARE to perform a full-scale MT survey in Antarctica. The wide-band MT system (Phoenix Ltd. MTU-5), which frequency range is 0.0055 Hz to 320 Hz, was used for the survey. The MT measurement was carried out at six stations around Richardson Lake. Among these, one station was on the middle of frozen Richardson Lake, and others were on moraine deposits. The ranges of the survey area were about 5km east and west, and 3km north and south. The acquired MT data were influenced by non-uniform source field contributions from the auroral electrojet. However, since impedance tensor and transfer function were obtained stably within the period of 100 s, we thought the influence is small and applied a usual MT analyses within that period. The survey area is surrounded by complicated coastline. There is Adams Fjord to the south and Amundsen Bay to the west. In order to estimate the coastline effect, we performed 3-D MT forward calculation by modeling the depth of surrounding sea. From this estimation, it is found that the observed induction arrows can be explained by coast effect roughly except 0.1 Hz to 1 Hz arrows which points to west strongly and the impedance tensors are not influenced so seriously within the period of 100 s. These MT sounding curves obtained at each station are roughly the same. The general features of the obtained one dimensional resistivity structure are high resistivity layer from surface to 8km depth, relatively low resistivity layer 8-28km depth and high resistivity layer below 28km depth. This feature of the resistivity structure may be similar to that of the other continental shields.

**GAI.08/08P/D-006** Poster **1400-141**

**THE CONDUCTIVITY STRUCTURE IN THE BACK-ARC REGION BENEATH JILIN AND LIAONING PROVINCE, NE CHINA**

Ji TANG<sup>1</sup>, Makoto UYESHIMA<sup>1</sup>, Hisashi UTADA<sup>1</sup>, Guozhe ZHAO<sup>2</sup>, Masahiro ICHIKI<sup>1</sup>, Minzhi MA<sup>3</sup>, Yuanchao LIU<sup>3</sup>, Xiuqing JIANG<sup>3</sup> (<sup>1</sup>Earthquake Research Institute, University of Tokyo, Japan, <sup>2</sup>Institute of Geology, China Seismological Bureau, China, <sup>3</sup>IFREE, JAMSTEC, Japan, <sup>4</sup>Seismological

Bureau of Jilin Province, China, <sup>5</sup>Seismological Bureau of Liaoning Province, China)

Long-baseline magnetotelluric (MT) and geomagnetic depth sounding (GDS) experiments have been conducted for studying the upper mantle electrical conductivity structure and understanding the geodynamic process of the Pacific back-arc beneath Jilin and Liaoning province, NE China since 1998. 9 sites MT responses were determined up to a period of 10<sup>5</sup> s by using telephone lines with baseline lengths of 10-40 km at 6 stations. GDS responses were obtained for the longer period ranges (up to 10<sup>6</sup>-10<sup>7</sup> s) at Changchun, Jilin province. RRRMT data processing method was employed for estimating both MT and GDS responses. Static shifts of MT responses were estimated and corrected with the aid of the rho+ inversion scheme which combines MT and GDS responses by assuming P<sub>1</sub> source for the GDS responses. The responses were then inverted by using the OCCAM inversion to determine a smooth 1-D conductivity structure. The conductivity models display several stable boundaries at the depth of about 20 - 30km, 100km, 400 km and 600 km which correspond to lower crustal high conductivity layer, the bottom of lithosphere and the transition zone between upper and lower mantle respectively. The electrical conductivity structures between southern and northern Changchun are different, especially, at the transition zone of the mantle. In the northern of Changchun, the transition zone is several times more conductive than that of the southern area. However the conductivity of the mantle transition zone beneath the investigation region is several times to one order more conductive than those of other tectonic settings obtained by Neal et al., 2000. One possibility is that the subsurface conductivity structure reflect existence or non-existence of the stagnant slab in NE China. Beneath north Changchun area, high conductivity of transition zone may correspond to the presence of a stagnant slab with fluid. \*: Ji Tang has backed to Institute of Geology, China Seismological Bureau, China, since may 30,2003 e-mail:jitang@163bj.com

**GAI.08/08P/D-007** Poster **1400-142**

**MAGNETOTELLURIC OBSERVATIONS IN THE WESTERN PART OF THE NORTH ANATOLIAN FAULT ZONE**

S. Bulent TANK<sup>1</sup>, Yoshimori HONKURA<sup>1</sup>, Yasuo OGAWA<sup>1</sup>, Naoto OSHIMAN<sup>2</sup>, M. Kemal TUNCER<sup>3</sup>, Masaki MATSUSHIMA<sup>4</sup>, Cengiz CELIK<sup>5</sup>, Elif TOLAK<sup>6</sup> (<sup>1</sup>Tokyo Institute of Technology, <sup>2</sup>Kyoto University, <sup>3</sup>Bogazici University)

Magnetotelluric (MT) surveys were carried out to investigate the deep resistivity structure in the western part of the North Anatolian Fault Zone (NAFZ), which was subject to a major rupture during the 17th August 1999, Izmit Earthquake. The geology of the study area is complex since it is positioned between the two branches of the North Anatolian Fault. MT is preferred as a method for investigating the crustal structure of the fault zone, because it is an efficient method for detecting the presence of fluid in a media by monitoring the resistivity. Recent observations state that there is high correlation between the earthquakes and fluids. Two-dimensional inversions were performed in four profiles by using the code developed by Ogawa and Uchida (1996). The frequency range for the inversions is between 320 Hz and 0.001 Hz, which is enough to resolve upper-crust structures. The results show that the area is getting more conductive approaching west. The aftershocks tend to occur on the highly resistive areas around the mainshock hypocenter. On the western profiles, on the other hand, aftershocks are occurring in relatively conductive areas. This property of the fault may be related to the heterogeneity of the fault. Here, in this poster presentation we are showing two-dimensional inversion models of two profiles.

**GAI.08/08P/D-008** Poster **1400-143**

**MANTLE CONDUCTIVITY STRUCTURE BELOW THE MARIANA ISLAND ARC**

Tada-nori GOTO<sup>1</sup>, Nobukazu SEAMA<sup>2</sup>, Masahiro ICHIKI<sup>1</sup>, Kiyoshi BABA<sup>1</sup>, Katrin SCHWALENBERG<sup>3</sup>, Noriko TADA<sup>4</sup>, Hisanori IWAMOTO<sup>4</sup>, Hisashi UTADA<sup>5</sup>, Kiyoshi SUYEHIRO<sup>6</sup>, Hiroaki TOH<sup>6</sup> (Japan Marine Science and Technology Center, <sup>2</sup>Research Ctr Inland Seas, Kobe Univ., <sup>3</sup>Univ. of Toronto, <sup>4</sup>Earth and Planetary Sci., Kobe Univ., <sup>5</sup>Earthquake Research Inst., Univ. of Tokyo, <sup>6</sup>Dept. of Earth Sciences, Toyama Univ.)

The Mariana Islands are located in the eastern part of the Philippine Sea. Typical island arc tectonics and backarc spreading characterize the region. Mantle upwelling zones exist below the Mariana Islands which form the recent magmatic arc, below the Mariana Trough in the backarc, and below the serpentine seamounts in the forearc. These upwelling zones are probably related to various tectonic features in the Mariana region. However, the deeper structure in this region is not clear, yet. Here, we make a preliminary report of a seafloor electromagnetic experiment in the Mariana region with special attention to the mantle conductivity below the Mariana island arc. The electrical conductivity of the upper mantle is known to be sensitive to temperature variation, the degree of partial melting, and/or the presence of water. Ten Ocean Bottom Electromagnetic instruments (OBEMs) were deployed in the Mariana region in October 2001 to image mantle upwelling zones and dehydration processes in context with the subducting plate. In 2002, five instruments were retrieved. Here, we present the results obtained from two OBEM sites in the vicinity of the Mariana Islands; one located near the arc axis and the other at the eastern edge of the Mariana Trough. At both sites, high quality EM data were recorded for about six months. We used the magnetotelluric (MT) sounding method and a 2-D inversion technique developed by Goto et al. (2003) to derive the conductivity structure below the Mariana island arc. The best fitting model shows on one hand a highly conductive mantle below the Mariana Trough (about 70km in depth). On the other hand, the mantle conductivity below the Mariana Islands is two orders of magnitude less than below the Mariana Trough. This abrupt change of conductivity implies that the conductive mantle wedge is not related to temperature, but to the presence of water in the mantle. We think that this possibly affects the backarc opening procedure in the Mariana Trough. The remaining OBEM sites are located in the Mariana Trough and will be useful to discuss the mantle conductivity structure there in more detail. Also, an international seismological survey has been started in 2001, and an international seafloor electromagnetic experiment will be conducted in 2005-2006. All these additional information will help us to infer the properties of the mantle wedge more clearly.

**GAI.08/08P/D-009** Poster **1400-144**

**ABOUT THE PHASE DIFFERENCE OF VERTICAL COMPONENT OF SQ FIELD IN THE CENTRAL JAPAN**

Masahiro ICHIKI<sup>1</sup>, Hisashi UTADA<sup>2</sup> (<sup>1</sup>IFREE, JAMSTEC, <sup>2</sup>ERI, University of Tokyo)

Rikitake et al. (1956) analyzed magnetic variation in Japan during a geomagnetically quiet period between 1952 and 1955, and pointed out that there is a phase progress in the vertical component of Sq field at Kakioka geomagnetic observatory (KAK) relative to those at other observatories. From this observation, they proposed a qualitative model in which the phase shift can be attributed to anomalous distribution of the mantle electrical conductivity. However, three-dimensional (3-D) numerical modeling has been realized and Kuvshinov et al. (1999) showed that this phase shift of Sq field variations at KAK can be explained by the induction in the oceans, where Schmucker(1985)'s 1-D conductivity model was used as the background. On the other hand, we analyzed the Sq field variations by the different data

processing. Using hourly values of 3 components of magnetic field in 1964 and 65, the transfer functions of each component of magnetic field at each observation site were calculated to a reference site. First, we reexamined the phase responses of transfer function for KAK and other observation sites in Japan. Irkutsk observatory in Russia was chosen as a reference site. At period of 24 hours, the phase response of vertical component at KAK tends to progress indeed and that of Memambetsu observatory also indicates the same tendency. These results consist with the study of Kuvshinov et al.(1999). However that of Kanoya observatory in Japan seems not to be anomalous behaviour, although it locates close to a coast. With regard to the influence from the tides, we calculated power spectrum density. The superimposed amplitude of P1, S1 and K1 is dominant relative to the amplitude of M1 and O1 for the vertical component at KAK.

**GAI.10**  
**ELECTROMAGNETIC INVERSION MODELING**  
 Location: Site A, Room 11

**Wednesday, July 9 AM**  
 Presiding Chairs: S.K. Verma, M.S. Zhdanov

**GAI.10/09A/A11-001** **0900**

**NEW FAST METHOD OF THREE-DIMENSIONAL INVERSION OF MAGNETOTELLURIC DATA**

Michael S. ZHDANOV, Nikolay G. GOLUBEV (Department of Geology and Geophysics, University of Utah)

Interpretation of magnetotelluric data over inhomogeneous geological structures is still a challenging problem in geophysical exploration. We have developed a rapid 3-D MT inversion method and a computer code based on full nonlinear conjugate gradient inversion and quasi-analytical (QA) approximation for forward modeling solution (Zhdanov and Hursan, 2000; Zhdanov, 2002). Application of the QA approximation in forward modeling and Fréchet derivative computations speeds up the calculation dramatically. However, in order to control the accuracy of the inversion, our method allows application of the rigorous forward modeling in the intermediate steps of the inversion procedure and for the final inverse model. The main distinguishing feature of this algorithm is application of the special stabilizing functionals that allow construction of both smooth images of the underground geoelectrical structures and models with sharp geoelectrical boundaries. The 3-D magnetotelluric inversion code has been carefully tested on synthetic models and applied to the practical MT data collected in an area with complex geology. The rapid inversion of the array magnetotelluric data (observed with the hundreds of multi-frequencies observation stations) can be done within a few minutes on a PC to generate the full 3-D image of subsurface formations on a large grid with the tens of thousands cells. The new fast 3-D MT inversion technique has been applied to three-dimensional MT data collected in the areas with the complex geology. We demonstrate that for such complex geoelectrical models the 3-D inversion can provide a much more adequate interpretation of the array MT data than conventional 2-D inversion.

**GAI.10/09A/A11-002** **0915**

**MAGNETOTELLURIC 2-D AND 3-D INVERSIONS USING MARKOV CHAIN MONTE CARLO (MCMC) :PRELIMINARY RESULTS**

Hendra GRANDIS<sup>1</sup>, Toru MOGF, Elena Y. FOMENKO<sup>2</sup> (<sup>1</sup>Dept. Geophysics and Meteorology - ITB, <sup>2</sup>Institute of Seismology and Volcanology, Hokkaido University, <sup>3</sup>Computer Science Center of Moscow State University)

A fully non-linear inversion scheme based on bayesian Markov Chain Monte Carlo (MCMC) algorithm has been developed for magnetotelluric (MT) 1-D and thin-sheet models. Application for both synthetic and field data from various scale showed satisfying results with reference to synthetic models and local geology. The paper will describe an attempt to apply the MT inversion algorithm to 2-D and 3-D cases. We incorporate existing 2-D and 3-D MT forward modelling algorithms to our inversion method. The 2-D and 3-D forward modelling are solved using finite-element and staggered grid finite-difference methods respectively. Tests using simple conductivity models showed that there are problems remain to be studied further : (i) equivalence or ambiguity, (ii) sensitivity or resolution in terms of "a priori" conductivity values. Additionally, efficient and faster forward modelling algorithm is needed since MCMC based inversion is a slow and computer intensive method. Partially resolving the forward modelling due to conductivity change of only one grid or cell might improve the algorithm. Nevertheless, the fact that the algorithm showed decreasing error or misfit is encouraging.

**GAI.10/09A/A11-003** **0930**

**PARAMETERIZATION AND FUNDAMENTAL MODELS FOR EM INVERSION**

Igor Ivanovich ROKITYANSKY (Institute of magnetism)

Inversion of any observational data into new knowledge about object under study implies three main stages: parameterization, approximation and optimization. Complex real object, the Earth, possesses infinite number of details, so its precise description is possible only by infinite quantity of numerical parameters. Observation data at any epoch are limited, contain uncertainty and therefore can define only limited number of parameters with limited accuracy. The rest remains undefined and can be selected arbitrarily. Parameterization aims to select the model of real object, adequate to the data in hand and all a-priori information. Parameterization is not formalized, it results from the guess-work of the investigator guided by knowledge of physical regularities, as well as by experience and intuition. The following stages of interpretation (approximation and optimization) are formalized and yield the result (model parameters) in computational regime, but they act only within framework of the parameterization chosen. If parameterization turns out to be unsuccessful, the computed model strongly differs from the real object. Therefore, the parameterization is of primary importance. Catalog of fundamental models (FM) is a useful tool to improve parameterization and therefore the interpretation of real data. FM is a simplified and generalized model of a set of real geoelectric structures, characterized by specific behavior of observed response functions (impedance, magnetic parameters, etc.) to be distinguishable from any other FM. The beginning of the catalog can be as follows: 1) 1D models; 2) 2-D models: 2a) Compact anomalies that are characterized by identical anomalous magnetic fields at long periods under the same longitudinal conductance, 2b) Edge of very wide conductor (e.g. sea, contacts), 2c) Transverse transparent anomalies, which are not seen in B-polarization but clearly seen in E-polarization, 2d) Transverse shunting anomalies when B-polarization apparent resistivity runs at long periods well below E-polarization; 3) Quasi-2D models: 3a)

Elongated anomalies of varying conductance that can be recognized by comparative analysis of MVP and MTS data even on a profile; 4) Local 3D on 1D background (local scatterers, not resolved spatially by data, are not included in model and considered as geological noise), 5) Local 3D on 2D background. As an example, the modeling results for S-form local structure with 2D continuation are presented, which can be used for 3D inversion. The knowledge of fundamental models helps to make right natural decomposition of inverse problem for a complex geoelectrical structure into a set of more simple problems. The outlined ideology is applied to real data.

**GAI.10/09A/A11-004** **0945**

**INVERSION OF AMT DATA FOR KIMBERLITE EXPLORATION**

Alexander K. SARAIEV<sup>1</sup>, Mikhail I. PERTEL<sup>1</sup>, Mikhail N. GARAT<sup>2</sup>, Alexander V. MANAKOV<sup>2</sup>, Yuri G. PODMOGOV<sup>2</sup> (<sup>1</sup>St. Petersburg State University, <sup>2</sup>ALROSA Co Ltd.)

Kimberlite fields are connected with linear tectonic zones, which appear as series of close on direction deep kimberlite controlling faults. These faults are filled usually by dolerite dikes and can be easily mapped using magnetic methods. Kimberlite pipes inside the kimberlite fields are located along faults of another type - kimberlite hosting, but mapping of them is more difficult, because they are not filled by dikes and do not create significant magnetic anomalies. These faults are appeared weakly at the Earth surface and only in depths more than of 400-600 m they are breccial zones. Kimberlite pipes have usually a low resistivity contrast in comparison with the hosting rocks. Overlying horizons have significant heterogeneity and include local conductive objects. These features of the kimberlite hosting faults and kimberlite pipes require the increased depth of investigations, high accuracy of measurements and reliability of data interpretation of used electrical prospecting methods. The audiomagnetotelluric soundings (AMTS) method has a good perspective for kimberlite exploration. A primary field in the AMTS has simple structure (plane wave) and using this model we can ensure the authentic data interpretation. Tensor measurements provide the obtaining of reliable results in heterogeneous media. The depth of investigation of the AMTS in the kimberlite fields makes usually from 50 to 1000 m. The surveys using the AMTS method with ACF-4 instrument were carried out for diamond prospecting in Yakutia and Archangelsk regions (10 pipes were investigated). Different character of appearance of the faults depending on the component of impedance tensor was shown. Both 1-D and 2-D inversions were used at the data interpretation. It was found that the upper parts of the faults in interval of frozen rocks from 0 to 300-400 m have a complicated structure. The dipper parts of them in interval from 500 to 1000 m correspond to breccial zones filled by mineralized water. They have the low resistivity of 2-6 Ohmm and can be confidently mapped on the AMTS data. When the search of the kimberlite pipes the low resistive parts of the pipes (2-10 Ohmm) were observed in the depths from 300 to 600 m. These intervals of pipes have the most noticeable resistivity contrast in comparison with hosting rocks. The frozen rocks at the pipes have the significant variability of thickness. This feature can be used for the search of sites, perspective for localization of kimberlite pipes or groups of the pipes. The surveys show the big informative value of studying of kimberlite hosting rocks in interval from 300 to 1000 m and the possibility to solve the problem of kimberlite exploration using the AMTS method.

**GAI.10/09A/A11-005** **1000**

**GLOBAL OPTIMIZATION OF MAGNETOTELLURIC FIELD DATA COLLECTED ACROSS THE ARCHAEOAN PROTEROZOIC CONTACT IN THE EASTERN INDIA USING FINITE ELEMENT FORWARD MODEL WITH ADVANCED LEVEL ELEMENTS**

Kalyan Kumar ROY<sup>1</sup>, N.S.R. MURTHY<sup>2</sup> (<sup>1</sup>Department of Geological Sciences, Jadavpur University, <sup>2</sup>Infosys Ltd.)

Two dimensional magnetotelluric forward modeling was done applying finite element method using eight noded isoparametric elements and Galerkin's weights. The source code written in C was used as a forward model to invert the magnetotelluric field data collected across the Archaean-Proterozoic contact near the northern margin of the Eastern Ghat Mobile Belt and the southern boundary of the Singhbhum Archaean craton. Genetic Algorithm(GA) and Very Fast Simulated Annealing(VFSA) was used for inversion of field data.25 pairs of initial models and 15 bit string for a single element are observed to be sufficient to handle two dimensional geoelectromagnetic problems with desired level of convergence. More than 250 generations of populations in GA and more than ten thousand iterations in VFSA were necessary to get complete convergence. Highly conducting crushed contact of the granulite facies rocks in the south and green schist facies rocks in the north could be mapped near Kamakshyanagar, Dt.Dhenkanol, Orissa, India. Plots of telluric vectors and induction arrows supported this observation.

**GAI.10/09A/A11-006** **1015**

**INVERSION OF MAGNETOTELLURIC DATA ALONG REGIONAL PROFILE IN THE NORTH-EAST OF RUSSIA**

Pavel Yu PUSHKAREV<sup>1</sup>, Mark N. BERDICHEVSKY<sup>1</sup>, Alexander V. LIPILIN<sup>2</sup>, Leonid L. FELDMAN<sup>3</sup>, Robert G. BERZIN<sup>4</sup>, Arsen K. SULEIMANOV<sup>4</sup>, Andrei G. YAKOVLEV<sup>5</sup>, Denis V. YAKOVLEV<sup>1</sup>, Elena V. ANDREEVA<sup>3</sup>, Igor M. SBORSHIKOV<sup>3</sup> (<sup>1</sup>Geophysical Department, Moscow University, <sup>2</sup>Ministry of Natural Resources, Moscow, Russia, <sup>3</sup>Department of Ministry of Natural Resources, Magadan, Russia, <sup>4</sup>Spetsgeofizika State Enterprise, Moscow Region, Russia, <sup>5</sup>North-West Limited, Moscow, Russia)

In order to study the deep geological structure of vast oil-producing and ore-bearing areas of Russia, complex geophysical surveys (including seismic, electromagnetic, gravimetric, magnetometric and geochemical investigations) are now conducted along a number of regional profiles. In particular, such geophysical surveys have been fulfilled along the profile, which crosses Magadan and Chukotka regions in the North-East of Russia. During 2001 and 2002 the southern part of the profile (830 km long) was studied. Three modifications of magnetotelluric (MT) method were applied here. Audio-frequency MT soundings were performed with a relatively small spacing between sites (1 km) to provide detailed information about near-surface structure. Standard (middle-range) and deep (low-range) MT soundings allowed to study the Earth's crust and upper mantle. They were fulfilled using larger spacings (3 and 12 km, respectively). Magnetovariational (MV) soundings played a key role in studying deep conductive zones. Phoenix Geophysics MTU-5 and Russian-made CES-M equipment were used. The remote reference data processing was carried out. The analysis of impedance tensor and tipper matrix revealed rather strong horizontal inhomogeneity of the medium and helped to choose the strike directions. In order to reduce near-surface distortions, the static shift correction of the apparent resistivity curves was performed. To obtain the geoelectric cross-section along the profile, a smoothed-structure 2D inversion of MT data using Geosystem WinGeoLink software was used. To verify the anomalies revealed, a number of inversions were performed using different data subsets and inversion parameters. 3D modeling was also accomplished to study the distortion effects caused by resistivity variations along the regional strike. The constructed geoelectric cross-section was considered together with seismic results, obtained at the same profile. Inside the Okhotsko-Chukotsky volcanic belt (near the coast of the Okhotskoye Sea) several deep

conductive zones have been discovered. It is remarkable that the seismic Moho boundary is not clearly seen in these zones. Therefore the possible explanation of the nature of these zones is that they are permeable and contain rising flows of mantle fluids. This information is important for the mineral deposits prognosis. Further to the North-East the profile crosses the Yano-Kolymskaya folded system. Here some shallower conductive zones have been outlined. They are associated with the increase of sediments thickness and tectonic activation.

**GAI.10/09A/A11-007****1100****IMPROVEMENT IN TARGET RESOLUTION BY JOINT INVERSION OF MT, SEISMIC, AND DC DATA**

Saurabh Kumar VERMA, Ajay MANGLIK (National Geophysical Research Institute, Hyderabad)

A numerical scheme is developed to jointly invert the seismic, MT, and DC electric data. The algorithm has the option of performing individual or joint inversion of any combination of: seismic refraction and reflection, amplitude and phase of MT fields, and DC resistivity data for any electrode configuration. For difficult targets like sandwiched low velocity layer or a thin resistive layer below a conducting overburden, examples are presented to demonstrate that the ambiguity in interpretation is significantly reduced in case of joint inversion. The range of possible solutions is increasingly constrained as more number of data sets is included. This is found to be valid even for noisy data with some vital data points missing. Efficacy of the algorithm is also demonstrated on data relating to: 1) detection of low velocity sediments below a thick layer (~ 1 km) of high velocity basalts, and 2) location of sea water - fresh water interface at shallow depths (< 50 m) in coastal areas.

**GAI.10/09A/A11-008****1115****APPROXIMATE JOINT INVERSION OF DC GEOELECTRIC AND REFRACTION SEISMIC DATA**Tamas ORMOS<sup>1</sup>, Michael DOBROKA<sup>1</sup>, Akos GYULAI<sup>1</sup>, Lothar DRESEN<sup>2</sup> (<sup>1</sup>Department of Geophysics, University of Miskolc, <sup>2</sup>Institute of Geology, Mineralogy and Geophysics, Ruhr University, Bochum)

One of the most important possibilities to reduce or abolish the uncertainty of measured VES data, occurring in a single inversion, is known as the joint inversion method. Many joint inversion schemes use 1D forward modelling in the integrated interpretation of various geophysical data. In extending the joint inversion approach to the investigation of 2D structures the discretization of the model parameters and the appropriate choice of the forward modelling procedure play very important role. This problem is closely related to the forward modelling algorithm, used in the inversion procedure. In the paper a seismic-geoelectric joint inversion method is proposed for the investigation of two dimensional near-surface geological structures. Assuming the model being layer-wise laterally inhomogeneous with curved boundaries, a quick ray tracing algorithm is used for the calculation of refraction seismic traveltimes data (Ormos, 2002). For the above mentioned reasons we use in the geoelectric forward modeling the locally 1D approximation with model parameters given by the Generalized Series Expansion method. This means, that in calculating the apparent resistivities - at the  $x_j$  measurement point - the (weighted) integral mean of the laterally varying thickness- and resistivity functions are used as local (quasi 1D) model parameters (Kis, 2001). The boundary surfaces and resistivities are written in the form of series expansion, the inversion algorithms are formulated for the expansion coefficients and the petrophysical parameters, as unknowns. The joint inversion method is tested using both synthetic and field data. The numerical examples show, that the method is quick and stable. It is shown, that relative to the independent geoelectric and refraction seismic inversion procedures, the joint gives better parameter estimation. The joint inversion of geoelectric and refraction seismic field data gives highly reliable and acceptable results demonstrating the validity of the (GSE) approximation used in the geoelectric forward modelling procedure. Ormos, T., 2002. Inversion of refracted travel-times for near-surface investigations, D-25, EAGE 64th Conference and Exhibition - Florence, Italy, 27-30 May, 2002. Kis, M., 2002. Generalized Series Expansion (GSE) used in DC geoelectric - seismic joint inversion. J. Applied Geophysics, 50, 401-416

**GAI.10/09A/A11-009****1130****JOINT INVERSION OF GEOELECTRIC- AND SURFACE WAVE SEISMIC DISPERSION DATA**

Michael DOBROKA (Department of Geophysics, University of Miskolc)

In the field of engineering and environmental geophysics, near-surface structures are traditionally explored by seismic and geoelectric methods. In order to overcome the ambiguity and non-uniqueness problems inherent in the independent inversion algorithms joint inversion methods are often applied. It was proved by various investigators, that - compared to independent inversion - the joint inversion methods give better parameter estimation in a more stable iterative procedure. In the paper the validity of this statement is extended to the joint inversion of surface wave dispersion data (group velocities) and DC geoelectric apparent resistivities. The laterally varying model parameters (thickness, body wave velocities and specific resistivity) are discretized using series expansion in terms of appropriately chosen base functions. The seismic guided waves are assumed to propagate along the dip direction of the 2D model while the and geoelectric measurement arrays are assumed to be parallel with the strike direction. The inversion algorithm proposed in this paper uses accurate forward modelling procedure in the calculation of the frequency dependent group velocity of the guided waves (1st order WKB approximation), while in the calculation of theoretical apparent resistivity data 1D approximation is used with the local value of the discretized thickness and, resistivity functions. The inversion algorithm is tested in the special case when the petrophysical parameters are constant and the thicknesses are functions of the lateral coordinates. In the numerical tests geoelectric data sets calculated by means of an FD method are used, while the dispersion data are calculated in the WKB approximation. Two inversion methods are used throughout the paper minimizing the L2 and the L1 norm of the vector of difference between the measured and calculated data, respectively. In the later case the method of Iteratively Reweighted Least Squares (IRLS) is applied. The inversion results are qualified in both the data and model spaces. A comparison is shown between the individual and joint inversion and also between the L2 and L1 inversion methods. It is proved, that the approximate joint inversion procedure is stable and accurate. The non-uniqueness and internal ambiguity problems can sufficiently be reduced by the use of seismic-geoelectric joint inversion. The joint inversion algorithms give much better parameter estimation in comparison with the independent evaluation (inversion) of the data sets measured at various measurement arrays.

**GAI.10/09A/A11-010****1145****SOLUTIONS OF THE INHERENT PROBLEM OF THE EQUIVALENCE IN DIRECT CURRENT RESISTIVITY AND ELECTROMAGNETIC METHODS THROUGH GLOBAL OPTIMIZATION AND JOINT INVERSION BY SUCCESSIVE REFINEMENT OF MODEL SPACE**Shashi Prakash SHARMA<sup>1</sup>, Saurabh Kumar VERMA<sup>2</sup> (<sup>1</sup>Department of Geology and Geophysics, IIT, Kharagpur, 721302, India, <sup>2</sup>National Geophysical Research Institute, Uppal Road, Hyderabad, 721302, India)

The problem of equivalence for the DC resistivity and electromagnetic methods for a thin resistive and conducting layer is well known. Attempts have been made in the past to resolve the problem of equivalence through joint inversion. However, it still remains an unresolved problem in electrical and EM geophysics. In the present study, effort is made to reduce the non-uniqueness due to equivalence using global optimization and joint inversion by successive refinement of the model space. A number of solutions derived using very fast simulated annealing (VFSA) global inversion that fit the observation equally well, follow the physical principle and show a definite trend. Model data from simply defined mean model of various VFSA solutions does not necessarily fit the observations. Study of multiple models satisfying equivalence show a definite trend. This trend is  $\rho_z/h_z = \text{constant}$  and  $\rho_z \cdot x_h = \text{constant}$  for conductive and resistive layer, respectively. Former representing a straight line while latter one represents rotated branch of a hyperbola. Logarithmic transformations of both represent straight lines such that mean model fit the observation always. Therefore, the mean model must be defined according to the trend of the non-uniqueness. The mean model defined by multiple VFSA solutions shows extremely large uncertainty (almost 100%) in the final solution after inversion of individual data sets. Uncertainty associated with the intermediate resistive and conducting layers is also very high after global optimization and joint inversion. In order to reduce the large uncertainty associated with the intermediate layer, the global optimization is performed again by reducing and redefining the search limits of model parameters according to the uncertainty in the solution. The new minimum and maximum limits are obtained from the uncertainty in the previous iteration. Though the misfit error reduces in the solution after successive refinement of the model space in individual inversion, it is observed that the mean model drifts away from the true model. However, successive refinement of the model space using global optimization and joint inversion of DC resistivity and EM data reduces uncertainty to a very low level in 4 to 5 iterations. This approach works very well in resolving the problems of equivalence for resistive as well as for conducting layers.

**GAI.10/09A/A11-011****1200****SIMULTANEOUS INVERSION OF ELECTRIC AND MT DATA IN 1-D SITUATIONS USING MCMC METHODS**Michel MENVILLE<sup>1</sup>, Michel ROUSSIGNOL<sup>2</sup>, Jean-Jacques SCHOTT<sup>1</sup> (<sup>1</sup>CETP, <sup>2</sup>EQUIPE D'ANALYSE ET DE MATHÉMATIQUES APPLIQUÉES, UNIVERSITÉ DE MARNE LA VALLÉE, FRANCE., <sup>3</sup>EOST, STRASBOURG, FRANCE)

In the Bayesian approach, the inverse problem solution can be obtained from a posteriori probability distribution of the model given the data and a priori information on model parameters. Stochastic algorithms based upon MCMC (Monte Carlo Markov Chain) methods have already been developed to solve the Bayesian inverse problems in both electric and MT 1-D situations. The domain under study is divided into a large number of thin horizontal homogeneous layers whose thickness is fixed, and the model parameters are the conductivity of each layer. We use an a priori law of the parameters which favour smooth models. For each layer, the a priori and a posteriori laws are digitised over a limited set of conductivity values. The Markov chain relies on updating the model parameters during successive scanning of the domain under study. For each step of the scanning, the conductivity is updated in one layer given the actual value of the conductivity in the other layers. Thus we designed an ergodic Markov chain, the invariant law of which is the a posteriori law of the parameters, provided the forward problem is completely solved at each step. The a posteriori marginal probability distributions are estimated from the simulated successive values of the Markov Chain. We present an application of this MCMC algorithm to the simultaneous inversion of electric and magnetotelluric data.

**GAI.10/09A/A11-012****1215****JOINT INVERSION OF MAGNETOTELLURIC AND SEISMIC DATA FROM SOUTHERN GRANULITE TERRAIN OF THE INDIAN SHIELD**

A. MANGLIK, K. NAGANJANEYULU, K. SAIN, T. HARINARAYANA, V. VIJAYA RAO, S.K. VERMA (National Geophysical Research Institute)

An integrated geophysical, geological study of the Southern Granulite Terrain (SGT) of the Indian shield was carried out along the Kuppam- Palani transect in order to delineate the crustal structure and understand the evolution of this Proterozoic crust. This 300-km long transect was covered by deep seismic reflection and refraction, and wide-band magnetotellurics studies besides other geophysical methods. The results indicate presence of a thick mid- crustal low velocity and electrically conducting layer. In the present study, a segment of this profile is selected where both MT and seismic data indicated layered-structure model. Individual inversions of these data sets for wide ranging initial guess models yield different results emphasizing the ambiguity of obtained models. Joint inversion of the two data sets leads to reduction of the range of this ambiguity.

Wednesday, July 9 PM

Presiding Chair: M. Dobroka

**GAI.10/09P/A11-001****1400****THREE-DIMENSIONAL ELECTROMAGNETIC MODELING BASED ON THE CONTRACTION INTEGRAL EQUATION METHOD**

Michael S. ZHDANOV, Gabor HURSAN (Department of Geology and Geophysics, University of Utah)

The integral equation method has been proven to be an efficient tool to model three-dimensional electromagnetic problems. Due to the full linear system to be solved, the method has been considered effective only in the case of models consisting of a strongly limited number of cells. However, recent advances in matrix storage and multiplication issues facilitate the modeling of horizontally large structures. Iterative methods are the most feasible techniques for obtaining accurate solutions for such problems. In this paper we demonstrate that the convergence of iterative methods can be improved significantly, if the original integral equation is replaced by an equation based on the modified Green's operator with the norm less or equal to one. That is why we call this technique the Contraction Integral Equation (CIE) method. We demonstrate that application of the modified Green's operator can be treated as a preconditioning of the original problem. We have performed a

comparative study of the convergence of different iterative solvers applied to the original and contraction integral equations. The results show that the most effective solvers are the BIGGSTAB, QMRCGSTAB, and CGMRES algorithms, equipped with preconditioning based on the CIE method. The high convergence rate of the iterative methods applied to the contraction integral equation is based on the fact that this new equation is the preconditioned form of the conventional integral equation with the preconditioning matrices determined by the conductivity distribution within the electromagnetic model. This form of the preconditioners is based on the fundamental radiation properties of the electromagnetic field, expressed by the energy inequality, which has a clear physical interpretation: the total energy of the anomalous electromagnetic field radiated outside the domain with the anomalous conductivity is always non-negative. This physical property of the electromagnetic field provides the mathematical convergence property of the iterative methods with the new preconditioners introduced in this paper.

**GAI.10/09P/A11-002** **1415**

**THREE-DIMENSIONAL INVERSION OF VERY LOW FREQUENCY (VLF) ELECTROMAGNETIC DATA**

Shashi Prakash SHARMA (Department of Geology and Geophysics, IIT, Kharagpur, 721302, India)

Three-dimensional inversion of VLF and VLF-R data measured along several profiles over an isolated conducting structure is considered. Generally numerical modeling and inversion of VLF data are performed considering 2-D structures where subsurface models are assumed on the basis of equivalent current density cross section. In the present study, equivalent current density cross-section over a 3-D structure is studied. The study shows that 2-D current density cross section over 3-D structure yields information useful to construct the subsurface model. These models are described using a set of variables in terms of geometrical and physical parameters. Various model parameters are then optimized (parametric inversion) to obtain best estimates that fit the observation. Apparent resistivity and phase data from E-polarization are used in inversion. The results show that the models thus obtained can also fit the real and imaginary anomalies. A number of models where profiles may or may not be perpendicular to the geological strike are inverted. Data from both E- and H-polarization are inverted together for a complex model that has azimuth as well as dip. Synthetic, noise-free, and noisy data from a number of models are inverted to show the efficacy of the approach.

**GAI.10/09P/A11-003** **1430**

**GLOBAL-SCALE ELECTROMAGNETIC INDUCTION: 3-D TEST COMPUTATIONS AND THE RESPONSE OF A REALISTIC STRUCTURE**

Ryokei YOSHIMURA, Naoto OSHIMAN (Research Center for Earthquake Prediction, Disaster Prevention Research Institute, Kyoto University)

We provide a new forward simulator based on an edge element finite element method (FEM) for calculating electromagnetic induction responses in a 3-D conducting sphere excited by an external source current for a variety of frequencies. The formulation is in terms of the magnetic vector potential. The edge element approach used in our simulator assigns the degrees of freedom to the edges rather than to the nodes of the element. In other words, the unknowns are the tangential components of the magnetic vector potential along the edges of the element. This edge element strictly satisfies the discontinuity of the normal boundary conditions across a material interface without considering the enforced normal boundary conditions that are usually practiced in a nodal element FEM. We also propose a new and efficient algorithm for mesh generation. The reason why we developed the algorithm is that little has been reported on tetrahedralization of the 3-D domain adopted to analyze geoscientific problems, although mesh generation is an essential pre-requisite for numerical solution. In comparison with the previous mesh generators, the algorithm presented here has an advantage that the generated tetrahedral element's shape is more appropriate for numerical analyses, especially solutions with the FEM. In order to verify our simulation code, we compare our results with those of other solvers for several test computations, corresponding to azimuthally symmetric and asymmetric thin shell models and a fully 3-D model. As a consequence, the test computations verify our formulation and simulation code, and derive the properties of our simulator. Finally, we plan to apply our code to calculate the response of a realistic mid-mantle structure.

**GAI.10/09P/A11-004** **1445**

**PROPERTIES OF THE TIME DOMAIN SURFACE GEOELECTRIC MODELED USING 3D EARTH MODEL AND REALISTIC IONOSPHERIC SOURCE CURRENT**

Antti A. PULKKINEN<sup>1</sup>, Martin ENGELS<sup>2</sup>, Ari VILJANEN<sup>1</sup>, BEAR WG<sup>3</sup> (Finnish Meteorological Institute, <sup>1</sup>University of Uppsala, <sup>2</sup>project leader: Toivo Korja, Geological Survey of Finland)

Geomagnetically induced currents (GIC) flowing in technological systems on the ground are known as ground effects of space weather. The primary driver of these currents is the surface geoelectric field which in turn is produced by rapidly varying ionospheric currents. The knowledge about the behaviour of the ionospheric source current and the surface geoelectric field is of great interest when trying to understand the GIC, and the induction phenomena in general. Traditional way to investigate GIC-related geoelectric fields is to use simplified earth models (e.g. 1D) or/and simplified ionospheric source models (e.g. line current and uniform current sheet). Although simplified models have provided valuable knowledge, the next natural step is to move toward more realistic Earth and ionospheric current models. In this paper, we first derive ionospheric equivalent currents using novel Spherical Elementary Current System method and the magnetic data from about 70 magnetometer sites of the BEAR experiment (June-July 1998). Fourier-transformed time series of ionospheric currents are then fed to the volume 3D code that uses crustal conductivity model based on all available data of the whole Fennoscandian Shield and surrounding areas. 3D code is run for relevant frequencies and the time domain geoelectric fields at the Earth's surface obtained via inverse Fourier-transforms are analyzed.

**GAI.10/09P/A11-005** **1500**

**INVERSION OF TDEM DATA IN POLARIZED AND SUPERPARAMAGNETIC MEDIUM**

Pavel O. BARSUKOV, Edouard B. FAINBERG, Eugeny O. KHABENSKY (Applied Electromagnetic Research, the Netherlands)

1D inversion program for time domain electromagnetic (TDEM) data registered in geological medium characterized by frequency dependence of electrical conductivity, dielectric and magnetic permeability is developed. The inversion algorithms are based on the direct problem solution in layered section with electromagnetic parameters which are complex functions of frequency. The models of frequency dispersion developed by Debye, Cola-Cola, Davidson and Neel in any combination for each analyzed layer of rocks are admitted in the program. Inversion is carried out by purposive enumeration of the layers' parameters by minimization the functional of experimental and theoretical data misfit. Efficiency of this

approach is shown by the examples of interpretation of experimental TDEM data containing single and multiple changes of a sign of the medium response (program TEM-RESEARCHER). The dispersion parameters of the medium received in result of inversion are used for mineral research, mapping of the environmental contaminations and tectonic dislocations of rocks as well.

**GAI.10/09P/A11-006** **1515**

**DERIVING MANTLE CONDUCTIVITY-DEPTH PROFILES FROM REGIONAL HARMONIC ANALYSIS OF GEOMAGNETIC VARIATIONS AT AURORAL OVALS**

J. Miquel TORTA<sup>1</sup>, Angelo DE SANTIS<sup>2</sup>, Lluís R. GAYA-PIQUE<sup>2</sup>, Santiago MARSAL<sup>1</sup> (<sup>1</sup>Observatori de l'Ebre, CSIC-URL, 43520 Roquetes, SPAIN, <sup>2</sup>Istituto Nazionale di Geofisica e Vulcanologia, Rome, Italy)

Deep electromagnetic sounding of the Earth can be obtained from the determination of an inductive response transfer function from a set of harmonic coefficients representing some measured geomagnetic field variations at or near the surface. Conductivity profile of the average Earth can be deduced from global analyses of the geomagnetic field variations. A reliable way to make regional estimations goes through isolating the distinct field variation over the restricted region by means of a tool that allow separating the external source field from the internally induced one. But, any regional method that is supposed to fit fields with intrinsic wavelengths much larger than the area covering the measurements suffers from an improperly external-internal separation. However, there are some conditions in which it is possible to carry out an analysis of some geomagnetic variations and rigorously separate internal and external fields, i.e. in those cases in which the area of existence of the variations is somewhat coincident with the region defining the analysis; or when some regional part of the global source field can be separated, because of its independence or symmetry, from the remainder of the variation source. In this work we present some applications of the method of Spherical Cap harmonic Analysis to polar cap and auroral fields which, in turn, present rather complex structures, and so more suitable to be fitted by inherently short wavelength basis functions, so that information about the mantle conductivity beneath the Arctic and the Antarctic can be readably extracted.

**GAI.10/09P/A11-007** **1530**

**TIME-DOMAIN INVERSION FOR THE RADIAL ELECTRICAL CONDUCTIVITY DISTRIBUTION OF THE EARTH'S MANTLE**

Yozo HAMANO (Department of Earth and Planetary Science, University of Tokyo)

A new time domain inversion method was applied to obtain a global radial distribution of the electrical conductivity of the Earth's mantle. In this method, sequential data sets of hourly mean values during a large magnetic storm from 57 geomagnetic observatories were used to separate the externally generated field and the induced field based on the spherical harmonic analysis. The separated external field is dominated by P10 component during the initial stage of the magnetic storm, but P21 component becomes significant in the later stage. As for the induced field, the self-induced field is dominant in degree 1 and degree 2 components, whereas the higher components ( $n > 2$ ) were largely contaminated by the secondary field caused by the interaction of the P10 source field and the strong surface heterogeneity due to the distribution of oceans and lands. Relative importance of the self-induced field and the coupled fields in each harmonic component was estimated by the forward calculation of the induction process for the 3-D heterogeneous earth (Hamano, 2002), in which the surface conductivity heterogeneity was assigned based on the surface topography of the earth. The result indicates that the degree 1 and 2 components are mainly due to the self-induced field and the secondary fields are negligibly small. On the other hand, in the higher degree components, coupled components are dominant during the initial stage of the magnetic storm. Hence, for the radial distribution estimate, the low degree components were used, although the higher degree component become important for the determination of the conductivity heterogeneity of the deep mantle. For the inversion, step response of the induced field (time variation of the internal field corresponding to the abrupt change of the external field), were first obtained by combining the external and the internal field. Then, the observed step responses were compared with the theoretical response function of a uniform sphere (Chapman and Bartels, 1940) to obtain the penetration depth,  $d(t)$ , and the average conductivity to the depth,  $s(t)$ , as a function of time. The relation,  $s(t) - d(t)$ , gives the radial conductivity structure  $s(d)$ . Since the present approach can utilize the signals with the time range between 1 hour and several days, the method is more sensitive to the mid-mantle structure (400 km - 1000 km) compared to the previous frequency domain approaches. It is also to be noted that the present approach can explicitly take into account the influence of the surface heterogeneity on the response functions.

**GAI.10-Posters**

**ELECTROMAGNETIC INVERSION MODELING**  
Location: Site D

**Wednesday, July 9 PM**  
Presiding Chair: A. Saraev

**GAI.10/09P/D-001** **Poster** **1615-120**

**ELECTRICAL AND GPR TOMOGRAPHIES FOR ARCHAEOLOGICAL INVESTIGATIONS AT MIT-RAHEINA VILLAGE, GIZA, EGYPT**

Abdel- Rady Ghareeb HASSANEEN<sup>1</sup>, Salah Sherif OSMAN<sup>2</sup>, Mohamed Abdel - Aal ABD - ALLAH<sup>3</sup>, Fathy Ahmed SHAABAN<sup>4</sup> (Prof. of Geophysics and Head of the Geomagnetic and Geoelectrical Dept. National research Institute of Astronomy and Geophysics, Helwan, Cairo, Egypt., <sup>2</sup>Assistant Prof. of Geophysics, <sup>3</sup>Lecturer of Geophysics, <sup>4</sup>Lecturer of Geophysics)

This work aims to investigate the near-surface sedimentary cover for tracing the buried archaeological relics, at Mit-Raheina village, Giza, Egypt. Resistance scanning and GPR profiles have been conducted in the investigated area. Resistance survey have been conducted, using the RM15 Resistance Meter (from the Geoscan Research Institute, England), at Tell El-Rabi'a (behind Hathour Temple). A total number of 12 square grids, with grid length of 20 m, are conducted. The field data are processed and illustrated using the GEOPLOT software. Sixty-five detailed GPR profiles were measured at Tell El-Rabi'a using the Surface Interface Radar, SIR-2000 instrument, and utilizing a 400 MHz antenna with a time window 100 ns. Two Way Time (TWT), 38 profiles are carried out east to Hathour temple, each profile has a length of 60 m with profiles apart of 1 m and 27 profiles are carried out north to the temple, each of them has a length of 40 m and profiles apart of 1 m. The analysis of the radar sections and the resistance measurements with the available excavation data allowed for identification and constructions of the shape and extension of

the expected archaeological targets beneath the earth surface.

**GAI.10/09P/D-002** Poster **1615-121**

**GEOELECTRICAL STUDY TO DELINEATE THE EFFECT OF GROUNDWATER INCREMENT IN ABU-SIR ARCHAEOLOGICAL AREA, EL- GIZA, EGYPT**

Abdel - Rady Ghareeb HASSANEEN<sup>1</sup>, El-Said Ahmed EL-SAYED<sup>2</sup>, Mamdouh Mohamed SOLIMAN<sup>3</sup> (Prof. of Geophysics and Head of the Geomagnetic and Geoelectrical Dept. National Research Institute of Astronomy and Geophysics, Helwan, Cairo, Egypt., <sup>2</sup>assistant Prof. of geophysics., <sup>3</sup>assistant Lecturer of geophysics)

Abu-Sir area has a great archaeological importance whereas, it includes the Sun Temple, three famous archaeological Pyramids, and many other tombs. The present study is concerned with mapping the groundwater aquifers, delineating the litho-facies distribution and the structural controls, and for studying the characteristics of the groundwater in Abu-Sir archaeological area. In the geoelectrical resistivity work, 45 VESes using Schlumberger configuration were carried out. In a primary step to interpret the present data qualitatively, the apparent resistivity data are used to construct iso-apparent resistivity maps and sections. From the qualitative interpretation, it is concluded that, the resistivity values increase with increasing AB/2 reflecting the presence of two bearing water zones (shallow and deep aquifers). The thicknesses of these aquifers increase to the east of the area under investigation and decrease gradually to the west of the area. The apparent resistivity data is processed and interpreted quantitatively using Zohdy (1989) and Resist (Velpen, 1988) programs. The interpreted resistivity data are used in constructing twelve geoelectrical cross-sections (two are given), two iso-pach maps for the two upper layers (zone A and B) and water level map for the deep aquifer surface (zone C). According to these cross-sections and maps, the area under investigation is divided into four geoelectrical zones. The upper zone has a thickness varying from 4 to 19 m and consists mainly of sandy gravel, while the second zone varies in thickness from 15 to 40m and varies in lithology from clay to sandy clay, and is underlain by a sandy zone intercalated with clay lenses having a thickness of about 50m. The fourth zone is a very high resistive zone, which is referred to limestone and marly limestone equiclude. It is also appeared from the groundwater map constructed based on the resistivity data and in the light of the previous hydrographs for the groundwater wells in and near the area under study that, there is slightly decrease in the groundwater level after the construction of the High Dam.

**GAI.10/09P/D-003** Poster **1615-122**

**MAPPING OF BURIED ARCHAEOLOGICAL RELICS USING GPR SURVEY AT THE ISIS TEMPLE AREA, BAHBEIT EL-HEGARA, EGYPT**

Fathy Ahmed SHAABAN<sup>1</sup>, Fouad Fawzy SHAABAN<sup>2</sup>, Abbas Mohamed ABBAS<sup>3</sup>, Abdel Aleem Hassan EL-ESSAWY<sup>4</sup> (<sup>1</sup>Lecturer of Geophysics, National Research Institute of astronomy and geophysics, Helwan, Cairo, Egypt., <sup>2</sup>Professor of applied Geophysics, Geology Dept., Fac. of science, Mansoura Univ. Egypty, <sup>3</sup>Lecturer of Geophysics, National Research Institute of astronomy and geophysics, Helwan, Cairo, Egypt., <sup>4</sup>Geophysicist, Schlumberger company)

The Interpretation of ground penetrating radar (GPR) surveying data on the archaeological site of Isis temple of Bahbeit El-Hegara area helped in tracing and mapping buried relics of that temple. Sixty-three GPR profiles were conducted at the southern and eastern parts of the temple area using the SIR (Surface Interface Radar) -2000 instrument and 400 MHz antenna with time window of 100 ns. A preliminary GPR profile was conducted on a partially buried granitic block stone of the destroyed temple for subsequent calibration and interpretation of the GPR sections and for the dielectric constant and velocity determination. The field GPR data are processed by using the Radan and Reflex programs. Analysis and interpretation of the GPR sections reveal anomalous relics of different shapes and dimensions buried at depths ranging from 1 to 5 m below the ground surface. These relics are either irregular stone blocks or regular building structures (probably walls and columns of the destroyed temple). On the other hand, the wave amplitude time slices were constructed illustrates the subsurface locations and extension of these delineated archaeological relics in the study area.

**GAI.10/09P/D-004** Poster **1615-123**

**GEOELECTRIC STRUCTURE ACROSS NARMADA-SON LINEAMENT ZONE, CENTRAL INDIA, FROM 2-D MODELING RESULTS**

Bantu Prasanta Kumar PATRO, Harinarayana T., Sastry R.S., Madhusudan Rao, Manoj C., Naganjaneyulu K., Sarma S.V.S. (National Geophysical Research Institute)

Magnetotelluric studies have been carried out with 25 soundings along NNE-SSW trending traverse from Edlabad-Khandwa across Narmada-son lineament (NSL), an important tectonic zone in peninsular India. The 130 km long traverse also passes through intense seismic tremor activity near Khandwa. The data were subjected to two different 2D inversion schemes- RRI and Occam. For better resolution, modelling of the data was carried out in two steps- first with the high frequency part of the data to get the shallow section and then with the data for the total frequency range. The model for the shallow section has brought out moderately resistive layer (30-150 Ohm.m) representing the exposed Deccan trap layer overlying a conductive layer (10-30 Ohm.m) corresponding to the subtrappean Gondwana sediments. The thickness of this subtrappean sediments amounts to as much as 2 km in the northern half of the profile. Further, the model has brought out well defined vertical conductive features, spatially coincide with Gavligarh, Tapti, Barwani-Sukta and Narmada south faults. The high resistive upper crust is relatively thick towards the southern end and tends to become thinner in the middle of the traverse. The lower crustal segment is conductive over a major part of the profile. The subsurface model integrated with the available regional gravity together with constraints from the nearby Ujian-Mohan DSS traverse, provided a better constrained crustal structure for the region. The relation of the crustal model to the seismotectonic significance of the NSL region is discussed.

**GAI.10/09P/D-005** Poster **1615-124**

**3-D MODELLING AND ANALYSIS OF THE DST C-RESPONSES IN THE NORTH PACIFIC OCEAN REGION, REVISITED**

Alexei KUVSHINOV<sup>1</sup>, Hisashi UTADA<sup>2</sup>, Dmitry AVDEEV<sup>1</sup>, Takao KOYAMA<sup>3</sup> (<sup>1</sup>Geoelectromagnetic Research Institute, Russian Academy of Sciences, 142190, Troitsk, Moscow region, Russia, <sup>2</sup>Earthquake Research Institute, University of Tokyo, 1-1-1 Yayoi, Bunkyo-ku, Tokyo 113-0032, Japan, <sup>3</sup>Japan Marine Science and Technology Center, Natushima, 2-15, Yokosuka, 237-0061, Japan)

We have performed detailed 3-D simulations in the model with a realistic inhomogeneous surface layer in order to understand, which one-dimensional 1-D upper mantle model beneath North Pacific Ocean from a bunch of those published in the last decade, is in a better agreement with a majority of available experimental data. Our main finding is that there exists persistent disagreement between experimental and 3-D modelled C-responses when

1-D sections of Lizarralde et al. (1995), Semenov (1998) or Neal et al. (2000) are considered as the upper mantle sections. Our 3-D model studies and reinterpretation of the experimental data confirms the inference of Utada et al. (2002) that upper mantle beneath North Pacific Ocean in depth range down to 400 km is much more resistive than it was guessed before. In particular our 1-D upper mantle models does not reveal astenosphere conducting layer. While 3-D modellings it was detected that there exists a systematic shift of experimental GDS C-responses at Honolulu observatory compared with the experimental C-responses at another observatories. It is still unclear what is the reason of such a shift. At least 3-D simulations in the model of the inhomogeneous surface layer even at a very detailed grid of 0.3°×0.3° don't exhibit notable ocean effect in the GDS C-responses at this site. An attempt has been made to reduce the misfit between experimental and modelled C-responses by incorporating into 3-D model the inhomogeneous lithosphere and upper mantle. However we could observe only slight changes in the behaviour of the model responses, because the ocean has much stronger induction effect than deep mantle heterogeneities. Routine simulations in realistic 3-D models became possible due to novel 3-D spherical forward solution that is also presented in this contribution. The solution combines modified iterative-dissipative method with Krylov subspace iteration and grid detailization scheme, and allows one to compute efficiently the EM fields in full 3-D spherical models with very high lateral contrasts of conductivity and at very dense grids.

**GAI.10/09P/D-006** Poster **1615-125**

**ANTENNA POLARIZATION EFFECT IN TDEM**

Pavel O. BARSUKOV, Edouard B. FAINBERG, Eugeny O. KHABENSKY (Geoelectromagnetic Research Institute RAS)

It is well known that sometimes TDEM responses in coincided antennas change a sign, forming negative anomalies. This phenomenon is usually associated with complex, frequency dependent resistance of rocks. However in some cases frequency dispersion cannot explain the features of really measured signals. For example, at late stages of responses the negative signal attenuates in time more slowly than  $\sim 1/t$  and depends on resistance of antenna's cable. On the basis of theoretical analysis of EM-field of antennas with dispersive capacity and resistance, laying on the surface of 1D layered medium with frequency dependent dielectric permeability, it is established, that at axisymmetrical excitation of magnetic field there are both vertical and radial components of an electric field, and signal decay in time with the speed depending on relaxation time of dielectric permeability of medium. The amplitude of the signal is proportional to a square of resistance of the antenna's wire and their capacity. This phenomenon was confirmed with numerous experiments and named as Antenna Polarization effect (AP-effect or AP). AP-effect makes it possible to explain registered negative TDEM anomalies which amplitudes depend on resistance of antenna's wire, their location above a surface of the ground, humidity of ground and air etc., abnormal slow decay in time of negative TDEM signals both in coincided and in loop-in-loop antennas.

**GAI.10/09P/D-007** Poster **1615-126**

**ON THE UNIQUENESS OF THE INVERSE PROBLEM SOLUTION FOR METHOD SQ-VARIATIONS**

Peter S. MARTYSHKO, Peter S. MARTYSHKO, Valentin A. PYANKOV (Institute For Geophysics)

As field magnetization it is suggested to use a field of Sq-variations. The research of effects of a field magnetization with the help of these variations is of interest in connection with a large deep of penetration of the field (that is not so solid for an artificial source), regular occurrence of Sq-variations and their wide circulation. For depths in the first kilometers the field magnetization field of Sq-variations practically is similar. The Sq-variations are generated by system of electrical currents in the top layers of an atmosphere (ionosphere). General distribution of vectors of variations to the earth surface depends on the fact that the system of currents, adequate for Sq-variations, embraces an arc (30) on a midday meridian and remains motionless in space between the Earth and Sun. The observer, rotating round this system, fixes during 24 hours all values of a vector of the intensity of the field, caused by the currents. Thus, we have a situation, similar to continuous moving of a source of a primary magnetization field. Therefore it is of interest to investigate questions of uniqueness of the inverse problem solution of magnetic exploration in case of a field magnetization by a similar field, continuously changing the direction. We showed the possibility of determination of parameters of the object in the form of an elliptic cylinder from results of monitoring of effects of a field magnetization by a field of Sq-variations. On a practical example we illustrated the opportunity of determination of parameters of an anomaly forming body on measurements data of a magnetic field, induced by Sq-variations. As a result of interpretation a basic opportunity of determination of the unique solution of a nonlinear inverse problem of a method of a field magnetization the rotating field of Sq-variations on data of synchronous differential supervision of the module of a complete vector T of a geomagnetic field is shown. The offered approach - methodical basis for operative interpretation of magnetic anomalies has, in comparison with earlier existing methods, the following advantages: a) With the help of a powerful source of a similar rotating field magnetization field (the Sq-variation) it is possible essentially to increase a depth of a method of a field magnetization and to lower its labor input; b) Application of the new interpretational apparatus allows simultaneously to determine boundary and magnetic susceptibility of an abnormal object, that within the framework of a method of variations was considered problematic.

**GAI.10/09P/D-008** Poster **1615-127**

**CHARACTERIZATION OF GEOTHERMAL RESERVOIR AROUND A HOT SPRING THROUGH INTEGRATED GEOPHYSICAL AND GEOCHEMICAL STUDIES**

Shashi Prakash SHARMA (Department of Geology and Geophysics, IIT, Kharagpur, 721302, India)

Geoelectrical, very low frequency (VLF) EM and ground magnetic surveys are carried out to characterize the geothermal reservoir around a hot spring in Nayagarh, Orissa, India. Vertical electrical sounding (VES) studies in the area reveal the presence of two to four prominent litho units. The weathered and fractured litho units constitute the main aquifer system. The results of geophysical survey coupled with the geochemical studies and well inventory show venting of thermal water into the regional aquifer system through the fractured and weathered rocks. As a result, fluoride contamination is occurring in villages around the hot spring. Fluoride concentration is observed to be very high in both the hot spring and the groundwater of Singhpur village compared to those in surrounding areas. Spatial distribution of apparent resistivities at different electrode spacings indicates the presence of a low apparent resistivity zone encompassing the hot spring and the fluoride contaminated villages such as Singhpur and Sagaragan. Fluoride concentrations of groundwater and hot spring water show an inverse relation with the apparent resistivity of the formation at different electrode spacings. Finally, detailed VLF and ground magnetic survey is carried out to find the fractures in the crystalline rocks and their direction to assess the movement of contaminated groundwater.

**GAI.10/09P/D-009** Poster **1615-128**

**ANALYSIS OF THE POSSIBILITIES OF LOCAL MAGNETOVARIAIONAL SOUNDING**

Pavel Yu PUSHKAREV, Mark N. BERDICHEVSKY, Vladimir I. DMITRIEV, Nina S. GOLUBTSOVA (Geophysical Department, Moscow University)

One of the most troublesome problems of magnetotelluric explorations is the correction of near-surface distortions. To avoid this difficulty, we turn to the local magnetovariational sounding, employing the magnetic field. It is well known that near-surface magnetic distortions attenuate with lowering frequency. Until recent times the interpretation of magnetovariational anomalies was constrained because of the insufficient understanding of its potentials. We think that the very important event was proof by professor Dmitriev of the uniqueness theorem for 2D magnetovariational inverse problem. This allows us to treat the magnetovariational sounding with its freedom from near-surface distortions at low frequencies as a base method of deep geoelectrics. A number of experiments involving 2D and 3D modeling and 2D inversion were performed in order to study the potentials and frontiers of the local magnetovariational sounding. Models containing several conductive and resistive bodies have been considered and the resolution of the magnetovariational sounding has been studied. It was shown that single conductive bodies manifest themselves separately if the distance between them considerably exceeds their depth. Criteria of structural quasi-two-dimensionality have been derived. It was shown that conductive and resistive three-dimensional structures allow for two-dimensional approximation of magnetovariational indicators if the aspect-ratio of the structures exceeds 10. The methodology of deep electromagnetic investigations combining the local magnetovariational sounding (basic information) with the magnetotelluric sounding (detailed information) has been considered. We suppose that the most efficient approach to the inverse multicriteria magnetotelluric inverse problem may be constructed using a sequence of partial inversions taking into account the different sensitivity and different robustness of magnetovariational and magnetotelluric indicators. Using this approach, several successful inversions of synthetic and field data have been performed.

**GAI.10/09P/D-010** Poster **1615-129**

**TWO-DIMENSIONAL MAGNETOTELLURIC INVERSION USING MONTE CARLO MARKOV CHAIN ALGORITHM**

Nugroho Dwi HANANTO<sup>1</sup>, Djedi Setyo WIDARTO<sup>2</sup>, Hendra GRANDIS<sup>3</sup> (<sup>1</sup>Research Center for Geotechnology, Indonesian Institute of Sciences, <sup>2</sup>Department of Geophysics and Meteorology, Institut Teknologi Bandung)

This paper describes the integration of two-dimensional magnetotelluric forward modeling into an inversion method based on a stochastic Monte Carlo Markov Chain (MCMC) algorithm. Effective exploration of model space is performed using biased sampler that is believed to have an ability to avoid local minima entrapment that frequently encountered in highly non-linear inversion problem. The Markov Chain relies on updating the model parameters during successive scanning of the domain under study. For each step of the scanning, the conductivity is updated in one element given the actual value of the conductivity in the other element. Thus we designed an ergodic Markov chain, the invariant distribution of which is the a posteriori distribution of the parameters, provided by the forward problem is completely solved at each step. Results from inversion of synthetic MT data show that the algorithm can reasonably resolve the true structure. Effectiveness and limitations of the proposed inversion method is discussed with reference to the synthetic data inversions.

**GAI.10/09P/D-011** Poster **1615-130**

**A FAST APPROXIMATE INVERSION PROCEDURE TO INTERPRET MAGNETOTELLURIC DATA**

Erno PRÁCSER<sup>1</sup>, Michael DOBROKA<sup>2</sup>, Márta KIS<sup>1</sup> (<sup>1</sup>Eötvös Loránd Geophysical Institute, Budapest, <sup>2</sup>Department of Geophysics, University of Miskolc)

In the presented simultaneous inversion algorithm a quick forward modeling is applied, which is approximate in the sense that the predicted data are calculated by means of formulae given for 1D geological models. In order to improve the often used 1D forward modeling approximation, the integral mean value of the horizontally changing model parameters (calculated along an appropriately defined interval) is introduced for giving a more complete lateral sight. Optimizing this interval and appropriately choosing the weight function, a new tool serves for decreasing the difference between 1D and 2D interpretation in the process. The approximate inversion method is tested by using synthetic and field data. During the numerical investigations a 2D model is defined and the synthetic data sets are generated by applying a real 2D forward modeling code. In order to simulate real data sets 1% random noise is added to the calculated data. A comparison is made between the results of a real 2D inversion procedure and the presented approximate inversion algorithm. It is shown, that the presented algorithm is quick, stable and accurate enough for practical work. Its reliability is demonstrated by using it in interpreting in-situ measured data. Using the approximate inversion procedure a problem –often arising in solving 2D inversion problems - can be answered: the higher reliability and stability of the simultaneous and/or joint inversion algorithms are not always achievable in case of more complicated geological structures. In order to find acceptable inversion results it is very important to use appropriate discretization method. Another important factor in choosing the discretization and the inversion methods is the computation time. Taking this into account –as a reasonable compromise- it is often useful to reduce the number of unknowns (in order to ensure the accurate and stable parameter estimation). Our results show, that the WGSE inversion algorithm can be considered as a good candidate to realise this compromise with acceptable accuracy and cost effective calculation speed.

**GAI.10/09P/D-012** Poster **1615-131**

**SOME PROBLEMS APPLYING THE 3D MODELING SCHEME TO PRACTICAL DATA**

Elena Yu. FOMENKO<sup>1</sup>, Tohru MOGF<sup>2</sup> (<sup>1</sup>Moscow State University, Moscow, Russia, <sup>2</sup>Institute of Seismology and Volcanology, Sapporo, Japan)

We applied a forward and inverse modeling scheme for CSMT and MT 3D data to the Usu volcanic area, Japan, to clear a resistivity structure. The Usu is an active volcanic area covered mostly by recent volcanic rock (lava or ocrastics). It is located near Usu-Shinzan fault. 2D-model in the part of this area was investigated by Ogawa et al., 1999 and Ballestracci and Nishida, 1987 (AMT data). The field data contained amplitudes and phases of impedance at 25 CSMT sites in the far zone (frequencies were in the range 0.6 - 5000 Hz) and 10 MT sites (0.0005 - 320 Hz). The data were essentially 3D and noisy. The impedances were obtained from measured Ens-Hew (Zxy) and Eew-Hns (Zyx). At first the data were smoothed and cut. Then 1D-inverse modeling scheme was applied both to the impedance amplitudes and phases taking in account the topography structure at each CSMT and MT site. Because data were essentially 3D, we used the invariant of impedance  $Z_{inv} = \sqrt{(Z_{xx} \cdot Z_{yy} - Z_{xy} \cdot Z_{yx})}$  and corresponding Rinv. Then we constructed 3D resistivity model.

At first the average algorithm was used to calculate apparent resistivity values at each Z-level for the given sites (1D). Second, the interpolation was applied in the central part of sites to convert irregular data grid to the non-uniform rectangular one at each Z-level, the extrapolation in the blank of data areas was made by using method of the nearest neighbor. The special areas (the sea, the lake Toya) were added to the 3D model manually. The constructed 3D resistivity model based on 1D-inversion data was investigated by using 3D forward modeling code based on 3D staggered grid finite difference approximation of the electrical field in the Maxwell equations (E. Fomenko, T. Mogi, 1999, 2002). This code was applied to the linear system of  $380,000 \times 3$  equations (for Ex, Ey, Ez) to calculate Rapp amplitudes and phases at the 91 frequencies (9 decades). The relative error of stopping iterative process for the relative residual  $r/r_0$  and divergence of the electric current  $DivJ / |J|$  was less than 1.E-6. Simulation was carried out at the PC with Pentium-III CPU, 500 MHz, 512 MB RAM. The calculation required from 20 minutes to 3 hours depending on frequency. Finally we obtained a 3D resistivity model of the USU area up to 5 km depth including topography, the spacing of sites were 100 m. After comparison 1D and 3D Rapp-inv the correction of 3D-resistivity model was made. Finally the difference between 1D, 3D and the field data Rapp were not less than 10-15%.

**GAI.10/09P/D-013** Poster **1615-132**

**IDENTIFICATION AND LOCALIZATION OF ARCHEOLOGICAL OBJECTS IN MAGNETIC SURVEY BY COMPLEX WAVELET ANALYSIS**

Gitnet SARACCO<sup>1</sup>, Pierre-Etienne MATHE<sup>1</sup>, Frederique MOREAU<sup>2</sup>, Daniel HERMITTE<sup>1</sup> (<sup>1</sup>CNRS-UMR 6635, CEREGE, Department of Geophysics, Aix-en-Pce, <sup>2</sup>CNRS-UMR 6118, Geosciences-Rennes)

We want to detect and localized buried structures like antik ovens from magnetic measurements performed on the Fox-Amphoux site (France). A well-know method to localize in depth sources, responsible of potential anomalies measured at the ground surface (magnetic or electric), is the real continuous wavelet transform (WT), with the Poisson analyzing wavelet. This wavelet is real by definition. We have here applied a position-scale analysis from complex analyzing wavelet to use complementary information carried by the phase of the wavelet transform. Complex wavelets are built by Hilbert transforms of the Poisson or derivative of the Poisson analyzing wavelet. We show that the phase of the WT provides additional information on the geometric and total magnetic inclination of potential sources, as the modulus allows to characterize their depth and heterogeneity degree. The phase compared to the modulus, is more stable in presence of noise and we can defined it, independently of the low level of energy of the signal. In this sense, information carried by the phase is more efficient to detect small objects or to separate close sources. Conjointly, a rock magnetic study including susceptibility and magnetisations (induced or remanent) measurements give a better constrain on the magnetic parameters we want to extract.

**GAI.10/09P/D-014** Poster **1615-133**

**COMPARISON OF 2-D AND 3-D MODELLING OF THE MT RESPONSE ALONG TRAVERSE IN COMPLEX TECTONIC REGIONS OF INDIA**

Nandini Nityananda NAGARAJAN<sup>1</sup>, Praveena M.<sup>1</sup>, S.G. GOKARN<sup>2</sup> (<sup>1</sup>National Geophysical Research Institute, <sup>2</sup>Indian Institute of Geomagnetism, Mumbai, India, 400 005.)

Two magnetotelluric traverses across tectonically complex regions, viz.; Narmada-Son Lineament (NSL) zone and the NW Himalaya were chosen to model using both 2-d forward modelling, incorporating topography where necessary and 3-d modelling with updated finite difference schemes. Effects of the boundary conditions on the responses were also obtained. Results for the NSL zone, indicate that the structures are significantly limited in depth when 3-d model responses are compared to the actual data. In the case of the NW Himalayan traverse, the topography was included in the 2-d model only. Even this exercise increased the complexity of the model significantly and responses for a relatively simple sub-surface structure were obtained. This is compared with the inversion of MT data along this traverse.

**GAI.10/09P/D-015** Poster **1615-134**

**3-D ELECTRICAL AND ELECTROMAGNETIC MODELING OF A KIMBERLITE PIPE**

Saurabh Kumar VERMA, Kushal Pal SINGH, K.P. PANTULU (National Geophysical Research Institute, Hyderabad)

Due to the presence of clayey minerals, the topmost regions of weathered kimberlites are often very good conductors. Such kimberlites provide good electrical/EM response even if they are concealed by an overburden layer. Considering a representative 3-D electrical model, DC electrical and multi-frequency EM responses are computed to study the role of various parameters like: overburden thickness and conductivity, conductivities of the pipe and host medium, size of the conductive pipe, etc. The study provides useful information on selecting optimum survey parameters for electrical and EM exploration of weathered kimberlite pipes. A field example from south India, considering DC electrical, multi-frequency and time-domain EM responses of a weathered kimberlite buried under a cover of black cotton soil, is presented. Three dimensional modeling of electrical and frequency EM data is done to compare the parameters of the kimberlite body as obtained by the two methods. Image sections based on frequency and time-domain EM responses reveal that the latter are comparatively less noisy. It is also found that the time domain EM response provides better resolution of the weathered kimberlite to a greater depth as compared to the frequency EM response.

**GAI.10/09P/D-016** Poster **1615-135**

**DEEP CRUSTAL IMPLICATIONS OF ELECTRICAL CONDUCTIVITY ON THE NORTHERN EDGE OF THE CONGO CRATON FROM AUDIO MAGNETOTELLURIC SOUNDINGS IN THE ABONG-MBANG/AKONOLING REGION, CAMEROON(CENTRAL AFRICA)**

Théophile Mbarga NDOUGSA, MBOM ABANE. S. (Department of Physics, Advanced Teachers Training College, University of Yaounde I)

Audio magnetotelluric (AMT) soundings have been carried out in the region of Abong-Mbang/Akonolinga (Cameroon Republic), along two profiles running approximately N-S each, over 35-40 km length. The station are located so as to cover laterally the extreme zones E and W of a vast region characterized by a remarkable E-W gravity anomaly. The principal directions along which the measurements were made, were determined by a rotation method with a scalar M.T instrument. The frequency range employed in this instrument is 4.1 to 2300 Hz, which in view of the large resistivities value of the metamorphic terrains encountered, is able to sound great depths. The analysis and interpretation of data reveal the existence of an extensive deep E-W fault, the Abong-Mbang fault. The resulting geoelectric model appears to be that of a structure of grabens and horsts in the basement, resulting from tectonic vertical movements reaching 3 km at Abong-Mbang.

This study is a preliminary report on a vast geophysical investigation on the deep structures on the border of the Congo Craton in Cameroon.

**GAI.10/09P/D-017** Poster **1615-136**

**DETERMINATION OF A TECTONIC NODE FROM THE INTERFERENCE OF STRUCTURAL DIRECTIONS ON THE BORDER OF THE CONGO CRATON AYOS REGION CAMEROON, BY USING THE AUDIO MAGNETOTELLURIC METHOD**

Mbom Abane S.<sup>1</sup>, Ndounga Mbarga T.<sup>1</sup>, Manguelle-Dicoum E.<sup>2</sup> (<sup>1</sup>Department of Physics, Advanced Teachers Training College, University of Yaounde I, <sup>2</sup>Department of Physics, Faculty of Science, University of Yaounde I)

The northern border of the Congo Craton shows important tectonic structures characterized by striking gravity anomalies, which remain to be precisely delineated. The existence of a major faulted structure known as the Abong-Mbang fault, has already been revealed along the 46°N latitude, thanks to a remarkable correlation between the gravimetric and the geoelectric signatures produced by it. The audio magnetotelluric (A.M.T) method has been used in a preliminary investigation of structures transversal to those suggested by the gravity map in the Abong-Mbang/Akonolinga region. Soundings in the Ayos zone give evidence of two structural directions, ENE-WSW and NNW-SSE, and confirm the continuity of the major E-W tectonic structure prevailing at Abong-Mbang/Akonolinga. Analysis and interpretation of the data enabled us to characterize these tectonic structures as concurring with those of the North Equatorial Pan African Chain. The present study reveals the existence of a major structural interference zone, the Ayos tectonic node, which requires further geophysical study.

**GAII.04**

**LIGHTNING-INDUCED TRANSIENT PROCESSES IN THE MIDDLE AND UPPER ATMOSPHERE AND THEIR IMPACT ON THE EARTH SYSTEM**

Location: Site A, Room 8

Monday, July 7 AM

Presiding Chairs: D.D. Sentman, H. Fukunishi

**GAII.04/07A/A08-001** Invited **0900**

**REALTIME GLOBAL MAPPING OF LIGHTNING USING WIDELY SPACED VLF RECEIVERS**

Craig J. RODGER<sup>1</sup>, Richard L. DOWDEN<sup>2</sup> (<sup>1</sup>Department of Physics, University of Otago, <sup>2</sup>Low Frequency Electromagnetic Research)

An experimental network of six radio receivers operating at Very Low Frequency (VLF; 3-30 kHz), stretching from Australasia to Japan, has been in operation since early 2002. Propagation at these very long electromagnetic wavelengths (up to 100 km) allows lightning strokes to be located in real time at up to 10,000 km from the receivers with a location accuracy that is estimated to be a few kilometres. True global mapping of lightning from widely spaced (a few Mm) ground-based receivers requires the use of frequencies below about 30 kHz. Lightning impulses in this frequency range suffer low propagation attenuation, and hence propagation in the Earth-ionosphere waveguide is possible over global distances. At each receiver site, some tens of lightning impulses ("sferics") are received each second. Propagation of the impulses inside the waveguide formed by the Earth and the lower boundary of the ionosphere disperses the impulses into wave trains, the first millisecond of which is processed to determine the time of arrival. These times of arrival are transmitted to a central station in Dunedin, New Zealand, for determining the lightning stroke location. The network is being expanded from the current 7 lightning receiver's located in the Western Pacific to ~16 receiver stations in locations spanning the whole world. All receiver stations are based on university campuses and consist of a short (1.5 m) whip antenna, GPS receiver and VLF receivers, plus a processing computer connected to the Internet. All our current and planned TOGA sites are in built-up areas unsuitable for use of magnetic loop antennas at VLF due to man-made noise such as power line harmonics which would dominate over the sferic magnetic field. This is not the case for the vertical electric field of the lightning impulses. The antenna's are mounted on ferro-concrete buildings, which are poor conductors at VLF and thus remain at ground potential, shielding the antenna from man-made electric noise generated within them. The processing of the lightning impulses at each receiver station is being upgraded to determine the signals time of group arrival (TOGA) rather than the threshold-based time of arrival. This will compensate for the dispersion of the lightning impulse, and increase the accuracy of the lightning locations determined by the network. A worldwide lightning detection network has a wide number of scientific and commercial applications, including those related to the studies of worldwide red sprite and elve observations. Current operation of the network is concentrated on Australasia and the Western Pacific area. The role of lightning in starting wildfires is being investigated in cooperation with Murdoch University and the Western Australian Government, and is partly funded by the Australian Research Council.

**GAII.04/07A/A08-002** **0925**

**ULF/ELF INTERFEROMETRY**

Martin FUELLEKRUG (Institut fuer Geophysik/Frankfurt am Main)

The electromagnetic radiation from natural atmospheric sources is recorded in the ULF/ELF frequency range from 1-200 Hz with a local magnetometer array. This array is used for beam forming of ULF/ELF radiation and for the development of noise reduction processing schemes, since the natural atmospheric electromagnetic radiation in the ULF/ELF frequency range is highly correlated on the local scale. The accuracy of the interferometry is tested prior to deployment for the arrival angle and the velocity. During the experiment, both parameters are recorded on a continuous basis and the temporal averaging results in a mean behaviour of the natural electromagnetic fields. Individual arrival angles are related to individual lightning flashes in the vicinity. The measured wave propagation velocities result from the continuous modification of the ionospheric D-layer and yields important information on local and short term ionospheric disturbances.

**GAII.04/07A/A08-003** **0940**

**RELATIONSHIP BETWEEN GLOBAL LIGHTNING ACTIVITIES AND CHANGES IN THE SPECTRAL POWERS IN THE SCHUMANN RESONANCE BANDS**

SATO MITSUTERU, Hiroshi FUKUNISHI (Department Geophysics, Tohoku University)

In order to identify the relationship between global lightning activities and changes in the spectral powers of the Schumann resonance (SR) bands, we have analyzed ELF magnetic field waveform data in the frequency range of 1-100 Hz obtained at Syowa station (69.0° S, 39.6° E) in Antarctica and Onagawa observatory (38.4° N, 141.5° E) in Japan. First, we have calculated dynamic spectra of the Syowa ELF data for both the geomagnetic north-south (H) and the east-west (D) component over the period between February 2000 and January 2002. Then, powers of first three SR modes at 8, 14, 20 Hz are extracted from each of the H- and D-component dynamic spectra as an indicator of global lightning activity. It is found that the SR power levels in the H-component are maximum for the time intervals of 5-13 UT and 18-01 UT from May to September. On the other hand, the SR power levels in the D-component are maximum for the time interval of 13-18 UT from September to May. It is found that these diurnal and seasonal variations of the SR power are caused by the latitudinal and longitudinal distributions of major lightning source regions located in North America, South America, Africa and South-East Asia. Power spectra of the SR power variations are calculated by the maximum entropy method. It is found that the power spectra show a distinct peak at ~27 days. Cross spectral analysis is made between the variations of SR power and each of the variations of F10.7 index, cosmic ray flux, sunspot number, relativistic electron and ion fluxes observed by the GOES-8 satellite, Kp index, and DST index. It is found that all these parameters have a distinct spectral peak around 27-32 days. However, coherence between variations of the SR power and other parameters are less than 0.3 in all cases. Using ELF magnetic field data obtained at Onagawa observatory for the period between October 2001 and January 2002, dynamic spectra and powers of first three SR modes are also calculated. Power spectra of changing SR levels at Onagawa also show a clear spectral peak at ~27 days. Coherence between the activity changes at Syowa and those at Onagawa is estimated to be 0.9. All these facts may imply that the changes in SR power are not due to the modulation of the upper reflection boundary at ~80 km altitude in the Earth-ionosphere cavity but due to that of the lightning activities themselves. Possible mechanisms of the 27-day modulation for global lightning activities will be discussed.

**GAII.04/07A/A08-004** Invited **0955**

**SPRITE-LIGHTNING STATISTICS, CLOUDTOP TEMPERATURES AND THE MESOSPHERIC BREAKDOWN ELECTRIC FIELD**

Fernanda T. SÃO SABBAS (Physics Department, University of Alaska Fairbanks)

A detailed statistical analysis of the temporal and spatial relationships between lightning and sprites shows that the distribution of time intervals between sprites and parent +CGs, centered in 10-20 ms, appears to characterize the time scale for the development of an individual electron avalanche into a streamer between ~70-85 km altitude, as given in the Pasko *et al.* [1998] model. Within the same analysis, the distribution of the distance between sprites and parent +CGs showed that sprites have the tendency to occur within 50 km lateral displacement from the CG, consistent with results previously reported by Wescott *et al.* [1998] and Lyons [1996]. Also studied was the relationship between IR cloudtop temperatures of the sprite-generating thunderstorm, as derived from GOES-8 satellite images, and lightning/sprite activity. The maximum sprite and -CG production of the system were simultaneously achieved at the time of maximum contiguous cloud cover of the coldest region ( $T_c < -52^{\circ}C$ ), ~ 2 hr before the system reached its maximum extent. It is suggested that the total -CG activity and dynamical development of the thunderstorm may be more tightly correlated with sprite activity than has previously been reported. This work establishes basic steps towards the development of a methodology to investigate sprite occurrence based on satellite images by themselves. This would permit studies of sprites in regions where ground lightning data is not available. In addition, a numerical simulation of electric breakdown conditions of the mesosphere based on the quasi-electrostatic model of Pasko *et al.* [1997] was performed. Inhomogeneities in the atmospheric conductivity were introduced in order to explain the lateral displacement of the sprite from the parent lightning discharge.

**GAII.04/07A/A08-005** **1015**

**OBSERVATION OF SPRITES OVER THE SEA OF JAPAN AND CONDITIONS FOR LIGHTNING-INDUCED SPRITES IN WINTER**

Masashi HAYAKAWA<sup>1</sup>, T. NAKAMURA<sup>1</sup>, Y. HOBARA<sup>2</sup>, E. WILLIAMS<sup>3</sup> (<sup>1</sup>Department of Electro-Engineering, University of Electro-Communications, <sup>2</sup>Laboratoire de Physique et Chimie de l'Environnement, CNRS, <sup>3</sup>Parsons Laboratory, Massachusetts Institute of Technology.)

We have succeeded in observing sprites for winter lightning in the Hokuriku area (Japan Sea side) of Japan in the winter of 2001/2002. The optical results on three days are compared with the corresponding characteristics of parent (causative) lightning with particular attention to the significant differences between Hokuriku winter lightning and the more widely studied continental lightning. Despite significant differences with Hokuriku winter lightning, we have found nearly the same sprite properties as already observed in the U.S. continent with a few significant differences. Then, we have also discussed the criteria for sprite occurrence. Specifically, two similar criteria are found : (1) cloud-to-ground discharges of positive polarity and (2) the presence of a certain threshold in vertical change moment (200-300C·km)(roughly consistent with that for the U.S. continent). Mesoscale convective systems are not necessary to store the charge necessary for sprites, but the parent Hokuriku winter clouds are substantially larger in area than ordinary summer thunderclouds. However, there may exit another condition such as clustering or self-organizing effect of thunderclouds for sprite production.

**GAII.04/07A/A08-006** Invited **1050**

**LOW-LIGHT VIDEO AND ELF OBSERVATIONS OF SPRITES ABOVE HAITI/DOMINICAN REPUBLIC THUNDERSTORMS**

Victor PASKO<sup>1</sup>, Steve CUMMER<sup>2</sup>, Mark STANLEY<sup>3</sup>, John MATHEWS<sup>1</sup>, Umran INAN<sup>4</sup>, Troy WOOD<sup>5</sup>, Earle WILLIAMS<sup>6</sup>, Robert BOLDI<sup>7</sup>, Mitsuteru SATO<sup>8</sup>, Yukihiko TAKAHASHI<sup>9</sup> (<sup>1</sup>Penn State University, University Park, PA 16802, USA, <sup>2</sup>Duke University, Durham, NC 27708, USA, <sup>3</sup>Los Alamos National Laboratory, Los Alamos, NM 87545, USA, <sup>4</sup>Stanford University, Stanford, CA 94305, USA, <sup>5</sup>Massachusetts Institute of Technology, Cambridge, MA 02139, USA, <sup>6</sup>Tohoku University, Aramaki-aoba, Sendai 980-8578, Japan)

In August-September 2001 an experimental campaign has been conducted in Puerto Rico to perform correlative studies of lightning and lightning-induced ionospheric effects. The campaign, which was sponsored by a Small Grant for Exploratory Research from the National Science Foundation to Penn State University, had a broad range of scientific goals including studies ionospheric effects of thunderstorms, studies of VHF-quiet positive leaders

and studies of large scale optical phenomena above ocean thunderstorms in tropics. As part of this program we conducted night time video recordings of lightning and large scale luminous phenomena above thunderstorms using a SONY DCR TRV 730 CCD video camera equipped with a blue extended ITT Night Vision GEN III NQ 6010 intensifier with 40 deg field of view. The intensifier provided a monochrome (predominantly green) image output. The video system was deployed at the Lidar Laboratory on the grounds of Arecibo Observatory, Puerto Rico (18.247 deg N, 66.754 deg W, elevation 305 m above the sea level). We report here low-light video and ELF recordings of 8 sprite events observed above a Haiti/Dominican Republic thunderstorm from Arecibo Observatory, Puerto Rico between 01:10 and 02:51 UT on September 3, 2001. The sprite producing thunderstorm system was located approximately 700 km from the observational site and had the cloud area exceeding 10<sup>4</sup> km<sup>2</sup>. Morphological features of the observed events closely resemble those observed in other parts of the globe and include, in particular, isolated columns, groups of two or more columns, 'dancing sprites', and small impulsive glows confined to higher altitudes. ELF recordings, performed at Duke University, at Rhode Island MIT site, and at Palmer (Stanford University) and Syowa (Tohoku University) Antarctic stations, identified the 7 of the observed events as to be clearly associated with positive cloud to ground lightning discharges (+CGs) involving the vertical charge moment changes ranging between +143 C km to +2520 C km. The observed QL=143 C km for the weakest sprite event is consistent with the experimentally established 120 C km minimum lightning charge moment change required for the initiation of a sprite [Hu et al., GRL, 29, 10.1029/2001GL014593, 2002]. One sprite event (02:05:49.561 UT) was confirmed in ELF records collected at all four observational sites as being produced by an impulsive CG lightning with negative polarity. The associated vertical charge moment change was estimated to be -278 C km in 1.2 ms.

**GAIL.04/07A/A08-007** Invited **1110**  
**GIGANTIC JETS BETWEEN A THUNDERCLOUD AND THE E-LAYER IONOSPHERE\***

Rue-Ron HSU<sup>1</sup>, H.T. SU<sup>1</sup>, Alfred B. CHEN<sup>1</sup>, W.S. HSIAO<sup>1</sup>, Y.C. WANG<sup>1</sup>, L.C. LEE<sup>2</sup>, M. SATO<sup>3</sup>, H. FUKUNISHI<sup>3</sup> (Department of Physics, National Cheng Kung University, <sup>2</sup>National Space Program Office, <sup>3</sup>Department of Geophysics, Tohoku University)

During Taiwan 2002 summer sprites campaign, five gigantic jets were observed above an oceanic thunderstorm, which was raging near Luzon Island, Philippines on 22 July 2002. The morphology of these jets was a hybrid of sprites and blue jets, which have a tree-like or carrot-like top but all have a blue jet-like body. The luminous period of these jets lasted from 300 ms to 500 ms, which is longer than typical sprites but is shorter than that of the gigantic jets observed by Pasko et al. in 2001 [Pasko et al., 2002]. At the fully developed stage, these jets extended from cloud top to 16 km to the E-layer ionosphere at 95 km. The luminous lengths were nearly 80 km, the lateral radius at the top of the jet was ~20 km, and the estimated illuminating volume was approximately 32,000 km<sup>3</sup>. From the existing lightning data, no cloud-to-ground strokes were found to be associated with these jets. However, Syowa station in Antarctica and Onagawa station in Japan both detected unmistakable signatures of these events in the ELF band. Thus it is highly probable that these gigantic jets were not CG-induced events, and they possibly are true lightning between a thundercloud and the ionosphere. In the talk, the dynamic behaviors, the ELF signatures, and the possible generating mechanism of these gigantic jets will be presented and discussed. Reference: Pasko, V.P., Stanley, M.A. Mathews, J.D., Inan, U.S. & Wood, T.G. Electric discharge from a thundercloud top to the lower ionosphere. Nature 416, 152-154 (2002). \*This work was supported in part by National Space Program Office and National Science Council in Taiwan under contract numbers NSC90-NSPO(B)-ISUAL-FA09-01 and NSC91-2111-M006-002.

**GAIL.04/07A/A08-008** Invited **1130**  
**TELESCOPIC IMAGING OF UPPER ATMOSPHERIC LIGHTNING-RELATED STREAMERS AND DIFFUSE GLOW**

Elizabeth A. GERKEN, Umran S. INAN (Electrical Engineering, Stanford University)

Telescopic imaging shows that decimeter-scale structure in luminous lightning-related electrical discharges above thunderclouds covers a wide range of morphologies and time scales. The Stanford University telescopic imager observed hundreds of sprites during deployments in New Mexico and Colorado in the summers of 1998-2000. The telescopic imaging system consists of a 41 cm diameter, f/4.5 reflecting telescope with an intensified CCD camera attached to its eyepiece, a bore-sighted wide field of view (FOV) camera mounted on its top, and both telescopic and wide field of view photometers. Electromagnetic signatures of causative lightning discharges known as radio atmospheric (or sferics) were recorded using crossed-loop magnetic antennas and ELF/VLF receiving systems located at Stanford and in Colorado. Certain categories of structures have been found to occur such as upward and downward branching, beading, propagating diffuse glow striations and streamer/diffuse glow transition regions. Propagating diffuse glow striations are observed to move slowly and are similar to the phenomenon observed in glow discharge tubes. A transition region between streamer formation and diffuse glow is observed at ~80 km altitude. Faint positive streamers are observed at the base of large bright sprites. Some sprites having branching positive streamers and non-branching negative streamers may be double-headed streamers initiated from plasma enhancements. While many streamers move at velocities greater than the time resolution of regular video rate imaging, some have been found to move as slowly as 10<sup>4</sup> m/s. Beads at the base of columns can glow for over 100ms while slowly drifting upward.

**GAIL.04/07A/A08-009** Invited **1150**  
**SPRITES, ELVES AND OTHER TRANSIENT LUMINOUS EVENTS (TLES) OBSERVED FROM THE SPACE SHUTTLE COLUMBIA DURING THE MEDITERRANEAN ISRAELI DUST EXPERIMENT**

Yoav Y. YAIR, Colin PRICE, Peter ISRAELVITCH, Meir MOALEM, Adam DEVIR, Joachim JOSEPH, Zev LEVIN, Ilan KOREN, Mustafa ASFUR (Department of Life and Natural Sciences, The Open University of Israel)

The Mediterranean Israeli Dust Experiment (MEIDEX) flew on-board the space shuttle Columbia in January 2003. During the night-side of 29 shuttle orbits there were dedicated observations of the Earth's limb, above forecasted areas of active thunderstorms. This was accomplished with a Xybion IMC-201 multispectral camera (860nm, 665nm, 380nm, 470nm), guided by the astronauts toward the storms with intent of capturing Sprites, Elves and Jets. Two VLF/ELF sites in Israel were simultaneously used to collect electromagnetic data, together with stations in Hungary, USA, Antarctica and Japan. The astronauts collected more than 9 hours of data, of which 7 hours were transmitted to the ground and saved. Initial analysis of the data from space shows many TLEs in the mesosphere above thunderstorms in Africa, Australia and the Pacific Ocean. Calculated heights, energies and dimensions will be presented. A possible relation with meteors that were observed in close proximity to the TLEs will be discussed.

**GAIL.04/07P/A08-001** Invited **1400**  
**COMPARISON OF TEMPORAL DECAYS OF DYNAMIC AND STATIONARY SPRITE FEATURES BASED ON 1-MS RESOLUTION OBSERVATIONS OF SPRITES**

Dana MOUDRY, Hans C. STENBAEK-NIELSEN, Dave D. SENTMAN (Geophysical Institute, Univ of Alaska Fairbanks)

A 1-ms resolution high speed imager deployed to Wyoming in the summer of 1999 by the Geophysical Institute at the University of Alaska Fairbanks provided good imagery of lightning-induced optical emissions in the upper atmosphere, such as multiple types of sprites, halos and elves (Stenbaek-Nielsen et al. 2000). The sprite images obtained on August 18, 1999 indicate that sprites are composed both of dynamic features previously identified - downward propagating tendrils and upward propagating branches (Stanley et al. 1999; Takahashi et al. 1996), and also of stationary features, such as columns, beads within the sprite body, and puffs above branches (Moudry et al. 2002). We compare the brightness decay of the individual sprite features with each other, with halos, and with an area-averaged brightness decay. The area-averaged brightness decay is more representative of real photometers. The comparison is made in order to find which sprite features may be responsible for the dominant photometer signal. We obtain the brightness decay curve by choosing areas on the 1-ms images which are fully within a particular stationary or dynamic sprite feature. The values of pixels within these areas are added to construct a signal from an imaginary photometer that would have the equivalent field of view as the chosen region. The stationary sprite features decay slower than dynamic sprite features, which in some cases resemble the decay of sprite halos. These characteristics are important for interpretation of photometers whose field of view includes more than one sprite feature. References: Moudry et al., Eos Trans. AGU, 83(47), Fall Meet. Suppl., A62D-04, 2002. Stanley et al., High speed video of initial sprite development, Geophys. Res. Lett., 26(20), 3201, 1999. Stenbaek-Nielsen et al., Sprites and possible mesospheric effects, Geophys. Res. Lett., 27(23), 3829, 2000. Takahashi et al., Temporal development of carrot-like sprites, Eos Suppl. 77(46), F69, 1996.

**GAIL.04/07P/A08-002** Invited **1425**  
**THE SPECTROSCOPY AND ENERGETICS OF RED SPRITES**

Jeff Stanley MORRILL (E. O. Hulburt Center for Space Research, Naval Research Laboratory)

During the past decade, the study of red sprites has evolved from the observation of their general physical properties and application of relatively simple models to detailed research into the fundamental nature of the morphology, chemistry, and energetics of this highly dynamic phenomenon. Spectroscopy is one area that has provided significant information on the energetics and chemistry of sprites. This includes observations from video spectrographs and narrow-band imaging and photometry. This talk will review spectroscopic and photometric observations and present recent results on ionization and electron energetics observed in sprites.

**GAIL.04/07P/A08-003** **1450**  
**MINIMUM ELECTRIC FIELDS REQUIRED FOR PROPAGATION OF POSITIVE AND NEGATIVE STREAMERS IN SPRITES**

Ningyu LIU, Victor P. PASKO (Department of Electrical Engineering, Penn State University)

Recent telescopic imaging of sprites revealed an amazing variety of generally vertical fine structure with transverse spatial scales ranging from tens to a few hundreds of meters [e.g., Gerken et al., GRL, 27, 2637, 2000]. The appearance of the fine structure in sprites has been interpreted in terms of positive and negative streamer coronas, which are considered as scaled analogs of small scale streamers, which exist at high atmospheric pressures at ground level [e.g., Pasko et al., GRL, 25, 2123, 1998; Raizer et al., J. Phys. D Appl. Phys., 31, 3225, 1998]. One of the important questions of the current sprite research, which directly relates to the evaluation of the total volumes of atmosphere affected by this phenomena and possible role of sprites in establishing a direct path of electrical contact between the tropospheric and mesospheric/lower ionospheric regions, is related to the determination of the minimum electric fields required for the propagation of streamers in air at different pressures. The minimum field required for the propagation of positive streamers in air at ground pressure has been extensively documented experimentally and usually stays close to the value 4.4 kV/cm [Allen and Ghaffar, J. Phys. D Appl. Phys., 28, 331, 1995], in agreement with recent results of numerical simulations of positive streamers [Babaeva and Naidis, IEEE Trans. Plasma Sci., 25, 375, 1997; Morrow and Lowke, J. Phys. D Appl. Phys., 30, 614, 1997]. The information about the absolute value of the similar field for the negative streamers at present is very limited. The existing sources indicate that this field is a factor of 2-3 higher than the corresponding field for the positive streamers [e.g., Raizer, Gas Discharge Physics, 1991, p. 361; Babaeva and Naidis, 1997]. We note that although from the streamer similarity laws one generally would expect the minimum fields required for streamer propagation to scale with altitude proportionally to the air neutral density N, the actual scaling for the altitude range of sprites has not yet been verified experimentally, and a limited amount of data currently available in the literature [Griffiths and Phelps, Q.J.R. Meteorol. Soc., 102, 419, 1976; Bazelyan and Raizer, Spark Discharge, 1998, p. 216] indicate possible deviations from the N scaling. A new two-dimensional model has recently been developed at Penn State for studies of dynamics of streamers for a wide range of air pressures corresponding to streamer dominated regions of sprites [Liu et al., Eos. Trans. AGU, Fall Meet. Suppl., 83, F137, 2002]. The model utilizes a modified Schaffetter-Gummel algorithm for solution of electron convection-diffusion equation [Kulikovskiy, J. Comput. Phys., 119, 149, 1995] and accounts for effects of photoionization on the streamer dynamics [e.g., Kulikovskiy, J. Phys. D: Appl. Phys., 33, 1514, 2000, and references therein]. In this talk we will discuss conditions required for the propagation of streamers in air at different pressures and will present corresponding results from the [Liu et al., 2002] model documenting the minimum electric field magnitudes required for the propagation of positive and negative streamers at sprite altitudes.

**GAIL.04/07P/A08-004** **1505**  
**FULL WAVE ANALYSIS OF ELVES CREATED BY LIGHTNING-GENERATED EMP**

Satoshi YAGITANI, Isamu NAGANO, Kazutoshi MIYAMURA, Satoshi MAKINO, Yoichi NAKAMURA (Graduate School of Natural Science and Technology, Kanazawa University)

Intense electromagnetic pulses (EMPs) radiated from lightning discharges interact with the ionosphere and create the transient optical flashes above thunderstorms referred to as elves at altitudes above 80 km. Corresponding to the EMP propagation up through the ionosphere, elves expand quasi-toroidally up to a few hundreds of km within 1 millisecond after lightning discharges. So far, several studies have modeled the EMP-ionosphere interaction to explain

the observed temporal and spatial aspects of elves with the unmagnetized ionospheric model. In this study, to investigate more exact spatial and temporal structures of elves, we calculate the propagation of lightning-generated EMPs in the magnetized ionosphere on the basis of a full wave analysis. Combining the full wave analysis with spatial and temporal Fourier analysis, we calculate rigorously the temporal and spatial evolution of a lightning-radiated EMP in a horizontally stratified magnetized ionosphere, free space and the ground. Actually in the creation of elves, the intense EMP first heats the ionosphere to enhance electron density and collision frequency there, which should then decay the EMP energy. The full wave analysis, however, cannot treat such temporal changes in ionospheric parameters because it is based on the solution of the linear wave equations in a temporally invariant cold plasma. Here, we approximately incorporate such an effect into the calculation by modifying the EMP propagation in the ionosphere, where the EMP, while going up through the heated region, is equivalently attenuated by the increase in the collision frequency. On the basis of the calculated evolution of the EMP, we evaluate the intensity of ionospheric optical emissions (elves) due to the first positive band of N<sub>2</sub> excited by the EMP. With a midlatitude nighttime ionospheric model and a +CG lightning discharge of 200 kA, calculated results show that the temporal and spatial evolution of elves is quite consistent with the so-far observed behavior of actual elves. It should be noted here that in this case the luminous ring of elves has the appreciable asymmetry in the north-south direction, which is caused by the whistler-mode propagation of the EMP along the geomagnetic field line. On the other hand, a more powerful lightning discharge radiates a more intense EMP, which furthermore enhances the ionospheric collision frequency. With such an over-enhanced collision frequency which is much higher than the electron cyclotron frequency, the whistler mode propagation of the EMP becomes impossible, so that the horizontal structure of the elves ring becomes more or less isotropic, as in the case of the unmagnetized ionosphere.

**GAI.04/07P/A08-005** Invited **1540**

#### THE RESULTS FROM THE 1999 SPRITES BALLOON CAMPAIGN

Edgar Andrew BERING, III<sup>1</sup>, Lekhnath BHUSAL<sup>1</sup>, James R. BENBROOK<sup>1</sup>, Jonathon A. GARRETT<sup>1</sup>, Amy M.P. JACKSON<sup>1</sup>, Eugene M. WESCOTT<sup>2</sup>, Dana R. MOUDRY<sup>2</sup>, Davis D. SENTMAN<sup>2</sup>, Hans C. STENBAEK-NIELSEN<sup>2</sup>, Walter A. LYONS<sup>3</sup> (<sup>1</sup>Department of Physics, University of Houston, <sup>2</sup>Geophysical Institute, University of Alaska, Fairbanks, Alaska, USA, <sup>3</sup>FMA Research, Inc., Yucca Ridge Field Station, 46050 Weld County Road 13, Ft. Collins CO 80524, USA)

A balloon campaign was conducted in summer, 1999, to measure the stratospheric electromagnetic fields associated with sprites. This paper will summarize some of the salient results of this work. The balloon payloads were instrumented with electric field detectors, magnetometers, an upward looking photometer, and other instruments. Ground observations for detection of sprites included low light level TV (LLTV) observations from three sites, Jelm Mt., WY, Bear Mt., SD, and Yucca Ridge, CO. The disagreements between models and these data will be discussed. The all-sky upward looking photometer data was examined by checking the trace at the times of cloud to ground (CG) strokes reported by the US National Lightning Detection Network (NLDN) to find transient luminous events (TLE's) that were missed visually. In total numbers, the number of -CG TLE's (presumably all halos) predominates over the number of +CG TLE's. 3602 events were analyzed in 4.1 hours of storm time. Threshold current moments of ~50 kA-km for the positive cloud to ground (+CG) TLE's and ~5 kA-km for negative cloud to ground (-CG) TLE's are found. Inclusion of the -CG events that are not seen from the ground raises mesospheric power input estimates by a factor of ~5-7. Including the mesospheric effect of CG's not associated with TLE's increases this estimate by a factor of 20.

**GAI.04/07P/A08-006** Invited **1605**

#### ELECTRODYNAMICS OVER SPRITE PRODUCING STORMS

Robert H. HOLZWORTH<sup>1</sup>, Michael P. MCCARTHY<sup>1</sup>, Timothy M. CHINOWSKY<sup>1</sup>, Jeremy N. THOMAS<sup>1</sup>, Michael J. TAYLOR<sup>2</sup>, Dominique PAUTET<sup>3</sup>, Osmar PINTO, JR.<sup>4</sup>, Iara PINTO<sup>5</sup> (<sup>1</sup>Earth and Space Sciences, University of Washington, <sup>2</sup>CASS, Utah State University, <sup>3</sup>DGE/INPE)

We present the latest results from a balloon campaign to measure electrodynamic, optical and X-ray properties of the middle atmosphere over sprite producing storms. The first flight was launched on 6 December 2002 from Cachoeira Paulista, Brazil during a period of active thunderstorms. The balloon floated within 50 km of 279 lightning network cataloged strokes and within 50 to 100 km of another 379 network detected strokes. The instrumentation consisted of optical flash detectors, x-ray spectrometers, and vector electric and magnetic field probes covering the frequency range from DC to 10 kHz. Two different electric field instruments were used in order to cover a wide dynamic range of 0.001 to 250 V/m. By the time of this presentation we expect to have had other successful balloon flights, now scheduled for Feb/Mar 03. Following the Sprite99 campaign (Bering, University of Houston), this campaign is the second effort to make near measurements of conductivity, the quasi-static electric field environment, and electromagnetic changes at sprite-producing thunderstorms. During preparations for the first flight in December 02 we made the first images of sprites from both the ground and airborne in Brazil. During that balloon flight we detected electric field transients related to both positive and negative strokes exceeding 100 V/m (largest detected was > 240 V/m). Interestingly the horizontal electric field component was about two times the magnitude of the vertical component.

**GAI.04/07P/A08-007** **1630**

#### STUDIES ON HYBRID TWEAK MODE WAVE

Koji KAWAKITA, Takeo YOSHINO (Graduate School of Electrical Engineering, Fukui University of Technology)

The author investigated the radiation mechanism of the hybrid tweak wave by means of the data observed at Awaro Space EM Phenomena Observatory of Fukui Univ. of Tech. between 1997 and 2000. Usual tweak wave has the guided mode propagation in wave guide consisting of the earth surface and the bottom region of ionosphere. It has a lower cutoff frequency produced by the dominant mode of wave-guide propagation characteristics at around 1.8 kHz. However, an unusual tweak wave propagates until zero order mode wave extended under the dominant cutoff frequency of usual tweak waves. The author accepted the name of the waves as Hybrid tweak mode wave. In our analysis results, we referred that the occurrence number ratio and the propagation distance of the hybrid tweak mode wave are tendency to affect with the geomagnetic activity. We found the most greatest radiated region of the hybrid tweak mode wave is tendency to concentrate in the geomagnetic 0 degrees dip. And we could obtain the analysis results of determination of source area of the Hybrid tweak wave is concentrated in the region of Borneo and New Guinea area. Accordingly, we considered the excitation characteristics of E.L.F. range (500 Hz) with the vertical components against a plane of the ionosphere by using of the Full wave analysis. At the n=0 mode propagation in the E.L.F. range, the analysing results is shown similar to the terrestrial wave-guide boundaries in the geomagnetic 0 degrees dip surrounded by the perfect conductors. And it is very difficult to apply to the E.L.F. electromagnetic wave components of the hybrid tweak mode wave which propagate to the all directions covered a wide range between the ionosphere and the ground by means of only the terrestrial wave-

guide mode theory. Therefore, we considered the refer to the feasible different propagation mode theory in which E.L.F. wave components has widely propagation path which are not depended on the wave-guide mode theory. As physical image of the Hybrid tweak mode wave propagation, the E.L.F. wave lower than cut-off frequency of the terrestrial dominant mode horizontally propagate along the boundary between the bottom of ionosphere and air as the surface mode, and the another natural radio wave components which higher than cut-off frequency propagate under the multi-reflections between the bottom of ionosphere and ground of the earth followed by the waveguide mode theory. This consideration means that the Hybrid tweak mode wave may be compared to "Hybrid propagation" which have both propagation mode of the surface mode and the waveguide mode. In analysis data, we considered the propagation characteristics in cases of the Hybrid tweak mode wave for E.L.F. wave propagate horizontally along the boundary between the bottom of ionosphere and air by surface mode. Although we could not progress into details about the propagation characteristics on E.L.F. electromagnetic wave which propagate by the surface mode propagation, We attempted to calculate the attenuation coefficients of the surface mode E.L.F. electromagnetic waves which are excited in the horizontal direction against plane of the ionosphere.

**GAI.04/07P/A08-008**

**1645**

#### SPATIAL SELECTIVITY OF THUNDERSTORM ACTIVITY (IMPACT OF LITHOSPHERE)

Igor Ivanovich ROKITYANSKY (Institute of magnetism)

In Ukraine, about 500 meteorological stations were in operation during second half of XX century, covering rather uniformly all the territory with typical spacing between stations 20 - 30 km. Thunderstorms were fixed by visual observations in an area around the station with radius approx. 10 km. Taking into account typical dimensions of thunderstorm clouds, we can expect that essential part of thunderstorms have been recorded. Annual quantity of thunderstorms observed at every station was used as initial data, this quantity averaged over several years (1986-1994) was termed as thunderstorm activity (TSA). The activity varied from 2 to 50, being for majority of stations in interval 20 - 30. Anomalous low TSA (<10) was observed at 28 stations and what is interesting this stations have a tendency to be arranged along several curve lines, some of them are rather long (up to 200 km). And three long lines of decreased TSA turns out to diverge from Chernobyl. When the processing of Ukrainian data was extended to earlier years (i.e. before 1986 - the year, when Chernobyl catastrophe happened), the picture of TSA anomalies turned out to be rather different. It lead to suggestion: Chernobyl catastrophe changed distribution of TSA. It can be explained as follows: radioactivity changes the conductivity of the air and than the conditions of thunderstorm/lightning formation. Comparison of TSA with geophysical, geological and geomorphological data does not reveal any significant correlation. In some books, it is written that TSA has anomalies over prominent geological structures, especially over deep faults, but no quantitative characteristics are given. Quantitative data were received in Siberia. Electrical power lines' pillars there were made usually of wood. Lightning strokes destroyed the pillars. Some pillars are frequently undergo lightning strokes, some - not frequently, some - never. The last ones are clustered into narrow strips, the first two are formed wide areas. It is exactly as were observed in Ukraine. This results suggest that thunderstorm/lightning spatial selectivity manifests some environmental characteristics of lithosphere origin, the most probable of which are: 1) Earth's conductivity which is very variable spatially, but not temporary, 2) Gases emanations from the Earth interior which are very variable both spatially and temporally. They (especially radioactive ones) influence electrical conductivity and other properties of the atmosphere from near the surface to ionosphere strata (which is manifested by earthquakes' precursor study) that should influence both the lightning discharge and thunderstorm cloud formation. Spatial ground selectivity of thunderstorm/lightning activity (lithosphere factor) is the essential aspect in the global electrical circuit study. Lightning spatial selectivity can and should be studied using the data of ground-based long-range detection systems (ZEUS in Europe) as well as satellite data.

**GAI.04/07P/A08-009**

**1700**

#### THIN WIRE REPRESENTATION OF A VERTICAL CONDUCTOR AND ANALYSIS OF ITS SURGE RESPONSE

Osman Md GONI, Hideomi TAKAHASHI, Eiji KANEKO (University of the Ryukyus)

The steel tower surge impedance is one of the basic parameters for the anti-lightning design. Therefore, since Jordan, a lot of experiments and theories are proposed, however, there are no established theories. This is the stumper which is known as "the vertical conductor problem" in the present-day electric engineering. In surge simulations, accurate modeling of a thin wire is necessary to represent transmission wires and steel frames of a building. Comparing the theories of FDTD and MoM, the former is more advantageous to handle 3-D currents in an imperfectly conducting medium. On the other hand, the latter is more advantageous to accurately represent the thin wire ("thin wire" is defined as a conductive wire of which the radius is smaller than the size of a discretized cell used in FDTD and segment length or wavelength in case with MoM). As for surge impedance on a tower model of a vertical conductor, we have a theoretical formula by Lundholm. The theory of Lundholm looks like to be a perfect theory, however, this formula does not coincide with the experimental results. Thus, there is the strange situation that the Jordan's formula of the wrong theory agrees with the experiments more correctly. Hara et al. derived experimental formula. Moreover, one of the authors proposed a theoretical formula of surge impedance; considering the existence of ground surface, and without ground surface. The former formula is very similar to the experimental formula of Hara et al. In this research, these theoretical formulas of surge impedance are examined by the simulation analysis of vertical conductor with the help of Numerical Electromagnetic Code (NEC-2) and the experimental results of that. In the measurement at an actual tower, however, it is difficult to stretch a current lead wire vertically from the tower top, where the current lead wire acts as a vertical lightning channel. Measurements on reduced-scale models are more economical than those on full-sized towers, and are flexible in setting up various experimental arrangements. It is, however, not easy to maintain the accuracy of the measurement, since the geometrical size of the measuring devices is larger relative to the measured system. The simulation and experimental analysis of surge response are carried out in the several arrangements of the current lead wire and the current source. In all the cases, the voltage measuring wire is placed at the perpendicular to the current lead wire. Each of the arrangement of the current lead wire affects the measured surge impedance of the vertical conductor and these will be explained in this research in detail. The experimental set up of the model to be analyzed in this paper is verified with the simulation result of the equivalent circuit model by the EMTP. Finally, this paper also shows a comparison study of FDTD method MoM for the calculations of the surge impedances of the vertical conductor.

**GAI.04/07P/A08-010**

**1715**

#### PROJECT OF MICROSATELLITE TARANIS

Elisabeth BlANC, Taranis team (Commissariat Energie Atomique, Laboratoire de Detection et de Geophysique)

Strong interactions between the middle and upper regions of the atmosphere and ionosphere are manifested by light emission in the middle and upper atmosphere, known as sprites and elves, gamma radiation of atmospheric origin, electromagnetic emissions recently observed above atmospheric storms. This direct coupling between active storm cells, the thermosphere and the ionosphere - and the considerable energies involved - gives rise to processes unsuspected until now regarding space plasmas as well as the chemistry and dynamics of the middle atmosphere. The electromagnetic and particle emissions could derive from the run away relativistic electrons initiated by the impact of cosmic rays on storm cells. These processes can have a significant effect on the Earth's magnetosphere, in particular by modifying the source terms and loss of the radiation belts. The microsatellite Taranis (Tool for the Analysis of RAdiations from lightNings and Sprites) proposes to study the coupling between atmosphere, ionosphere and magnetosphere during atmospheric storms. This has to be carried on a local and global scale in order to understand the physical mechanisms responsible for the impulsive transfers of energy between the neutral atmosphere and plasmas of the ionosphere and magnetosphere. The final goal is to establish the impact of these processes on the Earth's environment. The purpose of this presentation is to describe in a first part the project Taranis, his scientific objectives, the mission and the scientific payload. In a second part the first results of the experiment LSO (Lightning and Sprite Observations), on board of the International Space Station, will be presented. LSO is composed of two micro-cameras, fixed on a ISS window for observations at the horizon or at the nadir. One camera is equipped with a filter and measures the emissions from earth in a specific spectral window, the second works in the visible. The measurements allow the identification of sprites and lightning from space at the nadir. This measurement concept will be used for the camera observations in the future micro-satellite Taranis.

**GAIL.04-Posters**  
**LIGHTNING-INDUCED TRANSIENT PROCESSES IN THE MIDDLE AND UPPER ATMOSPHERE AND THEIR IMPACT ON THE EARTH SYSTEM**  
 Location: Site D

Wednesday, July 9 AM  
 Presiding Chair: H. Fukunishi

**GAIL.04/09A/D-001** Poster **0830-137**  
**ON THE DYNAMICS OF THE NORTH-SOUTH SEASONAL MIGRATION OF GLOBAL LIGHTNING**

Gabriella SATORI (Geodetic and Geophysical Research Institute, Csatkaï u. 6-8., H-9400 Sopron, Hungary)

The daily Schumann resonance (SR) frequency patterns are mainly determined by the lightning source-observer configuration. Four basic types of daily frequency patterns have been distinguished corresponding to the four seasons observed for each SR mode at Nagyecenk, Hungary. The number of days with similar daily frequency patterns (characteristic for a season) were very different. The similar daily frequency patterns (I. type) have been observed during 160-165 consecutive days from the beginning of November to the first part of April in any year of SR observations at Nagyecenk. This means that the position of global lightning, centered on the tropics and the Southern Hemisphere in these months, is rather stable with respect to the observer. The northward migration of lightning in the next season is very fast as only about 40-50 daily frequency patterns show similar characters (II. type) in the months April and May. The number of days with the daily frequency pattern of III. type is 90-100 covering the three summer months (June, July, August) in the Northern hemisphere. The migration of lightning is slower southward than in the opposite direction and it takes about 60-70 days as indicated by the daily frequency patterns of IV. type characteristic mainly in September-October. The dynamics of the north-south migration deduced from SR observations was compared with the dynamics of the mean land surface temperature variations measured in those latitudes of the Northern and Southern hemisphere lands where lightnings mainly occur and in the tropical Pacific. The temperature reaches the highest values and remains very stable in the south tropical Pacific for a rather long period just when the diurnal frequency pattern of I. type can be observed. "Cooling" (only about 1-2 degree C) occurs here in April when global lightning starts its migration to the Northern hemisphere as indicated by SR measurements. Duration of the migration back to the Southern hemisphere coincides with the warming up period in the south tropical Pacific and doesn't fit properly the warming up time in the Southern hemisphere lands. It seems that the dynamics of the north-south lightning migration follows oceanic (Pacific) thermodynamical properties in spite of the fact that the global lightning is mainly concentrated on the lands. This result is in accordance with the meridional redistribution of global lightning as a response to the temperature variations in the tropical Pacific on the ENSO time scale (Sátori and Zieger, 1999)

**GAIL.04/09A/D-002** Poster **0830-138**  
**LIGHTNING LOCATION WITH A SINGLE VLF EM RECEIVER**

Isamu NAGANO, Satoshi YAGITANI, Hisao KOMONMAE (Graduate School of Natural Science and Technology, Kanazawa University)

VLF radio pulses (spherics) generated by lightning discharges have been used to detect the locations of the discharges. As seen in the U.S. national lightning detection network (NLDN), one of the widely used systems utilizes the VLF receivers placed at a couple of stations to perform the direction finding and the time-of-arrival measurements of spherics. Such a system, however, requires to construct an expensive network of synchronized multiple electromagnetic sensors installed at different sites over a wide area. In this work, we have developed a simple and cheap system with just a single VLF electromagnetic (EM) receiver to locate lightning discharges, which can determine both the direction and range of each lightning returnstroke. With this system, we observe wave forms of two horizontal magnetic fields and of one vertical electric field of VLF spherics. The waveform of each VLF spheric usually consists of a couple of sequential pulses. The first pulse comes directly from a lightning returnstroke, and is used for the direction finding of the stroke. The second and later pulses represent the multiple reflections of the first pulse between the ionosphere and the ground. The difference in the time-of-arrival of each set of adjacent pulses is determined by the difference in their multi-hop propagation path lengths in the Earth-ionosphere waveguide. By using the time-of-arrival differences between two or more pulses, we can inversely estimate both the reflection height of the ionosphere and the range of the lightning stroke. In our developed system two orthogonal horizontal magnetic components and one vertical electric component of spherics are measured with two sets of loop antennas and a vertical wire dipole antenna, respectively. Their wave forms are band-limited between 1

and 14 kHz and then digitized, where the whole wave forms of individual spherics are automatically recorded. By extracting a sequence of pulses from each of the recorded spheric wave forms, the system calculates the direction and range of the corresponding lightning stroke. With this system installed at Kanazawa University, we have so far acquired thousands of lightning-generated spherics, including the +CG strokes in winter (characteristic of Japanese Hokuriku Region around Kanazawa) as well as the -CG lightning strokes in other seasons. Compared with the lightning location data provided by a local power company (which makes use of the conventional system with a couple of receivers set at different stations), it is confirmed that our system can locate each of the lightning strokes within several hundred km with fairly good accuracy. We are planning to apply this technique to develop a portable lightning detector carried, for example, by airplanes or ships cruising over remote areas with no lightning detection networks available.

**GAIL.04/09A/D-003** Poster **0830-139**  
**A DEVELOPMENT OF OBSERVATION SYSTEM AND INITIAL RESULTS FOR THE SIMULTANEOUS MEASUREMENT OF SPRITES AND HORIZONTAL ELECTRIC CURRENTS IN THE LIGHTNING DISCHARGE**

Atsushi OHKUBO<sup>1</sup>, Hiroshi FUKUNISHI<sup>1</sup>, Yukihiko TAKAHASHI<sup>1</sup>, Isamu NAGANO<sup>2</sup> (<sup>1</sup>Department of Geophysics, Tohoku University, <sup>2</sup>Department of Informations and Systems Engineering, Kanazawa University)

Sprites are atmospheric luminous events induced by cloud-to-ground discharges (CGs) at the altitude of 50-90 km, which are considered generated by quasi-electrostatic field caused by the CG. There are still many open questions on the occurrence and the generation mechanism of sprites and related phenomena. For example, what determine the horizontal distributions of sprite streamers and various sprite occurrence time lags from the parent CG. Horizontal electric current in intra-cloud discharge, cloud-to-cloud discharge and as a horizontal component of cloud-to-ground discharge are thought to be an explanation for these issues as suggested by some authors (ex. Cho et al., 2001; Bell et al., 1997). However, simultaneous observations of sprites and horizontal electric currents associated with lightning discharges have not been carried out up to now. In order to investigate the role of horizontal electric currents in sprite generation mechanism, we have developed a three-component dipole antenna system for an electric field measurement of spherics. These three electric field antennas are oriented in vertical, north-south and east-west directions, respectively. We operated this antenna system with two horizontal loop antennas for magnetic field at Iitate observatory, Fukushima (37.7°N, 140.7°E) in January 2003. On the other hand, we observed sprites by an image-intensified CCD imager and a multi-anode array photometer at the observatory. Further, we employed another two horizontal loop antenna system at Yamanashi Prefectural Science Center (35.40°N, 138.40°E), to determine the CG locations. The frequency range of electric field antenna system are from 10 Hz to 30 kHz and that of magnetic field antenna system are 1 to 30 kHz, covering VLF range in which spherics have the highest spectral power. The electric and magnetic field data of spherics are recorded in the audio channels of VHS videotape. We will present the detail description of the new system and initial observational results. Especially we will discuss about the identification of horizontal electric currents in lightning discharges.

**GAIL.04/09A/D-004** Poster **0830-140**  
**INVESTIGATION OF WINTERTIME SPRITES AND THEIR PARENT THUNDERSTORM SYSTEMS IN JAPAN**

Toru ADACHI, Hiroshi FUKUNISHI, Yukihiko TAKAHASHI (Department of Geophysics, Tohoku University)

Sprites are transient luminous events at the altitude of the mesosphere induced by cloud-to-ground discharges. To investigate the relationship between the sprites and their parent thunderstorm systems in winter of Japan, we have carried out the Wintertime Sprite Campaign for four winter seasons since 1998. During these periods, we captured 55 sprites with two multi-anode array photometers (MAPs), image intensified CCD cameras (IICCDs) and VLF spherics receivers. Each MAP has 16 channels arrayed in vertical and time resolution of 50 μs, which enables us to detect the rapid vertical motion of sprites. The result of data analysis demonstrates that winter sprites occurred above both the Sea of Japan and the Pacific Ocean. However, the characteristics of sprites observed in these two regions are different. That is, columniform sprites are observed above the Sea of Japan, while carrot sprites are observed above the Pacific Ocean. By combining the sprite data with GMS satellite infrared images, temperature profiles obtained from the observation of Rawinsonde or the MSISE-90 model and ground-based radar precipitation maps, we found that sprites above the Sea of Japan usually occur just above cold fronts. In minor cases, however, sprites occur after cold fronts have reached the Pacific Ocean. In both cases, it is likely that precipitation particles play an important role for sprite generation. Further, we classify winter sprites based on their occurrence regions, meteorological conditions, the characteristics of parent thunderstorms and cloud-to-ground discharges.

**GAIL.04/09A/D-005** Poster **0830-141**  
**SPRITES OBSERVATION IN NORTHERN SCANDINAVIA**

Yukihiko TAKAHASHI<sup>1</sup>, Mitsuteru SATO<sup>1</sup>, Satonori NOZAWA<sup>2</sup>, Hiroshi FUKUNISHI<sup>1</sup>, Ryoichi FUJII<sup>1</sup> (<sup>1</sup>Department of Geophysics, Tohoku University, <sup>2</sup>Solar-Terrestrial Environment Laboratory, Nagoya University)

It has been well known that the summer thunderstorm that has a large horizontal extent and a fairly high cloud top sometimes produce sprites and elves, transient luminous emissions induced by cloud to ground (CG) lightning discharges. Large amounts of charge removal by positive CG which often take place in a big thunderstorm are thought to be a requirement for sprites. However, in 1998 activities of sprites and elves were discovered in the west coast of Japan when a cold front passed over Japan. Now it has been recognized that these emissions occasionally appear also in the Pacific Ocean around Japan in wintertime. These facts strongly imply some occurrence of sprites and elves in other areas, such as Northern Scandinavia where large positive CGs are observed in wintertime like as in the west coast of Japan. If we can detect sprites and/or elves in the polar region, the interaction between the lightning-induced phenomena and the polar ionosphere/magnetosphere would be quite interesting. Computer simulation study shows an electron density enhancement by ~10 times associated with elves, suggesting a modulation of ionospheric currents. If the internal quasi DC current in sprite connects to field aligned current in the magnetosphere, an appearing aurora feature might be modified. Further, it is predicted that sprite-related CGs can make upward runaway electrons which incident into the magnetosphere. In order to search and investigate sprites and elves occurring in Scandinavia, we installed an image-intensified CCD camera at ESRANGE, Kiruna, Sweden in November 2002. The camera directed to the northwest covers 30 degree horizontally and its gain is adjusted automatically. The data are recorded in D-VHS videotapes. Actual operation of the camera and video recorder is conducted from Japan by an internet-controlled power supply, according to the weather information on web pages. Lightning data including location and peak current are provided by a Swedish company. Combining sprites and elves images with

EISCAT, ground-based magnetometer, and polar orbiting satellite data, we will examine the physical interactions between sprites/elves and the ionosphere/magnetosphere in detail.

**GAII.04/09A/D-006** Poster **0830-142**

**NUMERICAL MODELING OF SPRITES FOR THEIR ENERGETICS AND CHEMICAL EFFECTS ON THE MIDDLE ATMOSPHERE**

Yasutaka HIRAKI<sup>1</sup>, Lizhu TONG<sup>2</sup>, Hiroshi FUKUNISHI<sup>1</sup>, Ken-ichi NANBU<sup>2</sup>, Yukihiko TAKAHASHI<sup>1</sup>, Yasuko KASAI<sup>1</sup> (<sup>1</sup>Department of Geophysics, Tohoku University, <sup>2</sup>Institute of Fluid Science, Tohoku University, <sup>3</sup>Communications Research Laboratory)

Using our newly developed field and particle model, we have performed numerical simulations on the energetics and dynamics of sprites. In addition to ionization, dissociation and excitation processes, photoionization processes due to EUV emission, which are caused by high-energy electrons, are included in our model. We derived the non-Maxwellian energy distribution function of electrons accelerated by a large electric field in the middle atmosphere above thunderstorms. The temperatures of electrons can be estimated and are compared with the results of previous observations. Temporal evolution of optical emissions is also discussed, focusing our attention on the effect of photoionization processes, and the results are compared with observations. Further, we have investigated the chemical effects of sprites on ions and neutral species. Our preliminary results presented in the AGU Fall meeting in December 2002 are examined in details, using our particle simulation code. We estimated the total amount of ions and atomic neutrals produced by each sprite event. By substituting the calculated production rates of these particles into a 1-D chemical transport model, we will discuss the effect of sprites on the mesospheric ozone chemistry.

**GAII.04/09A/D-007** Poster **0830-143**

**THE EFFECTS OF THE THUNDERCLOUD OF REVERSE ELECTRIC POLARITY ON THE NIGHTTIME E REGION IONOSPHERE**

Vitalii P. KI M, Valerii V. HEGAI (IZMIRAN, Troitsk, Moscow Region, 142190 Russia)

The large thunderclouds of reverse polarity, with the negatively-charged upper part and the positively-charged bottom part, are frequently associated with intense upward electric discharges accompanied by sprites, elves, and blue jets. In this paper, we have modeled the effects exerted by the quasi-static electric field of the thundercloud of reverse electric polarity on the nighttime E region ionosphere. Calculations are made with and without allowance for the presence of metal ions. The results show that the electron density substantially increases in the middle part of the E region over the thundercloud. If the background ionospheric plasma contains a minor admixture of metal ions, the sporadic Es layer can be formed at about 120-km altitude.

**GAII.05-Posters**

**DATA ASSIMILATION TECHNIQUES FOR THE IONOSPHERE-THERMOSPHERE-MAGNETOSPHERE SYSTEM**

Location: Site D

Monday, July 7 AM

**GAII.05/07A/D-001** Poster **0830-017**

**GLOBAL ASSIMILATION OF IONOSPHERIC MEASUREMENTS (GAIM)**

Robert W. SCHUNK<sup>1</sup>, Ludger SCHERLISS<sup>1</sup>, Jan J. SOJKA<sup>1</sup>, Donald C. THOMPSON<sup>1</sup>, David N. ANDERSON<sup>2</sup>, Mihail CODRESCU<sup>3</sup>, Cliff MINTER<sup>2</sup>, Timothy J. FULLER-ROWELL<sup>2</sup>, Roderick A. HEELIS<sup>3</sup>, Marc HAIRSTON<sup>3</sup>, Bruce M. HOWE<sup>4</sup> (<sup>1</sup>Center for Atmospheric and Space Sciences, Utah State University, Logan, UT 84322-4405, <sup>2</sup>NOAA/Space Environment Center, Department of Commerce, 325 Broadway, Boulder, CO 84303, <sup>3</sup>W B Hanson Center for Space Sciences, University of Texas at Dallas, PO Box 830688, MS F022, Richardson, TX 75083-0688, <sup>4</sup>Applied Physics Laboratory, University of Washington, 1013 NE 40th Street, Seattle, WA 98105.)

The ionosphere is a highly dynamic medium that can vary significantly from day to day and from hour to hour at a given location, and these variations can have detrimental effects on military and civilian systems. In an effort to minimize or circumvent the detrimental effects, a physics-based data assimilation model of the ionosphere and neutral atmosphere is under development with funding from the Multi-Disciplinary University Research Initiative (MURI) program. Two university consortia are involved, with Utah State University (USU) and University of Southern California (USC) as the lead institutions. When completed, the GAIM model will provide specifications and forecasts on a spatial grid that can be global, regional, or local (50 km x 50 km). GAIM will use a physics-based ionosphere-plasmasphere-polar wind model and a Kalman filter as a basis for assimilating a diverse set of real-time (or near real-time) measurements. Some of the data to be assimilated include in situ density measurements from satellites, ionosonde electron density profiles, occultation data, ground-based GPS TECs, TECs between ground stations and LEO satellites with radio beacons, and line-of-sight UV emissions from selected satellites. The resulting specifications and forecasts will be in the form of 3-dimensional electron density distributions from 90 km to geosynchronous altitude (35,000 km). Auxiliary parameters will also be available, including  $N_e$ ,  $h_p$ ,  $N_e$ ,  $h_p$ ,  $N_e$ , and slant and vertical TEC. In addition, GAIM will provide global distributions for the ionospheric drivers (neutral winds and densities, magnetospheric and equatorial electric fields, and particle precipitation patterns), and in its specification mode, it will provide quantitative estimates for the accuracy of the reconstructed ionospheric densities. The overall program involves model construction, data quality assessment, data assimilation, construction of an executive system to automatically run the model, validation, and science. An initial form of GAIM already exists and recent results from the USU consortium will be presented. Also, there will be a discussion of the real-time data sources that will become available during the coming decade.

**GAII.05/07A/D-002** Poster **0830-018**

**HE+ DENSITY ISS-B SATELLITE DATA IN EMPIRICAL AND STATISTICAL TOPSIDE IONOSPHERE SIMULATION**

Larissa SIDOROVA (Institute of Terrestrial Magnetism, Ionosphere and Radiowave Propagation, Troitsk, Moscow region, 142190, RUSSIA, E-mail: lsid@izmiran.rssi.ru)

As repeatedly pointed out, there are serious shortcomings in the International Reference Ionosphere model (IRI) especially in upper topside and at high solar activity. The topside He+ density profiles, obtained at ~ 1100 km heights during 1978-1979 years (high solar

activity period) on ISS-b satellite data, were compared with IRI model data. The comparison reveals the large discrepancy in the regions of the low and, especially, middle latitudes, where the diurnal and seasonal He+ density profiles are overestimated in IRI by a factor of 10 and more. It seems the prominent feature of the topside ionosphere, as mid-latitude He+ density trough, LIT, is reflected in IRI topside model hardly. The present study deals with He+ density topside modeling at middle and low latitudes at high solar activity period. Since only He+ density was regularly measured onboard of ISS-b, He+ density profiles were under consideration. Mid-latitude He+ density troughs, LIT, and other distinct structure as He+ density subtroughs, located equatorward than LIT, are studied. The obtained He+ density characteristics are used for empirical and statistical simulation. (a) The He+ density profiles as functions of local time, season and longitude were obtained as empirical topside data in the different latitudinal areas. (b) The LIT occurrence statistics as function of local time, season, longitude and Kp activity was produced. For example, by day the He+ density LITs are seen more often in summer (P ~ 30%) than in winter (P ~ 5 to 10%). At night they do quite often occur in winter (P ~ 40 to 60%) than in summer (P ~ 35 to 55%). LIT probability is weakly dependent on magnetic activity. (c) The He+ density subtrough occurrence statistics as function of local time, latitude and season was obtained and mapped. Subtroughs are less frequent phenomena than LITs, but they are more frequent than it was expected from the literature analysis. So, according to ISS-b data, they were revealed in ~ 570 cases in ~ 4000 passes in a very broad latitudinal interval (25-58°A). For example, by day the subtroughs are observed rather seldom but stable in summer (P ~ 7 to 12%) and only in exclusive cases in winter. They are more often observed under nighttime conditions in winter (P ~ 30%) than in summer (P ~ 5-10%). Obtained empirical topside data and statistics could be very useful for further IRI development. For example, topside statistics is possible to use as empirical description in the IRI prediction scheme like the spread F occurrence statistics is used.

**GAII.05/07A/D-003** Poster **0830-019**

**SPECIFICATION AND PREDICTION OF DYNAMIC PROCESS IN IONOSPHERE**

Jian-shan GUO, Jiankui SHI, She-ping SHANG, Manlian ZHANG, Xigui LUO, Hong ZHENG (Laboratory for Space Weather, Center for Space Science and Applied Research, Chinese Academy of Sciences)

Specification and prediction of ionospheric weather are the key scientific pursuits of ionospheric physicists. However, not any arbitrary combination of a dynamic process and an observation system possesses possibility of specification and prediction for the dynamic process. Specification and prediction are essentially the state estimations of the dynamic process for current and beyond current time respectively from observation available at current time. This estimation procedure largely based on a random dynamic system, which consists of dynamic process, observation system and optimal estimation procedure. We attempt to give a complete framework in this paper under which the specification and prediction procedure carries through. Based on the procedure, the observability, the specificatability and the predictability of the dynamic process are discussed. We discuss some crucial issues as follows: modeling a specific dynamic process in the ionosphere as a random dynamic system in state space; state and its uncertainty estimation for the dynamic process; the observability of an observation system, the specificatability and predictability of the dynamic process. As an example, a second order dynamic system is discussed in a specific manner to illustrate the specification and prediction procedure, ranging from modeling the system, specification, prediction and their uncertainty calculation. The analysis shows that the key issue of specification and prediction are the state and parameter estimation for the dynamic process. Suppose the state and parameter of a dynamic process  $s(t+a)$  are estimated by output  $g(t)$  of the random dynamic system, the estimations are the specification as  $a=0$ , the prediction as  $a>0$ , and interpolation as  $a<0$ . The specificatability and predictability are determined by the possibility of retrieval of  $s(t+a)$  from  $g(t)$  as  $a=0$  and  $a>0$  respectively, and quantitatively defined by observable and controllable matrix of the system. The estimation technique, due to its optimization and integration features, could obtain better accurate results than those obtained by dynamic process, measurement or their statistical analysis alone. More attention for dynamic estimation procedure creation should be paid to transition matrix finding, which is usually not easy for practical ionospheric weather system. High performance computing hardware and software studies should be promoted further so as to meet the requirement of large storage and extensive computation in the optimal estimation. The random dynamic system discussed in the paper is in a very general form, so the main results are applicable to other dynamic fields such as atmosphere, space and geophysics in case of without difficulty for modeling the dynamic process in state space. The discussion in this paper is appropriate for the static or steady state or transition process of dynamic system. Many phenomena in atmosphere and space environment are unstable and chaos, so the dynamic study should include and integrate these two branches of learning. References: Jian-shan Guo, et al., Optimal assimilation for ionospheric weather: theoretical aspect, presented at World Space Environment Forum, July 22-25, 2002, Adelaide, Australia; accepted to be published in Space Science Reviews Goodwin, G.C. and Sin K.S., Adaptive filtering, prediction and control, Prentice Hall, 1984

**GAII.05/07A/D-004** Poster **0830-020**

**PLASMA TEMPERATURES FROM ACTIVE**

Ludmila TRISKOVA<sup>1</sup>, Vladimir TRUHLIK<sup>1</sup>, Jan SMILAUER<sup>1</sup>, Nella SMIRNOVA (<sup>1</sup>Department of Upper Atmosphere, Institute of Atmospheric Physics ASCR, <sup>2</sup>Space Research Institute, Russian Academy of Sciences)

Ion temperature (Ti) and related electron temperature (Te) distributions have been analyzed on the base of data measured by Radiofrequency Probe and Retarding Potential Analyzer onboard the main satellite of the ACTIVE mission (Interkosmos 24, perigee 500 km, apogee 2500 km, inclination 83 deg). Results from the period 1989-1991 have been analyzed. About 200000 I-V characteristics were evaluated so far. For each Ti value corresponding Te (from radiofrequency probe) was assigned. Only temperatures from intervals with both Ti and Te available were processed. Consistency of the obtained data is discussed. Measured Ti is compared with that modeled by IRI2001 (International Reference Ionosphere). Millstone Hill incoherent scatter results are also shown. At the altitude of 550km the measured Ti data and IRI model are in agreement, and both are relatively close to the Millstone-Hill ISR model. At higher altitudes during the daytime the IRI values are systematically higher than the measured Ti.

**GAII.05/07A/D-005** Poster **0830-021**

**THE ASSIMILATION OF GROUND AND SPACE GPS TEC MEASUREMENTS IN THE GLOBAL ASSIMILATIVE IONOSPHERE MODEL (GAIM)**

George A. HAJJ<sup>1</sup>, Xiaoping PI<sup>1</sup>, Gary ROSEN<sup>1</sup>, Paul STRUAS<sup>2</sup>, Chunming WANG<sup>1</sup>, Brian WILSON<sup>3</sup> (<sup>1</sup>University of Southern California, <sup>2</sup>Aerospace Corporation, <sup>3</sup>Jet Propulsion Laboratory)

As the number of ground and space-based receivers tracking the global positioning system (GPS) steadily increases, and ionospheric remote sensing data such as measurements of airglow become available, it is becoming possible to monitor changes in the ionosphere



continuously and on a global scale with unprecedented accuracy and reliability. This is best achieved by means of data assimilation using a 4-dimensional (4DVAR) scheme or a recursive statistical estimation approach such as the Kalman filter. Our presentation will review the development of a Global Assimilative Ionospheric Model (GAIM) at the University of Southern California and the Jet Propulsion Laboratory capable of assimilating various types of data including ground and flight GPS total electron content (TEC), ionosondes and airglow measurements. The recursive estimation technique is used to the determination of electron density with a relatively short data assimilation cycle of ~15 minutes. The 4DVAR technique is used to estimate the ionospheric driving forces with a longer data assimilation cycle of ~ 2 hours. The optimized ionospheric state variables and driving forces are then used in the forward model to produce new forecasts for ionospheric variables. The evaluation of either approach is first made through Observation System Simulation Experiments (OSSE) in which simulated measurements derived from forward model output are used. Our presentation will describe GAIM and examine its analyses by assimilating GPS TEC data from nearly 100 global ground stations and the currently operating GPS flight experiments, CHAMP, SAC-C, GRACE and IOX. A series of GAIM retrievals will be presented and validated by comparisons to: vertical TEC data from the TOPEX altimeter, UV measurements, slant TEC data from ground GPS sites not used in the assimilation, and a global network of ionosondes.

**GAIL.05/07A/D-006** Poster **0830-022**  
**ESTIMATION OF IONOSPHERIC DYNAMICAL DRIVERS USING A GLOBAL ASSIMILATIVE IONOSPHERIC MODEL**

Xiaoqing PI<sup>1</sup>, Chunming WANG<sup>2</sup>, George A. HAJJ<sup>1</sup>, Gary ROSEN<sup>2</sup>, Brian D. WILSON<sup>1</sup> (Jet Propulsion Laboratory, California Institute of Technology, <sup>2</sup>University of Southern California)

A global assimilative ionospheric model (GAIM) has been developed by the consortium of University of Southern California and Jet Propulsion Laboratory. The model is capable of assimilating various types of ionospheric measurements, such as line-of-sight total electron content (TEC) and satellite limb scans of ultraviolet airglow emission, to optimize the modeling of ionospheric volume densities. Among the assimilation techniques developed with GAIM, a 4-dimensional variational (4DVAR) approach allows the estimation of model drivers that satisfies the requirements of minimizing the difference between observations and model predictions on regional and global scales. Observation system simulation experiments (OSSE) have been conducted with the global positioning system (GPS) and the IGS global ground-based network. The experiment results show that using GAIM and the 4DVAR technique with the existing GPS observation system, it is promising to solve for simultaneously zonal electric field and thermospheric meridional wind that play key roles in the evolution of equatorial spread-F irregularities. Validation of the assimilative modeling techniques is also conducted in the Pacific and South America regions with multi-diagnostic observation techniques. The framework of the validation effort and preliminary results will be presented at the meeting.

**GAIL.05**  
**DATA ASSIMILATION TECHNIQUES FOR THE IONOSPHERE-THERMOSPHERE-MAGNETOSPHERE SYSTEM**  
 Location: Site A, Room 15

Tuesday, July 8 AM  
 Presiding Chair: R.W. Schunk

**GAIL.05/08A/A15-001** **0830**  
**SOLAR WIND DRIVEN RADIATION BELT RESPONSE FUNCTIONS: DATA ASSIMILATION METHODS FOR CHARACTERIZING RADIATION BELT DYNAMICS**

E. Josh RIGLER<sup>1</sup>, Daniel N. BAKER<sup>1</sup>, Dimitris VASSILIADIS<sup>2</sup> (<sup>1</sup>LASP/Univ. of Colorado at Boulder, <sup>2</sup>Goddard Space Flight Center)

Characterizations of radiation belt dynamics using linear prediction filters (LPFs) were first published by Nagai (1988) and Baker et al. (1990). These studies focused primarily on short-term predictions of daily-averaged radiation fluxes at geostationary orbit using global magnetospheric indices and the speed of the solar wind impinging on the earth's magnetosphere. More recent work by Moorer and Baker (2000) focused on 4-dimensional data assimilation methods to specify with very high accuracy the outer radiation belt fluxes at all spatial locations. Using solar wind data from the NSSDC OMNI database and SAMPEX 2-6 MeV omnidirectional electron fluxes at various magnetic L-shells, new analyses have used multi-input, adaptive local-linear response functions to describe the evolving response of relativistic radiation belt electrons to solar wind input. Physical interpretations and implications can be gleaned by applying this powerful data analysis technique. This can include a partial separation of adiabatic and non-adiabatic responses to changing solar wind conditions. Extension of present methods holds the hope of ingesting data from numerous operational spacecraft in real time and subsequently specifying (or forecasting) radiation properties at any chosen point in the Earth's magnetosphere.

**GAIL.05/08A/A15-002** **0850**  
**MAGNETOSPHERIC DATA ASSIMILATION**

Joachim RAEDER (IGPP, University of California)

Data assimilation (DA), that is, the ingestion of data into large-scale numerical models was first introduced into numerical weather prediction models in order to overcome the problem of insufficient data for model initialization. It is now a standard procedure that is used in all contemporary forecast models. Following the success in atmospheric models, DA has been introduced into oceanic, and most recently into ionospheric specification and forecast models. No serious attempts have yet been made to incorporate DA techniques into global magnetospheric models. The prime reason is the lack of sufficient data. However, there are also other issues. While DA in the before mentioned areas primarily addresses an initialization problem, the magnetosphere is much more a driven system with relatively short memory. The magnetosphere is also characterized by discontinuous field variables and other constraints, such as the requirement that divergence of the magnetic field vanishes. These issues make the application of standard DA procedures difficult. In this talk I shall outline the problems that lie ahead of us to introduce DA into global magnetosphere models and possible pathways for a successful DA implementation.

**GAIL.05/08A/A15-003** **0920**  
**IONOSPHERIC DATA ASSIMILATION IN GAIM**

Ludger SCHERLIESS, Robert W. SCHUNK, Jan J. SOJKA, Donald C. THOMPSON (Center for Atmospheric and Space Sciences)

With the significant increase in the number of ionospheric observations that will become available over the next decade, ionospheric data assimilation will provide a powerful tool toward an improved specification and forecasting of the global ionosphere, with an unprecedented accuracy and reliability. A physics-based data assimilation model of the ionosphere is under development as the central part of a DoD MURI funded program called GAIM (Global Assimilation of Ionospheric Measurements). The goal of this effort will be the development of an operational ionospheric assimilation model that will provide specifications and forecasts on spatial grids that can be global, regional, or local (50 km x 50 km). This specification/forecast will be in the form of 3-dimensional electron density distributions from 90 km to geosynchronous altitudes (35,000 km). GAIM will use a physics-based ionosphere-plasmasphere model and a Kalman filter as a basis for assimilating a diverse set of real-time (or near-real-time) measurements. In addition, to the physics-based Kalman filter, we have developed a Gauss-Markov Kalman filter model. For both of these models, we have assimilated several data types, including in situ electron density measurements from DMSP satellites, bottomside electron density profiles from the Air Force network of digisondes, GPS-TEC from a global network of more than 100 ground stations, and GPS-TEC from more than 300 stations in the CORS network (over the U.S.). In this paper we give an update on the model development and present initial results from the two models and a validation using independent data sources.

**GAIL.05/08A/A15-004** **0950**  
**NEW DATA SOURCES TO DRIVE AN ASSIMILATING MODEL FOR THE IONOSPHERE**

Robert P. MCCOY (Code 321SR, Office of Naval Research)

Existing operational models used to specify and forecast the global ionospheric electron density are either empirical or climatological and do not use data assimilation techniques. This is due to the relatively small amounts of data that have been routinely available. Ionospheric data types used operationally include a few ground-based digisondes, in-situ plasma data on weather satellites and total electron content (TEC) measurements using about three dozen land-based dual frequency GPS receivers. The sum of these measurements is small compared to the five million+ measurements assimilated daily into meteorological forecast models. This situation is about to change dramatically when the Defense Meteorological Satellite Program (DMSP) begins launching its next block of weather satellites (currently scheduled for Spring 2003). Each satellite will have a pair of ultraviolet spectrographs to produce images of ionospheric airglow in the both the limb and nadir cross-track directions. These images will be used to infer electron density profiles and nadir TEC measurements along the satellite orbits and should yield more than a million electron column measurements per day. Additional new ionospheric data sources, which should be routinely available in the near future, include GPS occultation measurements (e.g. COSMIC constellation) and computerized ionospheric tomography (CIT) using the existing Transit (and similar) dual frequency UHF radio beacons on low Earth orbiting satellites. With these new and large data sets in mind, the Office of Naval Research (ONR) is sponsoring the development of an assimilating model for the ionosphere. The sponsorship is in collaboration with the Director Defense Research and Engineering and the Air Force Office of Scientific Research. This new model will assimilate these data and other potential new data sources including a geosynchronous ultraviolet ionospheric imager currently under development.

**GAIL.05/08A/A15-005** **1040**  
**VALIDATION OF A GLOBAL IONOSPHERIC DATA ASSIMILATION MODEL**

Brian D. WILSON<sup>1</sup>, George HAJJ<sup>1</sup>, Chunming WANG<sup>2</sup>, Xiaoqing PI<sup>1</sup>, Gary ROSEN<sup>2</sup> (Jet Propulsion Laboratory, Caltech, <sup>2</sup>Dept. of Mathematics, University of Southern California)

As the number of ground and space-based receivers tracking the global positioning system (GPS) steadily increases, and the quantity of other ionospheric remote sensing data such as measurements of airglow also increases, it is becoming possible to monitor changes in the ionosphere continuously and on a global scale with unprecedented accuracy and reliability. However, in order to make effective use of such a large volume of data for both ionospheric specification and forecast, it is important to develop a data-driven ionospheric model that is consistent with the underlying physical principles governing ionosphere dynamics. A fully 3-dimensional Global Assimilative Ionosphere Model (GAIM) is currently being developed by a joint University of Southern California and Jet Propulsion Laboratory team. GAIM uses a first-principles ionospheric physics model ("forward" model) and Kalman filtering and 4DVAR techniques to not only solve for densities on a 3D grid but also estimate key driving forces which are inputs to the theoretical model, such as the ExB drift, neutral wind, and production terms. The driving forces are estimated using an "adjoint equation" to compute the required partial derivatives, thereby greatly reducing the computational demands compared to other techniques. For estimation of the grid densities, GAIM uses an approximate Kalman filter implementation in which the portions of the covariance matrix that are retained (the off-diagonal elements) are determined by assumed but physical correlation lengths in the ionosphere. By selecting how sparse or full the covariance matrix is over repeated Kalman filter runs, one can fully investigate the tradeoff between estimation accuracy and computational speed. Although GAIM will ultimately use multiple datatypes and many data sources, we have performed a first study of quantitative accuracy by ingesting GPS-derived TEC observations from ground and space-based receivers and nighttime UV radiance data from the LORAAS limb scanner on ARGOS, and then comparing the retrieved density field to independent ionospheric observations. A series of such GAIM retrievals will be presented and validated by comparisons to: vertical TEC data from the TOPEX altimeter, slant TEC data from ground GPS sites that were not included in the assimilation runs, and global ionosonde data (F0F2, HMF2, and bottom-side profiles where available). By presenting animated movies of the GAIM densities and vertical TEC maps, and their errors computed as differences from the independent observations, we will demonstrate the reasonableness and physicality of the climatology derived from the GAIM forward model, examine the consistency of the GPS and UV datatypes, and characterize the quantitative accuracy of the ionospheric "weather" specification provided by the assimilation retrievals.

**GAIL.05/08A/A15-006** **1100**  
**IONOSPHERE SOUNDING BY GPS MEASUREMENTS ON CHAMP**

Norbert JAKOWSKI<sup>1</sup>, Stefan HEISE<sup>2</sup>, Konstantin TSYBULYA<sup>1</sup>, Andreas WEHRENPENNIN<sup>3</sup> (<sup>1</sup>Deutsches Zentrum fuer Luft- und Raumfahrt (DLR), Institut fuer Kommunikation und Navigation, <sup>2</sup>GeoForschungsZentrum Potsdam (GFZ), Division 1, Telegrafenberg, Potsdam, Germany, <sup>3</sup>Hochschule Neubrandenburg, Neubrandenburg, Germany)

GPS measurements onboard the German CHAMP (CHALLENGING Minisatellite Payload) satellite provide a good possibility for operational sounding the ionosphere on global scale. Both the radio occultation measurements and the navigation measurements made by using the upward looking GPS antenna have a big potential to reconstruct the spatial and temporal distribution of the electron density in the ionosphere. To fulfill operational requirements, the Ionospheric Radio Occultation (IRO) data are processed in an automatically working processing unit that provides electron density profiles within 3 hours after data dump from CHAMP. More than 50000 vertical electron density profiles have been obtained since the beginning of ionospheric radio occultation (IRO) measurements on 11 April 2001 by using a model assisted retrieval technique. Although comprehensive validation work is not yet finished, IRO data products are made available to the international science community via the ISDC of the GFZ Potsdam. At present about 150 electron density profiles from global scale are retrieved by the processing system. Recent validation results are reported. To obtain a more comprehensive view on the spatial and temporal electron density distribution, the 0.1 Hz sampled dual frequency navigation measurements are used to derive the total electron content (TEC) along the ray paths between the CHAMP and GPS satellites. After assimilating these integral measurements into the Parameterized Ionospheric Model (PIM) of local electron density it is possible to reconstruct the spatial electron density distribution close to the CHAMP orbit plane. This technique has also the capability to run in an operational mode for providing near-real-time data into forecast models for space weather applications.

**GAIL.05/08A/A15-007****1130****AN ON-LINE DATABASE FOR IONOSPHERIC THERMAL PLASMA DATA FROM DMSP**

Marc R. HAIRSTON, William R. COLEY, R.A. HEELIS (Center for Space Sciences, University of Texas at Dallas)

Since 1987 the polar orbiting meteorological satellites in the DMSP program have carried a package of instruments for measuring parameters of the thermal plasma in the topside ionosphere (~840 km). This instrument package (known as SSIES) measures all three components of the bulk flow of the plasma, the ion and electron temperatures, the total plasma density and the fractional composition of O<sup>+</sup>, H<sup>+</sup> and He<sup>+</sup>. To date eight satellites (DMSP F8 through DMSP F15) have flown with the SSIES package on board returning a total of over 45 satellite-years of data which span one and a half solar cycles. This database provides a tremendous scientific resource for the ionospheric community and numerous research projects and papers have already been based on these data. However its usefulness has been limited because of the sheer volume of data and the difficulty in distributing these data easily to the community. To solve this, we have set up a web-based distribution service of a subset of these data covering the past solar maximum period of 2000 through 2002. (The URL is <http://cindispace.utdallas.edu/DMSP/>) This talk will outline the scope and usefulness of these data as inputs to various models and data assimilation routines. Emphasis will be placed on the automatic evaluation of the data quality in order to prevent bad data from being used in models or data assimilation routines. In addition the talk will cover the current state of the data distribution service and our plans to expand it to encompass both the historical data (back to 1987) and the ongoing acquisition of new data from the operational DMSP spacecraft.

**GAIL.05/08A/A15-008****1150****VALIDATION OF THE IONOSPHERIC DATA ASSIMILATION THREE DIMENSIONAL (IDA3D) ALGORITHM**

Trevor W. GARNER, Gary S. BUST, Thomas L. GAUSSIRAN II (ARL:UT)

Ionospheric tomography has been used for several years to create large-scale electron density maps for GPS or radio beacon TEC data. Recently, the computerized ionospheric tomography (CIT) algorithm [Bust et al., *Int. J. Imag. Syst. Technol.*, 5, 160, 1994] has been adapted into the Ionospheric Data Assimilation Three Dimensional (IDA3D) algorithm. IDA3D is a data assimilation algorithm, which incorporates all available electron density and electron content observations into a coherent picture of the synoptic or global scale ionosphere. IDA3D primarily uses slant total electron content (TEC) measurements from available GPS ground sites and radio beacon receiver arrays operated by the Applied Research Laboratories, The University of Texas at Austin (ARL:UT), but can easily use peak electron density measurements from digasondes, electron density profiles from incoherent scatter radar and satellite-based GPS-occultation measurements of the topside TEC. This study compares different electron density maps for the same time period. Individual maps are created for each data set and combination of data sets (for a total of thirty maps), and compared to those observations that not used in a given map. By comparing the IDA3D maps to withheld observations, this study determines the validity of IDA3D, the usefulness of a given data set, and regions where more observations are needed.

**GAIL.05/08A/A15-009****1210****SPLINE-BASED EMPIRICAL MODEL OF HIGH-LATITUDE IONOSPHERIC POTENTIAL**

Satoshi TAGUCHI (University of Electro-Communications, Japan)

During a couple of decades the characteristics of the high-latitude ionospheric convection have been understood well, and now several empirical models exist which cover a broad range of solar wind conditions. While these existing models predict some situations well, it appears that they do not show satisfactory reproduction in particular for the convection during positive IMF Bz, and for the one during a substorm including its development. For this kind of situations, the convection tends to be intensified in a relatively small region, and if the location of such convection is affected by an unknown parameter or with a time scale that is out of range considered for the modeling, the convection structure may be smoothed out in the model. In this study, an empirical potential model presented in which a potential structure having a latitudinal scale of down to about 500 km can be reproduced reasonably. We took the potential zero and peaks from each of about 2500 pass of DE 2, focusing on the above scale, and obtained empirical relations for the location and magnitude of these potentials with the IMF magnitude or solar wind electric field for each 30 degree IMF clock angle and 3 hr MLT bin. Then, we created a potential distribution for each condition using a data interpolation technique with spline. This modeling for positive IMF Bz shows that a reverse convection pattern appears in a broader range of IMF conditions than the one given by the existing convection models, and that the potential magnitude can be larger by a factor of 1.5. For substorms, a phase-dependent model was made in which the development of potential during a substorm as well as the IMF dependence can be represented, by categorizing DE 2 substorm passes into several groups in terms of AL index development. The potential model shows that early in the expansion phase, the positive potential that usually occurs in the postmidnight sector, starts to enter the poleward side of the negative premidnight potential, leading to the development of a distorted pattern. At the substorm maximum, the negative premidnight potential occurs at higher latitudes than in earlier stages, leading to a pronounced Harang discontinuity. Details of relations of the potential variations with IMF, which are used in the model construction, will be presented, and possibility of the prediction of potential maps for extremely large IMF with the extrapolation of

these relations will be also discussed.

Tuesday, July 8 PM  
Presiding Chair: L. Scherliess

**GAIL.05/08P/A15-001****1400****RADIO AND OPTICAL MEASUREMENT OF THE IONOSPHERE WITH OBSERVATIONAL NETWORKS IN JAPAN**

Akinori SAITO<sup>1</sup>, S. FUKAO<sup>2</sup>, M. YAMAMOTO<sup>3</sup>, K. SHIOKAWA<sup>1</sup>, Y. OTSUKA<sup>1</sup>, M. KUBOTA<sup>1</sup>, T. OGAWA<sup>1</sup> (<sup>1</sup>Department of Geophysics, Kyoto University, <sup>2</sup>Radio Science Center for Space and Atmosphere, Kyoto University, <sup>3</sup>Solar-Terrestrial Environment Laboratory, Nagoya University, <sup>4</sup>Communications Research Laboratory)

Observational networks of GPS receivers, all-sky imagers, ionosondes and magnetometers are continuously operated in Japan and provide a large data set on the Ionosphere-Thermosphere-Magnetosphere system in the midlatitude region. The GPS network of Geographical Survey Institute and the all-sky imager network of Nagoya University can measure the 2-D horizontal structures of the ionosphere, which cannot be detected with classical observational techniques, such as ionosonde. Combination of the two-dimensional measurements by these networks and the vertical measurements by the ionosonde network, the MU radar and occultation by satellite-borne GPS receivers enable to observe three-dimensional structures of the ionospheric electron density and its temporal variations. Measurements of the other physical parameters, such as the electric field, the neutral wind, and the electric current by the MU radar, coherent radars, Fabry-Perot interferometers and magnetometers are also important to clarify physical mechanisms that create the structures of the ionospheric electron density. The F-region Radio and Optical measurement of Nighttime TID (FRONT) campaign demonstrated the advantage of these cluster of the observational instruments in Japan to study ionospheric phenomena. In this campaign, about 1,000 GPS receivers, five of all-sky CCD imagers, two of Fabry-Perot interferometers, the MU radar, and ionosonde network was operated to investigate the physical mechanism of the medium-scale traveling ionospheric disturbances (MSTIDs) in the nighttime ionosphere. The MU radar observed the electron density profile in its incoherent scatter mode, and 3-m scale field-aligned irregularities (FAIs) in its coherent scatter mode. Comparison of the total electron content detected by the GPS receiver network and the 630nm band airglow detected by the all-sky camera network clarified that the modulation of the ionosphere by MSTIDs occurs mainly on the bottomside of the ionosphere. FAIs were found to embed in a certain phase of MSTIDs measured by the GPS network. This indicates that the polarization electric field is generated inside MSTIDs and causes small-scale plasma instabilities. The continuous observation of the GPS network and the optical instrument network in Japan has observed the equatorial anomaly and plasma bubbles besides TIDs under various conditions of the geomagnetic activity, local time and season. Comparison of these observational results detected by multi-instruments with IRI model and physical models reveals the physical mechanisms that determine behaviors of the ionosphere at low- and mid-latitudes.

**GAIL.05/08P/A15-002****1430****INCOHERENT SCATTER RADAR DATA AND FUTURE POSSIBILITIES FOR FURTHER EXTENDED REAL-TIME DATA AVAILABILITY**

Anthony VAN EYKEN<sup>1</sup>, John HOLT<sup>2</sup> (<sup>1</sup>EISCAT Scientific Association, <sup>2</sup>MIT Haystack Observatory)

Incoherent scatter radars have been operating for 40 years and continue to provide the most detailed ionospheric data available from the ground. While operational constraints have normally restricted incoherent scatter to relatively short duration data sets, recent developments in radar hardware, coding techniques, data processing and data distribution make the recording of extended datasets both practical and valuable. Both the EISCAT Svalbard Radar and Millstone Hill Radar have been developing the infrastructure to support long experiments and can already handle programmes with durations exceeding four weeks. Long duration experiments provide possibilities to study phenomena not normally accessible to these facilities and also provide datasets applicable to comparison with many ionospheric and atmospheric models. Using examples from recent extended operations, we illustrate how the ready availability of fully analysed data through WWW-based database tools allows these facilities to be easily exploited by a wide user community.

**GAIL.05/08P/A15-003****1500****OPTIMAL INTERPOLATION (OI) ANALYSIS OF HIGH-LATITUDE IONOSPHERIC ELECTRODYNAMIC VARIABLES USING EOF BASES AND MAXIMUM LIKELIHOOD METHOD FOR ERROR COVARIANCE ESTIMATION: JANUARY 9-11, 1997**

Tomoko MATSUO, Arthur D. RICHMOND, Gang LU (HAO/NCAR)

The Assimilative Mapping of Ionospheric Electrodynamics (AMIE) procedure, developed by Richmond and Kamide [1988], carries out an objective multivariate functional analysis of high-latitude ionospheric electrodynamic variables: electric fields, electric potential, ionospheric currents, and magnetic field perturbations. The scheme is essentially based on Optimal Interpolation (OI) theory [e.g., Lorenz, 1986]. In the current AMIE procedure, each variable is presumed to be expanded in a series of  $l$  basis functions, which are chosen as modified spherical harmonic functions. For the problems to which the AMIE procedure is usually applied the size of state vector ( $l \sim 244$ ) is smaller than the size of observation vector (300 to 1000). In this study some technical improvements upon the traditional implementation of the OI method are demonstrated for the storm period of January 9-11, 1997. One of the improvements is to use the set of 11 Empirical Orthogonal Functions (EOFs) of Matsuo et al. [2002] as basis functions ( $l = 11$ ). This extension incorporates realistic spatial coherence of the electric field on large scales into the analysis and also reduces the background error covariance to a diagonal matrix. Furthermore, both observational and background error covariances are parameterized with respect to 4 free parameters, and these parameters are estimated at each analysis time-step using the maximum-likelihood method [Dee, 1995]. As has been demonstrated by Dee [1995], the error covariance parameter estimation can be performed in the innovation covariance space by matching a covariance model to the actual innovation vector. As the size of the problem is relatively small, on-line covariance parameter estimation is feasible. In this way the state dependence of the background error covariance is incorporated systematically into the procedure without resorting to a dynamic data assimilation methodology such as Kalman-filter.

**GAIL.05/08P/A15-004****1520****RTMIE STATISTICAL VALIDATION RESULTS**

Aaron J. RIDLEY<sup>1</sup>, Eric KIHN<sup>2</sup> (<sup>1</sup>Center for Space Environment Research, University of Michigan, <sup>2</sup>NGDC/NOAA, Boulder, CO)

We present results from a validation study of the assimilative mapping of ionospheric electrodynamics (AMIE) technique and the real-time version of AMIE. The validation consists of comparing AMIE calculations of particle precipitation and Hall conductances to DMSP J4 data. We will present 2 years worth of AMIE results (1997-1998) and statistical comparisons between the data and measurements. It is found that when there is very little data in a sector, the AMIE technique relies heavily upon the background model, such that the differences between AMIE and DMSP are the same as the differences between the statistical model and DMSP. As more data is included, the agreement differences between AMIE and DMSP increases. This increase is quantified as a function of magnetic local time and activity level. In addition, statistical comparisons between the background model and the DMSP data are presented.

**GAIL.05/08P/A15-005 1600**

**CIRCUM-PAN PACIFIC MAGNETOMETER NETWORK OBSERVATIONS FOR STUDY OF IONOSPHERE-THERMOSPHERE-MAGNETOSPHERE COUPLING SYSTEM**

Kiyohumi YUMOTO, the CPMN Group (Space Environment Research Center, Kyushu University, Japan)

In order to understand couplings of the magnetosphere-thermosphere-ionosphere system, the STP group in Kyushu University, Japan is conducting the Circum-pan Pacific Magnetometer Network (CPMN) observations at 54 stations in the world. Especially, by using the magnetic data from the CPMN stations along the 210 magnetic meridians, we are making global patterns of the equivalent ionospheric current, which show a clear seasonal variation of Sq current patterns and couplings of the Sq dynamo current system at middle- and low-latitudes and the ionospheric and field-aligned current (FAC) current in the auroral region. We are also developing a simulation code, which can calculate a global distribution of ionospheric current vectors generated by the Sq dynamo in the thin model ionosphere and by the Region 1 and 2 FAC model in the auroral region. We used the two-dimensional model called 'thin shell model' in order to simulate the Sq current system. This model reproduces well the ionospheric current, if the equator vicinity is excluded. In the equatorial region, the vertical electric current which can not be expressed in 'thin shell model' exists. Then, the new conductivity model at the equatorial latitude was made to add the effect of vertical electric current in the equatorial region, and global ionospheric current was simulated. The conductivity and current density model in the Region 1 and 2 in the polar region are a function of the magnetic activity. Although more realistic neutral wind model in the lower latitude region, conductivity models at the equatorial and auroral latitudes, and FAC patterns in the auroral region are desired, in the near future we may establish the data assimilation technique for the Ionosphere-Thermosphere-Magnetosphere system by comparing the ground-based network observations and the simulation results.

**GAIL.05/08P/A15-006 1630**

**IONOSPHERIC DATABASE IN EU COST 271 ACTION- EFFECTS OF THE UPPERATMOSPHERE ON TERRESTRIAL AND EARTH-SPACE COMMUNICATIONS INCLUDING EUROPEAN REAL-TIME IONOSONDE NETWORK**

Bruno ZOLESI<sup>1</sup>, Ljiljana CANDER<sup>2</sup> (<sup>1</sup>Istituto Nazionale di Geofisica e Vulcanologia, <sup>2</sup>Rutherford Appleton Laboratory)

The ability to monitor, specify and forecast the impact of the variability of the space environment on terrestrial and Earth-space and satellite to satellite communications significantly depend on data sources, data quality and data assimilation modelling. The EU COST (Co-operation in the field of Scientific and Technical Research) Action 271 on Effects of the Upper Atmosphere on Terrestrial and Earth-Space Communications (EACOS) is a research program that provides scientific context to study: (a) Impact of the variability of the space environment on communications; (b) Assessment of space plasma effects for satellite applications; (c) Ionospheric effects on terrestrial communications; and (d) Space plasma effects on Earth-space are described and the most significant results of different working groups reviewed. Two important components of this action are a unified database of detailed ionospheric vertical sounding observations from across Europe and European real-time ionosonde network. This paper presents a review of current ionospheric database status and focus on its application in modelling and forecasting studies.

**GAIL.05/08P/A15-007 1700**

**REAL DATA ASSIMILATION INTO SATELLITE-BASED EMPIRICAL MODELS OF HIGH-LATITUDE IONOSPHERIC ELECTRODYNAMICS FOR EMULATION OF QUASI-SYNOPTIC OBSERVATIONS**

Vladimir PAPITASHVILI<sup>1</sup>, Daniel WEIMER<sup>2</sup>, Freddy CHRISTIANSEN<sup>3</sup>, Frederick RICH<sup>4</sup> (<sup>1</sup>SPRL, University of Michigan, <sup>2</sup>Mission Research Corporation, <sup>3</sup>Danish Meteorological Institute, <sup>4</sup>U.S. Air Force Research Laboratory)

Although ample data from various ground instruments and satellite missions allow us to study ionospheric electrodynamics globally and instantaneously in both the sunlit and dark polar caps, little is available for the day-to-day collection of synoptic observations in 'Geospace' needed for constraining of physics-based models of the near-Earth environment to reality. Here we report on a series of new empirical models of ionospheric convection and field-aligned currents constructed separately for both the northern and southern polar regions from the satellite-based data (DE 2, DMSP, Ørsted, and CHAMP). These models are parameterized by the IMF strength and 'clock angle' direction, as well as by the Earth's dipole tilt; they are constrained to the quiet and moderately disturbed conditions but not to geomagnetic storms. In this study, we tried to develop a technique which would modify our modeled patterns (for the given IMF parameters and season) by assimilating available satellite passes (from one to a few) into the pattern. (This approach is similar to the AMIE technique but it does not utilize ground-based data.) The outcome of that assimilation is a series of emulated 'synoptic observations' over high latitudes sampled by a cadence of the available satellite passes. This allows us to capture quasi-synoptic time series of various ionospheric parameters, which we believe can then be digested into the MHD codes for the adjustment of code's regimes for various 'space weather' conditions. The proposed technique requires a unified approach in modeling of the high-latitude ionospheric electrodynamics from various data sources.

**GAIL.05/08P/A15-008 1720**

**IONOSPHERIC DATA FUSION ALGORITHMS FOR SATELLITE BASED IONOSPHERIC SENSORS**

Robert E. DANIELL<sup>1</sup>, Douglas J. STRICKLAND<sup>2</sup> (<sup>1</sup>Boston Office, Computational Physics, Inc., <sup>2</sup>Computational Physics, Inc.)

We are in the process of developing data fusion algorithms intended to produce ionospheric specifications in the low latitude, midlatitude, and auroral regions using a wide variety of *in situ* and remote sensing data from space based platforms. The data to be "fused" include

thermal plasma properties (e.g., electron density, ion composition, electron and ion temperature), slant TEC (from GPS occultation sensors, beacons, and radar altimeters), topside electron density profiles (EDPs) from topside sounders, and UV radiances (day, night, and aurora; disk and limb) from FUV and EUV imagers. Because the UV radiances come in the form of both disk and limb images, they are potentially extremely important sources of information. For example, at night images of the 135.6 nm line of atomic oxygen (whether disk or limb) can be converted to integrals of  $n_e^2$  along the line of sight. In the daytime, photoelectron excitation of atomic oxygen greatly exceeds the recombination source (except in the low latitude region where the ionosphere is frequently lifted above the main dayglow emitting layer) making ionospheric information indirect, but still potentially useful. In the aurora, the FUV emissions from atomic oxygen and molecular nitrogen provide information on the energy flux and hardness of the electron and ion spectra that produce the auroral displays. These can be used to estimate the electron density in the auroral E-layer. The data obtained from this wide variety of sensors and measurement techniques is of variable quality and is unevenly distributed in both space and time, but the objective is to produce ionospheric specifications throughout the region visible to the UV imagers. We will present the results of a study of various three dimensional ionospheric reconstruction techniques (based on various optimal estimation methods) capable of ingesting this data and producing the desired ionospheric specifications. The study is based on simulations of both the data sources and generic sensor models, designed to be as realistic as possible. For example the thermospheric and ionospheric models will be modified ('by hand') to simulate traveling ionospheric disturbances (TIDs) so that the effect of this phenomenon on algorithm performance can be judged. Our goal is to select from the candidate algorithms those that are accurate, compact, fast, and robust under realistic conditions, and which degrade gracefully when the various data sources are absent. We also hope the study can be used as a test bed for various configurations of space environment sensors.

**GAIL.05/08P/A15-009 1740**

**IMPROVEMENTS IN GLOBAL IONOSPHERIC SPECIFICATION USING IONOSPHERIC OCCULTATION MEASUREMENTS**

Phillip Charles ANDERSON<sup>1</sup>, Paul R. STRAUS<sup>1</sup>, Ludger SCHERLISS<sup>2</sup>, Robert W. SCHUNK<sup>2</sup>, Jan J. SOJKA<sup>2</sup> (<sup>1</sup>Space Science Applications Laboratory, The Aerospace Corporation, Los Angeles, CA, <sup>2</sup>Center for Atmospheric and Space Sciences, Utah State University, Logan, UT)

GPS occultation measurements are a new and valuable tool for providing global information about the ionospheric structure to assimilative ionospheric models. One low-Earth orbiting satellite with a single GPS antenna makes measurements of ~500 occultations a day. These measurements provide a global specification of the ionosphere never before available. We will be reporting the results of the first large scale study to incorporate these measurements into an assimilative ionospheric model, specifically the GAIM model. GAIM (Global Assimilation of Ionospheric Measurements) uses a Kalman filter to assimilate various types of ionospheric data such as slant path total electron content (TEC) measurements made by GPS occultation receivers, ionosonde data, and satellite-based in-situ electron density measurements. We will report on the improvement of GAIM achieved with the inclusion of the occultation measurements during selected space weather events. The occultation measurements will be provided by the PICOSat (Polymer Battery Experiment/Ionospheric Occultation Experiment/Coherent Electro Magnetic Radio Tomography/Optical Precision Platform Experiment - Satellite), CHAMP (Challenging Minisatellite Payload for Geophysical Research and Application), and SAC-C (Satellite de Aplicaciones Cientificas) spacecraft. Modeling parameters tested will include the accuracy of the ionospheric density profiles and the drivers responsible for the development of ionospheric structure such as the ionospheric electric fields.

**GAIL.06**

**IONOSPHERIC IRREGULARITIES, FIELDS AND WAVES**

Location: Site A, Room 10

Wednesday, July 9 AM

Presiding Chair: J. Labelle

**LOW AND MID LATITUDS**

**GAIL.06/09A/A10-001 0900**

**OCCURRENCE AND SPECTRAL CHARACTERISTICS OF IONOSPHERIC IRREGULARITIES DERIVED FROM ROCSAT-1 OBSERVATIONS**

Huey-Ching YEH<sup>1</sup>, S.-Y. SU<sup>1</sup>, R.A. HEELIS<sup>2</sup>, H.-H. HO<sup>1</sup>, K.-Y. CHEN<sup>1</sup>, C.-H. LIU<sup>1</sup> (<sup>1</sup>Institute of Space Science, National Central University, <sup>2</sup>William B. Hanson Center for Space Sciences, The University of Texas at Dallas)

A large set of F-region ionospheric irregularities at low latitudes has been detected by the Ionospheric Plasma and Electrodynamic Instrument (IPEI) onboard the ROCSAT-1 satellite since early 1999. Over the passing four years IPEI has been collecting data by alternating operations of the NORMAL mode with a sampling rate of 32 Hz and the FAST/AUTO mode with a sampling rate of 1024 Hz at 100% duty cycle. The simultaneously high resolution data of ion density and the two cross-track ion velocity components allow us, never before from satellite ion drift data, to study the spectral characteristics of the irregularities to the smallest scale of 15 m along the satellite track. Here, we report some statistical features of these irregularities. In particular we show how their occurrences vary with local time, longitude (geomagnetic field configuration), season, as well as the evolution of storm-time disturbed electric fields. We present the threshold values of density gradients along the satellite path and of upward ion drift enhancement, which might be considered as the precursor signatures for the prediction of post sunset irregularities. Furthermore, in the efforts to identify the underlying processes (instabilities) that control the evolution of irregularity structures, we investigate the detailed spectral features such as spectral index, wavelengths of spectral breaks that differentiate various wave modes, and the correlation between density and velocity spectra for various types of irregularity. As an example, we present the comparisons of these spectral features between those of fast rising bubbles and those of descending or fossil bubbles, which are chosen to approximately represent the growing and the decaying stages of irregularity structures.

GAI.06/09A/A10-002

0920

**SIMULTANEOUS RADAR OBSERVATIONS OF THE EQUATORIAL SPREAD F AT 18 MHZ AT THE EQUATOR AND AT 53 MHZ AT OFF THE EQUATOR OVER INDIA**

Amit Kumar PATRA, D. TIWARI, Sripathi S., Rao P.B., Sridhran R., Devasia C.V., Viswanathan K.S., Subbarao K.S.V., Sekar R., Kherani E. (National MST Radar Facility)

In this paper, we present simultaneous observations of equatorial spread F on several nights made using the 18 MHz radar at Trivandrum, an equatorial station and 53 MHz radar observations at Gadanki, an off equatorial station. It may be mentioned that a good part of the F region over these two locations are well connected through the magnetic field lines. We present the morphology of ESF irregularities and characteristic differences of the two scales of irregularities observed at the two locations. For example, we have not observed more than 3 plumes and no post-midnight plumes at 18 MHz while multiple plumes have been observed at 53 MHz. Bottomside irregularities at Trivandrum are found to be weak and they are very rare at Gadanki. The observed velocities at 18 MHz are found to be remarkably less than that observed at 53 MHz. Taking advantage of the locations of the two radar systems, we have also studied the mapping efficiency in the spread F structures and velocity fields. Mapping efficiency is found to decrease with decreasing periods (proportional to wavelength). The results are discussed in the light of present understanding of the ESF irregularities at different scale sizes. We also discuss on the mapping of the structures and coupling between the equatorial and low latitude.

GAI.06/09A/A10-003

0935

**SIMULTANEOUS STUDY OF LARGE SCALE GRADIENT-DRIFT AND RAYLEIGH-TAYLOR INSTABILITY IN THE NIGHT-TIME EQUATORIAL IONOSPHERE**

Eshfan Alam KHERANI (Post-doc fellow, Planetary and Space Science division, Physical Research Laboratory)

This is an attempt to explain the large scale (~100 km) towering structures observed by VHF radars in the equatorial E region. In order to know the possible cause for such structures, the numerical simulation of Gradient drift instability (GDI) in the E region and Rayleigh-Taylor instability (RTI) in the F region are simultaneously performed for night-time equatorial ionosphere. In contrast to the present believe, the investigation reveals that the fringe-field associated with the RTI is inefficient to produce any structures in the E region. On the other hand, it is found that the GDI can excite the large scales in the E region itself. These scales develop as the towering structures and penetrate into the lower boundary of the F region. Though the local linear theory of GDI does not predict growth for such large scales, the non-local linear theory with proper altitude variation of scale height may provide the answer for growth of such scales.

GAI.06/09A/A10-004

0950

**THE TOPSIDE IONOSPHERE HE+ DENSITY SUBTROUGH AS IRREGULARITIES OF THE BUBBLE ORIGIN**

Larissa SIDOROVA (Institute of Terrestrial Magnetism, Ionosphere and Radiowave Propagation, Troitsk, Moscow region, 142190, RUSSIA, E-mail: lsid@izmiran.rssi.ru)

The comparison of the topside ionosphere He+ density subtrough statistics (LT/month) with the similar statistics for equatorial F-spread (ESF) over the Brazilian and Peruvian regions for the same solar activity period shows the surprising coincidence in the most features. The He+ density subtroughs as irregular structure of the topside ionosphere, occurred equatorward of the light ion trough, were studied on ISS-b satellite data (1978-79). They were detected in ~ 570 cases in ~ 4000 passes at ~ 1100 km heights over mid- and low-latitude ionosphere (25-58°N) during high/maximum solar activity period. One group of the subtroughs, mainly revealed at latitudes of L=2-4 and being in dependence on geomagnetic activity, demonstrates a distinct storm-time nature. Apparently, this group could be created by so-called «plasmatails» mechanism. But another group of the subtroughs, revealed deeply inside of the plasmasphere at L= 1.3-3, does not depend on geomagnetic activity practically at all. These subtroughs of «non-disturbed origin» show the above-mentioned similarity with ESF phenomena. They mostly occur in the evening-night sector (18-05 LT) in period from October till May like ESFs (or bubbles). Monthly mean subtrough occurrence probability, plotted in local time versus month and averaged on longitudes, shows the distinct December solstice maximum and equinoctial maxima like the ESF occurrence probability plot at the Brazilian and Peruvian longitudes for the same solar maximum years. Hence, the He+ density subtroughs and ESFs may be considered as phenomena of the same bubble origin, since ESF is often associated with plasma bubbles, produced by Rayleigh-Taylor instability mechanism. As it is known from plasma bubble dynamics, the bubbles could display themselves as plasma density depletions at latitudes far from equator. Bubbles, upward lifting to plasmasphere heights, tend to extend along magnetic field tubes. So extended bubbles, looked like «banana», reach by own end(s) the more low (ionosphere) heights and tend to latitudes away from equator. Probably, the obtained He+ density subtroughs occur at the topside ionosphere heights by the same way.

GAI.06/09A/A10-005

1005

**SEASONAL VARIATIONS IN THE SPATIAL STRUCTURE OF EQUATORIAL SPREAD F IRREGULARITIES**

Archana BHATTACHARYYA, Bharati ENGAVALA, Krishnamoorthy JEEVA (Indian Institute of Geomagnetism)

Evolution of spatial structure in the Equatorial Spread F (ESF) irregularities determines the distribution of coherence (50% de-correlation) scale lengths found in the ground scintillation patterns produced by the scattering of radio waves by these irregularities. Scintillation data usually consists of a time series of amplitude or intensity fluctuations recorded by a receiver as the ground scintillation pattern drifts across the receiver. Hence, the spatial scales in the ground scintillation pattern are converted into temporal scales and an estimate of the drift speed of the scintillation pattern is required in order to derive the coherence scale length of the ground scintillation pattern for a particular interval of the scintillation event. The drift speed varies throughout the course of a scintillation event, with rapid variations in the initial stages of ESF development, due to the perturbation electric field associated with the Rayleigh-Taylor instability, and generally slower variations after 22 LT when the irregularities simply drift with the ambient plasma. A recently developed method is used to circumvent the problem presented by a varying drift speed, in obtaining the distribution of coherence scale lengths in the ground scintillation pattern, from spaced receiver measurements of amplitude scintillations on a 251 MHz signal transmitted from a geostationary satellite and recorded at an equatorial station. The distribution of coherence scale lengths obtained during the period June 2001 to July 2002 shows distinct seasonal variations in the evolution of spatial structure in the ESF irregularities. The shortest coherence scale lengths are obtained in the month of August 2001. Distinctly shorter coherence scale lengths are obtained in September – October 2001, as compared to March – April 2002. Presence of shorter scale lengths in

the ground scintillation pattern does not necessarily imply the presence of shorter scale length irregularities. In the strong scintillation regime, theoretical calculations show that on the contrary, short spatial scale lengths in the scintillation pattern may occur due to focusing of the radio waves by irregularities with steeper power-law spectra, which indicate absence of short scale length irregularities. Seasonal variations in the power spectrum of the irregularities is explained in terms of differences in the height of the night-time F-region, as deduced from the drift speed of irregularities derived from the data. A possible precursory role of the daytime electrojet strength in the evolution of spatial structure in ESF irregularities is also examined.

GAI.06/09A/A10-006

1020

**ROLE OF THE MAGNETOSPHERIC AND IONOSPHERIC CURRENTS IN GENERATION OF THE EQUATORIAL F LAYER IRREGULARITIES DURING MAGNETIC STORMS**

Lilia Z. SIZOVA (Institute of terrestrial magnetism, ionosphere and radio wave propagation)

The available model of the magnetospheric ring current effects on the generation of the equatorial F layer irregularities have been hypothesized by Aarons in 1991. Since that time three basic effects of the ring current in the generation or inhibition of irregularities are much used. According to results of current statistical studies, in the literature one can see that Aarons's criteria provide to predict near 70% of scintillations using Dst index. To amplify Aarons's criteria or propose new criteria for better predicting of S4 and other characteristics of scintillations that is the question. The equatorial electrojet strength, Kp, Dst, AE, AU and AL indices reflected contribution of different magnetospheric and ionospheric currents are examined to test geomagnetic activity effect on the generation of ionospheric irregularities producing VLF scintillations. It is shown, that additional to Aarons's criteria, can use models explained relationship between equatorial ionospheric parameters as h'F, foF2 and equatorial geomagnetic variations with the auroral ionosphere currents and the solar wind parameters as Bz and By components of the IMF for prediction of the ionospheric scintillations. In the present phase of the experimental investigations of electron density irregularities in the ionosphere the new ways are opened up because in interaction of the solar wind-magnetosphere-ionosphere during magnetic storms have progressed greatly. From the modern point of view intensity of electric fields and currents at the Polar Regions as well as the magnetospheric ring current intensity are strong depended from variations of the IMF. The magnetospheric ring current can not directly penetrate to equatorial ionosphere. On the other hand, the equatorial scintillations can be observed in the absence of the magnetospheric ring current.

GAI.06/09A/A10-007

1035

**MULTI-POINT GROUND AND SATELLITE OBSERVATIONS OF NIGHTTIME MEDIUM-SCALE TRAVELING IONOSPHERIC DISTURBANCES AT MIDLATITUDES**

Kazuo SHIOKAWA, Yuichi OTSUKA, Tadahiko OGAWA (Solar-Terrestrial Environment Laboratory, Nagoya University)

We review our recent results of nighttime medium-scale traveling ionospheric disturbances (MSTIDs) from multi-point airglow imaging observations in Japan, Australia, and Indonesia. The typical wavelength, velocity, period, and amplitude of MSTIDs are 100-300 km, 50-100 m/s, 0.5-1.5 h, and 5-15%, respectively. The occurrence of MSTIDs has a major peak in summer and a minor peak in winter, which is opposite to that at American sector (Arecibo). They continuously move southwestward. From a campaign observation in the southern island (Okinawa), Japan, there seems to be a possible equatorward limit of MSTID propagation around 18 MLAT. Detailed investigation of a MSTID event of May 17, 2001 was performed using 630.0-nm and 777.4-nm airglow images, neutral wind from a Fabry-Perot interferometer, and ion drift and density data from the DMSP satellite. We found that the vertical wavelength estimated from the gravity wave dispersion relation was too small to explain the observed amplitudes of airglow intensity. On the other hand, an electric field oscillation of about 1.2 mV/m was sufficient to reproduce the observed airglow amplitudes in a simple ionospheric model. The DMSP satellite did observe oscillation of the polarization electric field correlated with the MSTID structure in the airglow image, suggesting that the polarization electric field plays an important role in the generation of MSTIDs. From conjugate airglow measurements between Japan and Australia, we found magnetic conjugacy of the MSTIDs, indicating field-aligned mapping of the electric fields between both hemispheres.

GAI.06/09A/A10-008

1110

**A SURVEY OF PRESENT KNOWLEDGE OF THE UNSTABLE SPORADIC LAYERS AT MIDLATITUDE**

Christos HALDOUPIS (Physics Department, University of Crete, Heraklion, Crete, Greece)

In recent years, and especially after the deployment of the MU radar in Japan, the interest in the study of midlatitude E-region coherent backscatter phenomena, that exist always in connection with unstable sporadic E layers (Es), has grown remarkably. This has become evident from the increased number of midlatitude VHF and HF coherent backscatter radar experiments and in situ rocket flights, the large number of relevant publications, and the interesting new scientific results obtained. Among the highlights of this intensive research are: 1) the observation of characteristic periodicities in backscatter with periods from a few minutes to about 30 minutes (QP echoes) which implied a dominant wave-like modulation mechanism of the midlatitude Es plasma, 2) the detection of pure Farley-Buneman waves (Type 1 echoes) which implied the existence at times of large electric fields at least an order of magnitude higher than the ambient electric fields at midlatitude, 3) the existence of large neutral winds reaching at times values higher than 150 m/s which can play a key role not only in forming Es but also in causing plasma destabilization, 4) the observation of long term periodicities in backscatter and Es occurrence with periods in the range from 2 to 10 days which implied a connection with planetary waves, and 5) the new conceptual ideas and models developed for the interpretation of the observations. This survey does not purport to give a complete account of the large volume of work done on this topic, but aims rather at presenting a synthesis of old and new experimental findings which leads to an integrated picture of our present physical understanding. In addition we update what we consider to be remaining problems that require further study.

GAI.06/09A/A10-009

1130

**MORPHOLOGICAL STUDY OF THE FIELD-ALIGNED E LAYER IRREGULARITIES OBSERVED BY THE GADANKI VHF RADAR**Chen-Jeih PAN<sup>1</sup>, P.B. RAO<sup>2</sup> (Institute of Space Science, National Central University, <sup>1</sup>National MST Radar Facility, Tirupati-517502, India)

We operated the Gadanki radar on the nights (18 to 06 LT) of June 17-20, July 15-18, and August 19-22 during 1998; on the nights of August 5-12 and August 16-19 during 1999. On the other hand, daytime (09 to 18 LT) observations were carried out on June 15-18, July 13-

16, and August 17-20 during 1998. The total observation periods are 161 hours for the nighttime and are 68 hours for the daytime observation. By examining the 15-day data set, we present the morphological features of the E region FAI observed by the Gadanki radar. We find:(1) There are two echoing regions: the lower region between 90 and 100 km ranges and the upper region between 105 and 120 km ranges.(2) Echoes observed in both the upper and lower regions are similar to type 2 echoes reported by other radars in the mid-latitudes.(3) Echoes of the lower region may occur in daytime as well as in nighttime. Although there is an observation break between 06 and 09 LT, noontime (11 to 14 LT) seems to be the minimum period of occurrence. QP echoes are commonly detected at the lower region no matter daytime or nighttime and are the so-called "LQP echoes". (4) The spectral characteristics of the lower region echoes differ from daytime and nighttime. The mean Doppler velocities are more variant than those of the daytime and the spectral widths are broader in the nighttime.(5) The upper region echoes appeared only in the nighttime with a maximum period between 23 and 05 LT. Typical QP echoes detected here are similar to those observed at mid-latitudes. (6) Unlike the value close to zero of the mean radial velocities of the lower E region echoes, a downward velocity is noticed at the upper E region. Both the mean Doppler velocities and the spectral widths are found larger than those of the lower regions. We also compare the features of the FAI echoes between Gadanki and Piura radars since the geomagnetic latitude of these two radars are close. Although the morphological distribution and spectral characteristics are very similar for those FAI echoes, daytime echoes and the LQP echoes are rarely reported by Piura. It is suggested that the neutral winds may play a role in this discrepancy since those echoes usually occur at the altitudes below 100 km.

**GAIL.06/09A/A10-010** Invited **1145**

**ION THERMAL EFFECTS ON E-REGION INSTABILITIES**

Meers M. OPPENHEIM, Yakov S. DIMANT (Center for Space Physics, Boston University)

The Farley-Buneman (FB) and gradient-drift instabilities frequently create strong radar returns from the E-region ionosphere. The FB instability theory, as typically applied, assumes that ions remain in isothermal equilibrium with the background neutral atmosphere. We present both simulations and theoretical studies showing that wave-driven ion heating, particularly at high altitudes within the E-region, can profoundly modify the behavior of FB instability growth and saturation. Using a fully kinetic 2-D simulation of a field-driven FB instability, we shall illustrate the importance of ion thermal effects in both the high-latitude and equatorial electrojet. For instance, when the driving field exceeds the FB instability threshold field by a factor of 4 then an ion thermal instability develops in place of the FB instability. These waves grow and saturate with characteristics different from those of FB waves and may account for many observational characteristics of high latitude irregularities. In another instance, where the driving field exceeds the instability threshold field by a factor of 2, then FB waves develop but are modified from pure FB waves due to ion thermal effects. We shall also show how linear fluid theory of the thermally modified FB instability can explain many features seen in the simulations. Furthermore, by adding ion thermal effects to the FB theory, we predict an extended altitude range in which waves will grow for a given driving field.

**GAIL.06/09A/A10-011** **1205**

**INTERFEROMETRIC OBSERVATIONS OF E REGION FIELD-ALIGNED IRREGULARITIES WITH THE PIURA VHF RADAR**

Jorge L. CHAU<sup>1</sup>, Danny SCIPION<sup>1</sup>, Luis A. FLORES<sup>2</sup> (<sup>1</sup>Radio Observatorio de Jicamarca, IGP, <sup>2</sup>Laboratorio de Física, Universidad de Piura)

Since 1991, we have measured echoes from E region field-aligned irregularities using the Piura VHF radar (~7° dip latitude, just outside the equatorial electrojet (EEJ)). These observations have been made with a monostatic (the same antenna for transmission and reception) system allowing us to get a good understanding of their diurnal and seasonal characteristics. These echoes occur mainly at night and are stronger during southern hemisphere summer months. However, we have not been able to get a good understanding of their spatial and short-term temporal characteristics with the monostatic setup, which could give us ambiguous results when, for example, coherent scatter from these irregularities arises from spatially compact regions of space rather than as volume scatter. In order to resolve this ambiguity, we have recently implemented an interferometry receiving system with multiple baselines. In this work, we will present the latest results obtained during this summer, including results from a north-south baseline (aligned with the magnetic field), and from multiple baselines in the east-west direction (transverse to the magnetic field).

**GAIL.06/09A/A10-012** **1225**

**RECENT PROGRESS OF THE CHUNG-LI RADAR GROUP IN THE STUDY OF ES IRREGULARITIES**

Yen-Hsyang CHU (Institute of Space Science, National Central University)

It has been ten years since the capability of the ionospheric observation was implemented at the Chung-Li VHF radar. In this report, we present the recent progress in the investigations of the ionospheric Es irregularities. With the interferometry technique, three-dimensional structures of the type 2 irregularities in the expected echoing region were reconstructed. It shows that the structure of the type 2 irregularities may be in a form of horizontal thin layer, or well-organized clump shape, or loose cluster. The plasma structure of the type 1 irregularities is also analyzed and the results show that the zonal extent of the spatial structure of the type 1 irregularities assembled in a form of thin layer with thickness of 1-2.5 km may be as large as greater than 12 km. The beam broadening effect on type 2 radar spectrum due to the drift of the type 2 irregularities is investigated theoretically and experimentally. We find that the Doppler spectral width of the Es field-aligned type 2 irregularities is not only the function of the transverse beam drift velocity, but also related to the zonal extent of the plasma structure. The interferometry measurements support the theoretical predictions.

**GAIL.06/09A/A10-013** **1245**

**QUASI-PERIODIC DRIFT MOTIONS OF METER-SCALE IRREGULARITIES OBSERVED AT THE CHUNG-LI VHF RADAR**

Chien-Ming HUANG (Institute of Space Science, National Central Univ.)

The observations of meter-scale, field aligned irregularities made at the Chung-Li VHF radar are presented. Applying radar interferometry, the temporal and spatial variations of backscatter positions show the appearance of quasi-periodic drift motions, with wavelengths of about 10-15 km, and wave frequencies close to the Brunt-Vaisala frequency. This periodicity also reflects the so-called QP echoes shown in the RTI (range-time-intensity) plots. In-beam images of scatters are also analyzed in this paper, results show that the scattering structures are mainly organized along wave fronts. But, in some cases, the quasi-

point target scatters are responsible for the striations in the RTI plots.

Wednesday, July 9 PM  
Presiding Chair: M. Yamamoto

**SEEK II**

**GAIL.06/09P/A10-001** **1400**

**MID-LATITUDE E-REGION IRREGULARITIES REVEALED BY THE SEEK-2 (SPORADIC-E EXPERIMENT OVER KYUSHU 2) EXPERIMENT**

Mamoru YAMAMOTO, Shoichiro FUKAO (Radio Science Center for Space and Atmosphere, Kyoto University)

Ionospheric irregularities in the mid-latitude E-region has been one of the study topics for more than ten years. The epoch was the discovery of the quasi-periodic (QP) structure in the E-region FAI (Field-Aligned Irregularity) echoes observed with the MU radar in Japan. We have been extensively studying the phenomena by using HF/VHF radars, ionosondes, optical instruments, sounding rockets, and computer simulation. The QP structures appear in the E-region FAI as a reflection of modulation pattern in the Sporadic-E (Es) layers. The structures are associated with polarization electric field, which suggests strong coupling process between the ionized and neutral atmosphere. Electrodynamic coupling of different altitudes of E-region ionosphere is also an important issue together with E- and F-region coupling processes. Detailed generating mechanism of the QP echoes is, however, still unresolved. In August 2002, we conducted SEEK-2 (Sporadic-E Experiment over Kyushu 2) campaign in Japan under collaboration with many scientists from Japan, USA and Taiwan. Since the SEEK-2 follows the achievements of the first SEEK campaign in 1996, it was extended in some aspects. The SEEK-2 consists of two sounding rockets of Institute of Space and Aeronautical Sciences that include in-situ experiment of electron density, electron temperature, electric field, plasma fluctuation and waves, and geomagnetic field as before. As a new rocket experiment, we conducted rocket-beacon experiment to measure TEC (Total Electron Content) of the Es-layers, and both up-leg and down-leg releases of TMA (Tri-Methyl Aluminum) to measure the neutral winds and waves. From the ground we measured the same observation region of the rockets with two radars of 24.5MHz and 31.6MHz, ionosonde network of Japan, an MF radar, several airglow imagers, and a GPS scintillation-receiver system. We observed intense QP echoes with radars after 23 LT (= UT + 9 hours) on August 3, 2002, and launched rockets into the E-region at 2324 LT and 2339 LT. The operation of the SEEK-2 was very successful as we could select a good event for the launches. All instruments on the rockets worked fine. From preliminary data analyses we are finding that the rockets detected multi-layered Es-layers at 103, 105 and 129km altitudes, and intense electric fields that approach ± 10 mV/m. The rocket-beacon experiment measured horizontal structures of the E-region TEC. The TMA release showed rippled structures which may prove existence of wave or instability in the neutral atmosphere. We now continue efforts for further data analyses. In the presentation we will show more results from the SEEK-2, and discuss newer view of the mid-latitude E-region FAI.

**GAIL.06/09P/A10-002** **1420**

**SEEK-2: OBSERVATIONS OF NEUTRAL WINDS AND TURBULENCE IN A REGION SPORADIC E AND QP STRUCTURE**

Miguel Folkmar LARSEN<sup>1</sup>, M. YAMAMOTO<sup>2</sup>, R. TSUNODA<sup>3</sup>, S. FUKAO<sup>2</sup> (<sup>1</sup>Dept of Physics, Clemson University, <sup>2</sup>Radio Atmospheric Science Center, Kyoto University, <sup>3</sup>SRI International)

A pair of rockets was launched into sporadic E conditions from Kagoshima Space Center in Japan on August 3, 2002, to measure the electric fields, electron densities, neutral winds, and other parameters in a sporadic E layer which had Quasi-Periodic (QP) radar echo structures. The neutral wind measurements were obtained from a trimethyl aluminum (TMA) chemical tracer release which covered the altitudes from approximately 85 to 120 km. The measurements show the presence of large shears and significant turbulence and wave structure along the trail, consistent with several earlier measurements. In the talk, the results from the SEEK-2 wind measurements will be presented, along with a discussion of the relationship between the new results and earlier results from measurements of winds associated with sporadic E.

**GAIL.06/09P/A10-003** **1440**

**SEEK2 RADIO BEACON IMAGING OF SPORADIC-E LAYERS**

Paul A. BERNHARDT<sup>1</sup>, C.A. SELCHER<sup>2</sup>, C.S. SIEFRING<sup>1</sup>, M. YAMAMOTO<sup>3</sup>, S. FUKAO<sup>3</sup> (<sup>1</sup>Plasma Physics Division, Naval Research Laboratory, <sup>2</sup>Information Technology Division, Naval Research Laboratory, <sup>3</sup>Radio Atmospheric Science Center, Kyoto University, Kyoto)

During SEEK2 (Second Sporadic-E Experiment over Kyushu), two-dimensional images of Sporadic-E layers have been produced using computerized ionospheric tomography (CIT). Two rockets were launched from the Kagoshima Space Center (KSC) on August 3, 2002 at 23:24:00 JST (14:24:00 UT) and 23:39:00 JST (14:39:00 UT). Each of the two SEEK 2 rockets carried a two-frequency radio beacon that transmitted to receivers located at four ground sites. Two of the sites, Uchinoura and Taramizu were in the plane of the rocket trajectories. The rockets flew through sporadic-E layers located near 105 km altitude. The apogees of the two rockets were 151.9 and 116.6 km, respectively. The TEC measurements were obtained using differential phase from the 150 and 400 MHz carrier signals from the beacon. Because the rocket trajectory provided continuous tracking of phase absolute TEC was obtained. Data correction was required to eliminate rocket spin effects, which produced a constant differential phase, offset along with spin modulation of the phase. The latter was eliminated using a 1 Hz low pass filter. The initial data interpretation provided electron density profiles when passing through E-Layer and vertical TEC mapped to 105 km altitude along the propagation path. As the radio beacons penetrated the E-layers, sharp increases in total electron content (TEC) was observed. These data were differentiated with change in slant path to yield profiles of apparent electron density as a function of rocket altitude. With these profiles as basis functions, tomography was used to reproduce the structure of the sporadic-E layers as a function of both altitude and horizontal range along the trajectory. Two other receivers located at Tanagashima and Tasaki were located 50 km on either side of the rocket trajectory. The data from these sites will be used to determine the three-dimensional structure of the sporadic-E layers. This experiment demonstrated the utility of a rocket-borne radio beacon sensor to detect irregularities along the propagation path between the radio beacon and a network of ground receivers.

**GAI.06/09P/A10-004** **1500**

**RADAR OBSERVATIONS OF FIELD-ALIGNED PLASMA IRREGULARITIES IN THE SPORADIC E EXPERIMENT OVER KYUSHU 2 (SEEK-2)**

Susumu SAITO<sup>1</sup>, Masato MARUMOTO<sup>1</sup>, Mamoru YAMAMOTO<sup>1</sup>, Shoichiro FUKAO<sup>1</sup>, Roland T. TSUNODA<sup>2</sup> (<sup>1</sup>Radio Science Center for Space and Atmosphere, Kyoto University, Japan, <sup>2</sup>SRI International, USA)

To understand the physical processes of Quasi-Periodic (QP) echoes found in the mid-latitude E region, the Sporadic E Experiment over Kyushu 2 (SEEK-2) campaign was conducted in this summer as the successive campaign of the SEEK in 1996. Two ionospheric radars were installed in Tanegashima to measure properties of field-aligned irregularities (FAIs) as well as to determine the launch timing of two rockets into the ionosphere. Lower Thermosphere Profiler Radar (LTPR, 31.57 MHz) and Frequency Agile Radar (FAR, 24.515 MHz) were installed in Minamitane town (30.37N, 130.97E) and Nishino-omote city (30.75N, 131.03E), respectively. Strong QP echoes were observed with both the radars when the two sounding rockets were launched into the ionosphere with 15 minutes interval. From the twin radar measurements, it was inferred that echoing regions were propagating in the South-West direction at about 30 m/s with spatial separations of 12 - 23 km. These results were compared with onboard measurements of electric fields and electron densities as well as with neutral wind velocity derived from meteor echoes measured by LTPR. Interferometric measurements of fine scale structures of QP echoes by LTPR will also be presented.

**GAI.06/09P/A10-005** **1515**

**ELECTRON DENSITY IRREGULARITIES IN THE NIGHT-TIME SPORADIC-E LAYERS OBSERVED BY A SOUNDING ROCKET S-310-31 DURING THE SEEK-2 CAMPAIGN PERIOD**

Hirota MORI<sup>1</sup>, Koh-ichiro OYAMA<sup>2</sup> (<sup>1</sup>Communications Research Laboratory, <sup>2</sup>The Institute of Space and Astronautical Science)

SEEK-2 (Sporadic E Experiment over Kyushu) was the second coordinated rocket and radar campaign conducted in August, 2002 to observe spatial structures and properties of the nighttime sporadic-E layer in the midlatitude E region over Kyushu, Japan and study the generation mechanism of the QP (Quasi-Periodic) structure of the sporadic-E layers which were previously found by the QP radar backscatter echoes. Two sounding rockets S-310-31, -32 were launched successively in 15 minutes at the same night on August 03, 2002 when the strong QP echoes were detected by a coordinated radar measurement. A fixed-bias Langmuir probe was installed on the first rocket S-310-31 launched at 23:24 JST to measure the plasma-density structure related to a sporadic-E layer. The fixed-bias probe can measure the electron current proportional to the electron density continuously by applying a fixed-bias of 5 V to a gold-plated spherical probe with a 5-cm diameter installed on top of the rocket. It has two measurement modes with different frequency bands to measure the km-scale density structure and the small-scale density irregularities generated in the structure, respectively. The rocket reached an apogee of 152km and the probe worked normally during the entire flight. The preliminary analysis of the data reveals the following results. A strong double-peak Es layer was observed at a height of 102-104 km during the upleg, and a single-peak Es layer was observed at 103 km during the downleg. Week Es layers were also found at higher altitudes separated by about 10 km during the both legs. Meter-scale irregularities were generated in the density gradient regions of these Es layers. These results will be compared with other onboard and ground measurements.

**GAI.06/09P/A10-006** **1530**

**OBSERVATION OF ELECTRON NUMBER DENSITY PROFILES AND VLF PLASMA WAVES BY USING S310 SOUNDING ROCKETS DURING THE SEEK-2 CAMPAIGN**

Makoto WAKABAYASHI, Takayuki ONO (Graduate School of Science, Tohoku University)

The SEEK-2 campaign has been carried out in early August 2002 in order to study on the generation mechanism of quasi-periodic radar backscatter echoes due to field-aligned irregularities accompanied with sporadic-E layers of the mid-latitude region, including rocket experiments and ground observations. Two sounding rockets (S310-31,32) were prepared for this purpose and launched toward east from Kagoshima Space Center, at 23:24 JST(S310-31) and 23:39 JST(S310-32) on August 3, 2002. In this campaign, altitude profiles of electron number density were measured by using the Impedance Probe installed on both the rockets. The maximum electron densities of about  $9 \times 10^5/cc$  (for S310-31), and  $2 \times 10^6/cc$  (for S310-32) were measured within an altitude range of 100-105km associated by several sub peaks. On the other hand, TMA experiment on board S310-32 was carried out to observe the neutral wind velocity profile of the ionosphere. The Plasma Wave Monitor, also installed on S310-32, has detected plasma wave signatures associated with the TMA release in the sporadic-E layer. Electron density profiles showed that sporadic-E layer consists of one or two main peaks ( $\sim 10^6/cc$ ) at 104-106km altitude and several small peaks existing above and below the main peaks. We compared these number density profiles with the results of Low Thermosphere Profiler Radar located on Minamitane and FAR on Nishinoomote. In comparison with LTPR data, peaks in the number density profiles well correspond with altitude profiles of intense echoes in the radar data. We propose a model of 2 dimensional distribution model of sporadic-E structure. In this model, sporadic-E layer patches distribute horizontally being associated with multi-layer structure of relatively weak densities. From each weak ionization region the field-aligned irregularities are possibly generated along the magnetic field lines. On the other hand, Plasma Wave Monitor data shows generation of plasma waves associated not only with the TMA release but also with the effect of the passage through the sporadic-E layer. The present results are able to contribute to understand the mechanism of quasi-periodic echoes, and generation mechanism of TMA lightning which was found in the present rocket experiment.

**GAI.06/09P/A10-007** **1545**

**STUDY OF GENERATION OF POLARIZATION ELECTRIC FIELDS ASSOCIATED WITH A SPORADIC-E LAYER**

Tatsuhiko YOKOYAMA<sup>1</sup>, Mamoru YAMAMOTO<sup>1</sup>, Shoichiro FUKAO<sup>1</sup>, Robert F. PFAFF<sup>2</sup> (<sup>1</sup>Radio Science Center for Space and Atmosphere, Kyoto University, <sup>2</sup>NASA/Goddard Space Flight Center)

The quasi-periodic (QP) radar echoes of the ionospheric irregularities in the midlatitude E-region was first observed with the MU radar studied for more than ten years. It has been revealed that the QP echoes tend to appear in the post-sunset period during the summertime with periods of 2-15 minutes and generation of the QP echoes are correlated with sporadic-E (Es) layers. Further, from the two rocket experiment, "SEEK" and "SEEK-2" conducted in 1996 and 2002, respectively, the intense electric field of more than 10 mV/m associated with the QP echoes was detected. Recently, the new model to explain such a large electric field by the internal structure of a Es layer was proposed. In the SEEK-2 campaign, we conducted the measurements of an electric field, an electron density, a neutral wind, a horizontal distribution of Es layers, etc., at almost the same time. With a computer simulation model, we can

examine the generation of polarization electric fields by taking other measured parameters into consideration. We will present the detailed results of the electric field measurements and other related observations in the SEEK-2, and the simulation study of generation of polarization electric fields.

**GAI.06/09P/A10-008** **1620**

**SOME ASPECTS OF SUMMERTIME LOW-ALTITUDE QUASI-PERIODIC ECHOES OBSERVED WITH THE MU RADAR**

Tadahiko OGAWA<sup>1</sup>, Yuichi OTSUKA<sup>1</sup>, Kazuo SHIOKAWA<sup>1</sup>, Fumiki ONOMA<sup>1</sup>, Mamoru YAMAMOTO<sup>2</sup> (<sup>1</sup>Solar-Terrestrial Environment Laboratory, Nagoya University, <sup>2</sup>Radio Science Center for Space and Atmosphere, Kyoto University)

Quasi-periodic (QP) radar echoes from midlatitude sporadic E layers (Es) in the summer night were first discovered in 1989 by using the 46.5-MHz middle and upper atmosphere (MU) radar at Shigaraki, Japan. They appear at altitudes of 100-130 km, have periods of 5-20 min perhaps due to short-period atmospheric gravity waves, and are believed to be caused by field-aligned electron density irregularities generated through plasma instabilities and/or neutral turbulence. In this paper we analyze data obtained in the summer of 2002 with MU to demonstrate some new aspects of QP echoes. First, we discuss low-altitude (90-100 km) QP echoes, here referred to as the LQP echoes, that have weak echo power and low Doppler velocity. These echoes are often connected with high-altitude (100-130 km) QP echoes (referred to as the HQP echoes), that have stronger power and higher velocity, with a gap of about 5 km in altitude. This fact suggests that (1) there exist two sporadic E layers; one at higher altitudes and the other at lower altitudes in the E region to cause the HQP and LQP echoes, respectively, and (2) both echo regions are electrically coupled through the geomagnetic field. Then, a case is studied in which HQP and LQP echoes are combined without the altitude gap to produce QP striations extending from 90 to 110 km. In association with this event, the Shigaraki 557.7-nm all-sky CCD imager, which is sensitive to the airglow at around 95 km altitude, detected very turbulent airglow patterns. Interestingly, when airglow intensity increases (decreases) gradually with time, the QP echo altitudes also increase (decrease) gradually, and temporal fluctuations of the airglow intensity are well correlated to those of the QP echo structures. The MU radar detected very high Doppler velocities exceeding 100 m/s even at around 90 km for a short period, which might be due to localized, unusual high neutral winds. In this event the Shigaraki 557.7 nm Fabry-Perot interferometer observed neutral winds over Shigaraki. The hourly winds are roughly consistent with irregularity motions below 100 km that were determined from the radar observations. Thus, the event gives a good opportunity to disclose the relationship between the irregularity generation and neutral gas dynamics.



**GAI.06/09P/A10-009** **1640**

**THE SPORADIC E LAYER INSTABILITY IN THE NIGHTTIME MIDLATITUDE IONOSPHERE**

Russell B. COSGROVE, Roland T. TSUNODA (SRI International Center for Geospace Studies)

Recently, it has been shown that the configuration of a midlatitude sporadic-E ( $E_s$ ) layer at a zonal wind-shear node is unstable at night. The instability is the result of a wind-shear driven polarization process that occurs when a plane-wave perturbation in altitude is imposed on the  $E_s$  layer. The growth rate of the instability depends on the azimuthal alignment of the plane wave distortion, a feature that is reminiscent of the Perkins instability. The plane wave nature of the growing modes, combined with the azimuthal dependence of the growth rate, suggests that the instability may provide an explanation for frontal structures observed in  $E_s$  layers, which are found to consistently adopt the same azimuthal alignment preferred by the instability. Simulations of the nonlinear evolution find that the instability generates significant polarization electric fields that structure the layer; yet, the structuring saturates without destroying the layer completely. Decreasing the wind shear decreases the polarization electric field, and increases the evolution timescale, but otherwise does not profoundly affect the structures that form in the layer. Increasing the  $F$  layer conductivity, which is assumed to map perfectly to the  $E_s$  layer, damps the instability. These results suggest the instability as a possible source of the so-called quasi-periodic (QP) echoes, which are coherent radar echoes found in the nighttime midlatitude ionosphere.

**GAI.06/09P/A10-010** **1655**

**KILOMETRIC PLASMA WAVES IN MIDLATITUDE SPORADIC E LAYERS**

David L. HYSELL (Earth and Atmospheric Science, Cornell University)

While the primary waves associated with sporadic E layers are generally assumed to be produced by gradient drift instabilities, nonlocal effects would seem to preclude the growth of midlatitude gradient drift waves with kilometer scale sizes. However, at middle latitudes, the dip in the Earth's magnetic field and the associated zero order field aligned conductivity gradients make the region unstable to a kind of resistive drift instability. This instability produces waves with finite parallel wavenumbers and with wavelengths between a few hundred meters and a kilometer, depending on the thickness of the underlying sporadic E layer. A three-dimensional numerical simulation with realistic background parameters shows that the instability occurs in sporadic E layers which are coupled to the F region which dominates the conductivity on the affected field lines. A simple linear local analysis recovers most of the important characteristics of the instability. The principle nonlocal effect in nature is saturation and stabilization brought about by vertical shear. Evidence that kilometer waves are found in nature will be summarized.

**GAI.06/09P/A10-011** **1710**

**THE VARIATIONS OF ES LAYER IN THE WESTERN PACIFIC REGION DURING THE SEEK-2 CAMPAIGN**

Chien-Chih LEE<sup>1</sup>, J.Y. LIU<sup>1</sup>, C.J. PAN<sup>1</sup>, C.H. LIU<sup>1</sup>, W.H. TSAI<sup>1</sup>, T. MARUYAMA<sup>2</sup>, L. LIU<sup>3</sup> (<sup>1</sup>Institute of Space Science, National Central University, <sup>2</sup>Hiraiso Solar Terrestrial Research Center, Communication Research Laboratory, Ibaraki, Japan, <sup>3</sup>Wuhan Ionospheric Observatory, Wuhan Institute of Physics and Mathematics, The Chinese Academy of Sciences, Wuhan 430071, China)

The SEEK-2 (Sporadic E Experiment over Kyushu) campaign was carried out in July-August 2002. In this campaign, we conducted the ionospheric observation with a 5-minute time resolution at five ionosonde stations to monitor the Es layer over the western Pacific region. These five stations consist of a digisonde portable sounder (DPS) at Wuhan (30.6°N, 114.4°E) and four ionosondes at Chung-Li (24.9°N, 121.1°E), Okinawa (26.7°N, 127.8°E), Yamagawa (31.2°N, 130.6°E), and Kokobunji (35.7°N, 139.5°E). We deduced the maximum frequency (foEs) and the lowest virtual height (h'Es) of the Es layer and cross-compared the two parameters between these stations. Results show that the Es layer drifts in zonal (east-west) direction. Time variations of the two parameters suggest that the traveling ionospheric disturbances (TIDs) and tides to be important.

**GAIL.06/09P/A10-012 1725**

**AN EXPECTED RESPONSE OF IONOSPHERIC IRREGULARITIES GENERATED BY NEUTRAL TURBULENCE TO CHANGES IN THE TURBULENT ENERGY DISSIPATION RATE**

Yuriy KYZYUROV (Department of Space Plasma Physics, Main Astronomical Observatory NASU)

Results of in-situ rocket and ground-based radar experiments have clearly shown that plasma irregularities in the lower ionosphere can be induced by neutral air turbulence. One of important parameters in turbulence is the energy dissipation rate that defines the rate at which energy is generated at the larger scales, cascaded through the inertial subrange, and finally is dissipated in the viscous subrange of the turbulent spectrum. In this report an expected response of the ionospheric irregularities to changes in the turbulent energy dissipation (TED) rate is discussed. The consideration is based on an expression for the power spectral density of the irregularities that was obtained by using a macroscopic description of the ionospheric plasma. It is shown that under fixed values of ionospheric parameters corresponding to 95 km altitude, an increase in the TED rate from 0.02 to 0.2 W/kg results in changes in the rms level of relative plasma-density fluctuations from 1.5 to 2.2 % (for irregularity length-scales 10 - 1000 m) in the case of ionospheric E-region without sporadic-E layer, and from 4 to 7 % in the case of sporadic-E of 2 km thickness. It is found that changes in the shape of the irregularity spectrum may be expected too. The changes are connected with decreasing the inner scale of turbulence (Kolmogorov scale) from 7 to 3.9 m under the mentioned increase in the TED rate. Results of this report can be tested in coordinated experimental campaigns that include measurements of the irregularity spectrum and parameters of the turbulent neutral wind.

**GAIL.06/09P/A10-013 1740**

**RAYLEIGH AND TSUNAMI IONOSPHERIC COMPANION WAVES**

Philippe LOGNONNE<sup>1</sup>, Philippe LOGNONNE<sup>1</sup>, Juliette ARTRU<sup>2</sup>, Vesna DUCIC<sup>1</sup>, Hiroo KANAMORI<sup>1</sup>, Makoto MURAKAMI<sup>1</sup> (<sup>1</sup>Departement de Geophysique Spatiale et Planetaire, IGP, France, <sup>2</sup>Seismological Laboratory, Caltech, Pasadena, USA, <sup>3</sup>Geographical Survey Institute, Ibaraki, Japan)

Rayleigh surface waves and tsunamis are producing vertical oscillations of the earth surface, which propagate upward and reach the ionosphere. We report here the observation of such ionospheric waves associated to Rayleigh Surface wave and quake generated tsunamis. These waves were detected by using the dense GPS networks of Japan and California, enabling an imaging of the ionospheric TEC variations every 30 sec. In both case, images of the wave are obtained and the propagation of the wavefront is observed. We present first results in the modelling of these waves using Normal Modes summation. The Normal modes are computed by a theory which take into account the coupling between the solid earth, the ocean and the ionosphere, as well as the energy loss at high altitude due to viscous and non-linear effects. This theory allows to compute either the Earth surface velocity or the ionospheric vertical velocities, and can be used for the computation of the transfer function between the ground and the ionosphere

Thursday, July 10 AM  
Presiding Chair: T. Nakamura

**HIGH LATITUDE AND METEORS**

**GAIL.06/10A/A01-001 0830**

**MILLSTONE HILL OBSERVATIONS OF COHERENT RADAR BACKSCATTER FROM THE SUB-AURORAL POLARIZATION STREAM**

John C. FOSTER, Phillip J. ERICKSON, Frank D. LIND (Haystack Observatory, Massachusetts Institute of Technology)

Observations of coherent backscatter made with the Millstone Hill 440 MHz radar during strongly disturbed conditions have been used to investigate the fine-scale spatial and temporal structure of the electric field in the auroral and sub-auroral E region. Previous observations at Millstone Hill [Foster and Erickson, GRL, 2000] have demonstrated that the backscattered logarithmic power and the irregularity phase velocity are proportional to the electric field which drives the two-stream waves. A ~20 mV/m electric field threshold for the onset of the coherent echoes was observed with ~380 m/s coherent phase speed. Coherent phase speed increased linearly with increasing electric field strength at the rate 8.5 m/s per mV over the electric field range 20 mV/m - 60 mV/m. Coherent backscatter amplitude (observed outside the saturation region) increased linearly with the electric field at the rate 25 dB per 30 mV/m. Fixed-beam experiments with high spatial resolution and data recording rate have been used to characterize the sharp spatial and rapid temporal variations of the electric field strength in the region of the sub-auroral polarization stream (SAPS [Foster and Burke, EOS, 2002]). Electric field gradients exceeding 4 mV/m per km are observed at the equatorward edge of the SAPS region and 50 mV/m changes in the longitudinally-aligned regions of intense electric fields are seen in temporally-brief intensifications of SAID electric fields. Rapid (60s) azimuth scans using a variety of radar pulse patterns, combined with pulse to pulse data sampling and the sidelobe sensitivity of the Millstone Hill steerable radar to the strong coherent-scatter cross section, permit the fine structure of the coherent power, the irregularity phase velocity, and the background (F-region) electric field to be measured across a 500 km by 500 km spatial area with 10-km spatial and 10-s temporal resolution. Observations made during an intense geomagnetic storm (April 5-6, 2000, and during the development phase of a moderate-disturbance on May 24, 2000) examine the dynamic variability of the electric field structure associated with the region of stormtime particle precipitation as well as the periodic modulation of the SAPS electric field as it expands equatorward in the dusk sector E region.

**GAIL.06/10A/A01-002 0850**

**ON THE THERMOELECTRIC ORIGIN OF ELECTRIC FIELD IN THE POLARIZATION JET**

Victor L. KHALIPOV<sup>1</sup>, A.E. STEPANOV<sup>2</sup> (<sup>1</sup>Space Research Institute of Russian Academy of Sciences, <sup>2</sup>Institute of Cosmophysical Research and Aeronomy, Yakutsk, Russia)

Long-lasting ground based measurements of a polarization jet (PJ) by the latitudinal chain of ionospheric stations in Yakutia ( $3 < L < 5$ ; MLT = UT + 9 h) and by 5 subauroral Russian stations and energetic ion observations by AMPTE/CCE in 1984 - 89 were analyzed. 25 cases were found when PJ was recorded simultaneously with the AMPTE/CCE observations. The data comparison shows that at least in the considered cases of strong magnetic substorms, PJ was accompanied by strong injection of ions with the energy of ~20 - 50 keV and intensity of ~106 cm<sup>-2</sup>sec<sup>-1</sup>ster<sup>-1</sup>keV<sup>-1</sup>. Close to the injection region in the near midnight sector no ion dispersion was observed, but in the evening sector nose events were detected. Measurements by ionosondes at different longitudes show that

the westward velocity of the front of PJ development is close to the gradient drift velocity of 20 keV ions forming nose events. Thus, the physical mechanism of PJ formation due to energetic ion injection during a strong substorm burst is experimentally confirmed. PJ was observed equatorward from the region of energetic ion penetration into the inner magnetosphere but not in the gap between the injected ions and plasmasheet. PJ develops almost along constant invariant latitude covering a sector from 60 to 130 degrees in longitude. This suggests that electric field responsible for the PJ formation is of thermoelectric origin. For the recorded ion energies the PJ electric field can be as high as 50 - 100 mV/m. The position of equatorial ion injection boundary in more than 180 orbits of the AMPTE/CCE satellite for different levels of geomagnetic activity is analyzed. The form of the boundary does not depend on local time and is also located along invariant latitude in sector 18.00 - 02.00 MLT.

**GAIL.06/10A/A01-003 0905**

**IONOSPHERIC PLASMA STRUCTURING IN THE CUSP AND THE POLAR CAP REGION DURING ENHANCED PLASMA CONVECTION**

Santimay BASU<sup>1</sup>, Sunanda BASU<sup>2</sup>, C.E. VALLADARES<sup>3</sup>, R.E. SHEEHAN<sup>3</sup> (<sup>1</sup>Air Force Research Laboratory (VSBXI), <sup>2</sup>National Science Foundation, <sup>3</sup>Boston College)

The evolution of large (hundreds of km) and small scale irregularities (tens of m) of electron density in polar cap patches during their transit from the cusp to the central polar cap has been investigated from satellite scintillation, and GPS total electron content (TEC) and phase fluctuation measurements. The cusp and the central polar cap observations of irregularity structures have been made at Ny Alesund, Svalbard and Thule, Greenland, respectively, by monitoring scintillation of 250 MHz signals from satellites in highly elliptic orbits and from measurements of TEC and large scale phase fluctuations from GPS observations. The source function of patches are investigated in terms of drainage plumes through the erosion of plasmasphere during ring current events as well as in the context of injection and transport of plasma in the cusp region similar to flux transfer events. The irregularity evolution in the cusp and the central polar cap has been examined in the context of the state of the magnetosphere-ionosphere coupling as defined by the interplanetary magnetic field orientations and the SuperDARN radar observations of plasma convection. The broad spectral characteristics of scintillation recorded in the cusp region indicate the presence of electric field turbulence in this region whereas in the central polar cap the scintillation spectra remains confined over a narrow band but are shifted to higher frequencies consistent with high anti-sunward convection. It is shown that under conditions of enhanced convection when the patch becomes unstable to the gradient-drift instability it is able to retain the integrity of meso- and medium- scale irregularities as the patch convects for long periods of time over long distances of several thousand kilometers. It is shown that recent three-dimensional nonlinear simulations of the gradient drift instability with variable ExB drift and ion inertial effects reproduce the observed results on patch integrity and variable levels of leading/trailing edge asymmetry in structuring and irregularity amplitudes.

**GAIL.06/10A/A01-004 0920**

**A YEAR IN REVIEW: HIGH LATITUDE IONOSPHERIC IRREGULARITY OBSERVATIONSWITH PASSIVE VHF RADAR**

Melissa G. MEYER, John D. SAHR, Dawn M. GIDNER, Chucai ZHOU (University of Washington Electrical Engineering)

We operate a passive radar in the FM radio band (100 MHz frequency range) with the purpose of studying turbulence in the high latitude ionosphere. Currently the only radar of its kind in the world, our system has been online almost continuously since November 2001. During the year 2002, we recorded E-region irregularities on 25 separate days. Here we will present those observations, summarizing characteristics of the data, identifying trends, and noting conditions under which their irregularities were detected. Our radar field of view covers approximately the geomagnetic latitudes from 56° up to 63°, a region over southwestern Canada. Though our system is too far south to regularly study the auroral oval, it is sensitive enough to detect E-region turbulence during disturbed conditions. We have detected events at ranges up to 1200 km, and as close as 400 km; the reported Kp index during our observations has been as low as 4.0 and as high as 7.0. We will present range-Doppler diagrams of some typical (and atypical) irregularities that we detect; we will also present summarized results from the analysis of these observations, including the Doppler characteristics of the echoes, the local time at which they occurred, the range at which they occurred, and their range extent, as well as interferometric information such as transverse size and structure. We are able to form simple images with our interferometer, and plan to show "movies" of sequential images, from which an approximate transverse drift speed can be inferred. We will also compare our observations with those of other coherent scatter radars in the area, and provide supplementary information from the times of our observed irregularities from other instruments, such as UVI images, magnetometer readings, and measurements of the solarwind, when available. We intend to demonstrate that our unique instrument provides data of high quality which is comparable to that of other radars of similar purpose and design, and which may be used as a link in understanding existing datasets.

**GAIL.06/10A/A01-005 0940**

**WESTWARD TRAVELING SURGES IN CRNA AND OPTICAL AURORA**

Pieter H. STOKER, Albertus WILSON (Unit for Space Physics, Potchefstroom University for CHE, Potchefstroom, SOUTH AFRICA)

Latitudinal and diurnal variations in auroral data show (Hartz and Brice, Planet. Space Sci. 15, 301-329, 1967) that there are two basic categories of energetic auroral electrons, the softer electrons (<10 keV) cause optical emissions in the E- and F-regions of the ionosphere and the harder (>10 keV) electrons ionize down into the D-region for cosmic radio noise absorption (CRNA). These two categories of auroral electrons were observed during the expansion phase of a magnetic substorm on the evening of May 1, 1997, from recordings of all-sky optical aurora and 64 beam imaging riometer at the Antarctic base SANAE IV (L=4.1). While the spatial absorption structure changed only slowly during the period of observation, the low level white light luminosities showed both fast localized and fast spatial fluctuations on one second time scale. The CRNA and auroral optical emissions could therefore not have been caused by the same electron precipitating flux. This implies that there are two quite different processes, one that is related to a softer electron flux, causing a high variability in auroral optical emissions, and another process that generates a more persistent flux of harder electrons. A CRNA westward traveling surge (WTS) was observed coincident with a surge in the all-sky optical data, together with a surge in the optical data leading the CRNA WTS by ~30-50 seconds. The CRNA WTS was ribbon-like, traveling westward at a speed of 2.3 km s<sup>-1</sup>. Both the optical surge leading the CRNA WTS and the CRNA surge should have started along the velocity shear zone of the Harang discontinuity closest to the neutral line in the magnetospheric tail region. But the softer electrons, causing E- and F- region optical emissions, may have been injected onto drift paths closer to Earth than the more energetic electrons, ionizing down into the D-region for

CRNA. These harder electrons could have been accelerated for later precipitation by an increasing dawn-to-dusk electric field arising from a reconfiguration of the tail magnetic field during the expansion phase of the substorm.

GAI.06/10A/A01-006

0955

## INVESTIGATIONS OF PMSE: A SURVEY OF RECENT EMPIRICAL RESULTS

Phillip B. CHILSON<sup>1</sup>, Jürgen RÖTTGER<sup>2</sup> (NOAA ETL and University of Colorado CIRES, <sup>3</sup>Max-Planck-Institut für Aeronomie)

The term Polar Mesosphere Summer Echoes (PMSE) is used to describe dramatic enhancements in the radar backscattering cross-section observed during the summer months at high latitudes near the mesopause. Since the discovery of PMSE over twenty years ago, numerous experimental efforts have been undertaken in an attempt to better understand the mechanism or mechanisms responsible for their occurrence. For example, numerous hours of radar observations have been completed over a wide range of operating frequencies. To investigate small-scale structures associated with PMSE, some of the radar experiments were conducted in interferometric or imaging modes. Additionally, several radar observations made in conjunction with measurements from other instruments such as lidars, rocket launches, riometers, ionospheric heaters, and satellites. In this talk we review some of the more recent experiments and discuss how they relate to prevailing theoretical models of PMSE.

GAI.06/10A/A01-007

1030

## MASS ESTIMATION OF FAINT METEORS FROM RADAR HEAD ECHOES COMBINED WITH OPTICAL OBSERVATIONS

Toru SATO<sup>1</sup>, Takuji NAKAMURA<sup>2</sup>, Shuichi TSUTSUMI<sup>1</sup>, Masumi NISHIO<sup>3</sup> (<sup>1</sup>Department of Communications and Computer Engineering, Kyoto University, <sup>2</sup>Radio Science Center for Space & Atmosphere, Kyoto University, <sup>3</sup>Graduate School of Human and Natural Environment Sciences, The University of Tokushima)

Impacts of meteors with spacecraft are widely recognized as one of major sources of possible hazard in the space environment. Although the average mass of meteor bodies is much less than artificial space debris, relative velocity of high-speed meteors against the earth are as high as 70 km/s, which far exceeds that of artificial objects. It is thus very important to establish statistics of meteors, especially those of the mass and velocity, along the earth's orbit around the sun in order to make reliable data base for designing large scale spacecraft such as space stations. We have developed a high-sensitivity combined radar-optical system consisting of the MU radar, which is a high-power VHF Doppler radar, and an ICCD video camera for the purpose of studying velocity and mass distributions of faint meteors. By combining the optical magnitude and the velocity and orbit data obtained by the radar, we can estimate the mass of individual meteor body based on some empirical equations. On the other hand, as our precise radar measurements also provide the deceleration due to atmospheric drag, it is possible to estimate the mass based on the radar data alone. Although similar attempts have already been made with the data obtained with Arecibo incoherent scatter radar (Mathews et al, 2001), application of the same method resulted in a few to several orders smaller estimates than the radar-optical estimates. We consider this difference as mainly due to the fact that the previous study took into account only the direct impact of atmospheric molecules to the meteor body. Here we propose an alternate procedure of estimating the mass from radar data by taking the effect of deceleration due to the high-density gas emitted from the meteor body also into account. We derived an empirical relationship between the density of such gas and physical parameters obtained by the radar observations so that the estimated mass agrees with the radar-optical estimates. Our procedure provides the mass estimates based on the radar data which agree with the radar-optical data within an order of magnitude. Since the radar has much higher sensitivity of about 15 magnitude than the optical sensor, and is suitable for continuous observations with automatic data analyses, it will enable us to make statistical study of the mass distribution of faint meteors.

GAI.06/10A/A01-008

1050

## METEOR ECHO STUDIES USING THE NOAA HF RADAR

Lung-Chih TSAI<sup>1</sup>, Frank Tom BERKEY<sup>2</sup>, T.-T. HSIAO<sup>3</sup> (<sup>1</sup>Center for Space and Remote Sensing Research, National Central University, <sup>2</sup>Institute of Space Science, National Central Univ., <sup>3</sup>Space Dynamics Lab., Utah State Univ.)

Numerous meteor-induced Es events have been observed using the Bear-Lake dynamometer (NOAA HF radar) sited at 41.9°N and 111.4°W. As a tool for meteor diagnostics, the dynamometer utilizes interferometric receiving techniques to provide high-resolution echo-location, line-of-sight Doppler velocity, and digital ionograms as routine fundamental data products (288 soundings/day). The observed duration of the meteor induced echoes at HF is several seconds, as compared to more conventional VHF meteor observations where the ionization decay time is on the order of a second. The meteor-induced Es events are most evident between the hours of local noon and late afternoon, are characterized by radio bandwidths up to several MHz and preferentially peak at ~100 km height. Determination of atmospheric motions can also be provided by measurement of coherent scattering from meteor trails. In this work, a three-dimensional velocity vector has been derived by fitting a set of a spatially distributed, wide-band echoes to the line-of-sight Doppler velocity measurements by means of the singular value decomposition technique.

GAI.06/10A/A01-009

1105

## PLASMA SIMULATIONS, RADAR OBSERVATIONS AND THEORY OF A NEW TYPE OF METEOR ECHO: THE NON-SPECULAR TRAIL

Lars P. DYRUD, Meers M. OPPENHEIM, Sigrd CLOSE, Stephen HUNT, Kelly MCMILLON, Licia RAY (Center for Space Physics, Boston University)

The Earth is continuously bombarded by extraterrestrial material in meteoric form. Since most of this mass flux is comprised of very small meteors (< 0.1 g), they are either undetected or measured only by radars. We present research that allows new ways to interpret radar observations of a previously poorly understood type of meteor radar echo, the non-specular trail. This new understanding allows researchers use these non-specular meteor echoes to understand both the meteor flux and its effect on the mesopause/E-region. Plasma simulations demonstrate that meteor trails are unstable to growth of gradient-drift Farley-Buneman (GDFB) waves that become turbulent and generate large B-field aligned irregularities (FAI). These simulations and our analysis indicate that the non-specular echoes, that can extend between 5-10 km in altitude range, are reflections from plasma instability generated FAI. Simulation and model results can explain a number of characteristics of these non-specular observations. 1) The observed altitudinal extent of their trail echoes. 2) Trail diffusion in the plane perpendicular to B that can be up to an order of magnitude larger than expected from ambipolar diffusion. 3) A curious, approximately 20 ms delay between head

echo observation and trail reflection. Additionally, we present model showing that the specific altitude range of trail instability depends on meteor and atmospheric properties. This variability will allow researchers to infer neutral temperature, neutral-ion collision frequencies, and meteoric velocity and composition in completely new ways. Finally, we demonstrate some of these non-specular diagnostic techniques using radar observations from the ALTAIR and Piura radar facilities.

GAI.06/10A/A01-010

1125

## IONOSONDE OBSERVATIONS OF THE LEONID METEOR SHOWER IN NOVEMBER 2001

Takashi MARUYAMA, Hisao KATO, Maho NAKAMURA (Communications Research Laboratory)

We applied ionosondes at four stations in Japan in their rapid-operation mode to make observations every minute for 102 hours during the period of the Leonid meteor shower in November 2001. Plenty of radio echoes that look like echo traces produced by sporadic-E reflection are seen in the ionograms, and this allowed statistical analysis in a single meteor shower event including discrimination of the backscattering by meteor trails from reflection by a horizontally stratified sporadic-E layer. The radio echoes seen in the ionograms were categorized into three types. The first are spontaneous echoes which were distributed across a wide range of virtual heights; at times during the period of maximum meteor activity, there was a statistically good correlation among the echoes seen at the four stations; the echoes of this type appear to be produced by Fresnel backscattering from meteor trails. The second are also spontaneous echoes seen during the shower period but persist for several ten minutes at the same virtual height as the typical sporadic-E layer and the top frequency of these echoes decayed with time; echoes of this type are thus attributed to the reflection from a meteor-induced sporadic-E patch. Echoes of the last type appear outside the period of maximum activity of the meteor shower in the same range of virtual heights as the conventional sporadic-E layer, and there was no time correlation between such events as observed at the four stations; these events are attributed to a periodical increase in foEs which is modulated by planetary-wave activity and have no relation with the meteor shower.

GAI.06/10A/A01-011

1145

## LOCALIZED IONOSPHERIC PC 3-4 WAVES OBSERVED BY THE ICELAND EAST HF RADAR

Yuichi SHINKAI<sup>1</sup>, Natsuo SATO<sup>2</sup>, Yukimatu Sessai AKIRA<sup>3</sup>, Toshihumi MUKAI<sup>4</sup>, Tohru SAKURAI<sup>5</sup>, Yutaka TONEGAWA<sup>6</sup>, Mark LESTER<sup>7</sup>, Stephen Eric MILAN<sup>8</sup>, Jean-Paul VILLAIN<sup>9</sup>, George SOFKO<sup>10</sup>, Brian James FRASER<sup>11</sup> (<sup>1</sup>Department of Polar science, Grad. Univ. Advanced Studies, <sup>2</sup>NIPR, <sup>3</sup>ISAS, <sup>4</sup>Tokai Univ., <sup>5</sup>Leicester Univ., <sup>6</sup>LPC/ENRS, <sup>7</sup>Saskatchewan Univ., <sup>8</sup>Newcastle Univ.)

On 12 February 2002 the SuperDARN Iceland East radar observed very clear 20 MHz ULF waves during the campaign of the SuperDARN/GEOTAIL simultaneous observation that conducted to observe the Pc 3-4 range ULF wave. In this campaign, the HF radar has run with CUTLASS "Stereo mode" which runs two different scan modes simultaneously, one is a high time resolution mode (3 sec) at fixed one beam and the other is a global scan mode (16 beams). The Doppler velocity data obtained by the HF radar showed very high coherency among 8 range gates, where each range gate is about 45 km. The phase shift of this wave among 8 range gates was about 50 degree, indicating that the wavelength of this ULF wave is at least longer than 2000 km. The ground based magnetometers (IMAGE, Iceland, Finland, SAMNET in northern hemisphere, and the Davis in Antarctica) showed that the same ULF wave signatures as the HF radar with time period about 50 seconds is observed only by the magnetometer in Iceland. On the other hand, we could not find such wave signature from other magnetometers. This result suggests that the wave is very localized phenomena.

GAI.06/10A/A01-012

1200

## OBSERVATION OF SHOCK INDUCED PI-1 PULSATIONS IN TOPSIDE IONOSPHERIC PLASMA AT 600 KM ALTITUDE ON APRIL 17, 2002 STORM DAY

Su SHIN-YI<sup>1</sup>, Chi-Kwan CHAO<sup>2</sup>, Huey-Chin YEH<sup>3</sup> (<sup>1</sup>National Central University, Taiwan, R.O.C.; <sup>2</sup>On sabbatical leave as NRC Senior Research Associate at NASA/JSC, Houston, Texas, U.S.A., <sup>3</sup>Institute of Space Science, National Central University, Taiwan, R.O.C.)

ROCSAT-1 orbiting at 600 km altitude observed a rare Pi-1 pulsation event in the topside ionospheric plasma during the April 17, 2002 storm period. The pulsations in the two perpendicular-to-field-line flow components begin shortly after the interplanetary shock impact on the magnetosphere. The initial response of the topside ionospheric plasma indicates that the ionosphere was compressed inward and toward the dusk side as ROCSAT-1 was located in the post-noon sector. The subsequent oscillations with a period of 19 seconds in the radial and the zonal flow components last for less than two minutes. A rotation in the oscillation polarization is noted to change from the dominant radial component to the zonal component. This rotation in the polarization axis should be caused by the non-linear coupling effect between the two components in a layered structure of the non-uniform ionospheric plasma distribution in the radial direction. The density oscillation, though responds to the shock impact with a small delay in comparison with the flow oscillations, indicates an out-of-phase oscillation with the zonal flow component. The observation will be explained with a simple MHD model.

GAI.06/10A/A01-013

1215

## WAVE STRUCTURES OBSERVED IN THE IONOSPHERIC F-REGION DURING LOW AND HIGH GEOMAGNETIC ACTIVITY

Petra SAULI<sup>1</sup>, Patrice ABRYS<sup>2</sup>, Josef BOSKA<sup>3</sup> (<sup>1</sup>Institute of Atmospheric Physics ASCR, Czech Republic, <sup>2</sup>Laboratoire de Physique, ENS de Lyon, France.)

The short-term ionospheric variation, in the period range 15 minutes to 4 hours, studied in time series consisting of electron densities shows clear enhancements of waves. The analysis is based on the vertical ionospheric soundings measurements at midlatitude station Pruhonic (Czech Republic, 49.9N, 14.5E). Data were collected during several campaigns and consists of vertical ionospheric sounding measurement with 5 min repetition time, that were carried out during periods of low (1996, 1997 years) and high (1991, 2001 years) Solar activity. Among random oscillations, wave-like structures are well developed. Diurnal variations of the AGW activity during period of low solar and geomagnetic activity show clear enhancement during and several hours after sunrise and sunset. Some of the observed wave structures of AGW type have significant vertical component of propagation through the ionosphere. The most probable source of these waves seems to be the Solar Terminator passages. During the periods of high Solar and geomagnetic activity (1991, 2001), the substantial intensification of AGW activity at longer and shorter periods, associated with response of the magnetosphere to the sharp increase of solar wind, was observed.

**GAIL.06-Posters**

**IONOSPHERIC IRREGULARITIES, FIELDS AND WAVES**

Location: Site D

Friday, July 11 PM

**GAIL.06/11P/D-001** Poster **1400-053**

**SIMULTANEOUS RADAR OBSERVATIONS OF THE ELECTROJET PLASMA IRREGULARITIES AT 18 AND 54.95 MHZ OVER TRIVANDRUM, INDIA**

Amit Kumar PATRA<sup>1</sup>, D. TIWARI<sup>1</sup>, Viswanathan K.S, Jyothi N, Devasia C.V, Subbarao K.S.V, Sridharan R (<sup>1</sup>National MST Radar Facility, <sup>2</sup>Space Physics Laboratory, VSSC, Trivandrum)

Observations of electrojet plasma irregularities made using a newly established 18 MHz coherent backscatter radar at Trivandrum are presented. Also presented are the simultaneous observations of the electrojet plasma irregularities made using a collocated 54.95 MHz radar. These correspond to 8.3 m and 2.7 m scale irregularities respectively. An interesting and new aspect of these observations is that the 8.3 m irregularities have significant anisotropy in the plane perpendicular to magnetic field in contrast to that reported for 3 m irregularities. While type-1 and type-2 could be distinctly observed at 2.7 m, it is rather difficult to distinguish at 8.3 m. The type-2 velocities are found to be pretty close to each other as expected from gradient-drift instability theory. Type-1 velocities are found to be quite close to each other only at altitudes of the peak electrojet when clear type-1 echoes are noted. But spectral widths are found to be remarkably different at the two scale sizes. The ratio of spectral width corresponding to 2.7 m to that at 8.3 m is found to be close to 1.4, quite similar to that reported earlier from Jicamarca. Ratio of spectral width to mean Doppler shift for 8.3 m at times is found to be much less than unity, even for small mean Doppler shift unlike at 2.7 m. Statistical characteristics of the spectral parameters measured at the two scale sizes are also presented and a detail comparison of these parameters have been made. The above observations are studied in the light of plasma instability theories and related simulation works.

**GAIL.06/11P/D-002** Poster **1400-054**

**ROLE OF E-REGION CONDUCTIVITY IN THE DEVELOPMENT OF EQUATORIAL IONOSPHERIC PLASMA BUBBLES**

Archana BHATTACHARYYA (Indian Institute of Geomagnetism)

It is well known that E-region conductivity has a major effect on the non-linear evolution of equatorial ionospheric plasma bubbles because field-aligned currents (FACs) couple the equatorial F-region with the conjugate E-regions. In recent years, a linear theory for the development of equatorial bubbles has been put forward using a transmission line analogy, in which the FACs are considered to be carried by oppositely propagating Alfvén waves that are launched in the equatorial F-region when a plasma bubble starts to grow. Here, the transmission line analogy is extended to study the effect of the conductivity of the conjugate E-regions on the non-linear evolution of the equatorial ionospheric bubbles. For this, a simple three mode system is considered, and a set of mode coupling equations which describe the non-linear evolution of plasma bubbles, taking into account their coupling with the conjugate E-regions through FACs, is derived. From these equations, which correspond exactly with the Lorenz equations that have been used to describe the evolution of the Rayleigh-Bendard instability, a condition for unstable fixed states is derived. This condition shows that the E-region resistivity and F-region polarizability introduce another time scale in the non-linear evolution of equatorial bubbles, which is the time scale for discharging the bubbles and thus destroying the perturbation electric field. This time scale is found to be inversely proportional to the flux tube integrated E-region conductivity and directly proportional to the length of the transmission line, which depends on the height of the F-region. When this time scale is shorter than the inverse of the linear growth rate of the Rayleigh-Taylor instability in the inertial regime, the fixed states are stable. With increasing solar flux, the E-region conductivity increases and hence the onset of chaotic evolution of the equatorial bubble can only occur for a proportionate increase in the length of the transmission line such that there is no decrease in the bubble discharge time. This provides an explanation for the past observation that the threshold value of the post-sunset upward drift of the equatorial F-region for the generation of strong early night irregularities increases with solar flux.

**GAIL.06/11P/D-003** Poster **1400-055**

**ESTIMATION OF A SIZES SPECTRUM OF THE INHOMOGENEITY THE LOWER IONOSPHERE ON THE DATA OF DOPPLER PHASE-GONIOMETRIC MEASUREMENTS**

Vadim Yurievich TEPLOV, Vladimir Vladimirovich BOCHKAREV, Inna Romanovna PETROVA (Department of Physics, University of Kazan)

In this work an estimation of a spectrum of the sizes of ionospheric inhomogeneity in the lower ionosphere are resulted. These estimations are received on oblique ionospheric sounding for several middle-latitude radiolines. Measurements were carried out by the method of spaced reception with small base. Array antenna included 4 vertical vibrators. Diameter antenna fields is 15 m. Mode separation was carried out in frequency area on Doppler frequency shift of a signal. Continuous measurements of exact times stations signals (Moscow) and broadcasting SW-stations with frequencies in a range from 5 up to 12 MHz located in Moscow, Saint Petersburg, Ekaterinburg (Russia), and Lamperthaym and Holchirhen (Germany) have been carried out. Measurements of various frequencies signals from several transmitters simultaneously also were carried out. The size spectrum of the scattering inhomogeneity is connected to a frequency power spectrum of a radio signal integrated Fredholm equation of 1-st type. Characteristic function of a speed field of the scattering medium is a kernel of this equation. That fact, that a speed field of a wind at heights of the lower ionosphere is essentially non-stationary represents significant difficulty. For radiolines on which measurements were carried out, the size of Doppler variations of frequency caused by regular large-scale movements in an ionosphere, can be more than variations, caused by irregular movements. The adaptive methods of the spectral analysis based on use of wavelet-transformation are applied for correct account of influence of regular wind structure. Opportunity on phase measurements on spaced - carried array antenna to estimate of angular distribution of a scattered signal is other moment allowing essentially to improve reliability of results. At this configuration the array antenna it is possible to achieve of single-valued definition of angle of arrival no more than for 2 mode of signal in each frequency filter. At a large quantity of scattering irregularity the problem can be solved only statistically. In cases when the dominating mechanism of formation of a signal is incoherent scattering on small-scale ionospheric inhomogeneity, the estimation of angular distribution of capacity of a signal can be found according to criterion of the maximal plausibility. Presence of angular distribution allows to reduce essentially uncertainty of an estimation of a corner of dispersion, and therefore, a spectrum of the scattering irregularity

sizes. In work examples of an estimation of a spectrum of irregularity are resulted by various methods of processing of a signal. The work was conducted under the support of grant RFBR 01-05-65251

**GAIL.06/11P/D-004** Poster **1400-056**

**INVESTIGATING TRAVELING IONOSPHERIC DISTURBANCES WITH THE DPS-4 IONOSONDE**

Konstantin G. RATOVSKEY, Andrey V. MEDVEDEV, Boris G. SHPYNEV, Dmitriy S. KUSHNAREV (Institute of Solar-Terrestrial Physics)

The DPS-4 digisonde, produced by the Center for Atmospheric Research, University of Massachusetts Lowell, USA, is among the most advanced and widely used ground-based ionospheric sounding facilities. The worldwide DPS network includes over 70 stations. DPS-4 ionosondes are used in two basic areas of ionospheric research. One involves the study of the behavior features of the electron density profile obtained from height-frequency characteristics. The other area encompasses the investigation of the ionospheric plasma drift velocity. Drift velocity calculations are based on measuring angles of arrival and the frequency Doppler shift; essentially, DPS-4 are used as a HF radar. The method for calculating the velocity assumes the presence of three echo signals as a minimum, i.e. an essentially inhomogeneous ionosphere. Thus the method provides better results for high-latitude stations when compared with mid-latitude stations where the inhomogeneous structure is much more poorly pronounced. On the other hand, even in the presence of a single echo signal, the possibility of measuring angles of arrival and the frequency Doppler shift allows for using DPS-4 in investigating traveling ionospheric disturbances. Measurements on several carrier frequencies make it possible not only to calculate the horizontal velocity of disturbances but also to investigate their height structure. In contrast to existing facilities for investigating traveling ionospheric disturbances, DPS offers improved spatial and temporal resolution and enables continuous measurements, i.e. monitoring. This paper presents the results derived from investigating traveling ionospheric disturbances with the Irkutsk DPS-4 ionosonde during January through June 2003, as well as the results of comparison with experimental data obtained with the Irkutsk incoherent scatter radar.

**GAIL.06/11P/D-005** Poster **1400-057**

**STRONG TURBULENCE STRUCTURES IN MODIFIED IONOSPHERE**

Andrey Valentinovich KOCHETOV<sup>1</sup>, Galina Ivanovna TERINA<sup>2</sup> (<sup>1</sup>Department of Physics and High Power Electronics of Institute of Applied Physics, RAS, <sup>2</sup>Department of Solar and Terrestrial Physics & Wave Phenomena of Radiophysical Research Institute)

The experimental and theoretical results of study of nonlinear dynamic structures exciting in ionospheric plasma under action of powerful electromagnetic emission are presented. The experimental results were obtained in the Nizhny Novgorod region at the heating facilities "Zimenki" and "Sura" by the method of sounding of artificially disturbed ionospheric plasma by probing radio pulses. Spatio-temporal evolution of amplitude and phase characteristics of caviton signal (CS) (G.I. Terina, J. Atm. Terr. Phys., 1995, v.57, p.273) and main signal (MS) of probing transmitter are considered. For theoretical interpretation of the characteristics of CS and MS the numerical solution of nonlinear Schroedinger equation with driven extension (DNSE) in nonuniform plasma are presented for the linear inhomogeneous plasma layer and for one with prescribed densities depletions. The simulation enables us to study spatial structures of electromagnetic field and plasma density, their time and spectrum characteristics at formation and relaxation states. The comparison of the experimental results with the simulation ones shows their qualitative agreement, namely: correspondence of the time phase evolution of the MS of probing transmitter to the calculated time dependencies of reflected wave phase and correlation of the time phase evolution of CS to the calculated time phase dependencies of the wave field at plasma resonance point. Moreover, the simulation results allow to interpret qualitatively the following characteristics of CS: periodic generation of CS; the dependencies of CS period on heating power and heating time; the travel of CS maximum height down the density gradient (A. V. Kochetov, V.A. Mironov, G.I. Terina, Advances in Space Res., vol. 29, pp. 1369-1373, 2002). Observed evolution of the phase characteristics of the main signal and CS as well demonstrate powerful radio wave penetration into overdense, in linear approach, plasma region at formation state. The obtained results show the excitation of strong turbulence structures and allow us to interpret CS characteristics, and so far inexplicable phenomena as "spikes" too (L. M. Erukhimov, et al., Geomagnetism and Aeronomia, (in Russian), vol. 23, pp. 433-439, 1983). The work is supported in part by the Ministry of Higher Education of Russia (Grant No. E02-3.2-90) and the Russian Foundation for Basic Research (Grant No. 02-02-17277).

**GAIL.06/11P/D-006** Poster **1400-058**

**STATISTICAL CHARACTERISTICS OF VHF RADAR OBSERVATIONS OF LOW-LATITUDE E REGION FIELD-ALIGNED IRREGULARITIES OVER GADANKI**

Amit Kumar PATRA<sup>1</sup>, Sripathi S<sup>1</sup>, Sivakumar V<sup>1</sup>, Rao P.B<sup>2</sup> (<sup>1</sup>National MST Radar Facility, <sup>2</sup>National Remote Sensing Agency, Hyderabad)

In this paper, we present the statistical characteristics of the low-latitude (6.30 north magnetic latitude) E region field aligned irregularities observed using the Gadanki MST radar. We present diurnal and seasonal characteristics of a variety of parameters (percentage of occurrence of signal, signal-to-noise ratio, mean Doppler velocity and spectral width). The echoes are observed both during day- and night-time, nighttime being more intense and larger in height extent than daytime. The thickness of the echoing region is minimum during noon and maximum during midnight. The echoes could be observed at altitudes as low as 87 km and as high as 160 km. The percentage of occurrence of signal is found to be as high as 95% during sunrise and 80% just before sunset. Further the E region echoes are stronger and occur more frequently during local summer, and weaker and occur less frequently in winter. We also present some characteristics of the sunset echoes, which we believe that they could be used for studies related to the onset of equatorial spread-F since some of the magnetic field lines of the E region over Gadanki connect to that of the F region over the equator. The mean values of the Doppler velocities above 102 km are about 10 m s<sup>-1</sup> upward during daytime and 10 m s<sup>-1</sup> downward during nighttime, representing the electrodynamic drift due to zonal electric field. The Doppler velocities below 102 km do not have any specific trend and they are driven mainly by meridional winds.

**GAIL.06/11P/D-007** Poster **1400-059**

**TO IMPROVE A REGIONAL IONOSPHERIC TEC MODEL OVER JAPAN ISLANDS**

Jinsong PING<sup>1</sup>, Akinori SAITO<sup>2</sup>, Yusuke KONO<sup>1</sup>, Koji MATSUMOTO<sup>3</sup>, Kosuke HEKI<sup>1</sup>, Nobuyuki KAWANO<sup>1</sup> (<sup>1</sup>Earth Rotation Division, National Astronomical Observatory, Japan, <sup>2</sup>Department of Geophysics, Graduate School of Science, Kyoto University, Japan)

The high density regional GPS (Global Positioning System) Earth Observation Network (GEONET) of Japan, with average distance between nearby receivers as 25 km, is a

powerful facility to monitor the ionospheric variation over Japan Islands. Based on the phases and codes observables of this network, the total electron content (TEC) distribution and variation with very high time and spatial resolutions can be obtained continuously. Ping et al. (2002) expanded the obtained GEONET TEC by using the spherical harmonic function method through a full 60x60 degrees and orders for each 10 minutes. In this report, this regional ionospheric TEC model (RIM) is upgraded by means of both the spatial and time resolutions. A RIM model of coefficients through 150x150 degrees and orders for each 5 minutes has been carried out. However, the attempt to improve of the resolution for this RIM by using spherical harmonic function expanding method is not successful. Of this RIM, a daily map time series are arranged in an array to show the TEC evolution. The evolution history of medium and short scales traveling ionospheric disturbances (MSTIDs and SSTIDs), i.e. the polarward intense TEC enhancement near the geomagnetic equator and an isolated TID of medium or small scale with extremely high TEC density, have been found in each month during the period of which the data is analyzed. The isolated TID is appears in either day time or in night with period of several hours. Reasonable explanation about the source and mechanism of this kind of phenomenon is looking forward to being discovered. The RIM model discussed at here will benefit the application of other fields, like s/c radio tracking and orbiting.

**GAIL.06/11P/D-008** Poster **1400-060**

**ANNUAL TEC VARIATION IN THE EQUATORIAL ANOMALY REGION DURING THE SOLAR MINIMUM: SEPTEMBER 1996 - AUGUST 1997**

Chin-Chun WU<sup>1</sup>, C.D. FRY<sup>2</sup>, J.-Y. LIU<sup>3</sup>, K. LIU<sup>4</sup>, C.-L. TSENG<sup>5</sup> (<sup>1</sup>CSPAR/The University of Alabama in Huntsville, <sup>2</sup>Exploration Physics, International, Inc., EXPI, 614 Nashua Street, #222, Milford, NH 03055-4917, <sup>3</sup>Institute of Space Science, National Central University, Chung-Li, Taiwan, ROC, <sup>4</sup>Johns Hopkins University, Apply Physic Laboratory, Laurel, MD 20723, USA, <sup>5</sup>Satellite Geoinformatic Research Center, National Cheng Kung University, Tainan, Taiwan, ROC)

The ionospheric total electron content (TEC) in the equatorial anomaly regions studied by analyzing dual-frequency signals of the Global Position System (GPS) acquired from a meridional chain of 9 observational sites clustered around Taiwan (21.9°-26.2°N, 118.4°-112.6°E). This relatively dense GPS chain observation provides a powerful tool for studying ionospheric total electron content in the northern hemisphere equatorial anomaly region with an unprecedented spatial resolution. Specifically, we studied seasonal and geomagnetic effects on the equatorial ionospheric anomaly during the solar minimum period between September 1996 and August 1997. It is found that the surveyed data indicated double peaks in the magnitude of TEC,  $I_p$ , at the anomaly crest in the equinoxes, similar to the semi-annual variation of geomagnetic activity. The values of  $I_p$  were found to maximize in April, 1997 and minimize in July, 1997. Statistical studies indicated that the monthly values of  $I_p$  do not correlate with the planetary magnetic  $K_p$  index ( $r=0.41$ ) but correlate well with the geomagnetic activity  $Dst$  index ( $r=0.72$ ), suggesting that variations of TEC are mainly driven by a low-latitude forcing. The most likely time for to occur was 1400 local time (~30%) at 20°N geographic latitude ~37% for the surveyed period.

**GAIL.06/11P/D-009** Poster **1400-061**

**A STUDY OF EQUATORIAL SPREAD F DURING A SOLAR MAXIMUM PERIOD, 1999-2000**

Chien-Chih LEE<sup>1</sup>, J.Y. LIU<sup>1</sup>, B.W. REINISCH<sup>2</sup>, W.S. CHEN<sup>1</sup>, F.D. CHU<sup>1</sup> (<sup>1</sup>Institute of Space Science, National Central University, <sup>2</sup>Center for Atmospheric Research, University of Massachusetts)

We examine the onset conditions of the equatorial spread F (ESF) using a digisonde and 5 GPS stations. One digisonde, located at Jicamarca (11.9°S, 76°W), gives the time,  $h'F$  (the lowest virtual height of the F-layer), and vertical drift velocity ( $dh'F/dt$ ) of the ESF onset. The GPS stations along 75°W provide the total electron content (TEC), the ionization strength and asymmetry indices ( $I_s$  and  $I_a$ ) of the equatorial ionization anomaly (EIA), and the phase fluctuation. We intercompare the  $dh'F/dt$ ,  $I_s$ , and  $I_a$ , and find that the vertical drift velocity is the most important factor for the ESF onset. Furthermore, we find that ESF of ionogram is not fully coincident with the phase fluctuation of GPS at the equator, which could be owing to the magnitudes of  $h'F$  and  $dh'F/dt$  of the ESF onset.

**GAIL.06/11P/D-010** Poster **1400-062**

**SIMULTANEOUS RADAR AND OPTICAL OBSERVATION OF E-REGION IRREGULARITIES AND F-REGION TRAVELING IONOSPHERIC DISTURBANCES**

Fumiki ONOMA<sup>1</sup>, Tadahiko OGAWA<sup>1</sup>, Yuichi OTSUKA<sup>1</sup>, Kazuo SHIOKAWA<sup>1</sup>, Mamoru YAMAMOTO<sup>2</sup> (<sup>1</sup>Solar-Terrestrial Environment Laboratory, Nagoya University, <sup>2</sup>Radio Atmospheric Science Center, Kyoto University)

On the night of August 6, 2002, the powerful 46.5-MHz middle and upper atmosphere (MU) radar with 5 beam directions at Shigaraki, Japan, observed typical quasi-periodic (QP) echoes from field-aligned electron density irregularities in the ionospheric E-region. The QP echoes exhibited a wavy structure that propagated southwestward at 100 m/s with a wavelength of 30 km. During this QP event, a 630.0 nm all-sky CCD imager at the MU radar site detected traveling ionospheric disturbances (TID) at altitudes of around 250 km in the F-region. The TID also propagated southwestward at 80 m/s with relative fluctuation amplitudes of 30-50% and a wavelength of 300 km. This propagation direction is very similar to the direction of the QP echoes movement. Also, a 630.0 nm Fabry-Perot interferometer at the radar site detected neutral winds ( $U$ ) of 106 m/s that generates an electric field of 4.5 mV/m through  $U \times B$ , where  $B$  is the geomagnetic field. From these observed values and average F-region electric field of 1.0 mV/m that is derived from previous MU radar observations in summer under high solar activity conditions, we estimate polarization electric fields associated with TID are 1.2-2.0 mV/m toward the northeast. When these polarization fields are mapped down along  $B$  without attenuation,  $E \times B$  plasma drift velocities of 28-47 m/s are induced in the E-region. In actual, drift velocities in the QP echoes observed with the MU radar was 42 m/s, which is very consistent with the values (28-47 m/s) estimated above. Moreover, the direction of the  $E \times B$  drift estimated is almost identical to that of the plasma drift in the QP echoes observed with the MU radar. Thus, the electric fields associated with the F-region TID seem to be closely coupled to those that generate QP echoes in the E-region.

**GAIL.06/11P/D-011** Poster **1400-063**

**THE STRUCTURE OF THE TMA-INDUCED OPTICAL EMISSION OBSERVED IN THE SEEK-2 CAMPAIGN**

Makiko ARAKAWA<sup>1</sup>, Hiroshi FUKUNISHI<sup>1</sup>, Yukihiro TAKAHASHI<sup>1</sup>, Mitsuteru SATO<sup>1</sup>, Takayuki ONO<sup>1</sup>, Mamoru YAMAMOTO<sup>2</sup>, Kazuo SHIOKAWA<sup>3</sup>, Akinori SAITO<sup>4</sup>, Masa-yuki YAMAMOTO<sup>5</sup>, M.F. LARSEN<sup>6</sup>, Ryuichi TAMURA<sup>7</sup> (<sup>1</sup>Graduate School of Science, Tohoku University, <sup>2</sup>Radio Science Center for Space and Atmosphere, Kyoto University, <sup>3</sup>Solar-Terrestrial Environment Laboratory, Nagoya University, <sup>4</sup>Graduate School of Science, Kyoto University, <sup>5</sup>Communications Research Laboratory, <sup>6</sup>Clemson University)

The SEEK-2 (Sporadic-E Experiment over Kyushu) campaign was carried out to investigate the Sporadic-E generation mechanisms. Two rockets (S-310-31 and 32) were launched successively toward the east-southeast at a 15 minutes interval on August 3, 2002 from Uchinoura (31.25° N, 131.08° E), Kagoshima, Japan. The S-310-32 rocket released trimethyl aluminum (TMA) over the altitude range from about 80 km to the apex of 117 km. Neutral wind profile can be derived based on the triangulation of TMA optical emission from the ground. On this campaign, we confirmed occurrences of TMA-induced artificial optical emissions, which were different from TMA emissions. We operated an image-intensified CCD (II-CCD) camera which captures image at the standard video frame rate (30 frames/sec) near the launch site. An all-sky imager with OI 557.7-nm, OI 630.0-nm, OH emissions (720 - 910 nm) and background (572.5 nm) filters was operated at Tanegashima. A film camera with an exposure of 5 minutes captured the TMA trails and the artificial emissions from Tengu-plateau (33.5°N, 133.0°E), which is located about 400 km northward of the rocket orbit. The artificial emissions were confined within a region just under the rocket orbit, though TMA trails moved following background neutral atmosphere winds. The artificial emissions appeared in the altitude range from about 90 km to about 110 km, with layer structures separated about 10 km in altitude to each other. These layers have a thickness of about 3 km, and appeared continuously during the upleg and downleg releases. The artificial emissions extend from the kinks of the TMA trails, corresponding to the wind shear of the neutral atmosphere and increase of electron densities. The artificial emission lasted more than 40 minutes. All filters of the all-sky imager confirmed the artificial emission, suggesting that the artificial emissions included continuum emission. We investigate the generation mechanism of these emissions by comparing the optical structure with the structures of electron densities, plasma waves and neutral winds measured by the same rocket. It is speculated the TMA-induced optical emissions are generated by some plasma processes in the sporadic-E layer.

**GAIL.06/11P/D-012** Poster **1400-064**

**RAPID-RUN IONOSONDE OBSERVATIONS OF SPORADIC-E DURING THE SEEK-2 CAMPAIGN**

Takashi MARUYAMA<sup>1</sup>, Hisao KATO<sup>1</sup>, Maho NAKAMURA<sup>1</sup>, Mamoru YAMAMOTO<sup>2</sup>, Shoichiro FUKAO<sup>2</sup> (<sup>1</sup>Communications Research Laboratory, <sup>2</sup>RASC, Kyoto University)

A quasi-periodic striation pattern appearing in range-time-intensity (R-T-I) maps of radar backscattering from the sporadic-E has been extensively studied by using VHF radars, rockets, ionosondes, and satellite radio beacons, in this decade. Their generation mechanism, however, is not clearly resolved yet. Coordinated observations including two rockets were conducted in Kyushu Island, Japan in August 2002 (SEEK-2) to study the generation mechanism of the striation pattern in R-T-I maps of the radar backscattering and related upper atmospheric disturbances. During the campaign, we ran the ionosonde in its rapid-run mode at Yamagawa that is close to the rocket launch site. Ionograms were obtained every minute and foEs, fbEs, h'Es, and foF2 were scaled. Rockets were launched when intense VHF radar signals were observed. An increase in foEs was observed in accord with the period of the intense radar backscattering. During this event, foEs and fbEs varied out of phase. At the onset of the radar backscattering, foEs increased and fbEs decreased both rapidly. Prior to the onset, foEs and fbEs varied, also out of phase, periodically with a period of 10 minutes. These findings strongly suggest that the spatial inhomogeneity of electron density in the sporadic-E layer and associated polarization electric fields play an important role in the generation of radar backscattering. Also periodic variations of sporadic-E parameters prior to the onset of radar backscattering suggest that there exists some kind of fluid instability such as K-H instability modulated by a wave activity.

**GAIL.06/11P/D-013** Poster **1400-065**

**HIGH RESOLUTION VHF RADAR OBSERVATIONS OF DAYTIME QP STRUCTURES IN LOWER E REGION OVER GADANKI**

Sripathi SAMIREDDIPALLE<sup>1</sup>, Amit Kumar PATRA<sup>1</sup>, Sivakumar V.<sup>1</sup>, Rao P. B.<sup>2</sup> (<sup>1</sup>National MST Radar Facility, Department of Space, <sup>2</sup>National Remote Sensing Agency, Hyderabad)

In this paper, we present high resolution observations of the daytime quasi-periodic (QP) structures of the lower E region irregularities made using the Gadanki VHF radar. The structures are found to display striations with negative altitude rates of ~ 10 m s<sup>-1</sup>, periods of 1 - 3 min and vertical wavelength of ~1 km. The Doppler velocities associated with these structures are found to be mostly in the range -20 - 10 m s<sup>-1</sup>. More importantly, these structures are found to be associated with a descending irregularity layer having descent rate of ~ 0.3 m s<sup>-1</sup>. The characteristics of these structures although resemble closely to that of nighttime low altitude structures observed earlier at Gadanki as well as at midlatitudes, the periodicities observed during daytime are found to be higher than that observed as few tens of seconds during nighttime. These observations are discussed in terms of their generation mechanism in the framework of the large scale Gradient drift instability and recently advanced theories on well known QP echoes based on atmospheric gravity waves and Kelvin Helmholtz instability. We believe that these structures are generated on the low altitude metallic ion layers formed at the node of the tidal wind field.

**GAIL.06/11P/D-014** Poster **1400-066**

**SOME CHARACTERISTICS OF THE VHF RADAR OBSERVATIONS OF THE LOWER E REGION IRREGULARITIES AS DIAGNOSTIC TOOL TO IDENTIFY THEIR GENERATION MECHANISM IN TERMS OF PLASMA INSTABILITIES OR NEUTRAL TURBULENCE**

Amit Kumar PATRA<sup>1</sup>, Sripathi S.<sup>1</sup>, Rao P.B.<sup>2</sup> (<sup>1</sup>National MST Radar Facility, <sup>2</sup>National Remote Sensing Agency, Hyderabad)

VHF radar observations of the lower E region (<95 km) irregularities over Gadanki are presented to address the characteristics difference of these echoes with that of the normal E region. We present several unusual observations of the lower E region echoes displaying slowly descending layer structures of 2-3 km thickness, resembling their characteristics to the low altitude tidal ion layers observed over Arecibo. These structures have been found to descend to altitudes as low as 86 km. We also compare the characteristics of these echoes with that of the intermittent echoes observed at this altitude region and down below in the mesosphere. The characteristics of these echoes show remarkable degree of aspect sensitivity representing their field alignment as compared to that expected from neutral turbulence. In this paper, we emphasize on the source mechanism of these echoes and present evidence in support of plasma related process than neutral turbulence as the causative mechanism.

**GAIL.06/11P/D-015** Poster **1400-067**

**HEIGHT DEPENDENCE OF GRAVITY WAVE ACTIVITY IN THE F-REGION IONOSPHERE**

Petra SAULI<sup>1</sup>, Patrice ABRY<sup>2</sup>, David ALTADILL<sup>3</sup>, Josef BOSKA<sup>4</sup> (<sup>1</sup>Institute of Atmospheric Physics ASCR, Czech Republic, <sup>2</sup>Laboratoire de Physique, ENS de Lyon, France, <sup>3</sup>Observatori de l'Ebre,

The height dependence of gravity wave activity is studied in the electron concentration in the F-region ionosphere. The analysis is based on data measured at two stations, Ebro (Spain, 40.8N, 0.5E) and Pruhonice (Czech Republic, 49.9N, 14.5E), mainly on the data collected during the world campaign HIRAC 23 April – 29 April 2001 (low, moderate and high geomagnetic activity in a period of high solar activity). Time series consists of vertical ionospheric sounding measurement with 5 min repetition time. The analysis is made for 5 corresponding days at two stations. From these measurements, a set of 1D time series are extracted, consisting of the fluctuations of electron concentration at various fixed heights (ranging from 155km to the altitude of the maximum electron concentration). The time series are analyzed using Wavelet Transforms. They are used to detect wave-like structures and to characterize them (with respects to occurrence times, phase and group velocity, etc). Preliminary studies give evidences of a change of the wave-like activity pattern at a height around 200 km. Below that altitude, a larger number (compared to above 200km) of wave-like structures are detected and they almost all have shorter periods. These findings are consistent for data measured on both stations. The characteristics measured for one wave-like structure detected on one station are compared to those obtained for the same structure on the other station.

**GAIL.06/11P/D-016** Poster **1400-068**

**LATITUDINAL VARIABILITY OF SPECTRA OF PLASMA IRREGULARITIES INDUCED BY TURBULENT MIXING IN THE LOWER IONOSPHERE**

Yurij KYZYUROV (Department of Space Plasma Physics, Main Astronomical Observatory NASU)

Rocket-borne probes and ground-based radar systems are powerful tools for study of plasma in the lower ionosphere of the Earth. Radar observations and in-situ rocket measurements at various latitudes have shown the presence of plasma irregularities induced by turbulent mixing in the ionosphere below the turbopause level. An investigation of spectra of the irregularities is very important for better understanding complicated coupling processes between neutral and ionized atmosphere. In this report a possible latitudinal dependence of the spectra is analyzed by using a formula that was recently derived for the 1D spectrum of plasma fluctuations formed in turbulent flow of weakly-ionized gas. The analysis is carried out for 3 directions of the possible spectral measurements: (a) the vertical direction along the gradient in the ambient plasma density, (b) the horizontal direction perpendicular to both the gradient and the geomagnetic field, and (c) the horizontal direction perpendicular to the gradient but along the horizontal component of the magnetic field. The case (a) can be realized in rocket measurements, while (b) and (c) in radar experiments, say, under the proper direction of the mean neutral wind. Using the assumption that parameters of the ionosphere and the neutral air turbulence are unchanged, a comparison of the irregularity spectra is made for different angles between directions of the mean plasma-density gradient and the geomagnetic field. It is shown that the slope of the spectrum which can be measured by rocket probes along the vertical direction has to increase with an increase in latitude; in the case of radar experiments under the zonal drift of the irregularities, the shape of the spectrum is unchanged, but for the drift in the meridional direction, the spectral slope has to decrease with latitude. The changes in the spectra have to appear mainly under large wavenumbers, i.e. for the small-scale fluctuations that resulted from interaction of plasma embedded in turbulent flow of neutral gas with the geomagnetic field.

**GAIL.06/11P/D-017** Poster **1400-069**

**E-REGION DOPPLER SPECTRAL BANDS DETECTED USING HF DIGISONDE AND MF RADAR AT SOUTHERN HIGH LATITUDES**

Ray MORRIS<sup>1</sup>, D.P. MONSELESAN<sup>1</sup>, D.A. HOLDSWORTH<sup>2</sup>, D.J. MURPHY<sup>1</sup>, P.L.DYSON<sup>3</sup> (<sup>1</sup>Australian Antarctic Division, <sup>2</sup>Atmospheric Radar Systems, <sup>3</sup>La Trobe University)

A HF digisonde and an MF radar were operated concurrently at the polar cusp station Davis (78.0°E, 68.6°S geographic, 74.6°S magnetic), Antarctica during the austral summer of 2002-03. The digisonde transmitted in a swept-frequency mode from 1.2 MHz to 2.7 MHz while the MF radar transmitted at a single frequency at 1.98 MHz. The two independent instruments were programmed to record E-region backscatter from ionospheric irregularities. This paper presents preliminary results from this novel campaign to observe Bragg scatter in the E-region from a multi-instrument campaign. Preliminary results from spectral signal analyses show evidence of Doppler spectral splitting in the respective HF digisonde and MF radar processed data. The backscattered signals as observed from these different radar techniques appear to originate from the same E-region heights. Moreover there is a remarkable tendency for such spectral splitting to occur during intervals of ionosphere slant Es condition (SEC) with lacuna. Earlier independent MF radar observations from Davis and HF digisonde observations from Casey (66.3°E, 110.5°S geographic, 80.4°S magnetic) augment and support these findings. The plausibility of these spectral splitting events being related to E-region ionosphere plasma instability processes will be discussed.

**GAIL.06/11P/D-018** Poster **1400-070**

**MERIDIONAL NEUTRAL WINDS DERIVED USING THE E REGION FIELD ALIGNED IRREGULARITIES (FAI) AS TRACERS OVER GADANKI AND A COMPARISON WITH MODEL AND HRDI DATA**

Sripathi SAMIREDDIPALLE<sup>1</sup>, Amit Kumar PATRA<sup>1</sup>, Rao P. B.<sup>2</sup>, Manas Ranjan PADHY<sup>1</sup> (<sup>1</sup>Department of Space, <sup>2</sup>National Remote Sensing Agency, Hyderabad)

We have derived the meridional neutral winds in the E region altitudes using the field aligned irregularities observed by the Gadanki VHF radar. It may be mentioned that wind information at this height region is limited and episodic and hence continuous measurements of winds at this height region are of significant value. The observations were made along the north bearing (130 off zenith) of the Gadanki radar beam that satisfies the perpendicularity condition with the earth's magnetic field lines at E region heights. Hence, the radar detects the secondary plasma irregularities present in the meridional plane transverse to the magnetic field. For the radar geometry used here, the irregularities especially in the collision dominated E region will be driven by both meridional neutral wind and the zonal electric field. Using the dispersion relation of the gradient drift instability and model values of the collision and gyro frequencies of the electrons and ions, we have estimated the zonal electric field and meridional neutral winds. While deriving meridional neutral winds, the contribution from the zonal electric field has been taken into consideration. The estimated winds have been compared with the model and UARS-HRDI satellite data. We found that the model wind amplitudes are quite low as compared to that observed here whereas the HRDI winds are found to be comparable. The results show that the semi-diurnal component is more dominant in comparison to that of the diurnal component. We also present the seasonal characteristics of these winds.

**GAIL.06/11P/D-019** Poster **1400-071**

**INHOMOGENEOUS STRUCTURE OF THE HIGH-LATITUDE IONOSPHERE AS OBSERVED AT EAST SIBERIA**

Yury V. LIPKO, Gely Aleksandrovich ZHEREBTSOV (Lipko Yury)

The results of investigation of the inhomogeneous structure of high-latitude ionosphere are presented. The observation were carried out at Norilsk (geomagnetic latitude and longitude 64.2 N and 160.4 E, and L=5.3) in the 1970s and 1990s years. Small-scale irregularities (SSI) (with lifetime of several seconds and spatial scale less than 5-7 km), and medium-scale travelling ionospheric disturbances (MS TID) (with period of 10-50 min, and the horizontal size of tens and hundreds of kilometres) were investigated under different geophysical conditions. The following results were obtained: 1. The average patterns of motions in F- and E-layers of the ionosphere for various season of the year and for levels of geomagnetic activity were obtained. There are two-cells pattern of plasma drift for winter and one-cell pattern for summer. 2. The dependencies of SSI and MS TID parameters on geomagnetic activity was obtained. Auroral activity has a significant effect on the propagation velocity of irregularities and some other parameters. 3. The propagation directions and velocities of small- and medium-scale irregularities are different. Medium-scale TIDs travel predominantly in a southward direction with velocities of 40-100 m/s. The prevailing direction of small-scale irregularities is eastward and westward, and their velocities lie in the range of from 100 to 200 m/s.

**GAIL.07**

**AERONOMY OF PLANETARY ATMOSPHERES INCLUDING COMPARATIVE ATMOSPHERES**

Location: Site A, Room 12

Friday, July 11 AM  
Presiding Chair: F. Taylor

**GAIL.07/11A/A12-001** Invited **0835**

**OBSERVATIONS OF VENUS UPPER ATMOSPHERE AND IONOSPHERE BY JAPANESE VENUS ORBITER**

Takumi ABE<sup>1</sup>, Takeshi IMAMURA<sup>1</sup>, Shinobu MACHIDA<sup>2</sup>, Masato NAKAMURA<sup>1</sup>, Takayuki ONO<sup>3</sup>, Koh-ichiro OYAMA<sup>4</sup>, Andrew W. YAU<sup>5</sup>, Ichiro YOSHIKAWA<sup>1</sup>, Kiyohumi YUMOTO<sup>6</sup> (<sup>1</sup>Institute of Space and Astronautical Science, <sup>2</sup>Department of Geophysics, Kyoto University, <sup>3</sup>Geophysical Institute, Tohoku University, <sup>4</sup>University of Calgary, Department of Physics and Astronomy, <sup>5</sup>Department of Earth and Planetary Sciences, Kyushu University)

We present a planned exploration of the Venus atmosphere and ionosphere carried out by the Japanese Venus orbiter (Planet-C), which will be launched in 2008 and arrived at Venus in 2009. Direct and/or indirect measurements of charged and neutral particles, plasma wave and magnetic field, as well as optical sounding (remote sensing) of the lower atmosphere, will be made in this mission. In this presentation, we concentrate on describing the principal scientific objectives related to the upper atmosphere and the ionosphere and discussing observation strategies for various phenomena occurring in these regions and the particle escape processes from Venus atmosphere. Despite extensive studies based on Pioneer Venus Orbiter observations, there still remain many unresolved issues of the plasma dynamics in the upper atmosphere and ionosphere on Venus: 1) global particle circulation, 2) plasma dynamics and characteristic structure in the nightside ionosphere (ion hole, patch, cloud, streamer etc.), 3) plasma transport processes in the ionosphere, and 4) mass and energy transfer mechanism through the ionopause. The observation of particle escape processes from Venus is one of the most important scientific objectives in this mission, given the important influence of these processes on the evolution of the Venus atmosphere and the critical lack of quantitative information on the total flux of the escaping particles. We are assessing the feasibility of installing several instruments on the spacecraft for the observation of these processes: 1) extreme ultraviolet imager, 2) nonthermal ion mass/spectrum analyzer and electron spectrum analyzer, 3) thermal plasma analyzer, 4) plasma wave analyzer and sounder, and 5) magnetometer. Considering that Planet-C will arrive at Venus during solar maximum period, a nominal operation period of 2-3 years will provide a significant data set of the Venus ionosphere, which is known to exhibit a remarkable dependence on the solar activity. We will discuss the current status of our feasibility study and the instruments and methodology necessary for understanding the key scientific issues.

**GAIL.07/11A/A12-002** **0905**

**THE IONOSPHERE OF VENUS**

Hiroyuki SHINAGAWA (Solar-Terrestrial Environment Laboratory, Nagoya University)

Venus has no intrinsic magnetic field, and the solar wind interacts directly with the ionosphere. Previous studies of Venus suggest that the ionospheric thermal pressure (Pi) and the solar wind dynamics pressure (Psw) are the most important parameters, which determine the nature of the solar wind-ionosphere interaction. When Pi is larger than Psw, the solar wind flow is deflected at high altitudes. The magnetic field pile-up region (the magnetic barrier) and the ionospheric plasma region are usually clearly separated by a sharp boundary, which is called the ionopause. When Psw is larger than Pi, the whole ionosphere is magnetized. Under such conditions, the ionopause tends to be thicker, and a magnetic field belt is formed in the lower ionosphere. Although the basic behavior of the Venus ionosphere could be reproduced by MHD models, recent theoretical studies suggest that kinetic processes also play an important role in the structure and dynamics of the ionosphere. The ionosphere of Venus is reviewed in light of previous observations as well as theoretical studies.

**GAIL.07/11A/A12-003** **0925**

**NUMERICAL MODELING OF THE INTERACTION BETWEEN THE SOLAR WIND AND VENUS IONOSPHERE**

Shinobu MACHIDA (Department of Geophysics, Kyoto University)

In this paper, the models of the interaction between the solar wind and the Venus ionosphere are reviewed. In particular, the electromagnetic hybrid model in which ions are treated as finite-size particles and electrons as a massless fluid is described. This model enables us to treat the kinetic effect of ions, especially the Finite Larmor Radius (FLR) effect,

which is significant because the Larmor radius of pick-up oxygen ions is comparable to the planetary radius. Immediately after the production of the pick-up ions, they are accelerated in the direction of the solar wind electric field. Hence, an asymmetric structure can be created depending on the direction of the solar wind electric field. Recently, a new 2-1/2 D electromagnetic hybrid code adopting the boundary fitted coordinates has been developed and this code was adopted to study the solar wind interaction with the Venus ionosphere [Terada et al., 2002]. This code allows us to treat the dynamics of the solar wind and Venus ionosphere self-consistently in available computer resources today by realizing the mesh size of ~10 km in the ionosphere and the mesh size of ~100km in the solar wind region keeping the total number of grid points to be small. They found a pronounced development of the Kelvin-Helmholtz (K-H) instability at the ionopause in the hemisphere to which the solar wind electric field directs, and a development of very long and small amplitude K-H waves in the opposite hemisphere. A notable detachment of the ionospheric oxygen cloud from the night side ionosphere was found to occur in the opposite hemisphere. They also found that a vortex generated by the K-H instability gives similar time variations in the velocity and magnetic field to the data obtained by Pioneer Venus Orbiter (PVO), which was formerly interpreted to be a flux rope. Also, there are challenging attempts to model the solar wind interaction with the Venus ionosphere employing 3D electromagnetic hybrid code. In a study performed by Shimazu [2001], the effect of two major processes, i.e., the charge exchange and the photo-ionization were examined. These two processes gave us opposite results in the thickness of the magnetosheath with respect to the solar wind electric field. It was found that the charge exchange is favorable to explain the observational result obtained by PVO, i.e., the thickness of the magnetosheath is enhanced in the hemisphere to which the solar wind electric field directs. Recent electromagnetic hybrid models including the kinetic effects such as the FLR effect and chemical effect give us a powerful tool to study elementary and fundamental processes operating in the solar wind and Venus ionosphere interaction.

GAIL.07/11A/A12-004

0945

#### IMAGING OF INTERACTION REGION BETWEEN VENUSIAN IONOSPHERE AND SOLAR WIND

Atsushi YAMAZAKI<sup>1</sup>, Ichiro YOSHIKAWA<sup>2</sup>, Naoki TERADA<sup>3</sup>, Miho KANAOKI<sup>4</sup>, Takumi ABE<sup>5</sup>, Masato NAKAMURA<sup>6</sup> (<sup>1</sup>Communications Research Laboratory, <sup>2</sup>Institute of Space and Astronautical Science, <sup>3</sup>Solar-Terrestrial Environment Laboratory)

Japanese Venus Climate Orbiter (the Planet-C spacecraft) will be launched in 2008, and will reach the orbit of Venus in 2009. We propose two eXtreme UltraViolet (XUV) imagers to take global 2-Dimensional snapshots of the Venusian ionosphere including the interaction region between the solar wind and the Venusian ionospheric plasmas. The imagers can detect the resonantly scattering emissions of oxygen ions (O II 83.4nm) and atoms (O I 130.3nm), and neutral helium (He I 58.4nm) and hydrogen (H Ly- $\alpha$  121.6nm). We estimate the intensity of these emission lines and discuss the requirement for the specification of the imagers and the available temporal and spatial resolution. Scientific goals of the XUV imagers are to investigate mechanisms of momentum and mass transfer across the ionopause, of convection in the upper atmosphere and ionosphere, and of atmospheric and ionospheric escape. Especially we emphasize that sequential images of the O II emission illustrate temporal evolution of the vortex produced by the Kelvin-Helmholtz (K-H) instability at the Venusian ionopause. Though it is known that the vortex structure due to the K-H instability is also generated at the terrestrial magnetopause, oxygen ions is too tenuous to take 2-D images of the evolution. On the other hand at the Venusian ionopause oxygen ions have enough density to detect the resonance emission, i.e., the Venusian ionosphere plays a role as a space laboratory for plasma physics.

GAIL.07/11A/A12-005

Invited

1035

#### ANALYSIS OF WAVE AND PARTICLE SIGNATURES OBSERVED IN PLASMA ESCAPE AT VENUS

Richard E. HARTLE<sup>1</sup>, Joseph M. GREBOWSKY<sup>1</sup>, Devrie S. INTRILIGATOR<sup>2</sup>, Dana H. CRIDER<sup>3</sup> (<sup>1</sup>NASA-Goddard Space Flight Center, <sup>2</sup>Carmel Research Center, Santa Monica, CA, <sup>3</sup>Catholic University, Washington, DC)

Atmospheric gases escape from Venus as neutral and ionized atoms and molecules. Ion escape, considered here, occurs through ion pickup or collective plasma processes. The latter can arise from upward flow of nightside ionospheric plasma into the ionotail, day to night ionospheric flow into the ionotail, and scavenging of ionospheric plasma by ionosphere-magnetosheath instabilities at the ionopause. These plasma processes produce differing signatures in ion velocity and energy distributions and in ULF waves in the magnetic field. Using plasma ion spectra measured by the Pioneer Venus Orbiter (PVO) Orbiter Plasma Analyzer (OPA) and magnetic field fluctuations observed by the PVO Orbiter Magnetometer (OMAG) along with the expected particle and field signatures, various ion escape processes occurring along Pioneer Venus orbits are identified. In particular, OPA ion energy distributions are used in parallel with magnetic field power spectra and wave phase angles derived from OMAG measurements to study the characteristics of escaping ions. The principle ions observed escaping the influence of Venus are H<sup>+</sup>, He<sup>+</sup> and O<sup>+</sup>. In the ion energy distributions of the OPA, pickup ions appear hot relative to the much cooler ions flowing away from Venus in the ionotail and in the plasma clouds detached from the ionopause. This energy contrast is particularly evident downstream when PVO crosses the ionotail boundary from the hot solar wind plasma to the much cooler plasma within the tail. Magnetic field signatures accompanying the escaping ions appear as peaks in the power spectra at the corresponding ion cyclotron frequencies. Also, coherent wave trains at the same frequencies are observed in the phase angle plots of magnetic field fluctuations about the mean field.

GAIL.07/11A/A12-006

Invited

1105

#### CLUES FAVOURABLE TO THE DRAPING MAGNETIC FIELD MODEL ON THE VENUS HOLE

Yoshihiro KAKINAMI<sup>1</sup>, Koh-ichiro OYAMA<sup>2</sup>, Shigetou WATANABE<sup>1</sup> (<sup>1</sup>Division of Earth and Planetary Sciences, Graduate School of Science, Hokkaido University, <sup>2</sup>The Institute of Space and Astronautical Science)

Formation of the hole in Venus ionosphere is still controversial. We intensively studied the data observed with Pioneer Venus orbiter (orbit 1 - 570) in order to find the clues for the formation mechanism. Especially we use the information on electron temperature Te, which was so far rarely used for the discussion. Our major findings are: 1. The X component of the magnetic field prevails around the terminator, while the direction scatters more toward midnight (SZA > 120). 2. Three cases exist for Te of Venus hole: Case 1, Te decreases toward the midst of the hole and elevates in the midst of the hole, and two other cases are that Te in the hole is lower and higher than that of the ambient plasma. Case 1 can be theoretically reproduced if energy is injected into the hole along the magnetic field. The case requires that the ion temperature in the hole should be lower than that of the ambient, which suggests that the hole of low ion temperature rises from the lower ionosphere where ion

temperature is lower than at higher altitude. Two other cases can be explained by controlling the amount of energy deposited in the hole whose Te is equal to that of the ambient. The above two features on the hole are favorable to one of the mechanisms which were proposed in the past "draping magnetic field". However energy should come from dayside ionosphere.

GAIL.07/11A/A12-007

Invited

1135

#### NATURAL SUPERROTATION OF A RAREFIED SLOWLY ROTATING PLANETARY ATMOSPHERE

Peter Alexeevich BESPALOV<sup>1</sup>, Olga Nikolaevna SAVINA<sup>2</sup> (<sup>1</sup>Institute of Applied Physics, Russian Academy of Sciences, <sup>2</sup>Nizhny Novgorod State Technical University)

We consider the kinetics of a rarefied slowly rotating planetary atmosphere. The spatial distributions of the atmospheric-gas density and mean angular velocity were determined by analyzing the exact solution of the two-dimensional kinetic equation. We show that the angular velocity of the gas at some distance from the planet could be higher than that in the initial layer starting from which the atmosphere is rarefied. Our model calculations elucidate the superrotation mechanism under consideration. Experimental studies of atmospheric flows carried out for Venus, Earth, and Mars have established the possibility of superrotation of their atmospheres at large heights. This superrotation is characterized by the ratio (more than one) of the angular velocities of the atmosphere and the planet. Several possible superrotation mechanisms have been discussed in the literature. Several mechanisms responsible for atmospheric superrotation were proposed, but none of them was universal. Here, we consider the kinetics of a rarefied atmosphere replenished with particles injected from a spherical surface inside which collisions are significant. As we show below peculiarities of the motion of a rarefied gas in the gravitational field of a slowly rotating planet can give rise to superrotation. It follows from the laws of motion that sufficiently fast particles can rise high and even recede to infinity. Because of the axial rotation of the planet, the particles whose velocity have the same direction as the rotational velocity of the planet will have a higher (in magnitude) initial velocity. Primarily these particles can recede appreciably from the planet to become its "satellites" due to weak collisions. Therefore, we have reason to expect that the mean angular velocity of the particles in the upper planetary atmosphere can exceed the angular velocity at its inner boundary. A quantitative analysis of this problem based on the exact solution of the kinetic equation. We have shown that one of the superrotation mechanisms for rarefied planetary atmospheres is the separation of particles: some of them fly away from the planet, while others become its satellites. Based on the proposed mechanism, we estimated the superrotation for the exospheres of Venus, Earth, and Mars. Our main results are as follows. (1) We found an exact solution of the boundary-value problem for the two-dimensional collisionless Boltzmann equation that includes particles with elliptical and hyperbolic orbits. (2) We obtained and analyzed the solution of the kinetic equation with weak elastic collisions. (3) We determined the spatial distributions of the atmospheric-gas density and mean angular velocity and established the possibility of exospheric superrotation. This study was supported by the Russian Foundation for Basic Research (project nos. 01-02-17796, and 00-15-966674).

Friday, July 11 PM

Presiding Chair: K. Oyama

GAIL.07/11P/A12-001

Invited

1400

#### THE MARTIAN THERMOSPHERE: A NEW PERSPECTIVE

Gerald M. KEATING<sup>1</sup>, Michael E. THERIOT<sup>2</sup>, Robert H. TOLSON<sup>3</sup>, Stephen W. BOUGHER<sup>2</sup>, Jeffrey M. FORBES<sup>3</sup>, Francois FORGET<sup>4</sup> (<sup>1</sup>The George Washington Univ. at NASA Langley, Hampton, VA, USA, <sup>2</sup>Univ. of Michigan, Ann Arbor, MI, USA, <sup>3</sup>Univ. of Colorado, Boulder, CO, USA, <sup>4</sup>Univ. of Paris, Lab de Meteorologie Dynamique, Paris, France)

Recently thousands of vertical structures have been measured from pole to pole of the Martian thermosphere by means of accelerometers aboard Mars Global Surveyor and Mars Odyssey 2001. Only three in situ measurements of vertical structure had been obtained previously. Measurements are directly obtained of atmospheric density and from analysis of vertical structures, scale heights, temperatures, pressures and other characteristics are determined. Analysis of this data has revealed latitudinal/seasonal variations, diurnal variations, aphelion/perihelion variations, persistent planetary-scale waves, dust storm responses, winter polar warming, asymmetries between the Northern and Southern Hemispheres, and strong coupling between the lower and upper atmospheres. Analyses have also been performed of the global lateral and vertical temperature structure from the accelerometer data. The observations will be compared with general circulation models and previous measurements.

GAIL.07/11P/A12-002

Invited

1430

#### LONGITUDINAL DISTRIBUTIONS OF THERMOSPHERE AND IONOSPHERE AT LOW LATITUDE OF MARS : COMPARISON WITH ACCELEROMETER AND RADIO MEASUREMENTS

Syed Aftab HAIDER (Physical Research Laboratory, Ahmedabad)

We have developed global AYS approach to calculate longitudinal distributions of photoelectron flux, ion production rates and electron densities in the dayside Martian ionosphere at two wavelength ranges 1.9 nm and 9-102.57 nm produced by soft X-ray and EUV radiation respectively. These calculations are carried out at solar zenith angle 75 degree between latitudes 0 and 25N in spring season with medium solar activity condition, appropriate for accelerometer and radio occultation measurements made by MGS in Phobos-2 aerobraking period. In these calculations, the neutral densities are derived from accelerometer data which were obtained by MGS at same latitude range during orbit # P0790-P0910 for one month period of December, 1998. The ionosphere produced by these two sources were compared with MGS radio occultation measurements made at high latitude in December, 1998 between solar zenith angle 78° and 81°. This measurement shows two peaks near altitudes 134 km and 110-112 km at most of the longitudes in the dayside ionosphere. These measured densities are in better agreement with AYS calculation using combined source of ionization (EUV + X-ray). However, lower peak is more visible in this calculation in comparison to MGS radio occultation measurements. In order to compare these calculations and measurements with other models, we have run MTGCM code which calculates neutral densities and ion/electron densities self consistently at three latitudes (2.5N, 22.5N and 67.5N) and nine East longitudes (0, 45, 90, 135, 180, 225, 270, 315 and 360) for same observational period. It has been found that the neutral densities calculated at latitudes 2.5N and 22.5N are in reasonable agreement with accelerometer measurements. The peak value of low latitude ionosphere produced by MTGCM is larger by a factor of 1.5-2.0 as compared to that calculated by AYS approach. This difference may arise due to different technique used in both model calculations. AYS approach calculates photoionization impact rates using ionization cross sections and solar flux corresponding to solar moderate condition. MTGCM uses parameterization method to

calculate photoionization, photoelectron production rates and solar EUV/UV/X-ray fluxes at 81-day average  $110.7 \text{ cm indices}$ . These differences may, however produce larger uncertainty in production rates and solar fluxes used in MTGCM. It should be noted that same chemical reactions, neutral ion and electron temperatures have been used in both calculations.

**GAIL.07/11P/A12-003** Invited **1500**

**CHARACTERISTICS OF THE MIGRATING DIURNAL TIDE IN THE MARTIAN ATMOSPHERE**

Yoshiyuki O. TAKAHASHI, Hitoshi FUJIWARA, Hiroshi FUKUNISHI (Department of Geophysics, Tohoku University)

We have investigated the basic characteristics of the migrating diurnal tide in the Martian atmosphere using our Mars general circulation model (GCM) and linear response model (LRM). The Mars GCM used in this study is a spectral model. This model covers from the ground up to about 120 km altitude. In this Mars GCM, almost all physical processes appropriate for the Martian atmosphere are incorporated. This Mars GCM has successfully reproduced the general characteristics of the Martian atmospheric circulation. The LRM used in this study is based on the linearized primitive equation system. The governing equations are solved by the spectral technique. The model covers almost the same vertical domain as the GCM. The heating rates for wave generation and the distributions of the zonal mean zonal wind and temperature are obtained from the GCM. Using the Mars GCM, we have performed numerical simulations in a low dust condition (dust optical depth at  $0.67 \mu\text{m}$  of 0.3). Furthermore, we have performed numerical experiments using the LRM to reveal the important processes characterizing the migrating diurnal tide. The GCM simulation shows that the vertical wavelength of the migrating diurnal tide in the low latitude region is about 45 km. This vertical wavelength is longer than the vertical wavelength of 25-35 km predicted from the classical tidal theory. This long vertical wavelength is caused by the effect of the zonal mean vorticity, in other words, latitudinal shear of the zonal mean zonal wind. It is suggested that the vertical wavelength of the migrating diurnal tide increases through the changes of the effects of the planetary rotation rate in the presence of the zonal mean vorticity. The amplitude of the migrating diurnal tide in the low latitude region is much smaller than that expected in an inviscid atmosphere. This small amplitude of the migrating diurnal tide is caused by the radiative process of the thin  $\text{CO}_2$  atmosphere of Mars. On the other hand, the eddy diffusion process does not change the amplitude and phase of the migrating diurnal tide. This ineffective eddy diffusion process may be caused by the effective radiative damping and the long vertical wavelength of the migrating diurnal tide depending on the zonal mean vorticity. At solstices, the structures of the migrating diurnal tide are strongly asymmetric around the equator. It is suggested that the effect of zonal mean vorticity as well as the Doppler shift by the zonal mean zonal wind play an important role in determining the wave structure at solstices.

**GAIL.07/11P/A12-004** **1530**

**WAVE STRUCTURES IN THE MARTIAN TOPSIDE IONOSPHERE OBSERVED BY MARS GLOBAL SURVEYOR**

Jing-Song Wang WANG<sup>1</sup>, Erling NIELSEN<sup>2</sup> (<sup>1</sup>Department of Geophysics, Peking University, <sup>2</sup>Max-Planck-Institut fuer Aeronomie)

We analyzed the Martian ionospheric electron density altitude profiles obtained by Mars Global Surveyor radio occultation observations, and its found that about 80% of the upper parts of these profiles displays significant wavelike structures with spatial scales of about some tens of kilometers. These structures appear like wave activities superposed on background electron density distributions that principally decrease with altitude exponentially. The relative density deviations in the wavelike structures to the background are scattered but most limited in  $\pm 50\%$ . Above  $\sim 145 \text{ km}$ , the wavelike structures are prominent and the background electron densities generally distribute according to a single scale height. Below  $\sim 145 \text{ km}$  altitude, the wavelike structures are much less striking and simple exponential distributions can not describe the profiles any more. The altitude of  $\sim 145 \text{ km}$ , the beginning altitude of transference from the photochemistry dominant region to the dynamics dominant region, appears also the lower boundary of both the wavelike structures and the exponential approximation to the ionospheric density distribution. Spectrum analysis is applied to those topside ionospheric profiles and it is found that the wavelength of  $\sim 38 \text{ km}$  is prevailing. With a modeled Martian ionosphere including wave activities with a constant wavelength of 38 km but random phase at different solar zenith angle, the processes of radio occultation observation and the followed inversion of the radio signals are simulated and electron density profiles similar to MGS measurements are obtained. The same spectrum analysis is applied to the artificial profiles and proves a reliable method to find out the prevailing wavelength. Those statistical features as well as the prevailing scale of the wavelike structures agree with that of the wave activities predicted by Wang and Nielsen [2002, 2003] very well, and it is very likely that the wavelike structure discussed here is the appearance of the predicted or similar waves. If so, the  $\sim 145 \text{ km}$  altitude is also the end to which the effects of the external dynamic disturbances out the Martian ionosphere can reach, and could be a physics lower boundary of the topside ionosphere.

**GAIL.07/11P/A12-005** **1620**

**MARS ATMOSPHERE AND ITS EFFECTS ON RADIO WAVE PROPAGATION**

Christian M. HO, Miles K. SUE, Steve D. SLOBIN (Jet Propulsion Laboratory, California Institute of Technology, Pasadena, CA, USA)

Because the Mars atmosphere is significantly different from Earth's in its composition and structure, the effects of the Martian environment on radio wave propagation are also expected to be different. We have done some preliminary studies in understanding the effects. The Martian atmospheric gaseous attenuations have been calculated as a function of radio frequencies using the abundance information of  $\text{H}_2\text{O}$  and  $\text{O}_2$ . It is found that Martian gaseous absorption is at least three orders of magnitude lower than at Earth. Radio noise at Mars are mainly from its surface emissions. For a downward-looking antenna, the total noise temperature is about the same as the Earth's for all frequency bands of interest with  $\pm 15\%$  deviations. For an upward looking antenna, the noise temperature is slightly below that of Earth. The sky noise temperature is the highest at UHF (about 55 K) and lowest at X- and Ka-band (about 5 K). It is also found that the Martian atmospheric radio refractivity is about two orders of magnitude smaller than that of Earth because of its lower atmospheric pressure. Mars ionospheric scintillation loss for UHF band is one tenth of Earth's, while the refractive index fluctuations in the Martian troposphere is only about 0.5% of that at Earth. The Martian clouds are similar to terrestrial high-level cirrus clouds. The total attenuation due to Martian clouds, fog and aerosols should be less than 0.3 dB at Ka-band. Dust storms in Mars can significantly affect a communication link. A large dust storm can cause a 3-dB loss at Ka-band (32 GHz) for a zenith path. Most large storms occur in the southern hemisphere during later spring and early summer.

**GAIL.07/11P/A12-006** Invited **1640**

**THE PLASMA ENVIRONMENTS OF THE GALILEAN SATELLITES OF JUPITER**

Arvydas J. KLIORE<sup>1</sup>, Andrew F. NAGY<sup>2</sup> (<sup>1</sup>JPL, California Institute of Technology, <sup>2</sup>SPRL, University of Michigan)

The Galileo spacecraft has been orbiting Jupiter since 1995. During that time it has provided several opportunities for the study of the plasma environments of the icy Galilean satellites Europa, Ganymede, and Callisto by means of radio occultation of its S-band (13.5 cm. Wavelength) signal. There have been five occultations each by Europa, Ganymede, and Callisto, however, one of the Ganymede and one of the Callisto occultations occurred near superior conjunction, and did not provide useful data. Analysis of these data revealed small excursions in frequency (of the order of 0.01 Hz, or about 4 parts in  $10^3$ ), which indicated the presence of tenuous plasma above the surfaces of these bodies. When observed, the maximum electron densities range from about 5 to about  $20 \times 10^3 \text{ cm}^{-3}$ . The apparent vertical structure of these plasma layers range from classical ionospheric profiles observed at Callisto on two occasions to multi-peaked structures observed at Europa. On several occasions no discernible plasma was observed. These observations could be explained by a process in which a tenuous neutral atmosphere (about  $10^{10} \text{ cm}^{-3}$ ) is created on the trailing hemisphere by sputtering from the icy surface by energetic particles of the Jovian magnetosphere. If the trailing hemisphere is also illuminated by the Sun, plasma is produced by photoionization and is observed by radio occultation. The configuration of this plasma is, however, determined by its interaction with the corotating Jovian magnetospheric plasma, which under certain geometries would lead to the observation of multip peaked structures.

**GAIL.07/11P/A12-007** Invited **1710**

**NEW RESULTS ON ATMOSPHERIC AND SURFACE FEATURES ON TITAN**

Athena COUSTENIS (LESIA, Observatoire de Paris-Meudon)

I will present new findings on Titan's atmosphere and surface composition derived from recent observations using artificial satellites (such as ISO) and large telescopes (such as the CFHT or the VLT) both in spectroscopy and imaging (essentially with adaptive optics). Titan is becoming a more and more intriguing place as we manage to uncover further information about its lower atmosphere and its ground. While we await the Cassini/Huygens mission arrival in 2004, we put to use all available means both from the ground and from space so as to (a) investigate this wonderful planetary-scale laboratory for studying primitive-Earth conditions and (b) optimize the return of the Cassini/Huygens mission. Among our recent results, we have found evidence for seasonal and diurnal effects in Titan's atmosphere (asymmetry inversion and morning fog) and we have evidence for cloud (or more probably vortex) formation close to the South pole. We have also gathered new information on the spectral behavior of the surface constituents. References: Combes et al (1997), Icarus 129, 482; Coustenis et al. (2001) Icarus 154, 501; Coustenis et al., (2003), Icarus 161, in press; Lellouch et al. (2003), Icarus, in press.

**GAIL.05**

**WHAT ARE THE STRUCTURES IN THE MAGNETOTAIL, WHY ARE THEY THERE, AND HOW DO THEY INFLUENCE ITS DYNAMICS**

Location: Site A, Room 6

**Monday, July 7 AM**  
Presiding Chairs: J.-A. Sauvaud, T. Mukai

**GAIL.05/07A/A06-001** **0900**

**PLASMA CONVECTION IN THE Y-Z CROSS-SECTION OF THE MAGNETOTAIL**

Kiyoshi MAEZAWA, Toshifumi MUKAI, Yoshifumi SAITO (Institute of Space and Astronautical Science)

Plasma convection pattern in the cross-section of the magnetotail is derived for the first time from the archive plasma dataset of the Geotail spacecraft. In this statistics, the measured ion velocities are first divided into two independent components, i.e. components parallel and perpendicular to the magnetic field, respectively, and only the result for the perpendicular component is discussed. Since Geotail has an equatorial orbit, only the portion of the tail close to the plasma sheet has been covered by Geotail, but still the result provides sufficient information to identify some of the interesting characteristics of the plasma convection in the y-z plane. Some characteristics are consistent with the standard view of the convection in the magnetotail, but others are not readily compatible with the standard view. Important findings are as follows. (1) The plasma convection is directed from the lobe toward the plasma sheet near the midnight meridian plane as is consistent with the standard theory. (2) Near the flanks of the magnetotail, however, the convection direction is reversed, that is, directed from the plasma sheet to the lobe. This means that two convection vortices are formed within the y-z plane for each hemisphere, and some of the plasmas convecting from high latitudes are deflected towards flanks before they reach the neutral sheet and finally return to the high-latitude portion of the tail along the flank magnetopause. (3) The sense of rotation for these plasma vortices is not apparently correlated with the sign of the z component of IMF. That is, the plasma convection always has a component directed toward the plasma sheet near the midnight meridian even in the case of northward IMF. This probably means that the conversion process of closed field lines to open field lines is occurring at the dayside magnetopause even during periods of northward IMF. The reverse convection expected for the northward IMF seems to be spatially limited to the higher latitude portion of the tail not covered by GEOTAIL observations. (4) The effect of the y-component of the IMF is visible as an intensification of one of the two vortices, whose dawn-dusk asymmetry is controlled by IMF-By. The effect is smaller than expected, and barely visible at the distances of  $x = -15$  to  $-25 \text{ Re}$ .

**GAIL.05/07A/A06-002** **0915**

**ENERGETIC ELECTRON TRANSPORT IN THE EARTH'S MAGNETOTAIL: THE DAWN-DUSK ASYMMETRY**

Shinsuke IMADA<sup>1</sup>, Masahiro HOSHINO<sup>1</sup>, Toshifumi MUKAI<sup>2</sup> (<sup>1</sup>Department of Earth and Planetary Science, University of Tokyo, <sup>2</sup>Institute of Space and Astronautical Science)

The particle acceleration and transport of energetic electrons are the essential and fundamental problems in space. To reveal the origin of energetic particles, several past

satellite observations contributed to understanding these problems. Both of the local structure such as magnetic reconnection and the global structure of the magnetotail which depend on the solar wind condition are important to understand the accelerating and transport mechanism of energetic electrons. We conduct a statistical and systematic study of the dawn-dusk plasma sheet/magnetosheath asymmetry using both the thermal/middle energy electrons of  $< 40$  keV (LEP) and the energetic electrons of  $> 38$  keV (EPIC) onboard the Geotail satellite. The dawn-dusk plasma sheet asymmetry can be confirmed for the energetic electrons of  $> 38$  keV, while the asymmetry is not clearly found for the low energy electrons of  $< 10$  keV. These results are consistent with the dawn-dusk plasma sheet asymmetry of energetic particles observed by the Interball [Sarafopoulos et al., 2001]. The similar energy dependence can be found for the magnetosheath plasma adjacent to the magnetopause. This result can be interpreted as the result of the leakage of plasma sheet electrons to magnetosheath. To confirm the above, we also studied the 60 magnetopause crossing events in detail. From the 60 magnetopause crossing events, we discuss from LLBL to magnetosheath energetic electrons. We find that the leakage process of energetic electrons from the plasma sheet to the magnetosheath is controlled by the local IMF Bz and magnetopause conditions, and energetic electrons flux intensity are decrease gradually through the magnetopause boundary layer which scale is defined by ion thermal. These results suggest that the energetic electrons effectively leak from plasma sheet to magnetosheath.

GAIII.05/07A/A06-003

0930

#### MAGNETOTAIL OBSERVATIONS DURING LONG INTERVALS OF SOUTHWARD IMF BZ: TRANSITION FROM LOADING-UNLOADING TO STEADY MAGNETOSPHERIC CONVECTION

E. TANSKANEN<sup>1</sup>, J.A. SLAVIN<sup>1</sup>, D.H. FAIRFIELD<sup>1</sup>, D.G. SIBECK<sup>1</sup>, T. MUKAF, T. NAGAI, A. IEDA<sup>2</sup> (Nasa Goddard Space Flight Center, Greenbelt, USA, <sup>1</sup>Institute of Space and Astronautical Sciences, Japan, <sup>2</sup>Tokyo Institute of Technology, Earth and Planetary Sciences, Japan)

In this study we have examined the response of the Earth's magnetotail to long intervals of southward interplanetary magnetic field (IMF B<sub>z</sub> < 0). Southward IMF B<sub>z</sub> is known to produce enhanced energy input into the magnetosphere. We used ACE interplanetary magnetic field (IMF) observations to identify prolonged (>2h, >3h, >4h, >5 hours) periods of southward IMF B<sub>z</sub> during the last four Geotail seasons in the magnetotail (November through April, 1998 through 2002). Geotail plasma sheet observations obtained during these intervals are classified as 'steady magnetospheric convection' or 'periodic loading-unloading'. Examples of both responses have been found and will be described. We will present statistical analyses of the frequency of the occurrence of both types of tail convection, estimate the relative contributions of each to the tail energy budget, and determine their relationship to the upstream solar wind and IMF conditions.

GAIII.05/07A/A06-004

0945

#### TAIL LOBE CONVECTION AS OBSERVED BY CLUSTER/EDI 2001-2002

Stefan MUEHLBACHER<sup>1</sup>, Hirotomo NODA<sup>2</sup>, Rumi NAKAMURA<sup>1</sup>, Wolfgang BAUMJOHANN<sup>1</sup>, Götz PASCHMANN<sup>1</sup>, Hans VAITH<sup>1</sup>, Pamela PÜHL-QUINN<sup>3</sup>, Roy B. TORBERT<sup>1</sup>, Jack M. QUINN<sup>4</sup>, Helfried K. BIERNAT<sup>1</sup>, Helmut O. RUCKER<sup>1</sup> (<sup>1</sup>Space Research Institute, Austrian Academy of Sciences, Schmiedlstr. 6, 8042 Graz, Austria, <sup>2</sup>National Astronomical Observatory of Japan, Tokyo, Japan, <sup>3</sup>Max-Planck Institute for Extraterrestrial Physics, Garching, Germany, <sup>4</sup>Institute of the Study of Earth, Oceans, and Space, University of New Hampshire, Durham, USA)

One of the major parameters influencing phenomena within the terrestrial magnetosphere is the orientation of the interplanetary magnetic field (IMF). This orientation is illustrated in the IMF clock angle. In this paper we study average tail lobe convection of the terrestrial magnetosphere as a function of the IMF clock angle and extend earlier work of the authors. For this we used drift velocity data from the years 2001 and 2002 measured in the Earth tail lobe by the Cluster Electron Drift Instrument. The data confirm the convection pattern toward the neutral sheet in the meridional (XZ) plane. As a result of the solarwind-induced electric field to the magnetotail lobe via dayside reconnection we find that the IMF B<sub>z</sub> component controls the convection direction in the perpendicular to the Sun-Earth line (YZ). The convection velocity becomes smallest for positive IMF B<sub>z</sub> and largest for negative IMF B<sub>z</sub>.

GAIII.05/07A/A06-005

Invited

1000

#### FORMATIONS OF THE CUSP AND PLASMA SHEET AS A PART OF DYNAMO PROCESS DRIVING THE CONVECTION

Takashi TANAKA (Department of earth and planetary science, Kyushu University)

Based on the magnetosphere-ionosphere coupling scheme, convection as a compound system is considered including the generation of plasma population regimes in the magnetotail. In these considerations, primary elements that must be set to a self-consistent configuration are convection flows in the magnetosphere and the ionosphere, field aligned current (FAC) systems, ionospheric currents, energy conversion processes, and plasma population. Then from the magnetohydrodynamic force balance controlling the convection, plasma population regimes such as the cusp and plasma sheet are shown to be indispensable to fulfill the self-consistency in the convection system. In the traditional Dungey model, the line-tying current which overlaps on the shoulder of the magnetosphere behind the cusp with the pure Chapman-Ferraro current drives the convection. This overlapping region must be the dynamo (J·E < 0) for the region 1 current system. However, it results in a peculiar current configuration in which same current simultaneously branches to the dayside Chapman-Ferraro current and region 1 current at the frank magnetopause. Therefore, the confinement of earth's magnetic field conflicts with the generation of region 1 FAC, resulting in a statement that the generation of open field lines and following stretching is the primary cause of magnetotail formation. In the present model, however, the confinement of earth's magnetic field by the dynamic pressure is the primary cause of the magnetotail formation. With negative IMF B<sub>z</sub>, the Chapman-Ferraro current is not directly connected with the region-1 FAC but connected with the neutral sheet current in the dayside merging region. As a consequence, tangential Maxwell stress on the magnetopause acts to increase plasma internal energy around the cusp. This configuration is also same to tail theta current system in which tangential Maxwell stress on the tail surface acts to increase plasma internal energy in the plasma sheet through the convection. The plasma internal energy accumulated in the cusp and plasma sheet further drives the region 1 and 2 FAC, respectively. Thus, mechanisms to drive the region 1 and region 2 current systems are the same two step process; the tangential Maxwell stress on the magnetopause pumps up plasma internal energy, then plasma internal energy drives the FACs.

GAIII.05/07A/A06-006

1025

#### DEDUCING THE LENGTH OF THE MAGNETOTAIL FROM GEOTAIL, POLAR, AND WIND OBSERVATIONS OF TAPERED TAIL LOW FREQUENCY BURSTS

Roger R. ANDERSON<sup>1</sup>, Roger R. ANDERSON<sup>2</sup>, Hiroshi MATSUMOTO<sup>3</sup>, Kozo HASHIMOTO<sup>3</sup>,

Hirotosugu KOJIMA<sup>4</sup>, Michael L. KAISER<sup>5</sup>, Jean-Louis BOUGERET<sup>6</sup>, Jean-Louis STEINBERG<sup>7</sup> (<sup>1</sup>Department of Physics and Astronomy, The University of Iowa, Room 615 Van Allen Hall, Iowa City, IA 52242-1479, USA (roger-r-anderson@uiowa.edu), <sup>2</sup>Radio Science Center for Space and Atmosphere, Kyoto University, Gokanoshō, Uji, Kyoto 611-0011, JAPAN (anderson, matsumoto, kozo, or kojima@kuras.kyoto-u.ac.jp), <sup>3</sup>NASA Goddard Space Flight Center, Laboratory for Extraterrestrial Physics, Code 695, Greenbelt, MD 20771, USA (kaiser@lepmilk.gsfc.nasa.gov), <sup>4</sup>LESIA, Observatoire de Paris-Meudon, F-91295 Meudon Cedex, FRANCE (Jean-Louis.Bougeret@obsparis.fr) Jean-Louis.Steinberg@obsparis.fr)

Among the more interesting phenomena detected by the GEOTAIL and POLAR Plasma Wave Instruments (PWIs) and the WIND Radio Science Experiment (WAVES) are the auroral kilometric radiation (AKR) low frequency (LF) bursts. These electromagnetic emissions are the low frequency extension of AKR and are most frequently observed during the most geomagnetically disturbed times. In the solar wind the LF bursts are observed to extend in frequency down to the local electron plasma frequency (F<sub>pe</sub>) with increasing time delay the lower the frequency. In the magnetosphere the LF bursts often display a tapered tail that has maximum time delay at a distinct frequency which we call F<sub>ft</sub>. The LF bursts then show increasing time delay as F<sub>ft</sub> is approached from frequencies above it and from frequencies below it. When one of the spacecraft is in the solar wind and another is in the magnetosphere during a LF burst observation, we see that F<sub>ft</sub> almost always appears equal to the solar wind F<sub>pe</sub> in the near past (some few hours). We speculate that AKR generated in the Earth's magnetospheric auroral region at frequencies below the magnetosheath plasma frequency (2F<sub>pe</sub> near the nose) is reflected and refracted down the tail since it cannot penetrate the magnetosheath directly. As it travels down the tail, AKR of a given frequency finally reaches a point where the tail magnetosheath plasma frequency is equal to it and it can propagate into the solar wind. F<sub>ft</sub> is believed to be the AKR frequency which is equal to the local solar wind plasma frequency at the point down the tail where the magnetosheath frequency and local solar wind plasma frequency are equal and where waves of this frequency are broadly scattered. Upstream in situ measurements of the solar wind F<sub>pe</sub> and the flow speed allow us to determine how far down the tail the local solar wind F<sub>pe</sub> and F<sub>ft</sub> are equal. The results so far have ranged from 200 Re to 2000 Re which is the same range found from other methods.

GAIII.05/07A/A06-007

1055

#### SUBSTORM ONSET BY PLASMA SHEET DIVERGENCE

Larry R. LYONS<sup>1</sup>, Chih-Ping WANG<sup>2</sup>, Tsugunobu NAGAI, John C. SAMSON<sup>3</sup> (<sup>1</sup>Department of Atmospheric Sciences, UCLA, <sup>2</sup>Department of Earth and Planetary Sciences, Tokyo Institute of Technology, <sup>3</sup>Dept. of Physics, University of Alberta)

Substorms have been an active research topic for over thirty years. However, there is as yet no general agreement on what causes the substorm expansion phase. To understanding the cause of the expansion phase, it is necessary to understand what cause the formation of the substorm current wedge. This can be shown to be equivalent to understanding what causes a reduction in equatorial plasma pressure within the current wedge and an azimuthal gradient in equatorial pressure. We first use Geotail spacecraft measurements obtained near the center of plasma sheet at  $r \sim 10$  RE to show that a reduction in equatorial plasma pressure is indeed a general feature of substorms. We also show that, when viewed as a function of the adiabatic invariant parameter for the plasma sheet, there is actually a reduction in particle fluxes at all invariant energies despite the flux enhancements seen when energetic particle fluxes are viewed at fixed particle energy. This shows that the expansion phase is associated with a significant reduction in the flux tube content of plasma sheet particles, and that this reduction in flux tube content gives the reduction of equatorial plasma pressure that leads to the formation of the substorm current wedge. After discussing the Geotail observations, we apply the continuity equation for plasma sheet particles derived by Heinemann [J. Geophys. Res., 104, 28,397, 1999]. We show that this equation can account for the growth-phase enhancement in plasma pressure that occurs after an increase in the strength of magnetospheric convection. It is now known that the majority of substorms are associated with reductions in the strength of large-scale convection that is imparted to the magnetosphere from the solar wind, and we apply the Heinemann continuity equation to show that diamagnetic drift should lead to a divergence of plasma sheet particles following a reduction in the strength of magnetospheric convection. We furthermore show that this divergence should lead to a reduction of flux tube content that is appropriate to account for current wedge formation and thus the initiation of the substorm expansion phase.

GAIII.05/07A/A06-008

1120

#### IMPLICATIONS OF THE DOUBLE OVAL FOR SUBSTORM DEVELOPMENT IN THE MAGNETOTAIL

Gordon ROSTOKER (Department of Physics, University of Alberta)

It is now clear that substorm activity develops in two separate regions of space. The onset occurs in the equatorward portion of the midnight sector auroral oval, mapping to the inner region of the plasma sheet. However, most of the dynamic variations in the later stages of the substorm occur at the poleward edge of the oval, mapping to regions considerably further out in the magnetotail. In this paper, I will summarize the evolution of a typical substorm as detected in the ionosphere. I will relate each of the ionospheric signatures to the regions of the magnetotail to which they must map, and in doing so identify changes in the tail plasma and fields which relate to the ionospheric observations. Particular attention will be paid to the relevance of bursty bulk flows to substorm features in the ionosphere.

GAIII.05/07A/A06-009

1135

#### CURRENT SHEET FORMATION, SUBSTORM ONSET AND DIPOLARIZATION

C.Z. CHENG, S. ZAHARIA (Princeton Plasma Physics Laboratory, Princeton University)

At the end of the substorm growth phase, the plasma pressure profile steepens and a thin current sheet is formed in the near-Earth plasmasheet around the local midnight with a finite radial and azimuthal domain. In the current sheet the plasma beta becomes about 50 or larger and magnetic field curvature is enhanced. We find that the kinetic ballooning instability (KBI) can be excited with amplitude localized at the maximum plasma beta region. The KBI explains the low frequency (about 1 min period) instability observed by AMPTE/CCE with period on the order of 1 min is observed about 2-3 minutes before the substorm onset [Cheng and Lui, GRL, 1998]. Recent observations by Geotail at X = -10 R<sub>E</sub> have also confirmed the low frequency instability before or during substorm expansion. The KBI is responsible for substorm onset because as it grows to a large amplitude with  $\delta B/B > 0.1$ , it causes an enhanced westward ion drift during the explosive growth phase that lasts about 30 sec. The KBI then excites higher frequency instabilities, and the plasma and magnetic field become strongly turbulent. The plasma transport in both radial and azimuthal directions caused by the turbulence relaxes the steep plasma pressure profile during the expansion phase. As the plasma pressure profile relaxes, the magnetic field configuration dipolarizes and returns to the pre-substorm more dipole-like geometry. Theories of current sheet formation, KBI mechanism and dipolarization will be presented along with numerical solutions of 3D

**GAIII.05/07A/A06-010 1150**  
**THE RELATIONSHIP AMONG NEAR-TAIL MAGNETIC RECONNECTION, GEOSYNCHRONOUS SAWTOOTH INJECTIONS, PERIODIC MAGNETOSPHERIC SUBSTORMS, AND SOLAR WIND VARIATIONS**

Chaosong HUANG (Haystack Observatory, Massachusetts Institute of Technology, Westford, MA 01886, USA)

Outstanding problems in magnetospheric substorms include what causes substorm onsets, whether substorms have some specific periodicity, and what determines the periodicity. We will present multiple space-based and ground based observations of solar wind, magnetospheric, and ionospheric parameters during two magnetic storms. Energetic plasma particle injections from the magnetotail to geosynchronous orbit are often periodic with periods of 2-3 hours during storms. We will show that there is a one-to-one correspondence among the near-tail reconnection onsets, particle injections at geosynchronous orbit, energetic neutral atom emissions in the inner magnetosphere, and auroral brightenings. The multiple measurements provide unambiguous evidence that the sawtooth injections at geosynchronous orbit represent true substorm onsets and that magnetospheric substorms can be indeed periodic. Solar wind variations may trigger the periodic substorms. However, the period of substorms is determined by the magnetosphere. We suggest that magnetospheric substorms have an intrinsic cycle time of 2-3 hours. If solar wind pressure oscillations with periods comparable to the substorm cycle time are imposed on the magnetosphere, some magnetospheric resonant state may be excited, and periodic substorms can be triggered. Otherwise, if the solar wind oscillates too fast, no enough energy is accumulated in the magnetotail for substorms to occur; if the period of solar wind pressure oscillations is too long, magnetospheric energy may be released through other processes including internally triggered substorms.

**GAIII.05/07A/A06-011 Invited 1205**  
**CLUSTER OBSERVATIONS OF MAGNETOSPHERIC SUBSTORM BEHAVIOR IN THE MID-TAIL REGION**

Daniel N. BAKER<sup>1</sup>, Robert L. MCPHERRON<sup>2</sup> (<sup>1</sup>Laboratory for Atmospheric and Space Physics, <sup>2</sup>IGPP/Univ. California Los Angeles)

The Cluster constellation of spacecraft has returned a wealth of new data on particle and field variations in the near- and mid-magnetotail region of Earth's magnetosphere. Using the Research with Adaptive Particle Imaging Detectors (RAPID) systems onboard the four Cluster vehicles, we have identified substorm-related energetic ( $E > 20$  keV) electron enhancement events during the period March 2001 through October 2001 in the geocentric radial range of 4 to 19 Earth radii. A similar seasonal interval has been examined for the Cluster tail passages of 2002. We have used concurrent data from other Cluster instruments as well as from the IMAGE, FAST, GPS, and geostationary orbit spacecraft in order to understand particle injection and transport phenomena throughout this key region of the magnetotail. Electron enhancements in the plasma sheet at intermediate radial distances have been studied in a global substorm context. We find evidence that Cluster was often very near the near-Earth substorm neutral line and that magnetic reconnection often is closely associated with the substorm auroral brightening of the expansive phase onset. Several examples of these relationships will be discussed.

**GAIII.05-Posters**

**WHAT ARE THE STRUCTURES IN THE MAGNETOTAIL, WHY ARE THEY THERE, AND HOW DO THEY INFLUENCE ITS DYNAMICS**

Location: Site D

Monday, July 7 PM

**GAIII.05/07P/D-001 Poster 1400-099**  
**A SELF-CONSISTENT TWO DIMENSIONAL CONFIGURATION FOR THE MAGNETOTAIL**

Devashis BANERJEE, Gurbax Singh LAKHINA, Satyavir SINGH (Indian Institute of Geomagnetism)

A physically plausible two-dimensional (say  $x$ - and  $z$ -dependent) equilibrium configurations for magnetotail, ignoring variations in the cross-tail direction ( $\partial/\partial y = 0$ ) is studied analytically. The asymptotic theories valid for tail configurations that vary only weakly in the antisolar direction. The magnetotail equilibria by using an asymptotic expansion parameter  $\epsilon$ , defined as the ratio of the characteristic lengths in  $z$  and  $x$  directions ( $\epsilon = LZ/LX$ ), upto  $O(\epsilon)$ . In the present analysis, the effects of directed flow are being neglected and pressure function is assumed to remain isotropic throughout in the tail configuration. The cross-tail magnetic field along with poloidal fields have been incorporated for the first time in the formulation to obtain a more realistic equilibrium configurations. The formulation is self-consistent in the sense that the kinetic pressure forces are taken as the same order as the stresses exerted by the magnetic field for any volume element in the framework of Vlasov's theory. The asymptotic expansion solutions are valid only for the tail region where the conditions  $\epsilon \ll 1$ ,  $|BZ| / |BX|_{\text{max}} \ll 1$ , and  $|BY| / |BX|_{\text{max}} \ll 1$ . The analytical forms of the solutions are determined for all three magnetic field components, particle density function, pressure function, all three components of the drift velocities and the corresponding drifted Maxwellian distribution function satisfying the Maxwell-Vlasov equation. These solutions can reproduce the one dimensional Harris solutions in the limiting case.

**GAIII.05/07P/D-002 Poster 1400-100**  
**3D FORCE-BALANCED MAGNETOSPHERIC STRUCTURES**

Sorin G. ZAHARIA, C.Z. CHENG (Princeton University, Plasma Physics Laboratory)

For most times, the average plasma flow energy in the Earth's magnetosphere is much smaller than the plasma thermal energy, therefore the magnetosphere exhibits a "quasi-equilibrium" between the Lorentz force  $\mathbf{J} \times \mathbf{B}$  and the plasma pressure force. Because the magnetic field configurations given by empirical models commonly in use in the magnetospheric physics community are not force-balanced states and because force-balanced states are crucial for many physical applications, it is necessary to find an alternate

way of obtaining magnetospheric configurations. Such a model is presented, in which 3D solutions are calculated for magnetospheric fields and currents in force balance with several pressure distributions observed by satellites (e.g. Geotail). The fully 3D magnetospheric states are obtained by expressing the magnetic field in terms of Euler potentials and numerically solving the equation of force balance in a flux coordinate system. The calculation domain includes both closed and open magnetospheric field regions, and its boundaries are dependent on external conditions such as the solar wind dynamic pressure and interplanetary magnetic field (IMF). The output of our model will be discussed for both quiet and active magnetospheric conditions. The emphasis of the discussion will be on the structure of the magnetotail and the plasma sheet in particular, where the plasma  $\beta$  is very large (typically  $\beta > 100$ ) and therefore the pressure crucially determines the magnetic field configuration. We will also discuss the appearance of thin cross-tail current sheets close to Earth ( $|X| < 10 R_E$ ) during active magnetospheric times, whose existence has been observationally confirmed. By gradually changing the boundary conditions and pressure profiles, the model also allows one to obtain a series of "snapshots" of the magnetosphere at different times, thus permitting for example the study of the slow temporal variations in the magnetotail during events such as the magnetospheric substorm onset.

**GAIII.05/07P/D-003 Poster 1400-101**  
**MAGNETOTAIL ASSIMILATION MODEL**

Simon WING, Patrick T. NEWELL (Applied Physics Laboratory, Johns Hopkins University)

Progress in space plasma physics requires coordinated analysis of multi-point observations and hence, many upcoming ionospheric and magnetospheric missions will consist of multispacecraft. With the launch dates of these missions only a few years away, there is an urgent need to develop a method that can assimilate the unprecedentedly large multi-point data sets in coherent and unified manners. We have recently developed a technique that integrates low-altitude ionospheric observations to create 2-D/3-D global images of the plasma sheet ion pressure, temperature, and density. This method relies on the plasma sheet plasma isotropy, which has a strong theoretical foundation as well as overwhelming observational supports. Previously developed algorithms are used to detect the plasma isotropy boundary and to detect and exclude acceleration events. The plasma properties obtained with this method compare favorably with previous in situ measurements in the magnetotail. The technique can be refined to include mid-altitude and high-altitude observations. Therefore, it can serve as a foundation for building a model that assimilates multi-point plasma observations from multi-spacecraft missions into globally coherent and unified images of the magnetotail, tailward of  $\sim 8-10 R_E$ . The power this method for magnetotail investigations is illustrated in two examples: (1) the dynamics of the 2D equatorial plasma sheet under northward and southward IMF orientations and (2) the quiet time plasma sheet ion pressure contribution to the field-aligned currents.

**GAIII.05/07P/D-004 Poster 1400-102**  
**ENHANCEMENT OF PLASMA SHEET DENSITIES DURING LOW-DENSITY SOLAR WIND INTERVALS**

Masaki N. NISHINO<sup>1</sup>, Toshio TERASAWA<sup>1</sup>, Masahiro HOSHINO<sup>1</sup>, Masaki FUJIMOTO<sup>2</sup>, Toshifumi MUKAI<sup>3</sup>, Yasumasa KASABA<sup>3</sup>, Hirotsugu KOJIMA<sup>4</sup>, Hiroshi MATSUMOTO<sup>4</sup> (<sup>1</sup>University of Tokyo, <sup>2</sup>Tokyo Institute of Technology, <sup>3</sup>Institute of Space and Astronautical Science, <sup>4</sup>RASC)

It has been known that density ( $N_{ps}$ ) and temperature in the near-earth plasma sheet are controlled by density ( $N_{sw}$ ) and velocity of the solar wind. Especially, during northward IMF (NIMF) intervals the near-earth plasma sheet is filled with a cold and dense plasma, for which  $N_{ps}/N_{sw}$  becomes as large as 20%. It is noted that the this ratio,  $N_{ps}/N_{sw} \sim 20\%$ , was obtained under the nominal NIMF solar wind condition where the  $N_{sw} > 1 \text{ cc}$ . It is of interest whether this percentage holds under the extremely low density solar wind condition, which has recently attracted massive attention (e.g., the May 1999 event of "solar wind disappearance"). We have made a search for low- $N_{sw}$  and NIMF intervals during (or shortly after) which Geotail measured the plasma sheet status. What we have found is quite remarkable: The ratio  $N_{ps}/N_{sw}$  could become as large as  $\sim 1$  during such intervals. We will discuss the physical implications of such large enhancement of  $N_{ps}/N_{sw}$  for the understanding of the plasma transport process from the solar wind to the plasma sheet.

**GAIII.05/07P/D-005 Poster 1400-103**  
**THE SPATIAL DISTRIBUTION AND TEMPORAL VARIATION OF THE TOTAL PRESSURE IN THE DISTANT MAGNETOTAIL**

Ayako MATSUOKA (Institute of Space and Astronautical Science)

The total pressure in the magnetotail depends on the distance from the earth and also on the solar wind condition. In order to study the dynamics of the magnetosphere, it is important to know the spatial distribution and temporal variation of the pressure. We statistically analyzed the total pressure measured by GEOTAIL in the distance between 30 and 220  $R_E$ . We found that the pressure at  $X > -150 R_E$  was mainly influenced by the dynamic pressure in the solar wind while that for  $X < -150 R_E$  was often determined by the static pressure in the solar wind. Moreover, we found that, when the solar wind condition quickly changed or the magnetotail condition was disturbed, the measured pressure is sometimes considerably different from the predicted one from our statistics. We investigated an observation on 941002 in detail where static pressure variations in the distant magnetotail lobe were caused by the passage of a plasmoid. The traveling speed of the plasmoid is estimated to have been faster than the concurrent magnetosonic speed in the lobe. The magnetic field variation along the maximum variance direction was linearly related to the variation in the field strength, which suggests that a magneto-hydrodynamic compressional mode might have occurred. The propagation direction of the variation is determined from the background field direction and the maximum variance direction of the field. Shortly after the passage of the plasmoid, the relation between the field and velocity variations is consistent with the fast mode. Pressure variation in the fast mode was possibly generated in the trail of the plasmoid to restore equilibrium. ACKNOWLEDGMENTS: We are grateful to Drs. T. Mukai and T. Nagai for providing the LEP and MGF data from Geotail.

**GAIII.05/07P/D-006 Poster 1400-104**  
**SLOW MHD WAVES AND DIAMAGNETIC PROCESSES IN THE MAGNETOTAIL PLASMA SHEET**

Aoi NAKAMIZO<sup>1</sup>, Takeshi IJIMA<sup>2</sup> (<sup>1</sup>Department of Earth and Planetary Sciences, Kyushu University, <sup>2</sup>Communications Research Laboratory)

We focused on the changes of three kinds of energy density (plasma kinetic energy density, plasma internal energy density and magnetic energy density) in the magnetotail plasma sheet, considering their primary importance, their relationship and their flux transport. Using the magnetic field and low-energy particle data measured by the MGF and LEP instruments on board the Geotail satellite, we investigated the disturbances occurred in the magnetotail

region with a geocentric distance of  $\sim 9$  to  $30 R_E$ . We divided the disturbances into the Pi2-range (with a period of  $\sim 40$ -150s) variations (hereafter magnetotail Pi2s) and the background disturbances on which the magnetotail Pi2s are superimposed. Confirmed characteristics were as follows: In magnetotail Pi2s, (1) magnetic pressure perturbation and thermal pressure perturbation vary exactly in out-of-phase. (2) The field-aligned energy fluxes due to the plasma pressure perturbation along the magnetic field and the magnetic tangential stress (i.e. the Poynting vector component along the magnetic field) are much larger than the energy fluxes due to the magnetic and plasma pressure perturbations perpendicular to the magnetic field. The substance of magnetotail Pi2 is the slow MHD wave. The Poynting vector component parallel to the magnetic field is often directed toward the ionosphere, indicating coexistence and/or the coupling of the slow and transverse Alfvén wave. In background disturbances,  $\langle 1 \rangle$  the internal energy density and the magnetic energy density are dominant in the energy balance (the contribution of the kinetic energy density is usually much weaker), and the time changes of them are always in out-of phase, in turn, the plasma thermal pressure and the magnetic pressure vary exactly in out-of-phase.  $\langle 2 \rangle$  The intensity of the energy flux is greater in the direction parallel to the magnetic field than in the direction transverse to it. These tendencies are similar to the characteristics of the magnetotail Pi2s. The nature of background disturbances indicates slow MHD disturbances. The plasma fluid clearly exhibits the diamagnetic properties. We suggest the importance (and/or dominance) of diamagnetic currents in the current system of magnetotail in terms of the time changes of its configuration and magnitude.

**GAIII.05/07P/D-007** Poster **1400-105**

**FAST FLOWS AND COMPRESSIONAL WAVES IN THE MAGNETOTAIL**

Martin VOLWERK<sup>1</sup>, Rumi NAKAMURA<sup>1</sup>, Wolfgang BAUMJOHANN<sup>1</sup>, Andrei RUNOV<sup>1</sup>, Zoltan VOROS<sup>1</sup>, Tielong ZHANG<sup>1</sup>, Karl-Heinz GLASSMEIER<sup>2</sup>, Rudolf TREUMANN<sup>2</sup>, Berndt KLECKER<sup>1</sup>, Andre BALOGH<sup>3</sup>, Henri REME<sup>4</sup> (1WFI/OEAW, Graz, Austria, 2TU Braunschweig, Germany, 3MPE, Garching, Germany, 4Imperial College, London, UK, 5CESR/CNRS, Toulouse, France)

Compressional waves are responsible for the main wave power in the Earth's current sheet [Bauer et al., JGR 100, 9605, 1995]. We now study 2 years of Cluster magnetotail crossings and search for prolonged (12 minutes) intervals in which the spacecraft are within or near the neutral sheet. We relate the results from spectral analysis of the (FGM) magnetic field data with the flow velocities measured by the (CIS-CODIF) plasma instrument. For fast flows in the neutral sheet ( $>150$  km/s) the power level of the turbulence in the frequency range  $0.08 < f < 1$  Hz, is greater than the noise level of the instrument. We will show that the spectral index for the compressional waves lies around 3, indicative of fully developed 2D turbulence. The finite extension of the current sheet in z determines the 2 dimensionality and it can be shown that its z-extent also determines the break in the powerspectrum at low frequencies. Using a proxy for the total power in this "high-frequency" turbulence we find that there is a linear relationship between flow velocity and power. We also integrate the total power in the Pi2 band, and relate that to the flow velocity. We find that pre-midnight sector of the magnetotail shows greater Pi2 power, albeit with a larger spread, than the post-midnight sector. The power in the turbulence and in the Pi2 are highly correlated.

**GAIII.05/07P/D-008** Poster **1400-106**

**CHARACTERISTICS OF ENERGY-DISPERSED ION SIGNATURES IN THE PLASMA SHEET OBSERVED BY GEOTAIL**

Yoichi KAZAMA<sup>1</sup>, Toshifumi MUKAI<sup>1</sup> (1Swedish Institute of Space Physics, 2Institute of Space and Astronautical Science)

Based on the Geotail observations, we have found unexpectedly frequent occurrence of the dispersed ions in the plasma sheet. We report characteristics of energy dispersed ion signatures in the magnetotail region by event study and statistical study. The dispersed ion signature observed in October 10, 1997 was studied in detail. It is found that dispersed ions can be categorized into two types by their source regions, such as the magnetosphere and the ionosphere. The analysis showed that magnetospheric ions were accelerated probably by fast flows in the plasma sheet at 20-30 Re down the tail. On the other hand, the ionospheric protons were launched nearly at the same time into the same flux tube with the magnetospheric ions. To investigate the dispersed ions statistically we selected 172 events from Geotail data by visual inspection. The results from the statistical analysis indicate that the dispersed events occur with the dipolarization signatures, fast bulk flows, electron parallel pressure enhancement, and magnetic field disturbances. The dispersed ion events accompanied with ionospheric ions occupy approximately 40% of the selected dispersed events, and hence are not of special cases in the near-Earth plasma sheet. To investigate the relation between the tail events and the ionospheric ones, 18 events are selected by criteria in which the events have clear dispersed signatures for both the ionospheric and the magnetospheric ions. The results show that the magnetospheric ions come mainly from a mid-tail region ( $\sim 40$ -50 Re down tail), but also from the distant tail (XGSM  $< 140 R_E$ ). The distance is rather unexpectedly far, and further study should be pursued. The results also indicate that some disturbances in the tail might cause the ionospheric ion acceleration into the same flux tube.

**GAIII.05/07P/D-009** Poster **1400-107**

**ANALYSIS OF THE GEOTAIL CLOSE ENCOUNTER DATA WITH THE MAGNETIC NEUTRAL LINE UTILIZING THE GENERALIZED OHM'S LAW**

Shinobu MACHIDA<sup>1</sup>, Tsugunobu NAGAI<sup>1</sup>, Masahiro HOSHINO<sup>1</sup>, Masaki FUJIMOTO<sup>2</sup>, Iku SHINOHARA<sup>3</sup>, Yoshifumi SAITO<sup>4</sup>, Toshifumi MUKAI<sup>1</sup> (1Department of Geophysics, Kyoto University, 2Dept. Earth & Planetary Sci., Tokyo Inst. Tech., 3Dept. Earth & Planetary Physics, Univ. Tokyo, 4Inst. of Space & Astronautical Sci.)

We have conducted an analysis of the Geotail data obtained at around 1750UT on December 10, 1996 with the use of the generalized Ohm's law. This is one of the best close encounter data of Geotail with the magnetic neutral line. By analyzing the time series of the y-component of E,  $V \times B$  and  $J \times B/qN$  contained in the generalized Ohm's law, we found that it is impossible to achieve a balance only with those three terms without invoking other terms that are related to the violation of frozen-in relation. Namely, the time series data of  $J \times B/qN$  term has the largest amplitude and a spiky structure, while the  $V \times B$  has the smallest amplitude and shows gradual time variation. This tendency becomes apparent when we take the Fourier spectrum of these data. The Fourier amplitude of the  $(J \times B)/qN$  does not attenuate in the high frequency domain and largely has a flat distribution although there are jerky structures. In contrast, the Fourier amplitude of  $(V \times B)/qN$  rapidly decreases as a function of frequency. The  $E_y$  has a moderate structure. The amplitudes of these three curves roughly agree in the very low frequency domain, i.e., below 0.002 Hz. The result of the Fourier analysis suggests that the actual  $E_y$ , an approximated electric field ( $-V \times B/y$ ) from ion flow, and  $-(V \times B)_y$  from electron flow roughly agree in the low frequency domain, but not in the high frequency domain. As a result, it is not possible to achieve a balance among E,  $V \times B$  and  $J \times B/N$  in the generalized Ohm's law without invoking other terms associated with the violation of the frozen-in relation between the magnetic field and plasma. We also found a correlated time variation between the wave electric field and  $(J \times B)/qN$  term, suggesting a

significance of the anomalous resistivity in the PSBL region. In the vicinity of the magnetic neutral line, the frozen-in relation seems to approximately hold. However, this relation should be violated at the real center of the neutral line. The combined analysis of the Geotail data with the generalized Ohm's law gives us a comprehensive tool for detecting and understanding the nature of the magnetic neutral line.

**GAIII.05/07P/D-010** Poster **1400-108**

**ELECTRIC AND MAGNETIC FIELD FLUCTUATIONS IN THE NEAR-EARTH MAGNETOTAIL ASSOCIATED WITH DIPOLARIZATIONS: GEOTAIL OBSERVATIONS**

Yukinaga MIYASHITA<sup>1</sup>, Shinobu MACHIDA<sup>2</sup>, Yohsuke KAMIDE<sup>1</sup>, Toshifumi MUKAI<sup>1</sup>, Yoshifumi SAITO<sup>3</sup>, Hajime HAYAKAWA<sup>3</sup>, Koichiro TSURUDA<sup>3</sup> (1Solar-Terrestrial Environment Laboratory, Nagoya University, 2Department of Geophysics, Kyoto University, 3The Institute of Space and Astronautical Science)

By using GEOTAIL data, we have studied electric and magnetic field fluctuations in the near-Earth magnetotail around  $X \sim 10 R_E$  just before and after dipolarization onsets. We focused our examination on a low-frequency range from 1 Hz to a few tens of Hz, including the lower-hybrid frequency. It was found that about 1-2 minutes before dipolarizations, electric field fluctuations from 1 Hz to about 20 Hz were observed in some events, while no fluctuations were observed in other events. There was a tendency for the plasma  $\beta$  to be larger in the latter events than in the former events. Then broadband electric field fluctuations in the range of 1-32 Hz and magnetic field fluctuations below the lower-hybrid frequency were observed in association with dipolarizations. The wave propagation angle was nearly perpendicular to the ambient magnetic field. Furthermore, electrons and ions were heated in the events in which the electric field fluctuations were seen before dipolarizations, while electrons were not very much heated in the events without the prior electric field fluctuations. We will discuss the role and generation mechanism of these pre-dipolarization electric field fluctuations for understanding the substorm triggering mechanisms.

**GAIII.05/07P/D-011** Poster **1400-109**

**STATISTICAL ANALYSIS OF THE RESPONSE OF THE SYNCHRONOUS MAGNETIC FIELD TO SUBSTORM EXPANSIONS**

Tung-Shin HSU, Robert L. MCPHERRON (Institute of Geophysics and Planetary Physics, UCLA, USA)

It is generally accepted that the synchronous magnetic field becomes more tail-like during the growth phase and more dipole-like during the expansion phase of magnetospheric substorms. However, a close examination of high resolution data reveals that the various components of the field do not always respond at the same time, and that there are significant delays in the onset of effects at different local times. In this paper we examine a number of substorms from the ISTEP era for which we have detailed information about the time history of activity. We utilize superposed epoch analysis to characterize the response of each component of the synchronous field as a function of the locations of the spacecraft from the center of the substorm current wedge. The center of the substorm current wedge is determined by the extensive ground observations and/or auroral images. We will attempt to interpret the observations in terms of various current systems thought to be present at substorm onset.

**GAIII.05/07P/D-012** Poster **1400-110**

**FORMATION OF THE SUBSTORM CURRENT WEDGE INSIDE OF THE GEOSYNCHRONOUS ORBIT: A CASE STUDY OF THE MAY 27, 1997, STORM-TIME SUBSTORM**

Tetsuya SHIRAISHI<sup>1</sup>, Hideaki KAWANO<sup>1</sup>, Kiyohumi YUMOTO<sup>2</sup>, Akira MORIOKA<sup>3</sup> (1Department of Earth and Planetary Sciences, Kyushu University, Japan, 2Space Environment Research Center, Kyushu University, Japan, 3Planetary Plasma and Atmospheric Research Center, Tohoku University, Japan)

It is well known that the substorm current wedge is formed in the region of  $-6.6 > X > -15 R_E$  during the expansion phase of isolated substorms. However, it has not been well studied where the substorm current wedge is formed during the expansion phase of storm-time substorms. We study the formation of the substorm current wedge in a storm-time substorm which took place on May 27, 1997. In this event, many substorm onset signatures were observed at various regions (auroral ionosphere, high, mid and low-latitude ground geomagnetic stations and geosynchronous orbit). POLAR/UVI showed that auroral breakup occurred at latitudes lower than 60 MLat, and 2200-2230 MLT at 0501:57 UT. A clear positive bay and an isolated Pi2 pulsation were observed at a low-latitude station EUS (0.1 MLat., 0230 MLT). A negative bay and an increase in the Z component (positive downward) were observed at a high-latitude CANOPUS station ISLL (64.7 MLat., 2240 MLT), and this implies that the westward auroral electrojet developed at latitudes lower than ISLL. The above features suggest that the substorm current wedge was formed much closer to the Earth than usual isolated substorms. At mid-latitude stations, Y component (positive eastward) increased at the time of a positive bay at the ground stations to the west of BSL (40.8 MLat., 2300 MLT) while it decreased at stations to the east of BSL. This feature suggests that the center of the newly formed substorm current wedge was located at 2300 MLT. The GOES 8 satellite which was located at 2400 MLT observed a clear dipolarization and an increase in the eastward component of the magnetic field. It is well known that a geosynchronous satellite which is located to the east of the center of a substorm current wedge often observes a decrease in the eastward component of the magnetic field because the substorm current wedge is often formed tailward of the geosynchronous orbit. However for our event, the GOES 8 satellite which was located to the east of the center of the substorm current wedge observed an increase in the eastward component of the magnetic field. Taking into consideration the above features, it is suggested that the substorm current wedge was formed inside of the geosynchronous orbit.

**GAIII.05/07P/D-013** Poster **1400-111**

**VALIDITY OF THE FLUID DESCRIPTION OF CRITICAL BETA AND ALFVEN TIME SCALE OF BALLOONING INSTABILITY ONSET IN THE NEAR-EARTH COLLISIONLESS HIGH-BETA PLASMA**

Akira MIURA (Department of Earth and Planetary Science, University of Tokyo)

For a realistic highly stretched 2-D tail configuration, in which the pressure gradient force is balanced with the curved field line tension force at the equator, the growth rates of the ideal and nonideal MHD ballooning modes, in which the nonideal MHD means that the Hall and the electron pressure gradient terms are included in the Ohm's law, the ion bounce frequency, the ion magnetic drift frequency, and the ion cyclotron frequency are calculated numerically at the equator as a function of X from the near-Earth tail ( $X = -15 R_E$ ) to the mid-tail ( $X = -30 R_E$ ). Contrary to the well-known dipole field case, in which the bounce frequency decreases with increasing  $|X|$ , the ion bounce frequency increases with  $|X|$  for the 2-D tail



configuration. The growth rates of the ideal and nonideal ballooning modes, which are nearly equal, are given by the Alfvén velocity divided by the field line curvature radius at the equator. The growth rates are larger than the ion bounce, ion magnetic drift frequencies and smaller than the ion cyclotron frequency in the near-Earth tail at  $X \sim -15$  Re for ions with a thermal velocity and with an average pitch angle at the equator. Also, the ion motion remains adiabatic and the magnetic moment is conserved in the near-Earth tail at  $X \sim -15$  Re. Therefore, it is a posteriori verified that the fluid or nonideal MHD description of the linear stability of the ballooning instability is valid and the critical beta and the Alfvén time scale of the ballooning instability onset obtained by the fluid theory are validated in the near-Earth tail as close as 15 Re from the Earth. Despite the plasma being collisionless and high-beta in the near-Earth tail, the subtle collisionless kinetic effects due to the field line curvature in a high-beta collisionless plasma are not significant enough to invalidate the fluid description in the near-Earth tail, although they become more and more important as  $|X|$  increases. The Alfvén time scale of e-folding growth of the nonideal MHD ballooning (drift ballooning) instability due to the Alfvén wave trapped within a field line curvature radius in the equatorial region is usually less than a few tens of seconds in the near-Earth tail. It is faster than the ion bounce time and can explain the observed rapid time scale of a substorm onset.

**GAIII.05/07P/D-014** Poster **1400-112**  
**TAILWARD PERPENDICULAR FLOWS IN THE NEAR-EARTH PLASMA SHEET AROUND SUBSTORMS**

Rui YAMAGUCHI<sup>1</sup>, Hideaki KAWANO<sup>1</sup>, Shinichi OHTANI<sup>2</sup>, Kiyohumi YUMOTO<sup>3</sup>, Kan LIU<sup>4</sup>, Ching MENG<sup>5</sup>, Toshifumi MUKAI<sup>6</sup>, Yoshifumi SAITO<sup>7</sup>, Hajime HAYAKAWA<sup>8</sup>, The CPMN Group<sup>9</sup> (Dept. of Earth and Planetary Sci. Faculty of Sci. Kyushu Univ., <sup>2</sup>The Johns Hopkins University Applied Physics Laboratory, USA, <sup>3</sup>Space Environment Research Center, Kyushu University, Japan, <sup>4</sup>Institute of Space and Astronautical Science, Japan)

Tailward flows in the plasma sheet are sometimes observed even in the near-Earth region ( $-15 < X_{\text{gsm}} [\text{Re}] < -8$ ), which have not been explained by conventional substorm models. In order to understand the cause and effect of these flows in the framework of substorms, we have investigated features of the perpendicular flows in the plasma sheet measured by GEOTAIL in terms of their occurrence positions, durations, relative timings to substorm onsets, motions, and structures. The timing of the auroral onset determined by Polar/UVI images has been used. We have so far found (1) the tailward flows are observed ubiquitously in the near-Earth plasma sheet and their average flow directions are approximately along the  $X_{\text{gsm}}$  axis, (2) their occurrence rate significantly rises after substorm onsets, and (3) the tailward flows are often preceded by earthward flows. The result (3) suggests that the tailward flows represent reflection of earthward flows or passage of vortical flows. Regarding the possibility of reflection, we have statistically estimated the length of traveling path of these flows, that is, the distance from GEOTAIL to the reflection point, as a function of the satellite position. As a result, the travel path length decreases as the observing position (i.e., at GEOTAIL) approaches the Earth, but thus estimated reflection point approaches the Earth as the observing position approaches the Earth; this is unreasonable, suggesting that reflections do not occur at a fixed point in the near-Earth region. As for the possibility of vortical flows, we have applied the minimum variance method to these flows. The result suggests that these flows may correspond to the vortices in the plasma sheet for some events. We have estimated a scale and motion of a vortex during a large substorm. The result shows that it is difficult to interpret this vortex to be a part of the wedge current system.

**GAIII.05/07P/D-015** Poster **1400-113**  
**CHARACTERISTICS OF THE GROUND MAGNETIC VARIATIONS AT LOW AND MIDDLE LATITUDE ASSOCIATED WITH THE SAWTOOTH EVENT ON APRIL 18, 2002**

Kentarou KITAMURA<sup>1</sup>, Hideaki KAWANO<sup>2</sup>, Shin-ichi OHTANI<sup>3</sup>, Akimasa YOSHIKAWA<sup>4</sup>, Kiyohumi YUMOTO<sup>5</sup>, The CPMN Group<sup>6</sup> (Space Environment Research Center, Kyushu University, <sup>2</sup>Department of Earth and Planetary Sciences, Kyushu University, <sup>3</sup>The Johns Hopkins University Applied Physics Laboratory)

During recovery phase of a magnetic storm which occurred on 18 April, 2002, quasi periodic variations of the low-energy electron flux are observed by the LANL satellites at the geosynchronous orbit, which is named 'sawtooth event'. On the other hand, on the ground, magnetic bays and Pi2 pulsations appeared corresponding to the variations of the particle flux, and they are usually typical magnetic variations during substorms. However, any northward-turnings of the IMF-Bz corresponding to the sawtooth event were not observed by the ACE satellite. In this study, we have used the ground magnetic data from the middle and low latitude stations, which widely spread in the longitudinal direction, selected from the CPMN (Circum-Pan Pacific Magnetometer Network) stations, and compared the magnetic variations during the sawtooth event with that of the typical substorm (Lester et al., 1984). As a result, local time distribution of the polarization axis of the Pi 2 pulsations show a good agreement with that of typical substorm. However, the magnetic variations of the magnetic bay did not show a tendency typical to usual substorms. From the above, it is suggested that the current wedge was formed during this sawtooth event, and generated the Pi 2 pulsations on the ground; however, the other current system (ex. partial ring current) may have been superposed on the current wedge, and made unclear the DC-component (magnetic bay) of the substorm-associated magnetic variations on the ground.

**GAIII.05/07P/D-016** Poster **1400-114**  
**CHARACTERISTICS OF IONOSPHERIC ECHOES WITH VERY NARROW SPECTRAL WIDTH OBSERVED BY THE SUPERDARN HF RADARS DURING GEOMAGNETICALLY ACTIVE PERIODS**

Nozomu NISHITANI<sup>1</sup>, Tadahiko OGAWA<sup>1</sup>, Mark LESTER<sup>2</sup>, Steve E. MILAN<sup>3</sup>, Jim WILD<sup>3</sup>, Stanley W.H. COWLEY<sup>4</sup>, Natsuo SATO<sup>5</sup>, Hisao YAMAGISHI<sup>6</sup>, Akira Sessai YUKIMATU<sup>7</sup> (STELAB, Nagoya University, <sup>2</sup>Dept. Phys. Astron., University of Leicester, <sup>3</sup>National Institute of Polar Research)

The spectral width of the ionospheric backscatter echoes obtained with the SuperDARN radars has been regarded as a useful tool for locating specific ionospheric regions such as the cusp. In this paper we report the presence of ionospheric echoes with high (> 450 m/s) Doppler velocity and very narrow (< 60 m/s) spectral width, observed by the CUTLASS and Syowa East and South SuperDARN radars. These echoes have the following characteristics. (1) They have a close correlation with geomagnetic activity such that as the Dst index decreases, the radars tend to observe ionospheric echoes with high Doppler velocity and very narrow spectral width more frequently. (2) Their existence does not depend on magnetic local time. (3) They are located preferably in the polar cap region, where anti-sunward convection prevails. (4) They sometimes exist over a large spatial extent, so they are more likely to be F-region rather than E-region echoes. The occurrence of these echoes during active periods is associated with the suppression of the electric field turbulence. We also show that the appearance of ionospheric echoes with very narrow spectral widths in the polar cap is associated with the highly tail-like configuration of the magnetotail, by using the geosynchronous satellites data and Cluster satellite data. This result is consistent with the statistical results and their interpretation by Golovchanskaya et al. [2002]. Detailed

discussion of the possible generation mechanisms of these echoes will be presented.

**GAIII.05/07P/D-017** Poster **1400-115**  
**MAGNETOTAIL STRETCHING AS A DIAGNOSTIC TOOL FOR AURORAL SUBSTORM ENERGY DEPOSITION**

Ching-I MENG, Kan LIU, Patrick T. NEWELL (The Johns Hopkins University Applied Physics Laboratory)

Enhanced magnetotail field stretching is a key feature in the near-Earth magnetotail during enhanced couplings between the solar wind and the magnetosphere. Therefore, the degree of the field stretching is likely controlled by the amount of solar wind energy coupled into the magnetosphere, and it can be used as a proxy for the magnetospheric energy input to the ionosphere. Recent studies have shown, indeed, a good correlation between the magnetotail stretching index,  $b_2i$ , and auroral power. For the purpose of space weather application this study focus on the relationship between the magnetotail stretching and auroral energy deposition during substorm periods. The data set consists of global auroral images acquired from Polar ultraviolet imager (UVI) and magnetic field data from GOES magnetometers. The strength of substorms in terms of auroral power is inferred from auroral luminosity in the long wavelength bands (160-180 nm) of molecular nitrogen Lyman-Birge-Hopfield (LBH) auroral emissions observed from UVI, whereas the degree of magnetotail field stretch is estimated by the magnetic field elevation angles in the solar magnetic coordinates system. Universal time and seasonal effects are removed by subtracting empirical model field from the observed field. The result indicates that the relationship between the two quantities is nonlinear. We will present quantitative relationship between the two quantities and discuss the potential use of the result in substorm intensity forecasting.

**GAIII.05/07P/D-018** Poster **1400-116**  
**AURORAL POLEWARD BOUNDARY INTENSIFICATIONS: THEIR TWO-DIMENSIONAL STRUCTURE AND THE ASSOCIATED DYNAMICS IN THE PLASMA SHEET**

Efthya ZESTA<sup>1</sup>, Larry R. LYONS<sup>2</sup>, Eric DONOVAN<sup>3</sup>, Harald U. FREY<sup>4</sup>, Tsugunobu NAGAI<sup>5</sup> (<sup>1</sup>Department of Atmospheric Sciences, UCLA, <sup>2</sup>Space Sciences Laboratory, University of California, Berkeley, <sup>3</sup>Department of Physics, University of Calgary, <sup>4</sup>Department of Earth and Planetary Sciences, Tokyo Institute of Technology)

Auroral poleward boundary intensifications (PBIs) have an auroral signature in ground meridional scanning photometer (MSP) data that appears as an increase in intensity at or near the magnetic separatrix. This increase is often seen to extend equatorward through the ionospheric mapping of the plasma sheet. PBIs are associated with plasma sheet flow bursts and are thus important to plasma sheet dynamics. We previously found that equatorward extending PBIs are either north-south (NS) aligned structures or east-west (EW) arcs that mostly propagate equatorward. We further investigate the plasma sheet dynamic structures associated with these two types of PBIs by combining data from the CANOPUS MSPs, auroral images from the IMAGE spacecraft, and magnetic field and plasma data from the Geotail spacecraft. We study a period on January 3, 2001, when a series of PBIs were seen in the MSP data for 2.5 hrs. From simultaneous IMAGE and Geotail data we find that: (a) PBIs correlate well with plasma sheet fast flows observed within the local time sector of the PBIs. There can be several PBIs over the longitudinal range of fast flows in the tail, (b) multiple PBIs can occur over the whole width of the plasma sheet or in a more restricted local sector (i.e. only pre-midnight). When PBIs are seen only in a local sector fast flows are seen only in that local sector as well. Where no PBIs are seen no fast flows are seen, (c) most of the observed PBIs were EW arcs that initiated near the poleward boundary and then propagated equatorward. They often tilted and became mostly NS structures as they propagated equatorward and duskward, (d) there is a local time dependence on the type of PBI structure. Most PBIs seem to be narrow structures and primarily aligned with a line that goes through the 02 MLT and 17 MLT sectors. This results in PBIs that are NS structures in the postmidnight sector and EW arcs in the dusk sector. In the pre-midnight sector (22-00 MLT) PBIs start as EW arcs that then tilt and become primarily NS structures. These results suggest that the same plasma sheet dynamics produce EW and NS PBI structures.

**GAIII.05/07P/D-019** Poster **1400-117**  
**TWO TYPES OF PSBL ION BEAMS OBSERVED BY GEOTAIL: THEIR RELATION TO LOW FREQUENCY ELECTROMAGNETIC WAVES AND COLD ION ENERGIZATION**

Taku TAKADA<sup>1</sup>, Kanako SEKI<sup>1</sup>, Masafumi HIRAHARA<sup>2</sup>, Toshio TERASAWA<sup>3</sup>, Masahiro HOSHINO<sup>4</sup>, Toshifumi MUKAI<sup>5</sup> (<sup>1</sup>STEL, Nagoya University, <sup>2</sup>Rikkyo University, <sup>3</sup>University of Tokyo, <sup>4</sup>Institute of Space and Astronautical Science)

The plasma sheet boundary layer (PSBL) in the Earth's magnetotail is a region where hot plasma in the plasma sheet borders on the cold lobe plasma. Plasma in PSBL often consists of counter streaming ion and/or electron beam components generated from the nightside reconnection site. Although this beam component is considered to be a main energy source of broadband waves in PSBL, the mechanism responsible for generation of low-frequency waves is not identified. On one hand, it is often seen that cold ions from the lobe are accelerated gradually up to the plasma sheet energies in PSBL [Hirahara et al., 1994]. There are many candidates of heating processes via the electrostatic [e.g., Dusenbery and Lyons, 1989] or electromagnetic waves [e.g., Gary and Winske, 1990]. However, relative contribution of electrostatic and electromagnetic instabilities to the acceleration and heating of these cold ions still remains to be understood. It is a purpose of this study to clarify the causal relation of the ion beams, waves and cold ion energization in PSBL. Using high-sampling (16 Hz) magnetic field (MGF) and 12-s low-energy particle (LEP) data of Geotail, here we investigate characteristics of low-frequency (10 mHz to 1 Hz) electromagnetic waves and their relation to changes in ion distribution functions in PSBL. Two types of the PSBL crossings are analyzed in detail: During the periods of enhanced auroral activities with southward IMF, a collimated freshly injected earthward beam is observed together with the large-amplitude electromagnetic waves having a peak around 25 mHz (~1/10 of the local ion cyclotron frequency). Cold ions are energized during the same period. Before the disturbed period, however, we observed counter-streaming thermalized beams with neither cold ion energization nor significant wave activities in the low frequency range. The thermalized beams may be generated from the distant magnetotail and have undergone thermalization before reaching the Geotail position of  $X \sim -30$  R<sub>E</sub>. These observations suggest that fresh beams from the near-Earth neutral line (NENL) play an important role in the cold ion energization. References: Dusenbery, P. B., and L. R. Lyons, J. Geophys. Res., 94, 2484, 1989. Gary, S. P., and D. Winske, J. Geophys. Res., 95, 8085, 1990. Hirahara, M., et al., Geophys. Res. Lett., 21, 3003, 1994.

**GAIII.05/07P/D-020** Poster **1400-118**

**CLUSTER RAPID IES OBSERVATIONS OF HIGH-ENERGY ELECTRONS IN THE MAGNETOTAIL**

Jackie A. DAVIES<sup>1</sup>, Malcolm W. DUNLOP<sup>1</sup>, Manuel GRANDE<sup>1</sup>, ChrisH. PERRY<sup>1</sup>, Martin K. CARTER<sup>1</sup>, Pat W. DALY<sup>2</sup>, Andre BALOGH<sup>3</sup> (<sup>1</sup>Rutherford Appleton Laboratory, <sup>2</sup>Max Planck Institute for Aeronomy, <sup>3</sup>Imperial College)

The RAPID instrument on each of the four Cluster spacecraft comprises both an imaging ion mass spectrometer (IIMS) and an imaging electron spectrometer (IES). The latter is capable of detecting electrons within the energy range of some 40 to 500 keV. When operated in burst mode, each IES instrument provides complete angular coverage every 4 seconds (spacecraft spin period). Such high energy electrons provide a useful diagnostic of the occurrence of acceleration processes during, for example, reconnection. Between July and October 2002, the orbit of Cluster was such that near apogee the spacecraft crossed through the night-side plasma sheet at large separation (5000 km), covering some 8 hrs of local time from the dawn to the dusk-side flank. For many of the crossings, the spacecraft were operating in burst mode. These RAPID IES burst mode observations have been examined, in conjunction with data from the fluxgate magnetometer (FGM), to identify and classify the regions of the magnetotail within and adjacent to the current sheet. The data have thus provided the multi-point information necessary to enable us to characterise the energetic electron signature under a variety of conditions, such as tail reconfiguration and substorm activity.

**GAIII.05/07P/D-021** Poster **1400-119**

**Z-MODE WAVE IN THE MAGNETOTAIL : GEOTAIL OBSERVATION**

Hironobu TAKANO<sup>1</sup>, Isamu NAGANO<sup>1</sup>, Satoshi YAGITANI<sup>1</sup>, Yasuhiro OKUDA<sup>1</sup>, Kozo HASHIMOTO<sup>2</sup>, Hiroshi MATSUMOTO<sup>2</sup> (<sup>1</sup>Graduate School of Natural Science and Technology, Kanazawa University, <sup>2</sup>Radio Science Center for Space and Atmosphere, Kyoto University)

Electromagnetic Z mode waves have been observed in the auroral region and the Jupiter's magnetosphere. The Z mode wave consists of two frequency components having different polarization. The lower frequency component from the L-O mode cutoff frequency ( $f_{L-O}$ ) to the electron plasma frequency ( $f_e$ ) is the left-handed polarization. On the other hand, the higher frequency component extended to the upper hybrid resonance frequency ( $f_{UH}$ ) is the right-handed polarization. The Z mode wave can freely propagate by a linear mode conversion into an L-O mode through a radio window at the plasma frequency. The Z mode wave observed in the auroral zone is converted into the L-O mode wave on the auroral plasma cavity wall, which is radiated as the Auroral Myriametric Radiation (AMR). The L-O mode wave converted from the Z mode wave observed in the Jupiter's magnetosphere is emitted as Jovian Continuum Radiation (JCR). Terrestrial Continuum Radiation (TCR) is also generated by the linear mode conversion from the upper hybrid wave via the teradion window at the geomagnetic equatorial plasmapause, and is emitted to the Earth's magnetospheric cavity. The low frequency CR, which is called as Lobe Trapped CR (LTCR), has been observed by GEOTAIL spacecraft in the distant magnetotail. The LTCR would be generated at the plasma sheet boundary layer (PSBL) and the low latitude boundary layer (LLBL) by the same mechanism of CR emitted from the plasmapause and JCR. The Z mode observation in the PSBL and LLBL of the distant magnetotail would be an evidence of LTCR generation by the linear mode conversion. However, Z mode wave has not been observed in such regions. In the distant magnetotail, the narrow banded emission near the local electron plasma frequency is sometimes measured by the Wave Form Capture (WFC), which is a subsystem of the Plasma Wave Instrument (PWI) onboard GEOTAIL. Although the magnetic field component of this emission cannot be observed because of the lack of sensitivity of magnetic search coils, we consider this emission is the electromagnetic wave mode by analyzing the spectral structure with WFC data. By using the wave form data of electric field components, the spectral and polarization analysis determine the propagation mode of this emission. We will show the detailed spectral structure and polarization of this emission, and discuss whether this emission is the Z mode wave related to the LTCR generation or not.

**GAIII.05/07P/D-022** Poster **1400-120**

**KELVIN-HELMHOLTZ TYPE MODES DRIVEN BY OXYGEN IONS IN PLASMA SHEET REGION**

A.P. KAKAD, S.V. SINGH, G.S. LAKHINA (Indian Institute of Geomagnetism, Colaba, Mumbai, 400 005, India)

The Kelvin-Helmholtz type modes can be excited by the streaming of ionospheric oxygen ions in the plasma sheet region. In three component plasma consisting of electrons, protons and oxygen ions, the linear dispersion relation is derived with velocity shear in each component. The dispersion relation is studied numerically for the case of oxygen ion beam passing through stationary electron-ion plasma. The effects of oxygen ion beam speed, velocity shear and oxygen ion temperature on the growth rate of the Kelvin-Helmholtz mode are investigated. The results are applied to understand the low frequency turbulence observed in the plasma sheet region during substorm processes.

**GAIII.05**

**WHAT ARE THE STRUCTURES IN THE MAGNETOTAIL, WHY ARE THEY THERE, AND HOW DO THEY INFLUENCE ITS DYNAMICS**

Location: Site A, Room 6

Tuesday, July 8 AM  
Presiding Chairs: L.C. Lee, S.-I. Ohtani

**GAIII.05/08A/A06-001** **0830**

**THREE-COMPONENT PSBL ION BEAMS OBSERVED IN THE DISTANT MAGNETOTAIL**

Yoshifumi SAITO<sup>1</sup>, Toshifumi MUKAI<sup>1</sup>, Toshio TERASAWA<sup>2</sup>, Shinobu MACHIDA<sup>3</sup> (<sup>1</sup>Institute of Space and Astronautical Science, <sup>2</sup>University of Tokyo, <sup>3</sup>Kyoto University)

The most conspicuous feature of the Plasma Sheet Boundary Layer (PSBL) in the Earth's magnetotail is the existence of high-energy ion beams. These ion beams have been observed by several satellites in the near-tail region of  $X_{GSE} > -25R_E$ . In spite of the previous observational and theoretical works, the source and acceleration mechanism of the PSBL

ion beams is still unclear. The insufficiency of the ion observation in the source region of the PSBL ion beams is one of the major reasons. The purpose of this paper is to identify the source of the PSBL ion beams by analyzing the data obtained by the GEOTAIL satellite in the distant magnetotail  $X_{GSE} < -40R_E$ . Detailed structure of the Plasma Sheet Boundary Layer (PSBL) in the upstream region of slow-mode shocks in the distant magnetotail is investigated using low energy particle data. The existence of the slow-shock plasma sheet-lobe boundaries bounding the magnetic reconnection region in the Earth's magnetotail has already been proved by the GEOTAIL observations. When the plasma sheet-lobe boundary is a slow-mode shock, magnetic field is connected between the upstream lobe region and the downstream plasma sheet region. Three-component ions: cold ions and two-component PSBL beam ions were observed in the PSBL. One of the two-component PSBL beam ions was observed in the outer region of the PSBL. Its distribution function looked like "kidney bean" shape. The energy of this component was higher than the energy of the other component while the temperature was much lower. The number flux of this component was comparable with the number flux of the cold ions observed simultaneously. The other beam ion component was observed throughout the PSBL. It had characteristics that its low energy cut off gradually decreased as the satellite approached the plasma sheet. The number flux of this component was much higher than the number flux of the cold ions. The source of the former component may be the current sheet accelerated lobe cold ions. Since current sheet acceleration is most effective around the X-type neutral line where  $Z_{GSE}$ -component of the magnetic field is weak, this component is observed mainly in the outer region of the PSBL whose magnetic field is connected to the region near to the X-type neutral line. The source of the latter component may be the ions leaked from the hot plasma sheet towards the lobe region along the magnetic field that is connected between the lobe region and the plasma sheet region. Our statistical study has also revealed that three-component PSBL ions were observed with 34% of the slow-shock plasma sheet-lobe boundaries identified in the distant magnetotail.

**GAIII.05/08A/A06-002** **0845**

**GEOTAIL AND CLUSTER OBSERVATIONS OF FLUX ROPES IN THE MAGNETOTAIL FROM X ~ -15 TO -200 RE**

James A. SLAVIN, Eija TANSKANEN (NASA GSFC)

In the distant magnetotail flux ropes with diameters of 10 to 30 Re were frequently observed by Geotail and ISEE 3 often in association with magnetospheric substorms. We refer to these flux ropes as being of the "plasmoid-type" due to their being embedded in high-speed flow down the tail. More recently Geotail and Cluster observations have been used to study the occurrence of flux ropes in the near-tail. Earthward of  $X \sim -25 R_E$  most of the flux ropes are immersed within earthward directed bursty bulk flows. They are referred to as being "BBF-type" flux ropes. These near-tail flux ropes have diameters that are just ~ 1 to 2 Re or one order of magnitude smaller than what is seen in the distant magnetotail. We will compare and contrast the observations and models of magnetic flux ropes in the near and distant tail. The formation of small diameter flux ropes in the near-tail will be discussed in terms of the "filamentation" of the thinned cross-tail current layer while several competing models will be presented for the formation of large plasmoid-type flux ropes in the distant tail. Finally, the implications of the Geotail and Cluster flux rope measurements for tail stability and dynamics will be discussed.

**GAIII.05/08A/A06-003** Invited **0900**

**CLUSTER MULTI-POINT OBSERVATIONS OF FAST FLOWS IN THE PLASMA SHEET**

Rumi NAKAMURA<sup>1</sup>, Wolfgang BAUMJOHANN<sup>2</sup>, Andrei RUNOV<sup>1</sup>, Martin VOLWERT<sup>3</sup>, Zoltan VOERGES<sup>4</sup>, Tielong L. ZHANG<sup>5</sup>, Berndt KLECKER<sup>2</sup>, Andre BALOGH<sup>6</sup>, Henri REME<sup>7</sup>, Lynn KISTLER<sup>8</sup>, Christopher MOUKIS<sup>9</sup> (<sup>1</sup>IWF/OEAW, <sup>2</sup>MPE, <sup>3</sup>Imperial College, <sup>4</sup>CESR, <sup>5</sup>UNH)

Fast flows in the plasma sheet are considered to play an essential role in the energy conversion process in the magnetotail. Cluster spacecraft, which traversed the plasma sheet from the north to south at an apogee around 19 RE, observed fast flows at different location of the plasma sheet and for various conditions of the magnetosphere. Using multipoint measurements, we examine the spatial structure of the fast flows in the vicinity of a thin current sheet, in a thick plasma sheet configuration, associated with expansion of the plasma sheet, and thinning of the current sheet. We discuss on possible mechanisms responsible for these variety of flux transport process and how these fast flows interact with the ambient field and plasma.

**GAIII.05/08A/A06-004** **0925**

**CLUSTER OBSERVATIONS OF THE DYNAMICS OF THE TAIL CURRENT DURING SUBSTORMS**

Robert L. MCPHERRON<sup>1</sup>, Daniel N. BAKER<sup>2</sup>, Scott THOMPSON<sup>3</sup>, Margaret G. KIVELSON<sup>4</sup>, Krishan KHURANA<sup>5</sup>, Andre BALOGH<sup>6</sup>, Henri REME<sup>7</sup> (<sup>1</sup>Institute of Geophysics and Planetary Physics, University of California Los Angeles, Los Angeles, CA 90095-1567, USA, <sup>2</sup>Laboratory for Atmospheric and Space Physics, University of Colorado, Boulder, CO, <sup>3</sup>Space and Atmospheric Physics Group, The Blackett Laboratory, Imperial College, Prince Consort Road, LONDON SW7 2BW, UK, <sup>4</sup>CESR BP4346, 9 avenue du Colonel Roche, 31028 TOULOUSE Cedex 04, France)

We have carried out a detailed examination of the behavior of the tail current during several substorms that occurred during Cluster tail passes on August 15 and 27, 2001. We contrast this behavior to that seen during a quiet pass without a substorm expansion on September 22, 2001. We use minimum variance analysis to transform the magnetic field observations to a more convenient coordinate system and then use a Harris current sheet model to remotely sense the properties of the tail current. On August 15 Cluster was Earthward of the x-line at all times and we find that the current sheet systematically thins during substorm growth phase and expands during the expansion phase. On August 27 Cluster was initially tailward of the x-line. Several minutes before the ground onset a flux rope passed Cluster reversing the flow and field in the manner expected for a tailward moving x-line. On September 22 a growth phase was in progress during the passage and the sheet was extremely thin and changing with time. In all three cases it is necessary to assume that the location of the center of the current sheet and its thickness are varying with time to obtain agreement between the total measured current and the lobe field strength. We interpret these observations in terms of the near-earth neutral line model which argues that the tail effects are consequences of magnetic reconnection caused by current sheet thinning.

**GAIII.05/08A/A06-005** **0940**

**CURRENT CARRIERS OF THE CROSS-TAIL CURRENT: GEOTAIL OBSERVATIONS**

Toshifumi MUKAI<sup>1</sup>, Yoshihiro ASANO, Yoshifumi SAITO (<sup>1</sup>Institute of Space and Astronautical Science, <sup>2</sup>Kwasan Observatory, Kyoto University)

The cross-tail current is a basic element to sustain the magnetotail, and the identification of its current carriers is important to study the structure and dynamics of the current sheet,

especially physical processes in the evolution of a thin current sheet during magnetospheric substorms. In the adiabatic case, the current perpendicular to the magnetic field can be expressed as a sum of two terms: One is the pressure gradient term, and the other is due to the pressure anisotropy term divided by the local radius of the magnetic field. The first term is dominant in a normal thick current sheet, but several researchers have also argued for the significance of the second term in a thin current sheet. It has generally been presumed that ions are the dominant carriers in either case, since their temperature is much higher than the electron temperature in the plasma sheet. In principle, the current carriers can be identified by the distribution functions of ion and electrons and their velocity moments. However, the estimation of the electron current has been considered to be notoriously unreliable, because of various spurious effects in low-energy electron data as well as because the ratio of the electron bulk velocity to thermal velocity is usually very small (order of 1%). We have challenged this hard work with special cares to remove the spurious effects, and in some cases, succeeded in estimating the current density from the velocity difference between ions and electrons. As the result, the validity of the above general view is confirmed, but we have found that thin current sheets in which electrons are the dominant carriers evolve in the mid-tail region in the course of substorms. It is also noteworthy that the electron dominated current sheets appear not in the neutral sheet but in the off-neutral region, and the thickness is order of the ion inertial length. In this situation, ions are unmagnetized while electrons are magnetized, and the electric field directing to the neutral sheet makes electrons drifting downward.

**GAIII.05/08A/A06-006** Invited **0955**

**CURRENT SHEET STRUCTURE AND DYNAMICS IN MAGNETOTAIL**

M. HOSHINO<sup>1</sup>, T. MUKAI<sup>2</sup> (<sup>1</sup>Department of Earth and Planetary Science, University of Tokyo, <sup>2</sup>ISAS)

The magnetotail plasma sheet is one of the key elements for understanding the dynamic phenomena in the earth's magnetosphere. The current sheet is usually of the order of a few Re with a single peak current sheet, but a thin current sheet with the thickness of the order of ion inertia length is also known to exist before and during active phase. The structure of the thin current sheet is very important to understand the onset of substorms which is probably linked to various plasma instabilities such as magnetic reconnection, ballooning instability and so on. The energy dissipation rate is believed to be crucially controlled by the current sheet structure as well. Recent high-quality and multi-point observation data on the current sheet structure by Geotail and Cluster satellites revealed that a thin and double current sheet structure often exists in the magnetotail. Namely, the electric current density has two maxima away from the neutral sheet, and are embedded in a thick plasma sheet. This stratified structure seems to be very important not only on local plasma instabilities at the current sheet but also on the global dynamics in the magnetotail. We review a wide variety of the current sheet structures and dynamics observed in the magnetotail, and we argue the plasma heating and acceleration focusing on plasma kinetic effects in the relation to the stratified current sheet in the magnetotail.

**GAIII.05/08A/A06-007** **1040**

**ACCELERATION AND HEATING OF IONOSPHERIC IONS IN THE MAGNETOTAIL**

Jean-Andre SAUVAUD<sup>1</sup>, H. REME<sup>2</sup>, P. LOUARN<sup>3</sup>, G. FRUIT<sup>4</sup>, L. KISTLER<sup>5</sup>, G.K. PARKS<sup>6</sup>, M. ANDRE<sup>7</sup>, A. BALOGH<sup>8</sup>, M. DUNLOP<sup>9</sup>, N. CORNILLEAU<sup>10</sup> (<sup>1</sup>CESR/CNRS, Toulouse, France, <sup>2</sup>UNH, Durham, USA, <sup>3</sup>SSL, Berkeley, USA, <sup>4</sup>SISP, Uppsala, Sweden, <sup>5</sup>Imperial College, London, UK, <sup>6</sup>RAL, Oxfordshire, UK, <sup>7</sup>CETP, Velizy, France)

We present a study of the dynamics of the terrestrial ions in the mid-plasma sheet (10-19 RE). The high time resolution measurements of H<sup>+</sup>, He<sup>+</sup>, O<sup>+</sup> ions made onboard Cluster allow to show that these ions are massively injected into the tail during substorms and dispersed by time of flight effects. A single oxygen injection being able to account for over 80% of the oxygen population of the mid-tail plasma sheet. Ionospheric protons can at times have a sufficient energy to be directly measured inside the lobes. However, this population is generally very cold, quite often not fully measurable by a charged spacecraft, except when the ions acquire a large drift motion. We show that this is indeed the case during frequent disturbances of the plasma sheet boundary layers. In accordance with previous works, this boundary is found to be instable, affected by perturbations associated with large pressure gradients and fast flows. The use of the four Cluster spacecraft allow a unique determination of the geometry of the perturbations. We show that these disturbances lead to the generation of shear Alfvén waves propagating earthward inside the lobes. The wave electric field modulate there the energy of the near mono-energetic O<sup>+</sup> ions flowing from the Earth and dispersed by convection and also reveal the presence of the cold proton lobe population of ionospheric origin. Finally using the four cluster satellites, we show how cold ionospheric oxygen ions gain parallel velocity inside the PSBL where they are heated by low frequency waves.

**GAIII.05/08A/A06-008** **1055**

**PARTICLE SIMULATION OF PLASMA RESPONSE TO INDUCTION ELECTRIC FIELD IN THE MAGNETOSPHERE**

Yoshiharu OMURA<sup>1</sup>, Masataka MATSUNAGA<sup>1</sup>, Takayuki UMEDA<sup>1</sup>, Walter J. HEIKKILA<sup>2</sup>, Hiroshi MATSUMOTO<sup>3</sup> (<sup>1</sup>RASC, Kyoto University, <sup>2</sup>Center for Space Sciences, University of Texas at Dallas)

We study response of thermal plasmas to an induction electric field via particle simulations. We assume a small segment of the magnetic field line in the magnetotail where a large scale of induction electric field appears due meandering of the current sheet. We first performed one-dimensional electrostatic particle simulations with a constant external electric field applied to the Maxwellian thermal plasma with isotropic electrons and ions. The electric field is assumed to be due to the magnetic induction which takes place with a much longer time scale compared to that of the microscopic plasma wave instabilities to be studied in the present simulations. Therefore, we assume the external electric field is constant in time for simplicity. In the presence of the external electric field, thermal electrons are accelerated to form an electron beam drifting against the thermal ions. We observed onset of the Buneman instability after the electron acceleration. In spite of the strong diffusion of electrons due to the Buneman instability, we found formation of an electron beam running away from the acceleration region. We also performed two-dimensional electromagnetic simulations with external electric field applied to a localized area in the simulation model. Electrons are accelerated along the magnetic field, and they are diffused by the Buneman due to nonlinear trapping inside the acceleration region, while the untrapped electrons escaping from the acceleration region induce the bump-on-tail instability which results in the electrostatic solitary waves as observed in the plasma sheet boundary layer. We discuss possible connection of these nonlinear processes with specific plasma waves observed in the magnetosphere.

**GAIII.05/08A/A06-009** **1110**

**CLUSTER OBSERVATIONS OF ELECTRON POPULATIONS DURING MAGNETOTAIL RECONNECTION: 3-D STRUCTURE AND DYNAMICS**

Christopher J. OWEN<sup>1</sup>, Andrew N. FAZAKERLEY<sup>1</sup>, Jason P. DEWHURST<sup>1</sup>, Yulia BOGDANOVA<sup>1</sup>, Malcolm W. DUNLOP<sup>2</sup>, James A. SLAVIN<sup>3</sup>, Jean-Michel BOSQUED<sup>4</sup>, Andre BALOGH<sup>5</sup>, Henri REME<sup>6</sup> (<sup>1</sup>Mullard Space Science Laboratory, University College London, <sup>2</sup>Rutherford Appleton Laboratory, UK, <sup>3</sup>NASA/Goddard Space Flight Center, USA, <sup>4</sup>CNRS/CESR, France, <sup>5</sup>Imperial College, London, UK.)

We report on multi-point observations made by the 4 Cluster spacecraft during the first two magnetotail seasons (autumn 2001 and autumn 2002). Although we present data from a number of instruments for contextual purposes, we concentrate primarily on observations by the PEACE Electron spectrometers on each spacecraft. In particular, we survey the 3-dimensional structure of the electron populations in the vicinity of a number of plasma sheet flow reversal signatures that have previously been reported by Cluster researchers as possible encounters with active reconnection X-lines. We test the form of the electron distributions for consistency with the predictions of models of this region, in which a system of Hall electron currents flows within the ion diffusion region and causes characteristic magnetic field perturbations in the surrounding medium. We also compare these results with observations made further from active X-lines, for example as the spacecraft sample the separatrix layers during the passage of a plasmoid/flux-ropes. In this way, we qualitatively assess the variation of the electron populations with distance from the X-line.

**GAIII.05/08A/A06-010** Invited **1125**

**QUICK RECONNECTION TRIGGERING AND CROSS-SCALE COUPLING IN THE MAGNETOTAIL CURRENT SHEET**

Iku SHINOHARA<sup>1</sup>, Masaki FUJIMOTO<sup>2</sup> (<sup>1</sup>Institute of Space and Astronautical Science, <sup>2</sup>Tokyo Institute of Technology)

Understanding cross-scale coupling between MHD and dissipation scales in collisionless plasmas is challenging. Magnetic reconnection is an impressive example of the cross-scale coupling. While there is observational evidence that the magnetotail current sheet thickness becomes as thin as comparable to the relevant ion inertia length, whether it thins further down to electron scale to initiate reconnection is an open question. Carrying out a large scale 3D full particle simulation, we have recently found that quick triggering of magnetic reconnection is possible even in an ion-scale current sheet. If one thinks of the two-dimensional tearing mode as the triggering agent of magnetic reconnection in a current sheet of the Harris-type, the current sheet has to thin down to the electron scale for the instability to grow quickly. When the third dimension in the current-wise direction is taken into account, we have found that reconnection can be triggered very quickly. For the quick triggering, the lower-hybrid drift waves excited at the edges of the current sheet is indispensable. This wave excitation brings about formation of a thin current layer sustained by accelerated electrons. The inductive electric field, which is generated through change of the current profile, can efficiently accelerate meandering electrons around the magnetic neutral sheet. As a result, electric current in the thin layer is mostly carried by non-adiabatic electrons. Thus, the electron acceleration is playing a crucial role in making the quick triggering available. The result shows that the cross-scale coupling process is essential to enable the quick triggering of magnetic reconnection in an ion-scale current sheet. In the presentation, we will briefly introduce a Japanese future project of the magnetospheric explorer, namely the SCOPE project, in the context of understanding the cross-scale coupling in space plasma.

**GAIII.05/08A/A06-011** Invited **1150**

**THE NATURE OF BURSTY BULK FLOWS AND THEIR INFLUENCE ON MAGNETOTAIL STRUCTURE AND DYNAMICS: A KEY SCIENCE TOPIC FOR THE MAGNETOSPHERIC CONSTELLATION MISSION**

Harlan E. SPENCE<sup>1</sup>, Thomas E. MOORE<sup>2</sup>, Larry KEPKO<sup>1</sup>, Charles GOODRICH<sup>1</sup> (<sup>1</sup>Center for Space Physics, Boston University, <sup>2</sup>NASA Goddard Space Flight Center)

Recently, 3D simulations of the magnetosphere have been shown to exhibit a behavior that appears to be a global realization of the MHD plasma bubble phenomenon discussed first by Chen and Wolf. Bubble formation and dynamics appears to be a candidate mechanism for the production of bursty bulk flows, a term that is derived purely from observations of lone spacecraft in the magnetotail. We explore the evidence which links the simulated phenomenon to such observations and then use the simulation results to quantify their predicted important contributions to magnetotail structure and dynamics. Ultimately, reaching closure between theory and observation for such a three-dimensionally structured, dynamic phenomenon will require constellation-class observations having extent and resolution in space and time commensurate with global simulations, i.e. ~1-2 RE and ~10 sec. We treat the phenomenon of MHD plasma bubbles as representative of the general class of important magnetospheric dynamical structures that can practically be studied only by a distributed constellation of spacecraft, in order to obtain vector field "streamline" movies of the magnetotail plasma flow, magnetic field, and energetic particle fluxes. Relevant capabilities of the NASA Magnetospheric Constellation Mission (MCM) needed to resolve these outstanding key science questions are summarized.

**GAIII.05/08A/A06-012** **1215**

**INHERENTLY THREE DIMENSIONAL MAGNETIC RECONNECTION: A MECHANISM FOR BURSTY BULK FLOWS?**

Michael Anthony SHAY<sup>1</sup>, James F. DRAKE<sup>2</sup>, Marc SWISDAK<sup>1</sup>, William DORLAND<sup>3</sup>, Barrett ROGERS<sup>3</sup> (<sup>1</sup>University of Maryland, <sup>2</sup>Dartmouth College)

We examine the development of mesoscale structure during 3-D magnetic reconnection which initiates from random perturbations. Reconnection develops as multiple, finite length (on the order of 1 - 4 Earth Radii) x-line segments corresponding to strong variation in the cross tail direction. Forrelatively wide initial current sheets (several ion inertial lengths), these finite length x-lines remain spatially isolated and drive reconnection which is strongly reminiscent of bursty bulk flows (BBFs) in the magnetotail. In narrower initial current layers the x-line segments merge together to a state in which large scale magnetic energy release takes place. Thus, the degree of compression of the magnetotail may ultimately determine if energy is released in local bursts or globally as a substorm.

## GAIII.06-Posters

## HOW IS THE INNER MAGNETOSPHERE DYNAMICALLY COUPLED TO OTHER REGIONS OF GEOSPACE?

Location: Site D

Monday, July 7 PM

GAIII.06/07P/D-001 Poster 1400-121

## A NUMERICAL SIMULATION OF A GEOMAGNETIC SUDDEN COMMENCEMENT

Shigeru FUJITA<sup>1</sup>, Takashi TANAKA<sup>2</sup>, Takashi KIKUCHI<sup>3</sup> (<sup>1</sup>Meteorological College, <sup>2</sup>Kyushu University, Graduate School of Sciences, <sup>3</sup>Communications Research Laboratory)

A MHD simulation technique is utilized in order to investigate dynamic behavior of the magnetosphere-ionosphere coupled system corresponding to the solar wind disturbances. In this talk, we present a numerical simulation of a SC, including a negative SC revealed from a global 3D MHD simulation of the magnetosphere-ionosphere coupled system. A SC is divided into three phases in the point of view of the magnetosphere-ionosphere coupling. The preliminary impulse, the first signal just appearing on the onset of a SC, is explained with a MHD wave propagation in the non-uniform magnetosphere. The MHD wave is originally the compressional mode, which is converted to the Alfvén mode with a FAC in a region of steep gradient of plasma density. Thus, we confirm the previous Tamao-Araki model of a PI. In this phase, the ionosphere does not play a role in the magnetospheric disturbance. Following the PI phase, the compressional signal in the magnetosphere is still propagating in the magnetosphere. Behind the wavefront of the compressional wave in the magnetosphere, plasmas are decelerated and excess kinetic energy is converted into electric current energy. This phase is called as the first stage of a Main Impulse. The ionosphere begins to control the magnetospheric plasma dynamics, but its behavior is complex and transient. In the last phase, the ionospheric convection and the magnetospheric convection are corresponding to each other. The magnetosphere-ionosphere current system is quite similar to the steady region 1 current system. However, the current generation mechanism is not related to the magnetic reconnection in the magnetopause, but compressional of the magnetopause in the nightside cusp region. A negative SC is regarded as a mirror image of a positive SC after Takeuchi and Araki [2001] from morphological study of observed data. Our simulation results support this conclusion. However, the first compression of the magnetopause in the positive SC and the first expansion of the magnetopause in the negative SC seem to yield different current generating mechanisms. We will discuss this in the talk.

GAIII.06/07P/D-002 Poster 1400-122

## MORPHOLOGY OF THE RING CURRENT DERIVED FROM IN-SITU MAGNETIC FIELD OBSERVATIONS

Guan LE<sup>1</sup>, C.T. RUSSELL<sup>2</sup>, K. TAKAHASHI<sup>3</sup> (<sup>1</sup>NASA/GSFC, Greenbelt, MD, USA, <sup>2</sup>IGPP, University of California, Los Angeles, CA, USA, <sup>3</sup>Johns Hopkins University, Applied Physics Laboratory, Laurel, MD, USA)

We use the magnetic field data in the inner magnetosphere observed by Polar, ISEE, and AMPTE/CCE spacecraft to study the morphology of the ring current distribution. The combined data set from 5-year Polar mission, 10-year ISEE mission, and 5-year AMPTE/CCE mission provides extensive coverage of the equatorial inner magnetosphere in L-values, local times, and the Dst index for quantitative study of the ring current. Using intercalibrated magnetic field data from the three spacecraft, we are able to construct the magnetic field maps and the corresponding current density maps for different range of Dst\*, the corrected Dst index by the solar wind dynamic pressure which represents the true ring current strength. In the results, both an eastward inner ring current at ~ 3 RE and a westward outer ring current at ~ 4-7 RE are evident for all ranges of Dst\*. There is a local time asymmetry for the westward outer ring current for all levels of magnetospheric disturbances. The peak of the westward ring current is around the local midnight during the quiet time. The local time asymmetry intensifies and the current peak shifts towards pre-midnight sector as the ring current strengths. During moderate magnetic storms (-100 nT < Dst\* < -80 nT) the peak of the westward ring current occurs at ~ 2000 local time.

GAIII.06/07P/D-003 Poster 1400-123

## INFLUENCE OF SUBSTORMS AND STORMS IN THE SAR ARC DYNAMICS. STATISTICAL ANALYSIS

Igor B. IEVENKO, Valery N. ALEXEYEV (Institute of Cosmophysical Research and Aeronomy, SD RAS)

Population growth and urban development, with the consequent requirement of improved supplies and development of new potential water resources, have increased the need of an accurate knowledge of hydrological phenomena at basin scale, such as runoff, erosion, sedimentation and mass movements, in order to assess the possible consequences of their future evolution on human activities. However, the prediction of these evolutionary trends is often difficult due to the lack of data concerning hydrological parameters. This problem can be mainly connected to the difficulties in the measurement of such data. In particular, mass transfer rates are generally measured at few chosen points along the main channels of the watershed. This approach usually leads to unsatisfactory results since sediment transfer is mainly controlled by scale invariant pulse processes which are spatially and temporally scattered everywhere within the watershed. Local point measurements unavoidably involve the loss of information on spatial variability generating averaged or lumped values. In this context the extraction of such information could benefit from the use of a remote sensing technique, characterized by large scale and low cost. Spaceborne SAR interferometry in the last few years has been successfully applied to reconstruct the topography of the observed scene and to measure with millimeter accuracy changes on the earth surface induced by different geophysical phenomena. The aim of the present work is to investigate the possible contribution of the interferometric technique in the retrieval of hydrologically-related geomorphic parameters. In particular, the attention has been focused on the possibility to obtain two different types of data: i) continuously updatable DEMs of basins with a suitable vertical accuracy and ii) quantitative spatially distributed estimates of sediment transfer among hillslopes and between hillslopes and channels. These information can be extremely valuable for the calibration of hydrological models as well as for a better understanding of the spatial and temporal distribution of the landscape sculpting processes in a wide range of scales within the basin. The method has been applied by using SAR data acquired by the ERS satellites on different test-sites located in the Italian Alps and Apennines.

GAIII.06/07P/D-004 Poster 1400-124

## WHAT IS HILDCAAS?

Kazuya YAGO, Yohsuke KAMIDE (Solar-Terrestrial Environment Laboratory, Nagoya University)

Data of magnetic disturbances at high latitudes and those at low latitudes are coupled for periods of HILDCAAs (High-Intensity Long-Duration Continuous AE Activity) during the recovery phase of geomagnetic storms. During HILDCAAs, highly fluctuate interplanetary magnetic field are seen, and Dst values do not fully recover to the pre-storm level for several days. This study addresses the question of what causes HILDCAAs and what are their effects on low-latitude magnetic disturbances.

GAIII.06/07P/D-005 Poster 1400-125

## A COMPARISON BETWEEN TAIL AND LOW ALTITUDE OBSERVATIONS DURING A LONG PERIOD OF ENHANCED GEOMAGNETIC ACTIVITY

Rune STADSNEs<sup>1</sup>, Knut SVENES<sup>2</sup>, Kjell AARSNES<sup>1</sup>, Finn SOERAAAS<sup>1</sup>, Kjellmar OKSAVIK<sup>1</sup>, Marita SOERBOE<sup>1</sup>, Marit Irene SANDANGER<sup>1</sup>, Kjartan OLAFSSON<sup>1</sup> (<sup>1</sup>University of Bergen, Norway, <sup>2</sup>Nowegian Defence Research Establishment)

A geomagnetically disturbed period commenced with a storm sudden commencement at about 19 UT on August 18 2002. The Dst went down to -30nT and stayed depressed at this level until 16 UT on August 20. At this time a prolonged period of southward IMF-Bz started, lasting for 23 hours. During this period Cluster was located in the magnetotail. The magnetotail data provided by Cluster and the low altitude data provided by the NOAA satellites constitute an excellent combination to study the correspondence between particle boundaries close to and distant from the Earth. The period with increased southward IMF-Bz caused the Dst to reach down to -96 nT. The whole period under consideration exhibits an enhanced AE-index almost continuously above 500 nT. The relation between the solar wind energy input to the magnetosphere (the Akasofu epsilon-parameter), the particles observed in the tail, and the particle energy dumped into the upper atmosphere is investigated. By comparing particle boundaries in the tail and in the ionosphere constraints on magnetic field line models are obtained.

GAIII.06/07P/D-006 Poster 1400-126

## DOMINANCE OF TOROIDAL OSCILLATIONS IN DAWN/DUSK SECTORS- A PLAUSIBLE EXPLANATION IN TERMS OF VARIATIONS IN SOLAR WIND DYNAMIC PRESSURE

Ashwini Kumar SINHA (Indian Institute of Geomagnetism, Colaba, Mumbai 400 005.)

The changes in the solar wind dynamic pressure produce the oscillations in surface currents at the magnetopause boundary in order to establish equilibrium. These currents cause compressional variations in the magnetic field within the magnetosphere. The response of transverse field line oscillations to such variations in the magnetic field has been computed in dipole field geometry in reflecting ionospheric conditions. The analysis clearly shows the dominant characteristics of fundamental toroidal modes in the dawn and the dusk sectors as revealed by the statistical studies of pulsations observed by the satellite AMPTE/CCE [Anderson *et al.*, 1990]. It is traditionally believed that such oscillations are mainly driven by Kelvin-Helmholtz (K-H) instability. Our analysis shows that the dominance of fundamental toroidal modes in the dawn and dusk sectors can also be explained in terms of response to impressed pressure impulses without invoking K-H instability. The analysis also shows that poloidal modes do not exhibit any longitudinal structures. These results are consistent with the observations [Anderson *et al.*, 1990]. **References:** Andersan, B. J., M. J. Engebretson, S.P. Rounds, L. J. Zanetti, and T. A. Potemra, A statistical study of Pc3-5 pulsations observed by the AMPTE/CCE magnetic fields experiment 1. Occurrence distributions, *J. Geophys. Res.*, 95, 10495, 1990.

GAIII.06/07P/D-007 Poster 1400-127

## A TEST OF THE MAGNETOSPHERIC SOURCE OF TRAVELLING CONVECTION VORTICES

Mai Mai LAM, Alan S. RODGER (Physical Sciences Division, British Antarctic Survey)

Travelling convection vortices (TCVs) are a powerful tool for probing the nature of the coupling between the solar wind, the magnetosphere, and the ionosphere. Existing theoretical models of their generation do not properly represent the coupling between the magnetosphere and the ionosphere. We use conjugate ground magnetometer data from the Greenland magnetometer chain and Antarctica to test the nature of the magnetospheric source of 18 TCV events associated with changes in the magnetopause dynamic pressure. This is achieved by statistically comparing two groups of TCV events, one containing events for which the conjugate ionospheres are of similar conductivity, the other containing events for which the conductivity of the conjugate ionospheres differs by an order of magnitude. We find that the TCV intensity has a similar magnitude in both hemispheres regardless of any difference in conductivity between the two hemispheres. We propose that this is evidence in favour of the magnetospheric source of TCVs being a constant current source.

GAIII.06/07P/D-008 Poster 1400-128

## ENERGETIC ION INJECTION AND FORMATION OF THE STORM-TIME RING CURRENT

L. XIE<sup>1</sup>, Z.Y. PU<sup>1</sup>, X.Z. ZHOU<sup>1</sup>, S.Y. FU<sup>1</sup>, Q.G. ZONG<sup>2</sup>, T.A. FRITZ<sup>3</sup>, Z.X. LIU<sup>4</sup> (<sup>1</sup>Department of Geophysics, Peking University, <sup>2</sup>CSP, Boston University, <sup>3</sup>CSSAR, Chinese Academy of Science)

In this paper we made an extensive study of storm-time ring current formation through 3-D test particle trajectory calculations (TPTCs). We focus our attention on injection of the energetic Oxygen ions whose abundance and energy density in the inner magnetosphere are extraordinarily high near the Dst minimum of the main phase of great storms. Two sources of Oxygen ions are considered: The Oxygen ion population of a few tens keV originally situated in the near-Earth magnetotail ( $L \leq 8$ ) or in the mid-magnetotail ( $L \sim 15$ ), and the thermal population ( $\leq 10$  keV) up-flowing from the Earth's ionosphere. Different convection electric field models, such as the uniform electric field, the Volland electric field model (Volland, 1978) and the Heppner-Maynard-Rich model (Heppner, Maynard, and Rich, 1990) are applied to incorporate, respectively, with the co-rotation electric field. The TPTC runs show that the intense magnetospheric convection electric field can effectively energize (within 2 to 3 hours) Oxygen ions which are initially located either in the near-Earth tail or in the mid-tail as they drift into the inner magnetosphere. Meanwhile, the thermal Oxygen ions can be considerably energized by the co-rotation electric field once they come closer to the Earth along a closed orbit. In addition to the convection and co-rotation electric fields, a semi-quantitative and time-independent shielding electric field model is included in a few studies. The calculated results demonstrate that the shielding electric field plays an important role in the formation of the symmetric ring current.

**GAIII.06/07P/D-009** Poster **1400-129**

**STUDY OF THE DST-AL CORRELATION DURING MAGNETIC STORMS**

Fiori-Anastasia I. METALLINO<sup>1</sup>, Ioannis A. DAGLIS<sup>2</sup>, Yohsuke KAMIDE<sup>3</sup> (Aristotle University of Thessaloniki, Department of Physics, Section of Astrophysics, Astronomy and Mechanics, GR-541 24 Thessaloniki, Greece, <sup>2</sup>National Observatory of Athens, Institute for Space Applications, GR-152 36 Penteli, Greece, <sup>3</sup>Nagoya University, Solar-Terrestrial Environment Laboratory, 442 Toyokawa, Japan)

A dispute on the role of substorms in storm development has emerged during the last few years; the community has not yet reached a definite conclusion. Our study assesses the storm-substorm relationship through an investigation of the geomagnetic indices SYM-H and AL for a number of magnetic storms. The data were provided by the World Data Center for Geomagnetism, Kyoto, and by STELab, Nagoya University. We have selected a group of magnetic storms with SYM-H values in the range between -50nT and -350nT. We have calculated the integrals of SYM-H and AL indices over the storm duration, aiming to get a proxy of the total intensity of the two phenomena (storm/substorm). The integrals of the two geomagnetic indices exhibit a linear correlation. The linear correlation method yields a correlation index of  $r=0.867$  for the SYM-H / AL pairs for the selected storm periods. We have also calculated the integrals of the SYM-H and AL squares, to represent magnetic field energy for the two associated processes. In this case the correlation index reaches a value of  $r=0.907$ . Our results imply a strong coupling between storm and substorm energy dissipation.

**GAIII.06/07P/D-010** Poster **1400-130**

**A STRATEGY FOR FUTURE EXPLORATION INTO DYNAMICS OF THE INNER MAGNETOSPHERE**

Kazuo SHIOKAWA<sup>1</sup>, Kanako SEKI<sup>1</sup>, Yoshizumi MIYOSHI<sup>2</sup>, Takayuki ONO<sup>2</sup>, Tsutomu NAGATSUMA<sup>3</sup>, Takahiro OBARA<sup>3</sup>, Masahito NOSE<sup>4</sup>, Yoshiya KASAHARA<sup>5</sup>, Masafumi HIRAHARA<sup>6</sup>, Takeshi TAKASHIMA<sup>7</sup>, Kazushi ASAMURA<sup>8</sup>, Y. Kasaba<sup>9</sup>, A. Matsuoka<sup>9</sup>, Y. Saito<sup>9</sup>, H. Saito<sup>9</sup>, K. Yumoto<sup>9</sup>, H. Kawano<sup>9</sup>, Y. Yoshikawa<sup>9</sup>, Y. Ebihara<sup>9</sup>, A. S. Yukimatu<sup>9</sup> and the inner magnetosphere section, Society of Geomagnetism, Earth, Planetary, and Space Sciences (Solar-Terrestrial Environment Laboratory, Nagoya University, <sup>2</sup>Faculty of Science, Tohoku University, <sup>3</sup>Communications Research Laboratory, <sup>4</sup>Faculty of Science, Kyoto University, <sup>5</sup>Faculty of Engineering, Kanazawa University, <sup>6</sup>Faculty of Science, Rikkyo University, <sup>7</sup>Institute of Space and Astronautical Science (ISAS), <sup>8</sup>Faculty of Science, Kyushu University, <sup>9</sup>National Institute of Polar Research (NIPR))

The Earth's inner magnetosphere (the radial distance from the Earth less than 10 Re) has been a "missing" region from scientific investigation, particularly for the plasma dynamics. This is because there have been few satellites that made simultaneous measurements of the plasma distribution function, composition, and magnetic and electric fields in the inner magnetosphere near the equatorial plane. The inner magnetosphere contains several interesting regions from the viewpoint of the plasma dynamics, i.e., the inner plasma sheet, ring current, radiation belts, and plasmasphere. In the radiation belts, the electrons have the highest energy in the Earth's magnetosphere. Various unresolved processes of particle energization have been proposed to explain generation of relativistic electrons in these regions. In order to examine each candidate mechanism, continuous energy coverage of electrons as well as observations around the magnetic equatorial plane is essential. Investigation of these energization processes in the inner magnetosphere will also provide important clues for understanding of plasma acceleration mechanisms in the dipolar magnetic field of other planets and stars. Identification of dominant acceleration mechanisms of radiation belt electrons is also important for the space weather. In this talk, we review current status and unsolved problems related to the plasma dynamics of the inner magnetosphere in order to address scientific objectives and strategy of a possible future satellite mission, which investigates the dynamics of the inner magnetosphere. The subjects will be covered are: 1) substorm dynamics and energetics, 2) radiation belt dynamics, 3) ring current dynamics, 4) ULF waves, 5) plasma waves inside and outside the plasmasphere, and 6) mass transport including heavy ions.

**GAIII.06/07P/D-011** Poster **1400-131**

**MULTI-POINT MEASUREMENTS OF PLASMA DRIFTS AND DENSITIES NEAR THE PLASMAPAUSE**

Harri E. LAAKSO, A. MASSON, P. ESCOUBET, R. GRARD, F. PITOUT (ESA/ESTEC/Code SCI-SH, Noordwijk, The Netherlands)

Erosion and recovery of the plasmasphere are important issues that are inherently related to the global dynamics and structure of the magnetosphere. The plasmapause is a highly dynamic region where the density decreases a few orders of magnitude over a relatively short distance and the plasma drift is switched from corotation into convection. Sometimes the changes occur suddenly, sometimes slowly, but under some conditions, the transitions are quite oscillatory. This paper presents a variety of plasmapause crossings by the four Cluster satellites. We utilize the measurements from the electric field experiments that measure both the plasma drift and total plasma density variations along the satellites' trajectories across the plasmapause. Such measurements show that the flow separatrix and density decline do not necessarily occur simultaneously. We show cases of a modulating plasmapause either via wave activity (of a few minute periods) or radial motion of the plasmapause. Occasionally outside the plasmapause, large-scale density enhancements are observed that are likely related to plasma tails.

**GAIII.06/07P/D-012** Poster **1400-132**

**GLOBAL 3D ELECTROMAGNETIC PARTICLE SIMULATION FOR SATELLITE OBSERVED SASH EVENT**

Xiaoyang YAN, Dongsheng CAI, Nishikawa K. -I, Bertrand LEMBEGE (University of Tsukuba)

We made our efforts to parallelize the global 3D HPF Electromagnetic particle model (EMPM) for several years and have also reported our meaningful simulation results that revealed the essential physics involved in interaction of the solar wind with the Earth's magnetosphere using this EMPM in our PC cluster and supercomputer. Sash phenomena was observed and reported in some satellite observation. And some MHD simulations for it was accomplished. We investigate it with this HPF EMPM and recently new simulation for it was run in the new VPP5000 supercomputer. In the new simulations were performed on the new VPP5000 supercomputer of Tsukuba University, we used larger domain size, 305x205x205, smaller grid size  $\Delta$ , 0.5RE (the radius of the Earth), more total particle number, 200,000,000 (about 8 pairs per cell). And other parameters used in this simulation are, solar wind speed is 0.5c, the mass ratio of ion to electron is 16, the position of the Earth is at  $x=100$ ,  $y=100$ ,  $z=100$ , electron thermal velocity is  $v_{the}=0.01$ , electron plasma frequency is about 0.01, the electron Debye length is about  $\lambda_{De}=1.0\Delta$ . The position of magnetopause is at about  $x=20$   $\Delta=10RE$ . At first, we run this code up to 1000 time steps

without IMF, and get the called quasi-stationary status; After the quasi-stationary status was established, we applied a northward IMF ( $B_z=0.4$ ), then run it for 800 time steps, at this time, the IMF arrives at about  $x=-50RE$ , and then we change the IMF from northward to dawnward ( $IMF B_y=0.4$ ). The results revealed that the groove structure at the day-side magnetopause, that causes particle entry into inner magnetosphere and the cross structure or S-structure at near magneto-tail are formed. Moreover, in contrast with MHD simulations, kinetic characteristic of this event is also analyzed self-consistently with this simulation. The new simulation provides new and more detailed insights for the observed sash event.

**GAIII.06/07P/D-013** Poster **1400-133**

**STORMTIME MAGNETOSPHERIC ELECTRIC FIELD MODELING USING ION DRIFT MEASUREMENTS IN THE IONOSPHERE**

Phillip Charles ANDERSON (Space Science Applications Laboratory, The Aerospace Corporation, Los Angeles, CA)

Knowledge of the magnetospheric convection electric field pattern is essential to any study of the inner magnetosphere. While a number of empirical and theoretical electric field models have been developed in the past, none of them contains a good description of the stormtime magnetospheric electric fields, in particular the electric fields that penetrate to low L-values as a result of the breakdown of the shielding near the inner edge of the ring current. The potential drop equatorward/earthward of the auroral oval/electron plasma sheet can exceed 60 kV, a substantial fraction of the total potential drop across the polar cap/magnetosphere. The Defense Meteorological Satellite Program (DMSP) spacecraft have been providing ion drift measurements in the ionosphere since 1988 as well as precipitating auroral particle measurements since 1982 and geomagnetic field measurements since 1994. At times, these measurements have been provided simultaneously by 5 separate spacecraft. We are in the process of developing an empirical, stormtime magnetospheric electric field model using the data from the DMSP spacecraft. We report the initial results of the development, focusing on the penetration electric fields associated with geomagnetic storms.

**GAIII.06/07P/D-014** Poster **1400-134**

**CAN THE SURFACE-IONOSPHERE WAVEGUIDE TRANSMIT CONVECTION CHANGES TO LOW LATITUDES?**

Robert J. STRANGWAY (IGPP, University of California, Los Angeles)

The frozen-in electron condition, which applies for the upper E- and F-region ionosphere, leads to the equivalence between mechanical and electromagnetic loads. As a consequence, the work done in moving the ionosphere against the neutral atmosphere equals the Poynting flux dissipated in the ionosphere. This implies that in general any motion of the ionosphere is driven by the magnetosphere, unless there is an excess of Poynting flux into the ionosphere. In that case, the excess Poynting flux is available to make the ionosphere appear to be a driver of magnetospheric convection. In order to assess how and if Poynting flux, and by implication changes in convection, can be transmitted via the ionosphere we have investigated wave propagation across the ionosphere with a Green's function analysis and through the ionosphere into the surface-ionosphere waveguide. The Green's function analysis shows that signals will tend to propagate across the ambient field at higher altitudes, with diffusion dominating at lower altitudes, although this analysis ignores the altitude dependence of the collision frequencies and Alfvén velocity. The analysis of vertical propagation demonstrates that the ionosphere tends to absorb most of the wave Poynting flux, implying that the surface-ionosphere waveguide is an inefficient means for transferring wave energy. An important aspect of the analysis is that the surface ionosphere waveguide is not simply a free space cavity, but electron collisions are still important down to about 40 km altitude. Thus the absorption is not restricted to the E- and F-regions only, but extends down into the atmosphere. Furthermore, in order that the surface-ionosphere waveguide by a means for transmitting convection information, the incident wave energy must overcome the Joule dissipation at both the entry and exit sites, further arguing against the waveguide as a means for driving magnetospheric convection.

**GAIII.06/07P/D-015** Poster **1400-135**

**TSUBASA(MDS-1) OBSERVATIONS OF HIGH-ENERGY CHARGED PARTICLES IN THE MAGNETOSPHERE**

Kiyokazu KOGA, Haruhisa MATSUMOTO, Hideki KOSHIISHI, Hitoshi MATSUOKA, Masao NAKAMURA, Tateo GOKA (Office of R&D, NASDA)

In-situ observations are required to investigate fully fluctuations in the radiation belt. Tsubasa (MDS-1) measures the magnetic field and high-energy charged particle fluxes (electron, proton, alpha-particle) in the equatorial plane from 500 to 36000 km, so that, particle flux, pitch angle distribution, phase space density and radial distribution can be measured. Information from these measurements is very useful for revealing the cause of the radiation belt fluctuations, particularly those of high-energy electrons and protons. Tsubasa was successfully launched by the H-IIA launch vehicle from the Tanegashima Space Center on February 4, 2002. It was then injected into a geostationary transfer orbit (GTO), with a spin rate of 5 rpm for attitude stabilization. We report magnetic field observations, particle flux and pitch angle distributions during magnetic storms, and examine these results in the light of relevant radiation belt fluctuation theory.

**GAIII.06/07P/D-016** Poster **1400-136**

**SC TRIGGERED PLASMA WAVE AND FIELD PHENOMENA OBSERVED BY THE AKEBONO SATELLITE IN THE PLASMASPHERE**

Atsuki SHINBORI<sup>1</sup>, Takayuki ONO<sup>2</sup>, Masahide IIZIMA<sup>3</sup>, Atsushi KUMAMOTO<sup>1</sup>, Hiroshi OYA<sup>4</sup> (<sup>1</sup>Geophysical Institute, Gradual School of Tohoku University, <sup>2</sup>Fukui University of Technology)

Since sudden commencements (SCs) are very clear isolated global signature, they have been recognized as important phenomena in understanding the response of the earth's magnetosphere, plasmasphere and ionosphere associated with a passage of solar wind discontinuity of density and velocity. In order to study on the propagation feature of SC disturbances in the plasmasphere, DC electric and magnetic field phenomena and the generation of plasma waves associated with SCs, plasma wave and field phenomena were analyzed in the relationship to the SCs based on the Akebono satellite observations which have been carried out more than 13 years since March 1989. For the present data analysis, plasma wave data of PWS (20 kHz-5.1 MHz), VLF (3.16 Hz-17.8k Hz) and ELF (0 Hz-80 Hz) were used. Within a period from January 1989 to December 2002, 2803 events of SCs have been identified in SYM-H data as a rapid increase with more than 5 nT per ten minutes, and 263 events were covered by the simultaneous observation records of the Akebono satellite. For accurate determination of the SC onset time, we referred the geomagnetic variation data with the time resolution of 1 sec obtained at Kakioka Magnetic Observatory. Within the simultaneous Akebono observation data of 101 SC events in the low latitude region, we found that plasma waves are enhanced with one-to-one correspondence to SCs in the

plasmasphere. The SC related plasma wave phenomena show clear spectral modulation and increase of the center frequency of whistler mode, LHR waves, and electromagnetic ion cyclotron waves. On the other hand, the response of DC electric field perturbations associated with SCs also shows peak amplitude of 1-30 mV/m followed by dumping oscillation of Pc3-4 ULF waves with a period from 40 seconds to 60 seconds in all geomagnetic local times. The ULF waves have continued for about 3 to 6 minutes after the SC onset with a damping. The initial variations of the electric field perturbations at the onset of SC's in space are directed westward. About 1-2 minutes later, the dawn-to-dusk convection electric field is also enhanced with the amplitude of 0.5-1.5 mV/m in the plasmasphere. The Poynting vector is directed earthward with the amplitude of 0.00041-0.00015 W/m<sup>2</sup>. This analysis indicates that a compressional wave propagates inside the plasmasphere with refraction. Difference between onset times of SC and plasma wave enhancement showed propagation characters of SC triggered disturbances from dayside to nightside regions. The distribution of the delay time of the plasma wave disturbances suggested that the propagation route of SC disturbance inside the plasmasphere locates near the geomagnetic equator region with a speed of about 350 km/sec.

**GAIII.06/07P/D-017** Poster **1400-137**

#### KILOMETRIC RADIATION ASSOCIATED WITH PLASMASPHERIC DISTURBANCES

Manabu SATO<sup>1</sup>, Takayuki ONO<sup>1</sup>, Masahide IIZIMA<sup>1</sup>, Hiroshi OYA<sup>2</sup>, Atsushi KUMAMOTO<sup>3</sup> (<sup>1</sup>Department of Geophysics, Graduate School of Science, Tohoku University, <sup>2</sup>Department of Space Communications, Faculty of Engineering, Fukui University of Technology)

Due to the unique orbital character of the Akebono satellite, it became possible to obtain detail characters of plasma and plasma waves inside the plasmasphere. For example, within an early period of data analysis phase of the plasma wave and sounder experiment (PWS) on board Akebono satellite, the "Donkey Ear" phenomenon (Oya, 1997) was discovered as a significant density depletion region inside plasmasphere near the equatorial region. On the other hand, plasma wave observation inside the density depletion region revealed radiation of electromagnetic waves within a frequency range of several hundreds kHz that seems to be trapped inside the density depletion region. Interesting fact is that the propagation mode of the majority of the kilometric radiations tends to show the right-handed polarized waves (R-X mode). The electromagnetic wave is named as kilometric radiation since the wavelength is the order of kilometric scale length. There are 578 events of the kilometric radiation found in the observation results of the Akebono satellite during the period from 1989 to 1999. It shows clear that association of "Donkey Ear" phenomena with 41.3% of kilometric radiation events. The observation region is concentrated within  $\pm 50$  degree geomagnetic range, and it appears in an altitude range more than 4,000km. The occurrence probability of the kilometric radiation showed clear relation with the variation of the solar activity and significant concentration near the geomagnetic equator. This nature suggested that the source region of kilometric radiation is located near the geomagnetic equatorial region. Kp and Dst dependences were also investigated; it became clear that the kilometric radiation occurred in a condition of large geomagnetic disturbances. 64% of radiation events showed relation to geomagnetic storms, with the magnitude more than 50nT in Dst. A correlation analysis of occurrence probability to the phase of magnetic storms showed that there is occurrence peak near the start time of the recovery phase of geomagnetic storms. The kilometric radiation is expected to spread outside of plasmasphere through a window where plasma density is low comparing with the radiation frequency. The kilometric continuum observed by GEOTAIL satellite (Hashimoto et al., 1999) may be a part of the kilometric radiations propagating outside plasmasphere through the window. The present results may support the model proposed by Green et al. (2002) that the origin of kilometric continuum is located in the bite-out structure of plasmasphere by using the data observed by IMAGE satellite.

**GAIII.06/07P/D-018** Poster **1400-138**

#### SOLAR WIND - PLASMASPHERE - IONOSPHERE COUPLING DURING GEOMAGNETIC STORMS

Galina A. KOTOVA<sup>1</sup>, V. BEZRUKIKH<sup>1</sup>, M. VERIGIN<sup>1</sup>, L. LEZHEN<sup>1</sup>, J. SMILAUER<sup>2</sup>, J. LEMAIRE<sup>3</sup> (<sup>1</sup>Space Research Institute of Russian Academy of Sciences, <sup>2</sup>Institute of Atmospheric Physics, Czech Academy of Sciences, Prague, <sup>3</sup>Institute d'Aeronomie Spatiale de Belgique, Brussels, Belgium)

The ALPHA 3 thermal plasma measurements obtained on INTERBALL 1 and 2, and subsatellite MAGION 5 in the plasmasphere of the Earth are analyzed in conjunction with simultaneous solar wind data and ground-based ionospheric measurements during geomagnetic storms. Previously it was found, theoretically unpredicted increasing of cold ion density in the dusk and dawn outer plasmasphere with increasing solar wind ram pressure probably connected to the overall magnetospheric compression. Enhancements in solar wind pressure frequently initiate the development of geomagnetic storm in the whole magnetosphere. In the present talk detailed case study of some strong magnetic storms occurred in 1999 and 2000 is performed. Dynamics of the plasmopause and thermal plasma parameters during geomagnetic storms is interpreted taking into account the overall coupling in solar wind-plasmasphere-ionosphere system.

**GAIII.06/07P/D-019** Poster **1400-139**

#### MEASUREMENTS OF THE SAPCE RADIATION ENVIRONMENT WITH SDOM

Haruhisa MATSUMOTO, Hideki KOSHISHI, Tateo GOKA (National Space Development Agency of JAPAN)

TSUBASA satellite was launched on February 2002. TSUBASA is placed in a geostationary transfer orbit having roughly a perigee of 500 km, an apogee of 36,000km, a 28.5 inclination, and a 645 minute period. The Standard Dose Monitor (SDOM) onboard TSUBASA has carried out measurements of energetic electrons, protons, and alpha particles. We report the dynamic feature of the radiation belt environment, and the change of pitch angle distribution of the radiation belt particles by the geomagnetic storm.

**GAIII.06/07P/D-020** Poster **1400-140**

#### MOLECULAR ION OBSERVED BY AKEBONO SATELLITE NEAR THE INNER MAGNETOSPHERE

Manabu YAMADA<sup>1</sup>, Shigeto WATANABE<sup>1</sup>, Takumi ABE<sup>2</sup>, Yoshizumi MIYOSHI<sup>4</sup>, Eiichi SAGAWA<sup>3</sup>, A.W. YAU<sup>5</sup> (<sup>1</sup>Division of Earth and Planetary Science, Graduate School of Science, Hokkaido University, Sapporo, Japan., <sup>2</sup>The Institute of Space and Astronautical Sciences, Sagami-hara, Japan., <sup>3</sup>Communications Research Laboratory, Koganei, Japan., <sup>4</sup>Planetary Plasma and Atmospheric Research Center, Tohoku University, Sendai, Japan., <sup>5</sup>University of Calgary, Calgary, Canada.)

The importance of the ionosphere as a source of magnetospheric plasmas has been confirmed by recent studies. The existence of heavy ion in the magnetosphere, such as O+

coming from the ionosphere, means that we have to investigate in detail the processes of ion heating, ion acceleration, ion outflow, ion dynamics in the magnetosphere and the wave-particle interactions. The suprathermal ion mass spectrometer (SMS) on Akebono satellite has observed the polar topside ionospheric ions of 1-64 m/q with low energy (0-25keV) over the long period more than one solar cycle. SMS data is, therefore, useful for the statistical analysis of thermal ion heating and outflow phenomena, and provide us important information on the dynamics of molecular ions such as N<sub>2</sub><sup>+</sup> and NO<sup>+</sup> in addition to O<sup>+</sup> in the inner magnetosphere. In this paper, we discuss in detail about the molecular ion outflow events and show the molecular ion flux and the occurrence frequency in the inner magnetosphere.

## GAIII.06

### HOW IS THE INNER MAGNETOSPHERE DYNAMICALLY COUPLED TO OTHER REGIONS OF GEOSPACE?

Location: Site A, Room 2

Tuesday, July 8 AM

Presiding Chair: T. Obara

**GAIII.06/08A/A02-001**

**0900**

#### DEPARTURES FROM COROTATION IN THE INNER MAGNETOSPHERE

Bill R. SANDEL, William T. FORRESTER, Robert A. KING (Lunar and Planetary Laboratory, University of Arizona)

Using maps of the distribution of singly-ionized helium in the plasmasphere made by the IMAGE Extreme Ultraviolet Imager, we investigate departures from corotation in the inner magnetosphere. We deduce the angular velocity of the plasma by tracking discrete, long-lived features within the plasmasphere. On the basis of first-order theory, we would expect the cold plasma that we observe (energy < 1 eV) to be locked by the Lorentz force to Earth's magnetic field and to corotate with it. In contrast, our analysis shows that the plasma in the range  $2 < L < 4$  most frequently rotates at a rate that is roughly 85-90% of the corotation rate. A particular feature may move at a constant or variable rate during its lifetime. It may move at the corotation rate for a time, and then begin to lag. Our analysis is based on features that persisted for times in the range 15-60 hours. We find a range of angular velocities (averaged over the lifetime of the features) that is 77% to 93% of the corotation velocity. Structures having large radial extent frequently maintain their shapes over the period of observation. In these cases, measurable shearing by an L-dependent corotation lag must therefore be absent. We investigate the implications of these measurements for our understanding of electric fields and plasma motions in the inner magnetosphere.

**GAIII.06/08A/A02-002**

Invited

**0915**

#### IMAGE EUV OBSERVATIONS OF PLASMASPHERIC EROSION: INDICATIONS OF PLASMASPHERE/RING-CURRENT/IONOSPHERE COUPLING

Jerry GOLDSTEIN<sup>1</sup>, Bill R. SANDEL<sup>2</sup>, Pontus CSON BRANDT<sup>3</sup>, Stanislav Y. SAZYKIN<sup>4</sup> (<sup>1</sup>Space Science Division, Southwest Research Institute, <sup>2</sup>Lunar and Planetary Lab, University of Arizona, <sup>3</sup>Applied Physics Lab, Johns Hopkins University, <sup>4</sup>Department of Physics and Astronomy, Rice University)

The IMAGE extreme ultraviolet (EUV) imager obtains global images of the He+ plasmasphere as seen in 30.4 nm light. EUV directly observes the effects of plasmaspheric erosion by capturing the motion of the plasmopause. Several erosion events have been identified in which the nightside plasmopause moves inward, while at the same time the dayside fills up with (presumably sunward-moving) plasma. This global transport of plasmaspheric material from the nightside to the dayside is generally accepted to be connected in some way to enhanced convection electric fields that arise during periods of increased geomagnetic activity following southward turnings of the interplanetary magnetic field (IMF). However, the precise chain of events between a southward IMF turning and the onset of plasmaspheric erosion has not been established. EUV data consistently indicate a time delay of about 30 minutes between a southward IMF turning at the magnetopause, and the onset of plasmaspheric erosion. One simple explanation for this 30-minute delay is that the global convection field requires some time after a southward IMF turning to reach a new configuration with well-established flows, and thus the inner magnetosphere would not experience the effects of enhanced convection until that new global configuration is established. There are strong indications that this simple picture is incomplete and that coupling (between the inner magnetosphere and other regions of the magnetosphere) plays a significant role. Partial ring currents at the inner edge of the plasmopause participate in the erosion process (to an unknown extent) by providing a dynamically-changing shielding layer and/or by coupling to the ionosphere to produce regions of intense azimuthal flows known as sub-auroral polarization streams (SAPS). This raises the possibility that the 30-minute delay may be explained as an interval of buildup of ring current pressure. We shall present a picture of this plasmaspheric erosion process from an observational and theoretical/simulation perspective.

**GAIII.06/08A/A02-003**

Invited

**0940**

#### ULF RESONANCE, EUV REMOTE SENSING, AND IN SITU PLASMASPHERIC OBSERVATIONS

Mark B. MOLDWIN, D. BERUBE, J. WEYGAND (Earth and Space Sciences, UCLA)

The location of the plasmopause and the density structure of the plasmasphere can be determined from ground-based ULF resonance techniques, in situ plasma wave receivers and particle detectors, and the EUV imager on the IMAGE spacecraft. We take advantage of the opportunity to make simultaneous observations from these variety of techniques in order to understand the global behavior of the plasmasphere in response to storms.

**GAIII.06/08A/A02-004**

Invited

**1005**

#### IMAGE OBSERVATIONS OF PLASMASPHERE/RING CURRENT INTERACTIONS

Dennis L. GALLAGHER<sup>1</sup>, Mark L. ADRIAN<sup>2</sup>, Joseph D. PEREZ<sup>3</sup>, Bill R. SANDEL<sup>4</sup> (<sup>1</sup>NASA Marshall Space Flight Center, <sup>2</sup>University of Alabama in Huntsville, <sup>3</sup>Auburn University, <sup>4</sup>University of Arizona)

Evidence has been found in IMAGE observations that overlap of the plasmasphere and the ring current may lead to enhanced loss of plasma into the ionosphere. It has long been anticipated that this mixing of plasma leads to coupling and resulting consequences on both

populations. Wave generation, pitch angle scattering, and heating are some of the consequences that are anticipated. IMAGE plasmasphere, ring current, and auroral observations will be presented and used to explore these interactions and their effects.

**GAIII.06/08A/A02-005** Invited **1045**

**FORMATION OF MAIN PHASE RING CURRENT AND RECOVERY PHASE RING CURRENT**

Yusuke EBIHARA<sup>1</sup>, Masaki EJIRI<sup>1</sup>, Hans NILSSON<sup>2</sup>, Ingrid SANDAHL<sup>2</sup>, Manuel GRANDE<sup>3</sup>, Joseph F. FENNEL<sup>4</sup>, James L. ROEDER<sup>4</sup> (<sup>1</sup>National Institute of Polar Research, Japan, <sup>2</sup>Swedish Institute of Space Physics, Sweden, <sup>3</sup>Rutherford Appleton Laboratory, UK, <sup>4</sup>The Aerospace Corporation, USA)

Data from the Polar/MICS instrument (1-200 keV) and results of a single particle simulation are used to investigate the formation of the proton ring current during both the storm main and recovery phases. We performed a numerical simulation that tracks bounce-averaged trajectories of particles under various magnetic field models (the dipole and Tsyganenko 1989 and 1996 models), electric potential models (the Volland-Stern type and Weimer 2000 models) and induction electric field models. Three different transport processes were tested to account for the formation of the main phase ring current; the convection electric field, the substorm-associated induction electric field and the radial diffusion. Data from Polar/MICS shows that during a storm main phase a dramatic enhancement of the proton differential flux is seen on the night side. No significant enhancement is, in most cases, found on the dayside when Dst decreases monotonically. This may exclude some physical hypotheses that are simulated to produce a rather symmetric ring current, that is, the substorm and the diffusion processes are probably a minor contributor to the ring current formation when the local time asymmetry of the enhancement appears during the main phase. The simulation under a time-dependent convection electric field model gives a fairly reasonable result in comparison with the Polar/MICS data. The recovery phase ring current is not simply understood to the result of decay of the ring current. According to the Polar/MICS data, high-energy population of the ring current (>100 keV), which is minor during the main phase, appears in the heart of the ring current (L=3-5) when the recovery phase starts. A simple convection electric field model does not account for this kind of development. The substorm and diffusion processes are also unlikely because they are thought to be more effective during the main phase than during the recovery phase. We discuss the possibility that an azimuthal electric field induced by the storm-associated increase in the ambient magnetic field of the ring current is important to produce the development of the high-energy portion of the ring current during the recovery phase.

**GAIII.06/08A/A02-006** Invited **1110**

**ANALYSIS OF RING CURRENT CONTROL OF ELECTRIC FIELDS IN THE INNER MAGNETOSPHERE DURING THE APRIL 2002 MAGNETIC STORMS**

Michael W. LIEMOHN<sup>1</sup>, Janet U. KOZYRA<sup>1</sup>, Aaron J. RIDLEY<sup>1</sup>, Jichun ZHANG<sup>1</sup>, Gang LU<sup>2</sup>, Darren L. DE ZEEUW<sup>3</sup>, Daniel M. OBER<sup>4</sup>, Phil C. ANDERSON<sup>5</sup>, Cynthia CATTELL<sup>6</sup>, Jerry GOLDSTEIN<sup>7</sup>, Pontus C. SON BRANDT<sup>8</sup>, M. F. Thomsen, A. J. Mannucci (<sup>1</sup>SPRL, University of Michigan, <sup>2</sup>National Center for Atmospheric Research, <sup>3</sup>Mission Research Corporation, <sup>4</sup>The Aerospace Corporation, <sup>5</sup>Department of Physics, University of Minnesota, <sup>6</sup>Department of Physics and Astronomy, Rice University, <sup>7</sup>Applied Physics Laboratory, Johns Hopkins University, <sup>8</sup>Los Alamos National Laboratory, <sup>9</sup>Jet Propulsion Laboratory)

Modeling results of the inner magnetosphere during the April 17-22, 2002, magnetic storms are presented, showing the importance of a self-consistent calculation between the electric field and the hot ion fluxes. In particular, the control of the subauroral electric fields by the ring current will be discussed, along with their impact on the ionospheric and magnetospheric plasma. Using a kinetic plasma transport code that highly resolves the velocity space distribution, results from several simulations with different input and boundary conditions are examined. Output from a global MHD code is also presented for context. These results are analyzed in combination with observations of the inner magnetospheric and subauroral plasma populations and electric fields. Thus the global spatial and temporal evolution during the event is determined from several methods and all of these are compared together. This comparison yields information about the accuracy of the assumptions built in to the various models (e.g., formulations, conductances, boundary conditions, magnetic field descriptions) as well as the ability of the various data sets to accurately reveal the development of the event. These findings are discussed in detail. The aeronomic consequences of the stormtime electric fields, including storm-enhanced densities in the ionosphere from the subauroral region to the polar cap, are also discussed.

**GAIII.06/08A/A02-007** Invited **1135**

**MAGNETIC FIELDS AND PLASMAS IN ACTIVE SUBSTORMS AND STORMS**

Thomas E. MOORE<sup>1</sup>, J.F. FENNEL<sup>2</sup>, M.-C. FOK<sup>1</sup>, M.B. MOLDWIN<sup>3</sup>, J.A. SLAVIN<sup>4</sup>, R.J. STRANGEWAY<sup>5</sup> (<sup>1</sup>Laboratory for Extraterrestrial Physics, NASA's Goddard Space Flight Center, <sup>2</sup>JGPP, University of California in Los Angeles, <sup>3</sup>The Aerospace Corporation)

In this paper, we review recent advances and the current state of knowledge of the inner magnetosphere, defined as the region within which the ionosphere is the dominant source of plasma, including the bulk of the ring current and at least the inner plasma sheet. To limit scope, we focus on the magnetic field and plasma description of this region, rather than on the electric field and current description, taking the latter to be complementary but to some degree redundant, and in any case, less readily observed. We consider the significant recent contributions of remote sensing and imaging to our knowledge of the inner magnetosphere, as well as the recent development of a Comprehensive Ring Current Model (CRCM) and radiation belt forecasting tools. These have given us the first system description to account for interactions with the ionosphere and thermosphere, including the enhancement of ionospheric outflows into the high latitude regions. Next, we consider recent developments in the acceleration of charged particles to form the dynamic ring current and radiation belt environment, including mechanisms involving interplanetary shocks, ULF pulsations, and compressive impulses originating in the plasma sheet. Finally, we summarize by presenting a case that future progress in inner magnetospheric weather forecasting will require more and better coordinated observations of magnetic fields and plasmas in active substorms and storms, to better define the environment within which such dynamical effects arise and develop.

**GAIII.06/08A/A02-008** **1200**

**THE RING CURRENT AND INNER MAGNETOSPHERE DURING STEADY MAGNETOSPHERIC CONVECTION EVENTS**

Calvin Robert CLAUSER<sup>1</sup>, M.W. LIEMOHN<sup>2</sup>, D.L. DEZEEUW<sup>3</sup>, J.U. KOZYRA<sup>4</sup>, J. GOLDSTEIN<sup>5</sup> (<sup>1</sup>Center for Space Environment Modeling, Univ. of Michigan, <sup>2</sup>Southwest Research Institute)

The behavior of the inner magnetosphere in response to an increase or decrease of the

convection electric field is examined during periods of so-called Steady Magnetospheric Convection events. These events are distinctive in their lack of substorm signatures during intervals of enhanced convection driven by large, quasi-steady southward IMF. The temporal and spatial development of the ring current is measured using LT-UT maps of the low latitude ground magnetic disturbance measured by a chain of about 20 magnetic observatories. Temporal and spatial variations of the plasmasphere are measured using images obtained from the Extreme Ultra Violet Imager (EUV) instrument on the IMAGE satellite. Results from the Michigan inner magnetosphere models are consistent with the observations in many ways. We discuss the physical interpretation of the combined analysis of the model and observational results.

**GAIII.06/08A/A02-009** **1215**

**EVOLUTION OF RING CURRENT ENERGY DENSITY DURING GEOMAGNETIC STORMS**

Natalia Yu. GANUSHKINA<sup>1</sup>, Yusuke EBIHARA<sup>2</sup>, Tuija I. PULKKINEN<sup>3</sup>, Masaki EJIRI<sup>4</sup>, Ted A. FRITZ<sup>5</sup> (<sup>1</sup>Department of Geophysical Research, Finnish Meteorological Institute, <sup>2</sup>National Institute of Polar Research, Tokyo, Japan, <sup>3</sup>Department of Astronomy, Boston University, Boston, MA, USA)

Changes in the ring current energy density during storm periods are studied. Ring current energy densities and total ring current energies are obtained using particle data from PolarCMMICE/MICS instrument during several storms during year 1997-1998. Four different energy ranges for particles are considered: total (1-200 keV), low (1-20 keV), medium (20-80 keV) and high (80-200 keV). Evolution of contributions from particles with different energy ranges to the total energy density of the ring current during different storm phases is followed. To model this evolution we trace protons with arbitrary pitch angles numerically in the drift approximation. Tracing is performed in stationary (T96, Volland-Stern) and time-dependent magnetic and electric field models. Time-dependent electric fields given by Gaussian electric field pulse with azimuthal field component propagating inward with constant velocity of 100 km/s. We model particle inward motion and energization by a series of electric field pulses representing substorm activations during storm events. We demonstrate that such fluctuating fields can effectively energize the plasma sheet particles and transport them inward to closed drift shells. Analysing the model contributions from particles with different energy ranges to the model total energy density of the ring current during different storm phases and comparing with observations we show that the formation of the ring current is a combination of large-scale convection and pulsed inward shift and consequent energization of the ring current particles.

Tuesday, July 8 PM  
Presiding Chair: I. Daglis

**GAIII.06/08P/A02-001** Invited **1400**

**CRITICAL TEST OF THE DST INDEX AS A MEASURE OF THE STORM INTENSITY**

Shin-ichi OHTANI, Pontus C. SON BRANDT, Donald G. MITCHELL (The Johns Hopkins University Applied Physics Laboratory)

The Dst (or Sym-H) index has been ideally regarded as a measure of the ring current intensity, and the development and decay of the magnetospheric storm have been conventionally addressed in terms of the change of this index. However, caution needs to be exercised since the tail current makes a significant contribution to Dst. In the present study we examine the storm event of August 12, 2000 and compare variations of the ENA flux measured by the IMAGE/HENA instrument with the associated variations of the Dst index. The result indicates that substorm-associated changes of the tail current and the ring current have the opposite effects on Dst, and the former overcompensates the latter. We statistically test this result by cross-examining the near-Earth tail magnetic field and Dst for storm-time substorms. Possibility of estimating the ring current intensity from Dst is also discussed.

**GAIII.06/08P/A02-002** Invited **1425**

**COUPLING BETWEEN THE INNER MAGNETOSPHERE AND THE IONOSPHERE DURING MAGNETIC STORMS AND SUBSTORMS**

Anthony T.Y. LUI (Applied Physics Laboratory)

The inner magnetosphere is an important geospace region for magnetic storms since it contains the storm-time ring current responsible for the worldwide magnetic depression in magnetic storms. A relatively new tool in investigating the dynamics of the ring current is the energetic neutral atom (ENA) emissions. In this study, we present evidence of coupling between the inner magnetosphere and the ionosphere during magnetic storms as well as substorms through ENA observations from Geotail. It is found that ENA oxygen emissions are temporarily enhanced during substorms in a magnetic storm interval, consistent with earlier reports of transient ionospheric oxygen ion outflow in association with substorm activity. The spectral evolution of ENA oxygen during the main phase of a magnetic storm is also used to examine the temporal coupling of the ionosphere to the inner magnetosphere during the development of the storm-time ring current.

**GAIII.06/08P/A02-003** Invited **1450**

**THE GLOBAL SCALE OF SAWTOOTH INJECTIONS AND IMPLICATIONS FOR MAGNETOSPHERIC AND IONOSPHERIC COUPLING**

Geoffrey D. REEVES, Michelle F. THOMSEN, Joe E. BOROVSKEY, Michael G. HENDERSON, Ruth M. SKOUG (Space and Atmospheric Sciences Group)

Sawtooth injections were first identified as an intriguing signature in the LANL geosynchronous energetic particle fluxes showing sharp increases in particle fluxes followed by gradual decreases which repeat roughly every 2-3 hours. The variations are similar to the standard dropout and injection of energetic particles seen in isolated substorms. However, unlike isolated substorms, after each injection a new dropout begins immediately, over a broad range of energies, producing the characteristic sawtooth profile. Space magnetometer data show that the dropouts and injections are produced by exceptionally strong stretching and dipolarization of the magnetic field and confirm that the stretching begins immediately after the preceding injection without an intervening recovery phase. However, ENA observations show that these events are true injections of fresh particles and not an adiabatic re-arrangement in response to the field changes. Auroral observations likewise show clear auroral onsets with each sawtooth injection, but those onsets can be embedded in ongoing auroral activity rather than distinct episodes separated by quiet intervals. It is not surprising that sawtooth activity is a subset of geomagnetic storm activity (intervals of large negative Dst). The quasi-periodicity and clear separation of each onset are not, however, characteristic of most geomagnetic storms. Additionally, each individual sawtooth is associated with an increase in the SYM-H component. One of the most intriguing

characteristics is that sawtooth signatures are seen at all local times, not just the near-midnight sector. By analyzing multi-satellite data we are able to determine the scale of these injection events. Data from up to 7 simultaneously-operating geosynchronous satellites show that the injections there frequently cover more than 12 hours of local time. They are more prominent in the dusk sector than in the dawn sector and frequently, perhaps even typically, extend well past the dusk terminator toward local noon. We will discuss the spatial extent of the sawtooth injections, the possible signatures of propagation, and the implications for global coupling to the ionosphere and other magnetospheric regions.

**GAI.06/08P/A02-004** **1515**

**DYNAMICS OF FIELD ALIGNED CURRENTS ASSOCIATED WITH GLOBAL QUASI-PERIODIC GEOSYNCHRONOUS PARTICLE INJECTION EVENTS**

Brian J. ANDERSON<sup>1</sup>, M. THOMSEN<sup>2</sup>, R. SKOUG<sup>2</sup> (<sup>1</sup>Space Department, The Johns Hopkins University Applied Physics Laboratory, <sup>2</sup>Los Alamos National Laboratory, Space and Atmospheric Sciences, Los Alamos, New Mexico, USA)

Quasi-periodic particle injection events, also called 'sawtooth events', have been reported in geosynchronous orbit particle observations. They are characterized by a recurring sequence of dropout and nearly dispersionless recovery or injection of 50 to 400 keV ions at multiple satellites with repetition intervals ranging from one to several hours. The events typically occur during geomagnetic storm-times and give the appearance of substorm injections except that they are dispersionless on a scale that often exceeds 12 hours in longitude. To help characterize the magnetospheric electrodynamics associated with these events we examine observations from engineering magnetometers of the Iridium satellite system. These data provide global scale, 2-hour local time resolution, estimates of the high latitude Birkeland currents with a time and latitude resolution of approximately 2-latitude-hours. For this study we use 30 minute windows which provide 4 degree latitude resolution to examine the dynamics of nightside field aligned currents (FACs) associated with sawtooth injections. The nightside FACs display a systematic sequence with each dropout-injection event. The period of minimum flux is associated with a FAC pattern consistent with the classical Iijima-Potemra statistical pattern in which the morningside upward region 2 current is contiguous with the duskside upward region 1 current. Particle injection is associated with disruption of this pattern in the region of the Harang discontinuity in which a downward FAC appears at latitudes of the most equatorward (region 2) upward current. This change is consistent with the appearance of a pair of field aligned currents, downward post-midnight and upward pre-midnight, consistent with a substorm wedge current system.

**GAI.06/08P/A02-005** **1530**

**MODELING THE INNER PLASMA SHEET PROTONS AND MAGNETIC FIELD UNDER ENHANCED CONVECTION**

Chih-Ping WANG<sup>1</sup>, Larry R. LYONS<sup>1</sup>, Margaret W. CHEN<sup>2</sup>, Richard A. WOLF<sup>3</sup>, Frank R. TOFFOLETTO (<sup>1</sup>Department of Atmospheric Sciences, UCLA, <sup>2</sup>Space Science Applications Laboratory, The Aerospace Corporation, <sup>3</sup>Department of Physics and Astronomy, Rice University)

To understand the evolution of the inner plasma sheet from quiet to disturbed conditions, we incorporate a modified version of the Magnetospheric Specification Model with a modified version of the Tsyganenko 96 magnetic field model to simulate the protons and magnetic field under an increasing convection electric field with two-dimensional force balance maintained along the midnight meridian. The local-time dependent model boundary proton sources are a mixture of hot plasma from the mantle and cooler plasma from the low latitude boundary layer. We previously used this model to simulate the inner plasma sheet under weak convection corresponding to a cross polar-cap potential drop (DFPC) equal to 26 kV and obtained two-dimensional quiet time equilibrium for proton and magnetic field that agrees well with observations. We start our simulation for enhanced convection with this quiet time equilibrium and increase DFPC steadily from 26 kV to 146 kV in 5 hours while keeping the boundary particle sources time independent. Simulations are also run separately to steady states by keeping DFPC constant after it is increased to 98 and 146 kV. The magnitudes of proton pressure, number density, and temperature and their increase from quiet to moderate activity (DFPC = 98 kV) are consistent with most observations. Our simulation at high activity (DFPC = 146 kV) underestimates the observed pressure and temperature. This disagreement indicates possible dependence of the boundary particle sources on activity and possible effects of solar wind dynamic pressure enhancements that have not yet been included in our simulation. The equatorial distributions of the simulated equatorial pressures, density, and temperatures and their change with activity agree qualitatively with the DMSP observations. The simulated proton flow speed at the equatorial plane increases with enhancing convection while the overall flow direction does not change significantly, a result of enhancement in both the earthward electric drift and azimuthal diamagnetic drift. The equatorial magnetic field strength decreases more in the near-Earth plasma sheet than at larger radial distances as DFPC increases, resulting in an increasing flat radial profile with enhancing convection. The feedbacks from diamagnetic drift and magnetic fields to increasing convection are found to restrain the pressure increase. Based on the good agreement between our results and observations at moderate activity, our magnetic field indicates the plasma and magnetic field in the plasma sheet can be in a state far from possible force balance inconsistency during periods of moderately enhanced convection. A scale analysis of our results shows that the frozen-in condition  $E = -v \cdot \nabla B$  is not valid in the inner plasma sheet for moderate activity.

**GAI.06/08P/A02-006** **1545**

**MAGNETOSPHERIC CONVECTION IN MHD SIMULATIONS AND THE INFLATION OF THE INNER MAGNETOSPHERE DURING STRONG, STEADY SOLAR WIND DRIVING**

Ramon E. LOPEZ<sup>1</sup>, Michael J. WILTBERGER<sup>2</sup> (<sup>1</sup>Department of Physics, University of Texas at El Paso, <sup>2</sup>NCAR/HAO)

The coupling between the inner and outer magnetosphere during periods of strong steady driving by the solar wind is a basic problem in magnetospheric physics. A fundamental issue that arises is how steady, adiabatic magnetospheric convection can occur when the consequence would appear to be either physically unrealistic plasma pressures in the inner magnetosphere, or the development of deep Bz minima that would lead to substorms, and hence unsteady convection. Our studies using the Lyon-Fedder-Mobarry global MHD simulation indicates that part of the solution is that the inner magnetosphere is inflated during such steady (or quasi-steady) convection periods so that the resulting compression of plasma as it convects into the inner magnetosphere is limited. We will present the results of those studies, along with a comparison to observations in order to validate the results of the simulations.

**GAI.06/08P/A02-007** **Invited** **1615**

**THE EARTH'S RADIATION BELTS: SOLAR WIND, MAGNETOTAIL AND ATMOSPHERIC CONNECTIONS**

Daniel N. BAKER (Laboratory for Atmospheric and Space Physics)

The time of solar (sunspot) maximum is characterized by frequent solar transient events and coronal mass ejections (CMEs). These aperiodic disturbances can cause very powerful geomagnetic storms (if the solar outputs strike the Earth). On the other hand, during the approach to sunspot minimum, the solar corona is characterized by large coronal holes that are the source of powerful high-speed solar wind streams. Such streams also produce geomagnetic storms (which often are recurrent with a 27-day period). CME-driven storms, and even more so, high-speed stream-driven storms, produce powerful enhancements of relativistic electrons in the Earth's outer radiation belt. We present analysis of multiple long-term data sets including those from SAMPEX, POLAR, GOES, and other radiation belt-monitoring missions. We discuss the highly dynamic variability of the radiation belts and we show how this variability relates to solar wind inputs and plasma sheet source populations. We also consider the precipitation loss of radiation belt electrons and the subsequent effects in the Earth's upper and middle atmosphere.

**GAI.06/08P/A02-008** **1640**

**RELATIVISTIC ELECTRON INCREASE AND LOSS DEPENDING ON OTHER PARTICLE POPULATION, GEOMAGNETIC ACTIVITY AND MAGNETOSPHERIC CONVECTION**

Takahiro OBARA<sup>1</sup>, Yoshizumi MIYOSHIF<sup>2</sup>, Akira MORIOKA<sup>2</sup> (<sup>1</sup>CRL, <sup>2</sup>PPARC, Tohoku University)

Geomagnetic storm is the most dramatic interval in which particle energization takes place greatly in the inner magnetosphere. With the start of the geomagnetic storm relativistic electrons in the outer radiation belt disappears. During the recovery phase of the geomagnetic storm the outer radiation belt is filled with plenty of relativistic electrons, which sometimes exceed pre-storm level. We have investigated outer radiation belt by means of Akebono satellite over 14 years and following results were obtained. 1) Loss of relativistic electrons during the main phase of the geomagnetic storm was due to the enhancement of the magnetospheric convection as well as the precipitation into the atmosphere. 2) Location of the outer belt was coinciding with plasma pause location and both locations had a strong dependence on the magnetic activity. 3) Sufficient supply of intermediate-energy electrons from the plasma sheet was made during and after storm main phase, and these electrons were accelerated up to the relativistic energy range during the storm recovery phase. 4) Increase in the intensity of outer belt electrons strongly depends on the magnetic activity during the storm recovery phase. Possible candidates for the acceleration would be chorus emissions. 5) In the super storm, a new belt was created in so-called slot region, which sometimes persisted more than months. Only the betatron effect accelerated electrons and no additional acceleration was observed with the lack of plasma wave activities in the vicinity of the new belt region.

**GAI.06/08P/A02-009** **1655**

**VARIATIONS OF ENERGETIC ELECTRON FLUXES AND MAGNETIC FIELD IN THE OUTER RADIATION BELT DURING MAGNETIC STORMS**

Masao NAKAMURA, Hitoshi MATSUOKA, Hideki KOSHISHI, Kiyokazu KOGA, Haruhisa MATSUMOTO, Tateo GOKA (Space Environment Measurement Engineering Group, Office of R&D, National Space Development Agency of Japan)

We have investigated energetic electron flux variations (> 0.4 MeV) and the magnetic field in the outer radiation belt obtained from the Standard Dose Monitor (SDOM) and the MAGnetoMeter (MAM) of the Space Environment Data Acquisition equipment (SEDA) onboard Tsubasa (Mission Demonstration Test Satellite (MDS)-1) launched on February 4, 2002. Since Tsubasa operates in geostationary transfer orbit (GTO), it has provided a rare opportunity for directly observing near-equatorial radiation belt plasma particles and the magnetic field during magnetic storms. Energetic electrons in the outer radiation belt are important contributors to the total radiation dose deposited on lightly-shielded electronics on board spacecraft in high-altitude orbits, and are known to display drastic flux variability associated with magnetic storms and high-speed solar wind streams. Sharp drops and subsequent slower recoveries that occur in the energetic electron flux in the outer radiation belt during magnetic storms are linked respectively to typical variations of the magnetic field. These observations could shed light on possible mechanisms for the depletion and subsequent recovery and/or build-up of energetic electrons in the outer radiation belt.

**GAI.06/08P/A02-010** **1710**

**MAGNETIC FIELD VARIATIONS AT GEOSYNCHRONOUS ORBIT AND THEIR RELATIONS TO THE RELATIVISTIC ELECTRON DYNAMICS**

Tsutomu NAGATSUMA, Takahiro OBARA (Applied Research and Standards Division, Communications Research Laboratory)

We have examined the characteristics of magnetic field variations at geosynchronous orbit (GEO) and its relations to the relativistic electron dynamics using magnetic field and particle data from GOES satellites located at different geomagnetic latitudes, and solar wind data from Wind and ACE satellites. The results of our data analysis suggest that the magnetic field variations at GEO strongly depend on the dynamic pressure of solar wind and pressure corrected Dst index (Dst\*). Dst\* dependence shows some difference between the cases of IMF Bz positive and negative. The Dst\* dependences of magnetic field variations derived from two different magnetic latitudes suggest that these magnetic field variations can be explained by the existence of equivalent westward current beyond the GEO. This means that magnetic field structure during storm time is highly stretched. Enhancement of the dynamic pressure also stretches magnetic field structure in the tail region. The flux of relativistic electrons at GEO drops off under the highly stretched magnetic field configuration. The timing of this drop off sometimes differ between the two GOES satellites. This difference indicates that the flux drop off start from the distant L-shells. The signature of the rapid drop off is often seen in the dusk sector. These suggest that the non-adiabatic loss mechanism is significant for the relativistic electron dynamics at GEO.

**GAI.06/08P/A02-011** **1725**

**VARIATION OF RADIATION BELT ELECTRONS AND O+ IONS OBSERVED BY FAST AT LOW LATITUDES DURING MAGNETIC STORMS**

K. SEKI<sup>1</sup>, R.C. ELPHIC<sup>2</sup>, M.F. THOMSEN<sup>3</sup>, G.D. REEVES<sup>4</sup>, J.P. MCFADDEN<sup>5</sup>, J.W. BONNELL<sup>6</sup>, E.J. LUND<sup>7</sup>, M. HIRAHARA<sup>8</sup> (<sup>1</sup>Solar-Terrestrial Environment Laboratory, Nagoya University, Honohara 3-13, Toyokawa, Aichi 442-8507, JAPAN, <sup>2</sup>Los Alamos National Laboratory, NIS-1, MS466, Los Alamos, NM 87545, USA, <sup>3</sup>Space Science Laboratory, UC Berkeley, Berkeley, CA 94720-7450, USA, <sup>4</sup>Space Science Center, University of New Hampshire, Durham, NH 03824, USA,



Previous observations have shown that the O<sup>+</sup> ion population becomes an important contributor to the ring current during large magnetic storms. Its importance in terms of energy density increases with increasing geomagnetic activity. On the other hand, the processes responsible for this dramatic composition change of the ring current are still under debate. Enhanced polar outflows during geomagnetically active periods are considered to be responsible for the composition change. However, the link between the outflows and high-energy ring current is not clear due to the lack of low-energy ion observations in the inner magnetosphere inside GEO (R~6.6 Re). Penetration of radiation-belt electrons into instruments makes direct observations of low-energy ions difficult in the inner magnetosphere. A correction method to remove this background is also one of key elements needed for inner magnetospheric missions in the future. The Electrostatic Analyzer (ESA) onboard the FAST satellite had been operated in the mid-latitude regions above ~45 degrees for the past 4 years and observed ions below 30 keV. Radiation belt contamination is quite uniform in energy. Utilizing this feature, we developed an automated method to subtract the radiation contamination from ESA data and estimated the background counts and ion moments during several magnetic storms. Comparison between the estimated background and energetic particle data at GEO orbits indicates that electrons with energies of 0.5-1.5MeV are the main contributor to the background. The background count variation during a magnetic storm from April 11, 2001 indicates that the outer radiation belt electron fluxes decreased dramatically during the storm main phase and recovered from the inner L shells (ILAT~53-55 degrees) during the rapid recovery phase. Finally, the peak flux of the penetrating population moved to higher latitudes, near to its pre-storm position. The data after the background correction enable us to monitor behavior of low-energy (<30 keV) ions as a function of ILAT in a particular MLT range. For example, O<sup>+</sup> ions appeared in the inner magnetosphere at the beginning of the April 11, 2001 storm and became the major ion component in the inner magnetosphere during the storm. Preceding the development of the O<sup>+</sup> ring current, large numbers of O<sup>+</sup> ions comprising multiple energy bands below 12 keV were observed at low latitudes (50-60 degrees). The ionospheric O<sup>+</sup> are transported to the inner magnetosphere during the storm, and the observation suggests that it contributes, at least partially, to the O<sup>+</sup> ring current during the large storm. On the basis of these observations, the supply mechanisms of O<sup>+</sup> ions to the storm-time ring current will be discussed.

**GAIII.06/08P/A02-012** Invited **1740**

**DYNAMICS OF LOWER-ENERGY (30-250 KEV) PROTONS IN THE INNER MAGNETOSPHERE**

Akira MORIOKA<sup>1</sup>, Yoshizumi MIYOSHI<sup>1</sup>, Yo-ichi MATSUMOTO<sup>1</sup>, Hiroaki MISAWA<sup>1</sup>, Fuminori TSUCHIYA<sup>1</sup>, Takahiro OBARA<sup>2</sup>, Tsutomu NAGATSUMA<sup>2</sup> (<sup>1</sup>Planetary Plasma and Atmospheric Research Center, Tohoku University, <sup>2</sup>Communications Research Laboratory)

Dynamics of lower-energy protons in the energy range from 30 to 250 keV was studied using data from NOAA satellites. During the main phase of magnetic storms, the spiky enhancement of proton flux in the energy range from 30 - 80 keV was always detected deep in the inner zone almost simultaneously with increase in the outer magnetosphere, and its lower boundary was less than L = 2 during large storms. The flux enhancement usually reached up to 100 folds at around L=2 and 1000 folds at around L=3.5. The time profile of the proton flux variation was quite similar to that of Dst. These observations suggest that ring current protons are injected not only in the outer region but also into the bottom region of the radiation belt. After the main phase, the spiky enhancement disappeared and an "inner-belt like" proton structure remained in the region around L=2. The structure was more clearly seen in the energy range from 80- 250 keV and seemed to be diffusing from the main proton belt to lower L shells during the recovery phase in the L-t diagram. The location of the "inner-belt like" structure was slightly different from that of the electron inner belt; proton peak was located near L=2.2 - 2.5, and the electron peak was near L=2.0 - 2.4. This newly observed proton belt might necessitate the modification of the proton dynamics in the lower L regions.

**GAIII.07**

**WHAT IS THE ROLE OF NON-LINEAR PROCESSES AND COMPLEX SYSTEM DYNAMICS IN DETERMINING MAGNETOSPHERIC BEHAVIOR?**

Location: Site A, Room 14

**Wednesday, July 9 AM**  
Presiding Chair: G.S. Lakhina

**GAIII.07/09A/A14-001** **0900**

**COMPLEXITY AND FSOC IN SPACE PLASMAS**

Tom T.S. CHANG (Center for Space Research, Massachusetts Institute of Technology)

Bak et al. suggested in 1987 that nonequilibrium stochastic systems have a general tendency to organize themselves into complex states similar (but not identical) to the static critical states in equilibrium phase transitions. They dubbed such phenomena as self-organized criticality (SOC). Since then the topics of complexity and SOC have become hot topics in nearly every field of science. The first definitive observation that provided convincing evidence indicating certain turbulent space plasma processes are in states of complexity and SOC was the discovery of the apparent power-law probability distribution of solar flare intensities. Recent statistical studies of complexity in space plasmas came from the AE index, UVI auroral imagery, and in-situ measurements in the solar wind and the Earth's magnetotail. In this review, we describe the physics and a companion theory of dynamical complexity and forced and/or self-organized criticality (FSOC) for space plasma systems far from equilibrium. We demonstrate that the sporadic and localized interactions of magnetic coherent structures are the origin of complexity and FSOC. Such interactions generate the anomalous transport, diffusion, acceleration, and evolution of the macroscopic states of the overall dynamical system. Several illustrative examples related to the magnetospheric system are considered. These include: the dynamical multi- and cross-scale interactions of the macro- and kinetic coherent structures in a sheared magnetic field, the Alfvénic flux tubes and coexisting propagating and non-propagating fluctuations in the auroral turbulence region, the onset of fluctuation-induced nonlinear instabilities that can lead to magnetic reconfigurations, and the resonant energization of charged particles by non-propagating fluctuations.

**GAIII.07/09A/A14-002** **0930**

**ANALYSIS OF GEOMAGNETIC STORMS USING FRACTAL THEORY**

Chandrasekar ENAMUNDRAM<sup>1</sup>, Mohan N. L.<sup>2</sup> (<sup>1</sup>Indian Institute of Geomagnetism, Dr. Nanabhoj Moos Road, Colaba, Mumbai - 400 005, India., <sup>2</sup>Centre of Exploration Geophysics, Osmania University, Hyderabad - 500 007, India.)

Geomagnetic storms exhibit a deterministic chaotic phenomenon. Fractal theory is a unique tool for better understanding of such chaotic phenomena in a broader perspective. In an attempt to characterize and scale the different phases of geomagnetic storms, both the sudden and gradual commencement storms having well-defined space-time characteristics have been selected for the present analysis. The selected data sets, corresponding to the solar active year, 2001, have been procured from Indian magnetic observatories. The Mellin-Fourier transform (MFT) technique is employed to formulate a mathematical model for chaotic nature of geomagnetic storms and determine the Fractal scales for different phases of geomagnetic storms. The MFT technique facilitates to determine unified values of scale parameters corresponding to different phases of geomagnetic storms. Further, to estimate global scale value corresponding to each of the well-defined phases of geomagnetic storms, the Lyapunov exponents are also computed. The results of this analysis will be discussed in the present paper.

**GAIII.07/09A/A14-003** **0950**

**SELF-ORGANIZED CRITICALITY IN EARTH'S MAGNETOTAIL DYNAMICS AND ITS IMPLICATIONS FOR SUBSTORM ONSET**

Vadim M. URITSKY<sup>1</sup>, Alex J. KLIMAS<sup>2</sup>, Dimitris VASSILIADIS<sup>3</sup>, Daniel M. BAKER<sup>4</sup> (<sup>1</sup>St. Petersburg State University, St. Petersburg, Russia, <sup>2</sup>NASA / Goddard Space Flight Center, <sup>3</sup>USRA / Goddard Space Flight Center, <sup>4</sup>LASP, University of Colorado, Boulder)

A recent analysis due to Uritsky et al. [JGR, 2002] of auroral emission bright spots in POLAR UVI images has revealed a remarkable set of scale-free power-law avalanche distributions for several of the spots' physical characteristics. The most straightforward and, at present, sole explanation for these distributions is that localized reconnection in the plasma sheet leads to a self-organized critical avalanching system that is scale-free over a broad range of scales. This analysis will be reviewed and a more recent study of the spreading dynamics of the auroral bright spots will be discussed. It will be shown that the spreading dynamics provides further evidence of self-organized criticality (SOC) in the plasma sheet. Based on these results plus an additional ongoing analysis of the UVI data, a new scenario for substorm onset will be proposed.

**GAIII.07/09A/A14-004** **1030**

**THE STATE TRANSITION MODEL OF THE SUBSTORM ONSET**

Takashi TANAKA (Department of earth and planetary science, Kyushu University)

The onset mechanism of substorm is investigated from a resistive magnetohydrodynamic (MHD) simulation under the assumption that the magnetotail becomes more diffusive as it goes further downtail. The calculation started from a stationary solution under a northward interplanetary magnetic field (IMF) condition with non-zero IMF By. After a southward turning of the IMF, the simulation results show the progress of plasma sheet thinning in the magnetosphere, together with increases in the size of the auroral oval and in the magnitude of the field-aligned current (FAC) in the polar ionosphere. This thinning is promoted by the drain of closed flux from the plasma sheet occurring under the enhanced convection. In this stage, the reconnection process in the plasma sheet which determines the flux piling up from the midtail to the near-earth plasma sheet is not so effective, since it is still controlled by the remnant of northward IMF. The substorm onset occurs as an abrupt change of pressure distribution in the near-earth plasma sheet and an intrusion of convection flow into the inner magnetosphere. After the onset, the simulation results reproduce both the dipolarization in the near-earth tail and the near-earth neutral line (NENL) at the midtail, together with plasma injection into the inner magnetosphere and an enhancement of the nightside FAC. Dipolarization is hastened by a northward re-turning of the IMF indicating that it is triggered off through the breakdown of dynamic stress balance in the near-tail plasma sheet established under the convection-controlling tail thinning. It is concluded that the direct cause of the onset is the dipolarization, which is not a mere pile up of the flux ejected from the NENL but the state (phase-space) transition of the convection system from a thinned state to a dipolarized state associated with a self-organizing criticality.

**GAIII.07/09A/A14-005** Invited **1100**

**SELF-ORGANIZED TURBULENCE, FRACTIONAL KINETIC PROCESSES, AND POWER-LAW FLUCTUATION SPECTRA IN THE EARTH'S STRETCHED MAGNETOTAIL**

Alexander V. MILOVANOV, Lev M. ZELNYI (Department of Space Plasma Physics, Space Research Institute)

The focus of the present study is on the structural stability properties of the Earth's stretched and thinned magnetotail, meaning vanishing component of the normal field and unmagnetized particles (ions) in the current sheet plane. Such conditions (that are the case in the distant tail, as well as near-Earth tail at the substorm growth phase) offer a fertile playground for kinetic instabilities driving turbulent dynamics of particles and fields. The multiscale interaction of nonlinear relaxation processes and self-organization mechanisms operating in the turbulent media customarily results in a transition to a nonequilibrium (quasi)stationary state (NESS) dominated by long-range correlations in space and time. We argue that the inherent dynamics of the NESS is manifested in the low frequency power law fluctuation spectrum 1/f. At higher frequencies, the spectrum has a steeper shape with exponent ~-7/3 and reflects the structural characteristics of the magnetotail turbulence. A self-consistent kinetic description of turbulent plasma and fields at the NESS is proposed. Our models based on a nonlinear fractional kinetic equation which helps include the marginal correlation (memory) effects on the microscopic particle dynamics in the magnetotail plasma sheet. We find that the particle energy distribution function contains a power law nonthermal tail with the slope ranging between -6 and -7. The formation of the tail is justified from thermodynamical arguments involving the issue of generalized entropy in the Tsallis sense. The results obtained are in close agreement with the spacecraft observations on the Earth's magnetotail.

**GAIII.07/09A/A14-006** **1130**

**GLOBAL AND MULTI-SCALE DYNAMICS OF THE MAGNETOSPHERE**

A. Surjalal SHARMA, Alexander Y. UKHORSKIY, Mikhail I. SITNOV (University of Maryland)

The magnetosphere is a large scale natural system driven by the turbulent solar wind, and exhibits both global and multi-scale characteristics. The global features arise mainly from the nonlinear nature of the plasma and the electrodynamic coupling between its

different parts. On the other hand, its open and driven nature is the source of many multiscale features. The magnetospheric substorms, which can be characterized as nonequilibrium transitions, exhibit both global and multi-scale behavior. The global nature of substorms is evident in many observations as well as simulations and has been quantified from time series data using nonlinear dynamical techniques in terms of low dimensional behavior. However, there are significant deviations from the low-dimensional picture and these multi-scale characteristics are evident in the power law nature of many variables. These two aspects of the magnetospheric dynamics can be unified in the framework of nonequilibrium phase transitions. The global dynamics, obtained by an averaging of the dynamical trajectories, is amenable to a mean field description and is represented by a first order phase transition. The multi-scale substorm activity resembles second-order phase transitions and is characterized by a critical exponent. This description of the nonequilibrium transitions in the magnetosphere provides a new approach in the study of global and multi-scale processes, and yields a basis for developing improved forecasting tools. The global features are predicted dynamically using a mean field approach and the multi-scale features, which lead to deviations from the dynamical predictions, are characterized by conditional probabilities computed using the solar wind input and the corresponding magnetospheric response.

**GAI07.09/A14-007 1150**

**A MINIMAL SUBSTORM MODEL THAT EXPLAINS THE OBSERVED STATISTICAL DISTRIBUTION OF TIMES BETWEEN SUBSTORMS**

Mervyn Paul FREEMAN (British Antarctic Survey, Cambridge, U.K.)

We propose a minimal model for the evolution of the global dynamical state of the magnetotail during the substorm, involving only three simple rules. Rather than concentrate on the physical nature of the substorm instability, we consider the instability in a more general sense. The substorm is modelled as an integrate-and-fire process in which integrated solar wind power input during the substorm growth phase is eventually released in whole or in part by a firing mechanism at substorm onset. We propose that this nonlinear property is because the magnetosphere is prevented from moving to the lowest energy state appropriate to the prevailing solar wind boundary condition by some configurational constraint involving the magnetic field. When this configurational constraint is overcome, a substorm occurs and the magnetosphere moves towards the minimum energy state appropriate for that time. When driven by a real solar wind power input, the minimal substorm model produces a probability distribution of times between substorm onsets that compares favourably with the distribution of 1001 inter-substorm intervals found by Borovsky et al. from observation. We discuss these results in terms of the distributions of first-passage times from the general class of integrate-and-fire processes, and propose possible further tests of the model.

**GAI07.09/A14-008 1210**

**MAGNETOSPHERIC DYNAMICS DRIVEN BY SOLAR WIND PRESSURE PULSE: SPATIO-TEMPORAL STRUCTURE FROM THE AVERAGE MUTUAL INFORMATION**

A. Surjalal SHARMA<sup>1</sup>, J. EDWARDS<sup>1</sup>, M.I. SITNOV<sup>1</sup>, Y. KAMIDE<sup>2</sup>, B.T. TSURUTANI<sup>1</sup> (<sup>1</sup>University of Maryland, <sup>2</sup>Solar Terrestrial Environment Laboratory, <sup>3</sup>Jet Propulsion Laboratory)

The magnetosphere exhibit complex behavior during substorms and such behavior have been widely studied using the well-known auroral electrojet indices. However, these indices suffer from the limitations due to the loss of information associated their definitions. The time scales of magnetospheric dynamics are studied using the high resolution time series data of the AL index and of the magnetic field data from the high-latitude magnetometers. Considering the inherent nonlinearity of the magnetosphere it is important to use measures that are appropriate for nonlinear systems. The average mutual information (AMI) of a nonlinear dynamical system yields the coherence or memory time before dynamical information is lost and are computed from the time series data. Considering the differences in the magnetospheric dynamics during quiet and active periods, the AMI for these periods are computed from the AL and the magnetic field measurements at 11 magnetometer stations. For active periods the coherence time for AL is less than 10 min and for the individual stations it ranges from 10 min to 30 min, thus showing considerable loss of information when AL is used instead of the magnetometer data. Studies of the magnetospheric response to sudden changes in the solar wind dynamic pressure show dominant features of the spatio-temporal structure not captured by linear functions.

Wednesday, July 9 PM  
Presiding Chair: Y. Omura

**GAI07.09/A14-001 1400**

**DOUBLE LAYERS AND THEIR ROLES IN MAGNETOSPHERIC PLASMA TURBULENCE**

Nagendra SINGH (University of Alabama in Huntsville)

Double layers provide a universal mechanism for supporting electric fields parallel to the ambient magnetic field in collisionless plasmas. Depending on the application and the plasma processes, the double layers could be strong or weak. Strong double layers produce energetic electrons and ions, like in the auroral plasmas. The electron and ion beams accelerated by the strong double layers generate a host of plasma instabilities. Nonlinear plasma structures resulting from such instabilities are now commonly measured by satellites; electron and ion phase-space holes are prime examples of such structures. In turn, these spatially localized laminar plasma structures radiate plasma waves. These waves are eventually absorbed by the thermal (low energy) plasmas, affecting the dissipation of the energy supporting the double layer. The generation of VLF saucers in the auroral plasma is an example of this chain of processes. Weak double layers are consequences of plasma instabilities (Buneman and ion acoustic) driven by currents in the plasma. The instabilities in their nonlinear stage generate density cavities, and the charging of the cavities gives rise to the weak double layers. When parallel currents in the plasma encounter naturally occurring plasma depletions or cavities, the charging leads to a spontaneous double layer formation and acceleration of charged particles, providing a mechanism for dissipating the electromagnetic energy associated with the current. This mechanism may be operative in dissipating narrow Alfvén wave structures, which carry a significant level of current.

**GAI07.09/A14-002 1430**

**NONLINEAR ELECTRON ACOUSTIC WAVES WITH NON-THERMAL DISTRIBUTION OF ELECTRONS**

Satyavir SINGH, Gurbax S. LAKHINA (Indian Institute of Geomagnetism)

Nonlinear propagation of electron-acoustic waves is studied in an unmagnetized, three-component plasma consisting of non-thermally distributed electrons, fluid cold electrons and ions. The analysis employs Sagdeev pseudo-potential techniques and is valid for any

arbitrary amplitude of the wave. The soliton amplitude and width are numerically obtained and are compared with the spiky structures observed by several spacecrafts in the Earth's magnetosphere.

1. GAI07.02. What is the Role of the Non-linear Processes and Complex System
2. Dynamics in Determining Magnetospheric Behavior
3. Nonlinear Phenomena, Electrostatic Structures
4. 016240, Dr. Satyavir Singh, Indian Institute of Geomagnetism, Dr. Nanabhai Moos Marg, Colaba Mumbai-400005, INDIA, Tel: 091-22-22189569, Fax: 091-22-22189568, E-mail: satyavir@iig.res.in. O6. PC/OH7. NO8. Satyavir Singh: YES and G.S. Lakhina: NO9. NONE

**GAI07.09/A14-003 1450**

**ELECTRON HOLES AND DOUBLE LAYER-LIKE STRUCTURES OBSERVED ALONG THE CLUSTER ORBIT: CHARACTERISTICS AND INFLUENCE OF THE MAGNETIC FIELD ON THEIR AMPLITUDES**

Jolene S. PICKETT, Li-Jen CHEN, Scott W. KAHLER (Dept. of Physics and Astronomy, The University of Iowa)

We present examples of isolated electrostatic structures observed by the four Cluster Wideband (WBD) Plasma Wave Receivers at various locations in the Cluster orbit. These locations include the magnetosphere at 5-8 Re along magnetic field lines that map to the auroral zone, the magnetosheath just downstream of the bow shock at 15-19 Re, the plasma sheet boundary layer at 17-19 Re and other boundaries crossed by Cluster. These electrostatic structures appear in the WBD waveform data in two primary forms: 1) as bipolar pulses with durations on the order of tens up to hundreds of microseconds and amplitudes of hundredths up to a few mV/m, and are interpreted as electron holes, 2) as continuous waveforms consisting of bipolar pulses immediately followed by a half-sinusoid in the direction of the initial pulse, interpreted as double layer-like structures. We provide the typical characteristics of these structures in the various regions in which they are encountered, i.e., amplitude and time duration, and the results of a cross correlation study, the purpose of which was to identify electron holes that have propagated from one spacecraft to another. Finally, we compare the observed characteristics of the electron holes to the theory of BGK electron solitary waves (electron holes) and the influence of the local magnetic field on their amplitudes.

**GAI07.09/A14-004 1510**

**PARTICLE SIMULATIONS OF ELECTROMAGNETIC EMISSIONS FROM ELECTROSTATIC SOLITARY WAVES**

Takayuki UMEDA, Yoshiharu OMURA, Hiroshi MATSUMOTO (Radio Science Center for Space and Atmosphere, Kyoto University)

We present particle simulations of electrostatic solitary waves (ESW) observed by the GEOTAIL spacecraft and recent spacecraft in the Earth's magnetosphere. Recent particle simulations have demonstrated that ESW are Bernstein-Greene-Kruskal (BGK) electron holes formed through nonlinear evolution of electron beam instabilities. Since an electron hole is coherent electrostatic potential structure, electron beam instabilities were conventionally studied by electrostatic particle simulations. However, the FAST spacecraft observed electromagnetic field signatures associated with ESW. To study interaction between coherent electrostatic potential and electromagnetic waves, we extend the previous electrostatic particle simulations to electromagnetic particle simulations. In a two-dimensional simulation, we found that multi-dimensional electron holes are accompanied by magnetic field components. On the other hand, one-dimensional electron holes do not have any electromagnetic signatures. Two-dimensional electron holes have perpendicular electrostatic fields  $E_y$ . Electrons lead to  $E_y \times B_z$  drift in the z direction, and the current density  $J_z$  is enhanced at perpendicular edges of two-dimensional electron holes. Magnetic fields  $B_x$  and  $B_y$  are enhanced around the current  $J_z$ . However, the current structure excited by the  $E_y \times B_z$  drift of electrons is not closed in the two-dimensional simulation. In the real space plasma, we expect that the current structure may form a loop along the perpendicular edge of a multi-dimensional electron hole. Such a closed current structure will be studied by a three-dimensional simulation. We also study electromagnetic emissions from such moving current loops.

**GAI07.09/A14-005 1530**

**GENERATION OF ELECTRON HOLES BY MAGNETIC TURBULENCE ON AURORAL FIELD LINES**

Gurbax S. LAKHINA<sup>1</sup>, Bruce T. TSURUTANI<sup>2</sup>, Jolene S. PICKETT<sup>3</sup> (<sup>1</sup>Indian Institute of Geomagnetism, Mumbai, India, <sup>2</sup>Jet Propulsion Laboratory, California Institute of Technology, Pasadena, California, USA, <sup>3</sup>Department of Physics and Astronomy, University of Iowa, Iowa City, IA, USA)

Electric bipolar pulses (electron holes) have been observed on auroral zone field lines at various altitudes ranging from close to the ionosphere, to magnetopause low-latitude boundary layer (LLBL) and cusp on the dayside, and to plasma sheet boundary layer on the nightside. High-resolution wave magnetic component data from Polar spacecraft show "magnetic noise bursts", Alfvén waves, and large amplitude ( $\sim \pm 14$  nT peak-to-peak) obliquely propagating proton cyclotron waves. On the other hand, high-resolution data of the electric field components indicate three types of intense electric signals, namely, solitary structures (with bipolar, monopolar and offset bipolar pulses), lower hybrid waves, and narrow-band waves near electron plasma frequency (most likely the upper hybrid resonance waves due to their perpendicular polarization). It is proposed that obliquely propagating nonlinear Alfvén and proton cyclotron waves could accelerate electrons parallel to the magnetic field. These field aligned electron beams could act as free energy source for several electron beam instabilities leading to the formation of electron holes.

**GAI07.09/A14-006 1610**

**CLUSTER OBSERVATIONS OF DYNAMIC PHENOMENA NEAR THE BOW SHOCK AND IN THE MAGNETOSHEATH**

Andre BALOGH, Timothy HORNBURY, Elizabeth LUCEK (Imperial College London)

The complexity of many magnetospheric phenomena at small scales is highlighted by the four-point observations made by the Cluster mission. In many cases, the observed phenomena are dominated by (ion and/or electron) dynamics at scales comparable or even smaller than the typical range of spacecraft separations between 100 km and 5000 km. This is the case at the bow shock and in the magnetosheath. In this paper, we present typical examples of the dynamic behaviour of the quasi-parallel bow shock and observations of Hot Flow Anomalies associated with the interaction of the quasi-perpendicular bow shock with discontinuities in the solar wind. In addition, we review the Cluster observations that have led to the determination of the anisotropic structure of mirror-mode waves in the



magnetosheath. We conclude by an overview of how the Cluster observations are capable of constraining the dynamic scale of phenomena and also the limitations due to the finite range (too small or too large) of the observations.

**GAI11.07/09P/A14-007** **1640**

**ELECTRON HEATING PROCESSES AT QUASI-PERPENDICULAR SHOCKS**

Tooru SUGIYAMA<sup>1</sup>, Masaki FUJIMOTO<sup>2</sup>, Yoshiharu OMURA<sup>1</sup>, Hiroshi MATSUMOTO<sup>1</sup> (<sup>1</sup>Radio Science Center for Space and Atmosphere, Univ. of Kyoto, <sup>2</sup>Earth and Planetary Sciences, Tokyo Institute of Technology)

The role of micro-instabilities in dissipation process in collisionless quasi-perpendicular shocks is investigated by a full-particle numerical code. It is well-known that an anomalous dissipation is necessary in the super-critical Mach number shock. The reflected ions are mainly considered to produce the dissipation. Recently, the contribution of electrons is also well discussed and many waves are listed-up for the candidate of the dissipation process: ion acoustic waves, upper hybrid waves, whistler waves, and so on. In the present study, we discuss the variation of the wave types depends on both the shock parameters (shock Mach number, upstream plasma beta) and time. We have taken a low mass ratio between ion and electron. This assumption allows us to see a strong interaction between ions and electrons even though the shock Mach number is not so large ( $<15$ ). Here, the reflected ions again act as an important role. The instability between the incoming ions and the reflected ions excites electrostatic waves in the ramp region. When the amplitude of the electrostatic wave is large, the incoming electrons are also reflected. This is the case that the Mach number is large, because the growth rate of the instability is large. The reflected electrons are also accelerated by the upstream motional electric field as reflected ions are accelerated. We can see another kinetic effect for electron heating process at collisionless shocks which is different from resonance interaction between particles and waves.

**GAI11.07/09P/A14-008** **1700**

**ORIGIN OF PHASE COHERENCE AMONG MHD WAVES IN THE SOLAR WIND**

Tohru HADA<sup>1</sup>, Daiki KOGA<sup>1</sup>, Eiko YAMAMOTO<sup>2</sup> (<sup>1</sup>E.S.S.T., Kyushu University, Fukuoka, Japan, <sup>2</sup>N.A.S.D.A., Ibaraki, Japan)

Large amplitude MHD waves are ubiquitous in the solar wind. Nonlinear interactions between the MHD waves are likely to produce finite correlation among the wave phases. For discussions of various transport processes of energetic particles, it is fundamentally important to determine whether the wave phases are randomly distributed (as assumed in quasi-linear theories) or they have a finite coherence. By comparing structure functions of original data and its phase-shuffled surrogates, we analyzed Geotail magnetic field data to evaluate the phase coherence among the MHD waves in the earth's foreshock region. We show that the correlation of wave phases does exist, indicating that the nonlinear interactions between the waves is in progress. Furthermore, by applying a wavelet filtering technique, we find that, although the turbulence consists of waves with a wide range of plasma rest frame frequencies, only the wave modes whose frequencies were lower than the ion gyrofrequency are responsible for generating the phase coherence.

**GAI11.07/09P/A14-009** **1720**

**CAUSAL THERMODYNAMICS OF MAGNETOFLUIDS**

Tadas K. NAKAMURA (Center for Arts and Sciences, Fukui Prefectural University)

Large scale phenomena in the magnetosphere are often successfully formulated with the MHD theory with phenomenological dissipation terms. However, this kind of dissipation terms are known to be inconsistent theoretically. For example, the heat conduction calculated with the second-order spatial derivative would result in infinite propagation speed. A controversy has arisen since 1970s on the dissipation terms of fluid dynamics in connection with the relativity. Straight-forward generalization of the Navier-Stokes theory would result in a pathological unrealistic instability, in addition to the infinite propagation speed mentioned above. There have been proposed so called "Casual Thermodynamics" to overcome these difficulties, however, there are several different theories in Casual Thermodynamics, and the final solution is still yet to come. The present paper propose a systematic way to handle the dissipation mechanisms based on the definition of relativistic thermodynamical quantities by *van-Kampen* (Phys. Rev. 1968). Using four-vector inverse temperature, we can regard the heat conduction and viscosity as components of a same tensor. Electromagnetic dissipation can be treated in the same way. Possible applications to the magnetospheric physics will be briefly discussed in the presentation.

**GAI11.07/09P/A14-010** **1740**

**FULLY NONLINEAR ANALYSIS OF AURORAL SOLITARY WAVES IN THE PRESENCE OF MAGNETIC FIELD**

Suktisama GHOSH, Gurbax S. LAKHINA (Plasma Group, Indian Institute of Geomagnetism)

Over the past two decades, several spacecraft observations have revealed solitary wave structures in different regions of magnetospheres. Besides low altitude rarefactive ion solitary waves, subsequent satellite observations have also reported fast moving electron solitary waves with positive potentials at higher altitudes of the auroral region. Though there were extensive analytical and numerical investigations, little attention has been given so far to explain their width-amplitude characteristics. Recent FAST and POLAR observations have showed that for both ion and electron solitary waves, the width tends to increase with increasing amplitude. A small amplitude theory thus remains inadequate for the process while a complete theory of large amplitude solitary waves is still lacking. It is proposed that the observed increase in the width with increasing amplitude is essentially an intrinsic characteristics of large amplitude rarefactive ion (electron) acoustic solitary waves which differs qualitatively from its small amplitude limits. In the present work, a fully nonlinear approach is adopted for a two electron (ion) temperature magnetized plasma. The overall width-amplitude profiles for rarefactive ion (electron) acoustic solitary wave solutions in the presence of ion (electron) beams are investigated for different parameter ranges. The characteristics of the complete width-amplitude profile of a rarefactive ion acoustic solitary wave appears to be very much consistent over all the parameter ranges including unmagnetized as well as magnetized plasmas. A similar analysis is also applied for an electron acoustic solitary wave. The outcome of the analytical investigations is compared with recent space observations.

**GAI11.07-Posters**

**WHAT IS THE ROLE OF NON-LINEAR PROCESSES AND COMPLEX SYSTEM DYNAMICS IN DETERMINING MAGNETOSPHERIC BEHAVIOR?**

Location: Site D

Thursday, July 10 PM

**GAI11.07/10P/D-001** **Poster** **1400-105**

**PARTICLE DYNAMICS IN FULL PARTICLE SIMULATION OF SLOW WAVES**

DongSheng CAI<sup>1</sup>, Bertrand LEMBEGE<sup>2</sup> (<sup>1</sup>University of Tsukuba, <sup>2</sup>CETP/UVSQ)

Magnetohydrodynamic theory predicts that the slow shock pairs should be generated by magnetic reconnection in the Earth magnetotail. One question is focussed on conditions/mechanisms responsible for the survival time of such waves. For this purpose, kinetic and nonlinear effects of the slow waves dynamics are analyzed with the help of a 1-2/2-dimensional electromagnetic full particle code (1-D in x-space and 3-D in velocity space) with periodic boundary conditions. At the initial time of the simulation, the particles are loaded with sinusoidal density perturbation (30% of its background value) in x-space with consistent sinusoidal magnetic field in z; these perturbations are provided by results issued from MHD equations. Magnetic field and density profiles have opposite phase as a slow wave nature. In the present report, trajectories of preselected self-consistent electrons (in contrast with the test particle approach) have been analyzed in order to determine the slow shock reflection condition. The particle is accelerated in Vpara direction in the Tsteepening, PIC and saturated after Tsteepening, PIC. The particle Vperp1 and Vperp2 is oscillated in ion gyroperiod. The particle gains the energy Ekpara and Ekperp after Tsteepening, PIC.

**GAI11.07/10P/D-002** **Poster** **1400-106**

**NONLINEAR EVOLUTION OF MIRROR-MODE INSTABILITY**

B.-J. WANG, L.-N. HAU (Institute of Space Science, National Central University)

Linear theory has shown that the mirror instability criterion derived from the double-polytropic MHD model with  $\gamma_L = 2$  and  $\gamma_e = 0.5$  is the same as the one from the kinetic theory (Hau and Sonnerup, GRL, 20, 1763, 1993). In this study we investigate the nonlinear evolution of mirror instability that is solved numerically based on the nonlinear double-polytropic MHD and Hall MHD equations. The results show that an initial sinusoidal mirror wave will evolve into soliton-like structure with increased density and decreased magnetic field. The effect of Hall current may lead to dispersive multiple solitons with thickness of a few ion inertial lengths.

**GAI11.07/10P/D-003** **Poster** **1400-107**

**NONLINEAR EVOLUTION OF WAVE PARTICLE INTERACTION BY A PARTICLE-IN-CELL NUMERICAL CODE**

Manashi Na ROY, G.S. LAKHINA (Indian Institute of Geomagnetism)

A plasma system comprising electrons, protons and oxygen ions is investigated by a particle-in-cell code. The initial configuration is nine protons, four oxygen ions and equal number of electrons per cell. The simulation box is two dimensional with velocities of all the particles having three components. A magnetic field is applied along one direction. The mass ratio of oxygen to proton is assumed to be 400. Periodic boundary condition is applied. The initial distribution of the particles is assumed to be beam plasma for the oxygen ions and a part of the protons. The electron distribution is assumed to be Maxwellian with a finite temperature. This system is allowed to develop in time with different parameters like the ratio of the ion temperatures to the electron temperatures etc. The field configuration shows the development of the waves similar to the beam plasma instabilities. The distribution functions of the particles show considerable departure from their initial configurations. The nature of these waves will be discussed as function of various initial plasma parameters. As these waves grow with time we investigate the nature of the evolution of both the wave characteristics as well as the plasma distribution. The possibility of generation of any localised structures will be explored. The results will be applied to observations at the auroral and the plasmasheet regions of the magnetosphere.

**GAI11.07/10P/D-004** **Poster** **1400-108**

**SIMULATION STUDY ON GENERATION MECHANISM OF ELECTRON/ION HOLES IN SPACE PLASMAS**

Keisuke NINOMIYA, Yoshiharu OMURA, Hiroshi MATSUMOTO (RASC, Kyoto University)

In recent spacecraft observations, it has been found that a variety of coherent potential structures exist along magnetic field lines of various regions of the magnetosphere. We assume that some of coherent potential structures are electron holes and ion holes corresponding to positive solitary potentials and negative solitary potentials, respectively. We performed one-dimensional electrostatic particle simulations of the Buneman instability, which occurs when beams of electrons and ions have a relative drift velocity. We used the real ion/electron mass ratio and performed simulations with boundaries are periodic boundaries and open boundaries. We varied thermal velocities of electrons and ions, and found that nonlinear evolution are mainly classified into two potential structures. One is an electron hole, other one is an ion hole. It is also found that electron holes and ion holes coexist and interfere with each other under some conditions. In the present study we first calculated linear growth rates and phase velocities in order to study dependence of the instability on the thermal velocities of ions and electrons in detail. The difference of nonlinear evolutions depends not only on the thermal velocities of beams but also on the maximum growth rate and the phase velocity of the waves at the initial stage. Especially, the phase velocity is an important parameter which determines characteristics of interaction between the waves, electrons and ions. It affects the final states of nonlinear evolutions significantly. The electron holes are generated through coalescence of waves generated at the initial state. This mechanism is the same as found in a two-stream electron instability or bump-on-tail instability. On the other hand, the generation mechanism of ion holes is different from that of electron holes. At first, a double layer potential is formed at some local position in the system. A negative potential becomes gradually bigger at the boundary of the layer. Finally, the potential grows to trap ions, resulting in an ion hole in the velocity phase space of ions. The ion hole is unstable and disappears after a time. New double layer potential is generated at other local position after the disappearance, then an ion hole appears again. The process repeats in the simulation system. While the negative potential

exists, some electrons are reflected by the potential and excite a two-stream instability with non-reflected electron. We will present detail analyses of electron and ion dynamics related to the generation of double layers and ion holes.

**GAIII.07/10P/D-005** Poster **1400-109**

#### EVALUATION OF PHASE COHERENCE AMONG MHD WAVES

Daiki KOGA, Tohru HADA (E.S.S.T., Kyushu University, Fukuoka, Japan)

Large amplitude MHD waves are commonly found in the solar wind, in particular, in the earth's foreshock. The waves within this region exhibit various peculiar waveforms, suggesting that nonlinear interaction between the waves is in progress (e.g., SLAMs, shocklets, etc.). When we Fourier analyze such data, usually more emphasis is placed on the power spectrum than the phase distribution of wave modes, although the latter contains important information on nonlinear coupling between the eigenmodes (e.g., synchronization of phases). We have recently developed a method to quantitatively evaluate the phase coherence of a given time series data, by comparing structure functions of original data and its phase-shuffled surrogates. In this presentation we discuss critically some fundamental properties of this method, and show how one should determine such basic parameters used in the method as the data length for getting the optimum results. Furthermore, we discuss some extensions of the method, including the analysis of 2-dimensional data obtained by simulations.

**GAIII.07/10P/D-006** Poster **1400-110**

#### AURORAS DYNAMICS AS STRANGE ATTRACTOR MANIFESTATION

Victoria G. VASILYEVA (Institute of Cosmophysical Research and Aeronomy)

Large scale visual data and rather localized aurora video registrations demonstrate multi-scale, sporadic and localized structure. It allows to estimate statistical parameters of power law distributions for global disturbance scales, which were proposed in our ensemble interpretation of Kp-indexes (JUGG, 1999). It is shown that for increased auroral injections we are to differ the differential (spectral) duration which became shorter and integral one increasing versus of activity growth. There were resume this temporal parameter duality is set by non-linearity of disturbance nature caused by non-divisional unity of global injection power and just local lifetime acceleration of non-homogeneity. The statistical modulus defines the integral scales (durations) distributions. Ensemble applications respond to its universality at all in complex systems drawings according to Prigogin's presentation (2002). It independently brought to low-dimensional modeling and now is consonant with SOC-model. We can conclude that an ensemble application is fruitful from physical and instrumental point of views. Since the resonance conditions by means statistical modulus and an elementary (some ideal) substorm have been founded as matter intermediate state between two virtual states (ensembles), the auroral oval dynamics may be considered like strange attractor manifestation. The investigation is presented in accordance with percolation conceptual approach (L. Zelenyi, A. Milovanov, 2000), T. Chang's proposals and foundations (1992, 1999), representations of N. Watkins, S. Chapman, M. Freeman (2000). For part of global activities it looks like we can to unify equilibrium phase transition and topological one. It is possible with "dynamic factor-spectrum of fractals", if the fractal initiator is related to the driver, basic cycle of the dissipative system and defines the generalized function. Then underlying statistical consideration at all may satisfy dynamic symmetry approach.

**GAIII.07/10P/D-007** Poster **1400-111**

#### NONLINEAR BUNEMAN INSTABILITY UNDER THE PERPENDICULAR MAGNETIC FIELD

Keisuke MERA, Masahiro HOSHINO (Department of Earth and Planetary Science, University of Tokyo)

The electron phase space hole excited by Buneman instability (BI) is essentially important for the heating and acceleration of electrons, in a perpendicular shock region. The dynamics of the electron phase space hole under perpendicular magnetic field, however, is not fully understood yet. To understand the relationship between the electron phase space hole and the perpendicular magnetic field, we studied the saturation mechanism of BI under a finite perpendicular magnetic field. We used the 1-dimensional full particle simulation code, with the condition of periodic boundary. In our simulation, cold ions drift in background cold electrons, in the state of uniform magnetic field perpendicular to the ion beam. In case of the null magnetic field, it is well known that the saturation level of electric field energy of BI is the order of 1/3 power of the mass ratio (electron mass per ion mass) of the initial electron drift energy. In case of introducing a weak magnetic field perpendicular to the ion beam, it is believed that the BI breaks down. But, we found that, up to the electron gyro frequency equal to the electron plasma frequency, the growth rate and the saturation level of the BI are almost the same as the electrostatic case. This result is really important to study the heating and acceleration of electrons in the perpendicular shock region.

**GAIII.08**

#### WHAT IS THE LIFE-HISTORY OF PARTICLES IN THE MAGNETOSPHERIC REGIONS?

Location: Site A, Room 16

Thursday, July 10 AM

Presiding Chairs: C.H. Perry, R. Winglee

**GAIII.08/10A/A16-001** **0830**

#### ON THE CONTRIBUTION OF IONOSPHERIC IONS TO THE EARTH'S MAGNETOSPHERE: INSIGHT FROM GEOTAIL OBSERVATIONS

Kanako SEKI<sup>1</sup>, Masafumi HIRAHARA<sup>2</sup>, Masahiro HOSHINO<sup>3</sup>, Toshio TERASAWA<sup>3</sup>, Toshiyuki MUKAI<sup>4</sup>, Richard C. ELPHIC<sup>5</sup> (<sup>1</sup>Solar-Terrestrial Environment Laboratory, Nagoya University, Honohara 3-13, Aichi 442-8507, JAPAN, <sup>2</sup>Department of Physics, Rikkyo University, Toshima, Tokyo 171-8501, JAPAN, <sup>3</sup>Department of Earth and Planetary Science, University of Tokyo, Tokyo 113-0033, JAPAN, <sup>4</sup>Institute of Space and Astronautical Science, Sagamihara, Kanagawa 229-8510, JAPAN, <sup>5</sup>Los Alamos National Laboratory, NIS-1, MS466, Los Alamos, NM 87545, USA)

It is well known that a large flux of terrestrial ions is flowing out from the polar ionosphere. While these ionospheric ions are considered to contribute to the magnetospheric plasma, their energization and transport mechanisms, i.e., how and where they contribute to the

magnetospheric plasma, are far from fully understood. A statistical study, which compares O<sup>+</sup> fluxes at low and high altitudes during a solar minimum period, shows that there is a large gap between average fluxes of polar ionospheric O<sup>+</sup> outflows (~43×10<sup>24</sup> ions/s) and O<sup>+</sup> observed in the magnetosphere (~5×10<sup>24</sup> ions/s). There are three possibilities to explain this discrepancy: One possibility is that there exists a significant return flux from the magnetosphere back into the low latitude ionosphere, because more than 90 % of observed O<sup>+</sup> outflows had energies less than 1 keV and many of them will be trapped in the near-Earth magnetosphere within the distant neutral line. The second candidate is the escape of cold O<sup>+</sup> ions at energies below 50 eV either to the magnetosheath or through the plasma sheet, which are difficult to observe in the magnetosphere without spacecraft (s/c) potential control. The third possibility is the charge exchange loss of ring current ions that become dominated by O<sup>+</sup> during large magnetic storms. In this study, we focus on examining the validity of the second candidate on the basis of GEOTAIL observations. A spacecraft in sunlight usually undergoes positive charging due to photoelectron emission from its sunlit surfaces, and this charging prevents positive ions with energies below the s/c potential from reaching detectors. However, there are several occasions we can detect cold ions without the s/c potential control. For example, under existence of the large-amplitude oscillations such as Pc5 and/or enhanced convection velocity, or during time intervals when the spacecraft enters the shadow of the Earth, we can examine whether the cold ions exist in the plasma sheet or not. On the basis of GEOTAIL observations of these cases, we will discuss on the fate of ionospheric ions in the magnetosphere.

**GAIII.08/10A/A16-002** **0850**

#### THE STRUCTURE OF THE PLASMA SHEET UNDER NORTHWARD IMF

Masaki FUJIMOTO (Department of Earth and Planetary Sciences, TITech)

The structure of the plasma sheet under northward IMF is studied by the data from Geotail. It is now well known that the plasma sheet becomes cold and dense (CD) during extended northward IMF. We show that such CD ions appear mostly more than 10 Re off to the flanks from the tail axis. The dawnside CD ions are found to have higher temperatures with some of them reaching the upper limit of 2 keV used to identify CD ions in this study. These "high temperature" CD ions are detected at smaller geocentric distances and are connected to hot and dense (HD) ions located in the further inner region. A survey shows that the HD ions under nominal solar wind dynamic pressure is a northward IMF phenomenon. These results altogether suggest that HD ions are the inner-extension of the CD ions in the dawn-flanks, while such a partner to the duskside CD ions cannot be found. This structure of the plasma sheet implies significant asymmetry in transport and heating in the magnetotail under northward IMF when the convection electric field is not dominating.

**GAIII.08/10A/A16-003** **0910**

#### FIELD-ALIGNED ACCELERATION OF O<sup>+</sup> IONS BY THE PONDEROMOTIVE FORCE. CASE STUDY: APRIL 12, 2001

Sachiko JOKO, Hans NILSSON, Rickard LUNDIN, Ingrid SANDAHL (Swedish Institute of Space Physics)

We have investigated the cause of field-aligned acceleration of O<sup>+</sup> ion in the case of April 12, 2001, 07:30 - 09:30 UT. Before around 08:30 UT acceleration due to a diverging magnetic field could explain most of the trend of increase of O<sup>+</sup> ion bulk velocity parallel to the magnetic field ( $v_{\parallel}$ ). On the other hand, to explain much more increase of  $v_{\parallel}$  after around 08:30 UT than that expected by only acceleration due to a diverging magnetic field, the ponderomotive force was estimated. The ponderomotive force in this case was considered to act on O<sup>+</sup> ions under the action of Alfvén waves as well as under the action of electromagnetic cyclotron (EMC) waves. As to the increase of  $v_{\parallel}$  after around 08:30 UT, the ponderomotive force calculated from spin-averaged (4 seconds) electric field data could explain the large scale trend of increase of  $v_{\parallel}$ , if the oscillation frequency of electric field ( $f$ ) is less than or approximate to 0.1 Hz which was independently estimated from power spectra using high-resolution electric field data (0.04 second-interval). On the other hand, the bursty increase of  $v_{\parallel}$  in fine scale structure can be explained by an amplitude of electric field in high-resolution.

**GAIII.08/10A/A16-004** **0925**

#### AURORAL ION OUTFLOWS AND CIRCULATION THROUGH THE MAGNETOSPHERE

James P. McFADDEN (SSL, University of California, Berkeley)

Magnetic storms and substorms are characterized by a large increase in the ion outflow from both the cusp and midnight polar cap boundary. Low energy ions from the cusp form the bulk of lobe plasma and become a primary seed population to the plasma sheet. These lobe ions are subsequently energized through interactions at the plasmasheet boundary layer and the neutral sheet. The cusp activity also increases the density of the low altitude plasma on polar cap flux tubes. When this low altitude polar wind plasma moves to the nightside auroral zone, it is energized forming a more energetic ionospheric component injected into the plasmasheet. Both the cusp and nightside outflows occur on recently reconnected flux tubes that have associated strong Alfvénic turbulence and intense counter streaming electrons. Both the cold cusp and hotter nightside ionospheric outflow contribute significant plasma to the plasma sheet. During a storm main phase, these ions are subsequently injected into the inner magnetosphere near midnight, with the inner edge of the plasmasheet shifting Earthward to as close as L=2.5. These ions subsequently drift through the inner magnetosphere and are observed at local times that depend upon ion energy and phase of the storm. An asymmetry in the inner magnetospheric drift is observed with low energy ions preferentially observed on the dawn side and energetic ions observed at dusk. Low latitude oxygen densities of 100-1000/cc and temperatures of several hundred eV are not uncommon in the inner magnetosphere during storms. These ions subsequently convect to the dayside magnetopause where they can dominate the magnetospheric density and may affect the physics of reconnection. During magnetic storms, oxygen accelerated at the magnetopause can be observed as a distinct peak in the cusp velocity dispersed ion signatures.

**GAIII.08/10A/A16-005** **0945**

#### SPATIAL AND TEMPORAL TEXTURE OF BURSTY BULK FLOWS AND THEIR ROLE IN PLASMASHEET TRANSPORT

Harlan E. SPENCE, Larry KEPKO, Shannon MCCURDY (Center for Space Physics, Boston University)

Localized high-speed flows (> 400 km/s), called bursty bulk flows (BBFs), occur frequently in the inner central plasma sheet of Earth's magnetotail. BBFs are observed to occur semi-periodically with a characteristic period of approximately 10 minutes. A large collection of BBF events from 1996 are identified using Geotail magnetic field and plasma data, at times when the spacecraft was located between 10 and 25 Earth radii in the anti-sunward

direction. An ensemble BBF time series is constructed using a super-posed epoch analysis of the magnetic field and bulk plasma properties of the individual events. Epoch time is defined by the initial sharp increase in sunward velocity during a BBF, rather than at the time of the peak flow. The super-posed analysis interval spans one hour pre-epoch time to two hours post-epoch time. Fourier analysis of the post-epoch BBF interval reveals strong periodicities in plasma velocity, temperature, and magnetic field. Results of the analyses characterizing these periodicities, as well as representative case studies of BBF events, will be detailed. Additional properties of BBFs, including their association with magnetic field turbulence will be explored. The significance of these properties to net plasma sheet transport will be examined.

**GAIII.08/10A/A16-006 1005**

**TRANSPORT AND ACCELERATION OF IONS DURING STORM-TIME SUBSTORMS**

Ioannis A. DAGLIS<sup>1</sup>, Fiori-Anastasia METALLINO<sup>2</sup>, Dominique DELCOURT<sup>3</sup>, John H. SEIRADAKIS<sup>4</sup> (<sup>1</sup>Institute for Space Applications, National Observatory of Athens, <sup>2</sup>Department of Physics, University of Thessaloniki, <sup>3</sup>Centre d'étude des Environnements Terrestre et Planétaires)

In this paper we intend to study life-history of particles in the magnetosphere in order to assess the role of substorm ion acceleration in storm-time ring current growth. Particle orbit tracing is performed in time-dependent electromagnetic fields to study the effects of substorm reconfigurations. The model can give insight on energy transfer processes, particle acceleration, and non-adiabatic effects of particle orbits. Mass-dependence effects on particle trajectories and energisation are also investigated. Particular emphasis is given on the impulsive transport and energisation of ionosphere-originating ions during substorms and on their subsequent injection into the ring current. The response of these ionospheric populations to the large electric fields induced by magnetic field line relaxation from tail-like to dipole-like configuration is of critical importance to storm evolution.

**GAIII.08/10A/A16-007 1040**

**FATE OF THE PLASMA SHEET IONS**

Yusuke EBIHARA<sup>1</sup>, Masaki EJIRI<sup>1</sup>, Ingrid SANDAHL<sup>2</sup>, Lars ELIASSON<sup>3</sup>, Hans NILSSON<sup>2</sup>, Manuel GRANDE<sup>1</sup>, Joseph F. FENNELLS<sup>4</sup>, James L. ROEDER<sup>4</sup>, Lynn M. KISTLER<sup>5</sup> (<sup>1</sup>National Institute of Polar Research, Japan, <sup>2</sup>Swedish Institute of Space Physics, Sweden, <sup>3</sup>Rutherford Appleton Laboratory, UK, <sup>4</sup>The Aerospace Corporation, USA, <sup>5</sup>University of New Hampshire, USA)

We investigate the possible fate of the plasma sheet ions with energy ranging between hundreds eV and tens keV by using results of a particle simulation and data from Polar/MICS, Equator-S/ESIC and NOAA/MEPED. The plasma sheet ions, previously trapped by a geomagnetic field line, undergo sunward drift motion, and flow into the region where the earth's dipolar magnetic field governs their drift motion. Some of them drift into the deep inner magnetosphere, and contribute to the ring current buildup. Some of them experience pitch angle scattering and fall into the atmosphere. Some of them experience charge exchange with neutral atoms, and become free from the magnetic field. We performed a particle simulation that tracks ion drift trajectories under various magnetic field models (pure dipole or Tsyganenko 89) and various convection electric field models (Volland-Stern or Weimer 2000). The simulation is designed to conserve the phase space density except for loss terms. The following topics are particularly focused on in terms of impact of the changes in the phase space density of the plasma sheet ions on the inner magnetosphere. (1) "Imaging" of meso-scale structure (~1Re) of the ions. This "imaging" technique utilizes structured energy dispersion of sub-keV ions (wedge-like dispersion) seen in the dayside magnetosphere, and enables us to "image" remotely the spatial distribution of the ions in the inner magnetosphere and the near-earth plasma sheet. (2) Importance of the phase space density of the plasma sheet ions as a driver of the storm-time ring current buildup. (3) Estimation of number of plasma sheet ions reaching different regions; the ionosphere, the dayside magnetopause, and somewhere with energetic neutral atoms. This estimation will clue us on the large-scale circulation of the ions in the magnetosphere.

**GAIII.08/10A/A16-008 1100**

**STORM-TIME NITROGEN IONOSPHERIC ION INJECTION INTO THE MAGNETOSPHERE**

Andrew W. YAU<sup>1</sup>, Takumi ABE<sup>2</sup> (<sup>1</sup>Dept of Physics and Astronomy, University of Calgary, <sup>2</sup>Institute of Space and Astronautical Science)

Composition studies of ionospheric ion injection to the magnetosphere often focus on the two most dominant components, H<sup>+</sup> and O<sup>+</sup>, and neglect the N<sup>+</sup> component, because of the latter's proximity to O<sup>+</sup> in the mass spectrum and the inability or difficulty of most ion mass spectrometers to resolve the two species; also, N<sup>+</sup> is often regarded as a minor ion species and assumed to have negligible influence on magnetospheric dynamics. We present ion composition observations of storm-time low-energy (<50 eV) ionospheric ion injections from the Akebono suprathermal mass spectrometer (SMS), which has a mass resolution of 0.07 and a sharp (exponential) mass line shape and is capable of resolving N<sup>+</sup> from O<sup>+</sup> over a wide range of N<sup>+</sup>/O<sup>+</sup> ratio. These observations were acquired during a number of magnetic storms in different phases of the solar cycle. They reveal the substantial enhancement of N<sup>+</sup> ions during large magnetic storms, when the N<sup>+</sup>/O<sup>+</sup> ratio sometimes reach or exceed unity. We discuss the origin of the enhancement and its possible influence on ring current decay, in terms of prolonged thermospheric heating and non-resonant charge exchange of N<sup>+</sup> with atomic hydrogen, respectively.

**GAIII.08/10A/A16-009 1115**

**SOLAR WIND DRIVING OF RING CURRENT RECOVERY: DAYSIDE OUTFLOWS AND PLASMA SHEET DROP OUTS**

Janet U. KOZYRA<sup>1</sup>, Michael W. LIEMOHN<sup>1</sup>, Michelle F. THOMSEN<sup>2</sup>, Joseph E. BOROVSKY<sup>2</sup>, Thomas H. ZURBUCHEN<sup>1</sup>, Ruth SKOUG<sup>2</sup> (<sup>1</sup>Space Physics Research Lab, University of Michigan, <sup>2</sup>Los Alamos National Laboratory)

As a reservoir of ring current particles, the plasma sheet is a key participant in magnetic storm dynamics. In general, the plasma sheet density is higher during active than quiet times; the ring current begins to decay when convection decreases due to northward turning of the IMF B<sub>y</sub>. For a number of magnetic storms, a drop in plasma sheet densities has been observed to trigger a recovery of the ring current/partial ring current (seen in Dst\*) even though the Earth was engulfed in a region of southward IMF from the passage of an intense interplanetary magnetic cloud. During the cloud passage, magnetospheric convection remained strong; the ring current decay, to first order, was a consequence of moving low-density plasma into the inner magnetosphere along open drift paths to replace high density plasma exiting these same open drift paths at the dayside magnetopause. In this presentation, LANL observations are examined to identify cases of plasma sheet density decreases during times of enhanced magnetospheric convection associated with magnetic storms. ACE observations are used to characterize the solar wind drivers. The impact on

ring current decay is determined using sym H and asym H indices along with ring current model results. Collected events will be examined individually and through superposed epoch analysis techniques to investigate: (1) the role of plasma sheet dynamics in triggering ring current recovery and (2) magnetospheric and solar wind drivers linked to the depletions in plasma sheet density in the ring current source region.

**GAIII.08/10A/A16-010 1135**

**LOGNORMAL FORM OF THE RING CURRENT ENERGY CONTENT**

Michael W. LIEMOHN, Janet U. KOZYRA (SPRL, University of Michigan)

It is shown that the stormtime ring current energy content, from kinetic simulations, has a lognormal distribution. This type of functional form naturally arises from the superposition of many processes with a common initiation event but with differing growth and decay timescales. For the ring current, such a situation occurs from the disparate timescales of energization and decay for the hot ions at various energies, pitch angles, and spatial locations. The summation of this plethora of small currents results in a single current system (the ring current, both partial and symmetric) that has a loss time scale that decreases and then increases during every storm. The consequence is that the stormtime Dst index, which also has a lognormal shape, can be (and in fact usually is) dominated by this single current system.

**GAIII.08/10A/A16-011 1150**

**THE LIFE HISTORY OF A 'KILLER': THE ORIGIN AND FATE OF RELATIVISTIC ELECTRONS**

Geoffrey D. REEVES (Space and Atmospheric Sciences Group)

Relativistic electrons in the Earth's radiation belts have sometimes been called "killer electrons" in the popular press because of their sometimes severe impact on spacecraft systems and satellite instruments. While relativistic electrons (E > .5 MeV) have been studied for decades, many questions about their origins, dynamics, and fate remain unanswered. New observations have added new uncertainties and new challenges. Among the questions to be addressed are: Where do the radiation belt electrons come from? The plasma sheet is an obvious source but there appears to be a sufficient population of electrons of the right energy only at certain times and the question of where energetic plasmasheet electrons come from remains an unanswered logical extension. How are untrapped plasmasheet electrons transported and to and trapped in the inner magnetosphere? We will examine the role of storms and substorms in this process. How are particles accelerated to energies of 10 MeV or more? What are the relative role of diffusive and stochastic processes and what are the evidence for and against each? When are electrons lost? How? And How Many? We will track the life history of this highly energetic population of magnetospheric electrons and highlight areas where recent investigations have shed light on these questions, where significant gaps in our understanding remain, and how future missions can ultimately solve these problems.

**GAIII.08/10A/A16-012 1210**

**OUTER PLASMASPHERIC CIRCULATION**

Mark B. MOLDWIN<sup>1</sup>, D. BERUBE<sup>1</sup>, M. THOMSEN<sup>2</sup>, B. SANDEL<sup>3</sup> (<sup>1</sup>Earth and Space Sciences, UCLA, <sup>2</sup>Los Alamos National Laboratory, <sup>3</sup>University of Arizona)

The behavior of the outer plasmasphere and plasmopause will be reviewed. Recent observations that have advanced our understanding of the outer plasmasphere, particularly those during extreme quiet and extreme active conditions will be highlighted. Studies that utilize combinations of ground based, in situ, and IMAGE EUV remote sensing data have shown the extreme variability of the structure of the outer plasmasphere, but emphasize the overall flow of plasmaspheric plasma to the dayside magnetopause.

**GAIII.08-Posters**

**WHAT IS THE LIFE-HISTORY OF PARTICLES IN THE MAGNETOSPHERIC REGIONS?**  
Location: Site D

Friday, July 11 PM  
Presiding Chair: T. Moore, S.A. Fuselier

**GAIII.08/11P/D-001 Poster 1400-072**

**NONLINEAR WAVE-WAVE INTERACTION AND CASCADES OF THE TURBULENCE SEEN IN THE POLAR CUSP BY PROGNOZ 8, INTERBALL 1 AND CLUSTER SATELLITES**

Jan S. BLECKI<sup>1</sup>, Sergey P. SAVIN<sup>2</sup>, Michel PARROT<sup>3</sup>, Nicole CORNILLEAU-WEHRLIN<sup>4</sup>, Roman WRONOWSKI<sup>1</sup> (<sup>1</sup>Space Research Centre, <sup>2</sup>Space Research Institute RAS, <sup>3</sup>LPC Orleans, <sup>4</sup>CETP/CNRS/Vélizy)

Polar cusp is the site in the Earth's magnetosphere where the conversion of the energy is very intensive process. Wave form of the magnetic and electric fields taken in this region by Prognoz 8, Interball 1 and CLUSTER satellites has been processed with using the wavelet and bispectral analysis. The results showing the cascade of turbulence and wave-wave interactions will be presented in this discussion.

**GAIII.08/11P/D-002 Poster 1400-073**

**ANALYSIS OF THE ENERGETIC PARTICLES DATA FROM DETECTORS ONBOARD 'ZY-1' SOLAR SYNCHRONOUS SATELLITE**

Zou XIAO, Hong ZOU (Department of Geophysics, Peking University)

Based on the knowledge and related theory of the earth's radiation belt, the data of energetic particles observed by detectors onboard 'ZY-1' satellite at a solar synchronous orbit during the past 4 years are summarized and analyzed. Energetic electrons and protons at this orbit are only appeared at polar and SAA regions. On average, fluxes on the southern polar region are larger than that at the northern polar region. Their latitudinal distributions are along the geomagnetic latitudes instead of geographic ones. At nearly the same longitudes of SAA, there is a clear gap of occurrence of flux events on the northern polar region. Proton events

in general only occur in South Atlantic Anomaly region while electron events appear at both SAA and polar regions. Electron flux of 0.5-2MeV in polar regions is dominant over that of electrons of higher than 2MeV, while at SAA, fluxes from the two channels are about the same. The particle radiation is very sensitive to solar proton events and always has a positive response, but the amplitudes of enhancements and detailed features at polar regions and SAA are dependent on the individual solar proton event. It is proved that the observational results are in agreement with the theoretical description of the radiation belt structures. Although at high latitudes the energetic particles are mainly located in three regions with a wide geographical latitudinal coverage, at each longitude the latitudinal coverage is much narrower and particles are along the geomagnetic latitude of about  $\pm 60^\circ$  (except at SAA). Analysis showed that in SAA, usually both electrons and protons are observed, which should come from inner radiation belt; in Polar regions only energetic electrons are observed under quiet condition, which belongs to the outer radiation belt. The distribution of outer radiation electrons is asymmetrical for northern and southern polar regions, also for longitudes. This asymmetry can be explained with the reflecting altitudes of the mirror points of charged particles at the same L shell. So, the measured variations of the energetic particles and their response to solar disturbances at this orbit are actually a manifestation of the morphological features of the earth's radiation belts.

**GAIII.08/11P/D-003** Poster **1400-074**

**EFFICIENCY OF THE MAIN MECHANISMS OF THE MAGNETOSPHERIC RING CURRENT DECAY**

Lilia Z. SIZOVA (Institute of terrestrial magnetism, ionosphere and radio wave propagation, 142190 Troitsk, Russia)

The principal magnetospheric ring current dissipation mechanisms are used for estimation of its characteristic lifetime. The characteristic lifetime is calculated in connection with the ion composition of the ring current. The values of the characteristic lifetime of ring current decay obtained from experiments and theory are compared. It is shown that during main and recovery phase of magnetic storm the different mechanisms can play main role in dissipation of the ring current. The characteristic lifetime of the ring current decay was calculated from Dst-variations during 80 magnetic storms. Dst-variations were corrected for the solar wind dynamic pressure and DR- variations were calculated from the equation:  $DR = 2/3Dst - DCF - DCFq$ . For determination of the ring current characteristic lifetime we used the ring current energy balance equation using 3-8 h intervals of  $Bz IMF > 0$ , i.e. the additional energy input to the ring current could be neglected. The results show that lifetime of the ring current differs essentially during the main and recovery phases of magnetic storms. Lifetime of the ring current particles determined by Coulomb scattering and lifetimes of the ring current particles determined by the charge-exchange processes for different ions:  $H^+$ ,  $He^+$ ,  $He^{++}$ ,  $O^+$  were also examined on the basis of the experimental cross-sections and the numerical models of the hydrogen geocorona. The theoretical characteristic lifetimes for these dissipation mechanisms were compared with the observed ones. The available ion composition data for L-shells make possible to assume that the rise of the ring current characteristic lifetime in the recovery phase of magnetic storms is accounted for the ion composition variations. These can attribute to the changing value (and hence position) of the ring current and/or to rising of energetic proton fraction on low L-shells. The short lifetime of the ring currents during main phase of magnetic storms possible to explain by the instability mechanisms.

**GAIII.09-Posters**

**HOW DOES ENERGY FLOW FROM THE SOLAR CORONA THROUGH THE MAGNETOSPHERIC REGIONS?**

Location: Site D

Thursday, July 10 PM

**GAIII.09/10P/D-001** Poster **1400-112**

**STUDY OF INTENSE GEOMAGNETIC STORMS**

Geeta V. JADHAV, Shobhana ALEX, G.S. LAKHINA (Indian Institute of Geomagnetism)

Availability of satellite measurements of various parameters involved in the development of geomagnetic storms provides a good platform for the better understanding of geomagnetic storms. The present study analyses intense geomagnetic storms ( $Dst > 100$  nT) with the aid of satellite and ground databases. The study intends to confirm the earlier results such as crucial role of southward IMF in triggering the storm main phase as well as controlling the magnitude of the storm. The effect of the impingement of the solar energetic particles (SEP) on the earth's magnetosphere leading to the development of major geomagnetic storms is studied. We also examine the time profile of the energy injection into the ring current. An attempt is made to identify the multi peak signature in the energy injection rate during main phase of the storm. The relationship between the intensity and the duration of the main phase is also examined. We discuss these results in terms of the existing concepts of geomagnetic storms.

**GAIII.09/10P/D-002** Poster **1400-113**

**RELATIONSHIPS BETWEEN MAGNETOSPHERIC DISTURBANCES AND SOLAR ACTIVITIES OBSERVED FROM APRIL 30 TO MAY 5, 1998**

Haruka ADACHI<sup>1</sup>, Tohru SAKURAI<sup>1</sup>, Katsuhide MARUBASHI<sup>1</sup> (<sup>1</sup>Department of Aeronautics and Astronautics, Tokai University, <sup>2</sup>Communication Research Laboratory)

Three magnetic disturbances occurred successively during 6 days from April 30 to May 5, 1998, in which the Dst index grew greatly to the minimum value of about -200 nT. These strong magnetospheric disturbances were brought by attacks of three successively shocked solar winds observed during this period. In this paper we examined the storm and substorm signatures, and their related magnetic disturbances including ULF wave activities observed on the ground and in the magnetosphere by the Geotail satellite and the Geosynchronous satellite, Goes 8 and 9. The storm activities appeared in the development of the Dst index. The first SSC was observed at 0930 UT on 30 April, which was not so strong. However, clear Psc ULF waves were observed on the ground from high to low latitude ground stations, and simultaneously very interesting excitation of Pc 5 ULF waves was observed by Geotail in the morning side outer magnetosphere. The second SSC was observed at 2200 UT on 1 May, which brought the first clear negative excursion of the Dst index to -100 nT. This magnetic disturbance was caused by the second high speed solar stream in excess of about 600 km/s. Magnetic disturbances observed on the ground were very severe with strong substorm activities. ULF waves observed on the ground were also enhanced. The third SSC

was observed at 0330 UT on 4 May, which appeared with a very steep decrease of the Dst without any clear initial phase, but with strong substorm activities with large amplitude Pc 3 and 5 ULF waves. The speed of the third shocked solar stream was in excess of 800 km/s, highest among the three solar streams. The travel time was estimated as being very short only with about 45 hours. We also examined the relationship of the magnetic structure between the magnetic cloud observed on 2 May and the CME on 29 April, and found that the orientation of the flux rope was good agreement with the orientation of the filament disappearance. Magnetospheric disturbances associated with these interplanetary disturbances are discussed in more detail.

**GAIII.09/10P/D-003** Poster **1400-114**

**HOW TO USE MODERN SPACE SCIENCE MODELS AT THE COMMUNITY COORDINATED MODELING CENTER**

Masha M. KUZNETSOVA, Lutz RASTAETTER, Michael HESSE, Kristi KELLER, Ayris FALASCA, John DORELLI (Community Coordinated Modeling Center, NASA/GSFC)

The Community Coordinated Modeling Center (CCMC) is offering runson request of space weather models residing at CCMC to a broadspace science community. Runson request support an open modelpolicy by providing community access to state-of-the-art researchmodels. They also facilitate model testing by a large number of researchers. Runson request can be used for education purposes as well as for comprehensive scientific research. We have developed user friendly Web interfaces for on-line run submission and visualization of the simulation results. At the present time, runson request are available for two global MHD magnetosphere models (BATS-RUS and UCLA-GGCM), two ionosphere/thermosphere models (SAMI2 and Coupled Thermosphere Ionosphere Plasmasphere model) and one inner magnetosphere model (Fok ring current model). We will present examples of successful research through the www. We will demonstrate the run on request submission mechanism. We will illustrate the features of the www interface for visualization, discuss the post-processing options, as well as tools, which facilitate comparisons between simulation results and satellite and ground-based observations.

**GAIII.09**

**HOW DOES ENERGY FLOW FROM THE SOLAR CORONA THROUGH THE MAGNETOSPHERIC REGIONS?**

Location: Site A, Room 11

Friday, July 11 AM  
Presiding Chair: T. Watanabe

**GAIII.09/11A/A11-001** Invited **0830**

**OBSERVING GLOBAL PROCESSES IN THE SUN-EARTH SYSTEM WITH SOLAR TERRESTRIAL RELATIONS OBSERVATORY (STEREO) AND THE INTERNATIONAL HELIOPHYSICAL YEAR**

Joseph Michael DAVILA, Nat GOPALSWAMY (NASA Goddard Space Flight Center)

The solar magnetic field is constantly generated beneath the surface of the Sun by the solar dynamo. To balance this flux generation, there is constant dissipation of magnetic flux at and above the solar surface. The largest phenomenon associated with this dissipation is the Coronal Mass Ejection (CME). The Solar and Heliospheric Observatory (SOHO) has provided remarkable views of the corona and CMEs, and served to highlight how these large interplanetary disturbances can have terrestrial consequences. STEREO is the next logical step to study the physics of CME origin, propagation, and terrestrial effects. Two spacecraft with identical instrument complements will be launched on a single launch vehicle in November 2007. One spacecraft will drift ahead and the second behind the Earth at a separation rate of 22 degrees per year. Observation from these two vantage points will for the first time allow the observation of the three-dimensional structure of CMEs and the coronal structures where they originate. An international research program, the International Heliophysical Year (IHY) will provide a framework for interpreting STEREO data in the context of global processes in the Sun-Earth system. In 1957 a program of international research, inspired by the International Polar Years of 1882-83 and 1932-33, was organized as the International Geophysical Year (IGY) to study global phenomena of the Earth and geospace. The IGY involved about 60,000 scientists from 66 nations, working at thousands of stations, from pole to pole to obtain simultaneous, global observations on Earth and in space. There had never been anything like it before. The fiftieth anniversary of the International Geophysical Year will occur in 2007. We propose to organize an international program of scientific collaboration for this time period called the International Heliophysical Year (IHY). Like its predecessors, the IHY will focus on fundamental global questions of Earth science. The STEREO mission will be a major contributor to IHY research objectives.

**GAIII.09/11A/A11-002** **0900**

**PROPAGATION AND CHARACTERISTICS OF EJECTA AT 1 AU USING HALO CME EXPANSION SPEEDS AND INTERPLANETARY OBSERVATIONS**

Alisson DAL LAGO<sup>1</sup>, Walter GONZALEZ<sup>2</sup>, Rainer SCHWENN<sup>2</sup>, Alicia Luiza CLUA DE GONZALEZ<sup>2</sup>, Luis Eduardo Antunes VIEIRA<sup>1</sup>, Ezequiel ECHER<sup>1</sup>, Fernando Luis GUARNIERI<sup>1</sup>, Laura BALMACEDA<sup>1</sup>, Nelson Jorge SCHUCH<sup>1</sup> (<sup>1</sup>Instituto Nacional de Pesquisas Espaciais, Brazil, <sup>2</sup>Max-Planck-Institut fuer Aeronomie, Germany, <sup>3</sup>Centro Regional Sul de Pesquisas Espaciais, Brazil)

The Large Angle and Spectroscopic Coronagraph (LASCO) has observed 38 halo coronal mass ejections that were correlated with interplanetary ejecta at 1AU during the period from January 1997 to April 2001. We have measured the lateral expansion speed of these CMEs using LASCO C3 images, and we used them as an indication of the sun-earth line initial speed. Interplanetary ejecta speed observations made by the Advance Composition Explorer (ACE) have given us the interplanetary counterparts of these CMEs, allowing us to construct models to predict their characteristics and their travel time to 1 AU. During this same period, 5 out of the 8 most intense geomagnetic storms ( $Dst < -200$ nT) were caused by this kind of interplanetary ejecta.

**GAIII.09/11A/A11-003** Invited **0920**

**CME-ASSOCIATED MAGNETIC CLOUD STRUCTURES IN ASCENDING PHASE OF SOLAR CYCLE 23**

Takashi WATANABE<sup>1</sup>, Haruka ADACHI<sup>1</sup>, Katsuhide MARUBASHI<sup>1</sup>, Yuko NAMIKI<sup>1</sup> (<sup>1</sup>Department of Environmental Sciences, Ibaraki University, <sup>2</sup>Department of Aeronautics and Astronautics, Tokai



CME images taken by SOHO/LASCO coronagraphs show that CMEs were tend to be formed along the magnetic neutral line on the source surface in the solar corona. This leads to a suggestion that the axial orientation of an interplanetary magnetic cloud (IMC) will be coincide with the local inclination of the magnetic neutral line near the sub-Earth point (e. g. Mulligan et al., GRL, 28, 891, 2001). According to an analysis of CME-associated IMC events observed in the ascending phase of the present solar activity cycle (1997-2000), general increase of the inclination of the IMC axis is seen following the increase of a meandering tendency of the source-surface magnetic neutral line(from Wilcox Solar Observatory). At the same time, we found a number of IMCs which did not follow the general law mentioned above. To establish the CME-IMC connection, it is necessary to find solar sources of relevant CMEs. To do this, we examine coronal images taken by EIT/SOHO and SXT/Yohko to find characteristic coronal phenomena, e.g. X-ray dimming (Sterling and Hudson, Astrophys. Lett., 491, L55, 1998), transient coronal holes (Watanabe et al., in Proc. 3rd SOHO Workshop, ESA SP-373, 269, 1994) and other signatures indicating the formation of CMEs. A provisional analysis showed that a large-scale change in EIT coronal images took place near the solar disc center, beneath the neutral line, we found a reasonable angular coincidence between the neutral line and the IMC axis. Detailed analysis is in progress.

**GAI09.09/11A/A11-004** **0950**

**TRACING THE SOLAR PARTICLE CHAIN IN APRIL 2002**

Daniel N. BAKER<sup>1</sup>, Richard A. MEWALDT<sup>2</sup>, Glenn MASON<sup>3</sup>, Shri KANEKAL<sup>3</sup>, Janet U. KOZYRA<sup>4</sup>, David S. EVANS<sup>5</sup>, Scott M. BAILEY<sup>6</sup>, M.J. REINER<sup>7</sup> (<sup>1</sup>Laboratory for Atmospheric and Space Physics, <sup>2</sup>California Institute of Technology, <sup>3</sup>University of Maryland, <sup>4</sup>University of Michigan, <sup>5</sup>National Oceanic and Atmospheric Administration, <sup>6</sup>University of Alaska Fairbanks, <sup>7</sup>Goddard Space Flight Center)

Soon after the RHESSI spacecraft observed an X-class solar flare early on 21 April 2002 a coronal mass ejection (CME) moving at ~2500 km/sec was observed by SOHO to emerge from near the west limb of the Sun. Almost simultaneously, Type-II and Type-III radio emission was observed by the Wind spacecraft, indicating the onset of particle acceleration near the Sun. The active region on the Sun responsible for this event was magnetically well-connected to the Earth, leading to a prompt enhancement at 1 A.U. of solar particles (E > 10 MeV) as seen by the ACE and SAMPEX spacecraft. Strong shock-related particle acceleration continued to occur as the CME propagated outward from the sun. The solar particle enhancement lasted from 21 April to 26 April (as seen by the NOAA/POES spacecraft) and included enhancement not only of solar protons and heavier nuclei extending to hundreds of MeV/nucleon but also solar electrons. The energetic particles produced near the sun, at this and preceding interplanetary shock waves, and deep within the Earth's radiation belts were all observed using TIMED and SNOE to produce substantial effects on the chemistry of the Earth's middle and upper atmosphere. We examine the impacts of this set of events on atmospheric heating and cooling rates and on ozone densities in the mesosphere. Using the remarkable constellation of available spacecraft, we are able to follow the particle chain from the Sun's surface all the way to the deep layers of Earth's atmosphere with unprecedented completeness.

**GAI09.09/11A/A11-005** **1040**

**SOURCES AND ACCELERATION OF PARTICLES AT SHOCKS FROM THE SUN TO THE EARTH**

Eberhard MOEBIUS, Harald KUCHARAK (Department of Physics and Space Science Center, University of New Hampshire)

Shocks at solar wind stream interaction regions, coronal mass ejections and magnetospheric obstacles have long been known for their intimate link with particle acceleration. Much enhanced capabilities to determine mass and charge composition on ACE and SOHO and to obtain detailed distributions with commensurate time resolution on Cluster have enabled us to track down sources and injection mechanisms for the resulting energetic particles and to take a closer look at the processes. It has become apparent that both solar wind and interstellar pickup ions are substantial sources for particle acceleration in CIRs and at CME driven shocks. The relative contribution of these ions in the energetic particle populations does not only reflect their abundance variations with location in the heliosphere, but also their injection efficiency into acceleration. Most recently a more detailed look into shock structure and particle acceleration processes has become possible at the bow shock with Cluster. The emergence of the accelerated ion population out of the low energy population in the ramp of quasi-perpendicular bow shocks has become visible. Because simulations have shown that also in the case of quasi-parallel shocks the shock forming waves produce quasi-perpendicular conditions locally, where then particles are accelerated, the observations at the simpler quasi-perpendicular shocks provide us with more general information.

**GAI09.09/11A/A11-006** **1110**

**ACCELERATED PLASMA FLOWS IN THE CUSP BOUNDARY LAYER: A CLUSTER-FAST-POLAR-SUPERDARN CONJUNCTION STUDY**

Charles J FARRUGIA<sup>1</sup>, E. LUND<sup>2</sup>, P.E. SANDHOLT<sup>3</sup>, E. MOEBIUS<sup>4</sup>, S.W.H. COWLEY<sup>5</sup>, J. WILD<sup>6</sup>, A. BALOGH<sup>7</sup>, M. DUNLOP<sup>8</sup>, C. MOKIS<sup>9</sup>, L. KISTLER<sup>10</sup>, H. REME<sup>11</sup> (<sup>1</sup>Space Science Center, University of New Hampshire, USA, <sup>2</sup>Physics Department, University of Oslo, Oslo, Norway, <sup>3</sup>Ionospheric Physics Group, University of Leicester, Leicester, UK, <sup>4</sup>Imperial College of Science and Technology, University of London, UK, <sup>5</sup>Rutherford Appleton Laboratory, Chilton, Didcot, UK, <sup>6</sup>Centre d'Etude Spatiale des Rayonnements, Toulouse, France)

Observations during a multiple magnetic conjunction CLUSTER-FAST-Polar-SuperDARN are examined. CLUSTER was on an outbound pass through the exterior cusp. The IMF pointed south-west throughout. A solar wind dynamic pressure release shifted CLUSTER into the cusp boundary layer at the poleward edge of the cusp. There it observed 5 flow bursts and magnetic perturbations which are Alfvénic in nature. We interpret these flow events as being due to a sequence of reconnected flux tubes passing over CLUSTER (i.e., flux transfer events, FTEs). This interpretation is further supported by the following: (i) The observation at FAST of a staircase cusp ion signature on magnetic field lines nominally connected to CLUSTER; (ii) The observation by the SuperDARN radars of a sequence of pulsed poleward enhancements of ionospheric flows (PIFS) which are (a) in one-to-one correspondence with the flow bursts at CLUSTER and which (b) are well known from previous work to be an ionospheric signature of FTEs; (iii) Observations of the ion flow bursts at Polar, situated in the magnetosphere further downstream of CLUSTER, whose directional characteristics are consistent with the interpretation proposed above. The work extends previous studies of magnetospheric signatures of FTEs and associated energy and momentum transfer by showing flow bursts due with reconnection at sub-cusp latitudes but which are seen behind the cusp.

**GAI09.09/11A/A11-007** **Invited** **1140**

**FLUX TRANSFER EVENTS OBSERVED BY DUAL SATELLITES: ISEE-1 AND ISEE-2**

Hideaki KAWANO (Department of Earth and Planetary Sciences, Kyushu University, Japan)

Flux transfer events (FTEs) are transient events observed nearthe dayside magnetopause, characterized by bipolar perturbationin the magnetic field component normal to the magnetopause.They are generally thought to be generated by transient daysidereconnection, which transports solar wind energy into themagnetosphere. We have analyzed magnetic field data from dualsatellites ISEE-1 and ISEE-2 (usually separated from each otherby several hundred kilometers), in an attempt to directly detectthe motion of FTEs. From ten years' data of ISEE, we haveidentified about thousand cases in which the two satellitesobserved the same FTE. Then, from the positions and observationtimes of each FTE at the two satellites, we have estimated thedirection of motion of the FTE. Preliminary results suggestthat the FTEs tend to move tailward, mainly in the east-westdirection, away from the subsolar point; this is inconsistentwith an east-west elongated structure caused by a transientreconnection at the (east-west elongated) equatorialeconnection line, but consistent with a flux-tube structurewhich has a small cross-section in the GSM XY plane.

**GAI09.09/11A/A11-008** **1210**

**ENERGY TRANSFER FROM THE SOLAR WIND INTO THE IONOSPHERE INSIMULATIONS OF THE EARTH MAGNETOSPHERE-IONOSPHERE SYSTEM**

Lutz RASTAETTER<sup>1</sup>, Maria M. KUZNETSOVA<sup>1</sup>, Michael HESSE<sup>2</sup>, Aaron RIDLEY<sup>3</sup>, Tamas I. GOMBOSF, Joachim RAEDER<sup>4</sup> (<sup>1</sup>Community-Coordinated Modeling Center, <sup>2</sup>CSEM, University of Michigan, <sup>3</sup>IGPP, University of California Los Angeles)

Due to their different design, global magnetospheric models can generate different results for the same solar wind input conditions. However, the average of a quantity obtained from concurrentsimulations provides an estimate of the level of geomagnetic activity and the differences between the model results may serve as an estimated error level. The ultimate goal, of course, is to obtain modeled results that are close to actual observations and minimize the differences between the different model results by the use of better input data,improved algorithms or increased spatial resolution. Physics-based magnetospheric models may eventually be run in an ensemble to obtain forecasts like in terrestrial weather forecasting. As a first step toward the goals outlined, we use simulation results obtained with the global magnetospheric models BATSRUS (UM) and UCLA-GGCM.As an example, we can determine the energy and mass transferred into the inner magnetosphere and the ionosphere and compare those transfers with the varying solar wind condition to get transfer rates and reaction time constants. Modeled results will be compared by in-situ measurements or remote-sensing observations for selected events.

Friday, July 11 PM  
Presiding Chair: B. Thompson

**GAI09.09/11P/A11-001** **1400**

**MULTIPLE SPACECRAFT MEASUREMENTS OF ENERGETIC IONS DURING A HIGH SOLARWIND PRESSURE EVENT**

Jiasheng CHEN, Theodore A. FRITZ (Center for Space Physics, Boston University)

On June 28, 1999, the WIND spacecraft (near L1) observed a suddenincrease (by more than one order of magnitude) of the solar windpressure at about 4:45 UT and an upstream ion event at 5:23-5:45 UT, the INTERBALL-1 spacecraft located upstream of the bow shock(X=22.4Re, Y=-15.7Re, Z=6.25Re in GSE) measured an upstream ionevent from 5:16 UT to 6:00 UT, while the POLAR satellite at 7 hoursmagnetic local time detected an energetic particle event in thehigh-altitude region associated with turbulent diamagnetic cavitiesfrom 5:12 UT to 6:30 UT. Energetic oxygen ions of both ionosphericorigin and solar wind origin were observed by the POLAR during thisevent period. The energetic ions and the associated turbulentmagnetic field are very similar to what found in the high-altitude dayside cusp region. The interplanetary magnetic field (IMF) wasdominant by its tailward component; the IMF By was almost duskward,while the IMF Bz was almost southward at 5:00-6:00 UT. For aduskward IMF component, a cusp diamagnetic cavity found at 7 hourslocal time is unexpected by current MHD models. The relationbetween the cusp and the upstream energetic ions and the relationof these energetic ions with the interplanetary conditions will be discussed.

**GAI09.09/11P/A11-002** **1420**

**OBSERVATIONS OF DISCRETE, GLOBALMAGNETOSPHERIC OSCILLATIONS DIRECTLY-DRIVEN BY SOLAR WIND DENSITY VARIATIONS**

Larry KEPKO, Harlan E. SPENCE (Center for Space Physics, Boston University)

In this paper we present six events in which both the timeseriesand the spectral content of solar wind number density fluctuations andmagnetospheric magnetic field observations were highly correlated for intervalsranging from a few to twelve hours. The fluctuations were periodic andoccurred at discrete frequencies which often matched the f=1.3, 1.9, 2.6, and3.4 mHz oscillations that have been attributed to global magnetospheric MHDcavity and/or waveguide modes. We also observed significant power in thesub-mHz region, with frequencies as low as f=0.1 mHz. We show that these fluctuations were first observed in the solar wind, far upstream from the earth, and argue that the convected density perturbations slowly alter the size of the magnetospheric cavity leading to the appearance of multiple, discrete magnetospheric oscillations. We argue that for these events the discrete frequencies were an inherent property of the solar wind, and were not related to a possible cavity or waveguide mode of the magnetosphere. We then show that the solar wind density fluctuations, when converted into length-scales, organize into scalesizes of L=23, 30, 45, and 80-100 RE. Finally, we speculate on and show some evidence for a possible solar source for these particularly geoeffective solar wind structures, thereby suggesting a meansby which plasma energy may flow from the Sun, be transported through the heliosphere, and ultimately, couple into and energize the magnetosphere.

**GAI09.09/11P/A11-003** **Invited** **1440**

**COUPLING OF ENERGY FROM THE SOLAR WIND INTO THE OUTER ZONE RADIATION BELTS THROUGH ULF VARIATIONS**

Scot R. ELKINGTON<sup>1</sup>, Michael J. WILTBERGER<sup>2</sup>, Anthony A. CHAN<sup>3</sup>, Yue FEI<sup>1</sup>, Daniel N. BAKER<sup>1</sup>, Mary K. HUDSON<sup>3</sup> (<sup>1</sup>Laboratory for Atmospheric and Space Physics, University of Colorado, <sup>2</sup>Department of Physics and Astronomy, Dartmouth College, <sup>3</sup>Department of Space Physics

and Astronomy, Rice University)

The outer zone radiation belts are comprised primarily of energetic (>200 keV) electrons geomagnetically trapped in orbits encircling the Earth. The bulk of the radiation lies at radial distances between 3-7 Earth radii, a region of particular significance due to the large number of spacecraft operating at these altitudes, and global society's increasing reliance on space-based technologies for communications, navigation, weather prediction, and a variety of other economic and geopolitical purposes. As spacecraft operating in this region have sometimes been found susceptible to "anomalies" related to changes in the local radiation environment, understanding the transmission of energy from the solar wind into the magnetosphere and radiation belts is of particular practical importance. Waves in the ULF spectrum, with periods of a few to tens of minutes, have been shown to be an effective means of transporting and energizing particles within the radiation belts. Recent work has also shown that variation in the solar wind often occurs on ULF timescales, suggesting a means by which energy could be effectively transmitted from the solar wind into the inner magnetosphere, and directly affect the global radiation environment. In this work we use 3D, global magnetohydrodynamic (MHD) simulations of the magnetosphere, driven by upstream solar wind observations, to examine the ULF mode and power structure in the inner magnetosphere. Radial and local time dependence of ULF wave power is examined, and implications for radiation belt acceleration and transport are discussed.

**GAIII.09/11P/A11-004 1510**

**SOLAR WIND DRIVING OF THE MAGNETOSPHERE: RING CURRENT AND MHD RESULTS**

Nieszcja E. TURNER<sup>1</sup>, Ramon E. LOPEZ<sup>2</sup>, Michael J. WILTBERGER<sup>2</sup>, Elizabeth J. MITCHELL<sup>1</sup> (<sup>1</sup>Department of Physics, Univ. of Texas at El Paso, <sup>2</sup>Dartmouth College)

We use MHD simulations and ring current data to investigate the magnetospheric response to different types of solar wind energy input. The MHD simulations show that the dissipation of energy in the magnetosphere-ionosphere system is very sensitive to solar wind density variations during time of strong driving, with large density pulses during southward Bz exhibiting significantly greater geoeffectiveness than strong Bz without such pulses. This suggests that solar wind kinetic energy flux may play a significant role during southward Bz. We compare this behavior with the behavior of ring current ions (using particle measurements and Dst) in order to determine whether the ring current shows this same response to different types of solar wind energy coupling. Initial results suggest that the ring current does indeed respond this way, and we present results showing the overall magnetospheric effect of these different solar wind drivers. This work is a part of the Center for Integrated Space weather Modeling (CISM) initiative.

**GAIII.09/11P/A11-005 1600**

**INTERPLANETARY SHOCKS AS A POSSIBLE TRIGGER OF SUBSTORM ONSETS: A STATISTICAL STUDY WITH POLAR ULTRAVIOLET IMAGER IMAGES**

Kan LIOU<sup>1</sup>, Patrick T. NEWELL<sup>1</sup>, Chin-Chun WU<sup>2</sup>, Ronald P. LEPPING<sup>3</sup>, Ching-I MENG<sup>1</sup> (<sup>1</sup>The Johns Hopkins University Applied Physics Laboratory, <sup>2</sup>CSPAR, University of Alabama, Huntsville, AL 35899, <sup>3</sup>Laboratory for Extraterrestrial Physics, NASA/GSFC, Greenbelt, MD 20771)

One of the outstanding issues in magnetospheric physics is the trigger mechanism(s) of the substorm expansion phase onset. There is a large body of evidence indicating that an impingement of the high solar wind dynamic pressure may lead to the expansion phase onset of substorms. When high solar wind ram pressure impinges upon the magnetosphere, it compresses the lobe magnetic fields and enhances the cross-tail currents. Reconnection or current disruption may occur and ultimately lead to substorm onsets. Note that the forming of a negative magnetic bay has been the main proxy for a substorm used in previous studies, and we now know that some magnetic bays are not substorms but convection bays associated with the enhancement of convection. Therefore, it is reasonable to cast doubt on the compression trigger mechanism. In this study we use the classical substorm onset, the "auroral breakup," as the most reliable substorm onset indicator. These are identified with global auroral images from the Polar ultraviolet imager (UVI), to investigate this issue. We examine 43 interplanetary shock events that occurred between 1996 and 1999 with simultaneous UVI auroral images and the auroral electrojet indices. It is found, indeed, that ~50% of the shocks produce magnetic bays (AL < -100 nT). While most of the shocks enhance auroral luminosities, less than only ~10% of events show auroral breakups preceded by SSCs. These results strongly indicate that interplanetary shocks can produce negative magnetic bays but not auroral breakups.

**GAIII.09/11P/A11-006 1620**

**ON THE PREDICTION OF MAGNETIC STORMS**

Mervyn P. FREEMAN<sup>1</sup>, Richard B. HORNE<sup>1</sup>, Matthew DAWES<sup>2</sup>, Paul S. WILSON<sup>2</sup> (<sup>1</sup>British Antarctic Survey, <sup>2</sup>University of Leeds, <sup>3</sup>Imperial College London)

Magnetic storms are globally coherent non-secular variations of the geomagnetic field that have been identified as a natural environmental hazard with adverse effects on radio communications, satellite operations, electrical power distribution, etc. Thus it is desirable to forecast the occurrence of magnetic storms to mitigate their impact. To this end, we have analysed the probability density function (PDF) of magnetic storm duration, non-storm duration, and waiting time between storm onsets, for two objective definitions of a magnetic storm based on historical precedent. In the first definition, a magnetic storm is defined as a classic extreme event - the interval for which a relevant geomagnetic measure (the Dst index) is above a given threshold, c. The PDF of storm duration, non-storm duration, and waiting time between storm onsets are all found to be truncated power laws, independent of threshold. Thus, under this definition, magnetic storms have no characteristic duration or recurrence time between 1h and 100h. In the second definition, we show evidence that the extreme events of the first definition are part of a longer coherent structure in the time series such that a magnetic storm can alternatively be defined as the interval for which the Dst index is above a given threshold b and the maximum Dst is above a second, higher threshold c. Over a region of the two-threshold parameter space (b, c), the PDF of waiting times between storm onsets in 3-year samples is found to be a random stationary (Poisson) process with a Poisson statistic that varies with the solar cycle, and the PDF of storm durations is peaked at 20 - 30h. The analysis raises an interesting general question as to the occurrence properties of abstract extrema (e.g., gale force winds) compared to those of physical extreme events (e.g., hurricanes?). Moreover, an interesting similarity between the occurrence pattern of repeatable magnetic storms and of solar flares is noted.

**GAIII.09/11P/A11-007 Invited 1640**

**EARTH IN THE THREE DIMENSIONAL SOLAR WIND FLOW**

Ken'ichi FUJIKI<sup>1</sup>, Masayoshi KOJIMA<sup>1</sup>, Munetoshi TOKUMARU<sup>1</sup>, Tomoaki OHMI<sup>1</sup>, Masahiro YAMASHITA<sup>1</sup>, Masaya HIRANO<sup>2</sup>, Bernard V. JACKSON<sup>2</sup>, Paul P. HICK<sup>2</sup> (<sup>1</sup>Solar-Terrestrial

Environment Laboratory, Nagoya University, Japan, <sup>2</sup>Center for Astrophysics and Space Science, UCSD, USA)

Ground-based remote-sensing using interplanetary scintillation (IPS) is a unique tool for the study of the global structure of the solar wind. This technique measures solar wind at locations that are difficult or impossible to access with in situ measurements. Recently we introduced a computer-assisted tomography (CAT) program to reproduce solar wind features and this has greatly improved the reliability of our IPS studies. We applied the CAT analysis to the IPS data obtained at heliospheric distances 0.1-0.9 AU over one solar cycle (1985-2002) and analyzed the variation of the solar wind structure during this period. We discuss several solar wind features found in these analyses. The solar wind consists of two velocity components (i.e. the solar wind is bimodal) not only around solar minimum but also in the rising and declining phases. The fast solar wind velocity is asymmetric between northern and southern hemispheres. Around solar maximum the solar wind structure evolved asymmetrically in both hemispheres, similar to the evolution of magnetic elements of the old/new polarity in the photosphere. Interplanetary disturbances are the other target of IPS observations, and their dynamics have been studied by using model-fitting analysis and a sophisticated time-dependent tomography method. We will report several results from these studies. We have started trial real-time solar wind forecasting using the IPS CAT analysis on a daily basis. The preliminary results of this trial will also be shown in this talk.

**GAIII.09/11P/A11-008 1710**

**WAVELET ANALYSIS OF INTERPLANETARY MAGNETIC FIELD AND AE INDEX FLUCTUATIONS DURING HILDCAA EVENTS**

Fernando Luis GUARNIERI<sup>1</sup>, Walter Demetrio GONZALEZ<sup>1</sup>, Bruce TSURUTANI<sup>2</sup>, Ezequiel ECHER<sup>1</sup>, Alisson DAL LAGO<sup>1</sup>, Luis Eduardo VIEIRA<sup>1</sup>, Alicia Luiza CLUA DE GONZALEZ<sup>1</sup>, Nelson Jorge SCHUCH<sup>3</sup> (<sup>1</sup>Instituto Nacional de Pesquisas Espaciais/DGE, <sup>2</sup>Jet Propulsion Laboratory - JPL/NASA, <sup>3</sup>Centro Regional Sul de Pesquisas Espaciais/INPE)

HILDCAA events (High Intensity, Long Duration, Continuous Auroral Activity) were firstly discovered by Tsurutani and Gonzalez, in 1987. These events are characterized by an intense activity in auroral region, measured by AE index, despite the absence of a strong geomagnetic storm. The interplanetary magnetic field during these events presents Alfvénic fluctuations. The events must follow some criteria to be considered a HILDCAA: they must reach, at least, 1000nT in the AE peak, they can not drop below 200 nT in AE index by a period greater than 2 hours, have a minimal duration of 2 days and occur outside the main phase of a geomagnetic storm. For HILDCAAs identification, it was used high resolution (1 minute) ACE satellite data and AE index. The data were plotted simultaneously, and the results were analyzed in order to identify the event occurrences. It was analyzed the 13 strongest events occurred during year 1998. Wavelet analysis was applied in the AE index and interplanetary magnetic field Bz during periods of HILDCAA occurrences. The results show that only large periods were observed along the whole AE series, while short periods occur only in some periods of each event.



**GAIII.10 1400**

**HOW CAN WE USE WAVES AS DIAGNOSTIC PROBES FOR SPACE WEATHER STUDIES?**

Location: Site A, Room 1

Thursday, July 10 PM  
Presiding Chairs: F.W. Menk, K. Yumoto

**GAIII.10/10P/A01-001 1400**

**USING ULF WAVES AS DIAGNOSTIC PROBES OF THE MAGNETOSPHERIC DENSITY**

Fred W. MENK<sup>1</sup>, Mark A. CLILVERD<sup>2</sup>, Bill R. SANDEL<sup>1</sup>, Don L. CARPENTER<sup>1</sup>, Ian R. MANN<sup>3</sup> (<sup>1</sup>School of Mathematical and Physical Sciences, University of Newcastle, <sup>2</sup>British Antarctic Survey, High Cross, Cambridge, CB3 0ET, U.K., <sup>3</sup>Lunar and Planetary Laboratory, University of Arizona, Tucson, AZ 85721, USA, <sup>4</sup>Space, Telecommunications and Radioscience Laboratory, Stanford University, Stanford, CA, <sup>5</sup>Department of Physics, University of York, Heslington, York, YO10 5DD, U.K.)

Ultra-low frequency (ULF; f~1-100 mHz) plasma waves distribute energy of solar wind origin throughout the Earth's magnetosphere and down to the ground, where they are recorded as pulsations of the geomagnetic field. The waves propagate through the magnetosphere in the fast magnetosonic mode and may couple to shear transverse mode field line eigenoscillations. The frequency of these field line resonances (FLRs) is determined by the field geometry and the plasma mass density near the equatorial plane. The FLRs occur during the local daytime and can often be observed for several hours. Ground-based measurements of the resonant frequency can therefore provide information on the plasma mass density near the field line apex in the dayside magnetosphere. An array of latitudinally-separated ground magnetometers allows the plasma density profile to be monitored throughout the magnetosphere. This may be compared with ground-based VLF electron density measurements, and satellite-borne particle and imager observations. The average properties of the magnetospheric plasma are well established. However, case studies demonstrate that the magnetosphere exhibits density features that have only been partially described and which are far from understood. Regions of particular interest are in the vicinity of the plasmapause, where complex structures and temporal variations are frequently observed, and the outer plasmasphere, where small-scale density perturbations may occur. These regions may be examined by ULF FLR techniques on a time scale of 30-60 min and a spatial resolution in the range 0.15-0.4 RE. We describe case studies of the magnetospheric plasma using FLRs, and compare the observed mass densities with spacecraft data and models. In particular, we present illustrative examples of the density profile for the following cases: (1). Quiet conditions, when only a vestigial plasmapause is present; (2). Several days after a moderate magnetic disturbance; (3). Disturbed conditions; and (4). Cases when there are sudden changes in solar wind pressure. (5). A magnetic storm cycle. In addition to observing the erosion and refilling of the plasmasphere, we can detect small localized depletions and enhancements, and monitor the effect of heavy ion contributions. We also outline experiments that can provide multi-instrument studies of the same flux tube. These use (a) closely-spaced ground magnetometers to record the field line resonance frequency and hence provide mass density information, (b) co-located VLF receivers that simultaneously monitor the electron density, (c) RPI and EUV data from the IMAGE spacecraft, providing in situ electron and helium density information, and (d) mathematical modelling of the constituent densities and temperatures for this flux tube. These measurements provide the first intercalibration of different ground-based and in situ techniques and lend new insight on plasma dynamics within the plasmasphere.

**GAIII.10/10P/A01-002 1420**

**PLASMASPHERIC MASS COMPOSITION DYNAMICS: IMAGE AND GROUND BASED RESULTS**

David BERUBE<sup>1</sup>, Mark B. MOLDWIN<sup>2</sup>, James L. GREEN<sup>3</sup>, Shing F. FUNG<sup>4</sup> (<sup>1</sup>Department of Earth and Space Sciences, University of California, Los Angeles, <sup>2</sup>Institute of Geophysics and Planetary Physics, University of California, Los Angeles, <sup>3</sup>NASA Goddard Space Flight Center, Greenbelt MD)

The dynamics of plasma composition in the inner magnetosphere is not fully understood. It is known that the concentration of heavy ions in the ionosphere increases during times of enhanced geomagnetic activity, with the highest concentrations occurring during severe storms. The equatorial plasma mass density of the inner magnetosphere can be inferred using pairs of ground based magnetometers by measuring field line eigenfrequencies and invoking a model of the plasma distribution along the field line. The Radio Plasma Imager (RPI) on the IMAGE spacecraft takes routine measurements of the electron number density in the plasmasphere and plasmatrough. Knowledge of the plasma mass density and electron number density allows us to track the average mass of particles in these regions as a function of geomagnetic activity, local time, and L shell. Using pairs of ground magnetometers from the MEASURE array and overflights of the IMAGE spacecraft from 2000 and 2001, we have constructed a database of average particle mass for field lines between  $L=1.75$  and  $L=3.12$  as functions of local time and magnetospheric conditions. Assuming the magnetospheric plasma consists only of hydrogen, helium, and oxygen, we are able to constrain the plasma composition.

**GAIII.10/10P/A01-003 1440**

**CO-ORDINATED IMAGE SATELLITE AND GROUND-MAGNETOMETER OBSERVATIONS OF AN ANOMALOUS CROSS-PHASE REVERSAL AT L = 3.2: THE SIGNATURE OF A STEEP PLASMAPAUSE?**

Zoe C. DENT<sup>1</sup>, Ian R. MANN<sup>2</sup>, F.W. MENK<sup>3</sup>, J. GOLDSTEIN<sup>4</sup>, L.G. OZEKE<sup>2</sup> (<sup>1</sup>University of York, Heslington, York, YO10 5DD, UK, <sup>2</sup>University of Alberta, Edmonton, Canada, T6G 2J1, <sup>3</sup>University of Newcastle, Newcastle, NSW, Australia 2308, <sup>4</sup>Rice University, Houston, TX 77005-1892, USA)

The cross-phase technique was applied to magnetometer data from a meridional chain of ground-based magnetometers from the SAMNET, IMAGE and BGS chains in the northern European sector. Between 0800 and 1200 UT (UT = MLT) on the 14th May 2001 a region of anomalous cross-phase reversal was observed by two sets of station pairs (ESK-LER and GML-LER) whose mid-points are located at  $L = 3.16$  and  $L = 3.33$ . On a conjugate pass by the IMAGE satellite the Radio Plasma Imager (RPI) instrument measured a sharp plasmopause signature close to this L-shell; a decrease of electron density by a factor of 8 being observed between  $L = 3.0$  and  $L = 3.25$  from 0840-0846 UT near the equatorial plane and within 90 minutes of LT of the reverse cross-phase signature observed on the ground. We believe that this event represents the first observation of a cross-phase reversal co-located with an in-situ measurement of a sharp plasmopause. Previous studies have looked for a reverse cross-phase plasmopause signature, however, such signatures are not routinely observed. Using a simple dipolar field model, we show that the density profile across the plasmopause must decay faster than  $L^{-6}$  in order for a turning point in Alfvén frequency to be developed across L-shells. The IMAGE RPI data shows that this criteria is satisfied for the satellite pass conjugate to the ground-based reverse phase signature on this day. As the cross-phase reversal only exists in the European sector magnetometer data between 0800 and 1200 UT, this suggests that local-time structure is present in the radial density profiles on this day. Moreover if plasmopause density profiles shallower than  $L^{-6}$  are more typical, then this may explain in part why observations of plasmapausal cross-phase reversals have remained so elusive.

**GAIII.10/10P/A01-004 1500**

**STORM TIME PLASMA MASS DENSITY ESTIMATED USING ULF WAVES OBSERVED BY CRRES**

Kazuo TAKAHASHI<sup>1</sup>, Richard E. DENTON<sup>2</sup>, Roger R. ANDERSON<sup>3</sup>, W. Jeffrey HUGHES<sup>4</sup> (<sup>1</sup>The Johns Hopkins University Applied Physics Laboratory, <sup>2</sup>Dartmouth College, <sup>3</sup>University of Iowa, <sup>4</sup>Boston University)

The frequency of standing Alfvén waves has been used to estimate the plasma mass density based on the fact that the Alfvén velocity depends on the density. This technique by itself provides no information on ion composition, but with additional information on the electron number density one can find the total contribution of heavy ions to the mass density. The capability to monitor the behavior of heavy ions is important in understanding the formation of the ring current. In this paper we estimate storm time ion mass density using ULF waves detected by the CRRES spacecraft. A 40-day period in August-September, 1991 is chosen for analysis because the spacecraft was located in the postnoon sector and routinely detected toroidal mode standing Alfvén waves. Dynamic spectra of the B and E fields are generated for each CRRES orbit for identification of the fundamental frequency of the toroidal waves. A numerical method similar to that of Denton et al. [J. Geophys. Res., page 29,915, 2001] is used to relate the frequency to the mass density at the position of the satellite. We define a mass factor by dividing the mass density (in units of proton mass per cc) by the electron number density determined from the CRRES plasma wave data. The mass factor is greater than 1.0 as expected and varies significantly with Dst. A positive correlation is found between the mass factor and the magnitude of Dst. By contrast, the electron number density is not correlated with Dst. This result implies that intensification of the ring current does not occur from the increase of the number of particles and that a large fraction of the storm-time ring current is carried by heavy ions.

**GAIII.10/10P/A01-005 1520**

**TRAVEL-TIME MAGNETOSEISMOLOGY: A NEW DIAGNOSTIC TOOL FOR SPACE WEATHER STUDIES**

Peter J. CHI, Christopher T. RUSSELL (Institute of Geophysics and Planetary Physics, UCLA)

In the last few years, the studies on the propagation of sudden impulses and that of impulsive ULF waves have led to a new remote sensing method that is similar to what seismologists use to probe the interior structure of the Earth. This method, dubbed "travel-time magnetoseismology", is to utilize the measurements of the signal arrival time at different locations, either on the ground or in space, to infer the plasma density that controls the propagation speeds of MHD waves. Not only does travel-time magnetoseismology provide a useful diagnostic tool of the state of the magnetosphere, it also closely ties with the physics of MHD waves propagation in the inhomogeneous magnetosphere. In this paper we present a comprehensive overview of the subject and discuss the directions of future development. We find that Tamao's theory of preliminary impulse arrival provides a good and easy-to-use forward model in travel-time magnetoseismology. The time of wave energy propagation can be approximated by the sum of the travel time of fast-mode propagation from the source to the field line of concern and that of the subsequent Alfvén-mode propagation to the point of

observation, both strongly dependent on the plasma density distribution in the magnetosphere. The characteristics of Tamao's travel time have been confirmed by recent MHD simulations, as well as by observations of various impulsive perturbations of magnetic fields, such as the preliminary impulse of sudden commencements, magnetic impulse events (MIEs), and the beginning phase of Pi 2 waves. In particular, the capability of inferring the nightside plasma density from the arrival time of Pi 2 enables the travel-time method to be complementary to the field line resonance method that is mainly effective for the dayside magnetosphere. We also developed a nonlinear optimization algorithm for inverting the parameters in plasma density distribution, and the results based on test data show that the procedure well determines the location of the plasmopause and the density in the plasmasphere. Also provided by the inversion is the source location of the signal, a valuable piece of information for understanding the generation mechanisms of these impulsive events. In the end, we will assess how the inclusion of spacecraft data enhances the accuracy of plasma density estimation, as well as the expanding capabilities of travel-time magnetoseismology in the future as ground magnetometer networks and multi-satellite missions proliferate.

**GAIII.10/10P/A01-006 1540**

**PLASMA DENSITY DIAGNOSIS BASED ON FIELD LINE RESONANCES IN 3D MAGNETOSPHERE**

C.Z. CHENG, S. ZAHARIA (Princeton Plasma Physics Laboratory, Princeton University)

Field line resonance (FLR) has been considered as a diagnostic tool for determining the density distribution in the magnetosphere. Most FLR theories are based on the cold plasma model which is limited in applicability to the low plasma beta region of the inner magnetosphere. In the plasma sheet and magnetotail, plasma beta can be significantly larger than unity and we have developed a new MHD FLR theory for the magnetosphere by allowing arbitrary isotropic pressure distribution in the equatorial plane as well as cold plasma density distribution. A new contribution due to the longitudinal pressure gradient and geodesic magnetic field curvature is found in the shear Alfvén FLR equation. This new term together with the coupling between shear Alfvén waves and slow magnetosonic waves due to high plasma beta causes the shear Alfvén FLR frequency to be reduced to the 1 - 4 mHz range observed at auroral latitudes. Numerical solutions of the FLR frequencies are presented for 3D magnetospheric field in force balance with plasma pressure as well as model magnetic fields such as Tsyganenko's models. The results can be employed to compare with FLR observations to obtain the distribution of cold and warm plasma densities and magnetic field in the closed field line region of the magnetosphere.

**GAIII.10/10P/A01-007 1600**

**MAGNETOSPHERE-IONOSPHERE-ATMOSPHERE-EARTH ELECTROMAGNETICALLY COUPLED MODEL FOR SPACE- WEATHER STUDY**

Akimasa YOSHIKAWA<sup>1</sup>, Kiyohumi YUMOTO<sup>2</sup>, Masahiro ITONAGA<sup>3</sup> (<sup>1</sup>Department of Earth and Planetary Sciences, Kyushu University, <sup>2</sup>Space Environment Research Center, Kyushu University, <sup>3</sup>Faculty of Education, Yamaguchi University)

To clarify the aspects of space weather in the earth environments, it would be indispensable to understand the self-consistent picture of magnetosphere-ionosphere coupling in the context of global and transient. To achieve this, we construct a comprehensive model for ionosphere-atmosphere-Earth electromagnetically coupled system which enable to describe the formation process of global ionospheric current caused by field-aligned current (FAC) closure via the ionospheric conducting and atmospheric displacement currents. In this model, the ionospheric slab (conductor) is separated by Earth's ground plane by atmospheric region forms a capacitor. Outgoing current flows in the ionospheric slab and return current flows on the ground plane, which forms an inductor. Thus, ionospheric slab act as if it has a capacitor in parallel to ground inductor in series. Electric field between ionospheric slab and ground plane stores energy in dielectric atmospheric region. Charge present in ionospheric slab and induced in ground plane creates a shunt self-capacitance. Magnetic field around current in ionospheric slab stores energy in magnetic field. The magnetic field links the loop formed by the conductor and ground plane and creates series self-inductance. Using this model, the roles of the FAC closure via the currents in the ionosphere-atmosphere-Earth electromagnetically coupled system especially in the ULF range are clarified. The FACs lose their stored electromagnetic energy in the ionosphere through Joule dissipation; this process is caused by the closure of the FAC via the ionospheric divergent Pedersen current carried by ions. On the other hand, the FAC closure via the divergent Hall current carried by electrons gives a growing energy of rotational Hall current, causing it to radiate Poynting fluxes that lead to the growth of a poloidal-type magnetic field in the magnetosphere and atmosphere. Furthermore, the FAC closure via the atmospheric displacement current provides Poynting fluxes for generation of non-local ionospheric current system. In this study, we will show the detail of physics of the redistribution process of FAC's momentum and energy into current in the ionosphere-atmosphere loading region.

**GAIII.10/10P/A01-008 1620**

**PROBING PLASMASPHERIC RESONANCES WITH TWO INDEPENDENT ULF TECHNIQUES**

Fred W. MENK<sup>1</sup>, Mark CLILVERD<sup>2</sup>, Keith YEARBY<sup>3</sup>, Gennadi MILNEVSKI<sup>4</sup>, Neil Thomson<sup>5</sup>, Mike ROSE<sup>6</sup> (<sup>1</sup>University of Newcastle, <sup>2</sup>British Antarctic Survey, <sup>3</sup>University of Sheffield, <sup>4</sup>Ukrainian Antarctic Centre, <sup>5</sup>University of Otago, <sup>6</sup>British Antarctic Survey)

Previously it has been shown that by using arrays of ground-based magnetometers it is possible to determine the resonant frequency of ULF waves in the inner magnetosphere using the paired response of the magnetometers to pulsations i.e. the cross-phase. It is also well known that the motion of plasmaspheric field aligned ducts can be observed by analysing the Doppler shift of ducted man-made whistler-mode signals. Both of these measurements tend to be single point, or at least single longitude. The pulsations are essentially a daytime probe, while the whistler-mode signals are more often observed during nighttime. At dawn they should be complementary. Previously, using a VLF Doppler system several field-aligned plasmaspheric ducts have been observed to oscillate at close to the fundamental oscillation frequency for  $L=2.5$  field lines. However no ground-based magnetometer data could be compared with these results as the nearby system was unable to resolve the  $<1$  nT pulsation amplitudes that were presumably occurring at the time. During Doppler pulsations the field line has an anti-node of motion in the equatorial plane and the Doppler shift is responding almost entirely to the radial component of the duct motion, and good correlations are expected with the H-component of the geomagnetic field measurements. Here we analyse Doppler shift pulsations from the USA 24.0 kHz VLF transmitter received with an aerial located in the Antarctic Peninsula. Data were collected at  $L=2.5$  during 2001 in the morning hours 08-12 UT (04-08 LT) when Pc3 field-line resonance was likely to occur. Magnetic pulsation information from an array of co-located magnetometers is compared to the Doppler pulsation data, and detailed resonance conditions inferred. We concentrate on several well-defined pulsation events using cross-phase analysis to conclusively identify resonance frequencies and associated harmonics,

comparing these with the pulsation frequencies observed in the VLF Doppler shift records.

**GAIII.10/10P/A01-009**

**1640**

**THE ROLE OF WAVES IN RADIATION BELT MODELING AND SPACE WEATHER STUDIES**

Danny SUMMERS (Department of Math and Stats, Memorial University of Newfoundland)

A full understanding of radiation belt physics is a prerequisite to successful modeling of the geospace environment and to accurate space weather forecasting. In addition to ULF wave driven cross-L diffusion, complete models of radiation belt electron transport should include wave-particle interaction effects, i.e., energy diffusion and pitch-angle diffusion. Electrons can be accelerated by stochastic gyroresonant interactions with VLF chorus, while electron precipitation losses can result from pitch-angle scattering by VLF and EMIC waves. In this paper we present a CRRES survey of VLF wave data in the outer zone during 26 geomagnetically-disturbed periods, and discuss the significance of these observations with respect to local stochastic electron acceleration. We further present a comprehensive analysis of EMIC wave observations from CRRES, and discuss the implications of the results for electron precipitation by strong diffusion scattering. The importance of incorporating the effects of wave-particle interactions in radiation belt modeling and space weather investigations is emphasized.

**GAIII.10/10P/A01-010**

**1700**

**STOCHASTIC TECHNIQUES FOR GLOBAL PLASMASPHERIC PROFILE ESTIMATION USING VLF WAVES**

Yoshitaka GOTO<sup>1</sup>, Yoshiya KASAHARA<sup>2</sup>, Toru SATO<sup>1</sup> (<sup>1</sup>Department of Communications and Computer Engineering, Kyoto University, <sup>2</sup>Department of Information and Systems Engineering, Kanazawa University)

The global electron density distribution in the earth's magnetosphere is one of the most important information for space weather studies. For such global distribution, however, there are limitations in a direct observation from a single satellite. Recently, several remote sensing techniques are proposed to obtain such global structures. In such techniques, global electron density distributions are generally represented by a parametric or nonparametric model and parameters in the model are evaluated by goodness-of-fit to observations. We have developed a determination technique of global electron density profiles in the earth's plasmasphere using VLF waves observed by a scientific satellite. Since the characteristics of VLF waves propagating in the plasmasphere reflect electron density distributions along their propagation paths, parameters in a global plasmaspheric model can be determined from continuous observation of the waves along a satellite trajectory. In the present study, we use wave properties of Omega signals and nonducted whistlers for the reconstruction of electron density profile in the plasmasphere. The time delay and wave normal directions of the Omega signals can be determined from the observed wave data. On the other hand, these properties can also be calculated by ray tracing under an appropriate electron density model. In the same way, the spectrograms of the nonducted whistlers are also calculated by ray tracing. By comparing the wave properties obtained observationally and theoretically, the parameters in the density model are determined. The realization of the algorithm requires an appropriate model to represent global plasmaspheric density profile. A desirable model should satisfy the following two conditions; (i) the model is represented by a function which has as small number of parameters as possible, and (ii) any plasmaspheric profile can be reproduced by choosing a set of appropriate parameters in the model. We introduce a new analytical model which consists of a stochastic differential model and a parametric model. By applying the semi-parametric model, the number of model parameters are drastically reduced but the flexibility of the model is considerably improved. The parameters of the model are evaluated by the goodness-of-fit between observed wave properties and theoretically calculated ones. In order to take the various possibilities of the wave properties at an observation point into account, we introduce an evaluation technique in which the wave properties are represented by stochastic variables with their own probability distributions. The evaluation index is derived from the stochastic variables. From the sensitivity analysis of the evaluation index for the estimation error of densities, we confirmed that the index is valid to reconstruct the global plasmaspheric density profiles. The Akebono satellite have already observed for 13 years in the inner magnetosphere, and the data are accumulated in a database. It is expected that the long term variation and average features of the global electron density profiles for one solar cycle are revealed by the developed method.

**GAIII.10/10P/A01-011**

**1720**

**THE AVERAGE ELF/VLF WAVE POWER RECEIVED ON THE GROUND IN ANTARCTICA, AND ITS DIURNAL, SEASONAL AND SOLAR-CYCLE VARIATIONS**

A.J. SMITH (British Antarctic Survey, Madingley Road, Cambridge CB3 0ET, UK)

Space-weather events such as large magnetic storms are associated with changes in ground-observed ELF-VLF radio waves. For a fixed receiver, the causes may be a combination of a source effect and source-receiver propagation effects. For a magnetospheric source, the latter will generally comprise magnetospheric, transionospheric and subionospheric segments. In order to interpret such changes in the context of models, and conversely to use the data for diagnostics, we need to know the average wave power levels and their variations on different time scales, diurnal, annual etc. These will then serve as a reference against which to assess the sporadic space-weather related effects. Although several empirical models of ELF/VLF noise levels have been constructed in the past for VLF radio engineering applications, they have generally been poor in the polar regions, where space weather effects maximise, because of lack of data. Here we report the results of a systematic study of the VLF/VLF waves observed at Halley station, Antarctica (76S 27W, L=4.3). We use a complete solar cycle (1992-2002) of nearly continuous (>95%) data from the VELOX instrument which comprise 1s resolution measurements of ELF/VLF wave power, arrival azimuth, polarisation and peak-mean-minimum ratios, in eight frequency bands from 500 Hz to 10 kHz, though for the present purpose we have used only the wave power data. The original data are 1s time resolution, but the wave intensities are highly variable on this time scale, so we have worked initially with one-hour averages. At each of the eight frequencies we have found the average wave power and the amplitude and phase of the 1-day, 1-year and solar cycle components. Three different regimes are exemplified by the 1 kHz, 3 kHz and 9 kHz channels. At the lowest frequency the transionospheric propagation absorption is low while the subionospheric absorption is moderate. The receiver has a effective large field of view. The dominant signals are ducted whistler mode waves such as chorus, originating from a large volume of the magnetosphere; the dawn chorus peak and the equinoctial maxima can be identified and quantified. At 3 kHz, the transionospheric absorption is moderate while the subionospheric absorption is high. The receiver has a small effective field of view, and activity is dominated by whistler mode signals propagating close to the Halley field line. At the highest frequency, no transionospheric absorption is high while the subionospheric absorption is low. magnetospheric signals are observed (except auroral hiss), and radio atmospheric from tropical thunderstorms dominate. The latter still have space weather diagnostic applications as their propagation is

affected by downcoming particle precipitation from the magnetosphere.

**GAIII.10/10P/A01-012**

**1740**

**NEAR-EARTH SPACE DIAGNOSTICS BY MF WAVES (ALTERNATIVE OF LF WAVES)**

Donat V. BLAGOVESHCHENSKY<sup>1</sup>, Olga MALTSEVA<sup>2</sup> (<sup>1</sup>St. Petersburg University of Aerospace Instrumentation, <sup>2</sup>Institute for Physics, University of Rostov-on-Don)

Instead of diagnostics of the solar wind-magnetosphere-ionosphere system by LF waves, we would like to propose the diagnostics of plasma structures of the mentioned system by hectometric waves (middle frequencies, MF) in the range 1-3 MHz. Novelty consists in experimental revealing the magnetospheric propagation of MF waves (along the plasmopause) and computer modeling the conditions of propagation in the magnetosphere. Present research is devoted to three problems as follows: a) discovery of the geophysical conditions under which magnetospheric channeling the MF waves from the Earth's surface is possible; b) working out the method to determine the location of the main ionospheric trough and the plasmopause during disturbed periods, which could be the basis to introduce an effective geophysical index describing a value of disturbance; c) elaboration of the diagnostics method to estimate an electron concentration in the magnetosphere by analysis of experimental data of sounding the magnetosphere with frequencies 1-3 MHz and by carrying out the modeling the MF waves propagation with the help of the ray tracing method. I. The insufficiently known phenomenon of MF-wave propagation from the Earth's surface through the ionosphere and magnetosphere (guiding) to conjugate hemisphere and back to the transmitter has been investigated. According to the observations at St. Petersburg's station (L = 3.2) the echo signals are characterized by a low level of absorption and there is practically no dispersion or Doppler shift. The guiding effect is caused by the electromagnetic wave propagation into the magnetosphere near the main ionospheric trough and the plasmopause. The effect of MF-wave guiding allows to model the conditions of the transionospheric propagation in order to obtain observational delays of waves and to study the influence of plasma parameters on the group time of propagation  $t_g = \tau$ . II. Computer modeling fulfilled on the basis of ray tracing showed that guiding was possible only from area of the main ionospheric trough. The preliminary results are as follows. 1) The particular trough may be a duct for MF waves ( $f = 1.8$  MHz) by means of which waves may be captured, guided and reflected back to a transmitter location with an observational delay  $\tau = 0.29$  s. 2) Magnetospheric ducting is connected with: (a) low  $f_oF_2$  ( $f \pm 0.3$  MHz), and (b) a low-altitude gradient of  $N_e$  along a magnetic field line. 3) Relations between the locations of the transmitter-receiver, trough and plasmopause were found to guide MF waves. The proximity of  $L_{min}$ ,  $L_e$  and  $L_{max}$  locations should take place. Thus, the effect of MF guiding is most useful for the diagnostics of the plasmopause, poleward edge of the trough and the diffuse precipitation boundary through different space weather conditions.

**Friday, July 11 AM**

Presiding Chairs: A.J. Smith, V.A. Pilipenko

**GAIII.10/11A/A01-001**

**0830**

**ULF WAVES AT VERY HIGH LATITUDES**

Viacheslav A. PILIPENKO<sup>1</sup>, Nadezda V. YAGOVA<sup>1</sup>, Olga M. CHUGUNOVA<sup>1</sup>, Mark J. ENGBRETTSON<sup>2</sup>, Louis J. LANZEROTTI<sup>3</sup>, Alan RODGER<sup>4</sup> (<sup>1</sup>Institute of the Physics of the Earth, <sup>2</sup>Augsburg College, Minneapolis, MN, <sup>3</sup>AT&T Bell laboratories, NJ, <sup>4</sup>British Antarctic Survey, Cambridge, UK)

The paucity of ULF studies at very high geomagnetic latitudes was partly due to a dominating view that the polar cap is a relatively quiet area and thus ULF variations in this region are merely a combination of residual cusp and auroral activity. Here we present two new classes of ULF pulsations specific for the polar cap that have been analyzed using the data of magnetometer array in Antarctica and still have no established physical understanding. The first class comprises the polar geomagnetic variations in the period range 4-20 min, that have been designated as the cap associated Pi-3 pulsations. Statistical 2D patterns of spectral power and coherence show an occurrence of intense, but low spatial coherent, variations near the cusp projection and in the night side auroral region. At the same time, low amplitude Pi-3 pulsations are very coherent throughout the polar cap and are decoupled from the auroral and cusp ULF activity. The primary sources of long-period polar pulsations are probably related to the magnetosheath turbulence or tail lobe oscillations. Though an occurrence of narrow-band Pc3-4 waves (periods about few tens sec) in the polar cap was not expected by the ULF community, the search using the data from the trans-Antarctic profile of magnetometers unexpectedly revealed two regions of the high Pc3-4 activity. The first region corresponds to the near-noon cusp, and the second one in the polar cap corresponds to the morning flank of the magnetotail lobe. These groups of Pc3-4 emissions have different characteristics, and, probably, are related to different mechanisms. Statistics of ULF features at polar latitudes and correlative relationships with the solar wind and IMF parameters confirms the occurrence of two sources of Pc3-4 activity. Besides traditional channels of propagation of upstream turbulence to the ground (via the equatorial magnetosphere and the cusp), additional path - via the lobe/mantle, in the region with open field lines, is possible. The occurrence of narrow-band Pc3-4 waves in the polar cap provides a challenge to the ULF physics, because so far no resonant conversion/filtering mechanism on the open field lines has been identified.

**GAIII.10/11A/A01-002**

**0845**

**CONJUGATE PHASE STUDIES OF ULF WAVES IN THE PC5 BAND NEAR THE CUSP**

Yonghua LIU<sup>1</sup>, Brian James FRASER<sup>2</sup>, Ruiyuan LIU<sup>1</sup>, Pasha PONOMERANKO<sup>3</sup> (<sup>1</sup>Department of Upper Atmospheric Science, Polar Research Institute of China, <sup>2</sup>Department of Physics, University of Newcastle, NSW, Australia)

Conjugation of geomagnetic field lines at magnetic high latitude is variable, depending on solar wind and interplanetary magnetic field conditions. In this paper the geomagnetic conjugate point of a location under closed field lines near the cusp has been determined dynamically by examining the conjugate phase relation of ultra low frequency (ULF) waves in the Pc5 band using magnetometer data from high latitude ground stations at Longyearben (LYR), Hornsund (HOR) and Hopen Island (HOP) in the northern hemisphere and Davis (DAV), Zhongshan (ZHS) and Mawson (MAW) in the southern hemisphere. Cross spectral and coherency analysis methods are used to select conjugate Pc5 events and derive phase relations. The results show that near the cusp the geomagnetic field lines resonate mainly in the odd mode with the D component out of phase and the H component in phase, when observed at the two ends of the field line. Assuming this phase characteristic, the conjugate of LYR is typically located in the DAV/ZHS-region, and mainly east of Davis by about 10° CGM longitude. In a reverse mapping analysis the conjugates of ZHS and DAV are located in the LYR region, mainly west of LYR by 10°. These results are qualitatively consistent with corresponding locations derived from the Tsyganenko 1996 (T96) model. The relationship of the longitude movement of the conjugate of LYR with respect to the variation of IMF By is quantitatively consistent with the T96 model. However, the expected position of the

conjugate site of LYR (DAV/ZHS) derived from Pc5 phase for  $B_z = 0$  is moved westward (eastward) by about 10 CGM in longitude or ~300 km from that predicted by the T96 model.

**GAIII.10/11A/A01-003 0900**

**CONJUGATE STUDIES OF ULF WAVES DURING MAGNETICALLY ACTIVE PERIODS: FIRST RESULTS FROM SAMBA**

Athanasios BOUDOURIDIS<sup>1</sup>, Eftyhia ZESTA<sup>1</sup>, Dave BERUBE<sup>2</sup>, Mark MOLDWIN<sup>3</sup>, Ricardo MONREAL MAC-MAHON<sup>3</sup>, Marina STEPANOVA<sup>4</sup> (<sup>1</sup>Department of Atmospheric Sciences, University of California, Los Angeles, <sup>2</sup>Department of Earth and Space Sciences, University of California, Los Angeles, <sup>3</sup>Universidad de Magallanes, Chile, <sup>4</sup>Universidad de Santiago de Chile, Chile)

We present initial results of ULF wave power during active periods from the newly installed South American Meridional B-field Array (SAMBA). SAMBA is a new low-latitude meridional chain of magnetometers installed along the coast of Chile and in Antarctica. It is also partly conjugate to the MEASURE (Magnetometers along the Eastern Atlantic Seaboard for Undergraduate Research and Education program) magnetometer chain along the eastern coast of the United States. The combination of these two chains presents a unique opportunity for conducting conjugate studies of ULF waves at low latitudes ( $L < 3$ ). We present our initial results for Pc3-4 and Pc 5 waves. We select periods of active magnetic conditions ( $Dst < -30$ ) during the last eight months of 2002 when the first SAMBA stations became operational. We investigate the occurrence, power, phase, polarity and latitudinal dependence (within our latitude range) as well as the conjugacy of these waves during geomagnetically active periods. Initial results indicate that although there is generally good conjugacy in the occurrence of the Pc3-5 pulsations the power can be distributed differently with respect to frequency in the two hemispheres. We also investigate the conjugacy of field line resonances (FLRs) by using conjugate pairs of stations in the two hemispheres.

**GAIII.10/11A/A01-004 0915**

**SOME CHARACTERISTICS OF EQUATORIAL PC3,4 PULSATIIONS AND THEIR SOLAR CYCLE DEPENDENCE**

Madhusudhan RAO, Svs Sarma Satyanarayana SREEPATI (MAGNETOTELLURICS DEPARTMENT, NATIONAL GEOPHYSICAL RESEARCH INSTITUTE,)

Based on the analysis of a long series of data set (1970-'89) spanning nearly two solar cycles (part of solar cycle No.20, solar cycle No.21 & part of cycle No.22) from two observatories, Choutuppal (Gm. Lat.: 70 28'N) and Etaiyapuram (Gm.Lat.: 0. 60S), India, equatorial characteristics of Pc3,4 pulsations and their long term stability are examined. Pc3,4 pulsations together constitute nearly 75% of the total pulsation activity observed in the equatorial region of India. While Pc3's exhibit a highly stable double-peak pattern with peaks around 06 and 13hrs. LT in their diurnal occurrence, Pc4 activity is characterized by a sharp and dominant peak around 07hrs. LT for the entire period from 1970-'89. The Pc3,4 pulsation activity does not show any well-defined pattern in its seasonal occurrence pattern over the period of study. The solar cycle variation pattern of Pc3,4 activity is characterized by enhancements during years falling in the declining/minimum phase of the sunspot cycle unlike the longer period Pc activity (Pc5) which is known to closely follow the sunspot cycle. Pc3,4 pulsation examples from Etaiyapuram, the station located on the Dip equator, show good correlation pulsations with concurrent ISEE satellite data. The results are discussed in relation to the existing theories on their generation through upstream waves in the bow-shock region and their radial propagation towards equatorial latitudes. Key words: Pc3,4 pulsations, Dip equator, solar cycle, upstream waves.

**GAIII.10/11A/A01-005 0930**

**THE LOCAL TIME DEPENDENCE OF P12 DOMINANT FREQUENCY OBTAINED BY SIMULTANEOUS OBSERVATION AT 5 LOW-LATITUDE STATIONS**

DeSheng HAN<sup>1</sup>, Toshihiko IYEMORI<sup>2</sup>, Yufen GAO<sup>3</sup>, Masahito NOSE<sup>4</sup>, Yasuharu SANOO<sup>4</sup>, Fuxi YANG<sup>5</sup>, Wansheng LI<sup>6</sup> (<sup>1</sup>Department of Geophysics, Kyoto University, <sup>2</sup>Data Analysis Center for Geomagnetism and Space Magnetism, Graduate School of Science, Kyoto University, Kyoto, Japan, <sup>3</sup>Institute of Geophysics, CSB, Beijing, China, <sup>4</sup>Department of Information Management, School of Business Administration, Asahi University, Gifu, Japan, <sup>5</sup>Urumqi Basic Seismic Station, Urumqi, Xinjiang Uygur Autonomous Region, China, <sup>6</sup>Yinchuan Geomagnetic Observatory, Yinchuan, Ningxia Hui Autonomous Region, China)

1-second digital data from 5 stations located at low-latitude for the period from October 2001 to October 2002 was used to confirm the local time dependence of the dominant frequency of Pi2 pulsations at low-latitude. By analyzing 183 Pi2 pulsation events simultaneously recorded at the 5 stations, we acquired some statistical results about the frequency properties of Pi2 pulsations at low-latitude. The dominant frequency of H component of the Pi2 pulsation is lower on the dusk side than that on the dawn side. The dominant frequency has a peak value at the postnight. According to these results, we infer that the surface wave mode is also a plausible mechanism for generation Pi2 pulsations at low latitude. For the events, which have a common frequency at the 5 stations, the phase difference between any two stations shows that the Pi2 pulsations have no phase difference along longitude. We also found that the frequency of different part of Pi2 pulsation, i.e., the dominant frequency for the initial part and rear part of pulsation, is different.

**GAIII.10/11A/A01-006 0945**

**MAGNETOSPHERE-IONOSPHERE CURRENT SYSTEM RESPONSIBLE FOR THE GROUND MAGNETIC PERTURBATIONS DURING THE GEOMAGNETIC SUDDEN COMMENCEMENT**

Takashi KIKUCHI (Communications Research Laboratory)

Araki (Planet. Space Sci., 25, 373, 1977) demonstrated that the preliminary reverse impulse (PRI) of the geomagnetic sudden commencement (SC) occurred simultaneously at the afternoon high latitude and at the dayside dip equator, suggesting that the polar electric field was transmitted to low latitudes almost instantaneously. Instantaneous transmission to low latitudes on the nightside was identified with simultaneous onset of the high latitude PRI and the HF Doppler frequency deviations at low latitude (Kikuchi, J. Geophys. Res., 91, 3101, 1986). To explain the instantaneous transmission of the polar electric field, Kikuchi et al. (Nature, 273, 650, 1978), Kikuchi and Araki (J. Atmos. Terrest. Phys., 41, 927, 1979) proposed the TM0 mode waves in the Earth-ionosphere waveguide. Kikuchi et al. (J. Geophys. Res., 106, 15,555, 2001) further suggested significant Biot-Savart's effects of the field-aligned currents on the ground magnetic perturbations at the dayside mid latitudes. Most of the ground magnetic perturbations during the SC are a result of the magnetic effects of the magnetosphere-ionosphere current system composed of the magnetopause current, polarization current, field-aligned current and ionospheric Hall and Pedersen currents (Araki, Geophysical Monograph 81, 183, 1994; Kikuchi et al., 2001). On the other hand, the PRI at

mid and low latitudes could be attributed to the Alfvén waves converted from the three-dimensional compressional waves launched at the subsolar point on the magnetopause, resulting in the earlier occurrence of the maximum amplitude of the PRI at lower latitude (Tamao, Rep. Ionos. Space Res. Japan, 18, 16, 1964; Chi et al., J. Geophys. Res., 106, 18857, 2001). In this paper we examine the times of the onset and of the maximum amplitude of the PRI recorded at two separate equatorial stations, showing that the onset is simultaneous but the maximum amplitude occurs earlier at higher latitude. The simultaneous onset does not match the scenario including the three-dimensional propagation of the compressional waves, but match the TM0 mode waves in the Earth-ionosphere waveguide. The latitudinal dependence of the time attained by the maximum amplitude is explained as caused by relative contribution of the components of the magnetosphere-ionosphere current system. To apply the TM0 mode to the transmission of the polar electric field under the nighttime ionosphere, we evaluate the attenuation of the TM0 mode using the three-layer model of Kikuchi and Araki (1979). The finite conductivity of the nighttime ionosphere causes an attenuation of 12 percent for the distance of 10,000 km, which is much less than the geometrical attenuation due to the finite size of the polar electric field. Consequently, the TM0 mode in the Earth-ionosphere waveguide plays a major role in the instantaneous transmission of the ionospheric electric field and current to low latitudes both on the dayside and nightside.

**GAIII.10/11A/A01-007 1000**

**HOW MUCH ENERGY IS CONVERTED INTO ALFVEN WAVES FROM COMPRESSIONAL DISTURBANCE?**

Dong-Hun LEE<sup>1</sup>, Kihong KIM<sup>2</sup> (<sup>1</sup>Department of Astronomy and Space Science, Kyung Hee University, <sup>2</sup>Department of Molecular Science and Technology, Ajou University)

When sudden perturbations in the solar wind or the magnetotail disturb the magnetosphere, this impact is expected to launch compressional wave power. Owing to the inhomogeneity of plasma density and magnetic fields, it is well known that part of compressional energy is converted into transverse Alfvén waves. We quantitatively investigate how much energy is possibly mode converted in various boundaries such as at the magnetopause and the magnetotail. By adopting the invariant imbedding method, we calculate the absorption, reflection and transmission coefficients of compressional waves in an exact manner when the compressional waves propagate across the boundaries which include both cold and hot plasma regions.

**GAIII.10/11A/A01-008 1015**

**SLOW MHD WAVES AS THE PRIMARY CAUSE OF MAGNETOSPHERE-IONOSPHERE DISTURBANCES**

Takeshi IJIMA<sup>1</sup>, Manabu SHINOHARA<sup>1</sup>, Aoi NAKAMIZO<sup>2</sup> (<sup>1</sup>Communications Research Laboratory, <sup>2</sup>Kyushu University)

By using the low-energy plasma and magnetic field data acquired with the Geotail Satellite, we investigated the MHD characteristics of disturbances that were observed widely in the magnetosphere. This is an extension of the preceding study by Nakamizo and Iijima (2002), in which they found that the substance of magnetotail Pi2s is the slow MHD wave. We have determined the dynamical and thermodynamical properties of the disturbances whose components correspond to three groups of the time scale, 40-150 s, 150-600 s, and 600-1200 s. Principal characteristics determined here include the following: (1) For all the three frequency ranges, the disturbances exhibit almost same properties; (2) Plasma thermal pressure and magnetic pressure changes are exactly in antiphase; (3) Energy flux (i.e. the work done by the plasma and Maxwell stress) shows much larger intensity parallel to the magnetic field than that perpendicular to the field; (4) Overall stress balance is primarily determined by  $V_p$  force and  $J \times B$  force; (5) Nature of the disturbances is the slow MHD waves (disturbances). We conclude that the primary cause (source) of disturbances occurring in the magnetosphere-ionosphere system is ascribable to the generation of slow MHD waves (disturbances), and also the generation of field-aligned currents (transverse Alfvén waves) coupled with the former. Energy and momentum changes associated with the slow MHD disturbances are transmitted to the ionosphere via field-aligned currents and contribute to cause the plasma flow, ionospheric currents and the energy dissipation in the collisional ionosphere.

**GAIII.10/11A/A01-009 1030**

**SURFACE WAVE MODEL OF THE MAGNETOSPHERIC RESONANCES**

Petko I. NENOVSKI<sup>1</sup>, Umberto VILLANTE<sup>2</sup>, Patrizia FRANCA<sup>3</sup>, Massimo VELLANTE<sup>2</sup>, Alexander BOCHEV<sup>3</sup> (<sup>1</sup>Geophysical Institute, 1113 Sofia, Bulgaria, <sup>2</sup>Physics Department, University of L'Aquila, L'Aquila, Italy, <sup>3</sup>Central laboratory for Solar-Terrestrial Influences, Sofia, Bulgaria)

The magnetospheric cavity resonances in the Pc5 range exhibit specific amplitude, phase and polarization characteristics observed both in the magnetosphere and on the ground. They have been explained in the frame of recent cavity mode theories. On the other hand, although the mode frequencies are stable, close relationship exists between the solar wind parameters and the magnetospheric resonance occurrence and their intensity and dynamics. A lot of wave properties as different polarization in the magnetosphere (linear) and on the ground (elliptical), polarization plane orientation in the magnetosphere (roughly at 45 degree to the Sun-Earth direction) and occupation from low- to high latitudes remains unexplained. These evidences require more general examination of the magnetospheric resonance properties taking into account free boundary conditions being ignored in previous cavity theories. We suggest a treatment of the problem in the framework of the theory of MHD surface waves. To simplify our problem we use slab geometry and homogeneous plasma environment. Additionally we take into account various plasma density distributions in the plasmasphere and simple reflection properties at the infinitely thin sheet ionosphere. We obtain dispersion equation of MHD surface modes that yields discrete set of frequencies close to those recorded from well-known ULF magnetic field experiments. We derive also complicated polarization properties of the MHD surface modes depending on phase changes occurring at the ionosphere heights. The theoretical results are used for comparison with data from both ground observatories (low- and high latitude) and satellite magnetic field measurements (Interball and POLAR).

**GAIII.10/11A/A01-010 1045**

**MAGNETOSPHERE-IONOSPHERE COUPLING BY ALFVEN WAVES AT MID- AND LOW-LATITUDES**

Robert L. LYSAK (School of Physics and Astronomy, University of Minnesota)

Most previous theories describing the interaction of Alfvén waves with the ionosphere have concentrated on the auroral region at high latitude where the magnetic field lines enter the ionosphere nearly vertically. However, a number of wave phenomena indicate that wave propagation between high latitudes and lower latitudes may be important. Pc1 oscillations

can travel for over a thousand kilometers across magnetic field lines in the ionosphere, and the variation of dipole tilt over such distances can be significant. Ionospheric propagation of ULF waves is likely also to play a role in the propagation of signals during storm sudden commencements (SC's) in which signals can rapidly propagate around the Earth on time scales too fast for propagation through the magnetosphere. In addition, the relationship between low- and high-latitude Pi2 pulsations remains an open question. These wave propagation effects must be taken into account when using wave observations as diagnostics of magnetospheric processes. First results from a model of Alfvén wave propagation in the magnetosphere-ionosphere system that takes into account the dipolar structure of the field lines at lower latitudes will be presented in an attempt to address these wave propagation problems.

GAIII.10/11A/A01-011

1100

#### FLUCTUATION ANALYSIS OF THE IONOSPHERIC AND GEOMAGNETIC PLASMAS, USING VLF SIGNALS

Tomoya SAKAI<sup>1</sup>, Shin SHIMAKURA<sup>2</sup>, Kenji OHTA<sup>3</sup> (<sup>1</sup>Institute of Media and Information Technology, Chiba University, Japan, <sup>2</sup>Science and Technology, Chiba University, Japan, <sup>3</sup>Faculty of Engineering, Chubu University, Japan)

Artificial VLF signals observed at the geomagnetic conjugate point of the transmission station is analysed experimentally and theoretically in order to monitor the ionospheric and magnetospheric plasma dynamics. Since the VLF waves are considered to propagate along magnetospheric ducts in whistler mode and penetrate the ionosphere under specific conditions in mid-latitude, information about the plasma dynamics and structures along the propagation paths between transmitter and receiver can be extracted from the artificial VLF signals received on the ground. In this paper, the VLF signals which have been transmitted from Khabarovsk and received at Ceduna (L=1.8) are analysed by correlations among the received signal power, propagation delay time, location and scale of the ionospheric exit region, wave polarisation, and the fluctuation of the geomagnetic field. The influence of the geomagnetic pulsations Pc 3-5 is briefly discussed. The ionospheric exit region and wave polarisation are estimated by the ground-based direction finding techniques. The wave distribution function (WDF) method and the multiple signal classification (MUSIC) method are applied to the received signals. As the result, the exit region is found within the distance of about 200km from the observation site. The polarisation of the non-whistler mode due to the sub-ionospheric propagation is appeared quasi-periodically. In order to clarify the penetration mechanism in the ionosphere and the Earth-ionosphere waveguide effect, numerical calculations of the wave field on the ground induced by the VLF wave radiated from the magnetospheric ducts are also performed by the full-wave analysis. The received signal attenuation and estimation error of the direction finding results are evaluated by the full-wave calculations for a detailed discussion.

GAIII.10/11A/A01-012

1115

#### MAGNETOSPHERIC VLF HISS OBSERVATIONS BY ALOW-ALTITUDE POLAR ORBITER FOR SPACE WEATHER STUDIES

Tadanori ONDOH (Space Earth Environment Laboratory)

Latitudinal variations of magnetospheric VLF hiss observed in the topside ionosphere represent integrated spectra of whistler-mode VLF hisses propagating along geomagnetic field lines from wide sources in the magnetosphere. Substorm changes of magnetospheric VLF hiss regions are analyzed by using 6 frequency narrow band VLF electric field (50Hz-30kHz) data received from ISIS-2 at Syowa station, Antarctica. In a geomagnetic quiet or weak disturbed period, a broad-band polar hiss normally appears at geomagnetic invariant latitudes from the middle of auroral zone to about 80° and a narrow-band mid-latitude hiss around 5 kHz occurs at invariant latitudes from about 50° to 65°. The polar hiss is interpreted as whistler-mode Cerenkov emissions generated from inverted-V electrons precipitating from the plasmasheet, and the mid-latitude hiss is whistler-mode waves generated by the electron cyclotron instability around the equatorial plasmapause. In a substorm period, the polar hiss region shifts to lower latitudes or to inner L-shells and joins the mid-latitude hiss region as the substorm develops. This implies that the polar magnetosphere or high latitude horns of inner plasmasheet, where the polar hiss is generated, comes closer to the plasmapause together with L-shells of inverted-V precipitating electrons as the substorm develops. So, observations of magnetospheric VLF hiss by low-altitude polar orbiters are useful means for space weather studies.

GAIII.10/11A/A01-013

1130

#### THE TEMPORAL EVOLUTION OF SUBSTORM ENHANCED WHISTLER-MODE WAVES; THE RELATIONSHIP BETWEEN SPACE BASED OBSERVATIONS, GROUND BASED OBSERVATIONS AND ENERGETIC ELECTRONS

Gary A. ABEL<sup>1</sup>, Andy J. SMITH<sup>1</sup>, Nigel P. MEREDITH<sup>2</sup>, Roger R. ANDERSON<sup>3</sup> (<sup>1</sup>Physical Sciences Division, British Antarctic Survey, <sup>2</sup>Mullard Space Science Laboratory, University College London, <sup>3</sup>Department of Physics and Astronomy, University of Iowa)

One of the defining characteristics of substorm onset is the injection of energetic electrons. The observed evolution of the energy spectra of these injected electrons has been well documented and is understood in terms of energy dispersed gradient-curvature drifts. A less defining, but often observed, characteristic is the enhancement of equatorial whistler mode wave amplitudes. Whilst studies have categorised the occurrence of these waves in terms of location and geomagnetic activity levels, to our knowledge no attempt has been made to document and explain the evolution of the whistler frequency spectrum as has been done with injected electrons. In this paper we address this problem by examining 22 case studies of CRRES observations of substorm enhanced whistler mode waves. These observations were made close to the geomagnetic equator and between 02:00 and 06:00 MLT. The frequency of the enhanced whistler waves is seen to vary strongly with magnetic field strength and for this reason we re-plot the data in terms of the equivalent parallel resonant energy of an electron in first-order cyclotron resonance with a wave of a given frequency. We can interpret our findings in terms of the injected electron population and resonant ellipses in velocity space. Furthermore, we relate the findings of our study to observations of ducted waves seen on the ground as Substorm Chorus Events (SCEs) and conclude that the frequency dispersion seen in SCEs is dominated by electric field effects.

GAIII.10/11A/A01-014

1145

#### ELECTROSTATIC ELECTRON CYCLOTRON HARMONIC WAVES OBSERVED IN THE EQUATORIAL REGION OF THE PLASMASPHERE

Takayuki ONO<sup>1</sup>, Hiroshi OYA<sup>2</sup> (<sup>1</sup>Graduate School of Science, Tohoku University, <sup>2</sup>Fukui University of Technology)

Within dynamic spectra of 12 years observation of the plasma waves and sounder experiment (PWS) on board Akebono satellite, electrostatic electron cyclotron harmonic

(ESCH) waves are frequently observed in the equatorial region (M-LAT < 30 deg.) of the plasmasphere within an altitude range from 5000km to the apogee of the satellite (about 10,000km). The equatorial-plasmasphere ESCH waves (named as EP-ESCH waves) which appear above the UHR frequency at lowest harmonic number branch of the maximum frequency of the electrostatic electron cyclotron waves (Warren and Hagg, 1968), are commonly observable even in the quiet state of the plasmasphere. The EP-ESCH waves are observable in all the local time sectors, however, the occurrence probability showed clear enhancement in the early morning sector of 01-03 MLT. Sometimes the EP-ESCH waves are associated with other branch of the ESCH waves below the UHR frequency revealing a property of nonlinear wave particle interaction with the odd half harmonics branch of ESCH waves coupled by the cyclotron wave-particle interaction of the order of  $n = 1$ . Based on the analysis of the dispersion relation of ESCH waves, supra-thermal plasma with the energy of several tens eV with high temperature anisotropy is likely to generate the EP-ESCH waves in the plasmasphere. The similar type wave-particle interaction has been already identified in the topside sounder ionograms (Oya, 1971) and many plasma wave observations in the magnetosphere (Oya, 1972, Shawhan, 1979, Kurth et al., 1979). It is interesting that intense wave-particle interactions are stimulated in the plasmasphere which has been recognized as a moderate region of clod plasma only associated with radiation belt particles of very high energy. The occurrence character of the ESCH waves showed that there is a constant activation or a constant flow-in of free energy to generate the strong plasma instability of ESCH waves near the midnight sector of the plasmasphere. Existence of ESCH waves as well as the nonlinear wave particle interaction revealed more active and turbulent nature of the plasmaspheric plasma than it has been believed.

### GAIII.10-Posters

#### HOW CAN WE USE WAVES AS DIAGNOSTIC PROBES FOR SPACE WEATHER STUDIES?

Location: Site D

Friday, July 11 AM

GAIII.10/11A/D-001

Poster

0830-075

#### PC1 BURSTS IN THE POLAR CAP AS AN INDICATOR OF THE DAYTIME RECONNECTION

Vladimir V. SAFARGALEEV, Anna V. SEREBRYANSKAYA, Elena V. PCHELKINA (Polar Geophysical Institute, Apatity, 184200, Russia)

The data of induction magnetometer installed at Barentsburg observatory in Spitsbergen archipelago are analyzed in combination with the data of two other magnetometers located in Scandinavian and Kola Peninsulas. We considered the intervals of very large negative IMF Bz when the cusp is assumed to be shifted at large distance south of its statistical position and Spitsbergen turns out in the polar cap. Altogether, eight intervals were considered. In all cases the DMSP data indicated that Barentsburg observatory was in the polar cap, whereas the location of two others might be associated with either cusp or llll or bps projections. The magnetic pulsations of Pc1 frequency range were observed around the local noon and in the polar cap only. They had a form of several short-living bursts and lasted for 15 minutes. In the cases when the CUTLASS data were available, the interval of Pc1 activity coincided well with the appearance and decay of fast ionospheric convection flow channel. We think that these pulsations are originated from the magnetosheath (namely, from the plasma depletion layer) where the plasma is anisotropic and undergoes the IC-instability. Due to impulsive reconnection, the unstable plasma turns out on the magnetic field lines connected with the Earth's ionosphere and IC-waves may be seen from the ground as the bursts of Pc1.

GAIII.10/11A/D-002

Poster

0830-076

#### THE PLASMAPAUSE DETECTION BY MULTIPLE GROUND MAGNETIC FIELD OBSERVATIONS AT DIFFERENT LOCAL TIMES

Shuji ABE<sup>1</sup>, Kiyohumi YUMOTO<sup>2</sup>, Hideaki KAWANO<sup>3</sup>, Akimasa YOSHIKAWA<sup>4</sup>, Yuki OBANA<sup>1</sup>, Stepan I. SOLOVYEV<sup>5</sup>, Dmitry G. BAISHEV<sup>6</sup>, John V. OLSON<sup>7</sup>, E.W. WORTHINGTON<sup>8</sup> (<sup>1</sup>Graduate School of Science, Kyushu University, Japan, <sup>2</sup>Space Environment Research Center, Kyushu University, Japan, <sup>3</sup>Faculty of Science, Kyushu University, Japan, <sup>4</sup>IKFIA, Russian Academy of Science, <sup>5</sup>Geophysical Institute, University of Alaska, Fairbanks, <sup>6</sup>College Observatory U. S. Geological Survey)

One of the useful techniques for identifying the eigenfrequency of ULF waves is the dual-station H-component amplitude-ratio method. In this method, dynamic spectral pattern observed within the plasmapause boundary layer is opposite to that observed inside and outside the plasmasphere. The pattern inside and outside the plasmasphere is that naturally expected for the Alfvén speed decreasing with increasing L-value, which is expected for the geomagnetic field strength decreasing with increasing L and the plasma density whose L dependence is not strong; such an Alfvén speed profile leads to the resonant frequency decreasing with increasing L, consistent with the observation inside and outside the plasmasphere. Our explanation for the pattern observed within the plasmapause boundary layer is as follows: In the plasmapause boundary layer, the plasma density drastically decreases, and thus the Alfvén speed increases, with increasing L. Thus, the resonant frequency there increases with increasing L; this L dependence is opposite to that outside the boundary layer, and is consistent with the pattern observed at the plasmapause. Thus, we can detect the plasmapause from the ground by using this method. In this study, we use this method and analyze two data sets whose local times differ. One station pair consists of Tixie (geomagnetic latitude = 65.65, geomagnetic latitude = 196.90, L = 5.98; it belongs to the Circum-pan Pacific Magnetometer Network) and Chokurdakh (64.66, 212.14; CPMN), and the other pair consists of Poker Flat (65.60, 260.90; it belongs to the Geophysical Institute Magnetometer Array) and College (64.80, 264.11, CPMN). Analysis results and discussion on the plasmapause detection will be presented.

GAIII.10/11A/D-003

Poster

0830-077

#### ON THE FIELD-LINE RESONANCE POLARIZATION

Petko I. NENOVSKI<sup>1</sup>, Massimo VELLANTE<sup>2</sup> (<sup>1</sup>Geophysical Institute, 1113 Sofia, Bulgaria, <sup>2</sup>Physics Department, University of L'Aquila, L'Aquila, Italy)

Ionospheric effects on the field-line resonances (FLR) polarization are examined. We have taken into account the source (compressional) part of the field-line resonance magnetic field and studied its transmission through the ionosphere. Our examination of the FLR polarization reveals strong ellipticity effect (that is sometimes close to circular polarization). It

is found that there is an asymmetry in the ellipticity effect, i.e. the both maxima of ellipticity are of different magnitude and placed away from the FLR amplitude peak at distance ranging 1-3 times its semi-width. These FLR polarization features are dependent on frequency, horizontal scale and ionospheric conditions. The theoretical results are compared to experimental evidences.

**GAIII.10/11A/D-004** Poster **0830-078**  
**ULF SIGNATURE OF FIELD-ALIGNED CURRENTS IN THE DUSK MAGNETOSPHERE BY INTERBALL-AU AND POLAR**

Alexander Z. BOCHEV<sup>1</sup>, Petko I. NENOVSKI<sup>2</sup> (<sup>1</sup>Central Laboratory for Solar-Terrestrial Influences, Sofia, Bulgaria, <sup>2</sup>Geophysical Institute, Sofia, Bulgaria)

The POLAR and INTERBALL-AU spacecraft magnetic field experiments allow investigation of the time-spatial variation of large-scale field-aligned current (FAC) structures (Regions 1 and 2) at mid- and high-altitudes. The study includes two intervals over north high latitudes in the dusk magnetosphere: (1) 10 January 09-11 UT (consecutive transits) and (2) 11 January 03-06 UT (nearly conjugate situation at ~ 04:30 UT). FAC Regions 1 and 2 and concomitant ULF wave events that belong in the Pc3-5 range are simultaneously observed on both spacecraft. On January 11 a ULF wave period of ~5 minutes is identified. Within the FAC regions the ULF wave polarization goes from linear to elliptical. A polarization plane rotation at ~90 degree is clearly detected at the POLAR satellite heights. It occurs at the moment of transition from linear to elliptical polarization and coincides to the Region 2-Region 1 transition. One possible explanation of these ULF wave properties is changes in the plasma distribution and ionospheric conditions existing between upward and downward FAC regions.

**GAIII.10/11A/D-005** Poster **0830-079**  
**SEVERAL FACTORS OF PC 3-5 AMPLITUDES OBTAINED BY THE COORDINATED CPMN STATIONS**

Yuki OBANA<sup>1</sup>, Akimasa YOSHIKAWA<sup>1</sup>, Ray J. MORRIS<sup>2</sup>, Brian J. FRASER<sup>3</sup>, Stepan I. SOLOVYEV<sup>4</sup>, Kiyohumi YUMOTO<sup>5</sup> (<sup>1</sup>Earth and Planetary Sci. Kyushu University, Japan, <sup>2</sup>Australian Antarctic Division, Australia, <sup>3</sup>University of Newcastle, Australia, <sup>4</sup>Inst. of Cosmophysical Research and Aeronomics, Russia, <sup>5</sup>Space Environment Research Center, Kyushu University, Japan)

In order to understand several factors, which affect Pc 3-5 magnetic amplitudes, Pc 3-5 magnetic pulsations at the coordinated Circum-pan Pacific Magnetometer Network (CPMN) stations were analyzed. Amplitudes of magnetic pulsations observed on the ground can be expressed by  $B=A F(MLT) f(LT) \sigma$  where A is amplitude of source wave, F(MLT) indicates magnetic local time dependence of amplitude in the magnetosphere, f(LT) is a function of ionospheric conductivities at local time of a station, and  $\sigma$  is an amplification factor for each stations (Chi et al, 1996). The geomagnetic data used here are from the CPMN stations at Chokurdakh (CHD; M.lat.=64.67 deg., M.lon.=212.12 deg., L=5.46), Kotzebue (KOT; 64.52, 249.72, 5.40), and Macquarie Isl. (MCQ; 64.50, 247.84, 5.40) during the equinox seasons of 1994 and 1995. In the equinox, northern and southern hemispheres asymmetry of ionospheric conductivities can be neglected, thus, power ratio between KOT and MCQ can be considered to include a component of the local time difference factor:  $f(LT+dLT)/f(LT)$ . By using the inversion method, contaminated information of F(MLT) and f(LT) can be derived from daily variation of power difference between CHD-KOT and CHD-MCQ. While, pure f(LT) component can be extracted from daily variation of power difference between KOT-MCQ, because they are geomagnetic conjugate points each other. From the analysis, the following results are obtained. The F(MLT) of H component of Pc 4 showed different diurnal variation by months and years. The f(LT) of H component of Pc 4 has the maximum around 6 and 18 LT, and minimum around 12 LT. The  $\sigma$  of Pc 4 normalized by  $\sigma$  at MCQ are 1.71±0.02 at KOT and 1.53±0.01 at CHD in the H component, and are 3.10±0.24 at KOT and 1.94±0.03 at CHD in the D component. The minimum of f(LT) around local noon implies that the H component of Pc 4 is shielded by high conductivity ionosphere around noon. The very stable values of  $\sigma$  are remarkable, because this result indicates a possibility that  $\sigma$  is a good index of geological effects on magnetic pulsations.

**GAIII.10/11A/D-006** Poster **0830-080**  
**FIELD-LINE RESONANCES TRIGGERED BY SSC ONSETS**

Harri E. LAAKSO<sup>1</sup>, A. MASSON<sup>1</sup>, K.-H. GLASSMEIER<sup>2</sup>, M.J. ENGBRETSON<sup>3</sup> (<sup>1</sup>ESA/ESTEC/Code SCI-SH, Noordwijk, The Netherlands, <sup>2</sup>Institut für Geophysik und Meteorologie, Braunschweig, Germany, <sup>3</sup>Department of Physics, Augsburg College, Minneapolis, MN)

One of typical consequences of storm sudden commencements (SSC) in the magnetosphere is the occurrence of large-amplitude wave activities, such as low-frequency field line resonances (FLR). They are triggered by compressional waves generated at the magnetopause by fast moving solar wind disturbances. During its lifetime, since February 1996, the Polar satellite has collected observations during a few hundred SSC's, and in many cases the satellite was appropriately located on dipolar field lines where the field-line resonances can occur, and so we can study statistically the occurrence rate and wave properties of FLR's during SSC's. More recently, the four Cluster satellites have collected valuable multi-point observations of the FLR's, and in one SSC event, occurred at 14:11 UT on August 30, 2001, the quartet was in the inner magnetosphere (at L = 4.3-5.5) at the moment of the onset. The SSC onset was immediately followed by strong field line resonances, persisting for an hour. During the time, Cluster 3 moved towards the perigee near L = 4, whereas the other three moved to higher L shells up to L = 7. This study will present details of the electric and magnetic field oscillations and the Poynting vector during the event. We particularly compare wave characteristics at four points as well as their L shell dependence.

**GAIII.10/11A/D-007** Poster **0830-081**  
**MONITORING OF THE PLASMA DENSITY IN THE EARTH'S PLASMASPHERE DURING MAGNETIC STORMS BY USING MULTIPLE GROUND OBSERVATIONS (L-1.3)**

Satoko TAKASAKI<sup>1</sup>, Hideaki KAWANO<sup>1</sup>, Yoshimasa TANAKA<sup>2</sup>, Akimasa YOSHIKAWA<sup>1</sup>, Masahiro SETO<sup>3</sup>, Masahide IIZIMA<sup>4</sup>, Kiyohumi YUMOTO<sup>5</sup> (<sup>1</sup>Department of Earth and Planetary Sciences, Kyushu University, Japan, <sup>2</sup>Venture Business Laboratory, Kyushu University, Japan, <sup>3</sup>Tohoku Institute of Technology, Japan, <sup>4</sup>Graduate School of Science, Tohoku University, Japan, <sup>5</sup>Space Environment Research Center, Kyushu University, Japan)

The field line resonance (FLR) below in the Earth's magnetosphere is caused by hydromagnetic waves. In ground-based observations of FLR phenomena, it is known that the amplitude of the H-component perturbation reaches a maximum at the resonant point, and that its phase jumps by 180 degrees across the resonant point. The cross-phase method and the amplitude-ratio method are useful for identifying these properties and determining the resonant frequency. The field line eigenfrequency is dependent upon the plasma density and the magnetic field intensity in the region of space threaded by the field

line, and the length of the field line. When we observe the eigenfrequency of the field line and assume models for the latitude profiles of the magnetic field and the plasma density (with the equatorial density as a free parameter), we can estimate the plasma mass density. Therefore, FLR is useful for monitoring temporal and spatial variations in the plasmaspheric density. In ground-based observations, we can identify FLR phenomena and measure the fundamental field line eigenfrequency by applying the cross-phase method and the amplitude-ratio method. We have installed three magnetometers at L ~ 1.3, and observed geomagnetic pulsations in the Pc3 range. Each adjacent stations are separated in latitude by 50 ~ 100 km. We have analyzed the magnetic field data from these stations by using the two methods, the amplitude-ratio method and the cross-phase method. As a result, we have identified FLR events and measured their frequencies; these data provide the plasma density at L ~ 1.3 varying with time. By using these data, we will discuss the temporary variation of the plasma density at L ~ 1.3 during magnetic storms. In addition, we note that the observed FLR frequency decreased with decreasing latitude: We interpret this feature to be the result of heavy ion (for example oxygen ions from the ionosphere) mass loading at low latitudes, which decreased the magnetic field line eigenfrequency there. It is possible that the plasma is mainly composed of heavy ions at L ~ 1.3. It deserves to be studied if the activity of this mass loading effect seen in the ground data, depend on the storm activity.

**GAIII.10/11A/D-008** Poster **0830-082**  
**DEDUCING PROPERTIES OF THE MAGNETOSPHERE USING HIGH LATITUDE PC 3-4 PULSATIONS**

Fred W. MENK, Timothy A. HOWARD (School of Mathematical and Physical Sciences, University of Newcastle)

It is now generally accepted that Pc 3-4 (10-50 mHz) pulsations recorded on the ground at low latitudes are the result of standing shear Alfvén mode field line resonances. At higher latitudes the resonance frequency moves into the Pc 5 (1-10 mHz) range. Although broadband activity extends into the Pc 3-4 part of the spectrum, narrowband signals are also recorded by ground magnetometers. The generation and propagation mechanism for these bandlimited pulsations is not clear. Using two months of IMAGE magnetometer data we have examined the amplitude, cross-phase and coherence of narrowband Pc3-4 pulsations as a function of latitude and longitude, and have determined the propagation velocity and coherence length of each event. Antarctic magnetometer data provided information on conjugate point phase and polarization of these events. The pulsations may have a number of generation mechanisms. One of these involves propagation of fast mode waves Earthward, coupling to travelling waves along field lines. Ground phase information then may provide information on the Alfvén velocity and hence magnetospheric density distribution. We illustrate this for specific events.

**GAIII.10/11A/D-009** Poster **0830-083**  
**THE DEPENDENCE OF SPATIAL STRUCTURES OF PC 3 PULSATIONS ON THE SOLAR WIND PARAMETERS AND GEOMAGNETIC INDICES**

Yoshimasa TANAKA<sup>1</sup>, Kiyohumi YUMOTO<sup>2</sup>, The CPMN Group<sup>3</sup> (<sup>1</sup>Venture Business Laboratory, Kyushu University, Japan, <sup>2</sup>Space Environment Research Center, Kyushu University, Japan)

We statistically studied two-dimensional spatial structures of the amplitude and phase of Pc 3 pulsations observed at the CPMN stations (L=1.0-5.5) on the ground. The obtained amplitude and phase structures indicated two characteristic components; one is strongly dependent on the magnetic latitude and the other is coherent over a wide range of latitude. It was concluded that the former is associated with the toroidal mode oscillations excited by the field line resonance (FLR) and the latter is likely to be global compressional mode oscillations. By mapping the obtained amplitude and phase structures onto the equatorial plane of the magnetosphere, we could see a twin-vortex structure of the magnetic perturbations in the magnetosphere. The centers of the vortices are located at 0600-800 LT and 1300-1400 LT around the plasmapause. It was interpreted that the vortex structure may be generated by the mode conversion from compressional waves, which propagate from the prenoon outer magnetosphere toward the Earth, to Alfvén waves around the plasmapause. In the present paper, we further investigate the dependence of the spatial structures of Pc 3 pulsations on the solar wind parameters and geomagnetic indices. Using the magnetic field data obtained from the CPMN stations during the period from March to September, 1994, the amplitude ratio, phase difference, coherence of Pc 3 pulsations are calculated by the fast Fourier transform (FFT) method. In the calculation, we use the H component of the sub-equatorial station, Guam (GUA, L=1.01), as a reference. The local time is divided into the 30-min intervals and each interval is categorized by the solar wind parameters and geomagnetic indices. The main results are summarized as follows. 1) Although the direction of the interplanetary magnetic field (IMF) is well correlated with the occurrence frequency, its effect on the phase structure of Pc 3 pulsations is small. 2) The phase structure is also independent of the IMF intensity. 3) The phase structure shows a weak dependence on the Kp and Dst indices. The FLR component statistically seen at L=2.1, 2.8 on the quiet geomagnetic condition is masked on the disturbed condition. It is supposed that the solar wind parameters and geomagnetic indices reflect conditions of the wave source and the magnetosphere, for example, the IMF direction and Kp index should be associated with the spatial distribution of upstream waves, which is one of major sources of Pc 3 pulsations, and the plasmapause position, respectively. Therefore, our results imply that the phase structure of Pc 3 pulsations is little affected by the source condition and is principally controlled by the magnetospheric condition.

**GAIII.10/11A/D-010** Poster **0830-084**  
**PROPAGATION OF ULF WAVES THROUGH THE IONOSPHERE IN THE PRESENCE OF OBLIQUE MAGNETIC FIELDS**

Colin WATERS, Murray SCIFFER, Fred MENK (Department of Physics, University of Newcastle and CRC for Satellite Systems)

Solutions for ultra low frequency (ULF; 1-100 mHz) wave fields that interact with the earth's ionosphere in the presence of oblique background magnetic fields are presented. The inductive shielding effect (ISE) reduces the wave amplitude on the ground and arises from the generation of an "inductive" rotational current in the ionosphere. The inductive response of the ionosphere is described by Faraday's Law and the ISE depends on the horizontal scale size of the ULF disturbance, its frequency and the conductivities. Previous descriptions of the ISE were developed within the context of a vertical background magnetic field which limits the application to high latitudes. In this presentation we have reformulated the description of the ISE in the ionosphere for oblique background magnetic fields so that the effect of an inductive ionosphere and the associated shielding of ULF waves for mid to low latitudes may be examined. It is found that the dip angle of the background magnetic field significantly affects the ground signature of ULF waves. Implications for inferring ULF wave properties in the magnetosphere from ground-based magnetometer measurements of ULF waves will be discussed.

**GAIII.10/11A/D-011** Poster **0830-085**

**FREQUENCY ESTIMATION OF IMPULSIVE Pc3 MAGNETIC PULSATIONS ON THE BASIS OF MODIFIED MEM**

Yoshihiro HIGUCHI (Department of Electronics and Information Engineering)

A modified method for estimating prediction error filter coefficients for a maximum entropy spectral analysis is presented. An averaged forward and backward prediction error power weighted by a window function is minimized and Levinson recursion is employed. Frequency shift for a truncated real sinusoid with additive noise can be reduced using a Blackman window function in computation of coefficient  $\gamma_{mm}$  in the  $m$ -th order prediction error filter. Spectra computed from a short truncated real sinusoid and compared with the Burg spectra show frequency resolution improvement and robustness of spectral peak locations. Modified maximum entropy spectral analysis is applied to make an accurate frequency estimation of impulsive Pc 3 magnetic pulsations observed at Yonezawa during morning hours. It is shown that the modified maximum entropy method using a Blackman window function can clearly resolve three components of spectral peak location at 30mHz, 55mHz and 85mHz.

**GAIII.10/11A/D-012** Poster **0830-086**

**DYNAMIC SPECTRA AND WAVELET STRUCTURE OF ULF WAVES IN THE MAGNETIC STORM OF JULY 15, 2000**

Olga Vasilievna KOZYREVA<sup>1</sup>, Natalia Georgievna KLEIMENOVA<sup>1</sup>, Jean-Jacques SCHOTT<sup>2</sup> (<sup>1</sup>Institute of the Earth Physics, 10.Bolshaya Gruzinskaya, Moscow, 123995, Russia, <sup>2</sup>Ecole et Observatoire des Sciences de la Terre, Strasbourg, France)

We studied the strong magnetic storm on July 15, 2000, caused by magnetic cloud (Bastille Day Event). The 1-3 mHz ULF waves, observed on the ground in the global scale, have been analysed by using 1-min sampling INTERMAGNET data. The analysis showed that strong IMF and ion density variations at the front edge of the magnetic cloud triggered the magnetic substorm and geomagnetic Pi3 range pulsations at the polar latitudes near the footprint of the open/closed field lines border. The dynamic spectra and wavelet structure of the polar Pi3 pulsation and IMF fluctuations showed a certain similarity. We suppose that ground pulsations, observed at polar latitudes, can be result of the direct penetration and nonlinear transformation of the interplanetary hydromagnetic waves into the polar cap. Another possibility can be attributed to the wave generation at ionosphere altitudes by the oscillations of the substorm electron precipitation, related to field aligned currents.

**GAIII.10/11A/D-013** Poster **0830-087**

**PI2 MAGNETIC PULSATION AT LOW LATITUDES**

Yu-fen GAO, Gui-ming LE (Institute of Geophysics, China Seismological Bureau)

Data of Pi2 magnetic pulsations obtained from SMALL (Sino-Magnetometer Array at Low Latitudes) are analyzed with wavelet. The spatial and temporal characteristics at low latitudes are presented. The results of typical events show that the maximal amplitudes are correlated with longitudes and the arrived time of maximal amplitude are correlated with latitudes. At the same time interplanetary parameters will be shown.

**GAIII.10/11A/D-014** Poster **0830-088**

**DETERMINATION OF ONSET TIMES OF LOW-LATITUDE PI2 MAGNETIC PULSATIONS**

Keiko FUKUYAMA<sup>1</sup>, Tomoyuki HIGUCHI<sup>2</sup>, Teiji UOZUMI<sup>3</sup>, Hideaki KAWANO<sup>4</sup>, Kiyohumi YUMOTO<sup>5</sup> (<sup>1</sup>Department of Earth and Planetary Sciences, Kyushu University, Japan, <sup>2</sup>Space Environment Research Center, Kyushu University, Japan, <sup>3</sup>The Institute of Statistical Mathematics, Japan, <sup>4</sup>the CPMN Observation Group)

Pi2 magnetic pulsations are observed globally and their occurrences are almost simultaneous with substorm onsets; therefore Pi2 has been known as a good indicator of onset of substorm. However, its trigger process, propagation mechanism and relationship with substorm have not been well understood. In addition, it is very difficult to objectively determine the onset times of Pi2 magnetic pulsations; a visual inspection for determining the Pi2 onset times could make its estimate biased. Therefore, it is necessary to establish an accurate and objective determination method. We have constructed and examined two procedures for an onset time determination of low-latitude Pi2 magnetic pulsations. The first method is based on such assumption that Pi2 is described by stochastically perturbed quasi-periodic oscillations. We applied the time-series analysis method developed for such data [Higuchi et al., 2002]. The second procedure that we developed relies on the definition in the literature [Saito, 1961] that Pi2 starts with  $dH/dt > 0$  in the middle or low latitude. We examined the differenced sequences of the H-component and identified a positive variation seen in them. Then, we have compared these results, and found that the results of the first method have time lag with 3-50 seconds behind those of the second one. This suggests that Pi2 has a non-periodic fluctuation at its initial stage and we have to determine the Pi2 taking account of this non-periodic fluctuation.

**GAIII.10/11A/D-015** Poster **0830-089**

**RELATIONSHIPS BETWEEN NEAR-EARTH TAIL SUBSTORM SIGNATURES AND GROUND PI 2S ONSETS**

Tohru SAKURAI, Yutaka TONEGAWA (Department of Aeronautics and Astronautics, School of Engineering, Tokai University)

Relationships between onsets of substorm signatures, such as dipole-like magnetic field changes, fast plasma flows and plasma injections observed in the near-Earth magnetotail in the midnight region and those of ground substorm/Pi 2's are studied. Present study is only a case study, in which a substorm event, consisting of successive two occurrences of plasma flows in the magnetotail is studied. The results are as follows, i.e., the first earthward plasma flow was observed with a high speed in excess of 570 km/s at L = 10 in the midnight magnetotail, which brought only an onset of Pi 2 oscillations on the ground only near the sub-auroral latitudes. While, the second plasma flow, which was observed 12 minutes later than the observation of the first plasma flow, brought at first an onset of negative bay at high latitude ground stations and successive development of substorm activity. However, the onset of the negative bay began about two minutes before the observation of the second plasma flow in the magnetotail at L = 10, and the onset of low latitude Pi 2 and/or a simultaneous occurrence of positive bay began three minutes later than the onset of the negative bay. From these results where the substorm should be triggered in the magnetotail, earthward or tailward compared with the observation point, i.e., the satellite location at L = 10, and onsets of substorm and/or Pi 2 on the ground from high to low latitudes are discussed in relation to the plasma flow in the magnetotail.

**GAIII.10/11A/D-016** Poster **0830-090**

**CORRELATIONS BETWEEN HIGH- AND LOW-LATITUDE PI 2'S AS A FUNCTION OF LONGITUDINAL DISTANCE RELATIVE TO THE AURORAL BREAKUP REGION**

Teiji UOZUMI<sup>1</sup>, Kiyohumi YUMOTO<sup>1</sup>, Hideaki KAWANO<sup>2</sup>, Akimasa YOSHIKAWA<sup>3</sup>, S. OHTANI<sup>4</sup>, S.I. SOLOVYEV<sup>5</sup>, E.F. VERSHININ<sup>6</sup>, K. LIOU<sup>7</sup>, C.-I. MENG<sup>8</sup> (<sup>1</sup>Space Environment Research Center, Kyushu University, <sup>2</sup>Department of Earth and Planetary Science, Kyushu University, <sup>3</sup>Applied Physics Laboratory, The Johns Hopkins University, <sup>4</sup>Institute of Cosmophysical Research & Aeronomy, <sup>5</sup>Institute of Cosmophysical Research & Radiowaves Propagation)

In order to investigate the generation and propagation mechanisms of Pi 2's in the magnetosphere, we made a comparative study between magnetometer data observed at high- and low-latitude CPMN stations and the ultraviolet image (UVI) data of aurora obtained by the Polar satellite. Correlation coefficients among H component of low-latitude Pi 2 and H, D component of high-latitude Pi 2 were calculated. Where, in this paper, we assumed and used high- and low-latitude Pi 2s as the manifestation of fast and Alfvén mode wave propagating in the magnetosphere, respectively. Results were classified by the relative position between each high-latitude station and the auroral breakup region. We then studied the dependence of the correlation coefficient of Pi 2s on the position relative to the auroral breakup region. In this paper we have found the following results. When high-latitude stations were separated longitudinally from auroral break up region larger than 1 hour, the average correlation coefficient between H component of low-latitude Pi 2 and H, D component of high-latitude Pi 2 became 0.86 and 0.87, respectively. On the other hand, when high-latitude stations were located in the same longitudinal span of auroral break up region, those coefficients decrease 0.69 and 0.63 respectively. We have found a tendency that, as the distance between a high-latitude station and the auroral break up region become larger, correlation coefficient between the H component of the low-latitude Pi 2 and the H (or D) component of the high-latitude Pi 2 increases. This means that the coupling between fast and Alfvén mode wave were observed clearly as away from auroral breakup region. This observational result suggested that high-latitude Pi 2's, which occur at a distance from auroral breakup region, are generated via mode conversion from fast to the Alfvén mode. That is, fast mode waves are first generated at the Pi 2 source region, propagate from there in a three dimensional manner, and then excite shear Alfvén mode waves via mode conversion. It suggests that generation of fast mode wave in the magnetosphere at the onset of substorm is the essential process for global Pi 2 occurrence.

**GAIII.10/11A/D-017** Poster **0830-091**

**LONGITUDINAL STRUCTURE OF LOW-LATITUDE PI2 PULSATIONS**

Masahito NOSE<sup>1</sup>, K. LIOU<sup>2</sup>, P.R. SUTCLIFFE<sup>3</sup> (<sup>1</sup>Data Analysis Center for Geomagnetism and Space Magnetism, Kyoto University, <sup>2</sup>Applied Physics Laboratory, Johns Hopkins University, <sup>3</sup>Hermanus Magnetic Observatory)

Recent studies have shown that when Pi2 pulsations were observed on the ground during nighttime, satellites that were inside the plasmasphere observed almost identical oscillations in the compressional and radial components of the magnetic field. Magnetic field oscillations in the plasma trough were less correlated with the ground Pi2 pulsations. This indicates that the plasmaspheric cavity mode resonance is a plausible mechanism for nighttime Pi2 pulsations. The plasmaspheric cavity mode is a wave mode in which fast mode waves emitted at a substorm onset bounce back and forth between two reflecting boundaries (the ionosphere and the plasmapause) and are radially trapped in the plasmasphere. This is likely to occur near the midnight meridian where substorms are thought to initiate, because the wave normal becomes nearly perpendicular to the reflecting boundaries there. On the contrary, waves may not be trapped for a long time on the flanks where the waves make oblique incident on the boundaries, resulting in no appearance of Pi2 pulsations. However, the longitudinal structure of the cavity mode resonance is yet to be investigated. In the present study we examined how characteristics of low-latitude Pi2 pulsations depend on longitude (magnetic local time), using ground data and auroral images from the Polar ultraviolet imager (UVI). The data period used in the study is from December 1996 through March 1997. The Polar/UVI images were used to identify the onset time and location of substorms as well as to infer auroral power enhancement. More than 500 events of auroral breakups with auroral power enhancement of >2.0 gigawatts are identified. Then we investigated variations of geomagnetic field in the Pi2 frequency band, using data from Kakioka (L=1.27, 208.5° geomagnetic longitude) and Hermanus (L=1.45, 82.2° geomagnetic longitude). We will present statistical results and discuss the longitudinal structure of the cavity mode wave.

**GAIII.10/11A/D-018** Poster **0830-092**

**ARE PI 2 MAGNETIC PULSATIONS A GOOD INDICATOR OF SUBSTORM ONSETS ?**

Kiyohumi YUMOTO<sup>1</sup>, Teiji UOZUMI<sup>1</sup>, Rui YAMAGUCHI<sup>2</sup>, Hideaki KAWANO<sup>3</sup>, Kan LIOU<sup>4</sup>, Ching -I MENG<sup>5</sup> (<sup>1</sup>Space Environment Research Center, Kyushu University, Fukuoka, Japan, <sup>2</sup>Department of Earth and Planetary Sciences, Kyushu university, Fukuoka, Japan, <sup>3</sup>The Johns Hopkins University applied Physics Laboratory, Laurel, USA)

Pi 2 magnetic pulsations recorded on the induction magnetogram appears at the beginning part of positive H-component bays on the ordinary magnetogram at mid- and low latitudes, starts with  $dH/dt > 0$ , and its onset had been believed to show one-to-one correspondence to individual bays. However, Yumoto et al.(2001) recently found non-perfect one-to-one correspondence between the auroral expansions identified by the Polar satellite and the Pi 2 pulsations, due to the wave characteristics of Pi 2s into low latitudes. In order to understand the role of Pi 2 magnetic pulsations in the substorm process, we re-examine one-to-one correspondence of low-latitude Pi 2s to magnetic bays observed at the CPMN stations, and auroral brightenings identified by the Polar ultraviolet images. At least 5 % of 119 multiple-onset Pi 2 events at the CPMN stations in the midnight sector of 2230-2330 LT, are found to occur without magnetic bays (and/or with bays of amplitude smaller than 0.4 nT at Guam) during magnetic quiet times of Kp-1. The Pi 2s without/with magnetic bays tend to occur  $\sim 10$ -40 s later than the start of N2 LBH-band auroral sudden brightenings. One-to-one correspondence of Pi 2s occurrence to auroral sudden brightenings (precipitations) is much better than that to magnetic substorm onsets (expansions). Pi 2s must be excited just as a manifestation of the coupling (intensification and/or formation of FAC) between the near-Earth magnetotail and the polar ionosphere. Pi 2s are still a good indicator of substorm onsets, but they should be used with care.

**GAIII.10/11A/D-019** Poster **0830-093**

**A NUMERICAL SIMULATION OF PI 2 PULSATIONS IN MIDDLE- AND LOW-LATITUDES**

Shigeru FUJITA<sup>1</sup>, Masahiro ITONAGA<sup>2</sup> (<sup>1</sup>Meteorological College, <sup>2</sup>Yamaguchi University, Faculty of Education)

The Pi2 pulsation shows a cavity-mode behavior in the middle- and low-latitudes. The present paper deals with the transient behavior of MHD perturbations in the inner



magnetosphere induced by an impulsive localized eastward current (source current) as a model of Pi2 pulsations. The magnetospheric model consists of a dipole magnetic field, plasmasphere, ionosphere with Pedersen conductivity, and a free outer boundary. The source current is an impulsive magnetospheric current at the onset of the substorm current wedge, and is distributed around the equatorial plane of  $L = 10$  with 2 hour longitudinal extent around midnight. The numerical results allow us to track variation in the expected Pi2 pulsation signals in both local time and  $L$ . The poloidal mode wave exhibits plasmasphere virtual resonance (PVR), resulting in large amplitudes around midnight, weakening towards dayside. The toroidal mode wave is excited as a field-line resonance immediately after the wave front of the poloidal mode wave crosses regions where the radial gradient of  $V_a$  is steep. The toroidal mode wave has largest amplitude at the local time of the east/west edge of the source current. The duration of this wave is about 5 min. In the middle plasmasphere where the radial gradient of the  $V_a$  is smaller, the poloidal mode wave tends to predominate over the toroidal mode wave. These numerical results are consistent with satellite observations, in so far as the day-night asymmetry of Pi2 pulsations and observation of transient toroidal waves. In addition to this simulation, we perform another simulation by using a plasmasphere model that is non-uniform in longitudinal direction. Power spectra of a plasmaspheric virtual resonance are calculated. It is shown that the spectra depend on longitude. Therefore, a cavity resonance mode can have local time depending spectra when the plasmasphere is non-uniform in a longitudinal direction. This fact concludes that the local time dependent peak frequencies of the mid- and low-latitude Pi2 pulsations discussed by Kosaka et al. [2002] are also explained by the cavity resonance model. We also discuss that the surface eigenmode can be a possible generation mechanism for Pi2 pulsations localized in a longitudinal direction.

**GAIII.10/11A/D-020** Poster **0830-094**  
**PROPAGATION STRUCTURE OF PI2 PULSATIONS DURING SMALL BAYS**

Yuko SEKI<sup>1</sup>, Rui YAMAGUCHI<sup>1</sup>, Teiji UOZUMI<sup>1</sup>, Hideaki KAWANO<sup>2</sup>, Akimasa YOSHIKAWA<sup>1</sup>, Shin-Ichi OHTANI<sup>1</sup>, Masahiro ITONAGA<sup>4</sup>, Kiyohumi YUMOTO<sup>2</sup>, the CPMN Group<sup>3</sup> (<sup>1</sup>Department of Earth Planetary Sciences, Kyushu University, Japan, <sup>2</sup>Space Environment Research Center, Kyushu University, Japan, <sup>3</sup>Applied Physics Laboratory, University of Maryland, U.S.A., <sup>4</sup>Faculty of Education, Yamaguchi University, Japan)

Pi2 magnetic pulsations are known to be excited at the substorm onset. However, Pi2s are observed even when magnetic bays do not develop well. In this paper we aim to study the effects of the ionospheric conductivities on the ground Pi2 amplitudes, but auroral particle precipitations strongly modifies the ionospheric conductivities in a time-dependent manner, which is difficult to describe by simple equations. Thus, using data from Circum-pacific Magnetometer Network's (CPMN) stations along 210-degree magnetic meridian, we have statistically studied Pi2's associated with "small bays", which are defined here as magnetic bays at a low-latitude station in Guam whose H-component did not increase more than 1 nT in 10 minutes after onsets. We have studied the latitude dependence of the Pi2 amplitudes during northern summer and winter, and found the following features: (1) When averaged for all seasons, the H-component amplitude is almost constant at low- (< 50 deg) latitudes, exponentially increases with latitude at mid- to high- (50 ~ 65 deg) latitudes, and is generally large at higher (> 65 deg) latitudes (where the latitude dependence is unclear). On the other hand, the D-component amplitude exponentially increases with increasing latitude. (2) The H-component amplitude is larger in the summer hemisphere than in the winter hemisphere at low- to mid-latitudes, while the D-component amplitude does not show a clear season dependence. (3) A case study shows that the dominant frequency of a Pi2 was constant at low- to mid- (< 50 deg) latitudes, suggesting the plasmaspheric cavity-mode wave. The above results, and comparisons of them with a model of the ionospheric conductivity and simulation results of the cavity-mode wave, suggest that the H-component perturbation of Pi2s in the nighttime low- to mid-latitudes is caused by an enhanced Pedersen conductivity in the nighttime F-layer and the east-west component of the electric field perturbations of the plasmaspheric cavity mode.

**GAIII.10/11A/D-021** Poster **0830-095**  
**A STATISTICS STUDY OF MAGNETOSPHERIC RESPONSE TIMES DURING QUASI-PERIODIC SOLAR WIND VARIATIONS**

Kei KAMIKAWA<sup>1</sup>, Kiyohumi YUMOTO<sup>2</sup>, Kentarou KITAMURA<sup>2</sup>, the CPMN Group<sup>3</sup> (<sup>1</sup>Department of Earth and Planetary Sciences, Kyushu University, <sup>2</sup>Space Environment Research Center, Kyushu University)

In May 1996, two types of DP 2 magnetic variations were observed at the Circum-pacific Magnetometer Network (CPMN) stations. One correlates with quasi-periodic variations of the IMF-Bz component, and the other correlates with changes of the solar wind Dynamic Pressure (SW Pd). The ionospheric equivalent current patterns are obtained by using the ground magnetometer data from the CPMN and WDC stations. The ionospheric equivalent current patterns show almost the same in the both cases of DP 2, that is, at high latitudes, clockwise and counter-clockwise current vortices appear in the morning and afternoon sector, respectively. Furthermore, we examined cross-correlation of the ground magnetic variations with the IMF and plasma changes at the WIND satellite, in order to determine time delays of the variations between the satellite and ground (magnetospheric response time). It is found that DP 2 caused by the IMF-Bz was about 15 minutes, and that by SW Pd was about 4 minutes. The magnetospheric response times must be an important clue to understand the global response of the magnetosphere for the quasi-periodic solar wind variations. In the present study, we statistically analyze magnetospheric response times of 61 DP 2 events during the period of April, 1999 - AEMarch, 2000. The following results are obtained. (1) DP 2s observed at the ground stations can be categorized into three types: one is correlated only with the IMF-Bz [Type A: 7 events], the second is correlated both Z-component of the IMF and solar wind velocity [Type B: 45 events], and the third is correlated with SW Pd [Type C: 6 events]. (2) The Magnetospheric response times are 25 (+/-) 6 minutes for Type A, 19 (+/-) 2 minutes for Type B, and 11 (+/-) 7 minutes for Type C.

**GAIII.10/11A/D-022** Poster **0830-096**  
**THE SEVEM PROJECT: TOWARDS STATISTICAL AND EMPIRICAL MODELS OF THE DISTRIBUTIONS OF VLF WAVES**

Fabien DARROUZET<sup>1</sup>, Walther N. SPJELDVIK<sup>2</sup>, Joseph LEMAIRE<sup>1</sup>, Georg GUSTAFSSON<sup>3</sup>, Pierrette M.E. DECREAU<sup>4</sup> (<sup>1</sup>Belgian Institute for Space Aeronomy (IASB-BIRA), <sup>2</sup>Department of Physics, Weber State University, <sup>3</sup>Swedish Institute of Space Physics (IRFU), <sup>4</sup>Laboratoire de Physique et Chimie de l'Environnement (LPCE/CNRS))

The long-term objective of the SEVEM project (Statistical ELF and VLF Environment Models) is, by examining and analyzing satellite electromagnetic magnetospheric data, to build statistical maps of the VLF, ELF and plasma wave distribution in the magnetosphere, and to develop empirical and statistical models of the 3-dimensional distribution of wave parameters such as amplitude, polarization and frequency. We present here the SEVEM Web site (<http://www.magnet.oma.be/sevem/>), which contains a comprehensive catalogue/table of all the missions/satellites in the terrestrial magnetosphere which are, or have been, equipped

with radio antennae and/or fluxgate magnetometers. The site contains a comprehensive description of each satellite, presenting, for example, country of origin, contact numbers, orbital parameters, description of experiments, bibliographical references concerning the experiments and preliminary results, location where the databases are archived, format of the data, hyperlinks to relevant web sites, etc... The statistical maps and models of ELF and VLF wave distribution are useful to evaluate the average, maximum and minimum electromagnetic noise levels at different frequency ranges (useful when designing antenna for future space missions). We report here the development of a data-based model of the electromagnetic power spectral densities in the VLF band (8-50 kHz) as surveyed onboard the Swedish Viking spacecraft in the high-latitude region in the northern hemisphere. The data have been sorted into bins in spatial location and wave frequency for different geomagnetic conditions defined by the Kp index. A preliminary statistical model is presented showing the mean electric power spectral density versus magnetic local time and versus invariant latitude at fixed height intervals and for fixed frequency bands within the VLF range. An empirical model fitting these averages with simple analytical functions is also proposed. We have also used wave measurements onboard the four Cluster spacecraft to complete the frequency and spatial coverage of this statistical study. Progress along these lines is reported.

**GAIII.10/11A/D-023** Poster **0830-097**  
**COSMIC RADIO NOISE ABSORPTION AND VLF BURSTS CAUSED BY THE SOLAR WIND SHOCK**

Alefina OSEPIAN<sup>1</sup>, Sheila Catherine KIRKWOOD<sup>2</sup> (<sup>1</sup>Polar Geophysical Institute, Murmansk, Russia, <sup>2</sup>Swedish Institute of Space Physics, Kiruna, Sweden)

Variations of cosmic radio noise absorption (SCA) and bursts of VLF-emission at sub-auroral and auroral latitudes at the time of sudden commencements (SC) of geomagnetic storms are studied. About 300 SC and SI events in absorption and 140 records of VLF-emissions are considered. It is found that the response of cosmic radio noise absorption and VLF-emission records to the passage of an interplanetary shock depends on the level of the planetary activity before the onset of the SC event and the amplitude  $\Delta B$  of the geomagnetic field perturbation at a given L-shell in the equatorial magnetosphere. For SC events observed against a quiet background, effects of the SC in absorption and VLF bursts can be seen only if the jump  $\Delta B$  of geomagnetic field caused by the solar wind shock exceeds a critical value  $\Delta B_c$ . The magnitude  $\Delta B_c$  depends on both latitude and time of SCA and VLF observations. It is shown that the existence of a threshold value  $\Delta B_c$  at a given L-shell can be explained by the existence of a threshold value  $\Gamma_c$  for the growth rate  $\Gamma$  of the whistler-mode waves which limits self-exciting waves and spontaneous generation of the cyclotron instability. Sharp and strong ( $\Delta B > \Delta B_c$ ) compression of the geomagnetic field increases the anisotropy index and the number of resonant electrons due to the effect of betatron acceleration and as a result leads to the growth of the wave increment to values  $\Gamma > \Gamma_c$  and to electron precipitation. With increase of the level of geomagnetic activity before the onset of the SC event, the magnitude of  $\Delta B_c$  decreases. SC events observed against an active background ( $K_p > 3$ ) are accompanied by bursts in the absorption and VLF-emission for any jump  $\Delta B$  of geomagnetic field.

**GAIII.10/11A/D-024** Poster **0830-098**  
**GENERATION MECHANISM OF THE FUNDAMENTAL AND THE SECOND HARMONIC TERRESTRIAL HECTOMETRIC RADIATION**

Masahide IIZIMA<sup>1</sup>, Hiroshi OYA<sup>2</sup>, Akira HOSOTANI<sup>1</sup>, Atsushi KUMAMOTO<sup>3</sup>, Takayuki ONO<sup>1</sup> (<sup>1</sup>Department of Astronomy & Geophysics, Tohoku Univ., <sup>2</sup>Department of Space Communication & Science, Fukui Univ. of Tech.)

In the spectra of terrestrial hectometric radiation (THR) observed by PWS onboard the Akebono satellite, intense discrete components have been frequently observed in two frequency bands, from 1.3MHz to 2.1 MHz (1.7MHz band) and from 2.6MHz to 4.2MHz (3.4MHz band) forming a harmonic relation in the frequency. Polarization measurements of such discrete THR have shown that the fundamental band emission shows the nature of the L-O mode wave and the second harmonics emission reveals the nature of the R-X mode wave. The same polarization characteristics have been found for the case of auroral kilometric radiation (AKR) (Oya, 1990), i.e., the fundamental and the second harmonic AKR are generated in the form of the L-O mode wave and R-X mode wave, respectively. This result suggests that there is a common polarization feature in the harmonic generation of the planetary radio emission. The polarization feature of the fundamental and the second harmonic THR and AKR can be understood by the linear and nonlinear mode conversion processes from UHR mode waves into L-O and R-X mode electromagnetic waves: That is, at first, the strong UHR mode waves whose wave normal directions are nearly perpendicular to the local magnetic field are excited in the auroral electron beams through the cyclotron type wave-particle interactions. Then, the UHR mode waves are converted into L-O mode electromagnetic waves through the linear mode conversion process. These waves are observed as the fundamental emission. The origin of the second harmonic radiation includes the nonlinear wave-wave interaction processes of excited UHR mode waves. The theoretical calculations of energy conversion rates in this nonlinear mode conversion process have shown that the energy conversion rates from UHR mode waves into R-X mode electromagnetic waves are 20dB larger than those of L-O mode waves; that is in good agreement with the observations. Thus, the observed polarization characteristics of the fundamental and the second harmonic THR and AKR can be explained by the linear and nonlinear mode conversion processes from UHR mode electrostatic plasma waves into L-O mode and R-X mode electromagnetic waves.

**GAIII.11**  
**HOW DO SPACECRAFT INTERACT WITH THEIR SPACE ENVIRONMENT?**  
 Location: Site A, Room 15

Wednesday, July 9 AM  
 Presiding Chairs: J.-J. Berthelier, H. Usui

**GAIII.11/09A/A15-001** **0900**  
**A REVIEW OF SPACECRAFT EFFECTS ON PLASMA MEASUREMENTS**

Alain HILGERS (ESA-TOS-EMA)

The spacecraft induced environment includes, secondary particles, generated by primary radiation, outgassing material, particles emitted by thrusters or emitters, spacecraft

generated electrical and magnetic fields. All of these components may severely affect the behaviour of sensors and especially scientific instruments. In this presentation the various effects are reviewed and method to copewith or to mitigate them are proposed.

**GAIII.11/09A/A15-002 0925**

**HIGH-ENERGY PARTICLES AND THREATS TO SPACECRAFT**

Joe H. ALLEN<sup>1</sup>, Daniel N. BAKER<sup>2</sup> (<sup>1</sup>National Oceanic and Atmospheric Administration, <sup>2</sup>LASP/Univ. of Colorado)

Adverse space weather is one of the principal threats to modern human technology. Solar coronal mass ejections, large solar flares, and high-speed solar wind streams often lead to sequences of damaging disturbances within the Earth's magnetosphere, in the atmosphere, and even on the Earth's surface. Powerful and long-lasting geomagnetic storms can develop following solar disturbances and enhancements of the highly relativistic electron populations throughout the outer terrestrial radiation zone can also result. High-energy protons and heavier ions arriving in near-earth space, or trapped in the magnetosphere and having clearest effect in the South Atlantic Anomaly (SAA), can damage satellite solar power panels, confuse optical trackers, and deposit harmful charges into sensitive electronic components. Recent international space science programs have made a concerted effort to study activity on the Sun, the propagation of energy bursts from the Sun to near-Earth space, energy coupling into the magnetosphere, and its redistribution and deposition in the upper and middle atmosphere. Extreme solar, geomagnetic and solar wind conditions can be observed by a large array of international satellites and ground-based sensors. We discuss many of the types of space weather-related problems that have been identified in recent years. We present examples of space weather-induced spacecraft (and ground-based) anomalies and failures. An important effort is to propose technical and operational solutions to space weather problems and we discuss this aspect of space weather in this talk.

**GAIII.11/09A/A15-003 0940**

**INVESTIGATION OF SPACECRAFT/PLASMA INTERACTIONS USING ASPOC AND PEACE**

Knut SVENES<sup>1</sup>, Bjorn NARHEIM<sup>1</sup>, Klaus TORKAR<sup>2</sup>, Andrew FAZAKERLEY<sup>3</sup>, Michael FEHRINGER<sup>4</sup>, Phillippe ESCOUBET<sup>5</sup> (<sup>1</sup>Norwegian Defence Research Establishment, <sup>2</sup>Space Research Institute, Austrian Academy of Sciences, <sup>3</sup>Mullard Space Science Laboratory, University College of London, <sup>4</sup>Research and Scientific Support Department, ESA/ESTEC)

The Cluster satellites are equipped with instruments to actively control the spacecraft potential relative to the ambient plasma. The instruments emit an Indium ion beam of 5 to 50  $\mu\text{A}$  (typically 10  $\mu\text{A}$ ), with energies between 5 and 9 keV centered on the direction of the spacecraft spin axis. The ion emitter ASPOC (Active Spacecraft Potential Control) and the electron spectrometer PEACE (Plasma Electron And Current Experiment) have been operating together in a large variety of plasma environments. The main objective of this scheme is twofold: By lowering the magnitude of the spacecraft potential the modification of the ambient plasma before it is measured by on-board sensors are kept at a minimum. Secondly, the controlled conditions allow the escape of a larger fraction of photo-electrons generated at the spacecraft surface into space, whereby the wear of micro-channel plates in the electron detectors due to high count rates is reduced. In addition, the low energy ion measurements by the Cluster Ion Spectrometer (CIS) also gain from active spacecraft potential control. The improvement of the energy resolution of the detectors at low energy is one of the important features for multi-point measurements. These improvements have been achieved on Cluster with negligible disturbance of the plasma environment by the ion beam. The purpose of this presentation of spacecraft/plasma interactions is to systemise the resulting improvement of the Aspoc ion emitter on Cluster observations. In particular, the emphasis is to examine the effects on the Peace electron measurements. This study will be divided into a number of examples showing the effects of Aspoc in various regions of the orbit during different levels of geomagnetic activity. The time period covered is 2001 and 2002.

**GAIII.11/09A/A15-004 0955**

**CHARGING OF THE METALIC ELECTRODE CAUSED BY ENERGETIC ELECTRONS**

Yuzo WATANABE (Space Instrument Section, The Institute of Space and Astronautical Science)

Three antarctic rockets S-310JA-3, 5 and 6 were launched at Syowa Station into the auroral ionosphere. Charging of the electrode caused by the energetic electrons precipitated from the magnetosphere was observed on the frequency spectra of the impedance-probe. The measurement of the probe capacitance shows that the ion sheath thickness around the probe increases with enhanced energetic electron flux. A detailed study of the impedance characteristics of the impedance-probe measurement conducted in Antarctica reveals that the charging of the electrode occurred due to energetic electron precipitation from the magnetosphere. The sheath thickness normalized by the local Debye length ( $S/\lambda_D$ ) increased with the increase of energetic electron flux as well as the increase of auroral intensity at 557.7 nm observed by the meridian-scanning photometer. Above is the main theme in this short report about charging phenomena on the Impedance-probe. The following is the similar bias effect on the metallic probe in the space plasma by the electron-beam emitted from the rocket to the space. Sudden potential drop of the Impedance-probe due to closed current loop formation with the electron-beam will be described at the oral session. S-310-24 rocket was launched from Kagoshima Space Center at 20 JST on the 11th day of February in 1996. Charging of the probe caused by the electron-beam emitted from the rocket to the space was observed in the frequency spectra of the Impedance-probe. The measurement of the probe capacitance shows that the ion sheath thickness around the probe increases when the electron-beam strikes the probe surface. Probe potential rapidly decreases just after reaching the electron-beam to the probe surface. This negative charging ( $\Delta Q$ ) can be estimated from both the injected electron-beam current ( $\Delta I$ ) to the probe surface and the charging time ( $\Delta T$ ) by the beam as ( $\Delta I \cdot \Delta T$ ). The probe potential ( $V$ ) is negatively biased to the level of  $\Delta Q/C_{eq}$ .  $C_{eq}$  denotes the equivalent probe capacitance in the vacuum.  $V$  is restricted to the minus voltage of the cathode which is used as the electron-beam source of the beam-gun. Above phenomena is interpreted by closed current loop formation, including the electron-beam. The probe is electrically connected with the cathode of the gun when the electron-beam flow from the cathode hits upon the probe surface. The probe potential becomes immediately to the minus voltage applied to the cathode at this moment and then the ion sheath region around the probe expands. Rough estimations will be presented with several figures.

**GAIII.11/09A/A15-005 1010**

**SPACECRAFT CHARGING ANOMALIES AND THEIR RELATION TO THE SPACE ENVIRONMENT**

Tateo GOKA<sup>1</sup>, Haruhisa MATSUMOTO<sup>2</sup>, Kiyokazu KOGA<sup>1</sup>, Hitoshi MATSUOKA<sup>1</sup>, Hideki KOSHIIISHI<sup>1</sup>, Masaki AKIOKA<sup>2</sup> (<sup>1</sup>Space Environment Measurement Engineering Group, Office of

R&D, National Space Development Agency of Japan, <sup>2</sup>Hiraso Solar Observatory, Communications Research Laboratory)

Data concerning satellite anomalies induced by the natural environment, and related space environment measurements obtained by GEO, GTO and LEO satellites in Japan are reviewed. Electrostatic discharges (ESD) in GEO satellites remain the most common cause of anomalies in our database. ESD anomaly statistics show seasonal variations mainly occurring in spring and autumn equinox seasons and also correlate with the solar cycle, mainly in the decline and minimum phase. NASDA has measured surface charging potentials on board ETS-V (GEO, 10 years), ETS-VI (GTO, 2 years), ADEOS (LEO-polar, 10 months). We compare observed surface charging potentials on board ETS-V with substorm onset time, and have found that they are 80% correlated. The semiannual (equinoctial) variations in substorm occurrence are explained by the Russell-McPherron effect. Solar cycle variation matches our observed annual electron fluence data obtained by ETS-V in GEO orbit for 10 years (almost one solar cycle). This could be explained by two mechanisms: solar wind modulation and/or outer belt electron variations. Many satellite anomalies (NOAA-13, ANIK-E1&E2, INTELSAT-K, GOES-8, METEOSAT-3, BS-3a) occurred in the last solar decline and minimum phase (1993-1994). We focus on an ESD anomaly that occurred on BS-3a (22 Feb.1994) as a case study, and conduct a cause-and-effect analysis (a.k.a., cradle-to-grave analysis) using ground-based solar optical and radio data, IMP-8 solar wind data, and ETS-V and Ulysses radiation particle data. We have found that solar wind enhancement occurred around the time of the anomaly, coinciding with the detection of a radiation particle cloud, suggesting that this was the cause. In conclusion, the next solar decline and minimum phase, due in 2005-2007, is expected to lead to electron enhancement in the outer belt, and therefore result in more ESD anomalies in GEO satellites. The history of satellite anomalies should be the basis for uncovering the cause of operational problems. Combining space environment measurement data with satellite anomalies is crucial.

**GAIII.11/09A/A15-006 Invited 1055**

**CRITICAL PROBLEMS OF SOLAR POWER STATION FROM SPACE PLASMA PHYSICS VIEW POINT**

Hiroshi MATSUMOTO (Radio Science Center for Space and Atmosphere, Kyoto University)

In the 21st century, human activities will expand to near-Earth space. This talk discusses the potential important physical problems to which space plasma and magnetospheric physics should contribute. One of them is an impact of a very large structure on geosynchronous orbit such as Solar Power Station (SPS) on the environment of the magnetosphere and the ionosphere. The impact comes partly from the ion injection of the electric propulsion of the carrier from LEO to GEO. Another interesting issue is a nonlinear behavior of space plasma environment in response to a high density electromagnetic power beam passing through the magnetosphere, ionosphere and atmosphere. The paper also discusses a plasma-body interaction caused by a large solar array and a big phased array antenna for power beaming. The background and state of art of the SPS research in Japan and in the US will also be given as a reference

**GAIII.11/09A/A15-007 1120**

**ANALYTICAL STUDY ON THE APPLICATION OF EXHAUSTED BEAM IONS FROM ION THRUSTER TO ENA OBSERVATION**

Yoshiki YAMAGIWA<sup>1</sup>, Yukitaka TANAKA<sup>1</sup>, Hitoshi KUNINAKA<sup>2</sup> (<sup>1</sup>Faculty of Engineering, Shizuoka University, <sup>2</sup>Institute of Space and Astronautical Science)

The density of neutral particles in the upper atmosphere can be estimated by using ENA (Energetic Neutral Atoms) observation. At present, the ENA observation is done by using the charge exchange collision between the neutrals in upper atmosphere and the ions in the magnetospheric ring current field that is activated by solar wind. But in this method, it is difficult to separate the informations between neutrals and ions from ENA data because the ions in the magnetospheric ring current field are the natural origin and their energies are not constant. In this study, we propose the new method of ENA observation that uses the ions exhausted from ion thrusters. The ions exhausted from ion thrusters are the artificial ones and are more suitable for ENA observation because their energies and densities can be controlled. We evaluate the possibility of application of exhausted ions from ion thrusters to ENA observation. Analytical results show the range of altitude and the operating conditions of ion thrusters that this method effectively can apply.

**GAIII.11/09A/A15-008 1135**

**COMPUTER EXPERIMENTS ON INTERACTION OF HEAVY ION BEAM FROM A LARGE-SCALE ION ENGINE WITH MAGNETOSPHERIC PLASMA**

Yoshiharu OMURA, Toshihiro SAKAKIMA, Hideyuki USUI, Hiroshi MATSUMOTO (RASC, Kyoto University)

We study effects of heavy ions injected from a large scale ion engine to be used to propel large scale space station such as space solar power station in the lowearth orbit to the geosynchronous orbit. We performed a series of hybrid code simulations where ions are solved as particles, while electrons are treated as a massless fluid. We assume a two-dimensional plane ( $x, y$ ) where the external magnetic field is taken in the  $y$ -direction. We inject an argon beam in the direction perpendicular to the magnetic field, i.e., the direction along the  $x$ -axis. We study responses of the surrounding plasma to the heavy ion beam injected with different the density and initial drift velocity. With a sufficiently large injection velocity and high density of the argon beam, there arises a fast shock as the initial response to the injection, followed by gradual formation of tangential discontinuity at the front surface of the ion beam cloud. At the tangential discontinuity we find generation of Alfvén waves that propagate along the magnetic field lines, heating up the background thermal protons. We will discuss parametric dependence of the plasma response.

**GAIII.11/09A/A15-009 1150**

**ARTIFICIAL DISTURBANCES OF THE IONOSPHERE OVER THE MILLSTONE HILL RADAR DURING DEDICATED BURNS OF THE SPACE SHUTTLE OMS ENGINES**

Paul A. BERNHARDT, Phil J. ERICSON, Frank D. LIND, Bodo REINISCH (Plasma Physics Division, Naval Research Laboratory)

Two of the Shuttle Ionospheric Modification with Pulsed Localized Exhaust (SIMPLEX) experiments were carried out over the incoherent scatter radar (ISR) located at Millstone Hill Massachusetts. These experiments used 10 seconds burns of the dual Orbital Maneuver Subsystem (OMS) engines to produce the injection of high speed molecules in the ionosphere near 380 km altitude. Charge exchange between the high speed exhaust molecules and the ambient oxygen ions produce molecular ion beams that disturb the natural state of the ionosphere. Radar scatter measurements are used to measure the ion



velocity distributions that result from the ion beam interactions. Ground based observations with the University of Lowell Digisonde recorded the ionospheric density depressions resulting from recombination of the molecular ions with electrons. Prompt signatures of a non-equilibrium ion distribution in the OMS engine plume are seen in the data taken during Space Shuttle Flights STS-108 and STS-110 show. The presence of the stimulation of plasma turbulence is seen in the short-time measurements with the ISR for about 30 seconds duration and large scale irregularities are detected by the Digisonde for up to 20 minutes after the engine burn. The SIMPLEX experiments provide localized simulations of naturally occurring disturbances in the ionosphere that can be studied under controlled conditions. The experiment conditions are similar to the strong convection seen with high-latitude plasma during geomagnetically disturbed times.

**GAIII.11/09A/A15-010** Invited **1205**

**ION PROPULSION INDUCED PLASMA INTERACTIONS: AN OVERVIEW OF RESULTS FROM DEEP SPACE 1**

Joseph J. WANG (Virginia Polytechnic Institute and State University)

NASA's New Millennium Deep Space One (DS1) is the first interplanetary spacecraft operated on solar electric propulsion. Using a 30cm diameter Xenon ion thruster as its primary propulsion system, DS1 successfully flew by asteroid Braille in July 1999 and Comet Borrelly in Sept. 2001. One of the primary investigations on DS1 is to characterize ion propulsion induced plasma interactions and their effects on spacecraft and solar wind measurements. DS1 carried an integrated set of ion propulsion diagnostics sensors, Ion Propulsion Diagnostics System (IDS), and a state-of-the-art plasma sensor, The Plasma Experiment for Planetary Exploration (PEPE). 3-dimensional particle-in-cell simulations were also performed to assist data analysis and interpretation. This paper presents an overview of ion propulsion induced plasma interactions based on the results from DS1 investigations. Specifically we examine three major interaction problems: beam neutralization, plume-spacecraft interaction, and plume-solar wind coupling. Both in-flight measurements and modeling results will be discussed.

**Wednesday, July 9 PM**

Presiding Chairs: A. Hilgers, P. Bernhardt

**GAIII.11/09P/A15-001** Invited **1400**

**ELECTRODYNAMIC TETHERS FOR IN-ORBIT PROPULSION: STATUS AND TECHNOLOGICAL ISSUES**

Brian E. GILCHRIST (Space Physics Research Laboratory, University of Michigan)

Electrodynamic (ED) tether "propellantless" propulsion is accomplished through a magnetic force acting on an electrical current in the conducting tether to transform between electrical and mechanical energy. Orbit raising, lowering and possibly inclination change are all possible. The efficiency with which this is accomplished depends heavily on the ability of the tether system to extract current from and inject into the local magnetoplasma while moving at mesosonic speeds relative to the plasma. The key technologies include the electron collector configurations and low-power, propellantless electron emission technologies, and low-loss, long-life tethers. Both space flight experiments and ground chamber testing using high speed plasmas are helping to reveal details of ED tether operations that will be important for specifying future ED tether system designs. Here, results from the NASA Propulsive Small Expendable Deployer System (ProSEDS) experiment will be described. ProSEDS uses a 5-km bare aluminum tether (multiple strands) deployed from a Delta II second stage. Overall and individual sub-system performance will be reviewed. Ground chamber plasma tests of representative (scaled) geometries of future bare tethers will be described. Other technological issues and representative applications will also be discussed.

**GAIII.11/09P/A15-002** **1425**

**GROUND EXPERIMENTS OF ELECTRODYNAMIC TETHER USING HOLLOW CATHODE PLASMA CONTACTORS**

Masaya KOZAKAI, Naoyuki HIROSE, Tetsuya AOYAMA, Haruki TAKEGAHARA (Department of Aerospace Engineering, Tokyo Metropolitan Institute of Technology)

Plasma contactors are proposed as making good electrical contact devices between spacecraft and ambient ionospheric plasma. Especially, it has been studied as the one of key components of electrodynamic tether. The performance of electrodynamic tether depends on these devices because the current through the tether form a closed loop via space plasma. In this study, hollow cathode plasma contactor was used for both electron emitter and collector. The largest advantage of using hollow cathode is that the same device can both emit and collect electrons. Thus, the electrodynamic tether, which mounts hollow cathode plasma contactors both ends of tether, is possible to change the direction of current and it can generate thrust force and drag force. Since electrodynamic tether system that include current path through the space plasma is very huge, it is necessary to consider a scaling law between space operation and ground experiments to simulate the electrodynamic tether system. This study aims for ground simulation of electrodynamic tether system that is considered near-field and far-field plasma interaction. There are many factors for design a scaling law, such as tether length, geomagnetic field intensity, plasma environment (electron density, neutral density, gas species, and vacuum level), plasma cloud size, etc. However, all of the conditions are not necessary to conduct the ground experiments. Most of study have not been met these conditions. It is necessary to distinguish the dominant factors. Effective electrical connection between collector and ambient ionospheric plasma via luminous plasma cloud is most dominant for gathering enough current. For the understanding of the physical phenomena in plasma contactor operation, the experiment used hollow cathode was conducted in 3.2 m length by 1.5 m in diameter cylinder vacuum chamber. Experimental apparatus consists of three plasma sources. Two of them are the hollow cathode plasma contactors that are connected each other and separated from ground potential. And the other device is plasma simulator used ion thruster without ion beam extraction that simulates ionospheric plasma environment. Xenon was fed to the plasma contactors but argon was fed to the plasma simulator to minimize the ionization of background neutrals. It was confirmed that two functions (electron emission or collection) with one device could be changed in the simultaneous operation experiments. Probe measurement, mass spectrometry and emission spectrometry were performed to verify the elements of plasma cloud at the electron collector. We will describe the constitution elements of plasma cloud and validity of the ground experiments.

**GAIII.11/09P/A15-003** **1440**

**DETERMINATION OF ESD GROUND TEST CONDITIONS FOR HIGH POWER GEO SATELLITE SOLAR ARRAY**

Mengu CHO, Toshiaki MATSUMOTO, Emanuel AMORIM, Kazuhiro TOYODA (Department of

Electrical Engineering, Kyushu Institute of Technology)

Since the last decade, the power level of Geosynchronous Orbit (GEO) satellite has increased dramatically to nearly 10 kW or even higher. To manage the large amount of power efficiently, the satellite bus voltage has increased to 100V. Nowadays many commercial telecommunication satellites employ solar arrays that generate the electricity at 100V. As the voltage of solar array increases to 100V, the problems of arcing during the substorm condition have been recognized as serious hazard that sometimes threatens the stable supply of the solar array power. In the present paper, we report the results of ESD (electrostatic discharge) test carried out on solar arrays for Japanese telecommunication satellites. We have placed solar array coupons made with the same procedure as the flight model inside a vacuum chamber, where we have irradiated a test coupon by high energy electron beam to simulate the charging condition during the substorm in GEO. The threshold for the trigger arc inception and the sustained arc formation has been studied. The dependence on the coverglass material has been also studied. We have also used test coupons made only with two solar cells but with different gap distances. We have used many of this coupon type to statistically determine the threshold condition for the sustained arc formation. The test result is used to derive the safety margin for the potential difference between adjacent cells. During the tests, the amount of external capacitance simulating the coverglass capacitance of solar array paddle has been changed and the effect of external capacitance on the test results has been studied. We have analyzed the magnetospheric plasma data collected by LANL satellites. From the data of plasma temperature, density, and satellite potential, the duration during which a satellite is under the inverted-potential gradient condition is estimated. Then the total duration of inverted-potential gradient during the operational life time of a satellite is calculated to give a reasonable test duration on the ground. These results are used to determine the appropriate ESD test condition for the ground test of solar array for GEO satellites.

**GAIII.11/09P/A15-004** **1455**

**EFFECT OF SPACE PLASMA ON HIGH VOLTAGE SOLAR ARRAY**

Koji TANAKA<sup>1</sup>, Minoru IWASA<sup>2</sup>, Susumu SASAKI<sup>1</sup>, Haruhisa FUJII<sup>3</sup>, Masahiro MORI<sup>3</sup> (<sup>1</sup>The Institute of Space and Astronautical Science, <sup>2</sup>Tokyo Institute of Technology, <sup>3</sup>NASDA, <sup>4</sup>Mitsubishi Electric CO.)

The design and operation of the spacecraft power system will be affected by elements of the space environments. Increasing with power requirements of the spacecraft, a solar array is required to generate high voltage in order to reduce a power loss in a cable and a power system. Especially, a solar power satellite (SPS) will be operated above several kV or several ten kV. Though SPS2000 is a relatively small SPS, its array modules were designed to generate 1kV. A conventional solar paddle of the spacecraft exposes interconnectors to the space environment. When solar arrays generate electricity, interconnectors of the photovoltaic cells collect electrons from the ambient plasma, and spacecraft potential is biased to negative voltage. When spacecraft is negatively biased, the ionospheric ions attack the spacecraft surface. Spacecraft is possibly caused serious damages by ion bombardments. Also, the discharge occurs when the solar array has a negative potential below -200 V with respect to the plasma. The discharge causes various undesired effects, such as electromagnetic interference and surface deterioration, and leads to the permanent loss of the spacecraft power. In this paper, we describe results of the laboratory experiments concerning the interaction between ambient plasma, which simulates the low earth orbit conditions, and the high voltage solar array. We made a two dimensional electrode array that was consisted one hundred electrodes (10x10) on the CFRP honeycomb panel that simulated a solar paddle of the spacecraft. The vacuum chamber with 4.0 m in length and 2.5 m in diameter was used in this experiment. The chamber had a diffusive argon plasma source located at one end, which generated plasma conditions of  $n_e \sim 1 \times 10^{10} \text{ m}^{-3}$  and  $kT_e \sim 3 \text{ eV}$ . Each electrode on the panel was biased up to 1.5 kV by the solar array simulator that was consisted of the high voltage DC power supplies and voltage dividers. Plasma current from each electrode that was grounded through a 1 kΩ resistance was measured under the same condition and acquired by a mobile computer through the multiplexer. Also, the chamber is equipped with a spherical Langmuir probe with a radius of 1 cm that can be moved in the three axes. Our preliminary results of the plasma experiments using the electrode array show that electron collection currents increase rapidly with increasing bias voltage over several hundred V and saturates in some conditions. These phenomena may be involved in growth of the electron sheath.

**GAIII.11/09P/A15-005** **1510**

**STUDY OF SPACECRAFT ARCING IN AMBIENT PLASMA ENVIRONMENTS**

Takahisa MASUYAMA, Masato NAGATA, Tatuo ONISHI, Hirokazu TAHARA, Takao YOSHIKAWA (Graduate School of Engineering Science, Osaka University)

Spacecraft are in a severe environment in space. Their surfaces are exposed to energetic and reactive particles, such as electrons, ions, protons and oxygen atoms and ultraviolet light, including particles exhausted from plasma thrusters, during space missions. Then, electrostatic interactions between the surface materials and the ambient plasma, such as negative or positive sheath creation, and charging and arcing phenomena, frequently occur. In satellites, the current generated by a solar array is leaked by impact of ions, and the solar array is still degraded by sputtering and arcing due to the collected ions. The electrical breakdown of negative charging on insulating surfaces causes intensive damages in the satellite systems. Furthermore, in plasma contactor operations, negative charging is expected to be mitigated by ions attracted from the plasma, resulting in surface degradation as well as in the case of high voltage solar arrays. The mechanism of the material degradation, the structure of electrical sheaths, and the charging and arcing processes must be understood. In Osaka University, a ground facility was developed for simulation of space plasma and material interaction. Using the simulator, the structure of an ion sheath created around a high voltage solar array and the degradation of surface materials near the array due to high energy ion bombardment were investigated. The mitigation of negative charging by plasma flow, i.e., the feature of plasma contactor operations, has also been studied. In the future, spacecraft will be larger and higher powered. Because of the balance of leakage currents through the ambient space plasma, they will have higher negative potential without plasma contactor operation. When spacecraft operate with higher voltage, more intensive arcing is suspected to occur on the surface. In this study, ground experiment and PIC plasma simulation were carried out to understand this phenomenon and to examine effects of the ambient space plasma on the arcing process. Plasmas were generated by electron cyclotron resonance (ECR) discharge. When arcing occurred, the time variations in arc current and bias voltage were measured. Both peak arc current and total charge emitted by arcing increased with bias voltage and plasma number density. The diameter of arc spots also increased. Neutral particles in addition to charged particles around spacecraft are considered to play the important role for expanding of arc plasma.

GAIII.11/09P/A15-006

1525

**COMPUTER EXPERIMENTS OF TRANSIENT CHARGING PROCESS OF A PLASMA EMITTING BODY**

Hideyuki USUI<sup>1</sup>, Ikko FUNAKI<sup>2</sup>, Hayato TASHIMA<sup>3</sup>, Hitoshi KUNINAKA<sup>3</sup>, Masaki OKADA<sup>4</sup>, Yoshinori NAKAYAMA<sup>5</sup> (<sup>1</sup>Radio Science Center for Space and Atmosphere, Kyoto University, <sup>2</sup>University of Tsukuba, <sup>3</sup>Institute of Space and Astronautical Science, <sup>4</sup>National Institute of Polar Research, <sup>5</sup>National Defense Academy)

For the assessment of the spacecraft with active plasma emission and its surrounding plasma environment, we are planning to propose a plasma experimental space platform for the JEM (Japan Experimental Module) exposed unit of the international space station (ISS). By using this platform, we will be able to examine the transient processes in non-steady interference with plasma and charging/discharge in association with turn-on/off or unexpected failure of the plasma emission facility. In order to design the new platform, we started testing the charging process of a floating body with active ion emission in a vacuum chamber. In parallel to the ground experiment, we also started performing computer simulations with Particle-In-Cell (PIC) model in order to examine the detail of the charging process. In the simulations, we particularly focus on the transient response of a floating ion-emitting body in a situation where a neutralizer which emits electrons from the body is abruptly turned off by accident. In the present paper, in addition to the brief introduction of the concept of plasma experimental module for JEM, we will show some results obtained in the PIC simulations and discuss the body charging process, the spatial distribution of emitted ions and the response of the background plasma.

GAIII.11/09P/A15-007

Invited

1540

**DEVELOPMENTS IN MINI-MAGNETOSPHERIC PLASMA PROPULSION**

Robert WINGLEE<sup>1</sup>, Tim ZIEMBA<sup>2</sup>, Peter EURIPIDES<sup>3</sup>, Louis GIERSCHE<sup>4</sup>, John SLOUGH<sup>5</sup> (<sup>1</sup>Dept. of Earth and Space Sciences, Univ. of Washington, <sup>2</sup>Aeronautics and Astronautics, Univ. of Washington)

Mini-Magnetospheric Plasma Propulsion (M2P2) seeks the creation of a large-scale (10 km radius) magnetic wall or bubble (i.e. a magnetosphere) by the electromagnetic inflation of a small-scale dipole magnet. The inflated magnetosphere will intercept the solar wind and thereby provide high-speed propulsion with modest power and fuel requirements due to the gain provided by the ambient medium. Magnetic field inflation is produced by the injection of plasma onto the dipole magnetic field eliminating the need for large mechanical structures and added material weight at launch. Results are presented from the laboratory prototype that show the production of plasma and in a dipole and the expansion of the magnetic field. It is shown that the observed characteristics are very close to that predicted by computational models. The outcome though is very dependent on the presence of chamber walls which are shown to be limit the expansion of plasma and magnetic field. Possible applications from extrapolating the laboratory and simulations results show substantial savings in mission times spacecraft with a much larger payload to fuel ratio.

GAIII.11/09P/A15-008

Invited

1620

**THE CLUSTER DOUBLE PROBE ELECTRIC FIELD EXPERIMENT (EFW)**

Arne PEDERSEN<sup>1</sup>, Mats ANDRE<sup>2</sup>, Andre BALOGH<sup>3</sup>, Anders ERIKSSON<sup>3</sup>, Per-Arne LINDQVIST<sup>4</sup>, Forrest MOZER<sup>5</sup>, Goetz PASCHMANN<sup>6</sup>, Henri REME<sup>7</sup>, Jack QUINN<sup>8</sup> (<sup>1</sup>Dept. of Physics, University of Oslo, <sup>2</sup>Swedish Institute of Space Physics, Uppsala, <sup>3</sup>Imperial College, London, <sup>4</sup>Alfvén Laboratory, Royal Institute of Technology, Stockholm, <sup>5</sup>Space Science Laboratory, University of California, Berkeley, <sup>6</sup>Max Planck Institute for Extraterrestrial Physics, Garching, <sup>7</sup>CESR/CNRS, Toulouse, <sup>8</sup>Space Science Center, University of New Hampshire, Durham)

Each of the four Cluster spacecraft has two double probes at the tips of four 44 m long radial booms. The experiments allow for high time resolution measurements of the quasistatic electric field component in the spin plane of the spacecraft. The full electric field vector can be calculated with knowledge of the magnetic field under the assumption that the parallel electric field can be neglected. EFW has the unique possibility to compare data with the Electron Drift Instrument (EDI) which has good measurements in the inner magnetosphere. This comparison has demonstrated agreements, but has also uncovered problems with EFW over the polar caps. Outflow of low energy ions, some of which do not reach the positively charged spacecraft, creates wakes which disturb EFW. Comparisons with  $\mathbf{v} \times \mathbf{B}$ , from the magnetic field and the ion experiment, has demonstrated good agreements in the plasmashet. The force of EFW is the high time resolution of the measurements and the capability to measure spiky large amplitude electric fields. In many studies it is necessary to consider data from all the above experiments as complementary in order to get the full information. Other capabilities of EFW is the high time resolution measurements of the spacecraft potential and its connection to plasma density. EFW also provides high quality wave data; this will be briefly outlined.

GAIII.11/09P/A15-009

1645

**RHEOMETRY EXPERIMENT OF THE WIRE ANTENNA ABOARD SCIENTIFIC SPACECRAFTS**

Tomohiko IMACHI<sup>1</sup>, Satoshi YAGITANI<sup>2</sup>, Isamu NAGANO<sup>3</sup>, Ryoichi HIGASHI<sup>1</sup>, Satoshi ESAKI<sup>1</sup>, Minoru TSUTSUMI<sup>4</sup>, Hiroshi MATSUMOTO<sup>5</sup> (<sup>1</sup>Department of information and system engineering, Faculty of engineering, Kanazawa University, <sup>2</sup>Kyoto Sangyo University, <sup>3</sup>Radio Science Center for Space & Atmosphere, Kyoto University)

Observation of plasma waves in the space is an important subject of scientific spacecraft missions. The sensor frequently used to measure the low frequency AC electric field of plasma waves is a wire antenna. It is necessary for an accurate measurement to estimate the effective length of each wire antenna accurately, because it is closely related to the gain of the sensor, and the inaccuracy of it affects greatly to the quantitative studies of plasma waves. The effective length of an ideal short wire antenna in free space is considered to be a half of its physical length when the wavelength is much longer than the antenna, because a theory of short dipole antenna informs that current distribution along the wire becomes a triangular in low frequencies. So far, in most researches related to plasma waves, the effective length of a wire antenna has been assumed to be a half of its physical length. However, on the other hand, when we measure electrostatic or quasi-static field, the intensity is calculated from a voltage between probes, placed at both tips of the antenna, divided by the distance between them. In this case the antenna effective length is treated as the same as the physical length of the wire. What makes difference between them? To investigate this problem, we estimated frequency dependency of the effective length in quasi-static frequency range, by using "rheometry experiment" [1]. Rheometry is an experimental method to determine the effective length of a short antenna by using a water tank. We generate a quasi-static electric field uniformly in the water tank. The intensity of the generated electric field is exactly known so that we can estimate the effective length of a small "scale-model" wire antenna in the water from its output voltage. It would not be possible to make such a measurement in the air, because the impedance of the antenna is

very high in the quasi-static frequency range, and the voltage at the antenna terminals would be changed when a voltmeter is connected. However we can make the impedance low in the water because of water conductivity, and the electric field in the water surrounded by the air becomes homogeneous because the dielectricity of the water is much higher than that of the air. A homogeneous quasi-static electric field can be used to simulate the electromagnetic plane wave observed by the antenna. The result shows that the effective length is a half of their physical length in higher frequencies (> several kHz). However, in very low frequencies (< several hundred Hz), it depends on the structure of the antenna. We will show the detailed result. [1] H.O. Rucker et al., Radio Science, Vol.31, No.6, pp.1299, 1996

GAIII.11/09P/A15-010

1700

**STUDY OF SPACECRAFT-PLASMA INTERACTION VIA 3D UNSTRUCTURED-GRID EM PARTICLE SIMULATION**

Masaki OKADA<sup>1</sup>, Hiroshi MATSUMOTO<sup>2</sup> (<sup>1</sup>National Institute of Polar Research, <sup>2</sup>Kyoto University)

We have developed a 3-dimensional electromagnetic particle simulation code with an unstructured-grid system. This code solves Maxwell's equations which is discretized with triangular elements in 3D simulation space. Plasma particles are also traced by solving the equations of motion with the Buneman-Boris method. The main advantage of this code is the adaptability of modeling more realistic shape of a spacecraft than the orthogonal grid code. Thus, this simulation code is suitable for analyzing the plasma environment in the vicinity of a spacecraft especially in the region within a Debye length from the surface of the spacecraft as well as the spacecraft charging phenomena. We will show the scheme of this code and also show a couple of results from the test simulation runs taking into account of a realistic shape of a spacecraft.

GAIII.11/09P/A15-011

1715

**COMPUTER EXPERIMENTS ON ANTENNA CHARACTERISTICS IN SPACE PLASMA**

Nobuyuki NAKAMURA, Hideyuki USUI, Hirotugu KOJIMA, Hajime KAISHIMA, Hiroshi MATSUMOTO, Yoshiharu OMURA (Kyoto University)

Antenna characteristics in a magnetized plasma such as input impedance, effective length and pickup factor are important in the plasma wave observation, particularly for calibration of wave data obtained from spacecraft. However, it is difficult to evaluate antenna characteristics in space plasma accurately because of complex interaction among antenna itself, plasma waves, background plasma and photoelectron sheath. For last several decades, many studies on antenna characteristics have been done. In terms of antenna impedance, theoretical analyses were done with the assumption of the antenna surface current. Simultaneously analysis of antenna impedance was carried out by real observation with spacecraft and antenna equivalent circuit which is parallel circuit of resistance and capacitance was used. However there are some discrepancy between the observational results and the analysis with antenna equivalent circuit, which may be caused by the effect of sheath and photoelectron. In the present study, we focused on a dipole antenna and examined its characteristics in space plasma by performing three dimensional electromagnetic PIC (Particle-In-Cell) simulation. In three dimensional PIC simulation as an antenna analysis we put a conducting dipole antenna immersed in a magnetized plasma and examine its impedance, effective length including plasma kinetic effects under a variety of plasma environments. Firstly, we performed simulations to obtain the antenna impedance. In these simulations impedance resonance at the plasma frequency was recognized and the resonance becomes duller as thermal velocity of background plasma became larger. These results were consistent with theory qualitatively and we will proceed to the quantitative analysis. Next, we performed simulations to obtain effective length. We investigated the effective length by using a receiving antenna and calculated effective length from antenna surface current under the circumstances an electrostatic wave was excited by the beam instability. When wave length was comparable to antenna length antenna surface current can be approximated as sine wave. However, if load impedance is far higher compared to the antenna impedance it can be considered that the current flowing over the antenna becomes very little and the voltage induced on antenna becomes dominant. We are investigating the association between effective length and current distribution on antenna. The above simulations are performed in only case that antenna length is larger than the local Debye length. Therefore we also focus on the situation where the local Debye length is larger than or comparable to the antenna length.

GAIII.11/09P/A15-012

1730

**PIC MODELLING OF THE PHOTO-ELECTRON CLOUD AROUND A SPACECRAFT**

Alain M.F. HILGERS<sup>1</sup>, Benoit THIEBAULT<sup>2</sup>, Julien FOREST<sup>3</sup>, Olivier CHANRION<sup>4</sup>, Philippe ESCOUBET<sup>5</sup>, Michael FEHRINGER<sup>6</sup>, Harri LAAKSO<sup>7</sup> (<sup>1</sup>ESA-TOS-EMA, <sup>2</sup>ESA-SCI)

Photo-electrons emitted from sunlit surfaces in space may affect plasma measurements by several processes, e.g., via the resulting (i) surface potential, (ii) space charge effects, or/and (iii) direct propagation to detectors. We have used a fully kinetic particle-in-cell code, PicUp3D which is now made available in public domain, for modelling in three dimensions the electrostatic sheath and photo-electron cloud around a conductive volume representative of a spacecraft like Cluster in a typical magnetospheric plasma environment. The model shows several features of key interest for the interpretation of the measurements and for optimizing the design of future instruments. It is found that photo-electrons fill a large volume around the spacecraft where they can dominate over the ambient environment and a significant part of photo-electrons propagates to the antisunward sector. The resulting space charge has been found to generate negative potential barriers under certain conditions. Also long wire booms which are generally used for mounting electrostatic sensors away from the influence of the spacecraft are found to induce significant transport of the spacecraft generated photo-electrons toward the boom mounted detectors. In this presentation the feature of the computer code and the results of the numerical model are reviewed and the implications for plasma instruments are discussed.

GAIII.11/09P/A15-013

Invited

1745

**ELECTRICAL CHARGING OF THE ROSETTA ORBITER, (1) NUMERICAL SIMULATION**

Jean-François ROUSSEL<sup>1</sup>, Jean-Jacques BERTHELIER<sup>2</sup> (<sup>1</sup>ONERA, DESP, <sup>2</sup>CETP/IPSL)

One of the objectives of the ROSETTA missions is to investigate the various processes which are responsible for the development and evolution of the cometary neutral and ionized atmosphere. The main problem in measuring the characteristics of the plasma in the coma stems from the very low energy of thermal particles, from less than 10 meV for the electrons to about 100 meV for the outflowing ions. Besides the instrumental difficulties, the possible charging of the orbiter appears of major concern. For this reason, we have undertaken a numerical simulation study of the electrical equilibrium of the ROSETTA spacecraft. The model takes accurately into account the photo-emission and the anticipated characteristics of the cometary plasma, in particular its outflow from the nucleus. It provides the floating

potential of the orbiter and the structure of the plasma sheath for the various conditions expected during the operational phase that mainly depend on the distance of the orbiter to the nucleus. The results of this study demonstrate that the electric equilibrium of the spacecraft is essentially controlled by the photo-electron current emitted by its very large solar panels, leading to a positive floating potential. Only very close to the nucleus is the expected plasma density high enough to allow the collected thermal electrons to maintain the floating potential within a few kTe from the plasma potential. At larger distances it will float positive and at high potentials compared to the characteristic energy of cometary particles thus making questionable to obtain reliable measurements of the thermal plasma. A possible way to circumvent this effect, disconnecting the sunlit surface of the solar panels from the spacecraft ground, was suggested by our results.

**GAI11.11-Posters**  
**HOW DO SPACECRAFT INTERACT WITH THEIR SPACE ENVIRONMENT?**  
 Location: Site D

Thursday, July 10 PM

**GAI11.11/10P/D-001** Poster **1400-115**  
**EFFECTIVE LENGTHS OF CROSSED WIRE ANTENNAS ONBOARD AKEBONO**

Ryoichi HIGASHI<sup>1</sup>, Tomohiko IMACHI<sup>1</sup>, Satoshi YAGITANI<sup>1</sup>, Isamu NAGANO<sup>2</sup>, Iwane KIMURA<sup>3</sup> (<sup>1</sup>Graduate School of Natural Science and Technology, Kanazawa University, <sup>2</sup>Faculty of Informatics and Technology, Osaka Institute of Technology)

The effective length of a dipole antenna designed to pick up low frequency electric fields onboard satellite has been assumed equal to a half of its physical length. However the effective length may change under the influence of plasma sheath surrounding the antenna. To observe the electric field accurately, we must estimate the accurate effective length of the antenna in space plasmas. In this study, we evaluate the effective lengths of crossed wire antennas onboard Akebono satellite by using in-situ observations of OMEGA signals. The VLF instruments onboard Akebono are designed to observe VLF plasma waves and to determine wave normal direction of the waves. Two pairs of wire dipole antennas (tip-to-tip 60m) crossing each other are used for the VLF electric field, and triaxial loop antennas and search coils are used for the VLF magnetic field [1]. The absolute intensities of the electromagnetic fields measured by these antennas are calculated from their induced voltages and effective lengths. However the effective lengths of the wire antennas in space are difficult to be estimated generally because of the plasma sheath surrounding the antennas. So we evaluate the effective lengths by making use of OMEGA navigation signals observed as the whistler mode waves in the magnetosphere and the theory of cold plasma. The frequency and transmitting sequence of OMEGA signals are exactly known. We obtain the electron cyclotron frequency from MGF and the plasma frequency from PWS. The k-vectors of OMEGA signals are calculated from only the wave magnetic field under a cold plasma approximation of whistler mode propagation. For an OMEGA signal, we can calculate its electric field components theoretically from its observed magnetic field components, k-vectors and plasma parameters using the dispersion equation of the cold plasma and Maxwell's equations [2]. Finally, by comparing such calculated values with the actually observed electric fields that have been calibrated using the assumed effective length, we can determine the effective lengths of each of the two dipole antennas separately. We calculate effective lengths of the two dipole antennas separately by using Australian OMEGA signals (10.2kHz) observed along the two paths, Dec. 14, 1989, and Aug. 3, 1990. Results show that each of their average effective lengths is almost a half of the actual length (60m) of the dipole antennas, 30.8m and 31.5m for x- and y-antennas for the data of Dec. 14, 1989, and 31.4m for both antennas for Aug. 3, 1990. We will present the more detailed analysis results and discuss them statistically. [1] I. Kimura, et al., "VLF Observation by AKEBONO satellite," *Geophys. Res. Lett.*, Vol.18, No.2, pp.313-316, Feb. 1991 [2] T. Imachi, et al., "Effective Lengths of the dipole antenna onboard GEOTAIL spacecraft," 2000 ISAP, Vol.2, pp.819-822, Aug. 2000

**GAI11.11/10P/D-002** Poster **1400-116**  
**INFLUENCE OF THE SHEATH IMPEDANCE OF THE BIASED PROBE ON THE MEASUREMENTS OF THE SPACECRAFT POTENTIAL**

Keigo ISHISAKA<sup>1</sup>, Yasumasa KASABA<sup>2</sup>, Toshihiro OKADA<sup>1</sup>, Hajime HAYAKAWA<sup>3</sup>, Toshifumi MUKAIF<sup>1</sup> (<sup>1</sup>Toyama Prefectural Univ., <sup>2</sup>Institute of Space and Astronautical Science)

The spacecraft potential is determined by the balance of the photoelectron current from the spacecraft surface and the incoming ambient electron current and is given by a function related to the photoelectron emitted from the surface and the ambient plasma density. Therefore the spacecraft potential has been used to derive the electron density surrounding the spacecraft in the magnetosphere and the solar wind. The spacecraft potential of the Geotail spacecraft is measured by the single probe system, which is one of the subsystems of the electric field detector (EFD). The single probe system measures the difference of potential between the spacecraft and the spherical probe at the top of long wire boom. The probe potential can be set nearly equal to the ambient plasma potential by feeding a proper bias current to the probe. Therefore the voltage measured by the single probe system is approximately equal to the spacecraft potential for ambient plasma. In order to measure the spacecraft potential accurately, the amount of the bias current is determined to reduce the impedance between the probe and the surrounding plasma below the input impedance of the electronics. However the bias current is determined experimentally in orbit and the bias current actually set -225 nA constantly, while the plasma density and temperature may change from place to place in the magnetosphere. In this case, due to the low density and high temperature of the magnetospheric plasma, the impedance between the probe and the surrounding plasma is very high, especially near the floating voltage at which no current flows between the probe and the plasma. It is difficult to measure the spacecraft potential using the probe technique because the probe potential cannot be measured accurately. In this study, using the data of the Geotail spacecraft measurement, we investigate the sheath impedance between the probe and the ambient plasma in the magnetosphere and solar wind when the bias current is changed variously. We discuss the influence of the sheath impedance of the biased probe on the measurements of the spacecraft potential and demonstrate the method of feeding the proper bias current in the various regions. The spacecraft potential can be measured accurately using the revised bias current. And furthermore, we demonstrate that the spacecraft potential measured by the revised bias current is very useful for obtaining the electron density in the magnetosphere and solar wind.

**GAI11.11/10P/D-003** Poster **1400-117**

**ELECTRICAL CHARGING OF THE ROSETTA ORBITER, (2) LABORATORY SIMULATION**

Jean-Jacques BERTHELIER<sup>1</sup>, Jean-François ROUSSEL<sup>2</sup> (<sup>1</sup>CETP/IPSL, CNRS, <sup>2</sup>ONERA, DESP)

One of the objectives of the ROSETTA missions is to investigate the various processes which are responsible for the development and evolution of the cometary neutral and ionised atmosphere. The main problem in measuring the characteristics of the plasma in the coma stems from the very low energy of thermal particles, from less than 10 meV for the electrons to about 100 meV for the outflowing ions. Besides the instrumental difficulties, the possible charging of the orbiter appears of major concern. For this reason, we have undertaken a numerical simulation study of the electrical equilibrium of the ROSETTA spacecraft. The model takes accurately into account the photo-emission and the anticipated characteristics of the cometary plasma, in particular its outflow from the nucleus. It provides the floating potential of the orbiter and the structure of the plasma sheath for the various conditions expected during the operational phase that mainly depend on the distance of the orbiter to the nucleus. The results of this study demonstrate that the electric equilibrium of the spacecraft is essentially controlled by the photo-electron current emitted by its very large solar panels, leading to a positive floating potential. Only very close to the nucleus is the expected plasma density high enough to allow the collected thermal electrons to maintain the floating potential within a few kTe from the plasma potential. At larger distances it will float positive and at high potentials compared to the characteristic energy of cometary particles thus making questionable to obtain reliable measurements of the thermal plasma. A possible way to circumvent this effect, disconnecting the sunlit surface of the solar panels from the spacecraft ground, was suggested by our results.

**GAI11.11/10P/D-004** Poster **1400-118**

**EXPERIMENTAL STUDY OF TRANSIENT CHARGING PHENOMENA OF A FLOATING BODY WITH ION BEAM EMISSION**

Ikko FUNAKI<sup>1</sup>, Hideyuki USUI<sup>2</sup>, Hitoshi KUNINAKA<sup>3</sup>, Masaki OKADA<sup>4</sup>, Yoshinori NAKAYAMA<sup>5</sup> (<sup>1</sup>Institute of Engineering Mechanics and Systems, University of Tsukuba, <sup>2</sup>Radio Science Center For Space and Atmosphere, Kyoto University, <sup>3</sup>Institute of Space and Astronautical Science, <sup>4</sup>National Institute of Polar Research, <sup>5</sup>National Defense Academy)

Since 1960s, there were many space plasma experiments that actively emit charged particles in such forms as electron- or ion-beam from the satellites. Among them, spacecraft charging experiment by such projects as SCATTA, ATS6, in which the first spacecraft charging, and even successful control by those plasma beams were completed. However, it is regrettable these experiments require a whole spacecraft system that is developed for the specific experiments and available for only a short-term mission period. If a platform for plasma experiment is continuously executable in ISS, international space station, these opportunities will place a great impact on both scientific as well as engineering point of view. Based on such an idea, we are proposing a plasma experimental module for Japanese Experimental Module (JEM), that utilizes JEM's unique feature, whose experimental module is directly exposed to space, accordingly, idealistic plasma experiment in semi-infinite space becomes possible. However, before realizing such a plasma experimental facility, strict assessment on the plasma environment around the plasma emitting device should be finished. Plasma experimental module onboard JEM, which we propose, is focused on such assessment, starting from a very small experiment on spacecraft to artificial plasma interaction. In this paper, the need and concept of the plasma experimental module for JEM are described with some initial test results, preliminary numerical analysis and future plans.

**GAI11.11/10P/D-005** Poster **1400-119**

**MHD SIMULATION OF THE EXHAUST PLASMA PLUME IN THE VASIMR ADVANCED PROPULSION CONCEPT**

Alfonso G. TARDITI<sup>1</sup>, John V. SHEBALIN<sup>1</sup>, Edgar A. BERING<sup>2</sup> (<sup>1</sup>Advanced Space Propulsion Laboratory, NASA Johnson Space Center, Houston, TX (USA), <sup>2</sup>Dept. of Physics, Univ. of Houston, Houston, TX (USA))

VASIMR (Variable Specific Impulse Magnetoplasma Rocket, [1]) is an electric propulsion concept currently under experimental development at the Advanced Space Propulsion Laboratory, NASA Johnson Space Center. An RF (Helicon) discharge generates plasma (typically ionized Hydrogen or Helium) confined by a solenoidal magnetic field. The plasma is then further heated by a RF booster (in the ion cyclotron resonance frequency range) and finally flows through a magnetic nozzle where the thermal plasma energy is converted into kinetic energy along the longitudinal direction, enabling plasma detachment to produce thrust. The system has no electrodes and the magnetic field ensures magnetic insulation of the plasma from the material surfaces. By powering the plasma source and the heating antenna at different levels it is possible to vary smoothly of the thrust-to-specific impulse ratio while maintaining maximum power utilization. A MHD simulation modeling effort (NIMROD code [2,3]) is being carried on to study the plasma parameters and the detachment process of the plasma plume in the magnetic nozzle. In the model, a plasma source feeds a continuous flow through a nozzle-shaped magnetic field. Profiles of plasma density, temperature and flow velocity are then recorded at different times, while the plasma plume is formed in the magnetic field. Current simulations are set to model the plasma environment up to few meters from the nozzle throat: at that distance the plasma exhaust parameters reach values comparable with the ionospheric plasma background [4]. First, two-dimensional results (in cylindrical geometry) from simulation runs specifically designed for obtaining comparisons with laboratory measurements of the VASIMR experiment and first simulations of the plasma exhaust in 3D are here reported. [1] F. R. Chang-Diaz, *Scientific American*, p. 90, Nov. 2000 [2] A. H. Glasser et al., *Plasma Phys. Control. Fusion*, 41, A74 (1999) [3] <http://www.nimrodteam.org> [4] A. V. Ilin et al., *Proc. 40th AIAA Aerospace Sciences Meeting*, Reno, NV, Jan. 2002

**GAI11.11/10P/D-006** Poster **1400-120**

**USING THE HISTORICAL RECORDS OF SPACECRAFT MALFUNCTION DATA TO STUDY THE IMPACTS OF FUTURE SPACECRAFT OPERATION IN THE SPACE PLASMA ENVIRONMENT VERSUS THE SPACE DEBRIS ENVIRONMENT**

Shin-Yi SU (NRC Senior Research Associate at NASA/JSC, Houston, Texas, U.S.A., On sabbatical leave from National Central University, Taiwan, R.O.C.)

There are many different kinds of spacecraft anomalies caused by the space environment. For the geosynchronous (GEO) satellites, the electrostatic discharge (ESD) has the most serious impact on the spacecraft operation. However, for the low Earth orbit (LEO) satellites, the impact of ESD has greatly diminished so that all the effects from the space plasma environment and the space debris environment will have equal impact. Although the published NASA/GSFC spacecraft operation records (Timmins, 1971; 1974; and 1975) have been studied with the Weibull distribution for the spacecraft operation lifetimes (Baker and

Baker, 1980), we have reanalyzed these records to obtain the average occurrence rate of malfunctions per satellite. A Monte-Carlo simulation is then performed to compare the malfunction occurrences in the space plasma environment with the impacts from the space debris environment. It is noted that although the current miniaturization of the electronic circuits in the spacecraft bus system will increase the vulnerability of the spacecraft operation in the space plasma environment as compared with the operation in the space debris environment, this report should still be valuable for comparison of the impacts from the two different environments to assess the future spacecraft operation.

**GAIIL.14**

**HOW DO THE MAGNETOSPHERES OF OTHER PLANETS AND THEIR SATELLITES COMPARE WITH THE EARTH'S MAGNETOSPHERE?**

Location: Site A, Room 12

Monday, July 7 AM  
Presiding Chair: L.G. Blomberg

**GAIIL.14/07A/A12-001 0930**

**THE IONOSPHERES OF VENUS AND MARS AND THEIR INTERACTIONS WITH THE SOLAR WIND**

Hiroyuki SHINAGAWA (Solar-Terrestrial Environment Laboratory, Nagoya University)

Both Venus and Mars have no significant intrinsic magnetic field, and the solar wind interacts directly with the ionospheres. Previous studies of Venus suggest that the ionospheric thermal pressure (Pi) and the solar wind dynamics pressure (Psw) are the most important parameters, which determine the nature of the solar wind-ionosphere interaction. At Venus, when Pi is larger than Psw, the solar wind flow is deflected at high altitudes. The magnetic field pile-up region (the magnetic barrier) and the ionospheric plasma region are usually clearly separated by a sharp boundary, which is called the ionopause. However, when Psw is larger than Pi, the whole ionosphere is magnetized. Under such conditions, the ionopause tends to be thicker, and a magnetic field belt is formed in the lower ionosphere. The solar wind interaction with Mars appears to be more complicated than that of Venus. The magnetometer and electron reflectometer (MAG/ER) on Mars Global Surveyor (MGS) obtained magnetic field and plasma data throughout the near-Mars environment, from the solar wind to the bottom of the ionosphere (~110 km). It is found that the surface magnetic field of core origin is likely to be smaller than about 5 nT, indicating that the global intrinsic magnetic field at Mars does not play an important role in the solar wind interaction with Mars. Instead, MGS detected fairly strong (B <= 1600 nT) magnetic anomalies which are considered to be of crustal origin. It is expected that the crustal magnetic field significantly affects the structure of the ionosphere. The ionospheres of Venus and Mars and their interactions with the solar wind are reviewed in light of recent observations as well as theoretical studies.

**GAIIL.14/07A/A12-002 1000**

**ELECTRIC FIELDS AT MERCURY**

Lars G. BLOMBERG<sup>1</sup>, Judy A. CUMNOCK<sup>1</sup> (<sup>1</sup>Alfvén Laboratory, <sup>2</sup>Center for Space Sciences, University of Texas at Dallas)

Returning to Mercury with the BepiColombo mission will provide a unique opportunity to obtain in situ information on the electric field in Mercury's magnetosphere. The electric field plays a crucial role for plasma transport in the magnetosphere, for transfer of energy between different parts of the system, and for propagation of information. Measuring the electric field, we will be able to better understand plasma motion and wave propagation in Mercury's magnetosphere. Together with knowledge of the magnetic field a better understanding will be derived of the magnetospheric current systems and their closure at or near the planetary surface. Further insight into possible substorms at Mercury will be gained. We summarize the scientific case for electric field measurements on BepiColombo and outline the instrument design which, because of the harsh environment, is a challenging task.

**GAIIL.14/07A/A12-003 1015**

**HYBRID SIMULATIONS OF THE INTERACTION BETWEEN SOLAR WIND FLOW AND THE HERMEAN MAGNETOSPHERE**

Pavel TRAVNICEK<sup>1</sup>, Petr HELLINGER<sup>1</sup>, David SCHRIEVER<sup>2</sup> (<sup>1</sup>Department of Space Physics, Institute of Atmospheric Physics, Czech Academy of Sciences, Bocni II. cp. 1401, 14131 Prague 4, Czech Republic, <sup>2</sup>Institute of Geophysics and Planetary Physics, University of California Los Angeles, Los Angeles, 90095-1567, U.S.A.)

We will examine the magnetosphere of Mercury using global three dimensional hybrid plasmasimulations. Hybrid simulations treat ions as particles and electrons as a fluid. Having ions as particles allows ion kinetic behavior and waves to be included in the physical treatment of the plasma as compared to magnetohydrodynamic (MHD) modeling that treats the plasma as a single magnetized fluid and does not include such kinetic effects. Kinetic effects are essential for understanding magnetospheric physics. Hybrid simulations scale to the ion inertial length and thus on a global scale are somewhat limited in spatial extent compared to an MHD simulation. The overall structure of the interaction between a magnetized obstacle in the solar wind flow is determined by few basic parameters (namely the solar wind density, background magnetic field, and the speed of solar wind, and also the strength of the magnetic dipole of the obstacle and its radius). The structure of the interaction of the solar wind flow with Mercury is to a large extent unique when compared to other planets. For example, the magnetic moment of the Mercury is over 1000 times smaller than that of the Earth and also the solar wind is stronger nearby Mercury than Earth's vicinity. The typical magnetospheric scales are comparable to the ion gyroradius and hence kinetic effects are important for the overall structure of the interaction between the Hermean magnetosphere and the solar wind. In this paper we shall focus on the study of structure of the bow shock formed in front of Mercury under different conditions of the solar wind flow. The existence of shocklets (multiple shocks) is well known from observations of comets and it was also noticed in the Martian bow shock measurements of Phobos spacecraft (not seen in Viking observations). The shocklets structure has been subject of several two and three dimensional numerical studies of considering mainly unmagnetized obstacles in the solar wind using hybrid code with different spatial resolution. We shall examine the overall structure of the Hermean magnetosphere describing most of the structures formed due to the interaction with the solar wind like the bow shock, proton foreshock, magnetopause, magnetosheath, northern and southern cusps and the current sheet.

**GAIIL.14/07A/A12-004 Invited 1050**

**THE INTRIGUING MAGNETOSPHERE OF MERCURY**

Michel MONCUQUET, Jean-Louis BOUGERET (LESIA, Observatoire de Paris)

The magnetosphere of Mercury is very different from all other known magnetospheres: Mercury has very rarefied atmosphere, with almost no ionosphere; he has also the smallest known magnetosphere (1/7 of that of Earth), that implies especially small scale size and short characteristic times of magnetospheric processes. The planet occupies a much larger fractional volume of its magnetosphere than the Earth, and other planets. The magnetosphere of Mercury is exposed to much denser and hotter solar wind plasma and more intense interplanetary magnetic fields than any other planetary magnetosphere. These particular aspects of the Hermean Magnetosphere will be reviewed and some of associated magnetospheric processes will be compared to those at work in the Earth Magnetosphere. We will finally discuss how the BepiColombo/Mercury Magnetospheric Orbiter (MMO), and especially the radio experiment, should answer some of the questions asked by this intriguing magnetosphere of Mercury.

**GAIIL.14/07A/A12-005 Invited 1115**

**ENERGETIC PARTICLE DISTRIBUTIONS IN THE VICINITY OF IO**

Richard M. THORNE<sup>1</sup>, Donald J. WILLIAMS<sup>2</sup> (<sup>1</sup>Atmospheric Sciences, <sup>2</sup>Applied Physics Laboratory)

The Galileo Spacecraft has made several close passages of the moon Io. Pronounced changes in the energetic particle distributions were observed during each encounter. Some of these changes can be explained simply as an adiabatic response to changes in the magnetic and electric fields surrounding the moon. The two passes over the polar cap region of Io clearly demonstrate that the Jovian magnetic field is connected to the poles of Io and that most energetic particles on such field lines are lost by collision with the moon. There is, however, a residual trapped population that mirrors between the enhanced field at the surface of Io and some point further up the field line towards Jupiter. A detailed analysis of the development of such trapped distributions indicates that the convective motion over the poles is dramatically reduced from that in the corotation flow upstream of the moon. Energetic electron beams arriving in a narrow cone from the direction of Jupiter indicate pronounced field-aligned acceleration in the region close to the planet. Such beams, which are found over each polar cap and within the wake region downstream of Io, provide an estimate of the spatial region of field-aligned currents that connect Io to Jupiter.

**GAIIL.14/07A/A12-006 1140**

**RELATION BETWEEN EXTENDED SODIUM DISTRIBUTION ORIGINATED FROM IO AND AROUND IO**

Shin TAKAHASHI, Akira MORIOKA, Shoichi OKANO, Hiroaki MISAWA, Hiromasa NOZAWA, Masato KAGITANI (Planetary Plasma and Atmospheric Research Center, Tohoku University)

We have performed imaging observations of the D-line emissions of logenic sodium atoms. The method of the observation is the 2-dimensional imaging observations whose field of views are 20Rj (narrow FOV) and 400Rj (wide FOV) around Jupiter. From these observations, we investigated the characteristics of the emission distribution and its time variation. Based on these observations, we have also performed model analyses to investigate source processes of sodium atoms and time variation of sodium distribution, and presented the comprehensive source process which can consistently reproduce the observed characteristics. From these studies, we concluded that the composition of both charge exchange and molecular ion destruction processes are appropriate as source mechanisms of extended distribution of sodium atoms. The initial conditions of released sodium atoms through these two processes depend on the plasma environment around Io, so that we can investigate interaction between Io and the Jovian magnetospheric plasma by using spatial and temporal variation of extended sodium distribution.

**GAIIL.14/07A/A12-007 1155**

**IMPLICATION FOR THE SOLAR WIND EFFECT ON THE IO PLASMA TORUS**

Hiromasa NOZAWA, Hiroaki MISAWA, Shin TAKAHASHI, Akira MORIOKA, Shoichi OKANO (Planetary Plasma and Atmospheric Research Center, Tohoku University, Aoba, Aramaki-aza, Aoba-ku, Sendai, 980-8578, JAPAN)

Jovian inner magnetosphere is characterized by strong magnetic field and fast rigid-rotation. Hence, it is considered that there is little solar wind effect in the inner magnetosphere and also around the Io plasma torus (IPT). However, the narrow band kilometric (nKOM) radio emissions whose sources are thought to be at the outer edge of the IPT showed solar wind dependence at the time of the Ulysses observation (Reiner et al. 2000). Therefore, it is suggested that there may be some relations between the solar wind and the IPT. Between September 4 and 22 in 1999, we carried out ground-based optical observation of the IPT. In this period, the Galileo orbiter was in the Callisto 23 Orbit and made observations of planetary radio emissions with the Plasma wave system (PWS) between September 13 and 27. From the comparison between the ground-based and Galileo/PWS observations, it was found that sudden enhancement of the IPT emission was concurrent with the appearance of nKOM. In addition, just prior to the IPT enhancement, we detected the enhancement of the hectometric (HOM) radio emission that would be related to the solar wind. From these evidences, it can be supposed that the IPT is affected by the solar wind.

**GAIIL.14/07A/A12-008 1210**

**OBSERVATION OF [SII] EMISSION IN IO PLASMA TORUS USING AN IMAGING FABRY-PEROT INTERFEROMETER**

Masato KAGITANI, Takeshi SAKANOI, Shoichi OKANO (Planetary Plasma and Atmospheric Research Center, Tohoku University)

Plasma originated from volcanic eruption on Jovian satellite Io forms a donut-shaped region of dense plasma along Io's orbit, which is called Io plasma torus (IPT). Spectral line emission from singly charged sulfur ions, [SII], at 671.6 nm and 673.1 nm in IPT is strong enough to be observable from the ground. Imaging observation of sulfur ion emission with sufficient spectral resolution will enable us to monitor two-dimensional distributions of ion temperatures, line-of-sight velocities of ions, and emission intensity. In order to attain such purpose, we have developed an imaging Fabry-Perot interferometer (IFPI) for continuous observation of Io plasma torus. The IFPI is coupled to a 60-cm Coude telescope of our Iitate observatory (37.7°N, 140.7°E). Fabry-Perot etalon of the IFPI is characterized by wavelength resolution of .01 nm and finesse of 40 at 671.6 nm. The gap of etalon is scanned in order to obtain two-dimensional distributions of above mentioned physical quantities, and spectral profile is recorded at each pixel of a CCD detector. Before starting actual observation, the best combination of observation parameters; the etalon scanning step, number of scanning



points, and exposure time, were determined based on simulation. Calibration of the IFPI was made using Ne spectral lamp, whose wavelength (671.704 nm) is within one free spectral range of the Doppler-shifted sulfur ion line, as a light source for determination of absolute wavelength, and a frequency stabilized He-Ne laser as a light source for determination of etalon finesse. Preliminary observation was made on November 23, 2002 (JST). Although the nature of observation is very preliminary, following results were obtained from analysis of the recorded data for the east ansa of IPT; (1) emission intensity at 6.05R<sub>J</sub> was 600R, (2) regarding line-of-sight velocity, slowing down from the corotation velocity at 6.05R<sub>J</sub> was 5 km/sec, (3) ion temperatures perpendicular to the field line showed increase from 5.7R<sub>J</sub> to 6.05R<sub>J</sub>, where the value was approximately 2x10<sup>4</sup>K. From these results, it has been shown that the method is encouraging and we are going to continue monitoring observation of IPT.

**GAI11.14/07A/A12-009 1225**

**A COMPARISON OF THE GANYMEDE MAGNETOSPHERE WITH THE EARTH'S MAGNETOSPHERE UNDER EXTREME SOLAR WIND AND IMF CONDITIONS**

Aaron J. RIDLEY<sup>1</sup>, K.C. HANSEN<sup>1</sup>, F.J. CRARY<sup>2</sup> (<sup>1</sup>Center for Space Environment Research, University of Michigan, <sup>2</sup>Southwest Research Institute, San Antonio, Texas)

Ganymede has an intrinsic dipolar magnetic field. Because of the orbit of Ganymede in Jupiter's magnetic field, it is constantly in an amagnetic field dominated plasma. Earth is sometimes in this type of flow also - when the solar wind density is quite low and the magnetic field is quite high. This talk will show MHD simulation results of Ganymede's magnetosphere in nominal conditions above and below Jupiter's current sheet, and compare those simulation results to MHD simulation results of the Earth's magnetosphere during very strong interplanetary magnetic field conditions. The relative size and structure of the different magnetospheres will be discussed. The solar wind and IMF conditions which produce a Ganymede-like Earth magnetosphere will be discussed. In addition, the frequency of such events at the Earth will be discussed.

**Monday, July 7 PM**  
Presiding Chair: K. Khurana

**GAI11.14/07P/A12-001 1400**

**THE MAGNETOSPHERES OF JUPITER AND THE EARTH: A COMPARATIVE ASSESSMENT**

Margaret G. KIVELSON (Inst. of Geophysics and Planetary Physics)

The planetary magnetic fields of Earth and Jupiter exclude the solar wind from large volumes of space, the magnetospheres that surround these planets. Our knowledge of the Earth's magnetosphere relies on many decades of data from orbiting spacecraft supplemented by data from ground-based instruments from which a basic description of the structure and dynamics of this plasma regime has evolved. Galileo has recently completed a survey of the field and plasma properties of the Jovian system over a large range of radial distances (6-150 R<sub>J</sub>) in the near equatorial regions and at all local times. These data, supplemented by remote observations of the aurora and complemented by data from previous spacecraft flyby missions, provide considerable insight into the structures and processes that control Jupiter's magnetosphere. After introducing selected salient features of both of these magnetospheres, I will first discuss the properties that these systems share in spite of the vast differences in their scale sizes and sources of plasma and energy. Next, I will touch on some features unique to each of the magnetospheres. I will discuss the roles of reconnection, planetary rotation and ionospheric conductivity in driving and maintaining plasma convection. The differences and similarities in the processes that generate aurorae in the atmospheres of these planets will also be examined. The evidence for intermittent processes that may be similar to terrestrial substorms in the magnetosphere of Jupiter will be presented and I shall comment on their relation to plasma convection and magnetospheric reconfiguration. I will first discuss the properties that these systems share in spite of the vast differences in their scale sizes and sources of plasma and energy. Next, I will touch on some features unique to each of the magnetospheres. I will discuss the roles of reconnection, planetary rotation and ionospheric conductivity in driving and maintaining plasma convection. The differences and similarities in the processes that generate aurorae in the atmospheres of these planets will also be examined. The evidence for intermittent processes that may be similar to terrestrial substorms in the magnetosphere of Jupiter will be presented and I shall comment on their relation to plasma convection and magnetospheric reconfiguration.

**GAI11.14/07P/A12-002 1430**

**MAGNETOSPHERE-IONOSPHERE COUPLING CURRENTS IN JUPITER'S MIDDLE MAGNETOSPHERE**

Jonathan D. NICHOLS, Stan W.H. COWLEY, Emma J. BUNCE (Department of Physics and Astronomy, University of Leicester)

The dynamics of Jupiter's plasma environment is dominated by the outflow of material originating from the moon Io, which orbits deep within the magnetospheric cavity. Breakdown of corotation associated with this radial transport results in the formation of a magnetosphere-ionosphere coupling current system which transfers angular momentum to the magnetospheric plasma and has been linked to the formation of the main jovian auroral oval. It has been shown that the amplitude and spatial distribution of the currents, and the related profile of the plasma angular velocity, depend on the values of the effective Pedersen conductivity of the jovian ionosphere and the mass outflow rate of ionogenic plasma. In this talk we compute self-consistent solutions for this current system based on steady plasma outflow from the Io torus, and present our latest results.

**GAI11.14/07P/A12-003 1445**

**DIPOLAR MAGNETOSPHERES: CHARACTERIZATION AND SCALES**

Nick OMDI<sup>1</sup>, Homa KARIMABADI<sup>1</sup>, X. BLANCO-CANO<sup>2</sup>, Christopher RUSSELL<sup>3</sup> (<sup>1</sup>UCSD, <sup>2</sup>UNAM, <sup>3</sup>UCLA)

Hybrid simulations (kinetic ions, fluid electrons) of solar wind interaction with dipoles of various strength are used to characterize the resulting magnetospheres and establish the scales associated with the formation of various magnetospheric boundaries and regions. It is shown that depending on the dipole strength, a spectrum of magnetospheric structures exist which can be characterized in terms of the distance ahead of the dipole where the magnetic field pressure balances the solar wind ram pressure (D<sub>p</sub>). At low dipole strengths, the magnetosphere is fairly simple and consists of whistler and/or magnetosonic wakes. Increasing the dipole field results in the formation of progressively more complex magnetospheres with a number of different plasma regions separated by various types of waves or discontinuities. When D<sub>p</sub> approaches ~ 20 ion inertial length, the resulting

magnetosphere exhibits a terrestrial type behavior. This result explains why despite their major differences in size, all magnetospheres in the solar system (e.g. Hermean and Jovian) have characteristics similar to the Earth's. Despite similarities, however, differences due to scale sizes are also expected. Implications of these results for the various bodies in the solar system ranging from magnetized asteroids to planets and moons are discussed.

**GAI11.14/07P/A12-004 1500**

**EXTERNAL AND INTERNAL CONTROL OF THE MAGNETOSPHERIC CONFIGURATIONS AND DYNAMICS AT THE EARTH AND JUPITER**

Raymond John WALKER<sup>1</sup>, Tatsuki OGINO<sup>2</sup> (<sup>1</sup>Institute of Geophysics and Planetary Physics and Department of Earth and Space Physics, UCLA, <sup>2</sup>Solar Terrestrial Environment Laboratory, Nagoya University)

At the Earth magnetospheric dynamics are largely controlled by the solar wind and interplanetary magnetic field. Internal processes contribute to the details of magnetospheric dynamics but the energy required to power the system comes from the solar wind. At Jupiter the dominant energy reservoir is within Jupiter's magnetosphere. That energy reservoir is Jupiter's plasma disk which is powered by Jupiter's rotation. The existence of the magnetodisk is a major difference between the Earth's magnetosphere and that at Jupiter. On the dayside it is located between the inner magnetosphere where Jovian effects are dominant and the outer magnetosphere or cushion region where the solar wind influence is great. We have used a three dimensional global magnetohydrodynamic simulation of the interaction of Jupiter's magnetosphere with the solar wind to investigate the structure of Jupiter's magnetosphere. The emphasis in this study is on the extent to which the solar wind affects the structure and dynamics of the magnetodisk. The plasma in the magnetodisk flows around Jupiter. The azimuthal flow is largest in a band from 1800 LT across the night side magnetosphere to noon and between 30R<sub>J</sub> and 50R<sub>J</sub> from Jupiter. Between noon and dusk the azimuthal flow decreases. The region of largest azimuthal flow is also characterized by smaller flows away from Jupiter with maximum outflow predawn. The region where the azimuthal flow decreases contains radial flow toward Jupiter. The simulated equatorial plasma sheet is much thinner in the morning magnetosphere than in the afternoon magnetosphere as has been inferred from observations. The plasma sheet is thickest where the radial flow is toward Jupiter. The configuration of the middle magnetosphere is only weakly dependent on solar wind dynamic pressure. However, the radial inflow decreases when the IMF turns from northward to southward.

**GAI11.14/07P/A12-005 1515**

**PARTICLE MOTION IN JUPITER'S MAGNETOSPHERE COMPARED TO THE EARTH'S CASE**

Norbert KRUPP<sup>1</sup>, Joachim WOCH<sup>1</sup>, Andreas LAGG<sup>1</sup>, Krishan KHURANA<sup>2</sup> (<sup>1</sup>Max-Planck-Institut f. Aeronomie, <sup>2</sup>IGPP, UCLA)

Comparing the motion of plasma and energetic particles in different planetary magnetospheres provides new insights into the physical processes of these large-scale plasma laboratories in space and extends our knowledge of the solar system as a whole. Especially important information is obtained about the steady-state configuration and the dynamic processes of these magnetospheres. In this paper the observational facts of particle motion in Jupiter's magnetosphere is reviewed and compared with the well known pattern in the Earth's case. This study is essentially based on in-situ measurements from Galileo which is orbiting Jupiter since 1995 obtaining the most complete data set of the Jovian system. For the first time it was possible to determine details about the particle motion in the equatorial plane of Jupiter's magnetosphere. These results will be compared with the well-known processes in the Earth's magnetosphere achieved over the last decades. A comparison of the particle motion in both magnetospheres revealed both similarities and significant differences. At Earth, magnetospheric convection is driven by the solar wind whereas in the Jovian case planetary rotation is far more important. Another very important difference lies in the particle sources and in the composition of magnetospheric plasma - solar wind and ionosphere in the Earth's case and mainly the moon Io for Jupiter. AE lead to completely different global flow pattern. Similarities are also found in the comparison between both magnetospheres. The well-known substorm scenario at Earth could have its counterpart at Jupiter where flow bursts together with magnetic field rotations and auroral emissions were observed. This suggests that substorm-like events (eventually internally triggered) have been observed at Jupiter.

**GAI11.14/07P/A12-006 Invited 1600**

**PLASMA SOURCES FOR SATURN'S MAGNETOSPHERE**

John d RICHARDSON, Slobodan JURAC (Center for Space Research, M.I.T.)

The magnetosphere of Saturn, in contrast to that of Earth, has numerous orbiting sources of plasma. The rings and inner icy satellites are sources of water group neutrals which become ionized and contribute to the plasma population. Titan's atmosphere is a source of H and N. The main sources of plasma in Earth's magnetosphere are the solar wind and ionosphere; while these sources provide plasma at Saturn, they provide only a small percentage of the total plasma. We present models of the sputtering of water from Saturn's orbiting icy bodies, formation of the neutral cloud surrounding Saturn, and the transport and energy balance of the plasma. The model results match well observations of OH by the Hubble Space Telescope and of plasmab by Voyager. The required source of neutrals is larger than sputtering theory predicts. A possible solution to this problem is suggested; a large number of small ice grains providing additional surface area for sputtering.

**GAI11.14/07P/A12-007 Invited 1625**

**PLANETARY AURORAE**

Renée M. PRANGE, Philippe ZARKA (LESIA, Observatoire de Paris)

The Voyager missions have revealed the presence of auroral features surrounding the magnetic poles for all the magnetized planets in the solar system which also possess an atmosphere. Since then, planetary aurorae have been thoroughly studied on Jupiter, from Earth orbit and by means of the visible camera and of the UV spectrometer on board the Jupiter orbiting Galileo spacecraft. Increased performances of the Hubble Space Telescope instruments have also recently allowed to take very good images and spectra of the UV aurorae on Saturn in the prospect of Cassini's arrival in the planet vicinity. At all planets counterparts of these auroral emissions are found, from earth-based receivers and from space, in the radio spectral range. Taking advantage of these two complementary diagnostic tools, I will give an overview of the morphology, temporal behavior, and suggested auroral processes in the magnetosphere for the Earth, Jupiter and Saturn, taking a comparative point of view approach.

**GAIII.14/07P/A12-008 1650**

**COMPARISON OF AURORAL PROCESSES ON JUPITER AND THE EARTH**

John T. CLARKE (Center for Space Physics, Boston University)

High resolution images of Jupiter's UV aurora obtained over the past 4-8 years have revealed with increasing detail and sensitivity the auroral patterns on that planet. We are now beginning to learn the relationships between the auroral emissions and other properties of Jupiter's giant magnetosphere. Jupiter's aurora include a main oval related to the breakdown of corotation of outwardly drifting plasma in the middle magnetosphere. This region is most analogous to the outer boundary of the Earth's plasmasphere. Jupiter also displays auroral emissions from the magnetic footprints of at least 3 satellites, for which there is no analogous process at the Earth. Finally, the polar regions of Jupiter's aurora, which are also the most rapidly variable, are most analogous to the Earth's auroral regions, in the sense that they must map to the general vicinity of the magnetosphere/solar wind boundary. The characteristics of Jupiter's polar emissions are nonetheless quite different from those of the Earth's aurora. These analogies will be discussed and expanded upon in this presentation, supported by images of Jupiter's aurora obtained from the Hubble Space Telescope.

**GAIII.14/07P/A12-009 1705**

**SPECTRUM OBSERVATION OF JUPITER'S SYNCHROTRON RADIATION AT THE FREQUENCIES OF 325, 929 AND 2295 MHz**

Hiroaki MISAWA<sup>1</sup>, Fuminori TSUCHIYA<sup>1</sup>, Yoshizumi MIYOSHI<sup>1</sup>, Akira MORIOKA<sup>1</sup>, Tetsuro KONDO<sup>2</sup> (Planetary Plasma and Atmospheric Research Center, Tohoku University, <sup>1</sup>Communications Research Laboratory, Independent Administrative Institution)

Jupiter's synchrotron radiation (JSR) is generated by the relativistic electrons trapped in Jupiter's radiation belt. Variation of JSR is, therefore, an important probe to investigate generation and dissipation processes of the relativistic electrons and deformation of their global distribution in Jupiter's inner magnetosphere. For more than 40 years since its discovery, JSR has been thought to be quite stable emission except for a long-term variation at a time scale of nearly the solar-cycle. However regular and systematic JSR observations have been made by several groups particularly after the event of the comet P/SL9 impacts to Jupiter, and revealed the existence of short term variations at a time scale of several days to months inferring some electro-magnetic activities in the inner magnetosphere. Nowadays it's the time to investigate the details of variation characteristics and origin of the time variation. A program of a multi-frequency observation for JSR has been started since 2001. The JSR spectrum measurements give us information of variations of pitch angle and/or characteristics of radial diffusion of the relativistic electrons. In this program three observation frequencies measured with different facilities are adopted; i.e., 325 MHz at Tohoku Univ. and Nagoya Univ., Japan, 929 MHz at EISCAT, and 2295 MHz at Comm. Res. Lab. (CRL), Japan. As for the 325 MHz observation, although the Tohoku Univ. system will start the regular JSR observation in the middle of 2003, the Nagoya Univ. system has made the JSR observations for about three months a year since 1995. The observation method has been already established at 2295 MHz using the CRL system by our group. On the other hand, we made test experiments for JSR using the EISCAT 929 MHz system in the autumn of 2001 and made ten successive day observation in the end of November of 2002. Now we plan to make the spectrum observation with these three frequencies in this autumn. In the presentation, outline of the spectrum observation and present status will be shown with the objectives of this program.

**GAIII.14/07P/A12-010 1720**

**ON THE ORIGIN OF THE POLARIZATION CHARACTERISTICS OF JUPITER'S DECAMETRIC RADIATION**

Hiroaki MISAWA (Planetary Plasma and Atmospheric Research Center, Tohoku University)

The lo-related Jupiter's decameter wave emission (lo-DAM) is known to show two clear occurrence characteristics. One is the occurrence periodicity and another one is the polarization characteristics. The former is that the lo-DAM events occur in specific geometric combinations of the central meridian magnetic longitude and lo phase angle. The latter is the theme of this study, and shows following somewhat unique nature. 1) The lo-DAM events show highly elliptical polarization, which is observed only for certain pulsars except lo-DAM. 2) The degree of polarization of one lo-DAM event doesn't show a significant time variation for a few hours. 3) Although the degree of circular polarization decreases slightly with frequency, in most cases, the degree of polarization changes very little with frequency. 4) The degrees of circular or linear polarization between lo-A and lo-B DAM events show slight difference; i.e., the lo-A events are slightly more circular than the lo-B events. The elliptical polarization of the lo-DAM events was explained by Melrose and Dulk [1991, 1993] based on the cyclotron maser theory and strong magneto-ionic mode coupling assumption in and near the source region: 1) the lo-DAM wave is generated at an angle ( $\theta$ ) of 60 to 80 degrees with respect to the local magnetic field and starts out in elliptical polarization. 2) the plasma in and near source region is quite tenuous, say less than 5 per cc, then, the elliptical polarization is retained during propagation. If the idea is correct, the expected axial ratio (AR) of an event is denoted as  $AR = \cos(\theta)$ . Misawa et al. [1997] examined this explanation by comparing the observed AR with the AR value calculated from the angle between the local magnetic field of the expected source region and the direction of an observer (the earth) for each datum, and showed that the observed AR values are not interpreted by the idea. Instead of the idea of Melrose and Dulk [1991], Shaposhnikov et al. [1997] took into account the effect of plasma continuity (weak or no mode coupling condition) in and near the source region and showed the possibility of polarization variation of the lo-DAM wave during ray propagation using a simple model of the Jovian magnetosphere and ionosphere. We have made a 3D ray tracing analysis for lo-DAM to investigate the observed occurrence periodicity and polarization characteristics of lo-DAM by using the GSFC VIP4 magnetic field model. In this study, we have evaluated polarization characteristic based on the assumption of plasma continuity in and near source regions and have traced variation of polarization along a ray path. Preliminary results show some possibilities for explaining some of the above mentioned unique polarization characteristics of lo-DAM with the assumption of plasma continuity.

**GAIII.14/07P/A12-011 1735**

**ELECTRIC FIELDS IN THE JUPITER'S MAGNETOSPHERE (COMPARISON WITH THE CASE OF THE EARTH)**

Elena Semenovna BELENKAYA (Institute of Nuclear Physics, Moscow State University)

In a constructed model of the jovian magnetosphere the magnetospheric magnetic field consists of Jupiter's dipole field, the magnetodisc field, and the field of the magnetotail current system. All magnetospheric magnetic fields are screened by the magnetopause currents. Interplanetary magnetic field partially penetrates into the magnetosphere. The

electric fields and plasma motions caused by the Jupiter's rotation and the solar wind MHD generator are studied. The comparison with the case of the Earth is fulfilled.

**GAIII.14-Posters**

**HOW DO THE MAGNETOSPHERES OF OTHER PLANETS AND THEIR SATELLITES COMPARE WITH THE EARTH'S MAGNETOSPHERE?**

Location: Site D

Tuesday, July 8 AM

**GAIII.14/08A/D-001 Poster 0830-145**

**WHAT CAN SEE A MAGNETOMETER ON NOZOMI MISSION AT THE VICINITY OF PHOBOS?**

Valentina G. MORDOVSKAYA, Victor N. ORAEVSKY (Institute of Terrestrial Magnetism, Ionosphere, and Radiowave Propagation (IZMIRAN))

In this communication, we examine in situ observations of the magnetic field in the vicinity of Phobos on the "Phobos-2" mission and give some analysis of the data during a unique experiment "Celestial Mechanics," which leads to the evidence of the Phobos magnetic field. In particular, it is suggested that the peculiarity of the solar wind interaction with Phobos and rotating direction of the magnetic field obtained on the circular orbits around Mars are the evidence for the existence of an intrinsic planetary field of Phobos. Vector magnetic field observations of the solar wind interaction with Phobos were acquired by MAGMA and FGMM during Phobos-2 mission in regions which have not been explored before. Phobos deflects the flow of the solar wind and the subsolar stand-off distance of the deflection is about 16-17 Phobos radii. Source with equivalent magnetic moment  $M = 10^{15} \text{ Am}^2$  in Phobos leads to the development of such an obstacle for solar wind flow around Phobos. 1. THE PECULIARITIES OF THE INTERACTION OF PHOBOS WITH THE SOLAR WIND ARE EVIDENCE OF THE PHOBOS MAGNETIC OBSTACLE (FROM PHOBOS-2 DATA). V.G. Mordovskaya, V.N. Oraevsky, and V.A. Styashkine-Print arXiv:physics/0212072 v1 19 Dec 2002 submitted to Adv. Space Res., 2002. 2. IN SITU MEASUREMENTS OF THE PHOBOS MAGNETIC FIELD DURING THE PHOBOS-2 MISSION. V.G. Mordovskaya and V.N. Oraevsky-Print arXiv:physics/0212073 v1 19 Dec 2002 submitted to Adv. Space Res., 2002

**GAIII.14/08A/D-002 Poster 0830-146**

**AN ENA INSTRUMENT FOR MERCURY MAGNETOSPHERIC ORBITER OF THE BEPICOLOMBO MISSION**

Yoichi KAZAMA<sup>1</sup>, Stas BARABASH<sup>2</sup>, Kazushi ASAMURA<sup>3</sup>, Andrei FEDOROV<sup>3</sup>, Peter WURZ<sup>4</sup> (<sup>1</sup>Swedish Institute of Space Physics, <sup>2</sup>Institute of Space and Astronautical Science, <sup>3</sup>Centre d'Etude Spatiale des Rayonnements, <sup>4</sup>University of Bern)

It is known that Mercury has an intrinsic magnetic field, which forms the Hermean magnetosphere. Energetic magnetospheric ions and the solar wind directly hit the surface, and sputter material to populate the exosphere. Since the spectrum of the sputtering neutral atom is relatively hard, neutrals with energies above tens eV are produced in large amount. Therefore the interaction region between precipitating ions and the Mercury surface is a strong source of low energy ENAs (energetic neutral atoms). Some exospheric neutrals are ionized by charge-exchange process with magnetospheric ions and the solar wind. Once a particle is ionized, the particle is accelerated immediately due to electric field up to keV range. The energetic particle strikes again the Hermean surface, constituting a cycloprocess. The energetic ions are re-neutralized with some probability, resulting in high-energy ENAs around Mercury. Mentioned above, the magnetosphere, exosphere, and the surface are tightly coupled through neutral particles at Mercury. Therefore, neutral particle measurement is one of the important targets of the BepiColombo mission to gain knowledge about the particle environment around Mercury. The solar wind ions injected from the tail in the sub-storm/storm alike processes as well as from direct penetration of the solar wind can be also charged-exchanged to ENA. Therefore, the ENA measurements provide magnetospheric imagery, that give us important information on the dynamics and structure of the Hermean magnetosphere, as has the terrestrial ENA. To observe ENAs comprehensively around Mercury, we propose an instrument on MMO in the BepiColombo mission. The instrument can cover neutrals in a wide range of energies, from sputtered particles to accelerated neutrals with sufficient time and angular resolutions. Following very tight mass budget the priority, however, will be given to the mass resolution capability of the instrument (ENA mass spectroscopy) to fully investigate magnetosphere-exosphere-surface relations taking place at Mercury. Neutrals entering the instrument are ionized by carefully produced surfaces at first, and then selected in energy by well-designed electrostatic multiple reflections, in which a huge number of solar photons are rejected. Mass analysis is done by permanent magnets, and finally the particle is detected by an imaging MCP detector.

**GAIII.14/08A/D-003 Poster 0830-147**

**THE MAGNETIC FIELD EXPERIMENT FOR BEPI-COLOMBO MMO**

Ayako MATSUOKA<sup>1</sup>, Wolfgang BAUMJOHANN<sup>2</sup>, The MERMAG-M CONSORTIUM<sup>3</sup> (<sup>1</sup>Institute of Space and Astronautical Science, <sup>2</sup>Institut für Weltraumforschung, Graz)

The MERMAG-M consortium is now preparing to propose a magnetic field experiment for Bepi-Colombo MMO. We have examined the design and performance of magnetometers to measure fields around Mercury with good accuracy. It consists of two sets of ring-core geometry sensor and electronic system with an extendible arm. One of the sensors (outboard) is mounted at the top of the arm and the another one (inboard) is at the 1/3 distance of the arm length from the top. The dual measurement enables not only good evaluation of the magnetic interference caused by the satellite body, but also a reliable redundancy of the measurement. Because the instruments on board MMO are expected to suffer acute radiation and heat inflow from the sun, measures against them without additional weight have been particularly examined. For the outboard sensor, the electronics is designed so that most signal processing is done digitally in the field programmable gate array (FPGA). It resolves the problem of the offset drifting which is caused by the change of temperature in the conventional analogue electronics. For the inboard sensor, the electronics is relatively similar to the conventional analogue circuit, but the robustness against the radiation is highly increased. An international collaboration has worked very well to proceed the examinations described above.

**GAIII.14/08A/D-004** Poster **0830-148**

**BEPICOLOMBO MISSION: SCIENTIFIC EXPECTATIONS AND CURRENT STATUS OF MERCURY MAGNETOSPHERIC ORBITER (MMO)**

Hajime HAYAKAWA<sup>1</sup>, Yasumasa KASABA<sup>1</sup>, Hiroshi YAMAKAWA<sup>1</sup>, Hiroyuki OGAWA<sup>1</sup>, Toshifumi MUKAI<sup>1</sup>, Masaki ADACHI<sup>2</sup>, Mercury Exploration WG<sup>3</sup> (<sup>1</sup>Institute of Space and Astronautical Science, <sup>2</sup>NEC-TOSHIBA Space Systems, Ltd.)

BepiColombo for the exploration of Mercury is the first collaborated mission between Europe (ESA) and Japan (ISAS). The aim of this mission is to clarify present and past of Mercury by investigating interior, surface, atmosphere, and magnetosphere, by 2 orbiters and 1 lander, which are MPO (Mercury Planetary Orbiter), MMO (Mercury Magnetospheric Orbiter), and MSE (Mercury Surface Element). Intensive contribution to this project is essentially expected for Japanese earth & planetary science community. ISAS will provide the MMO spacecraft. In this paper, we report our scientific expectations for and current status of the MMO mission study, which was conducted by the ISAS Mercury Exploration Working Group. Main scientific targets of MMO are 1) Structure and origin of Herman magnetic field, 2) Structure, dynamics, and physical processes of Herman magnetosphere, 3) Structure, variation, and origin of Herman Na atmosphere, 4) Macroscopic structure of Herman crust, and 5) Physical environment of inner solar system. For these targets, MMO will have 10 model payloads: Electron Spectrum Analyzer (ESA), Mass Spectrum Analyzer (MSA), Solar Wind Analyzer (SWA), High Energy Particle (HEP), Energetic Neutral Atoms (ENA), Magnetic Field sensor (MGF), Plasma Wave Instrument (PWI), Mercury Dust Monitor (MDM), and Mercury Imaging Camera for Atmosphere (MIC-A) & for Surface (MIC-S). For these targets, MMO, which weighs about 200kg, is as a spinning spacecraft at 15 rpm whose spin axis is perpendicular to the Mercury orbital plane. MMO will be at polar orbit with the period of 9.2hour, the perihelion of 400km and the apohelion of 12,000km (~6RM). It is selected for the observations of large regions in the Herman magnetosphere, mappings of magnetic field and surface, and macroscopic imaging of the Na atmosphere. The telemetry ability will be 20~160Mbytes/day (~40Mbytes/day [ave]). Data production rate will show large seasonal variation, because the data rate of in-situ plasma instruments is correlated to the duration staying in the magnetosphere and varies in 20~75MB/day. So basic policy of the operation is storing in the high-production term and reproducing in the low-production term. Mission life is 1 Earth year (~4 Mercury year). The specifications of the model instruments in this paper are for the basis of spacecraft investigations and not final ones. Actual selection of the instruments is based on the results of Announcement of Opportunity (A/O) in Japan and Europe. In the current plan (Jan 2003), the A/O for MPO (from ESA) and MMO (from ISAS) payloads will be issued in June 2003.

**GAIII.14/08A/D-005** Poster **0830-149**

**MERCURY MAGNETOSPHERE: EXPECTED PROGRESS BY BEPICOLOMBO/MMO**

Hajime HAYAKAWA, Yasumasa KASABA, Toshifumi MUKAI, Hiroshi YAMAKAWA, Hiroyuki OGAWA, Mercury WG (Institute of Space and Astronautical Science)

More than 25 years ago the Mariner 10 observations discovered the presence of the intrinsic magnetic field which was strong enough to stand off the solar wind and form the magnetosphere. According to the limited data from Mariner 10, the Mercury's magnetosphere has been drawn schematically by analogy from the Earth's one, so that it is apparently similar to the Earth's magnetosphere, being scaled down by a factor of 7-8 with normalization by the planetary radius, or by a factor of 20 in the real dimension. There have also been addressed several unique features, such as large occupation of the planetary body in the magnetosphere, no significant atmosphere and ionosphere, and the direct interaction of magnetospheric plasma with the planetary surface. Thus the Mercury has long been one of the most interesting objects in the field of comparative magnetospheric physics. For example, we should note that the scaling with the MHD viewpoint may not necessarily hold in the internal structure of the magnetosphere. There are difficulties to adopt the simple scaling-law to the Mercury's magnetosphere. Average solar wind dynamic pressure at Mercury orbit is 7-8 times larger than that of Earth orbit. This requires stronger magnetopause current which is same as plasma sheet current than earth's magnetosphere case, if flaring angle of the magnetosphere is same as earth's magnetosphere. Also thickness of the Mercury's plasma sheet expected from the scaling-law is only several hundred km which is comparable to the so-called "very thin plasma sheet" in the earth's magnetosphere. These facts suggest that the Mercury's plasma sheet current layer may be unstable if the scaling-law is correct, or the current sheet thickness is much larger than that expected from the scaling-law. Furthermore in the Earth's magnetosphere, when magnetic reconnection occurs, reduced cross tail current generates FAC and flows in the ionosphere to close the current circuit. But in the Mercury's magnetosphere this bypass circuit may not be possible since there is no ionosphere. The planetary body acts as a large plasma sink and the source of heavy ions, so this also provides us other ambiguous aspects. We do not know yet what is really happened in the Mercury's magnetosphere and how the structure is BepiColombo/MMO will reveal these mysteries and provide essential keys for the magnetospheric physics.

**GAIII.14/08A/D-006** Poster **0830-150**

**DEVELOPMENT OF IITATE PLANETARY RADIO TELESCOPE (IPRT) FOR THE INVESTIGATION OF THE JOVIAN INNER MAGNETOSPHERE**

Fuminoiri TSUCHIYA<sup>1</sup>, Hiroaki MISAWA<sup>1</sup>, Riichi KUDOU<sup>1</sup>, Yoshizumi MIYOSHI<sup>1</sup>, Takuo WATANABE<sup>1</sup>, Akira MORIOKA<sup>1</sup>, Tetsuro KONDO<sup>2</sup> (<sup>1</sup>Graduate School of Science, Tohoku University, <sup>2</sup>Communications Research Laboratory)

Iitate Planetary Radio Telescope (IPRT) which measures meter to decimeter radio waves has been developed at the Iitate village in Fukushima Prefecture, Japan. Primary purpose of IPRT is continuous monitoring of Jovian synchrotron radiation (JSR) and research of the dynamics in the Jovian inner magnetosphere by detecting short-term variations of JSR with the time scale of a few days to a few months. The short term variation reflects dynamic transport and acceleration processes of relativistic electrons in the inner radiation belt of Jupiter. The total flux observation of JSR by using a single dish telescope is a useful tool for the investigation of the acceleration and transport of relativistic electrons because the spectrum and polarization of JSR reflect energy spectrum and pitch angle distribution of the relativistic electrons in the Jovian inner radiation belt, respectively. IPRT is an offset parabola antenna whose physical aperture area of 1023 m<sup>2</sup>. The front-end receivers and normal half-wave dipole feed system for 325MHz were already set up. The test observations of some calibration stars showed that the noise temperature of the receiver system and the aperture efficiency of the telescope achieved 83K and 50%, respectively. The shape of IPRT is very unique; the primary reflector is composed of two separate but same-shaped parabolic rectangle sections and installed on one altitude-azimuth mount. In order to match a beam pattern of the feed system with the rectangular shaped reflector, we developed beam forming technique and applied it to a dipole feed system. The numerical simulation and the experiment in a radio anechoic chamber showed that the beam forming feed system achieved high aperture efficiency of 70%, which makes possible highly sensitive measurement radio emission of Jupiter and other radio stars. The back-end receiver system

for the total power measurement and the new beam forming feed system for 325 MHz will be set up in February 2003, and continuous monitoring of JSR will be started from this spring.

**GAIII.14/08A/D-007** Poster **0830-151**

**THE DUAL FREQUENCY INTERFEROMETER OBSERVATION FOR JOVIAN DECAMETRIC RADIATION**

Tomoyuki NAKAJO<sup>1</sup>, Takayuki ONO<sup>1</sup>, Masahide IIZIMA<sup>1</sup>, Hiroshi OYA<sup>2</sup> (<sup>1</sup>Department of Geophysics, Graduate School of Science, Tohoku University, <sup>2</sup>Fukui University of Technology)

For understanding the generation mechanism of the Jovian decametric radiation (DAM), identification of the propagation mode by clarifying the source location as well as the polarization character is one of the most important observations. Although a long baseline interferometry is a unique method to identify the source location directly (whether the DAM source is located in northern or southern ionosphere of Jupiter), the method is significantly suffered from the effect of irregularities of the earth's ionosphere. To solve this difficulty, we have developed the double frequency long baseline interferometer system. The new observation system has been developed in Tohoku university in Japan by employing three member stations, Zao, Yoneyama and Iitate. These stations are adequate to identify whether the DAM source is located in northern or southern ionosphere of Jupiter because the baseline length is ranging from 50 to 116km. The receiving system consists of three parts, i.e. the front-end, the main receiver and the data recording system. The front-end consists of a log-periodic antenna, a band pass filter whose passband is 20-30MHz, and a low noise wide-band pre-amplifier. The main receiver consists of two sets of double super-heterodyne receivers to carry out the double frequency observation and the received RF signal is converted into the frequency range from 5 to 15kHz and this output signals are digitized directly by the data recording system. The phase stability of the observation system is essentially decided by the stability of main receiver. The stability is achieved to be 1.0 (degree/C) by using Direct Digital Synthesizer (DDS) whose reference signal is fed by the cesium frequency standard (the phase stability of band pass filter and pre-amplifier is about 0.1degree/C). In order to evaluate the quality of the data, the temperature measurements and the phase calibration is carried out. From the results of performance evaluation by the simulation study, it has been estimated that this observation system will allow us to decide the source location of DAM with an accuracy of 25 arcsec (about 0.5 Jovian radii) under the condition of temperature fluctuation less than 5.0 degree under the condition of TEC fluctuation less than 1.0x10<sup>16</sup> [el/m<sup>2</sup>] which is typical for the observation time interval of DAM (within a few ten minutes).

**GAIV.02**

**COUPLING COMPLEXITY IN THE HELIOSPHERE**

Location: Site A, Room 7

**Monday, July 7 AM**  
Presiding Chairs: I. Cairns, B. Lembege

**GAIV.02/07A/A07-001** **0900**

**THE ORIGIN OF WHISTLER WAVES AT INTERPLANETARY SHOCKS**

Kouta NAKATA<sup>1</sup>, Toshio TERASAWA<sup>1</sup>, Nobue SHIMADA<sup>2</sup>, Hiroshi MATSUI<sup>3</sup>, Iku SHINOHARA<sup>4</sup> (<sup>1</sup>Department of Earth and Planetary Science, University of Tokyo, <sup>2</sup>Communication Research Laboratory, <sup>3</sup>University of New Hampshire, <sup>4</sup>Institute of Space and Astronautical Science)

Whistler waves are generally considered to play important roles in the electron dynamics at collisionless shocks. However, generation problem of these waves is not yet completely solved. In this report, we first introduce GEOTAIL observations of whistler wave enhancement in the foreshock region of several interplanetary CME shocks, where energetic electrons (several hundred eV - several tens of keV) are seen to be accelerated through the shock Fermi mechanism. Next we show that these whistler waves are responsible for pitch-angle scattering of low energy electrons (<~1keV), namely the injection process needed for the Fermi mechanism to work. For the origin of these whistler waves, we consider (1) generation at the shock front or in the downstream region and successive upstream propagation, as well as (2) the nonlinear cascading process of the lower frequency MHD waves, which are excited by nonthermal ions accelerated at the same CME shocks. We will discuss the relative importance of these two processes.

**GAIV.02/07A/A07-002** **0930**

**STRUCTURE, FORMATION AND DYNAMICS OF SHOCK WAVES**

Bertrand LEMBEGE (CETP/IPSL/UVSQ)

Collisionless shocks are quite common throughout the heliosphere in association to coronal mass ejection, to travelling and planetary bowshocks and to the outer heliosphere. These represent excellent energyconverters from bulk energy to particles kinetic energy. A large part of this conversion takes place at and/or around the shock front itself. For this reason, shocks are quite often invoked as attractive candidates for being responsible for particles acceleration; in a second step, some accelerated particles may reach energies large enough to represent noticeable sources of radiation. The difficulty is (i) to determine which acceleration process is dominant around the front and (ii) to verify whether appropriate conditions are satisfied for particles to get significant energies during the process of concern. Recent works based on numerical simulations and motivated by sophisticated mono- and/or multi-spacecraft missions (as CLUSTER-2) have clearly stressed that: (i) shocks front is highly nonstationary and nonuniform. The nonstationarity takes place over quite different spatial/time scales which have been partially identified at present time. Moreover, the mechanisms responsible for the nonstationarity totally differ from quasi-perpendicular to quasiparallel shocks. (ii) the efficiency of the particles acceleration strongly depends not only on the spatial width of the front itself but also on its nonuniformity features (i.e. front rippling) and on its nonstationary dynamics. This suggests that simplified stationary shock models are not appropriate and that multidimensionality plays an important role. This presentation will review results of these recent works and will try to identify the key questions which are still open.

GAIV.02/07A/A07-003

1010

**NONLINEAR REPLENISHMENT OF THE DISSIPATION RANGE AND STOCHASTIC ION HEATING IN THE SOLAR CORONA AND WIND**

Yuriy M. VOYTENKO, Marcel GOOSSENS (Centre for Plasma Astrophysics, K.U.Leuven)

The perpendicular energization of the ions in the solar corona and solar wind has been mainly attributed to MHD waves that undergo either turbulent cascade or cyclotron sweep, transporting the wave energy in the dissipation range of ion-cyclotron waves. However, the ion-cyclotron scenario is not free from difficulties and is not unique. We study an alternative possibility that the dissipation range is formed by the kinetic Alfvén waves, which have a sufficiently short wavelength across the magnetic field for the dissipative effects to become significant. The energy reservoir is provided by the large-scale MHD waves launched by the photospheric motions or magnetic restructuring at the coronal base. However, instead of following local nonlinear interactions among MHD waves, which are rather slow, we study the nonlinear excitation of KAWs which are already in the dissipative range [1]. We show that the presence of the finite-amplitude MHD waves, polarized in the sense of fast and/or Alfvén wave, gives rise to the nonlinear excitation of KAWs via three-wave resonant interaction (jump-like transport of MHD wave energy directly in the dissipation range). Short transversal wavelengths of the order of the proton gyroradius make KAWs accessible for the stochastic heating of ions if the wave/background magnetic field ratio exceeds a critical value, proportional to the charge-to-mass ratio  $q/m$  of the ion. The resulting ion energization is primarily in the direction perpendicular to the background magnetic field. This process provides an alternative to the ion-cyclotron explanation for the transverse energization of ions (in particular, observed by SOHO at 2-4 solar radii). References: [1] Voitenko Yu.M., Goossens M. Nonlinear excitation of small-scale Alfvén waves by fast waves and plasma heating in the solar atmosphere. *Solar Phys.*, 209, 37-60 (2002).

GAIV.02/07A/A07-004

1050

**MHD INTERACTION OF THE SOLAR WIND AND LISM**Haruichi WASHIMI<sup>1</sup>, Takashi TANAKA<sup>2</sup> (Shonan Institute of Technology, <sup>3</sup>Kyushu Univ.)

The global structure of the heliosphere under the interaction between the solar wind plasma and the local interstellar medium is studied by MHD computer simulation. A new type structure, i.e., a V-shaped gutter on the nose-cone surface of the heliopause caused by MHD processes is found in this simulation. The V-shaped gutter is also found on the termination shock surface, and both gutters are found to almost touch on the ecliptic. Hence the width of the heliosheath near the ecliptic becomes negligibly thin in our new model.

GAIV.02/07A/A07-005

1130

**SOLAR WIND ENCOUNTER WITH STRONGLY MAGNETIZED INTERSTELLAR MEDIUM: PURELY MHD AND MULTIFLUID MODELLING**Nikolai V. POGORELOV<sup>1</sup>, Vladimir FLORINSKI<sup>2</sup>, Gary P. ZANK<sup>3</sup>, Donald P. COX<sup>3</sup> (<sup>1</sup>Institute for Problems in Mechanics, Russian Academy of Sciences, Vernadskii Avenue 101-1, Moscow 119526, RUSSIA, <sup>2</sup>Institute of Geophysics and Planetary Physics, University of California, Riverside, CA-92521, U.S.A., <sup>3</sup>Physics Department, University of Wisconsin-Madison, University Avenue 1150, Madison, WI 53706, U.S.A.)

Uncertainties in the value of the magnetic field in the local interstellar cloud and its direction with respect to the solar system ecliptic plane stimulate the analysis of the solar wind (SW)--interstellar medium (LISM) interaction problem, where these quantities act as free parameters. The range of their variation is defined by available observational data interpreted on the basis of theoretical models describing the origin and evolution of the interstellar cloud. Most previously obtained results dealt with magnetic field values below 3 microgauss. Since the LISM flow is super-fast magnetosonic in this case, the heliospheric interface involves two shock waves: a SW termination shock and a bow shock. Conversely, for stronger magnetic fields Parker's solution for the supersonic source inflow into the uniformly magnetized interstellar gas at rest contains only a termination shock. Crossing it, the solar wind moves along the symmetry axis to infinity pushing aside magnetic field lines. There exist strong physical arguments in favor of substantially sub-Alfvénic LISM velocities nearly parallel to the magnetic field direction. We study an axially symmetric and a three-dimensional SW--LISM interaction under such conditions both in a purely MHD statement and in the framework of a newly developed four-fluid model. The latter includes protons and various populations of neutral hydrogen atoms. Simulation of a plasma-alone flow gives a solution in many aspects similar to Parker's. It is no longer correct if neutral atoms are added, since under certain circumstances the bow shock remains even in the case of a sub-Alfvénic LISM flow. Lyman-alpha absorption profiles are calculated in order to reveal consistency of the developed models with the currently available observational data.

GAIV.02/07A/A07-006

1200

**COMPLEXITY: NEW INSIGHTS FOR SPACE PHYSICS**

Tom T.S. CHANG (Center for Space Research, Massachusetts Institute of Technology)

"Complexity" has become a hot topic in nearly every field of modern physics. Solar wind plasmas are of no exception. Recently, Chang [2002], in analogy with theories developed for phenomena observed in the magnetotail and the auroral zone [Chang, 1999; 2001], demonstrated that the sporadic and localized interactions of magnetic coherent structures arising from plasma resonances could be the origin of "complexity" of the coexistence of non-propagating pseudo-2D spatiotemporal fluctuations and propagating modes in solar wind turbulence. Such coexistence of two types of fluctuations were detected in the solar wind by Matthaeus et al. [1990] in terms of the two-dimensional correlation as a function of distance parallel and perpendicular to the mean magnetic field based on the ISEE-3 magnetometer data. Other supporting evidences have been reported by Tu et al. [1989], Tu and Marsch [1990, 1991], Bruno and Bavassano [1991], Bavassano and Bruno [1992], Bruno et al. [2001], and others. The above observational results are also consistent with the conclusions obtained from 2D MHD numerical simulations [Matthaeus and Lamkin, 1986; Roberts and Goldstein, 1988; Goldstein et al., 1989; Roberts et al., 1991, and Roberts, 1992]. These findings have led Chang [2002] to suggest the following evolutionary scenario for the plasma turbulence in the generic fast solar wind. In and near the coronal hole base, the turbulent fluctuations are predominantly generated by pseudo-2D nonlinear interactions. As the fluctuations emerge from the coronal hole base, they propagate in the field-aligned direction primarily as Alfvén waves. At the same time, field-aligned coherent structures in the form of flux tubes are generated. "Alfvénic flux tubes" have been observed and reported recently by Bruno et al. [2001]. Then these flux tubes begin to interact nonlinearly and intermittently; thereby generating new pseudo-2D transverse fluctuations. Some of these fluctuations then propagate along the field-aligned direction as newly generated Alfvén waves. Other non-propagating fluctuations, on the other hand, begin to generate new coherent structures of varied sizes and new flux tubes are then formed. Ultimately, some sort of a balance of the non-propagating pseudo-2D fluctuations and field-aligned

propagating fluctuations is developed. Consequently, the Alfvén ratio of the fast solar wind turbulence generally will have a value less than one at the space range sufficiently far away from the coronal hole base. It has been demonstrated by Tam and Chang [1999; 2001; 2002] that resonant wave-particle interactions can be the primary driving mechanism for the fast solar wind. We suggest that the additional particle interactions with the non-propagating portion of the solar wind fluctuations near the coronal hole base may significantly increase the efficiency of the energization process as the solar wind emerges from the coronal hole base. The solar wind fluctuations in the solar wind generally may be accompanied by an electrostatic component. Both the electrostatic and electromagnetic fluctuations can energize the local charged particle distributions in magnetized plasmas selectively and intermittently, particularly in the transverse direction to the ambient magnetic field [Chang et al., 1981; Chang, 1993; Tam and Chang, 1999; Chang, 2002].

Monday, July 7 PM

Presiding Chairs: R. Winglee, H. Washimi

GAIV.02/07P/A07-001

1400

**MULTI-FLUID SIMULATIONS OF PLANETARY MAGNETOSPHERES**

Robert M. WINGLEE, Erika HARNETT, Carol PATY (Dept. of Earth and Space Sciences, University of Washington)

Planetary magnetospheres development substantial structure due to the presence of multi-ion species, some of which originate from the solar wind and some from the planet's ionosphere and in the case of the Jovian magnetosphere, from moons within the system. In these mixed plasma systems, ion cyclotron effects can lead to preferential acceleration of heavy ions, and velocity filtering effects can lead to mass fractionation and the formation of boundary layers as well limit access to key regions such as current sheets and reconnection regions. To date the most common tool to investigate the global structure of planetary magnetosphere is MHD simulations, but this method treats the plasma as a single fluid and ion cyclotron effects such as the formation of a ring current are missing. To address these issues on ion-cyclotron and ion-species effects, a full treatment of the fluid equations for the different ion components has to be developed. In this paper, we present such a formalism and show how these effects modify our understanding of tail reconnection in the Earth's magnetosphere, in association with the development of filamented flux ropes and the heavy ion hot spots on the dusk flank. For the Jovian magnetosphere, the heavy ions control the energy transport and like the Earth's magnetosphere, dawn/dusk asymmetries develop and modify the reconnection geometry in the near-Jovian region.

GAIV.02/07P/A07-002

1440

**THE PERIODICITIES OF SOLAR FLARES AND CORONAL MASS EJECTIONS DURING SOLAR CYCLE 23**

Ahmed Abdel HADY (Cairo University)

The Events of energetic particles from solar flares have been studied. The data were taken from National Geophysical data center (NGDC) in Boulder, Colorado, USA. The data of these events were given during the solar cycle 23rd. The 23rd cycle is the present one, started in April 1996, and its maximum was in May 2001, and will be decayed during year 2007. Power spectrum methods have been applied for analysis of the data given, to find the short and intermediate periodicities. The periodicity around 14 days has been appeared in this analysis. This has important implications for understanding and predicting the effects of solar activity on the Earth and earth's atmosphere. If a CME hit the Earth, it can excite a geomagnetic storm. Large geomagnetic storms have, among other things, will cause electrical power which damage satellites communications. In space CME typically drive shock waves that produce energetic particles that can damage both electronic equipment and astronauts that are outside the protection of the Earth's magnetic field. So, the prediction of the high energetic particle events is of vital importance for space navigation and airline disasters.

GAIV.02/07P/A07-003

1510

**THE EARTH'S BOW SHOCK AS A NONLINEAR PARTICLE ACCELERATOR**Toshio TERASAWA<sup>1</sup>, Hirotomo NODA<sup>2</sup>, Mitsuo OKA<sup>1</sup>, Yoshifumi SAITO<sup>3</sup>, Toshifumi MUKAI<sup>1</sup> (<sup>1</sup>Dept. Earth & Planetary Science, Univ Tokyo, <sup>2</sup>National Astronomical Observatory, Japan, <sup>3</sup>Institute of Space and Astronautical Science, Japan)

The earth's bow shock has been known to be an efficient particle accelerator in several different ways, such as shock-drift-acceleration of reflected ions/electrons, and diffusive-shock-acceleration (DSA) of diffuse upstream ions. From the view of nonlinear physics involved, the DSA process for diffuse ions is most prominent, since (1) the low frequency MHD waves self-excited by these diffuse ions have a large amplitude (10-50% of the background field), and show various kinds of nonlinear wave phenomena, and (2) the pressure exerted by the diffuse ions becomes non-negligible with respect to the solar wind ram pressure, and the internal structure of the bow shock transition region is modified by the existence of these ions ("Cosmic-Ray-Modified" nature of the bow shock). We will present our recent observational results on the above two properties, and discuss their relevance in the general study of nonlinear shock acceleration problems in cosmic shock environments. In addition, we will also discuss the dependence of the bow shock acceleration efficiency on the distance from the nose region of the bow shock. (The nose bow shock has the largest compression ratio than any other part of the bow shock, and thus has the largest acceleration efficiency.)

GAIV.02/07P/A07-004

1600

**RADIO EMISSIONS ASSOCIATED WITH SHOCKS: COUPLING MICROPHYSICS WITH MACROPHYSICS**

Iver H. CAIRNS, Peter A. ROBINSON, Stuart A. KNOCK, Zdenka KUNCIC, Jeremy J. MITCHELL (School of Physics, University of Sydney)

Type II solar radio bursts, radiation near the electron plasma frequency  $f_{pe}$  and near  $2f_{pe}$  from Earth's foreshock, and the 2-3 kHz radiation observed by the Voyager spacecraft in the outer heliosphere are well known examples of radio emissions associated with shocks. These are widely interpreted in terms of electron reflection at the shock, generation of Langmuir waves, and coupling of Langmuir energy into  $f_{pe}$  and  $2f_{pe}$  radio emission. Recent observations and simulations provide evidence that macroscopic shocks are rippled on scales ranging from the thermal ion gyroradius to those of the ambient MHD turbulence and the shock's driver itself. Ripples affect electron reflection and acceleration at the shock, resulting in time variable electron beams upstream, and lead to multiple simultaneous, time-varying foreshock regions upstream from the overall shock. Similarly, the observed Langmuir waves are bursty on small time and distance scales but persist with the driving electron beams for macroscopic distances. These characteristics and the observed field statistics are consistent with stochastic growth theory (SGT), which describes the development of a

macroscopic state near marginal stability that retains microscopic burstiness. Finally, the radiation is generated by nonlinear coupling and/or linear mode conversion of Langmuir waves, described using microphysical theory. This paper reviews quantitative analytic theories for type II bursts, Earth's foreshock radiation, and the 2-3 kHz emissions that combine the above microphysics to predict the properties of the electron beams and radio emission throughout the foreshocks of macroscopic rippled shocks.

**GAIV.02/07P/A07-005 1640**  
**ON THE RADIAL HELIOSPHERIC MAGNETIC FIELDS: VOYAGER 2 OBSERVATION AND MODEL**

Chi WANG<sup>1</sup>, J.D. RICHARDSON<sup>2</sup>, L.F. BURLAGA<sup>3</sup>, N.F. NESS<sup>4</sup> (<sup>1</sup>Lab. for Space Weather, Chinese Academy of Sciences, <sup>2</sup>MIT Center for Space Research, <sup>3</sup>NASA Goddard Space Flight Center, <sup>4</sup>Bartol Research Institute)

The heliospheric magnetic field (HMF) direction, on average, conforms well to the Parker spiral. However, numerous examples of events where the HMF is oriented in near-radial directions for many hours have been reported based on observations inside 5 AU from spacecraft such as ISEE-3 and Ulysses. The magnetic field data observed by Voyager 2 from launch in 1977 through the end of 1982 (i.e. between 1 and ~10 AU) were searched for all instances of radial fields with durations of 6 hours or more. Radial fields of significant durations at large distances are unusual as the Parker spiral is very tightly wound. The radial HMF events in the inner heliosphere typically occur at times when the solar wind speed is declining gradually, while they tend to be associated with steady wind speeds at distances beyond ~6AU. The durations of these events appear to be independent of distance and solar cycle, with an average duration of ~11 hours. They generally are not associated with interplanetary coronal mass ejections (ICMEs). Possible generation mechanisms of the radial field events related to speed variations near the Sun are investigated by use of a MHD model. We find that a noticeable low-speed plateau of limited duration in solar wind speed near the Sun can produce radial field events having durations of the order of 10 hours in the heliosphere as observed by Voyager 2.

**GAIV.02/07P/A07-006 1710**  
**FULL PARTICLE SIMULATIONS OF QUASI-PARALLEL SHOCKS AND SLAMS FORMATION: A PARAMETRIC STUDY**

Ken TSUBOUCHI, Bertrand LEMBEGE (CETP/IPSL/UVSQ)

The dynamics of quasi-parallel shocks and the formation of associated SLAMS (Short Large Amplitude Magnetic Structures) have been analyzed via a parametric study based on the use of 1D full particle simulation. Recent works (Tsubouchi and Lembege, 2003) have focused on the characteristics of the SLAMS which have been shown to be in good agreement with experimental space observations. These works have confirmed that typical SLAMS patterns result from the steepening of a nonlinear magnetosonic wave excited by reflected ion beam-ambient plasma instability as proposed by Scholer (1993) with hybrid simulations; when the wavelength of these waves is of the order of reflected ion density gradient, it shrinks to lower values which contributes to the wave steepening and leads to the SLAMS formation. The present parametric study is an extension of this previous work and shows that such structures are very sensitive to the shock regime. This could explain the variety of SLAMS (isolated, embedded) identified in experimental spacecraft observations; the form and the occurrence frequency of SLAMS strongly varies with Mach number. In addition, present results suggest that a small variation in the Mach regime not only has a strong impact in the mechanisms responsible for SLAMS formation, but may also contribute to make dominant some mechanisms other than ion beam-plasma instability; these mechanisms lead also to a large variety of off-field patterns. Some intermittent spiky (short time life soliton-like) patterns in the electrostatic field have been identified but not always in association with well formed SLAMS. The mixing of these field patterns varieties developing over quite different time scales could account for the turbulent dynamics of quasi-parallel shocks.

**GAIV.03**  
**MARS: MAGNETISM AND INTERACTION WITH THE SOLAR WIND**  
 Location: Site A, Room 16

**Tuesday, July 8 AM**  
 Presiding Chairs: A. Nagy, C. Mazelle

**GAIV.03/08A/A16-001 0830**  
**THE MAGNETIZED CRUST OF MARS - THE FINDINGS OF MARS GLOBAL SURVEYOR**

Mario H. ACUNA (NASA-GSFC)

Mars Global Surveyor discovered intense crustal magnetization associated with the ancient, cratered highlands and provided new and fundamental views into Mars' early history, its interior evolution, ionosphere, tectonics, the loss of volatiles from the atmosphere and the planet's interaction with the solar wind. In many respects the MGS observations have changed our basic understanding of the planet. Fundamental questions remain about the processes that led to the formation of the magnetic anomalies. We now know that Mars has lacked a global magnetic field for >4 billion years and solar wind erosion is believed to be an important and possibly the dominant atmospheric loss process. The crustal magnetic sources lead to the formation of "mini-magnetospheres" and a complex ionospheric structure. This paper will review the MGS magnetic field and electron observations and selected results obtained to date.

**GAIV.03/08A/A16-002 Invited 0900**  
**THE STRUCTURE OF THE MARTIAN PLASMA ENVIRONMENT: INTEGRATING MARS GLOBAL SURVEYOR AND PHOBOS-2 RESULTS**

Daniel WINTERHALTER<sup>1</sup>, Mario H. ACUNA<sup>2</sup>, Christian MAZELLE<sup>3</sup>, David MITCHELL<sup>4</sup>, Konrad SAUER<sup>5</sup> (<sup>1</sup>Jet Propulsion Laboratory, California Institute of Technology, 4800 Oak Grove Drive, Pasadena, CA 91109, USA., <sup>2</sup>NASA Goddard Space Flight Center, Code 695, Greenbelt, MD 20771, USA., <sup>3</sup>Centre d'Etude Spatiale des Rayonnements, 9 Avenue du Colonel Roche, Toulouse, 31028, France., <sup>4</sup>Space Science Laboratory, University of California, Berkeley, CA 94720, USA., <sup>5</sup>Max

Planck Institute for Aeronomy, Klatenburg-Lindau, Germany.)

For a number of years a great deal of uncertainty has existed concerning the nature of the solar wind interaction at Mars, because of the lack of relevant plasma and field observations. However, measurements by the Phobos-2 and the Mars Global Surveyor spacecraft, with different instrument complements and orbital parameters, led to a significant improvement of our knowledge about the regions and boundaries surrounding Mars. The main signatures, defined by the different plasma processes at work, can be summarized as follows: (1) The bow shock stands off an effective obstacle at a distance expected from gas-dynamic and/or magnetohydrodynamic approximations. (2) The Magnetic Pile-up Region (MPR) is a region dominated by planetary ions. The region is separated from the magnetosheath by the Magnetic Pile-up Boundary (MPB). (3) A plasma boundary is observed in the supra-thermal electrons (> 10 eV, MGS data), which hints at the existence of a boundary between the MPR and the ionosphere below. In this review the magnetosheath, the Magnetic Pile-up Region, and the Magnetic Pile-up Boundary will be discussed, as well as the observations of a possible ionopause.

**GAIV.03/08A/A16-003 Invited 0930**  
**THE MAGNETIC PILEUP BOUNDARY: A COMMON FEATURE FOR WEAKLY MAGNETIZED BODIES?**

Cesar L. BERTUCCI<sup>1</sup>, Christian MAZELLE<sup>1</sup>, Mario H. ACUNA<sup>2</sup> (<sup>1</sup>CESR, CNRS/UPS, France, <sup>2</sup>NASA GSFC, USA)

The lack of an intrinsic magnetic field at Venus, Mars and comets makes their interaction with the solar wind very similar, with the formation of a magnetic barrier in front of a highly conducting obstacle and an induced magnetic tail as their most characteristic peculiarities. The Magnetic Pileup Boundary (MPB) is the plasma boundary that marks the entrance into the magnetic barrier at Mars and comets. This boundary can be identified by clear observational signatures: a gradient in the magnetic field magnitude (often as a sharp jump) accompanied by a decrease in the magnetic field fluctuations, and a simultaneous drastic decrease in the solar wind electron and proton densities as the obstacle is approached. Recently, an enhancement of the magnetic field draping has been reported at the Martian MPB from Mars Global Surveyor magnetometer data as a new ubiquitous characteristic of this boundary. As a result of the application of the same technique to magnetometer data acquired near comets and Venus, we confirm that the MPB is the dayside counterpart of the magnetic tail boundary and present new evidence in favor of the existence of a MPB at Venus, where the boundary has never been reported.

**GAIV.03/08A/A16-004 1000**  
**THE MAGNETIC PILE-UP BOUNDARY AT MARS AND RELATED ION DYNAMICS**

Konrad SAUER<sup>1</sup>, Eduard DUBININ<sup>1</sup>, Christian MAZELLE<sup>2</sup> (<sup>1</sup>Max-Planck-Institut fuer Aeronomie, Klatenburg-Lindau, Germany, <sup>2</sup>CESR, Toulouse, France)

The recent magnetic field measurements aboard Mars Global Surveyor at Mars have clearly shown that a permanent plasma boundary exist between the bow shock and the ionopause which is characterized by strong magnetic pile-up. The evidence of this 'Magnetic Pile-up Boundary' (MPB) confirms the outcome of earlier Phobos-2 measurements in which the presence of an 'obstacle boundary' was seen by different instruments. Especially, the observed change of ion composition at this boundary by ASPERA and TAUS seems to be of great importance to understand the physical nature of the MPB. Hitherto unpublished Phobos-2 data of MPB crossings at large distances (~10 RM) are discussed. The results are compared with simple 2D bi-ion simulations considering exclusively electrostatic coupling between solar wind protons and newly generated planetary ions by the charge separation field. The good agreement with the observations indicate that the different dynamics of both ion populations is essentially for the sharp magnetic field increase at the MPB.

**GAIV.03/08A/A16-005 1040**  
**MARTIAN SHOCK AND MAGNETIC PILE-UP BOUNDARY POSITIONS AND SHAPES REVISITED AFTER MARS GLOBAL SURVEYOR**

Jean Gabriel TROTIGNON<sup>1</sup>, Christian MAZELLE<sup>2</sup>, Cesar BERTUCCI<sup>3</sup>, Mario H. ACUNA<sup>4</sup> (<sup>1</sup>LPCE/CNRS, Orleans, France, <sup>2</sup>CESR/CNRS/UPS, Toulouse, France, <sup>3</sup>GSFC, Greenbelt, Maryland, USA)

A lot of Martian bow shock and magnetic pile-up boundary crossings have been unambiguously identified in the Phobos-2 and Mars Global Surveyor, MGS, data. From these observations the positions and shapes of the bow shock and magnetic pile-up boundary, MPB, have been derived and modeled, using curve-fitting techniques. The models derived separately from the Phobos-2 and MGS data sets do not differ drastically, despite the different time and space data coverages. The purpose of the presentation is to show the results obtained in mixing the Phobos-2 and MGS data sets and to compare the derived bow shock and MPB models with the ones obtained in considering the two data sets separately. The underlying objective is to see whether it is possible to determine general bow shock and MPB models or not.

**GAIV.03/08A/A16-006 Invited 1100**  
**THE IONOSPHERE OF MARS**

Hiroyuki SHINAGAWA (Solar-Terrestrial Environment Laboratory, Nagoya University)

Observations relevant to the ionosphere of Mars have been made by a number of missions. It is expected that structure and dynamics of the ionosphere of Mars are significantly affected by the solar wind interaction. The Mars Global Surveyor has detected a fairly strong but localized magnetic field which is of crust origin. It was also found that the surface magnetic field is likely to be insignificant. Although the solar wind interaction with Mars is basically similar to the solar wind interaction with Venus or comets, the crustal magnetic field appears to play an important role in the structure and dynamics of the Martian ionosphere. To study the ionospheric processes at Mars, many theoretical studies have been done using various kinds of numerical models. Our current understanding of the ionospheres of Mars is reviewed, and outstanding problems to be solved are summarized.

**GAIV.03/08A/A16-007 1130**  
**PROBING MARS' CRUSTAL MAGNETIC FIELDS AND IONOSPHERE WITH THE MGS ELECTRON REFLECTOMETER**

David L. MITCHELL<sup>1</sup>, Christina O. LEE<sup>1</sup>, Sherry CHOU<sup>1</sup>, Robert P. LIN<sup>1</sup>, Henri REME<sup>2</sup>, Paul A. CLOUTIER<sup>3</sup>, Mario H. ACUNA<sup>4</sup> (<sup>1</sup>Space Sciences Laboratory, U.C.-Berkeley, <sup>2</sup>CESR, Toulouse,

France, <sup>3</sup>Rice University, Houston, Texas, <sup>4</sup>NASA Goddard Space Flight Center)

Mars' magnetic field is dominated by remanent magnetization of the crust, which is distributed non-uniformly over the surface. In the northern hemisphere, crustal magnetic fields are so weak that the solar wind interacts directly with the atmosphere and ionosphere in a manner similar to that observed at Venus and active comets. However, in the most strongly magnetized regions of the southern hemisphere, the crustal field is strong and coherent enough to stand off the solar wind up to altitudes of ~800 km, forming localized "magnetospheres," which are elongated in the east-west direction following the pattern of magnetization. In sunlight, these mini-magnetospheres contain trapped ionospheric plasma, and in some locations form cusps, where the crustal field is connected to the interplanetary magnetic field. In darkness (2 am local time), trapped populations persist only on field lines that are nearly vertically oriented at 400 km altitude, and thus extend far downstream of the planet. The Electron Reflectometer (ER) onboard Mars Global Surveyor (MGS) detected a plasma boundary between the ionosphere and the solar wind as the latter is diverted around and past the planet. Above this boundary the 10-1000 eV electron population is dominated by solar wind electrons, while below the boundary it is dominated by ionospheric photoelectrons. We show that this "photoelectron boundary," or PEB, is sensitive to pressure variations and moves vertically in response to changes in the ionospheric pressure from below and the solar wind pressure from above. The PEB is also sensitive to crustal magnetic fields, which locally increase the total ionospheric pressure and positively bias the PEB altitude. We have analyzed more than five million electron spectra obtained in the mapping orbit, spanning two Martian years. We have empirically modeled and removed systematic variations in the PEB altitude associated with the solar wind interaction, thus isolating perturbations caused by crustal magnetic fields. A map of these PEB perturbations closely resembles a map of the horizontal component of the crustal magnetic field measured at 400 km by the MGS Magnetometer. This technique allows us to extend the sensitivity of existing magnetic field maps and reliably identify crustal fields with an intensity of only ~5 nT at 400 km altitude.

**GAIV.03/08A/A16-008** Invited **1150**

**THE EFFECTS OF CRUSTAL MAGNETIC FIELDS AND THE PRESSURE BALANCE IN THE HIGH LATITUDE IONOSPHERE/ATMOSPHERE AT MARS**

Tamara K. BREUS, Norman F. NESS, Alexander M. KRYMSKII, Mario H. ACUNA, Jack E.P. CONNERNEY, David HINSON, Konstantin K. BARASHAYN (Space Research Institute, Moscow, Russia)

The intensely and nonuniformly magnetized crustal sources generate an effective large-scale magnetic field. Re-connection with the interplanetary magnetic field can possibly take place in many localized regions. This will permit solar wind (SW) and more energetic particles to precipitate into and heat neutral atmosphere in cusp-like structures. The strongest crustal fields are located in certain regions in the Southern hemisphere and lead to the formation of large-scale mini-magnetospheres. In the Northern hemisphere, the crustal fields are rather weak and usually do not prevent direct interaction between the SW and the Martian ionosphere/atmosphere. Exceptions occur in the isolated mini-magnetospheres formed by the crustal anomalies. Electron density profiles of the ionosphere of Mars derived from radio occultation data obtained by the Radio Science Mars Global Surveyor (MGS) experiment have been compared with the crustal magnetic fields measured by the MGS Magnetometer/Electron reflectometer (MAG/ER) experiment. A study of 523 electron density profiles obtained at latitudes from 67° to 77° has been conducted. The effective scale-height of the electron density for two altitude ranges, 145-165 km and 165-185 km, and the effective scale-height of the neutral atmosphere density in the vicinity of the ionization peak have been derived for each of the profiles studied. A significant difference between the large-scale mini-magnetospheres and regions outside of them has been found. The neutral atmosphere is cooler inside the large-scale mini-magnetospheres. It appears that outside of the cusps the strong crustal magnetic fields prevent additional heating of the neutral atmosphere by direct interaction of the SW. For the regions outside of the mini-magnetospheres the thermal pressure of the ionospheric plasma for the altitude range 145-185 km has been derived. The pressure balance in the high latitude ionosphere at Mars has been studied.

**GAIV.03/08A/A16-009** **1220**

**MHD SIMULATION STUDY ON IMF PENETRATION INTO THE IONOSPHERE OF MARS AND VENUS**

Hidekatsu JIN, Kiyoshi MAEZAWA, Toshifumi MUKAI (ISAS)

Since Mars and Venus do not have a global intrinsic magnetic field, the solar wind directly interacts with the ionosphere of these planets. PVO (Pioneer Venus Orbiter) observed a sharp boundary between the solar wind and Venus ionosphere when dynamic pressure of the solar wind does not exceed ionospheric pressure. But in the case where the solar wind dynamic pressure is large, ionopause becomes rather obscure with its altitude lower and its thickness thicker. During this phase, a large-scale magnetic field is observed in the subsolar region of the ionosphere. Recently, MGS (Mars Global Surveyor) also observed the IMF penetration into the Martian ionosphere. The large-scale field as well as the ionopause behavior have caught a great deal of attention and have been studied by many scientists. The altitude profile of the large-scale field has been explained by using the model in which the field is transported by downward convection and accumulated in collision-dominated region. There are, however, some problems that still remain unclear. Especially, the key physics behind IMF penetration into the ionosphere and its altitude profile is not well understood. For example, it is not obvious how the altitude profile of the vertical ionospheric flow is formed, which is important for the altitude profile of the field. We study the mechanism for the penetration of IMF into Venus/Mars ionosphere and the altitude profile of the large-scale field, by using a 2D global MHD simulation model. The purpose of our study is to understand key physics behind those phenomena. We will report effects of physical processes such as ionospheric production and loss, gravity, collision, and magnetic diffusion due to collision in detail. We will clarify the differences between the physical processes operating at Mars and Venus.

**Tuesday, July 8 PM**

Presiding Chairs: D. Mitchell, K. Maezawa

**GAIV.03/08P/A16-001** **1400**

**THE MARTIAN MAGNETOSPHERE BASED ON PHOBOS-2 - IMPLICATIONS FOR THE UPCOMING NOZOMI AND MARS EXPRESS MISSIONS**

Rickard N.A. LUNDIN, Stanislav BARABASH (Swedish Institute of Space Physics)

The solar wind interaction with Mars, its atmosphere, ionosphere and magnetosphere, was first investigated by the Soviet Mars-2, 3 and 5 orbiters in the 1970ies. It took until the late 1980ies (1989) before another mission to Mars, the Soviet Phobos-2, was able to carry out

more detailed measurements in the martian magnetosphere. The Phobos-2 mission provided detailed measurements on the Sun-Mars interaction during its 2 months in orbit around Mars, substantially improving our understanding of the martian magnetosphere morphology and the atmospheric outflow/escape from a nonmagnetized planet. However, the Phobos-2 mission also left us with a number of unsolved issues. Subsequent MGS-results of e.g. magnetization regions at Mars have added to the "mystique" on the evolution of Mars. The investigations on the two missions Nozomi and Mars Express were designed to specifically address the above unsolved issues. For instance the IMI experiment on Nozomi were designed to analyze the magnetospheric structure, the ionospheric escape mechanisms and the potential occurrence of charged dust near the Phobos and Deimos orbits. ASPERA-3 on Mars Express will focus on the overall plasma outflow and its correspondence with the energetic neutral atoms produced as a result of charge exchange. This report will discuss some of the unsolved issues about the solar wind interaction with Mars and how we plan to address these issues with Nozomi and Mars Express.

**GAIV.03/08P/A16-002** Invited **1430**

**GLOBAL HYBRID SIMULATIONS OF THE MARTIAN PLASMA ENVIRONMENT**

Gerard M. CHANTEUR<sup>1</sup>, Ronan MODOLO<sup>1</sup>, Allan P. MATTHEWS<sup>2</sup> (<sup>1</sup>CETP / IPSL / CNRS, <sup>2</sup>University of Natal, Durban, South Africa)

Two- and three-dimensional hybrid simulations of the global plasma environment of Mars, including the night side of the planet and the near wake, have been made on uniform grids with varying resolutions. The simulation code includes photoionisation and electron impact ionisation of neutral hydrogen and oxygen coronae although with a simplistic modelisation of the second process based on an adiabatic behaviour of the electron fluid. The densities of the neutral species are supposed to vary only with respect to the planetocentric distance according to theoretical profiles. The simulation model also includes charge exchange processes between protons and oxygen ions both with neutral hydrogen and oxygen. Both two- and three-dimensional simulations clearly exhibit a well-resolved bow shock, a pile-up region of the magnetic flux and a wake depleted of solar wind ions but partially filled with planetary ions. Spatial variations of densities of planetary or solar wind ions (protons and alphas) around the planet extend over four decades. The spatial scales of the simulated Martian environment are reasonable but due to a presently insufficient spatial resolution the bow shock, in the three-dimensional simulations, is located too far away from the planet but more realistic results are expected from simulations on supercomputers.



**GAIV.03/08P/A16-003** **1500**

**ANALYSIS OF THE MARTIAN OBSTACLE AND BOW SHOCK TERMINATOR ANISOTROPY ORIGINS USING PHOBOS 2 AND MGS DATA**

M.I. VERIGIN<sup>1</sup>, G. KOTOVA<sup>1</sup>, A. REMIZOV<sup>1</sup>, J. SLAVIN<sup>2</sup>, M. ACUNA<sup>3</sup>, T.-L. ZHANG<sup>3</sup>, K. SCHWINGENSCHUH<sup>4</sup>, K. K. SZEGO<sup>5</sup>, M. TATRALLYAY<sup>6</sup> (<sup>1</sup>Space Research Institute of Russian Academy of Sciences, <sup>2</sup>NASA Goddard Space Flight Center, Greenbelt, Maryland, USA, <sup>3</sup>Space Research Institute of Austrian Academy of Sciences, Graz, Austria, <sup>4</sup>KFKI Research Institute for Particle and Nuclear Physics, Budapest, Hungary)

The Phobos 2 and MGS data sets on positions of the Martian obstacle and bow shock are analyzed by uniform method for checking of their mutual consistency and for analysis of anisotropy of these boundaries. New Martian obstacle model dependent on the solar wind ram pressure and based on recently introduced ram pressure proxies, is used for the obstacle tracing to terminator plane in the period of MGS observations. This model as well as earlier obstacle model constructed for the period of Phobos 2 observations, is applied to trace the Phobos 2 obstacle crossings. MHD model of the planetary bow shock taking into account the obstacle shape, solar wind sonic and Alfvénic Mach numbers, and interplanetary magnetic field direction, is used to trace bow shock positions observed by both orbiters to terminator plane. Thus traced terminator obstacle and bow shock positions are studied for the search of MHD, picked-up ion, crustal magnetization effects on position of both boundaries. It is found that localized Martian crustal magnetization increases the height of the terminator obstacle by several hundreds of kilometers while the influence of MHD or ion pick-up effects on Martian obstacle position is small. Elongation of the Martian bow shock cross-section in the direction perpendicular to the interplanetary magnetic field and the shift of this cross section in the +Y direction of the Martian interplanetary medium reference frame were clearly observed while the shift of bow shock cross section in the direction of the interplanetary electric field was not revealed thus not conforming the idea that mass-loading play any role in this boundary controlling.

**GAIV.03/08P/A16-004** **1540**

**MAGNETIC FIELD INVESTIGATION OF THE VENUS PLASMA ENVIRONMENT: WHAT DO WE EXPECT FROM THE VENUS EXPRESS MISSION**

Wolfgang BAUMJOHANN, Tielong ZHANG (Space Research Institute, Graz, Austria)

The Venus Express mission is scheduled to launch in 2005. Among other instruments, it carries a magnetometer to investigate the Venus plasma environment. Although Venus has intrinsic magnetic moment, magnetic field measurements are essential in studying the solar wind interaction with Venus. Our current understanding of the solar wind interaction with Venus is mainly from the long lasting Pioneer Venus Orbiter observations. In this paper, we describe the magnetic field experiment of the Venus Express mission. We assess the current understanding and find out what we will achieve with the upcoming Venus Express mission.

**GAIV.03/08P/A16-005** **1610**

**SOLAR WIND CONTROL OF THE VENUSIAN AND MARTIAN IONOTAILS**

Naoki TERADA, Hiroyuki SHINAGAWA (Solar-Terrestrial Environment Laboratory, Nagoya University)

Comprehensive two-dimensional global hybrid (particle ions, massless fluid electrons) simulations of the solar wind interaction with the ionosphere of the unmagnetized planets, Venus and Mars, are conducted. The hybrid code successfully models the entire solar wind-planet interaction region including the planetary ionosphere, magnetosheath, and solar wind regions simultaneously by applying boundary-fitted coordinates to the particle-in-cell code. The model predicts strong dependence of the ionotail configurations on the solar wind dynamic pressure. Asymmetry in the ionotail configurations with respect to the direction of the solar wind motional electric field becomes prominent as the dynamic pressure increases. We will show that the momentum transfer between magnetosheath protons and pickup planetary ions as well as the asymmetrical terminator transport of ionospheric ions plays an important role in producing the asymmetrical ionotail configurations. Development of the ionotails appears quite dynamic. We will also discuss the time evolution of the ionotails.

**GAIV.03/08P/A16-006 1630**

**PLASMA EFFECTS OF INTERACTION OF SMALL BODIES WITH SOLAR WIND**

Valentina G. MORDOVSKAYA (Institute of Terrestrial Magnetism, Ionosphere, and Radiowave Propagation (IZMIRAN))

The last planetary explorations have witnessed an increase of importance of investigations of small bodies of the Solar System because its substance may carry the information on an origin and evolution of Solar system. Interplanetary spacecrafts have passed near asteroidal bodies: Gaspra, Ida, Braille, Eros, and Martian moons (Phobos and Deimos). The small characteristic sizes of the obstacle to the solar wind have to give specific signatures of the solar wind-asteroid interaction. The typical length of the free motion of particles of the solar wind is much more enhanced than the sizes of the bodies; therefore, a hydrodynamic formulation is invalid for such solar wind-asteroid interaction. It is necessary to use a kinetic theory for the consideration of phenomena near the bodies. As an application of the kinetic theory, the solar wind interaction with Phobos is studied in this work both from the theoretical standpoint and from using the data of Phobos mission. The size of Phobos and the solar wind ion gyroradius are alike. That leads to a large-scale structure of the plasma in the Phobos tail. Just the modulation is responsible for the phenomenon observed by spacecraft Phobos-2 on February 1, 1989. The speculations about the dust/gas nature of the phenomenon are erroneous.

**Wednesday, July 9 AM**

Presiding Chairs: D. Winterhalter, M.H. Acu

**GAIV.03/09A/A16-001 0900**

**THE SOLAR WIND INTERACTION WITH MARS**

Yingjuan MA, Andrew F. NAGY, Igor SOKOLOV (Dept. Atmos., Ocean, & Space Sci.)

We have modified our multi-species, 3D, MHD model of the interaction of the solar wind with Mars. We have moved from a Cartesian coordinate system to a spherical one, in order to achieve better radial resolution and to achieve a better fit to the shape of the ionosphere-magnetosheath interface in our calculations. This is especially important in order to assess the role of the interaction processes on the ionosphere and the inner magnetosheath. We will be presenting the first results of these new calculations, which also include the effects of the crustal magnetic field.

**GAIV.03/09A/A16-002 0930**

**EXAMINING THE CRUSTAL FIELD TOPOLOGY AT MARS WITH THE MGS MAG/ER DATA: COMPARISONS WITH A B-FIELD DEPENDENT TRANSPORT CODE**

Michael W. LIEMOHN<sup>1</sup>, David L. MITCHELL<sup>2</sup>, Andrew F. NAGY<sup>1</sup>, Stephen W. BOUGHER<sup>1</sup>, Jane L. FOX<sup>3</sup>, Jacki M. FRANK<sup>4</sup>, Tamara W. REIMER<sup>1</sup> (SPRL, University of Michigan, <sup>2</sup>Space Science Laboratory, University of California Berkeley, <sup>3</sup>Department of Physics, Wright State University, <sup>4</sup>Department of Physics, Harvey Mudd College)

We compare MGS MAG/ER data with results from a B-field dependent kinetic transport code for electrons in the 10-1000 eV energy range. The photoelectrons created on the dayside, in regions where crustal fields are strong, allow for the exploration of the magnetic topology. By comparing the observed velocity space distributions of the electrons with the simulation results, in particular the depth and structure of the trapped zone fluxes, the integral "scattering depth" can be determined. This constrains both the topology of the field line as well as the thermospheric/ionospheric densities in the upper atmosphere of Mars. Case studies of typical MGS mapping phase orbits through the strong crustal field region in the southern hemisphere of Mars are examined.

**GAIV.03/09A/A16-003 0950**

**INTERACTION BETWEEN THE SOLAR WIND AND A "MARS-TYPE" PLANET HAVING A SMALL-SCALE LOCAL MAGNETIC STRUCTURE ON ITS SURFACE**

Kiyoshi MAEZAWA, Hidekatsu JIN, Akinori SHIGA (Institute of Space and Astronautical Science)

We present the result of our MHD simulations on the interaction between the solar wind and a planet having small-scale magnetic structures as in the case of Mars. In order to see the influence of the spatial scale of the surface magnetic field, various forms of local magnetic fields are examined, including the cases with a single dipole(s) below the surface, the ones with linearly aligned magnetic structures, and the ones expressed by several different spherical harmonic functions. In order to see the effects of the magnetic field clearly, a very simple ionospheric model is adopted for a generic case, where MHD equations include only two ion species (ionospheric Oxygen and the solar wind proton). In addition, our model incorporates the effects of the mass-loading processes on the local/global-scale solar wind flow around the planet by assuming a hot Oxygen corona. Our simulation code is TVD with source terms and a polar coordinate mesh is used. We compare the results for individual magnetic models and show that the effect of magnetic reconnection on the global-scale flow structure around the planet is strongly dependent on the spatial scale of the magnetic field. We also comment on the difficulty of MHD simulations for some of the cases where a very high Mach number flow can be produced by magnetic reconnection in a low-temperature planetary plasma. We finally comment on the possibility of obtaining observational clues for the simulated interaction processes with the instruments flown on the Nozomi spacecraft.

**GAIV.03/09A/A16-004 1010**

**WAVES AT MARS: A TENTATIVE REVIEW**

Jean Gabriel TROTIGNON (LPCE/CNRS, Orleans, France)

Despite the great number of missions devoted to the exploration of the Martian environment, a very few space probes carried instruments designed to study waves. The best equipped spacecraft was indisputably Phobos-2 which allowed, in 1989, electric field in the 5 Hz-150 kHz frequency range and high temporal resolution DC magnetic field to be monitored. Unfortunately, the lowest Phobos-2 perigee altitude was too high, about 850 km, to allow investigation of the ionosphere of Mars. More recently, the high quality DC magnetic field measurements performed onboard the Mars Global Surveyor, MGS, spacecraft have been used to derive valuable information on low frequency waves upstream of the Martian bow shock. The subject of the presentation is to tentatively review the wave observations made by both the Phobos-2 and MGS spacecraft. In a next future, we hope that NOZOMI and Mars Express will increase our poor knowledge of waves at Mars.

**GAIV.03/09A/A16-005 1100**

**REFLECTED IONS UPSTREAM OF A CURVED QUASI-PERPENDICULAR SHOCK**

Ronan MODOLO<sup>1</sup>, Gerard M. CHANTEUR<sup>1</sup>, Allan P. MATTHEWS<sup>2</sup> (<sup>1</sup>CETP / IPSL / CNRS, <sup>2</sup>University of Natal, Durban, South Africa)

Self-consistent data from two-dimensional hybrid simulations are used to investigate the reflection of solar wind ions (protons and alphas) by a curved quasi-perpendicular shock created by a small planetary obstacle having typically the size of Mars or slightly larger. All incoming alpha particles are transmitted downstream of the shock and reflected alphas are not observed in these simulations. A few percent of incoming protons are reflected on one side of the shock depending upon the orientation of the motional electric field of the solar wind as expected from theoretical considerations. The localisation of the reflection process is illustrated by maps of the acceleration sites built from the analysis of the self-consistent motion of the ions. The flux of reflected protons versus energy is exponential with a characteristic energy depending mainly upon the velocity of the solar wind and only slightly upon the size of the obstacle for the investigated range of sizes. Coarse pitch-angle distributions of reflected protons will also be presented.

**GAIV.03/09A/A16-006 Invited 1120**

**STATIONARY NONLINEAR LF ELECTROMAGNETIC WAVES IN A BEAM-PLASMA: APPLICATION TO UPSTREAM PHENOMENA AT EARTH AND MARS**

Konrad SAUER<sup>1</sup>, Eduard DUBININ<sup>1</sup>, Christian MAZELLE<sup>2</sup> (<sup>1</sup>Max-Planck-Institut für Aeronomie, <sup>2</sup>CNRS, Toulouse, France)

Using the full nonlinear system of fluid and Maxwell equations for a beam-plasma configuration, where the beam is thought to be formed by shock-reflected protons or exospheric ions (at Mars), stationary nonlinear electromagnetic waves near and below the proton cyclotron frequency are described. Depending on the beam parameters, coherent structures in form of "oscillitons" (Sauer et al., 2002) and solitons have been obtained. The results are applied to different upstream phenomena seen at Earth and Mars.

**GAIV.03/09A/A16-007 Invited 1150**

**OBSERVATION OF THE MARTIAN UPPER ATMOSPHERE BY JAPANESE MARS ORBITER NOZOMI**

Yoshifumi SAITO, Hajime HAYAKAWA, Kiyoshi MAEZAWA (Institute of Space and Astronautical Science)

Japanese Mars Orbiter NOZOMI launched in 1998 from Kagoshima Space Center is now on its way to Mars. Fourteen science instruments are onboard the NOZOMI spacecraft in order to observe the interaction between the solar wind and the Martian upper atmosphere. At the moment, NOZOMI is expected to arrive at Mars in the end of 2003. Similar to Venus, Mars has no strong intrinsic magnetic field that makes the structure and dynamics of the Martian upper atmosphere quite different from that of the Earth. Strong intrinsic magnetic field of the Earth prevents solar wind to directly enter into the Earth's magnetosphere. On the contrary, Martian upper atmosphere is directly exposed to the solar wind. The interaction between the solar wind and Venus upper atmosphere has been intensively investigated using the data obtained by the Pioneer Venus Orbiter (PVO). Most of our knowledge concerning the interaction between the solar wind and the planets without strong intrinsic magnetic field is based on the results obtained by the research of the Venus upper atmosphere. However, even the piecemeal data of the Martian upper atmosphere so far obtained cannot be fully explained by our current knowledge based on the Venus upper atmosphere. The Phobos-2 spacecraft discovered the significant amount of the oxygen outflow in the Martian tail region. According to this observation, the oxygen in the Martian atmosphere will be fully replaced in 10<sup>8</sup> years. If the interaction between the solar wind and the Martian upper atmosphere causes this outflow, this interaction is very important to understand the history and evolution of the Martian atmosphere. Recently, Mars Global Surveyor (MGS) discovered the existence of the strong crustal magnetic anomaly in the southern hemisphere of Mars. The existence of the strong magnetic anomaly clearly differentiates Venus and Mars from the viewpoint of the solar wind interaction. The interaction between the solar wind and the localized magnetic field may be greatly different from the interaction between the solar wind and the global magnetosphere. There is a possibility that the localized magnetic field significantly affects the ion transport in the Martian upper atmosphere. So far, no systematic observation of the Martian upper atmosphere has been performed. The most important tasks of NOZOMI are to measure the basic plasma parameters of the Martian upper atmosphere, to elucidate the composition of the Martian neutral atmosphere, and to survey the magnetic field distributions in detail. In order to answer the several questions brought up by the previous observations, NOZOMI will systematically observe the key parameters of the Martian upper atmosphere.

**GAIV.03/09A/A16-008 1220**

**ABOUT A MAGNETIC TOPOLOGY OF THE MARS WAKE IN THE PLANE OF PHOBOS ORBIT**

Valentina G. MORDOVSKAYA, Victor N. ORAEVSKY (Institute of Terrestrial Magnetism, Ionosphere, and Radiowave Propagation (IZMIRAN))

The plane of the "Phobos-2" spacecraft orbit coincided with that of Phobos. This led to sophisticated magnetic signatures of the Mars wake, which were acquired by the spacecraft. The measurements made on the circular orbits demonstrated an influence of the Phobos magnetic field on the topology of the Mars wake. Depending on location of Phobos during manoeuvres, a filamentation of the Mars magnetic tail was observed. The magnitude of the magnetic field observed varied from several nT to tens nT. The adopted rule that the orientation of the field in the Martian wake is governed by the direction of the solar wind magnetic field is not confirmed by the data. To obtain the expected change in polarity of magnetic field components in the Mars wake we must except the data obtained near Phobos and consider only "pure" measurements of the magnetic field in the Mars wake. Three types of magnetic field lines, acquired by the "Phobos-2" spacecraft, are revealed in the Mars wake. They refer to 1. Phobos magnetic field. 2. The Mars magnetic field of an internal origin. 3. The observation of the draping of the interplanetary field around Mars or/and the induced magnetic field of Mars for two directions of the interplanetary field which is governed by the interplanetary magnetic field points away the Sun and toward the Sun.

**GAIV.03-Posters**

**MAGNETISM AND INTERACTION WITH THE SOLAR WIND**

Location: Site D

Wednesday, July 9 PM

Vernadskii Avenue 101-1, Moscow 119526, RUSSIA)

**GAIV.03/09P/D-001** Poster **1400-144**

**DISTRIBUTION OF CRUSTAL MAGNETIC FIELDS ON MARS: SHOCK EFFECTS OF BASIN-FORMING IMPACTS**

Lon L. HOOD<sup>1</sup>, Nicola C. RICHMOND<sup>1</sup>, Elisabetta PIERAZZO<sup>2</sup>, Pierre ROCHETTE<sup>3</sup> (<sup>1</sup>Lunar and Planetary Laboratory, University of Arizona, <sup>2</sup>Lunar and Planetary Institute, Tucson, Arizona, <sup>3</sup>University of Aix-Marseille, France)

Crustal magnetic fields on Mars are inhomogeneously distributed with the strongest fields occurring over the southern highlands in a longitude sector between approximately 130E and 240E. Here we investigate whether radially extended shock demagnetization associated with the Hellas and Argyre basin impacts (in addition to thermal demagnetization associated with the northern resurfacing event and the formation of the Tharsis volcanic complex) may largely explain this distribution. Using analytic approximations and empirical scaling laws, it is estimated that much of the weakly magnetized southern highlands (i.e., that between 110W and 130E) was shocked to pressures exceeding 1-2 GPa during the Hellas and Argyre impacts. Possible primary remanence carriers in the martian crust include iron oxides and iron sulfides (pyrrhotite). If pyrrhotite is the main remanence carrier, extensive demagnetization of crustal regions (about 90%) may occur at shock pressures of 2 GPa or more. Thus, at least for this remanence carrier, impact shock demagnetization can potentially explain the distribution of crustal fields in the southern highlands.

**GAIV.04**

**REPORTER REVIEWS**

Location: Site A, Room 16

Wednesday, July 9 PM

Presiding Chair: S.J. Schwartz

**GAIV.04/09P/A16-001** **1400**

**THE ORIGIN OF THE SOLAR MAGNETIC FIELD**

Arman R. CHOUDHURI (Dept of Physics, Indian Institute of Science)

One of the most outstanding questions in the field of solar system studies is to understand the origin of the Sun's magnetic field varying with a cycle of 22 years. Some of the fundamental ideas in dynamo theory were developed nearly half a century ago. However, one needs fairly detailed information about the flow and magnetic fields in the interior of the Sun to make a realistic model of the solar dynamo. Such information was not available till a decade ago. Two developments within the last one decade have changed the scenario completely. (1) Helioseismology has mapped the internal differential rotation of the Sun, which is now a crucial ingredient in developing dynamo models. (2) MHD simulations of sunspot formation have put important constraints on the magnetic field in the solar interior. Only very recently solar dynamo models are being built which address these issues. I shall present a review of where we stand now on this subject.

**GAIV.04/09P/A16-002** Invited **1435**

**RECENT ADVANCES IN THE STUDY OF SOLAR ACTIVITY: REPORTER REVIEW**

Barbara J. THOMPSON (NASA Goddard Space Flight Center, Greenbelt MD, USA)

Recent advances in the study of solar activity have been spurred by several new missions and ground-based research initiatives, as well as widespread collaboration of theorists and modelers. Progress has been made in our ability to anticipate and react to nearly all types of solar variability which impact the heliosphere and Earth; studies of the origin, flow, storage and release of energy have paved the way for significant advances in our predictive abilities. The review will cover advances ranging from deep into the solar interior, to the study of impulsive releases of energy such as flares and coronal mass ejections, to the interaction of energetic shocks in the inner heliosphere.

**GAIV.04/09P/A16-003** **1510**

**ORIGIN OF THE FAST SOLAR WIND: OUR CURRENT UNDERSTANDING AND HOW WE GOT HERE**

Joseph V. HOLLWEG (Space Science Center, Univ. of New Hampshire)

Before the discovery of the fast solar wind in the mid - 1970s, it was known that even the average solar wind could not be well explained by models in which electron heat conduction was the energy source and the electron pressure gradient was the principal accelerating force. The Alfvén waves discovered around 1970 were thought for a while to provide the sought - after additional energy and momentum, but their wave pressure ultimately failed to explain the rapid acceleration of the fast wind close to the Sun. By the late 1970s, various in situ data were suggesting that protons and heavy ions were being heated and accelerated by the ion - cyclotron resonance far from the Sun. This notion was soon applied to the acceleration region in coronal holes close to the Sun. The models which resulted suggested that the fast wind could be driven mainly by the proton pressure gradient (which is mainly the mirror force if the anisotropy is large), and that the high temperatures and flow speeds of heavy ions could originate within a few solar radii of the coronal base; these models also emphasized the importance of treating the extended coronal heating and solar wind acceleration on an equal footing. By the mid 1990s, SOHO, especially the UVCS (Ultraviolet Coronagraph Spectrometer), provided remarkable data which have given great impetus to studies of the ion cyclotron resonance as the principal mechanism for heating the plasma in coronal holes, and ultimately driving the fast wind. We will discuss the basic ideas behind current research, emphasizing the particle kinetics. We will discuss remaining problems such as the source of the ion - cyclotron resonant waves (direct launching, turbulence, microinstabilities), problems concerning OVI and MgX, the roles of inward - propagating waves and instabilities, the importance of oblique propagation, and the electron heating. Some alternatives, such as shock heating and turbulence - driven magnetic reconnection, will also be mentioned.

**GAIV.04/09P/A16-004** Invited **1615**

**THREE-DIMENSIONAL STRUCTURE OF THE OUTER HELIOSPHERE**

Nikolai V. POGORELOV (Institute for Problems in Mechanics, Russian Academy of Sciences,

The review is presented of modern three-dimensional models of the outer heliosphere that confines the solar wind (SW) during its interaction with the local interstellar medium (LISM). Among many reasons determining spatial features of the heliospheric interface, the most important are those related to asphericity of the solar wind, prominently manifesting itself during solar activity minima, inhomogeneities in the LISM, and the presence of the interplanetary and interstellar magnetic fields. Starting from the seminal work of E.N. Parker (1961), the SW-LISM interaction is analyzed in the framework of mechanics of continuous media. Once this assumption is made, the heliopause acquires the form of a tangential discontinuity separating two flows and various shock waves can originate. Due to collective processes occurring in plasma, normally only the plasma component of the winds has a mean free path considerably smaller than the characteristic size of the heliosphere. However, the neutral component of the LISM substantially modifies the interface by a charge exchange with plasma particles. This process strongly affects distributions of the plasma and neutral components and substantially changes geometrical parameters of the heliopause and stand-off distances of the principal shock waves from the Sun. The charge exchange also contributes to breaking the spherical symmetry of the solar wind ahead of the termination shock. We analyze the current state of knowledge on the above-mentioned phenomena and discuss interrelations between the Lyman-alpha absorption in directions to nearby stars and possible three-dimensional features of the heliospheric interface. Different theoretical models of the local interstellar cloud are reviewed in order to extract information on the interstellar magnetic field strength and direction. Galactic cosmic ray diffusion into the heliosphere is discussed from the viewpoint of its necessarily three-dimensional character in the presence of the interplanetary magnetic field. New theoretical and computational challenges are set forth, which are critical for obtaining adequate reliable information about processes occurring in the heliosphere.

**GAIV.04/09P/A16-005** Invited **1650**

**SOLAR WIND INTERACTION WITH WEAKLY MAGNETIZED PLANETS AND COMETS**

Christian MAZELLE (CESR / CNRS)

Among solar system bodies, planets like Mars and Venus on one side and active comets on the other side share both the lack of any measurable large-scale magnetic field and the existence of a dense expanding neutral atmosphere. Therefore, it is not surprising that, despite their obvious different physical nature and different characteristic scales, their interaction with the solar wind exhibits many similarities. The most important are the formation of a magnetic barrier in front of the highly conducting ionosphere and an induced magnetic tail, often described by models, e.g., in the frame of gas-dynamics, MHD or kinetic hybrid simulations. The review will cover recent advances in the understanding of this type of interaction with the solar wind both from recent observations, e.g. by Mars Global Surveyor within the Martian environment, and from recent modeling efforts.

**GAIV.04/09P/A16-006** Invited **1725**

**COLLISIONLESS SHOCKS AND MAGNETOSHEATH: RECENT RESULTS FROM MULTIPOINT MEASUREMENTS IN SPACE**

Vladimir KRASNOSELSKIKH (LPCE/CNRS-Universite d'Orleans)

Several problems of collisionless shocks physics felt the lack of direct measurements of crucial parameters. To study electron heating or acceleration in quasiperpendicular shocks one needs detailed information about spatial and temporal fine structure of electric and magnetic fields across the front of the shock. Until recently, there were only two attempts to evaluate the distribution of electric field potential across the shock front based on the data of ISEE 1,2. The fine spatial structure of the shock front and its time variations were intensively studied in 2D computer simulations but there were no serious effort to study these characteristics experimentally. Some problems such as shock front variations could not be studied using one satellite and even two satellites measurements, which were not sufficient to perform such a research program. Serious improvement of the electric field measurements and multipoint measurements by the Cluster satellites offered the possibility to get new important income to our knowledge of physical processes in the front of quasiperpendicular shocks. Electric field measurements onboard of the Wind satellite allowed to establish the presence of the small scale electric field structures similar to double layers in the ramp region of the quasiperpendicular shock. Similar measurements onboard of Cluster satellites have demonstrated the presence of the small scale electric field structures in the front of low Mach number quasiperpendicular shocks. Analysis of characteristic scales of electric and magnetic fields was performed for many shock front crossings by Cluster satellites. Several shock crossings were studied that gave an evidence of the nonstationary dynamics of the shock front of high Mach number quasiperpendicular shocks. Multiple crossings of quasiperpendicular shocks have allowed to study in more detail three dimensional characteristics of short large amplitude magnetic field structures (SLAMS). The detailed study of their role for the process of particle acceleration is still to be performed. The combination of the multipoint measurements with the modern methods of data analysis have allowed to perform wave identification in the magnetosheath region. It was unambiguously established the presence of mirror mode waves in the downstream region of the moderate Mach number high beta shock. Intensive theoretical studies of these waves have provided the possibility to perform more detailed comparison of wave characteristics with theoretical predictions. There were new interesting results obtained onboard of Ulysses satellite that clarify the special role of shocks in particle acceleration. It was clearly shown that the enhanced fluxes of energetic electrons are associated with the crossings of reversed shocks in the vicinity of corotating interaction regions (CIR).

**GAV.04**

**INTERNATIONAL DECADE OF GEOPOTENTIAL FIELD RESEARCH: FIRST FIVE YEARS - ADVANCES IN THE UNDERSTANDING THE GEOMAGNETIC FIELD (SEDI)**

Location: Site A, Room 11



**GAV.04/07A/A11-001** Invited **0900**

**SWARM, A CONSTELLATION MISSION TO IMPROVE OUR UNDERSTANDING OF THE GEOMAGNETIC FIELD**

Eigil FRIIS-CHRISTENSEN (Danish Space Research Institute)

A new era in geomagnetic research began with the launch of the Oersted satellite in February 1999. Oersted is the first of a series of geomagnetic mapping missions during the International Decade of Geopotential Research. CHAMP (launched in July 2000) and the Oersted-2 experiment on board the SAC-C satellite (launched in November 2000) will continue to deliver high-precision geomagnetic data during the first years of the new millennium. However, these three satellites have been conceived as single-satellite missions. Recent progress in geomagnetic research indicates that the limiting factor in the accuracy of present geomagnetic field models is the dynamic behaviour of the external current configuration. Single satellite missions are not able to take advantage of the impressive instrument improvement, which has been achieved during the last couple of years. Multiple satellite missions measuring simultaneously over different regions of the Earth offer the only way to take full advantage of this new generation of instruments. A proposal with exactly this aim was submitted to ESA's Earth Explorer Opportunity Mission programme and has been selected for an industrial Phase A Study to be conducted during 2003. The swarm concept consists of a constellation of four satellites in two different polar low altitude orbits. Each satellite will provide high-precision and high-resolution measurements of the vector magnetic field. A few additional instruments like GPS receivers, an accelerometer, and an electric field instrument provide supplementary information for studying the interaction of the magnetic field with other physical quantities describing the Earth system.

**GAV.04/07A/A11-002** **0930**

**THE SWARM END-TO-END SIMULATOR STUDY: SEPARATING THE VARIOUS CONTRIBUTIONS TO EARTH'S MAGNETIC FIELD USING SYNTHETIC DATA FROM A SIMULATED MISSION**

Nils OLSEN<sup>1</sup>, Eigil FRIIS-CHRISTENSEN<sup>1</sup>, Roger HAAGMANS<sup>2</sup>, Gauthier HULOT<sup>3</sup>, Hermann LUEHR<sup>4</sup>, Stefan MAUS<sup>5</sup>, Michael PURUCKER<sup>6</sup>, Terence SABAKA<sup>7</sup>, Pascal TARITS<sup>8</sup>, Alan THOMSON<sup>9</sup> (<sup>1</sup>Danish Space Research Institute, <sup>2</sup>ESA, ESTEC Earth Sciences Division, <sup>3</sup>Institut de Physique du Globe de Paris, <sup>4</sup>GeoForschungsZentrum Potsdam, <sup>5</sup>NASA GSFC, Geodynamics Branch, <sup>6</sup>Universite de Bretagne Occidentale, <sup>7</sup>British Geological Survey)

The *swarm* mission concept consists of a constellation of four satellites for studying the Earth's magnetic field and its interaction with the Earth environment. Each satellite will provide high-precision measurements of the magnetic field; in combination, they will provide the necessary observations that are required to separate the various sources of the geomagnetic field. GPS receivers, an accelerometer and an electric field instrument will provide supplementary information for studying the interaction of the magnetic field with other physical quantities characterizing the Earth system. *swarm* has been selected by ESA for a Phase-A study. In parallel with this Phase-A, an End-To-End simulation of the mission has started. The objective of this End-To-End simulator is to evaluate various mission and constellation scenarios. This will be done by analyzing synthetic data in much the same way that will be used regarding the real data. We will report on the various approaches used for this End-to-End study, and on first results.

**GAV.04/07A/A11-003** **0950**

**FIRST MAGNETOMETER RESULTS FROM THE AUSTRALIAN MICRO-SATELLITE FEDSAT**

Brian J. FRASER<sup>1</sup>, Fred W. MENK<sup>1</sup>, Colin L. WATERS<sup>1</sup>, Andrew BISH<sup>1</sup>, C.T. RUSSELL<sup>2</sup>, J.D. MEANS<sup>3</sup> (<sup>1</sup>Cooperative Research Centre for Satellite Systems, University of Newcastle, School of Mathematical & Physical Sciences, <sup>2</sup>IGPP/UCLA, Los Angeles, CA, USA)

In December 2002 FedSat, an Australian scientific microsatellite (58 kg) was launched from the NASDA Tanegashima Space Centre on the HIIA-F4 rocket. FedSat was placed in an 800 km altitude 98.7° inclination polar orbit, sun-synchronous at 10:30 LT. The primary scientific experiment is NewMag a triaxial fluxgate magnetometer designed to study magnetosphere-ionosphere coupling through measurements of the Earth's magnetic field and its variations. NewMag observes field aligned current structures in the auroral zones and ultra-low frequency (ULF) plasma waves in the upper ionosphere. This paper will describe the NewMag instrumentation, and initial data initial reduction. The FedSat orbit period is ~ 101 minutes and during this time NewMag passes through the auroral zone current systems four times. It is anticipated that initial results from NewMag showing field aligned current signatures in the geomagnetic field and ULF waves associated with field line resonance and compressional cavity mode waves, will be presented.

**GAV.04/07A/A11-004** Invited **1030**

**NET FIELD-ALIGNED CURRENT SYSTEMS AND THEIR EFFECTS ON THE GROUND**

Toshihiko IYEMORI<sup>1</sup>, Shin'ya NAKANO<sup>2</sup>, Satoru YAMASHITA<sup>3</sup> (<sup>1</sup>Data Analysis Center for Geomagnetism and Space Magnetism, Graduate School of Science, Kyoto University, <sup>2</sup>Geophysical Institute, Graduate School of Science, Kyoto University)

Field-aligned currents normally appear as a pair of upward and downward currents and close in the ionosphere. If the amount of upward and downward currents balances, the magnetic effects generated by the currents would be mostly confined in the current flowing region. However, if there exists some imbalance, i.e., 'net' field-aligned current, the magnetic effects reach to distant region. This effect appears even at mid- or low- latitudes in midnight and could be a source of significant errors in modeling geomagnetic main field. For example, a pair of net field-aligned currents which flow into the ionosphere on the dayside and flows out from night side generates east-west disturbance fields in middle latitudes. We present the net current systems estimated from satellites and ground geomagnetic field observations and estimate their quantitative effects.

**GAV.04/07A/A11-005** **1100**

**MODELLING OF POLAR FIELD-ALIGNED CURRENT SYSTEMS**

Peter STAUNING<sup>1</sup>, Dan WEIMER<sup>2</sup>, Vladimir PAPITASHVILI<sup>3</sup>, Freddy CHRISTIANSEN<sup>4</sup> (<sup>1</sup>Solar-Terrestrial Physics Division of Danish Meteorological Institute, <sup>2</sup>Mission Research Corporation, <sup>3</sup>SPRL, University of Michigan)

Compared to the earlier high-precision Magsat magnetometry mission (1979-80) the Oersted and CHAMP satellites have since 1999 provided much more complete coverage with respect

to local time and geophysical conditions. The Magsat satellite had a fixed dawn-dusk orbit and even with the added spread in local magnetic time Magsat still gave poor coverage of the noon and the midnight sectors. With data from Oersted and CHAMP in their drifting orbits it has been possible to investigate the important high-latitude field-aligned current (FAC) and ionospheric current systems, like the cusp currents and the substorm current systems, located in these sectors. The added local time coverage has enabled a more complete determination of the local time dependencies in further ionospheric, magnetospheric and field-aligned current systems like the auroral electrojet currents and the region 1 and region 2 high-latitude field-aligned current systems. With the abundance of high-quality data the comprehensive statistical basis has now enabled the development of sophisticated models for the current distribution and intensities in dependence of solar wind and magnetospheric parameters. Three models for the polar FAC distribution based on different procedures for relating the observed magnetic perturbations to FAC's shall be presented and their predictions will be compared to each other and to actual observations. There are still large uncertainties involved in using the new models primarily due to the lack of precise knowledge of the temporal development of the currents in relation to the highly variable solar wind parameters and the still unpredictable effects of magnetospheric substorms.

**GAV.04/07A/A11-006** **1120**

**MAGNETIC SIGNATURE OF MAGNETOSPHERIC SOURCES IN CHAMP DATA**

Judith SCHWARTE<sup>1</sup>, Aude CHAMBODUT<sup>2</sup>, Hermann LUEHR<sup>1</sup>, Mioara MANDEA<sup>3</sup> (<sup>1</sup>GeoForschungsZentrum Potsdam, Div. 2.3, <sup>2</sup>IPG Paris, Laboratoire Geomagnetisme)

For modeling the main and crustal fields it is necessary to describe the magnetic field contributions from large-scale magnetospheric current systems, as the ring current. In general, the satellite data are corrected using the  $D_{ST}$  index. However, a first parameterisation of the external magnetic fields using CHAMP scalar data suggests that some problems may occur with this common correction, specially near the poles and in modeling the local time dependences. For a better description of the effects caused by the ring-current, CHAMP vector data are used in a second approach. From time to time the satellite is flying in resonance with the Earth's rotation, and we just took advantage of these orbital repeat tracks. While the contribution of magnetospheric effects is emphasized, the lithospheric contributions and model errors are eliminated by this technique. The differences of such two successive repeat tracks are taken as input data. In order to minimize non-scalar potential contributions, before applying the SHA, we determine Ampere's law integral over one full orbit and correct the data over a region of  $\pm 20^\circ$  around the poles. The east component is not taken into account because it is strongly affected by the field-aligned currents. We present the used data and technique, and the obtained results in modeling internal and external magnetic fields in a dipole-axis/local time frame.

**GAV.04/07A/A11-007** **1140**

**PRELIMINARY CORRELATIONS OF SATELLITE AND GROUND MAGNETIC VARIATIONS TO ESTIMATE SCALE-LENGTHS OF INDUCING FIELDS**

Nandini NAGARAJAN<sup>1</sup>, Manoj C.<sup>1</sup>, Stefan MAUS<sup>2</sup> (<sup>1</sup>National Geophysical Research Institute, <sup>2</sup>GeoForschungsZentrum Potsdam, Telegrafenberg, 14473 Potsdam, Germany)

Natural electromagnetic fields are measured on the earth's surface to estimate the electrical resistivity of the sub-surface, by means of Magnetotellurics (MT). The phase and amplitude of the E/H ratios, as a function of frequency, are dependent on the Earth's subsurface electrical resistivity. MT long period source field (>1 second) is generated by the interaction of solar wind with earth's magnetosphere. Man-made as well as natural distortion corrupts these fields and may result in erroneous estimates of resistivity and phase. Many attempts have been made to reduce the effect of such noise in inducing fields on computed resistivity estimates. Recent studies have shown the coherence of MT magnetic field over distance >500 km. An attempt is made here to examine the coherency of simultaneous measurements of magnetic fields (>1sec period) on the ground and by the CHAMP satellite. Additionally data at a distant magnetic observatory are also examined. A few samples of data have been examined in this preliminary study. The present study, if successful, would aim at reducing noise in MT resistivity estimates using vector magnetic data from CHAMP and distant observatories. Additionally the study of changing time and length-scales of natural magnetic variations that form the inducing fields for all induction studies would be brought out in this study as there are recorded instances where the uniform inducing field changes its length-scale unexpectedly. With the time and effort spent in collecting electromagnetic time series for induction experiments it would be worthwhile to assess the effects of changes in external magnetic field variations as measured at a sufficiently distant source - such as satellite magnetic data.

**GAV.04/07A/A11-008** **1200**

**GLOBAL SCALE IONOSPHERIC IRREGULARITIES ASSOCIATED WITH THUNDERSTORM ACTIVITY**

Sergey A. PULINETS, Viktor H. DEPUV, Amando C. LEYVA (Institute of Geophysics, UNAM)

The potential difference near 280 kV exists between ground and ionosphere. This potential difference is generated by thunderstorm discharges all over the world, and return current closes the circuit in the areas of fair weather (so-called fair weather current). The model calculations and experimental measurements clearly demonstrate non-uniform latitude-longitude distribution of electric field within the atmosphere. The recent calculations show that the strong large scale vertical atmospheric electric field can penetrate into the ionosphere and create large scale irregularities of the electron concentration. To check this the global distributions of thunderstorm activity obtained with the satellite monitoring for different seasons were compared with the global distributions of ionosphere critical frequency (which is equivalent to peak electron concentration) obtained with the help of satellite topside sounding. The similarity of the obtained global distributions clearly demonstrates the effects of thunderstorm electric fields onto the Earth's ionosphere.

**GAV.04-Posters**

**INTERNATIONAL DECADE OF GEOPOTENTIAL FIELD RESEARCH: FIRST FIVE YEARS - ADVANCES IN THE UNDERSTANDING THE GEOMAGNETIC FIELD (SEDI)**

Location: Site D

Monday, July 7 AM

GAV.04/07A/D-001 Poster 0830-141

**MODELING OF THE GEOMAGNETIC FIELD FROM THE JERK ASSUMPTION**

Anahit Hovhannes SIMONYAN (Institute of Geophysics &amp; Engineering Seismology of the National Academy of Sciences, Armenia)

Elucidating the geomagnetic field behavior for the XX century with construction of up to second time derivatives accuracy models we get appropriate data basis for solving the reverse problem of magnetic hydrodynamics on description of mechanism of core fluid motion system reorganization, which originates the jerks in the Earth's magnetic field. For this goal we have screened out the extended set of geomagnetic field elements annual mean values from 153 worldwide magnetic observatories. In development of jerk investigations we have kept the conception that in large regional scale the geomagnetic field dynamics for a few decades is characterizing by constant values of accelerations, which suffer jump-like changes during the jerk events. Hence meaningful, from physics point of view, method of piecewise linear approximation has been applied to the series of geomagnetic field X, Y and Z strength components annual mean values first time derivatives series. Slopes of linear segments in nT a<sup>-2</sup> present the geomagnetic field values second time derivatives. These values are input constructing the spatial spherical harmonic models of geomagnetic accelerations field at each central epochs of stable state interval between the successive jerks on the globe. Four harmonic global models dated on 1901, 1909, 1922, 1931, 1943, 1955, 1963, 1975, 1982 and 1992 are constructed for the XX century. It would be noticed however that the model on 1901 has anomalous powerful energy spectrum and is deteriorated by incredible strong foci on south hemisphere, when mapping the accelerations field components computed from this model. Obviously lack of data series from main part of south hemisphere at the beginning of XX century prevent from construction of more accurate model. While power spectrums for all of remainder models are of reasonable amplitudes with domination of first two non-dipole harmonics energy. And on the maps from those models are observed reasonable magnitudes in changeable sign large regional foci, depicting internal nature of mapped field. Furthermore, despite of constant accelerations global models are repeated over a decade, regional patterns from one model to another are not changing everywhere, so well reflecting the observational data, by which in their regional feature the neighboring jerks are divided by more than one, or in majority over a three, or even more decades. Construction of 6-, 8-harmonic models for second half of century resulted the similar feature of foci distribution but depicted also small-scale peculiarities, which could not be supported by observational data accuracy and density in their distribution. Hence we rely the homogeneity and better accuracy in modeling the geomagnetic accelerations field while interrupted the expansion series at fourth harmonic. On the basis of IGRF-1980 and IZMIRAN-1985 for geomagnetic field, using the acceleration model on 1982 coefficients set for SV-1980 has been computed. Better accuracy of secular variation computed model is proved by its persistent correlation with data based IGRF and IZM-SV models for 1980. Then that with obtained second time derivative models were used for extension the IGRF-1980 field model forward and back during the XX century transferring from one jerk to another.

GAV.04

**INTERNATIONAL DECADE OF GEOPOTENTIAL FIELD RESEARCH: FIRST FIVE YEARS - ADVANCES IN THE UNDERSTANDING THE GEOMAGNETIC FIELD (SEDI)**

Location: Site A, Room 11

Monday, July 7 PM

Presiding Chairs: J. Schwarte, S. Maus

GAV.04/07P/A11-001 Invited 1400

**THE CONTRIBUTION OF MAGNETIC ANOMALIES TO UNDERSTANDING TECTONIC EVOLUTION AND CRUSTAL STRUCTURE**

Colin V. REEVES (International Institute for Geo-information Science and Earth Observation (ITC))

Since shortly after the invention of the electronic magnetometer in the 1940s, airborne systems have been used to map variations in magnetic total field strength (F) over the Earth's surface. From initial naAe ambitions of finding buried magnetite deposits of economic value, the technique has evolved into one of the most sophisticated (yet inexpensive) tools for rapidly mapping geology over large areas. Reconnaissance surveys of a technical standard achievable in the period until ~1990 cover over half the land area of the Earth and have been systematically compiled for many large (continent-sized) regions. But even the assembly of thousands of individual surveys on land and millions of km of shiptracks at sea, while giving a tantalizing new glimpse of the Precambrian mosaic of the continents, does not yet provide a complete global magnetic anomaly map. The elegant simplicity of the magnetic anomaly patterns over the ocean has, nevertheless, been seminal in the evolution of ideas on ocean-floor spreading and global tectonics. The global uniformity of coverage afforded by satellite magnetometry, meanwhile, is obviously highly attractive. Unfortunately, potential field theory predicts that the resolution of anomalies at satellite altitude will be no better than several hundred kilometres. And experience from Pogo and Magsat over 20 years ago shows that amplitudes of even the largest crustal anomalies are no more than 10-20 nT. Improved technology has overcome the problem of signal-to-noise ratio and hence anomaly reproducibility in the current generation of satellite-borne magnetometer systems. Improved resolution of detail can only be attempted as satellites descend into lower - ultimately fatal - orbit. The GFZ 'Champ' satellite mission has produced a stable picture of crustal magnetic anomalies and their reconciliation with crustal geology has commenced. One of the largest anomalies is coincident with an area of the Arctic Ocean that has a distinctive signature on the marine/aeromagnetic anomaly compilation - probably a large igneous province lying entirely below sea level. Three distinct anomalies, now situated above Early Cretaceous oceanic crust off South Africa, Antarctica and Argentina respectively, coalesce when ocean creation is reversed in computer animation, suggesting a common origin off the southern coast of Africa during the early stages of dispersal of the three continents, 120-140 million years ago. Several pairs of anomalies in the South Atlantic and Indian Oceans suggest a similar conjugate origin on now-opposing sides of their respective mid-ocean ridges. Anomalies over the continents at satellite altitude are less easily related to what is known of the Precambrian crust. Suggestions of ancient meteorite impacts are not easily verified from direct observation of the crustal geology, such as in the Bangui region of central Africa.

GAV.04/07P/A11-002 1430

**DEPTH OF THE MAGNETIC CRUST IN THE INDIAN SUBCONTINENT**

Mita RAJARAM, Anand P. SASHIDHARAN (Indian Institute of Geomagnetism)

Aeromagnetic anomaly map over Indian Peninsula (from 8 to 24 degrees North) is prepared and downward continued to ground level. This is merged with available marine magnetic data and available ground magnetic data to fill gaps in the aeromagnetic data set. Distinct structural trends are identified and some of the features within the continent continue into the offshore area. From the aeromagnetic data combined with the gravity anomaly of the region, the different tectonic blocks are identified. An analytical signal map of the aeromagnetic anomaly is prepared and the different source fields are located; the sources of the magnetic anomaly within the different blocks are distinctly different. The data are also subjected to high pass filtering process. The depths are calculated from the spectral plots, in order to peep into the source depth of the magnetic anomaly in the different blocks like the Southern Granulite Terrain (SGT), Dharwar region, Eastern Ghat Mobile belt, etc. In Dharwar craton the magnetic sources extend up to a depth of around 36 km, possibly reflecting the average Moho depth. Within the SGT the magnetic crust is thin and is confined to within the first 22 km, with the deeper levels not contributing significantly to the magnetic signatures. Kuppam-Palani seismic reflection / refraction profiles also depict a change in velocity around this depth in the SGT. We conclude that below the exhumed crust of the SGT there is a lithological / mineralogical change at around 22 km depth caused possibly by magmatic underplating or the Curie isotherm is shallow when compared to the Dharwar craton. Satellite magnetic anomalies contain information of the long wavelength structures of the magnetic lithosphere above the Curie isotherm. The integrated susceptibility map from Oersted data (Purucker, 2002) depicts a low in the SGT when compared to the Dharwar region. From the Standard Earth Magnetisation Model (SEMM) developed from the global POGO / Magsat data, crustal anomaly depth over the Indian subcontinent is derived. The SGT depicts low crustal thickness values when compared to the Dharwar region. There is a reasonably good comparison between the depth estimates for these two blocks from the satellite derived and aeromagnetic derived crustal depth values. The implications of the depth estimates of the entire region will be discussed.

GAV.04/07P/A11-003 1450

**3D GLOBAL INDUCTION EFFECTS ON GEOMAGNETIC FIELD VARIATIONS INFERRED FROM THE RESPONSE TO RING CURRENT AND AURORAL OVAL EXCITATION**Ikuko FUJII<sup>1</sup>, Adam SCHULTZ<sup>2</sup> (<sup>1</sup>Kakioka Magnetic Observatory, JMA, <sup>2</sup>Earth Science Dept., Cardiff Univ.)

We report on global-scale induction effects on the geomagnetic field at the surface of the Earth over several decades of observations. We developed a statistically robust form of empirical orthogonal function (EOF) analysis to analyze a spatially and temporally sparse data set. This has resulted in an improved compilation of the functions representing the geoelectromagnetic response of the Earth's mantle. Fujii & Schultz (2002) presented the first results and an updated version of the functions in the spatial coverage and quality is shown in the present study. The EOF method was applied to a newly assembled global catalogue of magnetic observatory hourly mean values. The analysis indicates that for periods longer than 5 days the geomagnetic field variation can be represented predominantly by a single eigenmode. We have identified that the primary source fields of the dominant mode consist of two current systems in the same direction: an equatorial ring current in the magnetosphere, and two conjugate auroral oval ring currents in the ionosphere. The influence of the auroral current system is seen at surprisingly low latitudes, 40 and 50 degrees for the vertical and northern components, respectively, which results in non-negligible bias in the conventional c response at latitudes higher than 40 degrees. To correct the auroral current effect on the dominant EOF mode, the geomagnetic field by conjugate ring currents at the auroral oval was computed at the surface of a conductive Earth. The height and amplitude of the currents were determined in the least squares sense. Having established the optimal geometry of the auroral currents, the estimated auroral effects were removed from the dominant EOF geomagnetic response mode. Unbiased c responses were obtained for data from more than 50 observatories at latitudes from 60 to 60 at periods from 5 to 106.7 days. A newly defined d response function, which constitutes a sensitive indicator of lateral heterogeneities in conductivity was also estimated. The c and d response functions show significant spatial variations and vary stably with frequency. This is consistent with the view that significant lateral variations of the conductivity are found in the upper- and mid mantle. These new sets of electromagnetic response information are expected to increase the resolving power of the 3D distribution of electrical conductivity in the Earth's mantle.

GAV.04/07P/A11-004 1510

**USING SATELLITE MAGNETIC DATA FOR PROBING THE ELECTRICAL STRUCTURE OF THE EARTH**

Pascal TARITS (UMR CNRS Domaines Oceaniques, IUEM/UBO)

The magnetic field of the earth results from two primary sources, convection in a conductive liquid core and the interaction between the planet and solar wind plasma, and from two secondary sources, the local magnetisation and electric currents induced in the planet by the transient magnetic fields of external origin. The external natural fluctuations (the primary source) of the magnetic field induce an internal response (the secondary source) that can be used to infer the electrical conductivity structure of the planet. The maximum depth resolved by the technique is a function of the longest period of variations of the external magnetic sources that may be recovered from the data. The external transient variations result from both the interactions between the planetary environment and the solar wind plasma. Traditionally, induction studies on Earth make use of magnetic data recorded continuously at stations set up at the Earth surface transitionally or permanently (the geomagnetic observatories). The successful launch of several magnetic satellite missions in the last few years (OERSTED, CHAMP, SAC-C) has triggered the interest of the electromagnetic induction community to use satellite data to investigate the electrical conductivity of the Earth. The satellite provides a complete coverage of the planet. Measuring the vector magnetic field in a satellite surveying the planet offers the unique opportunity to investigate at planetary scale the heterogeneous electrical conductivity structure of the Earth's mantle. Results using data from OERSTED and CHAMP are presented and a new approach to extract the internal induced anomalous magnetic field is discussed.

GAV.04/07P/A11-005 1530

**ELECTRIC AND MAGNETIC FIELDS GENERATED BY OCEAN FLOW**

Robert H. TYLER (Ocean Physics Dept., Applied Physics Laboratory, University of Washington)

Through magnetohydrodynamic interaction between ocean flow and the main magnetic field, secondary electric and magnetic fields are generated. It has recently been shown that the

ocean tides generate magnetic fields which are clearly evident in magnetic observations of the CHAMP satellite. We review these results together with other evidence, and discuss the opportunity for identifying other ocean signals in the magnetic records.

**GAV.04/07P/A11-006** Invited **1610**

**CORE DYNAMICS REVEALED BY SPACE MAGNETIC OBSERVATIONS**

Gauthier HULOT (Departement de Geomagnetisme et Paleomagnetisme, IPGP/CNRS)

Magsat in 1980, was the first satellite capable of mapping the Earth's magnetic field up to degree and order 13. Oersted, launched in 1999, is the second satellite with similar capability. This offered the first opportunity to study the detailed way the core field had changed in 20 years time (Hulot et al., Nature, 416, 620-623, 2002) and revealed several striking features. First, that the smallest visible scales of the core field can change with time scales as little as 50 years, second that most of the changes have occurred only at polar latitudes or beneath the Atlantic Hemisphere, while very little changes seem to have occurred below the Pacific Hemisphere. This asymmetry echoes the current asymmetric pattern also found in the field itself at the core surface, which displays strong normal polarity values below the Pacific hemisphere, and much weaker, sometimes reversed values below the Atlantic hemisphere. Thanks to the high resolution of the field changes seen between Magsat and Oersted, it is also possible to try and infer core flows accounting for those changes, in very much the same way than has been done with historical data, but with a better resolution. Those maps, together with those of the field and its temporal changes can then be used for comparison with results from recent dynamo simulations. This can lead to stimulating interpretations. However, care must be taken when carrying such comparisons. Numerical simulations are still being run in unrealistic parameter regimes. But also, core flow computations remain limited in resolution. The good news is that this limitation is no longer linked to the quality of the observations. Satellite observations now appear to provide good enough field models (and field change models) as soon as the satellites are up for more than two years (as has been the case since the launch of Oersted, joined more recently by Champ) The bad news is that the limitation is now linked to the fact that we may not have access to the smallest scales of the core field, hidden by the crustal field. This not only stops us from recovering the smallest scales of the core flow, but also means that we should avoid interpreting too much of the smallest scales of the field changes in terms of computable flows. As a consequence, it may for instance be that the weak changes seen below the Pacific Hemisphere could mainly be due to inaccessible small scale flows (Eymin and Hulot, in prep.). This somewhat negative note should however not hide the important fact that continuous observation of the Earth's magnetic field from space has now been proven to provide much better images of the time varying core field, with a temporal resolution already of the order of a couple of years. Smarter missions, such as the Swarm constellation, could help reduce this temporal resolution to less than a year. This will eventually offer the possibility to study short-term dynamics of the core in much more detail than was previously possible.

**GAV.04/07P/A11-007** **1640**

**SHORT-PERIOD SECULAR VARIATION AND CORE DYNAMICS**

Jeremy BLOXHAM, Mathieu DUMBERRY (Department of Earth & Planetary Sciences, Harvard University)

A large part of the short-period secular variation (which we define as the part that is unexplained by steady flow) can be fit by a small number of torsional oscillations in the core. In particular, torsional oscillations provide a simple though unexpected explanation of geomagnetic jerks: unexpected because torsional oscillations have strong symmetry properties (they are both axisymmetric about the rotation axis and symmetric about the equator) while geomagnetic jerks have a highly asymmetric geographical distribution. The fit of torsional oscillations to geomagnetic jerks is not perfect. Given that it is unlikely that separate physical phenomenon happens to combine with torsional oscillations to produce jerks, we hypothesize that the misfit most likely results from insufficient temporal and spatial complexity in our field and flow models. Here we examine what we can learn about the complexity of the field and flow at the core surface from requiring a more complete fit to the observations. From this we can hope not only to gain an understanding of the spectrum of the field and flow at the core surface, but also a more complete spectrum of torsional oscillations which will provide important insight into the dynamics of the core.

**GAV.04/07P/A11-008** **1700**

**CHAOS IN THE PRESENT EARTH MAGNETIC FIELD: A SYMPTOM THAT A REVERSAL IS IN PROGRESS?**

Angelo DE SANTIS<sup>1</sup>, Tozzi ROBERTA<sup>2</sup>, Luis R. GAYA-PIQUE<sup>3</sup> (1Istituto Nazionale Geofisica e Vulcanologia, Rome, Italy / Earth Science Department, G. D'Annunzio University, Chieti, Italy, 2Istituto Nazionale di Geofisica e Vulcanologia, Rome, Italy, 3Istituto Nazionale di Geofisica e Vulcanologia, Rome, Italy / Observatori de l'Ebre, Roquetes, Spain)

Understanding the spatial and temporal characteristics of the geomagnetic field would allow us to infer important properties of the dynamics in the outer terrestrial core, where the geomagnetic field **B** is produced and maintained. In this contribution we apply the concepts of Information Theory to the geomagnetic field, as represented by global models of the last 100 years, to investigate on the temporal behaviour of a very important quantity for a physical system: its information content. The results support the idea that **B** is in a chaotic state with characteristic times close to those related to the westward drift of the secular variation (~1000 yr) and to the convective overturn time in the outer core (~500 yr). We also show that the dipole field has a characteristic time equal to the time-span (~5000 yr) of a reversal (i.e. the change of polarity of the field), leading us to suspect that loss of memory about its, possibly chaotic, origins plays an important part on geodynamo mechanisms. The main consequence of these results, and of the comparable results obtained from the analysis of the secular variation, is the suggestion that a possible geomagnetic reversal is current in progress.

**GAV.04/07P/A11-009** **1720**

**MAGNETIC FIELD SECULAR VARIATION: THE SATELLITE PERSPECTIVE**

Benoit LANGLAIS (NAS/NRC at NASA/GSFC)

The temporal changes of the Earth's magnetic field are usually modeled using observational data. Indeed the secular variation models rely on long-term series of magnetic measurements. Up to now, only the observatories were able to provide such measurements. The first half of the Decade of Geopotential Research has seen the launch of three satellites, Oersted, CHAMP and SAC-C. These three satellites are dedicated to monitoring the space and temporal changes of the Earth's magnetic field. In this study we present the combined use of the vector and scalar measurements made on-board these satellites to model the secular variation. First, data are selected with respect to their local time and to the external activity

indices. These data are sorted so that their geographical distribution are as equiangular as possible. Then, secular variation models are derived using two approaches. In the first one, we solve for the main field and the secular variation Gauss coefficients together. In the second, we first derive short-time main field models, from which the secular variations are derived by subtracting the coefficients from consecutive models. Comparison of the methods is presented, in terms of rms behavior and field spectra. We also discuss the core properties inferred from these models, including the core radius estimation, and the diffusivity of the magnetic field.

**GAV.04/07P/A11-010** **1740**

**GLOBAL SPACE-TIME MODELLING OF THE GEOMAGNETIC FIELD UTILIZING NOISY DATA**

Vadim P. GOLOVKOV, Tatiana N. BONDAR, Svetlana V. YAKOVLEVA (IZMIRAN)

Most precise data are obtained from magnetic observatories. These data are continuous in time, but very irregular in space. Supposing that exact data from irregular network can be used for obtaining precise model, the noise level of data was investigated as a factor of obtained models distortion. It was shown, that random numbers, taken as pseudodata in the observatory network, produce false anomaly with magnitude two orders more than their rms over large empty areas. A method of randomization was developed to minimize these false anomaly and to increase, in this way, an accuracy of models obtained from analyses of data from uneven net of magnetic observatories.

**GAV.05**

**MODELING THE EARTH'S MAGNETIC FIELD ON GLOBAL AND REGIONAL SCALES (SEDI)**

Location: Site A, Room 11

Tuesday, July 8 AM  
Presiding Chairs: B. Langlais, M. Mandea

**GAV.05/08A/A11-001** Invited **0830**

**SWARM, A NEW OPPORTUNITY TO IMPROVE GLOBAL MAGNETIC FIELD MODELS**

Eigil FRIIS-CHRISTENSEN (Danish Space Research Institute)

The Oersted satellite launched in February 1999 was the first in a series of geomagnetic mapping missions during the "International Decade of Geopotential Research". The high accuracy of the observations from these missions resulted in great advancements in geomagnetic field modelling. It was also shown that now the quality of the geomagnetic field models is related to the sophisticated separation of magnetic contributions of internal and external origin. Due to the dynamic nature of the external magnetic field the only way to reduce this ambiguity is to use simultaneous high precision observations from multiple satellites around the Earth. The SWARM concept with a constellation of four satellites in two different polar low altitude orbits has been proposed in response to ESA's Earth Explorer Opportunity Mission programme and was selected for an industrial Phase A Study to be conducted during 2003. Recent investigations have shown the great advantage of modelling the Earth's main field and its secular variation simultaneously with ionospheric and magnetospheric contributions in a comprehensive approach by means of a joint inversion of ground-based and satellite magnetic field measurements. The ability of SWARM to obtain simultaneous measurements at different places in space will allow a better separation of internal and external sources, thereby improving geomagnetic field models. A decision to implement the mission will provide important new knowledge about the Earth's magnetic field and its variations and create a wealth of new scientific opportunities for the whole science community.

**GAV.05/08A/A11-002** **0900**

**IMPROVED SEPARATION OF SOURCES USING SATELLITE AND GROUND-BASED DATA AND DAILY DIPOLE ESTIMATES**

Susan MACMILLAN, Alan THOMSON, Vincent LESUR (British Geological Survey)

Using Oersted satellite data we investigate the effects on model misfits as a result of including ground-based data and daily dipole terms. In general, satellite data are well distributed in space but less so in time whilst observatory data are well distributed in time but poorly distributed in space. However, often only observatory annual and monthly mean values are used in global modelling, or, if hourly mean values are used, estimates of the rate of change of the internal field are made by fitting simple functions to a selection of values. In the models presented here we use observatory hourly mean values directly and solve for the crustal biases. We also make some comments about the use of other ground-based data, in particular repeat station data, for global modelling. In order to characterise the rapidly varying magnetospheric and induced contributions, the external and internal dipole Gauss coefficients are re-calculated for each day where there are sufficient data. This avoids using coefficients for annual and semi-annual periodicity and magnetic activity indices. Preliminary results indicate improvements to the fits of the data when this new technique is used. Thus, by combining satellite and observatory hourly mean data and improving the parameterisation, the resulting models should represent a better description of the contributing sources. In turn, this should lead to a better prediction of secular variation which is important for the IGRF.

**GAV.05/08A/A11-003** Invited **0920**

**A COMPARISON OF MAGNETIC FIELDS FROM THE LATEST COMPREHENSIVE MODEL AND OTHER EARTH MODELS, PARTICULARLY OF CORE AND LITHOSPHERIC ORIGIN**

Terence John SABAKA<sup>1</sup>, Nils OLSEN<sup>2</sup> (1Geodynamics Branch, Code 921, NASA/Goddard Space Flight Center, 2Danish Space Research Institute, Copenhagen, Denmark)

The terrestrial magnetic environment contains field contributions from several major current sources. There are several philosophies as to the best way to extract these constituent signals. Comprehensive models (CMs) parameterize fields from all these sources and estimate their coefficients; the premise being that the important cross-correlative information will allow proper partitioning amongst these signals. However, other methods have also enjoyed varying degrees of success. Of course, as the methods vary so do the resultant models. In addition to a brief description of the latest CM, this talk will attempt to

evaluate some of the differences which exist between these models with respect to the more commonly described portions of the field, such as the core and lithosphere.

**GAV.05/08A/A11-004** **0950**

**REALISTIC ESTIMATES OF THE VARIANCES OF SPHERICAL HARMONIC GEOMAGNETIC FIELD MODELS DERIVED FROM SATELLITE DATA**

Frank J. LOWES<sup>1</sup>, Nils OLSEN<sup>2</sup> (<sup>1</sup>University of Newcastle, <sup>2</sup>Danish Space Research Institute)

We show that conventional estimates of the variances of the spherical harmonic coefficients can be grossly wrong. Because the modelling ignores the presence of along-track serial correlation in the (largely magnetospheric) data 'noise' it underestimates the variances of the tesseral ( $m=n$ ) and near-tesseral coefficients by large factors (up to 20 for the Ørsted OSVM model). Conversely, other variances can be overestimated (by a factor of up to 4). Also, an approach which does not adequately model the effect of ionospheric currents can lead to there being large systematic errors in the zonal ( $m=0$ ) and near-zonal coefficients, together with an enhancement of the variances of these terms.

**GAV.05/08A/A11-005** **1010**

**TOWARD IMPROVING THE MODELING OF THE MAIN GEOMAGNETIC FIELD**

Crisan DEMETRESCU, Venera DOBRICA (Institute of Geodynamics, J.L. Calderon St., Bucharest 37, R-70201, Romania)

Annual mean values at geomagnetic observatories and annual values at repeat stations contain a well known but forgotten component, namely the solar-cycle-related (SC) variation. The SC variation in the annual means of the horizontal and vertical components of the geomagnetic field at European observatories is used to infer information on the magnetic and electric properties of the interior, characteristic to the observatory location, by identifying and analyzing the magnetic induction component and respectively the electromagnetically induced component of the SC variation. The obtained results and the method can be used to better constrain the anomaly bias in main field modeling. A similar treatment for the Romanian repeat stations network data is presented as well. The analysis of long series of geomagnetic data from several observatories reveals the presence of longer period components, namely the 22 and 80-90 years cycles, also related to the solar activity, which might bias the secular variation model viewed as a linear variation of the main field coefficients between two successive 5-years epochs of IGRF and DGRF.

**GAV.05/08A/A11-006** **1050**

**MODELING OF HIGH-LATITUDE GEOMAGNETIC FIELD DISTURBANCES AT SATELLITE ALTITUDES FOR VARIOUS IMF CONDITIONS**

Vladimir PAPITASHVILI<sup>1</sup>, Freddy CHRISTIANSEN<sup>2</sup> (<sup>1</sup>SPRL, University of Michigan, <sup>2</sup>Danish Meteorological Institute)

We present a new model of high-latitude geomagnetic field disturbances generated by the varying 3-D system of field-aligned and ionospheric currents at satellite altitudes. This model is based on the high-precision magnetic field measurements made onboard of the Ørsted and CHAMP satellites in 1999-2002. The model is parameterized by the interplanetary magnetic field (IMF) strength and direction, as well as by the Earth's dipole tilt angle. Specific attention is paid to determining a set of geomagnetic variations during quiet conditions for different seasons; that is, when IMF nears zero. The latter allows us to better understand how the high-precision magnetic field surveys over high latitudes can be utilized for the main geomagnetic field modeling. We compare our 'disturbance' models for various IMF conditions and seasons with the actual satellite measurements to estimate how well our statistical patterns mimic observations along the orbits.

**GAV.05/08A/A11-007** **1110**

**MAIN AND LITHOSPHERIC FIELD MODELS FROM CHAMP VECTOR DATA**

Stefan MAUS<sup>1</sup>, Monika KORTE<sup>1</sup>, George BALASIS<sup>1</sup>, Hermann LUEHR<sup>1</sup>, Mioara MANDEA<sup>2</sup> (<sup>1</sup>GeoForschungsZentrum, <sup>2</sup>IPGP)

With its low orbit, long life time, high-resolution magnetometers, dual head star camera, and an almost 100% data coverage, CHAMP determines the geomagnetic field with an unprecedented resolution and accuracy. The lithospheric fields now resolvable to 500 km wavelength, corresponding to spherical harmonics of degree 80. We argue that further improvements now hinge on the prediction and subtraction of the weak but significant fields generated by ocean flow. CHAMP is also particularly suited for main field studies. Having 2 star camera heads pointing into different directions significantly reduce the inherent uncertainty in satellite attitude, in particular the errors in the rotation angle about the star camera bore sight. The standard calibration scheme applicable for spinning satellites fails for CHAMP due to its stable attitude in the presence of non-potential fields. However, we show that by making use of the orbit characteristics and modelling the non-potential fields, CHAMP's star camera orientation is well constrained. As inferred from the degree spectrum, the secular variation of our main field model from CHAMP-vector-only data is reliable to degree 11. We plan to further constrain the satellite derived secular variation back in time by including earlier CHAMP scalar and Ørsted measurements. The results are verified against data provided by Intermagnet observatories.

**GAV.05/08A/A11-008** **1130**

**GLOBAL MODELS OF THE LITHOSPHERIC MAGNETIC FIELD FROM SATELLITE DATA**

Kathryn A. WHALER<sup>1</sup>, Michael E. PURUCKER<sup>2</sup> (<sup>1</sup>School of GeoSciences, University of Edinburgh, <sup>2</sup>Geodynamics Branch, Goddard Space Flight Center)

Several satellite missions have now provided high quality 3-component magnetic measurements of the Earth's field from low altitude orbits. Careful data selection and subtraction of models representing external, main and induced field sources give estimates of the magnetic field due to lithospheric sources. Consistent images of the lithospheric field have emerged from the different missions. Consistency is easier to judge, and the results easier to interpret, if the data are reduced to common altitude or modelled in terms of lithospheric magnetisation. We present models of the lithospheric field downward continued to the Earth's surface and magnetisation models. Both types of model are calculated using a Green's function basis, and we regularise the solutions. The computational effort of solving a linear system of dimension many tens of thousands is eased by the matrices relating the data to the model parameters being sparse; we are therefore able to employ the conjugate gradient iterative scheme. The resulting maps retain the full resolution of the original data. Our magnetisation models include both induced and remanent magnetisation, with the division between the two determined by the regularisation constraint. The component

consistent with induced magnetisation agrees well with induced magnetisation models based on equivalent source models. Global maps of the downward continued field and lithospheric magnetisation will be presented, and their interpretation discussed.

**GAV.05/08A/A11-009** **1150**

**MIX AND MATCH, MULTIPLE SATELLITE DERIVED, GLOBAL AND AUSTRALIAN REGIONAL MAIN FIELD MODELS**

Jon TURNER, David IVERS, Denis WINCH (School of Mathematics and Statistics, University of Sydney)

Concurrent satellites, which are widely spaced in orbital radius, offer an opportunity to separate the internal and external potentials of the Earth's main field with greater accuracy than normally achievable with a single data source. However, satellite derived global models of the Earth's main field are a necessary compromise fulfilling a least squares or least modulus criterion with data containing various attitude inaccuracies. A more accurate model may be possible with the inclusion of data from quality ground-based observatories especially when the model is to be used to predict main field evolution over continental sized areas. CHAMP and Ørsted have had attitude determination problems and SAC-C appears to have little chance of yielding vector data. It is possible to use these data in conjunction with data from ground based observatories in a variety of ways, such as excluding certain data in rotation or weighting according to confidence levels, and then compare results both globally and over the greater Australian region. As a test of the accuracy of the satellite attitude solution, some of the vector data can be 'scalarised' and then 'equatorially biased' if some knowledge of the dip equator is available. If secular variation is of prime interest then models based on net changes from some defined epoch may be of greater reliability.

**GAV.05/08A/A11-010** **1210**

**TWO LONG BALLOON PROFILES ACROSS THE PACIFIC OCEAN AT AN ALTITUDE OF 30 KM**

Yves COHEN, Ali LATROUS (Institut de Physique du Globe de Paris)

Stratospheric balloons can be used to measure the Earth magnetic field, at an altitude between 20 and 30 km, bridging the gap between satellite, aeronomic and surface measurements. A 50 kg scientific payload gathering a proton magnetometer, a GPS receiver, and a worldwide transmission system allow a precise determination of the anomaly field. Infra-Red Montgolfiers developed by CNES, can carry such payload over thousands of kilometers between 25 and 30 km altitude. The obtained East-West profiles provide new informations that complement those obtained by the polar orbiting satellites. Two experiments of this kind were launched from South America, and crossed the Pacific ocean along the equator at a mean 27 km altitude. The anomaly field is tentatively extracted from these profiles by subtracting the values of the IGRF computed along the profiles, as well as an estimate of the external field. The two profiles are presented and shown to evidence very similar anomalies, thus demonstrating the capacity of this technique. Two anomalies situated along the profiles at the longitudes of 110 and 130° West are clearly evidenced for the first time. The geophysical signal thus detected is shown to bring new information that are tentatively interpreted and modeled.

**Tuesday, July 8 PM**  
Presiding Chairs: K. Whaler, I. Wardinski

**GAV.05/08P/A11-001** **1400**

**Invited** **1400**  
**GEOMAGNETIC REFERENCE FIELD MODELS: A GIVEN TOOL TO DESCRIBE THE MAIN FIELD**

Mioara MANDEA (Institut de Physique du Globe de Paris)

The Earth's magnetic field is used as a basis for navigation, surveying and mapping, mineral exploration, probing the Earth's crust and deep interior, and understanding solar-terrestrial relationships. Geomagnetic data, indices of activity, numerical field and secular-variation models and charts, advice and information for the geomagnetic field models are prepared by a variety of organizations and countries, all differing somewhat in the manner of processing and in the selection of data for the model fitting (data from surface observatories, from special surveys over land and sea, and from satellites). After an exacting study of the various national field models, a select committee (Working Group 8, Division V) of the International Association of Geomagnetism and Aeronomy agrees upon the best compromise Gauss coefficients for the recorded measurements of the magnetic field about the Earth. That committee fixes what is called the "International Geomagnetic Reference Field" (IGRF) for every five-year epoch since 1900. An estimate of the change-per-year for each coefficient allows projection of the model to later years. If any IGRF model is subsequently adjusted by agreement, the replacement is called the "Definitive Geomagnetic Reference Field" (DGRF). A presentation of the IGRF/DGRF models over the 20th century is given and a brief report on where and how these models have been used.

**GAV.05/08P/A11-002** **1430**

**BGS CANDIDATE MODELS FOR DGRF1995 AND DGRF2000 AND A SECULAR VARIATION MODEL FOR 2000.0 TO 2005.0**

Susan MACMILLAN, Vincent B.F. LESUR, Alan W.P. THOMSON (British Geological Survey)

The BGS DGRF candidate models for 1995.0 and 2000.0 and a revised constant secular variation model for 2000.0-2005.0 are presented and discussed. We describe the selection and weighting of input satellite and ground data and the model solution process used. Some comparisons with other models for the same epochs are also presented.

**GAV.05/08P/A11-003** **1445**

**DGRF CANDIDATES BASED ON OBSERVATIONS FROM OERSTED, CHAMP AND SAC-C**

Nils OLSEN<sup>1</sup>, Terence SABAKA<sup>2</sup> (<sup>1</sup>Danish Space Research Institute, <sup>2</sup>NASA GSFC, Geodynamics Branch)

The present high-precision geomagnetic missions Ørsted, CHAMP and Ørsted-2/SAC-C provide a unprecedented possibility to derive models of the Earth's magnetic field. We present a candidate for DGRF 2000 that has been derived entirely from satellite data, and candidates for DGRF 1995 and 2000 that are derived by a combination of satellite and observatory data and are extracted from the latest version of our Comprehensive Model. We also outline the procedure that we plan to use for deriving a candidate for IGRF 2005.



**GAV.05/08P/A11-004 1500**

**GEOMAGNETIC FIELD MODELS FOR EPOCHS 1995 AND 2000**

Aude CHAMBODUT<sup>1</sup>, Mioara MANDEA<sup>1</sup>, Benoit LANGLAIS<sup>2</sup> (<sup>1</sup>Laboratoire de Geomagnetisme, Institut de Physique du Globe de Paris, <sup>2</sup>NAS/NRC at GSFC/NASA, Geodynamics Branch, Greenbelt, Md, USA)

The recent call for revision of the IGRF/DGRF models for 1995 and 2000 epochs provides an excellent opportunity for studying the global and regional structure of the main geomagnetic field and of its secular variation. Available datasets consist of new, high-quality, satellite measurements, and of time series of the global magnetic observatory network. A 2000.0 main-field model (up to degree/order 13) and secular-variation one (up to degree/order 8) are derived using Ørsted vector and scalar data spanning twelve months centered on the considered epoch. In order to minimize the diurnal disturbances linked to the Sun, only satellite measurements made in the shadow region were kept. Then data were selected with respect to the geomagnetic indices:  $Kp(h) \leq 1+$ ;  $Kp(h \pm 3) \leq 2+$ ;  $|Dst| \leq 5$  nT and  $|dDst/dt| \leq 3$  nT/h. A series of secular-variation models from 1995 to 2000 is also computed using observatory data, weighted by a scheme based on their geographical distribution. These resulting models are presented, as well as their comparison with other models for the same epochs.

**GAV.05/08P/A11-005 1515**

**NEW INSIGHTS INTO THE SECULAR VARIATION BETWEEN MAGSAT AND CHAMP/ØRSTED**

Ingo WARDINSKI<sup>1</sup>, Richard HOLME<sup>2</sup> (<sup>1</sup>GFZ Potsdam Section 2.3, <sup>2</sup>Dept. of Earth Sciences, University of Liverpool)

Over the two decades between 1980 to 2000, the secular variation of the Earth's magnetic field demonstrates rich behavior, most obviously magnetic jerks in 1991 and around 2000. The 1991 jerk is most clearly seen in the  $dY/dt$  at European observatories, raising questions about the geographical extent of this feature and the processes which might cause it. In this study we developed models for the secular variation over this period. Our method is based on an approach proposed by Bloxham and Jackson (1992); a decomposition of the magnetic potential in spherical harmonics and expansion in time of its coefficients on a basis cubic B-Splines. The essential new feature of our method is the use of main field models as constraints for the field at the endpoints, 1980 and 2000. These models were derived from high-quality satellite vector data. For the intervening period our most useful data are secular variation estimates derived from magnetic observatory measurements. External variation is significant, but simple parameterization of this in terms of a uniform external field proves inadequate, we investigate ways of mitigating the effects of external fields on our model, particularly those from the ring current. Our resulting models are in good agreement with the models developed by Bloxham and Jackson for 1980 until 1990, but reveals more small-scale secular variation structure.

**GAV.05/08P/A11-006 1530**

**SPACE-TIME MODEL FOR OBTAINING CANDIDATE MODELS FOR DGRF 95, AND IGRF SV 00-05**

Vadim P. GOLOVKOV, Tatiana N. BONDAR, Svetlana V. YAKOVLEVA (IZMIRAN)

Using DGRF 80 and Olsen's model of the field and SV for 2000.0 a parabolic model of the main field change in the span between satellite epochs. Comparing modeled and observed in magnetic observatories data an unsatisfaction of this model was shown. A space-time model obtained by use data from observatories better describes field changes over regions of a good density of observatories. Expansion of observatory time series in natural orthogonal components has shown that the reason of this phenomenon is a jerk about 1991. To avoid the false anomaly formation due to uneven distribution of observatories on the Earth's surface the space-time model was improved with adding a number of "artificial" observatories in South Pacific with values, obtained from the satellite parabolic model. This improved model allows calculation of the 1991 yr model. Taking into account the very high stability of the geomagnetic acceleration between the jerk epochs, new parabolic model was designed, using the field models of 1991 yr and Olsen's ones of 2000, including SV of Olsen's model. These parabolic models were used to obtain candidate models of DGRF 1995.0 and IDRF SV 2000.0-2005.0.

**GAV.05/08P/A11-007 1620**

**MODELING THE GEOMAGNETIC SECULAR VARIATION FIELD FOR A TERRITORY WITH A LONG AND IRREGULAR FORM AS VIETNAM**

Ha Duyen CHAU<sup>1</sup>, Nguyen Thi KIM THOA<sup>1</sup>, Jean-Louis LE MOUËL<sup>2</sup>, Armand GALDEANO<sup>2</sup> (<sup>1</sup>Department of Geomagnetism, Hanoi Institute of Geophysics, <sup>2</sup>Paris Institute of Physics of the Earth)

The construction of a geomagnetic secular variation model from the Vietnam magnetic repeat stations network meets a difficulties due to the irregular geometry of the territory; the shape of this territory looks indeed like an elongated "S" oriented in the North-South direction. Geomagnetic secular variation charts for magnetic elements D, I, H, X, Y, Z, T have been constructed from the 56 repeat stations of the Vietnamese network. At each station, the absolute measurements of the geomagnetic field are made in 1991 and 1997. The used method is based on an analytic approximation (a second degree polynomial) of the real magnetic secular variation field. The computation is based on the values from different number of secular variation stations, sparsely distributed all over the territory of Vietnam, and in addition, on some weighted values of IGRF 1995 outside the territory of Vietnam. One discusses this technique and infer some criteria to take into account the minimum number of added IGRF values. The characteristics of the magnetic secular variation field were shown for 4 elements T, X, Y, Z. The secular variation of the total magnetic field and of its components in Vietnam vary in the following ranges:  $20 \text{ nT/year} < \text{or} = dT/dt < \text{or} = 33 \text{ nT/year}$ ;  $-9 \text{ nT/year} < \text{or} = dX/dt < \text{or} = 14 \text{ nT/year}$ ;  $0 \text{ nT/year} < \text{or} = dY/dt < \text{or} = 28 \text{ nT/year}$ ;  $60 \text{ nT/year} < \text{or} = dZ/dt < \text{or} = 76 \text{ nT/year}$ .

**GAV.05/08P/A11-008 1640**

**ØRSTED/CHAMP-BASED SPHERICAL CAP MODEL FOR SOUTHERN AFRICA**

Pieter Benjamin KOTZE (Hermanus Magnetic Observatory, South Africa)

Vector magnetic field measurements by both the Ørsted and CHAMP satellites have been employed to derive a Spherical Cap Harmonic geomagnetic field model for the southern African region between 10° and 45° South in latitude and between 10° and 45° East in longitude. In the process only data obtained during geomagnetic quiet conditions ( $|Dst| \leq 10$ ) were selected for modeling purposes, enabling us to derive a field model with minimum

wavelength resolution approximately 1200 km. This model is compared with other global magnetic field models in terms of a fit to observatory and repeat station data over the southern African subcontinent where the Hermanus Magnetic Observatory conducts field surveys at regular intervals. In addition, this model will also be compared to other Spherical Cap models based on only Ørsted vector data and POGS scalar data respectively. The inclusion of ground magnetic field data will be discussed when deriving a regional magnetic field model, especially towards the borders of the cap where such a model is most sensitive to the lack of ground data.

**GAV.05/08P/A11-009 1700**

**SPHERICAL CAP HARMONIC ANALYSIS REVISITED**

Erwan THEBAULT<sup>1</sup>, Jean-Jacques SCHOTT<sup>1</sup>, Mioara MANDEA<sup>2</sup> (<sup>1</sup>Ecole et Observatoire des Sciences de la Terre, Strasbourg, France, <sup>2</sup>Institut de Physique du Globe de Paris)

Spherical Cap Harmonic modelling is an attractive regional modelling of the geomagnetic field, widely used since the pioneer work of Haines (1985). It should offer many of the properties of the global Spherical Harmonic Analysis, particularly a straightforward upper continuation allowing to incorporate easily satellite data in the modelling. Yet, it may be shown that the bases proposed by Haines are hampered by the following drawbacks: actually they are not suitable for upper continuation; they lead to relationship between global and local Gauss coefficients dependent on the radial distance. Yet, the calculation of such relations would be useful for estimating prior covariance for the local Gauss coefficients and, hence, would be helpful in the inverse problem consisting of estimating local Gauss coefficients from a set of data. Setting the problem as a Boundary Value Problem on a domain defined by the intersection of a cone and two spheres, and splitting it up into two sub-problems with simpler boundary conditions, we propose a new set of two bases which solves the difficulties mentioned above. One of them is one of the bases proposed by Haines, but the second one contains so-called conical or Mehler functions, with complex degrees. The decomposition of the initial problem is not unique, but it can be demonstrated that among all possibilities, there are only two which lead to the build up of two mutually orthogonal bases. Beside these theoretical aspects, numerical difficulties had to be solved in order to be able to compute accurately the generalized Legendre functions up to large degrees and order. The algorithm of Over and Smith has been incorporated into our routine for this purpose. The effectiveness of this formalism and numerical implementation may be shown by an accurate reconstruction of the main field on the conical domain, either using the main field as boundary condition or by the computation of the local Gauss coefficients from a set of main field data distributed on a regular three-dimensional grid. We will show also an application to the regional secular variation modelling on a small cap covering the French territory.

**GAV.05/08P/A11-010 1720**

**POLAR LITHOSPHERIC FIELD FROM MULTIPLE SATELLITE OBSERVATIONS**

Benoit LANGLAIS<sup>1</sup>, Michael PURUCKER<sup>2</sup>, Susanne VANNERSTRØM<sup>3</sup> (<sup>1</sup>NAS/NRC at NASA/GSFC, <sup>2</sup>Raytheon ITSS at NASA/GSFC, <sup>3</sup>Danish Space Research Institute)

Mapping the magnetic field of lithospheric origin is a key to better understanding the properties of the oceanic and/or continental lithosphere. Models are usually based on local, airborne surveys, or on satellite datasets. The first kind of data doesn't allow large scale anomalies to be well modeled. The second one usually relied on the scalar measurements of the POGO series, or on the short time mission MAGSAT. The launches of Ørsted (Feb. 1999), CHAMP (Jul. 2000) and SAC-C (Nov. 2000) gave a new opportunity for studying the magnetic field of the Earth from the satellite perspective. This mini-constellation, which can be considered as a small satellite observatory network, provides for the first time multiple, simultaneous field measurements at satellite altitude. Of particular interest is the data density above the North and South pole areas of the Earth. In this study, we use the equivalent dipole source method to model the lithospheric field over polar ( $\pm 60^\circ$ ) areas. We use multiple step approach. First, data are selected globally, with respect to the local time and external magnetic perturbations. Spherical harmonic (SH) models are built, using short-time data subsets. The core contributions are then removed from the measurements. The computed residuals are carefully selected, in order to remove as much external perturbations as possible. Because only the total intensity enters the SH model, it is possible to use the average of the component perpendicular to the main field direction to determine the quiet intervals. The sorted residuals are then used to infer the susceptibility of field-aligned dipoles located in the lithosphere. The modeled dipoles are finally used to predict the magnetic field of lithospheric origin at a constant altitude. A comparison with other studies is shown. A discussion with respect to the season (winter or summer) is presented, as well as a comparison between the North and South pole areas.

**GAV.05/08P/A11-011 1740**

**IMPROVEMENT OF THE ANTARCTIC GEOMAGNETIC REFERENCE MODEL BY USING NEW SETS OF DATA**

Luis R. GAYA-PIQUE<sup>1</sup>, Angelo DE SANTIS<sup>2</sup>, Joan Miquel TORTA<sup>3</sup> (<sup>1</sup>Istituto Nazionale di Geofisica e Vulcanologia, Rome, Italy / Observatori de l'Ebre, Roquetes, Spain, <sup>2</sup>Istituto Nazionale di Geofisica e Vulcanologia, Rome, Italy / Earth Science Department, G. D'Annunzio University, Chieti, Italy, <sup>3</sup>Observatori de l'Ebre, Roquetes, Spain)

The first Antarctic geomagnetic Reference Model (ARM) was published in 2002. This model was intended as an alternative to global models like IGRF to give account of the geomagnetic main field south of 60° South latitude, with the main practical purpose of reducing magnetic survey data obtained from 1960 onwards to a common epoch. The first version of the model was developed using observatory annual means and a selected but reduced set of Ørsted satellite data. In this work we use new sets of data to improve the quality of the model. Data coming from Pogo, Magsat, and Champ satellite missions are used, as well as a larger set of Ørsted measurements. A suitable selection of all these data was performed to minimize the effect of external fields. On the other hand, the updating of the observatory database and the inclusion of data coming from a stratospheric balloon platform, contributed to a better representation of the field measured near the Earth's surface.

**GAV.05-Posters**

**MODELING THE EARTH'S MAGNETIC FIELD ON GLOBAL AND REGIONAL SCALES (SEDI)**

Location: Site D

**GAV.05/09P/D-001** Poster **1400-145**

**A NEW THEORY ON THE EARTH'S MAGNETIC FIELD**

Eugene D. RICHARD<sup>1</sup> (<sup>1</sup>American Geophysical Union, Sigma Xi, <sup>2</sup>Sigmz Xi)

With the use of basic principals of electricity and magnetism, a new approach to the theory of the earth's magnetic field is given; this approach also lends itself to a new theory on the earth's magnetic reversals. This approach has been tested by the author by construction of a magnetic model which helped in the final approach to the theory presented. A mathematical model was derived from this model that yields six parameters which are described in the paper. A two and a three dimensional computer model are available and can be seen on the web site {www.earthsgeomotor.com or www.earths-magnetic-field-and-how-it-reverses-and-more.com}. For reversals, relativity was introduced and utilized to show that reversals were cyclic and controlled by the interior heat of the earth. In addition, the cycle from normal to reverse shown in the computer models were all equal in time, however in the earth where the internal heat of the earth is being altered by volcanoes, hot spots, and oceanic ridges the aborted reversals, short time between reversals, and delayed reversals could be explained. In conclusion, both of the above web sites have a free E-Book available which goes into the theory in detail and shows that the theory described is simple, complete, and has no reference to someone in the past, only well known laws of electricity and magnetism.

**GAV.05/09P/D-002** Poster **1400-146**

**NORTH MAGNETIC POLE MOTION: JERK OR REVERSAL?**

Vladimir V. KUZNETSOV

The velocity of drift of North magnetic pole has increased about five times through the last 20 - 30 years. What is a reason of this phenomenon: is it a usual cyclic process causing a stop of a pole in 2140, or the effect of Jerk-69, or is it a start of the geomagnetic field reversal? Since 1860 modern magnetic poles, as North, and South, are drifting towards each other along the paths peculiar to the drift of virtual magnetic poles through the reversal. The possible reasons of the phenomenon of poles acceleration are discussed. It is shown, that the measurements of the North magnetic pole location carried out during the nearest 3-5 years, would help to answer this question.

**GAV.05/09P/D-003** Poster **1400-147**

**TRACING BACK THE MAGNETIC JERK OF 1991 TO THE CORE-MANTLE BOUNDARY BY NUMERICAL EXPERIMENTS**

Ludwig BALLANI<sup>1</sup>, Dietrich STROMEYER<sup>2</sup>, Ingo WARDINSKI<sup>1</sup>, Hans GREINER-MAI<sup>1</sup> (<sup>1</sup>Dept. Geodesy and Remote Sensing, GFZ Potsdam, <sup>2</sup>Dept. Geoenineering, GFZ Potsdam, <sup>3</sup>GFZ Potsdam, Section 2.3)

New global magnetic data (Gauss coefficients up to degree and order 13 from 1980 to 2000) are processed with a recent non-harmonic downward continuation method. It solves the related inverse boundary value problem by approximating the solution (e.g. at the core-mantle boundary) of an equivalent Volterra integral equation with finite-dimensional minimum-norm solution. In an extended version the magnetic field components in the top layer of the fluid outer core can be determined if fluid velocities of special type are prescribed. Using a weakly conducting mantle and the high conducting fluid in the outer core we investigate the temporal structure of the jerk in 1991 calculating different field components in dependency of the depth beneath the core-mantle boundary (up to 100km) and for some types of assumed velocities.

**GAV.05/09P/D-004** Poster **1400-148**

**MODELLING THE EARTH'S MAGNETIC FIELD USING WAVELETS FRAMES**

Aude CHAMBODUT<sup>1</sup>, Mioara MANDEA<sup>1</sup>, Matthias HOLSCHNEIDER<sup>2</sup> (<sup>1</sup>Laboratoire de Geomagnetisme, Institut de Physique du Globe de Paris, <sup>2</sup>Universitat Potsdam, Applied and Industrial Mathematics, Potsdam, Germany)

Wavelets analysis has proven to be a powerful tool for numerical studies and signal processing. The use of a frame of wavelets to model the geomagnetic field, allows us to take advantage of the flexibility of frames (as opposed to the rigidity of orthonormal bases) and the localization properties of wavelets. Firstly, we describe a simple technique for constructing wavelets on the sphere with properties which are useful for applications in geomagnetism. Here we discuss how to optimize the choice of the wavelets basis, with special regard to the choice of the evolution of scales, the number of wavelets, etc. To illustrate the completeness of the wavelet frame we show how well the wavelets are able to reproduce the spherical harmonics. Once shown the potential of wavelets, we apply this technique to describe the geomagnetic field at global and regional scale. Finally, we report on some field models obtained when observatories or satellite data are used, and we conclude with discussions and future work.

**GAV.05/09P/D-005** Poster **1400-149**

**ANALYSIS OF THE REGIONAL MAGNETIC FIELD AND ITS SECULAR VARIATIONS OVER THE ROMANIAN TERRITORY**

Ligia-Narciza E. ATANASIU<sup>1</sup>, Mioara MANDEA<sup>2</sup> (<sup>1</sup>INSTITUTE OF GEODYNAMICS, 19-21 Jean-Louis Calderon St., Bucharest-37, Romania R-70201, <sup>2</sup>INSTITUT DE PHYSIQUE DU GLOBE DE PARIS, 4 Place Jussieu, 75252 Paris cedex 05, France)

Many geological features of the Earth's lithosphere create variation in the Earth's magnetic field that can be detected by satellites. The resulting magnetic anomaly maps can provide new insights into the tectonic features and broad structure of the lithosphere. By the combined analysis of data provide by satellite missions (Orsted, Champ), ground data and aeromagnetic data we created a database and we were able to calculate the components of the magnetic field (Declination-D, inclination-I, vertical intensity-Z, horizontal intensity-H, total intensity field-F) over the southeastern European territory (especially over the Romanian territory). We calculated all the components of the magnetic field at different epochs. We think that is very interesting because the possibility to study the evolution of the magnetic field in time and space. Taking into consideration that the Romanian territory is a very important part of the alpine-carpato-hymalaian belt we hope that the resulted data set may considerably improve to the knowledge on the tectonics and geodynamics of the southeast European zone and Romanian territory.

**GAV.05/09P/D-006** Poster **1400-150**

**REGIONAL MODEL OF THE GEOMAGNETIC ANNUAL CHANGES IN AND AROUND JAPAN ISLAND BASED ON NOC AND SCH ANALYSIS**

Mitsuru UTSUGI<sup>1</sup>, Hiroki SHIRAI<sup>1</sup>, Hideo HAMASAKI<sup>1</sup>, Teruaki NISHIKI<sup>1</sup>, Satoshi FUJIWARA<sup>2</sup> (<sup>1</sup>First Geodetic Div., Geodetic Dep., Geographical Survey Institute, <sup>2</sup>Ministry of Land, Infrastructure and Transport)

In G.S.I. (Geographical Survey Institute of Japan), continuous geomagnetic observation and repeat survey (we call it as the first class magnetic survey) were conducted from early 1950's. From these data, reference values of intensity and direction of the magnetic field in and around Japan Island was estimated, and these information were published in every 10 years (1980, 1990 and 2000). To extract more accurate information about the magnetic field distribution and annual change from the observed data, we started to consider the construction of the geomagnetic spatial-temporal model for the area of Japan Island and, partially, surrounding seas. Inside the Japan area, there are many geomagnetic stations continuously observing the geomagnetic field. For example, our institute has 2 observatories and 13 magnetic stations which observe the geomagnetic 3 components and total force, or only total force, continuously. So that, we configured the goal of our study to establish the scheme to construct the regional 3 components magnetic models using only the continuously observed magnetic data set which consists of X, Y, Z and F time series. For this purpose, we tried to combine the technique of NOC and SCH (Spherical Cap Harmonic) analysis. This is because, to use the total force data, it might be the very easy way to apply the potential analysis method. To estimate the expressivity and clarify some problems come up with practical use of NOC + SCHA method, we treated the IGRF synthesize time series (period 1990-2001 and time spacing is 0.25 year) as the input data. The magnetic stations that we assumed were 34 points (in 16 points, 4 components (X, Y, Z and F), and in 18 points, only total force data were given). The locations of each station are identical with that of the actual geomagnetic stations. Using NOC + SCHA (colatitudes of half angle of the spherical cap is 45 degree and maximum degree of Gauss coefficients is 4), we can explain the input data with accuracy of 2-3 percent of input data and this accuracy will be suitable for our purpose. Now, we are trying to construct the monthly 3 component model using continuously observed geomagnetic data in the period of 1996 to 2002. In our presentation, we will discuss about the expressivity and accuracy of our model.

**GAV.05/09P/D-007** Poster **1400-151**

**RAPID CHANGE OF THE GEOMAGNETIC SECULAR VARIATION FIELD AS REVEALED BY THE FIRST ORDER MAGNETIC SURVEY OF JAPAN**

Hideo SAKAI<sup>1</sup>, Naokatsu SUZUKI<sup>1</sup>, Toru YAMAGUCHI<sup>1</sup>, Hiroo MIZUNO<sup>2</sup> (<sup>1</sup>Department of Earth Science, Toyama University, <sup>2</sup>Pasco Co. Ltd., <sup>3</sup>Graduate School of Science and Engineering, Toyama University, <sup>4</sup>Department of Education, Kagawa University, ret.)

Annual change distributions of the geomagnetic three components X, Y and Z have been compiled at discrete two-year epochs on the basis of available results from the first order magnetic survey of Japan, and annual mean values from observatories as well. The annual change distributions and their temporal changes have been examined from various angles in order to offer evidence that they are of internal origin. In the early 1980's, an abrupt change in the annual rate of secular variation in the Y component was observed in western Japan. This event has been associated with a rapid and remarkable change in the trend of isopors. Along with this Y event, the annual rate of change in the Z component showed an appreciable increase over the previous epochs reaching more than 20nT/year. These changes observed in Japan are confirmed by comparing the secular variation fields from IGRF 1980 and 1985. A remarkable difference in the fields between these epochs can be seen in the Far East. The difference in the trend of isopors for the Y component is quite similar to that obtained from the surveys. Every isopor from IGRF 1980 intersects every isopor from IGRF 1985 nearly at right angles. Although the land of Japan is limited, still the progressive change of annual change distribution with time can be investigated by using observations repeated many times at more than fifty magnetic stations. The secular variation field over the entire surface of the earth can be reproduced by a set of changing radial dipoles on the surface of the core. Mizuno(1984) showed that an abrupt changes in Y and Z annual changes observed in Japan in the early 1970's could be attributed to the development of dipoles forming a line which was thought to have rapidly progressed from India through east China to Japan sea. These dipoles are directed radially inwards(positive dipoles). The same method has been applied to the event in the 1980's. Sets of core surface radial dipoles responsible for IGRF 1980 and 1985 secular variation fields have been derived. Comparison of these dipole distributions in and around Japan shows that the dipoles described above increased their strength and extended to the pacific side. This change in the distribution and strength of dipoles provides a possible explanation of the change in the annual change distributions in the 1980's. The time scale of the redistribution of dipoles must be very short. The change in the dipole distribution is episodic. A comparatively stable state with gradual changes continues for years, which is succeeded by an abrupt change. This is the character of the jerk. The jerk has been regarded as a global event. However, the consideration given here strongly suggests that it must be regional. Mizuno, H., rapid and episodic variation of the geomagnetic secular variation field., Bull. Geograph. Surv. Inst., Vol.29, No.1, p1-102, 1984.

**GAV.05/09P/D-008** Poster **1400-152**

**NATIONAL RESEARCH INSTITUTE OF ASTRONOMY AND GEOPHYSICS, HELWAN EGYPT**

Deebes Hanafy ALY, Ahmed F. M, EL. saed M., Arafa T. (National Research Institute of Astronomy and Geophysics)

A new geomagnetic survey during a period of two years (2000- 2001) was performed to cover Egypt satic factory . Using a proton magnetometer, the total intensity (F) of the Earth's magnetic field were measured in 2000 sites of third order, along profiles of total length 5 200 K.m. About quarter of those occupied in previous surveys were reoccupied to produce the secular variations . Reduction to epoch 2000.0 was done. The field data was used to produce 4 charts: a) the total intensity (F) chart of the Earth's magnetic field in n.T. over the surface of Egypt, b) the isoporic chart using the available old data, c) the Egyptian Geomagnetic Reference Field (EGRF) chart to the epoch 2000.0 .This chart is obtained, using computer, to produce both the observed data and the EGRF2000.0 every 1/4 degrees.

**GAV.05/09P/D-009** Poster **1400-153**

**LONG-WAVELENGTH OF GRAVITY AND MAGNETIC FIELDS WHILE THE STUDY OF THE URALS DEEP STRUCTURE**

Vsevolod SHAPIRO, Faina NIKONOVA (Institute of Geophysics)

The Ural mountains preserve a late Paleozoic collision that forms a 2500 kmsuture in the world's largest landmass, Eurasia. Several features of the mountain belt are atypical when



compared with other Paleozoic orogens such as Appalachians, Caledonides and Variscides. The problem of regional field extraction is of undoubted importance for the interpretation of gravity and magnetic data on long (1000 km and longer) profiles, aimed at the construction of density magnetic sections throughout the entire thickness of the crust. This problem became particularly significant in the last years when a complex of geophysical data became available from long geotraverses such as Granit, Rubin, Quarts and others. A special investigation of potential field in the region was fulfilled for establishing the relationship between the Urals and the East European, Siberian and Kazakhstan Cratons. The regional components of gravity and magnetic field bearing information on deep structure of the orogen were analyzed. The gravitational data was investigated for several sufficiently long (1000 km and more) E-W profiles crossing the South, Central and North Urals. The new technique was used for the extracting of the regional component of the gravitational field. The main feature of the revealed regional component is the appreciable low over the main Urals structures as compared with the adjacent platforms. The extent of the negative anomaly in the regional gravity field is of the order of 400-500 km, with the maximum amplitude about -30 mGal. This fact is particularly interesting, if one takes into account that the absolute gravity maximum is confined to the Urals structures. The special survey of long, multi-altitude aeromagnetic traverses across the Urals designed to ensure that the long-wavelength component of the magnetic field was properly sampled. The survey was flown in 1980-1988 in area between 52-68°N and 52-72°E. Seven E-W traverses, each 1000-1200 km long, and two meridional traverses were flown. After subtraction of the reference field, an anomalous field is left which contains only those wavelengths that are larger than about 1000 km. The main result of study is revealing the regional negative magnetic anomaly with the size about 300 km and amplitude about 150-250 nT, which spatially coincides with the negative anomaly in gravity field. Along each profile, the inversion results indicate a major depression of the magnetic basement beneath the Uralide orogen. The interpretation is that the contrast in between magnetic crystalline basement (of the East European Craton to the west and the Siberian Craton and Kazakhstan microcontinent to the east) and the intervening terranes, which appear to have significantly lower average magnetization. The mentioned gravity maximum is in reasonable agreement with location of number of very intensive local magnetic anomalies produced by well-known Uralian magnetite bodies. It appears that checking in space of negative gravity anomalies with less magnetic zone is in part composed of thick sequence of Riphean rocks which may have been accreted against the margin of the East European Craton in pre-Uralian times.

**GAV.06-Posters**  
**MODERN MAGNETIC SURVEYS FOR REGIONAL TECTONICS, GEOHAZARDS AND ENVIRONMENTAL INVESTIGATIONS**  
 Location: Site D

Wednesday, July 9 PM

**GAV.06/09P/D-001** Poster **1400-154**  
**GEOPHYSICAL SIGNATURE ON THE SUBSURFACE STRUCTURE OF THE AEOLIAN ISLANDS, ITALY**

Shigeo OKUMA<sup>1</sup>, Tadashi NAKATSUKA<sup>1</sup>, Mitsuhiro SUGIHARA<sup>1</sup>, Masao KOMAZAWA<sup>1</sup>, Shun NAKANO<sup>2</sup>, Ryuta FURUKAWA<sup>3</sup>, John Joseph ELENJIPARAMPIL<sup>2</sup>, Robert SUPPER<sup>4</sup>, Massimo CHIAPPINI<sup>5</sup> (<sup>1</sup>Geological Survey of Japan, AIST, <sup>2</sup>Adelaide University, <sup>3</sup>Geological Survey of Austria, <sup>4</sup>Istituto Nazionale di Geofisica e Vulcanologia)

We, under an international cooperation, have conducted various geophysical surveys to better understand the dynamics of volcanic activities of the Aeolian Islands, which are located between the southern tip of the Italian Peninsula and Sicily Island. Supper et al. (2001) conducted an aerogeophysical survey such as magnetics, VLF and gamma ray in 1999, which were supplemented by detailed ground geophysical measurements such as geoelectric and magnetic surveys to investigate the physical structure of Vulcano and Lipari Islands. They compiled a high-resolution aeromagnetic map and conducted a temporal magnetic modeling, suggesting subsurface intrusions beneath the older volcanic outcrops on the west coast of Vulcano. They also compared the data with the older regional data by AGIP (Barberi, 1994) and showed a difference during the 15 years period. Sugihara et al. (2002) conducted gravity measurements of around 400 points on Vulcano in 2000 with a positioning by a differential GPS, particularly along with the profile lines of geoelectric and ground magnetic surveys by Supper et al. (2001) and compiled a detailed gravity map with denser station spacing than previous studies (Bonasia et al., 1973; Iacobucci et al., 1977; Barberi et al., 1994). They discussed a relationship between geothermal activity and gravity anomalies on the island. They also found a local gravity high inside the Fossa crater and modeled a denser rectangular prism beneath the crater, implying the existence of the self-sealed volcanic rocks under which geothermal fluids circulate. Komazawa et al. (2002) added more gravity stations on Vulcano and Lipari in 2001 to recompile a gravity map of the area. The Bouguer anomaly map with an assumed density of 1.8 kg/m<sup>3</sup> indicates gravity highs on the southern half of Vulcano called Piano, corresponding to a lava lake suggested by geologic studies. We have had an additional aerogeophysical survey, mainly magnetics this time, in early November 2002 in spite of an eruption of Mt. Etna on Sicily. The survey was flown with a real-time differential GPS on the same line of the 1999 survey for the Vulcano-Lipari area and also extended the survey northeastward up to Stromboli Island, which is continuing periodical eruptions. The comparison between the magnetic anomalies of 1999 and 2002 surveys can be conducted on the common surface, which the anomalies are reduced onto by a mathematical calculation. The geophysical signature on the subsurface structure of the Aeolian Islands and the results of a magnetic comparison by our method will be discussed.

**GAV.06/09P/D-002** Poster **1400-155**  
**CONSISTENT GEOMAGNETIC IMAGES OVER THE SW MARGIN OF THE EAST EUROPEAN PLATE**

Lucian BESUTIU<sup>1</sup>, Mikhail I. ORLYUK<sup>2</sup>, Inna K. PASHKEVICH<sup>3</sup>, Georgeta BESUTIU<sup>3</sup>, Svetlana V. ELISEEVA<sup>4</sup>, Vasile NEAGA<sup>4</sup>, Andriy A. ROMENETS<sup>5</sup> (<sup>1</sup>Sabba S. Stefanescu Institute of Geodynamics of the Romanian Academy, <sup>2</sup>Institute of Geophysics NAS of Ukraine, <sup>3</sup>Geological Institute of Romania, <sup>4</sup>Institute of Geophysics and Geology NAS of Moldova)

Joining regional geophysical images crossover the state border has become a practice during the last years in an attempt to solve large scale tectonic problems. Eastern Romania, Republic of Moldova and SW Ukraine represent the area where East European Plate (EEP), Scythian Plate, Moesian Plate, Carpathian Alpine Orogen, and North Dobrogea folded zone met each other. The examination and understanding of their junctions is rather difficult to make because the almost part of the bedrock in the area is hidden by the thick Neogene to Quaternary post-tectonic cover. Magnetics represents an appropriate tool for investigating

such areas, but previously obtained geomagnetic information within each national territory has its individual peculiarities: instruments and methodology used for data acquisition and processing, survey epoch, geomagnetic datum, reference field, etc. Therefore, trying to construct common geomagnetic images cross over the borders, large discrepancies were found. UKROMM project represents a joint venture of several scientific organizations from Romania, Ukraine and Republic of Moldova mainly aimed to overcome such difficulties and join airborne magnetic maps of the three countries covering the SW margin of EEP. As a first step, some pilot-maps have been constructed for the low Danube region (MAGLONAN sub-project) in an attempt to solve various problems that occur during such a complex research. After completing the pilot-stage, research extended to the area of the SW margin of EEP. The paper is aimed to the achievement of several crossover the state border consistent geomagnetic images, as a result of UKROMM project. Integrating the national geomagnetic standards was one of the main tasks within the project. Common observations were made at the geomagnetic observatories Surlari (Romania), Stepanovka (Ukraine) in order to compare their datum, and particular studies were devoted to the secular variation (SV) evolution on the national territories of the three countries. A special geomagnetic reference network covering the study area was designed and achieved in order to remove SV effects from the previously achieved data. Additional ground observations were also added in order to fill up some gaps within the former Ukrainian airborne maps. Finally, a computer database for both topography and geomagnetic information on the study area was designed and achieved, and data were brought at the same datum. The accuracy of the joining operation was checked up by constructing a map of the horizontal gradient of the geomagnetic field, which is very sensitive to the presence of any data inconsistency, but no discontinuity was revealed along the state border zones. Based on thus achieved data, several consistent geomagnetic images were constructed for the area by using various reference fields in order to separate regional/local effects and emphasize some tectonic features. Brief preliminary geological considerations are also made.

**GAV.06/09P/D-003** Poster **1400-156**  
**PRELIMINARY INTERPRETATION OF THE MAGNETIC ANOMALIES OF THE EASTERN VIETNAM SEA AND RECENT REGIONS**

Hung Viet LUU, Minh Huy LE (Hanoi Institute of Geophysics, NCST of Vietnam)

In this paper we showed that with appropriate choice of the noise-signal ratio, the reduction to the pole at low latitude based on a Wiener filtering approach of Hassen and Pawlowski could be applied on the magnetic equator. Using this reduced-to-the-pole method, we have found that the geological boundaries determined from the reduced-to-the-pole magnetic anomalies of the Eastern Vietnam sea and recent regions (from the magnetic anomaly map of East Asia published by Geological Survey of Japan and Committee for co-ordination of joint prospecting for mineral in Asian offshore areas) correlate remarkably well with the major geological features, including major faults, seafloor spreading segments, volcanic or intrusive blocks... These results could be considered as very important informations to reconstruct the tectonic history of the region.

**GAV.06/09P/D-004** Poster **1400-157**  
**TIME CHANGES OF GEOMAGNETIC TRANSFER FUNCTIONS AT LUNPING, TAIWAN RELATED TO EARTHQUAKE OCCURRENCES**

Kuang-Jung CHEN (Department of Earth Sciences, National Taiwan Normal University)

Time change of the transfer functions for short-period geomagnetic variations at Lunping, Taiwan, Geomagnetic Observatory is examined in association with earthquake occurrences near Lunping from 1988 to 2000. Using the geomagnetic data with a sampling interval of one minute, traditional transfer functions for the frequencies from 0.1 to 10 cycles/hour are calculated day by day. The method of analysis is based on the power spectrum analysis as developed by Everett and Hyndman. Monthly means are statistically obtained from these daily values of transfer functions. Small fluctuations are likely to be accounted for by seasonal changes probably originating in the external magnetic disturbance. All the transfer functions show the significant anomalous frequencies at 2, 3, 4, and 6 cycles/hour. Some remarkable changes of transfer function Au, possibly related to the earthquakes which occurred near the Lunping Observatory are found.

**GAV.06/09P/D-005** Poster **1400-158**  
**COMPREHENSIVE MAPPING THROUGH THE DATABASE OF AEROMAGNETIC ANOMALIES OVER JAPAN**

Tadashi NAKATSUKA, Shigeo OKUMA, Rie MORIJI, Masahiko MAKINO (Geological Survey of Japan, AIST)

Aeromagnetic survey data have been accumulated over the Japanese islands. Aeromagnetic area survey was initiated in the Geological Survey of Japan (GSJ) by Dr. J. Suyama and colleagues in 1964. The activity of this area survey was mainly aimed at the evaluation of petroleum potential in continental shelf regions. In 1981-1983, the New Energy Development Organization (NEDO), Japan, had a large project of aeromagnetic surveys (so-called Curie Point Surveys) of inland parts. The data from two organizations above have enough coverage over the Japanese main land and surrounding sea areas. The data from surveys by GSJ are stored in files with three types of unified formats. Those from NEDO surveys were also recovered from magnetic-tape archives into another two types of formats. There was a problem that the discontinuity exists between IGRF residual maps of adjacent areas surveyed at different epochs. However, it is proven that this discontinuity can be mitigated by adopting the DGRF model, instead of tentative IGRF model, as a reference base, because the tentative model sometimes fails to predict the secular variation of the geomagnetic field. The aeromagnetic anomaly data are attributed to the geographic position, which is based upon a specific geodetic datum. In Japan, regulations on the geodetic system was revised in 2001, and the formal geodetic datum today is same as the global standard WGS (ITRF), while the old datum (Tokyo Datum) is still used widely. The difference between the two amounts to 500m of the apparent dislocation. We should therefore be careful that the data in different geodetic system are not confused. Former work on the compilation of similar data were done by Makino et al. (1992) to publish the "Magnetic map of the Japanese Islands", in which the upward continuation filtering was applied, and a linear trend was further removed in each survey area. Now the data manipulations of such filtering are easily realized in the database, and also some kind of inversion softwares are going to be implemented in the system.

**GAV.06/09P/D-006** Poster **1400-159**  
**DIGITAL COMPILATION OF MAGNETIC ANOMALY MAP OF THE NORTH PACIFIC OCEAN**

Takemi ISHIHARA (Geological Survey of Japan, AIST)

A new magnetic anomaly map of the Pacific Ocean east of 140 E of the northern hemisphere

was compiled. Marine magnetic data, which were collected by various research cruises and are available from the U.S. NGDC were utilized in this compilation. Bad navigation data were first edited: if anomalous ship's velocities were obtained by calculation from neighbouring navigation and date/time data, the navigation and date/time data were checked. Then magnetic anomaly values were recalculated using DGRF reference fields. If absolute values of the obtained anomalies > 5000 nT, they were removed. After these editing procedures, data biases for each tracklines were adjusted to minimize the cross-over errors, and a gridded data set was generated. The data coverage is still scarce except near Hawaiian Islands, Japan, Aleutian Islands, and the west coast of North and Central Americas. However, lineated anomalies due to past seafloor spreading are clearly visible in the compiled map, and the amplitudes of anomalies generally increase northwards.

**GAV.06/09P/D-007** Poster **1400-160**

**COMPARATIVE AEROMAGNETIC STUDY OF SEISMIC HAZARDS IN TWO PACIFIC RIM FOREARC BASIN SETTINGS: PUGET SOUND, WASHINGTON, AND COOK INLET, ALASKA**

Richard W. SALTUS, Richard J. BLAKELY, Peter J. HAEUSSLER (U.S. Geological Survey)

Puget Sound, Washington, and Cook Inlet, Alaska, both host forearc basins above active subduction zones. In both regions active compressional features are superimposed on the original subsidence strata. Both regions include major population centers--the greater Seattle/Tacoma area in Puget Sound and the much smaller Anchorage/Kenai area in Cook Inlet. In addition to the urban infrastructure, the Cook Inlet region has oil and gas production facilities and pipelines. Detailed, high-resolution aeromagnetic studies have been undertaken to assist in hazard assessment in both regions. Here we compare and contrast the results of separate studies in the two regions. The basins of the Puget Sound and Cook Inlet regions all overlie and are surrounded by volcanic rocks that provide significant magnetic sources. The generally basaltic Crescent Formation is uplifted to relatively shallow levels in fault blocks between the basins of the Puget lowlands and forms magnetic anomalies that trace the bounding faults (e.g., the Seattle fault, Tacoma fault, and south Whidbey Island fault). In the Cook Inlet, basement magnetic sources include the volcanic and volcanoclastic Talkeetna Formation, as well as a number of dioritic to mafic intrusions on the northwestern side of the inlet, and the very magnetic tonalites exposed along the Border Ranges fault on the southeastern side of the inlet. In contrast to the Puget Sound basins, magnetic basement rocks do not come to shallow levels in the Cook Inlet compressional structures. There is significant magnetic material within the shallow sedimentary sections of all these basins. In particular, the Blakely Harbor Formation in the southern Puget Sound contains abundant basalt pebbles shed from the Crescent Formation. Shallow offset of the Blakely Harbor Formation gives rise to magnetic anomalies that can be used to map the active strand of the Seattle fault, which lies beneath Seattle and produced a M7 earthquake 1100 years ago. In the Cook Inlet, Quaternary volcanic detritus shed off the generally magnetic Alaska Range appear to account for significantly magnetic horizons within the shallow Tertiary Sterling Formation and overlying Quaternary rock section. Folds and anticlinal truncations of these shallow magnetic layers result in a series of long, linear, short-wavelength anomalies that trace the likely horizontal extent of deeper blind thrusts. The common occurrence of generally magnetic, volcanic and volcanoclastic rocks and detritus in forearc settings makes it probable that both high angle and thrust faults will have some magnetic signature both at shallow and basement levels. This means that detailed aeromagnetic studies provide an effective way to map potentially hazardous structures in the basins of the Pacific Rim.

**GAV.06/09P/D-008** Poster **1400-161**

**IDENTIFICATION OF POSSIBLE DEEP PENETRATIVE FRACTURES ON THE SOUTHWESTERN COLORADO PLATEAU, U.S.A**

Mark E. GETTINGS (U. S. Geological Survey)

The Redwall limestone is thought by many to be the principal aquifer feeding the springs and seeps on the south side of the Grand Canyon in Arizona, U.S.A. The Redwall limestone is overlain by several impermeable shale units of the Colorado Plateau, and thus recharge to the aquifer is probably totally by seepage down penetrative fracture systems. The National Park Service has sponsored a two-year study by the U. S. Geological Survey to produce an initial map coverage showing the location of possible deep penetrative fractures that might be important in groundwater recharge of deep aquifers. The area of study was the Colorado Plateau south of the Grand Canyon and west of the Black Mesa area. The approach used was to assume that fractures penetrating to the Redwall limestone probably also penetrate into the underlying crystalline basement. A map of a minimal set of deep structures that may be fractures was obtained from analysis of persistent curvilinear features of the gravity and magnetic anomaly datasets. This was correlated with maps of major surficial fractures obtained from geologic, topographic, aerial photographic, and satellite imagery maps. The resulting maps define a sub-set of possible penetrative fractures because 1) not all deep fractures have magnetic or gravity anomalies detectable at the surface, 2) surface fractures may be missed or not identified from the surficial data, and, 3) some areas have very sparse data coverage in one or more of the necessary datasets. Nevertheless, the resulting penetrative fracture distribution maps constitute an objectively obtained, repeatable dataset. These maps constitute a benchmark from which additional studies can begin. The geophysical anomaly data were available at a 500m grid interval, and geologic mapping in large areas was only of reconnaissance nature, so the analysis was carried out at a scale of 1:250,000 over the study area. Most newly defined penetrative fracture locations paralleled known fracture or fold axes, which are dominantly northeast and northwest trending. A less pervasive, and more interrupted, north-south trend was also recognized. This north-south trend appears to be related to an old fabric in the basement rocks defined by north-south trending gradients of many magnetic and gravity anomalies. The analysis was carried out digitally, and the final product was a set of digital map layers suitable for use in a Geographical Information System.

**GAV.06/09P/D-009** Poster **1400-162**

**UTILITY OF SATELLITE MAGNETIC OBSERVATIONS FOR ESTIMATING NEAR-SURFACE MAGNETIC ANOMALIES**

Hyung Rae KIM<sup>1</sup>, Ralph R.B. VON FRESE<sup>1</sup>, Patrick T. TAYLOR<sup>2</sup>, Jeong Woo KIM<sup>3</sup> (<sup>1</sup>Dept. of Geological Sciences, The Ohio State Univ., <sup>2</sup>Code 921 Geodynamics branch, GSFC, NASA, Maryland, USA, <sup>3</sup>Dept. of Earth Science, Sejong Univ., Republic of Korea.)

Regional to continental scale magnetic anomaly maps are becoming increasingly available from airborne, shipborne, and terrestrial surveys. Satellite data are commonly considered to fill the coverage gaps in regional compilations of these near-surface surveys. For the near-surface Antarctic magnetic anomaly map being produced by the Antarctic Digital Magnetic Anomaly Project (ADMAP), we show that near-surface magnetic anomaly estimation is greatly enhanced by the joint inversion of the near-surface data with the satellite observations relative to conventional minimum curvature Ørsted observations are especially advantageous relative to the Magsat data that have order-of-magnitude greater

measurement errors, albeit at much lower orbital altitudes. CHAMP is observing the geomagnetic field with the same measurement accuracy as the Ørsted mission, but at the lower orbital altitudes covered by Magsat. Hence, additional significant improvement in predicting near-surface magnetic anomalies can result from the CHAMP data. Our analysis also suggests that considerable new insights on the magnetic properties of the lithosphere may be revealed by a further order-of-magnitude improvement in the accuracy of the magnetometer measurements at minimum orbital altitude.

**GAV.06/09P/D-010** Poster **1400-163**

**DISPLACEMENT OF THE GEOMAGNETIC EQUATOR STOPS AT THE DEFLEXION OF MACHUPICCHU AS PART OF THE TECTONIC PROCESS IN SOUTH AMERICA**

Teodosio Chavez CAMPOS<sup>1</sup>, Casaverde RIO<sup>2</sup>, Israel Chavez SUMARRIVA<sup>3</sup> (<sup>1</sup>Post-graduate school of system, University National of Engineering, <sup>2</sup>Scientific consultant, National Institute of Civil Defense, <sup>3</sup>National University of Engineering, Av. Pablo Carrquiry 451, Lima-27, PerAENa1-1=Mateo)

The magnetic field distribution of the earth's surface shows an important temporal variation, named secular variation (SV). The secular variation is one of the important characteristics of the geomagnetic elements. Recently it has been observed an extraordinary high speed variation of the phenomenon, compared with geological scale time, when the magnetic equator crosses Brazil towards northeast. The origin of this change could be a consequence of fluid motion in the outer core of the earth. The secular variation of the vertical Z component and so inclination I component) of geomagnetic field is particularly important. The geomagnetic equator, where the inclination (I) of the magnetic field is zero degrees, when it crosses at South America, stops in its southward motion between the years 1938-1939, at the latitude 13° - 14° S in Peru. This behavior has been calculated with the model of the IGRF (International Geomagnetic Reference Field) and proven with data of the Huancayo Magnetic Observatory (HMO). On the other hand in the zone of Brazil the magnetic equator move toward the northeast. This stopping of the geomagnetic equator in Central Peru is given in the zone of the deflexion of Machupicchu (or deflexion of Abancay), and it is due to the tectonic process between the Nazca and south american plates. Which generates a deep structure with characteristics still unknown. It is originated to beginnings from the derives continental when Sudamerica was separated from Africa, generating a depth structure in the direction of the large defects transformantes of the Atlantic middle. Besides it is a structural feature, important in South-america because its development morfoestructural, necessarily implies a control of tectonic process of large scales. The deflexion of Machupicchu is an area of seismic calm, to either side of this seismic discontinuity, and the inclination of the Benioff plane is different: weak to the north, strong to the south. The anomalies maps of Bouger (without topographical correction) it registers the deflexion, and the same thing happens with electric conductivity anomaly. The Nazca ridge is situated front of these anomalies.

**GAV.06/09P/D-011** Poster **1400-164**

**AEROMAGNETIC ANOMALY EXPLORATION BETWEEN YULE BAY AND MERTZ GLACIER (EAST ANTARCTICA)**

Bozzo EMANUELE<sup>1</sup>, Detlef DAMASKE<sup>2</sup>, Fausto FERRACCIOLI<sup>3</sup> (<sup>1</sup>Dipartimento per lo Studio del Territorio e delle sue Risorse, Univ. di Genova, Viale Benedetto XV,5, 16132 Genova ITALY, <sup>2</sup>BGR, Stilleweg 2, 30655 Hannover GERMANY, <sup>3</sup>British Antarctic Survey, High Cross, Madingley Road, Cambridge, CB3 0ET UK)

The GITARA VI aeromagnetic campaign was performed over George V-, Oates-, and Pennell Coasts during the joint 1999-2000 German-Italian GANOVEX VIII-ITALIANTARTIDE XV Antarctic campaign. The general aim of the survey was to explore crustal structure and tectonics of the northernmost Transantarctic Mountains and its "backside" component, which is in major parts unknown. Over northern Victoria Land the aeromagnetic survey provides new coverage of tectonic units involved in the Ross Orogen. These widely debated units are often referred to as accreted terranes, marking an Early Paleozoic active margin of the East Antarctic Craton. Over western Oates Land and George V Land the aeromagnetic survey area extends over the northernmost edge of the Wilkes Subglacial Basin. This basin has been interpreted either as a flexural depression in thick Precambrian crust, or conversely as a more recent rift basin floored by extended crust. We present total field magnetic anomaly maps along the Antarctic coast between Yule Bay and Mertz Glacier and highlight the location and character of the main aeromagnetic anomalies. Where possible, we contrast these anomalies against geology and magnetic susceptibility measurements to interpret their sources. The Lillie Glacier anomaly map reveals contrasting magnetic signatures over the Late Devonian-Early Carboniferous Admiralty Intrusives of the Everett Range and of Yule Bay. Geochemical data indicate that these rocks could indeed differ, since they may have assimilated different proportions of pre-existing continental crust. A near-circular anomaly overlies the enigmatic occurrences of volcanic rocks of Unger Island and Surgeon Island granite. These rocks have been inferred to represent remnants of an accreted terrane or basement to the Robertson Bay metasediments. The Oates Coast map displays a linear magnetic anomaly over the Matusevich Glacier. It reveals mostly buried Cambro-Ordovician(?) Granite Harbour Intrusives and ultramafic rocks. Such rocks are associated with a major fault zone or maybe with a hitherto unrecognised suture within the Wilson Terrane. Just west of the Matusevich Glacier, the highest-amplitude anomaly of the entire survey overlies the Archangel Nunataks gabbro. Magnetic anomalies along the George V Coast indicate that the 180 Ma Ferrar Large Igneous Province may extend along the northernmost edge of the Wilkes Subglacial Basin. Specifically, comparison with similar anomaly patterns detected about 1000 km further south of the present survey suggests that thick Jurassic intrusions may exist along the northeastern flank of the Wilkes Subglacial Basin. Finally, an anomaly break close to the northwestern flank of the Wilkes Subglacial Basin, could mark the unexposed boundary between the Precambrian East Antarctic Craton and the Ross Orogen. The anomaly itself is co-linear with a major fault detected from seismic data offshore Mertz Glacier.

**GAV.06/09P/D-012** Poster **1400-165**

**GANOVEX VIII: AN AEROMAGNETIC SURVEY ALONG THE ANTARCTIC COAST BETWEEN COMMONWEALTH BAY AND CAPE ADARE**

Detlef J. DAMASKE<sup>1</sup>, Heinz-Dieter MOELLER<sup>1</sup>, Emanuele BOZZO<sup>2</sup>, Fausto FERRACCIOLI<sup>3</sup>, Massimo CHIAPPINI<sup>3</sup> (<sup>1</sup>Bundesanstalt fuer Geowissenschaften und Rohstoffe, <sup>2</sup>Dipartimento per lo Studio del Territorio e delle sue Risorse, <sup>3</sup>Istituto Nazionale di Geofisica e Vulcanologia)

Aerogeophysical investigations make it possible to survey extended and inaccessible areas of mountain and glacier regions. Based on an areal coverage, the structural interpretation of magnetic anomaly patterns allows to recognize rocks or rock types and yields tectonic structures in the earth's crust. Moving from areas geologically known to the unknown, one can extrapolate results or compare with magnetic patterns of other regions. For two decades BGR has carried out aeromagnetic surveys over large areas of Victoria Land and the western Ross Sea in cooperation with institutions in Italy (DIPTERIS, ING) and in the United States (USGS, INSTAAR, Ohio State University). GANOVEX VIII continued this research by - extending the survey across the western shoulder - the Transantarctic Mountains (TAM) -

of the Ross Sea Rift to study the transition to the East Antarctic Craton, - selecting the Oates- and George V Coasts to investigate the apparently high basement area between the subglacial Wilkes Basin (paralleling the TAM) and the continental shelf towards the Pacific / Indian Ocean, - conducting aeromagnetic surveys of the northern (Pennell Coast) TAM for correlation of marine tectonic elements between Australia and the Antarctic with structures in northern Victoria Land. A total of 26575 km of survey lines were acquired over an area of 83800 km<sup>2</sup>. The complete coastal region from the Mertz Glacier to Yule Bay over a length of approximately 1000 km was surveyed for the first time.

**GAV.06/09P/D-013** Poster **1400-166**  
**PEOPLE AS BIOSENSORS FOR MAGNETIC STORMS AND SOLAR WEATHER DETECTION**

Olga Valerievna KHABAROVA, Mary Valerievna RAGULSKAYA, Eugeny Antonovich RUDENCHIK (Department of Solar-Terrestrial Coupling, IZMIRAN (The Institute of Terrestrial Magnetism))

The results of many biophysical experiments and data of medical statistics confirm that people are susceptible to changes of environment (particularly, to leaps of geomagnetic field strength – magnetic storms) and space weather. In this connection, an experiment for revealing of solar weather - human health linkage from physical point of view is carried out in IZMIRAN, Sector for Helio-Ecological Coupling from 1998(see <http://helios.izmiran.rssi.ru/helioecology/index.html>). The experiment is based on a method of measurements of acupuncture points electroconductivity; the measurements are led daily; number of tested people - 40. The values of electroconductivity of each point characterize the functional condition of corresponding organs. Statistical checks show that the hypothesis about the casualty of coincidence of human health's sharp changes with atmosphere pressure fluctuations, geomagnetic and solar activity growth can be rejected at the 0.01 level of statistical significance. It means that detected human reaction – change of health status in the time domain (±2 days) of the magnetic storm commencement is not causality. So, the question about the origin of such phenomenon is emerging. It was found out that the time of registration of human health status changes before the magnetic storms commencement always coincides with the increase of amplitude of magnetospheric oscillations with periods 4-250 min. It was shown that the applying of parametrical resonance theory at biological systems (in our case - living organisms) could explain this fact. In accordance to calculations, the frequencies of 4-250min diapason of periods are resonant with the own frequencies of human brain and endocrine system. It was found out, that bioeffective amplification of geomagnetic oscillations with mentioned periods before magnetic storm commencement can be consequence of simultaneous increasing of solar wind oscillations (see abstract by O.Khabarova, E.Rudenchik "The possibility of magnetic storms prediction due to analysis of solar wind data").

**GAV.06/09P/D-014** Poster **1400-167**  
**AEROMAGNETIC SURVEY OVER UNZEN VOLCANO**

Ayako OKUBO<sup>1</sup>, Yoshikazu TANAKA<sup>1</sup>, Naoto KITADA<sup>1</sup>, Mitsuru UTSUGI<sup>2</sup>, Hiroshi SHIMIZU<sup>3</sup>, Takeshi MATSUSHIMA<sup>3</sup> (<sup>1</sup>Dept. of Geophysics, Kyoto University, Japan, <sup>2</sup>Geographical Survey Institute, Tsukuba, Japan, <sup>3</sup>Faculty of Science, Kyushu University, Japan)

We conducted helicopter-borne magnetic surveys over Unzen Volcano, southwestern Japan on September 18, 2002 in order to investigate the subsurface structure of Unzen graben and the cooling process of the lava dome formed in the latest eruption spanning between 1991 and 1995. Unzen volcano started a phreatic eruption in November, 1990 at summit craters after a quiescence of 198 years. After intensive ash ejection in February 1991, a lava dome appeared at the eastern neighbor of the previous peak of Mt. Fugen in May, 1991. The lava dome, named Heiseishinzan, gradually grew on the eastern flank of Mt. Fugen and yielded frequent pyroclastic flows until the surface activity ended in 1995. The survey consists of three flights of 1 hour for each. The first flight covers an area over Futsu, Chijiwa, and Kanahama faults, the major normal faults that form Unzen graben system. The second and the third flights cover the summit area of Unzen volcano with spiral trajectories at altitudes of 1000 and 500 ft, respectively. The spacing between the survey lines is about 500 m. Geomagnetic total field was recorded by an optical pumping magnetometer (GEOMETRICS) and an Overhauser proton magnetometer (GEM) installed in and over the sensor bird, which is suspended with a wire of 20 m long under the airframe. The sampling intervals of these magnetometers are 0.1 sec and 0.5 sec, respectively. While real time navigation was achieved by a portable GPS receiver with a PC monitor, precise positioning data of the sensor bird was obtained by the differential GPS technique with a time resolution of 1 sec. Diurnal magnetic variations of extra-terrestrial origin were removed by subtracting the total field data recorded at a temporal station nearby. As a next step, we estimated the effect of surface topography using a statistical correlation method (Grauch, 1987) in order to model a deeper magnetic structure. In the present study, we propose a plausible model of magnetic structure beneath Unzen volcano. Main features of the magnetic map are positive anomalies on the summit area of the volcano (Heiseishinzan lava dome and Mt. Fugen) and a negative anomaly on Unzen hot-spring area.

**GAV.06**  
**MODERN MAGNETIC SURVEYS FOR REGIONAL TECTONICS, GEOHAZARDS AND ENVIRONMENTAL INVESTIGATIONS**  
 Location: Site A, Room 11

Thursday, July 10 AM  
 Presiding Chair: S. Okuma

**GAV.06/10A/A11-001** **0830**  
**HIGH-RESOLUTION AEROMAGNETIC DATA FACILITATE MAPPING AND CHARACTERIZATION OF CASCADIA EARTHQUAKE HAZARDS**

Richard J. BLAKELY, Ray E. WELLS (U.S. Geological Survey)

The Puget Lowland-Willamette Valley urban corridor (Washington and Oregon) lies within the Cascadia forearc and above the subducting Juan de Fuca plate. Northward migration and clockwise rotation of the forearc are accommodated in part by crustal faults, some capable of M 7 earthquakes. Crustal faults are known or suspected to underlie the major population centers of the urban corridor, yet the cover of vegetation, young surficial deposits, and urban development hampers study of these structures. Tertiary volcanic rocks of diverse origins, however, underlie the region and produce distinctive magnetic anomalies that facilitate geologic mapping and help identify hazardous structures. During the past

decade the USGS has systematically acquired high-resolution aeromagnetic data over 80,000 km<sup>2</sup> of the Cascadia forearc, including its highly urbanized areas. These data are useful at many scales: They help define the limits, thickness, and internal structure of the Cascadia forearc as a whole, but also serve to map crustal faults in exceptional detail. Here we present two case studies: The Seattle fault zone in western Washington extends east-west beneath Seattle and was responsible for a M 7 earthquake 1100 years ago. The fault zone accommodates uplift of regions to the south relative to the Seattle basin to the north, with 9 to 10 km of structural relief on the highly magnetic Eocene basement. Much of the fault zone is concealed beneath glacial deposits and water, but the volcanic basement produces distinctive magnetic anomalies that illuminate hanging-wall geology. Miocene conglomerates within the Seattle basin are also magnetic, generate distinctive magnetic anomalies where deformed, and thus constrain mapping of specific strands of the Seattle fault zone within narrow spatial limits. The active strand of the Seattle fault zone is interpreted to extend at least 50 km east-west and lie beneath the neighborhoods of greater Seattle, conclusions now being validated by ongoing paleoseismic investigations. In northwestern Oregon, the Portland Hills and Mount Angel faults form northwest-striking, right-lateral structural zones that in large part lie beneath thick surficial deposits of the northern Willamette basin. Basalt flows of the Miocene Columbia River Basalt Group underlie much of this region and now serve as post-Miocene strain markers that produce characteristic magnetic anomalies. A M 5.6 earthquake occurred in 1993 on the Mount Angel fault about 50 km from downtown Portland. Prior to the earthquake, the location and characteristics of the Mount Angel fault were known primarily through widely spaced wells and seismic-reflection profiles. Models of the fault based on new high-resolution aeromagnetic data provide a three-dimensional view of this structure, indicate how it kinematically links to other elements of the structural zone, and suggest that it extends >60 km and thus may be capable of M 6-7 earthquakes.

**GAV.06/10A/A11-002** **0850**  
**AEROGEOPHYSICAL SURVEY OVER IWATE VOLCANO, NORTHEAST JAPAN**

Shigeo OKUMA, Tadashi NAKATSUKA, Rie MORIJI, Shinichi TAKAKURA (Geological Survey of Japan, AIST)

A helicopter-borne electromagnetic survey (HEM) with simultaneous measurements of the Earth's magnetic field was conducted to better understand the subsurface structure of Iwate volcano, northeast Japan with a special reference to an increase of seismic and fumarole activities. The Quaternary volcano is geologically divided into two parts, i.e. an eastern part called the East-Iwate, which is a stratovolcano with a small summit crater and younger than the other in age, and a western part called the West-Iwate, which comes with an east-west elongated caldera of about 2km wide and is overlain by the volcanic products from the East-Iwate at the eastern edge. The HEM system is a modified DIGHEM-V model that is operated at five frequencies ranging from 220 Hz to 137,500 Hz with five-fold frequency increments. The survey was flown in late 2000 at an altitude of 70-100 m above terrain along north-south survey lines and east-west tile lines, spaced 100 m and 1,000 m apart, respectively. A post differential GPS system was employed for flight path recovery. The observed electromagnetic data were processed and apparent resistivity maps for each frequency and cross-sections of apparent resistivity profiles were created. Aeromagnetic anomalies were reduced onto a smoothed observed surface and a reduction to the pole anomaly map with a terrain correction was created. The characteristics of apparent resistivities and magnetic anomalies (reduction to the pole) are obviously different between the East- and West-Iwate volcanoes. In general, apparent resistivity highs (> 4,000 Ω·m) and magnetic highs (> 2,000 nT) lie dominantly in the East-Iwate, while apparent resistivity lows (< 250 Ω·m) and magnetic lows (< 200 nT) in the West-Iwate, corresponding to a difference in the geologic age and hydrothermal activities of the volcanoes. Concerning a recent increase of the volcanic activity on the ground in the West-Iwate, an apparent resistivity low of 5 - 15 Ω·m occupies on the divide on the half way to Mt. Ubakura from Mt. Kurokura, where severe fumarole activity was being observed during the survey. Although a magnetic high lie over the divide, the amplitude of the anomaly is decreasing with getting close to Mt. Kurokura, where the activity was the severest. Lava flows from sub volcanoes around the West-Iwate caldera can be recognized by a coincidence of magnetic and apparent resistivity highs on the northern slopes of Mt. Ubakura and Akakura-dake and southern slopes of Onigajyo and Kamakura-mori. On the contrary, magnetic lows (< 1400 nT) and apparent resistivity lows (< 30 Ω·m) can be seen in geothermal and/or altered areas mainly on the southern flank of the West-Iwate volcano, implying a usefulness of the HEM survey for detecting these parts.

**GAV.06/10A/A11-003** **0910**  
**HELICOPTER BORNE EM STUDIES OVER THE MOUNT USU REGION, JAPAN**

John Joseph E., Shigeo OKUMA<sup>2</sup>, Tadashi NAKATSUKA<sup>2</sup> (<sup>1</sup>School of Earth and Environmental Sciences, The University of Adelaide, <sup>2</sup>Institute of Geoscience, AIST/GSI, Tsukuba 305-8567, Japan)

Mount Usu in the northern part of Japan is an active volcano. Latest eruption of this volcano was in the year 2000. An airborne electromagnetic (AEM) survey was conducted in this region to study shallow subsurface electrical conductivity distribution and thereby investigate the geohazards and environmental settings. The reported survey was conducted in October 2000, while the volcanic eruption was still continuing. We used a modified helicopter borne system called DIGHEM-V. It is a multi-frequency system that contained within a 10m bird towed beneath the helicopter. This bird has 5 stand-alone transmitting-receiving coil pairs corresponding to 5 different frequencies such as 137500 Hz, 27500 Hz, 5500 Hz, 1100Hz and 220 Hz. Two coil pairs are oriented in the co-axial directions (i.e. with the axes of the flight direction) and three coil pairs in the horizontal coplanar direction (axes vertical). For obtaining precise positioning of the helicopter and flight altitude we used a combination of DGPS system, a radar altimeter and a Video camera, which were installed on the helicopter. There were 85 survey lines in the North-South direction with line spacing of 100m and 15 survey lines in the East-West direction with line spacing of 1000m. Airborne EM data were processed and data inversion were carried out to estimate the depth-resistivity distribution of the whole survey region. Since the EM signal frequencies used are very high, we could obtain the shallow (~0-150 m) resistivity distribution. Preliminary result shows the presence of a 3-layer resistivity structure with a top layer which is less resistive (<200 Ohm-m) followed by a high resistive layer (500-5000 Ohm.m) which is underlain by a low resistive layer (<500 Ohm.m). Central region of Mount Usu seems to be more resistive (400-2500W-m) than the surrounding region. By examining the resistivity distribution maps of lower frequencies, it is clear that a similar trend in resistivity persists downward. Selected transects of the depth-resistivity profiles clearly show the presence of a highly resistive body at a depth of 60-70m depth beneath the SW slope of the mount summit. This highly resistive body may be indicating the presence of avalanche deposits of the previous summit. A detailed discussion on data collection, processing and comparison with apriori geological and geophysical information will be presented.

GAV.06/10A/A11-004

0930

### HIGH RESOLUTION AIRBORNE MAGNETIC SURVEYS TO INVESTIGATE THE STRUCTURE AND SYSTEM CHANGES IN ACTIVE VOLCANIC REGIONS OF SOUTHERN ITALY

Robert SUPPER<sup>1</sup>, Shigeo OKUMA<sup>2</sup>, Massimo CHIAPPINI<sup>1</sup>, Riccardo DERITIS<sup>3</sup>, Iacopo NICOLOSI<sup>1</sup>, Christian STOTTER<sup>1</sup>, Ingrid SCHATTAUER<sup>1</sup> (<sup>1</sup>Geological Survey of Austria, <sup>2</sup>Geological Survey of Japan / AIST, <sup>3</sup>Istituto Nazionale di Geofisica e Vulcanologia)

In the years on from 1999, several high resolution airborne magnetic surveys were carried out by the Geological Survey of Austria in cooperation with different partner in active volcanic regions of southern Italy (Vesuvio, Campi Flegreii, Vulcano, AE). However within this presentation we focus on the airborne surveys conducted at the Eolian Islands (Italy) in a close cooperation with the Geological Survey of Japan and INGV Roma. Southern Italy is characterised by several active volcanic regions like Mt. Vesuvio, Campi Flegrei, Mt. Etna and the Eolian Islands. A few of these are surrounded by some of the most densely populated areas in Europe like Napoli and Catania or are popular tourist destinations, like Vulcano Island. Therefore in view of hazard mitigation it is very important to understand the structural and geological settings of these areas. The purpose of the airborne surveys was to map the geophysical anomaly structures of this area from a regional point of view and to correlate them, including other potential field data, with recent volcanic activities to find significant geophysical anomaly patterns caused by these activities. Moreover these data sets should provide a basis for future research activities including volcanic hazard monitoring. A first survey on Vulcano and Lipari Island was conducted in 1999. Within the 1999 airborne magnetic survey only a restricted area of the Vulcano/Lipari area has been covered. Therefore some of the structural important magnetic anomalies of this region could not be investigated in detail. Therefore, for a second airborne magnetic survey, conducted in 2002, the area under investigation was significantly enlarged, including also the regions of Panarea and Stromboli, which recently have shown an increasing volcanic activity. The detailed results of these surveys are shown, outlining the main structural trends of this region. Some first results of modelling are also given. Additionally, as one might expect that due to the geodynamics of this area, corresponding changes of the magnetic anomaly pattern may occur with time, the same lines measured in the 1999 survey were re-flown to get hints for changes in the magnetic field within the last three years. As both surveys were unavoidably conducted at slightly different flight altitudes, delicate field transformation algorithms had to be applied to make the data comparable without losing much information. The results show a decrease of the magnetic field in western parts of the Vulcano-Lipari complex. This results and limitation of this method to monitor changes in the volcanic system are also discussed.

GAV.06/10A/A11-005

0950

### AIRBORNE MAGNETIC ANOMALY IMAGES OVER STROMBOLI (AEOLIAN ISLANDS, ITALY)

Massimo CHIAPPINI<sup>1</sup>, Iacopo NICOLOSI<sup>1</sup>, Riccardo DE RITIS<sup>1</sup>, Shigeo OKUMA<sup>2</sup>, Robert SUPPER<sup>3</sup> (<sup>1</sup>Istituto Nazionale di Geofisica e Vulcanologia, <sup>2</sup>Geological Survey of Japan/AIST, <sup>3</sup>Geological Survey of Austria)

The recent volcanic activity at Stromboli Island has threaten the local population. Remotely-sensed data, such as magnetic anomaly data provide an important means for obtaining geological information on the area, helping to delineate tectonic features, and to characterize the area magnetically. Only the apical part of the large Stromboli edifice emerges from the sea, therefore spatial observations need to be extended offshore far enough to cover the whole structure. An international consortium has been established, and a high resolution aeromagnetic survey was conducted. The effort constitutes a considerable step ahead, with respect to the existing magnetic data in the area. In fact, the magnetic anomaly field shows the major known structural features; also it clearly reveals the presence of a high frequency magnetic pattern associated to tectono-volcanic elements.

GAV.06/10A/A11-006

1010

### ANALYSIS AND INTERPRETATION OF AEROMAGNETIC DATA OF RUNGWE VOLCANIC PROVINCE, SOUTHWEST TANZANIA

Isaac Muneji MAROBHE (University of Dar es Salam)

The Rungwe volcanic province lies at the triple junction of the East African Rift System in southwest Tanzania. The volcanic province consists of basalts, trachytes, tuffs and volcanic ash erupted along vents that were controlled by basement structures. The youngest eruption of Kiejo is believed to have erupted in 1800 AD. The volcanics overlie basement and sediments that range from Karoo to Neogene. The countrywide aeromagnetic data surveyed in 1976 to 1980 at flight spacing of 1 km and altitude of 120m above the ground has revealed subsurface structures that have not been mapped by conventional methods. The Data has been analysed by enhancing the anomalies using filtering methods in the frequency domain. Two prominent magnetic lineaments NE/SW and NW/SE are revealed from the data. NE/SW lineaments terminate against the Mbozi Block whereas the NW/SE runs parallel to the block. Based on magnetic relief and amplitude, the aeromagnetic data of the area show two distinct provinces. The two provinces coincide with the young and old volcanic provinces. Individual anomalies are dipolar in form and have amplitude ranging from 50 to 300 nT, however there is one anomaly that has an amplitude of 3500 nT. The individual anomalies have been interpreted to get body parameters whereas spectral analysis suggest that depth basement is as high as 9 km in some parts..

GAV.06/10A/A11-007

1050

### MAGNETIC ANOMALY ANALYSIS USING 3D SPACING GEOMAGNETIC VECTOR FIELDS

Nobuhiro ISEZAKI (Department of Earth Science, Faculty of Science, Chiba University)

I observed the vector geomagnetic fields at Niniu, Hokkaido, Japan by the magnetometer developed in my laboratory which consists of a flux-gate magnetometer, a ring laser gyroscope (RLG), CPU, a GPS receiver and memory storages. RLG measures attitude with the precision of 0.001-0.005 degrees for yaw, pitch and roll. I used a helicopter and towed magnetometer 30m behind it. A helicopter flew from 50m to 1000m above the ground with the speed of about 80km/h and sampling rate of 5Hz. Niniu is located in the Hidaka collision zone and there are outcrop of serpentinites in the eastern part of the surveyed area where strong magnetic anomalies are observed. I analyzed 3D spacing vector geomagnetic anomalies to get magnetization structure beneath the area assuming polyhedral prism structure. I adopted 3 different processes, 1: X,Y,Z ANOMALIES USED, N SOLUTIONS OBTAINED AT ALL OBSERVATION POINTS; 2: X,Y,Z COMPOSITE ANOMALIES USED, 1 SOLUTION OBTAINED; 3: INDIVIDUAL X,Y,Z ANOMALIES, 3 SOLUTIONS OBTAINED FOR X,Y, AND Z. In the process 1, for 1 magnetic structure there are 3 unknowns, namely  $m_x$ ,  $m_y$  and  $m_z$  (3 components of magnetization) while there are 3

component magnetic anomaly data at each observation point, then we have N (number of data points) solutions which will give us an information for general feature of magnetization distribution because each solution will represent the magnetization of small local area just beneath the observation point. I will show the results of 3 processes and most optimum magnetic structure of NINIU.

GAV.06/10A/A11-008

1110

### THE THREE-DIMENSIONAL MAGNETIZATION VECTOR INVERSION

Ryuji KUBOTA, Akinori UCHIYAMA (Kawasaki Geological Engineering Co., Ltd.)

A three-dimensional non-uniform magnetic modeling is proposed to obtain information about the oceanic crust and/or a seamount. Our method is different from the semi-norm method of Parker et al. (1987). The structure of the crust and/or a seamount body was divided into many blocks modeled by layered and rectangular prisms, and parameters were assigned to each block describing magnetic three components. Our data were the magnetic total force on the sea. A set of linear equations for data was formulated in terms of the direction cosines of magnetization for each block. The solution was obtained by using the conjugate gradients method because of its fast and accurate advantages of calculation. The magnetic intensity is inversely proportion to the third power of distance between an observation point and a source, and consequently coefficients for shallower blocks in the linear equations are large values compared with ones for deeper blocks. Therefore the observed sea surface anomalies were continued to several altitudes (upward continuation) in order to suppress effects of differences among those distances depending on the depth of each block, relatively. On the other hand, a common set of the three direction cosines was defined for several blocks to decrease the number of unknown parameters. A computer program has been tested with artificial data and applied to sets of data observed during the first phase of the Kaiko project carried out with the R/V JEAN CHARCOT in 1984.

GAV.06/10A/A11-009

1130

### DETERMINATION OF THE PARAMETERS OF COMPACT FERRO-METALLIC OBJECTS WITH TRANSFORMS OF MAGNITUDE MAGNETIC ANOMALIES

Daniela Ivanova GEROVSKA<sup>1</sup>, Marcos ARAUZO-BRAVO<sup>2</sup>, Petar STAVREV<sup>3</sup> (<sup>1</sup>Department of Earth Resources Engineering, Laboratory of Geothermics, Kyushu University, Fukuoka 812-8581, Japan, <sup>2</sup>Department of Electromechanical Engineering, University of Burgos, Burgos 09006, Spain, <sup>3</sup>Department of Applied Geophysics, University of Mining and Geology)

The transforms based on magnitude magnetic anomaly (MMA), or modulus of total magnetic intensity  $T$ , including the MMA itself, the modulus of the full gradient of the MMA,  $R$ , the half of the square root of the Laplacian of the square of the MMA,  $E$ , and the Laplacian of the MMA,  $L$ , are low sensitive to the direction of the source magnetisation vector and show high centricity. The shape of the anomalies of these transforms is ten times less strongly dependent on the magnetisation vector direction than the shape of the anomalies of the measured field. The transforms based on MMA, with only non-negative values, for a dipole source show displacement of the maximum of the anomaly from the epicentre, in respect to the depth of the causative body, of 25%, 20%, 15% and 8% for  $T$ ,  $R$ ,  $E$  and  $L$ , respectively. Their obtaining requires calculation of only first order horizontal derivatives of the component magnetic anomalies  $X$ ,  $Y$  and  $Z$ , obtained through transformation of the measured total magnetic anomalies (TMA). We studied the use of the magnetic transforms of the TMA based on the MMA of a dipole source and that of their ratios for determining the geometric and physical parameters of compact environmental ferro-metallic sources. Analytical formula for all the parameters of the magnetic dipole based on calculation of MMAs, their gradients and Laplacian, and their ratios, were obtained. The horizontal position of the dipole source is determined by the maximum of the Laplacian of the MMA, which is the transform with highest centricity. The depth to the source is determined by the maxima of ratios of the transforms based on MMA, producing depths, which are functions only of the depth and a magnetisation inclination factor. The least dependent on the magnetisation inclination factor was found to be the ratio of  $T$  and  $R$ , which makes it the most suitable ratio for the dipole depth estimation. We applied the approach on model data and on magnetic anomalies over environmental sources, represented by UXO and clutter, from the Badlands Bombing Range, USA. The obtained parameter values were compared with those estimated through Euler deconvolution using unprescribed structural index and linear model of the background. The comparison showed that both methods produce similar depth results for the objects with estimated structural index over and around 2.5, i.e., for the sources, which to a great extent can be approximated with a dipole.

GAV.06/10A/A11-010

1150

### A METHOD OF DELINEATING DEEP PENETRATIVE FRACTURES IN THICK SEDIMENTARY ROCK SEQUENCES

Mark E. GETTINGS (U. S. Geological Survey)

In many areas characterized by a thick surficial layer of sedimentary rocks, the mapping of deep penetrative fractures has become an important undertaking. Flat-lying sedimentary sequences often comprise significant portions of basins and plateaus, and if they contain regional aquifers such as shales, mudstones, siltstones, or some limestones, the vertical hydraulic conductivity is essentially zero except where broken by steeply dipping fractures. In these environments, the only significant recharge to deep aquifers is via deep penetrative fractures, and mapping their probable location is thus an important objective for groundwater studies. Here, it is assumed that the geologic environment is a thick section of sedimentary rocks (1-3 km) overlying a heterogeneous crystalline basement of contrasting units of magnetization and density. The sediments are assumed to be flat-lying or only gently deformed, so that bedding plane hydraulic conductivity is not a factor other than possibly providing horizontal conduits to fracture systems where the water can percolate to deep levels. The strategy is to map structures in the basement that are likely to generate fractures, mainly fault and fold axes, and to superimpose this map on a surficial fracture map derived from geologic and other shallow data. Coincidences of deep fracture candidates down-dip from surface fractures define the likely penetrative fractures. Maps of the likely deep fracture, fault, and fold axis locations are prepared by interpretation of curvilinearly persistent features of magnetic and gravity anomaly maps. A primary tool for this interpretation is the location of local analytic signal maxima. Modeling is usually required to resolve ambiguities in location of signal maxima with respect to the location of the actual fault, fracture, or fold axis. If magnetic horizons are present within the sedimentary section and if there is evidence of significant non-vertical dip of fracture systems, an intermediate depth layer must be utilized. Maps of surficial fractures are prepared from geologic maps to define known faults and fold axes. Fractures are obtained from aerial photographs, satellite images, topographic maps, and any other remote sensing data available. The deep and surficial fracture maps are then superimposed and candidate penetrative fractures defined from analysis of coincident or nearly coincident features. If there is significant dip to the surficial fractures, this must be taken into account using depth estimates computed from the gravity and magnetic anomaly data. There are several sources of difficulty with the method. For the deep fracture pattern, a lack of sufficiently precise or closely spaced magnetic and

gravity anomaly data will mean that not all anomalies will be detected and thus lineaments, especially subtle ones, will be lost. If fracture or fault systems do not juxtapose rocks with contrasting density or magnetization, there will be no anomaly. For the shallow fracture dataset, lack of sufficiently precise data is a limitation, and some anthropogenic factors may lead to false identifications. Shallow burial by surficial deposits may obscure fractures. The net result of these sources of error is that the set of penetrative fractures defined by this method is a lower bound.

**GAV.06/10A/A11-011** **1210**

**UTILITY OF COMPREHENSIVE MAGNETIC FIELD MODEL IN STUDYING THE EARTH'S LITHOSPHERE**

Dhananjay RAVAT<sup>1</sup>, Thomas G. HILDENBRAND<sup>2</sup> (<sup>1</sup>Department of Geology, Southern Illinois University Carbondale, <sup>2</sup>U.S. Geological Survey)

Near surface magnetic surveys are generally reduced using IGRF/DGRF and additional diurnal and regional corrections to meet specific survey needs. In preparing continental scale compilations, which involves surveys acquired at widely different times, the levels of derived magnetic anomalies from adjacent surveys do not often merge properly because of the failure of IGRF/DGRFs in representing correctly the secular variation of the geomagnetic field. Merging of these surveys is generally accomplished by warping individual surveys until discontinuities are minimal at the survey boundaries. The resulting field is often not the correct representation of the intermediate and long wavelength magnetic anomalies and can severely affect the interpretation of regional crustal magnetic sources, the Curie isotherm, and related properties of geodynamic interest. Models of geomagnetic field, continuous in space and time, such as the comprehensive model (CM) (Sabaka et al., 2002), are helpful in avoiding the poorly constrained or ad hoc warping step and preserving the magnetic anomaly signal. Using the CM and various near surface magnetic data sets over North America, we show that near surface magnetic anomalies based on such models can be better defined than those computed using the IGRF/DGRF and therefore they are more useful for exploration and scientific purposes. The CM also is useful in modeling some of the diurnal variations of the magnetic field.

Thursday, July 10 PM  
Presiding Chair: R. Saltus

**GAV.06/10P/A11-001** **1400**

**INDIAN TECTONIC STRUCTURE THROUGH AEROMAGNETIC DATA**

Mita RAJARAM, Anand SASIDHARAN (Indian Institute of Geomagnetism)

Available degree-sheet aeromagnetic maps, over India (from 8 to 24 degrees North), acquired from the Geological Survey of India, were rigorously reprocessed. These degree sheet maps include surveys carried out by different agencies at different epochs with different survey altitude (5000' / 7000' / 9500') and flight line directions but with a constant flight line spacing of 4 km. The data have not been corrected for the main field. Aeromagnetic surveys have not been conducted over the Deccan trap covered regions. These maps were digitized along contours, corrected for the main field, gridded at 2 km interval, reduced to a common altitude of 5000ft and merged. The crustal anomaly map thus prepared depicts very distinctive structural trends related to the different tectonic blocks of the region. The Southern Granulite Terrain (SGT), the Dharwar, Bastar, Singhbhum cratons, the Eastern Ghat Mobile Belt (EGMB) and the Central Indian Tectonic Zone are distinctly visible on the map. The data has been analysed to throw light on the various tectonic blocks of the region, ranging from the Archean to the present. The changing inclination ( $10 < I < 35$ ) of the main magnetic field makes it difficult to identify the magnetic sources directly from the anomalies; we therefore calculate the analytical signal. It dramatically maps the charnockites, the iron ore series (Bailadilla, Singhbhum, etc) and is able to delineate the orthopyroxene isograd, the Siluru Shear amongst others. A very striking feature is the long arcuate shaped shear that extends for over 1000 km in Central India across the Peninsula from west to east to mark the edge of the Eastern Ghat block, the Bastar craton and possibly the Dharwar craton. We call this as the Main Peninsular shear. Proposed geotectonic models are based on inadequate data and studies of relatively small regions and it is in this regard that the aeromagnetic data could provide very valuable information. From the aeromagnetic anomaly, its analytical signal and Euler solutions we bring out the subsurface structure of the region and redefine the tectonic elements especially in regions with large surface cover. Results of this study will be presented.

**GAV.06/10P/A11-002** **1420**

**ANALYSIS OF AEROMAGNETIC DATA OVER SINGHBHUM, INDIA, FOR IDENTIFICATION OF URANIUM DEPOSITS**

Anand P. SASHIDHARAN, Mita RAJARAM (Indian Institute of Geomagnetism)

Two distinctive types of Uranium mineralization occur in the Singhbhum Uranium Province (SUP) of the Indian subcontinent: 1) the early quartz-pebble-conglomerate type and 2) shear controlled hydrothermal type. The country's main Uranium producing mines (second type of mineralization) are located on the mapped Singhbhum Shear zone. Detailed high resolution aeromagnetic data was collected over SUP under Operation Hard Rock. The aeromagnetic survey was flown at a height of 61–122 m with a flight line spacing of 500m. Aeromagnetic data over a part of SUP covered under Operation Hard Rock has been analysed. The total field anomaly map prepared after applying necessary corrections depicted signatures of several known geological formations viz. the Singhbhum Shear zone (SSZ), the Dalma volcanics, Dhanjori lavas, etc. To identify the magnetic sources, the analytical signal map was prepared. The magnetic sources are clearly concentrated along the arcuate shaped Singhbhum Shear and also on the small part of the Barabhum shear zone that falls within the study area and can be explained as due to the magnetite present in this shear zone as accessory mineral in rocks hosting uranium mineralisation. To throw light on the depth, position and the nature of the magnetic sources, 3D Euler Deconvolution method has been adopted. The Euler solutions confirm that the SSZ turns EW in the southern part under the Tertiary gravels and alluvium. The region covered by Tertiary gravel and alluvium is deepest compared with the other regions. The sources within the Shear zones seem to be shallow, having an average depth of 300 ±45m, but can be as low as 100m. Distinctive magnetic sources have been identified in the Central part of the zone lying between the Dalma volcanics and the Chotanagpur Granitic Gneissic Complex. The sources in this zone are shallow and depict similar magnetic characteristics as the Singhbhum Shear Zone and may be a zone of concealed uranium deposit that can be explored in the future. The entire SUP is studied with respect to the aeromagnetic data of Central India and the results will be presented. The analysis shows the importance of conducting high resolution aeromagnetic surveys and how a proper and systematic analysis of aeromagnetic data can be useful in the identification of concealed mineral deposits.

**GAV.06/10P/A11-003** **1440**

**AEROMAGNETIC IMAGING OF THE JUTULSTRAUMEN AREA, WESTERN DRONNING MAUD LAND (EAST ANTARCTICA)**

Fausto FERRACCIOLI, Phil JONES, Mike CURTIS, Philip LEAT (Geological Sciences Division, British Antarctic Survey)

During the 2001/02 Antarctic campaign a combined aeromagnetic and aerogravity survey was performed over the Jutulstraumen area in western Dronning Maud Land (East Antarctica). This aerogeophysical survey was part of the MAMOG (Magmatism as a Monitor of Gondwana Break-up) project. This project aims at assessing driving forces of Gondwana break-up as Africa rifted away from East Antarctica, while investigating related Mesozoic magmatic and tectonic events. However, current Mesozoic break-up models are hampered by the lack of robust geophysical constraints on the magmatic and structural context of the Dronning Maud Land margin. Additionally, Dronning Maud Land was situated in the pivotal region, between East and West Gondwana during the transition from fragmentation to Gondwana amalgamation. Hence, new geophysical imaging of the Mid-Proterozoic to Early-Paleozoic tectonic structures of Dronning Maud Land was also required. The aeromagnetic survey over the Jutulstraumen area was flown on a 1 km line spacing grid, with tie line interval of 8-km, at a constant barometric altitude of about 2700 m. An area of about 15300 km<sup>2</sup> was covered. This is the first airborne aeromagnetic campaign over Antarctica with such detailed line spacing. Some long profiles were also flown to image longer wavelength features for aerogravity. Aeromagnetic data processing involved standard procedures: quality control, post-processing of GPS data, magnetic compensation, filtering, base station correction, IGRF removal, statistical levelling and microlevelling. The final processed data were gridded with a grid cell size of 250 m (1/4 of the line spacing). A 1: 250,000 scale shaded relief aeromagnetic anomaly map was produced, leading to the identification of the following major aeromagnetic anomaly features. A broad positive anomaly chain with amplitudes of about 250 nT is observed over the H.U. Sverdrupfjella. It likely images the Middle to Late Proterozoic Maudheim Province, though some higher frequency anomalies correlate with more recent granitoids of Pan-African age. Just to the west of the Sverdrupfjella anomaly, two discrete aeromagnetic anomalies reveal the extent of the Jurassic alkaline intrusions of Straumsvola and Tvorá. The aeromagnetic image shows that similar intrusions are unlikely beneath the inferred Jutulstraumen rift structure. However, a very high-amplitude (1000 nT) anomaly at Straumsvolane, along the inferred western flank of the rift, may reveal an unexposed mafic intrusion. The Jutulstraumen itself exhibits a pattern of distinct magnetic highs and lows that suggest a hitherto unrecognized complexity of the rift itself. High-frequency magnetic anomalies mark the Borgmassivet and Ahlmannryggen areas; they relate to mid-Proterozoic dolerites and to probable faults displacing them. Finally, by combining the new detailed aeromagnetic data with previous Russian data over adjacent areas, we shall discuss some new implications for Mesozoic and Proterozoic to Early-Paleozoic tectonics and magmatism.

**GAV.06/10P/A11-004** **1500**

**AIRBORNE AND GROUND GEOPHYSICS USED FOR REGIONAL TECTONIC ANALYSIS**

Sven G. AARO<sup>1</sup>, Håkan SJÖSTRÖM<sup>2</sup> (<sup>1</sup>Geological Survey of Sweden, <sup>2</sup>Department of Earth Sciences, Uppsala University)

The magnetic and gravity fields give in many case insights to brittle and ductile shear zones, fractures, folds and rock contacts. By determining the petrophysical properties of the constituent rocks the size, shape and orientation of the formations can be revealed. For Proterozoic and older rocks the best results will be given by integrating magnetic and gravity data with petrophysics, bedrock information, EM and seismic data if available. In Sweden and other countries where most of the bedrock is covered with till and swamps the geophysical information is of crucial importance for a meaningful bedrock mapping and naturally for exploration. The geophysical databases at the Geological Survey of Sweden (SGU) contain airborne measurements, gravity measurements and petrophysics as well as magnetic observatory data. Since 1960 the airborne measurements have been carried out at low altitude (ground clearance 30 or 60 m) and with 200 m line separation. The systematic gravity measurements started in the 1950's, in the ore-bearing regions in the northernmost part of Sweden, and petrophysical measurements in the 1960's. Today, systematic regional gravity measurements are normally made with a distance between the gravity stations of 1 to 2 km, but in areas with few outcrops and with a special magnetic signature a station distance of 0.5 to 11/2 km is used. The petrophysical data bases contain density, magnetic susceptibility and q-value information from about 60 000 samples, as well as radiometric information from in-situ and laboratory measurements. To illustrate the benefit of the geophysical information the Hassela shear zone (HSZ) in the central part of Sweden is discussed. The HSZ is interpreted as a Paleoproterozoic tectonic domain boundary across the Fennoscandian Shield. This zone is the most prominent of several, c. 1.8 Ga crustal-scale, dextral shear zones in central Sweden. These more or less transpressive zones are components of a structural evolution including the formation of E-W regional folds and variably dipping, E-W stretching lineations.

**GAV.06/10P/A11-005** **1520**

**THE OKAVANGO GIANT DYKE SWARM (NORTHERN BOTSWANA): INSIGHTS FROM COMBINED GROUND-LEVEL MAGNETIC AND AEROMAGNETIC DATA**

Jérôme DYMENT<sup>1</sup>, Gomotsang TSHOSO<sup>2</sup>, Charly AUBOURG<sup>3</sup>, Bernard LEGALL<sup>2</sup>, Jean-Jacques TIERCELIN<sup>4</sup>, Fred JOURDAN<sup>5</sup> (<sup>1</sup>CNRS UMR 7097, Institut de Physique du Globe, Paris, FRANCE, <sup>2</sup>CNRS UMR 6538, Institut Universitaire Européen de la Mer, 29280, Plouzane, FRANCE, <sup>3</sup>CNRS UMR 7072, Université de Cergy Pontoise, 95031 Cergy, FRANCE, <sup>4</sup>CNRS UMR 6526, Université de Nice-Sophia Antipolis, 06108 Nice, FRANCE)

The Okavango Giant Dyke Swarm (OGDS) is a 100 km wide dyke complex which cut across Northern Botswana on 1000 km along a N110 ° E direction. Although the dykes outcrop locally from the Kahalari sands in the river beds, the OGDS has so far been mapped using the dense aeromagnetic data available in Botswana. To complement such remote-sensing data, field work including a complete transect of the OGDS along the Shashe River (Northeastern Botswana) has provided rock samples, direct geological observation, and geophysical profiling. Rock samples, basalt and dolerite, were dated using Ar-Ar technique, leading the definition of two families, Karoo dykes (about 85%, 178.3 ± 1.1 to 179.3 ± 1.2 Ma) and Proterozoic dykes (about 15%, 758.2 ± 6.6 to 1223.8 ± 10 Ma), which otherwise are structurally indistinguishable. Rock magnetic measurements have been performed on some samples and show a dominant remanent magnetization of about 1 A/m. As for the direct geological observation, 171 dykes have been charted and described, although a significant amount remained hidden by the Kahalari sands. A typical dyke is vertical, 5 km-long and 20 m-thick, and exhibits a N110 °E direction. In addition, a high resolution magnetic profile, 100 km long, have been recorded along the same section using a portable land magnetometer. The altitude of measurements is 2 m above ground-level (5-10 m above the magnetic sources), and the maximum sampling interval is 10 m. Unlike the aeromagnetic data, the ground-level magnetic profile has a resolution sufficient to distinguish unambiguously the

signature of each dyke. Therefore, it allows the identification of 423 dykes, which compare to the 171 dykes actually seen on the section. The dyke thickness ranges between 5 and 70 m, (average 20 m). This would represent an extension of about 6-10%. The average skewness of the magnetic anomalies associated to dykes is 50°, in agreement with the location of paleomagnetic poles for Karoo ages. The skewness values show no clear difference between the two families of dyke. The range of magnetization intensity deduced from forward modeling (by adjusting the amplitude of synthetics to the observed anomalies) ranges between 0.35 and 8.82 A/m, with an average of 2.75 A/m in rough agreement with sample measurements. Again, no clear difference is observed in terms of magnetization intensity between the two families of dyke. A striking result is that almost all the dykes exhibit a constant, apparently normal magnetic polarity. Only 12 on a total of 423 dykes show an opposite behavior, all located in a very small area. As the mid-Jurassic was a period of high geomagnetic reversal frequency (about 2.5 reversal / Ma), this observation suggests that the Karoo dykes have formed in a very short time - 0.5 to 1 Ma. Such a rapid occurrence for Karoo volcanism, already suggested from radiochronological dating of Karoo extrusives in South Africa, is comparable to other flood basalt usually associated to the inception of plume head with the continental lithosphere.

**GAV.06/10P/A11-006****1600****DEEP-SEA MAGNETIC SURVEY OF RAINBOW HYDROTHERMAL SITE ON THE MID-ATLANTIC RIDGE: MAGNETIC SIGNATURE OF A HYDROTHERMAL SITE IN ULTRAMAFIC ENVIRONMENT**

Kaori NAKASE<sup>1</sup>, Jérôme DYMENT<sup>2</sup>, Kensaku TAMAKI<sup>1</sup>, Michiko YAMAMOTO<sup>3</sup>, Morgane RAVILLY<sup>4</sup>, Mitsuko KITAZAWA<sup>4</sup>, Yves FOUQUET<sup>5</sup> (<sup>1</sup>Ocean Research Institute, 1-15-1 Minamidai, Nakano-ku, Tokyo 164-8639, JAPAN, <sup>2</sup>CNRS UMR 7097, Institut de Physique du Globe de Paris, 4 place Jussieu, 75005 Paris, FRANCE, <sup>3</sup>GEOMAR, Wischhofstrasse 1-3, D-24148 Kiel, GERMANY, <sup>4</sup>CNRS UMR 6538, Institut Universitaire Européen de la Mer, 1 place N. Copernic, PlouzanAE FRANCE, <sup>5</sup>IFREMER Centre de Brest, B.P. 70, 29280 PlouzanAE FRANCE)

Most of the hydrothermal vent systems discovered so far on the Mid-Atlantic Ridge (MAR) lie on basaltic substratum. Major exceptions are Sites Logatchev and Rainbow, both located on outcropping ultramafic rocks. Cruise IRIS (Interdisciplinary Research for hydrothermal Interaction during Serpentinisation) of R/V L Atalante was designed to study the hydrothermal activity in ultramafic environment and its possible role in the early development of life. In May 2001, Site Rainbow (MAR 36° 14'N) was investigated through a variety of experiments using IFREMER deep-sea ROV Victor. Among these experiments, one dive was fully devoted to a Deep Sea Three Components Magnetometer (DSTCM) survey of the site area. A total of 22 lines, amounting for more than 16 km, were collected, among which 19 lines, 700-800 km long and 60 m apart, densely covered the whole site area. The magnetic data were acquired about 1 to 10 m above seafloor, providing an ultra-high resolution never achieved so far on a hydrothermal system in ultramafic environment. Both the magnetic effects from the ROV and the main geomagnetic field were evaluated and removed. The absolute magnetization of the seafloor was estimated in the following way: (1) synthetic magnetic anomalies were calculated along the ROV tracks, assuming a local 2D topography (as given by the immersion and altitude of the ROV) and a unit (1A/m) magnetization of the seafloor, (2) observed and synthetic anomalies were compared on sliding windows, and if the coherence between both signals is high, an estimate of the magnetization is given by the ratio between observed and modeled anomalies. Unlike the hydrothermal systems in basaltic environment, generally characterized by a lower magnetization as the result of pervasive alteration of the highly magnetized basalt layer, the Rainbow site exhibits a very strong magnetization (higher than 28 A/m). This observation can be explained by the formation of magnetite during the serpentinisation process. Local significant decreases in magnetization intensity may be associated to later stages of hydrothermal vent evolution, suggesting that the newly formed magnetite is further altered to less magnetized minerals (maghemite, clay minerals) during the continuing hydrothermal weathering.

**GAV.06/10P/A11-007****1620****SUBSURFACE STRUCTURE MAPPING OF QUSEIR AREA, NORTHERN RED SEA, EGYPT, USING HIGH-RESOLUTION AEROMAGNETIC DATA**

Abuelhoda Mahmoud ELSIRAFI<sup>1</sup>, Ahmed Said SALEMF<sup>2</sup>, Keisuke USHIJIMA<sup>1</sup> (<sup>1</sup>Professor, <sup>2</sup>Doctor)

Exploration in the Egyptian Red Sea has had little success in locating a hydrocarbon accumulation. The complex block faulting and Miocene salt structure are the main problems entailed the oil exploration. The complex basement block structure arises from the different ages of faults and the difficulty of determining the exact age relations. In an attempt to identify the possible subsurface structure framework, we designed and applied high-resolution aeromagnetic survey over Quseir area, Northern Red Sea, Egypt. A sensitive airborne system has been built that includes an airborne magnetometer of 0.001 nT sensitivity. Pdas-1000 data acquisition system with GPS satellite navigation for positioning was used. Geosoft Oasis software was used for all merging, correction, and editing functions. Digital manipulation of aeromagnetic data allowed the development of higher derivatives and analytic signal maps. The end result product was a map where geologic structures with magnetic expression were defined. The surveyed area is affected by sets of fault systems, which are mainly trending in the NNW-SSE, NE-SW to ENE-WSW directions. Moreover, structural interpretation of the surveyed data enabled delineation of promising areas for further oil exploration.

**GAV.06/10P/A11-008****1640****MAGNETIC AND SEISMIC STUDIES FOR DELINEATION OF THE SHAPE AND PARAMETERS OF EL HAMRA WATER RESERVOIR BURIED STRUCTURE, WESTERN DESERT, EGYPT**

Nasser Mohamed HASSAN<sup>1</sup>, Mohamed El-Saeed EL-BOHOTY<sup>2</sup>, Fathy Mohamed AHMED<sup>3</sup>, Taha Taha RABAH<sup>4</sup> (<sup>1</sup>Geophysics Dept., Fac. of Sc., AIN SHAMS Univ., <sup>2</sup>National Research Institute of Astronomy and Geophysics, CAIRO, EGYPT)

An intensive magnetic and seismic field surveys have been performed in EL Hamra area in the Western Desert of Egypt to delineate the subsurface tectonics controlling the occurring subsurface water reservoir and the surface salt lakes. The constructed total intensity magnetic map for the study area was reduced to the pole and the RTP map was subjected to application of linear wavelength, Walter and Mark method (1993) after modifications. Also two dimensional modeling and seismic interpretations were carried out. A comparative analysis was carried for the different filtered magnetic maps. It was found that the main tectonic trends are taking the directions NW-SE and NE-SW. The application of Walter and Mark (1993) method to the RTP magnetic anomaly map showed that there are three faults bounding El Hamra area from the east, west and south directions. The applied two dimensional modeling technique indicated that these faults are making a graben crossing El Hamra area. The seismic interpretations revealed two faults extending from the basement to the overlying sedimentary section. The El Hamra water spring flows along one of these fault lines. The depth of the fault reaches about 30 meters from the ground surface.

**GAV.07****MAGNETIC ANOMALIES AND ROCK PROPERTIES**

Location: Site A, Room 13

Monday, July 7 PM

Presiding Chair: V.J.S. Grauch

**GAV.07/07P/A13-001****1400****CAN WE ESTIMATE TOTAL MAGNETIZATION DIRECTIONS FROM AEROMAGNETIC DATA USING HELBIG'S FORMULAS?**

Jeffrey D. PHILLIPS (U.S. Geological Survey)

Helbig (1963, Zeitschrift für Geophysik) published integral equations for estimating the vector components (M<sub>x</sub>, M<sub>y</sub>, M<sub>z</sub>) of the total magnetization from the vector magnetic field components (ΔX, ΔY, ΔZ). Schmidt and Clark (1997, Preview) have advocated applying these integrals to modern total field aeromagnetic survey data by first converting the total field data to vector component data using linear transformations. According to Helbig, (1) the integrals over -∞ to +∞ of ΔX, ΔY, ΔZ, yΔX, and xΔY should all vanish, and (2) the integrals over -∞ to +∞ of xΔX, yΔY, xΔZ, and yΔZ should yield M<sub>z</sub>, M<sub>x</sub>, M<sub>y</sub>, and M<sub>y</sub>, respectively. To apply these formulas to gridded magnetic data, a quadrature algorithm using a 2-D trapezoidal rule was implemented in a moving window across the grid. If (1) is not satisfied within each window, the moments (2) will depend on the choice of origin. Therefore, within each window mean values are removed from ΔX, ΔY, and ΔZ to assure that their first three integrals of (1) are near zero, and planar surfaces are removed from ΔX, ΔY, and ΔZ to reduce the magnitudes of the remaining two integrals of (1). Continuous grids of magnetization inclination, I<sub>m</sub>, and declination, D<sub>m</sub>, are produced based on quadrature results at the center of each window. These grids must then be sampled at estimated source locations. Any location error translates into directional error, because the estimated inclination and declination tend to vary rapidly in the vicinity of a source. To locate the sources using a "closeness" algorithm, two different window sizes are used to estimate the magnetization parameters (I<sub>m</sub> and D<sub>m</sub>), then the grid cells where the two solutions are in close agreement are taken as the preferred source locations. Schmidt and Clark (1997), using an unspecified algorithm, have done a Helbig analysis on aeromagnetic data over the Black Hills North, South Australia. They report an estimated magnetization direction of I<sub>m</sub> = -32°, D<sub>m</sub> = -151°, which is within 22° of the measured total magnetization direction of I<sub>m</sub> = -20°, D<sub>m</sub> = -131° (Rajagopalan and others, 1993, Exploration Geophysics). Results from application of the closeness algorithm yield I<sub>m</sub> = -9°, D<sub>m</sub> = -130°, which is within 11° of the measured result. If results of the closeness method appear unreliable, it is possible to turn the method around and ask questions such as "Which grid cells correspond to sources that are consistent with induced magnetization?" or "Which grid cells correspond to sources that are consistent with magnetization in a given direction?" This approach worked well on aeromagnetic data near Albuquerque, New Mexico, where the volcanic centers and flows are Tertiary in age, so magnetization directions collinear with the present field could be assumed.

**GAV.07/07P/A13-002****1420****HIGH RESOLUTION DATING OF THE SEAFLOOR 40 YEARS AFTER VINE & MATTHEWS: INSIGHTS FROM MAGNETIC ANOMALIES, ROCK MAGNETIC PROPERTIES, AND PALEOINTENSITY MEASUREMENTS ACROSS THE CENTRAL INDIAN RIDGE, 19°S**

Jérôme DYMENT<sup>1</sup>, Annick CHAUVIN<sup>2</sup>, Helene HOREN<sup>3</sup>, Mitsuko KITAZAWA<sup>4</sup>, Christophe HÉMOND<sup>5</sup> (<sup>1</sup>CNRS UMR 7097, Institut de Physique du Globe, 4 place Jussieu, 75005 Paris, FRANCE, <sup>2</sup>CNRS UMR 6118, Géosciences Rennes, 35042 Rennes, FRANCE, <sup>3</sup>CNRS UMR 8538, Ecole Normale Supérieure, Paris, FRANCE, <sup>4</sup>Ocean Research Institute, University of Tokyo, Tokyo, JAPAN, <sup>5</sup>CNRS UMR 6538, Institut Universitaire Européen de la Mer, 29280, PlouzanAE FRANCE)

For 40 years, thanks to Vine and Matthews, marine geoscientists use magnetic anomalies to date the seafloor and reconstruct the history of oceanic basins. The extraordinary success of this technique relies on the irregular succession of geomagnetic polarity reversals and the ability of the oceanic basalt to record them. This method allows dating with a resolution of about 1 Ma for the recent times, quite sufficient to reconstruct basin history but much too low to properly address modern issues on the oceanic crust formation at mid-ocean ridge axes. Other dating methods, such as radiochronological techniques, are quite difficult to apply, because MORBs are generally depleted in the elements required by these techniques. Fortunately, recent investigations in different oceans show that the oceanic basalt are not only an excellent recorder of the geomagnetic polarity, but also a quite good recorder of the geomagnetic intensity. These results, from the slower Mid-Atlantic Ridge at 21° N (20 km/Ma full rate), the slightly faster (45 km/Ma) Central Indian Ridge at 19° S, and the ultrafast East Pacific Rise at 17° S (150 km/Ma), suggest that high resolution magnetic data can be used to date the seafloor with a much higher resolution, depending the spreading rate and the altitude of the measurements. To investigate this hypothesis, we have collected a large amount of magnetic data on two transects of the axial anomaly (from ridge axis to Brunhes-Matuyama transition on both ridge flanks) on the Central Indian Ridge at 19° S. These data include surface (2500 m above seafloor = asf), deep tow (500-1000 m asf), and submersible (1-10 m asf) magnetic anomalies, as well as rock magnetic properties and paleointensity determinations measured on about 150 samples collected by deep-sea submersible Nautile. The submersible anomalies are corrected for the submersible magnetic effects and absolute magnetization of the seafloor are determined by comparing the observed anomalies with synthetics computed for a constant magnetization using the real topography and dive path. Sea surface, deep tow, and submersible anomalies exhibit similar behavior with different resolutions: they compare well to the paleointensity records deduced from the sedimentary cores. The rock magnetic properties show the existence of two types of magnetic carriers: a rather large grain-sized titanomagnetite and a very small grain-sized magnetite. Thermomagnetic analysis (both in high and low magnetic field) indicates that titanomaghemite is present in all rocks samples. The paleointensity was determined by applying the original Thellier double-heating procedure to both the glassy margin and the crystalline part of pillow-lava. Paleointensity results obtained on the crystalline part are systematically higher (10 to 20%) than on glasses, a discrepancy possibly explained by a cooling rate effect on the thermomagnetic magnetization intensity. The magnetization estimated from submersible anomalies and from direct measurements are compared to these paleointensity determinations to investigate how well the magnetization reflects the geomagnetic field intensity.

**GAV.07/07P/A13-003**

**1440**

**SUBSURFACE STRUCTURE OF THE KITAKAMI PLUTONES, NORTHEAST JAPAN, CONSTRAINED BY PETROPHYSICAL AND GEOPHYSICAL DATA**

Shigeo OKUMA, Hiroshi KANAYA (Geological Survey of Japan, AIST)

The Geological Survey of Japan (GSJ), AIST has been measuring rock physical data mainly of granitic rocks in Japan under the same condition in laboratory for more than 30 years and has constructed a petrophysical data base called PB-Rock 21 (Petrophysical Data Base of Basement Rocks in Japan for the 21st Century; <http://www.aist.go.jp/RIODB/pb-rock21/>). As an example of a use of the petrophysical data to interpret geophysical data, we will show here a case study conducted in the Kitakami Mountains, northeast Japan, where the late-Cretaceous Kitakami granites intruded into Paleozoic and Mesozoic sedimentary rocks, which widely cover the surface. The Kitakami granites are composed of more than 50 named blocks, which are classified into six zones (Zone I ~ VI) based on their mode of occurrence, megascopical features and topography (Katada, 1974). The database indicates that the Kitakami granites are the most magnetic ( $> 0.01$  SI) on average among pre-Tertiary granites which outcrop in the Japanese Islands, whereas the intensity of Natural Remanent Magnetization (NRM) is relatively low. Consequently, Qn ratio is low ( $< 0.5$ ) and the effect of NRM can be negligible when interpreting magnetic anomalies caused by the rocks. On the contrary, Paleozoic and Mesozoic sedimentary rocks surrounding the Kitakami granites are almost non-magnetic in contrast to the magnetic granites. This means it is straightforward to estimate the dimensions of the Kitakami granites by interpretations of the magnetic anomalies in the area. As for the density of the Kitakami granites, the rocks are relatively dense (average dry and wet densities  $> 2.75$  kg/m<sup>3</sup>) and roughly equivalent to that of Paleozoic and Mesozoic sedimentary rocks, suggesting that it is not easy to interpret gravity anomalies caused by the granitic rocks. Petrophysical data vary in some amounts among each block. Generally, the more magnetic, the denser the specimens are. Granitic blocks, which belong to Zone IV and VI, are more magnetic and denser than the others, suggesting to a quantitative difference of mafic minerals. We conducted an interpretation of aeromagnetic anomalies over Mt. Himekami where the Himekami granites, one of the Kitakami granites outcrop, taking account of the rock magnetic data. The granitic block is composed of geologically and magnetically three sub-blocks. Assuming the horizontal dimensions by geologic maps, a three dimensional modeling to estimate the depths of the model was conducted by trial and error. The result suggests the bottom depth of the block is around 1.0 km below sea level, when the bottom surface is flat. Furthermore, we will show the results of other granitic blocks in the area including subsurface ones in our presentation.

**GAV.07/07P/A13-004**

**1500**

**RELATION OF MAGNETIC ROCK PROPERTIES TO AEROMAGNETIC CHARACTERISTICS OF AN ARCHEAN TTG-MIGMATITE AND GNEISS AREA, THE NORTHERN FENNOSCANDIAN SHIELD**

Meri-Liisa AIRO (Geological Survey of Finland)

Aeromagnetic interpretation of an area comprising Archean TTG-migmatites and gneisses in eastern Finland is complemented by information on rock properties for more than 14 500 samples. Statistical analysis of the magnetic property data (intensity of induced and remanent magnetizations) and rock densities of such a great number of samples representing diverse rock types, implies to classification and characterization of varied basement blocks and investigation of the structure of the uppermost crust. The magnetic anomaly field of the study area (100 km x 100 km) is decorated by 20-30 km broad regional magnetic anomalies, rising about 100 nT from the generally weakly magnetic surroundings, and local magnetic anomalies representing variation in mineral composition. A 2 km wide belt of N-S striking banded magnetic anomalies, caused by Archean greenstones, divides the area into western and eastern parts. These parts differ in their aeromagnetic character, referring to a change in deformation styles. The whole terrain is structurally fragmented by a network of Palaeoproterozoic mafic dyke swarms. Reasons for the dissimilar aeromagnetic characteristics are examined on the basis of the variation in the magnetic properties and densities for diverse rock types, and compared between the western and eastern parts. For example, the magnetic properties measured from the outcropping TTG-gneisses do not explain the magnetic field intensity in the eastern part. In the same way, there is no such change in the densities, which would explain the 12 mgal increase in Bouguer-anomaly from west to east across the greenstone belt. An explanation is, that denser, more intensively magnetic rocks below the surface, most probably representing a higher metamorphic degree must cause the observed regional effects in magnetic and Bouguer-anomaly fields.

**GAV.07/07P/A13-005**

**1520**

**AEROMAGNETICS- A DIRECT TOOL FOR THE DISCOVERY OF CARBONATITE PLUGS IN NORTHEASTERN INDIA**

Ram Babu Venkata HARI (NATIONAL GEOPHYSICAL RESEARCH INSTITUTE)

In the northeastern part of India, the Meghalaya plateau and the Mikir hills are occupied by Archean-Proterozoic gneissic complex with acid, basic and alkaline intrusives. The carbonatites are emplaced along a NE trending zone from Mawpuyt in Jaintia hills district to Barpung in the Mikir hills of the Karbi Anglong district of Assam, through Sung valley, Jasra, Samchampi, Sam Taran and Tarung area. The carbonatites of northeastern India are considered to be much younger (about 100 Ma) when compared to those occurring in other parts (except Ambadongar) of India. Due to their association with magnetizable minerals such as pyrite and magnetite, and due to large areal extent, these carbonatite complexes produce strong magnetic anomalies, which can be observed even at a height of 1000 m above ground. The Sung valley carbonatite complex in Meghalaya plateau is associated with an intense (3500 nT) aeromagnetic anomaly produced at a height of 2000 m. The anomaly is a predominant low, which is unusual at this magnetic latitude of 40° N. The change of polarity of the observed anomaly reveals the presence of remanence, which is an important clue to look for similar anomalies in other parts of the map. Similar type of anomalies could be seen near Jasra in the Meghalaya plateau and Tejpur in the Mikir hills region. While the anomaly near Jasra was proved to be due to a carbonatite plug, the other three anomalies are yet to be proved on ground. Based on palaeo-latitude calculations from the magnetic anomalies, the age of emplacement is identified to be Jurassic, which agrees well with the geo-chronological estimates. Thus the aeromagnetic data proved to be a direct tool for the discovery of carbonatite plugs in northeastern India.

**GAV.07/07P/A13-006**

**1600**

**GROUND MAGNETIC STUDIES OVER DECCAN VOLCANIC PROVINCE, MAHARASHTRA, INDIA**

Vinit C. ERRAM, Mita RAJARAM, Anand P. SASHIDHARAN (Indian Institute of Geomagnetism)

The enormous mass of basaltic rock known as the Deccan Trap is of great importance in the geological structure of the Indian Peninsula. It now covers about 200,000 sq. m., and

formerly extended over a much wider area. The maximum trap thickness is about 6000 ft. They form some of the most striking physical features of the Peninsula with many of the most prominent hill ranges having been carved out of the basaltic flows. The Deccan Volcanic Province (DVP) is one of the most important regions of continental flood basalts in the world, comprising a sequence of basaltic flows extruded through fissures in the crust from a large magma chamber during 65 Ma. The Deccan flood basalts may be major carriers of remanence and this will leave its signatures in the magnetic data. No aeromagnetic data has been collected over this region possibly because of the expected noise due to the trap cover. Ground magnetic studies were initiated over the DVP in Maharashtra, parts of Karnataka and Goa regions for deciphering the magnetic anomalies beneath the Deccan Traps and to study the source depth extent of the entire region. An area of around 25,000 sq.km. was surveyed using PPM and Fluxgate magnetometers for the magnetic total field F, and the vertical component Z. Due to the high topography and lack of road access the data distribution is skewed. The main trend shown in both the F and Z anomaly maps is NW-SE. It is very interesting to see that the NW-SE lineament is a continuation of the lineament seen in the aeromagnetic map in the southeast region from Chennai; this continues up to the coast and merges with a lineament evident in the marine magnetic anomaly. This long linear structure should have major implication on the tectonics of the area. The ground data were analysed to study the source depths and characteristics. Results of this study combined with the adjacent aeromagnetic and marine magnetic data will be presented.

**GAV.07/07P/A13-007**

**1620**

**MAGNETIC SURVEYS IN SABZEVAR OPHIOLITIC ZONE, IRAN**

Abolghasem KAMKAR-ROUHANI (Department of Mining and Geophysics, Shahrood University of Technology, Shahrood, IRAN)

Sabzevar ophiolitic zone with a long spread pattern of east-west is located in the northeast of Iran. Having a length of 300 km and a narrow width, this ophiolitic zone is famous for its chromite deposits of podiform type. These chromite deposits, which are scattered in the form of chromite lenses in the subsurface, are associated with mafic and ultramafic igneous rocks (e.g. peridotite) containing high amounts of magnetite. The magnetic anomalies over the chromite lenses are, in fact, related to magnetite contents of these kinds of igneous rocks. The results of microscopic studies on the polished sections, prepared from the ore samples taken from the zone, indicate that the magnetite contents of the samples vary in a wide range of 5 to 30 percent of the total volume of the samples. Airborne magnetic and radiometric surveys over the zone were conducted by Iranian Atomic Energy Agency (IAEA) along a regular flight lines pattern having a distance of 1 km between the parallel flight lines. The total field magnetic data, obtained from the airborne magnetic surveys, were processed in two steps: In the primary processing step, at first the raw magnetic data, obtained from the data acquisition stage of the airborne magnetic surveys, were checked, and then, the positioning coordinates corresponding to the magnetic data were exactly determined. A geographic positioning system (GPS) measuring instrument was used in the data acquisition stage to determine the coordinates of the places where the magnetic measurements were made. In the secondary processing step, a number of corrections such as drift, elevation, parallax, international geomagnetic reference field (IGRF), levelling and microlevelling corrections, and also necessary filters or transformations, were applied on the magnetic data. Based on the processed magnetic data, a total field contour map from the Sabzevar ophiolitic zone was provided in which large magnetic anomalies were considerable. Due to ambiguities in the interpretation of the aeromagnetic data or anomalies, locating the chromite lenses appeared to be difficult. The main point, arising an ambiguity in the interpretation stage, was that neither all of the magnetic anomalies, mainly due to high magnetite contents of the rocks, were related to the presence of the chromite lenses in the subsurface, nor all of the chromite lenses were associated with high amounts of magnetite producing considerable magnetic anomalies. As the results of both qualitative and quantitative interpretation steps of the magnetic data from the ophiolitic zone were not completely applicable to locate the chromite lenses, an integration of geological, geochemical and geophysical findings was used to determine the location of these chromite lenses in the subsurface.

**GAV.07/07P/A13-008**

**1640**

**RECOGNITION OF MAGNETIC ANOMALIES ASSOCIATED WITH ORE DEPOSITS USING GIS IN MAHNESHAN REGION, IRAN**

Abolghasem KAMKAR-ROUHANI (Department of Mining and Geophysics, Shahrood University of Technology, Shahrood, IRAN)

Mahneshan region, with an area of 2472 square kilometres in the northwest of Iran, is geographically located at latitude of 36:30 to 37 degrees north and longitude of 47:30 to 48 degrees east. There are a large variety of igneous, metamorphic and sedimentary rocks in the region. Although sedimentary rocks cover most of the region, the outcrops of igneous and metamorphic rocks are also remarkably seen in the east, south and west of the region. The results of dating tests on the rock samples, taken from the geological units and formations present in the region, also show that the rocks have been formed in a wide range of geologic time from the Precambrian to the Quaternary. Geological reports from the region indicate the presence of various mineralisations of gold, copper, lead, zinc, tin and tungsten associated with plutonic and metamorphic rocks. Based on airborne magnetic surveys carried out in the region, a total magnetic field contour map has been provided by Geological Survey of Iran (GSI). The map indicates higher total field values (magnetic anomalies) in the north, northeast, west and southeast parts of the region. The large magnetic anomalies in the north and northeast parts of the region are attributed to a shallow but thick bed rock or basement of igneous (or metamorphic) type overlain by a thin overburden of sediments covered the ground surface in these parts of the region. The west and southeast parts of the region, however, are covered by igneous and metamorphic rocks, and thus, the magnetic anomalies in these areas may be associated with metallic mineralisations. For reduction of ambiguities in the interpretation of magnetic data, and thus, locating ore bodies, a vertical first derivative transformation has been applied on the total field data. As a result, a first derivative magnetic anomaly map has been obtained in which local magnetic anomalies due to the metallic mineralisations can be recognised. Geographic information system (GIS) has also been used to manage the spatial magnetic data, and as a result, the first derivative magnetic data have been reclassified. Weighting operation has, then, been applied on different classes of the first derivative magnetic map using the weight of evidence feature in GIS. Thus, based on the two groups of contrast values (i.e. contrasts above 1 and below 1), a binary map of first derivative magnetic data from the region has been produced. This binary map indicates the locations of more likely mineralisations (i.e. those with contrast values above 1) with a different colour (e.g. red) from the rest of the map. Therefore, points or places with higher contrast values on the map can represent the locations of more possible ore deposits.

GAV.07/07P/A13-009

1700

**USING ROCK PROPERTY MEASUREMENTS TO UNDERSTAND AEROMAGNETIC ANOMALIES RELATED TO INTRABASIN FAULTS: A CASE STUDY FROM THE CENTRAL RIO GRANDE RIFT, USA**

V.J.S. GRAUCH, Mark R. HUDSON, Scott A. MINOR, Jonathan S. CAINE (U.S. Geological Survey)

Faults within sedimentary basins are commonly associated with low-amplitude aeromagnetic anomalies, but whether the anomalies are produced by tectonic juxtaposition or as the result of chemical processes along the fault zone has been poorly documented. We used rock-property measurements, geophysical analysis, and geologic information to confirm that the anomaly associated with the San Ysidro Fault near the west side of the central Rio Grande rift is primarily produced by tectonic juxtaposition of sedimentary units with differing magnetic properties. More than 1000 m of sedimentary section is exposed and offset 400-700 m across the northerly-striking, down-to-the-east normal fault, located ~30 km northwest of Albuquerque, New Mexico. A 10-20 nT aeromagnetic anomaly from a survey flown 150 m above ground closely follows the fault over most of its exposure. Magnetic susceptibility (k) measurements from 254 sites were used to characterize the magnetization of the stratigraphic units. The uppermost formation, consisting of poorly lithified rift-basin sediments, shows highly variable k values, with most in the range of 1-33 x E-04 (SI). k generally increases with increasing sediment grain size. The underlying formation, consisting of older rift-basin sediments, shows less variation in k, with most values in the range of 5-13 x E-04 (SI) and less correlation with grain size. The geometric mean of k sampled from the two lowermost formations, composed of pre-rift clastic sediments and sedimentary rocks, is 1.3 x E-04 (SI). We developed magnetic models along several profiles across the fault by assigning the characteristic k values to the units in geologically constructed cross-sections. Calculated responses from the magnetic models fit the observed curves to first order. Some differences between models in the assignment of k for units in the uppermost formation were required, which is expected based on its measured variability. Comparing the models to magnetic depth estimates from the observed data confirms that magnetic contrasts arise at several different juxtapositions of units along the fault and between the same juxtaposed units along strike. In addition, deviations in the anomaly gradient location from the mapped fault trace can be explained by differences in the depth to the shallowest contrast and by variations in fault dip. Thus, tectonic juxtaposition of different stratigraphic units is the primary cause of the aeromagnetic anomaly associated with the San Ysidro Fault. Further study should lead to a better understanding of the detailed relations between lithology, structure, magnetic properties, and aeromagnetic sources. This understanding will help us use aeromagnetic data to predict which lithologies are juxtaposed across buried faults and their structural configurations in other parts of the basin, which are important for understanding the alluvial basin aquifer system.

**GAV.07-Posters****MAGNETIC ANOMALIES AND ROCK PROPERTIES**

Location: Site D

Monday, July 7 PM

GAV.07/07P/D-001

Poster

1400-142

**MAGNETIZATION OF OCEANIC CRUST SUBDUCTING BENEATH THE JAPAN TRENCH**Yumiko NODA<sup>1</sup>, Toshiya FUJIWARA<sup>2</sup>, Yukari KIDO<sup>3</sup> (<sup>1</sup>Department of Earth Sciences, Toyama University, <sup>2</sup>Deepsea Research Department, Japan Marine Science and Technology Center, <sup>3</sup>Institute for Frontier Research on Earth Evolution)

We present characteristics of crustal magnetization around the northern Japan Trench, analyzed from magnetic anomalies. The northwestern margin of the Pacific Plate is being subducted beneath the northern Japanese Islands at the Japan Trench. In the northern part of this trench, the Pacific Plate has a series of parallel magnetic anomalies (Japanese Lineations), identified as chron M10-M7 (130-127 Ma). These anomalies are well lined and have high-amplitudes of ~500-1000 nT, peak-to-trough, in the seaward slope of the trench. The amplitudes of anomalies gradually decay to the landward from the trench axis, associated with the plate subduction. Crustal magnetization was calculated to correct for effects of increasing depth of subducting plate and seafloor topography. We used a three-dimensional inversion method. Upper surface of the magnetic source layer is assumed to be the surface of oceanic crust. In the seaward slope, ocean drillings and seismic reflection profiles indicate that the thickness of sediment layer is ~500 m. Meanwhile, densely distributed seismic refraction and reflection profiles in the study area enable us to constrain the surface of the subducting oceanic crust, in the landward of the trench. Uniform thickness of the magnetic source layer, and constant direction of magnetization within the source layer are assumed in this calculation. As the general trend of magnetization, the magnitude gradually decreases as the plate subduction proceeded. In the study area, temperature in the subducted oceanic crust is supposed to be still lower than 100 °C, deduced from heat-flow measurements, even at depth of 20 km beneath the seafloor. Thus, temperature effects to reduce the magnetization could be insufficient. Otherwise, low temperature chemical demagnetization is possible for reducing the magnetization. The apparent decay in magnetization would reflect some kind of destruction and mechanical disorganization of the topmost part of the subducting oceanic crust by friction along the plate boundary, resulting in progressive randomization of natural remanent magnetization of the magnetic layer. There appeared to be along-lineation variation in magnetization. The wakes of higher magnetization, sub-perpendicular to the strike of lineations, may suggest non-transform discontinuities that originated at a mid-ocean ridge, where the oceanic crust was formed.

GAV.07/07P/D-002

Poster

1400-143

**MARINE MAGNETIC ANOMALIES FOR SHIKOKU BASIN, NANKAI TROUGH**Yukari N. KIDO<sup>1</sup>, Toshiya FUJIWARA<sup>2</sup> (<sup>1</sup>IFREE, JAMSTEC, <sup>2</sup>DSR, JAMSTEC)

The Nankai Trough and Shikoku Basin, where the Philippine Sea plate subducts beneath the Eurasia plate, has a series of magnetic lineation patterns demonstrating a seafloor origin aligned NW-SE. They are clearly visible seaward of the trough but gradually disappear to the NW across the axis. The development of the Shikoku basin started in the late Oligocene (~25 Ma), splitting the proto Kyushu-Palau arc into two parts. The spreading direction changed to east-west at 23 Ma. From 23 Ma to the final stage of active eruption at 7Ma, several transform faults, fracture zones, off-ridge volcanism and other tectonic traces were produced. We collected marine magnetic data across Shikoku basin and the Nankai Trough together with MCS and OBS seismic structural data. We also use geomagnetic anomaly data provided by the GSJ's East Asia magnetic anomaly map, the Hydrographic

Department, and JAMSTEC. In this paper, we present forward and inverse magnetic modeling with slab depth distribution and discuss the decay process of magnetic anomalies from viewpoints of seismic stratigraphy and structure. The objectives of the study are: (1) to reveal the characteristics of the subducting plate with magnetic anomalies; (2) to identify geomagnetic properties with intensity variations and shape of magnetic layers; (3) to build a 3D magnetic crustal structure model in this region. We identify five categories from magnetic intensity distribution in the subducting northern Shikoku basin; the westernmost zone; Kyushu-Palau Ridge, the easternmost zone; Zenisu ridge, the middle; Kinan Seamount chain, the Ashizuri zone, and Kii Peninsula zone. Magnetic inversion analysis with slab depth observes cyclic intensity along the Kyushu-Palau and Zenisu ridge zones. Along the Kinan Seamount Chain and off the Kii Peninsula zone, intensity lineation along traces of segmentation and fracture can be seen. The magnetic lineation for Ashizuri is clear up to the trough axis, with rapid attenuation landward of the axis. The main component of total magnetic force is 300 nT at 50 km south of the trench axis, which can be modeled with a 2 km thick oceanic crust with 8 A/m magnetization. Along the trench axis track line, a 2 km thick crust with 7 to 2 A/m magnetization is required to explain the magnetic profiles. At 50 km north of the trench axis, non magnetic crust is needed. One potential mechanism for reducing the magnetic amplitude is low temperature chemical demagnetization. The other possibility is horizontal dislocation of oceanic crust along active faults; such as splay faults, heterogeneous structure and interaction between the decollement.

GAV.07/07P/D-003

Poster

1400-144

**MAGNETIC SIGNATURES OVER FOUR SEDIMENTARY BASINS OF EASTERN CONTINENTAL MARGIN OF INDIA**

Vinit C. ERRAM, Mita RAJARAM, Anand P. SASHIDHARAN (Indian Institute of Geomagnetism, Plot No. 5, Sector-18, Near Victoria Petrol Pump, Kalamboli (Highway), New Panvel (W), Navi Mumbai-410206.)

The Eastern Continental Margin of India (ECMI) is important from the point of view of oil exploration. Four petroliferous sedimentary basins were chosen from ECMI to the study long wavelength features: the Mahanadi basin of Orissa, Krishna-Godavari basin of Andhra Pradesh, Palar basin and the Cauvery basin of Tamilnadu. Ground magnetic data were collected over these four basins with a station spacing of 5 to 10 km and dictated by road access. The anomaly maps contain combination of trends and comparison with the marine magnetic data shows that the anomalies continue into the offshore region. The trends in the ground magnetic anomalies corroborates very well with the aeromagnetic maps and signatures of the Sileru shear, Nallamalai shear, contacts between the crystalline and the sedimentary basins etc are evident on the maps. To identify magnetic sources related to different depths, various transformations have been applied on the total field anomaly map of all the four basins. The second vertical derivative and downward continued map showed NE-SW and E-W trends related to ridges and depressions of all the four coastal basin implying that these are shallow features. The deeper features evidenced from upward continuation showed NW-SE trends only in Mahanadi and Krishna-Godavari basins. Thus these two basins are composed of two structural units associated with different tectonic events. The Palar basin, which separates the Cauvery basin towards south from the Krishna-Godavari basin and Mahanadi basins towards north, marks the transition region with two structural domains in the north and with single domain in the Cauvery basin south of Palar basin. The Orthopyroxene isograd separates the Southern Granulite Terrain (SGT) from the northern Dharwar craton and Eastern Ghat Mobile Belt (EGMB). The Palar basin lies within this transition zone and also brings out the two structural domains to the north with a single domain to the south. The Palar river fault appears to control the tectonic activity of the region. The analytical signal identifies the Charnockites as the main magnetic source of the area. The data were also filtered and euler depths calculated. Results of the analysis will be presented. A comparison with the magnetic data from Antarctica and Australia should help to build a tectonic model of the Gondwanaland separation.

GAV.07/07P/D-004

Poster

1400-145

**MAGNETIC AND ELECTRICAL STUDY IN ARCHEOLOGICAL SURVEY: THE FOX-AMPHOUX SITE (FRANCE)**

Daniel HERMITTE, Pierre-Etienne MATHE, Andre REVIL, Ginette SARACCO (CNRS-UMR 6635, CEREGE, Department of Geophysics, Aix-en-Pce)

A total magnetic field survey of the archeological site of Fox-Amphoux (Southern France) was performed by a G858 cesium vapor probe combined to electrical resistivity profiles in order to localize and characterize the archeological structures. Magnetic mapping was obtained using the kriging extrapolation method on a 1x2.5m grid step. A Wenner protocol (64 electrodes of 1m spacing) combined with classical RES2DINV software, was performed to obtain resistivity data as inversion results from potential measurements. This site is potentially constituted of several buried ovens, as suggested by the numerous decimetric fragments of artefacts lying on the field. These structures are embedded in a clayey soil on a carbonated substrate, outcropping at site boundaries. Both resistivity and magnetic method point out anomalies of two different wavelengths, above and below ten meters, which characterize respectively the main geological and archeological structures. Spatial distribution of resistivity and magnetic anomalies are in a good agreement. These methods appear complementary to localize and determine the nature of sources. Magnetic mapping allows an horizontal determination of archeological structure, while the resistivity method gives a better constrain on the burial depth. Similarly, the higher the resistivity (e.g. carbonates) contrasts the lower the susceptibility contrast is, and reverse. So archeological artefacts of various nature can be detected either by one or both of these methods. Further work will consist in an automatic characterization of archeological structure by position scale method (wavelet transform). The validity of the choice of the analyzing wavelet will be checked by using the petrophysical parameters obtained in this study.

GAV.07/07P/D-005

Poster

1400-146

**MAGNETIC PROPERTIES OF OIL-GAS-BEARING ROCKS OF THE CENTRAL PART OF DNIPER-DONETSK TROUGH**

Roman KUDERAVETS, Valentyn MAKSYMCHUK, Jurij GORODISKY (Carpathian Branch of the Subbotin Institute of the NAS of Ukraine)

Small amplitude positive local delta T anomalies were revealed by the results of high-accuracy magnetic prospecting in the Dniper-Donets trough over a series of oil-gas-bearing structures. Their nature can be explained by lithofacial and epigenetic rock magnetic variations in the oxidized-reduced zones of carbon deposits. Though, there is no trustworthy experimental data on magnetic properties of rocks in these zones. To study peculiarities of lateral and vertical magnetic perceptibility, mineral rock composition distribution within oil-gas-bearing areas in Dniper-Donetsk trough a series of investigations of these characteristics have been conducted for productive and unproductive holes. In general, the magnetic perceptibility of core from 19 holes, near oil-gas deposits and far from theirs as well were determined. A statistic analysis of the obtained cappa values was done, rock mineral composition in some holes was determined. The results make it possible to

## IAGA

conclude:1. The cut is composed mainly of terrigenous rocks and is characterized by a slight differentiation by the magnetic perceptability ( $0-150 \times 10E-5Si$ )2. Small values of rock magnetic perceptability ( $1-3 \times 10E-5Si$ ) and dispersion for low Visean substage of low carbon with which oil-gas-bearing of the region under study is closely connected were determined.3. Statistic analysis proved the existence of some types of cappa distribution within the hole in particular it differs within productive and unproductive formations.4. Larger values of cappa and their dispersion in comparison with analogical deposits in productive formations, were revealed.5. A series of secondary epigenic minerals: quartz, kaolinite, aragonite, ankerite, dolomite, pirite, hematite, siderite was determined in the deposit zone and out of it. The largest amount of ironminerals (ankerite, pirite, hematite, siderite) was found in terrigenous rocks (argillite) located over and under carbon deposits. The analysis of the outcomes testifies to the significant influence of carbon on magnetic perceptability distribution and mineral composition in the zones of oil-gas-bearing.

**HS01** **Tuesday, July 8 - Wednesday, July 9**

**EROSION PREDICTION OF UNGAUGED BASINS (PUBS):  
INTEGRATING METHODS AND TECHNIQUES (ICCE, ICRS AND  
ALL IAHS COMMISSIONS)**

Location: Site C, Room 29

**Tuesday, July 8 AM**

Presiding Chairs: W. Froehlich, T. Mizuyama

**HS01 /08A/C29-001**

**0950**

**MATHEMATICAL MODEL FOR PREDICTING SOIL EROSION THROUGH RUN-OFF  
FROM UNGAUGED WATERSHEDS**

Uttam C. SHARMA (Indian Council of Agricultural Research)

The northeastern region of India, having an area of 255090 sq km, is predominantly hilly. Though the region is endowed with rich natural resources of soil, water and vegetation, it has remained economically backward due to gross misuse and mismanagement of these resources. Prevalence of shifting cultivation, land ownership pattern, heavy precipitation, low accessibility due to hilly terrain, lack of proper infrastructural and marketing facilities are the major socio-economic constraints hindering judicious management of natural resources. Shifting cultivation alone results in deforestation and an annual loss of 88.3 million tonnes of soil and 10620, 370 and 6050 tonnes of N, P<sub>2</sub>O<sub>5</sub> and K<sub>2</sub>O. The practice was alright when the shifting cycle used to be 25 to 30 years and the land was rejuvenated with vegetation but with reduction in shifting cycle to 2 to 10 years, the surface soil gets washed away with rain water due to constant human interference on hill slopes. With increase in population from 10.5 million in 1951 to 40.0 million in 2001, there is tremendous pressure on land, water and forests. Heavy annual rainfall of 250 cm has caused unabated soil erosion in the hills and silting of river beds and floods in the plains. A soil erosion model was developed for describing the loss of soil in order to estimate the overall soil loss from ungauged watersheds with known parameters. The data used to develop the model was collected from long term study on eight gauged watersheds, undertaken at ICAR Research Complex, Barapani and Byrnhati, Meghalaya, India as well as also from some other gauged watersheds under different agro-climatic conditions and slopes. Four parameters viz slope of the land, rainfall, soil clay content and vegetation cover were taken as independent variables and soil loss through run-off as dependent variable, for developing the model. These parameters are mainly responsible for controlling the soil loss through run-off from the watersheds. The gauged watershed comprise only a minute fraction of the total ungauged area of the region which require soil erosion estimation on spatial and temporal basis. The vegetative cover was considered in the scale of 1 to 5, 1 being bare soil surface and 5, being the extremely dense forests with trees, bushes and grasses. The mathematical model is: Soil loss through run-off (tha<sup>-1</sup>) = 41.73 + 0.181 x slope (%) + 0.046 x rainfall (cm) - 0.387 x clay (%) - 8.125 x vegetation cover (1 to 5 scale). The model was applied to the data obtained from gauged watersheds during subsequent years for validity and was found quite effective in estimating soil loss through run-off from watersheds. However, further investigations are required for refinement of the model.

**HS01 /08A/C29-002**

**1010**

**A DISTRIBUTED HYDROSEDIMENTOLOGICAL MODEL FOR ESTIMATING SEDIMENT  
EROSION AND DEPOSITION IN YELLOW RIVER BASIN**

Zongxue XU, Kuniyoshi TAKEUCHI, Hiroshi ISHIDAIRA, Changming LIU (Institute of Materials & Environmental Technology, Graduate School of Engineering, Yamaguchi University)

Although great achievements have been made on hydrological research in the past several decades, the problem of how to predict reliably the sediment erosion and deposition in ungauged river basins has been still a great challenge for hydrologists. The objective to obtain available information on hydrological variables such as precipitation, streamflow, especially sediment erosion and transport is also a great challenge and a key issue for the integrated water resources management in the Yellow River basin, where streamflow and sediment erosion rate are not monitored in most part of the catchment, and it is therefore quite difficult to identify where and how much erosion or deposition of sediment has occurred in the study area. The simulation for the erosion, transport and deposition of sediment involves complex interactions among precipitation, surface and subsurface hydrologic processes, soil properties, land cover and topography. For this kind of complex spatial process, conventional conceptual rainfall-runoff model has its limits on the simulation ability. On the contrary, GIS and spatially distributed models provide great potential for improving mankind's capability to understand hydrological processes, especially those in ungauged basins. In this paper, a spatially distributed hydrosedimentological model for the simulation of water budget and estimation of the sediment erosion is proposed and applied to Wei River basin, one subbasin of the Yellow River in China. The total area of the basin is 139,000 km<sup>2</sup> and is subdivided into 48,146 grid cells with a horizontal spacing of approximately 2kmx2km. The unique characteristics of the strongly variable land use, soil, and geography are schematically represented through those square cells. The hydrological processes are simulated at the grid scale. DEM data is taken from GTOPO30 database. Daily precipitation, temperature, wind speed, and other climatologic data are taken from National Climatic Data Center (NCDC). A catchment digital elevation model is created through an automatic processing of the elevation data, streamlines, and soil and vegetation cover data by using Arc/View GIS software. Routing of the water and sediment to the catchment outlet is performed by simplified equations of continuity and motion for both water and sediment. The governing equations are integrated and calibrated on a daily time scale by using available field data on precipitation, climatological observations, and sediment data in the study area. The numerical simulations show that the proposed mathematical model is able to adequately simulate the water and sediment budgets in the catchment on a daily time scale. It also shows that the GIS and spatially distributed modeling have indeed greatly improved the capability for characterization of streamflow, erosion and transport of sediment at the basin scale.

**HS01 /08A/C29-003**

**1050**

**APPLICATION OF A RAINFALL-SEDIMENT-RUNOFF MODEL TO THE UPPER  
BRANTAS RIVER BASIN, INDONESIA**

Takahiro SAYAMA<sup>1</sup>, Kaoru TAKARA<sup>2</sup>, Yasuto TACHIKAWA<sup>2</sup> (<sup>1</sup>Graduate School of Civil Engineering, Kyoto University, <sup>2</sup>DPRI, Kyoto University & CREST, JST)

The circulation of water and substances is important to deal with environmental problems in river basins. Sediment is one of the significant substances that have a potential to change the environment of basins. Being covered with very fine volcanic ash, the Brantas river basin, East Java, Indonesia yields a lot of sediment, which will be deposited at dam

reservoirs and riverbeds, and these sediment movements increase flood risk and shorten the lifespan of dams. There are some measures to protect erosion and to decrease sediment deposits at dam reservoirs, such as forestation and Sabo dams. Accurate prediction of sediment movement in river basins and relevant evaluation of these measures are very important for integrated water and sediment management. Distributed hydrological models have been applied to investigate sediment movement in basins considering geographical conditions, meteorological information, and human activities. However, we often face to the problem that there are not many reliable data, especially related to sediment. Remote sensing and simple in-situ measurements for hydrological analyses could be useful tools for the compensation. This research constructs a distributed sheet erosion process model for sediment runoff prediction in a catchment scale. The model deals with spatial information such as flow direction, slope and land cover. GIS has generated a DEM from digitized contour map, and classified land cover based on ADEOS/AVNIR images acquired on June 4, 1997. Constructed here is a grid-cell based distributed rainfall-sediment runoff model. Surface and subsurface flows on each grid-cell are simulated by the Kinematic Wave model, and the transportation capacity of overland flow is calculated based on the unit stream power theory for modeling sediment yield and deposit processes physically. Sediment yielded in slope cells moves in the flow direction derived from the DEM to river grid-cells. For realistic simulation of riverbeds, bed load and suspended load in the channel are calculated in river grid-cells by incorporating elevation change caused by sediment movement. The model is applied to the Lesti River basin (625 km<sup>2</sup>) located in the upper Brantas River basin. The performance has been verified with historical hydrological data (hourly rainfall and discharge sequences during a rainy season from November 1995 to April 1996). The verification indicates that the model can reproduce the sedimentation record at the Sengguruh dam located at the junction of the Lesti River and the Brantas main reach. Further, the volume of eroded material at the cultivated hill slope of Mt. Semeru is found larger than other parts of the basin, which is analogous phenomenon to the natural physical process of sediment erosion. The model simulation gives us information to predict the risk of changing the circulation of substances in basins.

**HS01 /08A/C29-004**

**1110**

**PHYSICALLY-BASED MATHEMATICAL FORMULATION FOR HILLSLOPE SCALE  
PREDICTION OF EROSION AT UNGAUGED BASINS**

Hafzullah AKSOY<sup>1</sup>, M. Levent KAVVAS<sup>2</sup>, Jaeyoung YOON<sup>3</sup> (<sup>1</sup>Istanbul Technical University, <sup>2</sup>University of California, <sup>3</sup>University of California)

An explicit finite difference scheme for erosion and sediment transport on upland areas of a watershed is derived. The derivation is based on the unsteady state one-dimensional sediment continuity equation and the momentum equation simplified with the kinematic wave approximation. The derivation is ended up with a linear partial differential equation to be explicitly solved by a finite difference scheme. Hydrological part of the model uses a simplified scheme for which a linearized partial differential equation was developed. Outputs of the hydrological simulations are given as inputs to the erosion and sediment transport routine. Upland erosion is thought of as sheet erosion. Erosion due to rainfall and that due to runoff are considered. Rainfall erosion and runoff erosion include non-physical calibration parameters. Calibration of those parameters is of great importance for ungauged basins where data do not exist. In this study, at the end, a backward finite difference scheme is chosen to solve the resulting equation together with appropriate boundary and initial conditions. Hypothetical data sets are used in evaluating the applicability of the model developed in the study.

**HS01 /08A/C29-005**

**1130**

**CALIBRATING SEDD MODEL FOR SICILIAN UNGAUGED BASINS**

Vito FERRO<sup>1</sup>, Costanza DI STEFANO<sup>1</sup>, Mario MINACAPILLI<sup>1</sup>, Mario SANTORO<sup>2</sup> (<sup>1</sup>Dipartimento di Ingegneria e Tecnologie Agro-Forestali, University of Palermo, Italy, <sup>2</sup>Dipartimento di Ingegneria Idraulica ed Applicazioni Ambientali, University of Palermo)

Identifying areas of the landscape that are most sensitive or susceptible to erosion stimulated the study of within-basin variability of the sediment delivery processes and the use of spatially distributed models coupled with Geographical Information Systems. At first in this paper, for a basin divided into morphological units, a Sediment Delivery Distributed (SEDD) model based on the Revised Universal Soil Loss Equation (RUSLE), with different expressions of the topographic factors, and on the sediment delivery ratio SDR, of each morphological unit is briefly reviewed. In particular, the within-basin variability of the hillslope sediment delivery is modelled by a sequential approach. This approach follows the sediment mass in a Lagrangian scheme and applies appropriate delivery factors SDR, to each sequential modelling morphological unit. The sediment delivery factor SDR, is calculated by the relationship proposed by Ferro and Minacapilli (1995) in which a only parameter b appears. The model was applied using as morphological units the square cells (square size equal to 50 m) of a Digital Elevation Model realized by ARC-INFO software and using a topographic map on scale 1:25,000. The application of SEDD model was developed for five Sicilian basins having a reservoir at the basin outlet and an area ranging from 20 to 70 km<sup>2</sup>. All basic information for applying the model (rainfall erosivity, soil erodibility, topographic factors, travel time, etc.) were stored into the information layers of a GIS managed by ARC-INFO software. The application of the model at mean annual temporal scale allowed to calculate both the spatial distribution of the sediment yield (raster cover) and the sediment yield Y<sub>o</sub> at basin outlet, which is equal to the sum of the sediment yields Y<sub>i</sub> produced by all morphological units into which the basin is divided. For the five investigated Sicilian basin the sediment balance equation at the basin outlet, which equates the sediment yield measured Y<sub>o</sub> by reservoir sedimentation to the basin sediment yield Y<sub>o</sub> calculated by SEDD model, allowed to estimate the values of the only parameter b of the model. Finally, the b values obtained for the five monitored basins were used to establish an estimate relationship useful for applying the SEDD model to Sicilian ungauged basins.

**HS01 /08A/C29-006**

**1150**

**HYDROLOGICAL MODELING OF IMPERFECT GAUGED BASINS: A NEW CHALLENGE**

Jun XIA (Institute of Geographical Science & natural Resources Research, Chinese Academy of Science)

Many countries of the world have been facing increasing problems in managing their water resources. The imperative of the sustainable development puts several tasks on water management. China is an example of a country where water related problems are multifold and range from water shortage, eco-environment degradation to food safety, such as the courses drying up of low reaches of the Yellow River which almost became an annual events since 1972, and water crisis of the three river's alluvial plain in last two decades in terms of shallow groundwater depletion. In order to manage water resources in a sustainable manner, it was emphasized to study hydrological processes associated with water problems to understand causes of existing vulnerability of water resources and provide more information of water resources change in basin/regional scale to try to increase water safety. This paper address following problems:(1) Analysis of the time-space variation of the basin hydrological

cycle: To identify the fundamental characteristics of hydrological changes by using the basic information obtained from the hydrological processes and the analysis data from the multiple features of the time-space field. (2) Remote sensing information identification and parameterization of land-water interactions: To provide useful information for the construction of the hydrological model by making use of remote sensing data obtained from MODIS/TM combined with DEM and other GIS data layers, the mathematical model to be developed is required to capture the changes of types and coverage of vegetation, temperature in canopy layer and land surface, rate of reflection, soil water wetness, evapotranspiration capacity, and urbanization impact. Furthermore, through downscaling research, we aim to obtain the characteristic pattern of parameter variations of the basin-scale hydro-ecological model. (3) Modeling and verification of the time-space variation of the basin hydrological cycle: This covers the study on how the information obtained from unit dynamic processes of water cycle can be used to extract required information at basin scale by using nonlinear parametric regression techniques in statistics. We aim to build a hydrological cycle model based on the specific characteristics of the land and environmental conditions of Northern China. This model will help us understand the interrelationship between the information obtained from the experimental site and the entire study region. It will integrate the physical processes of and interactions between surface water and ground water, the changes in land use/cover and the remote sensing information obtained. Simulation studies will be performed to examine the effectiveness of the model, and to evaluate the impact of human activities on the water carbon cycle. Problem is "Can we do hydrological modeling & prediction in the imperfect gauged basin? How we can reduce uncertainty of hydrological modeling in large basin?". Hydrologists will have to face new challenges and opportunities that will be discussed in the Workshop.

**Tuesday, July 8 PM**

Presiding Chairs: A. Pietroniro, I. Douglas

**HS01/08P/C29-001**

**1400**

**THE APPLICATION OF AGRICULTURAL NON-POINT SOURCE POLLUTION (AGNPS) MODEL FOR THE SEDIMENT YIELD AND NUTRIENT LOSS PREDICTION IN DUMPUL SUBWATERSHED, CENTRAL OF JAVA, INDONESIA**

Sutopo Purwo NUGROHO (The Agency for the Assessment and Application of Technology)

Soil erosion in Indonesia is one of that nation's most serious environmental degradation problems. However, reliable measurement of erosion remains limited, and estimates of soil productivity are even rarer. Assessing the extent and seriousness of erosion, therefore, remains a difficult task. Nevertheless, identification and assessment of erosion problems could have an important role in influencing better land use and conservation practices. Watershed management plan should be done with use them AGNPS model. The model was used to identify critical areas within the watershed where land treatment should be focused to optimize result. Furthermore, the land and water conservation could establish on the critical areas according to bio geophysics of conditions from the watershed. The application of the AGNPS model in the Dumpul subwatershed, Central Java, resulted in a coefficient determination between AWLR and AGNPS of 0.94 when the latter model was for measuring sedimentation rates. Further analysis of the relationship between model versus measurement nutrient loss, phosphorous loss, and chemical oxygen demand loss has 0.98. Sediment yield, calculated by AGNPS model respectively nutrient loss, phosphorous loss, and chemical oxygen demand loss have 420.82 kg/ha, 6.83 kg/ha, 4.26 kg/ha, and 0.1 kg/ha respectively. The result of the model simulation at Dumpul subwatershed was get that land use change with farmstead would increase for peak runoff volume, peak runoff flow rate, sediment yield, nitrogen loss, phosphorous loss, and chemical oxygen demand concentration of about 36.5%, 39.8%, 118.1%, 87.4%, 90.6%, and 110% respectively. But, by the land and water conservation as crop contoured on all of watershed would decrease of about 33.3%, 29.8%, 57.2%, 45.9%, 46.6% and 41% respectively. At the same methods, crop contoured with combine terrace would decrease of about 52.1%, 51.4%, 77.4%, 68.2%, 68.5% and 72%.

**HS01/08P/C29-002**

**1420**

**EVALUATION OF CREAMS MODEL IN PREDICTING EROSION FROM AGRICULTURAL PLOTS IN BIRJAND, IRAN**

Nasser TALEBBEYDOKHTI (Department of Civil Engineering, University of Shiraz)

Agricultural soil considered being one of the most important natural resources for each country. Nowadays, erosion from agricultural land is a serious threat to human welfare and even a limiting factor in shaping human life. Erosion from agricultural land not only deteriorates top soil for which thousand of years are required for their creation, but also their accumulation in reservoir and transmission line may interfere with usual functioning of such hydraulic structures. This research is undertaken to further our understanding of erosion processes and delineate factors affecting erosion rate. To achieve the objectives cited in the study, four experimental plots with dimension 1.4\*2.0m and different physiographic settings were separated from adjacent land in Birjand region. After designing a field rainfall simulator, synthetic rainfall was applied to each plot and a set of rainfall-runoff and corresponding sediment load were gathered for further processing. Simulation of observed behavior was achieved via a continuous-based, distributed and physically based rainfall-runoff model so called CREAMS. After splitting the data set into two pieces, the first piece was used for model calibration, while the second piece was used for model verification. Results obtained from this research showed that (1) CREAMS hydrologic module is quite capable in replicating system response, while the erosion module was not successful partly because of uncertainty involved in data collection procedure and partly due to lack of calibrating this module. (2) Both sensitivity analysis and calibration of model is very sensitive to the selected state variable. Runoff calibration will trigger hydraulic conductivity and suction head while calibration for evapotranspiration will trigger some other calibrating parameters.

**HS01/08P/C29-003**

**1440**

**PROBLEMS OF MODEL SELECTION IN SEDIMENT YIELD PREDICTION**

Shou-shan FAN (Clarkson University)

Sediment yield from a watershed can be defined as the sum of all soil erosion less all sediment deposition within the entire watershed. Computer models have long been used by scientists and engineers in analyzing sediment yield from a watershed. Today in the United States, many computer models are available for use in predicting sediment yield. Unfortunately, all models are only approximations of the real world and are embedded with certain degrees of uncertainty. Therefore, the proper selection of models that would best fit a particular circumstance is always a critical and difficult task. While models are highly useful tools they can also be a source of misinformation for users and project managers who do not understand all the assumptions, capabilities, and limitations of a particular model. Unfortunately, this has been case in regulatory analysis. This paper is based on the author's experience working with a major Federal regulatory agency and an interagency sedimentation model evaluation group which consists of ten major agencies. It analyzes

several sediment yield approaches that have been used in the United States.

**HS01/08P/C29-004**

**1500**

**PARSIMONIOUS STATISTICAL MODELS FOR FAST ESTIMATION OF THE SUSPENDED SEDIMENTS DISCHARGES IN UNGAUGED BASINS**

Ionel HAIDU, Gavril PANDI (Dept. of Geography, Univ. of Cluj-Napoca)

In many parts of the world the hydrometrical network for suspended sediments measurements is still poor, but the need of information as regarding the erosion and the sedimentation rises continuously. In the other parts, because some economical reasons, the tendency is to reduce the existing network. In both cases the consequence is the necessity to explore much more the existing limited data. There are hydrological basins or regions having observations only on discharges or precipitations, and only a few stations having data on solid discharges, too. Therefore it is impossible to apply a deterministic model, or may be, it is too expensive to do it. This is the case when, for simple and fast estimation purpose, the statistical single input-output methodology could be applied. In Romania, at the beginning of the seasons there is a need for the information about the suspended alluvial in ungauged basins, in order to plan the erosion protection works, to assess the sedimentations rates in channels and in man made lakes and in order to plan the water resources managements. The 25 basins' monthly discharges and suspended alluvial discharges observed in the period 1960-2000 in Northwestern Romania (Tisza-Somes basin) were considered in order to check some statistical parsimonious models for simulation and forecasting. In order to get forecast or synthetic sequences of solid discharges in ungauged basins, we need a physical support capable to transfer the model on the length of the river or from a river to another. The physical support could be a mathematical relationship between the parameters of the model and any physiographical characteristic of the basin. Three models were tested: PARMA, Simplified Thomas-Fiering (STF) and the regression  $R=f(Q)$  model. In order to transfer the models from the gauged to the ungauged basins, GIS procedures were used, the results being parameters maps. Model tests on simulation as well as on forecasting were made according to the "split sample" principle. The simulation and the forecast performance of these models are compared using various measures of accuracy (RMSE, Cc, R2 etc). The stochastically models PARMA and STF give unexpected errors. The most valuable seems to be the  $R=f(Q)$  model which is a third order polynomial. The inferred law shows that the shape of regression curve (explained by the model parameters) is depending on the basin's size. There is possible to determine a coefficient of distortion of the curve on the length of the river. Therefore, the problem is reduced to the liquid discharge forecasting in the ungauged basins. In this paper is used the monthly rainfall-runoff model of Vrije Universiteit Brussels. Also, on the base of upstream and downstream curves shapes of  $R=f(Q)$  a similar curve for the ungauged basin has been estimated. This model gives good results on the length of the river but satisfactory results for the comparable rivers in the same region. Better results were obtained for the maximal season (power curve) and for the minimal season (modified exponential).

**HS01/08P/C29-005**

**1520**

**DEVELOPMENT OF AN INTERACTIVE EMBEDDABLE GEOGRAPHIC INFORMATION SYSTEM (E-GIS) PROGRAM FOR SOIL EROSION PREDICTION**

Ahmad MUNIR<sup>1</sup>, Muhammad Nurdin ABDULLAH<sup>2</sup> (<sup>1</sup>Faculty of Agriculture and Forestry Hasanuddin University,, <sup>2</sup>The Ministry of State for Research and Technology of the Republic of Indonesia.)

Erosion is a critical aspect in the overall water resources project and its properties are a dynamical phenomenon. A computer model was developed for simulating such dynamical phenomenon. The computer model is named E-GIS (Embeddable Geographic Information System) which is specially designed for soil erosion prediction. The model was programmed using Borland Delphi and MapObject component. It consists of five sub models. The first sub model is DATABASE, it is used for managing data for the model. The second sub modelis AKUISISI deals with data acquisition. The third sub model is RAMAL deals with forecasting simulation of erodibility and crop factor coefficients. The fourth sub model is SIMULASI, its main function is erosion simulation, this is the core of the model. The fifth sub model is E-GIS, deals with spatial erosion simulation. The sixth sub model is LAPORAN deals with spatial presentation of erosion variable. The model was tested and validated using recorded data at the Jeneberang Watershed, South Sulawesi, Indonesia.

**HS01/08P/C29-006**

**1600**

**SPACEBORNE RADAR INTERFEROMETRY: A PROMISING TOOL FOR EROSION ASSESSMENT IN UNGAUGED BASINS**

Filippo CATANI<sup>1</sup>, Paolo FARINA<sup>1</sup>, Sandro MORETTI<sup>1</sup>, Giovanni NICO<sup>2</sup> (<sup>1</sup>Department of Earth Sciences, University of Firenze, Via La Pira, 4 50121 Firenze - Italy, <sup>2</sup>National Research Council, Institute of Radioastronomy, c/o ASI/CGS, 75100 Matera - Italy)

Population growth and urban development, with the consequent requirement of improved supplies and development of new potential water resources, have increased the need of an accurate knowledge of hydrological phenomena at basin scale, such as runoff, erosion-sedimentation and mass movements, in order to assess the possible consequences of their future evolution on human activities. However, the prediction of these evolutionary trends is often difficult due to the lack of data concerning hydrological parameters. This problem can be mainly connected to the difficulties in the measurement of such data. In particular, mass transfer rates are generally measured at few chosen points along the main channels of the watershed. This approach usually leads to unsatisfactory results since sediment transfer is mainly controlled by scale invariant pulse processes which are spatially and temporally scattered everywhere within the watershed. Local point measurements unavoidably involve the loss of information on spatial variability generating averaged or lumped values. In this context the extraction of such information could benefit from the use of a remote sensing technique, characterized by large scale and low cost. Spaceborne SAR interferometry in the last few years has been successfully applied to reconstruct the topography of the observed scene and to measure with millimeter accuracy changes on the earth surface induced by different geophysical phenomena. The aim of the present work is to investigate the possible contribution of the interferometric technique in the retrieval of hydrologically-related geomorphic parameters. In particular the attention has been focused on the possibility to obtain two different types of data: i) continuously updatable DEMs of basins with a suitable vertical accuracy and ii) quantitative spatially distributed estimates of sediment transfer among hillslopes and between hillslopes and channels. These information can be extremely valuable for the calibration of hydrological models as well as for a better understanding of the spatial and temporal distribution of the landscape sculpting processes in a wide range of scales within the basin. The method has been applied by using SAR data acquired by the ERS satellite on different test-sites located in the Italian Alps and Apennines.

HS01/08P/C29-007

1620

**ASSESSING THE EFFECT OF LAND USE CHANGES ON RUNOFF IN THE TA-CHOU BASIN**

Pao Shan YU, Yu Chi WANG, Chun Chao KUO (Department of Hydraulics &amp; Ocean Engineering, National Cheng Kung University)

Land development and urbanization is significantly increasing these two decades because of population and economy development in Taiwan. The change of land use has caused the effect on hydrological processes. Unfortunately, almost areas are not suitably monitored such changes. Therefore, to investigate the influences of urbanizing on runoff hydrograph much depends on a distributed rainfall-runoff model, which can simulate the spatial hydrological processes. The Ta-Chou basin, in which there has a significant change on land use recently, is chosen as the study area. Both the Remote Sensing and GIS techniques are combined with a grid-based distributed Rainfall-Runoff model to assess the impact of land use change on runoff. As there are no any observed runoff data for model calibration, the calibrated model parameters from neighbor watershed are used in the studied area for runoff simulating. The 1972 LANDSAT MSS and 2000 SPOT satellite images are applied by using both traditional supervised and unsupervised classification methods to identify the land use types, and assess the land use changes from 1972 to 2000. It is found that impervious area is significantly increased and woodland is decreased in this period, the quantity is about 147% and 81% respectively. Finally, the land use, soil type, and basin characteristics obtained by using GIS and RS are input to the distributed rainfall-runoff model to simulate the influences of land use change on runoff. The results reveal that peak flow and runoff volume of 10 years return period is increased around 10% and 25%.

HS01/08P/C29-008

1640

**RUNOFF, SEDIMENT YIELD AND NUTRIENTS LOSS MODELING USING REMOTE SENSING AND ARCVIEW SWAT2000 ON AGRICULTURAL WATERSHED OF EASTERN INDIA**Vinay Kumar PANDEY<sup>1</sup>, Sudhendra Nath PANDA, Narendra Singh RAGHUWANSHI, S. Sudhakar SUDHAKAR (<sup>1</sup>Department of Agricultural and Food Engineering, Indian Institute of Technology, <sup>2</sup>National Remote sensing Agency, Department of Space, Hyderabad, India)

The accurate prediction of runoff and sediment yield is necessary for the design of conservation structures and to select the priority watersheds for implementing conservation and management programs. The potential change in agricultural management practices can have notable effects on hydrological processes at regional scale. To assess the current resource management system, a small agricultural watershed was selected in Jharkhand state of Eastern India with objective to evaluate the use of physically based, continuous hydrological model SWAT2000 for simulation of hydrological system and to investigate the potential of nutrient losses through runoff and sediment. Indian Remote Sensing Satellite (IRS-1D LISS-III) was used for land use/land cover classification. Initially the model was calibrated and then validated with different land use. The results revealed that the time to peak of simulated runoff matched consistently well with the measured values during the calibration period. The coefficient of determination ( $r^2$ ) of 0.92 and 0.96 for runoff and sediment yield, respectively, indicated a close relationship between measured and predicted runoff and sediment yield. Nash-Sutcliffe simulation efficiency (ENS) of 0.89 and 0.89 for runoff and sediment yield, respectively, also resulted the same trend. Overall percent deviation for runoff and sediment yield, respectively, indicated that the model was predicting satisfactorily results. Magnitude and temporal variation of simulated runoff matched closely with the observed runoff ( $r^2=0.94$ ) for the entire validation period. Nash-Sutcliffe simulation efficiency (ENS) of 0.941 and 0.927 and Dv of -8.369 and -0.927 % indicated that the model was accurately validated for predicting runoff and sediment yield from the watershed. A high value of  $r^2$  of 0.99, overall deviation of -9.25 % indicated that in general, the simulated monthly surface runoff and sediment yield compared well with measured monthly values. The observed and simulated mean of NO<sub>3</sub>-N, organic nitrogen, soluble phosphorous, and organic phosphorous were not significantly different at 95 % level of confidence. The values of % deviation (Dv) were found to be -11.45, 14.16, -16.36, 7.38 (in 2000) and -17.06, -11.702, 12.12, 16.39 (in 2001) respectively for NO<sub>3</sub>-N, organic nitrogen, soluble phosphorous, and organic phosphorous indicating that the model was predicting nutrient losses satisfactorily. The value of coefficient of determination ( $r^2$ ) of 0.82, 0.84, 0.81, 0.82 (in 2000) and 0.83, 0.82, 0.81, 0.82 (in 2001) respectively for NO<sub>3</sub>-N, organic nitrogen, soluble phosphorous, and organic phosphorous indicated close agreement between the observed and simulated values of nutrient losses. Thus, ArcView SWAT2000 can successfully be applied for accurate prediction of runoff, sediment yields and nutrient losses and thereby provide necessary database for developing suitable management plans with sound scientific basis.

HS01/08P/C29-009

1700

**LAND USE SCENARIO BASED GIS-MODEL FOR REDUCING SEDIMENTATION RATE AT BILI-BILI DAM INDONESIA**

Muhammad Nurdin ABDULLAH, Ahmad MUNIR, Syamsul Arifin ILYAS (Faculty of Agriculture Hasanuddin University Makassar)

This research deals with finding land use scenarios in order to reduce sedimentation at a watershed. This research was conducted at Bili-Bili Dam, South Sulawesi Indonesia. The land use scenario was formulated by using Erosion Model based Embeddable Geographic Information System. Input data for the model were collected from aerial photograph, satellite imagery and direct observation. Seven land use scenarios were developed for evaluating the most suitable land use at the Watershed. The land use simulation scenario shows that the land without conservation generates 2121.24 m<sup>3</sup>/km<sup>2</sup>/year. The fourth scenario (with conservation) can reduce sediment because 1472.76 m<sup>3</sup>/km<sup>2</sup>/year which is lower than the Dead Storage Sediment (DSS) of Bili-Bili Dam. This value should be maintained in order to maintain the function of dam within 50 years. It was found also that, the existing framework of the land use declared by the local government (Gowa Regency) generates erosion rate is higher than tolerable soil loss erosion (TSL). Therefore the existing land use should be changed in term of following the developed scenario.

Wednesday, July 9 AM  
Presiding Chairs: D. Higgitt, D. Walling

HS01/09A/C29-001

0900

**USE OF RECONNAISSANCE MEASUREMENTS TO ESTABLISH CATCHMENT SEDIMENT BUDGETS: A ZAMBIAN EXAMPLE**Desmond Eric WALLING<sup>1</sup>, Adrian Loric COLLINS<sup>1</sup>, Henry M. SICHINGABULA<sup>2</sup>, Graham J. LEEKS<sup>1</sup> (<sup>1</sup>Department of Geography, University of Exeter, <sup>2</sup>Department of Geography, University ofZambia, <sup>3</sup>Centre for Ecology and Hydrology, Wallingford)

A sediment budget is increasingly accepted as a key tool for understanding the sediment response of a drainage basin and thus for designing and developing catchment management and sediment control strategies. However, even where they exist, sediment measurement programmes are unlikely to provide the information necessary to construct a meaningful sediment budget for a catchment. There is a need to develop new approaches to assembling this information, avoiding the need for long-term, labour-intensive monitoring programmes. The authors have attempted to develop and test such approaches in the small (63 km<sup>2</sup>) Upper Kaleya catchment in southern Zambia. Sediment source fingerprinting techniques were used to provide information on the primary sources of the sediment exported from the study catchment. The potential sources identified were the surface soils of areas under the three main land use types, namely, communal cultivation, bush grazing and commercial cultivation, and erosion of channel banks and gullies. Measurements of caesium-137 and excess lead-210 activities in soil and sediment cores collected from the catchment were also used to estimate soil redistribution rates at representative locations within the study catchment under the three different land use types. These data were extrapolated to the entire catchment, in order to estimate rates of soil loss from the catchment slopes and the associated sediment delivery ratios. Cores were also collected from the floodplain areas bordering the stream in the lower portions of the catchment and caesium-137 measurements on these cores were used to estimate rates of overbank deposition on the floodplains and the associated conveyance losses. Integration of the data provided by the sediment source fingerprinting study, the information on rates of erosion and soil redistribution and associated sediment delivery ratios provided by the caesium-137 and excess lead-210 measurements and the available measurements of sediment yield afforded a basis for establishing a tentative sediment budget for the catchment. This indicated that the sediment delivery ratio for the catchment was relatively low, with only ca. 9% of the sediment mobilised within the catchment by erosion reaching the catchment outlet. Erosion of areas under bush grazing provided the major source of the sediment load of the river (63.7%), but erosion of areas under bush grazing (17.1%) and channel and gully erosion (17.2%) were also important sediment sources. The approach developed and successfully applied in the Upper Kaleya catchment should afford a viable mean of establishing sediment budgets in other study areas with limited sediment monitoring programmes.

HS01/09A/C29-002

0920

**SOIL EROSION ASSESSMENT FOR WATER RESOURCES MANAGEMENT IN SELECTED SOUTHERN AFRICAN RIVER BASINS USING THE EROSION RESPONSE UNITS APPROACH**Michael MAERKER<sup>1</sup>, Wolfgang Albert FLUEGEL<sup>2</sup>, Aleksey SIDORCHUK<sup>3</sup> (<sup>1</sup>Center of Environmental Systems Research, University of Kassel, Germany, <sup>2</sup>Geographical Institut, Friedrich-Schiller-University Jena, Germany, <sup>3</sup>Geographical Faculty, Moscow State University, Russia)

Soil erosion is one of the major environmental problems in southern Africa and is likely to become even more severe due to population growth and climatic changes. In situ land degradation caused by soil erosion includes the loss of fertile top soil, reduction of soil productivity as a result of lowered soil fertility, which may indirectly be perceived through decreased harvests. In addition the eroded soil material, viz. sediments, reduce the water quality in a river network. Apart from direct impacts such as reservoir sedimentation, such sediments are a carrier for chemical, physical and biological pollutants, which are stored by adhesion on their active surfaces. Consequently, such reduction in water quality must be viewed as being indirect impacts of soil erosion. Furthermore, progressive land degradation by erosion aggravate water management problems in semi arid regions of Southern Africa where water scarcity is frequent. This interactive dynamics generates the need for the evaluation of suitable methods of land use management that can lead to a reduction of soil erosion and, subsequent sediment yield in runoff. However, before remediation and prevention of excessive soil erosion can be undertaken, the spatial extent of the problem has to be established. An Integrated Water Resources Management in semiarid catchments of Southern Africa should enable managers and decision makers to improve the regional strategic planning of catchment water resources by optimising water use, thus satisfying the demands of competing stakeholders while protecting water and land resources. An innovative approach characterizing erosion processes caused by water and their integrated dynamics was introduced by Maerker et al. (1999, 2001) and Fluegel et al. (1999) with the concept of Erosion Response Units (ERU). The ERUs are used to identify areas subject to different erosion processes and as modelling entities for erosion simulations. Furthermore the ERU concept allows the regionalisation of erosion process dynamics. For the delineation of the ERU as well as for the modelling procedures remote sensing techniques provide spatial information, which is normally difficult to obtain, especially in developing countries of Southern Africa. Here remote sensing techniques were applied to get information about the distributed physiographic and anthropogenic catchment characteristics (land use, soil surface, digital elevation models, etc.). Furthermore the concept of Erosion Response Units (ERU) provides a fully distributed modelling structure. Thus, because the ERU contain detailed information concerning the erosion processes and intensities as well as the relative distribution of erosion processes and consequently allows the application as modelling entities. As already stated by several authors (see also Poesen et al. 1998, Bull & Kirkby 2000) especially the sediments derived from gully erosion cannot be simulated by RUSLE-type models. This was the reason for the development of a differentiated modelling approach to be able to simulate the specific erosion processes and dynamics.

HS01/09A/C29-003

0940

**THE USE OF GAVRILOVIC METHOD IN PREDICTION OF EROSION IN UNGAGED CATCHMENTS: ITS APPLICABILITY AND POSSIBLE DEVELOPMENT WITH NEW SPATIAL DATAMANIPULATION TECHNIQUES**

Lidija GLOBEVNIK, Danko HOLJEV, Josip RUBINIĆ, Gregor PETKOVŠEK (WATER MANAGEMENT INSTITUTE)

For the prediction of surface, deep and side erosion and sediment yield on the catchment scale, the Gavrilovic formula has been widely used in Slovenia and Croatia in the last 30 years. The formula has been developed for management practices in erosion protection, mainly in forest management and torrent control. The model, based on Gavrilovic formula is parametric distributed model, used for prediction of yearly quantities of eroded material and yearly sediment yield. It uses empirical coefficients (erodibility coefficient, protection coefficient, erosion coefficient) and a matrix of physical characteristics of catchment subunits. To analyse its applicability, we analyse erosion processes and river morphological changes between 1970 to 2000 on a 92 km<sup>2</sup> large catchment. GIS techniques can be used for preparing data from DTM and aerial photos, so we are developing Gavrilovic based model for erosion prediction.

HS01/09A/C29-004

1000

**PREDICTION OF ANNUAL SEDIMENT TRANSPORT IN A SMALL UNGAUGED TORRENTIAL BASINS IN SERBIA**

Stanimir C. KOSTADINOV (Department of Erosion and Torrent Control, Forestry Faculty of Belgrade University)

Torrents are two-phase watercourses that occur as the consequence of intensive processes of soil erosion in the watershed. They transport a large quantity of sediment. Previous engineering practice and experience shows that in the design of all structures on the streams loaded with sediment regime must be seriously studied. A very significant parameter of the sediment regime is the average annual sediment transport. The measurement of sediment transport in the torrents is very difficult and very expensive, and because of this practically all torrents in Serbia are ungauged. This is the reason that for the prediction of average annual sediment transport in ungauged torrential basins, in the watershed management practice of Serbia, the methods by Gavrilović and Polyakov were used. The new method used in latest years is the Modified Polyakov's method (method Polyakov-Kostadinov). The research of sediment transport in the experimental torrential watersheds in Serbia shows that the above methods, particularly that by Polyakov, deviate significantly from the results of field measurements. On the other hand, the results of the calculation by the modified Polyakov-Kostadinov method are quite close to measured data. The modification of Polyakov's method consists of the calculation of average annual turbidity of water based on the newly introduced parameter of pluvial-erosion index. This method is of regional character and it should be further tested for other regions in order to obtain the corresponding regional analytical correlation.

HS01/09A/C29-005

1020

**ESTIMATION OF SEDIMENT- AND DISSOLVED LOAD FROM GREENLAND**

Bent HASHOLT (Institute of Geography, University of Copenhagen)

Greenland, with an area of 2 million sq.km., has very few gauging stations determining the load into the sea. However, the influence on the neighbouring arctic seas is obviously strong. In order to estimate this load, no single method can provide a solution. The paper discusses the application of different types of methods of estimations. Estimation results are compared with results from the few existing gauging stations in order to find calibration procedures.

HS01/09A/C29-006

1040

**EROSION PREDICTION IN UNGAUGED GLACIERIZED BASINS**

Jim BOGEN, Truls Erik BØNSNES (Norwegian Water Resources and Energy Directorate)

The meltwater from glaciers often carries large amounts of sediment. Planning for hydropower development in glacierized areas thus needs sediment data as a basic input for the design and location of sand traps, sedimentation chambers or settling basins to prevent damage to waterways and machinery. Changes in sediment delivery may also affect the ecology of downstream reaches of regulated rivers, so sediment data is also needed to assess possible environmental impacts. Techniques for estimating sediment transport in ungauged glacier meltwater rivers may, however, be different from those employed in unglacierized basins. In this paper, methods are discussed for estimating sediment yields in unglacierized areas; the sediment load within ungauged parts of the Svartisen hydropower scheme in Northern Norway is estimated as a worked example. Long term measurements of sediment yields of various glaciers in Norway have revealed that erosion rates to a large extent are controlled by bedrock geology, glacial variables and the large scale morphology of each individual glacier. Measurements of bed load  $G_b$  and suspended load  $G_s$  of two glaciers gave a relation  $G_b = k G_s$ . Values of the constant  $k$  were found to be 0.5 at Nigardsbreen and 0.42 at Engabreen, an outlet glacier of the Svartisen ice cap. This relationship is due to the fact that suspended load is derived from abrasion and crushing of the coarser material supplied by subglacial quarrying processes. In the Svartisen power plant, water is collected through 45 intakes in a complex tunnel system totalling 100 km. Water is then transferred from the reservoir, or directly from the tunnels, to the power station. It was desirable to have estimates of both suspended load and bed load for all the intakes. The supply of bed load to each intake was computed employing an assessed value of  $k$  for each glacier. Direct measurements of sediment fluxes were carried out in a monitoring programme covering selected locations. The sediment yields of the remaining ungauged catchments were then estimated from a characterisation of each individual glacier and the underlying bedrock. The results indicate a total of 17,300 t/yr for the Southern tunnel complex and 11,000 t/yr for the Eastern one. The amount of sediment delivered by the glaciers draining directly into the reservoir was calculated to be 103,000 t/yr, applying sedimentation rates from dated sediment cores from the reservoir bed. The validity of measurements obtained from Norwegian glaciers is then discussed together with the applicability of the methods to other glacierized mountain areas.

HS01/09A/C29-007

1120

**FIRST-ORDER ESTIMATE OF OVERLAND FLOW BUFFERING IN A FRAGMENTED TROPICAL UPLAND BASIN**Alan D. ZIEGLER<sup>1</sup>, Thomas W. GIAMBELLUCA<sup>2</sup> (<sup>1</sup>Water Resources, Princeton University, <sup>2</sup>Geography, University of Hawaii)

We determine, for a fragmented upland watershed in northern Vietnam, the degree to which the current juxtaposition of land-cover mitigates the hydrological/geomorphological impact of accelerated surface runoff by the process of buffering (on down-slope patches) overland flow generated on upslope source areas. Our methodology relies on the following data and analyses techniques: (1) field measurements of infiltration-related soil properties, including saturated hydraulic conductivity (Ks), porosity, and soil texture; (2) one-minute rainfall data; (3) GIS analyses (at 30m x 30m resolution) of land-cover distribution, patch-related phenomena, and flow-transitions among the various land covers; and (4) diagnostic simulations of Horton overland flow (HOF) generation using the KINEROS2 runoff model. Using the above-mentioned data and simulation outputs, we develop an objective function to estimate basin-wide overland flow (BWOFF) for the 10 largest observed storms. We then compare the BWOFF values for the current land-cover arrangement with those of other fragmentation scenarios, including maximum/minimum fragmentation and random distribution of land cover. The comparisons show that the current land-cover distribution provides more buffering of erosion-producing HOF than the case where small land-cover patches are distributed at random (i.e., a higher degree of fragmentation). However, HOF-related impacts (including surface erosion, delivery of sediments to the stream system, change in the nature of storm response) could be further mitigated if land covers having relatively high Ks were intentionally positioned between swidden fields and the stream system.

HS01/09A/C29-008

1140

**CONSTRUCTION OF A SEDIMENT BUDGET FOR THE UPPER INDUS RIVER BASIN**

Khawaja Faran ALI, Dirk H. DE BOER (Department of Geography, University of Saskatchewan)

The rate of soil loss is ever increasing owing to natural and anthropogenic factors. This requires efficient monitoring and quantification methodologies so that effective land management strategies can be applied for controlling soil erosion. Construction of sediment budgets can be a useful technique since it provides a comprehensive accounting of the sources and disposition of sediments in the drainage basin. Sediment budget studies have mostly dealt with smaller catchments whereas larger basins pose challenges like the identification and contribution of different sediment sources. Sediment budgets studies are usually hampered by the inadequacy of data in quantity and quality. Not only the collection of such data is expensive and labour intensive, but also the data is collected only at a few points, which raises the question of representativeness. Remote sensing is emerging as a useful tool for larger areas in environmental applications. Soil erosion causes physical and visible changes in the surface properties of soil that can be measured in qualitative and quantitative terms, both spatially and temporally, using remote sensing techniques. GIS tools can be utilized further for combining spectral, spatial and temporal characteristics of remotely sensed data along with other available auxiliary data in erosion models for quantifying rates and patterns of soil erosion. The available historic hydrologic records can serve as control data for evaluating the contribution of sub-basins and balance calculation. A multidata type analysis approach, therefore, seems practicable for constructing sediment budgets for poorly-gauged large river basins. The Upper Indus is a unique, large river basin located in high Himalayan mountain areas exhibiting one of the highest rates of sediments transport. The greater Himalaya are a supreme example of young and rising mountain ranges where topography dominates the sediment dynamics. Sediment is contributed to the headwaters by the melt-water issuing from glaciers; by processes such as mass movement; by debris torrents; and by channel erosion during outburst floods from land-slide-, moraine-, and glacier-dammed lakes. The process is further accelerated by tectonic instability, high relief, steep slopes, heavy monsoon rainfall and runoff from glaciers in heavily ice-covered area. The Upper Indus is a poorly-gauged, data-sparse river basin. Since several water resources development schemes including high dams are planned, it is now important to conduct sediment studies in the region. This will help in understanding the characteristics of high sediment yield areas under natural environment and contribute for the better implementation of planned projects. For such a river basin, determining spatially distributed soil erosion using the classical techniques will be difficult, time consuming and expensive. It is, therefore, expected that a multidata type analysis approach of integrating remotely sensed data in a GIS framework supported by hydrologic and other auxiliary data will prove to be useful.

HS01/09A/C29-009

1200

**THE IMPORTANCE OF INSTITUTIONAL ARRANGEMENTS SHOWN BY EROSION EXAMPLES IN THE REPUBLIC OF MOLDOVA**Wolfgang SUMMER<sup>1</sup>, Wolfgang DIERNHOFER<sup>2</sup> (<sup>1</sup>International Commission on Continental Erosion, <sup>2</sup>IAHS - Hydrology 2020)

Due to the breakdown of the former Soviet Union, the centrally organised economic network collapsed, and the large-scale agricultural structures became obsolete as markets for agricultural products disappeared overnight. The Republic of Moldova was left with an energy- and cost-intensive agricultural infrastructure of single field sizes of several square kilometres. It was impossible to adopt the existing infrastructure to the regional needs of the country within a short period of time. After a decade of inappropriate agricultural management combined with natural processes such as drought, soil losses due to extensive landslides, wind erosion, degradation of soil fertility and many other negative erosion-related impacts, the country's economy is stressed. Agricultural productivity of the soils is threatened as well as agricultural economy and the wealth of the rural population. It is estimated that soil erosion in Moldova results in a financial loss of 45-55 million Euro annually. Institutional arrangements focusing on land management, the environment, hydrology and other related aspects are in a transition process. At the present, these arrangements are transformed from the previous Soviet system into a new national framework, following the legal rules and regulation of the Republic of Moldova. However, the lack of available information and data on natural processes as well as the lack of legal and strategic guidance to farmers during this transition period can be seen as the cause of the devastating situation of the country, thus, shows the environmental as well as socio-economic importance of properly based data acquisition as well as data and information management.

HS01/09A/C29-010

1220

**EVALUATION OF AN EROSION SIMULATION MODEL IN A SEMIARID REGION OF BRAZIL**Vajapeyam S. SRINIVASAN<sup>1</sup>, Ricardo de ARAGÃO<sup>2</sup> (<sup>1</sup>Department of Civil Engineering, Universidade Federal de Campina Grande, <sup>2</sup>Dept. of Civil and Environmental Engineering, Ehime University)

The northeastern region of Brazil is predominantly semi-arid and agriculture is the principal vocation of subsistence. The large spatial and temporal variations of the precipitation in the region provoke considerable land erosion. In order to evaluate the soil loss in these basins without any data on erosion, a predictive model that could be used needs to be calibrated and tested. This paper deals with this objective of testing an erosion simulation model for the region along with an analysis of the possible estimation of the calibrated parameters of the model. In order to evaluate the sediment production rates, several experimental plots of 100 m<sup>2</sup> with varying surface conditions and four micro-basins of about 0.5 ha were installed in an experimental basin located in a typically semi-arid region in the northeast of Brazil. The erosion plots were equipped with two collector tanks of 1000 liter capacity that would permit the determination of the total runoff and sediment erosion. In the case of the micro-basins, two of them were cleared bare and the other two were maintained with undisturbed native vegetation. In all the cases, the runoff and eroded sediments were directed to a collector tank equipped with automatic water level recorders, and a triangular weir. Cumulative samples of sediment-water mixture overflowing the weir were collected during each event along with the samples of the mixture in the tank. The collected data enabled the calculation of the total runoff and the sediment yield. Measurements of runoff and erosion were carried out between 1982 and 1991. A hydrodynamic model denominated as WESP was chosen for calibration and simulation of the processes of runoff and erosion involving essentially three parameters: the soil moisture tension parameter, the soil erodibility parameter and the channel erosion parameter. The calibration was carried out on an event by event basis. A large variation in the values of the parameters was noted due to the variation of the soil moisture condition at the beginning of each event. In order to obtain a better estimate of these parameters, they were related to an antecedent precipitation index. While the moisture tension parameter showed a reasonable relationship with the index, the other two parameters showed no such clear trend, but showed some dependency on the soil moisture parameter. These relationships were also used to estimate the values of the erosion parameters for each of the events. The validity of the calibrated model was tested by

comparing the results obtained from using the individually calibrated and estimated parameters in an adjacent micro-basin. The results show that the model simulated the runoff values well, but the calculated erosion values showed larger variations, underlining the complexity of the erosion process. However, the model could be considered a reasonable tool for obtaining the first estimates of erosion from basins without adequate data, but with similar characteristics.

Wednesday, July 9 PM

Presiding Chair: B. Hasholt

HS01/09P/C29-001

1400

**APPLICATION OF A PROCESS-BASED MODEL AS A PREDICTIVE TOOL FOR EROSION LOSS IN UNGAUGED BASINS**

Celso A.G. SANTOS<sup>1</sup>, Vajapeyam S. SRINIVASAN<sup>2</sup>, Carlos O. GALVAO<sup>3</sup> (<sup>1</sup>Department of Technology for Civil Engineering Constructions, Federal University of Paraíba, <sup>2</sup>Department of Civil Engineering, Federal University of Campina Grande)

Erosion of soil and its transport out of a hydrologic basin is a complex process that depends on several factors that can be divided into two groups. The first would be the climatic regime and the characteristics of individual precipitation events. The second would be the basin characteristics that include topography, soil characteristics and the vegetal cover. In order to produce a reliable predictive tool to estimate the soil loss from the basin due to erosion, a long and accurate data not only of the real amount of soil eroded and transported out of the basin, but also of the diverse variables of the afore mentioned groups will be necessary. In developing countries, in particular, such data are scarce and more often than not, must use the available data of a few basins for estimating the erosion loss from ungauged basins. Experimental basins specially installed and equipped for such purposes seem to be a highly practical and economic proposition. The data from these basins could be used to calibrate a suitable hydro-sedimentological model that can be used as a predictive tool either by a direct transposition of the parameters for basins of similar characteristics or for generating even empirical regional relationships for specific types of surface covers. In the semiarid northeast of Brazil, small and medium sized river basins have no monitoring devices that can help evaluate the erosion loss and the Experimental Basin of Sume was installed in early 80s with 4 micro-basins and 9 erosion plots to help understand the processes involved. The data collected till early 90s represent a unique and valuable field data about runoff and erosion in this region. A process-based event-oriented model - WESP, developed by Lopes (1987), has been successfully calibrated utilizing the data collected in the experimental basin. The calibrated model and data from erosion plots of the experimental basin were used to obtain an empirical regional soil loss equation of the type proposed by Musgrave. The results seem quite promising and the proposed method has the potential of being a reliable predictive tool for basins without data in the region.

HS01/09P/C29-002

1420

**IDENTIFICATION OF SOURCES OF SEDIMENT TO LAKE SAMSONVALE (NORTH PINE DAM) SOUTH-EAST QUEENSLAND, AUSTRALIA**

Grant Brian DOUGLAS<sup>1</sup>, Mark PALMER<sup>2</sup> (<sup>1</sup>CSIRO Land and Water, <sup>2</sup>CSIRO Mathematical and Information Sciences)

Lake Samsonvale (North Pine Dam - NPD) is a major dam of approximately 22km<sup>2</sup> with a capacity of 215000ML which supplies drinking water to Brisbane, the capital city of Queensland in eastern Australia. The catchment area of NPD is approximately 347 km<sup>2</sup>. The catchment of NPD is dominated by four major rock types: the Rocksberg greenstone (19%), Bunya Phyllite (39%), Neranleigh-Fernvale Beds (34%) and granitic rocks (the Mount Samson Granodiorite and the Dayboro Tonalite - 8%). Recent alluvium associated with major drainage networks constitutes approximately 5% of the catchment area. An important problem in the management of water supplies such as NPD is identifying the sources of sediment where there is little information on the composition or relative sediment loads of sub-catchments. This paper develops a Bayesian approach utilising end-member models to model the proportion of various sources in samples taken from NPD. This approach not only allows for the incorporation of prior knowledge about the geochemical signature (composition) of the sources (or end-members) but also allows for correlation between spatially contiguous samples and the prediction of the sediments composition at unsampled locations. Sediments sampled from the NPD in south-east Queensland are analysed to illustrate the approach. Results of the Bayesian end-member model suggest that the majority of sediment is derived from the Bunya Phyllite with important local contributions from the Rocksberg Greenstone and granitic rocks. Overprinting the primary geochemical signature of the catchment sediment sources, particularly in deeper sections of NPD, are enrichments of a number of elements including phosphorus which is strongly correlated with biogenic silica and iron and suggesting a combination of sediment diagenesis during transient periods of bottom water anoxia and the accumulation of algal detritus from the water column.

HS01/09P/C29-003

1440

**CHRONOLOGY OF ALLUVIAL SEDIMENT USING DATE OF PRODUCTION OF BURIED REFUSE: CASE STUDY IN AN UNGAUGED RIVER IN CENTRAL JAPAN**

Yoshimasa KURASHIGE<sup>1</sup>, Hajime KIBAYASHI<sup>2</sup>, Goro NAKAJIMA<sup>3</sup> (<sup>1</sup>School of Environmental Science, The University of Shiga Prefecture, <sup>2</sup>Biwako Broadcasting Co. LTD., <sup>3</sup>Nikken Technical Consulting Co. LTD.)

Alluvial terrace have been formed between embankments of the Inukami River which is one of the ungauged rivers in Central Japan. The date of sedimentation of each stratum of the terrace was determined in yearly resolution using date of manufacture of buried refuses combined with dendrochronological technique in 2000. A clear terrace with three layers (Layers 1, 2 and 3 from bottom to top) was found at 1.6 km upstream from the river mouth where alluvial meandering channel is formed. The border between two strata could be found by a humus-mixed layer. Many refuses (more than 100) were found from each stratum, whereas date of manufacture could be read only from two and six refuses in Layers 3 and 2, respectively. In contrast, from Layer 1, no refuse with its readable date of manufacture was found. From Layer 3, a beer bottle (made in 1990) and a beer can (June 1989) were found, showing that this layer was deposited in and after 1990. In contrast, two soft drink cans and four food packages (potato chips, chocolate, sweetmeat and noodle) were found from Layer 2, and the date of manufacture ranged from November 1984 to February 1987. This indicates that Layer 2 was deposited in and after 1987. On the other hand, some *salix* trees were found on the terrace surface. The trees which had age of 18 to 20 years slant to the river-flow direction, whereas the trees with age between 9 to 13 years stood straight. A tree with age of 20 years had germinated from the upper horizon of Layer 1, and trees with age of 13 years and 12 years from the upper Layer 2. In contrast, a tree germinated from upper Layer 3 had age of 9 years. These show that Layers 1, 2 and 3 were deposited in and before 1980, 1987 and 1991, respectively. The comparison between these two chronological results and meteorological data determined that Layers 1, 2 and 3 were deposited in 1980, 1987 and 1990. A clear terrace was also found at 2.0 km upstream of the

river mouth. Some refuses made before 1990 were found from its top layer, indicating that the top layer was deposited in 1990. In contrast, at a site 3.5 km upstream of the river mouth (i.e., on alluvial fan), many refuses could be found, but the date of manufacture could be read only from one food package (made in 1978). The composition of refuses at this site was significantly different from those at downstream sites. The top layer was thus determined to be deposited in late 1970s.

HS01/09P/C29-004

1500

**SEDIMENT YIELD ESTIMATION AND CHECK DAMS IN A SEMIARID AREA (SOUTH EDGE OF SIERRA DE GADOR, SOUTHERN SPAIN)**

Wenceslao Martin- ROSALES<sup>1</sup>, A. Pulido BOSCH<sup>2</sup>, J. GISBERT<sup>3</sup>, A. VALLEJOS<sup>2</sup> (<sup>1</sup>Department of Geodynamics, University of Granada, Avda., <sup>2</sup>Department of Hydrogeology, University of Almería, Spain)

Southeast of Spain has semi-arid climatic conditions. Rainfall has a high spatial and temporal variability, from less than 200 mm/year and 750 mm/year. This fact and the intensive human land use for centuries (mining, forestry uses, and fires) and a high topographic gradient, have induced an torrential hydrological behaviour. In the region of Almería (southern Spain), the carbonatic massif of Sierra de Gador constitute the natural recharge area of the Campo de Dalías aquifer system. The Campo de Dalías is a typical semi-arid sector with 200 mm/year average rainfall covered by some 20.000 ha of greenhouses of high economical interest. The uncontrolled development of this agricultural activity has produced an increasing in the flood risk, favoured by the location of several greenhouses on the dry stream beds. During intensive rainfall events run-off could reach high values. In 1977 the Spanish authorities carried out a soil and vegetation recovery program including 110 check-dams build up on 17 basins. They have an altitude between 3 and 14 m, with a drainage basin always less than 50 km<sup>2</sup>. The most obvious property of the drainage network is that flow is ephemeral, and the lack of observed data provides the major problem for runoff and sediment concentration modelling. Nevertheless a study has been carried out in order to evaluate the effectiveness of the check dams in trapping sediment. At the present, all the check-dam network has a global reservoir capacity of some 400.000 m<sup>3</sup>, 88% of its original capacity. From the volume of reservoir fill and the age of the check-dams we have estimate the annual sediment yield in the hole edge, using a coefficient of sediment retention of 35 %, deduced from a suspension sampling campaign in several check-dams during a run-off event. The sediment yield calculated is 59 m<sup>3</sup>/km<sup>2</sup>/year<sup>-1</sup>, although in some basins values of near 2100 m<sup>3</sup>/km<sup>2</sup>/year<sup>-1</sup> have been estimated, evidence of a high erodibility in the edge nowadays. With the study carried out we evidence the usefulness of this kind of infrastructure -so frequent and numerous in the Mediterranean area-, as a tool to reconstruct sediment yield histories and to estimate water erosion in small ungauged basins.

HS01/09P/C29-005

1520

**RECONSTRUCTING UPLAND SEDIMENT BUDGETS IN UNGAUGED CATCHMENTS FROM RESERVOIR SEDIMENTATION AND RAINFALL RECORDS CALIBRATED USING SHORT-TERM STREAMFLOW MONITORING**

David Laurence HIGGITT<sup>1</sup>, Victoria Jane HOLLIDAY<sup>1</sup>, Jeff WARBURTON<sup>1</sup>, Sue WHITE<sup>2</sup> (<sup>1</sup>Department of Geography, University of Durham, <sup>2</sup>Institute of Water and Environment, Cranfield University)

The estimation of sediment yield in upland environments is a difficult task, compounded by the scarcity of long-term monitoring. This is a significant problem when assessing sedimentation in upland reservoirs where there is a need to evaluate sediment budgets from limited information. Sediment is supplied differentially from variable sources within the catchment and the transfer of sediment is not related to rainfall or runoff characteristics in a simple linear fashion. Extreme events are likely to have a disproportionately large influence on sediment transfer. Furthermore, concerns about climate change and the likelihood of more frequent extreme events emphasise the need for predictive capability without reliance on gauging records. The results reported in this paper form part of a EU-funded programme (WARMICE) investigating the potential impact of sedimentation on water resource management in upland environments. Evaluation of the sediment transfer system of a representative reservoir catchment in the North Pennines, United Kingdom, has used reservoir core records to reconstruct sediment accumulation rates and changes in sediment supply. Short term monitoring of contemporary sediment transfer demonstrates that this is a supply-limited system where the majority of sediment is transported during storm events. Daily and seasonal rainfall records and synthetic discharge series can be correlated with the reservoir sedimentary archive and with field evidence of activity from the catchment. The paper examines how geomorphological evidence preserved within upland catchments can be related by extrapolating or constructing discharge series from other sources. It also demonstrates how recent climatic variations identified in the region have impacted on the sediment transfer system.

HS01/09P/C29-006

1540

**ESTIMATION OF EROSION AND SEDIMENT OUTFLOW IN OLD DAYS**

Takahisa MIZUYAMA<sup>1</sup>, Akitsu KIMOTO<sup>2</sup>, Yuji YASUDA<sup>3</sup>, Masaru TOUHEI<sup>4</sup>, Masaharu FUJITA<sup>4</sup> (<sup>1</sup>Division of Forest Science, Graduate School of Agriculture, Kyoto University, <sup>2</sup>Sabo Technical Center, <sup>3</sup>Kinki Regional Bureau, Ministry of Land, Infrastructure and, <sup>4</sup>Disaster Prevention Research Institute, Kyoto University)

Mountains surrounding Kyoto and its vicinity had been completely devastated about 100 years ago because of over logging for firewood. The areas are weathered Granite and there were no trees at that time. The mountains were white as covered with snow. A lot of sediment flowed out, to rise riverbed and to cause flood frequently. Intense hillside sabo works; terracing and plantation have been carried out for last 100 years. The areas are covered green almost completely these days. Erosion rate have been observed last 30 years in the area. The data are analyzed and an erosion prediction method was made out. The method contains rainfall, topography of slopes and basins and the condition of vegetation as parameters. The method is applied to the areas to estimate the erosion and sediment outflow 100 years ago. Riverbed elevation change is also estimated by a sediment routing method based on the estimated erosion as a boundary condition.

HS01/09P/C29-007

1600

**PREDICTING EROSION RATES IN SELECTIVELY LOGGED TROPICAL RAIN FORESTS**

Ian DOUGLAS (SCHOOL OF GEOGRAPHY, UNIVERSITY OF MANCHESTER)

The main damage to tropical rain forests under selective logging occurs from the construction of access roads and the opening up of log haulage lines from individual trees to log-loading points. These road building process create linear sediment sources that all too often are connected to stream channels or natural drainage lines. Once these tracks and roads become an effective extension of the drainage network they deliver large quantities of

sediment to channels and may, if unchecked, develop into gullies that continue to erode long after logging has ceased. Additional problems can arise several years after logging when hollow log culverts fail during exceptional storms and landsliding along cut and fill roads sends surges of sediment into the drainage system. Predicting the impact of such disturbance in ungauged catchments involves deriving suitable rates of erosion per unit length and width of road, estimating total road length within the catchment area, making allowances for road gradient and substrate, and calculating the potential sediment yield. Remote sensing can assist in these tasks, but identification of all roads and tracks, and their true widths, under a regenerating forest canopy requires considerable ground-truthing. Estimates derived for disturbed catchments can compare reasonably well with measured small catchment sediment yields determined by continuous flow and turbidity measurements calibrated against regular suspended sediment determinations on water samples. However, episodic mass movements that cause sudden slugs of sediment to move down small streams are often partially due to biotic phenomena, such as the collapse of trees or the decay of hollow log culverts, that are difficult to predict.

<b>HS01-Posters</b>	<b>Wednesday, July 9</b>
<b>EROSION PREDICTION OF UNGAUGED BASINS (PUBS): INTEGRATING METHODS AND TECHNIQUES (ICCE, ICRS AND ALL IAHS COMMISSIONS)</b>	
Location: Site D	

**Wednesday, July 9 PM**

<b>HS01/09P/D-001</b>	<b>Poster</b>	<b>1400-168</b>
-----------------------	---------------	-----------------

**ESTIMATION OF HYDROGEOMORPHOLOGICAL PARAMETERS OF A WATERSHED USING GIS**

Umamahesh Venkata NANDURI, Ramakrishna K. (Department of Civil Engineering, Regional Engineering College, Warangal)

Water is a primary source of life and sustains all human activities such as domestic needs, agriculture, industries etc. The allocation and management of water resources is becoming a difficult task due to increasing demands, decreasing supply & diminishing quality. This calls for judicious use of water resources. The geomorphology describes the environment in which the hydrological processes operate. A strong mutual correlation exists between geomorphological variables and hydrological characteristics. Such relationship can be applied to both surface and groundwater regime. Thus the linking of geomorphological parameters with hydrological characteristics of the basin provides a simple way to understand the hydrological behaviour of different basins and particularly of ungauged basins. During the last few years the Geographic Information System (GIS) technology has emerged as an extensively effective tool for analysing and prioritizing natural resource management alternatives. Because natural resource management problems are spatial in nature the GIS technology provides a tool for defining the extent of the problem, and facilitates the design and implementation of alternative management strategies. The flexible design of a GIS gives resource managers and planners the tools to effectively manage natural resources and to assess the implementation of regulatory policies before they are implemented. The present study describes the effective use of GIS in carrying out hydrogeomorphological study of a watershed in Warangal District of the state of Andhra Pradesh in India. The GIS is used to estimate the hydrogeomorphological parameters of the watershed, which can be used in watershed planning and management at micro and macro levels. The results of the study are used to infer the hydrological features like runoff potential, infiltration and groundwater recharge of the region. The PC ARC/INFO GIS software is used for the analysis.

<b>HS01/09P/D-002</b>	<b>Poster</b>	<b>1400-169</b>
-----------------------	---------------	-----------------

**SUSCEPTIBILITY OF ROCKS AND FORMATIONS TO EROSION AND SEDIMENT YIELD, LATIAN DRAINAGE BASIN, IRAN**

Sadat FEIZNIA<sup>1</sup>, Maryam ZARE-KHOSH EGHBAL<sup>1</sup> (Professor, College of Natural Resources, University of Tehran, Karaj, Iran, <sup>2</sup>Watershed Management Office, Ministry of Agriculture, Tehran, Iran)

Susceptibility of formations to erosion is important in conservation of watersheds. Iran is one of the world's countries that has high erosion and sediment yield production. There are different methods for investigation of susceptibility of formations to erosion, each having advantages and disadvantages. In this research, Selby method and factor K in USLE model were used to investigate sensitivity qualitatively and then by using sediment yield data, this matter was studied quantitatively. The studied area is Latian Drainage Basin, northeast of Tehran, located in 51.23 to 51.49 East longitude and 35.46 to 36.03 north latitude. This basin has eight subcatchments and six hydrometric stations with more than 20 years of water and sediment yield data. The main river is Jujrood River which originates from southern Alborz ranges. At the beginning, it was found that among all effective factors on erosion, geology, slope, land use and climate are the most effective ones in the studied area. Then the maps of four mentioned factors were prepared and were overlain to obtain the map of land units of the area. Then in each land unit, sensitivity of formations and rocks to erosion was obtained. To do so, in each land unit for pre-Quaternary formations, parameters of Rock Mass Strength Classification of Selby (1980) and in each Quaternary formation parameters of K factor in USLE method were obtained in the field and laboratory. In this way different formations and rocks of the drainage basin were ranked qualitatively according to susceptibility to erosion. For quantifying sensitivity of formations to erosion, first sediment yield data of four hydrometric stations were investigated. Then two variable regression analyses were performed between sediment yield data of each hydrometric station as dependent variable and four effective factors as independent variables. Then the regression analyses were added together and were classified and according to this classification, sensitivity map of formations to erosion was prepared. Then multi-variable regression analyses were performed between sediment yield data and qualitative coefficient of sensitivity, slope and climate and sediment yield of each land unit was calculated from these regressions.

<b>HS01/09P/D-003</b>	<b>Poster</b>	<b>1400-170</b>
-----------------------	---------------	-----------------

**THE MECHANISM OF WATER AND SEDIMENT DISCHARGES FROM GULKANA GLACIER, ALASKA: APPLICATION OF FILTER-SEPARATION AR MODEL**

Kazuhsa A. CHIKITA<sup>1</sup>, Kenta HIRAYAMA<sup>1</sup>, Rod S. MARCH<sup>2</sup>, Dennis TRABANT<sup>2</sup>, Daisaku KIDO<sup>1</sup> (Graduate School of Science, Hokkaido University, <sup>2</sup>U. S. Geological Survey)

The dynamics of englacial and subglacial drainage systems in Gulkana Glacier, Alaska was examined by analyzing the continuous data of water and sediment discharges obtained in a

proglacial river in the glacier-melt season of 2001. The plots of the data on a semi-log paper indicate that each of water discharge and sediment discharge can be separated into "fast" and "slow" components. The fast component corresponds to an englacial and subglacial, "channelized" drainage system downstream of snow line in the ablation area, while the slow component is related to a subglacial, "distributed" drainage system upstream of snow line. The hydrological and meteorological observations revealed that suspended sediment concentration (SSC) and water discharge both increased abruptly in ca. 2 days after the maximum air temperature was recorded. This suggests that a subglacial drainage system then changed drastically from the "distributed" to "channelized" drainage system toward the upglacier. This event is probably due to the great erosion of subglacial till under high water pressure in the distributed system. Flow separation by the AR model, using a numerical filter, was performed to the data sets of water and sediment discharges. As a result, for the slow component, there existed the highlinearity between SSC (mg/l) and water discharge (m<sup>3</sup>/s). The contributions of fast and slow components over the observation period were calculated at 48.2% and 51.8% for water discharge, and at 89.1% and 10.9% for sediment discharge, respectively.

<b>HS01/09P/D-004</b>	<b>Poster</b>	<b>1400-171</b>
-----------------------	---------------	-----------------

**THE RELATIONS BETWEEN SEDIMENT DISCHARGE AND FOREST COVER IN A WEATHERED GRANITE MOUNTAIN AREA**

Kazuhiro YABE (Department of Forest Science, Tokyo University of Agriculture)

In this study, the author applied the theory of sediment discharge to a mountain stream and examined its applicability for determining the sediment yield resulting from showers as well as the long-term applicability of the results for mountainous watersheds. Furthermore, using hydrological data obtained in the past 60 years and data of sediment yields, the author analyzed the influence of the process of forest recovery on sediment yield. Soil transportation by flowing stream can be expressed by the sediment discharge formula. Although such formula is generally applicable only for bedload, this study adopted one such formula, the Brown formula is considered applicable for bed material load (bedload and suspended load). As a result, the following expression was obtained at Shirasaka watershed (the weathered granite zone).  $Q_s = 0.38 Q_w^{1.40} Q_p$ . Sediment discharge,  $Q_s$ ; Runoff To verify this result, the author analyzed the relationship between the sediment yields and the runoff to the 1.40th power measured at 10-minute intervals for a significant period at Shirasaka watershed, and the two sets of data are observed to be well proportional.  $Q_s = 1.07 Q_w^{1.40}$ . It became clear that sediment yield in Shirasaka watershed is proportional to runoff to the 1.40th power. However, coefficient values obtained by observation and by calculation are different. This fact suggests that other factors, for example washload, may have a significant impact on sediment yield. Next, in order to test whether the Brown's formula is applicable for the same method was used at Ohora watershed (the new tertiary zone). As a result, the following expression was obtained  $Q_s = 0.17 Q_w^{1.31} Q_p = 0.16 Q_w^{1.31}$ . The result of the experiment was in beautiful agreement with the value that had been obtained by theoretical calculation. Because an outflow of washload is not recognized in the Ohora watershed, this fact suggests that Brown's formula may express equilibrium of sediment discharge. Next, using sediment data recorded in the past 60 years for Aichi forest and the result obtained from the sediment discharge theory, the author analyzed the relationship between sediment yield and the forest. Sediment yield has a tendency to decrease gradually. Although sediment yield is considerably influenced by precipitation, its tendency to decrease can be observed just as the changing size of the bare lands can be observed by aerial photos. Here, variations in the Erosion Index (E) was studied thoroughly, where "E" is the quotient when sediment yield is divided by runoff to the 1.40th power. Changes in the "E" align well with the changes in the bare-land ratio (L<sub>b</sub>). Thus as a result of having analyzed relation of "E" and "L<sub>b</sub>", it was expressed in an exponential function. It became clear that the Sediment yield could be expressed as a function of bare-land ratio.

<b>HS01/09P/D-005</b>	<b>Poster</b>	<b>1400-172</b>
-----------------------	---------------	-----------------

**VARIATION OF SEDIMENT YIELD RATE AFTER FOREST FIRE IN A STEEP HEADWATER CATCHMENT**

Tomohiro NARUOKA<sup>1</sup>, Shin'ichi ONODERA<sup>2</sup> (Graduate School of Biosphere Sciences, Hiroshima University, <sup>2</sup>Faculty of Integrated Arts and Sciences, Hiroshima University)

A mountainous area of 63 ha was burned by forest fire in August 2000 in southeast part of Setoda Island, Hiroshima Prefecture, Japan. The area caught fire from a superhighway construction site beside the area. To clarify the influence of forest fire on the variation of sediment yield rate, we investigated profiles of sediment accumulation at a sand guard dam at a steep headwater catchment in this area and monitored sediment discharge rate by a sediment trap at upper part of the dam. The sediment accumulation reached 160 cm in thickness beside the dam, and the profile could be classified into four layers. Surface layer, that was 20 cm in thickness, was composed of sands and coarse gravels. Second layer with 40 cm thick was composed of sands and gravels with ash. Black colored sandy silt layer, that was 20 cm thick, was accumulated as a third layer. And bottom layer with 80 cm thick was composed of sands and fine gravels. The black layer supposed to be derived from ash immediately after the forest fire. The dam was built in 1992 so the bottom layer had been accumulated for 8 years before the forest fire. The sediment accumulation of the bottom layer was 12m<sup>3</sup> and the sediment discharge rate was 1.5m<sup>3</sup>/yr. One year after the forest fire sediment accumulation reached 56m<sup>3</sup> and the rate of sediment yield became 44.0m<sup>3</sup>/yr. Sediment discharge rates were about 0.05 to 0.20 m<sup>3</sup>/month in 2001. The rates of sediment discharge became bigger during heavy rain events. Most of sediments were derived from rill and gully erosions on the side slope of the catchment. Denudation rates were 0.075mm/yr before the forest fire and 2.2mm/yr after the forest fire. After the forest fire the rate was about 30 times higher than that of before the fire. Results of this study determine the drastic acceleration of rill-gully erosion and sediment yield by forest fire at steep headwater catchments.

<b>HS01/09P/D-006</b>	<b>Poster</b>	<b>1400-173</b>
-----------------------	---------------	-----------------

**AN EXPERIMENT ON THE INFILTRATION RATE OF TEPHRA DEPOSIT FROM MT.USU, SOUTHWESTERN HOKKAIDO, IN 2000**

Yuki ICHIOKA<sup>1</sup>, Yuichi ONDA<sup>2</sup> (Graduate School of Life and Environmental Sciences, University of Tsukuba, <sup>2</sup>Institute of Geoscience, University of Tsukuba)

The overlandflow and debrisflow were found to occur frequently in hillslopes covered by the volcanic ash in the Usu eruption in 1977 and the Unzen eruption in 1990-95. After the eruption at Mt.Usu in 2000, nevertheless more rain fell than the 1977-eruption, little debris flow and gully erosion had occurred. The purpose of this study is to examine the mechanism of infiltration rate of the volcanic ash from Mt.Usu erupted in 2000. The large-scale sprinkling experiment and the permeability tests applying varying electrolyte concentration were conducted by using three kinds of ashes at Mt.Usu (total mass of about 2000 kg). The sprinkling experiment had two sizes of raindrops; misty raindrop (mean diameter of 0.24 mm) and larger raindrop (that of 0.80 mm). The experimental flume, 180-cm long, 48-cm wide was prepared, and the gradient of this experimental slope was 5 degrees. The volcanic ash

was air-falled through a 2-mm sieve until a thickness of 5 cm, overlain by coarse sand layers (10 cm). The rainfall was applied 30 minutes in each day for three days. We observed particle structures in several thin sections from the surface on an experimental slope (5-10 mm). When raindrop size is large, and the infiltration rate decreases rapidly to 15 mm/h in the first run. In the second and third run, the infiltration rate lowered to 6-7 mm/h. The soil pores are observed to be clogged by the effect of physical crusts. In the case of misty raindrop, the infiltrate decreases very slowly or remains high; the final infiltration rate varies from 9.81 to 29.35 mm/h after the third run. The pores are observed to be not clogged and no evidence of physical crusting. The effect of chemical crusts was examined by the permeability tests applying varying electrolyte concentration (0.5 N, 0.05 N, 0.005 N and distilled water). No well-defined tendency from electrolyte concentration was found, comparing the previous results of Unzen Volcano. Therefore, the effect of the chemical crust at the Usu eruption in 2000 is expected to be negligible. In addition, X-ray diffraction analysis shows the presence of clay mineral such as 'smectite'. This fact indicates the volcanic ash is originated from the mountain body and tends to swell with water. These indicate that if raindrop impact is strong, the impress of raindrop impacts to swollen soil produces clogged pores, but if the raindrop impact is weak, swollen soil disperse to vertical direction due to low raindrop compression. Above discussions suggest that after the Usu eruption in 2000, because the raindrop impact was not strong enough for clogging pores and the chemical crust effect was low, the infiltration rate of the volcanic ash from 2000-eruption remained high, so that no debrisflow occurs.

**HS01/09P/D-007** Poster **1400-174**

**ESTIMATION OF SEDIMENT LOAD VARIATION CONTROLLED BY RAINFALL AFTER FOREST FIRE DISTURBANCE IN SMALL MOUNTAINOUS CATCHMENTS, WESTERN JAPAN**

Naoyuki NISHIMUNE<sup>1</sup>, Shin-ichi ONODERA<sup>2</sup>, Tomohiro NARUOKA<sup>1</sup>, Tsutomu TAKEFI, Mitsuyo SAITO<sup>2</sup> (<sup>1</sup>Graduate School of Biosphere Sciences, Hiroshima University, <sup>2</sup> Faculty of Integrated Arts and Sciences, Hiroshima University)

Disturbance by forest fire in small mountainous catchments causes greatly increasing of sediment yield. Forest fire often occurs around Seto Inland Sea region, western part of Honshu Island, Japan, because of dry and hot climate in summer. But it is difficult to measure sediment load from all of the catchments around there. In order to estimate the sediment load to Seto Inland Sea, it is important to clarify the long-term variation in sediment yield process as well as sediment load. So, our objective is to confirm sediment yield during rainfall events at the disturbed catchments by the forest fire. Observed three catchments, IK, TB and TY, which were disturbed by forest fire in 2000, 1994, and 1978, respectively, are under different conditions of vegetation. These three catchments have non-vegetation, grasses and secondary forest, respectively. The other conditions such as annual precipitation, drainage area and mean gradient of slope are much the same, 1100mm, 2ha and 30 degrees, respectively. Thickness of sediment on the bottom of the upper stream is 2m in IK, 0.5m in TB, and 0.2m in TY, respectively. Firstly, we confirmed rainfall-runoff pattern in three catchments. In the IK, runoff had the high peak flow and base flow, as compared with that at TB. On the other hand, runoff characteristics changed to low peak flow and high base flow at TY. This result suggested that overland flow generated by strong water repellency on hillslope but a part of rainfall is stored in thick soil layer and valley bottom sediment at IK, as compared with that at TB and TY. Secondary, the annual sediment yield at IK was about ten times higher than the others. It means that sediment yield occurred by surface erosion on steep slope with much erodible soil. Meanwhile, at the other two catchments, sediment yield dominated more than 90% of annual amount during one rainfall event with daily rainfall of more than 100mm. This suggests that sediment yield at the heavy rainfall event determines annual sediment load at the catchment progressed for several years after the fire. Thirdly, we get clear relationships between daily rainfall and sediment yield at three catchments for estimation for sediment load with various conditions after forest fire. At IK, a remarkable increase of sediment yield was observed corresponding to daily rainfall, and it is suggested that sediment yield is active in the catchment immediately after a fire. Sediment yield at TB was larger than that at TY during the event with precipitation of less than 100mm, whereas they were inverted during the heavy rainfall. This suggests that fire disturbance kept high sediment yield from valley bottom sediment without soil erosion on hillslope for more than 5 years after the fire, despite the thin soil layer at TB with a little recovering of vegetation on a slope. When several decades passed after a fire, soil layer was recovered by growth of vegetation, the sediment yield process became active only during a heavy rainfall event.

**HS01/09P/D-008** Poster **1400-175**

**SEDIMENTATION IN THE RIVER GANGA: STATE-OF-THE-ART**

Ajai SRIVASTAVA<sup>1</sup>, Ajit K. SRIVASTAVA<sup>2</sup> (<sup>1</sup>Deptt. of Geology, Banaras Hindu University, Vanarasi. Pin-221 005, India, <sup>2</sup>Ecology Laboratory, Deptt of Botany, Banaras Hindu University, Vanarasi. Pin-221 005, India)

'Ganga', 'Gange', 'Gangeya' or 'Ganges', a symbol of purity has served as the cradle of Indian civilization. The river from time immemorial has been India's river of faith, devotion and worship and revered as a 'Goddess' and 'Mother' by millions of Indian. The river in the present time shrieking for her own liberation from the polyhedral monster of pollution due to industrial effluents, harmful and obnoxious chemicals, and domestic wastes generated from the 692 towns situated in its basin. Apart from this, sedimentation in the river channel is an equally serious matter for an environmentalists and sedimentologists. In the upper reaches of the river i.e., source region weathering and erosion are prominent. As a result of chemical and mechanical weathering, the pre-existing rocks are disintegrated and decomposed. As far as sediment transport is concerned the river is placed as the third largest sediment transporting river of the world; considering the sediment transport at Farakhka (744 million tonnes/year) as measures, after the Yellow and Amazon rivers. The sediment load of the river often rises to a level of 2 gm/litre of water i.e. 2000 ppm, about 2.4 billion metric tonnes/annum. The problem of siltation in the river has caused lateral migration of river channel, cutoffs of meander bends, the evolution of new channels and bars and several morphological changes. Silt deposited in the river raises the river bed which in its turn leads to floods. In 1970, the river carried a large amount of sediment/silt and thus resulted in excessive mortality of the fish at Har ki Pauri-Hardwar, where the fish population is normally high. Sedimentation has reduced navigability in several tracts, creates turbidity, degrades water needed for consumptive or other use. Some remedial measures have been given by ecologists. The role of vegetation in the upper reaches of the floodplain has been emphasized by most of the wetland specialists. Studies have been made on quantifying the degree of effectiveness of population and communities dominated by different herbaceous plants in conserving the soil against erosion. It was found that the fibrous roots of *Cynodondactylon*, *Saccharum benghalensis* and *Cyperus rotundus* conserved between 91 to 96% soil against simulated rainfall erosion. Through shoot clipping experiment, it was found that the relative role of roots is more than of shoots in preventing soil erosion. Besides, prevention of overgrazing in the upper reaches of the river is considered to be a prime factor in the reduction of silt load in the aquatic milieu of the river. It was observed in a study conducted to preserve the eco-system that species like *polygonum amphibium* helps in absorbing toxic load of the heavy metals from the polluted river water and sediments.

Keeping in view of the above, it is the high time that the problem of siltation in the river channel be given due significance in order to maintain an ecological balance.

**HS01/09P/D-009** Poster **1400-176**

**PRELIMINARY STUDY ON THE PREDICTION OF THE DEBRIS-FLOW PULSATION**

Hiroshi SUWA (Disaster prevention Research Institute, Kyoto University)

The 25-30 July 1997 debris flow attacked Kande, a small village on the fan of the Aa River, on sunny days and brought about significant disaster. The Aa River is one of upstream tributaries of Indus River. The author visited the village in the end of July 2000 to make field surveys, and unexpectedly encountered debris flows there. The debris flows were unpredictable there. The 27-30 July 2000 debris flow attacked the village and brought about significant disaster again. Debris flows at the Aa River occurred on sunny days, while debris flows usually occur under heavy rainfalls in temperate countries and tropical countries. We know that breaches of glacial moraine lakes in Himalayan Nepal would generate flash floods and debris flows. Some of the local residents believe in such glacial-lake breach at the Aa River. But we cannot find any lake in the Aa River basin. Debris flows may be generated by rapid melting of glacial ice due to the succession of hot sunny days. Exact processes of such features of debris flows are not known. The July 1997 debris flow consisted more than 20 surges over 6 days and the July 2000 debris flow more than 10 surges over 4 days. The phenomena consist of a series of debris-flow pulsation. Debris flows generally occur as an intermittent series of multiple surges with time interval of a few minutes. They are also the series of debris-flow pulsation. The time interval of debris flows at the Aa River is several hours which is much longer than general cases. This remarkable difference in the time interval may be caused by the difference in the mechanism of debris-flow initiation.

**HS01/09P/D-010** Poster **1400-177**

**LANDSLIDE DETECTION USING SATELLITE REMOTE SENSING IMAGERY**

Kwong Fai Andrew LO<sup>1</sup>, Hui-Chung YEH<sup>1</sup>, Ju-Chen HOU<sup>2</sup> (<sup>1</sup>Dept. of Natural Resources, Chinese Culture University, <sup>2</sup>Digital Earth Research Center, Chinese Culture University)

Landslide detection using satellite remote sensing images has been widely studied. This type of applications often involves either change detection or multi-spectral image classification methodologies. If there is only one set of satellite image, the change detection method has limited use. Collecting and analyzing training area data for image classification are costly and time consuming. This study, therefore, utilize only one SPOT satellite image data for estimating the normalized difference vegetation index (NDVI), and to segregate vegetated and non-vegetated areas of the Ta-An River Basin in Central Taiwan. The haze correction technique is applied to remove the effect of atmosphere. Slope factor and texture feature are then used to identify the landslide area. This study successfully demonstrates the capability of using one set of remote sensing image to map landslide area in a large river basin.

**HS01/09P/D-011** Poster **1400-178**

**USE OF ADVANCED REMOTE SENSING TECHNIQUES FOR RISK EVALUATION OF DEBRIS FLOW HAZARD AT TORRENTS AFTER VOLCANIC DISTURBANCES**

Takao YAMAKOSHI, Masaaki NAKANO, Masaaki WATARI (Erosion and Sediment Control Research Group, Public Works Research Institute)

Once a volcano erupts, hydrologic characteristics of the slope of the volcano might be completely altered. Usually, at torrents that originate from the erupted volcano, debris flows can be easily triggered even by a small rainfall. Therefore, it is difficult to evaluate risk of debris flow hazard at the torrents because the complete alteration of the hydrologic characteristics means that accumulation of debris flow occurrence data at the torrents before the eruption becomes almost useless. To re-evaluate the risk of debris flow hazard at the torrents after the eruption, damage of the basins of the torrents should be investigated quickly. However, rapid grasp of the damage by field surveys is almost impossible because of the danger of an erupting volcano and the widespreadness of the affected area. Consequently, remote sensing technique is highly expected to be applied because it enables us to investigate an erupting volcano safely and quickly. Authors tried to utilize recent remote sensing techniques, that is, satellite-borne hyperspectral sensor, air-borne laser scanner, and unmanned autonomous helicopter to know degree of the damage at the time of the 2000 eruption of Usu Volcano. As a result, the following were clarified. 1) Satellite-borne hyperspectral sensor could detect area of ash fall deposition by the eruption as an area where a vegetation index lowers. In the same way, thickness of the volcanic ash could be relatively evaluated through degree of lowering of the vegetation index. 2) Repeated measurements before and after the onset of the eruption by an air-borne laser scanner could show the thickness of mudflow deposit very precisely. However, the thickness of the volcanic ash deposit could not be detected because the significant crustal deformation occurred during the eruption and masked the subtle change of the ground elevation by the volcanic ash deposition. 3) Unmanned autonomous helicopter could give us information in detail even around the center of the volcanic activity, such as thickness of the volcanic ash deposit near the erupting vents. However, it took much time and effort to operate the helicopter, so that it should be utilized with the other remote sensing technique complementarily.

**HS01/09P/D-012** Poster **1400-179**

**COMPARING TWO INTERPOLATORS DETERMINING SPATIAL WATER BALANCES FOR UNGAUGED LOCATIONS ON SHIKOKU ISLAND**

Huaxia YAO<sup>1</sup>, Irena CREED<sup>2</sup>, Michio HASHINO<sup>3</sup> (<sup>1</sup>Shield EcoRegion, Environment and Resource Management, <sup>2</sup>Department of Biology, The University of Western Ontario, London, Ontario, Canada N6A 5B7, <sup>3</sup>Department of Civil Engineering, The University of Tokushima, Tushima 770-8506, Japan)

Simple methods for generating the spatial distribution of water balance components and discharges are required for water resources management of ungauged basins. This study evaluated statistical methods for interpolating the spatial distribution of precipitation (P), evapotranspiration (ET), and discharge (Q) from gauged data points to ungauged points on the Shikoku Island, Japan. Two methods were examined: a local spline interpolator where for a given point the function was fitted exactly to nearby gauged data points; and a global multivariate regression interpolator where the function was fitted to all gauged data points based on their topographic position (i.e., latitude, longitude, altitude). Local and global interpolators did not generate similar results for P and T (where T was used to calculate ET). The local interpolator produced good estimations of P and T, with high coefficient of determinations between observed and estimated (0.982 for P and 0.991 for T). In contrast, the global interpolator produced a less accurate estimation of precipitation P with coefficient of determination of 0.892, and an accurate estimation of temperature T with a coefficient of 0.998. Distributions of annual evapotranspiration and discharge were derived from interpolated precipitation and temperature, and they showed different accuracy against the

observed ones between the two interpolators. Discharges derived by spline interpolator were more agreeable to observed than that derived by regression interpolator. The number of gauged data points used in the interpolation affected the performance of the interpolators. For P, when the number of gauged data points included in the interpolation dropped from  $n=118$  to 8, both the local and global interpolators maintained a high coefficient of determination  $r(0.9)$  until  $n=37$ , after which  $r$  dropped rapidly. At any given number of gauged data points included in the interpolation, the local interpolator outperformed the global interpolator. Our findings indicate that local interpolators are more appropriate for predicting the spatial distribution of water balance components in mountainous regions similar to Shikoku Island.

**HS01/09P/D-013** Poster **1400-180**

**A TERRAIN BASED PARAMETERIZATION OF DRAINAGE BASIN RESPONSE: A CASE OF YEWA BASIN**

Olusegun Adebayo ADEAGA (Department of Geography, University of Lagos)

Uneven distribution of water resources over space and time within the environment constitutes concern in water resources management. The concern can be enlightened from varied degree of water resources uncertainty, most especially its distribution, potential and development among others. An in-depth study on basin system response provides the basic requirement needed for an effective water management and strategic plan options. Such plan is essential in order to make adequate mitigation plans towards administering severe hydrological extreme consequences which is paramount in most developing countries of the world. This is partly due to ill-defined water planning that characterizes developing countries' developmental processes. Also of importance is the need to balance disparity between water supply and water demand of the ever increasing population. A thorough study of water resources requires a timely, accurate and suitable data on various hydrological components in order to attain an effective and efficient operational hydrology plan. Such studies are being hampered by insufficient data set and numerous ungauged stations as well as poor river network scheme. In the developing world, ill-defined and erroneous information of basins' water resources potential and usage as a result of limited riverflow data set in relation to basin complexities, inconsistency and unrepresented data set as well as insufficiency of good quality data remains the major problem towards attaining a sound water resources assessment. In this study, geomorphological and hydrological parameters derived from Digital Elevation Model (DEM) morphological analysis formed the basis of transfer function generating within Yewa basin. Space discretization and Morphological transfer function techniques were used for the flow simulation estimation. Transfer time function is based on a pseudo-time while morphological indices like slope, drainage surface, basin cross sectional shape and roughness, channel width in respect of basin size and local slope and conventional flow lengths among others were used to evaluate resultant erosional processes within Yewa drainage surface and Instantaneous Geomorphologic Hydrograph (IGH) generation. IGH provides better understanding of the volume of water being generated and water resources system sensitivity to impulsive rain. Yewa basin lies within Ogun river basin; it is oval shape with a total catchment area of about 4000Km<sup>2</sup> with numerous ungauged stations and rich in surface water with flooding being one of the major hydrological hazards hampering socio-economic advancement of the basin. The above analysis were integrated into a GIS framework toward a sound flow estimation and profitable decision making processes for ungauged basin using different rain impulse towards a sustainable water resources management and environmental conservation measures.

**HS01/09P/D-014** Poster **1400-181**

**WATER EROSION IN A SMALL GRAZED SAHELIAN CATCHMENT: IDENTIFICATION OF SEDIMENT SOURCES**

Harouna KARAMBIRI<sup>1</sup>, Olivier RIBOLZI<sup>2</sup>, Anne COUDRAIN-RIBSTEIN<sup>3</sup> (<sup>1</sup>UMR SISYPHE, Laboratory of Applied Geology, University Pierre & Marie CURIE, <sup>2</sup>UR ECU 049, Institut de Recherche pour le Développement (IRD), <sup>3</sup>UMR Hydrosociences CNRS-UMII-IRD, Université Montpellier II)

The Sahelian part of Burkina Faso is nowadays undergoing serious problems of natural resources degradations, especially soil erosion, due to the aggressiveness of climatic factors and anthropogenic impacts. This study aims to quantify total soil losses at the outlet of a catchment and estimate the contribution of different sediment sources. To do this, surface water flow and associated solid matters were monitored during three years (1998-2000) on a small grazed catchment (1.4 ha) which is about 64% covered by permeable eolian sandy deposits (DRY soil surface type) supporting most of the vegetation, and about 34% by impermeable bare soils (ERO soil surface type). The annual rainfall amount was 518 mm in 1998, 486 mm in 1999 and 419 mm in 2000 with runoff coefficients of 34%, 23% and 38% respectively. The annual solid-matter export was more than 90% suspended sediment, varying between 4.0 and 8.4 t.ha<sup>-1</sup>. The bedload represented less than 10% of soil losses. The sediment yield reached 4.2 t.ha<sup>-1</sup> in one flood event (10-year return period). During the studied period, a small proportion (20 to 32%) of the floods was thus responsible for a large proportion (80%) of the solid transport. Seasonal variation of the suspended-matter content was also observed: high mean values (9 g.l<sup>-1</sup>) in June, decreasing in July and stabilizing in August (between 2 and 4 g.l<sup>-1</sup>). The changes in suspended-matter content at the outlet were analysed during a typical annual frequency event and the results showed high values (23 g.l<sup>-1</sup>) at the rising stage, followed by a strong and rapid decrease during the first fifteen minutes, and a stabilization around 2.5 g.l<sup>-1</sup> until the end of the rainstorm. To highlight the role and quantify the contribution of the two soil surface types in the sediment flow observed at the outlet, we used different techniques: sediment particle-size distribution, clay fraction mineralogy (kaolinite/quartz ratio) and physical-based modelling. The results indicated that the ERO surface type appeared to be the main source of sediment within the catchment.

**HS01/09P/D-015** Poster **1400-182**

**METHODOLOGY AND METHODS FOR ASSESSMENT OF HYDROLOGICAL CHARACTERISTICS IN UNGAUGED BASINS**

Lobanov Alexeevich LOBANOV (IAHS member, Leading Scientist)

Numbers of sites of hydrological observations are limited in space and time. As usual, the regular observations of hydrological characteristics needed for water projects and other aims are absent in such places. There are three main ways for a simulation and prediction of hydrological characteristics in these conditions: short-term field measurements (an unit measure, a season of observations, several years of record), site-analogies and regional models. In modern changing period the additional problem connects with an assessment of stability of all model's parameters over the time. It has been proved theoretically that the using of several methods and approaches for a determination of the same hydrological characteristic is better than only one but the best approach, because the random errors become less. Some empirical examples confirm this conclusion. One of them has been realized for using of several regional formulas for computation of design floods and the best decision has been obtained in the case of joint use of two methods. In any case when several methods and approaches are used for ungauged site the first step connects with a

determination of homogeneous region. Main criterion, which can be suggested, is the same climate change tendencies or their absent in time series of hydrological characteristics. Methods for an extraction of climate changes in hydrological time series, determination of their statistical efficiency, directions and contributions have been developed too. In selected homogeneous regions the main three approaches are applied and the particular methods have been developed for their realization. In the case of short-term field measurements, the regional relationships are created which connect the years with short-term data and other years of regular observations in the region. The problems of an averaging of simulated data are discussed as well as the estimation of random errors. In the case of regionalization, the methodology and methods for a development of models on the basis of empirical data have been developed which includes the following main parts: assessment of the kind of one-factor relationships, choice of effective structure of the models and computation of their parameters, analysis of remainders and assessment of stability of coefficients of the models and efficiency of simulated values taking into account a dynamic properties (time factor). Practical application of joint use of regional model and short-term data have been shown for maximum 1% design snowmelt discharge for the one of region in the Central part of Russia. The next question is connected with development of Territorial Construction Norms (TCN), which will be the main practical documents for hydrological computations in Federal regional units of Russia. These TCN will use all records of hydrological characteristics in the particular region and regional models, which will be developed on their basis. The particular GIS with data base of observed and extended time series, software for hydrological computations and regional models will be developed for a realization of TCN and their correction in modern changing conditions (monitoring). Block-scheme of such GIS is presented and discussed.

**HS01/09P/D-016** Poster **1400-183**

**ESTIMATING EROSION USING GIS FROM SMALL WATERSHED WITH PERENNIAL SPRING IN LOWER SHIWALIKS, PUNJAB, INDIA**

Amanjot SINGH (Dept. of Soil and Water Engineering)

The lower Shiwaliks, locally called KANDI area, used to be forest belt of Punjab, India. With the growing population, the forest lands are being brought under agriculture, which ultimately is changing the ecological system of the region. The Kandi area comprises of small watersheds (40-70 ha) and the agriculture mainly is dependent upon monsoon rains. Some of the watersheds have perennial springs flowing through them. The source of these streams has not yet been established but these are thought to be fed by base flow from the upper reaches of the Himalayas. The soil of these watersheds is medium to light in texture and is highly erodible. The groundwater is available in two strata. The upper is shallow perched aquifer of about 2-3 m depth and the lower is confined aquifer available at depth more than 75 m and is difficult to tap because of presence of hard clay layers. Since the monsoon has erratic behavior both in time and space and groundwater cannot be economically explored, it was thought to harvest perennial spring with check dam structure and use the stored water for life saving irrigation to the crops sown at the down stream end. The gullies in the catchments have been established to check the silt load. Now with the implementation of the conservation structure, it is required to monitor and assess the hydroecological changes in the region viz. changing surface flow and subsurface water conditions, and sediment redistribution. To meet the objectives, area has been sub-divided into three micro watersheds, i) the upstream of the check dam, ii) the middle area between upstream and cultivable down stream used for conveyance of water, and iii) the down stream agricultural land irrigated by harvested water. The watershed has been mapped and digitized in Geomedia Professional GIS package and different layers for each effecting parameters are being used for the estimation and redistribution of sediments in the catchment.

**HS01/09P/D-017** Poster **1400-184**

**RAINFALL CHARACTERISTICS AND SOME OF THEIR MANAGEMENT OPTIONS FOR IMPROVING SOIL PRODUCTIVITY IN NORTH-WESTERN TRACT OF INDIA**

Sanjay ARORA, M.S. HADDA (Department of Soils, Punjab Agricultural University)

The North-Western tract receives about 4.2 x 10<sup>6</sup> ha-m of rainwater which is sole natural water resource with deep to very deep underground water table. Some observations at 3-4 sites in the tract show that runoff varies from 35 to 45 per cent of rainfall and soil loss varies from 25-225 t/ha/yr on a small to large watersheds in the tract mostly in the summer monsoon months. It impairs the productivity of land which is not only physically based but more complex in nature. In order to improve the productivity of the land in the area, large scale development works are being proposed for water harvesting and erosion control. It was observed that a minimum rainfall depth of 10 mm is sufficient to cause runoff and overland flow in the area. These runoff producing rainstorms occur in 15-20 number and their duration varied from 1 to 16 hours. Their maximum fifteen minutes intensity and rainfall erosion index ranges from 4.25 to 240 mm h<sup>-1</sup> and 203.6 to 1523.5 m tons/ha cm/h, respectively. The mean rainfall aggressiveness for ten years (1990-2000) at Ballawal saunkhri, District Nawashahar was 224.8 thereby yielding an annual soil loss of 112.8 t/ha/yr. This placed it into a category that suffers from high erosion risk. Keeping these points in view, some of the proposed management options of rainwater at on-site and off-site are based in reducing the erosivity of rainfall by manipulating the soil surface, pre-monsoon ploughing, halodung, use of crop residues @ 6-8 t/ha through vertical mulching (band placement), timely and deep tillage operations and adoption of land verticalizing measures and provision of structures and vegetative barriers for safe disposal of excess runoff water at a non-erosive velocity. Also collecting harvested runoff water in suitable inverted, truncated and pyramid type of tanks or small tributaries in the vicinity of cultivated area. In this connection, a recent study conducted on farmers field showed an increase in yield of maize with the application of 50 % NPK+ 150 % FYM was at par with sowing of maize in raised bunds (15-20 cms). This suggests that sowing of maize in raised bunds could be practiced to economize on the use of chemical fertilizers and manures in the area.

**HS01/09P/D-018** Poster **1400-185**

**QUANTITATIVE ESTIMATION OF ALIAKMON BASIN DEGRADATION THROUGH THE USE OF G.I.S**

Dimitrios A. EMMANOULOUDIS<sup>1</sup>, Odysseas P. CHRISTOU<sup>2</sup>, Evangelos I. FILIPPIDIS<sup>3</sup> (<sup>1</sup>Department of Forestry, Technological Educational Institute of Drama, <sup>2</sup>GEOINFO, Applied Studies and Research, Gr. Lampraki 133)

The study of the three-fold phenomenon of erosion-transportation-deposition of sediment materials in the broader inner and outer basin area of the effusion basins of rivers and torrents is a scientific issue, which has been researched and analyzed in a great number of papers. Such studies and analyzes usually focus on both qualitative and quantitative estimations, via empirical methods or comparison models, which can be locally or universally applied. This paper deals with the definition of the annual potential degradation of Aliakmon riverbasin (the largest river in Greece). This degradation is the result of erosive processes that take place in the watershed subbasins. The products of this degradation, which are sediment materials, are transferred through the hydrographic system network and part of

them reaches the river exit in the plains, while another part remains in the mountain beds in the form of within-basin depositions. For the quantitative estimation of Aliakmon river basin degradation a new model was used. The stochastic model of Gavrilovic served as a starting point, which was further extended by initiating appropriate adjustments through the use of the G.I.S. In the case of the Aliakmon river basin, the average annual degradation has been calculated with a remarkably high precision. Using this new improved model, which for the first time was applied in an area of several thousand kilometres, a lot of maps were constructed and especially a total map of potential erosion. What is more important, is that this improved model of estimation may be applied to any basin, even extremely small mountainous watersheds up to very large river basins.

**HS01/09P/D-019** Poster **1400-186**

**PEAK DISCHARGE PREDICTION FROM REGIONAL CATCHMENT CHARACTERISTICS FOR EROSION MODELLING**

Andras BARDOSSY<sup>1</sup>, Istvan KONTUR<sup>2</sup> (Institute for Hydraulic Engineering, University of Stuttgart, <sup>2</sup>Technical University of Budapest)

Erosion and the solute transport is an important factor of water resources and the engineering planning. Erosion is a complicated process, which is seldom measured directly. Empirical formulae based on selected case studies are generalized and used for catchments with hydrological observations only. It is well known that erosion intensity, the volume of the eroded material is connected with the runoff especially of the peak discharges of the runoff. The purpose of this paper is to predict the frequency and magnitude of discharges which might cause erosion. For this purpose parameters of the stochastic process of discharges is related to the parameters of the precipitation process and the catchment characteristics. The Transfer of the parameters is based on an implicit assumption of the continuity supposing that similar catchments have similar runoff processes. The methodology is demonstrated on selected catchments in South-West Germany.

**HS01/09P/D-020** Poster **1400-187**

**PHOSPHORUS BEHAVIOUR IN A GRASSLAND CATCHMENT IN NORTHERN IRELAND DURING AND BETWEEN STORM EVENTS**

Wayne MENARY, Phil JORDAN, Richard DOUGLAS, Brian RIPPEY (University of Ulster)

Nutrient-suspended sediment interactions are complex and vary between and within storm events, according to the nutrient component (inorganic/organic) concerned and from one catchment to another depending on local mineralogy and upstream characteristics. Previous studies in Northern Ireland suggest that the process of phosphorus (P) loss to water from soils is via dissolution and desorption. There is evidence, however, to suggest that in some circumstances, the particulate P fraction may be the most mobile form during storm events. This project focused on the nature and controls of storm and non-storm period sediment-associated behaviour of P concentration fractions through detailed investigation on the Oona Water catchment, Co Tyrone, Northern Ireland. The research involved automatic storm-triggered hydrochemical monitoring at 3 different scales, ranging from 0.15km<sup>2</sup> to 88km<sup>2</sup>, in conjunction with a weekly discrete sampling monitoring programme at 6 different scales. Total and dissolved P were analysed in order to quantify the role of sediment-associated transport in the overall nutrient budget of the rivers. The study location is characterised by the homogenous nature of soil type (heavy clay over drumlins) within the catchment. This facilitates an examination of the effects of time, scale and season on hydrochemical fluctuations. The research has helped to clarify the behaviour of non-conservative P in the stream network by quantifying the magnitude of P losses and P transformations across different scales and time. It has also facilitated an interpretation of the relative contribution of P fractions from grassland soils to waters in the Oona Water catchment. The methodology employed and data obtained helped to fill knowledge gaps in the behaviour of non-conservative P from the micro to meso scale. Results show a dominant particulate P fraction across all 6 scales with total P to soluble reactive P ratios ranging from 1:0.14 to 1:0.24 whilst soil desorption experiments indicate a limited role for this theory of P loss. Despite typically low rainfall intensities for Northern Ireland on a global scale, erosion has to be considered an important factor explaining P loss to water from soils in the Oona Water catchment, given results revealing a dominant particulate P fraction across various scales, from the micro-scale through the meso-scale.

**HS01/09P/D-021** Poster **1400-188**

**MODERN CONDITION AND PROSPECTS OF DEVELOPMENT OF TOPOGRAPHICAL AND GEODETIC WORKS AT REALIZATION OF EROSION-PREVENTIVE MEASURES**

David Dato GUBELADZE<sup>1</sup>, Konstantine Kote BZIAVA<sup>2</sup> (<sup>1</sup>Department of Agricultural Land Reclamation, <sup>2</sup>Department of Agricultural Land Reclamation)

Georgia is one of strong erosive areas among the countries of former Soviet Union. Ravine erosion of soils is widely distributed in all soil and climatic zones. The natural conditions of the country (strongly dismembered relief of district, significant length and steepness of slopes, storm character of deposits, high percentage of tilled plots and small percentage of forest land) create danger formation of the new and active growth already of existing ravines. Unfortunately at present detailed survey of ravine-joint elements of a network are not completely stipulated, and to this day they are represented on a topographical basis with the large generalization. The scheduled network of a condensation is created by polygonometry in 2 categories. The high-altitude network is created by continuation of courses of technical geodesic leveling survey with application of geodetic level instruments of a modern type. The survey is made by a method of tachometry. The stationing register on all length of the ravine is made also. With occurrence of new devices such technology of works grows old. Today it is necessary to carry out construction of geodetic networks of a condensation in territories, which are subject to ravine erosion, on the basis of application of electromagnetic distance-meter allowing quickly, it is reliable and with high accuracy to measure significant distances. Use of such devices will enable to reduce terms of performance of works at the expense of automation of process of linear measurements and owing to application new, perfect circuit of construction of a geodetic substantiation, and also considerably will raise accuracy of definition of coordinates of items. The survey of ravine should be carried out by a tachometric way with application of the same devices. The reconnaissance should be carried out together with rodmen with simultaneous drawing up of an outline in duplicate, on which to render a sequence of points of a reflector that will allow to exclude lying of the odolite courses between basic marks and to reduce amounts of works. It is necessary to note, that with the help of these basic marks it is possible to carry out and number of research works, in particular - study of dynamics of growth of ravines and development new or perfection of existing settlement methods of the forecast of separate kinds of erosive processes. In result the made topographical plan will ensure with necessary accuracy of the following data general and private inclinations of slopes; an arrangement of places of concentration and direction of a drain in various parts of a slope; the detailed image of a relief with the instruction of a degree of its destruction by erosive processes; the area of the water collection; parameters of the ravine (length and width of the ravine in the certain intervals and depth of the ravine in characteristic points of cross section). All this will allow

increasing quality of designing of Erosion-preventive measures that in turn will enable to improve a condition of grounds usage in agriculture.

**HS01/09P/D-022** Poster **1400-189**

**CHARACTERISTICS AND TEMPORAL VARIABILITY OF LARGE WOODY DEBRIS TRAPPED IN A RESERVOIR ON THE RIVER RHONE (FRANCE) : IMPLICATIONS FOR RIVER BASIN MANAGEMENT**

Bertrand MOULIN, Hervé PIÉGAY (CNRS UMR 5600)

Woody debris is a structural element of river system which provides habitats for aquatic communities but may enhance flooding frequency and damage infrastructure. An abundant scientific literature highlights the role of the wood, particularly in the fields of ecology and geomorphology. In order to find a balance between woody debris preservation and reintroduced for ecological purposes and the need of channel clearing for risk management objective, more research is now needed to understand woody debris entrance, residence time and transport dynamic in regulated rivers. This work uses reservoirs which trap woody debris to determine its geographical origin and temporal variability in relation to the flow regime. This approach is illustrated by data collected on the Genissiat dam on the upper Rhône river (France) which trap all the woody debris even during high floods. The results show that the wood input increase with the flood frequency but also depend on the position of the flood event in the hydrological series. The wood load is significantly high and removed from the dam reservoir when the flood recurrency attains one for 1.5 years. Qualitative description of the wood extracted from reservoir indicates that 83 % of the pieces whatever the size have a natural origin (broken, cut by beaver) when 17 % have been cut by humans. The large pieces of wood (diameter > 12.5 cm) have a more frequently human origin (40 %). Large pieces with roots are unfrequent (10 %) underlining the low contribution of bank erosion. Most of the pieces are strongly smoothed, without any branches, roots and bark confirming the effect of physical breakage of high energy rivers. Amongst 503 samples, 45 % have a riparian origin (Populus, Fraxinus, Alnus).

**HS01/09P/D-023** Poster **1400-190**

**SOIL EROSION ESTIMATION WITH ARCVIEW GIS**

Guobin FU<sup>1</sup>, Shullin CHEN<sup>2</sup>, Donald MCCOOL<sup>3</sup> (<sup>1</sup>Department of Hydrology and Water Resources, Institute of Geographical Sciences and Natural Resources Research, Chinese Academy of Sciences, <sup>2</sup>Washington State University, <sup>3</sup>USDA-ARS-PWA)

ArcView GIS with the Revised Universal Soil Loss Equation (RUSLE) was used to estimate soil erosion in Pataha Watershed, a typical dryland agricultural watershed in southeastern Washington. With the aid of GIS, the L and S factors can be easily obtained from DEM, R factor from precipitation map, K factor from national SSURGO database, and C from crop rotation and land use map. Soil erosion in each piece of land then can be obtained with these available factors. In addition, the Sediment Delivery Distributed (SEDD) Model integrated with GIS was employed to transfer the soil erosion to sediment yield at the watershed scale. The coupling of GIS and soil erosion/ sediment yield models can supply the soil erosion/sediment yield spatial distribution and make procedure faster and more efficient.

**HS01/09P/D-024** Poster **1400-191**

**SEDIMENT YIELD MODEL FOR BHAKRA NANGAL DAM USING SATELLITE REMOTE SENSING DATA**

siddharth YADAV<sup>1</sup>, Ramesh P. SINGH<sup>2</sup> (<sup>1</sup>department of civil engineering, indian institute of technology ,kanpur , india 280016, <sup>2</sup>professor,department of civil engineering, indian institute of technology ,kanpur , india 280016)

Excessive siltation leading to drastic decrease in the water holding capacity and even damage to concrete hydraulic structures is a common problem in reservoirs. Erosion of top soil in the catchment area is influenced by natural and man-made factor that leads to increase sediment load. Bhakra Nangal dam, 255 m high, straight gravity dam (31.25N and 76.25E) is situated along the river Sutlej. The river Sutlej, originating from Mansarovar Lake on the Tibetan plateau at an elevation of 4572 m, flows in a southwest direction, cutting 915 m deep through the plateau and later entering India after traversing a distance of 320 km in Tibet. Gobind sagar reservoir covers 16867 ha at the FRL of 514 m above MSL and 5063 ha at the minimum water level. The reservoir has been designed to hold 9621 million m<sup>3</sup> of water, when full, and 2431 million m<sup>3</sup> at DSL. However, due to silt accumulation, the capacity has declined to 7118 and 1973 million m<sup>3</sup> respectively. The dam was designed for sediment load of 4.29 ha m 100 km-2 yr-1 but actual sediment load coming is 6.00 ha m 100 km-2 yr-1. In the present study, an attempt has been made to find locations using remote sensing data in Satluj river basin that are contributing more sediment to the river. Sediment yield in any basin depends upon parameters like soil moisture, extent of vegetation cover, surface temperature, soil type, snow thickness (if area is bounded by snow), surface precipitation rate, mean precipitation rate, drainage density, lineament density, lithology, slope of the area. For deducing these parameters optical as well as microwave remote sensing data have been used. Snow thickness has been calculated using SSM/I, for vegetation cover change detection using NOAA AVHRR and IRS -1D LISS -III, soil moisture using MSMR data. The mean precipitation and surface precipitation have been calculated using AVHRR NOAA data, evapotranspiration has been calculated using SSM/I and NOAA data and drainage and lineament density from IRS-1D LISS-III data. The basin area has been divided into different small zones and all the above numerous parameters responsible have been calculated and the locations contributing more sediment have been identified.

**HS02-Oral-Posters** Monday, July 7 - Friday, July 11

**WATER RESOURCES SYSTEMS: GLOBAL CHANGE, RISK ASSESSMENT AND WATER MANAGEMENT (ICWRS, ICASVR, ICSW, ICWQ)**

Location: Site C, Room 24

<b>HS02/07A/C24-001OP</b>	<b>Oral-Poster</b>	<b>0900</b>
---------------------------	--------------------	-------------

**IMPACTS OF ENVIRONMENTAL CHANGE AND POPULATION GROWTH ON THE WATER QUALITY AND WATER AVAILABILITY IN INDIA**

Shadananan K. NAIR (Department of Physical Oceanography, Cochin University of Science &amp; Technology)

Global environmental changes and demands of increasing population make water resources management a difficult issue in many parts of the world. This is especially true for a developing country like India with an exploding population, a weak economy that is related to agriculture and where there are disputes over sharing of water. Life of majority of the population in India depends on agriculture or related industries. Though India is rich in water resources and water resources development projects have helped attaining self-sufficiency in food, the fast increasing population and associated needs pose serious threat to water availability. Overuse, pollution and improper management have been seriously affecting the quantity and quality of water. Global climate models predict a possible change in the rainfall pattern and hence in the water resources of India in the coming decades. In this study, water balances of different States of India have been computed, incorporating the methods of Penman and Thornthwaite, to estimate the water deficiencies, surpluses and the per capita availability. Considering the rate of growth of population and predicted changes in temperature and rainfall patterns, the situation after two decades has been assessed. Study reveals that the present national per capita water availability of 2150m<sup>3</sup> will be drastically reduced to 972m<sup>3</sup> in few years. Even today, some states have no surplus water from precipitation annually, after meeting the requirements for evapotranspiration and soil moisture recharge. In almost all parts of India, water deficiencies show an increasing trend and surpluses show a decreasing trend. Though some climate models predict an increase in rainfall, it may not be able to compensate for the reduction in soil moisture due to rise in temperature. This will reduce the water level and runoff in rivers. This situation will surely add to the economic crisis. More investment will be needed in domestic supplies, irrigation, national waterways and for finding alternatives for cheap hydroelectric power. If the present population growth and urbanization continues, the country will find it hard to meet the requirements in domestic and industrial sector and after all in the agricultural sector that may need additional 200MCM water to feed more than 1.5 billion population. Guidelines for better management have been provided, considering socio-economic conditions and natural and man made environmental changes on water.

<b>HS02/07A/C24-002OP</b>	<b>Oral-Poster</b>	<b>0904</b>
---------------------------	--------------------	-------------

**ESTIMATION OF POTENTIAL WATER RESOURCES IN THE LOWER MEKONG RIVER BASIN**

NMNS Bandara NAWARATHNA, So KAZAMA, Masaki SAWAMOTO (Department of Civil Engineering, Tohoku University)

Availability of GIS data sets of watershed physical properties and the advancements gained in obtaining distributed meteorological variables with the help of GIS have stimulated the development of physically based hydrological models. The introduction of block wise approach to the TOPMODEL with Muskingum-Cunge flow routing methods (BTOPMC) has enhanced the applicability of TOPMODEL from hundreds of square kilometers to several ten thousands square kilometers. In this research work, BTOPMC is used to simulate hydrological processes in the effective watershed of 277,000 square kilometers from Luang Prabang to Pakse in Loas PDR along the Mekong River. It has become necessary to construct reservoirs to meet increasing water demand especially in agriculture and power supply in the lower Mekong river basin. However, with the ongoing debate on environmental aspects of dam constructions, a thorough study from a sound hydrological model is needed to ensure sustainable development. The watershed is divided into four rectangular blocks (250 km<sup>2</sup>/300 km) and the block wise average saturation deficit, which controls the depth to the saturation zone in each grid (1 km<sup>2</sup>/1 km), is calculated in each time step. Upstream observed runoff is used as a boundary condition of the model and four parameters namely, lateral transmissivity under saturated conditions, decay factor, maximum root zone storage, and flood plain Manning coefficient  $n$ , are estimated as a function of land use extracted from USGS (United States Geological Survey) global land cover characteristics database. Model parameters were calibrated based on the results at different gauging stations. Reservoir operations are taken into account using simplified routing curves depending on the purposes of the reservoir. Storages and releases from irrigated crop fields are taken into account by introducing required water level function to the relevant grids. Initially the most sensitive  $n$  values for different river reaches were estimated using the shape of simulated hydrographs without any rainfall input. The Mekong River, tributaries and flood plains were differentiated by introducing threshold values for the effective watershed area. Minimum value for the Mekong river basin at Pakse is identified as 0.0015. Annual evapotranspiration was estimated based on a pixel wise methodology related to potential evapotranspiration. The sub basins values ranges from 470 mm to 620 mm. Nash-Sutcliffe coefficient formula was used to evaluate the simulation efficiency. Lowest efficiency value for the year 1993 is 93.5%. Finally, potential water resources distributions at 100 square kilometer grid size were estimated. It has been found that there are sufficient water resources in mountainous area in Laos whereas flat irrigated fields in Thailand need to get water from nearest potential locations for a sustainable development.

<b>HS02/07A/C24-003OP</b>	<b>Oral-Poster</b>	<b>0908</b>
---------------------------	--------------------	-------------

**CLIMATE CHANGE AND WATER RESOURCES VULNERABILITY IN HEAD AREA OF CHANGJIANG AND HUANGHE**

 Shao-feng JIA<sup>1</sup>, Hua-yun YAN<sup>2</sup>, Run-jie LI<sup>3</sup> (<sup>1</sup>Department of Hydrology and Water Resources, Institute of Geographical Sciences and Natural Resource, <sup>2</sup>Bureau of Hydrology and Water Resources Survey of Qinghai Province, <sup>3</sup>Institute of Water Resources of Qinghai Province)

The head areas of Changjiang and Huanghe are called as Water Tower of China and have very important significance for water conservation and ecological integrity in Changjiang and Huanghe basins. Although the head area of Changjiang and that of Huanghe are connected together, runoff in two rivers showed different change patterns in recent 50 years. While runoff in head area of Changjiang didn't change evidently (only decreased by 1% compared to 1950's), runoff in head area of Huanghe had decreased by 10% in the same period. It's surprising that the annual precipitation in the head area of Huanghe didn't change obviously. Detail analysis indicated that the main reason of runoff decrease in the head area of Huanghe was the change of time distribution of precipitation i.e. the decrease of precipitation in summer. Perhaps the rising of temperature which may result in the increase of evaporation and transpiration was another reason. But an interesting phenomenon is that the recorded water surface evaporation in head areas of Changjiang and Huanghe decreased while temperature rose and sunlight time increased. In fact, this phenomenon occurred in Northwest China universally and so it worth being paid attention to. Because the main two factors influencing fresh water evaporation are temperature and wind, when temperature

rising, the sole factor inducing the decrease of water surface evaporation must be slowing of wind. Metrological records in those areas proved this deduction and showed obvious decline of annual average wind speed. So the rising of temperature will not certainly induce evaporation increase while wind speed descending. This make the relation between temperature and evaporation, further the relation between climate change and water resources, more complicated. Two phenomena in the head area of Changjiang and Huanghe—The dissimilar runoff change pattern (Changjiang's vs Huanghe's) in the same region when water and energy balance factors such as precipitation, sunlight time, temperature, wind speed and water surface evaporation are similar, and the complex relationship between temperature, wind speed and evaporation—make it very clear that there is still much uncertainty in the prediction of water resources change in the future in a global changing environment.

<b>HS02/07A/C24-004OP</b>	<b>Oral-Poster</b>	<b>0912</b>
---------------------------	--------------------	-------------

**AN ESTIMATION OF AVAILABLE WATER RESOURCES**

 Boris BERAKOVIC<sup>1</sup>, Marija BERAKOVIC<sup>2</sup>, Ksenija CESAREC<sup>3</sup> (<sup>1</sup>Water Research Department, Faculty of Civil Engineering, Univ of Zagreb, <sup>2</sup>Croatian Waters, <sup>3</sup>Meteorological and Hydrological Service)

Water management is a very complex activity and its successfulness depends on many factors and their reliability. In the paper the basic and most influential factors are described. A special attention is given to the estimation of available water resources as one of the basic elements influencing the effectiveness of water management. From the very beginning of water management activities information on water quantity and quality were its basic elements. Today, water balances are made routinely especially for larger areas, and the results obtained so are not sufficient for efficient water management planning. In the paper approval possibilities of estimation of available water resources in Croatia are suggested. Successfulness of water management could be improved by simultaneously improving some other influential factors, which are just mentioned in the paper.

<b>HS02/07A/C24-005OP</b>	<b>Oral-Poster</b>	<b>0916</b>
---------------------------	--------------------	-------------

**CHANGEMENTS CLIMATIQUES, RESSOURCES EN EAU ET SECHERESSES AU MAROC**

Mohammed-Said KARROUK (University Hassan II, Centre de Recherche de Climatologie)

En raison du changement climatique, l'environnement climatique actuel au Maroc subi une perturbation due au réchauffement du climat terrestre, qui peut violemment perturber presque tous les systèmes écologiques naturels et de nombreuses structures et institutions dont les marocains ont appris dépendre. Si les climats ne se sont que peu modifiés jusqu'ici, le pays est confronté dans les décennies venir, la perspective d'une accélération très forte du changement climatique. Les latitudes marocaines représentent les endroits les plus vulnérables aux effets négatifs de ce bouleversement climatique. Le secteur le plus touché par cette situation au Maroc est l'EAU d'eaux sèches prolongées et répétitives. Et ce en raison de la nouvelle distribution géographique du cycle de l'eau qui s'installe nos latitudes. Les ressources en eau au Maroc, dépendent principalement du retour des précipitations de la saison humide ou il pourrait pleuvoir. Cette précipitation qui connaît dans notre pays une instabilité accrue nous laisse en permanente inquiétude vis-à-vis de la disponibilité de cette denrée rare sur laquelle se base l'agriculture et la sécurité alimentaire au Maroc. La circulation atmosphérique est le principal mécanisme l'origine des changements dans les variables climatiques dont l'influence se fait sentir l'échelle régionale. Les fluctuations qui affectent nombre de ces facteurs sont fortement interdépendantes, cause des caractéristiques d'ensemble de la circulation atmosphérique et des interactions qui se produisent entre les surfaces terrestres et océaniques. Les précipitations et les températures ont changé au cours des 100 dernières années au Maroc. Au cours de cette période, les précipitations ont connu des variations substantielles et les fluctuations des tendances ont également été relativement importantes. Ces variations ont accompagné les grandes fluctuations des événements extrêmes observés dans la zone intertropicale « ENSO », qui se sont répétées sur les températures et surtout les précipitations au Maroc travers la circulation atmosphérique dominée par les transferts énergétiques. Un événement négatif « El Niño » se manifeste au Maroc par des sécheresses, et un événement positif « La Niña » par des précipitations. Ces fluctuations extrêmes au Pacifique sont devenues ces dernières décennies plus fréquentes et se manifestent par une violence « exceptionnelle ». Les sécheresses récentes au Maroc ont été très pesantes et catastrophiques (1983, 1995, 1998), et leur brève interruption s'est manifestée par des inondations (1986, 1996, 1997, 2000 et 2001). Cette instabilité accrue des événements océano-atmosphériques met en péril les ressources en eau au Maroc, l'agriculture et la sécurité alimentaire. Le Maroc, déjà sensible une variabilité climatique instable, est soumis aux effets du changement climatique dans plusieurs secteurs, savoir : • Le stress hydrique impose divers systèmes biologiques et secteurs socio-économiques, en raison de l'augmentation de la température et de l'évapotranspiration, entraînant un bouleversement du cycle hydrologique. • Les perturbations de l'écoulement de surface qui pourrait être excédentaire en cas de précipitations hivernales, et déficitaire dans les autres saisons. • La rentabilité agricole pourrait être altérée en raison des perturbations du cycle hydrique, ce qui poserait une sérieuse menace pour la sécurité alimentaire du pays. Des mesures draconiennes nécessaires devraient être entreprises pour s'adapter des éventuels bouleversements, lesquels représentent des facteurs limites pour la continuité en équilibre des écosystèmes et des systèmes socio-économiques.

<b>HS02/07A/C24-006OP</b>	<b>Oral-Poster</b>	<b>0920</b>
---------------------------	--------------------	-------------

**WORLD MAP OF HYDROGEOLOGICAL CONDITIONS AND GROUNDWATER FLOW**

Roald Gamidovich DZHAMALOV, Igor Semenovich ZEKTSER (Water Problems Institute, Russian Academy of Sciences)

The Map was compiled in accordance with special UNESCO Project and printed in the USA in 1999. The methods of groundwater flow assessment and mapping, legend of the map and its main contents were elaborated by Russian scientists (Principal editors Dr. R. Dzhamalov and Dr. I. Zektser). The Map was edited by a special International Editorial Board that included representatives from the Australia, Argentina, Brazil, China, Germany, USA, India, France, Indonesia and numerous other countries. World Map of Hydrogeological Conditions and Groundwater Flow (scale 1:10 mln.) is designed to provide specific and quantitative information for the following practical problems: a) to determine groundwater flow and natural groundwater resources in individual regions of the Earth to characterize water availability and to plan the use and protection of water resources; b) to determine groundwater recharge amounts to establish the regional water balance and existing water resources; c) to determine groundwater contribution to river runoff as it is the most stable portion of total river runoff, as well as to predict changes in river discharges under the effect of large scale groundwater withdrawal; and d) to determine the value of direct groundwater discharge to seas and oceans to establish groundwater contribution to water and salt balances of the seas. The World Map is a special, thematic hydrogeological map whose main content is information on the distribution of several quantitative characteristics of groundwater runoff as

well as geological and hydrogeological conditions of groundwater generation. In small-scale mapping of hydrogeological conditions selection of aquifer systems is a severe problem. It is necessary to distinguish principal groundwater flow media - types (subtypes) of rocks with common conditions of generation and spatial distribution of water-conducting properties. Besides of lithological composition of groundwater flow media on the Map the specific values of groundwater flow characteristics (modulus and coefficients) are presented. This combined representation of two quantitative characteristics appreciable improves the informativeness of the Map. Different colors are connected with groundwater flow media types, intensity of each color reflects modulus of groundwater flow or annual specific groundwater discharge values (from less than 0,1 to 10-20 l/s km<sup>2</sup>), and brown isolines represent coefficients of groundwater flow or ratios groundwater runoff to annual precipitation. The Map gives also information about special conditions of groundwater flow generation connected with human activities, intensive karstification, river channels with surface runoff losing, and rift zones and regional faults, and so on. Firstly in the hydrogeological mapping, the Map presents conditions of direct groundwater discharge to seas together with quantitative characteristics of this global process expressed in specific values. The results of quantitative estimation and mapping of groundwater flow make it possible to solve several problems of groundwater generation under different natural conditions on a completely new basis by introducing quantitative data into the analysis. The carried out research found the principle global and regional regularities and relation between groundwater recharge and the natural and climatic zonality.

**HS02/07A/C24-0070P** Oral-Poster **0924**

#### ASSESSING THE SUSTAINABILITY OF URBAN WATER RESOURCES

Matthias EISWIRTH (Department of Applied Geology, University of Karlsruhe)

With over 40% of the water supply of Western & Eastern Europe and the Mediterranean region coming from urban aquifers, efficient and cost effective management tools for this resource are essential to maintain the quality of life. Traditional water planning regularly concludes that future water demands will inexorably rise and eventually exceed water supplies available in any given location. However, the increasing concerns about the environmental impacts of water projects and their increasing economic costs mean that traditional planning concepts, which assume unlimited supplies of potable water, must be questioned. This includes the source of the water supplies and its appropriate use. With population densities increasing in urban areas and constraints on funding, it is becoming increasingly evident that the present management of urban water resources and systems will not be suitable models for service provision into the 21st century and that increased emphasis will be placed upon the use of groundwater reserves. Without an adequate knowledge base of the current status of urban water resources, and an understanding of the processes involved, the health and safety of the people who depend on urban groundwater as drinking water can not be assured. In spite of strong efforts initiated by the European Union and other international organisations in the past 20 years, groundwater pollution from industry, traffic, sewers and agriculture is still very high. The complex transport processes of groundwater flow are responsible for the wide distribution of recharged water and contaminants. There is evidence that urban downstream aquifers are contaminated by inorganic, organic and microbial pollution. With population densities increasing particularly in urban areas and the corresponding constraints on funding, it is becoming increasingly evident that present urban water systems will not be suitable models for service provision into the 21st century. The overall objective of a new European Commission funded initiative, called AISUWRS (Assessing and Improving Sustainability of Urban Water Resources and Systems), is to develop an innovative system to quantify and manage the problems from unsustainable urban water systems and assess the impact of pollution on the underlying groundwater resources. The overall scope of the AISUWRS initiative is to assess and improve the sustainability of selected urban water systems and resources with the help of computer tools and thus minimise the impact of pollution on the underlying urban groundwater resources. Parts of these model tools have been already developed to estimate the water flows and contaminant loads within the urban water system. This model represents water and contaminant flows through the existing water, wastewater and stormwater systems, from source to discharge point and have already been applied successfully in selected areas in Australia and Germany.

**HS02/07A/C24-0080P** Oral-Poster **0928**

#### ASSESSING VULNERABILITY OF WATER RESOURCES TO CLIMATE CHANGE IN MIDWEST

Hua XIE, Wayland J. EHEART (Department of Civil and Environmental Engineering, University of Illinois at Urbana-Champaign)

There exists much scientific evidence showing that our planet is undergoing a global climate change and that the climate change will threaten the status quo of regional water resources that support ecosystem and human society. An assessment was conducted to evaluate the vulnerability of water resources to climate change in the Mackinaw watershed in central Illinois, USA. In this study, the SWAT (Soil and Water Assessment Tool) model was used to predict stream flow and crop yields in a watershed under different future climate scenarios that represent possible climate outcomes predicted by well-known global circulation models. The potential effects of climate change and irrigation incurred by the change, if any, on low-streamflow and profitability of crop growing operations were investigated, for currently customary crops for the region and alternative crops.

**HS02/07A/C24-0090P** Oral-Poster **0932**

#### THE BASIC FEATURES OF TRANSFORMATION OF A REGIONAL CLIMATIC FIELD OF PRECIPITATION ON UKRAINE UNDER INFLUENCE OF GLOBAL WARMING

Volodymyr M. VOLOSHCHUK, Svetlana G. BOYCHENKO (Department of meteorology and climatology, Kyiv Taras Shevchenko University)

The main aim of this research is to obtain quantitative estimations of the basic tendencies of changes of the monthly sums of precipitation on Ukraine as a result of global warming and to work out scenarios of transformation of a climatic field of precipitation on Ukraine in first half of 21-th century on their basis. In this research were used the following methods:• Specific statistical analysis of empirical meteorological data which was worked out by authors specially for revealing very small climatic signal on a background of very large meteorological noise with use mainly of a space-time coordination and connectivity of climate fields;• The climatic theory of similarity of processes of formation of an atmospheric precipitation which was worked out by authors for construction of necessary semi-empirical models;• Comparison with known materials of regional climatic paleoreconstructions of warm epochs of the past. The following main features of transformation of climatic field of the monthly sums of precipitation on Ukraine under influence of global warming up to 2-3 K are established: •Increase of the monthly sums of precipitation for those regions and months of Ukraine for which meteorological norms of precipitation are below 50 mm per month;• Increase of the monthly sums of precipitation for those regions and months of Ukraine for which meteorological norms of precipitation are over 75 mm per month;• Decrease of the

monthly sums of precipitation for those regions and months of Ukraine for which meteorological norms of precipitation are over 50 mm but below 75 mm per month;• Space alignment of a climatic field of the annual sums of precipitation, but averaged on all territory of Ukraine the annual sum of precipitation does not practically change. The important methodological conclusion follows from the obtained results concerning dynamics of a climatic field of precipitation on Ukraine: incorrect averaging on various space-time scales of climatic field of precipitation can result in essential distortion concerning influence of global warming on intensity of regional precipitation. At construction of scenarios of transformation of a climatic field of precipitation on Ukraine two types semi-empirical models are used:• Variability and trends of precipitation as functions of meteorological norms;• Meteorological norms, variability and trends of precipitation as functions of seasons, geographical coordinates of a place and its height above the sea level. The scenarios constructed on the basis of such type of semi-empirical models are convenient for using at assessments of influence of global warming in various branches of economy of Ukraine, which are formulated as stochastic space-time functionals from meteorological parameters.

**HS02/07A/C24-0100P** Oral-Poster **0936**

#### FEATURES OF WATER RESOURCES SYSTEMS IN GEORGIA

Konstantine Kote BZIAVA<sup>1</sup>, David Dato GUBELADZE<sup>2</sup> (<sup>1</sup>Department of Land Reclamation and Engineering Ecology, <sup>2</sup>Department of Land Reclamation and Engineering Ecology)

The physical-geographical and climatic conditions promoted the large variety of hydrological features both as a whole in all Georgia, and in its separate areas. In Georgia the greatest drain of water (in comparison with the countries of former USSR), exceeding 3000 mm of water per year, however amplitude of fluctuations of this drain depending on territory and river pools is very high. Resources of fresh water of a region are composed from a superficial and underground component of a river drain; underground waters not participating in a river drains and getting directly in the sea; and also water of glaciers, lakes and bogs. The features of water resources of the country are defined by relief and climatic conditions, aridity of territory, mode and geography of a drain of the rivers, and also geographical isolation of Transcaucasia. All variety of natural resources depending on reproduction can be referred to two groups: renewed and not renewed. Now situation essentially has changed, as water has become scarce, and the former resources do not provide needs for it; besides it its quality considerably has worsened. In this connection there was a necessity besides the operational charges to carry out expenses for production of water accessible to use and on improvement of its quality. For example, at regulation of the river drain in reservoir water resources "sharply grow", and the clearing of water source from pollutants improves its quality, also increasing "water resources" etc. Proceeding from above told, it is possible to note, that in a long-term section "the water resources" as against "of water stocks" are variable size varying as quantitatively, and is qualitatively depending on the requirements showed to water. Now volumes of water used in industrial activity of the man and in a life, continuously grows. As a result of it the necessity of involving in activity of the man of all new and new water sources, i.e. transference "water stocks" in a category "of water resources" has appeared. The present stage of development of a human society is characterized by the tendency of increasing water requirement, and consequently, increasing of water resources. Though in absolute sizes, the specific parameters of water resources of East Georgia are not low in comparison with arid zones of other countries, but the conditions of their use are specific and difficult, since they play a main role in water requirement of neighboring Azerbaijan laying below on current of the river Mtkvari and using a transmitted drain from Georgia. This situation is aggravated also by that as East Georgia, and below laying grounds of Azerbaijan by the climatic conditions are sharply require irrigation up. Proceeding from above mentioned, the problem of water in East Georgia carries not only technical and economic character, but also social, as the development of a national economy of Azerbaijan and indirectly of Armenia depends on its decision, as the growing water consumption by Armenia also increases deficiencies in East Transcaucasia.

**HS02/07A/C24-0110P** Oral-Poster **0940**

#### STREAMFLOW VARIATION OF FOREST COVERED CATCHMENTS

Zoltán GRIBOVSKI, Mihály KUCSARA, Péter KALICZ (Department of Forest Opening Up and Hydrology, University of West Hungary)

Rainfall concentration and runoff, otherwise rainfall-runoff processes, which cause river water discharge fluctuation, is one of the basic question of hydrology. Looking for the answer is important because several social-economy demands have a strong connection with small or bigger rivers from the point of view both quantity and quality of the water. Gratification or consideration of these demands is complicated substantially that we have still poor knowledge about our stream-flow regime. Water resources mainly stem from upper watersheds. Rivers transported water discharge, which is potential usable, is an integral of streams take its rise in these small watersheds. These upper watersheds are the basis of the water concentration process, therefore we have to improve our knowledge about hydrological processes coming up in these territories. In this article we present runoff regime of three small catchments on the basis of one year data. Two catchments have a similar magnitude 0,6 and 0,9 km<sup>2</sup>, and one is bigger about 6 km<sup>2</sup>, which has a part other two above mentioned. We have been analyzed in detail from hydrological elements only features of rainfall, discharge, rainfall induced flooding waves, and basic discharge in rainless periods. Variances of these parameters have been analyzed in relation to catchments surface, vegetation coverage and forest management. Result data set well enforce our knowledge about *small catchments hydrological processes*. On the basis of these fundamentals we can plan more established the management of these lands (forest practices, civil engineering works, usage of natural water resources). Global change could change hydrological regime. These results can also utilize on the long term planning of land use and water demands gratification.

**HS02/07A/C24-0120P** Oral-Poster **0944**

#### FINGERPRINTING CLIMATE CHANGE DRIVEN DROUGHTS IN WESTERN CANADA

Lawrence Chima NKEMDIRIM (Geography and Earth Sciences, University of Calgary)

Some climate models forecast a higher frequency of drought events in western Canada due to an atmospheric greenhouse gas driven climate change. Because droughts are not uncommon there, it is necessary to differentiate events that are either wholly driven or intensified by climate change from "normal" events. Two trends currently identified with century-scale climate change appear to adequately fingerprint climate change inspired droughts in the region. They are (a) statistically highly significant increase in surface air temperature and (b) an equally significant decrease in sea level pressure. Fingerprint One (winter droughts- precipitation poor): Based on homogenized data from 114 stations, mean annual temperature rose at a rate of 2.7 C/century between 1953 and 1997. This trend was dominated by increases of about 5 and 6°C in the winter and spring respectively. Paralleling the trend was a highly significant reducing trend in surface air temperature especially during the two seasons. Observation and analysis showed that the Polar High Pressure, which dominates the region's winter climate had weakened and the temperature contrast between the Arctic and polar airmasses had declined. The resulting 'softening' of the polar front

correlated well with negative winter precipitation anomalies. Precipitation more than 2 standard deviations below normal were 20 percent more frequent in post 1975 winters than in pre-1975 ones and the difference was statistically significant at 95% confidence level. Additionally, the post-1975 two standard deviation events correlated well with both pressure anomalies and change in mean surface temperature. **Fingerprint Two (summer droughts-precipitation rich)**: The Canada Climate Center model predicted increases in precipitation for the region ranging from 15mm/year to 45mm. An energy balance model, in which all sources of energy including a strong advective component due to the Chinook (a mountain wind, which significantly impacts the temperature regime in the region) were fully specified, enabled a realistic assessment of the region's water balance under the present warmer regime. Water deficit ranging from 250mm above normal in the driest areas to 45 mm in the wettest parts was indicated for the post-1975 period. The Palmer Drought Index was used to identify recent drought events that were severer than they would have been under similar summer and rainfall and antecedent moisture. The frequency of such events increased 35% in the post-1975 period.

**HS02/07A/C24-013OP** Oral-Poster **0948**

**THE CONCEPT OF MODERN ARID ZONES OF HYDROGEOLOGY OF CENTRAL ASIA AND ITS PROBLEM**

Nasirdjan TAKHIROV, Shukhrat Saifullaevich RADJABOV (Department of hidrogeology, National University of Uzbekistan)

The hydrogeology as a science intensively developed within last century and its fundamental positions are already formulated. Especially, after 60th of the last century, the accomplishing of any type of hydro-geological researches was accompanied with the decision of a problem to manage the dynamics (changes) and chemical compound of underground waters within the limits of concrete borders. The requirement to a hydro-geological science after 70th has got rather complex character. These requirements follow from an ecological problematic of the regions. The underground hydrosphere is considered (examined) as the mainframe of the geocological environment and is one of the components for eco-system. So, it occurred the new situation connected to an intensification of technogenesis and gradually, the concept of a hydro-geological science has got the new maintenance (contents), providing an ultimate goal – management of underground hydrosphere within the framework of ecological requirements. The decision of hydro-geological problems in volume of its new concept demands the preliminary system analysis of hydro-geological situation. This work is feasible only in development of the further researches on a new scientific direction – technogenetic evolution of hydro-geological conditions of arid zones, rational use and resource management of underground waters: an ecological policy, balance, preservation, protection and the forecast. The object of research is underground water of hyper genesis zones, that is on a part of lytosphere where the active and slowed down water exchange is observed. Thus, the purpose of maintenance of the uniform concept, system, methodology and methods of management and operation of underground waters for needs of a national economy is pursued within the framework of ecological requirements. On the faculty of hydrogeology of National University of Uzbekistan, researches on the mentioned above new direction on Arid zones – Ustyurt, Aral Sea Region, Kyzilkum, Amu-Darya and Fergana artesian pools - are conducted. Researches on the given direction provide the following:- Revealing of scientific bases for development of underground waters under difficult ecological conditions in the arid zones of Uzbekistan and definition of their role in development of geo-ecological processes;- Identification of water problems and problems of social and economic development- Development of criteria for estimation of opportunities to use the resources of underground waters for social - ecological and technical needs- Development of long-term program to develop the water supply for drink, animal industries, technical needs and for infrastructures- Scheduling of the work on protection, management and rational use of underground waters according to the ecological requirements.

**HS02/07A/C24-014OP** Oral-Poster **0952**

**THE GLOBAL WATER SYSTEM PROJECT OF IGBP\*, IHDP\*, WCRP\*, DIVERSITAS**

Holger H. HOFF<sup>1</sup>, Holger HOFF<sup>2</sup>, Carlo JAEGER<sup>1</sup>, Denis LETTENMAIER<sup>2</sup>, Christian LEVEQUE<sup>1</sup>, Harry LINS<sup>1</sup>, Michel MEYBECK<sup>1</sup>, Madiodio NIASSE<sup>3</sup>, Charles VOROSMARTY<sup>4</sup> (PIK, <sup>1</sup>University of Washington, Seattle, USA, <sup>2</sup>Programme Environnement, Vie et Sociétés, Meudon Cedex, France, <sup>3</sup>U.S. Geological Survey, Reston, Virginia, USA, <sup>4</sup>Université de Paris 6, France, <sup>5</sup>IUCN-BRAO, Ouagadougou, Burkina Faso, <sup>6</sup>University of New Hampshire, Durham, USA)

The Global Water System (GWS) plays a central and integrative role in the dynamics of the Earth system. It is a regulator of biogeophysical and biogeochemical processes, and it is also essential for sustenance of human societies. The GWS is increasingly modified by humans and through climate effects (facets of it have moved well outside the range of natural variability) without adequate understanding of how the system works. For understanding the changes, feedbacks and potentially critical thresholds within the Earth system, and eventually for better managing the GWS, new synthetic knowledge is required. The Global Water System Project (GWSP) is a new activity being undertaken jointly by the World Climate Research Programme (WCRP), International Geosphere-Biosphere Program (IGBP), International Human Dimensions Program (IHP), and Diversitas. It will address the GWS in a comprehensive fashion at the global scale, building upon the emerging new consolidated Earth systems data sets, global monitoring tools, and predictive and coupled modeling capabilities. The central scientific question that motivates the GWSP is: "How are humans changing the global water cycle, the associated biogeochemical cycles, and the biological components of the GWS, and what are the social feedbacks arising from these changes?" GWSP will be structured around three "framing questions": a) What are the relative magnitudes of global-scale changes in the global water system that are attributable to changing human activities, and to environmental factors such as climate variability and change?; b) What are the main mechanisms by which human activities are affecting the global water system; and c) To what extent is the global water system resilient to global change? Examples of issues that might be addressed under each of these questions are provided.

**HS02/07A/C24-015OP** Oral-Poster **0956**

**MODELLING OF WATER AVAILABILITY IN GRASSLAND ECOSYSTEMS OF ARID ZONE DELTA PLAINS**

Natalia V. PENKOVA<sup>1</sup>, V.P. SINGH<sup>2</sup>, V.A. KHAYDAROVA<sup>3</sup>, N.M. NOVIKOVA<sup>4</sup> (<sup>1</sup>State Hydrological Institute, <sup>2</sup>Louisiana State University, <sup>3</sup>Water Problems Institute, Academy of Sciences of Uzbekistan, <sup>4</sup>Water Problems Institute, Russian Academy of Sciences)

For successful long-term planning and ecosystem management in river deltas of drought-prone regions, it is desirable to develop sufficiently rigorous but not very complex and data-extensive models which are easy to understand and can be used by a wide range of specialists and experts, not sophisticated in purely hydrological, ecological or biological scientific knowledge, for real decision-making. In the contribution, the most simple version of conductance-type combination equation (Budyko's combined method) is used to calculate within-the-year and long-term variations and trends in water availability (evapotranspiration

and soil water content) for grassland ecosystems in Syrdarya and Amudarya river deltas (Aral Sea basin), Volga and Terek river deltas (Caspian Sea basin) and Mississippi delta plain. The biological response to environmental conditions (atmospheric demand, precipitation intensity, ground water table, soil water properties), and to agrotechnology (fertilization, irrigation) by using non-linear multi-dimensional cubic splines approximations for "biological" parameter of the Budyko's equation is estimated for annual grass crops and perennial herbs, with particular emphasis on the vegetation condition (closed and sparse canopy, high and low productivity, etc.) (Khaydarova, Kucherova and Penkova, 1998). A comparison is made of the results with ones obtained by applying mechanistic volume type models (Singh, 1989), and resistance-type combination techniques (Penman-Monteith equation). The advantages and shortcomings of the models under analysis are highlighted. An application of the models for historical formation of water availability patterns and for possible climatic and economic conditions in the future is presented. The ecosystems of the deltas represent different natural self-development and man-induced stages - from the stage of drying, increasing of soil salinization and decreasing of meadowlands productivity (Aral basin) to the stage of humid-meadow lands restoration conditioned by rising the Caspian sea-level. Vegetation changes in the territories are of long-term cyclic nature, depending on climatic fluctuations and superimposed anthropogenic influences (Novikova, 1997). The superimpositions are investigated for different periods of economic development of states.

**HS02/07A/C24-016OP** Oral-Poster **1000**

**CLIMATIC VARIABILITY AND LAND RESOURCES VULNERABILITY IN THE FORCADOS RIVER ESTUARY**

Mayowa FASONA (University of Lagos)

The current climatic fluctuations and shift from global climatic normals is causing apprehensions across the blue planet. Data on global climatic indicators show that there has been a net increase in global surface temperature by between 0.30c and 0.50c over pre-industrial periods. Evidences of global warming have already been noted in glacial margin retreat, a rise in snowline, a rise in sea level, northward recession of the tundra margin in the arctic and the ferocious southward march of the Sahara in the tropics. It has also been estimated that an increase of between 10c and 4.50c over the current global temperatures is expected to trigger off accelerated sea level rise of between 0.2m and 1.4m, which have lots of catastrophic implications especially for the coastal ecologies and other low-lying areas of the world. This paper utilizes Remote Sensing and GIS techniques to assess likely implications of accelerated sea level rise on water and land resources of the areas around the estuary of the Forcados River. Current ecological and land resources data on the study area was generated from remotely sensed satellite imagery. This was overlaid with spatial data on elevation, soil, geology and water resources to generate floodable areas sensitivity map for this coastal environment. The implication of this for food security, sustainable water resources management and coastal resources management is also discussed.

**HS02** Monday, July 7 - Friday, July 11

**WATER RESOURCES SYSTEMS: GLOBAL CHANGE, RISK ASSESSMENT AND WATER MANAGEMENT (ICWRS, ICASVR, ICSW, ICWQ)**

Location: Site C, Room 24

Monday, July 7 AM

Presiding Chair: S. Franks

**HS02/07A/C24-001** **1045**

**SMALL HYDROLOGICAL BASINS IN DELTA REGIONS AND THEIR VULNERABILITY TO CLIMATIC CHANGE: THE CASE OF THE MARK-VLIET BASIN**

Victor Jan WITTER (Water Authority)

The paper gives an overview of changes in population, land use and economy, affecting the hydrology of the Dutch/Netherlands basin of the Mark and the Vliet. This is a relatively small hydrological basin (ca 140.000 has) situated in the Delta of the rivers Rhine, Meuse and Scheldt. The basin is of recent origin. Around the year 1000 the sea starts to penetrate what is now the Mark-Vliet basin and at that time was part of the vast peat-covered Delta of Rhine, Meuse and Scheldt. Consequently, the basin was shaped into its present form in the last 1000 years. The period of study starts in 1820, when sluices were built in the mouth of the rivers draining the basin, the Mark and the Vliet. Three periods can be discerned since then: 1820-1900, 1900-1960 and 1960-2000. Around the year 1900 radical changes land use took place in the southern part of the Mark-Vliet basin, because of large-scale colonization by farmers and forestation of fallow land. Around the year 1960 extensive land consolidation schemes and reconstruction works of water systems took place in the basin, with the objective to modernize agriculture. The changes in rural land-use and water management were accompanied by a rapid urbanization of the region. The period of study extends into the future period till 2050. Provisioned changes in climate and changes in population, land use and economy are analyzed with respect to their effect on water demand and supply and the region's hydrology. Changes are analyzed with respect to extremes of water levels and discharges, in mean conditions and in high flood and low flood conditions. The paper demonstrates (1) the profound changes that took place in the hydrology of small basins like the Mark-Vliet basin, changes that in large river basins are flattened out; (2) the magnitude of future changes in the hydrology of the region which will be needed to cope with autonomous developments and with the effects of climatic change; and (3) that the magnitude of future changes considerably exceeds that of changes in the past and possibly readjustment is needed of both magnitude of the changes as well as their direction. The results for the Mark-Vliet basin are generalized to small hydrological basins in Delta regions. It is argued that these basins are particularly vulnerable to climatic change.

**HS02/07A/C24-002** **1100**

**WATER PROBLEMS & SUSTAINABILITY IN THE NORTH CHINA**

Jun XIA (Institute of Geographical Science & natural Resources Research, Chinese Academy of Science)

Located in the semi-humid and semi-arid regions of eastern China, the North China Plain (NCP) is the largest alluvial plain in China with an area of about 32x104km2. The city such as Beijing, capital of China, is located in this area. Thanks to social-economic development and population growth, water shortage problem has become one of the most important issues in social & economic development. This paper focuses on water resources

sustainability in the Northern of China. Two key issues are presented, namely water cycle to environmental change, and carrying capacity of water resources in this area. The backgrounds will be introduced to show the causes from natural change and human activity impact. From these practical water issues, several interested mathematic problems on applied statistics and financial mathematics were proposed. Some of methods were presented to quantify water resources sustainability. It will be indicated that water is a highly precious resource and has become a key-limiting factor that plays a critical role in socio-economic development in the Northern of China. Besides necessary water diversion project from South to North, saving water will be a basic measurement. How to trade off conflicts of water supply and demand in the principle of environmental protection will be the big challenge in the 21st Century in this region.

HS02/07A/C24-003

1115

#### UTILIZATION OF WATER RESOURCES AND ITS EFFECTS ON HYDROLOGICAL ENVIRONMENT OF TARIM RIVER BASIN IN XINJIANG, CHINA

Changyuan TANG<sup>1</sup>, Shizuo SHINDO<sup>1</sup>, Xin LI<sup>1</sup>, Jianyao CHEN<sup>1</sup> (Graduate School of Science and Technology, Suzhou College of Urban Construction and Environmental Protection, Suzhou, China)

This paper describes the characteristics of water resources utilization in Tarim River basin in terms of both its quality and quantity. It is found that water cycle and water qualities have changed greatly because of human activities in last forty years. Many canals have been built to transfer almost all stream waters for irrigation and farmland salt-washed. For example, irrigation land has increased more than 4.0x10<sup>5</sup> ha at upstream of the Tarim River, which use almost 40% of the stream water for agriculture. According to the flow statistics of Tarim River in last forty years, the stream flows in middle stream and downstream decreased about 50% and 85%, respectively. As a result, water in downstream of the Tarim River decreased sharply and many lakes disappeared from the desert. Near half of farmlands had been abandoned. According to 52 sampling points of streams that flow from the south part of Tianshan Mountain, it was found that about 37% of streamwaters were Ca<sup>2+</sup>-HCO<sub>3</sub><sup>-</sup> type and more than 40% either Na<sup>+</sup>-Cl<sup>-</sup> type or Na<sup>+</sup>-SO<sub>4</sub><sup>2-</sup> type. The water of the former type was the stream water in natural hydrologic conditions, while the water of the later type was stream water affected by agriculture activities. Water use in Tarim river basin has two effects: one is the expansion of irrigated farmland, the improvement of land productivity; the other is the destruction of water balance, salt balance and ecological balance with desertification expanded rapidly in the lower reaches. From 1957 to 1996, annual runoff at Qiala reduced from 1.46 km<sup>3</sup> to 0.194 km<sup>3</sup>. Stream has run out till Alagan in 1972, and moved sand dune increased 20% there. Sand area has expanded 116km<sup>2</sup> since 1959, and desertification became seriously. The relationships among the water use, desertification and salinization were also discussed in the study region. It was found that desertification and salinity are twin problems that must be dealt with at the same time with respect to water balance. Desertification is closely related to water distribution along the river. However, when runoff in the tributaries of Tarim River reduced, water consumption in the upper reaches and middle reaches of Tarim River had increased. For instance, water consumption in the upper reaches was 14.77% of total flow in 1960's, and increased to 23.0% in 1994; in the middle reaches it was 61.54%, and 72.56% respectively; in the lower reaches, it was only 4.44% in 1994.

HS02/07A/C24-004

1130

#### WATER RESOURCES IN BULGARIA UNDER CLIMATE VARIABILITY AND CHANGE

Vesselin A. ALEXANDROV, Marin GENEV (National Institute of Meteorology and Hydrology)

The question of global climate variability and change is a major and important environmental issue facing the world at the beginning of the 21st century. Variability of water resources (e.g. precipitation, river runoff, groundwater) during the 20th century in Bulgaria were investigated. A special attention was paid on the drought period during the last two decades, where soil water content was also considered. Several GCM (global circulation model) climate change scenarios were created for the country. For example, some of the used GCM simulation outputs include the models from the Max-Planck Institute for Meteorology, UK Hadley Center for Climate Prediction and Research, Canadian Climatic Center Australian CSIRO model, Geophysical Fluid Dynamics Laboratory. According to the GCMs used in the study air temperature is expected to increase between 2 to 5°C till the end of the 21st century. In general, precipitation is expected to increase during the winter and to decrease during the warm half-year. It is obviously that there would be some changes in the water resources. Possible scenarios for air temperature, precipitation and annual runoff in Bulgaria assuming the current trends and also the last severe drought period were created, as well. Annual river runoff is expected to decrease up to 14% in 50 years and to be 0% at the end of the 21st century in respect to the current climate. In case that a severe drought period is also assumed within the study, the expected decrease of annual runoff in Bulgaria is between 39 and 45%. On the first hand total precipitation during the potential crop-growing season will increase due to projected increase of the duration of the potential crop-growing season caused by warming. On the second hand however, the total precipitation amount during the actual crop-growing season is projected to decrease due to the GCM simulated decrease of precipitation and because of shortening the actual crop-growing season caused also by expected warming. The Decision Support System for Agrotechnology Transfer DSSAT was used to simulate the impact of climate change scenarios on maize growth, development and yield formation and the parameters of the water balance during the maize growing season. The parameters of the water balance such as seasonal evapotranspiration, runoff, drainage and soil moisture at maturity were included within the analysis. Adaptation options and strategies in respect to irrigation under climate change are also discussed. The national program of the Bulgarian government on the adaptation measures under the current and expected drought tendencies in the country is also described.

HS02/07A/C24-005

1145

#### IMPLICATIONS OF CLIMATIC VARIABILITY AND CLIMATE CHANGE ON WATER RESOURCES AVAILABILITY AND WATER RESOURCES MANAGEMENT IN WEST AFRICA

Simon Oyediran OJO, Feyi ONI, Olatunde OGUNKUNLE (DEPARTMENT OF GEOGRAPHY, UNIVERSITY OF LAGOS)

This paper begins by examining trends in climatic variations and variability especially during the past three or four decades and their implications for water resources systems and water resources availability in West Africa. It then examines the impacts of the trends in climatic variability on the characteristics of climatic events (including floods and droughts), and the implications of these events on the characteristics of the hydrology and water supply systems. It emphasizes rainfall as a major factor of water resources availability, and the significance for surface and groundwater characteristics in the West African region. It also examines the impacts of climatic variability on the spatial and temporal characteristics of the water balance components with some detailed illustrations using locations and different ecological zones in West Africa. The results show that there were a lot of spatial and temporal variations in the characteristics of rainfall and the water balance components, and their implications for water availability and climatic events (including droughts and floods).

The results also show that the impacts of the trends in climatic variations and climate change on water resources availability have generally been more adverse and especially resulted in water stress in most parts of West Africa. In particular, most years within the study period have been characterized by water deficits and droughts, although flood events, which also have impacted adversely in many parts of the region, have been witnessed because of the general characteristics of climatic variations and variability especially as influenced man. Such human influences have for example, caused increased rates of deforestation and desertification processes, which have in turn resulted in rapid surface runoff and in many cases reduced water quality, and which in turn have affected potable water availability. Using the present knowledge of the characteristics of water supply-demand systems, the paper makes projection into the future of urban and rural water supplies for Nigeria, which is an epitome of West Africa, and using the projected population for the country. It also discusses the problems of acute shortage of freshwater and the prevalence of water stress currently experienced in most parts of West Africa, and whose characteristics would be worsened with the projected climate change, and which points towards the need to plan water resources development strategies and for coherent and effective policies and programmes of development and management of water resources. The paper then examines the two main categories of adaptation measures needed to improve water management and the extent to which they have been applied. The paper finally discusses the need to address a number of mechanisms for implementation of the various adaptation measures. In particular, the paper discusses the urgent need for (a) building capacity and manpower as part of the development of water institutions in the region (b) promoting education and public awareness on the various measures to be used (c) public participation and the involvement of stakeholders (d) the establishment of both national and regional co-operation and (e) the need for climate and other environmental data collection and monitoring.

HS02/07A/C24-006

1200

#### STRUCTURE OF ECOLOGICAL INDICATORS AND INDEXES FOR GROUNDWATER SUSTAINABLE DEVELOPMENT

Anna P. BELOUSOVA (Water Problems Institute of RAS)

A problem of preserving natural environment being of the same class as national security in many countries, is an important aspect of the global sustainable development problem. The main postulates of the problem have been first formulated at a top level in the Rio-de-Janeiro Meeting in 1992. In many developed countries the basic features of sustainable development are social and economic factors and the environment, that are characterized by special indicators and indexes series. By the present the underground part of hydrosphere (groundwater) as an environment component has undergone under intensive anthropogenic impact considerable qualitative transformations, that is dangerous for human health and environment. It is caused by the fact that due to the surface water pollution by industrial, agricultural and domestic waste water in many countries of the world, groundwater use for potable water supply has essentially increased. Qualitative characteristics for groundwater must be more deep and rich in content, i.e. they should specify processes of groundwater chemical composition changes under natural and anthropogenic factors impact in historical and contemporary time scale. As the groundwater being an environmental component is in a constant contact with its other components (atmosphere, lithosphere, biosphere and a sphere of anthropogenic activities), then its quality directly depends on complex physical-chemical processes, being a result of these contact. Thus, a complex assessment of groundwater quality is needed, using indicators and indexes of sustainability (indicators the environment). **Indicator** - is an attributive characteristic of the environment state (in our case it is hydrosphere underground part), fixing an impact on it and its response to this impact. **Index** - is a quantitative characteristic of indicator describing a degree of the environment sustainability to negative impact of natural and anthropogenic factors. The author has preliminarily elaborated a system of indicators and indexes of groundwater quality sustainability. A system of indicators (Pressure - State - Response) worked out by European Organization for Economic Co-operation and Development was taken as a basis, that was widened due to adding a new indicator of *foresight* and also subdividing all the indicators by time of their manifestation (present and future). Indicator of response is of a more complex structure, it indicates a level of accepted decisions (international, national, regional) and rate of response, planning (operation, perspective). Classification of groundwater sustainability indexes has been worked out for anthropogenic conditions. These indexes characterizing indicators of Pressure and State are subdivided by their content into the following groups: indexes of damage, indexes of pollution (chemical indexes), static indexes (hydrogeochemical indexes), dynamic indexes and indexes of interaction. Their assessing and compiling maps of groundwater sustainability using indicators and indexes has an advantage as to other methods due to its complexity and the fact that it is also a stage in a general structure of assessing sustainable development of the studied regions.

HS02/07A/C24-007

1215

#### ASSESSMENT OF THE VULNERABILITY OF WATER RESOURCES SYSTEM IN CHINA

Lihua XIONG, Shenglian GUO (Department of Hydrology and Water Resources, Wuhan University)

With the water resources becoming more and more vital to human existence on the earth, the reliability (or vulnerability) assessments of water resources system are increasingly recognized as the essential component of the integrated water resources management. These assessments should evaluate the combined effects of climate change and human activities on water resources at all scales from global to regional, with emphasis on the river basin scales. It is the strength of these effects and the watershed's hydro-climatological characteristics that ultimately determine the vulnerability of water resources system to any adverse impact. This paper is focused on one important question, i.e. how sensitive the watershed long-term runoff is to climate change. Based on the relationship of the watershed long-term runoff change rate with both the long-term precipitation and potential evaporation change rates, which is proposed by Dooge et al., the expressions of the sensitivity factor of watershed runoff to climate change are derived for the watersheds in China. The value of sensitivity factor depends on the long-term hydro-climatological conditions and the land surface properties of watershed. It is inferred that the larger the value of the sensitivity factor, the more vulnerable is the water resources system of watershed to climate change. According to the information of the average annual precipitation, potential evaporation, discharge and the information of the land surface properties of watershed, the sensitivity factors of runoff to precipitation for the nine major hydrological regions, eighty-two hydrological sub-regions of China have been calculated and ranked. It is found that the sensitivity factor of runoff to precipitation in the humid watersheds such as the southwest China is much smaller than that in the regions in need of water resources such as the Yellow river region. The vulnerability ranking of water resources system of all regions in China, which is based on the sensitivity factor of runoff, is very consistent with what the people have recognized in reality. It is hoped that this method of assessing the vulnerability of water resources system by the sensitivity factor of runoff will be useful in reasonably setting up the social and economic development plan in China.

**HS02-Oral-Posters Monday, July 7 - Friday, July 11****WATER RESOURCES SYSTEMS: GLOBAL CHANGE, RISK ASSESSMENT AND WATER MANAGEMENT (ICWRS, ICASVR, ICSW, ICWQ)**

Location: Site C, Room 24

**Monday, July 7 PM**

Presiding Chair: G. Bloeschl

**HS02/07P/C24-017OP Oral-Poster 1400****INFLUENCE OF CLIMATE WARMING ON ASIAN LAKES FROM VIEW POINTS OF WATER RESOURCES**

Hiroji FUSHIMI (The University of Shiga Prefecture)

Due to the climate warming, glaciers are rapidly melting and lakes are extremely expanding in the Nepal Himalayas, and the region faces further natural disasters including the glacial lake outburst flood and the related landslide phenomena. The water level of Lake Hovsgol in Mongolia has risen 60cm for the recent 20 years, so that the surrounding forests, pastures and the lakeshore town have been inundating year by year. Three causes of the water level rise could be noticed as follows: 1) the formation of a natural dam at the end of the lake caused by the sedimentation of sand and gravel which were transported from the tributary river at the time of heavy rain; 2) the thaw of permafrost around the lake where the ground temperature becomes higher with increases of the incoming radiation due to deforestation owing to the anthropogenic expansion of pasture and fired forest; 3) the thaw of permafrost caused by the global warming. When the average air temperature rises by 3.5 degrees Celsius in Lake Biwa basin in Japan, the amount of snow cover would significantly decrease to 60% of the average (1 billion tons) even if the precipitation exceeds by 20%. When the amount of snow cover is more than the average, the lowest dissolved oxygen concentration in the deep layer of Lake Biwa increases due to the density current of the oxygen-rich snowmelt. However, the dissolved oxygen concentration rapidly decreases, when the amount of snow cover is less than 1 billion tons. The climate warming will significantly decrease the amount of snow cover in Lake Biwa basin and the dissolved oxygen concentration in the deep layer of the lake, leading to further enhancement of eutrophication in the 21st century. There are numerous lakes in the inland mountainous regions and the coastal lowlands of Asia where the mighty rivers, such as Rivers Yellow, Yangtze, Mekong, Ganges and Indus, originate from and flow down to the megalopolises with the rapid population growth in the river mouth areas. At the first stage of the global warming, glaciers and permafrost layers melt, and the lake water increases. However, there comes the shortage period of water resources in the later stage of the global warming due to the shrinkage of glaciers and permafrost layers and this may lead to the serious environmental issues in Asia, when the water resources become scarce especially in the dry seasons. So, there is a need to create a new management system for the rational use of water resources taking into account the recent changes in glacial as well as limnological phenomena due to the climate warming.

**HS02/07P/C24-018OP Oral-Poster 1404****APPLICATION OF WATER BALANCE MODEL FOR REVEALING OF HIDDEN CYCLES IN THE CHANGES OF CHARACTERISTICS OF ENCLOSED LAKES (CASPIAN SEA AS A CASE STUDY)**

Alexey Vladimirovich BABKIN (Lab. of Hydroecological Research of Inland Water Bodies, State Hydrological Institute)

The specific inter-year variations of level, area and water balance components of large closed lakes are caused by quasi-periodical dynamics of global and regional natural processes. The global factors are directly or through Earth climatic system affect the water regime of the lakes and their catchment areas. The revealing of hidden cycles in the variation of lake's characteristics is acute for exploration of their relationships with global factors and for forecast of their possible changes in the future. {BR} The solution of differential equation of lake water balance permitted to elaborate a mathematical model, where dynamics of the mutually related Caspian Sea characteristics (level, water surface area, evaporation and flow of water to Kara-Bogaz-Gol gulf) are the response of inflow (river run off, precipitation and ground-water run off) oscillation. The oscillation of water inflow causes the variation of sea level, area and water balance components. The extremes of sea characteristics have a time lag, if compared with impact extremes. {BR} The amplitudes of variations of sea characteristics and the time of their delay from inflow were calculated for different values of inflow and for the large number of periods. The dependencies of amplitudes of sea characteristics and the time of their delay to inflow from period of variations are exposed on the special nomographs. {BR} The observation data on water inflow and sea level were approximated by periodic functions. The least sums of quadrates of differences of approximating sinusoids and the values of time series of level and water inflow were computed in dependence with the length of period. The cyclic qualities in variation of lake's characteristics are revealed near the periods where there are the minimums of sums of quadrates of differences of approximating sinusoids and values of time series of level and water inflow, and where the time delay of level to inflow and relation of their amplitudes of approximating functions are close to the model results. The application of water balance model for analysis of cyclic qualities in dynamics of lake's characteristics make its results more reliable and physically based than the use of statistical approaches only. {BR} The resemble research and modeling of dynamics of lake characteristics may be fulfilled for another large enclosed water bodies of the Earth.

**HS02/07P/C24-019OP Oral-Poster 1408****INDUSTRIAL WASTE WATER IMPACT ON WATER QUALITY OF ZARAVSHAN RIVER, UZBEKISTAN**Marina Stanislavovna MOLODOVSKAYA<sup>1</sup>, Raisa V. TORYANNIKOVA<sup>1</sup>, Nariman M. UMAROV<sup>2</sup> (<sup>1</sup>Central Asian Res. Hydrometeorological Inst., Dept. of Res. and Forecasts of Environmental Pollution, <sup>2</sup>State Spec. Inspection of Analytical Control of the State Com. for Nature Prot. of Uzbekistan)

Zaravshan River valley is one from the most important economical areas of Uzbekistan. The catchment area of Zaravshan River includes territories of several industrially developed areas of republic with the number of largest cities - Samarkand, Navoi, Bukhara, etc. In past, Zaravshan had been the confluent of Amu-Darya River (which is currently the main tributary of Aral Sea) but along with irrigation network development later it became the separated river system. Zaravshan belongs to rivers with the snow-glacial type of feeding. The Height of Flow Formation Zone is 2829 m.a.s.l.; Total Length is 2342 km; Total Catchment Area is 12,300 km<sup>2</sup>. In its low stream Zaravshan River is intensively withdrawn by channels network.

The Average Annual Discharge is 169 m<sup>3</sup>/s. About 96% of Total Runoff is used for agricultural irrigation. There are also 93 Industrial Enterprises, 52 Sewage Disposal Plants at the territory of river basin; 46 Water Intake and 46 Water Release points along the middle stream of Zaravshan River. Specific Human Water Demand in this region has increased in 1.5 times since 1975. Industrial and Domestic Wastes Inflows into Zaravshan River pose a serious threat for Water Quality and Public Health especially in urban zones with high population density. The ecological situation in region has been considerably deteriorating for recent years due to increasing fresh water demands for industrial and agricultural needs. In turn, it has led to the large-scale contamination of surface and ground water of Zaravshan River basin. The Water Quality Assessment after exposure by Waste Water is carried out using the comparison of hydrochemical data obtained from different points of Zaravshan River body with the Admissible Limits. The choice of Representative Hydrochemical Indexes was done with considering wastes composition and pollutants transformation. The main principles were formulated as following: • Representative Compounds(RC) must be specific about prevalent wastes composition; • RC must have Maximum Admissible Concentration (MAC) exceeding maximal over the other compounds; • Velocity of RC transformation after coming into water flow must be minimal. For Zaravshan there were chosen two groups of the RC. The first group is common for any type of water system: 1)BOD; 2)COD; 3)Dissolved Oxygen; 4)TDS; 5)Ammonium Ions; 6)Surface Active Substances (SAS); 7)Phenols. The second group is specific one and caused by the character of wastes: 1)Oil Products; 2)Fluorides; 3)Phosphates; 4)Nitrates; 5)Nitrites; 6)Copper; 7)Chromium; 8)Lead; 9)Cyanides; 10)Arsenic, etc. The Hydrological Indexes of Average Contamination and Total Loading of River Flow were calculated with using the average concentration of pollutants in river flow at the point lower than waste water release had been done. The duration of periods of Contaminated and Pure Runoff and their volumes (in shares of Annual Average Runoff or directly in m<sup>3</sup>/year) also were calculated using Representative Indexes. This methodology can be applied either to single observing point, or river section, or water subject as a whole.

**HS02/07P/C24-020OP Oral-Poster 1412****STATUS, TENDENCY AND PROBLEMS OF TRANSBOUNDARY WATER QUALITY MANAGEMENT IN ARAL SEA BASIN**

Raisa V. TARYANNIKOVA, Marina S. MOLODOVSKAYA (Central Asian Res. Hydrometeorological Inst., Dept. of Res. and Forecasts of Environmental Pollution)

The system of water use exploited in Aral Sea Basin for the last decades, had led to water deficiency, deterioration of surface and ground Water Quality (WQ) along with corresponding social and ecological disasters. It became one of constraining factors of region stable development. Moreover, many water subjects have lost their ecological and biotic functions as environment of aquatic flora and fauna; landscape-aesthetic shape and recreation abilities. The situation is typical one not only for Zones of Intensive Water Consumption (ZIWC) with the highest anthropogenic stress on reservoirs, but also for Water Formation Zone (WFZ) where Surface Water Quality (SWQ) has been always considered satisfactory. The analysis of long-term WQ information has shown the dangerous tendency of intensification of biological productivity, i.e. there is eutrophication and, as a result, deterioration of WQ in WFZ reservoirs. The tendencies of Surface Water Quality for the last ten years are indicated. The anthropogenic changing of surface runoff, disregarding the buffering water ecosystems and necessary ecological minimum of river water discharge negatively influence on their social and ecological features. Decreasing water discharges lower than Ecological Allowable Level infringes ecological equilibrium and WQ. The water warming-up increases and contents of Dissolved Oxygen reduces. The pollution density grows up even without their additional coming from outside and "hydrological" eutrophication and secondary contamination take place. In Central Asian region practically all large and numerous small-sized rivers are transboundary, i.e. they coincide with or intersect the boundaries between two or more States. Currently, the WQ management in region is represented as Complex Regional Program of interacting political, economic, technical and legal operations. That ensures the fulfillment of rules regulating and limiting harmful effect on water environment. The solution of such complicated and actual problems is possible only with coordination efforts of all Regional States, with mutual obligations on realization adequate both of water economic and water-security policies and responsibility of States for Transboundary Waters (TW) Quality state. However, nowadays in region there is not any regulating system of TW Resources Quality. Measures on protection and rehabilitation of Water Resources should be based on ecosystem approach with new understanding WQ problems. All water basins should be considered as single whole ecosystem, concerning which water economic activity is carried out. Just on the base of ecosystem approach it is possible to resolve the primary and challenge task of TW management – definition of quotas of dumping pollutants in TW for each State, appropriate agreements and responsibility for their fulfillment. In future, along with further population growth, urbanization of landscapes, social-economic development of region, anthropogenic influence on WQ will be increasing, especially within low-water years. It makes us fall to thinking about the preventive measures just now, not putting off until "afterwards", and to direct efforts for restoring and preservation of Natural Water Resources.

**HS02/07P/C24-021OP Oral-Poster 1416****STUDY ON THE MODELING METHOD OF LAND WATER QUANTITY AND QUALITY AND ECOLOGY COUPLING SYSTEM**Ge TAN<sup>1</sup>, Qiting ZUO<sup>2</sup>, Jun XIA<sup>1</sup> (<sup>1</sup>Hydrology Studio, Institute of Geographical Sciences and Natural Resources Research, CAS, <sup>2</sup>College of Water Resources and Environment, Zhengzhou University)

As the basic content of quantitative study on Management of Sustainable Water Resources, it is necessary, and difficult as well, to build water quantity and quality and ecology coupling system model. On the basis of application study, this paper puts forward a new method called "Multi-Box Modeling". This method's clue is definitude, calculation is simple, and model is reliable. It is confirmed by the authors that the built model can stand for "land water resources system construction connection" and can be used in quantitative study on Management of Sustainable Water Resources.

**HS02/07P/C24-022OP Oral-Poster 1420****SOIL DEGRADATION OF JAVA ISLAND**

Seno ADI (BPP Teknologi)

AbstractThe rapid population growth in Java island has caused the pressure to natural resources through intensive agriculture activity. Especially in the upstream region, this situation caused the soil degradation by heavily erosion lead to sediment deposition in the lower region as indicated by the sediment carried of over 10 million ton/year in one river basin in central Java. The land degradation in Java island is not only cause unproductive soil for agriculture development but also cause the disaster such as flooding as well as water crisis. The soil and water conservation activities have been introducing to carry out the land degradation. The Indonesian government under Forestry Department has such a program called reforestation and greening, however the farmers have their own interest for land management in relation to the farming commodity that may not take care the soil and water

conservation. The research institute has an important role to link and correspond the farmercommodity interest with the government program in such away the soil and water conservation could be implemented by conducting the appropriate technology thatfacilitate economic development for the farmers.

**HS02/07P/C24-0230P Oral-Poster 1424**

**ASSESSMENT OF THE IMPACT OF INDUSTRIAL EFFLUENTS ON WATER QUALITY IN KORBA AND ENVIRONS, CHHATISGARH, INDIA**

L.P. CHOURASIA (Department of Applied Geology,Dr. H.S. Gour Univ)

The effects of multiple industrial pollution sources on the groundwater system were evaluated in the industrial complex at Korbe of Chhatisgarh State of India. The quality of groundwater in the region has been affected negatively due to the discharge of effluents on open and land into ponds, tanks and streams. Water samples from surface water bodies and dug wells were analyzed for their major ion concentrations. The high values of electrical (EC) and concentrations of Na<sup>+</sup>, Ca<sup>2+</sup>, Cl<sup>-</sup> and HCO<sub>3</sub><sup>-</sup> indicate the impact of industrial effects on water quality. Based on the hydro chemistry, the groundwater is classified into various types such as sodium chloride, sodium-bicarbonate calcium chloride, and magnesium-chloride etc. Its suitability for drinking and irrigation purpose has been assessed. The groundwater quality in around Korba has become hazardous. Some possible remedial measure are suggested.

**HS02/07P/C24-0240P Oral-Poster 1428**

**WATER QUALITY IN NORTHERN KARNATAKA, INDIA - A CASE STUDY**

Ramaraju Hanumanahalli KAMBADARANGAPPA<sup>1</sup>, Rajkama<sup>2</sup>, Prasanna Kumar N. S.<sup>2</sup>, Ranganna G.<sup>3</sup> (<sup>1</sup>Dept. of Civil/ Environmental Engineering, Bangalore Univ., <sup>2</sup>Karnataka Rural Water Supply & Sanitation Agency, Rural Development & Panchayat Raj Dept.)

Of all kinds of pollution that are steadily degrading man's physical, environment. Probably the least recognised is the hidden deterioration in the quality of ground water. Diseases related to the use of contaminated ground water may be divided into those, which are caused by microorganisms, a biological agent (a pathogen), and those, which are caused by chemical substances those that are caused by chemical substances. However, these latter diseases are over shadowed in developing countries by the former, which are the main causes of disease and death. As a part of the preparatory work for the **JAL NIRMAL** Project, a Water Quality Analysis study was undertaken. The objective of this study was to access the nature, extent and severity of Water Quality problems in the project area and the underlying causes thereof. The study was under taken in three pilot districts viz. Belgaum, Dharwad, Gulbarga (and Gadag district as a special case study due to fluoride problem) and the primary data was generated on water quality. There are 281 existing water sources in the 24 villages (10 GP's), out of which 212 sources are in use. Some are not in use due to inadequate quantity and some due to meager quality. 204 samples were collected from all the sources in use and additional 26 samples were collected for analysis of pesticides. The results reveals 174 samples (85%) were found to be non potable. The full-length paper presents the Water Quality status and mitigative measures.

**HS02/07P/C24-0250P Oral-Poster 1432**

**INTEGRATING HIGH RESOLUTION SATELLITE IMAGERY AND WATER QUALITY STATISTICS FOR WATER RESOURCE MANAGEMENT**

Nandani Dhammika Kumari DAYAWANSA (Department of Agricultural Engineering, University of Peradeniya)

Water is an important natural resource and is a vital component of plant and animal life with two thirds of the earth being covered with water. Proper management of water resources is of paramount importance as the water quantity and quality deterioration is being widely reported all over the world. Scarcity and the low quality of water are serious problems that are faced by the disadvantaged communities in the less developed countries. With the above background, this study focussed on the use of multidisciplinary approach to handle the water-related issues in a cost effective and sustainable manner. The seasonal variations of the water availability in the reservoirs in a part of the dry zone of Sri Lanka are predicted with high-resolution (IRS LISS III) satellite imagery. At the same time the command areas of the reservoirs/ tanks are identified with the help of the same imagery. The water samples from the water bodies are selected to monitor the water quality status and the crop management information are gathered to be coupled with the water quantity data during different seasons of the year. The extracted information from remote sensing sources and field sampling is used to quantify the extent of water pollution and the contribution of agricultural and other anthropogenic activities on water quality deterioration. The output of the study can be used for policy formulation and determining guidelines for fertilizer and agrochemical use with a proper understanding of the uncertainty coupled with the information. The synoptic viewing capability and the quickness of gathering spatial information in remote sensing approach compared to the field surveying will be economically and technically feasible in sustainable water resource management in a rapidly changing environment.

**HS02/07P/C24-0260P Oral-Poster 1436**

**SEASONAL VARIATION IN WATER QUALITY IN ORLE RIVER BASIN, S.W. NIGERIA 2 CHEMICAL HYDROLOGY**

Catherine Imhangulaya IKHILE<sup>1</sup>, Stella Maris AKHIONBARE<sup>2</sup> (<sup>1</sup>Department of Geography and Regional Planning, <sup>2</sup>New Grass Technologies)

An investigation of the chemical conditions of water bodies in the Orle River Basin in Edo State, Nigeria was carried out in 1987 and 1997. The quality of the water in the drainage basin was compared between this ten years period for any possible variation due to global changes in climate and population pressure. The results reveal that in 1987, chloride, sodium, biochemical oxygen demand (BOD5) and dissolved oxygen (DO) varied significantly with the seasons. While chloride, DO, BOD5 and COD show increase in the wet season, sodium, potassium, calcium, magnesium, iron, aluminium, silica, nitrate, sulphate and total hardness increased in the dry season and decreased in the wet season. In 1997, while total hardness, silica, nitrate iron and COD increased in the wet season, chloride, calcium, magnesium, DO and BOD5 increased in the wet season and decreased in the dry season. The values of some of the parameters are beyond tolerable limits. The degree of pollution observed in the rivers constituting Orle River Basin is sufficiently significant to necessitate pre-treatment of the basin water prior to domestic and industrial uses. Presently, the natives treat the water with alum before use, but this practice is not sufficient chemical treatment required to make the water safe for consumption.

**HS02/07P/C24-0270P Oral-Poster 1440**

**CONCENTRATIONS OF URANIUM IN SURFACE WATER IN QINGHAI-TIBET PLATEAU**

Yuefang LI, Tandong YAO, Lide TIAN, Wusheng YU, Jianchen PU (Key laboratory of Ice Core and Cold Regions Environmental Research, CAREERI, CAS)

U is not also a natural radioactive element but a heavy metal. It has radio-activity and also do harmful to human health just like lead. So many studies pay attention to this element in recent years. Study showed that human mainly intake uranium from water. So it is important to know the content of uranium in natural water. In other hand, the distribution of uranium in water has significance in geochemistry exploration of uranium and water quality assessment. The Qinghai-Tibet plateau is affluent in water resources and some big rivers are the headwaters of some world rivers such as the Changjiang River and the Brahmaputra river etc. So it is important to know the distribution of U concentrations in waters in the plateau. We present here data on the dissolved U in surface waters as well as some ground waters in the plateau for the first time in most sites of Qinghai-Tibet plateau. The primary objective of our study is to identify the spatial distribution of U concentrations and establish the background value of uranium concentration in the water in the plateau. This study contributes new data on the U content in waters in China. Sampling equipment were pre-cleaned in clean room and concentrations of U were determined by the ultrasensitive inductively coupled plasma sector filed mass spectrometry (ICP-SFMS) technique in clean room conditions. The data show that the concentrations of dissolved U in surface waters are in the range of 0.17 to 6.53µg/L, with a mean value of 2.56µg/L. That is higher than that of World Rivers. The concentrations of U are changeable not only in the same water system but in the different water system and show an obvious spatial variations. The highest concentration was observed in a glacial melt water comes from Xixiabangma mountain located in Himalayan region, the southern part of the plateau. The lowest concentration was found in the west-middle part of the plateau.

**HS02/07P/C24-0280P Oral-Poster 1444**

**ISOTOPIC EVALUATION OF GROUNDWATER SYSTEMS FOR RISK ASSESSMENT AND MANAGEMENT DURING EXTREME EVENTS**

Partha Sarathi DATTA, Sunil Kumar TYAGI (Nuclear Research Laboratory, India Agricultural Research Institute)

In different parts of the world, increasing population, urbanization, and competition for economic development induced indiscriminate exploitation of groundwater and its contamination hamper groundwater management programs. Management strategies require scientific evaluation of groundwater vulnerability to depletion and pollution, and risk assessment, in relation to changes in landuse and other environmental conditions. In this context, the groundwater system in Delhi region has been described, using stable isotopes (<sup>2</sup>H, <sup>18</sup>O) distributions in groundwater and rainfall. The isotope signatures of Delhi rainfall (<sup>18</sup>O: -15.3 to +8.0‰ and <sup>2</sup>H: -120 to +55.0‰) generally fall along the world meteoric line, depleted <sup>18</sup>O is generally associated with heavy rainfall, and the rainfall deficient years are generally associated with relatively enriched <sup>18</sup>O in monthly rainfall. Changes in landuse result in variation in recharge from location to location, both in space and time, with a wide range of <sup>18</sup>O signatures in groundwater (<sup>18</sup>O: -2.8 to -8.6‰), both laterally and vertically, suggesting occurrence of an inhomogeneous stratified system. Groundwater renewal has a selection effect in favor of isotopically depleted rainfall, with most parts receiving less than 5% recharge. Imbalance in recharge with withdrawal resulted in decline in groundwater levels by 8-10m during the last decade. Distribution of <sup>18</sup>O and Cl in groundwater suggest occurrence of two main flow systems vertically: (i) Uppermost local flow, rapidly circulating, low salinity, more vulnerable to overexploitation, and (ii) Relatively slow circulating intermediate zone and more vulnerable to salinisation and depletion. The groundwater in different parts has also become considerably vulnerable to pollution, with a wide range of nitrate (30-1600 mg/l), fluoride F (1-16.0 mg/l), Zn (3-41 Mg/l), Cu (5-182 Mg/l), Fe (279-1067 Mg/l), Pb (31-622 Mg/l), Ni (<1-105 Mg/l), Cd (<1-202 Mg/l). Increase in groundwater contaminants levels, associated with enriched <sup>18</sup>O isotope, clearly suggests increasing risk of groundwater to pollution from localized infiltration of isotopically enriched (<sup>18</sup>O: -3 to -5‰) and highly contaminated agricultural and urban surface run-off water, through stagnant water pools. Governed by the zonal disparity in water supply and groundwater abstraction, many flowpaths of inter-mixing of contaminated water with fresh water bodies can be visualized from <sup>18</sup>O and Cl relationships. Risk of groundwater depletion and contamination are governed by rainfall pattern, recharge, withdrawal, and surface run-off characteristics, groundwater-surface water interactions, and sorption/desorption processes in the soil. For comprehensive assessment of risk associated with extreme events, more field research and scientific knowledge is needed on isotopic responses and dynamics of pollutants in the groundwater flow, aquifer's attenuation capacity for contaminants, under natural and exploited conditions, in relation to land use, wastes disposal and other environmental changes. Risk can be partly minimized or controlled by restricting migration of population from surrounding states, unplanned groundwater abstraction, and eliminating wastes disposal within the protection zones, through strict enforcement of regulatory measures.

**HS02/07P/C24-0290P Oral-Poster 1448**

**GROUNDWATER ISSUES IN PONDICHERRY COASTAL ZONE, INDIA**

S.S.SUNDARVEL RAGASAKTHI (IAHS)

The intense use of ground water has caused major water-level declines and significantly decreased the saturated thickness of aquifers in some areas. In many semi-arid to arid regions, ground water has been withdrawn at rates far in excess of recharge, leading to ground-water "mining." This is often accompanied by detrimental environmental side effects, such as reduced ground-water discharge to springs, streams, and wetlands, and land subsidence. Land drainage is a source of ground-water depletion, as the construction of drainage ditches and canals in surficial systems can lead to regional lowering of the water table. A significant component of the total depletion may come from low-permeability confining layers, but they are rarely monitored and usually overlooked. The magnitude of worldwide depletion of ground water in storage may be so large as to constitute a measurable contributor to sea-level rise. But the magnitude of depletion is poorly documented worldwide, particularly in developing countries. The management concept of "sustainable development" may offer a viable approach to dealing with overexploitation of ground-water resources, but its implementation has been largely subjective and sometimes arbitrary. The purpose of this paper is to document methods and examples that would help define the magnitude of the problem in Pondicherry Coastal Zone, India and explore local and regional management approaches to mitigate the problem or assure sustainable development.

**HS02/07P/C24-0300P** Oral-Poster **1452**

**THE STUDY FOR GROUNDWATER RESOURCES SYSTEM OF CHINA WITH THREE-RATED APPRAISING METHOD OF SUBAREA**

huajun hua LOU, Hong Hong WANGHONG, Jun Jun XIAJUN, XianFang Xian SONG (institute of geographic sciences & natural resources research, chinese academy of sciences(cas))

The study for groundwater resources system of china with three-rated appraising method of subarea Key word: Water resources; subarea; River valley; Hydrology geology unit; GIS databaseSummary: surface water and groundwater are important constituents of water resource system. Since the water transport and deposited in a different way within the medium between surface water and ground water, so the modeling and appraising method adopted are different. the first water resources appraising of China, only the one item of national groundwater resources' gross is to 10000 billion tons (occupy 1/8 of all the national groundwater resources or so), this data is equal to the data of the water transported from south to north one time or more. The author think that the main reasons for the total error of groundwater resource are:1) In the nature, groundwater and surface water frequently conversed and replenished with eachother. It is impossible to appraise them respectively. In the water resources' appraising of China, from one- rated subarea to three-rated subarea, the method of ground water modulus was divided with surface water. So, it can't be reflected clearly that the system of surfacewater and groundwater are oneness. 2) In the water resources' appraising, the computing methods of surface water and ground waterreplenishment and evaporation are not be united, the resource quantities' iteration principles different, leading to the inconformity of the result. 3) The basic data for water resource's evaluation of china come from the different managementsection respectively. Water conservancy department managed surface water and agricultural water. So relevant water data primarily come from the water conservancy section. Constructed department managed the water for city use. Relevant data mostly come from local constructsection. For a few years, the groundwater was managed by geologic and mining section. Meantime, the section can pursue a part of monitoring work. They have the accumulated data of many years. The data of above three sections are the foundation on which proceed the water resource's evaluations in China. So the problem of data unification should be resolved. The author think that in the first water resources evaluation of China, surface water wasevaluated according to River valley, while ground water was evaluated through Hydrology geology unit, which are the principal reason for the error of water resource's gross. Theconversed relation of four kind of water is complexity, which adopt the evaluation methodof river valley and hydrologic unites respectively. So the gross' error is unavoidable in water resources' appraising. In the thesis, the author brings up the project of three-ratedevaluation and subarea. In the groundwater resources' quantity evaluation, one and two-ratedsubarea method according to river valley are adopted. While three rated subarea according to groundwater unites is used to resolve the problem of the water resources' evaluation error.

**HS02/07P/C24-0310P** Oral-Poster **1456**

**ACID RAIN AND GROUNDWATER QUALITY**

Roald Gamidovich DZHAMALOV (Water Problems Institute, Russian Academy of Sciences)

The study of the effect of precipitation on acidification processes in groundwater for different combinations of natural and anthropogenic factors that control the response of hydrogeological systems to acidification and the development of methods for the risk assessment of groundwater pollution by acid fallout. On catchment areas in Moscow and Novgorod regions in Central Russia, field observations and analytical determinations were carried out (the sampling of rainwater, meltwater, surface water, soil water, and groundwater, as well as of water-bearing rocks) for the subsequent study and update of the data base on groundwater acidification under individual geological, hydrogeological, landscape, and geomorphological conditions and degree of acid load. The main attention was paid to the study of the hydrochemical regime of spring water and groundwater, which are most liable to acidification. In addition, the mineralogical composition of water-bearing rocks and clayey interlayers was analyzed to assess the degree of interaction between them and percolating acid waters. The data on the hydrochemical groundwater regime within individual catchment areas have been generalized over the period of last 30-40 years. These materials were used for verification and adaptation of the hydrodynamic and physicochemical models for estimating the areal extent and degree of groundwater acidification. The field and experimental studies, as well as simulations, were carried out with a special attention paid to studying the soil and rocks of aeration zone, since they buffer the effect of acid precipitation on groundwater. Stages in leaching the soluble minerals of soil and water-bearing rocks were determined as a function of the acid load and duration of exposure. The relationship was determined between the neutralizing capacity of rocks of aeration zone and amount of carbonate rocks, the rate of infiltration of acid precipitation, as well as the duration of physicochemical interaction in the water-rock system and the solid-to-liquid ratio. Possible forms of migration of constituents of rainwater, meltwater, surface water, and groundwater have been studied under various conditions of their formation and migration, as well as with allowance made for the duration of acidification process in the water-rock system. The analysis of the available criteria of acidification allowed developing new criteria of the degree of acidification of natural waters, which are based on the amount of acid load and its residence time in the water-rock system. Various phases of acidification of soil water and groundwater have been studied under a variety of conditions of their formation and under various hydrogeological regimes. The field and experimental studies, as well as the computer simulation allow us to establish several important particularities of groundwater acidification and contamination under atmosphere fallout.

**HS02/07P/C24-0320P** Oral-Poster **1500**

**HYDROGEOLOGICAL ANDHYDROGEOCHEMICAL ASPECTS OF THE NUBIAN SANDSTONE AQUIFER IN EAST OWEINAT AREA, SW EGYPT**

Esam EL SAYED<sup>1</sup>, K. DAHAB<sup>2</sup>, A. M. EBRAHEEM<sup>3</sup> (<sup>1</sup>Geology Department, Faculty of Science, Minia University, <sup>2</sup>Geology Department, Faculty of Science, Menofia Univ, <sup>3</sup>Geology Department, Faculty of Science, Assiut Univ)

East Oweinat area is currently a site of a major reclamation project, which totally depends upon the groundwater extraction from the Nubian Sandstone Aquifer; the only water resource in this area. This aquifer is composed of sandstone beds with minor intercalation of siltstone and kaolinitic sandstone. Groundwater in this aquifer occurs under unconfined conditions, while elsewhere it is under semi confined conditions as a result of the occurrence of clay intercalations within the aquifer materials. Generally, groundwater flow is from southwest to the northeast. The saturated thickness is ranging from less than 100 to 650 meters in the study area. The recent annual recharge to the aquifer system in this area is too low if compared to the present extraction rate and exclusively depends on the transmissivity of the aquifer material and its hydraulic gradient. Groundwater belongs to fresh water class whereas salinity content ranges between 302 and 876 ppm. It is of meteoric origin and belongs to alkali- chloride sulphate water type. Therefore, it is suitable for irrigation purposes for most of the soil types under ordinary conditions.

**HS02/07P/C24-0330P** Oral-Poster **1504**

**A STUDY OF HYDROGEOLOGICAL CONDITIONS OF THE NUBIAN SANDSTONE AQUIFER IN THE AREA BETWEEN ABU SIMBEL AND TUSCHKA, WESTERN DESERT, EGYPT**

Esam EL SAYED<sup>1</sup>, K. DAHAB<sup>2</sup>, A. M. EBRAHEEM<sup>3</sup> (<sup>1</sup>Geology Department, Faculty of Science, Minia University, <sup>2</sup>Geology Department, Faculty of Science, Menofia Univ, <sup>3</sup>Geology Department, Faculty of Science, Assiut Univ)

The Nubian Sandstone Aquifer in the area between Tuschka and Abu Simbil is small portion of the very well known Nubian Sandstone Aquifer System in the Eastern Sahara, which covers the entire area of southwest Egypt, southeast Libya, northeast Chad, and northern Sudan. Tuschka area is currently the site of intensive drilling and development for a huge land reclamation project. The drilling information was used to study the hydrogeological setting of the aquifer in the area. The obtained results indicate that the lithological characteristics and tectonic setting is strongly affecting the groundwater flow pattern as well as the aquifer potentiality of the Nubian Sandstone aquifer in the area. The aquifer potentiality in the study area is low if compared to that of east Oweinat, Dakhla, and Kharga areas. The aquifer is mainly composed of hard ferruginous sandstone with great shale and clay intercalation with a thickness ranging from 140 to 230 meters. The potentiometric surface is ranging between 102 and 170 meters above mean sea level. Depth to water ranges between 20 and 140 meters from the ground surface. Groundwater in this aquifer belongs to fresh to slightly brackish type (salinity is ranging from 240 to 2370 ppm). The predominant water type is sodium sulphate and sodium chloride. The groundwater is related to meteoric origin. The high concentration of sodium, chloride, and sulfates reflect leaching and dissolution processes of gypsiferous shales and clay as well as long residence time of water. Most of the collected groundwater samples are suitable for irrigation purposes in the study area.

**HS02/07P/C24-0340P** Oral-Poster **1508**

**GEOPHYSICAL EXPLORATION FOR GROUNDWATER IN THE TOLON-KUMBUNGU DISTRICT OF GHANA**

Jude Simon BAYOR, Aboagye MENYE (HYDROLOGY)

Geophysical exploration for groundwater has been carried out in seven communities the Tolon-Kumbungu District of the Northern Region of Ghana. The communities involved are Gbullung, Woribogu, Gun, Nyorong, Yoggu, Nyankpala-Tuunayili and Nyerishegu. These communities are mostly located in the south-eastern half of Tolon and lie in the Lower Voltaian Sedimentary Basin. The geophysical techniques involved were the Electromagnetic (EM) survey for ground profiling with the EM 34-3 ground conductivity meter and the dipole-dipole configuration in Vertical Electrical Sounding (VES) with the Swedish ABEM SAS 300C resistivity equipment. Results show that major aquifers are confined to hard, fractured sandstone formation. No water was found for weathered zone or fresh rock aquifers. Analysis of data also revealed several thin-bedded sequences of between 4 m and 10 m thickness of sandstone, mudstone shale and their intercalations to be the dominant formations here. Groundwater was confined to between 25 m and 45 m with major aquifers occurring approximately between 34 m and 45 m depths. Groundwater availability to beyond 55 m was not possible. The potential success rate is estimated at 75%. The surveys show conclusively that the EM method and the dipole-dipole array in VES when combined is an effective tool for the location of groundwater in the survey area of the Tolon-Kumbungu District.

**HS02/07P/C24-0350P** Oral-Poster **1512**

**A POLLUTION OF AQUIFERS BY HYDROCARBONACEOUS INCLUSIONS**

Nadezhda K. KORSAKOVA, Valentin I. PENKOVSKY (Siberian Division, Russian Academy of Science, Lavrentyev Institute of Hydrodynamics)

Damages of oil-pipe lines, liquid escape from gasoline storage and oil storage, petrol leak from filling station lead to percolation of immiscible with water fluids into water-bearing stratum occurs. At that closed hydrocarbonaceous inclusions are generated inside aquifers. Similar formations are able to be in dynamic equilibrium with groundwater flow. A water phase partially flows around and partially through such inclusions which are in stationary position under the influence of capillary forces. This phenomenon is called "internal capillary locking". The experiments were realized on transparent fill-up physical models of water-saturated bed contained circle oil inclusions under presence of gravity. It was observed the redistribution of saturation in oil spot under influence of gravity and oncoming flow of water. The limit dynamic equilibrium with water phase flow criterion was obtained for an inclusion. It was demonstrated that equilibrium stationary position was broken under excess over the criterion, and hydrocarbonaceous phase started moving. The mathematical model as a system of differential equations have been formed that allowed to describe in a hydraulic approximation a distribution of oil particles in three-dimensional inclusion been under action of a field of hydrodynamic forces and field of gravitation. A hydraulic pressure have been averaged over vertical component, consequently seepage became two-dimensional. But a distribution of oil particles remained as three-dimensional because of a gravity was taken into account. The condition of phase pressure jump on boundary of phases was taken into consideration too. The finite element method was used for solving of the two-dimensional ground water flow problem with an arbitrary given form of hydrocarbonaceous inclusion. The obtained numerical results are well agreed with the experimental data.

**HS02/07P/C24-0360P** Oral-Poster **1516**

**INTEGRATED GEOPHYSICAL INTERPRETATION FOR GROUNDWATER EXPLORATION AT NUKHL AREA, CENTRAL SINAI, EGYPT**

Abdel-Rady Ghareeb HASSANEEN<sup>1</sup>, Sultan Awad SULTAN<sup>2</sup>, Badr Saad MOHAMED<sup>3</sup> (<sup>1</sup>Prof. of Geophysics and head of the geomagnetic and geoelectrical dept., National Research Institute of Astronomy and Geophysics, Helwan, Cairo, Egypt., <sup>2</sup>Lecturer of Geophysics, <sup>3</sup>Geologist (Egyptian geological survey))

Different geophysical tools were carried out on the studied area to define the stratigraphic units, structural elements and the depth to the basement surface. These geophysical tools are geoelectric, magnetic and gravity methods. Quantitative interpretation of the vertical electrical sounding curves was done by using the two layer standard curves and generalized Cagniard graphs (Koefoed, 1960; Orellana and Money, 1966) to determine the thickness and true resistivities for each geoelectrical unit in order to obtain a preliminary models. All VES stations are re-interpreted as a final models using IPI-1D program to compute these final models. The interpretation of the magnetic data started with reduction to the magnetic pole, then depth to the upper surface of the basement was determined applying Euler deconvolution technique. The quantitative interpretation of Bouguer gravity anomaly map started with separation of residual and regional gravity anomalies applying high and low pass filter technique using Geosoft program (1994). The structural elements can be determined

from the residual gravity anomalies. Also, gravity modeling was carried out along three profiles to define the depth of water bearing Nubian sandstone aquifer and the upper surface of the basement using GM program (1995). The results of the geophysical interpretation show that, the subsurface section consists of six geoelectric units. The depth of upper surface of the Nubian sandstone(aquifer) ranges between 800 to 1000 m. The depth of the basement surface ranges between 1720 m at the northwestern part and 3600 m at the southwestern part of the studied area. There are normal faults whose directions are: N-S, E-W and NE-SW.

**HS02/07P/C24-0370P** Oral-Poster **1520**

**STUDY ON REMOVAL OF CADMIUM FROM GROUNDWATER BY ADSORPTION USING GAC, BAC & BIOFILTER**

Ramazan ali DIANATI TILAKI (Environmental Health Engineering Department, Mazandaran University of Medical Sciences)

The Contamination of groundwater by toxic heavy metals is a world-wide environmental problem. Rock and minerals containing heavy metals can increase concentrations of these elements in groundwater. Cadmium is a toxic element and can accumulate in the living organisms. Low concentration (below 5 mg/L) of Cadmium is difficult to treat economically using chemical precipitation methodologies. Ion exchange and reverse Osmosis while can guarantee the metal concentration limits required by regulatory standards, have high operation and maintenance costs. The goal of this research was to determination of efficacy of using GAC, Biofilm and BAC columns to treat low concentration Cadmium bearing water streams and was to determination of the effects of temperature and pH on the adsorption isotherms. Studies were conducted to delineate the effect of pH, temperature, initial Cd and adsorbent concentration on adsorption of Cd<sup>2+</sup> by GAC, BAC and Biofilm. Breakthrough curves for removal of 0.5 mg/L Cd<sup>2+</sup> by GAC, Biofilm and BAC columns at two contact times were plotted. Batch adsorption and column data are compared. pH is shown to be the decisive parameter in Cd removal for GAC but not for BAC or biofilter. Lagergren plots confirms applicability of first-order rate expression for adsorption of Cd by GAC, BAC and Biofilm. The adsorption coefficient (Kad) for BAC were 2 times greater than those with plain GAC. Bed Volumes of water containing 0.5 mg/L Cd<sup>2+</sup> treated at breakthrough for GAC, Biofilm and BAC columns were 45, 85 and 180 BV respectively. BAC is more efficient than GAC in the removing of Cd from water environment. Keywords: Cadmium, adsorption, GAC, BAC, Biofilter.

**HS02/07P/C24-0380P** Oral-Poster **1524**

**GROUND WATER ROLE IN THE ARAL SEA REGION PUBLIC WATER SUPPLY**

Abdulkhakim SALOKHIDDINOV, Khidoyat VALIEV (Tashkent Institute of Irrigation and Agricultural Mechanization Engineers)

The role of groundwater in public water supply has increased dramatically in many countries during the last decades. Surface water resources contamination (and often depletion) is a reason to use groundwater more intensively. In a number of regions, especially in Central Asia including the Aral Sea region, it reached a catastrophically large scale. At the same time in determining the perspectives of groundwater use, one should consider groundwater not only as a commercial deposit but also and above all as a part of water resources and an important component of the environment. Taking that into account it should be noticed that groundwater in many arid regions is an alternative and often the only possible source for public water supply that can provide terrestrial ecosystems with pure, safe drinking water of high quality. All the above-mentioned apply equally to Central Asia arid regions and in the first place to the Aral Sea basin, where water resources degradation assumed a catastrophic character. According to preliminary results of research it is established that the Aral Sea shrinking has direct impact on change of amudarya and aral complexes higherquaternary and modern sediments groundwater's level and chemical composition mainly within area of the dried Aral Sea bed.

**HS02a-Posters**

**Monday, July 7**

**WATER RESOURCES SYSTEMS: GLOBAL CHANGE, RISK ASSESSMENT AND WATER MANAGEMENT (ICWRS, ICASVR, ICSW, ICWQ)**

Location: Site D

**Monday, July 7 PM**

**HS02a/07P/D-001** Poster **1545-147**

**IMPACTS OF ENVIRONMENTAL CHANGE AND POPULATION GROWTH ON THE WATER QUALITY AND WATER AVAILABILITY IN INDIA**

Shadananan K. NAIR (Department of Physical Oceanography, Cochin University of Science & Technology)

Global environmental changes and demands of increasing population make water resources management a difficult issue in many parts of the world. This is especially true for a developing country like India with an exploding population, a weak economy that is related to agriculture and where there are disputes over sharing of water. Life of majority of the population in India depends on agriculture or related industries. Though India is rich in water resources and water resources development projects have helped attaining self-sufficiency in food, the fast increasing population and associated needs pose serious threat to water availability. Overuse, pollution and improper management have been seriously affecting the quantity and quality of water. Global climate models predict a possible change in the rainfall pattern and hence in the water resources of India in the coming decades. In this study, water balances of different States of India have been computed, incorporating the methods of Penman and Thornthwaite, to estimate the water deficiencies, surpluses and the per capita availability. Considering the rate of growth of population and predicted changes in temperature and rainfall patterns, the situation after two decades has been assessed. Study reveals that the present national per capita water availability of 2150m<sup>3</sup> will be drastically reduced to 972m<sup>3</sup> in few years. Even today, some states have no surplus water from precipitation annually, after meeting the requirements for evapotranspiration and soil moisture recharge. In almost all parts of India, water deficiencies show an increasing trend and surpluses show a decreasing trend. Though some climate models predict an increase in rainfall, it may not be able to compensate for the reduction in soil moisture due to rise in temperature. This will reduce the water level and runoff in rivers. This situation will surely add to the economic crisis. More investment will be needed in domestic supplies, irrigation, national waterways and for finding alternatives for cheap hydroelectric power. If the present

population growth and urbanization continues, the country will find it hard to meet the requirements in domestic and industrial sector and after all in the agricultural sector that may need additional 200MCM water to feed more than 1.5Million population. Guidelines for better management have been provided, considering socio-economic conditions and natural and man made environmental changes on water.

**HS02a/07P/D-002** Poster **1545-148**

**ESTIMATION OF POTENTIAL WATER RESOURCES IN THE LOWER MEKONG RIVER BASIN**

NMNS Bandara NAWARATHNA, So KAZAMA, Masaki SAWAMOTO (Department of Civil Engineering, Tohoku University)

Availability of GIS data sets of watershed physical properties and the advancements gained in obtaining distributed meteorological variables with the help of GIS have stimulated the development of physically based hydrological models. The introduction of block wise approach to the TOPMODEL with Muskingum-Cunge flow routing methods (BTOPMC) has enhanced the applicability of TOPMODEL from hundreds of square kilometers to several ten thousands square kilometers. In this research work, BTOPMC is used to simulate hydrological processes in the effective watershed of 277,000 square kilometers from Luang Prabang to Pakse in Loas PDR along the Mekong River. It has become necessary to construct reservoirs to meet increasing water demand especially in agriculture and power supply in the lower Mekong river basin. However, with the ongoing debate on environmental aspects of dam constructions, a thorough study from a sound hydrological model is needed to ensure sustainable development. The watershed is divided into four rectangular blocks (250 km<sup>2</sup>×300 km) and the block wise average saturation deficit, which controls the depth to the saturation zone in each grid (1 km<sup>2</sup>×1 km), is calculated in each time step. Upstream observed runoff is used as a boundary condition of the model and four parameters namely, lateral transmissivity under saturated conditions, decay factor, maximum root zone storage, and flood plain Manning coefficient *n*, are estimated as a function of land use extracted from USGS (United States Geological Survey) global land cover characteristics database. Model parameters were calibrated based on the results at different gauging stations. Reservoir operations are taken into account using simplified routing curves depending on the purposes of the reservoir. Storages and releases from irrigated crop fields are taken into account by introducing required water level function to the relevant grids. Initially the most sensitive *n* values for different river reaches were estimated using the shape of simulated hydrographs without any rainfall input. The Mekong River, tributaries and flood plains were differentiated by introducing threshold values for the effective watershed area. Minimum value for the Mekong river basin at Pakse is identified as 0.0015. Annual evapotranspiration was estimated based on a pixel wise methodology related to potential evapotranspiration. The sub basins values ranges from 470 mm to 620 mm. Nash-Sutcliffe coefficient formula was used to evaluate the simulation efficiency. Lowest efficiency value for the year 1993 is 93.5%. Finally, potential water resources distributions at 100 square kilometer grid size were estimated. It has been found that there are sufficient water resources in mountainous area in Laos whereas flat irrigated fields in Thailand need to get water from nearest potential locations for a sustainable development.

**HS02a/07P/D-003** Poster **1545-149**

**CLIMATE CHANGE AND WATER RESOURCES VULNERABILITY IN HEAD AREA OF CHANGJIANG AND HUANGHE**

Shao-feng JIA<sup>1</sup>, Hua-yun YAN<sup>2</sup>, Run-jie LI<sup>3</sup> (<sup>1</sup>Department of Hydrology and Water Resources, Institute of Geographical Sciences and Natural Resource, <sup>2</sup>Bureau of Hydrology and Water Resources Survey of Qinghai Province, <sup>3</sup>Institute of Water Resources of Qinghai Province)

The head areas of Changjiang and Huanghe are called as Water Tower of China and have very important significance for water conservation and ecological integrity in Changjiang and Huanghe basins. Although the head area of Changjiang and that of Huanghe are connected together, runoff in two rivers showed different change patterns in recent 50 years. While runoff in head area of Changjiang didn't change evidently (only decreased by 1% compared to 1950's), runoff in head area of Huanghe had decreased by 10% in the same period. It's surprising that the annual precipitation in the head area of Huanghe didn't change obviously. Detail analysis indicated that the main reason of runoff decrease in the head area of Huanghe was the change of time distribution of precipitation i.e. the decrease of precipitation in summer. Perhaps the rising of temperature which may result in the increase of evaporation and transpiration was another reason. But an interesting phenomenon is that the recorded water surface evaporation in head areas of Changjiang and Huanghe decreased while temperature rose and sunlight time increased. In fact, this phenomenon occurred in Northwest China universally and so it worth being paid attention to. Because the main two factors influencing fresh water evaporation are temperature and wind, when temperature rising, the sole facto inducing the decrease of water surface evaporation must be slowing of wind. Meteorological records in those areas proved this deduction and showed obvious decline of annual average wind speed. So the rising of temperature will not certainly induce evaporation increase while wind speed descending. This make the relation between temperature and evaporation, further the relation between climate change and water resources, more complicated. Two phenomena in the head area of Changjiang and Huanghe—The dissimilar runoff change pattern (Changjiang's vs Huanghe's) in the same region when water and energy balance factors such as precipitation, sunlight time, temperature, wind speed and water surface evaporation are similar, and the complex relationship between temperature, wind speed and evaporation— make it very clear that there is still much uncertainty in the prediction of water resources change in the future in a global changing environment.

**HS02a/07P/D-004** Poster **1545-150**

**AN ESTIMATION OF AVAILABLE WATER RESOURCES**

Boris BERAKOVIC<sup>1</sup>, Marija BERAKOVIC<sup>2</sup>, Ksenija CESAREC<sup>3</sup> (<sup>1</sup>Water Research Department, Faculty of Civil Engineering, Univ of Zagreb, <sup>2</sup>Croatian Waters, <sup>3</sup>Meteorological and Hydrological Service)

Water management is a very complex activity and its successfulness depends on many factors and their reliability. In the paper the basic and most influential factors are described. A special attention is given to the estimation of available water resources as one of the basic elements influencing the effectiveness of water management. From the very beginning of water management activities information on water quantity and quality were its basic elements. Today, water balances are made routinely especially for larger areas, and the results obtained so are not sufficient for efficient water management planning. In the paper improvement possibilities of estimation of available water resources in Croatia are suggested. Successfulness of water management could be improved by simultaneously improving some other influential factors, which are just mentioned in the paper.

**HS02a/07P/D-005** Poster **1545-151**

**CHANGEMENTS CLIMATIQUES, RESSOURCES EN EAU ET SECHERESSES AU MAROC**

Mohammed-Said KARROUK (University Hassan II, Centre de Recherche de Climatologie)

En raison du changement climatique, l'environnement climatique actuel au Maroc subi une perturbation due au réchauffement du climat terrestre, qui peut violemment perturber presque tous les systèmes écologiques naturels et de nombreuses structures et institutions dont les marocains ont appris dépendre. Si les climats ne se sont que peu modifiés jusqu'ici, le pays est confronté dans les décennies venir, à une perspective d'une accélération très forte du changement climatique. Les latitudes marocaines représentent les endroits les plus vulnérables aux effets négatifs de ce bouleversement climatique. Le secteur le plus touché par cette situation au Maroc est l'EAU d aux sécheresses prolongées et répétitives. Et ce en raison de la nouvelle distribution géographique du cycle de l'eau qui s'installe nos latitudes. Les ressources en eau au Maroc, dépendent principalement du retour des précipitations de la saison humide où il pourrait pleuvoir. Cette précipitation qui connaît dans notre pays une instabilité accrue nous laisse en permanente inquiétude vis-à-vis de la disponibilité de cette denrée rare sur laquelle se base l'agriculture et la sécurité alimentaire au Maroc. La circulation atmosphérique est le principal mécanisme d'origine des changements dans les variables climatiques dont l'influence se fait sentir à l'échelle régionale. Les fluctuations qui affectent nombre de ces facteurs sont fortement interdépendantes, cause des caractéristiques d'ensemble de la circulation atmosphérique et des interactions qui se produisent entre les surfaces terrestres et océaniques. Les précipitations et les températures ont changé au cours des 100 dernières années au Maroc. Au cours de cette période, les précipitations ont connu des variations substantielles et les fluctuations des tendances ont également été relativement importantes. Ces variations ont accompagné les grandes fluctuations des événements extrêmes observés dans la zone intertropicale « ENSO », qui se sont répétées sur les températures et surtout les précipitations au Maroc travers la circulation atmosphérique dominée par les transferts énergétiques. Un événement négatif « El Niño » se manifeste au Maroc par des sécheresses, et un événement positif « La Niña » par des précipitations. Ces fluctuations extrêmes au Pacifique sont devenues ces dernières décennies plus fréquentes et se manifestent par une violence « exceptionnelle ». Les sécheresses récentes au Maroc ont été très pesantes et catastrophiques (1983, 1995, 1998), et leur brève interruption s'est manifestée par des inondations (1986, 1996, 1997, 2000 et 2001). Cette instabilité accrue des événements océano-atmosphériques met en péril les ressources en eau au Maroc, l'agriculture et la sécurité alimentaire. Le Maroc, déjà sensible à une variabilité climatique instable, est soumis aux effets du changement climatique dans plusieurs secteurs, savoir : • Le stress hydrique impose divers systèmes biologiques et secteurs socio-économiques, en raison de l'augmentation de la température et de l'évapotranspiration, entraînant un bouleversement du cycle hydrologique. • Les perturbations de l'écoulement de surface qui pourraient être excédentaires en cas de précipitations hivernales, et déficitaires dans les autres saisons. • La rentabilité agricole pourrait être altérée en raison des perturbations du cycle hydrique, ce qui poserait une sérieuse menace pour la sécurité alimentaire du pays. Des mesures draconiennes nécessaires devraient être entreprises pour s'adapter des éventuels bouleversements, lesquels représentent des facteurs limites pour la continuité en équilibre des écosystèmes et des systèmes socio-économiques.

**HS02a/07P/D-006** Poster **1545-152**

**WORLD MAP OF HYDROGEOLOGICAL CONDITIONS AND GROUNDWATER FLOW**

Roald Gamidovich DZHAMALOV, Igor Semenovich ZEKTSER (Water Problems Institute, Russian Academy of Sciences)

The Map was compiled in accordance with special UNESCO Project and printed in the USA in 1999. The methods of groundwater flow assessment and mapping, legend of the map and its main contents were elaborated by Russian scientists (Principal editors Dr. R. Dzhamalov and Dr. I. Zektser). The Map was edited by a special International Editorial Board that included representatives from the Australia, Argentina, Brazil, China, Germany, USA, India, France, Indonesia and numerous other countries. World Map of Hydrogeological Conditions and Groundwater Flow (scale 1:10 mln.) is designed to provide specific and quantitative information for the following practical problems: a) to determine groundwater flow and natural groundwater resources in individual regions of the Earth to characterize water availability and to plan the use and protection of water resources; b) to determine groundwater recharge amounts to establish the regional water balance and existing water resources; c) to determine groundwater contribution to river runoff as it is the most stable portion of total river runoff, as well as to predict changes in river discharges under the effect of large scale groundwater withdrawal; and d) to determine the value of direct groundwater discharge to seas and oceans to establish groundwater contribution to water and salt balances of the seas. The World Map is a special, thematic hydrogeological map whose main content is information on the distribution of several quantitative characteristics of groundwater runoff as well as geological and hydrogeological conditions of groundwater generation. In small-scale mapping of hydrogeological conditions selection of aquifer systems is a severe problem. It is necessary to distinguish principal groundwater flow media - types (subtypes) of rocks with common conditions of generation and spatial distribution of water-conducting properties. Besides of lithological composition of groundwater flow media on the Map the specific values of groundwater flow characteristics (modulus and coefficients) are presented. This combined representation of two quantitative characteristics appreciably improves the informativeness of the Map. Different colors are connected with groundwater flow media types, intensity of each color reflects modulus of groundwater flow or annual specific groundwater discharge values (from less than 0,1 to 10-20 l/s km<sup>2</sup>), and brown isolines represent coefficients of groundwater flow or ratios groundwater runoff to annual precipitation. The Map gives also information about special conditions of groundwater flow generation connected with human activities, intensive karstification, river channels with surface runoff losing, and rift zones and regional faults, and so on. Firstly in the hydrogeological mapping, the Map presents conditions of direct groundwater discharge to seas together with quantitative characteristics of this global process expressed in specific values. The results of quantitative estimation and mapping of groundwater flow make it possible to solve several problems of groundwater generation under different natural conditions on a completely new basis by introducing quantitative data into the analysis. The carried out research found the principle global and regional regularities and relation between groundwater recharge and the natural and climatic zonality.

**HS02a/07P/D-007** Poster **1545-153**

**ASSESSING THE SUSTAINABILITY OF URBAN WATER RESOURCES**

Matthias EISWIRTH (Department of Applied Geology, University of Karlsruhe)

With over 40% of the water supply of Western & Eastern Europe and the Mediterranean region coming from urban aquifers, efficient and cost effective management tools for this resource are essential to maintain the quality of life. Traditional water planning regularly concludes that future water demands will inexorably rise and eventually exceed water

supplies available in any given location. However, the increasing concerns about the environmental impacts of water projects and their increasing economic costs mean that traditional planning concepts, which assume unlimited supplies of potable water, must be questioned. This includes the source of the water supplies and its appropriate use. With population densities increasing in urban areas and constraints on funding, it is becoming increasingly evident that the present management of urban water resources and systems will not be suitable models for service provision into the 21st century and that increased emphasis will be placed upon the use of groundwater reserves. Without an adequate knowledge base of the current status of urban water resources, and an understanding of the processes involved, the health and safety of the people who depend on urban groundwater as drinking water can not be assured. In spite of strong efforts initiated by the European Union and other international organisations in the past 20 years, groundwater pollution from industry, traffic, sewers and agriculture is still very high. The complex transport processes of groundwater flow are responsible for the wide distribution of recharged water and contaminants. There is evidence that urban downstream aquifers are contaminated by inorganic, organic and microbial pollution. With population densities increasing particularly in urban areas and the corresponding constraints on funding, it is becoming increasingly evident that present urban water systems will not be suitable models for service provision into the 21st century. The overall objective of a new European Commission funded initiative, called AISUWRS (Assessing and Improving Sustainability of Urban Water Resources and Systems), is to develop an innovative system to quantify and manage the problems from unsustainable urban water systems and assess the impact of pollution on the underlying groundwater resources. The overall scope of the AISUWRS initiative is to assess and improve the sustainability of selected urban water systems and resources with the help of computer tools and thus minimise the impact of pollution on the underlying urban groundwater resources. Parts of these model tools have been already developed to estimate the water flows and contaminant loads within the urban water system. This model represents water and contaminant flows through the existing water, wastewater and stormwater systems, from source to discharge point and have already been applied successfully in selected areas in Australia and Germany.

**HS02a/07P/D-008** Poster **1545-154**

**ASSESSING VULNERABILITY OF WATER RESOURCES TO CLIMATE CHANGE IN MIDWEST**

Hua XIE, Wayland J. EHEART (Department of Civil and Environmental Engineering, University of Illinois at Urbana-Champaign)

There exists much scientific evidence showing that our planet is undergoing a global climate change and that the climate change will threaten the status quo of regional water resources that support ecosystem and human society. An assessment was conducted to evaluate the vulnerability of water resources to climate change in the Mackinaw watershed in central Illinois, USA. In this study, the SWAT (Soil and Water Assessment Tool) model was used to predict stream flow and crop yields in a watershed under different future climate scenarios that represent possible climate outcomes predicted by well-known global circulation models. The potential effects of climate change and irrigation incurred by the change, if any, on low-streamflow and profitability of crop growing operations were investigated, for currently customary crops for the region and alternative crops.

**HS02a/07P/D-009** Poster **1545-155**

**THE BASIC FEATURES OF TRANSFORMATION OF A REGIONAL CLIMATIC FIELD OF PRECIPITATION ON UKRAINE UNDER INFLUENCE OF GLOBAL WARMING**

Volodymyr M. VOLOSHCHUK, Svetlana G. BOYCHENKO (Department of meteorology and climatology, Kyiv Taras Shevchenko University)

The main aim of this research is to obtain quantitative estimations of the basic tendencies of changes of the monthly sums of precipitation on Ukraine as a result of global warming and to work out scenarios of transformation of a climatic field of precipitation on Ukraine in first half of 21-th century on their basis. In this research were used the following methods: Specific statistical analysis of empirical meteorological data which was worked out by authors specially for revealing very small climatic signal on a background of very large meteorological noise with use mainly of a space-time coordination and connectivity of climate fields; The climatic theory of similarity of processes of formation of an atmospheric precipitation which was worked out by authors for construction of necessary semi-empirical models; Comparison with known materials of regional climatic paleoreconstructions of warm epochs of the past. The following main features of transformation of climatic field of the monthly sums of precipitation on Ukraine under influence of global warming up to 2-3 K are established: Increase of the monthly sums of precipitation for those regions and months of Ukraine for which meteorological norms of precipitation are below 50 mm per month; Increase of the monthly sums of precipitation for those regions and months of Ukraine for which meteorological norms of precipitation are over 75 mm per month; Decrease of the monthly sums of precipitation for those regions and months of Ukraine for which meteorological norms of precipitation are over 50 mm but below 75 mm per month; Space alignment of a climatic field of the annual sums of precipitation, but averaged on all territory of Ukraine the annual sum of precipitation does not practically change. The important methodological conclusion follows from the obtained results concerning dynamics of a climatic field of precipitation on Ukraine: incorrect averaging on various space-time scales of climatic field of precipitation can result in essential distortion concerning influence of global warming on intensity of regional precipitation. At construction of scenarios of transformation of a climatic field of precipitation on Ukraine two types semi-empirical models are used: Variability and trends of precipitation as functions of meteorological norms; Meteorological norms, variability and trends of precipitation as functions of seasons, geographical coordinates of a place and its height above the sea level. The scenarios constructed on the basis of such type of semi-empirical models are convenient for using at assessments of influence of global warming in various branches of economy of Ukraine, which are formulated as stochastic space-time functionals from meteorological parameters.

**HS02a/07P/D-010** Poster **1545-156**

**FEATURES OF WATER RESOURCES SYSTEMS IN GEORGIA**

Konstantine Kote BZIAVA<sup>1</sup>, David Dato GUBELADZE<sup>2</sup> (<sup>1</sup> Department of Land Reclamation and Engineering Ecology, <sup>2</sup> Department of Land Reclamation and Engineering Ecology)

The physical-geographical and climatic conditions promoted the large variety of hydrological features both as a whole in all Georgia, and in its separate areas. In Georgia the greatest drain of water (in comparison with the countries of former USSR), exceeding 3000 mm of water per year, however amplitude of fluctuations of this drain depending on territory and river pools is very high. Resources of fresh water of a region are composed from a superficial and underground component of a river drain; underground waters not participating in a river drains and getting directly in the sea; and also water of glaciers, lakes and bogs. The features of water resources of the country are defined by relief and climatic conditions, aridity of territory, mode and geography of a drain of the rivers, and also geographical

isolation of Transcaucasia. All variety of natural resources depending on reproduction can be referred to two groups: renewed and not renewed. Now situation essentially has changed, as water has become scarce, and the former resources do not provide needs for it; besides its quality considerably has worsened. In this connection there was a necessity besides the operational charges to carry out expenses for production of water accessible to use and on improvement of its quality. For example, at regulation of the river drain in reservoir water resources "sharply grow", and the clearing of water source from pollutants improves its quality, also increasing "water resources" etc. Proceeding from above told, it is possible to note, that in a long-term section "the water resources" as against "of water stocks" are variable size varying as quantitatively, and is qualitatively depending on the requirements showed to water. Now volumes of water used in industrial activity of the man and in a life, continuously grows. As a result of it the necessity of involving in activity of the man of all new and new water sources, i.e. transference "water stocks" in a category "of water resources" has appeared. The present stage of development of a human society is characterized by the tendency of increasing water requirement, and consequently, increasing of water resources. Though in absolute sizes, the specific parameters of water resources of East Georgia are not low in comparison with arid zones of other countries, but the conditions of their use are specific and difficult, since they play a main role in water requirement of neighboring Azerbaijan laying below on current of the river Mtkvari and using a transmitted drain from Georgia. This situation is aggravated also by that as East Georgia, and below laying grounds of Azerbaijan by the climatic conditions are sharply require irrigation up. Proceeding from above mentioned, the problem of water in East Georgia carries not only technical and economic character, but also social, as the development of a national economy of Azerbaijan and indirectly of Armenia depends on its decision, as the growing water consumption by Armenia also increases deficiencies in East Transcaucasia.

**HS02a/07P/D-011** Poster **1545-157**

#### STREAMFLOW VARIATION OF FOREST COVERED CATCHMENTS

Zoltán GRIBOVSKI, Mihály KUCSARA, Péter KALICZ (Department of Forest Opening Up and Hydrology, University of West Hungary)

Rainfall concentration and runoff, otherwise rainfall-runoff processes, which cause river water discharge fluctuation, is one of the basic question of hydrology. Looking for the answer is important because several social-economic demands have a strong connection with small or bigger rivers from the point of view both quantity and quality of the water. Gratification or consideration of these demands is complicated substantially that we have still poor knowledge about our stream-flow regime. Water resources mainly stem from upper watersheds. Rivers transported water discharge, which is potential usable, is an integral of streams take its rise in these small watersheds. These upper watersheds are the basis of the water concentration process, therefore we have to improve our knowledge about hydrological processes coming up in these territories. In this article we present runoff regime of three small catchments on the basis of one year data. Two catchments have a similar magnitude 0.6 and 0.9 km<sup>2</sup>, and one is bigger about 6 km<sup>2</sup>, which has a part other two above mentioned. We have been analyzed in detail from hydrological elements only features of rainfall, discharge, rainfall induced flooding waves, and basic discharge in rainless periods. Variations of these parameters have been analyzed in relation to catchments surface, vegetation coverage and forest management. Result data set well enforce our knowledge about small catchments hydrological processes. On the basis of these fundamentals we can plan more established the management of these lands (forest practices, civil engineering works, usage of natural water resources). Global change could change hydrological regime. These results can also utilize on the long term planning of land use and water demands gratification.

**HS02a/07P/D-012** Poster **1545-158**

#### FINGERPRINTING CLIMATE CHANGE DRIVEN DROUGHTS IN WESTERN CANADA

Lawrence Chima NKEMDIRIM (Geography and Earth Sciences, University of Calgary)

Some climate models forecast a higher frequency of drought events in western Canada due to an atmospheric greenhouse gas driven climate change. Because droughts are not uncommon there, it is necessary to differentiate events that are either wholly driven or intensified by climate change from 'normal' events. Two trends currently identified with century-scale climate change appear to adequately fingerprint climate change inspired droughts in the region. They are (a) statistically highly significant increase in surface air temperature and (b) an equally significant decrease in sea level pressure. Fingerprint One (winter droughts - precipitation poor): Based on homogenized data from 114 stations, mean annual temperature rose at a rate of 2.7°C/century between 1953 and 1997. This trend was dominated by increases of about 5 and 6°C in the winter and spring respectively. Paralleling the trend was a highly significant reducing trend in surface air temperature especially during the two seasons. Observation and analysis showed that the Polar High Pressure, which dominates the region's winter climate had weakened and the temperature contrast between the Arctic and polar air masses had declined. The resulting 'softening' of the polar front correlated well with negative winter precipitation anomalies. Precipitation more than 2 standard deviations below normal were 20 percent more frequent in post 1975 winters than in pre-1975 ones and the difference was statistically significant at 95% confidence level. Additionally, the post-1975 two standard deviation events correlated well with both pressure anomalies and change in mean surface temperature. Fingerprint Two (summer droughts - precipitation rich): The Canada Climate Center model predicted increases in precipitation for the region ranging from 15mm/year to 45mm. An energy balance model, in which all sources of energy including a strong advective component due to the Chinook (a mountain wind, which significantly impacts the temperature regime in the region) were fully specified, enabled a realistic assessment of the region's water balance under the present warmer regime. Water deficit ranging from 250mm above normal in the driest areas to 45 mm in the wettest parts was indicated for the post-1975 period. The Palmer Drought Index was used to identify recent drought events that were severer than they would have been under similar summer and rainfall and antecedent moisture. The frequency of such events increased 35% in the post-1975 period.

**HS02a/07P/D-013** Poster **1545-159**

#### THE CONCEPT OF MODERN ARID ZONES OF HYDROGEOLOGY OF CENTRAL ASIA AND ITS PROBLEM

Nasirdjan -TAKHIROV, Shukhrat Saifullaevich RADJABOV (Department of hydrogeology, National University of Uzbekistan)

The hydrogeology as a science intensively developed within last century and its fundamental positions are already formulated. Especially, after 60th of the last century, the accomplishing of any type of hydro-geological researches was accompanied with the decision of a problem to manage the dynamics (changes) and chemical compound of underground waters within the limits of concrete borders. The requirement to a hydro-geological science after 70th has got rather complex character. These requirements follow from an ecological problematic of the regions. The underground hydrosphere is considered (examined) as the mainframe of the geoecological environment and is one of the components for eco-system. So, it occurred

the new situation connected to an intensification of technogenesis and gradually, the concept of a hydro-geological science has got the new maintenance (contents), providing an ultimate goal – management of underground hydrosphere within the framework of ecological requirements. The decision of hydro-geological problems in volume of its new concept demands the preliminary system analysis of hydro-geological situation. This work is feasible only in development of the further researches on a new scientific direction – technogenetic evolution of hydro-geological conditions of arid zones, rational use and resource management of underground waters: an ecological policy, balance, preservation, protection and the forecast. The object of research is underground water of hyper genesis zones, that is on a part of lithosphere where the active and slowed down water exchange is observed. Thus, the purpose of maintenance of the uniform concept, system, methodology and methods of management and operation of underground waters for needs of a national economy is pursued within the framework of ecological requirements. On the faculty of hydrogeology of National University of Uzbekistan, researches on the mentioned above new direction on Arid zones – Ustyurt, Aral Sea Region, Kyzylkum, Amu-Darya and Fergana artesian pools - are conducted. Researches on the given direction provide the following: Revealing of scientific bases for development of underground waters under difficult ecological conditions in the arid zones of Uzbekistan and definition of their role in development of geo-ecological processes; Identification of water problems and problems of social and economic development- Development of criteria for estimation of opportunities to use the resources of underground waters for social - ecological and technical needs- Development of long-term program to develop the water supply for drink, animal industries, technical needs and for infrastructures- Scheduling of the work on protection, management and rational use of underground waters according to the ecological requirements.

**HS02a/07P/D-014** Poster **1545-160**

#### THE GLOBAL WATER SYSTEM PROJECT OF IGBP\*, IHDP\*, WCRP\*, DIVERSITAS

Holger H. HOFF<sup>1</sup>, Holger HOFF<sup>1</sup>, Carlo JAEGER<sup>1</sup>, Denis LETTENMAIER<sup>2</sup>, Christian LEVEQUE<sup>3</sup>, Harry LINS<sup>4</sup>, Michel MEYBECK<sup>5</sup>, Madiodio NIASSE<sup>6</sup>, Charles VOROSMARTY<sup>7</sup> (PIK, <sup>1</sup>University of Washington, Seattle, USA, <sup>2</sup>Programme Environnement, Vie et Sociétés, Meudon Cedex, France, <sup>3</sup>U.S. Geological Survey, Reston, Virginia, USA, <sup>4</sup>Université Paris 6, France, <sup>5</sup>IUCN-BRAO, Ouagadougou, Burkina Faso, <sup>6</sup>University of New Hampshire, Durham, USA)

The Global Water System (GWS) plays a central and integrative role in the dynamics of the Earth system. It is a regulator of biogeophysical and biogeochemical processes, and it is also essential for sustenance of human societies. The GWS is increasingly modified by humans and through climate effects (facets of it have moved well outside the range of natural variability), without adequate understanding of how the system works. For understanding the changes, feedbacks and potentially critical thresholds within the Earth system, and eventually for better managing the GWS, new synthetic knowledge is required. The Global Water System Project (GWSP) is a new activity being undertaken jointly by the World Climate Research Programme (WCRP), International Geosphere-Biosphere Program (IGBP), International Human Dimensions Program (IHDP), and Diversitas. It will address the GWS in a comprehensive fashion at the global scale, building upon the emerging new consolidated Earth systems data sets, global monitoring tools, and predictive and coupled modeling capabilities. The central scientific question that motivates the GWSP is: "How are humans changing the global water cycle, the associated biogeochemical cycles, and the biological components of the GWS, and what are the social feedbacks arising from these changes?" GWSP will be structured around three "framing questions": a) What are the relative magnitudes of global-scale changes in the global water system that are attributable to changing human activities, and to environmental factors such as climate variability and change?; b) What are the main mechanisms by which human activities are affecting the global water system; and c) To what extent is the global water system resilient to global change? Examples of issues that might be addressed under each of these questions are provided.

**HS02a/07P/D-015** Poster **1545-161**

#### MODELLING OF WATER AVAILABILITY IN GRASSLAND ECOSYSTEMS OF ARID ZONE DELTA PLAINS

Natalia V. PENKOVA<sup>1</sup>, V.P. SINGH<sup>2</sup>, V.A. KHAYDAROVA<sup>3</sup>, N.M. NOVIKOVA<sup>4</sup> (State Hydrological Institute, <sup>1</sup>Louisiana State University, <sup>2</sup>Water Problems Institute, Academy of Sciences of Uzbekistan, <sup>3</sup>Water Problems Institute, Russian Academy of Sciences)

For successful long-term planning and ecosystem management in river deltas of drought-prone regions, it is desirable to develop sufficiently rigorous but not very complex and data-extensive models which are easy to understand and can be used by a wide range of specialists and experts, not sophisticated in purely hydrological, ecological or biological scientific knowledge, for real decision-making. In the contribution, the most simple version of conductance-type combination equation (Budyko's combined method) is used to calculate within-the-year and long-term variations and trends in water availability (evapotranspiration and soil water content) for grassland ecosystems in Syrdarya and Amudarya river deltas (Aral Sea basin), Volga and Terek river deltas (Caspian Sea basin) and Mississippi delta plain. The biological response to environmental conditions (atmospheric demand, precipitation intensity, ground water table, soil water properties), and to agrotechnology (fertilization, irrigation) by using non-linear multi-dimensional cubic splines approximations for "biological" parameter of the Budyko's equation is estimated for annual grass crops and perennial herbs, with particular emphasis on the vegetation condition (closed and sparse canopy, high and low productivity, etc.) (Khaydarova, Kucherova and Penkova, 1998). A comparison is made of the results with ones obtained by applying mechanistic volume type models (Singh, 1989), and resistance-type combination techniques (Penman-Monteith equation). The advantages and shortcomings of the models under analysis are highlighted. An application of the models for historical formation of water availability patterns and for possible climatic and economic conditions in the future is presented. The ecosystems of the deltas represent different natural self-development and man-induced stages - from the stage of drying, increasing of soil salinization and decreasing of meadowlands productivity (Aral basin) to the stage of humid-meadow lands restoration conditioned by rising the Caspian sea-level. Vegetation changes in the territories are of long-term cyclic nature, depending on climatic fluctuations and superimposed anthropogenic influences (Novikova, 1997). The superimpositions are investigated for different periods of economic development of states.

**HS02a/07P/D-016** Poster **1545-162**

#### CLIMATIC VARIABILITY AND LAND RESOURCES VULNERABILITY IN THE FORCADOS RIVER ESTUARY

Mayowa FASONA (University of Lagos)

The current climatic fluctuations and shift from global climatic normals is causing apprehensions across the blue planet. Data on global climatic indicators show that there has been a net increase in global surface temperature by between 0.30c and 0.50c over pre-industrial periods. Evidences of global warming have already been noted in glacial margin retreat, a rise in snowline, a rise in sea level, northward recession of the tundra margin in the

arctic and the ferocious southward march of the Sahara in the tropics. It has also been estimated that an increase of between 10c and 4.50c over the current global temperatures is expected to trigger off accelerated sea level rise of between 0.2m and 1.4m, which have lots of catastrophic implications especially for the coastal ecologies and other low-lying areas of the world. This paper utilizes Remote Sensing and GIS techniques to assess likely implications of accelerated sea level rise on water and land resources of the areas around the estuary of the Forcados River. Current ecological and land resources data on the study area was generated from remotely sensed satellite imagery. This was overlaid with spatial data on elevation, soil, geology and water resources to generate floodable areas sensitivity map for this coastal environment. The implication of this for food security, sustainable water resources management and coastal resources management is also discussed.

**HS02a/07P/D-017** Poster **1545-163**  
**INFLUENCE OF CLIMATE WARMING ON ASIAN LAKES FROM VIEW POINTS OF WATER RESOURCES**

Hiroji FUSHIMI (The University of Shiga Prefecture)

Due to the climate warming, glaciers are rapidly melting and lakes are extremely expanding in the Nepal Himalayas, and the region faces further natural disasters including the glacial lake outburst flood and the related landslide phenomena. The water level of Lake Hovsgol in Mongolia has risen 60cm for the recent 20 years, so that the surrounding forests, pastures and the lakeshore town have been inundating year by year. Three causes of the water level rise could be noticed as follows: 1) the formation of a natural dam at the end of the lake caused by the sedimentation of sand and gravel which were transported from the tributary river at the time of heavy rain; 2) the thaw of permafrost around the lake where the ground temperature becomes higher with increases of the incoming radiation due to deforestation owing to the anthropogenic expansion of pasture and fired forest; 3) the thaw of permafrost caused by the global warming. When the average air temperature rises by 3.5 degrees Celsius in Lake Biwa basin in Japan, the amount of snow cover would significantly decrease to 60% of the average (1 billion tons) even if the precipitation exceeds by 20%. When the amount of snow cover is more than the average, the lowest dissolved oxygen concentration in the deep layer of Lake Biwa increases due to the density current of the oxygen-rich snowmelt. However, the dissolved oxygen concentration rapidly decreases, when the amount of snow cover is less than 1 billion tons. The climate warming will significantly decrease the amount of snow cover in Lake Biwa basin and the dissolved oxygen concentration in the deep layer of the lake, leading to further enhancement of eutrophication in the 21st century. There are numerous lakes in the inland mountainous regions and the coastal lowlands of Asia where the mighty rivers, such as Rivers Yellow, Yangtze, Mekong, Ganges and Indus, originate from and flow down to the megalopolises with the rapid population growth in the river mouth areas. At the first stage of the global warming, glaciers and permafrost layers melt, and the lake water increases. However, there comes the shortage period of water resources in the later stage of the global warming due to the shrinkage of glaciers and permafrost layers and this may lead to the serious environmental issues in Asia, when the water resources become scarce especially in the dry seasons. So, there is a need to create a new management system for the rational use of water resources taking into account the recent changes in glacial as well as limnological phenomena due to the climate warming.

**HS02a/07P/D-018** Poster **1545-164**  
**APPLICATION OF WATER BALANCE MODEL FOR REVEALING OF HIDDEN CYCLES IN THE CHANGES OF CHARACTERISTICS OF ENCLOSED LAKES (CASPIAN SEA AS A CASE STUDY)**

Alexey Vladimirovich BABKIN (Lab. of Hydroecological Research of Inland Water Bodies, State Hydrological Institute)

The specific inter-year variations of level, area and water balance components of large closed lakes are caused by quasi-periodical dynamics of global and regional natural processes. The global factors are directly or through Earth climatic system affect the water regime of the lakes and their catchment areas. The revealing of hidden cycles in the variation of lake's characteristics is acute for exploration of their relationships with global factors and for forecast of their possible changes in the future. The solution of differential equation of lake water balance permitted to elaborate a mathematical model, where dynamics of the mutually related Caspian Sea characteristics (level, water surface area, evaporation and flow of water to Kara-Bogaz-Gol gulf) are the response of inflow (river runoff, precipitation and ground-water runoff) oscillation. The oscillation of water inflow causes the variation of sea level, area and water balance components. The extremes of sea characteristics have a time lag, if compared with impact extremes. The amplitudes of variations of sea characteristics and the time of their delay from inflow were calculated for different values of inflow and for the large number of periods. The dependencies of amplitudes of sea characteristics and the time of their delay to inflow from period of variations are exposed on the special nomographs. The observation data on water inflow and sea level were approximated by periodic functions. The least sums of squares of differences of approximating sinusoids and the values of time series of level and water inflow were computed in dependence with the length of period. The cyclic qualities in variation of lake's characteristics are revealed near the periods where there are the minimums of sums of squares of differences of approximating sinusoids and values of time series of level and water inflow, and where the time delay of level to inflow and relation of their amplitudes of approximating functions are close to the model results. The application of water balance model for analysis of cyclic qualities in dynamics of lake's characteristics make its results more reliable and physically based than the use of statistical approaches only. The resemble research and modeling of dynamics of lake characteristics may be fulfilled for another large enclosed water bodies of the Earth.

**HS02a/07P/D-019** Poster **1545-165**  
**INDUSTRIAL WASTE WATER IMPACT ON WATER QUALITY OF ZARAVSHAN RIVER, UZBEKISTAN**

Marina Stanislavovna MOLODOVSKAYA<sup>1</sup>, Raisa V. TORYANNIKOVA<sup>1</sup>, Nariman M. UMAROV<sup>2</sup> (<sup>1</sup>Central Asian Res. Hydrometeorological Inst., Dept. of Res. and Forecasts of Environmental Pollution, <sup>2</sup>State Spec. Inspection of Analytical Control of the State Com. for Nature Prot. of Uzbekistan)

Zaravshan River valley is one from the most important economical areas of Uzbekistan. The catchment area of Zaravshan River includes territories of several industrially developed areas of republic with the number of largest cities - Samarkand, Navoi, Bukhara, etc. In past, Zaravshan had been the confluent of Amu-Darya River (which is currently the main tributary of Aral Sea) but along with irrigation network development later it became the separated river system. Zaravshan belongs to rivers with the snow-glacial type of feeding. The Height of Flow Formation Zone is 2829 m.a.s.l.; Total Length is 2342 km; Total Catchment Area is 12,300 km<sup>2</sup>. In its low stream Zaravshan River is intensively withdrawn by channels network. The Average Annual Discharge is 169 m<sup>3</sup>/s. About 96% of Total Runoff is used for

agricultural irrigation. There are also 93 Industrial Enterprises, 52 Sewage Disposal Plants at the territory of river basin; 46 Water Intake and 46 Water Release points along the middle stream of Zaravshan River. Specific Human Water Demand in this region has increased in 1.5 times since 1975. Industrial and Domestic Wastes Inflows into Zaravshan River pose a serious threat for Water Quality and Public Health especially in urban zones with high population density. The ecological situation in region has been considerably deteriorating for recent years due to increasing fresh water demands for industrial and agricultural needs. In turn, it has led to the large-scale contamination of surface and ground water of Zaravshan River basin. The Water Quality Assessment after exposure by Waste Water is carried out using the comparison of hydrochemical data obtained from different points of Zaravshan River body with the Admissible Limits. The choice of Representative Hydrochemical Indexes was done with considering wastes composition and pollutants transformation. The main principles were formulated as following: • Representative Compounds(RC) must be specific about prevalent wastes composition; • RC must have Maximum Admissible Concentration (MAC) exceeding maximal over the other compounds; • Velocity of RC transformation after coming into water flow must be minimal. For Zaravshan there were chosen two groups of the RC. The first group is common for any type of water system: 1)BOD; 2)COD; 3)Dissolved Oxygen; 4)TDS; 5)Ammonium Ions; 6)Surface Active Substances (SAS); 7)Phenols. The second group is specific one and caused by the character of wastes: 1)Oil Products; 2)Fluorides; 3)Phosphates; 4)Nitrates; 5)Nitrites; 6)Copper; 7)Chromium; 8)Lead; 9)Cyanides; 10)Arsenic, etc. The Hydrological Indexes of Average Contamination and Total Loading of River Flow were calculated with using the average concentration of pollutants in river flow at the point lower than waste water release had been done. The duration of periods of Contaminated and Pure Runoff and their volumes (in shares of Annual Average Runoff or directly in m<sup>3</sup>/year) also were calculated using Representative Indexes. This methodology can be applied either to single observing point, or river section, or water subject as a whole.

**HS02a/07P/D-020** Poster **1545-166**  
**STATUS, TENDENCY AND PROBLEMS OF TRANSBOUNDARY WATER QUALITY MANAGEMENT IN ARAL SEA BASIN**

Raisa V. TARYANNIKOVA, Marina S. MOLODOVSKAYA (Central Asian Res. Hydrometeorological Inst., Dept. of Res. and Forecasts of Environmental Pollution)

The system of water use exploited in Aral Sea Basin for the last decades, had led to water deficiency, deterioration of surface and ground Water Quality (WQ) along with corresponding social and ecological disasters. It became one of constraining factors of region stable development. Moreover, many water subjects have lost their ecological and biotic functions as environment of aquatic flora and fauna; landscape-aesthetic shape and recreation abilities. The situation is typical one not only for Zones of Intensive Water Consumption (ZIWC) with the highest anthropogenic stress on reservoirs, but also for Water Formation Zone (WFZ) where Surface Water Quality (SWQ) has been always considered satisfactory. The analysis of long-term WQ information has shown the dangerous tendency of intensification of biological productivity, i.e. there is eutrophication and, as a result, deterioration of WQ in WFZ reservoirs. The tendencies of Surface Water Quality for the last ten years are indicated. The anthropogenic changing of surface runoff, disregarding the buffering water ecosystems and necessary ecological minimum of river water discharge negatively influence on their social and ecological features. Decreasing water discharges lower than Ecological Allowable Level infringes ecological equilibrium and WQ. The water warming-up increases and contents of Dissolved Oxygen reduces. The pollution density grows up even without their additional coming from outside and "hydrological" eutrophication and secondary contamination take place. In Central Asian region practically all large and numerous small-sized rivers are transboundary, i.e. they coincide with or intersect the boundaries between two or more States. Currently, the WQ management in region is represented as Complex Regional Program of interacting political, economic, technical and legal operations. That ensures the fulfillment of rules regulating and limiting harmful effect on water environment. The solution of such complicated and actual problems is possible only with coordination efforts of all Regional States, with mutual obligations on realization adequate both of water economic and water-security policies and responsibility of States for Transboundary Waters (TW) Quality state. However, nowadays in region there is not any regulating system of TW Resources Quality. Measures on protection and rehabilitation of Water Resources should be based on ecosystem approach with new understanding WQ problems. All water basins should be considered as single whole ecosystem, concerning which water economic activity is carried out. Just on the base of ecosystem approach it is possible to resolve the primary and challenge task of TW management – definition of quotas of dumping pollutants in TW for each State, appropriate agreements and responsibility for their fulfillment. In future, along with further population growth, urbanization of landscapes, social-economic development of region, anthropogenic influence on WQ will be increasing, especially within low-water years. It makes us fall to thinking about the preventive measures just now, not putting off until "afterwards", and to direct efforts for restoring and preservation of Natural Water Resources.

**HS02a/07P/D-021** Poster **1545-167**  
**STUDY ON THE MODELING METHOD OF LAND WATER QUANTITY AND QUALITY AND ECOLOGY COUPLING SYSTEM**

Ge TAN<sup>1</sup>, Qiting ZUO<sup>2</sup>, Jun XIA<sup>1</sup> (<sup>1</sup>Hydrology Studio, Institute of Geographical Sciences and Natural Resources Research, CAS, <sup>2</sup>College of Water Resources and Environment, Zhengzhou University)

As the basic content of quantitative study on Management of Sustainable Water Resources, it is necessary, and difficult as well, to build water quantity and quality and ecology coupling system model. On the basis of application study, this paper puts forward a new method called "Multi-Box Modeling". This method's clue is definitude, calculation is simple, and model is reliable. It is confirmed by the authors that the built model can stand for "land water resources system construction connection" and can be used in quantitative study on Management of Sustainable Water Resources.

**HS02a/07P/D-022** Poster **1545-168**  
**SOIL DEGRADATION OF JAVA ISLAND**

Seno ADI (BPP Teknologi)

The rapid population growth in Java island has caused the pressure to natural resources through intensive agriculture activity. Especially in the upstream region, this situation caused the soil degradation by heavily erosion lead to sediment deposition in the lower region as indicated by the sediment carried of over 10 million ton/year in one river basin in central Java. The land degradation in Java island is not only cause unproductive soil for agriculture development but also cause the disaster such as flooding as well as water crisis. The soil and water conservation activities have been introducing to carry out the land degradation. The Indonesian government under Forestry Departement has such a program called reforestation and regreening, however the farmers have their own interest for land management in relation to the farming commodity that may not take care the soil and water conservation. The research institute has an important role to link and correspond the

farmercommodity interest with the government program in such away the soil and water conservation could be implemented by conducting the appropriate technology thatfacilitate economic development for the farmers.

**HS02a/07P/D-023** Poster **1545-169**

**ASSESSMENT OF THE IMPACT OF INDUSTRIAL EFFLUENTS ON WATER QUALITY IN KORBA AND ENVIRONS, CHHATISGARH, INDIA**

L.P. CHOURASIA (Department of Applied Geology,Dr. H.S. Gour Univ)

The effects of multiple industrial pollution sources on the groundwater system were evaluated in the industrial complex at Korbe of Chhatisgarh State of India. The quality of groundwater in the region has been affected negatively due to the discharge of effluents on open and land into ponds, tanks and streams. Water samples from surface water bodies and dug wells were analyzed for their major ion concentrations. The high values of electrical (EC) and concentrations of Na<sup>+</sup>, Ca<sup>2+</sup>, Cl<sup>-</sup> and HCO<sub>3</sub><sup>-</sup> indicate the impact of industrial effects on water quality. Based on the hydro chemistry, the groundwater is classified into various types such as sodium chloride, sodium-bicarbonate calcium chloride, and magnesium-chloride etc. Its suitability for drinking and irrigation purpose has been assessed. The groundwater quality in around Korba has become hazardous. Some possible remedial measure are suggested.

**HS02a/07P/D-024** Poster **1545-170**

**WATER QUALITY IN NORTHERN KARNATAKA, INDIA - A CASE STUDY**

Ramaraju Hanumanahalli KAMBADARANGAPPA<sup>1</sup>, RajkamaF, Prasanna Kumar N. S.<sup>2</sup>, Ranganna G.<sup>1</sup> (<sup>1</sup>Dept. of Civil/ Environmental Engineering, Bangalore Univ., <sup>2</sup>Karnataka Rural Water Supply & Sanitation Agency, Rural Development & Panchayat Raj Dept.)

Of all kinds of pollution that are steadily degrading man's physical, environment. Probably the least recognised is the hidden deterioration in the quality of ground water. Diseases related to the use of contaminated ground water may be divided into those, which are caused by microorganisms, a biological agent (a pathogen), and those, which are caused by chemical substances those that are caused by chemical substances. However, these latter diseases are over shadowed in developing countries by the former, which are the main causes of disease and death. As a part of the preparatory work for the **JAL NIRMAL** Project, a Water Quality Analysis study was undertaken. The objective of this study was to access the nature, extent and severity of Water Quality problems in the project area and the underlying causes thereof. The study was under taken in three pilot districts viz. Belgaum, Dharwad, Gulbarga (and Gadag district as a special case study due to fluoride problem) and the primary data was generated on water quality. There are 281 existing water sources in the 24 villages (10 GP's), out of which 212 sources are in use. Some are not in use due to inadequate quantity and some due to meager quality. 204 samples were collected from all the sources in use and additional 26 samples were collected for analysis of pesticides. The results reveals 174 samples (85%) were found to be non potable. The full-length paper presents the Water Quality status and mitigative measures.

**HS02a/07P/D-025** Poster **1545-171**

**INTEGRATING HIGH RESOLUTION SATELLITE IMAGERY AND WATER QUALITY STATISTICS FOR WATER RESOURCE MANAGEMENT**

Nandani Dhammika Kumari DAYAWANSA (Department of Agricultural Engineering, University of Peradeniya)

Water is an important natural resource and is a vital component of plant and animal life with two thirds of the earth being covered with water. Proper management of water resources is of paramount importance as the water quantity and quality deterioration is being widely reported all over the world. Scarcity and the low quality of water are serious problems that are faced by the disadvantaged communities in the less developed countries. With the above background, this study focussed on the use of multidisciplinary approach to handle the water-related issues in a cost effective and sustainable manner. The seasonal variations of the water availability in the reservoirs in a part of the dry zone of Sri Lanka are predicted with high-resolution (IRS LISS III) satellite imagery. At the same time the command areas of the reservoirs/ tanks are identified with the help of the same imagery. The water samples from the water bodies are selected to monitor the water quality status and the crop management information are gathered to be coupled with the water quantity data during different seasons of the year. The extracted information from remote sensing sources and field sampling is used to quantify the extent of water pollution and the contribution of agricultural and other anthropogenic activities on water quality deterioration. The output of the study can be used for policy formulation and determining guidelines for fertiliser and agrochemical use with a proper understanding of the uncertainty coupled with the information. The synoptic viewing capability and the quickness of gathering spatial information in remote sensing approach compared to the field surveying will be economically and technically feasible in sustainable water resource management in a rapidly changing environment.

**HS02a/07P/D-026** Poster **1545-172**

**SEASONAL VARIATION IN WATER QUALITY IN ORLE RIVER BASIN, S.W. NIGERIA 2 CHEMICAL HYDROLOGY**

Catherine Imhagulaya IKHILE<sup>1</sup>, Stella Maris AKHIONBARE<sup>2</sup> (<sup>1</sup>Department of Geography and Regional Planning, <sup>2</sup>New Grass Technologies)

An investigation of the chemical conditions of water bodies in the Orle River Basin in Edo State, Nigeria was carried out in 1987 and 1997. The quality of the water in the drainage basin was compared between this ten years period for any possible variation due to global changes in climate and population pressure. The results reveal that in 1987, chloride, sodium, biochemical oxygen demand (BOD5) and dissolved oxygen (DO) varied significantly with the seasons. While chloride, DO, BOD5 and COD show increase in the wet season, sodium, potassium, calcium, magnesium, iron, aluminium, silica, nitrate, sulphate and total hardness increased in the dry season and decreased in the wet season. In 1997, while total hardness, silica, nitrate iron and COD increased in the wet season, chloride, calcium, magnesium, DO and BOD5 increased in the wet season and decreased in the dry season. The values of some of the parameters are beyond tolerable limits. The degree of pollution observed in the rivers constituting Orle River Basin is sufficiently significant to necessitate pre-treatment of the basin water prior to domestic and industrial uses. Presently, the natives treat the water with alum before use, but this practice is not sufficient chemical treatment required to make the water safe for consumption.

**HS02a/07P/D-027** Poster **1545-173**

**CONCENTRATIONS OF URANIUM IN SURFACE WATER IN QINGHAI-TIBET PLATEAU**

Yuefang LI, Tandong YAO, Lide TIAN, Wusheng YU, Jianchen PU (Key laboratory of Ice Core and Cold Regions Environmental Research, CAREERI, CAS)

U is not also a natural radioactive element but a heavy metal. It has radio-activity and also do harmful to human health just like lead. So many studies pay attention to this element in recent years. Study showed that human mainly intake uranium from water. So it is important to know the content of uranium in natural water. In other hand, the distribution of uranium in water has signifi-cance in geochemistry exploration of uranium and water quality assessment. The Qinghai -Tibet plateau is affluent in water resources and some big rivers are the headwaters of some world rivers such as the Changjiang River and the Brahmaputra river etc. So it is important to know the distribution of U concentrations in waters in the plateau. We present here data on the dissolved U in surface waters as well as some ground waters in the plateau for the first time in most sites of Qinghai-Tibet plateau. The primary objective of our study is to identify the spatial distribu-tion of U concentrations and establish the background value of uranium concentration in the water in the plateau. This study contributes new data on the U content in waters in China. Sampling equipment were pre-cleaned in clean room and concentrations of U were determined by the ultrasensitive inductively coupled plasma sector filed mass spectrometry (ICP-SFMS) technique in clean room conditions. The data show that the concentrations of dissolved U in surface waters are in the range of 0.17 to 6.53µg/L, with a mean value of 2.56µg/L. That is higher than that of World Rivers. The concentrations of U are changeable not only in the same water system but in the different water system and show an obvious spatial variations.The highest concentration was observed in a glacial melt water comes from Xixiabanngma mountain located in Himalayan region,the southern part of the plateau.The lowest concentration was found in the west-middle part of the plateau.

**HS02a/07P/D-028** Poster **1545-174**

**ISOTOPIC EVALUATION OF GROUNDWATER SYSTEMS FOR RISK ASSESSMENT AND MANAGEMENT DURING EXTREME EVENTS**

Partha Sarathi DATTA, Sunil Kumar TYAGI (Nuclear Research Laboratory, India Agricultural Research Institute)

In different parts of the world, increasing population, urbanization, and competition for economic development induced indiscriminate exploitation of groundwater and its contamination hamper groundwater management programs. Management strategies require scientific evaluation of groundwater vulnerability to depletion and pollution, and risk assessment, in relation to changes in landuse and other environmental conditions. In this context, the groundwater system in Delhi region has been described, using stable isotopes (<sup>2</sup>H, <sup>18</sup>O) distributions in groundwater and rainfall. The isotope signatures of Delhi rainfall (<sup>18</sup>O: -15.3 to +8.0‰ and <sup>2</sup>H: -120 to +55.0‰) generally fall along the world meteoric line, depleted <sup>18</sup>O is generally associated with heavy rainfall, and the rainfall deficient years are generally associated with relatively enriched <sup>18</sup>O in monthly rainfall. Changes in landuse result in variation in recharge from location to location, both in space and time, with a wide range of <sup>18</sup>O signatures in groundwater (<sup>18</sup>O: -2.8 to -8.6‰), both laterally and vertically, suggesting occurrence of an inhomogeneous stratified system. Groundwater renewal has a selection effect in favor of isotopically depleted rainfall, with most parts receiving less than 5% recharge. Imbalance in recharge with withdrawal resulted in decline in groundwater levels by 8-10m during the last decade. Distribution of <sup>18</sup>O and Cl in groundwater suggest occurrence of two main flow systems vertically: (i) Uppermost local flow, rapidly circulating, low salinity, more vulnerable to overexploitation, and (ii) Relatively slow circulating intermediate zone and more vulnerable to salinisation and depletion. The groundwater in different parts has also become considerably vulnerable to pollution, with a wide range of nitrate (30-1600 mg/l), fluoride F (1-16.0 mg/l), Zn (3-41 Mg/l), Cu (5-182 Mg/l), Fe (279-1067 Mg/l), Pb (31-622 Mg/l), Ni (<1-105 Mg/l), Cd (<1-202 Mg/l). Increase in groundwater contaminants levels, associated with enriched <sup>18</sup>O isotope, clearly suggests increasing risk of groundwater to pollution from localized infiltration of isotopically enriched (<sup>18</sup>O: -3 to -5‰) and highly contaminated agricultural and urban surface run-off water, through stagnant water pools. Governed by the zonal disparity in water supply and groundwater abstraction, many flowpaths of inter-mixing of contaminated water with fresh water bodies can be visualized from <sup>18</sup>O and Cl relationships. Risk of groundwater depletion and contamination are governed by rainfall pattern, recharge, withdrawal, and surface run-off characteristics, groundwater-surface water interactions, and sorption/desorption processes in the soil. For comprehensive assessment of risk associated with extreme events, more field research and scientific knowledge is needed on isotopic responses and dynamics of pollutants in the groundwater flow, aquifer's attenuation capacity for contaminants, under natural and exploited conditions, in relation to land use, wastes disposal and other environmental changes. Risk can be partly minimized or controlled by restricting migration of population from surrounding states, unplanned groundwater abstraction, and eliminating wastes disposal within the protection zones, through strict enforcement of regulatory measures.

**HS02a/07P/D-029** Poster **1545-175**

**GROUNDWATER ISSUES IN PONDICHERRY COASTAL ZONE , INDIA**

S.S.Sundarvel RAGASAKTHI (IAHS)

The intense use of ground water has caused major water-level declines and significantly decreased the saturated thickness of aquifers in some areas. In many semi-arid to arid regions, ground water has been withdrawn at rates far in excess of recharge, leading to ground-water "mining" This is often accompanied by detrimental environmental side effects, such as reduced ground-water discharge to springs, streams, and wetlands, and land subsidence. Land drainage is a source of ground-water depletion, as the construction of drainage ditches and canals in surficial systems can lead to regional lowering of the water table. A significant component of the total depletion may come from low-permeability confining layers, but they are rarely monitored and usually overlooked. The magnitude of worldwide depletion of ground water in storage may be so large as to constitute a measurable contributor to sea-level rise. But the magnitude of depletion is poorly documented worldwide, particularly in developing countries. The management concept of "sustainable development" may offer a viable approach to dealing with overexploitation of ground-water resources, but its implementation has been largely subjective and sometimes arbitrary. The purpose of this paper is to document methods and examples that would help define the magnitude of the problem in Pondicherry Coastal Zone,India and explore local and regional management approaches to mitigate the problem or assure sustainable development.

**HS02a/07P/D-030** Poster **1545-176**

**THE STUDY FOR GROUNDWATER RESOURCES SYSTEM OF CHINA WITH THREE-RATED APPRAISING METHOD OF SUBAREA**

huajun hua LOU, Hong Hong WANGHONG, Jun Jun XIAJUN, XianFang Xian SONG (institute of geographic sciences & natural resources research, chinese academy of sciences(cas))

Surface water and groundwater are important constituents of water resource system. Since the water transport and deposited in a different way within the medium between surface water and ground water, so the modeling and appraising method adopted are different. The first water resources appraising of China, only the one item of national groundwater resources' gross is to 10000 billion tons (occupy 1/8 of all the national groundwater resources or so), this data is equal to the data of the water transported from south to north one time or more. The author think that the main reasons for the total error of groundwater resource are: 1) In the nature, groundwater and surface water frequently conversed and replenished with each other. It is impossible to appraise them respectively. In the water resources' appraising of China, from one-rated subarea to three-rated subarea, the method of ground water modulus was divided with surface water. So, it can't be reflected clearly that the system of surfacewater and groundwater are oneness. 2) In the water resources' appraising, the computing methods of surface water and ground water replenishment and evaporation are not be united, the resource quantities' iteration principles different, leading to the inconformity of the result. 3) The basic data for water resource's evaluation of china come from the different management section respectively. Water conservancy department managed surface water and agricultural water. So relevant water data primarily come from the water conservancy section. Constructed department managed the water for city use. Relevant data mostly come from local construction section. For a few years, the groundwater was managed by geologic and mining section. Meantime, the section can pursue a part of monitoring work. They have the accumulated data of many years. The data of above three sections are the foundation on which proceed the water resource's evaluations in China. so the problem of data unification should be resolved. The author think that in the first water resources evaluation of China, surface water was evaluated according to River valley, while ground water was evaluated through Hydrology geology unit, which are the principal reason for the error of water resource's gross. The conversed relation of four kind of water is complexity, which adopt the evaluation method of river valley and hydrologic unites respectively. So the gross' error is unavoidable in water resources' appraising. In the thesis, the author brings up the project of three-rated evaluation and subarea. In the groundwater resources' quantity evaluation, one and two-rated subarea method according to river valley are adopted. While three rated subarea according to groundwater unites is used to resolve the problem of the water resources' evaluation error.

**HS02a/07P/D-031** Poster **1545-177**

**ACID RAIN AND GROUNDWATER QUALITY**

Roald Gamidovich DZHAMALOV (Water Problems Institute, Russian Academy of Sciences)

The study of the effect of precipitation on acidification processes in groundwater for different combinations of natural and anthropogenic factors that control the response of hydrogeological systems to acidification and the development of methods for the risk assessment of groundwater pollution by acid fallout. On catchment areas in Moscow and Novgorod regions in Central Russia, field observations and analytical determinations were carried out (the sampling of rainwater, meltwater, surface water, soil water, and groundwater, as well as of water-bearing rocks) for the subsequent study and update of the data base on groundwater acidification under individual geological, hydrogeological, landscape, and geomorphological conditions and degree of acid load. The main attention was paid to the study of the hydrochemical regime of spring water and groundwater, which are most liable to acidification. In addition, the mineralogical composition of water-bearing rocks and clayey interlayers was analyzed to assess the degree of interaction between them and percolating acid waters. The data on the hydrochemical groundwater regime within individual catchment areas have been generalized over the period of last 30-40 years. These materials were used for verification and adaptation of the hydrodynamic and physicochemical models for estimating the areal extent and degree of groundwater acidification. The field and experimental studies, as well as simulations, were carried out with a special attention paid to studying the soil and rocks of aeration zone, since they buffer the effect of acid precipitation on groundwater. Stages in leaching the soluble minerals of soil and water-bearing rocks were determined as a function of the acid load and duration of exposure. The relationship was determined between the neutralizing capacity of rocks of aeration zone and amount of carbonate rocks, the rate of infiltration of acid precipitation, as well as the duration of physicochemical interaction in the water-rock system and the solid-to-liquid ratio. Possible forms of migration of constituents of rainwater, meltwater, surface water, and groundwater have been studied under various conditions of their formation and migration, as well as with allowance made for the duration of acidification process in the water-rock system. The analysis of the available criteria of acidification allowed developing new criteria of the degree of acidification of natural waters, which are based on the amount of acid load and its residence time in the water-rock system. Various phases of acidification of soil water and groundwater have been studied under a variety of conditions of their formation and under various hydrogeological regimes. The field and experimental studies, as well as the computer simulation allow us to establish several important particularities of groundwater acidification and contamination under atmosphere fallout.

**HS02a/07P/D-032** Poster **1545-178**

**HYDROGEOLOGICAL AND HYDROGEOCHEMICAL ASPECTS OF THE NUBIAN SANDSTONE AQUIFER IN EAST OWEINAT AREA, SW EGYPT**

Esam EL SAYED<sup>1</sup>, K. DAHAB<sup>2</sup>, A.M. EBRAHEEM<sup>3</sup> (<sup>1</sup>Geology Department, Faculty of Science, Minia University, <sup>2</sup>Geology Department, Faculty of Science, Menofia Univ, <sup>3</sup>Geology Department, Faculty of Science, Assiut Univ)

East Oweinat area is currently a site of a major reclamation project, which totally depends upon the groundwater extraction from the Nubian Sandstone Aquifer; the only water resource in this area. This aquifer is composed of sandstone beds with minor intercalation of siltstone and kaolinitic sandstone. Groundwater in this aquifer occurs under unconfined conditions, while elsewhere it is under semi confined conditions as a result of the occurrence of clay intercalations within the aquifer materials. Generally, groundwater flow is from southwest to the northeast. The saturated thickness is ranging from less than 100 to 650 meters in the study area. The recent annual recharge to the aquifer system in this area is too low if compared to the present extraction rate and exclusively depends on the transmissivity of the aquifer material and its hydraulic gradient. Groundwater belongs to a fresh water class whereas salinity content ranges between 302 and 876 ppm. It is of meteoric origin and belongs to alkali-chloride sulphate water type. Therefore, it is suitable for irrigation purposes for most of the soil types under ordinary conditions.

**HS02a/07P/D-033** Poster **1545-179**

**A STUDY OF HYDROGEOLOGICAL CONDITIONS OF THE NUBIAN SANDSTONE AQUIFER IN THE AREA BETWEEN ABU SIMBEL AND TUSCHKA, WESTERN DESERT, EGYPT**

Esam EL SAYED<sup>1</sup>, K. DAHAB<sup>2</sup>, A.M. EBRAHEEM<sup>3</sup> (<sup>1</sup>Geology Department, Faculty of Science, Minia University, <sup>2</sup>Geology Department, Faculty of Science, Menofia Univ, <sup>3</sup>Geology Department, Faculty of Science, Assiut Univ)

The Nubian Sandstone Aquifer in the area between Tuschka and Abu Simbil is small portion of the very well known Nubian Sandstone Aquifer System in the Eastern Sahara, which covers the entire area of southwest Egypt, southeast Libya, northeast Chad, and northern Sudan. Tuschka area is currently the site of intensive drilling and development for a huge land reclamation project. The drilling information was used to study the hydrogeological setting of the aquifer in the area. The obtained results indicate that the lithological characteristics and tectonic setting is strongly affecting the groundwater flow pattern as well as the aquifer potentiality of the Nubian Sandstone aquifer in the area. The aquifer potentiality in the study area is low if compared to that of east Oweinat, Dakhla, and Kharga areas. The aquifer is mainly composed of hard ferruginous sandstone with great shale and clay intercalation with a thickness ranging from 140 to 230 meters. The potentiometric surface is ranging between 102 and 170 meters above mean sea level. Depth to water ranges between 20 and 140 meters from the ground surface. Groundwater in this aquifer belongs to fresh to slightly brackish type (salinity is ranging from 240 to 2370 ppm). The predominant water type is sodium sulphate and sodium chloride. The groundwater is related to meteoric origin. The high concentration of sodium, chloride, and sulfates reflect leaching and dissolution processes of gypsiferous shales and clay as well as long residence time of water. Most of the collected groundwater samples are suitable for irrigation purposes in the study area.

**HS02a/07P/D-034** Poster **1545-180**

**GEOPHYSICAL EXPLORATION FOR GROUNDWATER IN THE TOLON-KUMBUNGU DISTRICT OF GHANA**

Jude Simon BAYOR, Aboagye MENYE (HYDROLOGY)

Geophysical exploration for groundwater has been carried out in seven communities the Tolon-Kumbungu District of the Northern Region of Ghana. The communities involved are Gbullung, Woribogu, Gun, Nyorong, Yoggu, Nyankpala-Tuunayili and Nyerishegu. These communities are mostly located in the south-eastern half of Tolon and lie in the Lower Voltaian Sedimentary Basin. The geophysical techniques involved were the Electromagnetic (EM) survey for ground profiling with the EM 34-3 ground conductivity meter and the dipole-dipole configuration in Vertical Electrical Sounding (VES) with the Swedish ABEM SAS 300C resistivity equipment. Results show that major aquifers are confined to hard, fractured sandstone formation. No water was found for weathered zone or fresh rock aquifers. Analysis of data also revealed several thin-bedded sequences of between 4 m and 10 m thickness of sandstone, mudstone shale and their intercalations to be the dominant formations here. Groundwater was confined to between 25 m and 45 m with major aquifers occurring approximately between 34 m and 45 m depths. Groundwater availability to beyond 55 m was not possible. The potential success rate is estimated at 75%. The surveys show conclusively that the EM method and the dipole-dipole array in VES when combined is an effective tool for the location of groundwater in the survey area of the Tolon-Kumbungu District.

**HS02a/07P/D-035** Poster **1545-181**

**A POLLUTION OF AQUIFERS BY HYDROCARBONACEOUS INCLUSIONS**

Nadezhda K. KORSAKOVA, Valentin I. PENKOVSKY (Siberian Division, Russian Academy of Science, Lavrentyev Institute of Hydrodynamics)

Damages of oil-pipe lines, liquid escape from gasoline storage and oil storage, petrol leak from filling station lead to percolation of immiscible with water fluids into water-bearing stratum occurs. At that closed hydrocarbonaceous inclusions are generated inside aquifers. Similar formations are able to be in dynamic equilibrium with groundwater flow. A water phase partially flows around and partially through such inclusions which are in stationary position under the influence of capillary forces. This phenomenon is called "internal capillary locking". The experiments were realized on transparent fill-up physical models of water-saturated bed contained circle oil inclusions under presence of gravity. It was observed the redistribution of saturation in oil spot under influence of gravity and oncoming flow of water. The limit dynamic equilibrium with water phase flow criterion was obtained for an inclusion. It was demonstrated that equilibrium stationary position was broken under excess over the criterion, and hydrocarbonaceous phase started moving. The mathematical model as a system of differential equations have been formed that allowed to describe in a hydraulic approximation a distribution of oil particles in three-dimensional inclusion been under action of a field of hydrodynamic forces and field of gravitation. A hydraulic pressure have been averaged over vertical component, consequently seepage became two-dimensional. But a distribution of oil particles remained as three-dimensional because of a gravity was taken into account. The condition of phase pressure jump on boundary of phases was taken into consideration too. The finite element method was used for solving of the two-dimensional ground water flow problem with an arbitrary given form of hydrocarbonaceous inclusion. The obtained numerical results are well agreed with the experimental data.

**HS02a/07P/D-036** Poster **1545-182**

**INTEGRATED GEOPHYSICAL INTERPRETATION FOR GROUNDWATER EXPLORATION AT NUKHL AREA, CENTRAL SINAI, EGYPT**

Abdel-Rady Ghareeb HASSANEEN<sup>1</sup>, Sultan Awad SULTAN<sup>2</sup>, Badr Saad MOHAMED<sup>3</sup> (<sup>1</sup>Prof. of Geophysics and head of the geomagnetic and geoelectrical dept., National Research Institute of Astronomy and Geophysics, Helwan, Cairo, Egypt., <sup>2</sup>Lecturer of Geophysics, <sup>3</sup>Geologist (Egyptian geological survey))

Different geophysical tools were carried out on the studied area to define the stratigraphic units, structural elements and the depth to the basement surface. These geophysical tools are geoelectric, magnetic and gravity methods. Quantitative interpretation of the vertical electrical sounding curves was done by using the two layer standard curves and generalized Cagniard graphs (Koefoed, 1960; Orellana and Money, 1966) to determine the thickness and true resistivities for each geoelectrical unit in order to obtain a preliminary models. All VES stations are re-interpreted as a final models using IPI-1D program to compute these final models. The interpretation of the magnetic data started with reduction to the magnetic pole, then depth to the upper surface of the basement was determined applying Euler deconvolution technique. The quantitative interpretation of Bouguer gravity anomaly map started with separation of residual and regional gravity anomalies applying high and low pass filter technique using Geosoft program (1994). The structural elements can be determined

from the residual gravity anomalies. Also, gravity modeling was carried out along three profiles to define the depth of water bearing Nubian sandstone aquifer and the upper surface of the basement using GM program (1995). The results of the geophysical interpretation show that, the subsurface section consists of six geoelectric units. The depth of upper surface of the Nubian sandstone(aquifer) ranges between 800 to 1000 m. The depth of the basement surface ranges between 1720 m at the northwestern part and 3600 m at the southwestern part of the studied area. There are normal faults whose directions are: N-S, E-W and NE-SW.

**HS02a/07P/D-037** Poster **1545-183**

**STUDY ON REMOVAL OF CADMIUM FROM GROUNDWATER BY ADSORPTION ON GAC, BAC & BIOFILTER**

Ramazan ali DIANATI TILAKI (Environmental Health Engineering Department, Mazandaran University of Medical Sciences)

The Contamination of groundwater by toxic heavy metals is a world-wide environmental problem. Rock and minerals containing heavy metals can increase concentrations of these elements in groundwater. Cadmium is a toxic element and can accumulate in the living organisms. Low concentration (below 5 mg/L) of Cadmium is difficult to treat economically using chemical precipitation methodologies. Ion exchange and reverse Osmosis while can guarantee the metal concentration limits required by regulatory standards, have high operation and maintenance costs. The goal of this research was to determination of efficacy of using GAC, Biofilm and BAC columns to treat low concentration Cadmium bearing water streams and was to determination of the effects of temperature and pH on the adsorption isotherms. Studies were conducted to delineate the effect of pH, temperature, initial Cd and adsorbent concentration on adsorption of Cd<sup>2+</sup> by GAC, BAC and Biofilm. Breakthrough curves for removal of 0.5 mg/L Cd<sup>2+</sup> by GAC, Biofilm and BAC columns at two contact times were plotted. Batch adsorption and column data are compared. pH is shown to be the decisive parameter in Cd removal for GAC but not for BAC or biofilter. Lagergren plots confirms applicability of first-order rate expression for adsorption of Cd by GAC, BAC and Biofilm. The adsorption coefficient (Kad) for BAC were 2 times greater than those with plain GAC. Bed Volumes of water containing 0.5 mg/L Cd<sup>2+</sup> treated at breakthrough for GAC, Biofilm and BAC columns were 45, 85 and 180 BV respectively. BAC is more efficient than GAC in the removing of Cd from water environment. Keywords: Cadmium, adsorption, GAC, Biofilter,

**HS02a/07P/D-038** Poster **1545-184**

**GROUND WATER ROLE IN THE ARAL SEA REGION PUBLIC WATER SUPPLY**

Abdulkhakim SALOKHIDDINOV, Khidoyat VALIEV (Tashkent Institute of Irrigation and Agricultural Mechanization Engineers)

The role of groundwater in public water supply has increased dramatically in many countries during the last decades. Surface water resources contamination (and often depletion) is a reason to use groundwater more intensively. In a number of regions, especially in Central Asia including the Aral Sea region, it reached a catastrophically large scale. At the same time in determining the perspectives of groundwater use, one should consider groundwater not only as a commercial deposit but also and above all as a part of water resources and an important component of the environment. Taking that into account it should be noticed that groundwater in many arid regions is an alternative and often the only possible source for public water supply that can provide terrestrial ecosystems with pure, safe drinking water of high quality. All the above-mentioned apply equally to Central Asia arid regions and in the first place to the Aral Sea basin, where water resources degradation assumed a catastrophic character. According to preliminary results of research it is established that the Aral Sea shrinking has direct impact on change of amudarya and aral complexes higherquaternary and modern sediments groundwater's level and chemical composition mainly within area of the dried Aral Sea bed.

**HS02** Monday, July 7 - Friday, July 11

**WATER RESOURCES SYSTEMS: GLOBAL CHANGE, RISK ASSESSMENT AND WATER MANAGEMENT (ICWRS, ICASVR, ICSW, ICWQ)**

Location: Site C, Room 24

**Tuesday, July 8 AM**  
Presiding Chairs: K. Musiake

**HS02/08A/C24-001** **0830**

**IMPACTS OF GLOBAL WARMING ON SEMI-LARGE SCALE LAKES**

Michio Dalai KUMAGAI<sup>1</sup>, Kanako ISHIKAWA<sup>2</sup>, Naoko ISHIGURO<sup>3</sup> (<sup>1</sup>Lake Biwa Research Institute, <sup>2</sup>Kyoto University, <sup>3</sup>Limoges University)

Global warming is now bringing serious problems on the semi-large scale lakes (100–1000 km<sup>2</sup> in area), because these sizes of lakes are not so much sensitive as small lakes and more reactive than great lakes over 1000km<sup>2</sup> in area. We have been studying such scale of lakes in the world, and found that some lakes are facing very much serious situation. Lac Leman of Swiss and France has lost oxygen in the hypolimnion, and it is rarely supplied now even if eutrophication stopped. Annual mean dissolved oxygen is less than 1mg/L for several years, and suddenly the level was recovered by winter overturning. This is clearly controlled by global climate change. Lake Huxian in Yunnan Province of China is also suffering from insufficient oxygen recovery in winter, and the local government is wondering what action they should take. As fresh water resource in China is very much limited, the deterioration of Lake Huxian is getting social problem now. Lake Biwa, the largest lake in Japan, looks still fine, but actually benthic ecosystem and water quality are getting worse year by year. The depletion of dissolve oxygen in Lake Biwa is caused by both decrease of oxygen supply in winter and increase of oxygen consumption in summer. As Lake Biwa is supplying drinking water to more than 13 million people in Osaka, Kobe, Nara, Kyoto and Shiga area, the well management of this lake is a big social demand. Even Lake Tahoe, which is one of most beautiful lakes in the world, is losing oxygen now in a deeper layer, and it depends on the deficiency of overturning due to global warming. When we compare the apparent oxygen consumption rate among several semi-large scale lakes, we found that Lake Biwa has highest value, and is most productive. Thus global warming is definitely changing water quality and ecosystem of semi-large scale lakes as well as eutrophication. In this study, we present current information of such lakes, and discuss what are happening at present and will occur in the future. As semi-large scale lakes play more important role to

maintain the human being society than others, those should be carefully monitored and managed wisely.

**HS02/08A/C24-002** **0845**

**ANALYSIS OF WATER RESOURCES IN THE YELLOW RIVER BASIN USING THE DISTRIBUTED HYDROLOGICAL MODEL**

Dawen YANG<sup>1</sup>, Toshio KOIKE<sup>2</sup>, Katami MUSIAKE<sup>3</sup>, Tetsuya KUSUDA<sup>3</sup> (<sup>1</sup> Department of Civil Engineering, Univ of Tokyo, <sup>2</sup>Institute of Industrial Science, Univ of Tokyo, <sup>3</sup>Faculty of Engineering, Kyushu University)

The Yellow River basin is the second largest basin in China. Due to recently fast development of economics, water shortage is becoming a serious problem. For better management of water resources in the Yellow River basin, water resources assessment is firstly important. This research develops a distributed hydrological model to simulate the spatial-temporal characteristics of hydrology in the Yellow River basin. Land uses, topography, geology and soil conditions, and artificial water uses (mainly agricultural irrigation) determine the complexity of hydrological characteristics in this basin. With the limited observation of the river discharge, it is impossible to develop a simple model for simulating hydrology in different sub-basins. Present research attempted to incorporate all available spatial information into the hydrological model by a distributed approach. Based on the physical governing equations, a comprehensive hydrological model has been developed. Using a 10-years metrological data set, the hydrological characteristics and distribution of water resources are discussed in the paper. Because the majority of water use is for agriculture irrigation, this research also tried to incorporate the irrigation water use with the hydrological model for exploring irrigation management.

**HS02/08A/C24-003** **0900**

**PATTERNS OF RUNOFF CHANGE IN BULGARIA**

Marin Gospodinov GENEV (National Institute of Meteorology and Hydrology)

We consider the geographical location of Bulgaria on the Balkan Peninsula and the impact of the complex mechanism of atmospheric circulation. We make statements regarding the cyclonic activity related to the rainfall situation in the country. We emphasise the importance of the Mediterranean cyclones, their formation and evolution, to rainfall. An overall climatic division of the country is also outlined. River runoff formation principles are also considered. The evolution of the runoff (a probabilistic process) is derived in terms of certain hypotheses introduced in the paper. Two approaches are employed in the analysis of river runoff pattern changes: determination of internal structural changes and of patterns in annual runoff change. For the purposes of the current investigation the country is divided into three runoff regions: Danubian, Black Sea and Aegean runoff basins. The climatic features of each of the basins are as follows: Danubian basin - moderate continental climate; the larger part of the Black Sea basin (its northern part) - Black Sea-influenced climate; its southern part is with a dominating Mediterranean climate (falling within a transitional zone); the northern part of the Aegean runoff region - a mixture of moderate continental and mountain climate, its southern part - under the influence of the Mediterranean climate. Each of these runoff basins had been formed by a raft of catchment basins, and can be characterized by the details of its temperature, precipitation and runoff changes. The patterns of runoff change are established by means of a complex approach allowing the combined determination of the principal climatic elements - temperature and precipitation. The raft of 1st and 2nd class meteorological stations enables us to set a space step, on a relatively uniform grid, of 25.6 km for the temperature, 19.2 km for the precipitation, and 27.3 km for the runoff. The analysis of the thus determined temperature, precipitation and runoff complex indicates the presence of specific structures giving rise the main phases of the main variation cycles. A trend analysis then determines the annual change patterns in the complexes. We observed a clear-cut phase of reduced rainfall and runoff beginning after 1981-82 and which has been active ever-since (2001). This shortage of precipitation caused droughts in each of the runoff basins. We assess this phase for each one of the complexes with respect to the recommended by the WMO norm. For the Danubian region the total decrease in runoff is in the order of 30-32 %, for the Black Sea of 43-46 % and for the Aegean - 35-39 %. It has to be noted that no such phase in the annual changes of river runoff and precipitation has previously been witnessed in Bulgaria.

**HS02/08A/C24-004** **0915**

**LONG TERM VARIATIONS IN RUNOFF AND CLIMATE IN SWEDEN**

Göran Johannes LINDSTRÖM, Sten BERGSTRÖM (Swedish Meteorological and Hydrological Institute)

Sweden, and many other countries, has experienced a large number of floods in recent years, e.g. in 1995, 2000 and 2001. The objective of the present paper is to study long term variations in runoff in Sweden, now that data from the whole 20th century is at hand. The runoff from the whole country, for the period 1901-2000, was estimated. The runoff during the period 1981-2000 was about 8 % higher than during the rest of the century. This wet period followed after the dry 1970s, which was the decade deviating the most from the rest of the century. The high runoff in recent years was most pronounced in the north. A substantial part of the increase in recent years occurred in the period January-June. However, the runoff in the 1920s was also high, and if isolated, the period 1920-1980 could be interpreted as having a falling tendency, whereas an increasing tendency appears from about 1950 to 2000. Seen over the whole century no significant changes were found. Extreme floods show a similar tendency as that of annual runoff, with many recent flood events, particularly in the northern part of the country. On the other hand, observations from the 19th century show that the runoff was even higher then. Trend tests suggest downward trends for two out of three of the long series in the analysis, the longest starting in 1807. The long records of runoff were analysed jointly with recorded precipitation, temperature and the NAO index. For the whole country, the latest ten years have been the wettest for more than 100 years and very warm. For southern Sweden, and in a longer time perspective, the high temperatures are more impressive than river runoff. The combination of high temperatures and high river runoff in recent years is quite different from the high runoff records in the 19th century, when temperatures were lower. The recent wet years have often been connected to winter periods with westerly winds. The past 20 years have undoubtedly been wet. It is nevertheless difficult to extrapolate a possible trend starting at about 1950 into the future.

**HS02/08A/C24-005** **0930**

**THE IMPACTS OF HUMAN ACTIVITIES ON THE HYDROLOGICAL PROCESSES IN THE ARID ZONES OF NORTHWEST CHINA IN RECENT 50 YEARS**

Genxu WANG, Guodong CHENG, Mingyuan DU, Yongping SHEN (Department of Water & Soil resources Research, Cold & Arid Regions Environmental and Engineering Research Institute, CAS)

Unlike other drylands in the world, arid zones in northwest China are characterized by

alternately distributed high mountains and plains. The mountain areas have abundant precipitation and glacier which forms surface water flow to plains and form numerous inland river systems. There were no runoff occurred in plains with precipitation of lower than 200mm, but complex transformation between surface water and groundwater. The hydrological regimes of groundwater and spring water, in a large extent, depend on the surface runoff. From several points of view, such as surface runoff dynamic changes out from mountain mouth and in lower reaches both in annual and inter-annual, the changes of groundwater table and the spring water volume, and temporal and spatial hydro-chemical regimes etc. were discussed in this paper for revealing the characteristics of hydrological changes resulted from human activities in recent 50 years. The inter-annual outflow of most rivers out from mountains exhibited an increase trend in recent 50 years, especially in the rivers that the recharges of the glacier and snow melt-water taken an important role by the component rate over 10.0%. However, river discharge in the lower reaches is decreasing, terminal lakes are contracting or drying up and water quality is getting worse due to expanding large-scale exploitation of water resources. Many small rivers disappear soon after flowing from mountain valleys, river courses are shortening, the spring water volume is continually reduced, and the groundwater table is falling in most parts of middle and lower reaches. These hydrological changes enhanced the water supply-demand paradox, and resulted to serious environmental problems. Understanding the characteristics of hydrological processes and regimes changes was important for driving the solutions of rational use of the limited water resources and the limiting of environmental degradation in the northwest China. Key word: Arid zone, hydrological process, water exploitation, impact, hydrological change

**HS02/08A/C24-006****0945****VARIATION FEATURES OF THE CLIMATE AND GLACIERS IN CHINA'S MONSOONAL TEMPERATE-GLACIER REGION SINCE THE LITTLE ICE AGE**Yuan Qing HE<sup>1</sup>, Zhonglin ZHANG<sup>2</sup>, Tuo CHEN<sup>3</sup>, Tandong YAO<sup>1</sup>, Hongxi PANG<sup>2</sup> (\*professor, <sup>2</sup>Dr.)

The collected climatic observation data, ice core records, tree ring index and recordation of glacier variations have been used and compared, to reconstruct the detailed history of climatic and glacial changes in the monsoonal temperate-glacier region of southwestern China during the past 400 years. All results indicate that the temperature in the region has increased in a fluctuating way since 20th century after the two cold stages of the Little Ice Age during the 17-19 century, corresponding to most of the retreating glaciers in a background of global warming. Differentially, the amount, variation amplitude and trend of precipitation in the region vary in different parts of the region. The climatic records in Dasuopu ice core, located in the Himalaya area and the western part of this region, show that the precipitation has trended to decrease since 1950's, in comparison with the tendency of increasing temperature during the same period. However, precipitation in Hengduan Mountains and other districts of this region display a rising and similar trend with that of temperature change. The different climatic variation feature may be associated with the varied atmosphere circulations over the region. As indicated by the analyzed data, the southwestern monsoon, which mainly controls China's temperate-glacier region, can be classified into two sections. One is called Indian Monsoon from Arabian Sea, passing through the Indian Peninsula, which mainly carries the vapor for precipitation to Himalaya district, the western part of region; the other is called Bengal monsoon from Bay of Bengal, passing over Bengal and Burma, which is the major source of precipitation in Hengduan Mountains and other areas, the eastern part of the region. Moreover, the eastern part of this region is also controlled by the southeast monsoon deriving from the western Pacific and in the west is manipulated by the southern branch of westerly circulation in winter. This complex atmospheric situation results in the variable patterns of precipitation in different parts of the region. The temperate glaciers distributed in the region is very sensitive to climate warming after the Little Ice Age and most of glaciers have been retreating successively since 20th century and the speeds have accelerated after 1980's and speeds of few advancing glaciers are alleviating. Although both temperature and precipitation influence the change of glaciers, further work is needed to confirm which one is major factor to affect present glacier change.

**HS02/08A/C24-007****1000****PREDICTION OF RIVER RUNOFF BY THE THE NORTH ATLANTIC OSCILLATION INDEX**

Joanna K. POCIASK-KARTECZKA, ZENON NIECKARZ, Danuta LIMANOWKA (Hydr. Dept., Institute of Geography, Jagellonian University)

The North Atlantic Oscillation has been identified as one of principal factor controlling the weather conditions over the middle and high latitudes of the Northern Hemisphere. It has controlled the regional temperature and precipitation variability (Bonsal *et al.* 2001, Hurrell & Van Loon 1997, Shabbar *et al.* 1997). The meteorological conditions in Poland are influenced also by the NAO (Wibig 2000). Therefore, it creates a possibility of a non-directly influence of NAO on the river runoff. This relationship has not received enough of scientific attention. Three river basins runoff was analysed: Skawa (835 km<sup>2</sup>), Dunajec (4 341 km<sup>2</sup>) and Wistula (31 846 km<sup>2</sup>). All basins are located in the Carpathian Mts. Data sets of long-term mean monthly, seasonal, minimum and maximum values of river discharge were available for 1951-2000 and taken into consideration. And, the winter Hurrell's NAO index and the Rogers's NAO indexes respectively. The NAO conditions over the period 1951-2000 were very differentiated, and two particular air-circulation epochs was analysed separately also: 1951-1970 and 1971-1995 (Marsz, Styszyńska 2001). On the base of analysis of the Rogers's and Hurrell's indexes and the Carpathian river discharge, some relationships were identified. The present analysis of the NAO Hurrell's and Roger's indexes and the Carpathian rivers discharge demonstrates very interesting large-scale connections: the positive NAO episode in winter are associated with low discharge in the summer and in the beginning of the autumn. The most remarkable relationships were obtained in the analysis performed over the atmospheric circulation epochs: mean annual NAO index explains 41% of variability of mean river discharge in summer time and 30% of variability of mean annual river discharge. There is a relationship between the winter NAO index and river discharge in August. Styszyńska (2002) stated similar relationship concerning NAO and the Warta Riv. (western Poland) discharge. She found also a link between winter NAO index and precipitation during late summer: the winter NAO index explains about 30% of precipitation variability in August next year (Styszyńska 2001). This delay of reaction of this part of Central Europe is noticeable. The article describes the possibilities of prediction of the river runoff in summer. Models of linear regression for estimation the river runoff in August were calculated. It may facilitate a prediction the August river runoff with a few months preceding. It may be stated that NAO plays an important role as indirect factor influencing river discharge.

**HS02/08A/C24-008****1045****UTILISATION COUPLEE DE MODELES HYDROLOGIQUES DE BILANS ET DE SIG POUR EVALUER LES RESSOURCES EN EAU MOBILISABLES ET LEUR EVOLUTION SPATIO-TEMPORELLE. APPLICATION A L'AFRIQUE DE L'OUEST**

Jean-Emmanuel PATUREL, Eric SERVAT, Gil MAHE, Alain DEZETTER, Mahaman OUEDRAOGO (Institute of Research for Development (formerly ORSTOM))

L'Hydrologie Régionale vise et permet de répondre aux besoins de ceux qui, gestionnaires de projet, d'aménagements, décideurs et autres, travaillent généralement une grande échelle d'espace. Celle-ci est, en effet, celle de la mobilisation et de la planification en termes de ressources en eau. Le travail présentici couple des modèles hydrologiques un Système d'Information Géographique, afin d'analyser l'impact de la péjoration climatique observée depuis plus de 30 ans en Afrique de l'Ouest sur ces lames d'eau écoulées et donc sur la ressource en eau disponible et mobilisable. En fonction de l'objectif visé une grille régulière de mailles de dimension 0.5°x0.5° et un pas de temps mensuel ont été retenus. Un travail préparatoire a abouti à la sélection de modèles Pluie-Débit de bilans simples et robustes (GR2M, Water Balance Model modifié Yates) nécessitant des données d'entrée peu nombreuses et assez facilement disponibles en Afrique : précipitation, évapotranspiration potentielle et des valeurs de capacité rétention en eau des sols. On simule alors, pour chaque maille et indépendamment les unes des autres, et pour chaque pas de temps, la lame d'eau écoulée totale. Les modèles de bilan hydrologique sélectionnés permettent d'atteindre des niveaux de performance très satisfaisants. Dans les tests réalisés, aucun des modèles ne présente une supériorité nette par rapport aux autres. Cependant, pour les modèles GR2M et WBM, les résultats obtenus sur certains bassins versants se révèlent difficilement transposables d'autres, non jaugés, et pour lesquels on ne dispose d'aucune information. Le modèle de Yates permet, quant lui, de prédéterminer les valeurs de ses paramètres sans aucune procédure de calage et validation. Il s'appuie sur le schéma de classification "climat-végétation" de Holdridge qui autorise une prédétermination des paramètres l'aide d'une méthode empirique précédemment appliquée à la région étudiée. La cartographie des lames d'eau écoulées mensuelles et annuelles rend possible, d'une part, de dresser une répartition spatiale des écoulements l'échelle régionale et, d'autre part, d'apprécier l'impact de la variabilité du climat sur les ressources en eau. En superposant ces grilles les contours des bassins versants, l'écoulement total l'exutoire d'un bassin est, en effet, obtenu par l'addition des contributions élémentaires pondérées des différentes mailles qui les constituent. Ce travail a permis de s'intéresser la sélection de modèles pluie-débit opérationnels en Afrique de l'ouest. Il a également conduit mener un travail de fond quant l'influence des données disponibles sur les résultats obtenus en aval d'une modélisation hydrologique. Cette étude a aussi souligné l'évolution des ressources en eau en Afrique de l'ouest durant les dernières décennies, mettant l'accent sur la baisse des ressources mobilisables, ce qui est particulièrement pénalisant dans des pays du Sud où l'économie repose principalement sur l'agriculture.

**HS02/08A/C24-009****1100****GLOBAL WATER RESOURCES ASSESSMENT UNDER CLIMATIC CHANGE USING TRIP**Taikan OKI<sup>1</sup>, Yasushi AGATA<sup>2</sup>, Shinjiro KANAE<sup>3</sup>, Katumi MUSIAKE<sup>3</sup>, Takao SARUHASHI<sup>1</sup> (\*Research Institute for Humanity and Nature, <sup>2</sup>JST/CREST, <sup>3</sup>Institute of Industrial Science, U of Tokyo, <sup>4</sup>The NEWJEC, Inc.)

Anticipated water scarcity in the first half of this century is one of the most concerned international issues to be assessed adequately. However, even though the issue has an international impact and world wide monitoring is critical, there are limited number of global estimates at present. In this study, annual water availability was derived from annual runoff estimated by land surface model using Total Runoff Integrating Pathways (TRIP) with 0.5 degree by 0.5 degree longitude/latitude resolution globally. Global distribution of water withdrawal for each sector in the same horizontal spatial resolution was estimated based on country-based statistics of municipal water use, industrial water use, and agricultural intake, using global geographical information system with global distributions of population and irrigated crop land area. The total population under water stress estimated for 1995 corresponded very well with former estimates, however, the number is highly dependent on how to assume the ratio how much water from upstream of the region can be considered as "available" water resources within the region. It suggests the importance of regional studies evaluating the water quality deterioration in the upper stream, the real consumption of water resources in the upper stream, and the accessibility to water. The last factor should be closely related to how many large scale water withdrawal schemes are implemented in the region. Further studies by an integrated approach to improve the accuracy of future projections on both the natural and social sides of the water resources should be promoted. About the future projection of the global water resources assessment, population growth, climatic change, and the increase of water consumption per capita are considered. Population growth scenario follows the UN projection in each country. Change in annual runoff was estimated based on the climatic simulation by a general circulation model by the Center of Climate System Study, U of Tokyo, and the National Institute for Environmental Studies, coupled with TRIP. The increase in unit consumption of water was related to the predicted growth of GDP. With the increase of population only, future population under strong water scarcity, with water scarcity index is larger than 0.4, will increase by 90% in 2050 compared to the current situation in 1995. Consideration of the climatic change due to the global warming will relax this situation, and only 74% will be under the strong water scarcity according to the future projection used in this study.

**HS02/08A/C24-010****1115****FORECASTING RUNOFF WITH COMBINED MODELS OF ATMOSPHERIC BEHAVIOUR AND RIVER BASIN RESPONSE: A CASE STUDY FROM SOUTHERN BRAZIL**CARLOS E.M. TUCCI<sup>1</sup>, Walter COLLISCHONN<sup>1</sup>, Pedro L. DIAS<sup>2</sup>, Robin T. CLARKE<sup>1</sup> (Instituto de Pesquisas Hidráulicas, <sup>2</sup>University of São Paulo, Brazil)

Over 90% of Brazil's energy demand is supplied at present by hydropower. It is therefore essential for purposes of future planning to have good estimates of reservoir inflows, and the longer the lead-time of streamflow forecasts, the more distant is the planning horizon for decisions concerning the costing, production and distribution of power. Whilst it is relatively easy to forecast river basin response to precipitation that has already fallen, forecasts for periods beyond this immediate response time must be based upon estimates of future precipitation. This paper describes the results of work which combines forecasts of future rainfall given by a model of global climate with a detailed, distributed model of river basin response in the Brazilian part of the River Uruguay basin, an area of intensive hydropower production. The work required close collaboration between meteorologists and hydrologists. Comparison of predicted and observed rainfall over the period of model calibration showed that it was necessary to apply a statistical correction to eliminate a spatial trend in predicted rainfall. Data from a two-year period was set aside for model validation. Results show that the combined use of models of climate and river-basin response has been successful for the River Uruguay basin, in that the root-mean-square error (RMSE), between observed flows

and flows predicted by the combined model, is substantially less than the RMSE between observed flows and the historic mean monthly flows.

HS02/08A/C24-011

1130

#### INVESTIGATION OF FEEDBACK MECHANISMS BETWEEN SOIL-MOISTURE, LAND USE AND PRECIPITATION IN WEST AFRICA

Harald G. KUNSTMANN, Gerlinde JUNG (Institute for Meteorology and Climate Research, Karlsruhe Research Center)

The ongoing intensification of agriculture in West Africa leads to a change in surface and subsurface characteristics, which directly affects evapotranspiration rates. If these changed evapotranspiration rates in turn affect regional rainfall patterns, rainfed and irrigated agriculture in West Africa may face changed boundary conditions because rainfall can decrease in specific areas due to feedback mechanisms between land use change, soil moisture change and subsequent precipitation change. To identify the feedback mechanisms between land surface (soil and vegetation) and atmosphere, an extensive numerical experiment was carried out. We applied the mesoscale meteorological model MMS for the investigation of soil-moisture-precipitation and landuse-precipitation feedback effects in West Africa and in particular the Volta Basin (which covers 400,000 km<sup>2</sup> and extends from Burkina Faso to Ghana, Togo, Ivory Coast). For that purpose, MMS was prepared for runs in West Africa; optimal parameterisations for microphysics, cumulus parameterisations and radiation scheme were determined and validation was performed for a 30 day period. Great differences in the ability to quantitatively describe the observed meteorological data were found between different model parameterisations. The determined optimal parameterisation was found to reproduce observations well. The main research question was to what extent regional (intra-domain) evapotranspiration determines rainfall within the domains. We concentrated on the estimation of lumped precipitation recycling ratio and precipitation efficiency. The effect of decreased and increased initial soil moisture on the total rainfall after a four weeks period in summer 1998 was investigated. Scale dependent, positive as well as negative feedback mechanisms were found: while in the Volta Basin itself, an increase in initial soil moisture led to decreased precipitation, in West Africa as a whole, an increase led to increased total precipitation. Moreover, nonlinear effects were observed. Sensitivity of precipitation with respect to soil moisture was found very variable over space and takes on negative as well as positive values. Recent research revealed that land use change in the Volta Basin is basically characterised by a transition from cropland woodland mosaic into shrub land and finally into grassland. To investigate the effect of such a transition for the simulation period, we computed the total rainfall distribution under the assumption of the proposed land use substitution for the simulation period, *ceteris paribus*. Similar to initial soil moisture sensitivity, the precipitation change response was found to be very variable over space. Investigation of a locally differentiating precipitation ratio, determined from an iterative algorithm, showed much larger values for the recycling ratio than the lumped approach. This discrepancy shows the current research need for concepts which do not assume perfect vertical mixing of water molecules. The approach we follow for this task is the "Evapotranspiration tagging" which follows the path and the phase transitions of water molecules from its origin as evapotranspiration to their "final" return to the surface as precipitation. Preliminary results of the approach are presented.

HS02/08A/C24-012

1145

#### THE EFFECT OF DOWNSCALING TECHNIQUES ON WATER RESOURCE SCENARIOS FOR CLIMATE CHANGE

Johan ANDRÉASSON, Sten BERGSTRÖM, Bengt CARLSSON, L. Phil GRAHAM, Göran LINDSTRÖM (Swedish Meteorological and Hydrological Institute)

The prospect of climate change is an issue of high importance regarding future water resources. About 50% of Sweden's electric power production is generated by hydropower, which raises questions about how a future climate will affect both the frequency of extreme runoff events and the seasonal river runoff. During the last decade there seems to have been more floods than experienced before, which furthermore adds to the question AELs this a result of climate change that we can see already today? Global Climate Models (GCMs) are used as a tool to create scenarios on what kind of changes in the future climate we might expect. However, the typical horizontal resolution of GCMs is 200-300 km, which tends to greatly smooth the geographical features of the earth's surface. There is therefore a need for more detailed information when studying the climate change effects on a regional scale, as is the case when one wants to estimate the effects on single catchments. Downscaling of GCMs, to increase the resolution over a limited region, can be done either by use of a regional climate model (RCM) or by statistical downscaling of the GCMs. Although all of these techniques are common, they are seldom compared. In this paper, water resources simulations are presented for three Swedish catchments, ranging in size from 3 665 km<sup>2</sup> to 4 646 km<sup>2</sup>. The simulations were based on direct GCM model output, dynamical downscaling and statistical downscaling. The GCMs used were the HadCM2 and ECHAM4. The regional climate model, RCA, was developed at the Rosby Centre of the Swedish meteorological and Hydrological Institute. The hydrological model used was the HBV model. The statistical downscaling used long time series of sea level pressure, temperature and precipitation to find relationships between the GCM control run (present climate) and apply them on the GCM scenario simulations to obtain a more regionally oriented future climate result. Preliminary results indicate that the orographic influence of especially high mountains described in the dynamical downscaling has an effect on the outcome of the water resources studies. The ensemble of simulations further provides a measure of the uncertainty in assessing the future water resources in a changing climate. **Acknowledgements** The authors are active participants in the Swedish Regional Climate Modelling Programme (SWECLIM), which is funded jointly by the Swedish Foundation for Strategic Environmental Research (MISTRA) and the Swedish Meteorological and Hydrological Institute (SMHI).

HS02/08A/C24-013

1200

#### GENERATION OF RAINFALL SCENARIOS USING DAILY PATTERNS OF CHANGE FROM GENERAL CIRCULATION MODELS

Timothy Ives HARROLD (CSIRO Atmospheric Research)

Climate change under global warming conditions can be simulated using General Circulation Models (GCMs), which give results at regional scales, with a grid square resolution typically of the order of 200km in each direction. However, it is changes in local climates, below the resolution of the GCM outputs, that will determine the impacts on water resources. Downscaling of the GCM outputs is therefore required to produce rainfall scenarios at scales relevant for hydrological impact studies. One of the simplest, and most widely used, techniques for generation of "climate change impacted" rainfall is to perturb observed records of point rainfall by the average change in GCM grid square rainfall from current to future conditions, calculated on a monthly basis. In this simple approach, all of the daily values occurring in a given month are scaled by the same percentage, regardless of the magnitude of the rainfall. This paper proposes a modification of the perturbation approach, that uses a daily pattern of change in the ranked rainfalls from the GCM, and then scales the

ranked point daily rainfall by this pattern of change. This new approach can produce sequences of "climate change impacted" point daily rainfall that are very different in magnitude to sequences that are produced by simpler perturbation methods, especially in terms of rainfall that will produce runoff. We argue that the proposed method is superior, because it produces sequences that are consistent with what the GCM is saying about changes in extreme daily rainfalls and changes in the frequency of wet days.

HS02

Monday, July 7 - Friday, July 11

#### WATER RESOURCES SYSTEMS: GLOBAL CHANGE, RISK ASSESSMENT AND WATER MANAGEMENT (ICWRS, ICASVR, ICSW, ICWQ)

Location: Site C, Room 24

Tuesday, July 8 PM

Presiding Chairs: D. Rosbjerg

HS02/08P/C24-001

1400

#### CAUSAL RELATIONSHIPS BETWEEN LAND USE CHANGES AND WATER QUALITY – A CASE STUDY FROM NIAH CATCHMENT, SARAWAK, EAST MALAYSIA

Tina Svan HANSEN (Institute of Geography, University of Copenhagen)

Over the past decades, successive waves of land use changes have taken place in the coastal zone of Sarawak, Malaysia. Large forest areas have been logged and gradually the same land areas have been converted into oil palm plantations. This paper presents results from an ongoing Ph.D. study in the Niah River Catchment, which is located in the northern part of the coastal zone of Sarawak. The study aims to relate different types of land use changes to water quality changes in the same catchment area. Land use changes are identified by means of satellite images, plantation maps and logging concession maps from the past thirty years. These land use data are related to historical data on water quality, which are provided by the institutions collecting data on water quality in Sarawak, i.e., Public Works Department, Department of Environment and the Natural Resources and Environment Board. The long-term historical data are supplemented with recent water quality data from individual local oil palm plantations in the catchment. In addition, water quality data are currently being collected from the major land use types in the area i.e. oil palm plantations, logged forest and shifting cultivation. Preliminary results show that over the past thirty years large forest areas have been logged and gradually replaced by oil palm plantations in the interior areas of the catchment. In 2001, oil palm plantations occupied more than 40% of the catchment area upstream of the local water treatment plant. In the same time period, the agricultural production in the local shifting cultivation and small scale farming systems have been intensified with the consequence of increased and more frequent use of fertilizers and herbicides. Preliminary results on changes in water quantity and quality indicate heavier and more frequent flooding down-stream after the 'emergence' of large oil palm plantations upstream in the mid eighties. In addition, a trend can be identified towards a decreasing pH-value and increased TSS and nutrients levels.

HS02/08P/C24-002

1415

#### CHEMICAL CHARACTERISTICS OF SURFACE WATER IN ORAMIRIUKWA AND ONUKWU RIVERS AZARAEBELU, OWERRI

Ibe Kasimir MADUABUCHI, A.I. EGBUJOR (Department of Geology, Federal University of Technology)

The catchment area of the Oramiriukwa and Onukwu Rivers are within the sandy formation of the coastal plain sands of the Benin formation (Miocene - Recent). Soil type is lateritic sand. The study has been carried out by conducting a short term hydrochemical analysis of the surface water (Oramiriukwa and Onukwu Rivers) and land pollution survey around the rivers. The partial distribution of contaminants/pollutants due to poor land use systems and human activities were investigated, thus emphasizing integrated planned development as a preventive measure for arresting pollution levels in fast-growing urban centers. Metallic, non-metallic ions, total dissolved solids, chemical oxygen demand and physical parameters were analysed for the surface water samples and the results were evaluated in the light of World Health Organisation standard (WHO) and found good/admissible for human consumption. They are also good for irrigation purposes.

HS02/08P/C24-003

1430

#### MODELING NITROGEN DYNAMICS IN AN AGRICULTURAL-FORESTED CATCHMENT

Baolin SU<sup>1</sup>, So KAZAMA<sup>1</sup>, Minjiao LU<sup>2</sup>, Masaki SAWAMOTO<sup>1</sup> (<sup>1</sup>Department of Civil Engineering, Tohoku University, <sup>2</sup>Department of Civil and Environmental Engineering, Nagaoka University of Technology)

A spatially distributed nitrogen simulation (DNS) model has been developed to simulate nitrogen dynamics in catchments. The model can simulate hydrological process and various nitrogen processes in grid cell level continuously by considering plant uptake, atmospheric wet depositions, fertilizer application, mineralization, nitrification and denitrification, and point sources if any. The hydrological component of DNS model is based on the distributed Xinanjiang (DXAJ) rainfall-runoff model, in which the whole catchment is divided into square grid cells and runoff generation component of the Xinanjiang model is applied to estimate the surface and sub-surface runoff in each grid cell. Rainfall input is distributed to each grid cell using distance-weighted rainfall, and evapotranspiration is adjusted to each grid cell considering air temperature variation depending on elevation. Parameters for runoff calculation are specified to land use level. An optimal routing order approach is used to implement the distributed routing through a routing order sequential file, which consists of information necessary for routing calculation, such as routing order, hydraulic attributes and hydrological connectivity of each grid cell. The nitrogen component of DNS model simulates daily average nitrate- and ammonium-nitrogen concentration of stream water considering key sources and sinks which are represented by a series of first order kinetic equations and various external inputs. In particular, plant growth indexes for land use class forest and agricultural lands are incorporated to simulate the plant uptake variation in according to seasonal vegetation cover variations. Model calibrations showed that there is a good agreement between simulated and observed stream nitrate-nitrogen concentration. Sensitivity analysis showed that the plant uptake is the key sink of nitrogen, whereas the agricultural fertilizer application is the key source of nitrogen during the fertilizer addition period. Wet deposition makes a small contribution to the stream nitrogen concentration.

HS02/08P/C24-004

1445

**ASSESSMENT OF GROUNDWATER QUALITY AND CLIMATIC WATER BALANCE STUDIES IN PAGERU RIVER BASIN, ANDHRA PRADESH, INDIA**

Shakeel AHMED (I.F.C.G.R., NATIONAL GEOPHYSICAL RESEARCH INSTITUTE,)

Pageru River is located in Cuddapah district, Andhra Pradesh, India. Cuddapah is a chronically drought prone area in terms of water resources with inadequate and highly erratic rainfall resulting poor groundwater potential. The scanty surface water resources for drinking and agriculture, has made no dispute to rely more on groundwater resources in the district. Total annual rainfall and its distribution in space and time of the season are responsible for a success. This means the intensity of rainfall and its variability both in kharif (June to September) and Rabi (October to January) seasons are guiding factors. Climatic water balance and droughts of Pageru River Basin has been prepared by using rainfall data of eight rain gauge stations located in and around the basin. The values of rainfall and temperature have been collected and the water balance parameters have been computed on the basis of Thornthwaite and Mather method. In addition 99 water samples were collected for both pre and post-monsoon seasons and analysed for major ions to assess the water quality in relation to agriculture and domestic uses in the basin. Total area of the basin is 480 Km<sup>2</sup> lies between Lat 14° 03' 04" and 14° 39' 51" N and Long 78° 09' 12" and 78° 41' 32" E. The drainage pattern of the basin is dendritic in nature. The rock formations of the study area are classified as Cuddapah super group and Kurnool group. The important rocks consist chiefly of quartzite, limestone and shale. The general climate of the basin is hot and semi-arid in nature. The temperature reaches high in the month of April and decreases gradually and reaches minimum in the month of December. The River Basin receives an average annual rainfall of 581mm with significant seasonal variations. The rainfall data for 105 years (1891-1995) of Kamalapuram station, which is located within the basin area, has been used to compute yearly water balance parameters, while for the remaining 7 stations monthly averages are used to compute the water balance parameters of the region. Based on computation of climatic water balance analysis indicates that the annual water deficit of the basin is 821mm. The maximum water deficit is observed during March and June months and it is minimum in the month of September. The analysis of the data revealed that the annual distribution is more controlled by the physiography of the region. A comparison of water balance and cropping pattern adopting in the villages indicate that the area under basin is only suitable for cultivation of drought resistant crops such as jowar (*Sorghum Bicolor*), ragi (*Eleusine Coracana*), bajra (*Pennisetum Typhoides*). Assessment of water samples from various methods proved that majority of the water samples is good either for drinking or for agriculture in both seasons.

HS02/08P/C24-005

1500

**EFFECT OF IRRIGATION ON GROUND WATER CHEMISTRY IN LOWER CHAMBAL COMMAND AREA, MADHYA PRADESH, INDIA**

L.P. CHOURASIA (Department of Applied Geology, Dr. H.S. Gour Univ)

The study area is a part of the Chambal and Sind river basin and falls Bhind and Morena districts of Madhya Pradesh, India. It is irrigated by the Chambal canal system. The area comprises of alluvium in which groundwater occurs under unconfined and semi-confined conditions. To determine the effect of irrigation on groundwater chemistry, forty-five ground water sample from non-irrigated area and forty five samples from irrigated area have been collected during. May June 1998 from the existing dug wells of the study area. The major cations and anions have been determined from the samples. The statistical analysis of these data suggests that the irrigations does have an effect on groundwater chemistry. At the 99% confidence level, the concentrations of the chemical constituents are much higher in irrigated area than the non-irrigated area. These areas are identical except in their agricultural development. Though most of groundwater of samples come under good water class for irrigation but some of them are unsuitable for irrigation. The processes associated with surface water irrigation involved in modifying the concentration of chemical constituents in groundwater are evaporation and transpiration, mineral dissolution, dissolution of fertilizers, mixing with existing groundwater, CO<sub>2</sub> uptake and ion exchange. In addition, Calcite precipitation is likely to be a control on Ca and HCO<sub>3</sub> concentrations at several stages. Although the method has only examined one "Snap Shot" in time, the approach to data analysis adopted here is simply enough to be incorporated as routine following field collection of data but it is representative of a longer-term average.

HS02/08P/C24-006

1515

**THE ORIGIN OF WATER SALINITY OF THE ANNABA COAST (N.E ALGERIA)**

Larbi DJABRI, R. LAOUAR, A. HANI, J. MANIA, J. MUDRY (11, Rue Asla Hocine, Annaba 23000, Algérie)

Water of wells located at the Annaba city coast are characterised by high salinity. The origin of this may be attributed to several factors such as the geological features of the region, the climate and the salted beach. A number of analyses have been carried out during October 1990, November 1998, December 1998, January 1999 and February 1999, in order to locate the origin of this high salinity. Principal component analysis show that the chloride-riche, Na-rich water is located nearby the sea. This indicate that seawater is the most likely contaminant of freshwater and that the sand can contribute highly to the observed high chloride contents. Our results also indicate that the salinity increases steadily when approaching the sea, and this indicates again the influence of marine water. Away from the coast, the observed Sr/Ca ratios (< 1) is due to the absence of the evaporitic formation which outcrops further south of the region.

HS02/08P/C24-007

1530

**LOWER NIGER DREDGING AND CUMULATIVE ENVIRONMENTAL CHANGE**

Shakirudeen Sule ODUNUGA, Tejuoso OLUFEMI, Fasona JOHNSON (University of Lagos)

The Niger-Benue waterway, with a cumulative water route distance of about 2,200km, provides a natural artery and has great potential for water transportation from the coastal area of Warri and port-Harcourt to the middle belt and from thence to the north-easter and north-wester frontiers of Nigeria. The long period of the neglect of the lower Niger has resulted in the blockage of the channel of the waterway. The blockage and seasonal fluctuation of the river has confined effective service of even small ferry to particular area and period of year. In view of these, the present project of dredging was conceptualized to improve the navigability of the water route so as to promote both local and international economic integration. Statistical measure of moments, regression and trend analysis were adopted for the understanding of the water resources dynamic of the lower Niger, while uncertainty in the water resource, processes as a result of large scale deforestation due to dredging activities was reduced through the adoption of water balance approach for the local catchment of the three selected stations (Onitsha, Lokoja and Baro). Ranges of parameters from about 20% to 15% reductive in Evapo-Transpiration contribution to rainfall at onitsha to

about 15% to 10% reductive of Baro were assumed. The response of the water resource to the expected change was estimated and the trend in water resources potential was properly determined. On the most critical issue of Least Available Depth (LAD's) for large scale shipping the water level duration analysis was adopted. The expected depths for the lower Niger at the three selection station were calculated / forecasted spatio-temporally and the freight movements for the forecasted water depth were suggested. The implication of the dredging on water demand, use and supply for the teeming population along the Niger valley was examined and suggestion were made for sustainable use.

HS02/08P/C24-008

1615

**IDENTIFYING HUMAN INDUCED PRESSURES AND THEIR IMPACT ON WATER RESOURCES - THE ASSESSMENT OF THE HYDROLOGICAL QUALITY IN RIVER BASINS**

Michael EISELE, Andreas STEINBRICH, Christian LEIBUNDGUT (Institute of Hydrology, University of Freiburg)

To maintain or establish a sustainable use of water resources the identification of human induced pressures on the hydrological system has to be combined with an assessment of its vulnerability. For this purpose assessment procedures, which integrate all relevant hydrological criteria on the catchment scale, are needed. The assessment procedure Hydrological Quality is a combination of tools, by which identification and quantification of human impacts on quantity and quality of water resources within a catchment can be carried out. Pressures on the hydrological system are assessed using criteria which are derived from commonly available data sets. Quantitative pressures on water resources are identified using criteria of land use structure, water use, water abstraction and transfer, storage volume of dams and reservoirs and river morphology. Pressures on water quality are characterized using criteria for land use, agricultural intensity, population density, sewage system and urban runoff. The vulnerability of the hydrological system towards quantitative pressures is described using stream flow coefficients and a spatially differentiated estimation of groundwater recharge. Additionally human induced alterations of runoff dynamics are evaluated using statistical methods and taking into account climatic effects. To link pressures on water quality with the chemical situation in surface and groundwater a spatially differentiated water and nutrient balance is calculated. Calibration and validation of parameter values (e.g. for nutrient losses) and model results (e.g. total runoff and concentration levels) are achieved using stream flow data and measured concentrations from rivers and groundwater wells. The procedure is applied in a set of meso-scale river basins (15 to 3000 km<sup>2</sup>) in South-West Germany. To examine the human impact, different scenarios (potential natural status, land use change, urban development) are calculated and compared to the actual status. To estimate the potential range of error in the predictions an uncertainty analysis is carried out based on the sensitivity of calibrated parameter values. In the paper an overview on the methodology and the results of the procedure will be presented. With the application of the assessment procedure Hydrological Quality a reliable estimation of the human impact on water resources can be achieved. Individual pressures on different parts of the hydrological system can be identified and quantified. Subsequently this information can be used to define options for the improvement of water resources management in a river basin.

HS02/08P/C24-009

1630

**ESTIMATING LAND COVER CHANGES AND ASSOCIATED ENVIRONMENTAL IMPACTS ON WETLANDS, BY COUPLING REMOTE SENSING AND HYDROLOGIC MODELING**

Ierotheos Z. ZACHARIAS, Elias DIMITRIOU, Theodoros KOUSSOURIS (NCMR)

Significant degradation occurred worldwide in ecologically significant wetland areas during the last century. Land use changes and associated hydrologic disturbances, mainly caused by human activities, is a common reason for this evolution. Thus, there is a need to identify and quantify potential impacts on wetlands from specific land use alterations in order to facilitate future environmental management and preservation activities. The particular scientific effort utilized remotely sensed data, GIS techniques and hydrologic modeling to estimate land use alterations during a 40-years period and simulate respective changes in hydrologic parameters such as overland and underground flow, infiltration, evapotranspiration and water storages on ground surface. Aerial photos of an intensely modified area from various human activities have been acquired concerning the years 1947 and 1986, elaborated with a GIS package and provided the land use maps for each period. These maps have been imported to MIKE SHE hydrologic model and two simulations have been developed (one for each period) by utilizing the same meteorological data so as to estimate and compare the differences in the aforementioned hydrologic parameters caused by the quantified land use changes. The results indicated significant variations in the hydrologic regime such as a considerable increase of agricultural land which caused a 6% increase in the annual evapotranspiration and a 10% increase in the water deficit of the soil profile. The urban development during the examined period, directed to an 11% increase in the annual overland flow and a 2% decrease in the underground flow towards wetland area. These indicative results together with the detailed modeling outputs illustrated substantial impacts on the regional hydrology and consequently on the wetland areas due to the observed land use changes.

HS02/08P/C24-010

1645

**A COMPARATIVE STUDY ON FLOW GENERATION MODELS FOR WATER RESOURCE PLANNING**Seung Yup RIEU<sup>1</sup>, Young-Oh KIM<sup>1</sup>, Dong Ryul LEE<sup>2</sup> (<sup>1</sup>School of Civil, Urban & Geosystem Engineering, Seoul National University, <sup>2</sup>Water Resource & Environmental Division, Korea Institute of Construction Technology)

The long-term water resource planning in Korea has been updated typically every 10 year based on so-called 'the water balance analysis. Predicting the water supply and demand for the basin being considered in a target year, the analysis simply estimates the possible water deficits within the basin, using a simulation model such as MODSIM. The common water resource performance criteria such as reliability, resiliency, and vulnerability can be calculated as the model output to assess the water deficit severity. The previous studies showed that the performance criteria were very sensitive to the choice of the future water demand and supply scenarios, especially the future streamflow scenario. Two approaches have been commonly used for the streamflow scenario in Korea. The first approach selected the driest year among the available 30-year historical data and calculated the performance criteria using this single series. For most of the Korean river basins, the lowest flow occurred in 1968. The second approach used the entire 30-year record and searched the worst criteria. For both approaches, the calculated criteria were considered as the 30-year water deficit indices but their uncertainties have been recognized to be large because the 30-year record is not long enough to overcome the sampling variability. Therefore, it becomes necessary to generate a large number of synthetic flow data in order to obtain reliable values of the performance criteria though the water balance analysis. In this study, we compare a



water and energy balances in mountain watersheds. However, the dependency of snow interception on tree species and the differences in the influence of snow interception on the energy and water balances are not well understood. In this paper, we discuss how intercepted snow above deciduous and coniferous forests affects water and energy balances. Intensive micrometeorological observations above and below the canopy were carried out in a deciduous (DF) and coniferous (CF) forest in mid-winter 1996-97 near Sapporo, on Hokkaido Island, Japan. The energy balances were analyzed based on the observations. The DF was composed mainly of ash and oak trees, and had a plant area index (PAI) of 0.9. The CF consisted of Yezo spruce, Akazeo spruce, and Todo fir, and the PAI was 5. The sensible heat fluxes above both the DF and CF were measured using the eddy correlation method, while the latent heat flux was evaluated using the band-pass eddy covariance method in the CF and the energy balance method in the DF. Since the amount of intercepted snow was large in the CF, but insignificantly small in the DF, the latent heat flux above the CF was larger than that above the DF, especially just after a snowfall. This demonstrated that variation in the amount of snow on a canopy due to differences in forest conditions affects the water and energy balances above the canopy. Furthermore, intercepted snow above the CF increased albedo, while the net all-wave radiation above the DF was larger than that above the CF. The effect of intercepted snow on the canopies caused more of the net all-wave radiation above the CF to be partitioned into the latent heat flux than into the sensible heat flux. Conversely, the net all-wave radiation at the DF was partitioned mostly into the sensible heat flux and snowmelt energy. This might cause differences in the location of energy exchange in CF and DF.

HS02/09A/C24-004

0945

## SOME PROBLEMS IN REGIONALIZATION OF INDIANA WATERSHEDS

A. Ramachandra RAO<sup>1</sup>, A. Ramachandra RAO<sup>2</sup> (<sup>1</sup>School of Civil Engineering, Purdue University, <sup>2</sup>Department of Civil Engineering, Indian Institute of Science, Bangalore - 560012, INDIA)

Because of the paucity of flood data, it is not always possible to use traditional methods of frequency analysis to arrive at estimates of flood values corresponding to specified recurrence intervals. Engineers use methods that are based on data from nearby stations. As watersheds in a region may have different responses to rainfall, hydrologists have sought to identify groups of watersheds that have similarity in flood producing mechanisms. The group of watersheds with similar hydrologic response constitutes a hydrologically homogeneous region. The procedure of identifying such regions is traditionally referred to as Regionalization. The basic objective of this paper is to address some problems concerning the use of cluster analysis methods for regionalization of watersheds. As no single procedure has been demonstrated to yield universally acceptable results, several methods of regionalization are in use. No information is available about the performance of these methods. In particular, problems which arose in the use of the Hybrid Cluster Analysis are discussed in this paper. Three hybrid-cluster algorithms, which are a blend of agglomerative hierarchical and partitioning clustering procedures, were tested in this study to determine their potential in delineating watersheds in Indiana, U.S.A., into regions that are homogeneous in hydrologic response. The hierarchical clustering algorithms considered for hybridization were Single linkage, Complete linkage and Ward's algorithms, while the partitioning clustering algorithm used is the hard K-means algorithm. The details concerning the data used for the study region are provided. The results from the hybrid cluster analysis models are reported and the problems encountered in deriving the final regions from the clusters are discussed. The results of the study are discussed and a set of conclusions is presented.

HS02/09A/C24-005

1000

## AN APPROACH TO CREATING LUMPED-PARAMETER RAINFALL-RUNOFF MODELS FOR CATCHMENTS EXPERIENCING ENVIRONMENTAL CHANGE

William Earl BARDSLEY<sup>1</sup>, Suxia LIU<sup>2</sup> (<sup>1</sup>Earth Sciences, University of Waikato, <sup>2</sup>Chinese Academy of Sciences.)

Many stream and river catchments are presently experiencing progressive hydrological change as a consequence of land use modification. The single-calibration approach to rainfall-runoff models is not appropriate in such circumstances because, in reality, the model parameter values will themselves be undergoing change through time. Such parameter trends can be incorporated readily in empirical statistical catchment models, but progressive recalibration of nonlinear lumped rainfall-runoff catchment models can be cumbersome because nonlinear model calibration remains something of an art. While still maintaining a link to physical hydrological processes, we present an approach to straightforward progressive model recalibration by way of a lumped-parameter finite-mixture distributional model for simulating hydrograph generation from rainfall events. The model contains just two nonlinear parameters and a large number of linear parameters. A single manual calibration is carried out to fix the values of the nonlinear parameters, with the linear parameters thereafter being progressively re-estimated over time by a standard automated procedure. This allows reliable convergence during recalibrations which implicitly incorporate the effects of catchment environmental changes via the linear parameter adjustments. The model might be applied, for example, as a flood warning technique for catchments with progressive land use change. Application of the model is illustrated with examples from river catchments in New Zealand and China which have experienced time-varying hydrological responses.

HS02/09A/C24-006

1045

## THE IMPACT OF CLIMATE VARIABILITY ON FLOOD RISK

Anthony S. KIEM, Stewart W. FRANKS (Department of Civil, Surveying and Environmental Engineering, University of Newcastle)

Recent research has highlighted the persistence of multi-decadal epochs of enhanced/reduced flood risk across New South Wales, Australia. Recent climatological studies have also revealed multi-decadal variability in the modulation of the magnitude of El Niño/Southern Oscillation (ENSO) impacts. In this paper, the variability of flood risk across NSW is analysed with respect to the observed modulation of ENSO event magnitude. This is achieved through the use of a simple index of regional flood risk. The results indicate that cold ENSO events (La Niña) are the dominant drivers of elevated flood risk. An analysis of multi-decadal modulation of flood risk is achieved using the inter-decadal Pacific Oscillation (IPO) index. The analysis reveals that IPO modulation of ENSO events leads to multi-decadal epochs of elevated flood risk, however this modulation appears to affect not only the magnitude of individual ENSO events, but also the frequency of their occurrence. This dual modulation of ENSO processes has the effect of reducing and elevating flood risk on multi-decadal timescales. These results have marked implications for achieving robust flood frequency analysis as well as providing a strong example of the role of natural climate variability.

HS02/09A/C24-007

1100

## COULD THE GLOBAL WARMING CAUSE THE LAST FLOODS OF TISZA RIVER?

Istvan KONTUR<sup>1</sup>, Andras BARDOSSY<sup>2</sup>, Balazs CZENTYÉ<sup>1</sup> (<sup>1</sup>Technical University of Budapest, <sup>2</sup>University of Stuttgart)

The last 4 years on the Hungarian part of the Tisza river there experienced the highest ever flood peaks of the more than 100 years of observations series. The purpose of this paper is to analyze the possible causes of these floods and establish methodologies for the assessment of design floods. The water system of Tisza has two main typical properties: its system is forked and has several subsidiary streams and the other is when the river gets on plain area the slopes of the riverbed reduces to a few centimeters on each kilometer. The watercourses forming a fan lean against the east-north-eastern crags of Carpathians collect precipitations water of fronts coming from south and west. A large amount of extreme situations is conceivable because each cyclone effects each part of catchments differently. The first task is to identify the common meteorological features occurring prior to floods. Large-scale atmospheric circulation patterns and specific humidity are considered for this purpose. The time series of these variables shows non-stationary behavior. On the other hand the Tisza river basin experienced major changes due to anthropogenic influences during the last 150 years. Substantial changes in the river course affected the flow times and the interactions of the flood waves coming from different subcatchments. Land use changes have also affected the flood production. The effects of these changes are quantified using simplified models. The time series of circulation patterns is investigated for the frequencies of the patterns and their durations. Further the Markov transition matrices are investigated to see if changes in typical circulation pattern sequences occurred. The relationship of the circulation patterns and discharge changes helps to identify the amount to which climate change or climate fluctuations are responsible for the unusual behavior of the Tisza river.

HS02/09A/C24-008

1115

## EXTREME PRECIPITATION AND FLOODS IN THE CHANGING WORLD

Zbigniew W. KUNDZEWICZ (Research Centre of Agricultural and Forest Environment, Polish Academy of Sciences, Poznan, Poland)

In recent decades, flood losses have shown a rapid rising tendency worldwide, which can be linked to socio-economic and climatic factors. Increase in the flood risk is also foreseen in the future. In the present contribution, existing information on changes in extreme precipitation and river flow has been reviewed, in the context of the past-to-present records and future scenarios. Several non-climatic factors exacerbate flood hazard, such as the land-use changes: deforestation and urbanization; and river regulation, which reduce the available water storage capacity. Demographic pressure causes encroachment of informal settlements into hazardous locations in floodplains, e.g., around mega-cities in developing countries. Over-reliance on the safety provided by flood control works enhances accumulation of wealth in endangered areas. However, when a levee breaks, flood losses are higher than they would have been in a levee-free case. Climate impacts contribute considerably to the increase of flood exposure. As the atmosphere's water holding capacity grows with temperature, the possibility of intensive precipitation also increases. Higher and more intense precipitation has been already observed in many areas of the globe and this trend is expected to be even more pronounced in a future, warmer world. In a number of studies, floods have been found to become more frequent and intense, and continuation of this tendency is foreseen for the future. Yet, it would be a gross oversimplification to state that floods have uniformly exhibited growing trends everywhere. Results of some well documented studies demonstrate reduction of flood flows in several locations, or else reduction in some amplitude categories, leading to the conclusion "generally wetter but less extreme". Adverse effects on floods have already been observed due to changing climatic variability, and they are also projected to amplify. The frequency and intensity of El Niño-Southern Oscillation (ENSO) have been unusual over the last decades. Warm phase of ENSO, i. e. El Niño, during which precipitation and floods in several locations occur more frequently, has become more frequent, persistent and intense. In general, changes in flood frequency are complex, depending on the generating mechanism, e.g., rainfall vs snowmelt. It is a robust finding that seasonality of floods has changed in the warmer world. Increase in floods in mid and high latitude winters (due to more frequent, and more intense, wet spells; with rain rather than snow), earlier high spring flows e.g., in Europe, and decreasing ice-jammed floods have been observed. Despite the considerable investments into flood protection, in many countries there is a rising vulnerability to floods, as the increase of exposure to floods is faster than the growth of the adaptive capacity.

HS02/09A/C24-010

1130

## TESTING TRENDS IN ANNUAL PEAK DISCHARGE SERIES IN ISRAEL

Arie BEN-ZVI<sup>1</sup>, Benjamin AZMON<sup>2</sup> (<sup>1</sup>Israel Hydrological Service, <sup>2</sup>Israel Hydrological Service, Haifa, ISRAEL)

It is commonly presumed that development enhances flood discharges. Therefore, use of statistical properties of past records, for flood predictions in areas under development, might underrate the predicted values. This may be particularly important for arid and semiarid regions, where the discharges are sensitive to land use changes. However, temporal variations in the statistical properties of high discharges are little dealt with in the scientific literature. In this respect, Israel, which is located in such a region and underwent a widespread development during the recent decades, can provide a suitable case study. Results of this study are presented here. The study encompasses annual peak discharges at 64 hydrometric stations whose period of available records is between 24 and 57 years, and on average it is 47 years. Effects of abrupt major changes in watersheds of a number of stations, such as construction of dams and transferring lake and swamp areas into an arable land, were excluded from the study by ignoring the records prior to the appropriate change. Values of the coefficient of variation, for annual peak discharge series in Israel, are about a unity. Such high values hinder distinction between random and systematic changes in magnitudes of peak discharges. To gain reliable conclusions, the data underwent a variety of parametric and non-parametric tests. These include trend analysis with respect to time and comparisons between statistical values computed for the first and the second half of the period of observation at each station. No general trend is found for annual peak discharges in most areas of Israel, although a few local trends are observed. An exception appears for the Upper Jordan Watershed, where an overall decline is found. This trend is statistically significant for a number of stations located in that watershed. The decline is conceptually attributed to changes in the meteorological causes of high discharges and to the intensified water use within the State of Lebanon, where major tributaries of the Jordan River are originated. Another general result is the lack of relatively high discharges from 1970 to about 1985, vs. the very frequent occurrences of floods during the 1990s. Consequently, the variability of annual maximum discharges during the 1970s-1990s is substantially larger than during the 1940s-1960s. This effect is assumed resulting from fluctuations in meteorological conditions that generate high discharges. Another effect, attributed to a shift in cloud tracks, is the appearance of opposite trends in two neighboring stations.

HS02/09A/C24-011

1145

**REGIONAL FLOOD RISK - WHAT ARE THE DRIVING PROCESSES?**

Ralf MERZ (Institute of Hydraulics and Hydrology, TU Vienna)

The assessment of flood risk under changed conditions, such as changed land-use, climate, and hydropower operation, is difficult as traditional flood frequency analysis relies heavily on black-box statistical methods that use observed historic flood peak data alone. Under changed environmental conditions it is likely that these simple methods will fail to provide realistic estimates. An alternative is to use a process based approach. The main advantage of a process based approach is that it allows to factor in the various controls on flood risk and to examine changed controls explicitly. However, at the regional scale the identification of flood processes is hampered by data limitations. Also, in the same catchment extreme floods can result from different processes. We propose an event based flood process classification method that combines a number of data sources to address the data problem. Maximum annual flood data are combined with event based information on the atmospheric forcing and the catchment state. The latter is estimated by running a soil moisture accounting scheme for all the catchments over the entire study period. The procedure allows us to identify five catchment-scale flood driving processes. These are: synoptic rainfall, short duration rainfall, flash floods, rain-on-snow, radiation melt. The identification procedure is manual based on expert judgment. For each event, the expert decides the process type, based on an examination of synoptic maps of the state variables and the atmospheric forcing, and a set of rules. For example, the rule for radiation melt is of the form 'snow water equivalent > 10 mm and snow melt > 3 mm/day and rainfall < 1 mm/day'. We applied the new method to 500 catchments in Austria. The catchments exhibit very diverse climate and land-use characteristics, from low-land to alpine characteristics. The data set consisted of up to 30 years of data which led to a classification of a total of 10 242 flood events. The method classified 43, 27, 4, 21, 3% of the events into synoptic rainfall, short duration rainfall, flash floods, rain-on-snow, and radiation melt, respectively. We analysed the severity of the floods belonging to each process type with respect to flood seasonality, event characteristics (e.g. precipitation depth, runoff coefficient) and catchment characteristics (e.g. land-use, scale). This analysis provided useful information on the regional behaviour of floods of different magnitudes. The process classification can also be used in a more quantitative way by constructing compound flood frequency curves. The results indicate that the compound curves that use information on both the flood peaks and the process types extrapolate more accurately to large return periods than curves that use only information on the flood peaks. Ongoing work examines the potential of an automated method of process classification based on fuzzy rules. Preliminary analyses suggest that the automated method can mimic the manual process classification well. It is suggested that the automated method is also applicable to flood regimes in other regions.

HS02/09A/C24-012

1200

**MAXIMUM PRECIPITATION VALUES?**

Gerd TETZLAFF, Michael BOERNGEN, Manfred MUDELSEE, Armin RAABE (Institut of Meteorology, University of Leipzig)

Recent flood events in Germany initiated an debate on the causalities. In many opinions the climatic change effects were held responsible for the clustering of catastrophes as recorded in the media. Looking at central European historic flood events exhibited that major floodings are not restricted to recent periods. However, there is very little material available on the frequency and its changes through times, including even the actual times. Indirectly, it was often postulated to suppress flood totally. This however means to estimate a maximum catchment areal precipitation. There are published methods to achieve such an estimation. For the river Main these results were compared against the major flood event of 1342, the highest flood recorded in central Europe since the medieval ages. From the river levels the precipitation was estimated in several steps, applying a precipitation model as well. Finally, the average precipitation for the catchment areas of more than 2000km<sup>2</sup> amounted to about 200 mm. This value is somewhat larger than the ones found in the recent river Elbe floodings.

HS02/09A/C24-013

1215

**THE SCENARIOS OF CHANGE OF REPEATABILITY OF THE CATASTROPHIC PHENOMENA IN UKRAINE UNDER INFLUENCE OF GLOBAL WARMING (ON THE BASIS OF HISTORICAL RECORDS AND ANNALS)**

Svetlana G. BOYCHENKO (Department of meteorology and climatology, Kyiv Taras Shevchenko University)

The main aim of this research is to obtain quantitative estimations of the basic tendencies of change of repeatability of the catastrophic phenomena in Ukraine as a result of global warming and to work out scenarios of possible increase or decrease of their repeatability in first half of 21-th century on their basis. In this research were considered data, which obtained on the basis of the analysis of various historical records and annals (manuscripts). These records were very carefully conducted and described in monasteries, which were placed, in particular, on all territory of Russian plain. The following phenomena were considered: droughts, rainy summers, floods and high waters, cold winters, late springs, colds at the beginning of a summer, catastrophic thunderstorms, catastrophic storms etc. Therefore we use the names of these events, which have accepted in historical records and annals (manuscripts). But most sharply expressed events both on space scales and ecological and social consequences were selected. For reduction of the mistake caused mainly with the psychological factor at records and statistical sample of the data methods of a respective centering and normalization of empirical time series of repeatability of the climatic catastrophic phenomena were used. The statistical analysis of these data shows that the long-term dynamics of repeatability of the climatic catastrophic phenomena in the territory of Ukraine was not an ordinary stationary Poisson's flux of events. For example, grouping of events is precisely traced for some periods. It means that there is a factor, which essentially influences repeatability of the considered events. The hypothesis was proved that the fluctuations of temperature of Europe possibly could be such factor. These fluctuations are closely connected to fluctuations of the global thermal regime of our planet. Therefore this hypothesis means that a global warming or a global cooling can essentially influence the repeatability of climatic catastrophic phenomena on the territory of Ukraine. It is found that the repeatability of the considered events is a non-monotonic function of temperature fluctuations, namely: repeatability (frequencies) of catastrophic climatic phenomena in the territory of Ukraine was higher, when the global temperature was deviating in either direction from some optimum level (at global warming or cooling from some optimum level of global temperature). In this research are constructed semi-empirical model for rating of intensity of climatic catastrophic phenomena in Ukraine as function of index of climatic anomaly. This semi-empirical model can be used as a scenario of possible dynamics of repeatability of climatic catastrophic phenomena in the territory of Ukraine at the further global warming. Unfortunately there is no certainty that global warming caused by various physical mechanisms will lead to analogous environmental consequences (it is possibly that the present global warming is caused by anthropogenic amplification of the global greenhouse effect).

HS02/09P/C24-001

1400

**DATA ASSIMILATION IN THE MIKE 11 FLOOD FORECASTING SYSTEM USING KALMAN FILTERING**Dan ROSSBERG<sup>1</sup>, Jesper DAMGAARD<sup>1</sup>, Frands Søbjerg HANSE<sup>2</sup>, Henrik MADSEN<sup>2</sup> (<sup>1</sup>Environment & Resources DTU, Technical University of Denmark, <sup>2</sup>DHI Water & Environment, Agerø)

In recent years major floodings have occurred in a number of countries world-wide, e.g. Poland, Czech Republic, Germany, UK, China, Bangladesh and Mozambique. To reduce the loss of life and the damage to property hydrological models to forecast flow and water level in the river systems are often implemented. Usually measurements of water level or flow are available at different locations throughout the river system. By using these measurements it is possible to update the model results and obtain a better estimate for the initial conditions in the river system at the time of forecast. The updating procedure in the 1-D hydrological model MIKE 11, developed by DHI Water & Environment, was examined. The existing iterative flood forecasting updating procedure (FF) was compared with a newly developed ensemble Kalman filter updating procedure (KF). Unlike the FF the KF pays respect to the uncertainty associated with the model results and the data used for updating. The user provides MIKE 11 with estimates of model and measurement uncertainty and KF weights the information to obtain an optimal result in the least square sense. Using data from the extreme flooding event in 1999 in the Sesia catchment in the Piedmonte region in the north-western part of Italy, FF and KF were compared with respect to their ability to assimilate and forecast water levels. It was verified that both methods produced similar results at and downstream of the measurement stations, but that the KF was also capable of correcting the flow upstream the measurement stations. In most cases the model results were improved upstream when using KF compared to using FF, but at the expense of significantly higher computational costs. The model uncertainty in the KF was placed on the catchment runoff determined from the deterministic, lumped, conceptual rainfall runoff model NAM. To get realistic estimates of the model uncertainty, studies of the catchment runoff from the NAM model as a function of the uncertainties in input data (precipitation and temperature) and model parameters were conducted using Monte Carlo simulations. Due to the highly heterogeneous geology and varying topography in the model area the study was conducted on both a low land and a mountainous sub-catchment within the Sesia catchment. It was found that the coefficient of variation of the uncertainty on runoff from a mountainous catchment was 25-35 % whereas the value was somewhat lower, 15-25 %, in a low land catchment due to the higher response time. Using these values in MIKE 11 reasonable uncertainty estimates of the predicted water levels in the river system were obtained.

HS02/09P/C24-002

1415

**A CONSENSUS REAL-TIME RIVER FLOW FORECASTING MODEL FOR THE BLUE NILE RIVER**Asaad Y. SHAMSELDIN<sup>1</sup>, Kieran M. O'CONNOR<sup>2</sup> (<sup>1</sup>Department of Civil Engineering, University of Birmingham., <sup>2</sup>Department of Engineering Hydrology, National University of Ireland, Galway, Galway)

The Blue Nile, one of the main tributaries of the River Nile, which is the longest river in the world, is a trans-boundary river. Originating in Lake Tana in the Ethiopian plateau, which is located in East Africa, it has a basin area of 324,530 km<sup>2</sup>. Contributing about 59 % of the annual flow of the River Nile, it is regarded as the main source of floods on that river. Such floods cause loss of life and massive scale damage to the agricultural sector and to property near the river. In the present paper, a consensus real-time river flow forecasting model for the Blue Nile River is presented. The essence of the consensus model concept is that the synchronous outputs (i.e. the discharge forecasts) of a number of structurally different river flow forecasting models are combined to provide an overall 'consensus' discharge forecast that would be more accurate and reliable than that of the best of the individual models contributing to the combination. The consensus model developed in the present paper uses the river flow forecasts of two individual real-time multiple-input single-output river flow routing models, the first of which is based on the structure of the linear transfer function model, the second having the structure of the multi-layer feed-forward neural network. Each of these two individual models uses the upstream inflows on the Blue Nile and the outflows of its major tributaries as inputs and has an in-built forecast updating procedure. The final outputs required are the real-time river flow forecasts on the Blue Nile upstream Khartoum, the capital city of Sudan. Both the weighted average method and the neural network method are used to combine the forecasts of these two models in order to produce the consensus real-time river flow forecasts. Nineteen years of daily flow data are considered in the study; the first thirteen years being selected for model calibration/training, while the remaining six years are used for model verification. The results indicate that the consensus model can successfully be employed for real-time river flow forecasting on the Blue Nile River, at Khartoum. The results also confirm that the forecasts of the consensus model are indeed better than those of the best individual model used in producing the consensus forecasts, thereby vindicating the consensus concept. Thus, the consensus model can be used as an effective tool for flood forecasting and hence as a component of a decision support system for the mitigation of the hazardous impacts of the floods of the River Nile.

HS02/09P/C24-003

1430

**PLICATION OF DYNAMIC-STOCHASTIC MODEL OF RUNOFF GENERATION FOR ESTIMATING OF EXTREME FLOOD RISK IN A BASIN WITH LAND-USE CHANGE**

Lev S. KUCHMENT, A.N. GELFAN, V.N. DEMIDOV (Water Problems Institute of Russian Academy of Sciences)

A coupling of a physically based model of runoff generation with the Monte-Carlo simulation of the model inputs is applied to obtain flood series and estimate flood characteristics frequencies for a river basin with changing land-use. The model of runoff generation is based on the finite-element schematization of river basin and includes the description of the following hydrological processes: snow cover formation and snowmelt, freezing and thawing of soil, vertical soil moisture transfer and evaporation, overland and channel flow. The Monte-Carlo simulation of snowmelt runoff is based on stochastic models of daily precipitation series, daily air temperature and daily air humidity deficit (for continuous modeling during autumn-winter-spring seasons) or statistical distributions of snow water equivalent, depth of frozen soil, and soil moisture content before snowmelt (for modeling during only snowmelt flood events). The daily precipitation consists of a model of daily precipitation occurrence (a first-order Markov chain is applied) and gamma distributions of daily precipitation amounts. Because of the strong autocorrelation in the air daily temperature series, for modeling the daily temperature the fragment method was applied. The histogram of daily air humidity deficit values was fitted by lognormal distribution. The distributions of snow water equivalent, depth of frozen soil, and soil moisture content before snowmelt were constructed on basis of calculations which were carried out with help of the

physically based model of snowmelt runoff generation. To simulate the rainfall runoff, the statistical distributions of precipitation amounts, precipitation durations, durations of dry periods, and mean air humidity deficit for dry periods were used. The case-study carried out for the Seim River basin situated in the south-western part of Russia (the catchment area is 7460 km<sup>2</sup>). The 20-years hydrometeorological measurement series have been used for calibration and verification of the dynamic part of the model (5 parameters have been calibrated); the 34-years series have been used for construction of the stochastic part. The calculated exceedance probabilities of the peak discharge were compared with ones calculated using 61-years runoff data. The good correspondence of the measured and calculated values have been obtained. The developed dynamic-stochastic model was applied for estimation of changing exceedance probabilities of runoff characteristics at three scenarios of land use in the Seim river basin (for the beginning of the twentieth century, for the present time, for future). Problems of uncertainty in estimating of extreme snowmelt flood characteristics have been investigated for continuous modeling of flood series and for event flood approach.

HS02/09P/C24-004

1445

#### DECISION SUPPORT SYSTEM FOR FLOOD CONTROL AND ECOSYSTEM UPGRADING IN RED RIVER BASIN

Martijn J. BOOIJ, C.B. VREUGDENHIL (Department of Civil Engineering, University of Twente)

Flood disasters cause massive losses of human lives and immense damage to the infrastructure and economic activities in the Red River basin in Vietnam and China. These disasters result not only from the climatological circumstances, but are also caused by human development. The ecosystem has been seriously disrupted by the rapid population growth and by the uncontrolled development of industrial and urban centres. This has led to deforestation and changes in the ecosystem, which in turn increased the flooding risk. The severity of the floods can be mitigated by adopting suitable measures for flood control and for preservation and sustainable upgrading of ecosystems. These measures should take into account the social, economical and ecological consequences. Short term measures include flood diversion, rescue actions and prevention of unexpected dyke break and inundation in important urban and industrial zones. Here, the emphasis is on the long term, with measures such as reforestation, the construction of reservoirs in upstream areas and a controlled development of urban and industrial centres. The objective is to develop and apply a system to support decisions concerning the selection of a suitable combination of measures, considering all important consequences. This objective is achieved by carefully selecting the most appropriate model environment for the decision support system (DSS). Next, the hydrological, hydraulic and socio-economic models were constructed in a consistent way taking into account the characteristics of the measures, spatial and temporal scales, future scenarios and the project objectives. The thus obtained DSS and its components were tested for a number of scenarios and time periods. Meteorological, hydrological, hydraulic and socio-economic data from several sources in Vietnam and China were used for this purpose. The main advantages of the chosen model environment are the spatial-temporal character, the built-in capabilities, the flexibility and the possibility to construct user interfaces appropriate for the model user. The DSS has a variable spatial resolution with a more coarse scale in the upstream part of the basin and a finer scale downstream, to account for example for the large spatial variability in flood damage in the river delta. The hydrological model is based on the concepts of the HBV model, while the hydraulic inundation model is a statistical parameterisation taking into account the elevation pattern, land use, dike location and water level. The socio-economic model is a conceptualisation of the socio-economic flows, allowing for migration between the economic sectors based on net revenues and land use. The appropriate measures are selected and optimised by evaluating their effects in the DSS and applying a simple linear programming model. Preliminary results suggest that a combination of measures in the upstream part together with dike heightening will be most preferable. However, large uncertainties complicate the distinction to be made between different measures.

HS02/09P/C24-005

1500

#### FLOOD CONTROL - ENVIRONMENTAL AND SOCIO-ECONOMIC ISSUES: A CASE STUDY IN THE DAY RIVER REGION IN VIET NAM

Dao Thi Anh PHAN<sup>1</sup>, Kaoru TAKARA<sup>2</sup> (<sup>1</sup>Institute of Meteorology and Hydrology, Hydro-Meteorological Service, Viet Nam, <sup>2</sup>Disaster Prevention Research Institute, Kyoto University, Japan)

Viet Nam has large systems of rivers and is one of the most disaster-prone countries in the world including river flooding. Viet Nam has appropriate policies, strategy and action to control floods and mitigate its damage and help people to recover after floods. Viet Nam also builds hydraulic works to prevent important zones of Viet Nam from floods. It leads to impact on changes of hydrological regime and water resources in some areas. Many researches on flood control have been done in Viet Nam. However, it is important to recognize that flood control has not been attached to the environmental and socio-economic issues in areas suffering from flood yet. This paper explores the environmental and socio-economic issues in areas suffered by floods including policy/strategy analysis related to flood control. Questions focused are: How floods affect the living, socio-economic development and environment? And how societies respond and adapt to the above problems? Based on these points, a case study in the Day River region, which belongs to the Red River Delta of Viet Nam will be discussed. The Day River region has an important position for socio-economic development in the Red River Delta. The area borders the capital city of Hanoi and many important cities, towns and economic, politic centers of the country. Therefore, a project on flood diversion in the Day River region was approved by the Viet Nam Government in 1999. The findings would provide comprehensive understanding about the environment and socio-economic condition based upon an integrated approach for the decision-makers and managers in planning/management and reasonable use of water resources and in the flood control in this region.

HS02/09P/C24-006

1515

#### RISK ASSESSMENT FOR DIVERSION OPEN CHANNEL CLOSURE OF THE THREE GORGES PROJECT IN THE YANGTZE RIVER

Caijun WANG<sup>1</sup>, Shenglian GUO<sup>1</sup>, Xiangrong TIAN<sup>1</sup>, Yonghua ZHU<sup>2</sup> (<sup>1</sup>College of Water Resources and Hydropower Engineering, WUHAN University, <sup>2</sup>College of Mathematics and Statistics, Wuhan University, Wuhan 430072 CHINA)

Three Gorges Project (TGP) located on the Yangtze River is the largest hydraulic project in the world. TGP commenced construction in 1994 and the diversion open channel will be closed in November 2002. The final closure will begin when the gap through which the river flows has been reduced along the axis of the fill to 120m by simultaneously dumping rock-fill from both banks. This paper mainly focuses on the assessment of the hydrologic and construction risks of the diversion open channel final closure. On the basis of daily flow data of Yichang hydrological station during 1877~2000 with 124 years of records and the different sampling methods, the Pearson type-III distribution, flow duration curve and Poisson procedure are proposed and applied to determine design flow discharge and assess the

hydrologic risks. The design flow discharges with 10300m<sup>3</sup>/s or 12200m<sup>3</sup>/s are finally recommended for diversion open channel closure. It is found that the maximum hydrologic risks are 15.47% (Nov. 23rd, 2002) and 14.31% (Nov. 16th, 2002) under the design discharge 10300m<sup>3</sup>/s or 12200m<sup>3</sup>/s respectively. The construction risk of the final closure is resulted from the randomness and uncertainty of some hydraulic variables, such as water head, flow velocity and discharge. The water head of the gap is regarded as the primary factor of the construction risk and a corresponding model is proposed and developed. One dimensional unsteady flow hydraulic model based on discharge and energy conservation laws are established and the value of water head, flow velocity and discharge is obtained for given design flow discharge. The water head of the gap is assumed as a random variable with normal distribution, and the construction risks of point and 95%-confidence interval estimate are calculated. The results show that the construction risk increases with the reduction of the gap width or water head increase. For 10300m<sup>3</sup>/s or 12200m<sup>3</sup>/s design flow discharges, the maximum construction risks (when the gap is 20m wide) are 18.6% or 13.6% respectively. These estimated hydrologic and construction risks are all satisfied Chinese guidelines of the Construction Design of Hydraulic and Hydropower Engineering. It is suggested the final closure be completed after Nov. 23rd, 2002 or during Nov. 16th to 23rd with 10300m<sup>3</sup>/s or 12200m<sup>3</sup>/s design flow discharge respectively. These recommendations have been adopted by the Three Gorges Project Development Corporation and used for the diversion open channel closure of TGP decision-making.

HS02/09P/C24-007

1530

#### GLOBAL CHANGE--RISK ASSESSMENT AND REAL TIME HYDROLOGICAL FORECASTING OF FOREST CONFLAGRATIONS FOR WATER MANAGEMENT

S. LOBANOV<sup>1</sup>, S. LOBANOV<sup>1</sup>, V. KULIK<sup>2</sup> (<sup>1</sup>Far Eastern Regional Hydrometeorological Research Institute (FERHRD), <sup>2</sup>CYPUM PTY LTD, P.O. Box 863, Canberra City, ACT, AUSTRALIA 2601)

The global change makes irrelevant many methods of risk assessment and forecasting. In particular, changing climate means a greater probability of forest conflagrations. This results in disabling of water supply watersheds and reservoir contamination. Old methods of meteorological forecasting of conflagrations will become less reliable, being based on correlations, obtained for a period of stable climate. EXISTING hydrological networks can be used for wild conflagration prediction. Runoff data allows the prediction of high fire danger earlier, with less overcaution, highlights the most dangerous watersheds and makes forecast more foolproof. In some cases hydroforecast improves the likelihood of prevention of a major disaster. This technique has certain DIFFERENCES from the standard meteorological methods: (1) It predicts bushfires not for an administrative or geographical region, but for a watershed-- so, a bushfire can be forecast for certain water supply reservoirs; (2) It allows forecast of the bushfire danger earlier and estimates of the amount of time available for active measures; (3) It is less overcautious, thus excluding most false alarm situations; (4) It is more accurate, simply because it uses hydrographical data, which is more representative than meteorological data; (5) It is more foolproof and less dependent on the errors of observations; (6) It depends less on the stochastic nature of summer rains and other meteorological elements. (7) It is simpler than any other method. There are two groups of PREDICTORS. (A) Early Predictors: (A1) Low flow; (A2) Change of the curvature of the recession curve from concave to convex (semi log paper); (A3) Accelerated recession. These early predictors can be used to estimate how many days there are before the critical fire danger starts (by an extrapolation of the recession curve). (B) Later Predictors: (B1) Stabilization of the runoff to a "zero flow" value; (B2) Steep rate of recession after intermediate minor rains; (B3) Convex recession after intermediate rains; (B4) Abrupt stabilization of the runoff to "zero flow" several days after a minor rain. The manifestation of these late predictors means that the probability of a bushfire has increased dramatically. This method allows a forecast of the CRITICAL fire danger, when a bushfire is almost inevitable. Experimental risk assessment and real time forecast were successful for water supply watersheds of Russia and Australia. Quite different tools may be used in any particular case, due to local customs, hardware and software. For example, in some cases a deviation from normal rainfall-runoff relationships (runoff-rainfall or water balance models) could be a good indicator. A conflagration is a very rare phenomenon and to collect sufficient amount of information for any development of the forecasting technique it is necessary simply to analyze more cases. We ask everybody who has in their disposal data on watersheds, affected by an intense bushfire, to try this simple technique, to develop it and to communicate their results.

HS02/09P/C24-008

1615

#### SUSTAINABLE GROUND-WATER EXPLOITATION

Hugo A. LOAICIGA (Department of Geography / UCSB Santa Barbara California 93106-4060 USA)

Sustainable ground-water exploitation defines indefinite extraction of potable ground water that preserves its quality, maintains its natural ecological functionality, and provides water for human use without creating environmental or geologic hazards. Sustainability is a difficult goal in view of local and global climate changes that might effect the rates of ground-water recharge and of population and economic growth that may change the rate of water extraction. Climate variability -and, in particular, protracted drought- pose additional challenges to sustainable ground-water exploitation. Several factors most coalesce in order to achieve sustainable ground-water management: (1) knowledge of the climate-recharge linkages that determine the status of storage in an aquifer; (2) understanding of the evolution of ground-water chemical, biological, and physical characteristics as a result of ground-water pumping; (3) development of alternative and substitute water sources to replace and supplement ground water; (4) creation of institutional and cultural practices of water use that are flexible and adaptable to changing conditions. This article provides examples of sustainable ground-water exploitation strategies in the United States. The examples cover physical (e.g., pumping, recharge) and non-physical (pricing, conservation) measures that have been implemented in stressed aquifers to maintain their integrity and yield in the long term.

HS02/09P/C24-009

1630

#### SUSTAINABLE WATER RESOURCES MANAGEMENT IN DRAGONJA CATCHMENT, SLOVENIA

Mitja BRILLY<sup>1</sup>, Lidija GLOBEVNIK<sup>2</sup> (<sup>1</sup>Faculty of Civil and Geodetic Engineering, University of Ljubljana, <sup>2</sup>Water Management Institute)

The Dragonja river catchment extends over two countries, Slovenia and Croatia. Historically, the area was important food supply area for the cities on the Trieste Bay shoreline. Due to intensive land use, erosion processes have been intensive. There have been more than 60 water mills on the area. Due to its weak socio-economic potential after the WWII, the area has been depopulated and agriculturally abandoned until recently. In 1991, the river Dragonja became the state border. Today, the area is developing again. There are a lot of conflict situations due to three doctrines that are being promulgated by different parties. The first doctrine is development of the area as drinking water supply and food production resource on sides, Slovenian and Croatian. The second is tourist development (airport extension, golf resort) of the valley. At the same time, the area is being planned to be

protected as Landscape Park. Though the processes of natural overgrowing have been intensive lately, the area still has not lost its traditional agricultural landscape character. There is a strong process of natural forestation on the abandoned agricultural lands on hill slopes. The hydrology of river change tremendously due landscape changes as impact of economical and social processes on the catchment. The river gained natural character due to abandonment of water mills and lack of any regulatory measures. At the same time there was strong impact of change of hydrological regime and lowering of erosion processes on the catchment surface and riverbank. The hydromorphological processes are different today due to past human involvement. Physical planning and use of natural resources should take into consideration trend analysis of river morphological character. This is even more important because the river is a bordering river between two countries. There are two main goals for promotion of sustainable development of water resources: analysis of scientific questions and development of national and international institutional and human resources capacities. The questions are long term impact of existing processes and impact of new development of the area, increasing of population and economical development. The issues are: 1) How to preserve the area as an important natural and cultural heritage area, manage sustainable development and protect the water resources. 2) How to manage river corridors and erosion spots to reasonably control hydrological characteristics and to protect endemic and other important flora and fauna species. 3) How to streamline and fulfill water demands in Slovenia and Croatia. 4) How to manage flood protection of coastal areas under development. and 5) How to propose suitable land use practices. The Slovenian and Croatian IHP Committees propose the Dragonja catchment for HELP initiative of UNESCO.

HS02/09P/C24-010

1645

#### CHANGES OF WATER RESOURCE AND COUNTERMEASURES IN CHINA

Yongjian DING, Jianping YANG, Rensheng CHEN (Cold and Arid Regions Environmental and Engineering Research Institute, Chinese Academy of Sciences)

As a country of monsoon climate, water resource supply depends on precipitation in the majority of China. General distribution of water resource is more south and less north in China. In ordinary monsoon and strong monsoon years, precipitation is plenty in north China. After the end of 1970s, due to remarkable climate warming, rapidly economic development after carrying out the reform and open policy, increasing population, quick urbanization process and so on, water resource in north China is in severe shortage conditions. Contradiction between supply and need of water resource is even worse. Economic loss took the shortage of water resource is significant Moreover the loss multiplies year after year. On the contrary, there occur flood disasters frequently because of excessive precipitation. In the face of the above conditions, on the one hand, measures took is as follows: to economize on water in everyday life, to develop saving rainfall style agriculture, and to utilize saving water technique in industry. On the other hand, surplus water in south China is transferred into north China to mitigate tense water resource in north China. At present the east line of the project of South Water North Transfer is constructing. The middle and west lines is discussing. Except for above the countermeasures, it is essential to pay attention on scientific management. If management and countermeasures took is inconsistent, the countermeasures cannot bring into play practical utility. So based on active assessment of water resource changes, effective countermeasures took, and enforcement of scientific management, limited water resources can be only used rationally and economic loss gave rise to by the shortage and the excessiveness of water resources can be only decreased as large as possible.

HS02/09P/C24-011

1700

#### MANAGEMENT OF INTERNATIONALLY SHARED GROUNDWATER RESOURCES IN SEMI-ARID AND ARID REGIONS ?THE NORTHERN AFRICAN AQUIFER SYSTEM

Tobias U. SIEGFRIED (Institute of Hydromechanics and Water resources Management)

Population growth, extension of irrigated agriculture, pollution of surface and groundwater and inefficient allocation are amongst the most prominent factors contributing to water shortage. The resulting stress on societies is multidimensional - from a non-equal distribution of water on the communal level to centre-periphery issues on the national level and up to international disputes over shared resources. What is needed is an intelligent management strategy of the water resources in order to prevent an escalation of existing and future conflicts of interest. This research project focuses on the Northern Saharan Aquifer System (SASS) shared between Algeria, Tunisia and Libya. In these countries agricultural policy in the last fifty years was largely determined by considerations of food security, self-sufficiency and import substitution practices. That, in addition to lacking political will to jointly manage the aquifer system as well as inadequate monitoring tools and sparse data have led to the present situation where global abstraction exceeds recharge approximately three times. According to planning provided by the individual states, this imbalance of the hydrological state of the system will further accentuate until 2050 where the ratio abstraction / recharge is estimated to surpass a factor of 15. With regard to quantity a simple "back of the envelope" calculation shows that the SASS constitutes a resource for exploitative use for many centuries to come. However any adherent of this position has to be aware that the approach of pursuing purely exploitative strategies comes at a price economically, environmentally and socially speaking. Therefore a systemic approach based on a basin-wide collaboration to achieve optimal allocation is presented. Within that, a physical quantification of the resource was combined with an economic quantification of costs and benefits and the evaluation of tradeoffs involved in different courses of action. Its objective is to maximize benefits resulting from groundwater abstraction while taking into consideration spatially distributed quantity and quality constraints. These constraints include: head constraints, gradient switching constraints in areas sensitive to backflow of brine from Chotts and Sebkhass and finally quantity constraints. A globally optimal allocation strategies will be presented that can be considered as a benchmark for differing strategies. However, such a strategy is not likely to be pursued by the three riparian states if the negative externalities associated with alternative management cannot be better understood and quantified and the potential of tradeoffs investigated. Previous research within the framework of non-cooperative differential games has extensively covered situations where symmetry between the player's interests existed. With regard to the highly diverse productive systems and greatly varying aquifer properties as well as economic potential of the three riparian states it is questionable whether this approach is appropriate. We follow a more natural method by representing the differential game with asymmetric economic players that act upon the SASS aquifer model. Results will be presented utilizing empirical data supplied from Algeria, Tunisia and Libya putting the Gisser-Sachez-effect in new light.

HS02/09P/C24-012

1715

#### WATER MANAGEMENT BUDGET AS A BASE FOR ASSESSMENT OF WATER PRIORITIES IN A CATCHMENT

Boris FASHCHEVSKY<sup>1</sup>, Tatyana FASHCHEVSKAY<sup>2</sup> (<sup>1</sup>International Sakharov Environmental University, <sup>2</sup>Department of Ecology, Ufa State Aircraft University)

In this article new approaches are discussed of priorities of integrated water resources

management in the river basins taking into account as the economical development of the territories as the environmental limitations by means of computation the retrospective and perspective water management budgets of the river basins. The computation of environmental flow is considered for example of the territories Russia and Belarus.

HS02/09P/C24-013

1730

#### WORLD WATER USE: TRENDS, SCENARIOS, CONSEQUENCES

Igor Alexeevich SHIKLOMANOV (Director of the State Hydrological Institute)

New results of the prognostic assessment of the world water use obtained at SHI in 2001 during the research made to improve the dynamics of the world water resources are presented. Using the materials which are being published in the monograph "World Water Resources at the Beginning of the 21st Century", prepared by SHI, as well as a new data on water use all over the world a new scenario has been developed and validated on the global water use before 2025, i.e. scenario of "Sustainable Development". This scenario is an alternative to that used in the monograph and known as "Conventional Scenario". A detailed critical analysis of the scenarios developed by the international group of experts (Scenario Development Panel) during 1999-2000 which were submitted to the Second World Water Forum in the Hague shows that all these scenarios give quite an optimistic picture of a perspective water use development; the basic prerequisites of these scenarios, however, are not realistic at all and they do not take into account the available opportunities of many countries. Besides, the "Conventional Scenario" forecasting a development of water use on the model of the previous decades is the most realistic one, but it gives a critical water situation in many regions in the future. "Sustainable Development" scenario takes into account the main factors determining possibilities, volumes and structure of the present water use in certain regions and it is oriented to a wide use of modern technologies for freshwater use, in irrigation and industries in particular. In accordance with computations by the scenario of the "Sustainable Development", the world water use before 2025 would be practically stable; before 2025 it would equal 3900 km<sup>3</sup>/year which would be greater than that in 1995 by 2.7 % only; moreover, industrial water use would be lower by 10%; agricultural water use would be practically the same, meanwhile the municipal water use would be by about 25% greater due to the developing countries. According to the new scenario, more significant changes of water use may be expected on the continents. In Europe, North America and Australia a reduced water use would be from 24 to 5 % compared with that in 1995. On other continents it would be from 33% to 12 % higher. Still greater differentiation in the dynamics of water use is expected in natural-economic regions of the world. Nevertheless, it should be noted that a stabilization and even decrease of water use in the future can significantly decrease a load on water resources, but would not greatly affect the specific water availability in most regions in the world due to population growth. Only effective projects on improvement of technologies of freshwater use together with projects on increase of the available water resources may cardinaly solve the problem of a perspective water supply in the world.

HS02

Monday, July 7 - Friday, July 11

#### WATER RESOURCES SYSTEMS: GLOBAL CHANGE, RISK ASSESSMENT AND WATER MANAGEMENT (ICWRS, ICASVR, ICSW, ICWQ)

Location: Site C, Room 24

Thursday, July 10 AM

Presiding Chair: C. Goldman

HS02/10A/C24-001

0830

#### ADJUSTABILITY AND FLEXIBILITY OF RESERVOIR SYSTEMS TO CHANGES IN DEMAND AND SUPPLY CONDITIONS

Carsten BRASS, Andreas H. SCHUMANN (Institute for Hydrology, Water Management and Environmental Engineering, Ruhr-University Bochum)

The future reliability of reservoir systems is subject to climate change, which induces variations in boundary conditions of the appropriate management policies. In order to retain the actual system performance mainly two options exist. First of all reservoir operation should be adapted to changes by optimization. If the results are not satisfying the second option would be structural changes of the reservoir system, e.g. by construction of new or extension of existing reservoirs. For both approaches reasonable forecasts of future requirements would be extremely helpful to initialize the complex planning and decision procedure for the necessary adoptions. As it becomes evident by the wide range of regional climate change assessments estimated by different GCMs (General Circulation Models), it seems to be impossible at the moment to make any quantitative prediction of future hydrological conditions. As a result it is infeasible to make assessments about the required changes of existing reservoir system in future. One option to cope with this problem consists in analyzing the range of thinkable climatic change scenarios in order to get an idea of the future behavior and necessary changes of reservoir systems with regard to its operation and their structure. In this paper a way to adapt reservoir systems to changes in demand and supply is presented. For this purpose a tool to optimize reservoir systems operation to changing demand and supply conditions by Flexible Stochastic Dynamic Programming (FSDP) was developed. It considers the inflow as first-order Markov process and generates management policies with a flexible time-step. The different objectives (release, drinking-water withdrawal, flow at a control-gauge downstream, energy production and storage-volume) can be varied interactively. They are combined in a weighted objective function. In order to estimate the combinations of weights which are suitable, a decomposition of the system into single reservoirs and a site-specific optimization with an automated variation of weights is proposed. An evaluation of the site-specific results is done by simulations with measured daily runoff-data. In this way the vulnerability of a reservoir system with respect to possible changes of the demand and/or supply conditions can be assessed. With the computed information weights of the different objectives for all reservoirs are chosen to optimize the future operation of the reservoir-system. System decomposition is used to cope with the "curse of dimensionality" to reduce the computational efforts. The applicability of the developed methodology is demonstrated by a case study.

HS02/10A/C24-002

0845

#### WATER ALLOCATION FOR MULTIPLE USES BASED ON PROBABILISTIC RESERVOIR INFLOW FORECASTS

Ashish SHARMA<sup>1</sup>, Upmanu LALL<sup>2</sup>, Sankar ARUMUGAM<sup>3</sup> (<sup>1</sup>School of Civil and Environmental Engineering, The University of New South Wales, <sup>2</sup>International Research Institute for Climate

Allocating water to downstream users is a traditionally conservative exercise. How much water to allocate is decided based on stringent assumptions about the sequence of likely reservoir inflows (in many cases assumed to be the worst on record), and a requirement that the amount allocated for each use be reliable. In practice, the inflows that actually occur are often a predictable function of catchment storage and longer scale climatic fluctuations, and the water supplied for each use has a reliability that is influenced by the relative socio-economic considerations that may be applicable. This paper presents a framework for water allocation that is different from the traditional in the following respects: (a) it allows for the specification of the reliability associated with each water use, allowing for the formulation of a process where water can be auctioned between competing uses and users with a pre-specified reliability and value, and (b) it uses probabilistic forecasts of the likely reservoir inflows that take into account both local-scale factors such as prior inflow and rainfall, and larger scale climate related influences, which in this study are identified through a careful selection of predictors from climate indices and globally distributed, gridded sea surface temperature anomaly data. The approach is demonstrated through an application to the Oros reservoir in the state of Ceara, Brazil, with a simplified formulation assumes the uses to be confined to irrigation, and municipal and industrial water supply. The performance of the probabilistic forecasts is compared with that of the climatological or un-conditional forecasts within the proposed water allocation framework, the comparison being performed by forecasting each year on record in a cross-validated manner. The results from this exercise point both to the usefulness of the relatively pragmatic water allocation framework proposed in this work, and to the use of climate based probabilistic forecasts that can lead to substantial savings of water in regions where the link to low-frequency climate variability is strong.

**HS02/10A/C24-003****0900****IMPROVED HEURISTIC RESERVOIR OPERATION USING CONTROL CURVES INCORPORATING THE VULNERABILITY NORM**

Adebayo Johnson ADELOYE (Civil and Offshore Engineering, Heriot-Watt University)

Control or rule curves are an essential aspect of reservoir management in that by showing target storage levels in reservoirs in different periods, usually months, they are meant to guide reservoir operation. They however do not prescribe the amount of water to release from the reservoir; such an information can only be provided by an operating policy. However, the derivation of an operating policy often involves more complex analyses than that required for the derivation of control curves. Furthermore implementing an operating policy requires a user with specialist expertise not required for the implementation of control curves. For these reasons, most reservoir operators have tended to rely almost exclusively on control curves for reservoir operation. Traditionally, control curve targets are developed using non-sequential reservoir planning analysis. Efforts are then made to operate the reservoir in such a way that its level in any month does not fall below the target for that month. If the level falls below the target, then action must be taken to reverse the trend by reducing the amount of water put into supply. The problem is that a traditional control curve does not give any guidance on the level of cut back required to reverse the trend and there is therefore no guarantee that this objective will be achieved. Too little cut back will only make the recovery impossible or longer to achieve, while too much supply reduction will place unnecessary hardship on water users. Therefore, one way to increase the effectiveness of control curves for reservoir operation while still benefiting from its relative ease of use is to introduce the vulnerability norm as one of its attributes. Vulnerability is a measure of water shortage and limiting the supply cut back during failures to the vulnerability should ensure that the reservoir level does not fall below the target. In the study reported here, control curves with the dual attributes of reliability and vulnerability were developed for seven separate reservoirs. The reservoir planning analysis used a sequential approach based on the modified sequent peak algorithm. Because the analysis was implemented within a Monte Carlo framework, uncertainty limits for the control curves were also developed. The derived control curves are then used to simulate the reservoirs, by which it was clearly demonstrated that by following the prescribed water shortage targets, future reservoir catastrophic failures are avoided. The results of the study are presented and ways by which the control curves can be used to improve the operation of reservoirs are discussed.

**HS02/10A/C24-004****0915****OPTIMAL SHORT TERM OPERATION OF MULTIPURPOSE RESERVOIRS SYSTEM UNDER LIMITED WATER SUPPLY**

Giuseppe GIULIANO, Antonino CANCELLIERE, Giuseppe ROSSI (Department of Civil and Environmental Engineering, University of Catania (Italy))

A methodology is presented for deriving operating rules of a multipurpose reservoirs system through application of optimization and neural networks techniques. In order to find operating rules well suited to different degrees of drought severity, different scenarios of water resources availability, irrigation and municipal demands were hypothesized. A combination of the multiobjective optimization  $\epsilon$ -constraints method and the weighting method was used to find nondominated solutions that represent the best trade-off between two competitive objectives, namely the sums of squared irrigation and municipal deficits. Then neural networks were built through adaptive techniques, calibrating the parameters in order to better model the data provided by the optimization model. In particular, irrigation releases were expressed as a function of the reservoirs storage volumes, irrigation demands and inflows. Effectiveness of the selected operating rules was assessed through simulation of the system operation on new data, on the basis of many operational indices. Results showed that operating rules obtained through neural networks can well model the output of the adopted multiobjective optimization model, and therefore can be effectively used for optimum short term operation.

**HS02/10A/C24-005****0930****SIMULATING THE DISCHARGE OF CHAO PHRAYA RIVER CONSIDERING RESERVOIR OPERATION**

Naota HANASAKI, Taikan OKI, Shinjiro KANAE, Katumi MUSIAKE (Institute of Industrial Science, University of Tokyo)

In order to simulate global river discharge, global river routing network models (GRRNMs) have rapidly developed over the past decade. They have digital global river network and calculate river discharge by routing runoff. One practical problem of current GRRNM, is that they do not deal with reservoir operation. However, large number of rivers is regulated by reservoirs, and their impacts on river discharge are sometimes too large to neglect. In this paper, simple reservoir operation model for Total Runoff Integrating Pathways (TRIP), which is one of the GRRNMs, is introduced. The improvement in global river discharge simulation will provide us more reliable seasonal distribution of global water resources and its inter-annual fluctuation. At first, the model calculates release/storage of each reservoir based on their capacity and hydrological feature, in order to reduce mean inter-seasonal difference of

discharge (Basic operation, i.e. store in high inflow season and release in low). Then, additional release/storage is calculated according to the purpose of each reservoir and drought/flood event (Unique operation). For example, if a reservoir's main purpose is irrigation water supply, additional release/storage is supplied for the shortage of rainfall in the irrigated area in the lower reach. The model has simple structure and its global parameters such as distribution of irrigated area or climatic rainfall are derived from published global data sets, aims its global application. The model is applied to Chao Phraya River in Thailand as a case study. The basin is under tropic monsoon climate and has vast irrigated paddy field in its lower reach. The model dealt with two large reservoirs in the basin, namely 'Bhumibol' and 'Sirikit'. The resolution of TRIP was  $1^\circ \times 1^\circ$  longitude-latitude and simulated period was two years from 1/Jan/1987 to 31/Dec/1988. The calculated release compared well with the observation, especially the release in dry season when supplying irrigation water for the second crop. Consequently the trend of discharge at the lower reach is dramatically improved compared with former version. It supports the usefulness of our model and possibility of global application. However due to the underestimated inflow to the reservoir, which is caused by runoff derived from LSMs, error occurred in simulation of storage. The performance of our reservoir operation model strongly depends on the inflow data, so the improvement of LSMs is a critical issue. For global application, development of additional model components is necessary to cope with climatic and regional variety. Also, collection of long-term, reliable reservoir operation data (at least daily inflow, release, storage) are indispensable, for modeling and validation.

**HS02/10A/C24-006****0945****EVALUATION OF ALTERNATE OBJECTIVE FUNCTIONS FOR OPTIMAL OPERATION OF AN IRRIGATION RESERVOIR UNDER MULTI-CROP ENVIRONMENT**

Umamahesh Venkata NANDURI (Department of Civil Engineering, Regional Engineering College, Warangal)

In India, irrigation is one of the important purpose for which most reservoirs are operated. Many times these reservoirs operate under conditions of deficit water supply. Hence the development of appropriate mathematical models for optimal operation of irrigation reservoirs should receive greater attention. The proper formulation of the objective function of the optimization model to operate a reservoir is very important. The success or failure of the modeling effort depends largely on the formulation of an objective function, which represents with sufficient accuracy the goals of the operating policy. In the present study, three stochastic dynamic programming (SDP) models with different objective functions are used to develop operating policy for an irrigation reservoir, namely, Sri Rama Sagar Reservoir on River Godavari in the state of Andhra Pradesh in India. The reservoir is a major project meeting the irrigation requirements over a large command area. The three SDP models model the objectives of the reservoir with different levels of mathematical complexity. The performance of the reservoir under these three operating policies is compared through simulation. Three criteria, namely reliability, resilience and average annual deficit of water supply are used to evaluate the performance of the reservoir under the alternate operating policies developed.

**HS02-Oral-Posters****Monday, July 7 - Friday, July 11****WATER RESOURCES SYSTEMS: GLOBAL CHANGE, RISK ASSESSMENT AND WATER MANAGEMENT (ICWRS, ICASVR, ICSW, ICWQ)**

Location: Site C, Room 24

**Thursday, July 10 AM**

Presiding Chair: C. Goldman

**HS02/10A/C24-001OP**

Oral-Poster

**1045****A TREE MODEL FOR RAINFALL PREDICTION**A.W. JAYAWARDENA<sup>1</sup>, Xu PENCHANG<sup>2</sup> (<sup>1</sup>Department of Civil Engineering, The University of Hong Kong, <sup>2</sup>Institute of Applied Mathematics, Chinese Academy of Sciences)

One of the unique characteristics of daily rainfall data in any region is that the time series contains a large number of zeros. This poses problems in modeling using either deterministic or stochastic approaches. In general, rainfall data has a deterministic behaviour in the large time scale and a stochastic behaviour in the small time scale. In this study, it is proposed to model daily rainfall by using tree models of average rainfall values and their transmitting probabilities. It is assumed that the average rainfall in a fixed long period of time in each year is similar, and in a short period within that long period, it is stochastic. The long term can be a season or a certain number of months. For simplicity in bifurcating at each successive level, a period of 64 days is considered as the long time scale (64 is a power of 2). If, for any given year, the 64 days average rainfall is considered as the root of a tree which has 2 branches which in turn has two branches until it comes to the daily rainfall. The next step is to determine the transmitting probability from the root to the branches in succession. The probability tree also will have a structure similar to that of the rainfall value tree. The probability tree can be obtained by defining the probabilities as functions of the values of rainfall at each level. With these two tree models, and knowing their root values, the rainfalls at all other levels can be estimated. This method is applied to simulate rainfalls at a number of stations in Hong Kong and in Thailand. The results are encouraging.

**HS02/10A/C24-002OP**

Oral-Poster

**1049****CHARACTERISTICS OF INTERCEPTION LOSS AND FORMULATION OF AN APPROPRIATE MODEL FOR THREE REGIONS WITH DIFFERENT CLIMATE AND FOREST CONDITION**Tae TOBA<sup>1</sup>, Tekeshi OHTA<sup>1</sup>, Nobuaki TANAKA<sup>2</sup> (<sup>1</sup>Graduate School of Bioagricultural Sciences, Nagoya University, <sup>2</sup>Frontier Observational Research System for Global Change, <sup>3</sup>Graduate School of Agriculture and Life Sciences, The University of Tokyo)

In the future, changes in the water cycle resulting from climate changes will seriously affect water resource management. Knowledge of the characteristics of interception loss on a regional scale is important for understanding changes in the water cycle and for water resource management. In forests, the percentage of gross precipitation lost to interception usually ranges from 10 to 40%. When considering interception losses on a regional scale, an understanding of forest structure and of climatic conditions, i.e. precipitation, is much more important than it is in analyses on a patch scale. Therefore, an interception loss model that is appropriate for various forest types is needed. We analyzed the characteristics of interception

loss at eight locations with different climate and forest conditions, in boreal (east Siberia), temperate (Japan), and tropical (Thailand) forests. We used an interception loss model (Toba and Ohta, 2002) that was calibrated using data for six locations in two of these regions, and validated this model with the results for the remaining two points in two regions. Three study sites were located at 62°N, 129°E in boreal forest, three at 39°N, 140°E and one at 35°N, 137°E in temperate forest, and one at 18°N, 98°E in tropical forest; the forests had plant area indexes (PAI) ranging from 2.8 to 11.1. The PAI reflects forest structure. Throughfall, stemflow, gross precipitation, and meteorological elements (air temperature, relative humidity, wind speed, etc.) at each site were observed. Compared with gross precipitation measured at open sites, the percentage lost to interception ranged from 10 to 20% in the boreal forest, 10 to 15% in the temperate forest, and was about 10% in the tropical forest. We have not analyzed the characteristics of interception loss for the tropical forest site in detail yet, but these results will be described later in a full paper. At the other sites there were clear relationships between interception loss and precipitation intensity, saturation deficit, and rainfall duration. The canopy storage capacity increased with the PAI. Parameters in the model were decided using the relationships of throughfall, stemflow, and gross precipitation. We then evaluated the characteristics of interception loss using this model.

**HS02/10A/C24-003OP** Oral-Poster **1053**

#### CHANGES IN THE HYDROLOGICAL CYCLE AND ITS EFFECTS ON THE ENVIRONMENT IN AN INLAND RIVER BASIN OF WETSREN CHINA

Jumpei KUBOTA<sup>1</sup>, Tomohiro AKIYAMA<sup>2</sup>, Yusuke YAMAZAKI<sup>3</sup> (Research Institute for Humanity and Nature, <sup>2</sup>Graduate School of Environmental Studies, Nagoya University, <sup>3</sup>Graduate School of Agriculture, Kyoto University)

This paper focuses the effects of changes in the hydrological cycle during the past fifty years caused by the water resource development on the environment in the Heihe River basin, an inland river of the arid region in the western China. The Heihe River basin consists of three parts, namely the upper mountainous area which is the source of the Heihe River by rather big amount of precipitation and glaciers, the middle oasis area like Zangye and Jiuquan, and the lower terminal arid area like Ejina. Each area has independent hydrological condition and ecosystem. Surface runoff from the upper mountain area by rain and melt water of snow and glaciers is the only source of water available in the middle oasis area and the lower arid area. The increase of water demand in the middle oases area mainly by irrigation for agricultural land has resulted in the decrease of surface water supply for the lower arid area. The degradation of vegetations and the difficulties of the usage of shallow groundwater in terms of not only quantity, but quality have become serious problems. Even in the middle oasis area, over 80% of the total discharge has been diverted from main river courses to many irrigation canals, resulting in not only the rise of groundwater level inside the cultivated oases, but also the increase of soil salinization area. At the same time, the decrease of discharges in the main river courses have formed deserted area. Developing a distributed hydrological model with the grid based information of land use and irrigation systems, the spatial distribution water budget in the Heihe River basin has been evaluated. The relationship between the water status and the degradation of vegetations and water quality were investigated. Based on this analysis, we found that the strategies of farm production in each area are closely related to hydrological status. Also, using several future scenarios including possible climate change and expansion of the economy of this area, the proper way to use the limited water resources minimize the degradation of the environment will be discussed.

**HS02/10A/C24-004OP** Oral-Poster **1057**

#### SUB-SURFACE WATER CONTRIBUTION TO SURFACE WATER USING STOCHASTIC DIFFERENTIAL EQUATION

Gouldaria K. NOURBAEVA, So KAZAMA, Masaki SAWAMOTO (Department of Civil Engineering, Tohoku University)

The scheme is proposed to analyze the distribution of soil water balance characteristics in a river catchment. The water movement processes are considered using stochastic differential equation (SDE) to obtain the dynamics of interrelated catchment parameters including water table depth, soil saturation and equilibrium soil moisture content. The SDE includes total prediction error modeled as a wideband stochastic process with zero mean. The non-stationary solution of SDE is derived by the efficient fourth order Runge-Kutta approximation method. The Van Genuchten-type relationship is used to obtain the soil water content values from water table predictions. The Kalman filter was used to calibrate the stochastic model to measured data. The discrete-time recursive routine such as Kalman filter gives a maximum likelihood criterion in terms of the differences between measurements and predictions. Aquifer screen variation for single location was modeled from measured data. The spatial distribution of water table depth is evaluated from contributing area concept based on the relationship between topographic index and water table depth. According this theory, soil moisture depends on the location on the hillslope at the catchment scale and the water table depth is a function of flow accumulating area and location slope. Under topographic index conception from hydrologic and topographic characteristics of catchment, the distribution of water table depths, equilibrium soil moisture content and specific discharge in each time step were predicted. The model has adapted to a specific character of the Natori River basin in Japan as mountain catchments. The spatially distributed data considered in the modeling are designed as raster data to be compatible with GIS software. The contributing area and slope for each location are calculated using digital elevation model of the catchment. Predictions are obtained as time series of digital maps with 1km grid scale. In the case of the scant sources observed data, described technique gives preliminary representation of full space-time distribution of water budget characteristic in the catchment. Proposed scheme can be useful for assessment of water resources redistribution in the river basin at temporal and spatial scale.

**HS02/10A/C24-005OP** Oral-Poster **1101**

#### EVOLUTION OF THE SOIL WATER STORAGE UNDER PRESENT AND CHANGED ATMOSPHERIC CONDITIONS

Urszula SOMOROWSKA (Faculty of Geography and Reg.Studies, Warsaw University, Krakowski Przedm.30,00-927 Warsaw, Poland)

The wetness status of land surface is an important element of the soil-plant-atmosphere systems. Traditional approach assumes that main factors affecting spatial and temporal patterns of soil water content include precipitation, evapotranspiration, groundwater levels, topography, vegetation and soil types. The soil water storage balances the temporal surplus of water supply from precipitation against the atmospheric demands for evapotranspiration. In case of shallow groundwater levels the volume of the soil water storage is dependent on the groundwater level fluctuations. This study is a search for interactions between soil water storage and precipitation - main factor responsible for recharge of the soil water resources. The focus is on the dynamic soil water resources of the lowland basin situated in the central region of Poland, in the protected area of the Kampinos National Park. The analysis is

based on field measurements of soil moisture conducted over the period 1995-2002 in fourteen representative sites. The measurements were conducted using Time Domain Reflectometry meter tracking the characteristic stages of soil water storage of shallow soil layers. Specific question to be answered is what is the basin's inertia that affects subsequent evolution of the soil moisture stages, and, in consequence, soil water storage. Enabling the answer to this question requires (i) understanding the soil moisture variability and interdependencies between soil moisture and key factors e.g. precipitation and evapotranspiration (ii) quantifying the effects of hazard atmospheric situations on the volume of soil water storage (iii) setting the scheme for predicting soil water storage under extreme atmospheric conditions. Range of natural variability of soil water storage was derived from the soil moisture profiles detected. Extreme and normal stages of the soil water resources were related to the antecedent precipitation. It was found that at least four months' antecedent precipitation has an influence on temporal stages of the soil water storage, thus the system has its memory. Inertia of soil water resources has been additionally investigated indirectly by applying autocorrelation function to the monthly minimum baseflow. Evolution of the soil water storage have been analyzed for the observation period of eight years. Additionally, the changes in the volume of the soil water storage have been estimated depending on the depletion of groundwater level in selected dry, wet and normal years over the period 1995-2002. In this case water storage decrease function was applied which is a simple correlation model allowing estimation of water deficits as an effect of groundwater level drop. Depletion of soil water storage was set as dependent from the deficit of precipitation (precipitation minus evapotranspiration). The relation was parameterized according to the logarithmic equation established for wet, dry and average years. Assuming exaggerated atmospheric conditions, the depletion of soil water storage can be predicted.

**HS02/10A/C24-006OP** Oral-Poster **1105**

#### CLIMATE, WATER AND ENERGY IN THE NORDIC COUNTRIES

Arni SNORRASON, Jona Finndis JONSDOTTIR (Hydrological Service, National Energy Authority)

In light of the recent IPCC Climate Change assessment and recent progress made in meteorological and hydrological modeling, the directors of the Nordic hydrological institutes (CHIN) initiated a research project **Climate, Water and Energy (CWE)** with funding from the Nordic Energy Research and the Nordic Council of Ministers focusing on climatic impact assessment in the energy sector. Climatic variability and change affect the hydrological systems, which in turn affect the energy sector, this will increase the risk associated with the development and use of water resources in the Nordic countries. Climate and hydrology are thoroughly intertwined through the hydrological cycle. In fact, one can claim that climatic change is nowhere more clearly manifested than in hydrological systems and processes. Changes in precipitation and temperature will have direct influences on runoff. Glaciers are especially vulnerable to climate change, for example increased temperature may result in increased runoff, at least temporarily. Climatic change may have a large influence on the temporal distribution of runoff within the year. The impacts on the hydropower industry are many and varied, many of which are directly linked to the hydrological changes. Climatic change will affect the hydropower sector in general. The changes will affect the total water available as well as both its spatial and temporal distribution. This will create both opportunities and benefits to the hydropower sector, but also problems and costs. In fact, it can be stated that the risk, in general, will increase due to increased hydrological uncertainty caused by climatic changes. New investment and design, as well as operational and management practices are needed to respond to these changes. The product of the project will be an in-depth analysis of the present status of research and know-how in the sphere of climatic and hydrological research. Furthermore it will be a synthesis and integration of present research with focus on the needs of the energy sector. It will also identify and prioritize key future research areas for the benefits of the energy sector. Finally it will provide comprehensive research proposals for top priority research areas. The Climate, Water and Energy project can create a platform for further scientific co-operation. Such co-operation could focus on issues concerning the interplay of climate and water in the Arctic region and could also be extended into a joint Nordic, European and North American research program focusing on the North Atlantic region and its role in the climate of the Northern Hemisphere, or the Globe as a whole. The role of e.g. the North Atlantic Oscillation (NAO) in climate variability, is thought to be of great significance for the meteorological and hydrological conditions in Europe as well as other regions.

**HS02/10A/C24-007OP** Oral-Poster **1109**

#### RAINFALL VARIABILITY AND ITS IMPACTS ON WATER RESOURCES DEVELOPMENT IN PART OF OGUN-OSUN RIVER BASIN

Olusegun ADEAGA (Department of Geography, University of Lagos)

Highly variable rainfall over space and time constitutes major constraints to water resources development most especially in developing countries of the world. Also, major consequences of extreme hydrological events (flood and drought) and low mitigation techniques and inadequate technological know-how threaten water resources development in developing region. Evaluating the nature of hydrological processes that affect water resources variability most especially rainfall in parts of Ogun-Oshun River Basin will provide adequate knowledge towards providing information on the amount, reliability and timing of available renewable water resources within the region. Such information is necessary; if problematic issues on water resources availability and production are to be resolved in a sustainable way. A safe transition to sustainability is crucial to meeting the increasing water demand per capita in Ogun-Oshun basin. In this paper emphasis was based on rainfall variability characteristics in Ogun-Oshun basin and the telecommunication of the El-Nino events and sea surface temperatures (SST) on rainfall distribution within Ogun-Oshun basin. Also, time series and probability analysis of extreme rainfall events frequency distribution and probability of occurrence was also carried-out. All the above analyzes was integrated into a Geographical Information System (GIS) framework for spatial analyses and scenario building. Finally, investigation was made on adequate measures to be taken towards extreme hydrological events prediction and planning.

**HS02/10A/C24-008OP** Oral-Poster **1113**

#### HEAT FLUX OBSERVATION ACROSS THE AIR/WATER INTERFACE OF A SMALL RIVER

Mohammed Aslam M.A.<sup>1</sup>, Akihiko KONDOH<sup>2</sup> (<sup>1</sup>Graduate School of Science and Technology, Chiba University, Chiba 263-8522, Japan, <sup>2</sup>Center for Environmental Remote Sensing (CEReS), Chiba University, Chiba 263-8522, Japan)

River water temperature information is very important in the studies of potential effects of climate change on freshwater system. The relationship between stream temperature and air temperature are always active. The linear regressions of river temperature versus air temperature are best fitted for this purpose. The applicability of linear regression has been verified in this study. The present study deals with water temperature and air temperature flux in a small river Kuriyamagawa, Chiba Prefecture, Japan, where long-term database is maintained by Chiba Prefecture Environment Department. Temperature data from 1976 to

1997 were employed for the analysis. The heat flux observation for water and air interface has been observed at three stations across the river covering both upstream and downstream at Arai-bashi (longitude 140.473E and latitude 35.696N), Kido-bashi (longitude 140.528E and latitude 35.622N) and Yohei-bashi (longitude 140.464E and latitude 35.687N) respectively. The inter-annual trend of river water temperature follows the trend of air temperature in these locations. The maximum temperature has been recorded for the month of August and that of the minimum for the month of January. The heat exchange processes that contribute to surface water temperature have been analyzed and related to the air temperature on a monthly time scale. This regression analysis strongly supports the linear relationship between the air and water temperature flux, which are based on the best autocorrelation structure of river water time series. This results has shown that water temperature ( $T_w$ ) and air temperature ( $T_a$ ) can be related by a linear regression as,  $T_w = 0.7941 T_a + 2.2392$  for this small river, where heat flux studies has been carried out. The river temperature and air temperature interface is very similar to the equilibrium temperature and air temperature relationship. Linear regression between river temperature and air temperatures are found to be accurate and are good for interpolation within the record length used in the analysis.

**HS02/10A/C24-009OP** Oral-Poster **1117**

**REPRESENTATION OF COMPLEX LOW-FREQUENCY FEATURES IN A DAILY RAINFALL MODEL**

Timothy Ives HARROLD<sup>1</sup>, Ashish SHARMA<sup>2</sup> (<sup>1</sup>CSIRO Atmospheric Research, <sup>2</sup>University of New South Wales)

Australian rainfall records contain complex low-frequency features that are associated with climate variability. Both the pattern of wet and dry days, and the average rainfall on a wet day, are linked to large-scale quasi-periodic variations such as the El Niño Southern Oscillation Index. These linkages are even more complex when wet days are treated in separate classes based on the number of adjacent wet days (i.e. solitary wet days; days at the start or end of a wet spell; and days in the middle of a wet spell). We present a stochastic model for generation of daily rainfall that considers these features in its formulation. We show that use of predictors that reflect the low-frequency variations can result in a more appropriate representation of rainfall variability at long time scales.

**HS02/10A/C24-010OP** Oral-Poster **1121**

**ASSESSMENT OF THE EFFECTS OF VEGETATION COVER CHANGES ON HYDROLOGIC REGIME**

Mohammad Javad POURAGHNAEI<sup>1</sup>, M. MAHDAVI<sup>2</sup>, B. SAGHAFIAN<sup>3</sup> (<sup>1</sup>Natural Resources Research Center of Semnan, <sup>2</sup>Professor of Tehran University, College of Natural Resources, <sup>3</sup>Associate Professor in Watershed management research of Tehran)

Hydrologic regime of watersheds has high importance and needs attention. Lack of management and planning in natural resources and land use, cause changes in hydrologic regime of watersheds and converting runoff to flood. To be aware of management feedbacks is necessary to have a successful management in a watershed. In this study, hydrographs of Neka Rud basin were compared for several land use conditions (1967, 1992 & 2000) according to 24 hours maximum precipitation of several return periods. At first, land cover maps of Neka Rud basin for different years (1967, 1992 & 2000) were provided. Old maps and aerial photographs of 1967, TM and ETM Landsat images of 1992 and 2000 were used to provide the land cover map of 1967, 1992 & 2000, respectively. Using area of each land cover (from land cover maps), area of each soil type of basin (from soil map of basin) and other necessary information for SCS method, curve number (CN) for each period was calculated (614.7, 65.5 & 67.1). For the next step, from rain gauge data and by use of hHyfa soft ware, 24 hours maximum precipitation for selected return periods was calculated. The hydrographs (spatial pattern) for each return period were drawn from inter basin stations data, using surfer software. Then weighted average of this hydrographs identified the 24 hours maximum precipitation in basin area. Average of temporal pattern (using IDF curves) of Babolsar and Gorgan rain gauges -in side of basin- was used for temporal pattern of Neka Rud basin and hourly temporal pattern was extracted. These data were used in Hydrologic Modeling System (HMS) to predict the hydrographs for each land use condition (1967, 1992 & 2000) and on the 24 hours Maximum precipitation of several return periods. This model needs to simulation, calibration and Validation steps for Neka Rud Basin situation before running for predict a hydrograph. The model was simulated by 3 real storm-runoff events that after optimization, each of them had special calibration coefficients (for initial absorption and lag time). An average of these calibration coefficients was used as the coefficient for Neka Rud basin. Validation was the last step before prediction. For this step a real storm run off event was used. The observed and predicted hydrograph had the same trends, this result was suitable and the calibration was valid. Finally, the calibrated model was used to predict the hydrographs of Neka Rud basin for various land cover conditions. After running of the model for each situation, the results showed an increasing trend for peak discharge and volume of runoff from 1967 to 2000.

**HS02/10A/C24-011OP** Oral-Poster **1125**

**MODELING THE INFLUENCE OF VARIATION IN ATMOSPHERIC PRECIPITATION ON THE HEAT AND WATER BALANCE COMPONENTS OF DRY AREAS**

Alexey Vladimirovich BABKIN (Lab. of Hydroecological Research of Inland Water Bodies)

The aim of the work is the development of the mathematical model for research of the moisture and water-thermal regime dynamics within arid and semi-arid areas. The base of model is the differential equations of water and heat balance of soil. The income of energy (absorbed solar radiation), water outcome components (evaporation and run-off) and energy outcome components (turbulent heat-exchange of ground surface with atmosphere, evaporation and effective radiation) were related through heat and water storage of soil. The relations between income-outcome characteristics and storage components permitted the soil water and heat balance equations to combine into the system. Its solutions were found for leap-pattern and linear changes of precipitation and for their variation simulated by periodic function. The increase of precipitation within arid and semi-arid areas causes the increase of soil water storage, evaporation and run-off and reduction of the heat storage and energy outcome for turbulent heat-exchange and effective radiation. The dynamics of characteristics of semi-arid area of Caspian Lowland and Western Kazakhstan was calculated for 50 mm/year leap-pattern increase of precipitation and for linear precipitation increase with the velocity of 5 mm/year. For leap-pattern change of precipitation the climatic and hydrologic characteristics of the territory reach the values of new equilibrium state for the time less than the year. Under linear precipitation increase the changes of area characteristics become linear for the time interval less than half of year. The oscillation of precipitation causes the variation of area characteristics. The extremes of climatic and hydrology characteristics of area have a time lag to the respective precipitation extreme. For the same variation period the time delay of area characteristics is different. After the precipitation extreme the evaporation reach its extreme value the first. The extremes of absorbed solar radiation, water storage of soil and run-off appear some time later. The heat

storage extreme of opposite phase is the last.

**HS02/10A/C24-012OP** Oral-Poster **1129**

**MODELING WATER QUALITY BY USING NEURAL NETWORKS**

Jian-Ping SUEN, Wayland J. EHEART (Department of Civil and Environmental Engineering, University of Illinois at Urbana-Champaign)

In this study, artificial neural networks (ANNs), are applied to estimating the nitrate concentration in a typical Midwestern river, i.e., the Sangamon River in Illinois. In Illinois, and throughout the Midwestern US, nitrate has recently become an increasingly important problem in drinking water quality. This is due to a somewhat recent change in the EPA nitrate standard and to the increasingly widespread use of chemical fertilizers in agriculture. Two ANNs, Back Propagation Neural Networks (BPNN) and Radial Basis Function Neural Networks (RBFNN), were compared with regard to their effectiveness in water quality modeling. BPNN uses a gradient descent method, modifying the weight by simulation errors to construct the neural network. RBFNN uses a fuzzy min-max network to do the first clustering part and multivariate regression method to construct the neural network. RBFNN is much faster than traditional BPNN and the results of RBFNN also appear to be more robust. The study compared these two types of ANNs to traditional regression and traditional mechanistic water quality modeling. Comparisons were based on overall accuracy and on the frequency of false-negative prediction, i.e., the frequency with which the model would predict the nitrate concentration to be below the standard when it actually exceeded it. The study showed that the RBFNN achieved the best results of all models in terms of overall accuracy, and both BPNN and RBFNN had the same false-negative frequency which has better than traditional models.

**HS02/10A/C24-013OP** Oral-Poster **1133**

**TIME SCALE ANALYSIS FOR INVESTIGATING STATIONARITY OF HYDROLOGIC TIME SERIES**

A. Ramachandra RAO<sup>1</sup> (<sup>1</sup>School of Civil Engineering, Purdue University, <sup>2</sup>Irrigation and Hydraulic Department, Faculty of Engineering, Cairo University)

To overcome the difficulties encountered in conventional spectral analysis, a different approach known as Wavelet analysis has been introduced during the past 10 years (Daubechies, 1992; Combes et al., 1990; Mallat, 1996; Meyer, 1993; Strang and Nguyen, 1996; Chui, 1992). In Wavelet analysis, a different type of basis functions, called Wavelets, are used. Wavelets, as opposed to sine and cosine functions, have a limited extent in time (a limited support), and are therefore localized in time as well as in frequency. In the theory of Wavelet transforms, the notion of 'frequency' is changed to an equivalent one of 'scale', where large scales correspond to low frequencies and small scales correspond to high frequencies. Wavelet analysis provides a technique for analyzing the structure of a time series by using variable size windows. In effect, by using the Wavelet transform the signal is decomposed into components of different scales. This offers a method for a local examination of the signal, a multi-scale outlook, and a time-scale analysis (Misiti et al., 1996). Wavelet analysis can be used as a tool for performing a wide range of tasks which include: detecting discontinuities in signals, detecting long-term evolution (trends), detecting self similarity (fractal signals), identifying pure frequencies (time-frequency analysis), suppression, and compression of signals. Wavelet analysis is used in this paper to investigate the stationarity of hydrologic and climatic time series as well as tree-ring series. Annual rainfall, runoff and temperature series from the Midwestern United States are used in the study. The results indicate the nonstationarities in these time series, thereby demonstrating the use of wavelets in the study of climatic variation. The time-scale structures in these time series are studied and the relationships between them are investigated. Also, Wavelet analysis is used for assessing similarities between different time series at different scales in the region under study. References Chui, C.K. 1992 An Introduction to Wavelets. Academic Press. Combes, J.M., A. Grossmann, Tchamitchian, Ph. eds. (1990) Wavelets, Time-Frequency Methods, and Phase Space. Springer. Daubechies, I. (1992) Ten Lectures on Wavelets. SIAM, Philadelphia, PA. Mallat, S. (1996) Wavelet Signal Processing. Academic Press, New York, NY. Meyer, Y. (1993) Wavelets: Algorithms and Applications. SIAM. Misiti, M., Y. Misiti, G. Oppenheim and J.M. Poggi. (1996) Wavelet Toolbox for use with MATLAB. The Mathworks, Inc., Natick, Mass. Strang, G. and T. Nguyen (1996) Wavelets and Filter banks. Wellesley -Cambridge Press, Wellesley, MA.

**HS02/10A/C24-014OP** Oral-Poster **1137**

**THE RELATION BETWEEN  $\delta^{18}O$  IN MONSOONAL PRECIPITATION AND AIR-SEA ACTIVITY, ASTRONOMICAL AND METEOROLOGICAL FACTORS**

Hongxi PANG, Yuanqing HE (Lab ice core, Cold and Arid Regions environmental and Engineering Research Institute, Chinses Academy Sciences)

The variations of isotopic content are different, with different locations and climatic types. The isotopic contents in precipitation vary complicatedly over monsoon regions in mid-latitude zones. The isotopic data in precipitation at New Delhi (the IAEA/WMO station; 28.58°N, 77.2°E), located in southwest monsoon region, are analyzed, suggested that the  $\delta^{18}O$  values vary in 11 years cycle, which is closely agreed with that of sunspot; the strong correlation between  $\delta^{18}O$  and T/P, a parameter by coupled temperature and rainfall; the remote positive correlation between  $\delta^{18}O$  and ENSO event induced by the interactions of coupled air-sea systems in tropical Indian Ocean and Pacific Ocean; and rainy drops evaporated is the key reason to lead the positive correlation between  $\delta^{18}O$  and zonal wind velocity at the height of 500mb while the amount and temperature effect strengthen this correlation.

**HS02/10A/C24-015OP** Oral-Poster **1141**

**SCALES OF HYDROLOGICAL CHANGES IN VOLGA RIVER BASIN POSSIBLE AT CLIMATE CHANGES**

Alexander GEORGIADI (Department of Hydrology, Institute of Geography, RAS)

Three main approaches for model using as tool for assessments of possible hydrological regime changes which differ from each other by type of model are developed. One of them is based on physically based water cycle models (including SVAT models) that are used for small site or rather small watershed (Georgiadi, Nazarov, 1997; Kashutina, 1999 and others). Simplified monthly water budget models that could be used for wide diapason of spatial scale (Georgiadi, Milyukova, 2001). Mean annual river runoff could be estimated on the basis of rather simple relationships between water budget components and climatic elements (Belyaev, Georgiadi, 1989, 1992; Georgiadi, 1991, 1993; Velichko et al., 1992; Georgiadi, Jai-Ho Oh, Yong Hee Lee, 2000). The paper presents the assessments of possible changes of spring flood and annual river runoff changes as well as changes of intraannual distribution of river runoff in Volga river basin (to Volgograd) at the Holocene Optimum (6 thou. years before present) as well as at a doubling of atmospheric CO<sub>2</sub>. The

data of experiments on a global climate model of Moscow State University (Kislov, 1992) and Geophysical Fluid Dynamics Laboratory (GFDL), Princeton University, USA were used as the scenario of climate change. The hydrological changes are determined on the basis of original model of monthly water balance. In the present work the model of formation of a monthly water balance for plain watersheds, allowing to estimate influence such important hydrological factors as potential evaporation, snow cover accumulation and snow melting, infiltration of water into the ground and its deep infiltration, soil moisture reserve change. The model allows to compute dynamics of runoff losses. This model could be used for calculate of rain and snow melting flow. The conditions of river runoff formation at various sites of watershed are non-uniform, at the same time there is a limited enough information on the soil hydrophysical characteristics, and as the rather rough estimations of some other characteristics of watersheds. Therefore for identification of some parameters of model the method of optimization was used. The calculations of a monthly river runoff for main part of Volga watershed for grid cells  $1^\circ \times 1^\circ$  were made. The following monthly average long-term data were used: precipitation, air temperature, soil moisture reserve at field capacity, river runoff. All calculations were made for monthly time steps, but were used approach based on using so called quasi-daily calculations.

**HS02/10A/C24-016OP** Oral-Poster **1145**

**THE DECREASE OF THE PRECIPITATION IN PERIODS OF THE YEAR AS A SIGN OF CLIMATIC CHANGE: CASES STUDIED IN PORTUGAL**

Maria Manuela PORTELA, Antonio de Carvalho QUINTELA (Instituto Superior Tecnico (IST))

A more irregular distribution of the precipitation within the year and a significant reduction of its amounts during some periods of the year are generally pointed out as consequences of the climatic change that seems to occur in Portugal. To be considered a sign of climatic change, the previous reduction must correspond to an increasing tendency persisting along the years. In order to detect variations having a persistent nature in temporal series of precipitation in Portugal, two procedures were applied: the classic method of moving averages and a procedure, expressly developed within the scope of the study that originated this article, based on a statistical comparison of the precipitation averages during certain intervals of time in which the recording periods were divided. The applications carried out for precipitation series in eleven gauging stations in Portugal denote that the amount of rain during the 2nd quarter of the hydrologic year (from January to March), and specially in March, is clearly decreasing.

**HS02/10A/C24-017OP** Oral-Poster **1149**

**CLIMATE CHANGE, GLACIER MASS BALANCE AND WATER RESOURCES**

David N. COLLINS, Oliver G. MACDONALD (School of Environment & Life Sciences, University of Salford)

Disproportionately large contributions of runoff arise from the portions of catchments overlying the high mountain areas of the world, as a result of the orographic increase of precipitation with elevation. At present, high specific discharges from glacierised high mountains are also generally enhanced by destocking of ice from the many thousands of often small glaciers which characterise ranges such as the western cordillera of the Americas, the Alps, and the Himalaya. River flows have often doubled, between the cool 1970s and warm 1990s, reflecting in the Alps, for example, summer air temperature increases of about  $2^\circ\text{C}$  over the same period. However, enhanced river flows can not go on for ever. As warming continues, glacier mass loss and diminishing glacierised partial areas of catchments will ultimately result in reduction of annual total discharge with greater variability from year to year. Glaciers will become reduced in size in most areas over a timescale of 20 – 50 years. Warmer air temperatures will result in the freezing level rising in the atmosphere so that where snow formerly fell precipitation will occur as rain. Winter snow pack will probably decline and snow cover duration shorten. Heavy rainfall whilst the transient snowline stood at high elevation resulted in severe summer flood events in the Alps and the Karakoram in the warm 1990s. Daily integration of air temperature and precipitation from results of the HadCM3Gga1 experiment for  $2.5$  latitude  $\times$   $3.75$  longitude degree grid square resolution are coupled with standardised glacierised basins, downscaled through derivation of statistical relationships between regional climate (NCEP/NCAR reanalysis project), and actual glaciologically-relevant meteorological observations obtained at mountain stations. In the short term, warming increases flow, but coupled with deglaciation, greatly reduced flows will have serious consequences for water resources, particularly where mountain runoff drains to neighbouring arid lowlands.

**HS02/10A/C24-018OP** Oral-Poster **1153**

**THE HIGHEST ALTITUDE ICE CORES IN THE HIMALAYAS RECORD ANTHROPOGENIC POLLUTION**

Tandong YAO<sup>1</sup>, Keqin DUAN<sup>2</sup>, Shucheng XIE<sup>2</sup>, Wenmian HUO<sup>2</sup>, Lide TIAN<sup>2</sup> (Prof., <sup>2</sup>Dr.)

High resolution, well-dated ice core records, especially low-latitude ice cores near the populated regions provide a unique tool to study and to evaluate the impact of anthropogenic activities on environment and climate. Recently ice cores were recovered at an altitude of 7200m on the Dasuopu Glacier located in the Xixiabangma Mountain. The high elevation of the coring site provides very good background to detect any anthropogenic pollution. Organic and inorganic methods are applied to the Dasuopu ice core analyses. The analyses detected petroleum residues from the ice core. Our study has concluded that the material is from the oil combustion in Kuwait and vehicle pollution in India. The measured lead concentration ranges from  $16 \times 10^{-12}\text{g/g}$  to  $161.7 \times 10^{-12}\text{g/g}$ . Lead concentration increases significantly since the 1940s. A very dramatic rise happened in the 1980s in which the mean lead concentration reached to  $161.7 \times 10^{-12}\text{g/g}$ . The organic and inorganic analyses indicated that the anthropogenic pollution has already impacted the environment at 7200m a.s.l. in the Himalayas.

**HS02/10A/C24-019OP** Oral-Poster **1157**

**ATMOSPHERIC METHANE OVER THE PAST 1000 YEARS FROM A SUB-TROPICAL ICE CORE**

Baigjing XU<sup>1</sup>, Tandong YAO<sup>2</sup>, Jerome CHAPPELLAZ<sup>2</sup>, Lonie THOMPSON<sup>2</sup>, Ninglian WANG<sup>2</sup>, Lide TIAN<sup>2</sup> (<sup>1</sup>Dr., <sup>2</sup>Prof.)

A high-resolution methane record from an ice core recovered above 7200m of altitude on the Dasuopu Glacier in the Himalayas, reveals similar trend of methane concentration fluctuations with the polar region records. The high degree of detail of the Dasuopu record over the last century allows revealing a significant period between the two World Wars when the anthropogenic methane increase was put to a halt. This sub-tropical methane record also allows quantifying for the first time the difference of methane mixing ratio between polar and sub-tropical latitudes during pre-industrial time. The average difference is 120 ppbv with Greenland and 160 ppbv with Antarctica. The record suggests that the tropical latitudes

might represent large percent of the global methane sources in pre-industrial time. In addition, the temporal fluctuation of the pre-industrial methane records suggests that Monsoon evolution incorporated with high methane input in the south Asia might be responsible for the relatively high methane concentration observed in the Dasuopu ice core around 1700 AD.

**HS02/10A/C24-020OP** Oral-Poster **1201**

**ICE TEMPERATURE VARIATION IN PUROUGANRI ICE FIELD ON THE TIBETAN PLATEAU**

Jianchen PU<sup>1</sup>, Tandong YAO<sup>1</sup>, Ninglian WANG<sup>2</sup>, Keqin DUAN<sup>2</sup>, Lide TIAN<sup>2</sup> (Prof., <sup>2</sup>Dr.)

Puruogangri ice field is located in the middle of the Tibetan Plateau, with a total area of 422.58km<sup>2</sup>. Four ice cores with a depth of 154m, 118m, 80m and 20m respectively. The ice temperature was measured in the 4 holes using resistance thermometer. The ice temperature shows same trend in the 4 holes. The ice temperature in the above 2m is intensively influenced by cold wave from the ice surface. Under that the ice temperature curve shows a warm-season type. The lowest ice temperature is  $-9.9^\circ$  measured at 12m depth. The ice temperature increase downwards in a linear manner under 12m, but the increasing ratio is lower than the decreasing ratio in the upper 12m. During the observation, the ice temperature decreased obviously in the upper 4m of the ice hole, and the decrease is vanished downwards. In the 80m ice hole, the ice temperature decreased  $0.62^\circ$  from 18:50 of October 18 to 14:40 of October 21, which a daily average of  $0.2^\circ$ . The ice temperature decreased  $1.15^\circ$  in the same period, with a daily average of  $0.3^\circ$ . There was no obvious variation in 12m depth.

**HS02/10A/C24-021OP** Oral-Poster **1205**

**THE INFLUENCE OF THE SNOW COVER AND CLIMATE INTERSECTION TO EXTREMELY HYDROLOGICAL SITUATIONS IN THE SNBMPUNTANE ZONE (NORTH SLOPE OS CAUCASUS AS AXAMPLE)**

Lev M. KITAEV (Department of climatology, Institute of Geography RAS)

The data bases of the snow thickness for the period 1966-1990 are compiled. In these bases 41 stations over the Great Caucasus ranges and 636 stations over the East European plain are included. The average snow thickness for the winter period (snowiness) is calculated. Their interannual changes in different regions in relation to atmosphere circulation are investigation. The coefficient of variation for the averaged values for all the plain and for all mountain stations is of the order 30%. For the single Caucasian stations with the high snowiness the coefficient of variation is about 30-45%, the maximum deviation is about 90%. For the single stations with the low snowiness the coefficient of variation is about 90-100% with 3-5 times maximum deviation. Over the East European plain with North Caucasian plain the snowiness was low over the period 1966-1977 and high over the period of 1978-1990. The zonal circulation prevailed in the first and the meridional one in the second period. The snowiness trend in 1966-1990 was positive. Cases of the high and low snowiness alternated incoherently over Grate Caucasus. The significant trend is absent. That is the result of different circulation factors of snow accumulation in dependence on the topography. In the high snowiness years over the Great Caucasus the frequency of the southern lows or the blocking high over the East European plain is above the average. During the blocking highs the western lows are concentrated the high southern periphery. In the half of years the anomalies signs for Caucasus and the plains are opposite. This has lead to the mutual compensation of melted run-off anomalies related to mountain and plash parts of the North Caucasian river basins. Combinations of extremely interannual maximal and minimal annual snow depth of Caucasus and its north submontane zone were generated. The potential contribution of a snow cover of extreme years to a river drain is revealed.

**HS02/10A/C24-022OP** Oral-Poster **1209**

**RISK ASSESSMENT OF FLOOD CONTROL SYSTEM OF THE YANGTZE CENTERED ON THE THREE GORGES PROJECT**

Shenglian GUO, Xiangrong TIAN, Caijun WANG, Honggang ZHANG, Pan LIU (Department of Hydrology and Water Resources, Wuhan University)

The Three Gorges project (TGP) is the largest hydropower project in the world. TGP possesses huge comprehensive benefits, including flood control, power generation, navigation improvement, etc. Flood control is the key and also the essential one with the largest ecological and environmental benefits. TGP's construction commenced in 1994 and the first turbine will generate hydropower in 2003 May, and the whole project will be completed in 2008. Based on the characteristics of flood control system of the Yangtze River centered on Three Gorges Reservoir (TGR), one and two dimensional hydraulic flood routing models and multiple-input single output linear system models were proposed and developed by using numerical methods and modern system engineering principles. Four inter-basins, Shashi, Luoshan, Hankou and Dongting Lake, are selected for flood simulation case study. The models were applied to these inter-basins and the simulated flood hydrographs were compared with those depicted from observed data. The river network in the lake region and the river-lake relationship are considerable complicated and investigated in detail. The results were satisfactory with high model efficiencies and low relative errors. The model will provide technical support and service for flood forecasting and flood dispatch decision as well as risk analysis in this region. The results show that under the condition of the 1998 large flood, if TGR conducting the compensation operation for the Jingjiang area, the highest water level in the Shashi, Luoshan and Hankou hydrological stations would decrease 0.86m, 0.78m and 0.44m respectively. The risk herein means that under different frequency of designed flood of TGR, how much is the risk corresponding to the flood control system of the Yangtze basin after the upstream flood is regulated by TGR. The 1954 large flood (with flood diversion) and the 1998 large flood (without flood diversion) are chosen as prototype for this study. The risk of flood control system in the Yangtze basin is analyzed based on the TGR operation regulations and flood detention area management rules. It is shown that with 22.15 billion m<sup>3</sup> of TGR regulating capacity and incorporating with embankment, flood diversion and other non-engineering measures, the bank failure along Jingjiang river reach due to heavy flood, which usually cause huge mortality and millions' homeless, can be effectively avoided. It can also protect millions people in downstream plain from flood menace and the consequent ecological and environmental destruction. The irreplaceable function of TGR for flood control will greatly ensure the harmonized development of social economy in the middle and lower reaches of the Yangtze.

**HS02/10A/C24-023OP** Oral-Poster **1213**

**CROSS-CORRELATION ANALYSIS BY KENDALL'S  $\tau$  BETWEEN CATEGORIZED SOI AND THE NONEXCEEDANCE PROBABILITY OF PRECIPITATION IN KOREA**

Young-Hoon JIN, Akira KAWAMURA, Kenji JINNO (Institute of environmental systems, Kyushu University)

El Niño/Southern Oscillation (ENSO) has influenced on the hydrological variables on global scale, but the influence of ENSO is not so clear in middle to high latitude including Korea and Japan. Especially, the quantitative influence of ENSO is difficult to be revealed in this region. There are several researches to reveal the correlation between Southern Oscillation Index (SOI) and the hydrological variables in Korea. Moon (2001) applied Multi-channel Singular Spectral Analysis (M-SSA) to the precipitation in Korea for identifying the coherent space-time patterns of low frequency harmonic element between SOI and the precipitation. Shin (2002) revealed the significant influence of El Niño/ La Niña on the flood and drought in Korea, using the statistical robust cross-correlation analysis. Kawamura et al. (2000) succeeded to detect the direct and significant correlation between SOI and precipitation/temperature in Fukuoka, Japan by categorizing SOI into five groups according to their magnitudes. Therefore we used the categorized SOI for revealing the relationship with the monthly precipitation at Pusan, Mokpo, and Incheon in Korea. In the kind of study, the appropriate transformation of the hydrological variables is often critical to obtain better results. It is difficult to normalize the precipitation data in the present study area because there are some months with no precipitation (less than 0.1 mm), whereas the precipitation data in Fukuoka were easy to be normalized by cubic root transformation. So in the present study we uniquely applied the nonexceedance probability transformation instead of the usual ones such as logarithmic and power transformations. We also applied Kendall's correlation coefficient ( $\tau$ ) when carrying out the cross-correlation analysis as well as the usual Pearson's correlation coefficient ( $r$ ). The Kendall's  $\tau$  is a rank-based procedure and is therefore resistant to the effect of extreme values and to deviations from a linear relationship. Most of all, this correlation coefficient can be applied to the data whose distribution is non-normal and unknown. These properties of Kendall's  $\tau$  are well suited for the data of the present study, because the used data cannot be easily transformed normally, as mentioned earlier. The results from these approaches which used the nonexceedance probability and the Kendall's  $\tau$  show that there are several significant correlations between the categorized SOI and precipitation in Korea. Especially, the correlation coefficients, which are significant at 1 % level in both Kendall's  $\tau$  and Pearson's  $r$ , were detected only at Pusan station under the "Strong La Niña" category with lag time four months. The correlation coefficients in both Mokpo and Incheon stations were obtained only at the 5 % significance level for various lag times. From these results, we can infer that the influence of SOI on the precipitation in Korea is stronger at Pusan than at both Mokpo and Incheon stations, and that the stronger the La Niña event, the less the precipitation four months later in Pusan.

HS02

Monday, July 7 - Friday, July 11

**WATER RESOURCES SYSTEMS: GLOBAL CHANGE, RISK ASSESSMENT AND WATER MANAGEMENT (ICWRS, ICASVR, ICSW, ICWQ)**

Location: Site C, Room 24

Thursday, July 10 PM

Presiding Chair: D. Rosbjerg

HS02/10P/C24-001

1400

**RESERVOIRS AND GLOBAL CHANGE - AN EVALUATION APPROACH**

Elke PETERSSON<sup>1</sup>, Manfred W. OSTROWSKI<sup>2</sup> (<sup>1</sup>Centre for Interdisciplinary Studies of Technology, Darmstadt University of Technology, <sup>2</sup>Institute for Hydraulics and Water Resources engineering, Darmstadt University of Technology)

The availability and quality of water have been crucial for the development of all human societies. On the other hand water bodies are integral parts of the natural environment. To satisfy societal water demands e.g. for domestic, industrial and agricultural uses, for electricity generation and to protect human settlements from extreme floods, systems for water storage and distribution have been developed over the centuries to balance the uneven distribution of water in space and time. Situated in the stream bed of a river, dams and reservoirs interrupt the natural hydrological cycle. Their dominant position in the hydrologic cycle makes them very sensitive to all kinds of changes in the catchment, among others global impacts on land use, climate, settlement structures or living standards. Vice versa dams strongly affect the spatially distributed, complex system of ecology, economy and society in the catchment both up- and downstream of the reservoir. The occurrence of negative impacts due to large dams led to serious conflicts about future dams. Nevertheless, water shortages due to climatic conditions and their changes, that are faced by enormous water and energy demands due to rising living standards of a growing world population, seem to require further dam construction, even if demand management is optimised. According to the American Society of Civil Engineers' sustainability criteria for water resource systems and the recent WCD report, the planning of a dam has to span its whole life cycle from options assessment to reassessment of an implemented project to decommissioning. The planning procedures of the future have to break up the rigidity of present day technology-focused planning assumptions, that are mainly based on information regarding actual and past conditions. In the long run this will open a greater scope, supporting the integration of supply security, risk issues, transience of the natural system and stakeholder acceptance. To reach a sustainable development in line with the WCD report the corresponding information and knowledge has to be carefully structured and evaluated. The highly complex and dynamical system of interrelated physical and non-physical processes that involves many different groups of stakeholders constitutes the need for a model-oriented decision support system. The major challenge is the development of a generic evaluation approach. In the given context the presentation will define the goals, the corresponding requirements as well as the difficulties of the evaluation approach. An integrated analysis and structure of the complex interrelations between dams, ecology, economy and society will be presented as the basis of the evaluation module. Furthermore potential users, their needs as well as the limits of computer-based evaluation procedures in the very specific context of dam construction will be identified. Special focus will be on the constraints arising from the need to jointly evaluate qualitative and quantitative aspects. In this regard the methodological potential of multi-criteria analysis will be investigated.

HS02/10P/C24-002

1415

**WATER MANAGEMENT IN INDIA'S NATIONAL WATER POLICY**

Sitharama Murty KOTTAPALLI (Coordinator of Geoarchives, International Commission on the History of Geological Sciences (INHIGEO))

The predominant source of water in India is the rainfall. The Himalayan rivers have an additional source in the glaciers which sustain a perennial supply. The peculiar climatic diversity the country has is also responsible for the variation in the water availability. The average annual precipitation by way of rain and snow over India's landmass is 4000 km<sup>3</sup>, but the annual water resources of the country have been estimated by the National

Commission as 1953 km<sup>3</sup>, including groundwater component of 432 km<sup>3</sup>. But the usable water resources as estimated by the Commission are 690 km<sup>3</sup> of surface water and 396 km<sup>3</sup> of groundwater, making up a total of 1086 km<sup>3</sup>. At present the resource used is about 600 km<sup>3</sup>. The growth in population, urbanization and demands from various sectors would find this insufficient. In fact, by the year 2050 this would be found inadequate as the total requirement of water would be between 973 to 1180 km<sup>3</sup> depending upon the projections. The National Water Policy, adopted in 1987 recommended that economic development and activities including agricultural, industrial and urban development should be planned with due regard to the constraints imposed by the configuration of water availability. It also stressed efficiency in the use of water and conservation consciousness in the minds of the people, through education, regulation, incentives and disincentives. Priority was accorded to drinking water. The inadequacies of the 1987 National Water Policy slowly began to be felt as a result of which the Central government recently announced a revised National Water Policy. Some major changes are: recognition of water as a part of a larger ecological system; rainwater harvesting is to be of much importance; watershed management through extensive soil conservation, catchment area treatment, preservation of forests and increasing the forest cover; drainage system recognized as an integral part of project planning; involvement and participation of beneficiaries and other stakeholders in the project planning stage itself and onwards; the need to get optimal productivity per unit of water; reclamation of water-logged / saline affected lands; monitoring and evaluating the performance and socio-economic impact of the projects undertaken. The National Perspective for Water Resources Development envisages a long-term plan of interlinking of rivers of the north to those in the south, that hopes to solve the problems of floods and drought etc. As per the constitution of India, Water is a State subject. The Supreme Court declared Water as a Fundamental Right. Any policy of management of water resources has to keep in mind these two basic points.

HS02/10P/C24-003

1430

**TOWARDS A NEW PARADIGMA FOR INTEGRATED WATER RESOURCES MANAGEMENT AND DEVELOPMENT IN INDONESIA**

Joesron LOEBIS (Research Coordinator on Water Resources)

By 1999 Indonesia is entering a whole new era by issuing and implementing the Law 22 on Regional Government. The spirit of the new law is to decentralizing the authority and responsibility from central to the regional government in aim to achieve more equals distributed welfare of the nation. Regional government are no more heavily dependent on central government policy. Instead now they have in their hand huge authority and responsibility to initiate the management of all self-nation resources. This covers all sectors, and water resources sector has no exception. Focusing on water resources sector, the effort taken in this time will concentrated on its management and development aspects regarding the strategic issue mention above. In order to achieve the objectives of efficiency and effectiveness of water supply to all stakeholders, it is a great urgency to implement the policy on 'one river basin, one plan and one integrated water resources management and development' This policies focusing on establishing proper institutional framework, exploring self-financial system management, legal aspect and water right in development and management. Here, establishing institutional framework is the main issue and priority, and indeed a very complex issue since intersecting domains of economic, society, law culture, science and technology. Thus, any consideration within this framework should involve an interdisciplinary analysis of all the above factors. Furthermore, it will cover several important activities that is modification of existing institutional and legal aspect on water resources related to present law and regulation, establishing networking on hydrological data collection, provided decision support system, conjunctive use on surface and groundwater at the local levels, water quality control and role shearing between central and regional government.

HS02/10P/C24-004

1445

**SOIL AND WATER CONSERVATION STRATEGIES IN THE LAKE OF RAWA DANO, WEST JAVA, INDONESIA**

Seno ADI (BPP Teknologi)

The Rawa Dano lake lies within the caldera of volcano in the west Java. Locally, Rawa Dano means swampy lake as indicated that the lake mostly covered by the swamp forest and water plantation in the elevation of 90's m above sea level. The lake ecosystem has a main role as a water supply for the Krakatau Industrial Estate as well as for the city of Cilegon, West Java. So the soil degradation in around this lake catchment as identified the sediment carried over 71 million ton/year or 3.32 ton/ha/year and water plant blooming is threatening of water resources availability. Therefore the soil and water conservation strategies are needed urgently to mitigate the erosion and nutrient loss to the lake. The civil engineering approach should be constructed by conducting the control dam, check dam, and gully plug/drop especially in the land slope of > 30% which is indicated by high erosion hazard. The vegetative approach then has to be implemented by conducting the minimum tillage farming, agroforestry, or farming forest. The establishment of the lake authority seems to be important to restore the hydrological function by controlling the forest encroachment, soil & water conservatin practice, and community development. Thus, the lake authority get the retribution from the water beneficiaries then the budget has to be reinvested for soil and water conservation practice.

HS02-Oral-Posters Monday, July 7 - Friday, July 11

**WATER RESOURCES SYSTEMS: GLOBAL CHANGE, RISK ASSESSMENT AND WATER MANAGEMENT (ICWRS, ICASVR, ICSW, ICWQ)**

Location: Site C, Room 24

Thursday, July 10 PM

Presiding Chair: D. Rosbjerg

HS02/10P/C24-001OP

Oral-Poster

1515

**ASSESSMENT OF IMPACT OF URBANISATION ON STORMWATER RUNOFF**

Rathnam Venkata ERVA, Jayakumar V. K. (Lecturer)

Increasing problems in urban stormwater management consequent to urbanization has been realized and appreciated in many hydrologic studies. Stormwater drainage and management systems are designed and constructed to cope up with the increase in runoff due to increased imperviousness of the land due to developmental activities. For the design of an adequate drainage system, it is essential to understand the changes in stormwater runoff quantity and quality with land use changes. Urbanisation usually results in increase in

volume and velocity of runoff, produces larger peak, decrease in the time to peak, downstream flooding and increase in pollutant loadings. The principal effects of land use change have been discussed by Geiger et al (1987), ASCE (1996) and Dunne and Leopold (1978), Overton and Meadows (1976), Urbanos and Stahre (1993) and many others. Runoff estimation techniques include: hydrograph methods and peak discharge methods. Many applications allow use of the peak flow analysis and the procedures are much less time consuming than the complete hydrograph method. The objective of the present study is to investigate the impact of land use changes due to urbanisation on stormwater runoff in part of Hyderabad city, in southern part of India. During the last 20 years, urbanisation has taken place at an alarmingly rapid rate in the Hyderabad city. Land use change maps and rainfall data for the period 1980-2000 are available. Using the available data, increase in built-up area and impervious surface with the progression of urbanisation are estimated. Design storms of different return periods 2, 5, 10, 25, 50 and 100- years are developed. SCS (NRCS) curve numbers and runoff coefficients are estimated. The generated runoff from different design storm is computed using a well documented package, SMADA, as well as the rational method, as to study how runoff volume is increasing with increase in impervious area. It is observed from the studies that the rational method gave higher peaks for all design storms, while the SMADA, which uses SCS hydrograph method resulted in increased runoff duration. An assessment is also made of possible expansion of built-up area with increased urbanisation in future and consequent storm runoff volume is investigated.

**HS02/10P/C24-0020P** Oral-Poster **1519**

**USE OF PHYSICALLY BASED MODEL FOR FLOOD ESTIMATION IN SMALL CATCHMENTS IN A DATA SCARCE ENVIRONMENT**

Jayakumar KANDATHIL VALAPPIL<sup>1</sup>, Ramaseshan S.<sup>2</sup> (<sup>1</sup>Regional Engineering College, <sup>2</sup>Indian Institute of Technology)

Estimates of flood are required for the design and economic appraisal of a variety of engineering works. When adequate and appropriate data area available for the basin, conventional methods like frequency analysis or use of unit hydrographs and other rainfall-runoff procedures may be applied to model the basin system. When this is combined with the design storm, the design flood may be derived. Data available for small catchments are generally inadequate for these approaches. Empirical approaches may be used to model such small catchments. Since generally adequate data are available for estimating design storms, it seems worthwhile to derive relationships between storm rainfall and runoff. The parameters of the model may then be related to the characteristics of the storm and physiographic features of the watershed to yield regional relationship between storms and floods. But a more realistic and alternate approach is to model the catchment runoff process according to physical principles. Information regarding physiography, soils, vegetation and drainage pattern of the catchment is used in the physically based models. The catchment is decomposed into a network of channels and overland flow segments. Using the physical characteristics of each component and appropriate hydraulic equations, the hydrologic processes are simulated using the distributed parameter model. Necessary values of the coefficients and constants are specified from physical characteristics of the watershed or are obtained from calibration of the model with observed data. The study reported is essentially a regional case study of flood estimation in small catchments in a part of North Brahmaputra basin, in the north-eastern part of India. The scope of the study is to apply, in a data scarce environment, a physically based model, DRRM and to study the regional variation, if any, of the parameter of the model and also to judge the validity for flood estimation. Data regarding catchment plan, cross section at the bridge sites and hourly rainfall and stage data for about 10 catchments in the region were available for the study for a very limited period of 3 to 4 years. The catchment area ranged from 7 km<sup>2</sup> to 215 km<sup>2</sup>. After preliminary analysis of the data for errors, only seven basins were found to be suitable for analysis. The results of the study indicated that a constant parameter physically based model for small catchments in the region is realistic. The design flood estimated using this model compared favourably with other approaches reported in the literature. The study shows that because of the easy availability of, and competence with computers and software in field organizations, it seems preferable to adopt a distributed parameter model with relevant field data rather than using empirical statistical relationships of questionable reliability.

**HS02/10P/C24-0030P** Oral-Poster **1523**

**PHYSICALLY-BASED MODELS FOR FLOODS MODELLING IN THE MEDITERRANEAN AREA**

Philippe GOURBESVILLE<sup>1</sup>, Vincent GUNOT<sup>2</sup> (<sup>1</sup>University of Nice- Sophia Antipolis, <sup>2</sup>International Institute for Infrastructural Hydraulics and Environmental Engineering - IHE)

Extreme hydrological events are characterised by the scarcity of data (in terms of spatial and temporal frequency). This problem becomes more acute when it comes to modelling the response of large catchments with small concentration times due to particular morphology or rainfall intensities. The classical approach to modelling, (that consists of trying of tuning the model parameters so as to bring the calculations as close as possible to the measurements) becomes highly questionable because it may turn out to be extremely harmful to the predictive power of the model. The present paper addresses uncertainty in modelling the flash flood of 05.11.1994 on the Var watershed (France, 2820 km<sup>2</sup>). This watershed, located in the French riviera, is characterised by steep slopes, narrow valleys and large topography curvatures, making the flow pattern extremely complex. Seven models of the catchment were built using the Mike She hydrological modelling system. These models have different structures, geometries, or parameter values. The analysis of the model results on the flash flood of 05.11.1994 leads to the following conclusion: - the physically based approach is efficient and the flood characteristics are well reproduced; - the main sources for uncertainty in model results are, by decreasing order of importance: (i) the model structure, i.e. the assumptions concerning the dominant phenomena and how they are modelled, (ii) the model geometry and (iii) the value of the model parameters. This shows that, for this particular case at least, it is much more important to have a good knowledge of the phenomena occurring on the catchment, as well as of the particular geometrical feature, than to try to calibrate the parameters of the model. On the contrary, blind calibration of the model may jeopardise its predictive capabilities.

**HS02/10P/C24-0040P** Oral-Poster **1527**

**FLOOD FORECASTING & MANAGEMENT IN PAKISTAN**

Shaukat A. AWAN (Pakistan Meteorological Department)

Floods in Pakistan are mainly caused by the heavy monsoon rains during the summer monsoon period from July to September. Meteorologically there are two situations which cause flood producing rains in the upper catchments of the rivers. The two meteorological situations in relations to different conditions of intensity and movement of low/depression may produce three categories of floods as described below. i) Meteorological Situation for Category-I Floods A situation when the seasonal low is a semi permanent weather system situated over south eastern Balochistan, south western Punjab, adjoining parts of Sindh get intensified (due to westerly wave) and causes the moisture from Arabian Sea to be brought

up to upper catchments of Chenab and Jhelum rivers resulting in heavy downpour along windward slopes of mountain ranges due to orographic lifting of moist air mass. ii) Meteorological Situation for Category-II & Category-III Floods Second flood generating meteorological situation is linked with monsoon low/depression. Such monsoon systems originate in Bay of Bengal region and then move across India in general west/north westerly direction arrive over Rajasthan or any of adjoining states of India. After this monsoon depression may take any one of following three courses. a) Continue moving straight west causing heavy wide-spread rains over Sindh/Balochistan. However, no river flooding shall occur in this case. b) Recurve in the north east direction towards upper catchments of Sutlej, Ravi and Chenab rivers causing extremely heavy rainfall and consequently floods first across border in India and then (within hours) at Rim Stations in Pakistan. This is Category-II flood situation. c) Continue moving in northerly direction (under the effect of a strong westerly over plains of Lahore/Gujranwala Divisions to finally end up over Rawalpindi/Hazara Divisions. Upper catchments of Chenab, Jhelum and Indus rivers come under its influence. Flood management process in Pakistan is multi-functional involving a number of different organizations. First step in the process is issuance of flood forecast/warning. This function has been assigned to Pakistan Meteorological Department (PMD) since basic cause of the floods in Pakistan is the rainfall which can be best predicted and monitored by PMD utilizing satellite cloud pictures and quantitative precipitation measurement radar data, in addition to the conventional weather forecasting facilities. For quantitative flood forecasting, hydrological data is obtained through Provincial Irrigation Department and WAPDA. WAPDA's telemetric system is an important source of hydrological data for flood forecasting purposes. A most modern 'S-Band' Doppler weather radar has recently been provided to PMD, while a new hydrometric data measurement and transmission system is being established by WAPDA. Furthermore, improved rainfall/runoff and flood routing models have been developed to provide more reliable and explicit flood information to flood prone population.

**HS02/10P/C24-0050P** Oral-Poster **1531**

**DETECTION ON RAINFALL VARIETY IN WESTERN TAIWAN**

Pao Shan YU, Chia Wen SUNG, Tao Chang YANG (Department of Hydraulics & Ocean Engineering, National Cheng Kung University)

Global climate change and its influence on water resource are the worldwide issues. This paper aims to investigate the variety of historical rainfall on Taiwan. This study on local climate change may provide the reference for climate change study on Asia region. As the area of Taiwan is too small, the GCM is not suitable for our investigation on climate change. Therefore, the statistical method of Mann-Whitney-Pettitt test was applied to detect the change points of annual rainfall depth in the historical records. Rainfall records from four meteorological stations of the Central Weather Bureau distributed over western Taiwan, including Taipei, Taichung, Tainan and Hengchunstations, were adopted as our data set which almost have one hundred years records. It is found that the change points at these four stations vary from 1956 to 1968. As the rain fall during May and June is important for the reservoir operation in Taiwan and the annual maximum daily rainfall has extreme influences on the rainfall design. Hence, the difference between rainfall characteristics, including the rainfall during May and June and annual maximum daily rainfall, before and after the change point for each station was investigated. This work found that the rainfall during May and June, and annual maximum daily rainfall in Northern Taiwan have increase trend. However, the rainfall characteristics in the Middle and Southern Taiwan have decrease trend. For example, the 100-year return period maximum daily rainfall estimated by using Log-Person type III in Northern Taiwan increases around 17%. There are decrease round 20% in the Middle and Southern Taiwan.

**HS02/10P/C24-0060P** Oral-Poster **1535**

**THE INTEGRATED RISK ANALYSIS OF OVER-STANDARD FLOOD FOR FLOOD CONTROL SYSTEM**

Xiang ZHANG<sup>1</sup>, Xinyu WANG<sup>2</sup>, Guowei LAI<sup>3</sup> (<sup>1</sup>Dept. of Hydrology and Water Resources, Wuhan University, <sup>2</sup>Institute of Planning and Design, Changjiang Water Resources Commission, <sup>3</sup>Dept. of Hydropower, Wuhan University)

The flood control system mainly consists of reservoir, levee and flood spreading area with a certain flood control standard. The natural flood is a stochastic event. No matter how high the flood control standard is, the probability that the flood exceeds the standard still exists. So the risk analysis for the over-standard flood is very important for the flood control planning and the construction of flood control system. The traditional flood risk analysis may mainly concern with the hydrological and/or hydraulic uncertainty. The engineering uncertainty, such as the reliability of dam and levee, is seldom considered combined with them. In fact, facing the over-standard flood, the reliability of dam and levee strongly influence the ability of flood control system resisting flood. So the integrated risk analysis, considering the hydrological and engineering risk, may provide more thoroughly the information about the ability of flood control system. For the hydrological risk analysis of over-standard flood, we apply the compound Poisson model. It is a kind of risk value model based on stochastic point process theory and is superior with the typical characteristic discussing the frequency problem in time domain. Its discharge threshold for the selection of sample can be very low, and the discharge or the flood peak exceeding the threshold may be selected as the samples. It has been used to study the annual over-standard flood risk of flood control system. The engineering risk is caused by the uncertainty factors that influence the safety of engineering structure, including the load and the mechanics characteristics of material. In this paper, we apply the reliability theory to evaluate the engineering structure safety. The methods for the engineering safety of gravity dam and earth bank are discussed respectively. In order to calculate the integrated risk rate, the hydrological and engineering risk are considered as compatible events. The Selective Probability is used to calculate the integrated risk rate of compatible events. The case study about the flood control system in the Lishui catchment is done. The objective of flood protection is to control that the designing flood of 50 year recurrence through the operation of flood control system is lower than the safety discharge of downstream channel at Sanjiangkou station, 12000m<sup>3</sup>/s. So we discuss the three different operating schemes by the hydrological risk analysis, and calculate the engineering safety of the three dams and levee in Lishui catchment. Through the integrated risk analysis, the optimal operating scheme and the weak link in the flood control system are suggested. The result illustrates that these methods are practical in integrated risk analysis of flood control system and the results of integrated risk analysis are useful in decision making for flood control planning.

**HS02/10P/C24-0070P** Oral-Poster **1539**

**LONG-TERM CHANGE IN DAILY RAINFALL CHARACTERISTICS AT OKAYAMA**

Hidetaka CHIKAMORI, Akihiro NAGAI (Faculty of Environmental Science and Technology, Okayama University)

Rainfall characteristics is said to change in recent decades. It is said that rainfall has concentrated in the shorter duration than before so that occurrence of extreme hydrological events like floods and droughts have become more frequent and the disasters related to

these events become more severe than before. The changes are attributed to global climate change like global warming and/or local environmental change like heat island effect. The purpose of this paper is to statistically clarify the long-term change in rainfall characteristics, that is, frequency distribution of rainfall depth, rainfall and no-rainfall duration and so on. A statistical analysis was performed for 100-year (1898-1997) daily rainfall record at Okayama Meteorological Observatory, Japan. In this analysis, we defined a storm as a succession of rainy days, and examined statistical characteristics of total rainfall and duration of a storm, storm inter-arrival time and interval between storms. The record was divided into two 50-year periods or three 33-year periods. In the two periods case, the period of 1898-1947 and that of 1948-1997 were named as  $I_{50}$  and  $II_{50}$  periods, respectively. In the three periods case, the period of 1899-1931, that of 1932-1964 and that of 1965-1997 were named as  $I_{33}$ ,  $II_{33}$  and  $III_{33}$  periods, respectively, where the record of 1897 was excluded for the analysis. First, we examined frequency distribution of annual maximum of a storm rainfall in each record period, and found that the storm rainfall with the equally probability is becoming larger year by year. Gumbel distribution was applied to each data of the record period, and the result shows, for example, that 100-year storm rainfall increases by 17% in the period  $II_{33}$  and by 67% in the period  $III_{33}$  comparing with that in the period  $I_{33}$ . Second, we examined frequency distribution of storm duration and found that the storm duration tends to decrease from year to year. Thus the more rainfall happens in the shorter duration so that average rainfall intensity in a storm tends to increase. Finally, we examined frequency distribution of interval between storms, and found that the interval tends to increase year by year. Gumbel distribution was applied to each data of the record period, and the result shows, for example, that 100-year interval between storms in the period  $III_{33}$  becomes five times larger than that in the period  $I_{33}$ . The results show the apparent change in frequency distribution of rainfall characteristics in recent decades. The change tends to shorten return period of the hydrologic design value such as design discharge or design rainfall of the water use or control plans designed before so that the risks of floods or those of droughts are both increasing. The fact suggest us necessity to reconsider magnitude of design floods and droughts for water resources planning and management.

**HS02/10P/C24-0080P Oral-Poster 1543**

**HYDROLOGICAL REGIONALIZATION USING THE TCEV METHOD WITH THE SUPPORT OF A GEOGRAPHICAL INFORMATION SYSTEM**

Cristiane M. FINZI, Iara Righi AMRAL, Bruno Rabelo VERSIANI (Centro de Pesquisas Hidráulicas e Recursos H<sub>2</sub>O Aricos - EHR - Escola de Engenharia - UFMG)

The analysis of a statistical model allows a better evaluation of the spatial variability of the hydro-climatological phenomena. The application of that model is called "regionalization". The paper focus the Two Component Extreme Value, TCEV Model, (Rossi et al., 1984), which tries to describe the extreme values of a statistical series, as maximum precipitation an maximum flood data. The regionalization method based on this model allows to identify hydrological homogeneous regions in a watershed, in terms of maximum values of precipitation and flood. The determination of those regions allows to evaluate realistic estimates for the involved variables, concerning studies and projects of water resources management, in the state of Minas Gerais, Brazil, mainly in a watershed where there is a lack of data. Previous studies applied the method in the southern portion of the Sao Francisco watershed. In this paper one compares the results when more data are included extending the study region. The statistical characteristics of maximum precipitation and flood determine the homogeneous regions. The methodology is developed in three stages: the first seeks the determination of the homogeneous regions according to the similarity of the coefficient of skewness and the second stage is the determination of sub regions where the coefficient of variation remains practically constant. The third stage is the determination of the index flood, based on the physical and climatic characteristics of the region. The results of the application of the methodology are the quantile estimates of the maximum values of precipitation and flood, specially in some regions with lack of data. In this application, one determine three homogeneous concerning maximum flood and five regions concerning maximum precipitation. In some of those areas the statistical regional curve is similar to the Gumbel model. In this case the TCEV method could not be applied. This means that the samples used in the calibration of the regional statistical model don't identify outliers values.

**HS02/10P/C24-0090P Oral-Poster 1547**

**WATER RESOURCES SUSTAINABILITY IN THE CONTEXT OF CLIMATE VARIABILITY AND INCREASING EXTREME EVENTS IN THE HIMALAYAN-INDO-GANGETIC PLAINS**

R. B. SINGH (Department of Geography, University of Delhi)

The Himalayan environment is subject to significant and uncertain changes. Variation in climatic conditions could result in large-scale changes in the Indo-Gangetic ecosystem. The Himalaya which is fragile and globally important ecosystem, is also known as the water towers of the earth surface and rich repositories of biological diversity. Variability in climatic conditions influence water resource sustainability of the plains. In the present paper an attempt has been made to analyse the impact of climatic variability and other mountain extremes particularly floods on the Indo-Gangetic plains. Paucity of observational data and analysis makes the study on mountain areas rather difficult. The issues of Himalayan - Indo-Gangetic plains interactions including the nature and quantities of materials transported from highland to valleys along with the dynamics of land use induced sediment erosion processes and floods attract particular attention at different temporal and spatial scales. The Indo-Gangetic plains include region of national significance in terms of dense and increasing human population. There exists very large and variable discharges of fresh water, suspended sediments and dissolved matter. The present pattern of flooding suggests that high productivity is no longer being sustained. Shrinking natural resource base (per capita availability of land/water devoted to agriculture) and declining quality of resources are increasing the risk to our ability to meet the basic needs of the growing population of the region. In addition a range of socio-economic factors emerging out of flood problems impact land use and the food security. Investments in irrigation development are unattractive and have declined. Competing uses for water would force shifts in crops/cropping pattern. Soil-characteristics as well as cropping system in the Indo-Gangetic plain region is largely uniform. There are, however, a number of variations within the region. There are 6 agro-ecological regions and 12 sub-regions. Irrigation facilities are available to the maximum extent in the north-west and minimum in the east. The size and distribution of the land holding varies from 3.6 hectares in the north-west to approx. 1 hectare in the Bengal Region. There are vast differences in actual and potential yields, earning from about 6-tons/hectare in the north-eastern region to as low as 2 tons/hectare in the east having frequent flood prone areas. Major sustainability issues require focus on the ecosystem functioning, agro-biodiversity (including soil biota), loss in soil fertility, hazards, declining water table and rising water table / water logging etc. Managing floods in one region often co-exists with managing droughts in another region. The need for a comprehensive watershed based planning integrating land and water resources is urgently felt so as to monitor and manage the water resources of this region optimally. The strategy reflects a major conceptual shift towards risk reduction i.e. culture of prevention.

**HS02/10P/C24-0100P Oral-Poster 1551**

**APPROACH FOR ASSESSMENT OF RISK AND CHANGES IN EXTREME HYDROLOGICAL CHARACTERISTICS**

Helen (Elena) Vladislavovna LOBANOVA (IAHS member, Senior Scientist)

One of the main practical application of hydrology is connected with a frequency analysis of extreme hydrological events such as floods and droughts. New Federal normative documents in Russia (Construction Norms and Rules, Code of Rules) take into account two kind of safety and risk assessment: -for existing water projects under some period of operation, -for future water projects. The first direction condition by the following reasons: short-term records in the past, new effective methods of computations which have been developed in last time, modern changes (climate change, man's impacts). These peculiarities lead to a necessity of possible re-computation of design hydrological characteristics for the existing hydraulic constructions and other water projects to increase their safety. The algorithm of assessment and re-computation includes the following main steps: -extraction of the components in time series which connect with "natural" conditions and with "pure" impact of existing constructions on the runoff; -assessment of stability of working existing hydraulic constructions and other water projects (analysis of man's activity component); -assessment of climate change in time series in "natural" conditions (extraction and analysis of modern long-term climate change component); -determination of design extreme values taking into account the last observation, new methods and changing conditions; -comparison of the determined design values with the same one, which have been obtained before the construction of this hydraulic structure and making the decision about the re-computation. Such scheme characterizes a monitoring of design hydrological characteristics for changing conditions. New methods have been developed for a realization of this algorithm and they are: -methods for extraction of runoff components connected with operation by existing hydraulic and other kind of constructions and under different availability of the information; -methods for extraction of climate variability and long-term climate change components; -methods for assessment of statistical efficiency and contributions of climate change and water management; -assessment of empirical probability of non-regular extreme events such as floods and droughts taking into account historical information; -decision the problems of non-homogeneity of the extreme data by statistical criteria for testing of outlying data and application of the composition of distribution functions for non-homogeneous records; -methods for assessment of random errors of design hydrological events taking into account short-term period of the regular observations, palaeo-restorations and long-term period of future operation in changing conditions. Application of developed approach and methods have been given for some different examples: -re-computation of maximum design discharges for the cascade of the Dnieper hydropower stations; -re-computation of design maximum water level for the Lena River - Lensk city; -assessment of long-term operation of main hydropower stations in Russia for different hydrological characteristics (water resources, extremes, etc); -using of palaeo-restoration of annual runoff in more than 4000 years for assessment of climate changes and random errors of design values; -assessment of changes in low flow for different regions of Russia under climate change.

**HS02/10P/C24-0110P Oral-Poster 1555**

**ASSESSMENT OF THE RISKS OF EXTREME RAINS OCCURENCE DEPENDING ON THEIR GENESIS**

Ionel Haidu (Dept.of Geography, Univ.of Cluj-Napoca)

Usually, in a study that has in view the rain falls that produce high floods, a single raw of maximum yearly values are to be analyzed, indifferently of the type from which those rains derive. It is to be appreciated that the rains with a maximum intensity are "covering", and there is no need to apply to diverse informative sources. This is a quantitative concept which refers only to the magnitude of the extremes (torrential rains, high floods) which would have unexpected hydrotechnical and social consequences. On the other hand, a qualitative approach, respectively the analysis of the extremes on genetic categories may reduce the uncertainties. It is possible that the set of the extremes (for instance, in the case of the rains with a yearly maximum intensity, but also in other cases) will lack the same statistical population as a source. Another example is given by the possible appearance in the observations raw of a value with an extraordinary magnitude, which is aberrant from a statistical point of view, and which must be removed by the analyst from the analyzed sample, in order to obtain "fair" adjustments. Thus, the historic maximum intensity of 8.5 mm/min registered at Borod station (west of Romania) that far exceeds the value of 2.77 mm/min, representing the average of those 28 years of observations, can not be explained by the statistics of extreme values. That's why it is useful to set up series of values on genetic categories, suspecting the possibility to find out many source-populations of the extremes. Besides the series of yearly maximum intensities, set up indifferent of the generating rain type (28 values), the succession of yearly maximum intensities produced by rains of thermic convection and the series of yearly maximum intensities produced by frontal rains, have been built. Were considered too, series having source couple of months: May-June typical of the most intense period of cyclonic activity and July-August specific for the most active period of thermic convection. For the length of the whole rainy season (April - September), in which the rains of thermic convection and the frontal rains can coexist, the monthly series of maximum intensities was also taken into consideration. While the frequency model of the series of yearly maximum values is, clearly, that of an exponential type, the genetic series are different. The maximum intensities generated by convective rains can be also adjusted through a lognormal model of 2 parameters though from the point of view of graphic correspondence, the best law is that of GEV type, on the theoretical curve being situated even the historical maximum of 8.5 mm/min. In the case of frontal rains, the candidate laws are Gumbel, Lognormal and exponential, and from those with 3 parameters, the GEV. The most adequate laws for the case of bimonthly and monthly series are also described. The paper approaches in its final part the possible genetic explanations of the extreme events, which can have different consequences as regards the high floods appearance.

**HS02b-Posters**

**Thursday, July 10**

**WATER RESOURCES SYSTEMS: GLOBAL CHANGE, RISK ASSESSMENT AND WATER MANAGEMENT (ICWRS, ICASVR, ICWS, ICWQ)**

Location: Site D

Thursday, July 10 PM

HS02b/10P/D-001 Poster 1630-121

**A TREE MODEL FOR RAINFALL PREDICTION**A.W. JAYAWARDENA<sup>1</sup>, Xu PENCHANG<sup>2</sup> (<sup>1</sup>Department of Civil Engineering, The University of Hong Kong, <sup>2</sup>Institute of Applied Mathematics, Chinese Academy of Sciences)

One of the unique characteristics of daily rainfall data in any region is that the time series contains a large number of zeros. This poses problems in modeling using either deterministic or stochastic approaches. In general, rainfall data has a deterministic behaviour in the large time scale and a stochastic behaviour in the small time scale. In this study, it is proposed to model daily rainfall by using tree models of average rainfall values and their transmitting probabilities. It is assumed that the average rainfall in a fixed long period of time in each year is similar, and in a short period within that long period, it is stochastic. The long term can be a season or a certain number of months. For simplicity in bifurcating at each successive level, a period of 64 days is considered as the long time scale (64 is a power of 2). If, for any given year, the 64 days average rainfall is considered as the root of a tree which has 2 branches which in turn has two branches until it comes to the daily rainfall. The next step is to determine the transmitting probability from the root to the branches in succession. The probability tree also will have a structure similar to that of the rainfall value tree. The probability tree can be obtained by defining the probabilities as functions of the values of rainfall at each level. With these two tree models, and knowing their root values, the rainfalls at all other levels can be estimated. This method is applied to simulate rainfalls at a number of stations in Hong Kong and in Thailand. The results are encouraging.

HS02b/10P/D-002 Poster 1630-122

**CHARACTERISTICS OF INTERCEPTION LOSS AND FORMULATION OF AN APPROPRIATE MODEL FOR THREE REGIONS WITH DIFFERENT CLIMATE AND FOREST CONDITION**Tae TOBA<sup>1</sup>, Tekeshi OHTA<sup>1</sup>, Nobuaki TANAKA<sup>3</sup> (<sup>1</sup>Graduate School of Bioagricultural Sciences, Nagoya University, <sup>2</sup>Frontier Observational Research System for Global Change, <sup>3</sup>Graduate School of Agriculture and Life Sciences, The University of Tokyo)

In the future, changes in the water cycle resulting from climate changes will seriously affect water resource management. Knowledge of the characteristics of interception loss on a regional scale is important for understanding changes in the water cycle and for water resource management. In forests, the percentage of gross precipitation lost to interception usually ranges from 10 to 40%. When considering interception losses on a regional scale, an understanding of forest structure and of climatic conditions, i.e. precipitation, is much more important than it is in analyses on a patch scale. Therefore, an interception loss model that is appropriate for various forest types is needed. We analyzed the characteristics of interception loss at eight locations with different climate and forest conditions, in boreal (east Siberia), temperate (Japan), and tropical (Thailand) forests. We used an interception loss model (Toba and Ohta, 2002) that was calibrated using data for six locations in two of these regions, and validated this model with the results for the remaining two points in two regions. Three study sites were located at 62°N, 129°E in boreal forest, three at 39°N, 140°E and one at 35°N, 137°E in temperate forest, and one at 18°N, 98°E in tropical forest; the forests had plant area indexes (PAI) ranging from 2.8 to 11.1. The PAI reflects forest structure. Throughfall, stemflow, gross precipitation, and meteorological elements (air temperature, relative humidity, wind speed, etc.) at each site were observed. Compared with gross precipitation measured at open sites, the percentage lost to interception ranged from 10 to 20% in the boreal forest, 10 to 15% in the temperate forest, and was about 10% in the tropical forest. We have not analyzed the characteristics of interception loss for the tropical forest site in detail yet, but these results will be described later in a full paper. At the other sites there were clear relationships between interception loss and precipitation intensity, saturation deficit, and rainfall duration. The canopy storage capacity increased with the PAI. Parameters in the model were decided using the relationships of throughfall, stemflow, and gross precipitation. We then evaluated the characteristics of interception loss using this model.

HS02b/10P/D-003 Poster 1630-123

**CHANGES IN THE HYDROLOGICAL CYCLE AND ITS EFFECTS ON THE ENVIRONMENT IN AN INLAND RIVER BASIN OF WETSREN CHINA**Jumpei KUBOTA<sup>1</sup>, Tomohiro AKIYAMA<sup>2</sup>, Yusuke YAMAZAKI<sup>3</sup> (<sup>1</sup>Research Institute for Humanity and Nature, <sup>2</sup>Graduate School of Environmental Studies, Nagoya University, <sup>3</sup>Graduate School of Agriculture, Kyoto University)

This paper focuses the effects of changes in the hydrological cycle during the past fifty years caused by the water resource development on the environment in the Heihe River basin, an inland river of the arid region in the western China. The Heihe River basin consists of three parts, namely the upper mountainous area which is the source of the Heihe River by rather big amount of precipitation and glaciers, the middle oasis area like Zangye and Jiuquan, and the lower terminal arid area like Ejina. Each area has independent hydrological condition and ecosystem. Surface runoff from the upper mountain area by rain and melt water of snow and glaciers is the only source of water available in the middle oases area and the lower arid area. The increase of water demand in the middle oases area mainly by irrigation for agricultural land has resulted in the decrease of surface water supply for the lower arid area. The degradation of vegetations and the difficulties of the usage of shallow groundwater in terms of not only quantity, but quality have become serious problems. Even in the middle oasis area, over 80% of the total discharge has been diverted from main river courses to many irrigation canals, resulting in not only the rise of groundwater level inside the cultivated oases, but also the increase of soil salinization area. At the same time, the decrease of discharges in the main river courses have formed deserted area. Developing a distributed hydrological model with the grid based information of land use and irrigation systems, the spatial distribution water budget in the Heihe River basin has been evaluated. The relationship between the water status and the degradation of vegetations and water quality were investigated. Based on this analysis, we found that the strategies of farm production in each area are closely related to hydrological status. Also, using several future scenarios including possible climate change and expansion of the economy of this area, the proper way to use the limited water resources minimize the degradation of the environment will be discussed.

HS02b/10P/D-004 Poster 1630-124

**SUB-SURFACE WATER CONTRIBUTION TO SURFACE WATER USING STOCHASTIC DIFFERENTIAL EQUATION**

Gouldaria K. NOURBAEVA, So KAZAMA, Masaki SAWAMOTO (Department of Civil Engineering, Tohoku University)

The scheme is proposed to analyze the distribution of soil water balance characteristics in a river catchment. The water movement processes are considered using stochastic differential equation (SDE) to obtain the dynamics of interrelated catchment parameters including water table depth, soil saturation and equilibrium soil moisture content. The SDE includes total prediction error modeled as a wideband stochastic process with zero mean. The non-stationary solution of SDE is derived by the efficient fourth order Runge-Kutta approximation method. The Van Genuchten-type relationship is used to obtain the soil water content values from water table predictions. The Kalman filter was used to calibrate the stochastic model to measured data. The discrete-time recursive routine such as Kalman filter gives a maximum likelihood criterion in terms of the differences between measurements and predictions. Aquifer screen variation for single location was modeled from measured data. The spatial distribution of water table depth is evaluated from contributing area concept based on the relationship between topographic index and water table depth. According this theory, soil moisture depends on the location on the hillslope at the catchment scale and the water table depth is a function of flow accumulating area and location slope. Under topographic index conception from hydrologic and topographic characteristics of catchment, the distribution of water table depths, equilibrium soil moisture content and specific discharge in each time step were predicted. The model has adapted to a specific character of the Natori River basin in Japan as mountain catchments. The spatially distributed data considered in the modeling are designed as raster data to be compatible with GIS software. The contributing area and slope for each location are calculated using digital elevation model of the catchment. Predictions are obtained as time series of digital maps with 1km grid scale. In the case of the scant sources observed data, described technique gives preliminary representation of full space-time distribution of water budget characteristic in the catchment. Proposed scheme can be useful for assessment of water resources redistribution in the river basin at temporal and spatial scale.

HS02b/10P/D-005 Poster 1630-125

**EVOLUTION OF THE SOIL WATER STORAGE UNDER PRESENT AND CHANGED ATMOSPHERIC CONDITIONS**

Urszula SOMOROWSKA (Faculty of Geography and Reg.Studies, Warsaw University, Krakowskie Przedm.30,00-927 Warsaw, Poland)

The wetness status of land surface is an important element of the soil-plant-atmosphere systems. Traditional approach assumes that main factors affecting spatial and temporal patterns of soil water content include precipitation, evapotranspiration, groundwater levels, topography, vegetation and soil types. The soil water storage balances the temporal surplus of water supply from precipitation against the atmospheric demands for evapotranspiration. In case of shallow groundwater levels the volume of the soil water storage is dependent on the groundwater level fluctuations. This study is a search for interactions between soil water storage and precipitation - main factor responsible for recharge of the soil water resources. The focus is on the dynamic soil water resources of the lowland basin situated in the central region of Poland, in the protected area of the Kampinos National Park. The analysis is based on field measurements of soil moisture conducted over the period 1995-2002 in fourteen representative sites. The measurements were conducted using Time Domain Reflectometry meter tracking the characteristic stages of soil water storage of shallow soil layers. Specific question to be answered is what is the basin's inertia that affects subsequent evolution of the soil moisture stages, and, in consequence, soil water storage. Enabling the answer to this question requires (i) understanding the soil moisture variability and interdependencies between soil moisture and key factors e.g. precipitation and evapotranspiration (ii) quantifying the effects of hazard atmospheric situations on the volume of soil water storage (iii) setting the scheme for predicting soil water storage under extreme atmospheric conditions. Range of natural variability of soil water storage was derived from the soil moisture profiles detected. Extreme and normal stages of the soil water resources were related to the antecedent precipitation. It was found that at least four months' antecedent precipitation has an influence on temporal stages of the soil water storage, thus the system has its memory. Inertia of soil water resources has been additionally investigated indirectly by applying autocorrelation function to the monthly minimum baseflow. Evolution of the soil water storage have been analyzed for the observation period of eight years. Additionally, the changes in the volume of the soil water storage have been estimated depending on the depletion of groundwater level in selected dry, wet and normal years over the period 1955-2002. In this case water storage decrease function was applied which is a simple correlation model allowing estimation of water deficits as an effect of groundwater level drop. Depletion of soil water storage was set as dependent from the deficit of precipitation (precipitation minus evapotranspiration). The relation was parameterized according to the logarithmic equation established for wet, dry and average years. Assuming exaggerated atmospheric conditions, the depletion of soil water storage can be predicted.

HS02b/10P/D-006 Poster 1630-126

**CLIMATE, WATER AND ENERGY IN THE NORDIC COUNTRIES**

Arii SNORRASON, Jona Finndis JONSDOTTIR (Hydrological Service, National Energy Authority)

In light of the recent IPCC Climate Change assessment and recent progress made in meteorological and hydrological modeling, the directors of the Nordic hydrological institutes (CHIN) initiated a research project **Climate, Water and Energy** (CWE) with funding from the Nordic Energy Research and the Nordic Council of Ministers focusing on climatic impact assessment in the energy sector. Climatic variability and change affect the hydrological systems, which in turn affect the energy sector, this will increase the risk associated with the development and use of water resources in the Nordic countries. Climate and hydrology are thoroughly intertwined through the hydrological cycle. In fact, one can claim that climatic change is nowhere more clearly manifested than in hydrological systems and processes. Changes in precipitation and temperature will have direct influences on runoff. Glaciers are especially vulnerable to climate change, for example increased temperature may result in increased runoff, at least temporarily. Climatic change may have a large influence on the temporal distribution of runoff within the year. The impacts on the hydropower industry are many and varied, many of which are directly linked to the hydrological changes. Climatic change will affect the hydropower sector in general. The changes will affect the total water available as well as both its spatial and temporal distribution. This will create both opportunities and benefits to the hydropower sector, but also problems and costs. In fact, it can be stated that the risk, in general, will increase due to increased hydrological uncertainty caused by climatic changes. New investment and design, as well as operational and management practices are needed to respond to these changes. The product of the project will be an in-depth analysis of the present status of research and know-how in the sphere of climatic and hydrological research. Furthermore it will be a synthesis and integration of present research with focus on the needs of the energy sector. It will also identify and prioritize key future research areas for the benefits of the energy sector. Finally it will provide comprehensive research proposals for top priority research areas. The Climate, Water and Energy project can create a platform for further scientific co-operation. Such co-operation could focus on issues concerning the interplay of climate and water in the Arctic region and could also be extended into a joint Nordic, European and North American research program focusing on the North Atlantic region and its role in the climate of the Northern Hemisphere, or the Globe as a whole. The role of e.g. the North Atlantic Oscillation (NAO) in climate

variability, is thought to be of great significance for the meteorological and hydrological conditions in Europe as well as other regions.

**HS02b/10P/D-007** Poster **1630-127**

#### RAINFALL VARIABILITY AND ITS IMPACTS ON WATER RESOURCES DEVELOPMENT IN PART OF OGUN-OSUN RIVER BASIN

Olusegun ADEAGA (Department of Geography, University of Lagos)

Highly variable rainfall over space and time constitutes major constraints to water resources development most especially in developing countries of the world. Also, major consequences of extreme hydrological events (flood and drought) and low mitigation techniques and inadequate technological know-how threaten water resources development in developing region. Evaluating the nature of hydrological processes that affect water resources variability most especially rainfall in parts of Ogun-Oshun River Basin will provide adequate knowledge towards providing information on the amount, reliability and timing of available renewable water resources within the region. Such information is necessary; if problematic issues on water resources availability and production are to be resolved in a sustainable way. A safe transition to sustainability is crucial to meeting the increasing water demand per capita in Ogun-Oshun basin. In this paper emphasis was based on rainfall variability characteristics in Ogun-Oshun basin and the telecommunication of the El-Nino events and sea surface temperatures (SST) on rainfall distribution within Ogun-Oshun basin. Also, time series and probability analysis of extreme rainfall events frequency distribution and probability of occurrence was also carried-out. All, the above analyses was integrated into a Geographical Information System (GIS) framework for spatial analyses and scenario building. Finally, investigation was made on adequate measures to be taken towards extreme hydrological events prediction and planning.

**HS02b/10P/D-008** Poster **1630-128**

#### HEAT FLUX OBSERVATION ACROSS THE AIR/WATER INTERFACE OF A SMALL RIVER

Mohammed Aslam M.A.<sup>1</sup>, Akihiko KONDOH<sup>2</sup> (<sup>1</sup>Graduate School of Science and Technology, Chiba University, Chiba 263-8522, Japan, <sup>2</sup>Center for Environmental Remote Sensing (CEReS), Chiba University, Chiba 263-8522, Japan)

River water temperature information is very important in the studies of potential effects of climate change on freshwater system. The relationship between stream temperature and air temperature are always active. The linear regressions of river temperature versus air temperature are best fitted for this purpose. The applicability of linear regression has been verified in this study. The present study deals with water temperature and air temperature flux in a small river Kuriyamagawa, Chiba Prefecture, Japan, where long-term database is maintained by Chiba Prefecture Environment Department. Temperature data from 1976 to 1997 were employed for the analysis. The heat flux observation for water and air interface has been observed at three stations across the river covering both upstream and downstream at Arai-bashi (longitude 140.473E and latitude 35.696N), Kido-bashi (longitude 140.528E and latitude 35.622N) and Yohei-bashi (longitude 140.464E and latitude 35.687N) respectively. The inter-annual trend of river water temperature follows the trend of air temperature in these locations. The maximum temperature has been recorded for the month of August and that of the minimum for the month of January. The heat exchange processes that contribute to surface water temperature have been analyzed and related to the air temperature on a monthly time scale. This regression analysis strongly supports the linear relationship between the air and water temperature flux, which are based on the best autocorrelation structure of river water time series. This results has shown that water temperature (Tw) and air temperature (Ta) can be related by a linear regression as,  $T_w = 0.7941 T_a + 2.2392$  for this small river, where heat flux studies has been carried out. The river temperature and air temperature interface is very similar to the equilibrium temperature and air temperature relationship. Linear regression between river temperature and air temperatures are found to be accurate and are good for interpolation within the record length used in the analysis.

**HS02b/10P/D-009** Poster **1630-129**

#### REPRESENTATION OF COMPLEX LOW-FREQUENCY FEATURES IN A DAILY RAINFALL MODEL

Timothy Ives HARROLD<sup>1</sup>, Ashish SHARMA<sup>2</sup> (<sup>1</sup>CSIRO Atmospheric Research, <sup>2</sup>University of New South Wales)

Australian rainfall records contain complex low-frequency features that are associated with climate variability. Both the pattern of wet and dry days, and the average rainfall on a wet day, are linked to large-scale quasi-periodic variations such as the El Nino Southern Oscillation Index. These linkages are even more complex when wet days are treated in separate classes based on the number of adjacent wet days (i.e. solitary wet days; days at the start or end of a wet spell; and days in the middle of a wet spell). We present a stochastic model for generation of daily rainfall that considers these features in its formulation. We show that use of predictors that reflect the low-frequency variations can result in a more appropriate representation of rainfall variability at long time scales.

**HS02b/10P/D-010** Poster **1630-130**

#### ASSESSMENT OF THE EFFECTS OF VEGETATION COVER CHANGES ON HYDROLOGIC REGIME

Mohammad Javad POURAGHNIAEI<sup>1</sup>, M. MAHDAVI<sup>2</sup>, B. SAGHAFIAN<sup>3</sup> (<sup>1</sup>Natural Resources Research Center of Semnan, <sup>2</sup>Professor of Tehran University, College of Natural Resources, <sup>3</sup>Associate Professor in Watershed management research of Tehran)

Hydrologic regime of watersheds has high importance and needs attention. Lack of management and planning in natural resources and land use, cause changes in hydrologic regime of watersheds and converting runoff to flood. To be aware of management feedbacks is necessary to have a successful management in a watershed. In this study, hydrographs of Neka Rud basin were compared for several land use conditions (1967, 1992 & 2000) according to 24 hours maximum precipitation of several return periods. At first, land cover maps of Neka Rud basin for different years (1967, 1992 & 2000) were provided. Old maps and aerial photographs of 1967, TM and ETM Landsat images of 1992 and 2000 were used to provide the land cover map of 1967, 1992 & 2000, respectively. Using area of each land cover (from land cover maps), area of each soil type of basin (from soil map of basin) and other necessary information for SCS method, curve number (CN) for each period was calculated (614.7, 65.5 & 67.1). For the next step, from rain gauge data and by use of hHyfa soft ware, 24 hours maximum precipitation for selected return periods was calculated. The hyetographs (spatial pattern) for each return period were drawn from inter basin stations data, using surfer software. Then weighted average of this hyetographs identified the 24 hours maximum precipitation in basin area. Average of temporal pattern (using IDF curves)

of Babolsar and Gorgan rain gauges -in side of basin- was used for temporal pattern of Neka Rud basin and hourly temporal pattern was extracted. These data were used in Hydrologic Modeling System (HMS) to predict the hydrographs for each land use condition (1967, 1992 & 2000) and on the 24 hours Maximum precipitation of several return periods. This model needs to simulation, calibration and Validation steps for Neka Rud Basin situation before running for predict a hydrograph. The model was simulated by 3 real storm-runoff events that after optimization, each of them had special calibration coefficients (for initial absorption and lag time). An average of these calibration coefficients was used as the coefficient for Neka Rud basin. Validation was the last step before prediction. For this step a real storm run off event was used. The observed and predicted hydrograph had the same trends, this result was suitable and the calibration was valid. Finally, the calibrated model was used to predict the hydrographs of Neka Rud basin for various land cover conditions. After running of the model for each situation, the results showed an increasing trend for peak discharge and volume of runoff from 1967 to 2000.

**HS02b/10P/D-011** Poster **1630-131**

#### MODELING THE INFLUENCE OF VARIATION IN ATMOSPHERIC PRECIPITATION ON THE HEAT AND WATER BALANCE COMPONENTS OF DRY AREAS

Alexey Vladimirovich BABKIN (Lab. of Hydroecological Research of Inland Water Bodies)

{BR}The aim of the work is the development of the mathematical model for research of the moisture and water-thermal regime dynamics within arid and semi-arid areas. The base of model is the differential equations of water and heat balance of soil. The income of energy (absorbed solar radiation), water outcome components (evaporation and run-off) and energy outcome components (turbulent heat-exchange of ground surface with atmosphere, evaporation and effective radiation) were related through heat and water storage of soil. {BR}The relations between income-outcome characteristics and storage components permitted the soil water and heat balance equations to combine into the system. Its solutions were found for leap-pattern and linear changes of precipitation and for their variation simulated by periodic function. The increase of precipitation within arid and semi-arid areas causes the increase of soil water storage, evaporation and run-off and reduction of the heat storage and energy outcome for turbulent heat-exchange and effective radiation. {BR}The dynamics of characteristics of semi-arid area of Caspian Lowland and Western Kazakhstan was calculated for 50 mm/year leap-pattern increase of precipitation and for linear precipitation increase with the velocity of 5 mm/year<sup>2</sup>. For leap-pattern change of precipitation the climatic and hydrologic characteristics of the territory reach the values of new equilibrium state for the time less than the year. Under linear precipitation increase the changes of area characteristics become linear for the time interval less than half of year. {BR}The oscillation of precipitation causes the variation of area characteristics. The extremes of climatic and hydrology characteristics of area have a time lag to the respective precipitation extreme. For the same variation period the time delay of area characteristics is different. After the precipitation extreme the evaporation reach its extreme value the first. The extremes of absorbed solar radiation, water storage of soil and run-off appear some time later. The heat storage extreme of opposite phase is the last.

**HS02b/10P/D-012** Poster **1630-132**

#### MODELING WATER QUALITY BY USING NEURAL NETWORKS

Jian-Ping SUEN, Wayland J. EHEART (Department of Civil and Environmental Engineering, University of Illinois at Urbana-Champaign)

In this study, artificial neural networks (ANNs), are applied to estimating the nitrate concentration in a typical Midwestern river, i.e., the Sangamon River in Illinois. In Illinois, and throughout the Midwestern US, nitrate has recently become an increasingly important problem in drinking water quality. This is due to a somewhat recent change in the EPA nitrate standard and to the increasingly widespread use of chemical fertilizers in agriculture. Two ANNs, Back Propagation Neural Networks (BPNN) and Radial Basis Function Neural Networks (RBFNN), were compared with regard to their effectiveness in water quality modeling. BPNN uses a gradient descent method, modifying the weight by simulation errors to construct the neural network. RBFNN uses a fuzzy min-max network to do the first clustering part and multivariate regression method to construct the neural network. RBFNN is much faster than traditional BPNN and the results of RBFNN also appear to be more robust. The study compared these two types of ANNs to traditional regression and traditional mechanistic water quality modeling. Comparisons were based on overall accuracy and on the frequency of false-negative prediction, i.e., the frequency with which the model would predict the nitrate concentration to be below the standard when it actually exceeded it. The study showed that the RBFNN achieved the best results of all models in terms of overall accuracy, and both BPNN and RBFNN had the same false-negative frequency which has better than traditional models.

**HS02b/10P/D-013** Poster **1630-133**

#### TIME SCALE ANALYSIS FOR INVESTIGATING STATIONARITY OF HYDROLOGIC TIME SERIES

A. Ramachandra RAO<sup>1</sup> (<sup>1</sup>School of Civil Engineering, Purdue University, <sup>2</sup>Irrigation and Hydraulic Department, Faculty of Engineering, Cairo University)

To overcome the difficulties encountered in conventional spectral analysis, a different approach known as Wavelet analysis has been introduced during the past 10 years (Daubechies, 1992; Combes et al., 1990; Mallat, 1996; Meyer, 1993; Strang and Nguyen, 1996; Chui, 1992). In Wavelet analysis, a different type of basis functions, called Wavelets, are used. Wavelets, as opposed to sine and cosine functions, have a limited extent in time (a limited support), and are therefore localized in time as well as in frequency. In the theory of Wavelet transforms, the notion of 'frequency' is changed to an equivalent one of 'scale', where large scales correspond to low frequencies and small scales correspond to high frequencies. Wavelet analysis provides a technique for analyzing the structure of a time series by using variable size windows. In effect, by using the Wavelet transform the signal is decomposed into components of different scales. This offers a method for a local examination of the signal, a multi-scale outlook, and a time-scale analysis (Misiti et al., 1996). Wavelet analysis can be used as a tool for performing a wide range of tasks which include: detecting discontinuities in signals, detecting long-term evolution (trends), detecting self similarity (fractal signals), identifying pure frequencies (time-frequency analysis), suppression, and compression of signals. Wavelet analysis is used in this paper to investigate the stationarity of hydrologic and climatic time series as well as tree-ring series. Annual rainfall, runoff and temperature series from the Midwestern United States are used in the study. The results indicate the nonstationarities in these time series, thereby demonstrating the use of wavelets in the study of climatic variation. The time-scale structures in these time series are studied and the relationships between them are investigated. Also, Wavelet analysis is used for assessing similarities between different time series at different scales in the region under study. References Chui, C.K. 1992 An Introduction to Wavelets. Academic Press. Combes, J.M., A. Grossmann, Tchamitchian, Ph. eds. (1990) Wavelets, Time-Frequency Methods, and Phase Space. Springer. Daubechies,

I. (1992) Ten Lectures on Wavelets. SIAM, Philadelphia, PA Mallat, S. (1996) Wavelet Signal Processing. Academic Press, New York, NY. Meyer, Y. (1993) Wavelets: Algorithms and Applications. SIAM. Misiti, M., Y. Misiti, G. Oppenheim and J.M. Poggi. (1996) Wavelet Toolbox for use with MATLAB. The Mathworks, Inc., Natick, Mass. Strang, G. and T. Nguyen (1996) Wavelets and Filter banks. Wellesley -Cambridge Press, Wellesley, MA.

**HS02b/10P/D-014** Poster **1630-134**

**THE RELATION BETWEEN  $\delta^{18}\text{O}$  IN MONSOONAL PRECIPITATION AND AIR-SEA ACTIVITY, ASTRONOMICAL AND METEOROLOGICAL FACTORS**

Hongxi PANG, Yuanqing HE (Lab ice core, Cold and Arid Regions environmental and Engineering Research Institute, Chinese Academy Sciences)

The variations of isotopic content are different, with different locations and climatic types. The isotopic contents in precipitation vary complicatedly over monsoon regions in mid-latitude zones. The isotopic data in precipitation at New Delhi (the IAEA/WMO station; 28.58°N, 77.2°E), located in southwest monsoon region, are analyzed, suggested that the  $\delta^{18}\text{O}$  values vary in 11 years cycle, which is closely agreed with that of sunspot; the strong correlation between  $\delta^{18}\text{O}$  and T/P, a parameter by coupled temperature and rainfall; the remote positive correlation between  $\delta^{18}\text{O}$  and ENSO event induced by the interactions of coupled air-sea systems in tropical Indian Ocean and Pacific Ocean; and rainy drops evaporated is the key reason to lead the positive correlation between  $\delta^{18}\text{O}$  and zonal wind velocity at the height of 500mb while the amount and temperature effect strengthen this correlation.

**HS02b/10P/D-015** Poster **1630-135**

**SCALES OF HYDROLOGICAL CHANGES IN VOLGA RIVER BASIN POSSIBLE AT CLIMATE CHANGES**

Alexander GEORGIADI (Department of Hydrology, Institute of Geography, RAS)

Three main approaches for model using as tool for assessments of possible hydrological regime changes which differ from each other by type of model are developed. One of them is based on physically based water cycle models (including SVAT models) that are used for small site or rather small watershed (Georgiadi, Nazarov, 1997; Kashutina, 1999 and others). Simplified monthly water budget models that could be used for wide diapason of spatial scale (Georgiadi, Milyukova, 2001). Mean annual river runoff could be estimated on the basis of rather simple relationships between water budget components and climatic elements (Belyaev, Georgiadi, 1989, 1992; Georgiadi, 1991, 1993; Velichko et al., 1992; Georgiadi, Jai-Ho Oh, Yong Hee Lee, 2000). The paper presents the assessments of possible changes of spring flood and annual river runoff changes as well as changes of intraannual distribution of river runoff in Volga river basin (to Volgograd) at the Holocene Optimum (6 thou. years before present) as well as at a doubling of atmospheric  $\text{CO}_2$ . The data of experiments on a global climate model of Moscow State University (Kislov, 1992) and Geophysical Fluid Dynamics Laboratory (GFDL), Princeton University, USA were used as the scenario of climate change. The hydrological changes are determined on the basis of original model of monthly water balance. In the present work the model of formation of a monthly water balance for plain watersheds, allowing to estimate influence such important hydrological factors as potential evaporation, snow cover accumulation and snow melting, infiltration of water into the ground and its deep infiltration, soil moisture reserve change. The model allows to compute dynamics of runoff losses. This model could be used for calculate of rain and snow melting flow. The conditions of river runoff formation at various sites of watershed are non-uniform, at the same time there is a limited enough information on the soil hydrophysical characteristics, and as the rather rough estimations of some other characteristics of watersheds. Therefore for identification of some parameters of model the method of optimization was used. The calculations of a monthly river runoff for main part of Volga watershed for grid cells  $1^\circ \times 1^\circ$  were made. The following monthly average long-term data were used: precipitation, air temperature, soil moisture reserve at field capacity, river runoff. All calculations were made for monthly time steps, but were used approach based on using so called quasi-daily calculations.

**HS02b/10P/D-016** Poster **1630-136**

**THE DECREASE OF THE PRECIPITATION IN PERIODS OF THE YEAR AS A SIGN OF CLIMATIC CHANGE: CASES STUDIED IN PORTUGAL**

Maria Manuela PORTELA, Antonio de Carvalho QUINTELA (Instituto Superior Tecnico (IST))

A more irregular distribution of the precipitation within the year and a significant reduction of its amounts during some periods of the year are generally pointed out as consequences of the climatic change that seems to occur in Portugal. To be considered a sign of climatic change, the previous reduction must correspond to an increasing tendency persisting along the years. In order to detect variations having a persistent nature in temporal series of precipitation in Portugal, two procedures were applied: the classic method of moving averages and a procedure, expressly developed within the scope of the study that originated this article, based on a statistical comparison of the precipitation averages during certain intervals of time in which the recording periods were divided. The applications carried out for precipitation series in eleven gauging stations in Portugal denote that the amount of rain during the 2nd quarter of the hydrologic year (from January to March), and specially in March, is clearly decreasing.

**HS02b/10P/D-017** Poster **1630-137**

**CLIMATE CHANGE, GLACIER MASS BALANCE AND WATER RESOURCES**

David N. COLLINS, Oliver G. MACDONALD (School of Environment & Life Sciences, University of Salford)

Disproportionately large contributions of runoff arise from the portions of catchments overlying the high mountain areas of the world, as a result of the orographic increase of precipitation with elevation. At present, high specific discharges from glacierised high mountains are also generally enhanced by destocking of ice from the many thousands of often small glaciers which characterise ranges such as the western cordillera of the Americas, the Alps, and the Himalaya. River flows have often doubled, between the cool 1970s and warm 1990s, reflecting in the Alps, for example, summer air temperature increases of about 2°C over the same period. However, enhanced river flows can not go on for ever. As warming continues, glacier mass loss and diminishing glacierised partial areas of catchments will ultimately result in reduction of annual total discharge with greater variability from year to year. Glaciers will become reduced in size in most areas over a timescale of 20 – 50 years. Warmer air temperatures will result in the freezing level rising in the atmosphere so that where snow formerly fell precipitation will occur as rain. Winter snow pack will probably decline and snow cover duration shorten. Heavy rainfall whilst the transient snowline stood at high elevation resulted in severe summer flood events in the Alps and the Karakoram in the warm 1990s. Daily integration of air temperature and precipitation

from results of the HadCM3Gga1 experiment for 2.5 latitude x 3.75 longitude degree grid square resolution are coupled with standardised glacierised basins, downscaled through derivation of statistical relationships between regional climate (NCEP/NCAR reanalysis project), and actual glaciologically-relevant meteorological observations obtained at mountain stations. In the short term, warming increases flow, but coupled with deglaciation, greatly reduced flows will have serious consequences for water resources, particularly where mountain runoff drains to neighbouring arid lowlands.

**HS02b/10P/D-018** Poster **1630-138**

**THE HIGHEST ALTITUDE ICE CORES IN THE HIMALAYAS RECORD ANTHROPOGENIC POLLUTION**

Tandong YAO<sup>1</sup>, Keqin DUAN<sup>2</sup>, Shucheng XIE<sup>2</sup>, Wenmian HUO<sup>2</sup>, Lide TIAN<sup>2</sup> (\*Prof., <sup>2</sup>Dr.)

High resolution, well-dated ice core records, especially low-latitude ice cores near the populated regions provide a unique tool to study and to evaluate the impact of anthropogenic activities on environment and climate. Recently ice cores were recovered at an altitude of 7200m on the Dasuopu Glacier located in the Xixiabangma Mountain. The high elevation of the coring site provides very good background to detect any anthropogenic pollution. Organic and inorganic methods are applied to the Dasuopu ice core analyses. The analyses detected petroleum residues from the ice core. Our study has concluded that the material is from the oil combustion in Kuwait and vehicle pollution in India. The measured lead concentration ranges from  $16 \times 10^{-12}\text{g/g}$  to  $161.7 \times 10^{-12}\text{g/g}$ . Lead concentration increases significantly since the 1940s. A very dramatic rise happened in the 1980s in which the mean lead concentration reached to  $161.7 \times 10^{-12}\text{g/g}$ . The organic and inorganic analyses indicated that the anthropogenic pollution has already impacted the environment at 7200m a.s.l. in the Himalayas.

**HS02b/10P/D-019** Poster **1630-139**

**ATMOSPHERIC METHANE OVER THE PAST 1000 YEARS FROM A SUB-TROPICAL ICE CORE**

Baiqing XU<sup>1</sup>, Tandong YAO<sup>2</sup>, Jerome CHAPPELLAZ<sup>3</sup>, Lonie THOMPSON<sup>2</sup>, Ninglian WANG<sup>2</sup>, Lide TIAN<sup>2</sup> (\*Dr., <sup>2</sup>Prf.)

A high-resolution methane record from an ice core recovered above 7200m of altitude on the Dasuopu Glacier in the Himalayas, reveals similar trend of methane concentration fluctuations with the polar region records. The high degree of detail of the Dasuopu record over the last century allows revealing a significant period between the two World Wars when the anthropogenic methane increase was put to a halt. This sub-tropical methane record also allows quantifying for the first time the difference of methane mixing ratio between polar and sub-tropical latitudes during pre-industrial time. The average difference is 120 ppbv with Greenland and 160 ppbv with Antarctica. The record suggests that the tropical latitudes might represent large percent of the global methane sources in pre-industrial time. In addition, the temporal fluctuation of the pre-industrial methane records suggests that Monsoon evolution incorporated with high methane input in the south Asia might be responsible for the relatively high methane concentration observed in the Dasuopu ice core around 1700 AD.

**HS02b/10P/D-020** Poster **1630-140**

**ICE TEMPERATURE VARIATION IN PUROUGANRI ICE FIELD ON THE TIBETAN PLATEAU**

Jianchen PU<sup>1</sup>, Tandong YAO<sup>2</sup>, Ninglian WANG<sup>2</sup>, Keqin DUAN<sup>2</sup>, Lide TIAN<sup>2</sup> (\*Prof., <sup>2</sup>Dr.)

Puruogangri ice field is located in the middle of the Tibetan Plateau, with a total area of 422.58km<sup>2</sup>. Four ice cores with a depth of 154m, 118m, 80m and 20m respectively. The ice temperature was measured in the 4 holes using resistance thermometer. The ice temperature shows same trend in the 4 holes. The ice temperature in the above 2m is intensively influenced by cold wave from the ice surface. Under that the ice temperature curve shows a warm-season type. The lowest ice temperature is -9.9° measured at 12m depth. The ice temperature increase downwards in a linear manner under 12m, but the increasing ratio is lower than the decreasing ratio in the upper 12m. During the observation, the ice temperature decreased obviously in the upper 4m of the ice hole, and the decrease is vanished downwards. In the 80m ice hole, the ice temperature decreased 0.62° from 18:50 of October 18 to 14:40 of October 21, which a daily average of 0.2°. The ice temperature decreased 1.15° in the same period, with a daily average of 0.3°. There was no obvious variation in 12m depth.

**HS02b/10P/D-021** Poster **1630-141**

**THE INFLUENCE OF THE SNOW COVER AND CLIMATE INTERSECTION TO EXTREMELY HYDROLOGICAL SITUATIONS IN THE SNBMPUNTANE ZONE (NORTH SLOPE OF CAUCASUS AS AN EXAMPLE)**

Lev M. KITAEV (Department of climatology, Institute of Geography RAS)

The data bases of the snow thickness for the period 1966-1990 are compiled. In these bases 41 stations over the Great Caucasus ranges and 636 stations over the East European plain are included. The average snow thickness for the winter period (snowiness) is calculated. Their interannual changes in different regions in relation to atmosphere circulation are investigated. The coefficient of variation for the averaged values for all the plain and for all mountain stations is of the order 30%. For the single Caucasian stations with the high snowiness the coefficient of variation is about 30-45%, the maximum deviation is about 90%. For the single stations with the low snowiness the coefficient of variation is about 90-100% with 3-5 times maximum deviation. Over the East European plain with North Caucasian plain the snowiness was low over the period 1966-1977 and high over the period of 1978-1990. The zonal circulation prevailed in the first and the meridional one in the second period. The snowiness trend in 1966-1990 was positive. Cases of the high and low snowiness alternated incoherently over Grate Caucasus. The significant trend is absent. That is the result of different circulation factors of snow accumulation in dependence on the topography. In the high snowiness years over the Great Caucasus the frequency of the southern lows or the blocking high over the East European plain is above the average. During the blocking highs the western lows are concentrated the high southern periphery. In the half of years the anomalies signs for Caucasus and the plains are opposite. This has led to the mutual compensation of melted run-off anomalies related to mountain and splash parts of the North Caucasian river basins. Combinations of extremely interannual maximal and minimal annual snow depth of Caucasus and its north submontane zone were generated. The potential contribution of a snow cover of extreme years to a river drain is revealed.

**HS02b/10P/D-022** Poster **1630-142**

**RISK ASSESSMENT OF FLOOD CONTROL SYSTEM OF THE YANGTZE CENTERED ON THE THREE GORGES PROJECT**

Shenglian GUO, Xiangrong TIAN, Caijun WANG, Honggang ZHANG, Pan LIU (Department of Hydrology and Water Resources, Wuhan University)

The Three Gorges project (TGP) is the largest hydropower project in the world. TGP possesses huge comprehensive benefits, including flood control, power generation, navigation improvement, etc. Flood control is the key and also the essential one with the largest ecological and environmental benefits. TGP's construction commenced in 1994 and the first turbine will generate hydropower in 2003 May, and the whole project will be completed in 2008. Based on the characteristics of flood control system of the Yangtze River centered on Three Gorges Reservoir (TGR), one and two dimensional hydraulic flood routing models and multiple-input single output linear system models were proposed and developed by using numerical methods and modern system engineering principles. Four inter-basins, Shashi, Luoshan, Hankou and Dongting Lake, are selected for flood simulation case study. The models were applied to these inter-basins and the simulated flood hydrographs were compared with those depicted from observed data. The river network in the lake region and the river-lake relationship are considerable complicated and investigated in detail. The results were satisfactory with high model efficiencies and low relative errors. The model will provide technical support and service for flood forecasting and flood dispatch decision as well as risk analysis in this region. The results show that under the condition of the 1998 large flood, if TGR conducting the compensation operation for the Jingjiang area, the highest water level in the Shashi, Luoshan and Hankou hydrological stations would decrease 0.86m, 0.78m and 0.44m respectively. The risk herein means that under different frequency of designed flood of TGR, how much is the risk corresponding to the flood control system of the Yangtze basin after the upstream flood is regulated by TGR. The 1954 large flood (with flood diversion) and the 1998 large flood (without flood diversion) are chosen as prototype for this study. The risk of flood control system in the Yangtze basin is analyzed based on the TGR operation regulations and flood detention area management rules. It is shown that with 22.15 billion m<sup>3</sup> of TGR regulating capacity and incorporating with embankment, flood diversion and other non-engineering measures, the bank failure along Jingjiang river reach due to heavy flood, which usually cause huge mortality and million's homeless, can be effectively avoided. It can also protect millions people in downstream plain from flood menace and the consequent ecological and environmental destruction. The irreplaceable function of TGR for flood control will greatly ensure the harmonized development of social economy in the middle and lower reaches of the Yangtze.

**HS02b/10P/D-023** Poster **1630-143**

**CROSS-CORRELATION ANALYSIS BY KENDALL'S  $\tau$  BETWEEN CATEGORIZED SOI AND THE NONEXCEEDANCE PROBABILITY OF PRECIPITATION IN KOREA**

Young-Hoon JIN, Akira KAWAMURA, Kenji JINNO (Institute of environmental systems, Kyushu University)

El Niño/Southern Oscillation (ENSO) has influenced on the hydrological variables on global scale, but the influence of ENSO is not so clear in middle to high latitude including Korea and Japan. Especially, the quantitative influence of ENSO is difficult to be revealed in this region. There are several researches to reveal the correlation between Southern Oscillation Index (SOI) and the hydrological variables in Korea. Moon (2001) applied Multi-channel Singular Spectral Analysis (M-SSA) to the precipitation in Korea for identifying the coherent space-time patterns of low frequency harmonic element between SOI and the precipitation. Shin (2002) revealed the significant influence of El Niño/ La Niña on the flood and drought in Korea, using the statistical robust cross-correlation analysis. Kawamura et al. (2000) succeeded to detect the direct and significant correlation between SOI and precipitation/temperature in Fukuoka, Japan by categorizing SOI into five groups according to their magnitudes. Therefore we used the categorized SOI for revealing the relationship with the monthly precipitation at Pusan, Mokpo, and Incheon in Korea. In the kind of study, the appropriate transformation of the hydrological variables is often critical to obtain better results. It is difficult to normalize the precipitation data in the present study area because there are some months with no precipitation (less than 0.1 mm), whereas the precipitation data in Fukuoka were easy to be normalized by cubic root transformation. So in the present study we uniquely applied the nonexceedance probability transformation instead of the usual ones such as logarithmic and power transformations. We also applied Kendall's correlation coefficient ( $\tau$ ) when carrying out the cross-correlation analysis as well as the usual Pearson's correlation coefficient ( $r$ ). The Kendall's  $\tau$  is a rank-based procedure and is therefore resistant to the effect of extreme values and to deviations from a linear relationship. Most of all, this correlation coefficient can be applied to the data whose distribution is non-normal and unknown. These properties of Kendall's  $\tau$  are well suited for the data of the present study, because the used data cannot be easily transformed normally, as mentioned earlier. The results from these approaches which used the nonexceedance probability and the Kendall's  $\tau$  show that there are several significant correlations between the categorized SOI and precipitation in Korea. Especially, the correlation coefficients, which are significant at 1 % level in both Kendall's  $\tau$  and Pearson's  $r$ , were detected only at Pusan station under the "Strong La Niña" category with lag time four months. The correlation coefficients in both Mokpo and Incheon stations were obtained only at the 5 % significance level for various lag times. From these results, we can infer that the influence of SOI on the precipitation in Korea is stronger at Pusan than at both Mokpo and Incheon stations, and that the stronger the La Niña event, the less the precipitation four months later in Pusan.

**HS02b/10P/D-024** Poster **1630-144**

**ASSESSMENT OF IMPACT OF URBANISATION ON STORMWATER RUNOFF**

Rathnam Venkata ERVA, JAYAKUMAR V. K. (Lecturer)

Increasing problems in urban stormwater management consequent to urbanization has been realized and appreciated in many hydrologic studies. Stormwater drainage and management systems are designed and constructed to cope up with the increase in runoff due to increased imperviousness of the land due to developmental activities. For the design of an adequate drainage system, it is essential to understand the changes in stormwater runoff quantity and quality with land use changes. Urbanisation usually results in increase in volume and velocity of runoff, produces larger peak, decrease in the time to peak, downstream flooding and increase in pollutant loadings. The principal effects of land use change have been discussed by Geiger et al (1987), ASCE (1996) and Dunne and Leopold (1978), Overton and Meadows (1976), Urbanos and Stahre (1993) and many others. Runoff estimation techniques include: hydrograph methods and peak discharge methods. Many applications allow use of the peak flow analysis and the procedures are much less time consuming than the complete hydrograph method. The objective of the present study is to investigate the impact of land use changes due to urbanisation on stormwater runoff in part of Hyderabad city, in southern part of India. During the last 20 years, urbanisation has taken place at an alarmingly rapid rate in the Hyderabad city. Land use change maps and rainfall data for the period 1980-2000 are available. Using the available data, increase in built-up

area and impervious surface with the progression of urbanisation are estimated. Design storms of different return periods 2, 5, 10, 25, 50 and 100- years are developed. SCS (NRCS) curve numbers and runoff coefficients are estimated. The generated runoff from different design storm is computed using a well documented package, SMADA, as well as the rational method, as to study how runoff volume is increasing with increase in impervious area. It is observed from the studies that the rational method gave higher peaks for all design storms, while the SMADA, which uses SCS hydrograph method resulted in increased runoff duration. An assessment is also made of possible expansion of built-up area with increased urbanisation in future and consequent storm runoff volume is investigated.

**HS02b/10P/D-025** Poster **1630-145**

**USE OF PHYSICALLY BASED MODEL FOR FLOOD ESTIMATION IN SMALL CATCHMENTS IN A DATA SCARCE ENVIRONMENT**

Jayakumar KANDATHIL VALAPPIL<sup>1</sup>, Ramaseshan S.<sup>2</sup> (Regional Engineering College, <sup>1</sup>Indian Institute of Technology)

Estimates of flood are required for the design and economic appraisal of a variety of engineering works. When adequate and appropriate data area available for the basin, conventional methods like frequency analysis or use of unit hydrographs and other rainfall-runoff procedures may be applied to model the basin system. When this is combined with the design storm, the design flood may be derived. Data available for small catchments are generally inadequate for these approaches. Empirical approaches may be used to model such small catchments. Since generally adequate data are available for estimating design storms, it seems worthwhile to derive relationships between storm rainfall and runoff. The parameters of the model may then be related to the characteristics of the storm and physiographic features of the watershed to yield regional relationship between storms and floods. But a more realistic and alternate approach is to model the catchment runoff process according to physical principles. Information regarding physiography, soils, vegetation and drainage pattern of the catchment is used in the physically based models. The catchment is decomposed into a network of channels and overland flow segments. Using the physical characteristics of each component and appropriate hydraulic equations, the hydrologic processes are simulated using the distributed parameter model. Necessary values of the coefficients and constants are specified from physical characteristics of the watershed or are obtained from calibration of the model with observed data. The study reported is essentially a regional case study of flood estimation in small catchments in a part of North Brahmaputra basin, in the north-eastern part of India. The scope of the study is to apply, in a data scarce environment, a physically based model, DRRRM and to study the regional variation, if any, of the parameter of the model and also to judge the validity for flood estimation. Data regarding catchment plan, cross section at the bridge sites and hourly rainfall and stage data for about 10 catchments in the region were available for the study for a very limited period of 3 to 4 years. The catchment area ranged from 7 km<sup>2</sup> to 215 km<sup>2</sup>. After preliminary analysis of the data for errors, only seven basins were found to be suitable for analysis. The results of the study indicated that a constant parameter physically based model for small catchments in the region is realistic. The design flood estimated using this model compared favourably with other approaches reported in the literature. The study shows that because of the easy availability of, and competence with computers and software in field organizations, it seems preferable to adopt a distributed parameter model with relevant field data rather than using empirical statistical relationships of questionable reliability.

**HS02b/10P/D-026** Poster **1630-146**

**PHYSICALLY-BASED MODELS FOR FLOODS MODELLING IN THE MEDITERRANEAN AREA**

Philippe GOURBESVILLE<sup>1</sup>, Vincent GUNOT<sup>2</sup> (<sup>1</sup>University of Nice - Sophia Antipolis, <sup>2</sup>International Institute for Infrastructural Hydraulics and Environmental Engineering - IHE)

Extreme hydrological events are characterised by the scarcity of data (in terms of spatial and temporal frequency). This problem becomes more acute when it comes to modelling the response of large catchments with small concentration times due to particular morphology or rainfall intensities. The classical approach to modelling, (that consists of trying of tuning the model parameters so as to bring the calculations as close as possible to the measurements) becomes highly questionable because it may turn out to be extremely harmful to the predictive power of the model. The present paper addresses uncertainty in modelling the flash flood of 05.11.1994 on the Var watershed (France, 2820 km<sup>2</sup>). This watershed, located in the French riviera, is characterised by steep slopes, narrow valleys and large topography curvatures, making the flow pattern extremely complex. Seven models of the catchment were built using the Mike She hydrological modelling system. These models have different structures, geometries, or parameter values. The analysis of the model results on the flash flood of 05.11.1994 leads to the following conclusion: - the physically based approach is efficient and the flood characteristics are well reproduced; - the main sources for uncertainty in model results are, by decreasing order of importance: (i) the model structure, i.e. the assumptions concerning the dominant phenomena and how they are modelled, (ii) the model geometry and (iii) the value of the model parameters. This shows that, for this particular case at least, it is much more important to have a good knowledge of the phenomena occurring on the catchment, as well as of the particular geometrical feature, than to try to calibrate the parameters of the model. On the contrary, blind calibration of the model may jeopardise its predictive capabilities.

**HS02b/10P/D-027** Poster **1630-147**

**FLOOD FORECASTING & MANAGEMENT IN PAKISTAN**

Shaukat A. AWAN (Pakistan Meteorological Department)

Floods in Pakistan are mainly caused by the heavy monsoon rains during the summer monsoon period from July to September. Meteorologically there are two situations which cause flood producing rains in the upper catchments of the rivers. The two meteorological situations in relations to different conditions of intensity and movement of low/depression may produce three categories of floods as described below. i) Meteorological Situation For Category-I Floods A situation when the seasonal low is a semi permanent weather system situated over south eastern Balochistan, south western Punjab, adjoining parts of Sindh get intensified (due to westerly wave) and causes the moisture from Arabian Sea to be brought up to upper catchments of Chenab and Jhelum rivers resulting in heavy downpour along windward slopes of mountain ranges due to orographic lifting of moist air mass. ii) Meteorological Situation for Category-II & Category-III Floods Second flood generating meteorological situation is linked with monsoon low/depression. Such monsoon systems originate in Bay of Bengal region and then move across India in general west/north westerly direction arrive over Rajasthan or any of adjoining states of India. After this monsoon depression may take any one of following three courses. a) Continue moving straight west causing heavy wide-spread rains over Sindh/Balochistan. However, no river flooding shall occur in this case. b) Recurve in the north east direction towards upper catchments of Sutlej, Ravi and Chenab rivers causing extremely heavy rainfall and consequently floods first across border in India and then (within hours) at Rim Stations in Pakistan. This is Category-II

flood situation. c) Continue moving in northerly direction ( under the effect of a strong westerly over plains of Lahore/Gujranwala Divisions to finally end up over Rawalpindi/Hazara Divisions. Upper catchments of Chenab, Jhelum and Indus rivers come under its influence. Flood management process in Pakistan is multi-functional involving a number of different organizations. First step in the process is issuance of flood forecast/warning. This function has been assigned to Pakistan Meteorological Department (PMD) since basic cause of the floods in Pakistan is the rainfall which can be best predicted and monitored by PMD utilizing satellite cloud pictures and quantitative precipitation measurement radar data, in addition to the conventional weather forecasting facilities. For quantitative flood forecasting, hydrological data is obtained through Provincial Irrigation Department and WAPDA. WAPDA's telemetric system is an important source of hydrological data for flood forecasting purposes. A most modern 'S-Band' Doppler weather radar has recently been provided to PMD, while a new hydrometric data measurement and transmission system is being established by WAPDA. Furthermore, improved rainfall/runoff and flood routing models have been developed to provide more reliable and explicit flood information to flood prone population.

**HS02b/10P/D-028** Poster **1630-148**

#### DETECTION ON RAINFALL VARIETY IN WESTERN TAIWAN

Pao Shan YU, Chia Wen SUNG, Tao Chang YANG (Department of Hydraulics & Ocean Engineering, National Cheng Kung University)

Global climate change and its influence on water resource are the worldwide issues. This paper aims to investigate the variety of historical rainfall on Taiwan. This study on local climate change may provide the reference for climate change study on Asia region. As the area of Taiwan is too small, the GCM is not suitable for our investigation on climate change. Therefore, the statistical method of Mann-Whitney-Pettitt test was applied to detect the change points of annual rainfall depth in the historical records. Rainfall records from four meteorological stations of the Central Weather Bureau distributed over western Taiwan, including Taipei, Taichung, Tainan and Hengchungstations, were adopted as our data set which almost have one hundred years records. It is found that the change points at these four stations vary from 1956 to 1968. As the rainfall during May and June is important for the reservoir operation in Taiwan and the annual maximum daily rainfall has extreme influence on the rainfall design. Hence, the difference between rainfall characteristics, including the rainfall during May and June and annual maximum daily rainfall, before and after the change point for each station was investigated. This work found that the rainfall during May and June, and annual maximum daily rainfall in Northern Taiwan have increase trend. However, the rainfall characteristics in the Middle and Southern Taiwan have decrease trend. For example, the 100-year return period maximum daily rainfall estimated by using Log-Person type III in Northern Taiwan increases around 17%. There are decrease around 20% in the Middle and Southern Taiwan.

**HS02b/10P/D-029** Poster **1630-149**

#### THE INTEGRATED RISK ANALYSIS OF OVER-STANDARD FLOOD FOR FLOOD CONTROL SYSTEM

Xiang ZHANG<sup>1</sup>, Xinyu WANG<sup>2</sup>, Guowei LAI<sup>3</sup> (<sup>1</sup>Dept. of Hydrology and Water Resources, Wuhan University, <sup>2</sup>Institute of Planning and Design, Changjiang Water Resources Commission, <sup>3</sup>Dept. of Hydropower, Wuhan University)

The flood control system mainly consists of reservoir, levee and flood spreading area with a certain flood control standard. The natural flood is a stochastic event. No matter how high the flood control standard is, the probability that the flood exceeds the standard still exists. So the risk analysis for the over-standard flood is very important for the flood control planning and the construction of flood control system. The traditional flood risk analysis may mainly concern with the hydrological and/or hydraulic uncertainty. The engineering uncertainty, such as the reliability of dam and levee, is seldom considered combined with them. In fact, facing the over-standard flood, the reliability of dam and levee strongly influence the ability of flood control system resisting flood. So the integrated risk analysis, considering the hydrological and engineering risk, may provide more thoroughly the information about the ability of flood control system. For the hydrological risk analysis of over-standard flood, we apply the compound Poisson model. It is a kind of risk value model based on stochastic point process theory and is superior with the typical characteristic discussing the frequency problem in time domain. Its discharge threshold for the selection of sample can be very low, and the discharge or the flood peak exceeding the threshold may be selected as the samples. It has been used to study the annual over-standard flood risk of flood control system. The engineering risk is caused by the uncertainty factors that influence the safety of engineering structure, including the load and the mechanics characteristics of material. In this paper, we apply the reliability theory to evaluate the engineering structure safety. The methods for the engineering safety of gravity dam and earth bank are discussed respectively. In order to calculate the integrated risk rate, the hydrological and engineering risk are considered as compatible events. The Selective Probability is used to calculate the integrated risk rate of compatible events. The case study about the flood control system in the Lishui catchment is done. The objective of flood protection is to control that the designing flood of 50 year recurrence through the operation of flood control system is lower than the safety discharge of downstream channel at Sanjiangkou station, 12000m<sup>3</sup>/s. So we discuss the three different operating schemes by the hydrological risk analysis, and calculate the engineering safety of the three dams and levee in Lishui catchment. Through the integrated risk analysis, the optimal operating scheme and the weak link in the flood control system are suggested. The result illustrates that these methods are practical in integrated risk analysis of flood control system and the results of integrated risk analysis are useful in decision making for flood control planning.

**HS02b/10P/D-030** Poster **1630-150**

#### LONG-TERM CHANGE IN DAILY RAINFALL CHARACTERISTICS AT OKAYAMA

Hidetaka CHIKAMORI, Akihiro NAGAI (Faculty of Environmental Science and Technology, Okayama University)

Rainfall characteristics is said to change in recent decades. It is said that rainfall has concentrated in the shorter duration than before so that occurrence of extreme hydrological events like floods and droughts have become more frequent and the disasters related to these events become more severe than before. The changes are attributed to global climate change like global warming and/or local environmental change like heat island effect. The purpose of this paper is to statistically clarify the long-term change in rainfall characteristics, that is, frequency distribution of rainfall depth, rainfall and no-rainfall duration and so on. A statistical analysis was performed for 100-year (1898-1997) daily rainfall record at Okayama Meteorological Observatory, Japan. In this analysis, we defined a storm as a succession of rainy days, and examined statistical characteristics of total rainfall and duration of a storm, storm inter-arrival time and interval between storms. The record was divided into two 50-year periods or three 33-year periods. In the two periods case, the period of 1898-1947 and that of 1948-1997 were named as  $I_{50}$  and  $II_{50}$  periods, respectively. In the three periods case, the period of 1899-1931, that of 1932-1964 and that of 1965-1997 were named as  $I_{33}$ ,  $II_{33}$  and  $III_{33}$

periods, respectively, where the record of 1897 was excluded for the analysis. First, we examined frequency distribution of annual maximum of a storm rainfall in each record period, and found that the storm rainfall with the equally probability is becoming larger year by year. Gumbel distribution was applied to each data of the record period, and the result shows, for example, that 100-year storm rainfall increases by 17% in the period  $II_{33}$  and by 67% in the period  $III_{33}$  comparing with that in the period  $I_{33}$ . Second, we examined frequency distribution of storm duration and found that the storm duration tends to decrease from year to year. Thus the more rainfall happens in the shorter duration so that average rainfall intensity in a storm tends to increase. Finally, we examined frequency distribution of interval between storms, and found that the interval tends to increase year by year. Gumbel distribution was applied to each data of the record period, and the result shows, for example, that 100-year interval between storms in the period  $III_{33}$  becomes five times larger than that in the period  $I_{33}$ . The results show the apparent change in frequency distribution of rainfall characteristics in recent decades. The change tends to shorten return period of the hydrologic design value such as design discharge or design rainfall of the water use or control plans designed before so that the risks of floods or those of droughts are both increasing. The fact suggests us necessity to reconsider magnitude of design floods and droughts for water resources planning and management.

**HS02b/10P/D-031** Poster **1630-151**

#### HYDROLOGICAL REGIONALIZATION USING THE TCEV METHOD WITH THE SUPPORT OF A GEOGRAPHICAL INFORMATION SYSTEM

Cristiane M. FINZI, Iara Righi AMRAL, Bruno Rabelo VERSIANI (Centro de Pesquisas Hidraulicas e Recursos Hídricos - EHR - Escola de Engenharia - UFMG)

The analysis of a statistical model allows a better evaluation of the spatial variability of the hydro-climatological phenomena. The application of that model is called "regionalization". The paper focus the Two Component Extreme Value, TCEV Model, (Rossi et al., 1984), which tries to describe the extreme values of a statistical series, as maximum precipitation an maximum flood data. The regionalization method based on this model allows to identify hydrological homogeneous regions in a watershed, in terms of maximum values of precipitation and flood. The determination of those regions allows to evaluate realistic estimates for the involved variables, concerning studies and projects of water resources management, in the state of Minas Gerais, Brazil, mainly in a watershed where there is a lack of data. Previous studies applied the method in the southern portion of the Sao Francisco watershed. In this paper one compares the results when more data are included extending the study region. The statistical characteristics of maximum precipitation and flood determine the homogeneous regions. The methodology is developed in three stages: the first seeks the determination of the homogeneous regions according to the similarity of the coefficient of skewness and the second stage is the determination of sub regions where the coefficient of variation remains practically constant. The third stage is the determination of the index flood, based on the physical and climatic characteristics of the region. The results of the application of the methodology are the quantile estimates of the maximum values of precipitation and flood, specially in some regions with lack of data. In this application, one determine three homogeneous concerning maximum flood and five regions concerning maximum precipitation. In some of those areas the statistical regional curve is similar to the Gumbel model. In this case the TCEV method could not be applied. This means that the samples used in the calibration of the regional statistical model don't identify outliers values.

**HS02b/10P/D-032** Poster **1630-152**

#### WATER RESOURCES SUSTAINABILITY IN THE CONTEXT OF CLIMATE VARIABILITY AND INCREASING EXTREME EVENTS IN THE HIMALAYAN-INDO-GANGETIC PLAINS

R. B. SINGH (Department of Geography, University of Delhi)

The Himalayan environment is subject to significant and uncertain changes. Variation in climatic conditions could result in large-scale changes in the Indo-Gangetic ecosystem. The Himalaya which is fragile and globally important ecosystem, is also known as the water towers of the earth surface and rich repositories of biological diversity. Variability in climatic conditions influence water resource sustainability of the plains. In the present paper an attempt has been made to analyse the impact of climatic variability and other mountain extremes particularly floods on the Indo-Gangetic plains. Paucity of observational data and analysis makes the study on mountain areas rather difficult. The issues of Himalayan - Indo-Gangetic plains interactions including the nature and quantities of materials transported from highland to valleys along with the dynamics of land use induced sediment erosion processes and floods attract particular attention at different temporal and spatial scales. The Indo-Gangetic plains include region of national significance in terms of dense and increasing human population. There exists very large and variable discharges of fresh water, suspended sediments and dissolved matter. The present pattern of flooding suggests that high productivity is no longer being sustained. Shrinking natural resource base (per capita availability of land/water devoted to agriculture) and declining quality of resources are increasing the risk to our ability to meet the basic needs of the growing population of the region. In addition a range of socio-economic factors emerging out of flood problems impact land use and the food security. Investments in irrigation development are unattractive and have declined. Competing uses for water would force shifts in crops/cropping pattern. Soil-characteristics as well as cropping system in the Indo-Gangetic plain region is largely uniform. There are, however, a number of variations within the region. There are 6 agro-ecological regions and 12 sub-regions. Irrigation facilities are available to the maximum extent in the north-west and minimum in the east. The size and distribution of the land holding varies from 3.6 hectares in the north-west to approx. 1 hectare in the Bengal Region. There are vast differences in actual and potential yields, earning from about 6-ton/ha in the north-eastern region to as low as 2 tons/ha in the east having frequent flood prone areas. Major sustainability issues require focus on the ecosystem functioning, agro-biodiversity (including soil biota), loss in soil fertility, hazards, declining water table and rising water table / water logging etc. Managing floods in one region often co-exists with managing droughts in another region. The need for a comprehensive watershed based planning integrating land and water resources is urgently felt so as to monitor and manage the water resources of this region optimally. The strategy reflects a major conceptual shift towards risk reduction i.e. culture of prevention.

**HS02b/10P/D-033** Poster **1630-153**

#### APPROACH FOR ASSESSMENT OF RISK AND CHANGES IN EXTREME HYDROLOGICAL CHARACTERISTICS

Helen (Elena) Vladislavovna LOBANOVA (IAHS member, Senior Scientist)

One of the main practical application of hydrology is connected with a frequency analysis of extreme hydrological events such as floods and droughts. New Federal normative documents in Russia (Construction Norms and Rules, Code of Rules) take into account two kind of safety and risk assessment: -for existing water projects under some period of operation, -for future water projects. The first direction condition by the following reasons: short-term records in the past, new effective methods of computations which have been

developed in last time, modern changes (climate change, man's impacts). These peculiarities lead to a necessity of possible re-computation of design hydrological characteristics for the existing hydraulic constructions and other water projects to increase their safety. The algorithm of assessment and re-computation includes the following main steps: -extraction of the components in time series which connect with "natural" conditions and with "pure" impact of existing constructions on the runoff; -assessment of stability of working existing hydraulic constructions and other water projects (analysis of man's activity component); -assessment of climate change in time series in "natural" conditions (extraction and analysis of modern long-term climate change component); -determination of design extreme values taking into account the last observation, new methods and changing conditions; -comparison of the determined design values with the same one, which have been obtained before the construction of this hydraulic structure and making the decision about the re-computation. Such scheme characterizes a monitoring of design hydrological characteristics for changing conditions. New methods have been developed for a realization of this algorithm and they are: -methods for extraction of runoff components connected with operation by existing hydraulic and other kind of constructions and under different availability of the information; -methods for extraction of climate variability and long-term climate change components; -methods for assessment of statistical efficiency and contributions of climate change and water management; -assessment of empirical probability of non-regular extreme events such as floods and droughts taking into account historical information; -decision the problems of non-homogeneity of the extreme data by statistical criteria for testing of outlying data and application of the composition of distribution functions for non-homogeneous records; -methods for assessment of random errors of design hydrological events taking into account short-term period of the regular observations, palaeo-restorations and long-term period of future operation in changing conditions. Application of developed approach and methods have been given for some different examples: -re-computation of maximum design discharges for the cascade of the Dnieper hydropower stations; -re-computation of design maximum water level for the Lena River - Lensk city; -assessment of long-term operation of main hydropower stations in Russia for different hydrological characteristics (water resources, extremes, etc); -using of palaeo-restoration of annual runoff in more than 4000 years for assessment of climate changes and random errors of design values; -assessment of changes in low flow for different regions of Russia under climate change.

**HS02b/10P/D-034** Poster **1630-154**  
**ASSESSMENT OF THE RISKS OF EXTREME RAINS OCCURENCE DEPENDING ON THEIR GENESIS**

Ionel HAIDU (Dept.of Geography, Univ.of Cluj-Napoca)

Usually, in a study that has in view the rain falls that produce high floods, a single raw of maximum yearly values are to be analyzed, indifferently of the type from which those rains derive. It is to be appreciated that the rains with a maximum intensity are "covering", and there is no need to apply at diverse informative sources. This is a quantitative concept which refers only to the magnitude of the extremes (torrential rains, high floods) which would have unexpected hydrotechnical and social consequences. On the other hand, a qualitative approach, respectively the analysis of the extremes on genetic categories may reduce the uncertainties. It is possible that the set of the extremes (for instance, in the case of the rains with a yearly maximum intensity, but also in other cases) will lack the same statistical population as a source. Another example is given by the possible appearance in the observations raw of a value with an extraordinary magnitude, which is aberrant from a statistical point of view, and which must be removed by the analyst from the analyzed sample, in order to obtain "fair" adjustments. Thus, the historic maximum intensity of 8.5 mm/min registered at Borod station (west of Romania) that far exceeds the value of 2.77 mm/min, representing the average of those 28 years of observations, can not be explained by the statistics of extreme values. That's why it is useful to set up series of values on genetic categories, suspecting the possibility to find out many source-populations of the extremes. Besides the series of yearly maximum intensities, set up indifferent of the generating rain type (28 values), the succession of yearly maximum intensities produced by rains of thermic convection and the series of yearly maximum intensities produced by frontal rains, have been built. Were considered too, series having source couple of months: May-June typical of the most intense period of cyclonic activity and July-August specific for the most active period of thermic convection. For the length of the whole rainy season (April – September), in which the rains of thermic convection and the frontal rains can coexist, the monthly series of maximum intensities was also taken into consideration. While the frequency model of the series of yearly maximum values is, clearly, that of an exponential type, the genetic series are different. The maximum intensities generated by convective rains can be also adjusted through a lognormal model of 2 parameters though from the point of view of graphic correspondence, the best law is that of GEV type, on the theoretical curve being situated even the historical maximum of 8.5 mm/min. In the case of frontal rains, the candidate laws are Gumbel, Lognormal and exponential, and from those with 3 parameters, the GEV. The most adequate laws for the case of bimonthly and monthly series are also described. The paper approaches in its final part the possible genetic explanations of the extreme events, which can have different consequences as regards the high floods appearance.

**HS02** Monday, July 7 - Friday, July 11

**WATER RESOURCES SYSTEMS: GLOBAL CHANGE, RISK ASSESSMENT AND WATER MANAGEMENT (ICWRS, ICASVR, ICSW, ICWQ)**

Location: Site C, Room 24

Friday, July 11 AM  
 Presiding Chair: Y. Sakura

**HS02/11A/C24-001** **0830**

**ENVIRONMENTAL FLOW REQUIREMENTS IN WATER RESOURCE PLANNING AND OPERATION**

Denis HUGHES (Institute for Water Research, Rhodes University)

Many rivers throughout the world are impacted by either upstream reservoirs, run-of-river abstractions or stream flow reduction activities, such as commercial afforestation. Against this background, the new South African Water Act of 1998 introduced the need to reserve a certain proportion of the natural flow regime of rivers to ensure in the long-term that all water resource developments are environmentally sustainable. A relatively simple model is described that has the following characteristics and benefits with respect to the determination of instream flow requirements.- The model is consistent with the current main South African approach to setting environmental flows (Building Block Methodology). - The

model is designed for use in gauged or ungauged basins.- The model can be used to support site specific determinations carried out by a group of freshwater ecology specialists, but can also be used to generate low confidence desktop estimates based on a set of regional parameters.- One of the outputs of the model is a time series of environmental flow requirements with the same length as the input natural time series of monthly flow volumes that is used to determine the patterns of variability in the requirements.-The model generates outputs that are consistent with the standard water resource system yield analysis models used in South Africa. It is therefore relatively straightforward to assess the degree to which the required environmental flows have an impact on system yields. It is also possible to assess the impact of system operating rules on river flows and whether environmental flow requirements will still be achieved.-The output from model can be used to assess the extent to which existing, or future, water use licences are likely to impact on environmental sustainability. A further simple procedure has been developed to be able to analyse such impacts in relatively small river basins which do not have major dam storage and where the application of a complex system yield model would be inappropriate.-The model is also designed to provide outputs that can be used in the operation of water resource schemes, although there are still a number of issues that have to be addressed before this can be considered a practical proposition.The paper will briefly describe the basis of the model, the origin of the regional parameters, explain its use under different situations and how it is associated with other standard methods of water resource management analysis in South Africa. The role that the model is currently playing in enabling the implementation of the environmental components of the new Water Act will also be discussed. The paper will also discuss possible ways in which new information on streamflow-biota relationships can be used to improve the confidence in the model results.

**HS02/11A/C24-002**

**0845**

**INTEGRATED WATER RESOURCES MANAGEMENT UNDER COMPLEX HYDRO-POLITICAL CONDITIONS- THE PALESTINIAN CASE STUDY**

Ayman Ismail RABI, Natasha George CARM, Abdelatif KHALED (Palestinian Hydrology Group)

Integrated water resources management in the Jordan River Basin is hindered by the complex hydro-political situation, which is characterized by natural water scarcity, shared nature of water resources, conflicting demands, and intensive development and use of resources. In addition, the lack of final water agreements defining the exact shares, roles and responsibilities of each riparian, especially the Palestinians, coupled with the lack of water laws, regulations and plans make it difficult to manage these resources efficiently, especially under the given uncertainties. The foremost significant uncertainty is the one related to climate change in general and to drought in particular. Changes in climate over the years have assisted in aggravating problems in water quantity and quality. Given that the region is characterized by a high variability in rainfall depth over time and space, the occurrence of a drought event is a random variable. The analysis of drought years over the past 50 years shows non-uniform return periods. In 1998/99, the rainfall record in the winter was the minimum in the past 100 yearlong history of rainfall records. This drought has led to a rise in the salinity & chloride concentration. In addition, there has been a decline in groundwater levels, a reduction in groundwater storage, an increase in the volume of water pumped, and a drop in the discharge of springs. Accordingly, water shortage has become very acute and available supply falls short in meeting demand. Under the foreseeable future scenarios of population growth and development needs, this water shortage is expected to intensify. The average population growth rate is estimated at 4% which, means that the population is expected to double in the coming two decades. In addition, nearly 50% of the population is young; i.e., new housing units and other infrastructure development will be needed to accommodate the growing needs. This paper will define, based on a case study, the various drought phenomena that play a major role in planning for the management of droughts and/or other uncertainties in a semi-arid environment. Furthermore, it will address the most crucial yet delegate water supply and demand issues under various development scenarios. In addition, the paper will highlight the role of ecosystem services in adopting the concept of resource sustainability while trying to meet the water use requirements of the various adverse uses. Finally, the paper will look into the foreseeable urban development and its likely impact on resource availability, both in terms of water quantity and quality.

**HS02/11A/C24-003**

**0900**

**RESTORATION OF URBAN WATER CYCLE WITH URBAN RENEWAL**

Srikantha HERATH<sup>1</sup>, Katumi MUSIAKE<sup>2</sup>, Sadayuki HIRONAKA<sup>2</sup> (<sup>1</sup>Institute of Industrial Science, University of Tokyo, <sup>2</sup>Institute of Industrial Science, The University of Tokyo)

Urban water cycle consists of natural water cycle components such as rainfall runoff processes, evapotranspiration, infiltration and subsurface processes as well as discharge components arising from human water use such as water supply and irrigation. In addition to complex interactions among these components, the urban water cycle is deeply influenced by the human intervention, especially the alteration of infiltration, evaporation and runoff processes associated with urbanization. The authors have clarified these complex interactions and quantified the urban water cycle through distributed hydrological modeling in a well-equipped urban catchment located in the suburbs of Tokyo, Japan, which has high-resolution spatial and temporal data accumulated for more than a decade. One of the major adverse effects of urbanization has been the increase of impervious areas that has resulted in an increase of flood runoff, both in volume and peak discharge, and the associated reduction of ground water recharge that leads to reduced river low flows deteriorating amenity functions and water quality. In order to restore the urban water cycle, artificial infiltration through infiltration facilities has been proposed, where infiltration trenches and collection boxes installed at residential areas collect rainwater and let it infiltrate recharging the ground water. During the past few years, a water cycle management committee has been set up in the study catchment with the participation of various stakeholders to improve the urban water cycle. One of the measures adopted has been to install infiltration systems systematically in all residential housing complexes within the catchment. A study has been carried out where a distributed hydrological model has been set up for the catchment at 50m spatial resolution coupled to a grid level infiltration facility modeling system. Long-term scenario analysis has been carried out for installation of infiltration systems covering 1%, 2% and 4% of dense urban areas, simulating hydrological processes at 1-hour time step resolution for a number of years. The results show that total runoff volume reductions of 63%, 54% and 47% can be achieved for a 5 yr return period rainfall, while improvements of .5 mm per day of low flow quantities can be expected from the infiltration system implementation. Next, installation of infiltration systems with urban renewal is considered. The Urban Development Corporation of Japan manages most residential housing schemes in the catchment where houses are replaced every 30 years whereas other residential and infrastructure too have a similar renewal practice. With the detailed information of the expected urban land cover changes and the urban renewal plans, it was possible to map the urban renewal and infiltration facilities installation options that gives a clear picture of the state of urban water environment and its restoration potential.

HS02/11A/C24-004

0915

**METHOD OF SATELLITE MONITORING OF RESERVOIR STORAGES FOR EFFICIENT REGIONAL WATER MANAGEMENT**Jun MAGOME<sup>1</sup>, Hiroshi ISHIDAIRA<sup>2</sup>, Kuniyoshi TAKEUCHI<sup>3</sup> (<sup>1</sup>Graduate Student, Yamanashi University, <sup>2</sup>Graduate School of Engineering, Yamanashi University)

More than 41,413 dams over the height of 15m are now in operation in the world serving for various important purposes in their region. Their efficient use, especially a group of reservoirs integrated in a region, is the most important subject in integrated water resources management. It necessitates the regional monitoring of water storage in reservoirs, especially its seasonal variation for strategic risk management. Since the ground observations of reservoir storages are often not available to the users due to lack of proper information transmission network as well as, in some cases, administrative barriers, it is desirable to develop technology to monitor water storage by the use of satellite remote sensing technique. In this study, we propose a new method of estimating water storage in reservoirs based on satellite observations and digitized topographical data. In the method proposed, the area of water surface (A) measured from satellite images is transformed into the volume of water storage (V) by using the relationship between the area of water surface (A) and the volume of water storage (V) (called as "A-V relation") derived from Digital Elevation Model (DEM). Other method which combines the area of water surface (A) measured from satellite images and water level derived from satellite radar altimeter is also shown. In order to identify the area of water surface of reservoirs (A), the satellites and sensors used are: JERS-1/SAR, SPOT/HRV, ADEOS/AVNIR. The radar altimeter system mounted on TOPEX/POSEIDON was used for deriving water level. These methods are applied to the Yagisawa-reservoir in Japan and Volta Lake of Akosombo dam in Ghana to verify the possibility of estimating the water storage in reservoirs. The derived average accuracy based on satellite images and DEM for Yagisawa-reservoir was, in terms of percentage error, 8.3% (SPOT/HRV and ADEOS/AVNIR: semi-automated), 8.2% (JERS-1/SAR: image reading) and 19.7% (JERS-1/SAR: semi-automated) as against observations at dam site. As for Volta Lake, since observations at dam site was not obtained, annual variation of water storage in reservoirs calculated from long term discharge data was used for verification. As a result, accuracy of both methods was relatively good. Consequently, the high potential of estimating reservoir storage from satellite and its use for regional water management were demonstrated.

HS02/11A/C24-005

0930

**INTERMITTENT UTILIZATION OF WATER RESOURCES IN AN OASIS REGION FOR THE LAST 2000 YEARS**

Masayoshi NAKAWO (Research Institute for Humanity and Nature)

A decrease in water resources has become a serious problem lately in the Heihe River basin, an oasis region, in western China. In the downstream region, in particular, groundwater level has decreased and the local ecosystem has become poorer and poorer. Lakes formed at the termini of the river have dried up and disappeared already. The local people, who are mainly living on nomadic activities, are facing to a water scarcity even for their drinking water, and to difficulties in keeping their animals. It was pointed out that the decrease of water resources is caused by an overuse of the river water upstream where agricultural development has become intense with irrigation systems in these days. Looking back the history of the region, however, we can find similar situations in the last 2000 years. In the Han Dynasty, many soldiers were sent by the government as colonial troops to this basin, and a vast area was cultivated through an introduction of irrigation systems, in order to fight against the Hunnu, a powerful nomadic people at that time. This seems to have taken place in the Tang Dynasty as well, but with smaller scale, which could have been stressed by the Toqquz Oghuz Empire. The empire, however, has collapsed suddenly, and many historians blamed a climate change for the collapse. In the era of the Xixia and Yuan Dynasties, nomadic troops have occupied the region, and an 'interdependent society appears to have been established, when the famous Heicheng City was in prosperity. The population in the region has drastically decreased during the Ming Dynasty, but again increased dramatically during the Qing Dynasty indicating that water utilization for agriculture must have increased extremely in this era. The water demand in the region has been evolved intermittently as mentioned above, in accordance with the evolution of the society such as changes of ruling government. During the last 2000 years, however, climate has also changed significantly, which would have affected the society of the region. The sudden collapse of the Toqquz Oghuz Empire can be one of the examples. For considering the environmental problems taking place now, it is necessary to examine both the natural changes and the changes in the society, and their interaction. We would be able to obtain a clue for solving the recent problems by examining what happened in the history.

HS02/11A/C24-006

0945

**EFFECTS OF CLIMATE CHANGE ON IRRIGATION ACTIVITIES: A CASE STUDY OF BENIN-OWENA RIVER BASIN IRRIGATION PROJECTS**Catherine Imhangulaya IKHILE<sup>1</sup>, George Ubuihoro IKHILE<sup>2</sup> (<sup>1</sup>Department of Geography and Regional Planning, <sup>2</sup>Scripture Union (Nigeria))

This study examines the effects of climate change on irrigation activities in Edo State under the Benin-Owena River Basin Irrigation project in SW Nigeria. Data was collected for Benin City on rainfall and temperature from 1960-2000 and on irrigation activities from 1990-2000. Results show that the annual rainfall pattern for Benin City showed a wide variation between 1960-1980. For example, in 1965, an annual total rainfall figure of 3000mm was recorded as against a figure of 1702.9mm in 1972, the highest monthly reading being in July 1965 (about 1000mm). The variation in rainfall between 1980-2000 is fairly less varied but generally much lower. The lowest annual total rainfall figure of 1227.6mm was recorded in 1986 as against the highest figure recorded in these decades which was 2773.8mm in 1992. The period, 1982-1986, showed the greatest downward trend in annual rainfall totals. There was a significant relationship between mean annual rainfall and temperature in this period at 0.01. The temperature conditions for the period is as shown below: Decade Mean Max range (°C) Mean min range (°C) Mean Annual range (°C) Decadal range (°C) The annual mean rose steadily from 1960 to 2000. During the 1960-1970 decade, it was 25.8°C to 27.0°C (decadal range: 1.2°C). During the 1971-1980 decade, it was 26.3°C to 27.5°C (decadal range: 1.2°C). During the 1981-1990 decade, it was 27.1°C to 27.6°C (decadal range: 0.5°C). In this decade, the climate of Nigeria was described as playing a climatic drama (Ojo, 1987). There were lots of fluctuations and the weather became more unpredictable. The farmers were a lot more confused and uncertain about their crops performance. The last decade, 1991-2000, has been the warmest with annual mean temperature ranging from 27.2°C to 28.2°C (decadal range: 1.0°C). The temperature appears to be on the increase in Edo State coupled with fluctuating rainfall. This is an indication of global warming and climate change. There is a significant relationship between mean annual rainfall and temperature in the study period at 0.01. This shows a gradual warming up of the environment from 1960-2000. The mean annual temperature rose steadily. This is an indication of global warming. These observed patterns of variation in rainfall and temperature

coupled with increasing population and other factors caused the farmers and policy makers in Nigeria to embark on massive irrigation programmes in Nigeria. From the analysis of irrigation projects in Edo State, it is observed that at the onset of the irrigation schemes in the 1990s, only a few projects were in operation. The total available irrigable land area was about 500 hectares and they were mostly small scale. By the year 2000, more irrigation projects had been embarked upon and the total land area involved was about 6295 hectares. Most of the former schemes have been upgraded to medium and large-scale schemes.

HS02/11A/C24-007

1000

**IMPACT OF GURARA RIVER (NIGERIA) INTERBASIN WATER TRANSFER SCHEME ON RIVER KADUNA AT SHIRORO DAM**

Onemayin David JIMOH, O. S. AYODEJI (Civil Engineering Department, Federal University of Technology)

River Kaduna is impounded at Shiroro for the purpose of generating electricity only. There is a persistent low reservoir level between November and June due to seasonal flow in the river. One of the aims of the Gurara River interbasin water transfer scheme is to transfer 1500 Mcu.m (which is about 10% of the mean annual inflow to Shiroro reservoir) of water from Gurara River between December and May to Shiroro reservoir. The interbasin water transfer is meant to stabilize the reservoir level at Shiroro dam. This paper examines the effect of the water transfer on the storage level at Shiroro. Fourteen years of daily inflow record was used to study the real-time operation of the reservoir. It was observed that the reservoir attained its maximum operating level in July and maintained it till September or October due to the transfer. Whereas, maximum operating level would have been attained in August without the transfer into the reservoir. Although the interbasin water transfer into Shiroro reservoir will enhance power generation, but there will be an increase in the frequency and severity of annual flooding of the downstream sector of the dam. Appropriate flood damage mitigation measures are recommended for Kaduna River basin, so as to optimize the benefit of the interbasin water transfer scheme.

HS02-Oral-Posters

Monday, July 7 - Friday, July 11

**WATER RESOURCES SYSTEMS: GLOBAL CHANGE, RISK ASSESSMENT AND WATER MANAGEMENT (ICWRS, ICASVR, ICSW, ICWQ)**

Location: Site C, Room 24

Friday, July 11 AM

Presiding Chair: Y. Sakura

HS02/11A/C24-0010P

Oral-Poster

1045

**MAXIMUM OVERLAND FLOW IN RIVER BASIN AND LANDUSE**

Elena ASABINA (Russian Research Institute for Integrated Water Management and Protection)

Present paper is the case of study of the basin where water resources for large city water supply are being formed. High economical activity in the basin transforms environment. Change of landuse structure such as transformation of forests into farmlands, meadows into pasture lands, bogs into meadows, etc. leads to changing of overland flow which presents the main component of river runoff. Solved problem is to assess how the values of overland flow depend on character of landscape. To prevent negative consequences of these processes for runoff regime it needed to reveal the areas in the basin where main quantities of overland flow are to be generated and to protect them against possible landuse. Values of precipitation were almost equal in different areas of studied basin. However, significant differentiation of overland flow in the space of the basin was found that is explained by differences of overland flow genesis such as characteristics of land surface. Character of landscape and soil type cause different conditions in the basin. Each of landscapes in combination with topography and soil can be considered as certain runoff-producing unit, which characteristic is uniform conditions of overland flow genesis. Hence, the river basin as a whole and its different areas were represented by combination of various runoff-producing units and overland flow was evaluated in different areas of the basin. Also, overland flow was assessed for different phases of hydrological regime such as winter low water, spring flood, and summer low water with rain floods. It was found that main amount of overland flow is being formed during spring flood and in upstream but not in downstream part of the basin as it was thought earlier. Obtained conclusion will allow providing optimal landuse practice in future.

HS02/11A/C24-0020P

Oral-Poster

1049

**ARTIFICIAL NEURAL NETWORK MODELING OF THE RAINFALL-RUNOFF EXTREME EVENTS**

Dionysia PANAGOULIA, Nikos MARATOS (Department of Water Resources, Hydraulics and Maritime Engineering, National Technical University of Athens)

An artificial neural network (ANN) is a reliable mathematical mechanism in modeling the complex nonlinear relationships between input and output timeseries. ANN models have been proven effective and efficient to model the rainfall-runoff relationship in situations where explicit features of the internal hydrological subprocesses are difficult to be described using physically based equations. A new algorithm using a combination of linear least squares and multistart simplex optimization is developed to show the mechanism and parameters of three-layer feed forward ANN models and the potential of such models for simulating and forecasting the high-and low-flow events over a mountainous catchment. The output "rain plus melt" from the snow accumulation and ablation model of the US National Weather Service (US NWS) applied on a medium-sized mountainous catchment. The Mesochora catchment in Central Greece was used as input to ANN model. The conceptual soil moisture accounting model (SMA) of the US NWS applied, as well, over the same catchment, for comparison of extreme values. The RMSE (root mean square error) and %VE (percent volume error) statistics, for each model, computed separately for flows above and below the 15-year meandaily flow and presented as a function of the total annual flow for each data year. Note that the five calibration years were the driest of the 15 data years. Clearly, RMSEA (root mean square error above-mean daily flow) performance of the SMA model is worse than that of ANN on all years. The results of the RMSEB statistic (root mean square error below-mean daily flow) indicate that ANN model performs best for all of the years. The %VEA (percent volume error for above-mean daily flow) statistic indicates that the ANN model consistently has the smallest bias, while the SMA performance is poor. The %VEB (percent volume error for below-mean daily flow) statistic shows the poor performance of SMA model. We should not point out that the poor performance of the SMA model does not

reflect so much on the ability of the model as it does on the calibration procedure used. In addition, an 'expert' would not allow the model error bias at various flow levels to deteriorate so much while minimizing the error variance. Although the ANN model developed here, by no means, could substitute a physically based conceptual model, the results indicate that the ANN model may provide best performance when only dry years of data are used for calibration.

**HS02/11A/C24-003OP** Oral-Poster **1053**

**DETERMINATION OF INSTANTANEOUS UNIT HYDROGRAPH WITH CLARK'S TECHNIQUE IN GIS**

Musa YILMAZ, Nurunnisa USUL (Water Resources Lab. Department of Civil Eng. Middle East Technical University)

Determination of unit hydrographs for the basins is very important for the design of hydraulic structures. When there are observed rainfall-runoff data for the storms they are obtained by using these data, but when there are no observed data they are obtained by using synthetic unit hydrograph methods. In this study one such method is used together with Geographical Information Systems techniques. Application of Clark's synthetic unit hydrograph technique with GIS technology requires the estimation of three parameters of the original methodology. Time of concentration,  $T_c$ , is derived from SCS lag equation, reservoir storage coefficient,  $R$ , from an observed storm hydrograph and the time-area histogram is determined from the Digital Elevation Model of the basin. The translation hydrograph is then derived from time-area graph by applying a unit excess rainfall over the basin. After performing a linear reservoir routing, the translation hydrograph is routed to the basin outlet and the Instantaneous Unit Hydrograph of the basin is obtained. It can be used to obtain any duration unit hydrograph and then storm hydrographs for this basin. Such a study is performed for two different size basins in Turkey and the results are compared with the observed unit hydrographs of the basins and a discussion is given.

**HS02/11A/C24-004OP** Oral-Poster **1057**

**ARIDIFICATION AND THE INCREASE OF FLOOD EVENTS IN CENTRAL EUROPE**

János RAKONCZAI, Katalin BÓDIS, Ferenc KOVÁCS (Department of Physical Geography, University of Szeged)

Hydrological events in Central Europe (including the more thoroughly analyzed Hungary) began to show a strange kind of controversy in the past decades. It is clearly visible through statistics that precipitation has decreased significantly (with about 10 %), at the same time however, the number of flood events shows a remarkable increase. In the year 2000 the situation was really peculiar, because in the beginning of a persistent drought significant flood prevention efforts had to be made along the Tisza river i. e. drought and flood at the same time! We demonstrate the characteristics and consequences of the aridification process from several aspects. Beginning as early as 1910 precipitation in Hungary is dropping constantly. Statistical analyses show that the reduction did not bring about the decrease of variability; fluctuation was merely transferred into a lower range of values, clearly showing the decrease in the average amount of precipitation. The persevering drop of precipitation has produced a significant decline in the amount of groundwater. This process became obvious since the early 0-s. We have determined through detailed GIS analysis the spatial and temporal changes in the level of groundwater and the total deficiency in subsurface waters. One of the most important consequences of the analysis is that in some areas even the significantly rainy years could not stop the decrease of groundwater meaning that the drop of precipitation clearly appears in subsurface waters. (It is important to bear in mind that the decrease of subsurface waters in closely connected to relief: in plain areas that are higher than their surroundings the decrease is more significant.) To determine the reaction of foliage to aridification we executed spatial analysis based on Remote Sensing methods. Throughout the world, floods became more frequent in the past decades. This is caused by both natural processes as well as the changes in social and economical structures. Extensive growth of agriculture became possible by creating arable lands through massive river regulation works. However population growth can also cause people to move into areas that are endangered by floods. Floods are thus just the products of natural processes in such areas. The truth is however, that due to human interventions, areas of potential flood-risk has expanded as well. The higher water levels in regulated rivers or the huge amount of water stored in large reservoirs both lead to flood risks to get higher than they would naturally be. In addition to the above, meteorological extremities also augment the possibilities for floods. The flood disasters of recent years all over the world and in Central Europe clearly demonstrate this as well. In this lecture we will, through demonstrating several floods, evaluate their natural and social background. It can be said that now floods can appear in any part of the year due to climatic changes, nature can produce quite peculiar extremities (extraordinary amounts of precipitation; record breaking flood levels along the Tisza river in four consecutive years), as well as the way human actions affect natural processes.

**HS02/11A/C24-005OP** Oral-Poster **1101**

**DEVELOPMENT OF NEW TECHNOLOGIES OF FLOOD SIMULATION AND FORECASTING IN REAL-TIME**

Sandra Gabriela GARCIA (Technical University of Cartagena. Department of Thermic Engineering and Fluids)

The flash floods constitute one of the main problems of the Mediterranean semi-arid zones of Spain. The convective storms of high intensity, typical of these zones, produce hydrological events that can turn out to be catastrophic. Due to the scanty existing time between the runoff hydrograph peak and the associated rainfall, the warning of flooding must be based on meteorological and hydrological forecasting. The coordination among the responsible authorities in the operational flood management, needs real-time operative decision support system. The use of Geographical Information Systems (GIS) in the development of these support tools, it constitutes a foreseeable direction. The GIS allow an efficient integration of information with a high spatiotemporal resolution, and spatially distributed hydrologic models oriented to runoff simulation and prediction in real time. The development of new methodologies and tools that allows the operative integration of radar rainfall fields and short term quantitative rainfall forecasting as input to distributed spatially rainfall-runoff models, are proposed. Finally, it is to be underlined that this work incorporates the use of new technologies (GIS, remote sensing, Digital Elevation Models) and the most recent developments in aspects of estimation and treatment of the spatial distribution of soil moisture and the flow in the unsaturated zone. The main objective is to improve the forecasts of flash floods applying a decision support tool in real-time named *Shyska*, developed with GIS-embedded functions.

**HS02/11A/C24-006OP** Oral-Poster **1105**

**SPATIAL-TEMPORAL APPROPRIATENESSES OF EXTREME PROCESSES FORMATION IN RIVERS SYSTEMS OF REGIONS WITH SHARP CONTINENTAL CLIMATE**

Leonid M. KORYTNYI, N. V. KICHIGINA (Institute of Geography Siberian Branch Russian Academy of Sciences)

Spatial-temporal appropriatenesses of floods and shallows formation in main basins of East Siberia- the Enisey, Angara, Lena rivers, Lake Baikal are researched. Genetic and statistical regional analysis considers the specific of physiography conditions and also the peculiarities of sharp continental climate that has a tendency to change for the last ten years. Long-term series of flow on 120 hydrological gauge lines are the basis. Floods and shallows characteristics are determined: causes of extreme situations, their recurrence, geophysical and hydroengineering factors. Zoning of East Siberia on floods risk is implemented and statistic analysis of flow' extremes and curves of maximum flow distribution as well. Researches are directed to decrease extreme situations in water resources' systems. Effectiveness of different gear of risk management, the system of ecological insurance in particular is considered. For a number of regions the risk areas in the valleys of main extreme flood rivers is marked out and regulations of economic activity in these valleys are worked out. In the base of regulations there is the combination of four types of arrangements: geocological, economical, engineering, and legal.

**HS02/11A/C24-007OP** Oral-Poster **1109**

**DEVELOPMENT OF WATERSHED RAINFALL-RUNOFF MODEL BASED ON THE PARTIAL CONTRIBUTING AREA CONCEPT**

Chin-Hsin CHANG<sup>1</sup> (<sup>1</sup>Department of River and Harbor Engineering, National Taiwan Ocean University, <sup>2</sup>Department of River and Harbor Engineering, National Taiwan Ocean University)

The objective of this study is to develop a rainfall-runoff model based on the partial contributing area (Betson, 1964; PCA) concept. The influence factors of the PCA phenomena were investigated. The size of the PCA during storm is derived from TOPMODEL theory and estimated by using a digital elevation model (DEM). The PCA concept was then combined with a kinematic-wave based geomorphic instantaneous unit hydrograph model (Lee and Yen, 1997; KW-GIUH) for rainfall-runoff simulation. In the KW-GIUH runoff simulation considering PCA concept, the surface runoff mechanism was simulated by Manning's formula, and the subsurface runoff was approximated by Darcy's law. The Hen-Chi watershed in northern Taiwan was used to demonstrate the capability of the proposed model. The PCA size and geomorphic factors of the study watershed were obtained using a DEM, and SPOT satellite images were adopted for land cover analysis to obtain the roughness coefficient. The results showed that significant improvements were found in the simulation of rising and recession hydrographs.

**HS02/11A/C24-008OP** Oral-Poster **1113**

**REAL TIME FLOOD FORECASTING: A CASE STUDY OF THE JHELUM RIVER, PAKISTAN**

Sajjad AHMAD (Department of Urban and Regional Planning, University of California, Irvine)

A modeling system is developed for real-time flood and reservoir inflow forecasting. It comprises a lumped conceptual rainfall runoff model, a hydrodynamic model for river routing, and an up dating procedure for real time operation of reservoirs. The model is implemented for the Jhelum River Basin in Pakistan, with watershed area of 14860 km<sup>2</sup> and the Mangla Reservoir situated at the down stream end. The model is calibrated and verified at five gauging stations using daily rainfall data from twelve rain gauges and daily discharge data from three stream gauging stations for the period 1985 to 1991. Statistical parameters are used to evaluate the performance of the model. Real time forecasts of historic floods of 1976 and 1992 are performed with 24 hour and 6 hour lead times respectively. Sensitivity analysis on quantitative precipitation forecast (QPF) is made. The model performance for short term forecasts that is, 6 to 24 hours indicate robust system behavior in real time inflow prediction. Results indicate that if the accuracy of precipitation forecast is greater than 60 %, the error in the forecasted stream flow is less than 25 % for huge flood events. Sensitivity analyses show that large historic floods are highly sensitive to QPF.

**HS02/11A/C24-009OP** Oral-Poster **1117**

**REVISITING 1992 FLOODS IN PAKISTAN: OPERATION OF MANGLA RESERVOIR**

Sajjad AHMAD (Department of Urban and Regional Planning, University of California, Irvine)

Occurrence of floods is a natural phenomenon all over the world. With the increase in population and human activity in the floodplains, flood damages represent escalating hazard in many countries, despite increasing investments in flood control measures. Reservoirs are important structural measures to reduce damages caused by floods. Reservoir operation during large flood events is crucial in utilizing reservoirs as flood damage reduction options. In 1992 a catastrophic flood passed through the Mangla Reservoir on the Jhelum River in Pakistan. Operation of reservoir resulted in severe flooding of down stream areas causing damages to lives and property. A reservoir operation model is developed for the Mangla Reservoir. Model is calibrated for the flood event of 1976. The simulation model is used to investigate the water levels in the Mangla reservoir that would have resulted in 1992 with releases of 5700 m<sup>3</sup>/s (safe passage down stream) and 8500 m<sup>3</sup>/s (high flooding conditions down stream). Simulations revealed that it was possible to accommodate a considerable volume of the 1992 flood in the reservoir. However, to operate the reservoir in this way, difficult decisions have to be made during the flood. This can only be done with a full overview of the flood situation and in close cooperation with the concerned agencies. It also requires that the procedures for the reservoir operation for such a situation be already developed.

**HS02/11A/C24-010OP** Oral-Poster **1121**

**STOCHASTIC MODEL OF THE RUNOFF FLUCTUATIONS OF THE RIVERS WITH A FLOOD FLOW REGIME**

Andrei V. KHRISTOFOROV<sup>1</sup>, Taras V. SAMBORSKY<sup>2</sup> (<sup>1</sup>Department of Hydrology, University of Moscow, <sup>2</sup>Department of Oceanology, University of Moscow)

The stochastic model of fluctuations of a runoff during a flood period is offered. It includes a stochastic model of the hydrograph of a flood season and stochastic model of the annual fluctuations of its characteristics. The stochastic model of the hydrograph is based on the approximation of the individual hydrographs of separate flood peaks and base flow and their superposition into the unit hydrograph of the whole flood period. The parameters of the approximation - base flow, number of flood peaks, dates of their passage, their maximums,

durations of the growth and intensity of recession. All these characteristics are considered to be the random variables. The sequence of flood peaks during a flood period is described by a model of Poisson process. The model of annual fluctuations includes the description of probability distribution of hydrograph elements, correlation between them, autocorrelation of their annual fluctuations, their probable climatic and man-made regular changes. The number of flood peaks is the major characteristic of flood season. It can be considered as an index of flood forming situations of the year. The realization of model includes the Monte-Carlo method and theoretical formulas suggested for transition from model elements to any river flow characteristics of flood season. In a case of some regular changes caused by climate or economic activity the principles of correction of the parameters of probability distribution of model elements are suggested. The adequacy of the model was successfully tested on a base of hydrologic data for 68 rivers of the world. These are the rivers of the Amur basin and Northern Caucasus in Russia, North Korea, Ukrainian Carpathians, Georgia, USA, Algeria and Surinam. The statistical stability of the model is rather high. The basic parameters of the model can be estimated with the errors no more than 5-10% already in a case of 10-15 years of hydrologic observations. The model is intended for the hydrologic computations of any characteristics of the river flow of flood season for a weakly studied rivers in a case when a lack of hydrometeorologic observations don't allows to use the models of river flow formation. The model permits to increase the accuracy of hydrological computations by a factor of 1.5 - 2 and more in comparison with normative methods used now. The application of the model is not limited by the traditional problems of hydrologic computations. This is confirmed by an example of model application for the analysis of the systematic increase of the annual river flow which was discovered for the rivers of Mid-Atlantic of USA from the beginning of 70-ties.

**HS02/11A/C24-011OP** Oral-Poster **1125**

**IMPACT OF POPULATION GROWTH AND THE CLIMATE CHANGE ON THE QUANTITY OF WATER RESOURCES IN NORTH EASTERN REGION OF INDIA**

Uttam C. SHARMA (Indian Council of Agricultural Research)

The north-eastern region of India, comprising seven states, has a geographical area of 255,090 sq km. The region is extremely rich in water resources but continuous increase in human interference and mismanagement has rendered these resources in fragile state. The region receives about 510 cubic km of water as annual rainfall. It has two major river basins viz. Brahmaputra and Barak, which drain 194413 and 78150 sq km area with an annual runoff of 537.0 and 59.8 cubic km, respectively. The region has a total surface and ground water potential of 1064.8 and 16.6 cubic km. The scenario appears to be quite encouraging but indiscriminate use of water resources has caused land and environmental degradation in the region. Against an irrigation potential of 3.68 million ha, only 10.6% has been exploited. The population in the region has increased from 10.5 million in 1951 to 40.3 million in 2001, that is, it has grown 4 folds in 50 years, thereby exerting tremendous pressure on land and water resources. More than 82% of the population is rural based, whose main occupation is agriculture. Prevalence of shifting cultivation has resulted in deforestation and annual soil loss of 88.3 million tonnes through run-off from hill slopes, causing silting of river beds and frequent occurrence of floods. Due to population pressure, more and more forest area is being brought under plough, putting whole ecology in peril. The declining trend in rainfall and frequent temperature fluctuations are a signal for climate change. The demand for water for domestic use has suddenly increased due to fast population growth and change in life lifestyle of the people. At present, about 2.9 and 20.0 cubic km of water is required for domestic and irrigation and 1.5 cubic km each for energy, industry and other miscellaneous uses. In towns, generally the raw rainwater is supplied for domestic use while the people in rural areas have to depend on stream or pond water collected during monsoon. Seasonal rainfall flushes the catchments earlier charged with polluted environment. This polluted water results in frequent occurrence of diseases like cholera, jaundice, diarrhea and typhoid. Water demand is high and the supply does not commensurate with it. Due to mismanagement of rainwater, about 3586 thousand ha of land has become prone to floods. Further, the quality of water has also deteriorated due to its being polluted with nitrates, chlorides and sulphates with increased use of fertilizers and pesticides in an effort to increase crop productivity in the region. If the rate of population increase remains unabated, the water resources are likely to dwindle further as also deterioration in the quality of water. A multidisciplinary study, based on watershed approach, is in progress since 1983, to evolve new farming system to replace shifting cultivation, judicious management of rain-water and monitoring of soil, nutrients and water yield through surface and base flows. Lot of useful data has been generated which will help in planning, developing and improving the water resources in the region.

**HS02/11A/C24-012OP** Oral-Poster **1129**

**MANAGEMENT OF WATER RESOURCES IN KANDI (DROUGHT PRONE) ZONE OF JAMMU PROVINCE FOR HIGHER CROP PRODUCTIVITY**

Vikas SHARMA (S.K. UNIVERSITY OF AGRICULTURAL SCIENCES AND TECHNOLOGY- JAMMU)

The *kandi* zone of Jammu province of Jammu and Kashmir state of India is characterized by low rainfall (<650 mm), deep water table, undulating topography, poor soil fertility with land surface full of sand stones, soil moisture stress, frequent droughts and acute scarcity of water for domestic use and crop production. The *kandi* zone has two major river basins viz. Chenab and Tawi, which pass through deep gorges and undulating terrain, draining entire Jammu region. About 3.5 to 5.0 km<sup>3</sup> of water is received as annual rainfall, mostly during July and August. Rest of the period during the year remains dry except few showers during winter. Rains are generally with high intensity, resulting in over flowing of seasonal streams, soil erosion and degradation. The entire zone has agriculture-based economy but is always deficient in food grains. Though, the farmers are hardworking, working most of the time in the field along with their spouse and children, they do not produce as much as to feed their family. In absence of optimum soil moisture and irrigation facilities; application of fertilizers, good crop seed and other inputs have little impact on crop productivity. The studies have shown that water management is the major factor, which can improve the crop productivity in the *kandi* zone. It is difficult to derive any benefit from the water from two rivers as they flow in hilly terrain and cost involved in lifting the water and construction of canals would be two high compared to the area available for irrigation in the immediate vicinity. Construction of small structures for rainwater harvesting during monsoon will be good preposition. Farmer's participation in the whole programme is necessary for achieving the desired goals. Construction of small check-dams to divert the water to ponds will not only reduce the soil erosion but water can be utilized for life saving irrigation during winter. Besides, there is need to introduce such cropping pattern, which may reduce the run-off and help in ground water recharge. The paper discusses the feasibility of the check-dams, water storage reservoirs, soil conservation measures according to topography and judicious utilization of available water for higher crop productivity, resource management and environment conservation in *kandi* zone of Jammu Province.

**HS02/11A/C24-013OP** Oral-Poster **1133**

**WATER RESOURCES MANAGEMENT AND PLANNING; THE NEED FOR MULTIDISCIPLINARY MODELLING APPROACHES**

Islam Hamza ABOU EL-MAGD, Trevor TANTON (Civil & Environmental Engineering Departement, University of Southampton)

Water is a finite resource and the rapidly growing population in many arid and semi arid countries is placing excessive pressure on the limited water resources of these Countries. Unfortunately, it is predicted that many of these arid and semi arid countries will be the most seriously effected by a decline in water resources as a result of global warming. In most of these countries irrigated agriculture is the main consumptive user of water and unless water management is improved there will be a dramatic reduction in food production as a result. Typically most large irrigation schemes have an unimaginable wastage of water, with crop evapotranspiration accounting for only 20-35% of the water supplied, the remainder being wasted. Global warming will result in both increased evapotranspiration and reduced water resources and it is clear that if productivity is to be maintained water will have to be used more efficiently. Water allocation for irrigation is traditionally based on theoretical estimations of crop water requirements and rough estimations of canal losses, with the result that water supply rarely meets demand. Remotely sensed data is capable of supplying the planners with up to date data on the crops in the field and in measuring crop water requirements and wetland losses. This paper explores how remote sensed data is presently being used to improve water resource management in large irrigated catchments. It investigates the potentiality of spatial modelling of the real time data from satellite images, crop water demand from climatic data and irrigation information from the field to accurately allocate the irrigation water need in large irrigation scheme.

**HS02/11A/C24-014OP** Oral-Poster **1137**

**THE SYSTEM FOR ECOLOGICAL AND ECONOMICAL ASSESSMENT OF USE, PRESERVATION AND RESTORATION OF URBAN WATER BODIES: ST. PETERSBURG AS A CASE STUDY**

Sergey A. KONDRATYEV (Prof.)

The water surface area of 106 water bodies of St. Petersburg city is equal to about 21 km<sup>2</sup>. The urban water bodies reflect the level of environmental pollution of St. Petersburg. At present time only 2% of water bodies can be referred to pure, 18% - to polluted, and 80% - to dirty. The State is the owner of water resources, including urban water bodies. Its interests are to stop deterioration of water quality and degradation of water ecosystems, and to find money for restoration of water bodies. The potential water-user can rent water bodies for the aim to get money income. In this case he should be interested in preservation or restoration of water bodies being a natural basis of his business. At present study there is discussed the problem of a choice of optimum variants of urban water resources use without deterioration of water quality and ecological status of water bodies, and with financial profit for water-user. The system for ecological and economical assessment of use, preservation and restoration of water bodies has been developed. The basic stages of the system are the following:- Data bases load and GIS development.- Assessment of the investment appeal of urban water body. High level of environment pollution, industrial enterprises located in catchment, high level of anthropogenic impact on water body are the reasons for negative assessment. The below mentioned stages take place only for positive assessment of the investment appeal of water body. - Assessment of present suitability of water body for various kinds of use. The basis of assessment is the result of comparison of present parameters of water quality with critical limits of chemical substances in water and sediments. High level of water and sediment pollution is the reason for negative assessment. - Economical assessment of water body restoration. Various kinds of restoration methods are considered: internal (chemical, biological and engineering) and external (catchment changes). - Optimisation of water body use on the basis of mathematical modelling. - Assessment of sensitivity of results of modelling to change of parameters of water body (depth, volume, area of recreation zone, etc.). Results of assessment are the information for choice of scenario of parameters changes for maximization of financial profit of water use.- Economical assessment of water body parameters change.- Economical assessment of monitoring.- Final ecological and economical assessment of water body use taking into account costs of restoration, parameters change and monitoring. Application of the developed system has been made for urban water bodies. Results of application show that it is possible to use a number of water bodies with financial profit for water-user and without deterioration of water quality and degradation of ecosystems. The lists of water bodies with maximal and middle investment appeal are carried out.

**HS02/11A/C24-015OP** Oral-Poster **1141**

**OPTIMAL PRESSURE CONTROL IN SUPERVISORY WATER DISTRIBUTION NETWORK USING SHUFFLED COMPLEX EVOLUTION ALGORITHM**

Haytham AWAD, Akira KAWAMURA, Kenji JINNO (Institute of Environmental Systems, Kyushu University, Fukuoka, Japan)

Obtaining an optimal control of the distribution of system service pressures in a municipal water distribution networks has always faced combinatorial problems due to its complexity, scale of the problem, variation of water demand and the difficulty in estimating the roughness coefficient of old pipes. Referring to the previous difficulties, the application of linear, non-linear, dynamic programming, simulated annealing and genetic algorithm have been investigated by many authors and used in recent years for the optimization programs of water distribution networks design, replacement and leakage minimization. Particularly, the application of genetic algorithm (GA) in water distribution networks optimization models has been known as the most successful method in this field. It works with a coding of the parameter set, direct the search to the improved solutions by probabilistic rules and working directly with the objective function requiring no additional knowledge. In this paper, we used an evolutionary optimization procedure known as Shuffled Complex Evolution - University of Arizona (SCE-UA) for searching for the optimal or near-optimal solution of valves setting for the pressure regulation of a water distribution network. The SCE-UA technique has been successfully used in the calibration of conceptual rainfall-runoff models and the identification of aquifer formation parameters in the area of surface and subsurface hydrology, respectively. However, this algorithm has never been used in the field of water distribution networks management and planning and this paper is our first attempt in this direction. The SCE-UA Method which is relatively new concept is a general purpose global optimization program which combines the strengths of the simplex procedure with (i) the concept of controlled random search; (ii) competitive evolution; and (iii) the concept of complex shuffling. The synthesis of these three concepts makes the SCE algorithm not only effective and robust, but also flexible and efficient. The main advantage of the SCE-UA method is that, for a given number of objective function evaluations, the SCE-UA have the highest probability of succeeding of finding the global optimum. To demonstrate the performance of the SCE-UA algorithm, a case study of a certain block of the supervisory Fukuoka City water distribution networks is presented showing the effectiveness of the algorithm to regulate the pressure at all the network nodes between upper and lower values and as near as a target

value. In Fukuoka City water distribution networks, electrically motor valves openings are adjusted by remote control to regulate pressures and flow rates on the basis of information provided by flow meters and pressure gauges attached to distribution pipes. Results show that pressures are well regulated by SCE-UA algorithm to a target value for a specified nodal demands and external inflows.

**HS02/11A/C24-0160P** Oral-Poster **1145**

**BANK FILTRATION SYSTEMS AS COMBINED TECHNOLOGY FOR GROUNDWATER AND SURFACE WATER**

Ekkehard O. HOLZBECHER (Humboldt University Berlin)

Bank filtration systems are of increasing importance for the supply of water for all kind of purposes. Worldwide water works extend old pumping well galleries, and increasingly new investments are directed to this technology. By bank filtration in most cases both surface water and groundwater resources are exploited, what has to be taken into account by the management of bank filtration facilities. Through the combination disadvantages of pure surface water or pure groundwater systems can be overcome. The technology of bank filtration makes the system less vulnerable to extreme events. The quality of the pumped mixture is higher than the water of the reservoir with lowest quality. Moreover surface water is significantly purified during the filtration passage from the surface water body to the pumping facility, so that the application of further water treatment may even become obsolete. An example is the water supply for the city of Berlin, Germany, which is studied in detail within the NASRI project (Natural and Artificial Systems for Recharge and Infiltration) since spring 2002. The aim of the project is to obtain a better understanding of such systems and to develop appropriate models and management tools - not only for the Berlin sites. The contribution to the conference provides an overview on the current state of the project. An introduction to the technology will be presented, followed by an overview on the activities of the NASRI project. Computer models will be demonstrated concerning the design and dimension of pumping well galleries and concerning the biogeochemical transformations during the passage of surface water through the porous medium. Finally follow some implications concerning the management of combined surface water and groundwater resources.

**HS02/11A/C24-0170P** Oral-Poster **1149**

**REDUCING SHALLOW - WELL CONTAMINATION IN UGANDA**

James MWAMI (Project Manager, Busoga Trust)

Despite an abundance of surface water in Uganda (18% of the land area), the predominantly rural (>70%) population relies almost exclusively on groundwater for a portable water supply. This dependence arises from the more widespread occurrence, superior quality and reduced susceptibility to contamination, of groundwater supplies compared to surface water resources. As a result, provision of safe water to rural communities in Uganda has depended primarily upon the construction of wells and protection of spring discharges. In Uganda, as with other regions in equatorial Africa, featuring extensive, weathered crystalline rocks, often referred to as the "basement complex" ground water development has targeted two main aquifer units: a deep aquifer of fractured bedrock and a shallow, muddy-sand aquifer comprising of detrital bedrock and alluvium. This paper depicts a case study taken in east and central Uganda. Particular attention has recently been directed at developing the shallow - well aquifer since the formation is less costly to develop and a recent study has found it to be more productive than the deeper, bedrock aquifer. However, monitoring of water quality in south eastern Uganda, a region of intense shallow - well development, shows that within months of installation, shallow groundwater commonly exhibit levels of coliform bacteria and nitrate exceeding W.H.O health guidelines. Human and livestock waste excreted in pit latrines, over land or in open-pit wells, called "scoop wells" may contain worms, protozoa, bacteria and viruses that if consumed, can lead to the contraction of hepatitis, typhoid, cholera and a variety of diarrhoea diseases. Wells and springs harvesting shallow groundwater are generally protected from these pathogens by a granular soil matrix which both filters bacteria, protozoa and worms due to their relatively large diameter (>0.5 um) in relation to the aquifer material, and adsorbs smaller viruses (0.07 um to 0.7 um) on account of their strong, negative surface charge. Despite this cleansing capacity, the presence of coliform group of bacteria in groundwater indicates that faecal contamination has occurred. The practice of siting shallow wells in the vicinity of existing scoop wells has been identified as a probable source of faecal contamination to shallow wells in Mukono District of South Eastern Uganda. Simulations of groundwater flow in the shallow aquifer indicate that a well head protection area of 60m between wells and contaminant sources such as scoop wells, pit latrines and swamps is required to ensure the sustainability of this vital, potable source of water to rural communities.

**HS02/11A/C24-0180P** Oral-Poster **1153**

**WATER MANAGEMENT ON MEDITERRANEAN ISLANDS UNDER CHANGING CONDITIONS**

Manfred A. LANGE (Center for Environmental Research, University of Muenster, Mendelstr. 11, D-48149 Muenster, GERMANY)

The availability of water in the Mediterranean in sufficient quantities and adequate quality represents a significant problem, particularly in light of possible changes in climatic conditions. This is due to a number of factors which include: the over-exploitation of existing aquifers by various users, insufficient recharge due to diminishing precipitation, excessive and inadequate use through agricultural activities or tourism, significant deficits in water management and distribution schemes and conflicting or unresolved demands and interests between various users, to name just a few. These problems are exacerbated on the islands in the Mediterranean because of their isolation and thus the impossibility to draw on more distant or more divers aquifers in general and because of the threat of saline intrusions, which reduce the utilisation of existing, near-shore aquifers in particular. While the availability, demand and distribution of water on each island are determined by specific conditions, there are a number of attributes common to all Mediterranean islands which call for the formulation of generic solutions to the above mentioned problems. Because most of these problems are mutually related and interdependent, solutions will only be obtained through holistic considerations that are carried out by an interdisciplinary research team. Equitable and acceptable strategies require a stakeholder-based participatory process that builds on the results of scientific investigations on the one hand and on the consent of major stakeholders on the other. These requirements are central to the EU-funded MEDIS project, which aims to contribute towards the sustainable use of water on islands of the Mediterranean where conflicting demand for water is combined with a wide range of hydrological, social and economic conditions. MEDIS is being carried out by a consortium of 12 institutions from seven countries and will involve detailed investigations in one typical catchment each on Corsica, Crete, Cyprus, Mallorca and Sicily. By carrying out this project on five islands that cover the Mediterranean from west to east and by enabling a dialogue between scientists and stakeholders as well as between principal stakeholders from each island, these recommendations will embrace generic solutions based on the collective

experiences of the residents on all islands. We will report on the results of the first year of MEDIS, which include an extensive review of current conditions pertaining to water management on each island and the specification of a typology of water demand and supply relationships for the islands of the Mediterranean. In addition, we will consider water supply under future climate scenarios derived through a regional model for the Mediterranean and/or downscaling of GCM results from models of the Max Planck Institute Hamburg, Germany. These results will give rise to a set of recommendations for improved water management practices that will have to be discussed, modified and agreed-upon through a participatory process involving key stakeholders on each island in the future course of the project.

**HS02/11A/C24-0190P** Oral-Poster **1157**

**RELIABILITY ANALYSIS OF THE INTEGRATED MANAGEMENT OF WATER QUANTITY AND WATER QUALITY FOR WATER TRANSFER SYSTEM**

Xiang ZHANG<sup>1</sup>, Jun XIA<sup>2</sup> (<sup>1</sup>Dept. of Hydrology and Water Resources, Wuhan University, <sup>2</sup>Department of Hydrology and Water Resources, Institute of Geographical Science & natural Resource)

Water consuming around the world increased sharply in order to meet the demands of the rapid economic development. On the other hand, it is the economic development that courses the degeneracy of eco-environmental system and the decrement of available water quantity, especially in the developing countries. It is necessary to consider the integrated management of water quantity and water quality in order to decrease the risk of water supply. In this paper, the integrated management of water quantity and water quality for the water transfer system is discussed. And based on the reliability theory, the method of reliability analysis is applied to assess quantitatively the operation reliability of water transfer system. Transferring water from the catchment with abundant water resources to the area in shortage of water, the water transfer system covering the different catchments plays an important role in solving the water shortage. Obviously it also influences the water quantity and water quality of the river in the water source area. In this paper, the importance and the method to consider the integrated management of water quantity and water quality are discussed and suggested. For the water quantity, the temporal and space variability of water resources in the water source area should be analyzed carefully in order to determine the amount of the available water. On the other hand, the influence to the water quality should also be considered thoroughly, including the pollutant source, the decrease of discharge in river resulting in the deterioration of water quality at the downstream and etc. In this paper, the environmental critical discharge, which is defined as the lowest required discharge to keep the water quality of the river to reach the standard of drinking water source, is used as a threshold for the management of water quality. It can be determined by using the river water quality mathematical model. At last, for the reliability of the integrated management of water quantity and water quality, the two reliability criteria, the temporal reliability and the volumetric reliability, are presented. The last part of this paper gives a case study about the water transfer system in Shenzhen city, Guangdong province. This system transfers water from the Dongjiang catchment to Shenzhen. Considering the integrated management of water quantity and water quality, not only the water quantity in the Xizhijiang and Dongjiang river is analyzed carefully, but the environmental critical flow is calculated. And the two reliability criteria are used to evaluate the operation of the system. The result shows the reliability analysis of the integration of water quantity and water quality can provide thorough decision making for the sustainable management of water transfer system.

**HS02/11A/C24-0200P** Oral-Poster **1201**

**LATERITE - LOW COST REMEDIAL OPTION FOR HIGH ARSENIC GROUNDWATER**

Rupa BHATTACHARYYA<sup>1</sup>, Debashis CHATTERJEE<sup>2</sup>, Yoshio TAKAHASHI<sup>1</sup> (<sup>1</sup>Department of Earth & Planetary Systems Science, Hiroshima University, <sup>2</sup>Department of Chemistry, University of Kalyani, India, <sup>3</sup>Department of Land & Water Resources Engineering, Royal Institute of Technology, KTH, Stockholm)

High arsenic groundwater has emerged as a nagging environmental problem in the recent decades. Elevated levels of groundwater arsenic (>50ppb) in the Bengal Delta Plain (BDP) threatens the lives of millions of people. Large scale uncontrolled groundwater development may play a key role for such human suffering. The present study deals with the adsorption pattern of AsO<sub>4</sub><sup>3-</sup> and AsO<sub>3</sub><sup>3-</sup>, the predominant arsenic species in groundwater using Red Earth (Laterite) for the supply of potable water. Laterite is an indigenous, abundantly available, natural geological material enriched with amorphous ferric hydroxide (HFO)/ oxides. The mineralogical study of Laterite exhibits the predominance of iron and aluminium secondary phases. Chemical composition reveals that Laterite contains 30 - 35% iron oxides. Batch experiments indicate the Langmuir adsorption isotherm. The pH<sub>Zpc</sub> of laterite is determined to be 8.5-8.6. The high pH<sub>Zpc</sub> value supports a high positive surface charge of laterite over a wide pH range. The material, therefore acts as an effective adsorbent for several anionic contaminants. On the basis of the lab as well as field scale studies, laterite is used as a fixed bed filter media in an earthenware pitcher with a view to supply drinking water on the household basis. The results interpret that the material is not only effective in adsorbing arsenic but also effectively removes iron from the groundwater. Cost calculated for the transportation of laterite approximates to Rs 750 /ton/km (US\$ 16) whereas the treatment process estimates to Rs30/100L(US\$ 0.6) contaminated water. Therefore fixed bed laterite can be successfully used for removal of arsenic from groundwater. Lab scale experiments are also executed to understand the efficacy of the system for removing heavy metals as well from the aquatic environment.

**HS02/11A/C24-0210P** Oral-Poster **1205**

**LARGE DIAMETER WELLS AS A SOLUTION AGAINST THE RISK OF CONTAMINATION IN THE SEMI-ARID WORLD USING THE FILTER FACTOR CONCEPT**

Sarma K. SEEMANAPALLI, Soniaeli P. CARVALHO, Silvestre L. NOBREGA, Alex M. NEYVES (Smith Research Corporation, Small Business Technological Center, LSU, Baton Rouge, LA)

Water is the life blood of living creatures on earth. Seventy percent of earth's surface is covered with water. Despite much information available, groundwater movement, its quantity and quality remain a mystery. Groundwater levels decline due to intensive pumping and yearly below-normal precipitations, that accelerate the downward trend in water levels. Natural groundwater quality is affected by the materials it passes through on its way to the groundwater reservoir. Human activities also cause water quality degradation, serious enough to prevent the use of water for human consumption. Well location is a crucial factor, a well downhill from a source of bacterial contamination running greater risk of contamination than that on the uphill of pollution source. Minimum separation distances from potential sources of contamination are to be maintained. Proper well design reduces the risk of pollution by sealing the well from contaminants that enter from the surface. Bacterial contamination which cannot be detected by sight, smell or taste can result from a number of sources. Shallow wells and wells that do not have water-tight casings can be contaminated by bacteria infiltrating through the soil near the well. Soil remediation is a difficult, time-consuming and expensive operation and environmentalists select the most appropriate

HS02

Monday, July 7 - Friday, July 11

**WATER RESOURCES SYSTEMS: GLOBAL CHANGE, RISK ASSESSMENT AND WATER MANAGEMENT (ICWRS, ICASVR, ICSW, ICWQ)**

Location: Site C, Room 24

Friday, July 11 PM  
Presiding Chair: G. Bloesch

HS02/11P/C24-001

1400

**ELEVATED DROUGHT RISK DUE TO MULTI-DECADAL CLIMATE VARIABILITY**

Anthony S. KIEM, Stewart W. FRANKS (Department of Civil, Surveying and Environmental Engineering, University of Newcastle)

A number of previous studies have identified changes in the climate occurring on decadal to multi-decadal timescales. Recent studies have also revealed multi-decadal variability in the modulation of the magnitude of El Niño/Southern Oscillation (ENSO) impacts on rainfall and streamflow in Australia and other areas. This study investigates the multi-decadal variability of drought risk by analysing the performance of a water storage reservoir in NSW, Australia, during different climate epochs defined using the Inter-decadal Pacific Oscillation (IPO) index. The performance of the reservoir is also analysed under three adaptive management techniques and these are compared with the reservoir's performance using current reactive management practices. Two of the three techniques investigated use climate indicators to alter management procedures and initiate them in advance of drier than average periods based on an ENSO forecast. The results indicate that IPO modulates both the magnitude and frequency of ENSO events. This dual modulation of ENSO processes has the effect of reducing and elevating drought risk on multi-decadal timescales. The results also confirm that adaptive reservoir management techniques, based on ENSO forecasts, can improve drought security and become significantly more important during dry climate epochs. These results have marked implications for achieving drought security, despite climate variability, for water storage reservoirs.

HS02/11P/C24-002

1415

**ON THE CAUSES OF TAIWAN DROUGHT EPISODES**

Fong-Chiau CHANG, Chung-Ho WANG (Institute of Earth Sciences, Academia Sinica, P.O. Box 1-55, Nankang, Taipei, Taiwan)

Droughts, prolonged deficit rainfall, affect the balance between water resources and demands. Atmospheric processes, sea surface temperature anomalies, land surface conditions, solar variability, sulfur-rich volcanic eruption and anthropogenic processes are all involved in their onset and maintenance. There is considerable debate on the role of anthropogenic process, natural forcing or natural variability in initiating droughts. Four major Taiwan drought episodes occurred during the 20th century. They are 1906-1910, 1961-1966, 1978-1982 and 1993-1995. These droughts appear synergistic phenomena with the 1907 Kusdach, 1963 Agung, 1980 St. Helen, and 1991 Mt Pinatubo eruptions. The higher frequency since 1960s seems related to both anthropogenic aerosols increases ensued from rapid economic development and urbanization in 1960s and four major sulfur-rich volcanic eruptions during the period from 1963 to 1991. This study examines 1) how monthly precipitation changes for each episode before and after the corresponding eruption, and 2) what are their respective characteristics.

HS02/11P/C24-003

1430

**THE CHARACTERISTICS OF BASE-FLOW RECESSON COEFFICIENT AND ITS LONG TERM CHANGE ON MOUNTAINOUS WATERSHED OF RAPID FOREST RESTORATION**

Junji SHIMOKURA, Hirofumi SHIBANO (Graduate School of Agricultural and Life Sciences, University of Tokyo)

This study aims at exploring the method that can directly assess water conservation by using watershed storage as an index, which is found from the base-flow recession coefficient; therefore this study only pays attention to the recession coefficient of discharge in non-precipitation terms. The influence of recession characteristics affected by evapotranspiration is taken into consideration in order to remove the influence of seasonal change. Properties of recession coefficient are analyzed through secular change and comparison between experimental watersheds. Ananomiya, Higashiyama and Shirasaka, experimental watersheds in the University Forest in Aichi, University of Tokyo, are elected as object watersheds for analysis. From the end of the 1800s, forests in the experimental watersheds and their surrounding areas had been cut. Consequently, forests including experimental watersheds had been denuded. When the observation started in 1923, the forest in each experimental watershed, especially in Ananomiya, was in bad condition. The recent research showing an increase of stand volume and reduction of bare land rate concludes that forest in experimental watersheds is in the process of recovery. However, soil is still unripe. In the experimental watersheds, no tree logging has been conducted except for work on several streams and artificial reforestation in denuded areas. In August 1959, water dispersion work was performed in a large scale as an experiment to intercept hillside runoff and make water penetrate into Ananomiya. Daily data of discharge and precipitation, over a period of 70 years, is used for analysis. Non-precipitation terms, defined as days there is no precipitation continuously for more than 7 days, are extracted from the long-term daily data to estimate the recession coefficient. An equation expressing the runoff from an unconfined aquifer is used to estimate it. Estimated coefficients are large in Ananomiya where the forest condition is poor and small in Higashiyama and Shirasaka where the forest condition is good (a large coefficient means discharge recesses fast and a small one means the contrary). The coefficient averaged every month has seasonal changes, i.e. it's large in summer and small in winter. Evapotranspiration in non-precipitation terms is estimated by the Penman-Monteith equation. The recession coefficient has seasonal change, i.e. it is large in summer and small in winter, similar to that of estimated evapotranspiration. And there is positive correlation between the recession coefficient and evapotranspiration. Secular change of recession coefficient, analyzed by dividing a year into two seasons, has a downward tendency, however it temporarily increases in Ananomiya in the 1960s and has increased in all watersheds since the 1980s. The downward tendency is caused by development of forest soil, and it can be easily estimated that water reservation in the watershed has increased. The temporary increase in the 1960s in Ananomiya is based on the influence of water dispersion work and the increase in the 1980s is a future examination subject.

technology for specific contaminated sites. Here-in is suggested one such method of soil remediation, using Large Diameter Wells (LDW) that are popular in the semi-arid world. The simplicity and low cost in the construction and operation of such wells make their use viable for rural communities. The LDW is a viable alternative to tube wells to alleviate the problem of draughts and the risk of contamination in Paraíba state, Brazil. The filter factor concept,  $f_f$ , conceived by Sarma (1997) considers the relative effects of transmission and passage of water through bricks and cement mortar. Values of  $f_f$  in function of well yield for given diameters and drawdown are presented. Criteria to avoid mutual interference due to simultaneous pumping of wells was also studied. Computer programs developed would prove useful in making the characteristics curves for LDWs constructed in aquifers with low transmissivity values. Unlike tube wells, in LDWs, water continues to get extracted from aquifer to the well even after the cessation of pumping, attesting LDWs as efficient in aquifers in the semi-arid world. Using field data, calibration was effected adopting a 14/16 mesh for the LDW. The numerical method adopted here-in was the volume element method. The flexibility of the method permits implantation of desired well-diameters, change the network in the computer program, thus permitting to evaluate the drawdown-discharge-diameter relationships. Regional characteristic curves drawn between the variables facilitate practical application of these by agriculturists and engineers to explore rightly the aquifers, avoiding thus the risk of contamination of LDWs.

HS02/11A/C24-022OP

Oral-Poster

1209

**REDUCTION OF RISK OF AGROTOXICS BY DRAINAGE IN AGRICULTURAL LANDS USING INTERCEPTOR DRAINS**

Sarma K. SEEMANAPALLI (Smith Research Corporation, Small Business Technological Center, LSU, Baton Rouge, LA)

About 80% of the sick and over 33% of the deaths in the third world countries are attributed to the clean water crises, caused by degradation in water quality. According to UNO, the disorderly distribution of available resources affects 20% of 3<sup>rd</sup> world countries. South America goes black-listed as a continent, threatened with water crisis. Brazil is however privileged because of its abundance of water, with its availability of 5000m<sup>3</sup>/year/capita, with a demand of only 200 m<sup>3</sup>/year in its NE region. Subsurface waters have distinct economic advantages over other components of the hydrological cycle. Groundwater can be used directly in most cases, without prior treatment. However, groundwater may also be polluted by way of natural or surface contamination. Because of the greater demand of groundwater, the confidence in the quality of potable water is posing doubts, its authenticity being questioned, once that major sources are already getting over-explored. Higher standards of water quality imply higher costs of water. Environmental scientists are concerned about groundwater contamination by way of agro-toxic substances entering the flow regime. The pollutants detected in shallow waters might reach the deeper strata of the aquifers. Here-in, an investigation is made about the effective use of interceptor drains in the irrigated perimeter in Sume in the Semi-arid Paraíba State in Northeast Brazil, in function of their geometric, hydraulic and hydro-geologic parameters. Effective removal of chemical pollutants from aquifers through the use of interceptor drains is suggested to contain and even to remove subsurface pollutants from shallow aquifers. Interceptor Drain is a gravel trench excavated into a relatively impermeable soil layer and installed to collect and remove groundwater as it flows across the impermeable layer, which is typically placed across a contour of a slight to moderate sloping area to intercept groundwater. The potential theory used here-in and the concept of ground water divide conceived proved helpful to quantify the efficiency of interceptor drains. These drains offer concrete solutions to the problem of the control of subsurface water pollution in shallow aquifers. Such drains are used to capture the contaminants and to delimit the spreading of hazardous chemicals. Finite difference scheme used here-in was developed by Sarma e Alex (1997). For the totally and partially penetrating drains studied to know the effectiveness of such drains, spacing, widths and depths of drains varied. The drain discharge is treated as a function of the number of tubes that effectively enter into the drain. Recharge played an important role in the control of the pollutant movement, in delimiting the configuration of the phreatic surface, an increase in recharge rate correspondingly increasing the depth of the groundwater divide. Such water divides help one to forecast the contaminant movement and to quantify the same.

HS02/11A/C24-023OP

Oral-Poster

1213

**WATER QUALITY MANAGEMENT FOR CONJUNCTIVE USE OF GROUND WATER AND WASTEWATER FROM AQUACULTURE : AN INDIAN OVERVIEW**

Lalitkumar Pandit CHAUDHARI (Institute for sustainable development and research)

Aquafarming has emerged as one of the more promising industries in the world with considerable growth potential expected to contribute around the quarter of global fishery the year 2000 AD. The aquafarming has a multidimensional in perspective agricultural growth. It is a tool for utilizing land and water more economically and optimally for increasing the productivity of both natural resources, land and ground water through sustainable agriculture. The countries in the Asia-Pacific region have vast and varied aquafarming resources. Oftenly these are these are main source of Irrigation in this region. The overexploitation of ground water causes salinity problem in many countries reducing the cultivating area resulting reduction in agriculture production. An attempt has been made in this paper to develop the plan for ground water management for the aquaculture and horticulture as well as drinking water from the river source adopting conjunctive use of irrigation water from Indian experience. The paper also evaluate the water quality criteria of ground water and irrigation water for increasing the agricultural productivity. The methodology is based on the economics of the conjunctive use of irrigation and ground water for horticulture and aquaculture and also for agriculture. The main aim is to utilize the ground water over saline land for aquafarming and to reduce the soil salinity in irrigated land to increase the productivity of the land and the water. Series of the observations were taken on the various aspects of irrigation and soil salinity management for aquafarming using different methods to maintain the quality of land and the ground water. Also the relative economics of aquafarming and horticulture system under alternative water conserving irrigation /rain water harvesting management options, has been compared with the resources available. The result obtain demonstrate the implication of increase in yield in horticulture including agriculture and indicate the necessity of optimal and suitable use of natural resources for increasing the agricultural productivity. The result signify that the soil salinity can be managed using ground water management practices and the additional area can be brought down under agriculture. The result obtained also suggest that significant economic gains can be had from adopting conjunctive use of ground water to maintain the quality criteria for increased production in horticulture and agriculture as well as for drinking water from the river source after discharge. Apart from results of drinking water quality, it also signifies that the increase in the production can be achieved through reuse of water alongwith the ground water as supplemental irrigation, reducing the soil salinity problems in command area.

HS02/11P/C24-004

1445

**IMPACT OF CLIMATE ON FLOW REGIMES OF THE UPPER REACHES OF STREAMS**

Hironobu SUGIYAMA<sup>1</sup>, Varawoot VUDHIVANICH<sup>2</sup>, Andrew C. WHITAKER<sup>1</sup>, Kosit LORSIRIRAT<sup>1</sup> (<sup>1</sup>Graduate School of Science and Technology, Niigata University, <sup>2</sup>Faculty of Engineering, Kasetsart University, Thailand, <sup>3</sup>Royal Irrigation Department, Thailand)

The objective of this paper is to compare flow regimes in the upper reaches of streams in the temperate zone (eastern Japan) and the tropical monsoon zone (western Thailand), and then to examine an index of low flow, aiming towards the synthesis of water resources evaluation. Research catchments were selected with the restriction that there are no regulation or diversion structures in the upper reaches of the streams. The range in catchment areas is 45.9-10,880 km<sup>2</sup>, and the range in record lengths is 15-43 years. Firstly, the flow regimes of the upper reaches of streams are stochastically evaluated by applying the stochastic flow duration (SFD) curve. In Japan, the nonexceedance probability value of 10% (10 year probability) of the discharge exceeded 97% of time (Q97<sub>10</sub>) has generally been recognized as a design flow for water resources facilities based on the severity of droughts. Then, by the comparison of values used from the SFD curve with the 10 year probability value, it is understood that the discharge exceeded 97% of time in the tropical monsoon zone is about one-fifteenth of the temperate zone. This difference indicates that this flow regime is uncomfortable for planning if a water resources planner evaluates a flow with the 10 year probability. It may be argued that a more severe probability of occurrence (i.e. longer than 10 years) should be adopted for the design of water resources facilities in the tropical monsoon zone. Secondly, the recession shape of the lower part of the flow duration curve is compared. From the examination of these shape characteristics, it is observed that the recession shape of the lower part of the flow duration curve is dependant on the strength of low flow persistence. By comparing the recession shape of the lower part of the flow duration curve, it is seen that the persistency of low flow in the temperate zone is stronger than that in the tropical monsoon zone. Finally, the index of low flow is discussed by examining the relation between the index used in Japan and that in the United States. In the United States, the value of the 10 year probability for annual minimum flow averaged over a consecutive period of 7 days (Q<sub>10,7</sub>) of a given year has been used as an index of low flow. The relationship between Q<sub>10,7</sub> and Q97<sub>10</sub> is strong. This aspect implies that the 10 year probability value for the discharge exceeded 97% of time can be recognized as an index of low flow.

HS02/11P/C24-005

1500

**ASSESSMENT OF DROUGHT IN THE CONDITIONS OF CLIMATE AND ECOSYSTEM CHANGES: CASE STUDY IN THE SOUTH - WEST REGION OF ROMANIA**

Gheorghe STANCALIE, Elena SAVIN, Vasile CRACIUNESCU, Simona CATANA, Anisoara IORDACHE (National Institute of Meteorology and Hydrology, Bucharest, Romania)

The physiographic and biophysical characteristics of many regions change through time, due to natural or anthropogenic factors, thus increasing or lessening sensitivity to climate impacts. Among the various suspected causes of climate variability land cover/use modifications and environmental degradation (overgrazing, deforestation) constitute a major focus of interest. In the last 2 decades, the increase of the aridization trends under the conditions of drought having affected certain regions in south of Romania, where the mean yearly temperature is over 10°C, the mean yearly precipitation is under 500 mm and the aridity "de Martonne" index is under 25. The south of the country with temperate continental climate undergoes also more severe hydrological drought as against the others regions. Injurious consequences of drought are felt going to exhaustion of water resources, drainage of rivers and diminution of crops. The area of interest corresponds to the Oltenia region, situated in the south-west of Romania in which eight very severe droughts years were recorded during the last 20 years, and the annual mean runoff was constantly at least 50% lower than multiannual mean runoff. In this region there is the coal basin Motru, chosen as a relevant example for emphasizing the modifications, which affected the active surface, due to the human intervention, and analyzed on the basis of cartographic documents, aerial and satellite images. From the analysis of processed remotely sensed data an updated representation of the topography, as well as of the land cover/use has resulted. The modifications occurred in the land cover and use, led obviously to the modifications of the structure of the radiative field at the local and regional scale, due to the redistribution of the albedo values of different surface types, that in this case have suffered a weak increase. In analyzing the drought phenomena, the lack of rainfall and the hydrological regime were mainly considered but other parameters were also taken into account, such as the maximum temperature over 25°C, the potential evapotranspiration and the aridity "de Martonne" index. Studying the meteorological and hydrological factors, a natural aridization tendency, associated with the climate variability at regional scale has been observed. An integrated monitoring system was designed and implemented in order to emphasize the trends, extent and future evolution of the drought and aridization phenomena. This approach allows the combination of thematic layers for the modeling of the interactions between the physiographic, climatic and anthropogenic factors as well as for the determination of some complex parameters facilitating the surveillance of the vegetation-soil system and the water resources during the drought periods. The main conclusion of the study is that in order to increase ecosystems resistance at long drought effects due to climate change, stress elements as anthropogenic ones must be decreased, if not eliminated.

HS02-Oral-Posters Monday, July 7 - Friday, July 11

**WATER RESOURCES SYSTEMS: GLOBAL CHANGE, RISK ASSESSMENT AND WATER MANAGEMENT (ICWRS, ICASVR, ICSW, ICWQ)**

Location: Site C, Room 24

Friday, July 11 PM  
Presiding Chair: G. Bloeschl

HS02/11P/C24-001OP

Oral-Poster

1515

**TOWARDS AN OPTIMUM WATER RESOURCES DEVELOPMENT IN THE NIGERIAN NIGER DELTA**

Adepoju D. OLUSEGUN (Geography Department, Faculty of Social Sciences)

Man's interaction and interference with the environment in order to satisfy his socio-economic needs without adequate management plan always result in environmental degradation either in the short or long term since the effects of his actions are registered in the atmosphere, accumulates and it is only a matter of time before its manifestation. The present water problem in the Niger Delta area of Nigeria is a combination of tripartite factors

of climate change, increasing population, and the global economy. The implication of the climate change is due to the fact that Nigeria through the Oil and gas activities especially flaring contributes a significant amount of carbon mono-oxides, carbon dioxides in the global atmosphere which play an important role in raising temperatures at both the local and regional levels; but the major effect of these is mostly felt by the local environment. One of the consequences of these actions is inundation through the saline water incursion into the freshwater environment thereby increasing water problem both in quality and quantity. Secondly, growing populations, associated urban development and intensifying pressures on small areas of land are creating new pressures on available water resources with conflicting water demands, occurring to a lesser extent across the Niger Delta area. The population continues to grow at an estimated 2.8 percent per annum while urbanisation increases even more rapidly at an estimated rate of 5.2 percent. A visible consequence of this is the increased competition between users leading to increased conflict between users. That Nigeria and in particular the Niger Delta is having a fair share of the impact of dynamic global economy cannot be overemphasised. Of the three standard categories of freshwater use - for Agriculture, industry, and domestic - industry ( processing, exploration, exploitation activities etc ) is dominating. As a result of Pollution of surface water from increasing oil exploration and exploitation, industrialisation, increased food production is reducing the quality and quantity of portable water thereby reinforcing the problem of scarcity. In this study monthly rainfall and temperature datasets from the period 1941-1990 was in order to evaluate climatic trends of basic water resources parameter useful for assessing proper water resources planning and development in the Niger Delta. Optimal strategic water resources scenarios was built towards a sound water resources of the Niger Delta using GIS techniques.

HS02/11P/C24-002OP

Oral-Poster

1519

**CURRENT CONSTRAINTS TO THE IMPLEMENTATION OF WATER DEMAND MANAGEMENT (WDM) IN URBAN CENTRES IN ZAMBIA**

Daniel C.W. NKHUWA (School of Mines, University of Zambia)

Water is more than just a commodity but also an essential element that supports all forms of life. It is also basic to many socio-economic activities. In this regard, it is imperative to recognise its economic value in all policy and sector activities so that wise and efficient use of the resource is initiated and promoted in all sub-sectors, particularly in the large urban centres. However, the provision of adequate water supply and sanitation to the rapidly growing urban populations is increasingly becoming a problem for most cities and towns in Zambia. The continuing expansion of the numbers of people who need water and sanitation services and who cannot readily get the services by self provision continue to exert continuous pressure on either investment to create additional production capacity or to stretch the available supplies to serve more people. The predominant approach towards meeting these increasing water demands has been towards supply augmentation schemes. Undoubtedly, the cost of developing these new sources will get higher and higher as most accessible water, in terms of quality and quantity, has already been tapped. In places like Lusaka, the country's capital, where demand has outstripped demand, citizens have taken to indiscriminate drilling of boreholes. In places, this has caused aquifer over-abstraction, which has initiated lowering of the water table. If this trend persists, pumping charges may go up, thereby heightening the cost of supply. This may eventually affect the availability of water to the poor who may not be able to afford the new rates. It is in this regard that water demand management (WDM) becomes the preferred alternative in meeting increasing water demand in order to improve efficiency and sustainable use of water resources taking into account economic, social and environmental considerations. However, there are a number of constraints that have inhibited successful implementation of WDM. These include: Inadequate knowledge by consumers and water utility staff of the socio-economic benefits of implementing WDM Unfavourable pricing mechanisms Poor revenue collection rates, which have caused the water utility companies so severe financial constraints that they are unable to finance some of the routine operation and maintenance operations to the existing conveyance networks. Consideration of WDM as an inferior alternative to the construction and extension of new conveyance systems. Inadequate policy and legal frameworks, overlapping responsibilities among the water and sanitation sector institutions. Lack of clear sector policies, compatible legal framework, clear division of responsibilities and mandates, which has resulted in low priority assigned to operations and maintenance within the water sector. This paper will attempt to highlight what measures must be adopted to overcome these and other constraints to the implementation of WDM.

HS02/11P/C24-003OP

Oral-Poster

1523

**PRECIPITATION ENHANCEMENT OPERATION ALONG THE YELLOW RIVER IN WESTERN CHINA BY WEATHER MODIFICATION METHOD**

Xueliang GUO<sup>1</sup>, Meiyuan HUANG<sup>1</sup>, Tiezheng LI<sup>1</sup>, Junsheng ZHANG<sup>2</sup> (<sup>1</sup>Institute of Atmospheric Physics, Chinese Academy of Sciences, <sup>2</sup>Yellow River Hydropower Co. of China)

This paper discussed the weather modification activities and their application to water resources management. The shortage of water supplies in the region along the Yellow River of western China has increased in recent years and is related to some decrease in annual precipitation, but mainly due to the increasing demand from the rapid growing population and industrialization in the region, which has seriously threaten the development of hydropower along the Yellow River. The precipitation enhancement activities have been conducted as an additional source of unconventional water supply for many years in the region. This work focused on clarifying the fundamental mechanism involved in precipitation enhancement by cloud seeding. We will introduce the climate condition that suitable for precipitation enhancement activities in the region as well as the efficacy of cloud seeding. In addition, a comparison study of cloud seeding was made with a current widely used seeding agent—silver iodide (AgI) and a newly developed seeding agent—liquid carbon dioxide (liquid CO<sub>2</sub>). Characteristics of cloud dynamics and microphysics and the interactions between them affected by the artificial seeding of AgI and liquid CO<sub>2</sub> are examined using a 3D stratocumulus cloud model with seeding processes. The model results show that the liquid CO<sub>2</sub> seeding in the region of high supercooled cloud water in the simulated cloud can generate shallow thermal convection and cause larger dynamic effect than that AgI seeding, and thus can significantly enhance surface precipitation. The seeded clouds by liquid CO<sub>2</sub> show two prominent increases in maximum updraft. The first increase is directly produced by liquid CO<sub>2</sub> seeding and the second is caused by downdraft outflow induced by falling precipitation in the boundary layer. The formed shallow thermal convection can produce many ice crystals. By the recirculation growth of these ice crystals transferred by the updraft of the thermal convection, they can consequently grow to precipitable particles such as snow and graupel.

HS02/11P/C24-004OP

Oral-Poster

1527

**WATER RESOURCE MANGEMENT IN THE UPPER REACH OF THE GORAI RIVER OF BANGLADESH**

Mohammad Monowar HOSSAIN, Mohammad Rashedul ISLAM (Department of Water Resources Engineering, Bangladesh University of Engg. & Technology)

Gorai river is the only distributaries of the river Ganges in Bangladesh. The Ganges is the second largest river in the Indian subcontinent. Gorai river is the prime source of freshwater to the South West Bangladesh, which covers an area of about 30% of area of the country. In recent times, the river was getting silted up at its mouth and for some distance downstream due to gradual decrease of the Ganges water. As a result very little water was available in the Gorai river during dry flow season. Tremendous environmental impacts were being felt in the Gorai dependent area due to this water shortage over the last few years. The Government undertook a program of dredging the Gorai for a distance of about 30 km from the mouth with a view to increasing the conveyance and attracting more flow in the river. The aim of this study is to examine the effectiveness of this dredging activity. The analysis has been conducted on the basis of dredge and post dredge observed bathymetry. The dredge bathymetry stands for the bathymetry measured immediately after the dredge and the post dredge bathymetry stands for the bathymetry after the passage of first year flood flows over the dredged Gorai. It is found from the analyses of these bathymetry that the normalized bed levels of the dredge bathymetry has been lowered all along the dredged Gorai while the bottom bed levels is found to have been raised. This implies that the pilot dredging has increased the high level conveying capacity of the Gorai while the low level conveying capacity has been decreased after the passage of first year flood flows over the dredged Gorai. Evidently this change in decreasing the low level conveying capacity of the dredged Gorai is due to the sedimentation in the deeper channel and therefore, the first year pilot dredging is not meaningfully effective in the sense of self-sustaining development for low flow augmentation. It is found that the bottom bed level of dredge channel has been raised close to the level of pre-dredge (post monsoon 1997) state after the passage of first year flood event over the dredged channel. Thus dredging may not be a sustainable means for management of water resources problems in the sediment-laden rivers of Bangladesh especially of the Gorai.

**HS02/11P/C24-0050P Oral-Poster 1531**

#### THE GENERAL PRINCIPLE FOR RESTORATION OF THE RIVER BASINS

Boris FASHCHEVSKY<sup>1</sup>, Tatyana FASHCHEVSKAY<sup>2</sup> (<sup>1</sup>International Sakharov Environmental University, <sup>2</sup>Ufa State Aircraft University)

The first step to restore any water body has to be the assessment of its ecological troubles on the scale "norm-pathology" here the criteria must be established determining the notions "the norm" and the "the pathology". The main among such criteria are the following: First, these are indices of the basic hydrological characteristics: maximum and minimum discharges and levels of water, inside-year distribution of a river flow in different years of water capacity -5, 25, 50, 75, 95 % frequency and average annual discharges and levels of water, duration of floodplain flooding, temperature and ice regime, flow of sediments. Second, these are indices of water quality, characterized by major ions, oxygen and pH concentration, biogenic elements, organic matters and heavy metals. Third, the important criterion in assessment of a river state is the character of channel process development, which in the result of economic activity can be changed greatly in the terms of hydrography (slopes of rivers and basins, drainage density, tortuosity, area of swamping, area of lakes, area of forests, area of ploughed lands, area of urban, etc) and morphology (increase and decrease of depths, narrow or widening of channels, damming of floodplains, extraction of building materials from channels, dredging of waterways, etc) of rivers and their basins. Forth and often (but not always) a main and completing component is a biotic one of the river ecosystem, the influence by the first three components and includes: bacteria and viruses, alga and higher aquatic plants, invertebrates, fishes, amphibia and aquatic reptiles, waterfowl and semi-aquatic birds, aquatic and semi-aquatic mammals. As the "norm" of a river ecosystem is its state before the beginning of a human activity in this basin or the state of the river-analogue that are situated in analogous natural conditions but untouched by a human activity must be accepted. All above-mentioned hydrological, hydrochemical, hydrographical, morphological and biotic components have to be accepted for the norm and recalculated for a restored basin in a special way. The restoration of a river basin can be produced: 1. Totally on all regime elements and bioproductivity of aquatic and semi-aquatic plants and animals. 2. Partially, only for the separate elements of regime and separate components of biotic ones. For example, restoration of only migratory fish, ignoring the phytoplankton species, which need an obligatory flooding of floodplain. 3. Artificial creation of a new ecosystem in a given river system by the way of introduction and acclimatization new species of plants and animals which have never occurred in a given river but if there are favorable conditions for reproduction these species. The experience of such developments has obtained a wide dissemination in the world, including Japan, China, Australia, Chile, Norway, France, Russia and others countries.

**HS02/11P/C24-0060P Oral-Poster 1535**

#### MAÎRISE ET CONFLITS LIÉS À LA GESTION DES RESSOURCES EN EAU DANS LA BASSE VALLÉE ET LE DELTA DU FLEUVE SÉNÉGAL

Alioune KANE (department of geography/ Faculty of Arts and Human Sciences/ University Cheikh Anta Diop)

L'intérêt porté à ces milieux de la zone tropicale sèche, caractérisés par l'extrême fragilité de leur équilibre écologique, se justifie par la demande en eau pressante d'une population en forte croissance, les saisons climatiques contrastées avec une irrégularité pluviométrique marquée, imposant des contraintes sévères à l'environnement et un caractère aléatoire à cette ressource dont l'exploitation traditionnelle était très souvent rythmée par le régime hydrologique du fleuve. Depuis deux à trois décennies, de grands programmes d'aménagements hydro-agricoles ont été développés. Les barrages de Diama et de Manantali, ont complètement artificialisé le régime hydrologique du Sénégal, permis le desserrement de la contrainte de mobilisation de la ressource en eau, le fonctionnement du système est désormais tributaire de la pluviométrie dans le haut bassin et du mode de gestion. Ces programmes se traduisent par des modifications radicales du fonctionnement hydrologique naturel et des transformations très importantes affectent l'environnement. Ces bouleversements peuvent prendre un caractère particulièrement grave, notamment lorsqu'ils se conjuguent à des modifications climatiques qui fragilisent encore un milieu sensible du fait de sa position en bordure du Sahara. Souvent ces programmes d'aménagement des bassins versants ont mal évalué les impacts écologiques et sociaux, engendrant des dysfonctionnements dans les rapports homme-nature, et compromettant l'instauration d'un développement durable. La maîtrise hydraulique est imparfaite, les parcelles sont souvent mal planées. La qualité des eaux de drainage est une préoccupation majeure, la capacité du réseau s'est avérée limitée et insuffisante pour assurer une bonne vidange. Les déversements d'eaux de drainage ne sont plus acceptables, le degré de toxicité de ces eaux et les volumes en jeu ne sont pas connus. La maîtrise des eaux et le développement de la riziculture ont mis en contact les populations avec l'eau douce stagnante et différents vecteurs de maladies. Le grand effet purgatif dû à l'invasion des eaux marines a disparu, les risques d'aggravation des maladies se sont multipliés. La prolifération de la végétation aquatique se pose. La construction des grands barrages ayant pour but d'atteindre l'autosuffisance alimentaire, se révèle mal maîtrisée. Les efforts de modernisation agricole ont porté sur une conquête de l'espace et un développement de la riziculture irriguée. Les modifications du milieu résultent de la création des aménagements hydro-agricoles et des réserves d'eau douce, avec une recomposition d'une société paysanne multiforme, sans

aucune technicité ni moyens financiers appropriés, les éleveurs peul sont les grands perdants. Le partage des ressources en eau est un problème difficile entre états riverains aux intérêts divergents avec la revitalisation des vallées fossiles du Sénégal. La vallée du Sénégal n'est pas une région d'irrigation traditionnelle. Les dysfonctionnements notés au plan de l'environnement, hypothèquent lourdement l'avenir des aménagements.

**HS02/11P/C24-0070P Oral-Poster 1539**

#### RAINWATER MANAGEMENT TECHNOLOGY FOR CONJUNCTIVE USE IN ARID REGION, INDIA

M. A. KHAN (Central Arid Zone Research Institute)

In Indian arid zone of Rajasthan and elsewhere several kind of rainwater harvesting structures have been in vogue since many centuries. At field level runoff has been collected in natural depressions or in dug-out structures such as ponds, tankas, and khadins. Till recently local wisdom, experiences and precedences guided the designing of such structures. However, for better storage, conservation and judicious use, CAZRI, Jodhpur provides details of design. Seepage proofing in ponds was found necessary in sandy soils where percolation rates are high. In western Rajasthan, dug-out ponds locally known as Nadi and tanka are used mainly for domestic water use and economically not viable option for surface irrigation. However, if recycling of rainwater primarily links more profitable cash yielding crops or tree component, potential water storage in these structures is likely to become highly attractive. Recently, tankas have been constructed on large scale in western Rajasthan for developing fruit orchards. Response of ber (*Ziziphus nummularia*) and pomegranate to supplemental irrigation from tanka was studied (1995-97) on a loamy soil at Jodhpur. Compared to control (no irrigation) increase in fruit yield with 2, 4 and 6 irrigation for ber was 46.4%, 80.3% and 124%, whereas in the case of pomegranate it was 69.8%, 112.5% and 191.7%, respectively. Tankas have also been found useful in raising forest nurseries and establishment of trees in watershed. Khadin is an other method of water resources development, conservation and utilisation for crop production even in very low rainfall 150-300 mm. Rocky catchments with adjoining valley-filled lands are converted in khadin farm by constructing earthen embankment at lower periphery of field with suitable spillway arrangement. The system is very popular in hyper arid region of Rajasthan. Due to low rainfall, the catchment to command ratio is rather high ranging from 8 to 15. On khadin farms, even without agronomical practices and with no application of fertilizer the average of yield ranges from 20-30 q ha<sup>-1</sup>. Anicut, percolation tanks and sub-surface barrier are very effective water harvesting and recharge techniques to improve ground resources in depleted aquifers. With the construction of anicut in Ujailan watershed in Jodhpur district, the annual increase in static water level in wells located in the zone of influence ranges from 1.8 to 2.2 m as compared to wells located in the adjoining area. In Pali district, due to the presence of anicut groundwater recharge has increased from 5.2 to 38.5%. Percolation tanks for inducing recharge is being practiced in parts of India. The average rate of percolation from percolation tanks constructed in different geological formation ranges from 10 to 72 mm day<sup>-1</sup>. Similarly with the construction of sub-surface barrier across an ephemeral stream at Chauri-kalan in Jodhpur district, the rate of depletion has been reduced from 1.2 m year<sup>-1</sup> to 0.3 m year<sup>-1</sup>, and water yield has increased from 60 m<sup>3</sup>year<sup>-1</sup> to 125 m<sup>3</sup> year<sup>-1</sup>. With the increased ground resources, over 15 ha area has been brought under well irrigation.

**HS02/11P/C24-0080P Oral-Poster 1543**

#### DECISION SUPPORT INFORMATION FOR WATERSHED MANAGEMENT OVER DROUGHT PRONE REGION

Nagarajan Ramakrishnan IYER (Center of Studies in Resources Engineering, Indian institute of Technology, Bombay)

An effective mitigation activity during drought situations offer support to the people, in carrying out their regular activities, without much stress on their existing water and food (if necessary) availability. Continuous monitoring of spatial and dynamic land resources and the vulnerable groups is important. Integrated analysis of rainfall, run-off and surface storage facilities and creation of demand and supply scenario during the summer months would help the water regulation planning. It is observed that some of the un-preparedness situation of the government agencies is mainly due to the lack of dynamic input into their preparedness planning. The individual subject experts broadly use deficit of rainfall amount, water supply, crop production and reduced purchase power in identifying a drought area. Even though meteorological drought is considered as the initiation of drought situation over an area, followed by deficit of water supply and crop production. A multi-criteria approach is warranted. An attempt has been made in the creation of drought intensity scenario (demand and supply approach) for group of settlements located in a watershed located in the semi-arid region using integrated analysis of static and dynamic information. This study has adopted a methodology based on the rainfall and water requirement, in aiding the crisis situation and sustainable planning at local level. Time series analysis of annual rainfall of 100 years was used in identifying critical period. The inter-rainfall gap analysis was carried on 10 years of daily rainfall. Based on these results and the reported physical situation, a threshold of annual rainfall (below which scarcity begins) was established. Surface run-off was calculated using SCS method and the surface cover information changes were collected from the orbital India remote sensing satellite data. The water spread of the irrigation tanks was demarcated and used in the water availability estimation. Ground water level fluctuation information was collected and used in establishing relationship with rainfall over the years. Crop area and type and their inter-seasonal (winter/summer) and annual changes were deciphered from temporal satellite Revenue village information on the human / animal population, crop type and area, water resources availability (ground water & surface water), natural vegetation cover, rainfall and temperature information, etc., were collected from the existing revenue records and updated from the interpretation of temporal IRS data. The demand from the crops (including the evapo-transpiration and transmission loss) and the settlements (human and animal) was calculated for individual settlement/villages. The supply position of the watershed by way of surface run-off and storage and their losses over seasons was estimated for a given rainfall event. A drought scenario situation for Jhod nadi watershed, tributary of Godavari River, located in Nanded District of Maharashtra, India, with an area of 196 km<sup>2</sup> was created. Probable drought severity of the settlements (about 40) was grouped in low to very High depending on their deficit percentage of demand-supply. An effective method for regular monitoring and preparedness is discussed in the paper.

**HS02/11P/C24-0090P Oral-Poster 1547**

#### USE OF GEOGRAPHIC INFORMATION AND REMOTELY SENSED DATA IN THE DECISION-MAKING SUPPORT SYSTEM FOR FLOOD MANAGEMENT IN ROMANIA

Corina PREDESCU, Gheorghe STANCALIE, Elena SAVIN (Remote Sensing and GIS Laboratory, INMH)

Floodings are an important risk in many areas around the globe and especially in Romania. In the latest years floodings occurred quite frequently in Romania, some of which isolated, others were affecting wide areas of the country's territory. The paper presents the elaboration of the cartographical documents on the flood risk regions over a pilot watershed

and the development of the GIS applications with a decision system for the crises management. A modern approach is used for the flooding risk indices estimation. These indices are associated to the physio-geographical, morpho-hydrographical and vulnerability characteristics of a region. The methodology was elaborated to determine the flooding risk, using risk indices at a scale compatible with a synthetic representation of the territory. There are stressed the facilities supplied by the Geographic Information System (GIS) and the remotely sensed data to manage flooding during their characteristic phases: before, during and after flooding. Accent is laid on the pre and post-crisis phases. An important research topic was the study of the parameters that can be extracted from satellite images in view of organizing a hierarchy of the geographical space versus the flooding risk. Information obtained from satellite images proved to be useful for the determination of certain parameters necessary to monitor flooding: hydrographic network, water accumulation, size of floodable surface, land impermeability degree, water absorption capacity over the basin surface, or resilience to in-soil water infiltration. The study encompassed both the risk degree levels related with various parameters, which influence and determine floodings and which takes into consideration the human presence in the sensitive areas. The application was developed for the Arges hydrographic basin in Romania, a critical area, keeping in mind that it withholds many localities, including the capital and also important economic centers. Advantages offered by this integrated system are: to manipulate and make available large databases, to easily update the information, to survey the temporary modifications, to establish the link between the measured/forecasted data and the GIS database. The database allows obtaining synthetic representations of the hydrologic risk for the Arges basin, through separate or combined use of the risk parameters as well as for interfacing with the hydrological models in view to improve them as regards recovering results and the possibility to achieve scenarios.

**HS02/11P/C24-0100P** Oral-Poster **1551**

#### VELOCITY DISTRIBUTION DUE TO LAUNCHING APRON AROUND ABUTMENT

Mohammad Monowar HOSSAIN, Mohammad Salzar HOSSAIN, Mohammad Faheem SADEQUE (Department of Water Resources Engineering, BUET)

Velocity distributions were measured in a small-scale riverbed model for vertical wall abutment constructed at the Hydraulics and River Engineering Laboratory of Bangladesh University of Engineering and Technology (BUET). A series of test run were conducted for five different apron-setting configurations and velocities were measured using a programmable 2-D electromagnetic liquid velocity meter. Comparison of velocity distribution in terms of velocity vectors with and without apron was made. It was observed that considerable displacement of velocity vectors occur due to different apron setting. Due to displacement of velocity vector, the scour depth was found to be affected significantly. Vertical velocity distribution at the maximum scour hole formed due to apron setting was also measured. The result obtained gives an indication of use of falling apron for protection of vertical abutment against failure due to scour.

**HS02/11P/C24-0110P** Oral-Poster **1555**

#### URGENT WATER SUPPLY INTO ZHALONG WETLAND IN 2001 AND 2002

Shiguo XU<sup>1</sup>, Lianwen DANG<sup>2</sup>, Heyue LF<sup>1</sup> (<sup>1</sup>Department of Civil Engineering, Dalian University of Technology, <sup>2</sup>Songliao Water Resources Commission)

Nen River basin is located in northeast of China, where belongs to monsoon precipitation zones. There usually are short summers and long winters with spring draught and summer floods. Around lower reaches of Nen River, there exist many big wetlands, such as Zhalong, Xianghai and Momoge wetlands. Zhalong wetland is the biggest one with the area of 2100km<sup>2</sup>, 468 species of vegetations and 236 species of birds belonging to 48 families. The main protected bird is Red Crown Crane. It is one of 7 wetlands earliest accepted by Ramsar convention in China. Water is very important for wetland evolution. As the water resource development is gradually actualized on the upstream of rivers that flow into Zhalong wetland, water shortage problem has endangered the wetland ecological environment. Farther more, after the big flood in 1998, Nen River basin faced a four-year long draught series. At the begin of 2001, the area of water surface in Zhalong wetland was only 130km<sup>2</sup>, much less than the average area 800km<sup>2</sup> and that in common dry year 300-400km<sup>2</sup>. The most part of the wetland draught up. Reeds couldn't grow up as usual. A lot of reed wetland became into grass wetland and the vegetal state degrades very seriously. It threatens the habitation condition of Red Crown Cranes that make their nests and hatch small cranes in every earlier summer here. So as to maintain the condition to keep basic function of the wetland, an urgent water supply project from Nen River to Zhalong wetland is put into practice. In the later autumn of 2001, supplied 357106 m<sup>3</sup> of water into the wetland, and from the spring to summer of 2002, 300x106 m<sup>3</sup> again. According to the investigation on site, water supply has achieved satisfactory results. In the end of April, the supplied water pours over the central area of the wetland. By recovering the ecologic condition of reed and fish, it helps Cranes and birds very much. This urgent water supply program provided a useful experience to rescue wetlands from a water shortage disaster. In the same time, an especial water resources plan of Zhalong wetland is under working to guarantee the water supply safety of it for a long term. A key project supported by National Natural Science Foundation of China is also come to operation, which studies the problems concerned with using floodwater to restore wetlands and using wetland to make floodwater a useful water resources.

**HS02c-Posters**

**Friday, July 11**

**WATER RESOURCES SYSTEMS: GLOBAL CHANGE, RISK ASSESSMENT AND WATER MANAGEMENT (ICWRS, ICASVR, ICSW, ICWQ)**

Location: Site D

**Friday, July 11 PM**

**HS02c/11P/D-001** Poster **1630-099**

#### MAXIMUM OVERLAND FLOW IN RIVER BASIN AND LANDUSE

Elena ASABINA (Russian Research Institute for Intergrated Water Management and Protection)

Present paper is the case of study of the basin where water resources for large city water supply are being formed. High economical activity in the basin transforms environment. Change of landuse structure such as transformation of forests into farmlands, meadows into pasture lands, bogs into meadows, etc. leads to changing of overland flow which presents the main component of river runoff. Solved problem is to assess how the values of overland flow depend on character of landscape. To prevent negative consequences of these

processes for runoff regime it needed to reveal the areas in the basin where main quantities of overland flow are to be generated and to protect them against possible landuse. Values of precipitation were almost equaled in different areas of studied basin. However, significant differentiation of overland flow in the space of the basin was found that is explained by differences of overland flow genesis such as characteristics of land surface. Character of landscape and soil type cause different conditions in the basin. Each of landscapes in combination with topography and soil can be considered as certain runoff-producing unit, which characteristic is uniform conditions of overland flow genesis. Hence, the river basin as a whole and its different areas were represented by combination of various runoff-producing units and overland flow was evaluated in different areas of the basin. Also, overland flow was assessed for different phases of hydrological regime such as winter low water, spring flood, and summer low water with rain floods. It was found that main amount of overland flow is being formed during spring flood and in upstream but not in downstream part of the basin as it was thought earlier. Obtained conclusion will allow providing optimal landuse practice in future.

**HS02c/11P/D-002** Poster **1630-100**

#### ARTIFICIAL NEURAL NETWORK MODELING OF THE RAINFALL-RUNOFF EXTREME EVENTS

Dionysia PANAGOULIA, Nikos MARATOS (Department of Water Resources, Hydraulics and Maritime Engineering, National Technical University of Athens)

An artificial neural network (ANN) is a reliable mathematical mechanism in modeling the complex nonlinear relationships between input and output timeseries. ANN models have been proven effective and efficient to model the rainfall-runoff relationship in situations where explicit features of the internal hydrological subprocesses are difficult to be described using physically based equations. A new algorithm using a combination of linear least squares and multistart simplex optimization is developed to show the mechanism and parameters of three-layer feed forward ANN models and the potential of such models for simulating and forecasting the high-and low-flow events over a mountainous catchment. The output "rain plus melt" from the snow accumulation and ablation model of the US National Weather Service (US NWS) applied on a medium-sized mountainous catchment. The Mesochora catchment in Central Greece was used as input to ANN model. The conceptual soil moisture accounting model (SMA) of the US NWS applied, as well, over the same catchment, for comparison of extreme values. The RMSE (root mean square error) and %VE (percent volume error) statistics, for each model, computed separately for flows above and below the 15-year meandaily flow and presented as a function of the total annual flow for each data year. Note that the five calibration years were the driest of the 15 data years. Clearly, RMSEA (root mean square error above-mean daily flow) performance of the SMA model is worse than that of ANN on all years. The results of the RMSEB statistic (root mean square error below-mean daily flow) indicate that ANN model performs best for all of the years. The %VEA (percent volume error for above-mean daily flow) statistic indicates that the ANN model consistently has the smallest bias, while the SMA performance is poor. The %VEB (percent volume error for below-mean daily flow) statistic shows the poor performance of SMA model. We should not point out that the poor performance of the SMA model does not reflect so much on the ability of the model as it does on the calibration procedure used. In addition, an "expert" would not allow the model error bias at various flow levels to deteriorate so much while minimizing the error variance. Although the ANN model developed here, by no means, could substitute a physically based conceptual model, the results indicate that the ANN model may provide best performance when only dry years of data are used for calibration.

**HS02c/11P/D-003** Poster **1630-101**

#### DETERMINATION OF INSTANTANEOUS UNIT HYDROGRAPH WITH CLARK'S TECHNIQUE IN GIS

Musa YILMAZ, Nurunnisa USUL (Water Resources Lab. Department of Civil Eng. Middle East Technical University)

Determination of unit hydrographs for the basins is very important for the design of hydraulic structures. When there are observed rainfall-runoff data for the storms they are obtained by using these data, but when there are no observed data they are obtained by using synthetic unit hydrograph methods. In this study one such method is used together with Geographical Information Systems techniques. Application of Clark's synthetic unit hydrograph technique with GIS technology requires the estimation of three parameters of the original methodology. Time of concentration,  $T_c$ , is derived from SCS lag equation, reservoir storage coefficient,  $R$ , from an observed storm hydrograph and the time-area histogram is determined from the Digital Elevation Model of the basin. The translation hydrograph is then derived from time-area graph by applying a unit excess rainfall over the basin. After performing a linear reservoir routing, the translation hydrograph is routed to the basin outlet and the Instantaneous Unit Hydrograph of the basin is obtained. It can be used to obtain any duration unit hydrograph and then storm hydrographs for this basin. Such a study is performed for two different size basins in Turkey and the results are compared with the observed unit hydrographs of the basins and a discussion is given.

**HS02c/11P/D-004** Poster **1630-102**

#### ARIDIFICATION AND THE INCREASE OF FLOOD EVENTS IN CENTRAL EUROPE

János RAKONCZAI, Katalin BÓDIS, Ferenc KOVÁCS (Department of Physical Geography, University of Szeged)

Hydrological events in Central Europe (including the more thoroughly analyzed Hungary) began to show a strange kind of controversy in the past decades. It is clearly visible through statistics that precipitation has decreased significantly (with about 10 %), at the same time however, the number of flood events shows a remarkable increase. In the year 2000 the situation was really peculiar, because in the beginning of a persistent drought significant flood prevention efforts had to be made along the Tisza river. i. drought and flood at the same time! We demonstrate the characteristics and consequences of the aridification process from several aspects. Beginning as early as 1910 precipitation in Hungary is dropping constantly. Statistical analyses show that the reduction did not bring about the decrease of variability; fluctuation was merely transferred into a lower range of values, clearly showing the decrease in the average amount of precipitation. The persevering drop of precipitation has produced a significant decline in the amount of groundwater. This process became obvious since the early 0-s. We have determined through detailed GIS analysis the spatial and temporal changes in the level of groundwater and the total deficiency in subsurface waters. One of the most important consequences of the analysis is that in some areas even the significantly rainy years could not stop the decrease of groundwater meaning that the drop of precipitation clearly appears in subsurface waters. (It is important to bear in mind that the decrease of subsurface waters in closely connected to relief: in plain areas that are higher than their surroundings the decrease is more significant.) To determine the reaction of foliage to aridification we executed spatial analysis based on Remote Sensing methods. Throughout the world, floods became more frequent in the past decades. This is

caused by both natural processes as well as the changes in social and economical structures. Extensive growth of agriculture became possible by creating arable lands through massive river regulation works. However population growth can also cause people to move into areas that are endangered by floods. Floods are thus just the products of natural processes in such areas. The truth is however, that due to human interventions, areas of potential flood-risk has expanded as well. The higher water levels in regulated rivers or the huge amount of water stored in large reservoirs both lead to flood risks to get higher than they would naturally be. In addition to the above, meteorological extremities also augment the possibilities for floods. The flood disasters of recent years all over the world and in Central Europe clearly demonstrate this as well. In this lecture we will, through demonstrating several floods, evaluate their natural and social background. It can be said that now floods can appear in any part of the year due to climatic changes, nature can produce quite peculiar extremities (extraordinary amounts of precipitation; record breaking flood levels along the Tisza river in four consecutive years), as well as the way human actions affect natural processes.

**HS02c/11P/D-005** Poster **1630-103**

**DEVELOPMENT OF NEW TECHNOLOGIES OF FLOOD SIMULATION AND FORECASTING IN REAL-TIME**

Sandra Gabriela GARCIA (Technical University of Cartagena. Department of Thermic Engineering and Fluids)

The flash floods constitute one of the main problems of the Mediterranean semiarid zones of Spain. The convective storms of high intensity, typical of these zones, produce hydrological events that can turn out to be catastrophic. Due to the scanty existing time between the runoff hydrograph peak and the associated rainfall, the warning of flooding must be based on meteorological and hydrological forecasting. The coordination among the responsible authorities in the operational flood management, needs real-time operative decision support system. The use of Geographical Information Systems (GIS) in the development of these support tools, it constitutes a foreseeable direction. The GIS allow an efficient integration of information with a high spatiotemporal resolution, and spatially distributed hydrologic models oriented to runoff simulation and prediction in real time. The development of new methodologies and tools that allows the operative integration of radar rainfall fields and short term quantitative rainfall forecasting as input to distributed spatially rainfall-runoff models, are proposed. Finally, it is to be underlined that this work incorporates the use of new technologies (GIS, remote sensing, Digital Elevation Models) and the most recent developments in aspects of estimation and treatment of the spatial distribution of soil moisture and the flow in the unsaturated zone. The main objective is to improve the forecasts of flash floods applying a decision support tool in real-time named *Shyska*, developed with GIS-embedded functions.

**HS02c/11P/D-006** Poster **1630-104**

**SPATIAL-TEMPORAL APPROPRIATENESSES OF EXTREME PROCESSES FORMATION IN RIVERS SYSTEMS OF REGIONS WITH SHARP CONTINENTAL CLIMATE**

Leonid M. KORYTNYI, N. V. KICHIGINA (Institute of Geography Siberian Branch Russian Academy of Sciences)

Spatial-temporal appropriatenesses of floods and shallows formation in main basins of East Siberia- the Enisey, Angara, Lena rivers, Lake Baikal are researched. Genetic and statistical regional analysis considers the specific of physiography conditions and also the peculiarities of sharp continental climate that has a tendency to change for the last ten years. Long-term series of flow on 120 hydrological gauge lines are the basis. Floods and shallows characteristics are determined: causes of extreme situations, their recurrence, geophysical and hydroengineering factors. Zoning of East Siberia on floods risk is implemented and statistic analysis of flow's extremes and curves of maximum flow distribution as well. Researches are directed to decrease extreme situations in water resources' systems. Effectiveness of different gear of risk management, the system of ecological insurance in particular is considered. For a number of regions the risk areas in the valleys of main extreme flood rivers is marked out and regulations of economic activity in these valleys are worked out. In the base of regulations there is the combination of four types of arrangements: geoeological, economical, engineering, and legal.

**HS02c/11P/D-007** Poster **1630-105**

**DEVELOPMENT OF WATERSHED RAINFALL-RUNOFF MODEL BASED ON THE PARTIAL CONTRIBUTING AREA CONCEPT**

Chin-Hsin CHANG<sup>1</sup> (<sup>1</sup>Department of River and Harbor Engineering, National Taiwan Ocean University, <sup>2</sup>Department of River and Harbor Engineering, National Taiwan Ocean University)

The objective of this study is to develop a rainfall-runoff model based on the partial contributing area (Betson, 1964; PCA) concept. The influence factors of the PCA phenomena were investigated. The size of the PCA during storm is derived from TOPMODEL theory and estimated by using a digital elevation model (DEM). The PCA concept was then combined with a kinematic-wave based geomorphic instantaneous unit hydrograph model (Lee and Yen, 1997; KW-GIUH) for rainfall-runoff simulation. In the KW-GIUH runoff simulation considering PCA concept, the surface runoff mechanism was simulated by Manning's formula, and the subsurface runoff was approximated by Darcy's law. The Hen-Chi watershed in northern Taiwan was used to demonstrate the capability of the proposed model. The PCA size and geomorphic factors of the study watershed were obtained using a DEM, and SPOT satellite images were adopted for land cover analysis to obtain the roughness coefficient. The results showed that significant improvements were found in the simulation of rising and recession hydrographs.

**HS02c/11P/D-008** Poster **1630-106**

**REAL TIME FLOOD FORECASTING: A CASE STUDY OF THE JHELMUM RIVER, PAKISTAN**

Sajjad AHMAD (Department of Urban and Regional Planning, University of California, Irvine)

A modeling system is developed for real-time flood and reservoir inflow forecasting. It comprises a lumped conceptual rainfall runoff model, a hydrodynamic model for river routing, and an up dating procedure for real time operation of reservoirs. The model is implemented for the Jhelum River Basin in Pakistan, with watershed area of 14860 km<sup>2</sup> and the Mangla Reservoir situated at the down stream end. The model is calibrated and verified at five gauging stations using daily rainfall data from twelve rain gauges and daily discharge data from three stream gauging stations for the period 1985 to 1991. Statistical parameters are used to evaluate the performance of the model. Real time forecasts of historic floods of 1976 and 1992 are performed with 24 hour and 6 hour lead times respectively. Sensitivity analysis on quantitative precipitation forecast (QPF) is made. The model performance for

short term forecasts that is, 6 to 24 hours indicate robust system behavior in real time inflow prediction. Results indicate that if the accuracy of precipitation forecast is greater than 60 %, the error in the forecasted stream flow is less than 25 % for huge flood events. Sensitivity analyses show that large historic floods are highly sensitive to QPF.

**HS02c/11P/D-009** Poster **1630-107**

**REVISITING 1992 FLOODS IN PAKISTAN: OPERATION OF MANGLA RESERVOIR**

Sajjad AHMAD (Department of Urban and Regional Planning, University of California, Irvine)

Occurrence of floods is a natural phenomenon all over the world. With the increase in population and human activity in the floodplains, flood damages represent escalating hazard in many countries, despite increasing investments in flood control measures. Reservoirs are important structural measures to reduce damages caused by floods. Reservoir operation during large flood events is crucial in utilizing reservoirs as flood damage reduction options. In 1992 a catastrophic flood passed through the Mangla Reservoir on the Jhelum River in Pakistan. Operation of reservoir resulted in severe flooding of down stream areas causing damages to lives and property. A reservoir operation model is developed for the Mangla Reservoir. Model is calibrated for the flood event of 1976. The simulation model is used to investigate the water levels in the Mangla reservoir that would have resulted in 1992 with releases of 5700 m<sup>3</sup>/s (safe passage down stream) and 8500 m<sup>3</sup>/s (high flooding conditions down stream). Simulations revealed that it was possible to accommodate a considerable volume of the 1992 flood in the reservoir. However, to operate the reservoir in this way, difficult decisions have to be made during the flood. This can only be done with a full overview of the flood situation and in close cooperation with the concerned agencies. It also requires that the procedures for the reservoir operation for such a situation be already developed.

**HS02c/11P/D-010** Poster **1630-108**

**STOCHASTIC MODEL OF THE RUNOFF FLUCTUATIONS OF THE RIVERS WITH A FLOOD FLOW REGIME**

Andrei V. KHRISTOFOROV<sup>1</sup>, Taras V. SAMBORSKY<sup>2</sup> (<sup>1</sup>Department of Hydrology, University of Moscow, <sup>2</sup>Department of Oceanology, University of Moscow)

The stochastic model of fluctuations of a runoff during a flood period is offered. It includes a stochastic model of the hydrograph of a flood season and stochastic model of the annual fluctuations of its characteristics. The stochastic model of the hydrograph is based on the approximation of the individual hydrographs of separate flood peaks and base flow and their superposition into the unit hydrograph of the whole flood period. The parameters of the approximation - base flow, number of flood peaks, dates of their passage, their maximums, durations of the growth and intensity of recession. All these characteristics are considered to be the random variables. The sequence of flood peaks during a flood period is described by a model of Poisson process. The model of annual fluctuations includes the description of probability distribution of hydrograph elements, correlation between them, autocorrelation of their annual fluctuations, their probable climatic and man-made regular changes. The number of flood peaks is the major characteristic of flood season. It can be considered as an index of flood forming situations of the year. The realization of model includes the Monte-Carlo method and theoretical formulas suggested for transition from model elements to any river flow characteristics of flood season. In a case of some regular changes caused by climate or economic activity the principles of correction of the parameters of probability distribution of model elements are suggested. The adequacy of the model was successfully tested on a base of hydrologic data for 68 rivers of the world. These are the rivers of the Amur basin and Northern Caucasus in Russia, North Korea, Ukrainian Carpathians, Georgia, USA, Algeria and Surinam. The statistical stability of the model is rather high. The basic parameters of the model can be estimated with the errors no more than 5-10% already in a case of 10-15 years of hydrologic observations. The model is intended for the hydrologic computations of any characteristics of the river flow of flood season for a weakly studied rivers in a case when a lack of hydrometeorologic observations don't allows to use the models of river flow formation. The model permits to increase the accuracy of hydrologic computations by a factor of 1.5 - 2 and more in comparison with normative methods used now. The application of the model is not limited by the traditional problems of hydrologic computations. This is confirmed by an example of model application for the analysis of the systematic increase of the annual river flow which was discovered for the rivers of Mid-Atlantic of USA from the beginning of 70-ties.

**HS02c/11P/D-011** Poster **1630-109**

**IMPACT OF POPULATION GROWTH AND THE CLIMATE CHANGE ON THE QUANTITY OF WATER RESOURCES IN NORTH EASTERN REGION OF INDIA**

Uttam C. SHARMA (Indian Council of Agricultural Research)

The north-eastern region of India, comprising seven states, has a geographical area of 255,090 sq km. The region is extremely rich in water resources but continuous increase in human interference and mismanagement has rendered these resources in fragile state. The region receives about 510 cubic km of water as annual rainfall. It has two major river basins viz. Brahmaputra and Barak, which drain 194413 and 78150 sq km area with an annual runoff of 537.0 and 59.8 cubic km, respectively. The region has a total surface and ground water potential of 1064.8 and 16.6 cubic km. The scenario appears to be quite encouraging but indiscriminate use of water resources has caused land and environmental degradation in the region. Against an irrigation potential of 3.68 million ha, only 10.6% has been exploited. The population in the region has increased from 10.5 million in 1951 to 40.3 million in 2001, that is, it has grown 4 folds in 50 years, thereby exerting tremendous pressure on land and water resources. More than 82% of the population is rural based, whose main occupation is agriculture. Prevalence of shifting cultivation has resulted in deforestation and annual soil loss of 88.3 million tonnes through run-off from hill slopes, causing silting of river beds and frequent occurrence of floods. Due to population pressure, more and more forest area is being brought under plough, putting whole ecology in peril. The declining trend in rainfall and frequent temperature fluctuations are a signal for climate change. The demand for water for domestic use has suddenly increased due to fast population growth and change in life lifestyle of the people. At present, about 2.9 and 20.0 cubic km of water is required for domestic and irrigation and 1.5 cubic km each for energy, industry and other miscellaneous uses. In towns, generally the raw rainwater is supplied for domestic use while the people in rural areas have to depend on stream or pond water collected during monsoon. Seasonal rainfall flushes the catchments earlier charged with polluted environment. This polluted water results in frequent occurrence of diseases like cholera, jaundice, diarrhoea and typhoid. Water demand is high and the supply does not commensurate with it. Due to mismanagement of rainwater, about 3586 thousand ha of land has become prone to floods. Further, the quality of water has also deteriorated due to its being polluted with nitrates, chlorides and sulphates with increased use of fertilizers and pesticides in an effort to increase crop productivity in the region. If the rate of population increase remains unabated, the water resources are likely to dwindle further as also deterioration in the quality of water. A multidisciplinary study, based on watershed approach, is in progress since 1983, to evolve new farming system to replace

shifting cultivation, judicious management of rain-water and monitoring of soil, nutrients and water yield through surface and base flows. Lot of useful data has been generated which will help in planning, developing and improving the water resources in the region.

**HS02c/11P/D-012** Poster **1630-110**

**MANAGEMENT OF WATER RESOURCES IN KANDI (DROUGHT PRONE) ZONE OF JAMMU PROVINCE FOR HIGHER CROP PRODUCTIVITY**

Vikas SHARMA (S.K. UNIVERSITY OF AGRICULTURAL SCIENCES AND TECHNOLOGY-JAMMU)

The *kandi* zone of Jammu province of Jammu and Kashmir state of India is characterized by low rainfall (<650 mm), deep water table, undulating topography, poor soil fertility with land surface full of sand stones, soil moisture stress, frequent droughts and acute scarcity of water for domestic use and crop production. The *kandi* zone has two major river basins viz. Chenab and Tawi, which pass through deep gorges and undulating terrain, draining entire Jammu region. About 3.5 to 5.0 km<sup>3</sup> of water is received as annual rainfall, mostly during July and August. Rest of the period during the year remains dry except few showers during winter. Rains are generally with high intensity, resulting in over flowing of seasonal streams, soil erosion and degradation. The entire zone has agriculture-based economy but is always deficient in food grains. Though, the farmers are hardworking, working most of the time in the field along with their spouse and children, they do not produce as much as to feed their family. In absence of optimum soil moisture and irrigation facilities; application of fertilizers, good crop seed and other inputs have little impact on crop productivity. The studies have shown that water management is the major factor, which can improve the crop productivity in the *kandi* zone. It is difficult to derive any benefit from the water from two rivers as they flow in hilly terrain and cost involved in lifting the water and construction of canals would be two high compared to the area available for irrigation in the immediate vicinity. Construction of small structures for rainwater harvesting during monsoon will be good preposition. Farmer's participation in the whole programme is necessary for achieving the desired goals. Construction of small check-dams to divert the water to ponds will not only reduce the soil erosion but water can be utilized for life saving irrigation during winter. Besides, there is need to introduce such cropping pattern, which may reduce the run-off and help in ground water recharge. The paper discusses the feasibility of the check-dams, water storage reservoirs, soil conservation measures according to topography and judicious utilization of available water for higher crop productivity, resource management and environment conservation in *kandi* zone of Jammu Province.

**HS02c/11P/D-013** Poster **1630-111**

**WATER RESOURCES MANAGEMENT AND PLANNING; THE NEED FOR MULTIDISCIPLINARY MODELLING APPROACHES**

Islam Hamza ABOU EL-MAGD, Trevor TANTON (Civil & Environmental Engineering Departement, University of Southampton)

Water is a finite resource and the rapidly growing population in many arid and semi arid countries is placing excessive pressure on the limited water resources of these Countries. Unfortunately, it is predicted that many of these arid and semi arid countries will be the most seriously effected by a decline in water resources as a result of global warming. In most of these countries irrigated agriculture is the main consumptive user of water and unless water management is improved there will be a dramatic reduction in food production as a result. Typically most large irrigation schemes have an unimaginable wastage of water, with crop evapotranspiration accounting for only 20-35% of the water supplied, the remainder being wasted. Global warming will result in both increased evapotranspiration and reduced water resources and it is clear that if productivity is to be maintained water will have to be used more efficiently. Water allocation for irrigation is traditionally based on theoretical estimations of crop water requirements and rough estimations of canal losses, with the result that water supply rarely meets demand. Remotely sensed data is capable of supplying the planners with up to date data on the crops in the field and in measuring crop water requirements and wetland losses. This paper explores how remote sensed data is presently being used to improve water resource management in large irrigated catchments. It investigates the potentiality of spatial modelling of the real time data from satellite images, crop water demand from climatic data and irrigation information from the field to accurately allocate the irrigation water need in large irrigation scheme.

**HS02c/11P/D-014** Poster **1630-112**

**THE SYSTEM FOR ECOLOGICAL AND ECONOMIC ASSESSMENT OF USE, PRESERVATION AND RESTORATION OF URBAN WATER BODIES: ST. PETERSBURG AS A CASE STUDY**

Sergey A. KONDRATYEV (Prof.)

The water surface area of 106 water bodies of St. Petersburg city is equal to about 21 km<sup>2</sup>. The urban water bodies reflect the level of environmental pollution of St. Petersburg. At present time only 2% of water bodies can be referred to pure, 18% - to polluted, and 80% - to dirty. The State is the owner of water resources, including urban water bodies. Its interests are to stop deterioration of water quality and degradation of water ecosystems, and to find money for restoration of water bodies. The potential water-user can rent water bodies for the aim to get money income. In this case he should be interested in preservation or restoration of water bodies being a natural basis of his business. At present study there is discussed the problem of a choice of optimum variants of urban water resources use without deterioration of water quality and ecological status of water bodies, and with financial profit for water-user. The system for ecological and economical assessment of use, preservation and restoration of water bodies has been developed. The basic stages of the system are the following:- Data bases load and GIS development.- Assessment of the investment appeal of urban water body. High level of environment pollution, industrial enterprises located in catchment, high level of anthropogenic impact on water body are the reasons for negative assessment. The below mentioned stages take place only for positive assessment of the investment appeal of water body. - Assessment of present suitability of water body for various kinds of use. The basis of assessment is the result of comparison of present parameters of water quality with critical limits of chemical substances in water and sediments. High level of water and sediment pollution is the reason for negative assessment.- Economical assessment of water body restoration. Various kinds of restoration methods are considered: internal (chemical, biological and engineering) and external (catchment changes). - Optimisation of water body use on the basis of mathematical modelling. - Assessment of sensitivity of results of modelling to change of parameters of water body (depth, volume, area of recreation zone, etc.). Results of assessment are the information for choice of scenario of parameters changes for maximization of financial profit of water use.- Economical assessment of water body parameters change.- Economical assessment of monitoring.- Final ecological and economical assessment of water body use taking into account costs of restoration, parameters change and monitoring. Application of the developed system has been made for urban water bodies. Results of application show that it is possible to use a number of water bodies with financial profit for water-user and

without deterioration of water quality and degradation of ecosystems. The lists of water bodies with maximal and middle investment appeal are carried out.

**HS02c/11P/D-015** Poster **1630-113**

**OPTIMAL PRESSURE CONTROL IN SUPERVISORY WATER DISTRIBUTION NETWORK USING SHUFFLED COMPLEX EVOLUTION ALGORITHM**

Haytham AWAD, Akira KAWAMURA, Kenji JINNO (Institute of Environmental Systems, Kyushu University, Fukuoka, Japan)

Obtaining an optimal control of the distribution of system service pressures in a municipal water distribution networks has always faced combinatorial problems due to its complexity, scale of the problem, variation of water demand and the difficulty in estimating the roughness coefficient of old pipes. Referring to the previous difficulties, the application of linear, non-linear, dynamic programming, simulated annealing and genetic algorithm have been investigated by many authors and used in recent years for the optimization programs of water distribution networks design, replacement and leakage minimization. Particularly, the application of genetic algorithm (GA) in water distribution networks optimization models has been known as the most successful method in this field. It works with a coding of the parameter set, direct the search to the improved solutions by probabilistic rules and working directly with the objective function requiring no additional knowledge. In this paper, we used an evolutionary optimization procedure known as Shuffled Complex Evolution - University of Arizona (SCE-UA) for searching for the optimal or near-optimal solution of valves setting for the pressure regulation of a water distribution network. The SCE-UA technique has been successfully used in the calibration of conceptual rainfall-runoff models and the identification of aquifer formation parameters in the area of surface and subsurface hydrology, respectively. However, this algorithm has never been used in the field of water distribution networks management and planning and this paper is our first attempt in this direction. The SCE-UA Method which is relatively new concept is a general purpose global optimization program which combines the strengths of the simplex procedure with (i) the concept of controlled random search; (ii) competitive evolution; and (iii) the concept of complex shuffling. The synthesis of these three concepts makes the SCE algorithm not only effective and robust, but also flexible and efficient. The main advantage of the SCE-UA method is that, for a given number of objective function evaluations, the SCE-UA have the highest probability of succeeding of finding the global optimum. To demonstrate the performance of the SCE-UA algorithm, A case study of a certain block of the supervisory Fukuoka City water distribution networks is presented showing the effectiveness of the algorithm to regulate the pressure at all the network nodes between upper and lower values and as near as a target value. In Fukuoka City water distribution networks, electrically motor valves openings are adjusted by remote control to regulate pressures and flow rates on the basis of information provided by flow meters and pressure gauges attached to distribution pipes. Results show that pressures are well regulated by SCE-UA algorithm to a target value for a specified nodal demands and external inflows.

**HS02c/11P/D-016** Poster **1630-114**

**BANK FILTRATION SYSTEMS AS COMBINED TECHNOLOGY FOR GROUNDWATER AND SURFACE WATER**

Ekkehard O. HOLZBECHER (Humboldt University Berlin)

Bank filtration systems are of increasing importance for the supply of water for all kind of purposes. Worldwide water works extend old pumping well galleries, and increasingly new investments are directed to this technology. By bank filtration in most cases both surface water and groundwater resources are exploited, what has to be taken into account by the management of bank filtration facilities. Through the combination disadvantages of pure surface water or pure groundwater systems can be overcome. The technology of bank filtration makes the system less vulnerable to extreme events. The quality of the pumped mixture is higher than the water of the reservoir with lowest quality. Moreover surface water is significantly purified during the filtration passage from the surface water body to the pumping facility, so that the application of further water treatment may even become obsolete. An example is the water supply for the city of Berlin, Germany, which is studied in detail within the NASRI project (Natural and Artificial Systems for Recharge and Infiltration) since spring 2002. The aim of the project is to obtain a better understanding of such systems and to develop appropriate models and management tools - not only for the Berlin sites. The contribution to the conference provides an overview on the current state of the project. An introduction to the technology will be presented, followed by an overview on the activities of the NASRI project. Computer models will be demonstrated concerning the design and dimension of pumping well galleries and concerning the biogeochemical transformations during the passage of surface water through the porous medium. Finally follow some implications concerning the management of combined surface water and groundwater resources.

**HS02c/11P/D-017** Poster **1630-115**

**REDUCING SHALLOW - WELL CONTAMINATION IN UGANDA**

James MWAMI (Project Manager, Busoga Trust)

Despite an abundance of surface water in Uganda (18% of the land area), the predominantly rural (>70%) population relies almost exclusively on groundwater for a portable water supply. This dependence arises from the more widespread occurrence, superior quality and reduced susceptibility to contamination, of groundwater supplies compared to surface water resources. As a result, provision of safe water to rural communities in Uganda has depended primarily upon the construction of wells and protection of spring discharges. In Uganda, as with other regions in equatorial Africa, featuring extensive, weathered crystalline rocks, often referred to as the "basement complex" ground water development has targeted two main aquifer units: a deep aquifer of fractured bedrock and a shallow, muddy-sand aquifer comprising of detrital bedrock and alluvium. This paper depicts a case study taken in east and central Uganda. Particular attention has recently been directed at developing the shallow - well aquifer since the formation is less costly to develop and a recent study has found it to be more productive than the deeper, bedrock aquifer. However, monitoring of water quality in south eastern Uganda, a region of intense shallow - well development, shows that within months of installation, shallow groundwater commonly exhibit levels of coliform bacteria and nitrate exceeding W.H.O health guidelines. Human and livestock waste excreted in pit latrines, over land or in open-pit wells, called "scoop wells" may contain worms, protozoa, bacteria and viruses that if consumed, can lead to the contraction of hepatitis, typhoid, cholera and a variety of diarrhoea diseases. Wells and springs harvesting shallow groundwater are generally protected from these pathogens by a granular soil matrix which both filters bacteria, protozoa and worms due to their relatively large diameter (>0.5 um) in relation to the aquifer material, and adsorbs smaller viruses (0.07 um to 0.7 um) on account of their strong, negative surface charge. Despite this cleansing capacity, the presence of coliform group of bacteria in groundwater indicates that faecal contamination has occurred. The practice of siting shallow wells in the vicinity of existing scoop wells has been identified as a probable source of faecal contamination too shallow wells in Mukono

District of South Eastern Uganda. Simulations of groundwater flow in the shallow aquifer indicate that a well head protection area of 60m between wells and contaminant sources such as scoop wells, pit latrines and swamps is required to ensure the sustainability of this vital, potable source of water to rural communities.

**HS02c/11P/D-018**

Poster

**1630-116****WATER MANAGEMENT ON MEDITERRANEAN ISLANDS UNDER CHANGING CONDITIONS**

Manfred A. LANGE (Center for Environmental Research, University of Muenster, Mendelstr. 11, D-48149 Muenster, GERMANY)

The availability of water in the Mediterranean in sufficient quantities and adequate quality represents a significant problem, particularly in light of possible changes in climatic conditions. This is due to a number of factors which include: the over-exploitation of existing aquifers by various users, insufficient recharge due to diminishing precipitation, excessive and inadequate use through agricultural activities or tourism, significant deficits in water management and distribution schemes and conflicting or unresolved demands and interests between various users, to name just a few. These problems are exacerbated on the islands in the Mediterranean because of their isolation and thus the impossibility to draw on more distant or more diverse aquifers in general and because of the threat of saline intrusions, which reduce the utilisation of existing, near-shore aquifers in particular. While the availability, demand and distribution of water on each island are determined by specific conditions, there are a number of attributes common to all Mediterranean islands which call for the formulation of generic solutions to the above mentioned problems. Because most of these problems are mutually related and interdependent, solutions will only be obtained through holistic considerations that are carried out by an interdisciplinary research team. Equitable and acceptable strategies require a stakeholder-based participatory process that builds on the results of scientific investigations on the one hand and on the consent of major stakeholders on the other. These requirements are central to the EU-funded MEDIS project, which aims to contribute towards the sustainable use of water on islands of the Mediterranean where conflicting demand for water is combined with a wide range of hydrological, social and economic conditions. MEDIS is being carried out by a consortium of 12 institutions from seven countries and will involve detailed investigations in one typical catchment each on Corsica, Crete, Cyprus, Mallorca and Sicily. By carrying out this project on five islands that cover the Mediterranean from west to east and by enabling a dialogue between scientists and stakeholders as well as between principal stakeholders from each island, these recommendations will embrace generic solutions based on the collective experiences of the residents on all islands. We will report on the results of the first year of MEDIS, which include an extensive review of current conditions pertaining to water management on each island and the specification of a typology of water demand and supply relationships for the islands of the Mediterranean. In addition, we will consider water supply under future climate scenarios derived through a regional model for the Mediterranean and/or downscaling of GCM results from models of the Max Planck Institute Hamburg, Germany. These results will give rise to a set of recommendations for improved water management practices that will have to be discussed, modified and agreed-upon through a participatory process involving key stakeholders on each island in the future course of the project.

**HS02c/11P/D-019**

Poster

**1630-117****RELIABILITY ANALYSIS OF THE INTEGRATED MANAGEMENT OF WATER QUANTITY AND WATER QUALITY FOR WATER TRANSFER SYSTEM**

Xiang ZHANG<sup>1</sup>, Jun XIA<sup>2</sup> (<sup>1</sup>Dept. of Hydrology and Water Resources, Wuhan University, <sup>2</sup>Department of Hydrology and Water Resources, Institute of Geographical Science & natural Resource)

Water consuming around the world increased sharply in order to meet the demands of the rapid economic development. On the other hand, it is the economic development that courses the degeneracy of eco-environmental system and the decrement of available water quantity, especially in the developing countries. It is necessary to consider the integrated management of water quantity and water quality in order to decrease the risk of water supply. In this paper, the integrated management of water quantity and water quality for the water transfer system is discussed. And based on the reliability theory, the method of reliability analysis is applied to assess quantitatively the operation reliability of water transfer system. Transferring water from the catchment with abundant water resources to the area in shortage of water, the water transfer system covering the different catchments plays an important role in solving the water shortage. Obviously it also influences the water quantity and water quality of the river in the water source area. In this paper, the importance and the method to consider the integrated management of water quantity and water quality are discussed and suggested. For the water quantity, the temporal and space variability of water resources in the water source area should be analyzed carefully in order to determine the amount of the available water. On the other hand, the influence to the water quality should also be considered thoroughly, including the pollutant source, the decrease of discharge in river resulting in the deterioration of water quality at the downstream and etc. In this paper, the environmental critical discharge, which is defined as the lowest required discharge to keep the water quality of the river to reach the standard of drinking water source, is used as a threshold for the management of water quality. It can be determined by using the river water quality mathematical model. At last, for the reliability of the integrated management of water quantity and water quality, the two reliability criteria, the temporal reliability and the volumetric reliability, are presented. The last part of this paper gives a case study about the water transfer system in Shenzhen city, Guangdong province. This system transfers water from the Dongjiang catchment to Shenzhen. Considering the integrated management of water quantity and water quality, not only the water quantity in the Xizhijiang and Dongjiang river is analyzed carefully, but the environmental critical flow is calculated. And the two reliability criteria are used to evaluate the operation of the system. The result shows the reliability analysis of the integration of water quantity and water quality can provide thorough decision making for the sustainable management of water transfer system.

**HS02c/11P/D-020**

Poster

**1630-118****LATERITE - LOW COST REMEDIAL OPTION FOR HIGH ARSENIC GROUNDWATER**

Rupa BHATTACHARYYA<sup>1</sup>, Debashis CHATTERJEE<sup>2</sup>, Yoshio TAKAHASHI<sup>3</sup> (<sup>1</sup>Department of Earth & Planetary Systems Science, Hiroshima University, <sup>2</sup>Department of Chemistry, University of Kalyani, India, <sup>3</sup>Department of Land & Water Resources Engineering, Royal Institute of Technology, KTH, Stockholm)

High arsenic groundwater has emerged as a nagging environmental problem in the recent decades. Elevated levels of groundwater arsenic (>50ppb) in the Bengal Delta Plain (BDP) threatens the lives of millions of people. Large scale uncontrolled groundwater development may play a key role for such human suffering. The present study deals with the adsorption pattern of AsO<sub>4</sub><sup>3-</sup> and AsO<sub>3</sub><sup>3-</sup>, the predominant arsenic species in groundwater using Red Earth (Laterite) for the supply of potable water. Laterite is an indigenous,

abundantly available, natural geological material enriched with amorphous ferric hydroxide (HFO) oxides. The mineralogical study of Laterite exhibits the predominance of iron and aluminium secondary phases. Chemical composition reveals that Laterite contains 30 - 35% iron oxides. Batch experiments indicate the Langmuir adsorption isotherm. The pH<sub>zpc</sub> of laterite is determined to be 8.5-8.6. The high pH<sub>zpc</sub> value supports a high positive surface charge of laterite over a wide pH range. The material, therefore acts as an effective adsorbent for several anionic contaminants. On the basis of the lab as well as field scale studies, laterite is used as a fixed bed filter media in an earthenware pitcher with a view to supply drinking water on the household basis. The results interpret that the material is not only effective in adsorbing arsenic but also effectively removes iron from the groundwater. Cost calculated for the transportation of laterite approximates to Rs 750 /ton/km (US\$ 16) whereas the treatment process estimates to Rs30/100L (US\$ 0.6) contaminated water. Therefore fixed bed laterite can be successfully used for removal of arsenic from groundwater. Lab scale experiments are also executed to understand the efficacy of the system for removing heavy metals as well from the aquatic environment.

**HS02c/11P/D-021**

Poster

**1630-119****LARGE DIAMETER WELLS AS A SOLUTION AGAINST THE RISK OF CONTAMINATION IN THE SEMI-ARID WORLD USING THE FILTER FACTOR CONCEPT**

Sarma K. SEEMANAPALLI, Soniaeli P. CARVALHO, Silvestre L. NOBREGA, Alex M. NEYVES (Smith Research Corporation, Small Business Technological Center, LSU, Baton Rouge, LA)

Water is the life blood of living creatures on earth. Seventy percent of earth's surface is covered with water. Despite much information available, groundwater movement, its quantity and quality remain a mystery. Groundwater levels decline due to intensive pumping and yearly below-normal precipitations, that accelerate the downward trend in water levels. Natural groundwater quality is affected by the materials it passes through on its way to the groundwater reservoir. Human activities also cause water quality degradation, serious enough to prevent the use of water for human consumption. Well location is a crucial factor, a well downhill from a source of bacterial contamination running greater risk of contamination than that on the uphill of pollution source. Minimum separation distances from potential sources of contamination are to be maintained. Proper well design reduces the risk of pollution by sealing the well from contaminants that enter from the surface. Bacterial contamination which cannot be detected by sight, smell or taste can result from a number of sources. Shallow wells and wells that do not have water-tight casings can be contaminated by bacteria infiltrating through the soil near the well. Soil remediation is a difficult, time-consuming and expensive operation and environmentalists select the most appropriate technology for specific contaminated sites. Here-in is suggested one such method of soil remediation, using Large Diameter Wells (LDW) that are popular in the semiarid world. The simplicity and low cost in the construction and operation of such wells make their use viable for rural communities. The LDW is a viable alternative to tube wells to alleviate the problem of draughts and the risk of contamination in Paraíba state, Brazil. The filter factor concept,  $f_f$ , conceived by Sarma(1997) considers the relative effects of transmission and passage of water through bricks and cement mortar. Values of  $f_f$  in function of well yield for given diameters and drawdown are presented. Criteria to avoid mutual interference due to simultaneous pumping of wells was also studied. Computer programs developed would prove useful in making the characteristics curves for LDWs constructed in aquifers with low transmissivity values. Unlike tube wells, in LDWs, water continues to get extracted from aquifer to the well even after the cessation of pumping, attesting LDWs as efficient in aquifers in the semi-arid world. Using field data, calibration was effected adopting a 14/16 mesh for the LDW. The numerical method adopted here-in was the volume element method. The flexibility of the method permits implantation of desired well-diameters, change the diameter in the computer program, thus permitting to evaluate the drawdown-discharge-diameter relationships. Regional characteristic curves drawn between the variables facilitate practical application of these by agriculturists and engineers to explore rightly the aquifers, avoiding thus the risk of contamination of LDWs.

**HS02c/11P/D-022**

Poster

**1630-120****REDUCTION OF RISK OF AGROTOXICS BY DRAINAGE IN AGRICULTURAL LANDS USING INTERCEPTOR DRAINS**

Sarma K. SEEMANAPALLI (Smith Research Corporation, Small Business Technological Center, LSU, Baton Rouge, LA)

About 80% of the sick and over 33% of the deaths in the third world countries are attributed to the clean water crises, caused by degradation in water quality. According to UNO, the disorderly distribution of available resources affects 20% of 3<sup>rd</sup> world countries. South America goes black-listed as a continent, threatened with water crisis. Brazil is however privileged because of its abundance of water, with its availability of 5000m<sup>3</sup>/year/capita, with a demand of only 200 m<sup>3</sup>/year in its NE region. Subsurface waters have distinct economic advantages over other components of the hydrological cycle. Groundwater can be used directly in most cases, without prior treatment. However, groundwater may also be polluted by way of natural or surface contamination. Because of the greater demand of groundwater, the confidence in the quality of potable water is posing doubts, its authenticity being questioned, once that major sources are already getting over-explored. Higher standards of water quality imply higher costs of water. Environmental scientists are concerned about groundwater contamination by way of agro-toxic substances entering the flow regime. The pollutants detected in shallow waters might reach the deeper strata of the aquifers. Here-in, an investigation is made about the effective use of interceptor drains in the irrigated perimeter in Sume in the Semiarid Paraíba State in Northeast Brazil, in function of their geometric, hydraulic and hydro-geologic parameters. Effective removal of chemical pollutants from aquifers through the use of interceptor drains is suggested to contain and even to remove subsurface pollutants from shallow aquifers. Interceptor Drain is a gravel trench excavated into a relatively impermeable soil layer and installed to collect and remove groundwater as it flows across the impermeable layer, which is typically placed across a contour of a slight to moderate sloping area to intercept groundwater. The potential theory used here-in and the concept of ground water divide conceived proved helpful to quantify the efficiency of interceptor drains. These drains offer concrete solutions to the problem of the control of subsurface water pollution in shallow aquifers. Such drains are used to capture the contaminants and to delimit the spreading of hazardous chemicals. Finite difference scheme used here-in was developed by Sarma e Alex (1997). For the totally and partially penetrating drains studied to know the effectiveness of such drains, spacing, widths and depths of drains varied. The drain discharge is treated as a function of the number of tubes that effectively enter into the drain. Recharge played an important role in the control of the pollutant movement, in delimiting the configuration of the phreatic surface, an increase in recharge rate correspondingly increasing the depth of the groundwater divide. Such water divides help one to forecast the contaminant movement and to quantify the same.

**HS02c/11P/D-023** Poster **1630-121**

**WATER QUALITY MANAGEMENT FOR CONJUNCTIVE USE OF GROUND WATER AND WASTEWATER FROM AQUACULTURE : AN INDIAN OVERVIEW**

Lalitkumar Pandit CHAUDHARI (Institute for sustainable development and research)

Aquafarming has emerged as one of the more promising industries in the world with considerable growth potential expected to contribute around the quarter of global fishery the year 2000 AD. The aquafarming has a multidimensional in perspective agricultural growth. It is a tool for utilizing land and water more economically and optimally for increasing the productivity of both natural resources, land and ground water through sustainable agriculture. The countries in the Asia-Pacific region have vast and varied aquafarming resources. Oftenly these are these are main source of Irrigation in this region. The overexploitation of ground water causes salinity problem in many countries reducing the cultivating area resulting reduction in agriculture reduction. An attempt has been made in this paper to develop the plan for ground water management for the aquaculture and horticulture as well as drinking water from the river source adopting conjunctive use of irrigation water from Indian experience. The paper also evaluate the water quality criteria of ground water and irrigation water for increasing the agricultural productivity. The methodology is based on the economics of the conjunctive use of irrigation and ground water for horticulture and aquaculture and also for agriculture. The main aim is to utilize the ground water over saline land for aquafarming and to reduce the soil salinity in irrigated land to increase the productivity of the land and the water. Series of the observations were taken on the various aspects of irrigation and soil salinity management for aquafarming using different methods to maintain the quality of land and the ground water. Also the relative economics of aquafarming and horticulture system under alternative water conserving irrigation /rain water harvesting management options, has been compared with the resources available. The result obtain demonstrate the implication of increase in yield in horticulture including agriculture and indicate the necessity of optimal and suitable use of natural resources for increasing the agricultural productivity. The result signify that the soil salinity can be managed using ground water management practices and the additional area can be brought down under agriculture. The result obtained also suggest that significant economic gains can be had from adopting conjunctive use of ground water to maintain the quality criteria for increased production in horticulture and agriculture as well as for drinking water from the river source after discharge. Apart from results of drinking water quality, it also signifies that the increase in the production can be achieved through reuse of water alongwith the ground water as supplemental irrigation, reducing the soil salinity problems in command area.

**HS02c/11P/D-024** Poster **1630-122**

**TOWARDS AN OPTIMUM WATER RESOURCES DEVELOPMENT IN THE NIGERIAN NIGER DELTA**

Adepoju D. OLUSEGUN (Geography Department, Faculty of Social Sciences)

Man's interaction and interference with the environment in order to satisfy his socio-economic needs without adequate management plan always result in environmental degradation either in the short or long term since the effects of his actions are registered in the atmosphere, accumulates and it is only a matter of time before its manifestation. The present water problem in the Niger Delta area of Nigeria is a combination of tripartite factors of climate change, increasing population, and the global economy. The implication of the climate change is due to the fact that Nigeria through the Oil and gas activities especially flaring contributes a significant amount of carbon mono-oxides, carbon dioxides in the global atmosphere which play an important role in raising temperatures at both the local and regional levels; but the major effect of these is mostly felt by the local environment. One of the consequences of these actions is inundation through the saline water incursion into the freshwater environment thereby increasing water problem both in quality and quantity. Secondly, growing populations, associated urban development and intensifying pressures on small areas of land are creating new pressures on available water resources with conflicting water demands, occurring to a lesser extent across the Niger Delta area. The population continues to grow at an estimated 2.8 percent per annum while urbanisation increases even more rapidly at an estimated rate of 5.2 percent. A visible consequence of this is the increased competition between users leading to increased conflict between users. That Nigeria and in particular the Niger Delta is having a fair share of the impact of dynamic global economy cannot be overemphasised. Of the three standard categories of freshwater use - for Agriculture, industry, and domestic - industry ( processing, exploration, exploitation activities etc ) is dominating. As a result of Pollution of surface water from increasing oil exploration and exploitation, industrialisation, increased food production is reducing the quality and quantity of portable water thereby reinforcing the problem of scarcity. In this study monthly rainfall and temperature datasets from the period 1941-1990 was in order to evaluate climatic trends of basic water resources parameter useful for assessing proper water resources planning and development in the Niger Delta. Optimal strategic water resources scenarios was built towards a sound water resources of the Niger Delta using GIS techniques.

**HS02c/11P/D-025** Poster **1630-123**

**CURRENT CONSTRAINTS TO THE IMPLEMENTATION OF WATER DEMAND MANAGEMENT (WDM) IN URBAN CENTRES IN ZAMBIA**

Daniel C.W. NKHUWA (School of Mines, University of Zambia)

Water is more than just a commodity but also an essential element that supports all forms of life. It is also basic to many socio-economic activities. In this regard, it is imperative to recognise its economic value in all policy and sector activities so that wise and efficient use of the resource is initiated and promoted in all sub-sectors, particularly in the large urban centres. However, the provision of adequate water supply and sanitation to the rapidly growing urban populations is increasingly becoming a problem for most cities and towns in Zambia. The continuing expansion of the numbers of people who need water and sanitation services and who cannot readily get the services by self provision continue to exert continuous pressure on either investment to create additional production capacity or to stretch the available supplies to serve more people. The predominant approach towards meeting these increasing water demands has been towards supply augmentation schemes. Undoubtedly, the cost of developing these new sources will get higher and higher as most accessible water, in terms of quality and quantity, has already been tapped. In places like Lusaka, the country's capital, where demand has outstripped demand, citizens have taken to indiscriminate drilling of boreholes. In places, this has caused aquifer over-abstraction, which has initiated lowering of the water table. If this trend persists, pumping charges may go up, thereby heightening the cost of supply. This may eventually affect the availability of water to the poor who may not be able to afford the new rates. It is in this regard that water demand management (WDM) becomes the preferred alternative in meeting increasing water demand in order to improve efficiency and sustainable use of water resources taking into account economic, social and environmental considerations. However, there are a number of constraints that have inhibited successful implementation of WDM. These include: • Inadequate knowledge by consumers and water utility staff of the socio-economic benefits of

implementing WDM Unfavourable pricing mechanisms Poor revenue collection rates, which have caused the water utility companies so severe financial constraints that they are unable to finance some of the routine operation and maintenance operations to the existing conveyance networks. Consideration of WDM as an inferior alternative to the construction and extension of new conveyance systems. Inadequate policy and legal frameworks, overlapping responsibilities among the water and sanitation sector institutions. Lack of clear sector policies, compatible legal framework, clear division of responsibilities and mandates, which has resulted in low priority assigned to operations and maintenance within the water sector. This paper will attempt to highlight what measures must be adopted to overcome these and other constraints to the implementation of WDM.

**HS02c/11P/D-026** Poster **1630-124**

**PRECIPITATION ENHANCEMENT OPERATION ALONG THE YELLOW RIVER IN WESTERN CHINA BY WEATHER MODIFICATION METHOD**

Xueliang GUO<sup>1</sup>, Meiyuan HUANG<sup>1</sup>, Tiezheng LI<sup>1</sup>, Junsheng ZHANG<sup>2</sup> (Institute of Atmospheric Physics, Chinese Academy of Sciences, <sup>2</sup>Yellow River Hydropower Co. of China)

This paper discussed the weather modification activities and their application to water resources management. The shortage of water supplies in the region along the Yellow River of western China has increased in recent years and is related to some decrease in annual precipitation, but mainly due to the increasing demand from the rapid growing population and industrialization in the region, which has seriously threaten the development of hydropower along the Yellow River. The precipitation enhancement activities have been conducted as an additional source of unconventional water supply for many years in the region. This work focused on clarifying the fundamental mechanism involved in precipitation enhancement by cloud seeding. We will introduce the climate condition that suitable for precipitation enhancement activities in the region as well as the efficacy of cloud seeding. In addition, a comparison study of cloud seeding was made with a current widely used seeding agent—silver iodide (AgI) and a newly developed seeding agent—liquid carbon dioxide (liquid CO<sub>2</sub>). Characteristics of cloud dynamics and microphysics and the interactions between them affected by the artificial seeding of AgI and liquid CO<sub>2</sub> are examined using a 3D stratocumulus cloud model with seeding processes. The model results show that the liquid CO<sub>2</sub> seeding in the region of high supercooled cloud water in the simulated cloud can generate shallow thermal convection and cause larger dynamic effect than that AgI seeding, and thus can significantly enhance surface precipitation. The seeded clouds by liquid CO<sub>2</sub> show two prominent increases in maximum updraft. The first increase is directly produced by liquid CO<sub>2</sub> seeding and the second is caused by downdraft outflow induced by falling precipitation in the boundary layer. The formed shallow thermal convection can produce many ice crystals. By the recirculation growth of these ice crystals transferred by the updraft of the thermal convection, they can consequently grow to precipitable particles such as snow and graupel.

**HS02c/11P/D-027** Poster **1630-125**

**WATER RESOURCE MANGEMENT IN THE UPPER REACH OF THE GORAI RIVER OF BANGLADESH**

Mohammad Monowar HOSSAIN, Mohammad Rashedul ISLAM (Department of Water Resources Engineering, Bangladesh University of Engg. & Technology)

Gorai river is the only distributaries of the river Ganges in Bangladesh. The Ganges is the second largest river in the Indian subcontinent. Gorai river is the prime source of freshwater to the South West Bangladesh, which covers an area of about 30% of area of the country. In recent times, the river was getting silted up at its mouth and for some distance downstream due to gradual decrease of the Ganges water. As a result very little water was available in the Gorai river during dry flow season. Tremendous environmental impacts were being felt in the Gorai dependent area due to this water shortage over the last few years. The Government undertook a program of dredging the Gorai for a distance of about 30 km from the mouth with a view to increasing the conveyance and attracting more flow in the river. The aim of this study is to examine the effectiveness of this dredging activity. The analysis has been conducted on the basis of dredge and post dredge observed bathymetry. The dredge bathymetry stands for the bathymetry measured immediately after the dredge and the post dredge bathymetry stands for the bathymetry after the passage of first year flood flows over the dredged Gorai. It is found from the analyses of these bathymetry that the normalized bed levels of the dredge bathymetry has been lowered all along the dredged Gorai while the bottom bed levels is found to have been raised. This implies that the pilot dredging has increased the high level conveying capacity of the Gorai while the low level conveying capacity has been decreased after the passage of first year flood flows over the dredged Gorai. Evidently this change in decreasing the low level conveying capacity of the dredged Gorai is due to the sedimentation in the deeper channel and therefore, the first year pilot dredging is not meaningfully effective in the sense of self-sustaining development for low flow augmentation. It is found that the bottom bed level of dredge channel has been raised close to the level of pre-dredge (post monsoon 1997) state after the passage of first year flood event over the dredged channel. Thus dredging may not be a sustainable means for management of water resources problems in the sediment-laden rivers of Bangladesh especially of the Gorai.

**HS02c/11P/D-028** Poster **1630-126**

**THE GENERAL PRINCIPLE FOR RESTORATION OF THE RIVER BASINS**

Boris FASHCHEVSKY<sup>1</sup>, Tatyana FASHCHEVSKAY<sup>2</sup> (International Sakharov Environmental University, <sup>2</sup>Ufa State Aircraft University)

The first step to restore any water body has to be the assessment of its ecological troubles on the scale "norm-pathology" here the criteria must be established determining the notions "the norm" and "the pathology". The main among such criteria are the following: First, these are indices of the basic hydrological characteristics: maximum and minimum discharges and levels of water, inside-year distribution of a river flow in different years of water capacity -5, 25, 50, 75, 95 % frequency and average annual discharges and levels of water, duration of floodplain flooding, temperature and ice regime, flow of sediments. Second, these are indices of water quality, characterized by major ions, oxygen and pH concentration, biogenic elements, organic matters and heavy metals. Third, the important criterion in assessment of a river state is the character of channel process development, which in the result of economic activity can be changed greatly in the terms of hydrography (slopes of rivers and basins, drainage density, tortuosity, area of swamping, area of lakes, area of forests, area of ploughed lands, area of urban, etc) and morphology (increase and decrease of depths, narrow or widening of channels, damming of floodplains, extraction of building materials from channels, dredging of waterways, etc) of rivers and their basins. Fourth and often (but not always) a main and completing component is a biotic one of the river ecosystem, the influence by the first three components and includes: bacteria and viruses, alga and higher aquatic plants, invertebrates, fishes, amphibia and aquatic reptiles, waterfowl and semi-aquatic birds, aquatic and semi-aquatic mammals. As the "norm" of a river ecosystem is its state before the beginning of a human activity in this basin or the state

of the river-analogue that are situated in analogous natural conditions but untouched by a human activity must be accepted. All above-mentioned hydrological, hydrochemical, hydrographical, morphological and biotic components have to be accepted for the norm and recalculated for a restored basin in a special way. The restoration of a river basin can be produced: 1. Totally on all regime elements and bioproductivity of aquatic and semi-aquatic plants and animals. 2. Partially, only for the separate elements of regime and separate components of biotic ones. For example, restoration of only migratory fish, ignoring the phytophilous species, which need an obligatory flooding of floodplain. 3. Artificial creation of a new ecosystem in a given river system by the way of introduction and acclimatization new species of plants and animals which have never occurred in a given river but if there are favorable conditions for reproduction these species. The experience of such developments has obtained a wide dissemination in the world, including Japan, China, Australia, Chile, Norway, France, Russia and others countries.

**HS02c/11P/D-029** Poster **1630-127**

#### MAÎRISE ET CONFLITS LIÉS À LA GESTION DES RESSOURCES EN EAU DANS LA BASSE VALLÉE ET LE DELTA DU FLEUVE SÉNÉGAL

Alioune KANE (département de geography/ Faculty of Arts and Human Sciences/ University Cheikh Anta Diop)

L'intérêt porté à ces milieux de la zone tropicale sèche, caractérisés par l'extrême fragilité de leur équilibre écologique, se justifie par la demande en eau pressante d'une population en forte croissance, les saisons climatiques contrastées avec une irrégularité pluviométrique marquée, imposant des contraintes sévères à l'environnement et un caractère aléatoire à cette ressource dont l'exploitation traditionnelle était très souvent rythmée par le régime hydrologique du fleuve. Depuis deux à trois décennies, de grands programmes d'aménagements hydro-agricoles ont été développés. Les barrages de Diama et de Manantali, ont complètement artificialisé le régime hydrologique du Sénégal, permis le desserrement de la contrainte de mobilisation de la ressource en eau, le fonctionnement du système est désormais tributaire de la pluviométrie dans le haut bassin et du mode de gestion. Ces programmes se traduisent par des modifications radicales du fonctionnement hydrologique naturel et des transformations très importantes affectent l'environnement. Ces bouleversements peuvent prendre un caractère particulièrement grave, notamment lorsqu'ils se conjuguent à des modifications climatiques qui fragilisent encore un milieu sensible du fait de sa position en bordure du Sahara. Souvent ces programmes d'aménagement des bassins versants ont mal évalué les impacts écologiques et sociaux, engendrant des dysfonctionnements dans les rapports homme-nature, et compromettant l'instauration d'un développement durable. La maîtrise hydraulique est imparfaite, les parcelles sont souvent mal planées. La qualité des eaux de drainage est une préoccupation majeure, la capacité du réseau s'est avérée limitée et insuffisante pour assurer une bonne vidange. Les déversements d'eaux de drainage ne sont plus acceptables, le degré de toxicité de ces eaux et les volumes en jeu ne sont pas connus. La maîtrise des eaux et le développement de la riziculture ont mis en contact les populations avec l'eau douce stagnante et différents vecteurs de maladies. Le grand effet purgatif dû à l'invasion des eaux marines a disparu, les risques d'aggravation des maladies se sont multipliés. La prolifération de la végétation aquatique se pose. La construction des grands barrages ayant pour but d'atteindre l'autosuffisance alimentaire, se révèle mal maîtrisée. Les efforts de modernisation agricole ont porté sur une conquête de l'espace et un développement de la riziculture irriguée. Des modifications du milieu résultent de la création des aménagements hydro-agricoles et des réserves d'eau douce, avec une recomposition d'une société paysanne multiforme, sans aucune technicité ni moyens financiers appropriés, les éleveurs peul sont les grands perdants. Le partage des ressources en eau est un problème difficile entre états riverains aux intérêts divergents avec la revitalisation des vallées fossiles du Sénégal. La vallée du Sénégal n'est pas une région d'irrigation traditionnelle. Les dysfonctionnements notés au plan de l'environnement, hypothèquent lourdement l'avenir des aménagements.

**HS02c/11P/D-030** Poster **1630-128**

#### RAINWATER MANAGEMENT TECHNOLOGY FOR CONJUNCTIVE USE IN ARID REGION, INDIA

M. A. KHAN (Central Arid Zone Research Institute)

In Indian arid zone of Rajasthan and elsewhere several kind of rainwater harvesting structures have been in vogue since many centuries. At field level runoff has been collected in natural depressions or in dug-out structures such as ponds, tankas, and khadins. Till recently local wisdom, experiences and precedences guided the designing of such structures. However, for better storage, conservation and judicious use, CAZRI, Jodhpur provides details of design. Seepage proofing in ponds was found necessary in sandy soils where percolation rates are high. In western Rajasthan, dug-out ponds locally known as Nadi and tanka are used mainly for domestic water use and economically not viable option for surface irrigation. However, if recycling of rainwater primarily links more profitable cash yielding crops or tree component, potential water storage in these structures is likely to become highly attractive. Recently, tankas have been constructed on large scale in western Rajasthan for developing fruit orchards. Response of ber (*Ziziphus nummularia*) and pomegranate to supplemental irrigation from tanka was studied (1995-97) on a loamy soil at Jodhpur. Compared to control (no irrigation) increase in fruit yield with 2, 4 and 6 irrigation for ber was 46.4%, 80.3% and 124%, whereas in the case of pomegranate it was 69.8%, 112.5% and 191.7%, respectively. Tankas have also been found useful in raising forest nurseries and establishment of trees in watershed. Khadin is an other method of water resources development, conservation and utilisation for crop production even in very low rainfall 150-300 mm. Rocky catchments with adjoining valley-filled lands are converted in khadin farm by constructing earthen embankment at lower periphery of field with suitable spillway arrangement. The system is very popular in hyper arid region of Rajasthan. Due to low rainfall, the catchment to command ratio is rather high ranging from 8 to 15. On khadin farms, even without agronomical practices and with no application of fertilizer the average of yield ranges from 20-30 q ha<sup>-1</sup>. Anicut, percolation tanks and sub-surface barrier are very effective water harvesting and recharge techniques to improve ground resources in depleted aquifers. With the construction of anicut in Ujalian watershed in Jodhpur district, the annual increase in static water level in wells located in the zone of influence ranges from 1.8 to 2.2 m as compared to wells located in the adjoining area. In Pali district, due to the presence of anicut groundwater recharge has increased from 5.2 to 38.5%. Percolation tanks for inducing recharge is being practiced in parts of India. The average rate of percolation from percolation tanks constructed in different geological formation ranges from 10 to 72 mm day<sup>-1</sup>. Similarly with the construction of sub-surface barrier across an ephemeral stream at Chauhi-kalan in Jodhpur district, the rate of depletion has been reduced from 1.2 m year<sup>-1</sup> to 0.3 m year<sup>-1</sup>, and water yield has increased from 60 m<sup>3</sup>year<sup>-1</sup> to 125 m<sup>3</sup> year<sup>-1</sup>. With the increased ground resources, over 15 ha area has been brought under well irrigation.

**HS02c/11P/D-031** Poster **1630-129**

#### DECISION-SUPPORT INFORMATION FOR WATERSHED MANAGEMENT OVER DROUGHT PRONE REGION

Nagarajan Ramakrishnan IYER (Center of Studies in Resources Engineering, Indian institute of Technology, Bombay)

An effective mitigation activity during drought situations offer support to the people, in carrying out their regular activities, without much stress on their existing water and food (if necessary) availability. Continuous monitoring of spatial and dynamic land resources and the vulnerable groups is important. Integrated analysis of rainfall, run-off and surface storage facilities and creation of demand and supply scenario during the summer months would help the water regulation planning. It is observed that some of the un-preparedness situation of the government agencies is mainly due to the lack of dynamic input into their preparedness planning. The individual subject experts broadly use deficit of rainfall amount, water supply, crop production and reduced purchase power in identifying a drought area. Even though meteorological drought is considered as the initiation of drought situation over an area, followed by deficit of water supply and crop production. A multi-criteria approach is warranted. An attempt has been made in the creation of drought intensity scenario (demand and supply approach) for group of settlements located in a watershed located in the semi-arid region using integrated analysis of static and dynamic information. This study has adopted a methodology based on the rainfall and water requirement, in aiding the crisis situation and sustainable planning at local level. Time series analysis of annual rainfall of 100 years was used in identifying critical period. The inter-rainfall gap analysis was carried on 10 years of daily rainfall. Based on these results and the reported physical situation, a threshold of annual rainfall (below which scarcity begins) was established. Surface run-off was calculated using SCS method and the surface cover information changes were collected from the orbital India remote sensing satellite data. The water spread of the irrigation tanks was demarcated and used in the water availability estimation. Ground water level fluctuation information was collected and used in establishing relationship with rainfall over the years. Crop area and type and their inter-seasonal (winter/summer) and annual changes were deciphered from temporal satellite Revenue village Information on the human / animal population, crop type and area, water resources availability (ground water & surface water), natural vegetation cover, rainfall and temperature information, etc., were collected from the existing revenue records and updated from the interpretation of temporal IRS data. The demand from the crops (including the evapo-transpiration and transmission loss) and the settlements (human and animal) was calculated for individual settlement/villages. The supply position of the watershed by way of surface run-off and storage and their losses over seasons was estimated for a given rainfall event. A drought scenario situation for Jhod nadi watershed, tributary of Godavari River, located in Nanded District of Maharashtra, India, with an area of 196 km<sup>2</sup> was created. Probable drought severity of the settlements (about 40) was grouped in low to very High depending on their deficit percentage of demand-supply. An effective method for regular monitoring and preparedness is discussed in the paper.

**HS02c/11P/D-032** Poster **1630-130**

#### USE OF GEOGRAPHIC INFORMATION AND REMOTELY SENSED DATA IN THE DECISION-MAKING SUPPORT SYSTEM FOR FLOOD MANAGEMENT IN ROMANIA

Corina PREDESCU, Gheorghe STANCALIE, Elena SAVIN (Remote Sensing and GIS Laboratory, INMH)

Floodings are an important risk in many areas around the globe and especially in Romania. In the latest years floodings occurred quite frequently in Romania, some of which isolated, others were affecting wide areas of the country's territory. The paper presents the elaboration of the cartographical documents on the flood risk regions over a pilot watershed and the development of the GIS applications with a decision system for the crises management. A modern approach is used for the flooding risk indices estimation. These indices are associated to the physico-geographical, morpho-hydrographical and vulnerability characteristics of a region. The methodology was elaborated to determine the flooding risk, using risk indices at a scale compatible with a synthetic representation of the territory. There are stressed the facilities supplied by the Geographic Information System (GIS) and the remotely sensed data to manage flooding during their characteristic phases: before, during and after flooding. Accent is laid on the pre and post-crisis phases. An important research topic was the study of the parameters that can be extracted from satellite images in view of organizing a hierarchy of the geographical space versus the flooding risk. Information obtained from satellite images proved to be useful for the determination of certain parameters necessary to monitor flooding: hydrographic network, water accumulation, size of floodable surface, land impermeability degree, water absorption capacity over the basin surface, or resilience to in-soil water infiltration. The study encompassed both the risk degree levels related with various parameters, which influence and determine floodings and which takes into consideration the human presence in the sensitive areas. The application was developed for the Arges hydrographic basin in Romania, a critical area, keeping in mind that it withholds many localities, including the capital and also important economic centers. Advantages offered by this integrated system are: to manipulate and make available large databases, to easily update the information, to survey the temporary modifications, to establish the link between the measured/forecasted data and the GIS database. The database allows obtaining synthetic representations of the hydrologic risk for the Arges basin, through separate or combined use of the risk parameters as well as for interfacing with the hydrological models in view to improve them as regards recovering results and the possibility to achieve scenarios.

**HS02c/11P/D-033** Poster **1630-131**

#### VELOCITY DISTRIBUTION DUE TO LAUNCHING APRON AROUND ABUTMENT

Mohammad Monowar HOSSAIN, Mohammad Salzar HOSSAIN, Mohammad Faheem SADEQUE (Department of Water Resources Engineering, BUET)

Velocity distributions were measured in a small-scale riverbed model for vertical wall abutment constructed at the Hydraulics and River Engineering Laboratory of Bangladesh University of Engineering and Technology (BUET). A series of test run were conducted for five different apron-setting configurations and velocities were measured using a programmable 2-D electromagnetic liquid velocity meter. Comparison of velocity distribution in terms of velocity vectors with and without apron was made. It was observed that considerable displacement of velocity vectors occur due to different apron setting. Due to displacement of velocity vector, the scour depth was found to be affected significantly. Vertical velocity distribution at the maximum scour hole formed due to apron setting was also measured. The result obtained gives an indication of use of falling apron for protection of vertical abutment against failure due to scour.

**HS02c/11P/D-034** Poster **1630-132**

**URGENT WATER SUPPLY INTO ZHALONG WETLAND IN 2001 AND 2002**

Shiguo XU<sup>1</sup>, Lianwen DANG<sup>2</sup>, Heyue LF (Department of Civil Engineering, Dalian University of Technology, Songliao Water Resources Commission)

Nen River basin is located in northeast of China, where belongs to monsoon precipitation zones. There usually are short summers and long winters with spring draught and summer floods. Around lower reaches of Nen River, there exist many big wetlands, such as Zhalong, Xianghai and Momoge wetlands. Zhalong wetland is the biggest one with the area of 2100km<sup>2</sup>, 468 species of vegetations and 236 species of birds belonging to 48 families. The main protected bird is Red Crown Crane. It is one of 7 wetlands earliest accepted by Ramsar convention in China. Water is very important for wetland evolution. As the water resource development is gradually actualized on the upstream of rivers that flow into Zhalong wetland, water shortage problem has endangered the wetland ecological environment. Farther more, after the big flood in 1998, Nen River basin faced a four-year long draught series. At the begin of 2001, the area of water surface in Zhalong wetland was only 130km<sup>2</sup>, much less than the average area 800km<sup>2</sup> and that in common dry year 300-400km<sup>2</sup>. The most part of the wetland draught up. Reeds couldn't grow up as usual. A lot of reed wetland became into grass wetland and the vegetal state degrades very seriously. It threatens the habitation condition of Red Crown Cranes that make their nests and hatch small cranes in every earlier summer here. So as to maintain the condition to keep basic function of the wetland, an urgent water supply project from Nen River to Zhalong wetland is put into practice. In the later autumn of 2001, supplied 35×106 m<sup>3</sup> of water into the wetland, and from the spring to summer of 2002, 300×106 m<sup>3</sup> again. According to the investigation on site, water supply has achieved satisfactory results. In the end of April, the supplied water pours over the central area of the wetland. By recovering the ecologic condition of reed and fish, it helps Cranes and birds very much. This urgent water supply program provided a useful experience to rescue wetlands from a water shortage disaster. In the same time, an especial water resources plan of Zhalong wetland is under working to guarantee the water supply safety of it for a long term. A key project supported by National Natural Science Foundation of China is also come to operation, which studies the problems concerned with using floodwater to restore wetlands and using wetland to make floodwater a useful water resources.

**HS03**

**Monday, July 7 - Tuesday, July 8**

**WEATHER RADAR INFORMATION AND DISTRIBUTED HYDROLOGICAL MODELING (ICSW)**

Location: Site C, Room 26

**Monday, July 7 AM**

Presiding Chair: B.E. Vieux

**ASSESSMENT OF UNCERTAINTY IN DISTRIBUTED HYDROLOGICAL MODELING**

**HS03/07A/C26-001** Invited **0900**

**A METHODOLOGY FOR ASSESSING THE UTILITY OF DISTRIBUTED MODEL FORECAST APPLICATIONS IN AN OPERATIONAL ENVIRONMENT**

Konstantine P. GEORGAKAKOS, Theresa M. CARPENTER (HYDROLOGIC RESEARCH CENTER)

Modern day deployment of weather radars in the US and abroad, and the availability of high-resolution distributed digital spatial databases have accelerated the development of a variety of new hydrologic models with distributed parameters and input. These models range from process-based to statistical and from time-continuous to event based. Distributed models have long been viewed as beneficial for hydrologic forecasting. However, errors in the precipitation data and model parameters may diminish any gains in prediction accuracy realized by accounting for the spatial variation of precipitation and parameters. Application of these models for the purposes of reliable flow simulation using observed spatially distributed precipitation data requires the resolution of the issue of balancing model complexity (as measured for example by the requirements for parameter estimation) with distributed-input uncertainty. The present paper exemplifies a probabilistic methodology to address this issue. A distributed model with components used in the operational forecasting of streamflow in the US is utilized to produce flow predictions for a typical catchment in a semi arid environment (Blue River in Oklahoma, USA). Models of uncertainty for input data and model parameters are identified, the latter based on consistent calibration procedures. Ensemble flow forecasts are produced at the outlet of the catchment for a number of forcing and parameter uncertainty scenarios and for a high and low spatial resolution model configuration. Kolmogorov-Smirnov test analysis is then performed to assess whether the results of the low and high resolution models can be distinguished at a given confidence level. Assessments of the implications regarding accuracy under operational forecast conditions are given.

**HS03/07A/C26-002** **0930**

**PROPAGATION OF PRECIPITATION UNCERTAINTY THROUGH FLOOD FORECASTING MODEL**

SHREEDHAR MASKEY<sup>1</sup>, VINCENT GUINOT<sup>2</sup>, ROLAND K. PRICE<sup>1</sup> (1)HE-Delft, PO Box 3015, 2601 DA, Delft, Netherlands, (2)Universite Montpellier 2, Maison des Sciences de l'Eau, 34095 Montpellier Cedex 5, France)

Over the last decade significant progresses have been made in quantitative forecast of precipitation by the use of sophisticated radar technology. The imprecision in the forecast precipitation however remains one of the major sources of uncertainty in real time flood forecasting. The uncertainty in the forecast precipitation generally comprises of (i) the imprecision in the quantity of forecast precipitation (P<sub>q</sub>), (ii) the imprecision in the temporal distribution of the precipitation over the forecast horizon (P<sub>t</sub>), and (iii) the imprecision in the spatial distribution of the precipitation over the watershed (P<sub>s</sub>). This paper presents a methodology for the propagation of precipitation uncertainty (P<sub>q</sub>, P<sub>t</sub> and P<sub>s</sub>) through a real time flood forecasting model. The imprecision P<sub>t</sub> is represented by assuming a 3-valued forecast precipitation (minimum, most credible and maximum) for the period of a forecast horizon. A typical triangular fuzzy membership function is constructed based on the 3-valued forecast. A number of precipitation patterns are considered representing the possible distributions of each forecast precipitation over the forecast horizon and over the sub-basins. This is meant to treat the uncertainty due to P<sub>t</sub> and P<sub>s</sub>. The uncertainty in the forecast flood

due to the uncertainty in the forecast precipitation is computed applying the extension principle of the fuzzy set theory assisted by a genetic algorithm (GA). The idea here is basically to search for the maximum and minimum possible model-simulated floods for the given range of forecast precipitation and for the given possible precipitation patterns distributed both in time and space. The methodology was applied to a watershed model for flood forecasting that was developed using the HEC-1 software. The result of the analysis comprises of a band of minimum and maximum flood values associated with the forecasted flood. This is analogous to the confidence intervals in the probability theory-based uncertainty analysis. The method also provides a fuzzy membership function of each forecasted flood. The result shows good potential of this method for modelling precipitation uncertainty in flood forecasting models.

**HS03/07A/C26-003** **0945**

**COMBINING PHYSICALLY BASED AND CONCEPTUAL APPROACHES IN THE DEVELOPMENT AND PARAMETERIZATION OF A DISTRIBUTED SYSTEM**

Victor I. KOREN, Seann REED, Michael SMITH, Ziya ZHANG (Department of Commerce, NOAA/NWS/OHD)

Gridded precipitation estimates from a radar-gage analysis (NEXRAD) are now available for operational use by the National Weather Service (NWS) of the United States. While these estimates provide high temporal and spatial resolution data, it is not clear how the NWS can most effectively utilize these data to improve its river forecasts. One possibility is to incorporate high resolution NEXRAD precipitation into an existing lumped modeling framework. Two such approaches were tested: use of dynamical distribution functions of precipitation in addition to a basin average rainfall, and downscaling a rainfall-runoff model to capture the spatial pattern of rainfall. The tests suggested that while these approaches have potential in capturing the spatial variability of precipitation, they failed to improve upon 'basic' lumped simulations consistently. At the same time, they increased requirements on parameterization procedures. Another possibility, use of fully distributed physically based models, is also not as strait forward. Most distributed models are based on point process equations, and their spatially variable parameters are less identifiable from hydrograph analysis because they represent local properties. Recently, the Hydrology Laboratory of the NWS has developed a grid-based Research Modeling System (HL-RMS) that combines lumped conceptual and distributed model features. The HL-RMS consists of a conceptual water balance model (well tested over wide range of basins and climates) applied on a regular spatial grid and physically based kinematic hillslope and channel routing models. GIS-based algorithms are used to derive grid connectivity, overland and channel slopes from a digital elevation model. Experience with lumped and distributed models suggests that practical benefit from any rainfall-runoff model depends significantly on the availability of advanced parameter estimation procedures. Such a procedure is being developed for the HL-RMS. The procedure is based on combined analyses of distributed basin properties and the integrated basin response at the outlet. Initial (a priori) water balance model parameter grids are generated using high resolution soil-vegetation data. Uniform adjustment of a priori parameter grids is performed using results of lumped calibration at selected outlets. To remove scale effects, further fine tuning is achieved comparing simulated and observed hydrographs by a trial-and-error process. Spatially variable channel routing parameters are estimated from discharge measurement information at the basin outlet and geomorphological properties at each grid cell. HL-RMS tests have been conducted for a few headwater basins which have hourly NEXRAD precipitation estimates for nine years with a 4x4 km resolution. The tests showed that while the HL-RMS yields results comparable to well calibrated lumped model simulations, it outperforms a lumped model over basins where the effect of rainfall variability is significant. Combining outlet information and spatially variable basin properties provides a reliable procedure to estimate distributed model parameters. While uniform adjustment of water balance model parameters provides reasonable results at basin outlets, the problem of removing scale effects in nested basins is still a challenge.

**HS03/07A/C26-004** **1000**

**IMPROVING A PRIORI ESTIMATES OF HYDRAULIC PARAMETERS IN A DISTRIBUTED ROUTING MODEL VIA VARIATIONAL ASSIMILATION OF LONG-TERM STREAMFLOW DATA**

Dong-Jun SEO, Victor KOREN, Seann REED (Hydrology Laboratory, National Weather Service)

Due to the typically very large dimensionality of the problem, exhaustive estimation of distributed parameters in hydraulic routing models is highly impractical (if not infeasible). For this reason, much attention has been given in recent years to improving, with the aid of GIS, estimation of a priori distributed parameters from all available spatial data sources. Such a priori estimates of distributed routing parameters, however, are subject to various sources of error, and hence may not necessarily be dynamically consistent in the hydraulic sense. The purpose of this work is to develop a procedure for systematic improvement, or refinement, of a priori distributed hydraulic parameters in a kinematic wave routing model via variational assimilation (VAR) of long-term streamflow observations. Conceptually, the task amounts to solving a distributed inverse problem of downscaling the sensitivity of the streamflow observations to hydraulic parameters from the basin scale (O(1,000 sq km)) to the model grid scale (O(10 sq km)) through the distributed routing model of choice. Calculation of the gradient (i.e., the sensitivity of the streamflow to some parameter at some grid) for the least squares minimization is obtained from the adjoint of the distributed kinematic wave routing model of the National Weather Service Hydrology Laboratory's (NWS/HL) Research Modeling System (RMS). To evaluate the marginal value of parameter improvement, the baseline distributed model in RMS consisting of a gridded Sacramento soil moisture accounting model with kinematic hillslope and channel routing is run with the a priori and the refined routing parameters for selected basins used in the Distributed Model Intercomparison Project (DMIP). The results are presented and the issues are described.

**HS03/07A/C26-005** **1015**

**DISTRIBUTED MODEL FLOW SENSITIVITY TO UNCERTAINTY IN RADAR RAINFALL INPUT**

Theresa M. CARPENTER, Konstantine P. GEORGAKAKOS (HYDROLOGIC RESEARCH CENTER)

The high spatial and temporal resolution of precipitation estimates afforded by weather radar has lead to increased research on distributed hydrologic models that can utilize these radar precipitation estimates, along with other high-resolution, spatial data on terrain, land use, land cover, and soil characteristics. HRCDDHM is a catchment-based, distributed model that ingests radar precipitation estimates from the U.S. National Weather Service's WSR-88D radar and produces runoff and channel flow estimates for sub-catchments of a watershed of interest. The sub-catchments are delineated through GIS-processing of digital terrain and land use/land cover databases. The focus in the development of HRCDDHM is on distributed hydrologic modeling suitable for use in an operational flow-forecasting environment. Thus, HRCDDHM assumes operationally available input databases and includes components based

on operational hydrologic models. The aim of the current research is to assess the sensitivity of flow simulations produced by the distributed model under various definitions of uncertainty in the radar rainfall estimates. The distributed model is applied to several watersheds in the Midwestern United States. Generally, the basins are mildly sloping, with silty-loam soils, and range in contributing drainage area from 1,000 to 2,500 km<sup>2</sup>. The catchment delineation yielded sub-catchments with average sizes on the order of 60-80km<sup>2</sup>. Hydrologic model parameters were calibrated based on uniform distribution of parameters within each watershed and with distributed rainfall input. This yielded good agreement with observed flow records, with cross-correlation of hourly flow on the order of 85% and small bias. Available soils databases were then used to distribute hydrologic model parameters with each watershed based on average soil properties such as available water content and permeability. Thus, the distributed model was applied with both distributed precipitation forcing and distributed hydrologic model parameters. The resulting variation of parameters across the study watersheds was not great, and the flow simulations with distributed parameters were similar to those with uniform parameters. A Monte Carlo simulation framework was used to examine the sensitivity of the flows produced by the distributed model to uncertainty in the radar rainfall estimates. For each watershed, various historical events were selected and modeled with 100 Monte Carlo simulation runs for each event and for various definitions of radar-rainfall uncertainty (uniform, exponential and radar-pixel scale). The variation in the resulting flow simulations were summarized in terms of the maximum range of simulated flow for several watershed locations including interior locations and the watershed outlet. These results consistently show scale-dependence in the flow prediction uncertainty for a given radar rainfall uncertainty definition.

**HS03/07A/C26-006****1045****DISTRIBUTED HYDROLOGICAL MODELING IN THE YATA WATERSHED USING THE WEP MODEL AND PROPAGATION OF RAINFALL ESTIMATION ERROR**

Yangwen JIA, Tsuyoshi KINOCHI, Junichi YOSHITANI (Hydrologic Engineering Team, Hydraulic Engineering Research Group, Public Works Research Institute)

Distributed hydrological modeling is highly required for hydrological prediction in watersheds with heterogeneous land surfaces, soils and aquifers under uneven distribution conditions of rainfall. A robust distributed hydrological model should be applicable to both long-term prediction of water budgets and short-term prediction of flood with satisfied accuracy. In this study, the WEP (Water and Energy Transfer Processes) model is applied to simulate the hydrological changes in the Yata watershed in the past 25 years (1976-2001) and the impact of rainfall estimation error and rainfall spatial distribution on river discharge prediction is also evaluated. The Yata watershed is located in the northwest of Ibaraki prefecture, Japan, and has an area of 166km<sup>2</sup> of which agricultural landuse and forest accounts for about 70%. Urbanization in the watershed started in 1970's with the development of the Tsukuba city, and now as a part of a new railway development plan, 5 regions with a total area of 13km<sup>2</sup> are scheduled for various kind of urban development. Though several institutions had ever carried out some field investigations of groundwater and river discharges in the watershed in 1970's, PWRI and the local government began to monitor water and heat fluxes, river discharges and groundwater levels in 1999 and periodically carry out field investigations of river water and groundwater quality. In comparison with the observed results of 1970's, it is found that the river peak discharges become bigger and the groundwater levels become a few meters lower. The WEP model is first validated using the observation data in 2000 and 2001 and then applied to the long-term simulation from 1976 to 2001 in a time step of 1 hour and a grid cell size of 100m. The simulation results have good matching with the observation ones in both low river flow and flood peaks. The simulation results also show the same trend of groundwater level changes with that of the observed results. The sensitivity analysis of soil hydraulic conductivity and time step of flow routing is also conducted. It is found that the time step of 10 minutes for flood routing of river flow and overland flow can give satisfied results in the watershed. Finally, the impact of rainfall estimation error and rainfall spatial distribution on river discharge prediction is also studied. The simulation shows that during typhoon seasons, spatial distribution of rainfall has a great impact on river discharge prediction in the watershed because of its unevenness even at sites a few kilometers away.

**HS03/07A/C26-007****1100****THE EFFECTS OF RADAR-DERIVED RAINFALL UNCERTAINTIES ON FORECASTS FROM A DISTRIBUTED HYDROLOGIC MODEL**

Jonathan J. GOURLEY<sup>1</sup>, Baxter E. VIEUX<sup>2</sup> (<sup>1</sup>National Severe Storms Laboratory, Univ. of Oklahoma, <sup>2</sup>Univ. of Oklahoma)

The advent of weather radar has provided the potential to estimate rainfall accurately at high spatial and temporal resolutions. When these estimates are input to a distributed hydrologic model, forecasts of stream flow may be used to anticipate and thus mitigate the potential hazards associated with a flash flood. In hydrologic modeling, forecast uncertainties have traditionally been a function of the uncertainty in the model parameters, and in some cases the model structure. The study presented here uses a physics-based, distributed hydrologic model (that is based on the University of Oklahoma's *r.water.fea* model with modifications) to address the impact of uncertainties in the input rainfall estimates on stream flow predictions. Specifically, extension of the Generalized Likelihood Uncertainty Estimation methodology allows us 1) to assess prediction uncertainties by including uncertainties in the rainfall estimates and 2) to evaluate the accuracy of different rainfall algorithms independently at the scale of an integrating watershed. The study plan and some initial results will be presented for several events in the U.S.

**HS03/07A/C26-008****1115****REAL-TIME ASSIMILATION OF RADAR-BASED PRECIPITATION DATA AND STREAMFLOW OBSERVATIONS INTO A DISTRIBUTED HYDROLOGIC MODEL**

DONG-JUN SEO, Victor KOREN, Neftali CAJINA (Hydrology Laboratory, National Weather Service)

Along with the uncertainty in Quantitative Precipitation Forecast (QPF), the uncertainties in Quantitative Precipitation Estimate (QPE) and in soil moisture states represent arguably the biggest source of error in real-time hydrologic prediction. To reduce the uncertainty in the soil moisture states, much attention has been given in recent years to state-updating techniques that assimilate streamflow observations in real time. Though a number of such techniques appear in the literature in the context of lumped modeling, it is not clear whether the applicability extends to situations of significant biases in radar-based QPE and to distributed models. The purpose of this work is to explore real-time assimilation of radar-based QPE and streamflow observations into a distributed hydrologic model using variational assimilation (VAR) techniques. Experience with VAR in a lumped setting indicates that, being a primitive non-recursive filter (compared to, e.g., Kalman filter), VAR is well-suited for assimilation of QPE that is subject to significant biases, and offers much insight into the formulation and parameterization of the assimilation procedure (be it VAR or Kalman filter). The VAR formulation in this work solves the inverse problem of perturbing the grid-specific initial model soil moisture states and the grid-specific QPE over the time window

commensurate to the basin response time, based on the real-time streamflow observations. The hydrologic model is the gridded application of the Sacramento soil moisture accounting model in the National Weather Service Hydrology Laboratory's (NWS/HL) Research Modeling System (RMS). To evaluate the technique, VAR-aided forecasts (under clairvoyant QPF) are compared with raw forecasts for selected basins used in the Distributed Model Intercomparison Project (DMIP). The results are presented and the issues are described.

**HS03/07A/C26-009****1130****IMPACT OF ONLINE CALIBRATION OF RADAR-MEASURED RAINFALL IN HYDROLOGICAL FORECASTING USING DISTRIBUTED HYDROLOGICAL MODEL**

Minjiao LU<sup>1</sup>, Norio HAYAKAWA<sup>2</sup> (<sup>1</sup>Dept. of Civil and Environ. Eng. Michigan State University, <sup>2</sup>Nagaoka University of Technology)

In order to find a more effective way to use both gauge-measured and radar-measured rainfall data in hydrological forecasting, a runoff analysis using a distributed hydrological model is carried out over Uono River basin (355 square kilometers), a tributary of Shinano River, the longest in Japan. In order to take into account the spatially distributed information on rainfall and hilly topography of the study basin, a distributed hydrological model is constructed by using our distributed hydrological modeling system. This model computes runoff generated in all grid cells, 100x100m square areas from rainfall data using XinAnJiang model, and routes the runoff from all grid cells to the basin outlet through a channel network delineated from a DEM (Digital Elevation Model). Calculated hydrographs can be derived at all interested grid points, central points of grid cells near by the hydrological stations. Before running the distributed model, the rainfall data derived by using operational radar constants are compared with rainfall data from rain gauges. It's shown that both point rainfall and the basin average rainfall from radar-measured rainfall data are over-estimated. This may be caused by radar constants determined improperly at logarithmic scale. In order to correctly consider the water budget over the basin, we determine the radar constants at normal scale using non-linear optimization. However, these constants are not always the best. The radar constants vary largely from storm to storm in all 16 selected heavy storms, and even vary largely during a storm. An algorithm is developed to make online calibration of radar-measured rainfall data by using gauge-measured rainfall data. The impact of this online calibration is investigated by using above distributed hydrological model. It is shown that online calibration can combine low-accuracy and high-density radar-measured rainfall and high-accuracy and low-density gauge-measured rainfall well and improve the accuracy of hydrological forecasting.

**HS03/07A/C26-010****1145****A NEW COMPOSITE APPROACH OF PHYSICAL AND GEOSTATISTICAL ASPECTS TO GROUNDWATER MODELING**

Toshio HAMAGUCHI (Disaster Prevention Research Institute, Kyoto University)

A new groundwater model in conjunction with spatial uncertainty is proposed in this paper. Modeling errors, which is typically included in spatial uncertainty components, cannot be completely covered by physical modeling in details. Geostatistical approaches using trend and random functions in space-time are founded on deterministic and stochastic models. Most of trend functions are, in general, represented as just a deterministic form based on the corresponding and well-known physical law, whereas a new additional component of uncertainty such as a geostatistical bias of a so-called "drift" is introduced in this approach. It consists of a constant in space but changes with the lapse of time. A random function at each time is indirectly described through a stochastic form of an appropriate error covariance model with spatial uncertainty. For the sake of the best agreement with actual behavior by physical modeling, parameter identification with high accuracy is needed. A highly efficient scheme for numerically solving inverse problems, the extended Kalman filter-FEM, is herein employed. This tool filters out uncertainty components as a set of system noises by using observed data. It can easily identify the most likelihood model that is represented by a set of the equivalent uniform materials in zones even though the true structure gets unknown. Attempts to estimate model parameters of permeabilities are numerically tested in some hypothetical aquifers, which are designed to allow testing various aspects of the modeling problem. The true and hypothetical aquifers of interest are subdivided into two, four and twenty constant-permeability zones, respectively. Convergence on the inverse solution can be achieved with high accuracy. The changes in the water levels to be calibrated are assessed in the several cases based on permeability zonation. The model errors at observed points are then obtained with uncertainty. It is now assumed that they have a geostatistical structure with a spatial bias. Their geostatistical distribution is mapped by a constant drift and the error covariance function, which is chosen a sphere type in this work. As mentioned above, the proposed method to eliminate modeling errors is demonstrated through all of the case studies. The greater effectiveness of the geostatistical bias in this work can be seen from a reciprocal of the absolute coefficient of variation in transition. The dependent relationship of such coefficients to a drift is investigated from their transient reciprocal, which gets larger in strongly depending on the drift term for the statistical model and becomes smaller in weakly depending on that. Finally all the results to be discussed can be then shown that the composite estimates are reasonable and successfully in best agreement with the true ones.

Monday, July 7 PM  
Presiding Chair: E. Nakakita

**WEATHER RADAR INFORMATION FOR HYDROLOGICAL PREDICTION****HS03/07P/C26-001****1400****EFFECT OF RADAR BEAM GEOMETRY ON RADAR RAINFALL ESTIMATION**

Siriluk CHUMCHEAN<sup>1</sup>, Alan SEED<sup>2</sup>, Ashish SHARMA<sup>1</sup> (<sup>1</sup>School of Civil and Environmental Engineering, The University of New South Wales, <sup>2</sup>Bureau of Meteorology and CRC for Catchment Hydrology)

The frequency, accuracy and resolution of hydrologic records is a major limitation in the accurate modelling of hydrologic events. The weather radar provides real-time spatially continuous measurements covering a large area at short time intervals. However, considerable uncertainty still remains in the procedures used to estimate the rainfall from weather radar observations. This uncertainty may be caused by the variability of raindrop size distribution, the variation of reflectivity with height and with range and the temporal and spatial resolutions adopted for sampling the radar reflectivity. This paper accounts for the effect of the radar beam geometry as a function of distance. The conical shape of the radar beam causes the observed volume to increase with range from the radar, leading to both bias and an increase in the standard error associated with the measured reflectivity as a

function of range. To remove the bias caused by the radar beam spreading, a simple-scaling transformation is proposed. The results show that the transformed reflectivity becomes relatively free from range dependent bias, which leads to more accurate relations with the measured ground rainfall than what is obtained otherwise. Formulation of relations between rainfall and reflectivity implicitly assumes that the reliability of the reflectivity measurements does not change with distance from the radar. This is far from true in practice. A procedure is developed to estimate the standard error associated with reflectivity measurements as a function of range. This is then used to develop reflectivity-rainfall relationships that take the uncertainty of reflectivity measurements specifically into account. A 6-month long rainfall-reflectivity record from the Kurnell radar at Sydney, Australia is used to illustrate the efficiency and applicability of the reflectivity scaling transformation and the consideration of reliability in reflectivity measurements, compared to radar rainfall algorithms used conventionally.

HS03/07P/C26-002

1415

#### EVALUATION OF DUAL POLARIZATION RADAR FOR RAINFALL-RUNOFF MODELING - A CASE STUDY IN SYDNEY, AUSTRALIA

Phillip W. JORDAN<sup>1</sup>, Alan W. SEED<sup>2</sup>, Tom D. KEENAN<sup>2</sup>, Peter T. MAY<sup>2</sup> (<sup>1</sup>Hydrology Unit, Bureau of Meteorology, Australia, <sup>2</sup>Bureau of Meteorology Research Centre, Australia)

The routine use of radar for rainfall measurement and short-term forecasting in flood forecasting and other hydrological applications is increasing. Dual polarisation radars have a theoretical advantage for rainfall rate estimation over conventional radars because the radiation returned by the horizontal and vertical polarised beams provide several additional parameters of the rainfall field that can be combined into an estimate of rainfall intensity. The Bureau of Meteorology Research Centre operated a 5.3 cm wavelength dual polarisation radar at Badgery's Creek, 44 km West of Sydney Australia, for the period from September 2000 to June 2001. The aim of this paper is to analyse and optimise the performance of a C-Band dual polarisation radar for forecasting of floods in rural and urban catchments. Hourly rainfall data from a network of 239 tipping bucket raingauges, located within 110 km of the radar, has been utilised in the analysis. The Bureau of Meteorology is responsible for preparing flood warnings for the Georges River, which flows through the Western suburbs of Sydney. The URBS semi-distributed rainfall runoff routing model is used to predict flood inflows from the 350 km<sup>2</sup> catchment area upstream of the urban area. Accurate measurement of rainfall across the catchment is critical for timely and accurate flood forecasts on the Georges River. The paper compares rainfall accumulation estimates across the Georges River catchment from: 1. raingauge networks of varying density, 2. single polarisation (reflectivity only) radar, 3. reflectivity with attenuation correction calculated using dual polarisation algorithms, 4. several multi-parameter algorithms that implement measurements from the dual polarisation radar, such as reflectivity at dual polarisation, attenuation and specific differential phase, and 5. single or dual polarisation radar combined with raingauge networks of varying density. The paper then goes on to analyse the effect of each of the rainfall measurement strategies on the accuracy of prediction of the flood hydrograph from the catchment. Inferences are drawn about selection and optimisation of parameter values for the rainfall runoff routing model for use with rainfall data from each of the various sources.

HS03/07P/C26-003

1430

#### RADAR RAINGAUGE WITH VOLUME SCANNING FUNCTION

Takeo KINOSHITA<sup>1</sup>, Minoru IRISAWA<sup>2</sup> (<sup>1</sup>The Representative of Suimon Kankyo, <sup>2</sup>Ministry of Land, Infrastructure and Transport)

CAPPI is the abbreviation of Constant Altitude PPI while PPI means Plane Position Indication of a radar. The radar equipped with CAPPI has been operated since 10 years ago at the top of Mt. Akagi which is about 100 km northwest of Tokyo. It can monitor rainclouds three-dimensionally every 15 minutes. It has 20 kinds of angles and observes rainfall 200 km radius. The authors try to develop the availability of the CAPPI radar for operational use, especially to operation of multi-purpose reservoirs. The followings show the steps of development of CAPPI radar application to reservoir operation and monitoring of heavy rainfall disasters. 1) Parameter development The empirical formula  $Z=BR^\beta$  is used for calculation of rainfall R from the radar reflectivity Z where B and  $\beta$  are determined by the observed data. The data for determination of B and  $\beta$  are selected from the adequate mesh point data of the radar and the good conditioned ground raingauge. 2) Selection of the altitude For monitoring of rainfall on the ground, the radar beam must be as low as possible. Since there are high mountains around Mt. Akagi, and the cloud producing heavy rainfall is more than 3000 m height, the 3000 m level is chosen as the best altitude. It may be changing season by season. 3) Variable B and  $\beta$  method The parameters B and  $\beta$  are revised every hour both by the reflectivity at the constant altitude and rainfall in raingauges. Every next hour the revised parameters are successively adopted for accurate estimation of rainfall. B and  $\beta$  are not fixed. 4) Bright band elimination A bright band sometimes appears in PPI observation. It is like a doughnut on the PPI picture because the radar beam forms a conic plane and a bright band exists at the 0° level of the atmosphere. The variable B and  $\beta$  method based on the CAPPI observation is not affected by the bright band because a) the reflectivity on the 0° level can be avoided by the selection of the advantageous altitude, or b) the variable B and  $\beta$  method can find the best B and  $\beta$  even if the bright band appears. 5) Vertical profile The vertical profile of the raincloud can be drawn at any section by CAPPI method due to three dimensional data acquisition. Therefore a winter storm, a Baiu rain, a thunderstorm etc are characterized by their cloud profile. This picture gives us the important information such as rainfall potential, heavy rainfall monitoring and prediction of a downburst. The authors developed the variable B and  $\beta$  method by using the CAPPI radar, then implemented successfully rainfall observation by the radar. They would like to improve in the future the software of CAPPI analysis for reservoir operation, and prevention of disaster caused by heavy rainfall.

HS03/07P/C26-004

1445

#### EVALUATION OF THE APPLICABILITY OF RADAR RAINFALL INFORMATION TO OPERATIONAL HYDROLOGY

Tadashi MATSUURA, Kazuhiko FUKAMI, Junichi YOSHITANI (Hydraulic Engineering Research Group, Public Works Research Institute)

This paper proposes a framework for evaluating usefulness of radar rainfall information by different usage, and discusses prospect and limitation of further development of the radar system. First, effectiveness of radar data online calibration for accuracy improvement was discussed. Second, an appropriate evaluation method for observation accuracy according to each usage purpose was suggested after reviewing various reports on evaluation methods. Radar usage purposes include weather forecast, flood forecast, sediment disaster warning, reservoir management, and traffic management. Last, the authors demonstrated case studies to show advantages of the use of different evaluation methods according to usage purpose and evaluated the usefulness of the radar rainfall system from multi-functional aspects. Two different online calibration schemes are commonly used in the present Japan.

The process of the development of the two schemes and their effectiveness for accuracy improvement were reviewed and analyzed in terms of difference in radar data usage intentions. Generally-used evaluation method of radar observation accuracy is comparison of the ground point rainfall and the mesh radar rainfall right above the ground station. Studies employing this comparison to show the accuracy of radar data have reported high correlation between hourly ground point rainfall and the radar mesh rainfall right above the station; correlation coefficient sometimes exceeds 0.8 in studies conducted in Japan. Another evaluation method is comparison of ground point rainfall and a mesh radar rainfall in the vicinity of the mesh right above the ground station. This evaluation could be better when falling raindrops in the atmosphere drift, and could avoid unreasonable judgment that the radar rain system has low accuracy and no use. For the purpose of flood forecasting, Matsuura et al. have proposed rainfall averaged over the river basin instead of ground point rainfall as an index to show the radar observation accuracy. They showed that radar observation for several extreme rain events including the devastating 2000 Tokai storm could be considered to have very high accuracy which could not be shown by comparison with ground point rainfall. Then, critics that flood forecasting with direct input of radar rainfall alone has less reliable than one with ground rain input could be reconsidered by checking the accuracy of radar rainfall by more appropriate index. In the same way, accuracy of radar rainfall data for each purpose was discussed. Synthesizing these accuracy evaluations from multi-functional aspects, the authors discuss the usefulness of the radar system.

HS03/07P/C26-005

1500

#### WEATHER RADAR DISTRIBUTED HYDROLOGIC MODEING, CASE STUDY IN INDUS BASIN

Shaukat Ali AWAN (Pakistan Meteorological Department)

Tropical cyclone and depression and associated rainfall over the catchment areas of the rivers which generates rainfall runoff resulting in flooding in the rivers. The radar rainfall estimation through echo reflectivity in decibels (dB) delineates heavy precipitation areas. The uncertainty occurs because of the beam width and the location of the vertex. The limited area calibration sensors help in ground truth and radar estimation. However, keeping in view the continuity equation for hydrological aspects better results can be obtained particularly in rainfall amounts in three categories i.e.; (a) Less than 50 mm, (b) 50 mm to 100 mm and (c) More than 100 mm. Doppler weather radar plays a significant role in tracking down the tropical storms and depressions. Since its effective hydrological range is 240 Km as such at least 1 to 2 days in advance the information with specific direction of movement and internal structure of the clouds embedded with heavy precipitation are obtained. The intensity of the rainfall as depicted quantitatively through decibel variations with Pseudo coloring technique can pinpoint the areas of intense rainfall, and with appropriate software CAPPI (Constant Altitude Plain Position Indicator) the volumex Analysis over a particular place (determined through Echotop capability) and its intensity value provides a time lapse and cumulative information in three dimensions which is extremely important for Hydrological/Flood Forecasting. With regard to catchment area of rivers which lies beyond our borders and from where hardly any ground information is available; this remote sensing equipment played extremely vital role for disaster monitoring i.e. Flood Forecasting and its assessment for subsequent mitigation as applied to Pakistan River basins on real-time basis. The vertical wind shear profiler coupled with X-Y cross-section gives the areal distribution of precipitation with altitude depiction pin pointing the potential vorticity area max (PVA max) essential for flash flooding giving a quantitative assessment essential for area under threat for issuing early flood alert. A consequential application of both Radar estimation and rainfall runoff was made in Indus River sub-basin, the runoff was with in an accuracy of 20 %. However it did save life, cattle and property particularly evacuation was carried out in riverbed areas. The flow channel was estimated 60,000 cusecs whereas the actual was 45,000 cusecs. Relief and Flood Mitigation authorities appreciated the community coordination.

HS03/07P/C26-006

1515

#### RADAR PRECIPITATION FOR WINTER HYDROLOGICAL MODELLING

Steven R. FASSNACHT<sup>1</sup>, Eric D. SOULIS<sup>2</sup>, Nicholas KOUWEN<sup>2</sup> (<sup>1</sup>Colorado State University, <sup>2</sup>University of Waterloo)

Weather radar has been successfully used for estimating rainfall to drive hydrological models for watersheds of numerous sizes, and has been applied to temporal resolutions from individual storm events to seasonal to annual periods. However, the use of weather radar for snowfall estimation has focussed primarily on short time intervals, such as hourly and sub-hourly, to single storm events lasting up to two days. The emphasis has been to improve radar estimates using ground-based measurements as truth. This paper illustrates the use of weather radar snowfall estimation for seasonal hydrological modelling purposes. In this paper weather radar data are used for winter precipitation estimation. The estimates are compared to gauge measurements (corrected for wind undercatch) to illustrate the improvement in the radar data as the length of accumulation increases. The radar data and interpolated ground based measurements are used to drive a physically based hydrological model (WATCLASS). Post-processing of the radar data has been undertaken to consider a local scaling issue, underestimation due to the use of winter radar coefficient for winter rain, and variability in reflectivity based on snow particle shape. The study area is the Upper Grand River Basin in central southwestern Ontario, Canada and the study period is the winter from 1993 through 1997. For four of the five year, the radar data provided precipitation estimates that were better than those provided by the gauge data, in terms of simulated runoff volumes. For the winter of 1995, the gauge data yielded better precipitation estimates for runoff volume modelling than the gauge data. The significant over-estimation of the radar data compared to gauge point estimates for 1995 was also observed by radar operating in Michigan, USA. Along with runoff volumes, peak streamflows were more closely estimated from radar precipitation than gauge precipitation. Gauge estimates consistently yielded lower than observed peak streamflows.

HS03/07P/C26-007

1545

#### NUMERICAL STUDY OF RAINFALL-TOPOGRAPHY RELATIONSHIPS IN MOUNTAINOUS REGIONS OF JAPAN USING A MESOSCALE METEOROLOGICAL MODEL

Yoshiharu SUZUKI<sup>1</sup>, Eiichi NAKAKITA<sup>2</sup>, Shuichi IKEBUCHI<sup>3</sup> (<sup>1</sup>Department of Architecture and Civil Engineering, Faculty of Engineering, Utsunomiya University, <sup>2</sup>Department of Global Environment Engineering, Graduate School of Engineering, Kyoto University, <sup>3</sup>Water Resources Research Center, Disaster Prevention Research Institute, Kyoto University)

From the standpoint of hydrological applications and water resources management, it has been required to determine the spatial and temporal structures of rainfall distribution with consideration to topographic properties in a watershed. Especially, it is much difficult to understand the nature of the relationship between rainfall distribution and topography in mountainous regions like in Japan. For the purpose of determining the mechanism of topographic effects on rainfall and making a stochastic model of rainfall distribution, this study researched the relationship through the following two approaches: analyzing long-term

rainfall information from a weather radar in Japan, and running numerical simulations of precipitation using the mesoscale meteorological model named MM5. First, for a quantitative estimation of topographic effects on rainfall distribution, rainfall-elevation relationships were determined through the analysis of data from a weather radar on the basis of the Dependence Line on Topographic Elevation (DLTE), one of the models which represent the correlation between rainfall distribution and topographic elevation. The condition required for establishing the relation of DLTE was determined by analyzing various cases of rainfall distribution which have various time scales of accumulation. Furthermore, some investigations were also conducted on the basis of DLTE to determine the temporal accumulation process of rainfall distribution (TAPR), which explains how properties of rainfall distribution fluctuate with temporal accumulation. It is one of important standpoints which should be taken into consideration to make a stochastic model of rainfall distribution. Next, DLTE and TAPR were analyzed by running numerical simulations using the MM5, which is the mesoscale model constructed in the Pennsylvania State University - National Center for Atmospheric Research (PSU-NCAR), to determine the mechanism of topographic effects on rainfall distribution. In testing simulations, it was verified by comparison with the raingauge data in some areas of Japan that rainfall distribution could be simulated with reasonable accuracy, and that the relation of DLTE and the process of TAPR were also hold in such numerical simulations. By running simulations under the topographic conditions which have various scales of resolution, it was investigated what influence the scales had on the process of TAPR. The relationship between the scales of topographic resolution and the degree of topographic effects was made clear, and it was found that the degree depended largely on the scale of mountains. On the other hand, an attention was focused on the slope of DLTE, and the relationship between the slope and the wind on a synoptic scale was investigated to determine the influence of wind speed and direction on rainfall-elevation relationships. It was found that linear correlation was hold overall between the slope of DLTE and horizontal wind speed although vertical wind speed and wind direction had no definite correlation with the properties of rainfall distribution.

**HS03/07P/C26-008****1600****SIMULATION OF PRECIPITATION CAUSED BY A BAIU FRONT: AN EVALUATION STUDY WITH RADAR DATA**

Soichiro SUGIMOTO, Hiromaru HIRAKUCHI (Central Research Institute of Electric Power Industry)

Remarkable improvements of a mesoscale model allow its potential applications for short-term precipitation forecasting to be wider range. The objective of this study is to investigate the capability of a mesoscale model to reproduce the spatial variability of precipitation and the associated wind field at mesoscale. To evaluate the ability of a mesoscale model, a simulation of precipitation system embedded in the Baiu (Mei-yu in Chinese) front is performed. A west-east oriented rainbelt along the front was prominent and a few precipitation centers were found in the event. Simulated results are compared with 3-h accumulated precipitation amount from Radar-AMeDAS, which is calibrated using operational C-band radar data and surface rainfall data collected by the automated meteorological acquisition system of Japan Meteorological Agency. Horizontal wind field in an orographic region estimated by the extended volume velocity processing (EVVP) using radial velocities from Doppler radar is also used for evaluation of wind field in meso-beta scale. The model for this study is the nonhydrostatic version of the Pennsylvania State University - National Center for Atmospheric Research Mesoscale Model version 5.3.4 (MM5v3.4). In all simulations, the coarsest grid has a spacing of 81 km, the middle grids 27 km and 9 km, and the finest grid 3 km. The model is initialized using both archived analyses from the European Center for Medium-Range Weather Forecasts (ECMWF) and Reynolds sea surface temperature (SST) from the National Oceanic and Atmospheric Administration (NOAA), from which first-guess fields are generated. 3- and 9-km domains are nested within a 27-km domain using one-way interfaces, and two-way interactive nested grid system is adopted between 27- and 81-km domains. Model results indicate that the MM5 can provide a general description of mesoscale features such as the rainbelt and more local strong precipitation centers of the frontal system observed by Radar-AMeDAS. The southward propagation of rainbelt and the eastward movement of the embedded system can be also well simulated by the model. The major deficiencies of the model are its underestimation of rainfall amount and to fail in reproducing localized rainbands in a mountainous region of Japan. These deficiencies are associated with the model's limit that the model cannot resolve the convergence zones of EVVP-based wind field affected by complex terrain. These findings suggest that mesoscale data assimilation should be required for additional improvements particularly in applying to mountainous regions and that radar data may represent a potentially valuable source of upper-air data suitable for four-dimensional data assimilation.

**HS03/07P/C26-009****1615****RAINSTORM CHARACTERISTICS IN TEMPERATE AREAS DERIVED FROM MULTIPLE TIME SERIES OF WEATHER RADAR IMAGES**

Gabrielle J.M. DE LANNOY, Inge L.M. DE JONGH, Niko E.C. VERHOEST, François P. DE TROCH (Laboratory of Hydrology and Water Management, Ghent University)

In order to define the spatial and temporal characteristics of rainstorms, 20 time series of weather radar images over The Netherlands and Belgium are analysed. The velocity of rainfall events and the direction of movement are determined for the 1632 available radar images using the cross-correlation technique. After a thorough statistical analysis, theoretical probability distribution functions could be fitted to the histograms of these two rainfall characteristics. To discriminate single rainstorms within a radar image, a new technique was developed. Spatial characteristics, like the area and the perimeter of the rainstorms are determined and theoretical distributions were fitted to the data. Different methods to define the dimension of a rainstorm are proposed and worked out. A statistical analysis revealed that the dimensions of rainstorms in the direction of the rainfall movement are significantly different from the dimensions in the direction perpendicular to the movement. Rainstorms are composed of several rain cells which are clustered together. Due to the spatial resolution of the radar images, individual rain cells cannot be identified. In order to describe the occurrence of cell clusters, a technique was developed for localizing cluster centra within a radar image. The method is based on level slicing the image and detecting connected areas which have a rainfall intensity above a preset threshold. A statistical analysis revealed that the positions of the cluster centra in the two perpendicular directions (i.e. along and across the rainfall movement) follow a Poisson distribution.

**HS03/07P/C26-010****1630****STOCHASTIC MODELING OF ERROR STRUCTURE OF REAL-TIME PREDICTED RAINFALL AND RAINFALL FIELD GENERATION**Yasuto TACHIKAWA<sup>1</sup>, Yoshimitsu KOMATSU<sup>1</sup>, Kaoru TAKARA<sup>1</sup>, Michiharu SHIIBA<sup>2</sup> (<sup>1</sup>Disaster Prevention Research Institute, Kyoto University, <sup>2</sup>Department of Civil Engineering Systems, Kyoto University)

To evaluate the uncertainty of a real-time river discharge prediction with a distributed rainfall runoff model, an error structure of real-time rainfall prediction by a translation model is modeled as a spatial random field and predicted rainfall fields are simulated according to the characteristics of the prediction error structure. At first, absolute prediction error fields and relative prediction error fields between radar observed rainfall and predicted rainfall by a translation model are statistically analyzed. Kolmogorov-Smirnov test shows that the relative prediction error of 1 hour ahead mean precipitation with 3km spatial resolution fits to a lognormal distribution. Also spatial correlation of relative prediction error is found to be modeled using Gaussian model and the correlation length takes almost same value during one precipitation term. Thereby a lognormal spatial random field is selected to represent the prediction error structure. Then a method to generate a lognormal spatial random field is developed, which uses a matrix factorization technique of a covariance matrix decomposition into its square root matrix approximately by using the Chebyshev polynomials. Finally, rainfall fields with the uncertainty having lognormal spatial random field characteristics are generated by using the method. The generated rainfall fields will be used to evaluate the uncertainty of real-time river discharge predictions with a distributed rainfall runoff model on a Monte Carlo simulation framework.

**HS03/07P/C26-011****1645****ON THE MODELING OF TEMPORAL CORRELATIONS IN SPATIAL-CASCADE RAINFALL DOWNSCALING**Assela PATHIRANA<sup>1</sup>, Srikantha HERATH<sup>2</sup>, Tadashi YAMADA<sup>1</sup> (<sup>1</sup>Chuo University, <sup>2</sup>University of Tokyo)

Using cascade theories to spatially-distribute global or mesoscale rainfall forcing for watershed scale run-off simulations, has a number of attractive features compared with the traditional approaches (e.g. Thiessen polygons), where the adequacy of the ability to mimic the spatial variability and discontinuity as in observed rainfall is a major concern. In last two decades, a number of multiplicative cascade based downscaling models and techniques have been developed. In spite of these numerous advances in cascading theories and techniques, the applications of the principal in run-off studies has been rare. A rainfall product needs to be accurate in the temporal-persistence, in addition to the spatial features for it to qualify as a candidate for run-off studies. Most of the past efforts of multifractal analysis and cascade modeling of rainfall have been limited to either temporal or spatial dimension. On the other hand, even a crude maintenance of both spatial and temporal correlations is a pre-requisite for distributed run-off modeling. Thus, the lack of reliable means of maintenance of the temporal-persistence in spatial models is perhaps a main reason for the lack of appeal to apply cascade downscaling to run-off studies. One theoretically attractive way of overcoming this inadequacy is to model rainfall as a full spatiotemporal process. This involves transformation of the temporal dimension in to a third spatial dimension by multiplying with a hypothetical velocity factor, derived empirically from observed rainfall. Alternatively, we propose that a simpler time-series approach combined with the cascade schemes can be used with relative ease, to model the temporal-correlations observed in rainfall in to spatial downscaling schemes. We interpret the scaling of rainfall in space as the combined effect of a spatial multiplicative cascade process based on large-scale forcing and a number of time-series processes that relate rainfall intensity at a given cascade level to that of the past time steps or the history. Thus, the model is capable of mimicking the temporal-persistence at all spatial scales involved in the problem at hand. We use a number of Markov processes to model the time-series process. The ability of a cascade scheme to treat the zero rainfalls explicitly (e.g. Over and Gupta 1996) may be of particular interest to the run-off analyst. In addition to the intensity, data analyses shows that zero rainfall at various spatial scales, also have a strong temporal correlations. In the present model, zero rainfall persistence is modeled based on a simple conditional probability scheme. After developing the theoretical framework for the proposal based on the features of spatial rainfall, the model is verified using hourly radar based spatial rainfall observations for the central part of Japan.

Tuesday, July 8 AM

Presiding Chair: K.P. Georgakakos

**ASSESSMENT OF PERFORMANCE IN DISTRIBUTED HYDROLOGICAL MODELING****HS03/08A/C26-001**

Invited

**0830****DISTRIBUTED HYDROLOGIC MODELING: WHAT ACCURACY IS ACHIEVABLE?**Baxter E. VIEUX<sup>1</sup>, Fekadu G. MOREDA<sup>2</sup> (<sup>1</sup>School of Civil Engineering and Environmental Sci., University of Oklahoma, <sup>2</sup>National Weather Service, National Atmospheric Administration)

Distributed parameter watershed models that are physics-based offer distinct advantages over conceptual rainfall-runoff models. Spatially distributed parameters derived from soil properties, land use/cover, topography, and input from radar rainfall require new methods of adjustment in order to minimize differences between simulated and observed hydrographs. Distributed hydrologic models based on conservation laws have identifiable optimal values and expected behavior and interaction during calibration. This paper describes a calibration method that exploits these model characteristics and presents results for two river basins: the Illinois River (2300 km<sup>2</sup>) and Blue River basins (1142 km<sup>2</sup>) in Oklahoma. The calibration scheme presented is an ordered physics-based parameter adjustment (OPPA) method. Two river basins are simulated with volume errors with good agreement in volume for a series of twenty storm events over each basin. Within a subset, high accuracy is achieved, while for other event subsets, departures of simulated from observed volume and discharge are much larger. Realistic parameter values are obtained for both basins using a storm subset. As storm events are added to the calibration set, stability in the optimal parameter set is examined.

**HS03/08A/C26-002****0900****MODEL BEHAVIOR OF DISTRIBUTED HYDROLOGICAL MODELING WITH DIFFERENT FORCING DATA RESOLUTIONS**

Roshan K. SHRESTHA, Yasuto TACHIKAWA, Kaoru TAKARA (DPRI, Kyoto University)

Hydrological modeling with distributed approach lacks popularity in practical application due to problems with data rather than modeling principles. On the other hand, the advantages of distributed modeling approach, for example its ability to evaluate the effects of spatially variable human and natural impacts, make it very attractive and an essential tool. General Circulation Models (GCMs) are one of the major data source in distributed hydrological modeling for gauged and un-gauged basins. However, the available grid resolution of GCM data should resemble to the need of hydrological model's spatial resolution, which largely depends on catchments size. Observing the behavior of spatial resolution in distributed

hydrologic modeling, data requirement criterion with respect to catchments size is investigated by evaluating IC Ratio (ratio between catchments area and input data resolution) expecting massive use of GCM data and coupled atmospheric and hydrologic model in near future. A macro scale distributed hydrological model is developed using object oriented hydrological modeling system (OHYMoS) and test simulations are conducted for the case of Huaihe River Basin (132000 sq. km.), in China and its two sub-basins Wangjiaba (29800 sq. km.) and Suiping (2093 sq. km.). A 10 minute spatial resolution data set is generated using the 1.25 degree GAME Reanalysis Data Version 1.1 referring the spatial pattern of 5 minute HUBEX EEWB Data, a field measurement based distributed data set. The newly created data has improved the modeling result. Later on, the generated 10 minute spatial data is converted to 20 minute, 30 minute and so on. Feeding these generated data into the model separately for discharge simulation keeping all other parameters same as before, its model performances are experimented. The change behavior of simulation result displayed a rapid improvement on model result with finer resolution. The improvement in model performance saturates afterward which suggests an existence of a threshold value of IC Ratio. Optimal simulation results are observed while the IC Ratios are around 1:10 ~ 1:20. Geo-statistics has revealed that the input data with greater spatial variability displays significant improvement in performance otherwise spatial pattern of input data has feeble sensitivity. Higher sensitivity in model performance due to spatial resolution is observed in smaller catchments in both presence and absence of routing models than that of larger catchments.

**HS03/08A/C26-003****0915**

#### INVESTIGATING THE EFFECT OF CATCHMENT CHARACTERISTICS ON THE RESPONSE TIME SCALE USING DISTRIBUTED MODEL AND WEATHER RADAR INFORMATION

Efrat MORIN<sup>1</sup>, Konstantine P. GEORGAKAKOS<sup>2</sup>, Uri SHAMIR<sup>1</sup>, Rami GARTY<sup>1</sup>, Yehouda ENZEL<sup>1</sup> (Hydrology and Water Resources, University of Arizona, Tucson, AZ 85721, <sup>1</sup>Hydrologic Research Center, 12780 High Bluff Drive, Ste. 250, San Diego, CA 92130, USA, <sup>2</sup>Civil Engineering and Nancy Grant Water Research Institute, Technion, Haifa 32000, Israel, <sup>3</sup>Soil Erosion Research Stations, Emek Hefer 40250, Israel, <sup>4</sup>Institute of Earth Sciences, The Hebrew University of Jerusalem, Jerusalem 91904, Israel)

The Response Time Scale (RTS) is a characteristic time scale of the catchment that represents the amount of smoothing performed by the hydrological system in transforming the rainfall input into runoff. The identification of the RTS involves analysis of time series of rainfall and runoff and does not require information about the hydrological system. In our study we use weather radar rainfall data, rain gauge data and runoff data to identify the RTS of five small catchments (10-150 km<sup>2</sup>) in Israel and Panama. The results indicate that the RTS is stable for a given catchment and it depends on the catchment characteristics. For example, the RTS of the urban and arid catchments is considerably lower than the RTS of the rural catchments. In order to study the relationships of the catchment characteristics to the RTS a physically based, non-calibrated distributed hydrological model is applied to one of the studied catchments. The radar rainfall data are used to obtain the computed runoff hydrographs, and these computed data are then used to derive the RTS of the modeled catchment. The effect of several catchment parameters (such as length, slope and roughness of hillslopes and channels) on the RTS is examined by altering each parameter and deriving the RTS for each case. The effect of the different parameters on the time scale characteristics of the catchment hydrological response is investigated. Special emphasis is placed on comparing hillslope vs. channel processes. The results indicate that the effect of hillslope processes on the response time scale is greater than the effect of the channel processes.

**HS03/08A/C26-004****0930**

#### EFFECT OF SPATIAL AND TEMPORAL RESOLUTION OF PRECIPITATION DATA ON ACCURACY OF THE LONG-TERM RUNOFF SIMULATION

Hiroshi ISHIDAIRA<sup>1</sup>, Kuniyoshi TAKEUCHI<sup>1</sup>, Zongxue XU<sup>1</sup>, Tianqi AO<sup>2</sup>, Jun MAGOME<sup>3</sup>, Makoto KUDO<sup>4</sup> (<sup>1</sup>Graduate School of Engineering, Yamanashi University, <sup>2</sup>Public Works Research Institute, <sup>3</sup>Graduate Student, Yamanashi University)

The precipitation is usually dramatically distributed with time and space within a basin. In physically-based distributed model, the precipitation data with rational resolution to represent the variability of precipitation is needed for accurate estimation of the river discharge. However, it is not yet clear that with what resolution will the runoff be estimated with rational accuracy at different time scales. The objective of this study is to identify the effect of spatial and temporal resolution of precipitation data on the accuracy of long-term runoff simulation. The hourly Radar-AMeDAS precipitation data with 5km x 5km spatial resolution is used in this study. The original Radar-AMeDAS data is averaged over different spatial and temporal scales, and both original and the averaged data are used as the input for hydrological model. The rainfall-runoff simulation is carried out in Fuji River basin by using the Block-wise use of TOPMODEL with Muskingum-Cunge method (BTOPMC). The difference between the simulated daily hydrographs using original precipitation and the averaged ones are investigated through the comparison of Nash efficiency and the total runoff volume ratio for each simulation. In addition, same analyses are also carried out for hydrographs at other time scales, and the influence of spatial and temporal resolution of precipitation data on the accuracy of the hydrological simulation was identified.

**HS03/08A/C26-005****0945**

#### EFFECT OF PRECIPITATION SPATIAL DISTRIBUTION ON THE HYDROLOGICAL RESPONSE IN THE UPPER TONE RIVER OF JAPAN

Dawen YANG, Toshio KOIKE, Hiro TANISAWA (Department of Civil Engineering, University of Tokyo)

Distributed physically-based hydrological models give a detailed and potentially more correct description of the hydrological processes in a catchment than do other model types. Moreover, they are able to make effective use of available information and knowledge concerning the catchment, and the Geographic information systems (GIS) and remote sensing have been widely used in the advanced hydrological modeling. Besides the information from land surface, the spatial distribution of precipitation is usually a key factor to the accuracy of hydrological simulations. With development of the weather radar technique, it is possible to incorporate the radar measurement with the distributed model for investigating on the hydrological response, especially for the flood events. This research aims at evaluating the effect of spatial rainfall distribution on the hydrological response in the upper Tone River basin of Japan. The spatial rainfall distributions are generated by two ways. One is the traditional Thiessen Polygon Method based on the point measurements. Another method is integration of the point observations and the weather radar measurements. The results are compared for the long term hydrological responses and several flood events.

**HS03/08A/C26-006****1000**

#### GRID-BASED DAM INFLOW PREDICTION ON A LARGE RIVER BASIN USING THIESSEN POLYGON AND SPATIALLY DISTRIBUTED RAINFALL DATA

Seong-Joon KIM, Hyung-Joong KWON, In-Kyun JUNG, Geun-Ae PARK (Department of Rural Engineering, Konkuk University)

The surface runoff and streamflow responses between Thiessen average rainfall controlled by rainfall stations (T) and spatially distributed rainfall that is cell by cell units (R) would be different each other. To identify the effects quantitatively, the grid-based kinematic wave storm runoff model (Kim, 1998; Kim et al., 1998) that predicts temporal variation and spatial distribution of overland flow, subsurface flow and stream flow, was adopted. The model adopts single overland flowpath algorithm and simulates surface and/or subsurface water depth at each cell by using water balance of hydrologic components. The model programmed by C-language uses ASCII-formatted map data supported by the irregular gridded map of the GRASS (USACERL, 1993) GIS and generates the spatial distribution maps of discharge, flow depth and soil moisture of the watershed. The model was tested for the above rainfall conditions to Yeoncheondam watershed (1,875 km<sup>2</sup>) that has just 4 available rainfall stations in South Korea. We found that there were big temporal and spatial surface runoff/discharge differences between T and R when the rainfall is moving from north to south direction rather than moving from east to west direction because the watershed width is relatively narrow in shape.

**HS03/08A/C26-007****1030**

#### APPLICATION OF RADAR-MEASURED RAIN DATA IN HYDROLOGICAL PROCESSES MODELING DURING THE IOP OF HUBEX

Liliang REN, Chunhong LI, Meirong WANG (Dept. of Hydrology & Water Resources, Hohai University)

On the basis of Digital Elevation Model (DEM) data, raster flow vectors, watershed delineation, and spatial topological relationship, are generated by Martz and Garbrecht method for the upper area of Huangnizhuang station in the Shihe Catchment with 805 sq. km. of area, intensified observation field for the HUBEX/GAME Project. Then, the Xin'anjiang Model is applied for runoff production in each grid element where rain data measured by radar at Fuyang Station is utilized as the input of hydrological model. Those elements are connected by flow vector to the outlet of drainage catchment where runoff is routed by the Muskingum method from each grid element to the outlet according to the length between each grid and the outlet. The Nash-Sutcliffe model efficiency coefficient is 92.41% from May 31st to August 3rd in 1998, and 85.64%, 86.62%, 92.57%, 83.91%, respectively for 1st, 2nd, 3rd, 4th flood event during the whole computational period. As compared with the case where rain-gauge data were used in simulating hourly hydrograph at Huangnizhuang station in the Shihe Catchment, the index of model efficiency improvement is positive from 27.56 % to 69.39 %. That justifies that radar-measured data is superior to rain-gauge data as the input of hydrological modeling. As a result, grid-based hydrological model provides a good platform for runoff computation, in which radar-measured rain data with highly spatiotemporal resolution are taken as the input of hydrological model.

**HS03/08A/C26-008****1045**

#### APPLICATION OF MODELS WITH DIFFERENT TYPES OF MODELING METHODOLOGIES FOR RIVER FLOW FORECASTING

Hapu Arachchige Prasantha HAPUARACHCHI<sup>1</sup>, Li ZHIJIA<sup>1</sup>, F. A. WOLFGANG<sup>2</sup> (Hohai University, <sup>2</sup>International Water Management Institute)

A number of watershed modeling methodologies are available at present. Basically they can be divided into three categories as conceptual modeling, distributed modeling and "black box" type modeling. In the present study, a conceptual model, a distributed model, and an artificial neural network (ANN) have been applied for river flow forecasting in the *Kalu* river upper catchment in Sri Lanka. The Xinanjiang watershed model, which is widely applied in China for flood and river flow forecasting has been used as a conceptual watershed model and the SWAT (2000) model has been used with spatial data as a distributed model. ANN has been applied as a "black box" type modeling methodology. Two types of ANN architectures, namely multi-layer perceptron network (MLP) and a radial basis function network (RBF) have been implemented. Based on the application results, it seems that the conceptual watershed model could perform slightly better than the distributed model and the ANN for this watershed. It was clearly noted that the performance of distributed models strictly depend on the quality of data. Therefore the application of distributed models is bounded to the availability and quality of data. ANNs are good in many practical situations where the main concern is with making reasonable predictions at specific locations where less data are available. On the other hand the performance of conceptual models strictly depend on the calibration and the input data. However the results obtained using above three methods are conceptually realistic and acceptable.

**HS03/08A/C26-009****1100**

#### EFFECTS OF SUB-BASIN SCALE ON RUNOFF SIMULATION IN DISTRIBUTED HYDROLOGICAL MODEL: BTOPMC

Tianqi AO<sup>1</sup>, Junich YOSHITANI<sup>1</sup>, Kuniyoshi TAKEUCHI<sup>1</sup>, Kazuhiko FUKAMI<sup>1</sup>, Tadashi MATSUURA<sup>1</sup>, Hiroshi ISHIDAIRA<sup>2</sup> (<sup>1</sup>Hydrologic Engineering Research Team, Public Works Research Institute (PWRI), <sup>2</sup>Institute of Material and Environment Technology, Graduate School, Yamanashi University)

It has been widely recognized that the scale problem of distributed hydrological models is a very difficult and serious question; it affects model accuracy and reliability a great deal, yet is far from any form of solution. Model parameter dependence on sub-basin and/or grid cell size selection is an example. In the case of physically based distributed hydrological model, BTOPMC (Block-wise use of TOPMODEL with Muskingum-Cunge method), topographic scale including both sub-basin and grid cell size is closely related to runoff to be generated. In this study their effects, particularly that of sub-basin scale on runoff simulation were investigated, attempting to identify the quantitative relationship between model parameters and basin characteristics, so that the model can be applied to large watersheds especially to ungauged/data-poor basins. In BTOPMC, runoff generation is based on TOPMODEL; flow routing is carried out by the Muskingum-Cunge method; drainage networks are generated using the Ao automated pit-removal method; study basins are automatically subdivided into either rectangular blocks or natural sub-basins over which groundwater balance was taken (the latter by the Pefafstetter numbering system); model parameters are automatically calibrated using the SCE-UA optimization algorithm (Shuffled Complex Evolution Method for Global Optimization-the University of Arizona). Using this BTOPMC, the 3,500km<sup>2</sup> Fuji-kawa basin and the 3,270km<sup>2</sup> Nakagawa basin of Japan were subdivided into natural sub-basins of different sizes. In order to focus on the effects of sub-basin scale, soil type and vegetation were assumed homogeneous. Hourly precipitation data and 30"X30" GTOPO30 DEM (digital

elevation model) were used for simulation. Simulated were the floods of the Fuji-kawa basin in September 1993 and its annual runoff of 1990-1991, and the flood of the Nakagawa basin in 1989. The preliminary results indicate that in the case of floods, smaller sub-basin scale will generally result in higher peak discharge, a little earlier peak time, larger base flow and larger total runoff. Such behavior is considered as an effect of averaging scale of the topographic index used in calculating surface and base flow in the model. On the other hand, in the case of annual runoff, the effects on peak discharges do not show any determined tendency; the effects on peak time, total runoff and flow components are not obvious or negligible. Furthermore, when average sub-basin size is smaller than about 1/150 of the entire basin (say, around 25km<sup>2</sup> for the two basins), simulation results seems stabilized, indicating that there may exist a proper sub-basin scale for BTOPMC, at which uncertainty due to topographic scale in modeling can be reduced to quite a low level. This sub-basin size might be used as a referential scale for catchment subdivision both in modeling large river basins and in establishing the relationship between model parameter values and basin features. Key words scale issue; model parameters; physically based distributed hydrological model BTOPMC model; Pfafstetter numbering; SCE-UA optimization; Fuji-kawa;Nakagawa

**HS03/08A/C26-010****1115****A GRID-CELL BASED DISTRIBUTED FLOOD RUNOFF MODEL AND ITS PERFORMANCE**

Toshiharu KOJIMA, Kaoru TAKARA (Disaster Prevention Research Institute, Kyoto University)

Distributed parameter runoff models are recently developed and expected to be used in practice. They can take into account spatial distribution of rainfall, land surface conditions and their changes, which affect the runoff from river basin. This paper introduces a grid-cell based distributed rainfall-runoff model that was developed by the authors in 1997. The model uses geographic information such as digital elevation models (DEM), land cover/use based on either the National Land Information developed by Geological Survey Institute (GSI) or remote sensing imageries. The model has the following features. 1) A d-m square area centering on a node point of a d-m DEM is a sub basin, which is called a cell, and many cells constitute a river basin. 2) A DEM produces a drainage path, and the discharge from a cell to another cell flows to only one direction. 3) In each cell, the total amount of outflows from upper cells is the inflow to the cell, and an outflow from the cell is calculated using the kinematic wave model. The objective of this paper is to compare this distributed runoff model with two models conventionally used in Japan: the storage function model and the slope-channel system kinematic wave model. This paper discusses some problems to improve the precision of the distributed runoff model and to put it to practical use, by comparing each model on the basis of the indices for the model parameter sensitivity, such as the difference in peak time, peak discharge and hydrograph shape between observed and simulated hydrographs. The slope-channel system kinematic wave model can reproduce the observed hydrographs well with the optimum model parameters, which are almost the same as the conventionally recommended values. Although the grid-cell based distributed model also can reproduce the observed hydrographs well, it has a tendency to give earlier peak than the observed one. Further investigation is necessary to improve this tendency by adjusting the roughness coefficient of channel much affecting the peak time. In the storage function model, the optimum parameters depend on flood events. Variation in optimum parameters is greater than other runoff models. This paper also discusses about the effect of spatial resolution of the grid-cell based distribution runoff model. The authors compare the 50-m grid-cell based runoff model with the 250-m model in terms of the model parameter sensitivity. The optimum model parameters of the coarse-resolution runoff model have a tendency to become larger than the higher resolution model, and the model parameters of the coarse-model are more sensitive than the high-resolution model.

**HS03/08A/C26-011****1130****EVALUATING LAND USE CHANGE EFFECTS ON FLOOD PEAK USING DISTRIBUTED RAINFALL RUNOFF MODEL IN YASU RIVER, JAPAN**Tumaini Anderson KIMARO<sup>1</sup>, Yasuto TACHIKAWA<sup>2</sup>, Kaoru TAKARA<sup>3</sup> (<sup>1</sup>Graduate School of Civil Engineering Kyoto University, <sup>2</sup>Disaster Prevention Research Institute Kyoto University)

The effects of land use changes on flood peaks in Yasu River basin are investigated using a distributed rainfall runoff model. The land use changes over a 20 year period are determined using 100 m spatial resolution data of 1976 and 1997. The main land use classes in the basin are forest, paddy fields, urban and water bodies. As compared to 1976 there is decrease in areal coverage by forests of 2.5% and paddy fields by 1.4%. The coverage of urban area increased by 2% and that of agricultural land by 0.2%. A new land use "Golf courses" emerged in 1997 covering 2.3% of mostly forested area in 1976. Simulation results shows that 1997 land use data produces higher flood peaks by 6% and faster travel times by 16 minutes as compared to 1976 land use data. The changes detected indicate the gradual effects of urbanization in the study basin.

**Tuesday, July 8 PM**

Presiding Chair: Y. Tachikawa

**APPLICATION OF DISTRIBUTED HYDROLOGICAL MODELS IN WATERSHED MANAGEMENT****HS03/08P/C26-001****1400****OPERATIONAL DEPLOYMENT OF A PHYSICS-BASED DISTRIBUTED RAINFALL-RUNOFF MODEL FOR FLOOD FORECASTING IN TAIWAN**Baxter E. VIEUX<sup>1</sup>, Jean E. VIEUX<sup>1</sup>, Chiarong CHEN<sup>2</sup>, Kenneth W. HOWARD<sup>3</sup> (<sup>1</sup>Vieux & Associates, Inc. Norman, OK 73072 USA, <sup>2</sup>Central Weather Bureau, Taiwan, <sup>3</sup>NOAA National Severe Storms Laboratory)

The Central Weather Bureau of Taiwan in cooperation with the Water Resources Agency, among others, seeks to improve technology used to forecast rainfall-runoff throughout Taiwan. Forecasting technology is needed for the specific hazards of floods, debris flow, and landslide for all of Taiwan. This initiative for the development of a flood alert and water resources system is expected to unify forecasting of floods on a single system enhancing the accuracy and efficiency of flood information for dissemination from the central government to the public, and to regional and local agencies. Operational deployment of a physics-based distributed rainfall-runoff model, coupled in real-time with quantitative precipitation estimates (QPE) from radar, satellite and rain gauges, allows distributed prediction of flooding at any location. Coupling and deployment of Vflo™ along with integrated quantitative precipitation estimates from multiple sensors provides unique opportunities for improved prediction of flood hazards. Addition of a rainfall-runoff model, Vflo™, coupled with quantitative precipitation estimates provides improved flood information in real-time. Vflo™ relies on digital elevation and other geographic information to predict discharge and stage at any selected location. This model relies on the QPE derived from a system developed by the US

NOAA-National Severe Storms Laboratory called QPESUMS. The Vflo™ system and QPESUMS were installed this year and was operational during Typhoon Rammasan as well as other events in 2002. One of the most damaging events of 2001, Typhoon Nari, is the subject of post-analysis event re-construction. Typhoon Nari left 93 dead and 10 people missing and caused extensive damage to the northern part of the island and to the City of Taipei. Besides an overview of the flood warning system design and operational features, a sensitivity study and simulation of river stage compared with observed stream flow will be presented.

**HS03/08P/C26-002****1415****APPLYING RADAR RAINFALL DATA IN BASIN HYDROLOGIC MODELING**

Oscar KALINGA, Thian Yew GAN, Jiancang Xie (Department of Civil and Environmental Engineering, University of Alberta)

To overcome the limitation of point measurements from rain gauges, there is a growing interest in utilizing radar data for basin-scale hydrologic modeling. Since radar rainfall data are derived from radar echoes, there is also a need to analyze errors associated with precipitation estimated from different radar processing techniques. This study uses the WSR-88D level III hourly rainfall estimates supplied by Hydrology Laboratory (HL) of the National Weather Service (NWS) office, USA, meteorological data of Oklahoma Mesonet, and a semi-distributed hydrologic model, DPHM-RS developed by Biftu and Gan (2001). Major sources of errors affecting the WSR-88D level III hourly rainfall estimates are radar electronic calibration, the Z-R relationship, rainfall attenuation, radar range effect, anomalous propagation, ground clutter, beam filling, and the radar sampling strategy, and techniques used to produce stage III data from stage II products, such as averaging the overlapping radar bins. In general, more spatially and temporally variable spring and summer convective rainfall is better represented by radar data than the sparse rain gauges, while the less variable stratiform winter precipitation could be well captured by sparse rain gauges. This study focuses on the following objectives: (1) To assess the advantage of basin-scale hydrologic modeling gained from using radar rainfall data as input over the standard input of gauge measurements in terms of basin subdivision and radar data resolution; (2) To integrate radar rainfall fields with gauged rainfall data via a statistical objective analysis scheme as an effort to reduce errors in terms of storm type (i.e. convective and stratiform storms), and storm size.

**HS03/08P/C26-003****1430****A DISTRIBUTED HYDROLOGICAL MODELING APPLIED TO HEIHE MOUNTAINOUS BASIN IN WESTERN CHINA**

Jun XIA, Wang GANGSHENG, Tan GE (Institute of Geographical Science &amp; natural Resources Research, Chinese Academy of Science)

The Western China Development is confronted with a quite serious and realistic problem on water resources because of the water cycle's district characteristics, the ecosystem's vulnerability and the increasing demand of water resources. Based on the traits and existent problem of water cycle in western China, the key scientific issues of water cycle in western China has been studied in this paper. Main contribution in this paper is to develop a distributed hydrological modeling coupled physical process grids with a Time Varian Gain Model (TVGM) that was developed for system approach in University College of Galway, Ireland for river flow forecasting (1995). This model has three advantages: (a) it can be available to the case of input information imperfection such as the lack of enough precipitation and evaporation observations for distribution modeling; (b) it can be coupled the present physical process units or conceptual models with hydrological system approach such as TVGM, where time variant gain factor, G(t), could be linked with RS information to extend easily to application of hydrological prediction in basin scale; (c) Parameter sets of the distributed hydrological model can be estimated in terms of system identification approach to reduce uncertainty. By preliminary application and examination in the Heihe River Basin of Guansu Province with area 1300km<sup>2</sup> in arid & semi arid region, it was found that this model is successful with more advantages than conditional distributed model applied in China. Moreover, the new problems were addressed in the paper.

**HS03/08P/C26-004****1445****DEVELOPMENT OF DISTRIBUTED RED SOIL RUNOFF MODEL USING RADAR DATA**Yutaka ICHIKAWA<sup>1</sup>, Katsuhiro NAKAGAWA<sup>2</sup>, Kazuki FUJIWARA<sup>1</sup>, Michiharu SHIIBA<sup>1</sup>, Shuichi IKEBUCHI<sup>3</sup> (<sup>1</sup>Graduate School of Global Environmental Studies, Kyoto University, <sup>2</sup>Okinawa Subtropical Environmental Remote-Sensing Center, Communications Research Laboratory, <sup>3</sup>Disaster Prevention Research Institute, Kyoto University)

Okinawa region is located at the south-west end of Japan and consists of a number of islands. The region has been suffering from the problems caused by severe red soil runoff. The red soil of Okinawa region is called as Kunigami Maaji. It is quite erosive and has medium hydraulic conductivity. Okinawa region has much rainfall and is often attacked by typhoons occurred at south sea, especially in summer and autumn. The heavy rainfall causes overland flow and soil erosion. The soil particle of Kunigami Maaji is very fine and will not sink once the soil is eroded and involved into water flow. The muddy water containing soil particles pollutes the shores and coasts, and it gives heavy damage to ecosystems of the sea, farming and tourism. The final goal of this study is to develop a distributed red soil runoff model using radar data, and to investigate the effective countermeasures to prevent or mitigate red soil runoff. As a preliminary study, we developed a distributed red soil runoff model based on a kinematic wave flow model and a digital topographic model. This model describes erosion process of plane soil surface due to overland flow. A study basin is described as a set of small rectangular plane. The kinematic wave flow model considering field capacity of surface soil layer is applied to each rectangular plane, and water flow is routed from upstream to downstream. This kinematic wave flow model is a model of subsurface flow - saturated overland flow and also describes a process that a part of water infiltrated into surface soil layer is captured by capillary force of the soil. The erosion of surface soil is assumed to occur at a point where overland flow occurs, and the rate of erosion is calculated by using the friction velocity at the point, which is determined from water depth of overland flow. The model was applied to Taiho River basin (24km<sup>2</sup>), which is located at the north part of Okinawa main island. The results of simulations showed good agreements with observations, while the model needed tuning of a parameter which greatly affected the rate of soil erosion. This model is now using rainfall data observed at rain gauges, however it can also use radar rainfall data as input. Then we are planning to use rainfall data obtained by a bistatic radar which is now being installed by Communications Research Laboratory (CRL). This radar will observe rainfall intensity and distribution of precipitation particle size. The latter will give us quite important information to model soil detachment process due to raindrop impact.

HS03/08P/C26-005

1500

**A FLASH FLOOD FORECAST MODEL FOR THE THREE GORGES BASIN USING GIS AND REMOTE SENSING DATA**

Yangbo CHEN<sup>1</sup>, Jiayi HU<sup>2</sup>, Jie YU<sup>3</sup> (<sup>1</sup>Department of Urban and Resource Planning, Sun Yat-sen University, <sup>2</sup>Department of Management, Three Gorges University, <sup>3</sup>Cascade Dispatching Center, CTGPC)

This paper presents a physically-based, distributed hydrologic model for the flash flood forecasting of Three Gorges Basin, which uses GIS technique and remote sensing data, including digital weather radar estimated precipitation and satellite sensed DEM and vegetation. This model is divided into several sub-models, which include the Basin Digitization Model(BDM), Precipitation Feeding Model(PFM), Evapotranspiration Model(EM), Runoff Production Model(RPM) and Runoff Routing Model(RRM). In the BDM, a Square-Grid Network DEM is employed to discretize the whole basin into a number of squared cells, and every cell is considered as a basin(called mini-basin), which is divided into three layers: the Canopy Layer(CL), the Soil Layer(SL) and the Underground Layer(UL). To every cell, there are unique vegetation type and leaf area index. The flow direction, flow accumulation, slope, flow length of every cell are calculated by ArcView based on the DEM. The PFM is used to treat the precipitation measured from both the digital weather radar and rain gauges. The input digital weather radar rainfall reflectivity is first transferred into the precipitation and assigned to every cell. The precipitation measured from the rain gauges is assigned to every cell using the Thiessen Polygon. In this study as the current digital weather radar can not cover the whole Three Gorges Basin, so the precipitation from both the weather radar and the rain gauges are used. The EM is used to calculate the cell evapotranspiration, which is down based on the vegetation type and the leaf area index. The RPM is used to determine the runoff produced upon the precipitation which is down by the Xinanjiang Model at the cell scale. That means the runoff will be and will only be produced after the soil is saturated. The runoff is then divided into surface runoff and underground runoff according to the steady infiltration rate. The RRM is used to route the runoff to the basin outlet. In this study as the focus is on the flash flood forecast, so the underground runoff is considered steady, and the runoff routing is mainly the surface runoff routing which is further divided into hill slope routing that routes the surface runoff at the cell, and the river routing that routes the surface runoff in the river channel. The routing is controlled by the runoff flow velocity, the river routing velocity is derived from the Manning equation, and the hill slope routing velocity is governed by the Darcy-Weisbach equation, and a equation for deciding the velocity is derived also. The 2001 summer flooding of Three Gorges Basin is studied using the model presented in this paper, and satisfactory results was found. This model mainly relies on the remotely sensed data to physically derive model parameters, so it is particularly useful in the ungauged or poorly gauged basins.

HS03/08P/C26-006

1515

**PERFORMANCE ASSESSMENT OF BTOPMC MODEL IN NEPALESE DRAINAGE BASIN**

Nawa Raj PRADHAN<sup>1</sup>, Raghunath JHA<sup>2</sup> (<sup>1</sup>DPRI, Kyoto University, <sup>2</sup>Department of Civil Engineering, Institute of Engineering, Pulchowk Campus)

Nepal, with an area of 147,181 sq. km. has more than 6000 rivers stretching from the Great Himalayas with an elevation of more than 8800m to the southern plain called 'Terai' with an elevation of 100m within a mere 200 km width. This provides a dense network of rivers with steep topographical conditions and concentration of 80% of the total annual rainfall in a relatively short period of about four months. These peculiar characteristics lead to a set of hazards including frequent floods. In view of the important role that water resource can play in Nepal and the need to harness it in a sustainable manner, it is essential to know the various facets of water resource. Depending on the situation, different approaches to its use needed to be designed, sometimes to 'keep the water away from the people' and the other times 'keep the people away from the water'. Suitably selected models can help to identify issues which are useful for planning various development projects with minimum risk of flood disasters, alerting people to keep away from such disasters in time and providing planners an information about water for use in various development projects like hydropower, irrigation etc. But at the same time, evaluation of rainfall-runoff models that incorporates all the challenges- non availability of hydrological data itself, rugged terrain, a large part of catchment lying in Tibetan Plateau where the information of the data is not available-become one of the most significant themes in the context of Himalayan kingdom of Nepal. More suitable types of model include distributed models but they are data demanding. BTOPMC - a physically based distributed hydrological model based on the blockwise use of TOPMODEL with Muskingum-Cung flow routing method- was selected to evaluate the applicability in Nepalese catchment. The major rivers of Nepal like the Sun Kosi river originates from the Tibetan plateau where the data information is not available. Thus to cope with this problem further modification in the model was suggested that lead to the development of BTOPMC version II. The quality of simulation is classically judged by comparing the simulated flow with observed flow. Sensitivity analyses was performed as an effective means of coping with the inherent complexities of catchment modeling, including the associated parameter uncertainties. Model performance was judged by a range of quantitative and qualitative measures of fit applied to both the calibration and validation periods. The regression analysis for saturation deficit and discharge was performed. The daily stream flow estimation in Sun Kosi river basin was promising. BTOPMC being a distributed hydrological model uses a few numbers of parameter and can simultaneously simulate low flow or flood runoff for multiple subcatchments in large watersheds with DEM and other GIS oriented data. BTOPMC can be successfully used as a tool for integrated water resources investigation in large watershed, mountain physiographic region, of Nepal.

HS03/08P/C26-007

1545

**COUPLING OF MODFLOW AND WATFLOOD IN HYDROLOGICAL MODELING OF A SMALL WATERSHED**

Sayed-Farhad MOUSAVI<sup>1</sup>, Nicholas KOUWEN<sup>2</sup> (<sup>1</sup>College of Agriculture, <sup>2</sup>Department of Civil Engineering, Univ of Waterloo)

In water resources assessment, coupling of watershed and groundwater models is a process to integrate surface water and groundwater components. In this research, the coupling process was performed by applying the recharge component of the WATFLOOD hydrologic model to the MODFLOW groundwater model in the Laurel Creek watershed, Ontario, Canada. Net groundwater leakage computed by MODFLOW was combined with WATFLOOD surface flow and interflow and routed down the creek. The flows obtained by the coupling of the two models were compared with flows computed by the WATFLOOD model. Several runs were performed using radar-rainfall data and the hourly-measured stream flow for the period of 1993-1999. The results showed that use of adjusted radar precipitation improved the predicted stream flows. Running the MODFLOW model for 28 years of consecutive data showed that it takes about 20 years for the system to reach equilibrium, regardless of the starting heads. A simple lower-zone function (in WATFLOOD) was substituted for the MODFLOW to predict the stream flows without degrading the

computed stream flow.

HS03/08P/C26-008

1600

**PREDICTION OF EVAPOTRANSPIRATION AND STREAM FLOW WITH A DISTRIBUTED MODEL OVER THE LARGE WUDING RIVER BASIN**

Xingguo MO<sup>1</sup>, Suxia LIU<sup>1</sup>, Zhonghui LIN<sup>1</sup>, Weimin ZHAO<sup>2</sup> (<sup>1</sup>Institute of Geographical Sciences and Natural Resources Research, Chinese Academy of Sciences, <sup>2</sup>Bureau of Hydrology, Yellow River Conservancy Commission)

A process-based distributed model, LISFLOOD, is used to simulate the temporal and spatial variation of evapotranspiration and discharge over the Wudinghe basin in China. The climate of Wudinghe basin is arid with an annual precipitation of 450 mm, but there are usually heavy storm in the summer that may cause disastrous flooding. The basin is divided into 32000 square grids with a resolution of 1 km x 1 km. Channel pattern and slope gradient derived from digital elevation data of the basin are corrected by real pattern in the Geographical Information System. Recordings of 40 rain gauges and 10 meteorological stations are spatially interpolated with an inverse distance square method to all the grids in the basin. Remotely sensed normalized difference vegetation index (NDVI) of NOAA-AVHRR and the land use/cover data are used to retrieve the distribution of vegetation leaf area index (LAI). The model is applied to predict the discharge and evapotranspiration in two time periods 1984-1986 and 1994-1996. The predicted daily discharges are compared with the observed at five sub-catchments. It is shown that predicted discharges agree well with the measured in most of the sub-catchments, but obvious biases exist in some extreme discharge conditions. In this large, arid basin, it is found that the contributions of discharge are mainly from subsurface runoff, rather than surface fast runoff. Spatial patterns of evapotranspiration and its components in these two periods are also compared to distinguish the effect of land cover change on the hydrological cycle in this basin.

HS03/08P/C26-009

1615

**A CATCHMENT SURFACE RUNOFF SIMULATION FOR LAND SURFACE MODEL STUDY**

Shufen SUN, Weiping DENG (LASG, Institute of Atmospheric Physics, Chinese Academy of Sciences)

The main focus of this paper is to numerically simulate the surface runoff process in a catchment in China based on the TOPMODEL. The catchment is located in western China with area of around 2300 km<sup>2</sup>. In the paper, the basic principle and relevant problems of the TOPMODEL will be described and discussed. The long term more than 40 years observation data in the catchment is used to compare with the model output and thus verify the TOPMODEL function. The result shows that there is a good agreement between the observation data and model prediction. It is indicated that the TOPMODEL can be extended for land surface model in the region with runoff process controlled mainly by topography.

HS03/08P/C26-010

1630

**APPROACHING REALISTIC SOIL MOISTURE STATUS WITH AN IMPROVED MESO-SCALE NUMERICAL WEATHER PREDICTION MODEL**

Suxia LIU<sup>1</sup>, Lance LESLIE<sup>1</sup>, Milton SPEER<sup>2</sup>, Rees BUNKER<sup>3</sup>, Russel MORISON<sup>1</sup> (<sup>1</sup>Institute of Geographical Sciences and Natural Resources Research, Chinese Academy of Sciences, <sup>2</sup>Bureau of Meteorology, Sydney, Australia, <sup>3</sup>Rural Fire Office, NSW, Australia, <sup>4</sup>Inst of Geographical Sciences and Natural Resources Research, Chinese Academy of Sciences, Beijing)

Much research has focussed on the development of high resolution Limited Area meso-scale weather Models (LAM) to improve operational guidance for the prediction of meteorological variables including those associated with high levels of bushfire risk. Forest Fire Danger Index (FFDI) in Australia is one of the main indices used as guidance by fire weather forecasters to issue fire weather warnings. Most schemes that calculate a fire danger index are based on values of air temperature, relative humidity, wind speed and a factor that represents the dryness of the vegetation based on the number of days since precipitation has occurred. However, few schemes have yet considered soil moisture status, especially root zone soil moisture status, which is a key factor to consider for the outbreak of bushfires. The weak link between the land surface scheme and the atmosphere in LAMs is one of the reasons for the deficiency. To address this deficiency, this paper outlines a method to couple a self-nested High Resolution meso-scale atmospheric LAM (HIRES) developed by one of the authors (LL) to a hydrological model. By considering the moisture status in the whole of the root zone with a five layer soil division, the Force-Restore scheme used in original version of HIRES is replaced with the Richards Equation, as used in other land surface process models. Attention is also focused on how to effect the correct two-way transfer of soil moisture in the nesting, the setting of suitable boundary conditions, and other processes in the LAM that are affected by soil moisture. The model is validated with both gauge-observed precipitation and weather radar information. Use of both rainfall records together with radar data is important for validation as it has been shown that the spatial pattern of precipitation over the Goulburn River catchment is very important in shaping the hydrograph. By applying the coupled HIRES modelling system to the Goulburn River catchment in the Hunter Valley, NSW, Australia prior to and following a large bushfire in the catchment (November 97/December 97) for a sufficiently long enough period, improvements in surface soil moisture values are investigated. By including the improved regional scale soil moisture field, improvements in the HIRES model predictions of FFDI over the fire weather season can then be assessed. In previous work there was no effect of 1997/98 fires found on streamflow in the Goulburn River catchment. This contrasts with conclusions reported from extensive studies on catchments by other authors who have reported an immediate increase in streamflow after fire based on a variety of techniques including experimental analyses, paired-catchment analyses and modelling studies.

HS04

Monday, July 7 - Tuesday, July 8

**METHODOLOGIES FOR RISK ASSESSMENT OF WASTE WATER RE-USE ON GROUNDWATER QUALITY (ICWQ)**

Location: Site C, Room 30

## KEY NOTE LECTURES

HS04/07A/C30-001

0910

**AGRICULTURAL USE OF TREATED WASTEWATER: THE NEED FOR A PARADIGM SHIFT IN SANITATION & TREATMENT**

Julius B. VAN LIER (Sub-department of Environmental Technology, Wageningen University)

Shortages in irrigation water in and around urban areas calls for alternative sources in particularly the (sub)tropical zones. Domestic sewage represents such alternative source and its nutritional value is known by the farmers since long times. In many situations, even (diluted) raw domestic sewage is used for agricultural purposes, especially in those areas that cannot afford sewerage and treatment systems. However, discharge or reuse of non-treated effluents, give rise to serious environmental problems, including human health threats. Nonetheless, in most cases, the master plan of big cities reveals the conventional approach to deal with domestic and municipal wastewater, i.e., the construction of large-scale sewage collection systems including pumping stations and ideally a centralised treatment system. Unfortunately, such approach is not affordable for most of the developing countries and solutions between needs, requirements and socio-economic feasibility are paralysed. Decentralisation will play an important role in looking for alternative solutions since large-scale infra-structural investment can be avoided. Also with respect to the available treatment techniques, economic sustainability is often disregarded in making the final choices. Amongst the available compact technologies for wastewater treatment, the anaerobic (pre-)treatment can be regarded as an appropriate technology of which its potential is hardly utilised. In addition, anaerobic treatment is ideal to be implemented in a decentralised mode, i.e., reducing the required sewerage. The products of anaerobic treatment consist of nutrient-rich effluents, stabilised digested sludge and energy rich biogas. Particularly, the former two can beneficially be used by the local farmers, whereas the produced biogas can be used on the site if it is produced in sufficient quantities. The key-note lecture discusses the various options for anaerobic (pre-)treatment, embedded in centralised and decentralised treatment & reuse concepts. Its cost-effectiveness may lead to a more rapid implementation of productive sewage reclamation, while the environmental problems are concomitantly addressed.

HS04/07A/C30-002

1005

**ASSESSMENT METHOD FOR RISK OF GROUNDWATER QUALITY DETERIORATION WHERE RECLAIMED WATER IS STORED IN AQUIFERS**Peter J. DILLON<sup>1</sup>, Russell MARTIN<sup>2</sup>, Simon TOZE<sup>1</sup>, Paul PAVELIC<sup>1</sup>, Karen RATTRAY<sup>1</sup>, Ray CORRELL<sup>1</sup>, Ros MILLER<sup>1</sup> (<sup>1</sup>CSIRO Land and Water, <sup>2</sup>SA Dept for Water, Land and Biodiversity Conservation)

A five year research project involving laboratory and field investigations of aquifer storage and recovery with municipal sewage effluent treated to a quality suitable for unrestricted irrigation is drawing to a close. This has involved studies of the fate of various components of injected water including natural organic carbon, nutrients, disinfection byproducts, and pathogens. Seventeen observation wells up to 160m deep enabled studies of heterogeneous aquifer properties, hydraulics, clogging, mixing, recovery efficiency and geochemistry, as well as attenuation of constituents over two periods when a total of 360,000 cu.m. of reclaimed water was injected. The results give clear support for an ecosystems view of attenuation processes and enable confidence in prediction of risk associated with fate of contaminants. Consequently a simple screening model has been developed to predict the risk of unacceptable water quality being recovered at production wells. The paper will focus on the development and application of this risk assessment tool as a means of predicting impacts of injection of reclaimed water on groundwater quality.

HS04/07A/C30-003

1130

**FATE AND TRANSPORT OF ORGANIC CONSTITUENTS DURING SOIL-AQUIFER TREATMENT LEADING TO INDIRECT POTABLE REUSE**

Jorg Eckard DREWES (Colorado School of Mines)

One major water quality issue associated with soil-aquifer treatment (SAT) leading to indirect potable or non-potable reuse of wastewater effluents is the fate and transport of organic constituents. The objective of this study was to investigate the fate and transport of bulk and trace organics associated with potential adverse health effects in reclaimed water used for indirect potable reuse. The fate of organics during SAT was investigated using controlled biodegradation studies in adapted soil-columns and full-scale infiltration facilities in Arizona and California. The study design followed a watershed guided approach considering hydraulically corresponding samples of drinking water sources, SAT-applied wastewater effluents, and subsequent post-SAT samples representing a series of different travel times in the subsurface. Extensive characterization of organic carbon in the different samples was performed using state-of-the-art analytical techniques and biomass/bioactivity measurements in order to distinguish between primary removal mechanisms (biodegradation vs. adsorption). The results generally demonstrated that naturally-derived and effluent-derived organic matter after SAT overlap extensively in molecular weight distribution, amount and distribution of hydrophobic and hydrophilic carbon fractions, and chemical characteristics based on elemental analysis and structural analysis. However, the residual portion of the DOC contained both effluent-derived organic matter and natural organic matter. The study revealed that the stimulant caffeine, analgesic/anti-inflammatory drugs and blood lipid regulators were efficiently removed to concentrations near or below the detection limit of the analytical method after retention times of less than 6 months during ground water recharge. The antiepileptics carbamazepine and primidone were not removed during ground water recharge under either anoxic saturated or aerobic unsaturated flow conditions during travel times of up to eight years. Organic iodine showed a partial removal only under anoxic, saturated conditions as compared to aerobic conditions and persisted in the recharged ground water.

## CASE STUDIES

HS04/07P/C30-001

1405

**ASSESSMENT OF RE-USE OF WASTEWATER FOR IRRIGATION: A CASE IN PUNJAB, PAKISTAN**Yutaka MATSUNO<sup>1</sup>, Jeroen ENSINK<sup>2</sup>, Robert SIMMONS<sup>2</sup>, Wim VAN DER HOEK<sup>2</sup>, Sarfraz MUNIR<sup>1</sup>, Rizwan ASLAM<sup>2</sup> (<sup>1</sup>Department of International Resources Management, School of Agriculture, Kinki University, <sup>2</sup>International Water Management Institute)

Farmers often take advantage of using wastewater for irrigation in arid regions of developing countries as it is a reliable water source and contains rich nutrients. However, its negative impact on health, environment, and sustainability needs to be taken into account. In addition, as a country develops, the risk of industrial pollution in irrigated fields increases. In most cities in Pakistan, untreated wastewater is used directly for irrigating crops in urban and peri-urban areas. A study to assess the environmental and health risks associated with using untreated wastewater for irrigation was carried out in two cities; Faisalabad and Haroonabad, in the Punjab province of Pakistan. The two cities have distinct characteristics: Haroonabad has a population of 67,000 and no major industries, while Faisalabad is one of the bigger cities in Pakistan with a population of over 2,000,000 and has major industries. In Faisalabad, inadequate and inconsistent original irrigation supply and in particular a significantly restricted command area due to drought/re-allocation induced reduction in flows has resulted in partial and in most cases 100% reliance on wastewater for irrigation. The study consisted of hydrological analysis of wastewater irrigation and chemical analysis of wastewater, soil, and groundwater, in addition to field inspections and interviews with farmers and officials from the respective Municipalities and the Irrigation Department. In order to establish management alternatives, the information collected was categorized to evaluate the risk of current practices and its impacts on the environment. The results confirmed that, due to an excessive application of wastewater, the nitrogen and phosphorus concentrations in the groundwater under the wastewater irrigated sites were much higher than those concentrations in fields irrigated with normal canal water. Soil heavy metal contents in wastewater irrigated areas of Faisalabad indicate significantly elevated heavy metal loading rates, which pose a risk for both sustainable production and human/livestock health. In comparison, soil heavy metal concentrations in Haroonabad were within internationally established 'safe' limits. Salinity problems have also been reported in some fields in Faisalabad due to the high content of salt in the wastewater. In addition, crop diversity and quality has steadily declined following long-term wastewater application. In Faisalabad and Haroonabad, positive impacts of wastewater utilization to farmers include the provision of a reliable source of irrigation and the ability to produce cash crops with high cropping intensity and less fertilizer inputs. Consequently in both cities, wastewater utilization is fundamental to maintaining current rural livelihoods. Owing to the present financial constraints and institutional settings of the cities, it is difficult to foresee an introduction of a treatment system in the near future. In this circumstance, it is very important to develop and apply comprehensive methods of wastewater irrigation management that would facilitate the sustainable use of soil and ground water resources, preserve environmental integrity and improve rural livelihoods on a long-term basis.

HS04/07P/C30-002

1435

**ON THE IDENTIFICATION OF NITRATE POLLUTION IN GROUNDWATER IN A WASTEWATER IRRIGATED FIELD**

Jianyao CHEN, Changyuan TANG, Yasuo SAKURA, Yanjun SHEN (Hydrology Group, Department of Earth Sciences, Chiba University)

Wastewater is widely used for irrigation in arid and/or semi-arid area, especially in the suburb of the big city. As a special water resource with respect to its nutrients and toxic chemicals, wastewater, particularly non-treated must be used with care to prevent nitrate pollution in groundwater. Luancheng County, nearby Shijiazhuang, the capital city of Hebei Province in the North China Plain, was selected as a case study area, where non-treated wastewater from a non-proof canal had been used for more than 40 years. Direct irrigation with wastewater and seepage from the canal flowing from the north to the south, were two approaches for contaminating the local aquifer. Local people use groundwater as drinking water without any treatment from the aquifer, which flows from the northwest to the southeast according to the groundwater table and topography. Field surveys and the measurement of major ions of groundwater show that hardness (Ca+Mg) in groundwater increases in recent years, indicating the effects of long-term wastewater irrigation. Groundwater table of the study area remains relatively stable and shows no seasonal fluctuation in comparison to the intensive seasonal change in the vicinity without exterior water. Though low hardness and no nitrate was found in the wastewater, nitrate was detected for all groundwater samples in the wastewater irrigated area with about 50% higher than the drinking water standard (45 mg NO<sub>3</sub>-N/l) of WHO. The concentration of NO<sub>3</sub> decreased with the distance from the canal and the highest of 124 mg NO<sub>3</sub>-N/l was found in a well near the canal. Good linear relationship between CL and NO<sub>3</sub> indicated that nitrate in groundwater in the area had the same source associated with a dilution process. Stable isotopes, O-18, D and N-15 were also used as tracers to identify the source of pollution and the related physical and chemical processes. In order to identify the sources and distribution of nitrate in groundwater, physical factors, such as water balance components and groundwater flow system ought to be integrated well with chemical contents and isotopes as well in a comprehensive manner.

HS04/07P/C30-003

1505

**LONG TERM EFFECT OF IRRIGATION WITH WASTEWATER ON NITRATE IN GROUNDWATER OF NORTH CHINA PLAIN**

Changyuan TANG, Jianyao CHEN, Yuanjun SHEN (Graduate School of Science and Technology)

Because urban wastewater or groundwater has been used for irrigation in the regions where water is scarce and re-use of wastewaters is a challenging possibility to manage regional water resources, it is important to re-assess the long-term impacts of wastewater irrigation practices on regional groundwater quality. As wastewaters contain elements and compounds that may damage environmental quality, if deposited at a wrong location and time at a too high rate, wastewater can be dealt with in terms of water cycle and chemicals migration in groundwater. At first, history of wastewater irrigation practices in North China Plain (NCP) after 1950s was reviewed. With the urbanization in NCP, huge tons of wastewater was disposal from cities as an alternative source of irrigation water for agricultural development. With its average annual precipitation less than 600mm, 80% of irrigation water used in the farmland near big cities of NCP is urban wastewater. As a result, surface water and groundwater quality problems have been very serious. Then, nitrate problem in groundwater quality caused by wastewater irrigation has been discussed. A case study in the North China Plain was shown. There are three ways for nitrate entering into the groundwater system, i.e.

seepage of wastewater at the bottom of the canal, infiltration of wastewater in the wastewater-irrigated croplands, and infiltration of fertilizers used in the groundwater-irrigated croplands. It was found that the wastewater canal controls the local groundwater flow system, and concentrations of nitrate in most wells with depths of less than 40 m are higher than the drinking water standard set by WHO. In the croplands irrigated by wastewater, NO<sub>3</sub>- concentration ranges from 50 to 130 mg/L, but in the croplands irrigated by pumping wells away from the canal, NO<sub>3</sub>- concentrations are less than 35 mg/L. Clustering analysis was used to classify the spatial distribution of nitrates resulting from the wastewater. Identification of chemical patterns is found to be effective for the comprehensive assessment of spatial distribution of groundwater quality. As a result, poor management of wastewater transport systems may cause leakage of wastewaters to groundwater resulting in a serious deterioration of its quality. Monitoring of the chemical composition of groundwater quality yields information that can be used to find trends in groundwater quality. Finally, statistical analysis was used to identify effects of pumping irrigation and wastewater irrigation on nitrate distributions in groundwater of the study region, respectively. It was found that there is a higher possibility of nitrate concentration detectable in wastewater irrigation area than that in pumping-irrigation. It is also emphasized that the wastewater controls nitrate distribution in groundwater, and should be used carefully to protect both soil and groundwater from nitrate pollution. Effluent-soil-plant system is necessary for the development of appropriate irrigation-fertilization-cropping management system.

**HS04/07P/C30-004****1555****DETERMINATION OF WATER QUALITY IMPROVEMENTS DUE TO THE ARTIFICIAL RECHARGE OF TREATED EFFLUENT**Simon TOZE<sup>1</sup>, Jon HANNA<sup>1</sup>, Tony SMITH<sup>1</sup>, Lindsay EDMONDS<sup>1</sup>, Adrian MCCROW<sup>2</sup> (CSIRO Land and Water, <sup>2</sup>Water Corporation WA)

An indirect wastewater reuse project was established at a wastewater treatment plant to determine the effectiveness of obtaining reclaimed water of suitable quality and low risk for the irrigation of parks and gardens. Treated sewage effluent was infiltrated to a shallow limestone aquifer and recovered by two recovery wells situated 80 and 100 m from the infiltration basins. A monitoring and research program was established to ensure that the water recovered from the production bores meet environmental and health guidelines for water reuse in irrigation. The monitoring program consisted of monthly sampling of the two production bores, an in-line water storage tank, treated effluent in the infiltration ponds and native groundwater. The collected samples were analysed for a range of physical, chemical and microbiological analytes. Results of the monitoring program indicated that the recovered water quality was well below the Western Australian guideline limits for effluent reuse and suitable for irrigation purposes. The reclaimed water was found to be physically, chemically and microbiologically different from both the treated effluent in the infiltration basins and the native groundwater. The reclaimed water had consistently low inorganic nitrogen and phosphate concentrations and significantly lower electrical conductivity than the native groundwater. Total organic carbon concentrations in the reclaimed water were much lower than in either the treated effluent or native groundwater. No bacteriophage or enteroviruses and only intermittent very small numbers of *E. coli* cells were detected in the recovered water at any time during the monitoring program. As these microorganisms were frequently detected in the treated effluent this indicated that there was removal during infiltration and in the aquifer. An assessment of the hydrogeology in the region of the infiltration ponds found that the limestone aquifer was highly transmissive, under tidal influences and had a very flat hydraulic gradient. Modelling of the groundwater flowpaths and the effect of secondary porosity in the aquifer determined that the infiltrated effluent would remain within the general limits of the wastewater treatment plant. An additional study of pathogen survival potential indicated that bacterial pathogens and indicators had very limited survival in the aquifer with 90% removal times within ten days. Viral pathogens had a greater survival potential than the bacteria but still had 90% removal times of less than 17 days. The results of this study have shown that indirect reclamation in shallow limestone aquifers within Western Australia is a viable means of obtaining reclaimed water of suitable quality for irrigation purposes and that there would thus, be a limited impact on groundwater quality in the surrounding area.

**HS04/07P/C30-005****1625****IMPACT OF UNINTENDED RECHARGE OF ASSAMRA WASTEWATER STABILIZATION PONDS ON THE SHALLOW AQUIFER IN WADI DHULEIL BASIN**

Nizar KLhalil AL-HALASAH (Environmental Research Centre, Royal Scientific Society)

This paper tackles the impact of Assamra Wastewater Stabilization Ponds (AWSPs) and the discharge effluent from the treatment plant on the groundwater quality of the shallow aquifer in the area. AWSPs is considered as one of the largest treatment plants in the world, it is located about (40 Km) northeast Amman. To study the impact of infiltrated wastewater on the groundwater, twelve wells were monitored during the period from March 1994 to March 2002. Two wells upstream the plant, six wells adjacent wadi Dhuleil where AWSPs discharge its effluent, and five wells to the south-east of plant. It is clearly noticed that wells adjacent to wadi Dhuleil contain higher concentrations of TDS, SO<sub>4</sub>, NH<sub>4</sub>, NO<sub>3</sub>, Cl, Na, TH, B, PV, in addition to TCC and TTCC than the wells located upstream and south-east the plant this trend attenuates along the groundwater flow direction (East-West). Physical, chemical and microbiological analyses show that there are several sources of pollution in the study area like, agricultural activities, overpumping rates and AWSPs.

**HS04/07P/C30-006****1655****TREATED URBAN WASTEWATER REUSE FOR IRRIGATION OF A GOLF COURSE AND IMPACT ON SOIL AND GROUNDWATER**Lucila CANDELA<sup>1</sup>, Jordi MAS<sup>2</sup> (Dep. of Geotechnical Engineering and Geoscience-UPC, <sup>2</sup>Dep. of Microbiology. UAB.)

Starting in July 2000, treated wastewater of urban origin has been used for the irrigation of the "Serres de Pals" golf course (Girona-Spain). To evaluate if the soil and the aquifer underneath are affected by the utilization of this type of water, samples have been taken along a period of several months from the wastewater treatment plant, the stabilization lagoon and soil profiles. Analyses have been performed for total coliforms and aerobic bacteria, soil water pressure and soil water content as well as chemical analyses of the irrigation water and water of the vadose zone. Soil profiles taken at several times during the study indicate the absence of coliforms except for a short period during summer. In the vadose zone and the aquifer a significant increase in salinity was detected 10 months after starting the application.

**MODEL DEVELOPMENT POLYCY****HS04/08A/C30-001****0905****THE NUTRIENT EXPORT RISK MATRIX (THE NERM) FOR STRATEGIC APPLICATION OF BIOSOLIDS TO AGRICULTURAL LAND**Louise HEATHWAITE<sup>1</sup>, Sean BURKE<sup>1</sup>, Paul QUINN<sup>2</sup>, David LERNER<sup>3</sup>, Paul WHITEHEAD<sup>4</sup>, Adrian SAUL<sup>1</sup>, Neil PREEDY<sup>4</sup> (<sup>1</sup>Department of Geography, University of Sheffield, <sup>2</sup>Department of Civil Engineering, University of Newcastle, <sup>3</sup>Department of Civil & Structural Engineering, University of Sheffield, <sup>4</sup>Department of Geography, University of Reading)

Diffuse phosphorus (P) export from land is a key driver of the eutrophication of surface waters (Dils & Heathwaite, 2000) and may contaminate groundwater resources. High risk diffuse P sources include animal manures and biosolids: both carry the enhanced environmental risk associated with microbial contamination of waters. Biosolids recycling to land in the UK is projected to double by 2006 but the security of this route is threatened by environmental concerns and health scares. Soil P saturation is already being documented in some areas and may further elevate P losses to surface and groundwaters. The SEAL Research Project: Strategic Management of Non-Point Source Pollution from Sewage Sludge is evaluating the environmental risk of contaminant export from biosolids recycling to land. Our basic premise is not all land has an equal risk of contributing diffuse contaminants to receiving waters. We believe high risk is associated with critical source areas of diffuse pollution where source and transport risks coincide (Heathwaite & Sharpley, 1999). We are focusing on colloid-size particles, which have been shown to be mobile in subsurface environments and important for virus and bacterial transport. We are investigating the extent to which colloids facilitate the transport of strongly sorbing pollutants such as P. This work is tied to the development of a predictive and spatially-sensitive semi-distributed model of critical thresholds for biosolids application that goes beyond traditional 'end-of-pipe' or 'edge-of-field' modelling, to include hydrological delivery to receiving waters from diffuse sources at the catchment scale. The research output from this project is being synthesised into a risk advice matrix (the Nutrient Export Risk Matrix or NERM) for our end-users on the project which include water utilities: Thames Water plc, North West Water plc, Yorkshire Water plc and their research arm: UKWIR (UK Water Industries Research), the Environment Agency and DEFRA (the Department of Environment, Food and Rural Affairs). The NERM will help determine the most appropriate form and frequency of spatially-sensitive biosolids application to land to achieve sustainable biosolids management without detriment to the environment and receiving water quality, whilst being of net benefit to farmers. Dils, R.M & Heathwaite, A.L. (2000). Tracing P movement in agricultural soils. In Foster, I. (Ed) Tracers in Geomorphology. Wiley, 259-276. Heathwaite, A.L. & Sharpley, A.N. (1999) Evaluating measures to control the impact of agricultural P on water quality. Water Science & Technology 39, 149-155.

**HS04/08A/C30-002****0935****VARIATION OF CHEMICAL SPECIES INFILTRATING TREATED SEWAGE WATER USING THE MULTI-COMPONENT SOLUTE TRANSPORT MODEL**

Gingging De Castro GUERRA, Kenji JINNO, Yoshinari HIROSHIRO (Institute of Environmental Systems, Kyushu University)

For the conservation of water resources, the re-use of treated sewage water should be considered. However treated sewage waters contain elements and compounds that may damage environmental quality. The relevant physical, chemical and biochemical processes in the soil must be understood in order to determine the state and movement of groundwater contaminants. To simulate the mechanisms responsible for the movement of chemical species through soils and aquifers predictive tools in the form of mathematical models have been developed by several researchers. This study deals on the processes and chemical transport in an aqueous soil similar to paddy field, where successive reduction reactions occur like denitrification, cation exchange reactions and oxidation and reduction reactions. Oxidation and reduction reactions play an important role in the spatial distribution of chemical species in soils like O<sub>2</sub>, NO<sub>3</sub><sup>-</sup>, Mn<sup>2+</sup>, and Fe<sup>2+</sup>. To examine the behavior of the different chemical species infiltrating secondary treated sewage water, a two-soil column experiment was conducted using columns of different thickness of plow layers. Glass beads were used as oxidized layer at 15 cm for both the two soil columns. Treated sewage water was constantly supplied up to 5 cm at the top of the soil column in order to reproduce the redox condition similar to paddy field situation. In order to more fully understand chemical and biochemical processes, a solute transport model that takes into consideration the biochemical reactions and cation exchange reactions was developed in this study. The multi-component solute transport model simulates solute transport and computes changes in concentration over time caused by the processes such as advection, dispersion, biochemical reactions and cation exchange reactions. The soil column experiment and solute transport model had produced interesting observations on the behavior of different chemical species infiltrating treated sewage water. The measured cation concentrations correlated fairly well with the simulated cation concentrations. The most rapid bacterial growth occurred at the top of the column where O<sub>2</sub> and CH<sub>2</sub>O concentrations are present. NO<sub>3</sub><sup>-</sup> concentration decreased due to denitrification while Mn<sup>2+</sup> and Fe<sup>2+</sup> increased due to dissolution of Mn- and Fe-hydroxides. The simulated concentrations approximately agreed with the measured concentrations and the sequences of reduction reactions can be reproduced by the developed solute transport model.

**HS04/08A/C30-003****1005****SATURATED MODELING OF EFFLUENT RECHARGE AND ITS IMPACT ON GROUNDWATER QUALITY**Shutang ZHU<sup>1</sup>, Gang ZHAO<sup>1</sup>, Yueqiang LIU<sup>1</sup>, Keke PENG<sup>1</sup>, Xuan ZHAO<sup>1</sup>, Xiaojing YANG<sup>1</sup>, Yuanle MA<sup>1</sup>, Yiping GAN<sup>2</sup> (<sup>1</sup>Institute of Nuclear Energy Technology, Tsinghua University, <sup>2</sup>Gaobeidian Wastewater Treatment Plant)

This paper presents numerical modeling on saturated flow and reactive transport of groundwater recharge with secondary effluent. To alleviate the shortage of water supply in North China and maintain the sustainable development, reuse of treated wastewater through groundwater recharge must be considered as an integral part of water and wastewater management. Based on such a background, a demonstration project of groundwater recharge with secondary effluent at Gaobeidian Wastewater Treat Plant (WWTP) will be implemented. As the wastewater may bring pollution to surface water, if the artificial recharge is dealt with improperly, it may also bring serious contamination to the groundwater. To avoid the effluent recharge bringing additional pollution to groundwater system and deteriorating the water quality, complex and deep-going investigations including laboratory experiments, numerical simulations as well as pilot tests are required before the practical operation. Processes of groundwater movement and contaminants transport

should be simulated while the impact on the quality of groundwater resource must be assessed. The present study focuses on the numerical model, which is used to simulate contaminants transport including convection-dispersion, adsorption / de-sorption, dissolve / precipitate and / or biodegradation and to assess the impact of such recharge on the quality of groundwater resource. The groundwater movement is modeled based on the saturated flow assumption and Bossinesq approximation. The soil field is divided into two zones with different characteristics: the inertial zone above the water table and the saturated zone below the water table. It is assumed that the effluent directly drops to the water table after recharged. A new method is developed to deal with the varying water table and the discretized matrix equation is solved using the Pre-conditioned Jacobi Conjugate Gradient method (PJCG). Operator-splitting techniques are applied to the reactive transport model while an implicit upwind finite difference scheme is developed to solve the convection-dispersion equations. Explicit solutions with small time step, which can be considered as exact solutions, are also computed to demonstrate the validity of the present method. With the numerical predictions, the scheme of practical operations for the demonstration project is drawn up. The detailed descriptions on the solution procedure for the reactive transport model are given in an accompanying paper (Zhu et al.)

## WASTEWATER RE-USE POLYCY

HS04/08A/C30-004

1100

### ASSESSMENT OF WASTE WATER GENERATION, MANAGEMENT PATTERN AND ITS RE-USE POTENTIAL IN URBAN INDIA

R. B. SINGH (Department of Geography, University of Delhi)

Cities and towns in India are exposed to water pollution. Indiscriminate discharge of domestic and industrial waste water has polluted water resources. Ground water reserves are under risk of pollution as a result of seepage of surface pollutants. Estimates of access to excreta disposal systems vary between 48 per cent to 70 per cent. Out of 300 cities having population of 100,000, about 70 have partial sewage systems and sewage treatment facilities. Levels of sewage treatment is very low. Thus the untreated and partially treated municipal waste water finds its way into precious water sources such as rivers, lakes and ground water, causing water pollution. Recently untreated such water is being used for urban agriculture etc. As per the study conducted by the central Pollution control Board during 1994-95, the total waste-water generated in 300 class-I cities is about 15,800 million litres a day (mld), while the treatment capacity is hardly 3,750 mld. In the 23 metropolitan cities, over 9000 litres of sewage is generated daily, of which about 60 per cent is generated in the 4 mega cities such as Mumbai, Kolkata, Delhi and Chennai. In the metro cities, only 30 per cent waste water is treated before disposal. Most of the cities have only primary treatment facilities. The situation of industrial waste water is also problematic. Waste water management system is the framework within which all activities associated with generation, storage, collection, transfer, processing and disposal of waste water. This includes other activities designed to reduce the amount of waste water at all points. Waste water can be categorized according to the sources from which it emanates such as household, commercial, institutional like hospitals and industrial etc. Waste water can be reduced through pre-consumer recycling (during production process, household level, transport, re-use and recycling. In Indian situation sustainability of waste water management includes minimization of waste water production, maximization of re-use and recycling and its financial viability, efficiency in terms of clean and healthy neighbourhood. Keeping within the absorption capacity of local sinks for waste water, level of facilities need to be improved for protection of soil and ground water from pollution. It is very important that waste water produced by enterprises should be re-use or recycled within the same. Public involvement through NGOs and DNGOs and resident association will go a long way in achieving the sustainability. Contents of linkages for partnership between local government and communities include discussions, consultations, negotiation, sharing of functions and decision taking power etc. The Central Pollution Control Board strengthened the monitoring of water quality of national aquatic resources through a network of 414 stations on rivers, 25 on ground water, 38 on lakes and 30 on canals, creeks, drains and ponds etc.

HS04/08A/C30-005

1130

### ASPECTS OF GROUND WATER ENRICHMENT BY WASTEWATER REUSE IN THE PALESTINIAN TERRITORIES

Rebby Ata EL SHEIKH<sup>1</sup>, Sami Mahmoud HAMDAN<sup>2</sup>, Ashraf Sobhy ABO SHAMMALA<sup>3</sup> (<sup>1</sup>Technical Directorate, Palestinian Water Authority, <sup>2</sup>Information department, Palestinian Water Authority, <sup>3</sup>Engineering Unit, UNDP)

The Palestinian population amounts to 1.2 Million in Gaza and 2.1 Million in the West Bank. Water is mainly supplied for Gaza Strip from the coastal aquifer at the rate of 130-135 MCM/year. The annual renewable quantity for the coastal aquifer is about 98MCM out of which 46MCM are infiltrated directly from rain water and the remainder is from the irrigation return flow, wastewater leakage and brackish trans boundary flow. This allows for sea water intrusion. In the West Bank the annual renewable quantities of groundwater in the Western, Northeastern, and Eastern basins in addition to springs are estimated at 691-811 MCM/year. Out of that only 143 MCM/year are accessible by the Palestinians in the West Bank due to the political situation. On the wastewater side, only 50% of the Gaza strip is covered by collection networks where only secondary treatment is available for 20%. Meanwhile more than 80% of the West Bank area is not sewered. Generally, the water quality is continuously deteriorating as a result of over abstraction and infiltration of both the wastewater and the return flow polluted with pesticides and detergents recharged from agriculture. Samples taken from the ground water aquifer down stream from wastewater treatment plants and in unsewered areas where septic tanks for sewage are used show relatively high Nitrate concentration. Although recovery wells drilled at a safe distance from the recharging sites indicate improved water quality, still a psychological barrier exists for local residents in the vicinity of a waste water treatment plant that the quality of extracted ground water is affected by the plant effluent infiltration. By the time recharge to the aquifer and reuse of treated wastewater in agriculture are key points in the Palestinian water sector policy especially since the agriculture sector consumes about 80% of the total abstraction, it is still not an easy task to apply on a large scale due to high investment requirements to improve the effluent characteristics, to build the required infrastructure and to overcome the psychological problem. Nevertheless a pilot project is under preparation in Gaza Strip.

HS04/08A/C30-006

1200

### GROUNDWATER QUALITY DETERIORATION - A MAJOR THREAT TO WATER RESOURCES

Hillel RUBIN (Department of Civil Engineering, Technion - Israel Institute of Technology)

About 50 years ago the Israeli Water Law was established, stating that all water resources available with the State of Israel belong to the nation. This law allowed the National Water Carrier and the Coastal Drainage that avoids loss of groundwater into the sea, etc. However,

presently the Israeli Water Law cannot compete with contemporary water quality problems. For many years cotton was the major crop irrigated by treated wastewater. Due to the government decision of raising the price of treated wastewater raising cotton disappeared, and large quantities of treated wastewater flow into the sea. A group of professors has claimed that irrigation with treated wastewater is extremely dangerous to groundwater quality, and only treatment to drinking water quality is acceptable. The Water Commission has no capability to compete with this issue. Eventually, this topic is of purely agricultural nature. Also here some examples indicate that often privatization with limited governmental control give results much better than provided by the big government. Some urban communities have been released from payments of the "balance payment" (is imposed by the Water Law) if they pump and reclaim groundwater contaminated by nitrate, micropollutants, etc. So, they built groundwater treatment plants. The Water Commission is presently pushing the construction of big desalination plants to overcome the water needs. However, in Florida many urban communities have built such plants with no government involvement. Why do Israeli urban communities need the Commissioner involvement? Why should not they obtain reclaimed groundwater? If the urban communities can sell treated wastewater to farmers for irrigation, why do they need the pricing of the Water Commission? The operation of the Coastal Drainage plant, resulted in a continuous increase of contaminants in groundwater. Mass conservation law implies such a result. Therefore, quantities of these contaminants should be taken out from the aquifer, to balance the mass input and output. It is appropriate to encourage use of reclaimed groundwater rather than desalination of sea water, wherever it is possible. The government should allow communities to choose the best option for their water supply source. Probably they will pick up the optimal solution much better than it can be done by the Water Commission. There are also good chances that communities have better capability than the Water Commission to avoid the contamination of their aquifer and to identify the individuals responsible for the contamination of groundwater.

HS04/08A/C30-007

1230

### CONSERVATION OF WATER RESOURCES IN BERLIN (GERMANY) THROUGH DIFFERENT RE-USE OF WATER

Birgit FRITZ<sup>1</sup>, Stephanie RINCK-PFEIFFER<sup>2</sup>, Thomas HEBERER<sup>3</sup>, Asaf PEKDEGER<sup>1</sup> (<sup>1</sup>Centre of Competence for Water Berlin, <sup>2</sup>Technical University Berlin, <sup>3</sup>Free University Berlin)

The inhabitants of Berlin, just about 3.4 million, are supplied with drinkingwater by its own groundwater resources exclusively. In order to conserve the natural available groundwater, it is enriched intensively by bank filtration from surface waters and artificial recharge. In addition, some of in the past intensively used sewage farms are still in function. Hence, the volume of the groundwater storage, its quality and the proportion of artificial recharged or bank filtered water are of significant importance for a sustainable water management in Berlin. A partly closed water cycle is a result of the usage the treatment and recycling of water in Berlin. Advanced treated wastewater is discharged into the surface waters. To predict increasing loads of nutrients in the surface water, phosphorus is removed upstream in a phosphorus removal plant (up to 0.02 mg/l). The production wells of the water supply system are located in a short distance (10-600 m away) around the lakes and rivers, which are affected by the input of the above described treated water. The surface waters are also used for artificial recharge through infiltration ponds. Nevertheless, there is no need for further treatment after abstracting the bank-filtered water. The only treatment consists of an aeration step for removal of manganese and iron. The natural pre-treatment in the aquifer (Soil-aquifer treatment) during bank filtration and artificial recharge is one of the most important parts within this water cycle. Intensive investigations started to study the efficiency of the removal processes. Former studies have shown that the oxygen consumption and the most important geochemical processes are taking place in the first few centimetres to meters in the aquifer. Redox sequences can be observed as described in the marine environment also in the groundwater, where oxygenated river water infiltrates to an anoxic aquifer. On of the main topics of this research programme is the removal of bacteria, drug residues, algae toxins and organics and the hydrogeochemical and biological interaction in the sediment/water layer. Mathematical models for flow and transport can be used to simulate possible changes of chemical loads, flow velocities or through the performance of the supply system.

H

HW01

Wednesday, July 9 - Thursday, July 10

### EFFECTS OF HUMAN ACTIVITIES ON HYDROLOGICAL AND BIOGEOCHEMICAL CYCLES (ICWQ)

Location: Site C, Room 26

Wednesday, July 9 AM

Presiding Chairs: K. Heal, N. Ohte

HW01/09A/C26-001

Invited

0910

### WATER AND SEDIMENT PATHWAYS FROM TERRESTRIAL TO FLUVIAL SYSTEMS: THE KEY TO ASSESSING LAND USE

Roy C. SIDLE (Disaster Prevention Research Institute, Kyoto University)

Understanding the pathways of water and sediment from the hillslope to the stream, and subsequently within stream systems is essential to evaluate the spatial and temporal effects of land uses. Headwater catchments are sources of sediments, nutrients, and biota for larger streams, yet the hydrologic pathways that transport these materials remain unclear. Most of the research on hydrologic and sediment modeling that has attempted to incorporate processes, still greatly simplifies the complexity of hydrologic and geomorphic pathways. To understand the movement of sediments and water from source to sink, it is necessary to link hydrologic processes with their respective geomorphic setting and vice versa. One paradigm that has been proposed is the hydrogeomorphic concept of stormflow generation, whereby catchments are partitioned into landform attributes based on their unique hydrologic response. For example, in steep forested hillslopes, storm runoff occurs largely as subsurface flow, comprised of dynamic proportions from the matrix flow and preferential flow paths depending on antecedent wetness. The relatively flat riparian corridor generates saturated overland flow due to the perennially high water table. The extent of saturated overland flow depends on the width of the riparian zone. Geomorphic hollows are also important dynamic sources of storm runoff, as well as landslide sediment, in many steep catchments. Runoff from hollows appears to initiate when a threshold on groundwater has accumulated and thus the timing of response is related to soil depth. Each of these three sources may have different chemical signatures, but sorting out the pathways based solely on these signatures can be misleading due to mixing and exchange that occurs as water moves to stream channels. Sediment pathways are more obvious than hydrologic pathways, but are still poorly understood. To assess the effects of land use practices on soil loss and

sediment transport, a clear distinction needs to be drawn between surface erosion processes (surface wash) and mass wasting. Surface erosion is typically initiated when contiguous areas of hillslopes are compacted and disturbed. In temperate forests where organic horizons are relatively thick, sites may be able to withstand a certain level of disturbance before surface erosion links directly to streams; however, in tropical environments where decomposition rates are high and in sparsely vegetated dry sites, such erosion linkages can be dramatic. Mass wasting occurs in many steep environments and often links directly to channels, but the dynamics of sediment loading to streams is difficult to assess due to the episodic nature of these processes. Geomorphic hollows are sites of recurrent landsliding and sometimes initiation of debris flows depending on failure volumes and channel linkages. Assessment of this suite of hydrogeomorphic processes and pathways is necessary for the planning of land use activities.

HW01/09A/C26-002

0930

#### IMPACT OF URBAN GROWTH ON INDIA'S SURFACE AND GROUNDWATER QUALITY

Sitharama Murty KOTTAPALLI (Coordinator of Geoarchives, International Commission on the History of Geological Sciences (INHIGE))

Urbanization has become a global phenomenon and its ramifications are more pronounced in developing countries. Natural growth of population, reclassification of habitation and migration trends are important factors contributing to the unmitigated increase of urban growth and population in India. Urban population of India was 217 million as per 1991 census, accounting for about 26 per cent of its total population, in 3768 urban agglomerations and towns. This is likely to rise in 442 million (38 per cent) of the country's population by 2006 - 2007 A.D. The first attempts at a survey of water supplies and sewerage systems in India was made in 1944 which revealed that the urban population as also the rural population that could bank upon safe water supplies was 6.6 per cent in Madras, 7.3 per cent in Bengal, and 4.1 per cent in U.P. It was then proposed that 90 per cent of the population should obtain water supply and sanitation facilities within 40 years. The number of metropolises increased from 12 in 1981 to 23 in 1991. In the initial period of planning (first five year plan) the outlay on urban drinking water was relatively substantial in relation to the urban population (17.3 % to 19.9 %). The outlay was 1.28 % which has risen to 1.38 %. Correspondingly, the outlay on rural water supply rose from 0.18 % to 2.47 % from 1951 to 1992 - 97 plans. In the eighth plan, an Accelerated Urban Water Supply Programme (AUWSP) was launched, targeted to small towns (population less than 20,000 - 1991), with a modest outlay of Rs. 500 million and 50:50 contribution by the Central and State Governments. Out of 2151 eligible towns project reports have been approved for 225 towns at an estimated cost of Rs. 2129.00 million. In India, the availability of water (both surface and ground) varies extremely in the various regions of the country. Rajasthan, for example, has 8 % of the country's population, but has only 1 % of the total water resources of the country, while Bihar with 10 % of the country's population has 5 % of the water resources. Until recently, an ordinary Indian was satisfied with availability of water, but today he wants water that is devoid of chemical and bacteriological contamination. Groundwater in the coastal tracts of Saurashtra is brackish due to over exploitation. Fluoride level is high in vast tracts of Andhra Pradesh, Haryana, Rajasthan, parts of Uttar Pradesh, Punjab, Karnataka and Tamil Nadu. Iron content is higher in major parts of northeastern States and many parts of Bengal have high arsenic content in the groundwater. The surface and groundwater sources have been affected by indiscriminate use of pesticides, release of wastes and industrial effluents into the surface and groundwater zones. A modified Model Bill of the Central Ministry of Water Resources in groundwater exploration is there for the consideration of the State Governments and many of them have enacted the necessary legislation.

HW01/09A/C26-003

0950

#### THE CHANGE OF SPRING WATER QUALITY CAUSED BY URBANIZATION IN UPLAND AREA

Atsuko TERAZONO<sup>1</sup>, Hiroo OHMORI<sup>2</sup> (<sup>1</sup>Graduate Student, Department of Natural Environmental Studies, The University of Tokyo, <sup>2</sup>Department of Natural Environmental Studies, The University of Tokyo)

In recent years, land use/cover changes due to urbanization have been followed by the changes in quality of spring waters and shallow groundwater, in the uplands and hilly lands, in metropolitan areas. The deterioration of hydrological environment has been emphasized, and it is needed to put forward an adequate policy for urbanization. However, the actual state of material loads from diffuse land use is still unclear yet. This study aimed to clarify the relationship between the spatial differences of spring water quality and various diffuse land use. The study area is the upland located in the northwest part in Chiba Prefecture. There various land uses have been developed. The landforms consist of upland surfaces with an altitude of 15-30m and alluvial lowland (2-9m). There are many water springs along the small rivers. The altitudes of spring points vary with upland and valley landforms. The upland consists of four units of geological strata, indicating that the aquifers of spring water are controlled by geology. A total of 60 springs were surveyed in Jul. 2002. In the field, water temperature, electronic conductivity, pH, and alkalinity were measured. Major ion concentrations were analyzed in laboratory by high performance liquid chromatography. Silica concentration was determined using spectrophotometer. Using the Detailed Digital Information maps, land use in drainage basin was analyzed. Firstly, basic water quality originated from geology was examined. Along the increase in relative height between spring points and upland surface, the silica concentration increases. Concentrations of inorganic ions show the same tendency. There is no relationship between the relative height and the land use in drainage basins. Thus, the basic water quality is formed in the process of groundwater flow through geology by dissolving of carbonate minerals in layers. The rest of the loads are controlled by land use development in drainage basins. The spatial difference of the additional loads is larger than that of the basic loads. There are clear relationships between the additional loads and land use. When forests occupy a large part of the drainage basin, the concentration of major ions is low. In the area with fields, the concentration and the proportions of Mg<sup>2+</sup>, Ca<sup>2+</sup>, SO<sub>4</sub><sup>2-</sup> and NO<sub>3</sub><sup>-</sup> are high. In residential area, the ion concentration is basically low but Mg<sup>2+</sup> and NO<sub>3</sub><sup>-</sup> show high proportion. Ca<sup>2+</sup> and HCO<sub>3</sub><sup>-</sup> concentrations become high for the developed drainage basins. When the land use consists of fields and residential area, the load is explained by taking the components of fields and residential area into account. Thus, the spring water quality is controlled mainly by land use in drainage basin.

HW01/09A/C26-004

1010

#### NITRATE TRANSPORT IN UNSATURATED ZONE NEAR A SMALL STREAM IN AN AGRICULTURAL AREA

Fumi SUGITA<sup>1</sup>, Michael ENGLISH<sup>2</sup>, Sherry SCHIFF<sup>3</sup> (<sup>1</sup>Chiba University of Commerce, <sup>2</sup>Department of Geography and Environmental Studies, Wilfrid Laurier University, Ontario Canada, <sup>3</sup>Department of Earth Sciences, University of Waterloo, Ontario Canada)

Nitrate contamination in groundwater and surface water caused by agricultural activities is

one of major environmental concerns in many countries. Due to non-point nature of the source distribution, the nitrate transport processes and its pathways in soil are not clearly understood. In this study, nitrate concentration of soil water in five different land uses near a small stream (Strawberry Creek) in an agricultural area were investigated and compared with that of stream water. The purposes of this study are to identify major nitrate contributing land-uses into underground in the watershed and also to estimate its major pathways to the stream. The study area is located approximately 100km southwest of Toronto, Ontario. The watershed (3.5km<sup>2</sup>) is covered mainly with various croplands, and also with patches of woodland and narrow stripes of uncultivated land along the creek. Intensive land use and very narrow riparian zone are resulted in high nitrate concentration in the stream water (NO<sub>3</sub>-N ≈ 10mg/l) in this area. In the growing season of 1999, several soil cores were obtained from 0.2m below the ground surface to the saturated zone which was around 1.2m below the surface in barely field, corn field, soy bean field, woodland and riparian zone along the creek. The soil water was extracted and was analyzed for NO<sub>3</sub><sup>-</sup>, NH<sub>4</sub><sup>+</sup>, Cl<sup>-</sup> and DOC concentrations. Stream water and groundwater beneath the streambed were also sampled and analyzed for the same components listed above. The differences between the stream water head and that of under streambed indicated groundwater was discharging into the creek in most part along the creek. The NO<sub>3</sub><sup>-</sup> concentrations typically found in the groundwater were lower than those found in stream water except small upstream part. The highest NO<sub>3</sub><sup>-</sup> concentrations were found at the top (0.2m below the surface) of the soil profiles of barely and cornfields and the concentration decrease with depth. The concentrations found in the rest of the field were relatively low, suggesting corn and barely fields were the main nitrates contributing area. Along with the groundwater in the upstream, the tile drains which are facilitated about 0.7m below the surface in some part of this watershed give shortcut for nitrate to flow from upper unsaturated zone to the stream and may be contributing to the high nitrate concentrations found in the stream water. Depletion of NO<sub>3</sub><sup>-</sup> with depth is mainly due to denitrification that could take place in anaerobic loam patches exist in the zone. The average denitrification rates obtained by curve fitting were 0.0108 mg/l/day for the barley and 0.0064 mg/l/day for the corn. Though these rates are almost one-order of magnitude smaller than most found in saturated zone, they suggest considerable denitrification is taking place even in unsaturated zone and this process is not negligible.

HW01/09A/C26-005

1030

#### EFFECTS OF LAND USE AND SOIL TYPE ON MANGANESE MOBILISATION FROM UPLAND SOILS

Kate Victoria HEAL<sup>1</sup>, Alasdair Macdonald HARDIE<sup>2</sup>, Allan LILLY<sup>3</sup> (<sup>1</sup>School of GeoSciences, University of Edinburgh, <sup>2</sup>Scottish Environment Protection Agency, East Kilbride, <sup>3</sup>Macaulay Land Use Research Institute, Aberdeen)

Concentrations of the trace metal manganese (Mn) in water supplies in excess of the drinking water standard of 0.05 mg L<sup>-1</sup> cause aesthetic and structural problems and have been linked with neurological health effects. The majority of Scotland's drinking water is supplied from upland catchments and Mn concentrations in a number of these water supplies appear to have increased since the 1970s. We investigated two hypotheses to explain the observed increases in Mn concentrations: 1) Land use change: recent extensive conifer afforestation in many upland water supply catchments could cause elevated Mn concentrations in surface waters, for example, by enhanced leaching from tree foliage and from soils due to increased acidification; 2) Changes in soil moisture regime: increased Mn concentrations are particularly evident during autumn following unusually dry summer conditions so Mn may be mobilised when rewetting of dried soils occurs. The two hypotheses were tested in the Ballochbeathies Burn catchment, a 0.86 km<sup>2</sup> sub-catchment of the Loch Bradan water supply reservoir, southwest Scotland, in which Mn concentrations frequently exceed the drinking water standard. Soil water chemistry and soil hydrology were monitored for 18 months at six locations in the catchment, selected to represent the major upland land uses of Sitka spruce (*Picea sitchensis*) plantation and a dwarf shrub/grass moorland and the major soil types found in upland Scotland (Histosols, Histic Gleysols and Histic Podzols). No significant difference was observed in Mn concentrations in soil water under Sitka spruce plantation and moorland, indicating that this land use change is not responsible for increased Mn concentrations in surface waters. There was no evidence of Mn release into soil water from the rewetting of dried soil but this was attributed to the absence of extended drying conditions during the field programme. Laboratory controlled experiments were conducted, using soil cores taken from the horizons of the soils investigated in the field, to examine whether Mn release into soil water would occur following prolonged drying. The experimental results showed that Mn mobilisation into soil water occurred in organo-mineral horizons two weeks after re-wetting. To determine whether catchment soils could have dried sufficiently to promote Mn mobilisation and account for elevated Mn concentrations measured in surface waters in autumn 1995, a process-based soil water simulation model (WAVE) was used to hindcast catchment soil moisture regime. The simulation results showed a greater degree of soil drying during 1995 than we measured in the field or in the soil core experiments, indicating that changes in soil moisture regime can account for elevated Mn concentrations in surface waters. Although the processes responsible for Mn mobilisation during the rewetting of dry upland soils are not known, these conditions may occur more frequently in the future due to increased climatic variability, resulting in drinking water supplies regularly exceeding the standard for Mn.

HW01/09A/C26-006

1110

#### EFFECTS OF LAND USE CHANGE ON HYDROLOGICAL CYCLE: A CASE STUDY ON CHAOBAIHE RIVER BASIN IN NORTH CHINA

Gang-sheng WANG<sup>1</sup>, Jun XIA<sup>2</sup> (<sup>1</sup>Institute of Geographical Sciences and Natural Resources Research, Chinese Academy of Sciences, China, <sup>2</sup>School of Water Resource and Hydropower, Wuhan University, 430072, China)

The issue of water shortage and related eco-environmental degradation in North China is one of the major emergency problems in China. As runoff generated from mountainous area is significantly decreased and water resources are over developed, serious water and eco-environmental problems have arisen, such as drying-up of river system, ground water decline, lake and wetland degradation, and water pollution in plain area, etc. Based on the traits and existent problem of water cycle in North China, a distributed hydrological modeling has been developed. This model, so-called DTVGM (Distributed Time Variant Gain Model), can be coupled the present physical process units or conceptual models with hydrological system approach such as TVGM (Time Variant Gain Model), where time variant gain factor,  $G(t)$ , could be linked with RS information to extend easily to application of hydrological simulation in basin scale. DTVGM picks up the information, such as the gradient of the slope, the direction of the slope, the water current path, as well as the boundaries of the river network and the watershed of the land surface units with DEM by establishing itself on the basis of GIS/DEM. It simulates the movement of the water in the soil-vegetation-atmosphere (SVAT) system, describes the relation between the cellular grids in the horizontal direction, and it performs mathematical calculations of the surface water and the subsurface water on the watershed cellular grids divided by DEM. DTVGM combines runoff generation process and flow routing process by soil moisture content. At present, the runoff generation process is divided into two layers in the vertical direction: the upper layer is the surface flow based on the concept of TVGM; the lower layer is the subsurface flow developed through a control

volume approach, including a water balance equation and a storage-outflow equation. On the other hand, the kinematic wave models are applied to simulate the flow routing process. DTVM can simulate the effects of human activities such as land use change on hydrological cycle by establishing the relationship between  $G(t)$  and land use types. A case study on Chaobaihe River Basin, controlled by Miyun Reservoir in North China, is implemented by applying DTVM. The basin, with area about 13,846 km<sup>2</sup>, is divided into 55,444 grid elements; and the grids are partitioned into different ranks for flow routing. The land use types of the basin include forest, meadow, river, reservoir, construction area, arable land area and naked land. By preliminary application and examination in Chaobaihe River Basin, it was found that DTVM is successful with more advantages than conditional distributed model applied in China; and the increase of forest area could cause the decrease of runoff in this basin. Moreover, the new problems were addressed in the paper.

HW01/09A/C26-007

1130

#### BIOMASS BURNING AEROSOLS AND RAINWATER CHEMISTRY IN SOUTHEAST BRAZIL

L.B.L.S. LARA<sup>1</sup>, P.B. CAMARGO<sup>1</sup>, P. ARTAXO<sup>2</sup>, L.A. MARTINELLI<sup>1</sup>, E.S.B. FERRAZ<sup>1</sup> (<sup>1</sup>Lab. Ecologia Isotópica, Centro de Energia Nuclear na Agricultura (CENA), <sup>2</sup>Instituto de Física, Universidade de Sao Paulo Brazil)

The acidification of precipitation by H<sub>2</sub>SO<sub>4</sub> and HNO<sub>3</sub> and subsequent high N deposition rates has been taken place in Southeast Brazil. Besides, the biomass burning, which occurs around 6 months in every year, has increased the inhalable particles as well as black carbon concentrations in this region. In order to understand how the anthropogenic activities could be changing the rainwater and aerosol chemical composition, during one year we have collected and analyzed aerosols and rainwater samples in three different sites in State of São Paulo (Southeast Brazil), with different kind of anthropogenic activities: pristine area with original forest, biomass burning and industrial activities and pasture area. The origin of the free acidity in rainwater is different in each site and come out to be linked to the land-use. Organic acids appear to control the acidity in pristine areas, while in other sites, mineral acids (mainly nitrate), dominate rainwater acidity. According to the Factor and Cluster Analyses, the composition of rainwater in the two sites appears to be controlled mostly by two sources: biomass burning and industrial emissions, and in the pristine area by biogenic emissions and marine influence, due to the proximity to the sea. High levels of pollutants have been measured during biomass burning season in southeast Brazil, the annual PM<sub>10</sub> concentration (57.1±45.2µgm<sup>-3</sup>) exceeds of the other urban and industrialized areas and the BC concentration is significantly higher during the biomass burning season - dry season (4.2±2.2 µgm<sup>-3</sup>) than the wet season (2.0±1.0 µgm<sup>-3</sup>). A detailed aerosol source apportionment study was performed in these three sites. A complex system of air pollution sources modulates the pollutants concentration in the Southeast Brazil. Principal component analysis results showed that the main source of fine aerosol is biomass burning which is generated into the State (sugarcane burning) or coming from fires in the Amazon Basin. The other main sources are soil dust, industrial emissions and oil combustion. Resuspended soil is the main source of coarse mode followed by industrial emissions. The sampling and analytical procedures applied in this study showed that the biomass burning and agricultural practices are dominating the chemical composition of the rainwater and aerosols in Southeast Brazil, possibly altering the biogeochemical cycles. Besides, if in the future, urbanization and industrialization process continues to grow in this rate we can expect significant climate changes.

HW01/09A/C26-008

1150

#### EFFECTS OF VEGETATION AND LANDUSE ON THE HYDROLOGIC CYCLE OF SEMI-ARID CANADIAN PRAIRIES

Masaki HAYASHI, Garth VAN DER KAMP (Department of Geology and Geophysics, University of Calgary)

In the semi-arid northern plains of North America there are millions of small wetlands, also called "prairie potholes" or "sloughs", which play an important role in the hydrology of the region and provide important breeding habitat for migratory waterfowl. At the St. Denis National Wildlife Area in the prairie region of southern Saskatchewan, Canada, water levels in over 100 wetlands have been monitored since 1968. Most of the wetlands, located in closed drainage basins, have no permanent inflow and outflow streams. As a result the water balance of the wetlands is primarily controlled by snowmelt runoff, summer precipitation, and evapotranspiration from open water and the riparian fringe. The underlying glacial deposits consist largely of clay-rich glacial till with low permeability. Therefore, groundwater flow is generally slow and represents a minor component of the water balance although it may play a decisive role in controlling the chemical mass balance. Between 1980 and 1983 about one-third of the 4 km<sup>2</sup> area was converted from cultivation to a permanent cover of brome grass in order to provide dense nesting cover for waterfowl. A few years after this conversion all the wetlands within the area of grass dried out and have remained dry since, while wetlands in adjacent cultivated lands have held water as before. Field measurements show that introduction of permanent grass reduces water input to the wetlands mainly through a combination of efficient snow trapping and enhanced infiltration into frozen soil. In winter the tall brome grass traps most of the snowfall whereas in the cultivated fields more wind transport of snow occurs, especially for short stubble and fallow fields. Single-ring infiltration tests were conducted during snowmelt while the soil was still frozen and again in summer. The infiltrability of the frozen soil in the grassland is high enough to absorb most or all of the snowmelt, while in the cultivated fields infiltration into the frozen soil is limited and significant runoff occurs. In summer the grassland maintains a much higher infiltrability than the cultivated land. The development of enhanced infiltrability takes several years after the conversion from cultivation to grass and is likely due to the gradual development of macropores such as root holes, desiccation cracks and animal burrows.

HW01/09A/C26-009

1210

#### INFLUENCE OF ANTHROPOGENIC ACTIVITY TO EROSION PROCESSES IN THE CHANNELS OF THE BELAYA AND UFA RIVERS

Tatyana FASHCHEVSKAYA<sup>1</sup>, Nicolay OSIPOV<sup>2</sup> (<sup>1</sup>Department of Ecology, Ufa State Aircraft University, <sup>2</sup>Hydrometeorological centre, Bashkirian hydrometeorological service)

The Belaya river is situated in limitations of South Ural and is one of main tributary of the Volga river with area catchment equal 142000 km<sup>2</sup>. The length of the Belaya river is 1430 km. The Ufa river is the main tributary of the Belaya river. Its length is 918 km. There are intensive economic activities at floodplain and at channels nowadays, especially at middle and lower reaches of river. As a result of these activities the river makes active erosion processes. First of all is extract of sand-gravel materials from channel that is used for production of asphalt-concrete mixture, roads repairing and for building. The depth and the width of some quarries may be compared with the depth and the width of rivers. The second direction of anthropogenic exploitation of river channels is intensive dredging for navigation. River transport development (carrying, intensity) promoted improvement of water ways and

increasing of navigation water depths. Every year much soil is withdrawn from river channel in order to restore or to support the fairway. Today the navigation distance in the Belaya River is 670 km, in the Ufa River - 305 km. The third important factor which increases river erosion activity considerably is construction of reservoirs. The intensive channel wash-out happens in downstream of reservoir. In 1961 year the Pavlovskoye reservoir was built at the Ufa River (water volume is 1,41 km<sup>3</sup>). The influence of the reservoir is being observed till inflow of the Ufa river into the Belaya River, i.e. 170 km. In that place the channel had been scoured and the water level was decreased till scale that could be compared with navigation water depth. The analysis of the dynamics of suspended load before and after building of Pavlovskoye reservoir showed considerable decreasing of entering of them into downstream because of accumulation them in the upstream. As a result of the research it became clear decreasing of water level while water discharge was invariable. In the Ufa River, where it inflows into the Belaya River the decreasing is 100cm, in the Belaya River is 156cm. As a result of the decreasing of water level we have: 1.Undertaking pipelines and intakes, those were made on the bottom of the river, became stripped, and their exploitation was violated; 2. Navigation conditions got worse; 3.Duration of the flooding of floodplain decreased, that is why the spawning grounds of fishes have degraded, the crop capacity of floodplain meadow reduced, the conditions nesting of birds and mammals have aggravated.

HW01-Posters

Wednesday, July 9

#### EFFECTS OF HUMAN ACTIVITIES ON HYDROLOGICAL AND BIOGEOCHEMICAL CYCLES (ICWQ)

Location: Site D

Wednesday, July 9 PM

Presiding Chairs: N.E. Peters, N. Ohle

HW01/09P/D-001

Poster

1400-192

#### MODELLING STREAM WATER CHEMISTRY USING RIVER BASIN LANDUSE CHARACTERISTICS

Chandra Sekhar MATLI, Surender REDDY (Department of Civil Engineering, Regional Engineering College)

The study of water quality is fundamental to understanding a water resource, as it gives insight into the benefits derived from water management. Urbanization and industrialization are recognized to be main causes for water quality degradation for quite some time. Hence, assessment of non-point (diffuse) pollution, which arises from the river basin, has to some extent been overshadowed by the urgent need for treatment of domestic and industrial wastewater (point sources). The River Krishna and its tributaries drain three important states of South India. The river water plays a very important role in the overall socioeconomic development of Andhra Pradesh. The river water is used for drinking, industry, power generation and predominantly for irrigation in the basin, which has a tropical climate. From available literature, it is evident that the river receives pollutants from non-point sources, in addition to point sources. In large river basins monitoring non-point sources pollution is rather difficult and expensive and is subjected to analytical errors. Hence, modeling water quality using landuse data of the basin is attempted in the present study. The results of the study indicated the impact of landuse on water quality of the tributaries of River Krishna. The seasonality in river flows and concentrations of dissolved solids is explained with the help of variations in flow patterns that is due to unequal rainfall distribution in the basin over the year. Agriculture is the dominant landuse in all the sub-basins. Correlation studies explain the relationships, between dissolved solids concentration and landuse of the basins. The multiple regression models accounted for significant variation in concentrations for majority of dissolved solids. The predicted concentrations are in good agreement with the observed values. However, some of the deviations can be explained by dynamic nature of the landuse patterns. The proposed models can be useful for planning landuse controls in integrated water quality management program. As water quality of flowing water is closely linked to the landuse in the basin, it is essential to include water quality management in future river basin planning.

HW01/09P/D-002

Poster

1400-193

#### THE BENEFIT BROUGHT BY SOIL AND WATER CONSERVATION IN CHINA

Ge TAN, Jun XIA (Hydrology Studio, Institute of Geographical Sciences and Natural Resources Research, CAS.)

Soil and Water Conservation (SWC) approach can reduce the runoff and sediments of rivers, these functions should be estimated and quantified. There are two kinds of traditional estimating ways: one is called hydrological way and the other is called water conservation way. Aimed at the biggest rivers of China, Yangtze River and Yellow River, two typical heavy eroded catchments are selected as study areas, these areas have been harnessed for some years, and can be choose as study object. In this paper, the Jialingjiang catchment (upper course catchment of Yangtze River) and middle course catchment of Yellow River will be studied to find out the influence of SWC approach on water resources. Though analyzing, we can make latter conclusions: The soil and water conservation can reduce more runoff and sediment of arid area than that of humid area. (1) With the implement of soil and water conservation measure, the condition of catchment runoff and sediment will be better. When the harness reaches a certain degree, there will be a balance of wash and silt. (2)The study of typical catchment show that: since 90s, reasons of the reduce of sediment amount included precipitation decrease and SWC, the former make 16% of the runoff and sediment reduce, the latter make the left 84% reduce. (3) Using the precipitation data, runoff data and sediment date of before-harness area to build a experience model, and then using this model to simulate the benefit of harness project, this is a better analysis method until now. The key point is whether the sediment rules of harnessed area can be really reflected by the experience model which is based on the data of before-harness area. According to the change of runoff of Yellow River under SWC influence: (1) Reservoir can adjust the river annual and year-to-year runoff. LongYangXia and LiuJiaXia reservoir made the runoff distribution change greatly, the runoff increased in low-water season and decreased in high-water season. According the observation data, the runoff increased 10~20% in low-water season. (2) Analyze from the aspect of water loss, because of the reservoir the water surface area is increased, the evaporation is increased accordingly. By statistic of the main reservoirs of China, the evaporation increased 77×108m<sup>3</sup>(not included plain reservoirs), account for 1.3% of the natural runoff of Yellow River. (3) According to the analyses of the change reason of the runoff in the Hekou-Longkou area and catchments of the Jinghe, the Luohe, the Weihe and the Fenne, the measurements of SWC is one of the elements which affect the amount water entering the Yellow River, which has decreased about 10.9×108 m<sup>3</sup>. The affections of SWC and the irrigation measurements are almost the same, but the irrigation measurement is the main means in catchments of the Jinghe, the Luohe, the

Weihe and the Fenhe, where the contribution of SWC approaches to reduce the runoff of Yellow River is about 10%.

**HW01/09P/D-003** Poster **1400-194**

**IMPACT OF INDUSTRIAL EFFLUENT ON WATER QUALITY IN KORBA AND ENVIRONS, CHHATISGARH, INDIA**

L. P. CHOURASIA (Department of Applied Geology, Dr. H.S. Gour Univ)

The impact of multiple industrial pollution sources on the groundwater system were evaluated in the industrial complex at Korba of Chhatisgarh State of India. The quality of groundwater in the region has been affected negatively due to the discharge of effluents on open land and into ponds, tanks and streams. Water samples from surface water bodies and due wells were analyzed for their major ion concentrations of Na<sup>+</sup>, Ca<sup>2+</sup>, Cl<sup>-</sup> and HCO<sub>3</sub><sup>-</sup> indicate the impact of industrial effects on water quality. Based on the hydro chemistry, the groundwater is classified into various types such as sodium chloride, sodium-bicarbonate calcium chloride, and magnesium-chloride etc. Its suitability for drinking and irrigation purposes has been assessed. The ground water quality in and around Korba has become hazardous. Some possible remedial measures are suggested.

**HW01/09P/D-004** Poster **1400-195**

**GROUNDWATER AS AN ALTERNATIVE SOURCE OF SUPPLY FOR URBAN AREAS IN RUSSIA**

Igor Semenovich ZEKTSER (Department of Hydrogeology, Water Problems Institute, Russian Academy of Sciences)

Groundwater represents a valuable source of public drinking water in many parts of the Russian Federation but its use varies widely across the country. In part this reflects differences in the hydrological and hydrogeological settings that govern groundwater recharge and safe groundwater yield. However, in some regions, groundwater development is constrained by water management organizations that simply ignore available and well-protected groundwater resources in favor of surface water supply. Locally, significant human impacts on groundwater quality and quantity have been documented. In many populated areas, for example, groundwater recharge has been artificially enhanced and safe yield has increased; in other cases, aquifers have been drained and safe yield has been depleted. It is important that these impacts be understood if future problems are to be resolved. In particular, a full knowledge of the extent to which human activity impacts groundwater resources is essential for adequate assessment of safe yield. Safe yield assessment allows changes in surface runoff and fluctuations of the water table to be predicted; however, an inadequate representation of human influences on annual recharge and discharge will lead to serious error. The depletion of groundwater resources and safe yield is generally localized. The effects of anthropogenic pollution on groundwater also tend to be local. Pollution is most prevalent in the uppermost aquifers, particularly in urbanized and agricultural areas and in river valleys. Deeper confined aquifers used for centralized withdrawal normally produce water of good quality. Where pollution of confined aquifers occurs, it is normally caused by inadequate protection of well capture zones or by the poor design of the water-supply wells.

**HW01/09P/D-005** Poster **1400-196**

**THE EFFECT OF LAND USE CHANGES ON FLOW REGIME**

Richard P. SILBERSTEIN, Tim GARGETT (IAHS)

Clearing of native vegetation for agriculture in Western Australia has resulted in enormous environmental problems. The irony is stark in a region generally considered dry and lacking in water for much of the year, we have a problem caused by too much water accumulating in local areas. The native deep rooted perennial vegetation used virtually all the available rainfall, and maintained a very deep water table or ensured there was no water table at all. Salt accumulated from the rainfall in the root zone in huge amounts. Shallow rooted annual agricultural crops and pastures do not use all the rainfall, and each winter a small amount drains through the soil until it reaches the now rising water table. The result on stream flow has been a complete change on flow characteristics, with ephemeral streams now flowing continuously, and with high salinity, so they are no longer drinkable. In catchments subject to detailed analysis there has been a much lesser impact on extreme flows than on low flows. Conversely, when cleared catchments are planted to trees, there is a reduction in streamflow, and potentially a big impact on water resources. This paper shows the extent to which flow regime has been modified by the rising water tables resulting from the clearing for agriculture. We discuss time scales for these changes to become apparent and for them to reach their maximum expression; and what impact might be expected of recovery attempts by reforestation catchments. In this work we seek a general solution to the prediction of changes to flow regime resulting from land use changes. Flow frequency and salinity frequency distribution curves are analysed and represented as parametric curves, with the parameters linked to catchment and climate characteristics.

**HW01/09P/D-006** Poster **1400-197**

**ENVIRONMENTAL CONDITIONS EFFECT ON THE FLUVIAL TRANSPORT CHANGES IN SOME CATCHMENTS OF THE VISTULA AND BUG INTERFLUVE**

Andrzej TUCKI, Andrzej SWIECA (Department of Regional Geography, Maria Curie-Skłodowska University)

The purpose of this study was to determine the influence of environmental conditions and economic activities on the nature and quality of solute and suspended sediment transported by the rivers in the middle and southern parts of the Vistula and Bug interfluvium. The above-mentioned problems were studied in the four catchments with different natural conditions and anthropogenic impact (Fig. 1). The upper Wieprz river catchment up-stream of the gauging station at Zwierzyniec (405 km<sup>2</sup>) is situated in Tomaszów Roztocze. Its geological structure is distinctly different; the Upper Cretaceous opokas and gajzes occur often on the surface as well as loess. The Quaternary sandy deposits are wide spatially extended too. The forestage is significantly high (36% of the catchment area), whereas arable land covers 59.9% of this area. The mean annual amount of drained off sewage during 1989-1992 was 0.2 million m<sup>3</sup>, which was 0.4% of the river yield. The Por river catchment - the Wieprz river left tributary - 590.3 km<sup>2</sup> in size - is situated mainly in Goraj Roztocze. The MWM gauging station at Sullow closes this catchment (571 km<sup>2</sup> - 96.7%). The Upper Cretaceous marl and opokas, mainly overlaid by loess are in the basement complex. The arable land in this catchment is 66.3%, whereas the forest - 18.7% of the catchment area. The amount of municipal and industrial wastewater is small. The mean annual amount of drained off sewage during 1989-1992 was 0.1 mln m<sup>3</sup>, which was 0.1% of the river runoff. The Labunka river catchment - the Wieprz right tributary - up-stream of the gauging station at Krzak is 416 km<sup>2</sup> in size - 81%; the catchment is 513.5 km<sup>2</sup>. It largely comprises the area of the Zamosc Basin. Of Quaternary formations, mineral-organic ones lining the valley bottom of the

Labunka river and its tributaries are the most widely-distributed. The cropland covers 79.3% of the area, in it meadows and grassland constitute 16.2%. Forests cover about 12.3% of the Labunka river catchment. During 1989-1992 the surface waters were polluted with 6.5 million m<sup>3</sup> of municipal and industry sewage. The Uherka catchment - the Bug river right tributary - up-stream of the MWM gauging station at Ruda Opalin is 432 km<sup>2</sup> in size, which constitutes 75% of the Uherka river catchment. The catchment is situated mainly in Lublin Upland and Polesie Plain. Soft limestones of the Upper Cretaceous rocks, which are related to spread depression, predominate in the basement complex. Whereas more resistant rocks of the same age (marl and marly opokas) are related to Inselberg heights. In the basin up-stream of the MWM gauging station at Ruda Opalin, forests cover 12% of area, meadows and grassland - 11%; whereas the arable land - 69%. The surface waters are polluted mainly with municipal and industry sewage (during 1989-1992 they were polluted with 7.7 million m<sup>3</sup> of sewage).

**HW01/09P/D-007** Poster **1400-198**

**CHARACTERISTICS, CHANGING TRENDS AND CLASSIFICATIONS OF NITRATE-NITRITE IN HOKKAIDO**

Xuan-Zhu YANG (Ueyama-Sisui Earth Consultant Co. Ltd)

Nitrogen (ammonium-, nitrite-, and nitrate-nitrogen) is inputted to the land from various sources (fertilizers, atmospheric deposition, animal wastes and wastewater) during the past decades years in Hokkaido. Most common drinking water pollutant in groundwater is caused by agricultural watersheds and wastewater of nitrogen. Elevated nitrate-nitrite concentration in groundwater have raised serious human-health and ecological concerns. The degree of pollution in agricultural and urban area is not easily determined because of overprinting by numerous subsequent processes. It is possible for us to determine that concentrations of nitrate-nitrite vary systematically with an increase in time. The purpose of study is that understand their characteristics and changing tendencies, and then suggest some countermeasures about pollution. The combined results of this study indicate that the nitrate-nitrite concentrations in Hokkaido have responded to increased or decreased nitrogen loads from various sources in agricultural and urban area over the last few decades. Six significant changing trends of nitrate-nitrite concentrations, corresponding to an increase of time, may be identified on the basis of mode of their characteristics in Hokkaido. Type 1 is characterized by lower concentration (<10ppm) and a gradual increase in nitrate-nitrite. Type 2 shows remarkable higher concentration (>10ppm) and a gradual increase in nitrate-nitrite. Type 3 is characterized by lower concentrations (<10ppm) and a gradual decrease in nitrate-nitrite. Type 4 show remarkable higher concentrations (>10ppm) and a gradual drop in nitrate-nitrite. Type 5 and Type 6 indicate that concentrations of nitrate-nitrite essentially is stable, although there may be slight concentration variation. Because of the severe environmental effects, removal of the various forms of nitrogen from soil, water and wastewater has become mandatory in recent years. The data presented in this study provide insights into such significant events as pollution countermeasure. The result of study indicates that pollution countermeasure is necessary to Type 1 and Type 2. It is suggested that previous survey of pollution conditions is very important before consideration of countermeasure. Nitrate-nitrite pollution must be controlled if we are to improve significantly nitrogen input to the land from various sources.

**HW01/09P/D-008** Poster **1400-199**

**GEOCHEMISTRY OF GROUNDWATER IN MINE-AFFECTED ZONES OF SALEM, TAMIL NADU, SOUTHERN INDIA**

Palanivel Periakali GOUNDER, Manavalan Sathya NARAYANAN (DEPARTMENT OF APPLIED GEOLOGY, UNIVERSITY OF MADRAS)

Mineralogical, hydrogeologic and geochemical data of ultrabasic - Peninsular gneiss rocks of Salem covering an area extent of about 194 sq.Km around Salem magnesite mine area were used to determine the source of solutes to groundwater and to assess the chemical weathering processes. The results indicate that the flux of dissolved solids from the abandoned mines are controlled by interaction between ultrabasic rocks and materials derived from local bedrock. Mass balance calculations indicate that dissolution of feldspar and ferromagnesian minerals release Na, Ca and Mg. The average denudation rate was found to vary from 0.3 to 4.2 tons/km<sup>2</sup>/yr for a discharge of 5.3 X 10<sup>8</sup> l/yr, and from 0.5 to 8 tons/km<sup>2</sup>/yr for a discharge of 10 X 10<sup>8</sup> l/yr. Mineral solubility study of Mg-phase in the system shows that serpentine is the dominant Mg<sup>2+</sup> contributor. The distribution of several dissolved species in groundwater over the ultrabasic rocks - Peninsular gneissic complex explain the significance of water-rock interactions. Input-output budgets for major chemical species show an increase in the concentration of (Na+K) and TDS towards downgradient. Weathering of plagioclase feldspar and biotite in the Peninsular gneiss could be the source of (Na+K) to the groundwater. There is a net export of major cations, silica and bicarbonate from the magnesite mine area, reflecting the weathering of bedrock. Bedrock in magnesite mine is ultrabasic rocks comprised of dunites, peridotites, shonkinites, missourites, yugites and syenites. While Ni and Co are within the tolerable limits in most of the area, the concentration of total Cr was observed to be about 3-4 times more than the permissible limit. Though chromium is an essential trace element in the metabolism of lipids and proteins and is vital for the maintenance of a normal glucose tolerance factor, excess of chromium uptake damages mucous membranes, causes renal damages and has been classified carcinogenic to humans by the International Agency for Research on Cancer. Our preliminary studies have shown, the incidence of breast cancer among the inhabitants in the study area. From the chromium speciation studies, it was observed that the trivalent chromium concentration was below the permissible level (50 ppb), but carcinogenic hexavalent chromium ranges from 0 to 228 ppb during summer and 3 to 186 ppb during winter. The concentration of hexavalent chromium is about three times greater than the permissible limit (50 ppb) rendering the groundwater unfit for drinking and domestic use. Hexavalent chromium shows positive correlation with pH and most of the major ions. Shaded colour contour diagram were prepared which showed that an area of 145 sq.Km was affected by hexavalent chromium contamination during summer and 132 sq.Km during winter.

**HW01/09P/D-009** Poster **1400-200**

**WATER QUALITY ENHANCEMENT THROUGH IN-LAKE MODIFICATION**

Byeong-Chan KIM, Sang-il LEE (Department of Civil and Environmental Engineering, University of Dongguk)

The quality of reservoirs and lakes is gradually deteriorating due to social and environmental changes. Since the construction of new dams gets increasingly difficult owing to environmental concerns, rehabilitation of existing water bodies become necessary. In order to achieve this scientifically challenging task, Herculean efforts are being made. This paper presents the issue of improving the water quality of a lake by modifying its shape. Lake Sihwa, located in the midwest of the Korean Peninsula, is an artificial water body created as a result of the construction of an embankment in 1994 to secure agricultural water for the region. Besides the freshwater lake having 56.5km<sup>2</sup> of surface area, a reclaimed land of 173km<sup>2</sup> and 330 million m<sup>3</sup> volume was also created. However, due to the cut-off of tidal

currents and the rapid increase of population and industrial waste loads from factories in the neighborhood, the water quality of Lake Sihwa has deteriorated immediately after the construction. Various measures based on both hydrodynamic and environmental approaches have been proposed and implemented thus far to improve the water quality of the lake. External measures include the creation of artificial marsh, conduit works for collecting stormwater, and the construction of treatment plants for wastewater from livestock. But these measures have intrinsic limitations both in technical and operational aspects. There also exists a practical need for an in-lake approach: the sluice gates at the embankment are being operated for the purpose of flood control and water quality improvement. Accordingly, seawater flows into the lake and the downstream part of the lake has lost the function of freshwater impoundment. Thus the plan of zoning and partial reclamation of the lake has been highlighted. While the waterway is channeled through reclamation, the water body is divided into three zones by two submerged dams. The middle zone is expected to supply some portion of water demand for the future industrial complex nearby. To estimate the daily inflow for a watershed where hydrologic data are insufficient, a methodology based on the inflow weight factor has been devised. Numerical analysis was performed for water quality prediction, utilizing the daily inflow estimates and biochemical information acquired from field measurements. Results showed that the water quality of modified Lake Sihwa would be enhanced up to the level of both agricultural and industrial use. Acknowledgment: This work was partially supported by a grant (H00018) from Korea Research Foundation.

**HW01/09P/D-010** Poster **1400-201**

#### EFFECT OF URBANIZATION ON FLOOD RUNOFF

Tokuo KISHII<sup>1</sup>, Michiko HAYANO<sup>2</sup>, Yasuhisa KUZUHA<sup>2</sup> (<sup>1</sup>National Research Institute for Earth Science and Disaster Prevention and University of Tsukuba, <sup>2</sup>National Research Institute for Earth Science and Disaster Prevention)

In this research, the change of flood runoff characteristics, that is, the flood runoff ratio and the time of concentration etc. are investigated, on the Shakujii River which flows from west to east on the Musashino Terrace in the northern part of Tokyo Metropolis. The basin area of the river is 48 km<sup>2</sup> in area with a total channel length of 19 km. The surface geology of the area is the volcanic ash of high permeability, called Kanto Loam. After 1950's, this basin has been urbanized rapidly and in 1975 it had over 50% of impermeable area and a population of 590 thousands. On this river there are available data of rainfall and discharge of floods which occurred through twenty years and the data have made it possible to investigate the change in flood runoff characteristics in these years. As a result, no considerable difference in runoff ratio was found between each year. From this it is considered that the surface geology of high permeability influences much more than the urbanization does. The time of concentration was reduced remarkably to about a half after urbanization. This is supposed to have been caused by the decrease of roughness in the basin and the channel. Concerning runoff coefficient of Rational Formula, no conspicuous difference is seen. Because the shortening on time of concentration causes high rainfall intensity the time of concentration and the increase of peak discharge, consequently, the runoff coefficient is not so different year by year. These results were derived only from data of the period of twenty years, in which period only a few floods were recorded. Further investigation of flood runoff ratio and runoff coefficient of Rational Formula with enough records of big floods is expected.

**HW01/09P/D-011** Poster **1400-202**

#### LOW COST TREATMENT TECHNOLOGIES FOR RECLAMATION OF CONTAMINATED SOILS AND POLLUTED GROUNDWATERS

Zareen KHAN, Anjaneyulu Y. (Center for environment, Jawaharlal Nehru Technological University)

Currently approximately 155 cubic yards of soil is contaminated with hazardous organics at Patancheru industrial estate, Hyderabad, (A.P.) India. These hazardous organic contaminants are frequently part of wastes disposed on land and the study of waste site interaction is key to assess the potential for onsite contamination of soil and groundwaters and their interference in the biogeochemical cycles. Phenol and substituted phenols are selected as the test contaminants in the present study. The data on nature of organics, soil organic content, free iron and aluminium oxides of soils which are known to influence the adsorption and desorption process of hazardous organics on soils are presented. Desorption isotherms of soil adsorbed hazardous organics exhibited hysteresis at higher initial concentration indicating the degree of irreversibility of adsorption-desorption process. Leaching potential of the hazardous organics decreases with their increasing hydrophobicity and soil organic content while their persistence in terms of half life time (DT50) increases. By adopting low cost treatment methods like bioremediation have demonstrated that phenols can be degraded by the concerted activity of microbial consortia under optimized conditions. Continuous monitoring of percent COD reduction, microbial count and hazardous organic concentration revealed that there is considerable decrease in the amount of organics.

**HW01/09P/D-012** Poster **1400-203**

#### STUDYING CONTAMINATION RISK TO A DRINKING WATER SOURCE THROUGH GROUNDWATER FLOW ACROSS A DYKE IN A GRANITIC AREA NEAR HIMAYATSAGAR, HYDERABAD, INDIA

Ratan L. DHAR<sup>1</sup>, S. SANKARAN<sup>2</sup>, R. RANGARAJAN<sup>2</sup>, M.R.K. SARMA<sup>2</sup>, V.S. SINGH<sup>2</sup> (<sup>1</sup>Groundwater Exploration & Management Group, National Geophysical Research Institute, Hyderabad, India, <sup>2</sup>National Geophysical Research Institute)

In order to examine the hydraulic behaviour of a dolerite dyke and its impact on the groundwater flow, multi-parameter geophysical and hydrogeological investigations were carried out. This would in turn reflect on the possibility of contamination of a drinking water source downstream of the dyke due to discharge of effluents from an oil industry. The investigations included water level monitoring, pumping tests, magnetic, electrical, resistivity and tracer studies. Groundwater flow inferred from the water level contour maps clearly indicates the existence of flow across the dyke. However, it was not possible to draw any conclusions from the pumping test because of (i) the large distance between the observation and pumping wells and (ii) pumping of the wells for irrigation is a continuous process in the area and interferes with the water level recovery monitoring in the observation wells. The tracer tests have also been inconclusive for the same reason. However, the similarity of background iodide levels of well water samples upstream and downstream side of the dyke suggests continuity of groundwater flow across the dyke. The groundwater electrical conductivity and chloride data wells located across the dyke also suggest a similar nature. Electrical resistivity and magnetic investigations have indicated that the dyke is weathered and, therefore, capable of transmitting groundwater. There is no significant contrast between the resistivity of the dyke and the surrounding granite. Low resistivity values are observed over parts of the dyke. Electrical resistivity soundings have revealed the weathered nature of dyke with the thickness of weathering varying from place to place. Magnetic studies also indicate the dyke to be weathered. The interpretation of magnetic and resistivity data estimate the depth to the hard dyke to be 6-31 m along the investigated profiles. The depth to the hard dyke could vary considerably from place to place and so also

the degree of weathering. From the results of multi-parameter investigations carried out in the area, it is concluded that hydraulic connectivity exists across the dolerite dyke facilitating the groundwater movement. A bore well drilled right into the dyke has been found to have a sustained yield. The oil industry located upstream of the drinking water source has been closed as a result of the findings of these investigations.

**HW01/09P/D-013** Poster **1400-204**

#### MONITORING OF WATER POLLUTION OF A HYDROMORPHIC ENVIRONS

Hari Shanker GUPTA (Department of Geography, University college, M. D. University, Rohtak 124 001, INDIA)

The future life support system of mankind is being threatened by the rate at which we deplete and degrade our fresh aquatic resources. The rise in human population exploits more of natural resources and this met through the growth of industries; chemical and petrochemical, urbanisation, desertification, deforestation and intensive agriculture. The industrial and urban solid and liquid waste is discharged into the rivers. The deforestation process itself aggravates the sedimentation transport into the streams. And use of chemicals in the crops contaminates groundwater through percolation, rivers and lakes through surface run-off. All these sporadic degrading activities have lead to gradual deterioration in the quality of surface and sub-surface water causing health hazards and death of human, livestock, aquatic lives, crop failure and loss of aesthetics. Keeping in view the importance of good water quality, the Central Pollution Control Board (CPCB) has initiated a series of integrated river basin studies, and established the water quality monitoring (WQM) network all over the country. The present study is taken up for measures of water pollution control in a hydrogeomorphic region (about 19388 km<sup>2</sup>, which is 7.2% of the total catchment area) with the help of GIS. A spatial GIS model has been put into analysis to monitor water quality. GIS database has been generated for storage and retrieval of attribute data for water quality. The hydrogeomorphic zonation has been suggested in terms of spatial coverage and pollution controls. Key Words: Pollutants, Hydromorphic unit, and Water Quality Monitoring

**HW01/09P/D-014** Poster **1400-205**

#### THE REDUCTION OF RADIOACTIVE CONTAMINATION FLOW BY A WATERWAY BEYOND THE BOUNDS OF THE CHERNOBYL NPP EXCLUSION ZONE

Dmitri I. GUDKOV<sup>1</sup>, Valery V. DEREVETS<sup>2</sup>, Sergey I. KIREEV<sup>2</sup>, Alexander B. NAZAROV<sup>2</sup> (<sup>1</sup>Department of Radioecology, Institute of Hydrobiology, <sup>2</sup>SSSPE Chernobyl Radioecological Centre)

In 1986 after the termination of aerosol emissions from destroyed unit of the Chernobyl nuclear power plant (NPP) the basic migration of radionuclides beyond the bounds of the exclusion zone occurs by a waterway. During 1986-2002 about 132 TBq (tera-bequerel) of caesium-137 and 159 TBq of strontium-90 has flow into Kiev reservoir by Pripyat River – the main waterway of the exclusion zone. Getting into reservoir radionuclides are distributed on all cascade of Dnieper River reservoirs. The flow of radionuclides into the rivers influences increase on radiation dose of the population of Ukraine at water consumption. In this connection the necessity of the careful control behind the radionuclide contents in water, estimation of its transference into Dnieper River reservoirs, and also for easting and prevention of such transference is obvious. The main purposes of the submitted researches were: the analysis of results of surface waters radioecological monitoring within territory of the Chernobyl NPP exclusion zone; the determination of the basic sources of radio active contamination of Pripyat River; the assessment of efficiency of operation mode of water-protection structures interfering of radionuclide flow into Pripyat River; the evaluation of radioactive contamination distribution beyond the bounds of the exclusion zone, as well as development and duly introduction of measures on its minimization. The greatest contribution in radionuclide contamination of Pripyat River and the formation of transference of radionuclides in Dnieper River reservoirs system brings in radionuclide migration from periodically flooded sites of Pripyat River flood-lands, with the basic inflows of the river, and also from cooling-pond of the Chernobyl NPP. To the basic sources concern also Uzh River, which flows into Pripyat River and Braginka River flowing into Kiev reservoir. The analysis of operation of water-protection structures and radiation condition of water objects within exclusion zone during postaccident period shows that apriority direction at realization of water-protection measures should be creation of dams, which protect the most contaminated territory from flooding and radionuclide flow into the river systems. To the basic tasks of radioecological monitoring of surface waters for the nearest period it is necessary to include the solution of problem of increased radionuclide flow from the territory of the left-bank flood-lands of Pripyat River due to over-wetting of these territories in connection with change of a mode of the flow natural formation. Not less important the development of the possible scripts of decrease of water level in a cooling-pond of the Chernobyl NPP and evaluation of impact of these measures on a radioecological condition of water objects is occurred.

**HW01/09P/D-015** Poster **1400-206**

#### ASSESSMENT OF THE HYDROLOGIC CYCLE CONDITION IN SAPPORO

Yoshinari HAMAHARA<sup>1</sup>, Makoto NAKATSUGAWA (<sup>1</sup>FUKUDA Hydrologic Center CO., LTD., <sup>2</sup>Civil Engineering Research Institute of Hokkaido)

The Toyohira River runs through Sapporo, Hokkaido. The upper reaches of the basin are densely forested, and the river merges at its lower reaches with the main stream. Sapporo (pop. 1.82 million) lies on an alluvial fan formed by the Toyohira River. The city has relied on the Toyohira for most of its water resources for drinking and hydroelectric power. However, population increases have necessitated the development of artificial elements in the hydrologic cycle, such as the public water supply system and the sewerage network. In recent years, rivers in northern Sapporo have experienced drought and have experienced water quality deterioration. We researched the hydrologic cycle in Sapporo toward finding solutions to these water environment problems, focusing on the artificial elements of the hydrologic cycle, such as the public water supply system and the sewerage network, for quantitative and qualitative assessment. The assessment revealed the following characteristics of the hydrologic cycle in Sapporo: 1) There are two dams at the upper reaches of the Toyohira River. Their presence makes for a ratio of annual mean discharge to 355 day discharge, which indicates dry stage, of 3.9, versus an estimated value of 6.7 if these dams were absent. This suggests that the dams contribute to stable supply of water from the Toyohira River. 2) The water quality (BOD) of the Toyohira River was assessed based on the per capita volume of organic matter in the municipal water system. Although the two dams mitigate drought, the BOD required for native fish species including salmon to live in the river and migrate up it is 3.0 mg/L or less. To meet this requirement, the river discharge must be approximately three times the wastewater discharge from the municipal water system, to allow the river water to dilute the municipal wastewater. For the Toyohira River to satisfy the above environmental requirement and to receive all the municipal water emitted from Sapporo, the catchment basin at the upper reaches would need to be 2.3 times its current size. 3) 2/3 the volume of wastewater discharge from the municipal water system is channeled into other rivers, and the remaining 1/3 into the Toyohira River. The load on the Toyohira River is reduced in this way to meet the above environmental requirement. 4) The Barato River, which runs through low flatlands in northern Sapporo, receives 1/3 the volume

of wastewater discharge from the municipal water system. Construction of sewerage facilities has enabled the reduction of organic pollutant emission, but eutrophication remains a problem. Based on the population and water hydrologic of Sapporo, we have clarified how the water environment in the river basin is maintained and the problems in maintaining that environment.

**HW01/09P/D-016** Poster **1400-207**  
**EFFECTIVENESS OF HYDROGEL IN WATER AND FERTILISER RETENTION**

Manta Devi NOWBUTH<sup>1</sup>, Nivedita GOKOOL<sup>2</sup> (<sup>1</sup>Department of Civil Engineering, Faculty of Engineering, University of Mauritius, <sup>2</sup>Faculty of Agriculture, University of Mauritius)

Hydrogels (gel forming polymers) were introduced in agriculture because of their water retaining properties. This particular study was carried out to evaluate the effectiveness of hydrogels with soluble fertilisers in highly permeable soils. Tests carried out on the hydrogels showed that the gels have a much lower absorptive capacity when dissolved salts are present in the solution. The tests carried out, clearly confirm that hydrogels do help significantly in retaining both water and fertilisers, and releasing them at a reasonable pace for the plant development. An experiment carried out under protected conditions, revealed that the best treatment for the particular soil, was obtained when the hydrogel was soaked in tap water and solid granular fertiliser was mixed separately in the soil. Though results indicate that there is not much increase in productivity, but as far as water requirement is concerned, the results do confirm that hydrogels extend irrigation intervals to a reasonably economic level. Destructive tests carried out at the end of the experiment noted that a higher concentration of fertilisers within the soil with the presence of hydrogels.

**HW01/09P/D-017** Poster **1400-208**

**THE IMPACT OF LAND-USE PATTERN ON GROUNDWATER RECHARGE AND ALTERNATIVES FOR MITIGATION**

Subrahmanyam KAMBHAMPATI (National Geophysical Research Institute)

Hyderabad, the capital city of Andhra Pradesh in India is underlain by hard rock aquifers. During the past three decades a lot of developmental activities took place, the most important being the construction of building complexes, establishment of new industries and increased demand for domestic water consumption. The rainfall data for more than two decades indicates that the average annual rainfall oscillates around 900 mm. Many foreshore areas of irrigation tanks are presently occupied by housing colonies. Thus urbanization of the city has lessened the scope for natural recharge and increased pollutant loads. There is a drastic decline in the natural recharge as observed from a network of observation wells. This has caused hydrological degradation, particularly over the last 30 years. Factors responsible for this hydrological degradation include: decreased agricultural areas, changes in land use, increased drainage and groundwater abstraction, and quality changes due to indiscriminate disposal of effluents into surface water structures. The changes in landscape include the destruction of hillocks, resulting in hydraulic head losses, causing more evaporation than run-off and infiltration. The situation is becoming alarming and the only alternative is monsoon water harnessing through roof-water collection, and construction of artificial structures for enhancement of recharge. The possible structures and mitigation methodologies are suggested.

**HW01/09P/D-018** Poster **1400-209**

**CARRYING CAPACITY BASED SUSTAINABLE DEVELOPMENT: A HOLISTIC TOOL AS APPLIED TO WATER RESOURCES FOR CENTRAL KERALA STATE**

Balchand N. ALUNGAL (IAPSO)

The State of Kerala on the west coast of Indian peninsular region is blessed with numerous rivers and waterways. The southwest monsoon (June September) mainly regulates the water balance for this region followed by a scanty northwest monsoon (October November) giving rise to a bimodal distribution. The 3000 mm rainfall on this tropical belt is no exception but that the steep slopes of Western Ghats run down major portion of the precipitation along the narrow width of the state and very shallow coastal plains to the Arabian Sea. Through decades, regarded very crucial are the transport of nutrient rich waters embedded with particulates that paves the way for high productivity coastal waters. More recently, events such as river sand mining, changes in catchments characteristics, damming of flow, inter-basin transfers, abstraction for human use and accelerated agricultural practices have upset the inter relations and periodic cycling processes of this region. The resultant impacts on the water resources are well reflected in supply demand mechanisms, inabilities in adjusting to mild climatic extremities, altered status of nutrient/particulate loadings and more importantly, the failure to resolve watershed issues by correct management techniques now warrant judicious, policy backed developmental initiatives. The matured techniques exemplified towards sustainable development based on the concepts of Carrying Capacity are applied to this region as a holistic tool such that (1) the multi decadal biogeochemical cycles and currently prevailing scenario are critically assessed (2) watershed management in the realm of water resources are re-defined (3) human activities stand quantified and impacts listed and (4) locally practiced traditional techniques are integrated with new technologies to utilize as well as conserve the waters which is backed by models in the structured carrying capacity approaches.

**HW01/09P/D-019** Poster **1400-210**

**ENVIRONMENTAL GEOCHEMISTRY OF DAMODAR RIVER BASIN: IMPACT EVALUATION OF COAL MINING AND ALLIED INDUSTRY ON WATER AND SEDIMENT QUALITY**

Abhay Kumar SINGH (Geo-environment Division, Central Mining Research Institute, Barwa Road, Dhanbad -826 001, India)

Geochemical cycling has received wide attention due to the need for understanding the pathways of pollutants through our present environment. River processes form a major link in the geochemical cycle. Nearly 90% of the natural weathered, as well as man-made materials that are transported both in dissolved and particulate phase are delivered to the oceans by rivers. Geochemical study of river basins thus reveals the nature of weathering on a basin scale and helps us to understand the exogenic cycles of elements in the continent-river-ocean system. The present study deals with the elemental chemistry of medium sized river basin – Damodar River. The Damodar River Basin is sub basin and part of the master Ganga River Basin, spreading over an area of about 23,370 km<sup>2</sup>. It flows through a vast track of rich mineralized zones of eastern India with variable topography and geology. The river flows through the countries richest coal bearing zones in its upper catchments and through alluvial and agricultural area in the lower stretch. A large number of coal based industries i.e.- coal washeries, steel plants, fertilizer, thermal power etc. are located in the Damodar basin, besides large mining activities. The major objective of the study is to evaluate the controlling factors and impact of coal mining and allied industry on the water

and sediment quality in the Damodar River basin. Na and Ca dominate the water chemistry of the Damodar River basin in the cationic abundance and HCO<sub>3</sub> and SO<sub>4</sub> in the anionic composition. Water chemistry strongly reflects the dominance of continental weathering aided by atmospheric and anthropogenic activities in the catchment area. High concentrations of SO<sub>4</sub> and PO<sub>4</sub> at some sites indicate impact of mining and anthropogenic on water quality. The high concentration of dissolved silica, relatively high (Na+K)/TZ+ ratio (0.2-0.4) and low equivalent ratio of (Ca+Mg)/(Na+K) indicates significant contribution of dissolved ions by the weathering of aluminosilicate minerals of crystalline rocks. The seasonal data show minimum ionic concentrations in the monsoon season, reflecting the influence of atmospheric precipitation on TDS contents. The suspended sediments show positive correlation with discharge and both discharge and suspended load reaches their maximum value during the monsoon season. The elemental composition of the sediments is characterised by the dominance of Si, Al, K, Fe and Na, constituting 75% of the elemental abundance. The suspended sediments show increased concentrations with respect to the bed sediments for the elements Al, Mg, Fe, Ti, and Ni and reduced concentrations with respect to Si, Na, Ca and K. The suspended sediments are finer and richer in multiple hydroxide coatings and heavy metal scavenging clays, so they carry higher heavy metals loads compared to the bed sediments. The concentration of heavy metals in the finer size fraction (<37 µm) is significantly higher than the bulk composition. The Igeo value calculated for Fe, Mn, Zn, Ni and Cr is well below '0' grade suggesting that there is no pollution with respect to these metals in Damodar River sediments.

**HW01/09P/D-020** Poster **1400-211**

**OCCURENCE AND CONSEQUENT HAZARDS OF EXCESSIVELY NUTRIENT SEDIMENT IN ARTIFICIAL RESERVOIRS**

Kazuo OKUNISHI (Japan Institute of Land and Environmental Studies)

Excessively nutrient sediment found in freshwater bodies of any dimension and in estuaries has been referred to as "Hedoro" in Japanese and has been translated in English simply as sludge. It is commonly muddy and very loose with much pore water which is in anaerobic condition. Hedoro was comprehensively recognized as different from natural nutrient mud at first in Japan when it occurred in the estuaries affected by an industrial complex in 1950's causing serious environmental hazards. Sometimes, hedoro involved such poisonous substances as organic mercury that caused Minamata Disease (mud hatter's disease). Hedoro has been frequently found in the freshwater bodies of different sizes that receive untreated sewage water. The hazards caused by hedoro in artificial reservoirs had been recognized only locally until the ecosystem of the Kurobe River, Japan, was badly spoiled by hedoro, when the sediment in one of the upstream dam was flushed in order to recover its storage capacity. Here I will compile the result of the research of Japan Institute of Land and Environmental Studies into the environmental problems of the hedoro that occur in the Tonoyma Reservoirs in an upstream reach of the Hiki River, Wakayama Prefecture, Japan. The Hiki River has recorded hazardous floods 11 times in 74 years between 1984 and 1957. After the construction of the Tonoyma dam, the equivalent floods occurred 22 times between 1958 and 2002, with the biological hazard caused by the hedoro involved in the flood water. A laboratory experiment proved that the ponding of water with hedoro suspended in it reduced the harvest of rice by 27% in weight while the ponding of clear water presented a reduction of 10%. Analysis of the composition of different species of diatom in the samples of hedoro taken from the flooded rice field in the downstream part of the drainage basin and from the bottom of the reservoir, and in the mud adhering the channel bed boulders in the tributary rivers showed that most of the diatom in the flood deposit in the downstream areas had come from the bottom of the reservoir, not from the tributary rivers or upstream rivers pouring to the reservoir. Although the samples of hedoro from the bottom of the reservoir contained relatively small amount of organic matter, the cavities commonly found in it suggest that the deposit was subject to the anaerobic fermentation with emission of methane. A local citizen group working in the area of Kurobe River has found that the collective deposition of sediment involves much quantity of fallen leaves, which becomes harmful to the aquatic ecosystem when disintegrated biochemically under anaerobic conditions. Taking this finding into account, the influx of organic material in excess of the oxygen supply needed for its aerobic disintegration can be a major cause of the generation of hedoro in the reservoir and consequent environmental hazards.

**HW01/09P/D-021** Poster **1400-212**

**WATER SHED DEGRADATION AND WATER CONSERVATION CHALLENGES IN RIAANA RIVER CATCHMENT WITHIN THE VICTORIA DRAINAGE BASIN IN KENYA**

George ONGWENYI, JOHN M. NYANGARA (Post-graduate programme in Hydrology, Faculty of Science, University of Nairobi)

Watershed degradation problems are worldwide in extent, leaving no continent unaffected. It is global in its environmental and socio-economic impacts. The need to address the global problem of watershed degradation is increasingly urgent as it is a major cause and mechanism of global loss of productive land resources in particular water resources. It can lead to economic instability and political unrest in the affected areas. The management of water resources possess several challenges to water resource planners, policymakers, politicians, researchers and academicians woldover-The major challengers include inadequate or lack of hydrological and hydrometeorological networks, leading to poor river regime forecasting and subsequent determination of water resource quantities. Technical mistakes during design and construction of water abstraction structures, upstream downstream water use conflicts, individual vs community, and institutional vs individual or community conflicts, legal and water pollution challenges adds to the long list of possible challenges. It is important that these challenges are addressed urgently to ensure availability of sufficient water for use by mankind. This paper addresses water management challenges to ensure in Kericho District in Western Kenya. Conclusive Recommendations for solving some of the challenges and the way-forward are suggested.

**HW01/09P/D-022** Poster **1400-213**

**CONTAMINANT ARRIVAL-TIME DISTRIBUTIONS FROM A RANDOM WALK MODEL OF HYPORHEIC TRANSPORT**

William Earl BARDSLEY (Department of Earth Sciences, University of Waikato)

A simple random walk model is used to approximate a pulse of conservative contaminant released into stream water which interchanges with sub-channel groundwater. It is assumed there is steady stream flow and minimal longitudinal channel variation between the release point and a monitoring point at some distance  $x$  downstream. In a unit of time a contaminant particle in the channel water either advances downstream a small fixed distance  $b$ , or moves vertically down into the hyporheic zone a small fixed distance  $c$ . The respective movement probabilities are defined as  $p$  and  $1-p$ . A contaminant particle which has previously entered the hyporheic zone moves the (vertical) distance  $c$  in unit time, upward or downward, which may or may not return the particle back to the channel. The upward and downward movement probabilities are respectively defined as  $p$  and  $1-p$ . No constraint is placed on the relative sizes of  $b$  and  $c$ , although  $c$  is likely to be small relative to  $b$ . The use of  $p$  in both

vertical and horizontal contexts gives rise to contaminant arrival-times which are mathematically equivalent to a simple 1-dimensional random walk model with probabilities of steps to the right or left of  $p$  and  $1-p$  respectively, where rightward movement represents the downstream direction. The resulting contaminant arrival-time distributions at the monitoring point are as follows: For  $p \neq 0.5$  the arrival-time distribution is inverse Gaussian, which tends toward a normal distribution limit for sufficiently large  $x$ . For  $p = 0.5$  the arrival-time distribution is a highly-skewed form which is distance-invariant and characterised by a long right tail with the log of contaminant concentration decreasing linearly with gradient  $-3/2$  against log of time. This is illustrated with an example data set from a tracer experiment. The skewed distribution corresponds to an equivalent model of Brownian particle arrival times with zero drift, which predicts that the waiting time for contaminant concentration to decline to less than a specified value will increase with travel distance as  $x^{2.5}$ . For  $p < 0.5$  some of the contaminant particles never escape the hyporheic zone and the proportion of permanently lost particles increases with travel distance as  $[1 - \exp(-kx)]$ , where  $k$  is a positive constant. The random-walk model is capable of further extension, such as placing a reflecting barrier at the base of the hyporheic zone.

**HW01/09P/D-023** Poster **1400-214**

#### STABLE ISOTOPES IN LEKE STECHLIN CATCHMENT AND ITS VICINITY

Ekkehard O. HOLZBECHER<sup>1</sup>, Andrea KNAPPE<sup>2</sup>, Asaf PEKDEGER<sup>3</sup>, Gunnar N-ZMANN<sup>1</sup>  
(<sup>1</sup>Humboldt University Berlin, <sup>2</sup>Free University Berlin)

An extended observation campaign was undertaken in the watershed of Lake Stechlin watershed and its vicinity, sampling several chemical species, including stable isotopes D and O<sup>18</sup>. Measurements are available from precipitation, from seepage water and groundwater at different depths, and from various surface water bodies. Data show that local meteoric and evaporation lines can be clearly identified in the  $\Delta O^{18}$ - $\Delta D$  diagram. A part of the hydrological cycle can be traced, following seepage water and groundwater to lake water - the lake is almost entirely fed by groundwater. The concentrations of stable isotopes ( $\Delta O^{18}$  = 2 per mille), measured in Lake Stechlin surface water, is unexpectedly high. It is still an open question, whether this can be attributed to the operation of the now abandoned atomic power plant. During operation of the plant the lake was utilized as part of the external cooling cycle. In the contribution it is attempted to answer this and other questions by a model, which is currently being set-up. The model takes advantage from the fact that a data-base of environmental parameters is available for Lake Stechlin from past observation campaigns and research activities, which accompanied already the planning of the power plant in the 1960s. Nevertheless, stable isotopes were neglected, and the newest measurements open the chance, to confront former assumptions and results with new data.

**HW01/09P/D-024** Poster **1400-215**

#### INFLUENCE OF INTENTIONAL WATER STORAGES AND RELEASES ON HYDROLOGICAL PROCESSES OF DIFFERENT REGIONS IN THE MEKONG RIVER BASIN

Nmns Bandara NAWARATHNA, So KAZAMA, Masaki SAWAMOTO (Department of Civil Engineering, Tohoku University)

Controlled water storage and release activities in reservoirs and irrigated crop fields affect the hydrological cycle of large-scale watersheds. Water storing devices have been constructed to meet water demands especially for agriculture and power supply with increasing population. However, some of those human activities have adversely resulted in insufficient water resources and harmful environmental impacts in downstream locations. Availability of Geographical Information System (GIS) data sets of watershed physical properties such as land use, soil types, geology and the advancements gained in obtaining distributed meteorological variables with the help of GIS have stimulated the development of physically based hydrological models. Introduction of block wise approach to the TOPMODEL with Muskingum-Cunge flow routing method (BTOPMC) has enhanced the applicability of TOPMODEL from hundreds of square kilometers to several ten thousands square kilometers river basins. In the block wise approach, a watershed is divided into blocks and local saturation deficit which controls the depth to the saturation zone is calculated with respect to the block average saturation deficit value. The optimum number of blocks, which results in maximum simulation efficiencies produces the maximum standard deviation of block average soil topographic index. The BTOPMC model is used to simulate hydrological processes in the effective watershed of 277,000 square kilometers from Luang Prabang to Pakse in Lao PDR along the Mekong River. Model parameters are assigned as functions of watersheds physical properties. Reservoir activities in the watershed are taken into account using simplified ruling curves determined by the purposes of the operation and catchment area. Water storages and releases from irrigated crop fields are taken into account by introducing desirable water level function to the relevant grids. The Manning's coefficient along the main stream and tributaries are assigned as a function of slope and the best Manning's coefficient value at the most downstream location. Average Manning's coefficient values found for both the main river and tributaries are 0.029 and 0.034, respectively. Nash-Sutcliffe coefficient was used to evaluate the simulation accuracy. The efficiency coefficients were estimated for five gauging stations along the main stream. The value ranges from 93.5% to 95.4%. Simulation accuracy has significantly improved after considering intentional water storages and releases activities in the watershed. Hydrological processes are thoroughly studied at different climatic regions of the basin. Sub-basins annual evapotranspiration ranges from 470 mm to 620 mm. It was found that in lesser rainfall areas, 95% of the days in a year produce daily runoff that is less than that of basin average. The figures are 88% and 57% for an average and higher rainfall areas respectively. It has been found that there is sufficient water resources in mountainous areas in Lao PDR whereas flat irrigated fields in Thailand need to get water from nearest potential locations to meet their requirement.

**HW01/09P/D-025** Poster **1400-216**

#### GENERATION OF DATA BASE FOR EROSION PREDICTION OF HYDROLOGICAL BASINS

Hari Shanker GUPTA (Department of Geography, University College, M. D. University, Rohtak, 124 001 India)

Geographic Information System (GIS) coupled with Remote Sensing has proved as a powerful tool in the field of land evaluation and management. Various studies have been reported across the world, illustrating the application of GIS in the evaluation and management of landform, soil and water resources. In the present study, GIS capabilities have been utilized to understand the erosion potential and slope stability characteristics of a small catchments zone from a highly important terrain segment of bio-diversity hot spots in peninsular India. A multi-thematic analysis based on different physical factors has been adopted to generate integrated maps on erosion proneness as well as on critical slope under a GIS platform for terrain evaluation. The spatial data on erosion proneness has demonstrated that 17.62 Square Km. Area, out of ~140 Square Km. in the catchments zone, needs careful attention for Eco-restoration. In the critical slope map four land stability

classes have been demarcated. The area represented as unstable and moderately stable is found to be important for slope stability problems. Temporal change as well as the extent of loss in the perennial status of tributaries has been recorded to evaluate the landform changes. A catchment's treatment plan has also been suggested. Key Words: Spatial Data, Critical slope, and Temporal change

**HW01/09P/D-026** Poster **1400-217**

#### AN ENHANCED MONITORING METHODOLOGY OF THE RIVERBED MORPHOLOGICAL CHANGES, APPLIED ON THE LOWER COURSE OF THE DANUBE RIVER

Constantin Stefan SAVA (National Institute of Marine Geology and Geocoology - GeoEcoMar, Bucharest - Constanta, Romania)

In the frame of the PHARE project 'Morphological Changes and Abatement of Negative Effects on a Selected Part of the Danube River' scientists and specialists from Austria, Bulgaria and Romania carried out a surveying experiment in the Zimnicea-Svistov research pilot sector. The main task of this project is the assessment of geo-morphological changes of the River Danube. For that purpose it is necessary to compare the situation in different epochs and to assess the occurring differences. This comparison can be done quantitatively by derivation of certain geometric properties (for instance volume differences) or qualitatively. Qualitative comparisons aim to detect if changes have occurred and if yes, what kind of changes. Quantitative assessment tries to give an exact measure of these changes. The aim of the experiment was the surveying and mapping of this selected reach of the river, applying new technologies, in order to establish the preconditions for remedial actions:- Development and application of modern methodology and technology including GPS use for surveying and mapping of the Danube River;- Generation of precise maps of the riverbed from historical and current measurements;- Assessment of morphological and hydrological situation and its development for planning of remedial actions based on a common view and perception of the major processes. It is proposed that all Danubian countries should use a uniform co-ordinate and height systems for all control points, benchmarks and gauges, situated along the river banks and on the islands. The bases of these systems are EUREF and EUVN. Results, such as maps of the Danube River, GIS-applications, etc. have to be prepared in Lambert conic map projection. This system is named System 2000. Optimal values of the parameters are derived.

**HW01/09P/D-027** Poster **1400-218**

#### MEASURING VERTICAL WATER FLUX AND CONVECTIVE SOLUTE TRANSPORT IN FOREST SOIL WITH CONTROLLED-SUCTION-PERIOD LYSIMETER

Ken'ichirou KOSUGI, Akihito YOSHINO, Masanori KATSUYAMA (Graduate School of Agriculture, Kyoto Univ.)

The unsaturated infiltration of rain and irrigation water and solute transport in the vadose zone are major processes in hydrological and biogeochemical cycles. They are important for understanding groundwater quality and material balances in ecosystem. Although the convective chemical transport in the vadose zone can be quantified by measuring both the unsaturated water flux and the solute concentration of flowing water, few studies have accurately measured convective chemical fluxes in the field. This is partly because the existing techniques for sampling unsaturated soil water are not necessarily appropriate, considering the mechanism of soil water flow. This study evaluated the long-term performance of a recently developed controlled-suction-period lysimeter in the field. The lysimeter consists of two tensiometers and a porous plate connected to a vacuum system. The soil matric pressure heads immediately above the horizontally-buried porous plate, and at the same depth in the natural soil profile, are measured at 3-second intervals. The vacuum system is automatically controlled so that the readings of the two tensiometers match. The lysimeter was installed at a sampling depth of 30 cm in a sparse mixed evergreen and deciduous broadleaved forest, and at a sampling depth of 50 cm in a evergreen coniferous forest. At both monitoring sites, the lysimeter succeeded in maintaining the soil moisture condition in the sampling profile as about the same as that in the natural soil profile for most of the monitoring period, and water extraction by the lysimeter did not cause remarkable convergence or divergence in the soil water flow. The water-loss due to evapotranspiration estimated from the water-sampling rate showed a reasonable seasonal trend, as compared with the evapotranspiration rate. Combining the soil water flux data measured by the lysimeter with the results of chemical analyses of the sampled water, convective chemical fluxes in the vadose zone were quantified. Since the lysimeter minimized the disturbance of soil moisture in the sampling profile, the physical soil environment in the sampling profile, which affects biological and chemical reactions, was maintained at a similar state to that in the natural soil profile. At the sparse mixed forest, a sinusoidal seasonal trend was found in the dissolved silica concentration of the sampled water which corresponded to the seasonal trend in soil temperature. Although no nitrate was detected in the sampled water at the sparse mixed forest, the nitrate concentration of the sampled water at the coniferous forest showed a seasonal trend affected by the balance between litter-decomposition and uptake by plants. As a result, data observed with the controlled-suction-period lysimeter could be used effectively to analyze material balances in the vadose zone, and to validate numerical simulations, thereby contributing to the prevention of soil and groundwater contamination.

**HW01/09P/D-028** Poster **1400-219**

#### STATISTICAL MODELLING AND ESTIMATING THE IRRIGATION AND MAN-MADE EFFECTS ON ANNUAL RUNOFF AND WATER RESOURCES

Natalie LOBODA (Department of Hydrology & Water Resources, Odessa State Environmental University (OSEU))

The modern land use activity and necessity of governing by complex water systems in order to provide a rational use stimulate so called the technological direction in the hydrology science. It is supposed a calculation and estimate of changing the river runoff due to the land use activity and anthropogenic effect. Use of the water resources for needs of collective farm, irrigation and other ones is possible due to the using the annual runoff of rivers which are regulated by the pond and water reservoirs. Differential estimate of the annual runoff changing due to the irrigate and artificial water reservoirs effect is possible under availability of sufficiently long sets of natural runoff and detailed information about dynamics of factors which determine the level of the watershed technological use. As a rule, such data are available only for large river basin. For little and middle rivers an account of the water use is carried out non systematically or absent entirely. So, it is of a great importance a carrying out the imitative numeric models for runoff on the basis of modelling runoff sets with the use of initially known parameters of the functioning technological water systems. In our paper a new techniques is developed to carry out modelling the pond, reservoir and irrigation effects on the statistical parameters of annual runoff time series and state of water resources. We started from new statistical models, which are presented in (Loboda, NATO Advanced Research Workshop, Moscow, 1998). An effect of the land use activity on the water resources is provided by nature factors (speech is about link with climate stochastic vibrations) and by the land use activity level. In order to model an influence of ponds and

reservoirs as artificial land shaft objects, it is used a modified balance equation for the annual runoff layer under availability of the ponds and reservoirs in the watershed. The key physical parameters are taken into account, in particular, ; parameters of the artificial water reservoirs, atmosphere precipitation, the watershed parameters etc. It is also considered more complicated and adequate balance approach, based on the generalized memory functions formalism. A modelling of the annual runoff sets is carried out on the basis of balance equation by means of the Monte-Carlo methods. Necessary parameters for the annual runoff set generation are the norm, variation and asymmetry coefficients and also information about inside set correlation. As example, we present the results of calculation for the effect of anthropogenic activity on annual runoff features for rivers of territory of Ukrainian south and republic of Moldavia. The effect of anthropogenic activity is in significant degree defined by the moisture of studied territories. Under consideration of the more acid territories the natural water resources are decreased and the anthropogenic factor role is increased.

**HW01/09P/D-029** Poster **1400-220**

**TRANSFORMATION OF GROUNDWATER QUALITY UNDER ACID RAIN IMPACT**

Anna P. BELOUSOVA (Water Problems Institute of RAS)

If in humid zones an evolution process in the direction of groundwater acidification under the impact of acid rain, then in semiarid zones in oil field this process develops successively in two opposite directions from alkalization to acidification of neutral groundwater. It is known that hydrocarbonate groundwater possesses a high protective natural geochemical potential, supporting neutralization of acid atmospheric precipitation. Natural hydrocarbonate water undergoes three stage of anthropogenic transformation caused by acid atmospheric precipitation over more than 50 years of oil field development. The first stage is transformation of neutral hydrocarbonate water into alkaline water and high alkaline water, accompanied by calcite precipitation and sodium carbonate dissolution from the unsaturated zone. The second stage is transformation of alkaline water into neutral hydrocarbonate water; the carbonate content, being less than the lower limit for background concentrations, showed reduced water buffering properties or protective potential relative to acid precipitation. The third stage is transformation of neutral hydrocarbonate water into acidic water, with a complete loss of protective geochemical potential. This unfavorable ecological situation with groundwater shows that even natural hydrocarbonate groundwater less protected from the impact of acid atmospheric precipitation an oil field in the semiarid zone.

**HW01/09P/D-030** Poster **1400-221**

**CHANGE OF GROUNDWATER REGIMES IN RESPONSE TO URBANIZATION**

Jiu J. JIAO (Department of Earth Sciences, University of Hong Kong)

Steep terrain in Hong Kong has forced around six million people to congregate in only about 165 km<sup>2</sup> near the coast, creating the highest population density and tallest buildings in the world. The construction of high-rise buildings requires extensive deep foundation and ground engineering work including large bored pilings and diaphragm walls. Consequently, the natural soil to depths of a few tens of meters, usually a zone with the most active groundwater flow, is largely replaced by concrete and other construction materials. This paper studies the change of extensively urbanized area of about 6 km<sup>2</sup> located on the north facing slopes of Hong Kong Island. This area consists of volcanic and granite rocks overlain by colluvium and residual soils and has a history of instability owing to the steep topography. A long history of engineering activities, including housing and road construction and slope work, has resulted in a wealth of data on the geology, hydrology, and geotechnical engineering of the area. A three-dimensional geological model is constructed based on information from over 400 boreholes. A review of the historical information indicates that numerous springs located in the lower part of the hillslope were extinguished in the process of urbanization. In recent 20 years, the seepage zone at the hillslope has moved uphill by several tens of meters to over 100 meters. A groundwater flow numerical model along a typical section is established and calibrated by comparing the simulated water levels with the observed ones. The modeling results show that the hydraulic conductivity in the shallow zone of the lower part of the slope is about one order of magnitude lower than that in the upper natural slope. The significant decrease in the hydraulic conductivity may reflect the modification of the natural aquifer system due to deep foundations of the extremely crowded buildings in the urbanized area. This paper goes on to discuss the possible undesirable engineering and environmental effects due to extensive urbanization, a process rapidly affecting many coastal areas of the world.

**HW01/09P/D-031** Poster **1400-222**

**DENUDATION AND TRANSPORT OF TERRESTRIAL MATERIALS FROM A TROPICAL (KAOPING) RIVER WATERSHED**

Jia-Jang HUNG, C.-Y. YANG (Institute of Marine Geology and Chemistry, National Sun Yat-Sen University)

Recent studies have demonstrated the importance of river fluxes from western Pacific islands in contributing to the global riverine material flux. The Kaoping River is a tropical, island-type river with the largest drainage area in Taiwan. In order to understand the denudation rates of river basin, the temporal and spatial distributions of hydrochemical parameters, total suspended matter (TSM), major ions, dissolved and particulate species of carbon in the Kaoping River were measured from August 1999 to August 2000. The total, physical and chemical weathering rates were estimated to be 7368, 5985 and 1383 g/m<sup>2</sup>/yr, respectively. Such physical and chemical weathering rates are much higher than those reported from world rivers. The generation of total carbon (DIC+DOC+PIC+POC) from the Kaoping drainage basin was about 176 gC/m<sup>2</sup>/yr. The yields of DIC, DOC, PIC and POC were 110 (63%), 2.27 (1.2%), 18.4 (10.4%) and 44.9 (25.4%) gC/m<sup>2</sup>/yr, respectively. These carbon yields are very high in comparison with ones obtained from the Langyang River in northern Taiwan and the other major rivers in the world. The annual fluxes of riverine DIC, DOC, PIC, POC and TC from the Kaoping River were about 34.5, 0.71, 6.02, 14.7 and 63.2 x 10<sup>10</sup> g C, respectively. Regarding the nutrient loads, the fluxes of total dissolved nitrogen (TDN) and phosphorus (TDP) were 2.3 x 10<sup>9</sup> and 3.4 x 10<sup>7</sup> mole/yr, respectively. More than 80% TDN and 60% TDP were derived from anthropogenic sources. Human activities appear to play a major role on affecting the generation, transport and transformation of terrestrial materials in the Kaoping drainage basin. This study confirms that small mountainous rivers may contribute significantly to global fluxes of terrestrial materials.

**HW01/09P/D-032** Poster **1400-223**

**STUDY ON TRANSPORT MECHANISM OF AL IN FOREST WATERSHED OF A SUB-URBAN FOREST IN JAPAN**

Min-Sik KIM<sup>1</sup>, Chisato TAKENAKA<sup>1</sup>, Kyoji YOSHIDA<sup>2</sup>, Ho-Taek PARK<sup>3</sup> (<sup>1</sup>Graduate School of Bioagricultural Sciences, Nagoya University, <sup>2</sup>Aichi Environmental Research Center, <sup>3</sup>Aichi science

and technology foundation, Aichi Industrial Institute)

Concentration of aluminum ion in soil water is considered as an indicator of soil acidification. Even so, the concentration decreases through infiltration process in soil layer with increase in pH value and reaches quite low level in stream water. In case of Foresta Hills in Aichi prefecture, high concentrations of aluminum (above 0.07mM) have been observed in the stream water although the pH value is almost neutral. In this work, in order to clarify the mechanism of aluminum runoff, spatial and temporal changes of chemical property of soil water and stream water were observed in Foresta Hills. Foresta Hills is located in Toyota city, Aichi-prefecture, Japan (137° 11' 27"E, 35° 02' 00"N.L.) and varies from 40m to 105m in altitude. The surveyed area belongs to a temperate secondary forest, where the dominant tree species are *Quercus serrata*, *Q. variabilis* and *Evodiapanax innovans*. The soil originated from granite bed rock. In the study area, the annual precipitation is 1272mm and the mean temperature is 16.8°C in 2001. The soil type is slightly dry brown forest soil (Bd). Sampling of stream water were done at 5 sites and that of soil water at one site. Performed sampling was once every week from May 9, 2002 to January 17, 2003 in Foresta Hills. Samples of stream water were collected at 20 m intervals from the sampling site of soil water. The pH and EC values were measured using a model WM-22WP (TOA, Japan). After filtration with a 0.45µm membrane filter, cations were analyzed using a Nippon Jarrell Ash IRLS Inductively Coupled Plasma Spectrophotometer (Na<sup>+</sup>, Mg<sup>2+</sup>, Ca<sup>2+</sup>, K<sup>+</sup>, Fe, Mn, Zn, Cu, Si, Al). Anions (Cl<sup>-</sup>, NO<sub>3</sub><sup>-</sup>, SO<sub>4</sub><sup>2-</sup>) were analyzed using a Shimadzu PIA-1000 Ion Chromatography. During the study period, pH values of stream water ranged between 6.14 and 6.99(average of 6.52) and had statistically a little difference among season. However, the pH values of soil water in the upper stream ranged from 5.73 to 6.54(average of 6.10) and were lower than those of stream water. The mean concentrations of aluminum in stream water and soil water were 0.046mmol/L and 0.063mmol/L respectively, and higher values were observed at high discharge event. The concentrations of aluminum decreased from upper-stream to down-stream by intervals. The aluminum concentrations showed significantly correlation with Fe and Si concentrations in stream water and soil water. These results indicate that the high aluminum concentrations were derived from the weathering of bed rock. Therefore, the chemical species of aluminum in the neutral stream water would be clarified.

**HW01/09P/D-033** Poster **1400-224**

**CHANGE OF SULFATE BUDGET AND FLUX BY PARTIAL DISTURBANCE WITH PINE WILT DISEASE**

Su-Jin KIM, Nobuhito OHTE, Masatoshi KAWASAKI (Division of Environmental Sciences & Technology, Graduate School of Agriculture, Kyoto University)

Sulfur is found in a wide variety of inorganic and organic forms in forest ecosystems. Sulfur is an important element in the biogeochemistry of forest ecosystems because its role as an essential plant nutrient, and the contribution of sulfate as a counter ion in altering the flux of other elements, especially basic cations in soil solutions. Overload of sulfuric deposition can disturb terrestrial ecosystems not only plant physiology, but nutrients dynamics in soil. With economic and populational growth of Asia, it is considered that release of this local S oxide increases to 44TgS/yr in 2020. This overload may affect the nutrient cycle in forested ecosystems in eastern Asia. However, there is little information on S dynamics in a forest ecosystem compare with other nutrient in Japan. To evaluate response of sulfate dynamics to partial disturbance with pine wilt disease in a temperate forest catchment, we conducted a series of field experiments. Sulfate concentration in soil solutions were increased after peak of nitrate concentration at disturbed area. It suggested that nitrate seasonality is originated by lost of uptake and the influence on nitrate leaching following the unusual decomposition associating with pine-wilt. It is also considered that these results were due to pH depression originated by increase of nitrate concentration way enhanced sulfate adsorption to anion exchange site. Sulfate budget in upper soil layers (0-30cm) were larger than deeper layers (40-100cm). Sulfate budget in surface soil layer at disturbed area was largest than other layers. It may assume that mineralization of organic S from humus and retention of inorganic sulfate by soil. Moreover, 20-30 cm layer at disturbed area was showed increasing of sulfate budget. Increases of sulfate budget suggested that result from decomposition of root, which is residue due to pine wilt disease. While, deeper layers were showed different trend comparing to surface layers. Sulfate budget in 90-100 cm layer at unsaturated area increased, however the same layer at disturbed area decreased. It suggests that increase of sulfate budget at unsaturated area resulted from retention of sulfate by adsorption, because adsorbed sulfate concentration in 90-100 cm layer at unsaturated area highly increased comparing to surface soil. Consequently, disturbed area has low retention ability resulting from low adsorption of sulfate, and has large movement of sulfate with soil water infiltration. Sulfate concentration increased with depth, whereas nitrate concentration decreased with the depth of the groundwater at saturated area. Discharges from high concentrations of nitrate in shallow groundwater increased stream nitrate. During the winter, when groundwater levels were low, stream flow was dominated by deeper groundwater, which increased streamwater sulfate concentration. These results suggest that hydrological processes are important to clarify sulfate discharge to forest disturbances.

**HW01/09P/D-034** Poster **1400-225**

**THE ROLE OF HORTONEAN OVERLANDFLOW IN STORM RUNOFF IN HINOKI PLANTATION, MIE, JAPAN**

Yuichi ONDA<sup>1</sup>, Maki TSUJIMURA<sup>1</sup>, Daiji Harada HARADA<sup>2</sup>, Taijiro FUKUYAMA<sup>3</sup> (<sup>1</sup>Institute of Geoscience, University of Tsukuba, <sup>2</sup>Department of Environmental Earth Science, Aichi University of Education, <sup>3</sup>Graduate School of Bioagricultural Sciences, Nagoya University)

The field evidence collected in the 1970's showed that in forested hillslopes, infiltration capacities almost always exceeds the rainfall intensities. In Japan, Hinoki (*Chamaecyparis Obtusa*) plantation distributes widely because of the expensive log price. In unmanaged Hinoki plantations, understory vegetation decreases and the litter of Hinoki is known to be likely to move downward. Therefore, from the field observation, Hortonian overlandflow may occur. In addition, the soil erosion in Hinoki plantation has been the serious problems in Japan. In this study, we monitored the runoff in small catchments in unmanaged Hinoki plantations to understand the importance of Hortonian overland flow for understanding the human impact on hillslope stormflow path in Japan. The study catchments locate in Ohmiya village, Mie Prefecture, central Japan. We installed two Parshall flumes in unmanaged Hinoki plantations, and one in broad leaf tree area. Electrical conductivity of runoff water is monitored continuously and in selected storm events, in situ water sampling was conducted 1 or 2 hour interval and dissolved ions were analyzed. When the rainfall intensities were high, runoff peaks coincide with rainfall peak in unmanaged Hinoki plantations, but runoff peaks were low and sometimes delayed to the rainfall peak in the broad-leaf forest. The storm hydrograph in Hinoki plantations were separated into two or three components, using electrical conductivity and Cl ions. When rainfall intensity was high, rainfall components occupied 49-67% of the storm hydrograph. This shows that the importance of the rainfall components in overland flow during rainstorm in unmanaged Hinoki plantations.

HW01/09P/D-035 Poster 1400-226

**SPATIAL VARIATION OF AEOLIAN AND BEDROCK MATERIALS IN THE SURFACE SOIL ALONG A SLOPE IN THE KAWAKAMI BASIN, CENTRAL JAPAN**Yoriko YOKOO<sup>1</sup>, Takanori NOKANO<sup>2</sup> (<sup>1</sup>Institute of Geoscience, University of Tsukuba, <sup>2</sup>The Graduate School of Life and Environmental Sciences, University of Tsukuba)

Elements in soil are partitioned into various phases such as soil minerals, organic matter, and soil solution. A-horizon with dominant organic matter constitutes an important soil component to elucidate and predict the response of recent changes of atmospheric environment on forest ecosystems, because it provides active sites for the interaction and circulation of elements between plants and exchangeable components in the soil. Soils on volcanic rock substrate, termed as kuroboku from its black color, are widely distributed in Japan. In order to evaluate the provenance of soil minerals and their relationship to vegetation, we determined Sr-Nd isotopic ratios and elemental compositions of andesite soils and their coarse-grained and fine-grained minerals along a small slope in the Kawakami forested basin of central Japan, which is divided by a valley in the lower and a woodland path in the upper. Sr and Nd in dehydrated soil is mainly contained in minerals and its <sup>87</sup>Sr/<sup>86</sup>Sr ratio varies widely from 0.7044 to 0.7070 along the slope. However, coarse-grained minerals (>20 μm) in the soil have relatively homogeneous <sup>87</sup>Sr/<sup>86</sup>Sr (0.7042-0.7046) and <sup>143</sup>Nd/<sup>144</sup>Nd (0.5125-0.5127). As the values are slightly higher than the <sup>87</sup>Sr/<sup>86</sup>Sr and lower than the <sup>143</sup>Nd/<sup>144</sup>Nd of original andesite (0.7040 and 0.5128) but are indistinguishable from those of strongly altered andesite, it is assumed that the coarse-grained minerals were largely originated from the chemical weathering of bedrock minerals through which the atmospheric Sr of high <sup>87</sup>Sr/<sup>86</sup>Sr (0.708 in the annual average) and REE were mixed. In contrast, the fine-grained minerals (<2 μm), mainly composed of illite and quartz, have high <sup>87</sup>Sr/<sup>86</sup>Sr (0.710-0.714) and low <sup>143</sup>Nd/<sup>144</sup>Nd (0.5122-0.5125) due to an incorporation of aeolian minerals (~0.720 and 0.5120) originated from arid areas in northern China. It is estimated that the proportion of the aeolian minerals in the fine-grained soil minerals and in the bulk soil range from 14 to 22% and 6 to 19%, respectively. These data indicate that the Sr-Nd isotopic compositions of aeolian minerals do not change in the soil environment, demonstrating their usefulness as provenance tracers. In the upper slope, the aeolian-mineral contribution tends to decrease systematically with elevations from 20% down to 10%. This systematic decrease is caused by the input of secondary minerals of bedrock origin which was supplied from the regolith discarded at the construction of woodland path. This is consistent with elemental patterns which show that elements (Si, Al, Ga, Cu) normalized to Ti, an immobile element, tend to increase upward. The <sup>87</sup>Sr/<sup>86</sup>Sr of vegetation and soil solution and their variation pattern along the slope are entirely different from those of soil minerals, showing no vital exchange of Sr and other elements between the two components.

HW01/09P/D-036 Poster 1400-227

**ANTHROPOGENIC EVOLUTIONS OF PEAT SOILS AND CHANGES OF THEIR HYDROPHYSICAL PROPERTIES**

Elena N. ROVDAN (Belarus, 10, Staroborisovsky tr., Minsk, 220114, BELARUS)

Natural evolution of the most ancient peat soils of Belarus Polesye took place during the last post-glacial period-holocene. Anthropogenic evolution of meliorated peat soil proceeds much quicker and going on no longer that 300 years and most often during last tens years. Drainage amelioration changed natural orientation of geochemical processes in soils, which are expressed in partial destruction of soils organogenic layer due to mineralization and erosion processes, humus content decrease and variation of its qualitative composition. Agricultural utilization of the soils leads to mixture the peat with underlying sand soils. As results the great territories of peatlands have been turned into anthropogenic organic-mineral formations, requiring both special study and special use methods. Genesis and properties of peat soils stipulate the unfavorable thermal regime for grow and development of plants on the organic soils as compare with mineral soils. The sand application to drained peat soils is one of the methods to protect these soils from fast decomposition of organic matter and to change their hydrothermal regime. In spite of wide usage of the method there is lack of investigations about affect of the sand application on hydrophysical properties of peat. Knowledge of soil hydraulic conductivity and water retention is required for quantitative description and prediction of water and solute transport processes, to quantify effects of land use, soil management on soil structure related processes, to predict the impact of human influences on the environment. The hydraulic conductivity of peat soils at different stages of organic matter transformation, peat, sand and their mixtures have been investigated by using TDR and instantaneous profile methods. Transformation of the peat soils as results of drainage and utilization leads to change in porosity, pore size distribution, bulk density, ash content, water retention, saturated and unsaturated hydraulic conductivity. Peat soils at aerobic conditions contain the greatest quantity of water at the saturation, but it gives its water more easily with increasing water potential. The water retention capacity of the drained peat soils which have reached a more advance stage of decomposition is lower, and the loss of water with increasing the water potential are also smaller. The surface peat layers do not show similar regularity with regards to their hydraulic conductivity as to deeper peat layers but the difference between the hydraulic conductivity is not large. Hydrophysical properties of peat sand mixtures are strongly depends from relation of organic and mineral parts. The most drastic changes in water retention of peat sand mixtures takes place in the region of the small quantity of organic matter content in systems (up to 20 % of organic matter content). The results obtained have been generalized using Mualem-Van Genuchten equation and parameters of the model have been defined.

HW01/09P/D-037 Poster 1400-228

**SPATIAL VARIABILITY OF HYDROCHEMICAL DYNAMICS IN WEATHERED GRANITE CATCHMENTS**

Masanori KATSUYAMA, Masayuki ITOH, Nobuhito OHTE, Hiroshi ITOH, Makoto TANI (Graduate School of Agriculture, Kyoto University)

To understand the differences of the hydrochemical processes between catchments, the variability of the catchment scales must be considered. In this study, the hydrochemical dynamics from headwaters to a 2-order catchment are examined at the Kiryu Experimental Watershed (KEW) located in Central Japan (34°58'N, 136°00'E). The entire area of KEW consists of weathered granitic rock and the vegetation mainly consists of afforested stands of Japanese cypress. Hydrochemical observations were conducted at the outlet of the KEW (K; 5.99ha), 4 subcatchments (A; 0.086ha, H; 0.40ha, M; 0.68ha, R; 1.75ha) and a 0-order hillslope plot within A catchment (AP; 0.024ha). The discharge rates in each catchment have been measured continuously and the streamwater for chemical analyses was sampled once two or three week. The discharges were perennial except for those of H and AP. The saturated throughflow generation processes during rainstorms have been observed at AP. Annual rainfall was 1179.4mm at 2002, much dryer than the mean value from 1972 to 2001 (1645.0mm). Some stonemasonry dams constructed here to prevent soil erosion. Upslope from the dam, the groundwater bodies are formed under the soil sedimentation areas in the headwater catchments (A, H, M, and R), and a small wetland is formed along the main

stream. The area of the wetland corresponds to 0.5% of the area of K. Considering the water budget from June to November 2002, the total discharge was increased in larger catchment. Based on the water budget at AP, a large proportion of rainfall seeped into the bedrock at hillslope and less contributed to the stream runoff at headwaters. The contributions of this bedrock groundwater to the stream runoff increased with increasing of catchment area. The SiO<sub>2</sub> concentrations of the streamwater of each catchment increased and NO<sub>3</sub><sup>-</sup> concentrations decreased at larger catchment. The bedrock groundwater has high SiO<sub>2</sub> concentrations and low NO<sub>3</sub><sup>-</sup> concentrations, thus, the variations of concentrations between the catchments depend on the contributions of this component. However, NO<sub>3</sub><sup>-</sup> concentrations in the K streamwater were increased again. NO<sub>3</sub><sup>-</sup> concentration of mainstream surface water decreased during passing through the wetland. NO<sub>3</sub><sup>-</sup> concentrations were nearly zero except for the surface in the vertical profiles of the wetland soilwater. Thus, the surface water NO<sub>3</sub><sup>-</sup> removed by instream processes such as denitrification under the reduced conditions. Therefore NO<sub>3</sub><sup>-</sup> increase at K streamwater was caused by the runoff component from the hillslope of the stream channel and instream hydrobiogeochemical processes. Depend on the catchment scales, the proportion of the constituent elements of catchment (hillslope, stream channel, wetland, etc.) may change. In addition, the existence of erosion control dams may form the wetlands along the stream. To clarify the hydrochemical mechanisms in various spatial scales, it is necessary considering the roles of the each constituent element.

HW01/09P/D-038 Poster 1400-229

**THE SPATIAL AND TEMPORAL VARIATION OF METHANE FLUX OF TEMPERATE FOREST WATERSHED**

Masayuki ITOH, Nobuhito OHTE, Masanori KATSUYAMA, Masatoshi KAWASAKI (Graduate School of Agriculture, Kyoto UnivUniversity)

Methane is considered to be one of the significant greenhouse gases, and is produced in soils as the end product of the anaerobic decomposition of organic matter. Soil methane emissions are taken place in the anaerobic soils such as natural wetlands, landfills, and rice paddies. On the other hand, under the aerobic conditions such as forest soil in hillslope, methane is oxidized to carbon dioxide. So it is believed that the forest catchments function as a sink for methane. However, in temperate forest region, there are usually wetlands in riparian zones around streams, ponds. And it is possible that methane emissions in such wetlands exceed uptake in forest soil. It still has been not fully understood whether the forest catchment site is a net sink or source for methane. The in site observation was conducted at wetlands and dry hill slope around wetlands in the Kiryu Experimental Watershed (KEW), central Japan, covered by mixed stands of secondary broad-leaved deciduous trees and planted coniferous trees. Several wetlands are located along the main stream in KEW. The area of KEW and the total area of wetlands are 59900 m<sup>2</sup> and 300 m<sup>2</sup> respectively. To elucidate the temporal and spatial variability of methane uptake and emission, methane flux was observed regularly by closed chamber method at both the hillslope sites and wetland sites, coupling with surveys on soil physical and nutrient status. Methane was emitted through the year in the wetlands and showed strong seasonality. The emission rate was strongly depending on soil temperature, showed highest in summer (330 mg-CH<sub>4</sub> m<sup>-2</sup> d<sup>-1</sup>) and lowest in winter (0.1 mg-CH<sub>4</sub> m<sup>-2</sup> d<sup>-1</sup>). Spatial distribution within the wetland was highly heterogeneous, depending on soil water content and ground water level. While methane emission showed strong seasonality, methane uptake showed almost constant rate through the year (0-0.2 mg-CH<sub>4</sub> m<sup>-2</sup> d<sup>-1</sup>), and independent of soil temperature change. Estimated methane flux in watershed-scale varied seasonally from 2.97 g-CH<sub>4</sub> d<sup>-1</sup> in Nov.2000 to 58.38 g-CH<sub>4</sub> d<sup>-1</sup> in June 2001. This indicates that a small wetland which shares 0.05% of entire catchment area play important role for controlling the watershed-scale methane budget.

HW01/09P/D-039 Poster 1400-230

**SPATIAL AND SEASONAL DISTRIBUTIONS OF DENITRIFICATION ZONE IN A FORESTED HEADWATER CATCHMENT IN CENTRAL JAPAN**Ken'ichi OSAKA<sup>1</sup>, Nobuhito OHTE<sup>1</sup>, Keisuke KOBA<sup>2</sup>, Takuo NAKAJIMA<sup>3</sup>, Masanori KATSUYAMA<sup>1</sup>, Masatoshi KAWASAKI<sup>1</sup> (<sup>1</sup>Graduate School of Agriculture, Kyoto University, <sup>2</sup>Graduate School of Informatics, Kyoto University, <sup>3</sup>Lake Biwa Research Institute)

To clarify nitrogen loss from the forested headwater catchment, we investigated spatial and seasonal distribution of denitrification process by measuring N<sub>2</sub>O concentration of soil gas and it's dissolved phase of groundwater in situ condition. Field investigation has been conducted at an unchanneled headwater catchment (0.68 ha) in the Kiryu Experimental Watershed (KEW) covered by mixed stands of secondary broad-leaved deciduous trees and planted coniferous trees. The concentrations of N<sub>2</sub>O in the soil gas and the groundwater were measured with temperature, moisture content that potentially affect denitrification. We measured gaseous and dissolved N<sub>2</sub>O at four site in the hillslope part of catchment, that is relatively shallow and wet soil layer above the groundwater body (G1), deep soil layer at the upper side of groundwater body (G34), deep and dry soil layer (G27), shallow and dry soil layer where saturated subsurface flow was occasionally generated during rainfall (G28). At the spring point, where the most wet part of catchment, we measured N<sub>2</sub>O emission by closed chamber method. In the groundwater body, concentration of dissolved N<sub>2</sub>O is generally higher in shallower portion than deeper portion. Correspondingly, the NO<sub>3</sub><sup>-</sup> concentration decreased with depth in the groundwater body. Especially concentration of dissolved N<sub>2</sub>O in groundwater was higher in July-August when it recorded the highest soil temperature: max concentration was 1296nM in shallowest groundwater. It was about 150 times higher than ambient concentration. The concentration of dissolved N<sub>2</sub>O in stream water was relatively equivalent to ambient concentration. At the spring point concentration of dissolved N<sub>2</sub>O was constantly high and emission of N<sub>2</sub>O was large with intense correlation to soil temperature. These indicate that N<sub>2</sub>O generated in shallower groundwater body was emitted at the spring point. At the hillslope part of the catchment, where covered relatively dry forest soil, the concentration of gaseous N<sub>2</sub>O in soil was relatively high at G1: max was 718ppbv in August. The concentration was gradually decreased with the decline of the soil temperature. On the other site in the hillslope, the N<sub>2</sub>O concentration was equivalent to ambient concentration. However at G28, where is generally dry part of the catchment, high concentration of dissolved N<sub>2</sub>O was detected when saturated subsurface flow was generated during rainfall. These observed results suggest that the complete saturation by water was one of the most critical factors for determining the denitrification zone of this catchment. Moreover, denitrification might be highly variable depend upon temporal changes of groundwater condition.

HW01/09P/D-040 Poster 1400-231

**THE ROLE OF FOREST VEGETATION ON THE SEASONALITY OF NITRATE CONCENTRATIONS IN STEEP HILLSLOPES**

Yuko ASANO, Taro UCHIDA, Nobuhito OHTE, Masatoshi KAWASAKI (Graduate School of Agriculture, Kyoto University)

Understanding the factors influencing nitrate concentrations in mountainous headwater streams is important for the stream ecosystem and water resources management. Land-use

can strongly influence N export from hillslopes, however, the interactions between land-use and hydrological processes on the stream nitrate concentrations have been poorly understood. Spatially intensive observations within a hillslope, which is recharging a small stream will be useful in understanding the relationship between land-use and N export. Here we compare the seasonality of nitrate concentrations in soil solution, groundwater, spring from bedrock fracture and stream for two adjacent granitic hillslopes with contrasting land use. One hillslope is poorly vegetated, almost bare with thin soils and no organic layer due to forest cutting more than 1000 years ago (Rachidani: disturbed hillslope, 0.18ha), and the other covered with undisturbed forest (mixed stand of cypress and oaks) with developed forest soils (Fudoji: mature forest, 0.1 ha), in Tanakami Mountains, central Japan. Previous studies showed that the dominant source of stream during baseflow was from bedrock in both hillslopes. Dissolved N in stream was dominated by nitrate. The dominant N species in those stream was nitrate. In mature forest, the mean nitrate concentrations in soil solution at 10 and 40 cm depths were 2.35 and 2.90 mg NO<sub>3</sub>-N L<sup>-1</sup> respectively, and quite variable. The concentration in transiently formed groundwaters ranged from 1.12 to 2.07 mg NO<sub>3</sub>-N L<sup>-1</sup>. The bedrock spring showed the lowest and least variable concentrations of 0.43 mg NO<sub>3</sub>-N L<sup>-1</sup>. The nitrate concentration in mature forest decreased with increasing sampling depth. Further, the nitrate concentration in stream was 0.67 mg NO<sub>3</sub>-N L<sup>-1</sup>, less than 60% of transient groundwater. In disturbed hillslope, the mean nitrate concentration in soil solution was 0.34 mg NO<sub>3</sub>-N L<sup>-1</sup> and concentrations in transient groundwaters ranged from 0.14 to 0.19 mg NO<sub>3</sub>-N L<sup>-1</sup>. The nitrate concentration slightly decreased with depth and the concentration in the stream (0.16 mg NO<sub>3</sub>-N L<sup>-1</sup>) was almost the same as the transient groundwater. Transient groundwater in mature forest showed relatively high nitrate concentrations in winter and low concentrations in summer, however, the stream showed no distinct seasonal pattern. In disturbed hillslope, both the transient groundwater and stream showed similar seasonality and stream nitrate concentration decreased with stream temperature. The seasonal patterns indicate the effect of biological activity, in particular, plant uptake of N during the growing season. In mature forest, nitrate concentrations in stream decreased with increasing bedrock groundwater contribution, which was estimated using SiO<sub>2</sub> concentrations. These results show that although disturbed hillslopes are covered with poor vegetation, plant uptake appears to play an important role in seasonal nitrate dynamics. In contrast, nitrate fluxes from the mature forest are strongly influenced by hydrological mixing. For mature forest, we suggest that signal of biological activity on N was extinguished in stream because of combination of two reasons, 1) large differences in nitrate concentrations between soil and bedrock water component, and 2) large contribution and variation of bedrock groundwater to stream.

**HW01/09P/D-041** Poster **1400-232**  
**THE GROUNDWATER RECHARGE MECHANISM REVEALED BY STABLE ISOTOPES AND CHEMICAL SOLUTIONS ANALYSIS IN AN ARID AREA, WESTERN CHINA**

Tomohiro AKIYAMA<sup>1</sup>, Masayoshi NAKAWO<sup>2</sup>, Jumpei KUBOTA<sup>3</sup>, Yutaka AGETA<sup>1</sup>, Yuki KONAGAYA<sup>1</sup> (Graduate School of Environmental Studies, Nagoya University, <sup>1</sup>Research Institute for Humanity and Nature, Kyoto, Japan, <sup>2</sup>National Museum of Ethnology, Osaka, Japan)

The objective of this study is to clarify the mechanism of groundwater recharge in an arid area, Heihe river basin, Gansu Province and Inner Mongolia, China. This river is typically an inland river in an arid area, which originates from glaciers in the headwaters and disappears in the lower reaches. The basin could be divided into three areas by the topography and the vegetation: the upper, the middle and the lower reaches. Field investigations mainly in the lower reaches were carried out in August to September 2001, January to February, and June 2002. Groundwater level was measured, and water samples, which are groundwater, river water, precipitation, and melt water of glacier, were collected. Stable isotopic compositions of oxygen and deuterium, and chemical compositions were analyzed for all samples. The results are summarized as follows. The depth of groundwater table in the desert area was shallower than that in the area along the river, whereas, altitude of groundwater table in the desert area was higher than that near the river. Therefore, it is suggested that groundwater in the desert area is never recharged by river water directly. There should be a boundary of aquifer at a depth of 60 to 100 m. The d-excess of deep groundwater, which is deeper than 100 m, was significantly lower than that of the meteoric water. So, it is drastically affected by evaporation. Nevertheless, estimated isotopic compositions of its origin were lower than that of melt water of glaciers in the basin. Consequently, it is considered that water, that originated from outer the basin, must contribute to the recharge of the deep groundwater. On the other hand, the origin of shallow groundwater, which is less than 60 m, can be separated corresponding to the surface condition. Groundwater near the river is originated from river water. Its chemical and isotopic compositions are concentrated by evaporation as it infiltrates. Groundwater in the desert area is completely supplied by some of precipitations with high intensity, not low intensity or river water. It is hardly affected by evaporation as it infiltrates. Hence, its isotopic compositions are little concentrated, but chemical compositions are significantly concentrated due to elution of salt accumulation. Therefore, the mechanism of groundwater recharge in the desert area is as follows. Precipitation with high intensity must be divided into two parts. One is evaporated completely near the surface so that salt can be accumulated. The rest part for infiltration, not being affected by evaporation, will recharge the groundwater. Salt accumulation is eluted due to precipitation so that it becomes of high salinity. As it is percolating and recharging the groundwater, chemical composition of the groundwater becomes high. However, isotopic composition is not concentrated, because it is hardly affected by evaporation in the infiltration process.

**HW01/09P/D-042** Poster **1400-233**  
**DRY DEPOSITION OF GASEOUS AND PARTICULATE MATTERS IN A JAPANESE CYPRESS FOREST**

Tomoko OBOTE, Nobuhito OHTE, Masanori KATSUYAMA, Makoto TANI (Graduate School of Agriculture, Kyoto University)

In the last decades, dry deposited gaseous and particulate matters has been recognized as a major process for input of anthropogenic or naturally originated chemical substances from atmosphere into terrestrial ecosystems. To evaluate the effects of dry deposited chemical substances on the nutrient cycle in a forest ecosystem, we observed ionic concentrations of inorganic constituents of incident precipitation, throughfall, stemflow (Na<sup>+</sup>, NH<sub>4</sub><sup>+</sup>, K<sup>+</sup>, Ca<sup>2+</sup>, Mg<sup>2+</sup>, H<sup>+</sup>, Cl<sup>-</sup>, NO<sub>3</sub><sup>-</sup>, SO<sub>4</sub><sup>2-</sup>, HCO<sub>3</sub><sup>-</sup>), some trace gases (SO<sub>2</sub>, HNO<sub>3</sub>, NH<sub>3</sub>, HCl, NO<sub>2</sub>) and ionic concentrations of water-soluble constituents of particulate matters (Na<sup>+</sup>, NH<sub>4</sub><sup>+</sup>, K<sup>+</sup>, Ca<sup>2+</sup>, Mg<sup>2+</sup>, Cl<sup>-</sup>, NO<sub>3</sub><sup>-</sup>, SO<sub>4</sub><sup>2-</sup>) from 1999 to 2001 in a Japanese cypress forest, in the Kiryu experimental watershed, located in the southern part of Shiga prefecture, Japan. To estimate dry deposited rates of inorganic ionic constituents of gaseous and particulate matters, we used two different methods. (1) TF (throughfall) method, which is based on the difference in wet deposition above and below the canopy, was used to estimate dry deposited rates of particulate matters. (2) A single-layer canopy model with a canopy conductance submodel was used to estimate dry deposited rates of gaseous matters. Canopy conductance for gaseous matters were estimated from that for water vapor which was determined based on the flux measurements by the eddy correlation method. Estimated annual dry deposition rates of inorganic ionic constituents were almost same as that of wet deposition, namely, the ratio of annual dry deposition rate versus that of wet deposition for Na<sup>+</sup> was 1.1, NH<sub>4</sub><sup>+</sup> was 0.9, K<sup>+</sup> was 1.0, Mg<sup>2+</sup> was 1.1, Ca<sup>2+</sup> was 1.1, H<sup>+</sup> was 1.9, Cl<sup>-</sup> was 1.6, NO<sub>3</sub><sup>-</sup> was 1.5, SO<sub>4</sub><sup>2-</sup> was

0.6 and HCO<sub>3</sub><sup>-</sup> was 1.0, respectively. And the percentage of each component of total atmospheric sulfate deposition was estimated, the deposits with incident precipitation (6.9-9.8 kg S ha<sup>-1</sup> yr<sup>-1</sup>) was about 60 %, particulate matter (1.4-2.1 kg S ha<sup>-1</sup> yr<sup>-1</sup>) was about 15 % and SO<sub>2</sub> (3.0-3.2 kg S ha<sup>-1</sup> yr<sup>-1</sup>) was about 25 %, respectively.

**HW01/09P/D-043** Poster **1400-234**  
**CHANGING OF STRAMN WATER CHEMISTRY AFTER THE DISTURBANCE OF CLEAR-CUTTING**

Naoko TOKUCHI<sup>1</sup>, Keitaro FUKUSHIMA<sup>1</sup>, Kouichi MOURI<sup>1</sup>, Nobuhito OHTE<sup>2</sup> (<sup>1</sup>Department of Forest Science, Kyoto University, <sup>2</sup>Division of Environmental Science and Technology)

**Introduction** There are many studies about the relation between nutrient cycling and forest management (ex. Bormann and Likens 1979). These studies showed that forest managements, clear cutting, thinning and pruning, had the large influences on nutrient cycling. However, it is difficult to detect the controlling factor for the influences, because the forest does not have the same characteristics of geology, slope direction and plant species composition etc.. Furthermore, the response and/or recovery of the forest sometimes show very slow and it takes long monitoring. In our study site, plantation forest is rotationally managed about 80 years interval and the unit of rotation is one watershed. Namely, there are more than 30 watersheds adjacent each other and it is almost same geology, slope direction, and the different age. It is very useful to understand the influences of the disturbance of forest management. In this study we introduce the experimental site and show the stream water chemistry after the disturbance of clear-cutting. **Study site and methods** Study site is Nara prefecture, Japan. There are 33 watersheds adjacent each other. Each watershed is the different age after the clear-cutting. The minimum age of the forest was 0 year, just after clear-cutting and planted, the maximum forest age was 87 years. Stream water samples were collected from each watershed every 2 weeks in 1998 and 2002. Precipitation was collected every week. Solution samples were kept under 4 °C until the analysis. Ion concentrations (Na<sup>+</sup>, K<sup>+</sup>, NH<sub>4</sub><sup>+</sup>, Ca<sup>2+</sup>, Mg<sup>2+</sup>, Cl<sup>-</sup>, NO<sub>3</sub><sup>-</sup>, SO<sub>4</sub><sup>2-</sup>) and total concentration of Si, Al, Mn, and Fe and dissolved organic C and N concentrations were determined. **Results and discussion** After the disturbance of clear-cutting, stream water chemistry dramatically changed. Especially, NO<sub>3</sub><sup>-</sup> concentration in stream water increased after the clear-cutting and reached to 0.05 meq L<sup>-1</sup> of 3 years after clear-cutting. Then NO<sub>3</sub><sup>-</sup> concentration in stream water decreased with the forest age. After 25 years NO<sub>3</sub><sup>-</sup> concentration in stream water showed the similar range to the concentration of 87 year-old forest. However, the deviation of NO<sub>3</sub><sup>-</sup> concentration in 25 year-old forest was larger than 87 year-old forest. These temporal changes of NO<sub>3</sub><sup>-</sup> concentration in stream water after the clear-cutting were very similar between 1998 and 2002. It suggests that the changes of stream water chemistry after clear-cutting is mainly controlled the local climate and geology.

**HW01/09P/D-044** Poster **1400-235**  
**HYDROLOGICAL TRENDS AFTER SUB-DRAINAGE AT THE HOVI EXPERIMENTAL CATCHMENT, SOUTHERN FINLAND**

Pertti Olavi SEUNA (Finnish Environment Institute)

In 1971 the drainage of the small agricultural catchment of Hovi was changed from open ditches to sub-drains. Due to that change the annual runoff increased by 15 %, spring maximum decreased by 9 % and summer maximum decreased by 36 % judging from the control basin study carried out. Total nitrogen and nitrate nitrogen concentrations increased strongly. During the 30-year period after the sub-drainage the percentage of surface runoff has increased considerably. Right after the sub-drainage the annual surface runoff was about 20 % of the total runoff, while in the late 90's this percentage exceeded 60. The respective trend was recorded for the summer maximum runoff; the surface runoff percentage grew from about zero to about 50 % of the total maxima. In the runoff maxima obtained from snowmelt the trend was not so clear due to the strong dependence on the soil frost. For the comparison it can be stated that according to the isotopic flow separation (oxygen-18) the percentage of the event water amounted to about 70 % of the total runoff on the annual basis, although a part of this event water came through the sub-drains. The nitrogen concentrations dropped by 50-60 % during the 30 years after the drainage change. A part of this trend can be explained by the decrease in fertilization by about 20-25 %. In general, it can be concluded that the trend towards higher surface runoff percentages may contribute to increased flooding on old sub-drainage basins.

**HW01/09P/D-045** Poster **1400-236**  
**NUTRIENTS RUNOFF FROM AN ABANDONED ARTIFICIAL FOREST OF CAMEACYPARIS OBTUSA DURING STORM EVENTS**

Junichiro IDE<sup>1</sup>, Osamu NAGAFUCHI<sup>2</sup>, Atsushi KUME<sup>1</sup>, Kyoichi OTSUKI<sup>1</sup>, Shigeru OGAWA<sup>1</sup> (<sup>1</sup>Research Institute of Kyushu University, Forest, <sup>2</sup>Fukuoka Institute of Health and Environmental Sciences)

Japanese archipelago is covered with forested hills about 67%. Recently, the commercial use of these forests nearly ceased, but public functions of forests (e.g. controlling rising water level, water purification) have been highly evaluated. These functions are thought to work well as forest management is conducted sufficiently. However, many of Japanese artificial forests are abandoned and forest management such as tree thinning is not sufficiently conducted. The artificial forests were about 44% of the total forested area. In the abandoned forests, the canopy becomes dense and thick, and the development of understorey vegetation is disturbed. In such forests, soil erosion is easily occurred during storm events because of bare soil surfaces. In the abandoned artificial forest of Japanese cypress, *Camaecyparis Obtusa*, which is one of the most typical forested species in Japan, the forest floor is denuded because the litter leaves of the tree are decayed on the forest floor soon after defoliation. The increase in the abandoned may decrease the water purification functions and increase the soil runoff during storm events. In order to estimate the water purification function of abandoned artificial forests, hydrological and hydrochemical survey was conducted in the small watershed covered by an artificial forest of Japanese cypress, and the flux budgets for total nitrogen (T-N) and total phosphorus (T-P) were investigated. In both T-N and T-P budgets, stream-water outcomes were greater than precipitation incomes. The concentrations of both T-N and T-P in the stream water increased during storm events. The concentration of phosphorus rapidly increased in the early stage of storm events because high-level particulate phosphorus (PTP) was flushed out together with suspended sediment (SS). The runoff of high-level PTP may coincide with soil erosion. These results suggested that the function of water purification of this watershed became dysfunctional because of soil erosion. We expect that the increase in the abandoned artificial forests will affect harmfully the watershed system in Japan.

**HW01/09P/D-046** Poster **1400-237**

**MONITORING STABLE ISOTOPE HYDROLOGY AT THE FU-SHAN FOREST RESEARCH CENTER, TAIWAN**

Jeffrey S. OWEN<sup>1</sup>, C.H. WANG<sup>2</sup>, Y.J. HSIA<sup>1</sup>, H.B. KING<sup>3</sup>, L.J. WANG<sup>4</sup> (<sup>1</sup>Taiwan Forestry Research Institute, <sup>2</sup>Institute of Earth Sciences, Academia Sinica, <sup>3</sup>National Dong-Hwa University, <sup>4</sup>National Taiwan University)

At the Fu-shan LTER (Long-Term Ecological Research) site in northeastern Taiwan, we have analyzed the  $\delta D$  and  $\delta^{18}O$  compositions of drainage waters from two study watersheds as part of a hydrological and ecological research program. Streamwater  $\delta D$  and  $\delta^{18}O$  values changed seasonally and probably reflected seasonal changes in precipitation isotopic composition. We intend to use differences between calculated fractions of event and pre-event water between the two adjacent watersheds were used to estimate the amount of water that likely does not flow through the outlet weir at one of these watersheds because of differing installation methods used. The results from this study are the first of this kind to include within event sampling in Taiwan and we hope to expand this research approach in the future.

**HW01/09P/D-047** Poster **1400-238**

**ANTHROPOGENIC CHANGE AND THE WATER CYCLE: OUR SEARCH FOR MAUNA LOA**

Charles J. VOROSMARTY (University of New Hampshire)

A careful monitoring of rising concentrations of atmospheric CO<sub>2</sub>, such as at the famous Mauna Loa observatory, has provided an important impetus for continued study of greenhouse warming and the carbon cycle. From the standpoint of predicted impacts on nature and society the concern is not difficult to justify. And, as a result of a clear global signature of change and an allied theory on global warming, substantial financial and intellectual resources are devoted to this topic. A postulated acceleration of the water cycle places hydrology stage center in the climate change debate. Case studies and regional analysis have been widely employed to assess the hydrological impact of climate change. Such vignettes provide an important start, but the global nature of water cycle changes has yet to be fully clarified. Hydrological changes embody many other impacts besides climate change including those associated with land cover change, hydraulic engineering, and pollution of inland waterways. I present a heuristic exploration how a hydrologically-oriented 'Mauna Loa curve' might appear, describing its features and exploring how human activities distort the nature of continental runoff. I provide evidence that such changes are now globally significant. Seeking a hydrological Mauna Loa curve raises several scientific, technical, and political issues. The adequacy of our capacity to monitor such changes, the need to inventory and understand human modification of the water cycle, and mechanisms to focus resources on the study of the more direct human interventions in the global water cycle.

**HW01/09P/D-048** Poster **1400-239**

**MASS TRANSPORT MODELING FOR ASSESSMENT OF GROUNDWATER POLLUTION IN BOLARAM INDUSTRIAL DEVELOPMENT AREA AND ENVIRONS, MEDAK DISTRICT, A.P**

Gurunatha rao VVGS, Subrahmanyam KAMBHAMPATI (National Geophysical Research Institute)

Bolaram Industrial Development area has been established during 1977 on the outskirts of Hyderabad city in Medak district, Andhra Pradesh, India. Bulk drugs and pharmaceutical industries form the main industries and a common effluent treatment plant has been commissioned to treat the wastewater. The effluents are let out in the open channels and minor irrigation tanks, which ultimately reach the tank in Krishnareddytpet village through Pamulavagu. The total dissolved solids (TDS) concentration of the effluent ranges from 2500 - 4500 mg/l. The TDS concentration of groundwater has reached concentrations of 1500 - 2000 mg/l along Pamulavagu stream and in the command area of the Krishnareddytpet tank during 1997. Water level and water quality monitoring was carried out during 1997-98 and also aquifer parameters have been estimated by carrying out pumping tests. Groundwater flow and Mass transport models have been developed to assess the extent of groundwater contamination that has occurred over the last two decades. The mass transport model has been calibrated for the year 1997 and the same has further been used to predict the contaminant migration for 2017 for present loading conditions in the area.

**HW01/09P/D-049** Poster **1400-240**

**PESTICIDE AND NUTRIENT LOADINGS IN THE RIANA RIVER WITHIN THE LAKE VICTORIA - DRAINAGE BASIN**

George ONGWENYI, John M. NYANGAGA (Post-graduate programme in Hydrology, Faculty of Science, University of Nairobi)

The use of modern Agricultural methods i.e the use of various varieties of Pesticide to control diseases and pests and chemical fertilizer to control diseases and pests and chemical fertilizers is now a pre-requisites of increasing agricultural productivity, world over. Despite the fact that this is a positive move, it has serious problems to water resource managers. After application, some of the pesticides and fertilizer residues get their way into surface and ground water bodies in various ways, i.e. through direct application to control aquatic pests, runoff from agricultural farmlands, soil erosion and sedimentation, which may lead to water pollution. The paper describes a 3 year period study on the effect of landuse on water quality and examines pesticide and nutrient (P&N) Loading And concentrations in Riana river catchment within the lake Victoria drainage basin. The common pesticides discussed include, Diazinon, malathion. Ambush, Aldrex, Furadan, D.D.T. and Ridomil. The study incorporated a detailed programme of water quality and riverflow, monitoring, landuse surveys, soil surveys and stream ecological surveys. The study gives unveiling challenges to planners particularly those in the water and agricultural sector.

**HW01/09P/D-050** Poster **1400-241**

**ASSESSMENT OF IRRIGATION IMPACT ON WATER RESOURCES OF PANGANI RIVER BASIN IN TANZANIA**

Simon Hosea MKHANDI, George Venance LUGOMELA (Department of WRE, University of DSM)

Pangani river basin is the second most important river basin in Tanzania in terms of water resources development. The major water users in the basin are for irrigation and hydropower generation. The effective management of the water resources of Pangani river basin is crucial to ensure sustainable development and elimination of conflicts between different water users. Usually, available water in a basin cannot satisfy all demands and consequently restrictions have to be imposed for the benefit of all the stakeholders. Since irrigation

transforms water into a form which makes it unavailable for other users, it is therefore important to quantify the amount of water required for irrigation purposes at present and in the future for Pangani basin. This paper investigates the present and future impact of irrigation on water resources of Pangani river basin in relation to the effect on the generation of hydropower downstream of the river. Irrigation water requirement are estimated using the Penman Monteith method. This approach is incorporated in the F.A.O program developed for irrigation management and planning known as CROPWAT. The paper gives the recommendations to reduce the strain in the competition for use of water between irrigation and hydropower generation in Pangani river basin.

**HW01/09P/D-051** Poster **1400-242**

**STUDIES ON THE EFFECT OF SOIL PROPERTIES ON RETENTION OF HAZARDOUS ORGANICS ON HAZARDOUS WASTE DUMPSITES**

Zareen KHAN, Anjaneyulu Y. (Center for environment, Jawaharlal Nehru Technological University)

Laboratory experiments were carried out on the field samples to study the effect of soil properties in retention of hazardous organics like phenol, p-nitro phenol, 2,4-dichlorophenol and 4-chloro,2-nitrophenol which are released in the waste waters and solid wastes of several industries in Patancheru industrial area, Hyderabad, (India). The parameters like organic matter, clay and iron and aluminium oxides which are known to influence the soil adsorption capacity are studied in the present work. Several soil samples in the entire industrial area were collected and characterized and the adsorption-desorption studies were carried out. The results clearly indicated the decrease in the adsorption capacity by 67% when organic matter was removed from the soils when compared to untreated soils indicating that soil organic carbon content plays a major role in the adsorption process of hazardous organics. Adsorption isotherm data reveal that the Freundlich constant K<sub>f</sub> and the distribution constant K<sub>d</sub> are significantly correlated with organic carbon content of the soils and hydrophobicity of organics while the K<sub>oc</sub>, the soil water distribution coefficient, per unit organic content varied for different hazardous organics. The CBD (citrate-bicarbonate-dithionite) treated soils exhibited a reduction of up to 24.2% in adsorption indicating the significant contribution of free iron and aluminium oxides which are reduced to lower levels. The clay destructed soils also showed a reduction in adsorption capacity up to 53.8%. From these studies it can be concluded that soils having more organic matter, clay and oxides of iron and aluminium content help in retention of hazardous organics in the soil thereby preventing their leaching into groundwaters. Thus the disposal of industrial wastes containing these hazardous organics can be made on soils containing high percentage of these components and further treatment can be accomplished by adopting cost effective methods like bioremediation and phytoremediation on the site.

**HW01/09P/D-052** Poster **1400-243**

**GROUNDWATER FLOW SYSTEM ESTIMATED BY WATER QUALITY**

Yusaku TAGUCHI (Geological Survey of Japan, AIST)

It is well known that groundwater quality has been gradually changed by ion exchange and other reactions with soil granules with keeping long residence time going through the process of groundwater flow. Conversely, there is some possibility that groundwater flow in a basin can be traced using groundwater quality as a tracer. Especially, groundwater quality will be the most important tool for estimating the groundwater flow system in the basin where an area distribution of hydraulic potential could not be clarified. The author proposed the method on how to estimate the groundwater flow system in the basin from the concept of evolution ratio of water quality, distance of groundwater flow, and pattern of groundwater quality. To verify this method, the author selected the Hayadegawa basin, located in Niigata Prefecture, Japan, where there is a lot of information on hydrogeology, as the area for this study. The result of groundwater flow system estimated by this method was harmonized with those known by previous hydrogeological studies. It means that this proposed method has a high possibility to be applicable for field surveys.

**HW01** Wednesday, July 9 - Thursday, July 10

**EFFECTS OF HUMAN ACTIVITIES ON HYDROLOGICAL AND BIOGEOCHEMICAL CYCLES (ICWQ)**

Location: Site C, Room 26

Thursday, July 10 AM

Presiding Chairs: E. Holzbecher, T. Paces

**HW01/10A/C26-001** **0830**

**CRITICAL ANTHROPOGENIC LOAD AND TEMPORAL TRENDS OF HEAVY METALS IN SOIL - WATER SYSTEM**

Tomas PACES<sup>1</sup>, Milan SANKA, Radek KADLUBIES, Milan ZAPLETAL, Petr CHROUST (<sup>1</sup>Department of Geochemistry, Czech Geological Survey, <sup>2</sup>Centre for Environment and Land Assessment, EKOTOXA, Horni nam. 2, 74601 Opava, , Czech Republic)

Accumulation or depletion of heavy metals in soil and water is result of a mass balance between natural and anthropogenic inputs and outputs. The mass balance of heavy metals is expressed by a differential equation  $P \cdot dt = Fatm + Fagr + Fwth - Fup - Frun$ , where  $dP/dt$  is the temporal change in the pool of the metal,  $F_x$  is flux of the metal by a transport mechanism  $x$ ;  $Fatm$  - atmospheric deposition,  $Fagr$  - application of agrochemicals,  $Fwth$  - dissolution of bedrock minerals,  $Fup$  - biological uptake,  $Frun$  - runoff of water. The integral of the equation from an initial pool  $P_0$  at the initial time to  $t$  is  $P = (Finput/k) - [(Finput/k - P_0) \exp\{-k(t - t_0)\}]$ , where  $Finput$  represents the sum of all inputs and  $k$  is the first rate constant of all outputs ( $Foutput = k \cdot P$ ). The critical load is calculated as a steady-state pool of the metal that is not yet harmful to the soil ecosystem ( $P_{critical}$ ) according to  $(Fatm + Fagr)_{critical} = k \cdot P_{critical} - Fwea$ . The exceedance of the critical load,  $EX$  is the difference between the real input from atmosphere and from agricultural chemicals and their critical values:  $EX = Fatm + Fagr - (Fatm + Fagr)_{critical}$ . The future trends of the soil pool of the heavy metals are defined using the difference between the present inputs and outputs  $d = Fatm + Fagr + Fwea - Fup - Frun$ , the ratio between present pool and critical pool of the metals  $r = P_0/P_{critical}$  and the critical time ( $t_{critical}$ ) when the critical pool will be reached. Four regions were defined in the Czech Republic: (1)  $r < 1$ ,  $d < 0$ , and  $t_{critical} < 0$ : no environmental problem is expected, (2)  $r < 1$ ,  $d > 0$ , and  $t_{critical} > 0$ : environmental problem is either not expected or it is expected that the critical limit will be reached in a distant time, (3)  $r > 1$ ,  $d > 0$ , and  $t_{critical} < 0$ : this is the worst case when the present soil pool is higher than its critical value and will still increase in future. The negative time is not significant because the pool will be always above the critical limit, (4)  $r > 1$ ,  $d < 0$ , and  $t_{critical} > 0$ : the present concentration is above the critical limit. It will

decrease in future if the present inputs prevail. The critical time indicates when the pool of the metal in soil reaches its critical level. The mass balance was calculated for various soils in the Czech Republic and maps of the critical loads of Pb, Cd and Cu were constructed. Other maps represent the exceedance of the critical load by present atmospheric and agricultural inputs, projected temporal trends and critical times when the critical pool will be reached. The maps and their environmental significance serve to decision-makers to locate regions where industrial emissions and agricultural inputs of heavy metals should be decreased in order to lower the dangerous contents of the metals in soils.

HW01/10A/C26-002

0850

#### CONSEQUENCES DU DRAINAGE AGRICOLE SUR LES ECOULEMENTS DE CRUE

Claude COSANDEY, Tatiana MUXART, Marie-Jos-PENVEN (C N R S, Lab de Géographie physique)

La question des conséquences du drainage agricole (par drains enterrés) sur l'ampleur des crues est une question largement controversée. Selon certains auteurs, le drainage agricole, obligeant l'eau à transiter par le sol, augmente le temps de transfert et modère donc les écoulements de crue. Pour d'autres pourtant, les processus de transferts résultent essentiellement de transmission de pression : l'eau qui tombe à la surface d'une parcelle drainée provoque rapidement une montée du niveau de la nappe ; cette montée rapide augmente la charge hydrostatique et entraîne une augmentation simultanée du débit des drains ; le temps que met l'eau à être évacuée de la parcelle n'est pas plus long que celui qui lui serait nécessaire par ruissellement dans une parcelle non drainée. L'étude des conséquences du drainage sur la formation des crues a été menée dans les terres loessiques du Bassin Parisien à partir de trois unités hydrologiques emboîtées : une parcelle drainée de 6.4 ha, un petit bassin agricole presque totalement drainé de 52.4 ha, et enfin un petit bassin versant rural de 20 km<sup>2</sup>. A l'échelle de l'événement pluvieux, le drainage se révèle parfaitement efficace pour assurer une apparition rapide de l'eau à l'exutoire de la parcelle (sans qu'il soit possible de savoir s'il s'agit de l'eau de pluie, ou d'eau préexistante, « chassée » par l'eau de pluie) ; de plus, le coefficient d'écoulement est proche de 100 % pour cette parcelle, alors qu'il est toujours sensiblement plus faible pour des territoires plus grands. Cette observation se retrouve pour l'ensemble de la période dite « de drainage intense » c'est à dire pendant la période d'hiver durant laquelle, la réserve hydrique étant reconstituée et les prélèvements de l'évaporation très faibles, l'essentiel des précipitations contribue au ruissellement. Dans ces conditions il semble bien que, au moins à l'échelle de la parcelle, le drainage agricole ne ralentisse ni la vitesse, ni le volume de l'eau qui rejoint le réseau hydrographique. Le drainage d'une région s'accompagne de travaux connexes que sont la remise en état de tout le réseau de collecteurs à ciel ouvert. C'est à ce niveau d'aménagement plus global que le drainage peut jouer un rôle positif sur les écoulements de crues, par la mise en action des processus dits de « ralentissement dynamique »

HW01/10A/C26-003

0910

#### APPROACH IN IDENTIFICATION HEAVY METAL POLLUTION SOURCES OF DNIESTER RIVER

Veru MUNTEANU (Aquatic Ecosystems National Institute of Ecology)

The Republic Moldova is a country located in the drainage basin of the Black Sea. Dniester River, a main water artery of the country, being a transboundary river with a total length of 1352 km, is of great importance for a wide variety of uses, especially drinking water purpose for about 10 mln. population of Moldova and Ukraine. In the last decades, however development of economic interests conflicts more and more with the ecological functioning of the ecosystem. On the both sides of the Dubasari reservoir, total length 125 km, total volume of 485 mln. m<sup>3</sup>, are located the Rezina-Rabnita industrial complex, consisting of 2 cement plants, with annual production of 4.4 mln.tonn/year and one metallurgical plant, 0.7 mln tonn/year, potential sources of heavy metal. Analysis of environmental parameters contamination requires a reliable, quantitative understanding of natural conditions. Seasons monitoring (2000-2002) have shown the highest concentration of mercury (Hg), cadmium (Cd), lead (Pb), copper (Cu) in river water (dissolved + suspended forms) and soils in the nearest zone of industrial complex, to compare with downstream part of the reservoir. For mercury and cadmium water contents are three times higher, for their contents in soils 8-11 times highest, respectively. Taking into account the erosion process (16 tonn/ha/year) from neighboring soils, the purpose of this study was to estimate the influence of heavy metal content from sediment on their contents in water, assessing that these parameters are in a linear interdependence. The mathematical processing of data demonstrated that metal content in dissolved form have a ration of  $r=0.95 - 0.99$  with its content in sediment and suspended matter, respectively. The presence of an interaction structure between model parameters is a typical feature of the classification of model realizations. It is known that the complex models have a lot of causes, which reduce their importance, the ecological processes being very hard to be described in an adequate way. The simple models now are not only satisfactory, but usually are recommended. This simple model has been developed to assess short-term prognostication of heavy metal content both in sediment and dissolved form. In case of dry season the predicted values correspond satisfactory with those measured and confirm the negative impact of industrial complex on heavy metal content in Dubasari aquatic ecosystem. The utilization of model for data interpretation in case of abundant atmospheric precipitations, decreases the errors between measured and calculated values and denote conclusive that the polluted soil from neighboring zone of industrial complex are the main source of heavy metal pollution of Dubasari aquatic ecosystem. Positive value of the parameter, describing the contribution of metal content from sediment on that in dissolved form indicates, for mercury and cadmium, transport direction downward-top, for all longitudinal reservoir direction, when for copper and lead, this process is observed only downstream, fact explained by low velocity of suspended particles sedimentation. Acknowledgement This work was supported by the research Support Scheme of the Open Society Support Foundation, grant N246/2000.

HW01/10A/C26-004

0930

#### LIQUID ANALOG MODELLING OF RIVER POLLUTION PROBLEMS

Parzhang MONADJEMI (Civil Engineering Department, School of Engineering, Shiraz University)

The idea of an analog model is to create a small scale, easily managed system that behaves in critical ways in the same manner as its prototype. Many examples could be given of the successful application of analogs to engineering problems. The main requirement of such models is that it be governed by the same differential equations. Almost all of the analog models are of electronic type. An exception is an analog model which uses liquid flow in a thin slot between two smooth plates. This is the Hele-Shaw model which is mathematically similar to the liquid flow in a two dimensional potential flow. It is the object of this paper to introduce and describe a novel and innovative liquid analog model of extremely simple construction which is able to model various problems of river pollution (A patent has been issued for this device). The model contains two basic elements: a reservoir unit (RU) and a linear friction unit (FU). There is also a terminal reservoir unit (TRU) which is a constant level overflow device. The following figure shows a liquid analog model which is capable of

modeling various river pollution problems. RU<sub>1</sub> & RU<sub>2</sub> are cylindrical shape with cross sectional area A. Initially all the valves in FU<sub>1</sub> & FU<sub>2</sub> are closed and the potential heads in RU<sub>1</sub> & RU<sub>2</sub> are respectively L<sub>0</sub> and D<sub>0</sub>. At time t = 0 the valves are opened. At time t water levels in RU<sub>1</sub> & RU<sub>2</sub> are L & D and a mass balance in RU<sub>1</sub> & RU<sub>2</sub> with q<sub>1</sub> flowing through RU<sub>1</sub> and q<sub>2</sub> flowing through FU<sub>2</sub> results in: Which is exactly the differential equation defining the oxygen sag curve. Experiments with the above model has given very good results which will be fully discussed in the final paper. It has been demonstrated that the liquid analog model can be used for river pollution studies where there are more than one concentrated loads where there are distributed loads along the river and where the deoxygenation rate K<sub>1</sub> and reaeration rate K<sub>2</sub> are not constant and change along the stream. The model described above can also be used for situations where BOD reaction is not first order and for many other complex situations. Experimental results with excellent fit will be described in the final paper. There are many advantages of the liquid analog modeling of river pollution problems. The primary advantage is that the input signals and response signals c.e. the solution to the problem is readily observable by the naked eye. Therefore the solutions may be sensed and visualized and even predicted. The visualization & actual observation of the solutions assigns a great value to this model as an instrument for educational and instructional purposes. There are many other advantages which will be discussed in the final paper.

HW01/10A/C26-005

0950

#### USING MAPS OF DOMINANT RUNOFF PROCESSES TO IDENTIFY AREAS THAT ARE SUSCEPTIBLE FOR PESTICIDE REMOVAL

Petra SCHMOCKER-FACKEL, Felix NAEF (Institute of Hydromechanics and Water Resources Management, Swiss Federal Institute of Technology Zurich)

Chemical compounds like pesticides, phosphorous, nitrate, etc. are applied to most agricultural fields in Switzerland. Considerable amounts of them do reach rivers and lakes and cause water quality problems. To be able to reduce these amounts, e.g. through change of land-use or change of farming practices, it is necessary to identify areas that are susceptible to compound removal. The percentage of a compound applied to a field that reaches a river depends on the chemical properties of the compound and the soil, as well as on the process of runoff formation on the field. In the following the process of runoff formation and its implication on pesticide transport will be discussed in more detail. Compounds like pesticides can be transported to a river by different runoff processes. One possibility is transport by surface runoff. Surface runoff results either because rainfall intensity exceeds the infiltration capacity of the soil (Hortonian overland flow, HOF) or because of saturation of the soil (saturated overland flow, SOF). In the first case, rainfall intensity and infiltration capacity are the critical parameters that determine time and amount of runoff, in the second one it is storage capacity of the soil and amount of rainfall. Another, less known runoff process that removes pesticides is fast preferential subsurface flow (subsurface flow, SSF). Here the density and capacity of preferential flow paths like macropores and tile drains are important parameters concerning runoff formation. Contrary to fast SSF, slow SSF in the soil matrix is not a relevant pesticide transport mechanism. Thus to understand and predict pesticide transport, the spatial distribution of the runoff processes in a catchment has to be known. A methodology was developed to map the dominant runoff process (DRP) using information about soil structure, geology, topography, land-use, etc. as well as from sprinkling and infiltration experiments. The dominant runoff processes were mapped in great detail for several small agricultural watersheds on the Swiss plateau, which react very differently to intense precipitation. The difference in hydrological reaction could be explained with the extend and distribution of the DRP in the catchments. Leu (2003) applied the pesticide atrazine plus a labelling substance to several corn fields in one of the catchments and measured their concentrations in runoff in high temporal resolution. The concentration curves of the pesticides were then compared with the estimated runoff from the respective fields. Fields with HOF or fast SOF as dominant runoff process contributed most to pesticide transport, followed by areas with retarded SOF and fast preferential SSF, while fields dominated by slow subsurface flow did not contribute at all. The delineation of areas that are hydrologically susceptible for pesticide removal is a prerequisite for taking measures to reduce pesticide load in rivers. This requires a detailed evaluation of the spatial distribution of runoff processes as proposed in this paper. Leu, Ch. (2003): Input of corn herbicides and metabolites from small agricultural fields to surface waters: A study in four sub-catchments of lake Greifensee, PhD thesis, EAWAG.

HW01/10A/C26-006

1050

#### AUTOMATIC STORM-TRIGGERED, CONTINUOUS AND DISCRETE HYDROCHEMICAL MONITORING ON A GRASSLAND CATCHMENT

Wayne MENARY, Jeff SHI, Phil JORDAN, Richard DOUGLAS, Brian RIPPEY (University of Ulster)

Sampling methodologies have to be developed which accurately qualify and quantify hydrochemical fluctuations. Sampling inaccuracies associated with discrete monitoring has led to the implementation of auto sampling. The advantage of such an approach is the ability to quantify whole storm loads and qualify the variations of chemicals and suspended sediment during and between storm events, thereby facilitating an examination of inter-storm patterns such as nutrient and sediment washout. We describe the application of automatic storm triggered hydrochemical monitoring on the Oona Water river catchment. Automatic and discrete sampling of phosphorus (P), suspended sediment (SS), volatile organic matter (VOM), ammonia (NH<sub>3</sub>), nitrate (NO<sub>3</sub>), iron (Fe), manganese (Mn), silica (Si), potassium (K), calcium (Ca) and sodium (Na) concentrations in the Oona Water river catchment began on 1 October, 2001 across 6 spatial scales ranging from 0.15 km<sup>2</sup> to 88 km<sup>2</sup>. This places phosphorus and suspended sediment runoff into the context of wider catchment processes such as other nutrient losses, soil erosion and chemical transformations. Furthermore, a YSI 6920 multi-probe sonde was deployed at the 88 km<sup>2</sup> site and continuously monitored pH, temperature, conductivity, dissolved oxygen and turbidity at a 15 minute resolution. This established total solids fluxes and the seasonal and diurnal effects of eutrophication. The turbidity data is highly correlated with suspended sediment concentration and had provided a high resolution series for sediment loads and associated nutrient loss. Data generated from the automatic samplers and discrete sampling programme show that SS varied from a minimum of -0.4 to a maximum of 342.7 mg/L, total P (from -0.072 to 1.468 mg/L), total soluble P (from -0.083 to 0.360 mg/L), soluble reactive P (from 0.008 to 0.200 mg/L), NH<sub>3</sub> (from -0.020 to 1.491 mg/L), NO<sub>3</sub> (from 0.0002 to 5.04 mg/L), Fe (from 0.162 to 2.935 mg/L), Mn (from 0.13 to 2.824 mg/L), VOM (from 6.25 to 96.55 %) across the 6 spatial scales. Sonde data reveals fluctuations for turbidity (from -1.6 to 1470.9 NTU), temperature (from 3.36 to 21.07 °C), conductivity (from 0.001 to 14.75 ms/cm), pH (from 5.8 to 8.73), DO (from 0.21 to 14.75 mg/L). The sonde also highlights the close relationship between suspended sediment and turbidity fluxes (r<sup>2</sup> = 0.91). Deployment of the YSI 6920 multi-probe sonde facilitated monitoring of selected parameters on a resolution not feasible for routine monitoring programmes. Analysis of the results generated permits a qualified estimation of how monitoring programmes should be undertaken, which parameters should be analysed and when.

HW01/10A/C26-007

1110

**CARBON BIOGEOCHEMISTRY IN A COOL-TEMPERATE FOREST WATERSHED IN NORTHERNMOST OF JAPAN**

Hideaki SHIBATA<sup>1</sup>, Kentaro TAKAGI<sup>1</sup>, Mutsumi NOMURA<sup>1</sup>, Kaichiro SASA<sup>1</sup>, Fuyuki SATOH<sup>1</sup>, Tatsuya FUKAZAWA<sup>2</sup>, Masazumi KAYAMA<sup>1</sup>, Karibu FUKUZAWA<sup>1</sup>, Mineko KOHNO<sup>3</sup>, Masami OHGI<sup>4</sup>, Yasumi FUJINUMA<sup>5</sup> (<sup>1</sup>Field Science Center for Northern Biosphere, Hokkaido University, <sup>2</sup>Graduate School of Engineering, Hokkaido Univ., <sup>3</sup>Graduate School of Agriculture, Hokkaido Univ., <sup>4</sup>Faculty of Agriculture, Niigata Univ., <sup>5</sup>Faculty of Agriculture, Hokkaido Univ., <sup>6</sup>Center for Global Environmental Research, National Institute for Environmental Studies)

The quantitative understandings of biogeochemical processes of carbon in forest-soil-stream ecosystem are very important to assess the ability of terrestrial ecosystem to sequester the carbon from atmosphere locally, regionally and globally. Human activities (e.g. climate change, forest harvestings and nitrogen deposition) sometimes disturbed such carbon cycling and budgets in natural ecosystems, motivating us to study the effect of the anthropogenic disturbance on the carbon biogeochemistry and to compare the carbon dynamics between disturbed and undisturbed conditions. We conducted the intensive monitoring of carbon cycling and budgets in a natural cool-temperate mixed-forest as a component of a comprehensive project (CC-LaG: Carbon Cycle and Larch Growth Experiment) to assess the effect of the clear-cut and following plantation on the carbon biogeochemistry in a forest watershed. We report the preliminary products related to the carbon cycles and budgets under the undisturbed condition before the clear-cut treatment. The study basin (1st order stream, 0.08 km<sup>2</sup>, 55-75 m.a.s.l) is located in Hokkaido University's Teshio Experimental Forest, northern Japan (45° 03' N, 142° 08' E). The vegetation is a natural mixed forest, mainly dominated by *Abies sachalinensis*, *Quercus crispula*, *Betula platyphylla* var. *japonica*, *Betula ermanii*, *Picea jezoensis*, *Kalopanax pictus* and *Acer mono*. The understory vegetation is mainly dominated by dense *Sasa senanensis*. The dominant bedrock and soil is Cretaceous sedimentary rock and Pseudogley brown forest soils, respectively. Annual precipitation and annual mean temperature in this region was ca. 1000 mm and 5.7 °C, respectively. We observed net ecosystem exchange (NEE) of carbon between canopy and atmosphere using eddy covariance methods (at 30 m height tower), particulate and dissolved carbon leaching from soil to the stream using intensive monitoring of soil solution and stream chemistry on annual basis. Stand biomass, litterfall, bulk deposition, throughfall, litterfall and soil respiration were also measured in the study basin. We quantified these carbon fluxes separately and established the carbon budgets in this watershed. Our result suggested the leaching of dissolved organic carbon to the stream is relatively important component for the carbon balance in a whole watershed compared to other Japanese forest basins in previous studies.

HW01/10A/C26-008

1130

**APPLICATION OF STABLE ISOTOPES TO IDENTIFY NITRATE CONTAMINATION SOURCES AND ALANYZE HYDROLOGIC TRANSPORT: A CASE STUDY IN A SHALLOW AQUIFER, KOREA**

Seong-Chun JUN, Kang-Kun LEE (School of Earth and Environmental Sciences, Seoul National University)

This study applied a hydrogeological field survey and isotope investigation to identify source locations and delineate pathways of groundwater contamination by nitrogen compounds. The study site is covered largely with agricultural fields and partly with residential sectors. The infiltration and recharge processes were analyzed with groundwater-level fluctuation data and oxygen-hydrogen stable isotope data. The groundwater flow pattern was investigated through groundwater flow modeling and spatial and temporal variation of oxygen isotope data. Based on the flow analysis and nitrogen isotope data, source types of nitrate contamination in groundwater are identified. Groundwater recharge largely occurs in spring and summer due to precipitation or irrigation water in rice fields. Based on oxygen isotope data and cross-correlation between precipitation and groundwater level changes, groundwater recharge was found to be mainly caused by irrigation in spring and by precipitation at other times. The groundwater flow velocity calculated by a time series of spatial correlations, 231 m/yr, is in good accordance with the linear velocity estimated from hydrogeologic data. Nitrate contamination sources are natural and fertilized soils as non-point sources, and septic and animal wastes as point sources. Seasonal loading and spatial distribution of nitrate sources are estimated by using oxygen and nitrogen isotopic data.

HW01/10A/C26-009

1150

**HYDROLOGICAL CONDITIONS AND ITS EFFECT ON NITROGEN DYNAMICS IN UNSATURATED LOAMY SOIL COVERING THE UPLAND SURFACE**

Baku OHJI, Hirohumi IWAMI, Changyuan TANG (The Graduate School of Science and Technology, Chiba University, Yayoi 1-33, Inage-ku, Chiba 263-8522 JAPAN)

One of the most important problem need to be evaluated is the effect of the agriculture activities on the groundwater quality. Based on these needs, the relationship between hydrological condition and nitrogen dynamics in unsaturated loamy(volcanic ash) soil was studied at different types of land use (coniferous-forested and cultivated sites). The study area is located in Ochi experimental watershed, Chiba prefecture, Japan. Nitrate concentration in groundwater of the study area has been increased and detected above the accepted level for safe drinking-water. Although groundwater table in upland area is relatively deep (about 20m below the ground surface), loamy soil with high moisture content (about 70%) is widely distributed over sandy upland surface. As soil moisture content is one of the most important factors which can control the biogeochemical cycle, therefore, in such loamy soil, it is important to investigate the role of special hydrological conditions which affect to the nitrogen cycle. In this study, porous cup samplers were set at different 11 depths in both forested and cultivated areas. Soil water chemistry and in situ various processes controlling it in loamy soil were monitored to the depth of 4m (the thickness of loam layer is about 3-4m). In coniferous-forested site, with increasing the depth, nitrate concentrations in the soil water decrease till approximately 0mg/L. The mechanisms of nitrate debilitating with depth, however, were complex and different by the depths. Vertical changes in NH<sub>4</sub><sup>+</sup> concentration and NO<sub>3</sub><sup>-</sup>/Cl<sup>-</sup> ratio suggest that there are three stages of processes controlling nitrate concentration: (1)uptake by plant and nitrification at depths of 0-1.0m below the ground surface. (2)nitrification and dilution caused by increase of soil moisture content at depths of 1.0-2.5m. (3)nitrate loss by the microbial reaction under anaerobic condition due to high soil moisture at depths of 2.5-4.0m. Nitrification is the main biochemical process at the most depths of loamy soil, in the cultivated site strongly affected by human activities such using the fertilizer, probably due to lower soil moisture content of the cultivated soil than that of the forested soil. These results suggest that although upland surface soil is generally considered as aerobic environment, loamy soil can make, in macro-scale level, anaerobic condition due to high soil moisture content under the forested sites. In this case aerobic/anaerobic zone boundary may exist at the depth of about 2.5m. In cultivated soil it was suggested that not only use of fertilizer but also soil moisture deficit caused by cultivation and/or vegetation can be one of the most important process as human impact to upland surface environment. Furthermore, the application of conceptual model

which had been proposed in previous studies on nitrogen cycling in near-stream environment to the upland surface soil was also examined.

HW01/10A/C26-010

1210

**N<sub>2</sub>O EMISSION FROM TEMPERATE MONSOON FORESTS IN JAPAN AS CORRELATED WITH STREAM NO<sub>3</sub><sup>-</sup> CONCENTRATION**

Muneoki YOH<sup>1</sup>, Yuji TAKESHIGE<sup>2</sup>, Eiichi KONOHIRA<sup>3</sup> (<sup>1</sup>Faculty of Agriculture, Tokyo University of Agriculture and Technology, <sup>2</sup>Shimadzu Techno-Research, Co., Ltd., 604-8436, Japan, <sup>3</sup>Graduate School of Environmental Studies, Nagoya University, 464-8601, Japan)

Terrestrial ecosystems act as an important source of atmospheric N<sub>2</sub>O, but uncertainties remain in not only their quantitative importance but the mechanics. The estimated emission from temperate forests has a wide range of 0.1-2.0 Tg yr<sup>-1</sup>. Actual effect of 'nitrogen saturation' on N<sub>2</sub>O emission as presumed by Aber et al. (1989) has little been clarified. In addition, few data on forest N<sub>2</sub>O emission are available for monsoon Asia that has characteristic climate and soil properties. Here, we present a correlation of annual N<sub>2</sub>O emission rate with corresponding streamwater NO<sub>3</sub><sup>-</sup>. N<sub>2</sub>O emission was measured in 5 forested watersheds in Japan using a closed chamber set at 10-15 places per watershed. A specially intensive research was made for deciduous forest near Tokyo, which has been demonstrated typically N-saturated (Yoh et al., 2001; Yoh, 2001). In this site, N<sub>2</sub>O fluxes showed a clear seasonal variation, having an onset in spring, a maximum in summer, and a decline in late autumn. A significant correlation was observed between the flux and soil temperature, which has scarcely been observed in Europe and North America. This seasonality may be reasonable considering that microbial activities have little limitation all the year round by water in soil, thus probably representing a feature of humid monsoon climate. Consequently, the change in fluxes at a site was successfully described as a function of soil temperature. Taking advantage of it, we estimated annual N<sub>2</sub>O fluxes in other less often studied forests, which are variable in region, altitude, or geological and ecological conditions. The results showed a large difference in N<sub>2</sub>O fluxes ranging 20-fold from 0.04 to 0.9 kg N /ha/yr. However, we found a linear correlation between the magnitude of annual N<sub>2</sub>O flux and stream NO<sub>3</sub><sup>-</sup> concentration of the corresponding watershed. This relationship implies that: (1) the large variability of N<sub>2</sub>O emission observed among watersheds is accounted for just by a factor reflected in stream water NO<sub>3</sub><sup>-</sup>, little by any others. (2) nitrogen saturation may really accelerate N<sub>2</sub>O emission from forest ecosystems as well as NO<sub>3</sub><sup>-</sup> leaching, indicating an increasing source for atmospheric N<sub>2</sub>O. (3) stream NO<sub>3</sub><sup>-</sup> concentration could be a powerful parameter that enables an easy estimation of N<sub>2</sub>O emission from a whole area of corresponding forested watershed. The emission factor of N<sub>2</sub>O calculated from annual N<sub>2</sub>O flux / annual NO<sub>3</sub><sup>-</sup> flux by stream outflow is 3.1 %. Seasonal variation in stream NO<sub>3</sub><sup>-</sup> concentration seems practically insignificant judging from its averaged CV as low as 25% through preceding seasonal observations on stream water chemistry (Yoh et al., 2001). Under similar climate condition at least, annual N<sub>2</sub>O emission from a watershed could be calculated from a single measurement of stream NO<sub>3</sub><sup>-</sup> concentration (C) from the following formula:  $N_2O \text{ (g N/ha/yr)} = 0.031^* 10000(m^2/ha)^* C \text{ (gN/m}^3)^* \text{Discharge (m}^3\text{/yr)}$ .

Thursday, July 10 PM

Presiding Chairs: R.C. Sidle, N.E. Peters

HW01/10P/C26-001

1400

**IMPORTANCE OF COMPARATIVE CATCHMENT STUDIES FOR UNDERSTANDING BIOGEOCHEMICAL CYCLES IN FORESTED ECOSYSTEMS: SUGGESTIONS FROM HYDROLOGICAL CONTROLS ON NITROGEN DISCHARGE**

Nobuhito OHTE, Naoko TOKUCHI (Graduate School of Agriculture, Kyoto University)

In studies of hydrological and biogeochemical cycles in forested ecosystems in humid regions, a key strategy is to define watersheds as ecosystem boundaries, because precipitation usually exceeds evapotranspiration in such regions, and many nutrients are transported by water flow through various pathways within a catchment. Therefore, the nutrient budget can be quantified directly by hydrologic observations coupled with chemical analyses, which means that nutrient cycling in a forest is an open system. For example, the quantity and quality of nitrogen in a forest ecosystem is controlled both by the within-system cycle among plants and soils, and by the exchange of nutrients between systems (catchments) via hydrological and meteorological transport. We emphasize the importance of catchment-scale studies focusing on the hydrological control of nutrient cycles for the following reason. Anthropogenic and chemical disturbances of forest ecosystems, such as the impact of acid rain, have been continuously investigated, beginning in the 1960s. Since the late 1980s, these studies have focused on the effects of heavy nitrogen deposition as one of the critical factors in nitrogen saturation in the forest ecosystems of the northeastern United States and northern Europe. In many cases of nitrogen saturation, high NO<sub>3</sub><sup>-</sup> loads in stream and lake water have been reported. In order to elucidate the mechanisms causing these problems, it is very important to recognize that the major substances related to nitrogen dynamics are usually transported by water flow, and the related microbiological activities are controlled by hydrological and meteorological conditions, since the responses to such disturbances occur very transiently and are spatially heterogeneous within a watershed. This paper reviewed previous experimental results regarding the effects of hydrological processes on N-related biogeochemical reactions, such as mineralization, nitrification, and denitrification, and the seasonal pattern of nitrogen discharge via drainage system in Japanese humid temperate regions. In addition to these review, we compare the discharge characteristics of NO<sub>3</sub><sup>-</sup> between watersheds in the northeastern United States and Japan, to evaluate differences in the status and process of nitrogen saturation, focusing on the hydrologic controls. From these geographical comparisons, following differences were pointed out. 1) High precipitation and runoff by Asian monsoon in warm summer caused higher NO<sub>3</sub><sup>-</sup> discharge in Japanese cases than the northeastern United States, even though high nitrogen demand by plants removes inorganic nitrogen vigorously from soil solution in summer. 2) High NO<sub>3</sub><sup>-</sup> discharge led to higher leaching of base cations to the drainage system instead of streamwater acidification, which was frequently found in the northeastern United States. These findings suggest that the comparative analysis on catchment biogeochemistry can obtain important information to approach a universal understanding of ecosystem response to environmental changes.

HW01/10P/C26-002

1420

**GEOCHEMICAL MASS BALANCES FOR WATERSHEDS OF THE USGS WATER, ENERGY, AND BIOGEOCHEMICAL BUDGETS (WEBB) PROGRAM, 1992-97**

Norman E. PETERS, James B. SHANLEY, Brent T. AULENBACH, Alex E. BLUM, Donald H.CAMPBELL, Robert F. STALLARD, Joseph W. TROESTER, John F. WALKER, Arthur F. WHITE (U.S. Geological Survey)

Geochemical mass balances for 1992-97 were evaluated for five relatively pristine watersheds of the WEBB Program to determine the primary regional factors controlling

yields of the major dissolved inorganic solutes. The sites, which vary markedly with respect to climate, geology, physiography, and ecology, are: Allequash Creek, Wisconsin (low-relief humid continental forest); Andrews Creek, Colorado (cold alpine, taiga/tundra, and subalpine boreal forest); Icaos River, Puerto Rico (lower montane, wet tropical forest); Panola Mountain, Georgia (humid subtropical piedmont forest); and Sleepers River, Vermont (humid northern hardwood forest). Average annual air temperature ranged from about 0°C in Colorado to 21°C in Puerto Rico. Likewise, hillslope gradients vary markedly among sites from extremely low slopes (average <1% associated with the groundwater dominated system in Wisconsin to very steep slopes (average = 66%) in Colorado. For the WEBB sites, annual precipitation ranged from 950 to 5,340 mm at the Wisconsin and Puerto Rico sites, respectively, and the associated annual runoff ranged from >500 to >4,000 mm at these sites. Atmospheric deposition was calculated from volume and solute concentrations of weekly wet-only precipitation data, which were linearly scaled for the estimated watershed precipitation. Streamwater solute fluxes were computed by integrating the product of discharge and streamwater solute concentration, which was estimated from an objective function for each solute that includes streamflow and time. The annual wet-only constituent deposition was comparable among continental sites typically varying by less than a factor of 5, and was much less than in Puerto Rico, which has very high annual precipitation that is dominated by sea salt. Wet-only deposition is a dominant source of N, S, and Cl in each watershed. Droplet deposition (fog and cloudwater) and dry deposition (gases and aerosols) probably contribute most of the remaining difference between outputs and inputs for these constituents, but were not measured at all sites. Bedrock type, residence time of water in the watershed, and temperature are important controls on the weathering contribution of other solutes to streamwater, as reflected by streamwater H<sub>2</sub>SiO<sub>4</sub> and alkalinity among sites. The highest average streamwater H<sub>2</sub>SiO<sub>4</sub> concentrations were in the warmest watersheds in Georgia and Puerto Rico and the lowest was in the coldest watershed in Colorado. The highest average alkalinity was at the groundwater-dominated site in Wisconsin and in the watershed in Vermont, which contains calcite in the bedrock.

**HW01/10P/C26-003****1440****INTERSITE COMPARISON AS MEANS TO QUANTIFY THE PRIMARY PROCESSES CONTROLLING HYDROLOGICAL AND BIOGEOCHEMICAL CYCLING AT THE HILLSLOPE SCALE**

Taro UCHIDA<sup>1</sup>, Jeffrey J. MCDONNELL<sup>2</sup>, Yuko ASANO<sup>1</sup> (<sup>1</sup>Graduate School of Agriculture, Kyoto University, <sup>2</sup>Department of Forest Engineering, Oregon State University)

Effects of land use and land use change on hillslope hydrology are usually made by quantification of the inter-site comparison of catchment response to rainfall or snowmelt. To date, most of these inter-comparison studies have dealt only with the timing and volume of stream flow. In the past several decades, tracer approaches and internal soil water and groundwater response observations have revealed complex runoff process behaviors. Nevertheless, the many different hillslope hydrological processes often seem to very similar hydrograph response. Here we compare stream flow response, tracer and internal pore pressure response data for two well studied sites; Maimai in New Zealand and Fudoji in Japan. These catchments share remarkably similar topography, soil depth, slope angles climate conditions. However, soil drainable porosities at Fudoji are much greater than that in Maimai. Maimai is also underlain by a firmly compacted poorly impermeable conglomerate, whereas Fudoji is underlain by permeable granite. Results show that baseflow recession curves in Fudoji hillslope discharge are significantly gentler than that of Maimai and mean residence time at Fudoji was > 200 % larger than Maimai. Mean residence time gradients at Fudoji increased vertically through the soil profile whereas mean residence time of soil water and transient groundwater increased in a predominantly downslope direction at Maimai. An examination of hydrograph shape and soil water potentials in medium size storms (total rainfall amounts ranges 20 to 60 mm) suggest that these sites are functionally similar. Nevertheless, event/pre-event water components for medium size storms at Fudoji were >3 times that of Maimai and the extension of subsurface saturation area at the Fudoji hillslope was significantly less than that of Maimai. While, during the heaviest storms (total rainfall amounts is greater than 60 mm), the quick flow rate in Fudoji was much greater than Maimai. We argue that a holistic approach to compare and contrast processes among watersheds should include multiple data constraints, including flow, tracers and internal pore pressure and groundwater responses.

**HW01/10P/C26-004****1500****REGIMES DE FLUX DES MATIERES SOLIDES EN SUSPENSION A L'ECHELLE DES PRINCIPAUX ECOSYSTEMES DU CAMEROUN : DIVERSITE CLIMATIQUE ET ACTIONS ANTHROPIQUES**

Gaston LIENOU<sup>1</sup>, Gil MAHÉ<sup>2</sup>, Luc SIGHA-NKAMDJOU<sup>1</sup>, Daniel SIGHOMNOU<sup>1</sup>, Georges Emmanuel EKODECK<sup>1</sup>, Felix TCHOUA<sup>1</sup> (<sup>1</sup>Faculté des sciences, Université Yaoundé, Cameroun, <sup>2</sup>IRD, 01 BP 182 Ouagadougou Burkina Faso, <sup>3</sup>Centre de Recherches Hydrologiques BP 4110 Yaoundé (Cameroun))

Situé en Afrique Centrale, le Cameroun couvre une superficie de 475 000 km<sup>2</sup>, étirée entre le 2° et 13° nord. Le pays est alors soumis à deux grands ensembles climatiques : Le climat équatorial à quatre saisons dans la partie sud et le climat tropical à deux saisons au nord. Le relief du pays, marqué principalement par la mégastucture tectonique de l'Adamaoua, et son exposition aux flux de mousson atlantique associent aux deux principaux climats des nuances maritimes et montagnardes. Le couvert végétal se différencie aussi dans le sens sud au nord, de la forêt dense humide à la steppe à épineux, en passant par les savanes de moins en moins boisées. La population, estimée à 15 millions d'habitants en l'an 2000 est très inégalement répartie sur le territoire, la densité variant de moins de 8 habts/km<sup>2</sup> à plus de 200 habts/km<sup>2</sup>. C'est donc par la combinaison déléments complexes : configuration donnant l'avantage à la latitude, localisation au golfe de Guinée, relief très différencié, population inégalement répartie, que le Cameroun affirme sa diversité, faite de nombreuses interférences entre climats zonaux et azonaux, et modes d'occupation de l'espace. Les mesures des matières en suspension dans les fleuves et rivières du Cameroun sont faites depuis la fin de la décennie 1950. Ces mesures, pour une unité hydrologique, ont souvent été limitées dans le temps. Mais l'ensemble constitue un support privilégié pour une approche globale des régimes des transports solides en suspension dans les différentes rivières. On tente d'appréhender l'intensité de l'érosion et d'en déterminer les principaux facteurs conditionnels à l'échelle des principales unités climatiques. L'activité humaine est mise en évidence. Il ressort que les fortes pentes, la densité de la population, les cultures et l'élevage en sont les facteurs primordiaux. La charge solide des rivières croît avec les latitudes de 20-40 g/m<sup>3</sup> vers l'équateur à 80-100 g/m<sup>3</sup> dans les zones de transition et à 150-160 g/m<sup>3</sup> en zone tropicale sec. Le choix de la taille du bassin versant pour la caractérisation du taux d'érosion effectif est indispensable. En effet, à l'échelle des grands (S > 5 10<sup>4</sup> km<sup>2</sup>), il y a une intégration des caractéristiques géomorphologiques, phytogéographiques, pédologiques et anthropiques hétérogènes en caractéristiques moyennes qui ne rendent plus compte de l'influence du milieu sur l'érosion. Mots clés : érosion, action anthropique, diversité climatique

**HW01/10P/C26-005****1520****SUBSURFACE HYDROLOGIC FLOWPATHS AND BIOGEOCHEMICAL CONTROLS OF NO<sub>3</sub>- TRANSPORT IN KAWAKAMI FORESTED HEADWATER CATCHMENT, CENTRAL JAPAN**

Kasdi Subagyono <sup>-1</sup>, Tadashi TANAKA<sup>2</sup> (<sup>1</sup>Center for Soil and Agroclimate Research and Development, Agency for Agricultural Research and Development, <sup>2</sup>Institute of Geoscience, University of Tsukuba, Tennoudai 1-1-1, Tsukuba, Ibaraki 305-8571 Japan)

NO<sub>3</sub> is important nutrient in agricultural and forested lands, yet the assessment of its dynamic behavior under controls of hydrologic pathways and biogeochemical characteristics is still under considerable debate. NO<sub>3</sub> concentration, hydrometric and biogeochemical characteristics were measured during storm event on August 21-22, 2001 and monthly during the period of August 2000 to August 2001 to define NO<sub>3</sub> mobility in Kawakami Experimental Basin (KEB), Central Japan, a forested headwater catchment with various soil depths overlying late Neogene of volcanic bedrocks. pH, electrical conductivity (Ec), dissolved oxygen (DO), and oxygen reduction potential (ORP) were also measured. Flux of NO<sub>3</sub> was obtained using the convection-dispersion model and its residence time was estimated from its mass divided by its flux. Change in NO<sub>3</sub> concentration agreed well with magnitude and direction of flow. Its concentration in deep riparian groundwater zone increased during low flow, and decreased during high flow. At early onset rain during storm event, its concentrations in deep riparian groundwater was 4.62 mg/L, which significantly differed with that in near surface riparian (0.16 mg/L) and hillslope soil water (0.26 mg/L) due to difference of residence time. At peak storm, its concentrations decreased more than 50% suggesting an occurrence of flushing high concentration of NO<sub>3</sub>. The NO<sub>3</sub> residence time (Tr) obey the following sequence: Tr (deep riparian groundwater) > Tr (near surface riparian) > Tr (hillslope soil water), which have positive correlation with its concentrations. The spatial distribution of NO<sub>3</sub> concentrations showed general patterns in which it increases away from the stream and decreases near the border between riparian and hillslope as well as at hillslope. Bivariate diagrams of stream chemistry show controls of Ca<sup>2+</sup> and Mg<sup>2+</sup> on the NO<sub>3</sub> transport to the stream channel. High concentration of NO<sub>3</sub> in permanent anaerobic deep riparian groundwater zone in some extent of considering an obvious downward flow and the flux of NO<sub>3</sub> (the flux ranges from 0.16 to 1.64 mg.cm-2.day-1) in this zone suggest that the rate of NO<sub>3</sub> accumulation is higher than that of transformation due to long residence time.

Thursday, July 10 PM

Presiding Chairs: R.C. Sidle, N.E. Peters

**HW01/10P/C26-006****1620****A PHOSPHORUS TRANSPORT MODEL FOR SCENARIO-BASED EUTROPHICATION ASSESSMENT IN CATCHMENTS**

Jonas OLSSON, Lotta ANDERSSON, Berit ARHEIMER, Göran LINDSTRÖM, Charlotta PERS, Jörgen ROSBERG (Swedish Meteorological and Hydrological Institute)

Several possible measures are available to reduce diffuse (non-point source) nutrient load to surface water and thereby reduce eutrophication. Such measures include changed arable practices and constructions of wetlands and buffer zones in the landscape, as well as managing lake ecosystems. For some measures, there is an intense debate regarding their nutrient reducing capability. Further, the combined effect of several measures in a catchment is not necessarily equal to their sum. Finally, scale effects (e.g. between fields and catchments) may significantly influence loadings. It is therefore important to apply a holistic and integrated catchment approach when applying and evaluating different management strategies. To facilitate such catchment analyses, the Swedish research program on water quality management - VASTRA - focuses on the development of modeling tools addressing both phosphorus (P) and nitrogen (N) dynamics in catchments. The program is a multidisciplinary effort and in Phase II of the program (2002-) in particular three urgent problem areas are tackled: stakeholders' participation and resolution of conflicts, modeling P transport for eutrophication control, and integrated tools for scenario analysis at the catchment scale. One sub-program aims at improving the description of nutrient flow in catchments by studies of three key landscape elements: (1) arable land - nutrient leakage under differing agricultural management practices will be assessed, (2) wetlands - crucial factors for nutrient reduction will be identified and a model for nutrient trapping in wetlands and buffer zones developed, and (3) lakes - operational scenario modeling including nutrient turnover routines of in-lake measures will be performed. Finally, the findings will be combined to build an integrated, predictive tool for catchment synthesis of nutrient fluxes. The current development of a P transport model builds on the successful decision support tools for N management in rivers and lakes, developed by the group within Phase I of the program. The N model is based on the conceptual, semi-distributed HBV hydrological model, equipped with routines for N transport and turnover. The HBV-N model has been used for estimation of natural retention and source apportionment of N in entire Sweden. Roughly, the P model is designed as an extension of the N approach, taking into account additional processes relevant for P transport such as P turnover in streams, streambank erosion, surface runoff, and sediment transport. The sub-routines for these processes are presently being tested in an experimental catchment in southern Sweden, where the effect of various reducing measures of diffuse nutrient release will later be demonstrated in scenario-based modeling. Further, extensive P transport data bases are being analyzed in order to optimize the sub-routines' design. The presentation will introduce the VASTRA program in general, and in particular present recent results from data analyses and the ongoing P transport model development.

**HW01/10P/C26-007****1640****PREDICTING THE IMPACT OF AFFORESTATION OR DEFORESTATION ON RECHARGE USING ONLY TIME SERIES SOIL MOISTURE DATA**

Joseph POLLACCO (School of Civil Engineering and Geosciences, University of Newcastle)

Modelling the impact of afforestation or deforestation on water resources is complex. Many factors need to be taken into account such as the microclimate, the soils, the underlying geology, the presence of macropores, the species and their age and density. Parameters used in modelling the different processes are traditionally determined individually from laborious and expensive measurements such as the evaluation of transpiration from branch bag; sap flow; eddy covariance method; the interception calculations of the precipitation differences next to and within the canopy. In this study a modelling approach is taken where the only input data required are time series precipitation and penman evapotranspiration. The SheLuc (System Hydrological European Land Use Change) model uses parameters describing interception, evapotranspiration and soil parameters (van Genuchten parameters). The novel aspect of the SheLuc model is that the parameters are determined solely from normalised time series soil moisture profiles measured by neutron probes. Thus the SheLuc inverse problem for calibration uses a minimum of parameters to describe the different processes which renders SheLuc a valuable tool to predict scenarios of climate and

HW02

Friday, July 11

**STREAM TEMPERATURE CHANGES AND EFFECTS (ICWQ)**

Location: Site C, Room 31

Friday, July 11 AM

Presiding Chair: B. Webb

HW02/11A/C31-001

0835

**SEASONAL VARIATION IN RIVER HEAT BUDGETS**

Bruce W. WEBB, Yu ZHANG (School of Geography and Archaeology, University of Exeter)

The nature of the seasonal variation in the non-advective components of river heat budgets has been investigated for four streams of different character in South-West England. These comprise an exposed upland tributary, a regulated water course, and tributaries shaded by deciduous and coniferous riparian woodland. The contribution of radiation (including short-wave and long-wave components), sensible heat, evaporation, bed conduction and friction to the heat energy gain and losses of the study streams has been determined from on-site hydrometeorological measurements conducted over a complete annual cycle (May 1995–April 1996) and is reported as monthly mean values. The results highlight how the river heat energy budget changes throughout the year, but also emphasise the effects of stream characteristics in influencing the seasonal march of energy budget components.

HW02/11A/C31-002

0900

**HEAT EXCHANGES AND TEMPERATURES WITHIN A SALMON SPAWNING STREAM IN THE CAIRNGORMS, SCOTLAND**David M. HANNAH<sup>1</sup>, Iain A. MALCOLM<sup>2</sup>, Chris SOULSBY<sup>3</sup>, Alan F. YOUNGSON<sup>3</sup> (<sup>1</sup>School of Geography, Earth and Environmental Sciences, University of Birmingham, UK, <sup>2</sup>Department of Geography and Environment, University of Aberdeen, UK, <sup>3</sup>Fisheries Research Services (FRS) Freshwater Laboratory, Pitlochry, UK)

Stream bed gravels are important spawning areas for salmonid fish, which bury their eggs in a redd (nest) within river bed sediments to a depth of 0.30 m. The rate of development of salmonid eggs is largely dependent upon temperature and dissolved oxygen profiles. Stream temperatures are often used to predict salmonid embryo development; but there are very few medium-term studies of the heat exchanges determining water column and bed temperatures. Furthermore, no research exists on the energy balance for subarctic Scottish rivers. Hence, this paper reports the results of a hydrometeorological study of a salmon spawning stream in the Cairngorms that aims: (1) to characterise seasonal and sub-seasonal stream energy budget and thermal dynamics and; (2) to explain these variations in terms of meteorological and hydrological factors. Field data were collected within a study reach of Girnock burn (Aberdeenshire, northeast Scotland) from salmon spawning (late October 2001) until estimated egg hatch (mid-April 2002). Energy budgets for the air-water column and river bed interface were estimated based upon hydrometeorological observations made above the river (automatic weather station) and within both the channel and river bed. Bed thermal profiles were monitored to 0.4 m depth. River discharge was approximated from records at the outlet of Glen Girnock and stage (water depth) was recorded for the study reach. All field data were recorded at 15 min intervals. In terms of average river energy flux contributions, net bed radiation (35.6%), sensible heat (24.9%), bed heat flux (23.8%) and friction at the stream bed and banks (15.7%) are heat sources; while latent heat (73.1%) and net radiation (26.9%) are heat sinks. All energy losses and 24.9% of heat gains occur at the air-water interface; and 59.4% of energy gains (75.1% including friction) take place at the water-channel bed interface. Typically, temperatures increase (+1.97°C) and show dampening of thermal response from the water column to depth in the stream bed. The most salient findings include: (1) the stream bed (atmosphere) is the dominant energy source (sink) for heating (cooling) channel water, which may be attributed to inferred heat advection by groundwater up-welling into the bed of this upland stream; (2) sensible heat is the primary atmospheric energy source due to limited net radiation; (3) friction at the stream bed and banks is an important heat source. Energy budget terms and temperatures exhibit sub-seasonal changes (daily and diurnal) in response to meteorological and hydrological conditions. This research may inform models of salmonid embryo development through physical process understanding of energy fluxes driving stream temperature dynamics.

HW02/11A/C31-003

0925

**STREAM TEMPERATURE AS AN INDICATOR OF HYDROLOGICAL CIRCULATION IN A STEEP FORESTED MOUNTAIN BASIN**

Andrew C. WHITAKER, Hironobu SUGIYAMA (Graduate School of Science and Technology, Niigata University)

Seasonal and short-term flood event changes in stream temperature are examined for a steep forested basin in the Asahi Mountains of Niigata Prefecture on the Japan Sea coast. Average annual precipitation is 3000–4000 mm with seasonal snow cover December–May, a rainy season June/July, summer typhoons, and a wet autumn season. Vegetation is mainly natural mixed beech with some planted cedar and larch. Stream temperature is monitored at three nested scales: (1) zero-order spring, (2) 1.32 km<sup>2</sup> second-order tributary, and (3) 19.45 km<sup>2</sup> third-order stream. Soil temperature is monitored to a depth of 1 m close to the spring and beside the tributary/main stream channel. The dependence of stream temperature on ambient air temperature is observed, although during freezing winter periods the stream temperature is maintained well above zero by deep groundwater contributions, including very stable temperatures of about 10°C at the spring. Seasonal changes in stream temperature are driven by strong variations in the seasonal climate and the occurrence of heavy rainfall and snowmelt runoff. Short-term flood event stream temperature dynamics, which are unrelated to air temperature patterns, may be explained by changes in the dominant streamflow generation mechanisms. A drop in stream temperature can often identify peak snowmelt contributions. However, in two successive years a dramatic though short-lived drop in stream temperature occurred during the peak flood event of the warm rainy season, slightly delayed on the early falling limb. A corresponding drop in soil temperature occurring only at the zero-order site (especially 80–100 cm layer) indicates rising water tables and a sudden increase in subsurface flow from these headwater hollows. In contrast, other summer rainstorms (intensities up to 50 mm/h) caused only a rise in stream temperature due to the apparent dominance of surface or near-surface flow paths. Simple monitoring of stream, source spring, and soil temperature is shown to be useful in identifying dominant mechanisms of hydrological circulation, although cases of contradictory evidence are also presented.

landuse change. SheLuc is the merger of two models, SHETRAN and Hyluc. The latter is a parsimonious parameter water balance model which predicts evaporation, interception, soil moisture deficit and recharge. Hyluc uses only the integrated soil moisture content within the upper 2 m of soil and employs the concept of field capacity and has been used on its own and in many studies to predict recharge. The only component of SHETRAN employed in this model represents the Richards equation for 1-dimensional flow through unsaturated porous media. A finite difference solution to the equation is calibrated using all of the soil moisture data to a depth of 9 m, and the method avoids the concept of the field capacity. SheLuc is being used as a Decision Support tool to estimate whether there will be an increase or decrease of recharge if the Midlands region of the UK is forested or deforested with pine or oak on current pasture grassland and heather landuse. SheLuc gives quantitative predictions that recharge would be greatest for pasture grass decreasing in the following order for Heather, Oak and then Pine.

HW01/10P/C26-008

1700

**THE EFFECTS OF 3-YEAR OLD ROAD NETWORK ON BIOGEOCHEMICAL RESPONSES OF A SMALL TROPICAL HEADWATER CATCHMENT TO STORM EVENTS IN PENINSULAR MALAYSIA**Junjiro N. NEGISHI<sup>1</sup>, Roy C. SIDLE<sup>2</sup>, Shoji NOGUCHI<sup>3</sup>, Robert STANFORTH<sup>4</sup>, Abdul Rahim NIK<sup>5</sup> (<sup>1</sup>Department of Geography, National University of Singapore, <sup>2</sup>Disaster Prevention Research Institute, Kyoto University, Japan, <sup>3</sup>Japan International Research Center for Agricultural Sciences, <sup>4</sup>Department of Chemical and Environmental Engineering, National University of Singapore, <sup>5</sup>Forest Research Institute Malaysia)

Tropical rainforests are generally characterized by being nutrient poor compared to temperate forests because the relatively high temperatures throughout the year and the large amounts of precipitation promote nutrient mobilization through higher decomposition rates of organic detritus as well as leaching from organic matter and inorganic minerals. However, continuous and efficient internal recycling of nutrients within tightly-coupled tropic levels enables exceedingly high productivity and biological diversity of tropical rainforests to be established. Construction of road networks for timber production is among the most devastation land uses related to nutrient cycling in forested catchments because it greatly alters the residence time and pathways of precipitation and runoff leading to the discontinuity of nutrient recycling. Compacted bare soil surfaces and intense rainfall promote occurrence of infiltration-excess overland flow and surface erosion, particularly on roads. Formation of artificially extended surface runoff networks on the roads not only cause a quick delivery of precipitation water and eroded sediment into stream systems, but also promotes a net loss of nutrients associated with runoff and eroded sediment due to a shortened residence time and decreased chance to be utilized by vegetation. Although the effects of logging operations on flow regime, sediment and water yields are somewhat understood, most of the previous studies have been based on the monitoring at catchment outlets. Therefore, our process-based understanding of how road networks influence nutrient pathways and how such intra-catchment processes are reflected in the outlet measurements is limited. In this study, biogeochemical responses of road systems to precipitation events were examined by collecting water samples over several storm events along with hydrological measurements in a small headwater catchment (13 ha) at Bukit Tarek Experimental Watershed, Peninsular Malaysia. The road networks were established within the catchment in 1999 when it was selectively harvested. We employed an experimental design in which a subcatchment (< 1 ha) is nested within the 13 ha catchment. Infiltration-excess overland flow generated on the road surface appeared to have consistently contained one of the highest concentration of dissolved organic carbon (DOC) and potassium (K) observed in the catchment. The concentrations of these elements did not significantly drop even during highly intense rainfall and also had a positive relationship with suspended sediment (SS) concentration. This observation suggests that these elements might originate from organic matter rich side cast materials that have been left on the road edges. At the catchment outlet, the trajectories of concentration level of DOC, K and SS appeared to be synchronized, suggesting their origin as the road surfaces. Our preliminary findings support our original hypothesis that road surfaces are the major source of elements such as DOC and K even 3 year after the road construction.

HW01/10P/C26-009

1720

**AQUATIC ECOSYSTEMS WITHIN THE CHERNOBYL NUCLEAR POWER PLANT EXCLUSION ZONE: 17 YEARS AFTER THE ACCIDENT**Dmitri I. GUDKOV<sup>1</sup>, Valery V. DEREVETS<sup>2</sup>, Mikhail I. KUZMENKO<sup>3</sup>, Alexander B. NAZAROV<sup>2</sup> (<sup>1</sup>Department of Radioecology, Institute of Hydrobiology, <sup>2</sup>SSPE Chernobyl Radioecological Centre)

The territories of the Chernobyl NPP exclusion zone are characterised by significant heterogeneity of radionuclide contamination, which is significantly reflected by the radioactive substances contents in aquatic ecosystem components. Primarily this is due to the composition and the dynamics of radionuclide emissions into the environment as a result of accident in 1986, as well as to the subsequent processes of radioactive substances transformation and biogeochemical migration in the soils of catchment basin and bottom sediments of reservoirs. Relatively low contents of radioactive substances are found in the river ecosystems. Due to high water change rate the river bottom sediments have undergone decontamination processes (especially during floods and periods of high water) and over the years that passed since the accident have ceased to play the essential role as a secondary source of water contamination. The main sources of radionuclides in rivers are currently the washout from the catchment basin, their flow from more contaminated water bodies, as well as the groundwater. On the other hand, the closed reservoirs, and in particular the lakes in the inner exclusion zone, have considerably higher levels of radioactive contamination caused by limited water change and by relatively high concentration of radionuclides deposited in the bottom sediments. Therefore, for the majority of standing reservoirs the level of radionuclide content is determined mainly by the rates of mobilization of radionuclide forms exchange between bottom sediment and water, as well as by the external wash-out from the catchment basin. In this paper will be considered: (1) the latest data on content of the most biologically hazardous radionuclides (Sr-90, Cs-137, Pu-238, Pu-239+240 and Am-241) in water, seston, bottom sediments and hydrobiota of the different trophic levels and ecological groups (higher aquatic plants, molluscs and fish); (2) the dynamics of radionuclide distribution in components of aquatic ecosystems; (3) the impact of hydrotechnical facilities within the Chernobyl NPP exclusion zone on hydrologic regime of flood-lands of the Pripyat River; the main water way of the exclusion zone; (4) the peculiarities of formation of vegetative communities from lakes within embankment territory of Pripyat River flood-lands and its impact on radionuclide distribution in aquatic ecosystems; (5) the major hydrochemical factors, which determine the behaviour of radionuclides in the aquatic ecosystems; (6) the possibility to use of hydrobiota of different trophic levels as biological indicators of radioactive contamination of water objects; (7) the seasonal dynamics of radionuclides content in macrophytes and the role of main aquatic plant associations in processes of radionuclides distribution in biotic component of biocenosis; (8) some biological effects (somatic and cytogenetic) of radiation exposure on hydrobiota living in water reservoirs with different levels of radioactive contamination; (9) the level of ecological risk for aquatic organisms within the Chernobyl NPP exclusion zone.

HW02/11A/C31-004

0950

**SPATIAL AND TEMPORAL STREAM TEMPERATURE DYNAMICS WITHIN AN ALPINE CATCHMENT: IMPLICATIONS FOR BENTHIC COMMUNITIES**

Lee E. BROWN, David M. HANNAH, Alexander M. MILNER (School of Geography, Earth and Environmental Sciences, University of Birmingham, UK)

Stream temperature is one of the key physical habitat factors influencing the distribution and diversity of macroinvertebrate taxa in alpine catchments. However, a limited number of studies have been conducted to determine temperature variations in alpine streams other than those fed primarily by glacial meltwater. Furthermore, the thermal regime of the hyporheic zone (i.e. the active streambed layer where surface water and groundwater interact) in alpine streams has received very little attention. Hence, the aims of this paper are: (1) to characterise the nature and dynamics of water column and bed temperature patterns within alpine streams and (2) to determine the key physical factors influencing spatial and temporal variability in alpine stream thermal behaviour. Field data were collected over the 2002 summer melt-season in the Taillon-Gabiétous catchment, French Pyrénées. The catchment contains four distinct and highly dynamic hydrological stores: (1) two cirque glaciers (Taillon and Gabiétous), (2) seasonally variable snowpacks, (3) a karst groundwater system, and (4) hillslope/alluvial aquifers. Water column temperatures were recorded at 8 sites: (A) the Taillon stream near the glacier snout; (B) 1 km downstream on the main Taillon stream, upstream of the confluence with C; (C) a karst groundwater spring; (D) the Taillon stream downstream of the confluence with C, upstream of the confluence with E; (E) a predominantly groundwater fed tributary (Tourettes) with a small glacial input; (F) the Taillon stream downstream of the confluence with E; (G) a hillslope groundwater stream that is a tributary of E; and (H) a large upwelling fed by alluvial groundwater. At three sites (D, E and F), bed temperatures (0.05, 0.20 and 0.40 m depth) and stream discharge were monitored. An automatic weather station was installed over the stream at Site D. All data were recorded at 15 min intervals. With the exception of streams fed directly by deep groundwater stores and at the Taillon Glacier snout, surface water temperatures were strongly influenced by air temperature, and inputs from tributaries. Bed temperatures in the Taillon (Tourettes) stream were on average, coldest (warmest) and most (least) variable. However, dynamic sub-seasonal contributions from different water stores resulted in short term deviations away from seasonal patterns. Hyporheic water temperatures were strongly influenced by the direction and extent of inferred groundwater-surface water interactions. In the Taillon stream, thermal regimes of surface and hyporheic waters were very similar with short lag times and limited vertical dampening of thermal response, indicating strong surface water downwelling. In the Tourettes stream, bed temperatures were colder than surface waters and hyporheic thermal responses to warming of surface waters were increasingly lagged and attenuated with depth, suggesting groundwater upwelling. In providing an insight into the controls upon water column and streambed temperatures, this research will inform ongoing hydroecological investigations in the Taillon-Gabiétous catchment and, more widely, the study of benthic communities in alpine catchments.

HW02/11A/C31-005

1045

**WATER-AIR TEMPERATURE RELATIONSHIPS AND THE ROLE OF FLOW**

Bruce W. WEBB, Paul D. CLACK, Des E. WALLING (School of Geography and Archaeology, University of Exeter)

The nature of the water-air temperature relationship, and its moderation by discharge, have been investigated for catchments ranging in size from 2.1 to 601 km<sup>2</sup> in the Exe Basin, Devon, UK and for data relating to hourly, daily and weekly time bases. The sensitivity and explanatory power of simple water-air temperature regression models based on hourly data were improved by incorporation of a lag, which increased with catchment size, while relationships became more sensitive and less scattered as the time base of data increased from hourly to weekly mean values. Significant departures from linearity in water-air temperature relationships were evident for hourly, but not for daily mean or weekly mean, data. A clear tendency for relationships between water and air temperatures to be stronger and more sensitive for flows below median levels was apparent, and multiple regression analysis also revealed water temperature to be inversely related to discharge for all catchments and timescales. However, discharge had a greater impact in accounting for water temperature variation at shorter timescales and in larger catchments.

HW02/11A/C31-006

1110

**EFFECTS OF RIPARIAN MANAGEMENT ON STREAM TEMPERATURE IN HEADWATER STREAMS, COASTAL BRITISH COLUMBIA, CANADA**Takashi GOMI<sup>1</sup>, R. Dan MOORE<sup>1</sup>, Amod S. DHAKAL<sup>2</sup> (<sup>1</sup>Department of Geography, University of British Columbia, <sup>2</sup>Department of Forest Resources Management, University of British Columbia)

Stream temperature is arguably the "master variable" in stream ecosystems. Forest harvesting can influence stream temperature regimes, and the potentially deleterious impacts of higher temperatures on salmonids and other species have generated significant debate. One common approach to protecting streams is to leave a riparian buffer to provide shade. However, little information has been collected on the effectiveness of different buffer widths. We report the results of a 6-year field experiment to evaluate the effects of riparian buffer widths on stream and riparian ecosystems, including stream temperature response, in headwater streams in coastal British Columbia. The experiment included 12 streams, of which three were assigned to each of four treatments, including no harvesting (80 yr-old second growth conifer riparian forest), 10 m and 30 m riparian buffers, and clear-cut harvesting with no buffer (no riparian overstory vegetation). Regression analysis was used to calibrate the pre-harvest data for each treatment stream with one of the control streams, to provide a basis for estimating post-harvest treatment effects. Autoregressive and heteroskedastic errors were included in the regression model, because stream temperature exhibited serial correlation and the error variance increased with stream temperature. Water temperature in the streams with 10 and 30 m buffers did not exhibit significant warming. Summer temperature increases averaged only 2 to 3 °C in the streams in the no-buffer treatment, compared to increases of up to 7 to 10 °C, or greater, found in previous studies. Because the headwater channels are narrow (bankfull width 1-3 m), both over and under-story vegetation provided shade and reduced direct input of solar radiation. In addition, ongoing research suggests that hyporheic flow through step-pool features formed by pieces of large woody debris may have a strong role in moderating water temperature increases in these steep headwater streams.

HW02/11A/C31-007

1135

**EVALUATION OF POTENTIAL ENERGY LOSS WITH DAM CONSTRUCTION**

Koshi YOSHIDA, Hajime TANJI (Graduate School of Agricultural and Life Sciences, The University of Tokyo)

This paper attempts to propose an idea of dam assessment, which aims after potential

energy of river water. It is easy way to estimate an impact of dam development by volume balance that many previous studies have employed for dam assessment. Generally dam for generating electricity has been regarded as non-consumptive water use in the past. Of course, that does not consume river water volume, however potential energy must be consumed for generating hydroelectricity. In this study, authors estimated potential energy loss based on the following two conversion theories. 1) The potential energy of river water must be converted into heat energy on non-dam condition. The change of river water temperature by dam construction was estimated to evaluate an impact to the heat environment. 2) The potential energy of river water must be converted into friction stress to erode the riverbed on non-dam condition. The change of soil erosion by dam construction was estimated to evaluate an impact of soil supply to the downstream area. Needless to say, soil is important medium to transport nutritive salts and the amount of soil supply must be considered to assess an ecological system in downstream area. The proposed model was applied to Nam Theun dam in Laos. Laos is blessed with topographical condition for dam site of hydroelectric power and recently converted an economic policy by the exportation of forest resources into by the one of electric power. Therefore the results of this study will give one solution to the adjustment between the dam development and the environmental protection in this area

HW02/11A/C31-008

1200

**TEMPERATURE-OXYGEN REGIMES OF SOME TROPICAL STREAMS IN SOUTH-WESTERN NIGERIA**Catherine Imhangeluya IKHILE<sup>1</sup>, Stella Maris AKHIONBARE<sup>2</sup> (<sup>1</sup>Department of Geography and Regional Planning, <sup>2</sup>New Grass Technologies)

The temperature-oxygen variations in seven rivers (Orle, Edion, Ojo, Owan, Ule, Obvoti, Oruen) located in the tropical rainforest area of Edo State, Nigeria were studied in the periods 1987 and 1997. In 1987, air temperatures ranged from 29.5-37.0 °C and water temperatures ranged between 21.0-34.0 °C. Values were lower for air temperatures in the dry season (29.5-37.0 °C) than in the wet season (30.0-37.0 °C); and water temperatures were generally higher in the wet season (range: 25.0-33.0 °C) than in the dry season (range: 21.0-34.0 °C). In 1997, the temperatures of the rivers ranged from 20.0-29.0°C while air temperatures ranged from 26.0-34.0 °C; being generally higher in the dry season than in the wet season. Dissolved Oxygen (DO) in 1987 was generally low (ranging from 2.1-36.8 mg/l), being lower in the dry than in the wet season while in 1997, DO for the rivers ranged between 0.30-2.20 mg/l and were generally low especially during the dry periods of the year. Various factors were attributed to the regimes of temperature and dissolved oxygen namely; (i) Effect of sunlight and cold harmattan winds that lower temperatures of air and water to different extents (ii) Effect of mixing and turbulence in the river flow of the dissolved oxygen as observed for River.

HW02-Posters

Friday, July 11

**STREAM TEMPERATURE CHANGES AND EFFECTS (ICWQ)**

Location: Site D

Friday, July 11 AM

HW02/11A/D-001

Poster

0830-133

**WATER TEMPERATURE VARIATION IN AUSTRIAN RIVERS DURING THE TWENTIETH CENTURY**Bruce W. WEBB<sup>1</sup>, Franz NOBILIS<sup>2</sup> (<sup>1</sup>School of Geography and Archaeology, University of Exeter, <sup>2</sup>Hydrographisches Zentralbuero, Bundesministerium fuer Land- und Forstwirtschaft, Vienna)

Trends in water temperature during the twentieth century have been investigated for 10 rivers in Austria, which range from small upstream tributaries strongly influenced by glacial and snow meltwater, to downstream locations on the River Danube, affected by regulation for H.E.P. generation. Monthly mean values for the period 1901 - 2000 have been investigated using LOWESS smoothing techniques to identify trends in annual and seasonal water temperatures, and to highlight different patterns of variation in catchments of different character. Variation in water temperature has also been examined in relation to the North Atlantic Oscillation Index as an indicator of climatic conditions during the twentieth century.

HW02/11A/D-002

Poster

0830-134

**EXPOSED RIVERINE SEDIMENT PATCHES: ENERGY FLUXES AND THERMAL PROFILES**

David M. HANNAH (School of Geography, Earth and Environmental Sciences, University of Birmingham, UK)

Exposed riverine sediments (ERS) represent important habitats along both natural and highly modified rivers. Furthermore, ERS have long been associated with rare and scarce invertebrates in the UK. Some ecologists have suggested faunal communities in these 'harsh' environments are influenced by abiotic factors. Heat transfer within ERS is a key determinant of physical habitat quality between disturbance (inundation) events. However, there is currently no information about ERS surface and subsurface microclimate (specifically vertical energy fluxes and thermal profiles) during these 'drying-out' periods. Hence, the primary aim of this paper is to determine the nature and dynamics of energy (heat) fluxes within ERS and, thus, to elucidate the key factors that control variations in surface and subsurface physical habitat in space and over time. Field observations were made during summer 1999 and 2001 on the Fiume (River) Tagliamento, Italy. Two study sites were instrumented to provide both alpine (upstream) and Mediterranean (downstream) hydroclimatic conditions and a complete range in ERS calibre from fine sand to coarse gravel. At each site, an area (e.g. gravel bar) of varied ERS patches was identified. An automatic weather station was set-up in the middle of each area to collect meteorological time-series at 15 min intervals from which the surface energy balance was estimated. Thermal profiles (0.05-0.3 m depth) were monitored for patches of different sediment calibre using synchronised miniature temperature dataloggers. Spot measurements of surface albedo and surface sediment calibre and mineralogy were determined for each patch. The results show net radiation (Q\*) is dissipated by latent (Qe), sensible (Qh) and ground (Qg) heat fluxes in descending order. Qe is dominant because of freely available water but as sediments dry-out Qh becomes more important. Typically, net daily Qg is a small heat gain (warming sediments) but under overcast conditions Qg supplies energy to the atmosphere (cooling sediments). Diurnal temperature cycles are attenuated and lagged with depth. Finer calibre sediments produce stronger near surface thermal response. Moist sediments exhibit a larger amplitude response at depth, although sub-surface temperatures are lower than adjacent dry patches due to channelling of Q\* into evaporation (Qe). Together, diurnal

fluctuations in energy fluxes and spatially variable sediment characteristics (i.e. size and mineralogy which control surface albedo and thermal conductivity) interact to govern the dynamic and heterogeneous physical habitat conditions found within areas of ERS.

HW03

Friday, July 11

### QUALITY ASSURANCE IN HYDROLOGICAL RESEARCH (ICWQ, ICSW, ICGW, ICWR, ICASVR, ICCE)

Location: Site C, Room 30

Friday, July 11 AM

Presiding Chairs: F.R. Naef, V. Krysanova

HW03/11A/C30-001

0830

#### QUALITY ASSURANCE IN ENVIRONMENTAL MODELS AND DATA: SCIENTIFIC AND ORGANIZATIONAL ASPECTS

Jacques JANSEN<sup>1</sup>, Harm HOUWELING<sup>2</sup>, Jünt HALBERTSMA<sup>1</sup>, Michiel JANSEN<sup>1</sup>, Hans HEESTERBEEK<sup>4</sup> (<sup>1</sup>Alterra Green World Research, Wageningen University & Research Centre, <sup>2</sup>Nature Policy Assessment Office, Wageningen Branch, <sup>3</sup>Biometris, Wageningen University & Research Centre, <sup>4</sup>Faculty of Veterinary Medicine, Utrecht University)

The Nature Policy Assessment Office Wageningen branch is an integrated part of The Environmental and Nature Policy Assessment Agency (MNP), a collaboration between the National Institute of Public Health and the Environment (RIVM) and Wageningen University and Research Centre. This organization acts as a centre of expertise for the national government in the development, monitoring and assessment of policies for the quality of environment and nature. Models and databases on various environmental disciplines and topics are important instruments in the MNP-toolbox. Quality assurance is crucial to provide policy makers, parliament and the public in general with reliable information. The paper presents and discusses the results of a recently finished research project by Wageningen University and Research Centre aiming at: 1) quality assessment of 27 individual models or databases and 2) development of a policy and organizational framework for quality assurance of models and data. The quality aspects examined in the individual audits are: a) scientific soundness of the model concepts, b) translation of these concepts into mathematical formula's and numerical procedures, c) statistical aspects including the treatment of uncertainties, in particular when models and databases are linked into chains, d) quality assurance of the procedures followed in building and using a model or database and e) communication of the results to policy makers and the public. The audits were designed and conducted on the basic principle that the quality of a model or database cannot be described as such but only in terms of fitness for a specific use, in this case the design and assessment of national environmental and nature policies. The central themes in the development of a methodology and organization for quality assurance of models and data are: a) roles and responsibilities in the process of quality assurance of models and data, b) development of sets of quality criteria and standards, c) integration of procedures for quality assurance and management (development, maintenance and operational use) of models and databases, d) incorporation in ISO-9001 procedures of the institutions involved and e) interaction with the MNP as the client for the assessment studies. Especially the conclusions and recommendations of this second part of the study, the development of a methodology and organizational framework for quality assurance, are relevant for other types of models and databases, other applications and other organizations.

HW03/11A/C30-002

0850

#### QUALITY ASSURANCE IN CATCHMENT AND RIVER BASIN MODELLING USING KNOWLEDGE ENGINEERING TECHNIQUES

Huub SCHOLTEN<sup>1</sup>, Jens Christian REFSGAARD<sup>2</sup>, George ZOMPANAKIS<sup>1</sup>, Ayalew KASSAHUN<sup>1</sup>, Costas GAVARDINAS<sup>1</sup>, Hans Jørgen HENRIKSEN<sup>2</sup>, Bill HARRAR<sup>3</sup> (<sup>1</sup>Wageningen University, the Netherlands, <sup>2</sup>Geological Survey of Denmark and Greenland, Denmark, <sup>3</sup>National Technical University of Athens, Greece)

Mathematical models have been applied for several decades in solving problems in many domains of water management. In the last decade a strong need for Quality Assurance has emerged among professionals in this field. A summary of reasons for this growing interest in Quality Assurance includes: a lack of mutual understanding between key-players (modellers, clients, auditors and the general public), malpractice (careless handling of input data, insufficient calibration/validation and model use outside of its scope), overselling of model capabilities, confusion on terminology and uncertainty on how to use model results in decision making. The aim of the HarmoniQuA project is to provide Quality Assurance support to key-players in model based water management. The complex process of modelling is decomposed into tasks that are defined at levels consistent with the conceptual understanding and action repertoire of the associated key-player. The body of knowledge describing these tasks has been compiled by experts within various domains of water management, discussed until consensus was reached and stored in a Knowledge Base (KB) with an ontology-based structure. The KB also contains a glossary of terms and concepts used in model based water management and is designed to allow easy maintenance and upgrading of the knowledge structure and content. In order to facilitate the ease of use of the KB, a toolbox has been developed that facilitates the use of the knowledge in the KB by key-players, who may be inexperienced in knowledge engineering. A *guideline tool* provides help for each task pertinent to specific key-players by defining tasks and offering information on methods and activities to solve these tasks. A *monitoring tool* stores the activities of each key-player in a model journal, the data structure of which is based on the same ontology as the KB. Other components of the HarmoniQuA tools suite offer a user demand driven *reporting tool* and an *advisor tool*, which enables modellers to use expertise accumulated during previous model studies and available through a model archive consisting of a set of model journals. A prototype of the KB and the toolbox are tested using two series of ten commercial case studies. These tests represent common model applications in various domains of model based water management throughout Europe. The prototypes are revised and improved after each test series. What's new? Existing guidelines for model based water management are generally written for modellers interested in a single domain. The static nature of these documents hinders their application, upgrading and consistency evaluation. HarmoniQuA provides the required knowledge and tools to support the whole modelling process for integrated studies applied in combinations of several domains in water management. The HarmoniQuA tools suite enables universal access to modelling knowledge, documentation of modelling activities, including client-modeller interaction, model development and review of the model study rendering the quality of modelling explicit.

HW03/11A/C30-003

0910

#### UNCERTAINTY ANALYSIS AND MULTI-CRITERIAL VALIDATION OF REGIONAL-SCALE ECOHYDROLOGICAL MODELS

Valentina KRYSANOVA, Fred HATTERMANN (Global Change and Natural Systems Dept., Potsdam Institute for Climate Impact Research)

The need for powerful validation techniques for distributed hydrological and ecohydrological models has often been pointed out. The validation has to be multi-scale, multi-site and multi-criterial, if the model has to be further used for regionalisation or global change impact assessment. While the primary idea of distributed hydrological modelling is to reproduce water fluxes in sub-basins and hydrotopes along with river discharge, the models are often validated using only observed river discharge, and multi-scale validation is rather exceptional. This is especially true for macro-scale basins. The river discharge is an integral characteristic of hydrological processes in the basin, but its correct representation by the model does not guarantee adequacy in spatial and temporal dynamics of all water components in the basin. The presentation will demonstrate a method to perform the multi-criterial and multi-scale validation of a regional-scale ecohydrological model based on uncertainty analysis performed in advance. The method enables to reproduce local hydrological processes like water table dynamics in sub-basins, using contour maps of the water table and observed groundwater level data. The study was carried out with the ecohydrological model SWIM (Soil and Water Integrated Model). The model integrates hydrological processes, vegetation/crop growth, erosion and nutrient dynamics at the basin and regional scale, and was developed for climate and land use change impact assessment in meso- to macro-scale river basins and at the regional scale. The study area is the German part of the Elbe River basin (about 100,000 km<sup>2</sup>). It is representative for semi-humid landscapes in Europe, where water availability during the summer season is the limiting factor for plant growth and crop yield.

HW03/11A/C30-004

0930

#### THE IMPROVEMENT OF A DISTRIBUTED HYDROLOGICAL MODEL BY USING CIP METHOD

Yasuhiro ISHIMINE, Yasuhisa KUZUHA, Tokuo KISHII, Tomonori MATSUURA (Disaster Prevention Research Group, National Research Institute for Earth Science and Disaster Prevention)

The improvements in a computer performance and the advances of geographic information systems (GIS) make numerical studies in hydrology more and more important. In particular, numerical simulations based on a distributed hydrological model are expected to provide useful information about flow characteristics. However, many of conventional distributed hydrological models have to be used with the optimization of the parameters to fit the calculation results with observed data. This implies that we need to make a further effort to improve these models. A key of hydrological process is the horizontal transport of water along the topography, and thus, it should be precisely calculated in distributed hydrological models. Nevertheless, some models bring unreliable results, such that the directions of flows are affected by the configuration of computational cells, because the calculation of the horizontal transport is not appropriate. The finer the computational cells we use, the more significant the effect of this drawback becomes. Thus, it is desirable to calculate the horizontal transport by a numerical scheme in which the configuration of computational cells little affect the flow directions. For the purpose, we have adopted the CIP method and developed a new distributed hydrological model. The CIP method is a kind of high-order upwind differencing schemes and has received much attention in the field of computational fluid dynamics since it proposed about twenty years ago. This method can obtain a fine structure of flows with a relatively small number of computational cells. In addition, the flows calculated by this method are little affected by the configuration of computational cells, despite that the CIP method is a finite differencing method using uniform rectangular computational cells. We have improved the original CIP method so as to conserve the total volume of water and applied to the distributed hydrological model. The calculation results of example problems with simple topography are satisfactory good. As is expected, the flow pattern obtained from the new model is little affected by the configuration of computational cells. In particular, the calculation of the flow spreading concentrically over the ground surface clearly shows the superiority of the new model.

HW03/11A/C30-005

0950

#### VALIDATION OF THE MODEL HBV TAKING INTO ACCOUNT THE UNCERTAINTY DUE TO THE SPATIAL INTERPOLATION OF THE RAINFALL

Radhia MCHIRGUI, Zoubeida BARGAOUI, Andreas BARDOSSY (Department of civil engineering, school of engineering of TUNIS)

The use of a hydrologic model for the simulation of the rainfall-runoff transformation is submitted to many uncertainties related to (i) accuracy of hydrometric, climatic and pluviometric data, (ii) to the model structure, and (iii) to the parameter estimation method. The scope of this study is to evaluate the effect of the uncertainties due to spatial interpolation of the rainfall data on the identification of the conceptual hydrologic model HBV. For simplification, only three parameters were identified during the calibration procedure, the other parameters being fixed. They have been selected because they are related to the soil function of the model. As an entry to the model, we have considered pluviometric fields simulated with the turning bands method. The application of the Turning Bands Method implies that we know the covariance function of the rainfall field. The application concerns the basin of TESSA, located in the North of Tunisia, having a total area of about 1950 km<sup>2</sup> and limited by the hydrometric station TESSA SIDI MEDIEN (coordinates). Available observations are used for the years 1974 to 1977: the maximum daily runoff registered in this period is of 528 m<sup>3</sup>/s. Respectively 11, 7 and 3 rainfall-runoff events with a point rainfall exceeding 30 mm have been observed each year (from 1975 to 1977). Two events were changed among calibration input sets. They are the most important from the chronology regarding the maximum runoff registered and the rainfall. The event of the 25/03/1975 is characterized by a maximum rainfall observed=40 mm, a mean rainfall=9 mm over a network of 23 stations in service with 9 zero observed values, which show a high intermittency of the rainfall field. The 17/11/1976 event is has a less intermittent field: one zero observed value among 12 rainfall stations in service, while its maximum rainfall=69 mm; its mean rainfall=31 mm; in both cases the maximal distance between two stations is of 86.5 km. In order to describe the covariance structure of the rainfall field, we have modelled the experimental variograms of the two events with spherical models: 25/03/1975 (Landing=120 mm<sup>2</sup>, range=30 km, Nugget effect=0); 17/11/1976 (Landing=300 mm<sup>2</sup>, Range=30 km, Nugget effect=0). This spatial structure is preserved during the simulations. We have achieved the kriging of the rainfall over a network of 2 km of side. Twenty fields have been then simulated for each event (Random seed=3, number of generating lines=16) and introduced as a part of the model inputs. Model calibration was performed for each input series. For the verification of adequation between observed and calculated runoff, we have used Nash criterion and the correlation coefficient between calculated and observed runoff during the events of 25/03/75 and 17/11/76 over a period of three days. For each simulation, we also compared the hydrographs of the observed and calculated discharges over the period 1975-1977. The optimal values are

respectively 400mm,130mm and 0.67. We have then obtained the probability distributions for each parameter in addition to the joined distributions of these parameters. Key-words :Uncertainty ;calibrating ;conditionalsimulation,parameter,spatial interpolation.

HW03/11A/C30-006

1030

#### WHY IS QUALITY ASSURANCE IN RAINFALL RUNOFF MODELLING SO DIFFICULT?

Feli Robert NAEF (Institute of Hydromechanics, Swiss Federal Institute of Technology, Zurich)

In the last decades, countless procedures and models to simulate parts of the hydrologic cycle have been developed. However, the benefits or superiority of these different approaches could not be assessed, mainly because a generally agreed scale how to measure quality was missing. In addition, the highly exaggerated expectations on the accuracies that could be reached with model simulations prevented a meaningful comparison. It probably started with the publication of the simulations of the Stanford Watershed Model in the sixties, which were already in a nearly perfect agreement with the observed hydrographs. Authors of later models felt obliged to present simulations that were at least as good or even better. The main thrust was therefore put to attain an optimal fit between the observed and simulated hydrographs. It can be shown, however, that an optimal fit does not guarantee an adequate representation of the catchment's response by a model. On the contrary, the errors from different independent sources should be reflected in the results of a suitable model. Basically, the errors from the different sources are independent. If an optimal fit is sought, they become interdependent and the model parameters are misadjusted in such a way, that the different errors compensate each other. To assess any research progress, it should at first be evaluated which results can be reached with the present day knowledge for each of the following areas. Any progress should then be measured against this background. Precipitation: The transformation of point measurements into an adequate representation of the time variant rainfall field is not yet solved satisfactorily and even larger gaps exist in determining rainfall fields with defined return periods. The error of the precipitation input using the methods available today can easily surpass 20 to 30%. Runoff production: Infiltration and retention capacity of the soil varies enormously throughout a catchment. Progress has been made in upscaling process knowledge from the plot to the catchment scale and to define infiltration parameters from field measurements. However, the uncertainty of these parameters is still considerable. Discharge measurements: Detailed evaluation of numerous stream gages showed that measurements during floods often contain large errors, putting in question results of studies that used these data without corrections. Extreme Floods: Hydrological research is often aimed to estimate floods with return periods of 100 years and more. As series of rainfall and discharge measurements hardly ever exceed 100 years, the magnitude of such floods is not well known.

HW03/11A/C30-007

1050

#### APPLICATION OF FUZZY MULTI-OBJECTIVE FUNCTION ON HYDROLOGICAL MODEL CALIBRATION

Tao-Chang YANG, Pao-Shan YU, Chen-Min KUO (Department of Hydraulics & Ocean Engineering ,National Cheng Kung University)

Storm event rainfall-runoff models are essential tools to simulate peak flows or design floods for many purposes in water resource projects. As the application of rainfall-runoff models is important for water resource projects, attention to further improve performances of rainfall-runoff models is increased. Successfully modeling the rainfall-runoff relationship depends on many factors, ranging from model input data (rainfall, geographic data, and runoff etc.), model structure, optimization technique to the selection of an objective function. This study proposed a fuzzy multi-objective function to improve model calibration, which has the capability of combining various objectives of features in storm hydrograph (such as time to peak, peak of discharge, total runoff volume, etc.). A grid-based distributed rainfall-runoff model was applied to simulate hydrological processes over each grid. Watershed boundaries, river network and geographic characteristics were determined by using the GIS technique based on the Digital Terrain Model (DTM). The images of the SPOT satellites were utilized for land use classification. The rainfall-runoff model was then calibrated by using the shuffled complex evolution global optimization method, in which the fuzzy multi-objective function proposed in this work was compared with a conventional single objective function. The basin of Pa-Chang Creek is located in southern Taiwan and has a drainage area of 475 km<sup>2</sup> and the main stream length of 87.1 km, in which seven bigger storm events were collected as the data set in which five of them were arbitrarily chosen for model calibration and the other two were used for model verification. The study results conclude that the fuzzy multi-objective function can calibrate the model more reasonably than the single objective function and have better hydrograph simulations.

HW03/11A/C30-008

1110

#### IDENTIFICATION OF THE HYDROLOGICAL PARAMETERS AS AN ILLUSTRATION WAY OF THE SEMI-EMPIRICAL MODEL DEVELOPMENT

Valentina A. KHAYDAROVA<sup>1</sup>, Natalia V. PENKOVA<sup>2</sup>, Evgenia L. PAK<sup>1</sup> (<sup>1</sup>Institute of Water Problems, Uzbek Academy of Sciences, <sup>2</sup>INENCO Centre of Russian Academy of Sciences, 14 Kutuzova Embankment, 191187 Saint-Petersburg, Russia)

In the hydrological cycle models a modeling subject is the water balance dynamic. Up today a lot of the heat and water balance models for description of the lands hydrological regime are suggested. The main difficulties of its application are connected with necessity for identification of a number of the combined empirical parameters, which are totally taking into account of the surface peculiarities (including vegetation) on evapotranspiration. Last years authors were conducting investigations on development of new modification of the Heat and Water Balances Model (HWBM) and its adaptation to arid and semi-arid regions in the framework of the INCO-COPERNICUS project "Adaptation of Efficient Water Use Criteria in Marginal Regions of Europe and Middle Asia with Scarce Sources Subject to Environmental Control, Climate Change and Socio-Economic Development". The obtained results show that the observation data from the complex network give wide possibilities of describing the combined parameters features and allows to extend knowledge about the heat and water balances components. The diagrams obtained by the using of the observation data from the complex network reflect all hypothetical possible combinations of factors affecting on the combined parameters. Therefore they must be considered as combinations of possibilities for the plants functioning. The non-linear multi-dimensional relationships between the heat and water balances components and characteristics of the plant growth conditions can broaden the possibilities of investigations of the limiting factors of plant's life under different (including extreme) conditions. The major feature of the semi-empirical submodels obtained for the heat and water balances of agricultural lands is that they are described by curves with saturation, i.e. reflecting the fundamental characteristics of the biogeocenoses functioning: appearance of the "negative" feedback to achieve the equilibrium state minimizing the external forcing effects on ecosystems. Taking into account features of the system of measurements of evapotranspiration and precipitation it is necessary to consider their values not as components of water balance, but as their indices. Systematic errors can be taken

into account by means of construction of empirical relations between elements of water exchange at stressing the most authentic characteristics. In this case such characteristic can serve the soil water content measured by a thermostat method. At such approach the non-accounted elements of water balance are considered as components of a total systematic error of measurement of basic elements. Researches cover the analysis of parameterized imitation models for heat and water regimes of regional and local ecosystems.

HW03/11A/C30-009

1130

#### ALES DU RESEAU PLUVIOMETRIQUE DU BASSIN VERSANT DU TESSA ETUDE DE LA VARIABILITE DU CHAMP PLUVIOMETRIQUE PAR KRIGEAGE ET VALIDATION CROISEE PLUIE-DEBIT

Radhia MCHIRGUI, Zoubeida BARGAOULI, Andreas BARDOSSY (Department of civil engineering,school of engineering of TUNIS)

Le bassin versant du TESSA situ au nord de la Tunisie et ayant une superficie avoisinant 1950Km<sup>2</sup> limit la station hydrométrique TESSA SIDI MEDIEN, présente une structure pluviométrique très particulière. Notre étude porte sur les années 1984 - 1992 et a pour objectif d'analyser les événements pluvieux de cette période afin de valider les observations dans le réseau pluviométrique constitué de 27 stations. Les événements sont choisis tels que la pluie est supérieure ou égale 30mm en l'une quelconque des stations , on a ainsi déduit 51 événements. Pour ce faire , nous avons établi d'abord les variogrammes spécifiques chaque événement pluvieux : la majorité de ces variogrammes est sphérique et a une portée variant entre 25 et 40km , avec un palier compris entre 300 et 4500mm<sup>2</sup>. Afin de dégager les singularités des observations pluviométriques , nous avons procédé par le krigeage par validation croisée , qui nous a permis de simuler l'effet du choix du voisinage dans l'incertitude des résultats. Nous avons alors calculé pour chaque événement les erreurs relatives de krigeage après élimination des stations une , puis comparé les lames brutes et écoulées. Cette comparaison nous a permis de dégager les événements du 01/08/90 , du 11/07/89 et du 15/10/90 , comme événements douteux. Puis , nous avons procédé par une validation pluie observée-pluie krigée , pluie-débit maximal , intensité de pluie-débit maximal, intensité de pluie-écart-type, intensité de pluie-lame écoulée. Toutes ces analyses nous ont permis d'avoir une critique bien fondée de la qualité des données de pluie et de conclure quant à la variabilité spatio-temporelle de la pluie dans la région. Mots-clés : Incertitude ; Variogramme ; Krigeage ; validation croisée ; variabilité.

HW03/11A/C30-010

1150

#### ANALOGOUS SIMULATION THE ANNUAL RUNOFF OF HEIHE RIVER (CHINA,QILIANSHAN)

Vladimir G. KONOVALOV<sup>1</sup>, Masayoshi NAKAWO<sup>2</sup> (<sup>1</sup>Institute of Geography, Russian Academy of Sciences, <sup>2</sup>Institute for Humanity and Nature, Kyoto, Japan)

In order to solve the entitled problem the criteria of river basin similarity are defined based on the conditions of runoff formation and its intra-annual distribution. Characteristic features of intra-annual distributions of climatic factors of runoff (precipitation and air temperature) were revealed for the Heihe river basin by data of meteorological stations. Calculated set of morphometry parameters of the Heihe river watershed includes: area of the basin, its average weighted altitude, function of the basin area distribution in relation with elevation above sea level, glaciers' area and its average weighted altitude. Role of mean weighted elevation of a watershed was shown as characteristic level to determine precipitation, air temperature and other meteorological variables equaled to their average values for the whole given area of a river basin. Thus calculation of the climate factors at the mean weighted elevation of a watershed allows using the water balance method for the simulation of the annual runoff within the Heihe and its analogy river basins. After selecting analysis, the Naryn river basin was adopted as basin-analogy for the Heihe watershed. Empirical formulae of good quality were obtained to calculate the annual sum of precipitation and average summer air temperature at the mean weighted elevation of the Heihe river and its basin-analogy. These variables were applied in the multiple regression equation obtained to compute the annual runoff coefficient for the Naryn river basin. Precipitation and air temperature were transformed to their normalized form in order to eliminate influence of different norms of climate factors within Naryn and Heihe river basins. The long-term range of Heihe river annual runoff for 1957-1993 was simulated as the results of applying the water balance method and the equation for calculating the annual runoff coefficient, obtained by means of the basin-analogy. Quality assurance of the computed runoff range was based on three different estimations: a) Comparison of calculated and measured long-term ranges of Naryn river runoff and their statistical parameters which demonstrates a rather acceptable quality of the simulation results based on water balance equation; b) Preparation of a diagram of temporal course for computed annual runoff within Heihe river and its neighboring basin (measured one). Its analysis showed synchronism of low and high water years for the compared watersheds. c) Calculation of input and output components of water balance for the Heihe river basin. Annual evapotranspiration was estimated for this basin. After solving the equation of water balance, we found that the difference was only 6 % between input (precipitation) and output (runoff + evapo-transpiration) parts of this equation.

HW03-Posters

Friday, July 11

#### QUALITY ASSURANCE IN HYDROLOGICAL RESEARCH (ICWQ, ICSW, ICGW, ICWR, ICASVR, ICCE)

Location: Site D

Friday, July 11 AM

HW03/11A/D-001

Poster

0830-135

#### PROBABILITY-STATISTICAL ANALYSIS DYNAMICS OF POLLUTION THE BELAYA RIVER

Tatyana FASHCHEVSKAYA, Natalya KRASNOGORSKA (Department of Ecology, Ufa State Aircraft University)

The Belaya river is situated in limitations of South Ural and is one of main tributary of the Volga River with area catchment is 142 000 km<sup>2</sup>. The volume of average annual flow is 29,2 km<sup>3</sup> in the year. The quality water doesn't remain as in time as in space that essentially is connected with disposition on the river banks the large industrial ecologically dangerous objects exert influence to the quality water. The basic loading to the river exerts the oil-refining, chemical and oil-chemical industry. These plants are concentrated in cities Ufa, Salavat, Sterlitamak, Meleuz etc. The main pollutants of wastewaters of the plants are oil-products, phenols, nitrogen of nitrite and nitrate, ammonia, phosphorus, copper, zinc, nickel

and suspended matters. Their mean yearly concentration in the river water is more than 5-10 maximum admissible concentration (MAC). We made probability-statistical analysis of dynamics of pollution in the Belaya River water using perennial data observations. The comparison of empirical and theoretical (asymmetrical binomial Pearson III type) frequency curves demonstrated possibility of their using for the investigation. The parameters of probability curves (norm, Cv, Cs) and scale of quality significance (frequency range: 10, 25, 50, 75 and 95%) were calculated through using perennial data series observations. For taking into account of the water availability under analysis of water quality is used not concentration of pollutants in water river (in mg/l) but recalculated values of mass pollutants in tons per year. The calculated data made by probability-statistical analysis perennial observations gives information about water quality not only during the moment of sample but in long-term period. Besides, they taking into account processes which are in a concrete water environment: migration, transformation and bioaccumulation of pollutants and ability of a concrete water body to be self-purified and assimilated. We considered the annual water quality change in the Belaya River during different seasons. We found out that non-point pollution (spring snowmelt flood surface washing off) put in pollution process a very big share. It is obtained links entering of pollutants to river between volumes for year and for period of the spring snowmelt, which could be used for forecasting of entering pollutants. For the long-term period contributions of the main industrial centers into pollution of the Belaya River are computed. So, Ufa gives over 64% oil-products, 56% phenols etc. These data could be used for compiling ecological passports of different regions, development of plans of ecological situation improving and reducing of discharges of wastewater into water bodies.

HW03/11A/D-002

Poster

0830-136

#### MONITORING THE GARONA RIVER WATER TABLE BY MICROGRAVIMETRY AND GPS

Jean-Pierre BARRIOT, Michel SARRAILH, Thierry FAYARD (UMR5562/CNES/BGI)

We show the first results of the monitoring of the superficial water table associated with the Garona river near Toulouse, in the south of France. We use two kinds of gravity meters: a Lacoste and Romberg model D and a SCINTREX CG-3, as well as two operators, and two different close sites, to avoid systematic effects (microgal level). The soil motion is separated by doing a simultaneous GPS surveying of the site altitudes at the mm level. The equation of state of the water table is written with respect to inputs and outputs of water, and expected and computed gravity signatures are compared.

HW03

Friday, July 11

#### QUALITY ASSURANCE IN HYDROLOGICAL RESEARCH (ICWQ, ICSW, ICGW, ICWR, ICASVR, ICCE)

Location: Site C, Room 30

Friday, July 11 PM

Presiding Chairs: J. Jansen, H. Scholten

HW03/11P/C30-001

1400

#### QUALITY ASSURANCE IN HYDROLOGICAL DATA

Takeo KINOSHITA (The Representative of Suimon Kankyo)

Background: In order to discuss about quality assurance in hydrological research, basic attention should be paid to quality assurance in original data. On the way to quality assurance, various kinds of unknown hydrological phenomena will be found in and around observation sites. Quality assurance is called researches by itself. In this report, several experiences obtained in Japan will be discussed for further development of quality assurance in hydrological community. A rating curve is commonly applied to calculate hourly discharge from hourly water stage. The author points out two major topics, field check and check of a rating curve. Field check: Field works at the gauging site are the most essential in quality assurance. Is the bench mark installed at clear place near the water gauge? Is the staff gauge set at the base line? The zero point must be levelled from the bench mark. Is the recording gauge operating? Is its sensor fixed deep enough to measure the lowest water. The observed value by the recording gauge must coincide with the staff gauge. The current meter site must be adequately selected. Distribution of measuring point must be correct. Is the current meter calibrated once a year? Drift rods must be properly used. Submerging length must be corresponding to the depth. Is there any unusual flow of a drift rod? Rating Curve: A rating curve, called an H-Q curve in Japan, is drawn by the least square method as  $Q=a(H+b)^2$ , where H is the water stage on the ordinate, Q is the discharge on the abscissa, a and b are empirical constants. When the H-Q curve makes a clockwise loop, some event, for instance a tide, is coming upstream. When it makes a counterclockwise loop, it means a flood. If not, careful inspection should be given to basic data, especially the stage velocity relation. When the rating curve makes a counterclockwise loop in the flood period, the surface gradient is useful to adjust the curve to a single-valued function. The adjusted discharge is written by  $Q_a=Q_o \sqrt{R} (I_a/I_o)$  where  $Q_o$  and  $I_o$  are observed discharge and surface gradient and  $I_a$  is an average gradient. The surface gradient must be calculated at two gauging sites separated each other several kilometers. A steady flow H-Q curve is proposed to check the observed H-Q curve and to extrapolate the curve slightly. Two parameters in a H-Q curve, a and b, are determined by  $a=v(1+p)^2/4A$   $b=2R/(1+p)-H$  where v is the mean velocity, p is the power of steady flow formula, B is the river width, A is the cross section, R is the hydraulic radius and they are all observed values. Conclusion: The author presents several experiences to assure hydrological data. All procedures have been developed at the operational work in water managements.

HW03/11P/C30-002

1420

#### INFERRING HIGH AND LOW TRANSMISSIVE ZONES AS WELL AS DISCONTINUITIES IN AN AQUIFER USING SPATIAL CORRELATION OF WATER LEVELS

Tanvi ARORA, Shakeel AHMED (INDO-FRENCH CENTRE FOR GROUNDWATER RESEARCH)

Water levels if measured accurately, reveal the most information about the dynamics of the aquifer system. The water levels, measured at some finite points/well are often used in drawing iso-lines with suitable interpolation and extrapolation. The gradients of water level then provide the knowledge of zonal transmissivity. However, several time data could not be used simultaneously as well as this procedure assumes inherent continuity in the aquifer system. The availability of the water level data from 51 observation wells for about 24 months period has allowed to carry our statistical studies and inferring high and low

transmissive zones in the Srikakulam district of Andhra Pradesh, India. The study area with an extent of 5837 sq. kms consists of khondalites, granite gneiss and charnolites. The normal annual rainfall is 1085.6 mm. The periodic changes in groundwater regime are monitored through measurement of water levels regularly in the monitoring dug wells distributed over the area. These wells are monitored 6 times in a year. Well depth varies from 6.3 m to 12.90 m. An effort was made to analyze the spatial correlation of the water table for a span of 11 years (time for which maximum data is available). Large number of correlation coefficient were calculated between two wells water level and the correlation matrix was prepared. The correlation coefficient varies from AE.001 to 0.91. From the study 21 wells show good correlation among each other and 10 wells shows intermediate to poor correlation. The correlation coefficients were plotted on the area map to demarcate the areas with high, moderate and poor correlation. With comparatively high rainfall and assuming a uniform rainfall recharge, the areas with high correlation coefficients were demarcated as having high transmissivity and with low correlation coefficient as low transmissivity or aquifer with possible discontinuity or geological barrier. The present method using a set of large time data provide more reliable estimates than the water level contours of individual time period.

HW03/11P/C30-003

1440

#### ANALYSIS OF NON-LINEARITY BETWEEN THE DESIRED ACCURACY AND THE DATA NETWORK DENSITY

Shakeel AHMED, Dewashish KUMAR (INDO FRENCH CENTRE FOR GROUNDWATER RESEARCH, N.G.R.I.)

A water level monitoring network in a small watershed of about 60 km<sup>2</sup> in a crystalline fractured aquifer under semi-confined condition has been optimized. Initially a network of about 56 wells fairly distributed in the area and based on the drainage system was selected. The monthly water-level measurement has been analyzed geostatistically. The standard deviations of the measured water levels have been on average 12 meters. There have been a number of constraints on measuring the water levels in the shortest period of time and it was decided to reduce the number of wells in the network without losing the benefit of measurements. Thus a monitoring network to have only 40 wells and providing a maximum standard deviation of the estimation error ( $\sigma_e$ ) of 8 meters was designed. In this paper, it has been studied that if the  $\sigma_e$  varied from the value of 8 meters what could be the effect on various norms of optimization and the final number of measurement points to make the network optimal. It has been found that for the same change in  $\sigma_e$  when  $\sigma_e$  has lower value the number of measurement points are much more compared to the same change in  $\sigma_e$  for the greater value of  $\sigma_e$ . The variation of other norms of optimization has also been studied with different values of  $\sigma_e$  and a non-linear relation was always found. Such an exercise provides the estimated water levels for example to calibrate an aquifer model in an unbiased way.

HW03/11P/C30-004

1500

#### ABOUT ASSURANCE TO THE QUALITATIVE PARAMETERS OF WATER RESOURCES IN RIVERS AND LAKES

Boris FASHCHEVSKY (International Sakharov Environmental University)

In this paper the qualitative parameters of water resources (physical, chemical, microbiological) are considered, with goal estimation of their reliability and trustworthy. It is determined that the main factors for achievement of these goals are: representativeness of disposition points of observation on locality, representativeness of sampling in points of cross-sections of rivers and lakes, in width and in depth, taking into account the frequency of sampling, taking into account the development of plants and animals into rivers and lakes and so ice phenomena, storm weathers and snowmelt and rainfall floods. It is necessary to notice that on the whole a statistical treatment of observed data with using probability (frequency) curves for estimation all diapason fluctuations of the qualitative characteristics of water resources is needed. One of the main factors for assurance of qualitative parameters of water resources in water bodies is rational disposition network of points of observations, taking into account sources of discharges of waste waters and development processes of self-purification in locality. The second important factor is representativeness of sampling in the cross-section of river (mean as a channel as a floodplain) or in lake, taking of a shallow zone and deep-water zone. In case a stratification of water column in epilimnion, metalimnion and hypolimnion depending on the frequency of this phenomenon. The field experiments on the Zapadnaya Dvina River have shown that for getting a real average estimation it is necessary to sample as minimum in three verticals across the water surface and two points (0.8H and 0.2H). The third factor is a time course. The presence practice of sampling (one-two samples in month) especially in small rivers leads to that enterprises discharge waste waters in the interval between measures. Such a bright example is the Svisloch River, flowing through city Minsk when of night many big plants discharge waste waters and ever rubbish. The fourth factor, disturbing the accuracy definition of a real quality of water, serves the development of plants and animals in water bodies, when in certain period all these organisms are dead, causing sharp worsening of ecological conditions. The fifth factor is the development of ice phenomena, including ice cover, ice drift, frazil drift, ice-jam and frazil-jam, etc. For rivers and lakes with developed floodplain, that is flooded for a long time it is necessary to samples from floodplain. The special attention would be attracted to disposition of sections for sampling upper and below of waste water discharge in order to estimate the influence of these discharges on water quality. However, only taking into account the above-mentioned factors the task of assurance of the qualitative parameters of water resources is not solve to the end. For the objective assessment of assurance on the whole we need the estimation of all diapason fluctuations of qualitative indices. For decision of this task it is necessary to use the probability-statistical methods of analysis. The application of probability or frequency curves allows to get an objective picture of the water body state.

HW03/11P/C30-005

1520

#### SPATIAL VARIABILITY OF VERTICAL PERMEABILITY OF THE SOIL COVER DETERMINED USING DOUBLE RING INFILTROMETER IN MAHESHWARAM WATERSHED IN A GRANITIC SEMI-ARID REGION

Dewashish KUMAR, Shakeel AHMED (INDO FRENCH CENTRE FOR GROUNDWATER RESEARCH, N.G.R.I.)

Ring infiltrimeters are commonly used for in situ measurement of soil hydraulic properties. The infiltration test was carried out specially to know the rate of percolation or rate of vertical flow from the surface to few ten's of centimeter below the ground. As the hard rock region is extremely heterogeneous system so as to understand the unsaturated zone specially the top layer, this infiltration test was very useful to have idea of vertical flow of fluid. The objective of the infiltration test has been understand the characteristics of the top layer zone and the vertical flow rate as well as characterize soil types, infiltration property of the tank beds and the behavior in the dug wells. In the present study infiltration test was carried out at 38 sites in a small watershed of about 60 km<sup>2</sup> in a crystalline hard rock terrain. Out of 38 sites: 16 tritium injection sites comprising different type of soils, 17 tank beds, 4 bottom of the dug

wells and 1 near the hydro-meteorological station. The infiltration test performed by double ring infiltrometer with a diameter of 30 and 60 cm respectively were placed on the surface of the ground and were firmly fixed few centimeters below the ground so as to avoid direct passage of water from the sides of the ring. A height of 5 cm was marked on the inner and outside of the inner ring. Water was added in both the rings simultaneously up to the mark and the level was maintained throughout the test period. Known amount of water was added to the inner ring subsequent to the fall of water level below the marked position. Throughout the test the level of water in the outer ring was also maintained up to the marked position so as to prevent the lateral flow of water into the ground from the inner ring. The result shows significant variation of the infiltration rate in different soil types, tank beds and dug wells. Different soil types shows different rate of infiltration at some place where the soil colour is light red, the infiltrate rate was found to be high. Some of sites do not show any percolation showing a thick siltation in the area. The infiltration rates vary from 848.8 to 1.7mm/hr, such a wide variation in rate again confirms the heterogeneity although it also depends on the initial soil moisture content. This infiltration results could be used for the correlation of the recharge measured with tritium injection and also these results has provided spatial variability of rainfall recharge an important input to the groundwater flow model.

HW03/11P/C30-006

1600

#### A NEW GEOSTATISTICAL APPROACH TO ANALYZE SPATIO-TEMPORAL VARIATION OF FLUORIDE IN GROUNDWATER AND OPTIMIZATION OF ITS MONITORING NETWORK

Shakeel AHMED (Indo-French Centre for Groundwater Research, NGRI, Hyderabad, India)

A small watershed in the granitic aquifer has shown increase in Fluoride content beyond the permissible limit of 1.5 mg/L. In the present study A simple and new method has been developed using the cross-validation technique of Geostatistics to analyse and optimize an existing network for monitoring Fluoride in Maheshwaram watershed, RR Dist. of Andhra Pradesh, India. Water samples from 60 wells fairly distributed in 60 Sq. km area of the watershed are available. They are analyzed for water chemistry and Fluoride. Using the result of the cross-validation of the variogram particularly jack-knifing, it has been possible to assign a priority index to all these measurement points and depending on the constraints such as financial and logistic, a network could be reduced without losing the outcome. A number of monitoring networks with less number of wells have been prepared and compared. A number of network with reduced size have been analyzed from the given measurements. The change in the mean value is not much. However, with the close observation, it is found that the mean is slowly reducing when the network is reduced from 60 until 50 or 45 but the difference is considerable when we further reduce the network. Iso-lines of fluoride were drawn based on the 60 and 30 measurements respectively coming from the network decided on the basis of the priority index. The two contours show more or less similar distribution and the regionalized picture is almost identical. Although, slow but fluoride is a time varying parameter, an optimal network will make the sample collection easy and in the shortest possible time. This optimal network will also be cost-effective and the priority index will be helpful to vary the network size depending upon the financial and logistic constraints. However, one should remember that a network of (say for example) 30 measurement points would obviously provide high variance of the estimation error at the remaining parts of the study area.

HW03/11P/C30-007

1620

#### HYDROECOLOGICAL MAPS OF BELARUS

Boris FASHCHEVSKY<sup>1</sup>, Anatolij SHARIKOV<sup>2</sup> (International Sakharov Environmental University, <sup>1</sup>Laboratory of Hydroecology, Central Research Institute for Water Resources Management)

It is considered principles of hydroecological maps compilation for the territory of Belarus. Assessment reliability of initial data for compilation of maps is done. In the basis of selection indices for compilation of hydroecological maps the following principles are put: -presence of the spatial-temporary series of observation for qualitative and quantitative characteristic for the long period; -degree of influence of the qualitative and quantitative changes of water resources on the natural background regime; -revealing of the most changing indices; - presence of discharges of pollutants in composition of wastewater's. In the result of carefully analysis the following indices have been chosen: the main ions (Cl, Mg, HCO<sub>3</sub>, Ca, SO<sub>4</sub>) and general mineralization, O<sub>2</sub>, BOD<sub>5</sub> and COD, phenols, surfactants, oil products, the main biogenic-phosphorus and nitrogen, salts of heavy metals (copper, lead, zinc, etc), temperature of water and suspended loads and as well annual, ecological and free flows, minimum and maximum flows. Dissolved substances and suspended loads are presented in a view of modules flow-kilograms and tons from square kilometer of catchment. Oxygen, BOD and Cod are presented in a view of mg/l. Mapping of dissolved substances were timed to the water availability of 75 % frequency. Modulus of suspended loads and temperatures were taken for the average year of water availability. Comparative analysis of the observed data with the data of discharges from point sources are greatly differed especially as for such indices as oil products, phenols, copper, nitrate and nitrite. If take into account a phenomenon of selfpurification then the real discharges of wastewater are reduced on average in 2 times. The experimental material shows that the share of surface inflow into rivers from urban and agricultural territories don't exceed more than 20-30 % of the whole pollution of water bodies. Hence, 70-80 % pollutants are discharged by enterprises without any control. The analysis distribution all above mentioned characteristics on the territory of Belarus is done.

HW03/11P/C30-008

1640

#### FRACTIONAL GOVERNING EQUATION OF GROUNDWATER FLOW: A NUMERICAL ANDEXPERIMENTAL STUDY

Kenta OKADA, Yuko HATANNO (Institute of Engineering Mechanics &amp; Systems, University of Tsukuba)

In the present study, we experimentally show the efficacy of a new governing equation of transport in the groundwater. Instead of the widely-used advection-dispersion equation (ADE), we use an equation with "fractional" derivatives. It is first introduced by Benson *et al.* (1998) and gradually gaining recognition (*e.g.* Sokolov *et al.*, 2002). The new equation utilizes the fractional derivatives (1.5th or 2.1th derivatives) in the diffusion term, such as  $\partial C/\partial t = D \partial^2 C/\partial x^2$ . This equation has an advantage over the classical ADE, since it does not depend on scales of heterogeneity of geologic media. In the presentation, firstly, we show the numerical solution of the fractional governing equation, calculated by the finite difference method, and discuss the profiles. Specifically, the concentration profiles show clearly different behavior from the classical ADE. The difference at the long-term or at the location distant from the source indicates that the evaluation with the classical ADE would result in underestimate for the risk assessment. The present numerical result could reproduce the concentration profiles with "tailing behavior", which the classical ADE didn't. We used the data of a column experiment, and found that the order of derivative is about 1.5. Secondly, we show the efficacy of the governing equation with experimental data. Since we still do not have the knowledge how we can determine the value of the index of derivative,  $\alpha$ , we do a

series of experiments in a sandbox, with different degree of heterogeneity. The experiment system is built based on Berkowitz *et al.*, (2000). The container is filled with *Tohoku keisa* (1000mm x 710mm x 120mm; with a channel switching machine, amplifier, and PC). Two tanks are installed at the both end of the test section, whose water heads are kept constant. We use a marriott tank for the inlet container. The solution of tracer (NaCl 3%) flows horizontally with the head difference between the inlet- and the outlet-tank. With the breakthrough curve of the experimental result, we discuss the value of the index of the fractional governing equation. In conclusions, we show that the new fractional governing equation can describe the phenomena called "subdiffusion" in geologic media.

HW03/11P/C30-009

1700

#### GEOSTATISTICAL ANALYSIS OF GROUNDWATER CONTAMINATION IN PAGERU RIVER BASIN AND TESTING THE ADEQUACY OF THE MONITORING NETWORK

P.D. SREDEVI, Shakeel AHMED (Indo-French Centre for Groundwater Research, NGRI, Hyderabad, India)

Pageru river basin lies in the drought prone areas of the south India as the aquifers are usually over exploited. The studied watershed covers an area of 480 Km<sup>2</sup> and forms the part of the Pageru river basin which is an ephemeral river. The groundwater resources are exploited through a large number of dug-wells and some bore-wells. About 99 dug wells fairly distributed in the area have been systematically monitored for water quality during pre and post monsoon seasons of 1996-97. The variographic analysis through calculation and modeling of experimental variograms as well as cross validation test show a large variation in the variability of chemical properties of the groundwater concluding the strong influence of anthropogenic activities such as use of fertilizers and pesticides on groundwater quality. The geostatistical analysis testing the adequacy of the monitoring network shows that with the variance of the data as the cut-off for monitoring network precision, the network remains adequate and rather dense. However, when the cut-off value is reduced to half of the respective variances, the network becomes inadequate and sparse for most of the parameters except pH.

HW04

Wednesday, July 9

#### SYSTEMS MODELING OF GLOBAL WATER DYNAMICS (ICWRS)

Location: Site C, Room 31

Wednesday, July 9 AM  
Presiding Chairs: T. Hori, T. Kojiri

HW04/09A/C31-001

0900

#### RISK ANALYSIS FOR WATER RESOURCE SYSTEM BY USING SYSTEM DYNAMICS: CASE STUDY IN YELLOW RIVER BASIN

Zongxue XU, Kuniyoshi TAKEUCHI, Hiroshi ISHIDAIRA, Zhifeng YANG (Institute of Materials and Environmental Technology, Graduate School of Engineering of Engineering, Yamanashi University)

Sustainable development issue has been received wide attention by scientists, politicians, and publics during the past decade. Sustainable water supply is particular a key problem in this century. With the development of economics and urbanization, this issue has become one of the greatest challenges both central and local government in China faces. Streamflow cessation and water curtailment, occurred in Yellow River several years ago, further aggravated the tension state of water supply in the study area. As the "cradle of Chinese civilization" and one source of humankind's civilization, the water resources issue in Yellow River basin has received great attention everywhere in the world. Water authorities in Yellow River basin has and will continue to face great challenges in meeting both in-stream flow and ecological requirements, and providing more water for the growing populations, industry and agriculture. On the purpose to evaluate the risk of the water resource system in Yellow River basin, a system dynamics model for water resources planning is developed to analyze the risk of water resources in Yellow River basin to climate change, population growth, and industrial development in the future. The objective of the model remains on simulating the water resources system and capturing the dynamic characteristics of the system. The existing and potential water supplies from surface water, aquifers and treated wastewater are estimated, and potential water demands for domestic, industrial and agricultural uses are projected. The model has been developed using STELLA Research 6.0, and may be used to identify preferred solutions to satisfy a variety of requirements relating to the development, environmental concerns and ecological needs of the water resources in the study area. It is an interactive, computer-based tool with friendly user interface, allowing users to explore how various water-supply objectives can be met for future scenarios. Water supply risk is then estimated with the combination of the observed streamflow data. From this result, the regions with high risk in shortage of water have been identified. It has shown that although the downstream of the Yellow River previously had the greatest risk in shortage of water, the risk in this region has been considerably decreased due to the construction and rational operation of the Xiaolangdi reservoir with an effective storage of 5.05 billion m<sup>3</sup>. It also shows that the river segment from Lanzhou to Hekouzen will take great risk if the present way of flooding irrigation can not be improved with more efficient irrigation techniques such as spray and drip approaches. The result provided in this study is helpful for the regionalization of the water supply. This also makes it possible to evaluate the impacts of large projects such as "South-to-north water transfer" on water resources in the Yellow River basin.

HW04/09A/C31-002

0920

#### SYSTEM DYNAMICS APPROACHE FOR REGIONAL WATER RESOURCES

Toshiharu KOJIRI, Nobuchika TAMURA (Disaster Prevention Research Institute, Kyoto University)

Recently, climate change and environmental issues have been the important problems in water resources development. However, hydrological process of precipitation and evapotranspiration due to climate change has so much relationship with regional development and economical activities. System Dynamics (SD) is the great power to represent this water behavior including the related factors. On the other hand, recently the distributed runoff model has been developed using the digital geographical data and land use data. The main purpose of this research is to develop an understanding of 1) the influence of water resources distribution on agriculture yield, economic activity, population change and so on, and 2) the influence of change in those distributions on nation's water resources demands. We are focusing on the closed region such as main island of Japan in

order to the regional water circulation, water utilization, population change and economic dynamics. Moreover, the proposed system will be connected with runoff model showing the detail water utilization processes. SD simulation is performed to model the changing circumstances in the area's water resources distribution. The proposed regional SD divided into ten regions; namely Tohoku-northwest, Tohoku-southeast, Kanto, Shinetsu, Hokuriku, Tokai, Chubu, Kinki, Sanin, and Sanyo and consists of ten sectors; namely population, land use, agriculture, industry, information technology, pollution, water quality evaluation, water quality treatment, climate and water balance. Through investigation of the environmental factors contributing to changes in the hydrological circulation, such as regional deforestation and heat island phenomenon, and through simulation of the effects of climate change and realization of social policies, a research tool capable of providing meaningful information, and aiding in reaching consensus regarding policies for the development and allocation of domestic water resources will be achieved.

**HW04/09A/C31-003** **0940**

**WATER RESOURCES DYNAMICS MODEL CONSIDERING REGIONAL INTERDEPENDENCIES**

Tomoharu HORI, Michiharu SHIBA, Toshiharu KOJIRI (Faculty of Global Environmental Studies, Kyoto University)

In recent years, water problems are getting one of the major issues of earth's human life in various levels of policy making: international, national, regional, municipal, etc. Water resources development and distribution to meet the predicted demand in a basin have been major issues in such decision levels for a long time since they requires a lot of time and money. People, however, are now getting aware that it is also important to take regional interdependencies about water resources in terms of transportation of various products. In highly networked environment, a water-related problem in a certain place or basin will affect social life in other regions through economic activities. Water resources assessment based on the dynamical environment would have a great importance for making water policy. One of the difficulties in water resources assessment in such a networked and dynamic circumstances is the complexity of water resources systems. They include various sectors such as consumers and providers: consumers comprise of agricultural, industrial and municipal sectors. System Dynamics approach is one of the powerful methodologies to model those complex systems. SD modeling was mainly applied to water demand prediction in Japan but its inherent flexibility to express the complex system structure will be good in modeling various water-related component and their interdependencies. In this study, we design a regional water dynamics model to analyze stability of water supply-consumption systems not only in a single city or basin but also in the interdependencies among regions. First, water users are categorized into agricultural, industrial and municipal sectors. In agricultural sectors, water demand is modeled by the use of depletion depth in paddy fields. In industrial and municipal sectors, water demand is expressed in terms of multiple regression models through the past industrial and water use statistics data in Japan. Next, water consumption sectors are connected to population sectors and regional water flow sectors. Emigration sectors are introduced to explain the movement of products in one region to others. Finally by putting all the sectors into one system dynamics model, the behavior of the water resources systems in Kinki-region in Japan is analyzed under the possible future scenarios.

**HW04/09A/C31-004** **1000**

**MODELING HYDROSYSTEM DYNAMICS OF MAE KLONG RIVER BASIN, THAILAND**

Ekasit KOSITSAKULCHAI<sup>1</sup>, Pierre CHEVALLIER<sup>2</sup> (<sup>1</sup>Department of Irrigation Engineering, Faculty of Engineering, Kasetsart University, Nakhon Pathom, Thailand, <sup>2</sup>Institut Languedocien de Recherche sur l'Eau et l'Environnement, Maison des Sciences de l'Eau, Montpellier, France)

Modeling of integrated water resources management of Mae Klong river basin (31,000 sq.km.) is based on the system approach. The variability of water resource and the increasing competition of water uses (irrigation, hydropower, urban water supply, seawater intrusion protection, and recreation) entail a cautious water management in highly developed hydrosystems. In order to tackle such a complex dynamical situation, simulation models that take into consideration the existing management rules play a crucial role. The system thinking coupling with System Dynamics modeling tool, Vensim®, offer double advantages in helping to learn and to represent complex systems. Firstly, a lumped rainfall-runoff model was developed in order to represent unregulated stream flows at various control points in the basin. Moreover, a water management decision model was elaborated. The latter model incorporates technical aspects of multi-purpose multi-reservoir operation, governing rules, and economic evaluation. This model can be considered as a tool supporting decision in water management processes. The diverse questions related to water management in the Mae Klong river basin can be clarified as a result of the applications of model.

**HW04/09A/C31-005** **1020**

**SOLVING URBAN REGIONAL WATER HOUSEHOLD AND QUALITY PROBLEMS UNDER GLOBAL CHANGE**

Volker WENZEL (Potsdam-Institute for Climate Impact Research)

Subject of investigations is the future optimization of water household and water quality conditions within the urban region of Greater Berlin driven by global change. The hierarchy of scales to be considered together with appropriate problem-oriented bridging strategies from global dynamics down to the water-related problems of Berlin is as follows: 1. Exogenous drivings of global change, 2. Elbe river basin: From divided Germany to globalization, 3. Landscape-specific upstream-downstream conflicts in the tributary Spree region, 4. Urban agglomeration and capital Berlin. Climate change and the new economic conditions caused by globalization are the components of global change considered in this context. The IPCC scenarios A1 and B2 serve as an orientation. The drastic structural changes since 1990 concerning values, administration and economy led also to a considerable restriction of the intensity of open-cast lignite mining in the upper Spree area. As a consequence, it has been stopped to pump into Spree river the ground water out of the mining holes of the abandoned mining places. At the opposite, all this holes need a lot of water for a rather demanding restoration process. Thus, we have a genuine water scarcity conflict and distribution problem, because downstream follows the Spreewald area with biotope quality to be protected. This is necessary even by economic reasons, taking into account the tourism and the specific agricultural production of this region. And further downstream follows Berlin where, in addition, the water quantity problems are causing serious water quality problems. 10 alternative strategies for water management in Berlin with options from 6 fields of activity including rain water management, additional water purification efforts, biotope protection measures etc. are defined under participation of about 10 interest groups or their stakeholders. The model fund for impact analyses comprises climate, sealing and runoff models, hydraulic and long range water management models, water quality and aquatic ecosystem models. For the realization of a specific epistemic aggregation, the manifold of single indicators delivered by those models, in analogy to the prenatal human ontogenesis process of the formation of organs and the potential realization of their functions, are then

combined to few relevant index variables and evaluation criteria, integrating ecological, economic, social and normative aspects. Finally, the results of corresponding multicriteria and equity analyses may be used for planning and decision support.

**HW04/09A/C31-006**

**1100**

**THE THEORETICAL MODEL OF OPTIMAL DIVISION OF WATER RESOURCES BETWEEN DIFFERENT COUNTRIES OF CENTRAL ASIA**

Andrei V. KHRISTOFOROV (Department of Hydrology, University of Moscow)

For the countries of Central Asia (Kazakhstan, Kirghizstan, Tajikistan, Turkmenistan and Uzbekistan) the problem of the division of water resources is very actual and difficult and many political, economical and social problems of this region are connected with it. For the scientific substantiation of political solution of this problem the theoretical model of optimal division of water resources between different countries of Central Asia is offered. The model is based on the principles of the market economy, which are rather new for these postsoviet republics. The main instrument of the model is a total economical effect of water resource utilization as a function of quantity and quality of water, which is used during a calculation period. Such functions must be determined not only for every country, but for their regions and districts too. The general type of these functions is offered. Every country, region or district is considered to be a participant of the market and can buy or sell some part of quote for the water utilization and pollution. The model determines the optimum strategy and gives the possibility to reach maximum profit. The model can be used for the scientific substantiation of quotes and expenses for the ecological monitoring and protection. The successful realization of this model can give an opportunity for the normalization of the political situation and for economically effective and ecologically safe utilization of water resources in Central Asia and other regions of the world.

**HW04/09A/C31-007**

**1120**

**MODELING IRRIGATION WATER REQUIREMENT USING FUZZY LOGIC**

Yutthana PANKAMOLSIN, Ekasit KOSITSAKULCHAI (Department of Irrigation Engineering, Faculty of Engineering, Kasetsart University, Nakhon Pathom, Thailand)

This paper proposes the fuzzy approach for representing the irrigation water requirement under the conditions of imprecise human decision and uncertain environment. The irrigation water requirement is the results of various processes at the field level, including crop evapotranspiration, changes in soil moisture storage and variations of irrigation supply. The input parameters of the model, based on daily time step, consist of temperature, crop development stages, sunshine duration and rainfall. The first three parameters are applied in the model for estimating the crop evapotranspiration. In order to assess the soil moisture states, the model takes into an account the rainfall data and the feedback information of irrigation supply in the previous days. The relationships between input and output variables were defined by fuzzy rules. These rules are established according to human reasoning and decision. The calibration and validation of model were performed by comparing the simulated results with the conventional method of soil water balance, and the recorded field data. The results of fuzzy model are highly correlated with those of soil water balance. Furthermore, the model is capable to estimate daily water requirement from monthly or annual mean data sets. The results of estimation are as reasonable as those of daily input data.

**HW04/09A/C31-008**

**1140**

**CONTINENTAL SCALE MODELING OF WATER BALANCE IN EAST EURASIA FOR EVALUATING AGRO-WATER RESOURCES**

Yasushi ISHIGOOKA, Hitoshi TORITANI, Tsuneo KUWAGATA, Shinkichi GOTO, Hiroyuki OHNO (Department of Global Resources, National Institute for Agro-Environmental Sciences)

In evaluating climatic agricultural productivity, it is important to recognize renewable water resources. In this regard, we should attend not only to the effective precipitation but also to the supply of water by irrigation systems. In order to estimate the potential available water for irrigation, it is necessary to comprehend water dynamics on a global or continental scale, with river discharges being one of its most important components. In this study, we attempted to construct a simple water balance model to estimate the discharges of the main river basins and to evaluate the agricultural water requirement as irrigation for cropland throughout East Eurasia. Our model is based on the aggregation of small drainage basins instead of rectangular grids, in order to eliminate the geographical disagreements between actual drainage basins and those defined by grids. The model consists of runoff model and river flow model; the former estimates the amount of runoff from basin according to the hydrological process, and the latter represents lateral movement of water through the network of river-channels. In runoff model, calculation was performed independently for every 6 type of land cover, and each hydraulic characteristics of soil and phenology of vegetation which expressed by seasonal variation of NDVI were used as the boundary conditions. Evapotranspiration was calculated as the sum of the evaporation and the transpiration, both of which were calculated by using FAO-56 method. In this process, the crop water requirement was estimated as the deficit of the actual transpiration against the transpiration without water-stress. In river flow model, the discharge of each stream was calculated by accumulating the runoff from the current contributing drainage basin and the flow from the upper streams. The model were implemented using published monthly climate data obtained from Climatic Research Unit (CRU), in which global historical various climatic data are constructed with 0.5 degree resolution from 1901 to 1995, as forcing data, and then the annual discharge of each stream was estimated. Observed discharge data from 118 selected gauging stations on several main rivers, which were obtained from GRDC and IHP/UNESCO, were used for the validation of the simulated discharges. In many cases, it was found that this model tended to underestimate the discharge in comparison with the observations. This tendency seemed to be more obviously at the area with sparse vegetation, which indicate that the model tend to overestimate the evaporation from bare soil.

**HW04/09A/C31-009**

**1200**

**ASSESSING THE SIGNIFICANCE OF GLOBAL SCALE WATER STRESS INDICATORS**

Martina FLOERKE, Petra DOELL (Center for Environmental Systems Research, University of Kassel)

Indicators are used for a clear illustration of complex results, for example those obtained with global models. We present two indicators of water stress that are based on water availability, water withdrawals, water consumption, and 90% reliable monthly discharge. All these quantities have been computed with the global water model WaterGAP (Water Global Assessment Prognosis), which has been described among others in Alcamo et al. (2002) and Doll et al. (2003). The first indicator is the commonly used withdrawals-to-availability ratio (w.t.a.), which is obtained by dividing the long-term average (30 years period) annual

withdrawals for the four main water use sectors (domestic, industry, irrigation, and livestock) by the long-term average annual availability on a drainage basin level (Alcamo & Henrichs, 2002). A drainage basin is assumed to be under medium water stress if  $0.2 < w.t.a. < 0.4$  and under severe water stress if  $w.t.a. > 0.4$ . The second indicator introduced here is the consumption-to-90% reliable monthly discharge ratio (C/Q90). Here the long-term average annual water consumption is divided by the long-term average 90% reliable monthly discharge on the drainage basin level. Under water consumption we understand the fraction of the withdrawn water that is lost by evaporation or evapotranspiration during its use. The 90% reliable monthly discharge Q90 is the discharge that is exceeded in 9 out of 10 months for the period under consideration, and can be considered as a typical design flow for surface water supply. The C/Q90 indicator considers not only the variability of the discharge but also the reduction of natural discharge by upstream consumptive use. With this indicator, we assume that a drainage basin suffers from severe water stress if  $C/Q90 > 1$ . For  $0.5 < C/Q90 < 1$  the basin is under medium stress. It should be kept in mind that this indicator, as calculated here, does not take into consideration the storage of water (neither surface water nor groundwater). Both indicators are computed for current conditions (1995) as well as for scenarios of the future. Due to the uncertainties in the calculation of the future precipitation, both indicators are computed using two different global climate models, HadCM3 (Hadley Center, UK) and ECHAM4-OPYC3 (MPI, Germany), to better assess the impact of climate change. Additionally, results for the SRES scenarios A2 and B2 (IPCC, 2001) in 2075 are included to analyse the influence of technological and structural changes on these indicators. The water stress results obtained using the two different indicators withdrawal-to-availability ratio and consumption-to-90% reliable monthly discharge ratio point out that there is no best indicator. Both indicators are complementary and illustrate different aspects of water stress. Each of them has its own advantages and disadvantages related to its significance and uncertainty.

**HW04/09A/C31-010****1220****STATISTICAL THE ASSESSMENT OF THE WATER RESOURCES ON METEOROLOGICAL EVIDENCE. FORECAST OF ANNUAL RUNOFF FOR DIFFERENT CLIMATIC SCENARIO**

Natalie LOBODA (Department of Hydrology & Water Resources, Odessa State Environmental University (OSEU))

The water-management transformation of runoff and prospective change of a global climate calls for the necessity of studying the climatic factors contribution to the runoff formation process. In present paper we consider and try to solve the problem of the "climate-runoff" interaction with the use of mathematical and computer modelling on the basis of the empirical orthogonal functions (EOF) and water-heat balance methods. The approach is illustrated by studying the north-west Black Sea region, where data about a runoff in a natural condition is not available and, therefore, it is necessary to develop methods of its account on basis of meteorological information. For modelling of natural annual runoff series the results of analysis of annual precipitation and maximally possible evaporation fields with the empirical orthogonal functions method are used. Spatial distribution of the first four weight expansion coefficients for annual flow can be considered as a result of the interaction between the climatic factors in the meso- and macroscale. For an evaluation natural (not infringing the economic activity) runoff in conditions of defect of the hydrological observations data there have been proposed the modification of method of water-heat balance, in which the meteorological data are used (Loboda, 1998b, 1999). Basis of water-heat balance method is joint solving of the equations of water and heat balances of an earthly surface, which contain a common component - total evaporation. The empirical orthogonal functions analysis of the annual precipitation, maximum possible evaporation and runoff data showed that the fields of main climatic factors (annual precipitation and maximum possible evaporation) and annual flow are formed under influence of the common physical processes, which can be reflected by the first components of the fields expansion on the empirical orthogonal functions. Spatial distribution of the first four weight expansion coefficients for the annual runoff can be considered as a result of the interaction between the climatic factors in the meso- and macroscale. For river, where there are no measurements of runoff, this coefficients can be calculated as linear functions of norms of annual precipitation and maximally possible evaporation by maps of isolines. The water-management transformation of annual runoff is excluded by fulfilling the filtration of initial data on the basis of the first components. Approach proposed opens the new perspective possibilities for the natural rivers runoff (runoff non-transformed by the economic activity) restoring problem solution. For regions where the meteorological studying is better than hydrological one, the average arithmetical values and average quadratic deviation of a natural runoff series (necessary for modelling within the empirical orthogonal functions formalism) can be determined by using the regional generalization of the climatic flow characteristics, calculated on the basis of meteorological information.

Wednesday, July 9 PM

Presiding Chair: Z. Xu

**HW04/09P/C31-001****1400****MODIFICATION OF RESERVOIR OPERATION RULES BASED ON MATHEMATICAL SIMULATION AND OPTIMISATION APPROACHES**

Manfred Walter OSTROWSKI (Department of Civil Engineering, Darmstadt University of Technology)

Reservoirs have substantial effects on society and the environment. While the construction of new reservoirs is still in progress, the functioning of existing reservoirs has to be re-evaluated for several reasons. Many of them are approaching their expected lifetime and it has to be decided whether and to what extent they should be maintained or re-constructed or even de-commissioned. Other reservoirs have to be operated under changing boundary conditions such as climate and to account for changing objectives such as satisfying new uses as well as meeting new ecological and socio-economic criteria. Existing reservoir operation rules often resulted from heuristic optimisation of purely economic objectives; only in a few cases mathematical optimisation was applied. At present, reservoir owners and operators tend to maintain the actual release rule as the development of modified rules is expected to be most complex, controversial and thus time consuming. To account for new objectives a different decision making approach is necessary to include the interests of a wider stakeholder community. This requires the use of decision support systems (DSS) to analyse multiple scenarios and to present these in an adequate form to decision makers and stakeholders. A gap can be observed between analysts, using advanced simulation and optimisation approaches and decision makers. The key problem is the translation of technical results into information to be evaluated and decided on by non technical people. The presentation includes a brief description of a simulation/optimisation package (TALSIM) as part of a DSS which has been applied to ten reservoir systems in Germany, Spain and East-Africa. Some of the case studies will be presented to make the problem transparent and to identify requirements for an improved interface between technology and decision maker/stakeholder. The simulation/optimisation package is a generic tool being solely controlled by input data, which does not need any sources code modifications. Case studies

stem from Namibia, Tanzania, Ethiopia, Spain and Germany.

**HW04/09P/C31-002****1420****URBAN HYDROLOGY AND RECLAMATION POTENTIAL OF URBAN STORMWATER**

Parviz MONADJEMI, N. VASSELLI (Civil Engineering Department, School of Engineering, Shiraz University)

Urbanization increases the volume of stormwater runoff, greatly amplifies its peak, and modifies its quality. The use of ponds detention of urban stormwater began to gain broad recognition only in the early 1970s. Nowadays stormwater detention ponds are being used in many countries, e.g., the United States, Australia, Sweden, Canada, etc. The purpose of such detention ponds in urban areas has been the mitigation of urban floods downstream and reduction of pollution. In these schemes the ultimate aim is stormwater disposal and not stormwater conservation. However a new and innovative approach to urban stormwater management is beginning to take shape. Many arid urban areas are looking to stormwater as a potentially valuable resource. Urban stormwater is being stored in detention ponds for immediate irrigation or is being transferred to appropriate places to be stored underground for later use. In this paper conservation and reclamation potential of urban stormwater is investigated. A systematic analysis is introduced using a detention ponds and diversion facilities to transfer stormwater for reclamation. Bander Abbas, a rapidly urbanizing & arid region located in the southern part of Iran was chosen for this study. The amount of stormwater reclaimed is a function of rainfall/runoff, characteristics of urban watershed and the size of detention ponds and diversion or reclamation facilities. The basic elements of detention and diversion of stormwater are shown below. Runoff is temporarily stored behind a small dam with height H. At the same time the water is diverted by gravity through outlet facilities e.g. a rectangular weir with width of W. Ten years of 10 - minute interval rainfall data and 14 years of daily rainfall data were disaggregated into 1 - hr data. All the rainfall data, basin data, loss rate data function, unit hydrograph data, river & reservoir routing data and diversion data blocks were prepared as input data file. HEC1 model was chosen to handle these data. In order to determine the reclaimed or diverted fraction of runoff for the chosen basin, the curve number CN, lag time, slope, roughness, flood plain geometry, main channel geometry and reservoir geometry were treated as fixed. A 20 meter long overflow dam was used. The total areas, of watershed was 22 km<sup>2</sup>. A Matlab based computer package was developed. 129 rainfall events, 11 values for the height of the dam and 4 values for the width of diversion canal were used to determine the amount of reclaimed stormwater. The results shown in the following figure. Stormwater reclamation potential for a 22 km<sup>2</sup> urban watershed in Bandar Abbas with an average annual rainfall of 179 mm could be as high as 1.4 million m<sup>3</sup> per year. This is a substantial amount and is highly desired for arid areas. Reclamation of stormwater in urbanized regions especially in arid climates e.g. Western China, Western United States, North Africa, Middle East, etc, is technically and economically feasible and environmentally desirable.

**HW04/09P/C31-003****1440****STORM LOSS STUDIES FOR THE BREMER RIVER CATCHMENT IN AUSTRALIA**

Mahbub ILAHEE, Rahman ATAUR (School of civil engineering, QUT)

The rainfall based design flood estimation techniques are commonly adopted in hydrological design, which require a number of inputs including storm loss characteristics. Storm loss or simply loss is the part of rainfall that does not appear to the stream during or immediately after the rainfall event. A conceptual loss model known as the "initial loss-continuing loss model" (AIE) is the most commonly used method in Australia. The loss that occurs in the beginning of the rainfall event, prior to the commencement of surface runoff is called initial loss. After initial loss is satisfied the continuing loss is the average rate of loss throughout the remainder of the storm. The current Australian design flood estimation technique is known as the Design Event Approach in that it is assumed that the design rainfall frequency can be preserved in the final design flood estimate by considering representative values of other model inputs such as rainfall temporal pattern and loss. In practical situations, losses show a wide variability and it is more logical to consider loss as a probability-distributed variable in design flood estimation. This paper examines losses for the Bremer River catchment located in southeast Queensland which has a catchment area of 130 km<sup>2</sup>. The study uses one pluviograph and one daily rainfall station having 33 and 80 years of data respectively to compute catchment average rainfall. The continuous streamflow record length at the Bremer River is 32 years. The paper focuses on continuing losses. Continuing loss estimates obtained from selected observed rainfall and streamflow events include errors arising from factors such as inadequacies of input design rainfall, flow rating and separation of baseflow from total streamflow. It has been found that continuing loss shows a wide variability and it is unreasonable to adopt a representative value (either mean or median) of continuing loss in design flood estimation. The paper examines the potential of adopting probability-distributed continuing loss in design flood estimation using a joint probability approach. It has been found that probability-distributed continuing loss can offer significant improvement in design flood estimation. Keywords: rainfall runoff modelling, flood estimation, probability-distributed losses.

**HW04/09P/C31-004****1500****A REMOVED DYNAMICAL MODEL OF A GEYSER INDUCED BY INFLOW OF GAS**

Hiroyuki KAGAMI (Wakkanai Hokusei Gakuen College)

Though some models of a geyser induced by inflow of gas has been proposed for a long time, a comparison between the model and observational data has not been made enough and as a result the mechanism of it, especially the dynamical one, has not been solved enough yet. Lately, model experiments of the geyser were tried to do (Katase et al. (1999)) based on observation of Hirogawara geyser (Yamagata) (Ishii et al. (1999)). These experiments showed that periods of spouting depend on various parameters height of a spout from the bottom, volume of a cave (under the ground), a supply rate of gas and so on. Then a mathematical model of the experiments was proposed by Kagami et al. (2000). The model qualitatively explained results of the experiments dependence of a period of spouting on each parameter, but the dynamics of spouting was not dealt with in this model. Then a dynamical model of a geyser induced by inflow of gas was proposed by Kagami (2001). The model assumes that structure of a natural geyser is essentially as same as that of the model experimental system. From the result of simulation using this dynamical model, it was found that the model reproduced characteristics of observational data of a natural geyser just before spouting the water level under a spout oscillates and it rising. In this meeting, we will introduce an improved dynamical model of the geyser and report minute results of simulation using the model dependence of a rate of spouting and a period of the water level's oscillation just before spouting on each parameter (height of a spout from the bottom, a diameter of a spout, volume of a cave under the ground, a supply rate of gas and so on. In the dynamical model, dynamical equations after the event that balance of power affecting a lump of water is lost, when pressure of gas under the ground becomes larger than the sum of power surface tension, gravitation and so on holding a position of the lump of water stable, are led. In the improved dynamical model, both effects of complex structure of the paths of

water under the ground and friction working between the wall's surface along the edge of the paths of water and water are taken into account. Through simulation, we will evaluate minutely above 2 new effects of the improved model comparing with results of the first model.

**HW04/09P/C31-005****1520****NEURAL NETWORKS & FRACTAL MODELLING THE FRUSTRATED AQUIFER SYSTEMS: ANNUAL RUNOFF ANALYSIS**

Natalie LOBODA (Department of Hydrology & Water Resources, Odessa State Environmental University (OSEU))

A new approach to the neural networks and multi-fractal modelling the frustrated hydrological systems (calculation of the river runoff fractal spectrum is developed and numerically realized. It is well known that hydrological (etc.) systems (and the dynamics of their key characteristics fluctuations) can be described as a mechanical dissipative multi-body systems, which are fundamentally non-linear (Davis, 1991; Kothiyari and Singh, 1999; Loboda, 1998; ). General non-linear parameter dependent dynamical dissipative systems very often have parameter ranges, in which the dynamics is chaotic. Chaotic behaviour in the sense of a fully deterministic evolution of the systems in time bounded in phase space with sensitive dependence on initial conditions, might therefore be expected to occur in above cited systems. Dissipative non-linear systems typically have a long-term behaviour, which is described by an attractor in phase space. At the same the chaotic dynamics in details is often unknown. It is well known that an attractor is called strange attractor if its dimension is non-integer, i.e. fractal. Non-linear systems of fractal objects like interfaces or time-series is their scaling property related to invariance under magnification. For uniform fractals the scaling is uniquely described by one-fractal exponents, the so-called fractal dimension. In last years studying the fractal properties of dynamical systems is of a great interest. In this paper we consider an effective method for treating the non-linear complex systems, based on the 'neural networks' and multi-fractal modelling (Glushkov *et al.*, 2001; Loboda, 1998; Loboda, 2001). Approach developed allows getting a possibility of forecasting the evaluation dynamics, including the extreme phenomena in non-linear complex systems. We apply these models to treating the chaotic dynamics and fluctuations of the annual runoff for natural rivers. As example, we present the time-series of the annual runoff fluctuations for the Pripyate, Southern Bug rivers (Ukraine; catchment squire 26.4·10<sup>3</sup> km<sup>2</sup>), received by us on the basis of processing the experimental data and calculating within the neural networks stochastic model. Non-uniform and multi-fractal objects can be more completely characterized by spectrum of  $D(q)$  fractal exponents, where  $q$  is a real number, the so-called generalized dimension, where the fractal dimension is equal to  $D(0)$  and the function  $D(q)$  is generally referred to as multifractal spectrum. We carried out numeral modelling of chaotic dynamics for studied systems and our analysis (annual runoff fluctuations) shows that the average fractal dimensionality is 1.3-1.9. The knowing of the multi-fractal spectra allows to reconstruct the natural annual runoff with reasonable degree of accuracy.

**HW04/09P/C31-006****1540****RELATIONSHIP ANALYSIS BETWEEN MULTI-YEAR SOIL MOISTURE AND CLMATE CHANGE OF NORTHWEST OF CHINA**

Mingguo MA (CAREERI,CAS)

Based on the SMM/I data, a set of skin soil moisture data were estimated for Northwest China from 1987 to 2001. The vegetation condition was calculated from AVHRR data during 1987 to 2001. The temperature data and precipitation data were also collected for our work. In this paper the relationship between soil moisture change and the above factors was analyzed.

**HW05****Thursday, July 10****GROUNDWATER RESOURCES FOR EMERGENCY SITUATIONS (ICGW)**

Location: Site C, Room 31

**Thursday, July 10 AM**

Presiding Chairs: M. Bolgov, N. Tase

**HW05/10A/C31-001****0830****PRESENT SITUATION AND ISSUES OF GROUNDWATER USE FOR EMERGENCY IN JAPAN**

Norio TASE<sup>1</sup>, Yoshizumi HOSONO<sup>2</sup> (<sup>1</sup>Institute of Geoscience, University of Tsukuba, <sup>2</sup>Department of Geography, Nara University)

There are two approaches to cope with groundwater issues for emergency situations. One is to use groundwater as supplementary sources when water supply systems are destroyed by disasters such as earthquakes and can not supply enough water. The other is to measure against destruction of natural groundwater systems by disasters when groundwater is used for water supply source. The former is common but the latter may be seldom considered. This paper introduces present conditions and issues on groundwater resources for emergency in Japan. Although groundwater accounts only for 30% of water use in Japan at present, it is recognized as important water resources for emergency situations, especially after the Great Hanshin-Awaji Earthquake(GHAE) in 1995, which revealed essentials of waters for extinguishing fires and domestic uses. Roles of groundwater for extinguishing fires have been decreased to 1.2% in 1995 because groundwater wells cannot always supply enough water for fire fighting. While, in Japan, many local municipalities are storing water in ground and underground tanks, installing emergency wells, or designating private wells as emergency ones. For example, Nerima Ward in Tokyo, with 675,000 population in area of 48.16 km<sup>2</sup>, has 22 deep wells with generators for potable water, and 103 shallow wells in public schools and more than 500 private shallow wells for domestic uses except drinking. Under other emergency situations such as droughts, floods, and volcanic eruptions, groundwater resources are also affected in various ways. Drastic changes of groundwater in quantity and quality due to earthquakes and volcanic activities have been reported in many cases such as GHAE and Mt. Miyake. Deterioration or destruction of groundwater resource systems due to disasters and its effects on water supply systems may not be evaluated yet. During droughts, groundwater has been used as a supplementary source mainly for irrigation, which brought drastic water decline and occasionally land-subsidence. Under very extreme droughts such in 1939, we do not know well what happens.

**HW05/10A/C31-002****0850****EVALUATION OF GROUNDWATER DAM SITES FOR EMERGENCY WATER SUPPLY**

Sang-il LEE, Byeong-Chan KIM (Dongguk University)

Global climate change accounts for frequent drought and flood occurrences in many regions over the world. The Far East including the Korean Peninsula is also experiencing ever-increasing extreme events, and Korea has seen eight years of drought during the last decade. About thirty cities and counties located in southern and eastern parts of the country suffer from chronic water shortage. In addition to the climate change, steady increase in population and economic development have yielded imprudent expansion of urban areas, sometimes resulting urban floods which, in turn, lead to emergency situations such as suspension of water supply in some regions. These circumstances have increased the overall hazard potential due to either natural phenomena such as flood and drought or side effects of excessive development. The resultant hazard might cause not only tremendous amount of costs but social instability. While the construction of dams are delayed or challenged on account of environmental concerns, groundwater having annual recharge of about 13 billion cubic meters can be a reliable source of water supply for emergency situations in some regions of Korea. The hydrogeologic conditions of most regions of the country, however, make the major development of groundwater infeasible. Thus environmentally friendly small-size groundwater dams are being considered as a solution for emergency situations as well as for sustainable water supply source. In this study twenty-one candidate groundwater dam sites, selected based on preliminary studies, are evaluated in terms of their suitability. Systematic quantification of the suitability as a reliable source of water supply in emergency situations is the goal of the evaluation. The process of evaluation involves various factors: they include hydrogeologic, environmental, social, and economic attributes. The possibility of groundwater use in conjunction with available surface water is one of the important assessment criteria. Since the evaluation incorporates both qualitative and quantitative aspects of the complex decision-making problem, AHP (Analytic Hierarchy Process) was adopted as an analysis tool. Various influence factors of the candidate locations were identified and weighted. Suitability index was defined as a function of weighted influence factors. As a result, candidate locations were ranked and categorized into three groups based on the quantified suitability index. The evaluation results showed some discrepancies in suitability and priority from the preliminary study in which only some parts of factors such as water shortage and hydrogeology were considered for qualitative judgment. We believe that the suitability index approach based on AHP could be used as a guideline for decisions such as prioritization of further site characterization or of investment for groundwater dams. Acknowledgement: This research was supported by a grant (code 3-4-1) from Sustainable Water Resources Research Center of 21st Century Frontier Research Program.

**HW05/10A/C31-003****0905****CONJUNCTIVE USE OF GROUNDWATER AND SURFACE WATER FOR DRINKING WATER SUPPLY BY USING IRRIGATION RESERVOIRS**

Takeshi HATA (Faculty of Agriculture, Kobe University)

There are lots of small-scale irrigation reservoirs in Japan, especially in Kinki, Chugoku and Shikoku districts, southwestern part of Japan. For example, their number is around 50,000 in Hyogo Prefecture in Kinki district. In the drought season irrigation reservoirs, which are close to the supplying system to a water purification plant, are to be used for drinking water by installing shallow or deep well to pump up groundwater. These systems are for the emergency and are used for municipal use as well as agricultural use. The conjunctive use of small-scale irrigation reservoirs and the large volume of groundwater resources will raise security of drinking water. The reservoirs especially in the urban areas became evacuation places where people hit by the great earthquake in Kobe and the surrounding areas in 1995 lived in sheltered tents for some period of time with getting necessary water there. Many of the reservoirs are now in the difficult situation in their maintenance and management, because of severe decrease in the number of farmers. Besides the irrigation water, these reservoirs have some important roles of recharging groundwater storage, flood mitigation, valuable biotope areas for the species of plant and animals with scarcity and so on. Especially paddy fields contribute so much to the recharge of groundwater throughout the wide areas of paddies. In these areas lots of irrigation reservoirs have been constructed since 5th century in Japan. These 40 years many of the local areas have been developed and changed their land use from paddies to residential zones, and many plant factories have been constructed. Introducing the drinking water use to an irrigation reservoir will contribute to the maintenance of reservoirs under the support by the residents of urban areas and also to maintain the paddies as the source area of groundwater recharge. These days the source of drinking water has been changed from groundwater to surface water by constructing dams. However, the construction of new dams and large-scale reservoirs has become difficult mainly by reason of its severe affects to the natural ecosystem. Therefore the broad use of irrigation reservoirs is to be more important. Detailed system of the conjunctive water use including its social support system is discussed in the paper, i.e. how the storage water in a reservoir is allocated to the multi-objective use, how to support the maintenance of a reservoir by the participatory approach. Concerning the relationship between groundwater and surface water, water logging and leaching water are important issues for the agricultural water use in the world. These issues also should be considered in the application of the system to the arid zone like in Africa.

**HW05/10A/C31-004****0920****CONJUNCTIVE USE OF SURFACE AND GROUNDWATER RESOURCES FOR WATER SUPPLY OF NUCLEAR POWER PLANTS DURING EXTREME LOW FLOW PERIODS**

Mikhail V. BOLGOV (Water Problems Institute, Russian National Committee for IAHS)

Using the one Nuclear Power Station (NPS) in Russia as an example, the complex of hydrological and water management problems arising when designing system of industrial water supply for such station was considered. A variant of joint use of surface water and groundwater was suggested. It consists in the intermittent exploitation of aquifers within the system of industrial water supply in the years with a water deficit. A method was developed that permits one to assess the degree of reliability of water supply for the nuclear power station under the condition of the preservation of aquatic ecosystems. The imitation model for investigation was created. Next conclusions were received. 1. Natural regulation of the runoff of lakes and strongly waterlogged rivers used for the water supply of NPS results in the tendency of low-water years toward grouping. Under such conditions, the reliable satisfaction of demands on water can be provided only if the proportion of utilised water resources is small. For a great proportion of utilised runoff, the system of water supply should comprise either several surface sources with asynchronous fluctuations of runoff or aquifers. 2. When using internal reservoirs and the rivers flowing out of them for the water supply of the nuclear power station, one should take into account the requirements for environmental preservation. 3. Presently, no unified method for the estimation of admissible disturbances of the hydrological regime of rivers exists. Thus, the restrictions on transformation of the natural hydrological regime should be substantiated individually in each

case. 4. When making water management calculation, one should correct water loss for additional evaporation (at the expense of heated wastewaters discharged into the lake). In addition, changes in the dates of freeze-up (later freezing and earlier break-up) should also be taken into account. 5. The calculations showed that the beginning of operation of the NPS based on the current system of water supply will be followed by violating the ecological requirements and serious failures in the operation of NPS. On average, the units of the nuclear power station should be stopped once every five years. 6. The system of water supply of NPS should be connected to additional ground water sources. For effective operation of this system, it is necessary to develop special rules.

**HW05/10A/C31-005****0935**

#### **SIGNIFICANCE OF GROUNDWATER EXPLORATION AND ITS DEVELOPMENT IN NORTH WEST INDIAN HIMALAYAS: IMPLICATIONS FOR FINDING EMERGENCY AND SUSTAINABLE SOLUTIONS**

Ritesh ARYA (Aqua Associates)

This paper emphasise the significance of groundwater exploration and its development to solve drinking water problem in the high altitude (>3000 meters above mean sea level), cold mountain (in winters, temperatures drop to -30°centigrade), deserts of northwest Indian Himalayas of Ladakh. Present findings are based on studying data from more than 500 boreholes drilled in the last 5 years in different hydrostratigraphic zones, identified by Arya(1996) along and across the Indian Himalayas. Prior to this study, entire system of water distribution and its management was based on surface water as the main source. Water was tapped from rivers/streams and distributed by water tankers to various places of habitation. Main problem with these water supply schemes was that in summers, due to snow melt ablation there was flashflooding. As a result water remained turbid, when it was most needed. Whereas in winters the surface water in rivers /streams freeze and sub surface temperatures drop down to +1°centigrade. Results from our present study shows that even in winters, when outside temperatures drop down to -30°centigrade, groundwater from the borehole always enjoys temperature difference of +4° centigrade over surface/sub surface waters. Therefore groundwater harvesting not only provides drinking water solutions on sustainable basis but also helps in finding emergency solutions to solve drinking water problem, arising due to extreme hydrological conditions (due to freezing of source in winters and turbidity due to flash flooding in summers) in the Ladakh, Indian Himalayas.

**HW05/10A/C31-006****0950**

#### **MEASURES, TAKEN FOR PREPARING UNDERGROUND WATER SOURCES TO BE USED IN CASE OF EMERGENCY**

Inom Sherovich NORMATOV (Institute of Water Problems, Hydroenergetics and Ecology, Academy of Sciences, Republic of Tajikistan)

In case of emergency (during earthquakes, floods), the problem of providing people with lodging, food, and clean potable water is becoming actual and requires immediate solving. In such cases the water supply will be submitted mainly from underground sources. Therefore one of urgent tasks is preliminary monitoring of underground waters, especially in the suburbs of densely populated cities and villages, industrial and agricultural sites. This is first of all the completing of measures to define: - the depth of underground water level; - the lithological contents and the capacity of water carrying horizons, water stress; - the feeding and unloading conditions of underground waters; - mineralization and chemical contents of underground waters; - contents of technogen pollutants and supposed polluting sources; - the underground waters regime and its defining factors; - the observing chinks on the site. According to above-mentioned characteristics there must be created GIS for every underground water source supposed to be used in case of emergency. Alongside, cartographic materials must illustrate the characteristics of underground waters. While constructing the underground water sources providing people with drinking water, the special attention should be paid to establishing the areas of sanitary security of water-intakes, their working ability in case of emergency, stability and lasting ability of constructions and auxiliary units.

**HW05/10A/C31-007****1005**

#### **MANAGEMENT OF DROUGHT EVENTS IN A SMALL ISOLATED ISLAND**

Manta Devi NOWBUTH<sup>1</sup>, Teeluck BHOWRUTH<sup>2</sup>, Farook MOWLABACCUS<sup>3</sup> (<sup>1</sup>Department of Civil Engineering, Faculty of Engineering, University of Mauritius, <sup>2</sup>Water Resources Unit, Ministry of Public Utilities)

Water is an inexhaustible and replenishable natural resource, which circulates through the hydrologic cycle. It is essential to meet several requirements of man starting from food to recreation. When demands exceed supply, there is naturally a scarcity of water in space and time, and this is generally referred to as 'drought'. Drought events can have impacts on both the social and economic sectors of a country. However, the impact of drought in isolated islands, is very critical, given that options to cater for deficits in water supply are not readily and economically available. This present study considers the management of water resources for Mauritius both during the normal and during a severe drought conditions. It places emphasis on the effectiveness of the short term measures taken to management water resources as well as the long term though expensive measures which had to be considered given the situation. The response of the public with regards to the campaign of the water authorities is analysed. The effectiveness of statistical analysis currently being used by the water authorities and the possibility of using other analytical methods that could provide sound basis to help in improving the management of severe drought events were compared. The results of the study indicated though there may be a number of measures that can be taken to manage water resources during drought events the actual measures which work efficiently is largely dependent on the understanding and sense of responsibility of the public. The local water authorities have over time develop a relatively quick and effective way of predicting drought events. However, with new development in the field of statistical methods such as the low flow frequency method, the run-sum analysis and the moving-average method, for drought predictions, can provide sound basis for decision making. It was found that the Run-Sum method of analysis is the most flexible approach for our region. It is advantageous, as both daily data for short droughts and annual data for multi-year droughts can be analysed. The use of a variety of different thresholds allows it to be applied over the whole range of flow regimes found in the region. For Mauritius, the Normal Flow or the Mean Flow can be used as threshold.

**HW05/10A/C31-008****1020**

#### **THE IMPACT OF REFUGEES ON GROUNDWATER RESOURCES IN KENYA**

Francis Mwaura MWANGI (Department of Geography)

Kenya receives an average annual rainfall of 567 mm which converts to approximately 322.8 billion cubic metres of water. The country is considered to be a water scarce area because it

has an annual freshwater per capita of about 700 m<sup>3</sup> compared to the world benchmark of 1000 m<sup>3</sup>. The country supports and maintains a large number of refugees from the war-torn countries of Somalia, Sudan and Ethiopia. The settlement of a large number of refugees can cause a wide range of environmental transformations including high consumption of natural resources including water. An Assessment of groundwater extraction in a dryland area of northern Kenya which supports a large number of refugees was undertaken for the last one-decade. The overall objective was to determine the effects of groundwater withdrawal on water levels and quality. A total of 13 boreholes were considered in the assessment. Six boreholes operating in Liboi Refugee Camp were found to have average yields in the range of 9-12 cubic meters per hour. The estimated daily discharge was approximately 660 cubic metres in a network of boreholes within an area covering 4 km<sup>2</sup>. Elsewhere, a total of six boreholes in the Ifo Refugee Camp were analyzed and found to produce upto 6 cubic metres per hour within a small area of about 6 km<sup>2</sup>. The Merti Aquifer which underlies about 35 000 km<sup>2</sup> of Northern Kenya was estimated to supply approximately 880 000 cubic meters per year to the refugee camps alone. The assessment of 4 boreholes in the Hagadera Refugee Camp indicated an average monthly water consumption of 25 621 cubic metres and 65% increase in production since the early 1990s. The analysis of groundwater levels did not show any tremendous variability in the water table. However, the analysis of water quality trends indicated that the chemical characteristics of water in the Merti Aquifer have been changing most likely as a result of increased withdrawal. A consistent increase in electrical conductivity was observed. The results indicated a need for close aquifer monitoring to capture the variability in terms of groundwater quality and quantity. There is also need for greater efforts towards water conservation and new alternative sources including the use of rainwater harvesting for the artificial recharge of groundwater aquifers.

**HW05/10A/C31-009****1055**

#### **GROUNDWATER RECHARGE BY LEAKING WATER SUPPLY NETWORK IN LARGE CITIES, JAPAN**

Masaya YASUHARA (Geological Survey of Japan)

Unconfined groundwater (phreatic water) in urban areas, whose importance had been disregarded due to its deteriorated quality, is now attracting a great deal of attention again as a potential source of water after catastrophic events like large earthquakes, when the water supply system can be broke down for a long period of time. The study was carried out for a better understanding of origin of unconfined groundwater in large urban cities. As well as reducing recharge by precipitation, urbanization creates new sources of groundwater recharge, including leaking water mains. It is widely recognized that most, if not all, of pipe networks leak and a large part or all of leakage flows vertically downward and recharge groundwater. The leakage and its interconnections with groundwater have rarely been quantified in Japan. The water supply data of 1995, published by the Japan Water Works Association, were examined mainly for 47 high-density prefectural capitals with large imported water supplies. The total water supply across the country was 16 x 10<sup>9</sup> m<sup>3</sup>/yr and 9.7% of supply, that is 1.6 x 10<sup>9</sup> m<sup>3</sup>/yr, was lost through leakage. For respective capitals, leakage rate (% of total water supply) ranges from 2% in Niigata to 22% in Gifu. A simplifying assumption was made that all leakage became recharge, and dividing the leakage quantity by the areal extent of water supply for each capital gave recharge flux as 8 mm/yr (Niigata) -214 mm/yr (Osaka). This recharge flux was compared with net precipitation, which was obtained by subtracting annual evapotranspiration based on the Thornthwaite method from annual precipitation. The ratio of recharge flux to net precipitation is found to be low, being below 5% for 43 out of 47 capitals due mainly to high precipitation (900-2,600 mm/yr) under the monsoon climate and relatively low leakage rate. However, the ratio is exceptionally as high as 16.1% for Osaka and 10.5% for Tokyo, the third largest and the largest city in Japan, respectively. For these highly urbanized cities with impermeable-surface ratio of 0.8 or more, net groundwater recharge by precipitation, calculated by multiplying net precipitation by permeable-surface ratio, becomes less than one-fifth of the net precipitation. Therefore, despite high precipitation and low leakage rate, in Tokyo and Osaka, leakage must be comparable in size with recharge by precipitation or already be a predominant source of groundwater recharge. With the decreased infiltration accompanying further progress of urbanization, it is highly probable that leakage comes to play a predominant role in recharge and preservation of unconfined groundwater even in other cities such as Kyoto and Kofu, where impermeable-surface ratio is still relatively low at present.

**HW05/10A/C31-010****1110**

#### **3D SOLID MODEL FOR GROUNDWATER AQUIFERS NORTH-EAST MOSUL**

Abdulghani A. HASAN (Saddam Research Center for Dams and Water Resources, University of Mosul)

The fact is producing a 3D solid model for Aquifer characteristics is very complicated and may produce inaccurate model, but with using a good finite elements numerical modeling technique and depending on a good lithological data for wells and data from electrical investigations a good model for representing geological aquifer dimensions could be produced. In this paper the data for the region north-east Mosul have been used to build a 3D solid model with an area about 1750 square kilometer and to depth about 250 m and the numbers of artesian wells are 87 and the numbers of electrical data points are 46. All geological layers have been connected with 3D finite elements to produce the final 3D solid model for aquifers in this region. After completing this model a horizontal and vertical sections are produced to declare the types and the shapes of different layers. The main objective from producing this model is to seek for a good isolated aquifer that could be used as a ground water basin in case of emergency.

**HW05/10A/C31-011****1125**

#### **EVALUATING THE GROUNDWATER VULNERABILITY DUE TO OVER EXPLOITATION IN WALAWE BASIN, SRI LANKA**

Ranjan Priyantha SARUKKALIGE<sup>1</sup>, Ashim Das GUPTA<sup>2</sup>, So KAZAMA<sup>1</sup> (<sup>1</sup>Department of Civil Engineering, Tohoku University, <sup>2</sup>School of Civil Engineering, Asian Institute of Technology, Thailand)

Walawe river basin is located in the southern part of Sri Lanka and major part of it is located in the dry zone, which is frequently face the water scarcity problems and droughts. The availability of surface water becomes limited in the area and the reserve of groundwater becomes an important source of water supply in drought periods. The over exploitation of groundwater resource will enhance its adverse effect like depletion of resources and degradation of groundwater quality. The increasing trend of anthropogenic stresses on groundwater resource has made it vulnerable. Adequately assessing the vulnerability of groundwater systems is important, since it is very costly to restore the resource once it reaches certain deterioration thresholds. One of the fundamental problems with the groundwater resources unlike surface water is that, the resource is not physically visible. Groundwater indicators therefore should provide a means to appraise the groundwater situation. Among the potential variables to be considered in evaluating vulnerability of

groundwater with respect to groundwater exploitation, groundwater level decline was used to indicate how various factors influence the susceptibility of the aquifer and cause future problems occur in Walawe river basin. Adams and MacDonalds (1995) produced a set of diagnostics, involving hydro-geological criteria, which could be used to indicate aquifer susceptibility and vulnerability. With regard to this diagnostic approach, a relative simple technique was developed to determine the susceptibility of aquifers to water level decline. According to the available data only the selected factors, hydraulic diffusivity, lateral heterogeneity and annual recharge were considered to determine the susceptibility of the aquifers in the study area. The technique was based on assigning numerical values for contributing factors and then summing to give an overall grade of susceptibility. Three grades were possible for each factor: high, moderate and low. These grades were estimated for each aquifer parameter with respect to the available data. Once the grades have been determined, the tables were used to determine the attribute numbers for each parameter, and then summed to get an overall score. This score was finally used to give a general indication of the vulnerability of the area with respect to groundwater quantity. Results of vulnerability assessment were portrayed on a map showing various homogeneous areas, which have different levels of vulnerability. The ultimate goal of the vulnerability map was a subdivision of an area into several units showing the differential potential for a specified purpose and use. It shows that the groundwater resource is highly susceptible for the excess use in lower part of the basin and it is less susceptible in the upper-west part of the basin. The groundwater exploitation in lower part of the basin is more susceptible than other areas. This methodology can be taken to prevent the decline of groundwater resource due to over exploitation, support decision making and making long term commitments to achieve sustainable groundwater usage.

**HW05/10A/C31-012****1140****ESTIMATION OF GROUNDWATER RESOURCES IN PAGERU RIVER BASIN, INDIA**

P.D. SREEDEVI, Shakeel AHMED (Indo-French Centre for Groundwater Research, NGRU)

Groundwater is the main source of supply for domestic and irrigation purposes in Pageru River Basin, India in the absence of even meager surface water resources. Thus a perceive groundwater balance and resource estimation is extremely important in the drought prone areas. Groundwater estimation has been made quantitatively by using hydraulic budget method in the study area. It is a quantitative measure of the balance between the total water gains and losses of the basin for a particular period of time. The hydrograph analysis clearly reveals the fluctuations in the water levels have direct relationship with the intensity and amount of rainfall in the catchment area. Groundwater balance studies are carried out by taking in to consideration aspects such as rainfall, runoff, percolation, evapotranspiration, groundwater recharge, discharge, change in soil moisture and changes in groundwater storage and by following the norms recommended. The total area of the basin is 480 km<sup>2</sup>. The basin area lies between latitudes 14o29'04" and 14o39'51" N and longitudes 78o19'12" and 78o41'32" E. The Pageru River Basin receives an average annual rainfall of 581mm with significant seasonal variations usually the region receives its first spell of rainfall from pre-monsoonal convectional showers in the month of May. But its occurrence is erratic. The intensity and amount of rainfall is unpredictable during the Southwest monsoon period (June to September). In fact, highest rainfall occurs in the basin during the Northeast monsoon period (October and November). The period between January and May is the main dry seasons and receives some rainfall due to convections or winter cyclonic disturbances. The hydrograph analysis clearly reveals the fluctuations in the water levels have direct relationship with the intensity and amount of rainfall in the catchment area. It is also noticed that the water table levels rises in the wells to a maximum in the months of November and December and starts declining from January to June. The total quantity of groundwater recharge per annum is estimated as 5434.5 ha.m, where as draft accounts for 4649.5ha.m with a net groundwater balance of 785 ha.m in the catchment area.

**HW05-Posters****Thursday, July 10****GROUNDWATER RESOURCES FOR EMERGENCY SITUATIONS (ICGW)**

Location: Site D

**Thursday, July 10 PM****HW05/10P/D-001**

Poster

**1400-155****UNDERGROUND WATER STUDIES IN THE CRYSTALLINE BASEMENT AQUIFERS OF SOUTHERN NIGERIA**

Omeimen E. UJUANI, Collins OSE INGBEDION (AMBROSE ALLI UNIVERSITY, EKPOMA.)

Increases in population and industrial activities during the past decade have increased the demand for water in the northern part of Edo State Nigeria. This study area is situated within the crystalline precambrian rocks, collectively known as the basement complex of Southern Nigeria. The survey is part of regional exploration programme at delineating the presence of diastrophic features like fractures within the study area. It was observed that the ground water flow pattern follows the fracture lines and the fracture lines in turn align themselves in the direction of the major foliations within the rocks.

**HW05/10P/D-002**

Poster

**1400-156****OCCURENCE OF GROUNDWATER IN HARD ROCK TERRAIN**

Faisal Kamal ZAIDI, Dewashish KUMAR (INDO FRENCH CENTRE FOR GROUNDWATER RESEARCH, N.G.R.I.)

Ground water is a distinguished component of the hydrologic cycle, however the uncertainty about the occurrence distribution and quality aspect of ground water and the energy required for its withdrawal impose certain restrictions on its exploitation. Fractured igneous, metamorphic and consolidated sedimentary rocks are distributed abundantly both in time and space. They occur principally in large areas called shields and smaller massifs and partly in cores of major mountain ranges. The extension of shield rock outcrop built usually by igneous and metamorphic rocks is estimated to be 20% of the present land surface. India is a vast country having diversified geological setting. Variation exhibited in the rock formation ranging from the Archean crystalline to the recent alluvia are as great as the hydro meteorological conditions. Almost the entire of south and central India is occupied by a variety of hard rocks with hard sediments in the intercratonic and river basins. The hard rock terrains, river valleys and abandoned channels, wherever having adequate thickness of porous material act as potential areas for groundwater storage and development, but the lack of primary porosity restricts the movement and storage of ground water in these hard

rock aquifers. Thus the ground water availability is dependant upon the development of secondary porosity caused by the weathering and fracturing of the rock matrix. The weathering reactions of granitoid rocks are affected by a number of factors but permeability to weathering solution and mineral composition appear to be the most important. The density of joints control permeability at the macro and meso scale. The extent of macro and micro fracturing depends directly on the thermal and stress history of rocks concerned. Rocks, which contain high proportion of quartz and potassium feldspars, are generally more resistant to weathering than rocks, which contain substantial amount of calcic plagioclase, biotite and other mafic minerals. One of the most important properties of hard rock aquifer is that the aquifer parameters like Storativity (S) and Transmissivity (T) often show erratic variation within short distances. Increasing amount of hydro geologic data due to increasing demand for water and improved drilling technology have simulated efforts to regionalize and generalize results from different fractured environments. Data on rock transmissivity, ground water resources and quality obtained from different methodological approaches offer excellent possibilities of correlative hydro geologic studies. Thus new important results have enabled better understanding of hydro geological studies of hard rocks both in local and regional scales and improvement of methodological approaches to be used there.

**HW05/10P/D-003**

Poster

**1400-157****WATER BALANCE STUDY AND ESTIMATION OF NATURAL RECHARGE IN THE BARIND AQUIFER OF BANGLADESH**Md. Monirul ISLAM<sup>1</sup>, Pintu KANUNGOE<sup>2</sup> (<sup>1</sup>Associate Specialist, Coastal Hydraulics Division, Institute of Water Modelling, H # 476, R # 32, New DOHS, Mohakhali, Dhaka-1206, Bangladesh, E-mail: mnr@iwmbd.org, <sup>2</sup>Senior Scientific Officer, Hydraulic Research Directorate, River Research Institute, Faridpur, Bangladesh, E-mail: rri@btb.net.bd)

In this paper, for the planning purpose, results of the study for preliminary estimation of the recharge rate as well as sustainable yield will be presented for the semi arid Barind Tract of Bangladesh. It is found from detailed water balance study for the area that natural recharge rate in the Barind Tract vary widely year to year. And for the same time period different method gives different result. In managing a groundwater basin efficiently and effectively, evaluation of the maximum annual groundwater yield of the basin that can be withdrawn and used without producing any undesirable effect is one of the most important issues. In investigating such recharge rate, introduction of certain terms, such as sustainable yield, safe yield, and perennial yield has been accompanied. Basically there is no significant difference between them. They are almost synonymous (Kashef, 1987). The Barind tract in North-West region of Bangladesh is characteristically dry (Semi arid region) and of elevated land feature covered with a thick clay layer although upto a depth of 30m in some places and underlying a sand layer which serve as the aquifer. Natural recharge in this region is quite uncertain because of the thick clay layer and the aquifer may be treated as the confined one (Ahmed and Burgess, 1993). Development of this area is closely related with the intensive use of vast land, which is now under utilization. Utilization of this land is possible only under insured irrigation. The Government has a plan to develop the irrigation facilities by optimum utilization of available ground and surface water (BWDB, 1989). The available surface water for irrigation purpose is very low in comparison with the demand. In this context under groundwater utilization programme, installations of huge amount of deep tube wells have been proposed (2000 in 1st phase and 3000 in 2nd phase). Installation of deep tube wells of the 1st phase was completed by June 1988 and 3000 deep tube wells of the 2nd phase have also been installed. The sustainability of this large-scale abstraction programme has been questioned by environmental scientists (Ahmed et al., 1995). The present rate of extraction for irrigation is 1.2\*10<sup>9</sup> m<sup>3</sup>/year, which may lead to exhaustion of the aquifer in nearly 53 years time (Khan & Sattar, 1995). The rivers around Barind Tract have an effluent character, which gain water from the aquifers throughout the year. The groundwater table is lowering rapidly and whole region is in the acute state of deforestation. Indiscriminate groundwater development may accelerate deforestation trend (Khan & Sattar, 1995). In this context estimation of actual natural recharge rate to the Barind aquifer will unquestionably assist in proper management and planning of environmentally viable abstraction schemes.

**HW05/10P/D-004**

Poster

**1400-158****ESTIMATING GROUNDWATER RECHARGE IN A VOLCANIC BASALTIC AQUIFER**Manta Devi NOWBUTH<sup>1</sup>, Satyajay Prayagsingh MOHUNGOO<sup>2</sup> (<sup>1</sup>Faculty of Engineering, Civil Engineering Department, University of Mauritius, <sup>2</sup>Faculty of Engineering, Civil Engineering Department, University of Mauritius)

Reliable estimates of recharge rates to an aquifer are often a pre-requisite to the development of efficient plans for the management of groundwater resource (Raper & Sharma, 1989). There are several methods commonly in use for estimating groundwater recharge and these methods vary in degree of complexity and their adaptability to a particular geological conditions. Review of relevant published literature revealed that for regional studies of highly complex geological formations, the common practice is to use simplified methods for estimating groundwater recharge. In the present study, a simple water balance method was used to estimate groundwater recharge in a complex geological formation, a volcanic basaltic aquifer. This method has been reported to perform reasonably well in similar geological formations. Results showed that about 23% total rainfall is annually converted to recharge in that particular area. This value correlated well with the predicted percentage recharge but was lower than those values used for past local studies in estimating potential of groundwater basins. The results therefore emphasised not only on the need for good recharge estimates but also on the consequences of water resources management locally.

**HW05/10P/D-005**

Poster

**1400-159****HYDROLOGIC CYCLE USING RADON CONCENTRATION AS AN INDICATOR OF GROUNDWATER IN THE SMALL CATCHMENT OF THE TOHTSURU MARSHLAND, EASTERN HOKKAIDO, JAPAN**Takeo TSUCHIHARA<sup>1</sup>, Satoshi NIHIRA<sup>2</sup>, Satoshi ISHIDA<sup>1</sup>, Masayuki IMAIZUMI<sup>1</sup> (<sup>1</sup>National Institute for Rural Engineering, <sup>2</sup>Hokkaido Development Agency)

A lot of wetlands have disappeared due to human activities such as drainage, reclamation and deforestation for cultivating agricultural land. Although the importance of wetlands has been widely recognized, the basic components of wetlands are not sufficiently understood. The hydrology of a wetland system is fundamentally involved with their formation and persistence. Nevertheless, the hydrology of wetland systems is complicated by geographical conditions. In particular, the groundwater input to a wetland is generally considered one of the most difficult components to quantify. The estimation of water balance in wetland hydrologic cycles has been requested strongly in order to take effective countermeasures for preservation of wetlands. In this study, investigation and analysis for hydrologic cycle using radon concentration as an indicator of groundwater revealed a hydrologic system with a 1.58 km<sup>2</sup> catchment area in Tohtsuru marshland, eastern Hokkaido. The hydrologic system consists of a swamp of 0.5km<sup>2</sup> surface area, 3 small recharge rivers and Uenbetsu

discharge river. Water flows between the Uenbetsu River and the swamp is interchanged due to difference between river and swamp levels. Radon-222 is a radioactive gas that is soluble in water. The concentration of radon dissolving in groundwater is extremely more than that in surface water because radium-224, which is the source of radon, is ubiquitously included in the material of aquifers such as soil and rock. This difference of solubility enables radon concentration to be an indicator to evaluate the contribution of groundwater in a hydrologic cycle. The measurement of radon concentration at survey points of a 100-m grid system in the swamp and every 100 m along small recharge rivers revealed the distribution of a spring in the marshland. Marshland basin model with a radon mass-balance equation is introduced to quantify the groundwater input to the swamp. The ratio of groundwater to the total recharge volume of the river was calculated at 73.7%. The water balance model with a three-layered tank model to calculate recharge from the 3 small rivers and an exchange model to calculate interchange of water between the Uenbetsu River and the swamp was constructed to confirm the results of the marshland basin model. The results of simulation show that the ratio of groundwater volume to this river volume was 74.7%. This good agreement between the results from the marshland basin model and the water balance model confirms the effectiveness of the investigation and analysis using radon concentration.

**HW05/10P/D-006** Poster **1400-160**

#### MODELING GROUNDWATER REMEDIATION

Khaled Ismail HAMZA (Department of Civil, The Hashemite University)

Assessment of contaminant migration and remedial options are crucial due to the increased environmental problems related with long term groundwater pollution. Groundwater flow simulation models are commonly used to simulate hydraulic conditions in an aquifer. They are also useful in the design of aquifer remediation system where the remediation technology used is pump and treat. To that end a two-dimensional vertical cross-sectional model is developed taking into account reference density concept. Governing equations are combined into two nonlinear coupled partial differential equations in only two variables namely, the concentration and the equivalent freshwater. Dispersion coefficient are taken to be scale and velocity dependent which increases the nonlinearity of the problem. The concept of variable-density fluid flow, in which the fluid density is affected by the presence of pollutant, is considered. Numerical integration is carried out using the Gauss method. The dispersion tensor is dependent on the velocity and is updated after each iteration. The model is able to simulate groundwater's aquifer cleanup using pump-and-treat method. It is capable to construct equi-concentration lines and equi-potential lines with different conditions under transient and steady state conditions. Polluted zone is clearly described.

**HW05/10P/D-007** Poster **1400-161**

#### CAUSES AND EFFECTS OF ARSENIC CONTAMINATION IN DRINKING WATER IN WEST BENGAL: A PUBLIC HEALTH ISSUE

Debashis CHATTERJEE, Joydev JANA, Sudip Jyoti SAHU, Rupa BHATTACHARYYA, Bibhas NATH, Sudipto CHAKRABORTY (Department of Chemistry, University of Kalyani, Kalyani, India)

High arsenic groundwater is widely reported in the Holocene sedimentary aquifers of the Bengal Delta Plain, BDP (West Bengal, India and Bangladesh) causing serious threat to the supply of safe drinking water. Manifestations of skin lesions, cancer and other toxic exposures are envisaged among the affected population. The arsenic content ( $>50 \mu\text{g/L}$ ) of the contaminated aquifers are far above the recommended Indian and Bangladesh drinking water standards ( $50 \mu\text{g/L}$ ) as well as the WHO guidelines ( $10 \mu\text{g/L}$ ). The scale of the problem is therefore serious and unprecedented. Groundwater chemistry demonstrates that the water is generally fresh exhibiting Ca-Mg- $\text{HCO}_3^-$  nature predominantly and the acid-base equilibrium of the system is well controlled. The nitrate and sulphate content is generally low to very low indicating the anoxic environment. High alkalinity of the groundwater in the contaminated wells is by and large associated with relatively high DOC reflecting the microbial degradation of organic matter in the sediment. Absence of dissolved oxygen and low to very low Eh further confirms the prevalent anoxic conditions in the system. This facilitates the anaerobic microbial processes favored by the relatively high groundwater temperature of the BDP. Arsenic and iron seldom shows a unique relationship. The vast majority of the arsenic contaminated water on regional basis exhibits positive correlation with high iron concentration. On the contrary, high iron enriched water does not necessarily contain high arsenic. Dissolved Fe(II) and As concentration show positive correlation with DOC. Therefore, arsenic may be derived as a consequence of desorption and dissolution of oxy iron hydroxides, originally precipitated as weathered product during land formation. The release of the sorbed arsenic into the groundwater occurs during iron reduction. The process is driven by microbial metabolism of sedimentary organic matter and locally developed reducing conditions. Arsenic is introduced into the alluvial aquifers in the soluble state during sediment transportation from upper catchment and subsequently deposited (mostly oxidized form) on secondary iron/aluminium/manganese phases in the deltaic plain. Grain size of the aquifer sediments, concentration and allocation of microbial activity as well as the role of terminal electron acceptors across the fluid interface of the mineral grains assist in the micro scale control and release of arsenic, the redox sensitive species. The microbial cycling of redox sensitive species (Fe(II) / Mn(II)) is the key player for such environmental processes.

**HW05/10P/D-008** Poster **1400-162**

#### GEOELECTRIC STUDY ON THE FACTORS CONTROLLING THE GROUNDWATER OCCURRENCE IN THE AREA NORTH OF NEKHL, CENTRAL SINAI, EGYPT

Nasser Mohamed HASSAN<sup>1</sup>, Talaat A. ABDELLATIF<sup>2</sup>, Mohamed Abbas MABRUK<sup>2</sup>, Abdallah El-Abasery ABDELRAHMAN<sup>2</sup> (GEOPHYSICS DEPT., FAC. OF SC., AIN SHAMS UNIV., GEOPHYSICAL EXPLORATION DEPARTMENT, DESERT RESEARCH CENTER, CAIRO, EGYPT.)

Exploration for groundwater in anisotropic aquifers, such as carbonates, requires accurate identification of the lithologic changes and delineation of the structural elements with the associated features. According to borehole data, groundwater exists within the carbonate rocks that dominate the area lying to the north of Nekhl, Central Sinai. The present geoelectrical sounding survey was carried out in two selected sites (Abu Hamth and El Bruk areas) lying to the north of Nekhl with the purpose of delineating the lithological and structural factors that contribute to the groundwater flow and accumulation in that area. A total of 58 vertical electric resistivity soundings (VES) were distributed along the selected sites. The resistivity sounding data has been qualitatively and quantitatively interpreted. The qualitative interpretation gave information about the number and continuity of the layers throughout the area. The data of the existing boreholes was used to construct the initial model for the quantitative interpretation. Electrical resistivity mapping was carried out at EL Hassana area with the purpose of verifying and delineating some marked features. Two-dimensional resistivity imaging profile (electrical tomography) was measured at EL Hassana area in NNW-SSE direction along a distance 246m in order to investigate the shallow structural elements that contribute to the groundwater occurrence in the study area.

**HW05/10P/D-009** Poster **1400-163**

#### THE CONTRIBUTION OF SHALLOW GEOPHYSICAL INVESTIGATIONS IN DELINEATING THE HYDROGEOLOGICAL MODEL FOR THE SHALLOW AQUIFER IN WADI EL NATRUN AREA, WESTERN DESERT, EGYPT

Nasser Mohamed HASSAN<sup>1</sup>, Ahmed Ragab ALLAM<sup>2</sup>, Ahmed Moustafa ABDEL GAWAD<sup>1</sup>, Abdallah Ibrahim AMMAR<sup>2</sup> (GEOPHYSICS DEPT., FAC. OF SC., AIN SHAMS UNIV., RESEARCH INSTITUTE FOR GROUNDWATER, MINISTRY OF IRRIGATION AND WATER RESOURCES, EGYPT.)

Wadi El Natrun area is located at the western part of the Nile Delta, about 86 km northwest of Cairo city, parallel to Cairo-Alexandria desert road. This area belongs to the arid zones, where the groundwater is considered the main water source. The present work deals with the building of the hydrogeological model of the study area based on the available hydrogeological data and the obtained geophysical results. Forty three vertical sounding stations were measured throughout the study area. Quantitative interpretations were done through the analysis of the field curves in terms of electric layers of specified thicknesses and resistivities, then constructing the geoelectric cross sections along the layout of the electrical profiles. The quantitative interpretations revealed the presence of five geoelectric layers forming the shallow section of the study area. The well log data of fifteen wells selected in Wadi El Natrun area were used for the evaluation of the encountered rock units; lithology, shale content, porosity and water saturation. Results were represented in different isoparametric maps for the encountered geoelectric layers. These maps were used for integrated subsurface geologic and hydrogeologic evaluation. Among the encountered five geoelectric layers, the second, third and fourth layers reflect the main water unconfined aquifer in the study area. The constructed hydrogeological model for the second layer, which is the best layer with the highest groundwater potentiality, revealed that the flow direction of groundwater is from the NE (high velocity) and from the SW (low velocity) toward the central part of the study area. Also the area will be dry gradually from the southwestern to the northeastern directions and its expected limitations will be from the southeastern and eastern directions. Recommendations were made for future production wells and pumping rates to avoid fast depletion of the shallow aquifer of Wadi El Natrun area.

**HW05/10P/D-010** Poster **1400-164**

#### THE EVOLUTION CHARACTERISTICS OF GROUNDWATER IN SHULE RIVER BASIN AND THEIR EFFECT ON ECO-ENVIRONMENT

hanzhang BAO, tangdong YAO, shiyin LIU, anxin LU (Laboratory of Ice Core and Cold Regions Environment, CAREERI, CAS)

Shule River Project, which supported by loan of World Bank, is an integrated project for agricultural development and immigrant allocation in Hexi Corridor, west of China. The whole construction will be built up in 2005a. In view of global climatic changes and the executing of the project, the change of water resources of the basin in space-time distribution and the interaction between surface water and ground water are more intensive. Based on the long-term hydrological, climate and regular groundwater observation data, the evolution characteristics of groundwater are studied by using water budget model and groundwater flow model in this paper. The results illustrate that groundwater system of the basin now is in a period of great variation. In the basin, hinge project of Changma reservoir and long-distance canals have been finished. The artificial hydraulic irrigating project took place of natural river system. Yield of groundwater heavily increases with the expanding of immigrant allocating areas and land reclamation. All these above lead to the recharge and discharge condition of groundwater changed obviously, and the process of circulation and conversion between surface water and groundwater are much faster than ever. So the quality and quantity of groundwater, dynamic characteristics of groundwater varied correspondingly. Furthermore, along with the adjustment of groundwater system, groundwater change has led to structural failure of region eco-environment. The main environmental problems in the basin, such as everglade atrophy, plant degradation and land desertification, which are all getting more and more serious, are also studied in this paper.

**HW05/10P/D-011** Poster **1400-165**

#### GENETIC ALGORITHM BASED DESIGN FOR DRAINAGE WELL ARRANGEMENT

Takeshi SATO<sup>1</sup>, Takao SUZUKI<sup>2</sup> (Dept. of Civil Engineering, Gifu University, Dept. of Civil Engineering, Gifu National College of Technology)

Genetic algorithm was applied to determining arrangement and number of deep wells for groundwater drainage from excavation area of an underground parking station construction. The site locates in central area of a downtown of which groundwater level stands near the surface. Environmental assessment required suitable drainage to minimize the impact of deep well technique for withdrawal of groundwater and decrease of the level. This is a case study of genetic algorithm application to engineering practices in decision making from some alternatives of arrangement and number of deep wells.

**HW05/10P/D-012** Poster **1400-166**

#### GROUNDWATER POLLUTION VULNERABILITY AND GROUNDWATER PROTECTION STRATEGY FOR THE OWERRI AREA, SOUTHEASTERN NIGERIA

Ibe Kasimir MADUABUCHI, G. I. NWANKWOR, S. O. ONYEKURU (Head, Department of Geology, Federal University of Technology)

The vulnerability to pollution of the Owerri regional water-supply in, Nigeria, was assessed as the basis for proposing an appropriate strategy for protecting the groundwater resources. The vulnerability assessment was accomplished using the LeGrand, GOD, SIGA, and DRASTIC computer models. Techniques of the models generally involve parameter-rating and point-count systems, based on the evaluation of various hydrogeologic parameters in relation to their capacity to influence the flow of contaminants in the groundwater system. The Owerri study area is generally flat and the amount of groundwater recharge is relatively high. The area is underlain by predominantly sandy strata in the north, which grade into gravelly sequences toward the southwest. The southeastern part of the area is underlain in part by a thick clayey facies that thins and interfingers into the gravelly strata. Effective hydraulic conductivity ranges from  $5.6 \times 10^{-9}$  -  $1.44 \times 10^{-3}$  m/s, the higher value being in the coarse sand and gravel units. The depth to the water table is about 60 m in the north and decreases southward, to less than 20 m; the hydraulic-head gradient is 9-22%. The southwestern part of the Owerri area including the Owerri metropolis have a high vulnerability, to groundwater pollution and therefore are areas where waste disposal site should not be located. The northern and southeastern have moderate and low vulnerabilities, respectively, and carefully parts, selected and engineered sites within those area could be considered for future waste disposal. Policies should be instituted to facilitate the closing of pollution sources in area of high vulnerability such as open disposal pits, leaking petrol stations, discharge of effluents from industries, and use of pit latrines and to locate future disposal site in areas of lower vulnerability.

HW06

Monday, July 7 - Tuesday, July 8

**ISOTOPE TRACERS IN WATER CYCLE MODELS (IAHS/ICT, IAEA)**

Location: Site C, Room 31

Monday, July 7 AM

Presiding Chair: J.J. Gibson

HW06/07A/C31-001

0910

**HOW TO ESTIMATE THE MEAN RESIDENCE TIME OF WATER IN A CATCHMENT? RESULTS FROM A MODEL COMPARISON AND THE SIGNIFICANCE OF ISOTOPE RECORDS**

Stefan UHLENBROOK, Falk SCISSEK (Institute of Hydrology, University of Freiburg)

The mean residence of the water is a crucial parameter to characterize a hydrological system. In a previous study, the spatial and temporal (event and seasonal time scale) variability of major runoff components and residence times in the mountainous Brugga basin (40 km<sup>2</sup>, Black Forest, Germany) were examined. For this purpose, time series of the tracers <sup>18</sup>O, <sup>3</sup>H, CFCs, dissolved silica and major anions and cations were analyzed over the period 1995-1998 (Uhlenbrook et al. 2002, WRR). Residence times were estimated using classical lumped-parameter approaches. It was found that the shallow groundwater is the predominant system and originates from the upper drift and debris cover. For this paper longer isotope records (1995-2002) could be analyzed and the following questions are examined: (i) What is the potential benefit of longer records to estimate the residence-time distribution and the mean residence time? (ii) What is the influence of the modeling time step (monthly vs. bi-weekly), generation of the isotope-input data, and different infiltration/recharge modeling approaches for the residence-time estimation? (iii) How good is the performance of simple estimation techniques, as for instance the amplitude-dampening method? (iv) What are the main reasons for the uncertainty of the residence-time estimation, and how could these be reduced? Using different lumped-parameter models, it was found that the analyses of the longer isotope records resulted in about the same residence-time estimations for the whole Brugga catchment (26 months) and the shallow groundwater (3 years). Thus, previous results could be confirmed. Using the longer records did not reduce the uncertainty interval of approximately ±6 months. The influence of shorter modeling time steps was negligible. It is interesting to note that the simple amplitude-dampening method resulted in only slightly different estimations of the mean residence times. This method is 'like the used lumped-parameter model' based on an exponential distribution of residence times. In addition, the significance of the infiltration/recharge modeling became obvious. In consideration of this fact, some shortcomings of the lumped-parameter approach were investigated, and the importance of a correct isotope input into the investigated hydrological systems was highlighted. For the study area, in particular, the problematic estimation of the spatially and temporally variable snowmelt input and soil-water movement caused uncertainties. Finally, new modeling strategies for isotope modeling that contain an improved process-realistic description of water movement in the investigated system are discussed.

HW06/07A/C31-002

0930

**EXAMINATION OF MRT MODELING CONCEPT THROUGH A FIELD MEASUREMENT OF SPATIAL VARIABILITY IN GROUNDWATER SEEPAGE ISOTOPIC COMPOSITIONS**Taro UCHIDA<sup>1</sup>, Shyusuke MIYATA<sup>1</sup>, Yuko ASANO<sup>2</sup>, Yuichi ONDA<sup>2</sup>, Takahisa MIZUYAMA<sup>1</sup> (<sup>1</sup>Graduate School of Agriculture, Kyoto University, <sup>2</sup>Institute of Geoscience, University of Tsukuba)

Mean residence time (MRT) modeling is a useful tool for characterization of catchment behavior. Kirchner et al. (2000, Nature, 403) showed that the residence time distribution of stream water had very long and fractal tail, suggesting that the stream water consists of diverse residence time water. This result suggests two possibilities; (1) there is underground large well-mixed reservoir in hillslopes and (2) diverse flowpaths contribute to rainfall-runoff process in hillslopes. However, the processes, which produced these residence time distributions, are poorly understood. While spatial aspects of flowpath dynamics have been examined, the classifications of flowpaths in hillslopes have been simple (i.e., a shallow soil flowpath, flow along the soil-bedrock interface and flowpath in the bedrock). Thus, most of previous studies have not paid attention to the diversity and the distribution of flowpaths in the hillslope that ultimately control residence time distribution. Here we measured the spatial and temporal variability of flow rate, dissolved silica concentration, temperature, and isotopic composition of groundwater seepage in a small first-order catchment in central Japan. Our measurements showed that there are large spatial variations in the recession curve of hydrograph, standard deviation of dD and amplitude of temperature in groundwater seepage. The spatial distribution of mean dissolved silica concentration ranged from 6 to 14 mg/L, although the seasonal variation of dissolved silica concentration at each groundwater seepage was relatively small (<2.5 mg/L). The recession curve of hydrograph, the standard deviation of dD and the amplitude of temperature decreased with increasing with the mean silica concentration, indicating that the longer mean residence time of the groundwater seepage had a deeper source. These results imply that there are diverse and discrete flowpaths in the hillslope, and that these flowpaths are not well mixed before entering the stream channel. We also measured the first-order streamflow hydrograph at five adjacent catchments. An examination of hydrograph shape would there was very small spatial variation of streamflow response, suggesting that would suggest that these catchments were functionally similar, suggesting that diverse and discrete flowpath systems may commonly control the stream flow response in this region. According to these results, it concluded that the very long and fractal tail of residence time distribution was produced by diverse and discrete flowpath.

HW06/07A/C31-003

0950

**EXAMINATION OF THE ASSUMPTIONS IN ISOTOPE-BASED HYDROGRAPH SEPARATION: A VIRTUAL EXPERIMENT APPROACH**

Jeffrey J. MCDONNELL, Markus WEILER (Dept. of Forest Engineering)

The assumptions for hydrograph separation associated with spatially invariant end members are well known. Unfortunately, due to expense and difficulty of collecting the large amounts of data necessary to understand the limitations of the approach, the assumptions are rarely examined in detail in experimental studies. We present a new set of 'virtual' hydrograph separations where isotope tracing is performed within a physically-based hydrologic model. The spatial and temporal variability of water components are examined in terms of how these result in mixing internal to the catchment. We define virtual experiments as numerical experiments with a model driven by collective field intelligence stemming from field-based isotope tracing experiments. We analyse how the depth distributions of saturated hydraulic conductivity and drainable porosity, soil depth variability, as well as mass exchange between

the saturated and unsaturated zone influence the results of hillslope and watershed scale investigations. We also show how these controls combine with the history of different rainfall signatures to produce observed hillslope and catchment mixing. We argue that this virtual isotope hydrograph separation experimental approach may provide a well-founded basis for defining the limitations of spatially invariant end member hydrograph separation and under what circumstances it may be best applied.

HW06/07A/C31-004

1030

**A NEW TRANSFER FUNCTION BASED HYDROGRAPH SEPARATION MODEL**Kevin James MCGUIRE<sup>1</sup>, Markus WEILER<sup>1</sup>, Brian MCGLYNN<sup>2</sup>, Jeff MCDONNELL<sup>1</sup> (<sup>1</sup>Department of Forest Engineering, Oregon State University, <sup>2</sup>Department of Land Resources & Environmental Sciences, Montana State University)

Isotope based hydrograph separation has been an important tool for defining water source components in headwater catchments. One major limitation to the further development of these techniques has been the often observed large temporal variations in rainfall isotope composition through the event. Here we present a new hydrograph separation approach (TRANSEP) that uses the temporal variability of the rainfall isotopic composition to more accurately determine hydrograph components and to provide transfer functions for both the tracer and runoff responses separately. TRANSEP overcomes many limitations of traditional two-component hydrograph separations (e.g. tracer travel time) by integrating the instantaneous unit hydrograph and isotope hydrograph separation techniques. Separate functions that describe the lumped transfer of runoff, event water, and pre-event water to the stream were derived and used to interpret hydrograph components. We argue that TRANSEP provides a new and better method for extraction of runoff generation information.

HW06/07A/C31-005

1110

**STABLE ISOTOPIC COMPOSITIONS OF SUBSURFACE WATER AND WATER VAPOR IN THE ATMOSPHERE AT FORESTED REGIONS**

Maki TSUJIMURA, Yuichi ONDA, Risa SASAKI, Tadashi TANAKA (Institute of Geoscience, University of Tsukuba)

The data on stable isotope in subsurface water and water vapor in the atmosphere from the field has not been enough for modeling of the water cycle and isotope processes at the local to regional scales. We have performed tensiometric observation and isotopic study of subsurface water in the slope to clarify the formation process of stable isotopic ratio profile of subsurface water in forested catchments. Isotopic analysis of deuterium and oxygen-18 for subsurface water in the slope revealed systematic trend in a vertical profile direction in catchments where vertical subsurface flow is dominant in hillslopes. The monthly observed isotopic ratios of subsurface water showed a large variation in response to the rainfall and evapotranspiration above the depth of 50 to 70 cm, and the isotopic ratio was homogenized and the temporal variation of observed data were dampened below the depth of 70 cm. Also, the average stable isotope ratios in subsurface water was a little higher than the volume weighted mean of rainfall because of evaporation from the soil surface, though the evaporation rate itself was low in the forested area. The stable isotope in water vapor in the atmosphere and soil water was monitored synchronously to investigate the stable isotope profile throughout the soil and atmosphere. Stable isotopic compositions in the water vapor at the height of 5 cm above the soil surface were affected much by the evaporation from the soil water. The contribution ratio of evaporated water vapor from soil surface to the atmosphere was estimated to be from 16 % to 55 % based on the observed stable isotopic ratio of water vapor and soil water under a humid condition in winter season. More data should be necessary for modeling the formation process of stable isotopic compositions in water near the soil surface in the forested regions.

HW06/07A/C31-006

1130

**CONTINUOUS SOIL WATER ISOTOPE OBSERVATIONS AND MODELING APPROACHES AT A FOREST METEOROLOGICAL EXPERIMENTAL SITE IN GERMANY**Paul KOENIGER<sup>1</sup>, Lutz JAEGER<sup>2</sup>, Helmut MAYER<sup>2</sup>, Christian LEIBUNDGUT<sup>1</sup> (<sup>1</sup>Institute of Hydrology, Albert-Ludwigs University Freiburg, Germany, <sup>2</sup>Meteorological Institute, Albert-Ludwigs University Freiburg, Germany)

At the forest meteorological experimental site Hartheim (Pinus sylvestris) in southwestern Germany, soil water isotope concentrations (deuterium and oxygen-18) were measured biweekly over a three-year period to investigate unsaturated water flow and recharge mechanisms. The study site is characterized by small amounts of rainfall and relatively high evapotranspiration. A human-influenced lowering of the groundwater level has led to the classification of the area as almost semi arid. The soil layer is characterized by a low water storage capacity and a high permeability. The root depth is about 40 cm. A distance of 7 m to the groundwater table suggests that capillary rise and groundwater uptake are negligible. Water extraction for isotope analyses was carried out using the toluene distillation method and soil water contents were analyzed gravimetrically. An estimation of isotope concentrations in rainfall and groundwater together with micrometeorological observations allow a qualitative and quantitative description of hydro-meteorological frame conditions. In order to complete the study and evaluate the influence of evapotranspiration on water movement, actual evapotranspiration was calculated using the Bowen Ratio Energy Balance method. Continuous isotopic observations at 2, 20 and 40 cm depth in the soil layer indicate a sharp decrease of seasonality with depth, allowing an estimation of the depth of dampening of the isotope signature, to a value of 1% by 200 cm. Flow velocities calculated using a sine curve fit resulted in values of 1-2 cm per day. These values indicate a rather slow matrix flow but correspond with investigations summarized by other authors. In contrast to the monitoring, two deeper profiles (150 cm) that were taken in August and November 1999 showed that the isotopic signal changed significantly. This leads to the conclusion that additional rapid water movement through macro pores was occurring to the entire depth of the profiles. An interpretation of the observed field data using a lumped parameter approach and sine wave fitting allows an discussion of flow velocities and transport processes. The results enlighten mechanisms that are usually not considered in regional and macro scale modeling approaches.

HW06/07A/C31-007

1150

**MINING LAKES AS GROUNDWATER DOMINATED HYDROLOGICAL SYSTEMS: ASSESSMENT OF THE WATER BALANCE OF LAKE PLESSA 117 (LUSATIA, GERMANY) BY USING ISOTOPE TRACERS AND SEEPAGE METER MEASUREMENTS**Hilmar HOFMANN<sup>1</sup>, Kay KNÖLLER<sup>2</sup>, Dieter LESSMANN<sup>1</sup>, Klaus JÖHNK<sup>1</sup>, Uwe GRUENEWALD<sup>1</sup>, Brigitte NIXDORF<sup>3</sup> (<sup>1</sup>Brandenburg University of Technology Cottbus, <sup>2</sup>UFZ-Center for Environmental Research Leipzig-Halle)

Lusatian mining lakes are characterised by extreme physical and chemical conditions, e.g. low pH (iron buffered), high conductivity, simply structured food webs, and primary

production limitation by phosphorus or inorganic carbon. These lakes are mainly fed by groundwater inflow. Due to their distinct hydrological regime, mining lakes differ considerably from natural lakes with consequences for mixis, hydrochemistry and biology. The aim of the study was to quantify the groundwater inflow for the assessment of water balance calculations by the use of isotope tracers and to estimate the influence of the groundwater on lake water chemistry. Both are of fundamental importance for the ecosystem. With a groundwater model and the results of seepage meter measurements, the groundwater inflow was calculated directly and compared with the results of the hydrological water balance from direct in- and outflow measurements. These results were verified using the environmental isotopes  $\delta^{18}\text{O}$  and  $\delta^2\text{H}$  by employing an autonomous water balance. Through separate sampling of the individual components, groundwater inflow and -outflow, surface in- and outflow and precipitation, the quantitative distribution of ground- and surface water in the lake was possible. It could be shown that the groundwater model and the environmental isotope water balance method lead to comparable results. The seepage meter data showed strong heterogeneity. The water balance results indicate that the direct groundwater inflow is about 60% of the total inflow to the lake. The groundwater outflow is around zero, which was also verified by the groundwater model. This represents the influence of the groundwater on the lake water chemistry.

HW06/07A/C31-008

1210

#### BLACK-BOX MODELS FOR THE INTERPRETATION OF ISOTOPE DATA IN DIFFERENT GROUND WATER SYSTEMS (MONO- AND BI-POROUS) TO DETERMINE SOME HYDROLOGICAL PARAMETERS

Piotr MALOSZEWSKI (GSF-Institute of Hydrology, D-85764 Neuherberg, GERMANY)

The paper presents different types of black-box models which are applicable for the interpretation of environmental tracer data in different ground water systems (mono- and bi-porous). Black-box models have found relatively wide application in isotope hydrology, mainly due to their simplicity and reduced number of fitting parameters. The use of these models requires the environmental tracer concentrations measured, in most cases as a functions of time, in the input (recharge zone, infiltration area) and in the output (i.e. springs, streams, pumping/observation wells, etc.) of the system. Generally, only limited hydrological and geological information about area under investigation is needed. However, this knowledge has to be sufficient to construct a conceptual model of water flow through the system and in turn, to decide which type of black-box model (or their combination) should be used. Each model is defined by its own transit time distribution function,  $g(t')$ . The function  $g(t')$  describes the whole spectrum of transit times of single tracer particle ( $t'$ ) on the pathway between input and output. Most frequently used are the models, which were developed for mono-porous mediums (fully saturated, include only mobile water). These models were constructed assuming piston-flow (PFM), exponential (EM), combined exponential-piston flow (PFM) or dispersive (DM) types of transit time distributions. When the isotope technique is used in so called bi-porous mediums then completely different models has to be applied. Bi-porous medium exists when the water flows through the unsaturated zone (mobile water in capillaries or channels and quasi stagnant water in the matrix), in fissured aquifers (mobile water in fissures and immobile in micro-porous matrix) and by water flow through aquifer (mobile water) surrounded by aquitard (immobile water). Near advection and/or dispersion in the mobile phase, the diffusive transfer of tracer mass between mobile and immobile water and diffusion process in immobile water have to be taken into account. The paper presents three black-box models which can be used in such a cases: Parallel Fissure Dispersion (PFDM), Single-Fissure Dispersion (SFDM) and Single-Fissure Piston Flow (SFPFM) model. Their parameters, limitations and applicability are discussed. The main parameter of all models is the mean transit time of water through the system. Other, additional, parameters, depend from the type of model used. All model parameters are determined by fitting the theoretical output concentrations (calculated for known input function) to the tracer concentration measured. By applying the model some additional practical information such a water velocity, volume of water in the system, portion of water flowing through macro-pores (channels) can also be found. The practical applications of a new models for the interpretation of isotope data obtained: (i) in lysimeter experiments within the unsaturated zone under natural flow conditions, and (ii) in the water flowing through the aquifer situated within the aquitard, are additionally shown.

Monday, July 7 PM

Presiding Chairs: J.J. Gibson, J. McDonnell

HW06/07P/C31-001

1400

#### A FORMATION PROCESS OF STABLE ISOTOPIC COMPOSITIONS OF OXYGEN AND HYDROGEN IN SOIL WATER AND ESTIMATION OF AVERAGE RECHARGE IN THE UNSATURATED ZONE OF THE KANTO LOAM, JAPAN

Shiho YABUSAKI<sup>1</sup>, Norio TASE<sup>2</sup>, Maki TSUJIMURA<sup>2</sup>, Atsuko SUGIMOTO<sup>3</sup> (Doctoral Program of Geoscience, University of Tsukuba, <sup>1</sup>Institute of Geoscience, University of Tsukuba, <sup>2</sup>Center for Geological Research, Kyoto University)

In recent years, it has become important to make clear the soil water movement for preventing the groundwater pollution and establishing sustainable water use. Using the stable isotopic compositions of oxygen and hydrogen has been pointed out as one of the effective methods to estimate the soil water movement. The soil water in the loamy soil were sampled at University of Tsukuba, Japan, eleven times from April to November in 2001, and groundwater and event precipitation are also collected. The  $\delta^{18}\text{O}$  and  $\delta\text{D}$  were analyzed for all samples, and the tritium analysis is carried out for samples of precipitation and groundwater. In the vertical profiles of isotopic compositions in soil water, the variations of isotopic composition near the soil surface are very large, because soil water is affected by the evaporation and precipitation. The variation, however, decreases gradually as the soil depth. Isotopic compositions become almost constant near the water table. Furthermore, some cyclic variations are observed in the vertical profiles of isotopic compositions of soil water. The time series variations of isotopic composition in soil water and precipitation suggest that the isotopically heavy peak of soil water was formed in summer period, and it moved downward during fall season when intensive rainfall happened. It is also indicated that the piston flow is dominant in this study site. Using the results of migration length of isotopic composition in soil water, average recharge is about 658 mm, which is close to other places of the loamy soil in Japan. The result from Displacement Flow Model explains the observed results well, and quantitative estimation of the groundwater recharge could be possible by the model. The data of isopleth indicate that groundwater recharge occur under the condition that rainfall amount exceeds 50 mm per event, which is agree with the result of  $\delta$  diagram of different size event precipitation and groundwater. The isotopic composition in soil water can be used for estimation of the soil water movement in these places such as depositing of loamy soil mainly in Japan.

HW06/07P/C31-002

1420

#### SUSTAINABLE GROUNDWATER ABSTRACTION BASED ON THE CALIBRATION OF NUMERICAL MODELS USING RESULTS OF AN ENVIRONMENTAL ISOTOPE MONITORING

Klaus-Peter SEILER (GSF-National Research Centre)

Safe groundwater abstraction is mostly based on management strategies elaborated by means of validated and calibrated mathematical models; to verify this mathematical prediction, as a rule this step is followed by a water quality monitoring, because calibration does not cover all necessary extrapolation stages. This procedure leads to three challenges: 1. Mathematical modeling has to face hydraulic and geologic uncertainties, which are often difficult to assess, and may lead to non-adapted decisions; 2. The monitoring results often lead to a passive assessment, because whenever the contaminant the exploitation site, it is too late for respective changes in the management strategies; 3. Traditional predictions often disregard the transient hydraulic behavior of many subsurface systems. All three challenges can be faced by an additional monitoring of environmental isotopes and by using the analytic results on environmental isotopes to recalibrate iteratively the existing mathematical model. This procedure was applied to elaborate an early warning system for bank-filtration and to better survey the sustainable abstraction of groundwater from the passive recharge zone, which is often transient over decades. To use this tool it is important to select the appropriate observation wells and the most sensitive environmental isotopes. In the case of deep groundwater abstraction, downstream areas proved to be more sensitive than upstream areas; with increasing observation depth,  $^3\text{H}$ ,  $^{39}\text{Ar}$  and than  $^{14}\text{C}$  in turn become the most sensitive parameter. In the case of bank-filtration, stable environmental isotopes can be used to calibrate the behavior of non-reactive and reactive contaminants as well and to set up base lines of contaminant concentration in the river to avoid groundwater contamination exceeding international health standards.

HW06/07P/C31-003

1440

#### CHARACTERISATION OF AQUIFERS IN KARSTIC TERRAIN USING STABLE ENVIRONMENTAL ISOTOPES

Ninad BODHANKAR<sup>1</sup>, K.M. KULKARNI<sup>2</sup> (School of Studies In Geology & WRM, Pt. Ravishankar Shukla University, Raipur 492010 INDIA, <sup>3</sup>Isotope Hydrology Section, International Atomic Energy Agency, Vienna AUSTRIA)

Hydrogeological investigations were carried out to study the groundwater condition and groundwater interconnections in karst terrain around Raipur. The ground elevation varies from 270 meters to 300 meters above mean sea level, and the average mean annual rainfall is about 1200 mm. The Chandi limestone of Raipur Group of Chhattisgarh Supergroup forms the major geological unit in the study area. Laterite/ shale cover, at places, overlies the limestone. Apart from conventional hydrogeological investigations, thirty-six water samples were collected from different sources like, dugwells (10), tubewells (21) and surface water bodies (05). The samples were analysed for major chemistry. Stable environmental isotope measurements for delta  $^{18}\text{O}$  and delta  $\text{D}$  were also carried out. The Piper trilinear plot reveals Ca-Mg-HCO<sub>3</sub> facies, which is characteristic of limestone aquifer. The delta  $^{18}\text{O}$  values vary from -3.14 to -0.98 for dugwells, from -3.75 to -0.7 for tubewells and from -3.2 to -0.68 for surface water bodies. The delta  $\text{D}$  values vary from -18.5 to -7.7 for dugwells, from -25.1 to -5.8 for tubewells and from -18.9 to -3.5 for surface water bodies. The coalesce of hydrogeological information, environmental isotope measurement along with chemistry data has helped to deduce a conceptual model of the hydrodynamic system as follows: (a) the soil cover over limestone, which varies from laterite to black soil, forms the shallow aquifer catering to the needs of dugwell. It extends up to a depth of 10 meters and at places is intercalated with yellow shale. The yellow shale is impervious thus forms an aquiclude, as deduced from the depleted delta  $^{18}\text{O}$  and delta  $\text{D}$  values for dugwell water, (b) weathered limestone zone, 2 meters thick, and (c) compact limestone at the bottom, which forms the major aquifer supplying to the tubewells. At places, the enriched delta  $^{18}\text{O}$  and delta  $\text{D}$  values for tubewell water is indicative of rapid recharge to the aquifer due to karstification. Thus, development of secondary porosity in limestone makes the hydrological situation more complex to understand and model the groundwater hydrodynamics.

HW06/07P/C31-004

1500

#### USING THE TRITIUM/HELIUM AGE DATING METHOD TO CHARACTERISE TWO RIVER RECHARGED AQUIFER SYSTEMS IN GERMANY

Massmann GUDRUN<sup>1</sup>, Juergen SUELTFUSS<sup>2</sup>, Andrea KNAPPE<sup>3</sup>, Asaf PEKDEGER<sup>1</sup> (Free University of Berlin, <sup>2</sup>University of Bremen)

The T-He age dating method uses the ratio of the concentration of radioactive tritium ( $^3\text{H}$ ) derived from atmospheric nuclear bomb testing and its decay product Helium ( $^3\text{He}$ ) in the groundwater to determine a groundwater age, i.e. the time passed since the water had its last contact with the atmosphere. At the Free University of Berlin, hydraulic and hydrochemical processes accompanying bank-filtration are currently examined at two very different locations: In metropolitan Berlin and the rural Oderbruch polder region. The city of Berlin enhances bank-filtration through well galleries located adjacent to the surface water system. The spatial and temporal development of the bank filtrate is studied in cooperation with the Berlin Waterworks and the Berlin Centre of Competence for Water at several exemplary piezometer transects. The system generally behaves highly transient due to continuously changing pumping regimes. At the gallery Lake Wannsee, the well filter screens are pumping water from 3 different glacial sand layers separated by aquitards. The well water is a mixture of very old deeper groundwater, medium old water from the middle layer and very young bank-filtered water. The Oderbruch is located north-east of Berlin aside the river Oder. Intensive melioration activities in the past 250 years converted the former swamp into a fertile, agricultural region and lead to the permanent infiltration of river water into the shallow, confined aquifer. Compared to Berlin, the infiltration is a long-term, very stable process. The groundwater is getting older with increasing distance and travel-time from the river. The concentration of "stable" tritium (sum of  $^3\text{H}$  and tritogenic  $^3\text{He}$ ) increase from the river inland reflecting the decrease of  $^3\text{He}$  in the atmosphere from the early 60's onwards. Peak concentrations are encountered in 2.1 km river distance whereas further inland (3.4 km river distance) old water which infiltrated prior to the nuclear bombing peak is encountered. In addition, the groundwater has a high radiogenic  $^4\text{He}$  concentration which also indicates that the groundwater is more than a few decades old. Even further inland, in the central polder areas, the groundwater is unconfined and continuously recharged to some extent by percolating water infiltrating through shrinkage fissures in the overlying dried alluvial loam. The water is a mixture of young seepage water and very old bank filtrate, the resulting "mixed" T-He age is getting younger again. The T-He method was successfully applied to support estimated groundwater ages derived from tracer analysis (e.g.  $^2\text{H}$ ,  $^{18}\text{O}$ , EDTA, Gd) at both locations. In the Oderbruch, the T-He ages were used to calibrate a flow model. The method also proved to be a very good indicator for the identification of mixing processes.

HW06/07P/C31-005

1520

## REGIONAL MODELLING OF ISOTOPE EXCHANGE DURING EVAPORATION

John J. GIBSON<sup>1</sup>, S. Jean BIRKS<sup>2</sup> (Water & Climate Impacts Research Centre, National Water Research Institute, P.O. Box 3050, University of Victoria, Victoria BC V8W 3P5 Canada, <sup>2</sup>Department of Earth Sciences, University of Waterloo, Waterloo ON Canada)

Tracking and modelling the stable isotope content of water as it passes through the continental water cycle requires use of algorithms to account for the well-known isotope enrichment effects that accompany open water and soil evaporation. While the primary forcings on the isotope enrichment processes have been well documented (Craig and Gordon 1965; Allison et al. 1983), model application at the continental scale has largely been limited by availability of regional isotopic datasets. This study demonstrates use of the Global Network of Isotopes in Precipitation database in combination with global climatological fields to obtain a first approximation of atmospheric conditions that control the isotope enrichment process and their global variability. This new conceptual model (Gibson 2002) predicts changes in the slope of the Local Evaporation Lines that are consistent with regional observations from north America and northern Eurasia. Although a simplified approach, the model helps to understand broad trends and systematic variability in evaporative enrichment using monthly potential evaporation, temperature, humidity, oxygen-18 and deuterium composition of precipitation. Results suggest that seasonality is a strong control on the slope of local evaporation lines in  $^2\text{H}$ - $^{18}\text{O}$  space, which is particularly important for explaining differences in enrichment behaviour in lakes across the polar regions. Allison, G.B., Barnes, C.J. and Hughes, M.W., 1983. The distribution of deuterium and  $^{18}\text{O}$  in dry soils. *J. Hydrol.*, Vol. 64, pp. 377-397. Craig, H. and Gordon, L.I., 1965. Deuterium and oxygen 18 variations in the ocean and marine atmosphere. *Stable Isotopes in Oceanographic Studies and Paleotemperatures*, E. Tongiorgi (Editor), Lab. Geologia Nucleare, Pisa, pp. 9-130. Gibson, J.J., 2002. A new conceptual model for predicting isotope enrichment of lakes in seasonal climates. *IGBP PAGES News* 10 (2): 10-11.

HW06/07P/C31-006

1540

## ISOTOPIC SIGNATURES OF SOURCE WATER AND RAIN FORMATION MECHANISM IN INDIAN MONSOON PRECIPITATION

Sourendra Kumar BHATTACHARYA, Pradeep Kumar AGGARWAL, Kshitij M. KULKARNI (Isotope Hydrology Section, International Atomic Energy Agency, Vienna)

The stable isotopic composition in precipitation reflects the composition of the moisture source and the fractionation associated with the mechanism of precipitation formation. Often these factors are too intricately linked to decipher the moisture source and identify the causes of seasonal and inter-annual variations in isotopic composition. In this context, isotopic data of New Delhi and Bombay rains (from GNIP database of IAEA) from the Asian monsoon region are investigated here to identify the signatures of moisture source and meteorological processes. In Bombay, rains occur mainly from June to September whereas New Delhi has precipitation throughout the year with peak rainfalls during July to September. The seasonal variation of Bombay rains show that isotopic ratios (in per mil) are heavier from December to May (-1 to +1) but decrease smoothly from June to September. The decrease in isotope ratio is initially associated with increase in precipitations suggesting an amount effect but later on, delta variation pattern deviates from the amount effect prediction. Co-variation plots of monthly rainfalls in New Delhi and corresponding  $\delta^{18}\text{O}$  values show that the two variables are poorly correlated. In contrast, the data for Bombay show quite different features. Though the September rainfall is much lower than July rainfall the mean monthly delta values from July to September are close to each other (~ -1.3). Interestingly, the delta values are quite low (-4.5 to -5.5) in October and November when precipitation is small. Above analysis shows that the mean isotopic compositions of monthly precipitation samples from New Delhi and Bombay do not correlate with the rainfall. Though both the stations belong to a region under the influence of the Asian Monsoon the rain forming mechanisms in these places are significantly different. The rainfall at New Delhi is controlled by north-west moving depressions with diverse routes and variable transit times over the land subsequent to their formation at the head of Bay of Bengal. The mean life-time of these stormy depressions seems to determine the rain isotopic composition through a Rayleigh mechanism. In contrast, the Bombay rains are caused by cyclonic vortices on the west coast of India with constant supply of oceanic moisture resulting in small isotopic variation over the rainy months. Analysis of the data reveals a dominant role of meteorological factors in controlling the rain isotopic composition and only a minor dependence on the amount of rain.

HW06/07P/C31-007

1600

## OBSERVATION ON RECYCLING OF WATER IN EAST SIBERIAN TAIGA

Atsuko SUGIMOTO<sup>1</sup>, Daisuke NAITO<sup>1</sup>, Kimpei ICHIYANAGI<sup>2</sup>, Naoyuki KURITA<sup>2</sup>, Yoshiyuki ISHII<sup>1</sup>, Tetsuo OHATA<sup>3</sup> (<sup>1</sup>Center for Ecological Research, Kyoto University, <sup>2</sup>Frontier Observation Research System for Global Change, <sup>3</sup>Institute of Low Temperature Science, Hokkaido University)

East Siberian taiga is a unique ecosystem, which is established on permafrost. Climate there is extremely dry (about 250mm of annual mean precipitation). Oxygen and hydrogen isotope ratios of precipitation, soil water, sap water of plants, river, surface water, and atmospheric water vapor were observed in deciduous boreal forest near Yakutsk, Russia, to investigate the water cycle in the ecosystem. Large inter-annual variation was observed in soil moisture and its stable isotopic composition, depending on summer rainfall. As we already reported, isotope signature of water in plants shows that snow melt water is essential for plants in early summer: the highest activities of plants soon after leaf unfolding in June are supported by the snow meltwater. In late summer, plants use summer rainwater when the amount of rainfall is enough, while, ice meltwater from permafrost is used as a direct water source for plants during drought. Namely, function of soil for water storage stabilizes transpiration, and it is very important for water cycle in this region. Discrepancy of the period of transpiration by plants (maximum in June) and soil thaw may also cause another time-lag for hydrologic cycle (Sugimoto et al., 2002, *Ecol. Res.*, 17; Sugimoto et al., in press, *Hydrological Processes*). Water used by plants for transpiration returns to the atmosphere. This "recycled water" may be very important as atmospheric water vapor. Since eastern Siberia is extremely far from the source area of water vapor, the isotopic composition of atmospheric water vapor is expected to show great variability depending on precipitation in the upstream area and recycling of water from the surface. Actually, the observed isotopic composition of water vapor varied largely. Oxygen isotope ratio was varied from -39 to -19 permil in delta value against SMOW, during the period from May to September in 2000. The value of d-excess of water vapor also varied: extremely high d-excess was observed during May in 2000. Isotopic variation of water vapor may reflect on the condition of surface and the isotopic composition of evaporated and transpired water vapor. Trend of oxygen isotope variation of water vapor was similar to that of transpired water by plants and precipitation. This result indicates that water in this area is on a recycling mode during summer. Isotopic composition of precipitation was also observed at Tiksi which locates near arctic ocean. Variation of the oxygen isotope ratio and d-excess in precipitation at Tiksi was also indicative of the difference in isotopic composition of water vapor. Isotopic composition of precipitation formed in the air from southwest (from inland area) was clearly different from that derived in

the air mass from northeast (from arctic ocean).

HW06-Posters

Monday, July 7

## ISOTOPE TRACERS IN WATER CYCLE MODELS (IAHS/ICT, IAEA)

Location: Site D

Monday, July 7 PM

Presiding Chairs: J.J. Gibson, J. McDonnell

HW06/07P/D-001

Poster

1400-185

## APPORTS DES TECHNIQUES ISOTOPIQUES A LA CONNAISSANCE DE LA DYNAMIQUE DES EAUX SOUTERRAINES DANS UN BASSIN TRANSFRONTALIER (BASSIN DE TAUDENNI)

Denis DAKOURE<sup>1</sup>, Ghislain (de) MARSILY<sup>1</sup>, Mustapha BESBES<sup>2</sup>, Henri SALVAYRE<sup>1</sup>, Martial DRAY<sup>1</sup> (<sup>1</sup>UNIVERSITE PIERRE ET MARIE CURIE, <sup>2</sup>ECOLE NATIONALE INGENIEUR DE TUNIS (ENT) TUNISIE, <sup>3</sup>MAS SARRAGOSSE)

La région sud-ouest du Burkina Faso partage avec le sud du Mali, un système d'aquifères sédimentaires transfrontalier, celui de la bordure sud-est de Taoudéni. L'extension ainsi que le fonctionnement de ces aquifères à forte potentialité d'exploitation demeurent imprécis, notamment en ce qui concerne l'origine, l'intensité de leur recharge et leur taux de renouvellement. A cette échelle (180.000 km<sup>2</sup> environ) la connaissance des écoulements se heurte à l'absence de piézométrie fine indispensable pour une meilleure exploitation et gestion des eaux souterraines. Cette absence est d'autant vraie qu'il existe peu ou presque pas de nivellement topographique adapté. Les circuits hydrogéologiques sont souvent longs, complexes et quelquefois profonds. La connaissance détaillée de ces circuits et de leur fonctionnement est indispensable pour en assurer une gestion optimale. Une bonne connaissance du circuit nécessite de répondre aux interrogations sur l'origine de l'eau (où), et sur la durée du circuit (quand). Les méthodes isotopiques se prêtent remarquablement à ce genre d'études. Une approche multicritère combinant entre autres techniques, la géochimie isotopique et l'hydrodynamique couplée à un essai de modélisation est utilisée pour comprendre le fonctionnement hydrogéologique de ce vaste bassin sédimentaire. Les études chimiques et isotopiques donnent une homogénéité de faciès qui ne dégage pas d'éléments convaincants pour envisager l'existence d'une circulation souterraine individualisée entre les différentes formations géologiques. Le bassin sud-est de Taoudéni dans sa grande partie contient des eaux qui se renouvellent lentement. Cette faiblesse de recharge est confirmée par l'esquisse de modélisation hydrogéologique. Cela hypothèque pour l'avenir le développement socio-économique de la région.

HW06/07P/D-002

Poster

1400-186

## ISOTOPE METHODS AND THEIR ROLE IN ANALYZING THE ALLOCATION OF WATER RESOURCES

Inom Sherovich NORMATOV (Institute of Water Problems, Hydroenergetics and Ecology, Academy of Sciences, Republic of Tajikistan)

In the conditions of hydrological situation and lack of hydrometric observations the isotope methods open wide perspectives to define more precisely the allocation of water resources. The applying of correlation of even uranium isotopes ( $\gamma = \text{U}^{234}/\text{U}^{238}$ ) and its general contents (C) in waters is perspective for defining more precisely the water balance characteristics of mountainous rivers. The waters formed or running in different hydrogeological conditions are distinguished by  $\gamma$  and C values. Having defined with the help of isotope dilution equations, the  $\gamma$  and C values in 2 merging flows before and after dislocating them, it is easy to evaluate the relative flowing part of every flow. During isotope surveying in different seasons (transition period), it is possible to evaluate the average annual flowing rate and to foresee the resources even for those rivers, which were not hydrometrically measured. We checked the advantages of uranium isotope method, having defined the forming of Panj River flowing.

HW06/07P/D-003

Poster

1400-187

## SEASONAL CHANGES IN STABLE ISOTOPE CONTENTS OF STREAM WATER IN A SMALL TUNDRA WATERSHED, EASTERN SIBERIA

Yoshiyuki ISHII<sup>1</sup>, Atsuko SUGIMOTO<sup>2</sup> (<sup>1</sup>Institute of Low Temperature Science, Hokkaido University, <sup>2</sup>Center for Ecological Research, Kyoto University)

As a part of the GAME-Siberia project, meteorological and hydrological observations concerning the basin water balance were carried out in the Siberian tundra region near Tiksi, in eastern Siberia, during the summer seasons in 1998 and 1999. To clarify how the snow meltwater and the ground-ice meltwater contribute to the hydrologic cycle in the arctic tundra basin, lateral inflow rate of the surface and subsurface water to the stream was evaluated by the hydrograph separation technique using the stable isotope contents (oxygen-18 and deuterium) and the major ion concentrations. Stream and rain waters were collected every morning around the base station, and snowpack, soil water, lake water, spring water, puddle water were also sampled at one or two times during the summer. Lake water was collected every evening in 1999 only. The oxygen-18 versus deuterium diagram of all sampled water shows that not only rainwater but also all other waters are distributed on the global meteoric water line (MWL) and d-values of those are nearly 15 per mil. This means that the isotope fractionation effect due to the phase change is small. The oxygen-18 content of rainwater shows high fluctuation with every storm event, ranging between -10 per mil and -25 per mil with an average of -16.6 per mil. These values are not depending on the intensity and the total amount of rainfall. Whereas, the oxygen-18 content of snowpack collected just prior to snowmelt season has a large minus value remarkably, ranging between -33.7 per mil and -35.5 per mil with an average of -34.4 per mil, and there is clear contrast between winter and summer precipitation. In the beginning of snowmelt season, stream water has a large minus value of the oxygen-18 content due to the extensive mixing of snowmelt water that has a larger minus value. As the season progresses, its minus value decreases due to the increase of mixing of summer precipitation, which has a small minus value. After the totally 10 to 20 mm storm event in the middle of August in both year, oxygen-18 content of stream water does not change during the storm event and it approaches to the value of soil water. According to the simple two-component model for hydrograph separation, summer rainwater occupied 40 to 45% of the total stream water in the typical storm event.

HW06/07P/D-004 Poster 1400-188

**STABLE ISOTOPE SIGNATURE OF SUMMER AND WINTER MONSOON RAINS IN SHALLOW GROUNDWATERS FROM INDIA**

Sourendra Kumar BHATTACHARYA, R.D. DESHPANDE, R.A. JANI, S.K. GUPTA (Planetary Geosciences Division, Physical Research Laboratory)

Isotopic character of groundwater can, in principle, be used to determine the relative influence of different vapour sources contributing to the local precipitation if post-precipitation modifications during groundwater recharge are small or can be quantified. In case of south India, the dominant vapour sources for the two rainy seasons, namely, Southwest Monsoon and Northeast Monsoon are respectively the north Indian ocean/the Arabian Sea and the Asian continental sources supplemented by moisture from the Bay of Bengal. Oxygen and hydrogen isotope ratios of groundwater and river water samples from the south Indian peninsula were measured to look for the influence of these two vapour sources in the rains. Our studies show that the groundwater oxygen isotopic ratios (in per mill) in the west coast of India are fairly uniform at a value of around -2 which is only slightly depleted compared to the mean rainwater ratio of about -1.5 based on the GNIP data set of Bombay rains. In contrast, the areas adjoining the east coast of India are characterized by depleted ratios ranging from -3 to -5 signifying sizeable contribution from depleted surface water of the Bay of Bengal and winter precipitation bringing Asian continental moisture. The distribution of the isotope ratios also signify the influence of the Western Ghat hills in shielding a large part of the southern peninsula from the Arabian Sea moisture. Assuming groundwater ratios as representative of rain water ratios and the fact that the isotope contours do not match the rainfall contours the role of the amount effect seems to be marginal. Rather, the isotopic distribution indicates strong influence of vapour sources, the orography and local re-evaporation component in some cases. Our earlier work on north Indian groundwaters, in contrast, showed influence of continental effect and contribution of evapotranspiration component. Rains in north India are caused by northward moving storms and depressions starting from the northern Bay of Bengal. As these systems move inland progressive rainout depletes the heavy isotopes. However, a good amount of the rainfall is returned back as evapotranspiration. Based on a simple box model incorporating the fluxes of moisture and isotopic changes during condensation using Rayleigh fractionation we estimated that about 30% of moisture is derived from evapotranspiration in this region. Monthly isotope monitoring stations in a few key locations in north and south India are required to confirm the above conclusions.

HW06/07P/D-005 Poster 1400-189

**DIVERSITY OF SR ISOTOPIC POSITIONS OF HOT SPRING AND VOLCANIC WATERS FROM ZAO VOLCANIC AREA, JAPAN**

Hiromasu ISHIKAWA, Hirokazu FUJIMAKI (Institute of Mineralogy, Petrology and Economic Geology, Graduate school of Science, Tohoku University)

$^{87}\text{Sr} / ^{86}\text{Sr}$  isotopic analyses were carried out for hot spring water, volcanic lake water, and some rocks in Zao volcanic area to investigate the origin of Sr and water-rock interaction. Based on Sr isotopic and major chemical compositions, various hot spring water and volcanic lake water in this area are divided into three types. Type I is characterized by high Mg-Ca-SO<sub>4</sub>-Cl abundances, and their  $^{87}\text{Sr} / ^{86}\text{Sr}$  ratios are around 0.7053. Zao hot spring water belongs to this type. Type II is characterized by high Ca-SO<sub>4</sub> concentrations, and their  $^{87}\text{Sr} / ^{86}\text{Sr}$  ratios range from 0.7039 to 0.7043. Waters from the volcanic lake and Shinfukiko hot spring belong to this type. Type III is characterized by high Na-Ca-HCO<sub>3</sub>-SO<sub>4</sub> contents, and their  $^{87}\text{Sr} / ^{86}\text{Sr}$  compositional range is 0.7070-0.7073. Waters from Gaga, Aone, and Togatta hot spring belong to this type. The  $^{87}\text{Sr} / ^{86}\text{Sr}$  ratio of basement pre-Tertiary granite is 0.7068, and the value of plagioclase separated from the granite is 0.7064. Whereas Tertiary sedimentary rocks show such a wide range of  $^{87}\text{Sr} / ^{86}\text{Sr}$  ratio as 0.7054-0.7202. The  $^{87}\text{Sr} / ^{86}\text{Sr}$  ratios of the Quaternary volcanic rocks range from 0.7038 to 0.7044. The  $^{87}\text{Sr} / ^{86}\text{Sr}$  ratio of Type I is similar to the average value of the pre-Tertiary granite and the Quaternary volcanic rocks. Therefore soluble Sr in Type I might have been derived from both the pre-Tertiary granite and Quaternary volcanic rocks. Sr in Type II might have been derived from the Quaternary volcanic rocks because the  $^{87}\text{Sr} / ^{86}\text{Sr}$  ratios of Type II are similar to these of the Quaternary volcanic rocks. The  $^{87}\text{Sr} / ^{86}\text{Sr}$  ratio of Type III is higher and it is within the range of Tertiary sedimentary rocks; they should be the source of the Sr of Type II. SO<sub>4</sub> / Cl ratio of Type I is lower than Type II. Judging from the chemical characteristic and geological structure of this area, Type I might be the residual liquid phase derived from hot water boiled in a reservoir. High SO<sub>4</sub> / Cl ratio of Type II can be explained by low Cl. Because Cl can be strongly partitioned into liquid phase while boiling.

HW06/07P/D-006 Poster 1400-190

**TEMPORAL VARIATION OF STABLE ISOTOPES IN PRECIPITATION AT THAILAND OBSERVED IN 2001**Kimpei ICHIYANAGI<sup>1</sup>, Manabu D. YAMANAKA<sup>2</sup> (<sup>1</sup>Frontier Observational Research System for Global Change, <sup>2</sup>Kobe Univ.)

Spatial and temporal variability of the stable isotope composition of precipitation in the Asia Pacific region was discussed based on the monthly dataset, and regional climatology and atmospheric circulation patterns were shown in Araguaas-Araguaas et al. (1998). However, the relationship between isotope signature of precipitation and climate in Tropics is not well understood, because the daily isotopic data in precipitation is limited. The purpose of this study is to understand the temporal variation of stable isotopes in precipitation at Thailand based on the daily observation. Stable isotopes (Oxygen-18, Deuterium) in precipitation and meteorological data were observed at Bangkok, Phuket and ChaingMai from August to December in 2001. Temporal variations of stable isotopes in precipitation were almost same features among three stations, ranged from -15 permil to 0 permil. Considering relationships between Oxygen isotopes and precipitation amount, there were positive correlations in three stations by the monthly basis. However, there was no correlation between them by the daily basis. In general, isotopic compositions are heavy in low precipitation and light in high precipitation caused by the amount effect. Conversely, observed isotopic compositions were opposite change at Bangkok in October 2001. In this study, this strange phenomenon will be considered with meteorological data.

HW06/07P/D-007 Poster 1400-191

**THE CONTRIBUTION OF WATER RECYCLING TO THE ISOTOPIC COMPOSITION OF RAINFALL OVER CENTRAL EURASIA**Naoyuki KURITA<sup>1</sup>, Koiti MASUDA<sup>2</sup>, Koji YAMAZAKI<sup>3</sup>, Naohiro YOSHIDA<sup>4</sup> (<sup>1</sup>Frontier Observational Research System for Global Change, <sup>2</sup>Frontier Research System for Global Change, <sup>3</sup>Graduate School of Environmental Earth Science, Hokkaido University, <sup>4</sup>Frontier Collaborative Research Center, Tokyo Institute of Technology)

The response of the isotopic ratio of summer precipitation over central Eurasia to recycled

water from land surface is estimated by examination of stable isotopic ratios in the summer precipitation and by evaluated continental precipitation recycling ratio. The isotopic composition of precipitation are collected at thirteen monitoring stations across Russia between 1996 and 2000, and determined the spatial and temporal isotopic variation. The result shows remarkable isotopic tendency more negative isotopic content farther inland, i.e., "continental effect" and these largely varied in time and space. The comparison with continental moisture recycling ratio and observed isotopic data shows that both temperature and moisture recycling explains more than half of the variability of spatial isotopic feature, however the anomalies of summer isotopic composition in each station are explained by neither temperature nor moisture recycling. The atmospheric moisture balance model is applied to air masses forming observed precipitation along trajectories and used to evaluate the factors that control the observed temporal variation of isotopes which is not explained by recycling ratio. The model extends Rayleigh descriptions of isotopes in precipitation by including effects of recharge to air masses by evapotranspiration from land surface. The water fluxes used in this model are based on National Center for Environmental Prediction (NCEP) reanalysis. The isotopic composition of recycled moisture is adopted as an input parameter in model calculation of observed isotopes in precipitation at each station. At inland stations where recycled moisture largely contributes to precipitation, total amount of precipitation and evaporation during air mass traveling across continent is balanced in each air masses, thus the evaluated temporal isotopic variation of precipitation primarily depends on the isotopes in recycled moisture. This suggests that the temporal isotopic variability of summer precipitation is controlled by the variation of isotopic composition from moisture source. Because the evapotranspiration is assumed to transfer soil water into atmosphere without isotope fractionation, the variability of soil moisture may result in isotopic variation of recycled moisture. Furthermore, in Siberia region, the fact that the isotopes in thaw water are lighter than other season's precipitation suggests that estimation of the contribution of thaw water to summer precipitation may be possible using isotopes.

HW06/07P/D-008 Poster 1400-192

**SULFUR ISOTOPE CONSTRAINT ON THE PROVENANCE OF SALINITY IN CONFINED AQUIFER SYSTEM. A CASE STUDY IN ESTUARINE AREA OF KISO RIVER, CENTRAL JAPAN**

Masaru YAMANAKA, Yoshihiro KUMAGAI, Hiroki TAKAMURA (Faculty of Geo-environmental Science, RISSHO University)

This study aims to comprehend the provenance of salinity in confined aquifer system in estuarine area of Kiso River, central Japan, by using water quality and sulfur isotopic ratios ( $\delta^{34}\text{S}$ ) as indicators. Groundwater samples were collected in July or August in 2002 from 29 wells which have single screen around 50m depth, and were used for chemical and sulfur isotopic analyses. High Cl content groundwater (>1000mg/L) is distributed in tongue-shape along Kiso River (where three rivers: Kiso, Ibi and Nagara Rivers flow into sea) and has fairly low SO<sub>4</sub>/Cl ratios and high  $\delta^{34}\text{S}$  values (~79 permil) than those of present seawater. Assuming that present seawater induces the salinization of confined groundwater, intruded SO<sub>4</sub> with Cl is expected to be reduced in confined aquifer where is in anaerobic condition. The  $\delta^{34}\text{S}$  values of the saline groundwater would be well explained by following Rayleigh distillation model, in which initial SO<sub>4</sub> has  $\delta^{34}\text{S} = 21$  permil of the seawater (Longinelli, 1989):  $\delta^{34}\text{S} = 21 + \epsilon \ln f$  (1) where  $\epsilon$  is the isotopic enrichment factor and  $f$  is the fraction of initial SO<sub>4</sub> remaining in groundwater. Based on previous field studies of sulfate reduction, -20 permil can be adopted as  $\epsilon$  for the model. The  $f$  is calculated by following equation using SO<sub>4</sub>/Cl content ratio of present seawater:  $f = \text{SO}_4 / (\text{Cl} \times 2700/19000)$  (2). A part of the saline groundwater along the Ibi-Nagara Rivers can be well explained by this Rayleigh model, in which volume contribution of present seawater in the groundwater is 10.7% as a maximum, whereas most of the saline groundwater plotted on smaller  $f$  field than theoretical line of the model on  $f - \delta^{34}\text{S}$  diagram. This is caused by overestimation of initial SO<sub>4</sub> contents (Cl × 2700/19000) on Equation (2), strongly indicating another Cl source without SO<sub>4</sub> besides present seawater. Fossil seawater trapped in aquiclude layer for hundreds years is the most plausible candidate for the Cl source, since SO<sub>4</sub> can be completely reduced in anaerobic stagnant conditions. Based on Equations (1) and (2), it is estimated that the volume contributions of present and fossil seawaters are 10.1% and 9.4% respectively, and the lost SO<sub>4</sub> content through sulfate reduction process is 350mg/L as maximums.

HW06/07P/D-009 Poster 1400-193

**CHARACTERIZING THE HYDROLOGY OF HEADWATER SYSTEMS USING RESIDENCE TIME DISTRIBUTIONS**Kevin James MCGUIRE<sup>1</sup>, Jeff MCDONNELL<sup>1</sup>, Carol KENDALL<sup>2</sup> (<sup>1</sup>Department of Forest Engineering, Oregon State University, <sup>2</sup>US Geological Survey, Menlo Park, CA)

The relationship between streamwater residence time and landscape character is poorly understood. Residence time distributions can be used to gain a better understanding of landscape organization, storage, and subsurface flow routing mechanisms. Few studies have yet examined explicit residence time relations at multiple nested watershed scales. We present new data for the H.J. Andrews Experimental Forest where we examine the relationship between rainfall and streamflow 180 for weekly data over the period October 2000 through February 2003 to estimate watershed residence time. Residence time distributions from hillslope (~0.3 ha) to watershed scales of 10, 100, 500, and 6,000 ha with varying degrees of geomorphic complexity are explored to clarify landscape unit (i.e. hillslopes and riparian zones) influence on runoff generation processes.

HW06/07P/D-010 Poster 1400-194

**IMPLEMENTATION AND TESTING OF WATER ISOTOPES INTO THE WEATHER RESEARCH AND FORECAST (WRF) MODEL**

Norman L. MILLER, Prudence N. FOSTER, Donald J. DEPAOLO (Earth Sciences Division, Lawrence Berkeley National Laboratory)

To date, atmospheric water isotope modeling has been performed on a global scale. The development of a stable water isotope scheme in a mesoscale model will lead to a simulated spatial distribution that will improve our understanding of present day climate variability, as well as historical climate patterns. The purpose of this study was to add water isotope tracers to the regional atmospheric model WRF (NOAA's Weather and Research Forecast model) in order to link existing global and basin-scale isotope models, and to work toward an improved understanding of the water budget at the ARM/CART site. In order to include isotopic processes in WRF, eight new prognostic variables were added to the model's dynamical core. These are the isotopic mixing ratios for water vapor, cloud liquid water, cloud ice, and rain for the stable isotopes O18 and deuterium. The isotopes are treated in a manner similar to the natural water vapor, cloud liquid water, etc. in terms of diffusion, advection, nudging, and filtering. Isotope fractionation and diffusion are handled using the approach of Gedzelman and Arnold (1994). Processes handled in this model are fractionation during deposition of water vapor onto cloud ice and condensation of water vapor onto cloud water, and also diffusive exchange of isotopes between vapor and falling rain drops. The bulk flux model of Hoffman et al. (1998) is used here as a first order

approximation for isotopic evaporative processes. For the runs to be discussed here, lateral boundary conditions were generated by the Melbourne University General Circulation Model. This GCM runs at a resolution of R21, and predicts values of the O18 and deuterium mixing ratios at each grid point. Results of preliminary model runs will be discussed.

HW06

Monday, July 7 - Tuesday, July 8

### ISOTOPE TRACERS IN WATER CYCLE MODELS (IAHS/ICT, IAEA)

Location: Site C, Room 31

Tuesday, July 8 AM

Presiding Chairs: J.J. Gibson, J. McDonnell

HW06/08A/C31-001

1040

#### CHANGE OF THE ISOTOPIC PARAMETERS OF RIVER WATER ALONG THE RIVER COURSE:- TO WHAT EXTENT CAN ONE USE IT AS A MEASURE OF THE WATER BALANCE IN THE RIVER BASIN?

Joel Robert GAT<sup>1</sup> (Environmental Science and Energy Res., Weizmann Institute of Science, <sup>2</sup>Center for Dryland Water Resources Research, Ben-Gurion University of the Negev)

The isotopic composition of an undisturbed flowing river represents the amount-weighted summation of the composition of its tributaries. Evaporative water losses along its course, be it from through-flow lakes, reservoirs or from overflow wetlands along the river banks, result in the enrichment of the heavy isotopes of both hydrogen and oxygen in the residual waters in addition to the increase of the salinity. In particular, the decrease of the d-excess value is a tell-tale indicator of such a process. In contrast, the extraction of water by means of the transpiration of water plants does not affect the isotope composition but adds to the accumulation of salinity in the residual waters whereas, obviously, the loss by outflow or pumping of the river water does not fractionate at all between the components of the system. These different attributes of these three processes form the basis for using the isotopic and salinity parameters for quantifying the river's water balance. The Isotopic River Continuum model (IRCM), developed within the framework of the Coordinated Research Program of the IAEA on "Isotope Studies in Large River Basins", provides both the conceptual and mathematical tools for quantifying the water balance along the river course. It follows the isotopic composition from the input by precipitation through the watershed and along the river course, accounting foremost for the seasonally changing input (including the effect of snow-melt), the "catchment effect" on the isotopic composition of the runoff to the river, the effect of holdup in lakes or reservoirs both in terms of water loss and mixing and, finally, the recycling of the river water following its use either in agricultural or urban activities. Due to the non-linear degree of the isotopic enrichment as a function of the fractional amounts of water lost by evaporation relative to the total amount of water, it is necessary to follow the evolution of both flow and isotopic parameters along the different sections of a river. The IRCM can then provide the monitoring scheme required for the purpose of both the water balance evaluation under steady state conditions, as well as in order to detect changes, climatic or anthropogenic in origin, in a river's water balance.

HW06/08A/C31-002

1100

#### REGIONAL ATMOSPHERIC WATER ISOTOPE MODELLING

Kristof STURM<sup>1</sup>, Georg HOFFMANN<sup>2</sup>, Bärbel LANGMANN<sup>1</sup>, Hans GRAF<sup>3</sup> (<sup>1</sup>Max-Planck-Institute for Meteorology, <sup>2</sup>Laboratoire des Sciences du Climat et de l'Environnement)

We introduce a new module handling the water isotope tracers  $H_2^{18}O$  and HDO in the atmospheric regional circulation model REMO, based on previous work with the ECHAM (ECHAM6 inspired, in HAMBURG enhanced climate model) atmospheric global circulation model. Preliminary results over Europe (from Moroccan coast to the Barents Sea and from the Egyptian coast to South-East Greenland) are analysed, with particular emphasis on the comparison with a regional isotopic precipitation climatology compiled from station measurements. The atmospheric models ECHAM-4 and REMO-5 use the same physics scheme, referred to as EC4-physics. An isotopic module was elaborated for ECHAM, accounting for isotope fractionating processes in stratiform and convective clouds, vertical diffusion, and evapo-transpiration from the surface with regard to sub-surface reservoirs: a centennial experiment was run in the T30 spectral truncature, corresponding to a horizontal resolution of 3.75°, i.e. ca. 450 km. This isotopic module was adapted for REMO, with a standard resolution increased to 0.5°, i.e. ca. 50 km over Western and Central Europe. A rotated grid was applied, providing an equal grid cell area over the entire study domain, with its longitudes and latitudes comprised in [50°E; 70°W] and [30°N; 75°N] respectively. The main aim of this study is an improved representation of the atmospheric processes, especially the hydrological cycle, contributing thanks to the increased model resolution to a better understanding of the measured isotopic signal. Preliminary results of REMO iso are compared to monthly mean of meteoric isotopic measurements from the Global Network for Isotopes in Precipitation (GNIP) over the study area. We focus on case studies in mountain areas during the BALTEX experiment, discussing the need of further downscaling of precipitation and related isotopic processes. Further investigations will test the model output against event measurements at several study sites in Germany monitored by the GSF, based at Neuberberg, Germany.

HW06/08A/C31-003

1120

#### APPLICATION OF STABLE ISOTOPES IN LARGE SCALE HYDROLOGICAL STUDIES

Balazs M. FEKETE<sup>1</sup>, Pradeep AGGARWAL<sup>2</sup>, John J. GIBSON<sup>3</sup>, Charles J. VOROSMARTY<sup>4</sup> (<sup>1</sup>Water Systems Analysis Group, Complex Systems Research Center, Institute for Earth, Oceans, and Space, University of New Hampshire, NH 03824 USA, <sup>2</sup>Water & Climate Impacts Research Centre, National Water Research Institute, P.O. Box 3050, University of Victoria BC V8W 3P5 Canada, <sup>3</sup>International Atomic Energy Agency)

Isotope tracers offer complimentary tools for hydrologists to study hydrological processes. Traditionally, application of isotope tracers has been limited to small scale hydrological studies due to the lack of isotope data in large catchments. New efforts initiated by the International Atomic Energy Agency (IAEA) and the World Meteorological Organization (WMO) pave the way for large-scale hydrological research by establishing complimentary networks for monitoring stable isotopes globally both in precipitation and large rivers. This effort has already resulted in valuable preliminary datasets such as Global Network for Isotopes in Precipitation (GNIP) and Global Network for Isotopes in Rivers (GNIR). The primary focus of current research and monitoring efforts is on 2H and 18O, which are naturally present in trace quantities within water, and systematically vary in components of

the water cycle due to fractionations that accompany phase changes and diffusion. These differences result in marked regional differences in the isotopic composition of precipitation and runoff. The new global data sets offer new opportunities for the testing of analysis tools and for assessing the applicability of stable isotopes in large scale hydrological studies. The present paper demonstrates the use of the newly emerging data sets representing the isotopic composition of precipitation and runoff in the context of a high resolution (6° longitude x latitude) gridded network. Simple GIS analyses were performed to assess the consistency between the isotopic composition of the precipitation and runoff. Further tests were carried out applying a modified version of the water balance and water transport modeling framework (WBM/WTM) developed at UNH. This modified version of WBM/WTM incorporated additional processes to track the migration of isotopes through the evapotranspiration and water transport processes. This modeling environment allowed the simulation of the key processes affecting the changes in the isotopic composition of the runoff at large scale. The modified WBM/WTM was tested using climatological climate forcings (e.g. air temperature, precipitation, vapor pressure, solar radiation, wind speed) at monthly time step. The results from the GIS analysis and the modeling exercise are presented demonstrating the potential of using isotopes as additional constraints in large scale hydrological modeling. The paper highlights the regional variations in isotopic composition of runoff and evaluates the representation of hydrological processes in the modified WBM/WTM with respect to the capturing changes in the isotopic composition of the runoff.

HW06/08A/C31-004

1140

#### SIMULATING SHORT-TERM 18O VARIABILITY WITH A RAYLEIGH-TYPE ISOTOPE CIRCULATION MODEL

Kei YOSHIMURA<sup>1</sup>, Taikan OKI<sup>2</sup>, Nobuhito OHTE<sup>3</sup>, Shinjiro KANAE<sup>1</sup> (<sup>1</sup>Institute of Industrial Science, University of Tokyo, <sup>2</sup>Research Institute of Humanity and Nature, <sup>3</sup>The Graduate School of Agriculture, Kyoto University)

Large spatial and temporal variability of stable water isotopes (D and  $^{18}O$ ) in precipitation are widely used to trace the global hydrologic cycle. Rayleigh-type models have first explained the spatial and temporal variability. Subsequently, studies that incorporate the isotopic physics into atmospheric general circulation models (AGCM) have examined the isotopic variability at monthly or annual scales. The causes of short-term (1-10 days) variability in precipitation isotopes, however, remain unclear. This study seeks to explain isotope variability quantitatively at such scale. Thus, a new water isotope circulation model on a global scale that includes a Rayleigh equation and the use of external meteorological forcings is developed. Transport and mixing processes of water masses and isotopes that have been neglected in earlier Rayleigh models are included in the new model. A control simulation of  $^{18}O$  for 1998 is forced with data from the GAME (GEWEX Asian Monsoon Experiment) reanalysis. The results are validated by GNIP (Global Network of Isotopes in Precipitation) monthly observations with correlation  $R=0.76$  and a significance level  $>99\%$ . The short-term isotopic variability is well reproduced comparing with daily observations at three sites in Thailand with similar correlation and significance. The present study also confirms that the impact of the amount of precipitation at the site, i.e., 'amount effect,' is insufficient to explain the short-term isotopic variability. The causes of short-term variability are quantitatively revealed for the first time in this study. Among three factors that cause isotopic variability, i.e., precipitation, evaporation, and moisture flux, the contribution of moisture flux is the largest, accounting for 37% at Chiangmai, and 46% in the global average. This highlights the importance of transport and mixing of air masses with different isotopic concentrations. Furthermore, sensitivity experiments reveal required temporal and spatial resolutions of each variable and enable to use different datasets. The more accurate GPCP (Global Precipitation Climatology Project) precipitation dataset yields improved model results at all three observation sites in Thailand. For example at Chiangmai, Thailand, the correlation increases to 0.80 from 0.76, and the root mean square error decreases to 2.9 per mill from 4.2 per mill comparing with the control simulation. In addition, data from the NCEP/NCAR (the National Centers for Environmental Prediction and National Center for Atmospheric Research) reanalysis allow the simulation to cover two years, reproducing reasonable interannual isotopic variability. In particular, the model reproduces the downward arch in seasonality over Thailand in 1998, and the upward arch in seasonality in 1999. The improved results from GPCP and the reasonable interannual reproduction from NCEP/NCAR support that the study appropriately models isotope circulation in an area influenced by the Asian Monsoon.

HW07

Thursday, July 10 - Friday, July 11

#### TOWARDS A SCIENCE PROGRAM FOR PREDICTION IN UNGAUGED BASINS (ALL IAHS COMMISSIONS)

Location: Site C, Room 25

Thursday, July 10 AM

HW07/10A/C25-001

Invited

0840

#### SCIENCE AND IMPLEMENTATION PLAN OF IAHS PUB: HERALDING EXCITING FUTURE FOR HYDROLOGIC SCIENCE AND PRACTICE

Murugesu SIVAPALAN (Centre for Water Research, University of Western Australia)

The IAHS Predictions in Ungauged Basins (PUB) initiative was launched at a workshop held in Brazil in November 2002. The central cross-cutting themes of PUB will be heterogeneity and its effect on uncertainty of hydrologic predictions. PUB is geared towards developing methodologies for assessing the uncertainty in hydrologic predictions arising from the heterogeneity in landscape properties and climate inputs, the uncertainty in the choice of model structure and methods of information transfer from gauged to ungauged catchments, and towards developing targeted methods to constrain and reduce these uncertainties. This talk will present for discussion the latest outlines of the science and implementation plan for PUB prepared by the Scientific Steering Group appointed by the IAHS to lead the PUB initiative. The PUB Science and Implementation Plan will be organized around the following thematic objectives: 1) Explore ways to characterize heterogeneity of landscape properties and climatic inputs; 2) Develop general model framework for heterogeneity and predictive uncertainty; 3) Carry out model inter-comparisons in selected gauged basins (PUB-HELP basins) to investigate the uncertainties due to choice of model structure; 4) Explore methods for the efficient assimilation of gauged and/or remotely sensed data in order to constrain predictive uncertainty; 5) Promote process studies and field experiments to advance process understanding and conceptualizations with a view to reducing predictive uncertainty; 6) Advance our understanding and predictions of the effects of hydro-climatological variability and change; and 7) transform the available global research products into the hydrological information useful for local and regional water resources management.

**HW07/10A/C25-002** Invited **1000**

**PUB FOR TRANSFORMING GLOBAL HYDRO-METEOROLOGICAL PRODUCTS INTO LOCAL WATER RESOURCES INFORMATION**

Kuniyoshi TAKEUCHI (Yamanashi University)

There are an abundant number of global research programs and their products in various institutes at freely accessible web sites encouraging a wide use. They are precipitation, cloud cover, temperature, radiation, soil wetness etc. It is, however, little, if not at all, heard about the examples used in local water resources planning and management. This is because the information is too crude and unreliable. While the reliability is essential and is the major scientific agenda, the downscaling/disaggregation of large scale information to local scale is another important subject. Even if the information is only a qualitative and with high uncertainty, if it is translated into the local condition, it is of great value for local water management, especially in ungauged basins. There are a number of downscaling/disaggregation techniques such as statistical methods and physical dynamic equation methods. In any case, the local topographic, land cover features and local land/water use are the main elements that determine the local variation. In the presentation, the experiences in the Mekong and the Yellow River basins studies will be reported.

**HW07/10A/C25-003** **1045**

**A METHODOLOGY FOR THE DYNAMICAL RECONSTRUCTION OF HISTORICAL TIME-SPACE PRECIPITATION DATA OVER UNGAUGED WATERSHEDS: APPLICATION/VALIDATION OVER TOKYO AREA**

M.L. KAVVAS<sup>1</sup>, Z.Q. CHEN<sup>1</sup>, M.L. ANDERSON<sup>1</sup>, J.Y. YOON<sup>1</sup>, J. YOSHITANI<sup>2</sup>, T. MATSUURA<sup>3</sup>, H. OKUMURA<sup>4</sup> (<sup>1</sup>Hydrologic Research Laboratory, Dept. of Civil & Envr. Engineering, University of California, Davis, <sup>2</sup>Hydraulics Engineering Research Group, Public Works Research Institute, 1-6 Minamihara, Tsukuba, 305-8516 JAPAN)

Water resources studies require precipitation input to hydrologic models. However, there are many ungauged watersheds around the world where precipitation data are completely lacking. There are also many watersheds where precipitation data are available at a few ground locations, yielding an unsatisfactory quantification of the spatial distribution of precipitation over such watersheds. Therefore, it is necessary to reconstruct historical precipitation data at fine spatial (~ 6km grids) and time (~1 hour intervals) resolutions over ungauged and sparsely gaged watersheds around the world. A methodology for dynamically downscaling the 1948 – 2002 historical atmospheric data of U.S. National Center for Environmental Prediction (NCEP) and U.S. National Center for Atmospheric Research (NCAR) at 2.5° latitude x 2.5° longitude spatial grid resolution over the whole globe at 6 hr time intervals, to any specified watershed at 6 km spatial grid resolution and 1 hr time intervals has been developed and successfully tested over the Tone and Arakawa river basins, draining to the Tokyo Area. This methodology consists of sequentially nesting the Integrated Regional Scale Hydrologic-Atmospheric Model (IRSHAM) first over a continental domain (in this study, the Eastern Asia continent) at 54 km grid resolution within the global domain of NCEP/NCAR atmospheric data, and then nesting IRSHAM over a country domain (in this study, the Japan Islands) at 18 km grid resolution within the continental domain IRSHAM. Then these nested models are run by means of initial and boundary conditions, provided first from the NCEP/NCAR atmospheric data (for the continental domain simulations), and then from the continental (Eastern Asia) domain IRSHAM to country (Japan) domain IRSHAM. Finally, for the reconstruction of precipitation data at 6 km grid resolution and 1 hr time intervals over a specified watershed (in this study, Tone and Arakawa watersheds), the MM5 non-hydrostatic regional atmospheric model of NCAR which is set up over that watershed, is nested into the country domain IRSHAM. Then the historical atmospheric simulations of country domain IRSHAM provide the initial and boundary conditions for the watershed domain MM5 model simulations of the historical precipitation data over the specified watershed. This methodology was applied to Tone and Arakawa watersheds that drain into the Tokyo Area. Over this region historical precipitation data were constructed for the 1994 – 2000 period at 6 km spatial resolution and 1 hr time intervals by means of the above methodology without using any of the available precipitation data over this region. Then the reconstructed historical precipitation data were compared against corresponding precipitation observations at daily and monthly intervals and for the historical extreme storm events. The comparison results are quite promising.

**HW07/10A/C25-004** **1100**

**USE OF SATELLITE REMOTE SENSING IN PREDICTION OF UNGAUGED BASINS**

Venkat LAKSHMI (University of South Carolina)

Ungauged basins pose a challenge to hydrological studies as they lack both calibration and validation data for the use of land surface models. Therefore, one has to use the satellite data that is available which describes the aspects/attributes of the basin from a hydrological perspective. Soil moisture is routinely mapped by the Advanced Microwave Scanning Radiometer (AMSR). Vegetation is characterized by MODIS (Moderate Resolution Imaging Spectroradiometer) and surface temperature is estimated using AIRS (Advanced Infra-Red Sounder) as well as MODIS. Precipitation is measured (in the tropical regions) from the TRMM (Tropical Rainfall Measuring Mission) Microwave Imager (TMI) with the Global Precipitation Mission (GPM) due to be launched in a few years. The synergistic use of these data sets along with hydrological models would help us to (a) input precipitation and vegetation information into a hydrological model and calculate the soil moisture and surface temperature using the water and energy balance equations (b) the measured soil moisture and surface temperature can be used in two ways (i) to calibrate certain model parameters (ii) to verify the output of the model through validation. The overland runoff from the hydrological model would be routed in the stream channel network (obtained from the Digital Elevation Data) to obtain the streamflow at the catchment outlet. This would help in estimation of the water resources for the catchment.

**HW07/10A/C25-005** **1115**

**ON THE COMBINED USE OF SURFACE AND AIRBORNE MEASUREMENTS FOR BASIN SCALE ASSESSMENT**

Yoram N. RUBIN<sup>1</sup>, Yoram N. RUBIN<sup>1</sup>, Katharine GROTE<sup>1</sup>, Susan HUBBARD<sup>2</sup> (<sup>1</sup>U.C. Berkeley, <sup>2</sup>Lawrence Berkeley National Laboratory)

Large scale monitoring of soil moisture dynamics is important for agricultural applications, for investigating the dynamics of ecosystems, and for basin-scale water resources budgeting. The current state-of-the-art in remote-sensing techniques is still unsatisfactory due to the limitations of low-resolution and the limited depth penetration. In this talk we propose to combine remote-sensing techniques with ground-based measurements in a way which allows to bypass these difficulties. Specifically, we propose to use geophysical techniques such as Ground-Penetrating-Radar (GPR) for measuring the soil moisture profile at the shallow subsurface and to correlate these measurements with remotely-sensed information.

GPR allows substantial depth penetration for a wide range of soil types, and accurate measurements of soil moisture over the rooting depth. Where depth-penetration is limited, such as in clay-rich soils, ground wave techniques can be used, augmented by physically-based mathematical models. These techniques allow to measure rapidly soil moisture over large areas, in a non-invasive manner, and over short periods of time. By correlating these measurements with airborne data, a correlation function can be developed which will allow us to conduct rapid and accurate interpretation of airborne surveys. This talk will report the principles and concepts of our approach, as well as applications to field sites.

**HW07/10A/C25-006** **1130**

**MULTISENSOR OBSERVATIONAL NETWORK OF RAINFALL FOR FIELD EXPERIMENTS ON THE PUB PROBLEM**

Witold F. KRAJEWSKI, Anton KRUGER (IHR-Hydroscience & Engineering, University of Iowa)

Experimental studies aimed at addressing prediction from ungauged basins require quantitative knowledge of space-time rainfall fields. These could be provided by specially designed observational systems. There are several requirements that such systems should fulfill. First, they have to be able to provide high space and time resolution rainfall estimates over a substantial area to enable scaling studies of rainfall. Second, they should be able to provide highly accurate estimates of ground rainfall with known measures of the associated uncertainty. Third, they should be relatively inexpensive in deployment and operation. Forth, they should be robust and redundant. The authors justify and elaborate on these requirements and demonstrate gaps in state-of-the-art of such systems. In particular they discuss rain gauge network design in terms of the network configuration, the sensor requirements, and the engineering design of the observational platforms. They also discuss issues of design and deployment of a network of small inexpensive X-band polarimetric radars. In particular, they discuss the issues of signal attenuation at X-band and development of rainfall estimation algorithms based on polarimetric radar data.

**HW07/10A/C25-007** **1145**

**MULTIFRACTAL SIMULATIONS OF RAIN, TIPPING BUCKET GAUGE NETWORKS AND RADAR REFLECTIVITIES**

Shaun M. LOVEJOY<sup>1</sup>, Daniel SCHERTZER<sup>2</sup> (<sup>1</sup>Physics, McGill University, <sup>2</sup>LMM, U. P. et M. Curie)

Measuring, modeling and predicting rain is essential for the success of PUB. Rain is a typical PUB variable: it displays extreme variability over huge ranges of space-time scales, yet it has the advantage that it is in some ways easier to measure and can thus be used as an exemplar for measurements of other fields. This is not to say that rain is at the present time reliably measured. There are currently no direct ways to measure the areal distribution of rain fields: gauges make measures at (nearly) spatial points, radars measure effective reflectivity factors which are non trivially related to the rain rate. Indeed, in order to interpret these measurements detailed assumptions are necessary about the structure of rain and (typically sparse) measuring networks; these are usually implicit, the usual one being some form of space-time homogeneity assumption. For example, classical geostatistics (e.g. Kriging) implicitly assume both the regularity of the network as well as of the other relevant measures with respect to the standard (Lebesgue) measure. This effectively rules out sparse fractal networks as well as all but the most trivial scaling behaviours in rain. At the same time, the standard interpretation of the fluctuating radar echo assumes a statistical homogeneous (Poisson) distribution of rain drops. During the last twenty years, the quality and quantity of rain data has improved, and systematic scaling analysis techniques have been developed and applied to rain and related fields. These have shown that - as predicted by cascade models - the statistics are multifractal implying systematic resolution dependence of rain. In this talk we show how to analyze and model these multifractal rain fields, carefully taking into account the strong stratification in the vertical as well as in space-time. We then show how these multifractal models can be used to simulate space-time rainfields, sparse gauge networks, tipping bucket gauge response to rain, and biases in the standard radar rain rates.

**HW07/10A/C25-008** **1200**

**PROPOSAL FOR AN INTERNATIONAL NETWORK OF MESOSCALE CATCHMENTS IN SUPPORT OF PREDICTION IN UNGAUGED BASINS (PUB)**

Patrick Enda O'CONNELL<sup>1</sup>, R.B. GRAYSON<sup>2</sup> (<sup>1</sup>School of Civil Engineering and Geosciences, University of Newcastle upon Tyne, UK, <sup>2</sup>Department of Civil and Environmental Engineering, University of Melbourne)

The vast majority of catchment experiments have been conducted at the small scale (< 10km<sup>2</sup>), and it has not generally been possible to transfer the understanding gained from these experiments to larger scales. However, it is at larger scales that predictions are required, and so the PUB (Prediction in Ungauged Basins) initiative has focussed on the problem of making reliable predictions in ungauged basins. However, to enhance the reliability of such predictions, a better understanding is needed of how the hydrological functioning of catchments changes with increasing scale across a wide spectrum of physiographic settings, and under different land use and climate change scenarios. Mesoscale catchments (100-1000km<sup>2</sup>) play an important role in determining the responses of larger catchments, and are frequently major sources of runoff and flooding. However, a major challenge in instrumenting such catchments is the difficulty of sampling the heterogeneity in hydrological response associated with the spatial variability in climate, topography, soils, vegetation, geology, and geomorphology encountered with increasing scale. Dealing with heterogeneity is a central theme of PUB. Mesoscale catchment experiments are now being undertaken in several countries, notably Australia, Brazil, New Zealand, the UK and the US, and some valuable understanding and experience has already been gained. To promote a coordinated approach to catchment experimentation within PUB, it is proposed to establish an international network of mesoscale catchment experiments involving a coherent experimental design approach, the networking of researchers, and the sharing of people, expertise, data and facilities. This would provide a major contribution towards achieving the scientific goals of PUB.

**HW07/10A/C25-009** **1215**

**AN AUSTRALIAN COLLABORATIVE NETWORK FOR LONG-TERM HYDROLOGICAL AND ECOLOGICAL MONITORING**

Richard P. SILBERSTEIN (IAHS)

Australian hydrology is in need of an injection of vitality and long-term vision. Continuing scientific input is essential to keep water management and natural resource management (NRM) at a high standard, and we have not kept pace with international developments. The ability to predict hydrological behaviour in ungauged basins depends absolutely on good data in basins that are gauged. While the goal is to make predictions with minimal data, we need data to test this ability. Since 1960 there has been a major review of hydrological

monitoring in Australia at least twice every 10 years. Each has concluded that long-term monitoring is essential, but needs focus and coordinated analysis to ensure its value. There is widespread recognition within Australian State and Federal agencies that long-term monitoring is essential for good NRM, and general recognition that the timing is good for renewed activity, partly because of frustration in the hydrological science community. In this paper I call for a significant improvement in the state of hydrological gauging and ecological monitoring networks, data processing, quality control and data sharing. Existing networks should be expanded to include ecological indicators. I seek new opportunities for funding and renewed collaboration between agencies on analysis of the data and hydrological and ecological research. We need to expand beyond our one link in the International Long-term Ecological Research Network, to establish catchments around the country that satisfy the criteria, and can contribute to international efforts in understanding the global bio-geochemical and hydrological cycles. A national workshop is proposed to establish: a) minimum levels of monitoring activity; b) common interests; c) collaboration between agencies; d) a reinvigoration of hydrology in Australia. It is aimed to generate a collaboration to establish links between data collection agencies, Universities, CSIRO, and other research agencies, industry, schools and the community, all participating at some level in the hydrological science activity through data collection, analysis, and reporting. Such an activity would have irreplaceable value to the Australian community if adequate monitoring is undertaken and well-designed. A model for this is the highly successful Australian Collaborative Land Evaluation Programme (ACLEP). Key threats to the project are insufficient funding for the basic science to maintain the enthusiasm of the key protagonists, complexity of the bureaucracy in funding and coordinating data collection and collation, and communication linkages. A major threat is the perception that computer models are now sophisticated enough to replace the need for data. This is very dangerous. It is the science (that is, understanding observations) in hydrology that generates new knowledge, and leads to better engineering and better land management. The Australian Commonwealth Government has launched a National Action Plan on Salinity and Water Quality that offers both opportunities and threats to this activity. There are potentially competing demands on the resources, with many monitoring sites chosen for their convenience of location and focussed on filling a regulatory requirement, rather than their scientific value. This project's mission could be to coalesce the regulatory requirements with scientific goals.

Thursday, July 10 PM

**HW07/10P/C25-001** Invited **1400**

**A PILOT STUDY FOR FLOODS IN THE WHITE-WATER RIVER BASIN, KANSAS USING A SCALING FRAMEWORK**

Vijay K. GUPTA (DEPT. OF CIVIL ENG. AND CIRES)

Our objective is to design a pilot study for floods in the White Water sub basin of Walnut River basin, KS, USA using the scaling framework. Special emphasis will be given to the role of scaling in space-time variable rainfall and spatially variable channel network structure in determining the scaling parameters of peak flows. We are first testing the scaling framework for peak flows using existing observations from the semi-arid Walnut Gulch basin, AZ, and for both peak- and low flows using existing observations from the humid Goodwin Creek basin, MS. Tests of physical hypotheses are being carried out using a GIS-based numerical simulation laboratory for these two basins. In addition, we will simulate peak flows in the White Water sub basin. From the simulation results, we will design a pilot study for strategically gauging the basin to test peak flow scaling. The scaling framework unifies spatial flood statistics with its physics, and thereby addresses a longstanding fundamental problem in hydrologic sciences and engineering. The body of new knowledge under scaling provides the scientific foundations for solving the long-standing global problem of prediction of floods and low flows from ungauged and poorly gauged basins. This is a cooperative interdisciplinary project involving scientists and engineers from the University of Colorado, Boulder, the U.S. Geological Survey and the University of Iowa. The proposed pilot study is also a first step to conduct large-scale cooperative field experiments in the future in the Walnut River basin, KS, which has been the site for cooperative atmospheric surface exchange studies (CASES) for nearly a decade. Recently, White Water sub basin is being used for the Department of Energy (DOE) Water Cycle Pilot Study involving five DOE laboratories. These on-going activities are complementary to our long-term goal of conducting large-scale cooperative field experiments.

**HW07/10P/C25-002** **1430**

**SCALING ISSUES IN PUB**

Daniel J.M. SCHERTZER<sup>1</sup>, Shaun LOVEJOY<sup>2</sup> (<sup>1</sup>Meteo-France and LMM, U. P. M. Curie, <sup>2</sup>Physics dept., McGill U.)

PUB problem is still unsolved because some fundamental questions have prevented its solution. Nonlinearity is at the core of the question of prediction and hydrological fields indeed display an extreme variability over a wide hierarchy of space-time scales. This variability is beyond the scope of classical mathematical and modeling methods which are forced to introduce scale truncations and ad-hoc parameterizations. These ad hoc procedures nevertheless lead to complex numerical codes: they are difficult to transfer from one basin to another one, or even to verify with data at a different scale. Tuning the model parameters is hazardous: predictions are often reduced to fitting existing observations. In contrast, in recent scaling approaches heterogeneity and uncertainties at all scales are no longer obstacles. It is viewed as a consequence of a scale symmetry which must first be analyzed and then exploited: small scale homogeneity assumptions are replaced by small scale heterogeneity assumptions that are verified from data covering a wide hierarchy of scale. PUB provides an unprecedented opportunity not only to test scaling concepts and techniques, but also to develop them further. The latter cross-cut PUB, since they are indispensable to evaluate: the information requirement, e.g.: which space and time scales are sensitive for a given prediction, what are the scaling regimes, the experimental requirement, e.g.: space and time resolution, outer/inner scale ratio, new data acquisition and processing methodologies to deal with wide range of space-time scales, strong variability, sparse networks, measurements at different scales and of different dimensionalities, implement a new modeling framework to incorporate the natural heterogeneity over a wide hierarchy of scales, use the latter to explore the heterogeneity and uncertainty in hydrologic predictions, maximise the yield of available hard and soft data by overcoming their mutual scale incompatibilities. We will illustrate the current state of the art on these questions and discuss their implementation in IAHS PUB initiative.

**HW07/10P/C25-003** **1445**

**MULTIFRACTAL METHODS OF FLOOD PREDICTIONS IN THE UNGAUGED BASINS**

Ioulia TCHIGUIRINSKAIA<sup>1</sup>, Pierre HUBERT<sup>2</sup>, Daniel SCHERTZER<sup>1</sup>, Hocine BENDJOU<sup>1</sup>, Shaun LOVEJOY<sup>2</sup> (<sup>1</sup>UMR Sisyphe, LGA, University P. et M. Curie, <sup>2</sup>UMR Sisyphe, CIG, Ecole des Mines, Paris, <sup>3</sup>Meteo-France & LMM, University Paris VI, <sup>4</sup>Physics Department, McGill University, Montreal)

River runoff phenomena reflect many complex interactions between diverse basin factors as well as meteorological and climatic fluctuations that strongly modify the precipitation input. Therefore the river runoff forecasting is a rather unresolved issue in hydrology. The question is even more puzzling for the areas where no actual flow measurements are available. Deterministic models based on various physical and/or statistical approaches are still face difficulties in capturing the phenomena of extreme precipitation and floods. It is well known that one of the main difficulties for the description of hydro-meteorological extremes is the colossal variability of their intensities over a wide range of space-time scales. To contribute to the PUB initiative, we use the multifractal framework not only to explain the power-law fall-off of probability distributions for hydrological-meteorological extremes, but also to explore a connection of the observed variability with the physics. We analyze space-time distributions of precipitation and discharges over different hydrological regions. A multifractal data analysis performed in the space-time domain produces - amongst other things - a physically-based tool for the clear distinction and multifractal description of flash-floods. We illustrate these methods on two recent flooding events in France: the Abbeville phreatic floods in 2001 and the flash floods in Gard in 2002.

**HW07/10P/C25-004**

**1500**

**APPLICATION OF A RANDOM CASCADE MODEL TO TEMPORAL AND SPATIAL PRECIPITATION DATA IN JAPAN**

Kunio TOMOSUGI<sup>1</sup>, Yasuhisa KUZUHA<sup>2</sup>, Tokuo KISHI<sup>1</sup> (<sup>1</sup>DPRI, Kyoto University, <sup>2</sup>National Research Institute for Earth Science and Disaster Prevention, and the Cooperative Graduate School, University of Tsukuba)

The theory of random cascades is useful for prediction of ungauged basins (PUBs) in the following contexts: 1) Multiscaling, which is one of the scale invariance properties resulting from spatial variability of precipitation, which can be reproduced by the theory of random cascades [e.g. Gupta, 1996], and the notion of scale invariance is very important for scaling, which is a powerful tool for PUBs in flood prediction. 2) The random cascade model is expected to be used as a tool for downscaling outputs from GCMs or radar data of precipitation and such downscaled data will be used as precipitation data of ungauged basins. Over and Gupta [1994] applied beta model to a meso-scale rain field and subsequently many researchers have investigated the theory of discrete random cascades. We applied the model whose generator is a beta model to temporal and spatial precipitation data in Japan. We applied the model to a long term's (8192 days) daily precipitation time series. Although the beta model is not adequate to reproduce the time series, we believe that a parameter  $p$  (see Over and Gupta, 1994), which governs the rate at which no-precipitation periods (pixels) appear in the time series, is meaningful in analyzing characteristics of the time series. Using the parameter, the meteorological observation sites are classified into two groups. One is along the Pacific and the other is along the Japan Sea. Time series of the former is relatively intermittent and the latter is less intermittent. Moreover, although both groups exhibit multifractal properties through convex function  $\tau(q)$ , the former exhibits a stronger multifractal property than the latter. Concerning spatial analyzing, we applied the beta model to many more scans than Over and Gupta. Because a rain field is affected by topography, we compared the data on 'land region' with those on 'sea region'. In respect to  $\log[\lambda_x]$  versus  $\log[f(\lambda_x)]$ , there is a difference between a land region and a sea region; for a land region, both positive and negative intercepts appear equally, but the positive intercept dominates in summer for a sea region. This results from the large spatial scale of a rain field. However, in respect to the correlation coefficient between  $\log[\lambda_x]$  and  $\log[M(q)]$ , both land and sea regions exhibit scale invariance in the range of 5 - 100 km, and random cascades can be applied to a land region as well as a sea region. We extracted some storms from the whole dataset and looked for a one-to-one relation between the spatial average of precipitation and parameter  $p$ . We concluded that the relation is a one-to-one function if we extract each 'individual' rain event, and the equation proposed by Over and Gupta [1994] is more appropriate than Over and Gupta [1996] for data in Japan. Gupta et al. (1996): J. Hydrology, 187, 81-104, Over and Gupta (1994): JAM, 33, 1526-1542. Over and Gupta (1996): JGR, 101, D21, 26,319-326,331.

**HW07/10P/C25-005**

**1515**

**PREDICTION IN UNGAUGED BASINS - DEVELOPMENT OF A COUPLED LAND SURFACE - CLIMATOLOGICAL MODEL FOR NEW SOUTH WALES**

Stewart William FRANKS (School of Engineering)

It is well known that Eastern Australia and New South Wales in particular experience one of the most variable climates at a range of timescales. Marked predictability of seasonal to interannual variability is governed by the occurrence of individual El Nino/Southern Oscillation (ENSO) events. In addition, recent research has also revealed multi-decadal modulation of both the magnitude and frequency of ENSO events, governed by a low frequency mode in midlatitude Pacific Ocean sea surface temperature (SST) anomalies. Given simple indices of ENSO and multi-decadal variability, a simple conceptual model of climate variability is shown to provide good explanation of the historic occurrence of every major drought and flood event across NSW, and may be used to anticipate future climate variability from seasonal to multidecadal timescales. With these insights, it is proposed that a coupled landsurface-climatology model is developed across NSW. The aim of such a model scheme is to provide prediction of a range of key hydrological variables under different multidecadal ENSO climate states. The utility of such a modelling scheme lies in its applicability to a range of users. This naturally necessitates a multi-objective conditioning approach (for instance, soil moisture, surface water, evaporative demand). To achieve a state-wide coupled model, regionalisation of both the climate and landsurface hydrological models is required. In this presentation, novel regionalisation methodologies to provide prediction in ungauged catchments are proposed. These include (a) conditioning a distributed rainfall model, (b) regional landsurface model structure assessment and identification and (c) the robust quantification of uncertainty.

**HW07/10P/C25-006**

**1545**

**GLOBAL ANALYSES OF SIMULATED HYDROLOGICAL BUDGET SENSITIVITY TO TEMPORAL CHARACTERISTICS OF PRECIPITATION**

Yukiko HIRABAYASHI<sup>1</sup>, Shinjiro KANAE<sup>1</sup>, Taikan OKP, Katumi MUSIAKE<sup>1</sup> (<sup>1</sup>Institute of Industrial Science, University of Tokyo, <sup>2</sup>Research Institute for Humanity and Nature)

Global numerical runoff simulation driven with global atmospheric data such as satellite estimation and output of atmospheric general circulation model (AGCM), is practical for providing probable runoff perspectives in ungauged basins. Since global atmospheric forcing which is indispensable for global hydrological simulation is limited in temporal resolution, several downscaling methods are proposed to obtain temporal characteristics of precipitation input, which has a large impact for hydrological budget estimation. In order to examine when and where the hydrological budget is estimated in the Land Surface Model (LSM) is sensitive to the temporal characteristics of precipitation input, two sets of off-line experiments are investigated. The first set of the experiments is global 1 x 1 degree simulation in 1987, which is driven by the same atmospheric forcing but different precipitation input, varying in temporal

scale from high(6-hourly) to low(deca-day or monthly).Low temporal precipitation is obtained by averaging original 6-hourlyprecipitation. Original 6-hourly and obtained deca-day averaged ormonthly averaged precipitation forcing are provided to the model and theresults are compared at each grid pixel.The results show that increases in surface runoff are obtained at mostof the grids with the low temporal precipitation, due to large increasein canopy interception.At the place where monthly LAI value is large and monthly precipitationis around 100 mm/month, the effects of the temporal scale of precipitationtend to be the largest.Another set of experiments is also 1 x 1 degree off-line simulation atone grid pixel using the accumulation of the observed precipitation.Three downscaling schemes for retrieving daily precipitation from the monthlyvalue are compared in terms of water balance calculated in the LSM.Both the number of days and intensity are shown to be important for thehydrological estimation in LSM.Thereby the water balance calculated in the experiment with a gammadistribution method shows fairly well accorded with the experiment usingobserved daily precipitation, and shows the applicability of the schemefor downscaling of daily precipitation from monthly data.

HW07/10P/C25-007

1600

**GLOBAL WETNESS PROJECT 2 AND PUB**

Taikan OKI<sup>1</sup>, Paul A. DIRMEYER<sup>2</sup> (<sup>1</sup>Research Institute for Humanity and Nature, <sup>2</sup>Institute of Industrial Science, University of Tokyo, <sup>3</sup>Center for Ocean-Land-Atmosphere Studies)

The Second Global Soil Wetness Project (GSWP-2) is the principalelement of the large-scale uncoupled land surface modeling actionin the Global Land-Atmosphere System Study (GLASS; Polcher et al. 2000)and a major element of the International Satellite Land-SurfaceClimatology Project (ISLSCP), both contributing projects of GEWEX.The overarching goal of GSWP is to produce as a community effortthe best model estimates of the global land-surface water and energycycles. This will entail an evaluation of the uncertainties linkedto the land surface schemes (LSSs), their parameters, the forcingvariables which drive them, and the spatial and temporal scalesto run the numerical simulations. The original pilot phase of GSWP covered the two-year period of theISLSCP initiative I data set (1987-1988), and proved the utility ofmodel comparison and sensitivity studies of the land surface at theglobal scale (Dirmeier et al. 1999).GSWP-2 will take advantage of the 10-year (1986-1995) ISLSCPInitiative II data set (<http://islsdp2.sesda.com/>) and LSS simulationswill be conducted at a spatial resolution of 1degree, sans Antarctica. LSSs calculate runoff and it can be compared with river dischargewith applying runoff routing models. Therefore GSWP can be consideredas PUB on global scales. Regional scales should be more focusedin PUB as hydrological science, nevertheless studies on global scale is also relevant since there are many places in the worldwhere global datasets of precipitation, landuse, soil types, etc.,are the only sources available for simulation and prediction ofriver runoff. Numerical experiments under GSWP2 is well designedto examine the uncertainties associated with the global offlinesimulations, and the outcomes should contribute for PUB studiesvery much. GSWP2 in PUB is also expected to identifyto what extent of temporal and spatial resolution predictingriver runoff can be estimated from global approach. Even though the major project under GSWP2 is the global approach,GSWP consists a few regional offline simulation, as well.Rhone-AGG experiment was carried out in the Rhone river basinwith gridded forcing data over Rhone river basin, and theeffect of the spatial resolution of the forcing data, suchas precipitation, radiation, on the energy balance estimationspecially river runoff by land surface models were evaluated.The scaling issues in land surface models particularly in terms of snow process and topography were addressed, and such anapproach can be expected to contribute for the PUB scaling issues.An intercomparison of regional offline simulations in the Chao Phrayariver basin in Thailand is planned under GSWP frame work,and it should also fit to be a suitable candidate for PUB basin.

HW07/10P/C25-008

1615

**IMPROVED MODELING OF CATCHMENT SCALE HYDROLOGICAL PROCESSES: BRIDGING THE GAP BETWEEN LOCAL KNOWLEDGE AND THE GLOBAL PROBLEM OF UNGAUGED CATCHMENTS**

Peter A. TROCH (Department of Environmental Sciences, Wageningen University)

Society is facing growing water resource needs (e.g. hazard mitigation) in a changing global environment. The postulated acceleration of the water cycle places hydrological science at the centre stage in the climate change debate. In IPCC reports, climate change predictions are more reliable for temperature as compared to precipitation, river flows and aquifer levels. This is due to the poor performance of hydrologic predictions at larger scales. Most hydrologic understanding is based at the point scale, whilst our needs for predictive modeling are at catchment scales. There is an urgent need for improved hydrologic predictions at that scale. Solving this spatial scaling problem requires a new approach along two lines of research. First, understanding the interaction between catchment characteristics and flow processes is of crucial importance. Recently, Troch et al. (2002a,b) developed storage-based dynamic equations able to capture the flow processes of complex landscapes by simple scaling laws pertaining to hillslope length, slope and form. Such a description will form the basis of a new generation of distributed catchment models that capture the essential behavior of the natural system but are low-dimensional and computationally efficient. Second, the complexity of the groundwater-surface runoff interaction forms a major challenge in catchment modeling. Due to the fact that the hydrologic system is heterogeneous and distributed, its identification is ill-posed. In this situation progress can be made by supplementing in-situ observation with remotely sensed soil moisture and evapotranspiration observations. By concentrating on the assimilation of remote sensing data in its broadest interpretation with the new strategy in catchment-scale hydrological modeling, this research aims at resolving the longstanding ungauged catchment problem.

HW07/10P/C25-009

1630

**MODELLING UNGAUGED CATCHMENTS USING THE REW APPROACH: DERIVATION OF REGIONAL SCALE CLOSURE RELATIONS USING HIGHLY RESOLVED, PHYSICALLY BASED SIMULATIONS**

Erwin ZEHE<sup>1</sup>, Murugesu SIVAPALAN<sup>2</sup> (<sup>1</sup>Institute of Hydraulic Engineering, University of Stuttgart, 70550 Stuttgart, Germany, <sup>2</sup>Department of Environmental Engineering, Centre for Water Research, The University of Western Australia, Crawley WA 6009, Australia)

Predicting the water balance of ungauged catchments is one of the most challenging tasks in hydrology. The Representative Elementary Watershed approach (REW) is a promising theoretical framework for that purpose. An REW is an abstract spatial object that shall be used as characteristic elementary unit to represent real world catchments in a model. Consequently it posses the most important properties of real catchments such as a saturated and unsaturated zone, saturated areas, a river net and a topography. The mass, energy and momentum balances in the individual zones of an REW are modelled using a set of coupled ordinary differential equations, that are derived from first principles using the second law of thermodynamics. The application of the REW approach to real catchments requires of course suitable parameterisations of the exchange terms of mass, energy and momentum across the boundaries between the different zones. The water and heat exchange between

the soil and atmosphere or between the unsaturated and saturated zone is determined by the subsurface thermal and hydraulic properties and their variability, due to the presence of macropores or strata in the soil or the aquifer. Appropriate closure relations have therefore to parametrise the main effects of the dominating subscale subsurface heterogeneity on the exchange of mass, energy and momentum. Thus, the concrete soil, geological and morphological properties of the region of interest come into play. A physically based model for catchment water and heat dynamics may explicitly account for the heterogeneity of hydraulic and thermal properties and therefore generate a suitable data base for deriving appropriate closure relations to parametrise the influences of subscale heterogeneity in the REW approach. Of course these relations are unique in the sense that the very details of the catchment properties are determined by unique details of a place. On the other hand catchments in the same landscape exhibit often similar geological, morphological and soil characteristics, which in turn affect the hydrological cycle in a way that is typical for that landscape. Due to this generality of places, the objective of our joint research is to derive closure relations for two typical regions in Australia and Germany, that reflect the typical subscale influences on the exchange of water and heat. To this end the water and heat dynamics of several typical catchments in each of the regions are simulated using a highly resolved, physically based model. Closure relations are derived, using appropriate measures for average quantities and their variation, and verified in a cross validation approach. By relating the closure terms to typical catchment characteristics, we hope to end at typical landscape specific closure relations. This would be significant progress towards the prediction of ungauged basins using the REW approach.

HW07/10P/C25-010

1645

**THE ROLE OF 'TOP-DOWN' MODELLING FOR PREDICTION IN UNGAUGED RIVER BASINS**

Ian Geoffrey LITTLEWOOD<sup>1</sup>, Murugesu SIVAPALAN<sup>2</sup>, Tony JAKEMAN<sup>3</sup>, Barry CROKE<sup>3</sup> (<sup>1</sup>Centre for Ecology and Hydrology, <sup>2</sup>Centre for Water Research, The University of Western Australia, Crawley WA 6009, Australia, <sup>3</sup>Integrated Catchment Assessment and Management Centre (iCAM), Australian National University, Canberra ACT 0200, Australia)

Following the 2002 Kick-off Meeting to mark the start of the Decade on Prediction in Ungauged Basins (PUB), an initiative of the International Association of Hydrological Sciences, various groups were commissioned to prepare position notes as contributions towards the development of Science Plan and Implementation Plan documents for PUB. In the context of the role of 'top-down' modelling in PUB, this paper is an extension of the notes prepared on that topic for that purpose. Top-down modelling is described and placed within the broad spectrum of modelling approaches that will be adopted for PUB. The merits of top-down modelling in hydrology, and its applications for assisting with prediction in ungauged basins, are discussed through relevant examples.

HW07/10P/C25-011

1700

**INVESTIGATION OF APPLICABILITY OF A PHYSICALLY BASED MODEL OF SNOWMELT RUNOFF GENERATION TO POORLY GAUGED BASINS**

Lev S. KUCHMENT (Water Problems Institute of RAS)

A physically based distributed model of runoff generation, including the description of snow processes, soil freezing and thawing, formation of runoff losses and infiltration, evaporation, overland and subsurface flow, water movement in the river channel system, has been applied to investigate capability of assigning a priori values of the model parameters for snowmelt flood modelling. The measured or calibrated parameters which had been obtained for the models of runoff generation for two experimental river basins (the Kontaknyy Creek basin with the catchment area 21 sq. km, and the Devitzka River basin with the catchment area 103 sq. km.), have been also used for modelling runoff generation in two large basins with similar physiographic conditions (the Kolyma River basin with the catchment area 100,000 sq. km. and the Seim River basin with the catchment area is 7500 sq. km., respectively). It has been shown that only 2-3 of the most important parameters should be recalibrated against runoff data for 2-3 years, whereas the values of the rest 10-12 parameters can be regionalized. Numerical experiments have been carried out to test ability of using different relationships between the most important parameters of the models under consideration and the measured basin characteristics for runoff modelling at absence of runoff measurements.

HW07/10P/C25-012

1715

**ACCURACY AND SENSITIVITY OF PHYSICS-BASED DISTRIBUTED MODELING USING FIRST-GUESS PARAMETER CHOICES DERIVED FROM GEOSPATIAL DATA**

Baxter Ernest VIEUX, Jean E. VIEUX, Eddie KOEHLER (School of Civil Engineering and Environmental Sci., University of Oklahoma)

Hydrologic predictions in ungauged basins can be approached by using a physics-based distributed hydrologic modeling framework. The objective of distributed hydrologic modeling is to better represent the spatial heterogeneity of a watershed and thereby increase the prediction accuracy. Accomplishing this by representing the spatial pattern of important parameters requires assembly of geospatial data from a variety of sources including geographic information system maps and remotely sensed data (GIS/RS). Models that make use of these worldwide geospatial datasets offer important prediction capabilities where limited data exists. For example, digital elevation models (DEM) of terrain are available worldwide at 1-km resolution, and locally at even higher resolution. Prediction accuracy related to resolution and data accuracy of the DEM, as well as other data, can limit the ability to model certain basin scales or processes. Other sources of prediction errors stem from precipitation inputs, land cover/vegetation, and soils. Together, the data and associated uncertainties affect model accuracy for predicting various components of the hydrologic cycle. Rainfall-runoff is particularly important for a variety of applications such as water supply, flood prediction, and hydropower. Modeling event-scale runoff provides important decision support for water quality and quantity management. While calibration of conceptual models depends on historical archives of flow rates and precipitation inputs; physics-base models can be applied with fewer or even no historical data. Physics-based models that rely on conservation equations have the advantage of having physically significant parameter values that can be estimated from physical watershed characteristics, some of which are derived from GIS/RS geospatial data. Within such a modeling framework, an important question remains: How accurately can hydrographs be simulated using first-guess parameter choices? Several case studies using a fully distributed physics-based rainfall-runoff model, called Vflo™ will be presented that demonstrate the first-guess accuracy within this framework. The accuracy that can be expected and the sensitivity to geospatial data resolution, accuracy, and ancillary channel hydraulics will be examined. Understanding model limitations and sensitivities in these cases provides guidance for application in ungauged basins. Case studies are derived from model applications for basins in Romania, Taiwan, and the US that demonstrate model accuracy for river basins on the order of 100-10000 km<sup>2</sup>. **Submitted under (iii) Methodological (Modelling) Frameworks**

HW07/10P/C25-013

1730

**EXPLORING THE POTENTIALITY OF PREDICTION IN UNGAUGED BASINS OF A PHYSICALLY BASED HYDROLOGIC MODEL**

Mario L.V. MARTINA<sup>1</sup>, Ezio TODINI<sup>1</sup>, Zhiyu LIU<sup>2</sup> (<sup>1</sup>Department of Earth Science, University of Bologna, <sup>2</sup>Hydrology Bureau, Ministry of Water Resources of P.R. China)

This work explores the potentiality of prediction in ungauged mesoscale basins of a physically based distributed rainfall-runoff model using some globally available data sets. The rainfall-runoff model TOPKAPI is characterized by a simple parameterization linked to the Digital Elevation Model, the soil type and land use maps of the catchment. The availability of these data at global scale makes possible to take advantages of information and results from gauged catchments for geomorphological and topological similar ungauged ones. The estimations of meteorological inputs from remote sensing campaigns are used either at their original scale or downscaled by means of a disaggregation technique which takes into account local variability (orographic effects). An application is presented for two morphological similar gauged catchments, one treated as ungauged.

HW07/10P/C25-014

1745

**A HYDROLOGICAL MODEL FOR UNGAUGED BASINS USING THE KINEMATIC WAVE APPROACH**

Amithirigala W. JAYAWARDENA, Pat J.-F. YEH (Department of Civil Engineering, The University of Hong Kong)

A physics-based distributed hydrological model that can be used for ungauged basins is proposed in this study. It can be thought of as a spin-off from an earlier study in which a catchment has been subdivided into strips of variable widths and the kinematic wave approximation used as the governing equation. With the availability of GIS techniques and digital elevations maps, the catchment topographical features can now be represented to a much higher degree of accuracy. The geometrical framework for the model would consist of a series of overland flow strips which will join the river network. Runoff would be simulated by assuming two layers of flow, one overland, and the other sub-surface, representing interflow, parallel to each other. The governing equations would be the kinematic wave equation for the overland flow, and the continuity equation coupled with Darcy's law for the sub-surface flow. The latter can also be expressed as a form of kinematic wave equation. Because of the kinematic wave assumption, this approach will be limited to steep catchments where hillslope hydrology dominates. The governing equations will have parameters that can be physically identified and therefore measurable at least in theory. Spatial variations can be accommodated to account for catchment heterogeneity. It is proposed to solve the governing equations within the distributed catchment framework using a numerical procedure based on the Finite Element Method. The Finite Element Method has the flexibility to accommodate uneven boundaries. The proposed technique will be applied to a small catchment in Southern China.

Friday, July 11 AM

HW07/11A/C25-001

Invited

0830

**NESTED CATCHMENT EXPERIMENTS: CONSTRAINING THE HYDROLOGIC UNCERTAINTY IN THE PREDICTION OF UNGAUGED BASINS**

Eduardo M. MENDIONDO (Escola de Engenharia de Sao Carlos, University of Sao Paulo, Brazil)

A central theme of the IAHS' PUB initiative (Prediction in Ungauged Basins) is to constrain the predictive uncertainty through improved ways to study the effects of heterogeneity, process understanding and through access to new data resources. This is a task in the IAHSAPUB Science Steering Group (<http://www.cig.ensmp.fr/~iahs/>), concerning experiences gained, lessons learned and perspectives on hydrologic uncertainty. Scientific questions are to be more developed in the forthcoming decade to constrain the predictive uncertainty in terms of the role of theory, basins, field experiments, process understanding and new data base required. Research pathways feasibly advanced on hydrologic uncertainty are here depicted, in order that regionalization thresholds could be grasped by practical methods of gauging. For instance, the Nested Catchment Experiment (NCE) sets up observational layouts of gauging catchments in nested spatial scales, i.e. from headwaters to lowlands. The NCE's focus is on multiple spatial gauges as well as on measurement of hydrologic parameters needed for modelling. By using NCE in representative basins it is better understood how space-time hydrologic variabilities occur and are related to basin heterogeneity of a specific world biome. Experiences gained with different NCE layouts sited in Brazil are presented, in terms of observational hydrology, modeling requirements and how they will be integrated into the entire PUB programme. Special attention of NCE layouts is outlined on the feedback from field hydrologists and water practitioners who are highly aware of the prior uncertainties in gauging station networks and experiments. NCE envisages new win-to-win opportunities in providing scientific underpinnings with UNESCO programmes like HELP and WWAP, as well with WMO. Summarized discussions look for lessons learned in those Brazilian NCE layouts showing what helpful yardsticks could collaborate with the IAHS' PUB Decade, assisting new kind of experiments to the constrain of predictive uncertainty in world biomes.

HW07/11A/C25-002

0900

**LESSONS LEARNT FROM TRACER AND CATCHMENT MODELLING STUDIES IN MESO-SCALE BASINS**

Stefan UHLENBROOK, Nils TILCH, Jens DIDSZUN, Bettina OTT (Institute of Hydrology, University of Freiburg)

Beside the prediction of water quantities the PUB initiative focuses also on the prediction of water quality, erosion, sediment etc. In addition, predictions for future conditions under changed circumstances (i.e. altered land use, changed climate) or extreme conditions are wanted. Therefore, processes-based approaches are required since extrapolations are not feasible using purely empirical approaches. Since 3 years comparative field and modeling studies are carried out in four meso-scale mountainous basins in Germany and the Austrian Alps. The catchment sizes vary between 1.5 and 258 km<sup>2</sup>. Land use and other physiographic characteristics (climate, geology, soils, topography etc.) are different in each basin. Within this research initiative, the authors carried out tracer studies in each basin and applied the process-oriented catchment model TACD to several (sub-)basins. The tracer aided catchment model (TACD, D = distributed) is a raster-based conceptual catchment model that works on an hourly base. This paper summarizes some fundamental results and lessons learnt from it. Specifically it addresses the following questions: (i) How can a meso-scale catchment be discretized from a process-based point of view into a set of response units? (ii) How can a better understanding of runoff generation mechanisms (incl. its heterogeneity and variability) at smaller scales be translated to an improved catchment modeling at larger scales? (iii) How can we use process knowledge and further hydrometric

measurements (tracers, snow cover, soil moisture, groundwater levels etc.) for model application and validation? (iv) What is the value of such data to reduce the predictive uncertainty in ungauged basins?

HW07/11A/C25-003

0915

**NEEDS AND CONSTRAINTS FOR HYDROLOGICAL BEHAVIOUR OF UNGAUGED BASINS: AN EXPERIENCE IN SWISS AND LUXEMBOURG CATCHMENTS**

Andre MUSY, Benoit HINGRAY, Markus NIGGLI (IAHS - CHy)

To provide operational methodological frameworks to institutions in charge of the sustainable management of water resources, various key issues have to be investigated and solved previously by the scientific community. Appropriated tools have to be identified for the various hydrological, climatic and physiographic contexts that are to be observed throughout the world. Hydrological models may be for example very different according to the scale of the catchment and to the dominant processes that govern the rainfall-runoff transformation. One challenging issue for the future decades is 1) to identify from the already available set of gauged catchments an exhaustive panel of the different kinds of possible hydrological behaviours, 2) to identify the dominant physical catchment and climatic characteristics that explain such behaviours and 3) to develop different criteria to identify for any ungauged catchment the catchment class it belongs to. The transposability of methodological tools that may be valid for a class of catchments has also to be explored. Dense experimental catchment networks are here of major interest as for these catchments the climatic context can be considered as homogeneous and as the hydrological behaviour variability observed between the different gauged catchments can be a priori explained by the variability of a small number of physiographic factors. The regional relationships that may be derived between the parameters of hydrological models and relevant physiographic features can be used afterwards for ungauged catchments. For the characterisation of some hydrological characteristics (floods, low flows, seasonality) of the ungauged catchments located in the 'swiss plateau' region (approximately 6000 km<sup>2</sup>, with homogeneous climatic and physiographic context), the Laboratory of Hydrology and Land Improvement (HYDRAM) tested a continuous hydrological model on 30 gauged catchments belonging to the region. The good performance of the modelling approach obtained for the 30 studied catchments as well as the reasoned and robust multilingual calibration procedure developed for the calibration of the model parameters permitted the development of the model regionalisation. For the homogeneous climatic context of the studied region, the variability of the model parameters could be actually explained, as expected, from the variability of relevant physical catchment characteristics such as the catchment slope and surface area, the nature of the soil and underground material. To improve the transposability of the model, this regionalisation procedure is also performed for other climatic and physiographic contexts: this regionalisation was successfully applied for example to the very dense discharge measurement network of the Alzette catchment, Luxembourg, and is being carried out for different mountainous catchments located in the upper Rhone catchment (swiss alps). These works especially permit to highlight other relevant physiographic variables for the explanation of the model parameters variability. The development of appropriated tools for ungauged catchments could thus benefit from the experiences derived from very dense networks as the ones already available in some regions of the world. Such experiences could actually provide afterwards relevant basis for extension to other regions with lower instrumental potential but high interest in efficient methodological tools for water resources management.

HW07/11A/C25-004

0930

**A SCIENTIFIC FRAMEWORK FOR MODEL EVALUATION WITHIN PUB**

Thorsten WAGENER, Hoshin V. GUPTA, Soroosh SOROOSHIAN (Department of Hydrology and Water Resources, The University of Arizona, USA)

A large number of modeling approaches is available for predictions in gauged and ungauged basins. Modelling approaches differ, for example, in the degree of detail described, the manner in which processes are conceptualized, requirements for input and output data, and possible spatial and temporal resolution. However, there exists little scientific guidance to what modeling approach might be suitable for what circumstances. The result is that a range of modeling approaches often appear equally likely for a specific study, and the selection process amounts to a subjective decision by the modeler. What kind of approach is suitable for what case is one of the challenges we face within PUB. Progress in this area can only be made through the combined efforts of a large number of scientists with different expertise. Here, we suggest a scientific framework for this task. The main (scientific) criteria for the selection of a particular modeling approach are the modeling purpose (e.g. simple vs. complex), the basin characteristics (e.g. arid vs. humid) and the available data (e.g. sparse vs. abundant). These three dimensions of the classification problem have to be split into cases representative for realworld situations. Recent advances in model evaluation techniques, such as multi-objective and adaptive approaches, could then be utilized as far as possible to classify modelling approaches. We outline the details of such a scientific framework for model evaluation and classification, including potential evaluation techniques to be used and open questions to be answered. Partial application examples for such a framework will be given. This effort can be an integrating element within PUB since it requires the contribution of scientists working on any element that contributes to hydrological predictions. The implementation of such an evaluation effort would mean significant progress in hydrological modeling and would also form a very valuable link between PUB and other existing initiatives such as MOPEX.

HW07/11A/C25-005

0945

**MOPEX'S LINK TO PUB**

John SCHAAKE, Qingyun DUAN (Hydrology Laboratory, NOAA/NWS/OHD)

The goal of the Prediction for Ungauged Basins (PUB) initiative is to gain scientific knowledge, acquire experimental data and routine observations, and develop application techniques to produce hydrologic predictions for basins where hydro-meteorological data are scarce or non-existent. Intercomparison of existing hydrological models, in a wide range of basins around the world, is identified as a key activity to achieve PUB goal. Model Parameter Estimation Experiment (MOPEX), an ongoing international project to develop a priori parameter estimation techniques for ungauged basins, can contribute the PUB initiative in several ways. First, MOPEX can contribute to PUB science as MOPEX leads to improved understanding of how model parameters reflects basin climatic and geophysiological properties and heterogeneities. Second, MOPEX has assembled a large number of basins worldwide that can facilitate the PUB model intercomparison study. Third MOPEX provides vehicles to transfer knowledge from gaged basins to ungauged basins.

HW07/11A/C25-006

1000

## ON ENVIRONMENTAL MODELS OF EVERYWHERE AS A TEMPLATE FOR PUB

Keith J. BEVEN (Lancaster University, UK)

The PUB initiative will span the period during which, at least in the developed world, integrated environmental models will be developed of whole countries. Initiatives in this direction have already been taken for hydrological purposes in Denmark, the Netherlands, France and elsewhere. These will, in the future, be developed to include other environmental processes that are the subject of legislation for sustainable development. The computer power already exists to do this and it will become cheaper to implement and maintain in future. The interesting question of such systems is, of course, that nearly all the landscape that will be modelled is, to some greater or lesser extent, "ungauged". Thus, however such models are implemented - whether as fully distributed discretisations or overlapping scale-dependent lumped landscape units - initial representations of every ungauged unit will be required. A viable PUB extrapolation methodology, from gauged sites to ungauged sites, is therefore initially essential. After that, however, the game will change to a process of learning about local places and, in particular, about local places where the initial representation turns out to be wrong. There will be places where that may not be important and uncertainty is acceptable, there will be other places where it is essential to have accurate predictions and uncertainty will need to be constrained. The really interesting question within the context of PUB is then how best to use sparse resources to constrain uncertainty at local places with their own unique characteristics.

HW07/11A/C25-007

1015

## ANALYSIS OF UNCERTAINTY IN FLOW PREDICTION FOR UNGAGED CATCHMENTS

Manfred Walter OSTROWSKI (Civil Engineering, Darmstadt University of Technology)

Both, simulated river flows in gaged and ungauged basins contain considerable uncertainty, however, uncertainty of estimated flows in ungauged basins is considered definitely higher. To identify and possibly quantify these uncertainties, they have to be categorised and analysed separately. Possible categories could be uncertainties of data (random and systematic errors), models (structural and application errors) and parameter estimation (methodological and application). Data errors include input data (geographic, geometric and meteorological) and data being used for parameter estimation and verification such as measured flows. At times, uncertainty of stage discharge relationships used to derive flows from water levels is known to be as uncertain as no flow data at all. Model errors include e.g. errors related to deviations between physically defined and conceptual approaches, application errors cover inadequate application of model, e.g. through limited knowledge of user. Parameter estimation errors can relate to inadequate application of an estimation method or to weakness of the method itself. With such a differentiation it is possible to isolate and quantify the effects of e.g. missing flow data for parameter estimation. It clarifies the probably non linear superposition of single uncertainties, which provides much more information than simply applying a model with and without measured flow data. The paper will present the background of the problem, and demonstrate a possible approach for a separated analysis of single categories. The approach is based on the estimation of error distribution functions from which values are drawn randomly for Monte Carlo Simulation. A case study will be presented when errors involved in erosion process analysis were investigated. The paper is meant to contribute to the discussion rather than presenting new results.

HW07/11A/C25-008

1045

## COLD REGIONS HYDROLOGY, UNCERTAINTY AND PREDICTION WITH MINIMAL INFORMATION

John W. POMEROY<sup>1</sup>, Lev S. KUCHMENT<sup>2</sup>, Alexander N. GELFAN<sup>3</sup>, Raoul J. GRANGER<sup>4</sup>, Donald M. GRAY<sup>5</sup>, Newell R. HEDSTROM<sup>6</sup> (<sup>1</sup>Institute of Geography & Earth Science, University of Wales, Aberystwyth, <sup>2</sup>Water Problems Institute, Russian Academy of Sciences, Moscow, Russia, <sup>3</sup>National Water Research Institute, Environment Canada, Saskatoon, Canada, <sup>4</sup>Division of Hydrology, University of Saskatchewan, Saskatoon, Canada)

The IAHS 'Decade for Prediction of Ungauged Basins' issues of predicting water resources in areas with poor or sparse observations have particular relevance to those interested in cold regions hydrology. The major hydrological events in cold regions are related to storage in and melt of snow, ice and frozen ground. However, observational networks of snowfall, snow depth, frozen ground, ice extent, and streamflow have never been particularly dense in cold regions, and recently have declined dramatically. The difficulties of measuring snow accumulation, interception, redistribution, frozen soil moisture content, and streamflow under ice have long meant that even routinely-gauged basins represent areas of high uncertainty in hydrological calibration and estimation. The transferability of regionally-developed modelling methods and parameters is of interest to improved water resource prediction in data sparse regions. Because of a long-standing problem of data availability in cold regions, there are several methods for applying physically-based models based on hydrological processes; the physical basis of these approaches may have relevance to improving more temperate hydrological applications as well as in the cold regions. Initial experiences suggest that physically-based snow process representations with parameters bounded by physical laws, field or analytical experiments rather than calibration show promise for inter-continental transferability of models, parameters and applications. Transferrability is most successful within similar biome types such as steppes, boreal forest, taiga and arctic tundra.

HW07/11A/C25-009

1100

## WATER-QUALITY PREDICTION IN UNGAUGED BASINS

Norman E. PETERS (U.S. Geological Survey)

To date (January 2003), the focus of the International Association of Hydrological Science's decadal initiative on the Prediction in Ungauged Basins (PUB) has been on water quantity (storage and fluxes). A primary interest of hydrologists and water resource managers, however, is water quality, particularly as affected by human activities, i.e., growing and pervasive water-quality degradation. The quality of freshwater at any point on the landscape reflects the combined effects of natural and anthropogenic processes along hydrologic pathways, for which the process relations may be cyclical (interdependent and/or periodic) and cascading. Local, regional, and global differences in human activities (e.g., mining, industry, agriculture, waste treatment and disposal), climate, and streamflow are considerable, and, in turn, cause varying effects on water quality and quantity. This paper explores answers to several questions about a water quality component of PUB. What do we know about the water quality of ungauged basins? What confidence do we have to predict parameter or constituent concentrations and loads (averages, medians and ranges)? What information is required to reduce the uncertainty in water-quality predictions? How can information from well-studied areas be used for predictions in poorly studied areas?

HW07/11A/C25-010

Invited

1115

## THE IMPERATIVE OF THE PUB APPROACH FOR SUSTAINABLE WATER MANAGEMENT IN WEST AFRICA

Lekan OYEBANDE, Olusegun ADEAGA (University of Lagos)

Rational water resources planning and development is being hampered by the problem of inadequate data and information in developing countries such as those of West Africa including Nigeria. An understanding of the spatial and temporal variation of hydrological phenomena and processes is crucial for sustainable water resources planning. Although great efforts have been made in the past at the national, regional and international levels in respect of hydrological monitoring and data bank creation as well as data dissemination. The status of gauging of the various basins is far from satisfactory and in many cases, worse that it was a decade ago. The hydrometeorological networks of the 1980s have fallen apart and there are doubts as to how many stations are actually functioning. Indeed the proportion of the established hydrometric gauging stations that may be functioning in the nine countries of the Niger basin represents as low as 45% in Niger and Nigeria to 50% in Mali and Burkina Faso. Only countries such as Benin, Cameroon and Cote d'Ivoire, which operated only 5-15 stations, have been able to keep those stations in operation. Efforts made to improve hydrological assessment of basins and their water resources in West Africa include those of the World Bank Sub-Saharan Hydrological Assessment, the HydroNiger a project consisting of 65 data collection platforms (DCPs) in the whole of the Niger basin with the technical assistance of WMO, OPEC Fund, EEC, and UNDP. The current and latest initiative is the West and Central African HYCOS being developed by WMO. It has inherited the DCPs used by the Niger Basin Authority's HydroNiger project and the WMO OCP/ONCHO. HYCOS involves 23 countries in West and Central Africa in its pilot phase launched in Dec 1999. In this study, the causes of the seeming failure of the past efforts and present status of hydrological monitoring and data base management task and data dissemination in West Africa are addressed. The imperative of adopting PUB as a complimentary tool for a better understanding of drainage basin dynamics and their aggravation by man's activities in these poorly gauged / ungauged basins is stressed. Ironically it is in such basins as the Niger that intensive and reliable data sets are more needed in order to understand the complexity of the basin hydrological systems. PUB is necessary if a policy-relevant science is to be adopted in this era of ever-reducing ground based conventional observation networks and wide spread ungauged basins. The paper examines the value that could be added by PUB through digital terrain modelling for a dynamic, if not near real time operational hydrological practice in the data-scarce basins of the Niger basin and West Africa.

HW07/11A/C25-011

1145

## THEORETICAL EXPLORATION OF CLIMATIC AND LANDSCAPE CONTROLS ON INTER-ANNUAL VARIABILITY OF RUNOFF AND FLOW DURATION CURVES

Murugesu SIVAPALAN<sup>1</sup>, Yoshiyuki YOKOO<sup>2</sup> (<sup>1</sup>Centre for Water Research, University of Western Australia, <sup>2</sup>Institute of Industrial Science, University of Tokyo)

The chief cause of the PUB problem is our inability to deal with the heterogeneity of climatic inputs and landscape properties, and their impacts on the space-time variability of streamflows. The main aim of this paper is therefore to present a theoretical framework with which to investigate space-time variability of runoff fields, with a view to eventually enabling us to interpret the space-time patterns in the variability of observed streamflows in terms of the underlying climate-soil-topography interactions. It is expected that the resulting understanding of the causes of observed variabilities will enable us to make improved predictions in ungauged catchments. In particular, the paper focuses its attention on two distinct signatures of such variability, namely the inter-annual (between years) and intra-annual (within year) variabilities of runoff. In this case we use a physically-based formulation of water balance developed that has been developed from first principles, directly at the scale of a representative elementary watershed (Reggiani et al., 2000), for an idealised catchment, and capable of including the effects of climate, soils and topography. The model is driven by synthetic realisations of precipitation events which are generated through a stochastic rainfall model but reflecting realistic conditions. The model simulations of catchment response are used to characterize the probability distribution functions of antecedent soil moisture content and storage, and within-year and inter-annual variabilities of runoff for various combinations of climate (including seasonality), and soil and topographic properties, and these will be interpreted in terms of key dimensionless similarity indices the climate, soils and topography (a dryness index, a storage index and a drainability index). Reggiani, P., M. Sivapalan and S. M. Hassanizadeh (2000). Conservation equations governing hillslope responses: Exploring the physical basis of water balance. *Water Resources Research*, Vol. 36, No. 7, pp. 1845-1864.

HW07/11A/C25-012

1200

## ESTIMATION OF ANNUAL RUNOFF STATISTICS IN UNGAUGED BASINS WITH PARSIMONIOUS EVALUATION OF CLIMATIC INDICES

Pierluigi CLAPS<sup>1</sup>, Giovanni LAGUARDIA<sup>2</sup> (<sup>1</sup>DTIC - Politecnico di Torino, <sup>2</sup>DIFA - University of Basilicata)

Relations between climatic parameters and hydrological variables at the basin and the regional scale are investigated, using climatic classifications as synthetic indices representing the average annual water budget. Precipitation, temperature and net radiation are the climatic variables required for evaluating the climatic indices in the formulations proposed by Thornthwaite, Emberger and Budyko. The spatial distribution of these variables has been studied in the 10,000 km<sup>2</sup> territory of the Basilicata region (southern Italy), to evaluate the possibility of their indirect estimation. Precipitation and temperature data was available for several stations within the region, while only measures of global radiation were available for few stations in a reasonable number of years. Simple, yet robust, literature methods for estimation of net radiation were adopted, to limit the ground data requirement to temperature, and relative heliophany. Temperature was, in turn, related to elevation and latitude in a statistical analysis performed earlier in a much larger area. Consequently, all of the climatic indices considered can have an approximate evaluation using only data of precipitation, elevation, latitude and relative heliophany. The above-mentioned climatic indices were evaluated after estimation of the mentioned variables over a grid of resolution of about 1 km. Satellite data of cloudiness were used in place of the relative heliophany. Lumped climatic indices computed on the gauged basins available in Basilicata were found to be clearly related to mean and variance of the measured annual runoff series. The Budyko index was the best in terms of symmetry of the frequency distribution, sensitivity to aridity and quality of the correlation with the moments of the annual runoff. To further substantiate the potential of synthetic climatic information to support a regional hydrologic studies, additional satellite data have been used, retrieved by NOAA-AVHRR. In particular, the normalized difference vegetation index (NDVI), obtained with the maximum value composite technique, has been compared to the above estimates of climatic indices. Dependency of the vegetation phenology from the available water and, as such, from the average water budget, support the connections found between NDVI and the estimated climatic indices. These initial results indicates that there are good premises in the task of reducing the

dependence of climatic mapping in a region from ground data, with special reference to the measure of precipitation.

**HW07/11A/C25-013**

**1215**

**SOME PERSPECTIVES ON REGIONALISED MODELS FOR WATER RESOURCES ASSESSMENT: FROM FLOW STATISTICS TO TIME-SERIES**

Andy R. YOUNG, Matt G.R. HOLMES, Alan GUSTARD, H.Gwyn REES (Centre for Ecology and Hydrology - Wallingford)

The estimation of river flows is a central component of water resources management, however management decisions are frequently required within catchments for which there are little or no gauged flow data. Since the 1970s this has led to many international examples of the development of regionalised hydrological models. Commonly these have been based on the development of empirical relationships between statistics of river flow and catchment characteristics. More recently, advances have been made in the science of regionalising parsimonious rainfall runoff models. From a regulatory perspective these recent advances have been primarily driven by the requirement for linking hydrological determinations with ecological assessments. Other drivers have been to improve the representation in land surface interactions within climate models and to improve our understanding of the scaling of hydrological processes. This paper will review the development of the science of regionalisation for water resources purposes within the United Kingdom from flow statistics to time series of river flows. The paper will discuss the drivers, the methods, data and will seek to identify some of the limiting factors and challenges that this area of research is faced by, using the UK as an example. The paper will conclude with an example of how similar principles have been used within the relatively data-sparse region of Nepal and the northern Indian state of Himachal Pradesh to elucidate relationships between river recession characteristics and basin characteristics.

Friday, July 11 PM

**HW07/11P/C25-001**

**1400**

**THE NEED FOR A NEW LOOK AT REGIONALIZATION BY REGRESSION ANALYSIS**

Robin Thomas CLARKE (IPH-UFRGS)

Regression analysis has long been used for the transfer of information from gauged to ungauged drainage basins. It is used not only for estimating (a) flow characteristics, such as mean annual flow, but also (b) extreme flows with given return period, and (c) estimates of parameters of rainfall-runoff models fitted to the hydrological data in gauged basins. As commonly used, the logarithm of the variable of interest (here termed  $Q$ ) is expressed as a linear multiple regression in terms of the logarithms of explanatory variables which include basin area ( $A$ ), together with other variables ( $S, P, \dots$ ) describing basin topography, climate, vegetation, geology and lake storage. Until better procedures are developed, regression-type relations will continue to be used in the future for imputing the hydrological behaviour of ungauged basins. However, statistical methods and computing software have developed rapidly over the last quarter century, and there are now many alternatives to expressing  $\ln Q$  linearly in terms of  $\ln A, \ln S, \ln P, \dots$ . This paper argues that there is a need to utilise existing data from gauged basins to explore the usefulness of the many alternatives to simple multiple regression, so as to (a) incorporate information on the spatial configuration of the gauged basins: namely, their degrees of spatial separation and orientation; (b) allow for the facts that the explanatory variables  $A, S, P, \dots$  are known to be subject to error, which can often be estimated; (c) explore the use of possibly more appropriate functions of  $Q, A, S, P, \dots$  than their simple logarithms; (d) allow for the correlation between different response variables  $Q_1, Q_2, \dots$ , where these are each to be estimated for an ungauged basin; (e) explore the use of robust regression procedures that are less susceptible to outliers in data than least-squares regression. Better empirical relations would not only be useful in their own right, but would also increase the value of prior information, where this is to be combined with limited data from an ungauged basin by Bayesian methods.

**HW07/11P/C25-002**

**1415**

**SIMPLE METHODS OF HYDROLOGICAL DATA PROVISION FOR UNGAUGED CATCHMENTS IN DEVELOPING COUNTRIES**

Vladimir SMAKHITIN (Hydrology and Eco-Hydrology, International Water Management Institute)

International Water Management Institute carries out a number of research projects in Asia and Africa, which are related to efficient water use in agriculture, food and environmental security. The quantification of hydrological processes under natural and modified conditions in study river basins, is a constant need, but often complicated by a decline of measuring networks in developing countries, limited quantity and poor quality of available data, and institutional barriers to data acquisition. These often necessitate the development and application of parsimonious methods of hydrological data provision. The paper will describe one group of such techniques, which are based on Flow Duration Curve (FDC). This methodology of pragmatic hydrological time series modeling includes: i) technique by which to establish FDCs at ungauged sites (primarily by means of hydrological regionalisation) and ii) techniques by which to convert the established FDCs into actual continuous hydrograph. The latter is a non-linear spatial interpolation technique based on the assumption that flows occurring simultaneously at sites in close proximity to each other correspond to similar percentage points on their respective FDCs. The technique is designed to work with either available flow or rainfall data from gauges in a catchment. Pragmatic hydrological modeling focuses exclusively on the generation of hydrological time series, has a limited number of parameters and unambiguous reasons for success or failure. It is simple to use, time efficient, not regionally restricted and is applicable for generation of both daily and monthly flow data. The paper presents examples of application of pragmatic time series modelling concept in several developing countries including South Africa, Sri Lanka and Nepal.

**HW07/11P/C25-003**

**1430**

**EXTREME-EVENT MODELING IN UNGAUGED BASINS BY REGIONAL ESTIMATION**

Taha B.M.J. OUARDA<sup>1</sup>, Alin A. CĂRSTEANU<sup>2</sup>, Hugo GINGRAS<sup>1</sup>, Bernard BOBÉE<sup>1</sup> (<sup>1</sup>Institut national de la recherche scientifique - Eau, terre et environnement, <sup>2</sup>Investav del IPN)

Regional estimation involves the identification of groups of hydrologically homogeneous catchments, as well as the regional estimation method used for information transfer from the homogeneous region to the ungauged site. We present, by means of a multi-method original software, the advantages of using neighborhoods in canonical correlation space, rather than geographically contiguous regions, for homogeneous-region identification purposes. The methods of index flood and multiple regression are used for regional estimation. A discussion is offered on the implications of scaling probability distributions of events, for these methods.

**HW07/11P/C25-004**

**1445**

**ON DEFINING WATERSHED SIMILARITY FOR REGIONAL ESTIMATION OF FLOODS AT UNGAUGED SITES**

Van-Thanh-Van NGUYEN<sup>1</sup>, Nelly PEYRON<sup>1</sup>, Ganesh R. PANDEY<sup>2</sup> (<sup>1</sup>McGill University, Department of Civil Engineering and Applied Mechanics, <sup>2</sup>State of California, Department of Water Resources, Division of Planning and Local Assistance)

Accurate estimation of flood flows from a watershed is essential for the design of many hydraulic structures (e.g., dams, culverts, bridges). However, flow records that are needed for this estimation are either limited or unavailable at the site of interest. In such cases, regional estimation methods, which use hydrological information from many sites, have been proved to be able to improve the accuracy and reliability of the flood estimates. However, the success of these procedures lies upon the appropriate identification of hydrologically similar basins (or homogeneous regions). While several methods of delineating homogeneous regions, such as index-flood procedure, cluster analysis, discriminant analysis, or region of influence approach, have been proposed in the literature, the criteria used in these procedures for determining regional homogeneity involve still a great deal of subjectivity and may not be suitable for the estimation of floods at ungauged locations. Therefore, the main objective of the present study is to propose an objective approach to delineation of homogeneous regions for improving the accuracy of flood estimation at locations with limited or without data. The proposed method is based on the scaling of statistical properties of floods with basin characteristics. More specifically, the analysis of the physiographic and hydrologic data for over 200 watersheds of different sizes (ranging from 100 km<sup>2</sup> to 90,000 km<sup>2</sup>) in Canada has indicated the scaling behaviour of the non-central moments of flood series with the basin areas. Based on this empirical evidence, a new definition of regional homogeneity of watersheds has been formulated. It was found that the grouping of homogeneous basins as proposed in this study formed well-defined geographical regions with distinct climatic characteristics. Further, it was recommended that the selection of regional probability distribution for the estimation of flood quantiles and the corresponding parameter estimation method should be made such that the scaling properties of the flood series were preserved. Finally, it has been demonstrated that, based on the proposed definition of regional homogeneity, the estimates of floods for ungauged sites could be more consistent and more accurate than those provided by existing methods.

**HW07/11P/C25-005**

**1500**

**ANALYSIS BY THEORETICAL AND DISTRIBUTED MODELS ON FLOOD FREQUENCY AND PROBABILITY DISTRIBUTION OF RUNOFF SOURCE AREAS**

Salvatore MANFREDA<sup>1</sup>, Vito IACOBELLIS<sup>2</sup>, Mauro FIORENTINO<sup>3</sup> (<sup>1</sup>Dipartimento di Ingegneria e Fisica dell'Ambiente, Università della Basilicata, <sup>2</sup>Dipartimento di Ingegneria delle Acque e Chimica, Politecnico di Bari)

Flood generation mechanisms depend on basin features as: soil type (soil water storage capacity and permeability), vegetation (surface coverage) and climate. These variables are spatially distributed, and we try to interpret their effects by using a distributed model. Such a model is physically based and capable to evaluate the runoff generation considering the influences of soil characteristics and local soil moisture conditions. The focus of this study is to identify the contributing areas to the peak flow and to underline the existing relations between the probability distribution of floods parameters, the physical characteristics of the watershed, and the contributing areas. By using the rainfall-runoff model Wetspa it is possible to evaluate the real contributing area to the peak flow. Synthetic rainfall series, generated by IRP model, were combined with the rainfall-runoff model, obtaining time series of discharge. Finally the annual maximum floods and the corresponding contributing area have been extracted from the discharge series and their frequency distribution has been analyzed to interpret and support on physical bases the theoretically distribution of floods recently proposed by Fiorentino and Iacobellis (2000). Such a theoretical model for analytical derivation of the flood frequency distribution is based on a simple rainfall-runoff model in which the peak flow  $Q_P$  is treated as a stochastic variable function of two other mutually dependent stochastic variables, namely the mean areal rainfall intensity  $i_a$  and the peak runoff contributing area  $a$ . The results validate the hypothesis of gamma distribution and show a strong correlation between the variable  $a$ , calculated by Wetspa, and the climatic and geomorphologic characteristics of the basin.

**HW07/11P/C25-006**

**1515**

**PREDICTING FLOWS USING CLIMATE AND LAND USE DATA FOR UNGAUGED CATCHMENTS IN THE MURRAY-DARLING BASIN, AUSTRALIA**

Barry FW CROKE (Centre for Resource and Environmental Studies, and the Integrated Catchment Assessment and Management Centre, The Australian National University)

Predicting flows in ungauged catchments using calibrated rainfall-runoff models requires determination of regional relationships between parameters and catchment attributes. This approach is only possible with parsimonious models (fewer than ~7 parameters). Even with such models, the uncertainties in the data used to determine the relationships between measurable catchment attributes and non-measurable parameter values generally results in poor predictive power. This paper presents three top-down approaches to improve the estimation of parameter values through regionalisation of three observable quantities: the runoff coefficient; shape of the flow duration curve; and the unit hydrograph. These approaches can be used separately or in combination to constrain model parameters depending on data availability and output requirements. Post et al (1999) found that constraining the parameter values using estimates of the runoff coefficient from similar neighbouring catchments improved the predictive power of this approach. This concept has been extended through development of a broad scale regionalisation of the runoff coefficient for the Murray-Darling Basin in Australia. The approach applied here is to estimate evapotranspiration (ET) using relationships developed by Zhang et al (2001), empirically corrected for variations in the potential evapotranspiration across the basin using gauged sites in the Goulburn-Broken and Upper Condamine catchments. The runoff coefficient is then derived assuming that the only significant terms in the water balance are rainfall, streamflow and ET. The performance of the model has been tested using gauged sites in the Upper Murrumbidgee and Wingecarribee catchments. A method of extending this to determine the relationship between catchment attributes and the shape of the flow duration curve is being developed. This method uses the linear form of the log-normal transformed flow duration curve, with the slope of the transformed FDC related to attributes such as land use, rainfall and potential evaporation. The third approach is to relate the shape of the unit hydrograph to catchment attributes. This is based on a technique to derive the unit hydrograph response curve directly from observed streamflow (Croke, 2003). These approaches constrain the model parameters and potentially increase the predictive power of the regionalisation approach. This work is part of the IHACRES component of PUB proposed by Littlewood et al. (2002) in Brasilia.

### TOWARDS A SCIENCE PROGRAM FOR PREDICTION IN UNGAUGED BASINS (ALL IAHS COMMISSIONS)

Location: Site D

Friday, July 11 PM

HW07/11P/D-001

Poster

1400-137

#### TOWARDS THE PREDICTION IN UNGAUGED BASINS – DATABASE DEVELOPMENT FOR A MESOSCALE RIVER BASIN IN TROPIC CLIMATIC ZONE

Taichi TEBAKARI<sup>1</sup>, Chanchai SUVANPIMOL<sup>2</sup>, Sukit SUANKUASAKOOL<sup>2</sup>, Tianqi AO<sup>3</sup>, Kazuhiko FUKAMI<sup>1</sup>, Junichi YOSHITANI<sup>1</sup> (<sup>1</sup>Public Works Research Institute of Japan, <sup>2</sup>Royal Irrigation Department of Thailand)

In general, a hydrological model applicable for PUB (Prediction in Ungauged Basins) should be capable of identifying model parameters directly on the base of basin features, and model performance is desired to be free from uncertainty resulted from scale problem. To develop and validate such models and carry out their inter-comparisons, particularly in establishing the relationship between model parameters and basin features, hydrological databases of various well-gauged study/experimental basins are essential. For a selected study basin, the accuracy of collected hydrological data has the same importance as model itself. It is desired that the stream flow discharge is not disturbed by human activities, the intensity of hydro-climatic gauge station is not too low and long-term hydro-climatic records are available. Also, corresponding to physically based distributed hydrological models, data of land use/cover, soil type, soil water content and geology are desired to be available. Moreover, such database is desired to be prepared for such representative river basins that locate in different climatic zones and have different hydrological response characteristics. For the Southeast Asia, selecting a well-gauged representative study basin for PUB is necessary, because in this area there exist many ungauged basins and their hydrological predictions are becoming more and more important to overcome the water crisis in the 21st century. In this study, prepared was the database of a mesoscale river basin that locates in tropic climatic zone, the Khlong Luang River basin of Thailand. This basin locates in the southeast of Thailand, 100 km far from Bangkok, has a drainage area of 433 km<sup>2</sup> and a mainstream of about 30 km. Its elevation is between 30-100 m and its topography is comparatively flat. There is not large dam and large city in the basin and no significant human made interruption to the natural stream flow. Its major land use is for agriculture; about 70% of the area is arable. Its surface soil is dominantly loam and clay. From 1965 to present, the Royal Irrigation Department of Thailand (RID) has been measuring water level, discharge, rainfall, and evaporation for the Khlong Luang River basin. The Public Works Research Institute of Japan (PWRI) and RID have carried out cooperative observation for soil moisture during 1994 to 1995. For the period of 1965-2001, the observed annual average rainfall is 1229.94 mm, the maximum and minimum are 1644.7 mm and 869.8 mm, respectively; annual runoff is 663.6-48.2 mm, and the annual runoff rate is between 43% and 5.5%. For the Khlong Luang River basin, the prepared hydrological database contains observed rainfall, stream discharge/water level, evaporation, land use, soil type, soil water content and geology. This database will open to PUB researchers who plan to apply watershed and rainfall data to a physically based distributed hydrological model and to verify the model with observed discharge data. The authors will report the analytical results using the BTOPMC (Block-wise use of TOPMODEL with Muskingum-Cunge method), for relating model parameters with physical features of the Khlong Luang River basin.

HW07/11P/D-002

Poster

1400-138

#### EXPERIMENTAL STUDIES ON RUNOFF AND SOIL EROSION OF BHETAGAD WATERSHED IN CENTRAL HIMALAYAS

Umesh Chandra KOTHYARI (Department of Civil Engineering)

Soil, water and nutrient conservation practices are increasingly being designed and adopted in almost every part of the world for enhancing the water availability and fertility of land surfaces as well as for curbing non-point source pollution from agricultural and other land usages. Therefore, in recent years there has been increasing demand for the need to include both water and sediment control strategies within the watershed management plans. The runoff and sediment discharge from a watershed is controlled by a complex functions of meteorological, ecological, climatic and geo-morphological processes. Compared to other parts of the world, the degree of controls affected by each of these factors is much different in the watersheds located in the region bounded by the Hindu-Kush Himalayan Region. The Himalaya is a fragile land and one of the greatest mountain systems of the world. In spite of the fact that Himalayas play the role of a water tower for the entire Indo-Gangatic planes in Indian subcontinent, the availability of water is a big problem for the Himalayan inhabitants themselves. Also millions of tons of eroded fertile soil generated through erosion in watershed areas in upper parts is transported to the downstream plain area every year by the mighty rivers like Ganga, Yamuna, Brahmaputra and the others. In the above context, it becomes absolutely necessary to have better understanding of the natural processes causing runoff and sediment generation and also in identifying the influence of human activity on the watershed in these areas. Using such knowledge one can more accurately estimate the upper bound capacity of the earth in these areas to sustain the burden due to population. To fully understand the system and the involved processes there is only little reliable data available within the region mentioned above and most of the river systems are ungauged. Therefore, long-term data is needed for the understanding of the dominant natural processes, resource assessment, possible changes and impacts. An extensive study on monsoon fed Bhetagad sub watershed in Hindu-Kush Himalayan area of the Garur Ganga, (tributary to river Gomti in the Ganga river system) watershed was started by the authors in the years 1997 for meeting above stated objective. Experiments both on plot scale and the watershed scale are being performed for investigating the rainfall – runoff – soil erosion processes in the study area, which lies in the Central Himalayan region having tropical climate. There are further plans for near future for gauging such macro size watersheds in the monsoon fed Shiwalk ranges of the Himalayas. These plans and the results obtained through earlier studies shall be presented in this paper.

HW07/11P/D-003

Poster

1400-139

#### THE DEVELOPMENT OF THE DETAILED CLIMATIC SCENARIOS FOR CENTRAL ASIA REGION

Inom Sherovich NORMATOV (Institute of Water Problems, Hydroenergetics and Ecology, Academy of Sciences, Republic of Tajikistan)

The Central Asia is a particularly bordered region. Almost all the climatic zones and high altitudes from the level of Caspian Sea to the highest peaks of Central Asia are located here.

The Aral Sea basin can be considered a closed one, as it has not any links with the World Ocean and borders with mountain chains of Tian Shan, Pamirs and Kopetdag on the south and the east. The only exterior factor, which influences the climate of this region is the atmosphere. In these conditions the most important of the main factors influencing the ecological situation in this region is the population increase and activation of human industrial activity, which intensifies ecological misbalance. In Tajikistan Republic over 10% of the territory is the zone of everlasting snow and glaciers. This territory requires strategic defense, as global anthropogenic increasing of temperature more perceptibly tells upon the regime of forming the river flow and activation of ice disintegration. Intense glaciers melting causes not only decreasing of the fresh water supply for Central Asia but also the formation of glacial lakes. Therefore there appears the danger of destructive mountain flows, which caused the human victims and land degradation not once. Under modern climatic conditions the area of the Pamirs and Alai's glaciers is decreasing annually by 1.2 sq. km. The observing network in Tajikistan Republic has a unique peculiarity, which differs it from similar networks in other countries. It is situated at the altitudes of 300 to 4,169 m, i.e. in the troposphere. All those stations were included into the world observing network. In Tajikistan numerous scientific works require proper processing. Today it is necessary to make systematization and scientific analysis of hydrometeorological data, accumulated for the last hundred years. Only the analysis of long observations data, obtained from the stations in mountains will allow to reveal the changing trends of climatic hydrometeorological parameters and to develop the prognosis method for the future perspective. This research work may contribute to fundamental international research on the program of global climatic changes. The foundation of the stations of the local and global monitoring of the greenhouse gases opens the wide perspective to establish the changing dynamics of green concentration according to the altitudes. It establishes the dependence of the snow and glaciers melting process and the formation of the river flows on the greenhouse gases concentration at the different heights, as well as the influence of the greenhouse gases on the flora and fauna. The results of conducted measurements, observations of the greenhouse gases influencing the environment will generate the research and practical works in developing modern technologies, which provide the essential decrease in the greenhouse gases emission and the wide use of untraditional energy carriers instead of organic fuels.

HW07/11P/D-004

Poster

1400-140

#### DATA AVAILABILITY PROBLEMS IN UNGAUGED BASINS OF DEVELOPING COUNTRIES - A TEST CASE

Syed Muhammad Saeed SHAH<sup>1</sup>, Hazael Firoton GABRIEL<sup>1</sup>, Ifiikhar AHMAD<sup>2</sup> (<sup>1</sup>Centre of Excellence in Water Resources Engineering, University of Engg. & Tech., Lahore, Pakistan, <sup>2</sup>Department of Mining & Geology, University of Engg. & Tech., Lahore, Pakistan)

For the prediction and design of hydrologic phenomena, long term hydrological data is needed in most of the cases. In this paper the main data issues and problems those are concerned with the hydrologic prediction and design in ungauged basins are investigated with special reference to developing countries. As a test case, Pakistan one of the developing countries is chosen for the study. The ungauged basins of the country are selected and problems and main issues are determined. The whole region has been divided into three areas, arid, semi-arid and humid differentiated on the basis of occurrence of precipitation. In arid areas the rivers remain dry in most of the time of a year and rainfall is scanty. The problems found to be different as compared to other two regions. In semi-arid parts, the ungauged basins have different problems and issues. In humid areas the rivers are perennial and have appreciable water potential. Due to this reason the water funding agencies have more inclination towards these areas. There problems are different as compared to the other two areas. In developing countries, due to little available funds, the basins are poorly gauged. This problem is more critical if the area lies in arid to semiarid regions. These have little or no gauging stations due to less water resources. The water authorities in Pakistan, perhaps have no plan for the installation of new gauging stations. The information regarding precipitation, land surface processes, stream flow, ground water flow, snow and ice, sediments and water quality is limited. Data availability in these basins is discussed in detail. The shortcomings in data collection, storing the field data and analysis are also discussed. Although the population is increasing rapidly, and need of water resources is increasing but the density of hydrologic gauging is towards decreasing side. These issues have been discussed, some new suggestions are proposed

HW07/11P/D-005

Poster

1400-141

#### REPRODUCTION OF DISTRIBUTED RAINFALL INTENSITY USING NUMERICAL MODEL AND SATELLITE DATA

Satoru OISHI<sup>1</sup>, Makoto AKAIKE<sup>2</sup>, Kengo SUNADA<sup>1</sup>, Kuniyoshi TAKEUCHI<sup>1</sup> (<sup>1</sup>Department of Civil and Environmental Engineering, University of Yamanashi, <sup>2</sup>Graduate School of Engineering, University of Yamanashi)

**Introduction** In order to prediction of ungauged basins, we will reproduce the distributed rainfall intensity in the Mekong river basin. The reason for the Mekong river basin is that the Mekong river is important international river without gauging the rainfall distribution. The Mekong river is important not only in hydrological aspect but in political and economical aspect. In order to investigate the hydrological process in the Mekong river basin, the distribution of rainfall is strongly required. Moreover, it is also required for flood disaster prevention. Therefore, we try to reproduce the distributed rainfall intensity by using a numerical weather forecasting model and satellite data. This research is basic investigation for nowcasting the real time rainfall distribution in the future. **Method** The target of this research is 1hr and 20km grid rainfall intensity data. For the reproduction, we use the MRI/NPD NHM as a numerical weather forecasting model and TRMM-PR as satellite data. MRI/NPD NHM is the Non-Hydrostatic numerical weather forecasting Model made by Meteorological Research Institute and Numerical Prediction Division both in Japan Meteorological Agency. MRI/NPD NHM can calculate the detailed meteorological situation including rainfall intensity by using the global assimilation data and nesting method. However, it is difficult to calculate the correct distribution of rainfall intensity by using numerical weather forecasting model. It is required to compare the result of numerical model and observed data. Moreover, the reproduced rainfall intensity data has to be modified by using satellite data. In the ungauged basins, the distributed rainfall intensity is obtained only from the satellite data. We use the TRMM-PR data as rainfall distribution data. TRMM-PR is Precipitation Radar onboard the Tropical Rainfall Measuring Mission satellite. Data from TRMM-PR is three dimensionally distributed rainfall data having good spatial resolution (horizontally 4.3km grid, vertically 250m grid). However, the temporal resolution of TRMM-PR is coarse (about twice a day). Therefore, it is necessary to interpolate the TRMM-PR data temporarily by using the numerical weather forecasting model. The method of reproduction of distributed rainfall intensity data is summarized in the following sentences: 1) to calculate the meteorological situation by using MRI-NPD NHM, 2) to compare and to modify the distributed rainfall intensity of the result of calculation by using TRMM-PR data, 3) re-calculating the modified rainfall intensity data by using MRI-NPD NHM, the result has the rainfall intensity of 1hr and 20km grid.

HW07/11P/D-006 Poster 1400-142

## SIMULATION OF HISTORICAL RAINFALL OVER INDOCHINA PENINSULA

Hiroshi OKUMURA, Taichi TEBAKARI, Tianqi AO, Junichi YOSHITANI (Public Works Research Institute)

An opportunity for PUB (Prediction in Ungauged Basins) exists in the assessment of causes of flood risk increase over the South-East Asia such as the lower Mekong river. The lower Mekong experienced massive deaths and serious damages by six floods in 1991, 1994, 1995, 1996, 2000 and 2001 in the last decade, while it experienced only once in 1984 in 1980's. The increased flood damage may be caused by increased frequency of floods due to climate variation, landuse/landcover change, or artificial control of water, or by other human activities such as urbanization. Scientific assessment of causes of increased flood damage is the basic knowledge for decision-making, but poor data has prevented assessment. PUB will be the breakthrough technology for providing the knowledge base. PUB comprises rainfall prediction as the first step and flow prediction as the second step. Public Works Research Institute of Japan and the University of California at Davis jointly developed a downscaling model named IRSHAM (Integrated Regional-Scale Hydrologic Atmospheric Model) to reconstruct historic rainfall over ungauged basins. Downscaling requires a sophisticated integrated hydro-meteorological model that requires no parameter fitting, and it is one of the key technologies in PUB (IAHS PUB initiative web site). The downscaling approach has the advantages of (1) the applicability to any basins in the world, because all necessary input data can be obtained from world available database, (2) the availability of reanalysis data; and (3) the applicability to completely-ungauged basins, while remote sensing always requires a few ground rainfall data. This reconstruction technology is now being applied to reconstruct rainfall over the South-East Asia and to scientifically assess frequent-occurring flooding in the past years. In this research, the authors carried out a numerical simulation to reconstruct historical rainfall over the South-East Asia on the 0.1-degree mesh. In this simulation, a non-hydrostatic numerical model has been improved and developed based on IRSHAM. From the standpoint of numerical simulation, a highly accurate non-hydrostatic numerical model is required in the reconstruction technology at the scale of 0.1-degree (mesoscale). To verify the simulated rainfall data, ground-based observed rainfall at about 800 points in the ChaoPhraya river basin (162,800km<sup>2</sup>) of Thailand will be used.

HW07/11P/D-007 Poster 1400-143

## HYDROLOGICAL ASPECTS OF THE RAINFALL VARIABILITY OVER KENYA: TREND AND PERIODICITY

Balla Paul MAGGERO (Kenya Meteorological Services)

Trends and periodicities in the seasonal rainfall of highlands and coastal climatic units are studied using 80 years database from a network of 25 stations. Standardized regional mean seasonal rainfall is determined in order to derive mean normalized anomaly index for each of the rain season eventually. Slight increasing tendencies are observed for the whole country during the long rains and over the Kenya high grounds areas during short rains. Slight decreasing tendencies are seen during the short rains in the whole region and the coastal. The Kenya high grounds and the coastal do not show any significant Trend. A general and statistically spectra can be seen. Peaks with a wavelength of about 3 to 4 years are prevalent in the Kenya series, Kenya high grounds and the coastal; this implicates a moderate variance. Peaks of about 4.5 to 5 periodicities are also conclusive, and they match the ElNino/Southern Oscillation (ENSO) phenomena. Both solar and the QBO are not exhibited from the analysis.

HW07/11P/D-008 Poster 1400-144

## PUB AS HYDROLOGICAL PARADIGM, FOOD SECURITY AND POVERTY REDUCTION IN HIMALAYAN RIVER BASINS

R.B. SINGH (Department of Geography, University of Delhi)

The Prediction in Ungauged basins (PUB) has emerged as important hydrological paradigms. The monitoring and prediction of ungauged basins open up vast possibilities in order to achieve food security and poverty reduction in India. Geographers can, and should make a variety of contributions to the important international hydrological project form both natural science and socio-economic perspectives. The study of ungauged basin is very appropriate for India due to severe paucity of hydrological data e.g., quality, quantity, stream-flow, sediments, snow-melt, pollution, etc. through space and time. A good number of medium and minor river basins are still ungauged. Whereas, the major ones are poorly gauged with respect to one or the other hydrological variables. Considering above issues, the following two types of river basins are important: 1. Poorly Gauged Basins: Many of the major river basins and a few medium river basins which have flood-data but lacks adequate data about other hydrological variables. These include mostly peninsular river of India. 2. Ungauged Basins: Most of the Himalayan rivers and rivers of North-East comes under this category. Besides minor river basins, a good number of medium river basins are also ungauged basins. To coordinate the comparative PUB study, detailed case studies at different settings provide the bases of understanding environmental changes in the ungauged basins of the Himalayan India. Emphasis has been done not only on recent data, but also on historical materials. Technical issues related to remote sensing data, such as classification and scale are also considered to be important. The basins of India, specially ungauged ones are facing a multitude of hydrological challenges including: 1) reliability of water supply (quantity) i.e., seasonality of river basins, 2) water quality i.e., concentrations of contaminants; nutrients, heavy metals, etc.; 3) space-time variability of the hydrological variables 4) problems of extreme events such flood and drought, etc., 5) differences in the attributes e.g., soil, vegetation, topography, climate, demography, etc., 6) lack of information infrastructure both in quality and quantity e.g., remote sensing, GIS, ground observation and gauging network, etc. The hydrologic response to be predicted depends on the nature of the problems including prediction of floods of a given return period, extent and frequency of floods, mean annual water yield reliability of water supply, crop fields, irrigation scheduling and water quality (concentrations of contaminants; nutrients, heavy metals). In general, the predicted hydrologic response can be a continuous time series of the quantity and quality of interest (e.g., storm hydrograph) or statistical measures of its variability in space or time (e.g., mean, variance, annual total), including extremes (e.g., annual maximum floods, droughts etc.). Thus PUB must take into consideration the identification and measurements of hydrological data/information in spatiotemporal variability of a Indo-Ganga Brahmaputra basins which are densely populated agricultural regions of India. Finally, the paper highlights water as driving force for food security and poverty alleviation in India.

HW07/11P/D-009 Poster 1400-145

## PROBLEMS OF UNGAUGED BASINS IN PAKISTAN(WITH REFERENCE TO HYDROLOGIC STUDIES)

Syed Muhammad Saeed SHAH<sup>1</sup>, Hazael Firoton GABRIEL<sup>1</sup>, Iftikhar AHMAD<sup>2</sup> (<sup>1</sup>Centre of Excellence in Water Resources Engineering, University of Engg. & Tech., Lahore, Pakistan,<sup>2</sup>Department of Mining & Geology, University of Engg. & Tech., Lahore, Pakistan)

**Why this presentation?** Although the problems of ungauged basins with reference to different hydrologic studies are worldwide, but the specific problems of a developing country like Pakistan, where most of the basins are ungauged, rarely highlighted in detail in any international forum. Due to socio-economic and political reasons the problems of developing countries are much more than developed countries therefore this kick-off workshop on PUBs is the right forum to listen and discuss the real life problems based on the experience of different hydrologic studies from the hydrologists of a developing country. **Problem** Most of the techniques developed for ungauged basins, based on data from the watershed of developed countries, are not applicable in true sense even after certain modifications/calibrations. **Possible Reasons**- Not all but in most of the cases hydrologists of developing countries got higher education from the Universities of the developed countries therefore in most of cases their basic training is not helping much to solve the problems. - Infra-structure and required funds, for further developments, are not available to those who gained little experience on the local problems.- Research outcome (published in different journals), in most of the cases, unfortunately, is not covering and highlighting the real issues to be investigated, in detail, due to reasons.- Aliens try to give solutions to the problems, in most of the cases, within their own point of views. **Issues to discuss** In this presentation, because of time limitation, selected problems would be highlighted under the following topics:- Flood estimation for ungauged watersheds- Rational Method- discussion regarding Runoff Coefficient (C)- Empirical Method- discussion regarding Regression formulae and Envelope Curves- Application of Regional - Frequency Curves to ungauged basins - discussion about transposition of floods- Typical problems associated with- SCS Method- Multiple Regression- Physically based Catchment Models

HW07/11P/D-010 Poster 1400-146

## THE PROBLEM OF UNGAUGED CATCHMENTS IN THE SUBHUMID TROPICS OF WEST AFRICA (BENIN)

Helge BORMANN, Bernd DIEKKRUEGER (Department of Geography, University of Bonn)

While predicting the hydrological behaviour of regional scale ungauged catchments in the humid tropics of West Africa in the future one is faced with diverse uncertainties. In addition to often non existing river gauge data one has to get by with coarse spatial data sets, sparse rainfall and climatic data and uncertain predictions of the expected future environmental changes. Before tackling the ungauged catchment problem, the standard data availability of ungauged catchments has to be defined: discharge data, climate and rainfall data and spatial data concerning soils, geology, and land use. Normally the data availability is dependent on the given scale as well as on the region. In the worst case one has to use globally available data sets (FAO soil map 1:5.000.000, USGS global ecosystems / Corine land cover data set for Europe, global digital elevation model of the USGS, HYDRO1K dataset; climate data from national services and remote sensing). Based on these data sets model predictions of many existing model approaches fail. Especially physically based models cannot be parameterised sufficiently. As calibration is precluded only those conceptual, but process based models remain applicable which represent the dominant water fluxes and consider the controlling land surface properties. As the predictive tools contributing to the PUB initiative focus on the support of management operations, the question has to be posed, at which scale which hydrological components or resources have to be managed and whether the proposed methods account to these resources. In this context also the usefulness of hydrographs for investigations concerning water and land use management has to be discussed. As the ratio of runoff to rainfall is small in subhumid to semiarid regions (smaller than 0.15), runoff and discharge have only a limited significance with regard to water management purposes (in arid regions almost no significance except for erosion processes). Groundwater resources for instance are much more significant. Because the reproduction of hydrographs is not important in such areas, the focus should be set on the optimisation of the internal model validity, especially for the use of models during scenario studies. Therefore an improved understanding of interactions between hydrological processes and catchment properties is required, which has to be translated into existing or new modelling approaches (Sivapalan, 2002). The uncertainties incorporated in this model application and validation process of course have to be accepted (Sivapalan, 2002), but also quantified. With regard to internal model validity the lack of gauges is only one of the numerous problems. In the presentation the questions describe before concerning ungauged catchments are discussed considering the background of water management issues in Benin (West Africa). The presentation focuses on the interactions between data availability, model restrictions and expected environmental changes with the objective of making realistic predictions of future water fluxes in ungauged catchments with regard to management options.

HW07/11P/D-011 Poster 1400-147

## ON THE SCIENCE FOR SUSTAINABLE DEVELOPMENT AND MANAGEMENT OF WATER RESOURCES IN UNGAUGED WATERSHEDS

Constantine C. MBAJIORGU (Department of Agricultural Engineering, University of Nigeria)

Access to water and improvement of water management have been directly linked to poverty eradication, biodiversity, public health, agricultural productivity, and environmental and world gender issues. Water is the essential and critical element, which ties together all these areas of sustainable development. Hydrologic science provides the analytical tools for water management, tools that shape and are used to evaluate management practices. Earlier, a shift in water management practice occurred with the development of Watershed Hydrology, when whole-of-the-catchment approaches replaced field and farm level understanding of hydrologic phenomena, and the watershed became a basic unit for water management. Now a new shift is imminent, as the paradigm of sustainable water management recognizes that the primary resource is the natural endowment of climate, geology and ecosystem processes in a given region. To determine the quantity, quality, timing and spatial distribution of the readily available water in a region, new methods of integrating the physical and climatic factors governing hydrologic processes with biotic processes over varied spatial and temporal scales are required. How can the unique composition of plants and animals in a given region, and its effect in retaining/utilizing water and nutrients, as well as the impacts of human activities, be integrated with climatic factors along with the physics and chemistry of hydrologic processes in order to determine the flow and distribution of water, sediments and nutrients across the landscape? The science providing an answer to this question will eliminate, to a large extent, the need for much of the gauged data required in calibration and validation of hydrologic models. Factors such as the effect of biotic communities on hydraulic processes and on water quality, e.g. moderation of nutrient loads and flood peaks, will need to be reflected in predictive models.

HW07/11P/D-012 Poster 1400-148

## WAYS TO USE THE DISCIPLINE OF COMMUNICATION TO MAKE A GREATER CONTRIBUTION TO THE PACE OF PUB

Natalia V. PENKOVA<sup>1</sup>, Anna KURTYCH<sup>2</sup>, Michael NARODOSLAWSKY<sup>3</sup>, Reva S. PETROVA<sup>4</sup>

(<sup>1</sup>State Hydrological Institute, Saint-Petersburg, Russian Federation, <sup>2</sup>Paris University (XIII), Paris, France, <sup>3</sup>Graz University of Technology, Graz, Austria, <sup>4</sup>Institute for Ecology of Natural Systems, Tatarstan Republic, Russian Federation)

An evolution of communications methodology began in the first quarter of the 20th century with the use of publicity tools to bring attention to social problems. It grew to a reliance on public relations, more recently, development and strategic communications took center stage. Several networks of professionals (social activists, academics, journalists, electronic communications experts, professional communicators, etc.), who test innovative communication concepts, committed to a new agenda for global communication that is empowering, horizontal versus top-down, gives voice to previously unheard, and has a bias toward local content and ownership. Modern communication programming has tended to fulfill three roles: to inform and persuade people to adopt certain beneficial practices; to enhance image and profile of the work of organizations involved in development; to enable community consultation over specific initiatives. All these roles are important within water development domain and are essential for PUB targets, but work on communication methodology in the field remains underfunded and undervalued. The "communication" is being understood as it was originally defined: as exchange of information. A general idea is being exploited that mass media play strategic role in promoting the process. However, researches show that mass media are not efficient, they may be considered both as an actor (with its own interests) and as tool for actors in public, political, scientific and economical spheres with which they interact. Mass media efforts would be complemented by other types of communication and education strategies in order to be reflected in resolving of water-related tasks. New fundamental advances in PUB are possible on the basis of research about particular communication dynamics around water in particular geographical settings under widening the concept for all exchange processes (exchange of matter, energy, information, culture, persons and/or capital) between different process units. The transfer of site-based knowledge (both scientific and indigenous) about past and present natural-climatic and man-induced hydrological and ecological regimes should attract main attention, especially in developing nations with scarce human and financial resources. So, a PUB science programme should include topic on interdisciplinary studies aimed at linking hydrological methodologies with those under development in Social science and Economics (theory of communication, concept of environmental responsibility, the "nature-friend" principle, eco-economy, etc.), in Ecology (concept of ecologically destabilized environment, reductionists approaches in Plant science, etc.), in Physical geography (Landscape science), and others. The "language" should be the main subject of concern: the notion of how to explain hydrological phenomena in terms that can be readily accessible and used by other professionals and general public as easily as by hydrologists. In the contribution, some innovative ways to change hydrologic research and observations methodology are cited, that may be considered as "starting points", with examples on different regions in Austria, Mexico, and Russia.

**HW07/11P/D-013** Poster **1400-149**

**GEOMORPHOLOGIC APPROACH TO HYDROGRAPH PREDICTION IN UNGAGED BASINS**

Praveen KUMAR, Kyungrock PAIK (Department of Civil and Environmental Engineering, University of Illinois)

The direct runoff hydrograph of a basin is a result of complex interaction between precipitation and runoff generation processes, and hillslope and channel dynamics. Both network and hydraulic geometry interact to shape the runoff process at the shorter time scales, while the runoff variability shapes the hydraulic geometry at the longer time scale. Evidence for the latter is provided by the widely observed fact that the bankfull channel geometry corresponds to a flow with a typical return period of one to two years. Flow transport equations with various degrees of approximation have been combined with the systematic organization of the planar network geometry, as characterized through the Horton's ratios, width function and self-similar trees. Recent work by Saco and Kumar [2002] has shown that the spatial variability of flow velocities, arising from the systematic downstream variations of hydrologic geometry, within a basin induce a dispersive effect that impacts the residence time of water and consequently the time to peak and peak flow of a hydrograph. They characterized this phenomenon as kinematic-geomorphologic dispersion to signify that it arises due to the interplay of the celerity variation arising from the variation of the hydraulic geometry and the stream network. This dispersion is the predominant mechanism, along with hillslope controls in determining the peak time and peak flow in a basin and is prevalent at all scales from very small to large basin sizes. Theoretical formulations that combine channel flow dynamics with the network and hydraulic geometry open up the possibility of addressing the long standing problem of "prediction in ungauged basins" for hydrograph prediction by taking advantage of the signatures of the streamflow variability as evidenced through the existing characteristics of planar network topology and (bankfull) hydraulic geometry. The network characteristics are relatively easy to extract using digital elevation model (DEM) data that are becoming widely available at high resolutions. However, the hydraulic geometry relations are not available as easily and they correspond only to the bankfull flow conditions when available. However, significant work has been done in the past to develop prediction equations for the hydraulic geometry. These include statistical estimates using data samples as well as theoretically predicted equations using hypotheses such as minimum entropy production, minimum variance, maximum transporting capacity, minimum stream power per unit channel length and minimum energy expenditure among others. These relationships are available for both at-a-station (i.e., variation at a specific location for different flows) and downstream (i.e., variation along the stream for flow with a specified return period) hydraulic geometry variations. We discuss how these can be used for hydrograph prediction in ungauged basins. Saco, P. M., P. Kumar, Kinematic Dispersion in Stream Networks, Part 1: Coupling Hydraulic and Network Geometry, Water Resources Research, 38(11), 1244, doi:10.1029/2001WR000695, 2002.

**HW07/11P/D-014** Poster **1400-150**

**STUDY ON A SYNTHETIC SEDIMENT ROUTING MODEL IN A WHOLE RIVER SYSTEM**

Kengo SUNADA<sup>1</sup>, Katsuhiko KOMATSU<sup>2</sup> (<sup>1</sup>Department of Civil and Environmental Engineering, University of Yamaguchi, <sup>2</sup>Engineering Section, Kokusai Kogyo Consultant Co., Ltd.)

It is needed to evaluate the complicated situations of water and material circulation in a basin for getting an appropriate way of better river basin management. In this study, in order to estimate the amount of sediment transport in a whole river system having poor information about sedimentation, a synthetic sediment routing model based on the river channel networks obtained from the digital elevation models is proposed. Authors have already developed an original basic sediment routing model which can take spatially distributed topographical feature of a basin into account, and it can also consider hydrological and geological response to strong storms in the basin system. Assumptions and procedures of the basic model are as follows. a) The digital terrain map is used for expressing basin topography. b) The steepest descent method is applied to tracing pseudo channel network. c) Width of channel element is calculated by an empirical equation. d) Significant riverbed variation is caused only if rainfall is stronger than 100mm a day. e) Runoff discharge at each channel element is estimated by the runoff function method with the heavy rainfall sequence.

f) Non-dimensional shear stress is computed using quasi uniform flow depth for the discharge at each time step. g) Sediment supply per unit area at each grid point is estimated by using another empirical equation. First, the basic model was examined from the viewpoints of model performance such as computational time interval, tuning hydraulic parameters, effects of computational mesh scale on the results of simulation of riverbed variation, channel network made from DEM and so on. Then in this study, further analysis regarding scale effects of pseudo stream channel element, distribution of sediment production area and channel width were carried out. Next, the model was applied to a couple of river basins, the Haya river (area: 509.1km<sup>2</sup>, tributary of the Fuji river) and the Abe river (area: 518 km<sup>2</sup>) both in the central Japan. The both river basins are producing large amount of sediment production because of the fragile rock due to the great geological default line through the basins. Through the applications using two kinds of scale of channel network element and the different catchments conditions, effects of these elements on the simulation of riverbed variation were discussed. The results of the simulations of riverbed variations in the two kinds of scale, 250m and 500m meshes, shows roughly same behavior except upper part of the basins. Last, the model was also applied to the larger river basin, the Fuji River basin (3,571km<sup>2</sup>) by using a new method of automatically tracing of channel networks. Results showed fairly good agreement between the calculated riverbed elevation and the observed one in the Fuji River. It is concluded that the model has possibility of practical application.

**HW07/11P/D-015** Poster **1400-151**

**MULTIFRACTAL DAM MANAGEMENT AND PREDICTION IN UNGAUGED BASINS**

Angelbert Chabi BIAOU<sup>1</sup>, Pierre HUBERT<sup>1</sup>, Daniel SCHERTZER<sup>2</sup>, Frederic HENDRICKX<sup>3</sup>, Ioulia TCHIGUIRINSKAAIA<sup>4</sup> (<sup>1</sup>CIG, Ecole des Mines de Paris, <sup>2</sup>Meteo France; LMM, Universite Paris VI, <sup>3</sup>EDF R&D, LNHE Chatou, <sup>4</sup>LGA, Universite Paris VI)

In order to get a more efficient production management of reservoirs, it would be helpful to apply long-term meteorological forecasts to hydrological models. Unfortunately, the explicit scales of present meteorological models are quite larger than those of hydrological models. Therefore it is indispensable to proceed to a downscaling of the output of the former in order to obtain an input for the latter. In this paper, we discuss a multifractal downscaling procedure. The site of the study is the area of Doubs basin, with the help of a dense local hydrological network, but in order to get a larger spatial scale ratio we extend our multifractal analysis to France, with the help of Météo-France PRECIP data base. We first argue that it is indispensable to consider a multifractal downscaling procedure in order to respect the scaling properties of the hydro-meteorological fields. We performed time, scale and time-space multifractal analysis of the available data and evaluate the corresponding universal exponents, as well as the dynamical exponent of the time-space generalized scale. We show that these exponents are quite robust and allow to perform space-time downscaling down to micro-scale of meso-scale data. We greatly acknowledge the financial support from Electricité de France, as well as Météo-France for providing access to its PRECIP data base.

**HW07/11P/D-016** Poster **1400-152**

**NEW SYSTEM OF HYDROLOGICAL COMPUTATIONS FOR UNGAUGED BASINS IN RUSSIA**

Vladimir Alexeevich LOBANOV, H.V. LOBANOVA, A.V. ROZHDESTVENSKY (IAHS member, Leading Scientist)

Hydrological computations for ungauged basins include two vectors of prediction: temporal (probabilistic limit for period of future operation of water project) and spatial (data interpolation or extrapolation on ungauged area). Problem of ungauged basins is the most actual for Russia reasons by its large area, rare hydrological network (in northern and eastern parts especially), which is reduced today. Therefore the large attention was given traditionally for a development of effective regional methods of hydrological computations for different climate conditions. In Russia two levels system of official documents for hydrological computations are developing in present time. The first level includes the federal guidebooks, such as Building Norms and Rules and Code of Rules, which consist of main general methods and their description. The documents of the second level is Territorial Building Norms (TBN), which will be developed for each region with the particular methods, databases and software for a realisation of new water projects and monitoring of the existing ones. TBN is represented in two forms: methodological (as a document) and computational (as regional GIS). General methodology of development of the models for ungauged basins includes two main steps: - determination of design hydrological characteristics in the site of observations (including restoration of long-term time series, assessment of homogeneity and stationarity, design values and their errors, etc); - transition from the information in observation sites to any ungauged basin on the basis of different kinds of models. System of methods and models has been used and developed, including deterministic and stochastic space models, regionalisation, analogues. New principle is suggested for generalisation of the results obtained by different models and field data. Assessment of impact of modern changing conditions (man's activity, climate change) on design hydrological characteristics in ungauged basins is discussed. The technological scheme of environmental GIS for regional hydrological computations is presented. Some examples of computations for ungauged basins are given in case study of different models and regions over the Russian area. Suggestions for the joint international programme of collaboration in frame of the PUB project have been developed and given for discussion, which include: - methodology, ways and approaches for transition from point to area (development of the general model); - different methods for temporal modelling in changing conditions; - main indexes of spatial classifications in modern changing conditions; - different methods of spatial generalisation and modelling in homogeneous regions; - methods for assessment of results and their generalisation.

**HW07/11P/D-017** Poster **1400-153**

**RIVER-LIKE GROUNDWATER FLOW PATTERNS AT THE JUDEA DESERT, THE DEAD SEA RIFT**

Haim GVIRTZMAN, Leehee LARONNE (Inst. of Earth Sciences, Hebrew University of Jerusalem)

The groundwater hydraulic gradient at the Eastern Judea Mountain aquifer (adjacent to the Dead Sea Rift Valley) is very steep, from approximately 400 m above sea level in the Jerusalem-Hebron area to 400 m below sea level near the Dead Sea, along a distance of about 30 km. A simple west to east flow direction would have caused a continuous groundwater leakage from the exposed aquifer along the base of the cliffs near the shore. However, such a leakage does not occur. The annual recharge of approximately 85 million cubic meters emerges through three large springs: Fescha, Kane and Samar, all located in the northern part of the Dead Sea. The scarcity of data at this region makes it very difficult to understand the subsurface flow field. Previous attempts to explain the flow field both conceptually and numerically using 2D flow simulations, have left unanswered questions. We claim that the geologic structural characteristics of the area plays a major role in the subsurface flow regime. Groundwater flows along the syncline axes towards the northeast, exhibiting a subsurface river-like flow pattern. Based on this conceptual model, we have

constructed a 3D hydrogeological model, for both the upper and lower sub-aquifers, using the MODFLOW code above the GMS platform. The model was calibrated using the few available boreholes. Thereby, we have quantified the water mass balance, including recharge amounts, leakages between sub-aquifers and between basins, as well as spring discharges and subsurface leakages towards the Dead Sea. Better understanding of the groundwater flow field would benefit both, Israeli and Palestinian water supply. Planning of better groundwater pumping schemes would now be possible.

**HW07/11P/D-018** Poster **1400-154**

#### HYDROLOGICAL FORECASTING USING DISTRIBUTED MODELS IN THE GREAT LAKES BASIN

Alain Claude PIETRONIRO<sup>1</sup>, Herman GOERTZ<sup>2</sup>, Paul PILON<sup>3</sup>, Harold RITCHIE<sup>3</sup>, Pierre PELLERIN<sup>3</sup>, Paul CAMPBELL<sup>2</sup>, Nick KOUWEN<sup>2</sup>, Paul FORD<sup>2</sup> (<sup>1</sup>National Water Research Institute, <sup>2</sup>Meteorological Service of Canada - Ontario Region, <sup>3</sup>Meteorological Service of Canada, <sup>4</sup>Department of Civil Engineering, University of Waterloo)

Hydrological models are integral components of water management and monitoring strategies. In particular, distributed hydrological models allow for detailed description of the hydrological and energy cycle and provide opportunities for dealing with forcing variables that fluctuate strongly in space and time, such as precipitation. Hydrologists and water resources specialists increasingly implement these models as a means to ameliorate the state of knowledge on basins of interest, and provide valuable information regarding hydrological state variables and potentially important distributed information on existing and future streamflow conditions. Also, there is increasing interest in using spatially distributed meteorological data from diverse sources such as weather radar, Numerical Weather Prediction (NWP) models and traditional rain gauge networks to drive these distributed models. This paper examines the feasibility of implementing a distributed hydrological model for estimating streamflow in unregulated basins and the accuracy of short-term hydrological-forecasting in the Great Lakes Basin of North America. The platform for hydrologic assessment in the Great Lakes Basin is the WATFLOOD hydrological forecasting system. The focus of this study is to provide initial testing of the hydrological model including calibration and validation of the model parameters using historic data. The meteorological forcing data sets include distributed Quantitative Precipitation Estimates (QPE) derived from rain gauge and ground-based radar data. NWP model input from the Canadian Global Environmental Multi-scale (GEM) model and nested high-resolution GEM runs during our initial testing phase (summer of the year 2000) for limited time periods of extreme precipitation also are used as forcing. Initial results to assess the applicability of distributed hydrological modeling and to provide the framework for testing the hydrological aspects of integrated hydrological and atmospheric models, are presented. Routing and regulation considerations including stream network conceptualization and lake routing are also discussed.

**HW07/11P/D-019** Poster **1400-155**

#### INVESTIGATING PEAK DISCHARGE FLOOD HYDROGRAPHS IN SELECTED UNGAUGED BASINS OF BALOCHISTAN (PAKISTAN)

Syed Muhammad Saeed SHAH<sup>1</sup>, Hazael Firoton GABRIEL<sup>1</sup>, Iftikhar AHMAD<sup>2</sup> (<sup>1</sup>Centre of Excellence in Water Resources Engineering, University of Engg. & Tech., <sup>2</sup>Centre of Excellence in Water Resources Engineering, University of Engg. & Tech., Lahore, Pakistan, <sup>3</sup>Department of Mining & Geology, University of Engg. & Tech., Lahore, Pakistan)

Balochistan is the biggest province of Pakistan in terms of its area. It lies in arid to semi-arid region where the rainfall is scanty. Due to little rainfall, most of its streams remain dry and flows only for a short period when the rainfall occurs. Due to high intensity of rainfall, these streams carry flash floods. Water is scarce in Balochistan and therefore these flash short duration floods are precious resource for the inhabitants and should be exploited through diversion structures or storage dams. Peak discharge flood hydrographs are required to design these structures. Due to lack of funds in developing countries like Pakistan, most of these streams are ungauged. But rainfall data and physical parameters/G.T sheets are available. Considering the limitations of hydrologic data availability in ungauged basins a technique is investigated that may be useful to derive peak flood hydrographs in ungauged basins. The procedure starts from evaluating quality of data, estimating the frequency of rainfall, volume of runoff and peak discharge flood hydrograph. The methods employed in the proposed procedure have four main components: outliers and consistency testing program, an autoregressive model, a statistical distribution analysis and a runoff computation program. To test the usefulness of the proposed procedure, it is used to estimate peak discharge rates in selected 18 ungauged basins of Balochistan. For the test cases, there is an indication that the proposed procedure is effective. The results obtained from proposed procedure is then used to investigate a simple equation that may be used to determine peak discharge rates in Balochistan basins with the help of easy to estimate physical parameters. One of the purposes to present this study is to explain the main difficulties to adopt the proposed procedure regarding the calibration of Rainfall Runoff computation program that was based on US Soil Conservation Services (US SCS) Curve Number method.

**HW07/11P/D-020** Poster **1400-156**

#### DESIGN FLOOD CALCULATION FOR UNGAUGED SMALL BASINS IN CHINA

Yuanfang CHEN<sup>1</sup>, Guoxing CHEN<sup>1</sup>, Zengchuan DONG<sup>1</sup>, Shenghua GU<sup>2</sup> (<sup>1</sup>Department of Hydrology and Water Resources, Hohai University, <sup>2</sup>SHANGHAI GENERAL HYDROLOGICAL STATION)

The two main methods to calculate the design flood in ungauged watershed are introduced in this paper. Concerning the rational method which is widely used in China, its design storm formula form and parameter estimation method, its derivation process of design peak flood Qmp rational formulae, and a case study in Jiangxi Province are introduced in details. Concerning the second method—the empirical formula method, a brief introduction is made. Some comments are also done in the final part of this paper. Keywords: Design flood calculation, ungauged basin, rational formula, empirical formula method, case study.

**HW07/11P/D-021** Poster **1400-157**

#### EFFECTS OF SPATIAL VARIETY IN INSTANTANEOUS UNIT HYDROGRAPH TYPES FROM FIRST-ORDER BASIN ON FLOOD PEAK IN SELF-SIMILAR RIVER NETWORKS

Yosuke KOMATSU<sup>1</sup>, Yasuhisa KUZUHA<sup>2</sup>, Tokuo KISHII<sup>2</sup>, Kunio TOMOSUGI<sup>2</sup> (<sup>1</sup>Disaster Prevention Research Group, National Research Institute for Earth Science and Disaster Prevention, <sup>2</sup>DPRG, National Research Institute for Earth Science and Disaster Prevention, and the Cooperative Graduate School, University of Tsukuba, <sup>3</sup>DPRI, Kyoto University)

Many hydrographs in first-order basins have been observed in the field catchments, although the physical and hydrological processes have not been completely revealed because many natural factors are involved in the complexity of water movements: soil, landform, lithology,

vegetation, and climate. Therefore, in this study, scaling exponents of flood peak generated on idealized self-similar networks are simulated using an experimental simplified instantaneous unit hydrograph from a unit-basin (IUHU), excepting physical processes on hillslopes from consideration. In addition, since Komatsu and Onda (1996) reported high spatial variability of discharge in a basin underlain by fractured rocks, we investigate the effects of distribution and combination of multiple IUHUs on scaling exponents of flood peak. The hydrologic response of a drainage network to impulsive net precipitation may be considered the function of travel time to the outlet of water distributed uniformly in space. This study applied a self-similar and deterministic Peano network, which has a ternary tree structure and is applied in many reports on flood analysis. A Peano network basin is divided into small similar unit basins. IUHUs are defined as various simplified rectangular hydrographs whose runoff ratio is 1, and the water reaches the basin outlet via the channel networks. We further assume that the relative velocity through the channel is constant and no water is stored in the network. A geometrical consideration of the peak flow properties via the width function maxima leads to a scaling exponent value of 0.7925. Width function is defined as the total number of channel links at a distance  $x$  from the outlet. The first experiment is simulated using only single rectangular IUHU. This assumption led to two regression lines between catchment area and peak flow, the scaling exponents were 1 and 0.7925AD. The latter value is governed by the geometric structure of a Peano network. The larger relative flow velocity through a channel:  $V_c$ , and longer duration of IUHU:  $T_d$ , make the join of two regression lines vary toward a smaller drainage areaAD. The travel times of water particles and all water depend on  $V_c$  and  $T_d$ , respectively. These results suggest that the effects of the two factors on peak flood are essentially synonymous with the effects of rainfall duration. The second experiment uses random distribution of two different IUHUs. Three regression lines were obtained; these scaling exponents were 1, a range from 0.7925 to 1, and 0.7925. The tendency of  $V_c$  and  $T_d$  was similar to the result of the first experiment.

**HW07/11P/D-022** Poster **1400-158**

#### METHODICAL APPROACHES TO PREDICTION AND COMPUTATION OF HYDROLOGICAL CHARACTERISTICS IN UNGAUGED BASINS

Tatyana FASHCHEVSKAYA<sup>1</sup>, Boris FASHCHEVSKY<sup>2</sup> (<sup>1</sup>Department of Ecology, Ufa State Aircraft University, <sup>2</sup>Department of Environmental Management, International Sakharov Environmental University)

This paper considers a perennial experience of development of computation methods of the different hydrological characteristics (maximum and minimum flow, average annual flow and its distribution in months, temperature water, ice regime and etc.) on the territory of the former USSR in ungauged river basins. Over recent 70 years hydrological predictions were developed for ungauged basins on the territory of the former USSR. This approach came into being as it was impossible to cover the vast territories with measurement, yet the knowledge of designed hydrologic characteristics was prerequisite for economic development (construction of bridges, roads, railways, settlements, etc.) The basic inputs to such predictions and computations are as follows: 1. Method of hydrological analogy that implies choosing another water body with analogous physical-geographical and hydrological conditions and having a long series of observations; 2. Method of hydrological characteristics mapping on the basis of their parameter distribution following the latitude zoning on the plain and the high-altitude zoning in the mountain areas. Theazonality factor is accounted for by introducing correction coefficients for fissured rocks, developed carst phenomena, etc. 3. Method of empirical formulas, in particular for maximum and minimum flows under homogenous natural conditions as based on the generalization of available observation series at separate river sections; 4. Method of maximum discharge determination on the high water marks, i. e. on the traces left upon natural and artificial objects: rocks, trees, buildings, pillars, etc. 5. Method of determination of annual and maximum flows in relation to climatic characteristics (precipitation, temperature, air humidity, height of firm line). 6. Method of remote sensing based on the simultaneous generalization of the hydrological regime characteristics and of aerial-space survey and generation of discharge-level and river-flooding relations. The report will be illustrated with different methods of forecasting and computing for various territories of Russia, Brazil and Belarus.

**HW07/11P/D-023** Poster **1400-159**

#### ENVELOPE CURVES OF FLOOD WAVE VOLUMES IN THE DANUBE RIVER BASIN IN CROATIA

Danko BIONDIC<sup>1</sup>, Darko BARBALIC<sup>1</sup>, Josip PETRAS<sup>2</sup> (<sup>1</sup>INSTITUTE OF WATER MANAGEMENT, CROATIAN WATERS, <sup>2</sup>UNIVERSITY OF ZAGREB, FACULTY OF CIVIL ENGINEERING)

The Danube River basin in Croatia comprises more than 35,000 km<sup>2</sup> which represents about 62 % of the country's land area, where approximately 69 % of the total population of the Republic of Croatia live (data from 2002). It is located in the Pannonian plain and its marginal areas, with the water divide separating it from the Adriatic catchment running through the Dinaric karst. A particular socio-economic significance of this area not only for the Republic of Croatia but also for a greater region requires efficient protection against flood and torrents. Gradual development of protection systems in the last four decades has significantly reduced potential damages, a fact proven by successful evacuation of numerous recent floods. The constructed systems are for the most part only partially completed, which leaves larger areas still at a significant risk of flooding. Further development and improvement of the flood and torrents protection system remains therefore one of the strategic tasks of Croatian water management. Basic hydrological informations for further planning and designing of flood control systems are maximum discharges, maximum volumes and maximum durations of flood waves of required return periods in adequate locations along the watercourses. Those can be estimated by applying stochastic methods for sufficiently long homogenous time series of measured discharges at gauged locations or by different PUB methods on locations where time series of measured data are insufficiently long or non-existent. Common hydrological practice also recognizes the use of various methods for evaluation of reliability of such calculated values. This paper presents comparison of Creager's and Francou-Rodier's envelope curves for evaluation of reliability of previously estimated flood wave volumes at subject area. Envelope curves were defined for average maximum annual volumes, for highest observed volumes, and for maximum annual volumes of the 10, 100 and 1000-year return periods over characteristic discharge thresholds ( $Q_{0.995}$ ,  $Q_{0.99}$ ,  $Q_{0.95}$ ,  $Q_{0.9}$  and  $Q_{0.5}$ ). Those are calculated on the basis of approximately a hundred available sufficiently long homogenous time series of measured daily discharges on gauging stations at investigated area. This work is a continuation of the investigations focused on maximum discharges in the Danube River basin in Croatia which were presented on the PUB Kick-off Workshop in Brasilia, 20-22 November 2002.

**HW07/11P/D-024** Poster **1400-160**

#### THE STATE-OF-THE-ART IN PREDICTING BLUE NILE LOW FLOWS: A STRATEGIC IMPORTANCE FOR THE WATER RESOURCES MANAGEMENT IN SUDAN

Anil MISHRA<sup>1</sup>, A.W. ABDELHADF<sup>2</sup>, Takeshi HATA<sup>3</sup>, O.E. HAMAD<sup>3</sup> (<sup>1</sup>Division of Regional Environment, Graduate School of Science and Technology, Kobe University, <sup>2</sup>Agricultural Research

The Blue Nile River originates from Lake Tana, in the Ethiopian Highlands and is one of the most important tributaries of the main Nile. The river provides a vital source of freshwater to the downstream riparian users, Sudan and Egypt. However, only a few studies in its upper basin within Ethiopia have been conducted and the information available on the climatic, hydrologic, topologic, and hydraulic characteristics of the river and the basin is incomplete. Thus the hydrologic assessment of the upper Blue Nile is dependent on downstream measurement. The Blue Nile is characterized by severe seasonality and about 70% of the runoff occurs between July and September. Peaking in August, after which the Blue Nile start to fall as rain water supply to the river begins to decline. Flow in the river rises again in March-May because of equatorial spring rains on the southern tributaries. There are two reservoirs in the Sudanese territory along the Blue Nile, Roseires and Sennar, with a combined storage capacity of 3 km<sup>3</sup>. The reservoirs are operated in series. Operating rules have been developed to minimize sedimentation and to optimize hydropower production in terms of water availability and irrigation demands. The problem is complex because energy demand increases during the recession time and doesn't coincide with irrigation releases. The water stored from the previous season in the two reservoirs is essential for irrigation and for hydropower generation. Thus the aim of the Sudanese authorities is to maximize irrigation, hydropower and water supply while minimizing sedimentation within the framework of Sudan's share in the 1959 River Nile water agreement between Egypt and Sudan. Since the combined capacity of the two reservoirs falls short of the total requirements the gap has to be supplemented from the natural river flow during the recession time. Several attempts have been made to forecast the Blue Nile low flows for this purpose. About two decades ago two methods were commonly used to forecast the recession flows: 'similar year' or a recession constant linking successive 10-days flows. Recently several models, which were derived from the linear and nonlinear storage-outflow relationship, were studied and applied to forecast the recession flow of the river. Similarly an autoregressive AR (2) model was also introduced to model the recession flow using parallel linear reservoir algorithm. This paper reviews 20-year efforts made in predicting recession flows and presents a comparison of reviewed models. The development of the recession modelling has greatly simplified the methodology and improved the forecasting accuracy. The study shows that the management of water resources in Sudan can be improved by better forecasting the low flows of the Blue Nile river, which can be achieved by the use of a more accurate, simple and reliable method.

**HW07/11P/D-025** Poster **1400-161**

**DISCHARGE PREDICTION USING COMPARISON OF CALCULATED-HISTORICAL DATA (CASE STUDY: KRAMAT MICRO-DAM, MADURA - INDONESIA)**

Tri Budi PRAYOGO (Department of Water Resources Engineering University of Brawijaya)

In the arid areas of Indonesia, the role of micro-dam for water domestic and irrigation supply is very significant. Micro-dam in Indonesia is called 'embung' is usually built in the small watershed and used to store rain water and/or river discharge. However, small watershed with very small river is usually not completed with rain gauge or hydrometric data recorder. Due to this limitation, hydrometric and hydrologic data for 'embung' design is usually calculated using stations outside the watersheds or predicted based on the discharge history. This paper aims to describe the process of discharge prediction in the design of 'embung' in the Kramat watershed, Madura Island, East Java, Indonesia. Discharges are modeled by using rainfall data and discharge data from the closest watershed called experimental watershed. Empirical Tank Model is used for the modeling. The adjustment for Kramat watershed discharge data is proceeded by comparing watershed characteristic data between Kramat watershed and the experimental watershed. The adjusted discharge data is furthermore compared with the daily discharge data predicted from the history discharges in the river. This history discharge data is predicted based on the descriptions from the people living near the watershed or based on the morphology exposure of the river. The adjusted discharge data is considered valid if it is not exceeded the historical discharge data.

**HW07/11P/D-026** Poster **1400-162**

**AN EMPIRICAL EQUATION FOR UNGAGED BASINS TO FIND THE MAXIMUM RUNOFF DISCHARGE**

Abdulghani A. HASAN, Anas M. RASHEED (Saddam Research Center for Dams and Water Resources, University of Mosul)

In this paper a numerical modeling technique using (finite elements) have been used to calculate the maximum runoff discharge for three ungauged basins, northern Iraq. All data results that produced from a very big number of rainfall depths have been used to find an empirical equations for these basins. Depending on basins characteristics and curve number the model calculations and discharge prediction has been achieved. This equation could be used in the future to calculate the maximum discharge produced from any rainfall depth that occur in those basins and maybe we can check its validity for other basins northern Iraq.

**HW07/11P/D-027** Poster **1400-163**

**APPLICATION WATERSHED MODELLING SYSTEM IN PREDICTING FLOWING SEDIMENT HYDROGRAPH, NORTH IRAQ**

Thair Mahmood AL-TAIEE<sup>1</sup>, Anas Mahmood RASHID<sup>2</sup> (Head of Water Resources Department in Saddam Research Center for Dams and Water Resources, <sup>3</sup>Water Resources Department, Saddam Research Center, Mosul University)

The watershed area of Fayda and Al-Baqaq wadies were selected as a case study in the eastern area of Saddam lake North Iraq to estimate the average sediment yield resulted from the surface erosion processes during rainfall and also to predict a standard unit sediment hydrograph flowing in those wadies. The research work introduce computer topographical and morphological simulation using Watershed Modeling System feeding this model with a hydrological and physiographical data concerning the case study area. Such model is defined as a simple compound system in which its behavior is represented by number of equations contribute with logical aspects and relations between the variables to predict the required results. The simulation process in the model is considered an alternative tool than carrying out comprehensive continuous field studies and experiments which is often be costly and difficult to use. An aspectable model for the case study area is used. This process is one of the essential steps in the whole modeling processes. The aspectable model is a simple representation for the study site throughout prediction of the watershed border and the surface runoff movement over the basin , in addition to the topography of soil type. Number of assumptions and simplifications to get this model where depended. A common world depended approaches were used to predict the sediment yield in the drainage basin. This is a useful tool for the evaluation of the future influences of the flowing sediments in those wadies on Saddam lake and may aid in the suggestion of many treatments to eliminate eroded sediment quantities from the drainage basin. Empirical relations to estimate runoff coefficient and peak discharges in addition to sediment yield related with peak discharges only were predicted. A non dimensional sediment hydrograph was

predicted to calculate the sediment curve for any rainfall storm on those wadies. Recommendation concerning performing field sediment transport measurement at the outlet of these wadies were suggested.

**HW07/11P/D-028** Poster **1400-164**

**INTRODUCTION OF SEASONALITY INTO A UNIFYING THEORETICAL FRAMEWORK FOR WATER BALANCE PREDICTIONS IN UNGAGED BASINS**

Yoshiyuki YOKOO<sup>1</sup>, Murugesu SIVAPALAN<sup>2</sup> (Institute of Industrial Science, University of Tokyo, <sup>2</sup>Centre for Water Research, University of Western Australia)

This paper addresses the role of seasonality on water balance prediction in ungauged basins and introduces a unifying theoretical framework through the use of a simple, physically based water balance model (Reggiani et al., 2000). Given measures of the basic properties of basins, such as soil type and depth, basin topography, as well as climatic features, it investigates the key roles of the climatic and landscape features on water balances. In particular, the paper focuses on the effects of seasonality of climate on the overall water balance. Precipitation and potential evaporation are assumed to vary seasonally with specified amplitudes and phase differences, mimicking realistic conditions. Results of the simulations demonstrate that the net effect of seasonality is to decrease annual evaporation and increase annual runoff, and with the largest impact occurring when seasonal variations of precipitation and potential evaporation were completely out of phase. These results confirm trends seen in observed data as well as results of previous simulation exercises. We also investigate the effects of storminess of climate, soil type and soil depth, and found that the effects of seasonality are amplified with more permeable and shallower soils, and with increased storminess. We also investigated the effects of these factors on mean monthly variation of water balance, including the magnitudes of seasonal fluctuations of both soil moisture and streamflow. These results are presented in terms of a number of dimensionless similarity indices: the climatic dryness index, a storage index, a drainability index, and a storminess index. Interpretation of the results in terms of these indices enables a more physically meaningful classification of catchments for first-order predictions in ungauged catchments. Reggiani, P., M. Sivapalan and S. M. Hassanizadeh (2000). Conservation equations governing hillslope responses: Exploring the physical basis of water balance. *Water Resources Research*, Vol. 36, No. 7, pp. 1845-1864.

**HW07/11P/D-029** Poster **1400-165**

**MULTIVARIATE ESTIMATION OF FLOODS**

Jose A. RAYNAL (Department of Civil Engineering, Universidad de las Americas, Puebla)

Flood frequency analysis has been carried out by using wide-known univariate probability distributions for the maxima. A few examples of that are: Three-parameter Log-Normal, Pearson Type III, Log-Pearson Type III, Wakeby and the Extreme Values Types I (Gumbel) and II (Frechet). The methods for estimating the parameters of such distributions vary from the old method of moments to new options like the probability weighted moments and maximum entropy methods. Multivariate extreme value models for flood and drought frequency analyses have been explored towards their application in hydrological problems. This is the case of the bivariate and trivariate extreme value distribution functions for the maxima which were explored towards their application in solving hydrological problems. The characteristics, properties and construction of the models are quite suitable to provide a powerful tool for flood frequency analysis. The selected method of estimation of parameters is the method of maximum likelihood. From the study reported here, it has been shown the suitability of using multivariate modeling of extremes when it is needed to improve the estimation of parameters and confidence limits of design values of gauging station with short records when gauging stations with longer records are available in its neighborhood. In the paper an example of application is given to show the suitability of the model in engineering practice.

**HW07/11P/D-030** Poster **1400-166**

**PREDICTION OF SEDIMENTGRAPH IN SMALL UNGAUGED BASINS**

Kazimierz BANASIK<sup>1</sup>, Mariusz BARSZCZ<sup>2</sup>, Marek MADEYSKI<sup>3</sup>, J.Kent MITCHELL<sup>3</sup> (<sup>1</sup>Dept. of Water Engineering and Environmental Reclamation, Warsaw Agricultural University, <sup>2</sup>Dept. of Water Engineering, Cracow Agricultural University, <sup>3</sup>Dept. of Agricultural Engineering, University of Illinois at Urbana-Champaign)

Estimates of sedimentgraphs (graphs of suspended sediment load associated with hydrographs caused by rainfall) are essential for sediment yield assessments, for providing input data for prediction models of sediment deposition in reservoirs, for designing efficient sediment control structures, and for water quality predictions. In these cases, and specially in the frequently considered non-point pollution models, in which sediment is a pollutant and a carrier for other pollutants, it is important to estimate sediment transport accurately during individual storms. The sedimentgraph model, which was developed for predicting ungauged basin response to heavy rainfall consists of two parts: a hydrological submodel and sedimentology submodel. The hydrological submodel uses the Soil Conservation Service CN method to estimate effective rainfall, and the instantaneous unit hydrograph (IUH) procedure to transform the effective rainfall into a direct runoff hydrograph. The sedimentology submodel uses a form of modified universal soil loss equation to estimate the amount of suspended sediment produced during the rainfall-runoff event, and the instantaneous unit sedimentgraph (IUSG) procedure to transform the produced sediment into a sedimentgraph. The instantaneous unit sedimentgraph (IUSG) has been developed by using the concept of instantaneous unit hydrograph (IUH) and dimensionless sediment concentration distribution (DSCD). New equation of IUSG is presented, and a procedure for estimating sediment routing coefficient, which is a key parameter of the IUSG, based on measured data of rainfall-runoff-suspended sediment (i.e. based on lag times), is applied. Field data from small basins of three different locations (south and centre of Poland and Central Illinois, USA), and different land management, were used to investigate lag times. The analysis of rainfall-runoff-sediment yield data from small basins shows that (i) a significant linear relationship exists between the lag time for hydrographs LAG and lag time of the sedimentgraphs LAGs, (ii) the values of LAGs/LAG are for most cases smaller as 1.

**HW07/11P/D-031** Poster **1400-167**

**CLIMATE AND LANDSCAPE CONTROLS ON SPATIAL (SUB-BASIN) VARIABILITY OF WATER BALANCE WITH CHANGING TIME SCALES: APPLICATION OF THE DOWNWARD APPROACH**

Darren FARMER, Murugesu SIVAPALAN (Centre for Water Research, University of Western Australia)

The south-west of Western Australia has a semi-arid, Mediterranean climate with cold, wet winters and hot, dry summers. Both the climate and the landscape feature significantly in a highly heterogeneous regional hydrology. Local hydrological understanding and prediction is

hampered by irregular gauge data for rainfall and streamflow. This paper deals with the application of a "downward" or top-down approach for the systematic analysis of space-time variability of observed streamflows across the region. The analysis identifies the key climatic and landscape (soils, topography and vegetation) controls on runoff variability, with a view to quantifying local runoff characteristics for varying landscapes across a region. The downward approach involves the use of conceptual (storage based) water balance models of increasing complexity with decreasing timescales (annual, monthly daily etc.) to investigate discrete signatures of streamflow variability at various timescales. Parameters extracted a priori from measurable landscape features are evaluated in order to infer local sensitivities and thus establish local landscape parameterization needs. A benefit of the approach is the ability to derive this knowledge from gauged locations removed from the area of immediate interest. The paper uses the 7,000 sq. km Murray River Basin (WA) to demonstrate how the method is used to evaluate significant east-west trends driven by climate variability, soils, topography, vegetation and land use. The systematic analysis clearly identifies local requirements for parameter variability and permits appropriate parameter sets to be determined for local ungauged catchments in order to portray variability in sub-catchment runoff generation and basin contribution.

**HW07/11P/D-032** Poster **1400-168**

#### WIDE UNCERTAINTY OF STEEP UNGAUGED INDUS BASIN

Shaukat A. AWAN (HYDROLOGICAL ADVISOR OF PAKISTAN WITH WMO (PAKISTAN MET DEPARTMENT))

In South-Asia since Indus basin is very widespread (970,000 KM<sup>2</sup>) with drainage basin located in (HKH) Hindu Kush Himalayan region. The upper reaches and tributaries, which are located in populated areas, have gauges site for river flows and telemetric station for precipitation reporting for effective flood forecasting. The Ungauged basin area in Indus Basin (Main) is 46410 KM<sup>2</sup> and its tributaries sub-basins Jhelum (23000 KM<sup>2</sup>), Chenab (24000 KM<sup>2</sup>), Ravi (5000 KM<sup>2</sup>) and Sutlej (13000 KM<sup>2</sup>). The hilly and inaccessible stations being ungauged a very tricky problem both for rainfall and channel runoff reporting. This problem is further compounded by the fact that upper drainage basin are located across the boarder, where the slope is of the order of 20 to 30 m/km, which often causes flash flows thus giving a time lag of only 3 to 4 hours for peak flow to buildup and enter the country over the rim station. Normally dam/reservoir authority and river regulating authority are caught unaware. Flood forecasting division has been entrusted with the responsibility to predict the flash flows for whole of the country. Knowing the equipment limitations ungauged, unmanned and inaccessible basin a methodology has been devised with some empirical/statistical relationship. The technique for gauging the ungauged basin is twofold, which is being practically implemented by this organization. One of them is the Radar-Based and the other is isohyetal analysis based. The S-band radar and C-band radar are both used. The reflectivity in dB (decibel) is calibrated with precipitation rate are mm/hr. The enormous ungauged basin of the tributaries is further sub-divided in the sub-basin areas. The precipitation rate in each sub-basin is integrated and hence an average rainfall rate is calculated and translated into runoff by keeping the previous rainfall runoff relationship. Also VIL feature (vertically integrated liquid content in Kg/m<sup>3</sup>) is used. This methodology has been of great success in the limited time period and has been actually used in the current flood season 2002. In extreme flashy and sloppy drainage basin isohyets are also used by first locating the precipitation recording station encircling the ungauged basin area and later on give a reasonable idea of flood causing precipitation and resultant channel flow. In the recent flood season a new situation was found where in the cloud cell detected by the radar, gave no rainfall at the recording stations but gave rainfall in between the recording stations, this made the gauged basin appear as ungauged basin. Consequently the technique used for ungauged basin was applied here also with considerable success. This new technique has yet to be put in full practice to make it more effective in both gauged and ungauged basin area.

**HW07/11P/D-033** Poster **1400-169**

#### ESTIMATION OF DESIGN DISCHARGE IN UNGAUGED BASINS USING GIS

Umamahesh Venkata NANDURI, Naga Malleswara RAO (Department of Civil Engineering, Regional Engineering College, Warangal)

Rainwater harvesting through indigenous methods has been the tradition in Warangal District in the State of Andhra Pradesh, India, developed and practiced by the rulers of Kakatiya Dynasty about 800 years ago. Unfortunately many of these techniques are forgotten today. Warangal District is semi-arid and drought prone. The water harvesting techniques have helped in sustaining the agriculture activity even under drought conditions. But today the district faces severe water crisis along with the problem of soil erosion in agricultural lands. The local government has taken up watershed development project in many parts of the district to tackle these two problems. The objective of this project is to revive the water harvesting techniques practiced earlier and to protect the agricultural lands from erosion. Planning and construction of water harvesting and soil and water conservation structures requires estimation of the quantity of runoff and peak discharges. Most of the watersheds where these structures are constructed are ungauged and do not have any records of runoff. During the last few years the Geographic Information System (GIS) technology has emerged as an extensively effective tool for analyzing and prioritizing natural resource management alternatives. The present paper describes the use of GIS in estimating the peak discharge from an ungauged watershed. The study is taken up in six villages of Warangal District covering an area of about 6000 hectares. The daily rainfall data of 30 years is available, which is used to develop the intensity-duration-frequency relationship. Spatial database of the study area is developed from digitized maps pertaining to topography, soils, land use and land cover, drainage system and hydrogeomorphology. The GIS created from these data is used in estimating the peak flow from the watershed. Three methods are used for estimating the peak flow. The first method is based on SCS curve number technique. In the second method a synthetic unit hydrograph is developed based on the technique developed by Central Water Commission, New Delhi. In the third method the various geomorphological parameters are estimated and these parameters are then used to construct Geomorphological Instantaneous Unit Hydrograph (GIUH). The peak runoff at different sites are computed using these three methods and they are compared.

**HW07/11P/D-034** Poster **1400-170**

#### REGIONALIZED REGRESSION RELATIONSHIPS FOR STREAMFLOW ESTIMATION IN UNGAUGED BASINS OF COASTAL KARNATAKA, INDIA

Lakshman NANDAGIRI, Ram Mohan RAO (Department of Applied Mechanics & Hydraulics, NITK, Surathkal, India)

The need for estimating streamflow arises in situations where water resources projects are planned at ungauged locations. Although several methods have been developed for streamflow prediction in ungauged basins (PUB), practicing engineers in India still prefer to use simple regionalized rainfall-runoff relationships that were developed during the colonial era. Such equations will continue to remain popular till such time as recently installed

networks and proposed ones begin to provide hydrometeorological data at desired spatial and temporal scales for operational hydrological models to be used. Therefore, the immediate task is to improve the predictive capabilities of this approach by re-formulating such relationships considering smaller hydroclimatic regions and using more recent measurements of streamflow and rainfall. In this study, we undertook the task of developing Regionalized Regression Relationships (RRR) for the hydroclimatically homogeneous coastal districts of Dakshina Kannada and Udipi of Karnataka state, India. Our approach involved developing linear regression models between daily streamflow and basin average daily rainfall for eight gaged basins in the region using data for the period from 1970 onwards. Two linear regression models, one relating streamflow on any day to rainfall of the same day and, the second including an additional term for rainfall lagged by one day, were developed. For each basin, such relationships were derived for each month of the monsoon season (June to September) and also for the monsoon season as a whole. Fairly reasonable model performances were noted both during the calibration and validation phases. Statistically significant relationships (both linear and non-linear) were then established between the regression coefficients of these linear models and physical characteristics of the basins. Regionalized regression relationships developed in this manner were validated and found to perform well. In spite of their simplicity, these relationships will provide reasonably accurate estimates of daily streamflow in ungauged basins in the region. As part of the IAHS Decade on Prediction in Ungauged Basins (PUB), work needs to be initiated to develop such simple prediction tools in other regions of India and also in other countries possessing sparse data networks.

**HW07/11P/D-035** Poster **1400-171**

#### A NEW WEIGHTED FUNCTION MOMENT METHOD BASED ON L-MOMENT FOR PEARSON-III DISTRIBUTION

Yuanfang CHEN<sup>1</sup>, Shenghua GU<sup>2</sup>, Zhigui SHA<sup>3</sup>, Shengbin XU<sup>1</sup> (<sup>1</sup>Department of Hydrology and Water Resources, Hohai University, <sup>2</sup>SHANGHAI GENERAL HYDROLOGICAL STATION, <sup>3</sup>BUREAU OF HYDROLOGY, YANGTZE RIVER COMMISSION)

The defect of a weighted function moment method for Pearson-III distribution developed by Chinese hydrologist MA Xiufeng is that the parameter of  $C_v$  is negatively biased, especially when the population parameter  $C_v$  is large. In order to overcome it, a new weighted function moment method is proposed, where the parameter  $C_v$  is estimated by L-moments method. A lot of Monte-Carlo calculation shows that the new weighted function moment method based on L-moment is better than the conventional one in the bias of the quantiles and the parameter  $C_v$ , but the effectiveness of the quantiles and the parameter  $C_v$  of above two estimation methods are almost the same. Key words: Weighted function moment method; L-moment; bias, effectiveness; Person-III distribution.

**HW07/11P/D-036** Poster **1400-172**

#### APPLICATION OF REGIONAL FLOOD FREQUENCY ANALYSIS METHOD BASED ON L-MOMENT IN THE REGION OF MIDDLE AND LOWER REACHES OF YANGTZE RIVER

Yuanfang CHEN<sup>1</sup>, Qingrong WANG<sup>1</sup>, Zhigui SHA<sup>2</sup>, Jiangchi CHEN<sup>2</sup> (<sup>1</sup>Department of Hydrology and Water Resources, Hohai University, <sup>2</sup>BUREAU OF HYDROLOGY, YANGTZE RIVER COMMISSION)

The regional flood frequency analysis method based on L-moment proposed by Hosking in 1997 is applied to the flood frequency analysis of annual maximum flood volume for five hydrological stations, including Yichang, Shashi et al., in the middle and lower reaches of Yangtze river. The method of Hosking is a new one for Chinese traditional regional flood frequency analysis. The calculated results show that the five stations could be considered as in an homogenous region for frequency analysis, so the index-flood method is used to calculate design values for each station, and the Wakeby distribution is recommended to be population grow-curve (or distribution), because the others distribution, i.e., Pearson-III, GLO, GEV, GPA, and GLN are not accepted by Z statistics test.

**HW07/11P/D-037** Poster **1400-173**

#### A TENDENCY OF COEFFICIENT OF VARIATION (CV) OF ANNUAL FLOOD AND IMPROVEMENT OF EAGLESON'S CLASSIC MODEL

Yasuhisa KUZUHA<sup>1</sup>, Yosuke Komatsu<sup>2</sup>, Kunio TOMOSUGI<sup>1</sup>, Tokuo KISHII<sup>1</sup> (<sup>1</sup>National Research Institute for Earth Science and Disaster Prevention, and the Cooperative Graduate School, University of Tsukuba, <sup>2</sup>National Research Institute for Earth Science and Disaster Prevention, <sup>3</sup>DPRI, Kyoto University)

Regional flood frequency analysis is a useful method of predicting flood discharge from ungauged basins. According to Gupta and co-workers [1998], flood discharge data in a snow-melt dominant region exhibit simple scaling, and those in a storm dominant region exhibit multiscaling. We confirmed this using data in Japan by moment-based and quantile-based analyses. Mean annual flood versus catchment area and CV versus catchment area for Japan exhibit the same tendency as shown by Smith [1992] and Bloschl and Sivapalan [1997]; CV increases below a critical catchment area and decreases above the critical value with area. Even if this tendency were not true (namely; there is not a critical area), decreasing tendency with area seems to be natural. However, if we calculate CV using Eagleson's classic model, CV increases with area [Kuzuha et al. 2000]. To investigate the reason for this we developed a simple precipitation-runoff model consisting of a square catchment and a channel along the diagonal. Flow velocity is assumed to be 3 (non dimension) on the slope and unity in the channel. We carried out numerical integrations and obtained mean and CV using their definitions, namely; without the assumption of Gumbel distribution, which Eagleson assumed. Note that we converted the distribution for annual exceedance series into annual maximum series. The result shows an increasing tendency for small basins and constant tendency for large basins. First, we thought that this tendency, which is not consistent with observations, results from the simplicity of the model, namely; this model doesn't include a channel network; and so we introduced the Peano network. The result indicated that the scale exponent is about unity for small basins and 0.7925 for large basins, which is a characteristic value for Peano basins, but the decreasing tendency could not be reproduced. Secondly, we assumed that rainfall intensity obeys a kind of Gamma distribution whose CV decreases with increasing area. As a result, we could reproduce the increasing-decreasing tendency of CV. According to Robinson and Sivapalan [1997], increasing CV for a small basin results from PDR (peak discharge response) function's behavior. Eagleson's classic model and our model take account of this PDR's effect. On the other hand, because the classic model assumed the exponential distribution for rainfall intensity, the model could not reproduce decreasing CV. To improve the classic model, a different type of distribution for rainfall intensity is necessary, and the simplicity of the model, (namely; not including channel network) is not the main reason for being inconsistent with observations. Bloschl and Sivapalan (1997): WRR, 2967-2980, Eagleson (1972): WRR, 878-898, Gupta and Waymire (1998): in Scale Dependence and Scale Invariance in Hydrology, Kuzuha et al. (2000): Ann. J. Hydraul. Eng., JSCE, 7-12, Robinson and Sivapalan (1997): WRR, 1045-1059, Smith (1992): WRR, 2993-2999.

**HW07/11P/D-038** Poster **1400-174**

**LONG TERM WATER BALANCE PREDICTION OF POORLY GAUGED MOUNTANEOUS BASIN IN THAILAND**

M. Husni IDRIS<sup>1</sup>, Kuraji KOICHIRO<sup>2</sup>, Kowit PUNYATRONG<sup>3</sup>, Thada SUKHAPUNNAPHAN<sup>4</sup>, Suzuki MASAKAZU<sup>1</sup> (<sup>1</sup>Department of Forest Science, The University of Tokyo, <sup>2</sup>University Forest, Graduate School of Agricultural and Life Sciences, The University of Tokyo, <sup>3</sup>The Royal Initiative and Security Project Division, National Park, Wildlife and Plant Conservation Department, <sup>4</sup>Hydrological Center 1, Royal Irrigation Department)

The long-term water balance of poorly gauged basin in mountainous area in Northern Thailand has been described. The Mae Chaem watershed with catchment area 3853 km<sup>2</sup> was selected as study area. The relatively dense rainfall gauges in the watershed is available for the last three years, while only few gauges are exist for long-term rainfall record. Discharge data have been continuously collected at the outlet of the whole watershed by Royal Irrigation Department (RID) Thailand. This study involved spatial rainfall distribution and long-term rainfall analyses. Spatial rainfall over whole basin were developed using 11 rain gauges of the present intensive measurement. The basin was divided into grids with about 1 km in size. Several interpolation methods (e.g. linear regression, inverse distance, Thiessen polygon and krignings) were applied to provide rainfall at all grids. Cross validation that allow the calculation of root mean square error (RMSE) was used to compare the performance of each interpolator. Long-term basin average rainfall was estimated based on (1) a relationship between rainfall at long-term observation site and rationally interpolated basin average rainfall during intensively observed period and (2) an appropriate interpolation from long-term rainfall data recorded at outside the basin. Long-term water balance were assessed from the estimated average rainfall and observed discharge. Result on spatial rainfall distribution during dense rain gauge measurement period showed that linear regression between rainfall and elevation gives simple and a good prediction for annual rainfall rate. The interpolators considering the effect of elevation (e.g. linier regression, linier regression and simple kriging and external drift kriging) have small and slightly different in RMSE. On the other hand, the interpolator, which regardless the effect of elevation (e.g. inverse distance, ordinary kriging and thiessen polygon, arithmetic mean) resulted in higher RMSE and inadequate water budget which shows too large in evaporation rate.

**HW07/11P/D-039** Poster **1400-175**

**AN APPROACH FOR GROUNDWATER PROSPECTING**

Sanjeev KUMAR<sup>1</sup>, Shakeel AHMED<sup>1</sup>, Anand JOSHI<sup>2</sup> (<sup>1</sup>F.C.G.R., NATIONAL GEOPHYSICAL RESEARCH INSTITUTE., <sup>2</sup>KURUKSHETRA UNIVERSITY KURUKSHETRA, INDIA)

Groundwater resources are extremely important in Rajasthan as almost the entire region lies in arid/semiarid tropics of Rajasthan especially in the hard rock areas. The recharge is less due to scanty rainfall. The study has revealed the advantages of remotely sensed data in identifying the prospect of groundwater in geologically and structurally complex terrain. Remote Sensing & Geographic Information System (GIS) is a dynamic tool for facilitating the generation and use of thematic information, has been applied to groundwater potentiality of the Upper Kali Sindh Chauhi watershed in the Jhalawar district of Rajasthan, India. The role of different parameters namely geology, geomorphology, structures, lineaments, slope, land use & land cover, digital elevation model, digital terrain model etc. have been emphasized for delineation of the groundwater potential zones. The groundwater potential zone map was prepared based on the visual interpretation of satellite Geocoded data of IRS-1D, LISS III, FCC and the topographic map (54D/2, 54D/3, 54D/6, and 54D/7) on 1:50,000 scales. In the study area major lineaments are identified from the satellite data interpretation, which are surface manifestation of some structural features in the bedrocks as fractures and joints. The study areas divided into mini-watershed and micro-watershed on the basis of area and stream channels. Groundwater prospects are controlled by the lineaments/joints, as the lithology is not much suitable for groundwater development. Ultimate groundwater prospecting map indicate a variable groundwater potentiality in the area i.e. *good, moderate, limited, and poor* and based on these categorization the depth of wells for drilling are suggested.

**HW08** Monday, July 7 - Wednesday, July 9

**PARAMETER ESTIMATION TECHNIQUES (IAHS/WMO WORKING GROUP ON GEWEX WITH THE SUPPORT OF ICSW AND ICASVR)**

Location: Site C, Room 28

Monday, July 7 AM

Presiding Chairs: Q. Duan, H. Gupta

**DEVELOPMENT AND APPLICATION OF MODEL CALIBRATION TECHNIQUES**

**HW08/07A/C28-001** Invited **0900**

**ADVANCES IN AUTOMATIC CALIBRATION OF WATERSHED MODELS**

Hoshin V. GUPTA<sup>1</sup>, Soroosh SOROOSHIAN<sup>1</sup>, Thorsten WAGENER<sup>1</sup>, Jasper A. VRUGT<sup>2</sup> (<sup>1</sup>Department of Hydrology and Water Resources, The University of Arizona, <sup>2</sup>Institute for Biodiversity and Ecosystem Dynamics, University of Amsterdam)

There is an urgent need to develop reliable automatic methods for the identification of watershed models. The goal of such research should be to develop strategies that explicitly account for all of the following - a priori model uncertainty, input, state, structure, parameter and output uncertainties, and multiple sources and types of information, while allowing recursive processing of data as they become available, and providing quantified (perhaps probabilistic) estimates of model output uncertainty. The 'Turing Test' of such a strategy would be its ability to provide reliable model performance that is indistinguishable from, or demonstrably superior to what can be obtained by an expert hydrologist. Traditional automatic methods based on techniques of non-linear regression fail in this regard. Major weakness include their underlying assumption that the model structure is correct, an inability to handle various sources of uncertainty, a dependence on a single aggregate measure of model performance, and an emphasis on identifying a unique optimal parameter set. The multiple-criteria approach offers a way forward by emulating the ability of manual-expert calibration to employ a number of complementary ways of evaluating model performance, thereby compensating for various kinds of model and data errors, and extracting greater

amounts of information from the data. The outcome is a set of models that are constrained (by the data) to be structurally and functionally consistent with available qualitative and quantitative information and which simulate, in an uncertain way, the observed behavior of the watershed. Additionally, Bayesian methods allow a progressive reduction of model (and hence forecast) uncertainty through stepwise recursive (in time) processing of the input-output data as they become available. We will present the historical development of current perspectives on calibration and raise questions for further investigation.

**HW08/07A/C28-002** **0930**

**APPLICATIONS OF THE NEW REDUCED RANK SQUARE ROOT KALMAN FILTER TO THE PROBLEM OF PARAMETER ESTIMATION IN HYDROLOGICAL MODELS**

Dimitri TREEBUSHNY (Department of Environmental Modeling, Institute of Mathematical Machines and System Problems, NAS Ukraine)

It is known, that parameter estimation problem can be reformulated in terms of Data Assimilation approach. The augmented stochastic model is able to correct parameters of interest but becomes nonlinear in general case, even if the initial model is linear one. From the other hand, hydrological models are known to be large-scale or very large-scale ones. There are two Kalman filter based approaches able to deal with large-scale nonlinear models: Ensemble Kalman filter (EnKF, Evensen, 1994) and reduced rank square root filter (RRSQRT, Verlaan, 1995). The reduced rank square root filter is a special formulation of the Kalman filter used for Data Assimilation in large-scale models. In this formulation, the covariance matrix of the model state is expressed in a small number of modes, stored in a lower rank square root matrix. The RRSQRT algorithm includes a reduction part that reduces the number of modes if it becomes too large in order to ensure that the filter problem is feasible. In the classical implementation the problem of proper normalisation of the square-root matrix arises in the reduction step when variables of different scales are considered in the model, which is the case for parameter estimation problems. A new filter with more appropriate truncation procedure is presented. According to this approach one completely avoids normalisation problems, and, even more, the new truncation step needs much less computational time than the original procedure. The filter is applied for parameter estimation in the pollution transport model RIVTOX and verified against the Ensemble Kalman filter. RIVTOX one-dimensional model of pollutant transport based on advection-dispersion equation. The basic model's parameters are dispersion coefficient and the coefficients of the pollutant exchange between solute and solid phases. Some synthetic experiments are conducted for the verification. It is shown that the new filter is capable to estimate the system parameters and to predict the evolution of the system with about the same accuracy that the EnKF while consuming less computational time.

**HW08/07A/C28-003** **0950**

**DEVELOPMENT OF A HYBRID GENETIC ALGORITHM (HGA) TRANSFER FUNCTION MODEL FOR RAINFALL-RUNOFF PARAMETER ESTIMATION**

Sohrab HAJJAM (Department of Space Physics, University of Tehran)

In this paper an extensive investigation the application of genetic algorithms to the rainfall-runoff transfer function model has been presented. A new parameter estimation technique (Hybrid Genetic Algorithm) has been developed by combining conventional procedures with a genetic algorithm. The HGA has been successfully used both in identification (calibration) and simulation (updating) of the TF model. The new genetic algorithm techniques of interview and scaled procedures as well as random bit mutation and multiple crossover are included in HGA. Furthermore, both binary and real numbers encoding techniques have been used. Finally four software packages including two packages for the model identification phase both in binary and real number encoding and two packages for model updating phase have been developed. Extensive development and testing has shown that the performance of HGA is more accurate and powerful than conventional procedures and HGA guarantees that model estimation error will be less than current method because it is programmed that the RMSE of HGA to be less than RMSE of current method. **Keywords:** rainfall-runoff, genetic algorithm, transfer function, parameter estimation, simulation.

**HW08/07A/C28-004** **1010**

**EVALUATION OF PARAMETER CONSISTENCY IN THE TANK MODEL OPTIMIZATION**

Haruya TANAKAMARU (Graduate School of Science and Technology, Kobe University)

In this study, the parameter consistency was evaluated in the Tank Model optimization. The Tank Model is a conceptual rainfall-runoff model developed by Sugawara. The model for long-term simulation consists of four tanks and has 16 parameters including 4 initial storage depths. The previous study (Tanakamaru and Burges, 1996) showed that the SCE-UA method (Duan et al., 1992) and the multi-start Powell method provided superior performance to six other algorithms of local and global search in the numerical experiments of the Tank Model optimization using synthetic data. Thus, the SCE-UA method and the multi-start Powell method were compared in the following historical data study. The root mean square error (RMSE) and the root mean square of relative error (RR) of simulated daily runoff hydrograph, which show obvious trade-off relationship, are adopted as objective functions and these objectives are minimized under the constraint of the permitted water balance error. The 131.5 km<sup>2</sup> Eigenji Dam basin in Japan was chosen for a study basin and hydrological data (daily mean inflow, daily precipitation and monthly evaporation) of 4 years are used for parameter calibration. At first, the performance of single-objective optimization using RMSE and RR was examined. 100 independent trials with different initial search points were run to evaluate the consistency of estimated parameters. Results showed that the SCE-UA method is obviously superior to the multi-start Powell method in the consistency of estimated parameters and the parameter consistency in the trials using RMSE were relatively higher than that using RR. Secondly, the optimization using multi-objectives of RMSE and RR was also examined. The multi-objective problem can be converted into a single-objective problem by the weighting method. The weighting method using the SCE-UA single-objective scheme was applied here for solving the multi-objective problem because the good parameter consistency of the SCE-UA method is an important advantage for estimating reasonable parameter space of Pareto solutions. In the ordinary use of the weighting method, one optimization run is required to obtain one Pareto solution (it is called the ordinary Pareto solution, here). But, in this study, 100 independent optimization trials were run for one Pareto solution and the best one which has the minimum objective function value were adopted in order to calculate strict Pareto solutions. Here, 21 strict Pareto solutions were obtained changing the weight value and these solutions were compared with the ordinary Pareto solutions to evaluate effectiveness and consistency of the optimization. Some of ordinary solutions did not satisfy the necessary conditions of non-dominated solutions due to small fluctuation in the single-objective optimization. But, in the objective space, the Pareto front of the ordinary solutions were almost same with that of the strict solutions. Therefore, the multi-objective optimization using the weighting method and the SCE-UA scheme are considered to be approximately effective and consistent.

HW08/07A/C28-005

1030

**AUTOMATIC PARAMETER ESTIMATION FOR A DISTRIBUTED HYDROLOGICAL MODEL AND APPLICATION TO AN ALPINE WATERSHED**

Harald G. KUNSTMANN, Jan C. KRAUSE (Institute for Meteorology and Climate Research (IMK-IFU), Karlsruhe Research Center)

Efficient parameter estimation techniques are a basic prerequisite for the successful application of distributed hydrological models to questions of sustainable water management, such as assessments on water availability, flood risk or hydrological impact analysis of regional climate change. Even in physically based hydrological models, a set of parameters generally remains that must be calibrated. Lumped parameters (like e.g. storage coefficients) even must be calibrated for each subcatchment, which can be a tremendous effort. Against this background, we combined the nonlinear parameter estimation tool PEST with the distributed hydrological model WASIM. PEST is based on the Marquardt-Levenberg method, a gradient based nonlinear parameter estimation algorithm. WASIM is a fully distributed catchment model using physically based algorithms for most of the process descriptions. WASIM solves the Richards-equation for water fluxes in the unsaturated zone and couples to a 2-dimensional groundwater model as lower boundary condition. Beside of meteorological input data it requires gridded information on soil properties, land use and topography. We applied WASIM to the alpine/prealpine catchment of the river Ammer (Southern Germany, 700 km<sup>2</sup>). It is characterised by physiographic heterogeneity in terms of geology, pedology and land use and shows complex orography (the difference of elevation is around 1600 m). Using the developed PEST-WASIM interface, the hydrological model was calibrated by comparison of simulated and observed runoff at eight gauges for the hydrologic year 1997. For each subcatchment four parameters had to be calibrated: the storage constants of direct runoff and interflow, the drainage density, the recession constant for decrease of saturated hydraulic conductivity with depth, and the hydraulic conductivity of the uppermost aquifer). Additionally, three snow-melt specific parameters were calibrated for the entire catchment. PEST successfully fitted the observed runoff curves and showed tremendous time saving against the default manual "trial and error" calibration. Additional a-priori information (e.g. from flood hydrograph analysis) narrowed the parameter-space of the solutions and improved the non-uniqueness of the fitted values.

HW08/07A/C28-006

1110

**ON ESTIMATING BASIN PARAMETERS FOR OPERATIONAL HYDROLOGICAL MODELLING**

Sandra G. GARCIA (Department of Thermic Engineering and Fluids, Technical University of Cartagena)

In hydrological modelling, the most limiting factor does not correspond to the ability to characterize the hydrological processes but to the methodology to determine the suitable parameters of the models. The Geographical Information Systems (GIS) present digital data analysis techniques, which greatly facilitate this task. The development and application of methodologies to achieve a priori estimates of hydrological and geomorphological parameters, is fundamental in ungauged basins. In this paper, different methodologies and automatic processing tools for raster Digital Elevation Models for the topographical parameterisation of hydrological models are presented, together with examples of their application. In hydrometeorological alert situations in the Mediterranean basins characterized by flash flood type events, decisions have to be taken in short periods of time. It is absolutely vital to be able to make use of systems which act as a support when taking decisions in real-time. This type of system should combine the latest information treatment technologies with the most efficient and precise simulation and parameterisation techniques. Currently, we are researching the exploitation of satellite information for the analysis of soil moisture spatio-temporal evolution and its influence on flash flood hydrographs. The main objective is to improve the forecast of flash floods applying a decision support tool in real-time named *Shyska*, developed with GIS-embedded functions. New spatial analysis modules oriented to estimate and treat the spatial distribution of soil moisture and the flow in the unsaturated zone, are being studied for their integration in the *Shyska* environment. One of the objectives of this new research project, is the development and application of methodologies that facilitate the real (or near real) time decision taking on the most suitable parameters of hydrological models oriented to flood forecasting in South-East Spain. Finally, the results of spatially distributed rainfall-runoff transformation models, where inputs partially come from a real-time flood warning system, are presented.

HW08/07A/C28-007

1130

**PARAMETER ESTIMATION OF RAINFALL-RUNOFF MODELS USING THE EVOLUTION STRATEGY**Yoichi FUJIHARA<sup>1</sup>, Haruya TANAKAMARU<sup>1</sup>, Takeshi HATA<sup>2</sup>, Akio TADA<sup>2</sup> (<sup>1</sup>Graduate School of Science and Technology, Kobe University, <sup>2</sup>Faculty of Agriculture, Kobe University)

In this study, we discuss the use of the Evolution Strategy (ES) (Schwefel, 1977, 1995), which is one of the non-linear optimization methods, for the estimation of rainfall-runoff model parameters. The algorithm of the ES is similar to the Genetic Algorithm (GA) in the respect that multipoint search and recombination used in the GA are also adopted. But, the main feature of the ES is that its principal search procedure of the ES is mutation, which is conducted by adding perturbation of normal random variable to decision variable, and the standard deviation of random variable, which is a mutation parameter, is updated by self-adaptation. First, we apply the ES to the single-objective optimization of the Tank Model, which has 16 unknown parameters including 4 initial storage depths. The Eigenji Dam Basin and the Osaka Dam Basin in Japan were chosen as study basins. The data of 4 consecutive water years were used for the estimation of rainfall-runoff model parameters. The root mean square of relative error (RR) was used as an objective function. We also obtained the parameter estimates using the SCE-UA method (Duan et al., 1992). 100 runs with different initial populations were conducted for those two methods to check the consistency of optimization results. The calibration results of the ES and the SCE-UA method are compared. Results show that the search ability of the ES is equal or superior to that of the SCE-UA method in the consistency of estimated parameter values and the ES is effective in single-objective optimization of rainfall-runoff model parameters. Next, we apply the ES to the multi-objective optimization of the Tank Model parameters. The root mean square error (RMSE) and RR were used as objective functions. Before the application of the ES, we obtained the Pareto-optimal solutions using the weighting method with the SCE-UA method. For the purpose to search strict solutions, 100 optimization runs with different initial populations were conducted for one of the weight parameters and the run of minimum function value was adopted. Consequently, it was needed about 21x10<sup>7</sup> function evaluations to obtain 21 strict Pareto-optimal solutions. In the ES algorithm for the multi-objective optimization, we adopted the Pareto ranking suggested by Goldberg (1989) as fitness evaluation like the MOCOM-UA method (Yapo et al., 1998). In the application of the ES, when the number of function evaluations reached 10<sup>8</sup>, the optimization run was terminated and about 200 Pareto-optimal solutions were obtained. Results show that parameter estimates by the ES are almost the same as parameter estimates by the weighting method

and a large number of Pareto-optimal solutions are obtained by relatively small amount of calculation. Therefore, the ES is considered to be also effective and efficient in multi-objective optimization of rainfall-runoff model parameters.

HW08/07A/C28-008

1150

**APPORT D'UN CRITERE A PAS VARIABLE AU CALAGE DES PARAMETRES D'UN MODELE JOURNALIER A PARTIR DE DONNEES ANNUELLES**Antoine HREICHE<sup>1</sup>, Claude BOCQUILLION<sup>1</sup>, Wajdi NAJEM<sup>1</sup>, Eric SERVAT<sup>2</sup>, Alain DEZETTER<sup>2</sup> (<sup>1</sup>Ecole Supérieure d'Ingenieurs de Beyrouth, Saint-Joseph University - Lebanon, <sup>2</sup>Institut de Recherche et de Développement - IRD - France)

La modélisation conceptuelle des bassins versants comporte un certain nombre de paramètres identifiés généralement avec un critère de choix à partir de séries de mesures de pluie et de débit du bassin à un pas de mesures défini. Une des difficultés de cette démarche est souvent liée aux problèmes d'équifinalité : des jeux de paramètres différents sont « équivalents » en termes de comparaison de valeurs simulées par le modèle aux valeurs mesurées. Cette équifinalité a été mise en évidence sur le modèle à 4 paramètres, MEDOR, spécifique au climat méditerranéen, comportant : une production ne dépendant que de la pluie et de l'état hydrique et privilégiant ce dernier par rapport aux variables climatiques, et un transfert modélisé par deux réservoirs en parallèle. Elle est détaillée sur le bassin libanais du Nahr-Beyrouth et a été vérifiée sur huit bassins méditerranéens. L'analyse exhaustive de la fonction critère dans l'espace des 4 paramètres a montré l'existence de relations d'équifinalité entre paramètres de production (REP) d'une part, et de transfert d'autre part. L'indépendance des paramètres de production vis à vis de ceux de transfert permet de déterminer les paramètres de production préalablement et indépendamment de ceux de transfert. L'ajustement des bilans simulés - mesurés sur des pas variables avec un critère « Nash aggloméré » permet de réduire l'information nécessaire au calage. Au pas journalier, ce critère est le Nash habituel, et permet de déterminer une REP journalière. L'analyse à pas variable montre que cette REP est indépendante du pas, jusqu'au pas annuel, pour lequel le transfert est éliminé. Au pas annuel, les écarts de bilans ont des valeurs successives indépendantes et une répartition gaussienne. Le critère de Nash aggloméré annuel maximum entraîne une moyenne nulle des écarts et un écart type minimum. La REP annuelle, donc journalière, est confondue avec la relation de bilan global nul. La zone d'adéquation liée à l'intervalle de confiance du critère peut être définie à partir de l'expression de l'écart type des bilans. En conclusion, on a défini une méthodologie de recherche des paramètres de production du modèle journalier à partir de la seule connaissance des bilans annuels. Le problème de la détermination a priori des paramètres de production est reporté sur celle de la connaissance des bilans, plus simple à régionaliser.

HW08/07A/C28-009

1210

**OPTIMIZATION OF SOIL HYDRAULIC PARAMETERS FROM IN-SITU DATA**

Kun YANG, Toshio KOIKE (River Lab., Department of Civil Engineering, University of Tokyo)

As an important component of water cycles, soil moisture is often observed in field experiments for hydrological studies, while corresponding laboratory experiments are not always carried out for determining soil hydraulic parameters. This study presents an inverse system to optimize soil hydraulic parameters from observed soil moisture and temperature data. The system consists of a land surface model to predict soil moisture profile, and an optimization method to minimize an objective function, which is defined as the discrepancy between observed and model predicted values of soil moisture and surface temperature. The value of an objective function is affected by soil thermal parameters, hydraulic parameters and observation errors, which have to be optimized simultaneously. The objective function is highly nonlinear and contains many local minima, so we use simulated annealing algorithm to search the global minimum among many local minima of the objective function. Idealized case studies show that the system can estimate soil hydraulic parameters and correct systematic errors of moisture measurement, and the optimized parameters are not sensitive to model errors and small disturbances. Because the inverse method avoids tedious and expensive laboratory experiments, it is attractive in field experiments whenever soil moisture data are available.

HW08

Monday, July 7 - Wednesday, July 9

**PARAMETER ESTIMATION TECHNIQUES (IAHS/WMO WORKING GROUP ON GEWEX WITH THE SUPPORT OF ICSW AND ICASVR)**

Location: Site C, Room 28

Monday, July 7 PM

Presiding Chairs: A. Hall, S. Franks

**REVIEW OF MODEL PARAMETER ESTIMATION EXPERIMENT WORKSHOP RESULTS**

HW08/07P/C28-001

1410

**GEOELECTRICAL PARAMETERS ESTIMATION IN HYDROGEOLOGICAL INVESTIGATION USING FUZZY LOGIC TECHNIQUE**

Moruffdeen Adedapo ADABANIJA (Department of Pure and Applied Physics, Ladoko Akintola University of Technology, Ogbomoso, Nigeria.)

Fuzzy logic technique was designed, implemented using MATLAB and applied to estimate the geoelectrical parameters in terms of linguistic variables high, medium, low and very low for hydrogeological investigation. This was accomplished by hydrogeological and geoelectrical characterization of the subsurface earth layers using the layering parameters inferred from the approximate and computer assisted interpretation of the vertical electrical sounding curves; synthesis and fuzzification of rules and antecedents of the subsurface layering characteristics; and eventual defuzzification of the rules. The procedure yielded degree of membership graph for each geoelectrical parameter from which their degree of fulfillments (DOFs) and the actuated data range in the form of linguistic variables high, medium, low and very low were established. With this approach, hydrogeological appraisal of an area can be instantly carried out for optimum groundwater prior to holes/wells boring.

**HW08/07P/C28-002** Invited **1430**

**OVERVIEW OF MODEL PARAMETER ESTIMATION EXPERIMENT (MOPEX)**

Qingyun DUAN, John SCHAAKE (Hydrology Laboratory, NOAA/NWS/OHD)

How to estimate model parameters that vary spatially and are unique to each computational element is a key issue in all computer-based hydrological modeling. An international Model Parameter Estimation Experiment (MOPEX) was established to develop techniques for the a priori estimation of the parameters used in land surface parameterization schemes of atmospheric models and in hydrological models. The major effort to achieve this goal involves assembling a large number of historical hydrometeorological data sets and river basin characteristics data sets for a wide range of river basins representing different climatic and hydrologic conditions throughout the world. These data sets are intended for developing model parameter estimates and for developing relationship between model parameters and basin characteristics. This paper presents the rationale, science strategy and MOPEX's links to other international programs such as Global Energy and Water Cycle Experiment (GEWEX), Predictions for Ungauged Basins (PUB) and Coordinated Enhanced Observations Period (CEOP).

**HW08/07P/C28-003** Invited **1500**

**REVIEW OF RESULTS FROM THE SECOND MOPEX WORKSHOP IN TUCSON, AZ, APRIL 8-10, 2002**

Qingyun DUAN, John SCHAAKE (Hydrology Laboratory, NOAA/NWS/OHD)

The Second International MOPEX Workshop was held in Tucson, Arizona, April 8-10, 2002. This workshop was designed to bring together interested US and international hydrologists and land surface modelers to exchange experience in developing techniques for a priori estimation and calibration of hydrologic model parameters. Participants of the MOPEX project were given data for 12 basins selected in the Southeastern United States and were asked to carry out a set of numerical experiments using a priori parameters as well as calibrated parameters developed for their respective hydrologic models. More than 30 scientists from 8 countries directly participated in the workshop and a few more have submitted results of their hydrologic model simulations to the workshop. The results from the workshop are summarized in this presentation. Attempts are made to understand the differences in the results from different models. It is also hoped that we learn how to use model calibration to enhance a priori parameter estimation and to benefit from the expertise from different modeling groups.

**HW08/07P/C28-004** **1550**

**DEVELOPMENT AND TESTING OF A PRIORI PARAMETER ESTIMATION METHODS FOR DISTRIBUTED-PARAMETER MODELS: A COMPARISON AMONG 20 HYDROLOGIC LANDSCAPES DEFINED FOR THE UNITED STATES**

George H. LEAVESLEY, Lauren E. HAY, Roland J. VIGER, Steven L. MARKSTROM, Thomas C. WINTER (U.S. Geological Survey)

Model over-parameterization, ungauged basins, and the assessment of the impact of land-use and climate change are a few of the problems that limit the use of calibration techniques for distributed-parameter models. One approach to addressing these problems is the use of a priori parameter-estimation procedures to minimizing the number of parameters to be calibrated, or to obtain parameter values where calibration is not possible. A set of modeling and analytical tools is being developed using the US Geological Survey's Modular Modeling System to facilitate the development and evaluation of objective a priori methods. Initial testing of these tools is being conducted using multiple basins in each of the 20 hydrologic landscapes defined for the United States. Hydrologic landscapes provide a conceptual framework for describing and classifying landscapes in terms of land-surface slope, hydraulic properties of soils and geologic framework, and the difference between precipitation and evapotranspiration. A priori parameter estimates were made for the USGS distributed-parameter model PRMS using available digital datasets of terrain, soils, vegetation type and density, and climatological data. Parameter sensitivity and model performance are being evaluated within and among the hydrologic landscapes at incremental levels of calibration ranging from no calibration to the calibration of all sensitive parameters. A total of 67 basins are currently included in the evaluations. Twelve of these 67 basins are MOPEX basins. Tools, techniques, and results will be presented to facilitate workshop discussion.

**HW08/07P/C28-005** **1610**

**AN ATTEMPT TO RELATE THE MOPEX BASIN FEATURES WITH THE BTOPMC MODEL PARAMETERS**

Kuniyoshi TAKEUCHI<sup>1</sup>, Tianqi AO<sup>2</sup>, Hiroshi ISHIDAIRA<sup>1</sup>, Junichi YOSHITANI<sup>1</sup>, Kazuhiko FUKAMI<sup>1</sup>, Hiroshi OKUMURA<sup>3</sup>, Taichi TEBAKARI<sup>1</sup> (<sup>1</sup>Department of Civil and Environmental Engineering, Yamaguchi University, <sup>2</sup>Hydrologic Engineering Team, Hydraulic Engineering Research Group of Public Works Research Institute, Japan)

For physically based hydrological models, it is desirable that the model parameters are identified from physical features of river basins without calibration. This is essential for prediction in ungauged basins (PUB) and for simulating the effects of watershed development scenarios. In practice, however, such quantitative relationship is not available as most of physically based model parameters are immeasurable. The identification of model parameters is a major challenge for any hydrological modelers. BTOPMC is a physically based distributed hydrological model developed for large river basins. A modified TOPMODEL is used for flow generation at each grid cell and the Muskingum-Cunge method for flow routing. Watershed is described by drainage networks and automatically subdivided into either rectangular blocks or natural sub-basins. Model parameters are manually calibrated or automatically optimized by the SCE-UA algorithm, and a reference table is used in preparation relating the basin features with model parameters. In this study, the MOPEX (<http://www.nws.noaa.gov/oh/mopex/>, Model Parameter Experiment) basins were analyzed. The a priori estimation procedure that was suggested by MOPEX was used to explore the possibility of parameter transferability between different basins; the strategy for inverse problems was used for relating parameters with basin characteristics and some information on the scale dependent reference table is identified through the trial.

**HW08/07P/C28-006** **1630**

**A ROBUST TECHNIQUE FOR MODEL STRUCTURE IDENTIFICATION AND CALIBRATION**

Emiel E. VAN LOON, Paul TORFS, Peter A. TROCH (Department of Environmental Sciences, Wageningen University)

Using the MOPEX data sets for 12 basins, a technique for model-structure identification and

calibration is demonstrated. The technique is based the decomposition of a model in separately identifiable parts, such as a fastflow component, a slow flow component, soil moisture storage (recharge minus actual evapotranspiration and drainage) - all conditioned on rainfall. Each model part is characterized by one dependent variable that is a function of one to three independent variables. This function is represented by a sum of Gaussian kernels (as such, it is a probability density function). The different model parts are related via the dependent variables. This relationship is also described by a sum of Gaussians. The fact that each model component can be identified separately, makes that structurally different models can be composed and evaluated. For each of the twelve MOPEX basins, the best model structure is determined. Next, the MOPEX basins are subdivided into three main classes on the basis of corresponding model structures. For each of the main classes the identification technique is repeated, leading to a limited number of generalized models. The success of the identification technique is based on the predictive strength of the independent variables chosen. The fact that predictive strength can be evaluated separately for each model component as well as the fact that a sum of Gaussians gives a very general and flexible function representation, makes the proposed technique robust.

Tuesday, July 8 AM

Presiding Chairs: G. Leavesley, A. Young

**PARAMETER ESTIMATION AND MODEL DIAGNOSTIC TECHNIQUES**

**HW08/08A/C28-001** Invited **0830**

**IDENTIFICATION AND EVALUATION OF HYDROLOGICAL MODELS**

Thorsten WAGENER<sup>1</sup>, Hoshin V. GUPTA<sup>1</sup>, Jasper A. VRUGT<sup>2</sup>, Terri S. HOGUE<sup>1</sup>, Howard S. WHEATER<sup>1</sup>, Soroosh SOROOSHIAN<sup>1</sup> (<sup>1</sup>Department of Hydrology and Water Resources, The University of Arizona, USA, <sup>2</sup>Institute for Biodiversity and Ecosystem Dynamics, University of Amsterdam, NL, <sup>3</sup>Department of Civil and Environmental Engineering, Imperial College London, UK)

Hydrological modeling requires the identification of a suitable model structure mainly based on current hydrological understanding and the estimation of parameter values (and their uncertainty), usually through calibration against observed data. The reduction of uncertainty in current modeling procedures is hindered by a lack of objective approaches to evaluate parameter sets and model structures while making optimum use of the information present in time-series data. This is further complicated by the increasing awareness of model structural inadequacies. There has been recent progress in the form of multi-objective optimization algorithms, improved adaptive techniques, wavelet analysis and the use of field (soft) data. The general idea behind these approaches is to make better use of the available information to yield models which are not optimal in a statistical sense, but are consistent with our understanding of the hydrological system. Application examples of these approaches are multi-objective optimization algorithms and adaptive approaches. Multi-objective algorithms enable the comparison of individual model components instead of just the overall model performance. Adaptive approaches allow periods of high information content for specific parameters to be identified and model structures to be evaluated with respect to the failure of individual components by tracking parameter variation in time. In this talk we explore the historical development of current perspectives on model evaluation and highlight opportunities for future research. Examples of the areas of rainfall-runoff and land surface modeling are used to demonstrate some of the recent developments.

**HW08/08A/C28-002** **0900**

**A TOOL FOR DIAGNOSING THE SIGNALS IN HYDROLOGIC TIME SERIES**

John SCHAAKE, Qingyun DUAN (Hydrology Laboratory, NOAA/NWS/OHD)

It is essential to develop improved diagnostic tools to get every possible piece of information from hydrologic time series. Such tools are also necessary to understand the differences between simulation results and observations and between simulation results from different models. A diagnostic tool, called Variance Decomposition, is developed for such a purpose. The basic idea of variance decomposition is to use a transformation in this case a wavelet transformation -- to decompose a time series into different temporal frequency components and then to compute the seasonal variance of each frequency component. This produces a 2-dimensional pattern showing how the total variance of a time series depends on frequency and season and that can be visualized graphically. Variance decomposition can be applied to any time series (e.g. precipitation, streamflow, evaporation, soil moisture, base flow, surface flow, or differences between observed and simulated flow). Functions of variance decomposition can illustrate how input variance is transferred to model output variance. They can be used to show how the Nash-Sutcliffe efficiency for a given model varies with both frequency and season. This can be used as the basis of a filter to post-process model output to improve its validation statistics. This presentation describes how variance decomposition method works. Its use is demonstrated by some examples from the evaluation of results from the second international workshop on Model Parameter Estimation Experiment (MOPEX).

**HW08/08A/C28-003** **0920**

**SIMULATION OF HYDROLOGICAL PROCESSES BY THE LAND SURFACE MODEL SWAP USING AN A PRIORI ESTIMATED MODEL'S PARAMETERS FOR BOREAL CATCHMENTS**

Yeugeniy M. GUSEV, Olga N. NASONOVA (Institute of Water Problems, Russian Academy of Sciences)

The boreal zone is characterised by a cool and cold climates with low temperatures during the cold season, deep seasonal snow cover and frozen soil. These circumstances complicate the problem of modelling hydrological processes especially with respect to the forested areas where the problem is much more complicated due to a lack of measured characteristics of hydrological regime as well as appropriate soil and vegetation parameters. The aim of this work is to investigate the ability of the land surface model SWAP (Soil Water - Atmosphere - Plants) to simulate hydrological processes occurring in boreal regions on a catchment and river basin scales using a priori estimated model's parameters. On a small catchment scale, the validation of SWAP was performed using a set of hydrometeorological data measured during 18 years (1966-1983) at the Tayozhnyy catchment (covered by boreal forest, mainly composed by spruce) and the Usadievskiy catchment (grassland), both situated in the central part of Valdai Hills, Russia. On a river basin scale, the validation of SWAP was performed for the Polomet river basin (1215 km<sup>2</sup>), also situated in Valdai and covered by mixed forest and grass vegetation. The river basin area was divided into 14 cells (small catchments) with different soil, vegetation and geomorphological characteristics. In this case a set of hydrometeorological data (excluding precipitation), measured at the Usadievskiy catchment during the period 1966-1971 was used. The data on precipitation

were taken from 13 gauges located within the Polomet river basin. None of soil and vegetation parameters (soil hydraulic conductivity at saturation, Clapp-Hornberger B-parameter, soil water potential at saturation, depth of soil root zone, annual dynamics of leaf area index, etc.) was measured at the catchments. Soil parameters were computed empirically using information about soil texture and density. Vegetation parameters were estimated using literature data, experience of the authors and information about vegetation type. For the Tayozhniy and the Usadievskiy catchments, simulations of different characteristics of heat and water regime, in particular, snow water equivalent, snow surface temperature, evaporation from snow cover, water yield of snow cover, depth of soil freezing and thawing, soil water storage, daily surface and total runoff from the catchment, monthly evapotranspiration from the catchment, and precipitation intercepted by spruce forest on an annual and monthly basis were validated against observations. As to the validation on a basin scale, daily discharge, measured by 7 gauges from 1966-1971 within the Polomet river basin, was used. The results of validation have showed that the model SWAP is able to reproduce hydrological processes in the boreal zone on a catchment and river basin scales quite reasonable using an a priori estimated model's parameters.

**HW08/08A/C28-004****0940**

#### ON SEMI-DISTRIBUTED RAINFALL-RUNOFF MODELLING: 'SATURATION PATH' PERSPECTIVE ON TOPMODEL AND VIC

Dmitri KAVETSKI, George KUCZERA, Stewart W. FRANKS (School of Engineering, University of Newcastle)

The conceptual foundation, behaviour and implementation of semi-distributed models such as TOPMODEL and VIC are revisited from a 'saturation path' perspective. A general family of models is analysed, based on the assumptions that i) an event-invariant relationship between the saturated area and catchment storage exists (which may include hysteretic and stochastic components) and ii) quickflow is generated from precipitation on the saturated areas. The VIC and TOPMODEL equations are obtained by substituting particular constitutive functions describing the saturation mechanism, as well as applying specific numerical approximations. In general, the saturation path perspective leads to compact model equations in canonical ODE form, making the behaviour of the models, including ill conditioning due to parameter correlations and non-robust numerical implementations, very transparent. Avenues for substantial improvements in computational performance are detailed, yielding substantial reduction of model runtime and increased stability and robustness. Moreover, the generality of the proposed 'saturation path' modelling is demonstrated by a 'non-parametric' fit of constitutive relationships.

**HW08/08A/C28-005****1000**

#### ON THE PARAMETERIZATION OF DISTRIBUTED MODELS

Fekadu G. MOREDA, Ziya ZHANG, Victor KOREN, Seann REED, Michael SMITH (Office of Hydrologic Development, National Weather Service)

The Hydrology Lab (HL) of the National Weather Service (NWS), Office of Hydrologic Development is currently developing and testing the HL Research Modeling System (HL-RMS). HL-RMS is a modeling framework for testing fully distributed, semi-distributed, and lumped modeling approaches. The system is designed in such a way that different models can be used to generate runoff. Currently, the system has two surface runoff models: the Sacramento Soil Moisture Accounting (SAC-SMA) and the Continuous Antecedent Precipitation Index (CONT-API). The NWS Antecedent Precipitation Index model is one of the earliest conceptual rainfall runoff models and has been operational in a few NWS River Forecasting Centers (RFCs) in the United States. This study deals with the derivation of distributed parameters of the CONT-API model. For some of the parameters, a priori estimates have been derived in other research efforts. For the remaining parameters, we derive initial parameters based on the calibrated parameters of the lumped CONT-API. Results using initial lumped parameters of eleven subbasins in the Juniata River Basin (8687 km<sup>2</sup>) located in Pennsylvania show that the shape and timing of the hydrographs are captured well. However, as expected, direct use of lumped parameters in each of the grid cells results in oversimulation at the subbasin outlets. Techniques to adjust these initial parameters in order to obtain accurate simulation of runoff at the subbasin outlets are presented. The relationship between the final calibrated and initial parameter estimates will also be discussed.

**HW08/08A/C28-006****1040**

#### RESEARCH OF THE HYDROLOGICAL MODELING IN NORTHERN REGION

Xieyao MA<sup>1</sup>, Yoshihiro FUKUSHIMA<sup>2</sup>, Tetsuzo YASUNARI<sup>1</sup> (<sup>1</sup>Frontier Research System for Global Change, <sup>2</sup>Research Institute for Humanity and Nature, <sup>3</sup>Hydrospheric Atmospheric Research Center, Nagoya University)

A combined model considered the climate phenomenon of cold region like snow-cover, river frozen and permafrost was built in order to understand the hydrological cycle processes of a river basin in northern cold region. The model is composed of four components: one-dimensional soil-vegetation-atmosphere transfer (SVAT) model, runoff formation model, river ice model and river routing model. The SVAT model is a simple biosphere model, in which the land surface is described by a big-leaf and a soil layer. The SVAT model provides estimation of latent and sensible heat fluxes between the land surface and the atmosphere, and thermal regimes in the snow-cover and soil layer. A conceptual model is used to determine the formation of runoff for a grid box. It is a reservoir system representing each of the four runoff components, which are saturated land surface runoff, infiltration runoff from the topsoil zone, base runoff and direct runoff from the water surface. In order to consider the permafrost condition, a parameter-related mean effective soil depth was designed as a function of the active layer depth. A simple method using accumulated degree-days is used to determine river ice growth and decay processes. The flow velocity in the river network is set as a constant and the number is depended on the depth of runoff. In the paper, we would like to introduce the results of the model application to the Lena River basin located in east Siberia, the Selenge River basin in Mongolia and the Yellow River basin in China.

**HW08/08A/C28-007****1100**

#### ESTIMATION OF HYDROLOGIC PARAMETERS RELATED TO SOIL AND VEGETATION USING REMOTELY-SENSED DATA AND GIS - AN EXPERIENCE AT MOUNTAINOUS WATERSHEDS IN JAPAN

Kazuhiro FUKAMI<sup>1</sup>, Kazuhiko FUKAMI<sup>1</sup>, Yoko HIROSE<sup>2</sup>, Takuya OKADA<sup>3</sup>, ZhiQiang CHEN<sup>4</sup>, M. Levent KAVVAS<sup>5</sup>, Junichi YOSHITANI<sup>1</sup> (<sup>1</sup>Hydrologic Engineering Research Team, Public Works Research Institute, Japan, <sup>2</sup>Kokusai Kogyo Co.,Ltd., <sup>3</sup>Asia Air Survey Co.,Ltd., <sup>4</sup>University of California at Davis)

Distributed models are now indispensable for hydrologists to understand hydrologic environment considering basin-wide interactions among hydrologic processes in a variety of

temporal/spatial scales. However, the distributed models are still regarded as difficult to apply to operational hydrologic problems because of the existence of many parameters. Here, a priori estimation of parameters related to land-atmosphere interactions, i.e. soil and vegetation system, are tried using GIS analysis. This is based upon the idea that real situations near ground surface are relatively easily reflected in GIS with in situ and/or remotely-sensed data. This study focuses on hydrology in mountainous forest-covered watersheds in Japan and consists of two experiences there in long-term riverflow simulation and in flood (dam-reservoir inflow) forecasting. In the long-term riverflow simulation study, a new version of PWRI distributed hydrologic model (PWRI model), a conceptual distributed model, was applied to two small mountainous forest-covered watersheds in the Kanto district, the Kusaki-dam watershed (254km<sup>2</sup>) and the Shiobara-dam watershed (120km<sup>2</sup>). The former watershed consists of old geologic condition and the latter has relatively new volcanic geology. The PWRI model seems a kind of tank model, but the land-atmosphere interactions are modeled on the basis of Noilhan and Planton (1989) scheme. The scheme requires some geophysical & biophysical parameters. LAI was estimated by Ishi et al. (1999) method with Landsat-TM images. The satellite images were also used to update land-use (forest cover) conditions. Soil hydraulic parameters were grouped into three categories based on soil map and sample data. Parameters for groundwater were set based on the system of the old version of PWRI model, which had been optimized for several Japanese rivers. Flow network was estimated by DEM. The long-term riverflow simulations of the two watersheds were both quite successful by just one-parameter tuning. The flood forecasting study was made at the Shiobara-dam watershed with a physically-based Watershed Environmental Hydrology (WEHY) Model. The model requires not only the similar information such as topography, soil hydraulics, vegetation but also soil-depth distribution for each hillslope modeling computational unit (MCU). A soil-depth ranking matrix table was created on the basis of empirical knowledge about the relationship among soil-depth, topographical feature, slope, land use (vegetation type), the soil and in-situ soil depth measured at 36 points for each ranking-category of soil-depth. The flood simulations using the parameters were also successful. The method to estimate areal distribution of soil depth was tested at the Kusaki-dam watershed as well. According to the results, the parameter estimation methods above are expected to be applicable at least to the regions around the Kanto district of Japan.

**HW08/08A/C28-008****1120**

#### CLIMATE CHANGES IMPACT ON THE WATER RESOURCES

Cvetanka POPOVSKA (Department of Hydraulics, Hydrology and River Engineering, Faculty of Civil Engineering, University of Ss. Cyril and Methodius)

Climate changes as a result of global warmth will cause significant changes in the hydrological cycle and water resources. Republic of Macedonia is small, but geologically and climatically variable country. Until now, climate changes impact on the water resources and hydrology in the Republic of Macedonia, has not been carried out. This paper deals with some results obtained within the UNDP Project: "Vulnerability of the Climate Changes and Adaptation Measures in the Republic of Macedonia". Climatic factors are presented with the rainfall characteristics and evaporation components and with their time and space distribution. Hydrological parameters have been analyzed with historical measured data of the selected hydrological stations in the representative river basins for the period 1950-2000. Trend lines of the annual discharges and water levels in the main rivers and natural lakes, have been obtained. Besides analysis of the real parameters, the simulating scenarios have been investigated to predict the future influence of the climate changes on the water balance components. According to the performed analysis it can be stated that the climate changes as a result of global warmth will cause significant changes in hydrology and water resources and with that in water economy planning as well. Droughty seasons are more frequent and with longer duration and floods are with rare re-appearance. The most vulnerable segments in water economy have been identified and adaptation measures have been proposed. Action plan of the climate changes impact should be carried out on the national level and adaptation measures should be implemented with priorities. The action plan should present the knowledge in investigation methodologies, measurement techniques and management of the water resources. Achievement of those goals will help the long-term planning of water resources utilization and will provide public, professional and open discussion of all partners in the society.

**HW08/08A/C28-009****1140**

#### A METHOD FOR PARAMETER ESTIMATION IN URBANISED CATCHMENTS

Dirk MUSCHALLA, Manfred OSTROWSKI (Inst. of Hydraulic and Water Resources Eng., Section for Hydrology and Water Management, Darmstadt University of Technology)

The prediction of surface runoff from small urbanised catchments depends on the correct choice of the degree of imperviousness. As fast flow reactions from impervious areas are disturbing receiving water bodies hydraulically and pollution wise, the investment for storm water retention measures and treatment facilities is immense in Germany and elsewhere to reduce these negative impacts. In most cases this investment is based on modelling results, performed with storm water modelling techniques. In the past, the water administration authorities considered a system acceptable, when it did not exceed a threshold value. As neither flows are measured under normal planning conditions, nor exact values for impervious areas were available e.g. from airborne or ground surveying, imperviousness had to be estimated. At the end of a decade of planning and construction, a large sample of data sets was available for most of the communities in the Federal State of Hesse, Germany. This sample has been analysed and distribution functions for sensitive parameters (imperviousness, population density, domestic waste water, etc.) have been derived. Assuming that the expectation value corresponds to the arithmetic mean, outliers and implausible values can now be identified and questioned. In addition, interrelationships between single parameters could be identified. This supports the approving authorities which have to check incoming planning proposals and a model data set for plausibility and correctness. Finally, the distribution functions determined were used for Monte Carlo Simulations and an existing deterministic pollution load model was enhanced to an hybrid model by means of stochastic components. Input values were randomly drawn from the functions to produce a distribution output function for overflow volumes and pollution loads.

**HW08/08A/C28-010****1200**

#### DETERMINATION OF NON PHYSICAL VAN GENUCHTEN PARAMETERS IN HETEROGENEOUS SOILS

Joseph POLLACCO (School of Civil Engineering and Geosciences, University of Newcastle)

Modelling the highly heterogeneous unsaturated zone (vadose zone) is difficult especially with the presence of macropores. The usage of well logging is well suited to determine van Genuchten parameters used in studies of soil moisture activities. In the study we determine the impact of afforestation through the usage of time series neutron probe data. An inverse modelling technique was developed to determine the non physical van Genuchten parameters. Given the equifinality of the van Genuchten parameters and that no measured

values of the soil parameters are available, two soil parameters are redundant therefore they are presently kept fixed. A calibration procedure enables the replacement of residual soil moisture parameters for each of the 40 soil layers by only two parameters, by using compiled data from the observed soil moisture. The finding of the optimum soil parameters is complicated due to presence of macropores. A temporary and synthetic solution to this macropore modelling problem is to optimise the different layers, where the layers are optimised at first in large groups then split into individual layers. It was shown by successive trials that optimising from top-to-bottom produces satisfactory results. This provides an approach to represent these processes at a scale appropriate to calculate total recharge through the vadose zone. Once the heterogeneous unsaturated zone is modelled to a satisfying level, an attempt will be made to remove the heterogeneity and to build the simplest model that will be representative catchment scale processes by using well logging techniques in a more efficient way.

Tuesday, July 8 PM

Presiding Chairs: S. Franks, G. Leavesley

### UNCERTAINTIES IN MODELING AND INFORMATION IN DATA

HW08/08P/C28-001 Invited 1400

#### TEASING OUT UNCERTAINTIES IN THE MODELLING PROCESS

Keith J. BEVEN, Jim FREER (Lancaster University, UK)

It has been a common assumption in parameter calibration that all of the model error can be treated as if it were measurement error. In this way, the powerful tools available for statistical inference can be used directly. Such a simple assumption has served to hide some very real problems with calibration based on such methods because the implication is, therefore, that the model is a true representation of the processes under study. In most environmental modelling situations this is evidently not the case with the result that model and parameter uncertainties are generally underestimated in calibration. This may be important when derived variables (that do not have independent calibration data) are required to be predicted. However, neither environmental modellers nor statisticians have done much towards developing methods to deal with model structural error in parameter calibration. The different source of error in the modelling process - initial and boundary condition error, model structural error and true measurement error - are commonly recognised in discussions of modelling methodologies but have proved to be very difficult to tease out in practice. Teasing out sources of error requires strong a priori assumptions and the results will depend on the nature of those assumptions. The discussion of these problems will be illustrated by some representative examples from rainfall-runoff modelling.

HW08/08P/C28-002 Invited 1430

#### CONFRONTING UNCERTAINTY IN ENVIRONMENTAL MODELLING

Dmitri KAVETSKI, Stewart W. FRANKS, George KUCZERA (School of Engineering, University of Newcastle)

The majority of environmental models require calibration of some or all of their parameters before meaningful predictions of catchment behaviour can be made. Despite the importance of reliable parameter estimates, there are growing concerns about the ability of objective-based inference methods to adequately calibrate environmental models. The problem lies with the formulation of the objective or likelihood function, which is currently implemented using essentially ad-hoc methods. We outline limitations of current calibration methodologies, including least squares, multi-objective, GLUE and Kalman filter schemes and introduce a more systematic Bayesian Total Error Analysis (BATEA) framework for environmental model calibration and validation. BATEA imposes a hitherto missing rigour in environmental modelling by requiring the specification of physically realistic uncertainty models with explicit assumptions that can and must be tested against available evidence. Distinguishing between the various sources of errors will reduce the current ambiguity about parameter and predictive uncertainty and enable rational testing of environmental model hypotheses. A synthetic study demonstrates that explicitly accounting for forcing errors leads to immediate advantages over traditional least squares methods that ignore rainfall history corruption and do not directly address the sources of uncertainty in the calibration. We expect that confronting all sources of uncertainty, including data and model errors, will force fundamental shifts in the model calibration/verification philosophy.

HW08/08P/C28-003 1500

#### PROBABILISTIC STREAMFLOW PREDICTIONS IN UNGAUGED WATERSHEDS

Jasper A. VRUGT<sup>1</sup>, Thorsten WAGENER<sup>2</sup>, Hoshin V. GUPTA<sup>3</sup>, Willem BOUTEN<sup>1</sup>, Soroosh SOROOSHIAN<sup>2</sup> (<sup>1</sup>Institute for Biodiversity and Ecosystem Dynamics, University of Amsterdam, NL, <sup>2</sup>Department of Hydrology and Water Resources, The University of Arizona, USA)

Conceptual rainfall-runoff models can be applied to ungauged watersheds by developing statistical relationships between model parameters and watershed characteristics. However, the predictions will contain uncertainties which are likely to be considerably larger than for gauged watersheds. While probabilistic predictions in gauged watersheds can be commonly found, predictions in ungauged watersheds are almost always given as simple point estimates, ignoring the large uncertainty involved. New Monte Carlo Markov Chain optimization algorithms produce reliable estimates of posterior parameter distributions in gauged watersheds. These probabilistic estimations of parameter distributions in gauged watersheds can be transferred to ungauged watersheds while considering the additional uncertainty through the regionalisation process. We analyze options for regionalisation approaches which allow for the propagation of these distributions into predictions for ungauged watersheds. This stochastic estimate of the hydrological response of the watershed is more useful for decision-making since it considers the confidence in the model predictions. The approach is demonstrated in a pilot study using MOPEX data and a rainfall-runoff model structure with typical conceptual components.

HW08/08P/C28-004 Invited 1520

#### IDENTIFYING HYDROLOGIC MODEL PARAMETERS FROM INTRA-ANNUAL STREAMFLOW ANALYSES

Eylon SHAMIR, Eylon SHAMIR, Efrat MORIN, Bisher IMAM, Hoshin V. GUPTA, Soroosh SOROOSHIAN (Department of Hydrology, University of Arizona)

Current efforts to estimate physically plausible model parameters focus on incorporating a priori information from the observed data, into the parameter estimation process. Our study extracts intra-annual information on streamflow indicators that were tested to be intrinsic and representative of the basin hydrological response. These indicators are implemented in

parameter estimation to initial a plausible parameters space that ensures the indicators values in the simulation for consistent model performance. Minimal conditions have to be met in order to favor a streamflow indicator: (a) easy to derive from raw streamflow data with minimum presumptions; (b) have a strong central tendency with small dispersion when evaluated in a range of climatic conditions to represent basins property; (c) sensitive enough to vary among basins and behave as a unique description of a basin. Four indicators that satisfy the above requirements and are dominated by different hydrological processes were selected for this study. The validity of the indicators was evaluated using long-term daily streamflow data from multiple mid-size unregulated headwaters in the US. Subsequently, the parameter posterior distribution of the Sacramento Soil Moisture Accounting (SAC-SMA) model was derived for each indicator. The combine posterior distributions show a significant reduction in the plausible range of some parameters while other parameters were not sensitive to the streamflow indicators.

HW08/08P/C28-005 Invited 1600

#### CONSTRAINING PARAMETER VALUES WITH SOFT DATA: AN EXPERIMENTALIST'S VIEW OF PARAMETER ESTIMATION

Jeffrey J. MCDONNELL<sup>1</sup>, Kellie B. VACHE<sup>1</sup>, Jan SEIBERT<sup>2</sup> (<sup>1</sup>Department of Forest Engineering, <sup>2</sup>Swedish Agricultural University)

Multi-criteria calibration of runoff models using continuous time series of streamflow and groundwater well data has been proposed as a way to constrain parameter values and to ensure the realistic simulation of internal variables. Nevertheless, in many cases the amount of such available 'hard data' is limited. We argue that experimentalists working in the catchment 'to be modeled' often have much more knowledge of catchment behavior than is currently used for model calibration and testing. While potentially highly useful, this information is difficult to use directly as exact numbers in the calibration process. We present a framework whereby these 'soft' data from the experimentalist are made useful through fuzzy measures of model-simulation and parameter-value acceptability. The use of soft data is an approach to formalize the exchange of information and calibration measures between experimentalist and modeler. This dialog may also greatly augment the traditional and few 'hard' data measures available. We illustrate the value of 'soft data' with the applications to watersheds in New Zealand, Oregon and Alaska. We show how these techniques may allow one to make a priori parameter estimates (and thereby to simulate streamflow effectively) for watersheds encompassing different climatic and physiographic regions.

Wednesday, July 9 AM

Presiding Chairs: A. Hall, E. O'Connell

### A PRIORI PARAMETER ESTIMATION AND REGIONALIZATION OF MODEL PARAMETERS

HW08/09A/C28-001 Invited 0900

#### REGIONALIZATION OF HYDROLOGICAL MODEL PARAMETERS

Guenter BLOESCHL, Ralf MERZ (Institute for Hydraulics, Hydrology and Water Resources Management, Vienna University of Technology)

In this talk I will present recent results of a comprehensive test of parameter estimation methods for both gauged and ungauged basins. In a case study we analysed more than 500 catchments in Austria. 30 years of daily data (runoff, precipitation, air temperature, air humidity) were analysed. A spatially lumped, conceptual, HBV style soil moisture accounting scheme was used which involved 11 calibration parameters including snow processes. Prior information on the parameters was included in terms of a beta distribution. In a first step the calibrated parameters from two independent calibration periods of 11 years each were compared. These comparisons suggest that some of the parameters (such as the recession parameters and the degree-day-factor) are quite stable and hence well identifiable while others (such as the routing parameters) are not. The more reliable parameters were spatially clustered and these clusters could be interpreted on hydrological grounds. This lends additional credence to these parameter values. In a second step we examined the median Nash-Sutcliffe efficiency of a number of regionalisation methods for finding model parameters for ungauged basins. The performance of the methods was evaluated by jack-knifing where gauged basins were treated as ungauged and the streamflow simulated using the regionalised parameters was compared with observed streamflow. When using preset parameters (based on a prior guess without using any streamflow data), the model efficiency was 0.15. When using the same parameter value for all catchments equal to the mean of the calibrated values, the efficiencies for the calibration and verification periods were 0.19 and 0.19, respectively. When using multiple regression with catchment attributes (such as land use, geology and topography), the efficiencies were 0.32 and 0.32, respectively. When using Kriging for transposing the parameters in space (without the use of catchment attributes), the efficiencies were 0.44 and 0.41, respectively. When using the average of the calibrated parameters of the upstream and the downstream neighbours, the efficiencies were 0.46 and 0.42, respectively. These results imply that spatial distance is a better predictor than catchment attributes. This adds a caveat on the reliability of "physically based" models at the regional scale. Even though the comparisons suggest that most of the spatial variability of the (identifiable) model parameters is a result of real physical controls rather than an artefact of the calibration procedure, very little of it can be explained by those catchment attributes that are usually available at the regional scale. The challenge is to identify those controls, perhaps by using data that are not routinely available to date. It is likely that soil depths, stream-aquifer connectivity and the degree of fracturedness of the bedrock are important controls but these variables are difficult to come by at the regional scale.

HW08/09A/C28-002 0930

#### ESTIMATION OF HYDROLOGICAL MODEL PARAMETERS USING REGIONAL INFORMATION

Andras BARDOSSY (Institute for Hydraulic Engineering, University of Stuttgart)

Catchments with similar characteristics show a similar hydrological behaviour. Therefore a regionalisation of the hydrological model parameters on the basis of catchment characteristics is plausible. However due to the non-uniqueness of the parameters (equifinality) a procedure of parameter estimation by model calibration and a subsequent function fit is not appropriate. In this paper different regionalisation functions are estimated simultaneously for a set of different catchments. A generalised likelihood as in the GLUE methodology is assigned to each regionalisation function. The likelihood of a function is calculated from the likelihood of the corresponding parameters for the different catchments. The methodology consists of the following steps:

- definition of a similarity measure for the catchment characteristics,
- the choice of the parametric form of the regionalisation function,

- the assessment of the likelihood function for the different catchments,
- the estimation of the regionalisation function parameters and
- the assessment of the likelihood of the regionalisation function.

Using the regionalisation functions hydrological parameter sets and their likelihood can be estimated.

The methodology is applied to selected mesoscale subcatchments of the Rhine catchment.

**HW08/09A/C28-003****0950**

#### REGIONALISATION OF RAINFALL-RUNOFF MODELS: IDENTIFIABILITY ANALYSIS, MODEL SELECTION AND CATCHMENT CHARACTERISTICS

Neil Robert MCINTYRE<sup>1</sup>, Howard S. WHEATER<sup>1</sup>, Hyosang LEE<sup>1</sup>, Andrew R. YOUNG<sup>2</sup>, Thorsten WAGENER<sup>3</sup> (<sup>1</sup>Department of Civil and Environmental Engineering, Imperial College London, <sup>2</sup>Center for Ecology and Hydrology, Wallingford, UK, <sup>3</sup>SAHRA Hydrology and Water Resources, University of Arizona)

Recent developments in modelling tools provide a powerful analytical capability to support rainfall-runoff model development and application. Stochastic methods are now available to explore model structure and parameter uncertainty, and hence the trade-off between model complexity, performance and identifiability. Dynamic identifiability analysis has been developed to track parameter variability and identifiability through time. The information content of hydrological data has been increased by the use of multiple objectives, which in turn provide further insight into model structures and performance. These developments provide support for the regionalisation of rainfall-runoff models for application to ungauged catchments, and recent work has led to the formalisation of a general methodology for regional analysis. Analysis of the trade-off between performance and identifiability has led in the UK to the development of parsimonious local rainfall-runoff models capable of regionalisation. An important question concerns the selection of appropriate local model structures for regional application. Are different model structures required to represent different catchment types? And what are appropriate criteria to find catchment clusters which can be represented by particular model structures? A formal experiment has been designed, based on a data set of 277 UK catchments and sampling from a three-dimensional space of catchment characteristics, to address these questions. Results will be presented, based on 12 candidate parsimonious model structures. Calibration and validation performance is evaluated with respect to model complexity, identifiability and internal consistency, using different performance criteria. This is a precursor to further work to develop the theoretical framework for regional analysis, and for full use of the database in regional analysis.

**HW08/09A/C28-004****1010**

#### A PARAMETER ESTIMATION OF VIC MODEL FOR RIVER BASINS IN CHINA

Zhenghui XIE, Fengge SU (Institute of Atmospheric Physics, Chinese Academy of Sciences)

Research has shown that land surface schemes perform well when their model parameters are appropriately estimated based on calibrations with observations, but perform poorly when their parameters are not calibrated properly. In this work, soil and vegetation parameters needed by the land surface scheme VIC (Variable Infiltration Capacity) model for the mainland area of China are given to predict the discharge of the major river basins in China where the new surface runoff parameterization of VIC that represents both Horton and Dunne runoff generation mechanisms with the framework of considering subgrid spatial scale soil heterogeneity is applied. The mainland area of China is represented by 2604 cells with a resolution of 60km×60km for each cell. The VIC model is applied to each grid cell over each basin. A routing scheme is run offline which takes daily VIC surface and subsurface runoff as input to obtain model simulated discharge at the outlets of study basins. The VIC discharge simulations over Huaihe, Yellow river, and Yangtse river basin will be presented and compared with the observations.

**HW08/09A/C28-005****1030**

#### REGIONALIZATION OF WATER BALANCE MODEL PARAMETERS FROM GEOGRAPHIC INFORMATION AND ITS PROCESS-BASED VERIFICATION

Yoshiyuki YOKOO<sup>1</sup>, So KAZAMA<sup>2</sup>, Masaki SAWAMOTO<sup>3</sup> (<sup>1</sup>Institute of Industrial Science, University of Tokyo, <sup>2</sup>Graduate School of Environmental Science, Tohoku University, <sup>3</sup>Graduate School of Engineering, Tohoku University)

This research suggested a regionalization method of lumped water balance model parameters. We developed this method assuming that precipitation data were available as well as geographic information. An international project named "Prediction of Ungauged basins (PUBs)" is running from 2002 under the International Association of Hydrological Science (IAHS) at the present. Our method, for runoff predictions in runoff-ungauged basins, can contribute to this project. Firstly, we suggested a regionalization method of a water balance model parameters. The regionalization was based on multiple regression analysis between tank model parameters and geographic characteristics in 12 Japanese basins. The model employed in this study was Sugawara's tank model, which had a vertical series of 4 tanks. The modified Powell method optimized tank model parameters in the basins. Geographic data set in Japan provided the geographic characteristics of the basins. The characteristics included areal ratios of 9 land use types, 3 soil types, and 3 geology types, as well as basin area and a representative gradient of a basin. The representative gradient was a ratio calculated by the elevation difference between maximum elevation on the basin boundary and dam top over the horizontal distance between these two points. The 9 land use types consist of rice paddy, field, orchard, shrub and orchards, forest, waste or vacant or naked land, building, road or railroad, and water body (river or lake). The classifications of soil types and geology were on the basis of contribution degrees of soil and geology to subsurface flow and base-flow, respectively. The extracted regression equations performed well to simulate runoff only from rainfall data and geographic characteristics in two test basins, indicating the applicability of the regionalization method. Secondly, we conducted process-based verifications on the multiple regression equations that relate tank model parameters with geographic characteristics of a basin. These verifications utilized a physically distributed runoff model, which is developed in this research as a quasi-three dimensional model that consists of one-dimensional channel runoff model and vertically two-dimensional slope element models placed along the channel runoff model. Numerical experiments verified the effects of a single geographic parameter of the distributed model on hydrographs. The geographic parameters contained surface roughness, hydraulic conductivities, basin area, and representative gradient mentioned above, which corresponded to geographic characteristics used in the regression analysis. Representations of the hydrograph by tank model derived the relationships between distributed model parameters and tank model parameters, and the relationships partially supported the physical meanings of 6 multiple regression equations. A series of numerical experiments with respect to basin area concluded that the multiple regression equations for tank modeling were applicable for the basins up to 1,000 km<sup>2</sup>.

**HW08/09A/C28-006****1050**

#### REGIONALIZATION OF RAINFALL-RUNOFF MODEL PARAMETERS: APPLICATION TO NORTHEASTERN OHIO, USA

Richard M. ANDERSON, Victor I. KOREN, Seann M. REED, Michael B. SMITH, Vadim KUZMIN (NOAA/National Weather Service)

Regionalization of hydrologic model parameters is an active area of research. It is important in efforts to obtain a priori estimates of model parameters in order to model the rainfall-runoff process in ungauged catchments, predict hydrologic effects of land use change, and model the hydrologic land surface component in global atmospheric models. Previous efforts to regionalize model parameters have been hampered for a number of reasons. For example, uncertainty in the quality of data used in model calibration leads to additional, unquantified uncertainty in relationships between landscape attributes and model parameters. Recent research within the National Weather Service (NWS) takes the approach of first using physical reasoning to obtain a priori estimates of model parameters. This should provide the starting point for subsequent statistical or calibration approaches to constrain and improve parameter estimates. This approach has been applied to the Sacramento Soil Moisture Accounting (SAC-SMA) model by using a multilayer soil characteristics dataset for the conterminous USA, which was derived from the State Soil Geographic Database (STATSGO) developed by the U.S. Department of Agriculture. First, this paper discusses efforts to improve such starting point a priori estimates by using data of finer resolution, such as that available within the Soil Survey Geographic Database (SSURGO) that uses county-level survey data. Though not currently available in a centralized national format, availability of this data is increasing rapidly. A priori model parameters for SAC-SMA, a conceptual model, are derived using finer scale SSURGO data, and improvements compared to previous NWS results are presented. Second, model parameters for IHACRES (Identification of unit Hydrographs And Component flows from Rainfall, Evaporation and Streamflow data), a model that uses a transfer function/unit hydrograph approach, are regionalized using a regression approach based on the same SSURGO data. Performance improvements relative to the STATSGO case as well as significance of region characteristics for establishing regional relationships are discussed. Both models are applied within the same region in the Lake Erie basin in northeastern Ohio, USA.

**HW08****Monday, July 7 - Wednesday, July 9**

#### PARAMETER ESTIMATION TECHNIQUES (IAHS/WMO WORKING GROUP ON GEWEX WITH THE SUPPORT OF ICSW AND ICASVR)

Location: Site C, Room 28

**Wednesday, July 9 PM**

Presiding Chairs: M. Sivapalan, H. Gupta

#### MOPEX'S CONTRIBUTION TO PUB AND MOPEX FUTURE PLAN AND DIRECTION

**HW08/09P/C28-001**

Invited

**1420**

#### MOPEX'S CONTRIBUTIONS TO PUB: FROM GAGED TO UNGAGED BASINS

John SCHAAKE, Qingyun DUAN (Hydrology Laboratory, NOAA/NWS/OHD)

One of the most important issues in making predictions for ungauged basins is how to transfer information from gaged to ungauged areas. Predictions are made using data as input to an appropriate model. All models are imperfect. All models have parameters (coefficients and exponents) that must be specified and that control the model's approximation of the real world. The primary goal of the International Model Parameter Estimation Experiment (MOPEX) is to develop improved approaches to estimation of parameters of hydrologic models that can be applied to ungauged areas. This paper presents the implementation strategy for MOPEX, some results of recent workshops and suggestions for how MOPEX can contribute to the development of the science strategy for PUBs and subsequent achievement of PUBs objectives.

**HW08/09P/C28-002****1450**

#### RIVER FLOW SIMULATION WITHIN UNGAUGED CATCHMENTS; THE UTILITY OF GENERALISED MODELS

Andy R. YOUNG (Centre for Ecology and Hydrology - Wallingford)

Access to daily stream flow data, at the river reach scale is a central component of many aspects of water resource and water quality management. However, the majority of river reaches are ungauged and hence there is an operational requirement for a quick, consistent and reliable method for simulating historical stream flow records within ungauged catchments. Furthermore, the coupling of hydrological models into land-surface schemes for Regional Climate Models (RCM) is central to improving the utility of these models in predicting the potential impacts of future climate change and variability on river flows. The information content of hydrological data has been increased by the use of multiple objective functions which lead to trade off strategies during model calibration. Uncertainty within input data, model calibration and structure and parameter regionalisation schemes all led to uncertainty within model simulations when used as predictive tools. However, model success and failure is commonly determined not by abstract fit statistics but by the sensitivity of subsequent analyses to the uncertainty in the simulated stream flow data. Our paper will explore some of these issues using the results from a UK case study on generalising model parameters based on a catchment data set of 277 catchments. The paper will compare the impact of parameter uncertainty on stream flow simulations obtained using calibrated model parameters with that observed when using regionalised parameter sets. These uncertainties will then be compared with the strength of signals observed in model output data when the historical input data are perturbed using scenarios for predicted changes in precipitation and evaporation for the 2020s derived using a RCM. The paper will conclude with some comment about the utility of regionalised hydrological models for evaluating the impact of potential climate change scenarios and outline future directions for work in this area.



**MI03** **Tuesday, July 8**

**CHEMISTRY-CLIMATE INTERACTIONS (COVERS OZONE INTERACTIONS) (ICACGP, IOC, ICCI)**

Location: Site B, Room 18

**Tuesday, July 8 AM**

Presiding Chairs: D. Wuebbles, H. Akimoto

**MI03/08A/B18-001** **0830**

**ATMOSPHERIC CHEMISTRY DATA AT THE NASA GODDARD EARTH SCIENCES DAAC**

James E. JOHNSON<sup>1</sup>, Suraiya P. AHMAD<sup>1</sup>, Steven J. KEMPLER<sup>2</sup> (<sup>1</sup>NASA/GSFC/SSAI, <sup>2</sup>NASA/GSFC)

The NASA Goddard Earth Sciences Distributed Active Archive Center (GES DAAC) includes a vast collection of atmospheric chemistry data. Among the holdings are data from various heritage and current sensors. Among these are ozone products from the Backscatter Ultraviolet (BUV) instrument flown on Nimbus-4, the Solar Backscatter Ultraviolet (SBUV) and Solar Mesospheric Explorer (SME) instruments aboard Nimbus-7, and the Shuttle Solar Backscatter Ultraviolet (SSBUV) instruments. The Nimbus-7 Limb Infrared Monitor of the Stratosphere (LIMS) instrument measured profiles of O<sub>3</sub>, H<sub>2</sub>O, NO<sub>2</sub> and HNO<sub>3</sub>. The Spacelab-3 Atmospheric Trace Molecule Spectroscopy (ATMOS) data provide profiles of over 25 atmospheric species, including CO and halogenated hydrocarbons. The Total Ozone Mapping Spectrometer (TOMS) data set spans an impressive 25 years from instruments flown on Nimbus-7, Meteor-3 and ADEOS 1, as well as the still operational TOMS Earth Probe instrument. The comprehensive 10 year Upper Atmosphere Research Satellite (UARS) mission includes atmospheric chemistry data products from four of its 10 instruments: the Cryogenic Limb Array Etalon Spectrometer (CLAES), the Halogen Occultation Experiment (HALOE), the Improved Stratospheric and Mesospheric Sounder (ISAMS), and the Microwave Limb Sounder (MLS). The UARS atmospheric chemistry data products include mixing ratio profiles of O<sub>3</sub>, H<sub>2</sub>O, CH<sub>4</sub>, HF, HCl, chlorofluorocarbons, and various nitrogen and chlorine compounds. Of these UARS instruments, HALOE is still actively taking measurements under the UARS expanded follow-on mission. The EOS Aura satellite, to be launched into Earth orbit in early 2004, will expand upon atmospheric chemistry observations made during the UARS mission. Aura or the EOS chemistry mission includes four instruments: the High Resolution Dynamics Limb Sounder (HIRDLS), a Microwave Limb Sounder (MLS), the Ozone Monitoring Instrument (OMI), and the Tropospheric Emissions Spectrometer (TES). The first three instruments will focus on measuring various chemical species in the stratosphere and will be archived at the NASA Goddard Earth Sciences DAAC, while TES will measure pollutants and trace gases in the troposphere and will be archived at the NASA Langley DAAC. This presentation will provide an overview of the atmospheric chemistry data available at the NASA GES DAAC, including applications and services provided by the DAAC in support of users of these data. All data products from the NASA GES DAAC are available free to the public (see <http://daac.gsfc.nasa.gov/>).

**MI03/08A/B18-002** **0850**

**SAGE III FIRST YEAR OF MEASUREMENTS: OVERVIEW OF THE MISSION AND EARLY RESULTS**

William P. CHU<sup>1</sup>, Chip R. TREPTE<sup>1</sup>, Joe M. ZAWODNY<sup>1</sup>, Larry W. THOMASON<sup>1</sup>, Mike C. PITTS<sup>1</sup>, Mike S. CISEWSKI<sup>1</sup>, Didier F. RAULT<sup>1</sup>, Ghassan TAHA<sup>2</sup>, J.R. MOORE<sup>3</sup>, Allan D. RISLEY<sup>4</sup> (<sup>1</sup>NASA Langley Research Center, <sup>2</sup>University of Arizona, <sup>3</sup>SAIC)

The Stratospheric Aerosol and Gas Experiment III/Meteor (SAGE III) mission is part of the NASA EOS program to provide vertical profile measurements of key constituents of the atmosphere such as ozone, aerosol, water vapor, NO<sub>2</sub>, NO<sub>3</sub>, OClO, and atmospheric temperature. The SAGE III instrument was successfully launched on a Russian Meteor 3M spacecraft from Baikonur, Kazakhstan on December 10, 2001. After initial commissioning phase activities, it began routine solar occultation measurements by March 2002. During the first year of operation, additional measurement capabilities such as lunar occultation and limb scattering were successfully implemented with the SAGE III instrument. This paper will present a summary of the various data sets gathered from the SAGE III instrument during the first year of operation. Measurements of ozone, aerosol, and nitrogen dioxide from solar occultation, lunar occultation, and limb scattering techniques will be presented and discussed.

**MI03/08A/B18-003** **0910**

**POLAR CHEMISTRY BY THE 4D-VAR CHEMICAL DATA ASSIMILATION OF MIPAS OBSERVATIONS**

Frank W.R. DAERDEN<sup>1</sup>, Dominique FONTEYN<sup>1</sup>, Quentin ERRERA<sup>1</sup>, Simon CHABRILLAT<sup>1</sup>, Stijn BONJEAN<sup>1</sup>, Niels LARSEN<sup>2</sup> (<sup>1</sup>BIRA-IASB, Brussels, Belgium, <sup>2</sup>DMI, Copenhagen, Denmark)

The Belgian Assimilation System of Chemical Observations from Envisat (BASCOE) is a four dimensional chemical data assimilation system in which a chemistry and a transport module are coupled to a detailed microphysical model (N. Larsen, DMI). This microphysical model describes the formation and evolution of four types of polar stratospheric cloud (PSC) particles, and its coupling to the chemistry module allows an interactive calculation of chlorine activation and denitrification that are responsible for polar ozone destruction. After a study of CRISTA (1994) and MLS (1995-1996) observations, we are currently following the Envisat mission from the start. BASCOE is processing the MIPAS observations in an operational set-up. In this talk we will present results from both the 2002 Antarctic winter (including the exceptional splitting of the polar vortex) and the 2003 Arctic winter. The added value of chemical data assimilation is demonstrated with an analysis of various fields in function of equivalent latitude.

**MI03/08A/B18-004** **0930**

**CLIMATE IMPLICATIONS OF MOVEMENT OF THE UPPER TROPOSPHERE FRONTS DEDUCED FROM TOTAL OZONE DATA**

Robert D. HUDSON, Marcus F. ANDRADE, Melanie B. FOLLETTE, Alexander D. FROLOV (Department of Meteorology, University of Maryland)

Analysis of the total ozone field obtained from the TOMS and Dobson data sets has shown that one can deduce the movement of the upper troposphere subtropical and polar fronts as a function of time. It has been shown, for example, that between 1980 and 1992 both fronts

moved northward. Any such movement implies that the weather patterns associated with these fronts will also have moved northward, i.e. that a climate change has taken place. In this paper, the movement of the fronts between 1965 and 2002 will be compared with climate indices. Initial results indicate a solar cycle dependence of the movement of both the polar and subtropical fronts. The subtropical front also shows a correlation with both the Quasi-Biennial Oscillation, and the Southern Oscillation.

**MI03/08A/B18-005** **1030**

**NOX PRODUCTION BY LIGHTNING OVER THE INDIAN REGION**

Suvarna Sushil KANDALGAONKAR, Md. Iqbal Rasul TINMAKER, Asha Shashi NATH (Indian Institute of Tropical Meteorology, Pune 411 008)

The importance of NO<sub>x</sub> production by lightning over the Indian region covering from 8 to 30 deg. N has been assessed by using satellite lightning measurements from the Lightning Imaging Sensor (LIS) and Optical Transient Detector (OTD). The lightning data from LIS/OTD for 4/5 year (1998-2001)/(1995-1999) period are analysed and partitioned, based on the latitude, to obtain the number of cloud to ground (CG) and cloud to cloud (CC) flashes. The annual total lightning counts by LIS/OTD during the period of study are 1.12 x 10<sup>17</sup> / 7.12 x 10<sup>16</sup> respectively. Similarly, the annual IC and CG lightning count during 4/5 year period from two different sensors (LIS/OTD) are 9.4 x 10<sup>16</sup> / 5.9 x 10<sup>16</sup> and 1.8 x 10<sup>16</sup> / 1.15 x 10<sup>16</sup> respectively. The total lightning count and the differential count from two different sensors are employed to calculate the production of NO<sub>x</sub>. We obtain the total annual lightning NO<sub>x</sub> production of 0.175 Tg N<sub>2</sub>O<sub>5</sub> by LIS and 0.1105 Tg N<sub>2</sub>O<sub>5</sub> by OTD over this latitudinal region, using the representative values of NO production and energy as 10<sup>17</sup> molecules and 6.7 x 10<sup>9</sup> J. The NO<sub>x</sub> production values obtained by using differential count are 0.028 Tg N<sub>2</sub>O<sub>5</sub> from IC flashes and 0.018 Tg N<sub>2</sub>O<sub>5</sub> from CG flashes by using LIS Sensor and 0.146 Tg N<sub>2</sub>O<sub>5</sub> from IC flashes and 0.0913 Tg N<sub>2</sub>O<sub>5</sub> from CG flashes by using OTD sensor. The results of this study suggests that though the orbiting period of OTD satellite is more than the LIS satellite by 19%, OTD could record 37% less lightning activity in total and corresponding NO<sub>x</sub> yield is also ~37% less than the NO<sub>x</sub> produced by LIS. Similar feature has also been observed from the differential count of each sensor. The NO<sub>x</sub> value obtained in the present study are more or less comparable with the values reported (displayed) by Bond et al., 2002 for the Indian region. The observed difference in NO<sub>x</sub> from the two sensor may be due to lower detection efficiency (40-60%) of OTD sensor. Thus LIS is perhaps the best lightning sensor with a high detection efficiency.

**MI03/08A/B18-006** **1050**

**LIGHTNING AND OTHER INFLUENCES ON TROPICAL TROPOSPHERIC OZONE: EMPIRICAL STUDIES OF COVARIATION**

Robert B. CHATFIELD<sup>1</sup>, Hong GUAN<sup>2</sup>, Anne M. THOMPSON<sup>3</sup>, Robert D. HUDSON<sup>4</sup>, Jacquelyne C. WITTE<sup>5</sup> (<sup>1</sup>NASA (Ames Research Center), <sup>2</sup>BAER Inst. and NASA (Ames), <sup>3</sup>NASA (Goddard Space Flight Center), <sup>4</sup>Univ. of Maryland, <sup>5</sup>SSAI and NASA (Goddard))

Tropical and subtropical tropospheric ozone are important radiatively active species, with particularly large effects in the upper third of the troposphere. Temporal variability of O<sub>3</sub> has proved difficult to simulate day by day in process models. Thus, individual roles of lightning, biomass burning, and other pollution in providing precursor NO<sub>x</sub>, radicals, and chain carriers (CO, hydrocarbons) remain unquantified by simulation, and it is theoretically reasonable that individual roles are magnified by a joint synergy. We use wavelet analysis and Burg algorithm "maximum entropy" spectral analyses to describe time-scales and correlation of ozone with proxies for processes controlling its concentration. Our empirical studies link time variations apparent in several datasets: the SHADOZ (Southern Hemisphere Additional Ozone Sonde) network stations (Nairobi, Fiji), and auxiliary series with power to explain ozone-determining processes, with some interpretation based on the TTO (Tropical Tropospheric Ozone) product derived from TOMS (the Total Ozone Mapping Spectrometer). The auxiliary series are The OTD/LIS (Optical Transient Detector/Lightning Imaging Sensor) measurements of the lightning NO<sub>x</sub> source, the OLR (Outgoing Longwave Radiation) measurement of high-topped clouds, and standard meteorological variables from the United States NCEP and Data Assimilation Office analyses. Concentrating on equatorial ozone, we compare the statistical evidence on the variability of tropospheric ozone. Important variations occur on approximately two-week, two-month (Madden-Julian Oscillation) and annual scales, and relations with OLR suggest controls associated with continental clouds. Hence we are now using the Lightning Imaging Sensor data set to indicate NO<sub>x</sub> sources. We report initial results defining relative roles of the processed mentioned affecting O<sub>3</sub> using their covariance properties.

**MI03/08A/B18-007** **1110**

**A SIGNIFICANT INCREASE OF CARBON MONOXIDE TROPOSPHERIC CONCENTRATION IN THE NORTHERN HEMISPHERE DETECTED BY TOTAL COLUMN AND SURFACE LAYER MEASUREMENTS IN 1998**

Thomas BLUMENSTOCK<sup>1</sup>, Evgeny GRECHKO<sup>2</sup>, Yutaka KONDO<sup>3</sup>, Justus NOTHOLT<sup>4</sup>, Paul NOVELLI<sup>5</sup>, Curtis RINSLAND<sup>6</sup>, Ralf SUSSMANN<sup>7</sup>, Hiroshi TANIMOTO<sup>8</sup>, Leonid YURGANOV<sup>9</sup>, Rodolphe ZANDER<sup>10</sup> (<sup>1</sup>IMK, Forschungszentrum Karlsruhe, Germany, <sup>2</sup>Obukhov Institute of Atmospheric Physics, Russia, <sup>3</sup>University of Tokyo, Japan, <sup>4</sup>Institut fuer Meteorologie und Klimaforschung Atmosphaerische Umweltforschung, Germany, <sup>5</sup>Institute of Astrophysics and Geophysics, Belgium, <sup>6</sup>University of Bremen, Germany, <sup>7</sup>Frontier Research System for Global Change, Japan, <sup>8</sup>Langley Research Center, NASA, USA, <sup>9</sup>Climate Monitoring and Diagnostic Laboratory, NOAA, USA, <sup>10</sup>National Institute for Environmental Studies, Japan)

Carbon monoxide in the troposphere of Northern Hemisphere was investigated using two different measurement approaches. First, absorption spectra of the total atmospheric depth using the Sun as a light source were measured at the Network for Detection of Stratospheric Change (NDSC) in USA, Switzerland, Germany, Sweden, Japan, Spitsbergen (Norway), and Russia. Total column amounts of CO above the measurement stations were retrieved from the spectra. Second, CO mixing ratios were measured in the surface layer using continuous instruments or by regular grab sampling and gas chromatography analysis at the CMDL laboratory in Boulder, Colorado. Sites of sampling were located between 31 N and 82 N in North America, Europe, Asia, Arctic, and North Pacific. All the data show abnormally high CO abundances in 1998. The CO "anomalies" i.e., monthly means, divided by the average over 1996, 1997, 1999 - 2001 for corresponding months. The anomalies for all the stations reached maximum between August and October 1998. It was found that the average hemispheric mean maxima for total column and surface anomalies amounted to 1.4 and 1.7, respectively, during late summer/fall 1998; the effect decreases with the altitude. The measurements at mountain stations (e.g., Niwot Ridge and Jungfraujoch) confirm lower enhancements in the free troposphere. The column CO anomaly diminished exponentially between September 1998 and July 1999 with the time constant of 2-5 months, presumably due to a removal by OH. Monthly means of the atmospheric extra burden of CO in the NH were calculated by averaging all the available data. A "top-down" estimate for an additional CO source was obtained using a box model for a reservoir between 30 N and 90 N. This source had 2 maxima, in April and in August, 1998 and total annual magnitude between 70



and 140 Tg CO (for assumed life times 4.7 and 2.3 month, respectively). Extremely strong forest fires took place in 1998, especially in Siberia. The report indicates that the fires significantly affected the CO total column over the whole hemisphere in 1998.

**MI03/08A/B18-008** **1130**

**SEASONAL PERSISTENCE OF MIDLATITUDE TOTAL OZONE ANOMALIES**

Vitali FIOLETOV<sup>1</sup>, Theodore SHEPHERD<sup>2</sup> (<sup>1</sup>Meteorological Service of Canada, <sup>2</sup>University of Toronto)

The seasonal persistence of interannual variations in total ozone is investigated by analyzing temporal autocorrelations of monthly mean total ozone anomalies over the 35-60S and 35-60N latitude bands. It is found that anomalies established in the wintertime midlatitude ozone buildup persist (with photochemical decay) until the end of the following autumn, and then are rapidly erased once the next winter's variability begins. The photochemical decay rate is found to be identical between the two hemispheres. Particularly in the northern hemisphere, there is high predictability of ozone through late summer based on the late-spring values. In the northern hemisphere, extending the 1979-2001 springtime ozone trend to other months through regression based on the seasonal persistence of anomalies (with the trend removed) captures the seasonality of the long-term ozone trends remarkably well. This suggests that the northern hemisphere trends in all months can be understood in terms of trends in the wintertime buildup. In the southern hemisphere, this mechanism only accounts for part of the summertime trends. There is a strong correlation between the ozone anomalies in northern hemisphere spring and those in the subsequent southern hemisphere spring, but not the converse. This suggests that some of the southern hemisphere variability is driven by the same mechanism as the northern hemisphere variability, or even by the northern hemisphere variability itself.

**MI03/08A/B18-009** **1150**

**THE DETECTION OF THE POLAR ORIGIN AIR AT WAKKANAI, JAPAN, SECOND REPORT. FROM THE OBSERVATION OF VERTICAL OZONE PROFILE AT WAKKANAI, JAPAN FROM FEBRUARY 15 TO 24, 2001**

Shigeru CHUBACHI<sup>1</sup>, Kouji MIYAGAWA<sup>2</sup> (<sup>1</sup>Atmospheric environment and applied meteorology Division, Meteorological Research Institute, <sup>2</sup>Ozone and radiation Division, Aerological Observatory)

In order to get better understandings of the ozone layer in the northern hemisphere, the observation of vertical ozone profiles at Wakkanai (45.4N, 141.7E), the northernmost city in Japan was conducted during the period from February 15 to 24, 2001 (Chubachi et al. 2002). In this paper, we report that the air mass detected at Wakkanai in Japan, though Wakkanai is located in the middle latitude, has the same characteristics of the air mass which is originated over polar stratosphere. In addition, TOMS data showed that the low ozone (below 250 DU) area appeared over Europe (around 55N, 20E) in February 14, one day before the observation taken at Wakkanai. We showed that the high latitude air mass on the 700K potential temperature surface moved to Europe with the low ozone area on February 14, further moved over to Wakkanai on February 19 at 700 potential temperature surface. We present the results based on the ozone sonde data set for the period February 14 to 24 through potential vorticity analysis technique. Finally, we suggest that it is possible to detect or observe the polar air at Wakkanai, in Japan, if we conduct dense and careful observation at Wakkanai, Japan. Reference Chubachi, S., Y. Sawa, T. Sekiyama, Y. Makino, and K. Miyakawa, Preliminary results of vertical ozone soundings at Wakkanai, Japan, Polar Meteorol. Graciol., 16, 149-164., 2002.

**Tuesday, July 8 PM**  
Presiding Chair: H. Graf

**MI03/08P/B18-001** **1400**

**MODELLING TROPOSPHERIC AND STRATOSPHERIC CHEMISTRY IN THE UM**

Peter BRAESICKE, Guang ZENG, John PYLE (Centre for Atmospheric Science, University of Cambridge)

We will present results from a hierarchy of chemistry modules used with the Met Office Unified Model (UM) to model the chemistry of the troposphere and stratosphere. Problems studied include the role of dynamics in middle latitude ozone decline and the change in oxidising capacity of the Troposphere. The tropospheric setup comprises a comprehensive chemistry in a 19 level version of the UM and is used to predict future changes in surface ozone and changes in the ozone budget. The stratospheric setup is based on the 58 level version and can be used with either a simple stratospheric chemistry for sensitivity studies on longer timescales, or a comprehensive chemistry for seasonal ensemble integrations. We amalgamate results from all model systems in consideration of the UT/LS region. We find that changes in ozone in the LS are crucial for the future development of tropospheric ozone. Changes in ozone in the LS do not have a large dynamical feedback on stratospheric ozone.

**MI03/08P/B18-002** **1420**

**CAN HETEROGENEOUS CHEMISTRY ON CLOUDS INCREASE THE OXIDIZING ABILITY OF THE TROPOSPHERE**

Azadeh TABAZADEH<sup>1</sup>, Robert J. YOKELSON<sup>2</sup>, Hanwant B. SINGH<sup>1</sup> (<sup>1</sup>Earth Science Division, NASA Ames Research Center, <sup>2</sup>University of Montana, Dept. of Chemistry)

It is well known that heterogeneous chemistry in the polar stratosphere leads to the formation of the Antarctic ozone hole. However, very little is known about the effect of heterogeneous chemistry on the composition of the troposphere. Methanol is the second (methane is the first) most abundant organic trace gas found in the Earth's atmosphere, and there appears to be a large mismatch between atmospheric concentrations and estimated sources, indicating the presence of major unknown removal processes. Using trace gas and aerosol data from the SAFARI 2000 experiment, taken in clouds impacted by biomass burning, we show clouds may provide a major sink for methanol removal through a number of plausible heterogeneous chemical processes. Further, rapid heterogeneous chemistry on cloud surfaces, involving methanol, may also cause production of photochemically active species (i.e. formaldehyde) in cloud-processed air, affecting the oxidizing ability of the atmosphere on a global scale.

**MI03/08P/B18-003** **1440**

**SIMULATING ANTARCTIC STRATOSPHERIC OZONE LOSS IN A GCM: VARIABILITY**

Stephen R. BEAGLEY<sup>1</sup>, Jean DE GRANDPRE<sup>2</sup>, Victor I. FOMICHEV<sup>1</sup>, John C. MCCONNELL<sup>1</sup>, Theodore G. SHEPHERD<sup>3</sup> (<sup>1</sup>York University Toronto, <sup>2</sup>McGill University, Montreal, <sup>3</sup>University of Toronto, Toronto)

Simulation of polar ozone loss within a GCM for time-slice conditions permits the exploration of the interaction between radiation, dynamics and chemistry which can produce varying ozone loss for the same climate conditions. Dynamical variability influences springtime polar ozone abundance through both ozone transport and temperature-induced variability in PSC formation and consequent chemical ozone loss. Results using the Canadian middle atmosphere model (CMAM) for low and high chlorine loading scenarios will be presented to explore the model's capability in describing the dynamical and chemical evolution of lower stratospheric polar springtime events, and to explore the variability inherent in coupled chemistry-climate model simulations of ozone loss.

**MI03/08P/B18-004** **1500**

**QUANTIFYING THE TROPOPAUSE MIXING BARRIER IN THE CANADIAN MIDDLE ATMOSPHERE MODEL**

David SANKEY, Theodore G. SHEPHERD (Department of Physics, University of Toronto)

Mixing barriers in the atmosphere play an important role in shaping the large-scale dynamical circulation, and greatly affect the transport of chemical species. While some success has been achieved in identifying the edge of the tropical pipe and the wintertime polar vortex barrier, finding the location of the tropopause mixing barrier has proven to be much more elusive. In this study, various methods are applied to identify the tropopause mixing barrier in the Canadian Middle Atmosphere Model, a three-dimensional coupled chemistry GCM. AGCM is used partly to provide a dynamically self-consistent data set, and partly because it is an important exercise in itself to assess the extent to which such models represent the tropopause mixing barrier. The methods studied include Nakamura's effective diffusivity, age of air, PDFs of chemical species, seasonal evolution of ozone, and investigating the balance between radiative heating and cooling. In addition to quantifying the tropopause mixing barrier in the model, comparison of the different methods sheds light on their commonalities and differences.

**MI03/08P/B18-005** **1520**

**THE SEPARATE CLIMATE EFFECTS OF THE STRATOSPHERIC AND THE TROPOSPHERIC CO2 INCREASE AS SIMULATED WITH THE MA-ECHAM4 MODEL**

Michael SIGMOND<sup>1</sup>, Peter Christiaan SIEGMUND<sup>2</sup>, Hennie KELDER<sup>2</sup>, Elisa MANZINI<sup>3</sup> (<sup>1</sup>Eindhoven University of Technology (TUE), <sup>2</sup>Royal Netherlands Meteorological Institute (KNMI), <sup>3</sup>Max-Planck-Institut für Meteorologie)

The effect of the separate stratospheric and tropospheric CO2 increase on, respectively, the troposphere and the stratosphere has been investigated with the middle atmosphere version of the ECHAM climate model. Here, the CO2 is separately doubled in, respectively, the troposphere, the middle atmosphere and the entire atmosphere, and the results are compared to a control run. In addition, the linearity of the results is investigated. The results show that the tropospheric CO2 doubling causes a significant increase in the residual circulation in the stratosphere, leading to an increase in the stratospheric temperatures at high latitudes. The stratospheric CO2 doubling causes a significant increase in the tropospheric extratropical zonal wind. Results from an additional experiment show that also the doubling of CO2 above 10 hPa, which is close to the top of many GCM's, significantly influences the tropospheric climate.

**MI03/08P/B18-006** **1610**

**SIMULATION OF FUTURE DISTRIBUTIONS OF TROPOSPHERIC OZONE AND SULFATE AEROSOL: IMPACTS OF EMISSION CHANGE AND CLIMATE CHANGE**

Kengo SUDO<sup>1</sup>, Masaaki TAKAHASHI<sup>1</sup>, Toru NOZAWA<sup>2</sup>, Hiroshi KANZAWA<sup>2</sup>, Hajime AKIMOTO<sup>3</sup> (<sup>1</sup>Center for Climate System Research, University of Tokyo, <sup>2</sup>National Institute for Environmental Studies, Japan, <sup>3</sup>Frontier Research System for Global Change, Japan)

We performed experiments of future tropospheric chemistry involving ozone (O<sub>3</sub>) and sulfate aerosol with a coupled chemistry general circulation model (GCM). Future change in tropospheric ozone and aerosols distributions is of critical importance both for climate and atmospheric environment. Ozone and aerosols in the troposphere, having much short residence times relative to other principal greenhouse gases, are controlled by emissions of precursors and also by natural meteorological conditions (temperature, humidity, transport, etc.). In this study, we conducted simulations of tropospheric ozone and sulfate distributions for the next hundred years to 2100 using a coupled chemistry GCM (the CHASER model) which has been developed in the framework of the Center for Climate System Research/National Institute for Environment Studies (CCSR/NIES) atmosphere GCM. To evaluate impacts of emission change and of climate change independently, two kinds of experiments were carried out. In the first experiment (Exp1), the GCM simulates present-day meteorological conditions using constant greenhouse gases, but in the second experiment (Exp2) it simulates climate change based on the IPCC SRES A2 scenario. Trace gas emissions of CO, NO<sub>x</sub>, methane (CH<sub>4</sub>), non-methane hydrocarbons, and SO<sub>2</sub> in both experiments are prescribed by the SRES A2 scenario. In Exp1 with no climate change, global tropospheric ozone burden increased almost linearly from 325 Tg in 1990 to 397 Tg (22%) in 2050 and to 467 Tg (+44%) in 2100, showing significant increases in the low to midlatitudes in the Northern Hemisphere including eastern Asia (+53% in 2100). In Exp2 with climate change, the ozone increases predicted in Exp1 are generally reduced 10-20% in the lower troposphere after around 2050, due to water vapor increases causing more efficient ozone destruction. However, Exp2 calculates additional ozone increases of 5-10% in the boundary layers around the polluted regions as eastern Asia relative to Exp1 (after 2050), showing more enhanced ozone production due to temperature and water vapor increases. Exp2 also predicts additional increases in upper tropospheric ozone in the midlatitudes as a result of enhanced ozone transport from the stratosphere due to intensification of the Hadley Circulation and stratospheric circulation in the model. The model predicted an increase in the sulfate burden from 0.55 TgS in 1990 to 0.91 TgS in 2050 with showing pronounced increases in India and China. This experiment indicated that the sulfate formation in liquid phase was enhanced by the increases in H<sub>2</sub>O<sub>2</sub> after around 2050 particularly in the low latitudes as in India. Global mean methane concentration increased to about 4 ppmv in 2100 with emission change only (Exp1), but to 3.3 ppmv with climate change as well (Exp2), reflecting the impact of temperature and water vapor increases on the CH<sub>4</sub> lifetime against the reaction with OH. In Exp1, CH<sub>4</sub> lifetime increases from 9.2 years in 1990 to 11.4 years in 2100, whereas Exp2 shows reduction in CH<sub>4</sub> lifetime (8.6 years in 2100).

**MI03/08P/B18-007** **1630**

**CHANGES IN THE STRATOSPHERIC OZONE EQUILIBRIUM CAUSED BY GREENHOUSE GAS INCREASES BETWEEN 1979 AND 2060**

Michel S. BOURQUI<sup>1</sup>, Chris P. TAYLOR<sup>2</sup>, Keith P. SHINE<sup>2</sup> (Institute for Atmospheric and Climate Science, ETH Zurich, <sup>2</sup>Dept of Meteorology, University of Reading)

The depletion of stratospheric ozone due to chlorine emissions which started in the early eighties is now slowing down and is expected to end up near the 2050s thanks to emission cuts that followed the ratification of the Montreal Protocol. Stratospheric ozone may however recover towards a distribution substantially different from the pre-depletion one because of the concurrent increase in greenhouse gases (GHG). Here, a new coupled three-dimensional chemistry - general circulation model has been developed. The new chemistry model FASTOC (FASt STRatospheric Ozone Chemistry) represents the chemistry of stratospheric ozone in terms of constituent relationships derived from an accurate chemical box model. The circulation is performed by the IGCM (Intermediate General Circulation Model) of the University of Reading. This model is used in its T21 version with 26 levels from the surface up to 0.1 hPa. The thrust of this coupled model is the combination of a high computational speed and a realistic representation of ozone chemistry. In this study, changes in the stratospheric ozone equilibrium due to GHG increases between 1979 and 2060 are investigated in the context of time-slice experiments using our new coupled model. The emphasis is placed on the understanding of the three ways along which the GHG increase affects ozone chemistry: (i) by chemically and (ii) thermodynamically interacting with the ozone production/loss chemistry, and (iii) by changing the constituents circulation.

**MI03-Posters** **Wednesday, July 9**

**CHEMISTRY-CLIMATE INTERACTIONS (COVERS OZONE INTERACTIONS) (ICACGP, IOC, ICCI)**

Location: Site D

**Wednesday, July 9 AM**  
Presiding Chairs: D. Wuebbles, H. Akimoto

**MI03/09A/D-001** **Poster** **0900-244**

**INITIAL DATA COMPARISON OF SAGE III AND VARIOUS SATELLITES, GROUND-BASED AND BALLOON MEASUREMENTS**

William P. CHU<sup>1</sup>, Chip L. TREPTE<sup>1</sup>, Joe M. ZAWODNY<sup>2</sup>, Larry W. THOMASON<sup>1</sup>, Ghassan TAHA<sup>2</sup>, J.R. MOORE<sup>3</sup> (NASA Langley Research Center, <sup>1</sup>University Of Arizona, <sup>2</sup>SAIC)

The Stratospheric Aerosol and Gas Experiment III (SAGE III), which was launched on Dec 10, 2001 on the Russian spacecraft Meteor 3M, is an important part of NASA's Earth Observing System (EOS) mission to develop an understanding of the total Earth system and the effects of natural and human-induced changes on the global environment. The instrument makes use of solar occultation observations to provide high resolution vertical profiles of multi-wavelength aerosol extinction, the molecular density of ozone, nitrogen dioxide, and water vapor, as well as profiles of temperature, pressure, and cloud presence. The instrument is also capable of performing lunar occultation and limb scattering measurements. In this work, the latest SAGE III solar and lunar occultation measurements will be presented. In an early evaluation of the measurements, comparisons will be made between SAGE III level 2 solar products (version 2.0) and SAGE II, HALOE, POAM III, and GOMOS satellites. Comparisons also include balloon and ground-based measurements.

**MI03/09A/D-002** **Poster** **0900-245**

**DIURNAL VARIATION ON THE SUBTROPICAL BRO**

Manuel GIL, Olga PUENTEDURA, Margarita YELA (INTA. Dep. de Observación de la Tierra: Teledetección y Atmósfera)

A BrO column measurements programme by zenith sky UV spectroscopy at the Northern Subtropical belt (Izana Observatory, 28°, 16°W, 2370 m.a.s.l.) started on December 2001. The instrument set up and parameters used for BrO retrieval followed the recommendations by Aliwell et al. Data show a clear signature of the BrO cross sections structures in the recorded spectra but retrieved amounts are lower than at higher latitudes. The shape of the diurnal variation in the slant column display a marked seasonal dependence. Values are generally larger in the morning twilight, being the largest am-pm asymmetry in the summer solstice. This behaviour cannot be reproduced by the gas phase photochemical models assuming all the BrO in the stratosphere. Additionally, Langley plots at solar zenith angles between 60° and 85° yields values of the vertical column above 5x10<sup>13</sup> molec.cm<sup>-2</sup> in mid summer, while estimated stratospheric column for the same seasons below 2x10<sup>13</sup> molec.cm<sup>-2</sup>. The difference between both, larger than 3x10<sup>13</sup> molec.cm<sup>-2</sup>, is attributed to BrO residing in the free troposphere. This significant amount of tropospheric BrO is also inferred from the shape of the column around twilight, and from limited off-axis measurements.

**MI03/09A/D-003** **Poster** **0900-246**

**LONG TERM TRENDS OF NITROGEN DIOXIDE LEVELS OBSERVED AT MID- AND HIGH-LATITUDE STATIONS FROM GROUND-BASED SPECTROMETER DATA**

Daniele BORTOLI<sup>1</sup>, Andrea PETRITOLF<sup>1</sup>, Giorgio GIOVANELLF<sup>1</sup>, Ivan KOSTADINOV<sup>2</sup>, Fabrizio RAVEGNANI<sup>3</sup>, Ana Maria SILVA<sup>4</sup> (Geophysics Centre of Evora, University of Evora, <sup>2</sup>ISAC-CNR, via Gobetti 101, Bologna, Italy, <sup>3</sup>STIL-BAS, 6000, Stara Zagora, Bulgaria)

The interactions between mid- and high-latitude atmospheric changes are going to be one of the main issues for the future of stratospheric and tropospheric chemistry research. A more detailed study of the ozone trends and those of the chemically-related compounds (NOx, chlorine and bromine oxides) as well as a greater comprehension of their interactions at lower and higher latitudes, are important issues which should be addressed to build-up a more detailed picture of possible scenarios which we may have to face in the near future. Nitrous oxide (N<sub>2</sub>O), an important greenhouse gas, has been increasing since 1980 at a rate of about +3% per decade. Recently, a notably greater rate of increase of about +5% per decade since 1980 was reported for measurements of stratospheric nitrogen dioxide (NO<sub>2</sub>). However, since N<sub>2</sub>O is the dominant source of odd-nitrogen compounds in the stratosphere, including NO<sub>2</sub>, a more complex approach would seem to be necessary. These apparently conflicting trends are, in fact, generally consistent when viewed within a wider framework with the inclusion of concurrent trends in stratospheric ozone and halogens. GASCOD spectrometers (Gas Analyzer Spectrometer Correlating Optical

Differences) have been installed at the "Ottavio Vittori" Research Station at Monte Cimone, Italy (44.11N, 10.42E, 2165 m asl) since June 1993, at the Italian Antarctic Station, Terra Nova Bay (74.69S, 164.12E) since December 1995 and at the STIL-BAS station at Stara Zagora, Bulgaria (42.42N, 25.63E) since 1999. The instruments measure zenith scattered solar radiation between 407 and 464 nm (occasionally measurements at 330-390 nm are performed) and the nitrogen dioxide total column is retrieved with Differential Optical Absorption Spectroscopy. The seasonal trend of NO<sub>2</sub> v<sub>c</sub> values is reported and it shows the expected behaviour: maximum values during the summer period with the minima occurring during the winter season in both hemispheres. A typical behaviour of the AM/PM ratio at high latitudes is highlighted. The application of a simple photochemical model confirms that the NO<sub>2</sub> AM/PM ratio can be modelled with temperature at the NO<sub>2</sub> bulk altitude, the ozone concentration at the same altitude and the hours of darkness. A Fourier analysis is proposed as a tool to investigate the long-term components of stratospheric nitrogen dioxide levels. Results are presented and the NO<sub>2</sub> trend is shown and discussed. Measurements such as these are essential for identifying global change and provide a lesson in understanding it: careful simulation of the time, location, and geometry of measurements must be combined with concurrent trends in related chemical species and climatic parameters. **ACKNOWLEDGEMENTS** The author Daniele Bortoli gratefully acknowledges financial support from the Subprograma Ciência e Tecnologia do 3º Quadro Comunitário de Apoio. The Quantification and Interpretation of Long-Term UV-Vis Observations of the Stratosphere (QUILT) project supported this research.

**MI03/09A/D-004** **Poster** **0900-247**

**MOVEMENT OF THE SUB-TROPICAL AND POLAR FRONTS DEDUCED FROM TOTAL OZONE RECORDS**

Melanie B. FOLLETTE, Marcos F. ANDRADE, Alexander D. FROLOV, Robert D. HUDSON (Department of Meteorology, University of Maryland)

Analysis of the ozone field in the Northern Hemisphere outside of the polar vortex, using both TOMS and Dobson data, has shown that the total ozone field can be separated into three distinct meteorological regimes. These are defined as (1) the tropical regime - between the equator and the upper troposphere subtropical front (2) the midlatitude regime - between the subtropical and polar fronts, (3) the polar regime - between the polar front and the polar vortex. Within each regime, the daily mean total ozone value is relatively constant, with a clearly separate value for each regime. It has also been shown both from rawinsonde and ozonesonde measurements, that the tropical, mid-latitude, and polar regimes are identified with a distinct tropopause height. The trends in total ozone between 1979 and 1992 within each regime are much less than the overall mid-latitude trend obtained from zonally averaged data. Much of the observed zonal trend is due to the movement of the subtropical and polar front northward, causing more low ozone in the tropical regime, and less high ozone in the polar regime, to be included in the zonal average. This paper presents an analysis of the movement of the polar and sub-tropical fronts for the period between 1965 and 2002 deduced from both the TOMS and Dobson data sets.

**MI03/09A/D-005** **Poster** **0900-248**

**MODELING THE EFFECT OF A PINATUBO LIKE VOLCANIC ERUPTION WITHIN THE NEXT DECADE USING A COUPLED CHEMISTRY-CLIMATE MODEL**

Hamish STRUTHERS<sup>1</sup>, John AUSTIN<sup>2</sup> (National Institute of Water and Atmospheric Research, New Zealand, <sup>2</sup>The Met Office, UK)

A future major volcanic eruption, if it were to occur within the next decade, could potentially have a significant impact on stratospheric ozone amounts, due to the activation of halogen compounds on the surface of the volcanic aerosol cloud (Tabazadeh et al 2002). Accurately modeling the response of the stratosphere to a major volcanic eruption is difficult (Bodeker et al 2001, WMO 2002). Coupled chemical-dynamical models are required to simulate radiative-chemical feedbacks present in the atmosphere (Rosenfield et al 1997, Al-Saadi et al 2001). We use the UMETRAC, coupled chemistry-climate model (Austin et al 2001) to simulate a Mt. Pinatubo like volcanic eruption (Knight et al 1998), starting the model from 2010 initial conditions and future boundary forcing (sst, ice, stratospheric halogen loading etc). Comparisons will be made with a control run of the model to clarify the impact of stratospheric sulphate loading on ozone and temperature. Al-Saadi J., Pierce R., Fairlie T., Kleb M., Eckman R., Grose W., Natarajan M. and Olson J., Response of middle atmosphere chemistry and dynamics to volcanically elevated sulfate aerosol: Three-dimensional coupled model simulations, *J. Geophys. Res.* 106, 27,255-27,275, 2001 Austin J., A three-dimensional coupled chemistry-climate model simulation of past stratospheric trends, *J. Atmos. Sci.*, 59, 218-232, 2002 Bodeker G., Connor B., Liley J. and Matthews W., The global mass of ozone: 1978-1998, *Geophys. Res. Lett.*, 28, 2819-2822, 2001 Knight J., Austin J., Grainger R. and Lambert A., A three-dimensional model simulation of the impact of Mt. Pinatubo aerosol on the Antarctic ozone hole, *Q. J. R. Meteorol. Soc.*, 124, 1527-1558, 1998 Rosenfield J., Considine D., Meade P., Bacmeister J., Jackman C. and Schoeberl M., Stratospheric effects of Mount Pinatubo aerosol studied with coupled two-dimensional model, *J. Geophys. Res.*, 102, 3649-3670, 1997 Tabazadeh A., Drdla K., Schoeberl M., Hamill P. and Toon O., Arctic ozone hole in a cold volcanic stratosphere, *Proc. Nat. Academy Sci.*, 99, 2609-2612, 2002 World Meteorological Society (WMO), Scientific assessment of ozone depletion: 2002, Executive summary.

**MI03/09A/D-006** **Poster** **0900-249**

**VALIDATION OF THE NEWLY DEVELOPED CLIMATE-CHEMISTRY MODEL (SOCOL) AGAINST OBSERVED CLIMATOLOGY**

Tatiana A. EGOROVA<sup>1</sup>, Eugene V. ROZANOV<sup>1</sup>, Thomas PETER<sup>2</sup>, Werner SCHMUTZ<sup>3</sup> (PMOD-WRC, Davos and IAC ETH Zuerich, Switzerland, <sup>2</sup>IAC ETH Zuerich, Switzerland, <sup>3</sup>PMOD-WRC, Davos, Switzerland)

Predictability of climate and ozone changes in the future is one of the important and challenging problems in modern science that requires the development, implementation and validation of very sophisticated, computationally efficient, three-dimensional climate models with interactive chemistry (CCM). Here we present a newly developed CCM SOCOL (model tool for evaluation of the SOLar-Climate-Ozone-Links), which is a combination of MAECHAM-4 GCM with atmospheric chemistry and transport model developed in Switzerland. This spectral global model has T30 horizontal representation and 39 levels in the vertical direction. SOCOL enables simulating of the temperature, dynamics and photochemistry of the troposphere, stratosphere and lower mesosphere up to 85 km. When the development of such a complicated model is completed it is important to verify how well it reproduces observed climatology. With SOCOL we have performed a 40-year long simulation with prescribed sea surface temperature, sea ice and greenhouse gas distributions. The simulated winds, temperature, ozone and other trace species have been validated against available observations obtained from different satellite instruments and compared with other CCMs results. The comparison showed that SOCOL simulates photochemistry, temperature and dynamics of the troposphere, stratosphere and lower mesosphere reasonably well and can be used to address chemistry-climate interaction issues.

**MI05** **Wednesday, July 9 - Friday, July 11**

**LARGE SCALE PATTERNS OF ATMOSPHERIC VARIABILITY: DYNAMICS, CLIMATE IMPACTS, AND ROLE IN RECENT CLIMATE CHANGE (ICC)**

Location: Site B, Room 17

**Wednesday, July 9 AM**

Presiding Chairs: D. Thompson, M. Hori

**MI05/09A/B17-001** **Invited** **0900**

**ON THE PHYSICAL REALITY OF ANNULAR MODES**

Walter A. ROBINSON (Department of Atmospheric Sciences, University of Illinois at Urbana-Champaign)

Several authors have recently challenged the physical reality of annular modes. The crux of these challenges is that the low-frequency component of the atmospheric flow is not annular (zonally symmetric), and that the annular modes are, therefore, an artifact of empirical orthogonal function (EOF) analysis. The flow during individual annular mode events, periods when the projection on the annular mode EOF is unusually strong (positive or negative), displays zonally localized structures (Cash et al. 2002), as do teleconnection patterns obtained from one-point correlation analyses (Deser 2000). Here, it is argued these results are insufficient to show that annular modes are not real. While they are consistent with the absence of physical annular modes, they are also consistent with a system wherein annular and strong non-annular variability coexist. If annular and non-annular variability are mutually independent, then the presence of robust non-annular variability makes the annular modes no less real. In a very simple system (a coarsely resolved two-level model on the sphere) the annular and non-annular variability are nearly, but not completely, independent. For this model, at least, the annular mode is a physically useful concept. This independence requires, first, that the annular modes have only weak direct interactions with non-annular low-frequency variability, a condition unlikely to be satisfied in the Northern Hemisphere (DeWeaver and Nigam 2000), and, secondly, that interactions of both annular and non-annular low-frequency variability with transient eddies are approximately linear in the strength of the low-frequency flow. Again, this is true for the two-level model, but perhaps not in better-resolved models or in nature. If the above conditions are violated, it may still prove useful to focus on annular variability, if the annular ( $m=0$ ) components of originally localized disturbances are more persistent than non-annular components, and if this annular residual is significant in organizing weather at longitudes remote from the initial disturbance. Based on experiments with the two-level model, model experiments and diagnostic analyses are proposed that could be used to assess the physical reality and utility of annular modes in more realistic models and perhaps in nature. Cash, B.A., P.J. Kushner, and G.K. Vallis, 2002: The structure and composition of the annular modes in an aquaplanet general circulation model. *J. Atmos. Sci.*, 59, 3399-3414. Deser, C., 2000: On the teleconnectivity of the "Arctic Oscillation." *Geophys. Res. Lett.*, 27, 779-782. DeWeaver, E., and S. Nigam, 2000: Do stationary waves drive the zonal-mean jet anomalies of the Northern Winter? *J. Climate*, 13, 2160-2176.

**MI05/09A/B17-002** **0940**

**BUDGET OF OMEGA ANGULAR MOMENTUM: ANOTHER WAY TO ASSESS THE DYNAMICS OF THE ANTARCTIC AND ARCTIC OSCILLATIONS**

Jin-Song VON STORCH (Institute of Meteorology, University Hamburg, Germany)

Both the Antarctic and Arctic Oscillations (AO and AAO) reveal notable anomalies of axial angular momentum. When decomposing these anomalies into a part related to Omega angular momentum (the matter term) and apart related to relative angular momentum, one finds that the former is much larger than the latter. The large anomalies of Omega angular momentum result from mass conservation constraint. The mass (zonally averaged pressure) anomalies related to the AO and AAO reveal a meridional dipole structure such that the mass in the high-latitude center is equal to and has opposite size of the mass in the mid-latitude center. This structure makes the global Omega angular momentum be significantly non-zero, as the high-latitude mass is relatively close to the rotation axis. Given the significance of mass anomalies, the budget equation of omega angular momentum is used to study the maintenance of the two modes. Three types of mass transports are identified. The first one emerges from geostrophic flow in conjunction with tropospheric eddies. The second one, which is related to the friction torque, results from meridional Ekman velocities. The last one, which gives rise to the mountain torque, is induced by meridional geostrophic flow within mountainous barriers. The first two types of mass transport are directly related to the structure of zonal-mean zonal flow. They tend to balance each other and result in a persistence dipole structure in mass (pressure). This is the situation observed for the AAO. The emergence of the third type of mass transport destroys the balance between the first two mass transports. The dipole structure in pressure anomalies is much less persistent. This is the situation observed for the AO. The consideration of mass transports suggests that the AAO and AO are two internal modes of the atmosphere, which are differently modified by the lower boundary conditions.

**MI05/09A/B17-003** **1000**

**ANALYSIS AND MODELING OF THE ARCTIC OSCILLATION USING A SIMPLE BAROTROPIC MODEL WITH BAROCLINIC EDDY FORCING**

Hiroshi L. TANAKA (Institute of Geoscience, University of Tsukuba)

In this study, a numerical simulation of Arctic Oscillation (AO) is conducted using a simple barotropic model that considers the barotropic-baroclinic interactions as the external forcing. The model is referred to as a barotropic S-model since the external forcing is obtained statistically from the long-term historical data, solving an inverse problem. We have integrated the barotropic S-model for 51 years under a perpetual January condition and analyzed the dominant EOF modes in the model. The results are compared with the EOF analysis of the barotropic component of the real atmosphere based on the daily NCEP/NCAR reanalysis for 50 years from 1950 to 1999. According to the result, the first EOF of the model atmosphere appears to be the AO similar to the observation. The annular structure of AO and the two centers of action at Pacific and Atlantic are simulated nicely by the barotropic S-model. Therefore, the atmospheric low-frequency variabilities have been captured satisfactorily even by the simple barotropic model. The EOF analysis is further conducted to the external forcing of the barotropic S-model. The structure of the dominant forcing shows the characteristics of synoptic-scale disturbances of zonal wavenumber 6 along the Pacific storm track. The forcing is induced by the barotropic-baroclinic interactions associated with baroclinic instability. The result suggests that the AO can be understood as the natural variability of the barotropic component of the atmosphere induced by the inherent barotropic

dynamics which is forced by the barotropic-baroclinic interactions. The fluctuating up-scale energy cascade from synoptic-scale disturbances to the zonal motion plays the key role for the excitation of the AO.

**MI05/09A/B17-004** **1020**

**VERTICAL STRUCTURE OF THE ARCTIC OSCILLATION AND COLD OCEAN WARM LAND REGIMES AND THEIR ROLE IN CLIMATE CHANGE**

Susanna CORTI (ISAC Institute of Atmospheric Sciences and Climate, CNR National Research Council)

When examined in terms of diagnostics of the atmospheric circulation, recent climate change may be interpreted in terms of increases or decreases in the frequency of occurrence of pre-existing preferred modes of atmospheric behaviour rather than a simple linear shift in the mean climate with superimposed noise. This contrasts with the characteristics of the observed changes in temperature-related diagnostics, which appear much closer to the simple linear picture. While not necessarily inconsistent, the implications of these two views of the nature of climate change need to be explored. In this framework the main purpose of this paper is to use a 40-yr NCEP reanalysis dataset in order to explore the vertical structure of circulation regimes and (at the same time) illustrate the potential role of weather regimes and non-linearity in the emerging anthropogenic signal. An empirical orthogonal function (EOF) analysis is first applied in order to define, for each variable, a reduced phase space based on the leading modes of variability. Then a simultaneous analysis of the four fields is carried out performing a further EOF analysis in the subspace spanned by the leading EOFs of each field. This produced a multi-variable EOF picture of the large-scale vertical (and thermal) structure of the atmosphere. With the three-dimensional structure available, it is possible to assess whether the observed temperature changes are consistent with an increase in certain regime frequencies. Moreover the hypothesis that regime frequency change more than regime structure is checked by performing a regime analysis separately on the first and last 25-yr periods.

**MI05/09A/B17-006** **1110**

**DYNAMICAL PROTOTYPE OF THE ARCTIC OSCILLATION AS REVEALED BY A NEUTRAL SINGULAR VECTOR**

Masahiro WATANABE (Department of Ocean and Atmospheric Science, Hokkaido University)

Toward understanding dynamical origin of the Arctic Oscillation (AO), a dynamical analysis was conducted by means of a linear primitive equation model. This work is to extend our previous results (Kimoto et al. 2001, GRL) in which singular vectors have been computed for a zonal mean part of the linear dynamical operator that incorporates feedback from anomalous stationary eddies. In order to verify a hypothesis that the AO essentially originates from the zonally inhomogeneous time mean state, we again computed singular vectors of the dynamical operator but now linearized about the non-zonal winter climatology; that is, the operator includes both the zonal flow-wave interaction and the wave-wave interaction. The leading singular mode, which is close to neutral and dominates over others under stochastic forcing, has a considerable resemblance to the observed AO. Several processes, such as an interaction with transient eddies and a thermal forcing either in the stratosphere or at the surface, may preferably excite the AO, the singular vector analysis performed here strongly suggests that the origin of the AO resides in dynamics of a slowly-varying, non-zonal time mean state in the troposphere. Further diagnoses were made to the singular mode to clarify the role of zonal flow-stationary wave interaction, divergence in the upper troposphere, and so on.

**MI05/09A/B17-007** **1130**

**TOPOGRAPHIC EFFECTS ON ANNULAR VARIABILITY IN A COUPLED ATMOSPHERE-OCEAN GCM**

Seiya NISHIZAWA<sup>1</sup>, Shigeo YODEN<sup>1</sup>, Akio KITOH<sup>2</sup> (<sup>1</sup>Department of Geophysics, Kyoto University, <sup>2</sup>Meteorological Research Institute, Tsukuba, Japan)

Thompson and Wallace (1998, 2000) pointed out that the most dominant mode of low-frequency variability in the extratropical troposphere is the "annular mode" both in the Northern Hemisphere (NH) and the Southern Hemisphere (SH). Although the annular mode in the both hemispheres has some similar structures, there exist differences between the two hemispheres due to the surface conditions. Nishizawa and Yoden (2003) noted that annular variability depends on the number and spatial structure of storm tracks in a simplified global circulation model with some idealized topographic conditions. In this study, we examine the topographic effects on the annular variability with a coupled atmosphere-ocean GCM (MRI-CGCM2). The control run (M10) was integrated for 50 years with realistic land-sea distribution and topography (Kitoh 2002). In the M0 run, the worldwide mountain height was set to zero, but keeping the land-sea distribution. Similarly 20% of the topography in the M0 run were assumed in the M2 run, and 40%, 60%, 80%, 120% and 140% were in the M4, M6, M8, M12 and M14 runs, respectively. The monthly averaged data in winter season of the last 40 years for the eight runs are analyzed. An EOF analysis is done for the sea-level pressure field in the NH. Some characteristics of EOF1 depend on the amplitude of the topography, and there are switchings in the order of the EOFs. The leading EOF1 shows annular pattern except in the M0 and M4 runs, and second mode of EOF shows annular pattern in these two runs. It is noted that contribution rate of the first two EOFs are very similar in the M0 run; 22% and 21%. The switching in the M4 run is similar to that in the previous work with simple model. EOF analysis for the zonal-mean zonal wind field from the surface to 50hPa in the NH also shows dependence on the topographic amplitude. Latitude of the node of the EOF1 tends to shift equatorward with increasing the amplitude. The domain of the EOF analysis for the sea-level pressure field was swept by changing the latitude of northern boundary in the NH (cf. Itoh 2002). In the M8 run, the leading two EOFs for the domain without the polar region are dominant over the Pacific or the Atlantic sector, respectively. These two modes are well separated, although the leading mode of the hemispheric EOF shows annular pattern. In the other runs, the hemispheric EOF and the midlatitude EOF have similar pattern. Same analyses are also done for the SH, and the difference of the amplitude dependence between the NH and the SH is identified to understand the annular variability in the real atmosphere more clearly.

**MI05/09A/B17-008** **1150**

**DECOMPOSITION OF THE ARCTIC OSCILLATION INTO INDEPENDENT COMPONENTS**

Atsushi MORI<sup>1</sup>, Nobuaki KAWASAKI<sup>2</sup>, Kensuke YAMAZAKI<sup>3</sup>, Meiji HONDA<sup>4</sup>, Hisashi NAKAMURA<sup>5</sup> (<sup>1</sup>Department of Astronomy and Earth Science, Tokyo Gakugei University, <sup>2</sup>Senior High School at Otsuma of Tsukuba University, <sup>3</sup>Department of Mathematics and Informatics, Tokyo Gakugei University, <sup>4</sup>Institute for Global Change Research, Frontier Research System for Global Change, <sup>5</sup>Institute for Global Change Research, Frontier Research System for Global Change, and Department of Earth and Planetary Science, University of Tokyo)

Arctic Oscillation(AO) is known to be the most dominant variability over the northern hemisphere in winter(Thompson and Wallace, 1998). However, recently, physicality of AO comes into question from various points of view. One of the major questions is whether there exists a linkage between the North Atlantic and the Pacific, because the correlation between the signals at the North Atlantic and the North Pacific are quite weak(Deser, 2000; Ambaum et al., 2001; Itoh, 2002). We propose another way to check the validity and identify independent modes from a view point of statistical independence. The method, called "Independent Component Analysis(ICA)," is developed in the field of neuro-science and, now, it is widely used for multi-variate analysis(e.g. Hyvarinen and Oja, 2000). In principle, ICA differentiates independent components according to the shape of distribution function on the assumption that the probability of any natural independent component must be a non-Gaussian distribution, though the conventional EOF analysis relies on the amplitudes of the components. Applicability of ICA to artificial simple AO data proposed by Itoh(2002) is studied and the result is quite successful. Applying ICA to the real observed monthly-mean sea level pressure data(NCEP/NCAR reanalysis data), it is strongly suggested that AO is in fact a superposition of two statistically independent modes. In spite of the low correlation between the SLP data of the Atlantic and the Pacific, both two modes seem to have tight linkage between the two oceans. One of them corresponds to a saw-tooth-like relation between the intensities of the surface Aleutian and Icelandic lows(Honda et al., 2001); the relation accounts for most of the variation of AO(Honda and Nakamura, 2001). The other mode has in-phase relations between the two lows. A notable trend in the AO time series as noted in Thompson and Wallace(1998) and Thompson et al.(2001) may be a manifestation of this second mode that represents the recent long-term deepening of the two lows.

Wednesday, July 9 PM  
 Presiding Chairs: Y. Kosaka, M. Ogi

**MI05/09P/B17-001** Invited **1400**

**THE NAM AND PNA-LIKE PATTERNS AS A FRAMEWORK FOR INTERPRETING WINTERTIME LOW FREQUENCY ATMOSPHERIC VARIABILITY**

Roberta QUADRELLI, John M. WALLACE (Department of Atmospheric Sciences, University of Washington, Seattle)

The NAM and PNA-like patterns, as defined by the two leading EOF's of the monthly sea-level pressure field, together define a two-dimensional phase space that provides a framework for interrelating some of the more important patterns of Northern Hemisphere wintertime low-frequency variability. We show that these two modes have a significant influence on the atmospheric variability observed in the 1958-99 record over a range of frequencies. For example, they affect the occurrence of extreme cold events in 5 and 10-day mean temperature data. These two modes also have a strong impact on longer term variability. For example, they account for the most of the hemispheric sea level pressure and surface temperature trends observed during this period. The non-linear interactions between these modes, as well as their dependence on the mean state are also addressed. The ENSO cycle is shown to significantly affect the structure of the NAM on the intraseasonal timescale. Warm winters of the ENSO cycle account for a disproportionate share of the strong SLP and SAT trends observed during the past four decades.

**MI05/09P/B17-002** **1440**

**UNDERSTANDING ANNULAR VARIABILITY IN THE TROPICS**

David W.J. THOMPSON<sup>1</sup>, David LORENZ<sup>2</sup>(<sup>1</sup>Dept of Atmospheric Science, Colorado State University, <sup>2</sup>Dept of Atmospheric Science, University of Washington)

The Northern and Southern Hemisphere annular modes are associated with marked anomalies in the circulation of the tropics. Their high index polarity is characterized by westerly wind anomalies in the eastern tropical Pacific, and by negative temperature anomalies throughout the tropical troposphere with distinctive subtropical cooling maxima. The dynamics and climate impacts of the remote linkages are examined. It is argued that the tropical signature of the annular modes reflects the impact of waves propagating from the extratropical NH. Evidence is presented that suggests the tropical signature of the annular modes reflects a preferred pattern of variability of the tropical circulation.

**MI05/09P/B17-003** **1500**

**THE SYNOPTICS INDIVIDUAL PNA EVENTS**

Steven B. FELDSTEIN (EMS Environment Institute, The Pennsylvania State University)

The synoptic characteristics of individual PNA events are investigated by examining potential temperature on the nominal tropopause (the 2 potential vorticity unit surface). This variable is calculated from the NCEP/NCAR Reanalysis dataset for the winter season. Both PNA phases evolve from breaking synoptic scale waves. The wavebreaking is cyclonic for the positive phase, and anticyclonic for the negative phase. There are also differences in the longitude of the wave breaking for the two phases. For the positive phase, this wave breaking occurs off the Asian coast, and for the negative phase the wave breaking takes place off the west coast of North America. For both phases, it is the remnants of the breaking wave that comprise the optimal structure in the North Pacific which then evolves into the PNA teleconnection pattern. Throughout the wave breaking, North Pacific anomalies become increasing circular in spatial structure. These structural changes are followed by dispersion downstream over North America. These results are also compared with those of individual NAO events. The main similarities between the PNA and NAO are that both teleconnection patterns arise from the breaking of synoptic scale waves. Key differences include the much stronger dispersion and the relative absence of replenishing synoptic-scale waves for the PNA. Plausible explanations for these differences are presented.

**MI05/09P/B17-004** **1520**

**ATMOSPHERIC BLOCKING - A DYNAMICAL PERSPECTIVE ON CLIMATE MODES?**

Cornelia SCHWIERZ, Mischa CROSI MASPOLI, Huw C. DAVIES (Atmospheric and Climate Science, ETH Zuerich)

Persistent large-scale anomalies of the west to east flow in the mid-latitudes with a weakening and meridional splitting of the jet are specified as atmospheric blocking. Blocking anomalies significantly affect downstream weather and climate conditions. From a synoptic perspective blocked flow situations are long-lived (up to several weeks) and therefore singular strong events can determine a (monthly) climate index value (e.g. NAOI). The dynamical mechanisms contributing to the establishment, maintenance and breakdown of blocking are still not completely understood. Also, their prediction remains a major task for medium-range and seasonal forecasting and challenging feature under potential climate change. In an attempt to relate processes on synoptic and planetary scales, insight is sought here into the connection of the blocking phenomenon with the dominant planetary-scale patterns of

atmospheric variability as well as with relevant synoptic-scale processes. The investigation is conducted over the period 1979 to 2001 using ECMWF (re-)analysis data by applying both Lagrangian and Eulerian diagnostics. A potential vorticity (PV) perspective is adopted and blocking is regarded as persistent anomaly of low PV in the upper troposphere. Our analysis seeks to shed more light on the relative importance of Rossby-wave breaking and diabatic heating which both can modify the upper-level PV structures. Together the results provide novel synoptic insight into the dynamics of modes of atmospheric variability.

**MI05/09P/B17-005** **1610**

**STORM TRACKS AND PATTERNS OF CLIMATE VARIABILITY**

Brian HOSKINS<sup>1</sup>, Kevin HODGES<sup>2</sup> (<sup>1</sup>Dept. of Meteorology, University of Reading, <sup>2</sup>ESSC, University of Reading)

An objective feature tracking methodology has been applied to several of the recent re-analysis data sets to produce diagnostics of the NH winter storm tracks over the 79-present period. Many fields have been used and many diagnostics obtained to explore the effect of large scale patterns of variation on the storm tracks from the weather system perspective. The track ensembles have been stratified with respect to various teleconnection indices before the calculation of diagnostics such as track density and mean intensities which are the main diagnostics considered here. The calculation of the statistics makes use of the teleconnection indices in a more objective way than has been done in the past. The patterns considered are NAO, AO, PNA, Scandinavian pattern (SCN) and NINO3. The NAO and AO are found to produce very similar results. Their N Atlantic storm-track signatures are consistent with previous results and also highlight some new aspects. The PNA signatures are significant in the N Atlantic as well as in the N Pacific whilst the NINO3 signature is weak with only some coherence over the southern US which is also the only region that the NINO3 results have any correspondence with the PNA. Also considered is the impact of the stratospheric index of Baldwin and Dunkerton on the storm tracks and its relationship to NAO.

**MI05/09P/B17-006** **1630**

**THE TRANSITIONAL PROCESSES OF THE SOUTHERN HEMISPHERE ANNULAR MODE**

Hideo SHIOGAMA<sup>1</sup>, Toru TERAOKA<sup>2</sup>, Hideji KIDA<sup>3</sup>, Tatsuya IWASHIMA<sup>4</sup> (<sup>1</sup>Disaster Prevention Research Institute, Kyoto University, <sup>2</sup>Faculty of Informatics, Osaka Gakuin University, <sup>3</sup>Graduate School of Science, Kyoto University)

The effects of low- and high-frequency eddies (time scales longer and shorter than 10 days, respectively) on the transitional processes of the Southern Hemisphere annular mode are investigated, based on NCEP/NCAR daily reanalysis data for the period 1979-1999. At first, the poleward transitional processes are studied. Special attention is focused on the zonal asymmetry and temporal evolution of the eddy forcing. The effects of low-frequency eddies precede those of high-frequency eddies in driving the transitional events. The low-frequency eddies are regarded as quasi-stationary Rossby waves propagating along the polar jet, with wavelengths of 7000 km. The waves dissipate equatorward over the central and eastern Pacific Ocean, while they originally come from the Indian Ocean through the waveguide associated with the polar jet. This anomalous equatorward dissipation of wave activity induces an anomalous poleward momentum flux, which is responsible for changes in the polar jet over the Pacific Ocean during the beginning stage: the polar jet expands eastward and becomes separated from the subtropical jet over Australia and New Zealand. After the initial stage, momentum forcing anomalies due to high-frequency eddies rapidly appear. This forcing continues to drive the core of the polar jet poleward, while the low-frequency eddies have completed their role of inducing the anomalous poleward momentum flux during the earlier stage. Next, the equatorward transitional processes are examined. Special efforts are made to detect the precursors and the trigger processes of the equatorward transitional events. The well observed precursors of the transitional events are found to be positive height anomalies south of Australia. Those anomalies are associated with frequently observed blocking anticyclones. The transitional events are triggered by quasi-stationary Rossby waves with wavelength of 7000 km emitted by them. The wave activity of those Rossby waves propagates eastward along a waveguide over the Pacific Ocean. The forming and breaking of the Rossby waves over the Pacific Ocean directly disturb westerly circulation around Antarctica, kicking off the transitional events. After the start of the equatorward transitional events, high-frequency eddy forcing is responsible for the equatorward migration of the polar jet. These results make an important suggestion: the transitional processes of the Southern Hemisphere annular mode are essentially zonally asymmetric processes.

**MI05/09P/B17-007** **1650**

**THE ARCTIC OSCILLATION AS A RESPONSE TO TROPICAL FORCING**

Hai LIN, Jacques DEROME (Department of Atmospheric and Oceanic Sciences, McGill University)

A primitive equations dry atmospheric model is used to investigate the atmospheric response to a diabatic forcing that is linearly associated with the second EOF of SST in the tropical Pacific. Analysis is made for 51 winter seasons (DJF) from 1948/49 to 1998/99. For each winter a time-averaged model forcing is first calculated empirically from the NCEP/NCAR reanalyses. Regression coefficients of this forcing field upon the Principal Components (PC) of the second EOF of SST in the tropical Pacific are calculated. By multiplying the regression coefficients with yearly values of the PC, we obtain time series of the forcing anomalies at each grid point that represents a linear fit of the forcing to this tropical SST pattern. With this forcing anomaly for each winter, an ensemble of 30 integrations of 120 days are performed with different initial conditions. EOF analysis of the ensemble mean of the 90-day averaged SLP after a 30-day spinup shows that the leading mode of the forced variability resembles the Arctic Oscillation (AO), and its interannual variability is significantly correlated with that of the observed AO.

**MI05/09P/B17-008** **1710**

**OBSERVED INFLUENCES OF AMAZON RAINFALL ON NORTH ATLANTIC OSCILLATION AND THE WINTER CLIMATE OVER NORTH ATLANTIC AND ADJACENT CONTINENTS**

Rong FU, Mingxuan CHEN, Hui WANG (Georgia Institute of Technology)

We suggest based on an analysis of state-of-art satellite observations that a change of South American wet season rainfall can contribute to the NAO during boreal winter. Specifically, an increase of the South American rainfall is followed by stronger atmosphere circulation patterns associated with the NAO several days later. This influence occurs for both positive and negative phases of the NAO. This correlation is established on a synoptic time scale and after the Pacific influences on both regions are largely removed. Thus, it is not dominated by changes of sea surface temperature over Atlantic and atmospheric convection over tropical Pacific. The maximum correlation coefficients between NAO index



and lagged anomalous South American rainfall by 2-7 days are much stronger than those leading the latter. The upper troposphere streamfunction anomalies lagging the anomalous South American rainfall as shown to resemble those simulated by a time-dependent barotropic model, so apparently are carried by the latitudinal propagation of Rossby waves in the upper troposphere. An influence function analysis also suggests that effect of the anomalous South American rainfall on the extratropical North Atlantic and neighboring continents is about a half of that exerted by disturbances over the North Pacific-North American region.

**MI05/09P/B17-009** **1730**  
**INTRASEASONAL INFLUENCES OF TROPICAL CIRCULATIONS ON THE NORTHERN ANNULAR MODE**

Shuntai ZHOU, Alvin J. MILLER (NOAA/NCEP/Climate Prediction Center)

Based on 21 northern hemisphere winter-spring seasons (1979-1999) of pentad data, including outgoing longwave radiation, zonal wind, velocity potential, etc., tropical and extratropical interactions on the intra-seasonal time scale are studied in the context of the Arctic oscillation (AO) and the Madden-Julian Oscillation (MJO). By using a similar terminology to the AO, a high (low) MJO phase is defined as that strong (suppressed) convective activity over the Indian Ocean. It is shown that the high (low) AO phase occurs more frequently in the high (low) MJO phase. The AO pattern of sea level pressure anomaly is subtly affected by the MJO. When the AO and the MJO are in the same phase, the Atlantic action center becomes much weaker. When the AO and the MJO are in opposite phase, the Pacific action center becomes weaker and even broken apart. The coupling or decoupling of the two modes has different influences on the weather anomalies, such as surface air temperature and precipitation, downstream of the MJO activity. In the upper troposphere, the east-west oscillations of tropical and subtropical systems regulate local eddy momentum flux either poleward or equatorward, which may affect the phase of the northern annular mode.

**Thursday, July 10 AM**  
 Presiding Chairs: E.-J. Cha, M. Baldwin

**MI05/10A/B17-001** **Invited** **0830**  
**SOME ISSUES IN STRATOSPHERE-TROPOSPHERE COUPLING**

Theodore G. SHEPHERD (Department of Physics, University of Toronto)

There has been considerable recent interest in the possibility that stratospheric variability may significantly affect tropospheric variability. Given the rapid timescale of the apparent linkages, any such stratosphere-troposphere coupling must be essentially dynamical in nature. Possible mechanisms that could lead to such coupling will be described, and the current evidence from both observations and idealized modelling studies reviewed. The emphasis will be on developing testable hypotheses to identify well-defined mechanisms, assess their robustness, and quantify their significance.

**MI05/10A/B17-002** **0910**  
**PREDICTABILITY OF THE ARCTIC OSCILLATION**

Mark P. BALDWIN<sup>1</sup>, David B. STEPHENSON<sup>2</sup>, Timothy J. DUNKERTON<sup>3</sup>, David W.J. THOMPSON<sup>4</sup>, Andrew J. CHARLTON<sup>2</sup>, Alan O'NEILL<sup>1</sup> (<sup>1</sup>Northwest Research Associates, <sup>2</sup>University of Reading, <sup>3</sup>Colorado State University)

We use an empirical statistical model to demonstrate significant skill in forecasts of the monthly-mean Arctic Oscillation (AO). Forecast skill derives from long-lived circulation anomalies in the lowermost stratosphere and is greatest during the winter season. A comparison to the Southern Hemisphere, together with modeling evidence, indicates that both the timescale and predictability of the AO depend on the presence of long-lived circulation anomalies just above the tropopause. These circulation anomalies appear to affect the troposphere through a mechanism involving changes to synoptic-scale and planetary-scale waves in the upper troposphere, which induce surface pressure changes corresponding to the AO. We find that the timescale of the AO is much longer during winter than in other seasons and we hypothesize that this longer timescale is related to both the size and persistence of Northern Annular Mode (NAM) anomalies in the lowermost stratosphere, and is not caused primarily by tropospheric processes or an enhanced annual cycle. Under this hypothesis NAM anomalies in the stratosphere are caused mainly by upward-propagating planetary scale waves of tropospheric origin, which interact with the stratospheric flow. We use linear regression, based on the present values of the NAM in the troposphere and stratosphere, to predict the monthly-mean AO 10-40 days in the future. The long timescale of the AO during winter provides some forecast skill simply from persistence, but we find that best forecasts use the NAM in the lowermost stratosphere (150 hPa). Forecasts that use stratospheric NAM values and account for ~20% of the variance of the monthly-mean AO during December - February and substantially better than AO forecasts based on persistence. The effect of NAM anomalies in the lowermost stratosphere is to cause a bias toward tropospheric NAM anomalies of the same sign. On average the AO during winter tends to be of the same sign as the NAM in the lowermost stratosphere. The AO time series during winter can be viewed as a linear combination of short-time scale tropospheric processes (with an autocorrelation function similar to that seen outside the winter season) and the 150-hPa NAM (which has a much longer time scale). Our results also have implications for numerical extended-range weather forecasting. Forecast models that do not resolve the stratosphere (or that do not have realistic NAM anomalies in the lowermost stratosphere) will likely not be able to simulate the stratosphere-troposphere coupling and the effect on the AO. On longer timescales, our hypothesized mechanism would presumably allow stratospheric signals (e.g., greenhouse gas and ozone changes, solar/UV variations, and the quasi-biennial oscillation) to affect surface climate. Observations show that in both hemispheres that stratospheric and tropospheric annular mode time series are correlated on interannual timescales, and our results provide a mechanism for trends in the stratospheric NAM to be reflected in the AO index.

**MI05/10A/B17-003** **0930**  
**PROBABILISTIC SEASONAL FORECASTS OF THE NORTH ATLANTIC OSCILLATION INDEX**

Christof APPENZELLER, Wolfgang MUELLER, Mark Andrea LINIGER (Federal Office of Meteorology and Climatology (MeteoSwiss))

The North Atlantic Oscillation (NAO) explains a substantial part of the inter-annual variability in European winter climate. In this work the seasonal forecast system II of the European Centre for Medium Range Weather Forecast (ECMWF) was used to examine the skill of NAO predictions and its impact on European temperature. The system used was a fully coupled ensemble prediction system consisting of 40 operational ensembles members and a

hindcast database covering the period 1987 to 2001. The results were interpreted in terms of the ensemble median and in probabilistic space using the ranked probability skill score. First the leading mode in the model climate hindcast data was defined by an EOF analysis of the DJF mean z500 geopotential field. The spatial structure found agrees favourably with the observed NAO pattern. The seasonal NAO Index forecasts were calculated by regressing the observed pattern to each ensemble member. Correlation between the predicted ensemble median and the observed index reach weakly significant values for the first 3 integration months and subsequently decrease to non significant values. The skill based on the ranked probability measure suggests a prediction benefit of about 15% for forecasts started in December. Predictions started in September show no benefit relative to the climatology. The spatial impact of the NAO on the European 2 metre temperature distribution was also recovered in the hindcast data. Although the skill of the grid point based forecasts is low in the extra-tropics, it seems that weakly positive skills are collected in coherent areas of maximum NAO correlation. Finally the potential predictability of the NAO within the probabilistic framework of the RPSS was examined.

**MI05/10A/B17-004** **0950**  
**ROLE OF THE POLAR-NIGHT JET OSCILLATION ON THE FORMATION OF THE ARCTIC OSCILLATION IN THE TROPOSPHERE**

Yuhji KURODA, Kunihiko KODERA (Meteorological Research Institute)

Slow variability of the zonal wind, characterized by the poleward and downward movement of the zonal-mean zonal wind and called the Polar-night Jet Oscillation (PJO), is known to exist in winter stratosphere. On the other hand, in the troposphere of the northern hemisphere, hemispheric variability known as the Arctic Oscillation (AO) exists. Though these are different mode of variability, there appears strong interaction between these two modes in winter of northern hemisphere. Downward propagation of the annular mode (AM) signal from the stratosphere to surface is such example. We have examined from the observational data, how the PJO and AO are related each other in the northern winter. It is shown that the AO of specific phase preferably appears corresponding with the appearance of the PJO of specific phase. It is also found that the AO tend have longer life time when the coupled PJO have sufficiently large amplitude. Although there are some exceptions, these results suggest the existence of strong interaction between the stratospheric variability (PJO) and the AO. To see how the PJO influence the polarity of the AO, we have examined the change of the E-P flux, wave forcing and the meridional circulation due to the time evolution of the PJO. It is suggested that the change of the zonal wind in the lower stratosphere due to the PJO and the resultant change of the wave propagation and the formation of the wave forcing in the upper troposphere around 60N are keys for the formation of the AO.

**MI05/10A/B17-005** **1040**  
**SIMULATING THE SOUTHERN ANNULAR MODE RESPONSE TO STRATOSPHERIC OZONE DEPLETION**

Nathan Peter GILLET<sup>1</sup>, David THOMPSON<sup>2</sup> (<sup>1</sup>School of Earth and Ocean Sciences, University of Victoria, Canada, <sup>2</sup>Department of Atmospheric Sciences, Colorado State University, USA)

Recent observations indicate that climate change over the high latitudes of the Southern Hemisphere is dominated by a strengthening of the circumpolar westerly flow that extends from the surface to the stratosphere. Here we demonstrate that both the seasonality and structure of the observed climate trends are simulated in a state-of-the-art climate model run with high vertical resolution that is forced solely with prescribed stratospheric ozone depletion. As in observations, the modelled tropospheric response reflects a shift in the Southern Hemisphere annular mode towards stronger circumpolar westerly flow that peaks several months after the most pronounced ozone depletion.

**MI05/10A/B17-006** **1100**  
**THE ROLE OF LARGE-SCALE TOPOGRAPHY IN THE NORTHERN HEMISPHERE ANNULAR MODE**

Koji YAMAZAKI<sup>1</sup>, Atsushi OGASAWARA<sup>1</sup>, Rui NAKAZAWA<sup>2</sup>, Hitoshi MUKOUGAWA<sup>3</sup> (<sup>1</sup>Graduate School of Environmental Earth Science, Hokkaido University, <sup>2</sup>Hewlett-Packard Japan, Ltd., <sup>3</sup>Disaster Prevention Research Institute, Kyoto University)

Effects of large-scale topography on the Arctic Oscillation (AO) or the NH annular mode are examined using an atmospheric general circulation model under the perpetual January condition. Four experiments are done with and without North American orography and Eurasian orography. All experiments show a AO-like variation pattern as the first EOF of the 30-day mean sea level pressure field of the Northern Hemisphere. The AO in Himalaya experiment which includes only Eurasian orography is the most dominant and that in No-mountain experiment is the least. The teleconnectivity analysis reveals that the teleconnectivity over the Atlantic, i.e., the North Atlantic Oscillation (NAO), is robust in all experiments. Connection between the troposphere and the stratosphere is strong in Control and Himalaya experiments, while it is weak in other two experiments. This indicates that planetary waves generated by large-scale topography, especially by Eurasian topography, are indispensable for the troposphere-stratosphere connection. Overall, the Himalaya experiment shows similar variability to the Control run, probably because the climate in the Himalaya experiment reasonably simulates Icelandic and Alutian lows, while Rockies experiment and No-mountain experiments show a poor simulation for these lows.

**MI05/10A/B17-007** **1120**  
**LIFE CYCLE OF NORTHERN HEMISPHERE STRATOSPHERIC POLAR WARMING**

Varavut LIMPASUVAN<sup>1</sup>, David W.J. THOMPSON<sup>2</sup> (<sup>1</sup>Coastal Carolina University, <sup>2</sup>Colorado State University)

The present observational study examines the dominant structure of the atmospheric flow and wave fluxes related to the climatological life cycle of stratospheric sudden warming in the Northern Hemisphere. Following the pre-conditioning of the polar stratosphere, poleward heat and momentum flux anomalies (of mainly zonal wavenumber 1) in the upper stratosphere greatly intensify as wave activity is confined over the pole and the vortex weakens. Stratospheric wave activity significantly declines when the vortex eventually recovers. Through wave-mean flow interactions, zonal wind, temperature, and geopotential height anomalies over the pole exhibit downward descent from the upper stratosphere during the vortex's demise. As these anomalies reach the upper troposphere, significant growth of anomalous equatorward momentum flux and anomalous poleward meridional flow occurs near 300 hPa. Concurrently, anomalous equatorward meridional flow increases near the surface. Associated mainly with zonal wavenumber 3 and greater disturbances over the North Atlantic, the equatorward momentum flux anomalies and corresponding wave forcing promote amplification of the negative Northern Hemisphere Annular Mode (NAM) phase during which the entire atmospheric flow becomes dominated by zonal symmetry. The accompanying meridional winds are results of anomalous mean meridional circulation that

maintains zonal wind anomalies near the surface. Overall, a 15-day day lag exists between greatest polar warming at 10 hPa and strongest negative NAM index.

**MI05/10A/B17-008 1140**

**VERTICAL STRUCTURES OF ANNULAR-MODE VARIABILITY AND THE CONTRASTING ROLES OF EDDY MOMENTUM AND HEAT FLUXES**

Timothy J. DUNKERTON, Mark P. BALDWIN, David A. ORTLAND (NorthWest Research Associates)

Lag-zero regression of Eulerian mean meridional circulation with respect to the annular-mode index of surface pressure demonstrates that this circulation opposes the mean-flow anomaly in the upper troposphere and stratosphere, implying that eddy fluxes are responsible for maintenance of the annular mode, as first suggested by Thompson and Wallace. The sense of induced circulation responsible for the transport of mass is nevertheless consistent with the surface pressure anomaly over the polar cap. This 'static' picture of annular-mode anomalies of mean flow, induced circulation and surface pressure -- with troposphere and stratosphere apparently acting in concert -- can be uniquely explained by eddy momentum fluxes. More detailed examination of observations and model simulations demonstrates a richer spectrum of annular-mode behavior variously characterized by in-phase, delayed, and out-of-phase relationships between tropospheric and stratospheric anomalies. An out-of-phase relationship is uniquely explained by eddy heat fluxes, representing a flux of wave activity from troposphere to stratosphere, or vice versa. According to the theorem of Charney and Drazin, vertical fluxes of wave activity into the stratospheric polar vortex are limited to the gravest zonal wavenumbers of planetary scale. On the other hand, synoptic-scale waves contribute significantly to the horizontal flux of wave activity in the troposphere. The role of synoptic-scale waves in amplifying and maintaining the tropospheric annular-mode anomaly is discussed. At times when anomalies in the troposphere and stratosphere are coupled via planetary-wave propagation, as in winter, the synoptic-scale waves may play an important, if not essential, role in producing the predominant 'in-phase' relationship of anomalies in the two layers.

**MI05/10A/B17-009 1200**

**INTERANNUAL VARIATIONS OF PLANETARY WAVE ACTIVITY IN THE NORTHERN HEMISPHERE WINTER AND THEIR RELATIONS TO THE NAM AND SST**

Wen CHEN<sup>1</sup>, Masaaki TAKAHASHI<sup>2</sup>, Hans-F. GRAF<sup>3</sup> (<sup>1</sup>Institute of Atmospheric Physics, Chinese Academy of Sciences, <sup>2</sup>CCSR, University of Tokyo, <sup>3</sup>Max-Planck-Institute for Meteorology)

With NCEP-NCAR reanalysis data from 1958 to 1998, two teleconnection patterns in the EP flux divergence field due to planetary waves with wavenumbers (WNs) 1 to 3 were studied in the Northern Hemisphere winter. After the data are detrended by subtraction from linear trends, the interannual variations indicate that both appear as dipole structures with divergence of EP flux in the north and convergence in the south, or vice versa. One dipole evolves mainly in the stratosphere and is referred to as the stratospheric interannual oscillation (SIO). The other evolves mostly in the troposphere and is referred to as the tropospheric interannual oscillation (TIO). The TIO and the SIO are shown to be associated with anomalous meridional planetary wave propagation in the troposphere and stratosphere, respectively. Meanwhile the upward and poleward refraction of planetary waves into the polar waveguide across the tropopause is shown to be closely linked to the meridional propagation of planetary waves in the troposphere. Examination of individual waves indicates that the tropospheric dipole of EP flux divergence comes basically from WN 3, whereas the stratospheric one comes totally from WNs 1 and 2. And the reduced refraction of planetary waves into the polar waveguide across the tropopause associated with positive TIO index is dominantly contributed from both WNs 1 and 2. Regression and correlation analyses suggest that the TIO is mainly an internal mode of the atmosphere and is closely related to the Northern Annular Mode (NAM). In the winter, this atmospheric process has a significant influence on the sea surface temperature (SST). The regressed SST upon the TIO index exhibits clearly a sandwich pattern in the North Pacific and a tripole pattern in the North Atlantic, and these patterns can persist to the following season especially in the North Atlantic. On the other hand, the SIO is shown to be closely associated with anomalous zonal mean winds in the subtropics of the mid-upper stratosphere and has a moderate correlation with an augmented PNA pattern in 500hPa geopotential height. Significant correlation of SIO with tropical SST (basically the ENSO pattern) reveals that tropical SST is leading the SIO by up to around 9 months, which suggests a strong impact of ENSO on the SIO. Planetary waves tend to be bent poleward (equatorward) in the middle and upper stratosphere when there is a warm (cold) event.

Thursday, July 10 PM

Presiding Chairs: J. Cherry, I. Mares

**MI05/10P/B17-001 Invited 1400**

**A NEW INTERPRETATION OF THE PACIFIC SOUTH AMERICAN PATTERN AND ITS ROLE IN ENSO TELECONNECTIONS**

Carlos Roberto MECHOSO<sup>1</sup>, Andrew W. ROBERTSON<sup>2</sup>, Gabriel Cazes BOEZIO<sup>3</sup> (<sup>1</sup>Department of Atmospheric Sciences, University of California, Los Angeles, USA, <sup>2</sup>International Research Institute for Climate Prediction, Palisades, New York, USA)

Studies of the Southern Hemisphere extratropics based on Empirical Orthogonal Functions (EOFs) have found in the South Pacific structures that are referred to as the Pacific South American (PSA) patterns by similarity with the well-know Pacific North American pattern. There are two PSAs corresponding to the leading EOFs: PSA1 and PSA2. The phases of PSA1 and PSA 2 are approximately in quadrature, which has led to the suggestion that they represent a propagating wave. It is argued that this suggestion is not supported by analyses of observational data for the South Pacific in view of quasi-stationary circulation regimes and of oscillatory behavior. One of the regimes has a structure that consists of a meridionally elongated ridge centered near 110oW flanked by troughs to the west and east, thus resembling PSA1. Other regimes resemble the opposite phase of PSA1 and PSA2. It is shown that during southern spring, the frequency-of-occurrence of the PSA1-like regime and that of its opposite are positively correlated with the warm and cold phases of ENSO, respectively. Therefore, it is proposed that PSA1 and PSA2 represent nearly stationary circulation regimes, of which the former is associated with ENSO and the latter is not. It is further conjectured that the impact of ENSO over southern South America is through the preference for development of particular nearly stationary circulation regimes over the South Pacific and downstream effects associated with the regime evolution.

**MI05/10P/B17-002 1440**

**DYNAMIC RELATIONSHIP BETWEEN THE ANOMALIES OF THE ZONAL AND MERIDIONAL WINDS IN THE LOWER TROPOSPHERE OVER THE WESTERN EQUATORIAL PACIFIC DURING THE EL NINO ONSET PERIOD**

Kyung-On BOO, Gyu-Ho LIM (School of Earth and Environmental Sciences, Seoul National University)

Westerly wind anomalies over the western equatorial Pacific (WEP) during boreal winter and spring are known as an important indicator related to the onset of El Niño (EN) events. Comparing the evolutions of zonal wind anomalies over the WEP and Niño-3 SSTA, it is evident that the positive SSTA is closely related to westerly anomalies over the WEP by a time lag of almost three months with the maximum correlation lag of 0.51. These westerly anomalies which are an element of the monsoon circulation of the Asia-Australian region are attributed to the frequent appearance of the energetic active westerly wind occurrence. Therefore, the horizontal wind anomalies originated from the monsoon system revealed to be related to the SST evolution over the Pacific Ocean and determine the onset time of EN events. Here there was a previous document suggested as the precursor of the westerly anomalies strengthening the condition that northerly anomalies from the western North Pacific converge with southerly anomalies from the northeast coast of Australia. But the study did not deal with the detailed dynamical structure of the circulation itself. So, we aim to examine the dynamic relationship between the zonal and meridional wind anomalies over the WEP at 850 hPa and investigate whether the meridional convergent flows tend to increase the westerly anomalies or not. The datasets are the monthly mean 850 hPa wind, geopotential height, the sea surface temperature field derived from the NCEP/NCAR reanalyses data with a horizontal resolution of 2.5° x 2.5°. To estimate the dynamic balance, we evaluate the zonal momentum budget based on the monthly mean values of wind and geopotential anomalies relative to the climatological annual cycle. Then composite map is constructed by calendar month from February (0) to July (0) during the EN onset year 1965, 1972, 1982, 1991, and 1997. From our results, the coriolis force as well as zonal momentum flux convergence decrease the westerly anomalies driven by the pressure gradient force. The easterly acceleration increased in proportional to the speed of the meridional wind anomalies. That is, meridional wind anomalies emanating from the monsoon system are apparently related to the EN onset. But the meridional wind anomalies are formed to maintain dynamic balance in response to the zonal wind anomalies development rather than intensify the westerly anomalies.

**MI05/10P/B17-003 1500**

**SEASONAL CYCLE AND EL NIÑO TERMINATION**

Gabriel Andres VECCHI<sup>1</sup>, D.E. HARRISON<sup>2</sup> (<sup>1</sup>JISAO, University of Washington, <sup>2</sup>NOAA/PMEL/OCRD)

We explore the processes that lead to the termination of El Niño events, and propose a mechanism in which the seasonal cycle of solar heating drives changes in the meridional location of anomalous winds, resulting in the end of the events. The focus is on the 1997-8 El Niño event, as well as on comparing that event to others in the historical record, developing a generalized mechanism for El Niño termination, and applying the generalized mechanism to the current 2002-3 El Niño event. The characteristics of El Niño termination are explored using satellite, in situ and operational model data; and the impact of the proposed mechanism is tested using an ocean general circulation model (OGCM). The termination of the 1997-8 El Niño event was characterized by strong changes in the meridional structure of the wind and convective anomalies, corresponding to the seasonal evolution of solar heating. These meridional changes - though not incorporated in the dominant published mechanisms for El Niño phase transition - drove oceanic changes that resulted in the characteristic termination of the 1997-8 El Niño event. Similar changes in the meridional structure of anomalies, associated with the seasonal migration of maximum solar insolation, have been evident in every El Niño on record. These results suggest that the interaction between the seasonal cycle of solar heating and anomalous conditions during El Niño events is fundamental to their termination. We have developed a generalized conceptual theory of the role of the seasonal cycle in El Niño termination. This new mechanism for El Niño termination argues that the phase transition from warm to normal conditions in the tropical Pacific results from forcing external to the coupled ocean-atmosphere system, thus - in this view - El Niño is an event. The effect of the seasonal cycle on El Niño termination is evident in the evolution of the 2002-3 El Niño event, and suggests strong predictability of the termination of El Niño events once they are underway.

**MI05/10P/B17-004 1520**

**1997-98 EL NINO AND THE INDIAN MONSOON: A CASE STUDY**

Sooraj K. P. Rajan C.K. (Dept. of Atmospheric Sciences, Cochin University of Science and Technology)

The World Meteorological Organisation reported that the 1997-1998 El-Niño was the strongest of the 20th century. The estimated average surface temperature for land and sea worldwide was 0.80F (0.4oC) higher than the 1961-1990 average of 61.7°F (16.50C). 1998's temperature anomaly of 1.2°F (0.70C), above the long-term (since 1880) mean of 56.9°F (13.830C), is the 20th consecutive year with an annual global mean surface temperature higher, than the long-term average. Based on this fact, a case study has been carried out for the monsoon season of 1998, by analyzing parameters such as Total Precipitable Water Vapour (TPW), Sea Surface Temperature (SST) and wind (Ocean Surface) over the Indian Ocean using the Tropical Rainfall Measuring Mapping- Microwave Imager (TMI)(1998-2002) data to get the effect of this, on these parameters. In situ measurements and recent satellite data have revealed that the Bay of Bengal (BOB) exhibits large-amplitude variations in SST on subseasonal timescales (Bhat et al., 2001; Hareesh Kumar et al., 2001; Vecchi and Harrison, 2002). These SST variations occur in association with changes in monsoon circulation. In connection with this, time series of space averaged SST over the BOB and Arabian Sea (AS) is analysed. While the SST over AS shows no well-marked oscillation, BOB SST exhibits a prominent 10-12 days oscillation. Hovmuller diagram of SST in the longitudinal belt of 60-75E is used to get SST distribution and hence in turn meridional gradient. During the initial stages of the monsoon onset, the diagram exhibits a strong meridional gradient over the AS, while over the BOB (80-90E) belt, the diagram reveals a weak north-south gradient. It is also observed that the convection forms over an area, where SST had large north-south gradient, as suggested by Lidzen and Nigran (1987). Anomaly of 1998 SST (from 1998-2002 SST climatology) is also plotted to see the SST behaviour. It is inferred that the anomalous rise of SST may be due to the 1997-98 El Niño. Time series of space averaged TPW over the AS shows the existence of a well-marked oscillation of 10-12 days and 30-40 days. It also appeared on the surface wind. The cycle around 30-40 days shows the active/break cycle of the monsoon. This oscillation propagates northward towards India, after originating from the Equatorial Indian Ocean. It is also suggested that this cycle might be related to the date of onset of the monsoon. The former cycle appears to be associated with a westward propagating mode north of the equator.



**MI05/10P/B17-005 1610**

**INTER EL NIÑO/SOUTHERN OSCILLATION (ENSO) VARIABILITY IN THE SUBTROPICAL AMERICAS**

Tercio AMBRIZZI<sup>1</sup>, Victor MAGANA<sup>2</sup> (<sup>1</sup>Department of Atmospheric Sciences, University of Sao Paulo, <sup>2</sup>Center for Atmospheric Sciences, National Autonomous University of Mexico)

During boreal winter, the occurrence of El Niño/Southern Oscillation (ENSO) reflects an enhanced precipitation in various regions of the Americas. Anomalous convective activity in the central-eastern Pacific forces quasi-stationary Rossby waves following paths to North and South America. The so-called Pacific-North American (PNA) pattern forces a southward shift in the mean position of the subtropical jet, as well as ascending motion and enhanced precipitation over California and around the Gulf of Mexico. From December through February a weak quasi-stationary wave train is observed over southeast South America, resulting in enhanced precipitation around southern Brazil, northern Argentina and Uruguay. Finally, in Central America and northeast Brazil, the effects of enhanced subsidence associated with ENSO inhibit the development of deep convection and produce precipitation deficit and drought. Changes in the phase and amplitude of the quasi-stationary Rossby waves over the subtropical Americas from one ENSO event to another result in inter El Niño variability. Ray tracing analyses were performed and they showed how the characteristics of quasi-stationary waves are mainly affected by the structure of the mean flow. However, numerical experiments with a baroclinic model indicate that the location and horizontal structure of the anomalous convective forcing in the central Pacific may also affect the phase and amplitude of these quasi-stationary circulations. Using output from the NCAR Community Climate Model (CCM3), forced with observed monthly sea surface temperatures, it is shown that errors in simulations of the mean flow affect the phase of the quasi-stationary waves and result in poor long-term precipitation predictions during El Niño boreal winters. The importance of these analyses for long term predictions of regional climate in the subtropical Americas is discussed.

**MI05/10P/B17-006 1630**

**RECENT CLIMATIC CYCLES IN ASIAN SOUTHWESTERN-MONSOON REGION AS INDICATED BY THE SPECTRUM ANALYSIS OF DIFFERENT CLIMATE DATA**

Zhonglin ZHANG, Yuanqing HE, Hongxi PANG (Cold and Arid Regions Environmental and Engineering research Institute, Chinese Academy of Sciences)

Observed temperature and precipitation in China and India, ice core records, tree ring index and other proxy data has been used for spectrum analysis, to recover different scale of climatic cycles in Asian southwestern monsoon region including southeastern Tibetan plateau and northern India during the recent 400 years. Some parameters, such as the regional climate and topography conditions, sea surface pressure, the earth surface temperature ENSO events, have been considered for the analysis. The results indicate that there are apparent temporal and spatial variations of the monsoon intensity in the southwest-monsoon system, with different scale cycles. There is an apparent 2-3 year periodic change for temperature, with a similar pattern in different parts of whole region. However, precipitation varies more complexly, in 2-3 years, the shortest sub-cycle, 10-11 years and 22 years, and with non-uniform pattern in the region, corresponding to the periodic solar activities, special events on earth's surface, varied atmospheric circulations and vapor sources. Some drought and wet stages are evident in the analyzed sequences. In addition, analyzed results suggest that the study region are influenced not only by the southwest monsoon from Indian Ocean, the major source for precipitation, but also by the westerly circulation especially in winter and the southeast monsoon from the Pacific with partial vapor. Accordingly, the relation between temperature and precipitation is unclear.

**MI05/10P/B17-007 1650**

**WHY DOES EL NIÑO EVENT OCCUR IN APRIL 2002**

Xuexiang YANG<sup>1</sup>, Zhen CHEN<sup>2</sup>, Dianyou CHEN<sup>3</sup>, Qiyuan QIAO<sup>4</sup> (<sup>1</sup>Department of Geo-exploration, University of Jilin University, <sup>2</sup>Department of Computer, University of Jilin University, <sup>3</sup>Department of Mathmas, University of Jilin University, <sup>4</sup>2. National Astronomical Observatory, Chinese Academy of Science, Beijing100012, P. R. China)

The closed North Pacific Ocean and opened South Pacific Ocean are the tectonic basis of El Niño. It makes thermal energy amass in the North Pacific Ocean and disappear in the South Pacific Ocean. The harmonious effect caused by strong tide is the excitation mechanism of El Niño. Strong tide can increase the horizontal mixing of the seawater, drawing warm seawater from the North Pacific Ocean to the South Pacific Ocean. When the sun, the moon and the earth are in a line, and the moon is at perigee, tidal is the strongest and El Niño would occur at the time. It is shown by the calculation that half day tide caused by the moon at the equator makes the troposphere, hydrosphere and liquid core move westwards around the solid earth at the volumes of 54181864, 43257, and 3103 km<sup>3</sup> respectively. Moreover, the lithosphere and lower mantle expand and contract with volumes of 2745 km<sup>3</sup> and 10599 km<sup>3</sup> respectively. These are the driving forces for partial melting mass to flow, swell up and erupt. The sway of the sun between the tropic of Capricorn and Cancer relative to the earth results in the vibration and mixing of fluid in the south and north direction relative to the solid. The flattening of the earth is in its maximum status at vernal equinox and autumnal equinox. At the time, the strongest equator tide is formed and the air, seawater and fluid from the core liquid at high latitude area and two poles areas move towards equator through the critical latitude (35°) with their volume 6605998, 5251 and 368 km<sup>3</sup> respectively. There are 6-8 months from strong tide to weak tide. Solar eclipse and moon eclipse make it stronger. Since 1980, the two strongest El Niño events occurred in 1982-1983 and 1997-1998, and in both the amplitudes of interannual variation in day-length change and tidal strength change were larger. Using astronomical data, strong tide and El Niño will occur in end of April 2002 and develop in September 2002. The strongest El Niño from 1982-1983 and from 1997 to 1998 make Ozone Hole over the South Pole expand and the El Niño in 2002 will make the South Pole Ozone Hole expand in September, too. In front and behind of El Niño event, the oceanic water in East Pacific Ocean and West Pacific Ocean may rise or fall 40cm oppositely, which make oceanic crust fall or rise 13cm. It is the reason that El Niño events are interrelated with the earthquakes and volcanoes. This phenomenon is just like "seesaw". This paper is supported by National Natural Science Fund of China(No.49774228).

**MI05/10P/B17-008 1710**

**ENSO SIGNATURE IN NORTH EUROPEAN TIME SERIES OF ICE CONDITIONS DETECTED BY SINGULAR SPECTRUM ANALYSIS AND WAVELET TRANSFORM**

Svetlana JEVREJEVA<sup>1</sup>, John Christopher MOORE<sup>2</sup>, Aslak GRINSTED<sup>3</sup> (<sup>1</sup>Proudman Oceanographic Laboratory, Birkenhead, UK, <sup>2</sup>Arctic Centre, University of Lapland, Rovaniemi, Finland)

Variability in long-term time series of ice conditions in the Baltic and Barents Seas is examined within the context of atmospheric circulation. The study involves analysis of both

modern (instrumental), historical and proxy data covering 300 years and application of new advanced statistics techniques - Monte Carlo Singular Spectrum Analysis (MC-SSA) and Wavelet Transform (WT) to these climatological time series. We develop methods of assessing statistical significance and confidence intervals of crosswavelet power and wavelet coherence phases. Crosswavelet power for the time series indicates that the times of largest variance in ice conditions are in excellent agreement with significant power in the AO at 2.2-3.5, 5.7-7.8 and 12-20 year periods, similar patterns are also seen with the Southern Oscillation index (SOI) and Niño3 sea surface temperature (Niño3) series. Wavelet coherence shows in-phase linkages between the 2.2-7.8 and 12-20 year period signals in both tropical and Arctic atmospheric circulation and also with ice conditions in the Baltic and Barents Seas. These results are consistent with GCM simulations showing dynamical connections between high latitude surface conditions, tropical oceanic sea surface temperatures mediated by tropical wave propagation, the wintertime polar vortex and the AO, and with models of sea ice and oceanic feedbacks at decadal periods.

**MI05/10P/B17-009 1730**

**BIENNIAL AND LOWER-FREQUENCY VARIABILITY IN THE MERIDIONAL FLUCTUATION OF BAIU FRONT**

Tomohiko TOMITA<sup>1</sup>, Takao YOSHIKANE<sup>2</sup>, Tetsuzo YASUNARI<sup>3</sup> (<sup>1</sup>Department of Environmental Science, Faculty of Science, Kumamoto University, <sup>2</sup>Frontier Research System for Global Change, Institute for Global Change Research, <sup>3</sup>Hydropheric Atmospheric Research Center, Nagoya University, <sup>4</sup>Institute of Geoscience, University of Tsukuba)

The interannual meridional fluctuation of Baiu front and the related large-scale circulation are examined using empirical orthogonal function (EOF) analysis and composite or correlation analyses based on the EOF time coefficients. The first EOF mode, which explains 37.8% of the total variance, indicates the low-frequency fluctuation with a period of four to five years (LF mode) appearing to the south of 35°N. The development is concurrent with the horseshoe SST anomalies (SSTAs) in the entire tropical Pacific that are associated with the El Niño/Southern Oscillation (ENSO). The most west SSTAs control the anomalous southward expansion of Baiu front in the LF mode through the modification of convection around 20-30°N in the western Pacific. On the other hand, the second EOF mode explaining 32.5% is characterized by the meridional seesaw-like fluctuation with a node around 28°N and by the timescale of biennial oscillation (BO mode). The SSTAs again show the horseshoe pattern but with the different spatial phase in the tropical western Pacific. The teleconnection similar to the Pacific-Japan pattern controls the meridional seesaw fluctuation of anomalous Baiu precipitation, in particular, through the convection along 20°N in the western Pacific. The anomalies associated with the BO mode tend to appear in the tropical western Pacific, while the signals of LF mode rather expand in the entire basin, suggesting that the biennial oscillation is the aborted ENSO confined in the western Pacific.

**MI05-Posters Thursday, July 10**

**LARGE SCALE PATTERNS OF ATMOSPHERIC VARIABILITY: DYNAMICS, CLIMATE IMPACTS, AND ROLE IN RECENT CLIMATE CHANGE (ICCI)**

Location: Site D

Thursday, July 10 PM

**MI05/10P/D-001 Poster 1400-167**

**THE CONNECTIVITY OF WINTERTIME NORTH ATLANTIC OSCILLATION (NAO) WITH SUMMERTIME ATMOSPHERIC AND OCEANIC CONDITIONS**

Masayo OGI<sup>1</sup>, Yoshihiro TACHIBANA<sup>2</sup>, Koji YAMAZAKI<sup>1</sup> (<sup>1</sup>Graduate School of Environmental Earth Science, Hokkaido University, <sup>2</sup>International Arctic Research Center, Frontier Research System for Global Change/Liberal Arts education Center, Tokai University.)

It is widely known that the North Atlantic oscillation (NAO) is closely related to the wintertime surface air temperature field over the Eurasian continent. We investigate the persistency of the temperature anomaly from winter through following summer. Our findings show that when the wintertime NAO is in a positive phase, the summertime sea level pressure (SLP) over the Eurasian continent, especially in Western Europe, central Siberia, and eastern Siberia is higher. These patterns of SLP are similar with those of at higher levels geopotential heights and surface air temperature. The summertime SST anomalies surrounding the northern Eurasian continent after the winter of the positive NAO are also positive. The snow-cover anomaly over Siberia in early summer and the sea-ice concentration and the SST anomaly in the Barents Sea in early summer after the winter of the positive NAO are also negative. These results suggest that the wintertime NAO is memorized in the sea ice, the ocean surface and the snow, and then these memorized anomalies influence the interannual variation of the summertime atmospheric circulation over the Eurasian continent.

**MI05/10P/D-002 Poster 1400-168**

**TESTING OF THE NAO AND ENSO IMPACT ON THE WINTER CLIMATE ANOMALIES IN ROMANIA**

Ileana MARES<sup>1</sup>, Constantin MARES<sup>1</sup>, Mihaela MIHAILESCU<sup>2</sup> (<sup>1</sup>National Institute of Meteorology and Hydrology, <sup>2</sup>Agricultural Science University)

In the present paper, there has been tested the simultaneous influences of the ENSO and NAO events upon the monthly temperature and precipitation anomalies in Romania for January, February and March. The NAO used in this study is defined (Jones et al., 1997) as the difference of normalised pressure between Ponta Delgada (Azores) and Reykjavik (SW Iceland). The ENSO events have been quantified both by means of the Southern Oscillation Index (SOI) and by using the Trans Nino Index (TNI), defined by Trenberth and Stepaniak (2001). There have been analysed through canonical regressions and composite analyses, function of El Niño, La Niña and the positive neutral and negative NAO. The classification of NAO is achieved according to Bonsal et al. (2001). The predictands for Romania have been considered the first principal components of the EOF decomposition of the temperature and precipitation anomalies for the period 1950-1997. Another predictand at the level of Romania, has been also represented through the values of a drought index, calculated by means of the first EOF of temperature and precipitation anomalies. This index is similarly with Palmer drought severity index. For all the three months, a general characteristic feature for the temperature field is the fact that a cold phase of the ENSO event associated with a normal state of the North Atlantic Oscillation may favour positive temperature anomalies, especially in the central and western part of Romania. For the pluviometric field, the results

depend on the month, for instance for March, for which the moisture state is very important for the agricultural sector; the highest anomalies are recorded in the intercarpathian areas in the case of the El Nino phenomenon associated with the negative NAO phase. El Nino in the positive NAO case favours positive precipitation anomalies in the southeast country and negative in the rest. **References** Bonsal, B., Amir Shabbar and Kaz Higuchi, 2001: Impacts of low frequency variability modes on Canadian winter temperature. *International Journal of Climatology*, 21, 95-108. Jones, P.D., T. Jonsson and D. Wheeler, 1997: Extension to the North Atlantic Oscillation using early instrumental pressure observations from Gibraltar and South-West Iceland. *International Journal of Climatology*, 17, 1433-1450. Trenberth, K.E. and Stepaniak D.P., 2001: Indices of El-Nino evolution, *J. Climate*, 14, 1697-1701.

**MI05/10P/D-004** Poster **1400-169**

**EAST EURASIAN SNOW COVER TRIGGERING THE NORTHERN ANNULAR MODE ?**

Eun-Jeong CHA (Center for Climate System Research, University of Tokyo)

A sequence of cold waves hit the East Asian countries in early winter of 2000/01 as a result of cold waves, a number of low-temperature and snowfall records were broken. It is noted that a large increase in snow cover over the East Eurasia occurred in early October and continued to November 2000 prior to the 2000/01 winter. Then, negative SLP anomalies prevailed over the East Eurasia and the North Pacific concurrently, positive height anomalies were located around the Arctic Ocean in December-February 2000/01. Such anomaly configuration characterized by a dipole between middle and polar latitudes resembled well the negative phase of the Arctic Oscillation (AO). The 2000/01 case suggests that the AO like anomalies could be triggered by the autumnal snow cover. Therefore the winter of 2000/01 is a good example of the contradiction proposed earlier, i.e., how could the AO both originate in the lower troposphere and mid-upper stratosphere? Furthermore, it is noted that smaller than normal snow cover appeared in October 1988 succeeded by SLP anomalies over the midlatitudes in 1988/1989 winter; namely, the autumnal snow cover and winter height anomalies in 1988/89 were opposite to the those of 2000/01 and in the case of 1976/77 was similar to those of 2000/01, except for SST distribution, the mature phase of El Nino. These contrasting and similar cases have been chosen to examine predictability of the leading mode of winter by observational analyses and model experiments. The main features reproduced by 10 ensemble experiments for the 1976/77, 1988/89 and 2000/01 cases show general similarities to the observation. The polarity between the polar region and midlatitudes is captured well by the simulation, except for over the North Atlantic. The results of run for 50-year with the monthly varying SSTs also show quite resemble anomalies to the observation.

**MI05/10P/D-005** Poster **1400-170**

**DOWNSCALING ANALYSIS FOR DAILY AND MONTHLY VALUES USING CLIM.PACT-V.1.0**

Rasmus E. BENESTAD, Ole Einar TVEITO (Department of Climatology, Norwegian Meteorological Institute)

An analysis tool, clim.pact, has been developed for empirical downscaling and analysis of local and regional climate on both a daily and a monthly basis. This tool is built in the dataanalysis environment R, and consists of a contributed package. The R-software is freely available (A "GNU version of Splus") from the internet (URL: http://cran.r-project.org), and runs on both Linux and Windows platforms. Since R and Linux require no license, this approach provides a low-budget tool for data-analysis. The clim.pact package is tested with both monthly and daily data and a number of different scenarios are compared. Empirical downscaling has been carried out with clim.pact on January mean temperature in Bergen, Copenhagen, Helsinki, Oslo, Stockholm, and Tromsø using single field as well as mixed-field predictors and with predictors that cover different regions. The package can easily employ a new common EOF approach for empirical downscaling. A comparison has been made between the various results in order to study the robustness of the method. Furthermore, the residuals from the model calibration has been examined for remaining trends or biases. These tests indicate that clim.pact skillfully reproduces local climate variations with a linear model when these are near-normally distributed. Tests with skewed data such as daily precipitation show that a linear model does not give a good description of the local series. New models, however, are easily incorporated in the clim.pact framework, such as analogs and conditional weather generators. The empirical downscaling is fast, and clim.pact hence facilitates downscaling analysis on multi-model ensembles.

**MI05/10P/D-006** Poster **1400-171**

**NAO IMPACT TOWARDS THE SEASONAL EVOLUTION OF THE EURASIAN CONTINENT DURING THE NORTHERN HEMISPHERE SPRING**

Masatake E. HORI (Environmental Science, University of Tsukuba)

The impact of North Atlantic Oscillation (NAO) towards theseasonal evolution of the Eurasian continent is examinedbased on 51 years of NCEP/NCAR reanalysis data. While there has been many studies of NAO impact towards thesurface temperature in the downstream Eurasian continent during winter, its impact towards the transition period of winter through spring is not well known. Such seasonal evolution is essential in understanding the recent high correlation between the Eurasian surface temperature and the Asian monsoon. Composite analysis of seasonal evolution in NAO indices during five strong monsoon years show a positive NAO condition during the seasonal march of January through March. Snow cover composite for these years show an early snow retreat over Europe in January. Such anomaly is localized in a window region where the temperature anomaly accompanying a strong NAO condition is able to penetrate the seasonal evolution of the snow line to retreat earlier than normal. This window region is signified with a warmer troposphere and increased surface temperature which leads to more warm advection to flow into this region, thus advancing the snow line 2-3 weeks earlier than normal year throughout the following season. Following March and April shows a negative snow cover anomaly over central and eastern Europe and also in western Siberia. It is shown that such anomaly in the surface snow cover condition is accompanied by an early surface heating in the region acting as an apparent heat source. The atmosphere adjusts to such forcing with a northward shift in the subtropical jet. Also the blocking effect of the Tibetan region creates an anticyclonic anomaly over the Tibetan plateau and the surrounding region. In the following spring, composite analysis shows a wave guide like disturbance pattern along the southern slope of the Himalayas, creating an east-west temperature contrast over the Tibetan plateau. Such prominent seasonal evolution is triggered by a positive NAO extreme and has been dominant during 1978-1998, whereas its effect is not as clear during 1958-1978 period. Principal component analysis of these two period shows that the zonal structure of the temperature anomaly accompanying an NAO extreme has changed over the years, where in the recent years the Annular structure has become stronger, thus enabling the window region in western Europe to be directly influenced through such NAO extreme. Apparent correlation of the surface temperature and monsoon index may be a result of such change in seasonal evolution over the years. Relationship with the Siberian high and the activity of the EU

pattern will also be shown during the poster session.

**MI05/10P/D-007** Poster **1400-172**

**THE INFLUENCE OF THE BASIC WIND ON THE PROPAGATION OF PJ-LIKE ROSSBY WAVETRAIN**

Yosuke KOSAKA, Yoshihisa MATSUDA (Department of Science, University of Tokyo)

The influence of the convective activities in the subtropics on the northern hemisphere summer circulation is studied. In the time-scale of the interannual variation, there is positive correlation between the convective activities in the subtropical western Pacific around Philippines, and the height field in East Asia. Moreover, in the time-scale of the intraseasonal variations, we can see the barotropic wavetrain which is generated in subtropical western Pacific and propagating over the North Pacific to North America. This is called PJ pattern. It takes about 5 days or a week for this wave to arrive at North America (Nitta, 1987). It is also known that PJ pattern appears more frequently in the East Asian mid-summer than in the rainy season (TsuYuki and Kurihara, 1989). We have examined the impact of the heating around the subtropical western Pacific, using a numerical model. The linear and stationary model on the northern hemisphere is adopted. In this model, quasi-geostrophic approximation is assumed. When the observed zonal wind around the East Asia is used as the basic field, a Rossby wavetrain is generated by the heat source placed on Philippines, but its anomaly is cyclonic around Japan. This is opposite to the observed PJ pattern. Moreover, it is shown by the comparison of the results calculated with the wind fields in the East Asian rainy season and the mid-summer that the amplitude of the wavetrain is larger in the rainy season. Further, we have studied the relationship between the baroclinic forcing and the barotropic wavetrain, using the model with some idealized basic field. It is found that for the appearance of PJ pattern as stationary wavetrain, the following condition should be satisfied: the westerly wind in the lower layer in the subtropics is strong, and connected with the mid-latitude westerly region, so that the stationary Rossby wave can propagate into the mid-latitudes. When the ideal basic wind field that satisfies the above condition is used, the PJ-like Rossby wavetrain is obtained. Since PJ pattern is observed as intraseasonal variations, the validity of the stationary model is questionable. Hence, we reexamine PJ pattern with linear, quasi-geostrophic and prognostic model. In the results with this model, there appears the Rossby wavetrain, whose sign is opposite to PJ pattern, again. On the other hand, when the ideal basic wind field mentioned above is used, the PJ-like Rossby wavetrain is obtained again. These calculations suggest the following possibility: for the appearance of PJ pattern, in addition to active cumulus convection in subtropical western Pacific, it is required that in the mean wind field the lower layer westerly in the subtropics connects with the mid-latitude westerly.

**MI05/10P/D-008** Poster **1400-173**

**IMPACTS OF THE THERMOHALINE CIRCULATION ON ATMOSPHERIC VARIABILITY OVER THE NORTH ATLANTIC**

Pascal YIOU<sup>1</sup>, Pascale BRACONNOT<sup>1</sup>, Masa KAGEYAMA<sup>1</sup>, Yvonnick LE CLAINCHE<sup>2</sup>, Olivier MARTI<sup>1</sup> (<sup>1</sup>Laboratoire des Sciences du Climat et de l'Environnement, <sup>2</sup>Institut Maurice-Lamontagne)

The northward heat transport associated to the thermohaline circulation (THC) largely affects the North Atlantic region climate. We investigated the impact of a change of the THC on climate variability around the North Atlantic, with a particular emphasis on the North Atlantic Oscillation and the associated atmospheric circulation. We used a 250 yr control simulation of the IPSL coupled model with low resolution and a thermodynamic sea ice parameterization, as well as reanalysis data. This simulation offers the peculiarity of a sudden jump of the THC (from 15 Sv to 30 Sv) after 140 yr of run. This jump is observed through a shift of the convection zone from the Greenland-Iceland-Norwegian Sea to the Labrador Sea. To a first order, the mean climatic impact is mostly localized in the Labrador region. We focused our study on variability diagnostics like frequency spectra, statistics of extremes in temperature and precipitation, and weather regimes around the North Atlantic. Thus in this simulation, the THC might have a negligible effect on mean regional climates such as Western Europe, but its impact is potentially important on the description of climate variability and the statistics of short lived events. This study addresses the interactions between a mean state and variations around the mean.

**MI05/10P/D-009** Poster **1400-174**

**ANALYSIS OF THE CLIMATOLOGY OF EXTREME WEATHER EVENTS AFFECTING BARROW, ALASKA**

Elizabeth Noel CASSANO, Amanda H. LYNCH, Melinda R. KOSLOW, Casey THORNBRUGH (CIRES, University of Colorado)

Barrow, Alaska is located on the northernmost tip of Alaska at the intersection of the Beaufort and Chukchi Seas. The coastal geography of this region makes Barrow quite vulnerable to extreme weather events, which can result in significant flooding and erosion. This study is an analysis of high wind events in Barrow in the context of the synoptic climatology of the Western Arctic. The analysis uses the Self-Organizing Map (SOM) algorithm - an unsupervised learning process that groups large, multivariate datasets onto a 2-dimensional array or map. A strength of this algorithm is there are no assumptions made as to the structure of the clusters of the data. The SOM algorithm is used here to produce a synoptic climatology of sea level pressure patterns for 53 years for the Western Arctic. The same clustering is used to examine the decadal variability of the synoptic climatology, and relate this to the observed variability in temperature, circulation and other climatic parameters. Using this methodology, we study the extreme events that affect Barrow by including local variables, such as Barrow winds and fetch to the ice edge, in the SOM analysis. The highest winds and greatest fetch events can be weighted in order to find the patterns that cause the most significant damage. Hence, a map can be constructed that is representative of the synoptic patterns that produce extreme events in Barrow. It is intended that such an analysis will allow an assessment of the likely temporal variability of extreme events in Barrow into the future.

**MI05/10P/D-010** Poster **1400-175**

**CLIMATE ON ABNORMAL OCCURRENCE OF WILDLAND FIRE IN SIBERIA**

Keiji KIMURA<sup>1</sup>, Hiroshi HAYASAKA<sup>2</sup>, Koji YAMAZAKI<sup>3</sup>, Masami FUKUDA<sup>4</sup> (<sup>1</sup>Department of Geography, Tokyo Metropolitan University, <sup>2</sup>Graduate School of Engineering, Hokkaido University, <sup>3</sup>Graduate School of Environmental Earth Science, Hokkaido University, <sup>4</sup>Institute of Low Temperature Science, Hokkaido University)

A great many wildfires occurred in Siberia and Mongolia in 2002 summer. Especially in Mongolia, the Prime Minister declared that the whole area should be ready for civil defense to assist fighting the wildfires from August 16. Generally speaking, the wildfires are caused by extreme hot and dry conditions, but few analyzed climatic data can be seen as the reason. For example, in Ulaanbaatar, the capital of Mongolia, it rained only 10mm (it rains 68mm in



normal years) in July, 2002: the monthly mean temperature was 21.7 degreeC (the average is 17.7 degreeC). We can see the similar phenomenon was happened in 1998 recently, and we suspect that it will occur once in some years. Now we can use the climatic data of 1998, but cannot use the data of this year yet. Today, we have presentation about the analysis of 1998 summer. We use the dataset below: (1) Global Surface Summary of Day Data compiled by NCDC (2) ECMWF Reanalysis Data (3) JMA Historical Map (4) Wildfire Area Data analyzed by Remote Sensing data As we can use ECMWF Data from 1987 to 2001 (not yet in 2002), mainly we start analyze the summer in 1998. And we can get the Hot Spot Data around Yakutsk, Siberia by Dr. S. Tashilin. Now we have started to analyze around Yakutsk. Dr. S. Tashilin analyzed wildfires as Hot Spots from the satellite image data around Yakutsk. His analysis area is 58N-66N: 122E-136E. Indeed, in 1998 summer it was high temperature and little precipitation, and it was hotter and drier than that of 2002 summer. We can see the pressure distribution in August, 1998. The ridge at 500hPa level is seen from 80N, 0E strait to 50N, 130E over Yakutsk. It corresponds to the high pressure area at Sea Level. It is considered as the blocking high centered around 65N, 110E. It changed to abnormal circulation. Next, seasonal change in summer, 1998 is picked up. Wildfire had seasonal change. Every component of the climate was changed seasonally. Sometimes it rains, but like as from Aug.10 (Day Number=222) to Aug.27 (DN=239) no precipitation continued even 18 days. During this period, the SLP had been high level, and southern component of wind continued to blow. This phenomenon means hot and dry condition was kept. As typical case study, wildfires grew from Aug.12 to Aug.14, 1998. How was the climatic condition in this period? We analyze about the SLP, relative humidity and wind distributions. It was illegible high pressure around Yakutsk, but one after another low RH air mass attacked this area.

**MI05** **Wednesday, July 9 - Friday, July 11**

**LARGE SCALE PATTERNS OF ATMOSPHERIC VARIABILITY: DYNAMICS, CLIMATE IMPACTS, AND ROLE IN RECENT CLIMATE CHANGE (ICC)**

Location: Site B, Room 17

**Friday, July 11 AM**  
 Presiding Chairs: P. Yiou, E. Cassano

**MI05/11A/B17-001** **0830**

**NORTH ATLANTIC OCEAN-ATMOSPHERE INTERACTIONS IN TWO COUPLED MODELS**

Laurent Z.X. LI, Sebastien CONIL (LMD)

The Northern Hemisphere climate variability is dominated by some few preferred modes of the atmospheric circulation like the North Atlantic Oscillation and the Pacific/North America pattern. These major teleconnections are the dominant internal variability patterns of the atmosphere as shown by a number of study using atmospheric GCM's. External forcing such as ENSO tropical diabatic heating or anthropogenic influence is thought to modify natural and preexisting forms of internal variability. However the relationships of these dominant patterns of atmospheric variability with the underlying oceans is still unclear with the current scientific knowledge. Recent results using lead/lagged Singular Value Decomposition technique confirm that, in the North Atlantic basin, oceanic variability is mainly controlled by atmospheric forcing. But they also show a significant relationship between SST anomalies preceding by few months the atmospheric anomalies, reflecting the forcing of the NAO by the extratropical Atlantic ocean (Czaja and Frankignoul, 2002). In this study, the same methodology (delayed SVD) is employed to analyse extratropical air-sea interaction in two ocean-atmosphere fully-coupled climate models. The two models share a common oceanic component but they use two different state-of-the-art atmospheric general circulation models. A sequence of 100 years is extracted from both models and used to study the relationship between extratropical oceanic and atmospheric variability. In addition we use 100 years of Sea Surface Temperature and Sea Level Pressure reanalysed data from CRU. These two GCM's reproduce well the dominant teleconnections patterns of the Northern Hemisphere. We focus on the North Atlantic basin where extratropical local ocean-atmosphere coupling is particularly strong. The ability of the two models in reproducing the main behaviours of the North Atlantic ocean-atmosphere interactions is evaluated through a comparison with observations. The same analysis is also applied to the North Pacific where El Nino Southern Oscillation signal acts as a perturbation for the local extratropical processes.

**MI05/11A/B17-002** **0850**

**TRANSIENT RESPONSE OF AN ATMOSPHERIC GCM TO NORTH ATLANTIC SST ANOMALIES**

Laurent Z.X. LI, Sebastien CONIL (LMD)

A high-resolution atmospheric General Circulation Model (GCM) is used to evaluate the atmospheric response to North-Atlantic Sea Surface Temperature (SST) anomalies. The transient evolution of the response is studied in detail. The linear and non-linear effects can thus be contrasted and separated by their different time scales. Baroclinic patterns related directly to the surface anomalies reach quickly their maximum manifestation. Barotropic patterns related to the mid and upper troposphere eddy vorticity fluxes however have longer time scales with much more important amplitude, able to replace the initial baroclinic response. This study thus provides a comprehensive picture to reconcile the two types of response in GCM.

**MI05/11A/B17-003** **0910**

**MECHANISMS FOR THE NAO RESPONSES TO THE NORTH ATLANTIC SST TRIPOLE**

Shiling PENG<sup>1</sup>, Walter A. ROBINSON<sup>2</sup>, Shuanglin LI<sup>1</sup> (<sup>1</sup>NOAA-CIRES Climate Diagnostics Center, <sup>2</sup>Department of Atmospheric Sciences, University of Illinois)

Large (100-member) ensembles of GCM experiments reveal that the North Atlantic SST tripole, with warm anomalies off the US coast flanked by cold anomalies off Newfoundland and in the subtropics, can induce a significant NAO response in late winter (Feb-Apr) when the model's intrinsic variability projects strongly on the NAO. The tripole-induced NAO response exhibits an intriguing asymmetry about the sign of the SST anomaly, manifested in the weaker and more wavelike response to the positive tripole in contrast to the stronger and more zonally-elongated response to the negative tripole. Mechanisms for developing and maintaining these GCM responses are elucidated through diagnostic experiments using a linear baroclinic model and a statistical storm track model based on GCM intrinsic variability.

The NAO-like symmetric response is primarily maintained by a dipolar anomalous eddy forcing that results from interactions between the heating-forced anomalous flow and the Atlantic storm track, as expected from an eddy-feedback mechanism. To account for the asymmetry of the responses about the sign of the SST tripole, a nonlinear eddy-feedback mechanism is proposed that extends the previous mechanism to include the nonlinear self-interaction of the heating-forced anomalous flow and its effects on transient eddy feedbacks. Results of idealized model experiments demonstrate that, due to its nonlinear self-interaction, the tripole heating induces a much weaker response in the positive phase than in the negative phase. Interactions of these nonlinear heating-forced anomalous flows with the Atlantic storm track result in asymmetric eddy vorticity forcings that in turn sustain asymmetric eddy-forced anomalous flows in the two cases.

**MI05/11A/B17-004** **0930**

**A NEGATIVE FEEDBACK BETWEEN THE NORTHERN HEMISPHERE SEA ICE AND THE NAO**

Kentaro YAMAMOTO<sup>1</sup>, Yoshihiro TACHIBANA<sup>2</sup>, Meiji HONDA<sup>3</sup>, Jinro UKITA<sup>3</sup> (<sup>1</sup>University of tokai, <sup>2</sup>Frontier Research System, <sup>3</sup>NASA)

Temporal and spatial variability of sea ice in the northern hemisphere is a critical component of the global climate. This study presents a hemispheric scale modal structure in wintertime sea ice variability on interannual time scales and discusses its interaction to the NAO. The leading spatial structure given by an EOF analysis for the SMM/R-SSMII satellite dataset of the sea ice shows a seesaw (an out-of-phase) pattern in the field of hemispheric scale sea ice concentration. The seesaw consists of one polarity in Eurasian side, i.e., from the Sea of Okhotsk through Barents Sea, and the other polarity in American side, i.e., the Bering and Labrador Seas. A regression map of the time series of the EOF leading mode of the sea ice onto the global atmosphere in December and January are remarkably similar to the NAO pattern, whereas the regression of the time series of the ice EOF with the SLP field in February and March shows no connection to the NAO. We further execute an ideal AGCM in order to isolate the influence of the hemispheric ice seesaw upon the global atmosphere. In the model, an ideal seesaw-like sea-ice distribution based on the EOF leading mode is used as the surface boundary condition. The response of the SLP pattern to the sea-ice seesaw is similar to the NAO pattern, however the phase is opposite to the pattern shown above. These results suggest that in the first half of the winter the hemispheric ice seesaw is built in response to the NAO, whereas in the latter half of the winter, the ice seesaw destroys the NAO. Therefore, a possible cause of the less persistency of the NAO through the winter is in the negative feedback between the NAO and the hemispheric sea-ice seesaw.

**MI05/11A/B17-005** **0950**

**ATMOSPHERIC RESPONSE TO ZONAL VARIATIONS IN MID-LATITUDE SST: TRANSIENT AND STATIONARY EDDIES AND THEIR FEEDBACK**

Masaru INATSU<sup>1</sup>, Hitoshi MUKOUGAWA<sup>2</sup>, Shang-Ping XIE<sup>3</sup> (<sup>1</sup>Graduate school of Environmental Earth Science, Hokkaido University, <sup>2</sup>Disaster Prevention Research Institute, Kyoto University, <sup>3</sup>International Pacific Research Center/SOEST and Department of Meteorology, University of Hawaii)

We have investigated midwinter storm track and stationary eddy response to zonal variations in mid-latitude sea surface temperatures (SSTs) conducting atmospheric general circulation model experiments under the conditions with an aqua planet of the whole surface covered by water and with the perpetual January of isolation fixed at January. Zonal wavenumber-one SST variations with a meridionally confined structure are placed at various latitudes. Having these SST variations centered at 30N leads to a zonally localized storm track, while the storm track becomes nearly zonally uniform when the same SST forcing is moved further north at 40N and 50N. The zonally localized storm track prefers high baroclinicity zone in the planetary boundary layer. Following to high-frequency eddy kinetic energy (EKE) budget analysis, large (small) baroclinic energy conversion north of the warm (cold) SST anomaly near the axis of storm track (near 40N) is responsible for the large (small) storm growth. The equatorward transfer of EKE by the ageostrophic motion and the mechanical damping are important to diminish the storm track activity in the zonal direction. Significant stationary eddies form in the upper troposphere, with a ridge (trough) northeast of the warm (cold) SST anomaly at 30N, while they are much weakened with the SST forcing shifted more northward. Heat and vorticity budget analyses indicate that zonally localized condensational heating in the storm track is the major cause for these stationary eddies, which in turn exert positive feedback to maintain the localized storm track by strengthening the vertical shear near the surface. These results indicate an active role of synoptic eddies in inducing deep tropospheric-scale response to mid-latitude SST variations. We finally discuss the application of the model results to the real atmosphere, especially to the Southern Hemisphere.

**MI05/11A/B17-006** **1010**

**LARGE-SCALE INTERANNUAL CHANGES IN OCEAN WIND WAVES OVER THE NORTH ATLANTIC AND NORTH PACIFIC: LINKS TO THE NORTHERN HEMISPHERE CYCLONE VARIABILITY**

Sergey K. GULEV<sup>1</sup>, Vika GRIGORIEVA<sup>1</sup>, Olga ZOLINA<sup>2</sup> (<sup>1</sup>P.P. Shirshov Institute of Oceanology, <sup>2</sup>University of Bonn)

Variability in the characteristics of the wind waves over the Northern Hemisphere is studied on the basis of the Global Climatology of Ocean Waves, derived from the Voluntary Observing Ship (VOS) data for the period from the end of 19th century to present. Waves observations in VOS are taken visually by marine officers, and in a lesser degree than winds are influenced by historical changes in observational practices. An outstanding feature of visual wave observations is the availability of separate estimates of the wind sea, associated with the local wind, and swell, integrating the wind forcing over the larger domain. Traditionally analysed from the model and satellite data significant wave height (SWH) results from these two components and does not allow for the understanding of mechanisms driven the variations on surface roughness. We studied long-term trends in wind sea, swell, and SWH for the period from 1880 to 1940s along major ship routes and from 1950s to present over the whole North Atlantic and North Pacific. Decadal scale variations were studied for the last 50 years using EOF and SVD analysis. Special attention is given to the effects of sampling errors in variability of ocean waves. Wind sea and swell demonstrate different patterns of variability, associated with the North Atlantic Oscillation (NAO) and Pacific Oscillation. In particular, swell variability is clearly associated with the storm frequency, while wind sea reflects the local wind signal. In order to project the NAO signals onto wave variability, joint analysis of the climate variability in the characteristics of atmospheric cyclones over the Northern Hemisphere and of the wind wave parameters has been performed.

**MI05/11A/B17-007** Invited **1050**

**MULTI-DECADAL MODULATION IN THE ALEUTIAN-ICELANDIC LOW SEESAW AND RELATED MODULATIONS IN THE EOF STRUCTURE OF THE NORTHERN HEMISPHERE TROPOSPHERIC VARIABILITY**

Hisashi NAKAMURA<sup>1</sup>, Shozo YAMANE<sup>2</sup>, Meiji HONDA<sup>3</sup> (<sup>1</sup>IGCR, Frontier Research System for Global Change, also in Department of Earth, Planetary Science, University of Tokyo, <sup>2</sup>IGCR, Frontier Research System for Global Change)

It has recently been argued that interannual variability in the tropospheric circulation over the wintertime North Atlantic, including the intensity of the surface Icelandic Low (IL), is strongly influenced by the Northern Hemisphere annular mode (NAM). As recently found by the authors, the North Atlantic circulation is also under the significant influence of the North Pacific in the form of a late-winter seesaw between the IL and the Aleutian Low (AL). In recent decades the NAM and the upper-tropospheric manifestation of the AL-IL seesaw (i.e., a combination of the PNA pattern and NAO) were the most dominant anomaly patterns in the early and late winter periods, respectively, but their dynamics are fundamentally different. Unlike the NAM, the seesaw formation is through propagation of stationary Rossby wave trains across North America with strong feedback forcing from storm tracks, as clearly seen in the seesaw formation that occurred in late January of 2002. Which of the two dominant anomaly patterns is more dominant in the tropospheric variability has been changed on multi-decadal scales during the last century. The NAM was predominant and the seesaw formation was unlikely in the 1950s and 1960s, during which the first EOF of sea-level pressure (SLP) includes no significant AL anomalies. After that the seesaw became more dominant. The first EOF of SLP includes strong AL anomalies, and the PNA-NAO combination characterizes the wintertime first EOF in the free troposphere. In the 1930s and 1940s the seesaw was as dominant in the SLP variability as in the period since the 1970s. In those periods of the seesaw domination, the IL anomalies in a month of the seesaw completion were significantly correlated only with the AL anomalies with the opposite sign in the previous month, but not with the IL anomalies. The multi-decadal modulation observed in the AL-IL co-variability during the postwar period seems to be related to the corresponding modulation in the effectiveness of the atmospheric teleconnection across North America in the presence of a strengthening tendency of the midwinter planetary waves over the western hemisphere. Before the 1970s the midwinter westerlies were more zonal over the western hemisphere with weaker diffluence of the Pacific jet. Anomalies developing in the exit of the Pacific jet tended to be isotropic and a substantial fraction of Rossby wave activity emanated from those anomalies was dispersed into the lower latitudes. Since the 1970s, anomalies developing in the strongly diffluent westerlies over the North Pacific tended to be more zonally elongated and thus more persistent. The westerlies strongly meandered in such a way that most of the Rossby wave activity emanated from those anomalies tended to advected effectively into the IL region across North America.

**MI05/11A/B17-008** **1130**

**ALEUTIAN-ICELANDIC LOW SEESAW BEHAVIOR IN AGCM ENSEMBLE SIMULATIONS**

Meiji HONDA<sup>1</sup>, Yochanan KUSHNIR<sup>2</sup>, Hisashi NAKAMURA<sup>1</sup>, Shozo YAMANE<sup>1</sup>, Stephen E. ZEBIAK<sup>3</sup> (<sup>1</sup>IGCR, Frontier Research System for Global Change, <sup>2</sup>LDEO, Columbia University, <sup>3</sup>Department of Earth and Planetary Science, University of Tokyo, <sup>4</sup>January 1, 1990IRI, Columbia University)

Behavior of an interannual seesaw-like oscillation between the surface Aleutian and Icelandic lows (AL and IL, respectively) is investigated on the basis of 50-year AGCM climate simulations, by separating them into an external part due to the variability of sea surface temperature (SST) forcing and an internal part due to atmospheric dynamics only. Our study is based on 24-member ensemble hindcast runs forced by observed SST anomalies with different atmospheric initial conditions. The external variability defined as the ensemble mean of the 24 members is characterized as significant negative correlation between the AL and IL intensities in late winter (it reaches -0.8 in March). The seesaw is gradually formed toward March through a PNA-like wave train development by a remote influence of ENSO and its extension to the North Atlantic. However, the amplitudes of the North Atlantic anomalies are nearly half of the corresponding Pacific anomalies. Signal to noise ratio estimated as the SST-forced variance to the total variance does not exceed 15% over the North Atlantic. On the other hand, the internal part of 24 ensemble members defined as deviations from the ensemble mean is characterized by weak, but still significant, negative correlations between the AL and IL anomalies through winter (December to March). This suggests that the AL and IL anomalies associated with the internal variability are not mutually independent, either. It is confirmed that, whenever the AL-IL seesaw occurs, the IL anomalies are formed through eastward propagation of wave activity released from the AL anomalies in the form of stationary Rossby wave trains. Downstream influence of the North Pacific on the North Atlantic is still important for formation of the AL-IL seesaw as the internal variability. The most important trigger for the seesaw formation seems to be persistent AL anomalies lasting more than one month over the North Pacific so as to sustain eastward wave-activity propagation to the North Atlantic.

**MI05/11A/B17-009** **1150**

**A SIMULATED SEESAW BETWEEN THE ALEUTIAN AND ICELANDIC LOWS AND MULTI-DECADAL MODULATIONS**

Shozo YAMANE<sup>1</sup>, Hisashi NAKAMURA<sup>2</sup>, Meiji HONDA<sup>1</sup>, Wataru OHFUCHI<sup>3</sup> (<sup>1</sup>IGCR, Frontier Research System for Global Change, <sup>2</sup>Department of Earth, Planetary Science, University of Tokyo, <sup>3</sup>Earth Simulator Center)

The authors have recently found that the variability associated with a late-winter seesaw between the surface Aleutian and Icelandic Lows (AL and IL, respectively) was predominant over the last 30 years in upper-tropospheric interannual variability over the wintertime extratropical Northern Hemisphere. Here, we examine how realistically the seesaw is simulated in an AGCM and how significantly its appearance is modulated on multi-decadal scales. The AGCM integrations are composed of a set of seven 50-year control experiments with global SST fixed to the climatological seasonal march and another set of thirteen 50-year hindcast experiments forced by global SST anomalies observed since 1949. The NCEP/NCAR reanalysis data for 1948-2000 are also used. Though not necessarily significant, negative correlation was found between interannual anomalies of the AL and IL intensities for any winter month in any member of the AGCM ensemble. In many of the members the seasonality of the seesaw formation is not as distinct as observed in the recent decades. Still, some of them exhibit a clear tendency in the negative correlation becoming stronger towards the latter part of the winter as observed. In the real atmosphere, multi-decadal modulations were apparent in the strength and seasonality of the seesaw signature. The negative AL-IL correlation has been strongest in late February since the 1970s, but it was so in January before the mid-1950s. In the 1960s, the negative correlation was almost diminished. Our hindcast integrations were, however, unable to reproduce the observed modulated behavior, exhibiting no systematic multi-decadal tendency in the AL-IL correlation. Interestingly, clear multi-decadal tendencies in the correlation were found in

some of the control runs. Reflecting those tendencies, the leading EOF for the wintertime Northern Hemisphere defined for each of the mutually overlapping 15-year periods changes its structure from a more zonally-symmetric pattern representing the annular mode to a wavier pattern representing the AL-IL seesaw or the other way around. The leading wintertime EOF for any of the 15-year periods based either on the observation or simulations can be interpreted as a linear combination of the annular mode and the seesaw. Our AGCM experiment suggests that the remote ENSO influence does not set a necessary condition for the seesaw formation, which is possible solely through the internal atmospheric dynamics. It will be discussed in the presentation whether the simulated multi-decadal modulation in the seesaw is related to modulated behavior of wave-activity propagation across North America and, if so, it is attributable to any modulations in waveguide structure and the least dumped mode of the basic state.

**MI05/11A/B17-010** **1210**

**FORMATION MECHANISM OF VORTICITY ANOMALIES ON THE SUBTROPICAL JET IN THE MIDSUMMER NORTHERN HEMISPHERE**

Naoki SATO, Masaaki TAKAHASHI (Center for Climate System Research, University of Tokyo)

Some previous studies revealed that stationary Rossby waves over the North Pacific are related to the midsummer climate over Japan. In the present study, EOF analyses were performed for midsummer pressure anomaly patterns near the tropopause around Japan, so that a Rossby wave train which propagates from east Asia to North America was detected on the subtropical jet. The analyses detected a series of wave train which continues from Europe to North America through east Asia. Examination of the time evolution of the anomaly by calculating lag regressions revealed the propagation of a wave packet from west to east. The wave packet slowly develops eastward in the region with a small gradient of absolute vorticity (or PV) to the west of Caspian Sea. Then, it fast propagates eastward on the Asian jet where the PV gradient is large. From these results, we can interpret the wave-like anomaly pattern as a stationary Rossby wave train on the subtropical jet. The EOF analyses don't detect a wave-like pattern which is shifted by a quarter wavelength from the original anomaly pattern mentioned above. Only a wave-like anomaly with a certain phase is likely to appear on the jet. In order to understand a mechanism of this phase dependency, barotropic energy conversion from the basic field to the anomaly field is estimated near the jet entrance around the Caspian Sea. A net positive energy conversion is estimated from the climatological field to the wave-like anomaly pattern. On the other hand, no significant energy conversion is detected when we use a wave-like pattern which is virtually shifted zonally by a quarter wavelength. Another estimation is performed between the smoothed climatological field and the original anomaly pattern. Here, the climatological field is spatially smoothed by a low pass (total wavenumber  $K \leq 8$ ) filter. No significant conversion is obtained in this case. From these results, it is deduced that the phase dependency is caused by the energy conversion corresponding to a smaller-scale distortion of the basic field. The distortion of the basic field seems to help an anomaly pattern with certain phase to grow through barotropic energy conversion. This mechanism can be interpreted as a wave-wave interaction between the basic and anomaly fields. The small-scale distortion of the climatological vorticity field near the jet entrance may be related to the "monsoon-desert dynamics" or the "Silk Road pattern". In other words, it is possible that the diabatic heating related to the Indian monsoon plays an important role in forming the distortion of the basic field.

Friday, July 11 PM

Presiding Chairs: O. Tveito, K. Kimura

**MI05/11P/B17-001** **1400**

**CHANGES IN ARCTIC RIVER DISCHARGE FROM A CATCHMENT MODEL AND THE INFLUENCE OF ATMOSPHERIC MODES OF VARIABILITY**

Jessica Ellen CHERRY, Marc STIEGLITZ, Stephen DERY (Lamont-Doherty Earth Observatory, Columbia University)

A snow model is used to estimate Arctic precipitation from multi-decadal snow depth station data. The derived precipitation record is then used to drive a catchment hydrological model. Spatial and temporal patterns of river discharge, and their association with the dynamics of the North Atlantic Oscillation, Pacific North American pattern, and global climate change, are described, including differences between coastal and inland regions. Finally, mechanisms are proposed which could explain the observed changes in Arctic river discharge as a response to variability in atmospheric dynamical modes.

**MI05/11P/B17-002** **1420**

**RECONSIDERATION OF TRUE VERSUS APPARENT ARCTIC OSCILLATION**

Hisanori ITOH (Department of Earth and Planetary Sciences)

Extending Itoh (2002), the reality of the Arctic Oscillation (AO, or annular mode) is reconsidered. Data used are the monthly-mean values of the 500hPa and 30hPa geopotential height and the 850hPa temperature, in addition to the sea level pressure (SLP). First, considering the relationship between NAO (North Atlantic Oscillation)-PNA (Pacific/North American Oscillation) and AO-NCM (negative correlation mode between the Atlantic and the Pacific) in the simplest version of the 3-point seesaw system, a schematic figure is presented. From this figure, we can visually understand why AO-NCM is extracted from NAO-PNA by EOF (Empirical Orthogonal Function) analysis. Although NAO-PNA (apparent AO-NCM) and true AO-NCM give the same 3-point EOF, the time coefficients of the first and second EOF modes (PC1 and PC2) are differently distributed. Namely, PC1 and PC2 for apparent AO-NCM are dependent on each other, while those for true AO-NCM are independent. We then arrange the issues about the configuration of NAO-PNA and true AO-NCM in phase space and the possibility of their discrimination. It is explained that the discrimination is possible in principle irrespective of the configuration, and two-point or midlatitude EOF is a method to extract true AO-NCM on a different plane in phase space, if it exists, from NAO-PNA. In order to examine the significance of NAO-PNA obtained by midlatitude EOF, the sensitivity is checked for real data. The result shows that mistake of true AO-NCM on a different plane in phase space for NAO-PNA never occurs, and NAO-PNA is considerably robust. It is ascertained from several pieces of evidence that NAO-PNA and AO-NCM are located on the same plane in phase space in the real world. This means that NAO-PNA and AO-NCM have the same variations on the plane in common, implying that when NAO-PNA is real, AO-NCM is unlikely to be real. Next, we extend analysis fields other than the monthly-mean SLP field. First, we treat the winter-mean SLP field, for which EOF does not show AO-NCM but NAO-PNA. This may come from the fact that the winter-mean NAO and PNA patterns have little spatial correlation. Second, using the 500hPa height and the 850hPa temperature, it is considered how hemispherically dominant modes should be interpreted; the synthesis of NAO and PNA can explain larger hemispheric variations than the regression of AO and NCM. Finally, midlatitude EOF analysis is carried out for the Northern stratosphere and the Southern troposphere, where it is said that there are similar



annular patterns. Then, the annular modes can be reproduced there. The peculiarity of the Northern troposphere, where AO is not reproduced by midlatitude EOF, is thus clarified. All the above results show that almost all characteristics of AO-NCM can be explained from those of NAO-PNA, hence concluding again that AO is almost apparent, which is extracted by EOF analysis from almost independent variations of NAO and PNA.

**MI05/11P/B17-003 1440**

**A POSSIBLE CAUSE OF THE ANTARCTIC OZONE HOLE DIMINISHING IN 2002**

Pavel N. VARGIN, Evgeni N. JADIN (Central Aerological Observatory, Dolgoprudny, Russia)

Analysis of the total ozone and stratospheric circulation changes is performed for August-October 1998 (year with the large ozone hole in the Antarctic) and 2002 (year with the very small ozone hole) using the daily means of geopotential height and zonal wind (NCEP reanalysis) and total ozone (TOMS). Obtained results showed that the stratospheric circulation over the southern polar region during August-October 2002 characterized by high activity of planetary quasi-stationary wavenumber 1 (hereafter wave 1) and eastward traveling wavenumber 2 (wave 2). The maximum intensities of both planetary waves were observed simultaneously 22-28 September 2002. Wave 1 displayed eastward shift from ~50W longitude 20 September to ~50E longitude 5 October 2002 and peaked at 80-70S. Traveling wave 2 moved eastward with the period of ~20 days and maximized nearly 65S. Analysis of spatial structure of wave 1 and wave 2 showed the phases of both waves overlapped when its largest amplitudes occurred. As it known 24 September 2002 the Antarctic ozone hole split into two holes for the first time since satellite measurements have been taken. The stratospheric angular momentum (SAM) determined as the atmospheric angular momentum above 100 hPa was calculated as the identifier of stratospheric circulation and wave activity variations. Strong nonlocal correlations were indicated between the total ozone and SAM anomalies outside the polar vortex in the Antarctic by means of the singular valued decomposition (SVD) of these fields. Westerly (easterly) SAM anomalies are dominated during August-October 1998(2002) at 60S-40S. This result is in good accordance with those obtained by Jadin (1996) for the monthly mean total ozone and SAM anomalies in 1979-1992. A cause of the unexpected ozone hole diminishing in September-October 2002 might be associated with the V-shaped decadal propagation of the strong easterly SAM anomalies which arose nearly the equator in 1990-1991 and then propagated toward the middle-high latitudes during subsequent decade (Jadin, 2002a). Relations of the ozone layer changes with the Arctic and Antarctic Oscillations and sea surface temperature (SST) anomalies are discussed (Jadin, 2002b). Reference. 1. Jadin, E.A., 1996: Long-term propagation of zonal mean anomalies in the stratospheric dynamics, *Meteorology and Hydrology*, 7, 36-48. 2. Jadin, E.A., 2002a: Is Ozone Hole over Antarctic diminishing? *Ecology and Russian Industry*, December, 27-29. (<http://ecip.newmail.ru>) 3. Jadin, E.A., 2002b: Arctic and Antarctic Oscillations, Ozone Changes and SST anomalies, Abstracts of Inter. Symp. on Stratospheric Variations and Climate, Kyushu University, Fukuoka, Japan, 16-19.

**MI05/11P/B17-004 1500**

**POTENTIAL VORTICITY INTRUSION INDICES AND CLIMATE VARIABILITY OF SURFACE TEMPERATURE**

Ming CAI (Department of Meteorology, University of Maryland)

Daily pressure fields on a constant potential vorticity (PV) surface (PV = 2.5 unit) are analyzed using NCEP/NCAR reanalysis II (1979-2002) dataset. Potential vorticity intrusion (PVI) indices are developed to measure the mean latitudinal position, area, and intensity of the subtropical and polar front zones, as well as the equatorial convection zones. It is found that the polar front indices are closely related to the interannual and decadal variability of the cold air temperature anomalies over the high latitudes. In general, more (fewer) of extreme cold surface air temperature episodes in high latitudes coincide with a high (low) extratropical PVI index. The interannual variability of the extratropical PVI index exhibits a strong QBO-like signal. The high (low) PVI index prevails when the equatorial zonal mean zonal wind at 50 hPa is easterly (westerly). The composite anomaly surface air temperature maps of high versus low extratropical PVI indices exhibit a pattern resembling to the familiar regression map against the AO index found in Thomson and Wallace (1998). However, the composite maps of surface pressure anomaly show a different pattern: the circulation anomalies over the north Atlantic basin are very like NAO but the anomaly pattern over the Pacific shows a dipole that is out of phase with the pattern over the Atlantic basin. The probability distribution map of PV intrusion activities shows a shift of the preferred regions of frontogenesis from the oceans to the continents when the extratropical PVI index is high. This explains directly why more extreme cold events are observed over the northern Eurasian and Northern America continents when the PVI index is high or the QBO is in the easterly phase. The equatorial PVI indices exhibit a pure QBO signal as one may expect. It shows that in the easterly phase of QBO, the equatorial air expands while subtropical front moves equatorward and polar frontogenesis area increases and intensifies. This is particularly evident in the Northern Hemisphere. The reverse is observed in the westerly phase. It is found that the observed warming trend in the high-latitudes in the last two decades can be explained an upward trend of the PVI index of subtropical fronts.

**MI05/11P/B17-005 1520**

**CLIMATE CHANGE IN THE NORTH PACIFIC REGION OVER THE LAST THREE CENTURIES**

Kent MOORE<sup>1</sup>, Gerald HOLDSWORTH<sup>2</sup>, Keith ALVERSON<sup>3</sup> (<sup>1</sup>Department of Physics, University of Toronto, <sup>2</sup>Arctic Institute of North America, University of Calgary, <sup>3</sup>PAGES International Project Office)

The relatively short length of most instrumental climate records restricts the study of climate variability, and it is therefore essential to extend the record into the past with the help of proxy records. Only since the late 1940s have atmospheric data been available that are sufficient in quality and spatial resolution to identify the dominant patterns of climate variability such as the Pacific North America pattern and the Pacific Decadal Oscillation. Here we present a 301-year snow accumulation record from an ice core at a height of 5,340 m above sea level, from Mount Logan, northwestern North America, which is closely linked with the Pacific North America Pattern for the period of instrumental data availability. Our record extends the instrumental data back in time, covering the period from the closing stages of the Little Ice Age to the warmest decade in the past millennium. We find a positive, accelerating trend in snow accumulation after the middle of the 19th century. This trend is paralleled by a warming over northwestern North America which has been associated with secular changes in both the Pacific North America pattern and the Pacific Decadal Oscillation.

**MI05/11P/B17-006 1610**

**NAO AND ENSO PROJECTION ON IRAN CLIMATE PREDICTABILITY**

Iman BABAIYAN, Javad BODAGHJAMALI, Sohaila JAVANMARD, Leili KHAZANEDARI (Climatological Research Institute (CRI), I. R. of Iran Meteorological Organization (IRIMO), P. O. Box 91735-491, Mashhad, I. R. of Iran)

North Atlantic Oscillation (NAO) is the dominant mode of Variability over the Atlantic-European region. A number of studies have shown that most of cooling in the northwest Atlantic and the warming across Europe and Over Eurasia since the mid 1970s results from changes in the NAO. Besides, the EL Nino-Southern Oscillation (ENSO) exerts a profound on global weather and climate patterns. A great deal of time and effort here been spent investigating the phenomenon with benefits in terms of economics public safety and the environment. However, a more detailed regional projection of NAO and ENSO related climate fluctuations and predictability is still needed. In the present research, NAO and ENSO signal impacts on precipitation and other related elements, over I. R. of Iran in Climatological Research Institute (CRI), have been carried out. We choose 36 synoptic station of IRAN for this study. We found that for the El Nino events with SOI <-5 the mean annual rainfall of Iran increase about 63 percent, and for Lanino events with SOI >-5, the rainfall decreases about 67 percent. We found that there is a weak and reliable correlation between NAO and annual rainfall of Iran, which is about 20 percent.

**MI05/11P/B17-007 1630**

**DYNAMICS OF INTRA-SEASONAL VARIABILITY OF THE SIBERIAN HIGH**

Koutarou TAKAYA<sup>1</sup>, Hisashi NAKAMURA<sup>2</sup> (<sup>1</sup>Institute for Global Change Research, Frontier Research System for Global Change, <sup>2</sup>Department of Earth and Planetary Science, University of Tokyo)

The Siberian high is a cold, semi-permanent surface anticyclones residing over the Asian continent in winter. The high is known as one of the crucial factors for wintertime climatic condition over the Far East and Northwestern Pacific, as it influences the strength of the winter monsoon. However, our understanding is rather limited with respect particularly to the mechanism how the surface cold high develops under the influence of circulation anomalies in the upper-troposphere. In this study, time evolution and dynamical mechanism of intraseasonal amplification of the high are investigated on the basis of the circulation data observed over the 40 recent years. For each grid point over Siberia, a composite analysis was performed for the 20 strongest anticyclonic events separately at the 1000- and 250-hPa levels. At every location, a surface high was found to amplify in association with formation of a blocking ridge aloft. The evolution of the upper-level blocking was found quite different between the east and west of the climatological upper-level trough over the Far East. To the west, what may be called "wave-train type" is common, in which a blocking ridge forms near the leading edge of a quasi-stationary Rossby wave train propagating eastward across the Eurasian continent. To the east of the trough, in contrast, what may be called "Pacific-origin type" dominates, in which a blocking ridge forms in association with a westward extension of anticyclonic anomalies from the North Pacific. We have shown through "potential vorticity (PV) inversion" technique that an interaction of the upper-level wave train with pre-existing surface cold anomalies is essential for the extreme amplification of the surface high of the "wave-train" type. Surface circulation anomalies induced by upper-level PV anomalies associated with the wave train acts to reinforce the pre-existing cold anomalies by inducing anomalous cold advection, which counteracts the tendency of the surface anomalies to migrate eastward as "surface thermal Rossby waves". The surface cold anomalies thus intensified, in turn, act to induce anomalous circulation in the upper troposphere that reinforce the blocking ridge and cyclonic anomalies downstream. The above mechanism may be viewed as kind of thermal destabilization of barotropic Rossby waves. Similar interaction mechanisms between the upper-level and surface anomalies were found instrumental also in amplification of a surface high of the "Pacific origin" type. Regardless of a type of upper-level blocking formation in the upper troposphere, a cold-air outbreak tends to occur, once anomalously cold air reaches the northeastern slope of the Tibetan Plateau. Pre-existing cold anomalies at surface are found essential for the extreme amplification of the Siberian high. Extreme blocking events without pre-existing cold anomalies at surface can cause rather weak amplifications of the high and cold-air outbreaks.

**MI05/11P/B17-008 1650**

**NORTH ATLANTIC OSCILLATION PREDICTABILITY IN THE CLIMATE CHANGE PERSPECTIVE**

Roxana A. BOJARIU (Research Department of Dynamic Meteorology and Climatology, National Institute of Meteorology and Hydrology)

The magnitude of the recent observed upward trend in the North Atlantic Oscillation (NAO) index is inconsistent with the results obtained from control run experiments of global climate models implying that either the models are deficient or that external forcing is responsible for this variation. In this study, observational evidence is presented for the role of boundary variables such as Eurasian snow cover, Arctic sea-ice extent and Atlantic sea surface temperature (SST) in the NAO variability of the last decades. The analysis of boundary variables and NAO index suggests a pattern of change which has modified the NAO predictive potential in the last half century. Predictive signals are identified based on this pattern and a methodological framework is built to predict the NAO phase on interseasonal time scales in a hindcast experiment. The methodological framework uses the climate state vector concept of Barnett and Preisendorfer to select analogs in the interval 1973-2002.

**MI05/11P/B17-009 1710**

**ASYMETRIES IN THE TEMPERATURE PATTERN ASSOCIATED WITH THE NORTHERN ANNULAR MODE**

Judah Levi COHEN (AER, Inc.)

Since the influential paper of Hurrell (1995), and reinforced by the paper of Thompson and Wallace (1998) and subsequent papers by the same authors, it has been widely accepted that the negative (positive) phase of the NAO/AO produces cold (warm) temperatures across all the major land areas of the mid-high latitudes of the Northern Hemisphere, including Europe, Siberia and eastern North America, giving the appearance of annularity. We demonstrate that this temperature pattern is mostly an artifact of multi-year averaging, which results in the superpositioning of two distinctive patterns. In fact a negative (positive) NAO can also produce sub-seasonal warm (cold) temperatures for Europe, Siberia and eastern North America depending on the dynamic evolution of the NAO/AO. Separation of the two patterns allows for more accurate representation of temperature anomalies associated with the NAO/AO and introduces a spatial and temporal resolution in seasonal forecasts previously not possible.

**MI06-Posters** **Tuesday, July 8**

**THE DYNAMICS OF MID-LATITUDE AND POLAR WEATHER SYSTEMS OVER THE OPEN OCEAN (ICPM, ICDM)**

Location: Site D

**Tuesday, July 8 AM**

**MI06/08A/D-001** **Poster** **0830-152**

**CHANGES IN PROPAGATION PATH OF UPPER-LEVEL SYNOPTIC EDDIES AND INTERANNUAL VARIATIONS IN WINTERTIME STORM TRACK ACTIVITY OVER THE NORTH PACIFIC**

Takeaki SAMPE, Hisashi NAKAMURA (Department of Earth and Planetary Science, University of Tokyo)

In the wintertime Northern Hemisphere, activity of synoptic-scale eddies with subweekly periods is mostly confined in two major 'storm tracks'. The eddy amplification has been interpreted based on linear theory of baroclinic instability; i.e. the growth rate of baroclinic waves increases with the vertical shear of the mean westerlies. As already pointed out, however, the storm track activity over the North Pacific tends to be suppressed in midwinter despite the enhancement of the upper-level jet and associated lower-level baroclinicity, as opposed to the theory. One of the possible mechanisms suggested is changes in eddy structure under the strong subtropical jet, which act to reduce conversion of available potential energy from the basic state to the eddies. In this study, using reanalysis data, we examine how the propagation path of upper-level eddies changed in association with variations in the Pacific subtropical jet intensity, and how those changes are related to the observed modifications in eddy structure. Upper-level subweekly eddies are found to enter the North Pacific storm track mainly from Siberia, and their propagation path over the Far East and Northwestern (NW) Pacific is found sensitive to the intensities of the planetary-wave trough and subtropical jet aloft. In midwinters with suppressed storm track activity over the Pacific during the early and mid-1980s, upper-level eddies propagating from Siberia were steered southeastward by the deepened trough and tended to be trapped into the subtropical jet core with extremely tight potential vorticity (PV) gradient. Since the jet core was located at around 32°N and at 12 km above the surface, the eddies propagating through the mid-latitude tropopause into the jet core were lifted up by ~3 km and kept ~800 km away from the surface baroclinic zone that was anchored at ~40N by the oceanic subarctic frontal zone. The trapping thus hindered those eddies from interacting with the surface baroclinic zone, acting to distort eddy structure and weaken near-surface wind fluctuations and lower-tropospheric poleward eddy heat fluxes. In this manner, midwinter storm track activity tended to be suppressed in the presence of the deep upper-level trough and excessively strong subtropical jet. In addition, reduced near-surface baroclinicity over the anomalously cold continental surface acted to weaken synoptic disturbances coming into the NW Pacific storm track. Since the late 1980s, the winter monsoon was weakened and both the subtropical jet and associated PV gradient were relaxed. Thus, under the reduced trapping effect by the subtropical jet, synoptic eddies coming from Siberia could propagate through mid-latitude tropopause right over the surface baroclinic zone even in midwinter as in spring and autumn. In fact, poleward shift of the Pacific storm track axis was observed in the late 1980s. Consequently, strong interaction were likely between the upper-level eddies and the surface baroclinic zone, leading to enhanced storm track activity over the North Pacific, observed as the disappearance of the midwinter minimum of that activity since the late 1980s.

**MI06/08A/D-002** **Poster** **0830-153**

**AN EXCITEMENT OF THE GRAVITATIONAL AND ACOUSTIC WAVES IN THE EARTH ATMOSPHERE CAUSED BY HORIZONTAL AND VERTICAL SHEAR FLOW**

Tamara A. PATARAIA<sup>1</sup>, Avtandil D PATARAIA, Tamara A PATARAIA (<sup>1</sup>department of Plasma Physics, Tbilisi State University, <sup>2</sup>1. Centre for Plasma Astrophysics, abastumani Astrophysical Observatory, 2a Al. Kazbegi Ave., Tbilisi, 380060, Georgia)

In the paper is investigated the excitement of the gravitational and acoustic waves in the earth atmosphere in linear approximation. The atmosphere is assumed to be ideally non-isothermally stratified and waves are excited by horizontal and vertical shear flow. Calculations are made in a local Cartesian frame with the unit vector along x in the horizontal direction, the unit vector along z in the vertical direction. The x component of velocity has linear dependence on y and z components, y and z components of the velocity are zero.

**MI06** **Wednesday, July 9**

**THE DYNAMICS OF MID-LATITUDE AND POLAR WEATHER SYSTEMS OVER THE OPEN OCEAN (ICPM, ICDM)**

Location: Site B, Room 20

**Wednesday, July 9 PM**

**MI06/09P/B20-001** **1400**

**ANALYSIS OF THE UPPER COLD LOW IN THE SUMMER NORTH PACIFIC**

Kei SAKAMOTO, Masaaki TAKAHASHI (Center for Climate System Research, University of Tokyo)

Upper cold lows (UCLs) are generated near the tropopause in the midlatitude westerlies. These cyclonic circulations are seen at upper level. UCLs have a warm core around 150hPa, a cold core around 200~250hPa and have cirrus clouds (Shimamura, 1981). But the generation mechanism of UCLs have not been clear yet. Nishimori and Ishihara (1997) showed that UCLs came close to Japan when the Tibetan High and the subtropical high are toward north. Using ECMWF Operational datasets, the UCLs generated in 1999 in the summer north Pacific were analyzed. In June and July, the Tibetan High was toward north, UCLs traveled westward along 25~30°N latitude and 4 UCLs came close to Japan. One of UCLs in Aug 1999 was studied in detail. High PV was extended by advection at west of a synoptic disturbance and anti-cyclonic circulation was intensified at east of high PV. Then the tip of high PV was cut off and the UCL was generated. The UCL structure of cyclonic circulation, warm and cold cores and cirrus clouds are identified. The UCL had updraft in the

direction of movement. Convective clouds were seen at north of the UCL. To investigate the role of cirrus clouds and convective clouds in the UCL, the UCL and clouds were simulated using a meso model. Cirrus clouds were not so important for the UCL. But a cold core of the UCL was weakened by latent heat of convective clouds and the UCL was separated because of the cold core weakness.

**MI06/09P/B20-002** **1420**

**NUMERICAL STUDIES OF ATMOSPHERIC KELVIN WAVES OFF THE WEST COAST OF GREENLAND**

Rebekah E. MARTIN, G.W.K. MOORE (Department of Physics, University of Toronto)

Atmospheric Kelvin waves have been tracked and studied in the marine boundary layer of coastal regions of South Africa, the west coast of North America, and Australia. One characteristic of these regions that is crucial for the propagation of these waves is that the height of the boundary layer is below that of the coastal topography, which becomes the wall against which the Kelvin wave is trapped. With its very high topography, the west coast of Greenland is a good candidate for the development of atmospheric Kelvin waves. In particular, an atmospheric Kelvin wave would propagate northwards along this coast. This sense of propagation is actually retrograde to the prevailing winds in the region, which are directed southwards along the coast. As a result, a northward traveling mesoscale low pressure region could be the signature of a Kelvin wave. In this presentation we will show one such example of a weather system. On December 28, 1997 a synoptic-scale low collided with the southern tip of Greenland, and subsequently was split into two separate lows. The remains of the synoptic-scale system on the west side of the island spanned a polar low in the Davis Strait and excited a disturbance that propagated northwards along the west coast of the island. Both station data and high-resolution numerical simulations with MM5 show the propagation of the wave along the coast in the pressure, temperature, and wind fields.

**MI06/09P/B20-003** **1440**

**ATMOSPHERIC RESPONSE TO MID-LATITUDE THERMAL FORCING: IMPLICATIONS FOR CLIMATE REGIMES**

Peter G. BAINES (CSIRO Atmospheric Research)

In mid-latitudes the atmosphere is dominated by the zonal mean circulation forced by the latitudinal heating distribution, and large synoptic scale eddies that are attributable to its instability. It is also influenced by local topography and heating. On the quasi-geostrophic scale, the effects of the latter are manifested in forced barotropic and baroclinic Rossby waves. In this presentation I describe the effects of periodic and isolated thermal forcing in realistic sheared mid-latitude wind profiles, and the associated wave and flow fields that are produced. Typically, this consists of lee-side Rossby waves, and columnar upstream motions that may be identified with observed quasi-stationary high pressure systems, such as those upstream of Australia and in the Great Australian Bight, particularly in summer. The analysis shows that when the atmosphere is highly sheared and the mean flow near the ground is reduced to small values ( $< 1 \text{ ms}^{-1}$ ), as it is in the mid-latitude zonal high pressure belt, higher order vertical modes may become subcritical (that were formally supercritical). This means that they will form part of the stationary response to thermal forcing from the Australian continent, or parts of it. In these conditions, a reduction in the mean surface wind speed due to a movement in the latitude of the high pressure belt, may cause abrupt changes in the flow field. In particular, this may cause a change in the direction of the forced surface wind from, say, southerly to northerly. The systematic effects of such changes at particular times of the year may result in effective changes in climate and rainfall. Hence, a systematic change in the mean position of the high pressure belt may cause abrupt changes in regional wind fields, for given seasons.

**MI06/09P/B20-004** **1500**

**ON THE ROLE OF SYNOPTIC DISTURBANCES AND LOW-FREQUENCY VARIATIONS IN BLOCKING FLOWS**

Miki ARAI, Hitoshi MUKOUGAWA (Disaster Prevention Research Institute, Kyoto University)

We examine the formation and maintenance mechanism of blocking flows by using a  $\beta$ -channel barotropic model with an isolated topography. In particular, we focus upon the role of synoptic disturbances and low-frequency variations to the blocking formation in this model. This model has stationary solutions and periodic solutions with dominant zonal wavenumber 4 components for  $h=900 \text{ m}$  in the range of  $10 \text{ m/s} < U < 20 \text{ m/s}$ , where  $h$  and  $U$  denote the topographic height and the prescribed uniform zonal wind speed, respectively. Several time integrations are performed with an imposed eddy forcing representing synoptic scale disturbances just downstream of the topography. In the range of  $10 \text{ m/s} < U < 15 \text{ m/s}$ , distinct diffuent flows similar to the blocking frequently appear and persist more than 10 days. In fact, the EOF analysis to 10-day low-pass filtered streamfunction field for  $U=14 \text{ m/s}$  reveals that the most dominant variability associated with the EOF1 component is closely related to the occurrence of the distinct diffuent flow. Thus, we define the blocking event when the projection of the streamfunction field to EOF1 for  $U=14 \text{ m/s}$  and  $h=900 \text{ m}$  becomes greater than one standard deviation of the corresponding principal component variability. By using this definition, we find that the formation of the blocking event in this model crucially depends on the prescribed uniform zonal wind speed  $U$ . The time evolution of the streamfunction field decomposed into the high- and low-frequency part is examined based upon the vorticity equation. This analysis indicates that the advection of relative vorticity associated with the high-frequency eddies by the low-frequency flow field is the most important for the formation of the blocking flow. On the other hand, the development of the low-frequency field reveals that the eddy straining mechanism due to high-frequency eddies is not essential for the formation of the blocking event, but plays an important role for the maintenance of the diffuent flow after the onset of the blocking event. Thus, this study indicates that the effectiveness of the eddy straining mechanism crucially depends on the basic flow, and suggests the important role of the low-frequency variability to trigger the onset of the blocking.

**MI06/09P/B20-005** **1520**

**ANALYSIS OF THE ORIGIN STRUCTURE AND MOVEMENT OF THE MEDITERRANEAN DEPRESSIONS**

Farhang AHMADI-GIVI, Mohammad Ali NASR ESFAHANI (Department of Space Physics, University of Tehran)

A climatological analysis of Mediterranean cyclones and their impacts on the Middle East weather patterns is carried out. The diagnostic tools used in this study are the monthly mean geopotential height and relative vorticity at 850 and 500 mb as well as the monthly mean 1000-850 mb thickness. Using an objective method about 30 cyclones were identified that occurred in the Mediterranean region for a period of one year (July 2001- July 2002). The characteristics of each cyclone, such as duration, intensity, path, source region and its

dynamic were examined. The results show that the strength and the number of cyclones in the whole Mediterranean region are significantly decreased during the period of early June by the end of September, largely due to the movement of the subtropical highs to the higher latitudes. Also, the Persian Gulf pressure trough, which is an extension of the southwest Asian monsoon, acts to weaken the intensity of cyclogenesis and slow down its eastward movement in the eastern Mediterranean region. During early October until the end of January, as the effect of subtropical high seems weak in the northern Mediterranean, cyclogenesis activity increases over the Aegean Sea and the Gulf of Genoa. Since these cyclones move northeastwards, their effects are rather weak in the Middle East weather. From February to May, the cyclonic occurrences in the northern Africa increase, largely due to the strong temperature gradient between the North Africa coast and the southern Mediterranean. As these cyclones move eastwards over the Saudi Arabia and the Red Sea, the Middle East weather is affected.

**MI06/09P/B20-006 1540**

**POLAR LOW GENESIS OVER THE EAST COAST OF ASIAN CONTINENT SIMULATED IN AGCM**

Kozo NINOMIYA, Teruyuki NISHIMURA, Takeshi ENOMOTO, Tuneaki SUZUKI, Shinji MATUMURA (Frontier Research System for Global Change)

This report presents cases of polar low genesis over the eastern coast of the Asian Continent simulated in the seasonally varying climatological SST run by an AGCM (atmospheric general circulation model: T42L52 and T106L52). We study the simulation in January of the fourth and seventh year integration after the 10-year period of the spin-up. We compare features of these polar lows with the features described in several observational studies. In the simulations, the polar low is formed over the coastal sea area ~1500 km west of the major extratropical cyclone that developed over the Northwestern Pacific Ocean, under the influence of a short wave trough, which propagates along the rim of the large-scale upper cold low. The polar low genesis takes place first as the deepening of the surface trough, which extends westward from the major cyclone. The deepening of the surface trough in the zone of strong low-level thermal gradient over the coastal sea area suggests the important role of the low-level baroclinicity for the polar low genesis. The strong heating due to the energy supply from the sea surface contributes for the genesis of the polar low through the decreasing of the vertical stability and the sustaining the thermal gradient. Meanwhile, the heating around 700 hPa associated with the precipitation concentrated within the polar low indicates the influence of the condensation heating for the development of the polar low. Aforementioned various processes work together to generate and develop the polar low. The structure and the evolution process of the simulated polar low are consistent with those of the observed polar low. It is concluded that the realistic polar low genesis takes place in the AGCM, when the large-scale phenomena such as the upper cold low, the short-wave trough, parent major cyclone and polar air outbreak are reasonably simulated. The present study has significant meaning in presenting the AGCM simulation of polar low for the first time.

**MI06/09P/B20-007 1620**

**SHORT-WAVE BAROCLINIC DEVELOPMENT OVER A WARM OCEAN**

Maurizio FANTINI (ISAC - CNR)

Baroclinic waves can be unstable in a saturated environment at wavelengths much shorter than the common midlatitude cyclones. The presence of sensible and latent heat input from a warmer oceansurface reduces the length of possible growing baroclinic perturbations maintaining the saturatedenvironment necessary, and further by providing an additional source of energy. The mechanism by which this additional energy is made available to baroclinic development is studied in a PE model in simplified geometry.

**MI06/09P/B20-008 1640**

**DEFORMATION AND MOBILE TROUGH SUPPRESSION OVER EAST ASIA**

Boksoon MYOUNG, John W. NIELSEN-GAMMON (Department of Atmospheric Sciences, Texas A&M University)

The midwinter suppression of baroclinic activity over the North Pacific storm track is a paradox that tests our understanding of the role of baroclinic instability in the atmosphere. Existing theories for midwinter suppression have assumed that the suppression mechanism is local, through a jet-induced change in the linear or nonlinear instability characteristics or an alteration of the structure and role of moist processes. We examine the hypothesis that suppression is caused by a lack of suitable upper-tropospheric triggering disturbances due to extreme stretching deformation in the entrance region of the North Pacific storm track. A statistical climatology shows that upper-tropospheric mobile troughs approaching the western North Pacific are weaker in winter than in fall and spring, but that they intensify more rapidly than in the fall and spring when they reach the open ocean and interact with surface baroclinic zones. However, their more rapid intensification is insufficient to overcome their initial intensity deficit. We also show that the magnitude of this initial intensity deficit is strongly correlated to the strength of the background stretching deformation over Asia.

**MI06/09P/B20-009 1700**

**CYCLONES OVER THE FRAM STRAIT**

Burghard BRUEMMER, Gerd MUELLER (Meteorological Institute, University of Hamburg)

The Fram Strait between Greenland and Spitsbergen is the main gate of water mass exchange between the Arctic Ocean and the Atlantic Ocean. Per annum about 3,000 km<sup>3</sup> of freshwater in form of sea ice drift into the Atlantic. This freshwater supply into the world ocean is only surpassed by the Amazon river. The interannual variation is large and amounts to +/- 50 per cent. The Fram Strait is also a region of high cyclone activity. The variability of the cyclone activity may be one reason for the variability of the Fram Strait sea ice transport. This hypothesis is investigated by statistical methods and cyclone case studies. The case studies are based on measurements in two Fram Strait cyclone experiments, called FRAMZY 1999 and FRAMZY 2002, in which in situ measurements by aircraft, ship and an array of automatic sea ice buoys as well as satellite imagery (NOAA AVHRR, Radarsat, SSM/I) were taken. Generally, Fram Strait cyclones moves from south to north through the region. Most cyclones develop at the ice edge of the East Greenland Current and finally decay over the Arctic sea ice. The cyclones are small (diameter of a few hundred km) but can be very intense with wind speeds of more than 25 m/s. The horizontal temperature contrast between the warm and cold side of the cyclone can be up to 30 K, but is confused to a rather shallow layer of about 500 m. Comparing the in situ cyclone measurements with operational weather forecast models and analyses shows that some cyclones were not simulated by the models. In one extreme case, weak surface pressure differences around 1025 hPa were forecasted (24 h forecast) but a cyclone with wind force 7 was found by the aircraft. Such discrepancies have severe consequences for coupled of uncoupled sea ice-

models.

**MI06/09P/B20-010 1720**

**COMPARATIVE CLIMATOLOGY OF SYNOPTIC AND MESO-SCALE CYCLONIC EDDIES OVER NORTHERN AND SOUTHERN ICE OCEANS**

Victor E. LAGUN, Eduard I. LOUTSENKO (Arctic and Antarctic Research Institute, Air-Sea Interaction Department)

Increasing in recent time interest to synoptic eddy-wave activity in atmosphere is explained by the significant role which the synoptic disturbances play in formation of climatic fields and of their anomalies. Changes in seasonal variations of extreme values of synoptic climatology parameters are used as indicators and possible predictors of low-frequency climatic variability. On the base of twice-daily NCEP reanalysis data set for period 1967-2000 the spatial distribution and temporal variations of extra-tropical cyclone parameters in global atmosphere are calculated. Using satellite imageries of cloudy cover for 1981-2000 the statistical characteristics of sub-synoptic and of polar low type meso-scale eddies are estimated. The original methods for mean sea level pressure and geopotential fields analysis were developed to indicate the cyclone position. Applied numerical methods are based on the synoptic meteorology traditional definition: eddies boundaries are considered as first external closed isobaric line. As a result, the time frequency, pressure anomaly, cyclones square and corresponding horizontal squared mean scale, drift speed, cyclones form parameters, total cyclone number, duration, Hemispheric cyclone parking parameters, mean cyclonic trajectories and their variability are estimated as monthly, seasonal, annual and decadal values. For meso-scale eddies the frequency, shape parameters, number and linear size are estimated. The tendency of the cyclonic parameters variability for atmospheric warming condition is shown. Possible connection between synoptic climatology parameters and ENSO, Arctic and Antarctic Oscillations events and sea ice extent variation and air-sea interaction processes are discussed. The results demonstrate that the number of mature extratropical cyclones is increasing under global warming conditions. The possible reasons of cyclonic eddy activity increasing over Northern and Southern Ocean are discussed.

**MI06/09P/B20-011 1740**

**UPPER-LEVEL DYNAMICAL EFFECTS OF A HURRICANE UPON THE EXTRATROPICAL DOWNSTREAM EVOLUTION**

Cornelia SCHWIERZ, Olivia MARTIUS, Huw C. DAVIES (Atmospheric and Climate Science, ETH Zuerich)

In the beginning of November 2001 the transition of a hurricane from the tropics into the extra-tropics in the western Atlantic triggered (by way of upper-level downstream development) a succession of dynamically notable phenomena. The event is examined from the potential vorticity (PV) perspective, and both Lagrangian and Eulerian techniques are applied using 6-hourly ECMWF analysis data. The northwards moving storm system acted as a significant source of diabatic processes. Downstream of the area of the most intense diabatic heating a large negative PV anomaly was built up that extended up to the tropopause level and covered an area encompassing Greenland and the eastern North Atlantic. The severe storm also led to increased warm-SST advection and enhanced heat fluxes that helped in the intensification of a rapidly deepening Icelandic cyclone. Downstream of the upper-level low-PV ridge the formation of a meridionally elongated intrusion of stratospheric PV (i.e. a PV-streamer) was initiated at tropopause level over Europe. Intense rainfall over northern Algeria caused severe floods that were accompanied by and linked to the wrapping-up of the upper level streamer's tip over the southern Mediterranean and the concomitant formation of a low-level cyclone. During the whole episode an upper-level jet streak propagated downstream along the band of enhanced PV gradient, following the ridge and the streamer. The evolution of this feature is tracked further along the dynamical tropopause to examine a dynamical link between the observed positive wind velocity anomaly over Europe and a strong jet over Japan two days later.

**MI07-Posters Thursday, July 10**

**CLIMATE INTERACTION AT THE LAND-ATMOSPHERE INTERFACE Location: Site D**

Thursday, July 10 PM

**MI07/10P/D-001 Poster 1400-176**

**COMBINED PASSIVE/ACTIVE MICROWAVE REMOTE SENSING APPROACH FOR SURFACE PARAMETER RETRIEVAL FROM TROPICAL RAINFALL MEASURING MISSION (TRMM)**

Khil-Ha LEE, Emmanouil N. ANAGNOSTOU (Department of civil and Environmental Engineering, University of Connecticut)

The backscattering measured by radar technique and the emission measured by a radiometer show significant promise for the estimation of the surface parameters such as near surface soil moisture, vegetation characteristics. Both the dual-polarized 10GHz (X-band) Tropical Rainfall Measuring Mission (TRMM) microwave imager (TMI) and 13GHz (Ku-band) precipitation radar (PR) data are used for the estimation of the near surface soil moisture and vegetation properties, which leads to the potential advantage of simultaneous active/passive observations. In turn the retrieved complementary information included in both the emission and backscattering can retrieve the surface roughness properties. A simple Fresnel model for soil and modified simple model for vegetation are used to estimate the microwave emission and a theoretically based Geometric Optics Model (GOM) for soil and the semi-empirical water-cloud model for vegetation are used to estimate the backscattering signal of the land surface. The model parameters required to specify the nature of the soil and vegetation are not usually available from the data taken in the field experiments. Thus the parameters are optimized using either numerically derived or remotely sensed data. This study presents the combined active/passive approach is a good tool to estimate the surface parameters.

**MI07/10P/D-002** Poster **1400-177**

**WATER-USE EFFICIENCY OF LAND-ATMOSPHERE CARBON EXCHANGE IN THE WORLD'S MAJOR RIVER BASINS: A SIMULATION STUDY**

Akihiko ITO (Ecosystem Change Research Program, Frontier Research System for Global Change)

Water-use efficiency (assimilation of atmospheric carbon dioxide per unit water loss by evapotranspiration) is a physiologically, ecologically, and agriculturally important index of terrestrial vegetation. As freshwater is less accessible in the future, due to human utilization, water pollution, and climate change, the water-use efficiency (WUE) becomes more and more important for the sustainability of natural and cropland ecosystems. In this study, WUE of the world's major river basins is estimated with a process-based terrestrial model (SIM-CYCLE), which incorporates not only carbon dynamics (i.e. photosynthesis, allocation, respiration and decomposition) but also energy and water budget (i.e. evaporation, transpiration, and runoff). Based on datasets of actual biome, soil property, topography, and long-term climate, we estimate carbon and water budget of terrestrial ecosystems globally, at a 0.5-degree (longitude and latitude) horizontal resolution. At the present condition, global annual carbon assimilation rate (GPP) and net primary production (NPP) are estimated as 131.8 and 63.7 Pg C, respectively, at the cost of evapotranspiration (ET) by 69200 km<sup>3</sup>. Then, average WUE (=NPP/ET) is calculated as 0.92 g C per kg H<sub>2</sub>O. This is smaller than the instantaneous WUE (=GPP/transpiration) of leaf stomatal gas exchange, 3.55 g C per kg H<sub>2</sub>O. Here, the global basin maps are adopted to aggregate the global results for the world's major 53 river basins: for example, Amazon, Mississippi, Lena, and so on, covering about 40 % of the world land area. In this study, three different river basin maps, developed independently by the University of Texas, University of New Hampshire, and University of Tokyo, are used and compared. In the river basin analysis, it is apparent that the Amazon basin has the largest contribution to the atmosphere-biosphere exchange of water and carbon: 8.3 % of global GPP and 11.8 % of global ET. Among the river basins, dryer ones (i.e. precipitation < potential evapotranspiration) have higher values of WUE (approximately 5 g C assimilated per 1 kg transpiration) than moist/wet ones. The difference in WUE among the river basins is attributable to the differences in stomatal aperture of leaves and composition of C3/C4 plant species. The global and basin-specific results are validated by comparing with observations of stream discharge, which is strongly affected by vegetation activity. In spite of a simple representation of soil water with 2-layer model, the model shows good performance to capture broad-scale water budget. At last, the model study carries implications for management of water and carbon yields from terrestrial ecosystems. For example, when we plant to sequester 1 Pg of atmospheric carbon by increasing plant assimilation, it may require on average 280 km<sup>3</sup> of water for solely transpiration.

**MI07/10P/D-003** Poster **1400-178**

**COMPARISON OF WATER AND HEAT BALANCE ON GRASSLAND AND FOREST IN CENTRAL YAKUTIA, EAST SIBERIA**

Hironori YABUKI<sup>1</sup>, Yoshiyuki ISHIF<sup>2</sup>, Tetsuo OHATA<sup>3</sup> (<sup>1</sup>Frontier Observational Research System for Global Change, <sup>2</sup>Institute of Low Temperature Science, Hokkaido University, <sup>3</sup>Frontier Observational Research System for Global Change / Institute of Low Temperature Science, Hokkaido University)

Siberian region is an area dominated by taiga forest but the percentage of it is 70%, other being bare land, grassland and water bodies such as rivers and lakes. These regions were underlain by permafrost. Especially, in right bank of the Lena River region which is the opposite side of the Yakutsk City, there are many concave landform called "alas". An alas is formed after the forest has been cleared by natural collapse and forest fire, cultivation in an area where the ice content of permafrost was high. The alas occupying up to 20% of this area. Most alas have lakes and marshes near the center, and the surround of lake is covered in the grassland. When we consider the water and heat circulation of this region, it is necessary to clarify water and heat characteristics of the forest and grassland. In this study, the water and heat flux observation was carried out in the forest and grassland area, and the water and heat balance characteristics was compared. Until now, the simultaneous measurement of sensible heat and latent heat fluxes in forest and grassland was little, where weather condition seemed to be almost similar. Observation site in the right bank of the Lena River is called "Ulakhan Sykhan", located 50km north east part of the Yakutsk city. The field observation was carried out from April to September 2000. In forest site, we install observation tower in a flat larch forest. The stand density was 4200 tree ha<sup>-1</sup>. The mean basal diameter of tree was 7.6cm. The mean stand height was 7.6m. The maximum stand height was 17.3m. In grassland site, we installed observation mast in the center of alas. This alas has oval shape and 0.64km<sup>2</sup> area including a 0.1km<sup>2</sup> lake at the center. The tower and mast were used 1-D scale flux observations of forest canopy and grassland, respectively. Both sites have separated as a distance about 2km. Air temperature and humidity were measured at 22m and 17m in forest site, and 2m and 0.5m in grassland site, respectively. We measured the downward and upward short-wave/long-wave radiation on top of tower and upward short-wave/long-wave radiation at grassland. Latent heat and sensible heat fluxes were obtained by the BOWEN ratio method. And those fluxes were compared with between forest and grassland sites. At the grassland the sensible heat flux was smaller and latent heat flux larger than those at the forest site. PAI in forest and grassland were 3.5 and 3.2, respectively, this value of the grassland was smaller than that of the forest site. However, the area of trunk and branch at forest were big, LAI of the forest which contributes to the evapotranspiration was 2.0, this value was smaller than grassland. The difference of this LAI seems to appear the difference in the latent heat of the forest and the grassland.

**MI07/10P/D-004** Poster **1400-179**

**NET CO<sub>2</sub> EXCHANGE OF CANOPY AND FOREST FLOOR OF A LARCH FOREST IN NORTHERN JAPAN**

Ryuichi HIRATA<sup>1</sup>, Takashi HIRANO<sup>1</sup>, Junichi MOGAMI<sup>1</sup>, Naishen LIANG<sup>2</sup>, Yasumi FUJINUMA<sup>3</sup>, Nobuko SAIGUSA<sup>1</sup>, Susumu YAMAMOTO<sup>1</sup> (<sup>1</sup>Graduate School of Agriculture, Hokkaido University, <sup>2</sup>CGER, National Institute for Environmental Studies, <sup>3</sup>National Institute of Advanced Industrial Science and Technology)

CO<sub>2</sub> flux measured above a forest ecosystem is the sum of net CO<sub>2</sub> exchanges occurring between surrounding air and each part of the forest, such as canopy, understory, and soil, with a different physiological and structural function. The CO<sub>2</sub> exchange should be measured separately to investigate CO<sub>2</sub> dynamics in the forest and to establish a model for evaluating the CO<sub>2</sub> balance of the forest. We measured CO<sub>2</sub> flux above and below a larch forest in Hokkaido, northern Japan and evaluated the contribution of net ecosystem CO<sub>2</sub> exchange of the forest floor (NEEF) including understory and soil to that of the whole forest ecosystem (NEEw). The study site is a larch plantation (42o44'N, 141o31'E) with an area of 100 ha and a canopy height of 15 m. Understory consists primarily of fern with a height of 0.5 ~ 0.8 m in summer. Soil is an immature volcanic soil with high water permeability and poor nutrients. The maximum LAI was measured at 2.3 and 3.0 for canopy and understory, respectively, in June. CO<sub>2</sub> and energy fluxes have been measured at heights of 27 and 2 m by the eddy-covariance technique with an open-path CO<sub>2</sub>/H<sub>2</sub>O analyzer, for about seven months between April and November in 2002. After larch leaves emerged in mid-April, daily NEEw changed gradually from positive (upward direction) to negative (downward direction),

and daytime NEEw became more negative rapidly with leaf expansion in May. The change in daytime NEEw became smaller as LAI approached a peak value of 2.3, and it increased in mid-June. Daytime NEEf was negative in late-April when solar radiation penetrated into the forest floor and soil temperature was still low because photosynthesis of ferns with expanded leaves was larger than soil respiration. NEEf increased gradually with increases in canopy LAI and soil temperature from May to July, in spite of an increase in understory LAI; understory photosynthesis decreased by insufficient light condition and soil respiration increased. However, a significant diurnal variation in NEEf with the minimum around noon was observed, while the minimum NEEf was still positive. Daytime NEEf never returned to be negative even in fall when canopy was opened by defoliation and soil temperature decreased. In total for the seven months, about 35 % of the CO<sub>2</sub> absorbed by canopy leaves was originated from the forest floor. In particular, the percentage increased up to 70.0 % in summer when soil respiration was large.

**MI07/10P/D-005** Poster **1400-180**

**SEASONAL AND INTERANNUAL VARIATIONS IN CARBON DIOXIDE EXCHANGE AND CARBON BALANCE IN A COOL-TEMPERATE DECIDUOUS FOREST IN SAPPORO, JAPAN**

Yuichiro NAKAI, Kenzo KITAMURA, Satoru SUZUKI (Hokkaido Center, Forestry and Forest Products Research Institute)

Net ecosystem carbon dioxide exchange (NEE) was measured in a secondary deciduous broadleaf forest for three years (2000-2002) using eddy covariance technique. The study objectives were to document how NEE and its major component processes-gross photosynthesis (GPP) and total ecosystem respiration (RE)- vary seasonally and interannually. Annual NEE's were -269(gC m<sup>2</sup> y<sup>-1</sup>) in 2000, -420(gC m<sup>2</sup> y<sup>-1</sup>) in 2001, and -508 (gC m<sup>2</sup> y<sup>-1</sup>) in 2002. Annual mean air temperature were 17.5 (deg.C) in 2000, 16.2 (deg.C) in 2001, and 15.7 (deg.C) in 2002. In general, RE highly depends on temperature and its annual values were in the same order as the air temperature and were 1067 (gC m<sup>2</sup> y<sup>-1</sup>) in 2000, 990 (gC m<sup>2</sup> y<sup>-1</sup>) in 2001, and 932 (gC m<sup>2</sup> y<sup>-1</sup>) in 2002. On the other hand, annual GPP values were in the inverse order to RE and were 1336 (gC m<sup>2</sup> y<sup>-1</sup>) in 2000, 1410 (gC m<sup>2</sup> y<sup>-1</sup>) in 2001, and 1440 (gC m<sup>2</sup> y<sup>-1</sup>) in 2002. Various factors as the timing of leaf expansion, the photosynthesis available radiation in the growing season, and etc. were examined how GPP's were determined. However, critical factors have not narrowed down to a few issue.

**MI07/10P/D-006** Poster **1400-181**

**CO<sub>2</sub> AND ENERGY EXCHANGE OF A TROPICAL PEAT SWAMP FOREST IN A DEVASTATED PEATLAND IN CENTRAL KALIMANTAN, INDONESIA**

Takashi HIRANO<sup>1</sup>, Hendrik SEGAF<sup>2</sup>, Tania JUNE<sup>3</sup>, Suwido LIMIN<sup>2</sup>, Ryuichi HIRATA<sup>1</sup>, Mitsuru OSAKI<sup>1</sup> (<sup>1</sup>Graduate School of Agriculture, Hokkaido University, <sup>2</sup>Faculty of Agriculture, University of Palangkaraya, <sup>3</sup>Faculty of Mathematics and Natural Science, Bogor Agricultural University)

Tropical peatlands exist under the condition of permanent waterlogging and acidification in the tropics. Indonesia contains the largest area of tropical peatlands, and Kalimantan has the area of 6.7 Mha in lowlands. Tropical peatlands usually coexist a forest and have accumulated a large amount of carbon as organic matter for over thousands of years. Recently, however, deforestation in tropical peatlands is advancing rapidly owing to a growing demand for timber and farmlands. In addition, droughts caused by the El Niño event devastated tropical peatlands by the promotion of peatland fires. In Central Kalimantan a large area of peatlands was deforested to develop farmlands in late 1990's, and channels excavated for drainage dried the peat. The devastation of peatlands promotes decomposition of the peat through the disturbance of micrometeorology and water condition. The promoted decomposition increases the release of carbon fixed in tropical peat to the atmosphere as CO<sub>2</sub>. This suggests that tropical peatlands will be a major CO<sub>2</sub> source for the atmosphere in the near future. Thus we have measured CO<sub>2</sub>, water vapor, and energy fluxes over a tropical peat swamp forest (2° 20' 41.6" S, 114° 2' 11.3" E) in a devastated peatland in Central Kalimantan, Indonesia since November 2002. The existence of the rainy season in southern-hemisphere summer and the dry season in winter was confirmed from precipitation pattern. Findings from the first eight months of the measurements, from December 2002 to July 2003, were as follows. 1) Although precipitation was quite different, diurnal variation in net ecosystem exchange of CO<sub>2</sub> (NEE) was similar between the rainy and dry seasons. Monthly-mean daytime negative peak in NEE was about 20 μmol m<sup>-2</sup> s<sup>-1</sup>, and nighttime NEE was almost constant at about 10 μmol m<sup>-2</sup> s<sup>-1</sup>; this nighttime NEE was about twice as large as that of typical temperate forests. 2) Latent heat flux was considerably larger than sensible heat flux both in the rainy and dry seasons. 3) Monthly sum of NEE was negative in December, February, May, and July, However, it was positive in January and March, and almost zero in April and June. As a result, cumulative NEE for the eight month was only -3.6 mol m<sup>-2</sup>, which is equivalent to carbon fixation of 43 gC m<sup>-2</sup> by the forest ecosystem. 4) Monthly sum of evapotranspiration (ET) was between 100 and 140 mm. Difference in ET was much smaller than that in precipitation on a monthly basis. Cumulative ET for the eight months was 914 mm, which is about 75 % of the cumulative precipitation.a

**MI07** Friday, July 11

**CLIMATE INTERACTION AT THE LAND-ATMOSPHERE INTERFACE**

Location: Site B, Room 18

Friday, July 11 AM  
Presiding Chair: N.O. Jensen

**I07/11A/B18-001** **0830**

**A MODELLING STUDY OF THE CLIMATIC IMPACTS OF VEGETATION IN THE TROPICS: SENSITIVITY TO THE SPECIFICATION OF SOIL CHARACTERISTICS**

Tom OSBORNE<sup>1</sup>, David LAWRENCE<sup>1</sup>, Julia SLINGO<sup>1</sup>, Chris TAYLOR<sup>2</sup>, Tim WHEELER<sup>1</sup> (<sup>1</sup>NCAS Centre for Global Atmospheric Modelling, University of Reading, <sup>2</sup>NERC Centre for Ecology and Hydrology, Wallingford, <sup>3</sup>Department of Agriculture, University of Reading)

Vegetation is known to have a strong influence on land-atmosphere interactions, and major changes in tropical land cover, associated primarily with deforestation, have been shown to have significant impacts on the local climate, for example over South America. This paper describes a series of sensitivity experiments with the Hadley Centre atmospheric GCM (HadAM3) in which the effects of vegetation in the tropics on the mean climate and its variability are explored. An important part of the study has been an investigation of the dependence of these effects on the specification of soil characteristics. The processes



through which vegetation modifies the climate and in particular the soil hydrology will be described. It will be shown that there are large regional differences in the degree to which vegetation influences the mean climate and its variability. The sensitivity of the results to the specification of soil characteristics, involving soil hydraulic parameters, has been investigated by exchanging the standard soils dataset in HadAM3 with one derived from the IGBP-DIS soil data task. The results have shown that the climatic effects of land cover change depend critically on the specification of the soil characteristics. This emphasises the importance of improving the representation of soil hydraulic parameters in climate models used to predict the effects of land use/cover change.

**MI07/11A/B18-002** **0850**

**NUMERICAL STUDY OF THE IMPACT OF VEGETATION CHANGES ON CLIMATE IN ASIAN TROPICAL REGION**

Kazuo MABUCHI<sup>1</sup>, Yasuo SATO<sup>1</sup>, Hideji KIDA<sup>2</sup> (<sup>1</sup>Meteorological Research Institute, <sup>2</sup>Kyoto University)

A land surface model (Biosphere-Atmosphere Interaction Model: BAIM) has two vegetation layers and three soil layers, and for each layer predicts the temperature and stored moisture. In the presence of snow cover, the snow layer is divided into a maximum of three layers, with the temperature and amount of snow and water stored in each layer being predicted. Use of BAIM can result in estimates of not only the energy fluxes, but also the carbon dioxide flux between terrestrial ecosystems and the atmosphere. The photosynthesis processes for C3 and C4 plants are adopted in the model. The model can also predict the accumulation and melting of snow on the ground, and the freezing and melting of water in the soil. BAIM was incorporated into a spectral general circulation model. This general circulation model has a triangular truncation at wave number 63 (T63) and has 21 vertical levels. The horizontal grid interval is about 200 km (192 × 96 grids). The vegetation type of each grid point is specified and the interactions between the land surface vegetation and the atmosphere are estimated by BAIM at each grid point. The integration time step interval is about 20 minutes. To estimate the initial values of soil water content, including the ice content in the soil and soil temperature, over 10-year spin-up run was carried out. Using the initial values in the soil obtained by the spin-up run, the experimental control time integration was continued for 20 years under the actual global vegetation condition. After the control time integration, 3 type vegetation change integrations were performed. The vegetation types of Southeast Asia and India areas were changed to the bare soil (BS) at the first impact integration, secondly to the C4 grass (C4), and then to the vegetation without green (NG). In each impact experiment, a 10-year spin-up run was performed, and then the experimental impact time integration was continued for 20 years under the changed vegetation condition. In these integrations, the climate SST values were used. The results of the impact experiments were compared with the results of the control. From these investigations, it was found that the regional circulation patterns in Southeast Asia and surrounding area were significantly changed by the vegetation changes. The morphological and physiological effects of vegetation in Asian tropical region are very important for the formation of climate in Monsoon Asia.

**MI07/11A/B18-003** **0910**

**TOPIC: THE IMPACT OF CONGO BASIN DEFORESTATION ON PRECIPITATION AND OTHER CLIMATE PARAMETERS (A COMMON LAND MODEL SIMULATION.)**

Willis Otieno SHEM (Earth and Atmospheric Sciences, Georgia Institute of Technology)

**ABSTRACT:**Deforestation is the clearing of large spaces in the natural forest mostly through anthropogenic activities as the expanding human populations seeks to exploit the forested areas for its own comfort and 'survival'. The international community has in the past few decades campaigned vehemently against deforestation of tropical rain forest especially after most studies indicated a negative impact of this process on some climate parameters like rainfall and runoff. Despite these efforts deforestation has to a large extent persisted and more so in areas like the African tropical forests where the quest for modern living styles are quickly encroaching. The reasons for this activity range from the need for more land for agriculture, livestock and habitat to commercialization of forest products for the manufacture of paper and other wood works. In Central Africa many landless people have been moving into the once forested areas and are quickly converting them into cultivated plots using simple slash and burn methods to create more space. For the period 1980-1990 the tropical forest of the world are estimated to have been disappearing at the rate of 17 million ha annually (Lanly et al., 1991). This figure is known to have increased to 20 million ha annually in the early 1990s (Lal, 1995). While the accuracy of these figures may be open to debate, there has been a deluge of publications giving specific and vivid descriptions of environmental changes wrought by deforestation (Proctor, 1989). These publications have led many to automatically associate tropical deforestation with negative impacts like: lower rainfall; lower water yields from springs and streams; major floods; extreme sedimentation and hence the choking of reservoirs and irrigation canals, etc. Deforestation will add Carbon dioxide (CO<sub>2</sub>) into the atmosphere through biomass burning and hence increase the greenhouse effect, it will increase the surface albedo and will alter other climatic parameters like evaporation. This study seeks to confirm or counter (for the Congo Basin) some of these conclusions and to quantify the magnitude of these impacts on the regional rainfall regimes. The paper will also look at the impacts of deforestation on other climate parameters like temperature, evaporation, sensible and latent heat flux and runoff. The impact of this process on the Carbon-dioxide cycle will not be included in this study. Complex interactions between the soil-vegetation system plus changes in radiation and cloud regimes take place as a result of large-scale deforestation and therefore the General Circulation Models (GCMs) come in handy as a tool for simulating different climate- change scenarios. To take care of the land process that contribute to the general circulation, land surface models have been embedded in these GCMs with remarkable success. This study uses the Common Land Model (CLM2), embedded into the community climate model (CCM3), to simulate the climate change scenarios in the Congo basin when the land surface type is altered from evergreen broad leaf forest to short grassland.

**MI07/11A/B18-004** **0930**

**SEASONALITY OF GLOBAL LAND-ATMOSPHERE INTERACTION IN NCAR COMMUNITY CLIMATE MODEL COUPLED WITH THE COMMON LAND MODEL**

Wanru WU, Robert E. DICKINSON (Earth and Atmospheric Sciences, Georgia Institute of Technology)

The coupled land-ocean-atmosphere climate system is characterized by substantial amounts of spatial and temporal variability on wide range scales. To obtain a better description of this variability and the physical mechanisms responsible for it is critical in climate research [Delworth and Manabe, 1993]. Observations have provided a description of the soil moisture profile variability in terms of amplitude damping, phase shift, and persistence increasing with soil depth. In particular, the dryness signal penetrates more deeply than the wetness signal; the phase shift with soil depth is going deeper with longer time scales; and its seasonal variation is amplified in the drought-year composite, with the phase shift increased. Such variability as a function of soil depth couples to climate variability. Meanwhile, off-line

modeling study has implied the importance to simulate the soil moisture in the context of time scales rather than the soil wetness field itself. With the understanding of the soil moisture profile variability through integrated observational and off-line numerical experiments, this study explores the seasonality of global land-atmosphere interaction with an emphasis on the soil moisture variability and its impact on such seasonality. The NCAR Community Climate Model (CCM3) coupled with the state-of-the-art Common Land Model (CLM) is used for the study. The singular value decomposition (SVD) analysis is applied to the key hydrologic components, i.e., soil moisture, precipitation and evapotranspiration, to obtain the dominant modes of their heterogeneous correlations and corresponding spatial patterns. The time series for performing the SVD analysis are derived from the 10-year simulation of the CCM3-CLM model when its equilibrium status is reached.

**MI07/11A/B18-005** **0950**

**THE INFLUENCE OF LAND EVAPOTRANSPIRATION ON CLIMATE VARIATIONS**

Jan SUN<sup>1</sup>, Guoxiong WU<sup>2</sup> (<sup>1</sup>Chinese Academy of Meteorology Science, <sup>2</sup>National Key Laboratory of Numerical Modeling for Atmospheric Sciences and Geophysical Fluid Dynamics (LASG), Institute of Atmospheric Physics, Chinese Academy of Sciences)

A coupled numerical model of the global atmosphere with a qualified biosphere (GOALS/LASG) has been used to assess the nature of and physical mechanisms for land-atmosphere interactions, and the impacts of the Asian/North American land-surface evapotranspiration on the regional and global climate. This sensitivity study suggests that the simulated climate would be relatively larger sensitive to land surface evapotranspiration, especially over the Asian regions. The removal of evapotranspiration in Asia would create a warmer and drier climate to a certain degree. Furthermore, the surface evapotranspiration anomalies would make a substantial contribution to the formation and variation of subtropical anticyclones through the changes in monsoon precipitation and the β-effect, but also make a large contribution to the variations of the atmospheric circulation in the Northern and even global Hemisphere. Therefore, besides the traditional perception that we have generally emphasized on the influence of subtropical anticyclones activities on the boreal summer precipitation over the regions of eastern China, the surface evapotranspiration anomalies, however, also have substantial impacts on the subtropical anticyclones through the changes in monsoon precipitation. For this reason, the variation in the internal heating sources of the atmosphere caused by the land surface evapotranspiration and the vapor phase change during the boreal summer is an important external factor forcing the weather and climate.

**MI07/11A/B18-006** **1050**

**SURFACE ENERGY BALANCE STUDIES USING ASTER THERMAL INFRARED DATA**

Andrew FRENCH<sup>1</sup>, Thomas SCHMUGGE<sup>2</sup>, William P. KUSTAS<sup>3</sup>, John PRUEGER<sup>4</sup>, Frederic JACOB<sup>5</sup> (<sup>1</sup>Hydrological Sciences Branch, NASA Goddard Space Flight Center, Greenbelt, MD, 20771, <sup>2</sup>USDA/ARS Hydrology & Remote Sensing Lab, Beltsville, MD, 20705, USA, <sup>3</sup>USDA/ARS National Soil Tilth Lab, Ames, Iowa, USA, <sup>4</sup>Ecole Supérieure d'Agriculture de Purpan, Toulouse, France, 31076)

Knowledge of the relationship between the accuracy of surface energy balance estimates and remote sensing resolution is important for the integration of instantaneous satellite observations with regional and global scale hydrological models. Higher resolution thermal infrared (TIR) imagery, such as the 90 m data from the Advanced Spaceborne Thermal Emission and Reflection (ASTER) radiometer on NASA's Terra satellite, provide the needed observations to distinguish between hydrological end-member conditions and are expected to be more accurate than imagery with resolutions >1 km. But higher resolution observations are instantaneous and usually not repeatable at time intervals less than 2 to 4 weeks. On the other hand, lower resolution TIR imagery from sensors such as those on the geostationary GOES satellite, in combination with hydrological assimilation models, can estimate the diurnal variations in surface energy balance. To assess the relative merits of resolution vs. imaging frequency, we have collected a series of 10 ASTER observations, between May and November 2002 over the arid Jornada Experimental Range in New Mexico, and modeled the surface energy balance. Estimates of the energy components are made from the original resolution (90 m) up to an aggregated resolution of 4 km. These estimates are compared with ground based flux observations, and then compared with each other. Loss in range of data and expected biases due to resolution effects will be discussed.

**MI07/11A/B18-007** **1110**

**EARLY RESULTS OF THE ILAS-II ONBOARD THE ADEOS-II SATELLITE**

Hideaki NAKAJIMA, Takafumi SUGITA, Tatsuya YOKOTA, Hiroshi KANZAWA, Hirokazu KOBAYASHI, Yasuhiro SASANO (National Institute for Environmental Studies)

The Improved Limb Atmospheric Spectrometry-II (ILAS-II) onboard the Advanced Earth Observing Satellite-II (ADEOS-II) was successfully launched on 14 December, 2002 from National Space Development Agency of Japan (NASDA)'s Tanegashima Space Center. ILAS-II is a solar-occultation atmospheric sensor which will measure vertical profiles of O<sub>3</sub>, HNO<sub>3</sub>, NO<sub>2</sub>, N<sub>2</sub>O, CH<sub>4</sub>, H<sub>2</sub>O, ClONO<sub>2</sub>, aerosol extinction coefficients etc. with four grating spectrometers. After the checkout period of the ILAS-II which is scheduled in January-February, 2003, ILAS-II will make routine measurements from early April. An initial checkout (ICO) operation was done on 20-23 January, 2003. Preliminary data taken during the ICO period suggest good quality of the ILAS-II data. A validation campaign is scheduled to be taken place in Kiruna, Sweden in 2003, when several balloon-borne measurements are planned. Current status of the ILAS-II sensor and preliminary results using ILAS-II data for both northern and southern polar regions processed with the latest data retrieval algorithm will be presented.

Friday, July 11 PM

Presiding Chair: N.O. Jensen

**MI07/11P/B18-001** **1400**

**SURFACE ENERGY BALANCE OF BOREAL FOREST: DEPENDENCY ON SEASON, WEATHER AND SOIL MOISTURE**

Anders LINDROTH<sup>1</sup>, Achim GRELE<sup>2</sup>, Meelis MOLDER<sup>1</sup> (<sup>1</sup>Department of Physical Geography and Ecosystems Analysis, Lund University, P.O. Box 118, 221 00 Lund, <sup>2</sup>Faculty of Forestry, Swedish University of Agricultural Sciences, Box 7077, 740 07 Uppsala)

This paper focuses on which factors that are controlling the exchange of energy between a 100-years-old boreal forest and the atmosphere. The 8-year data series from the Norunda area in central Sweden with almost continuous measurements with half-hourly time resolution was used as a basis for the analysis. Surface fluxes were measured by three eddy covariance system located at different height above the canopy from 35 m up to 102 m above ground. The storage of sensible and latent heat in the stand air was measured by a

profile system comprising 12 levels. Rate of change of heat storage in the biomass was estimated from a large number of temperature measurements in branches and trunks in two different stands adjacent to the flux tower. Soil heat flux was estimated from soil heat flux plates located in the top-soil and from temperature profiles in the soil. The long-term data was used to analyse the seasonal dependency of all components of the energy fluxes including short- and long-wave radiation. The surface and aerodynamic resistances were calculated in order to assess the controls of the partitioning between sensible and latent heat fluxes. Short-term data of sap-flow and total evaporation during optimal and sub-optimal soil water conditions were used to estimate the effect of drought on the energy fluxes. The analysis showed a weak tendency of decreasing net radiation over time. The latent heat flux showed highest correlation with the net radiation on a monthly basis and the annual variation was to some degree correlated with the number of dry days.

**MI07/11P/B18-002**

**1420**

**DEVELOPMENT OF SVAT MODEL'S PARAMETERIZATION OF HEAT, WATER AND CARBON EXCHANGE PROCESSES WITHIN FOREST SYSTEMS OF THE BOREAL ZONE: SWAP MODEL**

Yeugeniy M. GUSEV, Olga N. NASONOVA (Institute of Water Problems, Russian Academy of Sciences)

The boreal zone determines significantly the intensity of climatic processes on the planet and effects on stability of the Earth as a global ecological system. For these reasons, problems related to modelling of heat, water and carbon exchange within ecosystems of the boreal zone get the special importance and topicality. The goal of the present work is improving one of SVAT models, namely SWAP, developed earlier by the authors. Among the sciences questions concerned in this work are: - (1) what is the ability of the SWAP model to reproduce correctly mutual formation of heat, water, and carbon budget within boreal forest system? - (2) are the SWAP model able to reproduce the observed sink (or source) of carbon for this system? Evergreen coniferous forests represents high vegetation, including overstory and understory. That is why, two active surfaces were used to schematize the heat, water and carbon exchange within forest: a surface of crowns of trees and understory or underlying surface of the forest floor. It was taken into account that trees extinguish incoming radiation, produce longwave emission in all directions, that turbulent heat exchange between the forest floor and the forest crowns exists as well. When the water balance of forest was calculated, snowpack formation at the forest floor was simulated considering the water-ice transfer within snow cover as well as the water yield from snow located on crowns. When the carbon budget was simulated, the processes of photosynthesis (of both forest overstory and understory), autotrophic (including leaf, sapwood and root) respirations, as well as heterotrophic (produced by microorganisms related to turnover of roots, detritus production from aboveground litterfall, and humus mineralization) respiration were considered. The quality of simulation of heat and water regime of boreal forest by SWAP model was validated by the comparison of calculated and measured characteristics of heat and water exchange using observation data of the Valdai research laboratory (Russia) for Tayozhnyi catchment (1966-1983, spruce forest) on precipitation, snowpack, soil water stores, ground water level, runoff. The availability of the model to treat carbon exchange processes was verified on the basis of numerical experiment of almost 100-years history of forest formation on site Loobos (Nederland, vegetation cover is a scots pine) using experimental data of "Euroflux" program network as well as the data on net ecosystem exchange of carbon on this site (1997-1998). SWAP model was provided by forcing data, soil and vegetation parameters for objects selected due to participation of authors at different stages international geophysical project PILPS, literature data, as well as own experience of authors. The validation of the SWAP model have shown that it treats hydrological and carbon exchange processes satisfactory for all selected objects.

**MI07/11P/B18-003**

**1440**

**PROGNOSTIC CANOPY AIR SPACE SOLUTIONS FOR LAND SURFACE BIOPHYSICAL EXCHANGES**

Pier Luigi VIDALE, Reto STOCKLI (Institute for Atmospheric and Climate Science ETH)

The importance of the correct representation of land surface processes has been progressively recognized in atmospheric sciences: several generations of land surface models have been developed, which include increasing levels of complexity. The latest, the third generation formulations, incorporate photosynthesis and physiological responses to environmental CO<sub>2</sub>. A new set of prognostic equations, providing a new solution core for one such land surface model, SiB2, is introduced here. The new equation set makes use of canopy air space variables which are prognostic and allow for the storage of heat, water and carbon at that level, providing both a new memory for the coupled system and a better representation of observed canopy processes. Results from off-line simulation using FLUXNET data from North America and Europe, over a range of very heterogeneous environmental and climatic conditions, indicate that the new solution core is able to represent land surface exchanges with equal or better characteristic than the set it replaces. At the same time, this new formulation provides a simplified mathematical framework, more suitable for further model development.

**MI07/11P/B18-004**

**1500**

**VALIDATION OF SSIB MODEL OVER GRASSLAND WITH CHERES FIELD EXPERIMENT DATA IN 2001**

Lan SUN<sup>1</sup>, Yongkang XUE<sup>2</sup> (<sup>1</sup>Chinese Academy of Meteorology Science, <sup>2</sup> Department of Geography, University of California)

The simplified Simple Biosphere model (SSiB) has been validated in off-line simulations against field measurements from the China Heavy Rainfall Experiment and Study (CHeRES) over a grassland site in summer of 2001. When initialized and driven by the observed atmospheric forcing over the lower reaches of the Yangtze River, the model reproduced the observed surface energy fluxes and surface skin temperature realistically. The model ably simulated the tendency of soil water content well too. The sensitivity experiments showed that the leaf reflectance were found to be most significant parameters in improving large overestimation of surface albedo during both wet and dry periods. This study can be confirmed that the model is capable of assessing the main impact of physical processes related to land-atmosphere interaction over monsoon regions in eastern Asia and the SSiB model can provide realistic surface heat fluxes for mesoscale atmospheric models.

**MI07/11P/B18-005**

**1540**

**HOW DOES THE PARTITIONING OF EVAPOTRANSPIRATION AND RUNOFF BETWEEN DIFFERENT PROCESSES AFFECT THE VARIABILITY AND PREDICTABILITY OF SOIL MOISTURE AND PRECIPITATION?**

Robert E. DICKINSON<sup>1</sup>, Guiling WANG, Xubin ZENG, Qingcun ZENG (<sup>1</sup>Georgia Institute of Technology, <sup>2</sup>University of Connecticut, <sup>3</sup>University of Arizona, <sup>4</sup>Institute of Atmospheric Physics, Beijing)

Water stored as part of the land surface is lost to evapotranspiration and runoff on different time scales and the partitioning between these time scales is important for modeling soil water in a climate model. Different time scales are imposed on evapotranspiration primarily because it is derived from different reservoirs with different storage capacities, from the very rapid evaporation of canopy stores to the slow removal by transpiration of rooting zone soil moisture. Runoff likewise ranges in time scale from rapid surface terms to the slower base-flow. The longest time scale losses of water determine the slow variation of soil moisture and hence the longer time scale effects of soil moisture on precipitation. We show with a simple analysis how shifting the partitioning of evapotranspiration between the different reservoirs affects the variability of soil moisture and precipitation. In particular, we conclude that a shift to faster time scale reservoirs shifts variance of precipitation from that which is potentially predictable to unpredictable.

**MI07/11P/B18-006**

**1600**

**EFFECT OF ROOT TEMPERATURE ON WATER UPTAKE AND TRANSPIRATION OF VEGETATION**

Tsuneo KUWAGATA<sup>1</sup>, Mari MURAI<sup>2</sup>, Takahiro HAMASAKI<sup>3</sup> (<sup>1</sup>National Institute for Agro-Environmental Sciences, <sup>2</sup>National Agricultural Research Center for Tohoku Region, <sup>3</sup>National Agricultural Research Center for Hokkaido Region)

Water uptake by plant root is one of the key processes for the land-atmosphere interaction over vegetated surface. This process not only controls the evapotranspiration, but also influences the CO<sub>2</sub> exchange, because stomatal behavior is sensitive to plant water status. It is commonly known by plant physiologists that the ability of roots to uptake water depends on root temperature. However, there have been few studies focusing on the effects of root temperature on the interaction between vegetation and atmosphere. In this study, we examined how the root temperature could affect water uptake, plant water status, and transpiration, in order to demonstrate an important role of root temperature on the energy and water exchange over vegetated surface. Rice plants were chosen as a plant material and were grown hydroponically in a growth chamber. The transpiration rate,  $E_r$  and the leaf water potential,  $\psi_l$  were measured under various root-temperature conditions with constant air temperature at 25 °C ( $\psi_l$  can be used as an indicator of plant water status). Over a range of root temperature,  $T_r$  from 35 °C to 10 °C,  $E_r$  and  $\psi_l$  gradually decreased with decreasing  $T_r$ . Below a critical root temperature 10 °C,  $E_r$  and  $\psi_l$  abruptly decreased with decreasing  $T_r$ , which is due to an abrupt increase in hydraulic resistance of plants. We also found that the dependency of transpiration rate on humidity became weaker below the critical root temperature. Stomatal conductance is one of the key parameters for modeling the energy and water exchange over vegetated surface. The bulk stomatal conductance of whole rice plants under experimental conditions, which was estimated from the measured transpiration rate and atmospheric conditions, could be parameterized as a unique function of only  $\psi_l$ . Finally, we constructed a simple model for the energy and water exchange of vegetation, which consists of the energy balance equation for plant leaves and the water transport equation by the root. This model simulated the experimental results fairly well. As shown in the present study, the root zone temperature has a significant impact on the energy and water exchange over vegetated surface through the changes in hydraulic resistance of plants. We suggest that the root temperature effect on the water-uptake ability should be taken into account, in order to improve present Soil-Vegetation-Atmosphere-Transfer (SVAT) models.

**MI07/11P/B18-007**

**1620**

**CHANGES, CONTROLLED BY A CLIMATE, IN VEGETATIVE COMMUNITIES OF EUROPEAN NORTH OF RUSSIA**

Svetlana Vladimirovna VIDYAKINA<sup>1</sup>, Alexander Andreevich MININ<sup>2</sup> (<sup>1</sup>Center for ecological research, Pomor State University, <sup>2</sup>Department of Social-Ecological Systems, Institute for a Global Climate and Ecology of RAS&Rosgidromet)

A characteristic of a climate of last decades is warming (IPCC, 1996). A global increase of annual air temperature for the 20th century is 0,6 °C, in the Northern hemisphere temperature has increased on 0,8 °C. Most actively the warming was shown here from the middle 1970th, and 1990th -s became the warmest for all period of instrumental supervision. Distinctive features of the contemporary warming of the climate are speed of changes and its spatial - temporary heterogeneity. So substantially the warming has touched winter and spring months, the night temperatures increased faster. In the present work the results of study of phenological reactions of trees in the territory of European north of Russia (ENR) are submitted. The analysis of a low-frequency component of the meteorological long-term data also shows heterogeneity of changes. Changes of air temperatures in XXth century (1901 - 1990 years) allocate groups of stations with dominant periodic component close to 80 years and to 30 - 40 years. The changes of air temperatures in XXth century (1901 - 1990 years) allocate groups of stations with a dominant periodic component close by 80 years and to 30 - 40 years. General contemporary increase of annual air temperatures since 60 - 70th to 1990, makes up 0,3 - 1 °C. The contemporary increase of temperatures is fixed on the data of measurements of temperatures at different depths in the soil for the Arctic stations ENR (Arkhangelsk, Hoseda-Hard and Kandalak-sha), 0,5 - 1,2 °C. The results of processing of the amount of atmospheric precipitation for the period from 1901 to 1990 tend to increase last decades. The condition of abiotic and biotic components of the biosphere is closely connected to variations of the climate. The long-term linear tendencies of the dates of coming phenological phenomena serve important indicators of changes, occurring in nature. We researched spatial - temporary regularities of changes of dates of leaf unrolling and leaf-fall of common birch (*Betula pendula* Roth.), breaking into bloom of bird cherry (*Prunus avium* Mill.), mountain ash (*Sorbus aucuparia* L.), for the period from 1966 to 1995 years. In a course of research the following conclusions are received: 1) The coordination of changes of linear phenological trends with occurring warming of the climate on ENR is revealed, earlier spring and late autumn terms of the phenological phenomena are established, the duration of the vegetation period for 10-20 of days increased; 2) For long-term series of dates of breaking into bloom of bird cherry, mountain ash in conditions of city are revealed more brightly expressed trends, than in a wild nature; 3) The most sensitive to the contemporary climatic changes in the region are the phenological phase: leaf unrolling and leaf-fall of common birch (*Betula pendula* Roth.), breaking into bloom of bird cherry (*Prunus avium* Mill.).

**MI07/11P/B18-008**

**1640**

**INFLUENCES OF ELEVATED CO2 (FACE) ON TRANSPIRATION, PHOTOSYNTHESIS AND MICROMETEOROLOGY IN A RICE PADDY FIELD**

Hiroki OUE<sup>1</sup>, Mayumi YOSHIMOTO<sup>2</sup>, Tsuneo KUWAGATA<sup>2</sup>, Kazuhiko KOBAYASHI<sup>1</sup> (<sup>1</sup>Faculty of Agriculture, Ehime University, <sup>2</sup>National Institute for Agro-Environmental Sciences)

Micrometeorological conditions within and above a rice canopy, stomatal conductance (gs), transpiration (Et) and photosynthesis (CER) of single leaves were observed in paddy fields under the free air CO<sub>2</sub> enrichment (FACE) and the ambient (AMB) conditions at three growing stages of rice. Plant area index (PAI) was larger in FACE plot than in AMB plot until heading stage. Observed gs was lower in FACE than in AMB influenced by higher CO<sub>2</sub> CER



of single leaves were larger in FACE than in AMB. Et of single leaves were lower in FACE than in AMB. However, Et from a whole canopy was a little larger in FACE than in AMB or quite the same level in both conditions owing to larger leaf area in FACE. Observed leaf surface temperature (Ts) and air temperature (Ta) within and just above the canopy in daytime were higher in FACE than in AMB especially in the upper canopy layer, which was influenced by two processes; one is less transpiration of a single leaf caused by lower gs and the other is larger radiative energy absorbed by larger leaf area in FACE. In order to evaluate effects of elevated CO<sub>2</sub> and the difference of leaf area on Et and CER of a whole canopy and on micrometeorological conditions separately, a multilayer energy and mass exchange model was developed. The model could reproduce observed datasets of micrometeorological conditions within and above the canopy successfully. An example of simulation revealed that Et of a whole canopy would be 15 % smaller and CER of a whole canopy would be 40 % larger in elevated CO<sub>2</sub> and that Ts and Ta would be up to 3 K and 1 K higher in elevated CO<sub>2</sub> for the same leaf area canopy.

**MI07/11P/B18-009** **1700**

**THE EFFECTS OF FACE (FREE-AIR CO<sub>2</sub> ENRICHMENT) ON CANOPY EVAPOTRANSPIRATION AND TEMPERATURE IN RICE PADDY ECOSYSTEM**

Mayumi YOSHIMOTO<sup>1</sup>, Hiroki OUE<sup>2</sup>, Kazuhiko KOBAYASHI<sup>1</sup> (<sup>1</sup>National Institute for Agro-Environmental Sciences, <sup>2</sup>Ehime University)

The understanding of terrestrial ecosystem processes is important to predict the global change precisely. It is well known that elevated CO<sub>2</sub> concentration causes the partial stomatal closure and the decrease of transpiration of each leaf, which may cause the reduction in canopy evapotranspiration (ET) and plant water requirements. However, the decrease in ET causes the leaf temperature, which stimulates the evapotranspiration through the increase in water vapor pressure deficit between leaves and the atmosphere. The change of plant growth caused by elevated CO<sub>2</sub>, also, affects the canopy evapotranspiration. The interactive effects between the atmospheric micrometeorology and plant response makes it difficult to evaluate the energy balance and temperature of terrestrial ecosystems. FACE (free-air CO<sub>2</sub> enrichment) experiment provides us a good opportunity to examine the interaction, since their effects of elevated CO<sub>2</sub> can be measured in open field condition without any artificial change in microclimate. FACE experiment was conducted at rice paddy field in Shizukuishi, Iwate, Japan, from 1998 to 2000. In order to evaluate the effects of FACE on heat balance and micrometeorology, we had measurements of radiation; soil heat flux; profiles of air temperature and humidity etc., at both control (ambient CO<sub>2</sub>) and FACE (elevated CO<sub>2</sub>) plots. Stomatal conductance (gs) profiles were parometrically measured at each growing stage. gs at FACE plot were usually smaller than that at control plot, whose difference was the largest in earlier growth stage and became smaller as rice growing stage progressed. gs was modeled as a function of solar radiation, water vapor deficit of the air, leaf height and growing stage, at both control and FACE plots. The gs-model was combined to bulk energy budget model, which gives 2 stream energy flow from vegetation and soil layers to the atmosphere. Bulk canopy conductance for water vapor transfer at FACE plot was smaller by 10 to 20% than control. The elevated CO<sub>2</sub> effect on bulk conductance was more significant when the air was dry and wind speed was high. The canopy temperature increased by 0.3 to 0.5 degree in daily mean by FACE, which caused the increase in water vapor pressure deficit between canopy and the atmosphere (LVPD), by 5 to 10%. The canopy evapotranspiration as multiplication of bulk conductance by LVPD, decreased by 5 to 10% by FACE. Seasonal trend of the FACE effect on canopy evapotranspiration was different from that of leaf conductance. Leaf area index at FACE was larger in earlier growing stage, but became a bit smaller after heading period, which caused the cancellation for the FACE effect on leaf stomatal conductance. Simulation in case that LAI was the same, showed that the cancellation effect by plant growth stimulation was about 20%.

**MI08** **Monday, July 7**

**LABORATORY STUDIES ON ATMOSPHERIC ISSUES (ICCP, ICACGP, IRC)**

Location: Site B, Room 18

**Monday, July 7 PM**

Presiding Chairs: C. Knight, Y. Furukawa

**MI08/07P/B18-001** **Invited** **1500**

**KINETIC LIMITATIONS TO CLOUD DROPLET GROWTH AND EVAPORATION: EXPERIMENTAL STUDIES WITH AN ENVIRONMENTALLY CONTROLLED LEVITATION CELL**

Dennis LAMB (Department of Meteorology, Penn State University)

Electrodynamic levitation affords a unique opportunity to observe individual aqueous-solution droplets throughout their lifetimes without influences from chamber walls, thus permitting simulations of direct relevance to atmospheric phenomena. A combination of AC and DC voltages on the six faces of a cubic cell gives complete control over droplet position in space and measures of the forces needed to keep the droplet centered against gravity and aerodynamic drag in the imposed gas flow. Each droplet is observed optically as it evaporates under disequilibrium conditions, precise measurements of droplet size (+/- 0.06 micron) being derived from data captured on video tape of the structural-resonances (Mie-scattering patterns) induced by illumination from an argon-ion laser. The experimental data (drop radius versus time), taken over a range of temperatures (-35 to 25 C) and pressures (200 to 1000 hPa), are analyzed by fitting them to theoretical condensational growth models, using the mass accommodation coefficient and ambient humidity as free parameters. The evaporation/growth of pure water droplets is best characterized by a mass accommodation coefficient of 0.2 +/- 0.1 at temperatures near -35 C. The mass accommodation coefficient of nitric acid evaporating at 22 C from solution droplets with initial acid weight percent between 5 and 22 was found to be 0.1 +/- 0.05. Nitric acid additionally lowers the water activity in the solution droplets, thereby causing the time scales for evaporation of solution droplets to be much larger than those of pure water droplets. The findings from these laboratory experiments suggest that the growth/evaporation of atmospheric haze and cloud droplets are likely to be kinetically limited under some environmental conditions, especially when the saturation ratio changes rapidly. The moderately large mass accommodation coefficients for water and nitric acid mean that only the smaller droplets (i.e., haze and CCN) will be substantially influenced by surface-kinetic effects. However, it may well be the cloud droplets that are affected by the presence of nitric acid vapor in the lower atmosphere, because of the larger solubility of nitric acid in more dilute solutions. Modeling studies are being initiated to explore the impacts of kinetic and thermodynamic limitations on the early drop size distribution of clouds, radiation balances, and precipitation initiation.

**MI08/07P/B18-002** **Invited** **1530**

**LABORATORY STUDIES OF THE INFLUENCE OF CLOUD MICROPHYSICS ON THUNDERSTORM ELECTRIFICATION PROCESSES.**

Clive P. R. SAUNDERS, Holly A. BAX-NORMAN (Physics Department, UMIST)

It is generally accepted that an important thunderstorm charging process involves collisions between vapour grown ice crystals and small hail pellets accreting supercooled water. The sign and magnitude of the charge transfer has been investigated in many studies over the last 50 years and with each investigation more details are discerned concerning the dependence of the sign and magnitude of the charge transfer on the microphysical conditions within the cloud. These results are interpreted in terms of a mechanism of charge transfer involving the surface properties of the interacting ice crystals and riming graupel pellets. The latest laboratory cloud studies in UMIST involve comparisons between two approaches to the method of simulating the conditions inside natural clouds. One method essentially involves ice crystals growing in the same cloud of supercooled droplets from which the droplets and ice crystals gain their vapour. This simulates certain regions of growing clouds where the particles are well mixed and able to mutually influence growth, or evaporation rates. This well mixed cloud is then used to impact the ice crystals and droplets on a riming target representing a falling graupel pellet in a growing cumulus cloud. The second method also involves the growth of ice crystals in a supercooled droplet cloud, but before the crystals and droplets impact upon the target, a second source of supercooled droplets is introduced to the cloud. The supplementary droplets have not been influenced by the presence of a growing cloud of ice crystals and so this freshly mixed cloud has a higher supersaturation than the well-mixed cloud described above. This study simulates the mixing of two cloud sources from different origins as may happen across the updraught/downdraught boundary - a region long identified with charge separation in thunderstorms. The new results from these studies show clearly how the cloud conditions influence the charge transfer. For example, the single source well mixed cloud causes the simulated riming graupel to charge positively at high droplet accretion rates and negatively at low accretion rates at all temperatures. However, in the two-cloud mixing case, the rimer charges positively above about -10 C at all cloud liquid water contents, but at lower temperatures, the sign of the charge depends on the droplet accretion rate with negative rimer charging at intermediate accretion rates. These results are consistent with a well established but recently developed charge transfer hypothesis involving the relative diffusional growth rates of the interacting ice surfaces. The experiments point clearly to the importance of using an appropriate methodology in these cloud simulation experiments. Most importantly, the role of cloud supersaturation is shown to have a dominant influence on the charging behaviour of soft hailstones in thunderstorms.

**MI08/07P/B18-003** **1600**

**ATMOSPHERIC ICE CRYSTALS BETWEEN -20 C AND -70 C: A NEW HABIT DIAGRAM**

Matthew P. BAILEY, John HALLETT (Division of Atmospheric Sciences, Desert Research Institute)

The ground breaking laboratory studies of ice crystal growth by Nakaya and others, along with the crystal classification scheme of Magono and Lee, provided the first comprehensive view of ice habits at temperatures relevant to snow and ice particles observed at ground level and in the lower troposphere. While the laboratory results generally showed good agreement with in situ observations for temperatures between -2 °C and -18 °C, the habit results of some studies were skewed by the use of artificial nucleating agents and control of supersaturation, especially when the laboratory measurements were extended to colder temperatures. A new method which combines static diffusion and expansion chamber techniques has been used to nucleate and grow ice crystals under realistic atmospheric conditions of temperature, pressure, and ice supersaturation. Linear, projected area and volume growth rates as well as habit frequency and distribution have been determined for crystals growing between -20 °C and -70 °C. This method has yielded results which are in excellent agreement with the vast majority of in situ observations for temperatures from 0 °C to -70 °C, reproducing the well established habits observed between 0 °C and -18 °C. Contrary to what is often stated in the literature though is confirmed by in situ observations, the crystal habit between -20 °C and -40 °C is not columnar but is instead dominated by plate-like polycrystals, columnar forms generally appearing with low frequency unless "seeding and feeding" from colder overlying clouds is present. Low ice supersaturation (1-2%) habits constitute a special class of crystals dominated by compact polycrystals, thick plates and short columns, nearly independent of temperature between -20 °C and -60 °C. The region of bullet rosette nucleation has been determined to begin at temperatures below -40 °C where a new habit transition from predominantly plate-like to columnar habit forms has been identified. In situ habit observations for temperatures warmer than -40 °C have at times yielded erroneous correlations between habit and temperature since regions near cloud top may include this habit transition or clouds at even colder temperatures. The growth histories and modification of habit for crystals which nucleate at columnar growth temperatures below -40 °C and subsequently fall to warmer plate-like growth temperatures have been simulated and remarkably reproduce the unique in situ characteristics of bullet rosettes and columns which have been observed in the atmosphere after falling to temperatures between -20 °C and -40 °C. All these results demonstrate the continuing utility and importance of laboratory simulations under controlled conditions which are critical to the correct interpretation of in situ observations and a better understanding of atmospheric processes in glaciated clouds.

**MI08/07P/B18-004** **1620**

**NEW IPSL EXPERIMENTS ON GLAZE ICE ACCRETION ON A STATION POST INSULATOR**

Wladyslaw J. RUDZINSKI<sup>1</sup>, Edward P. LOZOWSKI<sup>1</sup>, Masoud FARZANEH<sup>2</sup> (<sup>1</sup>Department of Earth and Atmospheric Sciences, University of Alberta, <sup>2</sup>NSERC/Hydro-Quebec/UQAC Industrial Chair on Atmospheric Icing of Power Network Equipment (CIGELE), University of Quebec in Chicoutimi, Quebec, Canada)

Dealing with ice build-up on outdoor insulators is of key importance for maintaining the reliability of power networks in many northern countries. Glaze ice accretion, with numerous icicles formed during freezing rain, is the most severe type of ice accretion for insulators, since it can considerably reduce their performance. When icicles are formed and conductive unfrozen liquid flows along the ice surface, electrical discharges and flashover can occur, frequently resulting in power failure. It is important to understand glaze ice formation in order to improve insulator design and thereby reduce flashover occurrence. Our research focuses on laboratory modelling of glaze ice accretion on a non-energized station post insulator. A series of laboratory icing experiments has been undertaken in the Icing Precipitation Simulation Laboratory (IPSL) of CIGELE at the University of Québec in Chicoutimi. The influence of air temperature, wind speed, precipitation rate and drop size on the shape, dimensions and mass of the ice accretion on the station post insulator has been investigated. The experimental results have been used to verify a novel high-resolution, full-scale 3D discrete particle model of ice accretion on a station post insulator. This model, also called a morphogenetic model, predicts the morphology of ice accretion by building it up one

particle at a time. The model is capable of predicting the shape, mass and mass distribution of the glaze ice accretion at a station post insulator. While the model predictions are in acceptable agreement with the results of the laboratory experiments, their comparison has led to revealing insights into the physics of glaze ice accretions on insulators.

**MI08/07P/B18-005**

**1640**

**STUDIES ON REACTION AND PHOTODISSOCIATION PROCESSES IN THE ATMOSPHERE USING A VACUUM ULTRAVIOLET LASER INDUCED FLUORESCENCE TECHNIQUE**

Yutaka MATSUMI, Kenshi TAKAHASHI (Solar-Terrestrial Environment Laboratory, Nagoya University)

We have studied reaction and photodissociation processes in the atmosphere using a vacuum ultraviolet laser-induced fluorescence (vuv-LIF) technique in our laboratory. Numbers of important atoms and radicals in atmospheric chemistry can be detected only by using vuv wavelength light. We have detected Cl(<sup>2</sup>P), O(<sup>1</sup>P), O(<sup>1</sup>D), O(<sup>3</sup>S), N(<sup>3</sup>S) and H(<sup>2</sup>S) atoms, and ClO(X<sup>2</sup>I) and CO molecules using tunable vuv laser light. For example, for the detection of O(<sup>1</sup>P), the necessary tunable vuv radiation is generated by two photon resonant four-wave difference frequency mixing ( $2\omega_1 - \omega_2$ ) in krypton gas, using two tunable dye lasers pumped simultaneously by an XeCl excimer laser. The frequency-doubled light of the first dye laser yield  $\omega_1 = 212.56$  nm, which is two-photon resonant with the atomic transition of Kr. The second dye laser is operated to generate  $\omega_2 = 578.1, 572.8,$  and  $570.6$  nm which, when mixed with two  $\omega_1$  photons, correspond to the appropriate vuv frequencies for detecting O(<sup>1</sup>P) atoms with  $j = 2, 1,$  and  $0$ , respectively. O(<sup>1</sup>D) atoms are detected by vuv-LIF at  $115.22$  nm. Radiation at this wavelength is generated by phase-matched frequency tripling of the output from a single XeCl pumped dye laser (345.66 nm) in a xenon / argon gas mixture. Xenon, krypton and mercury gases have been used as non-linear optical mixing media for the four-wave mixing ( $2\omega_1 \pm \omega_2$ ) and tripling to generate tunable vuv laser light in various wavelength ranges. There are several superior advantages for the usage of the vuv laser over conventional atomic lamps. The narrow band width of the vuv laser allow us to measure populations among the spin-orbit levels of Cl(<sup>2</sup>P) and O(<sup>1</sup>P) independently and to measure accurate concentrations of the atoms. Doppler profiles of the atoms can be measured with the narrow band width vuv laser light, from which we can determine the product states, for example, O(<sup>1</sup>D) + O<sub>2</sub>(a<sup>1</sup>Δ<sub>g</sub>) or O(<sup>1</sup>D) + O<sub>2</sub>(X<sup>3</sup>Σ<sub>g</sub><sup>-</sup>) in the photolysis of O<sub>3</sub>. Since the time resolution between photolysis and probe vuv laser pulses is high, we can measure nascent distributions of the products and also can measure precise reaction rate constants. Representative of our studies using the vuv laser system is the measurements of O(<sup>1</sup>D) quantum yields in the photolysis of O<sub>3</sub> at various uv wavelengths (230 - 330 nm) and at various temperatures (227 - 295 K). We have measured photofragment excitation spectra for both O(<sup>1</sup>P) and O(<sup>1</sup>D) in the uv photolysis of O<sub>3</sub> using the vuv-LIF technique. We have determined the precise absolute O(<sup>1</sup>D) quantum yield values which are functions of the O<sub>3</sub> photolysis wavelength and temperature. We have also revealed the contributions of the hot-band excitation and spin-forbidden dissociation mechanisms in the photolysis of O<sub>3</sub>.

**MI08/07P/B18-006**

**1700**

**THE LABORATORY INVESTIGATION OF CORONA DISCHARGE FROM ICE CRYSTALS**

Matthew P. BAILEY<sup>1</sup>, John HALLETT<sup>1</sup>, Danyal PETERSEN<sup>2</sup>, William BEASLEY<sup>2</sup> (<sup>1</sup>Division of Atmospheric Sciences, Desert Research Institute, <sup>2</sup>School of Meteorology, University of Oklahoma)

The initiation of lightning is likely to involve corona discharges from ice hydrometeors coupled with some mechanism whereby the local field is enhanced up to breakdown values. This process may depend on the enhancement of propagating positive streamers when the ambient electric field exceeds a certain critical value. Experimental results from Griffiths and Latham concerning the corona emission from ice crystals appeared to indicate that positive streamer emission was extinguished below approximately -18 °C, possibly related to a rapid drop in ice conductivity. However, those results were obtained under conditions of low humidity rather than near water saturation as is found in much of the ice growth regions of thunderclouds. Additionally, the crystals used for those experiments were several millimeters to over a centimeter in size which is considerably larger than the majority of large ice crystals found in clouds. A new experiment investigating the corona emission of positive streamers by crystals grown at ice supersaturations close to water saturation has been performed with crystals ranging in size from 0.3-3 mm over a range of temperatures and pressures relevant to thundercloud conditions. Positive streamer emission was directly observed with an image intensifier. Positive streamer emission was observed to occur for field strengths which ranged from approximately 450 kilovolts/meter for needles at -4 °C and a pressure of 850 mb to approximately 650 kilovolts/meter for thick plates at -30 °C and a pressure of 400 mb. Bipolar emission from thick plates was observed to begin below approximately -35 °C and a pressure of 350 mb for field strengths around 750 kilovolts/meter. Threshold field strengths varied greatly with crystal habit, thick crystals generally requiring lower threshold field values than thin crystals. Thin plates, thin plate-like polycrystals and dendritic forms growing between -15 °C and -22 °C typically required higher threshold field values than thicker forms at both lower and higher temperatures. While the mechanism of field enhancement has yet to be determined, these measurements place new limits on the field values for positive streamer emission in thunderclouds as a function of temperature, supersaturation, and crystal habit.

**MI08/07P/B18-007**

**1715**

**CAPACITANCES OF LABORATORY GROWN ICE CRYSTALS: A TEST OF THE ELECTROSTATIC MODEL OF CRYSTAL GROWTH**

Matthew P. BAILEY<sup>1</sup>, John HALLETT<sup>1</sup>, Alexei KOROLEV<sup>2</sup>, George ISAAC<sup>3</sup> (<sup>1</sup>Division of Atmospheric Sciences, Desert Research Institute, <sup>2</sup>Sky Tech Research, <sup>3</sup>Cloud Physics Research Division, Meteorological Service of Canada)

The electrostatic model of ice crystal growth from the vapor is constructed from the analogy between a conductor in an electric field and an ice crystal in a vapor field. This approach approximates the shape of a thick plate as an oblate spheroid and a column as a prolate spheroid, more complex forms generally not being addressed. While this model has been in the literature for sometime, there have been few attempts to verify the model through laboratory experiments. In a recent crystal growth experiment (Bailey and Hallett, this conference), average volume growth rates have been obtained for crystals with maximum sizes between 150-300 microns that were grown between -20 °C and -70 °C at ice supersaturations and pressures representative of the real atmosphere. Additionally, the time dependent growth rates for some of these crystals have been determined for crystals which grew from approximately 100 microns to 1000 microns in maximum dimension. Volume growth rates were converted to mass growth rates and were then used to calculate the crystal capacitances for several different habit types including bullet rosettes. In another experiment, drops frozen between -4 °C and -15 °C at various ice supersaturations were then allowed to grow for tens of minutes under controlled conditions. From these growth experiments, it was found that the electrostatic capacitance analog accurately predicts the spherical growth of frozen drops, somewhat adequately represents the growth of very thick

plates and short columns, but typically overestimates the growth of thin plates, long columns and bullet rosettes by a factor of three to four. Complex polycrystals exhibit capacitances with great variability that are typically less than those predicted by the electrostatic model for simple habit forms. Time dependent measurements indicate that the capacitance changes as a function time and crystal size, however not in the simple manner predicted by the electrostatic analogy. These measurements clearly indicate that the boundary conditions for crystals in a vapor field are not analogous to those of a conductor in an electric field except in limited cases. However, these measurements provide effective capacitances which more accurately reflect the interaction of crystals with the vapor field as a function of crystal size and habit and are more appropriate for use in crystal growth models.

**MI08-Posters**

**Monday, July 7**

**LABORATORY STUDIES ON ATMOSPHERIC ISSUES (ICCP, ICACGP, IRC)**

Location: Site D

**Monday, July 7 PM**

**MI08/07P/D-001**

Poster

**1400-195**

**PRECISE DETERMINATION OF THE QUANTUM YIELD FOR O(<sup>1</sup>D) PRODUCTION IN THE UVPHOTOLYSIS OF O<sub>3</sub>**

Kenshi TAKAHASHI, Takayuki SUZUKI, Tomoki NAKAYAMA, Yutaka MATSUMI (Solar-Terrestrial Environment Laboratory, Nagoya University)

The photodissociation reaction of O<sub>3</sub> following photoabsorption of the solar ultraviolet radiation produces the electronically excited oxygen atom, O(<sup>1</sup>D), that is highly reactive and has important roles in the chemical processes in the terrestrial atmosphere. For instance, the chemical reaction of O(<sup>1</sup>D) with H<sub>2</sub>O is a primary source of the OH radical in the stratosphere and troposphere. The O(<sup>1</sup>D) reaction with N<sub>2</sub>O produces NO that affects significantly the stratospheric ozone concentration. Therefore, it is quite important to know the quantum yield for O(<sup>1</sup>D) production in the solar uv photolysis of ozone. In this study, we determined the O(<sup>1</sup>D) quantum yield values in the wavelength region of 306-314 nm where the yield increases drastically from near-zero values around 330 nm to near-unity values around 300 nm and the solar actinic flux shows a strong wavelength dependence. The calculated atmospheric O(<sup>1</sup>D) production rate is very sensitive to changes in the quantum yield for its production in the uv photolysis of O<sub>3</sub> in this region and the uncertainty associated with the yield. We performed laboratory studies to determine precisely the quantum yield of the O(<sup>1</sup>D) atoms produced in the 306-314 nm photolysis of O<sub>3</sub>, by means of a high-sensitive technique of laser-induced fluorescence spectroscopy. The results are compared with the data recommended for use in atmospheric modeling. We also present that the uncertainties associated with the yields have been reduced significantly as compared to the current recommendation data. Our new values will be helpful to calculate more precisely the OH and NO<sub>x</sub> production rates in the atmosphere.

**MI08/07P/D-002**

Poster

**1400-196**

**THE STUDY OF SEEDING EFFICIENCY OF SOME NATURAL MATERIALS IN COLD CLOUDS**

Seyed Alireza SADEGHI HOSSEINI, Atoosa FERDOSIN NAJAFABADI (Institute of Geophysics University of Tehran, P. O. Box: 14155-6466, Tehran, Iran)

Despite many successes in the field of freezing nucleation during the last two decades, there are still uncertainties and questions that have been of special interest to cloud physicists. Due to the wide variety of nucleation processes, most of the concepts expressed to describe the subject, could not bring forward comprehensive explanations. Using cold plate and fishing line apparatus, the immersion freezing nucleation rates of some natural materials such as, distilled water, smog, clay and leaf mould have been studied. The seeding efficiency of natural material solutions have been studied through spraying them over the drops of distilled water suspended on the fishing line. The experimental results confirm the time-temperature dependence of freezing rate due to heterogeneous nucleation (Vali, 1994). They also show that a good cloud seeding agent can be easily produced from bacterial biogenic nuclei as effective nucleation materials. By deduction the effect of contact freezing, the biogenic nuclei are found to have maximum activity at -5°C and their seeding efficiency is about 80% at -9°C. These results are more acceptable than those of mineral substances such as Silver Iodide. The performance of these experiments in a clean weather or the use of the bacteria incubation method, leads to more accurate and reliable results. Performing such low-cost experiments, not only could bring out a better understanding of the freezing nucleation process, but it is also possible to decrease the expenses of cloud seeding projects as well as the dangers of airplane accidents inside the clouds.

**MI08/07P/D-003**

Poster

**1400-197**

**AEROSOL FLOW TUBE STUDIES ON THE HETEROGENEOUS REACTION OF HNO<sub>3</sub> AND N<sub>2</sub>O<sub>5</sub> ON MINERAL AEROSOL**

Friedrich HANISCH, Heleen DE CONINCK, John N. CROWLEY (Max-Planck-Institute for Chemistry, Dep. of Atmospheric Chemistry)

A recent study estimates that 1600-2000 Tg of mineral aerosol are emitted annually into the atmosphere (Ginoux et al., 2001). As shown by modelling studies (Zhang et al., 1994; Dentener et al., 1996), mineral aerosol can strongly influence atmospheric chemistry, especially the budgets of NO<sub>x</sub>, HO<sub>x</sub> and O<sub>3</sub>. These modelling studies revealed the need for reliable data quantifying the heterogeneous uptake of trace gases onto mineral dust particles. Earlier laboratory studies determining uptake coefficients for the interaction between trace gases and dust were using the Knudsen reactor technique (e.g. Börensén et al., 2000; Hanisch and Crowley, 2001). The main disadvantages of this technique, however, are the use of bulk substrates instead of airborne particles and the inability to simulate atmospheric relative humidities. These problems are overcome by the use of the aerosol flow tube technique. In this study we present results for the uptake of HNO<sub>3</sub> and N<sub>2</sub>O<sub>5</sub> onto airborne mineral aerosol, using an aerosol flow tube coupled to a chemiluminescence detector and an optical particle counter for the determination of the concentrations of NO<sub>y</sub> and mineral aerosol, respectively. Uptake coefficients for this reaction were measured and the influence of relative humidity on the reaction was investigated. References Börensén, C., U. Kirchner, V. Scheer, R. Vogt, and R. Zellner, 2000: Mechanism and kinetics of the reaction of NO<sub>2</sub> or HNO<sub>3</sub> with alumina as a mineral dust model compound. J. Phys. Chem. 104, 5036-5045. Dentener, F.J., G.R. Carmichael, Y. Zhang, J., Lelieveld, and P.J. Crutzen, 1996: Role of mineral aerosol as a reactive surface in the global troposphere. J. Geophys.



Res. 101, 22869-22889. Ginoux, P., M. Chin, I. Tegen, J.M. Prospero, B. Holben, O. Dubovik, and Sh.-J. Lin, 2001: Sources and distribution of dust aerosols simulated with the GOCART model. *J. Geophys. Res.* 106, 20255-20273. Hanisch, F. and J.N. Crowley, 2001: The heterogeneous reactivity of gaseous nitric acid on authentic mineral dust samples, and on individual mineral and clay mineral components. *Phys. Chem. Chem. Phys.* 3, 2474-2482. Zhang, Y., Y. Sunwoo, V. Kotamarthi, and G.R. Carmichael, 1994: Photochemical oxidant processes in the presence of dust: An evaluation of the impact of dust on particulate nitrate and ozone formation.; *J. Appl. Meteorol.* 33, 813-824

**MI09** **Tuesday, July 8 - Wednesday, July 9**

**NEW INSTRUMENTS AND TECHNOLOGY, ADVANCES IN REMOTE SENSING**

Location: Site B, Room 22

**Tuesday, July 8 PM**

**MI09/08P/B22-001** **1400**

**DEVELOPMENT OF A 400 MHZ-BAND WIND PROFILER RADAR AT OKINAWA IN THE WESTERN PACIFIC SUBTROPICS**

Tatsuhiko ADACHI (Okinawa Subtropical Environment Remote-Sensing Center, Communications Research Laboratory)

Okinawa Subtropical Environment Remote-Sensing Center of the Communications Research Laboratory has developed a new 400 MHz-band Wind Profiler Radar (400M-WPR) at Okinawa Island, Japan, located in the Western Pacific Subtropics, where we can observe active atmospheric phenomena such as typhoons, Asian monsoon, and Baiu fronts induced by thermal input from the warm ocean. This WPR is a monostatic Doppler radar operating at 443 MHz with peak and average transmission power of 20 kW and 2 kW, respectively. The antenna is square-shaped with sides of 10.4 m, consisting of orthogonally aligned 24-element linear arrays, which can electronically steer a radar beam in the meridional- and zonal-vertical plane. The key feature of our WPR is the enhancement of height coverage in RASS (Radio Acoustic Sounding System). In the RASS observations using a monostatic WPR, the wave number vector of transmitted radio waves must be 1/2 that of transmitted acoustic waves, according to the Bragg condition. However, the space that satisfies the Bragg condition is not always at its zenith, but mostly limited to the windward direction, because the acoustic wavefronts are distorted by the background wind velocity profile. Therefore, we have to steer the antenna beam to an appropriate direction satisfying the Bragg condition to enhance the height coverage. To realize this adaptive beam steering according to the background wind field, the whole antenna field of the WPR is mounted onto a turntable so that the antenna beam can steer in any azimuth directions. We calculate in advance the propagation path of the acoustic wave, based on the background wind velocity and the temperature field. We then extend the altitude of the observation by predicting the space region in which the Bragg condition is satisfied and by scanning the antenna beam in that direction. We built the Ogimi Wind Profiler Facility (128.16E, 26.68N, 225 m MSL) as a base for operating various atmosphere-observation devices. Apart from a 400 MHz-WPR, this Facility is equipped with a 1.3 GHz-WPR, a Doppler Sodar, a GPS radiosonde, an ultrasonic anemometer, an optical rain gauge, a disdrometer, and a ground-based weather observation system. The 400M-WPR has continued wind velocity profiling in a few minutes' interval with an altitude range from approximately 400 m to typically 13 km, and 10 km in summer and winter, respectively. We were successful for the wind profiling up to 16 km near the center of a typhoon Nari approached in September 2001. We were successful of preliminary RASS observations up to about 3 km, which indicated the importance of appropriate beam steering and geometric configuration between the acoustic transmitter and radar antenna in RASS.

**MI09/08P/B22-002** **1420**

**VERTICAL WIND OBSERVATIONS USING DOPPLER SPECTRA OF VERTICALLY POINTING W-BAND RADAR**

Yuichi OHNO (Communications Research Laboratory)

W-band radars are very useful instruments for cloud observations because of their higher sensitivity compared with lower-frequency radars and their higher penetrability of thick cloud layers compared with lidars. On the other hand, W-band radars have a disadvantage for rain observations because of larger attenuation compared with lower-frequency radars. However, Lhermitte (1988) found that a vertically pointing W-band radar can measure vertical wind in rainy environment using Mie scatter theory. His method uses the dip of a rain echo Doppler spectrum as an index of the specific size of raindrops that corresponds to Mie resonance. Using a relationship between drop-size and falling velocity, the Doppler velocity of the dip in still air condition is obtained. The environment air velocity can be estimated from the discrepancy between observed Doppler shift of the dip and its velocity in still air. Information of vertical air velocities is necessary to measure accurate drop-size distributions of rain from the vertically pointing radar. In 1997, Communications Research Laboratory developed a W-band (95.04GHz) cloud profiling radar called "SPIDER". SPIDER was mostly operated as an airborne radar, and even in the case of ground-based measurements, velocity was determined using the pulse-pair method before. In Dec 2002 and Jan 2003, SPIDER was operated pointing vertically from the ground and Doppler spectra were obtained during a few rain events. When a low pressure system passed over Japan in January, vertical winds during rain were observed by SPIDER using Lhermitte's methods up to 1 km over 5 hours. The measured vertical winds show clear vertically coherent oscillations that have a 1 m/s amplitude and a 5-6 minute periods. The oscillation is probably related to gravity waves, but the cause of the oscillation is still unknown. By comparing these data with data from a disdrometer as well as a vertically pointing L-band radar, we will be able to verify this method and investigate the change in drop-size distribution affected by vertical air motions.

**MI09/08P/B22-003** **1440**

**MST RADAR VOLUME-IMAGING OF THE LOWER ATMOSPHERE**

Richard M. WORTHINGTON<sup>1</sup> (<sup>1</sup>RASC, Kyoto University, <sup>2</sup>Physics Department, University of Wales Aberystwyth)

Measurements by wind profiler often assume that the background 3-d wind vectors uniform over horizontal distance of ~1km, and refractivity structures move with the wind. Volume imaging radars can remove these assumptions, by measuring full 3-d structure and dynamics of the atmosphere, on spatial scale ~0.1-10 km and time scale ~5 seconds. UHF spaced-

antenna and VHF beam-steering radar both exist for volume imaging. UHF systems are generally smaller, more transportable, and sensitive to insect and birds, whereas VHF systems offer higher power and work in all weather - and so the two are complementary, benefiting together from subtly different views of the same atmosphere. The MU radar at Shigaraki, Japan, can be used for volume imaging, a DBS mode allowing measurement in 64 directions in effect simultaneously. The moving and evolving structure of rain clouds, convective cells, waves, instabilities and deep convection can be visualised. Bird echoes are similar to rain, but discrete and moving in mostly horizontal trajectory instead of continuously down. With sufficient power, measurement height can be increased from the boundary layer and troposphere, to the tropopause region and stratosphere. In addition to the fraction revealed visually by clouds, 3-d structure and dynamics of their invisible atmosphere can be observed.

**MI09/08P/B22-004** **1500**

**ANALYSIS OF TURBULENCE STRUCTURE, WIND, AND WIND SHEAR USING SPACED ANTENNA OBSERVATIONS**

Gernot HASSENPFUG, Mamoru YAMAMOTO, Shoichiro FUKAO (Radio Science Center for Space and Atmosphere, Kyoto University)

Correlation lengths are important characteristics for the study of atmospheric turbulence and the mechanisms causing it. However, the small-scale turbulence structure scales are difficult to observe by remote sensing methods. On the other hand, the effect of small-scale structures has been evident as aspect-sensitive radio-wave scattering at VHF frequencies (Röttger, 1980). Spaced antenna (SA) observations (Röttger and Vincent, 1978) with the 46.5 MHz Middle and Upper atmosphere radar located at Shigaraki, Japan (34.85°N, 136.10°E) using the method of Doviak *et al* (1996) and Holloway *et al* (1996, 1997) permit direct estimates of horizontal correlation lengths, assumed to be due to turbulence, independent of the antenna parameters or baseline configuration. This is a major improvement over spaced antenna techniques that estimate only the ground diffraction patterns. Estimates of these assumed turbulence structure correlation lengths and associated turbulence intensities in the troposphere and lower stratosphere obtained at range resolution of 150 meters and time resolutions of between 26.2 seconds and approximately 5 minutes are compared with background wind and vertical shear of the horizontal wind determined by either SA or Doppler beam swinging (DBS) data. It is shown that enhanced turbulence decreases the size of scatterers without markedly affecting the horizontal anisotropy. We examine this anisotropy of the turbulence structures defined by the direction of the correlation ellipse major axis, the axial ratio, and its relationship to the background wind and wind shear directions. In the comparison, the wind and wind shear information obtained from both SA and DBS data is used, while turbulence intensity estimates derived from SA measurements are used to avoid the necessity of removing beam-broadening effects from DBS spectral widths. The comparison of DBS winds and shear with the turbulence structure size and orientation over several data sets showed consistent anisotropy with ratio of major and minor axis correlation length having values between 1.3 and 1.7, and average major axial lengths of approximately 20 meters. The direction of the major axis of the correlation ellipse tended to be aligned with the wind shear vector to within 30 degrees, while a difference of between 10 and 50 degrees existed for the wind vector. Enhancements in the shear intensity were correlated with a decrease in the scatterer correlation lengths and with a corresponding increase in the turbulence intensity. We observe the relationship of correlation ellipse and wind in an altitude range between two scattering layers where Richardson numbers close to 0.25 occur. Based on these results, we illustrate the usefulness of correlation ellipse parameters in studying turbulence scattering and atmospheric turbulence itself. The results also support the hypothesis that the anisotropic turbulence which is seen during the observations was possibly created by Kelvin-Helmholtz instabilities related to vertical shear of the background horizontal wind field.

**MI09** **Tuesday, July 8 - Wednesday, July 9**

**NEW INSTRUMENTS AND TECHNOLOGY, ADVANCES IN REMOTE SENSING**

Location: Site B, Room 22

**Tuesday, July 8 PM**

**MI09/08P/B22-005** **1600**

**CONTINUOUS MONITORING OF HUMIDITY PROFILES WITH THE WIND PROFILER RADAR-RASS OBSERVATION**

Jun-ichi FURUMOTO<sup>1</sup>, Kenji KURIMOTO<sup>2</sup>, Satoshi IWAI<sup>1</sup>, Toshitaka TSUDA<sup>1</sup> (<sup>1</sup>Radio Science Center for Space and Atmosphere, Kyoto University, <sup>2</sup>Now at Mitsubishi Electric Corporation)

Simultaneous observations of wind velocity, temperature and humidity are essential to study the detailed structure of atmospheric thermodynamics. A three-dimensional wind field can be observed by the wind profiler radar, while temperature profiles can be monitored by RASS (radio acoustic sounding system) with good time and height resolution. However, humidity profiles have not previously been continuously monitored with radar remote-sensing techniques. This study developed a remote-sensing technique to use radar to estimate humidity, which is aimed at enabling the simultaneous observation of wind velocity, temperature and humidity. The variation of the echo power intensity of clear air Doppler radars mainly depends on variation in the vertical humidity gradient. Then, humidity profiles can be estimated using this strong dependency. In order to achieve stable estimation of the humidity profiles, our method refers to complementary measurements such as precipitable water vapor obtained through simultaneous GPS measurement. The MU (middle and upper atmosphere) radar located in Shigaraki, Japan (36.51°N, 146.06°E, 375 m MSL) was used for the test of the method. The MU radar is a clear air atmosphere radar which can monitor three-dimensional wind velocity profiles, and combining RASS with the MU radar (MU radar-RASS) measures temperature profiles in the troposphere and lower stratosphere with good time and height resolution. Humidity profiles were estimated with the MU radar-RASS data obtained in July, 1999. The time-height structure of the radar-derived humidity agreed well with simultaneous radiosonde results obtained every three hours, although the radar-derived humidity revealed short-term fluctuations which could not be observed by the intermittent radiosondes. The hourly fluctuation of radar-derived humidity was consistent with the movement and the development or decay of the rain clouds as monitored by the meteorological radar. We are attempting to apply this method to other radar, such as the equatorial atmosphere radar (EAR) in the west Sumatra, Indonesia and the lower troposphere radar (LTR). This new approach is also presented.

MI09/08P/B22-006

1620

**DIFFERENTIAL ABSORPTION LIDAR SYSTEM FOR VERTICAL PROFILING OF ATMOSPHERIC OZONE**

Devara China Sattilingam PANUGANTI, Raj Ernest P., Pandithurai G., Dani K. KUNDAN (Indian Institute of Tropical Meteorology, Pune - 411 008, India)

Ozone plays a pivotal role in stratospheric chemistry and the radiative balance of the atmosphere. Stratospheric ozone protects life on Earth from harmful UV radiation and controls energy balance, temperature and wind system. In the lower stratosphere and upper troposphere ozone becomes a powerful greenhouse gas and forcing function for climate change. In the lower troposphere, it is a pollutant, created through complex photochemical reactions with anthropogenic gases and sunlight, affecting humans and plants. The gradual increase of the tropospheric ozone concentration has recently given rise to research programs. Continuous monitoring of atmospheric ozone vertical distribution would be of great importance, particularly over tropics where convective circulation and dynamical processes influence the spatio-temporal distributions of chemical constituents, including those originating from the anthropogenic effects, besides high photochemical activity in this region. Such measurements are very scanty in the tropical region. Vertical profiles of ozone are generally retrieved from ground-based, balloon-sonde, rocket-sonde and satellite-borne techniques. Recently, advanced active remote sensing systems utilizing the Differential Absorption Lidar (DIAL) technique have successfully been used for measurements in the stratosphere / troposphere. Of these, excimer (XeCl) lasers provide substantially higher pulse energies and repetition rates and thus allow averaging times of just a few minutes. In this paper, we describe an ultraviolet (UV), rare-gas halide, excimer-Raman laser-based lidar system that is being developed at the Indian Institute of Tropical Meteorology (IITM), Pune (18°43'N, 73°51'E, 559 m amsl), India for vertical distributions of ozone and to investigate their possible impact on environment and climate. The system essentially operates in the differential absorption lidar (DIAL) mode with the laser emission at 308 nm as well as reference wavelength of 353 nm generated by stimulated Raman shifting the 308 nm radiation in hydrogen. The receiving system consists of a 30-cm diameter cassegrain telescope tailored with a detection and data acquisition / processing system with 5 ns multi-channel scaler / averager. The methodology, data inversion algorithms for retrieving altitude profiles of ozone from a lidar return signal profiles and some results obtained on typical experimental days are briefly described. The potential applications of the lidar to studies in atmospheric chemistry and its interaction with aerosols and climate in the tropical region are presented.

MI09/08P/B22-007

1640

**HIGH-SENSITIVE INSTRUMENT FOR IN-SITU MEASURING ATMOSPHERIC NO2 AND SO2**

Yutaka MATSUMI, Hiroyuki SHIGEMORI, Kenshi TAKAHASHI (Solar-Terrestrial Environment Laboratory, Nagoya University)

A new *in-situ* NO<sub>2</sub> instrument has been developed using a laser-induced fluorescence (LIF) technique. The wavelengths for the peak and bottom features of NO<sub>2</sub> around 440 nm are used for the fluorescence excitation of NO<sub>2</sub>, while previous studies used features at 564 and 585 nm. The usage of 440 nm for the excitation has several advantages over the longer wavelength excitation at 564 and 585 nm: (1) The efficiency of the photo-excitation of NO<sub>2</sub> is higher, since the value of the peak photo-absorption cross-section multiplied by the peak-bottom cross section ratio at the features around 440 nm is several times larger than those around 564 and 585 nm. (2) The detection efficiency of the NO<sub>2</sub> fluorescence using a low-noise photomultiplier with a multi-alkali photocathode is higher than the longer wavelength excitations, since the fluorescence emits in the shorter wavelength range where the quantum efficiency of the photomultiplier is high. (3) The peak and bottom features in the absorption spectrum of NO<sub>2</sub> is more separated (100 cm<sup>-1</sup>) than those around 564 and 585 nm (< 0.1 cm<sup>-1</sup>). This makes it possible to use a broad-band OPO laser which are an all solid-state system. (4) Since the broad-band laser can interact with many rotational states of NO<sub>2</sub>, the saturation level of the laser excitation is high and strong fluorescence signal can be obtained. The NO<sub>2</sub> instrument developed in this study has the following features: (1) single-point, *in-situ* measurement, (2) high sensitivity of the 30 pptv in 10 s and S/N = 2, which is high enough for measurements under remote air conditions, (3) high selectivity for NO<sub>2</sub> using the two-wavelength measurements and no possibility of interferences by other species even with photodissociation processes, (4) wide range signal linearity from a few 10 pptv to sub ppmv levels, (5) fast response of less than 1 s, and (6) simple and easy-to-operate laser system. These features suggest the NO<sub>2</sub> instruments developed is suitable for the ground and air-borne measurements in clean remote and urban areas. The inter-comparison between the LIF instrument and a photo-fragmentation chemi-luminescence (PF-CL) instrument was made in the laboratory. The good linear correlation between the LIF and PF-CL instruments was obtained. We also have developed a new *in-situ* SO<sub>2</sub> instrument using almost same apparatus with that of the LIF detection of NO<sub>2</sub>. The light source is the second harmonics of the OPO laser. The sensitivity of the SO<sub>2</sub> system which we have developed is higher than systems using other measurement techniques.

MI09/08P/B22-008

1700

**AUTOMATIC TWILIGHT PHOTOMETER FOR MONITORING METEOR SHOWERS AND VERTICAL PROFILES OF AEROSOLS**

D.B. JADHAV<sup>1</sup>, B. PADMAKUMARI<sup>1</sup>, D.R. JADHAV<sup>1</sup>, H.K. TRIMBAKE<sup>1</sup>, P.R. PATIL<sup>2</sup> (Indian Institute of tropical Meteorology, Pune, India, <sup>1</sup>Y C college of Science, Karad, 415124, India)

A twilight photometer consisting of 15-CM diameter light collecting lens, Red filter centered at 670 NM with 50 NM HBW and Photomultiplier Tube as detector is developed. The photometer is controlled by microcontroller based data acquisition system for zenith sky observations during twilight period. The dark current of the photomultiplier is recorded by moving aperture at focal plane of the light-collecting lens. The variations in the zenith sky level is accommodated in the observation level of 2 to 10 volts output level of the amplifier by changing PMT output voltage by feedback loop system. The multiple stages in parallel combination amplifier is developed for PMT output current measurements, which reduces the amplifier noise considerably to measure the low light level studies. The observations of zenith sky spectra during clear sky condition are taken automatically during morning and evening twilight period for 90 to 100 degree solar zenith for deriving information regarding meteor shower dust at 70 to 120 km altitude and vertical profile of the aerosols up to 150 km altitude. The photometer is controlled by microcontroller based data acquisition system and data is stored in Personal Computer. The presence of observer is not required and the photometer is fully automatic. Preliminary observations for Leonoid meteor shower during 2002 are also presented in this paper.

MI09-Posters

Tuesday, July 8

**NEW INSTRUMENTS AND TECHNOLOGY, ADVANCES IN REMOTE SENSING**

Location: Site D

Tuesday, July 8 PM

MI09/08P/D-001

Poster

1400-154

**A LOWER TROPOSPHERE RADAR: L-BAND ACTIVE PHASED-ARRAY TYPE WIND PROFILER WITH RASS**

Hiroyuki HASHIGUCHI<sup>1</sup>, Shoichiro FUKAO<sup>1</sup>, Toshio WAKAYAMA<sup>2</sup>, Shinichiro WATANABE<sup>3</sup> (Radio Science Center for Space and Atmosphere, Kyoto University, Japan, <sup>2</sup>Mitsubishi Electric Corporation, Japan)

Transportable L-band (1357.5 MHz) Lower Troposphere Radar (LTR) was developed for lower troposphere observations. The Japan Meteorological Agency (JMA) installed their wind profiler network, called Wind Profiler Data Acquisition System (WINDAS), which consists of 25 LTRs, covering Japan. The unique design of the LTR includes a large active phased array antenna with 4 m x 4 m square shape. The antenna can be divided into four sub-panels, and this realizes transportability of the radar system. The array antenna is composed of 96 low-cost coaxial dipole elements, and 24 solid-state transmitter-receiver (TR) modules drive them. The LTR is the first active phased-array type wind profiler in the 1.3 GHz-band. An antenna beam can be steered toward five directions (zenith, east, west, north, and south) with arbitrary zenith angle in order to measure 3-dimensional wind vectors. Total transmitting peak power is 2 kW. In addition, we use 8-bit pulse compression, and hence average transmission power becomes 16 times as large as that of the conventional L-band boundary layer radar (BLR) we have developed. The technique of Spano's optimized complementary codes realizes data acquisition from low altitude, as well as it suppresses range sidelobes. Atmospheric winds in the lower troposphere including the atmospheric boundary layer are obtained with high time and height resolutions in real time. We confirmed the accuracy of the LTR in wind field measurement from the simultaneous observation results with the MU (middle and upper atmosphere) radar. Observations of atmospheric temperature are also possible using the radio acoustic sounding system (RASS) technique with speaker horns.

MI09/08P/D-002

Poster

1400-155

**THE EQUATORIAL ATMOSPHERE RADAR (EAR): SYSTEM DESCRIPTION AND INITIAL RESULTS**

Hiroyuki HASHIGUCHI<sup>1</sup>, Shoichiro FUKAO<sup>1</sup>, Mamoru YAMAMOTO<sup>1</sup>, Toshitaka TSUDA<sup>1</sup>, Takuji NAKAMURA<sup>1</sup>, Masayuki K. YAMAMOTO<sup>2</sup>, Toru SATO<sup>3</sup>, Masahiro HAGIO<sup>4</sup>, Yoshiyuki YABUGAKI<sup>5</sup>, Munir MUZIRWAN<sup>6</sup>, Mahdi KARTASASMITA<sup>7</sup> (Radio Science Center for Space and Atmosphere, Kyoto University, Japan, <sup>2</sup>Graduate School of Informatics, Kyoto University, Japan, <sup>3</sup>Mitsubishi Electric Corporation, Japan, <sup>4</sup>National Institute of Aeronautics and Space (LAPAN), Indonesia)

The western Pacific region is a center for intense atmospheric motions that are closely associated with global atmospheric changes. The world's most active convective clouds are generated in this region, and directly induce the global circulation. We established the Equatorial Atmosphere Radar (EAR) at the equator near Bukittinggi, West Sumatra in the Republic of Indonesia (0.20S, 100.32E, 865 m above sea level), in June 2001. The EAR uses a quasi-circular antenna array with a diameter of approximately 110 m (corresponding to antenna beam width of 3.4 deg), which consists of 560 three-element Yagi antennas. It is an active phased-array system with each three-element Yagi antenna driven by a solid-state transmitter-receiver module (TR module). With this system configuration, the antenna beam can be steered electrically, on a pulse-to-pulse basis, by controlling phase shifters in the TR modules. The beam can be steered within 200 micro sec, i.e. up to 5,000 times per second. Its operating frequency is 47.0 MHz with a bandwidth of 4 MHz. The maximum peak and average radiation powers are 100 kW and 5 kW, respectively (the maximum duty ratio is 5%). A subpulse width as short as 0.5 micro sec, corresponding to the range resolution of 75 m, can be accommodated by the 4-MHz bandwidth of the system. The EAR is now being continuously operated and provides valuable data day by day. The high-resolution observations with the EAR that have never been realized before must play an important role in various studies of the equatorial atmosphere and ionosphere. It is expected that the EAR will be operated in collaboration with other existing networks of radars and other instruments including satellites, and proceed to study the hierarchical structure of atmospheric variations in the equatorial region using the data from these networks. This paper presents the system description of the EAR, including observational results of the equatorial atmosphere made for the first time with an altitude resolution of 150 m.

MI09/08P/D-003

Poster

1400-156

**VALIDATION OF THE WINDOW EMISSIVITY ESTIMATES FROM MULTI-SPECTRAL THERMAL INFRARED DATA AND ITS POTENTIAL EFFECT TO EARTH RADIATION BUDGET**

Kenta OGAWA<sup>1</sup>, Thomas SCHMUGGE<sup>2</sup>, Frederic JACOB<sup>3</sup>, Andrew N. FRENCH<sup>3</sup> (USDA/ARS Hydrology and Remote Sensing Lab, and Hitachi Ltd, <sup>2</sup>USDA/ARS Hydrology and Remote Sensing Lab, <sup>3</sup>Hydrological Science Branch, NASA Goddard Space Flight Center)

Land surface window (8-12 micrometer) emissivity is an important parameter for estimating the long-wave radiation budget. With the successful launch of the NASA EOS Terra satellite in 1999, data from the Advanced Spaceborne Thermal Emission and Reflection (ASTER) radiometer became available for observing land surface emissivity. ASTER has five channels in the 8 to 12 micrometer band with 90 meter resolution. These data can be used to estimate the temperature and surface emissivity variations when used with the Temperature Emissivity Separation (TES) algorithm. We used multiple regression to relate the window emissivity to the five ASTER emissivities. This regression was developed using 257 emissivity spectra from two spectral libraries: ASTER Spectral Library and MODIS Emissivity Library. The approach was validated using a field radiometer, CIMEL CE312, which has approximately the same five channels as ASTER and a window channel. The measurements were performed during field experiment of the Jornada Experimental Range and White Sands National Monuments, New Mexico, USA. The Jornada site is typical of a desert grassland where the main vegetation components are grasses and shrubs and White Sands National Monument is large dunes of gypsum sand. The measured window emissivity are in qualitative agreement with the estimated values using the multiple regression of the five channel emissivities. The bias was 0.003 and the RMS error was 0.0095 for 71 measurements in the range of 0.87 to 0.95. We applied this approach to produce maps of window emissivity over a 400 x 1200 km area for a desert region of North Africa using over 200 scenes of ASTER acquired in 2000 to 2002, which is the subject of another paper being



**MI09** **Tuesday, July 8 - Wednesday, July 9**  
**NEW INSTRUMENTS AND TECHNOLOGY, ADVANCES IN REMOTE SENSING**  
 Location: Site B, Room 22

**Wednesday, July 9 AM**

**MI09/09A/B22-001** **0900**  
**NEW INFORMATION TECHNOLOGIES IN GEOECOLOGICAL MONITORING**

Sergey Zinovievich SAVIN, Nicolay Eduardovich KOSYKH (Computing Center of Far East Branch of the Russian Academy of Sciences)

Ecosystems are characterized by interweaving of nonlinear and accidental dynamic processes inseparably connected with the genetic program of the population and the influence of the environment. There exist various approaches, in this country and in the world, to the construction of information systems of similar complexity based on multi-layer spatial models of an object, e.g. so called geoinformational systems, where the problems of matching and manipulating graphic and attributive data in the framework of a unified integrated model are to some extent solved. However, in order to solve geoeological and medico-biological tasks, it is necessary to search for an adequate ideology, and the creation of adequate instrumental means of descriptive analyses is just beginning. The systems of computer-aided reconstructive tomography, neural networks, computer radiography and the system of rendering of three-dimensional models are widespread at present. They are used for conducting "virtual" surgeries and for the automation of diagnostics in clinical research. A specialized character of such processing systems doesn't allow using them as an instrument for developing new applications. The ideology of informational modelling of animate nature objects based on game-theoretic approach to the tasks of image identification, axonometric principles of creating specialized data bases and logical-semantic ideas of an organism's vital activity, was developed as early as in late 1980s in the laboratory of medical informatics of Computing Center of the FEBRAS. The topicality of such approach to biological information systems (BIS) is connected with the possibility of a wide use of modern computer engineering and informational environment for health care purposes, the use of Internet information environment for improving the effectiveness of prophylaxis, diagnostics and treatment of illnesses, especially in remote districts. In this connection, the problem of adaptation of wellknown visual modeling means, approaches to organizing visual data, means of identifying half-tone images used in other fields of earth science, geoeological monitoring technology, geology, manufacturing and management to medico-ecological tasks seems important. The scientific significance of the project is connected with the development of a universal approach to creating a unified BIS for prospective research of ecological physiology of humans and animals, geoeology, physiological mechanisms of human activity, development and stability of human population, development biology, and also in the theoretical field of neurocomputer development, neurophysiology and neurobionics.

**MI09/09A/B22-002** **0920**  
**REAL TIME PROCESSING OF COLLECTED PARTICLES: MEASUREMENT OF PARTICLES AND PARTICLE FLUXES BY THE CLOUDSCOPE AND THE HOTPLATE**

John HALLETT<sup>1</sup>, Roy RASMUSSEN (<sup>1</sup>Division of Atmospheric Sciences, <sup>2</sup>National Center for Atmospheric Research)

Immediate heating and melt/evaporation of cloud and precipitation particles on collection provides a convenient way of measuring particle mass through latent heat requirement. Instruments using this technique may maintain the substrate at constant temperature during collection and particle evaporation, the power required providing a measure of the evaporation rate. The incremental density is inferred for individual ice particles from the resulting incremental change of volume from video images obtained from a video system back-viewing the collected particle. An instrument (the cloudscope) has been developed for aircraft use whereby a window (size millimeter to centimeters) faces the airstream and is maintained at a temperature sufficient to evaporate incoming particles individually and video record the particles with resolution down to a few microns. Another instrument (the hotplate), developed jointly between DRI and NCAR, measures total mass flux at the ground (precipitation rate both as rain and/or snow over a plate 10 centimeter diameter). The principle of each instrument requires a reference surface free of collecting particles to compensate for the ambient conditions - temperature, air density and air speed. Such surface also provides a direct measure of air/wind speed and also turbulence levels and momentum flux. The instruments are designed and constructed to respond at less than 0.1 seconds at typical flight speed and some 25 seconds for surface precipitation. Data is collected and processed in situ and is readily adapted to provide derived products as precipitation rate, distribution and frequency. Data from several instruments at different locations may be combined to provide precipitation gradients in the vertical (as blowing snow) and horizontal.

**MI09/09A/B22-003** **0940**  
**CONTRIBUTION OF HOT-SPOT EFFECT TO LAND SURFACE ALBEDO**

Alexander P. TRISHCHENKO<sup>1</sup>, Yi LUO<sup>2</sup>, Rasim LATIFOVIC<sup>1</sup>, Zhanqing LI<sup>1</sup> (<sup>1</sup>Canada Centre for Remote Sensing, Natural Resources Canada, <sup>2</sup>University of Maryland)

Surface albedo is an important parameter that influences solar radiation budget, hydrological cycle and defines many important surface biophysical properties. Good knowledge of surface bi-directional reflectance distribution function (BRDF) is required in order to obtain surface albedo. We analyzed data from several sensors (MISR, MODIS, VGT, AVHRR and Landsat-7) to study the variability and dynamics of the BRDF shape in various spectral bands. According to the Landsat ETM high-resolution image, several small areas with homogenous vegetation land cover (cropland, natural grassland/savannas, forest etc) were identified. Combined datasets that include multi-angular and multi-platform observations for different times of the year were generated for these areas, thus providing an opportunity to study the seasonal dynamics of the BRDF properties. Three types of the BRDF models for medium-resolution sensors (MISR, MODIS, VGT and AVHRR) were tested. They are the modified-Rahman (MISR), Ross-Li (MODIS), and model developed at Canada Centre for Remote Sensing. We will present and discuss the results of comparison between these models and their ability to reproduce shape of BRDF function is the hot-spot area. Contribution of hot-spot effect to hemispherical albedo is evaluated numerically and compared with observational data available from CERES broadband radiometer. The

optimized approach for BRDF reconstruction is proposed and applied to generate consistent surface spectral albedo/BRDF data sets.

**MI09/09A/B22-004** **1000**  
**INITIAL FLIGHT OF THE GEOSTATIONARY EARTH RADIATION BUDGET INSTRUMENT: FROM LAUNCH TO OPERATIONS**

Jennifer HANAFIN<sup>1</sup>, J.E. RUSSELL<sup>1</sup>, S. KELLOCK<sup>1</sup>, E. SAWYER<sup>2</sup>, B.C. STEWART<sup>2</sup>, M.J. BATES<sup>2</sup>, D.J. PARKER<sup>2</sup> (<sup>1</sup>Imperial College London, <sup>2</sup>Rutherford Appleton Laboratory)

Initial flight of the Geostationary Earth Radiation Budget instrument: from launch to operations Mission The Geostationary Earth Radiation Budget (GERB) instrument, launched in 2002 on the MeteoSat Second Generation satellite mission, provides a new perspective on the earth-atmosphere radiation system. This instrument is providing measurements of spectrally integrated radiation over a disk on the earth centred at 0°N, 10°W every 15 minutes. Such high temporal resolution allows us to study the evolution of the effects of clouds on the net radiation leaving the earth-atmosphere system. This is an area of major uncertainty in our current knowledge of the system and is potentially a very important climate feedback process. The instrument is also ideally positioned to study radiative properties of the site of origin and much of the subsequent pathway of atlantic hurricanes and Saharan dust storms. Instrument design Measurements are made over the total (0.3-30µm) and shortwave (0.3-4µm) wavelength ranges and the longwave channel is obtained by subtraction. As the satellite is spin-stabilised, GERB uses a despun mirror rotating in the opposite direction to the spacecraft to direct radiation into the optics. An array of 256 detectors records a N-S strip of the earth, building up full total and shortwave scans every 5 minutes, which is then averaged to produce a 15 minute level 1 product. Spatial resolution is 50km<sup>2</sup> at the sub-satellite point. On board calibration includes an internal blackbody for the longwave and an integrating sphere for the shortwave range. Post-launch results and initial data The commissioning period of the instrument was in late 2002 and early 2003. It was carried out by collaboration between the instrument team at Rutherford Appleton Laboratory, Oxford and the operations team at Imperial College, London. A number of tests were implemented during this time and data was acquired in different instrument modes, allowing different elements of the system and their operating status to be examined. The results of these show that in-flight operation of the instrument is as expected and is similar to operation during ground calibration even under the 18G environment imposed by the rotation of the satellite. The results of these analyses and further tests to determine data quality will be presented. Initial data product validation analysis is underway and preliminary results will be discussed.

**MI09/09A/B22-005** **1050**  
**ASTER: A NEW TOOL FOR ESTIMATING LAND SURFACE EMISSIVITY**

Thomas SCHMUGGE<sup>1</sup>, Kenta OGAWA<sup>2</sup>, Frederic JACOB<sup>1</sup>, Andrew N. FRENCH<sup>3</sup>, Ann HSU<sup>1</sup>, Jerry RITCHIE<sup>1</sup> (<sup>1</sup>USDA/ARS Hydrology & Remote Sensing Lab, <sup>2</sup>USDA/ARS Hydrology & Remote Sensing Lab and Hitachi Ltd. Tokyo, 101-8010, Japan, <sup>3</sup>Hydrological Sciences Branch, NASA/GSFC, Greenbelt, Maryland, USA.)

The multispectral thermal infrared data obtained from the Advanced Spaceborne Thermal Emission and Reflection (ASTER) radiometer on NASA's Terra satellite have been shown to be of good quality and provide a unique new tool for studying the land surface. ASTER has 5 bands in the 8 to 12 micrometer waveband with 90 m spatial resolution, when the data are combined with the Temperature Emissivity Separation (TES) algorithm the surface emissivity over this wavelength region can be determined. This paper will present some quantitative emissivity results obtained over test sites in southern New Mexico, USA; the Jornada Experimental Range and the White Sands National Monument which are compared with ground measures. The Jornada site is typical of a desert grassland where the main vegetation components are grass and shrubs with a large fraction of exposed soil while the White Sands site is mainly dunes of gypsum sand which provides a good relatively homogenous emissivity target. More than a dozen ASTER scenes over these New Mexico test sites have been acquired since the launch of Terra in December 1999. There were simultaneous field campaigns in May of 2000, 2001 and 2002 and September/October 2001 and 2002. Also, MASTER (MODIS-ASTER airborne simulator) coverage was obtained for several of the dates. In spite of the 90 m resolution, the results appear to be in good quantitative agreement with laboratory measurements of the emissivity for the quartz rich soils of the Jornada with values < 0.85 for the 8 - 9 micrometer channels. For the longest wavelength channels little spatial variation of the emissivity was observed with values of 0.96 +/- 0.005 over large areas. Emissivity values from the ASTER data for the gypsum at White Sands were in good agreement with values calculated from the lab spectra for gypsum and with each other. Gypsum has a strong emissivity minimum centered on the ASTER 8.63 micrometer band, and the satellite results for this band agree within 0.01 of the value calculated from the laboratory spectra.

**MI09/09A/B22-006** **1110**  
**AN END-TO-END MODELING STUDY TO GENERATE SYNTHETIC DATA CUBES FOR IMAGING SPECTRAL SENSING APPLICATIONS**

Chih-Yue Jim KAO, William Scott SMITH, Jon M. REISNER (Applied Physics Division, Los Alamos National Lab)

An airborne IR hyperspectral imaging sensor based on the Fourier transform spectrometer technique has been used for studying atmospheric gaseous plumes under the auspice of US Department of Energy. Model generated synthetic data of spectral intensity associated with the plume and the surface background is useful in terms of performing trade studies as well as testing new algorithms. To cope with the highly turbulent and transient atmospheric boundary layer where plume emissions and evolution are embedded, we have used a high-resolution (at the scale of 1 m) time-dependent Navier-Stoke atmospheric hydrodynamic code, HIGRAD, to replace the Gaussian/multi-fractal approach in the original package of the Los Alamos End-to-End Modeling of Imaging Spectral Sensing Applications (EMISSA). The output from HIGRAD is then used for calculations of radiance reaching the sensor through the Fast Atmospheric Signature Code (FASCODE) with a spectral resolution of 1 cm-1 or less. The modeled plume structure in concentrations and associated plume images in radiance bear great resemblance to the commonly observed phenomenology. The 3-D data cubes of spectral intensity are used to test a plume contrast model for its capability in quantifying the column densities of chemical species. The synthetic data produced through our approach proves to be effective in evaluating our understanding of the thermal infrared imaging process.

**MI09/09A/B22-007** **1130**  
**COMBINING CROP GROWTH MODELS AND REMOTE SENSING DATA FOR CROP YIELD PREDICTION: FROM FIELD TO REGIONAL SCALES**

Yanxia ZHAO (Research Center of Agrometeorology and Remote sensing Application, Chinese

It has been widely recognized that global change on some extent are attributable to human activities; many human systems are sensitive to global change, and some are vulnerable. Agriculture is one of the most vulnerable. Food security has been attracting more and more attentions. The studies on crop yield prediction are therefore very significant in providing information to policy makers and government and keeping sustainable development. There are many methods of crop yield estimation. Among them, the most promising method is combining crop growth models and remote sensing data to estimate crop yield. The different ways for integrating crop models with remote sensing data can be generally classified into two groups: the forcing strategy and the 're-initialization/re-parameterization' strategy. The forcing strategy is to update at least one state variable in the crop model using remote sensing products as the values of some variables. The crop model runs at a constant time step (e.g., daily), but it is very difficult to acquire remote sensing imagery at such high-resolution temporal steps. The common practice is to fit an empirical curve to the estimate values from remote sensing observations and then carry out the interpolation according to the model time step. The 're-initialization/re-parameterization' strategy minimizes the difference between the values from remote sensing and the predicted ones from crop models by adjusting model parameters or the initial conditions. One method is to use the derived variables from remote sensing data to recalibrate crop model by optimization procedures. Another method is to directly use the observed radiometric information directly re-parameterize or re-initialize a crop model, which needs to couple the radiative transfer models with crop models. This assimilation of remote sensing data leads to the retrieval of one initial condition, subsequently it allows to use the model more confidently over an area where no ground information is available. Some case studies have been conducted using the strategies such as combining SOYGRO, AFRCWHEAT2, SUCROS or WOFOST crop models and remote sensing data. The results show that the accuracy and scale of crop yield estimation are improved when remote sensing information is used in the crop models. I tried to couple DASSAT crop model and MODIS remote sensing data to predict China wheat yield and obtained a result which was much better than that without using remote sensing.

Wednesday, July 9 PM

MI09/09P/B22-001

1400

**TM IMAGE CLASSIFICATION OF ZHALONG WETLAND (CHINA) USING NEURAL NETWORK**

Min HAN<sup>1</sup>, Lei CHENG<sup>1</sup>, Qingyu ZHOU<sup>2</sup> (<sup>1</sup>Dalian University of Technology, <sup>2</sup>Songliao Water Resources Commission)

Remote sensing images usually distinguish land cover information by the brightness of pixels. Different brightness of pixels indicates the different information of spectrum. Therefore, an important application of remote sensing images is to understand the land cover state by classification techniques. Traditionally, the ways to classify land cover information are based on the Bayesian classifier. It is well known that the Bayesian classifier is theoretically optimal if the assumptions about the probability density functions (PDFs) are correct. A poor performance may be obtained if the true PDFs are different from those assumed by the model. This limits the application of the method. Maximum likelihood classification is one of examples based on the Bayesian classifier. Artificial neural network has already been applied in the field of classification of remote sensing images, especially back-propagation neural network classifier. Compared with traditional methods, neural networks do not need a probabilistic distribution pattern. They have strong adaptive learning ability. Owing to parallel processing, adaptive learning and nonlinear procedure, neural networks can classify TM Images more efficiently and precisely. This paper applies neural networks to classify land cover information from the TM images of Zhalong wetland. An adaptive back-propagation algorithm based on a robust error function is introduced to build a four-layer neural network. Zhalong wetland, one of important National Natural Reserves and Ramsar sites, is located in northeast of China, 70 km long and 40 km wide. The total area of the wetland is 2100 km<sup>2</sup> and the water surface is about 800 km<sup>2</sup>. Considering the especial natural condition and the management demand, TM image analysis is expected to be useful technique in the water resources and ecosystem management of the wetland. In this paper, 7 categories of land cover information are classified, that is, water, marsh, farmland, woodland, grassland, residential area and salina. Comparing classification results of the four-layer neural network with three-layer neural network and the maximum likelihood classifier, conclusion can be summarized as follows: (1) the structure of the four-layer neural network and the adaptive back-propagation algorithm based on the robust error function is effective to classify TM image data; (2) the four-layer neural network adopted in this paper succeeded in building a complex model of TM image, and it avoided the great storage problem of remote sensing data, and (3) the adaptive back-propagation algorithm speeded up the descending of error. Above all, the four-layer neural network is superior to the three-layer neural network and the maximum likelihood classifier in the accuracy of the classification.

MI09/09P/B22-002

1420

**BALLOON-BORNE ALL SKY/ GROUND IMAGING OBSERVATION AND ITS APPLICATION TO THE VERIFICATION OF RADIATIVE-TRANSFER COMPUTATION**

Daren LU, Wen xin ZHANG, Juan HUO (Institute of Atmospheric Physics, Chinese Academy of Sciences)

For validation of satellite remote sensing of surface reflectivity (albedo) and atmospheric aerosol characteristics, one of common procedures is to conduct ground truth observation for both surface and atmospheric observation. Since in optical wavelengths, multiple scattering and surface inhomogeneity as well as bi-directional reflectivity play important role, complete radiance measurements from both all sky and all direction of surface are ideal ground truth database. So far, separate observations of surface reflectance and sky radiance are used. Usually these measurements are not for all sky/ground. In this paper, we used a balloon-borne facility to simultaneously observe all-sky and all ground images. A pair of digital cameras with fish-eye lens is put on a specially designed tethered balloon with parallel opposite field-of views. With geometric and radiative calibration, we may have the all sky/ground directional radiance. Tethered balloon-borne facility makes the measurements at different height levels. Thus it is not just useful for "bulk" validation but for analyzing the difference and their causes. Also this kind of observation will be a useful database for strict verification of radiative transfer algorithm. The primary experimental results and the comparison with some RT algorithms will be introduced in this paper.\*This work was supported by NSFC project No. 40027002 and Dept. of Science and Technology Project No 2001CCA02200

MI09/09P/B22-003

1440

**AESMIR: A NEW NASA AIRBORNE MICROWAVE IMAGER**

Edward KIM (NASA Goddard Space Flight Center)

The NASA Airborne Earth Science Microwave Imaging Radiometer (AESMIR) is a versatile new airborne instrument. The AESMIR design is unique in that it will perform imaging at all standard passive microwave frequency bands (6--90 GHz) using a single mechanical package, providing an efficient solution for a wide variety of Earth science applications (snow, soil moisture/land parameters, precipitation, ocean winds, sea surface temperature, water vapor, sea ice, etc.). Using parallel filter banks, AESMIR provides simultaneous outputs matching the channel sets of AMSR-E, CMIS, Windsat, GPM, SSM/I, SSM/IS, and TMI. In addition, all bands except the 23-GHz sounding band incorporate fully-polarimetric (4-Stokes) receivers with parallel analog polarization combining as well as high-speed digital correlators, for a total of 54 output channels. The microwave radiometers themselves will incorporate state-of-the-art receivers, with particular attention given to instrument calibration for the best possible accuracy and sensitivity. The arbitrary 2-axis gimbal can perform conical and cross-track scanning, as well as fixed-beam staring. An L-band option is also feasible, again using the same scanner. Thus, simultaneous imaging from 1.4 to 90 GHz will be feasible. When paired with its millimeterwave sister instrument, CoSMIR, synchronized imaging up to 183 GHz is feasible. The single-package design of AESMIR makes it compatible with high-altitude aircraft platforms such as the ER-2 and the Proteus as well as lower-altitude aircraft such as the P-3, DC-8, C-130, and even ground-based deployments. Thus AESMIR can provide low-, mid-, and high-altitude microwave imaging while leaving maximum space for other instruments--optimizing opportunities for synergistic science and field campaign effectiveness.

MI09/09P/B22-004

1500

**NETWORK OF VECTOR ELECTRIC FIELDMILS FOR THUNDERSTORM WARNING AT ROCKET LAUNCHING STATIONS**

Dattatraya B. JADHAV<sup>1</sup>, R. VIJAYAKUMAR<sup>1</sup>, D.R. JADHAV<sup>1</sup>, G.V. RAMA<sup>2</sup> (<sup>1</sup>Physical Meteorology and Aerology Division, Indian Institute of Tropical Meteorology, <sup>2</sup>SHAR Centre, Sriharikota, India)

Weather radar can not be used before and during launch operations, as field generated due to these radiations may trigger any accidental activity or may damage the important electronic systems. Also the electric fields due to charge clouds may introduce similar errors. Hence for taking precautionary measures for giving field warnings, a three-vector electric fieldmill system measuring Vertical, North-South and East-West component is developed. Four stations located ~10 km apart measuring the three vectors of electric field are utilized to locate the charge centers in 70 km diameter region. A single sensor is consists of two half-metallic cylindrical plates mounted on Fiberglass cylinder. The two metallic plate's signal is collected through rotating condenser and amplified by the bridge amplifier. The field sensed by single sensor of two metallic plates is utilized to sense two vectors perpendicular to the direction of rotation of sensor plates using optointerrupters and phase sensitive detection system. These three vectors gives the direction of the charge centers in space due to charges in the cloud, which is indicator of thunderstorm development. Each station consists of two sensors mounted perpendicular to each other to measure the three vectors of electric fields, signal-conditioning system, Interfacing unit and PC based data acquisition and transmission system. The data is transmitted to the Central processing system via telephone lines. The data received is processed for locating charge centers in space and time for giving three different warning levels. The algorithm is developed to calculate the orientation of the charge centers in space and time. The central processing system displays information regarding the location of the charge centers on the map of rocket launching station in the diameter of 70 km. All the systems consisting of sensor, signal conditioning system, Microcontroller based data acquisition and instrument health monitoring system, software required for data acquisition, data display and data processing is developed indigenously. Similar systems can be utilised as thunderstorm warning system at airports, ships, power establishments ... etc. Preliminary results are presented in this paper.



MC02

Monday, July 7 - Tuesday, July 8

**TYPHOONS IN ASIA: THEIR UNIQUE FEATURES (ICDM)**

Location: Site B, Room 20

Monday, July 7 AM

Presiding Chairs: P.S. Chu, J. Matsumoto

**TYPHOON VARIABILITY**

MC02/07A/B20-001

0945

**CLIMATOLOGICAL CONDITION OVER THE WESTERN NORTH PACIFIC BASIN**

Yoshio KURIHARA (Frontier Research System for Global Change)

Tropical cyclones that are observed in the Western North Pacific basin are called typhoons. This basin is defined as an area west of the date line of the North Pacific, including the South China Sea. A typhoon usually spends its entire life, from formation to decay, in this area. In the present talk, climatological condition of the atmosphere and ocean in this basin is described. Needless to say, the condition is strongly influenced by geographical features, including the global distribution of landmass. Relatively high sea surface temperature and strong conditional instability of the atmosphere in the tropics in this basin are conducive to typhoon genesis. The Pacific High pressure, monsoon trough and Tropical Upper Tropospheric Trough characterize the mass and wind field. Variability of these features at different time scales is an issue of importance. Formation of individual tropical disturbance can take place through combination of various factors. Increase above climatological mean in the low level vorticity and moisture in a broad area is certainly among them. It can be brought by transient features such as the Madden Julian Oscillation, mixed Rossby gravity waves, westerly wind burst along the equator, surge of southerly wind across the equator. The South China Sea is a loosely closed region, where formation and reintensification of typhoons are observed. The track of a typhoon is dependent on the large-scale wind surrounding the vortex as well as the flow associated with storm's structure. The so-called environmental wind at mid to high latitudes is strongly influenced by the behavior of synoptic scale systems in these latitudes. A typhoon may move westward and onto land to undergo structure change. If a typhoon moves northward, it may be transformed into an extratropical storm. The climatological condition in the northern part of the Western North Pacific basin is favorable for such transition. Specifically, it is featured by the existence of the jet stream at

upper levels, implying strong baroclinicity, large gradient of sea surface temperature, dry air over the land west of the basin, and so forth.

**MC02/07A/B20-002 1005**  
**INTERANNUAL VARIABILITY OF TROPICAL CYCLONE FREQUENCY OVER THE WESTERN NORTH PACIFIC DURING THE LATTER HALF OF THE 20TH CENTURY**

Michiaki YUMOTO, Tomonori MATSUURA (National Research Institute for Earth Science and Disaster Prevention)

Interannual variability of tropical cyclone (TC) frequency over the western North Pacific (WNP) during the latter half of the 20th century was investigated. Based on the time series of the TC frequency removed the interdecadal trend, nine years (1952, 1955, 1958, 1967, 1971, 1974, 1978, 1981, and 1994) are regarded as "prolific years" having an abundance of TCs. Six years (1963, 1969, 1973, 1987, 1995, and 1998) are recognized as "infertile years" in which the TC activity is low. Medians of TC frequencies in the prolific years and the infertile years were 32 and 21, respectively. The internal variability of TC frequency was related to the monthly frequencies in the boreal summer. Comparisons of atmospheric and oceanic summer conditions between the prolific years and the infertile years showed characteristics of the interannual variability of TC frequency. The atmospheric environments in prolific years were (1) westerly winds in the low-level troposphere, (2) low sea-level pressure, (3) divergent environments in the upper-level troposphere, and (4) high precipitation rate over the WNP, in comparison with the infertile years. Difference of the sea surface temperatures (SSTs) over the WNP showed the east-west contrast pattern. That is, the SSTs in the prolific years were warmer in the eastern part of the WNP and cooler in the western part than that in the infertile years. Finally, we will discuss the contributions of El Niño-Southern Oscillation and/or the Indian Ocean Dipole mode event, as the background of large-scale environmental changes, to the interannual variations of TC frequency.

**MC02/07A/B20-003 1025**  
**SEASONAL AND INTER-ANNUAL VARIATIONS OF TROPICAL CYCLONE APPROACHING INDOCHINA**

Hideaki SHOJI, Jun MATSUMOTO (Department of Earth and Planetary Science, University of Tokyo)

The seasonal and inter-annual variations of the number of tropical cyclone approaching Indochina (TCIC) have been investigated for the period 1951-2000 by utilizing Typhoon track data analyzed by the Japan Meteorological Agency. In order to understand the mechanism of large inter-annual variabilities of the number and tracks of tropical cyclones (TCs), large-scale flow patterns in abundant tropical cyclones approaching Indochina (ATCIC) and in no tropical cyclones approaching Indochina (NTCIC) months have been compared by utilizing NCEP re-analysis wind data. Also analyzed is the state of the sea surface temperature (SST) fields. (BR)1 The results obtained in the present study are summarized as follows: (BR)1 The number of annual total TCIC shows no long-term trend. On the other hand, the number of TCIC in June and July, and that in October and November shows slight increasing trend. (BR)2 Clear differences of the birth places and major courses of tropical TCs are recognized between ATCIC and NTCIC months. Generally speaking, more TCs are generated in the SCS in ATCIC months, and the courses of TCs direct more northward in NTCIC months. (BR)3 When abundant TCs approach Indochina in June to September season, the anomalous easterly wind is observed at 500hPa over the South China Sea (SCS), which will favor the more westward tracks of TCs. (BR)4 In October and November at 850 hPa, the westerly monsoon flow from the Indian Ocean across the Malay Peninsula and the northeasterly monsoon flow over South China and the northern SCS are both stronger in ATCIC months. The effect of Asian monsoon activity on the TC genesis and courses in the western North Pacific may be more important in the post-monsoon season in October and November. At 500 hPa, northerly and easterly anomaly is apparent over the East China Sea and the SCS, respectively. (BR)5 In ATCIC months SST fields show El Niño pattern in August and September, while, they present La Niña pattern in October and November.

**MC02/07A/B20-004 1105**  
**INTERANNUAL VARIABILITY OF TROPICAL CYCLONE FREQUENCIES FROM AN ENSEMBLE CLIMATE SIMULATION WITH THE NCAR CCM3**

Junichi TSUTSUI, Hideyuki KITABATA (Central Research Institute of Electric Power Industry)

The western North Pacific and the North Atlantic are both major tropical cyclone (TC) basins, for which reliable TC records are available over a period of more than 50 years. Such long-term TC records show large variability with interannual and interdecadal timescales associated with naturally occurring climate changes, and the characteristics of the variability is different between the two basins. El Niño and Southern Oscillation (ENSO) is one of the contributory factors to affect the variability. In the North Atlantic, an anomalous increase in upper tropospheric westerlies during ENSO warm events inhibits TC activity by increased tropospheric vertical wind shear, and less anticyclonic upper level winds. In the western North Pacific, although the relationship between TC activity and ENSO is not as evident as in the North Atlantic in terms of the annual number of TC formations, ENSO events can modulate the location of formation area or seasonal activity. Considering this characteristic behavior of TCs in the two basins, we are investigating impacts of sea surface temperature (SST) variations associated with ENSO on TC activity by numerical experiments. The present study adopted the National Center for Atmospheric Research (NCAR) Community Climate Model version 3 (CCM3) including a modification in the moist convection schemes. This modification is an implementation of an inhibition mechanism for the deep convection scheme in the model, and allows the model to produce TC-like disturbances with a realistic frequency. Since the model shows large interannual variability even with climatological SST data as a boundary condition, we've been conducting an ensemble climate simulation to reduce such model-inherent variations. Currently, we have completed seven climate simulations using observed SST from 1979 through 1989. Time integrations will be extended to the end of the 1990s. In the 1980s, two ENSO warm events occurred. Observed TC records show some responses to the events such as decreased frequencies during the periods. In the western North Pacific, it is remarkable that the observed response was delayed more than several months. Although the simulated interannual variations indicate some features of observed tendencies, the reproducibility in the western North Pacific is not as good as in the North Atlantic. In particular, the model shows scattering results among the ensemble members regarding the observed delayed response. This result implies that SST variations associated with ENSO affect TC activity rather directly in the North Atlantic, and that more climatological factors are indirectly involved in the TC activity in the western North Pacific.

**MC02/07A/B20-005 1125**  
**A MECHANISM OF INTERDECADAL VARIABILITY OF TROPICAL CYCLONE ACTIVITY OVER THE WESTERN NORTH PACIFIC**

Tomonori MATSUURA, Michiaki YUMOTO, Satoshi IIZUKA (National Research Institute for Earth

Science and Disaster Prevention)

Tropical cyclone (TC) activity in the western North Pacific (WNP) has changed interdecadally with an approximately 20-year period between 1951 and 1999 (Yumoto and Matsuura 2001). The cause and mechanism of interdecadal variability of TC frequency in the WNP is investigated using NCEP/NCAR reanalysis and the result obtained from a high-resolution coupled general circulation model (CGCM). The interdecadal variability of TC activity in the WNP correlates with long-term variations in sea surface temperatures (SSTs) in the tropical central Pacific and with those of westerly wind anomalies associated with the monsoon trough that appears over the tropical WNP during the typhoon season of July to October. The westerly wind anomalies at near 10°N show positive feedback with the SST anomalies in the central Pacific. Therefore, the interdecadal variability of TC frequency is related to long-term variations in atmosphere-ocean coupling phenomena in the tropical North Pacific. A 50-year long-run simulation using the high-resolution CGCM showed the robustness of interdecadal variability of TC frequency.

**MC02/07A/B20-006 1145**  
**DECADAL VARIABILITY OF TROPICAL CYCLONE ACTIVITY OVER THE WESTERN NORTH PACIFIC**

Hsin Hsing CHIA<sup>1</sup>, Pao-Shin CHU<sup>2</sup>, Chet ROPELEWSKI<sup>1</sup> (<sup>1</sup>Central Weather Bureau, Taiwan, <sup>2</sup>University of Hawaii, U.S.A., <sup>3</sup>Columbia University, U.S.A.)

Time series of tropical cyclone (TC) counts over the Western North Pacific from 1965 to 2001 are analyzed by a statistical change-point analysis. This method identical to that used recently to identify decadal variations of tropical cyclone activity over the central North Pacific (Chu, 2002). For the western North Pacific, results reveal two epochs of activity. The epoch during 1989-1997 is marked by high activity in contrast to the low activity during 1968-1988. Large-scale environmental conditions conducive to cyclone activity during the peak typhoon season (July through October) for the active (1989-1997) and inactive (1968-1988) epochs are investigated. The parameters considered include sea surface temperatures, sea level pressures, relative vorticity at the lower troposphere, and vertical wind shears between the lower (850 hPa) and upper (200 hPa) troposphere. The source of the data comes from the NCEP/NCAR reanalysis product and the horizontal resolution of the reanalysis dataset is 2.5 deg latitude/longitude. Relative to the inactive epoch, a warmer ocean surface over the region where TCs are generally formed in the western North Pacific is found in the active epoch, although this warming is rather small (<.2 deg C). The region bordered between 10N-20N and 130E-155E (Chia and Ropelewski, 2002) is referred to as the major genesis area (MGA). Lower sea level pressures are also found over the MGA in the active epoch compared to the inactive epoch. More interestingly, large anomalies of low-level cyclonic vorticity are observed over the MGA during the active epoch in contrast to the inactive epoch. Independently, streamline analysis reveals a huge anomalously cyclonic circulation gyre, similar to the monsoon gyre, with strong equatorial westerly anomalies over the western North Pacific when the inactive period is subtracted from the active epoch. Weaker vertical wind shears over the MGA are found during the active epoch as opposed to the inactive epoch. Although some of the aforementioned changes are small (e.g., sea level pressures), variations in each individual environmental field work in the proper sense and collectively favor more cyclone incidences as observed during the recent epoch. Research is underway to determine whether the changes in environmental conditions during the active and inactive epochs are statistically significant and to explore variations in other key parameters (e.g., upper-level divergence). References: Chia, H.H., and C.F. Ropelewski, 2002: The interannual variability in the genesis location of tropical cyclones in the northwest Pacific. *Journal of Climate*, 15, 2934-2944. Chu, P.-S., 2002: Large-scale circulation features associated with decadal variations of tropical cyclone activity over the central North Pacific. *Journal of Climate*, 15, 2678-2689.

**MC02/07A/B20-007 1205**  
**IMPACTS OF SST WARMING AND CO2 INCREASE ON TROPICAL CYCLONE FREQUENCY**

Jun YOSHIMURA<sup>1</sup>, Masato SUGI<sup>2</sup> (<sup>1</sup>Global Warming Research Program, Frontier Research System for Global Change, <sup>2</sup>Japan Meteorological Agency)

For realistic numerical simulation of tropical cyclones (TCs), it is generally thought that high-resolution models are required. Simulating greenhouse gas-induced warming with high-resolution atmospheric general circulation models (AGCMs), sea surface temperatures (SSTs) are usually prescribed (as 'time-slice experiments'). But it is difficult to predict global-mean SST warming exactly in response to given CO2 increase (such as doubling), based on current scientific understanding. Moreover, if global climate is in a transient state after rapid CO2 increase (due to human activity, for example), global-mean SST should be significantly lower than that of equilibrium value. We have studied about decrease in simulated TC frequency due to greenhouse warming, using high-resolution AGCMs (e.g. Sugi et al. 2002). In the present study, we investigate impacts of SST warming and CO2 increase separately, using a T106 atmospheric model (JMA-GSM8911) with prescribed SST. It is shown that, in response to CO2 increase without changing SST, TC frequency reduces globally. This change may be caused by decrease in convective precipitation in the tropics, and the change in convective heating is balanced with weakening of long-wave radiative cooling in the lower troposphere. On the other hand, SST warming without changing CO2 does not have large impacts on global TC frequency.

**Monday, July 7 PM**  
 Presiding Chairs: I. Ginis, J. Tsutsui

**TYPHOON STRUCTURE**

**MC02/07P/B20-001 1400**  
**USE OF QUIKSCAT DATA IN STUDYING THE EVOLUTION OF TROPICAL CYCLONE STRUCTURE**

Johnny C.L. CHAN, Cleo YIP (Laboratory for Atmospheric Research, Dept. of Physics & Mat. Sci., City University of Hong Kong)

Since the launch of the QuikScat in 1999, valuable ocean-surface wind data have been available for the study of tropical cyclone structure. In this paper, we will present results from detailed analyses of these data around tropical cyclones over the western North Pacific (WNP) for the period 1999-2002. Because of possible contamination near the center, the focus is on the outer-wind structure. Temporal evolutions of the size (radius of 15 m/s winds) and outer-wind strengths will be presented. The size variations are found to be consistent with those found in previous studies. An interesting finding is that the average size during this period over the WNP generally tends to be smaller than those from other years. This result is explained in terms of the environmental flow patterns (typical of La Niña

conditions) in which the tropical cyclones were embedded. Such an observation further emphasizes the control of the environment on the size evolution of a tropical cyclone. The evolution of the outer-wind strength as well as the entire outer-wind structure for different tropical cyclones can be classified into several types, each of which can be explained in terms of the changes in the environmental flow patterns. In some cases, internal dynamics apparently also has an important contribution.

**MC02/07P/B20-002 1420**

**ON THE FORMATION OF CONCENTRIC VORTICITY STRUCTURE IN TYPHOONS**

Hung-Chi KUO<sup>1</sup>, Lee-Yaw LIN<sup>1</sup>, Chih-Pei CHANG<sup>2</sup>, R. Terry WILLIAMS<sup>3</sup> (<sup>1</sup>Department of Atmospheric Sciences, National Taiwan University, <sup>2</sup>Department of Meteorology, Naval Postgraduate School)

During 25-26 September 2001, Typhoon Lekima moved northwestward near the southern tip of Taiwan. At 0900 local time 25 September, the typhoon possesses a small and strong central core vortex (of  $10^3$  to  $10^2$  s<sup>-1</sup> vorticity field) with a huge area of convection southwest of the vortex. Subsequent revolution as indicated by radar reflectivity suggests that the huge area of convection stretched and wrapped around the central vortex to form a concentric eyewall structure in less than 10 hours. In this work we use a nondivergent barotropic model to test a hypothesis that the formation of the concentric eyewall in Typhoon Lekima may be in part due to the vorticity advective dynamics. In this hypothesis we postulate that the concentric eyewall is a result of the shearing out of the huge area of convection into a band surrounding the central vortex. We test the hypothesis by considering the interaction between a small and strong inner vortex (the tropical cyclone core) and a larger and weaker outer vortex (the vorticity induced by the moist convection outside the central vortex of a tropical cyclone). The formation of the concentric eyewall is studied in terms of the separation distance, the vorticity strength ratio, and the radius size ratio of the two vortices. In general, the formation of the concentric vorticity structure requires a very strong core vortex (at least 4 times stronger than the neighboring vorticity), a larger area of the weaker vorticity field (2 times larger in size), and a separation distance of 2 to 3 times of the inner vortex radius. The evolution in Typhoon Lekima appeared to meet these conditions. The negative vorticity anomaly between the two vortices serves as a shield to impose a barrier to the inward mixing of the outer vorticity field. If the separation distance is too close, the resultant evolution most likely leads to either a merger or a tripole vortex formation. The central core vortex has to be strong to maintain itself against any deformation field from the environment due to the outer vortex. In addition, the stronger vortex induces a differential rotation across the weaker vortex to strain out the latter into a vorticity band surrounding the former. The change of sign of vorticity gradient across the band satisfies the Rayleigh necessary condition for instability. However, the band is stabilized by the Fjortoft sufficient condition for stability because the strong inner vortex can cause the wind at the inner edge to be stronger than the outer edge, allowing the vorticity band and therefore the concentric structure to be sustained.

**MC02/07P/B20-003 1440**

**DETECTABILITY OF TYPHOON EYES OVER OCEANS IN TRMM PR AND IR OBSERVATIONS**

Yasu-Masa KODAMA, Takuya YAMADA (Department of Earth and Environmental Sci. Hiroasaki University)

Satellite cloud images have been utilized for detecting typhoon centers and for evaluating typhoon intensity (e.g., Dvorak method). However, internal structure of typhoons, especially eyes, sometimes cannot be observed by cloud images, when typhoons are covered by upper cloud shields. TRMM (Tropical Rainfall Measuring Mission) launched in late 1997 realized space-borne precipitation-radar (PR) observations. PR of TRMM can observe the internal structure of typhoons under upper cloud canopy. Since TRMM also mounted IR imager in the atmospheric window, we can compare the internal structure of typhoons observed by PR and the configuration of typhoons shown in IR cloud images. In this study, we examined detectability of typhoon eyes in PR observations (rainfall intensity at 3km ASL) and IR observations (TBB in 12 $\mu$ m channel) of TRMM and studied their statistical relation to the typhoon intensity and life-stage, for 71 cases between 1998 and 2000, when the central portion of typhoons fall into the PR observation swath (~ 220km). In 55% of the whole 71 cases, eyes were detected not in IR but only in PR observations. Eyes were detectable in both PR and IR for ~ 32% of the whole cases, while not detectable in neither PR nor IR for 13% of the whole. There were no cases in which eyes were detected only in IR. Maximum wind speed of typhoons averaged for the cases when both IR and PR detected the eyes was ~ 20 knot larger than that for the cases when only PR detected. In the developing stage of typhoons, eyes were obscure in both IR and PR observations for 24% of the cases in this stage, and detectable in only PR for 62% of the cases. Eyes were detectable in IR only for 13% of the cases. In the mature stage, most of typhoons (97%) have eyes detected in PR observations, while only minor part of typhoons (35%) has eyes detected in both PR and IR. In the decaying stage, the detectability of typhoon eyes in IR is largest (detectable for 45% of the cases in this stage), while eyes were obscure in both IR and PR for 20% of the cases. We need remark that typhoon eyes cannot be observed in IR in many cases due to upper cloud shields extended over typhoon eyes. Typhoon eyes are obscure even in the PR observations in a small part (1/3-1/4) of the cases in developing and decaying stages. Detectability of typhoon eyes in IR observations increases larger in the later stage of typhoon life cycle.

**MC02/07P/B20-004 1500**

**TEMPORAL AND SPATIAL VARIATIONS OF PRECIPITATION OF LANDFALLING TYPHOONS IN TAIWAN**

JONG-DAO Ben JOU (DEPARTMENT OF ATMOSPHERIC SCIENCES, NATIONAL TAIWAN UNIVERSITY)

This study examines the temporal and spatial variations of precipitation structure within 300 km radius of the typhoon center by using reflectivity data taken by Doppler radars in Taiwan during landfall. Four typhoons with different tracks and intensity were analyzed. The gird-averaged reflectivity data in four quadrants were used to show the evolution of the eyewall, the rainbands in the annular area outside the eyewall, and area extended to 300 km from the center of the eye. More than 50 hours radar data with time interval of 6 minutes were analyzed in this study. The contraction of the eyewall, the outward propagating spiral rainbands, and the organized convective precipitation areas were identified. The asymmetric characteristic of the precipitation structure of typhoons was documented and the effect of Taiwan topography on the nature of these precipitation features was also discussed.

**MC02/07P/B20-005 1540**

**DIURNAL VARIATION PATTERNS OF THE LOW TBB AREA OF TYPHOONS**

Fumi UENOBE, Masaki ISHIWATARI, Atsui NUMAGUTI (Graduate School of Environmental

Earth Science Hokkaido University)

Diurnal variation patterns of cloud area of 37 typhoons in 1999 and 2000 are observed. The percentage ratio of cloud area with Tbb < 203 K to the circular area whose radius is 10 degree from each typhoon center (hereafter referred to as low Tbb percentage coverage) is analyzed. All previous studies (eg. Muramatsu 1983) show that "one maximum peak and one minimum peak pattern (O-pattern)" dominates in higher Tbb area. In lower Tbb area, various patterns appear: O-pattern, double-peaked pattern (D-pattern), multiple pattern (M-pattern). As a cause of D-pattern, Muramatsu (1983) suggests ground heating in daytime. However, there are three problems in previous studies. Firstly, since the number of storms analyzed by previous studies is not large, whether the other kind of patterns exist or not is unclear. Moreover, the incidence of each pattern cannot be determined. Secondly, since the method of composite analysis is commonly used, the question which of the environment and the characteristic of each storm determines the diurnal pattern is not considered. The third problem is the effect of ground heating. Muramatsu (1983) finds that, for two cases, D-pattern appears when typhoons pass over an island. The analysis of much more cases is needed. In this study, diurnal pattern of cloud area of tropical storms is reconsidered. Tbb horizontal distribution is calculated from Visible and IR Spin Scan Radiometer data (VISSR) of the GMS-5. In order to determine the typhoon center, best track data in Weather chart published by Japan Meteorological Agency. NGDC ETOPO5 global gridded elevation data is also used in order to define land area in this study. Observation of time series of low Tbb percentage coverage shows that there exist 4 kinds of diurnal pattern. They are O-pattern, D-pattern, M-pattern, and one maximum peak and flat pattern. The last one is not shown in any previous studies, therefore, is a new kind of diurnal pattern. Variety of diurnal patterns is always recognized in each time series if typhoons are not in decaying phase. Even in one time series of particular typhoon, more than one pattern appear. O-pattern has the highest incidence. In order to reconsider the effect of ground heating, time series of low Tbb percentage coverage of typhoons which exist on the ocean and those which stay in land area for at least one day. In time series of low Tbb percentage coverage of both types of typhoons, there appear D-pattern and O-pattern. Therefore, contrary to the discussion of Muramatu (1983), it is suggested that the effect of ground heating is not necessary for occurrence of D-pattern.

**MC02/07P/B20-006 1600**

**TROPICAL CYCLONES WITH AN ELLIPTICAL EYE OBSERVED AROUND THE SOUTHWESTERN ISLANDS IN JAPAN**

Toshihisa ITANO, Gen'ichi NAITO (Department of Earth and Ocean Sciences, National Defense Academy)

Tropical cyclones with an elliptical eye are occasionally observed around the Southwestern Islands in Japan. Such an elliptical eye was first reported in Typhoon Cora(T6618) during its passage around the Miyakojima Island. This typhoon is known as one of the hardest tropical cyclones which have ever hit Japan, and caused severe damages on that island. At this time, the maximum instantaneous wind of 85.3m/s, which is the historical record of a surface wind officially observed in Japan, was measured at the Miyakojima observatory under the tip of the longer axis of the elliptical eyewall. This implies the investigations of elliptical eyes of tropical cyclones are great importance from the view point of both meteorological interest and disaster prevention. One of the peculiar phenomenon analyzed in the elliptical eye of Typhoon Cora is that it followed the azimuthal wave number two structures of pressure, wind and other meteorological fields, which were quite similar to those observed in tornadoes taking a multiple vortex structure. This seems to indicate the phenomenon appeared with the elliptical eye is a multiple vortex phenomenon occurred in a typhoon-scale vortex. However, scarcity of the following studies prevents the further statement on this phenomenon. In the present study, we try to investigate several tropical cyclones with an elliptical eye which passed through the Southwestern Islands in 1990s. Results indicate the azimuthal wave number two structure as was observed in Typhoon Cora in all cases. This may confirm the reliability and reproducibility of the phenomenon, and also support the idea that the elliptical eyes are manifestation of the multiple structure observed in tropical cyclones.

**MC02/07P/B20-007 1620**

**COMPARISON OF THE SPATIAL DISTRIBUTION OF RAINFALL IN TROPICAL CYCLONES OF THE WEST PACIFIC AND OF OTHER OCEANIC BASINS**

Manuel LONFAT<sup>1</sup>, John A. KNAFF<sup>2</sup>, Frank D. MARKS<sup>3</sup>, Shuyi S. CHEN<sup>1</sup> (<sup>1</sup>RSMAS/MPO, University of Miami, <sup>2</sup>CIRA/Colorado State University, <sup>3</sup>NOAA/AOML/Hurricane Research Division)

The goal of this study is to characterize the spatial structure of rainfall in Tropical Cyclones (TC). We focus in particular on typhoons and on how their rainfall distribution differs from those of TCs in other areas. Surface estimates of rainfall are obtained from the Tropical Rainfall Measuring Mission (TRMM) passive microwave (TMI) instrument. Our database extends over the 3-year period from 1 January 1999 to 31 December 2001, and includes more than 2000 instantaneous observations of the TC rainfall. TRMM global coverage allows us to compare the distributions in various geographical areas, and the passive instrument has good enough resolution to derive significant information on the asymmetric structure of the rain. In this study, the rainfall asymmetry is constructed using a first order Fourier analysis on the rainfall estimates in four quadrants around the center. We compute the asymmetry in 50-km wide annuli, outward to 300 km. The analysis is conducted both in a reference system aligned with the storm motion direction and in a system based on the environmental wind shear vector. We define the vertical shear as the wind difference between the 200 and 850 mb levels. The shear information is obtained from the Statistical Hurricane Intensity Prediction Scheme (SHIPS). The asymmetry is located ahead of the storm center in motion-relative coordinates. The global analysis shows larger asymmetries in the shear-relative coordinate system. The asymmetry develops down-shear left in the North Hemisphere basins. The North West Pacific distribution, which includes all observations north-west of the dateline, shows a similar asymmetry location as the global average. The asymmetry is located down shear-left, but shifts cyclonically with radial distance. By 275 km, the asymmetry is along the shear direction. West Pacific storms however are the most symmetric storms, globally. Differences will be shown to relate to the intensity distribution of TCS in the West Pacific as well as to the general environmental wind conditions that prevail. Our study provides insights on the physical mechanisms that may alter the TC rainfall structure. By addressing differences among various basin TC distributions, the relative importance of processes such as associated to the vertical shear can be addressed.

**MC02/07P/B20-008 1640**

**EFFECTS OF ROLL VORTICES ON THE STRUCTURE OF THE MARINE BOUNDARY LAYER IN TROPICAL CYCLONES**

Isaac GINIS<sup>1</sup> (<sup>1</sup>University of Rhode Island, USA)

Recent observations in tropical cyclones using high-resolution synthetic aperture radars clearly demonstrate secondary circulations in the atmospheric boundary layer (roll vortices)



in the region between the main rainbands. These roll vortices with the horizontal scale of 2-4 kilometers are not resolved by present tropical cyclone models, either research or operational. Nevertheless, they may contribute significantly to the vertical exchange of momentum, heat, and moisture in the boundary layer. We investigate here the mechanisms of their formation and effects on the structure and dynamics of the marine boundary layer in high wind conditions typical for tropical cyclones. A non-hydrostatic model of the marine boundary layer with the horizontal resolution of 50 m is presented that explicitly calculates the two-way interaction of convective motions and background flow. The model simulations indicate the development of roll vortices in the boundary layer on a time scale of a few hours and a spatial scale of ~2-3 km that are superimposed on the mean wind field. They are generated mainly by dynamic instability in the boundary layer induced by the strong wind shear and air-sea heat and moisture fluxes. The roll layer is coincided with the depth of the boundary layer. The associated convective fluxes affect greatly the vertical profiles in the boundary layer and air-sea fluxes.

**MC02/07P/B20-009** **1700**  
**THE GENERATION MECHANISM OF THE MESOSCALE PRESSURE DIP WITHIN THE TROPICAL CYCLONE**

Hironori FUDEYASU<sup>1</sup>, Taiichi HAYASHI<sup>2</sup> (<sup>1</sup>Department of National Research Institute for Earth Science and Disaster Prevention, <sup>2</sup>Kyoto University, Japan)

One of the interesting phenomena within the tropical cyclones (hereafter denoted by TC), which are approaching the Japan Islands, is the low-pressure area occurring away from the TC center called as Pressure dip (hereafter denoted by PD). This PD has been recognized as a meso-β-scale disturbance with the horizontal scale of more than 100 km and the duration of more than 10 hours. The barographs during the passage of the TC sometimes show the sudden pressure drop in several stations during the passage of the PD. In this present study, the numerical simulation using the PSU/NCAR MM5 was performed to reveal the details of the spatial structure of the PD. The mesoscale trough (hereafter denoted by MT) was detected in the northwest quadrant of the TC, similar to the observed PD. Above the MT, the local strong downward wind was recognized in the whole troposphere. The dry air-intrusion was generated by this strong downward wind, and the warm-air anomaly was formed corresponding to the dry-air intrusion. The generation mechanism of the warm-air anomaly region above the MT was investigated by the backward trajectory analysis. The warm air came from the upper-troposphere of the northwest of the TC. The dry air was advected to the west of the TC by the upper-level westerly wind at the slope of the isentropic surface. When the TC moved northward, the dry air was brought to lower-troposphere by this strong downward wind. The descending dry air formed the warm-air anomaly through the adiabatic and diabatic warming process. The warm-air anomaly causes the pressure drop. Using the theoretical equation assuming the hydrostatic balance, the amount of the pressure drop was estimated using the temperature and depth of anomaly layer. The calculated amount of the pressure drop (-5 hPa) by theoretical equation was roughly reasonable with amounts of observed PD. The present study on the PD suggested the structure change of the TC in the mid-latitude baroclinic zone around the Japan Island.

**MC02-Posters** **Monday, July 7**

**TYPHOONS IN ASIA: THEIR UNIQUE FEATURES (ICDM)**  
 Location: Site D

**Monday, July 7 PM**

**MC02/07P/D-001** **Poster** **1400-198**  
**THE EFFECT OF ENTRAINMENT IN A CUMULUS PARAMETERIZATION ON THE SIZE OF A SIMULATED TROPICAL CYCLONE**

Akihiko MURATA, Mitsuru UENO (Typhoon Reserch Department, Meteorological Research Institute)

The effect of cumulus parameterization on the size of a tropical cyclone is investigated using the Meteorological Research Institute / Numerical Prediction Division unified Nonhydrostatic Model (MRI/NPD-NHM) with 20 km horizontal resolution. The model includes the Arakawa-Schubert cumulus scheme with a prognostic closure assumption. Sensitivity experiments are conducted with varying the degree of entrainment in the scheme. First of all, the scheme is modified so that fractional entrainment rate can vary with height instead of being set constant, which is based on recent observational and numerical studies. The magnitude of the cloud-base entrainment rate, which is the closure of the modified scheme, is changed ranging from two to ten times of that of the original scheme. The size of the simulated tropical cyclone, defined as the radius of 15m/s azimuth-averaged surface wind, decreases with increases in the cloud-base entrainment rate. The size difference between the cases manifests itself in the form of the difference in the radial profile of axisymmetric tangential velocity on the surface. The tangential velocity profile seems to be linked to the radial profile of precipitation, which also depends on the entrainment rate; the rainfall amount over the radii outside the 200 km radius, measured from the storm center, drops with increasing the entrainment rate. The less rainfall in the larger entrainment rate cases are accounted for by relatively little mass flux in the scheme, suggesting that vertical static instability over the outer radii is not eliminated so much as those of the smaller entrainment rate cases. In fact, vertical static stability over the outer radii decreases as the entrainment rate increases. In order to clarify the mechanism that regulates the size of the simulated tropical cyclone, an equation for axisymmetric tangential wind tendency is used. The temporal and vertically mass-weighted average of the tendency over the outer radii decreases with increases in the cloud-base entrainment rate, which is consistent with the result mentioned above that the storm size shrinks with increasing the entrainment rate. Over the outer radii, the difference in axisymmetric inflow and updrafts are mainly responsible for that in the axisymmetric tangential wind tendency. Since the inflow in lower and middle troposphere, where the absolute vorticity is positive, is stronger in the smaller entrainment cases, the flux of the vorticity due to the inflow is larger, which brings larger tangential wind tendency. As for the axisymmetric updrafts, the magnitude in the smaller entrainment cases are greater in middle and upper troposphere under the condition of the negative vertical shear in the tangential wind. The situation leads to greater vertical advection of the tangential wind by the updrafts, thereby more rapidly intensifying the tangential wind.

**MC02/07P/D-002** **Poster** **1400-199**  
**TRMM SCIENTIFIC DATA AT THE GES DAAC AND THEIR APPLICATIONS TO MONITORING TROPICAL CYCLONES**

Hualan RUI<sup>1</sup>, Bill TENG<sup>2</sup>, Long CHIU<sup>3</sup>, Zhong LIU<sup>3</sup> (<sup>1</sup>GES DAAC, GSFC, NASA, <sup>2</sup>George Mason

University)

More than five years of data from the Tropical Rainfall Measuring Mission (TRMM), an US-Japan joint mission, are available at the Goddard Earth Sciences Distributed Active Archive Center (GES DAAC). These data have been used for a variety of applications throughout the world, including monitoring tropical cyclones. These tropical cyclones, particularly the strong ones such as hurricanes or typhoons, bring strong winds and heavy rainfall along their paths and, when over land, cause tremendous human and economic loss and damage. For tropical cyclones initiated over the oceans, it is difficult to monitor them and to forecast their intensity change, since there are not sufficient observations over the oceans. TRMM has yielded invaluable information on rain intensity and distribution, rain type, and storm depth. With the first space-borne Precipitation Radar, TRMM has provided dramatic three-dimensional views of storm structures of many past tropical cyclones, including typhoons Phanphone, Sinlaku, and others. With the use of TRMM data, tropical cyclone forecasts and tracks are likely to continually improve, leading to better preparation for hurricanes/typhoons and a reduction in unnecessary evacuations during hurricane/typhoon season. Since TRMM's launch in November 1997, its standard products have been processed by the TRMM Science Data and Information System (TSDIS) and archived and distributed to general users by the GES DAAC. These standard data products, discussed in this paper, are available at <http://lake.nascom.nasa.gov/data/dataset/TRMM/>. The TRMM Online Visualization and Analysis System (TOVAS), [http://daac.gsfc.nasa.gov/hydrology/TRMM\\_analysis.html](http://daac.gsfc.nasa.gov/hydrology/TRMM_analysis.html), developed by the GES DAAC, provides users with a friendly web-based interface for quick exploration, analysis, and visualization of TRMM gridded rainfall products for tropical cyclone and other features. A new Experimental TRMM Real-time Multi-satellite Precipitation Data Set, created by G.J. Huffman et al. of the GSFC Laboratory for Atmospheres and the TSDIS, recently became available to the general public via the TOVAS. The real-time aspect of this data set could significantly increase the capability of TRMM real-time applications, such as monitoring tropical cyclones and forecast modeling.

**MC02/07P/D-003** **Poster** **1400-200**  
**TYPHOON SPIRAL BAND STRUCTURES OBSERVED WITH A WIND PROFILER NETWORK**

Michihiro TESHIBA<sup>1</sup>, Manabu D. YAMANAKA<sup>2</sup>, Hiroyuki HASHIGUCHI<sup>1</sup>, Yoshiaki SHIBAGAKI<sup>1</sup>, Yuichi OHNO<sup>3</sup>, Shoichiro FUKAO<sup>3</sup> (<sup>1</sup>Radio Science Center for Space and Atmosphere, Kyoto University, <sup>2</sup>Graduate School of Science and Technology, Kobe University / Frontier Observational Research System for Global Change, Japan, <sup>3</sup>Osaka Electro-Communication University, Japan, <sup>4</sup>Communications Research Laboratory, Japan)

We have investigated the characteristics of the wind behavior associated with Typhoon 0221 (Higos), which was observed with the wind profiler network and data acquisition system (WINDAS), which consists of 25 L-band boundary layer radars (BLRs), of Japan Meteorological Agency (JMA) and a L-band BLR of Communications Research Laboratory, simultaneously. This typhoon passed from the south of Japan to the north along the east side of Japan islands, and landed at 20 LST (11 UTC) on October 1, 2002. The central pressure of this typhoon was about 960 hPa at the typhoon's landing. So the typhoon remained strongly while the typhoon passed. We found from the averaged horizontal winds obtained by 6 BLRs that there were inflow and outflow below and above 2 km in height during the typhoon center's approaching, and there existed outflow below 6 km in height and strong counter-clockwise winds within 300 km in distance from the typhoon center after the center's passing, whose features are similar to the previous results obtained by a VHF wind profiler, the MU radar. We also found that the fluctuating component of the radial wind was nearly strong around the rainbands, and the fluctuation of the wind was coming to the typhoon center with a counter-clockwise rotation. We will discuss the relationship between this fluctuation and the rainbands and/or the moving speed of the typhoon. We could reveal these characteristics for the first time by using the data of the wind profiler network.

**MC02/07P/D-004** **Poster** **1400-201**  
**RADAR OBSERVATIONS OF TYPHOON 9807(VICKI)**

Noriyuki KAWANO<sup>1</sup>, Yoshiaki SHIBAGAKI<sup>1</sup>, Shoichiro FUKAO<sup>1</sup> (<sup>1</sup>Radio Science Center for space and atmosphere, Kyoto University, <sup>2</sup>Osaka Electro-Communication University)

In east Asia, tropical cyclones are called Typhoon. We conducted the Doppler radar observation during the passage of Typhoon 9807(Vicki) on Sep. 1998 with the middle and upper atmosphere (MU) radar located in the central region of the Japan Islands (at Shigaraki). The center of T9807 passed about 40 km northwest of the MU site. T9807 caused much damage by strong wind, and MU radar observation was also interrupted due to power cut by strong surface wind. A remarkable downdraft exceeding 6 m/s was found at the low level just before power cut, at which time also a rainband was observed by a meteorological radar operated by Japan Meteorological Agency (JMA). Global objective analysis produced by JMA shows that cool-dried air advected in the tail of the Typhoon on the middle troposphere, we also confirmed this cool-dried air by means of a radiosonde launched at the MU observatory, and the rainband was located in front of this cool-dried air. In our presentation, we will show a case study observation for the Typhoon at mid-latitude in east Asia, and discuss the relations among the cool-dried air, the rainband, and the strong wind.

**MC02/07P/D-005** **Poster** **1400-202**  
**WINDSTORM CATASTROPHES IN EUROPE AND JAPAN - CURRENT LOSS ANALYSES IN THE PERIOD 1990 - 2002**

Peter MIESEN (GeoRiskDepartment, Munich Re)

Vulnerability is a crucial parameter in the windstorm risk (= hazard x vulnerability x exposed values). For this reason it has been the subject of repeated analyses performed in the past 25 years by Munich Re's Geo Risks Research Dept. on the basis of empirical loss data from major windstorm catastrophes and is one of the essential quantities in studies for estimating loss potentials. The identification of possible changes in the vulnerability of insured objects – for example on account of new construction materials and architectural developments – is essential for risk carriers. On the one hand, it is necessary to have as realistic picture as possible of future losses when allocating risk capital in order to avoid being hit by unexpected accumulation losses should a catastrophe event occur. But fairness towards insurance clients also requires that any changes that may occur in loss expectancy are considered too when calculating prices that are commensurate with the risk. The studies presented here compare the behaviour of buildings during the winter storms in Europe in 1990 and 1999 and during the typhoons in Japan in 1991 und 2002. During this period, the loss ratios were subject to changes that were in some cases quite considerable, for which an initial explanation is suggested.

**MC02/07P/D-006** Poster **1400-203**

**EXTRATROPICAL TRANSITION OF TROPICAL CYCLONES IN THE WESTERN NORTH PACIFIC: THEIR FRONTAL EVOLUTION**

Naoko KITABATAKE (Typhoon Research Department, Meteorological Research Institute)

The major islands of Japan, which is located in the mid-latitude, are hit by several tropical cyclones (TCs) every year. These TCs are often at the extratropical transition (ET) stage. According to the Best Track data of the RSMC Tokyo-Typhoon Center, 21 TCs out of 57 were transformed to extratropical cyclones in the western North Pacific in 2001-2002. Particularly, 25 TC translated northward beyond the 30N, and the 20 cases out of them transformed into extratropical cyclones. Sometimes the frontal rainband associated with a TC at the ET stage brings a torrential rainfall and the subsequent flood. The variation of the translation speed may contribute to a forecast track error and disasters due to the strong winds. We examined the frontal structure of the 21 ET cases in 2001-2002 using the objective analysis dataset of JMA. The fronts are defined by the thermal front parameter of Renard and Clarke (1965), although the 925-hPa equivalent potential temperature was used as a thermal variable. Three types of the ET were found: 1) the warm occlusion pattern, 2) the cold advection pattern, and 3) the open wave pattern. Nine cases out of 21 ETs were classified as the warm occlusion pattern. When a TC moved northward and approached to the mid-latitude baroclinic zone, a warm front became obvious, extending eastward from the cyclone center. A rather weak cold front was formed 12-24 hours later south of, but not in the vicinity of, the cyclone center. This frontal structure included some features similar to the frontal fracture of Shapiro and Keyser (1990). Although the horizontal temperature gradients increased near the cyclone center in the lower troposphere, the cyclone still had the warm core structure. The warm-core structure and the shear deformation contributed to the warm frontogenesis and the cold frontolysis in the vicinity of the cyclone center. The TC followed a northward track and increased its translation speed, and subsequently organized into an occluded extratropical cyclone, decreasing the translation speed. These cyclones dissipated in 48 hours after the transformation. The cold-advection pattern was such that a TC moving ENE-ward approached to a preexisting cold front. Two cases out of 21 were classified as this type. They transformed into weak frontal cyclones in an environment of strong cold advection, and subsequently dissipated. In the other 10 cases, the TCs transformed into open-wave extratropical cyclones. Most of them were not well organized and dissipated in 36 hours, whereas three cases began reintensification as an extratropical cyclone in 24 hours after the transformation. As the aforementioned warm-occlusion pattern, a warm frontogenesis preceded the cold frontogenesis, although the cold frontogenesis occurred also in the vicinity of the cyclone center. Moreover the TCs did not lose their translation speed.

**MC02/07P/D-007** Poster **1400-204**

**APPLICATION OF STEERING WEIGHT CONCEPT TO TYPHOON SAOMAI IN 2000**

Mitsuru UENO, Akihiko MURATA (Typhoon Research Department, Meteorological Research Institute)

In an attempt to diagnose the mechanism by which a typhoon moves through vertically sheared environmental flows with keeping its vertical coherency, a series of idealized numerical simulations of typhoon are carried out and eventually a new approach termed "steering weight concept" is proposed based on the numerical results. The steering weight is a set of weighting factors mathematically derived from the surface pressure tendency equation and can be a measure of how much sensitive the storm motion is to the steering flow at each vertical level. The overall movements of simulated typhoons are well explained by taking into consideration not only so called "steering flow" but also the steering weight. The new concept is also applied to real typhoon cases such as Typhoon Saomai in 2000 to see the validity of the concept in real situations. The experiments are performed using a 20km version of MRI/NPD nonhydrostatic model which includes an Arakawa-Schubert cumulus parameterization scheme. It is found from the experiment that the simulated motion of Saomai is sensitive to and systematically changed with the tuning parameters of the scheme such as entrainment rate and relaxation time in a consistent manner with the foregoing idealized simulations, suggesting a strong correlation between steering weight and storm motion in real situations. The steering weight concept will be outlined at the conference putting stress on the results from real typhoon cases now in process.

**MC02/07P/D-008** Poster **1400-205**

**TROPICAL CYCLONE ASSIMILATION AND PREDICTION. PART II: COMPARISON BETWEEN THE NORTHWEST PACIFIC AND OTHER TROPICAL CYCLONE BASINS**

Lance M. LESLIE<sup>1</sup>, Seon Ki PARK<sup>2</sup> (<sup>1</sup>School of Meteorology, The University of Oklahoma, <sup>2</sup>Ewha Womans University, Seoul, South Korea)

In this study a comparison is made of the performance of a tropical cyclone assimilation and prediction system applied to the northwest Pacific basin, compared with its performance in four other tropical cyclone basins. The assimilation and prediction system used in the study is the HIRES (from High RESolution) system developed over the past decade at The University of New South Wales, Sydney, Australia and presently at The University of Oklahoma, USA. The four other tropical cyclone basins to which the HIRES system is applied include the north Atlantic, southwest Pacific, southeast and north Indian Ocean basins. The HIRES system was run at a horizontal resolution of 10km and employed several assimilation technique including 4D-Var, I3D-Var or intermittent cycled assimilation. Each assimilation procedure was applied over the 24 hour period leading up to the commencement of the forecast period. A total of 20 northwest Pacific cases (see the companion conference paper by Park and Leslie) were selected, together with a total of 30 cases from the other four tropical cyclone basins. The performance assessment focused on mean absolute and rms errors in track and intensity predictions. The forecasts were evaluated at 12 hour intervals out to 96 hours. Error statistics for the northwest Pacific basin were compared with those from the other basins. It was found that although a total of 50 tropical cyclones were used for the comparison, most of the storms investigated followed regular tracks, being either "straight runners" or tropical cyclones recurving in a classical path, such as around a sub-tropical ridge. Tests of statistical significant difference revealed no difference between the error statistics for the northwest Pacific and the other regions at the 5% confidence level. It was therefore decided to focus only on tropical cyclones that exhibited unusual behavior and, as a consequence, are regarded as difficult storms to forecast accurately. A total of five cases were chosen from the northwest Pacific and five from the other basins. Detailed case studies were carried out on all these ten tropical cyclones. It is well-known that each of the tropical cyclone basins investigated here has different characteristics, both for genesis and for the factors dictating the subsequent motion and intensity of the tropical cyclone. The results of these case studies therefore will be described in the context of the impact of these differing basin characteristics on the performance of the HIRES system.

**MC02/07P/D-009** Poster **1400-206**

**DEVELOPMENT OF A TWO-WAY MULTIPLY-NESTED MOVABLE MESH TYPHOON MODEL**

Wataru MASHIKO, Chiashi MUROI (Meteorological Research Institute)

In order to get better prediction of typhoon track, intensity, heavy rainfall and strong wind distribution, and inner structure, we are on the way to develop a two-way multiply-nested movable mesh typhoon model based on Meteorological Research Institute/Numerical Prediction Division unified nonhydrostatic model of the Japan Meteorological Agency (MRI/NPD-NHM; Saito et al., 2001). MRI/NPD-NHM has been used to simulate various cases of mesoscale phenomena. However, numerical experiments of typhoon in high resolution have rarely been conducted due to the limited computer resources. For the precise prediction of typhoon, enormous computer resources are needed because environment fields around a typhoon largely affect the typhoon evolution and therefore a large model domain is needed. Moreover, since each convective cloud plays an important role to a typhoon, fine mesh (horizontal grid size; less than 1-2km) that represents convection is desirable especially near the typhoon center. The major advantage of the two-way nested model is that it can effectively reduce computational time and memory requirements because both the large domain and high resolution can be accomplished together by arranging fine mesh over the typhoon area and coarse mesh over the environment. The main procedures of the two-way interactive mesh refinement scheme are (1) construction of an interface between coarse mesh and fine mesh, (2) interpolation that is used to provide initial and boundary values of fine mesh, (3) feedback from fine mesh to coarse mesh, and (4) boundaries conditions for fine mesh. We employed monotone advection algorithms for the interpolation procedure(2) and one point feedback with a smoother-desmoother for the feedback procedure(3) used in Penn State/NCAR Mesoscale Model (MM5). As for boundaries conditions(4), we adopted the radiative-nesting boundary conditions considering the difference between coarse and fine mesh's values (Chen 1991). Some Fortran90 modules concerning two-way nesting were added to MRI/NPD-NHM in such a way that minimizes the change of its original source code. To check the dynamical core of the model, we performed three-dimensional numerical simulations of a mountain flow with the model. The two-way nested model that covers the near-mountain area with fine mesh and elsewhere with coarse mesh produced almost the same results as those from the model with fine mesh all over the model domain and no erroneous wave reflection was excited near the boundaries. And computational time could be reduced, compared with the model covered with all area fine mesh. The impact of the two-way nesting and the case study of typhoons in the Western North Pacific will be shown at the symposium.

**MC02/07P/D-010** Poster **1400-207**

**DEVELOPMENT OF TYPHOON-OCEAN COUPLED MODEL AT METEOROLOGICAL RESEARCH INSTITUTE IN JAPAN METEOROLOGICAL AGENCY**

Akiyoshi WADA (Department of Typhoon, Meteorological Research Institute)

For the purpose of one of the attempts to improve typhoon prediction, 'Typhoon-ocean coupled model' has been developed at Meteorological Research Institute (MRI) in Japan Meteorological Agency (JMA). As an ocean part of the coupled model, a mixed layer model with turbulent mixing processes has been constructed using reference from Bender et al. (1993) (Wada 2002). The ocean model with global analysis data every 6 hours and Rankin vortex from JMA best track data could successfully reproduce about 3°C cooling of sea surface temperature (SST) observed by R/V Keifu Maru after the passage of Typhoon REX on August 29, 1998. As an atmospheric part of the coupled model, the typhoon model (TYM) routinely used in JMA was transferred to MRI. The horizontal resolution in the typhoon center has been revised from 24km to 20km in the present work. A numerical prediction using Typhoon-Ocean coupled model was conducted for Typhoon BILIS of which the initial time was at 12UTC on August 20, 2000. Computed SST cooling by Typhoon BILIS can be found on the right of the running typhoon. The maximum SST cooling during 72 hours reaches to 2.8°C after 39 hours from the initial time, while minimum sea level pressure (MSLP) of the coupled model, 936.hPa, rises to nearly 17hPa compared with that of TYM, 920.0hPa at that time. The maximum wind speed of the coupled model decreases and its region moves outside compared with the original typhoon model. The coupling effects are confirmed in horizontal distributions of sensible plus latent heat fluxes and precipitation. We should note that it is difficult to compare directly the best track MSLP of Typhoon BILIS in JMA with computed MSLP because the initial observed MSLP is not always equal to the initial bogus MSLP. Nonetheless, correlation coefficients of 6-hour MSLP tendency over 27 samples during 2000-2002 seasons indicate that MSLP tendency of the coupled model agrees better with that of JMA best track MSLP than with that of TYM MSLP. However, SST cooling after the passage of Typhoon BILIS by the coupled model is indeed insufficient compared with about 5°C observed SST cooling by TRMM/TMI. This is because TYM and the coupled model tends to estimate the intensity weaker than that in JMA best track data so that forcing from the atmosphere and the ocean by models becomes weaker. The fundamental problem may exist in the atmospheric boundary processes or cumulus parameterization as well as in the oceanic processes.



**MC02** Monday, July 7 - Tuesday, July 8

**TYPHOONS IN ASIA: THEIR UNIQUE FEATURES (ICDM)**

Location: Site B, Room 20

**Tuesday, July 8 AM**  
Presiding Chairs: C.-P. Chang, M. Ueno

**TYPHOON FORMATION**

**MC02/08A/B20-001** **0900**

**TROPICAL CYCLONE ENERGY DISPERSION AND CYCLOGENESIS IN THE WESTERN NORTH PACIFIC: OBSERVATIONS AND SIMULATIONS**

Tim LI, Yongti ZHU, Yuqing WANG, Bing FU, Xuyang GE, Bin WANG (University of Hawaii)

Using the QuikSCAT and TRMM satellite data, we identified tropical cyclone (TC) genesis processes during the western North Pacific (WNP) typhoon seasons in 2000 and 2001. Our particular focus is on the processes associated with the TC energy dispersion and easterly wave forcing. Among 34 TCs generated in the WNP during the two seasons, there are 7 TC genesis cases associated with easterly wave forcing and 6 cases associated with TC energy dispersion. It is noted that not all TCs have a clear Rossby wavetrain pattern in their wake. The wavetrain is more likely to appear in the wake of intense TCs. The TC induced Rossby

wavetrain is well simulated in a 3-D high-resolution model. While a TC moves northwestward in a beta plane, its energy propagates southeastward, forming a synoptic-scale wavetrain of alternating regions of anticyclonic and cyclonic vorticity perturbations. The maximum strength of the TC energy dispersion is found in the lower troposphere at 850 hPa. Experiments with both explicit and mass-flux convective heating schemes showed that a new TC could not be generated in the Rossby wavetrain of a preexisting TC in the resting environment. An anomaly baroclinic model was developed to understand the role of the WNP mean monsoon flow on the TC genesis. In the model an idealized or realistic basic-state field is specified, which does not change with time. Under the basic-state patterns similar to the monsoon gyre and the monsoon shear line, the model successfully simulates the TC formation associated with the Rossby wave energy dispersion of a preexisting TC. The physical mechanism responsible for the TC genesis is argued to be associated with the scale contraction of the synoptic-scale wave due to the concentration of the perturbation vorticity by convergent mean monsoon flows. Because of this scale contraction, the synoptic-scale wavetrain with a large meridional wavelength is organized into vortex-scale circulation and convection, leading to the formation of a new TC. The generated new TC has realistic dynamic and thermodynamic structures such as spiral cloud bands, asymmetric maximum winds and the warm core/eye wall structure. Further sensitivity experiments indicate that anomalous warm SST may greatly enhance the cyclogenesis process.

**MC02/08A/B20-002 0920**  
**A STUDY OF TROPICAL CYCLONE FORMATION IN THE WESTERN NORTH PACIFIC**

Cheng-shang LEE (Dept of Atmospheric Sciences, National Taiwan University, Taipei, Taiwan)

Observations have shown that significant changes in the environmental circulation pattern often occurred during the formation of a tropical cyclone. This study attempted to investigate the evolution of the circulation pattern during tropical cyclone formation in the western North Pacific using the EC grid point data and the QuikSCAT data. Results showed that about 40% of all tropical cyclones might be affected by the trade wind surges or the cross-equatorial surges during their formation stage. The PSU/NCAR MM5 was used to simulate the formation process of four cases. Model results were analyzed to examine the structure evolution and to address the important physical processes responsible for the formation of these systems. The role of tradewind surges and the cross-equatorial surges on tropical cyclone formation in the western North Pacific will be discussed. Results also showed that during 1950-2001, there were about 4.1 tropical cyclones formed in South China Sea (SCS) each year (about 27 for the whole western North Pacific basin). Among these systems, 17.3% formed in early season (May-June). This percentage was much higher than the 9.5% for the rest of the western North Pacific basin (east of 120E). In this study, the environmental circulation pattern during tropical cyclone formation in SCS during different seasons will also be examined. In the early season of 2002, there were two tropical cyclones formed on stationary fronts located at the northern part of SCS. One system formed in late May and only maintained as a tropical depression (TD06). The other formed in early June and reached tropical storm (Typhoon Noguiri) intensity. In this study, the formation process of these two systems will be examined and tropical cyclone formation under the baroclinic environment will be discussed.

**MC02/08A/B20-003 0940**  
**TYPHOON VAMEI: AN EQUATORIAL TROPICAL CYCLONE FORMATION**

Chih-Pei CHANG<sup>1</sup>, Ching-Hwang LIU<sup>2</sup>, Hung-Chi KUO<sup>3</sup> (<sup>1</sup>Naval Postgraduate School, <sup>2</sup>Chinese Culture University, <sup>3</sup>National Taiwan University)

Due to the diminishing Coriolis effect, the belt 300 km either side of the equator has been considered tropical cyclone-free. Typhoon Vamei, which developed near Singapore on 27 December 2001, was the first recorded tropical cyclone formation within 1.5 degrees of the equator. It caused damages to the carrier USS Carl Vinson and an accompanying ship. The development was the result of two interacting systems, a weak Borneo vortex that drifted into the southern tip of the South China Sea and remained there for four days, and a strong and persistent cold surge that created the large background cyclonic vorticity at the equator. The development process is similar to the spinning of a top played by a child. The probability of a similar equatorial development is estimated to be once every 100-400 years.

**MC02/08A/B20-004 1000**  
**RECENT OBSERVATIONAL STUDIES ON TROPICAL CYCLONE FORMATION IN THE WESTERN NORTH PACIFIC**

Kevin K.W. CHEUNG, Russell L. ELSBERRY (Department of Meteorology, Naval Postgraduate School, Monterey, California, U.S.A.)

Since a tropical cyclone (TC) may form and reach a mature stage within five days, an understanding and ability to predict TC formation is necessary to make skillful five-day forecasts. The goal of the observational study is to understand the physical processes during TC formation, and possible interactions with environmental systems with different spatial scales. Through examination of historical TC cases, detailed values and distributions of the environmental parameters such as relative humidity, convective instability and vertical wind shear associated with formations may be identified, that can be used as the basic reference in operational forecast situations. However, the character as well as the environment of the TC seedling (monsoon depression, waves, etc.) and the presence of mesoscale convective systems (MCSs) might also play an important role in TC formation. Therefore, the statistical properties and evolution processes of MCSs are also studied using both analyses and satellite data. The focus will be on how MCSs are controlled by tropical circulations of different time scales (from those with period less than one month to the longer-period Madden-Julian oscillation that are both correlated with TC formation to certain degree), and whether there are specific MCS configurations during the early-stage intensification of TCs. Much can also be learned from verifying the skill of operational global numerical weather prediction (NWP) models in predicting TC formation since many of these models are capable of spinning up circulations that have quite realistic TC structures. In particular, knowledge on the physical conditions in determining a TC formation (certainly limited by the finite resolution of the models and their physical parameterizations) can be obtained in comparing the real TCs generated in the NWP models and the spurious vortices (false alarms). Some effort along this idea on the U.S. Navy Operational Global Atmospheric Prediction System (NOGAPS) has already been finished. Verifications will be extended to the NCEP Aviation model, Taiwan's CWB global forecast system, German Meteorological Institute's global model, and Japan's global spectral model. Progress from the above observational studies will be presented during the Symposium.

**MC02/08A/B20-005 1100**  
**MESOSCALE ANALYSIS OF FORMATION PROCESS OF TYPHOON OVER THE WESTERN NORTH PACIFIC**

Kazumasa MORI (Meteorological Research Institute)

Mesoscale features of convection organized in the formation process of typhoon (TY) Rex (19804) on 21 August 1998 and around low-latitude low pressure area (L) on 4 November 1999 over the western north Pacific were investigated using mainly research vessel Keifu Maru(I) radar data. Two MCSs were formed successively in a mesoscale (400 km) low-level cyclonic circulation (LLCC) around the central area of the forming TY Rex. Mesoscale convection organized as the first MCS once decayed. However, the mesoscale LLCC which appeared to have been intensified corresponding to the formation of the first MCS remained. After the decay of the first MCS, near the center of the residual mesoscale LLCC, meso- $\gamma$ -scale intense convection was newly initiated. The meso- $\gamma$ -scale intense convection evolved into the second MCS associated with further intensification of the mesoscale LLCC, which was a kernel structure of the pre-TY Rex evolving from tropical depression (TD) to tropical storm (TS) stage. The low pressure area (L) was a pre-disturbance which developed to TD. A low-level confluent line made by west-northwesterly and west-southwesterly flow was detected by tracking of cell echoes. Several MCSs organized within the L. Among the MCSs, an eastward moving squall-line like MCS formed to the north of the confluent line (CL) and an east-northeastward moving squall-line like MCS formed to the south of the CL merged each other around the CL. On the process of the MCSs merger, individual two intense convective lines off the leading edges of MCSs were also merged sustaining their intensity and changed from line to area of about 30 km horizontal scale. By about three hours after the merger, large stratiform echo with horizontal scale about 500 km formed and spread to the southwest of the mesoscale intense convective area and LLCC appeared to be initiated around the area. The first case of TY Rex formation is one example of mesoscale process of typhoon formation by successive and mutual intensification of MCSs and LLCC chained through an implied release of latent heat and consequent decrease of surface pressure on mesoscale associated with the intense convection within the MCSs. The second case of low-latitude L implies the role of MCSs merger for formation of intense mesoscale convection on the process of TY formation.

**MC02/08A/B20-006 1120**  
**TYPHOON GENESIS IN GLOBAL HIGH-RESOLUTION SIMULATIONS ON THE EARTH SIMULATOR**

Mayumi K. YOSHIOKA<sup>1</sup>, Takeshi ENOMOTO<sup>2</sup>, Yoshio KURIHARA<sup>3</sup> (<sup>1</sup>Earth Simulator Center, Japan Marine Science and Technology Center, <sup>2</sup>Frontier Research System for Global Change)

Cumulus clusters in the tropics sometimes evolve into tropical depressions, which can eventually develop to typhoons. While such a process may be autonomous, it has also been argued that it is necessarily associated with the presence of favorable background conditions. Utilizing simulation results from aFES (Atmospheric global circulation model For the Earth Simulator), we attempt to study formation mechanism of tropical mesoscale systems. The effect of cumulus convection is treated in the model by the simplified Arakawa-Schubert parameterization scheme. Two different resolutions are used: one with horizontal resolution T1279 and 96 vertical levels (T1279L96) and the other with T319 and 24 levels (T319L24). In the case for June situation, a tropical cyclone is generated over the Warm Pool at both resolutions in the surf region of westward propagating equatorial waves. However, the one in the T1279L96 simulation becomes much more intense, apparently due to enhanced convections associated with a westerly burst. This wind burst is not found in the T319L24 simulation. In the case for September situation, four typhoons are simulated during the integration period in the T1279L96 simulation, but three in the T319L24 simulation. An investigation for this case will also be shown focusing on the differences of the background fields in two resolutions.

**MC02/08A/B20-007 1140**  
**RECENT MESOSCALE MODELING STUDIES ON TROPICAL CYCLONE FORMATION IN THE WESTERN NORTH PACIFIC**

Kevin K.W. CHEUNG, Russell L. ELSBERRY (Department of Meteorology, Naval Postgraduate School, Monterey, California, U.S.A.)

To complement the observational studies being carried out in our research group, modeling studies are also performed following two strategies. One is to simulate historical TC formation cases to further our understanding of the physical mechanisms during formation. For example, the NCAR/PSU MM5 model has been used to simulate the formation of Typhoon Robyn (1993) that occurred during the Tropical Cyclone Motion (TCM-93) field experiment. Observations during the intensive observational periods of TCM-93 are nudged into the model fields and high-resolution analyses are used to evaluate the simulations. The essential features associated with Robyn's formation can be realized in the 27-km resolution fine grid using the Betts-Miller cumulus parameterization. However, the intensification of the tropical cyclone is found to be highly sensitive to the model configurations, such as choice of cumulus scheme, boundary layer parameterization, number of model levels, and size of the nested domain. Diagnostic studies are being performed to understand these model sensitivities and to find a better model configuration for TC formation prediction. Future efforts will include a high-resolution simulation (with 9-km fine grid resolution or less) of the same case, so that the structure of the associated mesoscale convective systems is better predicted in the model. The second strategy is to study near real-time predictions of TC formations in the western North Pacific (WNP). To truly measure the skill of dynamical predictions of TC formations after the model is tuned specifically for the WNP, U.S. Navy Coupled Ocean/Atmosphere Mesoscale Prediction System (COAMPS) is used. Since TCs may form over a large domain in the WNP, a single grid with 27-km resolution is being tested with cases during the 2002 season. After the preliminary set up work is completed, forecasts of up to 144 h will be obtained. After verifications and evaluations of the results from the 2002 cases are done, modifications to the model configuration and/or model physics will be made. Focus will be paid on the effects of assimilation of various kinds of satellite products on the skill of predicting TC formation.

**MC02/08A/B20-008 1200**  
**NUMERICAL STUDY OF THE EVOLUTION OF A BAY OF BENGAL TROPICAL CYCLONE AND THE IMPACT ASSESSMENT**

Bhaskar Rao Venkata DODLA (Department of Meteorology and Oceanography, Andhra University)

A tropical cyclone crossed the East Coast of India at around 20 N latitude between 0430-0630 UTC on 29th October 1999 causing enormous damage to the coastal region of Orissa State. The India Meteorological Department has named this cyclone as 'super cyclone' as the estimated minimum central surface pressure attained was 912 hPa and associated maximum sustained winds of 155 knots. In this study an attempt has been made to simulate

the evolution of this cyclone using a NCAR MM5 mesoscale model. The evolution has been simulated using a two way nested two-domain model integration with horizontal resolutions of 30 km and 10 km. The model has been integrated for five days using the initial and boundary conditions taken from NCEP 1-degree daily data from 25th October 1999. The model could successfully simulate the evolution satisfactorily with the intensification and movement agreeing with the observations. The evolution of mesoscale convective features associated with the developing cyclone has been analysed. The model could produce the rainbands agreeing with the observations. The locations of the maxima of convection as the cyclone is evolving are well obtained by the model. The rainfall intensity and distribution at different stages of the cyclone are also well predicted. This study shows the usefulness of NCAR MM5 for the study of tropical cyclones over the north Indian Ocean and to understand the physical mechanisms associated with the mesoscale convective systems associated with tropical cyclones. However, the model underpredicted the ultimate strength with a minimum central surface pressure of 960 hPa which may be due to the limitations of horizontal resolution and sensitivity to physical parameterization schemes of convection and boundary layer. An impact assessment of the above cyclone is made in terms of the loss of life and damage to property. The collected data indicates the loss of 10,000 human lives and 400,000 cattle and nearly a million of other live stocks. The total estimated loss to the agriculture sector alone is about 2000 crores of Indian rupees or 400 million US dollars. Added to this there has been extensive damage to telecommunication network, power supply, building structures and the roadways. A storm surge of 5-6 meters above the astronomical tide of 2.5 meters has been reported which lead to tidal inundation up to 35 km inland from the coast of Paradeep. Some preliminary results of the impact assessment of the tropical cyclones along the East Coast of India will be presented. A statistical analysis of all the available cyclone data that crossed the coastal region of Andhra Pradesh along the East Coast of India is made. The damage associated with these cyclones is discussed in terms of the loss of life and property. The damage due to different aspects such as high winds, torrential rainfall and storm surge will be discussed. The study emphasises the usefulness of numerical modeling studies to predict the strength and movement of the cyclones and to assess their impact.

Tuesday, July 8 PM

Presiding Chairs: C.-C. Wu, S. Ishijima

**EFFECTS OF ENVIRONMENT, TYPHOON MODELING**

**MC02/08P/B20-001 1400**

**INTERACTION OF POTENTIAL VORTICITY ANOMALIES IN EXTRATROPICAL TRANSITION OF TYPHOON BART (1999)**

Jun YOSHINO, Hirohiko ISHIKAWA, Hiromasa UEDA (Disaster Prevention Research Institute, Kyoto University)

In recent years, considerable concern has been raised about *extratropical transition of tropical cyclones*. Once a tropical cyclone reaches at the mid-latitude baroclinic zone, it drastically changes its structure and strength. Mid-latitude tropical cyclones are expected to be influenced by surrounding systems (e.g. synoptic troughs, ridges and jet stream). Typhoon Bart (1999) has undergone a rapid weakening (a central pressure change of +50hPa/day) around Japan Islands and, after that, an unexpected re-intensification (-15hPa/day) over the Sea of Okhotsk. The purpose of this study is to investigate the detailed structure, dynamics and transitional process of mid-latitude Typhoon Bart using the mesoscale modeling system PSU/NCAR MM5. Furthermore, employing the gridded datasets from the successful simulation, a piecewise potential vorticity (PV) inversion is performed to determine the relative contributions of discrete pieces of the PV to the Bart's decaying and intensification. Bart simulated by MM5 shows good agreements with the JMA best track for Bart and GMS-5 images. The cloud field of Bart has changed from axisymmetric pattern to asymmetry in its transitional process. Although Bart in the cyclolysis phase was far from an upstream synoptic trough composed of a high PV anomaly at upper levels, it began to come under the influence of the lower-level dry and cold air mass and upper-level negative PV anomaly. The cold air mass intrusion in Bart led to contribute to the large positive value of frontogenesis along the cold front. According to the results of the piecewise PV inversion, the upper-level negative PV anomaly, which would be generated by the diabatic heating in cloud, caused a rapid surface cyclolysis. The cloud activity associated with Bart resulted in the self-decaying with the generation of the negative PV anomaly aloft. However, a low-level positive PV anomaly associated with the Bart's warm core remnant was the most significant contribution to the deepening rate, despite of the development of the negative PV anomaly. In the re-cyclogenesis stage, the simulated Bart wrapped typhoon cloud bands spirally and became an axisymmetric pattern again like its mature stage. The simulated PV field indicates that the upper-level high PV anomaly originating in high-latitude stratosphere, was vertically coupling with the low-level positive PV anomaly formed in the remnant of Bart. The spiral cloud bands in Bart produced the strong ascending motion resulting from the lifting of the tropopause, and accomplished the vortex stretching of Bart, and developed the divergent flow near the tropopause. The static piecewise PV inversion analyses showed that the upper-level dry positive PV anomaly with the synoptic perturbation was a minor contribution to the surface cyclogenesis, but it was essential factor to act on a positive feedback of cyclogenesis. The negative PV anomaly aloft, to the north of Bart, that had decreased its surface cyclonic activity in the weakening stage, played in an important role in evolving the outflowing jet streak and accelerating the positive feedback of cyclogenesis, resulting from the steeper PV gradient near the tropopause.

**MC02/08P/B20-002 1420**

**SEA SURFACE COOLING WITH THE PASSAGE OF TYPHOONS IN THE NORTHWESTERN PACIFIC OCEAN**

Chul-hoon HONG (Pukyong National University)

The ocean response to typhoons in the Northwestern Pacific Ocean is studied using the Buoy Data from Japan Meteorological Agency during 1982 to 2000 and a three-dimensional primitive model (POM). Sea Surface Cooling (SSC) response is emphasized, analyzing 27 typhoons. SSC at Buoy 21004 (29°00 N, 135°00 E) is observed in all cases, ranging from -6 to -3 °C. The amplitude of SSC is correlated with typhoon strength, track, and translation velocity. SSC after the passage of strong typhoons preserves more than about 10 days. The intense SSC occurs well in the cases of typhoon-tracks leftward from the Buoy 21004 (when viewing the typhoon from behind). A three-dimensional numerical model of which domain covers most of the Northwestern Pacific Ocean (24°N to 52°N) including the East China Sea, the Yellow Sea, and the East (Japan) Sea is implemented to simulate Typhoon Abby, August in 1983, and identifies well SSC with about ~-4 °C. The model suggests that a cyclonic eddy with a diameter of a few hundred kilometers occurs behind the typhoon, and SSC is greatly influenced by the eddy behavior.

**MC02/08P/B20-003 1440**

**A CLIMATOLOGICAL STUDY OF BINARY TROPICAL CYCLONES IN THE WESTERN NORTH PACIFIC BASIN**

Suguru ISHIJIMA (NPO Okinawa Typhoon Center)

A climatological study was made on the occurrences of the binary tropical cyclones in the western North Pacific and the feature in their relative and actual tracks was investigated. The analysis of JMA meteorological observation data covering for the period of 45 years (1952-1996) indicates that the binary tropical cyclone system (BTS) occurs at the rate of nearly twice a year in the months of May through November with the total of 90 cases. Their occurrences are most abundant from their initial center-positions orienting in the E-W direction in the open oceanic region south of Japan and east of the Philippines. The relative rotation sense of the binary tropical cyclones and the separation distance between them in the period of analysis were featured with Cyclonic Approaching (CA), Cyclonic Approaching and anticyclonic Departing (CAD), primarily Anticyclonic rotating (aC), nearly Stationary (ST) and Compound (CM) modes. The CA mode only occupies 22% of the whole number of BTS with its nearly half merged into one tropical cyclone and the majority belongs to CAD mode. The aC mode exists only by 10%. The averaged separation distance between the binary tropical cyclones of CA modes which merged into one cyclone is as short as 430 km while those CA modes which showed no merging could only approach as close as 700 km. The CAD modes featured with the anticyclonic rotation in the later stage could only approach up to 830 km. The averaged intensity ratio defined as a ratio of the intensity of one weaker pair against the other stronger pair is 0.65. The intensity and the size ratios are discussed as the effective parameter in determining a critical merging separation distance and the mutual interaction behavior. Some unique features found in the tracks of individual pairs of BTS will be presented.

**MC02/08P/B20-004 1500**

**A NEW LOOK AT THE BINARY INTERACTION: POTENTIAL VORTICITY DIAGNOSIS OF THE UNUSUAL SOUTHWARD MOTION OF TROPICAL STORM BOPHA (2000) AND ITS INTERACTION WITH SUPERTYPHOON SAOMAI (2000)**

Chun-Chieh WU, Treng-Shi HUANG, Wei-Peng HUANG, Kun-Hsuan CHOU (Department of Atmospheric Sciences, National Taiwan University)

Tropical Storm Bopha (2000) showed a very unusual southward course parallel to the east coast of Taiwan, mainly steered by the circulation associated with Supertyphoon Saomai (2000) to Bopha's east. The binary interaction between the two typhoons is well demonstrated by the potential vorticity (PV) diagnosis. With the use of the piecewise PV inversion, this paper quantitatively evaluates how Bopha moved southward due to the binary interaction with Saomai. A newly proposed centroid-relative track, with the position weighting based on the steering flow induced by the PV anomaly associated with the other storm, is plotted to highlight such binary interaction processes. Note that the above analysis can be well used to understand the more complicated vortex merging and interacting processes between tropical cyclones either from observational data or numerical experiments. The results also shed some light on the prediction of nearby tropical cyclones.

**MC02/08P/B20-005 1550**

**ASSIMILATION AND PREDICTION OF TROPICAL CYCLONES. PART I: PERFORMANCE IN THE NORTHWEST PACIFIC**

Seon K. PARK<sup>1</sup>, Lance M. LESLIE<sup>2</sup> (<sup>1</sup>Department of Environmental Science and Engineering, Ewha Womans University, South Korea, <sup>2</sup>School of Meteorology, University of Oklahoma, U.S.A.)

The northwest Pacific basin is one of the most active tropical cyclone (TC) regions in the world. It also is one of the most populous regions, so the accurate prediction of tropical cyclone tracks is of great importance. Almost all east Asian countries are affected by TCs, and active research programs are part of weather centers in many countries including Japan, PRC, South Korea and Taiwan. In this study, we present numerical results obtained for TCs over the northwest Pacific based on a high resolution limited-area assimilation and prediction system, called HIRES (High REsolution model), which is developed at Univ. of New South Wales, Australia and Univ. of Oklahoma, U.S.A. Numerical experiments for a total of over 20 TC cases have been performed by employing advanced assimilation techniques such as four-dimensional variational analysis (4D-Var) and inverse 3D-Var (I3D-Var), followed by high resolution (10 km) predictions of track, intensity and precipitation. The cases focused on landfalling TCs affecting Hong Kong, Japan, PRC, the Philippines, South Korea, Taiwan, and Vietnam. The assimilation used all available data, including satellite and radar observations for three TCs that hit Hong Kong in 1999. Additional focus has been on the 2002 season, especially TCs affecting Japan and South Korea in both the Pacific and the East/Japan Sea regions. Results will be presented concentrating on a number of aspects of the numerical experiments. The impact of assimilating nonconventional data using both 4D-Var and I3D-Var methods will be discussed. In addition, a comparison made of the two approaches, relative to control forecasts using no assimilation will be described. Other aspects of the forecasts that are assessed include tracks, intensity and quantitative precipitation forecasting for several storms that produced flooding after nearing or making landfall. Planned future work includes the hybrid application of I3D-Var and 4D-Var techniques, given the large gains in efficiency provided by the I3D-Var approach.

**MC02/08P/B20-006 1610**

**IMPROVING TROPICAL CYCLONE INITIALIZATION WITH APPLICATION OF QUIKSCAT DATA**

Chi-Sann E. LIOU<sup>1</sup>, Yi JIN<sup>2</sup> (<sup>1</sup>Naval Research Laboratory, <sup>2</sup>Science Applications International Corporation)

Due to lack of observations, tropical cyclone initialization for numerical model forecast remains a difficult problem. For Pacific Ocean region, the initialization is even more difficult since there is no reconnaissance flight and the majority of available observations near typhoon centers are single-level, remote-sensed satellite observations. At Naval Research Laboratory, we initialize tropical cyclones for operational model forecast through the use of synthetic observations. The synthetic observations are generated according to the latest observed position, structure, and intensity of tropical cyclones. These observed parameters reported in warning messages are, in general, determined by forecasters using available observations. We have developed a method to enhance the accuracy of the observed structure parameters by objectively retrieving these structure parameters from Quikscat satellite data. The method gathers Quikscat data within 600 km radius of a tropical cyclone, screens out poor quality data, and computes azimuthally averaged wind speed in every 15 km at 4 quadrants. Radii of 34 and 50 knot wind are then retrieved from the averaged wind speed at each quadrant by least square fitting the wind speed to a fifth-order polynomial. The retrieved 34 and 50 knot radii are weightily averaged with the radii included in the warning message to become the structure parameters used in constructing the synthetic



observations. Numerical experiments have been conducted to evaluate high-resolution tropical cyclone forecast in the Coupled Ocean/Atmosphere Mesoscale Prediction System (COAMPS™) with and without the application of Quikscat data. Preliminary results show that the cyclone track and structure forecast are improved with the application of Quikscat data, and for some cases the improvement is quite significant. The paper presented at the symposium will discuss the retrieval method as well as the evaluation results from the numerical experiments.

**MC02/08P/B20-007 1630**

**A PILOT STUDY ON THE SURVEILLANCE OF TYPHOONS NEAR TAIWAN USING GPS DROPSONDE**

Chun-Chieh WU<sup>1</sup>, Po-Hsiung LIN<sup>1</sup>, Tien-Chiang YEH<sup>2</sup> (<sup>1</sup>Department of Atmospheric Sciences, National Taiwan University, <sup>2</sup>Central Weather Bureau, Taipei, Taiwan)

Due to the important potential value of the GPS dropsonde data, a pilot study will be conducted on the aircraft surveillance of typhoons near Taiwan using GPS dropsonde. This work will not only improve the atmospheric data surrounding typhoons, but (also) promote the research on data assimilation and adaptive observation. This is a pioneering research work led by scientists in Taiwan to conduct typhoon surveillance experiments in the western Pacific, with international participants from the NCEP, HRD, FNMOS of U.S., and the MRI of Japan. The project will use aircrafts to perform experiments on typhoons in the northwestern Pacific Ocean for the first time in up to 15 years. Researchers will fly above typhoons approaching Taiwan and release GPS dropsondes to obtain environmental data from areas of interest around the typhoon periphery. Data will be transmitted to the Central Weather Bureau in real time and compared with the results of numerical prediction models. Apart from increasing our understanding of the typhoon structure, the project will improve forecasting of typhoon track, intensity, and wind and rainfall distribution. The typhoon surveillance experiments will be conducted when the first typhoons of the 2003 season threaten Taiwan. The project is expected to yield impressive breakthroughs in typhoon research, forecasting, and observation when it is completed.

**MC03 Wednesday, July 9 - Friday, July 11**

**DYNAMICS AND VARIABILITY OF MONSOON SYSTEMS (ICDM)**

Location: Site A, Room 7

**Wednesday, July 9 AM**  
Presiding Chair: Y. Xue

**MC03/09A/A07-001 Invited 0900**

**SEASONALLY VARYING AIR-SEA INTERACTION IN THE AUSTRALIAN-INDONESIAN MONSOON**

Harry HENDON (BMRC)

Dry season rainfall anomalies across Indonesia are spatially coherent, strongly correlated with local SST, and tightly coupled to El Niño/Southern Oscillation (ENSO). Broad-scale Indonesian rainfall and SST anomalies tend not to persist from the dry season into the wet season and rainfall in the heart of the wet season tends to be uncorrelated with SST and spatially incoherent. Seasonally varying feedback between Indonesian SST, winds and rainfall explains the growth, persistence and coherence of the local anomalies during the dry season and their decay or change in sign once the wet season commences. During the dry season anomalous surface easterlies, remotely driven by warm SSTs in the central Pacific during El Niño, act to increase local wind speed, cooling the ocean surrounding and to the east of Indonesia and thereby increasing the anomalous SST gradient across the Pacific. Hence, local rainfall and the Walker circulation are further reduced. Once the climatological surface winds across Indonesia shift from southeasterly to northwesterly associated with onset of the Australian summer monsoon, the anomalous surface easterlies act to reduce the wind speed. The initial cold SST anomaly is damped, reducing the negative rainfall anomalies and surface easterlies. These eastern Indian Ocean SST changes are driven largely by induced surface heat flux variations (primarily changes in latent heat flux and net short wave radiation). Biennial variations in the Indonesian region may also be induced by this seasonally varying air-sea interaction associated with ENSO.

**MC03/09A/A07-002 0930**

**MECHANISMS BY WHICH SEA SURFACE TEMPERATURE ANOMALIES PERTURB THE WEST AFRICAN MONSOON SYSTEM**

Kerry Harrison COOK, Edward Kalman VIZY (Dept. Earth and Atmospheric Sciences, Cornell University)

Statistical analyses of observations demonstrate that the West African monsoon is sensitive to anomalies in sea surface temperature (SST), and that this sensitivity is related to the interannual variability of the system. An analysis of model simulations (GCM and mesoscale climate model) and the NCEP/NCAR reanalysis is used to understand how this sensitivity comes about when the SST anomalies are relatively close to the African continent. In general, the West African monsoon is more sensitive to SSTAs in the Gulf of Guinea than in the eastern Atlantic off the west coast of Africa. The reason for this difference is the background atmospheric state. In response to a warm SST anomaly, for example, the presence of large meridional temperature gradients at higher latitudes allows the atmosphere to advect cool air to balance the heating. In the tropics, however, with much smaller horizontal temperature gradients, anomalous heating is balanced in large part by adiabatic cooling, i.e., rising air. As the air rises, water vapor condenses heating the air more and amplifying the response. Because of this feedback, the sensitivity to warm SSTs is greater than the sensitivity to cold SSTs. Anomalous precipitation maxima associated with warm SST anomalies in the Gulf of Guinea do not occur over the warm SST anomalies, and they do not weaken the monsoon even though they reduce the land/sea temperature contrast. Rather, they tend to enhance the monsoon precipitation over West Africa by the introduction of higher water vapor amounts into the on-shore flow. Large-scale sinking in the middle-troposphere over the Gulf suppresses convection over the ocean and allows the moisture to accumulate in the atmosphere and be transported into the monsoons system over the land surface.

**MC03/09A/A07-003 0950**

**TROPICAL PRECIPITATION PATTERNS IN RESPONSE TO A LOCAL WARM SST ARE REPLACED AT THE EQUATOR OF AN AQUA PLANET: AN ENSEMBLE STUDY**

Kensuke NAKAJIMA<sup>1</sup>, Yukiko YAMADA<sup>1</sup>, Masaki ISHIWATARI<sup>2</sup>, Yoshi-Yuki HAYASHI<sup>1</sup> (<sup>1</sup>Department of Earth and Planetary Science, Faculty of Sciences, Kyushu University, <sup>2</sup>Graduate School of Environmental Earth Science, Hokkaido University, <sup>3</sup>Division of Earth and Planetary Sciences, Graduate School of Science, Hokkaido University)

For the purpose of examining the initial development of the atmospheric response to a warm SST anomaly placed at the equator, an ensemble switch-on experiment is conducted with an aqua planet GCM. An ensemble average of the size of 128 satisfactory reduces the transient noise caused by both small scale convective activity and large scale intraseasonal variability. A convection center develops on the SST anomaly within three days after the switch-on. As a barotropic (or Lamb-wave like) response to the heating, pressure increases globally outside the low pressure region around the warm SST area. The response after this initial global pressure rise is just as expected from Gill (1980); a warm Kelvin wave-like anomaly is emitted to the east of the convection center, and a warm Rossby wave-like anomaly is emitted to the west. The Kelvin wave-like signal propagates at a speed quite slower than that expected from its vertical wavelength, suggesting that the signal is a "moist" Kelvin wave. Transient decrease of precipitation occurs at the front of the signal; the coupling of convection and vertical motion is consistent with its slow propagation. After several days, precipitation to the east of the warm SST begins to recover because of the surface frictional convergence associated with the Kelvin wave-like equatorial low pressure anomaly. On the other hand, precipitation to the west decreases monotonically. It seems that the continuous reduction of precipitation in the western area is caused by the equatorial surface frictional divergence associated with the relatively high pressure anomaly at the equator of the Rossby wave structure. Throughout the duration of the integration period, 50 days after the switch-on, zonally averaged surface pressure in the tropics continues to rise. At the same time, zonal mean flow in the upper troposphere in the tropics is accelerated to become westerly. This mass redistribution, presumably related to the wave momentum flux caused by planetary wave emission toward the mid-latitudes generated at the heat source on the SST anomaly, contributes about a half of the amount of time-mean positive pressure anomaly to the west of the warm SST area.

**MC03/09A/A07-004 1030**

**DOES THE ANOMALOUS SST LEAD TO THE CONTRASTING CHARACTERISTICS OF THE 1993 AND 1994 EASM?**

Huang-Hsiung HSU, Wen-Shung KAU, Ren-Tzeng CHEN (Department of Atmospheric Sciences, National Taiwan University)

East Asian summer monsoon (EASM) in 1993 and 1994 exhibits contrasting characteristics, which resulted in the 1993 drought in Taiwan and the 1994 drought in Japan, respectively. During July and August 1993, an anomalous anticyclonic circulation and below-normal precipitation appeared over Taiwan and the Philippine Sea, while an anomalous cyclonic circulation and above-normal precipitation appeared over Japan. The reversed situation was observed in 1994. The most contrasting sea surface temperature anomalies (SSTA) were observed in the extratropical Pacific in a zonally elongated area extending from the Japan Sea to the dateline. The relationship between the SSTA and circulation anomalies differs from that often observed in the tropics. For example, the cyclonic (anticyclonic) circulation anomaly was located above the negative (positive) SSTA in 1993 (1994). The anomalous atmospheric circulation and surface heat fluxes several months before the appearance of the extratropical SSTA were in a distribution that could result in the increase and drop of the SST in 1993 and 1994, respectively. The anomalous atmospheric circulation in the extratropical Pacific during the spring and early summer might have led to the changes in SST. Two General circulation models (i.e., NTUGCM and ECHAM4) were used to simulate the contrasting 1993 and 1994 EASM by prescribing the observed SSTA. The NTUGCM was able to simulate the contrast to some extent. However, the significant difference between the ten ensemble members indicate that the different initial conditions can result in larger fluctuations than those forced by the anomalous SST. Interestingly, the ECHAM4 produced precipitation and circulation anomalies that were in opposite phase to the observed. These results suggest that the anomalous SSTA in the extratropics was more like a response than a forcing. It follows that the AMIP-type climate simulation may produce incorrect results when and where the effect of SSTA forcing is relatively insignificant. Mechanisms other than the oceanic effect seem to be responsible for the contrasting 1993 and 1994 EASM. Our recent study indicates that the anomalous circulation may be related to the anomalous heating over the Tibetan Plateau instead of over the ocean.

**MC03/09A/A07-005 1050**

**INTERANNUAL INDIAN RAINFALL VARIABILITY AND INDIAN OCEAN SST**

Gabriel Andres VECCHI, D.E. HARRISON (JISAO, University of Washington)

Understanding and predicting interannual variability of Indian rainfall during the southwest monsoon has potential social and economic benefits, and is also a topic of scientific interest; much effort has been made to understand and predict nation-wide measures of Indian monsoon variability (e.g. All-India Rainfall). We suggest that a two-regional approach offers a useful alternative framework for understanding the interannual variability of the Indian monsoon. Indian rainfall is concentrated in two regions, each with strong area-average mean and variance in precipitation: the Western Ghats and the Ganges-Mahanadi Basin region. Over the past 23 years, rainfall over these two regions together explains 90% of the interannual variance of All-India rainfall, and interannual rainfall anomalies in each region are significantly correlated with All-India Rainfall. However, the time series of rainfall anomaly averaged over each region are uncorrelated with each other, suggesting that the interannual variability in each region is controlled by different mechanisms. We also explore statistical relationships between Indian Ocean sea surface temperature anomalies (SSTA) and precipitation anomaly over these two regions. We find strong simultaneous and leading correlations involving distinct Indian Ocean SSTA patterns, with the SSTA patterns preceding the southwest monsoon by up to nine months. Enhanced southwest monsoon precipitation in the Western Ghats is associated with warm SSTA in the Arabian Sea at the onset of the monsoon, while enhanced Ganges-Mahanadi Basin precipitation is associated with cool SSTA off the coasts of Sumatra and Java at the onset of the monsoon. Both regions are associated with leading SSTA patterns in the southern Indian Ocean, with the Western Ghats (Ganges-Mahanadi Basin) associated with warm (cool) SSTA patterns. The correlations with Western Ghats rainfall anomaly are generally robust; these relationships may contribute useful statistical forecast skill for rainfall in this region. The six and nine month lead correlations with Ganges-Mahanadi Basin rainfall are also generally robust. However, the zero-lag correlations with Ganges-Mahanadi Basin rainfall anomalies result primarily from one year with very strong SSTA and rainfall anomaly - this is not a robust statistical connection. The regional rainfall anomaly/SSTA connections are much stronger than those of All-India rainfall anomaly/SSTA. The mechanisms behind the connection at zero lag between warm Arabian Sea SSTA and enhanced Western Ghats precipitation have

been explored in the literature, but it still remains to explain the other observed relationships between SSTA and rainfall variability in these two centers of action.

**MC03/09A/A07-006**

**1110**

**OCEAN ROLES IN THE TRANSITION PHASES OF THE BIENNIAL INDIAN-AUSTRALIAN MONSOON TENDENCY**

Jin-Yi YU<sup>1</sup>, Shu-Ping WENG<sup>2</sup>, John D. FARRARA<sup>3</sup> (<sup>1</sup>University of California, Irvine, <sup>2</sup>Central Weather Bureau, Taiwan, <sup>3</sup>University of California, Los Angeles)

This study uses a series of CGCM (coupled atmosphere-ocean general circulation model) experiments to examine the roles of the Indian and Pacific Oceans in the transition phases of the biennial Indian-Australian monsoon tendency. In each of the three CGCM experiments, air-sea interactions are restricted to a certain portion of the Indo-Pacific Ocean by including only that portion of the ocean in the ocean model component of the CGCM. The results show that the in-phase transition from a strong (weak) Indian summer monsoon to a strong (weak) Australian summer monsoon occurs more often in the CGCM experiments that include an interactive Pacific Ocean. The out-of-phase transition from a strong (weak) Australian summer monsoon to a weak (strong) Indian summer monsoon occurs more often in the CGCM experiments that include an interactive Indian Ocean. The associated sea surface temperature (SST) anomalies are characterized by an ENSO-type pattern in the Pacific Ocean and basin-wide warming/cooling in the Indian Ocean. The Pacific SST anomalies maintain large amplitude during the in-phase monsoon transition in the northern autumn and reverse their sign during the out-of-phase monsoon transition in the northern spring. On the other hand, the Indian Ocean SST anomalies maintain large amplitude during the out-of-phase monsoon transition and reverse their sign during their in-phase monsoon transition. These seasonally dependent evolutions of Indian and Pacific Ocean SST anomalies allow these two oceans to play different roles in the transition phases of the biennial tendency in the Indian-Australian monsoon system.

**MC03/09A/A07-007**

**1130**

**CAN THE SST IN THE WESTERN NORTH PACIFIC AFFECT THE INTENSITY OF BAIU PRECIPITATION?**

Sophie FUKUTOME, Christoph FREI, Christoph SCHÄR (Atmospheric and Climate Science, ETH)

Precipitation during the Japanese rainy season, named Baiu, undergoes large interannual fluctuations that justify the search for physical and dynamical processes regulating its intensity. The purpose of the present study is to examine the role played by the sea surface temperature (SST) in the Western North Pacific (WNP; 120-160°E, 20-60°N) in the interannual variability of Japan's summer precipitation, with particular regard to its influence on lower tropospheric dynamics. To this end, numerical experiments are carried out with a regional climate model forced at its lower boundary by sea surface temperature anomalies corresponding to opposite regimes (wet or dry) of the interannual variability. Two pairs of summers with opposite behavior on the interannual scale are simulated, and subsequently repeated with exchanged SST evolutions. To assess the significance of the response signal with respect to the chaotic variability of the model, each experiment consists of a three-member ensemble with slightly modified initial atmospheric conditions. It is found that the response to SST forcing is non-linear. A wet summer forced by the SST of a dry summer experiences a decrease in precipitation over Japan of up to nearly 30%, while the opposite experiment yields no significant increase. This study demonstrates that the effect depends upon the relative position of the SST anomalies with respect to the low-level jet. While the SST distribution is unable to alter the course of the low-level jet, it can, if adequately placed, greatly affect the precipitation rate by influencing the jet's baroclinicity, and the moisture convergence into the Baiu frontal zone. Thus, a wet summer, during which the Baiu front is located above Japan, reacts sensitively to the underlying SST, while a modification of the large-scale circulation would be necessary to bring about an equivalent response in dry years.

**MC03/09A/A07-008**

**1150**

**IMPACT OF INDIAN OCEAN DIPOLE AND MONSOON VARIABILITY OVER SOUTH AND EAST ASIA : OBSERVATIONAL AND MODELING ASPECTS**

Jai Ho OH, R.H. KRIPALANI, J.H. KANG (Dept. of Env. & Atmos. Sci., Pukyong National Univ., Busan, Korea)

The influence of the Indian Ocean Dipole on the summer monsoon rainfall over South Asia (India) and East Asia (China, Korea, Japan and Mongolia) has been investigated using simple statistical procedures. Long period data varying from 1869 to 2000 have been used applying correlation and composite techniques. While the observed rainfall data are used as a measure of rainfall activity, the NCEP-NCAR Reanalysis data are used to examine the circulation features associated with the extreme Dipole and the Monsoon phases over the India subcontinent, the East Asian-North Pacific sector and over Eurasia. Results reveal that the positive phase of the Dipole is favorable for following year's rainfall activity over India, China and Mongolia, but is unfavorable for the following year's monsoon activity over Korea and Japan. The relationships are more consistent and stronger for the remote Korean and Japan regions, rather than for the near Indian Ocean region. The positive (negative) phase intensifies (weakens) the monsoon circulation over the India subcontinent. Further the positive phase is associated with the weakening of the Tibetan High during the same year and the North Pacific Subtropical High in the following year. The circulation and snow distribution over Eurasia are also affected following an extreme dipole event. It is proposed to examine the physical and dynamical processes associated with the above observed teleconnections through a General Circulation Model. The model will examine the impact of the extreme phases of the Indian Ocean Dipole and the El Nino Southern Oscillation phenomenon on monsoon variability.

**Wednesday, July 9 PM**  
 Presiding Chairs: E.H. Berbery, G. Wu

**MC03/09P/A07-001**

**Invited**

**1400**

**THE INDIAN SUMMER MONSOON-MEDITERRANEAN DYNAMICAL CONNECTION: THE CAUSE OF EUROPEAN FLOODS IN 2002?**

Mike BLACKBURN, Brian HOSKINS (Department of Meteorology, University of Reading)

Our previous research has suggested that the ambient descent and lack of rain in the summer in the Mediterranean region is a dynamic response to the diabatic heating occurring in the Indian Monsoon. In the summer of 2002, the Indian Monsoon rainfall was much below normal and there was anomalous rain in Europe, with some occurring where it is normally suppressed and exceptionally heavy rain in many parts of southern and central Europe. Historical data does indeed show a correlation between summer Indian rainfall and the

intensity of the descent over southern Europe. However the correlation with southern European rainfall is less apparent. The latter is strongly correlated with North European blocking. The Indian Monsoon - Mediterranean relation will be assessed further using experimentation with idealised models.

**MC03/09P/A07-002**

**1440**

**MAINTENANCE OF SUMMER MONSOON CIRCULATIONS: A PLANETARY-SCALE PERSPECTIVE**

Tsing-Chang (Mike) CHEN (Professor of Meteorology, Iowa State University)

The monsoon circulation, which is generally considered to be driven by the landmass-ocean thermal contrast, like a gigantic land-sea breeze circulation, exhibits a phase reversal in its vertical structure; a monsoon high aloft over a continental thermal low are juxtaposed with a mid-oceanic trough underlaid by an oceanic anticyclone. This classic monsoon circulation model is well matched by the monsoon circulation depicted with the observational data prior to the First GARP Global Experiment (FGGE). However, synthesizing findings of the global circulation portrayed with the post-FGGE data, we found that some basic features of major monsoon circulations in Asia, North America, South America, and Australia differ from those of the classic monsoon circulation model. Therefore, a revision of the classic monsoon theory is suggested. With four different wave regimes selected to fit the horizontal dimensions of these monsoon circulations, basic features common to all four major monsoons are illustrated in terms of diagnostic analyses of the velocity potential maintenance equation (which relates diabatic heating and velocity potential) and the streamfunction budget (which links velocity potential and streamfunction) in these wave regimes. It is shown that a monsoon circulation is actually driven by the east-west differential heating and maintained dynamically by a balance between a vorticity source and advection. This dynamic balance is reflected by a spatial quadrature relationship between the monsoon divergent circulation and the monsoon high (low) at upper (lower) levels.

**MC03/09P/A07-003**

**1520**

**DYNAMICS OF THE ATMOSPHERIC CIRCULATION ANOMALIES ASSOCIATED WITH THE NORTH AMERICAN MONSOON VARIABILITY**

Mingfang TING, Renu JOSEPH (Department of Atmospheric Sciences, University of Illinois at Urbana-Champaign)

The year-to-year fluctuations of the Arizona/New Mexico (AZNM) precipitation during the month of July are examined in this study to identify the North American monsoon variability. Using the AZNM precipitation index for the years 1979 to 1998, we identified three wet (1984, 88, 90) and three dry (1994, 95, 97) monsoon years for analysis in this study. The atmospheric circulation anomalies for the wet (dry) monsoon years contain an anticyclonic (cyclonic) anomaly over the western United States at the upper troposphere. For the divergence field, there is a distinctive low level convergence (divergence) anomaly over the AZNM region associated with the wet (dry) monsoon years and opposite polarity anomalies over the central US. The maintenance mechanisms of these anomaly fields are further examined using a linear and a nonlinear stationary wave model. The relative importance of the orographic forcings and the diabatic effect will be examined within the stationary wave model framework. The analysis will be extended to earlier years to increase the sample size and statistical significance.

**MC03/09P/A07-004**

**1540**

**RESPONSE OF THE ASIAN SUMMER TO CHANGES IN ENSO PROPERTIES**

H. ANNAMALAI, P. LIU (IPRC/SOEST)

Of all the boundary forcings, the SST anomalies associated with ENSO have been the most dominant forcing of ASM variability. In comparison to the period 1950-75, despite the occurrence of prolonged El Nino conditions during 1991-95 and the two very strong El Ninos (1982 and 1997), the period 1977-2001 experienced weak ENSO-ASM relationship. We hypothesize that ENSO forced regional air-sea interaction in the Indian Ocean counteracts the suppressing effect of El Nino and therefore results in a weak ENSO-ASM association. The hypothesis is verified by diagnosing atmospheric reanalysis products and conducting sensitivity experiments with an Atmospheric General Circulation Model (AGCM). We show that during 1950-75 El Nino induced subsidence weakens the ASM for the entire monsoon season (May through October) but in sharp contrast during 1977-2001, El Nino induced air-sea interaction in the eastern equatorial Indian Ocean favors a stronger ASM during July-August while El Nino induced subsidence weakens it during May-June and September-October. We argue that the ENSO-ASM linkage is returning based on response of the ASM during the developing phase of the 2002 El Nino.

**MC03/09P/A07-005**

**1620**

**THE ROLE OF THE ATMOSPHERIC HEATING OVER THE TIBETAN PLATEAU IN THE FORMATION OF THE MONSOON WESTERLY**

Kenji TANIGUCHI, Toshio KOIKE (Department of Civil Engineering, University of Tokyo)

This study focuses on the role of the atmospheric heating over the Tibetan plateau especially in early summer (this period is supposed to be the onset season of the Asian summer monsoon). The daily atmospheric temperature averaged from 500hPa to 300hPa layer is derived from the NCEP/NCAR reanalysis dataset. Lag correlation analysis between the time series of the air temperature over the western part of the Tibetan plateau and 850hPa p-velocity during the period of 16th march to 31st may for 1981-2000(20years) were conducted. Those results showed that there is a strong positive correlation over the Indian sub-continent and negative areas over the Arabian Sea and the Bay of Bengal. These areas with significant correlation values evidently emerge in case of positive lag, or the air temperature changes in advance of the p-velocity. These results indicate that downward flow is formed in the positive area after the heating of the Tibetan plateau and downward flow in the negative correlation areas. The same analysis were applied between the air temperature over the western part of the Tibetan plateau and 850hPa geopotential height. The results showed that strong negative correlation region is formed in the northwestern part of the Indian subcontinent after the heating of the plateau. There is a strong atmospheric low in the monsoon season (called Monsoon trough) and the above-mentioned result indicates that the heating in the upper atmosphere over the Tibetan plateau can induce the formation of the monsoon trough. This low pressure region can affect the strength of the monsoon circulation and, in consequence, monsoon rainfall. At the same time, the vertical and horizontal flow were investigated by using NCEP/NCAR long term mean wind data. The seasonal progression of the Latitude-Altitude cross section averaged between 80-85E showed that a subregional circulation is formed over the Indian subcontinent, an upward flow related to the monsoon trough in the north (just below the Himalaya), and the subsidence in the south during the heating period. After the heating, this subsidence disappears. The Longitude-Altitude cross section along 15N showed that the monsoon circulation, low level westerly, is



formed in the lower atmosphere after the disappearance of the downward flow over the southern India. These results give a speculation about the formation of the monsoon westerly as follows: 1) the heating of the Tibetan plateau occurs, 2) the monsoon trough and a locally vertical small circulation (like Hadley circulation) are formed, there is a downward flow over the southern India, 3) the subsidence disappears, 4) the monsoon westerly emerges. But how the Hadley-like circulation is formed and the subsidence disappears have to be investigated in more detail.

**MC03/09P/A07-006 1640**  
**THE ROLE OF MONSOON CIRCULATIONS IN THE DYNAMICS AND TRANSPORT OF THE TROPICAL UPPER TROPOSPHERE AND LOWER STRATOSPHERE IN NORTHERN HEMISPHERE SUMMER**

Timothy J. DUNKERTON<sup>1</sup>, Andrew GETTELMAN<sup>2</sup> (<sup>1</sup>NorthWest Research Associates, <sup>2</sup>National Center for Atmospheric Research)

Rotational circulations associated with convective heating in the Asian and North American summer monsoons maximize near the tropopause and are evident in stratospheric velocities and constituent transport to at least 30 hPa. Monsoon circulations also transport stratospheric air into the tropical upper troposphere owing to a relatively weak jet stream and PV gradient in NH summer. These unique circulation features are due, in part, to the large off-equatorial displacement of convective heating, and contrast sharply with the more equatorially symmetric circulation response in SH summer. While the North American monsoon in some ways is a microcosm of the Asian summer monsoon, the latter is stronger and more extensive in horizontal scale, resulting in deeper stratospheric penetration. Interesting (and provocative) differences in the distribution of water vapor and ozone are observed in connection with the two monsoon systems. Over South Asia, the monsoon creates a large pool of ozone-poor air and a moist anomaly slightly downstream. Over North America, a similar moist anomaly is observed, but ozone appears to be controlled by potential vorticity as the latter is influenced by a large-scale wave. The NH summer's unique combination of off-equatorial displacement of heating, warm ambient environment, vigorous deep convection of continental type, and forced evanescent planetary waves in creating the observed water vapor and ozone anomalies is examined with observations and a realistic CTM. Implications of these results for the water vapor tape recorder signal, upper tropospheric composition, climate and long-term trends are discussed.

**MC03/09P/A07-007 1700**  
**INTERACTIONS AMONG HADLEY, WALKER AND MONSOON CIRCULATIONS OVER THE INDONESIAN MARITIME CONTINENT**

Manabu D. YAMANAKA<sup>1</sup>, Noriko OKAMOTO<sup>2</sup>, Jun-Ichi HAMADA<sup>3</sup>, Tien SRIBIMAWATI<sup>4</sup> (<sup>1</sup>Graduate School of Science and Technology, Kobe University, Japan / <sup>2</sup>Frontier Observational Research System for Global Change, Japan, <sup>3</sup>Graduate School of Science and Technology, Kobe University, Japan, <sup>4</sup>Frontier Observational Research System for Global Change, Japan, <sup>5</sup>Agency for Assessment and Application of Technology, Indonesia)

The Indonesian 'maritime continent' has two climatological aspects. One is that this region itself plays a role of the major heat source due to equatorial strong solar radiation (sensible heat) and high humidity from the Indo-Pacific warmwater pool (latent heat). The convection center generated there induces both meridional (Hadley-like) and zonal (Walker-like) circulations. The other aspect is that the region is located in the middle of the annually-oscillating Asia-Australian monsoon circulation induced between the two hemispheres. The in total three-types of circulations mentioned above are interacted with each other. The convection center is shifted north-southward pursuing the subsolar latitude, and the winter-hemispheric Hadley-like cell is intensified by the monsoon circulation with the same direction. The monsoon circulation is intensified with a Walker-type cell induced in the western side of the convection center in the summer hemisphere. The activity of the convection center (or the updraft region of the Hadley- and Walker-like circulations mentioned above) varies highly due to intraseasonal variations (ISV) propagating eastward by about 1000 km/day. The monsoon blows from the west in the backward (western) side of the first super cluster generated in southern-hemispheric summer, which opens the rainy season in the Sunda Archipelago (Jawa, Bali and Nusa Tenggara). From the viewpoint of these interactions among the Hadley-like, Walker-like and monsoon circulations through ISVs, interannual variations such as the El Niño southern oscillation (ENSO) in the Pacific, the so-called dipole mode events (DME) in the Indian Ocean and some quasi-biennial-oscillation (QBO) like variations are discussed.

**MC03/09P/A07-008 1720**  
**A COUPLED GCM STUDY ON THE EFFECT OF MOUNTAIN UPLIFT ON ASIAN MONSOONS**

Akio KITOH (Climate Research Department, Meteorological Research Institute)

Asian monsoon is greatly affected by the existence of mountain. To study the effect of progressive mountain uplift on East Asian climate, a series of coupled GCM experiments were performed. We used eight different mountain heights: 0% (no mountain), 20%, 40%, 60%, 80%, 100% (control run), 120%, and 140%. The MRI-CGCM2 has been integrated without flux adjustments for 50 years for each run, for which the last 40 years data are analyzed. Systematic changes in precipitation pattern and circulation fields as well as sea surface temperature (SST) appeared with progressive mountain uplift. In the summertime, precipitation area moves inland of Asian continent with mountain uplift, while the Pacific subtropical anticyclone and associated trade winds become stronger. The June mean precipitation in Asia was most close to the observations at the 80% mountain height case. The model has reproduced a reasonable Baiu rain band at the 60% case and higher. There was saturation in precipitable water amount over the Asian monsoon region at the 80% case. This is associated with the maximum western Pacific warm pool SST at the 80% case due to compensating effects of ocean dynamics and evaporative heat loss, thus warranting an importance of air-sea coupling and a need for use of coupled models for such sensitivity studies.

**MC03/09P/A07-009 1740**  
**RELATIONSHIPS BETWEEN WINTER AND SUMMER MONSOONS OVER EAST ASIA**

Man Chi WU, Johnny C.L. CHAN (Laboratory for Atmospheric Research, Dept. of Physics & Mat. Sci., City University of Hong Kong)

The relationship between winter and summer monsoons over East Asia is examined using 40 years of NCEP/NCAR reanalysis data as well as station data of rainfall. The intensity of the winter monsoon is labelled as strong, normal or weak based on the unified monsoon index defined by an earlier study while the summer monsoon is classified into one of three patterns. Beginning with each winter, the summer patterns before and after are then identified so that a number of groups can be established. In general, a strong winter

monsoon is preceded (followed) by a summer pattern in which rainfall is generally more abundant over southern and northern China (the Type I pattern used by Chinese meteorologists). However, for a weak winter monsoon, the preceding summer pattern is not unique. After a strong winter monsoon, the following summer is likely to be one in which rainfall is above normal in central China or south China Type II or III). On the other hand, the summer following a weak winter monsoon is likely to have the Type I pattern, and thus a quasi two-year cycle. However, this cycle can be modified by the occurrence of the El Niño or La Niña.

Thursday, July 10 AM  
 Presiding Chair: K. Cook

**MC03/10A/A07-001 Invited 0830**  
**POTENTIAL PREDICTABILITY OF THE SOUTH AMERICA SUMMER MONSOON**

William K. LAU, Kyu-Myong KIM (Laboratory for Atmospheres, NASA/GSFC, Code 910)

We have developed a canonical ensemble correlation (CEC) methodology to maximize potential predictability from various predictors based on hindcast skills. In this paper, we use CEC to estimate and to explore the We have developed a canonical ensemble correlation (CEC) methodology to maximize potential predictability from various predictors based on hindcast skills. In this paper, we use CEC to estimate and to explore the dynamical controls of potential predictability of seasonal rainfall over South America, with particular emphasis on the South American Summer Monsoon (SASM). It is found that the tropical eastern Pacific and the tropical Atlantic contribute by far the largest fractions of the potential predictability in the tropical land regions (north of 20° S). Potential predictability is highest over the northeastern region during MAM, with the dominant contribution coming from the tropical Atlantic associated with meridional SST across the equator. The second highest potential predictability is found in the northwestern region including Columbia, Venezuela and northern Brazil in DJF with most of the contribution from the tropical Pacific, associated with El Niño. In the La Plata Basin (LPB), potential predictability is derived from the tropical Pacific in NDJ, associated with the onset of the SASM. Interestingly, during DJF and JFM, the dominant influence on LPB rainfall switches to the South Pacific, suggesting the influence of teleconnection wave trains associated with the fluctuation of the SACZ. Compared to aforementioned continental scale regions, much reduced potential predictability in seasonal rainfall is found in the interior of the Amazon in all seasons, and along the west coast region of Chile in the subtropics and extratropics for all seasons. The dynamical controls on potential predictability for the SASM, including remote forcing, as well as interactions with and among regional feedback processes will be discussed.

**MC03/10A/A07-002 0910**  
**REGIONAL MODULATIONS OF THE SOUTH AMERICAN MONSOON PRECIPITATION**

Ernesto Hugo BERBERY<sup>1</sup>, Estela A. COLLINI<sup>2</sup> (<sup>1</sup>Department of Meteorology, University of Maryland, <sup>2</sup>Servicio de Meteorología de la Armada Argentina)

The South American monsoon precipitation is part of a complex climate system that affects large portions of southeastern South America. A second precipitation regime further south tends to show an inverse relation with the core monsoon, so that an increase of precipitation in one implies a reduction of precipitation in the other. This out-of-phase variability or dipolar behavior has been observed in a broad range of frequencies, from daily to interannual. Moreover, it has important consequences for the hydrology of La Plata, a basin in southeastern South America, since the location and character of the floods depends on whether one or the other regime is more active. A multiyear data set of Eta model short-term forecasts is employed as a proxy of regional analyses to investigate the mesoscale processes contributing to the functioning of the dipole and its seasonality. The Low-level Jet (LLJ) east of the Andes has a significant role in this pattern modulation as it experiments lateral shifts during the warm season. When the LLJ has an eastward shift, it can supply moisture directly to the monsoon region, and increased precipitation is detected over the northern part of the La Plata basin. Meanwhile, the moisture supply to the center of the basin becomes weaker and a simultaneous decrease of precipitation is found. When the jet shifts west, its core acquires a southward direction, effectively reducing the moisture supply to the monsoon but increasing it to the other center of the dipole with the corresponding changes in precipitation. Land surface-atmosphere interactions that modulate the precipitation dipole are inspected using short and long term simulations of the Eta model. On time scales of about two weeks and longer, increased soil moisture is associated with a decrease of the sensible heat and an increase of the latent heat, which results in a lower Bowen ratio (increased evaporative fraction) and increased precipitation. The above sequence suggests a positive feedback between soil moisture and precipitation.

**MC03/10A/A07-003 0930**

**SALLJEX-BRASIL: THE BRAZILIAN COMPONENT OF THE SOUTH AMERICAN LOW LEVEL JET (SALLJEX) FIELD EXPERIMENT DURING DECEMBER 2002-FEBRUARY 2003**

Jose A. MARENGO<sup>1</sup>, Tercio AMBRIZZI<sup>2</sup>, Iracema Fonseca CAVALCANTI<sup>3</sup>, Manoel Alonso GN<sup>1</sup>, Gilberto Fernando FISCH<sup>4</sup>, Luiz Augusto MACHADO<sup>5</sup>, Marcelo Enrique SELUCHI<sup>1</sup>, Maria Assuncao SILVA DIAS<sup>2</sup>, Pedro Leite SILVA DIAS<sup>2</sup>, Javier TOMASELLA<sup>1</sup> (<sup>1</sup>CPTEC/INPE, <sup>2</sup>IAG/USP, <sup>3</sup>IAE/CTA)

The SALLJEX-Brasil field experiment is part of a broader international research agenda of the Variability of American Monsoon Systems (VAMOS) and its component Monsoon Experiment in South America (MESA), which are sponsored by the Climate Variability and Predictability (CLIVAR). The field experiment is also relevant to the observational and scientific activities in the continental scale experiment basins of the hydrographic basins that includes the Amazon and La Plata River basins. In the context of VAMOS and MESA, the regional experiment on South American Low Level Jet East of the Andes (SALLJEX) is basically dedicated to field observations and modeling studies of moisture transport between the Amazon and La Plata basins. There are some observational evidences as well as modeling studies that show that the Low Level Jet East of the Andes (hereafter, LLJ) is responsible for most of the moisture and energy transport between these two basins. The SALLJEX field experiment has regional components in each country involved (Argentina, Bolivia, Chile, Paraguay, Peru, Uruguay and United States). This abstract describes SALLJEX-Brasil, and the observational and modeling studies developed during the December 2002-February 2003 campaign. A science team involving scientists from Brazil, USA, Bolivia, Argentina, Paraguay and Peru is working on the analysis of series of detailed and high resolution surface, upper-air and remote sensing observation, in order to answer this science question: What is the role of the LLJ on the moisture transport from the Amazon to the La Plata basins? More specific science issues include: the synoptic variability of the LLJ; the spatial structure and time variability from diurnal to intraseasonal time scales; the role of the LLJ in the intraseasonal variability of precipitation along the South Atlantic Convergence Zone; the role of the LLJ in the dynamics of the Mesoscale Convective

Complexes over the La Plata Basin; the interannual variability of the LLJ; the dependence of the LLJ in relation to SST anomalies in the Pacific and Atlantic; the representation of the LLJ in atmospheric models; and the coupling between the occurrence or not of LLJ episodes and rainfall in the Andean region, east of the Andes, and southern Brazil-northern Argentina. The extension and upgrading of the current observational network will allow for better and more frequent surface and upper-air directed towards a better understanding of the LLJ, based on a combination of observation and monitoring of circulation and fluxes associated to the LLJ, complemented by regional and global models.

**MC03/10A/A07-004 0950**

**LA NINA IMPACT ON SUMMER MONSOON IN BRAZIL: LARGE-SCALE INFLUENCES, REGIONAL PROCESSES AND ATLANTIC SST VARIATIONS**

Alice Marlene GRIMM (Department of Physics, Federal University of Parana)

The rainy season in most of Brazil is associated with the summer monsoon regime in South America. The quality of this season is important because it rains little during the rest of the year over most of the country. In this study, the influence of La Nina events on the summer monsoon circulation, rainfall and temperature is analyzed with seasonal and monthly resolution, using data from a dense network of stations, giving a comprehensive view of the impact of these events. The expected precipitation percentiles during the monsoon season of La Nina events are calculated, as well as anomalies of surface temperature and thermodynamic parameters. This information is analyzed jointly with anomaly composites of several circulation parameters. There are abrupt changes of anomalies within the summer monsoon season, suggesting the prevalence of regional processes over remote influences during part of the season. In spring there are positive precipitation anomalies in north and central-east Brazil and negative ones in south Brazil. These precipitation anomalies are favored by the perturbation in the Walker and Hadley circulation over the eastern Pacific and SA, and by a Rossby wave-train over southern South America. Northerly moisture inflow from the Atlantic is favored into northern South America, and diverted towards the mouth of the Amazon by the low-level cyclonic anomaly north of the equator. In December (0) and January (+), probably triggered by anomalous surface cooling during the spring, there is an anomalous low-level divergence and an anticyclonic anomaly over southeast Brazil. This anomalous circulation directs moisture flux towards south Brazil, causing moisture convergence in part of this region and part of central-west Brazil. The thermodynamic structure in central-east Brazil does not favor precipitation over this region, and the wet anomalies in north Brazil are displaced northward. The dry anomalies in south Brazil almost disappear and even turn positive. In February (+), after the strongly below normal precipitation of January, the surface temperature anomalies turn positive over southeast. The low-level anticyclonic anomaly is much weaker than in January (+). There are positive rainfall anomalies in north Brazil and in the SACZ, and negative ones return to south Brazil. The intraseasonal variations of the La Nina impact are accompanied by SST variations off the southeastern coast of Brazil. It is not clear whether surface-atmosphere and land-ocean interactions favor the predominance of regional circulation anomalies over large scale perturbations in January or whether the atmospheric basic state in January is conducive to perturbations different from the other months in summer, leading to enhanced rainfall in Central-East Brazil.

**MC03/10A/A07-005 1030**

**INFLUENCE OF LAND SURFACE ON TRANSITION FROM DRY TO WET SEASON OVER SOUTH AMERICA**

Rong FU, Wenhong LI (Earth & Atmospheric Sciences, Georgia Institute of Technology)

Our analysis of the fifteen years of European Center for Medium Range Forecast (ECMWF) reanalyses suggests that the transition from dry to wet season in the Southern Amazon is mainly driven by increases of surface latent flux and consequently local thermal-driven precipitation. The latter triggers the reversal of the cross-equatorial flow, leading to large-scale net moisture convergence to the Southern Amazon. The analysis of early and late wet season onsets on an interannual scale shows that a longer dry season with a lower rainfall causes lower surface latent flux in the dry and earlier transition periods, compared to those observed before a normal wet season onset. This results in a higher Convective Inhibition Energy (CINE) and a lower Convective Available Energy (CAPE). These delay the increase of local thermal-driven rainfall in the initiating phase of the transition and consequently wet season onset. Conversely, a wetter dry season leads to a higher surface latent flux and weaker CINE. These promote an earlier increase of local thermal-driven rainfall and thus an earlier wet season onset. Our results imply that removal of the Amazon rainforest, which probably leads to a much drier surface during dry and transition seasons, could significantly delay the wet season onset and prolong the dry season.

**MC03/10A/A07-006 1050**

**DYNAMICS AND VARIABILITY OF THE SOUTH AMERICAN MONSOON SYSTEM**

Carlos Roberto MECHOSO (Department of Atmospheric Sciences, University of California, Los Angeles, USA)

The warm season circulation over South America includes the second largest monsoon system in the world. This South American monsoon (SAM) affects large parts of the continent over which it develops, their population, agriculture, and economies. As in all monsoons, ocean-continent contrasts are of fundamental importance. This presentation starts with SAM's climatology. The evolution during spring and summer of the region of intense convection over South America, establishment of the monsoon high over Bolivia, and development of the South Atlantic Convergence Zone (SACZ) are described. A strong low-level jet along the eastern slopes of the Andes is introduced and shown to be a key contributor to the moisture flux from the tropics to the mid-latitudes. The role of South American orography on the dynamics of outstanding monsoon components is discussed. Next the presentation focuses on SAM's variability. There is compelling evidence that ocean-atmosphere interactions involving the Pacific and Atlantic oceans play a major role in determining the variability of SAM in several time scales, particularly the interannual but also in the interdecadal. In reference to the SACZ, its variability is linked to sea surface temperature anomalies in the tropical Pacific and North Atlantic, and in the southern subtropics of this ocean.

**MC03/10A/A07-007 1110**

**A POSITIVE FEEDBACK PROCESS FOR MAINTAINING THE PRECIPITATION OF THE SACZ**

Yasu-Masa KODAMA (Department of Earth and Environmental Sci. Hirosaki University)

The SACZ (South Atlantic convergence zone) is a significant precipitation zone which stretches from the active rainfall area developed over the Amazon Basin in summer. The SACZ is one of the elementary features of the South American monsoon system (Zhou and

Lau, 1998). The rainfall over the Amazon, which is a strong atmospheric heat source, largely contributes to maintaining the SACZ (Kodama, 1993; Figueroa et al., 1995; Matthews, 1996). In this paper, we'd like to remark that the SACZ is not a simple slave of the Amazonian rainfall, but the rainfall along the SACZ also may play as a heat source to maintain the SACZ. Low-level northerly along the western edge of the subtropical high over the South Atlantic is important for maintaining the SACZ, because the northerly supplies much moisture and forms low-level convergence (Kodama, 1993). The northerly is considered as a part of monsoon circulation surrounding the monsoon heat low over the South America (Kodama, 1992). We performed vorticity budget analysis using the NCEP reanalysis data. The results suggest that the strong atmospheric heating along the SACZ also may intensify the low-level northerly. The heating maintained by the rainfall along the SACZ forms an updraft along the SACZ. This updraft intensifies the cyclonic vorticity in the lower troposphere by the stretching process. Actually a low-level weak trough is observed along the southwestern side of the SACZ. SLP gradient, and combined northerly, are then intensified along the northeastern side of the SACZ. Note that the low-level trough is not strong in spite of the strong heating. This is because the vorticity generation by the stretching is canceled out by southward advection of lower absolute vorticity from the tropics by the northerly. This suggests that the northerly is partly maintained by the updraft along the SACZ, as a result of vorticity balance between the stretching and the poleward vorticity advection. A positive feedback may exist in rainfall activity of the SACZ, because the moisture supply by the northerly intensifies the rainfall, and the combined updraft, which may intensify the northerly. We will also show some results of AGCM experiments to reinforce this idea.

**MC03/10A/A07-008 1130**

**ANALYSIS AND FORECAST OF THE MONSOON SYSTEM DURING A PERIOD OF THE SOUTH AMERICA LOW LEVEL JET EXPERIMENT IN JANUARY 2003**

Iracema Fonseca CAVALCANTI<sup>1</sup>, Pedro Leite SILVA DIAS<sup>2</sup>, Maria Assuncao SILVA DIAS<sup>2</sup>, Celeste SAULO<sup>3</sup>, Matilde NICOLINI<sup>3</sup>, Jose Antonio MARENGO<sup>3</sup> (<sup>1</sup>CPTCE/INPE, <sup>2</sup>IAG/USP, <sup>3</sup>UBA)

The monsoon system over South America is analyzed for January 2003, mainly for the period of 22-29 January 2003, during the South America Low Level Jet Experiment (SALLJEX). During this period there were several typical events, such as development of a CCM associated with LLJ over northern Argentina and with the passage of a frontal system; occurrence of the SACZ; occurrence of the Upper Level Cyclonic Vortex (ULCV) over Northeast Brazil; and prediction for a LLJ in the beginning of February. The synoptic situation during the period and the model forecasts are discussed based on results of several global and regional models (ETA, RAMS, LAM-CIMA, NCEP, NASA, UK MetOffice and CPTCE). The variability of the monsoon system can be seen, alternating cases of SACZ and LLJ as part of the intraseasonal cycle. In the beginning of the period a CCM developed ahead of a frontal system over Argentina. A LLJ case could be detected in the analysis. The ULCV started the development over Northeast and the frontal system moved toward southeastern Brazil, when strong southerlies developed over Argentina and Bolivia, reaching the Amazon Region. Another period of SACZ occurred, after a cyclogenesis development over Southern Brazil. The cloudiness band was well organized over central South America and the southern region had clear skies. This is consistent with several studies which show the opposite sign between central-east and southern South America. At the end of the period, there was a strong amplified trough over South America, and the Bolivia High continued displaced westward over the Pacific Ocean. The models were predicting the occurrence of a LLJ in the beginning of February, when the SACZ dissipates. Forecast models in general were able to forecast the general characteristics of the systems. However, there are significant differences in timing and intensity which are described and analysed.

**MC03/10A/A07-009 1150**

**MODEL SIMULATION OF MOISTURE CONVERGENCE IN THE NORTH AMERICAN MONSOON**

David A. SALSTEIN (Atmospheric and Environmental Research, Inc.)

From simulations over North America, we examine the ability of atmospheric general circulation models, principally those participating in the second phase of the Atmospheric Model Intercomparison Project, to reproduce observed moisture patterns in the regions of interest to the North American Monsoon Experiment (NAME): Precipitation, as well as overall moisture convergence start in the spring in low latitudes, and advance northward through western Mexico and reaching part of the southwest United States, with a maximum northward extent in August. This moisture convergence pattern then retreats back to its original location by the middle of the autumn. The AMIP models under consideration have mixed success in simulating this monsoon circulation, and the ability of a model to simulate the intensity and extent of the advance/retreat of the monsoon appears to be tied at least in part to its land surface scheme. Over a broader region, that is the conterminous United States, the summer season is instead a period when it is a moisture source region, and moisture divergence then is well captured by the ensemble of AMIP models there. In the NAME regions, the interannual variability of the moisture divergence simulation is of comparable magnitude to that of the observed but the phase is difficult to capture; the broader US area appears related to the phase of the El Niño-Southern Oscillation, and easier to simulate by the general circulation models, which react more successfully to large-scale forcing. Higher resolution models when available will be compared to additional observational data sets with the goal of establishing a relationship between resolution and success in capturing details of moisture divergence patterns of the monsoon circulation.

Thursday, July 10 PM  
Presiding Chairs: K. Cook, M. Ting

**MC03/10P/A07-001 1400**

**SUBTROPICAL MONSOONS IN EASTERN NORTH AMERICA AND EAST ASIA**

Brian E. MAPES (Climate Diagnostics Center)

East Asian monsoon rains in late spring (known as Mei-Yu, Baiu, and Changma in China, Japan, and Korea) have a little-known analogue in southeastern North America. Both monsoon systems extend offshore many thousands of kilometers, but the western end of the east Asian monsoon system affects east Asian lands and hence has been extensively studied. The corresponding North American system is almost totally located offshore, affecting only Caribbean islands and the southern half of Florida. A comparative depiction of these two eastern-continent monsoon systems is presented. The subtropical circulation systems associated with the rains involve a complex blend of tropical and extratropical dynamics. The relative roles of circulation features at upper levels (jets and their secondary circulations) and lower levels (subtropical highs in the western oceans) are still unclear. We attempt to deduce more about the dynamics of these subtropical monsoons from the mean annual cycle in observations and 13 GCMs, as well as from observed interannual variability.

**DATA ARCHIVES TO SUPPORT MONSOON SYSTEMS RESEARCH**

Scott M. LOEHRER<sup>1</sup>, Steven F. WILLIAMS<sup>1</sup>, Jose G. MEITIN<sup>2</sup> (Joint Office for Science Support, University Corporation for Atmospheric Research, <sup>1</sup>National Oceanic and Atmospheric Administration/National Severe Storms Laboratory)

The University Corporation for Atmospheric Research/Joint Office for Science Support (UCAR/JOSS) supports data management activities for a variety of monsoon related field projects around the globe. These include the Pan American Climate Studies (PACS), Variability of the American Monsoon Systems (VAMOS), East Pacific Investigation of Climate Processes in the Coupled Ocean-Atmosphere System 2001 (EPIC2001), and the proposed North American Monsoon Experiment (NAME). To support these projects UCAR/JOSS conducts a variety of data management activities ranging from the planning and preparation of data management plans, to the data collection, processing, quality assurance, archival and dissemination to support project researchers. In addition UCAR/JOSS is providing support to the World Climate Research Programme (WCRP) Coordinated Enhanced Observing Period (CEOP) project. One of CEOP's scientific objectives is to document the seasonal march of the monsoon systems, assess their driving mechanisms, and investigate their possible physical connections. To support this objective CEOP has identified a number of well instrumented "reference sites" in tropical regions. UCAR/JOSS takes the data from each of these reference sites and develops a quality assured hourly resolution "composite" data set in a uniform format. The initial data set for CEOP covers the period from 1 July to 30 September 2001 and three additional annual cycle data sets are planned to follow over the period from October 2001 to September 2004. This presentation will summarize these activities and provide an overview of these various project databases.

**NORTH AMERICA MONSOON WINDS AS SEEN FROM QUICKSCAT**

Simona BORDONI<sup>1</sup>, Bjorn STEVENS<sup>1</sup>, Timothy LIU<sup>2</sup> (<sup>1</sup>Department of Atmospheric Sciences, University of California Los Angeles, Los Angeles California, USA, <sup>2</sup>Jet Propulsion Laboratory, Pasadena California, USA)

Northward surges of relatively cool, moist maritime air from the Tropical Pacific into the Southwestern United States occur along the Gulf of California every summer during the North America monsoon season. These surges are believed to be strongly connected to the amount of convective activity in Arizona and northwestern Mexico. Lack of adequate lower tropospheric observations over northern Mexico and southwestern Arizona has hampered a definitive assessment of the role that gulf surges play in controlling the onset, the intensity and the variability of the NAM. In this paper, we use three year High Resolution QuickScat Data to study surface winds over the Gulf of California, to identify surge events and to study their relationship to monsoon activity. The 12.5-km resolution data set used in this study, derived from range compressed backscatter measurements, using the Direction Interval Retrieval with Threshold Nudging (DIRTH) method, have better spatial resolution and are more conducive to coastal studies than the standard QuickScat wind products (25 km resolution). Previous observations mainly collected during the SWAMP campaign have suggested the existence of a persistent time-mean southerly wind over the Gulf of California, believed to be the primary means of moisture transport to the arid southwest deserts. At odds with these observations, high resolution QuickScat data reveal a weak mean northerly flow over the Gulf of California during the monsoon months, with an up-slope component to the Western Flank of the Sierra Madre Occidental. Gulf Surges are identified with abrupt wind reversals from northerly to southerly flow. This result seems to suggest that the primary mechanisms by which moisture is transported into the monsoon region is through transient processes rather than through the average mean flow and supports the hypothesis that gulf surges are strongly related to the beginning of monsoon bursts periods. Given such predominant role of transient effects, we propose a new Monsoon Index, based on the frequency and intensity of gulf surge occurrences from QuickScat winds. Such index can be viewed as a measure of the overall strength of the North America Monsoon and can be used to identify the monsoon onset and to highlight the monsoonal variability, both on intraseasonal and inter-annual time scales.

**VARIABILITY IN EAST PACIFIC MONSOONAL CONVECTION OBSERVED IN EPIC2001**

David J. RAYMOND<sup>1</sup>, G.B. RAGA<sup>2</sup>, Christopher S. BRETHERTON<sup>3</sup>, Simon DESZOEKE<sup>3</sup>, John E. MOLINARI<sup>4</sup> (<sup>1</sup>Physics Department, New Mexico Tech, <sup>2</sup>Centro de Ciencias de la Atmosfera, Universidad Nacional Autonoma de Mexico, <sup>3</sup>Dept. of Atmospheric Sciences, Univ. of Washington, <sup>4</sup>Dept. of Earth and Atmospheric Sciences, SUNY Albany)

A strong cross-equatorial sea surface temperature (SST) gradient occurs in the east Pacific during the northern summer and fall, with warmer SSTs north of the equator. During the late winter and early spring this gradient relaxes to near-zero, but does not reverse. The result is a cross-equatorial atmospheric circulation which varies seasonally, giving it a monsoon-like character, but not a complete reversal on a seasonal basis. In other words, there is a strong SW monsoon, but little or no NE monsoon. The low-level cross-equatorial flow up the SST gradient is remarkably steady in the northern summer. However, the convection observed over the Mexican warm pool in the monsoonal region is quite unsteady. One of the goals of the EPIC2001 field program was to understand the origin of this variability. Intensive observations were made of convection in a 4 degree by 4 degree box centered on 95 W, 10 N in September and October of 2001. Under normal circumstances this region is shielded from the NE trade winds by the high terrain of southern Mexico and Central America, resulting in light surface winds. Little deep convection occurs under these conditions, even though SSTs can be 28 C or greater. However, EPIC2001 observed two situations in which ample deep convection can occur: (1) Under certain conditions strong flows through gaps in the high terrain to the north and east can impinge on warm pool. Such events have been studied extensively by Joe Zehnder and colleagues. (2) Westerly winds above the boundary layer are associated with the northward extension of the southwesterly monsoon flow, which results in stronger than normal winds over the Mexican warm pool. This apparently occurs because the geostrophic pressure gradient associated with these westerlies adds to the SST-induced pressure gradient which drives the climatological cross-equatorial flow -- easterlies have the opposite effect of suppressing the southwesterlies over the warm pool. Both of these situations result in stronger than normal total surface heat flux, which has been shown to be the primary forcing mechanism for deep convection in this region. Examination of time series of zonal winds near 850 mb at 95 W, 10 N shows that westerly wind pulses at 5-6 day intervals are associated with westward-moving tropical wave disturbances, many of which intensify into tropical storms. However, such tropical wave activity appears to be modulated at longer timescales by episodes of easterly and westerly winds, possibly associated with the MJO or other eastward-moving disturbances, as noted by Molinari and colleagues and by Maloney and Hartmann. EPIC2001 was able to observe both easterly and westerly phases of this modulation. During the easterly phase, the low-level southwesterlies terminated further south than normal and little tropical wave activity occurred.

**ROLE OF LAND SURFACE PROCESSES IN MONSOON DEVELOPMENT: EVIDENCE FROM EAST ASIAN AND SOUTH AMERICAN MONSOON SIMULATIONS**

Yongkang XUE<sup>1</sup>, Hann-Ming JUANG<sup>2</sup>, Weiping LI<sup>3</sup>, Fernando DE SALES<sup>4</sup>, C. Roberto MECHOSO<sup>5</sup>, Stephen D. PRINCE<sup>6</sup>, Ruth DEFRIES<sup>7</sup>, Carlos NOBRE<sup>8</sup> (<sup>1</sup>Department of Geography, Department of Atmospheric Sciences, University of California, Los Angeles, <sup>2</sup>Department of Geography, UCLA, USA, <sup>3</sup>Department of Atmospheric Sciences, UCLA, USA, <sup>4</sup>NCEP, NOAA, Camp Springs, USA, <sup>5</sup>Department of Geography, University of Maryland, USA, <sup>6</sup>CPTEC/INPE, Brazil)

Monsoonal systems provide the water for agriculture in the world's most populous regions, yet an understanding of the mechanisms that govern the development of monsoons has been elusive. We present evidence for the importance of exchanges of water and energy between the land surface and the atmosphere for simulations of precipitation and circulation for the 1987 East Asian (EA) and South American monsoon systems (SAMS). We compare simulations by a NCEP general circulation model (GCM) coupled with two different land surface parameterizations, a two-layer soil model with no explicit vegetation representation (Referred to as SOIL), and a more comprehensive biophysical model (SSiB). The results show that feedbacks between vegetation and the atmosphere are crucially important for proper simulation of intra-seasonal monsoon evolution, including its intensity, the spatial distribution of precipitation, and associated circulation at the continental scale. In the EA monsoon simulations with the NCEP GCM/SOIL model, the moisture transport and precipitation at the monsoon onset were too strong. During the monsoon evolution, although its simulation generally produced a wet season, an important EA monsoon feature, the abrupt monsoon northward jump, was missing. With the coupled GCM/SSiB model, the monsoon evolution process, including the abrupt northward jump, was correctly simulated. SSiB produced very different surface thermal heating than SOIL. The longitudinal gradients of sensible heat flux at surface and temperature at low atmospheric levels were much stronger in GCM/SSiB simulations than in GCM/SOIL, which caused differences in moisture transport and may have triggered the jump. SAMS starts developing in Central America and then moves southeast towards the Amazons in South America. Afterwards, the largest precipitation moves northward and eventually retreats northwest. NCEP GCM/SOIL and NCEP GCM/SSiB also produced substantially different evolution and spatial distributions of SAMS. In the SAMS simulation, the GCM/SOIL model did not produce a clear southward movement of the precipitation in pre-monsoon season. Instead, it produced a very strong and early northward SAMS movement. The precipitation in the wet season monsoon was also too intense. The coupled GCM/SSiB model correctly simulated the monsoon evolution. To understand the mechanisms that contributed to the differences in the SAMS simulations, the surface energy and water balances were analyzed. The NCEP/SSiB produced different spatial distributions of surface sensible and latent heat fluxes than the NCEP GCM/SOIL. These differences were consistent with changes in the circulation and the improvements in the simulation of SAMS. In the pre-monsoon stage, land surface processes influenced the flow divergence over Central America. In the monsoon maturation stage, they also influenced the simulations in South Atlantic Convergence Zone. The results reveal that in addition to low frequency mean forcings, such as the monthly mean albedo, from the land surface that affect the atmosphere, the perturbation processes of vegetation forcing that have much shorter time scales, which are described by a biophysical model, are also important to the simulation of the monsoon system. The results suggest that processes affecting these feedbacks such as land cover change can, in turn, alter the timing and spatial patterns of monsoons.

**THE DIURNAL CYCLE OF CONVECTION OVER THE NORTHERN SOUTH CHINA SEA DURING SCSMEX**

Richard H. JOHNSON, Steven L. AVES (Department of Atmospheric Science)

During May and June 1998, the South China Sea Monsoon Experiment (SCSMEX) was conducted to study the onset of the East Asian monsoon. As part of SCSMEX, a special radar and sounding network was established over the South China Sea (SCS) to document characteristics of convection and changes in the circulation accompanying the monsoon onset. There were two rainy periods during SCSMEX, each approximately ten days long, one in mid-to-late May at the time of onset and the other in early June. Data from the BMRC C-POL radar were available for all of the first of these periods, but only for a portion of the second. Six-hourly soundings taken at a number of sounding sites in the northern SCS have been used to determine the kinematic fields, apparent heat source, and apparent moisture sink over the northern SCS during the monsoon onset as well as to partially resolve the diurnal cycle of convection. Preliminary analyses of SCSMEX data over a large area in the northern SCS reveal a morning maximum in rainfall, consistent with findings for other tropical oceanic regions. The findings show good agreement between estimates of rainfall rate from the moisture budget and those from NASA's Tropical Rainfall Measuring Mission (TRMM) precipitation radar (PR) and microwave imager (TMI). However, further analysis reveals that this diurnal cycle is not so simple. Specifically, there is a variation in the phase from an early-morning maximum near the South China coast to a mid-day maximum near Dongsha Island about 200 km to the south (as observed by C-POL land rain gauge data). Thus, there is a propagation of convection southward away from shore, as has been observed over the Bay of Bengal by Yang and Slingo (2001) and Zuidema (2002). This propagation is seen in both the radar and Japanese GMS satellite datasets. We will explore whether this propagation is consistent with the idea recently put forth by Mapes et al. (2002) that offshore convection is a response to a diurnal gravity wave generated by the diurnally oscillating heat source of the daytime mixed layer over the land of south China, a wave which propagates offshore at 15--20 m/s. Thermodynamic and wind data from the six-hourly soundings along the south China coast and Dongsha Island should help analysis of the wave structure, if it exists. Alternatively, it is possible that the propagation is a result of downdraft outflows from deep convection, i.e., gravity current dynamics. Changes in the structure of the convective systems as the propagation offshore will be explored using the radar dataset.

**CASE STUDY OF THE BAY OF BENGAL MONSOON CONVECTION ON THE ONSET OF THE SOUTHERN CHINA SEA SUMMER MONSOON**

Yimin LIU<sup>1</sup>, JOHNNY C.L. CHAN<sup>2</sup>, Jiangyu MAO<sup>1</sup>, Guoxiong WU<sup>1</sup> (<sup>1</sup>LASG, Institute of Atmospheric Physics, <sup>2</sup>Laboratory for Atmospheric Research, Department of Physics and Materials Science, City University of Hong Kong)

Assimilated analysis fields from the South China Sea Monsoon Experiment and the outgoing longwave radiation data from the National Center for Atmospheric Research (NCAR) have been employed to describe the large-scale and synoptic features of the subtropical circulation during the Bay of Bengal (BOB, 6-20°N, 80-100°E) and South China Sea (SCS, 7-20°N, 110-120°E) monsoon onsets in 1998. The results show that the Asian monsoon onset during May 1998 exhibited a typical eastward development from the BOB region to the SCS domain. The weakening and retreat of the subtropical anticyclone from SCS were preceded by the intrusion of westerlies and the development of convective activities over the northern

part of the SCS (NSCS, 15-20°N, 110-120°E). As the vertical shear of zonal wind changes in sign, the ridge surface of the subtropical anticyclone tilted northward and the summer pattern was established over the SCS. Based on these observational results, version 4 of the NCAR climate model (CCM3) is used to investigate the physical link between the convection associated with BOB monsoon vortex and the SCS summer monsoon onset, as well as the mechanism of the evolution of the low-level subtropical anticyclone over the SCS. Introduction of heating over the BOB results in vigorous convection over the BOB, and the BOB monsoon onset, as well as the development of westerlies and vertical ascent over the NSCS region due to an asymmetric Rossby-wave response. Together with the low-level moisture advection, convection is induced over the NSCS. It is the condensation heating over the NSCS that causes the overturning of the meridional gradient of temperature over the SCS. Consequently the subtropical anticyclone in the lower troposphere over the SCS weakened gradually. Eventually as convection develops over the entire SCS domain, the subtropical anticyclone moves out of the region.

**MC03/10P/A07-008 1720**

**DIURNAL CYCLE OF MOVEMENT OF CONVECTIVE CLOUD SYSTEMS OVER SUMATERA ISLAND**

Namiko SAKURAI<sup>1</sup>, Fumie MURATA<sup>1</sup>, Manabu D. YAMANAKA<sup>2</sup>, Hiroyuki HASHIGUCHI<sup>1</sup>, Suiyuchi MORI<sup>1</sup>, Jun-Ichi HAMADA<sup>3</sup>, Yudi Iman TAUHID<sup>4</sup>, Tien SRIBIMAWATI<sup>5</sup>, Budi SUHARDI<sup>6</sup> (<sup>1</sup>Graduate School of Science and Technology, Kobe University, Japan, <sup>2</sup>Frontier Observational Research System for Global Change, Japan, <sup>3</sup>Radio Science Center for Space and Atmosphere, Kyoto University, Japan, <sup>4</sup>Agency for the assessment and application of technology, Indonesia, <sup>5</sup>Indonesian Meteorological and Geophysical Agency, Indonesia, <sup>6</sup>Graduate School of Science and Technology, Kobe University, and Frontier Observational Research System for Global Change, Japan)

Diurnal cycles are especially dominant in the tropics. This presentation introduces a diurnal cycle of movement of convective clouds over Sumatra Island in Indonesia and surroundings analyzed with GMS IR data from May 2001 to April 2002. Sumatra Island is about 1,500km in length in the northwest-southeast direction across the equator, and there are mountainous districts in the western part and plains in the eastern part. Convective activities start getting active in the western part of Sumatra Island in the afternoon, and the areas where convections are active migrate westward and/or eastward at a distance of several hundreds kilometers from midnight to morning. Such diurnal cycle of migration in both directions is different from diurnal cycles, system travels in either direction, observed in other areas, such as Indochina peninsula (Satomura, 2000), the east of Tibet Plateau (Asai et al., 1998), and north and south America continents (Wallace, 1974, Riley et al., 1986, Carbone et al., 2002, Mapes et al., 2002). The westward migration is found almost every month except for August. The eastward migration is found mainly near the ITCZ, which is shifted northward and southward with an annual cycle.

Friday, July 11 AM  
Presiding Chair: W.K. Lau

**MC03/11A/A07-001 Invited 0830**

**UNDERSTANDING AND PREDICTION OF THE ASIAN MONSOON ONSET**

Guoxiong WU, Jiangyu MAO, Anmin DUAN, Yimin LIU, Xin LIU (LASG, Institute of Atmospheric Physics)

Monsoon onset is characterized by the reversal in the direction of prevailing wind and the abrupt intensification of precipitation. As seasons evolve from winter to summer, the thermal contrast between ocean and land is changed, the aloft atmospheric temperature gradient between land and ocean is reversed, the atmospheric circulation pattern is transformed from winter type to summer type, and the monsoon onset occurs. In the boreal winter, the ridge line of the subtropical anticyclone at 500 hPa is zonal located by 120°N, and the ridge surface tilts southward with increasing height. In summer while its tilting keeps unchanged over other longitudes, it tilts northward over the Asian monsoon area because the air over Asian Continent is warmer than over Indian Ocean. Therefore the ridgelines of the subtropical anticyclone in the lower troposphere are broken over the monsoon area. During the seasonal transition the tilting of the ridge surface of the subtropical anticyclone changes from southward to northward. At the time when the ridge surface becomes perpendicular to the surface, the meridional temperature gradient vanishes, implying the replacement of the wintertime gradient by the summertime gradient, and the occurrence of monsoon onset. A "monsoon onset axis" (MOA) is then defined as the axis at the ridge surface of the subtropical anticyclone that is perpendicular to the earth's surface. Based on the NCEP/NCAR analysis data, it is shown that the MOA appears firstly over the eastern Bay of Bengal (BOB) in early May, which indicates the start of the Asian monsoon onset process, then propagates gradually eastward. It passes South China Sea (SCS) few days before May 20, and reaches the western Pacific in early June. The severe deep condensation heating accompanied with the SCS monsoon onset extends northward quickly and contributes to the development of the South Asian High (SAH) over the south of the Tibetan Plateau. The westerly jet in the upper troposphere then retreats to the north of the Plateau, and strong divergence appears to the southwest of SAH. These help the development of convection over the region of Arabian Sea and India and the monsoon onset over South Asia in early June. To this end, the whole process of the Asian monsoon onset is completed, and the general circulation has transformed to its summer pattern. Based on these, the time series of the Asian monsoon onset are constructed and correlated with meteorological variables. Particular efforts are made in understanding the impacts of the Tibetan Plateau on the seasonal transition in the area. Results show that the BOB monsoon onset is well correlated with the ENSO events and the springtime thermal status over the Tibetan Plateau. The possibility in qualitative prediction of the BOB monsoon onset is then discussed.

**MC03/11A/A07-002 0910**

**PREDICTABILITY ANALYSIS OF THE BAY OF BENGAL SUMMER MONSOON ONSET**

Anmin DUAN, Guoxiong WU, Jiangyu MAO, Yimin LIU (LASG, Institute of Atmospheric Physics)

Based on thermal-wind relation and the fact that the essence of summer monsoon onset is a result of the change in land-sea thermal contrast, the relation between monsoon onset and the variation of the subtropical anticyclone is studied, and the concept "monsoon onset axis" is defined. The axis appears firstly over the eastern Bay of Bengal (BOB), then propagates regularly eastwards to the western Pacific by early June. Whenever the axis arrives at a region, the in situ lower-layer wind direction and the sign of meridional temperature gradient (MTG) in the upper-layer are changed, and monsoon onset occurs. Furthermore, the time required to overturn the MTG depends on the initial MTG as well as the averaged meridional differential heating before the monsoon onset. Based on these results, the daily and monthly NCEP/NCAR reanalysis data during March to May from 1980 to 1999 were used to explore the predictability of the BOB monsoon onset. Results show that qualitative prediction of the BOB monsoon onset is possible by using the initial MTG and the climate mean meridional differential temperature variations. Moreover, there is significant correlation between the

spring-time monthly-mean air temperature over the Tibetan Plateau and the BOB summer monsoon onset. This provides additional clue for predicting the monsoon onset. These two methods have been utilized to predict the qualitative BOB monsoon onset in 2000 and 2001 correctly. However, detailed examination reveals that a satisfactory prediction of the BOB monsoon onset requires the consideration of the low-frequency variability of the atmospheric circulation.

**MC03/11A/A07-003 0930**

**THE SIGNIFICANCE AND THE PERSISTENCE OF PRECURSORY SIGNALS OF THE ASIAN SUMMER MONSOON**

Kuniko EGAWA, Masaki ISHIWATARI (Graduate School of Environmental Earth Science, Hokkaido University)

The significance and the persistence of precursory signals associated with the Asian summer monsoon circulation are examined with NCEP (National Center for Environmental Prediction) reanalysis data set of 1948 to 1999. These precursory signals are defined as anomalies appearing over the Asian region during several seasons prior to summer of strong or weak monsoon years. The patterns of anomalies reverse according to the intensity of the summer circulation. The most discussed precursory signal is zonal wind anomaly at the level of 200 hPa. Composite anomalies of zonal wind, temperature, geopotential height, surface temperature, surface pressure, soil moisture and outgoing long radiation (OLR) are analyzed for strong and weak summer monsoon years which are defined based on Webster-Yang index (Webster and Yang, 1992). In 200 hPa zonal wind, the significant signals emerge in winter of strong monsoon years and in spring of weak monsoon years. The persistent anomaly patterns are found in 200 hPa zonal wind from winter to spring, though they are insignificant. For both strong monsoon years and weak monsoon years, anomaly patterns persist from winter to spring in some years but not in other years. For OLR and 850 hPa temperature, the significant signals appear in winter and spring of strong and weak monsoon years. In these composite fields, anomaly patterns persist from winter to spring, but regional shifts of significant anomalies are observed. In all strong and weak monsoon years, similar anomaly patterns generally persist over the most Asian regions from winter to spring. In other fields, anomaly patterns in winter often differ from those in spring. Anomaly patterns in strong years don't show opposite patterns to those in weak years. The correlations between Webster-Yang index and each field during the period 1948 to 1999 are also examined. The correlation coefficient with 200 hPa zonal wind in spring is -0.48. The largest value of correlation coefficient, -0.66, is given by OLR in spring. The correlation coefficient of other fields are close to or less than that of 200 hPa zonal wind. Above results suggest that, contrary to discussions of previous studies, the precursory signals does not always persist during several seasons. There remains difficulty in predicting the Asian summer monsoon by use of these precursory signals.

**MC03/11A/A07-004 0950**

**GLOBAL WIND PATTERNS AND ASSOCIATED SNOW ANOMALIES OVER EURASIA: PREDICTABILITY AND INFLUENCE ON LARGE SCALE MONSOON CIRCULATION**

Susanna CORTI<sup>1</sup>, Franco MOLteni<sup>2</sup>, Cedo BRANKOVIC<sup>3</sup> (<sup>1</sup>ISAC Institute of Atmospheric Sciences and Climate, CNR National Research Council, <sup>2</sup>ICTP International Centre for Theoretical Physics)

In this study we focus on (the relationship between): (i) the global long-lasting (persisting from winter to the early summer) upper tropospheric anomalous circulation; (ii) the tropical SST anomalies (which can determine the kind of flow (i)); (iii) the snow depth anomalies over Eurasia (which can be determined by (ii) through (i)); (iv) and the large scale monsoon circulation in the following summer (related to (i), (ii) and (iii)). The dataset is the 40-year record (1958-98) of NCEP/NCAR re-analyses for sea surface temperatures and upper air fields, while, for snow depth fields, the Historical Soviet Daily Snow Depth dataset (based on observations at a series of 284 World Meteorological Organization (WMO) stations throughout the Former Soviet Union) is used. First the leading variability patterns of the atmospheric flow are searched for by calculating empirical orthogonal functions (EOFs) of seasonal anomalies. The Eurasian snow depth anomalies and SST anomalies associated with the leading circulation patterns are then identified by computing, for each season, the covariance between the principal components (associated with the EOFs) and the snow/SST anomaly time series. The relationship with the large scale monsoon circulation is evaluated through (lagged) correlations with the Webster and Yang index.

**MC03/11A/A07-005 1030**

**STRUCTURE AND EVOLUTION OF SOUTHERLY SURGES ON THE SUBMONTHLY TIMESCALE OVER THE EASTERN INDIAN OCEAN DURING AUSTRAL WINTER**

Yoshiki FUKUTOMI<sup>1</sup>, Tetsuzo YASUNARI<sup>2</sup> (<sup>1</sup>Frontier Research System for Global Change, JAMSTEC Yokohama Institute for Earth Sciences, <sup>2</sup>Hydropheric Atmospheric Research Center, Nagoya University and <sup>3</sup>Frontier Research System for Global Change, JAMSTEC Yokohama Institute for Earth Sciences)

Meridional wind surges from extratropics to tropics have been recognized as one of major regulators of tropical convective activity in many observational studies. The aim of this study is to confirm that the southern hemisphere (SH) meridional surge which is a form of extratropical forcing play a considerable role in modulating the tropical atmospheric and oceanic variability in the equatorial Indian Ocean neighboring the South Asian monsoon region. We explore the low-level surges on the submonthly (6-25 day) timescale occurring over the eastern Indian Ocean and associated tropical convection and large-scale atmospheric fields during the SH winter (June-August) season. For this study, the NCEP-2 reanalysis and NOAA/CDC OLR data on the daily basis for the 23-yr period from 1979-2001 are used, and composite analysis is carried out. A low-level surge index has been calculated using the 850hPa meridional component of wind over a key region where a local maximum of submonthly scale variance locates (17.5-2.5S, 87.5-97.5E). A total of 54 surge events are selected from the 6-25-day band-pass filtered index. Then, composites of various atmospheric and surface elements are generated based on this index to establish the relationships between the surge events and the large-scale fields. From the composites, the low-level meridional wind surges appear to be initiated by the mid-latitude Rossby wave passages along the mean westerly flow over the southern Indian Ocean and South Pacific. As the mid-latitude wave propagates eastward and develops in the entrance of the mean subtropical jet to the east of Australia, the low-level southerly surge blows through the subtropics into the equatorial region. The amplified wave and surge signals lead to a cold dry air incursion from the extratropics to the tropics. 2 to 4 days later with the surge peak, negative OLR anomalies develop near the key region, which is indicative of the local flare up of convection in the SH side equatorial region. This occurrence of convection can be explained by the influence of the incursion of cold and dry air accompanied by the southerly surge event. The enhanced southerly cold dry air flows from the mid-latitude into the tropics increase latent and sensible heat flux from the sea surface, which charges the low-level moist static energy in the near equatorial region. As a result of these processes, local unstable condition is set up in the lower troposphere, and subsequent convective motion is triggered. The potential roles of such surge events produced by the SH mid-latitude wave



passages on preconditioning the atmosphere for convection will be discussed in terms of the extratropical forcing and air-sea interaction.

**MC03/11A/A07-006 1050**  
**THE 10-20-DAY VARIATION OVER THE SOUTHEAST ASIA IN 1998 RAINY SEASON**

Satoru YOKOI, Takehiko SATOMURA (Department of Geophysics, Graduate School of Science, Kyoto University)

Intraseasonal variations (the 30-60-day variation and the 10-20-day variation) of convective activity and circulation pattern over Southeast Asia in 1998 rainy season are investigated using TMD rain gauge data, GMS5 IR1 data and GAME reanalysis data. Wavelet analysis of precipitation data in 1998 shows that the 30-60-day variation had its maximum amplitude in late June while the 10-20-day variation in middle August. Using IR1 data, it is shown that the latter variation had westward phase speed of about 5.6m/s. The circulation pattern with this 10-20-day variation is investigated using GAME reanalysis data. Lag correlation method shows that the horizontal circulation pattern in the lower troposphere resembled that of the equatorial Rossby wave of the gravest meridional mode very well. Namely, in the maximum rainfall stage of the 10-20-day variation over Indochina Peninsula, two cyclonic vortices were found whose centers were at 95E,10N and 85E,15S. These positions were about 10 degrees south of the positions that previous studies pointed out. This difference is probably due to one of the peculiarities in 1998 that the distribution of convection was south of climatological one. Besides, low height anomalies existed at the almost same positions as these cyclonic vortices. The westward phase speed and period are estimated to be 6.4 m/s and 12 days, respectively. From these two values, it is calculated that the equivalent depth is 64 m, which is consistent with the latitudinal scale of these vortices estimated by the linear theory. The vertical structures of this mode were as follows. Height anomalies in the upper troposphere were out of phase with that in the lower troposphere and a node existed at 300 hPa level. In the upper troposphere, the maximum amplitude was observed at 200 hPa level, while in the lower troposphere, it was at 700 hPa or 850 hPa level. These characteristics of vertical structures were also found in stream function anomalies. Lag correlation analysis also shows that anomalies of height and stream function in the lower troposphere were larger than that in the upper in the west of 120E, while anomalies in the upper were larger than that in the lower in the east. This fact indicates that as this wave moved west, its vertical structure changed such that the layer in which the maximum amplitude was observed changed from the upper troposphere to the lower troposphere. The background vertical shear of zonal wind is westerly (easterly) over the Western Pacific (the Bay of Bengal). Possibly this east-west distribution of the background vertical shear is important for this vertical structure change.

**MC03/11A/A07-007 1110**  
**SEASONAL CHANGE OF THE MOISTURE TRANSPORT TOWARD EAST ASIA AND THE WESTERN PACIFIC REGION DURING THE ASIAN SUMMER MONSOON**

Miki HATTORI, Kazuhisa TSUBOKI (Hydrospheric Atmospheric Research Center, Nagoya University)

East Asia and the western Pacific regions are the northernmost and easternmost parts of the Asian summer monsoon region. East Asian region has a wet climate and has a large amount of precipitation especially in the Baiu/Meiyu season. In order to show how the abundant moisture and the wet climate are maintained, seasonal change of the moisture transport from the Indian Ocean to the western North Pacific and East Asia during the Asian summer monsoon is investigated. Zonal and meridional moisture fluxes which calculated from the 6 hourly data of the NCEP/NCAR reanalysis averaged from 1978 to 1998 were examined from May to September. It is found that there are three typical northward moisture transport areas: the western equatorial Indian Ocean, the Bay of Bengal and the South China Sea. Two typical eastward moisture transport areas were also found: the tropical Indian Ocean and Baiu/Meiyu region in East Asia. Characteristics of seasonal change of these moisture transports are summarized as follows. In May, there are small eastward moisture fluxes around the equatorial Indian ocean and to the south of Japan whereas little northward moisture flux in the Indian ocean and South China Sea. In June, a strong northward moisture flux accompanied with Somali jet are found in the western Indian ocean and it last until August. It is also found that an intensification and northward spread of the eastward moisture flux in the northern Indian Ocean toward the Arabian sea and the Bay of Bengal around 20N. In the Bay of Bengal, strong northward moisture flux is also found from June to August. In the South China Sea, there are strong eastward and northward moisture fluxes from June to August. They connect to the intense eastward moisture flux area around the eastern China sea and Japan during June and July. In August, the eastward moisture flux increases and reaches to the east of the Philippines, then moisture convergence to the east of the Philippines reaches maximum of the year. On the other hand, northward moisture flux toward the mid-latitude decreases because of the relatively dry southeasterly anticyclonic moisture flux which accompanied by the subtropical Pacific high. In September, the eastward moisture flux in the north Indian Ocean shifts southward and weakens. This study indicates that the moisture transport from the tropics and subtropics toward the mid-latitude around Asian summer monsoon regions are closely related to the zonal moisture transport around the northern Indian ocean and the South China Sea and that studying variation and interaction of these moisture transports are needed to understand the water circulation of the East Asian summer monsoon.

**MC03/11A/A07-008 1130**  
**THE PRECIPITATION PATTERNS OVER AUSTRALIA AND EAST ASIA DURING THE SEASON OF AUSTRALIAN SUMMER MONSOON**

Mong-Ming LU, Ru-Jun MAY (Central Weather Bureau, Taiwan)

The spatial and temporal variability of the precipitation patterns over the vast area from Australia to Northeast Asia (100°-150°E, 40°S-40°N) is investigated. Three data sets are used in this study: the surface observed global land precipitation monthly anomalies in 1920-1995 (Dai et al. 1997), CPC Merged Analysis Precipitation (Xie and Arkin 1997) in 1979-2001, and NCEP-NCAR reanalysis monthly data set in 1949-2001. The station data in Taiwan during 1920-2001 is intensively used for verifying the results. Three pronounced precipitation patterns over the area from Australia to East Asia are identified. The patterns are determined based on three key areas, namely, south China and Taiwan, the Philippine Sea and northwestern Australia. Pattern-one has wet anomalies over south China, Taiwan, and Japan but dry anomalies over the Philippine Sea and northwestern Australia. Pattern-two has opposite anomalies to the pattern-one in aforementioned key areas. Pattern-three has wet anomalies over the Philippine Sea but dry anomalies over south China and northwestern Australia. After performing composite, EOF and regression analyses to the data sets, we find that pattern-one is mainly a response to El Niño and the warm SST anomalies over the Indian Ocean. Pattern-two is a response to cold SST anomalies over the equatorial central Pacific, the marginal seas of Asian continent from the South China Sea to the East China Sea, and the subtropical northwestern Pacific. Associated with the cold SSTs, there are compensating warm SSTs over the eastern south Indian Ocean, the Philippine Sea and the subtropical north Pacific. The SST anomalies associated with pattern-three are similar to

pattern-two in the tropics, but distinctly different over the northwestern Pacific, particularly in the subtropics. The contrast in the precipitation patterns and the associated large-scale fields suggests that the subtropical SST anomalies can influence the precipitation patterns in the region of study through a global-scale teleconnection mechanism. When the SSTs are warmer over the Philippine Sea and subtropical northwestern Pacific, the convection is stronger in that area, which subsequently enhance the downstream Rossby wave train that can subsequently enhance the intensity of the Asian winter monsoon. The intensity of the Asian winter monsoon makes directly impact on the phase relationship between the precipitation over south China, the Philippine Sea and the northwestern Australia.

**MC03/11A/A07-009 1150**  
**PRINCIPAL COMPONENT ANALYSIS OF PRECIPITATION REGIMES OVER INDIAN SUBCONTINENT**

Anu SIMON, Mohankumar K. (Dept. of Atmospheric Sciences, Cochin University of Science and Technology)

In a tropical country like India, the economy essentially depends on agriculture, which in turn depends mostly on the seasonal rains. The amount of rainfall however, undergoes variations from place to place and also from time to time. It will be of great importance to know whether this variability exhibits any identifiable pattern or whether the variation is purely random. As the monsoon is known to be organized spatially on a large scale and is persistent in time for several months, it will be useful to study the rainfall variability on a few optimal scales. However, since the optimal time and space scales of rainfall is not yet defined, the existence of rainfall patterns are to be investigated in an empirical manner. Eventhough, the south-west monsoon (June-September) is the major rainfall season of India, the post-monsoon season or north-east monsoon (October-December) is equally important for the southern peninsula. A study on the spatial patterns of the rainfall distribution is important. The present paper is concerned with both spatial and temporal variation of rainfall by composing the large scale data into empirical orthogonal functions (EOF) in space and principal components (PC) in time. The main emphasis of the study is to explain the spatial structure of rainfall considered and to bring out information about the seasonal, intraseasonal and interannual variability. The similarity between the western and central parts of India appears to be the most dominant feature of the annual precipitation regime. This mode of variability accounts for 50% of the total variance. The well recognized feature of the monsoon rainfall where excessive rainfall over Western Himalayas and deficient rainfall over the plains of north-west India associated with the movement of a western disturbance is brought out as a second component which explains 8% of the total variance. Monthly transitions of rainfall shows that September rainfall is an indicator for the rainfall during the first month of the northeast monsoon.

**MC03/11A/A07-010 1210**  
**INTRA-SEASONAL VARIABILITY OF THE INDIAN MONSOON AS EXAMINED FROM THE NCMRWF ANALYSES AND GLOBAL MODEL SIMULATIONS**

Sarat Chandra KAR, Shyam Vir SINGH (National Centre for Medium Range Weather Forecasting)

The Indian summer monsoon exhibits considerable intra-seasonal variability (ISV) during the summer monsoon months (June, July, August and September, referred to as JJAS hereafter) over India and its neighborhood. Intra-seasonal variability is not only seen in the spatial and temporal patterns of rainfall, it is also noticeable in observed wind patterns. Most predominant modes of ISV are popularly known as variability in 10-20 days and 30-50 days. There is also significant year-to-year variations of the ISV. At NCMRWF, global analyses are prepared on an operational basis using a global data assimilation forecasting system at T80L18 resolution, since 1994. In the present study, intra-seasonal variability of the Indian monsoon has been studied using these data for the JJAS months along with CMAP rainfall data (pentad). It was noticed that during 1998 monsoon season, considerable intra-seasonal variability existed in the sea surface temperatures (SST) over the Bay of Bengal (from TMI data and Buoy data). The NCMRWF analyses also showed similar trend as far as the atmospheric variables are concerned. In order to examine the air-sea coupling, the NCMRWF global model was run for this season using NCEP monthly SST, weekly SST, and TMI daily SST. The model could simulated observed intra-seasonal variability. This study shows that intra-seasonal variability in the Indian monsoon region could be a strongly coupled air-sea interaction process.

Friday, July 11 PM  
 Presiding Chair: M. Ting

**MC03/11P/A07-001 1400**  
**FOUR DIMENSIONAL RAINFALL AND LATENT HEAT RELEASE DISTRIBUTION WITH THE ASIAN SUMMER MONSOON CIRCULATION: THE RELATIONSHIP BETWEEN THE NORTH AND THE SOUTH OF THE PLATEAU**

Akiyo YATAGAI (Research Institute for Humanity and Nature)

The Asia monsoon system is, in a sense, characterized with the existence of a huge landmass, namely the Tibetan Plateau, comparing with the other monsoon systems. The southern foot of the Tibetan Plateau (Himalayas), Assam-Bengal and west of Western Ghats are well known as huge-rainfall regions because of orographic rainfall in the summer monsoon season. The latent heat release over these regions is a major energy source of the monsoon circulation. However detailed structure of the heavy rainfall has not clarified yet, and satellite remote sensing data is expected to investigate in such kind of the regions. Therefore, the four-dimensional rainfall pattern over south Asia in summertime is studied, using Precipitation Radar (PR) data acquired by the Tropical Rainfall Measuring Mission (TRMM). We used three years (1998, 1999 and 2000) rain rate and near surface rain products and made composite rainfall pattern for both diurnal and Indian-monsoonal active/break cycles, in order to overcome a weak point of sampling error of TRMM/PR. For comparison latent heat release is computed with ECMWF operational with 0.5 grid resolution dataset for the same period. Since the plateau exerts a significant influence on mid-latitude arid climate as well as very wet climate in the South Asia, we analyze the above mentioned variations with respect to the relationship between the north and the south the Tibetan Plateau. It is well-known that most part of land area shows precipitation maximum in the evening (afternoon hours), however strong convective precipitation along the foot of the Himalayas (Nepal, Bhutan, and Assam region) is seen at around the mid-night (18 UTC, 00 LST) to the morning (00 UTC, 06 LST). Latent heat release by ECMWF data shows roughly corresponding diurnal cycle with 1km order in the altitude and 500 km order in the horizontal scale. The independent upper tropospheric humidity estimated from GMS-5 water vapor channel reveals more moisture in the morning than that in the evening tat around the Tibetan Plateau (over the foot of Himalayas, Taklimakan Desert and west part of Chinese plain region) with a ring structure about 500 km in horizontal scale. So we conclude the strong convective precipitation observed along the foot of Himalayas in the mid-night to the morning, heat the mid-troposphere more than that in the daytime, and vertically transport

moisture to the upper troposphere more than that in the daytime. In the active phase of the Indian monsoon, precipitation mainly occurs over the whole part of India, Bay of Bengal, and west of the Western Ghats, while in the break phase very strong precipitation is seen in the foot of the Himalayas and over Bangladesh. Although summer precipitation at the Himalayas and at the Western Ghats is almost the same, the averaged storm height is around 5km around the west of Western Ghats in the active phase, while in the south of Himalayas, it reaches almost 10km in altitude in the break phase. Related atmospheric circulation, atmospheric heating, and their interannual variability are also shown at the conference.

**MC03/11P/A07-002 1420**

**SEASONAL AND DIURNAL VARIATION OF SURFACE TEMPERATURE OVER THE TIBETAN PLATEAU USING GMS DATA**

Yuichiroh OKU, Hirohiko ISHIKAWA (Disaster Prevention Research Institute, Kyoto University)

In the progress of Asian summer monsoon, the Tibetan Plateau has been thought to play an important role as an elevated heat source/sink protruded into the middle of troposphere. All the thermal effect from the Tibetan Plateau to atmosphere is passing through the near surface and boundary layer to free atmosphere. During the GAME (GEWEX Asian Monsoon Experiment), surface sensible and latent heat fluxes were measured at some sites with eddy covariance technique. From the surface measurements of GAME/Tibet, it has revealed that the boundary layer is characterized by its strong diurnal cycle. Although the land surface atmosphere interaction is experimentally revealed at these sites, they only represents fluxes in a patch scale around the measurement site. Thus, it is necessary to estimate the diurnal change of surface fluxes, and integrate the patch scale knowledge to the regional scale understanding over the plateau. Remote sensing from satellites offers the possibility to derive regional distribution of various surface meteorological elements in combination with sparse field experimental stations. For this purpose it is required to use the continuous data observed by geostationally satellite. For the Tibetan Plateau the GMS-5 provides continuous measurements from June 1995. The advantage of GMS is to observe the earth from a stationed position to monitor the change of meteorological phenomena at short time intervals. This advance makes it possible to analyze intra-diurnal variation over large area. We develop a methodology to retrieve one of important surface parameters, the land surface temperature, using GMS/VISSR images. The surface temperature retrieval method, infrared split-window algorithm, for NOAA/AVHRR measurements is applied with some modifications. The results of comparing estimated surface temperature from GMS data using this algorithm with in-situ surface measurements shows high correlation coefficient, it is nearly 0.8 or over. Almost 7 years, from 1996 to 2002, hourly surface temperature data is prepared. Analysis using this data shows the difference of diurnal variation of surface temperature between the eastern plateau and the western, which caused by the difference of surface condition. In the western plateau, the falling ratio of surface temperature in spring nighttime is about 1 K per hour, which is twice as quick as that in the eastern. In the morning, although it is less of obvious, the heating is faster in western than eastern. This seems to be caused by the difference of surface condition between the western plateau and the eastern. The western part of the Tibetan Plateau is relatively dry, so that the radiative cooling in the nighttime expects to become much stronger than the eastern. Also, the ground surface of the western plateau is easy to be heated and cooled. Thus, diurnal range of surface temperature is about 5 K greater in the western plateau than in the eastern.

**MC03/11P/A07-003 1440**

**ATMOSPHERIC WATER VAPOR AT KOTOTABANG DURING DIFFERENCE PERIODS OF SEASONAL RAINFALL**

Yudi Iman TAUHID<sup>1</sup>, Manabu D. YAMANAKA<sup>2</sup>, Tien SRIBIMAWATI<sup>3</sup>, Mori SUICHI<sup>1</sup>, Hamada JUN-ICHI<sup>1</sup>, Peiming WU<sup>1</sup>, Taichi SASAKI<sup>1</sup>, Noriko OKAMOTO<sup>2</sup>, Fumie MURATA<sup>3</sup>, Namiko SAKURAI<sup>1</sup> (FORSGC, JAMSTEC, <sup>1</sup>Agency for the Assessment and Application of Technology (BPPT), Jakarta, Indonesia, <sup>2</sup>Graduate School of Science and Technology, Kobe University, Japan)

Atmospheric water vapor is an important parameter governing various processes of hydrological cycle ranging from global to local. It becomes more crucial in humid tropical region, since this area has the greatest water vapor amount corresponding to the equatorial strong solar radiation and high temperature through the year. In particular, the Indonesian maritime continent area plays a role of the major latent heat source due to high humidity evaporated from Indo-Pacific warm water pool. This paper will describe the temporal and vertical variation of atmospheric water vapor and wind related to the seasonal rainfall amount of this region. Atmospheric water vapor at Kototabang (0.2° S, 100.3° E, 864 MSL), West Sumatra-Indonesia has been observed intensively during different seasons (May-June, August and November 2001), mainly with GPS rawindsondes (508 launches) and GPS water vapor soundings. Concerning seasonal variation of rainfall amount, each period (28 days continuously) has been designed as transition, dry and rainy seasons respectively. Vertical variations of specific humidity (q) in the three periods show values of q are the highest (10-18 g/kg) at below 2 km heights and gradually decrease as increasing the height (at 8 km above surface then q values are less than 2 g/kg). Daily variations of q seem more clearly during transition season than other seasons, especially near surface (below 2 km). Meanwhile, between 3-7 km heights, variations of q are less variable during rainy season than the other seasons. Estimated precipitable water by GPS rawindsondes (PWR) and by GPS water vapor soundings (PWG) have showed good agreement. Higher values of PWR are related to higher values of PWG as well as higher rainfall amounts. Mean diurnal variations of PWR during transition periods have larger variations (35-42 mm) than dry (33-37 mm) or rainy (37-40 mm) seasons, but each maximum values appear at similar local time, around 19 LT for all seasons. There is a seasonal shifted of diurnal cycle of PWG which is coincided with seasonal variation of diurnal cycle of moisture fluxes in both zonal and meridional. Concerning the seasonal variation of zonal moisture flux in the lower atmosphere (approximately below 6 km), eastward moisture fluxes become stronger, maximum values are increasing from transition (50-60 g/kg.m/s) to rainy (90-100 g/kg.m/s) seasons. Not only the maximum values but also the duration (more longer) and height (more higher) of large fluxes are increasing. On the contrary, in the upper layers (6-10 km heights), westward moisture fluxes are weaker. It was confirmed that the lower level moisture fluxes come from Indian Ocean (which can bring abundant of water vapor) into the study area (associated with westerly and southerly) dominantly during rainy season.

**MC03/11P/A07-004 1520**

**SURFACE HEAT AND WATER BALANCE TRENDS IN EASTERN ASIA IN THE PERIOD 1971-2000**

Jianqing XU<sup>1</sup>, Shigenori HAGINOYA<sup>2</sup>, Kazuyuki SAITO<sup>3</sup>, Ken MOTOYA<sup>1</sup> (<sup>1</sup>Frontier Research System for Global Change, <sup>2</sup>Meteorological Research Institute)

Climatic variations over Eastern Asia, including the Tibetan Plateau, were analyzed using meteorological data for 32 points in the period 1971 to 2000. Changes in heat and water balances were examined using potential evaporation and a wetness index as suggested by Kondo and Xu (1997a, 1997b). Climate zones in Eastern Asia identified by the wetness index matched well with the distribution of vegetation. Average monthly temperatures

increased over the 30 years, with the sharpest increase in February. The data showed that diurnal temperature ranges have decreased, but the range of ground surface temperature increased in recent years. Vapor pressure shows increase trends in most of the stations, this is due to the temperature increase. But the trends of relative humidity are decreased in most of the stations. It is suggested that although the water vapor become abundant in the atmosphere, but it is harder to condense to cloud because of the temperature increase. We also noticed that the cloud amount shown a decrease trend in the most of the stations. From the Tibetan Plateau, through central China, to southern Northeast China, there has been an increase in potential evaporation and pan evaporation, which may be related to higher temperatures and a lack of surface water.

**MC03/11P/A07-005 1540**

**MODES, MECHANISMS AND TELECONNECTION OF TROPICAL NORTH AFRICA CLIMATE VARIABILITY**

Abebe YESHANEW (National Meteorological Services Agency)

Modes of tropical North African hydroclimate variability are investigated based on rainfall and Nile River stream flow data (1950-1998/7) using continuous wavelet transform (CWT). It is found that Sahelian climate is characterised by ENSO timescale and decadal rhythm. The mountainous and equatorial regions are attributed by high frequency and interannual signals. The mechanisms that control this broad spectral mode of tropical North Africa climate are studied based on NCEP/NCAR ocean-atmospheric reanalysis and is found that large-scale east-west overturning of Atlantic and Pacific drive the hydroclimate swing of the North Africa through the upper-level velocity potential dipole and convection polarity. The ENSO mode determines the pole and the strength of the polarity between North Africa and South America through these zonal circulations. The tropical North Africa climate teleconnection with regional atmospheric circulation corroborates with long record that Pacific Walker Circulation-Atlantic Zonal Circulation are pivotal large-scale circulations that control the tropical North Africa climate variability. Integrated global angular momentum and quasi-biennial oscillation also play a significant role. Locally, the African Easterly Jet associated to Indo-Pacific SST determines the rainfall dipole configuration between Sahel and Guinea Coast.

**MC03/11P/A07-006 1600**

**SOME RECENT STUDIES OF THE CHARACTERISTICS OF WEATHER SYSTEMS (INCLUDING THE MONSOON SYSTEMS) OF WEST AFRICA USING SATELLITE DATA**

Simon Oyediran OJO (Department of Geography, University of Lagos)

In most previous writings on West African weather, there have been problems obtaining data for accurately examining the characteristics and consequences of patterns of the weather systems. With the recently available satellite data in Nigeria, it has become a big challenge for meteorologists and climatologists to use this satellite data and information to critically examine the characteristics and patterns of the weather and climate systems and their implications for the characteristics and consequences of environmental change in the region, and for better understanding of the weather systems in general and the monsoon systems in particular. It is the purpose of this paper, therefore, to examine the characteristics and consequences of ocean-atmospheric interactions and their consequences for the weather systems, and with special emphasis on the monsoon systems during the rainy season. Satellite data for 1998 and 1999 rainy seasons were used for detailed illustrations, and with respect to (a) the beginning of the rainy season (b) the middle of the rainy season (c) the little dry season and (d) the end of the rainy season. The paper first discusses the main factors usually associated with the characteristics and consequences of the weather systems, including the intertropical discontinuity (ITD) and the ocean factor, winds, topography, land and sea contrasts, which are especially significant for local scale systems and the characteristics and consequences of the disturbances during the period of study. The paper then discusses the various characteristics and consequences of the weather systems as they relate to meso and micro scale systems in West Africa, and the significance of the dynamic controls, particularly the relative significance of topography and land and sea contrasts as major factors in the potential predictability of the monsoonal systems, and developing prediction models for West Africa. The results of the study show that (a) although the ITD and the ocean factor are significant for inducing significant changes in the characteristics and patterns of change in the air-sea interactions, it is becoming clearer that (a) the influence of topography and micro scale land and sea contrasts are very significant factors influencing and initiating evolution of the weather systems, while the ocean and other factors influence the changes in the patterns of movement of the weather systems and (b) the characteristics of the variations and change in the patterns of movement of the weather systems are also significantly affected by the weather systems in other parts of the world especially by the European weather. The implications of the results for improving forecasting and prediction of weather and climate in West Africa are then discussed, particularly as regards (a) the need for consideration and inclusion of most of the significant factors in developing models for the region (b) the need for adequate considerations of the three scales of operations of weather and climate systems, namely macro, meso, and micro scales, in developing such regional models and (c) the need for continued acquiring of satellite and other data and information for continuous monitoring of the weather systems and their implications.



**MC03-Posters Friday, July 11**

**DYNAMICS AND VARIABILITY OF MONSOON SYSTEMS (ICDM) Location: Site D**

Friday, July 11 PM

**MC03/11P/D-001 Poster 1400-176**

**SEVERAL DAYS VARIATION OF TEMPERATURE INVERSIONS OVER THE PRE-MONSOON IN INDIA AND THEIR EFFECTS ON THE TRANSITION TO MONSOON ONSET**

Shin-Ya OGINO<sup>1</sup>, Yoshihiro TACHIBANA<sup>2</sup>, Masato NODZU<sup>1</sup>, Eisho AZUMA<sup>3</sup>, Yoshinori KAMATA<sup>3</sup>, Yuku KAMIAKITO<sup>3</sup> (<sup>1</sup>Graduate School of Science and Technology, Kobe University, <sup>2</sup>Liberal Arts Education Center, Tokai University, <sup>3</sup>Graduate School of Science, Tokai University)

Characteristics of several days variations of temperature inversions which frequently appear over the Indochina Peninsula in the late dry season were described and physical mechanism of the variations were examined based on the thermodynamic equation. We have found that

the vertical advection of temperature is one of the important processes which cause the several days variations of inversion heights. The background and purposes of this study are described below in detail. The Indochina peninsula is the peculiar region where the rainy season starts earliest among the other Asian monsoon regions. To clarify the reason for this peculiarity is one of the most important issues among the Asian monsoon studies. Several factors which control the beginning of the rainy season over the Indochina peninsula are reconsidered: large scale subsidence, temperature inversion, transported humid air from the ocean, sensible heat flux, synoptic scale disturbances propagating from mid-latitude, and so on. For example, the inflow of the humid air may activate convections, while the large scale subsidence may have an effect to suppress convections. Among these factors, the role of temperature inversion is of our interest. We noticed that strong temperature inversions appear at 3-4 km height in the late dry season over Thailand. Our preliminary analysis using worldwide radiosonde data clearly showed that the region from the northern part of Indochina peninsula to the southern part of China is one of the peculiar region where the strong and high-level inversions appear in the late dry season. We consider a possibility that these inversions play an important role on the seasonal transition from dry to rainy seasons. The temperature inversion may suppress convections, because the inversion is a quite stable layer. This is an essential role due to the inversion. However, the suppression of convections may result in the separation of the air above and below the inversion. As a result, some atmospheric quantities and matters, such as heat, water vapor and aerosols, may be accumulated below the inversion. The accumulation of heat and water vapor below the inversion may decrease the atmospheric stability, which can rather activate convections. The accumulation of aerosols below the inversion may affect the radiation budget and cloud generation process. But, it is not obvious whether these effects would activate or suppress convections, because which strongly depends on the property of the aerosols. In any case, the essential and accompanying effects of the temperature inversion possibly modulate or control the seasonal march of the thermodynamic fields and the beginning of the rainy season. Based on the abovementioned preliminary considerations, we have started to study the temperature inversions over the Indochina peninsula in the dry season. The objectives are (1) to understand the physical mechanisms of the generation, maintenance and disappearance of the temperature inversions and (2) to understand the role of the inversion on the seasonal transition over the Indochina peninsula. It is expected that this study would provide us physical understanding on the transition process from dry to rainy seasons over the Indochina peninsula.

**MC03/11P/D-002** Poster **1400-177**

**FINE VERTICAL STRUCTURE OF THE HORIZONTAL DIVERGENCE OVER THE ASIAN SUMMER MONSOON REGION**

Noriyuki NISHI (Graduate School of Science, Kyoto University)

Fine vertical structure of tropical circulation in the middle and upper troposphere was investigated, particularly paying attention to (horizontal) divergence and vertical wind. It is still difficult to make direct observation of large-scale (>1000km) divergence; precise data was limited to several special intensive periods and regions (e.g. TOGA COARE IOP 1992-93). Lack of direct observation results in poor reliability of divergence field in global objective analysis. Data analysis of divergence in some global analyses was conducted to detect meaningful regional fine structure. To get supporting evidence for the reality of patterns detected in global analysis, some indirect physical variables which were observed rather directly and precisely were also analyzed. In most part of the tropics (15S-15N), the sign of climatological divergence at a point is same throughout the upper troposphere (300-150hPa) in global analysis datasets (ECMWF, NCEP Reanalysis and JMA). However, complicated vertical change of sign is detected in some specific regions and seasons; the most remarkable patterns were detected in Asian monsoon region in JJA, south Indian Ocean in JJA and around Philippine in DJF. Sounding data and remote sensing data by satellites were used to confirm the reality of detected patterns. In this presentation, results on the pattern in Asian monsoon region in JJA are presented with using TRMM satellite data and GMS5 data. The most typical case was detected in ECMWF operational analysis during the period of 18-22 June 1998. In this period, clear western edge of cumulus activity was almost fixed at 85E. Westerly with speed of more than 15m/s were dominant in the lower troposphere, whereas easterly with speed of 30-50m/s at 70-100E along 10N at 100-200hPa. Though upward motion in ECMWF analysis dominated from the sea surface to the tropopause height in the east of 85E, the height range of upward motion was gradually confined to the top of upper troposphere as shifting to the west: it confined above 400hPa at 82.5E and only around 200hPa at 80E. In GMS infrared image, each cluster remained several hours; convective part of each cluster was stagnant or moved slowly to the east. In most of the clusters, the high cloud top (less than 210K) in TRMM Virs Channel 4 (IR) image extended 200-500km west of the western edge of near-surface precipitation in TRMM TMI. Observed shallow pattern of divergence with several kilometer scale in the upper troposphere results from horizontally extended upper tropospheric stratiform clouds in the extremely strong wind shear in Asian monsoon region.

**MC03/11P/D-003** Poster **1400-178**

**THE CHARACTERISTICS OF INDIAN OCEAN DIPOLE MODE - PRELIMINARY STUDY OF THE MONSOON VARIABILITY IN THE WESTERN PART OF INDONESIAN REGION -**

Edy HERMAWAN (The Indonesian National Institute of Aeronautics and Space (LAPAN))

Prediction of El-Nino and Southern Oscillation (ENSO) phenomena in Indonesia, generally is corresponded to the Sea Surface Temperature anomaly (SSTa) and Southern Oscillation Index (SOI) along West to East Pacific Ocean between Darwin (Australia) and Tahiti (Hawaii Islands). This phenomena is assumed having a good correlation with the moving average of convective activity, especially in the western part of Indonesia region which always covered by giant clouds like Cumulonimbus (Cb). Since only a few atmospheric and oceanography data in this region, we tried to investigate in this paper the preliminary results of the characteristics of Indian Ocean Dipole (IOD). We used the Sea Surface Temperature (SST), Sea Level Pressure (SLP) and Outgoing Longwave Radiation (OLR) of Dipole Mode Index (DMI) anomaly. By applying the spectrum method, we found that the most predominant peak of these parameters are three months oscillation such as on SST and SLP data analysis. While, for OLR data, the most predominant peak is six months oscillation. We suspect these phenomena are correspond the transition season from dry to rainy season for SST and SLP, and Monsoon season for OLR.

**MC03/11P/D-004** Poster **1400-179**

**DIURNAL VARIABILITY OF THE PRECIPITABLE WATER OVER THE EAST ASIA DURING GAME-IOP**

Nobuhiko ENDO (Frontier Research System for Global Change)

The water cycle of the Asian summer monsoon has many influences on agriculture, economy and human life over the broad Asian region. GAME and SCSMEX were conducted over the Asia in the early summer of 1998. One of the objectives of the both projects is to investigate the water and energy cycle in the Asian summer monsoon system. Diurnal

variability of convective activity over the western Pacific, the Southeast Asia and the Tibetan plateau have investigated by several researchers. However the diurnal variability of precipitable water (PW) has not been understood well. In this paper we will describe the seasonal change of the precipitable water (PW) and the diurnal variability of the water vapor over the East Asia using the GAME and SCSMEX data sets. Enhanced upper-air observation was carried out during the GAME and SCSMEX IOPs. The frequency of upper-air soundings is about two to four times per day. However the enhanced observation period is different from region to region. For example the enhanced observation was made from May to June around the South China Sea while the enhanced observations were conducted from May to August over the Tibetan plateau. PW is evaluated by the trapezoidal formula using with the significant level data. We define the daily mean of PW is average of the data at 00 UTC and that at 12 UTC for describing the seasonal change of PW with twice daily routine upper-air observation data, although twice daily sampling of upper-air soundings have some biases (Dai et al., 2002). In May, the daily mean of PW is about 50 mm in southern China and is about 10-20 mm in northern China. Over the Tibetan plateau, PW is less than 10 mm. As the Meiyu frontal zone and/or monsoonal flow advance to the north, PW is increased over central and northern China. Seasonal change of PW is relatively small around the coast of the South China Sea. Diurnal variability of PW is investigated with fourth daily soundings and objectively analyzed data. During the monsoon season the daily maximum of PW was appeared at 18 UTC (about 02 local time) over central and southern China. Although the surface evapotranspiration is vigorous in the daytime, the daily minimum of PW was observed at 06 UTC (about 14 local time). The amplitude of the diurnal variability is about 4-5 mm in central China. The fraction of the diurnal variability is extremely large over the Tibetan plateau, although the diurnal range of PW is less than that at lower altitudes. Diurnal variability of PW and its relationships to the monsoonal flow are discussed.

**MC03/11P/D-005** Poster **1400-180**

**CLIMATOLOGY AND TRENDS OF LOW LEVEL CLOUD IN THE EAST ASIA DURING SUMMER**

Nobuhiko ENDO (Frontier Research System for Global Change)

Clouds play important roles in water cycle and have influences on the radiation budgets. Houghton et al. (2001) summarized many aspect of the global change. It is considered that increased surface temperature may induce enhancement of water cycle. Sun and Groisman (2000) and Sun et al. (2001) reported the change of the frequency of low-level cloud in Former USSR and United States. However climatology and trends of low-level cloud in the East Asia are not well understood. In this paper we will present climatology and trends of frequency of low-level cloud appearance for the East Asia. The Extended Edited Cloud Report Archive (EECRA; Hahn and Warren, 1999) for the period of 1971-1996 is main data sets of this study. We selected the stations met following conditions: the stations are in the region from 70E to 135E and from 15N to 55N, and have at least 100 reports for each month of each year. Although the low-level cloud codes have 9 cloud types, we re-categorized cloud codes into four cloud types (St/Sc/Cu/Cb). The frequency was obtained for each month of each year at each station. Climatology of the frequency of the low level cloud was obtained for 26-yr data. Dominant low level cloud type is cumulus over northwestern, northern and central China in JJA. Cumulonimbus is frequently observed in the Former USSR and over the Tibetan plateau. In Korean peninsula, northeastern China and Thailand, stratocumulus is dominant in low-level cloud during JJA. Dominant low level cloud type in southern China is stratocumulus in May, while Cumulus cloud frequency tends to become predominant in July. Linear regression analysis and the nonparametric Mann-Kendall rank test were employed to detect the trend of frequency of low level cloud. Cumulus cloud frequency has decreasing trends before the monsoon season over the most of China, and the frequency of cumulonimbus also tended to decrease in Thai and the coast of South China Sea in May for the period of 26-years. On the other hand Stratocumulus frequency increased in Thai, the coast of the South China Sea, eastern Tibetan plateau, northeastern China and Mongolia. The trends for the other months also have same features. Trends of surface specific humidity and precipitable water and its relations to the trends of the low-level clouds are also discussed.

**MC03/11P/D-006** Poster **1400-181**

**THE WITHDRAWAL OF THE BAIU CAUSED BY MID-LATITUDE WAVES**

Shin-ichi SUZUKI (Disaster Prevention Research Group, National Research Institute for Earth Science and Disaster Prevention)

The Baiu is a rainy season in early summer around the East Asia. Compared with the onset of the Baiu season, the withdrawal of the Baiu is an abrupt seasonal march in Japan. Usually, the Baiu front, a precipitation belt in the Baiu season, disappears in late July as a high pressure anomaly area appears around Japan. Ueda et al. (1995) explained this high pressure anomaly as a Rossby-wave propagation excited by the convective heating in subtropical western North Pacific. However, such a relationship between the withdrawal of the Baiu and convective activity in subtropical region is not always evident. In our study, the formation mechanism of the high pressure anomaly, which appears around Japan in the process of the withdrawal of the Baiu, is analyzed during the past 23-year from 1980 to 2002, using NCAR/NCEP reanalysis data. Assuming that these high pressure anomalies are formed by propagation of Rossby-waves in our analysis, we calculate wave-activity flux (Takaya and Nakamura, 1997) to analyze the propagation of Rossby-waves. In climatological data, a pair of low pressure anomaly in the subtropical western North Pacific and high pressure anomaly around Japan clearly appears in late July at the lower troposphere, as shown by Ueda et al. (1995). This situation corresponds to the withdrawal of the Baiu in climatological data. However, the results of the analysis of individual cases indicate that such a clear pattern of the wave propagation from subtropical region hardly appear at the withdrawal stage of the Baiu. On the other hand, over half of high pressure anomalies are associated with various kinds of disturbances in midlatitude, such as stationary Rossby-waves, non-stationary Rossby-waves, synoptic disturbances, and so on. There is no withdrawal of the Baiu related to the disturbances in midlatitude in our analysis of climatological data.

**MC03/11P/D-007** Poster **1400-182**

**INTRASEASONAL RAINFALL VARIATIONS IN A MOUNTAINOUS REGION OF SUMATERA, INDONESIA**

Jun-Ichi HAMADA<sup>1</sup>, Manabu D. YAMANAKA<sup>2</sup>, Shuichi MORI<sup>1</sup>, Yudi Iman TAUHID<sup>3</sup>, Tien SRIBIMAWATI<sup>4</sup> (Frontier Observational Research System for Global Change / Japan Marine Science and Technology Center, <sup>1</sup>Frontier Observational Research System for Global Change / Japan Marine Science and Technology Center, and Kobe University, <sup>2</sup>Indonesian Agency for the Assessment and Application of Technology)

Localities of intraseasonal variations in a mountainous region of Sumatera, Indonesia are examined by using pentad rainfall data at 46 stations in 1992. The most remarkable characteristic of rainfall variations is the contrast between the coastal and the inland mountainous region. Annual rainfall amounts are more abundant in the coastal region (more

than 3,000 mm/year) than in the inland region (1,000-3,000 mm/year). As for the intraseasonal variations, three types in which rainfall is distributed mainly near the coast, mainly in the inland area and over the whole region are found. Intraseasonal variations are dominant for the occurrence of the coastal / the whole active type rainfall patterns, whereas seasonal variations with southern-hemispheric summer maximum is predominant for the inland type rainfall. From correlation and composite analyses, rainfall variations in the coastal region are well related with large-scale cloud disturbances over the Indian Ocean accompanying with low-level westerly wind. Whereas, inland rainfall variations are related with convection near large islands such as the southern part of Sumatera, Kalimantan and Jawa (in the central part of the maritime continent) mainly during easterly wind period. It may be suggested that coastal rainfall is governed by the large-scale cloud disturbance over Indian Ocean (intraseasonal variations) and inland rainfall is mainly caused by local circulation (diurnal variation). Besides, rainfall variations in a mountainous region of Sumatera may be controlled by the interaction between surface topography and monsoon.

**MC03/11P/D-008** Poster **1400-183**

**THE CONVECTIVE ACTIVITY IN PRE-MONSOON OVER THE INDOCHINA PENINSULA**

Masashi KIGUCHI, Jun MATSUMOTO (Department of Earth & Planetary Science, University of Tokyo)

The convective activity in Pre-monsoon over the Indochina Peninsula was investigated using the daily mean reanalysis data, the OLR data and rainfall data in 1998. In early April, middle April and early May (Pre-monsoon season), the lower OLR region extended southward from the mid-latitude zone to the Indochina Peninsula. The interval of southward extension was about 10-20 days. After the periodic convective activity, the lower OLR region migrated northward from the low-latitude zone in middle May. After that, the major part of the Indochina Peninsula was under the lower OLR area. The spatial scale of the periodic convective activity before the monsoon onset was not local, but synoptic. The southward extension of the cold air at 600hPa occurred periodically in accordance with the periodic convective activity. According to the time series of specific humidity in the inland area of the Indochina Peninsula (12.5-22.5N, 100-110E) and zonal wind along 110E (12.5-22.5N) at 850hPa, peaks of specific humidity from April to early May coincided well with the periodic convective activity over Thailand. During this period, when zonal wind was easterly from the South China Sea specific humidity increased. On the other hand, after the monsoon onset, specific humidity increased when zonal wind was westerly. Furthermore according to the distribution of the specific humidity and wind at 850hPa from 1st to 3rd April in 1998, the moisture inflow from the South China Sea came along the edge of the North Pacific high. We calculated the time-latitude section of lapse rate between at 700hPa and at 600hPa, and between at 850hPa and 700hPa, respectively. Between at 700hPa and at 600hPa, the unstable conditions existed at the periodic convective activity. It was suggested that weakening of strong inversion layer. While between at 850hPa and at 700hPa, it was found that the unstable condition of the lower layer was cyclic in pre-monsoon season. The unstable conditions existed before the periodic convective activity. Then after the rainfall the lower layer became stable. But after the monsoon onset, such unstable conditions did not exist at the lower layer. It was found that the cold air extended southward before the periodic convective activity. Further it was clear that the easterly belong the edge of the North Pacific high from the South China Sea brought in the increase of moisture in the inland area of the Indochina Peninsula. It was suggested that the periodic convective activity in pre-monsoon season was related with the southward extension of cold air from the mid-latitude zone and the increase of moisture in the inland area of Thailand from the South China Sea. Furthermore, according to investigate the unstable condition, the unstable condition of the middle layer (about 3-4km) and of the lower layer (about 1.5-3km) existed at and before the periodic convection, respectively. We suggested that the heating of the surface and the inflow of the cold air produced the lower and the middle unstable condition, respectively.

**MC03/11P/D-009** Poster **1400-184**

**DIURNAL LAND-SEA RAINFALL PEAK MIGRATION OVER SUMATRA ISLAND, INDOONESIAN MARITIME CONTINENT OBSERVED BY TRMM SATELLITE AND INTENSIVE RAWINSONDE SOUNDINGS**

Shuichi MORI<sup>1</sup>, Jun-Ichi HAMADA<sup>1</sup>, Yudi I. TAUHID<sup>1</sup>, Manabu D. YAMANAKA<sup>1</sup>, Noriko OKAMOTO<sup>2</sup>, Fumie MURATA<sup>3</sup>, Namiko SAKURAI<sup>4</sup>, Tien SRIBIMAWATI<sup>5</sup> (<sup>1</sup>Frontier Observational Research System for Global Change (FORSGC), Japan Marine Science and Technology Center (JAMSTEC), <sup>2</sup>Graduate School of Science and Technology (GSST), Kobe University, Japan, <sup>3</sup>FORSGC, JAMSTEC and GSST, Kobe University, Japan, <sup>4</sup>Agency for the Assessment and Application of Technology (BPPT), Jakarta, Indonesia)

Diurnal cycle of rainfall and its regional variation around Sumatra Island, Indonesian maritime continent are examined mainly using TRMM satellite Precipitation Radar (PR) and intensive rawinsonde observations. Based on the advantages of PR sensor that can detect raindrops directly regardless of the ground and cloud conditions, and distinguish rainfall into stratiform and convective types, following characteristics are found regarding the rainfall variation over this area.1) Convective rainfall in the late evening is predominant over the land region of Sumatra Island, whereas rainfall in the early morning composed of both stratiform and convective types almost evenly is predominant over the surrounding sea region of the island.2) A rainfall peak in the daytime and that in the nighttime migrate with time starting from the southeastern coastline of the island into the inland region and into offshore region, respectively. The total distance of migrations is up to approximately 1,000 km per day that equals to roughly 10 ms<sup>-1</sup> of average migration speed.3) Using intensive rawinsonde observation data, it is also found that remarkable diurnal variations appear also in the middle troposphere corresponding to the migrating rainfall peaks over both the inland and coastal sea regions.4) Finally, a mechanism of the rainfall peak migrations is discussed comprehensively using TRMM PR, rawinsonde, Equatorial Atmospheric Radar (EAR), Geostationary Meteorological Satellite (GMS), and ground based observation data.

**MC03/11P/D-010** Poster **1400-185**

**FORMATION PROCESS OF THE PRECIPITATION SYSTEMS IN THE MEIYU FRONT ON THE CHINA CONTINENT DURING GAME/HUBEX 1998**

Takeshi MAESAKA<sup>1</sup>, Hiroshi UYEDA<sup>1</sup>, Teruyuki KATO<sup>2</sup>, Masanori YOSHIZAKI<sup>3</sup> (Hydrospheric Atmospheric Research Center, Nagoya University, <sup>2</sup>Meteorological Research Institute, Japan Meteorological Agency)

The Meiyu front is a part of activities of the East Asian summer monsoon. In this paper, the characteristics and detailed structures of the precipitation system in the Huaihe River Basin during the Intensive Observation Period (IOP) of the GAME (GEWEX Asian Monsoon Experiment)/HUBEX (Huaihe River Basin Experiment) 1998 were investigated with dual Doppler radar, heat and moisture budget analysis, and numerical simulation to clarify the formation process of the precipitation systems in the Meiyu front on the China Continent. During the IOP, severe precipitation associated with the Meiyu front was brought on 29 June and 2 July 1998. The precipitation event on 29 June was associated with the Meiyu front moving northward in the subtropical air mass (ISA type), while the precipitation event on 2

July was associated with the Meiyu front which located on the polar front (OPF type) and moved southward. The ISA-type Meiyu front moved northward, and two types of precipitation systems formed in this front. One was the organized pair of the convective precipitation system on the convergence line near the ground, and the stratiform precipitation system formed to the north of the convective precipitation system. The other was the linear convective precipitation system to the south of the convergence line near the ground. In the former precipitation area, the stratiform precipitation system generated a cold pool near the ground. This cold pool intensified the local temperature gradient to maintain the Meiyu front, although there were only weak or reversed thermal gradient in the subtropical air mass. In the latter precipitation area, because the air near the ground was very moist, weak cold pool was enough to cause the condensation to create successive linear convective precipitation system in the leading side. The OPF-type Meiyu front had the temperature and moisture gradient and moved southward, since the polar air mass spread to 30 °N in latitude. This Meiyu front also accompanied with the organized pair of the convective and stratiform precipitation systems to the north of the convergence line on the ground. However, there was not any precipitation system to the south of the convergence line, since the lifting condensation level (LCL) was higher than that in the ISA type; therefore, a new convective precipitation system was generated with the synoptic convergence. The difference of the precipitation processes between two types of Meiyu fronts was caused by the difference of the LCL to the south of the front, and the difference of the LCL associated with the latitudinal front motion.

**MC03/11P/D-011** Poster **1400-186**

**SIMULATION OF HEAVY RAINFALL EVENTS DURING INDIAN SUMMER MONSOON USING A MESOSCALE MODEL**

Sijkumar S<sup>1</sup>, Mohankumar K<sup>2</sup>, Joseph V. PORATHUR<sup>3</sup> (<sup>1</sup>Research Student, <sup>2</sup>Professor, <sup>3</sup>Visiting Professor)

During south west monsoon season the west coast of India observes heavy rainfall events. One of the reason for these events is the formation of off-shore vortex. Offshore vortices are mesoscale in character with linear dimensions of the order of 100 km or even less and their presence is detected by weak easterly winds at coastal stations. The peculiarity of the rainfall associated with these vortices is that the rainfalls over the coast are heavier than those over hill stations just few kilometers east. Identification is the greatest difficulty in the study of these vortices because of the lack of mesoscale data. They form when the monsoon is normal or strong over the Arabian Sea. They are very small both horizontally and vertically and can be located at present by coastal surface winds only. As part of our study we tried to reproduce a case of intense rainfall more than 40 cm that observed during 1980-1990 using PSU / NCAR mesoscale model MM5. The objective of the study is to find whether a small scale vortex can be simulated using a high resolution mesoscale model. We examined four cases with input data from NCEP / NCAR reanalysis project. The model is run on triple nested domains at 90, 30 and 10 km resolutions. Simulations are done for 48 hours. After 6 hrs of integration there is a trough formed along the coast. The trough intensified into a vortex and is more clear on 950 hPa level. The predicted vorticity at this level are very high and the values can be attributed to the predicted mesoscale vortex. Above 850 hPa level the intensity of vortex becomes less. The vortices first formed over the east Arabian sea and afterwards it moves west northwestwards. The simulations are also done with uniformly flattened terrain to study the role of Western Ghats in the formation of these vortices.

**MC03/11P/D-012** Poster **1400-187**

**DEVELOPMENT OF A HIGH-RESOLUTION ASSIMILATED DATASET FOR SOUTH AMERICA REGION**

Dirceu Luis HERDIES, Jose A. ARAVEQUIA, Rosangela CINTRA, Jose P. BONATTI (Center for Weather Forecasting and Climate Studies, National Institute for Space Research)

This work is concentrated on the period from September 2002 to January 2003, when the DRY-TO-WET/LBA (LBA is one of the regional continental field experiments of the GEWEX-Global Energy and Water Cycle Experiment) campaign took place in southwestern Amazon and VAMOS (Variability of American Monsoon Systems) Experiment, which is sponsored by the International CLIVAR (Climate Variability) Office, EXPERIMENT occurred in Argentina, Bolivia, Brazil, Chile, Unites States, Paraguay, Peru and Uruguay. The experiments measured temperature, moisture and wind profiles from rawinsondes, surface fluxes, soil parameters, precipitation, etc. The Regional ETA/PSAS Data Assimilation System (ETA/RPSAS), implemented at CPTEC in 1999, was used to produce a high resolution reanalysis (40 km) for this pilot period. The circulation over South America obtained with this reanalysis are in good agreement with the observations and shows a more detailed structure. On a longer time scale, this regional system will be the engine for a regional South American Project which will serve the purpose of refining the data products available with recent reanalysis from NCEP, ECMWF and DAO/NASA. These regional data assimilation datasets represent an advancing in our understanding of the South American climate and synoptic climatology, given its high resolution and utilization of observational data not yet available to the global reanalysis aforementioned. This work will also serve as a proof of concept for a longer term reanalysis project for the South America.

**MC03/11P/D-013** Poster **1400-188**

**SUMMERTIME ENSO TELECONNECTIONS OVER THE EURASIA**

Eun-Jeong CHA (Center for Climate System Research, University of Tokyo)

The atmosphere over the extratropical regions thousands of kilometers remote from the equatorial Pacific is sensitive to the warming of those waters during El Niño. It is apparent, however, that not all extratropical regions are sensitive to El Niño, nor is its impact uniform throughout the year. Furthermore, different El Niño events have been accompanied by an assortment of climate anomalies in the extratropics. Within the NH, a distinct annual cycle of ENSO-related teleconnections occurs, with a strong response in boreal winter. Compared to the influence of El Niño on the global climate system in winter time, those in summer has received little attention specially the East Asia, upstream region with respect to the midlatitude westerlies. According to the correlation, it is not highly correlated between SST in Niño 3.4 and observed mean surface temperature over Korea both JJA and DJF. Although the correlation coefficients are low or the marginal value, it is easily recognized by probability density function (PDF). It is obvious that the PDF shifts toward negative in JJA El Niño and positive in JJA La Niña regimes when the Niño 3.4 SST anomalies are positive and negative, respectively. During El Niño developing summer, the anomalies in the boundary layer are displayed the three noticeable areas with significance. The wide positive temperature anomalies are centered over the equatorial eastern Pacific Ocean in response to the basinwide warming, while the negative temperature anomalies are relocated in the western tropical Pacific. In addition, the other negative anomalies are located over the west part of Tibetan Plateau and the East Asian region. These anomalies have a barotropic structure from the lower to the upper troposphere and zonally elongated from North Africa reached to the East Asia it applies to only El Niño summer. Further interestingly, the anomalies have near zonally uniform symmetric structure about the equator. The distinct anomalies

developing summer of ENSO implies that different teleconnection mechanisms are at work.

**MC03/11P/D-014** Poster **1400-189**

**SEASONAL CHANGES OF SUB-TROPICAL FRONTAL ZONE OVER EAST ASIA**

Hiroaki TAKAHARA, Jun MATSUMOTO (Department of Earth & Planetary Science, University of Tokyo)

Over East Asia, Sub-Tropical Frontal Zone (STFZ), including so-called Baiu (Mei-yu) and Akisame (autumn rain) frontal zone, exists throughout the year and changes its latitudinal position and frontal activity with seasonal march. So, STFZ is one of the most important components of East Asian monsoon system, and characterizes East Asian climate. In this study, we made surface front database by using daily surface weather charts analyzed by the Japan Meteorological Agency (JMA) for 22 years (1979-2000) and examined the seasonal changes of STFZ over East Asia. The surface front database is constructed by recording a latitude (per 1 degree) and kind (stationary, warm, cold, or occluded) of a front at an intersection of each front and each circles of longitude (per 5 degrees, 110E-150E) on JMA surface weather charts at 0900JST every day. Time-latitude sections of 5-day mean frequency of all kinds of front and stationary front are made at each longitude. There is large difference of seasonal changes between in China (115E) and around Japan (140E). In China, the Mei-yu season (from late May to late July) is an only season with very primary frontal frequency, and spring rainy season (from late February to middle May) is also recognized as secondary high frequency. In autumn frontal frequency is not so high as in spring. Around Japan, on the other hand, not only Baiu season (from late May to early August) but also Akisame season (from early September to late October) has very high frontal frequency. In spring, frequency of all kinds of front is rather high, but frequency of stationary front is not so high as in China. A comparison of seasonal changes of latitudinal position and frontal activity of STFZ is made between El Nino (La Nina) years and all 22 years. About latitudinal position, in El Nino (La Nina) years, STFZ shifts southward (northward) in summer and northward (southward) in winter at each longitude. About frontal activity, there are some differences between in China and around Japan. In China, STFZ is intensified in spring rainy season and late Mei-yu (in early Mei-yu and autumn) in El Nino (La Nina) years. Around Japan, on the other hand, STFZ is intensified from late Baiu to Akisame (in early Baiu) in El Nino (La Nina) years. Especially in autumn, frontal activity anomalies of STFZ in El Nino (La Nina) years are quite different between in China and around Japan.

**MC03/11P/D-015** Poster **1400-190**

**DETECTION AND DYNAMICS OF THE PRINCIPAL MODE OF ASIAN SUMMER MONSOON VARIABILITY**

Natsuko YASUTOMI, Masahide KIMOTO (Center for Climate System research, University of Tokyo)

Principal modes of Asian summer monsoon variability are identified. To extract principal modes, vertically integrated moisture flux components are used. The separation of principal modes obtained from this analysis is better than those of conventional analyses using precipitation and OLR. The mechanism of the formation and maintenance of the most dominant mode is also pointed out. The spatial pattern regressed against the principal component of the first empirical orthogonal function mode of moisture flux components shows an anomalous circulation over the Philippines and northeast-southwest dipole convective anomaly centers over western subtropical Pacific and eastern Indian Ocean. This mode is dominant from intraseasonal to interannual variability. We shall call this anomalous circulation pattern "Indo-Pacific dipole pattern". The Indo-Pacific dipole pattern is weakly correlated to simultaneous monthly sea surface temperature. This pattern also represents large proportion of the total variance of AGCM control run whose lower boundary condition is fixed to climatological SST. This is the pattern which can be excited without any external forcings. To understand dynamics of formation and maintenance of the principal mode, linear responses of summer basic state to random thermal forcings given in Asian monsoon region are solved. The most dominant response to those random forcings is extracted. It contains anomalous circulation over the Philippines in the lower level, and its vertical structure corresponds to that of Indo-Pacific pattern calculated from reanalysis dataset. Indo-Pacific dipole pattern is preferred mode of atmosphere in Asian monsoon region in summer. Vorticity and moisture budget analyses indicate that moisture converges over the western Pacific and diverges over the Indonesia when the cyclonic circulation anomaly over the Philippines is formed. The convection over the western Pacific is activated by vertically unstable atmosphere and the convection over the eastern Indian Ocean is suppressed. The dipole convection strengthens the cyclonic circulation over the Philippines in turn. It is true of the anticyclonic circulation over the Philippines. This feedback mechanism maintains Indo-Pacific dipole pattern, preferred mode of basic state in summer.

**MC03/11P/D-016** Poster **1400-191**

**THE 2000/2001 SUMMER DROUGHT OVER BRAZIL AND ITS ASSOCIATION WITH SST ANOMALIES**

Anita Rodrigues de Moraes DRUMOND, Tercio AMBRIZZI (Department of Atmospheric Sciences; Institute of Astronomy, Geophysics and Atmospheric Sciences; University of Sao Paulo)

Precipitation deficits were observed over the Southeast, Northeast and Center-West Brazilian regions during the austral summer of 2001 and contributed to the worsening of the energy crisis that was occurring in the Country. A low level anomalous anticyclonic circulation observed over eastern of Brazil enhanced the deviation of moisture transport which usually occurs from the Amazon basin to the Southeastern of Brazil and inhibited the occurrence of South Atlantic Convergence Zone (SACZ) events in that period. However, an anomalous low level northerly moisture flux was observed over La Plata Basin and positive precipitation anomalies occurred over Bolivia, Paraguay, northeastern Argentina and southern Brazil. These anomalous features were accompanied by the anomalous activity of the upper-tropospheric cyclonic vortices over Northeast Brazil, the enhanced convection over the Indonesia and the re-intensification of La Niña conditions. Using the ensemble technique a numerical study was carried out to investigate the role of different observed Sea Surface Temperature (SST) forcings over the 2001 January-February-March anomalous South American atmospheric circulation. Reynolds SST monthly means were used as boundary conditions to study the influence of South Atlantic, South Indian, South Pacific and Equatorial Pacific oceans. The simulations were run from September/2000 to April/2001 using the Community Climate Model version 3.6 (CCM3.6/NCAR) General Circulation Model. Ten integrations using different initial conditions (IC) were done to each experiment. These ICs were extracted from a 10 years Control Integration which used the repetition of the climatological SST annual cycle as boundary condition. Numerical experiments suggested that the combined influence of South Pacific and Equatorial Pacific oceans could be responsible for the observed drought. These experiments simulated the low level anticyclonic anomaly observed over eastern Brazil. The positive precipitation anomalies observed in the subtropics were fairly reproduced by the South Pacific experiment. However, both experiments have poorly reproduced the anomalous low level northerly moisture flux observed over La Plata Basin. Therefore, the intensity of the precipitation anomalies over the

subtropical regions was much weaker. For the South Indian experiment no significant signal was observed. The South Atlantic experiment presented a weak precipitation anomaly and opposite signal for some regions when compared to the observational data. It could be that the formation of an anomalous cyclonic circulation over the positive SST anomalies has contributed to this result. This anomalous circulation may have favoured the anomalous low level NW-SE moisture flux over the center of Brazil, enhancing the occurrence of SACZ events.

**MC03/11P/D-017** Poster **1400-192**

**ORGANIZATION MECHANISM AND HEATING EFFECTS OF MESOSCALE CONVECTIVE SYSTEMS RELATED TO THE ACTIVITY OF EQUATORIAL WAVES**

Chiharu TAKAHASHI<sup>1</sup>, Hiroshi UYEDA<sup>1</sup>, Masayuki MAKI<sup>2</sup>, Koyuru IWANAMI<sup>1</sup>, Ryohei MISUMI<sup>1</sup>, Thomas D. KEENAN<sup>3</sup> (<sup>1</sup>Hydrospheric Atmospheric Research Center, Nagoya University, <sup>2</sup>National Research Institute for Earth Science and Disaster Prevention, <sup>3</sup>Bureau of Meteorology Research Centre, Victoria Australia)

The relationship between organization of mesoscale convective systems (MCSs), their heating effects to the environment in the Australian region and the activity of the Madden-Julian oscillation (MJO) and the equatorial Rossby wave (ERW) is investigated. The study mainly uses the observed Doppler radar data, NCEP-NCAR reanalysis data and outgoing longwave radiation (OLR). The changes into the "active" or "break" monsoon conditions of the atmospheric circulation and convection are primarily associated with eastward propagation of convective anomaly from the Indian Ocean to the western Pacific in the austral summer November through March during the dominant intraseasonal oscillation. However, the daily precipitation and clouds amount observed over the northern Australian region are not necessarily to be consistent with phase and amplitude of seasonal anomaly on the MJO mode extracted by long period bandpass-filtered OLR and wind field. It is indicated that amplitudes of short-periods-filtered convective seasonal anomaly is larger than those of MJO and peak days of those conversely exhibits enhancement of precipitation. Therefore, these precipitation variance occurred by deep convection followed with westward-moving depressions to the around of observation area, which are usually clear over the sea off northeastern coast. This is further suggested that occurrence of the convective gyre is probably due to ERW. In most cases of continental origin MCSs (CMSCs) the isolated squall lines types composed of a leading convective line and trailing stratiform region, which occurred and developed in large low level wind shear, resulting from very strong low-level convergence accompanied with a disturbance like cyclone located over the northern ocean off continent, this is attributed to be the peak of "break" or transitioning "break" to "active" phase in midlevel dry situations as lately and low-level easterly. It was further characterized that convectively generated cold pool that could trigger new cells converged with moisture sea breeze, consequently enhanced rear inflow jet. On the other hand maritime origin MCSs (MMSCs) was usually formed and developed in large wind shear between low-level and upper-level, on the contrary small in low-level, during early "break" phases in moderate westerly, the consequently peak of "active" in transitioning easterly to westerly or lately "active" in strong westerly. It is also indicated that MMCSs is formed on convective moistening condition, therefore makes it more favorable for next convection. Indeed some new convective lines evolved during short time interval, where the cool low-midlevel backyard moist outflows from self-produced stratiform region converged with developing strong rear inflow jet with a maximum of wind speed between 2 and 4 km, suggested a positive feedback between water vapor and convection. One of the most important roles of MCSs is the heat and moisture transport. The vertical structures of convective-stratiform heating and vertical wind motions such as maximum height and magnitude were also estimated, which change according to the regimes and stages of MCSs evolution. It is found that the heating rates normalized by rainfall amount is significantly large within MMSCs stratiform rainfall region in the middle-upper troposphere. These findings suggest to the possibility of improving in parameterization of numerical models.

**MC03/11P/D-018** Poster **1400-193**

**EFFECTS OF AEROSOLS AND GREENHOUSE GASES ON THE SOUTHEAST ASIAN MONSOON SYSTEM**

Beate Gertrud LIEPERT<sup>1</sup>, Johann FEICHTER<sup>2</sup> (<sup>1</sup>Lamont-Doherty Earth Observatory, <sup>2</sup>Max-Planck Institute for Meteorology)

Air pollution increased drastically during the 1950s to 1980s and decreased slightly at the end of the 1990s in Southeast Asia. At the same time greenhouse gases warmed the surface by about 0.6K globally. We investigate the effects of these changes on the Southeast Asian monsoon system with two sets of climate simulations. The atmospheric model is the ECHAM4 general circulation model coupled to a mixed layer ocean of the Max-Planck Institute for Meteorology in Hamburg. One set of experiments simulates the direct and indirect aerosol effect on the energy budget of the surface and the second the set of experiments simulates the effects of both greenhouse gas forcing and direct and indirect aerosol effect. The model responds to these forcings is a change in the surface energy budget of the Indian Ocean and a change in moisture transport to the continent. Results of these simulations will be presented and discussed.

**MC04** Thursday, July 10 - Friday, July 11

**PLANETARY ATMOSPHERES AND THEIR EVOLUTION (ICPAE)**

Location: Site B, Room 22

Thursday, July 10 PM  
Presiding Chair: T. Imamura

**MC04/10P/B22-001** Invited **1400**

**VOLATILE ABUNDANCES, CLOUD STRUCTURE, AND ORIGIN OF JUPITER'S ATMOSPHERE**

Sushil K. ATREYA (University of Michigan at Ann Arbor)

Cassini-Huygens spacecraft flew by Jupiter at a distance of 140 RJ (10 million km) on 30 December 2000. Spectral features of ammonia ice were identified at 10 micron [1]. Discrete ammonia ice clouds were also identified in the equatorial region and the GRS turbulent wake using diagnostic wavelengths near 1.6 and 2.74 microns in the Galileo near infrared mapping spectrometer observations [2]. We suggest the discrete clouds of ammonia are transient, and they overlie a near ubiquitous cloud of ammonia ice whose spectral signature may be masked by photochemical haze and micrometeoritic dust falling from above.

Thermochemical models predict clouds of ammonium hydrosulfide and water below the ammonia clouds [3]. However, Galileo probe failed to detect a water cloud, and only a tentative association of the tenuous cloud seen at 1.3 bar with ammonium hydrosulfide-ice can be made [3]. The meteorologically anomalous region where the Galileo probe entered, a 5-micron hotspot, is a region of downdraft where the jovian air is dry. Although the near absence of clouds in the Galileo probe entry site is consistent with the depleted condensible volatiles measured by the mass spectrometer [3], the missing information on the abundance of water in deep well mixed atmosphere is critical to the models of the formation of Jupiter and its atmosphere [4,5]. The icy planetesimal hypothesis [4] and the clathrate hydrate hypothesis [6] have been invoked to explain the enrichment of heavy elements in Jupiter's atmosphere. Continued exploration of Jupiter, especially with multiprobes, is needed to answer unambiguously such fundamental questions as the accretion of Jupiter and the evolution of its atmosphere. References: [1] M.H. Wong et al., PSS, 2003, submitted. [2] Baines et al., Icarus 159, 74, 2002. [3] Atreya et al., PSS 47, 1243, 1999. [4] Owen et al., Nature 402, 269, 1999. [5] Atreya et al., PSS 51(2), 107, 2003. [6] Gautier et al., Ap. J. 550, L227, 2001.

**MC04/10P/B22-002 1430**

**NUMERICAL MODELING OF JUPITER'S MOIST CONVECTION LAYER: SENSITIVITY TO DEEP WATER CONTENT**

Kensuke NAKAJIMA<sup>1</sup>, Shin-ichi TAKEHIRO<sup>1</sup>, Masaki ISHIWATARI<sup>1</sup>, Yoshi-Yuki HAYASHI<sup>2</sup> (<sup>1</sup>Department of Earth and Planetary Science, Faculty of Sciences, Kyushu University, <sup>2</sup>Division of Earth and Planetary Sciences, Graduate School of Science, Hokkaido University, <sup>3</sup>Graduate School of Environmental Earth Science, Hokkaido University)

'Moist convection' i.e., convection associated with the phase change and the cloud physics of water, is supposed to occur in Jupiter's atmosphere. Nakajima et al (2000) examined the structure of the moist convecting layer by running a large-domain two-dimensional fluid dynamical model for a long time. Their result shows that the water condensation level acts as a dynamical and compositional boundary. The convection below the condensation level is Benard-like and water mixing ratio is homogeneous. Above the condensation level, transient convective clouds develop and water mixing ratio is highly inhomogeneous. The horizontal average of mixing ratio decreases rapidly with height just above the condensation level, resulting in a distinctive stable layer at 5 bar. These features do not match the observation by the Galileo probe showing dry layer extends down to as deep as 20 bar level, but they did not take the discrepancy seriously because the Galileo probe entered a rather special place where the humidity is considered to be exceptionally low. Nakajima et al (2000) assumed that the mixing ratio of water vapor in deep levels to be the value computed from the oxygen content in the solar atmosphere. However, a recent theory of solar nebula suggests that the water content in Jupiter may be 9 times the amount in the solar atmosphere (Gautier, 2001), which is consistent with the large value implied by the fast propagation speeds of the wavy features observed after the impacts of the nuclei of Comet Shoemaker-Levy in 1994 (Ingersoll and Kanamori, 1995). If the deep water mixing ratio is so large, the water condensation can occur at much lower levels. Then the deep dryness observed by Galileo probe may be global feature of Jupiters atmosphere. Considering the wide uncertainty of the deep water vapor content, we repeat the numerical experiment of Nakajima et al (2000) with different values of deep water mixing ratios assumed. The results shows that, until a certain critical value of deep water mixing ratio, which corresponds to about 5 times the "solar" value, the convective clouds develop from the water condensation level, which moves to deeper levels with the increase of water vapor. At the same time, the activity of convective clouds becomes more vigorous because larger amount of latent becomes available. However, with still larger amount of water vapor, the clouds around the condensation level becomes stratiform; convective clouds develop from a higher levels. This behavior results from the heavy molecular weight of water compared with "dry" component of Jupiter's atmosphere (Guillot, 1995). The present result implies a possibility as well as a limitation of the diagnoses of deep water content from the structure of atmosphere that is remotely observable from space.

**MC04/10P/B22-003 1445**

**NUMERICAL MODELLING OF EQUATORIAL JETS ON JUPITER AND SATURN**

Y.H. YAMAZAKI, D.R. SKEET, P.L. READ (Department of Physics, University of Oxford)

Using a new general circulation model of Jupiter and Saturn, we investigate the origin of the super-rotating equatorial jets with off-equatorial 'shoulders' that are observed at the cloud top level of Jupiter and Saturn. We have recently developed a general circulation model for the stratosphere and troposphere of Jupiter and Saturn. It uses the dynamical core of the Unified Model of the UK Meteorological Office, which has been employed for both operational weather forecasts and climate research in and outside the United Kingdom. The three-dimensional, nonlinear numerical model is an implementation of a generalized primitive equations set that handles all components of the Coriolis force due to the planetary rotation, and geometrical terms that are associated with the finite thickness of the atmosphere. The generalization was introduced to the Unified Model to improve the model accuracy in the tropics of the terrestrial atmosphere, but it also provides a significant advantage for investigations of the Jovian and Saturnian tropospheres, which are expected to be deep and weakly stratified. The origin of the Jovian jets has been of great interest for centuries, and a debate of deep convection versus shallow weather layer models has been active since Busse introduced his cylindrical convection model in 1976. Recent numerical experiments with deep Boussinesq spherical shell models have had some success in producing an equatorial jet of reasonable wind speed, but shallow 'weather-layer' models tend to have difficulty in producing a superrotating jet near the equator. This is not a surprising result because of the conservation of angular momentum in an axisymmetric model. In order to overcome this difficulty within the context of the weather layer model, we investigate the plausibility of the wave-induction model by Maxworthy (1975). His idea is that a vertically propagating equatorial Kelvin wave will deposit a prograde momentum to the mean flow as it travels upward. This will produce a superrotating jet of roughly Gaussian shape along the equator. A further interesting feature of the equatorial jets is the presence of off-equatorial peaks in the westerly winds in both the Jovian and Saturnian atmospheres. However, neither the cylindrical convection model nor the simple wave-induction model can explain these characteristics. We introduce a Hadley-type meridional-vertical circulation, which by itself produces a pair of narrow jets off the equator primarily because of the conservation of the angular momentum. We superimpose a differential heating in the latitudinal direction to force the Hadley type circulation and successfully generate the off-equatorial jets. When this mechanism is combined with the Kelvin-wave induction, we reproduce the equatorial prograde jets with shoulders for both Jupiter and Saturn. The origin of this additional Hadley mechanism will also be discussed.

**MC04/10P/B22-004 Invited 1500**

**AEROSOL STRUCTURE IN JUPITER'S POLAR STRATOSPHERE**

Robert A. WEST (Jet Propulsion Lab, Caltech)

Images obtained by the Cassini Imaging Sub-System (ISS) during approach to Jupiter over a 2.5-month period beginning October 1, 2000 show the motion and evolution of stratospheric haze features and circumpolar Rossby waves. Of particular interest is a large dark oval seen only in ultraviolet wavelengths (most prominently in filter UV1, effective wavelength 263 nm). This oval is seen to form at the beginning of the period. After several weeks it appears to be about the same size and shape as Jupiter's Great Red Spot. It continues to evolve by stretching in longitude and compressing in latitude. The contrast which produces this feature is probably caused by auroral-related gas-phase chemistry or/and by very small (radius smaller than ~ 0.1 micro-meter) particles. It is not seen in near-infrared images which are sensitive to larger aerosol particles. A movie superposing the UV images and the 890-nm methane images shows that the large oval sits on the boundary of the morphologically smooth polar stratospheric haze seen in the 890-nm methane filter. These data provide interesting clues to the nature of Jupiter's polar vortex and will help to motivate a quantitative dynamical/chemical/microphysical model. This work was performed by the Jet Propulsion Laboratory, California Institute of Technology.

**MC04/10P/B22-005 1530**

**THE SYSTEMATIC CALCULATION OF ADIABATIC STRUCTURE OF JOVIAN PLANET ATMOSPHERES**

Ko-ichiro SUGIYAMA, Masatsugu ODAKA, Kiyoshi KURAMOTO, Yoshi-Yuki HAYASHI (Division of Earth and Planetary Sciences, Hokkaido Univ.)

We investigate vertical profiles of adiabatic lapse rate, amount of condensed species, and static stability of the Jovian planet atmospheres by using a newly developed calculation method. Our method consists of three procedures as follows: (1) equilibrium composition is calculated by minimizing Gibbs free energy for various temperatures and pressures, (2) entropy is calculated for the equilibrium composition, and (3) adiabatic curve  $dS = 0$  is obtained by seeking the temperature and pressure relationship under which the value of entropy is conserved. In our method, it is not necessary to consider the details of corresponding chemical reactions. Therefore, one of the advantages of our method is that modification of numerical code is almost unnecessary when different elemental compositions and potential temperatures are given. In previous studies, the adiabatic profile of Jovian planet atmospheres has been obtained by direct calculation of entropy conservation for ascending air parcel according to given chemical reactions (Weidenschilling and Lewis, 1973, *Icarus*, 20, 465-476). We estimate dependency of vertical profiles of adiabatic lapse rate, amount of condensed species, and static stability on elemental composition for each Jovian planet atmosphere. In this series of calculations, the initial abundances of condensable species are taken from the solar abundance to several ten times the solar. The results of these calculations systematically reveal the effect of atmospheric composition on structure of atmosphere, which are useful for consideration not only of vertical distribution of cloud layers, but also of dynamics of cloud convection within the Jovian planet atmospheres.

**MC04/10P/B22-006 Invited 1615**

**NEW RESULTS ON TITAN FROM GROUND-BASED OBSERVATIONS**

Athena COUSTENIS<sup>1</sup>, Mathieu HIRTZIG<sup>1</sup>, Eric GENDRON<sup>1</sup>, Olivier LAFF<sup>1</sup>, Michel COMBES<sup>1</sup>, Emmanuel LELLOUCH<sup>1</sup>, Pascal RANNOU<sup>3</sup>, Pierre DROSSART<sup>1</sup> (<sup>1</sup>LESIA, Observatoire de Paris-Meudon, <sup>2</sup>CFHT, Hawaii, <sup>3</sup>Serv. Aéronomie, Univ. de Versailles, France)

I will present new insights on Titan's atmosphere and surface composition derived from recent observations using large telescopes (such as the CFHT or the VLT) both in spectroscopy (ISAAC) and imaging (PUEO, NAOS, OASIS). Our 2001 atmospheric images show some interesting phenomena: besides the well-known Titan "smile" observed at wavelengths between 1 and 1.3 micron, we find the situation to be currently changing, with a clear reversion of the asymmetry found in our Fell (1.64 micron) and Kcont (2.26 micron) filters, sounding higher atmospheric levels (in the stratosphere). We believe this is seasonal phenomenon, following the previously reported "loss of the smile" (Lorenz, 2001). This inversion is progressing and we are redefining its signature in our new images of 2002 at wavelengths of 2.16 (BrGamma), 1.64 (Fell), 2.06 (J2). Another atmospheric phenomenon, the limb brightening reported in our 1998 images - interpreted as a first detection of possible diurnal effects in Titan's atmosphere - something like a morning fog, observed after condensation processes have enhanced in condensates the atmospheric levels between 70 and 100 km (Coustenis et al., 2001) -, could not be firmly confirmed in our new data (although there is some indication for it) because the 2001 images were acquired in mediocre conditions (seeing of 0.5-1 arcsec). A third new feature is observed at wavelengths probing the atmosphere around 2 micron: a bright feature spanning about 2 by 4 pixels in latitude and longitude respectively (0.07x0.14 arcsec or roughly 9x18% of the projected disk) is seen attached to the Southern Pole of Titan and appears stable. This feature could be indicative of an atmospheric (cloud or more likely a vortex) phenomenon or a surface feature (polar cap?). After subtracting the atmosphere from the images sounding the CH4 windows, we recover information on the surface of Titan. We find the equatorial spot to be bright again in all the filters investigated from 1 to 2 micron and at the position expected with respect to the orbital phase. A preliminary study of the 2002 images already show pieces of evidence that the asymmetry inversion is still at work, furthermore at deeper altitudes than detected in 2001. Since we have observed at consequent nights around the GEE and the GWE, we expect to be able to trace the location (and the displacement) of the features observed and to check the bright zones found in the trailing hemisphere images of Titan (Combes et al., 1997). I shall also discuss recent findings in Titan's 5 micron spectrum. References: Combes et al (1997), Icarus 129, 482; Coustenis et al. (2001) Icarus 154, 501; Lorenz et al (2001), Geoph. Res. Letters 28, 4453; Lellouch et al. (2003), Icarus, in press.

**MC04/10P/B22-007 1645**

**MODELS OF COMET 19P/BORRELLY DURING THE DEEP SPACE 1 ENCOUNTER**

Daniel C. BOICE<sup>1</sup>, R. WEGMANN<sup>2</sup> (<sup>1</sup>Space Science Division, Southwest Research Institute, <sup>2</sup>Max-Planck-Institute für Astrophysik)

The Deep Space 1 Mission (DS1) successfully encountered comet 19P/Borrelly on 22 September 2001, returning a wealth of images and in situ plasma measurements. A coma model for 19P/Borrelly is presented that consistently represents the cometary environment from the nucleus surface to the solar wind interaction region. Neutral gas and plasma dynamics and spatial distributions of various cometary species are presented for interpreting in situ plasma measurements obtained during the encounter. The major findings can be summarized as follows: (1) Using estimates of the solar wind conditions and the gas production rate at the time of encounter, a bow shock is expected at a distance of about



60,000 to 80,000 km along DS1's trajectory, however, DS1 will not penetrate the contact surface. (2) At closest approach, the plasma speed steadily decreases to about 2 km/s, with an ion temperature of about 200,000 K and electron temperature of about 20,000 K (dominated by photoelectrons), and an ion number density of about 100/cm<sup>3</sup>. and (3) model abundances of water-related ions, O<sup>+</sup>, OH<sup>+</sup>, H<sub>2</sub>O<sup>+</sup>, and H<sub>3</sub>O<sup>+</sup>, are 1%, 7%, 82%, and 10% of the total water-related fraction, respectively, at the time of closest approach. An initial analysis of the DS1 measurements will be presented within the context of the model results.

**MC04/10P/B22-008 1700**

**PHYSICAL AND CHEMICAL PROCESSES IN COMETARY COMAE**

Daniel C. BOICE (Space Science Division, Southwest Research Institute)

The quantity and quality of high-resolution spectra and images of recent comets provide a unique opportunity to advance our knowledge of cometary parent molecules and thereby gain clues to understand the origin of the solar system. In order to successfully interpret the extensive observations in the UV, visible, IR, and microwave regions, the relevant physico-chemical processes must be identified to provide the framework within which comets can be understood and inferences about their composition can be made. Analyses of observations of recent comets (e.g., Kudo-Fujikawa, Borrelly, LINEAR WM1, Hale-Bopp, Hyakutake) have provided valuable insights into the intrinsic properties of their nuclei (e.g., composition, active surface fraction, surface properties, temperature) and the important physical and chemical processes that occur in their comae. The latest results are discussed detailing these processes, concentrating on the collision-dominated inner coma. i.e., thermodynamics (e.g., temperature and velocity structure), photo- and gas-phase chemistry (e.g., composition, gas and electron energetics), interactions between gaseous species and dust (composition in distributed sources, gas-grain reactions, mass-loading and energy balance of both gas phase and dust particles), role of electrons in the coma (e.g., inelastic collisions with primarily neutrals, distribution function and its moments for energy spectrum), optical depth effects and issues related to radiative transfer within the coma, and other topics (e.g., water clusters, near-nucleus boundary layer, transition to free molecular flow). Special consideration is given to the determination of "parent" species from the plethora of molecules and atoms seen in cometary comae, concentrating on observations of S<sub>2</sub>, CH, CN, CS, C<sub>2</sub>, C<sub>3</sub>, NS, and HCN/HNC, to gain clues for understanding the origins of the solar system and possibly life.

**MC04/10P/B22-009 Invited 1715**

**THE EFFECTS OF ION-DRAG ON GRAVITY WAVE HEATING AND COOLING IN JUPITER'S THERMOSPHERE**

Michael P. HICKEY<sup>1</sup>, Gerald SCHUBERT<sup>2</sup>, Richard L. WALTERSCHEID<sup>3</sup> (<sup>1</sup>Department of Physical Sciences, Embry-Riddle Aeronautical University, <sup>2</sup>Department of Earth and Space Sciences, Institute of Geophysics and Planetary Physics, University of California, Los Angeles, CA 90095-1567, USA, <sup>3</sup>Space Science Applications Laboratory, The Aerospace Corporation, Los Angeles, CA 90009, USA)

We use a full-wave numerical model to study the propagation and dissipation of two gravity waves in Jupiter's thermosphere. The present treatment differs from our previous study of these two waves by the addition of ion-neutral collisions (ion-drag dissipation) in the model. A Chapman profile is used to model the electron density profile with parameters adjusted to provide a fit to observations. We determine that one of the modeled waves is not significantly affected by the inclusion of ion-neutral collisions because it is viscously damped at low altitudes where electron and ion densities are small. At higher altitudes where significant ion densities occur this wave has a small amplitude. The inclusion of ion-neutral collisions is found to have a significant effect on the dissipation of the second gravity wave (wave 2) because it is viscously damped in the same region where maximum electron and ion densities occur. The Joule dissipation of the currents driven by this gravity wave provides a heating that, in addition to the viscous heating, dominates over the cooling associated with the divergence of the sensible heat flux and leads to a net heating of the thermosphere. We now find that with the inclusion of ion-drag dissipation the contribution of gravity waves like wave 2 can make a significant contribution to the heating required to explain the high thermospheric temperatures.

**MC04/10P/B22-010 1745**

**LEADING ATMOSPHERES EVOLUTION**

Therese SCHNECK (Ph.D.1977)

The synchronous rotation of the Moon around the Earth is caused by an unsymmetrical distribution of mass in the Moon. Interaction on the Moon slows the Earth rotation about two milliseconds per century. The dust obscuration, the plasma that filled the early universe during its first years was opaque to electromagnetic radiation. The solar system rotates every two hundred forty million years in the Milky Way at one thousand two hundred kilometers per second relative to the Microwave Background Radiation(1). Actually, atomic clocks on board GPS satellites are stable within one second in thirty two thousand kilometers at speed of light as the effect of the Earth's passage on plasma(2). Since the Cretaceous-Tertiary boundary sixty five million years ago, the error on the position of the Earth in space around the sun is more than one earth diameter. Mars had a magnetosphere at the Noachian between 4.4 and 3.8 billion years ago, related to oceans and high carbon dioxide content. A titanium rich-layer was produced by crystallisation of a huge ocean of magma that surrounded the Moon when it formed(3). Oceans, atmospheres and continents where in place by 4.3 billion years on Earth. Meteorites accumulated during early Ordovician at a rate two orders of magnitude higher than today. The carbonate chondrite Tagish Lake meteorite reflect infrared light better than visible light(4). The study of the evolution of the partial pressure of atmospheric oxygen over phanerozoic time supports the hypothesis of high atmospheric content during the Carboniferous. The fluctuations in primary fluid inclusions in marine halites are in phase with oscillations in sea floor spreading rates, volcanism and global sea level. Location of strewnfields associated with tektites crossing the atmosphere and major asteroid impact is aeolian and arid related to sunspots cycle(5) or to interactions between the atmosphere and deep ocean circulation. Maunder minimum refers to a period of particularly low number of sunspots at little ice age from 1645 to 1745. Lidar observations revealed that metals are deposited by meteor ablation at height of one hundred kilometers in Earth atmosphere. The upper stratospheric maximum temperatures increase with ozone depletion. Ionospheric parameters change in sixnight hours when a solar flare triggers a geomagnetic storm(6). The cyclone average of 1.5 per year was exceeded in 1995 for the first time since 1964 and reached 3.8 between 1995 and 2000(7). Laser cooled clock Parcs(8) are going to be installed on the ISS, where gravity is weaker than at Earth's surface, in late 2005 and would keep time within one second every 300 million years, apparently nearer to the accretion time of matter. The Earth's atmosphere dynamic filters out natural hazards as meteorites and cyclones below critical conditions. Earth climate and atmosphere seems more at the new clocks atomic times. GPS are operational since fifty years in a pre-evolving Milky Way. Ref:(1)Penzias and Wilson. (2)On the Electrodynamics of moving bodies. (3)J.Van Oman and T.L.Grove. (4)T.Hiroi. (5)Utah Water Laboratory. (6)Arecibo Observatory. (7)USGS. (8)NASA.

**MC04/11A/B22-001 Invited 0830**

**PRESENT STATUS OF JAPANESE VENUS ORBITER**

Masato NAKAMURA, Takeshi IMAMURA, Takumi ABE, Nobuaki ISHII, Hiroshi YAMAKAWA, Ichiro NAKATANI, Koichiro OYAMA (Institute of Space and Astronautical Sciences)

We have proposed a Venus orbiter which will arrive at Venus in 2009 to the Institute of Space and Astronautical Sciences (ISAS). This mission is now go and we will start the internal Phase B study at ISAS in the fiscal year of 2003. The main purpose of this mission is to reveal the details of the atmospheric motion on Venus and approach the dynamics of the Venusian climate. The angular position of the spacecraft on its orbit (300km x 13Rv with 172 degrees inclination and 30 hours orbital period) is synchronized for 20 hours at its apoapsis with the global atmospheric circulation at the altitude of 50km, thus the snap shots taken every 2 hours will be the images of the same side of the atmosphere. We have 4 cameras to take such snap shots of the planets in different wave lengths. In addition to these 4 cameras, we have a Lightning and Airglow camera (LAC) in visible range. This will be operated when the orbiter is close to the planet. Several other instruments to measure the plasma environment are seriously considered. They are 1)extreme ultraviolet imager, 2)nonthermal ion mass/spectrum analyzer and electron spectrum analyzer, 3)thermal plasma analyzer, 4)plasma wave analyzer and sounder, and 5)magnetometer We expect that the orbiter will survive after the next solar maximum in 2011 and the comparison of plasma environments around Venus before and after the solar maximum should be quite exciting.

**MC04/11A/B22-002 0900**

**METEOROLOGICAL OBSERVATION BY JAPANESE VENUS ORBITER**

Takeshi IMAMURA, Masato NAKAMURA, Venus Exploration Working Group (Institute of Space and Astronautical Science, Japan)

The PLANET-C Venus orbiter will be launched in 2008 by the Institute of Space and Astronautical Science, Japan, to explore the Venus atmosphere, with emphasis on the study of the general circulation. Atmospheric circulation is one of the key issues in the study of the Venus climate, and moreover, understanding the Venusian wind system which differs largely from the terrestrial one is a long-lasting issue in planetary meteorology. Although the rotation of Venus is slow with the period of 243 days, the stratosphere near the cloud top circles around the planet with the period of 4.7 days. The mechanism of this wind system, called the super-rotation, is unknown. The delay of the Venusian meteorological research is attributed to the lack of meteorological data within and below the clouds. The Venus mission will bring about a breakthrough by utilizing the near-infrared windows (1.0, 1.7, 2.3, 2.4 micron) at which we can view the sub-cloud atmosphere from space. Successive high-resolution global images of the atmosphere and clouds at such near-infrared wavelengths will enable us to trace atmospheric motions at several discrete altitude levels. Cloud images at long-infrared (10 micron) and ultraviolet (280, 350 nm) wavelengths are also used for this purpose. Radio occultation will yield vertical temperature profiles which are complementary to the optical observations. The detection of lightning discharges by a high-speed detector will give clues to the convective activity in the cloud layer. With these comprehensive meteorological data, we will construct a three-dimensional view of the atmospheric dynamics and investigate the outstanding issues, such as the mechanism of super-rotation, the structure of meridional circulation, meso-scale meteorology, and cloud physics.

**MC04/11A/B22-003 0915**

**VENUSIAN EQUATORIAL KELVIN WAVE IN MERIDIONAL CIRCULATION**

Takeshi IMAMURA (Institute of Space and Astronautical Science, Japan)

The influence of the Hadley-like meridional circulation on the Venusian Kelvin wave, which propagates in the super-rotating stratosphere, is investigated, using an equatorial beta-plane primitive equation model. The Kelvin wave has been observed in ultraviolet cloud images as a planetary-scale albedo feature. The meridional circulation has also been observed in cloud images: clouds drift poleward at a speed of 1-10 m/s in the mid-latitude in both hemispheres. Such a fast meridional circulation should influence the Kelvin wave, since the wave has a deformation radius of 2000 km and extends to the mid-latitude. The model result shows that the wave is modified to have a non-zero meridional wind disturbance, which is absent when the background atmosphere is at rest. The combination of the meridional and zonal winds induces a meridional flux of zonal momentum in the upstream direction of the background north-south flow. In the upper branch of the Hadley circulation, the wave transports zonal momentum equatorward. The theoretical background is reported in another session (MC05 Middle Atmosphere Science). The predicted momentum redistribution should contribute to the maintenance of the super-rotation, since a direct cell transports angular momentum upward whenever equatorial regions of the atmosphere have an angular momentum surplus relative to high-latitude regions. It is also suggested that the deformation of the Kelvin wave in the meridional circulation may explain the shape of the albedo feature which is called the "dark horizontal Y".

**MC04/11A/B22-004 0930**

**CHALLENGE TO DETECT VENUS LIGHTNING BY LAC ONBOARD PLANET-C**

Yukihiro TAKAHASHI<sup>1</sup>, Jun YOSHIDA<sup>1</sup>, Masaki TSUTSUMI<sup>2</sup>, Tomoo USHIO<sup>3</sup> (<sup>1</sup>Department of Geophysics, Tohoku University, <sup>2</sup>Arctic Environment Research Center, National Institute of Polar Research, <sup>3</sup>Department of Aerospace Engineering, Osaka Prefecture University)

Whether lightning is occurring in Venus or not is still under controversy, although extensive studies have been made using data obtained by optical and wave instruments onboard spacecrafts and from ground for almost 20 years. In order to conclude the discussion, we plan to install a lightning and airglow camera (LAC) at the Venus orbiter, PLANET-C, which will be arrived in 2009. Lightning discharge is a phenomenon that reflects the dynamics and material characteristics in the planetary atmosphere. Charge separation in the thundercloud is considered to be caused mainly by frictions between ice crystal and hail, which are closely related to atmospheric motion especially for vertical convection. Therefore, the lightning activity is an excellent quantitative indicator for the activity of atmospheric convection. In the Earth it is pointed out that the lightning activity is very sensitive to the global atmospheric temperature and H<sub>2</sub>O density at high altitude, one of the significant molecules causing the green house effect. It can be inferred that also in Venus the lightning are generated mainly by the vertical convection and the global observation of lightning is a good method to get information on the atmospheric activities and characteristics of cloud particle in the planet with a good time resolution. The lightning in Venus may be similar to sprites or elves observed in the Earth's middle and upper atmosphere. Since the distance between the cloud deck and the ground in Venus is considerably large (about 45 km) and the atmospheric pressure is quite high, the discharge from cloud top to the ionosphere may be more likely

than cloud to ground discharge. Development of LAC is now under design of a proto model (PM). A multi-channel photo-multiplier tube or an avalanche photodiode (APD) with 8 by 8 matrix pixels is adopted as a detector of LAC, which enables us to detect lightning flash at high time resolution of 20 microsecond. The sensitivity shall be determined in order to sense lightning flashes with an optical intensity of 1/100 of average in the earth's lightning. The data will be stored with time interval of 0.1 second for each flash event using pre-triggering data acquisition. Wavelength of OI 777 nm is chosen for the lightning detection based on the laboratory experiment. To reduce the stray lights from the sun and scattered sunlight in Venus dayside, Optical unit is placed on the surface of spacecraft body and an isolated vane unit will be used. To cross-check the existence of Venus lightning, simultaneous wave measurements are planned in a frequency range from DC to several MHz. Especially, the recording of waveform around 100 Hz, being triggered by optical emissions, might be essential.

**MC04/11A/B22-005 0945**

**POWER SPECTRUM ANALYSIS OF VENUSIAN CLOUD IMAGES**

Manabu SHIMOYAMA, Takeshi IMAMURA (The Institute of Space and Astronautical Science, Japan)

A Venus exploration project (Planet-C) is in progress for the purpose of elucidating the Venusian meteorology. In this project, the distribution of clouds and minor gases at different heights are continuously measured by using several cameras which differ from each other in observation wavelength. As a preparation, we have analyzed the cloud images of Venus which were taken by previous missions in order to examine methods for analysis and demands for observations. The cloud images used are the ones taken by the SSI onboard GALILEO at the time of Venus flyby. Observation wavelengths are violet and near-infrared. According to the past examinations, it is thought that the pattern of violet images indicates the distribution of the violet absorption matter, which exist at cloud top height, and near-infrared images reflect the structure of lower cloud at the height of about 50 km. In the beginning we have calculated spatial power spectra for equatorial and mid-latitude regions of those images to investigate the dependence of turbulent structure on latitude and height. Although this kind of analyses has been carried out for the data sets obtained by Pioneer Venus and Mariner, it has not been done for the data sets of Galileo. Moreover the data obtained by Galileo has higher spatial resolution and therefore covers smaller spatial scale which we have never seen. The results are as follows. 1) The power of violet images for equatorial region is bigger than that for mid-latitude region regardless of spatial scale, whereas that of near-infrared images have no dependence on latitude. 2) The slope of the power spectra for near-infrared images is smaller than that of violet images. These results indicate that the production and loss processes of turbulence and the mechanism which connect various scale phenomena vary with height. In this report, the slopes of the power spectra are also compared with the case of the Earth.

**MC04/11A/B22-006 1000**

**SUPERROTATION IN A VENUS-LIKE AGCM**

Masaru YAMAMOTO\*, Masaaki TAKAHASHI\* (\*Faculty of Education, Wakayama University, \*Center for Climate System Research, University of Tokyo)

A maintenance mechanism of Venusian superrotation is investigated by using a CCSR/NIES Venus-like atmospheric general circulation model. For a T10L50 experiment, a zonally uniform solar heating is used. The superrotation with velocities faster than 100 m/s is formed near 60 km altitude and a maximum of total angular momentum density is located at 21 km. The strong poleward flow over 10 m/s is seen above the cloud top (> 70 km) where the zonal flow steeply decreases with height. The upward flow of about 1 cm/s at the equator and the downward flow at the poles are seen near the cloud top (65-70 km). The vertical flow is formed continuously in the height range from the surface to the middle atmosphere. The meridional circulation of a single cell is predominant in the model atmosphere and effectively pumps up angular momentum from the lower to the middle atmosphere. The angular momentum is transported poleward by the meridional circulation, and a part of the transported momentum is returned back to low-latitude regions by vortical and divergent flows of various waves. Rossby, mixed Rossby-gravity, and gravity waves transport the angular momentum equatorward. Vertically propagating gravity waves predominantly transport the angular momentum downward. The zonal-flow deceleration by the gravity waves enhances the meridional circulation above the cloud top. The results support the Gierasch mechanism (Gierasch 1975; Matsuda 1980; 1982), as was simulated in previous Venus-like AGCMs (e.g., Del Genio and Zhou 1996). Although barotropic waves are emphasized in the previous AGCM studies supporting the Gierasch-Rossow-Williams scenario (Gierasch 1975; Rossow and Williams 1979), various waves play important roles in formation and maintenance of the superrotation in the present study. Large horizontal eddy diffusion required in the Gierasch mechanism corresponds to the equatorward momentum flux caused by not only barotropic waves but also other various waves. The eddy downward angular momentum flux, which corresponds to the small vertical eddy diffusion in the Gierasch mechanism, is caused by vertically propagating gravity waves. The dynamical process simulated by our Venus-like AGCM is one of possible mechanisms of Venusian superrotation. For a T21L50 experiment, fast equatorial waves of  $c > U$  ( $c$ : phase velocity,  $U$ : longitudinally averaged zonal flow) also contribute to upward eddy transport of angular momentum. Since the upward vertical momentum fluxes by the fast equatorial waves of  $c > U$  cancel the downward fluxes by vertically propagating gravity waves of  $c < U$  in low latitudes, the downward angular momentum transport by waves is ineffective in the equatorial region. Thus the cloud-top superrotation is enhanced in the T21 model.

**MC04/11A/B22-007 Invited 1045**

**THE MYSTERIOUS ATMOSPHERE OF VENUS, AND THE EUROPEAN EXPRESS MISSION**

Fred W. TAYLOR (Oxford University)

In November 2002, the European Space Agency approved a new mission to the planet Venus that will launch in November 2005. The spacecraft is a polar orbiter, which uses a slightly modified version of the bus developed for the Mars Express mission, which launches in May 2003. The scientific payload includes sophisticated infrared spectroscopic and imaging instruments that can operate in the near-ir 'windows' and sound the atmosphere down to the surface. This paper will describe the scientific objectives of the project, which include the investigation of the composition, chemistry, cloud structure and dynamics of Venus' atmosphere. Specific questions posed by our current knowledge and limited understanding of the Venus environment will be described, and the key measurements to help resolve them discussed.

**MC04/11A/B22-008 1100**

**THE INCEPTION OF THE OCEANS AND THE MISSING CO2 ATMOSPHERE OF THE EARTH**

Lin-gun LIU (Institute of Earth Sciences, Academia Sinica)

The oceans started to grow when the surface temperature of the Earth cooled to below about 450 oC, if the terrestrial planets were covered by 'magma ocean' after accretion. As envisaged and supported by earlier studies, a CO2-dominated atmosphere probably existed in the early history of the Earth. Carbon dioxide was removed away from the air mainly by dissolving into water during condensation (or the growing ocean), and then forming carbonate rocks in early geological history. The role of the green organisms in removing CO2 from the air is probably minor, though all sedimentary rocks contain a very large amount of reduced carbon of biogenic origin. A large-scale hydrosphere probably never existed on Venus, and not for long on Mars. Thus, the atmospheres of these latter planets are composed mainly of carbon dioxide.

**MC04/11A/B22-009 1115**

**STABILITY OF MEAN ZONAL FLOW IN CYCLOSTROPHIC BALANCE**

Masahiro TAKAGI, Yoshihisa MATSUDA (Department of Earth and Planetary Science, University of Tokyo)

In the mean zonal flow in cyclostrophic balance (e.g. the superrotating zonal flow in the Venus atmosphere), there is a possibility that the baroclinic instability arises (Matsuda, 1984; Young et al., 1984). Since the cyclostrophic balance with the hydrostatic approximation is equivalent to the balance between the buoyancy due to the meridional temperature difference and the centrifugal force due to the mean zonal flow with vertical shear, there exists available potential energy, which may be converted to kinetic energy of disturbances. Young et al. (1984) shows that the so-called baroclinic instability occurs at the cloud level in the Venus atmosphere. It should be noted, however, that the disturbance generated in the cyclostrophic flow is not necessarily similar to the baroclinic wave in the terrestrial atmosphere, because the local Coriolis parameter (Coriolis parameter defined in the coordinate rotating with the mean zonal flow at a certain altitude) is highly dependent on the altitude. To investigate stability of the mean zonal flow in cyclostrophic balance in the wider parameter range than those of the previous studies, 2D and 3D models are developed. In the result of the 2D model, it is found that the unstable modes are similar to those of the usual baroclinic instability when the Rossby number (Ro) is small. When Ro is large and the vertical shear (the centrifugal force) is small, the baroclinic wave cannot spread over the whole vertical region, and separates into two modes propagating in the east and west directions to the mean flow at the mid-altitude. When the vertical shear is large, the unstable mode similar to the usual baroclinic instability appears again even if Ro is large. Applying the 3D model on the sphere to the middle Venus atmosphere including the cloud layer, the result of Young et al. (1984) can be confirmed. In the case of the lower Venus atmosphere (from the ground to 40 km), the unstable mode whose phase velocity is in the direction of the mean flow appears. This mode has the amplitude in the lower latitudes, and may have some role in the vertical transport of zonal momentum (Yamamoto and Tanaka, 1997).

**MC04/11A/B22-010 Invited 1130**

**SUBMM DETECTABILITY OF MOLECULAR SPECIES IN PLANETARY ATMOSPHERES WITH GREAT AND HIFI**

Paul HARTOGH, Christopher JARCHOW (Max-Planck-Institut fuer Aeronomie)

In the near future two new instruments will help to improve our knowledge about the structure and composition of planetary atmospheres. The German REceiver for Astronomy at THz frequencies (GREAT, from 2004) on the Stratospheric Observatory For Infrared Astronomy (SOFIA) and the Heterodyne Instrument for the Far Infrared (HIFI, from 2007) on the Herschel Space Observatory will sound planetary atmospheres in ranges of the sub-millimeter-wave spectrum not accessible from ground. Since the sensitivity of these instruments is very high, a large number of new species may be detected during so-called deep line surveys. In case of good signal-to-noise ratios, altitude profiles of the detected molecules can be retrieved using the information of the pressure broadening and the optical thickness of the lines. Among others the vertical profiles of water vapor and its isotopes in the lower and middle atmosphere of Mars and the upper atmosphere of the giant planets are of great interest. In this talk we will present simulations of molecular spectra as they may be detected by GREAT and HIFI, taking into account the absorption of the Earth middle and upper atmosphere (GREAT only), nadir and limb emissions and absorptions of the planets, the instrument specific parameters including telescope size, sensitivity of the heterodyne receivers, efficiency of the observations modes, calibration and finally the frequency resolution of the spectrometers. We define a detection of a line, if the line amplitude is larger than 3 times the measurement noise (RMS). This detection can provide information about the column density of the species. In case the lines are much stronger they may contain information about the vertical distribution of the molecule in the planetary atmosphere. We will present a number of inversion calculations of our radiative transfer model. These retrievals will show which altitude resolution of a vertical profile can be expected as a function of the signal-to-noise-ratio of the simulated lines.

**MC04/11A/B22-011 Invited 1200**

**APPLICATION OF NONLINEAR OPTIMAL PERTURBATION TO THE STUDY OF THE INSTABILITY AND ASSOCIATED PREDICTABILITY OF PLANETARY ATMOSPHERIC MOTIONS**

Mu MU, Zhiyue ZHANG (LASG, Institute of Atmospheric Physics, Chinese Academy of Sciences)

Instability problems and associated predictability problems are central ones in the study and numerical prediction of planetary atmospheric motions. Linear singular vector (LSV) and linear singular value (LSVA) has been adopted to study these problems for the atmosphere of the earth. In this approach it is assumed that the initial perturbation is small enough such that its evolution can be governed by the tangent linear equations of the original nonlinear equations. This essential assumption limits the applicability of the method to study the effects of nonlinearity on the instability and predictability of atmospheric motions. Mu (2000), Mu et al (2001), Mu et al (2002) proposed new concepts of nonlinear singular vector (NSV) and conditional nonlinear optimal perturbation (CNOP), which are the natural generalizations to LSV. Results of both theoretical and numerical analysis demonstrated the nonlinear effects can be better treated by NSV and CNOP. In this study, we first apply LSV, NSV and CNOP to the study of stability and instability of barotropic motions of Jupiter's atmosphere. Particular attention is paid to the stability of Great Red Spot. Then the associated predictability is investigated by LSV, NSV and CNOP too. The importance of using nonlinear approach rather than linear ones is clearly demonstrated. The results also show that NSV and CNOP are useful tools to the investigation of instability and related predictability of planetary atmospheric motions.



**MC04/11P/B22-001** Invited **1400**

**TEN YEARS OF THE 'EUROMARS' CLIMATE MODEL**

Peter Leonard READ<sup>1</sup>, Stephen LEWIS<sup>1</sup>, Claire NEWMAN<sup>1</sup>, Luca MONTABONE<sup>1</sup>, Henning BÖTTGER<sup>1</sup>, Francois FORGET<sup>2</sup>, Frédéric HOURDIN<sup>3</sup>, Monika ANGELATS I COLL<sup>4</sup>, Miguel LOPEZ-VALVERDE<sup>5</sup>, Jean-Paul HUOT<sup>6</sup>, Marie-Christine DESJEAN<sup>7</sup> (Department of Physics, University of Oxford, <sup>1</sup>LMD-CNRS, Paris, <sup>2</sup>Instituto de Astrofísica de Andalucía, Spain, <sup>3</sup>ESA-ESTEC, CNES)

2003 marks the tenth anniversary of a collaboration between Oxford University and Laboratoire de Météorologie Dynamique du CNRS in Paris, whose objective has been to develop a comprehensive and detailed numerical circulation model for the atmosphere of Mars. Despite an inauspicious start, following the loss of the Mars Observer spacecraft in 1993, and thanks to consistent support from PPARC in the UK and CNRS in France (and more recently from ESA and CNES), this project has gone from strength to strength, culminating in the present suite of models which are capable of capturing many aspects of the observed meteorology and climate of Mars in considerable detail. In the present talk, we will review the current status of development of the 'Euromars' model, now involving an additional collaboration with the Instituto de Astrofísica de Andalucía in Spain. In the present configuration, Oxford and LMD run their own dynamical solvers (pseudo-spectral and finite-difference in the horizontal, respectively), whilst sharing a common library of physical parametrizations of all of the main physical processes which cannot be resolved by the model grids. These are now of comparable sophistication to those in use for long-term climate modelling studies of the Earth, and results generally compare very well with the increasingly extensive range of observations becoming available from missions such as NASA's Mars Pathfinder lander, Mars Global Surveyor (MGS) etc. Recent developments include a reasonably full representation of the transport cycles of dust and water in the Martian climate system, including an emerging ability to simulate the autonomous and spontaneous initiation of regional dust storms at appropriate phases of the seasonal cycle. Some examples of recent achievements will be presented, and compared with available observations. In new developments, the LMD version of the model is being extended into the thermosphere. In the latest efforts, a full meteorological data assimilation scheme has been implemented and interfaced with the Oxford version of the Euromars GCM. Results indicate that Mars's atmosphere is highly amenable to assimilated analyses of synoptic mapping observations e.g. from the TES instrument on MGS. To date, a first pass of the entire MGS/TES dataset has been completed, allowing the recovery of a detailed synoptic, day by day determination of the fully three-dimensional state of the Martian atmosphere for nearly two Mars years. The talk will conclude with an overview of this dataset, some highlights from the MGS mapping period, and an outlook for the future.

**MC04/11P/B22-002** **1430**

**A NUMERICAL STUDY OF VERTICAL EDDY MIXING DUE TO GRAVITY WAVES GENERATED BY THERMAL CONVECTION IN THE MARTIAN ATMOSPHERE**

Masatsugu ODAKA<sup>1</sup>, Kiyoshi KURAMOTO<sup>1</sup>, Kensuke NAKAJIMA<sup>2</sup>, Yoshi-Yuki HAYASHI<sup>1</sup> (<sup>1</sup>Division of Earth and Planetary Sciences, Graduate School of Science, Hokkaido University, <sup>2</sup>Department of Earth and Planetary Sciences, Faculty of Sciences, Kyushu University)

CO<sub>2</sub>, the major constituent of the Martian atmosphere, is dissociated into CO and O by ultraviolet radiation in the Martian middle atmosphere. However, the observed concentrations of CO and O in the Martian middle atmosphere are much smaller than those predicted by simple photochemical equilibrium. In a one-dimensional photochemical model, the observed concentrations are explained by the contribution of vertical mixing process (McElroy and Donahue, 1972); the HO<sub>2</sub> catalytic chemical reaction which promotes recombination of CO and O is enhanced by the vertical eddy transport of its source, H<sub>2</sub>O, from the lower to the upper atmosphere. The intense eddy diffusion coefficient assumed in the one-dimensional photochemical model may be explained by a strong mixing due to wavebreaking. One of the candidates for the waves is the vertically traveling internal gravity waves generated by the thermal convection in the lower atmosphere. In order to estimate the efficiency of possible mixing due to gravity wave breaking, we have performed a direct numerical simulation of generation, vertical propagation and breaking of internal gravity waves caused by the thermal convection under dust-free condition. The numerical model utilized is the two-dimensional anelastic model developed by Odaka et al. (2001). The computational domain extends to 51.2 km horizontally and 50 km vertically. The horizontal boundary condition is cyclic. Both horizontal and vertical grid intervals are 200 m except for the lowermost 200 m layer where the vertical resolution is enhanced. The solar flux at the top of the model atmosphere changes diurnally with the condition of Ls = 100 at 20N. The initial condition is a motionless atmosphere with horizontally uniform temperature. The numerical integration is started at LT = 6:00, and is performed for 24 hours. The numerical results show that the horizontal and vertical wavelengths of the internal gravity waves in the stratosphere are from 15 to 20 km and about 10 km, respectively. The temperature deviation associated with the waves is about 10 K around 40 km height. The effective vertical diffusion coefficient, K<sub>e</sub>, can be diagnosed as the vertical heat flux associated with the wave motion divided by the vertical gradient of the horizontal mean potential temperature. The horizontal mean values of K<sub>e</sub> above 25 km height have the same order of magnitude as that used by the one-dimensional photochemical model of Nair et al. (1994). This suggests that the internal gravity waves generated by thermal convection in the Martian lower atmosphere contribute greatly to the vertical mixing in the Martian middle atmosphere.

**MC04/11P/B22-003** **1445**

**DEVELOPMENT OF A GENERAL CIRCULATION MODEL FOR THE EARTH TYPE PLANETARY ATMOSPHERES: THE GFD DENNOU CLUB ATMOSPHERIC GENERAL CIRCULATION MODEL VERSION 6**

Masatsugu ODAKA<sup>1</sup>, Masaki ISHIWATARU<sup>1</sup>, Shin-ichi TAKEHIRO<sup>2</sup>, Keiichi ISHIOKA<sup>3</sup>, Eizi TOYODA<sup>4</sup>, Yoshi-Yuki HAYASHI<sup>1</sup> (<sup>1</sup>Division of Earth and Planetary Sciences, Graduate School of Science, Hokkaido University, <sup>2</sup>Graduate School of Environmental Earth Science, Hokkaido University, <sup>3</sup>Department of Earth and Planetary Sciences, Faculty of Sciences, Kyushu University, <sup>4</sup>Graduate School of Mathematical Sciences, University of Tokyo, <sup>5</sup>Japan Meteorological Agency)

The GFD Dennou Club Atmospheric General Circulation Model version 6 (AGCM6) is now being designed and developed as a tool that helps us to construct an understanding of dynamics and perform a comparative study of the planetary atmospheres. The major target of AGCM6 is to develop a software structure which enables us to change the model geometry and to build in or remove physical and/or dynamical processes with ease. This means that AGCM6 will be actually a series of virtual models which cover the dynamical hierarchy from a simple geophysical fluid dynamical model to a full GCM and also cover the planetary parameters ranging from Venus, Earth to Mars. Also aimed are 1) to incorporate anetwork transparent and self-descriptive data structure, and 2) to keep portability which guarantees execution on various types of computers. In these days, GCMs of the Martian and Venus

atmospheres have been developed by various groups to simulate, to a certain extent, the characteristic features observed in each atmosphere, respectively. However, from the viewpoint of understanding the simulation results and making a comparative study of the planetary atmospheres, current GCMs, to say nothing about GCMs of the terrestrial atmosphere, are becoming too complicated and/or specialized in each planet. Now, we have developed a spectral primitive equation model which is a prototype model of AGCM6 dynamical core. The source code is written by Fortran 90 and follows the Japan Meteorological Agency Fortran 90 coding rule (Muroi et al., 2002). For spectral transformation in the model, we use ISPACK library (Ishioaka, 2002) and SPMODEL library (Takehiro et al., 2002). ISPACK is a toolkit library for developing spectral numerical model, and SPMODEL enables us to improve readability of the source code. We are proceeding to develop the AGCM6 dynamical core which is incorporated with the network transparent and self-descriptive datastructure. The data format follows the gtool4 netCDF convention (Toyoda et al. 2000), and gtool4 Fortran 90 library (Toyoda et al. 2002) is used for constructing data input/output subroutines. We are performing Held-Suarez test with AGCM6 dynamical core and considering a suitable program structure which makes it easy to apply for the planetary atmospheres and to generate reduced system models. References AGCM6: <http://www.gfd-dennou.org/arch/agcm6/>, GFD Dennou Club. Ishioaka 2002: <http://www.gfd-dennou.org/arch/ispack/>, GFD Dennou Club. Muroi et al. 2002: Tenki 49, 91-95 (in Japanese). Takehiro et al. 2002: <http://www.gfd-dennou.org/arch/spmodel/>, GFD Dennou Club. Toyoda et al. 2000: <http://www.gfd-dennou.org/arch/gtool4/>, GFD Dennou Club. Toyoda et al. 2002: <http://www.gfd-dennou.org/arch/gtool4/>, GFD Dennou Club.

**MC04/11P/B22-004** **1500**

**MERIDIONAL CIRCULATIONS IN THE PLANETARY ATMOSPHERES**

Manabu D. YAMANAKA (Graduate School of Science and Technology, Kobe University, Japan / Frontier Observational Research System for Global Change, Japan)

Meridional circulations in the planetary atmospheres are overviewed theoretically. In the steady axis-symmetric linear problem, the meridional flow is given by the external forcing (including effects of nonlinear terms) which is approximated by a Rayleigh-friction-like term proportional to the zonal flow. The vertical flow is given by the external (diabatic) heating/cooling which is approximated by a Newtonian-cooling-like term proportional to the temperature anomaly from a radiatively-equilibrated temperature field. Substitutions of these formulas into the (two-dimensional) continuity equation in the meridional plane give a first-order differential equation in terms of the zonal flow and the temperature anomaly. This equation and the so-called thermal-wind relationship are essentially equivalent to the Cauchy-Riemann equations for the analytical functions. Using this set of equations, the meridional circulations and their balanced zonal-flow and temperature fields are discussed generally. Comparisons with the actual atmospheres in Venus, Earth, Mars and Jupiter and expectations for planets outside our solar system are also discussed.

**MC04/11P/B22-005** Invited **1515**

**SOME REMARKS ON THE THEORY OF MULTIPLE EQUILIBRIA IN THE ATMOSPHERE**

Jianping LI<sup>1</sup>, Shouhong WANG<sup>2</sup> (<sup>1</sup>National Key Laboratory of Numerical Modelling for Atmospheric Sciences and Geophysical Fluid Dynamics (LASG), Institute of Atmospheric Physics, Chinese Academy of Sciences, <sup>2</sup>Department of Mathematics, Indiana University, Bloomington, IN 47405, USA)

The phenomenon of multiple flow equilibria in the atmosphere is a basic characteristic of the atmospheric circulation. However, the necessary conditions of multiple equilibria in the atmosphere are an important and still unsolved problem. Theoretically, this problem is equivalent to find the conditions of multi-solution existed in stationary equations of the atmosphere. Based on the full primitive equations of stationary atmospheric motion the problem is discussed in this paper. Through studying three simplified equations of the atmospheric stationary equations, the linearized equations, adiabatic dissipative equations and forced non-dissipative equations, we prove that for the stationary equations of the atmosphere their stationary solution is either unique or non-existent in the absence of any one of nonlinearity, dissipation and external forcing. Therefore, the joint action of nonlinearity, dissipation and external forcing is the source of multiple equilibria in the atmosphere.

**MC04/11P/B22-006** **1615**

**HYDRODYNAMIC WAVES IN THE MARTIAN TOPSIDE IONOSPHERE: THEORY, SIMULATION AND EVIDENCE**

Jing-Song WANG<sup>1</sup>, Erling NIELSEN<sup>2</sup> (<sup>1</sup>Department of Geophysics, Peking University, <sup>2</sup>Max-Planck Institut fuer Aeronomie)

The dispersion relation for hydrodynamic waves in an ionosphere with almost a weak magnetic field shows, that acoustic-gravity wave (AGW) as well as hydrodynamic hybrid waves may be excited in the topside ionosphere of Mars and Venus owing to fluctuations in the solar wind pressure. The hybrid waves result from coupling between two different hydrodynamic wave modes. One of these modes is the AGW mode, and the other is excited independent of gravity, but depends on the presence of horizontal gradients in the background plasma pressure and density. The latter mode propagates horizontally but can also propagate vertically if there is a vertical gradient in the horizontal velocity. This new mode is therefore called Background Gradient Wave (=BGW). The hybrid waves will cause fluctuations with a wavelength of tens of kilometers in the vertical plasma altitude profiles when they propagate vertically. The period of the waves will be of the order of 10<sup>3</sup> s. Further properties of possible AGW-BGW waves in Mars and Venus ionospheres are given. A one-dimensional simulation of the amplitude and phase of these waves reveals that disturbances induced in the topside ionosphere can penetrate the ionosphere downward and excite waves propagating vertically in the ionosphere. Although the characteristics of the waves depend on the strength of the initial disturbance, some critical parameters of the waves do not depend significantly on the excitation force and are also found to be quite independent of solar zenith angle. The frequency of the excited waves is about 10<sup>3</sup>~10<sup>4</sup> Hz and the vertical wavelength of about 60 km is prevailing. Both agree well with and provide numerical support to the theoretical predictions. Spectrum analysis is applied to MGS observations, and structures very similar to the waves described above are found in the electron density altitude profiles, suggests that these structures are very likely the predicted waves.

**MC04/11P/B22-007** **1630**

**THE EFFECT OF OBLIQUITY AND SURFACE CONDITION ON THE WATER CIRCULATION AND FREEZING CONDITION OF A PLANET: IMPLICATIONS ON HABITABILITY AND PALEO-MARS ENVIRONMENT**

Yutaka ABE<sup>1</sup>, Ayako ABE-OUCHI<sup>2</sup> (<sup>1</sup>Department of Earth and Planetary Science, University of Tokyo, <sup>2</sup>Centre for Climate System Research, University of Tokyo)

To discuss habitability on extrasolar planets we investigated the water circulation and the condition for the occurrence of a completely frozen state (a "snow-ball" state) with a general circulation model for both a land planet case (a wet planet without fixed ocean) and an aqua planet (a planet entirely covered by an ocean). We particularly concerned about the effect of obliquity, because a chaotic change of planetary obliquity is suggested from dynamics. Since availability of liquid water is a necessary condition for life, water circulation is an important controlling factor of habitability. The complete freezing gives severe restrictions on the types of life, even though it may not sterilize the planet. Effects of obliquity and the surface condition are also important issues for understanding the environment of paleo-Mars, which likely experienced active hydrological cycle and large obliquity change. In addition, it has good chance to fall in a frozen state owing to the faint radiation of the young Sun and the large orbital radius. The results are summarized as follows. **1.** There are different regimes of hydrological cycle depending on obliquity. We call them as "Upright" and "Oblique" regimes. **2.** A land planet shows stronger resistance to the complete freezing than an aqua planet. **3.** Both land and aqua planets in the oblique regime show stronger resistance to the complete freezing than those in the upright regime. **4.** There is a good chance of low-latitude-only freezing (freezing of low latitude without freezing the entire planet) of a land planet with high obliquity. On the other hand, low-latitude-only freezing is unlikely on an aqua planet. From these results, following implications are obtained for habitability on an extrasolar planet and climate of paleo-Mars: **1.** A land planet with some water may be a better place for life than an aqua planet, because an aqua planet easily falls in a frozen state. **2.** It is a difficult question whether high or low obliquity planet is preferable for life, because former is resistive to the complete freezing, but the latter shows mild seasonal change. **3.** To keep a wet ground at the low latitude area of paleo-Mars, it must be in the oblique regime, or with oceans. Under such conditions, however, the low latitude is relatively easily covered by permanent snow. Thus, unfrozen wet surface on low latitude requires larger greenhouse gas than that required for unfrozen condition at the present obliquity. **4.** If the obliquity changed significantly while the average temperature was decreasing steadily, there must have been a period while only the low latitude area is covered by permanent snow. It is an interesting question whether we can find such evidence from geological records.

**MC04/11P/B22-008 1465**

**ROLE OF CO<sub>2</sub> CONDENSATION IN THE SURFACE ENVIRONMENTAL EVOLUTION ON MARS: PART I. CLIMATE TRANSITION BY ATMOSPHERE-ICE CAP MASS EXCHANGE**

Tokuta YOKOHATA, Masatsugu ODAKA, Kiyoshi KURAMOTO (Division of Earth and Planetary Sciences, Graduate School of Science, Hokkaido University)

A significant process in forming the Martian surface environment is the condensation of CO<sub>2</sub>, the main component of the atmosphere. In this study, we investigate the climate transition by the atmosphere-ice cap CO<sub>2</sub> exchange. Mars is a cold planet at present. However, several lines of evidence suggest that climate warming and cooling have repeated during its history. In order to study the stability and evolution of Martian climate, we constructed a 2-dimensional (horizontal-vertical) energy balance climate model. The long-term CO<sub>2</sub> mass exchange process between the atmosphere and CO<sub>2</sub> ice caps is investigated with particular attention to the effect of planetary ice distribution on the climate stability. Based on the analysis of the climate stability, we made numerical simulations of the climate transition between warm and cold climate taking into account the evolution of CO<sub>2</sub> ice cap topography (areal extent and altitude). Our model calculation suggests that high atmospheric pressure presumed for past Mars would be destabilized if H<sub>2</sub>O ice was widely prevailed. As a result, cold climate state might have been achieved by the condensation of atmospheric CO<sub>2</sub> onto ice caps. We call this process "collapse condensation". On the other hand, the low atmospheric pressure, which is buffered by CO<sub>2</sub> ice cap near the present pressure, would be destabilized if the CO<sub>2</sub> ice albedo decreases. This might have led the climate into a warm state with high atmospheric pressure owing to complete evaporation of CO<sub>2</sub> ice cap. We call this process "runaway evaporation". The time scale for the completion of collapse condensation and runaway evaporation is about 10<sup>3</sup> year, which is geologically very short. The pressure drop in the collapse condensation is larger for the larger H<sub>2</sub>O ice coverage and lower solar luminosity. The pressure would decrease from 10<sup>2</sup> Pa to 10<sup>1</sup> Pa due to collapse condensation at 3.8 Gyr ago. Areal extent of CO<sub>2</sub> ice cap formed by the collapse condensation would be larger (toward the latitude of 70-80 degree) than the present one (about 85 degree). On the other hand, runaway evaporation could occur if the albedo of CO<sub>2</sub> ice cap decreases enough. Through albedo feedback mechanisms of H<sub>2</sub>O and CO<sub>2</sub> ices in the atmosphere-ice cap system, Mars might have experienced warm and cold climates episodically in its history. The glaciated terrains observed in the middle latitude might be a signature of the past extension in H<sub>2</sub>O ice coverage. Polar layer deposits around the present ice cap might be traces of the past CO<sub>2</sub> ice cap formed by the collapse condensation.

**MC04/11P/B22-009 1700**

**ROLE OF CO<sub>2</sub> CONDENSATION IN THE SURFACE ENVIRONMENTAL EVOLUTION ON MARS: PART II. STABILITY AND GREENHOUSE EFFECT OF THE ICE CLOUD**

Tokuta YOKOHATA<sup>1</sup>, Yoshiyuki KOSUGITA<sup>2</sup>, Masatsugu ODAKA<sup>1</sup>, Kiyoshi KURAMOTO<sup>1</sup> (<sup>1</sup>Division of Earth and Planetary Sciences, Graduate School of Science, Hokkaido University, <sup>2</sup>Hitachi Software Engineering Co.,Ltd)

Geomorphological evidence suggests that Martian climate was warm enough for liquid water to be stable about 3.8 Gyr ago. However, the solar luminosity at that time may be too weak to allow the existence of liquid water even if several bars of CO<sub>2</sub> existed in the atmosphere, because the temperature lapse rate is decreased by the CO<sub>2</sub> condensation at the upper region of the atmosphere. Recently, it is widely accepted that the radiative effect of CO<sub>2</sub> ice clouds may resolve this enigma. This theory suggests that CO<sub>2</sub> ice clouds have a strong warming effect because the backward scattering of infrared radiation by the clouds would be more effective than that of the solar radiation. However, studies on the scattering greenhouse effect of CO<sub>2</sub> ice cloud so far have several problems. The effects of the radiative absorption by the clouds remain poorly investigated, even though the scattering effects of the cloud layer are well studied. In this study, therefore, we construct a one-dimensional atmospheric radiation model to investigate the stability and greenhouse effect of CO<sub>2</sub> ice clouds on early Mars. We particularly pay attention to the effect of radiative absorption by the cloud. Our numerical results suggest that the cloud particles are condensable in the cloud layer even though they receive the radiative warming. The column density of the cloud layer can be estimated on the basis of the mass balance between the CO<sub>2</sub> condensation and the particle loss due to gravitational settling. In addition, we can also calculate the cloud particle radius from the condensation mass flux and residence time, assumed for the particle number density. Our estimates yield that the cloud particle radius is about 10 micron and the column density is about 1 kg per square meter for the cloud number density same as that of the terrestrial cirrus cloud. Cloud layers most adequate for the greenhouse effect have particle radius of 10-20 micron, because backward scattering of infrared radiation is most effective at these particle size. However, the cloud layers with these particle sizes can also cause anti-greenhouse effect when the column density is larger than about 1 kg per square meter. This is because the effect of infrared absorption lowers the infrared backward scattering. Our estimate of the particle radius satisfies a necessary condition for the greenhouse effect, but that of the column density suggests that the cloud might have anti-greenhouse effect. However, the column density may not be so large enough to cause an

anti-greenhouse effect, since our estimate of the column density corresponds to the highest one by neglecting the effect of the surface infrared radiation.

**MC04/11P/B22-010 1715**

**EVOLUTION OF RESIDUAL CO<sub>2</sub> ICE CAP AND CLIMATE CHANGES ON MARS**

Kaoru TAKAYAMA, Tokuta YOKOHATA, Masatsugu ODAKA, Kiyoshi KURAMOTO (Division of Earth and Planetary Sciences, Graduate School of Science, Hokkaido University)

Abundant geological evidence including the outflow-channels and polar deposits strongly suggests that Mars has experienced significant climate changes through its history. Partitioning of CO<sub>2</sub> among the atmosphere, polar-caps and regolith plays an important role in controlling the state of martian climate. Such climate changes would be caused by the variability of CO<sub>2</sub> partitioning, which may be triggered by changes of boundary conditions such as the solar flux, obliquity and total CO<sub>2</sub> mass on Mars. In the past studies, residual CO<sub>2</sub> ice cap has been treated as a reservoir with infinite capacity or constant thickness without considering the formation processes, having inhibited the quantitative treatment of CO<sub>2</sub> partitioning. In this study, we construct a new climate model which can calculate the ice cap topography consistently. We apply this model to the partitioning of CO<sub>2</sub> on Mars, and discuss the past climate change and evolution of polar topography. CO<sub>2</sub> is assumed to be partitioned among the atmosphere, ice caps and regolith, which is dependent on the latitudinal surface temperature profile. Atmospheric bottom temperature and surface temperature are calculated as a function of latitude and atmospheric pressure using a two dimensional energy balance model. The topography of ice cap is calculated by solving the equation of mass conservation taking into account CO<sub>2</sub> condensation, evaporation and ice flow. Let us examine first the responses of ice cap extent for various atmospheric pressures. The CO<sub>2</sub> ice caps extend to lowest latitude of 40 degrees when the atmospheric pressure is about 10<sup>1</sup> Pa. The lower the latitude of ice cap extent, the larger the ice cap elevation at poles (about 15 km for maximum height). CO<sub>2</sub> partitioning is dependent on the total CO<sub>2</sub> mass on the martian surface. When the total CO<sub>2</sub> mass is large enough, most of CO<sub>2</sub> is partitioned into the atmosphere. As the total CO<sub>2</sub> mass decreases, the atmospheric pressure and surface temperature also decrease. Subsequently the growth of ice caps becomes possible due to the condensation of atmospheric CO<sub>2</sub>. Once the ice caps are allowed to form, its growth is rapid due to acceleration by the effect of ice albedo and ice flow, eventually massive CO<sub>2</sub> ice caps are formed. The mass and topography of such ice caps are estimated to have ice line latitude of about 80 degrees and polar elevation of about 1.5 km. This extent is similar to that of the observed polar deposits.

**MC05 Monday, July 7 - Friday, July 11**

**MIDDLE ATMOSPHERE SCIENCE (ICMA)**

Location: Site A, Room 9

**Monday, July 7 AM**  
Presiding Chair: T. Hirooka

**MC05/07A/A09-001 Invited 0900**

**STRUCTURE OF THE POLAR VORTEX AS REVEALED BY ILAS OBSERVATIONS OF MINOR-CONSTITUENTS AND METEOROLOGICAL DATA**

Hiroshi KANZAWA (National Institute for Environmental Studies)

The structure of the stratospheric polar vortex is investigated using minor-constituents data (O<sub>3</sub>, HNO<sub>3</sub>, NO<sub>2</sub>, N<sub>2</sub>O, CH<sub>4</sub>, H<sub>2</sub>O, aerosol) for November 1996 - June 1997 of ILAS (Improved Limb Atmospheric Spectrometer), a solar occultation sensor aboard ADEOS (renamed "Midori" after the launch), and meteorological analysis data of UKMO and ECMWF. A main advantage of ILAS is to provide longitude - height cross-sections of trace species at a latitude per day in both polar regions: it covers the stratosphere with altitude resolution of 1 km (see the details in the ILAS Special Section papers of J. Geophys. Res.-Atmospheres, Vol. 107, D24, 2002). The 1996/1997 Arctic winter is a characteristic winter because the polar vortex was maintained until the beginning of May 1997, that is, the polar vortex was stable and maintained abnormally long. This brought about abnormally low total ozone in March 1997 (e.g., Newman et al., 1997). The ILAS measurement latitude in the Arctic changed around 65 degrees North in December 1996 to around 70 degrees North in March 1997. ILAS measured the inside, the edge, and the outside of the polar vortex because the polar vortex developed in winter is not symmetric with respect to longitude. ILAS thus gives basic information on the structure of the polar vortex that is one of the main factors determining ozone distribution. The speed of downward motion in the polar vortex is regarded as an index of degree of isolation of the polar vortex. Using long-lived tracer (CH<sub>4</sub>, HF, and H<sub>2</sub>O) data of HALOE (Halogen Occultation Experiment) aboard UARS (Upper Atmosphere Research Satellite), several authors have carried out estimates of downward motion for the Antarctic polar vortex (Russell et al., 1993; Schoeberl et al., 1995; Kawamoto and Shiotani, 2000). No work of the kind has been carried out for the Arctic polar vortex because it is not so much stable as the Antarctic one and because frequency of HALOE measurements in high latitudes is low. Using long-lived tracer data of ILAS, we try to make an estimate of downward motion speed in the stable polar vortex of 1996/1997 Arctic. The mixing of the polar vortex air in the "horizontal" direction is also estimated to evaluate the degree of isolation of the polar vortex. For the evaluation, plots of ILAS data in cross-sections of potential temperature - potential vorticity based equivalent latitude are carried out. Moreover, a new method named time threshold diagnostics (TTD), having been developed by Sugata (2000) for estimating effective flux of air parcels across given boundaries, was applied with use of ECMWF data. The Antarctic vortex is also investigated using data from ILAS and possibly ILAS-II now in orbit on ADEOS-II which was launched on 14 December 2002.

**MC05/07A/A09-002 Invited 0930**

**FINE SCALE STRUCTURES IN THE DYNAMICS AND THE CHEMISTRY OF THE POLAR VORTEX: SIMULATIONS WITH THE CHEMICAL LAGRANGIAN MODEL OF THE STRATOSPHERE (CLAMS)**

Rolf MUELLER<sup>1</sup>, Paul KONOPKA<sup>1</sup>, Jens-Uwe GROOSS<sup>1</sup>, Gebhard GUENTHER<sup>1</sup>, Baerbel VOGEL<sup>1</sup>, Hildegard STEINHORST<sup>2</sup>, Daniel S. MCKENNA<sup>2</sup> (<sup>1</sup>ICG-I, Research centre Juelich, 52425 Juelich, Germany, <sup>2</sup>NCAR, ACD, Boulder Colorado, USA)

The chemical Lagrangian model of the stratosphere (CLaMS) is a chemical transport model that simulates the full stratospheric chemistry including heterogeneous reactions and represents transport employing an Lagrangian scheme. That is advection is represented through trajectory calculations and mixing is implemented via a novel scheme that allows control over both the intensity and the location where mixing occurs depending on the

properties of the atmospheric flow. Through this design, CLaMS is particularly useful to represent smaller scale features in the atmosphere and thus useful to be applied to the interpretation of observations. Here, we focus on observations in the polar and midlatitude region of the Northern hemisphere in 1999-2000 (when the SOLVE-THESEO 2000 experiment was conducted). CLaMS calculations in conjunction with balloon-borne and aircraft measurements show that the chlorine chemistry and ozone loss in late winter 2000 is in general well described by the model calculations. Some exceptions will be discussed. Furthermore, fields of long-lived tracers are well reproduced by the model calculations, including filamentary structures observed by in-situ aircraft measurements. An assessment of the relative role of chemistry and mixing in of outside vortex air on chlorine deactivation in winter 2000 was possible through model calculations. These show that deactivation is almost exclusively due to chemistry, the mixing effect not exceeding a few percent. Finally, first model results on the dynamics and chemistry of the split vortex in Antarctica in September 2002 will be shown.

**MC05/07A/A09-003** Invited **1000**

**SEASONAL VARIATIONS IN CHEMICAL TRACERS IN THE UPPER TROPOSPHERE/LOWER STRATOSPHERE BASED ON HALOE OBSERVATIONS AND MODEL SIMULATIONS**

Mijeong PARK<sup>1</sup>, William J. RANDEL<sup>2</sup>, Douglas E. KINNISON<sup>2</sup>, Rolando R. GARCIA<sup>2</sup>, Wookap CHOI<sup>1</sup> (<sup>1</sup>School of Earth and Environmental Sciences, Seoul National University, <sup>2</sup>National Center for Atmospheric Research, Boulder, Colorado)

The seasonal variations of methane, water vapor, ozone, and nitrogen oxides (NO<sub>x</sub>) are examined in the upper troposphere/lower stratosphere (UTLS) based on 10 years measurements by the Halogen Occultation Experiment (HALOE). The observed variations are compared with the output of the Model for Ozone and Related chemical Tracers (MOZART). Tropical methane at the 136 hPa level shows maxima in the Northern Hemisphere (NH) summer in both HALOE and MOZART, which implies enhanced stratosphere-troposphere exchange (STE) and mass transport into the stratosphere, especially in the Asian monsoon region. Another, weaker maximum in methane is observed in NH winter in HALOE but not in MOZART. The tropical seasonal cycles of water vapor derived from HALOE and MOZART are in good agreement except during the 'wet' phase of the 'tropical tape recorder' which is somewhat moister in MOZART. The annual cycle of water vapor correlates well with the tropical tropopause temperature and the summer monsoon circulation. Moist monsoon air entering the lower stratosphere becomes a direct source of moisture and contributes to the moist phase of the 'tape recorder' signal over the equator, especially in MOZART. In the annual cycle of ozone both HALOE and MOZART show strong tropical upwelling in NH winter. The seasonal cycle of NO<sub>x</sub> in the tropics observed by HALOE shows a maximum in NH winter, whereas a minimum is calculated with MOZART. This minimum seems to be due to inadequacies in the parameterizations for convection and lightning, which are responsible for transport and chemical generation of NO<sub>x</sub>, respectively. The seasonal variations of methane, water vapor, and ozone point to the importance of the NH summer monsoon region for transport of these constituents into the lowermost stratosphere.

**MC05/07A/A09-004** Invited **1100**

**THE REANALYSIS FOR STRATOSPHERIC TRACE GAS STUDIES (RESTS) PROJECT**

Steven PAWSON (UMBC GEST Center)

The "Reanalysis for Stratospheric Trace Gas Studies" (ReSTS) project intends to provide a state-of-the-art meteorological dataset for use in chemistry-transport models (CTMs). The initial focus is on the period from May 1991 until April 1995, which encompasses the initial few years of observations from NASA's Upper Atmosphere Research Satellite (UARS) as well as the abrupt increase and slow decay of volcanic aerosol loading from Mount Pinatubo. The reanalysis is being performed using NASA's operational "GEOS-4" data assimilation system. The results presented in this paper will begin with an overview of the meteorology of the ReSTS period, validating the ReSTS data against independent analyses, followed by an evaluation of the system statistics (the "Observation minus Forecast" for different input data types). Some sensitivities to the assumptions made in the assimilation process will be presented, including aspects of the forecast model and the statistical model used in the observation-forecast merging. Aspects of trace-gas transport will be discussed, focusing on the on-line water vapor distribution (which is a quasi-inert trace gas in the stratosphere), off-line transport studies of ozone and selected long-lived species, as well as assimilated ozone. The results will be discussed in the context of transport studies and our ability to use reanalyzed datasets to examine long-term variations in the meteorology and composition of the middle atmosphere.

**MC05/07A/A09-005** **1130**

**A COMPARISON OF ISENTROPIC TRANSPORT IN THE STRATOSPHERE**

Diane PENDLEBURY, Timothy J. DUNKERTON (NorthWest Research Associates)

Two-dimensional chemical transport models can be very useful in studying trends in climate and long-lived chemical species. However, it is important in these models to properly characterize the transport of tracers and other chemical constituents, since the full three-dimensional winds are not used to transport the chemical species in these models. Previous work has shown that it is sufficient to use the residual circulation in regions where the flow is linear and steady, and the waves are non-breaking. However, this relationship quickly breaks down in regions of even weak nonlinearity. Vertical transport in most of the stratosphere is naturally described by cross-isentropic motion, since potential temperature is conserved (except for diabatic heating/cooling of air which indicates an actual change in the particle position), and isentropic surfaces are monotonically increasing with height. A similar coordinate for describing meridional transport is potential vorticity (PV), since it is also conserved following the motion. However, potential vorticity surfaces are not monotonic in latitude, particularly in the region of the surf zone. PV equivalent latitude solves this problem by grouping air parcels by PV value, however, in doing so it ignores the spatial distribution of distinct air masses. This may be important if polar vortex air is entrained into the surf zone. By the PV equivalent latitude label, this air still belongs to the polar vortex, but it is now photochemically distinct from the polar vortex. Particle advection is used to analyse transport off PV contours on an isentropic surface. Particular attention is paid to motion within the surf zone, where PV gradients are very weak, and to motion across transport barriers (the edges of the surf zone), where PV gradients are relatively strong. Particles are initialized along constant PV surfaces in an already developed surf zone so that instantaneous velocities may be computed. The residual velocity, Lagrangian mean velocity, the particle transport velocity and the modified Lagrangian mean velocity will be calculated and compared. All quantities agree reasonably well in regions of linear waves, but not within the surf zone where PV contours overturn and are highly distorted. Discrepancies between these quantities and the meaning of each in different regions will be discussed. The possibility of labelling distinct air masses while making use of the PV equivalent latitude will be discussed.

**MC05/07A/A09-006** **1150**

**STRATOSPHERIC CHEMISTRY MODELLING USING ERA-40 METEOROLOGICAL FIELDS**

Pascal SIMON<sup>1</sup>, Franck LEFEVRE<sup>2</sup>, Vincent-Henri PEUCH<sup>1</sup>, Hubert TEYSSÈDRE<sup>1</sup> (<sup>1</sup>Météo-France, <sup>2</sup>CNRS-SA)

The MOCAGE model is a Chemistry-Transport Model (CTM) that has recently been developed by Météo-France on the basis of the REPROBUS stratospheric CTM (Lefevre et al, 1994). The main innovations of this new model are 1) the possibility to run the model with several nested grids and 2) its high degree of flexibility, with several options for the chemistry, physics and dynamics. It is thus possible to use the MOCAGE CTM for a large range of scientific applications, from studies of regional tropospheric pollution to studies of the stratospheric ozone hole phenomenon. The version of the model we will present here is the "climate" version, that has been developed specifically for long-term integrations and chemistry-climate interaction studies; it includes a parametrization of the important tropospheric dynamical and physical processes, such as convective transport, dry and wet deposition, and an explicit representation of tropospheric and stratospheric chemistries using about 80 species and 200 reactions. In this presentation, we will show results from a validation experiment with this version of the MOCAGE CTM, in which it is forced by the ERA-40 meteorological fields over the 1990-2000 period. ERA-40 is the reanalysis project of the European Center for Medium-range Weather Forecast (ECMWF) of the 1958-2001 period, that is about to be completed; compared with earlier reanalysis made at ECMWF (ERA-15, for the 1978-1993 period), one specificity of the ERA-40 experiment is that the model top level has been placed in the mesosphere, so that ERA-40 also provides an analysis of the stratosphere in addition to the more conventional tropospheric analysis. The first part of the talk will be devoted to a presentation of the climatology of ERA-40 in the stratosphere and its comparison with operational analysis and ERA-15 climatologies. Focus will be put on the temperature field and on the Stratosphere-Troposphere Exchange, as both features are important factors influencing the representation of stratospheric chemistry. In the second part of the talk, we shall present MOCAGE results, with emphasis put on the ozone field, that will be compared with several observation datasets available for the 1990-2000 period: satellite data (TOMS, MLS, ...), ground-based (WOUDC) and in-situ (MOZAIC) measurements.

Monday, July 7 PM  
Presiding Chair: S. Pawson

**MC05/07P/A09-001** Invited **1400**

**TESTING MIDDLE-ATMOSPHERIC OZONE PHOTOCHEMISTRY WITH TIMED SATELLITE OBSERVATIONS**

Daniel R. MARSH, Anne K. SMITH (National Center for Atmospheric Research)

Factors that affect the distribution of ozone in the mesosphere and lower-thermosphere (MLT) include solar ultra-violet fluxes, transport processes on scales from molecular to planetary, the distribution of water vapor and other hydrogen species, and the temperature dependence of key reaction rates. Theoretically, these factors can be incorporated into global models that allow prediction of ozone concentrations throughout the MLT. The paucity of ozone observations, in particular extended observations during both day and nighttime, has made testing of these models problematic. With the launch of the Thermosphere, Ionosphere, Mesosphere, Energetics and Dynamics (TIMED) satellite, we now are able to rigorously test our understanding of ozone photochemistry. We present comparisons of TIMED observations of composition, airglow and dynamical fields with simulations from ROSE, a 3-dimensional mechanistic chemical transport model. The ability of this model to simulate a variety of MLT observations on diurnal and seasonal timescales is evaluated.

**MC05/07P/A09-002** **1430**

**OZONE PERTURBATIONS IN THE ARCTIC SUMMER LOWER STRATOSPHERE AS A REFLECTION OF NOX CHEMISTRY AND PLANETARY-SCALE WAVE ACTIVITY**

Hideharu AKIYOSHI<sup>1</sup>, Takafumi SUGITA<sup>1</sup>, Hiroshi KANZAWA<sup>1</sup>, Nozomi KAWAMOTO<sup>2</sup> (<sup>1</sup>National Institute for Environmental Studies, Tsukuba, 305-8506 JAPAN, <sup>2</sup>National Space Development Agency/Earth Observation Research Center, Tokyo, 105-8060 JAPAN)

Ozone concentration perturbations in the high latitude lower stratosphere were observed by Improved Limb Atmospheric Spectrometer (ILAS) after the polar vortex breakdown at the beginning of May 1997 and until the end of June of that same year. Simulations and a passive tracer experiment using the CCSR/NIES nudging CTM show that the low-ozone perturbations observed in May were caused by the Arctic polar vortex debris, while those after the end of May resulted from a dynamical elongation of the polar low-ozone air mass developed by NO<sub>x</sub> chemistry in the summer polar stratosphere. These low-O<sub>3</sub> air masses of different origin were advected or extended from the polar region to the ILAS measurement points. An episodic event of a dynamical O<sub>3</sub> perturbation in June 1997 on a chemically induced meridional O<sub>3</sub> gradient is presented. These results show that a timing of the polar vortex breakdown may affect the O<sub>3</sub> background gradient in the summer lower stratosphere at mid and high latitudes. The O<sub>3</sub> distribution will be discussed comparing with N<sub>2</sub>O distribution, which shows the polar vortex debris with the low concentration for a few months after the polar vortex breakdown in 1997.

**MC05/07P/A09-003** **1450**

**ANALYSIS OF YEAR-TO-YEAR OZONE VARIATION OVER THE SUBTROPICAL WESTERN PACIFIC REGION USING EP\_TOMS DATA AND CCSR/NIES NUDGING CTM**

Libo ZHOU<sup>1</sup>, Hideharu AKIYOSHI<sup>1</sup>, Kohji KAWAHIRA<sup>2</sup> (<sup>1</sup>National Institutes for Environmental Studies, <sup>2</sup>Fukui Prefectural University, Kenjojima, Yoshida-Matsuoka Fukui 910-1195)

Most recently, Kawahira et al. [2002] found that the total ozone less than 225 DU was located around (200N, 130oE) over the subtropical western Pacific by EP-TOMS observation in December 2001. They also showed that a total ozone less than 200 DU was observed by the ground based measurement at Hongkong (22.22oN, 114o19'E), China and Naha (26.12oN, 127o40'E), Japan in the subtropical western Pacific for a few days in December, and with the lowest value below 190 DU. Such a local low ozone value stimulates us to study the ozone variation and its mechanism over the subtropical western Pacific. The year-to-year ozone variation over the subtropical western Pacific region is studied, especially the ozone lows in the 1996/97, 1998/99, and 2001/02 winters, using the Earth Probe Total Ozone Mapping Spectrometer (EP\_TOMS) ozone data from August 1996 to July 2002. Using the regression methods developed by Ziemke et al. [1997], the signals included in the total ozone over the subtropical western Pacific region were analyzed. The results show that (1) the total ozone includes the seasonal variability, solar, QBO, ENSO signals, and MSU temperature variation; (2) the seasonal variability is dominant among them; and (3) the QBO-

associated regression fit contributed greatly to the unusual ozone lows in the winters of 1996/97, 1998/99, and 2001/02. A nudging chemical transport model (CTM) is used to simulate the year-to-year ozone variation and explain the mechanism for ozone lows from a 3-D ozone field. The CTM was developed using the Center for Climate System Research/National Institute for Environmental Studies Atmospheric General Circulation Model (CCSR/NIES AGCM) and introducing a nudging process for temperature and horizontal wind velocity. The ozone lows over the subtropical western Pacific are well simulated. The year-to-year variation in the total ozone is closely related to the position of ozone minimum, which is largely controlled by the QBO cycle. However, the discrepancies between the calculated ozone and observation show that the heterogeneous reaction processes may have some influence on the ozone variation over the subtropical western Pacific. Further comparison of two models with and without considering the NAT and ice formation shows a heterogeneous loss of about 3 DU of total ozone. Since the calculated loss may be overestimated, results show that the heterogeneous reaction processes may have smaller influence on the total ozone compared to the influence by the dynamical processes.

**MC05/07P/A09-004** Invited **1510**

**DYNAMICAL INFLUENCES ON OZONE CHANGES**

Theodore G. SHEPHERD (Department of Physics, University of Toronto)

The stratospheric ozone distribution represents a balance between dynamics and chemistry, with processes of both kinds playing a first-order role. Thus, while the stratosphere has been chemically perturbed over the last few decades by increased halogen loading as well as long-term changes in other trace species, the effects of these perturbations need to be considered together with dynamical influences, which act together with chemical processes in a coupled manner. Dynamical changes over decadal time scales may arise from the ozone changes themselves, from long-term climate change, or from natural variability. This talk will assess our current understanding of dynamical influences on ozone changes, both in midlatitudes and in polar regions, with an emphasis on the northern hemisphere.

**MC05/07P/A09-005** Invited **1610**

**CHEMICAL SPECIES MAPPING ON TRAJECTORIES (CSMT): A NEW SCHEME OF CHEMICAL OZONE LOSS ANALYSIS USING A BOX MODEL ALONG TRAJECTORIES**

Sachiko HAYASHIDA<sup>1</sup>, Akiko KAGAWA<sup>1</sup>, Sachiko KAWASE<sup>2</sup>, Nao IKEDA<sup>2</sup> (<sup>1</sup>Faculty of Science, Nara Women's University, <sup>2</sup>Graduate School of Human and Culture, Nara Women's University)

We propose a new scheme to create synoptic maps of stratospheric minor species from asymptotic satellite measurements by utilizing a photochemical box model and trajectory analysis. Kagawa and Hayashida [submitted to J. Geophys. Res.] named it Chemical Species Mapping on Trajectories (CSMT). The CSMT incorporates: trajectory mapping; [Morris et al., 1995, 2000] with a photochemical box model. Minor constituents are time-integrated in a photochemical box model along trajectories that start from satellite measurement points until a target time. Combining a chemical model with trajectory mapping allows creation of synoptic maps of short-lived species as well as long-lived species. We applied CSMT to study the mechanism of Arctic ozone loss in the late winter and early spring of 1997, combined with Improved Limb Atmospheric Spectrometer (ILAS) data. The ILAS instrument was developed by the Environmental Agency of Japan (EA) on board the Advanced Earth Observing Satellite (ADEOS) that was launched in August 1996. ILAS successfully observed ozone and ozone-related species such as nitric acid, nitric dioxide, nitrous oxide, water vapor, methane and aerosols over both polar stratosphere during from November 1996 through June 1997 [Sasano et al., 1999]. The CSMT approach with initialization by ILAS-observed ozone, nitric acid, and nitrous oxide made it possible to map long- and short-lived minor species over the polar stratosphere. Comparison with ozonesonde and/or satellite data validated CSMT-derived ozone and other data, proving reliability of the scheme. The chemical ozone loss amount was estimated by using the chemical model, resulting the maximum rate of ozone loss being about 34 ppbv/day in late February, and the integrated ozone loss from 13 January to 31 March 41 %, when averaged over the polar vortex. The derived ozone loss rates and integrated ozone loss are fairly consistent with the results of other studies. The CSMT scheme is a simple but useful method to make assimilated maps of chemical species, and has a good potential to various applications including detailed analysis of chemical mechanisms in the atmosphere. [References] Kagawa, A. and S. Hayashida, Analysis of ozone loss in the Arctic stratosphere during the late winter and spring of 1997, using the Chemical Species Mapping on Trajectories (CSMT) technique, submitted to J. Geophys. Res. Morris, G.A. et al., J. Geophys. Res., 100, 16491-16505, 1995. Morris, G.A. et al., J. Geophys. Res., 105, 17825-17894, 2000. Sasano, Y. et al., Geophys. Res. Lett., 26, 197-200, 1999.

**MC05/07P/A09-006** **1640**

**ON THE INFLUENCE OF THE LARGE-SCALE EDDY FLUX VARIABILITY ON INTERANNUAL AND DECADEAL OZONE CHANGES**

Axel GABRIEL, Gerhard SCHMITZ (Leibniz-Institut fuer Atmosphaerenphysik an der Universitaet Rostock e.V.)

The influence of the variability of large-scale eddy heat and momentum fluxes on interannual and decadal changes in the zonal mean ozone distribution is investigated based on a two-dimensional (2D) circulation model with interactively coupled transport and chemistry. The model is a 2D version of the 3D GCM ECHAM. The large-scale eddy fluxes are prescribed in terms of monthly mean eddy mixing coefficients that are derived from ECMWF ReAnalysis (ERA). The results show that the eddy-forced changes in the lower stratospheric residual circulation and eddy mixing processes induce coherent interannual and decadal changes in temperature and ozone that covers much of the observed temperature and ozone variability at mid- and polar latitudes. The seasonal and vertical structure of the observed northern hemispheric zonal mean ozone trend is captured in a remarkable way. It is shown that the induced midlatitude ozone changes are mainly related to the changes in the eddy mixing processes, and that the induced polar ozone changes are mainly related to the induced changes in the lower stratospheric temperature. It is also shown that the feedback of the varying zonal mean ozone to the zonal mean temperature play an essential role in reproducing realistic decadal temperature changes at polar latitudes.

**MC05/07P/A09-007** **1700**

**CHEMICAL OZONE LOSS AND TRACER EVOLUTION IN THE ELEVEN ARCTIC WINTERS BETWEEN 1991/92 AND 2001/02 DERIVED FROM HALOE OBSERVATIONS**

Tilmes SIMONE<sup>1</sup>, Rolf MUELLER<sup>1</sup>, Jens-Uwe GROOSS<sup>1</sup>, Ulrich SCHMIDT<sup>2</sup>, James M. RUSSELL III<sup>3</sup>, Yasuhiro SASANO<sup>4</sup> (<sup>1</sup>Institute of Stratospheric Research (ICG-I), Juelich, Germany, <sup>2</sup>University Frankfurt, Germany, <sup>3</sup>Hampton University, Hampton, USA, <sup>4</sup>National Institute for Environmental Studies, Japan)

Chemical ozone loss in the eleven Arctic winters between 1991/92 and 2001/02 is calculated from HALOE satellite measurements using the ozone-tracer correlation technique. First results of the winter 2002/03 will also be shown. The early winter ozone-tracer reference function is deduced from HALOE and ILAS measurements and balloon observations for nine out of eleven years. Additionally a constant temporal relation function between two long-lived tracers CH<sub>4</sub> and HF valid for the entire lifetime of the vortex is derived for eleven years between 1991/92 and 2001/02 from HALOE. An evolution of the early winter ozone-tracer reference functions between 1991/92 and 2001/02 is apparent as well as the evolution of the relation functions between CH<sub>4</sub> and HF. Thus, the growth rate of HF at different stratospheric altitudes can be estimated from HALOE observations. Using of the growth rate of CH<sub>4</sub> and HF for each year to combine early vortex observations from several winters, an early winter reference function is calculated for two winters (1997/98 and 2000/01) where no observations are available inside the early vortex. The chemical ozone loss is deduced from deviations of the early winter ozone-tracer reference function in the course of the spring. The relation between the area of possible existing PSCs (A<sub>PSC</sub>) in the Arctic vortex and calculated ozone loss in eleven years indicates, that A<sub>PSC</sub> and ozone loss are related. However, we do not find a simple linear relationship.

**MC05/07P/A09-008** **1720**

**CHEMICAL OZONE LOSS MECHANISM IN WINTER/SPRING OF 1997 OVER THE ARCTIC DERIVED BY CSMT ANALYSIS: ON RELEVANCE TO DENITRIFICATION**

Sachiko HAYASHIDA<sup>1</sup>, Akiko KAGAWA<sup>1</sup>, Sachiko KAWASE<sup>2</sup>, Nao IKEDA<sup>2</sup> (<sup>1</sup>Faculty of Science, Nara Women's University, <sup>2</sup>Graduate School of Human and Culture, Nara Women's University)

Chemical Species Mapping on Trajectories (CSMT) is a new technique combining a chemical box model and trajectory analysis [Kagawa and Hayashida, submitted to JGR]. The CSMT incorporates Trajectory Mapping [Morris et al., 1995, 2000] with a photochemical box model, and minor constituents are time-integrated in a photochemical box model along trajectories that start from satellite measurement points until a target time. (See also our companion paper on CSMT scheme). The photochemical box model was generated by the tool developed by the Atmospheric Chemistry Division of the National Center of Atmospheric Research (ACD/NCAR). The chemical solver called RODAS was applied with 59 chemical species, 101 gas-phase reactions, 48 photodissociations, and 7 heterogeneous reactions. We also included PSC growth governed by the temperature change along trajectories. Super-cooled ternary solutions (STS) and nitric acid trihydrate (NAT) are summed based on thermodynamic equilibrium. Though there are many uncertainties in the PSC formation mechanism and our PSC scheme is still preliminary, our model can involve denitrification implicitly, because actual data of denitrified gaseous nitric acid can be used as initial values. In this study we utilized Improved Limb Atmospheric Spectrometer (ILAS) data to investigate the effects of denitrification on chemical ozone loss. ILAS could observe ozone and ozone-related species including nitric acid, nitric dioxide, nitrous oxide, water vapor, methane and aerosols over both polar stratospheres from November 1996 through June 1997. Irie et al. [2001] derived a significant denitrification of 43 % at 19 km (near 475 K) in late February of 1997 over the Arctic. In our study the chemical box model was initialized by ILAS-observed ozone and nitric acid, and the chemical ozone loss rate was estimated based on the chemical model along with the change in nitric acid. The ozone loss rates in late February are scattered considerably with high and low values in late February, indicating that denitrification caused two opposite processes: (1) prolonged activation of chlorine due to less NOx and (2) low additional activation of chlorine due to less PSC formation. Recently version 6 of ILAS data was released including ClONO<sub>2</sub> as a new product. ClONO<sub>2</sub> can be used to identify each air parcel as activated or deactivated in the form of chlorine. Preliminary analysis shows CSMT-derived ClONO<sub>2</sub> well correlated to the ILAS-observed ClONO<sub>2</sub>. CSMT-based analysis incorporating actual nitric acid and ClONO<sub>2</sub> data will throw new light on chemical processes in polar ozone destruction. [References] Irie, H. et al., J. Geophys. Res., 106, 23139-23150, 2001. Morris, G.A. et al., J. Geophys. Res., 100, 16491-16505, 1995. Morris, G.A. et al., J. Geophys. Res., 105, 17825-17894, 2000.

**MC05/07P/A09-009** **1740**

**DYNAMICAL INVESTIGATION OF OZONE MINI-HOLES DURING WINTER OF NORTHERN HEMISPHERE**

Koki IWAO, Toshihiko HIROOKA (Department of Earth and Planetary Sciences, Kyushu University)

Ozone mini-holes are localized and transient (several days) depletion phenomena of column ozone amount which often appear over northern Europe. Especially on 30 November 1999, a extremely low total ozone value of 165 DU was recorded between Scotland and southern Scandinavia with the Total Ozone Mapping Spectrometer. This value is the lowest in mid- to high-latitudes of the Northern Hemisphere since the observation started in 1979. These ozone mini-hole episodes are known to be caused mainly by dynamical processes rather than chemical processes. In order to reproduce approximate total ozone distribution in the data-missing region, the dynamical reconstruction of 3D ozone was performed. From 3 kinds of satellite ozone data and daily potential vorticity (PV) distributions, the relationship between ozone mixing ratio and equivalent latitude (EL) can be calculated on 16 isentropic surfaces. We reconstruct the ozone 3D distribution on 30 November 1999 from the spatial EL distribution and this relationship averaged for 2 months. On the basis of the reproduced 3D ozone data, we examine several dynamical processes contributing to ozone mini-holes, i.e., air uplift in the lower stratosphere and adiabatic advection of ozone-poor air. The local uplift of airmass throughout this level contributes to form these mini-holes by driving ozone-rich stratospheric air out of the column. Quantitative analyses on this effect explain about a half of total ozone depletion for the event on 30 November 1999. Remaining half depletion is due to horizontal advection on isentropic surfaces: The displacement of polar vortex toward Europe in the middle stratosphere and polarward intrusion of low-latitude air due to Rossby wave breaking around tropopause transport ozone-poor air to the mini-hole region. Similar results are obtained for other severe mini-hole cases.

**MC05-Posters** **Monday, July 7**

**MIDDLE ATMOSPHERE SCIENCE (ICMA)**  
Location: Site D

**MC05/07P/D-001** **Poster** **1400-208**

**CLIMATOLOGICAL FEATURES OF STRATOSPHERIC STREAMERS SIMULATED WITH THE BERLIN CLIMATE MIDDLE ATMOSPHERE MODEL (FUB CMAM)**

Kirstin KRUEGER, Ulrike LANGEMATZ, John Lee GRENFELL (Institute for Meteorology, Free University Berlin)

**Monday, July 7 PM**

Stratospheric processes and their role in the development of the future ozone layer are an essential aspect in climate change. Besides the fundamental chemical processes, transport processes are an important factor determining the global distribution of atmospheric trace gases, such as ozone. The influence of dynamical processes on strength and variability of the observed total ozone decrease at mid-latitudes, especially in the northern hemisphere, is still an open question. The purpose of this study is to investigate the influence of air mass exchange through streamers/tongues on ozone at mid-latitudes. The occurrence of streamers can determine the amount of total ozone in mid-latitudes, whether through transport of natural low ozone from the tropics to the mid-latitudes (tropical-subtropical streamer) or chemically processed air from polar to mid-latitudes (polar vortex streamer). For this reason a streamer climatology has been produced to investigate the frequency of both types of streamers with a 10-year climatology of the Berlin Climate Middle Atmosphere Model.

**MC05/07P/D-002** Poster **1400-209**

**A CONNECTION THE STRATOSPHERIC QUASI-BIENNIAL OSCILLATION WITH APPEARANCE AND VANISHMENT OF EL NIÑO / LA NIÑA EVENTS**

Makoto INOUE (Department of Earth Information Mathematical Sciences, The Graduate School of Integrated Basic Sciences, Nihon University, 3-25-40 Sakurajousui Setagaya-ku Tokyo 156-8550 JAPAN)

It is widely recognized that the existence of the quasi-biennial oscillation(QBO)changes westerly and easterly wind in the stratosphere above the Tropics on average every 27 months. Many papers describe the cause of El Niño events. For example, it is widely known that westerly wind bursts weaken easterly wind over the tropical Pacific and consequently lead to El Niño events, and this view enabled forecast of 1997 El Niño event. On the other hand, appearance of El Niño was also predicted in 2002. But behavior which was apparently seen in 1997 El Niño event was hard to appear and appearance of 2002 El Niño event was unexpectedly delayed. Although finally El Niño event has occurred in 2002, it seems appearance and vanishment of ENSO events can not be predicted accurately even if researchers continue to observe only the ocean and troposphere as usual. There is a study interannual variations of temperature at the tropical tropopause associate with both ENSO and QBO, but few studies refer to direct connection QBO with ENSO. This study takes notice of the connection appearance/vanishment months of ENSO events with vertical structure of equatorial zonal wind. First of all, in 1982 Walker circulation was weakened because a stratospheric easterly component propagated into the upper troposphere in May and an El Niño event has started. But easterly component propagation from stratosphere to the upper troposphere would not always cause El Niño events. This necessary condition is to form the critical fields in the troposphere whether is likely to become El Niño events by means of westerly bursts etc. or not. On the other hand, since a strong stratospheric westerly component propagated into troposphere in May 1998, it obliged to finish an El Niño event and simultaneously caused a La Niña event. Speaking to May 1998, Yangtze River Severe Floods started in earnest. This El Niño / La Niña events before and after change are large-scale and representative. The stratospheric QBO contributed to change from an El Niño event to a La Niña event. This change seems to have disturbed atmospheric circulation above the Tropics and caused East Asia local downpours and severe floods unprecedented in history. It was a significant factor that the lower stratospheric zonal wind component in May which is monsoon change time propagated into the upper troposphere, since few ENSO events appeared when they propagated in another months.

**MC05/07P/D-003** Poster **1400-210**

**IMPROVED SAGE II WATER VAPOR INVERSION**

Larry W. THOMASON<sup>1</sup>, Nina IYER<sup>2</sup>, S.P. BURTON<sup>2</sup> (NASA Langley Research Center, <sup>2</sup>Science Applications International Corporation)

Public versions of SAGE II water vapor data exhibit some problems, including strong sensitivity to enhanced aerosol and seasonal variability unlike other stratospheric data sets as well as an apparent bias near the hygropause. A new modification to the water vapor inversion technique has been developed which addresses these problems. Water vapor is measured with the SAGE II instrument using a single filter-based channel, nominally at 935 nm. It is hypothesized that the spectral response of the filter underwent a significant change in the first few years after launch. This is in accordance with evidence that the physically similar NO<sub>2</sub> channel, nominally at 448 nm, also underwent a change in wavelength after launch. The NO<sub>2</sub> retrieval was reworked and resulted in significant improvement in NO<sub>2</sub> in version 6.1. A similar change in the water vapor channel would affect the apparent strength of the water vapor feature as well as the contributions of other components such as molecular and aerosol scattering. It was found that a single constant wavelength adjustment is adequate to yield reasonable agreement with a water vapor climatology from HALOE for the period of 1986 through the present except immediately following the Pinatubo eruption when aerosol interference remains a problem. An additional improvement is made by allowing slightly different aerosol clearing models for the post-El Chichon period and the post-Pinatubo period. Water vapor data in this newest version show marked improvement over earlier versions.

**MC05/07P/D-004** Poster **1400-211**

**ESTIMATION OF TURBULENT OZONE FLUXES FROM THE MIDDLE ATMOSPHERE THROUGH THE TROPopause OVER SHIGARAKI, JAPAN**

Nikolai M. GAVRILOV<sup>1</sup>, Shoichiro FUKAO<sup>2</sup> (Saint-Petersburg State University, Atmospheric Physics Department, Petrodvorets, St. Petersburg, 198504, Russia, gavrilov@pobox.spbu.ru, <sup>2</sup>Kyoto University, Center for Atmospheric and Space Research, Uji, Kyoto 611, Japan, fukao@kurasc.kyoto-u.ac.jp)

A numerical simulation has been used to verify the hypothesis about the influence of sharp change of vertical temperature gradient near the tropopause on the increase of the amplitudes of IGWs propagating upward from the troposphere, wave breaking and generating of increased turbulence, which may make the middle latitude tropopause more transparent for the transport of admixtures between the troposphere and stratosphere. An increase in the turbulent diffusivities at altitudes near and above tropopause is usually observed with the MU radar in Shigaraki, Japan (35 N, 136 E). Turbulent diffusion coefficient calculated and measured with the MU radar are of 1 - 10 m<sup>2</sup>/s in indifferent seasons. They lead to the estimation of vertical ozone flux from the stratosphere to the troposphere of the order of (1 - 10) 10<sup>-4</sup> m<sup>2</sup> s<sup>-1</sup>, which is comparable with usually supposed ozone downward transport with the general atmospheric circulation. Therefore, local enhancements of IGW intensity and turbulence at tropospheric altitudes over mountains due to their orographic excitation and due to other wave sources may lead to the changes in tropospheric ozone and the total ozone over different regions.

**MC05/07P/D-005** Poster **1400-212**

**STRATOSPHERIC SUDDEN WARMINGS IN THE SOUTHERN HEMISPHERE : A COMPARISON BETWEEN EVENTS IN 2002 AND 1988**

Akiko MORI, Akiko SAKAI, Toshihiko HIROOKA (Department of Earth and Planetary Sciences, Kyushu University)

In late September 2002, an unprecedented major stratospheric sudden warming occurred in the Southern Hemisphere. This warming was accompanied with the split of the polar vortex as well as the Antarctic ozone hole. Moreover, the seasonal march of the winter in 2002 was very unusual: Planetary wave activities were very strong and an oscillatory change of the polar night jet with a typical time scale of about 10 days was observed throughout the winter season prior to the sudden warming. Correspondingly, ozone hole was not so much developed. Similar features were also observed in the winter of 1988, although such a split of the polar vortex didn't occur. It is very interesting to see the similarity as well as the difference between the two winters in terms of ozone distributions as well as stratospheric dynamics. Hence, we compare observational features of the events in 2002 and 1988 by using the NCEP/NCAR reanalysis data and the NOAA/TOMS total ozone data. We find that the planetary wave of zonal wavenumber 1 was very active in the stratosphere for both the winters; the strong wave activity in 2002 was seen from the beginning of the winter season, whereas that in 1988 was seen only after the end of July. The wavenumber 2 component was also active in 2002, whereas it was relatively weak in 1988 through the winter season. Such strong wave activity of wavenumber 2 brought about the split of the polar vortex. As a result, the above-mentioned periodic oscillation of the polar night jet was more conspicuous in 2002; the major warming occurred in late September in 2002, whereas an intense but minor warming occurred in the end of August in 1988. On the other hand, the intensity of ozone hole in terms of ozone hole areas and minimum column ozone amounts was weak in both the years; it was weaker in 1988. However, the area of low temperature less than 195 K, which is a threshold value for the formation of polar stratospheric clouds (PSCs), was almost the same in the two years. Nevertheless, we can say that the impact of the warmings to the general circulation and the ozone hole intensity seems to be larger in 2002, if taking account of the trend during the last two decades towards a stronger, colder and stable polar vortex.

**MC05/07P/D-006** Poster **1400-213**

**THE OZONE MINIMUM OVER THE SUBTROPICAL NORTHWESTERN PACIFIC IN WINTER**

Han JIANYU<sup>1</sup>, Koji YAMAZAKI<sup>1</sup>, Masanori NIWANO<sup>2</sup> (<sup>1</sup>Graduate School of Environmental Earth Science, Hokkaido University, <sup>2</sup>Dept. of Geophysics, Kyoto University)

The total ozone amount is generally low in the tropics and the zonal minimum lies in the Northern subtropics (20N, 140E) in winter. Over the subtropical northwestern Pacific, the prominent ozone minimum less than 235 DU is clearly seen. Since there is few studies on this ozone minimum, we examine the vertical structure of this ozone minimum. Using TOMS and HALOE/JARS data we found there is two distinct ozone minima in stratosphere, one at 10-15hPa and the other at 40-60hPa. Two vertical ranges are responsible for the northwestern subtropical ozone minimum. Although the middle stratospheric minimum (10-15hPa) is stronger than the lower stratospheric minimum (40-60hPa), but the lower stratospheric contribution for the total ozone is larger than the middle stratosphere because of density effect. The minimum in the lower stratosphere is probably caused by northward advection of an ozone-poor air from the equatorial region, which is brought from the troposphere (Randel et al., 2001). In the lower stratosphere, the ozone mixing ratio increases with latitude. Thus northward advection from the equator to the subtropics reduces the ozone in the subtropics. In the middle stratosphere, the ozone maximum is located at about 10S and the ozone density decreases toward northern high-latitudes. The northern subtropical tropical Pacific is located to the south of Aleutian High and it is a reasonable hypothesis that this anticyclonic circulation brings an ozone-poor air to the subtropical Pacific. A simple 2-dimensional chemical-transport model confirms this hypothesis.

**MC05/07P/D-007** Poster **1400-214**

**CHARACTERISTICS OF INERTIO-GRAVITY WAVES OVER THE SOUTH PACIFIC OCEAN**

Miho YAMAMORI<sup>1</sup>, Kaoru SATO<sup>2</sup> (<sup>1</sup>Center for Climate System Research, University of Tokyo, <sup>2</sup>Arctic Environmental Research Center, National Institute of Polar Research)

It is now widely recognized that the atmospheric gravity waves play a crucial role in determining the global-scale fields of wind and temperature in the middle atmosphere. However, our knowledge of the gravity waves over the ocean is limited, because of lack of observations. A radiosonde observation campaign MeSSO2001 (a meridional scan of the stratosphere over the ocean in 2001) was performed over the middle Pacific, during about 1 month cruise of Hakuho-maru, the research vessel of Ocean Research Institute of the University of Tokyo, in December 2001. By launching Vaisala RS80-15GH radiosondes, vertical profiles of temperature, horizontal winds and humidity were successfully obtained in a latitude range from 28N to 48S at almost the same interval of 1 degree. In this study, characteristics of inertio-gravity waves in the upper troposphere and lower stratosphere in the sub- and extra-tropics over the South Pacific Ocean were investigated by using the horizontal wind and temperature data at 31 points from 17 to 48S along the 160W meridian. We defined gravity wave components as those extracted by a bandpass filter having cutoff wavelengths of 500 m and 5 km. The magnitude of potential energy associated with the gravity waves was about one fourth of that of kinetic energy on average. The kinetic energy was large around 35S and 15-20 km. Wave parameters were estimated by hodograph analysis together with the dispersion relation. It was noted that enhanced kinetic energy was often due to near-inertial waves. The dominant direction of horizontal propagation was southward (poleward), with bias of eastward. The probability that the propagation direction was between 120 and 210 clockwise from north was about 40% above 18 km. Sources of gravity waves were estimated for distinctive cases based on the group velocity vectors with the aid of the operational analysis data and IR image of geostationary satellite. The northward (equatorward) propagating waves having relatively large vertical group velocity observed in the sub-tropical lower stratosphere were possibly associated with a cutoff cyclone existing to the south of the vessel at those times. The southward propagating waves with large amplitudes observed in the sub-tropical upper troposphere were likely generated in association with a vigorous convection in the South Pacific Convergence Zone.

**MC05/07P/D-008** Poster **1400-215**

**SEMI-ANNUAL OZONE VARIATION IN THE MESOSPHERE OBSERVED OVER TSUKUBA, JAPAN**

Tomoo NAGAHAMA<sup>1</sup>, Hideaki NAKANE<sup>2</sup>, Yasumi FUJINUMA<sup>1</sup>, Hideo OGAWA<sup>3</sup>, Akira MIZUNO<sup>3</sup>, Yasuo FUKUP<sup>3</sup> (National Institute for Environmental Studies, <sup>2</sup>Department of Earth and Life Sciences, Osaka Prefecture University, <sup>3</sup>Department of Astrophysics, Nagoya University)

We present results of continuous observations of the vertical ozone profiles between 38 and 76 km in altitude, which have been made with the millimeter-wave radiometer at the National Institute for Environmental Studies (NIES) in Tsukuba, Japan (36.1N, 140.1E) since October 1996. We analyzed temporal variations of ozone at various altitudes and newly revealed the features of a semi-annual variation between 56 and 68 km. The ozone mixing ratio in this region peaks in January and July, and the amplitude of the semi-annual variation at 60 km was estimated to be 13% of the annual average, which is about half the value of 28% observed at 76 km. The phase of the semi-annual variation from 56 to 76 km inverts suddenly at 68 km, suggesting that these semi-annual variations of ozone are not induced by the downward propagation of a single dynamical wave, but are caused by different mechanisms in the regions above and below 68 km. The ozone mixing ratio at 60 km correlates well with the inverse of the temperature at 65 km, indicating that the semi-annual variation of ozone at 60 km is mainly caused by the corresponding variation in temperature. Further details of the ozone temporal variations and comparison with physical properties are presented.

**MC05/07P/D-009** Poster **1400-216**

**SIMULATION OF INERTIAL INSTABILITY IN APRIMITIVE EQUATIONS MODEL**

Diane PENDLEBURY, Timothy J. DUNKERTON (NorthWest Research Associates)

Equatorial inertial instability simulated in middle atmosphere models is characterized by vertical grid-scale structures in the zonal-mean winds and temperature. This paper will examine the three-dimensional structure of the instability. It will be shown that the instability has a zonal wavenumber dependence that is selected by the winter-hemispheric planetary waves impinging upon the zero-wind line. The breakdown of the unstable region will be examined, along with the effects on the zonal-mean state. Modification of the potential vorticity gradient on the summer side of the equator by inertial instability creates a region of barotropically unstable flow that leads subsequently to the excitation of two-day waves. It will be demonstrated that the inertial instability also generates small-scale travelling waves. Examination of the dispersion relation suggests that these are upward propagating gravity waves. The possible effect of these waves on the mesospheric circulation due to critical layer absorption and generation of Eliassen-Palm flux convergences will be shown.

**MC05/07P/D-010** Poster **1400-217**

**SENSITIVITY OF STRATOSPHERIC OZONE TO MEAN CIRCULATION IN AN OZONE REANALYSIS SYSTEM BASED ON A CTM**

Kazuyuki MIYAZAKI<sup>1</sup>, Toshiki IWASAKI<sup>1</sup>, Kiyotaka SHIBATA<sup>2</sup>, Osamu CHIBA<sup>2</sup>, Tsuyoshi SEKIYAMA<sup>2</sup>, Kotato ORITO<sup>1</sup> (<sup>1</sup>Department of Geophysics, Graduate School of Science, Tohoku University, Japan, <sup>2</sup>Meteorological Research Institute, Japan)

To reproduce global ozone distribution, we are developing an ozone reanalysis system based on a CTM. This system showed realistic temporal variations but did systematic error. We studied impacts of changing meteorological parameters to be nudged into GCM. Nudging temperature field in addition to horizontal wind field weakens the mean meridional circulation and degrades reanalyzed ozone.

**MC05/07P/D-011** Poster **1400-218**

**FORCING MECHANISMS OF THE STRATOPAUSE SEMIANNUAL OSCILLATION**

Hiroshi KUBO (Department of Earth and Planetary Sciences, Kyushu University)

The stratopause semiannual oscillation(SAO) in low latitudes is well known phenomena. It is also well known that the zonal momentum forcing by the meridional wind and the easterly eddy momentum deposition by planetary waves play an important role in the SAO. However, the contribution of Kelvin waves and gravity waves to the zonal wind acceleration of the SAO is still uncertain. In this study, forcing mechanisms of the SAO are investigated by using UKMO assimilated data(1992-2001). The momentum balance is diagnosed by using the TEM momentum equation. The results are as follows. The easterly acceleration in the equatorial region during the solstice is mainly due to planetary waves and the meridional advection. On the other hand, the westerly acceleration during the equinox is likely due to the gravity wave drag. International variation of the SAO is also examined. It is clearly seen that the interannual variation in the SAO is related to the phase of the underlying quasi-biennial oscillation(QBO). Our result shows that the EP-flux divergence due to planetary waves and Kelvin waves plays an important role in the interannual variation of the SAO. Namely, during the westerly phase of the QBO at 20hPa, the easterly acceleration due to the EP-flux divergence in the equatorial stratopause is relatively strong. The role of gravity wave drag in the SAO is examined by using a general circulation model(GCM) developed at Kyushu University. In the GCM, the gravity wave drag parameterization by Hines is used to calculate effects of the gravity wave. The contribution of the gravity wave drag to the SAO will be discussed.

**MC05/07P/D-012** Poster **1400-219**

**OZONE DEPLETION OBSERVED AT TSUKUBA, JAPAN IN FEBRUARY 2001**

Isao MURATA<sup>1</sup>, Nobutaka KOBAYASHI<sup>1</sup>, Hideaki NAKANE<sup>2</sup>, Hiroshi FUKUNISHI<sup>1</sup> (<sup>1</sup>Department of Geophysics, Graduate School of Science, Tohoku University, <sup>2</sup>National Institute for Environmental Studies)

Considerable ozone depletion has been observed in the Arctic polar vortex since 1990s. Because of strong planetary wave activity in the Arctic region, the edge of the polar vortex occasionally attains to mid-latitudes. We investigated the effect of the Arctic ozone depletion in the mid-latitude region from the correlation analysis of O<sub>3</sub>, HCl, HNO<sub>3</sub> and HF vertical column densities observed at Tsukuba, Japan (36.0°N, 140.1°E) with a high-resolution Fourier transform infrared spectrometer (FTIR). This FTIR has been operated since December 1998. The spectral resolution of the FTIR (Bruker 120M) is 0.0035 cm<sup>-1</sup>. The spectral fitting algorithm to derive the vertical column densities is based on the SFIT program developed by Rinsland and is improved with a vertical shift procedure of the initial profile to minimize the residual of the spectral fitting. The derived O<sub>3</sub> vertical column densities agree with those measured by the Dobson spectrometer at the nearby (1 km apart) station within differences of 2 to 3 %. The spectra measured from December 1998 to October 2001 are used in this analysis. Correlations of column density variations between pairs of O<sub>3</sub> and HF, HCl and HF, and HNO<sub>3</sub> and HF are good indicators of the chemical changes of O<sub>3</sub>, HCl, and HNO<sub>3</sub>. These four species are all distributed mainly in the stratosphere. One of these species, HF is chemically very stable and hence a good tracer of the transport process. The other species, O<sub>3</sub>, HCl, and HNO<sub>3</sub>, are also relatively stable in the chemical processes in mid-latitudes. Therefore, variations in the column densities of these three species and HF usually show positive correlations. The correlations of O<sub>3</sub> and HCl to HF on February 20 to 23, 2001 are found to be lower than in other periods. It is indicated that O<sub>3</sub> and HCl on these days were chemically depleted. However, the correlation between HNO<sub>3</sub> and HF showed no significant variations. A potential vorticity analysis showed that Tsukuba was located in the

boundary region of the polar vortex on these days. The backward trajectory analysis indicated that the observed air masses at the potential temperatures of 475 K and 550 K came from inside the polar vortex. It is suggested that the chemically perturbed air masses arrived above Japan due to the distortion of the polar vortex.

**MC05/07P/D-013** Poster **1400-220**

**CORRELATION BETWEEN OZONE AND POTENTIAL TEMPERATURE AND ITS DEPENDENCE ON SEASON AND LATITUDE**

Katsuyuki NOGUCHI, Takeshi IMAMURA, Koh-ichiro OYAMA (The Institute of Space and Astronautical Science, Japan)

The seasonal and latitudinal variations of the correlation between the small-scale structures of ozone mixing ratio and potential temperature are investigated using ozonesonde data. Ozone distribution in the lower stratosphere is disturbed mainly by atmospheric motions since the chemical lifetime of ozone in this region is on the order of several months. Recently the backward trajectory method with the aid of meteorological assimilation data has successfully explained that the distinct structures of ozone profiles are mainly caused by horizontal advections associated with planetary waves. Ozone structures with vertical scales of <1km are less focused, due to the limit of the vertical resolutions of assimilation data, although they appear more frequently in the vertical profiles of routine ozone observations. The present study investigates the role of vertical and horizontal advections in creating small-scale structures of ozone profiles with statistical methods. We extract small-scale (< 2km) structures of ozone, temperature, and wind velocity from the ozonesonde data distributed by the World Ozone and Ultraviolet Radiation Data Centre. The contributions of vertical and horizontal advections are inferred from the statistical analysis of the correlation between ozone mixing ratio and potential temperature. The candidates for the dynamical processes that cause those advections are also discussed.

**MC05/07P/D-014** Poster **1400-221**

**EFFECT OF A CONVECTIVELY INDUCED GRAVITY WAVE DRAG PARAMETERIZATION ON HEAVY RAIN CASES SIMULATED BY MESOSCALE MODEL(MM5)**

So-Young KIM, Hye-Yeong CHUN (Department of Atmospheric Science, Yonsei University)

Vertically propagating gravity waves can accelerate or decelerate the mean flow at the levels where wave breaking occurs. Convection is one of important sources of gravity waves. Even though mesoscale models for numerical weather prediction are developed with high resolutions, gravity waves forced by individual convective cloud cannot be entirely resolved. Therefore convectively induced gravity wave drag is better to be parameterized in the mesoscale model. In this study, a parameterization of gravity wave drag induced by cumulus convection (GWDC) proposed by Chun and Baik (1998) is implemented in the PSU/NCAR mesoscale model MM5, and effect of the GWDC on numerically simulated heavy precipitation cases in Korean peninsula is investigated. Two heavy rain events associated with Janigma front on 23-25 June 1997 and convection bands on 5-6 August 1998 are considered. The numerical experiments are conducted in a two-way nested grid system with horizontal grid spacings of 45km in an outer domain and of 15km in an inner domain. In order to investigate effect of the GWDC, two types of simulations with (GWDC) and without (CTL) the parameterization are performed. In the GWDC simulation, cloud-top wave stress is distributed in major convective regions. The magnitudes of diabatic heating rate and resultant cloud-top wave stress are large where deep cumulus cloud exists under relatively weak wind and stability condition. Impact of the GWDC parameterization in horizontal wind field is strong along the main convective regions. The magnitude difference between the GWDC and CTL is significant at the levels above clouds, and it extends down to the lower atmosphere through the change of horizontal divergence/convergence pattern. The impact of the GWDC parameterization is stronger in the inner domain mainly by the large value of diabatic heating rate. Improvement of the model performance by including the GWDC parameterization will be presented by comparison of the model results with observations.

**MC05/07P/D-015** Poster **1400-222**

**STRATOSPHERE DYNAMICS OBSERVED BY MST RADARS.**

Hubert LUCE<sup>1</sup>, Michel CROCHET<sup>1</sup>, Francis DALAUDIER<sup>2</sup>, Shoichiro FUKAO<sup>1</sup>, Mamoru YAMAMATO<sup>3</sup> (<sup>1</sup>LSEET, Toulon-Var University, La Garde, France, <sup>2</sup>Service d'Aeronomie du CNRS, Verrieres le Buisson, France, <sup>3</sup>Radio Science Center for Space and Atmosphere, Kyoto University, Kyoto, Japan)

Mesosphere-Stratosphere-Troposphere (MST) pulsed radars are powerful remote sensing tools for the study of the lower atmosphere dynamics from synoptic scale of motion down to the small scale of turbulence. They are particularly well adapted for the monitoring of the tropopause and its foldings, and for the tracking of mesoscale structures such as meteorological fronts via reflectivity and wind observations at high spatio-temporal resolution. They are also proper instruments for continuously observing mountain and inertia-gravity waves and turbulence up to about 20-25 km. Such abilities are of interest for providing estimates of the vertical transport of mass and energy through the lower atmosphere and for a better understanding of the contribution of the meso and small scale processes on atmospheric chemistry, for example. This paper is devoted to report results of ST radar measurements, mainly with the Japanese Middle and Upper (MU) atmosphere radar in different observational modes. Attention is drawn to observations performed during a radar-balloon campaign called MUTSI which took place in 2000 near the MU radar. Careful comparisons between both of the observations permitted us to validate the performances of the ST radars for wind measurements with high accuracy and spatio-temporal resolution. The paper also deals with stability, gravity wave and turbulence observations by MU radar discussed in light of high resolution (10 cm) temperature profiles measured by balloon. Such high-resolution profiles also give direct information on disturbances from waves down to the smallest scales of turbulence. They permitted us to analyze in detail the relationship between the characteristics of the radar echoes and the reality of the temperature field. In particular, it was found that turbulent mixing structures such as those revealed by the temperature profiles give rise to intense isotropic radar echoes in the tropopause region. These turbulent layers clearly arise through either gravity-wave breaking or instabilities produced by stratified shear flows resulting from the passage of a meso-scale wind disturbance at the jet-stream height. Similar turbulent events have been found within the stratosphere. Even though the structures are less extended vertically, they seem also to arise through shear instabilities. In most cases, these dynamic instabilities seemed to be triggered by a dominant gravity wave, classically observed at the MU radar latitude. The turbulent mixing was also identified as one of the sources of the generation of strong temperature gradients. They are so thin that they cannot be resolved using standard radar modes of observation. Dual and multiple frequency domain interferometry techniques are presently developed and offer the possibility to improve the radial resolution performances of the ST radars. Some results from the MU radar and the Equatorial Atmosphere radar (Indonesia) are shown. They clearly indicate that the ST radars tend to be a complete instrument for observing directly from the largest down to the smallest scales at all latitudes.



**MC05** **Monday, July 7 - Friday, July 11**  
**MIDDLE ATMOSPHERE SCIENCE (ICMA)**  
 Location: Site A, Room 9

**Tuesday, July 8 AM**  
 Presiding Chair: R. Garcia

**MC05/08A/A09-001** **Invited** **0830**

**MODEL THERMAL RESPONSE TO MINOR ENERGY SOURCES AND SINKS**

Victor I. FOMICHEV (Department of Earth and Atmospheric Science, York University)

The original middle atmosphere radiative scheme of the Canadian Middle Atmosphere Model (CMAM) included solar heating due to absorption by O<sub>2</sub> and O<sub>3</sub> and infrared cooling in the 15 micron CO<sub>2</sub> and 9.6 micron O<sub>3</sub> bands. During the past few years this scheme has been updated by inclusion of such processes as chemical heating, infrared H<sub>2</sub>O cooling, sphericity effect in solar heating, and solar heating in the near-infrared CO<sub>2</sub> bands. All of these energy sources/sinks can be considered as minor ones either in terms of their magnitude, or in terms of the limited height region where they are of importance, or both. To examine the thermal response of the middle atmosphere, a version of the CMAM with an interactive gas-phase chemistry scheme has been used in a series of multi-year experiments for conditions of perpetual July. Contribution of each of the minor sources/sinks to the energy budget of the middle atmosphere, thermal response of the model and its statistical significance will be presented in the paper.

**MC05/08A/A09-002** **Invited** **0900**

**CHANGES IN TROPICAL UPWELLING: A POSSIBLE CAUSE FOR CHANGES IN STRATOSPHERIC WATER VAPOR**

Karen H. ROSENLOF (NOAA Aeronomy Laboratory)

Increases have been noted in Northern Hemisphere middle latitude stratospheric water vapor over an extended period of time. However, over the past two years, a substantial decrease has been observed in tropical HALOE data in the 100-70 hPa layer. Similar decreases in the lower stratosphere are also seen in the frost point balloon observations taken by the NOAA Climate Monitoring and Diagnostics Laboratory in Boulder, Colorado, USA. (~40N) The decrease in water vapor appears to be the result of significant decreases in tropical tropopause temperatures as noted in assimilated model output (NCEP/NCAR reanalysis, UKMO/JARS analysis). There are also indications in the operational radiosonde data that there has been a decrease in tropical cold point temperatures. The recently observed decrease in lower stratospheric water vapor is confined vertically to pressures higher than 50 hPa. Increases are still apparent in water vapor in the middle and upper stratosphere as observed by HALOE and the Boulder water vapor sonde data. Possible changes in the mean meridional circulation in the tropics will be presented as a mechanism to explain temporal changes in observed stratospheric water vapor.

**MC05/08A/A09-003** **Invited** **0930**

**COUPLED MODELING OF THE DYNAMICS AND CHEMISTRY OF THE MIDDLE ATMOSPHERE**

Byron A. BOVILLE, R.R. GARCIA, D. KINNISON, D.R. MARSH, R.G. ROBLE, F. SASSI (National Center for Atmospheric Research)

There are many fascinating scientific questions which require models that span the atmospheric domain from the surface to the thermosphere and include both dynamics and chemistry. Several such models are either already in use or are being developed. One of these is the Whole Atmosphere Community Climate Model (WACCM2), which simulates the atmosphere from the surface to the lower thermosphere (140 km) and includes coupled dynamical and chemical models. The dynamical model is an upward extension of the Community Atmosphere Model (CAM2) using the Lin and Rood finite volume dynamical core. The chemical model incorporates a comprehensive middle atmosphere ozone chemistry based on MOZART III. Differences will be discussed between simulations using observed climatological ozone; prognostic ozone; and ozone prescribed from the climatology of the prognostic run. The emphasis will be on the interactions between dynamics and chemistry. Both the effects of dynamics on the chemical evolution and the effect of chemistry on the dynamics will be discussed.

**MC05/08A/A09-004** **Invited** **1000**

**INVESTIGATION OF CHEMICAL AND DYNAMICAL COUPLINGS USING THE WHOLE ATMOSPHERE COMMUNITY CLIMATE MODEL (WACCM)**

Douglas Edward KINNISON, Rolando G. GARCIA, Byron A. BOVILLE, Fabrizio SASSI, Dan R. MARSH, Ray ROBLE (Atmospheric Chemistry Division, National Center for Atmospheric Research)

An accurate prediction of future global change must account for the changes in the middle atmosphere chemical system (e.g., O<sub>3</sub> and H<sub>2</sub>O distributions). Until recently, climate models have represented chemical processes in an overly simplified or decoupled manner. At the National Center for Atmospheric Research (NCAR), the Whole Atmosphere Community Climate Model (WACCM) has been developed to address the impact of dynamical and chemical couplings relevant to the stratosphere, mesosphere, and lower thermosphere. This model includes a detailed representation of middle atmosphere chemical processes. The chemical mechanism includes 48 species and approximately 120 chemical and photochemical reactions. The species are included within the OX, NOX, HOX, ClOX, and BrOX chemical families; along with CH<sub>4</sub> and its degradation products. Heterogeneous processes on sulfate aerosols and polar stratospheric clouds (Type 1a, 1b, and 2) are included. Dehydration and denitrification on these aerosols are also represented. In this study we will describe the WACCM model and show results from a multi-year simulation that couples dynamics and chemistry. Detailed model and data comparisons will be shown representing diurnal and seasonal distribution of key middle atmosphere constituents. These results will be contrasted with a control simulation where model-derived constituents, particularly ozone, are replaced with climatological distributions.

**MC05/08A/A09-005** **Invited** **1050**

**MIXING AND DEHYDRATION NEAR THE TROPICAL TROPOPAUSE: INFERENCES FROM RECENT WORK**

Steven C. SHERWOOD (Yale University)

Debate continues on the role of convection in mixing and/or dehydrating the region near the tropical tropopause. Superficial attempts to infer how high above the surface tropical convective mixing remains important yield conflicting results, depending on the constituent examined. A previous model (Sherwood and Dessler, 2001), was able, however, to correctly predict features in the vertical distributions of water vapor, ozone, and cloud using an explicit overshooting-mixing scheme. Here I will discuss the likely details by which dehydration in convective elements would occur. I will also present more recent model simulations that examine the seasonal cycle and transport of isotopes of water. These new simulations remove the most troubling obstacles to convection's being a dominant dehydration process. Although the simulations cannot rule out alternative dehydration mechanisms, they do show that convective fluxes must at least reach closer to the cold point than many have assumed.

**MC05/08A/A09-006** **Invited** **1120**

**A STRATOSPHERIC SPRINKLER OVER THE MARITIME CONTINENT - AN APPROACH BY TRAJECTORY CALCULATION**

Koji YAMAZAKI<sup>1</sup>, Hiroaki HATSUSHIKA<sup>2</sup> (<sup>1</sup>Graduate School of Environmental Earth Science, Hokkaido University, <sup>2</sup>Central Research Institute of Electric Power Industry)

A trajectory analysis by the AGCM-simulated three dimensional wind and temperature is done for investigating the path of the air with low water vapor from the tropical troposphere into the tropical stratosphere in the boreal winter. Tropospheric parcels are advected upward to the bottom of the tropical tropopause layer (TTL) mainly from the troposphere over the maritime continent and the western tropical Pacific, namely the "stratospheric fountain" region. Around the tropopause, there are strong easterlies and the cold ascent region tilts eastward with height. A down-slope flow over the upward bulged isentropic surface produces the downward -velocity over Indonesia. In addition, reduction of longwave heating over deep convection suppresses upward motion. Because of the time-mean downward motion over the maritime continent around the tropopause, it seems to be hard to ascend directly to the stratosphere in this region. Strong anticyclonic circulation tends to trap air parcels in the tropical western Pacific and it makes parcels pass the equatorial cold region several times during the slow ascent in the TTL. This slow spirally ascending motion (sprinkler) brings about low humidity in the stratosphere. In addition, transient disturbances, especially low frequency disturbances, produce intermittent upward motions over the fountain region and they dehydrate the air effectively. Both the spiral ascent and the transient mechanisms are the keys of the dehydration process around the TTL. An interannual variation of entered water vapor mixing ratio into the tropical lower stratosphere with the ENSO signal is also estimated. The La Nina years are more dehydrated than the El Nino years.

**MC05/08A/A09-007** **Invited** **1150**

**THE INTERFACE BETWEEN THE TROPICAL TROPOSPHERE AND STRATOSPHERE**

Ian A. FOLKINS (Dalhousie University)

The tropical troposphere is often thought of as well mixed by deep convective overturning up to about 17 km, the height of the highest cloud tops. However, the upper tropical troposphere exhibits a number of properties that we commonly think of as being stratospheric: lapse rates that strongly deviate from moist adiabatic, aseasonal temperature cycle that is in phase with the Brewer Dobson circulation, ozone mixing ratios that increase with height, and positive clear sky radiative heating rates. It may therefore be appropriate to think of the boundary between the tropical troposphere and the stratosphere as a layer rather than a discrete boundary. In this way of thinking, the detrainment rate plays an important role in characterizing the decrease in convective outflow as you approach the stratosphere from below, and in interrelating the emergence of the various stratospheric properties.

**Tuesday, July 8 PM**  
 Presiding Chair: M. Baldwin

**MC05/08P/A09-001** **Invited** **1400**

**BALLOON-BORNE OBSERVATIONS OF OZONE AND WATER VAPOR IN THE TROPICAL TROPOPAUSE LAYER - RESULTS FROM SOWER CAMPAIGNS**

Masato SHIOTANI (Radio Science Center for Space and Atmosphere, Kyoto University)

In view of the lack of ozone and water vapor observations in the tropical upper troposphere and lower stratosphere (UT/LS), the Soundings of Ozone and Water in the Equatorial Region (SOWER)/Pacific mission has been conducted. This is intended to improve our knowledge on the ozone and water vapor distributions by making coordinated balloon borne observations in the Pacific region along the equator. The SOWER bases are at San Cristobal, Galapagos, Ecuador and Christmas Island, Kiribati supplementing the on-going program at Watukosek, Indonesia. The observations have been started as a basis of campaigns, the first of which was realized in March 1998. Since then, roughly two-week long campaigns have been conducted mostly in the period of February-March and September-October to capture the atmospheric behavior during local rainy/dry seasons and strong/weak pumping from the extratropical stratosphere. For the ozone measurement, we use the meteorological balloon-borne electrochemical concentration cell (ECC) ozonesondes. For the water vapor measurement, we use three different balloon-borne sensors (often at the same time), i.e., 1) the relative humidity sensor of the meteorological radiosonde, 2) a Swiss-made commercial chilled-mirror hygrometer named "Snow White", and 3) a US-made chilled-mirror hygrometer developed at National Oceanic and Atmospheric Administration (NOAA). So far our results from these campaigns have been contributing to the understanding of the stratosphere-troposphere exchange, especially on issues of the tropical tropopause layer. These results are briefly summarized in the following and will be detailed in the talk. i) Our water vapor soundings have revealed for the first time the seasonal and regional characteristics of water vapor distributions in the tropical UT/LS region. For example, observations at San Cristobal show that in March-April, water vapor concentrations are low and nearly saturated around the tropopause, but that in September the concentrations are high and often sub-saturated. ii) Soundings in the Galapagos provided an observational evidence that the equatorial Kelvin wave around the tropopause acts as a dehydration pump for the stratosphere. This process may be one of the important mechanisms that control the stratospheric water vapor concentrations, hence the stratospheric photochemistry. iii) We have been making several intercomparison campaigns of the three water vapor sensors as introduced previously. This is very important for the current scientific community because we now have no established water vapor sensor for monitoring the tropical UT/LS regions. We

are focusing especially on the "Snow White" hygrometer for this purpose and improving this sensor.

**MC05/08P/A09-002 1430**

**HOW DO AIR AND HUMIDITY ENTER THE STRATOSPHERE?**

Andrew GETTELMAN<sup>1</sup>, Tim J. DUNKERTON<sup>2</sup> (<sup>1</sup>National Center for Atmospheric Research, <sup>2</sup>Northwest Research Associates)

It is well accepted that air and humidity enter the stratosphere around the tropical tropopause. Exactly how, when and where are not well understood. This limits our prognostic ability to understand changes to the stratosphere. Some of the important processes for determining how air and humidity enter the stratosphere are: convective transport, horizontal motions and stratospheric transport. For water vapor, cold temperatures and cirrus ice clouds are also important. But which are the dominant processes of interest on various timescales? In this study it is argued that the basic features of troposphere to stratosphere exchange can be understood on a global scale through the use of large scale models, and some parameterizations of small scale processes. A suite of models tied to observations are used to explore how air enters the stratosphere. A 3D chemical transport model with realistic chemistry and idealized tracers is used to examine the spatial and temporal locations that contribute to the stratospheric 'tape recorder' in humidity. The sensitivity of the stratosphere to changes in the driest (tropical western Pacific in December-February) and wettest (Asian Monsoon region in July-September) regions of the Tropical Tropopause Layer is analyzed and the source regions of the 'tape recorder' signal are decomposed. These simulations are compared to observations of clouds, water vapor, ice, and stable isotopes of water vapor. The simulations are also compared to more detailed models and observations of the tropopause region and the lower stratosphere. The implications for trends in stratospheric water vapor, as well as stratosphere-troposphere exchange of water vapor and other trace species around the tropopause are examined.

**MC05/08P/A09-003 1450**

**OBSERVING THE TROPOPAUSE TRANSITION LAYER IN THE TROPICS WITH THE HIGH RESOLUTION DYNAMICS LIMB SOUNDER (HIRDLS) ON NASA'S AURA SPACECRAFT**

John C. GILLE<sup>1</sup>, Alyn LAMBERT<sup>1</sup>, Douglas KINNISON<sup>1</sup>, Aaron LEE<sup>2</sup>, Kenneth STONE<sup>3</sup>, John BARNETT<sup>1</sup> (<sup>1</sup>NCAR, <sup>2</sup>University of Colorado, <sup>3</sup>Oxford University)

The High Resolution Dynamics Limb Sounder (HIRDLS) will be launched on the Aura spacecraft in early 2004. It has been designed to achieve higher vertical and horizontal resolution in retrieved quantities than has previously been available. The vertical resolution results from a narrow (~1.2 km) vertical field of view, oversampling, and low noise which allows deconvolution of fine scale structure. In addition, correcting for gradients along the line of sight results in results with high accuracy. We illustrate this with simulations of operational retrievals of 3-D model fields over the W. Pacific, showing the capability to retrieve temperature and water vapor structures in the vicinity of the tropopause only a few hundred meters in thickness.

**MC05/08P/A09-004 1510**

**INTRASEASONAL VARIATIONS OF HUMIDITY AND THIN CIRRUS CLOUDS IN THE TROPICAL UPPER TROPOSPHERE**

Nawo EGUCHI<sup>1</sup>, Masato SHIOTANI<sup>2</sup> (<sup>1</sup>Graduate School of Environmental Earth Science, University of Hokkaido, <sup>2</sup>Radio Science Center for Space and Atmosphere, University of Kyoto)

Distributions of upper tropospheric humidity, thin cirrus clouds and meteorological fields associated with the intraseasonal oscillation are investigated using UTH (Upper Tropospheric Humidity) data from MLS (Microwave Limb Sounder) on board UARS (Upper Atmosphere Research Satellite) at 215 and 146 hPa. The presence of thin cirrus clouds is inferred from the UTH data when relative humidity is over 100%. This is justified by comparing with the UARS CLAES (Cryogenic Limb Array Etalon Spectrometer) aerosol data. Five intraseasonal oscillation events are clearly observed during the two boreal winters from October 1991 to April 1993. Composite analyses on the distributions of humidity and thin cirrus clouds for these episodes are performed on the basis of the bandpass filtered outgoing longwave radiation (OLR) data with a period of 20-80 days. Eastward moving high humidity regions with a phase speed of about 5 m/s are found over the central Indian ocean and near the date line. The high humidity region at 146 hPa exists in the western hemisphere and expands more horizontally than at 215 hPa. When convection is mature, the thin cirrus cloud frequency becomes larger in the tropical Western Pacific and its high frequency region moves around the globe. Temperature anomaly field consists of zonal wave-number 2 or 3 components at both levels. The positive (negative) region at 215hPa (146hPa) precedes (moves behind) the convective area with about 10 degrees (5 degrees). The correlation between temperature anomalies and water vapor anomalies at 215hPa (146hPa) is positive (negative) over the convective area. The structure of temperature anomalies associated with the intraseasonal oscillation resembles that due to the Kelvin wave. The negative anomalies are over the convective area and tilt eastward and upward. The temperature anomalies change sign at 200 hPa over the convective area. The enhanced humidity area extends to near the tropopause by the deep convection. Then it extends further westward and northward from the convective area because of the horizontal transport. There are drier regions of subsidence on each side of the convective region.

**MC05/08P/A09-005 1530**

**SEASONAL AND INTERANNUAL VARIATIONS OF THE TROPOPAUSE TEMPERATURE AND HEIGHT OVER INDONESIA**

Noriko OKAMOTO<sup>1</sup>, Manabu D. YAMANAKA<sup>2</sup>, Shin-Ya OGINO<sup>1</sup>, Hiroyuki HASHIGUCHI<sup>1</sup>, Noriyuki NISHI<sup>1</sup>, Tien SRIBIMAWATI<sup>3</sup> (<sup>1</sup>Graduate School of Science and Technology, Kobe University, Japan, <sup>2</sup>Graduate School of Science and Technology, Kobe University, Japan, and Frontier Observation Research System for Global Change, Japan, <sup>3</sup>Radio Science Center for Space and Atmosphere, Kyoto University, Japan, <sup>4</sup>Graduate School of Science, Kyoto University, <sup>5</sup>Agency for the Assessment and Application of Technology, Indonesia)

Seasonal and interannual variations of tropospheric and lower stratospheric temperature including CPT (Cold Point Tropopause) have been investigated based on operational rawinsonde data at 11 stations over Indonesia and 22 stations in surrounding region during 1992-1999, and comparisons with NCEP reanalysis data are also made. Upper tropospheric and lower stratospheric temperature over Indonesia has annual variation which has lower (higher) in northern winter (summer) and peak to peak difference is approximately 5 K. This annual variation is the same as that at other equatorial region reported in previous studies. CPT over Indonesia is usually lying between 100hPa and 70hPa. In longitudinal direction, CPT temperature is almost uniform in northern summer but has difference of about 4 K which is lower in eastern part (130E) and higher in western part of Indonesia (100E) in

northern winter. In latitudinal direction, CPT temperature is highest over 0-5S and lower in higher latitudes (15N and 15S), and the temperature difference between over the equator and higher latitudes is larger in northern winter (about 3 K) than in northern summer (about 2 K). Similar latitudinal structure is clearly seen at 100 hPa level, and temperature has symmetrical structure about the equator. However this symmetrical structure is not appeared in NCEP reanalysis data especially in northern summer, and difference from rawinsonde data becomes larger with southward (4 K in 15S). As interannual variations, two kinds of variation are clearly confirmed. One is the variation correlated with ENSO, and the other is monotonical change. During normal (non-El Nino and -La Nina) period from July 1992 to April 1997, temperature below than 100 hPa altitudes increases year by year and the increasing rate becomes maximum (0.23 K/year) at 200 hPa level. On the other hand, lower stratospheric temperature decreases year by year and increasing rate is especially low at 50 hPa (-0.84 K/year) and 70 hPa (-0.82 K/year). During thus period, CPT temperature varies in inverse phase with CPT height correlated with QBO, and decreases year by year keeping with longitudinal structure mentioned above. However after the period, El Nino situation started in May 1997, both CPT temperature and height have positive anomaly and longitudinal structure also becomes unclear. In the troposphere, large positive anomaly appears in October 1997 (when El Nino came to mature stage) and continues until the end of the El Nino.

**MC05/08P/A09-006 1620**

**POSSIBLE CROSS-TROPOPAUSE TRANSPORT PROCESSES IN THE TROPICS OBSERVED BY THE EQUATORIAL ATMOSPHERE RADAR IN INDONESIA**

Shoichiro FUKAO, Masatomo FUJIWARA, Masayuki K. YAMAMOTO, Takeshi HORINOUCHE, Hiroyuki HASHIGUCHI (Radio Science Center for Space and Atmosphere, Kyoto University)

Dynamical transport across the tropical tropopause region directly or indirectly controls the stratospheric photochemistry and the Earth's radiative balance by determining the concentrations of minor constituents and particles there. However, the mechanism has not been well understood yet due to scarcity of observations. In this paper, we discuss two processes that seem to be related to this mechanism, Kelvin-Helmholtz instability and breaking of an equatorial Kelvin wave, obtained with the Equatorial Atmosphere Radar in Indonesia (EAR; 0.20°S, 100.32°E, 865 m above sea level). First, the EAR observed a persistent strong eastward wind shear (10-50 m/s/km) of westward wind in November 2001, and the radar echo layer tilted downward to the west in the region 0-1 km above the tropopause. The vertical wind was always upward in the same region. During the same period, the Richardson number was continuously less than 0.5 and occasionally less than 0.25, indicating that the Kelvin-Helmholtz instability frequently occurred there. The existence of the tilted radar echo layer can be explained by KHI billows. Also, the observed updraft has been found spurious, being caused by the KHI-induced tilted echo layer in the strong westward wind. Second, a significant enhancement of turbulence was observed with the EAR in the tropopause region intermittently for about 5 days during November 19-23. The turbulence intensity estimated from the power spectral width during the period was up to a factor of five times larger in kinetic energy than that in other periods. Further analyses have confirmed that the enhanced turbulence was convectively generated in the breaking phase of an equatorial Kelvin wave. Between July and December 2001, we observed three more prominent cases of the turbulence generation by the same breaking Kelvin waves in the tropopause region.

**MC05/08P/A09-007 1640**

**OBSERVATIONS IN THE TROPICAL TROPOPAUSE REGION WITH THE EQUATORIAL ATMOSPHERE RADAR**

Masayuki YAMAMOTO<sup>1</sup>, Masayuki OYAMATSU<sup>1</sup>, Takeshi HORINOUCHE<sup>1</sup>, Masatomo FUJIWARA<sup>1</sup>, Hiroyuki HASHIGUCHI<sup>1</sup>, Mamoru YAMAMOTO<sup>1</sup>, Shoichiro FUKAO<sup>1</sup>, Manabu YAMANAKA<sup>2</sup> (<sup>1</sup>Radio Science Center for Space and Atmosphere, Kyoto University, <sup>2</sup>Graduate School of Science and Technology, Kobe University/Frontier Observational Research System for Global Change)

Now there are many controversies about the airmass motions in the tropical tropopause layer (TTL). The Equatorial Atmosphere Radar (EAR), located at the equator in West Sumatra, Indonesia (0.2 degrees south, 100.32 degrees east, 865 m above mean sea level), is a 47-MHz clear-air Doppler radar. The EAR has been observing three-dimensional wind velocities and the intensity of turbulent eddies with half the radar wavelength (about 3m) in the troposphere and the lower stratosphere (2-20km) since July 2001 [Fukao et al., 2003]. So far, the EAR has been observed the enhancement of turbulence due to an equatorial Kelvin wave [Fujiwara et al., 2003] and the frequent occurrence of the Kelvin-Helmholtz instability (KHI) around the tropical tropopause [Yamamoto et al., 2003]. In this paper, we show that the EAR has the ability of determining the tropopause height and the observational result especially in the region 0-1km above the tropopause. A clear-air VHF Doppler radar receives the strong echo around the tropopause due to the rapid increase of static stability in the region. The scattered signals in the region comes from the horizontally stratified echo layer (Frenel reflection). By using these properties, we determined the tropopause height (Radar Tropical Tropopause: RTT) from the height profiles of echo power and echo power aspect ratio. The height of RTT was compared with the height of lapse-rate tropopause determined by the radiosonde soundings at Kototabang, and its correspondence was excellent. The height of RTT was almost corresponding to the maximum of the westward wind (20-35m/s), and the strong vertical shear of zonal wind (10-50m/s/km) was observed in the region 0-1km above RTT. The spectral width, which indicates root-mean-square turbulent motion of the 3-m eddies, increased in the region (0.5-0.9 m/s in northward beam and 0.7-1.2 m/s in eastward beam). The spectral width observed in the zonal direction was greater than that in the meridional direction, because the vertical shear of horizontal wind generates turbulence and the vertical shear of zonal wind was stronger than that of meridional wind. Yamamoto et al. [2003] showed that vertical wind measured with the vertical beam was continuously upward in the region 0-1 km above the tropopause in November 2001, and it contained a spurious updraft component caused by the tilted echo layer generated by the KHI billows and the strong westward wind. Upward wind measured with the vertical wind in the region 0-1 km above the tropopause was observed throughout July-December 2001, which suggests the frequent occurrence of KHI not only in November 2001 but also in the long term. To avoid the effects of spurious vertical wind component caused by tilted echo layer generated by KHI billows and the strong westward wind, vertical wind was calculated with two symmetric meridional beams (NS vertical wind), which is little affected by the tilted echo layer and the horizontal wind to the vertical wind measurement. The NS vertical wind also showed updrafts with the magnitude of 1-5 cm/s.



**WATER VAPOR AND AEROSOL EXTINCTION VARIATIONS ASSOCIATED WITH THE EQUATORIAL KELVIN WAVE IN THE TROPICAL TROPOPAUSE LAYER AS OBSERVED IN HALOE DATA**

Masanori NIWANO (Department of Geophysics, Kyoto University)

The occurrence of cirrus clouds and dehydration in the tropical tropopause layer (TTL) has a close relationship with seasonal cycle and an increasing trend of water vapor in the stratosphere. Water vapor and aerosol data from the satellite, balloon and lidar measurements have documented variations in the distribution of cirrus clouds within the TTL on a broad range of timescales. However, the spatial variation of cirrus clouds related to large scale intraseasonal variations, such as the equatorial Kelvin wave or the Madden-Julian Oscillation (MJO), has received little attention in the TTL. This work examines the occurrence of cirrus clouds associated with the short term variations in the TTL, using water vapor and aerosol extinction data (version 19) from the Halogen Occultation Experiment (HALOE) measurement. Temperature data are taken from rawinsonde measurements over Singapore to validate the occurrence of cirrus clouds. The cirrus cloud altitude is here defined by the log-pressure height where the vertical gradient of extinction at  $5.26 \mu\text{m}$  ( $d \log_{10} \beta / dz$ ) exceeds  $0.28 \text{ km}^{-1}$  with altitude decreased. The analysis is focused on two tropical measurements of 20 to 28 January 1993 (case 1), and 23 December 1998 to 1 January 1999 (case 2), during which cirrus clouds tied with the equatorial Kelvin wave appear just above the tropopause. Both in the two cases, the isolines of water vapor and aerosol extinction shows longitudinal distribution with planetary zonal wave number  $\sim 2$  and its maximum vertical displacement of about 6 km (from 70 to 150 hPa) around the TTL. The longitudinal structure tilts eastward with height, so that its vertical wave length is  $\sim 18 \text{ km}$ , which is identified with the equatorial Kelvin wave connected to the outgoing longwave radiation (OLR) anomalies. Over Singapore, temperature perturbation is descending with time with a period of 20-25 days, and cirrus clouds correspondingly appear in the region of cold temperature anomalies. It is stressed that, in case 2, a water vapor decrease by 1-2 ppmv and an extinction enhancement by an order of  $\sim 1$  are simultaneously observed up to 60 hPa where wet anomalies of water vapor of 4.5-5 ppmv exist. The occurrence of cloud top around 60 hPa nearly coincides with the upper extension of the region less than 195 K due to the equatorial Kelvin wave perturbation. This result demonstrates the tight connection between planetary scale variation and the occurrence of cirrus clouds in the TTL, suggesting the potential role of the equatorial waves in dehydration and ozone destruction on the cirrus clouds within the TTL.

**TROPOSPHERE- STRATOSPHERE INTERACTION DURING A TROPICAL CYCLONE PASSAGE OVER INDIA**

Mrudula G. Mohan Kumar K (Department of Atmospheric Sciences, Cochin University of Science and Technology)

Zonal and meridional momentum flux transport during the passage of a tropical cyclone over Indian sub-continent has been studied. The cyclonic storm, which formed on October 14, 2001 in the west central Bay of Bengal developed into a deep depression on October 15<sup>th</sup> morning. This system further intensified into a cyclonic storm on same day evening, crossed over MST radar site at Gadanki (13.5°N, 79.2°E), India, on October 16<sup>th</sup> morning. The MST radar daily observations of 30-minute duration (0930-1000 hrs LT) from 11 – 21 October 2001 and special observations of 1 hour duration from October 15<sup>th</sup> at 0930 hrs LT to October 16<sup>th</sup> at 1630 hrs LT between 3.75 and 21 km with an altitude resolution of 150 m have been used for the study. The horizontal velocity components show considerable changes in the upper troposphere and lower stratosphere during the passage of the cyclonic storm, whereas the vertical velocity shows strong upward motion in the 11 -12 km region. The zonal wind anomalies observed prior to the formation of the tropical cyclone seems to propagate upwards from the middle troposphere to the lower stratosphere. The transport of zonal and meridional momentum fluxes is calculated and presented. The zonal momentum transport is generally downward before the arrival of the tropical cyclone over Gadanki. Upward transport of zonal momentum flux starts in the middle troposphere (8 km) from October 13<sup>th</sup> onwards in association with the approach of the storm. As the cyclonic intensity increases the upward transport also extend to greater heights even upto the stratosphere. The maximum upward transport of zonal momentum flux is noted at the tropopause level on October 16 during the time of the overhead passage day of cyclone at the station. Before the development of the cyclone the meridional momentum flux transport is downward and changes to upward in lower levels from October 11<sup>th</sup> onwards, which becomes stronger as the storm approaches the station. The upward transport of meridional momentum flux is also maximum ( $\sim 18 \text{ m}^2 \text{ s}^{-2}$ ) at the tropopause level on the day of passage of cyclone over the station. After the passage of the cyclone the vertical transport of momentum fluxes returned to its prevailing downward direction.

**VHF RADAR OBSERVATIONS OF TROPICAL TROPOPAUSE AND ITS TEMPORAL VARIABILITY**

Siddarth Shankar DAS<sup>1</sup>, Mrudula G<sup>2</sup>, Pramod Kumar KHANDAPAL<sup>3</sup>, A.R. JAIN<sup>1</sup> (<sup>1</sup>National MST Radar Facility, <sup>2</sup>Cochin University of Science and Technology, <sup>3</sup>University of Allahabad)

Entrance of various chemical compositions and minor constituents from troposphere to stratosphere and vice-versa take place through tropical tropopause, which play a significant role in the troposphere-stratosphere exchange/dynamics. This makes the study of temporal and spatial variation of tropical tropopause so important to understand its various dynamical properties. Generally height of tropopause is determined from Radiosonde measurement, but it is limited in time resolution, since observations are taken only twice per day (0000 GMT & 1200 GMT). Thus the studies related to short period variability of tropical tropopause, which is important for the small-scale stratosphere-troposphere exchange are not possible by using existing conventional method. Also it is very difficult to get Radiosonde observation during convection and cyclone period, which play a major key role in Stratospheric-Tropospheric exchange (STE). At these situations detection of tropopause height by using remote-sensing technique, such as atmospheric radar, which are applicable in any of the above-mentioned weather condition can be adapted. In this paper we have used two different methods for the determination of tropopause height by using VHF-radar and compared each of them with the conventionally detected tropopause height derived from Radiosonde. These methods show consistency for both diurnal and day-to-day variation in tropopause height. Diurnal variation of tropopause during monsoon period is correlated with the tropopause temperature. The present results shows the minimum in both tropopause height as well as tropopause temperature at  $\sim 0400$  hrs (LT). There is a simultaneous change in the environmental lapse rate, which is observed to be minimum during that period. Our results show the net upward mass-flux during the diurnal cycles at tropopause level. The detailed results of these studies will be presented in this paper.

**MODEL EVALUATION ON EFFECTIVE TRANSPORT ACROSS THE EXTRATROPICAL TROPOPAUSE USING TRACER RELATIONSHIPS**

Jennifer Chu-Feng WEI<sup>1</sup>, Laura L. PAN<sup>2</sup>, Douglas E. KINNISON<sup>2</sup>, Rolando GARCIA<sup>2</sup>, Donald J. WUEBBLES<sup>2</sup> (<sup>1</sup>Department of Atmospheric Sciences, University of Illinois at Urbana-Champaign, <sup>2</sup>National Center for Atmospheric Research)

There remain significant uncertainties in understanding the chemical and physical processes that controls ozone and other constituents in the upper troposphere and lower stratosphere (UT/LS), or the tropopause  $\pm 2 \sim 3 \text{ km}$  region. One way to understand the transport characteristics associated with a wind field is to study the long-lived tracer distribution produced by the wind field through advection and mixing. The primary focus of our calculations is to examine the correlation of chemical tracers, such as N<sub>2</sub>O, O<sub>3</sub>, CO, NOy, H<sub>2</sub>O and CH<sub>4</sub>, in the UT/LS region using the new fully coupled troposphere, stratosphere and mesosphere version of the three-dimensional global scale chemical-transport model, MOZART 3 (Model for OZone And other Related Tracers, version 3). Studies are particularly aimed at evaluating the model transport in comparison with available measurements made by satellite instruments and by various aircraft campaigns, ozonesondes, and balloon experiments. Our intention is to carry out a comprehensive and systematic analysis of the UT/LS region in order to understand the relative roles of chemistry and transport for the distribution of key chemical constituents like ozone and water vapor in the UT/LS region.

**TROPOSPHERE-TO-STRATOSPHERE EXCHANGE AND THE WATER VAPOUR BUDGET IN THE EXTRA-TROPICAL LOWERMOST STRATOSPHERE**

Michiel S. BOURQUI, Heini WERNLI, Michael SPRENGER (Institute for Atmospheric and Climate Science, ETH Zurich)

The net downward transport across the extra-tropical tropopause is, in asymptotic perspective, the result of upward fluxes of tropospheric air and, to a larger extent, downward fluxes of stratospheric air. As far as watervapour is concerned, it is necessary to separate these two opposite fluxes because they have very different concentrations of H<sub>2</sub>O. The total upward transport of moist tropospheric air across the tropopause may have important implications for the water vapour budget of the lowermost stratosphere. The tropospheric contribution to the water vapour budget in this region is however not clearly understood yet and is the focus of this study. The problem is addressed here using a Lagrangian perspective of the flow. The technique, based upon ECMWF re-analysis data, enables to systematically trace air parcels and identify cross-tropopause exchange events. In the first part of the talk, the estimation of an upper bound for the mass of water vapour transported from the troposphere to the stratosphere based upon the temperature at exchange locations will be discussed. And in the second part, first results will be shown from a water vapour budget estimated by investigating the history of the air parcels found in the lowermost stratosphere.

**MIDLATITUDE CROSS-TROPOPAUSE TRANSPORT OF WATER VAPOR AND TRACE CHEMICALS BY DEEP CONVECTIVE STORMS**

Pao K. WANG (Department of Atmospheric and Oceanic Sciences, University of Wisconsin-Madison)

This paper shows the simulation results of cloud top plume transport process using a 3-D cloud dynamical model with explicit microphysics. The plume above thunderstorm phenomenon often observed by higher resolution satellite visible and IR images is successfully simulated. Analysis of the model results indicates that water vapor can be transported from the cloud into the stratosphere when the gravity waves caused by vigorous convection in the storm break. The breaking waves send water vapor through isentropic surfaces that are strongly distorted already by the updrafts. Characteristics of the simulated plumes and that observed by satellites show good agreement that lends strong support for the proposed process. This finding indicates that water vapor can be transported through the tropopause that is often considered impenetrable due to the strong stability of the overlying stratosphere. This could have important implications in global climate process and atmospheric chemistry. Water vapor is the most important greenhouse gas in the atmosphere and its radiative effect in the stratosphere is orders of magnitude higher than in the troposphere. In addition, water vapor at the stratospheric level serves as the source for strong oxidants such as OH and HOX radicals that are related to ozone destruction. Recent observational studies indicate that the lower stratospheric water vapor concentration increased by 1 to 1.5% annually in the midlatitudes in the last 35 years. The mechanism proposed here may serve as a key process in the possible explanations for the observed trend. Transport of inert chemical species that are less susceptible to the freeze-drying effect of the cold tropopause temperatures are also investigated. A preliminary simulation using the same model but for inert tracer transport by these storms show that this is indeed the case.

**CHANGE IN STRATOSPHERE/TROPOSPHERE EXCHANGE IN A DOUBLED CO<sub>2</sub> CLIMATE**

Warwick NORTON<sup>1</sup>, Alan IWF<sup>2</sup> (<sup>1</sup>Atmospheric Physics, University of Oxford, <sup>2</sup>Rutherford Appleton Laboratory)

A middle atmosphere GCM coupled to a slab ocean has been used to examine changes in stratosphere/troposphere exchange in a doubled CO<sub>2</sub> climate. Changes in transport from the troposphere to stratosphere of water vapour and tropospheric source gases, and transport from the stratosphere to troposphere of ozone, are diagnosed. Hence predictions are made of possible future changes in stratospheric water vapour and tropospheric ozone. Changes in the Brewer-Dobson circulation, Hadley circulation, tropopause temperature, and eddy mixing across the tropopause are analysed to understand the changes in transport.

**ASYMMETRY IN TRACER VARIATIONS DURING THE WESTERLY AND EASTERLY SHEAR PHASES OF THE QBO IN THE TROPICAL STRATOSPHERE**

Wookap CHOI<sup>1</sup>, Hyunah LEE<sup>2</sup> (<sup>1</sup>Seoul National University, <sup>2</sup>NCAR)

Concentrations and distributions of stratospheric aerosol, hydrogen fluoride and ozone from

the Halogen Occultation Experiment (HALOE) on the Upper Atmosphere Research Satellite (UARS) are used to investigate features associated with transport by the secondary meridional circulation induced by the quasi-biennial oscillation (QBO). The points of maxima in the divergence and convergence of the QBO-induced meridional velocity at the equator are identified from the meridional gradients of the tracers. Such points can be identified from the tracer fields in the westerly shear zones but not in the easterly shear zones. There are features of tracer fields associated with asymmetry between the easterly and westerly shear phases. The asymmetry seems to be mainly due to reversal of the direction of the secondary vertical motion. The temporal variation of tracer concentration at the equator is determined mainly by vertical advection, which is significantly larger during the westerly shear phase of the QBO than during the easterly shear phase, since the QBO-induced equatorial sinking motion amplifies the vertical gradient. Thus, the vertical advection associated with the secondary circulation has a stronger influence on the equatorial tracer variation during the westerly shear phase than during the easterly shear phase.

**MC05/09A/A09-006 1120**

**SEASONAL AND QBO VARIATIONS OF ASCENT RATE IN THE TROPICAL LOWER STRATOSPHERE AS INFERRED FROM HALOE TRACE GASES**

Masanori NIWANO<sup>1</sup>, Koji YAMAZAKI<sup>2</sup>, Masato SHIOTANI<sup>3</sup> (<sup>1</sup>Department of Geophysics, Kyoto University, <sup>2</sup>Graduate School of Environmental Earth Science, Hokkaido University, <sup>3</sup>RASC, Kyoto University)

Mean meridional circulation in vertical velocity is indirectly estimated from the calculations of radiative heating rates or wave forcing, while the accurate calculation can not be achieved in the equatorial lower stratosphere due to uncertainties in the both two kinds of calculations. Water vapor data from the satellite and in-situ measurements give us an opportunity to estimate ascent rate in the tropical lower stratosphere. The extensive studies of vertical velocity using trace gases succeeded to derive seasonal cycle and the quasi-biennial oscillation (QBO). However, there is no systematic analysis of ascent rate as a function of altitudes, latitudes, and frequency. In this study, time and spatial variations in ascent rates are investigated, using water vapor (H<sub>2</sub>O) and methane (CH<sub>4</sub>) data from the Halogen Occultation Experiment (HALOE) measurements since 1991. The ascent rate is inferred from the ascending seasonal variations of [H<sub>2</sub>O] + 2[CH<sub>4</sub>] (H). By calculating a vertical lag-correlation between the H profiles at a certain and the adjacent time steps, the ascent rate is estimated for every latitude, altitude and time. The ascent rate variations are not the same as variations of the actual vertical velocity, but a good indicator of the actual one within the subtropical barriers. The derived ascent rate exhibits two kinds of dominant variations within ±15° of the equator: the one is seasonal cycle and the other is interannual variation with a period of nearly two years, being consistent with the QBO variations. The amplitudes of the seasonal and QBO components are relatively similar (0.05-0.10 mm s<sup>-1</sup>), but exhibit quite different meridional structures. The seasonal cycle shows vertically in-phase variations with northern a winter maximum (0.2-0.4 mm s<sup>-1</sup>) and a summer minimum (0.15-0.2 mm s<sup>-1</sup>) between 20-60 hPa, and the ratio of ~2 in the range of 20-40 hPa. The latitudinal distribution is characterised by 1) an early appearance of the well-known subtropical summer maximum of ascent rate and 2) a double peak structure around 10-15°N and S during the northern winter. On the other hand, the QBO component of ascent rate shows tropically confined variations and a rapid downward propagation, whereas mass attenuation estimated from vertical mass flux presents much slower downward propagation. The phase dependency of the QBO anomalies is observed, such that the descent anomalies exhibits a structured variation symmetric about the equator, while the ascent anomalies have a tendency to propagate latitudinally. This can be tightly connected with the phase dependency of the QBO acceleration. An examination of amplitude and phase of variations in the ascent rate and temperature emphasizes that the radiative damping timescale is considerably long (40-100 days) below 40 hPa.

**MC05/09A/A09-007 1140**

**THE QUASI BIENNIAL OSCILLATION: ANALYSIS OF THE NEW ERA-40 DATA AND A GCM STUDY**

Charlotte PASCOE<sup>1</sup>, Lesley GRAY<sup>2</sup> (<sup>1</sup>Rutherford Appleton Laboratory, <sup>2</sup>The University of Reading)

The new 40-year ECMWF reanalyses and a stratosphere resolving global circulation model have been used to investigate the influence of the equatorial quasi biennial oscillation (QBO) on stratospheric and tropospheric circulation and variability. The model is a 64 level version of the UK Met Office Unified Model 4.5 with a top level at 0.01 hPa. The model has been used to perform three simulations. The first simulation imposes a QBO momentum forcing of specified period which has been confined to the lower stratosphere below 35 km. The second, deep QBO, simulation has equatorial QBO momentum forcing throughout the depth of the stratosphere. The third simulation is a control run where no modification of the equatorial wind has been made. In this way we can test the relative influence of the lower and upper equatorial stratosphere. The response of the wintertime polar stratospheric vortices to the three equatorial wind regimes will be discussed and validated using the new ECMWF era-40 data. Tropospheric circulation changes in response to the equatorial forcing will also be addressed.

**MC05/09A/A09-008 1200**

**KELVIN WAVE IN MERIDIONAL CIRCULATION AND LATERAL TRANSPORT OF ZONAL MOMENTUM**

Takeshi IMAMURA<sup>1</sup>, Takeshi HORINOUCHE<sup>2</sup> (<sup>1</sup>Institute of Space and Astronautical Science, Japan, <sup>2</sup>Radio Science Center for Space and Atmosphere, Kyoto University, Japan)

The solution of the equatorial Kelvin wave in the meridional circulation was obtained for the first time, using a perturbation theory, based on the primitive equations on the equatorial beta-plane. In this study, the meridional circulation is supposed to exist in the basic state and is not neglected in the linearized wave equations, in contrast to the conventional linear wave theories which assume meridional circulation to be the second order with respect to the wave amplitude. The wave solution was obtained analytically, after separating the vertical dependence from the horizontal dependence under the assumption that the mean flow is independent of height. The result shows that the wave is modified to have a non-zero meridional wind disturbance, which is absent when the background atmosphere is at rest. The combination of the meridional and zonal winds induces a meridional flux of zonal momentum in the upstream direction of the background north-south flow. When a Kelvin wave is present in a cross-equatorial circulation, the wave transports momentum from the winter hemisphere to the summer hemisphere. In the upper branch of the Hadley circulation, the wave transports zonal momentum equatorward. It was also shown that the non-acceleration theorem does not hold in the presence of a non-negligible meridional circulation: the EP flux divergence can be non-zero even when the wave transience and dissipation are absent. Implication of the results for the terrestrial and Venusian atmospheres is discussed.

**MC05/09P/A09-001 Invited 1400**

**QUASI-STATIONARY PLANETARY WAVES IN THE UPPER MESOSPHERE**

Anne K. SMITH (National Center for Atmospheric Research)

Observations and models indicate that quasi-stationary planetary waves extend as high as the mesopause. They occur more regularly in the winter hemisphere and can have large amplitude even above the altitude where the mean zonal wind reverses. Numerical modeling results indicate that two processes are responsible: 1) propagation of planetary waves forced in the troposphere into both the winter and summer mesosphere, and 2) in situ generation by gravity wave drag perturbations associated with filtering by variations in stratospheric winds.

**MC05/09P/A09-002 Invited 1430**

**WHAT DAMPS THE VERTICALLY PROPAGATING DIURNAL TIDE IN THE MESOSPHERE AND LOWER THERMOSPHERE?**

Charles MCLANDRESS (University of Toronto)

The Canadian Middle Atmosphere Model (CMAM) is a comprehensive general circulation model that extends from the Earth's surface to approximately 200 km and contains all important physical processes relevant to the region up to and including the lower thermosphere. Since the model generates a broad spectrum of waves in the troposphere, as a result of solar radiative heating and the release of latent heat by convection, it is a useful tool for examining the mechanisms which couple the troposphere and lower thermosphere. In particular, the model has been shown to be able to reproduce the observed seasonal behaviour of the vertically propagating migrating (Sun-synchronous) diurnal tide. In this presentation we will focus on the mechanisms responsible for damping the tide in the mesosphere and lower thermosphere, by examining the effects of convective instability and wave-wave interactions. As in earlier studies with the CMAM, a mechanistic tidal model is found to be useful in interpreting the general circulation model results.

**MC05/09P/A09-003 1500**

**GLOBAL DISTRIBUTIONS OF DIURNAL AND SEMI-DIURNAL TIDES: OBSERVATIONS FROM HRDI-UARS OF THE MLT REGION AND COMPARISONS WITH GSWM 2002 (MIGRATING, NON-MIGRATING TIDES)**

Alan H. MANSON<sup>1</sup>, Chris MEEK<sup>1</sup>, Maura HAGAN<sup>2</sup>, Xiaoli ZHANG<sup>2</sup>, Yi LUO<sup>3</sup> (<sup>1</sup>ISAS, University of Saskatchewan, <sup>2</sup>NCAR, Boulder, CO, U.S., <sup>3</sup>Canada Centre for Remote Sensing, NRCan, Ottawa, Canada)

HRDI (High Resolution Doppler Interferometer-UARS) winds data have been analyzed in 4°-latitude by 10°-longitude cells at 96 km to obtain global contour maps of solar-tidal amplitudes and phases, and also mean winds. The solstices June-July (1993), December-January (1993 - 1994), and one equinox (September-October, 1994) are shown. The 24-h Diurnal tide maximizes near 20-25° latitude, has significant seasonal changes with equinoctial maxima, and very clear longitudinal variability. Maxima are very clear over the oceans. In contrast the 12-h Semi-diurnal tides maximize near 40-55° latitude, have very strong seasonal changes with winter maxima, and more modest longitudinal changes. The similarities with MLT (mesosphere-lower thermosphere) radar observations (90 km) are satisfactory. Mean winds are consistent with expectations and show clear poleward flow from summer to winter hemispheres in the solstices. A tidal zonal wavenumber spectral analysis has been applied. For the Diurnal tide, as well as the dominant s=1 migrating component, there are spectral peaks at s=2, 0, -2, -3; and for the Semi-diurnal tide, as well as the dominant s=2 migrating component, there are more frequent non-(solar) migrating spectral peaks at s=4, -2. Comparisons are made with the Global Scale Wave Model (2002/3), which now incorporates migrating and non-migrating tides, and offers monthly outputs. For the Diurnal tide the strongest non-migrating spectral feature (94 km) is at s=-3, while for the Semi-diurnal tide spectral peaks are frequently at s=4, -2. There is a detailed discussion of the spectral features, their seasonal variations, and the similarities with the HRDI tidal data.

**MC05/09P/A09-004 1520**

**THE GENERATION OF STATIONARY WAVES AND NONMIGRATING TIDES IN THE UPPER ATMOSPHERE**

Elsayed R. TALAAT<sup>1</sup>, Hans G. MAYR<sup>2</sup>, Jeng-Hwa YEE<sup>3</sup>, John S. MENGEL<sup>4</sup>, Ruth S. LIEBERMAN<sup>5</sup>, James M. RUSSELL III<sup>6</sup>, H.S. PORTER<sup>7</sup> (<sup>1</sup>The Johns Hopkins University Applied Physics Laboratory, <sup>2</sup>Goddard Space Flight Center, <sup>3</sup>Science Systems & Applications, <sup>4</sup>Colorado Research Associates, <sup>5</sup>Furman University, <sup>6</sup>Furman University)

Nonmigrating tides are planetary-scale waves of periods that are integer fractions of a day (diurnal, semidiurnal, etc.) and are not sun-synchronous (migrating). Nonmigrating tides in the upper mesosphere are traditionally thought to be mostly forced from below through solar radiation absorption by tropospheric water vapor and stratospheric ozone. Modeling studies have suggested that nonlinear interactions between the migrating tide and stationary planetary waves may generate nonmigrating tides of greater or equal strength to those forced from lower atmosphere heating. We investigate the different forcing mechanisms using a Planetary Spectral Model that incorporates Hines AEDoppler Spread Parameterization for small-scale gravity waves. We further examine recent satellite measurements for the relationship between stationary waves and nonmigrating tides.

**MC05/09P/A09-005 1540**

**ON THE EASTWARD TRAVELLING WAVENUMBER TWO IN THE NORTHERN STRATOSPHERE**

Kirstin KRUEGER<sup>1</sup>, Steven PAWSON<sup>2</sup> (<sup>1</sup>Institut fuer Meteorologie der Freien Universitaet Berlin, <sup>2</sup>UMBC GEST CENTER)

Disturbances in the middle atmosphere are often interpreted in the framework of waves superimposed on a zonal-mean flow. This paper presents an analysis of travelling waves in the northern hemisphere stratosphere, concentrating on planetary wavenumber two (W2). Space-time spectral analysis reveals the existence of a substantial eastward-travelling planetary W2 at high latitudes in winter. While a similar feature is well documented in the southern hemisphere stratosphere, where it is observed in most winters, this northern hemisphere counterpart is less common and has not been examined in detail. A climatology of occurrence of the wave is given for the northern stratospheric winter. It is denoted as the quasi-16-day eastward-travelling W2, because of its dominant periodicity, which ranges from about one to three weeks. Although the wave has some similarities with the southern hemispheric wave, there is much larger interannual and intraseasonal



variability in the northern hemisphere. The paper will emphasize the variations in the spatial and temporal structure of this wave, as isolated in meteorological analyses of radiosonde and satellite data. The possible role of these travelling waves in preconditioning the stratosphere as a precursor to sudden stratospheric warmings in both hemispheres will be discussed.

**MC05/09P/A09-006 1600**

**INTERACTION BETWEEN MEDIUM-SCALE TROPOPAUSAL WAVES AND SHORT-PERIOD DISTURBANCES TRAPPED AROUND THE POLAR VORTEX EDGE**

Yoshihiro TOMIKAWA<sup>1</sup>, Kaoru SATO<sup>2</sup> (<sup>1</sup>Research Center for Advanced Science and Technology, University of Tokyo, <sup>2</sup>National Institute of Polar Research)

Tomikawa and Sato [2003] has first described the characteristics of short-period (< 1 day) disturbances with zonal wavelengths of about 2,000 km observed around the polar-night jet. They are considered to be Rossby waves latitudinally trapped in the large potential vorticity gradient around the polar vortex edge. In this presentation, the horizontal distribution of short-period disturbances is interpreted in terms of interaction with medium-scale tropopausal waves that have zonal wavelengths similar to the short-period disturbances [Sato et al., 1993]. The horizontal distributions of those disturbances exhibit a high positive correlation from May through August, suggesting that there is a relationship between those disturbances. The form of their interaction is diagnosed using three-dimensional wave activity flux. It shows that there is a net vertical convergence of wave activity flux around the polar-night jet throughout the year, indicating the transport of wave activity from the upper troposphere into the lower stratosphere due to those disturbances. The baroclinic coupling between those disturbances is suggested as a possible mechanism for upward transport of wave activity and amplification of short-period disturbances in the lower stratosphere. The other possible mechanisms and their characteristics will also be discussed in the presentation.

**MC05/09P/A09-007 1640**

**ISENTROPIC EXPRESSION OF ELIASSEN-PALM FLUX**

Toshiki IWASAKI, Daisuke TANAKA (Graduate School of Science, Tohoku University)

We are developing a diagnostic scheme of wave-mean-flow interactions and meridional circulation based on mass-weighted isentropic zonal mean states. This is a full extension of the transformed Eulerian mean (TEM) to exactly represent finite-amplitude effects of waves and to solve lower boundary conditions. This work demonstrates capability of diagnosing objective analyses, such as NCEP/NCAR reanalysis, and basic characteristics of isentropic expressions. A most significant difference from the TEM is in the vertical component of the EP flux near the lower boundary at mid-latitudes. In the free atmosphere, the isentropic Eliassen-Palm (EP) flux is almost similar to that of TEM. However, an exception is found around the polar vortex, where finite-amplitude effects may not be negligible. In case of the TEM, enormously large vertical flux comes out from the ground surface, because small amplitude approximations break down due to intersection of isentropic surfaces with the ground. In case of the new scheme, it becomes the mountain torque at the lower boundary, increases with height up to the middle troposphere and decreases above. The low level divergence and upper level convergence drive the extratropical direct circulation in the troposphere. In the NH winter, the EP flux is composed mainly of stationary ultra long waves (wave number 1-3) and transient long waves (wave number 4-7). A part of ultra long waves propagate through the tropopause and drive the direct circulation in the stratosphere. The EP flux of the transient waves is consistent with linear solutions of baroclinic instability waves. In the SH winter, on the other hand, stationary ultra long waves are not active. Thus, we can make a consistent analysis of the EP flux from the ground surface to the stratosphere. The energetics of the mass weighted isentropic zonal mean states is formulated. The potential energy of the zonal mean states is converted into the zonal mean kinetic energy, by driving the direct mean meridional circulation. Zonal mean kinetic energy is converted into eddy potential energy and kinetic energy through wave-mean flow interactions. Thus, we can get very straightforward interpretation of energy conversions among zonal mean parameters.

**MC05/09P/A09-008 1700**

**INTRASEASONAL OSCILLATIONS OF THE ZONAL WIND NEAR THE MESOPAUSE OBSERVED WITH MF AND METEOR RADARS IN THE TROPICS**

Fusako ISODA<sup>1</sup> (<sup>1</sup>Radio Science Center for Space and Atmosphere (RASC), Kyoto Univ., <sup>2</sup>Department of Physics and Mathematical Physics, University of Adelaide, <sup>3</sup>Indonesian National Institute of Aeronautics and Space (LAPAN))

We studied the behavior of intraseasonal oscillations (ISO) of the zonal wind in the equatorial mesosphere and lower atmosphere (MLT) using simultaneous observations during 500 days from January 1, 1996 with a meteor radar at Jakarta (6oS, 107oE) and two medium frequency (MF) radars at Pontianak (0oN, 109oE) and Christmas Island (2oN, 157oW). Phase difference of the ISO between Pontianak and Christmas Island is very small in spite of the longitudinal difference of about 90o, which suggests that the ISO in the equatorial MLT region is a variation of zonal mean flow. At Jakarta, the amplitude of the ISO of the zonal wind is smaller than that observed at other two equatorial sites. The peak of the ISO amplitude appears at 82-84 km at Jakarta, while it was at 88 km at other two sites. We also investigated long-term variation of the ISO of the zonal wind using Jakarta meteor radar data observed from January 1993 to October 1999. Inter-annual variation is dominant in the ISO amplitude. A relation between the ISO of the zonal wind and zonal amplitude variations of the diurnal tide is suggested. However, gravity wave activity in the MLT region did not correlate with the ISO in the zonal wind. The outgoing longwave radiation (OLR) in the tropical troposphere, which can be considered as an index for excitation intensity of the atmospheric waves, is compared with the Jakarta data in the MLT region. A relationship between the OLR and the ISO of the mean zonal wind is also suggested.

**MC05/09P/A09-009 1720**

**A THEORETICAL STUDY OF IONIZATION DURING NOCTILUCENT CLOUD**

Dipak K. CAKRABARTY (Centre for Environment Survey)

Noctilucent cloud (NLC) occurs mostly in the high latitude region during summer. Several campaigns have been conducted by various authors to understand this phenomenon. These have revealed the existence of many interesting features. Important among them is bite-out of electrons without any change in positive ion density but increase in water molecules in the clustered ions. It is now established that NLC contains ice particles. Measurements have also revealed that there is a drastic decrease in temperature and a decrease in atomic oxygen density. It is likely that there would be an increase in ozone and water vapor density and a decrease in OH density. In this paper, first, available observed information is briefly mentioned. Then this information is plugged in an ion chemical scheme in which both positive

and negative ions are included. It is shown that atomic oxygen blocks the detachment of electrons from O<sub>2</sub><sup>-</sup>, the precursor negative ion. A decrease in temperature further reduces the detachment of electrons from other negative ions. This causes the decrease of electron density or electron bite-out at the altitude of NLC. Positive ion density is, however, not affected. It is shown that if there is a sufficient decrease of temperature (by less than ~ 20K), then in the following reactions forward reaction rate *f* becomes fast and back reaction rate *r* become very slow making cluster ions with *n* as large as 50.

**MC05/09P/A09-010 1740**

**CHEMICAL AND DYNAMICAL RESPONSE OF HIGH LATITUDE MIDDLE ATMOSPHERE TO SOLAR PROTON EVENT: 3D MODEL STUDY**

Alexei A. KRIVOLUTSKY<sup>1</sup>, Tatyana Yu. VYUSHKOVA<sup>1</sup>, Anna V. KLYUCHNIKOVA<sup>1</sup>, Adolf EBEL<sup>2</sup>, Alexander A. KUMINOV<sup>1</sup>, Georgy R. ZAKHAROV<sup>1</sup> (<sup>1</sup>Department of Atmospheric Chemistry and Dynamics, Central Aerological Observatory, <sup>2</sup>Institute for Meteorology and Geophysics, University of Cologne)

3-D middle atmosphere general circulation model (developed in Cologne and installed now at CAO), and 3-D chemical global transport model developed at CAO were used to calculate the response of ozone (and other species), wind and temperature regime after one of the strongest solar proton event (SPE) of 23rd solar cycle. This event occurred in November 2001. It was assumed in photochemical scheme that each pair of ions created at high latitude middle atmosphere by solar energetic protons born approximately one molecular of NO and two molecular of OH, which disturb photochemical system in the stratosphere and mesosphere. Corresponding ionization rates caused by SPE has been calculated using high time-resolution satellite measurements of solar proton fluxes from the board of GOES-10. Calculated ionization rates showed that the maximum of ionization placed in the mesosphere and conserved about three days after the beginning of SPE. 3-D photochemical calculations showed that ozone was strongly reduced in the mesosphere region (about 80% with minus), but corresponding "tail" of disturbances existed more than 10 days after SPE. Some difference between ozone response over south and north polar regions have been revealed by simulations. Calculated ozone response has been introduced into dynamical model. Such ozone depletion caused by SPE leads to the disturbances of heating and cooling. The results of general circulation model simulations which used the results of photochemical calculations showed that calculated changes in zonal wind caused by SPE equaled about 2 m/s in the mesosphere, and corresponding changes in temperature equaled less than 1 K in this region. Some difference in dynamical and temperature response between north and south polar region have been revealed also in model simulations.

Thursday, July 10 AM  
Presiding Chair: H.-Y. Chun

**MC05/10A/A09-001 Invited 0830**

**STRATOSPHERIC SUDDEN WARMING IN THE SOUTHERN HEMISPHERE IN 2002 AND ITS PREDICTABILITY**

Toshihiko HIROOKA<sup>1</sup>, Akiko MORI<sup>1</sup>, Hitoshi MUKOUGAWA<sup>2</sup> (<sup>1</sup>Department of Earth and Planetary Sciences, Kyushu University, <sup>2</sup>Disaster Prevention Research Institute, Kyoto University)

In late September 2002, there occurred an unprecedented major stratospheric sudden warming in the Southern Hemisphere. The abrupt elongation and subsequent spectacular split of the stratospheric polar vortex was observed during the time sequence of the event. Such enhancement of the zonal wavenumber 2 component is very rare in the Southern Hemisphere stratosphere. Hence, by using the stratospheric assimilated data operationally produced by the Japan Meteorological Agency (JMA), we investigate dynamical features of the event, paying the special attention to the vertical linkage between the upper troposphere and stratosphere. It is found that planetary waves of both wavenumber 1 and 2 were very active in the upper troposphere and vertical propagation of planetary waves frequently occurred throughout the winter season prior to the major warming. Correspondingly, zonal mean westerlies in the upper troposphere were generally weaker than the usual through the period. Such vertical propagation of planetary waves brought about periodic deceleration of the westerly polar night jet with a typical time scale of about 10 days in the stratosphere. Among them, the deceleration occurred after the end of July were relatively large and gave rise to the sequential occurrence of minor warmings. As a consequence, the polar vortex were gradually weakened and became more vulnerable to planetary wave activities. Eventually, the major warming occurred in late September; the conditions necessary for the major warming were in fact the results of several minor warmings during mid-to-late winter. Moreover, we examine the predictability of the event by the use of operational one-month forecast data set based upon the JMA Numerical Weather Prediction Model. We also discuss precursor agents promoting the upward propagation of planetary waves and triggering the major warming event by comparing the predicted field with the observation.

**MC05/10A/A09-002 0900**

**WHY DID THE 2002 SOUTHERN HEMISPHERE WARMING HAPPEN?**

Richard SWINBANK<sup>1</sup>, Adam SCAIFE<sup>1</sup>, Neal BUTCHART<sup>2</sup>, David JACKSON<sup>1</sup>, Michael KEIL<sup>1</sup>, Hazel THORNTON<sup>3</sup> (<sup>1</sup>NWP, Met Office, <sup>2</sup>CR, Met Office)

In late September 2002, a major sudden warming was observed in the Southern Hemisphere for the first time since records began. The evolution of the warming was captured well by the Met Office stratospheric analyses. During the event the polar vortex was split into two, in a similar way to a northern hemisphere wavenumber-2 warming. In the classic picture, a stratospheric warming is preceded by pulse of wave activity from the troposphere that decelerates the winds in the vortex. In 2002 unusual conditions persisted throughout most of the preceding months, with vacillations in the zonal wind of amplitude about 20m/s. By contrast, in most previous winters the stratospheric westerlies varied much more gradually, and vacillations only occurred for limited periods, if at all. These vacillations are very similar to what is seen in idealized experiments with steady troposphere and suggest that stationary wave forcing may have been larger than usual. We suggest that the unusual vacillating regime preconditioned the stratosphere and made it more susceptible to the pulse of wave activity that led to the major warming.

**MC05/10A/A09-003 0920**

**ON THE TROPOSPHERIC ORIGINS OF UPWARD PROPAGATING ROSSBY WAVE TRAINS INVOLVED IN THE 2002 SOUTHERN HEMISPHERE MAJOR WARMING EVENT**

Kazuaki NISHII, Hisashi NAKAMURA (Department of Earth and Planetary Science, Graduate School of Science, University of Tokyo, Hongo 7, Bunkyo-ku Tokyo, 113-0033 Japan)

As unusual event of major stratospheric sudden warming occurred in the Southern Hemisphere in late September of 2002, leading to breakdown of the polar vortex and the

subsequent shrinking and breakup of the Antarctic hole. Time evolution of the warming is studied in this study through diagnosing the NCEP/NCAR reanalysis data, with particular emphasis on the three-dimensional structure and propagation of planetary waves. In our analysis two specific forms of a phase-independent pseudomomentum flux were utilized for depicting the propagation of quasi-stationary Rossby waves. One is Plumb's flux that is defined for the zonally uniform westerlies and therefore suited for instantaneous depiction of the propagation of the planetary waves as a whole. The other defined by Takaya and Nakamura for the zonally varying westerlies is suited for instantaneously depicting the propagation of a quasi-stationary Rossby wave trains that consist of circulation anomalies. Fluctuations associated with fast-moving synoptic-scale disturbances have been removed by applying 5-day moving average to the data time series, and anomalies are defined as departures of the 5-day running means from 31-day running means that represent the slowly varying seasonal cycle. In that year, the 20-hPa polar-night jet (PNJ) was unusually weak already in early August. Three minor warming events that occurred intermittently during the period of late August through mid-September gave rise to further weakening of the stratospheric PNJ. A diagnosis based on the two wave-activity fluxes indicates that a tropospheric blocking ridge persistent around the Drake Passage was likely the primary source of upward propagating Rossby wave trains involved in those minor warming events. The upward wave-activity emanation was enhanced in association with the intensification of the ridge. The breakdown of the polar vortex in late September immediately followed the upward propagation of a strong quasi-stationary Rossby wave train through the moderately strong PNJ that had been occurring since 19 September from the tropospheric blocking ridge developing over the southeastern Atlantic. In association with that wave train, streamfunction anomalies exhibited an apparent westward tilt with height between the blocking ridge and anticyclonic anomalies that formed in the lower stratosphere. Wave activity was injected into the developing blocking anomalies from a tropospheric quasi-stationary Rossby wave train propagating eastward from the South Pacific into the South Atlantic.

**MC05/10A/A09-004 0940**

**PREDICTABILITY OF STRATOSPHERIC SUDDEN WARMINGS**

Hitoshi MUKOUGAWA<sup>1</sup>, Hirokazu SAKAI<sup>2</sup>, Toshihiko HIROOKA<sup>3</sup> (<sup>1</sup>Disaster Prevention Research Institute, Kyoto University, <sup>2</sup>Graduate School of Environmental Earth Science, Hokkaido University, <sup>3</sup>Department of Earth and Planetary Sciences, Kyushu University)

Although the basic mechanism of the stratospheric sudden warmings(SSWs) was shown by Matsuno (1971), our understanding on the events is still incomplete. Among others, the comprehensive theory on the amplification of tropospheric planetary waves, which has been frequently documented before the onset of SSWs has not been established as yet. Moreover, very few studies examined the predictability of SSWs by using operational weather prediction models(e.g. Mechoso et al., 1985). In this study, by using the operational one-month forecast data set based upon the Japan Meteorological Agency(JMA) Numerical Weather Prediction Model (NWP) we examine the predictability of wavenumber 1 major SSW events occurring in December 1998 and December 2001. The forecasts are performed on every Wednesday and Thursday by conducting ensemble integrations from 13 initial conditions (one control run without initial perturbation and 12 perturbed runs). The associated triggering process in the troposphere and the dynamical influence on the tropospheric circulation during the SSW events are also investigated. At first, the time evolution of the Root Mean Square Error on the 10hPa height field over the Northern Hemisphere for the control forecasts as a function of forecast day shows linear growth suggesting a prolonged predictability of the stratospheric circulation, in contrast with the troposphere. In fact, these SSW events are correctly predicted by the NWP initialized more than two weeks before the warming peaks. Moreover, for the SSW in December '01 with the warming peak on 25 December, we find a distinct variation in the sensitivity of the prediction for the warming to the initial condition prior to the SSW event: Forecast spread between ensemble members starting from 6 December was extremely large while that from 12 December was small and all the members succeeded in predicting the occurrence of the SSW event. The forecast spread prior to the SSW in December '01 is studied in detail. The principal spatial pattern of the spread corresponds to a barotropic zonal-mean zonal wind variation with maxima around 80N and 60N in the troposphere. This variation is intimately connected with the enhancement of the upward propagation of the wavenumber 1 planetary wave, which in turn gives rise to the SSW. We also discuss the relation between the tropospheric zonal flow variation and the blocking revealed by the analysis on the ensemble forecast.

**MC05/10A/A09-005 1000**

**LONG-TERM VARIABILITY OF THE ANTARCTIC VORTEX AND OZONE HOLE: HOW CLOSE IS THE UM TO PRODUCING A SH MAJOR WARMING?**

Peter BRAESICKE, John PYLE (Centre for Atmospheric Science, University of Cambridge)

The unprecedented Antarctic ozone hole of 2002 raises a number of important questions including the likelihood of such an event and the role of chemistry in producing it. We analyse four twenty year integrations with the Met Office Unified Model (UM) using a simple stratospheric chemistry. One integration uses the modelled ozone interactively in the radiation scheme, the other three experiments are sensitivity integrations using climatological ozone. We will describe the differences in southern hemisphere (SH) winter variability between the experiments. Even though there is no major warming in the SH (as defined by WMO) in the 80 years modelled, we find one exceptionally early and strong warming in the integration with interactive chemistry. This warming is analysed in detail to establish the role of the interactive ozone scheme in producing the warming.

**MC05/10A/A09-006 1040**

**QUASI-PERIODIC VARIATIONS OF THE POLAR VORTEX DUE TO WAVE-WAVE INTERACTION IN THE SOUTHERN HEMISPHERE STRATOSPHERE**

Yasuko HIO, Shigeo YODEN (Department of Geophysics, Kyoto University)

In the Southern Hemisphere (SH) stratosphere, quasi-stationary planetary wave of zonal wavenumber 1 (hereafter Wave 1) and eastward traveling Wave 2 with the period around 15 days are active in late winter. Instability of the polar night jet is believed to be an important process for the generation of Wave 2, while Wave 1 is generated in the troposphere and propagated into the stratosphere. We investigate the behaviors of Wave 1 and Wave 2 in the SH winter stratosphere focusing on the wave-wave interactions. With the NCEP/NCAR Reanalysis dataset for 24 years (1979-2002), we could extract some typical interaction events and find some common features. The observed transient Wave 1 for these events travels eastward with the same angular velocity as that of Wave 2 changing its amplitude periodically. The transient Wave 1 has a nodal structure in mid-latitude. The traveling Wave 1 and Wave 2 are in phase with the stationary Wave 1 simultaneously. The traveling Wave 1 has its minimum amplitude, when it is in phase or out of phase with the stationary Wave 1. Furthermore, the transient Wave 2 has a maximum amplitude when the three waves are in phase. These phenomena are seen in the periods when the zonal mean PV gradient is nearly zero in mid-latitudes and both amplitudes of the stationary Wave 1 and traveling

Wave 2 are large. The mechanism of the periodic amplification of these waves is investigated with a global barotropic model with zonal-flow forcing and dissipation. Sinusoidal surface topography is assumed with a single zonal wavenumber 1 in the model SH and the prescribed zonally symmetric equilibrium state is set so as to satisfy the necessary condition of barotropic instability. In some parameter range, the eastward traveling Wave 2 due to barotropic instability are dominant, as well as the stationary Wave 1 generated by the topographic effect. As a result of the interaction between these waves, similar eastward traveling Wave 1 is found as to both the periodicity and the latitudinal structure observed in the real atmosphere. The correspondence between the observation and the model experiment confirms that the observed phenomena are due to the wave-wave interaction between the stationary Wave 1 and the traveling Wave 2 and that the generation of the traveling Wave 2 is strongly connected with the jet profile.

**MC05/10A/A09-007 Invited 1100**

**NEW MESOSPHERE WIND MEASUREMENTS AT THE SOUTH POLE: A LOOK AT THE ANTARCTIC MESOSPHERE RESPONSE TO A STRATOSPHERIC WARMING**

Susan Kathryn AVERY<sup>1</sup>, James AVERY<sup>1</sup>, Scott PALO<sup>1</sup>, Robert VINCENT<sup>2</sup>, Damian MURPHY<sup>3</sup>, Richard WALTERSCHEID<sup>4</sup> (<sup>1</sup>University of Colorado, <sup>2</sup>University of Adelaide, <sup>3</sup>Australian Antarctic Division, <sup>4</sup>Aerospace Corporation)

A new meteor radar was established at the South Pole and has been operational for one year. The radar is at an ideal location for providing ground-based information in support of the TIMED satellite mission as well providing an excellent opportunity to more thoroughly examine the dynamics of the Antarctic through an integrated analysis with other Antarctic radar observations. Preliminary data analysis has focused on the characterization of various wave motions observed in the wind data. Additional analysis is focused on the mesosphere response to the stratospheric warming that peaked 25 September 2002. This presentation will provide a description of the wave motions present at the South Pole during the stratospheric warming event. An initial analysis incorporating additional Antarctic radar data will also be presented.

**MC05/10A/A09-008 1130**

**PLANETARY WAVE ACTIVITY IN THE MIDDLE ATMOSPHERE ABOVE DAVIS, ANTARCTICA DURING THE 2002 AUSTRAL SPRING**

Andrew R. KLEKOCIUK<sup>1</sup>, Andrew J. DOWDY<sup>1</sup>, Robert A. VINCENT<sup>2</sup> (<sup>1</sup>Australian Antarctic Division, <sup>2</sup>Department of Physics and Mathematical Physics, Adelaide University)

The development of unusually strong planetary wave activity in the Antarctic stratosphere during late August 2002 led to the rapid warming and dramatic erosion of the polar vortex over the subsequent two months. Measurements of temperatures and winds over particular altitude regions from the ground to the mesopause above Davis Antarctica (68.6°S, 78.0°E) using a variety of techniques, combined with analysis of global NCEP/CPC operational data and NOAA/POES temperature soundings, have been used to investigate the characteristics and extent of the atmospheric disturbance during this event. At Davis, the signature of a 12-day wave in temperature was apparent throughout the atmosphere, including the mesopause region and surface, with peak amplitudes near the 20hPa level (~25km altitude). NCEP/CPC stratospheric data suggest that the wave was primarily associated with a zonal wavenumber 1 planetary wave at high southern latitudes which also received periodic intensification from a wavenumber 2 feature. During late September, Davis balloon-sonde wind data in the lower stratosphere showed a reversal in the zonal flow and a strong poleward meridional flow. These characteristics common to Sudden Stratospheric Warmings of the Arctic winter atmosphere, but which are rarely seen in the Antarctic. Rayleigh lidar temperatures between 30km and 70km altitude indicate that the 12-day wave penetrated into the lower-mesosphere, and was associated with a vertical disturbance having a dominant wavelength of approximately 50km. The lidar measurements also revealed several smaller scale vertical wave-like temperature perturbations with downward phase progressions in the stratosphere and lower mesosphere during this time. The most significant of these included an inversion of amplitude ~10K in the lower mesosphere during late August, and a warm perturbation of amplitude ~20K and vertical extent (FWHM) of 5km during mid-September. The relationship between these features and the planetary wave activity in the lower stratosphere, with particular regard to implied heating rates, is examined. In addition, the middle atmosphere conditions above Davis during the Austral spring of 2002 are compared with previous years.

**MC05/10A/A09-009 1150**

**A PARAMETER SWEEP EXPERIMENT ON THE EFFECTS OF THE QBO PHASE ON STRATOSPHERIC SUDDEN WARMING EVENTS**

Yoko NAITO, Shigeo YODEN (Department of Geophysics, Kyoto University)

The occurrence of stratospheric sudden warming (SSW) events is a dominant component of the intraseasonal variability of the wintertime stratospheric circulation in the northern hemisphere. Observational studies have shown that a time-mean state of the winter stratosphere is influenced by the equatorial quasi-biennial oscillation (QBO). The aim of the present study is to investigate the effect of the QBO on the occurrence of SSWs by analyzing daily data obtained in long time integrations of a simple global circulation model. An idealized zonal mean zonal momentum forcing is assumed in the equatorial stratosphere in the model to investigate QBO effects on the intraseasonal variability. Phase of the perpetual "QBO-wind" forcing is changed as an experimental parameter in the present study, by contrast with our previous study (Naito et al., accepted to JAS) in which magnitude of the forcing was changed. Eight integrations are performed for 12,000 days under perpetual winter condition. Polar temperature in the upper stratosphere shows that SSWs occur more frequently in the easterly phase than in the westerly phase, consistent with the observational result. Increase of the occurrence of SSWs from the westerly phase to the easterly phase through the easterly shear phase is relatively gradual compared with the decrease through the westerly shear phase. Composite analysis of SSW events also shows dependence on the phase of the QBO. Propagation of planetary waves based on the Eliassen-Palm flux analysis is discussed with estimation of statistical significance.

**MC05/10A/A09-010 1210**

**MESOPAUSE DYNAMICS FROM THE SCANDANAVIAN TRIANGLE OF RADARS WITHIN THE PSMOS-DATAR PROJECT**

Alan H. MANSON<sup>1</sup>, C.E. MEEK<sup>2</sup>, C.M. HALL<sup>3</sup>, S. NOZAWA<sup>4</sup>, N.J. MITCHELL<sup>5</sup>, D. PANICHEVA<sup>6</sup>, W. SINGER<sup>7</sup>, P. HOFFMANN<sup>8</sup> (<sup>1</sup>Institute of Space and Atmospheric Studies, University of Saskatchewan, Canada, <sup>2</sup>Tromsø Geophysical Observatory, University of Tromsø, Norway, <sup>3</sup>Solar-Terrestrial Environment Laboratory, University of Nagoya, Japan, <sup>4</sup>Department of Electronic and Electrical Engineering, University of Bath, UK, <sup>5</sup>Leibniz-Institute of Atmospheric Physics, KAElungsborn, Germany)



The 'Scandinavian Triangle' is a unique trio of radars within the DATAR Project (Dynamics and Temperatures from the Arctic MLT (60-97km) region): Andenes MF radar (MFR, 69N, 16E); Tromsø MF radar (70N, 19E) and Esrange MW radar (MWR, 68N, 21E). The radar-spacings range from 125-270 km, making it unique for studies of wind variability associated with small-scale waves, comparisons of large-scale waves measured over small spacings, and for comparisons of winds from different radar systems. As such it complements results from arrays having spacings of 25 km and 500 km that have been located near Saskatoon. Analyses show that while the wind speeds from the two MFRs are within 5%, the MWR speeds are larger (median annual factors of 1.6 at 97km, 1.1 at 85km), consistent with earlier studies at Tromsø-Andenes. The ratios vary with height and season. Wind directions and tidal phases agree very well across the Triangle. Annual climatologies for the year 2000 of mean winds, solar tides, planetary (PW) and gravity waves are presented, and as expected, are very similar in general features across the Triangle. The 12-h tide has a climatology very similar to that at middle latitudes, but with smaller amplitudes e.g. factors of 1-2 during the autumn maximum. The 24-h tide has amplitudes about half the size of the 12-h tide, and the climatology indicates the increasing dominance of the evanescent S(1,-1) mode. Comparisons with the latest version of the GSWM are included. Variabilities of these climatologies across the Triangle are somewhat greater than those of the Canadian-500km Triangle. The 16-d and 2-d PWs are discussed in some detail. In particular the 2-d PW winter activity is greater than in summer. There are again modest, but statistically significant, differences between the contour plots/climatologies for the three radars, indicating spatial and temporal intermittency of the local wind oscillations associated with these global scale PW structures.

Thursday, July 10 PM  
Presiding Chair: C. McLandress

**MC05/10P/A09-001** Invited **1400**

**ON THE INFLUENCE OF THE QUASI BIENNIAL OSCILLATION IN THE UPPER EQUATORIAL STRATOSPHERE**

Lesley J. GRAY<sup>1</sup>, Sarah SPARROW<sup>2</sup>, Charlotte PASCOE<sup>1</sup> (<sup>1</sup>Meteorology Dept., Reading University, U.K., <sup>2</sup>Oxford University, U.K., <sup>3</sup>Rutherford Appleton Laboratory, U.K.)

The quasi biennial oscillation (QBO) in the lower equatorial stratosphere has been observed for many years from radiosonde data. However, the characteristics of the QBO in the equatorial upper stratosphere above 35km are less well known. Recent modelling work and analysis of a 24-year period of rocketsonde data have suggested that the QBO in the upper equatorial stratosphere is relatively small but appears to have a significant influence on the frequency and amplitude of stratospheric sudden warmings in the northern winter-time. The height region of this QBO influence (35-50 km) is also the region dominated by the semi-annual oscillation (SAO). Recent model and rocketsonde data analysis will be summarised. Further analysis of the upper equatorial QBO in the newly available 40-year ECMWF re-analysis will be described, with particular emphasis on its influence on the strength and timing of the SAO. Model studies, including both a stratosphere mesosphere model and a full GCM will be explored to investigate possible mechanisms for the equatorial influence on the northern high latitudes in winter.

**MC05/10P/A09-002** Invited **1430**

**ISSUES IN STRATOSPHERE/TROPOSPHERE DYNAMICAL COUPLING**

Mark P. BALDWIN (Northwest Research Associates)

Although variability in the stratosphere is driven mainly by planetary-scale waves that originate in the troposphere, some of the most interesting aspects of stratosphere / troposphere coupling involve feedbacks in which the tropospheric circulation is affected by conditions in the stratosphere. These feedbacks are important on two timescales: intraseasonal and long-term trends. Over periods of one week to two months, observations show a strong statistical relationship between circulation anomalies in the lowermost stratosphere and changes to the phase of the Arctic Oscillation. Following changes to the circulation of the lowermost stratosphere, the Arctic Oscillation tends to be biased for up to two months. The effect only happens during the extended winter season, when planetary-scale waves are able to create large circulation anomalies in the stratosphere. The effect on the Arctic Oscillation could be useful not only for statistical forecasts, but could, in principle, be incorporated in numerical extended-range weather predictions. If the stratospheric circulation changes due to increasing greenhouse gasses, ozone loss, or other effects, how will the troposphere be affected? This remains an open question, in part because data records are not long enough to answer the question and in part because climate models do agree on the trends within the stratosphere. Most climate models are forecasting a trend toward a more positive Arctic Oscillation, but the reasons for this trend are model dependent; the trend in the Arctic Oscillation could be driven by either tropospheric or stratospheric processes. A related question that has not been answered is whether or not it is necessary for climate models to fully resolve the stratosphere. If a fully-resolved stratosphere is necessary to simulate future tropospheric climate, what are the implications of using, as we do today, climate models that have limited representations of the stratosphere?

**MC05/10P/A09-003** Invited **1500**

**STRATOSPHERIC- AND TROPOSPHERIC MODES IN THE ARCTIC OSCILLATION**

Kunihiko KODERA, Yuhji KURODA (Meteorological Research Institute)

The leading EOF of the sea-level pressure in the northern hemisphere is known as the Arctic Oscillation (AO). The AO is first considered as a seesaw in the geopotential height field between the polar region and midlatitudes from the surface to the stratosphere. However, the AO signal in the troposphere is not necessarily related to the stratospheric circulation. There exist two types of the AO: the one (stratospheric type) is connected to the stratospheric circulation and the other (tropospheric type) is trapped within the troposphere. Both types can also be characterized as a seesaw in zonally averaged zonal wind field, but one is a seesaw between 35°N-65°N involving the polar-night jet, and the other is in lower latitudes 30°N-55°N more related to the subtropical jet. Development of patterns during the winter is also very different. Anomalous zonal-mean zonal winds propagate down from the stratosphere for the stratospheric type, but anomalies develop in from the Pacific sector of the troposphere for the tropospheric type. Because of the similarity in spatial structure of these modes in the troposphere, in particular in the Atlantic sector, it is not always easy to separate by conventional techniques. However, occurrence frequency of the two modes might be dependent on the basic state, which can be affected by changes in external forcings or boundary conditions. Accordingly the two modes of variability are studied by stratifying winters according to the phase of the solar and ENSO cycles.

**MC05/10P/A09-004** **1530**

**DOWNWARD PROPAGATION IN THE SOUTHERN HEMISPHERE**

David W.J. THOMPSON<sup>1</sup> (<sup>1</sup>Department of Atmospheric Sciences, Colorado State University, <sup>2</sup>Northwest Research Associates)

In this talk, I will discuss the observed relationships between the strength of the Southern Hemisphere (SH) stratospheric circumpolar flow and the circulation of the troposphere. It will be demonstrated that: 1) large amplitude events in the SH stratosphere frequently propagated downwards to tropospheric levels where they are reflected as a bias in the SH annular mode; 2) that the observed coupling between the SH stratospheric and tropospheric circulations has implications for both weather prediction and climate change over the high latitudes of the SH; and 3) that the breakdown of the SH stratospheric polar vortex during the sudden stratospheric warming September 2002 was accompanied by pronounced anomalies in the SH annular mode that persisted for more than a month.

**MC05/10P/A09-005** Invited **1620**

**ON THE RELATIONSHIP BETWEEN THE WINTER STRATOSPHERE AND THE TROPOSPHERIC ARCTIC OSCILLATION**

Rolando R. GARCIA, Byron A. BOVILLE, Fabrizio SASSI (National Center for Atmospheric Research)

Recent work on large-scale patterns of atmospheric variability indicates that the state of the stratosphere during northern winter is significantly correlated, at positive lag, with the tropospheric Arctic Oscillation (AO). Specifically, periods when the polar night vortex is strong are followed by periods of positive AO index, and vice-versa. Because this relationship has predictive potential for tropospheric circulation patterns it is important to understand how it is produced. We examine several multi-year integrations of the Whole Atmosphere Community Climate Model (WACCM) to show that the stratosphere/AO relationship is present in the model, and we analyze the behavior of Eliassen-Palm fluxes and other circulation diagnostics in an attempt to establish a causal connection between the stratosphere and the AO.

**MC05/10P/A09-006** Invited **1650**

**LARGE ENSEMBLE EXPERIMENTS ON THE STRATOSPHERE-TROPOSPHERE COUPLED VARIABILITY**

Shigeo YODEN (Department of Geophysics, Kyoto University)

We have performed numerical experiments with an idealized troposphere-stratosphere global circulation model to investigate internal variability of the winter stratosphere which arises from the vertical dynamical coupling (Taguchi, Yamaga and Yoden, 2001; Taguchi and Yoden, 2002a,b,c). Although the model is simplified in some ways, it explicitly describes dynamical processes related to the vertical coupling: excitation of planetary waves by the surface topography and their interaction with baroclinic eddies in the troposphere as well as their upward propagation and interaction with the mean zonal flow in the stratosphere. Recently similar model was also used to study the effects of equatorial QBO on stratospheric sudden warming events (Naito, Taguchi and Yoden, 2003). Recent progress in computing facilities enabled us to perform some parameter sweep experiments in which many trials of computations in parameter space were done by sweeping the value of a control parameter (Yoden, Taguchi and Naito, 2002). For example, the sign and intensity of the equatorial zonal wind forcing were swept in 9 runs in Naito et al. (2003). In addition, it became much easier than before to make long time integrations. They obtained over 1,150 examples of stratospheric sudden events in total in contrast to the number of the observed major warming events (about 20 in the past 50 years). A large number of such ensembles makes it possible to use a large sample method in statistical tests instead of a small sample method with Student's t-test, so that it is not necessary to assume the equality of the variances of two populations. This kind of "new" statistical approach based on large ensemble experiments, which is new in a sense that it has become possible very recently for ordinary people, might be applied for the discussion of the rarity of the stratospheric sudden warming event in the southern hemisphere in September 2002. If we use the dataset of 1,000-year integrations by Taguchi and Yoden (2002c), extreme warm events over 3 times [standard deviation] might appear about 28 years in 1,000 years because the probability distribution is highly skewed. If it were Gaussian distribution, the events over 3 times [standard deviation] is less than 2 years in 1,000 years.

**MC05/10P/A09-007** **1720**

**UPWARD AND DOWNWARD INJECTION OF ROSSBY WAVE ACTIVITY ACROSS THE TROPOPAUSE: A NEW ASPECT OF TROPOSPHERE-STRATOSPHERE LINKAGE**

Hisashi NAKAMURA, Kazuaki NISHII (Department of Earth, Planetary Science, University of Tokyo)

Behavior of quasi-stationary anomalies observed in the lower stratosphere of the Southern Hemisphere during austral late winter of 1997 is studied. The anomalies are defined as daily lightly-low-pass-filtered departures from the seasonal cycle of that year. A wave-activity flux and refractive index for stationary Rossby waves are utilized, both defined locally for the zonally varying westerlies under WKB-type assumptions. Unlike the conventional one, our framework enables us to pinpoint the tropospheric origin, if exists, of particular lower-stratospheric anomalies. We adopt this framework, recognizing that in the lower stratosphere the mean polar-night jet (PNJ) exhibits a clear zonal asymmetry in the presence of zonal-wave number 1 component of planetary waves. In our framework, the persistent component is included in the basic state in which slowly varying anomalies are embedded. Therefore propagation of stationary Rossby wave trains that constitute those anomalies may be either upward or downward, depending upon location and time. Though only in a qualitative sense, the validity of the WKB-type assumptions may be given a posteriori with reasonable geographical correspondence between wave packets and local waveguides. Submonthly fluctuations in the lower stratosphere were often associated with a zonally confined wave train emanating upward from localized, quasi-stationary anomalies in the troposphere including a blocking ridge. Three-dimensional propagation of the wave train is found sensitive to the local waveguide structure. The distribution of the lower-stratospheric submonthly variability thus exhibits significant zonal asymmetries, reflecting those in the PNJ structure and in the distribution of tropospheric disturbances. Seasonal evolution of the PNJ and that in the tropospheric intraseasonal variability strongly modulated the activity of lower-stratospheric subseasonal fluctuations. Specifically, local overlapping of the stratospheric PNJ with a tropospheric subpolar jet forms a localized vertical waveguide that acts as a "chimney" through which wave activity accumulated in the troposphere is allowed to propagate upward into the stratosphere, followed often by the formation of a wave train propagating eastward along the lower-stratospheric PNJ. If another such chimney forms in the exit of the PNJ, wave activity associated with a lower-stratospheric wave train would be allowed to propagate downward into the troposphere, contributing to blocking formation or

large-scale cyclogenesis. Typical examples of that local downward influence of stratospheric anomalies include an event of large-scale, quasi-stationary cyclogenesis that occurred around August 10 off the Antarctic coast to the south of Australia. A substantial contribution was made to that cyclogenesis through downward wave-activity injection from a lower-stratospheric Rossby wave train that had emanated from a tropospheric blocking ridge far upstream over the southwestern Pacific. Another example is given where wave-activity injection from lower-stratospheric cyclonic anomalies contributed positively to the formation of a blocking ridge southwest of New Zealand in late September.

**MC05/10P/A09-008** **1740**

**EFFECTS OF POLAR VORTEX PERTURBATIONS ON TROPOSPHERIC WINTER CIRCULATION**

Kevin HAMILTON<sup>1</sup>, Georgiy STENCHIKOV<sup>2</sup>, Mark BALDWIN<sup>3</sup> (<sup>1</sup>IPRC, University of Hawaii, <sup>2</sup>Rutgers University, <sup>3</sup>Northwest Research Associates)

Interest in the dynamical influence of the circulation in middle atmosphere on the troposphere has had a resurgence largely due to recent observational studies that find evidence for downward propagation of large-scale perturbations in the extratropical circulation from the stratosphere to the troposphere. In particular, anomalies in the Arctic Oscillation (AO) index tend to propagate downward so that, on average, a weak vortex (warm pole) condition in the stratosphere is followed later by a positive AO index in the tropospheric circulation. The same general tendency is also found in control integrations of at least some atmospheric GCMs. The existence of a significant downward dynamical link of this sort would have implications for both seasonal prediction and sustained climate change. However, there is no guarantee that the tendency for downward propagation of anomalies across the tropopause reflects an actual physical effect of the stratospheric flow on that in the troposphere. In geophysics there are numerous examples of phenomena showing phase progression actually opposite to the physical propagation of disturbances. This paper will report first on results from a series of model integrations performed with initial conditions that are perturbed from those in a control run, but with the perturbation restricted to the extratropical stratosphere. In particular, the GFDL "SKYHI" model is applied in a series of winter seasonal integrations, each with initial condition taken from early winter in one year a long control run, but with a strong perturbation arbitrarily added to the stratospheric polar vortex. Another somewhat different set of experiments has been undertaken with a version of the model which includes an extra zonally-symmetric momentum source in the tropical stratosphere. The momentum source is designed to force the tropical stratospheric circulation to resemble that actually observed for the period 1978-1999. The results of these experiments will be examined to see if the imposed QBO in the tropics has a detectable effect on the extratropical tropospheric circulation.

Friday, July 11 AM  
Presiding Chair: T. Tsuda

**MC05/11A/A09-001** **0830**

Invited

**SIMULATIONS OF THE EFFECT OF SOLAR VARIABILITY ON THE TROPOSPHERE AND MIDDLE ATMOSPHERE**

Kiyotaka SHIBATA, Kunihiko KODERA (Meteorological Research Institute)

Solar irradiance is not constant but varies with various time scales. One of the most distinct variations is the 11-year cycle, in which irradiance change amplitude is, on average, by about several percent in ultra-violet region, while it varies little in longer wavelength region. Irradiance variations in ultra-violet region affect radiative heating and ozone concentration around the stratopause and above, which in turn affects underlying atmosphere through dynamical processes. This study investigates the effects of solar maximum and minimum on the stratosphere and troposphere using MRI/JMA98 GCM. The model is a T42L45 version, which is triangularly truncated at 42 total wavenumber in horizontal and has 45 layers from the surface to 0.01 hPa (about 80 km) in vertical. Experiment are made for solar maximum, normal and solar minimum conditions, respectively, over 21 years. Solar irradiance changes are incorporated in the radiationscheme, while ozone change is prescribed in the model. Two data are taken from 2-D chemical transport models (GISS and Imperial College) used separately. Other experiment are also made to investigate the effects of model top height and interactive chemistry.

**MC05/11A/A09-002** **0900**

Invited

**OBSERVED HIGH FREQUENCY GRAVITY WAVES IN THE MESOSPHERE; SEASONAL VARIATION OF THEIR DIRECTIONALITY AND DAMPING**

Gary R. SWENSON, Alan Z. LIU (Electrical and Computer Engineering, U of Illinois)

Dissipation of Atmospheric Gravity Waves (AGWs) is a dominant driver for the summer to winter meridional circulation in the mesosphere. Airglow observations from U of I and other groups around the globe are gathering information on the high frequency (HF) portion of the AGWs regarding directionality and wave amplitudes. Significant differences are being observed in winter versus summer, at mid and low latitudes. In addition, correlative studies at Maui, HI have begun to investigate the wave damping with altitude of HF waves, from which accelerations with altitude are calculated. Considering the observed seasonal difference in wave directionality as well as the altitudes and magnitudes of wave induced acceleration, we are beginning to gather insight into the roles AGWs play in the process of driving the residual circulation. These combined effects will be discussed.

**MC05/11A/A09-003** **0930**

Invited

**GLOBAL OBSERVATIONS OF GRAVITY WAVE PROPERTIES AND CONSTRAINTS FOR GCMs**

M. Joan ALEXANDER (NorthWest Research Associates, Inc., Colorado Research Associates Division)

Global models require parameterization of the effects of gravity waves that are either not resolved or not accurately generated in these models. The parameterizations require input parameters that describe the properties of the waves such as their phase speeds, propagation directions, and horizontal wavelengths. These input parameters have been poorly constrained allowing a very broad range for "tuning" these parameterizations and the effects of the parameterized waves in middle atmosphere models. In recent years, a variety of global data sets from satellite and balloon measurements have provided new information on the global properties of gravity waves in the lower stratosphere that should aid in constraining parameterizations. Each observation and data analysis technique includes a corresponding unique set of observing constraints that make each sensitive to only a portion of the gravity wave spectrum that may be present in the lower stratosphere. In addition, gravity waves tend to be generated at intermittent intervals, and this intermittency introduces

an additional observational bias that favors the observation of slow vertical group speed waves. These slow vertical group speed waves tend to carry smaller momentum flux than their high vertical group speed counterparts, rendering them potentially far less important to the net momentum budget for parameterized gravity waves than the observations would imply at face value. This talk will summarize some of these recent global gravity wave data sets and the constraints for gravity wave parameterization input parameters that they can provide.

**MC05/11A/A09-004** **1000**

**GRAVITY WAVE DRAG ESTIMATION USING A VARIATIONAL METHOD. TECHNIQUE DESCRIPTION AND TWIN EXPERIMENTS**

Manuel PULIDO, John THUBURN (Department of Meteorology, University of Reading)

The stratospheric circulation is strongly influenced by the drag from breaking and dissipation of gravity waves. Numerical global atmospheric models can not resolve these waves, so they must be parameterised. Progress in developing parameterisations requires information about the actual drag field in the atmosphere. However it is very difficult to infer the climatology of the actual drag field from observations, and so far budget studies have given information only on the zonal mean of the zonal component of the drag on seasonal time-scales. Here, the authors present a new technique to estimate the drag term. Using variational data assimilation principles, a cost function which measures the mismatch between the observed variables (e.g temperature or wind fields) and the model variables is minimised. The control variable which is varied to minimise the cost function is the three dimensional field of wave drag. Thus, the optimal value which minimises the mismatch is the estimated forcing field. The adjoint model used to obtain the gradient of the cost function has recently been developed from a three-dimensional dynamical model of the stratosphere. The model is based on the fully nonlinear, hydrostatic primitive equations, with an isentropic vertical coordinate and a hexagonal-icosahedral horizontal grid. Other features are the potential vorticity is used as a conserved prognostic variable, and it has a realistic parameterisation of radiative transfer. In this work we present the adjoint model description and a series of twin experiments where the observed fields are obtained from the model evolution with a prescribed forcing term. This prescribed drag term corresponds to simple analytical functions. The details of the minimisation process in a case study are presented. By means of the twin experiments the sensitivity of the final state to different forcing configurations is analysed (this implies not only how well the technique can estimate the drag field but also how important it is for numerical models to have a good estimation of the parameters). The quality of the estimation as a function of the temporal window length is examined. The preliminary results shows that the technique has the potential to diagnose three-dimensional time varying fields of zonal and meridional components of gravity wave drag from observations.

**MC05/11A/A09-005** **1050**

**GLOBAL DISTRIBUTION OF GRAVITY WAVE MOMENTUM FLUX DERIVED FROM CRISTA SATELLITE DATA**

Manfred ERN<sup>1</sup>, P. PREUSSE<sup>1</sup>, M.J. ALEXANDER<sup>2</sup>, S.D. ECKERMANN<sup>3</sup> (<sup>1</sup>ICG I, Forschungszentrum Juelich, Juelich, Germany, <sup>2</sup>Colorado Research Associates, Boulder, USA, <sup>3</sup>Naval Research Laboratory, Washington, USA)

Based on temperature altitude profiles measured by the CRISTA satellite amplitudes, vertical wavelengths and phases of gravity waves (GWs) were retrieved by a combination of maximum entropy method and harmonic analysis. Furthermore, the horizontal wavelengths of the GWs were derived by comparing the phases of GWs in adjacent altitude profiles. From these results altitude profiles of the absolute value of the vertical flux of horizontal momentum have been estimated. There are significant differences between distributions of the temperature variance and distributions of the momentum flux. For example, global maps of the momentum flux show a pronounced northward shift of the equatorial maximum whereas temperature variance maps of the tropics/subtropics are nearly symmetric with respect to the equator. Similar results can be found at different altitudes. These findings point out that the distributions of horizontal and vertical wavelength are very important for global structures of the momentum flux. Vertical profiles of momentum flux are presented and compared to GW models on the basis of regional averages.

**MC05/11A/A09-006** **1110**

Invited

**CONVECTIVELY FORCED INTERNAL GRAVITY WAVES AND THEIR PARAMETERIZATION IN GENERAL CIRCULATION MODELS**

Hye-Yeong CHUN, In-Sun SONG (Department of Atmospheric Sciences, Yonsei University)

Characteristics of gravity waves induced by mesoscale convective storms and the gravity wave sources are investigated by simulating two-dimensional squall lines using a cloud-resolving numerical model. In the convective storms, there are two types of wave sources: nonlinear sources in the form of the divergences of momentum and heat flux, and diabatic source. The magnitude of the nonlinear source is 2-3 times larger than the diabatic source, especially in the upper troposphere. However, the magnitude of waves in the stratosphere induced by each wave source is comparable, with similar spectral characteristics of vertical wavelength (6.6-9.9 km), horizontal wavelength (10-100 km), and period (8-80 min). This is because the vertical propagation condition of linear internal gravity waves, in both the troposphere and stratosphere, restricts wave sources in the horizontal wavenumber and frequency domain, and therefore all of the forcing cannot generate gravity wave that can propagate up to the stratosphere. Compared with the diabatic sources, the nonlinear sources are inefficient in generating linear gravity waves that propagate vertically into the stratosphere. A formulation of cloud-top wave momentum flux induced by diabatic source with respect to different phase speed is derived analytically, and effects of basic-state wind shear and magnitude of cloud-top wind on the momentum flux is investigated. Wave filtering by critical level and wave propagation condition will be discussed.

**MC05/11A/A09-007** **1140**

**CONVECTIVELY GENERATED MESOSCALE GRAVITY WAVES SIMULATED THROUGHOUT THE MIDDLE ATMOSPHERE**

Takeshi HORINOUCI (Radio Science Center for Space and Atmosphere, Kyoto University)

A three-dimensional simulation was conducted with a cloud-resolving model to investigate mesoscale convectively-generated gravity waves that propagate to the middle atmosphere. The model covers a horizontal domain of 200 km x 200 km with a 1.5 km resolution with the cyclic boundary condition for both dimensions. The vertical coverage is from the surface to 120 km with the top 20 km being the sponge layer, and the vertical resolution is 0.5 km above the mid troposphere. This is the first cloud resolving modeling covering the whole vertical range of the middle atmosphere. In order to simulate under a realistic background condition, a horizontally uniform forcing is added based on radiosonde observations during



the TOGA COARE Intensive Observation Period. The surface is assumed to an ocean with a uniform temperature. It is found that both individual convective turrets and mesoscale convective systems excite gravity waves, resulting in a broad scale distribution. Waves excited by the former have conically shaped phase surfaces as previously reported and are conspicuous up to around the stratopause. Waves excited by the latter dominate in the MLT region. Frequent wave breaking is found above 85 km, where convective instability is found typically in the initial stage, leading to unstable shear with billows resembling the ripple-type structures observed frequently in airglow imaging. The sensitivity of the results is investigated by using higher resolution runs and by changing subgrid-scale turbulence parameterization. We are currently conducting numerical experiments with a significantly larger horizontal domain, and the results will be presented in the talk.

**MC05/11A/A09-008 1200**

**SEASONAL VARIATIONS OF GRAVITY WAVE VARIANCE OBSERVED BY CLAES**

Peter PREUSSE<sup>1</sup>, M. ERN<sup>1</sup>, S.D. ECKERMAN<sup>2</sup>, M.J. ALEXANDER<sup>3</sup>, J.L. MERGENTHALER<sup>4</sup> (<sup>1</sup>ICG-I, Forschungszentrum Juelich, Juelich, Germany, <sup>2</sup>Naval Research Laboratory, Washington, USA, <sup>3</sup>Colorado Research Associates, Boulder, USA, <sup>4</sup>Lockheed Martin Advanced Technology Center, Palo Alto, USA)

Gravity wave variances in CLAES temperature data are isolated by a 0-6wavenumber Kalman filter. Resulting vertical profiles of temperature residuals are analyzed by a combination of Maximum Entropy Method (MEM) and harmonic analysis for gravity waves (GWs). This is the same method previously employed to study GWs in CRISTA data. We obtain nearly 1.5 years of continuous GW data between 34S and 34N and good coverage at higher latitudes depending on UARS yaw maneuvers. Results are compared to CRISTA data and interpreted for different wave sources. A time series of zonal mean GW variance shows quiet summer and enhanced winter values at mid and high latitudes, the shift of the tropical maximum of GW variance around the equator and a burst of wave variance at stratopause altitudes in February of both years investigated, i.e. 1992 and 1993.

Friday, July 11 PM  
Presiding Chair: K. Hamilton

**MC05/11P/A09-001 Invited 1400**

**GRAVITY WAVES IN A GENERAL CIRCULATION MODEL**

Masaaki TAKAHASHI, Yoshio KAWATANI (Center for Climate System Research, University of Tokyo)

Gravity waves have important roles in the general circulation of the middle atmosphere. There are many observational studies of gravity waves. But, the global characteristics of gravity waves are still unknown, because gravity waves have small time and special scales. In the present study, numerical results of gravity waves in a high resolution general circulation model are discussed. The model is a CCSR/NIES atmospheric general circulation model. The horizontal resolution is T106 with about 100km resolution. Then, several hundreds km scale gravity waves are resolved. The vertical resolution is 60 layers from the surface to about 50 km altitude with about 550m resolution in the upper troposphere and lower stratosphere. The cumulus convective parameterization is Arakawa-Schubert scheme. The model is run for 2 years and gravity wave activity for 11-16 June is analyzed. Model output data is each one hour for the analysis. Gravity waves in the lower stratosphere are examined. Recently, satellite data about potential energy of gravity waves are obtained. Then, we can see the global features of potential energy of gravity waves in the lower stratosphere. There are special places of strong gravity wave potential energy. There are also special places of strong gravity wave kinetic energy in higher latitudes. We will present why the strong gravity wave energy in each place is produced.

**MC05/11P/A09-002 1430**

**GRAVITY WAVE DISTRIBUTION ALONG THE EQUATOR IN A HIGH RESOLUTION AGCM**

Koichiro TSUJI, Masaaki TAKAHASHI, Yoshio KAWATANI (Center for Climate System Research, University of Tokyo)

It is recognized that the quasi-biennial oscillation in the equatorial lower stratosphere (QBO) is mainly maintained by upward propagating gravity waves excited by cumulus convection in the troposphere. Although the QBO is a global-scale phenomenon along the equator, gravity waves affecting the QBO have smaller horizontal scales. Therefore, gravity wave activities in the equatorial region are not expected to be uniform along the equator. It is interesting to study the local characteristics of the equatorial gravity waves and their contribution to the QBO. Up to now, there have been no observational data which enable us to analyze short scale (~1000km wavelength, ~1day period) gravity waves globally and continuously. In this study, numerical experiments were performed in order to investigate the gravity wave distributions and its effects on the zonal wind in the equatorial lower stratosphere using a high resolution GCM (CCSR/NIES AGCM ver.5.6) with 3 hours output interval. As a result, at the easterly accelerating phase of the QBO, remarkable un-uniform distribution was seen in the vertical wave momentum flux  $u'w'$  in the equatorial lower stratosphere. Eastward wave momentum fluxes were located mainly over the Indian monsoon region. On the other hand, westward wave momentum fluxes were located mainly over the Eastern Pacific and the Atlantic. Therefore, the waves over the Eastern Pacific and the Atlantic mainly contribute to the production of the simulated QBO in this season. Spectral analysis showed that the westward propagating gravity waves having the period of about 1-2days are dominant in this region.

**MC05/11P/A09-003 1450**

**A SIMULATION STUDY OF GRAVITY WAVES GENERATED BY TYPHOON WINNIE**

Zeyu CHEN<sup>1</sup>, Peter PREUSSE<sup>2</sup>, Michael JARISCH<sup>3</sup>, Manfred ERN<sup>3</sup>, Dirk OFFERMANN<sup>1</sup> (<sup>1</sup>Department of Physics, University of Wuppertal, <sup>2</sup>Research Center Juelich, ICG-I)

During the CRISTA II mission (08 to 16 August, 1997), a super typhoon Winnie (hereafter referred to as Winnie) was evolving over the tropical north west pacific ocean. Over Winnie a stratospheric temperature perturbation is observed by CRISTA and believed to be gravity waves (GWs) as the feature matches the dispersion relation of GW. To study the relation between Winnie and the temperature perturbation, a numerical simulation with the Penn/NCAR MM5 model was carried out. We observe two kinds of GWs generated in the simulation. First we find wave generation due to horizontal wind shear at altitudes range of 16-25 km, in which tropical west wind reversed to east wind at 5N latitude. Simulation results show that GWs were generated from the convergent area relating to the wind shear and propagated in two opposite directions, southwestward in the equatorial westerly background and northeastward in the easterly wind northward of the wind shear. Corresponding

structures are found in the CRISTA data. Second we consider waves generated by Winnie. Simulations start after the evolving stage of Winnie (UT 00:00, 7 August). Winnie was classified as typhoon after UT 00:00 10 August. The critical features of the real typhoon have been captured by the simulation, including moving trend, intensity, and evolving stages. After Winnie had developed into typhoon state, model results show pronounced GWs in the stratosphere, and the wave amplitudes grow with upward propagation. The waves show a curved front propagating radially away from the storm center. In the easterly background flow eastward propagating waves are amplified and prominent at higher altitudes (25 km latitude). It is indicated that the waves are generated by the interaction between the stratospheric background flow and the typhoon related 'obstacle effect'.

**MC05/11P/A09-004 1510**

**EFFECTS OF HURRICANES ON THE STRATOSPHERE: EVIDENCE OF GRAVITY WAVE ACTIVITY FROM CAMEX-4 IN SITU MEASUREMENTS AND MESOSCALE MODELING**

Eric A. RAY<sup>1</sup>, Karen ROSENLOF<sup>1</sup>, Erik RICHARD<sup>1</sup>, Ken KELLY<sup>1</sup>, M.J. MAHONEY<sup>3</sup>, Joan ALEXANDER<sup>4</sup> (<sup>1</sup>NOAA, Aeronomy Lab, <sup>2</sup>CIRES, University of Colorado, <sup>3</sup>Jet Propulsion Laboratory, <sup>4</sup>Colorado Research Associates)

In situ and remote measurements from the ER-2 aircraft during the CAMEX-4 mission contain features which suggest the stratosphere is disturbed by wave activity above hurricanes. The predominant waves produced by hurricanes are thought to be gravity waves. The propagation of gravity waves above tropical convective storms inferred from radiosonde data has been shown to have a significant impact on the energy balance of the lower stratosphere in several previous studies. However, very few measurements exist in the stratosphere above hurricanes. In this study we use ER-2 in situ and microwave temperature profiler measurements as well as NCAR/PSU MM5 simulations of Hurricanes Erin and Humberto to deduce the gravity wave activity and impact on the stratospheric energy balance above the hurricanes.

**MC05/11P/A09-005 1530**

**WAVE ACTIVITY IN THE TROPICAL TROPOSPHERE AND LOWER STRATOSPHERE OBSERVED WITH THE EQUATORIAL ATMOSPHERE RADAR**

Fumitaka TSUJINO, Masayuki YAMAMOTO, Masatomo FUJIWARA, Hiroyuki HASHIGUCHI, Mamoru YAMAMOTO, Shoichiro FUKAO (Radio Science Center for Space and Atmosphere, Kyoto University)

The tropics is the region where convective activities are very active, because of a strong solar heating and water vapor supply from the ocean. These convective activities generate equatorial waves, which have a significant influence on the global-scale atmospheric circulation. Especially, equatorial Indonesia is one of the regions where convective activities are very prominent in the tropics. The Equatorial Atmosphere Radar (EAR), which is newly installed at Kototabang, West Sumatra, Indonesia (0.2 degrees south, 100.32 degrees east, 865m above mean sea level), can observe three-dimensional wind velocities in the whole troposphere and the lower stratosphere (2-20km) with good time and height resolution of about 85 sec and 150m, respectively. The EAR has been continuously operated since July 2001. The purpose of this research is to clarify the seasonal variations of the equatorial waves in the troposphere and lower stratosphere over equatorial Indonesia. The principal data used for this study are three-dimensional wind velocities obtained with the EAR for the period from July to December 2001. We classified four height regions for the wind spectral analysis: lower troposphere (2-5km), middle troposphere (5-10km), upper troposphere (10-15km) and lower stratosphere (15-20km). At the lower troposphere, spectral peaks at 1 day were seen at all wind components. Spectral densities of meridional and zonal wind components at 1 day increased during the observational period. Spectral peaks of meridional and zonal wind components at 4-5 days matched the typical period of mixed Rossby-gravity waves. These spectral densities at 4-5 days decreased during observational period. The magnitude of spectral densities of zonal wind component was large at the period of > 15 days. This enhancement of spectral densities was considered to be associated with Intraseasonal Oscillation (ISO). At the lower stratosphere, spectral peaks at 1 day were also seen at all wind components. Spectral peaks at 4-5 days were also seen at meridional and zonal wind components. The time variations of spectral peaks at 4-5 days were almost the same as at the lower troposphere. The magnitude of spectral densities of zonal wind component was large at the period of > 6 days, while enhancement in meridional wind component was not seen. Thus it is considered that this spectral enhancement was associated with the equatorial Kelvin waves. In order to see the relation of equatorial waves and cumulus convection, we investigated infrared equivalent blackbody temperature (TBB) and wind data by National Centers for Environmental Prediction reanalyses (NCEP wind). There was a good correlation between TBB and NCEP vorticity at 500hPa. The daily variations of TBB were large when spectral peaks at 1 day at the lower troposphere were large. It is also noticed that NCEP westward wind at 300hPa and 70hPa over the Western Pacific agreed well with the spectral peaks at the period of > 6 days period. When NCEP westward wind at 300hPa and 70hPa over the Western Pacific became weak, spectral densities at the period of > 6 days decreased.

**MC05/11P/A09-006 1620**

**CHARACTERISTICS OF ATMOSPHERIC WAVES OBSERVED WITH RADIOSONDES DURING DAWEX CAMPAIGNS**

Toshitaka TSUDA (Radio Science Center for Space and Atmosphere (RASC), Kyoto University)

As one of the international observation campaign of SPARC, DAWEX (Darwin Area Wave Experiment) was conducted in October-December, 2001 to observe characteristics of atmospheric gravity waves excited by tropical convection. We conducted radiosonde campaigns with a duration of 120 hours for 3 times on October 13-18, November 15-20 and December 11-16, 2001. During these IOPs we launched radiosondes every 3 hours from 3 sites; Garden Point on the Tiwi islands (Pirangimpi) (11.4S, 130.3E), the Darwin weather station of BOM (12.4S, 130.9E) and a civilian airport in Katherine (14.5S, 132.5E). This paper is concerned with the behavior of atmospheric gravity waves analyzed by using intensive radiosonde observations during DAWEX. In the lower stratosphere at 15-20 km strong wind velocity fluctuations with a period of about 84 hours were detected in the 3 campaign periods. Gravity waves with a vertical scale shorter than about 3 km were enhanced at 15-20 km and above about 25 km, showing coherent downward phase propagation between the 3 sites. However, the wave activity was significantly depressed at 20-25 km. We will discuss a relation between the height variations of gravity wave intensity and the background conditions

**MC05/11P/A09-007 1640**

**DAWEX EXPERIMENT: OBSERVATIONAL ANALYSIS OF WAVES AT DIFFERENT SCALES**

Alejandro DE LA TORRE<sup>1</sup>, Toshitaka TSUDA<sup>2</sup> (<sup>1</sup>Departamento de Fisica, FCEN, Universidad de Buenos Aires, ARGENTINA, <sup>2</sup>Radio Science Center for Space and Atmosphere, Kyoto University, Uji, Kyoto, JAPAN)

A set of radiosoundings launched simultaneously from three stations in Northern Territory, Australia (Darwin Area Wave Experiment, DAWEX Experiment) is analysed. During the experiment, three periods were considered: (1) October 13-18, (2) November 15-20 and (3) December 11-16, 2001. Eight launches per day and site were released, and a total of 360 profiles during this experiment. The possible existence of critical levels interacting with quasi stationary waves and mixing layers found near the tropopause is analyzed. The significance of cloud-top mixing driven by radiative cooling across the top of anvils in these mixing layers is considered. A systematic wave structure observed in the altitude intervals (15, 20) and (25, 30) km and a negligible variance between them is observed. The wave amplitudes are larger in the meridional wind and a systematic near to zero mean wind around the tropopause is appreciated. A spectral analysis reveals two prevailing low frequencies in the wave structure. A wave selection near the tropopause and possible trapping and reflexion effects there are considered.

**MC05/11P/A09-008 1700**

**GRAVITY WAVE ACTIVITIES OVER A SMOOTH SURFACE WITH LITTLE CONVECTION**

Yoshio KAWATANI<sup>1</sup>, Masaaki TAKAHASHI<sup>1</sup>, Surendra Kumar DHAKA<sup>2</sup>, Toshitaka TSUDA<sup>3</sup> (<sup>1</sup>University of Tokyo, <sup>2</sup>Department of Physics, Rajdhani College, University of Delhi, <sup>3</sup>Radio Science Center for Space and Atmosphere, Kyoto University)

In order to understand the climate variability and atmospheric general circulation, it is important to consider the dynamical interaction between troposphere and stratosphere through gravity waves. Recently, satellites provided the global characteristics of the gravity waves by extracting the temperature disturbances (cf., Tsuda et al. 2000). In general, large potential energy (Ep) is found in tropical regions between 20°N and 20°S. Interestingly, they noticed regions around the tropical Atlantic (~ 0°-30°W, 0°-10°S) with large Ep. This is a region with little convection or topographic source of gravity waves. The mechanism for the formation of this energy remains uncertain. It is difficult to investigate all physical quantities simultaneously in observations. In this study, we used an atmospheric general circulation model with the resolution T106L60 in order to understand the mechanism for the presence of high-energy over the Atlantic Ocean. We investigate the activity of gravity waves for one week in June, when the Indian summer monsoon is typical and intense. The model well simulated the distribution of the precipitation such as the separation between ITCZ and SPCZ, and the Baiu front (cf. Kawatani and Takahashi 2003). The simulated global distribution of Ep is quite similar to that observed in the GPS/MET experiment, and large Ep is also found over the Atlantic Ocean (cf., Tsuda et al., 2000, Kawatani et al., 2003). It is found that gravity waves with a time period of 24 hours are excited around the Bay of Guinea in a region of large moist heating extending vertically up to 10-13 km. The gravity waves propagate upward from this region with a bias toward the south and are manifested as large energy fluxes in the cross equatorial region. Enhanced energy fluxes are therefore simulated at 20-30 km altitude over a region with no significant source of gravity waves.

**MC05/11P/A09-009 1720**

**OBSERVATIONAL FILTER FOR GRAVITY WAVE CHARACTERISTICS OBTAINED FROM GPS RADIO OCCULTATION SOUNDINGS**

Christian MARQUARDT (Met Office)

Retrievals of GPS based radio occultation soundings provide stratospheric temperature profiles with high vertical resolution. Consequently, data from, e.g., the GPS/MET mission have been used to infer about the global distribution of gravity wave characteristics and vertical wave number spectra in the stratosphere. The standard "dry temperature" retrieval which is usually implemented, however, suffers from a high sensitivity to measurement noise. This makes the distinction between gravity wave signal and instrumental noise difficult. Also, no "observational filter" for gravity wave observations with radio occultation soundings is currently known. A high-resolution variational retrieval of radio occultation data which allows the estimation of gravity wave parameters in the lower stratosphere is presented. Compared to the standard approach, the variational framework provides a more detailed understanding of the signal-to-noise issue. The gravity wave observational filter for the variational retrieval is discussed. Preliminary results of a 2 year climatology of the global distribution of gravity wave activity obtained from the German satellite CHAMP are presented.

**MC05/11P/A09-010 1740**

**A MODEL SIMULATION OF MOUNTAIN WAVES IN THE MIDDLE ATMOSPHERE AND ITS COMPARISON WITH MICROWAVE LIMB SOUNDER OBSERVATIONS**

Jonathan H. JIANG, Stephen D. ECKERMANN, Dong L. WU, Jun MA (Jet Propulsion Laboratory)

Topography-related wintertime stratospheric gravity waves in both Northern and Southern Hemisphere are simulated using the Naval Research Laboratory Mountain Wave Forecast Model (MWFModel). The results agree well with the observations from Upper Atmospheric Research Satellite Microwave Limb Sounder (MLS). Both the MWFModel simulation and MLS observations found strong wave activities over the high-latitude mountain ridges of Scandinavia, Central Eurasia, Alaska, southern Greenland in Northern Hemisphere, and Andes, New Zealand, Antarctic rim in Southern Hemisphere. These mountain waves are dominated by wave modes with downward phase progression and horizontal phase velocities opposite to the stratospheric jet-stream. Agreements of minor wave activities are also found at low- to mid-latitudes over Zagros Mountains of Middle East, Colorado Rocky Mountains, Appalachians, and Sierra Madres of Central America. Some differences between the MWFModel results and MLS data are explained by different horizontal resolution between the model and observation, and the fact that MLS may also see the non-orographic wave sources, such as mesoscale storms and jet-stream instabilities. The findings from this model-measurement comparison study demonstrate that satellite instruments such as MLS can provide global data needed to characterize mountain wave sources, their inter-annual variations, and to improve gravity wave parameterizations in global climate and forecast models.

**MC08 Monday, July 7**

**FUTURE CHANGES IN GLOBAL AND REGIONAL CLIMATE (ICDCI)**

Location: Site B, Room 17

**Monday, July 7 AM**  
Presiding Chairs: D. Frame, D. Sexton

**MC08/07A/B17-001 0930**

**THE EARLY CENTURY WARMING IN THE ARCTIC - A POSSIBLE MECHANISM**

Lennart BENGTTSSON<sup>1</sup>, Vladimir SEMENOV<sup>1</sup>, Ola M. JOHANNESSEN<sup>2</sup> (<sup>1</sup>Max-Planck-Institut fuer Meteorologie, <sup>2</sup>Nansen Environmental and Remote Sensing Center)

The huge warming of the Arctic that started in the early 1920s and lasted for almost two decades is one of the most spectacular climate events of the 20th century. During the peak period 1930-1940 the annually averaged temperature anomaly for the area 60°N-90°N amounted to some 1.7°C. Whether this event is an example of an internal climate mode or externally forced, such as by enhanced solar effects, is presently under debate. Here we suggest that natural variability is the most likely cause with reduced sea ice cover being the main reason of the warming. A robust sea ice-air temperature relationship was demonstrated by a set of four simulations with the atmospheric ECHAM model forced with observed SST and sea ice concentrations. An analysis of the spatial characteristics of the observed early century surface air temperature anomaly revealed that it was associated with similar sea ice variations. We have further investigated the variability of Arctic surface temperature and sea ice cover by analyzing data from a coupled ocean-atmosphere model. By analyzing similar climate anomalies in the model as occurred in the early 20th century, it was found that the simulated temperature increase in the Arctic was caused by enhanced wind driven oceanic inflow into the Barents Sea with an associated sea ice retreat. The magnitude of the inflow is linked to the strength of westerlies into the Barents Sea. We propose a positive feedback sustaining the enhanced westerly winds by a cyclonic atmospheric circulation in the Barents Sea region created by a strong surface heat flux over the ice-free areas. Observational data suggest a similar series of events during the early 20th century Arctic warming including increasing westerly winds between Spitsbergen and the northernmost Norwegian coast, reduced sea ice and enhanced cyclonic circulation over the Barents Sea. It is interesting to note that the increasing high latitude westerly flow at this time was unrelated to the North Atlantic Oscillation, which at the same time was weakening.

**MC08/07A/B17-002 1000**

**WHY DOES PRECIPITATION DECREASE INITIALLY IN TRANSIENT RESPONSE TO CO2 DOUBLING?**

Akira NODA<sup>1</sup>, Kazuki YAMAGUCHI<sup>2</sup>, Takao UCHIYAMA<sup>1</sup>, Sachiko YAMAKI<sup>1</sup> (<sup>1</sup>Climate Research Department, Meteorological Research Institute, <sup>2</sup>Tokyo Electric Power Company)

Precipitation decreases just after CO2 concentration of the atmosphere is doubled. This response is opposite to what is expected from equilibrium response to CO2 doubling. Two mechanisms have been proposed to explain the decrease in precipitation for the transient response: - The heat content of land is much smaller than that of ocean, so that the heat loss will be dominant over land, providing subsiding air over ocean to suppress the evaporation from the sea surface. (Land-sea effect) - The main effect of CO2 on longwave cooling in the troposphere is to reduce the longwave cooling due to water vapor through the spectral overlap at 15 micron band, resulting in the reduction of convective heating to keep the heat balance in the troposphere. (CO2 effect) In the radiative convective one-dimensional atmosphere, evaporation and precipitation decrease due to CO2 effect because no land-sea effect exists. In the three dimensional atmosphere both effects can work. In order to identify the relative importance, ensemble experiments have been made with doubling CO2 and with 2% increase in solar constant. As a result, the globally averaged land-sea effect is estimated to be twice larger than the CO2 effect in the initial response as estimated from precipitation averaged over ocean grids. However, the reduction in precipitation lasts only about one year due to the former effect. After this initial response, the latter effect remains to suppress the precipitation over oceans more than five years. Finally enhanced greenhouse effect of water vapor evaporated from the ocean surface dominates the tropospheric response and precipitation increases to maintain the heat and mass balances in the troposphere.

**MC08/07A/B17-003 1015**

**ESTIMATING UNCERTAINTY IN THE RESPONSE TO DOUBLED CO2 USING A LARGE ENSEMBLE OF GCM VERSIONS**

David M.H. SEXTON, James MURPHY, David N. BARNETT, Mark J. WEBB (Hadley Centre, Met Office)

For a given emissions scenario, GCM predictions of climate change are subject to uncertainties arising from the representation of climate system processes in the model and the effects of natural variability. These uncertainties imply a probability distribution of outcomes for a given climate variable, which must be specified before quantitative risk assessments can be made. In principle such distributions can be estimated from large ensembles of GCM predictions. In practice this has not hitherto been possible due to a lack of computing power with the result that only crude uncertainty estimates are currently available, based on a handful of models run at different centres. Another stumbling block has been a lack of objective methods of assessing the reliability of predictions from different models, or of identifying plausible model versions in the first place. Preliminary results will be presented from a new project aimed at addressing these issues. Frequency distributions of changes in the equilibrium response to doubled CO2 will be illustrated using an ensemble of versions of the Hadley Centre's coupled atmosphere/mixed layer ocean model, each distinguished by a change to a parameter controlling a key atmospheric process. This will be compared to distributions obtained from an ensemble of predictions produced using the same version of the model with varying initial conditions, thus allowing the relative uncertainties associated with natural variations and process uncertainties to be estimated. The effect of weighting model versions according to simulation quality will be discussed.

**MC08/07A/B17-004 1030**

**THE GLOBAL STATIONARY WAVE RESPONSE TO CLIMATE CHANGE IN A COUPLED GCM**

Mingfang TING<sup>1</sup>, Renu JOSEPH<sup>1</sup>, Paul J. KUSHNER<sup>2</sup> (<sup>1</sup>Department of Atmospheric Sciences, University of Illinois at Urbana-Champaign, <sup>2</sup>GFDL/Princeton University, Princeton, New Jersey)

The stationary wave response to global climate change in the Geophysical Fluid Dynamics Laboratory's "R30" coupled ocean-atmosphere GCM is studied. An ensemble of climate change simulations that use a standard prescription for time-dependent increases of greenhouse gas and sulfate aerosol concentrations is compared to a multiple-century control simulation with these constituents fixed at pre-industrial levels. The primary response to climate change is to zonally the atmospheric circulation, that is, to reduce the amplitude of the stationary waves in all seasons. This zonalization is particularly strong in the boreal summer over the tropics. In January, changes in the stationary waves resemble that of an El Niño, and all months exhibit an El Niño-like increase of precipitation in the central tropical Pacific. The dynamics of the stationary wave changes are studied with a linear stationary wave model, which is shown to simulate the stationary wave response to climate change remarkably well. The linear model is used to decompose the response into parts associated with changes to the zonal mean basic state and with changes to the zonally asymmetric "forcings" such as diabatic heating and transient eddy fluxes. The decomposition reveals that at least as much of the climate change response is accounted for by the change to the zonal mean basic state as by the change to the zonally asymmetric forcings. For the January response in the Pacific North-American sector, it is also found that the diabatic heating forcing contribution dominates the climate change response, but is significantly cancelled and phase-shifted by the transient eddy forcing. The importance of the zonal mean and of the diabatic heating forcing contrasts strongly with previous linear stationary wave models of the El Niño, despite the similarity of the January stationary wave response to El Niño. In particular, in El Niño, changes to the zonal mean circulation contribute little to the stationary wave response, and the transient eddy forcing dominates. The conclusions from the linear stationary wave model apparently contradict previous findings on the stationary wave response to climate change response in a coarse resolution version of this model.

**MC08/07A/B17-005 1045**  
**THE EFFECT OF AEROSOLS ON GLOBAL WARMING ESTIMATED FROM MULTI-CGCM RUNS AND MULTI-EMISSION SCENARIO RUNS**

Akira NODA, Takao UCHIYAMA, Sachiko YAMAKI (Climate Research Department, Meteorological Research Institute)

We have examined the effect of the negative radiative forcing due to the direct effect of sulfate aerosols on global warming by comparing results from common scenario runs with 7 coupled atmosphere-ocean general circulation models (CGCMs) and from multi-scenario runs with a new version of MRI-CGCM. Each result from common scenario runs is consist of a run forced by increases in CO2 alone and that obtained by increasing CO2 and aerosol concentration exactly or approximately following IPCC IS92a scenario. The future scenario assumes that the atmospheric equivalent CO2 concentration increases at a compound annual rate of about 1%, while the atmospheric aerosol concentration almost levels off after 2050, so that the CO2 forcing alone increases linearly at the same rate between the two runs during the second half of the 21st century. A comparison is made for the difference in trend and mean during the period. The most dominant geographical response due to the cooling effect of aerosols appears as a reduction of the magnitude of global warming patterns simulated with the CO2 only forcing. During the second half of the 21st century, a significant larger warming trend in surface temperature is found for the aerosol plus CO2 run than for the CO2 only run in winter over the polar region in the Northern Hemisphere. For the multi-scenario runs we have estimated three-dimensional atmospheric sulfate aerosol distributions due to anthropogenic emissions for the present and for SRES scenarios (A1B, A1T, A1F1, A2, B1 and B2), where a chemical transport model (MASINGER) developed at MRI (Tanaka et al., 2003) was used off-line. Since the model intercomparison shown above indicates that the primary effect of aerosols depends on global mean radiative forcing, we have calculated the radiative forcing for each scenario. Some preliminary results from the multi-scenario runs suggest that the scenario dependency of spatial global warming pattern is weak.

**MC08/07A/B17-006 1120**  
**REGIONAL CLIMATE CHANGE PROJECTION OVER JAPAN IN WINTER DUE TO GLOBAL WARMING USING AN MRI-CGCM1/ REGIONAL CLIMATE MODEL NESTING SYSTEM**

Yasuo SATO<sup>1</sup>, Kazuyo MURAZAKI<sup>1</sup>, Hidetaka SASAKI<sup>1</sup>, Seiji YUKIMOTO<sup>2</sup>, Akira NODA<sup>3</sup>, Ayako TAKEUCHI<sup>1</sup>, Shinya KOBAYASHI<sup>1</sup> (<sup>1</sup>Atmospheric Environment and Applied Meteorology Research Department, Meteorological Research Institute, Japan Meteorological Agency, <sup>2</sup>Climate Research Department, Meteorological Research Institute, Meteorological Research Institute, Japan Meteorological Agency, <sup>3</sup>Climate Prediction Division, Climate and Marine Department, Japan Meteorological Agency)

A regional climate model (RCM) experiment was performed to obtain regional climate change projection over Japan in winter due to global warming using the MRI/JMA regional climate model, whose lateral boundary conditions were supplied from the results of a transient CO<sub>2</sub> experiment performed by the MRI-CGCM1. The horizontal resolution of the atmospheric part of the MRI-CGCM1 is 5° by 4° in the longitudinal and latitudinal directions and 15 levels in the vertical. That of the oceanic part has 21 vertical layers, 2.5° longitudinal resolution, and variable latitudinal resolution ranging from 0.5° at the equator to 2.0° at 12° latitude and further poleward. The MRI/JMA regional climate model with 40 km resolution is integrated in a time-slice manner only in January for 20 years for both control (1xCO<sub>2</sub>) and doubling CO<sub>2</sub> conditions using the results of the Asian regional climate model with 120 km resolution which was generated by outputs of the MRI-CGCM1 transient CO<sub>2</sub> experiment with an increasing CO<sub>2</sub> concentration of 1%/year compound rate. Results over the Japanese Islands are analyzed only for winter. The RCM results with 40km resolution are much improved especially on precipitation distribution in comparison with 40 km-interpolated CGCM results. A regional climate change projection on precipitation shows a decrease along the Japan Sea side of the Japanese Islands, on one hand an increase along the Pacific Ocean side of them, which can be interpreted that cold air outbreak from the Siberian High in winter is weakened under the doubling CO<sub>2</sub> condition. At the same way, snowfall amount decreases along the Japan Sea side. On the other hand, precipitation off the south coast of the Japanese Islands increases under the doubling CO<sub>2</sub> condition because of increasing of the storm track precipitation, that is, the northward shift of the storm track in winter in a climatological sense.

**MC08/07A/B17-007 1135**  
**IMPACT OF POSSIBLE FUTURE CLIMATE ON COASTAL WINDS, STORM SURGES AND WAVE CONDITIONS IN THE NORTH SEA**

Hans VON STORCH, Frauke FESER, Amt PFIZENMAYER, Burkhardt ROCKEL, Ralf WEISSE, Katja WOTH (Institute for Coastal Research, GKSS Research Center, Geesthacht, Germany)

Using time slice simulations with T106 global models (EU project STOWASUS) as well as a regional climate model (EU project PRUDENCE) detailed scenarios of plausible future wind conditions in the North Sea and in the Baltic Sea are presented. The impacts of the changing wind statistics on water levels, storm surge severity and wave conditions are

discussed. The results are used to discriminate between present natural variations and first indicators of anthropogenic climate change.

**MC08/07A/B17-008 1150**  
**SOUTH WEST AUSTRALIA PAST AND FUTURE RAINFALL TRENDS**

Bertrand Olivier TIMBAL (Bureau of Meteorology Research Centre)

A statistical method, based on the idea of analogous synoptic situations, is used to study the observed rainfall trends in South West of Western Australia. The method has been developed and optimised by relating patterns of atmospheric field (predictors) to stations records of rainfall (predictands) in the South West of Western Australia, for both rain occurrences and daily rain amounts. When tested on observational data, the analogue method is able to reproduce partially the observed trend and inter-annual variability observed during the past 50 years, showing the sensitivity of the analogue approach to changed climatic conditions. Similar results are obtained over the entire record period and when data are splitted into a development and a validation period to ensure a proper cross validated examination of the method's skill. Among the parameters considered, the set of predictors has one of the most important impacts on results. It is demonstrated that moisture fields explain an important part of the observed trend. The model is then applied to three state-of-the-art coupled models' simulation of the current climate. The improvement when using the statistical downscaling tool over direct model grid-average outputs is shown to be substantial. Most of the model biases are removed and realistic probability distribution functions at station level are obtained. The method is then applied to altered climate conditions; the impact of large scale model uncertain responses and model sensitivities are quantified using the various coupled models. Future trends for rainfall estimated by direct GCM outputs are compared with downscaled projections. A general agreement is found; uncertainties are smaller amongst projections when the downscaling technique is used. All projections agree on a reduction of total rainfall in winter and spring for most stations in this part of the continent following global climate change.

**MC08/07A/B17-009 1205**  
**REGIONAL REGIMES WITH DROUGHT AND EXTREME WET CONDITIONS: POSSIBLE CHANGES IN XXI CENTURY FROM MODEL SIMULATIONS**

Igor I. MOKHOV<sup>1</sup>, Jean-Louis DUFRESNE<sup>2</sup>, Vyacheslav Ch. KHON<sup>1</sup>, Herve LE TREUT<sup>2</sup>, Vladimir A. TIKHONOV<sup>1</sup> (<sup>1</sup>A.M.Obukhov Institute of Atmospheric Physics RAS, <sup>2</sup>Laboratoire Meteorologie Dynamique du CNRS)

Possible regional changes of drought and extreme wet conditions in the XXI century relative to the XX century from simulations of a coupled atmosphere-ocean general circulation model IPSL-CM2 with a carbon cycle for the 1860-2100 period are analysed. The scenario with the carbon dioxide emissions due to fossil and land use from observations up to 1990 and the IPCC SRES98-A2 emission scenario from 1990 to 2100 in these simulations were used. Model simulations of extremal meteorological conditions were tested in comparison with observations in spring-summer from the end of the XIX century up to the end of the XX century in the European and Asian regions at the middle latitudes. An analysis is performed in terms of different indices characterizing anomalously warm and dry (or cold and wet) conditions. The changes in characteristics of the drought and wet regimes in summer between XXI and XX centuries were estimated from model simulations for East (EER) and West (WER) European regions. Model results display that the increase of temperature in the XXI century is accompanied in both regions by the decrease of precipitation and wet regime index and by the increase of drought indices. There are remarkable differences in changes for EER and WER. Model simulations show the interannual variability increase in the XXI century for temperature in both regions and for precipitation in WER, while the variability decrease for precipitation in EER. Drought indices display the general variability increase, while wet conditions index shows the interannual variability decrease.

Monday, July 7 PM  
 Presiding Chairs: I.I. Mokhov, Y. Sato

**MC08/07P/B17-001 1400**  
**THE FUTURE CHANGE OF THE VARIABILITY AND EXTREMES OF DAILY RAINFALL EVENTS DURING THE INDIAN SUMMER MONSOON SIMULATED IN A GLOBAL TIME-SLICE EXPERIMENT**

Wilhelm MAY (Danish Meteorological Institute)

The possible future change in the variability and extremes of daily rainfall during the Indian summer monsoon as a consequence of the anticipated increase in the concentrations of the important greenhouse gases is investigated. This is done on the basis of a global time-slice experiment with the ECHAM4 atmospheric GCM at a high horizontal resolution of T106, corresponding to a grid spacing of about 120 km. The first time-slice (period: 1970-1999) represents the present-day climate and the second (2060-2089) the future climate after roughly a doubling of the atmospheric CO<sub>2</sub> concentration relative to present-day values. During the two time-slices monthly mean values of the sea surface temperatures, the sea-ice extent and the sea-ice thickness originating from a transient climate change simulation with the ECHAM4/OPYC coupled model at a low horizontal resolution of T42 (corresponding to a grid spacing about 300 km) have been prescribed as lower boundary forcing to the atmospheric GCM. In addition to some basic properties, such as the frequency of wet days (defined as days with precipitation) as well as the mean and the variability of rainfall occurring on wet days, the characteristics of extreme daily rainfall events are investigated by means of percentiles as well as via theoretical distributions, namely the Generalized Extreme Value and the Generalized Pareto distributions. For the future, the time-slice experiment predicts an increase in the rainfall associated with extreme daily rainfall events in the entire Indian region, except for the central part of the Indian peninsula. This future increase is to about the same extent related to an increase in the intensity of extreme rainfall events and to an increase in the frequency of such extreme events. The magnitude of the future change in the rainfall originating from extreme rainfall events (relative to the change in the overall rainfall) varies conspiringly from region to region. This indicates the need to explicitly assess the future changes in the extremes of the monsoon rainfall, rather than inferring them from changes in the mean rainfall. The comparison with observational rainfall data (GPCP) shows that ECHAM4 is able to simulate the variability as well as the extremes of daily rainfall during the Indian summer monsoon under present-day climate conditions quite well. Therefore, the future changes in extreme daily rainfall events predicted in the time-slice experiment have a high degree of credibility.

**MC08/07P/B17-002 1415**

**FUTURE PROJECTIONS OF EAST ASIAN CLIMATE USING MULTI-MODEL ENSEMBLES OF IPCC SRES SCENARIO SIMULATIONS**

Seung-Ki MIN, E-Hyung PARK, Won-Tae KWON (Climate Research Laboratory, Meteorological Research Institute, Korea)

Future climate over East Asia (20-50°N, 100-145°E) is projected using multi-model ensemble of selected coupled climate model (CCM) simulations based on IPCC SRES A2 and B2 scenarios. Analyzed variables include annual and seasonal mean temperature and precipitation over East Asia. Before projecting future climate, model performances are evaluated with the simulations of present-day climate (defined as 1961-1990). Multi-model ensemble projections are constructed from high-performance CCMs, which are selected considering bias, RMSE and Taylor diagram analyses. After removing models with large bias and RMSE, CCMs which have a higher similarity to observations in spatial pattern and variability amplitude, are selected in the Taylor diagrams. As a result of model evaluation, CSIRO Mk2, ECHAM4/OPYC, GFDL\_R30\_c, and HadCM3 are selected as high-performance models for the simulation of temperature and precipitation over East Asia. Multi-model ensemble projections from high-performance CCMs show that East Asia will experience warmer and wetter climate in the 21st century. Area-averaged temperature changes for three 30-year periods (2020s, 2050s, and 2080s) simulated by A2[B2] scenario ensemble are 1.2[1.3], 2.4[2.3], and 4.0[3.0]°C and precipitation changes are -0.5[0.5], 2.0[1.8], and 6.1[3.3]%, respectively. Spatial patterns indicate that both temperature and precipitation increases are larger over the continental area than the ocean. In general, the areas with a large inter-model variability are in accord with the areas of large climate change, and there is too large inter-model variability in precipitation change patterns such that its amplitude is as much as ensemble mean. A marked difference (larger than inter-model variability) in projected patterns between A2 and B2 scenario ensembles appears in the 2080s temperature field with a larger amplitude located in the northern continental area. However, no significant differences can be found between precipitation patterns of A2 and B2 scenario ensembles because of a dominant inter-model variability.

**MC08/07P/B17-003 1430**

**PROJECTIONS OF CLIMATE CHANGE OF EXTREME EVENTS IN THE 21ST CENTURY OVER EAST ASIA**

Zong-ci ZHAO<sup>1</sup>, Akimasa SUMI<sup>1</sup>, Chikako HARADA<sup>1</sup>, Toru NOZAWA<sup>2</sup> (<sup>1</sup>Center for Climate System Research, University of Tokyo, <sup>2</sup>National Institute for Environmental Studies, Tsukuba, Japan)

In the recent years, four new IPCC scenarios of emission such as SRESA1, SRESA2, SRESB1 and SRESB2 have been inputted to the CCSR/NIES climate model system. The projections of climate change over East Asia in the 21st century have been calculated. In this research, we concentrated on the projections of several extreme climate events in the 21st century such as maximum and minimum temperatures, frequency of strong rainfall, extra-tropical cyclones, tropical cyclones and typhoons over East Asia. As projected by the CCSR/NIES model system, comparing to 1961~1990, the significant warming of 3.0~14.3C for SRESA1, 3.0~15.6C for SRESA2, 2.0~10.1C for SRESB1 and 2.0~11.6C for SRESB2 in the last 30 years (2071~2100) of the 21st century over East Asia has been noticed. The distributions of precipitation change for 2071~2100 minus 1961~1990 by the different scenarios were more complicated than the temperature change. It might be getting drier over the most part of Japan and the lower branch of Yangtze River of China as simulated by the model with SRESA2. It might be getting wetter in the most north and west parts of East Asia have been found. Both Tmax and Tmin over East Asia increase obviously due to the human activities in the 21st century. To compare the last 30 years (2071~2100) with 1961~1990, SRESA2 caused the warmest situation by about 3.5~13.9C in East Asia and SRESB1 responded for a smallest warming by about 2.5~8.9C among four scenarios. In this research, the frequency of strong rainfall, extra-tropical cyclones, tropical cyclones and typhoons over East Asia have been also investigated.

**MC08/07P/B17-004 1445**

**THE INTENSIFICATION AND SHIFT OF THE NORTH ATLANTIC OSCILLATION IN A GLOBAL WARMING SCENARIO SIMULATION**

Zeng-Zhen HU, Zhaohua WU (Center for Ocean-Land-Atmosphere Studies)

The impact of global warming on the spatial and temporal character of the North Atlantic Oscillation (NAO) is investigated with a ECHAM4/OPYC3 CGCM global warming scenario simulation. It is shown that the meridional pressure gradient over the North Atlantic is significantly strengthened, and the two centers of action of the NAO, the Icelandic low and the Azores high, are intensified and shifted northeastward by 10° to 20° in latitude and 30° to 40° in longitude in the global warming scenario. The strengthened meridional pressure gradient results in a tendency toward a positive phase of a modified NAO index and an enhancement of its intensity. The shift of the centers of action leads to a failure in capturing the NAO change with the traditional definition of the NAO index. The intensification of the NAOs tied up with zonal mean state change, and the changed zonal mean state alters stationary wave propagation that is associated with the shift of the centers of action of the NAO. In addition, it seems that the variances and frequencies of NAO variation at inter-monthly to interannual timescales are not affected much by the global warming. Warmed tropical oceans and intensified stratospheric polar vortex are the candidate mechanisms to interpret the NAO change in the global warming scenario.

**MC08/07P/B17-005 1520**

**THE CHANGE OF THE GLOBAL WATER CYCLE AROUND 2050 SIMULATED BY THE MRI GCM**

Masahiro HOSAKA<sup>1</sup>, Akio KITO<sup>1</sup>, Yasuhiro MURATA<sup>2</sup>, Yukimasa ADACHI<sup>1</sup> (<sup>1</sup>Meteorological Research Institute, <sup>2</sup>Graduate School of Science, Hokkaido University)

We conducted the simulations under the conditions of 1980-2000 and 2040-2060 with the MRI AGCM, and compared the results with respect to the global water cycle. The differences of the conditions are the prescribed distributions of the SSTs and the aerosols, and the amount of the greenhouse gases. The SSTs are obtained from the SRES A2 scenario simulation of the MRI coupled GCM. The 6 hourly data output are stored and analyzed. As in the coupled GCM cases, the surface air temperature becomes warmer over the high latitude regions than the low latitude regions, and the amount of the precipitation increases mainly over the middle-high latitudes. There is positive high correlation between the pattern of the precipitation and that of the soil moisture in the annual mean values. As for the seasonal march, the length of the snow-covered season gets shorter because of the warming. By using the 6 hourly data, we analysed changes in extreme precipitation events such as rainfall days, drought duration, heavy precipitation and changes of probability distribution of precipitation. It is found that there are areas such as East Asia where continuous no-rainfall days increase although in spite of the increase in mean precipitation by global warming.

**MC08/07P/B17-006 1535**

**REGIONAL CLIMATES UNDER DIFFERENT WARMING SCENARIOS: EFFECTS OF DYNAMICS AND THERMODYNAMICS**

Pier Luigi VIDALE, Cornelia SCHWIERZ, Daniel LUETHI, Christoph FREI, Christoph SCHAER (Institute for Atmospheric and Climate Science ETH)

The effects of climate change near elevated terrain still represent a very open research question, since the climate of elevated terrain regions is modulated by the interaction of the atmospheric circulation with orography at several temporal and spatial scales. In Europe, processes over the Alps, for instance, also influence the climate of neighboring regions through low-level blocking, lee cyclogenesis, the alteration of large scale storm tracks and induced advection/convection/subsidence patterns. In this climate change study we address the European regional impacts of these processes by performing multi-year sensitivity experiments, using the CHRM Regional Climate Model, forced at the lateral boundaries with data from different large scale analyses. In the first experiment we drive the model with data from a surrogate warming scenario, in which dynamical processes are left unchanged (i.e. the storm amount and tracks are kept fixed); in the second experiment we force the model with large scale analysis from a GCM simulation, integrated under a full SRES A2 scenario. By contrasting these experiments, and analyzing in reference to a standard current climate simulation (driven with perfect lateral boundary data from the ECMWF Re-Analysis project), this approach allows us to distinguish climate features and processes that can be attributed to different dynamical and thermodynamical processes in the region. The main results are analyzed in terms of changes in storm tracks, together with precipitation and cyclone frequency/intensity climatologies. We then turn to the long-term statistics of daily precipitation over the Alpine region, currently an important theater of intense storms, also associated with extreme events. The variability of these processes on the monthly and seasonal time scale are also discussed.

**MC08/07P/B17-007 1550**

**SIMULATION OF THE RECENT ANTARCTIC PENINSULA WARMING IN THE IPSL-CM2 COUPLED GCM**

Sebastien CONIL<sup>1</sup>, Claudio MENENDEZ<sup>2</sup>, Carolina VERA<sup>3</sup> (<sup>1</sup>LMD, <sup>2</sup>CIMA Buenos Aires)

Over the second half of the 20th century, Antarctic Peninsula stations show a strong warming trend, while stations in other areas of Antarctica show no significant trend or slight cooling. This recent warming correlates with the major reduction in sea-ice extension in the Bellingshausen Sea. The collapse of a large portion of the Larsen B ice shelf seems to be another consequence of this unprecedented warming. This observed positive trend of the Antarctic Peninsula temperature has been a critical climatic change with an order of magnitude greater than global mean warming. It is essential to understand the main processes controlling the climate in this region and to represent these in climate models in order to anticipate whether the trend will remain in the next 100 years. The main issue of this study is to examine the ability of a realistic global climate model to reproduce the main features of the Antarctic Peninsula climate and the observed regional change. We assess two different possible mechanisms that could be responsible of this change. The first is related with changes in the large-scale atmospheric circulation over the Southern Ocean while the second is related with changes in the sea-ice cover and the oceanic circulation and their interactions with the atmosphere. We use a state-of-art ocean-atmosphere general circulation model (IPSL/CM2) which includes coupled-to-land and -ocean carbon models to simulate the evolution of climate from 1860 to 2100 with no flux corrections. Two 241-y simulations were carried out, a control and a scenario simulations. The control run displays no significant drift of the global mean surface temperature while the scenario run present an increase of the global temperature consistent with the observations. Furthermore the most important features of the Southern Hemisphere climate are also well reproduced by the model in the control simulation as well as in the scenario simulation. Moreover, the two simulations present close realistic representations of the leading patterns of SH circulation low-frequency variability. The dominant modes of the simulated atmospheric variability is the well known Antarctic Annular Oscillation or High Latitude Mode while the second leading pattern is similar to the Pacific South American pattern. The response of the SH circulation to transient anthropogenic greenhouse warming mainly consists in an increase of the meridional pressure gradient between the high and mid latitudes, modulated by a wave-3 like pattern. That structure, which characterizes the linear trend of the SH circulation resembles the leading mode of interannual variability. The model is also able to reproduce some of the observed warming in the vicinity of the Antarctic Peninsula contrasting with the slight cooling of the East Antarctica. The regional change in the near surface temperature simulated around the Antarctic Peninsula is related to the modification of the mean atmospheric circulation but also to change in its leading modes of variability. The reduction of sea ice cover in this region and the local ocean-atmosphere-sea ice interactions also contribute to amplify the regional climate change.

**MC08/07P/B17-008 1605**

**CLIMATE CHANGE SCENARIOS FOR THE ARCTIC REGION BASED ON COUPLED GLOBAL CLIMATE MODEL SIMULATIONS**

Stanislav V. VAVULIN (Voeikov Main Geophysical Observatory, Saint-Petersburg, Russia)

Global coupled Atmosphere Ocean General Circulation Models (AOGCM) are widely acknowledged as the principal, most promising, and fast developing tools for simulating the response of the global climate system to increasing green-house gas (GHG) concentrations. Current AOGCMs « provide credible simulations of climate, at least down to sub-continental scales and over temporal scales from seasonal to decadal » (IPCC, 2001), and, as a class, provide useful projections of the future climate. The main sources of uncertainty in climate scenarios based on AOGCM projections are : (1) uncertainties in future emissions of GHG and aerosols (emissions scenarios), and in conversion of the emissions to atmospheric concentrations and to radiative forcing of the climate ;(2) uncertainties in the global and regional climate responses to emissions from different GCM simulations ; and (3) uncertainties due to inaccurate representation of regional and local climate, and application of different methods of regionalising AOGCM results . Scenarios are presented of the 21st century climate change based on simulations with five AOGCMs forced with the IPCC SRES B2 emission scenario. The simulations cover late 20<sup>th</sup> and entire 21<sup>st</sup> centuries. Surface air temperature, precipitation and sea level pressure over the northern polar region are considered. The three 20-year time slices are focuses in the 21<sup>st</sup> century : 2011-2030, 2041-2060, 2071-2090. The time slices centered at 2020, 2050 and 2080 are representing correspondingly the near-term, mid-term, and longer-term outlooks for future changes. References: McAvaney, B.J., C. Covey, S. Joussaume, V. Kattsov, A. Kitoh, W. Ogana, A.J. Pitman, A.J. Weaver, R.A. Wood, Z.-C. Zhao, 2001 : Model Evolution. In : Climate Change 2001 : The Scientific Basis. Contribution of working Group I to the Third Assessment Report of the Intergovernmental Panel on Climate Change (Houghton, J.T., Y. Ding, D.J. Griggs, M. Noguer, P.J. van der Linden, X. Dai, K. Maskell, and C.A. Johnson (eds)). Cambridge University Press, Cambridge, United Kingdom and New York, NY, USA, 881 pp.

**MC08/07P/B17-009** **1640**

**STATISTICAL DOWNSCALING OF GENERAL CIRCULATION MODEL OUTPUT FOR DRAINAGE DESIGN PURPOSES**

Yiping GUO (Department of Civil Engineering, McMaster University)

Climate simulation with general circulation models (GCMs) incorporating increased greenhouse-gas concentrations indicates that a warmer climate could result in an increase in extreme precipitation events. Engineered drainage facilities for urban and rural areas are designed for the safe passage of flood flows resulting from extreme rainfall events. The impact of climate change on the functioning of our drainage systems may need to be assessed using output from GCMs. The current GCMsAEoutput has a temporal resolution of a day. This temporal resolution is not adequate for urban and rural catchments with response times in the order of minutes to hours. A statistical downscaling approach is proposed for estimating the intensities of rainfall with durations appropriate for drainage facility design from those predicted by GCMs with daily time steps. Using the proposed approach, intensity-duration-frequency (IDF) relationships representing future climate conditions can be developed from GCM predicted precipitation time series for a location of interest. These IDF relationships can be used to assess the adequacy of existing drainage systems under future climate change and to assist in the development of mitigation and adaptation alternatives.

**MC08/07P/B17-010** **1655**

**ARE THE REGULARITIES IN CLIMATE CHANGE FIELDS?**

Roman M. COROBOV (Institute of Geography, Moldavian Academy of Sciences)

The main challenge of climate change modeling - downscaling of General Circulation Model (GCM) projections - is proposed to address through identification of some regularities in climatic variables expected change. Using Moldova as a case study, it is shown that these regularities exist and they may be used both for spatial and temporal downscaling. As GCM projections, Australian, Hadley and Canadian modeling centers' experiments were selected. To identify spatial regularities, dependencies of surface air temperature and precipitation changes on geographical latitude and longitude were studied. As a rule, there is a statistically significant, strong correlation between latitude and these variables' projections. This correlation is described very well by the second order polynomials, the form and parameters of which are different for each variable, month, GCM, and time-slice. Mathematically formalized dependence of variables change on latitude was used for development of an algorithm for constructing the climate change fields with the different level of resolution. For temporal downscaling, or transition from GCM monthly projections to the daily ones, the annual course of the first was studied. The best approximation of temperature curves is the fourth degree polynomial (adjusted coefficients of determination are 97-99% with statistical significance less 0.001). For precipitation curves these values, depending on modeling experiments and time horizons, are from 50 to 80% with smaller statistical significance but less than 0.05-0.10. Availability of such temporal regularities gives an opportunity to calculate likely temperature and precipitation values for every day that is a reliable alternative to weather generators.precipitation values for every day that is a reliable alternative to weather generators.

**MC08/07P/B17-011** **1710**

**ON THE DEVELOPMENT OF A REGIONAL CLIMATE MODEL FOR THE CENTRAL EUROPE**

Tomas HALENKA<sup>1</sup>, Radan HUTH<sup>2</sup>, Ladislav METELKA<sup>3</sup>, Richard MLADEK<sup>4</sup>, Ales FARDA<sup>1</sup>, Stanislava KLIEGROVA<sup>5</sup>, Jan KYSELY<sup>2</sup>, Lucie POKORNA<sup>2</sup>, Zuzana HUTHOVA<sup>4</sup>, Martin JANOUSEK<sup>6</sup> (<sup>1</sup>Department of Meteorology and Environment Protection, Fac. of Mathem. and Physics, Charles University, <sup>2</sup>Institute of Atmospheric Physics, Prague, Czech Republic, <sup>3</sup>Czech Hydrometeorological Institute, branch Hradec Kralove, Hradec Kralove, Czech Republic, <sup>4</sup>Czech Hydrometeorological Institute, Prague, Czech Republic)

The project with the aim to develop a regional climate model (RCM) for the territory of central Europe, which has been overlooked by regional climate modelling studies recently has been launched in 2001 in the Czech Republic. The RCM is being developed by modifications of the numerical weather prediction (NWP) model ALADIN, run operationally at the Regional Centre of LACE (Limited-Area Modelling in Central Europe) in Prague. It concentrates on the area of central Europe and is intended in close future to serve as a source of climate change scenarios on a regional and local scales for countries in that region, especially for the Czech Republic. The uniqueness of the RCM is in its very fine horizontal resolution of about 20 km, which is at the high end of current RCMs. The ALADIN model proves to be integrable for longer time periods, far beyond its current operational use (up to 48 hours), after only minor modifications of rather a technical nature are implemented as well as the first attempts with modification of physical parameterizations. The presentation will summarize validation of recent experimental runs of the RCM, nested in the operational assimilations by the ARPEGE NWP global model, representing observed conditions, both for monthly experiments in summer and winter seasons and for one year simulations. The influence of a treatment of lower boundary conditions, interpolation at lateral boundaries, the effects of repeated restarts of the RCM as well as some sensitivity tests of parameterization are studied. The validation concerns (i) the upper-air fields, (ii) surface temperature and precipitation at the dense station network in the Czech Republic, as well as against continental-scale gridded climatologies, and (iii) vertical cross-sections. During the development, supporting tests were completed with the RegCM2 concerning the modelling sensitivity to geometry of the model area. Moreover, we use the RegCM2 to test the methodology for planning and organizing the experiments. Finally, to understand the ability of RCM's to describe the extremes the distribution of climate parameters based on longer period experiments are compared to real ones.Future activities in the development of the RCM will also be outlined in the presentation.

**MC08-Posters** **Tuesday, July 8**

**FUTURE CHANGES IN GLOBAL AND REGIONAL CLIMATE (ICDCI)**

Location: Site D

Tuesday, July 8 PM

**MC08/08P/D-001** **Poster** **1400-157**

**CHANGES IN EXTREME TEMPERATURES IN NORTHERN CHINA SINCE 1951 AND ITS RELATIONSHIP TO REGIONAL WARMING**

Zhuguo MA, Congbin FU, Xiaobo REN (Institute of Atmospheric Physics, Chinese Academy of Sciences)

Based on observed daily mean surface air temperatures from 110 stations in China, changes in the frequency and intensity of extreme temperatures of northern China in the period 1951-2000 have been analyzed. Results indicate that the frequency with which minimal temperature are attained decreases remarkably, but that this trend begins at different times across the region. The frequency and magnitude of maximal temperatures has no obvious trend up to the 1990s; after that time, an increase in the frequency can be found. Results of annual maximaltemperatures show no trends over the dataset period in most regions of northernChina except for a decreasing trend in the west of northwestern China. There isdramatic reduction of total days below 0oC surface temperature in northern China, with delayed seasonal freezing and earlier seasonal warming. Regionally, the reduction in frequency of extreme temperature minima, and an increase in annualtemperature minima in northern China is closely related to the current warming trend since the 1990s.

**MC08/08P/D-002** **Poster** **1400-158**

**FLUX ADJUSTED COUPLED MODELS FOR CLIMATE CHANGE EXPERIMENTS**

Nicholas E. FAULL<sup>1</sup>, David STAINFORTH<sup>1</sup>, Myles ALLEN<sup>1</sup>, Jamie KETTLEBOROUGH<sup>1</sup>, James MURPHY<sup>1</sup> (<sup>1</sup>Atmospheric, Oceanic and Planetary Physics, University of Oxford, <sup>2</sup>Rutherford Appleton Laboratory, Didcot, <sup>3</sup>Hadley Centre, Met Office)

Quantifying uncertainty in climate change prediction requires large ensembles that deal with model uncertainty. Such "perturbed physics ensembles" require the initialisation of large numbers of drift-free coupled climate models. The ocean component of a coupled model typically requires a long spin-up period in order to reach equilibrium. We demonstrate a technique for obtaining approximately drift-free coupled models without the need for a new ocean spin-up when the fast components of the model (atmosphere, land-surface scheme) are perturbed. Using the flux adjusted Hadley Centre model, HadCM3L, we apply a linear correction to the atmosphere-ocean fluxes analogous to that of the standard "flux-correction" method used in coupled models. This approach enables us to investigate a much wider range parameter space than would otherwise be possible if we were to spin-up models individually. Flux adjusted coupled models may be used as a basis to form a perturbed physics ensemble of coupled models which could then be used for climate change experiments.

**MC08/08P/D-003** **Poster** **1400-159**

**WEATHER AND FOREST FIRES NEAR YAKUTSK (EAST SIBERIA) IN 2002**

Hiroshi HAYASAKA<sup>1</sup>, Sergey TASHCHILIN<sup>2</sup>, Abushenko NIKOLAY<sup>2</sup>, Keiji KIMURA<sup>3</sup> (<sup>1</sup>Hokkaido University, <sup>2</sup>Institute of Solar Terrestrial Physics Irkutsk, <sup>3</sup>Tokyo Metropolitan University)

The Taiga of Siberia is one of the largest contiguous forest areas in the world. In 2002, a large number of forest fires occurred in taiga near Yakutsk, the eastern part of the Russian Federation. Forests in taiga become very flammable from spring to fall because total precipitation amount is only less than 300mm. In addition, temperature rise due to global warming will make good conditions for forest fire. From now on, fire incidence in high latitude will likely increase due to ongoing global warming. To protect taiga from unnecessary forest fires, it is important to investigate the trends and characteristics of not only forest fire occurrences but also weather conditions in this area. This paper describes one of the causes of the unprecedented occurrence of forest fires near Yakutsk in 2002. Weather conditions in Yakutsk such as temperature, rainfall, humidity, wind direction, and wind speed were analyzed in detail, and a strong correlation between fire occurrence and weather conditions was established. Fire occurrence was determined by processing satellite images. Daily satellite images for the area around Yakutsk were processed to show how the forest fires spread in the Yakutsk forest region. The results imply that ongoing global warming may promote the frequency of the forest fires occurring near Yakutsk. There are a few reports describing recent fire trends around Yakutsk from the viewpoint of climate. There are several papers that describe forest fire trends in Russia. Unfortunately, the papers did not provide much detail of the relationship between fires and climate. M. D. Flannigan and B. M. Wotton indicated that forest fires are strongly linked to weather in a review paper. However, they did not refer to Russian fires and weather, and there are no papers related to Russia in the references. The following conclusions may be drawn from discussion of forest fires in Yakutsk. 1. Fire season (from May to September) precipitation amount has shown a gradual decrease from 1994. Daily mean precipitation amounts in the fire season reduced to half in the past nine years. Forest fires in Yakutsk would become active under these precipitation trends. At the same time, winter (from October to April) precipitation amounts increased suddenly from 1999. These anomalous trends may be due to the ongoing global warming. 2. Relatively strong, dry, and high temperature winds from the south would be a cause of fires in May. 3. Once fires occur, they would spread via spotting fires. 4. Under conditions of small precipitation amounts, fires can survive until the end of the fire season, and smoldering combustion in the forest floor may play an important role to sustain fires. 5. Catastrophic fires may occur when stable high pressure weather with low dew points are established by a stationary ridge above Yakutsk.

**MC11** **Thursday, July 10 - Friday, July 11**

**CLIMATE MODEL EVALUATION: HOW WELL DO MODELS REPRESENT OBSERVATIONS (ICCI)**

Location: Site B, Room 19

Thursday, July 10 AM

**MC11/10A/B19-001** **0830**

**DEVELOPMENT OF AN INDEX TO QUANTIFY CLIMATE MODEL PERFORMANCE AND ITS APPLICATION TO PREDICTING CLIMATE CHANGE**

David M.H. SEXTON, James MURPHY, David N. BARNETT, Mark J. WEBB (Hadley Centre, Met Office)

GCM predictions of climate change are subject to uncertainties in their presentation of the climate system by the model, as well as uncertainty due to natural variability and emission scenarios. To assess the uncertainty due to model physics in the equilibrium response to doubled CO<sub>2</sub> levels, we have run a large ensemble of coupled atmosphere/mixed-layer ocean integrations forced by 1x and 2x CO<sub>2</sub> concentrations. Each member of the ensemble differs from the Hadley Centre's standard configuration, HadSM3, by perturbing one of the model parameters that controls one of its key atmospheric processes. This ensemble provides a good starting point for estimating the probability distribution of equilibrium response to doubled CO<sub>2</sub>. However, an important issue in estimating such a probability distribution is that we need an objective method to ensure that the more realistic ensemble members have a greater relative contribution. We present a preliminary version of an index designed to measure how well a climate model simulates present-day mean climate. The index is based on 32 different climate variables which cover a broad range of features in the atmospheric climate. The effect of weighting the probability distribution to simulation quality will be discussed. The present ensemble will eventually be extended to include members whereby several parameters are simultaneously perturbed, so that our ensemble samples the parameter space more thoroughly. But this must be done in a cost-effective manner. We will also demonstrate a method that uses the index to predict integrations of multiple parameter perturbations that are likely to well simulate the mean present-day climate and are therefore worth running. For a model to be used for prediction of climate change, it is a necessary but not sufficient condition for it to simulate the mean climate well. We will discuss further development of the index so that it can measure more precisely the ability of the model to predict climate change.

**MC11/10A/B19-002 0900**

**EVALUATION OF AMPLITUDE-PHASE CHARACTERISTICS OF SURFACE AIR TEMPERATURE ANNUAL CYCLE: CLIMATE MODELS VERSUS REANALYSES**

Alexey V. ELISEEV<sup>1</sup>, Maria S. GUSEVA<sup>2</sup>, Igor I. MOKHOV<sup>1</sup>, Konstantin G. RUBINSTEIN<sup>3</sup> (<sup>1</sup>A.M.Obukhov Institute of Atmospheric Physics RAS, <sup>2</sup>Geophysical Faculty, M.V.Lomonosov Moscow State University, <sup>3</sup>Russian Hydrometcentre)

Climatology and interannual variability of the amplitude-phase characteristics (APC) for surface air temperature (SAT) are studied using two ensembles of atmospheric general circulation models (AGCMs) and coupled climate models (CMs) and compared with the data of NCEP/NCAR and ERA reanalyses for 1958-1998 and 1979-1993 respectively. The first ensemble consists of the AGCMs (HadAM3, RHMC-T21 and RHMC-T40) forced by the prescribed interannually varying sea surface temperatures. The second ensemble consists of the coupled CMs (ECHAM4/OPYC3, HadCM3 and IAP RAS CM) which are forced by the observed greenhouse gases and sulphate atmospheric loading for the XIX-XX centuries. The APC studied are amplitudes of the annual and semiannual AC harmonics, moments of zero- and pi-phases (when SAT equals its annual mean value in spring and autumn, respectively) and interval of exceeding (the period when SAT is higher than its annual mean value). The data of reanalyses show the distinct features of SAT AC APC in different regions (e.g. in the regions of the atmospheric centres of action and in the region near the snow-ice boundary). Generally, two studied reanalyses show the results which agree to each other except in the polar regions. The studied AGCMs ensemble generally reproduces the gross peculiarities of the SAT AC APC except in the polar regions. For RHMC AGCM the higher spatial resolution resulted in the improved simulation of the characteristics of the SAT annual cycle. Among the studied CMs, ECHAM4-OPYC3 and HadCM3 also generally reproduce the climatology and variability of SAT AC APC. The features found for the latter model are very similar to those exhibited by the atmosphere-only version (HadAM3) in the experiment with prescribed sea surface temperature. IAP RAS CM simulates well this climatology over the continents but fails over the oceans.

**MC11/10A/B19-003 0920**

**FINE STRUCTURE OF THE ANNUAL CYCLE: A DISCRIMINATING TEST OF MODELS**

Brian E. MAPES<sup>1</sup>, In-Sik KANG<sup>2</sup> (<sup>1</sup>Climate Diagnostics Center, <sup>2</sup>Seoul National University)

The annual cycle is an ideal test of climate models. Its radiative forcing is strong and precisely known, with a dominant annual harmonic and slight semiannual harmonic. The response of the climate system to this forcing is complex, and poses a graduated set of challenges for climate models. Unlike subtler forms of climate variability, the annual cycle is strong enough that small ensembles and short runs suffice to define model performance. Every serious model has a credible representation of some "easy" aspects, such as the annual harmonic of low-level temperature. Harder issues, such as the semiannual variation of subtropical jets and angular momentum, or the dominant ter-annual cycle of surface pressure over the oceans, begin to separate better from worse models -- but still within the context of a phenomenon common to all. Similarly, monsoons and other rainfall features provide both easy and harder tests of moist physics. The mean annual cycles of 13 climate models at daily or pentad resolution, from both AMIP-type runs and coupled ocean-atmosphere simulations, have been probed with harmonic and wavelet analysis tools for features seen in reanalyses and other observational data sets. Both easy and hard phenomena have been examined. A selected set of discriminating tests (not too easy, not too hard) will be shown in an attempt to define the forefront of model accuracy. A PC with a comprehensive, interactive analysis tool and all data sets will be on hand for demonstration, allowing real-time "coffee-break science."

**MC11/10A/B19-004 0940**

**COMPARISON OF RECENT RE-ANALYSES USING OBJECTIVE FEATURE TRACKING OF SYNOPTIC SCALE WEATHER SYSTEMS: HOW BELIEVABLE ARE THE RE-ANALYSES?**

Kevin HODGES<sup>1</sup>, Brian HOSKINS<sup>2</sup>, Lennart BENGTTSSON<sup>3</sup>, Jim BOYLE<sup>4</sup> (<sup>1</sup>ESSC, University of Reading, <sup>2</sup>Dept. of Meteorology, University of Reading, <sup>3</sup>Max Planck Institute for Meteorology, <sup>4</sup>PCMDI, Lawrence Livermore)

In order to use atmospheric re-analyses for evaluating climate model behaviour it is important to understand which aspects of the re-analyses are robust. An objective feature tracking analysis has been applied to four recent re-analyses to identify synoptic scale weather systems and compare their representation in the different re-analyses. The four re-analyses that are explored are ERA15, NCEP/NCAR, NCEP/DOE and NASA/GEOS1. The comparison is conducted using spatial statistics for storm distributions and mean attributes. In addition a direct track-by-track comparison is made between the track ensembles from the different re-analyses. Differences are discussed in the context of the model-assimilation combination used for each re-analysis. In general the results for the NH winter, lower troposphere show that the different re-analyses compare well for systems identified in both MSLP and vorticity at 850hPa with very similar distributions of storms. The spatial mean intensities indicate that ERA15 is weaker around the main orography related to the use of an orographic parameterization not used in the other re-analyses. The direct ensemble comparison shows that there are a core of systems that correspond well amongst all the re-analyses with a good correspondence in intensity and position together with a number of

weaker systems that correspond less well and which are sensitive to the available observations and the way they are assimilated. These weaker systems appear to have a small contribution to the mean attributes although they may be cumulatively important hydrologically. In the SH winter the comparison highlights the greater uncertainty in the representation of weather systems associated with the sparser observational database. Also the diagnostics for MSLP indicate differences with the circumpolar pressure trough in the SH in the different re-analyses. Above 500hPa the representation of weather systems are found to be sensitive to the assimilation methodology as indicated by the use of optimal interpolation in ERA15. This manifests itself by the poor representation of systems at the tropopause compared with the other re-analyses which used more sophisticated assimilation systems. In the tropics there is also considerable uncertainty highlighted by the large differences in the Easterly Wave activity amongst the re-analyses, in particular for NCEP/DOE compared with NCEP/NCAR with the introduction of a new boundary layer parameterization. In addition we have conducted experiments with the ERA40 re-analyses system to explore the impact of different observing systems and their impact on the re-analyses. This includes experiments with a satellite only, terrestrial only and surface only observing system. Results of applying the tracking analysis shows the relative importance of these observing systems in particular the equal importance of the satellite and radiosonde observations and the dominance of the satellite system in the SH. In general the surface only observing system leads to a poor representation of the weather systems. If time permits a comparison with AMIP models will also be presented.

**MC11/10A/B19-005 1000**

**DEVELOPING A NEW CLIMATE MODEL FOR THE MET OFFICE - HADGEM1**

Gill MARTIN, Vicky POPE, Rachel STRATTON (Hadley Centre, Met Office)

The Met Office has undertaken an ambitious programme of model development to produce their next generation of numerical models for weather forecasting and climate research. The project is well advanced. This study will show the first results from the climate version of the model, focussing on the atmospheric component. The new atmospheric model includes substantially improved representations of physical processes, increased functionality and higher resolution. Major improvements are the use of semi-Lagrangian instead of Eulerian dynamics to advect both dynamical and tracer fields, new boundary layer, convection, gravity wave drag and microphysics schemes, and major changes to the land surface (including tiled surface characteristics) and cloud schemes. Processes available in the standard version of the model for the first time include the direct and first indirect radiative effects of aerosol, RG12 the sulphur cycle, atmospheric chemistry, dynamic vegetation. The results of a preliminary evaluation of the new atmospheric model will be shown. Early results indicate improvements in cloud-radiative properties, boundary-layer properties and the representation of tracers. Sensitivities to horizontal and vertical resolution, and the impact of particular physics changes will be described. The problems associated with combining so many new features will also be discussed.

**MC11/10A/B19-006 1040**

**VALIDATING THE PHYSICS OF HADLEY CIRCULATION SEASONALITY IN MODELS**

Kerry Harrison COOK (Dept. Earth and Atmospheric Sciences, Cornell University)

The validation of model processes and mechanisms is needed to support model improvement and the evaluation of a model's ability to properly simulate climate change. This paper reports on an investigation of the Hadley circulation dynamics, and examines the physical processes that cause the observed seasonality of the MMC. The Hadley circulation has a well-know seasonal cycle, consisting of alternating solstice states with a dominant winter cell and equinox states with two cells of comparable strength divided by the equator. Applications of axisymmetric models of the atmospheric circulation associate this seasonal behavior with differences in the applied zonally uniform forcing. In particular, the strength of the Hadley circulation in axisymmetric models is enhanced when the heating is off the equator, and also when it is more concentrated. The Hadley circulation in an AGCM with realistic, prescribed surface features does not duplicate these axisymmetric model results. The correlation between the latitude and concentration of the heating in the axisymmetric models occurs because the applied heating distribution is unrealistic, being too sharply peaked near the equator. This heating shape causes a primary response in the vertical velocity field, as the diabatic heating is balanced by adiabatic cooling. In contrast, the GCMs heating is more broadly distributed through the tropics and is not zonally uniform. The response to such heating involves horizontal advection and the influence of a significant Coriolis force. The driving mechanisms of the MMC seasonality are similar to those in the GCM, and not similar to the axisymmetric model.

**MC11/10A/B19-007 1100**

**EXPLORING THE DIURNAL CYCLE OF PRECIPITATION IN AN AQUAPLANET MODEL: A POTENTIAL TESTBED FOR MODEL PARAMETRIZATIONS?**

Stephen WOOLNOUGH<sup>1</sup>, Brian HOSKINS<sup>2</sup>, Julia SLINGO<sup>3</sup> (<sup>1</sup>NCAS Centre for Global Atmospheric Modelling, <sup>2</sup>Department of Meteorology, University of Reading)

The diurnal cycle is a strongly forced mode of the atmosphere, yet the diurnal cycle of precipitation in the Tropics is poorly represented in most GCMs. The processes that determine the diurnal cycle of precipitation are not well understood and the extent to which the important processes are represented in GCMs is not clear. This paper will explore the oceanic diurnal and semi-diurnal harmonics of tropical precipitation in an aquaplanet GCM, representing the simplest forcing conditions for the diurnal cycle of precipitation. The performance of the model will be compared to the limited observations of the diurnal and semi-diurnal harmonics of tropical convection over the open ocean and the processes that determine the diurnal cycle of tropical convection in the model will be examined. In particular, the relationship of the precipitation signal to the diurnal and semi-diurnal pressure tides will be considered. The dependence of the representation of these harmonics (both phase and amplitude) on the closure of the convection scheme will be described. The extent to which the different representations of the diurnal cycle of precipitation can be used as a measure of the relative performance of convection schemes in the light of forthcoming improvements in the observations of the diurnal cycle of tropical convection will be discussed.

**MC11/10A/B19-008 1130**

**USING AN AQUA-PLANET MODEL TO INVESTIGATE MODEL SENSITIVITIES**

Rachel A. STRATTON (Hadley Centre, Met Office)

During the development of the Met Office's new climate model, HadGEM1, an aqua-planet version of the atmospheric model proved a useful tool to help investigate and understand the model's behaviour in the tropics. HadGEM1 differs significantly from the previous Hadley Centre model HadAM3. Not only are the model dynamics completely different (semi-Lagrangian, semi-implicit instead of Eulerian, split-explicit) but so are the horizontal and



vertical resolutions and most of the physical parametrisations. Aqua-planet runs exploring, in particular, the sensitivity of the convection scheme in HadGAM1 were compared with HadAM3 to understand differences in the tropical precipitation. The sensitivity of the HadGAM1 simulation to horizontal resolution and timestep were also investigated. Initially most of the aqua-planet runs were done using sea surface temperatures which were symmetrical about the equator. Further sensitivity studies have looked at the model's response to an idealised warm pool, an idealised cold tongue on the equator and the impact of adding tropical islands.

**MC11/10A/B19-009** **1150**  
**PROBABILISTIC CLIMATE FORECASTING USING DISTRIBUTED COMPUTING**

Dave FRAME (University of Oxford)

The current generation of atmosphere-ocean general circulation models (AOGCMs) are capable of simulating many large-scale features of present-day climate and recent climate change with a high degree of accuracy. However, these models contain large numbers of adjustable parameters whose values are poorly constrained by the available data and which are known, individually, to have a significant impact on simulated climate. We do not know the extent to which a different choice of parameter-settings, or entire parameterization schemes, may provide an equally realistic simulation of 20th century climate but a different forecast for the 21st century. In principle, the problem is simple: vary these "underdetermined" parameters and repeat the simulation and forecast in order to obtain a spread of forecast climates that are consistent with recent climate change. The challenge of such a perturbed-physics ensemble is that the number of underdetermined parameters is large (potentially in the hundreds, although expert judgement can be used to prioritise a few dozen). The chaotic nature of AOGCMs precludes the use of linearisation techniques to identify 'pathological' parameter-perturbations, and it has already been shown that the impact of multiple perturbations is not additive. This leaves no alternative to a 'brute-force' exploration of a high-dimensional parameter-space requiring potentially very large numbers of long integrations of the climate model. Currently available supercomputing resources are completely inadequate for such a full-scale perturbed-physics ensemble climate forecast. Fortunately, distributed computing (utilising idle processing capacity on personal computers volunteered by businesses and the general public) provides an effective alternative for this kind of large-scale Monte Carlo simulation. The climateprediction.net project aims to harness the power of idle home and business PCs to make the first fully probability-based 50-year forecast of human induced climate change using a full-scale 3-D atmosphere-ocean climate simulation model.

Thursday, July 10 PM

**MC11/10P/B19-001** **1400**  
**VALIDATING AND UNDERSTANDING THE RADIATIVE AND DYNAMICAL FEEDBACKS IN THE NCAR CCSM**

De-Zheng SUN, Tao ZHANG, John FASULLO, Andres ROUBICEK (Climate Diagnostics Center, NOAA-CIRES)

Climate feedbacks determine the sensitivity of the climate system to an external perturbation, affect the mean climate, and control the amplitude of natural variability. Thus validating and understanding climate feedbacks in climate models are of critical importance. Here we compare the radiative and dynamical feedbacks from the two most recent versions of the atmospheric component of the NCAR CCSM—the NCAR CAM1 and CAM2—with those from observations over the equatorial Pacific cold-tongue. The observational data are from ERBE and the NCEP reanalysis. The model data are from simulations with the observed-time-varying SST as the boundary conditions. Both the CAM1 and CAM2 capture the positive feedbacks from the greenhouse effect of water vapor and clouds. The water vapor feedback in both the CAM1 and CAM2 is somewhat larger than that from observations. The feedback from the greenhouse effect of clouds is stronger than observations in CAM1, but weaker than in observations in CAM2. Larger errors are found in the feedback from the short-wave forcing of clouds. While observations show a strong negative feedback from the short-wave forcing of clouds (-7.8 Wm<sup>-2</sup>), the feedback from the short-wave forcing of clouds in CAM2 is positive (+3.4 Wm<sup>-2</sup>K<sup>-1</sup>). The sign of the feedback from the short-wave forcing in CAM1 is correct, but the strength is less than half of the observed value (-3.0 Wm<sup>-2</sup>K<sup>-1</sup>). Consequently, the net atmospheric feedback in both CAM1 and CAM2 over the cold-tongue region are strongly positive (+5.1 Wm<sup>-2</sup>K<sup>-1</sup> in CAM1 and +6.7 Wm<sup>-2</sup>K<sup>-1</sup> in CAM2) while in the real atmosphere it is strongly negative (-6.4 Wm<sup>-2</sup>K<sup>-1</sup>). Both the CAM1 and CAM2 captures the strong negative feedback from the atmospheric transport (the vertically integrated transport of total energy), though the feedbacks from the models are somewhat weaker. The feedback from the atmospheric transport is closer to observations in CAM1 than in CAM2. A further analysis with the aid of the ISCCP data suggests that the apparent errors in the cloud feedbacks may be related to an excessive response in the upper level clouds to changes in the SST. Causes for the model-data discrepancies are further explored by comparing the feedbacks with those from a GFDL model.

**MC11/10P/B19-002** **1420**  
**EVALUATING CLOUD RESPONSE TO CLIMATE CHANGE**

Keith D. WILLIAMS<sup>1</sup>, M.A. RINGER<sup>1</sup>, C.A. SENIOR<sup>1</sup>, A. SLINGO<sup>2</sup> (<sup>1</sup>Met Office, Hadley Centre, <sup>2</sup>ESSC, University of Reading)

It is widely believed that the radiative feedback from clouds remains as one of the largest uncertainties in determining the climate sensitivity to increasing greenhouse gas concentrations. Many model evaluation studies determine the performance of a general circulation model's (GCMs) simulation of mean climatology with little evaluation of physical processes. Whilst it is certainly desirable that a climate model should accurately simulate the current climatology, this ability alone does not necessarily imply an accurate simulation of climate change. This study proposes a possible methodology for evaluating the cloud response to climate change simulated by GCMs. By using compositing techniques, the method attempts to identify the primary processes which are associated with the amount of cloud of a particular height and optical depth. Stratifying model data through such techniques permits the simulated climate change cloud response to be considered as a change in the population of the compositing bins. Compositing satellite observations of cloud using the same method allows the cloud amount in each bin to be evaluated and hence, an assessment can be made of the confidence in the cloud response resulting from a change in bin population. The method is illustrated using the Met Office's Hadley Centre atmosphere GCM coupled to a mixed-layer (slab) ocean.

**MC11/10P/B19-003** **1440**  
**TROPICAL CUMULUS CONVECTION AND UPWARD PROPAGATING WAVES IN MIDDLE ATMOSPHERIC GCMS**

Takeshi HORINOUCHI<sup>1</sup>, S. PAWSON<sup>2</sup>, K. SHIBATA<sup>1</sup>, U. LANGEMATZ<sup>3</sup>, E. MANZINI<sup>4</sup>, M.A. GIORGETTA<sup>5</sup>, F. SASSI<sup>6</sup>, R.J. WILSON<sup>7</sup>, K. HAMILTON<sup>8</sup>, J. DE GRANPRÉ<sup>9</sup>, A.A. SCAIFE<sup>10</sup> (<sup>1</sup>Radio Science Center for Space and Atmosphere, Kyoto University, <sup>2</sup>Data Assimilation Office, NASA GSFC, Greenbelt, MD, USA, <sup>3</sup>Meteorological Research Institute, Tsukuba, Japan, <sup>4</sup>Freie Universität Berlin, Berlin, Germany, <sup>5</sup>Max-Planck-Institut für Meteorologie, Hamburg, Germany, <sup>6</sup>NCAR, Boulder, Colorado, USA, <sup>7</sup>GFDL, Princeton, New Jersey, USA, <sup>8</sup>University of Hawaii, Honolulu, Hawaii, USA, <sup>9</sup>York University, Toronto, Ontario, Canada, <sup>10</sup>Met Office, Bracknell, UK)

It is recognized that the resolved tropical wave spectrum can vary considerably among general circulation models (GCMs) and that these differences can have an important impact on the simulated climate. A comprehensive comparison of the waves is presented for the December-January-February period using high-frequency (three-hourly) data archives from eight full GCMs and one slightly simple model participating in the GCM Reality Intercomparison Project for SPARC (GRIPs). Quantitative measures of the structure and causes of the wavenumber-frequency structure of resolved waves and their impacts on the climate are given. Space-time spectral analysis reveals that the wave spectrum throughout the middle atmosphere is linked to variability of convective precipitation, which is determined by the parameterized convection. The variability of the precipitation spectrum differs by more than an order of magnitude between the models, with additional changes in the spectral distribution (especially the frequency). These differences can be explained primarily by the choice of different cumulus parameterizations: quasi-equilibrium mass-flux schemes tend to produce small variability, while the moist-convective adjustment scheme is most active. Comparison with observational estimates of precipitation variability suggests that the model values are scattered around observational estimates. This result indicates that a significant portion of the forcing of the equatorial quasi-biennial oscillation (QBO) is provided by waves with scales that are not represented in present-day GCMs, since only the moist convective adjustment scheme (which has the largest transient variability) can force a QBO in models that have no parameterization of non-stationary gravity waves. Parameterized cumulus convection also impacts the nonmigrating tides in the equatorial region. In most of the models, momentum transport by diurnal nonmigrating tides in the mesosphere is larger than that by Kelvin waves, being more significant than has been thought. It is shown that the westerly accelerations in the equatorial semi-annual oscillation in the models examined are driven mainly by gravity waves with periods shorter than three days, with at least some contribution from parameterized gravity waves; the contribution from the ultra-fast zonal wavenumber-1 Kelvin waves is negligible. These results provide a state-of-the-art assessment of the links between convective parameterizations and middle atmospheric waves in present-day middle atmosphere-climate models, giving physical insight into the processes of wave generation and the indirect importance of the cumulus scheme to the climate of the middle atmosphere.

**MC11/10P/B19-004** **1500**  
**EVALUATION OF MIDLATITUDE CLOUD PROPERTIES IN A WEATHER AND A CLIMATE MODEL: DEPENDENCE ON DYNAMIC REGIME AND SPATIAL RESOLUTION**

George TSELIODIS<sup>1</sup>, Christian JAKOB<sup>2</sup> (<sup>1</sup>NASA/GISS, Columbia University, <sup>2</sup>Bureau of Meteorology Research Centre, Melbourne, Australia)

In this study, the midlatitude cloud fields produced by a climate (GISS) and a weather (ECMWF) model are evaluated against satellite observations. Monthly ensembles of model cloud property distributions for the four seasons are compared with similar ensembles from satellite retrievals. The weather model is run in both forecast and 'climate' mode in order to evaluate the importance of the exact representation of the atmospheric conditions in these ensemble comparisons. The weather and climate models are evaluated at different resolutions that cover the range used in today's climate and weather prediction simulations. Cloud property evaluations are separated into broadly defined dynamic regimes that cover the range of large-scale midlatitude motions. Quantitative evaluation tables are produced that rank the performance of the different model versions used in the study. The evaluation analysis reveals several common features between the two models. Those are the overestimation of cloud optical depth in all dynamic regimes, the underestimation of cloud cover in the large-scale descent regime and the underestimation of cloud top height in the large-scale descent regime. It is also shown that, in the radiative balance calculations, the models compensate for the overestimation of cloud optical depth through the underprediction of cloud cover. The comparison of the forecast and 'climate' runs of the ECMWF model shows remarkably similar statistical properties of the clouds in the two runs. The analysis of runs with different resolutions reveals large improvement when going from a 4x50 9-layer to a 2x2.50 32-layer run with the GISS GCM, much of which is caused by the increase in vertical resolution. A comparison of a T42 and a T106 run of the same vertical resolution with the ECMWF GCM does not show considerable differences between the two model versions.

**MC11/10P/B19-005** **1550**  
**A STATISTICAL COMPARISON OF ECMWF FORECASTED CLOUD FIELDS WITH EARTH OBSERVING SYSTEM (EOS) SATELLITE OBSERVATIONS**

Kuan-Man XU (Atmospheric Sciences)

Climate model simulations are usually validated against gridded monthly-mean satellite observations. Numerical weather forecasts are validated against surface observations, at least, at the daily time scale. In both types of validations, the gridded data are used, which represent an area over hundreds of kilometers in the horizontal direction. In this study, a new approach is proposed to validate subgrid-scale statistical properties of mesoscale cloud systems against those identified from Earth Observing System (EOS) satellite data. The forecasted cloud fields from the European Center for Medium-range Weather Forecasts (ECMWF) are validated in this study. A large set of cloud, radiation and precipitation data that are matched with simultaneous atmospheric state data from ECMWF is used for this purpose. A "cloud object" technique has been deployed to produce such a data set at the NASA Langley Research Center. Specifically, this technique classifies EOS satellite data into distinct cloud systems over contiguous regions of the Earth for a given type of cloud systems (e.g. trade cumulus, transition stratocumulus, solid stratus, and deep convection). These regions can be thought of as snapshots of cloud systems. The ECMWF data contain a set of forecasted cloud fields, which includes the vertical profiles of cloud water mixing ratio, cloud ice mixing ratio and cloud fraction. Since the ECMWF grid size (0.5625x 0.5625 degrees) is much larger than the footprint size of satellite data (an average size of 23.5 km x 4.6 km), each ECMWF grid is further divided into smaller subgrids (30 of them) in order to properly compare the statistics of ECMWF forecasted cloud fields with the satellite observed cloud systems. A major assumption for facilitating this comparison is that the maximum-random overlap assumption is used to distribute the ECMWF cloud fields horizontally and vertically (Klein and Jakob 1999). The broadband radiative fluxes and cloud optical properties of each ECMWF subgrid column are obtained using radiative transfer

parameterization from the Fu-Liou radiation code (Fu and Liou 1993). The same criteria used for identifying satellite cloud systems are then used to select the ECMWF subgrids for computing probability density functions (PDFs) of cloud properties and radiative fluxes. Preliminary results indicate that most PDFs of cloud properties and radiative fluxes of deep convection for ECMWF agree with those of satellite observations to some extent. The ECMWF forecasted clouds tend to be deeper and cooler than those observed, at least, for the March 1998 period. The ECMWF does not produce the dependence of PDFs on the cloud-system sizes as revealed by the satellite data. More detailed results will be presented for other cloud-system types and other periods.

**MC11/10P/B19-006 1610**

**EVALUATE CLOUD SIMULATION ASSOCIATED WITH MIDLATITUDE CIRCULATION SYSTEMS IN A CLIMATE MODEL**

Cheng-Ta CHEN (Department of Earth Sciences, National Taiwan Normal University)

Cloud fields and concurrent dynamical structures associated with extratropical cyclones in a general circulation model are investigated during the cool season (October to March). An ensemble approach is used for constructing the respective anomaly patterns in the storm track region of the northwestern Atlantic. The simulated composite patterns are in many respects similar to those derived from satellite cloud data and operational weather analyses. The results agree also reasonably well with traditional conceptual frameworks for the organization of clouds in the vicinity of warm and cold frontal zones. The vertical structure and wave characteristics of various dynamical, thermal and hydrological fields reveal the typical patterns found in observed baroclinic wave disturbances such as a westward tilt with height of pressure anomalies and an eastward displacement of the upper tropospheric clouds relative to the center of largest upward motion at 500 hPa. However, this displacement is not as distinct as in the observations. Similar to indications from surface weather reports, the largest precipitation anomalies are simulated westward of the reference site defined by the largest anomaly in cloud water path and cloud optical thickness, respectively. The changes in cloud cover, cloud water, humidity and temperature during the passage of a synoptic scale weather disturbance have a distinct impact on the energy budget with a pronounced seasonality in all components except for the longwave radiation. Due to changes in the fluxes of sensible heat, latent heat and shortwave and longwave radiation, the atmospheric column in most parts of the cyclonic systems is cooled in winter and heated in summer. On the other hand, extratropical cyclones cause anomalous surface heating in winter and cooling in summer.

**MC11/10P/B19-007 1630**

**EVALUATION OF UPPER TROPOSPHERIC WATER VAPOR IN THE NCAR CCM3 COMMUNITY CLIMATE MODEL USING MODELED AND OBSERVED HIRS RADIANCES**

Michael J. IACONO, Jennifer S. DELAMERE, Eli J. MLAWER, Shepard A. CLOUGH (Atmospheric and Environmental Research, Inc.)

Upper tropospheric water vapor (UTWV) simulated by the National Center for Atmospheric Research Community Climate Model, CCM3, is evaluated by comparing modeled, clear sky, brightness temperatures to those observed from space by the High-resolution Infrared Radiation Sounder (HIRS). The climate model was modified to utilize a highly accurate longwave radiation model, RRTM, and a separate module simulating HIRS radiances, both developed for the Atmospheric Radiation Measurement (ARM) Program. The radiance module applies physics that are consistent with RRTM to calculate brightness temperatures in the NOAA-7 HIRS 6.7 micron water vapor channel (CH12) and the 14.2 micron temperature channel (CH04). The utilization of radiation models that are evaluated with ARM measurements addresses the objective of improving radiative transfer in general circulation models and enhances the effectiveness of evaluating GCMs with observations. Simulations with CCM3 were performed for the period 1982-1984 following the Atmospheric Model Intercomparison Project (AMIP) protocol to provide a basis for evaluating the water vapor distribution over a wide range of atmospheric conditions. Brightness temperature differences of 2 K or less in CH04 indicate that CH12 differences are primarily due to water vapor rather than cloud effects or temperature variations. Regionally, CCM3 exhibits considerable positive and negative differences of 5-10 K in CH12 that are apparent in both convective and dry sub-tropical areas. This suggests that significant moist and dry discrepancies in UTWV amount of 50 percent or more are present in CCM3. Comparison to HIRS radiances provides a considerably more effective and comprehensive means of globally evaluating GCM-simulated UTWV on various time scales than surface-based water vapor measurements.

Friday, July 11 AM

**MC11/11A/B19-001 0830**

**TOWARD EXPLOITING COMMUNITY STANDARD EXPERIMENTS FOR CLIMATE MODEL EVALUATION**

Peter GLECKLER, K. SPERBER, K. TAYLOR (Program for Climate Model Diagnosis and Intercomparison, Lawrence Livermore National Laboratory)

Evaluating the overall performance of climate models is a difficult challenge. General circulation models of the atmosphere (AGCM) and the ocean (OGCM) are becoming increasingly complex and exhibit a wide range of strengths and weaknesses. Additionally, untoward complications arise when these models are coupled together, necessitating diagnosis of the component models to isolate the source of the errors. Numerical experimentation, often in the form of sensitivity experiments, is the fundamental approach toward understanding an individual model's behavior. As a complement to this approach, the examination of a collection of different models can help to distinguish which model biases are unique to a particular model from those that are commonplace. Additionally, collective evaluation of models helps to monitor improvements in state-of-the-art climate models. At PCMDI, we are exploiting a hierarchy of community-standard experiments to assess model behavior and performance. Making use of our open-source diagnostic tools, we are producing comprehensive diagnostic reports on simulations endorsed by working groups of the World Climate Research Programme (WCRP). The experiments analyzed include the Aqua-Planet Experiment (APE), Atmospheric Model Intercomparison Project (AMIP), and Coupled Model Intercomparison Project (CMIP), each of which are experiments that are complementary for understanding land/ocean and air/sea interaction. We will describe our approach toward synthesizing a wealth of diagnostics for evaluating the overall performance of climate models.

**MC11/11A/B19-002 0850**

**STATUS OF MIDDLE ATMOSPHERE-CLIMATE MODELS: RESULTS FROM SPARCGRIPS**

Steven PAWSON<sup>1</sup>, Kunihiko KODERA<sup>2</sup> (<sup>1</sup>UMBC GEST Center, <sup>2</sup>Meteorological Research Institute)

The middle atmosphere is an important component of the climate system, primarily because of the radiative forcing of ozone. Middle atmospheric ozone can change, over long times, because of changes in the abundance of anthropogenic pollutants which catalytically destroy it, and because of the temperature sensitivity of kinetic reaction rates. There is thus a complex interaction between ozone, involving chemical and climatic mechanisms. One question of interest is how ozone will change over the next decades, as the "greenhouse-gas cooling" of the middle atmosphere increases but the concentrations of chlorine species decrease (because of policy changes). A major obstacle when addressing this question concerns the climate biases in current middle atmosphere-climate models, especially their ability to simulate the correct seasonal cycle at high latitudes, and the existence of temperature biases in the global mean. This paper will present a summary of recent results from the "GCM-Reality Intercomparison Project for SPARC" (GRIPS) initiative. A set of middle atmosphere-climate models has been compared, identifying common biases. Mechanisms for these biases are being studied in some detail, including off-line assessments of the radiation transfer codes and coordinated studies of the impacts of gravity wave drag due to sub-grid-scale processes. An overview of recent results from the ensemble of models will be presented, along with numerical experiments undertaken with one or more models, designed to investigate the mechanisms at work in the atmosphere. The discussion will focus on dynamical and radiative mechanisms in the current climate, but implications for coupled ozone chemistry and the future climate will be assessed.

**MC11/11A/B19-003 0910**

**ASSESSMENT OF GCM-CALCULATED RADIATIVE FLUXES BASED ON LAND-BASED OBSERVATIONS**

Martin WILD (Institute for Atmospheric and Climate Science ETH)

Many uncertainties still exist regarding the distribution of radiative energy within the global climate system, and its representation in General Circulation Models (GCMs). This study uses surface observations taken from the Global Energy Balance Archive (GEBa, WCRP-Water Project A7) and Baseline Surface Radiation Network (BSRN/WCRP) located at the author's institute, in order to identify systematic errors in GCM-calculated radiative fluxes within the framework of the Atmospheric Model Intercomparison Project (AMIP II). The presentation will summarize recent results from the AMIP II diagnostic subproject No. 32 "Surface and atmospheric radiative fluxes". To date, these include an excessive insolation at the land surface in the GCMs, typically in the range of 10-20 Wm<sup>-2</sup>, which is particularly pronounced at low latitudes. Additional comparisons with top-of-atmosphere fluxes from the Earth Radiation Budget Experiment (ERBE) collocated with the surface radiation sites, suggest that the excessive surface insolation is predominantly related to an underestimated absorption in the GCM atmospheres rather than to errors in the planetary albedo. Evidence is presented that a lack of absorption in the cloud-free atmosphere contributes to the underestimated absorption of solar radiation in the atmosphere. This is based i) on direct comparisons of the GCM clear-sky surface fluxes with observed clear-sky climatologies at selected sites and ii) on off-line validations of the GCM radiation schemes for clear-sky conditions. Furthermore, in heavily polluted areas, the inadequate representation of absorbing aerosol in GCMs contributes to the lack of shortwave absorption in the GCM atmospheres. This is evidenced using radiation sites in Equatorial Africa during the biomass burning seasons, where the model biases are further enhanced by up to 30-40 Wm<sup>-2</sup> regionally. Within the longwave radiation components, the downward flux at the surface is affected with the largest uncertainties in the models. New observational data from BSRN suggest that the longwave downward radiation is typically underestimated in GCMs and Reanalyses at higher latitudes, but less so at lower latitudes. This results in a too strong meridional gradient in the model-calculated longwave downward radiation. These findings are consistent with offline calculations performed with the GCM radiation codes under clear sky conditions, suggesting that the emission of the cloud-free atmosphere is responsible for much of these biases. A common problem in many GCMs is therefore an excessive surface insolation, which is compensated by underestimated longwave downward radiation, leading to a superficially correct net radiation by error cancellation. This error cancellation no longer applies on zonal, regional, seasonal or diurnal scales, causing substantial problems in the simulated surface climates.

**MC11/11A/B19-004 0930**

**USING AMIP MODELS TO SIMULATE THE EARTH ROTATIONAL PROPERTY OF POLAR MOTION**

David A. SALSTEIN<sup>1</sup>, Jolanta NASTULA<sup>2</sup> (<sup>1</sup>Atmospheric and Environmental Research, Inc., <sup>2</sup>Space Research Center of the Polish Academy of Sciences)

Monthly mean results from 19 different general circulation models from the second phase of the Atmospheric Model Intercomparison Project, covering the period 1979-1995, based on the protocol of forcing only by a prescribed set of sea surface temperatures, are used to study the relationship of the atmosphere to the wobble of our planet as it rotates on its axis. Using surface pressure fields, we calculate the models' excitations for the Earth's polar motion. This motion has been tied strongly to changes in the atmospheric mass distribution, though the ocean plays a role as well. Parallel to the conservation of angular momentum in the axial direction that links atmospheric angular momentum to length-of-day variations, the values of angular momentum in the equatorial plane would be related to these polar motions, which are determined by a number of modern space-geodetic methods. Both global and regional values of polar motion excitation have been determined. We investigate the seasonal and interannual variability of the polar motion excitation term, including the spread among models, the standard deviation of which appears to vary by up to a factor of two. We check how well do models represent observations by comparing model-based excitations with those based on the NCEP-NCAR reanalyses for the same period, as well as directly with geodetic excitations, when taking account the ocean as well. Our earlier regional results of atmospheric excitations in the reanalysis revealed that such atmospheric excitations are particularly strong over certain land regions like Siberia and North America, and so we examine such geographic regions for similar variability in the AMIP-2 models. Different physical properties, including land surface parameterizations, are used for the various models and we seek, as part of a diagnostic effort within AMIP, to determine the most effective set of physical modeling mechanisms for the (three-dimensional) fields of angular momentum and the related Earth rotational parameters of interest.



**MC11/11A/B19-005 0950**

**INTERCOMPARISON OF STATIONARY WAVES IN AMIP-2 GCMS AND THEIR MAINTENANCE MECHANISMS**

Mingfang TING, Renu JOSEPH (Department of Atmospheric Sciences, University of Illinois at Urbana-Champaign)

Atmospheric and coupled ocean-atmosphere general circulation models (GCMs) are used extensively in understanding climate change and in making seasonal predictions. However, differences in model physics and numerics cause different GCMs, and sometimes the same GCM at different resolutions, to produce different atmospheric circulation patterns. In particular, climatological stationary wave simulations in GCMs differ considerably from each other, and quite often, from observations. Stationary waves and their changes are closely related to the local climate and climate change. It is therefore crucial to assess and understand how well climatological stationary waves are simulated in the various models and the sensitivity of stationary wave simulation to different parameterization schemes and model resolutions. In this study, we have compared the seasonal cycle of the climatological stationary waves in several AMIP-2 models. Considerable differences were found in the stationary wave spatial structure as well as amplitude throughout the seasonal cycle among the different models and between each model and the NCEP/NCAR reanalysis. Furthermore, the maintenance mechanisms of the climatological stationary waves in six of the AMIP-2 models have been examined using a nonlinear stationary wave model and compared to the NCEP/NCAR reanalysis. In general, diabatic heating has been the primary forcing mechanism in them consistent with the reanalysis. The relative importance of the orographic forcing and the diabatic forcing varies among different models and that of the reanalysis. This is mainly due to discrepancies in the surface zonal mean zonal wind simulations. We will show that some models may have obtained a better overall simulation of the stationary waves due to compensating errors in the orographic forcing and the diabatic forcing.

**MC11/11A/B19-006 1010**

**AMIP II SIMULATIONS OF SURFACE AIR TEMPERATURE AND PRECIPITATION: VALIDATION AND INTERCOMPARISON**

Jeong-Woo KIM<sup>1</sup>, Jeong-Hyun PARK<sup>2</sup>, Ho-Jeong SHIN<sup>1</sup> (<sup>1</sup>Department of Atmospheric Sciences and Global Environment Laboratory, Yonsei University, <sup>2</sup>Remote Sensing Division, Korea Meteorological Administration)

The observed and AMIP II-simulated normal annual mean, seasonal mean, and seasonal difference of surface air temperature and precipitation are shown on the scatter and Taylor diagrams for the globe and East Asia. The following questions are pursued in particular: Is the Gaussian distribution the rule over the ensemble of the AMIP II simulations? To what extent can the confidence in the ensemble average be ascertained through inter-model structure of simulations? Present inter-model differences among the ensemble members seem to be an impediment to our understanding of the climate system. We will discuss on the suggestions that effort should be exercised in the reduction of the inter-model differences an improved understanding.

**MC11/11A/B19-007 1050**

**ON THE PERSISTENT MOISTURE DIVERGENCE DURING COOL FROM THE INDIAN SUBCONTINENT**

Ho-Jeong SHIN, Jeong-Woo KIM (Department of Atmospheric Sciences and Global Environment Laboratory, Yonsei University)

According to recent studies (e.g. Shin et al. 2003), both NCEP/DOE and ECMWF reanalyses data show persistent moisture divergence during cooler two-thirds of a year, but most AMIP II models fail to reproduce this feature. We have analyzed this problem, and would like to present probable reasons for this discrepancy.

**MC11/11A/B19-008 1110**

**THE EFFECT OF CONVECTIVE TRIGGERING IN THE TROPICAL ATMOSPHERE SIMULATED BY ATMOSPHERIC GCM**

Tsuneaki SUZUKI, Seita EMORI, Teruyuki NISHIMURA, Shinji MATSUMURA (Frontier Research System for Global Change)

The convection does not always occur, even if the atmosphere is conditionally unstable. It is necessary that certain mechanisms lift the air parcel to the level of free convection. The convective trigger function expresses such subgrid-scale behavior of air parcel. Although the triggering process is one of essential processes in convection, the cumulus parameterizations for atmospheric general circulation models (AGCM) ignore the convective triggering. However, recent studies show that the introduction of simple convective triggering such as relative humidity criterion improves the tropical intraseasonal oscillation (ISO) and the distribution of tropical precipitation simulated by the AGCMs. In order to investigate the role of convective triggering in the simulation by AGCM, we introduce the convective trigger function similar to that proposed by Hong and Pan (1998). The convection trigger function is formulated on the basis of the obvious physical mechanisms, i.e., surface inhomogeneities (SI), turbulence-induced buoyancy (TB), large scale convergence (divergence) in source layer (LS). In addition, we consider the effect of the convective triggering caused by gust front (GF) using the model of Qian et al. (1998). Therefore, we are able to understand the influence of each convective triggering mechanism separately. The AGCM used in this study is developed at the Center for Climate System Research (CCSR) of the University of Tokyo and the National Institute for Environmental Studies (NIES), and adopts the simplified prognostic Arakawa-Schubert scheme as a cumulus convection parameterization. The simulations are performed with T106 horizontal resolution and 20 levels in the vertical (T106L20). We investigated the result of simulations, especially, the tropical ISO and the variation of precipitation in the monsoon regions. The CCSR/NIES AGCM with the resolution of T106L20 simulates the ISO well except for the coherence of the signal. The ISO becomes more coherent by introducing the LS or GF triggers with the trigger by SI. The LS trigger enhances the seasonal variability of the ISO. However, the signal of the ISO is suppressed, when the effect of LS or GF becomes larger in convective triggering. The simple homogeneous trigger only by SI intensifies the strength of the ISO regardless of season. The time-longitude diagram of observed precipitation in the monsoon regions reflects the westward traveling wave. In the simulation without convective triggering, the monsoon precipitation tends to stagnate at certain longitude and the structure of wave propagation does not appear clearly in the precipitation pattern. The precipitation obviously reflects the westward traveling wave by introducing only the simple trigger of SI. The prevailing period of wave found in the precipitation diagram changes by the addition of other triggering mechanisms. The effect of LS enhances the appearance of longer-period wave in the precipitation pattern and the effect of GS favors shorter-period wave.

**MC11/11A/B19-009 1130**

**EFFECT OF MICROPHYSICAL PROCESSES ON THE SIMULATION OF THE MADDEN-JULIAN OSCILLATION (MJO) IN GCM**

William K. LAU, H.T. WU (Laboratory for Atmospheres, NASA/GSFC, Code 910)

Recent studies have shown that the propagation and structure of MJO in GCMs are strongly dependent on the parameterization of physical processes. In this paper, we validate the Sundquist cloud water parameterization in the GEOS-GCM against TRMM observations, with focus on the effects on the propagation and structure of the model MJO. Based on joint probability distribution function of rainrate and columnar cloud liquid water from TRMM, we estimate an autoconversion time scale of about 200-1000 s and a critical cloud liquid water content of 0.5 AE.2 mm. The GEOS-GCM indicates an autoconversion of order of 1500-3600 s and a critical cloud liquid water content of less than 0.2 mm. This suggests that the GEOS-GCM has less efficient rain production than observed. The reduced rain conversion results in higher cloud liquid water content in the tropical atmosphere, less pronounced eastward propagation, and stronger stationary component. On the other hand, bring the rainfall efficiency closer to the observation leads to a more robust eastward propagating signal, and time scale for super-cloud clustering closer to the observed. The causes of the sensitivity of the dynamical regimes to the microphysics parameterization in the GCM and the need to better understand microphysical processes in the simulations of MJO, and the global hydrologic cycle will be discussed.

**MC11/11A/B19-010 1150**

**HOW WELL DO MODELS REPRESENT OCEANIC FORCING OF NORTH ATLANTIC CLIMATE?**

Mark John RODWELL<sup>1</sup>, Claude FRANKIGNOUL<sup>2</sup>, Holger POHLMANN<sup>3</sup>, Martin STENDEL<sup>4</sup>, Rowan T. SUTTON<sup>5</sup>, Laurent TERRAY<sup>6</sup> (<sup>1</sup>Hadley Centre, UK Met Office, <sup>2</sup>LODYC, Université Pierre et Marie Curie, Paris, France, <sup>3</sup>Max-Planck-Institut fuer Meteorologie, Hamburg, Germany, <sup>4</sup>Danish Meteorological Institute, Copenhagen, Denmark, <sup>5</sup>CGAM, Department of Meteorology, Reading University, UK, <sup>6</sup>CERFACS, Toulouse, France)

Lagged covariance analyses suggest that North Atlantic sea-surface temperatures (SSTs) have forced a signal in the observed North Atlantic atmospheric circulation. A similar analysis of the Hadley Centre's HadAM3 atmospheric model reveals very similar forced circulation patterns although these are possibly too weak in the cold half of the year. To get a better understanding of the strength and uncertainty of the instantaneous forcing by North Atlantic SSTs, a carefully controlled experiment using several atmospheric models has been conducted. The models used were two versions of the HadAM3 (one with a perturbed Charnock parameter), Meteo-France's ARPEGE3 model and the Max Planck Institut fuer Meteorologie's ECHAM4 and ECHAM5 models. The SST anomaly forcing patterns for each month were derived from a lagged maximal covariance analysis of the observations in order to optimise the anticipated strength of the atmospheric signal. The difference between two 20-year simulations of each model was calculated, one simulation with a negative version of the SST anomaly pattern. The results are remarkably similar for all models throughout the annual cycle. This gives some confidence that the models represent quite well the North Atlantic forcing of climate. European surface temperature anomalies of 2K and southern US and South American precipitation anomalies of 1mm per day are quite robust across models. An increase in the Charnock parameter appears to increase the temperature response over Europe. Surface latent heat flux anomalies over the entire North Atlantic respond to the imposed SST anomalies although precipitation anomalies are much stronger in the tropics. For autumn, winter and spring, HadAM3 experiments with just the tropical SST anomalies produce similar extratropical responses, although the autumn response is somewhat weaker. The latent heat fluxes forced by extratropical SST anomalies appear to re-enforce the precipitation anomalies induced by the tropical SST forcing. Extratropical SST anomalies appear to play a stronger local role in summer although the models agree well in the precise response pattern.

**MC11/11A/B19-011 1210**

**MODELLING OF EXTRATROPICAL ENSO TELECONNECTIONS AND THE LINK WITH TROPICAL PRECIPITATION**

Hilary SPENCER, Julia SLINGO (Centre for Global Atmospheric Modelling, Department of Meteorology, University of Reading)

There is much evidence that El Nino and La Nina lead to significant atmospheric seasonal predictability across much of the globe. However, despite successful predictions of tropical Pacific SSTs, atmospheric seasonal forecasts have had limited success. In particular, the observed, perhaps non-linear, atmospheric response to ENSO in the North Pacific/ North America region is not modelled accurately by many atmospheric models. However, the high signal to noise ratio in this region makes diagnosing the errors difficult. This study investigates model errors in the atmospheric model, HadAM3, by analysing composites of similar El Nino and La Nina events at their peak in December to February (DJF) and through their decay in March to May (MAM). Composites of very similar El Nino and La Nina events at their peak in December to February (DJF) are created in order to find the statistical significance of the difference between the model and observations in the tropics and extratropics. The large scale tropical ENSO teleconnections are modelled accurately by HadAM3 during DJF but the strongest extratropical teleconnection, that above the North Pacific during winter, is modelled inaccurately. The Aleutian Low is frequently observed to shift eastwards during El Nino but the modelled response always consists of a deepening of the low without shifting. This is traced to small errors in the sensitivity of precipitation to SST in the tropical Pacific, which does not display enough variability so that the precipitation is always too high over the warmest SSTs. The errors in both the tropical Pacific precipitation and North Pacific response are found to reduce dramatically when vertical resolution is increased from 19 to 30 levels. This improvement leads to the possibility for more useful studies of the linearity of the response and the influence of SST anomalies in different regions on the extratropical response. In MAM, following the peak of an El Nino or La Nina, atmospheric anomalies are observed to decay rapidly. The modelled ENSO response in DJF persists into MAM, making the extratropical anomalies in MAM too strong. This inaccuracy is again likely to be due to the high modelled sensitivity of tropical Pacific precipitation to SST which is not significantly improved with enhanced vertical or horizontal resolution in MAM.

Friday, July 11 PM

**MC11/11P/B19-001 1400**

**EVALUATING AMIP2 MODEL SIMULATIONS OVER THE AUSTRALIA REGION**

Huqiang ZHANG<sup>1</sup>, A. HENDERSON-SELLERS<sup>2</sup>, P. IRANNEJAD<sup>3</sup>, S. SHARMEEN<sup>4</sup>, T. PHILLIPS<sup>5</sup>, K. MCGUFFIE<sup>6</sup> (<sup>1</sup>BMRC, Melbourne, Australia, <sup>2</sup>ANSTO Environment, Sydney, Australia, <sup>3</sup>PCMDI, Livermore, CA, USA, <sup>4</sup>Applied Physics, UTS, Sydney, Australia)

Sixteen AGCM model simulations from the Atmospheric Model Intercomparison Project II (AMIP2) are analyzed over the Australian region as part of Diagnostic Subproject 12. This work is focused on assessing how well surface climate and fluxes over this region are simulated in current AGCMs and the possible impact of land-surface modelling on model predictability. Observational datasets are used in the model validation and the Linear Error in Probability Space (LEPS) score is calculated in assessing the skill of the models in simulating surface climate anomalies for the 17-year period (1979 to 1995). Numerous differences are found among the models and between models & observations. Some of these can be linked to the complexity of land-surface schemes used. Results reveal that the characteristics of climatic memory gain from land-surface processes (e.g. soil moisture) exhibit different features in the sixteen models. Specifically, models with simple bucket-type soil hydrology schemes, which tend to exhibit rapid decay of soil water anomalies, exhibit too weak an influence on forecasts of surface climate anomalies resulting from changed soil moisture conditions.

**MC11/11P/B19-002** **1420**

**EVALUATION OF THE REGIONAL ETA/SSIB MODEL IN MODELING NORTH AMERICAN CLIMATE**

Yongkang XUE<sup>1</sup>, Ratko VASIC<sup>2</sup>, Zavisla JANJIC<sup>3</sup> (<sup>1</sup>Department of Geography, Department of Atmospheric Sciences, University of California, Los Angeles, <sup>2</sup>Department of Geography, UCLA, CA, USA, <sup>3</sup>NCEP, NOAA, Camp Springs, MD, USA)

This study evaluates the North American climate simulations of the Regional Eta/SSIB model using observational and reanalysis data. It is important to understand the predictability of the regional climate model and the dominant factor(s), which may affect its predictability. To achieve these goals, a series of sensitivity studies has been designed to explore the role of variety of factors in regional climate simulations. These factors include domain size, horizontal resolution, different lateral boundary conditions (NCEP reanalysis, ECMWF reanalysis, NOAA GCIIP reanalysis, GCM outputs), sea surface temperature (SST) and its diurnal variation, deep soil conditions, and convective parameterizations. The summer of 1998 is selected for the experiments. In this study, we mainly focus on the model simulations of the precipitation and other relevant hydro-meteorological variables. The results show that the domain size, SST, and lateral boundary conditions have the crucial impact on the simulations. In the domain size experiment, a set of domains has been selected for testing. The domain that covers only continental U.S. produces the best simulations in the temporal evolution and the spatial distribution of the precipitation. When the domain is expanded to the oceans, although the model is still able to produce reasonable large-scale circulation, the simulation of the intensity and the spatial distribution of the precipitation deteriorate dramatically when the ocean areas become large. The lateral conditions are also crucial for simulations. Only the GCM lateral boundary conditions produce the proper precipitation over ocean. In addition, the sensitivity study reveals that the diurnal variation of SST could also improve the simulation for precipitation over ocean. The change of horizontal resolutions from 80km to 48 km does not make significant differences in the model simulation. The impacts of these factors on other climate variables, such as wind, humidity, and temperature will also be presented.

**MC11/11P/B19-003** **1440**

**PRECIPITATION OVER COMPLEX TOPOGRAPHY: AN EVALUATION AND INTERCOMPARISON OF REGIONAL CLIMATE MODELS**

Christoph FREI, Juerg SCHMIDL (Institute for Atmospheric and Climate Science, ETH)

Regional Climate Models (RCMs) are promising tools for climate downscaling from General Circulation Models. Accurate downscaling of precipitation is of primary interest in applications, but modeling the involved processes is demanding, especially over complex topography. This study evaluates and compares 5 RCMs with regard to their representation of the precipitation climate over the 1100x700km mountain range of the European Alps. Four limited area models and one variable-resolution global model are considered, all with a grid spacing of 50 km. The model integrations extend over a 15-year period and are forced by reanalyses at their boundaries. The observational reference is based on 6400 rain gauge records (10-50 stations per model grid box) over the same period, from which objective analyses have been generated that are compatible with the resolution of the climate models. Evaluation statistics encompass seasonal mean precipitation and several statistics characteristic of drought and heavy precipitation. Results are discussed with regard to the climatological bias and the skill in the reproduction of interannual variability. The results point to remarkable differences in the model performance in summer. Three of the models underestimate summer mean conditions significantly. Though more accurate in the mean, the two other models exhibit compensating errors in the precipitation frequency distribution. Interestingly, the model errors are very similar between the two models with the same dynamical core (but different parameterizations) and they differ considerably between the two models with similar parameterizations (but different dynamics).

**MC11/11P/B19-004** **1500**

**SENSITIVITY OF THE EAST ASIAN SUMMERTIME CLIMATE TO SURFACE WATER CAPACITY DISTRIBUTION**

Hyung-Jin KIM, Jeong-Woo KIM (Department of Atmospheric Sciences and Global Environment Laboratory, Yonsei University)

Soil moisture is one of the major sources of the atmospheric water vapor, and affects the land surface characteristics such as albedo, heat capacity and evapotranspiration (Smith et al. 1994), thus relating to the net surface energy balance. Therefore using realistic surface water capacity in GCMs should be relevant to simulating seasonal and longer time scale climate (Fennessy and Shukla 1999). At present, however, a number of AGCMs (for examples, 11 of 33 AMIP II AGCMs) use a single-layer bucket model to deal with soil moisture, and a constant maximum water capacity is uniformly prescribed in about two-thirds of these AGCMs including YONU AGCM. In this paper, we will present some of the salient results on our experiments in which our model runs with field capacity varying with surface types. We will discuss the sensitivity of the East Asian summertime climate to various distributions of the maximum water capacity over the region of East Asia. In particular, the summertime thermal low, and water and energy budget over the East Asia will be examined.

**MC11/11P/B19-005** **1520**

**PREDICTABILITY AND UNCERTAINTY IN A REGIONAL CLIMATE MODEL: LESSONS FROM PERFECT MODELS AND PERFECT DATA**

Pier Luigi VIDALE, Daniel LUETHI, Christoph FREI, Sonia I. SENEVIRATNE, Christoph SCHAER (Institute for Atmospheric and Climate Science ETH)

The evaluation of the quality and usefulness of climate modeling systems is dependent upon an assessment of both the limited predictability of the climate system and the uncertainties

stemming from model formulation. In this study a methodology is presented that is suited to assess the performance of a regional climate model (RCM), based on its ability to represent the natural interannual variability on monthly and seasonal time scales. The methodology involves carrying out multi-year ensemble simulations (to assess the predictability bounds within which the model can be evaluated against observations) and multi-year sensitivity experiments using different model formulations (to assess the model uncertainty). As an example application, experiments driven by assimilated lateralboundary conditions and sea surface temperatures from the ECMWF re-analysisproject (ERA-15, 1979-1993) were conducted. While the ensemble experiment demonstrates that the predictability of the regional climate varies stronglybetween different seasons and regions, being weakest during the summer andover continental regions, important sensitivities of the modelingsystem to parameterization choices are uncovered. In particular, compensating mechanismsrelated to the long-term representation of the water cycle are revealed, in whichsummer dry and hot conditions at the surface, resulting from insufficient evaporation, can persist despite insufficient net solar radiation (a result of unrealistic cloud-radiative feedbacks).

**MC11-Posters** **Friday, July 11**

**CLIMATE MODEL EVALUATION: HOW WELL DO MODELS REPRESENT OBSERVATIONS (ICCI)**

Location: Site D

**Friday, July 11 PM**

**MC11/11P/D-001** **Poster** **1400-194**

**HOW MUCH THE ADVECTION SCHEME AFFECTS CLIMATE SIMULATION WITH AGCM**

Xindong PENG<sup>1</sup>, Feng XIAO<sup>2</sup> (<sup>1</sup>Earth Simulator Center, <sup>2</sup>Tokyo Institute of Technology)

Spectral method is widely used in global AGCM model; the Legendre transform is proved to be very expensive when apply to high resolution climate simulation in the AFES (AGCM For Earth Simulator) T1279, though it achieved a 26.58 TFLOPS of operation speed. Also, the spectral discretization introduces oscillation or dispersion error. An alternative, by adopting the Conservative Semi-Lagrangian scheme with Rational function (CSLR), is considered to improve the transport computation. As the first step, tracer quantities (water vapor and liquid water) are implemented with the CSLR to improve the model accuracy and computational efficiency. In the frame of AFES T106L20, some simplified advection tests and a real general circulation run are carried out. In the asymmetric non-divergence current, passive advection tests show that the spectral leap-frog (SLF) type discretization always express a local message with global information. For a sharp distribution, oscillation in concerning with SLF is very large; positive definite is got in the CSLR tests, however. With Arakawa-Schubert cumulus parameterization, two 20-year integrations of T106L20 model of AFES with the SLF and CSLR were run over the Earth Simulator. Seasonal precipitation, with CMAP data as reference, shows a great improvement of global rainfall pattern by the CSLR, especially the tropical rainfall distribution in ITCZ. The ITCZ band in both the eastern Pacific and western Atlantic oceans is well reproduced with the new scheme; and the precipitation in the Indian ocean is also refined somewhat. With the model resolution rising, vapor distribution will be sharply simulated with the mesoscale effects in the model. The local characters of model atmosphere become more important for climate simulation. The sophisticated transport scheme helps us to produce more realistic numerical productions. For a further understanding of the impact of advection scheme, T319L32 runs with both the SLF and CSLR. The ITCZ rainfall shows a similar pattern as in T106; and the CSLR indeed improved the seasonal climate simulation largely. Some mesoscale impact on weather systems, such as Meiyu (Baiu) fronts and tropical cyclones is being analyzed. It is worthy noting that the application of the CSLR is not only to extend integration time step, but also to provide accurate treatment of advection. Because the present scheme CSLR is a conservative one, global quantity conservation is ensured for the integration, which is important for climate simulation. A summary of the simplified advection tests and the real general circulation run show that the realistic transport of water vapor with sophisticated scheme affects the model results evidently.

**MC11/11P/D-002** **Poster** **1400-195**

**ANALYSIS OF REGIONAL CLIMATE MODEL PERFORMANCE FOR THE ARAL SEA AREA. COMPARISON WITH OBSERVATIONS**

Elisaveta Lazarova PENEVA, Emil Vassilev STANEV (Dept. of Meteorology and Geophysics, University of Sofia, Sofia, Bulgaria)

The Aral Sea level changes during the last 40 years present one of the most drastic example globally about the possible consequences of man-induced environmental changes. From numerical point of view this region presents a good opportunity to study the model performance and complicated atmosphere-land-sea interactions in desertification areas, where the model parametrization and schemes are not well tuned. Meteorological observations in Aral Sea region exist only in several locations and has irregular time resolution, in particular for the last decade of 20th century, thus model results are very usefull if applicable for this area. In this study we use NCAR/PSU regional climate model (RegCM2) and the initial data and boundary forcing is based on the 6-hour NCEP reanalysis data, including air temperature, wind and humidity, surface pressure and sea surface temperature. Several numerical experiments are run for one winter and one summer months with horizontal resolution of 50 and 30 km. Additional experiments have been run, using the option to couple RegCM2 with a lake model in order to represent more adequately the Aral Sea surface temperature, e.g. thermal air-sea exchange. The results from different experiments are validated against regional climatic data, including air temperature and precipitation, measured in several meteorological stations during the period 1961-1990 and the skill of the model in representing the climate specifics is analysed.

**MC11/11P/D-003** **Poster** **1400-196**

**GCM SIMULATIONS OF THE HEAT AND WATER BUDGETS OVER MAJOR RIVER AND THE CASPIAN SEA WATERSHEDS**

Petr V. SPORYSHEV, Valentin P. MELESHKO, Tatyana V. PAVLOVA, Veronika A. GOVORKOVA (Dynamic Meteorology Department, Voeikov Main Geophysical Observatory)

The aim of the study is to assess performance capability of the AMIP-II GCMs in simulation of surface heat and water budget seasonal cycles over major watersheds of the world. The progress was also evaluated in development of GCMs for the last decade on the basis of intercomparison of model performance under the first and second phases of AMIP. Seventeen models were selected for the intercomparison that participated in the both

phases of AMIP, and their outputs were available for analysis: CCCma, CNRM, COLA, DNM, ECMWF, GISS, GLA, JMA, MGO, MPI, NCAR, NCEP, SUNYA, UGAMP, UKMO, UIUC. Eight watersheds were considered in the study: the Amazon, the Baltic basin, the Congo, the Mississippi, the Volga, the Ob, the Enisei, and the Lena. A comparison with observations indicates that AMIP-II models are more successful in simulation of seasonal variations of the surface radiation and temperature fields over most of watersheds as compared to AMIP-I. The intermodel scatter of surface air temperature (SAT) seasonalities distinctly reduced in AMIP-II models. The scatter of precipitation is also smaller in AMIP-II, although the improvement is less pronounced than that of the SAT. Correlation of the computed precipitation fields with observation is generally less than that for the temperature. It is important to note that observed precipitation datasets produced from different sources differ significantly, and for some watersheds the differences between them are of the same magnitude or even larger than that of the model simulations. A special attention was given to the Caspian Sea basin. The sea is located in a large continental depression about 27 meters below the global mean sea level with no surface outlets. Its water level is sensitive to climatic variations, and can serve as an indicator of long-term climatic trends. We discuss not only the accuracy of model simulation of climatic seasonal cycle, but also the model ability to reproduce longterm and interannual variability of the hydrological regime of the region. The results of the 11-member ensemble of 50-year experiments with the MGO GCM forced by observed SST, are used here as additional support. The experiments were performed in accordance with the requirements of the C20C (the Climate of the 20-th Century) project.

**MC11/11P/D-004** Poster **1400-197**

**AN ASSESSMENT OF SEASONAL PREDICTABILITY IN SUMMER BY USING THE NCC/IAF COUPLED ATMOSPHERE-OCEANIC GENERAL CIRCULATION MODEL**

Yihui DING, Qingquan LI, Zuqiang ZHANG (National Climate Center, China Meteorological Administration)

Seasonal predictability is investigated using a global atmosphere-ocean coupled model at National Climate Center, China Meteorological Administration. Seasonal hindcast experiments and validations of the abnormal climate in China during the summertime of 1982-2000 were conducted by using this coupled model. More than six months' ensemble integrations were performed from three consecutive days of initial condition preceding target summer season of each year. A set of indexes characterizing different predictive skills was used to assess systematically and quantitatively the predictive performance of the model. The model verification has indicated that the model has some certain capability in predicting seasonally the rainfall and temperature over China as well as the large-scale circulation in the North Hemisphere in summertime. The model prediction is better than climatological prediction and persistence prediction. During 1982-2000, the Hit Rate of Anomaly Sign scores of the seasonal predictions of the summer rainfall over China range between 40% and 70%; the Root Mean Square Skill Scores are all above zero; the Operational Skill Scores range from 55 to 80; the Skill Scores are all above zero; and 19-year average of Anomaly Correlation Coefficient of rainfall is 0.02. In the Asian monsoon region, except that the rainfall forecast for Iran has relatively large error (about 8%-12%), rainfall anomaly percentages usually range from to in other regions. The model performances of summer rainfall prediction vary in different regions of China. In general, the prediction of rainfall tendency in both East China and West China are reasonable. Among the five sub-regions of East China, the model predictive skills are higher in the Big Bend of the Yellow River and North China than in Northeast China, South China and the Yangtze and Huaihe River Basin. In view of anomaly correlation coefficient, the model skill in seasonal prediction of the summer temperature are relatively higher in West China, North China, the regions between the Yangtze River and the Yellow River, as well as the southeast part of Northeast China. The model's capability to reproduce the large-scale summer circulation in the Northern Hemisphere and the global sea surface temperature were also investigated. The averaged anomaly correlation coefficient of 500hPa geo-potential height over Asian monsoon area (50°E-160°E, 0-30°N) in summer is 0.45. The correlation coefficients of 4-6 month lead forecast of summer (JJA) sea surface temperature anomaly are relatively high in the tropical Pacific Ocean, Indian Ocean, and Atlantic Ocean as well as some regions of the Northern Pacific and the Northern Atlantic Ocean.

**MC11/11P/D-005** Poster **1400-198**

**THE MODELING OF OROGRAPHICAL EFFECT ON THE FORMATION OF DRY CLIMATE IN NORTHEASTERN ASIA**

Tomonori SATO<sup>1</sup>, Fujio KIMURA<sup>2</sup> (<sup>1</sup>Japan Science and technology corporation / University of Tsukuba, <sup>2</sup>Institute of Geoscience, Tsukuba University and Frontier research system for global change)

Broadly spread arid regions exist between 15 degree and 35 degree in both northern and southern hemisphere. The subsidence branches of Hadley circulation are believed to have the relation with the formations of these arid regions. In Northeastern Asia, however, arid and semi-arid climate distribute over remarkably higher latitude, namely from 30 degree to 50 degree, characterized as Steppe in Central Asia or Mongolia, Taklimakan desert and Gobi desert. Broccoli and Manabe (1992) investigated the influence of Tibetan plateau upon the maintenance of the dry climate in midlatitude Asia using GCM. They concluded that the plateau is the main reason for these arid/semi-arid areas although its mechanism depends on the season. It is well known, however, that the seasonal variations of precipitation are different in Midlatitude Asia, especially between the eastward and westward regions from the Tian-Shan mountain range. Large unknown part still remains in the mechanism which maintains dry climate in Northeastern Asia. A Regional Climate Modeling System (RAMS) is used to simulate the precipitation in Northeastern Asia in warm with (CTL) and without eastward topography of the Tian-Shan and the Altai Mts. (NOM). The model simulates the synoptic disturbances during each whole month of June and January of 1998, by using NCEP/NCAR reanalysis as a boundary condition. The convection parameterization and microphysical parameterization are used together to predict the synoptic scale disturbances in high spatial resolution. The arid region with small amount of precipitation, less than 10 mm/month, is produced in CNT run, which corresponds well with satellite estimated data of GPCP. The water vapor transported into the arid region is mainly supplied from the northwestern part of Tian-Shan mountain ranges, although the amount of water vapor seems evidently decreased when it is going over the mountain ranges. Thus, the mountain ranges looks as if they act as a moisture sink in warm season. Nevertheless, the monthly precipitation of MON run shows that the arid region still exists, even though the mountain ranges were omitted in the model so that the water vapor is allowed to be brought into the arid region. This means that the reason of warm season aridity in the Taklimakan desert is not always cause by the trap of moisture by the mountain range. The meridional-time cross section of vertical motion at 85E reveals the prominent diurnal variation of upward motions over Kunlun Mts., while gentle downward motions are found over Taklimakan desert. A couple of upward and downward motion is emphasized when the synoptic scale front are passing through this region, which causes the enhanced subsidence over the Taklimakan desert. The subsidence results to decrease the precipitation there.

**MC11/11P/D-006** Poster **1400-199**

**ORDER IN THE LOW-FREQUENCY PLANETARY WAVE DYNAMICS**

Dmitry Mikhailovich SONECHKIN, Nadejda Nazarovna IVACHTCHENKO (Hydrometeorological Research Center of Russia)

The hydrostaticity and geostrophicity phenomena are well known during many times. But until quite recently nobody knew is there any specific order in the atmospheric low-frequency dynamics (within the inverse energetic cascade of the atmospheric macroturbulence) in addition to the above phenomena. Experiments with very long integrations of some atmospheric toy-models (Sonechkin, 1984: Stochasticity in the atmospheric general circulation models, Hydrometeoizdat, L., 280 pp.- in Russian) shown that an essential reduction of the dimension of the model attractors in comparison with the dimension of the model state-space itself is caused by temporal synchronizations of the phases and amplitudes of the modeled planetary waves, i.e. the model attractors are constructed from the only synchronized motions (SM). The nonsynchronized motions (NSM) are also possible in the models, but because of their great instability these are observable during rather short initial time periods of the model integration. Later, SM has been recognized in the real-world planetary wave dynamics in the geopotential height fields of the Northern Hemisphere. A fingerprint of the phenomenon is even seen in the day-to-day planetary wave motions as a rather high correlation between pairs of instantaneous values of the wave phases and amplitudes. But, the phase synchronization looks like an almost functional relationship for 5-day mean geopotential height fields. Another kind of the order in the low-frequency atmospheric dynamics consists of geographical localization of wave phases. This phenomenon is well known for the ultra-long waves. But, it turns out that a similar localization is a property of the short synoptic waves too. This latter phenomenon may be explained as an effect of the prevalence of the topographic instability in comparison with the baroclinic one for these waves. A hypothesis has been brought up that NSM and nonlocalized motions, which are excited in forecasting models as a result of artificial nonadjustments of initial data, are one of the basic sources of the weekly predictability loss in the present-day forecasting models. Thus, a forced synchronization and localization must help to overcome this limit. A model (called quasi-synchronous) developed at the Hydrometeorological Research Center of Russia confirms this hypothesis.

**MC12** Monday, July 7 - Tuesday, July 8

**THE CLIMATE OF THE HOLOCENE (ICCI)**

Location: Site B, Room 19

Monday, July 7 AM  
Presiding Chair: V. Masson-Delmotte

**MC12/07A/B19-001** Invited **0930**

**CLIMATE, VEGETATION, AND CO2 DYNAMICS IN THE HOLOCENE: EXPERIMENTS WITH CLIMATE SYSTEM MODEL OF INTERMEDIATE COMPLEXITY**

Victor BROVKIN, Martin CLAUSSEN, Eva BAUER (Climate System Department, Potsdam Institute for Climate Impact Research)

Multiple proxy data reveal that the early to middle Holocene, ca. 8 to 6 kyr BP, was warmer than the pre-industrial period in most regions of the northern hemisphere. This warming is presumably explained by the higher summer insolation in the northern hemisphere owing to changes in the orbital parameters. Subsequent cooling in the late Holocene was accompanied by significant changes in vegetation cover and an increase in atmospheric CO2 concentration. The essential question is whether it is possible to explain these changes in a consistent way accounting for the orbital parameters as the main external forcing for the climate system. We investigate this problem using the computationally efficient model of climate system, CLIMBER-2, which includes models for oceanic and terrestrial biogeochemistry. We found that changes in climate and vegetation cover in the northern subtropical and circumpolar regions can be attributed to the changes in the orbital forcing. Externally driven climatic changes in these regions have been amplified by climate-vegetation feedbacks. Explanation of the atmospheric CO2 record requires an additional assumption of excessive CaCO3 sedimentation in the ocean during the Holocene. For the last 1,000 years, reconstructions of external natural and anthropogenic forcings (solar activity, volcanism, CO2 emissions, land cover changes) are much more precise than for the previous part of the Holocene. We extended the Holocene simulation by applying these additional forcings during the last millennium. Simulated surface air temperatures for the Northern Hemisphere correlate reasonably well with reconstructed temperatures (Mann et al., 1999). The long-term decrease in temperature from approx. 12 to 17th century within the model is largely attributed to changes in the solar forcing. Anthropogenic forcings impose significant climate changes after 1800. A warming due to elevating CO2 concentration is attenuated by the cooling due to historical land cover changes. Results suggest that the land cover forcing contributed to a stabilisation of the temperature during the second half of the 19th century, and has damped the warming in the 20th century.

**MC12/07A/B19-002** **1000**

**NATURAL AND ANTHROPOGENIC CLIMATE CHANGE OVER THE PAST 300 YEARS: THE ROLE OF HISTORICAL LAND COVER CHANGE**

H. Damon MATTHEWS, Andrew J. WEAVER, Katrin J. MEISSNER (School of Earth and Ocean Sciences, University of Victoria)

The effect of natural and anthropogenic influences on global climate over the past three centuries is explored using the UVic Earth System Climate Model. The initial focus is on a detailed sensitivity analysis of the radiative forcing of climate by historical land cover change. Two independent historical land cover datasets are used to force the model under varying model configurations, making use of a simple land surface model. These runs are then compared to results using a more comprehensive land surface and dynamic vegetation model. The effect of historical land cover change is further compared to the effects of natural influences (solar orbital and insolation changes and volcanic aerosols) and other anthropogenic influences (greenhouse gasses and sulphate aerosols) on the climate system. These processes are all combined in a series of transient climate simulations to generate a complete picture of global climate change over the past 300 years.

**MC12/07A/B19-003 1015**

**INFLUENCE OF LAND SPECIFICATION TO THE BERINGIAN CLIMATE OF THE EARLY HOLOCENE**

Aaron R. RIVERS<sup>1</sup>, Amanda H. LYNCH<sup>2</sup>, Patrick J. BARTLEIN<sup>3</sup> (<sup>1</sup>CIRES/ University of Colorado, <sup>2</sup>PAOS/ CIRES/ University of Colorado, <sup>3</sup>University of Oregon)

The sensitivity of the simulated climate to postulated surface conditions during the early Holocene in Beringia is studied with a single column model (SCM) and regional climate model (RCM). Climate metrics important to vegetation development, including summer mean temperature, soil moisture availability, and the timing of the spring thaw, are used to identify feedbacks between surface conditions and paleoclimate. The SCM is forced with output from a GCM simulation representing 11 ka, and a range of surface conditions, including vegetation, thaw lakes, and soil type, are varied to determine surface parameters most strongly influencing the simulation. These results are used in RCM simulations to further identify three-dimensional feedbacks that are absent in the SCM experiments. An analysis of the sensitivity of the climate to the land specification identifies important features of the Beringian landscape for paleoclimate simulations.

**MC12/07A/B19-004 1030**

**HOLOCENE VARIATIONS IN TREE COVER AND LEAF AREA INDEX IN NORTH AMERICA**

John W. WILLIAMS (National Center for Ecological Analysis and Synthesis, University of California Santa Barbara)

Understanding the consequences of Holocene land cover change upon climate history and variability requires accurate and quantitative maps of the Holocene vegetation. Biome-based descriptions of the vegetation are adequate for analyzing atmosphere-vegetation feedbacks at global scales, but at smaller spatial extents, within-biome heterogeneity in vegetation structure can significantly affect climate. By calibrating modern pollen samples against AVHRR-derived maps of tree cover and leaf area (LAI), quantitative estimates of LAI and tree cover for simple plant functional types have been produced for boreal and eastern North America for the past 21,000 years at a 50 km resolution and a thousand-year time step. A 'hierarchical analog technique' enables tree cover reconstructions even for times and places where fossil pollen samples are compositionally unlike any modern pollen samples, by condensing pollen taxa to plant functional types and rechecking for analog matches. Cross-validation analyses for the modern pollen data show that the hierarchical analog technique reproduces the present-day distribution of needleleaved and broadleaved tree cover with a high degree of accuracy. Total tree cover and LAI has increased in North America since the last glacial maximum, particularly in the eastern forests as both needleleaved and broadleaved tree coverages have increased. Holocene shifts in land cover include a continued infilling of the northern forest, leading to a connection between the eastern and western boreal forest by 6,000 years ago. This new generation of land cover products for the late Quaternary enables increasingly detailed examinations of vegetation-atmosphere feedbacks at regional to continental scales.

**MC12/07A/B19-005 1100**

**BETULA POLLEN IN THE LAPTEV SEA SHELF SEDIMENTS AS HOLOCENE CLIMATIC INDICATOR**

Olga D. NAIDINA<sup>1</sup>, Henning A. BAUCH<sup>2</sup> (<sup>1</sup>Department of Biostratigraphy, Institute of the Lithosphere of Marginal Seas, Russian Academy of Sciences, <sup>2</sup>Department of Paleoceanography, Alfred-Wegener Institute for Polar and Marine Research)

Absolute pollen analysis with morphological investigation of pollen indicators using scanning electron microscopy (SEM) was carried out on sediment samples of the core PS51135 from the eastern Laptev Sea. Several AMS dates indicate that deposits accumulated since 11142 cal.ka to 5301 cal.ka. The pollen record of the core PS51135 could be separated into several zones. From alternating birch pollen values these diagram can be divided into several cooling and warming events. SEM analysis of birch pollen from the Holocene deposits in the Laptev Sea suggest that it is possible to reliably separate shrub birch-type pollen from tree birch-type pollen. The main component of birch pollen from the core PS51135 belong to shrub birch from taxa typical of tundra zones. Given the close relationship between oscillations in birch shrub/tree-line and mean summer temperature in Arctic Siberia, it should therefore provide a valuable proxy summer temperature indicator for the Holocene in northern Yakutia.

**MC12/07A/B19-006 1115**

**SIMULATION OF NATURAL MILLENNIAL-SCALE CLIMATE VARIABILITY FROM THE EARLY HOLOCENE (8 KYR BP) TO THE PREINDUSTRIAL PERIOD (1700 AD) USING THE MCGILL PALEOCLIMATE MODEL**

Yi WANG<sup>1</sup>, Lawrence A. MYSAK<sup>1</sup>, Zhaomin WANG<sup>1</sup>, Victor BROVKIN<sup>2</sup> (<sup>1</sup>Department of Atmospheric and Oceanic Sciences, McGill University, <sup>2</sup>POTSDAM INSTITUTE FOR CLIMATE IMPACT RESEARCH (PIK))

Multiple proxy data reveal that the middle Holocene (6 kyr BP) was warmer than the early Holocene (8 kyr BP) as well as the preindustrial period (1700 AD) in most regions of the Northern Hemisphere. This warmth is somewhat counterintuitive because the summer insolation was decreasing during this time. Cooling in the late Holocene (after 6 kyr BP) is hypothesized to be due mainly to the astronomical forcing. This cooling was also accompanied by significant changes in vegetation cover (i.e., treeline retreat from northern high latitudes; the desertification of the Sahara/Sahel region) and a small but gradual increase of atmospheric CO<sub>2</sub> concentration (from 260 ppm to 280 ppm). The early-to-middle Holocene warming, on the other hand, is hypothesized to be due in part to ice-albedo feedback in Northern America, associated with decreases in the Laurentide ice sheet, which completely disappeared by 6 kyr BP. The snow-vegetation-albedo feedback is also hypothesized to have played a role in this early warming event. To test the above hypotheses, the earlier geophysical McGill Paleoclimate Model has been coupled to the vegetation model known as VECODE (VEgetation COntinuous DEscription, one of the simpler dynamic global vegetation models), and a number of sensitivity experiments have been performed. The model results illustrate the role that Northern Hemisphere land cover changes played in explaining the natural millennial-scale climate variability from the early Holocene (8 kyr BP) to the preindustrial period (1700 AD).

**MC12/07A/B19-007 1130**

**MESOSCALE MODELING OF THE AFRICAN HUMID PERIOD**

Kerry Harrison COOK, Nicholas J. NEARY (Dept. Earth and Atmospheric Sciences, Cornell University)

During the last glacial period, dry conditions prevailed over Saharan and Sahelian Africa, somewhat drier than today. But beginning around 14.5 ka BP, the region became progressively more moist. Numerous large lakes dotted the landscape of what is now the Sahel until about 5.5 ky BP, and the Sahara/Sahel boundary was about 5 farther north. The African Humid Period occurred at a time of higher summertime insolation in the Northern Hemisphere, and this forcing has been associated with an intensification of the African monsoon. However, GCM simulations suggest that a consideration of additional factors and/or feedbacks within the climate system is required to fully understand the African Humid Period. A mesoscale climate model (MCM) is developed for studying the African Humid Period. By modeling climate on smaller space scales (10's of kilometers) than is possible with a GCM, the space scale of the modeling is brought close to that of the geological record. This provides a better opportunity for model validation, and for the modeling to aid in the interpretation of geological evidence. Also, the MCM provides an improved simulation of the present day climate of northern Africa, since the physical parameterizations can be optimized for the region and the strong surface moisture and temperature gradients that characterize this region are resolved. A series of MCM integrations is used to compare the African climate of 6 ky BP with today's climate, and to explore the sensitivity to various assumptions about the surface boundary conditions. Unlike GCM simulations of the African Humid Period, the MCM produces excessive precipitation over the present-day Sahel and Sahara regions with 6 ky BP solar insolation, surface vegetation, and atmospheric CO<sub>2</sub> levels. The addition of colder sea surface temperatures off the west coast, as suggested by ocean cores, improves the model's agreement with geological reconstructions. There is some evidence that colder water occupied the Gulf of Guinea during the African Humid Period, but the MCM simulation suggests that this is inconsistent with the reconstructions of higher lake levels in Ghana.

Monday, July 7 PM

Presiding Chair: M. Mann

**MC12/07P/B19-001 Invited 1415**

**LATE HOLOCENE CLIMATE VARIATIONS AND THEIR RELATIONSHIP TO FORCING MECHANISMS**

Raymond Stuart BRADLEY (Department of Geosciences, UMASS, Amherst)

Numerous paleoclimatic records indicate that climate changed significantly around ~4,000 ± 500 years B.P. In some cases, the change is essentially a step function ("abrupt climate change"); elsewhere, the change is more gradual. Here, a set of well-dated records from a wide geographic network are used to assess the nature of large-scale climatic changes over this period, and to place those changes in the context of probable forcing factors.

**MC12/07P/B19-002 1445**

**REGIME OF CAUCASUS MOUNTAIN GLACIERS DURING HOLOCENE OPTIMUM: FIRST EXPERIENCE OF ESTIMATION**

Maria Dmitrievna ANANICHEVA, Natalia V. DAVIDOVICH (Department of glaciology, Institute of geography, Russian Academy of Sciences)

For the first time an estimation of regime and condition of mountain glaciers in the periods of interglacial (the extensive warming) is presenting. All existing global paleo-climatic maps show the mountain countries as a field of simple interpolation of the data referring to the surrounding plains and foothills without account for mountain specificity and in particular high-mountainous glacio-nival zone. On an example of the Bolshoy Caucasus during Holocene optimum (5-6 thousand years ago) the calculations and analysis, carried out by the authors, show that the deviations of the high mountains characteristics and that of mountain belts located lower, appreciably differed. In comparison with present time the B. Caucasus high mountains are characterized by better expressed humid climate, and foothills and bottom zones of mountains – by more dry one. And it is important that warming was stronger at the center of the mountain country, than on its periphery or foothill plains. Therefore the methodological conclusion is: it is illegitimate to use the temperature-humidity anomalies of continuous plains' climate without additional amendments at any paleo-glaciologic reconstruction. With the help of glacio-climatic method, developed by the authors (which is practically the only possible for the periods of climate optimum, when there were not any geomorphologic traces of the former glaciers survived) the reconstruction of mass balance, altitudes of glacio-morphological levels, temperature of air over the glacier zone is conducted. The main conclusion consists of the statement that in conditions of significant warming the glacial belt did not disappear, yet shifted upwards. The increase of the equilibrium line might reach 150-200 m, and the glaciers' terminuses – 300-400 m. Despite of a higher values of these parameters, summer air temperature enhanced as much as 1-1.50C, and the mass exchange intensity increased at 20-30 % compared to the present time conditions.

**MC12/07P/B19-003 1500**

**A CARBONATE MOUND POPULATION ON THE WESTERN MARGIN OF THE PORCUPINE BANK: EVIDENCE FOR NORTH ATLANTIC PALAEOCLIMATIC CONTROLS ON A COLD-WATER CORAL ECOSYSTEM**

Brian M. O'REILLY<sup>1</sup>, Peter W. READMAN<sup>2</sup>, Patrick M. SHANNON<sup>3</sup> (<sup>1</sup>Dublin Institute for Advanced Studies, 5 Merrion Square, Dublin 2, IRELAND, <sup>2</sup>Department of Geology, University College Dublin, Dublin 4, IRELAND)

Coral reefs are normally associated with warm water tropical regions of the Earth, but during the last decade or so large-scale carbonate build-ups, which resemble tropical reefs in many respects, have been recognized in the northeast Atlantic stretching from Norway to Iberia. The cold-water coral species *Lophelia pertusa* and *Madrepora oculata*, are the main framework constructors of these build-ups and unlike tropical corals flourish far below the photic zone at water temperatures of between 4° and 12° C. They are a significant reservoir or sink for excess carbon dioxide and their growth is potentially important in regulating climate change. The detailed structure of one such cold-water carbonate mound population was resolved along the western margin of the Porcupine Bank, west of Ireland, during a deep-tow TOBI (Towed Ocean Bottom Instrument) sidescan sonar survey, undertaken on behalf of the Irish Petroleum Infrastructure Programme. They are circular to elliptical in shape and range in size from 50 to 850 m across and are up to 300 m high and large-scale sedimentary bedforms at 700-900 m water depth envelope the larger mound structures. The bedforms are produced by the strong NE-flowing contour-parallel currents. A change to a more elliptical shape as the size of the mounds increases suggests that streamlining effects caused by the strong pole-ward bottom currents influence the geometry of the mound structures. The frequency distribution of the mound sizes is close to a power law and there is a systematic tendency for them to become gradually more elongate as they increase in size. The distribution is ultimately determined by the biological growth rate of the mound frameworks and the rate at which the coral framework builders colonise the substrate. Initially bottom currents are important in establishing a suitable environment for the growth of carbonate mounds and the establishment of embryonic mound settlements as they transport



nutrients into the framework and keep it free of sedimentary debris. There are also negative feedback effects on coral growth from fluid drag forces. The development of streamlined elliptical forms in the evolving mound population minimises the inhibiting effects of these forces. A model for the development of the population, incorporating the effects of bottom currents, allows its age structure to be derived. There is an interesting coincidence between certain properties of the observed distribution of mounds, the age structure of the entire population predicted by the model, and climatic change in the late Pleistocene and Holocene. This suggests that there is a subtle but well-defined correlation between the growth and colonization patterns of the biological species, comprising the mound population, with climate change and related variations in the strength (and perhaps direction) of these bottom currents.

**MC12/07P/B19-004 1515**

**TRANSIENT SIMULATION OF ABRUPT CLIMATE CHANGE INDUCED BY FRESHWATER INPUT FROM LAURENTIAN ICE SHEET TO THE NORTH ATLANTIC OCEAN**

Pavel Alekseevich TOROPOV<sup>1</sup>, Alexander Victorovich KISLOV<sup>1</sup>, Sergey Nikolaevich MOSHONKIN<sup>2</sup> (<sup>1</sup>Lomonosov Moscow State University, <sup>2</sup>Institut of the Numerical Mathematics of the Russian Academy of the Science)

Records from different proxies suggest that large and abrupt changes of climate occurred during both glacial and postglacial periods; clear example is the Younger Dryas (YD) cold event. Broecker (1990) speculated that these changes result from changes in the thermohaline circulation of the Atlantic Ocean, which were caused by the release of large amounts of melt water from continental ice sheet. It is important that these phenomena were not explicitly influenced by Milankovitch orbital variations of solar energy input. Manabe and Stouffer (1995,1997) demonstrated that events like YD could be simulated if tremendous freshwater flux (1 Sv during 10-yr period or 0.1 Sv during 500-yr period over the latitude belt between 50 and 700 in the North Atlantic Ocean) was prescribed. Here we describe an attempt to explore this phenomenon using the oceanic Global Circulation Model (GCMO) and realistic freshwater input. Our aim is to evaluate could the phenomenon like YD be simulated. The GCMO of INM RUS is a finite-difference technique with a regular grid system which has horizontal spacing of 40 latitude x 50 longitude and 11 vertical sigma-levels. At first the control experiment during a 1,000-year time integration was carried out. Stable-state fields were used as initial conditions for the freshwater experiment. The runoff of St. Lawrence river paleohydrology reconstructed as 0,35 Sv during 4-year period (... 2000) was used to create the salinity anomaly in the two grid points of GCMO near the river mouth. Although the flux was turned off at the end of fourth year, the time integration is performed over a period of 300 years. The reduction of salinity is accompanied by the development of circulation phenomenon (cyclone-anticyclone dipole) on the southeast from the input region. Its intensity is ~5% from strength of surface current. This dipole is long living structure. During 4 years it has been penetrating into seasonal thermocline and it was clearly evidenced during ~200 years after the time when freshwater flux was turned off. The change of thermohaline circulation of the North Atlantic in response to the appearance of fresh water spot was very small, insufficiently to induce just a little temperature anomaly. This is the principal result: the real melt water flux does not create strong (like YD) climate anomaly (but by the way the modelled anomaly is stronger than modern "Grate Salinity Anomaly"). Our result is quite different from mentioned above the conclusion of Manabe and Stouffer (1995,1997), but their successful simulation of strong climate change are explained by the fact that unrealistic freshwater flux was used.

**MC12/07P/B19-005 1545**

**BIOGEOCHEMICAL EVIDENCE OF VEGETATION CHANGES IN THE TROPICAL WETLAND DURING MID-LATE HOLOCENE**

Shafi Mohammad TAREQ<sup>1</sup>, Noriyuki TANAKA<sup>2</sup>, Keiichi OHTA<sup>3</sup> (<sup>1</sup>Division of Earth and Environmental Sciences, Graduate School of Environmental Studies, Nagoya University, Furo-cho, Chikusa-ku, Nagoya 464-8601, Japan, <sup>2</sup>Frontier Research System for Global Change, International Arctic Research Center, University of Alaska, Fairbanks, USA, <sup>3</sup>School of Environmental Science, The University of Shiga Prefecture, 2500 Hassaka-cho, Hikone, Shiga 522-8533, Japan)

Evidence of changing vegetation in the tropical wetland (Rawa Dannau, west Java, Indonesia) over the past 7428 years is illustrated by the ratio of lignin CuO-oxidation products as well as carbon preference index (CPI) and mean carbon number (MCN) of hydrocarbon, together with stable carbon isotope ( $\delta^{13}C$ ) and bulk organic geochemistry. The vertical profile of lignin phenol ratios (S/V and C/V) and lignin phenol vegetation index (LPVI) with calibrated radiocarbon ( $^{14}C$ ) ages showed that there were four major vegetation change events in the Rawa Dannau during mid-late Holocene. Periods of the vegetation change event displayed significant changes in organic carbon flux in the Rawa Dannau wetland, which might reflect dilution by enhanced influx of siliclastic material. The CPI of hydrocarbons (C21-C33) closely corresponded with the LPVI. The MCN calculated from hydrocarbon data (C27-C31) significantly related with other profiles (CPI and LPVI) and the signature of elemental carbon. Pollen data of a few number of pre-selected sections showed that grasses dominated during vegetation-change events. These vegetation changes in tropical area might occur due to forest fire and/or regional climate changes.

**MC12/07P/B19-006 1600**

**RECONSTRUCTION OF HISTORY OF FOREST FIRE RECORDED IN PEAT DEPOSIT IN RAWA DANAU, WEST-JAVA, INDONESIA DURING MID-LATE HOLOCENE**

Hiroyuki TSUJI<sup>1</sup>, Noriyuki TANAKA<sup>1</sup>, Shafi Mohamad TAREQ<sup>2</sup>, Keiichi OHTA<sup>3</sup>, Muhamad Rahman DJUWANSAH<sup>4</sup>, Hisashi NARITA<sup>1</sup> (<sup>1</sup> Graduate School of Environmental Earth Science, Hokkaido University, <sup>2</sup>Hydrospheric Atmospheric Research Center, Nagoya Univ., <sup>3</sup>Research center for Geotechnology, Indonesian Institute of Sciences)

The woody peat core (3.62m length) collected in Rawa Danau, West-Java, Indonesia (Lat. 6°8.978' S Long. 105°58.909' E) was analyzed for elemental carbon (EC) contents, C/N ratios and stable carbon isotope composition in order to reconstruct forest fire history involved in past climate change during mid-late Holocene. The EC contents ranged 0.00 to 0.06% and the six distinct peaks were found in the core. These peaks could be ascribed to frequent and extensive forest fire events. The relatively heavy stable carbon isotope compositions clearly coincided with high EC content. It was striking that the EC content peaks around 164.6-190.4cm depth (3000-3800 yr BP) corresponded to the heaviest  $\delta^{13}C$ . It also agreed with the rapid C/N ratio decreases. Considering the climate change in the other region around 3000-3800 yr BP, there were extensive forest fire events around Rawa Danau, West-Java, Indonesia, which were probably caused by the regional climate system shifts such as distinctive dry season.

**MC12/08A/B19-001 Invited 0930**

**THE CLIMATE OF THE HOLOCENE: A GLACIOLOGICAL PERSPECTIVE**

Georg Paul HOFFMANN<sup>1</sup>, Martin WERNER<sup>2</sup>, Gavin SCHMIDT<sup>3</sup>, Jean JOUZEL<sup>1</sup> (<sup>1</sup>LSCE, <sup>2</sup>MPI for Biogeochemical Cycles, Jena, Germany, <sup>3</sup>Goddard Institute for Space Studies, New York, USA)

There is an increasing number of ice cores documenting climate variability on time scales from a couple of hundred years to glacial/interglacial cycles. Regionally, this important source of information is no longer restricted to polar areas. Many tropical and subtropical sites have been added in the last years providing us with a more detailed picture of climate dynamics. In this contribution I'll give an overview on the existing stable water isotope records from various sites in high and low latitudes. The common variability on a millennial to centennial time scale will be discussed and compared with our information stemming from other types of archives. Furthermore, results from studies with GCMs which were fitted with water isotope diagnostics will be presented. These GCMs were integrated in a time slice mode throughout the Holocene and, on a shorter time scale, over the last century. Analysing these results allowed us to answer 1- how to interpret the water isotope records in term of local temperature and precipitation changes and 2- in what regions the isotopes react particularly sensitive to climate phenomena such as El Nino or the Arctic Oscillation.

**MC12/08A/B19-002 1000**

**HOLOCENE CLIMATE VARIABILITY RECORDED IN WATER STABLE ISOTOPES FROM ANTARCTIC AND GREENLAND ICE CORES**

Valérie MASSON-DELMOTTE<sup>1</sup>, S.J. JOHNSEN<sup>2</sup>, J. JOUZEL<sup>1</sup>, V.I. MORGAN<sup>3</sup>, B. STENNI<sup>4</sup>, J.W.C. WHITE<sup>5</sup>, F. VIMEUX<sup>1</sup> (<sup>1</sup>IPSL/CEA-CNRS LSCE, <sup>2</sup>University of Copenhagen, Denmark, <sup>3</sup>Antarctic CRC, Hobart, Australia, <sup>4</sup>University of Trieste, Italy, <sup>5</sup>University of Colorado, Boulder, USA)

We use water stable isotopes (dD, d18O) measured along several Antarctic and Greenland ice cores to discuss (i) Holocene trends which can be related to local glaciological effects (elevation of the ice sheet) and insolation-related climatic changes; (ii) millennial scale isotopic variability; (iii) high frequency periodicities. For different polar locations, isotopic modelling is used to quantify isotopic fluctuations in terms of site and source temperature changes.

**MC12/08A/B19-003 1020**

**ARGON AND NITROGEN ISOTOPES OF TRAPPED AIR IN GREENLAND ICE CORES AS A PALEOTHERMOMETER: APPLICATION TO ABRUPT CLIMATE CHANGE AT ~8200 YEARS BP**

Takuro KOBASHI, Alexi M. GRACHEV, Jeffrey P. SEVERINGHAUS (Scripps Institution of Oceanography, University of California, San Diego)

Recently the nitrogen and argon isotopic composition of trapped air in ice cores has been developed and utilized as a paleothermometer to investigate the past abrupt climate changes (e.g., Severinghaus et al., Nature, v. 391, 141, 1998). Within the firn layer (snow layers above the air bubble close-off depth), two types of isotopic fractionation occur: "gravitational fractionation" and "thermal fractionation". Thermal fractionation is induced by the temperature difference between the surface and bottom of the firn layer. Owing to the long atmospheric residence time of inert gases (nitrogen and argon), any deviation of the isotopic composition of trapped air from that of present air must be due to these processes. The combined analyses of nitrogen and argon isotopes ( $^{15}N/^{14}N$  and  $^{40}Ar/^{36}Ar$ ) allow us to separate these two processes, and to reconstruct the past abrupt temperature changes. In addition, temperature information from trapped air solves a long-standing problem of ice age - gas age difference, allowing a direct comparison between temperature change and trace gas concentration changes (e.g., CO<sub>2</sub> and CH<sub>4</sub>). We are developing a new method to process air for the simultaneous analysis of nitrogen and argon isotopes using a new mass spectrometer with 8 cups (Finnigan Delta XP). Previous methods required two separate analyses for argon and nitrogen. Therefore, this new method will reduce the time and ice for each analysis. We use copper at ~500 °C to remove oxygen (O<sub>2</sub>), which isobarically interferes with  $^{36}Ar$ , and we obtained a precision of 0.002 per mil for nitrogen, and 0.012 per mil for argon for 18 preliminary measurements of La Jolla air. We plan to apply this method with the experimentally determined constants (Grachev and Severinghaus, Geochim. et Cosmochim. Acta, v. 67, 345, 2003) to an abrupt climate change that happened ~8,200 years before present using the GISP2 ice core from Greenland. This event is especially important since it occurred during the relatively warm climate conditions of the Holocene, which may be a good analogue for possible future abrupt climate change induced by global warming.

**MC12/08A/B19-004 1055**

**CHANGES IN THE SEASONAL CYCLE- IMPLICATIONS FOR PALEOCLIMATOLOGY**

Philip D. JONES, Keith R. BRIFFA, Timothy J. OSBORN (Climatic Research Unit, University of East Anglia, Norwich, NR4 7TJ, UK)

Instrumental temperature averages for the Northern Hemisphere show significant changes in the seasonal cycle since the 1850s. Earlier than this the only proxy climatic source capable of providing independent seasonal reconstructions is historical documentary information. Summer and winter reconstructions from this source are compared for Europe and the Far East (China, Japan and Korea), the only two regions of the world where such evidence potentially exists. All available series indicate that long-term trends in calendar-year average temperatures are dominated by changes in the winter reconstructions. Summer series from documentary sources reveal hardly any century-timescale changes. With much paleoclimatic evidence of past temperatures coming from trees, ice cores and lakes being dominated by summer conditions, millennial-scale trends are potentially being underestimated by summer-responsive proxies.

**MC12/08A/B19-005 1115**

**QUANTIFYING SVALBARD CLIMATE VARIABILITY SINCE 1100 THE PRESENT, LITTLE ICE AGE AND MEDIEVAL WARM PERIOD**

John C. MOORE, Lomonosovfonna Ice Core Group (Arctic Centre, University of Lapland, Rovaniemi, FINLAND)

Ice cores from the relatively low-lying ice caps in Svalbard have not been widely exploited in climatic and environmental studies due to uncertainties about the effect of melt water percolation. However a well-dated ice core with high-resolution chemical and water isotopic

data from Lomonosovfonna show the history of temperature, accumulation, and atmospheric circulation patterns influencing the Svalbard archipelago for the past 900 years. The Little Ice Age (LIA) is well documented in the ice core and the sudden termination of the event around 1920 (associated with a decrease in sea ice extent in the Barents Sea) is the single clearest signal in the ice core chemical record. The  $\delta^{18}O$  data from the ice core suggests that the 20th century was the warmest century during the past 600 years. The earliest part of the core shows a gradual decrease in temperatures as the climate entered the Little Ice Age. The period 1100-1400 is marked by intervals that suggest relatively similar temperatures and conditions as the present period - these indicators include isotopic and chemical species ratios. We discuss several "time windows" for how the climate looked like at Lomonosovfonna during specific periods that are interesting, such as specific warm periods as the present, 1920s, 1930s, 1950s, 1750s and the MWP; and cold periods such as 1960s 1680s, 1780s, 1860s, 1880s. The similarity of the MWP to the 1930s or 1950s and present and the transitions between "climate types" i.e. around 1500 and 1920 are also discussed, as are comparisons with other reconstructions of high latitude climate variations over the past millennium.

**MC12/08A/B19-006 1130**

**A NEW CALIBRATION OF THE 200-YEAR TEMPERATURE SERIES FROM ARMAGH OBSERVATORY, NORTHERN IRELAND**

Christopher John BUTLER, Chloe MORRELL, Ana Maria GARCIA SUAREZ (Armagh Observatory)

Armagh Observatory has maintained three independent temperature series for extended periods of time: (1) a twice daily set of readings from an externally mounted thermometer (1796-1882), (2) a daily series of maximum and minimum temperatures (1844-2003), and (3) a series of wet and dry temperatures measured twice daily from 1833. A careful reassessment and recalibration of the data from this site has recently been completed. The data from Northern Ireland are particularly useful because of their longevity, the lack of any appreciable urban effects and the strong influence of the Atlantic Ocean. We discuss the usefulness of this long temperature series and compare it with similar series from European sites. The importance of such long term data for extending the global instrumental temperature series prior to the mid-19th century and how they may affect our understanding of the causes of global warming is discussed.

**MC12/08A/B19-007 1145**

**A NEW SOURCE OF PROXY DATA FOR DAILY AND MONTHLY CLIMATIC RECONSTRUCTIONS**

Dennis WHEELER, Jose Manuel Suarez DOMINGUEZ (University of Sunderland)

Several thousand logbooks of the British Navy have survived from the period c.1650 to 1850. They contain daily, sometimes hourly, non-instrumental, observations on wind and weather for many of the World's oceans. For waters close to the British Isles, the possible series of data is unbroken from 1685. A recently concluded project has examined the nature of these data and derived a climatology for the most intense phase of the Little Ice Age (LIA) from 1685 to 1700. The data consist of information on wind force, wind direction and general observations on the weather. The latter two categories of data were described in terms consistent with those in use today. The former, however, provided problems of interpretation, and many terms, such as 'gale' had a different meaning in late eighteenth century English. A 'dictionary' was produced using content analysis that allowed archaic terms to be re-expressed in Beaufort Scale equivalents. The abundance of logbooks permitted replicate sampling that confirmed the internal consistency of the records. The vocabulary was found to be limited but common between recorders, opening the way for numerical analysis. The data were of high quality, with a sub-daily scale of temporal resolution not matched by other contemporary sources. The derived daily data were aggregated to produce monthly summaries of wind force, wind direction, gale frequency, snow and rain. While no thermometer records were kept, the logbook entries also included usable information on the extent and intensity of cold periods and days. Correlation and principle component analysis using additional independently provided NAO indices, Central England Temperature (CET) data and contemporary pressure data, confirmed the consistency of the logbook data through their general agreement with the independent series. The data (seventeen variables) were reduced to four principal components, on all of which the logbook data were heavily loaded. Thermal, wind direction, and pressure field components were clearly identified in the structured data set; the former tending to dominate over the latter, but the balance shifting between seasons and months. The overall results provided partial confirmation of existing theories of weather patterns during the LIA, but challenged some other aspects. They added finer, daily, detail and extended the knowledge base to include observations made at sea, where hitherto there has been very little information. It is found that the period in question was one of measurably more marked storm activity, particularly for the summer months, than is currently the case. Furthermore, the derived patterns of wind directions do not wholly support the popular theory that the LIA was a period of notable meridionality. The reconstructed picture reveals meridionality to be notable during the late winter and spring, but only sporadically so at other times of the year. The presence of quantifiable degrees of 'easterliness' was nonetheless strongly associated with the coldest months in the CET series. The procedures are suggested to provide an excellent model on which longer term, detailed studies can be based using derived quantifiable data from an important non-instrumental source that is abundant, but hitherto overlooked.

**MC12/08A/B19-008 1200**

**CLIWOC: A DATABASE FOR THE WORLD'S OCEANS 1750-1850: OVERVIEW AND PRELIMINARY RESULTS**

Ricardo GARCIA-HERRERA<sup>1</sup>, Dennis WHEELER<sup>2</sup>, Gunther KONNEN<sup>3</sup>, Maria PRIETO<sup>4</sup>, Philip D. JONES<sup>5</sup> (<sup>1</sup>Universidad Complutense de Madrid, <sup>2</sup>University of Sunderland, UK, <sup>3</sup>KNMI, The Netherlands, <sup>4</sup>Instituto de Ciencias Humanas y Sociales, <sup>5</sup>Climatic Research Unit, University of East Anglia, Norwich, UK)

From the earliest days of deep sea sailing mariners have kept logbook accounts of their voyages. By 1750 the keeping of logbooks was almost universal amongst the officers of European ships. Although not prepared with this purpose in mind, the logbooks and the detailed observations that they contain are today of great scientific value. One of the factors that a ship's officer needed to take into account in the successful navigation of his vessel was the weather. It required that wind force and wind direction be carefully recorded, the data being then used to determine the drift, or 'leeway', made by the ship. Mariners tended also to keep a careful note of other weather phenomena such as rain, thunder, fog and snow even though they had little direct influence on navigation. Many logbooks failed to survive the rigours of life at sea, but tens of thousands have been preserved to the present day. Some date from as long ago as the seventeenth century, and they become more abundant as time goes by. Most frequent amongst the survivors are the logbooks of vessels in the state service and in particular those of the armed services. These have now been gathered together in a number of important national archives. Those of the UK, France, Spain and the

Netherlands all possess notable collections. The observations in the ship logs of these four countries comprise in the pre-1850 period the bulk of the observations that have been taken over the world oceans. CLIWOC is a project funded by the European Union with partners from Spain, the UK, the Netherlands and Argentina. Its principal objective is to produce a database of daily oceanic weather observations between 1750 and 1850. It will be completed by December 2003. At that time, the CLIWOC database will be ready for integration with the I-COADS world database of meteorological observations 1784-present. This will significantly augment I-COADS in its early period. The CLIWOC database utilises daily observations from logbooks that represent all the World's major oceanic areas, the North and South Atlantic, the Indian and the Pacific Oceans. The original data are being processed and presented using terms that conform to present-day usage and understanding. Information is based on the most frequently recorded elements of wind strength and direction, but data will also be provided on a wider range of commonly recorded phenomena that include rain and snow, thunder, fog and even the incidence of sea ice cover. A meta-database will also allow enquirers to consult the original sources. By December 2002, more than 175,000 observations had already been included in the database, and constitute the dataset at this presentation, which will describe the space coverage reached so far, as well as the first results obtained in the quality control process. Particular attention will be paid to the consistency of the observations from ships of the same and different nationalities and the comparison with present day climatology.

Tuesday, July 8 PM  
Presiding Chair: P. Jones

**MC12/08P/B19-001 Invited 1415**

**THE MEDIEVAL COOL PERIOD AND THE LITTLE WARM AGE IN THE CENTRAL TROPICAL PACIFIC? FOSSIL CORAL CLIMATE RECORDS OF THE LAST MILLENNIUM**

Kim M. COBB<sup>1</sup>, Chris CHARLES<sup>2</sup>, Hai Cheng<sup>3</sup>, R. Lawrence EDWARDS<sup>4</sup> (<sup>1</sup>Dept. of Geological and Planetary Sciences, California Inst. of Technology, <sup>2</sup>Scripps Inst. Of Oceanography, <sup>3</sup>University of Minnesota)

Proxy climate records from around the globe indicate that climate of the last millennium was characterized by substantial low-frequency variability, yet the mechanisms that underlie such variability remain controversial. Progress towards a mechanistic understanding of low-frequency climate change involves reconstructing the global footprint of interannual to centennial climate change over the last millennium. The tropical Pacific is potentially a key player in low-frequency climate change, given the global reach of the El Niño-Southern Oscillation (ENSO). However, sparse proxy data coverage in the tropical Pacific prior to ~1600 A.D. means that the role of this potent climate system in shaping low-frequency variability remains unknown. We present well-dated, monthly-resolved coral records from Palmyra Island (6°N, 162°W) that capture interannual to centennial climate change in the central tropical Pacific (CTP) over the last millennium. The U/Th-dated coral-based oxygen isotopic ( $\delta^{18}O$ ) records, many of which overlap in time, cover 40-150yr-long intervals during the 10<sup>th</sup>, 12<sup>th</sup>, 14<sup>th</sup>-15<sup>th</sup>, 17<sup>th</sup>, and 20<sup>th</sup> centuries. Together they document a wide range of ENSO characteristics - the most frequent, intense ENSO activity occurs in the mid-17<sup>th</sup> century, during the Little Ice Age (LIA), and the least frequent ENSO activity occurs during the 14<sup>th</sup> century. The background climate state in the central tropical Pacific, as reflected in mean coral  $\delta^{18}O$ , remained relatively stable over the last millennium, with two exceptions - relatively cool, dry conditions may have persisted early in the millennium and a trend towards warm, wet conditions began in 1976 A.D. By comparing the Palmyra coral timeseries to existing proxy data from other regions of the globe it is possible to extract valuable information about large-scale patterns of low-frequency climate variability over the last millennium. For example, the Palmyra coral data can be compared to proxy records from the western tropical Pacific to address whether the zonal sea-surface temperature (SST) gradient in the tropical Pacific changed during the LIA. West Pacific corals point to cooler, saltier conditions during the LIA, while the Palmyra corals imply little SST change in the CTP, such that the Pacific's zonal SST gradient may have decreased during the LIA. The MWP presents a greater challenge, because high-resolution proxy records of marine origin are no available for comparison. However, when combined with evidence of cool, dry conditions in the CTP from the Palmyra corals, select proxy records from ENSO-sensitive regions are consistent with a La Niña-like configuration of the Pacific during the MWP. If the Pacific alternated between El Niño- and La Niña-like mean states over the last millennium, then the associated changes in the pattern of large-scale atmospheric circulation would have affected temperature and precipitation patterns around the globe. Of course, this discussion does not address the origin of such low-frequency variability in the tropical Pacific, rather it suggests that the mechanisms that underlie centennial-scale variability likely involve the tropical Pacific.

**MC12/08P/B19-002 1445**

**TOWARD RECONCILING CLIMATE CHANGE RECONSTRUCTIONS FROM BOREHOLE TEMPERATURES AND PROXY DATA: THE ROLE OF SNOW**

Marshall Grant BARTLETT, David S. CHAPMAN, Rob N. HARRIS (University of Utah)

Borehole temperature-depth profiles contain information about surface ground temperatures a region has experienced in the past, and therefore provide complementary information to the more customary surface air temperature record of climate change. Using temperature-depth measurements from boreholes, researchers have been able to extend local, regional, and hemispheric estimates of surface temperature variations by several centuries prior to the onset of instrumental records of air temperature changes (Harris and Chapman [2001], Pollack and Huang [2000]). The borehole method of pre-observational climate reconstruction differs from proxy-based methods (tree ring growth patterns, coral growth, pollen counts, etc.) in two important ways. First, the physics of heat conduction in the earth is better understood than the empirical transfer functions used in proxy methods. Second, the estimated amount of warming the Earth's surface has experienced since the pre-industrial period based on the borehole record is significantly different from estimates based on proxy methods. Borehole reconstructions suggest that this warming has been on the order of 1.1 °C with approximately half of the warming occurring prior to 1850; more traditional proxy methods indicate a warming closer to 0.7 °C with most of the warming taking place in the 20th century (Pollack and Huang [2000], Mann et al [1999]). One of the suggested possibilities for reconciling these two records is that transient snow cover may bias the borehole record by introducing a spurious long-term warming signal into the ground temperature record. We have developed a simple model to investigate this possibility and have applied it on the local scale (Bartlett et al [2002]). We here extend our analysis to the regional scale by modeling snow events over the past century in the United States based on the snow and air temperature data available from the United States Historical Climatology Network Daily Temperature, Precipitation, and Snow Data for 1871-1997 (NOAA-NCDC NDP-070). The snow model is used to predict transient warming or cooling of the surface ground temperature due to changes in the onset, duration, and depth of snow events over the years of record in the dataset. Results illustrate that while there are some local trends in changes of onset time and duration in the snow record, these are insufficient to reconcile the



borehole and proxy reconstructions of climate change.

**MC12/08P/B19-003 1500**  
**PATTERNS OF NORTHERN EMISPHERE MID-LATITUDE TEMPERATURE VARIABILITY IN A 500-YEAR CLIMATE SIMULATION WITH VARIABLE RADIATIVE FORCING**

Piero LIONELLO<sup>1</sup>, Simona DE ZOLT<sup>2</sup>, Eduardo ZORITA<sup>3</sup> (<sup>1</sup>univ. of Lecce (I), <sup>2</sup>univ. of Padua (I), <sup>3</sup>GKSS Forschung Zentrum (D))

This study is based on a 500-year long simulation carried out with an AOGCM which computes the climate evolution from the 15th to the end of the 20th century. The simulation includes a VRF (Variable Radiative Forcing) which accounts for variations of the solar activity, volcanic eruptions and recent increase of GHG (Green House Gases) concentration. The results are compared with a 1000-year long CTR (ConTRol) simulation which is based on a constant radiative forcing, corresponding to the 1990 level. The model, called ECHO-G model, consists of the globalatmospheric model ECHAM4, at T30 resolution, and of the ocean circulation model HOPE-G, at 2.8 degs resolution. A clear (seasonal) signature of the radiative forcing variability on the temperature distribution is identified from the analysis of the fields associated with extreme radiative forcing values. The effect is present, though smaller, also on the sea level pressure fields. The dynamics behind these temperature and sea level pressure patterns are described and their importance for the temperature of the mid-latitudes in the Northern hemisphere is shown.

**MC12/08P/B19-004 1515**  
**CLIMATE CHANGES DURING THE PAST MILLENNIUM**

Michael E. MANN<sup>1</sup>, Scott RUTHERFORD<sup>1</sup>, Gavin A. SCHMIDT<sup>2</sup>, Drew T. SHINDELL<sup>3</sup> (<sup>1</sup>Department of Environmental Sciences, <sup>2</sup>Goddard Institute for Space Studies and Columbia University)

We will review recent progress in both the empirical reconstruction and modeling of climate changes in past centuries. Recent empirical reconstructions of Northern Hemisphere mean temperature changes over the past several centuries to millennium will be reviewed and compared, with an emphasis on the sensitivity of the reconstructions to the actual "proxy" data used as predictors, the statistical reconstruction methodology employed, and the seasonality, and spatial domain of emphasis in the reconstruction. The influence of these factors will be discussed in the context of the seasonally and spatially-specific nature of the response to known external climate forcings such as solar irradiance and explosive volcanism as revealed through recent climate modeling experiments. Implications for the scale and magnitude of climate anomalies associated with the so-called "Little Ice Age" and "Medieval Warm Period" will be discussed.

**MC12/08P/B19-005 1535**  
**A RECONSTRUCTION OF THE GLOBAL TEMPERATURE OVER THE LAST 10 THOUSAND YEARS**

Jorge Sesma SANCHEZ (Hidrometeorologia, Inst.Mex.Tecn Agua)

In order to provide a long-term perspective of climate, we need to be focussed on its evolution in the last thousands of years. Such a perspective encompasses the period before large-scale contamination of the global atmosphere and global-scale changes in land-surface conditions. By studying past climate variability, we can establish how the climate system varied under "natural" conditions, before human effects became significant on a global scale. There is considerable uncertainty about the future warming which may occur as a result of human activities, and we have to consider that it would be superimposed on a background of natural climatic variations. Although the climate of the past millennia, has been reconstructed by the integration of information taken from different sources, there are several caveats about these reconstructions. This paper will describe the techniques and data for an alternative reconstruction of the global climate over this period. The main sources of information for this reconstruction are instrumental global temperature records over the last 13 or 15 decades. Complementary information is taken from historical, biological and geophysical sources (archives, tree rings, ice acidity, sea levels, glacier extensions, isotopes densities, etc.). The reconstruction method is based on a linear regression done with smoothed proxy records in several stages of calibration. To estimate the parameters in each stage, a multiple linear regression is performed using the least squares method. This regression is assumed valid for the entire interval where the record is available. The calibration sequence is given by the record length. The shortest proxy record is first calibrated. The calibration process continues until the longest natural record has been calibrated. The proposed method also permits us to evaluate a range of the reconstructed values in each stage. The results obtained from two independent reconstructions, show an interesting, reliable and objective natural climate variability. The Medieval Climate Optimum, the Little Ice Age, the Industrial Period, and other interesting periods are associated with mean, minimum and maximum values of global temperatures. However, when these results are compared with previous results, great differences arise. Therefore, this study concludes with a discussion of these differences and the reliability of the available global temperature records both instrumental and reconstructed.

**MC12/08P/B19-006 1610**  
**TOWARDS AN ABSOLUTE CHRONOLOGY FOR THE MARINE ENVIRONMENT: THE DEVELOPMENT OF A 1000 YEAR RECORD FROM ARCTICA ISLANDICA**

Graham T.W. FORSYTHE<sup>1</sup>, James SCOURSE<sup>1</sup>, Ian HARRIS<sup>2</sup>, Chris A. RICHARDSON<sup>1</sup>, Phil JONES<sup>3</sup>, Keith BRIFFA<sup>4</sup>, Jan HEINEMEIER<sup>5</sup> (<sup>1</sup>School Of Ocean Sciences, University of Wales - Bangor UK, <sup>2</sup>Climate Research Unit, University of East Anglia UK, <sup>3</sup>AMS Laboratory, University of Aarhus, Denmark)

Time-series of environmental change using geochemical (stable isotope, trace element) proxies from annually-banded marine sclerochronological (coral, mollusc) records have hitherto been constrained to the life span of live-collected individuals or to floating chronologies of approximate age constrained by independent dating methods, notably radiocarbon or uranium-series dating. The construction of a long, absolute, time-series beyond the individual life-span demands statistically significant cross-matching of time-series from different specimens or individuals. We present the first cross-matched marine sclerochronological record for NW Europe based on annual growth bands of the ocean quahog *Arctica islandica* (Bivalvia, Mollusca). Using live- and dead-collected specimens from the Fladen Ground, North Sea, long shell growth records of over 100 years have been cross-matched between individuals demonstrating a common external environmental signal driving the growth curve of individual shells within a community. We have identified some very long-lived individuals with over 250 annual growth bands and one with 268; this is the longest-lived mollusc known to science. The cross-matching of growth-series is critical since this is the only statistically reliable way to identify missing bands or multiple bands within a single year. We have successfully cross-matched dead series (with inter-shell correlation

coefficients of up to 0.68); AMS radiocarbon dates from the umbo and tip of these series support the cross-matched chronology at the one standard deviation level. These dates indicate that this cross-matched chronology covers the period between AD 1128 (range AD 1066-1182) and AD 1392 (range AD 1335-1411) within the Medieval Warm Period. We have dated shell specimens which potentially link this dated floating time-series with the cross-matched chronology of 211 years (AD 2002 to AD 1791) from live-collected specimens, and anticipate the construction of a 1000-year absolute cross-matched chronology for this area of the North Sea soon. This will enable radiocarbon dating of marine material of known absolute age to derive a continuous curve of marine reservoir change for this location through time. We also have specimens from this area which have been dated to various phases of the Holocene and into the Late-glacial, raising the probability that we will be able to construct a 10,000-year absolute chronology in the future. The successful cross-matching of *Arctica islandica* is a breakthrough which will transform our understanding of both spatial and temporal radiocarbon reservoir changes in coastal and shelf seas and which will provide an absolute chronological template for geochemical proxies of marine environmental change.

**MC12/08P/B19-007 1630**  
**YEAR-BY-YEAR RECONSTRUCTION OF CLIMATE IN THE CENTRAL KOLA PENINSULA (NORTH-WESTERN RUSSIA) SINCE AD 862 BASED ON DENDROLOGICAL AND ISOTOPE DATA**

Yury M. KONONOV<sup>1</sup>, Tatjana BOETTGER<sup>2</sup>, Michael FRIEDRICH<sup>3</sup>, Konstantin V. KREMENETSKY<sup>4</sup> (<sup>1</sup>Institute of Geography, Russian Academy of Sciences, <sup>2</sup>Department of Isotope Hydrology, UFZ Centre for Environmental Research Leipzig-Halle, <sup>3</sup>Institute of Botany, University of Hohenheim)

More than 300 samples of living tree cores and subfossil slices of *Pinus sylvestris* L. have been taken in the course of joint Russian-German field investigations in the Khibiny low mountains in the central part of the Kola Peninsula (ca. 67-68°N, 33-34°E). The collected samples permitted to compose a continuous chronological series 1139 years long, from AD 2000 to 862. At present, it is the longest chronological sequence in the region. A comparison between annual ring width and instrumental climatic records over period of 1923 to 2000 revealed a high correlation between index of annual wood growth and summer air temperature. Besides, a 10 samples of cores taken from living trees were studied by annually isotope analysis ( $\delta^{13}C$  and  $\delta^{18}O$ ) in their late wood cellulose. Analysis of those isotopes is most promising with view to climatic reconstructions. At present a significant relationship has been established between proportion of  $^{13}C$  isotope and mean summer temperature. That formed the basis for reconstructions of main warming and cooling periods over the period under consideration. Altogether there were 12 considerable cooling, each of about 10 to 20 years long. As for warmings, they were less in number (7), but longer (about 40 to 90 years long). Very strong coolings occurred twice. First one was from the beginning of the studied interval to AD 884. In all probability, it was termination of the previous, still colder period, when weather prevented any tree growth. The second cooling was in 1641 to 1654; there is a good reason for believing that it was local manifestation of the Little Ice Age.

**MC17-Posters Thursday, July 10**

**PROPAGATION MECHANISMS FOR THE MADDEN-JULIAN OSCILLATION (MJO) (ICDM)**  
 Location: Site D

Thursday, July 10 AM

**MC17/10A/D-001 Poster 0830-182**

**INTRASEASONAL OSCILLATIONS IN LENGTH OF THE DAY AND POLAR MOTION VARIABILITY. ASSOCIATION WITH CLIMATIC AND SOLAR ACTIVITY INDICES**

Daniel GAMBIS, Abarca del RIO (Observatoire de Paris)

We re-investigate Length of day and Polar motion variations and their excitation at intraseasonal time scales (Madden and Julian Oscillation and other modes at these time scales). Taking advantage of long time series provided by International Earth Rotation Service, we search for an association at these scales with tropical and extratropical indices for a better understanding of its origin. We mainly investigate its modulation in phase and amplitude and their association with tropical and extratropical indices. We also search for statistical links at these time scales with other indices like solar activity which was shown to be linked to the phenomena. We also investigate a possible triggering effect of the MJO upon the large scale ENSO.

**MC17/10A/D-002 Poster 0830-183**

**INTRASEASONAL OSCILLATIONS IN THE SACZ: OBSERVATIONS AND SIMULATION WITH A BAROCLINIC MODEL**

Simone Erotildes FERRAZ<sup>1</sup>, Tercio AMBRIZZI<sup>1</sup>, Alice Marlene GRIMM<sup>2</sup> (<sup>1</sup>Department of Atmospheric Sciences, University of Sao Paulo, <sup>2</sup>Department of Physics, Federal University of Parana)

The austral summer (DJF) is the rainy season over most of Brazil and South America (Argentina, Paraguay and Uruguay). The knowledge of the intraseasonal oscillations of the summer precipitation with alternating dry and wet phases is important for some applications and can indicate procedures that allow its prognostic. Many studies have shown that the summer precipitation exhibits a large intraseasonal variability, indicated by the analysis of the outgoing longwave radiation (OLR) (e.g., Paegle and Mo (1997); Liebmann et al.(1999); and Paegle et al. (2000)). In general, these works emphasize that the intraseasonal variations in the Madden Julian Oscillation (MJO) time scales, over the region of the South Atlantic Convergence Zone (SACZ), exhibit a dipole pattern where enhanced precipitation over the SACZ is accompanied by decreased rainfall in southern South America. This study reports observational and numerical results of the signal of the MJO in South America precipitation. The baroclinic model used in the present study is based on Hoskins and Simmons (1975), and has been used in various studies of large scale circulation. The model was integrated for 15 days and perturbed with a heating source in the west Pacific (120°E - 10°S). As initial conditions in the baroclinic model are used the meridional and zonal wind, air temperature and geopotential of December 1981. The basic data come from the NCEP-NCAR reanalysis. The results are characteristic of a propagation in wave form, with maximum signal in South America (between 5°S and 15°S) after 12 days. Lag correlations between OLR (in the same region of the forcing heating) and global meridional wind at 250 hPa confirm the numerical results.

**MC17 Thursday, July 10 - Friday, July 11**

**PROPAGATION MECHANISMS FOR THE MADDEN-JULIAN OSCILLATION (MJO) (ICDM)**

Location: Site B, Room 23

**Thursday, July 10 PM**

Presiding Chairs: A. Matthews, T. Nakazawa

**MC17/10P/B23-001 Invited 1400**

**PROPAGATION OF MJO IN ASSOCIATION WITH MOISTURE SIGNALS OVER THE WESTERN HEMISPHERE AND ITS RECURRENCE MECHANISM DURING THE BOREAL WINTER**

Yukari N. TAKAYABU, Kazuyoshi KIKUCHI (Center for Climate System Research, University of Tokyo)

Since the discovery of the Madden Julian Oscillation (Madden and Julian, 1971,72), its slow propagation (~5m/s) coupled with convection in the eastern hemisphere and a fast propagation (~20m/s) in the western hemisphere have been a focus of numerous numbers of studies. Various efforts have been put to explain its propagation properties either by modifying the Kelvin wave with moist processes, or by considering effects of surface flux. However, all had some kinds of shortcomings, so could not complete the theory. Recent studies emphasize the modification of atmospheric stability through moisture processes (e.g. Kamball-Cook and Weare, 2001), as well as the air-sea interactions (e.g. Zhang 1996) in the convective phase. On the other hand, a faster Kelvin wave mode (30-40m/s) is rediscovered by Millif and Madden (1996). Matthews (2000) suggested its role in the dry phase to connect the disturbance to the next cycle. However, the mechanism of the recurrence is not clear yet. In this study, we reexamined the propagation features of MJO, especially over the western hemisphere where the atmospheric disturbance is decoupled with active convection and may be triggering the next cycle of MJO. We focused our analysis on the moisture signal, utilizing the total precipitable water data retrieved from SSM/I by Wentz algorithm. In total precipitable water data, we could find a moisture signal propagating eastward in association with MJO not only over the eastern hemisphere but also over the western hemisphere, and circulate all the way around the equator. Over the western hemisphere, the moisture signal was accompanying the fast free Kelvin wave mode (30-40m/s). It was shown that moisture build up is associated with the surface convergence in phase with the lower tropospheric easterly wind anomalies of the fast Kelvin wave. Elevated topographies in South America and in Africa prevent this fast mode from propagating smoothly in the lower troposphere but stop it for a while, until at last the surface signal catches up with the preceding upper tropospheric signal. Since the front of the Kelvin wave disturbance consists of surface easterly wind anomaly, it converges the near-surface moisture effectively to the east of the continent as soon as the surface signal overcomes the topography. Moisture accumulation is favored by active convection, which restarts emanating the equatorial waves. This obstruction-restart propagation of the fast mode results in the propagation speed of ~20m/s in average over the western hemisphere. After all, over the western Indian Ocean, as the Kelvin wave overcome the African topography, new convective activity connects to the next cycle of the MJO with ubiquitous supplies of moisture over the warm pool region eastward. Some results from analyses of GMS Tbb and TRMM satellite data will also be presented.

**MC17/10P/B23-002 1430**

**PROPAGATION AND THE VERTICAL STRUCTURE OF THE MADDEN-JULIAN OSCILLATION**

Kenneth Robert SPERBER<sup>1</sup>, Julia Marie SLINGO<sup>2</sup> (<sup>1</sup>Lawrence Livermore National Laboratory, PCMDI, <sup>2</sup>NERC Centre for Global Atmospheric Modelling, University of Reading)

The Madden-Julian Oscillation (MJO) controls tropical variability on timescales of 30-70 days. During the boreal winter/spring it is manifested as an eastward propagating disturbance, with a strong convective signature over the eastern hemisphere. We describe the space-time structure of the MJO using the National Centers for Environmental Prediction/National Center for Atmospheric Research Reanalysis, Advanced Very High Resolution Radiometer Outgoing Longwave Radiation, observed sea surface temperature, and the Climate Prediction Center Merged Analysis of Precipitation. Empirical orthogonal function analysis is used to identify the convective signature of the MJO, and regression is used to identify key relationships with the convection. Compared to analyzing contiguous years of data, the selection of years of strong MJO activity results in a more robust lead/lag structure and an increase in explained variance. The MJO exhibits a rich vertical structure, with low-level moisture convergence being well defined when the convective anomalies are strong. The westward vertical tilt is most apparent over the western Pacific. Over the Indian Ocean the system is more vertically stacked, principally due to the strong subsidence of the inactive phase of the MJO, which lies to the east of the convection. As the Kelvin wave decouples from the convection near the dateline, a sea-level low-pressure surge, previously discussed in Matthews (2000), transits the eastern Pacific and Atlantic Oceans. Here we link the zonal wind stress and low-level divergence to the pressure surge. The gradient gives rise to westerlies that propagate rapidly to the east. The pressure surge may play an important role in the development of the MJO convection in the western Indian Ocean, which occurs in an easterly basic state, and conditions not consistent with the low-level moisture convergence paradigm.

**MC17/10P/B23-003 1445**

**THE DEVELOPMENT OF ORGANIZED CONVECTION ASSOCIATED WITH THE MADDEN-JULIAN OSCILLATION (MJO) DURING TOGA COARE**

Kazuyoshi KIKUCHI, Yukari N. TAKAYABU (Center for Climate System Research, University of Tokyo)

To understand the eastward migration mechanism of the Madden-Julian Oscillation (MJO), the development of organized deep convection associated with an MJO during Tropical Ocean Global Atmosphere (TOGA) Coupled Ocean-Atmosphere Response Experiment (COARE) intensive observation period (IOP) was studied in details. We focused on an event in January to February, 1993, which showed a prominent eastward propagation. Using GMS IR histogram data, a composite life cycle of the organized deep convection associated with the MJO is constructed and categorized to stages. Some upper air stations over the Maritime Continent were located along the path of the organized convection, and their soundings are also utilized for the composite. Five convective stages are subjectively identified: 1) suppressed stage with no apparent large scale forcing and scarcely any cloud activity observed, 2) shallow convection stage where most clouds populated below the melting level with a duration time of 2-3 days, 3) developing stage with penetrating convective clouds (4-8 days), 4) mature stage where most clouds are concentrated in the upper tropospheric level of

about 240 K or less (4-6 days), and 5) decaying stage that most clouds exist from 240 K to 290 K level (5-7 days). Through shallow convection stage to developing stage, there exists boundary layer convergence associated with easterly anomalies in the lower troposphere. In the shallow convection stage, moist regions are mostly confined below ~700 hPa, in association with a weak stable layer around 700 hPa. In the developing stage, the moist layer starts to penetrate above the melting level. In the transition from the shallow convection stage to the developing stage, abrupt decrease of the convective available potential energy (CAPE) is observed, ensuring the existence of penetrating convections in the latter stage, and leaving the atmosphere almost neutral for mature stage. Mature stage can be divided into two sub-stages. In the former sub-stage, about 2-3 days in the beginning, the area is covered with various types of high clouds. Apparent heat source (Q1) in the mid-troposphere attains maximum at this substage, suggesting that convective activity is the strongest, so that it is the convective center of this MJO. Lower-level zonal wind changed to westerly at the beginning of this substage, and boundary layer convergence starts to decrease. In the latter sub-stage, the following 2-3 days, histogram shows high concentration of very cold cloud of about 220 K and vertically integrated Q1 changes signs to negative values. It suggests that the area is covered with anvil shields and the convective center moved away. These results suggest the crucial roles of clouds in moistening the atmosphere, besides a large-scale boundary convergence. Therefore, efficiencies of moisture convergence and modification of atmospheric stratification by clouds may control the propagation speed of MJO.

**MC17/10P/B23-004 1500**

**SURFACE CONVERGENCE AND THE MADDEN JULIAN OSCILLATION: CROSS-SPECTRAL CONFIDENCE INTERVALS FROM A PROBABILITY DISTRIBUTION FOR THE SURFACE WINDS**

Ralph F. MILLIFF<sup>1</sup>, Timothy J. HOAR<sup>2</sup>, Christopher K. WIKLE<sup>3</sup>, Roland A. MADDEN<sup>2</sup> (<sup>1</sup>Colorado Research Associates Division, NWR, Boulder, CO, USA, <sup>2</sup>National Center for Atmospheric Research, Boulder, CO, USA, <sup>3</sup>Department of Statistics, University of Missouri, Columbia, MO, USA)

Noise inherent in high-resolution observations of the surface wind field is often amplified in calculations of surface convergence; i.e. the spatial derivative of an already noisy process. Nonetheless, we are interested in investigating lead-lag relations between surface convergence and other variables of the Madden Julian Oscillation (MJO) propagation (e.g. SST, OLR anomaly, etc.). Traditional methods to extract reliable convergence signals from the noisy background rely upon composites of several MJO events. The MJO composites are often based on subjective criteria to align similar phases of the MJO in the presence of the different background states for each event in the composite (e.g. season, ENSO cycle, large-scale flow and SST distributions, etc.). In this paper we composite convergence field estimates derived from several realizations of the surface wind field for the same MJO event in the Indian and Western Pacific Ocean. The realizations derive from a Bayesian Hierarchical Model that blends QuikSCAT scatterometer wind retrievals with coincident surface wind analyses from the NCEP FNL model. Surface wind realizations in the posterior distribution from this model are consistent with high-resolution variability in the scatterometer winds (likelihood), as well as with the propagating normal modes of the equatorial beta-plane (prior). Cross-spectral confidence intervals (e.g. for coherence squared and phase as functions of frequency) are reduced by averaging over several surface convergence realizations.

**MC17/10P/B23-005 1515**

**THE MJO AND MOISTURE SENSITIVITY OF CONVECTION**

David J. RAYMOND (Physics Department, New Mexico Tech)

Cumulus parameterizations in large-scale models lead to an unstable mode when the precipitation produced by convection is sensitive in a realistic way to the saturation deficit of the low to middle troposphere. This instability, in conjunction with the dynamics of near-equatorial convection, leads to a large-scale disturbance that looks very much like the Madden-Julian oscillation (MJO; Raymond, D. J., 2001: A new model of the Madden-Julian oscillation. *J. Atmos. Sci.*, 58, 2807-2819). Ordinary surface moisture fluxes over tropical oceans, i. e., outside of tropical storms, take 1-5 days or more to moisten an initially dry atmosphere. If deep convective precipitation is insensitive to the moisture content of the atmosphere, this in turn leads to an instability mechanism if convection itself causes moistening -- a process which has been shown to occur under certain circumstances. Excess convection caused by a moisture anomaly can thus cause further moistening of the atmosphere, which in turn leads to more convection. Radiative feedbacks can enhance this instability, at least in models. Unlike more dynamically generated instability modes, disturbances operating via the above moisture instability are likely to propagate slowly, if at all, relative to the low-level winds. Sobel and Horinouchi suggest that this mechanism is responsible for tropical depression-like phenomena. Sustained deep convection near the equator tends to produce lower tropospheric, counter-rotating, cyclonic gyres on opposite sides of the equator. Air swept around these gyres into the equatorial regions comes from the subtropics, and is therefore likely to be dry. This air begins to moisten as a result of strong equatorial surface fluxes resulting from the strong, gyre-related equatorial westerlies and the warm equatorial sea surface temperatures. However, moistening is slow enough that this air mass can only support deep convection at the exit region of the equatorial westerly jet according to the model of Raymond. This is to the east of the previous convection responsible for creating the existing gyre system, so the whole gyre pattern shifts to the east. According to Raymond's results, the resulting eastward propagation is of order 5 m/s, which is typical of the rate of eastward propagation of the MJO seen in the western Pacific. Furthermore, the moistening time of the atmosphere helps set the characteristic length scale of the active part of the MJO of many thousands of kilometers. Thus, the length scale, propagation speed, and structure are explained by this model.

**MC17/10P/B23-006 Invited 1600**

**SEASONALLY-INDEPENDENT EASTWARD PROPAGATION OF THE MJO**

Harry HENDON, Matthew WHEELER (BMRC)

Traditionally, the MJO is defined as a convectively coupled baroclinic disturbance that propagates eastward along the equator. With this definition, the MJO is most prominent during northern summer. During northern summer, the dominant intraseasonal variability exhibits poleward propagation in the Asian monsoon, while eastward propagation is less apparent along the equator. Because of these dramatic seasonal differences, some researchers reserve the name MJO for the southern summer phenomena and treat the northern summer variability as another type of "intraseasonal oscillation", governed by different dynamics. The MJO is thought to result from coupling of equatorial waves modes with convection, while interactions with land and ocean are thought to govern the poleward propagating phenomena in northern summer. By discriminating to eastward propagating activity along the equator, we show that the dominant intraseasonal variability in both northern and southern summer possesses similar equatorial structure and eastward propagation,

despite dramatically different off-equatorial behavior. Furthermore, by removing that part of the wind and convective variance that is coherent with the equatorial eastward propagating component, we show that the remaining northern summer intraseasonal variability occurs at high frequency (periods less than 30 days) and on small spatial-scales. Nonetheless, poleward propagation is still evident, suggesting that mechanisms of poleward propagation are independent from that of eastward propagation. We further demonstrate that the MJO can be efficiently identified using an aseasonally-independent index that discriminates to equatorial eastward propagation.

**MC17/10P/B23-007 1630**  
**PROPAGATION OF INTRASEASONAL CONVECTIVE PERTURBATION OVER THE INDIAN OCEAN**

Jean Philippe DUVEL, Remy ROCA (Laboratoire de Meteorologie Dynamique, Paris, France)

The intraseasonal variability of the convection over the Indo-Pacific region is a highly intermittent phenomenon. The propagation of these intraseasonal perturbations presents very different patterns depending on season but also from one event to another for a given season. The variability of these propagation characteristics from 1975 to present is studied using a Local Mode Analysis. It appears that the propagation characteristics during the northern hemisphere winter are much more reproducible over the Indian Ocean compared to the Pacific Ocean. The mechanism of the propagation of the perturbation over the Indian Ocean is further analysed in term of interaction between the convective perturbation, the large-scale dynamical perturbation and the SST. For a case study in January 1999, we also analyse the different convective systems embedded in the intraseasonal perturbation and the effect of these systems on the surface fluxes.

**MC17/10P/B23-008 1645**  
**THE SECOND ONSET OF INDIAN SUMMER MONSOON: A DIAGNOSTIC STUDY**

Hanza VARIKODEN, Babu C. A., Joseph P. V. (Dept. of Atmospheric Sciences, Cochin University of Science And Technology)

Monsoon onset over Kerala marks the beginning of a large convective heat source on the ITCZ in the northern hemisphere tropics extending from the Arabian Sea to the West Pacific Ocean that lasts for hundred days. Accompanying it is a strong inter-hemispheric low level jet stream with peak wind speed at about 850 hPa level that transports moisture to maintain this heat source. In this paper, we have studied the surge of monsoon that occurs about 30 - 52 days after the monsoon onset that we call the "second onset". It has several characteristics different from the monsoon onset although the second onset is also associated with a convective cloud band close to the equator. Analysing 20 years (1979 - 1998) of data it is found that the mean and standard deviation of the date of the second onset is 13 July and 8 days respectively. This equatorial cloud band moves northwards faster than at onset and merges with the monsoon trough convection. The low level jet stream as at onset time is directed south-eastward from central Arabian Sea and it passes south of India to the Western Pacific, but it extends much more into the Pacific Ocean. The Arabian Sea heat source is weaker than at onset. Part of the cause for the weakening of the Arabian Sea heat source is the rapid cooling of the Arabian Sea SST after monsoon onset. The conditions in atmosphere and oceans at the time of the second onset are studied. At the second onset, the Arabian Sea branch of monsoon, its cross equatorial flow off the East African coast and the easterly trades south of the Arabian sea at 850 hPa are stronger than at the time of onset by about 15 m/s, 5 m/s and 8 m/s respectively. There is not much change over the Bay of Bengal in the wind flow. SST has cooled from onset to second onset through about 3°C in the western Arabian Sea to 1°C in the Bay of Bengal in the latitude band 10°N - 20°N. Equatorial Indian Ocean has cooled through less than 0.5°C but a band of cold water is seen between latitudes 5°N and 10°N and longitudes 70°E and 90°E due to the oceanic upwelling around the southern peninsula India and Sri Lanka and the spreading eastwards of this cold water. Convection (OLR) is apparently affected by the ocean cooling. There is a tongue of reduced convection in the latitude band equator to about 15°N in the Arabian Sea and the Bay of Bengal at second onset compared to the monsoon onset. However there is increased convection from the equator to 10°S latitude, which is the initial location of the second onset cloud band. Pre Monsoon Rain Peak, Monsoon Onset and the Second Onset are distinct events in the intra-seasonal oscillation of monsoon where east-west oriented cloud and wind anomalies are found to move northwards from the equatorial region at intervals of 30 - 50 days.

**MC17/10P/B23-009 1700**  
**NORTHWARD DEVELOPMENT AND PROPAGATION OF TROPICAL AND SUBTROPICAL 30-60 DAY OSCILLATION OVER THE WESTERN PACIFIC**

Chih-Hua TSOU, Pang-Chi HSU (Department of Earth Sciences, National Taiwan Normal University)

This study attempts to investigate the relative role of adiabatic (vorticity, thermal, and static stability advection) and diabatic heating on the development and propagation of 30-60 day oscillation over the Western Pacific by using a three-dimensional streamfunction tendency equation. The results showed that the northward development and propagation of a 30-60 day wave train in the region from the equatorial Western Pacific to East Asia was primarily contributed by the effect of diabatic heating and vorticity advection. They caused cyclonic vorticity ahead (northwestward) of the 30-60 day precipitation and cyclonic circulation, and anticyclonic vorticity behind (southeastward) the 30-60 day precipitation where the subsidence and anticyclonic circulation appeared. Their combined contribution enhanced the cyclonic vorticity ahead of the precipitation and led the cyclonic circulation and precipitation to develop and propagate northwestward. As the precipitation reached maximum intensity over the South China Sea/Western Pacific, the static stability effect associated with the adiabatic cooling and cooling of SST associated with the cloud-radiation effect would inhibit the development of the cyclonic circulation. The cyclonic circulation and precipitation weakened as they reached maximum intensity over the South China Sea/Western Pacific. The land-atmosphere interaction further decreases the intensity of diabatic heating by cutting off the moisture supply from the ocean.

**MC17/10P/B23-010 1715**  
**CONTRASTING CHARACTERISTICS BETWEEN THE NORTHWARD AND EASTWARD PROPAGATION OF THE INTRASEASONAL OSCILLATION DURING THE BOREAL SUMMER**

Huang-Hsiung HSU, Chun-Hsiung WENG, Cheng-Han WU (Department of Atmospheric Sciences, National Taiwan University)

This study investigates the characteristics of the evolution and structure of the eastward- and northward-propagating ISO in the Indian Ocean and the western Pacific during the boreal summer. Along the equator, the near-surface moisture convergence located to the east of

the deep convection region appears to result in the eastward propagation of the ISO, consistent with the frictional Wave-CISK mechanism proposed in previous studies. The eastward propagation is characterized by the sequentially downstream development of deep convection occurring mainly in certain regions such as 60°E, 95°E, 120°E, 145°E, and the dateline. While the northward propagation of deep convection can be attributed to the low-level moisture convergence located to the north, this convergence is not confined in the boundary layer as suggested in previous studies. Instead, it is a deep structure extending from surface to the middle troposphere. Near-surface convergence appears only after the systems approach the land mass in the north. It is suggested that both the deep convergence in the lower free atmosphere and in the boundary layer contribute to the northward propagation. While the near-surface convergence can be attributed to the frictional convergence embedded in Rossby wave, the lifting effect of the sloping terrain and the stronger surface frictional effect over the land in South Asia may also contribute to induce the convergence leading the deep convection. The northward propagation occurs sequentially from west to east in the following order: the Arabian Sea, the Bay of Bengal, and the South China Sea. A mechanism is proposed to explain this downstream occurrence of northward propagation. It is also found that surface sensible heating may also contribute to the northward propagation, especially in the Arabian Sea, by making the lower troposphere less stable. Latent heat flux is released to the atmosphere in the region located to the southwest of the deep convection and does not directly contribute to the destabilization of the lower troposphere ahead of the deep convection. In contrast, during the eastward propagation the surface heating does not seem to precondition the lower troposphere to the east of the deep convection. Frictional convergence is seemingly the dominant factor in the eastward propagation.

**MC17/10P/B23-011 1730**  
**A STUDY ON THE ANNUAL CYCLE OF THE TROPICAL INTRASEASONAL OSCILLATION**

Min DONG, Chidong ZHANG (Department of Meteorology and physical oceanography, University of Miami)

Using the 20 year NCEP data and CCM3 (with MCRAS convection scheme) the annual cycle of the tropical intraseasonal oscillation (TIO) is studied. It is found that: 1. From the spectral and wavelets analysis on the NCEP data it is found that there are obvious annual cycle in the tropical intraseasonal variability. In winter and early spring the power of TIO has its maximum. After that the power decreases and gets its minimum in summer. From the summer to winter the TIO power gets stronger again and finishes an annual cycle. 2. The TIO also exhibit a unique spatial distribution characteristics. Throughout whole year the TIO are active in the region from 60E through 140W, but in winter the most active TIO activities are in the south hemisphere while in summer it moves to the north hemisphere and it shift back to south hemisphere again in winter. 3. The CCM3 with MCRAS convection scheme can pretty well simulate the tropical intraseasonal variation though there are still some weakness in the ability to simulate this event. The Model can capture the main spectral characteristics and also can give an annual cycle of the tropical intraseasonal oscillation. But the simulated TIO signal is weaker than the observation and the phase of the annual cycle is a little bit earlier than the observation. 4. The simulated TIO is sensitive to the SST forcing and also to the monsoon circulation which is closely linked to annual cycle of the radiation change. 5. The model experiment shows the higher SST tends to produce more stronger TIO signal. The experiment also shows there are some linkage between the TIO annual cycle and the monsoon circulation.

Friday, July 11 AM  
 Presiding Chair: Y. Takayabu

**MC17/11A/B23-001 Invited 0830**  
**PROPAGATION MECHANISMS OF THE INTRASEASONAL OSCILLATION**

Bin WANG, Xiuhua FU, Kemball COOK (Department of Meteorology and International Pacific Research Center, University of Hawaii)

The physical processes that determine the eastward propagation of the Madden-Julian Oscillation are discussed. These processes include the interaction between precipitation heating and various vertical modes of equatorial waves, the coupling between moist Rossby and Kelvin waves, wave dispersion of equatorial wave packet induced by boundary layer friction, and atmosphere-ocean interaction. The boreal summer northward propagation in the Indian Ocean sector and the northward propagations of intraseasonal disturbance are depicted using finite domain wavenumber-frequency spectral analyses. The mechanisms of the northward and off-equatorial westward propagation during boreal summer are discussed. The role of sea-air interaction in boreal summer ISO in the Indian Ocean has been studied using coupled ECHAM-4 AGCM and UH intermediate ocean model. Four 15-yr integrations were made. In the first integration, the model lower boundary conditions were observed monthly mean sea surface temperatures, and, in the second, the AGCM was coupled to the ocean model. In the third and fourth simulation, the SST climatology generated in coupled run was used to create daily and monthly mean SSTs, respectively, which were then used to drive the AGCM in an uncoupled configuration similar to the first run. The coupled run shows pronounced northward propagation of convection and circulation anomalies over the northern Indian Ocean, as in observations, while northward propagation is very weak in the uncoupled run. The northward propagating ISO is strongly coupled with underlying SST. On the one hand, the intraseasonal atmospheric convection changes the SST through the solar radiation, latent heat flux and mixed-layer base entrainment. On the other hand, the intraseasonal SST significantly feeds back to the intraseasonal convection by increased low-level convergence into the positive SST anomaly ahead of the convection anomaly. The prevalent northward rather than southward propagation of the ISO is attributed to the interactions between the summer mean state and the atmospheric disturbances in the air-sea coupling context. The stand-alone atmospheric model even forced with the daily SST generated in the coupled run is unable to reproduce the intraseasonal oscillation in the coupled run. In the coupled system (or in nature), the intraseasonal SST is both a result and a force of the intraseasonal atmospheric convection. The SST has a quadrature phase relationship with the convection. However, in the stand-alone atmospheric system, the SST is only a boundary force. The resultant atmospheric convection has almost the same phase with the underlying SST. The intensity of the SST-forced intraseasonal convection in the stand-alone atmospheric model is also much weaker than that in the coupled model. In the coupled model, the movement of the off-equatorial convection in the northern Indian Ocean is not necessarily related to the equatorial eastward-moving Madden-Julian Oscillation. On the other hand, it well follows the local SST perturbations. The positive/negative SST perturbations in the northern Indian Ocean lead active/break phases of the intraseasonal oscillation by about 2 pentads (10 days). Therefore, the SST perturbation on the intraseasonal time scale over the northern Indian Ocean is potentially a useful index to forecast the active/break spells of the south Asian summer monsoon.

**MC17/11A/B23-002 0900**

**PROPAGATION OF THE MJO IN A COUPLED GENERAL CIRCULATION MODEL**

Peter INNESS, Julia SLINGO (NCAS Centre for Global Atmospheric Modelling)

The eastward propagation of the convection associated with the MJO has never been realistically represented in an atmosphere-only general circulation model (GCM). Evidence from observations suggests that there is a link between MJO convection and sea-surface temperature (SST) anomalies, which may partly explain the phase speed of the eastward propagation of the convection. Taken together, these two pieces of evidence suggest that we need to use coupled GCMs, in which the SST can respond to forcing associated with intraseasonal variations in convection, in order to adequately represent the propagation of the MJO. This study will present a comparison of the eastward propagation of the MJO in a coupled GCM with that simulated by the atmospheric component of the GCM forced with seasonally varying SSTs. The coupled GCM produces eastward propagating convection on MJO time-scales whereas the atmosphere-only version does not. The mean climate of the GCM in the Indo-Pacific region is found to be crucial in determining whether the MJO convection extends into the West Pacific.

**MC17/11A/B23-003 0920**

**THE STRUCTURE AND PROPAGATION CHARACTERISTICS OF THE MJO IN MRI COUPLED GCM: COMPARISON WITH OBSERVATION AND ATMOSPHERE-ALONE GCM**

Kavirajan RAJENDRAN, Akio KITOH (Climate Research Department, Meteorological Research Institute, Tsukuba, Ibaraki, Japan)

The Madden-Julian Oscillation (MJO) is the dominant mode of tropical variability on intraseasonal time scales. The simulation of propagation and spectral characteristics of the equatorially trapped waves associated with the MJO in the new version of MRI coupled GCM (MRI-CGCM) is analysed. The role of coupling in modulating the characteristics of these waves are also investigated by performing an additional integration using its atmosphere-alone component. The slowly varying boundary condition, SST, used in this integration is derived from the coupled simulation. A composite structure of the MJO is studied by applying extended EOF (EEOF) analysis. Air sea coupling is found to have improved both propagation and spectral characteristics on intraseasonal time scales. Thus, the simulated MJO in the coupled model shows more realistic propagation characteristics. However, the space-time spectral analysis shows that, in the coupled model, the maximum eastward power on intraseasonal time scales for wavenumber 1 occurs at a slightly higher frequency compared to the observation. In the coupled GCM, the complex interaction between the sea surface and the boundary layer appears to result in more realistic MJO. Besides, the better simulation of MJO in the coupled GCM is also associated with a realistic simulation of climatological mean, onset and evolution characteristics of Asian summer monsoon. This implicates that the skill of the model in the simulation of seasonal mean and intraseasonal variation are associated.

**MC17/11A/B23-004 0940**

**THREE-DIMENSIONAL STRUCTURE AND ITS MODIFICATION OF INTRASEASONAL VARIATIONS OVER THE INDONESIAN MARITIME CONTINENT**

Manabu D. YAMANAKA<sup>1</sup>, Toshiki OKUDA<sup>2</sup>, Noriko OKAMOTO<sup>3</sup>, Fumie MURATA<sup>1</sup>, Shuichi MORI<sup>1</sup>, Hiroyuki HASHIGUCHI<sup>4</sup>, Tien SRIBIMAWATI<sup>5</sup> (<sup>1</sup>Graduate School of Science and Technology, Kobe University, Japan / <sup>2</sup>Frontier Observational Research System for Global Change, Japan, <sup>3</sup>Graduate School of Science and Technology, Kobe University, Japan, <sup>4</sup>Frontier Observational Research System for Global Change, Japan, <sup>5</sup>Radio Science Center for Space and Atmosphere, Kyoto University, Japan, <sup>6</sup>Agency for Assessment and Application of Technology, Indonesia)

Intraseasonal variations over the Indonesian maritime continent are analyzed based on almost daily operational rawinsonde data through a year (1995). Composite analysis around maxima of the whole-Indonesia-mean, vertical-mean humidity shows a reversal from easterly to westerly in the lower troposphere and another one from westerly to easterly in the upper troposphere, suggesting a convergence of zonal wind around the humidity maximum associated with the intraseasonal variation with a zonal wavelength larger than the zonal width (about 5,000 km) of the Indonesian maritime continent. This structure is clear in particular in the southern-hemispheric side of this region. Over such a tropospheric variation another zonal-wind variation with downward phase progression is found in particular near the equator. These structures are compared with theories/models of the tropospheric intraseasonal variations and the lower-stratospheric Kelvin waves. Differences of the structures between stations are discussed in view of the modification of intraseasonal variations over the Indonesian maritime continent, which is also suggested from our recent intense observations in Sumatera Island using 3- and 6-hourly rawinsonde launches and other instruments.

**MC17/11A/B23-005 Invited 1030**

**THE ROLE OF SEA SURFACE TEMPERATURE FORCING IN THE ORGANISATION AND EASTWARD PROPAGATION OF MJO CONVECTIVE ANOMALIES**

Adrian J. MATTHEWS (Schools of Environmental Sciences and Mathematics, University of East Anglia)

The role of sea surface temperatures (SST) in the organisation and eastward propagation of deep tropical convective anomalies within the Madden-Julian oscillation (MJO) is examined using an atmospheric general circulation model. In an ensemble of initial value experiments forced with observed composite time-dependent MJO SST anomalies, a significant response in deep convection developed within a few days, with enhanced convection over the region of positive SST anomaly. The convective anomalies then propagated eastward along with the SST forcing. This supports the theory that atmosphere-ocean coupling is important in maintaining the MJO, at least in this particular model. The implied feedback of the atmosphere onto the ocean through changes in the surface short wave and latent fluxes and surface wind stress is presented and compared with observed anomalies. The response time of the tropical atmosphere to the SST anomalies, in terms of the development of convective anomalies and their subsequent forcing of a dynamical atmospheric (equatorial wave) response, is the same order of magnitude as the time scale of the MJO SST anomalies themselves, and the dependence of the atmospheric response and of the implied ocean-atmosphere coupling to the periodicity of the SST forcing is discussed. Observed latent heat flux anomalies within the MJO are attributable to a modulation of synoptic-scale weather systems by the MJO as well as to the slowly varying MJO wind anomalies themselves. The ability of the model to reproduce this modulation and its sensitivity to the SST forcing is also discussed.

**MC17/11A/B23-006 1100**

**WAVE-ZONAL FLOW INTERACTION IN THE MADDEN-JULIAN OSCILLATION**

Masahiro WATANABE (Department of Ocean and Atmospheric Science, Hokkaido University)

A possible interaction between planetary-scale waves and zonal mean flow associated with the Madden-Julian Oscillation was examined by means of the so-called aqua-planet experiments with and without 'warm pool' of tropical sea surface temperature. In the presence of the warm pool the model produces a broad spectral peak on intraseasonal timescale in the zonal mean wind. It was found that the zonal flow fluctuations are generated and maintained by eastward propagating waves that accumulate westerly momentum toward the equator in one phase of the MJO while emanate it toward the subtropics in the other phase. The anomalous zonal mean flow in turn encourages the convective anomaly moving eastward, but such a feedback may account only for about 10% of the propagation tendency of wave fields. The wave-zonal flow interaction in the MJO therefore appears virtually one-way from waves to the zonal mean flow.

**MC17/11A/B23-007 1120**

**MJO-LIKE SYSTEMS IN IDEALIZED AQUAPLANET SIMULATIONS**

Mitchell W. MONCRIEFF, Wojciech W. GRABOWSKI (MMM/NCAR)

Interaction between equatorially-trapped disturbances and tropical convection is investigated using a global model which applies the Cloud-Resolving Convection Parameterization (CRCP, a.k.a. super-parameterization). The CRCP represents sub-grid scale physical processes by embedding an east-west oriented two-dimensional cloud-resolving model in each column of a global model. Convection is represented explicitly. The modeling setup is a constant-SST aquaplanet, the size and rotation-rate of Earth, maintained in radiative-convective quasi-equilibrium. No large-scale organization of convection occurs outside the equatorial waveguide. Within the waveguide coherent structures characterized by deep convection at the leading edge with strong surface westerly winds to the west (westerly wind bursts) occur spontaneously. These structures resemble the Madden-Julian Oscillation (MJO) and occur in simulations with prescribed radiation and simulations with interactive radiation. Sensitivity simulations suggest that the coupling among deep convection, free-tropospheric moisture, and the large-scale flow is essential for coherence of the MJO-like structures. When large-scale fluctuations of convectively-generated free-tropospheric moisture are removed on a time-scale of hours, MJO-like structures do not develop and, if already present, disintegrate rapidly. The systems are weaker and structurally different when the two-dimensional cloud-resolving models are oriented north-south instead of east-west, suggesting that convective momentum transport is important. MJO-like structures also develop when CRCP is replaced by a traditional convection parameterization (Emanuel scheme). However, with parameterized convection the coherence is sensitive to parameters of the convection scheme. An idealized nonlinear dynamical model is formulated in order to examine the MJO-like structures at a basic level. The model analytically couples a Rossby-gyre circulation with organized convection dynamics and provides a simple analytic formula for the propagation speed of the MJO-like systems. This is distinct from formulae derived from tropical wave theory. The dynamical model reproduces the vertical and meridional transports of zonal momentum, and the atmospheric super-rotation in the global model. These quantities are analytic functions of the propagation speed of the MJO-like systems.

**MC17/11A/B23-008 1140**

**MODELING THE DISTINCTION BETWEEN THE MJO AND MOIST KELVIN WAVES**

Richard Brian NEALE, Brian E. MAPES (Climate Diagnostics Center)

Space-time spectral results of Wheeler and Kiladis clarify that the Madden-Julian oscillation (MJO) and moist Kelvin waves are distinct phenomena, both of which occur in nature. This distinction has not been recognized in much of the modeling literature. For example, studies which conclude that a model has a too-fast MJO may actually indicate that the model lacks an MJO, but has a reasonable moist Kelvin wave. Further confusion springs from quoting round-the-world periods rather than phase speeds in aqua-planet models with a zonally symmetric equatorial warm pool. We have undertaken to construct a model, of minimal complexity and satisfying diagnosability, exhibiting both moist Kelvin waves and a slower, MJO-like phenomenon. Our working hypothesis is that tropospheric wave (density) dynamics, involving the second vertical mode of the troposphere, contain the dominant propagation mechanism in the former, while the latter is associated with a slower time scale involving moisture storage and discharge. This slow moisture time scale may involve frictional convergence in the boundary layer, and certainly must involve an interplay between shallow convection (which mixes moisture vertically and has low precipitation efficiency) and precipitating deep convection. A key question involves hysteresis: how can deep convection persist and dry out the atmosphere, even as large-scale thermodynamic conditions become apparently less favorable than those prevailing before it began?

**MC17/11A/B23-009 1200**

**MECHANISM OF INTRASEASONAL OSCILLATION IN THE SOUTH ASIAN SUMMER MONSOON REGION**

Hae-Kyung Lee DRBOHLAV, Bin WANG (Department of meteorology, University of Hawaii)

The mechanism of boreal summer intraseasonal oscillation is examined with the zonally averaged intermediate atmospheric model (2D model). Without the ocean mixed layer, the barotropic and baroclinic mode of atmosphere can produce the oscillation in 2D model. The propagation of convection in 2D model is caused by the phase relationship between convection and barotropic divergence in the atmosphere. Most importantly, in the northern hemisphere, the vertical advection of July-mean easterly wind shear in regions of convection induces barotropic divergence (convergence) to the north (south) of convection. The resulting moisture convergence in the boundary layer induces the northward propagation of precipitation. The initiation of convection is also produced by the barotropic divergence in the atmosphere. Especially, the strong July-mean vertical motion at 10S causes convergence in the boundary layer between 10S and the equator. The baroclinic mode, on the other hand, acts to enhance existing convection.



**MC17/11P/B23-001 1400**  
**SUBSEASONAL ATMOSPHERIC VARIABILITY AND EL NIÑO**

Gabriel Andres VECCHI<sup>1</sup>, D.E. HARRISON<sup>2</sup> (JISAO, University of Washington, <sup>2</sup>NOAA/PMEL/OCRD)

The importance of atmospheric variability in the sub-seasonal band for El Niño/Southern Oscillation (ENSO) is an active area of research. In particular, it has been suggested that equatorial Pacific surface wind variability associated with the Westerly Wind Events (WWEs) and Madden-Julian Oscillation (MJO) are important in both the onset of El Niño warming, and in the termination of El Niño periods. We use a systematic definition of WWEs and a global index of MJO variability, based on 850-mb zonal wind, to investigate the structure of the average MJO and relationships between the MJO, WWEs and ENSO. As reported by others, there is no correlation between MJO activity and eastern equatorial Pacific sea surface temperature (SST) anomalies, for the period 1982-2002. We find that WWEs are very strongly connected to waveguide warming in the Pacific both statistically and in an ocean general circulation model, independent of their relationship to the MJO. When the eastern equatorial Pacific SSTs are close to climatology, western and central equatorial Pacific WWEs drive strong waveguide warming in the east. When the eastern equatorial Pacific SSTs are warmer than normal WWEs act to maintain the warm SSTs, which tend to disappear in their absence. We find, however, that we can only build a statistical or model-based connection between waveguide warming and the MJO when they co-occur with a westerly wind event. Statistical and OGCM connections between waveguide warming and the MJO are weak, and within the uncertainty in the statistics and the model parametrization. Small changes in OGCM parametrization can lead to the MJO driving either warming or cooling in the east Pacific. MJO events occurring with an equatorial WWE are associated with waveguide warming of the same magnitude as that associated with a WWE without an MJO. When an MJO with an embedded WWE is imposed on the model ocean the changes are not distinguishable from those produced by an independent WWE. Thus, the occurrence of WWEs should be the focus of interest in examining the relationship between subseasonal variability and ENSO waveguide warming. Further, we examine the relationship between WWEs and the MJO and find that there is very strong statistical case for MJO modulation of WWE activity on intraseasonal timescales, but on non-intraseasonal timescales WWEs appear to be independent of MJO. That is, the MJO redistributes the probability of WWEs within an MJO, but the occurrence of an MJO does not increase the probability of WWEs.

**MC17/11P/B23-002 1420**

**A STATISTICAL ANALYSIS OF WESTERLY WIND BURSTS IN THE EQUATORIAL TROPICS AND THEIR INTERRELATIONSHIP WITH ENSO AND INTRASEASONAL VARIATIONS**

Ayako SEIKI, Yukari N. TAKAYABU (Center for Climate System Research, University of Tokyo)

Observational features of westerly wind Bursts (WWBs) over the equatorial latitudes at all longitudes and their interrelations with MJO (Madden-Julian oscillation) and ENSO are studied, using ECMWF objective analysis data and satellite data for the period of 1979-2001. We defined WWBs, using surface 10-m zonal wind anomalies from 91-days-running-mean climatology averaged between 2.5°N-2.5°S, with cases which satisfy following criteria: anomalous westerlies exceed 5ms<sup>-1</sup>, extend more than 10 degrees longitude, and last at least 2 days. Total number of WWBs identified in 23-year analysis period was 279. WWBs are found over the Indian Ocean and the Pacific Ocean, but not over the Atlantic Ocean. Annual composite analysis revealed that over the Indian Ocean, WWBs frequently occur with seasonal intensification of westerlies in May and around November, which are also influenced by ENSO. On the other hand, WWB occurrences over the Pacific Ocean coincide with eastward migration of the warm pool controlled by ENSO. WWBs over the Indian Ocean occur where the mean surface westerly is largest, while those over the Pacific Ocean occur most frequently where the vertical shear of the zonal wind changes from the easterly shear to the westerly shear. Significant correlations between WWB frequencies and ENSO are found by lag-correlation analysis. WWB occurrences over the Indian Ocean are seen in lag 0 month which corresponds to La Niña peak, or in lag -15 months preceding El Niño. WWBs over the western Pacific Ocean are found around lag -4 months, leading El Niño peak. WWBs occur simultaneous with El Niño over the eastern Pacific Ocean. These results suggest that WWBs occur under the preferable environment prepared by ENSO. At last, composite analysis based on WWB maximum intensity as well as subjective examinations of individual cases revealed that most of WWBs are associated with slow downs of MJO with intensification of Rossby wave response. On the other hand, in terms of MJO phase which is determined with band pass filtered 200hPa velocity potential, largest numbers of WWBs occur in the latter half of MJO convective phase. This also implies that WWBs occur in association with MJO, though there exist some regional differences in timings. Considering that most of MJO do not bear WWBs, on the other hand, we suggest that ENSO controls the environment which is preferable for structure transformations from MJO to WWBs to occur. Structure transformation mechanisms will be addressed in future studies.

**MC17/11P/B23-003 1440**

**THE STRUCTURES OF DEEP CONVECTIONS AND THEIR ENVIRONMENT OBSERVED DURING THE ACTIVE PHASE OF MADDEN-JULIAN OSCILLATION OVER THE EQUATORIAL WESTERN PACIFIC**

Hisayuki KUBOTA<sup>1</sup>, Ryuichi SHIROOKA<sup>1</sup>, Tomoki USHIYAMA<sup>1</sup>, Jingyang CHEN<sup>1</sup>, Takashi CHUDA<sup>1</sup>, Kensuke TAKEUCHI<sup>1</sup>, Kunio YONEYAMA<sup>2</sup>, Masaki KATSUMATA<sup>2</sup> (Frontier Observational Research System for Global Change, Japan Marine Science and Technology Center)

The structures of deep convections and their environment were examined during the active phase of the Madden-Julian oscillation (MJO) using fine time resolution of the research vessel Mirai observation data. During the intensive observation period, MJO associated with deep convections passed through the observational area. Strong westerly wind also appeared during the active phase of MJO. Vertical structures associated with convective activity were detected using lag correlations of atmospheric parameters. Convective activity included deep convections, with a nocturnal maximum and another peak 12-18 hours earlier. Deep convections associated with the first peak developed in the daytime and decayed within a few hours. These daytime deep convections transported water vapor from lower to middle troposphere, making the environment more favorable for the more intensive deep convections that developed during the night. Westerly winds were accelerated in lower layers during both deep convections.

**MC17/11P/B23-004 1500**

**MODULATION OF TROPICAL CYCLONE BY MADDAN-JULIAN OSCILLATION**

Congwen ZHU<sup>1</sup>, Tetsuo NAKAZAWA<sup>2</sup> (Chinese Academy of Meteorological Sciences, China, <sup>2</sup>Meteorological Research Institute, Japan)

The modulation of tropical depression (TD)/storm(TS) over the Indian-western Pacific Oceans by the Madden-Julian Oscillation (MJO) has been explored for the period of September 1996 to June 1997. The present study showed that there are more (fewer) TD/TSs formed in the wet (dry) phase of the MJO except over the west North Pacific, where the TD/TS can be alternatively modulated by the eastward or westward propagating MJO. Singular Vector Decomposition (SVD) analysis has demonstrated that, coupled to the enhanced (suppressed) tropical convective anomalies, a pair of the east-west elongated cyclonic vortex in the northern (southern) hemisphere and the anti-cyclonic vortex in the southern (northern) hemisphere at 850 hPa appears over the tropical regions in both hemispheres with the westerly (easterly) wind anomalies along the equator in between. The westerly wind burst and its eastward progression, associated with the MJO, could result in a series of the tropical cyclogenesis with several day interval during the wet phase of the MJO. There are two cases of twin cyclone generation, modulated by the MJO, one in the Indian Ocean in October 1996 and another over the western Pacific in May 1997. The analysis shows that the equatorial westerlies and super cloud cluster are responsible for the twin cyclogenesis.

**MC17/11P/B23-005 1540**

**A FURTHER STUDY ON ZONAL PROPAGATION OF TROPICAL INTRASEASONAL OSCILLATION (MJO)**

Chongyin LI (Institute of Atmospheric Physics, Chinese Academy of Science)

The data analyses have shown clearly that the eastward propagation is a main feature of zonal propagation in the tropical (10N-10S) atmosphere, i.e., the MJO, but sometimes the westward propagation of the MJO can be seen there. The seasonal variability is another feature of zonal propagation of the MJO. Generally, eastward propagation of the MJO is more advantageous in the Northern winter than that in the Northern summer. Other hand, the data analyses and numerical simulation also show that zonal propagation of the MJO will occur anomalously due to the impacts of some processes. For example, the MJO propagates eastwards very obviously in the El Niño summer. The MJO still reveal anomalous propagation westwards in the tropical Pacific area when there is abnormal strong heating field over the equatorial eastern Pacific.

**MC17/11P/B23-006 1600**

**OBSERVATIONAL RESULTS FOR RELATIONSHIP BETWEEN LOWER TROPOSPHERIC WESTERLY AND RAINFALL AT KOTOTABANG, WEST SUMATERA, INDONESIA**

Fumie MURATA<sup>1</sup>, Manabu D. YAMANAKA<sup>1</sup>, Shin-Ya OGINO<sup>1</sup>, Masatomo FUJIWARA<sup>1</sup>, Hiroyuki HASHIGUCHI<sup>1</sup>, Shoichiro FUKAO<sup>2</sup>, Shuichi MORI<sup>3</sup>, Jun-Ichi HAMADA<sup>4</sup>, Yudi Iman TAUHID<sup>5</sup>, Tien SRIBIMAWATI<sup>6</sup>, Budi SUHARDI<sup>7</sup> (Graduate school of science and technology, Kobe University, Jpn, <sup>2</sup>Frontier observation research system for global change, Japan, <sup>3</sup>Radio science center for space and atmosphere, Kyoto University, Japan, <sup>4</sup>Agency for the assessment and application of technology, Indonesia, <sup>5</sup>Indonesian meteorological and geophysical agency, Indonesia)

A relationship between low tropospheric westerly and precipitation at Kototabang (100°E, 0.20°S, 865 mMSL), West Sumatera, Indonesia has been investigated. Kototabang is located on mountainous region along west coast of Sumatera Island. A Boundary layer radar have been operated there since August 1998. Besides, rawinsonde observation campaigns have been conducted therefor several times. Dominant lower tropospheric zonal wind at Kototabang was weak westerly, and strong westerly more than 10 m/s sometimes observed. Most of these strong westerlies associated with MJOs. Rainfalls at Kototabang tended to occur when westerlies was weak, and occupied most of total rainfalls. They tended to occur in the afternoon from local cloud systems developed along mountainous region. These results different from observations in Western Pacific region, where MJOs bring active convections. This implies the importance of complicated topography on making clouds. In two rawinsonde observation campaigns strong westerlies corresponded to the appearance of both low equivalent potential temperature and low specific humidity below 5 km altitude, and precipitations at Kototabang did not occur in the periods of dry air.

**MC17/11P/B23-007 1620**

**MANIFESTATION OF MJ OSCILLATION IN THE TROPICAL ATMOSPHERIC BOUNDARY LAYER OVER AN INLAND STATION**

P.K. KUNHIKRISHNAN, Praveena KRISHNAN, S. Muraleedharan NAIR (Space Physics Laboratory Vikram Sara Bhai Space Centre)

The Madden Julian Oscillation (MJO) is a planetary scale wave that traverses from west to east in roughly 40 days. It has the largest amplitude in the equatorial latitude and is discernible over the tropics and subtropics. Its signature is seen in most variables, such as the sea level pressure, zonal wind and divergent circulation. The lower atmospheric wind profiler established at National MST Radar Facility, Gadanki (13.5°N, 79.2°E) provides a continuous high resolution wind data in the first few kilometers of the atmosphere. The LAWP wind data was collected for the period March 1999 to September 2000. Analysis of the wind data collected during the period was carried out to see the signatures of MJ oscillations in the wind. The horizontal wind components (u and v) were classified into S-W monsoon (May, June, July, August and September) and winter monsoon (November, December, January, February and March) periods. The horizontal wind components were subjected to Fast Fourier transforms and wavelet analysis. Spectral analysis of data clearly shows the presence of synoptic scale oscillations and 40 to 50 day oscillation in the zonal wind. The 40 to 50 day oscillation is strong during S-W monsoon period compared to that at winter monsoon period. The 40 to 50 day oscillation is not seen in the 'v' component of horizontal wind. These long period oscillations are more prominent in the higher heights in the ABL than that in the surface layer. Wavelet analysis clearly show the temporal variation of these oscillations. When the synoptic scale oscillation and the MJ oscillations are in phase more rain is recorded in the region.

**MC17/11P/B23-008 1640**

**AN OBSERVATIONAL STUDY ON INTRASEASONAL VARIATIONS WITH EQUATORIAL ATMOSPHERE RADAR IN WEST SUMATERA, INDONESIA**

Tri Handoko SETO, Masayuki YAMAMOTO, Hiroyuki HASHIGUCHI, Masatomo FUJIWARA, Mamoru YAMAMOTO, Shoichiro FUKAO (Radio Science Center for Space and Atmosphere, Kyoto University)

The equatorial atmosphere over Indonesia seems to play an important role upon global change of the earth's atmosphere. In order to observe the phenomena in the whole troposphere and the lower stratosphere (2–20 km) in the equatorial region, we installed the equatorial atmosphere radar (EAR) in Kototabang, West Sumatra, Indonesia (0.20°S, 100.32°E). The EAR has good time and height resolutions of about 85 sec and 150 m, respectively, and has been continuously operated since July 2001. Intraseasonal variations, which is one of the most dominant variations in the tropics, has been studied using the EAR in Indonesia. Eastward propagating super cloud cluster (SCC) known as intraseasonal variation (ISV) or Madden-Julian oscillation (MJO) clearly appeared in GMS IR data ( $T_{bb}$ ) over the radar site (0.2°S) during June 2002. There was a good correlation between  $T_{bb}$  and 2–4 km averaged daily zonal wind obtained with the EAR on that period. Namely, when enhanced convection existed in the west side of the EAR site, easterlies or weak westerlies were observed with the EAR, and conversely when enhanced convection was situated in the east side of the EAR site, westerlies were observed. We investigated the relation between 2–4 km averaged zonal wind and variance of vertical wind obtained with the EAR. Strong variance of vertical wind was observed when easterlies or weak westerlies were observed, and conversely weak variance of vertical wind was observed during strong westerlies. Regardless of the direction of 2–4 km averaged zonal wind, variance of vertical wind weakened above the tropopause height (about 16 km).

MC17/11P/B23-009

1700

#### INTRASEASONAL VARIABILITY OVER TROPICAL AFRICA DURING NORTHERN SUMMER

Adrian J. MATTHEWS (Schools of Environmental Sciences and Mathematics, University of East Anglia)

The intraseasonal variability over Africa during northern summer was analyzed, using 25 years of NCEP/NCAR reanalysis and satellite data. The dominant pattern of variability was one of enhanced deep convection over the whole African monsoon region. It appeared to arise as a remote response to the intraseasonal (Madden-Julian) oscillation over the warm pool sector. Twenty days prior to the maximum in convection over Africa, there was no signal over Africa but convection was reduced over the equatorial warm pool. An equatorial Kelvin wave response to this change in warm pool convection propagated eastward and an equatorial Rossby wave response propagated westward and between them they completed a circuit of the equator and met up twenty days later over Africa, where the equatorial ascent in the Kelvin wave front and the off-equatorial ascent in the Rossby wave front favoured deep convection. Over West Africa, the Kelvin wave component contained lower-tropospheric westerly anomalies which acted to increase the boundary layer monsoon flow and moisture supply. The westerly anomalies also increased the cyclonic shear on the equatorward flank of the African easterly jet, leading to enhanced African easterly wave and transient convective activity, which then contributed to the enhanced convection over Africa on the longer intraseasonal time scale. The implications of this intraseasonal mode for predictability over Africa is discussed.

MC17/11P/B23-010

1720

#### IMPACT OF FREE-TROPOSPHERIC HUMIDITY ON DEEP CONVECTION

Steve DERBYSHIRE<sup>1</sup>, Wojciech W. GRABOWSKI<sup>2</sup>, Isabelle BEAU<sup>3</sup>, Peter BECHTOLD<sup>4</sup>, Jean-Yves GRANDPEIX<sup>5</sup>, Jean-Marcel PIRIOU<sup>1</sup>, Jean-Luc REDELSPERGER<sup>1</sup>, Pedro SOARES<sup>6</sup> (Met Office, Bracknell, <sup>1</sup>NCAR, USA, <sup>2</sup>Meteo-France, Toulouse, France, <sup>3</sup>ECMWF, Reading, UK, <sup>4</sup>LMD, Paris, France, <sup>5</sup>University of Lisbon, Portugal)

Humidity of the free troposphere has been long recognized as an important factor modulating moist convection. The most spectacular example is the impact of dry intrusions on the tropical convection. By moistening its immediate environment, convection renders it more favorable for future convection because clouds growing in a more humid environment lose their positive buoyancy (as a result of entrainment of dry environmental air) more slowly than clouds growing in a drier environment. However, convective parameterizations, which have to be used in traditional large-scale weather prediction and climate models, are often quite insensitive to the environmental free-tropospheric humidity. This presentation consists of two parts. First, we will present results from European Community project EUROCS which, among other themes, aimed at i) documenting impact of free-tropospheric humidity on moist convection using cloud-resolving modeling approach, and ii) using these results to improve sensitivity of traditional convective parameterizations to free-tropospheric humidity. Second, we will present results from idealized numerical simulations illustrating the impact of free-tropospheric humidity on large-scale organization on tropical convection. This can be understood as a feedback process which involves moist convection, free-tropospheric moisture, and the large-scale flow. This feedback causes perturbations in moist convection to strengthen perturbations of the free-tropospheric moisture, which, in turn, affect the spatial distribution of moist convection. The large-scale circulation, which develops in response to spatial fluctuations of convective heating, plays an important role in this feedback because, through the effect of the large-scale subsidence, it makes areas with suppressed convection even drier. Intraconvective radiative transfer strengthens this feedback loop considerably because more radiative cooling, and thus more subsidence, occurs in dry cloud-free areas. We will argue that problems in representing this feedback loop may explain the weak intraseasonal variability observed in many large-scale weather and climate models.

M



SS03

Monday, July 7

## TECTONOPHYSICS AND CRUSTAL STRUCTURE

Location: Site A, Room 2

Monday, July 7 AM

Presiding Chairs: P. Suhadolc, S. Das

SS03/07A/A02-001

0900

## SURFACE WAVE STRUCTURE STUDY USING A HIGH DENSITY NETWORK

Toshiro TANIMOTO, Kenton PRINDLE-SHELRAKE (Department of Geological Sciences, University of California, Santa Barbara)

Development of high density broadband seismic network provides new opportunities for structure study. In this paper, we report the use of surface waves for structure study under the network. We report our results for TriNet, a dense seismic network in Southern California, and report our new results on the three-dimensional S-wave velocity structure that was constructed from Rayleigh and Love wave phase velocity data. Two station method was used for the phase velocity measurement, using spectral fitting technique through perturbation of S-wave velocity structure, specifically developed for this project. The total number of paths are about 5500 for Rayleigh waves and 2000 for Love waves. We have taken into account some finite frequency effects in our analysis. The S-wave velocity maps show some large-scale features that are much more distinct than previous tomographic results in Southern California. There are some notable features when considering large-scale tectonics in this region; first, there is a clear seismic velocity contrast between the Pacific plate and the North American plate. The North American plate side is systematically slower than the Pacific plate side and this velocity contrast extends at least down to the depth of about 60 km. There is no question that this contrast exceeds the Moho. In the northern part, this contrast in the upper mantle is fairly vertical (abrupt) and is almost exactly under the San Andreas Fault. In the southern part, the contrast is under the Elsinore and the San Jacinto Fault area, somewhat west of the San Andreas Fault. Secondly, fast velocity under the transverse range is much more pronounced in the western part of the transverse range, rather than the part that the Pacific plate and the North American plate directly collide. A common interpretation of downgoing tongue, originally proposed by Humphreys et al., may require some modification in order to understand this feature. There is also another distinct fast velocity anomaly under the northern end of the Peninsular Ranges toward south. This fast velocity anomaly appears to be almost as large as the one under the Transverse Ranges. Thirdly, under the Eastern California Shear Zone, there are distinct slow velocity anomalies, suggesting higher temperature and lower viscosity in the lower crust.

SS03/07A/A02-002

0915

## THREE-DIMENSIONAL FAULT ZONE STRUCTURE AND EARTHQUAKE LOCATIONS AT PARKFIELD, CALIFORNIA

Clifford H. THURBER<sup>1</sup>, Steven ROECKER<sup>2</sup>, Peter MALIN<sup>3</sup>, William ELLSWORTH<sup>4</sup> (<sup>1</sup>Department of Geology and Geophysics, University of Wisconsin-Madison, <sup>2</sup>Rensselaer Polytechnic Institute, <sup>3</sup>Duke University, <sup>4</sup>U.S. Geological Survey)

Arrival-time data from about 650 local earthquakes and numerous shots are inverted for earthquake locations and 3-dimensional Vp and Vp/Vs structure of the San Andreas fault (SAF) zone near Parkfield, CA. Included are data from a temporary array of surface seismic stations installed around the SAFOD site as well as from a vertical array of geophones installed in the 2-km-deep San Andreas Fault Observatory at Depth (SAFOD) Pilot Hole, drilled in summer 2002. The primary features of the velocity models are generally consistent with those from previous local earthquake tomography studies, but with much finer detail. The P-wave structure is dominated by the velocity contrast across the SAF, with the southwest side about 20-25% faster than the northeast side. A low-Vp zone adjacent to the fault trace penetrates to a depth of as much as 9 km. Nearly all the earthquakes occur almost directly beneath the surface trace of the SAF, although to the southeast of the Pilot Hole the fault appears to step southwestward at depth. Regions of anomalously high Vp/Vs (> 2.0) are found at shallow depths along and northeast of the SAF. These high-Vp/Vs anomalies can be associated with low-resistivity features in a magnetotelluric model that are interpreted to represent fluid-saturated zones. We locate a magnitude 1.9 earthquake at a depth of 2.7 km below the surface with an epicenter within about 50 m of the surface fault trace that is a potential target event for drilling of the main SAFOD hole. Tests using "virtual earthquakes" (borehole receiver gathers of picks for surface shots) indicate that our event locations near the borehole are accurate to about 50 m in both the horizontal and vertical directions.

SS03/07A/A02-003

0930

## SEISMIC VELOCITY STRUCTURE IN THE MARGIN OF THE SOUTHWESTERN JAPAN SEA OFF TOTTORI BY OCEAN BOTTOM SEISMOGRAPHIC OBSERVATION

Takeshi SATO<sup>1</sup>, Seiichi MIURA<sup>2</sup>, Gou FUJIE<sup>3</sup>, Koichiro OBANA<sup>3</sup>, Aki ITO<sup>3</sup>, Dong-Hyo KANG<sup>3</sup>, Shuichi KODAIRA<sup>3</sup>, Kiyoshi SUEHIRO<sup>3</sup>, Yoshiyuki KANEDA<sup>3</sup>, Takaya IWASAKI<sup>1</sup>, Team Shikoku 2001 (<sup>1</sup>Deep Sea Research Department, JAMSTEC, <sup>2</sup>FREE, JAMSTEC, <sup>3</sup>KIGAM, <sup>4</sup>ERI, Univ. of Tokyo)

Deep seismic structure model across a subduction zone including the island arc and back-arc basin enables us to infer the geometry of the subducting plate, the deep structure in the seismogenic zone and the formation process of the island arc in the southwestern Japan arc, from an integrated wide-angle seismic survey in 1999, it is imaged that a subducting seamount is colliding with the arc and that it may have controlled the rupture process of the 1946 Nankaido earthquake (Kodaira et al., 2000). Furthermore, the geometry of the subducting Philippine Sea plate beneath Shikoku Island is also imaged (Kodaira et al., 2002; Kurashimo et al., 2002). However, there are few seismic structure surveys from the Japan island arc to the back-arc basin in the Japan Sea. The purpose of this study is to reveal detailed information about the geometry of the subducting Philippine Sea plate and the transitional structure, which is concerned with the formation process of the Japan Sea. In August to September of 2002, an integrated onshore-offshore wide-angle seismic survey was carried out from the Shikoku Island to Japan Sea off Tottori (Oki Trough, Oki Ridge and southwestern Yamato Basin). Thirty-five ocean bottom seismographs (OBSs) were deployed with a spacing of about 6 km along the offshore survey line (about 170 km). Seismic signals from an airgun array (200 liter) and ten land-explosives (50, 100, 300, and 500 kg) were recorded by OBSs. Also, multi-channel seismic (MCS) reflection data were acquired along the line. In this presentation, we report a model on the crustal structure beneath the Japan Sea off Tottori using these data. The OBSs recorded signals from an airgun array and a part of land-explosives with high signal-to-noise ratio in the entire offshore survey line. On OBSs record sections, first arrivals with a velocity of about 8.0 km/s appear greater than 75 km. The result shows that the sedimentary layer in the southwestern Yamato Basin consists of

three layers, with velocities 1.6 km/s, 2.1 km/s and 2.4 km/s. The thickness of the sedimentary layer is about 1 km in the southwestern Yamato Basin. This sedimentary layer is interpreted as marine sediments from lower Miocene to Quaternary (Leg 127 Shipboard Scientific Party, 1990). The thickness of the crust beneath the southwestern Yamato Basin can be estimated about 12-14 km from the preliminary analysis. It is supposed that Moho deepens towards the southwestern Japan island arc.

SS03/07A/A02-004

0945

## SEISMICITY, TOMOGRAPHY AND ACTIVE TECTONICS IN CENTRAL TAIWAN

Francis T. WU<sup>1</sup>, Harley M. BENZ<sup>2</sup>, Chien-Hsin CHANG<sup>3</sup>, Y-h-Min WU<sup>4</sup> (<sup>1</sup>Department of Geological Sciences, State University of New York, <sup>2</sup>USGS, <sup>3</sup>CWB, Taiwan)

The background seismicity in central Taiwan between 23°N and 24.5°N had been relatively low before 1999, but the occurrence of the September 20, 1999, Chi-Chi earthquake changed the scene. Within the first ten days after the Chi-Chi mainshock more than 8000 aftershocks were recorded. These and 20,000+ later events in the area have been located by the CWB network since then. As a response to orogenic stresses these crustal earthquakes, their location and focal mechanism, reveal the response of the crust to the stresses, possibly the dislocation surfaces, and perhaps the state of the crustal materials, brittle or ductile. For these purposes precise location of the background seismicity and the aftershocks is the most important task to be performed. The Double difference method, aiming at removing both the source- and receiver-side bias, has been shown to be effective in refining locations (Waldhauser and Ellsworth, 2000). Using the catalog arrival times of P and S waves and the event locations as input, we relocated all M>2.0 events from 1993 through 2001 with this method. The spatial patterns of the relocated events appear to be much better organized than those from the HYPO71 output; diffused hypocenters coalesce into narrow belts and seismic and aseismic areas more sharply defined. The Chi-Chi aftershock data also allow us to tomographically image the same region in greater detail. In combination with focal mechanisms from the Broadband Array for Taiwan Seismology (BATS) (Kao, 2002) we can decipher a consistent orogenic process that include the upwelling of the middle crust, the down-thrusting of the lower crust as well as pervasive thrust faulting in the upper crust of western Central Taiwan.

SS03/07A/A02-005

1030

## SHEAR VELOCITY STRUCTURE IN THE AEGEAN AREA OBTAINED BY INVERSION OF RAYLEIGH WAVES

Eleni E. KARAGIANNI<sup>1</sup>, C.B. PAPAACHOS<sup>1</sup>, D.G. PANAGIOTOPOULOS<sup>1</sup>, P. SUHADOLC<sup>2</sup>, A. VUAN<sup>3</sup>, G.F. PANZA<sup>4</sup> (<sup>1</sup>Geophysical Laboratory, Aristotle University of Thessaloniki, Greece, <sup>2</sup>Department of Earth Sciences, University of Trieste, Italy, <sup>3</sup>Centro Ricerche Sismologiche, Istituto Nazionale di Oceanografia e di Geofisica Sperimentale, Trieste, Italy, <sup>4</sup>The Abdus Salam International Centre for Theoretical Physics, SAND Group, Trieste, Italy)

The main target of the present study is to derive a 3D tomographic image of the shear-wave velocity structure of the crust-uppermost mantle in the Aegean area using the group velocities of Rayleigh wave fundamental mode. The database consists of 185 regional earthquakes recorded at broad-band stations that were installed for a period of six months in the Aegean area within the framework of a large-scale experiment. For each epicenter-station ray path an averaged group velocity has been determined using the method of frequency time analysis (FTAN) and the data are used in order to determine the local group velocities for different periods over the area covered by the seismic ray paths. Taking into account the resolution of the local group velocities, a grid of 0.5 degrees was adopted for the Aegean area and a local dispersion curve was defined for each grid point. More than 80 local dispersion curves were finally inverted using a non-linear inversion approach, deriving the corresponding 1D shear-velocity models. The interpolation of these models results in a 3D S-wave tomographic image of the crust and uppermost mantle in the broader Aegean area. In the Southern Aegean Sea, as well as in a part of the Central Aegean Sea a thin crust of approximately 20-22 km is observed, whereas the remaining Aegean Sea area exhibits a crustal thickness less than 28-30 km. On the contrary, a crustal thickness of 40-46 km is observed in western Greece along the Hellenides mountain range, whereas in the eastern continental Greece the crust has a typical thickness of about 30-34 km. Strong lateral variations of the shear-wave velocities are found throughout the Aegean area. For shallow depths (<10 km) low S-wave velocities are observed in the sedimentary basins of the North Aegean Sea, of the gulf of Thermaikos and western Greece. At depths ranging from 10 to 20 km low S-wave velocities are mainly found in western Greece under Peloponnesus as well as in Rhodes. In the Southern Aegean Sea very low S-wave velocities (3.6-4.0 km/sec) are observed at depths of about 30-40 km just below the Moho discontinuity, while in the rest of the inner Aegean Sea and the continental Greece the uppermost mantle is characterized by velocities around 4.3-4.4 km/sec. This low-velocity zone in the Southern Aegean Sea can be associated with the presence of a partially melt mantle wedge in the Southern Aegean subduction zone in agreement with previous studies.

SS03/07A/A02-006

1045

## LOW-FOLD SEISMIC REFLECTION IMAGE OF THE OUTER ZONE, SW JAPAN

Hiroshi SATO<sup>1</sup>, Tanio ITO<sup>2</sup>, Takaya IWASAKI<sup>1</sup>, Naoshi HIRATA<sup>1</sup>, Steven HARDER<sup>3</sup>, Kate MILLER<sup>3</sup>, Masazumi ONISHI<sup>1</sup>, Yoshiyuki KANEDA<sup>3</sup> (Earthquake Research Institute, The University of Tokyo, Tokyo 113-0032, Japan, <sup>2</sup>Dept. Earth Sci., Chiba Univ., Chiba, 263-8522 Japan, <sup>3</sup>Dept. Geological Sciences, Univ. Texas El Paso, El Paso, TX 79968-0555 USA, <sup>4</sup>Japex Geoscience Institute Inc., Tokyo, 112-0012 Japan, <sup>5</sup>Japan Marine Science and Technology Center, Natsushima 2-15, Yokosuka, 237-0061, Japan)

The outer zone of SW Japan is a classical example of accretionary complex. Deep seismic reflection profiling by low-fold reflection method, were carried out along three seismic lines in the outer zone of SW Japan; MTL 1999, Shitara 2001 and Shikoku 2002. Many seismic profiles of the toe portion of subducting system have been published, however, the internal structure of the backstop is not fully understood. To obtain detailed seismic image of the outer zone of SW Japan is important to assess the risk of large mega-thrust earthquake such as Nankai earthquake of 1946 (M 8.0) and also for understanding processes of continental growth. This experiment was performed as a part of a larger scale seismic experiment of island arc transect conducted by the Japan Marine Science and Technology Center and Joint Japanese University teams. The low-fold seismic reflection profiling was carried out using explosive sources (30 AE500 kg). The receiver intervals were 50 to 120 m. The length of seismic lines is 12 km in MTL 98, 27 km in Shitara 2001 and 110 km in Shikoku 2002. Recording system used were CDP-cable system and Texan recorders. The geologic structure of outer zone of SW Japan shows strong similarity along the trench parallel direction. Based on the three seismic sections, the detailed crustal structure of outer zone of SW Japan were synthesized. The upper surface of the subducting Philippine Sea Plate are clearly imaged by flow-fold seismic reflection profiles. In the fore arc side of central Japan and Shikoku, the northward (back-arc side) dipping reflectors in the upper crust are dominated, interpreted as deeper extension of geologic boundaries of the accretionary complex. The outstanding feature is the existence of trench-ward dipping reflector in the

lower crust and above-mentioned northward dipping reflectors are converged to the trenchward dipping reflector forming wedge-thrust structures. This crustal structure demonstrated by reflection pattern suggests that the main part of the accretionary material is injected into the mid-crust of the overlying plate associated with wedge-thrusting since the late Cretaceous.

SS03/07A/A02-007

1100

#### CRUSTAL SECTION ACROSS THE HIDAKA COLLISION ZONE, HOKKAIDO, JAPAN, AS INFERRED FROM SEISMIC REFRACTION/REFLECTION PROFILING

Takaya IWASAKI, Research Group of HOKKAIDO TRANSECT (Earthquake Research Institute, the University of Tokyo)

The Hidaka collision zone, central part of the Hokkaido Island, Japan, is known as an ongoing collision zone between Kuril Forearc(KA) and the Northeast Japan Arc (NJA) since middle Miocene. A multidisciplinary project of Hokkaido Transect in 1998-2000 revealed various scale structural heterogeneity across this collision zone by seismic refraction/reflection profiling and very dense earthquake observation. A 227-km long refraction profile was undertaken to determine the whole crustal structure from NJA to KA. A series of seismic reflection lines, whose total length is 138 km, were concentrated in the central part of the refraction line to get a clear image of crustal deformation associated with the collision. The data obtained elucidated a complicated collision structure. In the eastern part of the profile, KA is covered with 0.3-4km thick highly deformed sedimentary layer, beneath which two eastward dipping reflectors are imaged in a depth range of 10-20 km, probably representing obducting middle or lower crust of KA. Actually its outcropped part has a relatively higher velocity and Vp/Vs than those of the surrounding part. Beneath these reflectors, another flat and westward dipping reflectors are situated at 25 and 25-27 km depths respectively. The obtained layer geometry forms wedge-like (crocodile) patterns, probably expressing that the crust of KA is delaminated into two or three segments beneath the Hidaka Mountains. The western part of the profile (NJA), which belongs to the fold-and-thrust belt of the collision zone, is characterized by a very thick (more than 5-10 km) sedimentary package including two or more velocity reversals. Beneath this package, the crystalline crust of NJA is traced with a slight eastward dip down to 20-25 km. The crustal image obtained is much complicated as compared with that in the southernmost part of the collision zone, where the crust of KA is delaminated into to segments forming a single wedge structure, indicating a significant regional difference in style of crustal deformation.

SS03/07A/A02-008

1115

#### CRUSTAL STRUCTURE AROUND THE NORTHERN PART OF THE ITOGAWA-SHIZUOKA TECTONIC LINE (ISTL), CENTRAL JAPAN, FROM REFRACTION/WIDE-ANGLE REFLECTION DATA

Tetsuya TAKEDA, Takaya IWASAKI, Hiroshi SATO, Shin'ichi SAKAI, Takashi IIDAKA (Earthquake Research Institute, University of Tokyo)

The Itoigawa-Shizuoka Tectonic Line (ISTL) is a major structural boundary and one of the most active faults, which divides SW and NE Japan. To reveal the crustal structure around northern part of ISTL is important for better understanding of the development of Japanese islands and estimation of strong ground motion produced from deeper extension of ISTL active fault system. To reveal the crustal structure around the northern part of ISTL, the refraction/wide-angle reflection data from three seismic lines obtained in 1967-1991 were re-analyzed with adding a new seismic data carried out in Itohizu 2002. The three dimensional feature of velocity structure of upper crust around northern part of ISTL is clearly demonstrated. Some reflectors located in the middle to lower crust were obtained by wide-angle reflection data. From a wide view, crustal structure is different between the eastern and western sides of ISTL. It is said geologically that ISTL played an important role in the Miocene opening of the Sea of Japan and bending of Japan island arc. It means that the difference of reflector distribution bounded by ISTL indicates the possibility of horizontal movement in the opening of the Sea of Japan or crustal deformation undergone by igneous activity. In the velocity structure, the layer with 4km/sec is found to have 4km depth in the western side of ISTL. It is consistent with the fact that sedimentary rocks since Miocene is thickly distributed in this area. ISTL is found to be east-dipping from gravity and reflection data. To take account that ISTL is lifting up in the east as a reverse fault at present, we think that ISTL was formed as east-dipping normal fault in mid-Miocene during initial phases and has been reactivated as a reverse fault owing to subsequent crustal shortening. Additionally, by analyzing travel times of micro-earthquakes below ISTL, we expect to obtain more detailed structure of the eastern side of ISTL, which is deformed strongly owing to crustal shortening.

SS03/07A/A02-009

1130

#### REFRACTION AND WIDE-ANGLE REFLECTION STUDIES BY USE OF MCS AND OBS IN MARMARA SEA, TURKEY (SEISMARMARA 2001)

Hideki SHIMAMURA<sup>1</sup>, Anne BÉCEL<sup>2</sup>, Jean-Claude LÉPINE<sup>2</sup>, Tuncay TAYMAZ<sup>3</sup>, Yoshio MURAI<sup>1</sup>, Philippe CHARVIS<sup>1</sup>, Yuichi NISIMURA<sup>4</sup>, Mireille LAIGLE<sup>5</sup>, Alfred HIRN<sup>6</sup>, Serdar OZALAYBEY<sup>7</sup> (<sup>1</sup>ISV, Hokkaido University, <sup>2</sup>Sismologie Expérimentale, Institut de Physique du Globe de Paris, <sup>3</sup>ITU, Istanbul Technical University, Maslak, Istanbul, <sup>4</sup>IRD-Géosciences Azur, Villefranche, <sup>5</sup>TUBITAK-MAM, Marmara Research Center, Gebze)

The SEISMARMARA survey 2001 was carried out as a multi-method approach of seismic structure and activity, in the frame of the Turkish-French-Japan cooperation on the Marmara Sea, Turkey, after the 1999 Izmit earthquake occurrence on the North Anatolian Fault. MCS survey was made by the French N/O Nadir of Ifremer, and 37 OBS of ISV Hokka?Eo were deployed, in order to record airgun shots and natural earthquakes, and recovered by a Turkish vessel MTA-Sismik 1. We present the first results of modelling proceeds on the two longest, East-West lines of Leg 1. . In order to assess effects of off-line propagation in this region of strong 3D structural variation, North-South cross-lines of the MCS grid can be drawn in as well. Another E-W line along the southern rim of the Trough is modelled, tying in with the Marmara-1 borehole that reached the Upper Cretaceous limestone, the basement to the evolution of the Trough. The 8100 cu. in. capacity of the 12-airgun array of N/O Nadir, and its shooting in single-bubble mode, provided for signal strength, low frequency with relatively short signal duration. The main regional line, striking E-W along the axis of the North Marmara Through, is 120 km long and has 13 OBS. The corresponding MCS stack with 15-fold coverage, obtained at normal incidence with the 4.5 km long 360-channels digital streamer, is used for structural constraints for the shallow part in the refraction modelling. The airgun array was also shot at 20 seconds interval to give a higher, 45-fold coverage for MCS meant at finer resolution, and the comparison with velocity control given by the streamer recording in shallow water will be used too Basement topography and structure of the lower crust is sampled and modelled by these data sets. In the case of the line on the rim of the Trough, the velocity model can be compared to the MCS which gives a reasonable structural image through the whole crust. On the axial line, new critical constraints are provided on the basement and deep structure across the succession of basins and highs, where the normal-incidence MCS image is complicated by strong multiples

and off-line echoes. These results will contribute to the analysis of the structural evolution of the Marmara trough with respect to the North Anatolian Fault, and bring constraints on the depth limits of the seismogenic layer involved in earthquakes to occur in the Marmara sea part of the North Anatolian Fault. Derivation of the velocity structure provides a frame necessary to refine earthquake location procedures in general. More specifically, the analysis of shot data on the 3 components of OBSS, give prime control on the local P and S velocity heterogeneity under the OBS which will be used as input in a detailed study of the local earthquakes also recorded on these same OBSS.

SS03/07A/A02-010

1145

#### REFLECTION OF THE CHANGES OF THE PHYSICAL PROPERTIES OF THE EARTH CRUST IN THE BULK-SOUND AND SHEAR WAVE-SPEED VARIATIONS

Alexei GORBATOV<sup>1</sup>, Brian L.N. KENNETH<sup>2</sup> (<sup>1</sup>Pacific Region Data Centre, IFREE, JAMSTEC, <sup>2</sup>Research School of Earth Sciences, ANU, Australia.)

Examination of bulk-sound and shear wave speed variations at the active boundaries of the tectonic plates may provide valuable information about the compositional or physical properties of the Earth material and mechanic of collision processes because this information can be directly compared with the results of laboratory experiments. Detailed global and regional tomographic inversions have been carried out using the arrival times for P and S wave ray paths with comparable coverage. The inversion was performed directly for bulk-sound and shear wave speed variations in the Earth's mantle. Global inversion was performed using cells with sides of 2 by 2 degrees while for the regional tomography cells from 0.5 to 2 degrees were chosen. A simultaneous inversion was undertaken for both the regional and global structures to minimize the influence of surrounding structures on the regional image. The nonlinearity of the inverse problem was taken into account by using a scheme which iteratively applied three-dimensional ray tracing and linearized inversion. Detailed regional tomography of the Western Pacific region reveals prominent correlation between bulk-sound and shear wave speed balance within the slab and the average age of the subducting lithosphere in the uppermost mantle of the subduction zones. Plates older than ~90Ma are more prominent on the shear wave speed images while younger slabs are more distinctive in the bulk-sound wave speed. The 90Ma break would correlate with the subduction of the full thickness of oceanic lithosphere and hence a mature thermal regime at the trench. However this correlation can be strongly altered by thermo-mechanical process affecting the subducting slab such as in the case of back-spreading and consequent roll back of the trench. This effect is well illustrated by subduction of old slab below Tonga-Kermadec. Roll-back of the trench is high below Tonga diminishing toward the Kermadec subduction zone. Subducted slab below Tonga is dominated by bulk-sound anomalies while the shear wavespeed becomes more prominent below Kermadec. This behavior of bulk-sound and shear wave speed anomalies detected on the regional tomography of Western Pacific is consistent with the images on the global scale for the Pacific region in general. However, the most peculiar feature in this area is the strong anticorrelation between bulk-sound and shear wavespeed anomalies for the San Andreas Fault system where the zone of strongly positive bulk-sound anomalies correspond to negative shear wave speed perturbations. Observed anticorrelation may be explained by strong fracturation and partial water saturation of this zone.

SS03/07A/A02-011

1200

#### MELT GENERATING PROCESSES AT THE SOUTHEARN EAST PACIFIC RISE REVEALED BY THE ELECTRICAL CONDUCTIVITY STRUCTURE

Kiyoshi BABA<sup>1</sup>, Alan D. CHAVE<sup>2</sup>, Rob L. EVANS<sup>3</sup>, Greg HIRTH<sup>4</sup>, Randall L. MACKIE<sup>5</sup> (<sup>1</sup>Institute for Frontier Research on Earth Evolution, Japan Marine Science and Technology Center, <sup>2</sup>Woods Hole Oceanographic Institution, <sup>3</sup>GSY-USA, Inc.)

Electrical conductivity structure models allow us to discuss mantle dynamics based on melt and water distribution beneath a mid-ocean ridge system. The electromagnetic data from the Mantle Electromagnetic and Tomography (MELT) experiment have been re-inverted for two survey lines. The major line crosses the East Pacific Rise at 17°S where the ridge segment is thick suggesting an abundant magma supply. The northern line crosses at 15°45'S to the north of an overlapping spreading center on a magma-starved ridge segment. The data are inverted for a two-dimensional anisotropic conductivity structure that incorporates correction for three-dimensional topographic effects on the magnetotelluric responses. The model space allows for different conductivity values in the along-strike, cross-strike, and vertical directions along with imposed constraints that the model be smooth and that the three conductivities be as close together as possible. The strength of these constraints is variable, and hence a range of models from isotropic to anisotropic can be explored. For the southern line, two end-member models (one isotropic and one anisotropic) were obtained which yield similar RMS misfits. Both models have a major gross feature which is also seen in previous MELT inversions: an asymmetric conductivity structure with higher values to the west of the ridge axis. In addition, the anisotropic model is more conductive in the cross-strike direction to the east of the rise at depths of 60-150 km, is quite resistive above 60 km, and has a narrow, highly conductive pipe in the vertical conductivity located immediately beneath the ridge axis. First two features are well resolved required by the data. The last feature is not strongly required by the data. But some tests show that it seems to be something real. The anisotropic model is more consistent with other geophysical and laboratory data, and hence is preferred. These results suggest that melt exists over a wide region, but may be more highly concentrated and connected in the vertical at the ridge axis. The deep (>60 km) conductive region to the east of the ridgecrest is probably due to the preferred orientation of olivine under wet conditions. The flat resistive-to-conductive boundary at 60 km agrees well with the inferred depth of the dry solidus of olivine. These results suggest that the extraction of water from olivine due to partial melting substantially reduces mantle conductivity. The northern line data have been analyzed in the same manner as the southern line data. The resulting conductivity structure will be compared with the structure of the southern line. The comparison may reveal along axis variation of the melt generation and transportation system.

SS03/07A/A02-012

1215

#### THE SIMULATOR EARTH'S CRUST MAKE BY BASE OF THEORY COVER

Stanislav G. DOLGIKH (Dep. Atmosphere and Ocean)

Today, be many simulator of Earth, but all are not describe processes, which run at crust, mantle and surface marking. We developed simulator earth's crust base by theory cover. This is multi-ply spherical shell with real parameters of earth's crust/ Shell laded outside and internal forces. The model is flexible, that is why we may take into many processes which run on Earth (variation of pressure, natural oscillations of reservoirs? Wave processes of ocean and so on). When we will take into a count all this processes, we can count a stress of shell. We will get exertions, deformations, transference, so whale shell, and so this is values at a specific dot. In the upshot, we receive physical consistent dynamic model multiply shell. If we will take into distributed load (atmospheric and mantle pressure), we will can get significance elastic parameters earth's crust and significance fundamental frequencies

its lays. Later, we will examine extra periodic load (vibrations and waves of ocean, atmosphere and lithosphere), impulsive force (earthquake, convulsion of nature, explosions and so on). In that case, we will get elastic parameters, all vibrations and its amplitudes of earth's crust.

Monday, July 7 PM

Presiding Chairs: R. Clowes, A. Gorbатов

SS03/07P/A02-001

1400

**ORIGIN OF GREAT DEPTHS OF THE PALAU AND YAP TRENCHES**

Kazuo KOBAYASHI (Prof. emeritus, Univ. of Tokyo)

Water depths of the Palau and Yap Trenches situated in the southeastern margin of the Philippine Sea plate appear to be extraordinary in a frame of general rule that the trench is deeper as the rates of convergence are larger and ages of subducted plate are older. Water depths of these Trenches amount to 8000 m in spite of their extremely small subduction rates (0 to 6 mm/yr at Palau and 6 to 12 mm/yr at Yap) and ages of subducting Caroline plate younger than 30 Ma. Morphology of these trenches does not seem to be a relic of past tectonic activity, because repeated submersible observation verified that their landward walls are frequently collapsed to provide plenty of slumped debris toward the axial bottom of the trenches. Observed topographic and seismic profiles show thin cover of sediment, implying that slumped materials have been subducted. Abnormally close proximity of the Palau and Yap Islands to the trench axis cannot be explained by collisional mechanism, as the trench in front of the islands is so deep. A simple quantitative model of viscous mantle beneath the horizontally moving plate accompanied with short subducted slabs is postulated to elucidate the present configuration of these trenches and arcs on the basis of the GPS data indicating fast horizontal motion of the Philippine Sea plate together with the Palau and Yap trench-arc systems. Reasonable values of downward frictional stress on the frontal surface of the subducted slab derived from the hydrodynamic model may be able to explain a new type of tectonic erosion, while appreciable amount of upward (buoyant) pressure acting at the edge of the overlying plate appears to be sufficient to hold the island arcs (Palau and Yap).

SS03/07P/A02-002

1415

**VOLCANIC-HYDROTHERMAL ACTIVITIES AND SEGMENTATION STRUCTURE OF THE AXIAL RIFT IN THE WESTERN OKINAWA TROUGH**

Takeshi MATSUMOTO<sup>1</sup>, Mamoru NAKAMURA<sup>2</sup>, Jean-Claude SIBUET<sup>1</sup>, Chao-Shing LEE<sup>3</sup>, Ryuichi SHINJO<sup>4</sup>, YK00-06 Scientific Party (Marine Science Department, Nippon Marine Enterprises, Ltd., <sup>1</sup>University of the Ryukyus, <sup>2</sup>FREMER, <sup>3</sup>National Taiwan Ocean University, <sup>4</sup>Japan Marine Science and Technology Center)

The western Okinawa Trough which is characterised by an active rifting of the eastern margin of the Asian continent and is one of the key areas to describe the tectonics and dynamics of the initiation and evolution of backarc basins was surveyed by R/V YOKOSUKA and DSV SHINKAI6500 in July-August 2000 (Lequios Cruise: Cruise ID = YK00-06 Leg2) after the succession of the previous l'Atalante cruise in 1996 in the SPOT Area (east of Taiwan). The major objectives of the cruise were: (i) formation and evolution of the central rift axes, (ii) volcanic and hydrothermal activity in the trough area, and (iii) regional tectonics and dynamics of the study area. Two active hydrothermal sites were newly located through 10 dives in the study area. One is located in the SPOT area and the other on the axial zone of the Okinawa Trough off the northern coast of Miyako Island. Maximum temperature was 170C in the former case and 150C in the latter case. Both sites are characterised by active chimneys associated with sulphide deposits and chemosynthetic communities. Regional topography surveyed by the SEABEAM2112 system shows the clear segmentation of the central graben. The eastern hydrothermal site is located on the junction of the two different segment ends. The SPOT hydrothermal site is also located at the segment end of the Yonaguni Graben. On the other hand, there were no signs of recent active magmatism or hydrothermalism in the segment centres. The central knoll on the Yaeyama Graben was precisely surveyed by both SEABEAM2112 bathymetry and seafloor observation by SHINKAI6500. The result showed that the knoll is rather old although it has an E-W trending rift valley on the summit. The seafloor surrounding the knoll deforms as if an elastic bending due to the load of the knoll is taking place. It suggests that no more active rifting is taking place at the axis of the segment of the graben. Back-arc rifting seems to be immature and it is now in the stage of cessation of rifting and only arc volcanism with a couple of focussed magma chamber at the segment boundaries is predominant. A couple of remarkably meandering channels were located at the westernmost part of the study area on both sides of the trough axis. The most remarkable is located in the SPOT area. These are apparently developed on levees derived from sediment supply from the continent and/or the Ryukyu island arc. The active erosion along the channel is not taking place any more according to the result by a previous ROV cruise in 2000. This might be due to mass wasting along the pre-existing levees towards the trough axis due to a local seafloor current which took place when the area was shallow.

SS03/07P/A02-003

1430

**NUMERICAL SIMULATION OF TECTONIC DEFORMATION WITH DISCRETE ELEMENT METHOD (DEM)**

Yasuhiro YAMADA<sup>1</sup>, Atsushi TANAKA<sup>2</sup>, Toshi MATSUOKA<sup>3</sup> (JAPEX Research Center, <sup>1</sup>Kyoto University)

Sandbox modelling, a physical modelling technique using granular materials, can simulate the brittle behaviour of the upper crust, thus has been successfully applied to a number of geologic structures in various scales. The sandbox models can also be done as numerical simulation (digital modelling) with the Discrete Element Method (DEM), because the DEM also approximates that the geologic body as an assembly of particles. As an example of DEM simulation of large-scale tectonic deformation, the collision process of the Indian subcontinent to the Eurasian Plate was examined. We employed the geologic model by Tapponier et al. (1976) and compared our simulation results with their analogue experiments. The overall geometry and progressive development of major fault systems associated with secondary basins showed similarity between the two techniques. The fragmentation of continental blocks, a characteristic feature in the analogue models, was also reproduced by the simulation. The secondary fault systems seen in the experiments were, however, unclear in the simulation, because the size of the particles may be too large. In addition, we have extracted information of each particle, such as velocity vectors and stress fields. These can be compared with GPS and in-situ stress data, which express present deformation of the eastern Asian region. Despite the technique needs further refinements in the input parameters, application of the DEM to geologic deformations can be a powerful tool to simulate fault related structures and to analyse the deformation quantitatively.

SS03/07P/A02-004

1445

**CRUSTAL GROWTH AND RECYCLING: AN OVERVIEW OF RESULTS FROM THE CANADIAN LITHOPROBE PROGRAM**

Ron M. CLOWES (LITHOPROBE and Dept. of Earth and Ocean Sciences, University of British Columbia)

The North American continent has grown through the progressive accretion, dispersal and re-aggregation of continental lithosphere in tectonic cycles spanning Archean to present times. The preserved crustal record in Canada ranges from the 4025 Ma Acasta gneisses in the northwestern Slave Province of the Northwest Territories to present oceanic crustal formation at the Juan de Fuca ridge off the west coast. The basic building blocks of the continent include: significant Middle to Late Archean crust preserved in supracrustal belts and plutonic rocks of the core of the continent (the Superior, Nain, Slave, Rae, Hearne and Wyoming cratons); the Paleoproterozoic orogenic belts that permanently welded the Archean cratons together (Trans-Hudson, New Quebec, Torngat, Wopmay, Thelon-Taltson, and Penokean); and the Mesoproterozoic Grenville, Paleozoic Appalachian and Mesozoic-Cenozoic Cordilleran orogenies that border the Paleoproterozoic nucleus of the continent. In the southern part of the amalgamated continent, Laurentia, the Keweenaw rift system almost split the continent about 1100 Ma. LITHOPROBE transects have focused scientific studies on almost all of these primary features of Canada's landmass and offshore continental margins. From the new geophysical, geological and geochemical data generated by these studies, enhanced understanding of these features has been achieved. By contrasting and comparing results among the many transects, new understanding of the processes associated with crustal growth, recycling and preservation also is being derived. Accreted oceanic terranes or collages of such terranes, comprising ocean floor basalts, oceanic arcs and back arc assemblages, are fundamental building blocks in the development and growth of evolving orogens. Throughout the LITHOPROBE studies, examples abound among transects and regions ranging from Archean to Cenozoic. Subduction zones can be responsible for crustal growth through subduction underplating. Two prominent examples of such underplating have been demonstrated in western North America. Collisional processes associated with orogenic development contribute to crustal growth, but the direct evidence for the sutures resulting from the collisions is often very cryptic, as they have been metamorphosed, reworked by later deformation and intruded by marginal (Andean-type) arc magmas. These magmas, derived from subducting slabs and the mantle wedges above them, form the impressive and extensive granitoid batholiths occupying the hinterlands of orogens. LITHOPROBE studies encompass a number of these. Magmatic underplating is a known process for continental growth, but one that often is difficult to identify and establish, as the effects of the process are usually manifest in the lower crust or upper mantle. High seismic velocities, as inferred from refraction experiments and generally poor seismic reflectivity, can indicate such underplating. Lithospheric delamination and transfer of lower crust and uppermost mantle to deeper parts of the mantle is one primary process by which crustal material is recycled into the mantle. Vast volumes of crustal material are recycled and reorganized through erosion and subsequent sedimentary deposition. LITHOPROBE has some outstanding examples of these processes.

SS03/07P/A02-005

1500

**BIFROST PROJECT: FENNOSCANDIAN CRUSTAL STRAIN RATE FROM CONTINUOUS GPS OBSERVATIONS AND SEISMICITY**

Hans G. SCHERNECK<sup>1</sup>, Ruediger HAAS<sup>1</sup>, Ronald ARVIDSSON<sup>2</sup>, Sten BERGSTRAND<sup>1</sup>, Jan JOHANSSON<sup>1</sup>, Glenn A. MILNE<sup>3</sup> (<sup>1</sup>Chalmers University of Technology, <sup>2</sup>Uppsala University, <sup>3</sup>University of Durham)

Postglacial rebound appears to be the dominant component of recent crustal motion in the Fennoscandian shield. From 3000 daily solutions of GPS data in the BIFROST network we have derived a map of strain rates in the interior of the shield with values typically below 10 nano/year. Examination of the strainfield by means of a glacial isostatic adjustment model suggests that elastic extension is the dominant style of deformation in the lithosphere, controlled by horizontal displacement. Shear exists between a major axis oriented in NW-SE and a minor strain axis, that are both extending. The major and minor strain rates stand in a proportion of 2:1. We also find that vertical motion and bending have little direct importance for strain. The NW-SE orientation of the horizontal strain rate field remains fairly constant within the formerly glaciated area. Superposition of a plate tectonic stress field on the stress change inferred from our study suggests that the fault stability margin for primary faults is increasing.

SS03/07P/A02-006

1515

**SOME PECULIARITIES OF THE STRUCTURE OF THE EARTH'S CRUST IN THE CENTRAL ASIA (A REGIONAL PROFILE-ROMITAN-DARBAZATAOU IS TAKEN AS AN EXAMPLE)**

Oleg Petrovich MORDVINTSEV (Uzbekgeophysic)

Seismic profile Romitan-Darbazataou is located within the three main region's structures: Karakum-Tadjik massif, Southern Tien Shan geocline folded system, Kuramin-Fergan intermediate massif. The section is characterized by the presence of a large number of seismic boundaries of different extent. The inclination boundaries are located principally in the upper part of the Earth's crust, about 20km deep. A system of rupture disturbances covering practically the entire geological section has been revealed. The results of physico-geological modelling showed that the Earth's crusts structure has blocky-stratified character. One of the main features of the section is its heterogeneous basement: in Karakum-Tadjik massif. Its depth is 5-7km; in Southern Tien Shan- from 1km up to the surface; in Kuramin-Fergan intermediate massif- from 2 to 3km. The Earth's crusts deep horizons structure along the section is blocky, with intensive breaking, and differentiation of physical properties of rocks. The unique feature of the section is the presence of strong unconsolidated zones. The Moho transition zone, which thickness is 2.5 to 6km, is distinguished above the Mohorovichich section. Its density varies from 3,05 to 3,1 g/cm<sup>3</sup>. The upper mantle density increases towards Southern Tien Shan (from 3,23 to 3,26 g/cm<sup>3</sup>). The revealed rupture disturbances often reach Moho. Very often rupture disturbances form, very complicated systems, in which various tectonic structures are found.

SS03/07P/A02-007

1600

**A POSSIBLE DEEP, LONG-TERM SOURCE FOR WATER IN THE NORTHERN SAN ANDREAS FAULT SYSTEM AND OTHER BROAD PLATE-BOUNDARY ZONES: A GHOST OF SUBDUCTION PAST?**

Stephen Homer KIRBY<sup>1</sup>, Kelin WANG<sup>2</sup>, Thomas M. BROCHER<sup>1</sup> (<sup>1</sup>U.S. Geological Survey, <sup>2</sup>Geological Survey of Canada)

Previous work suggests that forearc mantle is serpentinized in warm-slab subduction systems because the subducting slab cools the forearc and because water from slab

dehydration of the mafic crust is released into the forearc mantle above it at depths of 40 to 80 km (See review in Kirby, Nature News & Views, 2000). Recent work by others shows that the Moho is not expressed in the Cascadia forearc of western Oregon and Washington and suggests this is because the mantle is partially or completely serpentinized by this mechanism. Rick Blakely of the USGS has also identified a margin-parallel magnetic anomaly in Oregon at the expected position of the serpentinized forearc mantle. Magnetite, an accessory mineral in serpentinites, may be the source of this magnetic anomaly. The continental margin of northern and central California south of the Mendocino triple junction is made up of former forearc crust and mantle of the Cascadia system. We propose here that this relic serpentinized wedge in the former forearc mantle has relevance to the San Andreas fault (SAF) system to the south because this initially cold, serpentinized region is not stable after the Mendocino triple junction moves north and subduction ceases. This broad (about 100 km) wedge-shaped region should heat up by conduction and hence is expected to dehydrate over time and release water into the overlying crust. Numerical thermo-petrologic simulation of this water evolution suggests that it takes from 10 Ma to greater than 20 Ma for water source to be exhausted. The distance between the center of this unstable mantle serpentinite wedge and the fossil trench or deformation front is determined by the distance at which slab depth is about 60 km. Allowing for the breadth of this region and for the possibility of variations in original slab dip (12 to 25°), the wedge should be at a distance ranging from 50 to 250 km from the former trench. This range brackets with the range of distances between the base of the California continental slope (positioned as the former position of the trench) and the traces of faults of the SAF system, suggesting that the San Andreas fault system may be positioned above this dehydrating mantle wedge. The total volume of water stored in the wedge is huge, estimated to be 0.6 to 1.2 Gm<sup>3</sup>/m of margin. Its release over time provides a deep source of water, possibly reducing the effective normal stress across this fault system, reducing the resistance to frictional sliding and, in turn, explaining the inferred low regional stresses and the lack of a heat-flow anomaly. The dehydrating wedge may also be a deep source region for serpentinite slivers that occur along the SAF System. The effectiveness of this water source in elevating pore pressures to near lithstatic (and hence lowering effective pressure and sliding resistance) depends on the distribution of permeabilities of the crust above the wedge relative to the water release rate.

SS03/07P/A02-008

1615

#### EARTHQUAKE ACTIVITY IN THE MESSINA STRAIT AREA, SOUTH ITALY, POSSIBLE INTERPRETATIONS AND HAZARD IMPLICATIONS

Giancarlo NERI<sup>1</sup>, Graziella BARBERI<sup>2</sup>, Barbara ORECCHIO<sup>1</sup> (<sup>1</sup>Department of Earth Sciences, University of Messina, <sup>2</sup>Istituto Nazionale di Geofisica e Vulcanologia, Sezione di Catania, Italy)

We analyzed the recent (1978-2001) crustal seismicity of northeastern Sicily and surroundings using the local and national instrumental seismic network data. The analysis allowed us to determine the space distribution of seismogenic stress and seismic strain in the study area and to obtain information on the faults active during the investigation period. The results evidence a clear transition from an extensional regime in the Messina Strait area (maximum magnitude 7 in historical times) to a north-south compressional regime to the west (max. magnitude 6), in agreement with the regional geodynamic model assuming that north-south slow plate convergence coexists with subduction slab southeastward rollback in the study area. Based on the joint examination of (i) recent seismicity, (ii) earthquake activity in historical times and (iii) information from geology and paleoseismology taken from the literature, we evaluate the possible evolution of earthquake activity in the study area, including the possibility that the temporal cluster of strong earthquakes of 1783, 1905 and 1908 has not yet ended, in opposition to what has been recently suggested by other investigators.

SS03/07P/A02-009

1630

#### LITHOSPHERIC DELAMINATION AND BUOYANCY-DRIVEN DEFORMATIONS IN THE CENTRAL APENNINES, ITALY

Abdelkrim Aoudia<sup>1</sup>, Alik T. ISMAIL-ZADEH<sup>2</sup>, Giuliano F. PANZA<sup>3</sup> (<sup>1</sup>SAND Group, Abdus Salam International Centre for Theoretical Physics & Dept. of Earth Sciences, University of Trieste, Trieste - Italy, <sup>2</sup>Geophysikalisches Institut, Universität Karlsruhe, Karlsruhe, Germany & International Institute of Earthquake Prediction Theory and Mathematical Geophysics, Russian Academy of Sciences, Moscow, Russia)

The coexistence of two end-member deformation mechanisms (contraction and extension) has been recognized in different geodynamic frameworks worldwide, but well exposed at the surface and active nowadays only in the Italian Peninsula. Several models, invoking mainly external forces, have been formulated to explain the complex pattern of the regional deformations, observed by geophysical and geological studies. These models appeal to interactions along plate margins or at the base of the lithosphere such as back-arc extension or shear traction from mantle flow or to subduction processes such as slab pull, roll back or retreat and detachment or break-off. We combine seismic data from Central Italy to image the crust and upper mantle and to understand the complex lithospheric deformations observed in the Apennines. The well-developed low velocity zone in the uppermost mantle between the crust and the underlying continental lithosphere supports the lithospheric delamination beneath the peninsula and provides a new background for the genesis and age of recent magmatism. A finite-element modeling of deformation and tectonic stress in the imaged lithosphere shows that buoyancy solely can explain the enigmatic juxtaposed crustal contraction and extension and the unusual intermediate-depth seismicity distribution.

SS03/07P/A02-010

1645

#### PORE PRESSURE RELATED SEISMICITY IN CRITICAL EARTH - A MODEL OF THE PHENOMENON AND APPROACHES TO THE MEDIUM CHARACTERIZATION

Serge A. SHAPIRO, Susanne RENTSCH, Elmar ROTHERT, Miltiadis PAROTIDIS (Fachrichtung Geophysik, Freie Universität Berlin)

Processes of pore fluid substitutions or borehole fluid injections influence stress states of rocks. Such processes are typical for developments of hydrocarbon or geothermic reservoirs. Recently they obtained also a central place in different scientific programs like carbon sequestrations or investigations of large scale fault systems. The observation of microseismicity occurring during such borehole fluid injections or extractions has large potential in understanding of physics of the seismogenic process as well as in obtaining detailed information about reservoirs at locations as far as several kilometers from boreholes. We show that principal spatio-temporal signatures of fluid injection induced microseismicity are very often in agreement with the hypothesis that the triggering of this seismicity is caused by a diffusive process of the pore pressure relaxation in porous (or fractured), fluid saturated rocks. If this hypothesis is correct, then there should be two physical parameters which control the spatio-temporal distribution of the induced seismicity. One parameter characterizes the criticality of the geological medium. It can be represented as a statistic field of critical porous pressure necessary for initiating sliding on preexisting cracks. The second parameter is the hydraulic diffusivity. Theoretically and numerically we show which signatures of the spatio-temporal distributions of the seismic events must be expected and

how they are related to the critical porous pressure and to the diffusivity. We show also that these signatures are observed in many cases of artificial and natural pore pressure perturbations in rocks. In such situation our model of the induced seismicity provides a possibility to infer an information about hydraulic properties of rocks and their criticality using passive seismic monitoring data. Estimates of hydraulic diffusivity tensors on large spatial scales as well as imaging of its distributions in space can be of significant importance for industrial applications and understanding of physical properties of geological structures. From the other hand, a characterization and animation of the medium criticality open new possibilities in studies of seismogenic processes. We results of applications of our approach to microseismic data obtained in different crystalline and sedimentary rocks.

SS03/07P/A02-011

1700

#### RHEOLOGY OF THE LITHOSPHERE INFERRED FROM POSTSEISMIC DEFORMATION IN NORTHERN JAPAN AND WESTERN US

Takuya NISHIMURA<sup>1</sup>, Wayne THATCHER<sup>2</sup> (<sup>1</sup>Geographical Survey Institute, <sup>2</sup>U.S. Geological Survey)

We have modeled the postseismic deformation of the 1959 M<sub>7.3</sub> Hebgen Lake earthquake which is a normal faulting event in the northern Basin and Range province, USA and the 1993 M<sub>7.8</sub> Hokkaido-Nansei-Oki earthquake which is a thrust faulting event in northern Japan. The broad uplift in the epicentral area of the Hebgen Lake earthquake is measured by leveling. The transient deformation decaying after the 1993 Hokkaido-Nansei-Oki earthquake is observed by a continuous GPS network. To fit the observed deformation we calculate synthetic postseismic deformation using the relaxation response of a gravitational viscoelastic Earth to the earthquake. For a model with an elastic plate overlying a viscoelastic half-space (hereafter called two-layer model), we estimated the elastic thickness and the half-space viscosity. In the case of the Hebgen Lake earthquake, we find the elastic thickness is 38±8 km. The half-space viscosity is estimated at 4×10<sup>18</sup> Pa s. The observed broad uplift cannot be explained by a physically plausible model of afterslip on and below the coseismic fault. However, local deformation across the coseismic surface rupture requires shallow afterslip reaching the surface. In the case of the Hokkaido-Nansei-Oki earthquake, both an afterslip model and a viscoelastic relaxation model can explain the observed horizontal deformation. The observed broad uplift ~100km east of the coseismic fault requires viscoelastic relaxation model. However, leveling data on Okushiri Island which is located just east of the coseismic fault show tilt of the island toward NNE and favor the afterslip model. When we assume the two-layer model, the elastic thickness is 32±12km with the half-space viscosity of 2.5×10<sup>18</sup> Pa s for the data set excluding Okushiri Island. We need a dual model of viscoelastic relaxation and afterslip to explain all the data. The elastic thickness in both regions is approximately equal to the local crustal thickness. We applied more complex viscoelastic structures with weak lower crust and/or strong uppermost mantle to fit the observed deformation from both earthquakes. However the residual misfit is not significantly smaller than the simple two-layer model. The postseismic deformation induced by the estimated viscoelastic structure decays exponentially with a time constant of a few decades. Because of coupling between the elastic layer and the viscoelastic substrate this relaxation time is significantly longer than the Maxwell relaxation time of the viscous half-space itself (a few years). Our result suggests the importance of postseismic relaxation in interpreting high precision GPS velocities. For example, our model results suggest that postseismic transient velocities from both the 1993 Hokkaido-Nansei-Oki and the 1983 M<sub>7.7</sub> Japan Sea earthquakes in northern Japan are currently as large as 8 mm/yr.

SS03/07P/A02-012

1715

#### STRAIN ACCUMULATION MODEL ON THE ATOTUGAWA FAULT SYSTEM, AN INLAND ACTIVE FAULT SYSTEM, LOCATED IN THE HIGH-STRAIN RATE ZONE, CENTRAL JAPAN

Kazuro HIRAHARA, Mamoru HYODO, Yoichi OOI (Graduate School of Environmental Studies, Nagoya University)

Recently, GEONET, a nation-wide GPS network by GSI, Japan, has revealed a high-strain rate zone, NKTZ, in central Japan (Sagiya et al., 2000). Around the Atotsugawa fault located within this zone, we set a dense GPS network. In addition to GEONET observations, our 5-year-observations elucidate the detailed strain accumulation on this fault system. Here, based on numerical simulations using GeoFEM (Iizuka et al., 2002), a parallel FEM code, we present a quantitative model of strain accumulation both regionally in the 100-km-wide NKTZ and locally in the Atotsugawa fault system within NKTZ. In a regional scale, the strain accumulation in NKTZ is basically explained by the model proposed by Iio et al. (2002). They propose that the eastward subduction of the Pacific plate (PAC) beneath the Japan trench, which is located far from NKTZ, produces the strain accumulation in NKTZ beneath which the crust is weakened by water content in the lower crust. Hyodo and Hirahara (2003) execute numerical simulations in models consisting of the 30km-thick elastic crust, the viscoelastic upper mantle wedge and the subducting elastic PAC, and find another requirement to explain the observed small strain rate in the Kanto region and to produce a long-range transfer of the effect of the subducting PAC. That is, there are no large interplate earthquakes during a period enough longer than the relaxation time of the whole viscoelastic system. Long-term plate coupling of PAC without any rebounds due to interplate earthquakes produces the relaxed viscoelastic upper mantle and the uniformly strained elastic crust. Actually, there are almost no large interplate earthquakes off the Kanto, while the Tohoku region has smaller recurrence interval of earthquakes and the large strain is accumulated in the ocean side. We seek the local thickness of elastic crust beneath NKTZ so as to produce the observed strain rate in this zone, and obtain the thickness of 5 km. In this zone, there are micro-earthquakes and the cut-off depth is around 15 km. Thus 5km-thick elastic crust is not realistic. Recent explosion seismology suggests a possibility of low-velocity zone beneath NKTZ, and the elastic crust in NKTZ will have smaller rigidity than in the surroundings. If this is the case, using the 15km-thick weak elastic crust, we can produce the observed strain concentration. In a local scale close to NKTZ, the rate the direction normal to the strike of the Atotsugawa fault is changing within a width of 100km, and the rate change is symmetric against the center. The fault-parallel rate change with a width of 40 km, however, is not symmetric, but the larger change appears in the northern size where the Atotsugawa fault system exists. And our dense GPS observations show the fault-parallel rate change occurs across the Atotsugawa fault and across the northern Ushikubi one, which seem to be creep. These features of observed rate field are explained by the model consisting of lateral structural changes within NKTZ, the weak region of the Atotsugawa fault system.

SS03/07P/A02-013

1730

#### CRUSTAL STRUCTURE BENEATH THE YINGGEHAI BASIN AND ADJACENT HAINAN ISLAND, AND ITS TECTONIC IMPLICATION

Shimin WU<sup>1</sup>, Xuelin QIU<sup>1</sup>, Gangping ZENG<sup>2</sup>, Di ZHOU<sup>1</sup>, Kanyua XIA<sup>1</sup>, Saijun LIU<sup>2</sup>, Sanyu YE<sup>1</sup> (<sup>1</sup>South China Sea Institute of Oceanology, CAS, <sup>2</sup>State Seismological Bureau, Hainan Branch, Haikou 570203, China, <sup>3</sup>GEOMAR, Research Center for Marine Geosciences, Kiel D-24148, Germany)

In the autumn of 1996, a joint team of Sino-German scientists carried out a wide-angle seismic experiment in the northwestern part of South China Sea. Two NE-SW trending wide-angle seismic profiles were surveyed across the Chinese side of the Yinggehai basin (YGHB) with Ocean-Bottom-Hydrophones (OBH) and piggyback recorded by onshore stations on Hainan Island. Detailed velocity-depth models were obtained through traveltimes modeling and partially constrained by amplitude calculations. The more than 10 km thick Tertiary sedimentary infill within the YGHB can be divided in three layers with distinct velocity-depth distribution. The top layer has overall a high velocity gradient with 3.8-4.1 km/s at its bottom, consistent with advancing compaction and diagenesis. Its thickness increases gently towards the basin center, reaching 4.5 km along the southern profile. The middle layer is characterized in its most part as a pronounced low velocity zone with velocity as low as 3.0 km/s. Its thickness increases from 3.0 km to over 4.5 km from NE towards SW. The velocity at the top of the lower layer is estimated about 4.5 km/s. Despite of strong energy source used (4x12L airgun array) no seismic signals, particularly not even the highly anticipated reflection from the basement, can be observed from deeper crustal level within the basin. Towards the NE the basin is bounded sharply by a clear and deep basement fault, the so called Fault No. 1. The bordering continental crust has a constant thickness of 28 km and shows no sign for crustal thinning towards the basin center, giving clear evidence that the eastern basin boundary, Fault No. 1, is a strike-slip fault. The crustal structure obtained in this study favors clearly the hypothesis that the YGHB is a narrow pull-apart basin formed by the sinistral strike-slip faulting of the Red River Fault Zone.

SS03/07P/A02-014

1745

#### POST SEISMIC CRUSTAL DEFORMATION IN KUTCH REGION OF GUJARAT, INDIA

Chappidi D. REDDY<sup>1</sup>, Kaoru MIYASHITA<sup>2</sup>, Teruyuki KATO<sup>3</sup> (<sup>1</sup>Indian Institute of Geomagnetism, <sup>2</sup>Department of Environmental Science, Ibaraki University, Mito 310-0903, Japan, <sup>3</sup>Earthquake Research Institute, The University of Tokyo, Tokyo 113-0032, Japan)

The Bhuj Earthquake occurred on January 26, 2001 was a major intra-plate event in the Indian sub-continental plate. In order to estimate the distribution of strain accumulation rate and understand the physics of the earthquake processes, five GPS campaigns were made in Kutch region of Gujarat during 2001-2002. The data collected at 14 sites were organized into 24 hours segments covering a UTC day and were processed using the GAMIT/GLOBK software to estimate the velocity vectors at each site in the ITRF2000 reference frame. The velocity field clearly portrays anomalous velocity at two sites viz. Dhamdkapur and Ratanpar which fall either side of the epicentral track region. Compressional strain of about 0.1 micro-strain/yr has been estimated in the vicinity of the source region. Finite element modeling is attempted to facilitate interpretation of neo-tectonic movements that can generate repeated earthquakes. The results are discussed in conjunction with the geo-tectonics of the study region and other geophysical studies such as GDS, MAGSAT, magnetic etc.

SS03-Posters

Tuesday, July 8

#### TECTONOPHYSICS AND CRUSTAL STRUCTURE

Location: Site D

Tuesday, July 8 AM

Presiding Chairs: R. Clowes, A. Gorbатов, S. Beck, W.-Y. Kim

SS03/08A/D-001

Poster

0830-160

#### P-P REFLECTIVITY MAPPING OF THE PLATE BOUNDARY IN THE JAPAN TRENCH SUBDUCTION ZONE

Gou FUJIE<sup>1</sup>, Junzo KASAHARA<sup>2</sup>, Ryota HINO<sup>3</sup>, Masanao SHINOHARA<sup>2</sup>, Kiyoshi SUYEHIRO<sup>1</sup> (<sup>1</sup>JAMSTEC, <sup>2</sup>Earthquake Research Institute, University of Tokyo, <sup>3</sup>Faculty of Science, Tohoku University)

In the Japan Trench area, many destructive earthquakes, as well as microearthquakes, have occurred. The Pacific plate is subducting beneath the Japanese island arc at this Trench. It is considered that most of the earthquakes are caused by plate subduction motion. Therefore, it is extremely important to clearly characterize the physical state of the plate boundary in order to understand theseismic activity in this region. In this subduction zone, there is a low seismic region with 100km-long and 30km-wide south of latitude 39 degrees N, and we conducted seismic refraction and reflection experiments there. We discovered an interesting feature that implies that the P-P reflectivity of the plate boundary correlates with seismicity: we observed distinct large amplitude reflected waves from the aseismic plate boundary located around 13km deep from the oceanic surface. This intense reflection implies the presence of low velocity materials along the subduction plate boundary. There is another low seismic region to the north of latitude 39 degrees N. This low seismic region is narrower than the one to the south. We placed a dense Ocean Bottom Seismometers (OBSs) with two dimensional array: Twenty-seven OBSs were deployed in a 10km x 40km area with 5km spacing. This dense OBS network enabled us to image the reflection phase from the plate boundary in 2D space. First, we analyzed the P-wave velocity structure with a traveltime inversion method using traveltimes of the first arrival and several reflection phases. Then, we computed reflected waves from the plate boundary and determined the reflection points and traveltimes. Using this information, we created a Move-out Seismic Record Section to image the plate boundary reflection waves using a method like the Normal Move Out (NMO) method often used in conventional MCS analysis. In this presentation, we will show the seismic record sections of the plate boundary. Although the reflections from the northern low seismic region are not as intense as the southern region, we observe clear reflection phases from the northern low seismic region in these sections. This result also implies seismicity correlates well with characteristics of the plate boundary.

SS03/08A/D-002

Poster

0830-161

#### LOW INTENSITY CHARACTERISTIC OF PLATE-BOUNDARY S-S REFLECTIONS WITHIN A REGION OF INTENSE P-P REFLECTIONS AND LOW SEISMICITY ALONG THE JAPAN TRENCH SUBDUCTION ZONE

Kimihiko MOCHIZUKI<sup>1</sup>, Junzo KASAHARA<sup>1</sup>, Mikako NAKAMURA<sup>1</sup>, Ryota HINO<sup>2</sup>, Minoru NISHINO<sup>3</sup>, Tomoaki YAMADA<sup>1</sup>, Asako KUWANO<sup>2</sup>, Toshinori SATO<sup>2</sup>, Yasuyuki NAKAMURA<sup>4</sup>, Peyman Poor MOGHADDAM<sup>5</sup>, Toshihiko KANAZAWA<sup>1</sup> (<sup>1</sup>Earthquake Research Institute, University of Tokyo, <sup>2</sup>Tohoku University, <sup>3</sup>Chiba University, <sup>4</sup>Ocean Research Institute, University of Tokyo)

It has been pointed out that space distribution of microearthquakes along the forearc slope of the Japan Trench in northeast Japan is not uniform. A location map of the microearthquake epicenters determined by Tohoku University show clustered seismically active zones, which are oriented perpendicular to the trench axis. One of the clear seismic-aseismic boundaries

can be identified in latitude 39 degrees north. A seismic velocity structure survey was conducted in 1996 with one experiment line running over the boundary and parallel to the trench axis. A P-wave velocity structure model was obtained by travel-time inversion for the line (Fujie, 1999). A quite good anticorrelation between plate-boundary-reflected P-P wave intensity and seismicity was found: strong plate-boundary P-P reflected waves were observed in a region where seismicity is quite low, and vice versa (Fujie et al., 2002). They discussed that a thin layer with its thickness up to a few hundred meters and with its velocity of 3-4 km/s could explain the intense reflections at the plate boundary. Results of finite-difference waveform calculations support this estimation (Moghaddam, 2002). Understanding the characteristics of S-S reflection at the plate boundary as well as S-wave velocity structure in addition to those of P-wave would greatly help put better constraints on the physical properties along the plate boundaries. We carried out a seismic experiment in 2001 in the same region as the 1996 experiment. Thirty-nine OBSs were deployed along seven survey lines within a 30 km x 50 km region. One of the lines (Line 3) closely overlaps a part of the 1996 NS-line. Airguns were used as artificial seismic sources, and their total chamber volume was ~57 liters. Absolute orientations of OBS horizontal-component seismometers were determined using horizontal-component waveforms of the direct water-wave arrivals of the airgun shootings (Yoneshima, 2001). Substantial P-to-S conversion at the base of the sediment layer was observed by most of the OBSs. S-wave velocity structure in terms of Vp/Vs ratio along Line 3 was determined as regarding that P-wave velocity structure along Line 3 does not change much from that of Fujie et al. (2002). Velocity structure of the sedimentary layers above the acoustic basement was determined by observing the tau-p mapping of the OBS horizontal-component waveforms. The Vp/Vs ratios within the sediment layers were obtained as 5.2 and 2.3 from top to bottom. The Vp/Vs ratios within the deeper structure were assumed to be 1.8 to 1.74 as Vp varies from 4.5 km/s to 8.0 km/s. The computed travel times with respect to this Vs structure explain well the observed travel times of P-S converted refraction arrivals. Expected arrival times of the plate-boundary S-S reflected waves were calculated with respect to the obtained Vs structure. Such intense amplitude as observed for the plate-boundary P-P reflections were not identified for the S-S reflections. Although the plate-boundary P-P intense reflections could be explained by putting a thin low-velocity layer, some additional features for S-S reflections along the plate boundary may be required, such as very low Q values for S-wave propagation.

SS03/08A/D-003

Poster

0830-162

#### SPATIAL RELATION BETWEEN INTERPLATE SEISMIC ACTIVITY AND THE SEISMIC REFLECTOR BENEATH THE EAST OFF BOSO PENINSULA INDICATED BY P-S CONVERTED WAVES

Hisanori KIMURA, Keiji KASAHARA (National Research Institute for Earth Science and Disaster Prevention, Japan)

For the purpose of damage mitigation in Tokyo metropolitan region of Japan, it is important to study the characteristics of large interplate earthquakes that occur, repeatedly, around Kanto district. Almost all events occurring in the shallower part of this region have thrust type focal mechanism solution with P-axis corresponding to the direction of relative plate motion between Philippine Sea plate (PHS) and Kanto district. And thus, these events are thought to be interplate seismic activity caused by the PHS plate subducting from Sagami trough and extending beneath Kanto district. In the east off Boso peninsula, a few multi-channel seismic surveys were conducted by NIED and JNOC (Japan National Oil Corporation). By analyzing those data (Kimura and Kasahara, 1997; Kimura and Kasahara, 2001) major reflectors have been found dipping northward along the survey line coincident to the plate boundary between PHS plate and landward plate. The candidates of these reflectors may be the upper and lower boundary of oceanic crust of PHS plate or rocked sediment layer which is observed east off Izu peninsula. The profile near Sagami trough support the possibility of latter and these reflectors are observed, too. In Kujukuri region, two-way travel time of the reflected wave is about 6.0sec and 7.5sec suggesting that depth of the reflector is about 14 and 18 km which is close to earthquake hypocenters. To evaluate detailed spatial relation of major reflectors and earthquakes, we investigate the waveform data of micro-earthquakes around Kujukuri region, in detail. As a result, a remarkable phase is detected below S wave. The radial component is dominant, for this phase, and its travel time difference from that of P is slightly dependent on the change of depth and hypocentral distance. Comparing the observed travel time and calculated one we conclude that this phase corresponds to P-S converted wave at the discontinuity just above hypocenters. This interpretation is also supported by the radial component dominating of this phase. Travel time difference between S-wave and this phase is 0.2-0.3 sec for shallowest event indicating that earthquakes occur just beneath the discontinuity and do not occur exactly at the major discontinuity. From the past research such as Sekiguchi, 2000 indicates that depth of earthquakes is close to that of lower reflector. Supposing that the discontinuity corresponds to lower reflector in consideration of travel time difference between S and this phase, at the depth of upper reflector, reflected waves are excited but converted waves are not. As a cause of upper reflector, the water layer which was generated there due to plate motion could be suggested in this case. Anyway, the fact that earthquakes occur just close to discontinuity would be important to study the characteristics of interplate seismicity.

SS03/08A/D-004

Poster

0830-163

#### DEEP SEISMIC PROFILING OF METROPOLITAN AREAS IN JAPAN FOR STRONG GROUND MOTION EVALUATION: PRELIMINARY RESULTS OF BOSO 2002 AND SAGAMI 2003

Hiroshi SATO<sup>1</sup>, Naoshi HIRATA<sup>1</sup>, Tanio ITO<sup>2</sup>, Takaya IWASAKI<sup>1</sup>, Kazuki KOKETSU<sup>1</sup>, Keiji KASAHARA<sup>1</sup>, Kiyoshi ITO<sup>3</sup>, Takeshi IKAWA<sup>3</sup>, David OKAYA<sup>4</sup>, Steven HARDER<sup>5</sup>, Kate MILLER<sup>6</sup> (<sup>1</sup>Earthquake Research Institute, The University of Tokyo, <sup>2</sup>Dept. Earth Sci., Chiba Univ., Chiba, 263-8522 Japan, <sup>3</sup>National Res. Inst. for Earth Science and Disaster Prevention, 3-1, Tennodai, Tsukuba 305, Japan, <sup>4</sup>Disaster Prevention Res. Inst. Kyoto Univ., Gokasho, Uji, Kyoto 611-0011, Japan, <sup>5</sup>Japex Geoscience Institute Inc., Tokyo, 112-0012 Japan, <sup>6</sup>Dept Earth Sciences Univ. of Southern California, Los Angeles, CA 90089-0740, USA, <sup>7</sup>Dept. Geological Sciences, Univ. Texas El Paso, El Paso, TX 79968-0555 USA)

The metropolitan areas in Japan, such as Tokyo and Osaka, have high risk of seismic hazards. For example, if present Tokyo is attacked by the great earthquake same as Kanto earthquake of 1923 (M7.9), the most pessimistic estimation of the economic loss reaches to 1 - 3 trillion USD. The Headquarters for Earthquake Research Promotion Japan determined to start the new program targeting the reduction of seismic hazard in the metropolitan areas. As a part of this program, the project to reveal the regional characterization of metropolitan area, including the deep seismic profiling, began from 2002 as a basically five years AE project. A long-term goal is to produce a map of reliable estimations of strong ground motion. This requires accurate determination of: source, propagation path, ground motion response. This projects focuses on identification and geometry of: source faults, subducting plates and mega-thrust faults, crustal structure, seismogenic zone, sedimentary basins, 3D velocity properties. Reconstruction of source fault and velocity models allow for more realistic 3D EQ wave simulations. All of these information will be synthesized and provided to communities involved in probabilistic hazards analysis, risk assessment and societal response. In the fiscal year of 2002, deep seismic profiling was carried out along the

Boso peninsula and along the Sagami bay. The target of the experiments was the imaging of upper surface of the Philippine Sea plate and its spray faults. In Boso 2002, the image of the toe portion of subduction mega thrust was obtained using four vibroseis trucks and deeper portion were obtained by low-fold reflection profiling method using total 2,500 channels and 12 explosive sources. The obtained image clearly demonstrates the upper surface of the Philippine Sea plate. In the Sagami 2003, due to the severe traffic noise the air-gun signals were used as seismic source and signals were recorded by land geophones.

**SS03/08A/D-005** Poster **0830-164**

**OCEAN BOTTOM SEISMOGRAPHIC OBSERVATION IN THE SOURCE REGION OF THE 1952 OFF TOKACHI EARTHQUAKE (M8.2)**

Tetsuo TAKANAMI<sup>1</sup>, Yoshio MURAI<sup>1</sup>, Ryou HONDA<sup>1</sup>, Yuichi NISHIMURA<sup>1</sup>, Kei KATSUMATA<sup>1</sup>, Hideki SHIMAMURA<sup>1</sup>, Seizo HASEGAWA<sup>1</sup>, Hisanaga UKI<sup>2</sup> (Institute of Seismology and Volcanology, Graduate School of Science, Hokkaido University, Kita 10, Nishi 8, Kita-ku, Sapporo 060-0810 JAPAN, <sup>1</sup>Hokkaido National Fisheries Research Institute, Fisheries Research Agency, Katsurakoi 116, Kushiro 085-0802 JAPAN)

We have deployed 10 pop-up type OBSs (Ocean Bottom Seismographs) in the source region of the 1952 off Tokachi earthquake (M8.2), off Hokkaido Island in the period from July 20 to September 20, 2002. The observation area is located 50 ~ 100km landward of the southern Kuril trench where Pacific plate is subducted toward Hokkaido Island. The current seismic activity in this area is extremely low in contrast with the adjacent trench areas. On the other hand, the seismic activity off Urakawa and the Hidaka mountains, which are close to the source region of the 1952 off Tokachi earthquake, are always high owing to the collision between the Kuril and the northeast Japan arcs. Namely, it is well explained by the westward lateral migration of the Kuril forearc sliver. In order to reveal the relationship between the collision structure and the earthquake occurrence, in summer of 1999 we have deployed 21 pop-up type OBSs off Urakawa and off Tokachi of Hokkaido Island and we have merged the earthquake data with the catalog data from the dense seismological network, which was composed of 87 land stations consisting of 41 permanent and 46 temporary stations, has been maintained by the study group of seismologists in Japan Universities for the period from August 1999 to July 2001. The tomographic inversion by using a vast of picking data from the combined earthquake catalog demonstrates the clear image suggesting a delaminating structure, which is probably produced by a collision (Murai et al., 2002<sup>\*</sup>). However, the tomographic inversion failed to image the structure for the source region in the 1952 off Tokchi toward the southern Kuril trench because of a sparse earthquakes occurring in the source region. By adding these picking data to the newly data from the seismological network of the present 10 OBSs, the current seismicity would be cleared and a three dimensional structure would be imaged precisely. This quiescent area off Tokachi has been recently paid attention from the viewpoint of earthquake prediction. <sup>\*</sup>Murai et al., 2002, Delamination structure imaged in the source area of the 1982 Urakawa-Oki earthquake, Program & Abstract, 74th Annual Meeting, Eastern Section of Seismological Society of America, 25.

**SS03/08A/D-006** Poster **0830-165**

**HOLOCENE SLIP RATE OF THE SUBDUCTION ZONE MEGA-THRUSTS ALONG THE SAGAMI TROUGH, CENTRAL JAPAN, ANALYZING THE HEIGHT DISTRIBUTION AND AGES OF EMERGED SHORELINE INDICATORS**

Masanobu SHISHIKURA, Shinji TODA (Active Fault Research Center, Geological Survey of Japan/AIST)

Two major historical earthquakes of the 1703 Genroku Kanto Earthquake (*M* 8.2) and the 1923 Taisho Kanto Earthquake (*M* 7.9) occurred along the Sagami Trough where the Philippine Sea Plate subducts beneath the North American Plate. As a result of the coseismic crustal movements associated with these earthquakes and repeated pre-historical earthquakes, Holocene emerged shoreline indicators (e.g. emerged wave-cut bench, fossilized mollusk etc.) are observed on about 10 or more levels along the coast of the Miura Peninsula and the Boso Peninsula. The height distributions of the lower two levels of them in the Miura Peninsula indicate more than 1 m of uplift during both the 1703 and 1923 events. In the Boso Peninsula, although geodetic data show up to 2 m of uplift during the 1923 event, historical documents and the height distribution of emerged shoreline indicators suggest that the coseismic crustal movement during the 1703 event had resulted steep northward tilting accompanied with uplift of more than 5 m in the southernmost area and subsidence of ca. 1 m in the central area. According to above results, it is inferred that the fault source model of the 1703 event is composed of dual fault system (fault A and B). The fault A is same as the model of the 1923 event which has already been estimated by Ando (1974). The uplift of the Miura Peninsula (both the 1703 and 1923 events) and the Boso Peninsula (only the 1923 event) can be explained by about 6.7 m slip of the fault A. The fault B is low angle dip thrust located off the southeast of the Boso Peninsula. The unique 1703 coseismic crustal movement in the Boso Peninsula has been derived from about 12 m slip of the fault B. <sup>14</sup>C ages of the older paleo-shorelines above two recent levels indicate that the characteristic earthquake generated from the fault A has been occurred repeatedly about every 400 years. One of several events is the 1703 type earthquake accompanied with the slip of fault B. Recurrence interval of this type is 2000-2700 years. Therefore, the slip rate of these faults are estimated to be 16.8 mm/year (fault A) and 5.2 mm/year (fault B) respectively. These value are greatly different each other and smaller than the back-slip rate (30 mm/year) estimated from GPS data (Sagiya, 1998).

**SS03/08A/D-007** Poster **0830-166**

**HIGH INTRA-SLAB SEISMIC ACTIVITY AND HORIZONTAL SLAB TEARING IN SOUTHWESTERN KURIL TRENCH**

Hiroaki TAKAHASHI<sup>1</sup>, Kenji HIRATA<sup>2</sup>, Isao HASHIMOTO<sup>3</sup>, Masayoshi ICHIYANAGI<sup>1</sup> (Institute of Seismology and Volcanology, Hokkaido University, <sup>2</sup>Deep Sea Research Department, Japan Marine Science and Technology Center, <sup>3</sup>Sapporo District Meteorological Observatory, Japan Meteorological Agency)

We have tried to re-examine the intra-slab earthquakes occurred in southwestern Kuril trench. This region has of recent experienced several intra-slab events in the subducting Pacific plate; 1994 Sikotan (M8.2, Dep=60km), 1993 Kushiro (M7.8, Dep=100km), 1987 Hidaka (M7.0, Dep=120km), 1981 Hidaka (M7.1), and 1978 Kunashiri (M7.7, Dep=120km). From the end of 1970's, Hokkaido University (HU) began to establish a seismic network in Hokkaido Island with more than 50 stations. In 1997, HU and Sapporo District Meteorological Observatory of Japan Meteorological Agency (SD) started the real-time waveform exchange to determine the hypocenter since 1997. Our advanced seismological networks have revealed the aftershock distribution of these intra-slab events. From the hypocenter catalogue, we can identify the following features associated with the intra-slab earthquakes. Most of them have occurred on the horizontal fault plane in the subducting Pacific plate. Aftershocks clearly indicate the occurrence of faulting on the plane from the lower plane of the double seismic zone to the upper ones. Though the slab unbending is one of the candidates for the cause of these intra-slab events, some events had been occurred in the

trenchward region as the 1994 Sikotan event. We think there are some other factors that control the occurrence of the intra-slab events in this region. It should also be noted that precise aftershock distribution is one of the powerful data used to clarify the property of the intra-slab events. In the beginning, we have tried to determine the precise hypocenters of aftershocks of the 1994 Sikotan event, for which the fault plane is still in debate, by combining the seismological data of both HU and SD. The result will give the clue to understand the intra-slab events that have occurred in this region.

**SS03/08A/D-008** Poster **0830-167**

**THREE DIMENSIONAL SEISMIC STRUCTURE BENEATH THE SOUTHERNMOST PART OF THE HIDAKA COLLISION ZONE, HOKKAIDO, JAPAN**

Noriko TSUMURA<sup>1</sup>, Shinsuke KIKUCHI<sup>1</sup>, Katsuko SUZUKI<sup>2</sup>, Takuro KAZUKA<sup>1</sup>, Tanio ITO<sup>1</sup>, Takeshi KOZAWA<sup>1</sup>, Takeshi IKAWA<sup>3</sup> (Faculty of Science, Chiba University, <sup>2</sup>Schlumberger LTD, Japan, <sup>3</sup>JGI Inc., Japan)

To better understand the three dimensional structure beneath the arc-arc collision and subduction system, we carried out seismic reflection survey in the Hidaka collision zone(HCZ), which is located at the junction of the northeastern Japan arc and the Kuril arc, in 2000. In this area, previous study revealed that a delamination-ledge structure has been formed due to the arc-arc collision[Tsumura et al.(1999), Ito et al.(2000)] and the Pacific plate is subducting beneath the two arcs. However the detailed geometry of the arcs and the subducting plate remained unclear. In this survey, two lines were set in the direction of NW-SE(parallel to the subduction trend of the Pacific plate), and NE-SW( parallel to the arc-arc collision). Since CMP is distributed in the 2-dimensional area because of the spatial relationship between shots and receivers, we set several stacking lines in the subduction-parallel and in the arc-arc collision-parallel directions and made quasi-three dimensional seismic profiles. From the profiles, we detected some distinctive reflections in the deeper part. Northwest-dipping strong reflections are seen around the two way travel time (TWT) 13-14s(group 1). These events are considered to be associated with the subducting Pacific plate, and it can be seen only in the shallower part of the subduction. Tentative reflections(group 2) exist just above the TWT where no significant reflections are seen although the upper boundary of the subducting plate is expected to pass through. These events are weak but have the similar character with those which are seen in the delaminated Kuril arc crust. The other events(group 3) are also seen in the TWT 7-10s. The origin of the reflectors( group 2 and 3) is not clear. From the geologic studies on the eastern part of the Hidaka metamorphic zone, detachment faults are expected to exist in the depths of 12-15kn. And group 3 events might show the shear zone associated with suchdetachment faults in the intruded arc's crust. On the contrary, group 2 events exist in the extension part of the descending delaminated lower crust of the Kuril arc. It means the descending delaminated crust meets the subducting plate and lay on it beneath the survey lines.

**SS03/08A/D-009** Poster **0830-168**

**CYCLIC RIDGE SUBDUCTION AT AN INTER-SEISMIC LOCKED ZONE IN THE EASTERN NANKAI TROUGH DEDUCED FROM ONSHORE - OFFSHORE WIDE-ANGLE SEISMIC SURVEY**

Shuichi KODAIRA<sup>1</sup>, Ayako NAKANISHI<sup>1</sup>, Jin-Oh PARK<sup>1</sup>, Aki ITO<sup>1</sup>, Tetsuro TSURU<sup>1</sup>, Yoshiyuki KANEDA<sup>1</sup>, Takashi IIDAKA<sup>2</sup>, Eiji KURASHIMO<sup>2</sup>, Hiroshi SATO<sup>2</sup>, Takaya IWASAKI<sup>1</sup>(IFREE, Japan Marine Science and Technology Center, <sup>2</sup>Earthquake Research Institute, University of Tokyo)

There are significant variations in the size, especially lateral extensions, of the co-seismic rupture zones and inter-seismic locked zones. Obvious factors controlling them are still unsolved questions, even though several geophysical studies have suggested possible candidates of structural factors. In the summer of 2001 we acquired onshore - offshore integrated seismic data at the edge of the rupture zone of the 1944 Tonankai earthquake in the eastern Nankai trough. The wide-angle seismic profile is designed as total 477 km long profile, 262 km onshore and 215 km offshore. Five 500 kg and one 100 kg explosion sources were shot onshore, while 187.5 L air gun array was shot at every 100 m interval offshore. 391 land seismic stations and 70 ocean-bottom stations were recorded the seismic signal both from the land explosions and the air-gun array. Qualities of data are generally good. We can trace first arrivals from the air-gun array more than 250 km offsets. A refraction tomography is applied for the all observed first arrivals to obtained seismic velocity image. In order to obtain a seismic reflectivity image, we also applied pre-stack depth migration for the offshore data, while only NMO correction is applied for the onshore data. From the both seismic velocity and reflectivity images, we successfully obtain two trough-parallel ridge systems, i.e. cyclic ridge subduction, with thickness of 13 ~ 20 km and wavelength of 35 ~ 50 km. This remarkable feature is recognized from iso-velocity contours in the seismic velocity image and reflectors in the seismic reflectivity image, i.e., the iso-velocity contour of 4 ~ 7 km/s shows repeated broader and narrower width and the reflectors show bulges at the same positions. By comparing the location of the subducted ridge and an inter-seismic locked zone estimated by GPS data, it is recognized that the deeper subducted ridge, which is subducted beneath the back stop of the present day accretion process, is located exactly at the inter-seismic locked zone. As a conclusion, our seismic images demonstrate that the rupture during the 1944 Tonankai earthquake did not extend to the east due to strongly locking caused by the ongoing cyclic ridge subduction; i.e., this study first proves the "subducted seamount - strongly locking" hypothesis where a large scale ridge or seamount is subducted beneath a back stop in an accretion dominant subduction zone. The locked region may rupture when accumulating stress exceeds the critical strength of locking. This idea could explain why the recurrence interval of the great earthquake in the Tokai segment is longer or more obscure than the other segments. We also propose that the subducted convex shape would not produce strong coupling when the convex is located under young accretionary sediment, presumably a weaker material.

**SS03/08A/D-010** Poster **0830-169**

**MICRO-SEISMICITY AROUND THE RUPTURE AREA OF THE 1944 TONANKAI EARTHQUAKE REVEALED BY OCEAN BOTTOM SEISMOGRAPH OBSERVATION**

Koichiro OBANA, Shuichi KODAIRA, Yoshiyuki KANEDA (Institute for Frontier Research on Earth Evolution, Japan Marine Science and Technology Center)

Along the Nankai trough, southwestern Japan, the Philippine Sea plate is subducting beneath the Eurasian plate with a convergence rate of about 4 cm/year. Great interplate earthquakes caused by the subduction of the Philippine Sea plate have occurred repeatedly. Records of the great earthquakes can be seen in historical documents from the seventh century and the recurrence interval is about 100-200 years. The latest great event at the eastern Nankai Trough is the 1944 Tonankai Earthquake (Mw=8.1). On the other hand, seismicity around the rupture area of the 1944 Tonankai Earthquake is very low and hypocenters are not determined accurately by the on-land seismic network. Micro-seismicity observation is one of the ways to monitor the state of stress in the seismogenic zone. We performed a micro-seismicity observation around the rupture area of the 1944 Tonankai Earthquake. The purpose of this study is to examine the relation between the micro-seismicity, crustal structure, and seismic rupture of the great interplate earthquake. In this

observation, we used free-fall and pop-up type ocean bottom seismographs (OBS). We deployed 26 OBSs in November 2001 and 24 OBSs were retrieved in February 2002. Clock drifts during the observation period were corrected for 13 OBSs. Arrival times of P- and S-waves at these corrected OBSs are used for the hypocenter determination. Since the other 13 OBSs could not be corrected for their clock drifts, only the time differences between P- and S-wave arrivals were used for the hypocenter determination. Earthquakes are located using a 2-D seismic velocity structure model. This model is based on an OBS-airgun seismic survey performed in our seismicity observation area [Nakanishi et al., 2002]. Around the rupture area of the 1944 Tonankai earthquake, seismicity is locally active at the toe of the accretionary prism. Hypocenters of them are located at the seaward limit of the coseismic slip area of the 1944 Tonankai earthquake. Although the depths of these earthquakes are not constrained well, they are considered to be shallower than the subducting oceanic crust. Next OBS observation is planned to improve the accuracy of the hypocenters around the toe of the accretionary prism. On the other hand, micro-seismicity in the rupture area of the 1944 Tonankai earthquake is very low. The recent GPS survey shows a fully coupled plate interface along the Nankai Trough seismogenic zone. Analyses of the seismic and tsunami waves show a uniform distribution of the coseismic slip during the 1944 Tonankai Earthquake. These facts imply an existence of a large asperity with a uniform interplate coupling.

**SS03/08A/D-011** Poster **0830-170**

**INTERPLATE EARTHQUAKE GENERATION IN THE NE-JAPAN AND THE IZU-BONIN REGIONS: WATER RELATED MINERAL PHYSICS**

Junzo KASAHARA<sup>1</sup>, Gou FUJIE<sup>2</sup>, Kimihiro MOCHIZUKI<sup>1</sup>, Mikako NAKAMURA<sup>1</sup>, Aya KAMIMURA<sup>3</sup>, Peyman Poor MOGHADDAM<sup>4</sup>, Ryota HINO<sup>5</sup> (<sup>1</sup>Earthquake Research Institute, University of Tokyo, <sup>2</sup>Japan Marine Science and Technology Center (JAMSTEC), <sup>3</sup>National Research Institute for Earth Sciences and Disaster Prevention, <sup>4</sup>Research Center for Prediction of Earthquakes and Volcanic Eruption, Graduate School of Science, University of Tohoku)

In order to understand the physical basis of earthquake generation along subducting plate boundaries, it is important to know the asperity distribution, the physical properties of rocks, and the presence of water and hydrous phases at the plate boundary. Three seismic experiments in the Japan Trench and the Izu-Bonin Trench were carried out between 1996 and 2001. This paper describes these results and discusses plausible materials to have physical properties obtained by the comparison between observed waveform and synthetic seismogram simulation. The former survey revealed a strong correlation between aseismic zones in the Japan Trench and the intensity of seismic reflections from the subduction plate boundary. Synthetic seismogram analysis suggested that the plate boundary causing the strong seismic reflections contains a thin (~100m thick), low velocity (VP= 2-4km/s and/or low Vs) layer. Water, hydrous clay minerals such as smectite, and/or low-temperature serpentine in the subducting plate boundary may cause intense seismic reflections. The latter survey indicated the presence of chrysotile (low temperature phase of serpentine) at the subducting plate boundary. These materials may act as a lubricant. We propose three types of subduction zones around the Japan arc with different earthquake generation characteristics. Earthquake occurrence in the three typical subduction types may be controlled by the presence of water, clay minerals and serpentines along the subduction boundaries. Dehydration of hydrous phases introduces other conditions related to earthquake generation.

**SS03/08A/D-012** Poster **0830-171**

**INDUCED SEISMICITY STUDIES AT GEHEYAN RESERVOIR**

Yun sheng YAO, Shi Jun GO, Zhong HUANG (Institute of seismology, China seismological bureau)

At Geheyuan reservoir in the Qinjian Rive, Hubei Province, China, the water-induced earthquake activity's frequentness and strength have had very good synchronous relation with reservoir's water level since 1994. The intensive areas of three main earthquakes are became on the earthquake space distributes. By the research of seismogeological environment term, induced earthquake characteristic, reservoir's water level and earthquake activity etc in reservoir area, we detect that the intensive areas of three main earthquakes have the good condition to permeate and to store the groundwater. The process of reservoir to store water lead to the variety of the particular environment condition of hydrology geology, and cause the occurrence of the area's reservoir induced earthquake. Besides some few of larger earthquakes have result to the crack or the layer glide, most of microearthquake swarm belong to the falling earthquake of the karst type. BR Before happing big induced earthquake, the earthquake activity's frequentness and b value as well as the P wave distribute of beginning move etc, all of them show the certain earthquake precursor. BR On the whole, water-induced earthquake activity at Geheyuan reservoir belongs to the preface row of small earthquake cluster. Its energy releases on time is even. The position of epicenters is not relation with main fault activity inside reservoir area, but it is relation with limestone district and stress field being made by the weight carry of reservoir water. It is the typical sensitive-respond type's reservoir induced earthquake in really.

**SS03/08A/D-013** Poster **0830-172**

**POSSIBILITY OF THE SERPENTINIZED MATERIAL AT THE IZU-BONIN SUBDUCTION ZONE AROUND 31°N BY COMPARISON BETWEEN OBSERVATION AND FDM-SIMULATION**

Aya KAMIMURA<sup>1</sup>, Junzo KASAHARA<sup>2</sup> (<sup>1</sup>National Research Institute for Earth Science and Disaster Prevention, <sup>2</sup>Earthquake Research Institute, University of Tokyo)

The main characteristics of the Izu-Bonin subduction zone are the presence of a chain of serpentine seamounts which is exposed at the forearc slope of trench axis, and few large earthquakes (>M7.0) at shallow depth (0-100km) in spite of many large ones at greater depth (>400km). To study the causes of these characteristics we carried out a seismic refraction-reflection study at the forearc slope of the Izu-Bonin subduction zone around 31°N using chemical explosions and airgun shots. As the results of forward and inversion modeling in the study, two velocity structures were obtained along E-W and N-S survey lines which is perpendicular to and parallel to the trench axis, respectively (Kamimura et al., 2002). The result of E-W line which was designed to transect the summit of a serpentine seamount shows a low velocity area on a subducting oceanic slab and this area connects to the serpentine seamount. The interpretation of Kamimura et al. (2002) is as follows. Dehydration of hydrated oceanic crust supplies water to the wedge mantle, and peridotites of the mantle wedge were serpentinized. The serpentinized peridotites moved on the oceanic slab and were diapiric to the serpentine seamount. The serpentine on the plate boundary might act as a lubricant and decrease seismic activity along the subduction zone, and this can explain the characteristics of seismicity in this area. We calculated synthetic seismograms using the P-wave and S-wave velocity structures (2D) of Kamimura et al. (2002) and compared those to the observed seismic records. In this presentation we will show a result of the comparison. We used the "E3D" code (2D/3D elastic finite-difference wave propagation code, developed by Dr. Shawn Larsen) for the calculation of the synthetic seismograms. Grid spacing is 30 m in x and z and 1.5 msec in time. Appropriate Q structure is assumed for the general structure. Five-Hz and 0-phase Ricker wavelet was used as

source. In this result there must be a low-Q area just below the serpentine seamount, to explain the observed seismic records. It is very important to understand where serpentinites of the seamounts came from to explain the characteristics of seismicity at the Izu-Bonin subduction zone. In this presentation we are going to explain an interpretation that serpentine moved through the plate boundary and reached just below the serpentine seamount, using an existence of the low-Q area.

**SS03/08A/D-014** Poster **0830-173**

**CONFIGURATION OF SUBDUCTING PHILIPPINE SEA PLATE BENEATH SOUTHWEST JAPAN REVEALED FROM THE RECEIVER FUNCTION ANALYSIS**

Katsuhiko SHIOMI<sup>1</sup>, Kazushige OBARA<sup>1</sup>, Haruo SATO<sup>2</sup> (<sup>1</sup>NIED, <sup>2</sup>Tohoku University)

The detailed configuration of the Philippine Sea (PHS) plate subducting beneath southwest Japan is revealed from the receiver function (RF) analysis of teleseismic waveforms. We analyze data recorded at 120 stations of the High Sensitivity Seismograph Network (Hi-net) in the Chugoku-Shikoku district, western part of Japan. More than 200 earthquakes with magnitudes 5.5 or higher and epicentral distances between 27 and 90 degrees are selected for the analysis. Considering the response characteristics of the Hi-net system and the ground surface reflection, we analyze the waveform data, which are band-pass filtered in frequency range from 0.1 to 0.6 Hz. To discuss the depth of the velocity discontinuity, the RFs, which are originally estimated as time series, are converted to depth by using the IASP91 earth model. Due to the contamination by multiple reverberations in RFs, we limit the depth of the target structure to less than 60 km in this analysis. After the direct P-phase in each RF, we find remarkable later phases, suggesting the existence of the velocity discontinuities. The high density of Hi-net stations enables us to investigate the spatial continuity of a specific later phase. The results show a clear velocity discontinuity beneath the Shikoku Island. This discontinuity subducts from the south toward the north with a low dip angle. The depth of this discontinuity is 30 km beneath southern Shikoku, 45 km beneath the Seto Inland Sea and continued down to the north at about 60 km beneath center of Chugoku district. Then, we interpret this discontinuity as the upper boundary of the high velocity layer (HVL) of the PHS plate. To investigate the relationship between the spatial distributions of the discontinuities and local seismicity beneath Shikoku region, we construct the depth contour of the upper boundary of the HVL of the PHS plate. The depth contour suggests a rather complicated feature with a few ridges. These ridges are located in the extension of sea terraces of the PHS and the most significant ridge is located around the longitude of 133°E, west of which the contours are basically directed north-south, and change to west-east in the east side of it. Local earthquakes occurred beneath the western part of this ridge are located above the HVL of the PHS plate, while earthquakes mainly occur within the slab mantle area in the eastern part. Although we don't use data of local earthquakes to construct the detailed configuration of the HVL of the PHS plate, we found that the local seismicity in the study region is strongly correlated with that.

**SS03/08A/D-015** Poster **0830-174**

**GEOMETRY OF THE UPPER SURFACE OF THE SEISMIC PHILIPPINE SEA SLAB SUBDUCTED BENEATH SOUTHWEST JAPAN**

Takayuki MIYOSHI, Katsuhiko ISHIBASHI (Department of Earth and Planetary Sciences, Kobe University)

We inferred precisely the geometry of the upper surface of the seismic slab of the Philippine Sea plate (PHS) subducted beneath southwest Japan based on hypocentral distribution. Despite the importance of the slab geometry for the subduction zone seismotectonics, the shape of the PHS slab had been obscure and controversial so far. We selected well-determined hypocenters for the period since Oct. 1997 from the integrated hypocenter database prepared by the Japan Meteorological Agency. Firstly, we made depth-slice hypocenter distribution maps for every 5 km depth and drew first-trial isodepth contours of the upper surface of the PHS slab assuming that the upper boundary of slab earthquake distribution roughly coincide the slab upper surface. Then, in many areas we made vertical cross sections of hypocenter distribution in the direction of inferred dip-direction of the slab, and revised isodepth contours. The main results are as follows: (1) In the region to the east of Lake Biwa, northwestward gently-dipping PHS slab reaches around the depth of 40 km, in which the disastrous 1819 slab earthquake (Ishibashi, 1999) presumably took place. To the northeast it continues to the slab beneath the central Tokai district, but to the southwest it looks separated from the slab beneath the eastern Kii Peninsula. (2) There is double seismic zone beneath the middle part of the Kii Peninsula. The slab earthquakes in this area seem to occur in oceanic crust and slab mantle. (3) The slab here is torn into two parts, with the southwestern part being underlain beneath the northeastern part. (4) In the west part of the Kii Peninsula no slab earthquake occurs deeper than 45 km, whereas just in this area a remarkable shallow crustal swarm earthquake activity exists. (5) Beneath Shikoku the slab is being subducted with gentle dip angle and forms a broad ridge. The slab looks continuous from Shikoku to Kyushu at least in the depth range shallower than 45 km, although the seismicity is low beneath the west part of Shikoku. Recently the PHS slab geometry, mainly for the shallower part than about 30 km, has been investigated by seismic refraction/reflection profiling. Those results show slab upper surface shallower than ours by 5 to 10 km in the Kii peninsula and by more than 5 km in Shikoku. In order to clarify the true slab geometry it is essentially important to know in which part of the slab, oceanic crust or mantle, the slab earthquakes are taking place in each region. We relocated slab events in the eastern Shikoku using velocity structure proposed by a seismic profiling (Kurashimo et al., 2002) and found inconsistency that the shallower main activity lay in the mantle with deeper remarkable events beneath it.

**SS03/08A/D-016** Poster **0830-175**

**THREE-DIMENSIONAL VELOCITY STRUCTURE OF THE PINGTUNG AREA**

Li-Chuin HU<sup>1</sup>, Cheng-Hong LIN<sup>2</sup>, Horng-Yuan YEN<sup>3</sup>, Chau-Huei CHEN<sup>4</sup> (<sup>1</sup>Institute of Geophysics, National Central University, Taiwan, <sup>2</sup>Institute of Earth Sciences, Academia Sinica, Taiwan, <sup>3</sup>Institute of Seismology, National Chung Cheng University, Taiwan)

The Chaochou fault in the Pingtung area is one of the most important faults in southern Taiwan, and is located between the Pingtung Plain and the Central Range. According to previous studies, the Chaochou fault is considered to be a high-angle fault that dips eastward to the Central Range. From a tectonic point of view, regional stresses in the Pingtung area are controlled by two tectonic forces. The first force is the compressional stress related to the arc-continent collision between the Philippine Sea Plate and the Eurasian Plate; the second is the extensional stress related to the opening of the South China Sea to the South. Under these two mechanisms, the crustal structure beneath the Pingtung area has a complex formation. However, in examining earthquakes greater than magnitude 3 that occurred in the years between 1991 and 2001, we discover that the seismicity in southwestern Taiwan in this period was low. The question as to why this is the case is what first inspired our interest in studying this particular area. This study makes use of data collected by the Institute of Earth Sciences, Academia Sinica between August 2001 and January 2002 at 24 temporary seismic stations located near the Chaochou fault, as well

as velocity structures collected through tomography in the foothills of the Pingtung area. We hope that this study will teach us more about crustal structure of this area and will enable us to understand the reasons for low seismicity there.

**SS03/08A/D-017** Poster **0830-176**

**SEISMICITY IN HYUGA-NADA BY TEMPORARY SEISMOLOGICAL OBSERVATION BOTH OF SEA AND LAND AREA**

Kenji UEHIRA<sup>1</sup>, Hiroshi SHIMIZU<sup>1</sup>, Norimichi MATSUWO<sup>2</sup>, Minoru NISHINO<sup>3</sup>, Ryota HINO<sup>4</sup>, Kimihiro MOCHIZUKI<sup>1</sup>, Kodo UMAKOSHI<sup>1</sup>, Hiroshi YAKIWARA<sup>5</sup>, Hiroki MIYAMACHI<sup>6</sup> (<sup>1</sup>Kyushu University, <sup>2</sup>Tohoku University, <sup>3</sup>University of Tokyo, <sup>4</sup>Nagasaki University, <sup>5</sup>Kagoshima University)

Seismic activity of the Philippine Sea plate differs notably Hyuga-nada and near Shikoku. Although usual microearthquake activity is active in Hyuga-nada, it is inactive near Shikoku. On the other hand, although the great earthquake ( $M > 8$ ) has occurred repeatedly in near Shikoku at intervals of about 100 years, in Hyuga-nada, smaller earthquakes (M7 class) has occurred at intervals of about dozens of years. Moreover, it was discovered that aseismic slip has occurred from GPS data in Bungo channel, between Hyuga-nada and near Shikoku (Hirose et al., 1999). Thus, styles of earthquake occurrence differ notably in the adjoining area. As mentioned above, plate coupling of the Philippine Sea plate change from near Shikoku to Hyuga-nada, but this reason is not yet known well. As one method of know the reason, it is important to investigate the details of the seismic activity in Hyuga-nada. So, we performed extraordinary observation in east coast of Kyushu and Hyuga-nada for two months in April, 2002 to June. 23 OBSs were deployed above hypocentral region of Hyuga-nada and 4 data loggers were deployed in east coast of Kyushu in order to compensate a regular seismic network on land. We calculated the highly precise focus distribution and the earthquake mechanism solution. Consequently, we found that reverse fault type earthquake and normal fault type earthquake have occurred by the almost same frequency, and that normal fault type earthquake has occurred so that a reversed fault type earthquake may be inserted up and down. It is suggested that normal fault type earthquake has occurred both side of plate boundary; we acquired important information about what determine the intensity of coupling between plates.

**SS03/08A/D-018** Poster **0830-177**

**INFLUENCE OF SEISMIC CYCLES IN KURILE-KAMCHATKA AND JAPAN SUBDUCTION ZONES ON CRUSTAL STRESS CHANGES AND SEISMIC ACTIVITY IN THE BAIKAL LAKE REGION (SIBERIA)**

Pyotr G. DJADKOV (Institute of geophysics SB RAS)

Very interesting connections between seismic processes in intracontinental region (the Baikal rift which located in Central Asia at western border of the Amur plate) and the Kuril-Kamchatka and Japan subduction zones were found. The distance between the Baikal region and the West-Pacific subduction zones is 2500-3500 km. As rule the rise of seismic activity in the Baikal region took place 2 – 5 years before the seismic active period with very strong earthquakes,  $M > 7.5 - 8$ , in the subduction zones near the eastern border of the Amur plate. Similar scenarios took place in 1949-1953, 1957-1962, 1966-1973, 1989-1995. Sometimes during the period of high seismic activity in subduction zones the second stage of seismic activity rise in the Baikal region happened (for example, 1994-1995). During seismic active period (1989-1995) in the Baikal rift zone we observed very unusual phenomenon in results of geophysical monitoring and data of focal mechanisms namely the compression episode (1992-1993) (Djadkov et al., 2000). We consider this episode as evidence of significant accumulation of potential elastic energy in this period in the earth crust of the Amur plate near the West-Pacific subduction zone. This could cause the essential change of crustal stress field in the Baikal region. The end of this episode was a beginning of energy release by means of the strong seismic events with  $M = 7.5-8.1$  in 1993 – 1995 near islands Hokkaido, Shikotan, Honshu, Sakhalin. Thus seismic active periods and regional changes of crustal stress fields in the Baikal region can be indicators of quantity of crustal elastic energy accumulated at the eastern border of the Amur plate near the Kuril-Kamchatka and the Japan subduction zones. Possibly these seismic active periods and crustal stress changes in the Baikal region can be long- and middle-time prognostic criteria for prediction of seismic process development in the West-Pacific subduction zones. Research is supported by RFBR, grant 03-05-65418, and Programmes of Integration Research of SB RAS.

**SS03/08A/D-019** Poster **0830-178**

**THE 1971 SOUTH YAKUT EVENT AND ITS EFFECTS**

Imaev Valeriy S., Ludmila P. IMAEVA, Boris M. KOZMIN (Institute of diamond and precious metal Geology Siberian Branch of Russian Academy of sciences)

THE 1971 SOUTH YAKUT EVENT AND ITS EFFECTS Imaev Valery S. 1, Imaeva Lyudmila P. 1, Koz'min Boris M. 1. 1. Institute of diamond and precious metal Geology, Siberian Branch, Russian Academy of Sciences, Lenin pr., 39, Yakutsk, 677891, Republic Sacha (Yakutia), Russia. Instrumental observations made in the 20 th century revealed the existence along the southern boundary of the Siberian platform of the Baikal-Stanovoy seismic belt stretching from lake Baikal toward the sea of Okhotsk, in which over 300 thousand seismic events have been recorded. The belt forms the boundary between the Eurasian and Chinese (Amur) lithospheric plates. It includes the Baikal rift and the Stanovoy fold area. Within the Stanovoy fold area (South Yakutia), the strongest over the last 20 years the South Yakutian earthquake occurred on the 20 th of April, 1989. The magnitude of the event (Ms) is 6.5 and the depth of focus is 27 km. The intensity of the event in the epicenter is 8 or the modernized Mercalli scale. The event was felt within radius of 800 km from the epicenter. For example, in Yakutsk and Blagovescensk its intensity attained 3 on the Mercalli scale. Macroeffects of magnitude 3 to 7 were observed over an area of 1.4 million sq. km in Yakutia, Buryatia, as well as the Irkutsk, Chita and Amur regions. The distribution of earthquake epicenters in South Yakutia until 1989 showed that within a radius of 200 km from the city of the future focus a seismically silent zone was observed where only solitary small events with  $M=1-3$  were recorded, while large ones were absent. Analysis of the modern topography showed distinctly that features of the local drainage system tend to be confined to active faults in this area. For example, the Tungurcha river has a characteristic step-like bend, coinciding with the northern and southern benches of the Tungurcha left-lateral strike-slip fault. The territory between the benches, acts as a compression duplex divided, by a system of sublongitudinal local faults. All the blocks have the same southnorthward topographic gradient as evidenced by the watercourtes of Tungurcha tributaries. It may be assumed that the topographical "anomalous" Usmun block was a large "concentrator" of tectonic stress originated under the influence of northeastward compression, the removal of which produced the South Yakut earthquake. It seems that compressive stress field, that formed before the main shock, led to a sharp increase in the rate of deformation of the earth's crust, which caused ionization state of atmosphere above the epicentral zone and the appearance of geodetic and geophysical precursors.

**SS03/08A/D-020** Poster **0830-179**

**TOMOGRAPHIC IMAGING OF VP AND VP/VS IN EASTERN TAIWAN: CONSTRAINS ON EARTHQUAKE NUCLEATION?**

Win-Bin CHENG (General Education Center, Jin-Wen Institute of Technology)

Abstract Tomographic inversion of P- and S-wave arrival times from events occurred in eastern Taiwan is used to produce three-dimensional images of subsurface Vp and Vp/Vs structures. The target area consisted of a  $130 \times 148 \times 50 \text{ km}^3$  volume divided into  $15 \times 25 \times 14$  grids. 2459 events recorded by the CWBSN during 1991 to 1999 providing 26350 P- and 15089 S-arrivals for inversion. As the preliminary results indicated a large volume of high velocity zone is observed in the middle- to lower-crust between the Central Range and Luzon arc in eastern Taiwan. This high velocity zone extends northwards to at least  $24^\circ \text{N}$  and can be interpreted as the oceanic crust of the Philippine Sea plate. The plate boundary between the Philippine Sea and Eurasian plates is generally outlined by a sharp across fault velocity variation, which is a primary feature in the 3-D Vp structure. This study also presents one of the first Vp/Vs tomography for eastern Taiwan. It is well known that Vp/Vs serves as an efficient indicator for a particular set of properties, e.g. temperature, pressure, saturation, porosity, crack geometry and lithology. Significant Vp/Vs perturbations appear to correlate with rupture properties of great earthquakes. Preliminary study showed a feature that the forearc high Vp body is almost coincident with less seismic area delineated by two sub-parallel seismic zones. However, this study indicates the high Vp/Vs anomalies occur at or near nucleation sites of at least five main shocks with magnitude greater than 6.5. Those locations of high moment release events appear to correlate well with the low Vp, high Vp/Vs volume, which may be due to fractured rock matrix, fluid-filled, over-pressurized near the bottom of theseismogenic zone. The existence of over-pressurized fluids beneath the seismogenic zone may affect the long-term structural and compositional evolution of the Longitudinal Valley fault, change the strength of the fault zone.

**SS03/08A/D-021** Poster **0830-180**

**AFTERSHOCKS AND SEISMOTECTONIC IMPLICATIONS OF THE SEPTEMBER 13, 2002 EARTHQUAKE (MW 6.5) IN THE ANDAMAN SEA BASIN**

Jnana Ranjan KAYAL, S.G. GAONKAR, Gautam Kumar CHAKRABOR, Om Prakash SINGH (Geological Survey of India)

A medium size earthquake, main shock (MW 6.5), occurred on September 13, 2002 (22h 28m 31s GMT) in the Andaman sea, about 20 km off shore Diglipur, north Andaman Island. The epicentre at  $13.0870^\circ \text{N}$  and  $93.1120^\circ \text{E}$  and centroid depth at 31 km were estimated (USGS). The main shock occurred by a reverse faulting. Four digital seismograph stations were established in the Andaman Islands to monitor aftershocks. About 200 aftershocks ( $M_d > 1.0$ ) were recorded during a period from September 19 to October 7, 2002. The epicenter map shows a NW-SE trending aftershock cluster in an area of about  $140 \times 70 \text{ km}^2$ , which reflects the rupture area of the main shock. The aftershocks occurred mostly at a depth range 5-20 km, except one at 38 km. The moment tensor solutions (USGS) of the main shock and the largest aftershock (MW 5.8), which occurred 22 hrs after the main shock, revealed consistent reverse faulting. The NE dipping NW-SE trending nodal plane, which is comparable with the aftershock trend, is inferred as the fault plane. The NE-SW compressional stress (P- axis), obtained by the fault-plane solutions, is conformable with the NNE movement of the Indian plate. The main shock and the two well located largest aftershocks, located by the USGS, occurred within the subducted plate. One composite fault-plane solution is obtained for the shallower aftershocks recorded by the temporary network. The solution shows a normal faulting with a NE-SW tensional (T) axis. These aftershocks occurred off the subducted plate at a much shallower depth ( $< 10 \text{ km}$ ), and are caused due to local tension in the overriding plate.

**SS03/08A/D-022** Poster **0830-181**

**THE MOST RECENT PERIOD OF SEISMIC ACTIVITY IN DINAVAR SEGMENT OF MAIN RECENT FAULT, ZAGROS MOUNTAINS OF WESTERN IRAN**

Noorbakhsh MIRZAEI

Following a period of relative quiescence after September 1958, a series of violent shocks on 24 April 2002 strongly affected the district of Dinavar in Kermanshah province of western Iran. The shocks completely destroyed 10 villages and damaged another 60. The largest event was a moderate earthquake of  $m_b=5.2$ ,  $M_s=5.2$  (USGS). The earthquake was associated with considerable surface rupture that runs for at least 15 kilometers. The surface rupture follows the trend of Dinavar segment of the Main Recent Fault. Pattern of developed shear fractures confirms right-lateral strike-slip movement in this event. The main shock proceeded by a foreshock of  $m_b=4.8$  just five minute before, and was followed by many aftershocks. In the first week after the main shock seven aftershocks was recorded teleseismically and in a seismographic station in Kermanshah, about 60 kilometers far from the epicenter, fifty aftershocks was recorded in the same time period. The number of aftershocks decreased gradually but continued to December 2002, when another damaging earthquake of  $m_b=5.0$  (USGS), on 24 December 2002, strongly affected the same region causing more property damages. It seems a new period of seismic activity is started in an area that has a well known history of devastating earthquakes, with magnitudes as large as  $M_s=7.0$ .

**SS03/08A/D-023** Poster **0830-182**

**SEISMOLOGICAL CONSTRAINTS ON THE STRUCTURE AND COMPOSITION OF THE WESTERN DECCAN VOLCANIC PROVINCE FROM CONVERTED PHASES**

Mohan GOLLAPALLY<sup>1</sup>, Ravi Kumar MANGALAMPALLY<sup>2</sup> (<sup>1</sup>Department of Earth Sciences, Indian Institute of Technology Bombay, Mumbai, India, <sup>2</sup>National Geophysical Research Institute, Hyderabad, India)

Receiver function analysis (RF) of teleseismic data recorded during the period 1998-2002 by a ten station seismic network comprising of one broadband (BB) and nine short period (SP) stations, deployed in a  $50 \text{ km} \times 100 \text{ km}$  area near Mumbai, in the western part of the Deccan Volcanic Province (DVP) of India, reveals a crust with thickness varying from 35.5 km to 38.8 km. Comparable results obtained from BB and SP data recorded at a common site enabled the application of the RF technique to SP data recorded by the network, with reliable results. The crustal thickness was effectively constrained by using the Poisson's ratio determined from the crustal multiples recorded by the BB station. Strong conversions were observed from the base of the traps and the Moho and a weak conversion from an intracrustal layer observed at eight stations which exhibit a relatively thick crust. The Poisson's ratio is determined to be 0.26 which indicates the felsic nature of the crust. Neglecting the traps, the crustal thickness, Poisson's ratio and the average shear velocity ( $3.7 \text{ km/s}$ ) are all similar to those observed for the Archean shield, implying that the crust in this region does not appear to carry any significant imprints of the basic volcanism.

SS03/08A/D-024 Poster 0830-183

**THE TOPOGRAPHY OF THE MOHO-DISCONTINUITY AND TECTONIC PROCESSES IN THE AREA OF THE REPUBLIC OF MACEDONIA**

Todor B. DELIPETROV, Deljo P. KARAKASEV (Department of geology and geophysics, Faculty of Mining and Geology, Stp. University "Sts. Cyril and Methodius" Skopje, Republic of Macedonia)

Tectonic processes in an area depend on the forces surrounding the area as well as those causing effects on local level. The local forces influencing the Earth's crust in the territory of the Republic of Macedonia are related to the complex topography of the Moho-discontinuity. According to the tectonic regional setting and the geophysical investigations carried out by the present authors the area under investigation can be divided into three zones: the Western Macedonian, the Vardar and Eastern Macedonian zones. In an area of 25 000 km<sup>2</sup> and a distance of less than 100 km the Moho-discontinuity shows a variation of 17 km. The fairly complex structure of the boundary M is directly influenced by block displacement comprising the three zones. Depending on the shape of the Moho-discontinuity two structural models are possible: a horizontal and inclined boundary. If the depth of the Moho-discontinuity beneath the block is constant then its topography does not generate tangent forces (thus the plates are stable). An analysis of the map of the Moho-discontinuity for the Republic of Macedonia and investigations carried out made it possible to draw the conclusions as follows: the Moho boundary in the area of the Western Macedonian zone buries to the west that causes the blocks in the zone to be affected by tangent forces of the east - west general strike. The tangent force generated in the Vardar zone by the boundary M is either the lowest or absent. The Moho-boundary in Eastern Macedonia buries to the east generating tangent force that affects the blocks with a general strike to the east. Vertical tectonic movements are caused by gravitation forces. With regard to the M boundary, vertical movements are possible if the blocks do not affect the boundary or if their relationship is not in consolidated state. Vertical displacements take place within the Earth's crust during the processes of subsidence and reconsolidation of the material which is not related to the M boundary.

SS03/08A/D-025 Poster 0830-184

**MOHO DEPTH VARIATION IN SOUTH IBERIAN PENINSULA**Inmaculada SERRANO<sup>1</sup>, Jose Benito MARTIN<sup>1</sup>, Jose MORALES<sup>1</sup>, Federico TORCAL<sup>2</sup> (<sup>1</sup>Andalusian Institute of Geophysics, Granada University, Spain, <sup>2</sup>Pablo Olavide University, Sevilla, Spain)

The steep transition in the Moho depth between the Betic Cordilleras (southern Spain) and Alborán Sea (the western termination of the Mediterranean Sea), has been the focus of widespread debate in the last decades. Numerous authors have studied this interesting region, attempting to relate the continental collision, the late extension and the relationships between these two processes with the intermediate and deep seismicity. In recent years several hypothesis have been proposed to explain its origin, evolution and present-day structure. Crustal thickness variations are of essential importance to comprehend the tectonic evolution of a region. Because of the large seismic velocity contrast between the lower crust and upper mantle, seismology provides the most direct measurement of crustal thickness. The main available information concerning to the crustal thickness in southern Iberian Peninsula includes some early works of seismic profiles during the 70 decade. However, although seismic surveys can provide very detailed pictures of crustal structure along linear profiles, they are expensive and do not always succeed in penetrating to Moho depths. Results from gravimetry, magnetic, magnetotelluric and heat flow have provided additional and valuable information, suggesting, for this region, that the petrologic Moho discontinuity differs from the seismic Moho. In this work the Moho depth variation is investigated in southern Iberian Peninsula by applying methods of refraction and reflection to the local earthquakes of the region. Although recent studies have obtained low Pn velocities in the western Mediterranean region, we try to improve resolution by using the new broadband stations installed recently by the Granada University, Spain. The crustal thickness and upper mantle velocities results from Pn phases are compared with those obtained from Moho-reflected phases, PmP. The results are correlate with major tectonic features and previous geophysical observations. On the other hand, mantle seismic anisotropy is a direct indicator of mantle strain history, and it constitutes an important tool in the study of the tectonic of any region. The first contrasts of the anisotropy beneath the different crustal domain of the Iberian Peninsula have been established from the analysis of teleseismic shear-wave splitting observed. The result inferred for a seismic station located in south Iberian domain is clearly different from those observed in the Alboran domain; the origin of which has to be related to the different geodynamic evolution. However, these results do not agree with those obtained from others authors, presumably owing to their low resolution because of the absence of broad-band seismic stations. In this work new shear-wave splitting observations are made possible by the deployment of the recent broadband seismic network in southern Spain.

SS03/08A/D-026 Poster 0830-185

**SIGNIFICANT EARTHQUAKES IN THE UK OVER THE PAST 25 YEARS**

Lars OTTEMOLLER, Alice WALKER, Brian BAPTIE (British Geological Survey)

The UK is an area of low to moderate seismicity with around 200 earthquakes detected each year and a recurrence rate for events of magnitude 5 of approximately 10 years. Historically, the largest earthquake to affect the United Kingdom occurred in 1931 and had a magnitude of 6.1 ML. It was located on the Dogger Bank, in the North Sea, and caused minor damage on the east coast of England. The diffuse temporal and spatial pattern of seismicity observed is consistent with other examples of intraplate continental deformation. However, no historical or instrumentally recorded earthquake has produced a surface rupture, therefore, it is difficult to relate a given earthquake to displacement along a specific fault on land. In the North Sea, however, broad correlations can be seen between the graben structures and offshore seismicity. Over the past 25 years, 11 earthquakes with magnitudes > 4.0 ML have been recorded instrumentally in the UK. In this study, we use data from the UK seismograph network to determine source parameters for these earthquakes and their aftershocks, which include: Carlisle, 1979 (4.7 ML); Lleyen Peninsula, 1984 (5.4 ML); Bishop's Castle, 1990 (5.1 ML); and Dudley, 2002 (4.8 ML). The network has evolved over the past 35 years and currently consists of 146 stations with an average spacing of 50 km, allowing the detection and location of all seismic events greater than 2.0 ML. Hypocentral depths for these earthquakes are typically in the upper crust and are rarely deeper than 15-20km. However, in some cases the depth constraint is poor. For these, we constrain depth using waveform modelling for simple crustal models. Focal mechanisms for individual earthquakes show a variety of source mechanisms but are generally compatible with the regional stress regime for northwestern Europe due to compression from the Mid-Atlantic ridge. Source parameters are determined from the observed displacement spectra, after correction for geometric spreading and attenuation, to examine the relationship between earthquake size and stress drop for these events.

SS03/08A/D-027 Poster 0830-186

**THE STRESS FIELDS DUE TO RECENT SEISMIC EVENTS IN THE CENTRAL APENNINES, ITALY**Michele DRAGONI<sup>1</sup>, Antonello PIOMBO<sup>1</sup>, Stefano SANTINI<sup>2</sup>, Andrea TALLARICO<sup>3</sup> (<sup>1</sup>Dipartimento di Fisica - Universita' di Bologna, <sup>2</sup>Istituto di Fisica - Universita' di Urbino, <sup>3</sup>Dipartimento di Geologia e Geofisica - Universita' di Bari)

The Central Apennines, Italy, are characterized by moderate seismic activity on normal faults, oriented in directions parallel to the Apenninic chain. The subject of this study is the Umbria-Marche Apennine, a segment approximately 200 km long, where three main seismic events occurred in the last three decades. The 1979 Norcia earthquake was a M = 5.8 event, taking place at the south end of the considered segment. The 1984 Gubbio earthquake was a M = 5.3 event which took place at the north end. The 1997-98 Colfiorito sequence was made of 8 main shocks with magnitudes between 5 and 6 and epicenters comprised between the Gubbio and the Norcia earthquake areas. A model made of an elastic half-space is considered, where the seismic sources are represented by rectangular dislocations having the appropriate values of source parameters, and the stress field produced by each event is calculated. The superposition of the different stress fields and of an assumed regional tensile stress gives the time evolution of the stress field in the area. The analysis of Coulomb failure stress as a function of time gives information as to the role played by coseismic stress transfer and fault interaction during the past three decades in the region.

SS03/08A/D-028 Poster 0830-187

**BOHEMIAN MASSIF ANISOTROPY AND HETEROGENEITY: - BOHEMA EXPERIMENT**

Michael KORN, BOHEMA WORKING GROUP (Dept. of Geophysics and Geology, University of Leipzig)

A passive seismic experiment is currently carried out in the western part of the Bohemian Massif close to the border between Germany and the Czech Republic. A network of 90 temporary stations in addition to 60 permanent stations in the region has been set up in a joint effort by Czech, French and German institutions and is expected to run until June 2003. The network is concentrated around the crossing of the Eger Graben and the Marianske Lazne fault zone, an area which is characterized by the periodic occurrence of earthquake swarms as well as CO<sub>2</sub> and He gas emanations in mineral springs and mofettes. The scientific aim is to use all available techniques such as high-resolution tomography, receiver function analysis, 3D anisotropy studies and investigation of xenoliths to image the crust and upper mantle to depths of about 250 km. Results of the experiment will shed light on the causes of the swarm earthquakes and the role of fluids triggering them, as well as on the location of a hypothetical deep seated source of the gas emanations. Preliminary results will be presented with respect to Moho depth variations from receiver function analysis, resolution studies of local traveltimetomography and the development of regional 1D velocity models

SS03/08A/D-029 Poster 0830-188

**WAVEFORM MODELING TO ESTIMATE THE SEISMIC WAVE ATTENUATION IN THE CRUST, IN THE VRANCEA (ROMANIA) SEISMIC AREA**

Luminita Angela ARDELEANU (National Institute for Earth Physics, P.O. Box MG-2, 76900 Bucharest, Romania, email: ardel@infp.ro)

Due to its tectonic setting, the Vrancea region (Romania) is an area with a complex structure, which should be described by a 3-D inhomogeneous model. Although the construction of such a complex model is still in early stages, 1-D crustal models designed for various seismic stations are already available; they were constructed as realistically as possible, on the basis of geologic and seismic data, and approximate the local structure for an area of a few km<sup>2</sup> around the recording stations. Since we have no local evaluations of the quality factor, in the present paper we propose average models for Q, suitable for the area located at the major bend of the Eastern Carpathians. For each station a pair of extreme, reasonable Q models (one corresponding to high Q-values, the other to low values) is considered. The most appropriate Q model, for various azimuths, is selected by comparing the local, short period records of a set of crustal low magnitude earthquakes with the synthetic waveforms computed for pairs of structures, which differ by the quality factor only. Two zones - one with high attenuation, the other with low attenuation - are evidenced, which determine decisively the optimum Q model for the rays crossing them.

SS03/08A/D-030 Poster 0830-189

**SEISMIC AMPLITUDE VARIATIONS DUE TO SITE AND AZIMUTHAL EFFECTS IN THE LOS ANGELES BASIN**

Allen LeRoy HUSKER, Monica KOHLER, Shirley BAHER, Paul DAVIS (Department of Earth and Space Science, University of California, Los Angeles)

Seismic amplitude variations are examined for the 1994 Northridge Earthquake and a first order model for wave propagation through the Los Angeles Basin is presented. The Northridge Earthquake caused greater damage and more violent shaking in Santa Monica than areas closer to the epicenter. An aftershock and Vibroseis study of amplitudes and travel times suggest a deep structure causes higher-frequency seismic energy from a northerly back-azimuth to focus in Santa Monica. We develop an empirical model for amplitude variations throughout the LA and San Gabriel Basins. The model incorporates geometrical spreading, magnitude, soil effects at the surface, and azimuthal effects. The model is compared to data from the LA Basin Passive Seismic Experiment (LABPSE). LABPSE involved running a passive seismic experiment of 18 seismic stations along a line crossing LA and San Gabriel basins for a period of 9 months during which local, regional and teleseismic earthquakes were recorded. The data consist of spectral amplitudes from 37 events for P waves and 39 events for S waves. The parameters of the model are fit to the data using a non-linear least-squares inversion. The spectral amplitudes are broken into frequency bands to determine frequency dependence of model parameters. Focusing by geological sub-structure is expected to be frequency and azimuth dependent. The results indicate that our model is a good first order approximation to the amplitude variation. We resolve statistically significant azimuthal amplitude variation, which we relate to the geologic sub-structure.

SS03/08A/D-031 Poster 0830-190

**ASPERITY DISTRIBUTION OF THE 1964 GREAT ALASKA EARTHQUAKE AND ITS RELATIONTO SUBSEQUENT SEISMICITY IN THE REGION**Stefano SANTINI<sup>1</sup>, Michele DRAGONI<sup>1</sup>, Giorgio SPADA<sup>2</sup> (<sup>1</sup>Istituto di Fisica - Universita' di Urbino, <sup>2</sup>Dipartimento di Fisica - Universita' di Bologna)

The 1964 Alaska earthquake was one of the largest seismic events in the 20th century. We study the slip distribution on the fault plane on the basis of surface coseismic deformation. To this aim we decompose the fault plane in a large number of small square asperity units with a side of 25 km. In the first stage, each asperity unit is allowed to slip or to remain locked, providing the geometry of the dislocation surface that best reproduces the observed displacements. To this purpose a large number of slip distributions has been tried by the use of a Montecarlo method. The slip amplitude is the same for all the asperities and is equal to the average fault slip inferred from the seismic moment. In the second stage, we evaluate the slip distribution in the dislocation area determined by the Montecarlo inversion; in this case we allow unit cells to undergo different values of slip in order to refine the initial dislocation model. The results confirm the previous finding that the slip distribution of the great Alaska earthquake was essentially made of two dislocation areas with a higher slip, the Prince William Sound and the Kodiak asperities. Analysis of the post-1964 seismicity in the rupture region shows a strong correlation between the larger earthquakes ( $M > 6$ ) and the distribution of locked asperities following the 1964 event, which can be considered as an independent test of the validity of the model. Our model confirms the results of recent studies by a different methodology defining the distribution of asperities on the fault plane, using only the fault geometry, the geodetic data and the seismic moment of the 1964 Alaska earthquake.

**SS03/08A/D-032** Poster **0830-191**

**SEISMOGENIC ZONE STRUCTURE ALONG THE MIDDLE AMERICA TRENCH: RESULTS FROM THE COSTA RICA SEISMOGENIC ZONE EXPERIMENT**

Heather R. DESHON<sup>1</sup>, Susan Y. SCHWARTZ<sup>2</sup>, Susan L. BILEK<sup>3</sup>, Andrew V. NEWMAN<sup>4</sup>, LeRoy M. DORMAN<sup>5</sup>, J. Marino PROTTI<sup>6</sup> (Department of Earth Sciences, University of California-Santa Cruz, <sup>2</sup>Department of Geological Sciences, University of Michigan, <sup>3</sup>Los Alamos National Laboratory, <sup>4</sup>Scripps, University of California-San Diego, <sup>5</sup>OVSICORI-UNA)

Large or great subduction zone thrust earthquakes commonly nucleate within the seismogenic zone, a region of unstable slip along the converging plate interface. A better understanding of the mechanical, thermal and hydrothermal processes controlling seismic behavior in these regions requires accurate earthquake locations and focal mechanism determinations. The Costa Rica seismogenic zone experiment (CRSEIZE), a collaborative effort between UCSC, OVSICORI-UNA, UCSD/Scripps, Univ. of Miami, and GEOMAR, combined broadband and short-period land and ocean bottom (OBS) arrays, oceanic fluid fluxmeters, and GPS measurements in order to better understand the geometry and mechanical behavior of the seismogenic portion of the plate interface. Subduction of the Cocos Plate beneath Caribbean plate beneath western Costa Rica generates large earthquakes (to around Mw 7.6), but the nature of seismicity is highly variable along strike. We focus on results from two seismic experiments, deployed on and offshore the southern Osa Peninsula and the northern Nicoya Peninsula from Sept.-Dec. 1999 and Dec. 1999 - June 2001 respectively. On August 20, 1999 an Mw 6.9 underthrusting interplate earthquake occurred offshore central Costa Rica. The magnitude was consistent with the highest magnitudes (Mw 7.0) recorded on the central Costa Rica margin, and the aftershock sequence was predicted to rupture much of the seismogenic zone. We record and locate interplate aftershocks, intraplate oceanic and continental activity, and outer rise events. The aftershock rupture area encompasses 400 km<sup>2</sup> and illuminates the seismogenic zone from 10 km depth, 30-35 km from the trench to 30 km depth, 95 km from the trench. Thereup area spatially correlates with the down dip extension of the oceanic Quepos Plateau, suggesting the morphology of the incoming Cocos plate heavily influences seismicity patterns offshore central Costa Rica. The 1999 earthquake possibly represents rupture of a seam or basement high at depth, and aftershocks reflect complexities caused by asperities in the region. Current results identify a significant deepening in up dip seismicity (from 10 - 20 km) occurring along a transition in subducting plate origin, Cocos-Nazca Spreading Center versus East Pacific Rise (EPR) origin. This change in up dip seismicity may be partially controlled by thermal differences in the downgoing crusts; significant crustal hydrothermal circulation in the EPR cools the crust and deepens the up dip limit. Further evidence for crustal hydrothermal circulation comes from fluid flux meters located on OBS as part of the CRSEIZE experiment. Flux meters recorded a number of fluid flow excursions on both the toe of the forearc wedge and on the incoming Cocos plate. Initial comparisons to local and regional seismicity rate suggests a causal link. We present a more detailed analysis of local and regional seismicity, focusing on comparisons of the datasets.

**SS03/08A/D-033** Poster **0830-192**

**SEISMOTECTONIC AND SEISMIC ANOMALIES IN NORTH WESTERN OF SOUTH AMERICA**

Carlos A. VARGAS-JIMENEZ<sup>1</sup>, Lluís G. PUJADES<sup>2</sup>, Arantxa UGALDE<sup>3</sup>, Jose A. CANAS<sup>4</sup> (<sup>1</sup>Departamento de Geociencias, Universidad Nacional de Colombia, <sup>2</sup>Universitat Politècnica de Catalunya, <sup>3</sup>Observatori de l'Ebre, Roquetes, Spain)

Stress inversion from focal mechanisms  $M_w > 5.5$  (NEIC, 1992-2000) correlated with geodetic data of several campaigns (CASA project, 1993-1999) and shear wave splitting analysis with data from Seismological Network of Colombia (1992-1999), suggests the presence of a cortical anomaly that causes a change of convergence direction of the Nazca Plate against South American Plate near to 77°W - 4°N. In this sector lateral variations of  $V_p$  are detected and they agree with  $Q_c$ , gravimetric and thermal flow anomalies that are product of local distribution of compressives NNW-SSE stress generated by the micro-plate ChocA against the Andean Block of Colombia and that it generates permanent destructive seismicity in this sector along transpressive right-lateral faults. The presence of predominantly intrinsic attenuation towards south of 77°W - 4°N and scattering attenuation towards north, allow to deduce greater angles in the subduction processes towards the north.

**SS03/08A/D-034** Poster **0830-193**

**A FIRST STEP TOWARD INTEGRATED GEOPHYSICAL AND GEOLOGICAL STUDIES IN URBAN AREAS: PRELIMINARY RESULTS ON NEOTECTONICS IN THE SOUTHERN KYOTO BASIN**

Takanobu YOKOKURA<sup>1</sup>, Naomi KANO<sup>2</sup>, Kazuo YAMAGUCHI<sup>1</sup>, Akiko TANAKA<sup>1</sup>, Toshiki OHTAKI<sup>1</sup>, Shinobu ITO<sup>1</sup>, Masao KOMAZAWA<sup>1</sup>, Yoshinori MIYACHI<sup>1</sup>, Tomio INAZAKI<sup>1</sup> (<sup>1</sup>Institute of Geoscience, Geological Survey of Japan, AIST, <sup>2</sup>Construction Technology Research Department, Public Works Research Institute)

We started integrated geophysical and geological studies on urban areas in order to provide precise and integrated geoscientific information that leads to mitigation of disasters and suitable public and industrial utilization of land. We have selected the southern Kyoto basin as a model field for the study. Large earthquakes have frequently attacked Kyoto historically. However the area has been very and abnormally quiet since 1830, except small damages by the 1995 Hyogo-ken Nanbu earthquake. Immediate collection and accumulation of geoscientific information is needed in this area. For the first step to do so, we have started to conduct deep and shallow seismic reflection surveys, detailed gravity survey, collection and

digitization of boring data, and so on. Shallow high-resolution reflection surveys, compared with some shallow boring data, revealed distribution of a gravel layer that has N-value of about 30-40 and corresponds to a bearing layer for construction in this area. Deep reflection surveys have revealed that the pre-Neogene basement is relatively flat and lies at about 700-800m in depth at the basin side, and becomes rapidly shallow toward the hill (called Yawata hill or Tanabe hill) side. There is a fault between the basin and the hill. Gravity data analysis, combined with the basement depth controlled by reflection seismic sections, has provided detailed basement structure of the southern Kyoto basin. The vertical slip rate of the fault between the basin and the hill can be estimated using precisely dated marine clay beds in the Plio-Pleistocene Osaka Group; indicating about 0.1m/ky during 0.4 to 0.9Ma and negligibly small before 0.9Ma. In the neighboring areas, some kinds of tectonic changes also occurred around 1Ma, such as uplift of Shikoku coastal mountains, unconformity beneath the Kii channel, activation or reactivation of faults, and so on. The activity change of this small fault may also reflect a drastic tectonic event around 1Ma in this region, which may be related to the change of subduction direction of the Philippine Sea Plate.

**SS03/08A/D-035** Poster **0830-194**

**SHALLOW FAULT GEOMETRY AND SLIP PARTITIONING ASSOCIATED WITH THE IWATE-KEN NAIRIKU-HOKUBU EARTHQUAKE OF 1998 (M6.1), NORTHERN HONSHU, JAPAN**

Shin KOSHIYA<sup>1</sup>, Tomonori KAWAMURA<sup>2</sup>, Hiroshi SATO<sup>2</sup>, Masaru NODA<sup>1</sup> (Department of Civil and Environmental Engineering, Iwate University, <sup>2</sup>Earthquake Research Institute, University of Tokyo)

It is important to estimate slip partitioning on each segment of fault system, when the possibility of earthquake in active faults is evaluated based on paleoseismic events. The Iwate-ken Nairiku-Hokubu earthquake (M6.1) of September 3, 1998, northern Honshu, Japan, caused some parallel surface ruptures and flexures, suggesting the contemporaneous motion of main fault and its branched faults. These faults, generally with north to south strike, comprise Nishine Fault System. This study is aimed at revealing the geometrical relationship between these faults and estimating displacement on each fault, by high-resolution shallow seismic profiling and geological survey. Seismic exploration experiment was carried out across the southern extension of Nishine Fault System. The seismic source of our experiment was Mini-vibrator (T-15000, IVI Inc.), and digital telemetry seismic recording system (GDAPS-4, JGI Inc.) was used for collecting seismic data. The geological structure around the experimental line is characterized by four faults, called F4, F3, F2 and F1 faults from west to east, and folds associated with these faults. F4, F2 and F1 faults are thrusts dipping to west, and F3 is a thrust dipping to east. F4 fault is a major fault, and F1, F2 and F3 faults are branches of F4 fault. F3 fault is a back thrust. The formations are strongly folded as an anticline in the western part of F4 fault, while small syncline and anticline folds develop between F4 and F1 faults. The shallow seismic profiling shows the large vertical displacement of remarkable reflectors on F1 faults and small ones on F2 and F3 faults. Particularly the displacement on F2 fault appears to be very small. Preliminary simplified balanced cross section, including F1, F3 and F4 faults, suggests that the total slip on F4 fault accumulated through geologic time is the largest and more than several times of the total slip on F1 fault. According to the section, these faults are presumed to be active together, because F4 and F1 faults have a common low-angle detachment fault plane in the section. Leveling survey reveals that the vertical displacement on F4 fault is almost the same as that on F2 and F3 faults at the earthquake. This implies that F1, F2 and F3 are still younger than F4, though they are all active.

**SS03/08A/D-036** Poster **0830-195**

**ACTIVE FAULT DRILLING RESEARCH ON STRESS, ELECTRICAL AND BASE ROCK STRUCTURE - FAULT ZONE STRUCTURE OF GOFUKUJI FAULT, CENTRAL JAPAN -**

Kentaro OMURA<sup>1</sup>, Ryuji IKEDA<sup>2</sup>, Tatuo MATSUDA<sup>3</sup>, Yukihiro MIZUOCHI<sup>4</sup> (<sup>1</sup>Solid Earth Res. Gr., National Research Institute for Earth Science and Disaster Prevention, <sup>2</sup>Division of Earth and Planetary Sciences, Hokkaido University, <sup>3</sup>Sumiko Consul. Co., Ltd.)

"Active fault drilling" is an effective method to investigate the physical and chemical state in and around an active fault zone, such as, stress and strength distribution, geological structure and materials properties. In a present study, we did down hole measurement, geophysical prospect and core recovery at a Gofukuji Fault, central Japan, that is considered to have activated about 1200 years ago. Longer duration has passed since the last earthquake occurred as compared with other active faults we have already drilled: Nojima fault which appeared on the surface by the 1995 Great Kobe earthquake (M=7.2), the Neodani fault which appeared by the 1891 Nobi earthquake (M=8.0), the Atera fault, of which some parts have seemed to be dislocated by the 1586 Tensyo earthquake (M=7.9). A 400m depth borehole was drilled at a distance of about 350 m west from the surface trace of the fault. Recovered cores show the lithology beneath the surface is conglomerate from an alluvial fan and sand/mud stone as a bed rock including aeolian deposit in spots. Logging data show that the apparent resistivity is about 100 ohm-m, density is about 2.5g/cm<sup>3</sup> in conglomerates but by 0.1 g/cm<sup>3</sup> denser in sand/mud stones. P wave velocity is approximately 3.0 to 3.5 km/sec. By the BHTV logging, the vertical fractures were detected which fractured by hydraulically due to the mud pressure in the borehole. The vertical fractures indicate the orientation of maximum horizontal stress is N45°W. Its shear stress component seems to act on the fault plane. The situation is contrast to the case of Nojima fault where the maximum horizontal stress was nearly perpendicular to the fault plane. We suggested the Nojima fault is "weak". The Gofukuji fault may be recovered in strength and not weak after long duration since the last earthquake. Electrical prospecting and CSAMT survey were performed with transects normal to the fault surface trace. The measuring line of electrical prospecting was about 1 km. Electrodes were set in the borehole as well as at ground surface and tomographic analysis was applied. CSAMT survey had two measuring lines which were about 3 km length. The electrical conductivity structure at the Gofukuji fault indicates the high conductive region is obscure associated with a fault fracture zone. This is not the case for the Atera fault where a broad fault fracture zone was estimated by an electrical image. The electrical image beside the Gofukuji strike slip fault is suggestive of the existence of vertical displacement in a bed rock. Considering other drilling data, such as well logging and core observation, the reverse fault may exist in the vicinity of the Gofukuji fault. We claim that the drilling method is effective to investigate physical and chemical features of active faults and compare with each other.

**SS03/08A/D-037** Poster **0830-196**

**FAULTING AND CREEP BEHAVIOR OF COMPLICATED STRIKE-SLIP FAULT SYSTEM - A CASE OF THE ATOTSUGAWA FAULT SYSTEM, CENTRAL JAPAN**

Bateer HASI, Akira TAKEUCHI, Yuki MATSUURA (Department of earth sciences, Toyama University)

In this study, we focused on the Atotsugawa fault system (AFS), a main strike-slip structure of central Japan. The AFS is composed of three NE-E striking faults, characterized by high seismicity of micro-earthquakes along the fault traces, is the most active zone of right-

lateral strike-slip faults in north-central Japan. To reveal the faulting history and present motional behavior, we carried out comprehensive studies on the fault system, and achieved some interesting features of the faults of AFS. Geological and geomorphological studies clarified detailed geometry of the AFS: The two main faults, Atotsugawa fault (AGF) and Ushikubi fault (UKF) parallel with each other and formed a rectangular block between the two faults. On the surface, the AGF extends continuously whereas the UKF shows right step <len echelon>. And the another member of the AFS, the Mozumi-Sukenobe (MSF) fault branches from the eastern end of the AGF and towards the UKF, so the activity of the Mozumi-Sukenobe fault is subordinate to the AGF. This geometric feature may indicate reorganization of local stress field near the fault system. We carried out seismo-geological studies on the fault system in three sites. One is in the central western part of the master AGF, one is at the end, and another is on the branching MSF. Trenching surveys on the eastern portion of the AGF revealed the faulting history of the AGF within recent 22,000 years. The results demonstrated a maximum recurrence interval of 3,000 years of the fault, which is similar to that of the central portion of the AGF, an interval of about 2,500 years that calculated by previous studies. This might indicate a uniform behavior in the seismogenic zone of the main AGF, despite the apparent segmentation by seismicity and creep motion in the shallower AGF. Another geo-slicing survey at MSF depicted a scarce interval of 13,500 years. Two simultaneous events on both the AGF and the MSF occurred in 1858 A.D. (Ansei Earthquake), and at about 17,300 years ago, suggesting an intermittent cooperation between the master and branch faults of the AFS. Geodetic data by dense GPS array across the fault system revealed a possible creep movement of the AGF and UKF, across a broad zone between those two faults. It shows that the creep is possibly occurring on the central eastern portion of the AGF and UKF. The creep behavior of the AFS suggests unique crustal phenomena beneath the AFS, such as presence of fluid chamber. Some future studies are necessary to reveal the mechanism of the strain partitioning concerning creep and strong earthquakes along each single fault, AGF and UKF.

**SS03/08A/D-038** Poster **0830-197**

#### GEOPHYSICAL AND GEOLOGICAL STRUCTURE OF THE ATERA ACTIVE FAULT, CENTRAL JAPAN

Tatsuo MATSUDA<sup>1</sup>, Kentaro OMURA<sup>1</sup>, Ryuji IKEDA<sup>2</sup> (<sup>1</sup>National Research Institute for Earth Science and Disaster Prevention, <sup>2</sup>Division of Earth and Planetary Sciences, Hokkaido University)

The Atera fault system runs NW-SE for about 70 km in central Japan. The fault system mainly consists of left-lateral strike-slip faults with NE-side-up reverse component. The Atera fault is one of the main faults of them. Its total lateral displacement is about 8 km and the average slip rate is estimated as 3-5 m per 1000 years. Its activity is very high. In some previous studies, the Atera fault had been regarded as one of the precaution faults for the lack of the evidence for the most recent paleoseismicity. But some other studies show that it is in the period of dormancy during a seismic cycle. In either case, we need more information about its various aspects. So we have conducted integrated investigations by surface geophysical surveys and drilling in and around the Atera fault. Six boreholes were drilled from the depth of 400 m to 630 m. Four of these boreholes (HATAJIRI, FUKUOKA, UENO, KAWAUE) are located on a line crossing in a direction perpendicular to the Atera fault. The Atera fault runs along the boundary between the Nohi rhyolite and the Naegi-Agematsu granite formations on the surface. In the Kawaue well, mostly fractured and alternating granitic rock continued from the surface to the bottom at 630 m. We did coring and investigated the mineral assemblages of the core using by X-ray powder diffraction (XRD). We detected quartz, feldspar, biotite in the parent rock (granitic rock), but also kaolinite, smectite, calcite and chlorite, which are related to hydrothermal alteration. This fracture zone is also characterized by the logging data such as low resistivity, low P-wave velocity, low density and high neutron porosity. Gravity measurements have been conducted at 242 points using the Lacoste G-260 gravity meter. A two-layer model is assumed in this study. The linear arrangement of the gravity low shows "S" geometry. These fabrics are similar to the strain field in the shear zone. A controlled source magnetotelluric (CSMT) survey has been carried out. Sixty measurement points were lined on two lines, A and B, of approximately 10 km length in direction perpendicular to the Atera fault. The high resistivity zone in the deeper part corresponds to mainly granite and a wide fractured zone like a flower-like structure was found out in some parts. In-situ stress measurements by the hydraulic fracturing method were conducted within selected intervals by the well logs, a borehole televiwer and rock core in four test holes (HATAJIRI, FUKUOKA, UENO, KAWAUE). Measurement results suggest that the stress magnitude increase with depth in each hole, however the stress gradient and the differential stress value are different from each other. And the stress magnitude decreases in the area closer to the center of the fracture zone. We are now under consideration to integrate of all these results to understand the activity of the Atera fault more clearly.

**SS03/08A/D-039** Poster **0830-198**

#### DEVELOPING PROCESS OF ACTIVE FAULT SYSTEM IN THE INNER ZONE OF WEST-CENTRAL JAPAN: A CASE OF THE ATERA FAULT BELT

Ken-ichi YASUE<sup>1</sup>, Akira TAKEUCHI<sup>2</sup> (<sup>1</sup>Graduate School of Science and Engineering, Toyama University, <sup>2</sup>Department of Earth Science, Toyama University)

This study clarified a developing process of active fault systems in the inner zone of west-central Japan (IWCJ) from the both viewpoints of geomorphology and geology. In the IWCJ, many active faults with a strike-slip and a reverse dip-slip are observed. In particular, the Atera fault belt, which limits the southwestern border of the Northern Japan Alps, is one of the most prominent strike-slip faults in Japan. This study clarified a time-space vicissitude of Quaternary faulting in the Atera fault belt as a case study, and then discussed it comparatively with the fault history in IWCJ. Quaternary development of the Atera fault belt was divided into three time-space systems; "initial system" (an initiation stage of a present faulting style), "decline system" (a slowed up stage of fault activity partly), and "growth system" (an extending stage of faulting). The initial system had been situated not only in the southeastern half of current Atera fault belt but also in the southeastern prolongation. Then a southeastern domain of the Early Pleistocene system, that is the initial system, became inactive as a decline system and has not been reactivated as a part of the same fault belt at all. While, a growth system occurred on the northwestern prolongation of the Middle Pleistocene system. An activating process of faulting in the Late Quaternary period might have worked in the fault segment ranging from the north-central part to the central of Atera faults. In short, the northwestward shift of three systems in the Atera fault belt demonstrates a style in evolution of the Quaternary fault province. In the wider area of the IWCJ, activated fault-domain also shifts northwestward in the individual fault belt as well as the Atera fault throughout the Quaternary period. The "initial IWCJ system" has dated in the Early Pleistocene from about 1.5 Ma in the southeastern district and 0.8 Ma in the almost whole area, and then has been observed in the middle to northwestern district. The time-space vicissitude of Quaternary faulting in the IWCJ also evidences northwestward shift of fault activation. The phases of the initial IWCJ system are synchronous with those of volcanism in the eastern margin of west-central Japan. The process will be of great value in interpreting changes in relative motion among the concerning plates. Based on the time-space distribution and characteristics of neotectonics, we attribute such critical ages as 1.5 Ma and 0.8 Ma to the change in subducting direction of the Philippine Sea plate and a jump of the

eastern boundary of Eurasian plate into the eastern margin of the Japan Sea, respectively.

**SS03/08A/D-040** Poster **0830-199**

#### BLIND THRUST FAULTS BENEATH METROPOLITAN OSAKA, SOUTHWEST JAPAN, CONSTRAINED BY TECTONIC GEOMORPHOLOGY AND SEISMIC REFLECTION PROFILES

Tatsuya ISHIYAMA<sup>1</sup>, Yuichi SUGIYAMA<sup>1</sup>, Karl J. MUELLER<sup>2</sup>, Masaki SUEHIRO<sup>3</sup>, Hiroshi YOKOTA<sup>4</sup> (<sup>1</sup>Active Fault Research Center, Geological Survey of Japan, <sup>2</sup>University of Colorado, <sup>3</sup>Hanshin Consultants, Co. Ltd)

We present structural models constrained by tectonic geomorphology, surface geologic mapping and high-resolution seismic reflection profiles to define the kinematic evolution and geometry of active fault-related folds along the Uemachi fault zone (UFZ) and Ikoma fault zone (IFZ) beneath Osaka metropolitan area. The UFZ and IFZ are active intraplate fault systems in southwest Japan, and are defined by 45-km-long arrays of active, west-verging reverse faults. We focus on the northern half of the UFZ and IFZ where we use the kinematic evolution of active fault-related folds to constrain rates of slip on underlying blind thrusts since early Quaternary time. Rocks uplifted in the hangingwall of the IFZ are composed of late Cretaceous granitic rocks that form the stripped cores of basement-involved folds which override a thick sequence of Neogene sediments in the Osaka basin. Numerous secondary, bedding-parallel thrusts also deform the Neogene sediments and late Quaternary fluvial terraces and are interpreted to form by flexural-slip folding that acts to consume slip on the primary blind thrusts across synclinal axial surfaces. The best-fitting trishear model for the forelimb geometry above the IFZ imaged on the seismic section requires a 56° east-dipping thrust fault with a 38° apical angle. This solution provides a 0.7 mm/yr of slip rate on the IFZ based on an age of shallow marine deposits folded across the forelimb identified in the borehole. Very subtle, Holocene fold scarps that deform alluvial fan deposits marked by changes in drainage channel networks coincide with the projected surface trace of the thrust tip. Fluvial terraces folded across the west-dipping forelimb, and east-dipping backlimb of the frontal UFZ suggest that it grows above an active, east-dipping thrust. The seismic sections across the northern UFZ and nearby borehole profiles show that the core of the basement-involved fold also overrides onto the lower portion of the thick Neogene sediments in the Osaka basin. Trishear solution for the northern UFZ suggests that the forelimb geometry has formed above the propagating tip of a 40° east-dipping thrust. A 458 m of slip for the retrodeformed horizon (shallow marine sediments Ma-1) provides a slip rate of 0.38 mm/yr, which corresponds well with a rate of vertical separation estimated on numerous, dated shallow marine horizons across the UFZ.

**SS03/08A/D-041** Poster **0830-200**

#### LATE HOLOCENE EARTHQUAKE EVENT ON AN 80-KM-LONG BLIND THRUST FAULT SYSTEM BENEATH GREATER METROPOLITAN TOKYO

Kiyohide MIZUNO<sup>1</sup>, Yuichi SUGIYAMA<sup>1</sup>, Yuichiro FUSEJIMA<sup>1</sup>, Toshihiko SUGAI<sup>2</sup>, Takashi HOSOYA<sup>3</sup>, Haruo YAMAZAKI<sup>4</sup> (<sup>1</sup>Active Fault Research Center, GSI, AIST, <sup>2</sup>Graduate School of Frontier Sciences, University of Tokyo, <sup>3</sup>Chuo Kaihatsu Corporation, <sup>4</sup>Graduate School of Science, Tokyo Metropolitan University)

Trenching and continuously-cored boring surveys identified a late Holocene earthquake event on an 80-km-long blind active fault system in the greater Tokyo metropolitan area. The NW-striking Fukaya fault system is located along the northwestern margin of the Kantō plain where greater metropolitan Tokyo is expanding. The fault system consists of an 80-km-long array of four left-stepping west-side-up reverse faults, and several subsidiary east-side-up back thrusts on the west. The west-side-up reverse faults appear as monoclines or fault-related folds on the ground surface. They are widely concealed beneath thin young Holocene fluvial deposits, and partly modified into steeper scarps by fluvial erosion. The maximum long-term uplift rate of the monoclines is estimated to be more than 0.3 mm/y based on tectonic geomorphology, seismic reflection profiles and boring data. For clarifying recent activity of the Fukaya fault system, we dug 14 continuously-cored boreholes across a monocline above the 35-km-long central (third from the north) west-side-up blind thrust, and excavated two trenches on its east-side-up back thrust about 4 km long. The boring survey showed that the most recent growth of the monocline took place after deposition of silt-sand beds dated 5500-6100 yBP. The excavation exposed a sharp north-dipping reverse fault that displaces 5300-5600 yBP soils by about 1 m along the fault plane. A radiocarbon age of 1700 ± 50 yBP was obtained from soils overlying the reverse fault. These data suggest that the most recent earthquake event with major surficial deformations occurred between 5.3 and 1.7 ka on the central geometrical segment of the Fukaya fault system. Historical documents and archaeological evidence indicate that a large ( $M \geq 7.5$ ) earthquake occurred in AD 818 and caused strong shaking in the area adjacent to the Fukaya fault system. However, no archaeological evidence of a large earthquake in the early Jomon to Yayoi Period (about 6 to 1.7 ka) is known in the adjoining area. In order to solve this discrepancy, we reinvestigate the timing of this geologically-identified late Holocene earthquake event.

**SS03/08A/D-042** Poster **0830-201**

#### ACTIVE TECTONICS ON THE MIDDLE PART OF TOKACHI-PLAIN FAULT ZONE, HOKKAIDO, WESTERN EDGE OF KURILE FORE-ARC SLIVER, JAPAN

Wataru HIROSE, Sunao OHTSU, Jun TAJIKA, Masazo TAKAMI (Geological Survey of Hokkaido)

Tokachi-Plain Active Fault Zone exists at the eastern side of Tokachi Plain, and consists of westernmost edge of Kurile fore-arc sliver. They would be appeared at least from Neogene and still active until now. Detailed survey of these faults has started by Hokkaido Local Government until 2001. At the middle part of Tokachi-Plain Active Fault Zone, reverse fault uplifted onto the western side. Pliocene AEPleistocene sedimentary rocks had been steeper by the fault. At least two liner flexure scarps appeared at the river terrace. Their slip rate could be estimated 0.2 m / ka or smaller. Shallow seismic reflection survey have done to investigate the subsurface structure of the middle part of Tokachi Active Fault Zone. Obvious flexure zone exist at the eastern side of the survey line. This flexure is 500 m wide and uprise at eastern side. This subsurface flexure agree with the bouguer anomaly survey, that increase at the eastern side on the flexure. On the other hands, reflection data indicates that the weak westward tilting exists at western edge of the survey line. This tilting may correspond to the western frontal deformation zone of the faults.

**SS03/08A/D-043** Poster **0830-202**

#### SOUTHERN EXTENSION OF SUMATRAN FAULT AND ITS TECTONIC SIGNIFICANCE, OFF SUNDA STRAIT

Wonn SOH<sup>1</sup>, Yusuf S. DIAJADIHARDJA<sup>4</sup>, Christoph GAEDICKE<sup>3</sup>, Saneatsu SAITO<sup>1</sup>, Yasutaka IKEDA<sup>2</sup> (<sup>1</sup>Japan Marine Science and Technology Center, <sup>2</sup>University of Tokyo, <sup>3</sup>Federal Institute for Geosciences and Natural Resources (BGR), <sup>4</sup>Agency for the Assessment and Application of Technology, BPPT)

Slip partitioning between closer-to-trench normal thrusting and trench-parallel strike-slip faulting has been postulated mainly from the study of earthquake slip. Offshore of Sunda Strait is one of the most appropriate areas in the world to examine the strain partition recorded in overlying fore arc. However there is no dependable geomorphic data yet although an attention for offshore of the Sunda Strait has been paid for a long time to the junction of the regimes between normal subduction off Java and oblique subduction off Sumatra. A single channel and bathymetric data were obtained by R/V Yokosuka, YK01-02/YK02-07 cruises provide quite different geomorphologic view to the expected previously. Namely we can identify the southern extension of Great Sumatran Fault as an active fault. Shinkai 6500 dive enables to show a few meter vertical topographic displacement along the fault associated with a significant shear zone. The junction area is occupied by a bundle of tectonic blocks, well demarcated by SSE- and east-trending lineaments. A few amount of mud diapir mounds are recognized along the east-trending thrust that propagates from the southern extension of the GSF, where corresponds to significant negative Bouguer anomaly zone (approx. -150 mgal). Of course the morphologic feature is different to the transtensional graven in the Sunda Strait, it tells us that the strain partition in a fore arc does not uniformly stretched in the entire fore arc but localized (or concentrated) in specific area such as this area.

**SS03/08A/D-044** Poster **0830-203**

#### SUBSURFACE STRUCTURE BENEATH SUNDA STRAIT INFERED FROM MARINE SEISMIC REFLECTION SURVEY

Nugroho Dwi HANANTO<sup>1</sup>, Hariadi PERMANA<sup>1</sup>, Wahyu TRIYOSO<sup>2</sup>, Sonny WINARDHIE<sup>2</sup> (<sup>1</sup>Research Center for Geotechnology, Indonesian Institute of Sciences, <sup>2</sup>Department of Geophysics and Meteorology, Institut Teknologi Bandung)

Sunda strait is a unique area located at transition between frontal subduction of Indian-Australian plate and Eurasia plate to the south of Java and oblique subduction to the west of Sumatra. The Sunda strait has been developed since last 15My (Later Cenozoic) caused by clock wise rotation of Sumatra relative to Java and displacement to the north-northwest of southern block of Sumatra along Semangka fault. The Sunda strait supposed as the axis during the rotation. The peak of this geological event occurred at 5My. This was characterized by extension and subsidence that builds Sunda strait. Upper part of the subducted plate is 21 km depth whilst the moho is 28km depth and bordered by volcanic products of different ages. Most of the islands within this strait consist of volcanic products covered by recent coral reefs in their flanks. Fault line pattern develops at Sunda strait that controlled Krakatau complex is supposed to NW-SE direction, parallel to Sumatra fault system and interpreted as normal fault with dip direction to SW, but gravity data shows no indication of continuation to the east of Sumatran fault across the Sunda strait. Along NW-SE trending, there are situated some volcanic centers and islands that are supposed to be volcanic centers. These include Rajabasa volcano, Sebuku Island, Sebesi Island, Islands of Krakatau Complex, Panaitan Island and Payung volcanic center in Ujung Kulon Peninsula. Around the southern tip of Sumatra Island and Sebuku Island can be found outcrops of andesite lava that mostly presenting sheeting joints. These rocks are supposed to be Pliocene in age. The Rajabasa volcano and Sebesi volcano (that construct the Sebesi Island) are also situated in the same areas with the former ones. The latter are constituted of lavas, breccias and tuffs of andesitic to basaltic compositions, and they are classified as Young Volcanic Deposits of Quaternary ages. The Krakatau Complex consists of Panjang, Anak-Rakata, Rakata, Sertung and Ombudsmen islands. The rock of this complex consists of lava, lava breccias and pumiceous tuffs having of dacitic, andesitic and basaltic composition. Oldest volcanic products are andesitic in composition and then followed by those of basaltic ones. We have conducted shallow marine seismic survey on northern part of Krakatau Complex and in the front of Semangka Bay. This survey was aimed to study the subsurface structure beneath the Krakatau Complex and to delineate the continuation of Sumatran Faults Zone to Sunda Strait. The seismic images revealed from this research shows, layered sediment and fault structures that indicate the lineament of Sumatra Fault Zone to Sunda Strait and subsidence event of this region.

**SS03/08A/D-045** Poster **0830-204**

#### QUANTITATIVE EVALUATION OF INLAND SEISMIC ACTIVITY IN JAPAN BY USING GIS

Satoshi ITABA<sup>1</sup>, Kunihiro WATANABE<sup>1</sup>, Ryohei NISHIDA<sup>2</sup> (<sup>1</sup>Research Center for Earthquake Prediction, Disaster Prevention Research Institute, Kyoto University, <sup>2</sup>Faculty of Technology, Tottori University)

It is important for quantitative evaluation to estimate the seismic activity; however, this evaluation has been seldom performed. It has been often determined by subjectivity until now. On the other hand, the assessment of active faults is the general public requirement today. We proposed a GIS (Geographic Information System)-method of quantitative evaluation of seismic activity (Nishida et al, 1999). By this method, the activity of inland active faults in Japan is estimated. We used in this investigation 2,324 active faults listed in "ACTIVE FAULTS IN JAPAN" (University of Tokyo Press). The shallow inland earthquakes of JMA catalogue from Oct.1997 to May 2002 are analyzed. By applying GIS to these fault traces, a buffered zone can be made, which is the zone within a distance between Ri and Ri+1 from the fault. The earthquakes included in each buffered zone can be chosen. The seismic activity of the zone is expressed by using three parameters, namely, number of events, accumulated fault surfaces and released energy. Dividing total amount of these quantities by the area of the corresponding zone, the density of seismic activity can be obtained for each buffered zone. Considering the relation between those activity density and the distance from the fault trace, the effective distance can be estimated, in which the seismic activity is influenced by the existence of the fault. By adopting the effective distance obtained above, we can examine the seismic activity of each fault. For some faults, the seismic activity decreases in proportion to distance from the fault, but not for others. Generally speaking, the correlation between seismic activity and the distance from the fault is not so high. Inland seismic activity of southwest Japan is generally higher than that of northeast Japan. There may be two reasons. First, the main pattern of fault movement in Northeast Japan is dip-slip, and that in Southwest Japan is strike slip. Dip slip type fault needs much tectonic energy to move than strike slip ones. Second, it may be caused by the difference of coupling factors.

**SS03/08A/D-046** Poster **0830-205**

#### A COMPREHENSIVE SIMULATION OF LITHOSPHERE DEFORMATION WITH FAULT SLIP USING A COUPLED METHOD OF FINITE ELEMENT METHOD WITH SPRING-BLOCK MODEL

Hanjing HONG, Yong YU, Xiuzhen ZHENG, Peixun LIU, Wei TAO (Institute of Geology, China Seismological Bureau)

A numerical method of finite element method (FEM) coupled with spring-block model (SBM) is developed to simulate the system of lithosphere with faults. The slip of intra-plate fault was studied using a spring-block system sandwiched in between two lithosphere blocks. Stress

and displacement exchange between FEM and SBM is engaged to couple these two methods in every time step. The resulting displacement from FEM was imposed on SBM as the boundary constrain of fault, and resulting stress, getting from SBM, was used as the intra-boundary constrain of FEM. The lithosphere is buildup using a heterogeneous two-layer viscoelastic model with different viscosities. With constant stress and constant velocity boundary conditions, stress transfers from the ductile layer to the brittle layer, and the heterogeneous rheology of ductile layer also affects the stress distribution in the brittle layer. As a result, the brittle-ductile regime provides an efficiency mechanism of stress transfer in the crust, and the deep-seated heterogeneous ductile layer resulting stress concentration in the brittle layer. The stress evolution of this coupled model can be divided into two stages: accumulation stage and critical stage. During the stage of accumulation, the stress build up in both lithosphere and fault, during the stage of critical, the stress fluctuated in a steady level in both lithosphere and fault, and the amplitude of stress alteration is much less than the steady level. Most earthquake events occur in the critical stage. Earthquake recurrence period, the correlated characteristic magnitude, seismic stress drop, Gutenberg-Richter law can be observed from the results of this coupled simulation. The modeling rupture process can be compared with geophysical inversion of seismic wave. The rupture process initiates from the nucleation node, spreads outward to both two sides. As the initial node, the stress state of this slider-block controls the time and place of the rupture, but it cannot affect the magnitude. Instead of the stress of initial node in the fault, the elastic energy of crust blocks play an important role to affect the magnitude of earthquake. Spatial distribution of major earthquakes in the Chuanbian area was studied using this coupled simulation. Fault segments are put into the coupling model of boundary faults, and the simulated earthquake sequence is compared with the historical catalogue in this area.

**SS03/08A/D-047** Poster **0830-206**

#### THE ROLE OF PORE FLUIDS IN THE MECHANISM OF SEISMIC SEQUENCES

Antonello PIOMBO, Michele DRAGONI (Dipartimento di Fisica, University of Bologna)

It is generally agreed that the occurrence of seismic sequences implies a kind of interaction between different fault segments. The coseismic stress transfer produced by each dislocation is the most obvious component of such an interaction. However the time intervals elapsing between subsequent events in a sequence indicate that the coseismic stress is not sufficient to trigger other seismic events by itself. We investigate the possibility that the coseismic stress field may induce flow of pore fluids, altering the pore pressure distribution in the region. The flow velocity depends on the pressure gradient and the permeability of the medium. We consider a porous, elastic medium and study under which conditions the change in pore pressure induced by a fault dislocation may lead to a significant decrease in friction on adjacent fault segments. A gradual decrease of friction on a fault segment, which was already loaded as a consequence of stress transfers by previous dislocations in the seismic sequence, might lead to the failure of the segment itself, after the time required for pore fluid diffusion to take place.

**SS03/08A/D-048** Poster **0830-207**

#### PRECISE SUPERVISION OVER MOTIONS OF THE EARTH SURFACE AND UNDERGROUND SITES

Mstislav N. DUBROV<sup>1</sup>, Vladimir A. ALYOSHIN<sup>1</sup>, Viktor A. VOLKOV<sup>2</sup>, Anna V. KALININA<sup>2</sup>, Rostislav F. MATVEEV<sup>1</sup>, Sergei A. MOISEENKO<sup>1</sup> (<sup>1</sup>Institute of Radio-engineering and Electronics, Russian Academy of Sciences, <sup>2</sup>Institute of Physics of the Earth of RAS, Moscow, Russia)

The test of natural and artificial geological processes which change the statics and dynamics of stress-deformed state of medium are in consideration. It is the straight method of an estimation of hazard during both the creating and the using of an engineering or energetic buildings, plants etc. The crustal processes in continental areas as active seismicity and recent fault motion make the safety problems being over important. The special place in associated risk decrease is occupied by real time supervising over system: building - basis - geological medium. The precise geophysical methods of this system check are discussed. Horizontal and vertical motions of the earth surface and parts of underground construction are measured by the high accuracy laser strainmeters and capacitive seismo-gravimeters. Three types of load actions on medium were explored: (1) immediate mechanical loading, (2) change of mode of the water wells operation, (3) action of sharp differences of atmospheric pressure. Laser strainmeter measure the relative displacements of two points at the earth surface or buildings on which the interferometer is anchored. The accuracy of the order of 10(-3) nm is achieved at basis 1-100 m. Seismo-gravimeters are supplemented by inertial properties high-sensitive accelerometers. The devices with resolution of 0.5 uGal to vertical biases about 1 um in a seismic frequency band. (1) We test the load affection of the earth surface by measuring the linear deformations of a ground under activity of the traffic motion. It is accompanied by 3-D spatial strains: vertical and horizontal tensions from which elastic modules of the medium are defined. (2) Changes of a mode operation of underground water wells cause the locality of ground strains up to 10-20 um per hour. The absence of instrumental check of medium status during a heavy use of underground waters give a raise of hazard from such phenomena as the sedimentary of building bases, development of landslides etc. (3) The connection of intensive variations of atmospheric pressure and motions of the earth surface are explored on distances between observation sites of 45 km. We obtained the synchronous records of pressure, gravity acceleration and the earth strains. The dynamic perturbations in the atmosphere have undular microstructure and are accompanied by motions of the earth surface as enough complicated superposition of horizontal strains and vertical displacements. These perturbations are precisely delineated over phase structure and are spread along a demarcation of the Earth - atmosphere with the velocities of 30-50 km per hour.

**SS03/08A/D-049** Poster **0830-208**

#### TECTONIC DEFORMATIONS DOMINATED BY NONLINEAR VON KÁRMÁN EQUATIONS

Tomoaki CHIBA, Hiroyuki NAGAHAMA (Department of Geoenvironmental Sciences, Graduate School of Science, Tohoku University)

Mechanical behaviour of tectonic deformations under the infinitesimal elastic deformations is linear behavior and therefore Curie symmetry principle, which is the law of causality for symmetry, is always preserved. On the other hand, breaking of Curie symmetry principle has already observed in several nonlinear phenomena. Such nonlinear systems are mathematically proved to be dissymmetrical by functional analysis and group theoretical bifurcation analysis. Von Kármán equations can describe such nonlinear systems, i.e. bending and buckling of thin elastic plates studied in engineering. We point out a few kinds of tectonic deformations (e.g., laccolith mounting, multilayer deflection and plate bending) can be also described by von Kármán equations. Von Kármán equations can also explain crack pattern formations (e.g., formations of echelon crack and c-surface in S-C mylonites) by using an analysis of the group theoretical bifurcation method. The analysis exhibits that von Kármán equations can allow to break Curie symmetry principle. Hence Curie symmetry principle cannot be used blindly to infer the past events from the rests now on the earth. The

group theoretical bifurcation analysis reveals that the nonlinear system behaves nonlinearly only at singular points on the solution path and that the system behaves linearly at ordinary points consisting most part of the solution path on the other hand. Therefore, Curie symmetry principle is still useful to interpret the history of tectonic deformations. With the new constraint for nonlinear dissymmetrical deformations, we can use Curie symmetry principle properly to consider nonlinear systems in tectonic deformations.

**SS03/08A/D-050** Poster **0830-209**

**VELOCITY AND STRESSES DURING TECTONIC DEFORMATION; INSIGHTS FROM DISCRETE ELEMENT SIMULATIONS**

Yasuhiro YAMADA<sup>1</sup>, Atsushi TANAKA<sup>2</sup>, Toshi MATSUOKA<sup>2</sup> (JAPEX Research Center, <sup>1</sup>Kyoto University)

Discrete Element Method (DEM) approximates the geologic body as an assembly of particles similar to sandbox experiments, thus can simulate the brittle behaviour of the upper crust appropriately. We have applied the method to a modelled collision process of the Indian sub-continent to the Eurasian Plate, and have extracted velocity vectors and normal/shear stress fields of each particle for every short time interval during deformation. Since the method is a forward modelling technique, progressive development of strain and stress can be examined during the collision process. The results show that the velocity distributions and the stress fields of the particles are quite unstable. This may be due to the brittle behaviour of the particle assembly corresponding to the upper crust, in which localisation of the stress and its release by faulting are clearly observed. In particular, shear stress concentration was commonly generated along a broad shear band and was released by faulting causing a large velocity anomaly in two opposite directions. The velocity distribution and normal stresses of the particles correspond to GPS and in-situ stresses respectively when applied to real geology. The GPS vectors and the directions of in-situ stresses of the eastern Asian region, however, show overall continuous curvature from the Himalayan Mountains. Thus such a large-scale tectonics may be primarily controlled by ductile deformation of the lower crust and its substrates.

**SS03/08A/D-051** Poster **0830-210**

**COMPARING GEODETIC AND GEOLOGIC DEFORMATION RATES AND PATTERNS IN SOUTHERN CALIFORNIA, U.S.A.**

Noah P. FAY, Eugene D. HUMPHREYS, Ray J. WELDON (Department of Geological Sciences, University of Oregon)

We present a comparison of geodetic and geologic-based deformation models for southern California, U.S.A. Contemporary surface deformation, which is accommodated by a diffuse zone of predominantly strike slip motion (the San Andreas fault system), is well characterized by a dense array of geodetic stations (mostly those of SCIGN, the Southern California Integrated GPS Network). Geodetic data tend to be spatially averaged and temporally discrete and are commonly used to determine long-term slip rates via simple kinematic models, such as an elastic halfspace. Alternatively, geologic data (e.g., paleoseismic trench studies, offset alluvial fans, etc.), which are spatially discrete and temporally averaged, provide an independent measure of the same long-term slip rates on active faults. In this study we have constructed a kinematic forward model, driven largely by geologically determined slip rates. Model faults creep below seismogenic depths of ~ 13 +/- 3 km and are locked above to simulate interseismic strain. Surface velocity and strain rates are calculated using the linear elastic half-space solutions of Okada (1992). In general the surface deformation observed by GPS and predicted by the geology-based kinematic model agree, to within 95% confidence. In other words, the residuals, or differences between the observed and predicted, are not significantly different from zero. The residual RMS (Root Mean Square) is ~ 5 mm/yr. There are, however, three regions where significant differences exist between the two data sets: along the San Andreas fault at Parkfield, CA; the Mojave Desert, north and east of the "Big-Bend" section of the San Andreas fault; and the greater Salton Trough area, between the San Andreas and San Jacinto faults from ~ 33.5N to the US/Mexico border. We offer some possible solutions to reconcile these differences.

**SS03/08A/D-052** Poster **0830-211**

**PSINSAR AS A RESOURCE FOR TECTONIC MODELLING IN SUBDUCTION AREAS**

Roger M.W. MUSSON<sup>1</sup>, Mark HAYNES<sup>2</sup>, Julian J. BOMMER<sup>3</sup>, Alessandro FERRETTI<sup>1</sup> (<sup>1</sup>British Geological Survey, <sup>2</sup>NPA Group, <sup>3</sup>Dept Civil Engineering, Imperial College, London, <sup>4</sup>TeleRilevamento Europa)

PSInSAR is a new technique for Earth Observation derived land motion measurement which relies on permanent scatterers, and offers the possibility of measurements of ground displacements to a degree of accuracy, and over periods of time, previously unobtainable from conventional interferometry. This technique has been developed by TeleRilevamento Europa of the Politecnico di Milano in Italy. By using at least 30 satellite radar scenes of the same place acquired over many years, a network of highly reflective pre-existing ground features (permanent scatterers) are identified against which sub-mm measurements of motion can be made. These permanent scatterers can be any large, permanent angular object, such as building roofs, metallic structures, and even large boulders. Using these data, very accurate displacement histories can be obtained for the period 1991 to the present. Calibration with GPS data show good agreement, but the PSInSAR data are less noisy. A unique attribute of PSInSAR is that the history of displacements over the last nine years (length of the SAR data archive) can be extracted for any part of the globe with data coverage. We present here the results of a test monitoring study for the Tokai area of Japan. The data are similar to those derived by other means (GPS, levelling) but much denser (291,000 data points between Hamamatsu and Ito). Such data provide a resource for studies such as the modelling of impending subduction earthquakes using the ABIC method. This work results from a European Space Agency (ESA) "Earth Observation Market Development" project entitled "Developing markets for EO-derived land motion measurement products", involving, NPA (lead), the British Geological Survey (UK), Imperial College (UK), TeleRilevamento Europa (Italy), ImageONE (Japan), the Geographic Survey Institute (Japan), Oyo Corporation (Japan), Fugro (Netherlands) and SARCOM (ESA data distributing entity).

**SS03/08A/D-053** Poster **0830-212**

**TIDAL COMPONENTS IN GROUNDWATER LEVEL OBSERVED AT OSAKAYAMA OBSERVATORY, KINKI DISTRICT IN JAPAN**

Kunihiro SHIGETOMI, Masatake HARADA (Research Center for Earthquake Prediction, Disaster Prevention Research Institute, Kyoto University)

Continuous monitoring of groundwater level has been carried out since December 1976 at Osakayama observatory in order to investigate relations between changes in groundwater level and strain changes and earthquake occurrence. To verify availability of continuous

monitoring of groundwater level for geodynamics studies, it is necessary to know fundamental characteristics of observation well in various frequency bands. The response of groundwater level for the earth tide is the most fundamental signal. In 1980's, as a result of the frequency analysis using the self-registering record by the float adopted as an observation system since the beginning, M2 and O1 tidal components were clearly distinguished. And it was clarified that the daily variation of groundwater level was the tidal variation caused by tidal potential. For the digitizing of the self-registering record, however, there was a limit at the accuracy of amplitude and time resolutions, and it was insufficient for discussing amplitude and phase of the tidal variation precisely. From 2001, we therefore applied the pressure detection type groundwater level indicator together in the same well. From this instrument, the accuracy of amplitude and time resolutions of the record was improved. In this study, we analyzed tidal variation which appears in groundwater level using new type indicator record. And we investigated relation between groundwater level and strains. Furthermore, we checked temporal variations of tidal factors associated with the earthquake (M=5.1, Δ=25km). As a result of tidal analysis, it became clear that groundwater level and strain observed with extensometer corresponded well. Comparing groundwater level with cubic dilatational strain predicted by GOTIC2, which was program to compute the global tidal deformation, we obtained these interaction coefficients about 2.5 mm/E-8strain in M2 constituent and about 2.0 mm/E-8strain in O1 constituent. And temporal variations of tidal factors revealed that the changes of groundwater level were seen to appear before about 10 days of the earthquake.

**SS03/08A/D-054** Poster **0830-213**

**TECTONIC MOTION OF THE RYUKYU ARC, SOUTHWEST JAPAN INFERRED FROM GPS VELOCITY FIELD AND EARTHQUAKE MECHANISM**

Tsuyoshi WATANABE<sup>1</sup>, Takao TABEL<sup>2</sup> (<sup>1</sup>Graduate School of Science, Kochi University, <sup>2</sup>Department of Natural Environmental Science, Kochi University)

Ryukyu Arc is a NE-SW trending islands arc connecting Taiwan and Kyushu, southwest Japan. At its southeastern boundary, the Ryukyu Trench, the Philippine Sea plate subducts at a rate of 6-8cm/yr. Japanese nationwide continuous GPS array has illustrated trenchward extrusion of the islands at a rate of 2cm/yr in the northeastern part and larger than 4cm/yr in the southwest. Tectonic movement of the Ryukyu Arc may be characterized by low plate coupling (loose constrain) at the Ryukyu Trench and backarc opening (or rifting) at the Okinawa Trough, the active backarc basin on the northwest. Though the movement of the Ryukyu Arc looks like a block motion rather than an internal elastic deformation, more details are not clear because GPS stations have been deployed nearly parallel to the Ryukyu Trench and the Okinawa Trough. At first we divide the region into several blocks based on spatial variation of earthquake focal mechanism and GPS velocity field, and determine Euler vector of each block. As the first approximation, tectonic movement in this region can be reproduced by the motion of five blocks, with an average discrepancy of about 5mm/yr between the observed and predicted velocities. Second we introduce moment tensor solutions of shallow earthquakes and translate them into strain rates in order to quantify plate coupling at the Ryukyu Trench. Plate coupling estimated is about 30% off Kyushu, then steeply decreases to a few percent in the central (near Okinawa Island), and again increases up to about 50% east off Taiwan. However, velocity discrepancy between observation and prediction still remains even after taking the plate coupling into consideration. Current GPS and earthquake data strongly suggest a trenchward motion of the Ryukyu Arc, divided into several tectonic blocks and probably driven by the backarc opening at the Okinawa Trough, accompanying small internal deformation.

**SS03/08A/D-055** Poster **0830-214**

**MULTI-DISCIPLINARY STUDY OF EARTHQUAKE SOURCE AREAS AND GAPS ALONG THE EASTERN MARGIN OF JAPAN SEA, OFF HOKKAIDO**

Yukinobu OKAMURA<sup>1</sup>, Kenji SATAKE<sup>2</sup>, Ken IKEHARA<sup>1</sup>, Kohsaku ARAI<sup>1</sup>, Akira TAKEUCHI<sup>1</sup> (<sup>1</sup>Institute for Marine Resources and Environment, AIST, <sup>2</sup>Active Fault Research Center, AIST, <sup>3</sup>Faculty of Science, Toyama University)

The eastern margin of the Japan Sea has been a zone of major E-W contraction during the last 2-3 million years. Four large earthquakes (M > 7.5) have occurred along this margin during the 20th Century. The largest earthquake is the 1993 Hokkaido-Nansei-oki earthquake (M 7.8) that was caused by rupture of 140 km long fault along the Okushiri Ridge. Abundant seismological, tsunami and geodetic data made it possible to construct the detailed model of source faults of this earthquake. In contrast to the 1993 earthquake, the 1940 Shakotan-oki earthquake (M 7.5) that occurred about 160 km north of the 1993 earthquake has been studied based on insufficient data. Because the location and size of its source area has been controversial, it is not clear if there is a seismic gap between the 1993 and 1940 earthquakes. To confirm the source area of the 1940 earthquake, we have conducted detailed marine surveys in and around the inferred source area of the 1940 earthquake. Seismic and bathymetric surveys have shown that there are two overlapping rows of several structural ridges in the area. The northeastern row is composed of three ridges including the Oshoro seamount which is located just on the epicenter of the earthquake. The southern ridge terminates at about 50 km north of the source area of the 1993 earthquake. The southwestern row of the ridge consists of the Kaiyo seamount and ridges extending to the south, which continues to the Okushiri ridge at the source area of the 1993 earthquake. Dive surveys provided us important data about the recent activities of the active faults. Dives in the source area of the 1993 earthquakes observed wide-spread sea-bottom disruption; open cracks, collapse and debris flow deposits. They indicate that ancient earthquakes have been geologically recorded as the sea-bottom disruptions. Several dive surveys were conducted in the source area of the 1940 earthquake. Fresh disruptions were observed on the Oshoro seamount and ridges to the north and south of the seamount, whereas disruptions were covered with thin muddy sediments in the Kaiyo Seamount. The observations suggest that Oshoro seamount possibly belong to the source area of the 1940 earthquake. The Kaiyo seamount can not be a source area of the earthquake, while it is active and could be a source area older earthquake. These sea-bottom observations and geologic structure also suggest that there is a seismic gap between the 1940 and 1993 earthquakes. The width of the gap is inferred to be longer than 50 km. Tsunami simulation from the 1940 earthquake will be updated based on the geologic structure and compared with the observed tsunamis.

**SS03/08A/D-056** Poster **0830-215**

**COLLISION STRUCTURE IN THE SOUTH OF HOKKAIDO REGION, JAPAN, DEDUCED FROM OBSERVATIONS WITH OCEAN BOTTOM SEISMOGRAPHS AND DENSE NETWORK OF LAND STATIONS**

Yoshio MURAI<sup>1</sup>, Satoshi AKIYAMA<sup>1</sup>, Kei KATSUMATA<sup>1</sup>, Tetsuo TAKANAMI<sup>1</sup>, Tadashi YAMASHINA<sup>2</sup>, Tomoki WATANABE<sup>3</sup>, Ikuo CHO<sup>2</sup>, Masayuki TANAKA<sup>3</sup>, Asako KUWANNO<sup>4</sup>, Naoto WADA<sup>1</sup>, Hideki SHIMAMURA<sup>1</sup> (<sup>1</sup>Institute of Seismology and Volcanology, Graduate School of Science, Hokkaido University, <sup>2</sup>National Research Institute for Earth Science and Disaster Prevention, <sup>3</sup>Japan Marine Science and Technology Center, <sup>4</sup>Geo-Research Institute, <sup>5</sup>Seismological and Volcanological Department, Japan Meteorological Agency, <sup>6</sup>Research Center for Prediction of

In the south of Hokkaido region, Japan, the Kuril arc is considered to collide with the northeast Japan arc. Arc-arc collisions are important process for the growth from an island-arc crust to a new continental crust. Such a collision is responsible for the uplift of the Hidaka Mountains, high seismic activity and large earthquake occurrence such as the 1982 Urakawa-oki earthquake ( $M_s$  6.8) in this region. It is important to image the 3-D structure of crust and uppermost mantle in order to clarify the collision tectonics and understand the mechanism of earthquake occurrence. We conducted observations of microearthquakes with a dense network of land stations and ocean bottom seismographs to reveal the relation between the collision structure and earthquake occurrence. 630 hypocenters were determined during the period from August 7 until September 30, 1999. We determined 3-D P wave velocity model using travel time tomography. From the tomographic images, low-velocity anomalies are detected to extend from the western side to the central part of the Hidaka Mountains in the depth from 9 to 25 km. These low-velocity anomalies are running parallel to the Hidaka Mountains from 42°N to 42.8°N. They are considered to be the crust of the northeast Japan arc. High-velocity anomalies are found just beneath the crest of the Hidaka Mountains. They stretch in the NW-SE direction so as to overlie the low-velocity anomalies stated above. They are considered to be the lower crust of the Kuril arc obducted towards the west. In the eastern side of the Hidaka Mountains, we find the lower crust of the Kuril arc is delaminated by the collision and the lower part of it is dipping gently southwestward from east of the Hidaka Mountains to the source area of the Urakawa-oki earthquake in the depth from 35 to 45 km. The faulting mechanism of the Urakawa-oki earthquake shows a thrust type solution with a compressional axis in NE-SW direction and the maximum stress axes estimated by the stress tensor inversion method and focal mechanism solutions of many microearthquakes show NE-SW direction in the western side of the Hidaka Mountains. The direction of the earthquake-generating stress is consistent with our collision model. The delaminated lower crust appears to collide with the upper boundary of the subducting Pacific plate. Our model well explains why the seismicity is high even in such a deep crust in this region. The length of the delaminated lower crust estimated here is consistent with the total crustal shortening length between the two island-arcs evaluated from geological data. Our model suggests the geometry of the delamination structure has a strong effect on earthquake occurrence and the Urakawa-oki earthquake was caused at the front of the delaminated lower crust.

**SS03/08A/D-057** Poster **0830-216**

**STRAIN PARTITIONING BETWEEN THE SURUGA TROUGH AND THE ZENISU THRUST: NEOGENE TO PRESENT TECTONIC EVOLUTION IN THE ONLAND AND OFFSHORE TOKAI DISTRICT, JAPAN**

Tetsuro HIRONO (Deep Sea Research Department, Japan Marine Science and Technology Center)

The Tokai district, central Japan, is located close to the convergent boundary between the Philippine Sea and Eurasian plates. Historical documents show that large interplate earthquakes have repeatedly occurred in this district along the Nankai-Suruga Trough. Recent events in the Tokai district include the 1707 Hoei ( $M_8.4$ ), 1854 Ansei-Tokai ( $M_8.4$ ) and 1944 Tonankai ( $M_8.0$ ) earthquakes. On the basis of the distribution of seismic intensities, coseismic crustal movements and tsunami waves, Ishibashi (1977, 1984) concluded that the faulting areas of the former two events covered the Nankai and Suruga Troughs, whereas that of the last event did not reach the Suruga Trough. Therefore, the area extending from the Cape Omaezaki to the northern end of the Suruga Bay can be regarded as a seismic gap, where tectonic stress has been accumulating since the 1854 Ansei-Tokai earthquake. Since this urgent warning against an impending 'Tokai earthquake', spatially and temporally dense observations of various kinds, such as seismic activity, crustal movements, electrical resistivity, and hydrological and geochemical changes, have been conducted to detect premonitory phenomena of a future Tokai earthquake, and to improve prediction of its occurrence. In addition to such geophysical methods, comparison of the present tectonic activity with past-movement, and to assess whether the tectonic movements in the Tokai district are now active or inactive, are also important. In this study I reconstruct quantitatively the spatial and temporal tectonic evolution of the eastern Tokai district based on a geological survey, and discuss the past and future degree of activity in this district. The geological survey and some interpretations of seismic profiles in the eastern Tokai reveals the tectonic evolution quantitatively. The horizontal crustal shortening strain and the strain-rate since the Neogene are calculated as 12 % and 2 x 10<sup>-6</sup> %/yr, respectively. The present interseismic horizontal crustal strain and strain-rate around the Omaezaki area are approximately 4 x 10<sup>-7</sup> % and 4 x 10<sup>-9</sup> %/yr. By comparing these rates, the present tectonic horizontal movement in the eastern Tokai has been becoming less active. This imply progressive transition of tectonic activity into low strain field. Since the tectonics around the Izu Peninsula have been strongly related to the collision of Izu to Japan, this phenomenon may result from the strain partitioning between the Suruga Trough and the Zenisu Thrust.

**SS03/08A/D-058** Poster **0830-217**

**TRANSCURRENT MOTIONS AND DEFORMATION ON THE FORE-ARC OF NORTHEAST JAPAN**

Yasuto ITOH<sup>1</sup>, Tetsuro TSURU<sup>2</sup> (<sup>1</sup>Dept. of Earth Sci., CIAS, Osaka Prefecture University, <sup>2</sup>Japan Marine Science and Technology Center)

Multi-channel seismic survey gives a new insight for deformation mode along an active margin. Geologic structure on the northern part of the fore-arc of northeast Japan has been understood in relation with late Cenozoic compressional stress regime as a result of subduction of the Pacific Plate and / or collision of the Kuril Arc. Recently acquired seismic data combined with reprocessed sections do not accord with such theory, but prefer NNW-SSE trending deformation zone bounded by large transcurrent faults. Contrast in geophysical properties (density, seismic velocity, magnetic anomaly, etc.) and geologic structure across the western fault strands implies considerable rearrangement of the crust associated with fault motion. Because lateral motions in the same azimuth since the Cretaceous time have been reported from the southern fore-arc of the island arc, deformation observed in the study area is to be linked with regional tectonic events along the eastern Eurasian margin. We also confirmed fault displacements in surface sediments using single-channel seismic profiles, suggesting recent activity on the NNW-SSE faults, on which some epicenters of shallow strike-slip aftershocks of the 1994 Sanriku-oki earthquake are located. Several en echelon topographic bulges are aligned on the fault trends, and interpreted as a growth right-lateral wrench deformation zone, since the bulges consist of deformed late Cenozoic sedimentary units. Unlifted characteristic remanent magnetization of the Paleogene core samples in a borehole on the fore-arc shelf shows a significant easterly deflection indicative of a clockwise rotation as a result of dextral wrenching. Thus transcurrent motions and related deformation have been dominant on the fore-arc of northeast Japan. It is noteworthy that some remarkable tectonic events such as back-arc opening of the Japan Sea and subduction erosion on the Japan Trench occurred during the course of the long-standing motions of the fault zone, easternmost strand of which seems to converge into the collision front between northeast Japan and Kuril Arcs to the north. Age determination of activity and quantitative estimate of displacement on the faults are essential

for reconstruction and understanding of tectonic processes going on the convergent plate boundary.

**SS03/08A/D-059** Poster **0830-218**

**TRANSITION OF NEOTECTONICS IN THE KUROMATSUNAI LOWLAND FAULT ZONE, SOUTHWEST HOKKAIDO, RELATED TO STARTING OF CONVERGENCE ALONG THE EAST MARGIN OF THE SEA OF JAPAN**

Takashi AZUMA<sup>1</sup>, Koji OKUMURA<sup>2</sup>, Koichi SHIMOKAWA<sup>1</sup>, Yuichi SUGIYAMA<sup>1</sup>, Akira SANGAWA<sup>1</sup>, Takuichiro KUWABARA<sup>1</sup> (<sup>1</sup>Active Fault Research Center, AIST, <sup>2</sup>Hiroshima University)

Kuromatsunai lowland, located in the southwestern part of Hokkaido, is N-S-trending narrow basin filled with sediments in Pliocene to Quaternary. This area is one of the fault-and-thrust belts adjoining the convergent boundary between the Eurasian and Okhotsk plates in the Japan Sea. The outline of the lowland topography seems to be the remnant of the Early Pleistocene depression while the structures of the Quaternary sediments indicate that the basin has been uplifted under E-W compression since Middle Pleistocene. This change represents the convergence along the eastern margin of the Japan Sea began to affect this area. In topographical, fluvial terraces have developed well in central part of the basin and marine terraces fringe along the Sea of Japan coast and the Pacific coast. These terraces are divided in five groups and are dated by several volcanic ash markers. Fluvial terraces, formed during Middle to Late Pleistocene, are deformed cumulatively by N-S trending fault scarps and folds. The folds on these terraces are characterized by the short wavelength (1 to 2 km), whereas the structure of Pliocene sedimentary rock has folds with rather long wavelength (5 to 10 km). The reverse faults are observed on the wing of the folds and they are seemed to be related to the growth of the folds. Marine terraces along the Sea of Japan coast and the Pacific coast show different pattern of the crustal movement across the lowland. Along the Sea of Japan, >30 km wide east-dipping monocline concordant with bedrock structure deformed Middle to Late Pleistocene marine terraces, but there is no differential movement across the lowland. On the other hand, along the Pacific, the west side of the lowland has been stably uplifted while the eastern side shows overall subsidence since Middle Pleistocene. We will discuss the neotectonic significance of the active structures in the lowland in terms of shortening tectonics in the convergent plate boundary along the eastern margin of the Japan Sea, as well as seismic potential in this area.

**SS03/08A/D-060** Poster **0830-219**

**SLAB ABUTMENT: A KEY TO THE ORIGIN OF THE BROAD BEND IN THE TRENCH LINE OF THE PHILIPPINE TRENCH SYSTEM AT 6°N LATITUDE**

Bautista Caparas BAUTISTA<sup>1</sup>, Maria Leonila Pascual BAUTISTA<sup>2</sup>, Ishmael Clarino NARAG<sup>3</sup>, Jane Tampoc PUNONGBAYAN<sup>1</sup>, Raymundo Santiago PUNONGBAYAN<sup>1</sup> (<sup>1</sup>Philippine Institute of Volcanology and Seismology, <sup>2</sup>Department of Science and Technology - Philippine Institute of Volcanology and Seismology (DOST-PHIVOLCS))

Broad bends along the trench lines of subduction zones are usually caused by collision and partial subduction of buoyant features such as microcontinental plates, island arc chains or seamounts and extinct mid-oceanic-ridges at the trench line. These bends develop as a result of the stoppage or slowing down of the subduction of the slab. The plate, instead of being subducted is just pushed towards the arc causing a broad bend to develop. The Philippine Trench System, a very active subduction system located east of the Philippine archipelago, exhibits a broad bend in its trench line at around 6°N latitude. There is, however, no obvious presence or traces of buoyant features mentioned above that could impede subduction process and form the broad bend in the trench line. The reason for the development of this broad bend is presently not so well known. In this study, we will try to seek an answer to the above problem by characterizing the geometry of the slabs comprising the complex subduction system in southern Mindanao, Philippines using earthquake data. Seismicity and focal mechanism maps at different depth ranges and cross-sections showing vertical distribution of seismicity and focal mechanisms are drawn in order to have a three-dimensional visualization of the geometry and stress regimes of seismogenic zones. A model to explain the said phenomenon is proposed. Southern Mindanao is a geologically and tectonically complicated region. One of the features found in this area is a 250-km wide zone called Molucca Sea Plate collision zone. This zone resulted from the continued westward subduction of the Molucca plate beneath the Sangihe island arc and the eastward subduction of the same plate beneath the Halmahera arc. Earthquake hypocenters beneath this zone show oppositely-dipping Wadati-Benioff zone that defines an inverted U-shape slab. In Mindanao island, collision is believed to be complete. Aside from this collision zone, the presence of two other trenches further complicates the tectonic setting in this area. The subduction of the Philippine Sea Plate along the Philippine Trench and the Celebes Sea Plate along the Cotabato Trench forms a complicated configuration with the subducted slabs of the Molucca plate. In this study, we will use the complex configuration of these subducted slabs to argue for the reason for the development of the broad bend in the trench line of the Philippine Trench. Using earthquake data, we will propose abutment at depth of the Philippine Trench slab and the Halmahera east dipping slab as the reason for the impediment of subduction process and the subsequent formation of the bend. This theory is further supported by steepening of the slab dip of the Philippine trench southward towards the bend.

**SS03/08A/D-061** Poster **0830-220**

**ZAMBOANGA PENINSULA, PHILIPPINES: COLLISION, OPHIOLITE EMPLACEMENT AND MELANGE FORMATION IN A CONTINENTAL MARGIN SETTING**

Graciano P. YUMUL, JR., Rodolfo A. TAMAYO, JR., Carla B. DIMALANTA, Victor B. MAGLAMBAYAN, Herve BELON, Mireille POLVE, Rene MAURY (IAVCEI)

Field mapping and geological investigations were conducted in the northern, central and southern portions of the Zamboanga Peninsula, Mindanao, Philippines over a 4-year period. Zamboanga Peninsula is underlain by Cretaceous to Paleogene ophiolite and metamorphic basement rocks, pre-Miocene to middle Miocene melanges, Miocene volcanic and sedimentary rocks with associated intrusive bodies and Pliocene to Quaternary volcanic and sedimentary rocks. Several ophiolite and ophiolitic masses, exhibiting back-arc basin to supra-subduction zone geochemical signatures, were found to be distributed along major shear zones that trend NW-SE in northeastern Zamboanga and NE-SW in the central and southwestern portions of the Peninsula. Regionally metamorphosed basement rocks often outcrop in proximity to the ophiolite and ophiolitic complexes. Tectonic and sedimentary melange units mapped are bounded by major strike-slip thrust faults which represent environments that range from subduction to transform fault settings. New whole rock K-Ar isotopic and paleontological ages constrain the temporal and spatial relationships of the different rock formations. The most widely distributed rocks in the Peninsula are the volcanic-plutonic and sedimentary rocks that overlie the basement sequences. Pyroclastic and lavafloes that were dated support the existence of a Middle Miocene volcanic arc in the Peninsula. The Miocene sedimentary sequences were deposited in a bathyal environment (northeast Zamboanga Peninsula) to a shallow marine

environment(southwest Zamboanga Peninsula). This suggests shallowing of the Peninsula from the northeast towards the southwest during the Miocene. The Peninsula could have either been rifted from China or Borneo.

**SS03/08A/D-062** Poster **0830-221**

**FORMATION OF DOUBLE FOREARC BASINS AT THE INITIAL PHASE OF ARC-CONTINENT COLLISION OFFSHORE SOUTHERN TAIWAN: INSIGHTS FROM PHYSICAL AND NUMERICAL MODELING**

Wei-Hau WANG<sup>1</sup>, Ruey-Cheng WEN<sup>1</sup>, Shu-Hao CHANG<sup>2</sup> (<sup>1</sup>. Institute of Applied Geophysics, National Chung Cheng University, <sup>2</sup>. Institute of Seismology, National Chung Cheng University)

The transition from a subduction phase in Philippines to arc-continent collision phase in Taiwan have been creating a unique bathymetry offshore southern Taiwan, where the North Luzon trough northwardly splits into two parallel forearc basins (the Southern Longitudinal Trough and the Taitung Trough) separated by the Huatung Ridge with folded and faulted strata. We have conducted both physical and numerical models to demonstrate that this characteristic is due to northward increase of strength of the accretionary wedge in front of the Luzon arc by lithification and accretion. The lithified accretionary wedge has been acting as a backstop and deforming the sediments in the forearc basin. As a result, a new outer-arc high and a pair of forearc basins appear at the northward extent of the North Luzon Trough. This deformation and shortening of the forearc basin offshore southern Taiwan resulted in transfer faulting at the place of the forearc-basin split.

**SS03/08A/D-063** Poster **0830-222**

**A NEW TECTONIC MODEL OF GORONTALO BASIN AND COLO VOLCANO, NORTHERN SULAWESI, INDONESIA**

Haryadi PERMANA<sup>1</sup>, Nugroho Dwi HANANTO<sup>1</sup>, Safri BURHANUDDIN<sup>2</sup>, Ray BINNS<sup>3</sup>, Joanna PARR<sup>3</sup> (<sup>1</sup>Research Center for Geotechnology, Indonesian Institute of Sciences LIPI, <sup>2</sup>. Marine and Fishery Department, Jakarta-Indonesia, <sup>3</sup>. Exploration and Mining, CSIRO, Sydney-Australia)

A new data on geology (petrology and geochemistry), single beam seismic, gravity and bathymetric were collected during IASSHA 2001 cruise surround Colo volcano and Gorontalo basin, Northern Sulawesi, Indonesia. The Gorontalo basin is dominated by a steep graben-like structure east-west direction. To the north of the graben lies the Sulawesi north arm and to the south lies part of the East Sulawesi Ophiolite Complex and Old Mélange Complex. It is suggested that the Gorontalo basin formed as the result of opening and rotating of northern Sulawesi. Flat-lying, undeformed sediments fill the basin and lack of seismic evidence for the Gorontalo fault suggests that the fault has not been active since prior to the opening and rotation of northern Sulawesi. Una-Una island (gulf of Tomini) where the Colo volcano located is structurally controlled by NE-SW and NW-SE graben like structure that are bounded by hilly morphology features. Normal faults cut recent sediments that indicate the structures are still active. The Colo volcanic product is potassic rocks with negative anomaly in Nb and enrichment of LILE indicates that Colo is produced in subduction environmental. The present of dunite in Colo volcanic product is explained that the magma source had through an oceanic material that possibly is part of East Sulawesi Ophiolite Complex (ESOC). The seismological data show two different patterns beneath the Colo volcano. The first pattern, at 100 to 200Km depths related to the southeast subduction of Sulawesi Sea Plate and the second, directly beneath the Una Una island at 70 to 100Km depths expected as northwest dipping subduction of Banggai-Sula micro-continent. We proposed a model where the Banggai-Sula micro-continent going down beneath oceanic crust that interpreted as part of the ESOC and caused Colo volcano activity. High concentration of K and lower MgO/FeO\* of Colo volcanic product explained that the magma source is a micro-continent associated.

**SS03/08A/D-064** Poster **0830-223**

**ANALYSIS OF REGIONAL STRESS TENSOR IN TONGONAN, LEYTE, PHILIPPINES**

Jane T. PUNONGBAYAN<sup>1</sup>, Louis DORBATH<sup>2</sup>, Henri HAESSLER<sup>3</sup>, Catherine DORBATH<sup>4</sup> (<sup>1</sup>Philippine Institute of Volcanology and Seismology, C.P. Garcia Avenue, U.P. Diliman, Quezon City 1101, Philippines, <sup>2</sup>Institut de Physique du Globe de Strasbourg, 5 rue RenéDescartes, 67084 Strasbourg, France)

In June and July 1997, an experiment on hydraulic stimulation of faulting in a geothermal exploration well that cuts across the active Philippine Fault in Tongonan, Leyte, Philippines was conducted. Seismicity before, during and after fluid injection was monitored with a temporary seismic network composed of 18 stations. Information on earthquake distribution and seismic tomography of the area were obtained via a simultaneous inversion for the earthquake location and the 3-D velocity structure underneath the network. Using results of these earlier reports as well as the raw data of observed polarities, we proceed in studying the regional tectonic stress regime in the area by performing a simultaneous inversion for the local stress tensor and the fault plane solutions of well-constrained events before and after the fluid injection. Events considered in this inversion had a minimum of eight (8) polarities for both pre-injection and injection periods. Seismicity for all observation periods showed that recorded microearthquakes were well related to hydraulic stimulations in the study site. The microearthquakes had magnitudes lower than 2 and with depths ranging from 1000-5000 m. Results for the data before, during and after the hydraulic experiment showed a well-constrained stress tensor explaining 91.2% of the observed polarities with a maximum likelihood of 97.7%. After the injection, the minimum principal stress tensor  $\sigma_3$  remained quasi-horizontal with a direction of N168° (pre-injection: N179°). The maximum principal stress tensor,  $\sigma_1$ , became more vertical with a dip of 57° (pre-injection: 41°) and showed a slight change in the direction towards N287° (pre-injection: N283°). The direction of  $\sigma_2$  did not change remarkably before (N74°) and after injection but its dip decreased to 27° from its pre-injection dip of 45°. The stress tensors that we obtained before and after the fluid injection in Tongonan, Leyte are in agreement with the left-lateral strike-slip character of the Philippine Fault and thus comply with the tectonic context of the region. Injection of fluids had the principal effect of increasing the pore pressure, facilitating fault rupture. The isotropic component of the stress tensor can be modified but not the deviatoric component, which was what was accessible to us (shape factor R). It is thus normal that our results for the tensors before and after injection be similar. The slight difference could be attributed to perturbations of thermoelastic stress provoked by the injection of cold fluids.

**SS03/08A/D-065** Poster **0830-224**

**GENETIC ALGORITHM - FINITE ELEMENT INVERSION OF STRESS FIELD IN CONTINENTAL CHINA**

Shoubiao ZHU, Yaolin SHI ( Department of Earth Sciences, The Graduate School of the Chinese Academy of Sciences)

We use the observed stress field data in Continental China as constraints, and apply the genetic algorithm - finite element method (GA-FEM) to evaluate the relative contribution of

boundary conditions and intraplate stress sources to the stress field by geophysical inversion. Boundary displacement, lower crust drags and topographic forces (represented as equivalent nodal forces) are inverted. Pseudo-3-D elastic simplification is made for a thin spherical elastic shell at 15 km depth. The vertical stress is assumed to be the lithostatic pressure at the depth, and the horizontal stresses are calculated by Finite Element computation. The studied area of continental China is divided into 1993 bilinear quadrilateral shell elements. The Young's modulus is chosen as 70GPa, and Poisson ratio as 0.25. Constraints for the modeling are provided by orientations of the maximum horizontal compressive stress derived mainly from focal mechanism and fault types which are related to the stress regime. The objective function for optimization in the inversion is the square root of the summation of square of the differences between observational orientation of maximum compressive stress and the calculated one. Models of different kinds boundary conditions and nodal forces are tested through a statistical F-test. An optimum model which gives best fit of orientation data is found step by step. Although there are no direct data on the magnitude of stress in the crust, the stresses are limited by the strength of faults by Byerlee's Law. Therefore, we further use the observation of fault types of normal, inverse or strike-slip, to roughly constrain the magnitude of stress, by linearly adjusting the magnitude of the stresses in the optimum model. Such a procedure does not change the fit of orientation data, but give a better fit to the fault type data. In our final optimum model, 54 parameters in total have been used in inversion, in which 32 boundary displacements and 22 equivalent nodal forces simulating basal drag and topographic forces. The results show that the stresses in Continental China are produced mainly by the collision of India plate, and action of the Philippine plate. Topographic highs and lower crust drag forces also play an important role in Tibetan Plateau of local significance. A very interesting suggestion of the optimum solution is that beneath the Tibetan Plateau, the ductile lower crust seems flow more easily than the brittle upper crust. The direction of the lower crust drag force to the upper crust is NE at the central Tibetan Plateau, and SE in the eastern Tibetan Plateau. We further use the GPS data as an independent observation to check the validity of the inverted optimal model. It is found that the displacement calculated from the model deduced from a long term stress data also fits well with the transient data of GPS velocity.

**SS03/08A/D-066** Poster **0830-225**

**THE USE OF THE MONTE-CARLO INVERSION METHODS IN THE DISTRIBUTION OF DENSITY MODELS OF THE AFRICAN CONTINENT TO A DEPTH OF THE ASTHENOSPHERE**

Adedeji Adegoke ADETOYINBO, Ebum Olufunmilayo ONI (Department of Physics, University of Ibadan, Nigeria.)

In the computation of the earth's gravity field with respect to the African continent lying between Latitude 400N-400S and Longitude 300W-600E, the zonal harmonics to J21 computed by Kozai were used as starting values. Fully normalised coefficients of the spherical harmonic expansion of degree 112 and order 112 were also used in the computation. The results of this computation were applied to a 3-Dimensional model of the Lithosphere and Asthenosphere of the African continent. The technique employed for this interpretation is the Monte-Carlo Inversion Method. This method uses a random generator at any stage. In applying the method, five hundred models were examined out of which only nine passed all tests. As far as we know, this is the first time that the technique is applied to the Lithosphere and Asthenosphere of the African continent. Although, the problem of uniqueness of earth structures obtained by this inversion of geophysical data, is still unsolved, the many models generated from the set of data using the inversion method agree with geological interpretation of the continent. Also, results from the interpretation using the Monte-Carlo inversion technique shows that the density range within the Asthenosphere is in agreement with other authors.

**SS03/08A/D-067** Poster **0830-226**

**MICROEARTHQUAKE CHARACTERISTICS AT THE SLOW SPREADING REGIONS; CASES OF THE LAASQORAY-SHARMAR SEGMENT OF THE GULF OF ADEN AND THE JOURDANNE SEGMENT OF THE SOUTHWEST INDIAN RIDGE**

Tomoaki YAMADA<sup>1</sup>, Kensaku TAMAKI<sup>2</sup>, Hiromi FUJIMOTO<sup>3</sup>, Kimihiro MOCHIZUKI<sup>1</sup>, Kazuo NAKAHIGASHI<sup>1</sup>, Toshihiko KANAZAWA<sup>4</sup> (<sup>1</sup>Earthquake Research Institute, University of Tokyo, <sup>2</sup>Ocean Research Institute, University of Tokyo, <sup>3</sup>Faculty of Science, Tohoku University)

We present the results of two microearthquake experiments conducted at the along axis of two ultra-slow spreading segments, the Laasqoray - Sharmar segment at 49 degrees E of the Gulf of Aden and the Jourdanne segment at 64 degrees E of the Southwest Indian ridge. The Gulf of Aden is a small ocean basin between Arabia Peninsula and Africa, and the continental rifting occurred around Early Miocene. The full spreading rate is 2.1 cm/year. The morphology of western part is affected by the Afar plume, however the Laasqoray - Sharmar segment of eastern Gulf of Aden shows a typical segment structure of slow spreading ridges as Mid-Atlantic ridge. The morphology has the axial valley and the segment center is higher relief with a narrow to axial valley whereas the segment ends are lower relief with wide axial valleys. For the experiment, we selected the Laasqoray - Sharmar segment as a typical young and slow spread rift zone. Otherwise, the Southwest Indian ridge is one of the ultra slow spreading ridges, and the full spreading rate is 1.4 cm/year. The northeastern section, especially, does not resemble any other known mid-ocean ridge in the morphology and geophysical and geochemical data. This section is characterized by a low melt supply, and further, underlain by cold mantle (Cannat et al., 1999). This also characterized by very high-relief segments with very strong mantle Bouguer anomaly lows, spaced every 200 km. The high-relief of these segments is inferred to result from large volcanic constructions (Cannat et al., 1999). The Jourdanne segment is one of the high-relief and highly focused magmatic segment. We selected this rarely segment for the experiment. Microearthquake observations were conducted in 2000 around the Laasqoray - Sharmar segment at 49 degrees E of the Gulf of Aden using 10 ocean bottom seismometers (OBSs) and in 1997 around the Jourdanne segment at 64 degrees E of the Southwest Indian ridge using 10 OBSs. In the Gulf of Aden, we got 20days continuous records, and more than 1400 earthquakes were located using arrival times of both P and S wave. The seismic activities were concentrated at three regions. One was the segment center, the others were fracture zones near the segment ends, westward and eastward the fracture zone. The earthquake focal depths were clearly shallow in the segment center whereas the focal depth of fracture zones were limited to deeper zone. In the Southwest Indian ridge, we got one week continuous records from 6 OBSs, and 814 earthquakes were located using arrival times. The pattern of hypocentral distributions was similar to the Gulf of Aden, and the segment center and non-transform offsets near the segment end were high seismicity regions. The focal depth along the ridge axis seems to decline to segment ends as seen in some segments of the other slow spreading ridges, but the lower limit of focal depths is relatively deep. It is consistent with cool temperature.

**SS03/08A/D-068** Poster **0830-227**

**PROBABLE EXTENSION OF NARMADA-SON LINEAMENT**

Gautam GUPTA, Vinit C. ERRAM, Bhisham Prasad SINGH (Indian Institute of Geomagnetism, Plot

No. 5, Sector-18, Near Victoria Petrol Pump, Kalamboli (Highway), New Panvel (W), Navi Mumbai-410206)

The Narmada-Son Lineament (NSL) is one of the most prominent features in the western-central India, characterized by numerous tectonic structures and complex geophysical signatures. The west of the western Ghats may be a belt of active rifts. The best-developed part of this rift system is observed in the Cambay-Kutch area. Transformation of the ground magnetic data in the Cambay basin in west coast of India delineated the Narmada-Son lineament, which appears to turn around and extend beyond the Gulf of Cambay towards the west. Magnetotelluric studies in central India have shown a high conductivity layer in the deep crust below the Vindhyan region. The total thickness of the Vindhyan sediments is about 5 km. Two crustal conductors with a resistivity of about 30  $\Omega$ -m are delineated below the Deccan volcanics. The high conductivity may be due to the presence of crustal fluids. The outburst of the Reunion plume on the western India landmass would have had strong effects on the geothermal state of the deep crust in the Vindhyan region, the Cambay basin, and the adjoining Arabian Sea. This is evident from the high Bouguer anomalies, deep-seated electrical conductivity, high heat flow, seismicity and significant high seismic velocity over the NSL and adjoining regions. This process may have had significant contribution to the wide spread intrusive activity. The conductive features noticed in central India over NSL might be associated with transform fault associated with rifts in this region. These studies suggest that the NSL is a typical rift like structure and is a part of the worldwide rift system joining the Indonesian arc to the east and extending on west coast to Carlsberg ridge and may have a probable extension in the northern Madagascar extending into Africa, Somalia and Ethiopia.

**SS03/08A/D-069** Poster **0830-228**

#### EARTHQUAKE RELOCATION AND THREE-DIMENSIONAL VELOCITY STRUCTURE IN THE NORTHEAST INDIA REGION

Pankaj Mala BHATTACHARYA, J.R. KAYAL, R.K. MAJUMDAR, S.G. MUKHUPADAAAYA (Geological Survey of India)

A detailed three-dimensional seismic velocity structure of the crust and upper mantle upto a depth of 60 km beneath the northeast India region is estimated using the local earthquake tomography method. A total number of 4850 seismic phases, 2698 P arrivals and 2152 S arrivals, from 700 selected events recorded by 77 standalone/telemetric stations are used. The tomography images show heterogeneous structures in the crust and upper mantle with a substantial horizontal velocity variations in the region. Seismogenic structures are well reflected in the tomography images. Most of the earthquakes have occurred in the high velocity, high Vp/Vs zones. The lateral heterogeneities have been the source area for stress concentration. The Kopili lineament / fault, is mapped with high Vp, high Vs and low Vp/Vs. Relocation of the earthquakes is very much improved with significant reduction in average rms and errors in horizontal and vertical directions.

**SS03/08A/D-070** Poster **0830-229**

#### STUDIES OF INTRAPLATE DEFORMATION IN THE NORTHERN INDIAN PLATE

Ranjit Kumar MAJUMDAR (Department of Geological Sciences, Jadavpur University)

Seismicity map has been prepared for the period 1963-1999 using epicentre listing of International seismological centre (ISC), U.K.; Indian Meteorological Department (IMD) and USGS earthquake data file. It shows a widely dispersed diffuse intraplate seismicity in the Bay of Bengal and adjoining Peninsular India in comparison to the clearly defined higher seismicity at the eastern plate boundary. Several geophysical evidences and observations indicate that the northern Indian plate including the Bay of Bengal and Peninsular India has experienced extensive deformation. From the fault plane solution study it appears that almost all intraplate earthquakes in the Bay of Bengal and coastal areas of Peninsular India exhibit thrust faulting mechanism having consistent north dipping fault plane and more or less N-S directed (range of variation NNW-SSE to NNE-SSW) pressure or compression axis. Composite plot of pressure and tension axes of focal mechanism solution of intraplate earthquake of this region suggest that this region is also experiencing N-S compression. Small scale seismic profiling in southern Bay of Bengal also suggests N-S compressive deformation apparently by folding of upper sedimentary layer and high angle reverse faulting of acoustic basement of oceanic crust having E-W orientation. Pre-existing zones of weakness like rift valley or fault is rejuvenated in response to N-S intraplate stress and ultimately leads to seismic activity in Peninsular India. Latur earthquake (1993) in India seems to be one of such example which occurs in a low Bouguer gravity anomaly in rift valley area.

**SS03/08A/D-071** Poster **0830-230**

#### SURFACE GRAVITY SURVEY AND GEOPHYSICAL INTERPRETATION OF GRAVITY FIELD DATA TO STUDY STRUCTURAL AND TECTONIC CHARACTERISTIC OF PARTS OF ARCHEANS, SATPURAS AND CHHATTISGARH BASINS AROUND MANDALARAIPUR DISTRICTS, M. P., INDIA

Daya SHANKER<sup>1</sup>, V.P. SINGH<sup>2</sup>, R. SINGH<sup>3</sup> (<sup>1</sup>Department of Earthquake Engineering, Indian Institute of Technology Roorkee, <sup>2</sup>Department of Geophysics, Banaras Hindu University, Varanasi-21005, INDIA, <sup>3</sup>Marine Wing (Geophysics Division), DK-6, Bhu Bigyan Bhavan (9th floor) Salt Lake, Kolkata-64, INDI)

Out of all geophysical investigations have been used to derive the structural and tectonic characteristics of large areas, gravity method play a major role in understanding the problems of the earth crust. Owing to technological development, most gravity surveys currently carried out are designed for reconnaissance of large unexplored areas to delineate faults, structural details, depths of intrusive bodies. The gravity method is best suited for mapping the basement configuration and intrusive bodies in them. Nowadays gravity data are being extensively used for study geological structures, tectonics, depths of Conrad and Moho and detailed structural investigations of the crust. For detail geological mapping and crustal structures dense network of gravity observations are required. A number of intracratonic sedimentary basins are existing in Indian subcontinent. The Cuddapah, Vindhyan, Kaladgi and Chhattisgarh basins are most important one. Detailed surface gravity surveys with the station spacing of 2 to 5 km over parts of Archeans, Satpuras and Chhattisgarh basins belonging to different ages around Mandala-Raipur region has been carried out. Detailed investigations provide depth of gravity sources, basement structural trend, nature of intrusive bodies and thickness of sediments in the basins. The basement structural trend along the seven profiles in Archeans (FF'), Satpuras (CC', DD', EE', FF', and GG'), Chhattisgarh (CC', DD', EE', FF', and GG') and Deccan Trap (AA' and BB') have been derived which ranges from 2.0 to 3.5 km. In Satpura region a positive anomaly of 12 mgal is observed indicating 2 km thick high density material at a depth of 3 km. Negative gravity anomaly of the order of -13 mgal at one place below the Deccan trap suggests thickness of sediments to be 2.5 km extending towards north-west. Thus the present analysis describes the detailed mapping of the local features of the region which may be useful in formulating evolution model of the various formations across NSL and nearby

areas.

**SS03/08A/D-072** Poster **0830-231**

#### INTRAPLATE SEISMICITY AND GRAVITY FIELD ANOMALIES OF THE CONTINENTAL CRUST

Boris Petrovich RYZHI<sup>1</sup>, Nikolay Ivanovich NACHAPKIN<sup>1</sup>, Svet Yurievich MILANOVSKY<sup>2</sup> (<sup>1</sup>Geophysical Institute of Ural Branch of RAS, Ekaterinburg, <sup>2</sup>Institute Physics of the Earth RAS, Moscow)

According developed concept the areas heightened intraplate seismicity are connected with the increased silica contents in the rocks, i.e. with patterns of acidic composition and, accordingly, with negative Bouguer gravity anomalies. Done statistical analysis of intraplate allocation of earthquakes on territory of Russia, Africa, Australia, South and North America has confirmed effect of correlation of their position with areas of negative Bouguer anomalies. For Russia analyzed the position of plate seismicity and it's relation with: (1) silica content, obtained from DSS observation with VP and VS waves (Egorkin, 2000); (2) Bouguer gravity field. The analysis shows that zones of higher seismicity are associated with 'acidAEcrustal blocks. The interplate earthquakes with magnitude 4-6 take place 6 times more often in 'acidAEcrustal blocks in comparison with 'basicAEones. The earthquakes with magnitude more than 6 happen only in 'acidAEcrustal blocks. The amount of earthquakes in areas with negative Bouguer field is in seven times more than in areas with positive Bouguer field. The outcomes of a statistical analysis testify that practically all earthquakes in Africa are associated with the areas with negative values of Bouguer gravity field. Thus in areas with values of a field -160 mgal to -100 mgal there was 80 % of all earthquakes. It is necessary to note, that the mean value of the field for the African continent is -70 mgal. For Australia was obtained, that in areas with negative values of Bouguer field from AE0 mgal up to -20 mgal 73 % of all earthquakes (average level of the field for continent is -17 mgal) is massed. If Bouguer anomalies are mainly related to morphology and composition of structural complexes of Earth crust, the isostatic anomalies, as a rule, are connected with acting tectonic forces and characterize a modern stress of Earth crust. In South America regions with negative values of Bouguer anomalies, smaller than its mean for the Platform (-30 mgal), there occur 70% of all earthquakes. The correlation of a magnitude and depth of a hypocenter of earthquake is supervised depending on the value of Bouguer anomalies in its epicenter. In regions with positive values of isostatic anomaly, larger its mean magnitude for the Platform (1 mgal), there occur 77 % of all earthquakes. For North America, from 383 events 288 (75 %) has taken place in areas with negative values of Bouguer anomalies and 95 (25 %) - with positive values. Thus, the amount of earthquakes recorded in a negative gravitational field, in 4 times exceeds an amount of earthquakes in a positive field. At values of isostatic anomalies close to normal (-10 - 10 mgal) there was 55 % of all earthquakes and 41 % - recorded in isostatically disturbed regions at values of a field from -60 up to -10 mgal. Therefore, the areas of intraplate seismicity are characterized predominantly by negative values of Bouguer anomalies, and also negative or normal values of isostatic anomaly. This work was supported with RFFI grant N 00-05-65067

**SS03/08A/D-073** Poster **0830-232**

#### NEW INTERPRETATIVE GRAVITY FOR LITHOSPHERE

Yury Ya. VASHCHILLOV, Natalia K. GAIDAI, Olga V. SAKHNO (North-East Interdisciplinary Scientific Research Institute FEB RAS)

**New interpretative gravity (NIG)** is independent and self-sufficient., and at this stage of the geologic-geophysical study of the Earth is better in many situations than other geophysical methods with stable reputation, for example, seismology. Large areas of land, seas and oceans are already covered by the gravimetric survey. The NIG use makes possible to obtain structural-substantial parameters of lithosphere by financing only the interpretation. Earlier many of such parameters could be obtained only by the seismologic study. Two principles form the theoretical and practical basis of NIG. They are as follows: 1) an idea about the essentially block nature of the anomaly sources, and 2) revealed regularities in combination of layers and density heterogeneity in the form of blocks. The latter was experimentally proved that the lower and upper limits of blocks coincide with major quasihorizontal surfaces of lamination. Mathematical interpretive methods of NIG was developed on the basis of 3-dimensional (3D) block sources of the gravity anomaly. Based on this method, NIG study makes possible to determine the depths of the lamination surfaces (boundaries of Moho (M), lamination of lithosphere, crust and sedimentary strata), of roots and penetration upwards of the faults and blocks irrespectively of the other geophysical data. It also enable one to interpret by methods lithosphere density «probing», to make gravity tomography according to the systems of horizontal sections, make 3-dimensional density models and give their geological-petrological interpretation (western and central Siberia, north-east and Far East of Russia, region of studies after the DECORP-2 SOUTH Project, Azov, Black, Norwegian and other seas, etc). The depth of investigations is determined by the lithosphere thickness of 60-20 km. **Necessary** condition of the strict quantitative interpretation of the gravity (and other geophysical) anomalies is the similarity with the given precision of gravity values, obtained by measurements, and calculated (theoretical). For mentioned purposes, gravity map and theoretical (model) gravity maps are compared. The interpretation has the total character. During the interpretation, local anomaly are divided between each other, and also we distinguish between the local and regional anomalies. The determination of velocity of seismic waves and distinguishing of the vertical faults are the serious problem in seismology. The use of NIG decreases a sharpness of mentioned problem. During the interpretation of the gravity anomaly, horizontal density jumps at vertical limits of density heterogeneity-blocks are determined. Their values reach the tenth-hundredth g/cm<sup>3</sup>. They also like the absolute density values, obtained at the interpretation, are easily calculated into the jumps and full velocity of seismic waves.

**SS03/08A/D-074** Poster **0830-233**

#### INSTRUMENTAL SEISMICITY AND SEISMOTECTONICS IN CENTRAL ALBORZ

Mohammad ASHTARI JAFARI (Institute of Geophysics - University of Tehran)

Alborz Mountains show structural axes trending approximately NE-SW in its eastern part and NW-SE axes in its western part. Central Alborz is the meeting point of the eastern and western trends. The overall structure is the site of shortening due to the compression against Eurasia and contains a high density of active faults. Most faults are longitudinal and follow the arcuate structure of the Alborz Mountains. Although an important horizontal component exists on the earthquake faults of this region, reverse faulting seems to be the main process of mountain building. I have used Central Alborz earthquakes from 1900 to 2001 to study seismicity patterns and focal mechanisms of the earthquakes in this region. Within several numerical methods to solve the focal mechanism problem based on the polarity of the first motion of P wave, I have used a least squares grid search procedure which minimizes the number of discrepant first motions to compute mechanisms. Focal mechanism results are divided into two groups: I) mechanisms based on the single fault plane solutions II) mechanisms based on the joint fault plane solutions. Well located earthquakes with good coverage around the focal region are within the first group. Where it is not possible to

compute well determined single solutions, joint fault plane solutions are calculated. The mechanisms reflect a range of faulting from strike-slip to reverse.

**SS03/08A/D-075** Poster **0830-234**

#### ACTIVE DEFORMATION IN CENTRAL ALBORZ

Mohammad ASHTARI JAFARI<sup>1</sup>, Farokh TAVAKOLI<sup>2</sup>, Hamid Reza NANKALI<sup>3</sup>, Faramarz NILFOROUSHAN<sup>2</sup> (Institute of Geophysics - University of Tehran, <sup>2</sup>National Cartographic Center of Iran)

Alborz Mountains are northern branch of Alpine-Himalayan orogeny in Iran. This range is characterized by a broad arch of parallel folds, reverse faults and nape forming imbricate structures verging both towards and away from the Caspian Sea. Within northern parts of Alborz faults dip southwardly representing underthrusting of the South Caspian basin and in its southern parts faults dip northwardly. Alborz seems to accommodate to the overall motion between the Eurasia and Central Iran that involve oblique left lateral shortening. Central Alborz is the connecting point of eastern and western parts of Alborz. In this study we have surveyed 18 GPS stations two times during 2000 and 2001. In each survey we have measured GPS stations with dual frequency receivers for at least three consecutive days. These measurements are processed based on the routine GPS processing methods to produce daily solutions. Then daily solutions are suitably combined to provide single session solutions. Single session solutions are stacked to produce multi session solutions as the final solution. The results from final solution are used to calculate horizontal velocities and strain rates in Central Alborz and to resolve regional active deformation. It is also tried to constrain direction and style of strain by using mechanism of medium-small sized earthquakes.

**SS03/08A/D-076** Poster **0830-235**

#### CRUSTAL MOTIONS IN A SLAB-DETACHED AREA (SE-CARPATHIANS)

Victor I. MOCANU<sup>1</sup>, Boudewijn C. AMBROSIUS<sup>2</sup>, Wim SPAKMAN<sup>3</sup>, Andrevd HOEVEN<sup>3</sup>, Gunter SCHMITT<sup>4</sup> (University of Bucharest, <sup>2</sup>Technical University Delft, <sup>3</sup>University of Utrecht, <sup>4</sup>University of Karlsruhe)

The Carpathian-Pannonian system has had a long geological history culminating in the past 16 Ma in the subduction of an ocean basin. The subduction process seems nearly completed. There is tomographic evidence, which delineates a localized slab (down to 350 km) below Vrancea. Below the remainder of the Carpathian arc no slab is found in the tomography. However, at large depth (> 500 km) a huge "pan-cake" of high seismic velocity material is detected which is interpreted as the remnant of detached slab [Wortel and Spakman, Science 2000]. One basic question regarding the Vrancea slab is whether it is still attached to surface lithosphere, or already detached, or in the process of being detached. To answer this question we have embarked on a project to measure the crustal motions in this region using both continuous and campaign style GPS observations. In 2001/2002 four permanent stations have been installed. In addition, a large GPS campaign was carried out in 2002, during which a network of 50 stations was observed including many points which were already occupied in previous campaigns. We present the network design and initial results on the data acquisition and data quality.

**SS03/08A/D-077** Poster **0830-236**

#### GEOPHYSICAL INVESTIGATION OF THE TRANSIT ZONES TECTOSPHERE ASIA - PACIFIC AND INDIAN OCEANS

Evgenya Lvovna MAZO, Adonis GAINANOV, Andrey BULYCHEV, Sergey BOLDYREV, Dolores GILOD, Vyacheslav MELIKHOV (Moscow State University, Geology faculty)

Geoid heights and gravity anomalies field maps were constructed based on combine altimeter and onboard data. There are several reductions of anomalies in the set of the maps for the investigation areas: transit zone Asia - Pacific and Indian oceanic. By original method of the authors we calculated Clenny reduction for the geoid heights field. Anomalies fields were transformed by striped methods with the deferent deep descriptions. Analyze all set gravity maps combine other geology-geophysical data allows to construct tectonic-structural scheme and allocated edge zone, boundary blocks earth crust type, transform zones, trending structures elements. Based on the seismic data and gravity anomaly field 2-D density models of the earth crust, lithosphere and asthenosphere (tectonosphere) were calculated for the basic tectonic structures of the transit zone Pacific and Atlantic (Arabian sea) types. The earth crust and lithosphere thickness was calculated by geochronology data. The minimum thickness of the earth crust (10 km) is obtained under the oceanic basin Far East sea. The minimum thickness of the lithosphere (20 km) is obtained under the festoon islands. The lithosphere thickness under the older basins Okhotsk, Japanese, Philippines seas is up to 70 km. Maximum thickness of the asthenosphere is 80-140 km is obtained under the young basins Far East marginal seas. Simultaneous thickness is up, asthenosphere density in low by 0,02-0,06 g/cm<sup>3</sup>. Earthquakes and seismogenic zones are the indicators of the geodynamic processes. Seismotectonic phenomena are the most effective in the continental - ocean transit zones. The earthquakes upper then 60 km are located in belt width about 250 km. Source earthquakes deeper then 60 km are located in the narrow lay conical form which is loaded under continent to 600-700 km. Boundary zone of these bokes date for shelf and continental slope deepwater trough. Region 150 S - 400N; 900 E-1500 E is very interesting. There are group Festoon island structures on the boundary Pacific and Indian oceans. Curvature of these structures is oriented in the different sides. Complexes are not completed by continental masses. They are appear like a special conglomerate. Deeper processes in it probably control the development lithosphere. There is intersection continuous transform zones Earth system Oceanic Ridge. Level of the seismic activity Zonde ridge chain on the east flank (in triple junction zone festoon island systems) - Zoned, Philippine, NewGweney, 130 0 E - is one order more then on the north flank, when seismoactivity zone is continued under the continent. Seismofocal zones Zoned and Philippine earthquakes slope toward each other. Seismic activity Philippine and Marian basins is present rare shallow-focus earthquakes with is located to the ridge Kusu-Palau. Research is support by Russian Fond Of Fundamental Investigations, project ' 01-05-64328, ' 02-05-64212.

**SS03/08A/D-078** Poster **0830-237**

#### MANIFESTATION OF TIBETAN PLUME STRUCTURE AND SEISMICITY OF HIGH ASIA IN REGIONAL GEOPHYSICAL FIELDS

Valentin POGREBNOY<sup>1</sup>, Tamara SABITOVA<sup>2</sup> (<sup>1</sup>Applied Research Center, KRSU, Leading geophysicist, <sup>2</sup>Institute of seismology NAS of Kyrgyz Republic)

This paper represents the results of complex analysis of High Asia geophysical fields in regional scale which show peculiarities of tectonic structure and ongoing in the region geodynamic processes. Based on juxtaposition of maps of following regional fields like geoidal undulations, anomalous magnetic and gravity fields, heat flow, shear wave attenuation, the Raleigh wave group velocities distributions for periods 0-10-70 s, Pn-wave velocity distribution in upper mantle of High Asia we guess that all of those are caused by

anomaly body which might consist of deconsolidated and hot material and hereafter named by authors as Tibetan plume. There was suggested its structure. According to quantitative and qualitative interpretation of geophysical fields, the Tibetan plume represents a steep ellipsoidal body (horizontal projection) where the longer axis size is approximately 2500 km and the shorter axis is 1000 km with narrow branches on the west side. Its depth extension is traced, as a through column, down to >300km from day surface. Judging by geographical location, a great extent both in spread and depth as well as geophysical fields which display it, the Tibetan plume is an independent formation but not consequence of continental plate collision. From comparison of seismicity and geophysical fields, it was made inference about correct correlation between seismic events and of geophysical field structure. High gradients zones of geophysical fields were found to be indicators of possible strong event zones. This criterion can be used for solution of a problem of revelation of seismogenous zones in seismic zoning of certain High Asia regions. It is noted that the location of such large deconsolidated body in High Asia which formed, most likely, due to ejection of a large amount of hot and deconsolidated substance onto upper layers of the High Asia tectonosphere, has an influence on dynamic processes in this region. Dynamic processes in High Asia region are guided with combination both of collision between Indostan and Eurasia lithospheric plates and ongoing development of Tibetan Plume. This investigation was carried out with support by International Science and Technology Center (ISTC), Project KR-214.

**SS03/08A/D-079** Poster **0830-238**

#### COMPRESSIVE DEFORMATION IN THE KACHCHH BASIN, GUJARAT, INDIA

Malay MUKUL, Sridevi JADE, Imtiyaz Ahmed PARVEZ, M.B. ANANDA, P. Dileep KUMAR, Vinod GAUR (CSIR C-MMACS)

The Kachchh Rift Basin (KRB), the site of the 2001 Bhuj earthquake, has been recognized as a rift basin that opened around 150 Ma and was subject to NNE-SSW directed compressive stress around 20 Ma. North-dipping Kathiawar fault and the south-dipping Nagar Parkar fault are extensional faults that form the southern and northern boundaries of the KRB, respectively. The NNE-SSW compression has resulted in the formation of two systems of thrust faults within the KRB. The northern Allah Bund system of thrust faults are NNE-dipping, with transport direction from NNE-SSW, whereas the southern Kachchh Mainland Fault system of faults dip to the SSW and have SSW to NNE transport direction. The zone of transition between the two systems of faults lies almost entirely in the Great Rann. Fault propagation folding dominates the geometry of the sheets carried by the major faults. Palaeoseismic data and the recent seismicity in the KRB indicates that both the systems of thrusts are active. Great Trigonometrical Survey (GTS) points were measured in 1857 and were reoccupied using GPS in 2001 and 2003. GTS (1857)-GPS (2001, 2003) baselines oriented at different angles to the regional transport direction in the thrust systems and the fault propagation structures are examined to work out the translation, vertical axis and horizontal axis rotations and elongation/shortening components of the total displacement vectors associated with the neotectonic deformation in the KRB over the period 1857-2003 and gain an insight into which geological structures are active in the basin and the earthquake hazard associated with it.

**SS03/08A/D-080** Poster **0830-239**

#### CRUSTAL DEFORMATION IN THE CHAMOLI REGION OF HIMALAYA INFERRED FROM GPS MEASUREMENTS

Ponraj MALLAPPAN, Amirtharaj SAMUEL, Sunil P. S. (Indian Institute Of Geomagnetism)

Following the Chamoli earth quake of March 29, 1999 (Magnitude 6.8 on Richter scale), three campaigns of Global Positioning System (GPS) measurements were made in Chamoli region of Garhwal Himalaya during 1999 to 2001 in reoccupation mode to estimate the horizontal crustal deformation rate. The study area (30° 13' to 30° 31' N and 78° 12' to 79° 31' E) includes many important thrust zones viz. Main boundary thrust (MBT), Main central Thrust (MCT) and some local upwarps. Estimated horizontal velocity vectors in ITRF 2000 are in the range of 35 to 57 mm/yr. Many Geophysical and strain measurements have suggested that about 14 mm/yr crustal shortening is taking place across this region. This paper presents a study relating to the tectonic interpretation of the crustal strain rate in the region.

**SS03/08A/D-081** Poster **0830-240**

#### NAPPE TECTONICS AND METAMORPHISM OF THE NEPAL HIMALAYA

Kazunori ARITA (Department of Earth and Planetary Sciences, Hokkaido University)

The Himalaya is a fold-and-thrust belt formed in the northern margin of the Indian continent after the India-Eurasia collision around 50 Ma. It is divided into three tectono-lithostratigraphic units by a series of foreland propagating thrust system; from north to south, the Higher Himalayan zone (HH) and the overlying Tethys Himalayan zone (TH), the Lesser Himalayan zone (LH) and the Sub-himalayan zone (SH). The HH consisting of high-grade metamorphic rocks sometimes overlap by the TH is thrust southward along the Main Central Thrust (MCT) zone over the LH which is composed of non- to less metamorphosed rocks. The MCT zone is of most significance in the Himalayan tectonics and is a ductile and brittle shear zone with various thickness in places. Its distribution, nature and tectonic role are still in debate. The HH extends southward for 100 km up to near the Main Boundary Thrust (MBT), by which the LH is thrust over the SH, and forms nappe and klippe in the southern part of the LH. In Nepal Himalaya there are four nappe and klippe structures; lam nappe in eastern part, the Kathmandu nappe and the Arkha klippe in central part and the Karnali klippe in western part. The lam nappe composed of Ky-Sil gneisses and granitic gneisses with no Tethyan sediments covers widely the LH to extend up to the MBT and makes tectonic bridge and window. The Karnali klippe consists of the Ky-Sil gneisses of over 8 km thickness with the Tethyan sedimentary cover and continues westward to the Almora klippe in Kumaon, India. On the other hand, the Kathmandu nappe consists of a thick pile of the Tethyan sediments in the upper part and garnet-grade metamorphic rocks in the lower part. The metamorphism of the Kathmandu nappe looks to be lower in grade than the rocks of the northern root zone of the nappe which represent Ky and Sil grade. Therefore, it is proposed that the Kathmandu nappe is another thrust sheet which underlies the Higher Himalayan rocks in the northern root zone. But this idea is unacceptable, because the MCT zone occurs along the southern margin of the Kathmandu nappe and underlie the nappe. The MCT zone likely continues northward to that in the northern root zone, although the Kathmandu nappe is cut by an out-of-sequence thrust in the northern part and separated from the northern root zone. In the Arkha klippe in central Nepal, the Tethyan sequence rests directly on rocks of the MCT zone without the intervening Higher Himalayan crystallines. This, as well as changing of thickness of the Higher Himalayan crystallines in places, suggests that the MCT zone cuts obliquely the structure of the overlying rocks, therefore the hanging-wall of the MCT zone is different in lithology and metamorphic grade in different localities; deeper Ky-Sil grade rocks of the HH in the root zone of the nappe and shallower Grt grade rocks of the LH and even the TH in the frontal part of the nappe.

**SS03/08A/D-082** Poster **0830-241**

**SEISMOTECTONIC STUDY OF THE KOYNA-WARNA SEISMIC ZONE BASED ON FAULT SEGMENTATION AND VELOCITY STRUCTURE**

Sunil Kumar SINGH<sup>1</sup>, Srinagesh DAVULURI<sup>2</sup> (<sup>1</sup>ONGC, Karaikudi, <sup>2</sup>NATIONAL GEOPHYSICAL RESEARCH INDIA, HYDERABAD)

A seismic tomographic experiment with 20 short period 3 component digital stations was mounted in Koyna-Warna region to investigate the tectonics and seismogenic character of the area. 634 events comprising of 4487 P-wave and 3689 S-wave arrivals were inverted simultaneously for the hypocentral parameters and the minimum 1-D P and S wave velocity model. The 1-D P and S wave reference velocity model is continuously increasing with depth. 3-D P wave tomography and teleseismic travel times reveal presence of lateral velocity variations. The seismogenic volume is associated with higher velocity anomalies (2% to 4%) that extend into the lower crust. This high velocity is inferred as a region of competent lithology. The seismicity patterns and focal mechanism studies reveal three distinct segmented and intersecting fault systems. The competent lithology together with intersecting geometry of faults could be the possible cause for the sustenance of seismogenic stress accumulation in the Koyna-Warna region.

**SS03/08A/D-083** Poster **0830-242**

**ACTIVE TECTONICS AND RECENT GEODYNAMICS OF CAUCASUS-EASTERN ANATOLIA AND NORTHERN IRAN REGION**

Mher AVANESYAN<sup>1</sup>, Ashot AVANESYAN<sup>2</sup>, Levon GYURJYAN<sup>2</sup>, Ruben STEPANYAN<sup>3</sup> (<sup>1</sup>Yerevan State University, Department of Geology, <sup>2</sup>Armenian National Survey of Seismic Protection)

The recent structure of the region has a heterogeneous mosaic-bloc nature. Such structure is conditioned by its position in the zone of tectonic collision of the Arabian and Eurasian plate. Non-uniformly scaled active blocks of the Earth crust are distinguished, the borders of which are different oriented active faults of different ranks and morphological types. The recent structure of the Arabian and Eurasian plate collision zone is a result of multistage formation during a long period of geological epochs. Every other period of tectonic activation, inheritance of the main structural units as well as their imposition in space happens, in qualitative and morphological plan. Such appearance of recent structure and active tectonics is confirmed by nature of seismicity, GPS data observation and analyses of vertical motion. The recent geodynamics of the region is determined by the northern drift of the Arabian plate (18+ 2 mm/yr). As a result of the effect of the Arabian plate from the South non-uniformly scaled blocks of the region with different speeds of horizontal displacement move in North-East and North-West direction. And the speed of horizontal is notable lower than that of the Arabian plate. The differences of speeds are indemnified by vertical motions. On the basis of the analysis of the neotectonics and recent geodynamics, the zones of high gradients of vertical and horizontal motions are distinguished. From the point of view of geodynamics they represent zones of compression, of relative extension, right-lateral and left-lateral slip. Rotation of the active blocks is also distinguished, on hour and counter-clockwise. Taking into consideration that the zone of high gradients of horizontal and vertical motion of active blocks represents areas of the greatest concentration fields of tension and at a definite moment can be transformed into zones of destruction and rupture emergence, they can be marked as potential seismically hazardous.

**SS03/08A/D-084** Poster **0830-243**

**NEOTECTONICAL AND PETROLOGICAL FACTORS OF FORMING OF LANDSLIDE SITUATION WITHIN EAST PONT - MINOR CAUCASUS REGION**

Arthur V. BOYNAGRYAN (Faculty of Geology, Yerevan State University)

The observed region unites echelon joint folding systems of East Pont, Adjar-Trialet and Minor Caucasus and makes up a part of Pont-Minor Caucasus-Elbrus belt of meganticlinorium. It's situated within tectonically active belt, is distinguished by high seismicity, break of Earth crust into the blocks of different sizes and their differentiated vertical displacements. A situation of region by numerous fault infringements, zones of fissuring and breaking of rocks, their hydrothermal change (often till the clay state); the dissected mountain relief; an abundance of springs, concussions of slopes at the earthquakes create the favourable conditions for the landslides' forming. The petrological state of rocks of the region has a great importance, i.e. their chemical and mineralogical peculiarities, structure and texture, conditions of occurrence and others, which have an essential influence on the process of their weathering and preparation to the landslide displacements. The landslides in the sections of spreading of porphyrites, loess loams, clays and etc. are lightly formed. There are a great number of large seismogenic landslides that are formed at the strong earthquakes (7 points and more) in the region. They are clearly marked out in the relief of locality as well as in the aerophotos and maps of large scale (more than 1:100 000). They are distinguished by large horizontal displacements from ordinary landslides.

**SS03/08A/D-085** Poster **0830-244**

**ABOUT CORRELATION BETWEEN THE EARTH'S STRUCTURE AND GEODYNAMIC PROCESSES IN SOME REGIONS OF ARMENIA**

Aram Artavazd GRIGORIAN<sup>1</sup>, Stepan B. ABOVIAN<sup>2</sup>, Amazasp A. BABADJANIAN<sup>3</sup> (<sup>1</sup>Advanced Research Laboratory, ARSAT Center, <sup>2</sup>Laboratory of Mineralogy, Institute of Geological Sciences NAS, Yerevan, Armenia, <sup>3</sup>Institute of Geophysics and Engineering Seismology NAS, Yerevan, Armenia)

The paper concerns with correlation carried out for the Earth's structure, changes in properties of rock minerals, affected by high strain and temperature, and global geodynamic process, occurring in Armenia and continuing to other regions of the Lesser Caucasus. The folding and block structure of the territory of Armenia were formed as a result of intensive submeridian horizontal compression, caused by movement of rigid northern wedge of the Arabian plate to the North. The process of deep fault formation as well as formation of the ophiolite zones are considered as a result of consecutive periods of the Earth's crust spreading and compression. Petrography and mineral analysis of mafic and ultramafic intrusive rocks and their serpentinised variety show high degree of deformation in ophiolites, indicating a process of pressing-out the mantle rocks upward to the Earth's surface. Rock density distribution is compared with geophysical data. Anomalies in gravitational and magnetic field data are discussed and compared with the data on geological investigations. Seismic activity is discussed in relation with structure of the Earth's interior of the region and local tectonic processes. Intrusive rocks of mafic and ultramafic composition are associated with the ophiolites. Simultaneously with the ophiolites, the intrusive rocks were formed in a zone being the Tethys oceanic basin of a riftogene trough type in the Jurassic time. The troughs were formed in result of lifting the mantle diapire and development of deep ruptures under spreading, deepening and thinning of the Earth's crust

accompanying by formation of rift with new ophiolite (oceanic) crust. Under further compression caused by movement of the Arabian plate in the north direction, mafite and ultramafite intrusives have been involved into folding processes, and then they were protrusively embedded into stratigraphically higher levels in the Cretaceous time and the Eocene. By the same processes, the intrusives have been deformed, broken in blocks and separated. The deep fault consists of a set of sub-parallel ruptures manifested as scraps and fractures within the Cretaceous-Palaeocene rocks. The seismo-gravitation formations in a form of large blocks and stepwise landslides appeared along the old gravitational seismic ruptures. According to known conception of global plates tectonics, earthquakes are related to tectonic processes and often confined the contact zones (deep faults) of lithosphere plates. Regional geodynamical, geological and geophysical situation described above, support the main statements of the mechanism of earthquake origin, suggested earlier.

**SS03/08A/D-086** Poster **0830-245**

**SEISMOGENIC LANDSLIDES AS ONE OF THE VARIETIES OF GEOLOGICAL DANGERS OF ARMENIA**

Vladimir R. BOYNAGRYAN (Faculty of Geography, Yerevan State University)

Armenia is situated within tectonically active Alpine-Himalayas belt and represents the mountain country with the dissected relief, complex geological structure, high seismicity, wide spreading of dangerous geological processes, where the landslides take the special place. More than 3500 landslides of different size, activity and different genesis are fixed by us in Armenia. On the whole they are spread in the basins of the Aghstev, Getik, Vedi, Arpa, Pambak rivers, in the vicinities of Yerevan, Dilijan, Kapan, separate sections of Yerevan, Vokhchaberd village suffer from the landslides very much. For the last years the activation of some old landslides took place and the new ones appeared. Thus, in 1992 Odzun landslide-collapse near the Sanain railway station recovered the railway Yerevan-Tbilisi for some days. In Yerevan the Nubarashen landslide caused the considerable destructions in the territory of the town cemetery; the middle rate of its displacement for 10 years made up 0.07-0.13m a year, and maximum was 1.4m. Near the Haghartsin village (basin of the Aghstev river) the activation of surface parts of the old seismogenic landslide because of slope cutting caused the destruction of railway bed and landslide masses throw off into the Aghstev river bed, creating a threat of cover (displacement of surface parts of this landslide occurs with a rate of 1-1.5m a month). State of anxiety has occurred in Vokhchaberd village, where in nowadays about 80% of houses are in a state of emergency and 44 houses are completely destroyed because of activation of the large seismogenic landslide with a size of 2.5x1.3 km<sup>2</sup>, frustrated and displaced along the line of reversed fault. The amplitude of vertical displacement of this landslide block is 200-225m and horizontal one is till 500m and more. The first destructions from the landslide motions were fixed here as far back as 1982, but for the last years the landslide "revived" and actively wins over the new lots of village. The motions become stronger after the spring snow-thawing and rain. Among the landslides of Armenia the ancient huge landslide-blocks and landslide-flows are especially marked out, those are complex tectonical-seismogravitational displaced bodies formed during the strong earthquakes. All of them are related to the zones of faults and high fissuring of rocks. The damage from landslides in Armenia makes up tens of thousands of dollars a year.

**SS03/08A/D-087** Poster **0830-246**

**STRUCTURES AND SEISMOTECTONICS OF SOUTH EASTERN GHANA EARTHQUAKE ZONE**

Anang Solomon ANUM (IASPEI)

B > Ghana lies on the southeastern margin of the West African Craton, far from the major earthquake zones of the world that mark the present lithospheric plate boundaries. However, there are historic records (The Accra Earthquake of 22nd June 1939), which show that earthquakes occur in the south of and southeast of Ghana from time to time. Geological, Geophysical and Seismological study in Southeastern Ghana shows that the occurrences of earthquakes in Ghana is due to movements along the Coastal Boundary Fault (CBF) and the Akwapim fault Zone (AKZ). Although studies on these fault zones is still in the elementary stage we believe that the reported seismic activities could be attribute to the crustal instabilities with geodynamic stress along the CBF and AFZ. In the last few decades, earthquake with epicenters located along the intersection of the two faults.

**SS03/08A/D-088** Poster **0830-247**

**KINEMATICS ENGINE OF THE ONGOING DEFORMATION FIELD AROUND CAIRO, EGYPT**

Ahmed BADAWEY, Sayed EL-ESSAWY, Gamal HASSAN, Ali TEALEB (Seismology Dept., National Research Institute of Astronomy and Geophysics (NRIAG))

Abstract Kinematics engine of the ongoing deformation field around Cairo, Egypt have been investigated from earthquakes, repeated GPS and gravity observations. First results provided from this combined strategy are presented, by focusing on both stress field and surface kinematics. The spatio-temporal distribution of earthquakes reveals that Cairo region has suffered not only from interplate earthquakes but also from inland seismic dislocations. Earthquake focal mechanisms indicate that the stress field around Cairo is dominated by a transtensional stress regime (normal faulting with strike-slip component). Repeated gravity measurements around Cairo proved an existence of considerable temporal variations of gravity. These non-tidal changes could be explained by dynamics processes within the upper crust related to the development of local stress conditions. The comparison between the observed GPS and gravity shows a remarkable agreement and provides a convincing explanation for the observed fluctuations with seismic activity. The results of deformation analysis indicate three different deformation zones in the investigated area. The northern part dominates as a compressional area with a magnitude of 0.19 ppm/year. The compressions in this area are generally in NW-SE direction. However, an extensional area with a magnitude of 0.21 ppm/year in the NE-SW direction has been observed in the southern part. The central part of the investigation area seems to be in a state of no significant deformation.

**SS03/08A/D-089** Poster **0830-248**

**MESOZOIC BASIN DEVELOPMENT IN THE NORTH ATLANTIC AREA AROUND IRELAND: SOME CONSTRAINTS FROM POTENTIAL FIELD STUDIES?**

Peter W. READMAN, Brian M. O'REILLY (Dublin Institute for Advanced Studies, 5 Merrion Square, Dublin 2, IRELAND)

Multiphase rifting episodes during the early to late Mesozoic Era associated with the break-up of Pangaea led to the formation of a global assemblage of sedimentary basins distributed across the entire North Atlantic region from eastern North America to the European Platform. The region around and to the west of Ireland lies at the centre of this regional assemblage and in this area tectonic re-activation of a strong NE-SW trending Caledonian basement

fabric partly controlled the siting of the basins. The syn-rift phase of basin development was contemporaneous with continental rifting and the onset of sea-floor-spreading within the Atlantic south of the Charlie Gibbs and Azores Fracture Zones. In this study a compilation of marine and satellite gravity data is primarily used to produce a regional interpretation of the tectonic fabrics in the region around Ireland and extending westwards and southwards into the Rockall and Porcupine Basins. A series of gravity models across the various sedimentary basins including the Celtic and Irish Sea Basins are used with interpretations of vertical incidence and wide-angle seismic data, where available, to define crustal structure and its relationship with basin geometries. End-member sedimentary basin types are identified and a regional preliminary model for Mesozoic basin development is outlined. The deep-water Rockall and Porcupine Basins overlie North Atlantic lithosphere where large amounts of extensional strain were focused into the upper and mid-crust producing greater amounts of syn-rift subsidence. Within the inboard shallow water shelf sea basin areas of the Celtic and Irish Sea generally smaller strains occur within all levels of the lithosphere and this strain is distributed across wide regions of the lower crust and mantle lithosphere. The model for the regional structuring of sedimentary basins requires that the strain field varies erratically within the upper to mid-crust across the North Atlantic but varies more smoothly in the lower crust and lower mantle lithosphere. The changes in the pattern of strain in the upper to mid crust are accommodated by rotation of continental crustal blocks (about vertical axes) and also by large-scale crustal transfer fault systems that penetrate at least to a lower crustal level. These fault systems may have been important in controlling fluid flow at a lithospheric scale locally hydrating the upper mantle.

**SS03/08A/D-090** Poster **0830-249**

#### GEODYNAMIC ANALYSIS OF THE ROMANIAN TERRITORY BY A SET OF GEOTEMATIC MAPS

Ligia-Narciza E. ATANASIU (INSTITUTE OF GEODYNAMICS, 19-21 Jean-Louis Calderon St., Bucharest-37, Romania, R-70201)

The Romanian territory is a very important part of the alpine-carpato-himalayan belt. We mention only two specific elements: First the Romanian territory placed at the border of the East European Platform is a region of complex geological structure dominated by the presence of the Vrancea active seismic zone, located in the bending area of Romanian Carpathians. Three tectonic plate/sub-plate seem to join in this region: East European plate, Moesian sub plate and Intra Alpine plate. During the years, Vrancea active seismic area has been subject to much research trying to better understand the mechanism of its intermediate-depth seismicity. Second, on the Romanian territory we find the contact between Central European Platform (Epi-Paleozoic Platform) and East-European Platform (Precambrian Platform) so called Tornquist-Teisseyre zone, which is reflected by the different kind of geophysical maps. Our work is represented by the visualization and plotting of a set of thematic maps with geophysics, topographic and tectonic information on the Romanian territory, offering the possibility of a quick correlation and analysis of this huge amount of data. We hope that the resulted data set may considerably improve the knowledge on the tectonics and geodynamics of the Romanian territory and contributed to a better understanding of the natural hazards on the regional frame.

**SS03/08A/D-091** Poster **0830-250**

#### GEOPHYSICAL CONSIDERATIONS ON PLATE TECTONICS WITHIN THE ROMANIAN TERRITORY AND INTERMEDIATE DEPTH SEISMICITY

Lucian BESUTIU, Dorel ZUGRAVESCU (Sabba S. Stefanescu Institute of Geodynamics of the Romanian Academy)

During the time various models for plate tectonics on the Romanian territory were constructed mainly based on geological arguments, without taking into account the geophysical behavior of a plate boundary. The paper attempts to outline lithosphere blocks boundaries and their dynamics as inferred from geophysical data interpretation. Gravity, magnetics, geomagnetic soundings, heat flow, deep seismic investigations (DSS), magnetotelluric soundings (MTS), borehole breakouts, etc. were used on purpose. Consequently, a three-plate tectonic model for the Romanian territory was considered: East European Plate (EEP), Moesian micro-plate (MoP), and the Intra-alpine micro-plate (IaP). They are separated by large lithosphere discontinuities: Tornquist-Teisseyre (TTZ) compressional zone, Peceneaga-Camena (PCF), and the Trans-Getica (TGF) transform faults. Past to recent dynamics of the tectonic plates on the Romanian territory is discussed with special emphasize on the consequences of the Black Sea opening. It seems that crust extension related to the W Black Sea basin opening split the MoP into several crustal slivers, which relatively move each to another, thus generating normal earthquakes along their wedges. After the Black Sea ended its evolution, active rifts in SW Arabian Plate seem to offer the necessary driving forces for the present dynamics of these blocks. Back to the Black Sea opening, crust shortening took place in various environments. East Carpathians, crust expelled met the inclined boundary of TTZ and came into an oblique subduction to which the peculiarities of volcanism in the southernmost Harghita Mts. seem to be related. South Carpathians, crustal slivers faced the vertical margin of the IaP and provoked a lithosphere buckling, well reflected in the lowest gravity low on the Romanian territory, which lies in front and not beneath the highest mountains in the country. During the years, numerous attempts, mainly based on the hypothesis of a subduction in the area, have been made to explain the strange peculiarities of the intermediate-depth seismicity within the bending zone of East Carpathians. In the authors opinion, the strictly confined hypocenters location in the Vrancea area seems to be due to the presence of a continental unstable transform-transform-compression triple junction. Thereafter, the lithosphere block squeezed between MoP, EEP and IaP wedges was pushed down by tectonic forces driving the three plates. Statistics of the Vrancea intermediate earthquakes occurred after the major event of November 1940 showed a systematic SW migration of the seismogenic zone, advocating for the triple-junction actual slight displacement under the above-mentioned tectonic forces. The penetration of a colder lithosphere block into the hotter upper mantle led to an obvious thermodynamic disequilibrium. During the temperature accommodation various phenomena such as convective cells, phase transform, and devolatilization add new sources to the intermediate seismicity in the area.

**SS03/08A/D-092** Poster **0830-251**

#### ACCRETION TECTONICS OF NORTH PACIFIC AND FRACTAL DIMENSION OF TERRANES

Vladimir S. ZAKHAROV, Vsevolod N. VADKOVSKY (Moscow Lomonosov State University)

The forming continental crust on active zones has been connected with interaction between oceanic and continental lithosphere in convergent plate-boundaries. Different inhomogeneities (fragments) of the oceanic crust such as seamounts, island arcs, oceanic plateaus and fragments of craton, becomes continental margin due to subduction and collision processes (present time and in the past). Other fragments created during these processes such as accretionary complexes and subduction zone terranes. Terrain may be defined as tectonic and stratigraphic unit which distinct from adjacent units separated by

faults. The size of terrain is undefined: from some micrometers up to thousand kilometers. We used data from detailed digital geological map (GIS compilation on Geophysical, Geologic and Tectonic data for Circum –North Pacific. Eds.: W.Nokleberg and M.Diggles. Open file report 99-422, version 1.0, 1999) To calculate fractal dimension D set of terranes we take  $\ln(S)/\ln(P)$  relation where S-area and P- perimeter of the individual terrane. Fractal dimension  $D=2/B$  where B defined as slope of the straight-line approximation (LSQM) these ratio for set of terranes (Mandelbrot, Lovejoy). For set of terranes of the Russian Far East  $D=1.377$ ,  $r=0.977$  whereas for Northwest of the USA and Canada  $D=1.202$ ,  $r=0.974$ . The range of variation S and P includes many orders. Set of terranes is self-similarity. We investigate variations of fractal dimension of terranes sets in geologic time, when terrain had been added to the active continental wedge for two regions. This small variability of D may be connected with terrain rigidity which didn't deformed during accretion process and its geologic life. Recent seismicity and GPS measurements for these regions confirm this point of view.

**SS03/08A/D-093** Poster **0830-252**

#### EVIDENCE OF DEEP SEISMOGENIC DEPTH IN STABLE CONTINENTAL REGIONS

Won-Young KIM (Lamont-Doherty Earth Observatory of Columbia University)

Well-documented recent earthquakes that occurred in Eastern North America and in other stable continental regions (SCR) provide an opportunity to appraise the seismicity and hazard in this kind of tectonic environment through new data and analysis methods. One important question is the occurrence of SCR earthquakes at depth --down to lower-crust (15 to 30 km depth). Deep crustal earthquakes in old cratonic environments such as, Scandinavia and Canadian shield, have been interpreted as brittle rupture at depth due to low heat flow coupled with favorable rheology. Another question is, are pre-existing faults in the crust is pertinent to SCR seismogenesis? Recent detailed studies of SCR earthquakes in Eastern North America indicate that deep seated former rift system acted as pre-existing zone of weakness and some part of those may have been reactivated. In this paper, I will show evidence of such deep seismogenesis in the Eastern North America using the data from recent earthquakes. Regional and teleseismic waveform data from the June 18, 2002, Evansville, Indiana earthquake ( $M_w = 4.6$ ) indicate that the main shock occurred on a steeply dipping fault at a depth of about 18 km. The source mechanism determined from the regional waveform inversion is predominantly strike-slip along near-vertical nodal planes, striking NNE and WNW. The focal depth is well constrained by regional and teleseismic waveform modeling as well as the accurate location of an aftershock recorded by portable local stations deployed following the main shock in the epicentral distance range 5 to 9 km. This earthquake sequence occurred in the Wabash Valley fault zone in the Illinois Basin Indiana. A large number of subsurface faults are identified in the Wabash Valley fault zone from over 6,000 petroleum test wells in the basin. The close proximity of the main shock and aftershock epicenters to the trace of the compound Caborn fault, and a strong correlation between the trend and dip of the Caborn fault and source mechanism of the June 18, 2002 event, suggest that the earthquake may have occurred on that fault. Downward continuation of the Caborn fault as well as other major faults mapped in the shallow subsurface of the Wabash Valley fault zone (to at least 7 km depth), and the focal depth of the June 18, 2002 event suggest that the seismogenic depth in the fault zone extends to at least 18 km depth. Its focal mechanism -- vertical strike-slip faulting at depth -- may suggest that faults associated with a possible Precambrian rift system are being reactivated by the contemporary NE-E trending regional compressive horizontal stress.

**SS03/08A/D-094** Poster **0830-253**

#### THE CAMPBELL PLATEAU, NEW ZEALAND: ITS CRUSTAL EVOLUTION AND BREAK-UP PROCESS

Karsten GOHL<sup>1</sup>, Bryan DAVY<sup>2</sup>, Daniel BARKER<sup>3</sup>, Fred DAVEY<sup>2</sup>, Gabriele UENZELMANN-NEBEN<sup>1</sup> (<sup>1</sup>Alfred Wegener Institute for Polar and Marine Research, Bremerhaven, Germany, <sup>2</sup>Institute of Geological and Nuclear Sciences, Lower Hutt, New Zealand)

The Campbell Plateau is a large submarine continental plateau lying to the southeast of New Zealand and separated from the landmass of New Zealand by a series of deep extensional sedimentary basins and morphological deeps. Prior to about 110 Ma, the region (with New Zealand) formed part of Gondwana, fitting adjacent to eastern Ross Sea and western Marie Byrd Land, and coincident with an active subducting continental margin. At about 110 Ma, subduction at the margin ceased and extension of the region commenced. This extension continued until about 82 Ma when active seafloor spreading commenced forming the Southern Ocean. The Campbell Plateau has probably remained essentially submerged (presently at depths of about 500 m to 1000 m) since that time as extension has continued and little sedimentation has occurred on the Plateau due to the remoteness of sediment supply and ocean currents. The southeast margin of the Plateau, the conjugate margin to the western Marie Byrd Land margin of West Antarctica, has little sediment cover. Although the timing of break-up is relatively well documented, the processes that led to break-up and the subsequent evolution of the continental fragment forming Campbell Plateau are not well understood. The reason for the very steep southeastern margin is not known. Was it fast break-up, oblique break-up or erosion? Is a submarine plateau passive margin different to continental passive margin or just a result of differences in sediment supply? On the basis of potential field data, the Plateau can be divided into a series of crustal segments with varying crustal parameters. The Stokes and Campbell magnetic anomaly systems indicate extensive magmatic crustal provinces. What was the role of magmatism during break-up and subsequently? To answer these questions on the evolution of submarine continental plateaus, a geophysical survey was conducted across the Campbell Plateau in January-February 2003. The survey carried out a seismic (OBS) transect and a series of crustal seismic reflection lines from the South Island to and across the southeast margin of the Campbell Plateau. It crossed the Great South Basin and several poorly known east-west trending inferred extensional basins on the Campbell Plateau and defined the change in structure across the southeast margin of the Plateau. Preliminary results of this project are presented here.

**SS03/08A/D-095** Poster **0830-254**

#### EVOLUTION AND DYNAMICS OF THE PACIFIC MARGIN OF WEST ANTARCTICA

Karsten GOHL<sup>1</sup>, Graeme EAGLES<sup>1</sup>, Robert D. LARTER<sup>2</sup> (<sup>1</sup>Alfred Wegener Institute for Polar and Marine Research, POB 120161, 27515 Bremerhaven, Germany, <sup>2</sup>British Antarctic Survey, High Cross, Madingley Road, Cambridge CB3 0ET, UK)

The Pacific continental margin of West Antarctica has undergone a diverse evolution from a rifted passive margin in the SW Pacific to a converted active-to-passive regime in the SE Pacific sector. While the western margin developed as a result of rifting between greater New Zealand and Marie Byrd Land, the eastern margin evolved after the collision of the Pacific-Antarctic ridge with the subduction trench. While this general scheme has been known for some time, the detailed evolution of the margin and its adjacent ocean basins has become clearer only for the last few years with the gathering of more geophysical data. A distinct boundary between the two different West Antarctic margin types is marked by a

crustal-scale convergence zone in the western Bellingshausen Sea. This zone extends from oceanic to continental crust perpendicular to the margin and can be interpreted as the former eastern Bellingshausen plate boundary. The margin west of it and north of Thurston Island developed as a classical passive one after break-up from Chatham Rise (NZ). The Pine Island Bay and the NW-extension of its main trough across the shelf seem to form another boundary. The margin west of it evolved after separation from Campbell Plateau (NZ) and shows abundant volcanic structures. Although newest plate-tectonic reconstructions of the South Pacific places Pine Island Bay conjugate to Bounty Trough (NZ), it is still speculative to assume that both systems formed as a continuous rift. The data coverage in this remote area is still somewhat sparse. But by integrating seismic information with satellite altimetry and ship/airborne potential field data, we are able to show an improved model for the evolution of the West Antarctic margin.

**SS03/08A/D-096** Poster **0830-255**  
**NUMERICAL AND FUNCTIONAL REPRESENTATIONS OF REGIONAL HEAT FLOW IN SOUTH AMERICA**

Valiya M. HAMZA, Fernando J.S. SILVA DIAS (IASPEI)

An updated database incorporating results of recent geothermal investigations has been setup for the purpose of examining regional trends in heat flow in South America. These include recent conventional heat flow measurements at nearly 40 sites in the southeast coastal area of Brazil and new BHT heat flow estimates for nearly 150 sites in the sub-Andean basins in the west-central parts of the continent (in Bolivia, Chile, Colombia, Ecuador and Paraguay). The present continental data base consists of 793 heat flow values, giving an overall data density of 45 per million square kilometers and a representative mean of  $63 \pm 36$  mW/m<sup>2</sup>. Comparison with previous compilations indicates that there has been some improvements in data quality. Thus, results obtained by conventional methods constitute a significant part of the data set in the central and eastern parts of the continent. The geographic distribution, however, continue to be non-uniform, there being several areas where data density is low, and some for which heat flow data are not altogether available. The updated database was employed in generating numerical surfaces of regional heat flow pattern in several parts of the South American continent. In addition, polynomial methods were employed for examining regional scale variations in heat flow over the continent. Specifically, a general purpose least square solution was used to determine coefficients of up to sixth order in latitude and longitude. Examination of meansquare residuals indicates that higher order polynomials are unwarranted. Maps of regional trends and residual anomalies reveal the existence of several systematic patterns in regional heat flow. Thus cordilleran regions of the Andes are, in general, characterized by relatively high heat flow (with values  $> 75$  mW/m<sup>2</sup>), compared with the western coastal regions and the Pre-Cordilleran basins to the east. In the eastern part of the continent, heat flow is low to normal (with values  $< 60$  mW/m<sup>2</sup>), the exceptions being the Mesozoic rift basins (Potiguar, Recôncavo and Taubaté), areas of Cenozoic alkaline intrusions and some isolated localities in the Precambrian terrain in the central parts of Brazil. Problems arising from low data density allow only limited insights into the nature of heat flow variations along and across the main tectonic units. Thus only large-scale trends associated with changing tectonic patterns and subduction-related magmatism can be identified in polynomial representations of the regional heat flow field. Prominent among these are east-west trending belts of low heat flow in northern Peru and in central Chile, as well as the high heat flow belts in northern Chile (extending into the Altiplano of Bolivia) and southern Chile (extending into northwestern Argentina). The low heat flow belts are found to coincide approximately with zones of sub-horizontal subduction, while high heat flow belts are situated in regions of high angle subduction. The results also indicate that further improvements in polynomial and numerical representations of regional thermal fields can be achieved only through acquisition of new good quality geothermal data in areas of low data density.

**SS03/08A/D-097** Poster **0830-256**  
**VOLCANIC CENTRE DISTRIBUTION FABRIC AS INDICATOR OF FINITE INCREMENTAL STRAIN IN SOUTHERN CENTRAL ANDES**

Guillermo Hector RE<sup>1</sup>, Maria Silvia JAPAS<sup>2</sup>, Silvia Patricia BARREDO<sup>1</sup> (<sup>1</sup>Dpto. Geología - Universidad de Buenos Aires, <sup>2</sup>CONICET - Argentina)

The Andes chain is built as a consequence of the subduction of the Nazca plate under the South American plate, without continental collision involvement. This fact has made of the South American Pacific margin a typical example of ocean lithosphere subduction under a continental plate. The Cordillera de los Andes system lies parallel to the Peruvian-Chilean trench, which delineates the meet zone between the subducted oceanic plate and the continental plate; and their evolution is linked to the particular characteristics shown by the Nazca Plate subduction and, associated to it, the subduction of the Nazca, Iquique and Juan Fernández ridges under the South American Plate. The main characteristic of the current Andean orogen, and possibly also of the previous evolutionary stages of the South American convergence system, is a persistent, in terms of space and time, longitudinal segmentation of the tectonic, geodynamic and morphological elements that make up the continental margin. The present work is centered in the study of the segment understood between the 20° and the 33° of south latitude. In this sector the analysis of the volcanic centers distribution fabric has permitted to characterize the incremental strain of the Andean system for Miocene to Recent times. The results of this analysis confirm the existence of two sets of localized non-coaxial regional structures that exerted a structural control on the volcanic placements, and in the periods of activity of these volcanic centers. These structures consists in NNE and NNW trending extensional megashears zones which play an important role in the Andean evolution. NW secondary wrench structures locally control volcanic bodies location and would represent transtensional features, en-echelon arranged. In close relationship with the volcanism and the kinematics of the orogen, the salt deposits of borates, geysers and hot springs of the Argentinean Puna would also undergo the tectonic control exercised by these megashears. Beginning with the integrated analysis of the tectonic fabrics, the time interval in which any of these structures was active has been delimited with even more precision; and confirm the importance that the shears extensional of regional character exercise in the control of the evolution Andean tectonics. Therefore, it was possible to determine that the system evolution of progressive deformation (type *c/c'*), developed in an transpressive tectonic environment, has played a fundamental role in the structuring and kinematics evolution of this section of the central Andes.

**SS03/08A/D-098** Poster **0830-257**  
**LOW-VELOCITY OCEANIC CRUST AT THE TOP OF SUBDUCTING PLATES RESOLVED BY A TOMOGRAPHIC METHOD WITH SPATIAL CORRELATION**

Makoto MATSUBARA, Shutaro SEKINE, Kazushige OBARA, Keiji KASAHARA (National Research Institute for Earth Science and Disaster Prevention)

The detailed velocity structure beneath Japan arc is obtained by applying the tomographic method (Zhao *et al.*, 1992) with spatial correlations (Matsubara *et al.*, 2001) to 1,061,936 *P*-wave arrival times from 19,943 earthquakes recorded at NIED Hi-net of 664 stations. The

target region is the crust and the upper mantle beneath Japan arc (29-46°N, 129-146°E, 0-200 km depth). The horizontal spacing of the grid nodes is 0.125° in the crust and 0.25° in the mantle, 2.5 km. That in the vertical direction is 2.5-5 km in the crust and 7.5-15 km in the mantle. The corresponding resolution is twice as grid interval, say, 0.25° in the crust and 0.5° in the mantle, horizontally. A low velocity zone exists within depths of 30-50 km beneath the northeastern Japan arc corresponding to the upper boundary of the subducting Pacific plate. In Kanto region, two low-velocity zones have been found at depths of 40-100 km in the southern part and around 30 km in the western part. The deeper section corresponds to the upper boundary of the Pacific plate and coincides with the S-wave reflector (Obara and Sato, 1988). The shallower one indicates the upper boundary of the subducting Philippine Sea plate and supports the results of Ohmi and Hurukawa (1996). We conclude that these low velocity zones are the oceanic crusts that exist at the top of the subducting Pacific and Philippine Sea plates. We also found the low velocity zones along the volcanic front beneath the northeastern Japan arc and back-arc side in the upper mantle. These zones are parallel to the subducting Pacific plate. The high velocity zone indicating the subducting Philippine Sea plate beneath the eastern Kyushu district, western edge of Japan arc is also shown clearly.

**SS03/08A/D-099** Poster **0830-258**  
**DEEP CRUSTAL STRUCTURE EXPLORATION IN HYPOCENTRAL REGION OF THE 2000 TOTTORI-KEN SEIBU EARTHQUAKE**

Shintaro ABE<sup>1</sup>, Yasuhira AOYAGI<sup>1</sup>, Katsuyoshi MIYAKOSHI<sup>1</sup>, Daiei INOUE<sup>2</sup>, Yoshiya ODA<sup>2</sup> (<sup>1</sup>Geosphere Environmental Science Department, Central Research Institute of Electric Power Industry, <sup>2</sup>Tokyo Metropolitan University, <sup>3</sup>Central Research Institute of Electric Power Industry)

The Tottori-ken Seibu earthquake of October 6, 2000 was a large earthquake exceeding Mj 7. However, active fault was not pointed out on the existing map in hypocentral region of this earthquake. This fact is very important in order to argue about the validity of predicting the magnitude of great or large earthquakes generated in the target area based on the results of earth scientific investigation. We carried out dense earthquake observation in which we installed 44 points in order to grasp the detailed form of earthquake source fault. Furthermore, we carried out seismic reflection prospecting of 3 observation lines which cross the earthquake source fault of main shock. We clarify the relevance of earthquake source fault and lineament. Principal Results 1. Low velocity zone detected in the crust by velocity analysis. We interpreted S-P interval of the seismic wave obtained by earthquake observation, and carried out velocity analysis using travel time seismic tomography method. Low velocity zone was detected in the depth of about 2 km of hypocentral region as a result of the analysis. The low velocity zone is distributed on earthquake source fault presumed from aftershock distribution. Generally fall in seismic wave velocity is caused by fall of rigidity. That is, it is thought that the low velocity zone was formed from destruction of the crust by fault activity. 2. Flower structure recognized by seismic reflection prospecting. In the place where lineament and an observation line cross, two faults have been recognized in seismic reflection prospecting line-B. These faults seem to converge toward the depths. This geological structure is called flower structure, and it is characteristic underground structure formed of accumulation of lateral displacement. In this area, we were also carrying out aerial photograph interpretation and trench excavation. As a result, the geological proof that the lineaments were formed of left-lateral fault was acquired. That is, both underground structures and deformations of surface have lateral fault features. 3. Aftershock distribution and region crushed by faults recognized by seismic reflection prospecting. Faults recognized by seismic reflection prospecting and region crushed by the faults are located in the upper part of earthquake source fault presumed from aftershock distribution. However, the scale is too large if this crushed region was formed only by fault activity of the 2000 Tottori-ken Seibu earthquake. That is, it suggests that earthquakes with the same mechanism as the 2000 Tottori-ken Seibu earthquake occurred in this area repeatedly in the past. Reference Shintaro Abe, 2002, Seismic Reflection Survey around the 2000 Tottori-ken Seibu Earthquake area, The Society of Exploration Geophysicists of Japan, Proceedings of the 107th SEGJ Conference (Japanese only).

**SS03/08A/D-100** Poster **0830-259**  
**SEISMIC STRUCTURE OF THE CRUST AND UPPERMOST MANTLE BENEATH KYUSHU, JAPAN AS INFERRED FROM RECEIVER FUNCTION ANALYSIS**

Takumi MURAKOSHI<sup>1</sup>, Hiroshi TAKENAKA<sup>1</sup>, Sadaomi SUZUKI<sup>1</sup>, Hiroshi SHIMIZU<sup>2</sup>, Kenji UEHIRA<sup>3</sup> (<sup>1</sup>Department of Earth and Planetary Sciences, Faculty of Sciences, Kyushu University, <sup>2</sup>Institute of Seismology and Volcanology, Faculty of Sciences, Kyushu University)

Kyushu is one of the typical active subduction zones where the Philippine Sea plate goes northwestward beneath the Eurasian plate. For understanding its tectonic features we studied seismic structure of the crust and uppermost mantle beneath Kyushu by use of receiver function analysis. The data used for receiver function are three-component broadband records of the teleseismic events occurring in the epicentral distance of 30-100 degree observed by 17 stations in and around Kyushu. We obtained 10-80 high quality receiver functions for each station. And we applied SVD filtering to the receiver functions of multi-channel for each station to emphasize the coherent phases. Most of the filtered functions show the Moho-boundary phase converted from P to S. We also found the phases of negative amplitude which means the existence of low-velocity layers in the crust and uppermost mantle. We applied the receiver function inversion using genetic algorithm (GA) to estimate the detailed velocity structures beneath the stations. For estimating the both of shallow and deep structures with high accuracy we applied a new approach by separately using the high-frequency and low-frequency receiver functions. After calculating the receiver function inversion for each station, we estimated the three-dimensional velocity structures beneath Kyushu by using a migration technique. The results reveal the followings. (1) The depths of the Moho-boundary beneath Kyushu are 25-35 km. The Moho of western Kyushu in backarc tends to be shallower, whereas the Moho of northeastern Kyushu and western Chugoku which locate at the junction of the Southwest Japan Arc and the Ryukyu Arc are deeper. The Moho depths beneath the active volcanoes tends to be slightly deeper. (2) The top of the subducting Philippine Sea plate is imaged clearly in the range of depth from 40 to 70 km beneath eastern Kyushu. (3) Low velocity layers are visible at the crust and uppermost mantle beneath the active volcanoes in Kyushu; for instance, at the upper crust under northern Kuju and eastern Aso volcanoes, at the lower crust and uppermost mantle under western Aso volcano, and at the upper crust and uppermost mantle near Sakurajima island in the western Kyushu. It may show the partially melting by the mantle upwelling in the backarc of Kyushu.

**SS03/08A/D-101** Poster **0830-260**  
**SEISMIC STRUCTURE OF INTERPLATE SEISMOGENIC ZONE IN THE SOUTHERN JAPAN TRENCH FROM SP CONVERTED PHASES**

Minoru NISHINO<sup>1</sup>, Ryota HINO<sup>1</sup>, Masanao SHINOHARA<sup>2</sup> (<sup>1</sup>AOB, Tohoku University, <sup>2</sup>ERI, University of Tokyo)

Evident later phases often appear about 1-3 second after the P first arrivals on seismograms of the interplate earthquakes occurring in the southern part of the Japan Trench subduction zone recorded by the land seismic network in the NE Japan arc. If these arrivals (X-phase) are converted or reflected waves at an interface in the deeper part of the interplate seismogenic zone, it is important to locate the conversion or reflection points to clarify the seismic structure. The results of preliminary analyses on the particle motions and arrival time differences, X-P times, versus offsets indicate that X-phase is possibly a SP converted wave at an interface located near the hypocenter. For accurate estimation of the point of conversion, it is very important to determine the hypocenters of the earthquakes with the SP arrivals. In this study, we relocate the hypocenters of the offshore interplate earthquakes by using ocean bottom seismographic data. Our data set consists of two groups: 1) nine events occurred in 1997 when a dense OBS array was deployed and 2) earthquakes taking places since 1995 when a permanent offshore seismic station was put into operation. The OBS array in 1997 observation was in operation for over three weeks and detected about 900 microearthquakes. 94 of them were recorded also by the land stations and nine were observed with the evident SP phase. Detailed inspection of the OBS waveform records, the SP phase was also recorded at OBSs. Using a seismic velocity structure model determined by an airgun-OBS seismic experiment (Nishino et al., 1999), we relocated both the hypocenters and the point of SP conversion simultaneously, from P and SP arrival times at the land and OBS stations. The estimated SP conversion points are located just above the cloud of the microseismicity defining the location of the subduction interface. Therefore, the nine earthquakes are not actually the interplate events and the observed X-phase was interpreted as the S to P conversion at the plate interface. We are now analyzing the data set 2) and the conversion points also seem to be located along the plate boundary. If our interpretation that X-phase is the plate boundary SP from the intraplate events is true, X-phase can be a good marker to identify intraplate events. Since it is difficult to distinguish whether an earthquake actually occurs along the plate boundary only from its hypocenter location, our X-phase analyses is important not only to clarify the geometry of the plate boundary but also to understand the 'thickness' of the interplate seismogenic zone.

**SS03/08A/D-102** Poster **0830-261**

**CRUSTAL STRUCTURE OF CENTRAL JAPAN OBTAINED FROM SEISMIC SURVEYS - ROLE OF STRUCTURE IN MEGATHRUST EARTHQUAKE OCCURRENCE**

Yoshiyuki KANEDA<sup>1</sup>, Shuichi KODAIRA<sup>1</sup>, Jin-Oh PARK<sup>1</sup>, Ayako NAKANISHI<sup>1</sup>, Takashi IIDAKA<sup>2</sup>, Eiji KURASHIMO<sup>2</sup>, Hiroshi SATO<sup>2</sup>, Takaya IWASAKI<sup>1</sup> (FREE, JAMSTEC, ERI, Univ. Tokyo)

Among subduction zones, the Nankai subduction zone off southwest Japan is known as one of the best-suited convergent plate margins for studying subduction zone earthquakes. Historic, large subduction thrust earthquakes have occurred with a recurrence interval of 100-200 years along the Nankai Trough. The last two large earthquakes that occurred off the Kii Peninsula were the 1944 Tonankai (M 8.1) and 1946 Nankai (M 8.3) events. Seismic imaging of deep structure is a very important seismological method and may help explain the mechanisms that control megathrust earthquake occurrence around the Nankai Seismogenic Zone. Results of seismic studies from 1997 to present include the presence of a subducting seamount that acted as the barrier in 1946 Nankai earthquake, an imaged splay fault which may have controlled the rupture process in 1944 Tonankai earthquake and cyclic ridge subduction in Tokai district. Remarkable results are summarized as follows. 1) Multichannel seismic (MCS) reflection profiles obtained in 2001 show splay faults in the rupture area of the 1944 Tonankai earthquake. This splay fault may have experienced slip during the 1944 Tonankai event. 2) In 2001, onshore-offshore wide-angle seismic data were acquired along a profile from the western edge of the Izu arc to the northern coast of central Japan crossing the Tokai district. Results from refraction tomography and pre-stack depth migration of the offshore wide-angle data reveals the structures are immediately outside of the rupture zone during the 1944 Tonankai earthquake; i.e. a cyclic ridge subduction in the non-rupture zone. The model shows the repeated crustal thickening with thickness of 13 - 20 km and wavelength of 35 - 50 km between the western edge of the Izu arc and the Tokai district. This structure is interpreted as the cyclic ridge subduction beneath the Tokai district. In recent seismic experiments, we have succeeded in imaging high resolution irregular characteristics of the subducting plate and coseismic slip zone such as a subducting seamount, subducting ridge, offshore splay faults and strong reflectors onshore. In analyses of historical earthquakes, the high energy asperities obtained around the subducting seamount area indicates that the seamount acts as a complementary asperity in the 1946 and 1707 megathrust earthquakes. These results suggest that irregular structure may control rupture asperities by acting as a rupture inhibitor or high slip zone during the megathrust earthquake cycle.

**SS03/08A/D-103** Poster **0830-262**

**CRUSTAL STRUCTURE OF THE MID-IZU-OGASAWARA ARC FROM WIDE-ANGLE SEISMIC DATA**

Kentaro KANEDA<sup>1</sup>, Azusa NISHIZAWA<sup>1</sup>, Tsuyoshi YOSHIDA<sup>1</sup>, Osamu YOKOO<sup>1</sup>, Shin TANI<sup>1</sup>, Ayako NAKANISHI<sup>1</sup>, Shuichi KODAIRA<sup>2</sup>, Narumi TAKAHASHI<sup>2</sup>, Wonn SOH<sup>2</sup>, Yoshiyuki KANEDA<sup>2</sup>, Kiyoshi SUYEHIRO<sup>2</sup> (Hydrographic and Oceanographic Department, Japan Coast Guard, Japan Marine Science and Technology Center)

A wide-angle seismic experiment was conducted as a joint operation between the Hydrographic and Oceanographic Department, Japan Coast Guard (HODJ) and the Japan Marine Science and Technology Center (JAMSTEC) in April-May, 2002, to construct a crustal structure model of the Izu-Ogasawara (Bonin) arc, which can be a clue to clarify the evolution process of the intra-oceanic island arc. The Izu-Ogasawara arc is located on the Philippine Sea plate along with the Izu-Ogasawara Trench, and shifts to the Mariana arc at its southern end. In this investigation, we deployed 25 ocean bottom seismographs (OBS) at 20-30 km of intervals along about 800 km track-line at 30-31°N from the Pacific Basin at its eastern end, through the Shichito-Iwojima Ridge and Kinan Escarpment, to the center of the Shikoku Basin at its western end, except for the Izu-Ogasawara Trench area exceeding 6000 m depth. The deployment and retrieval of OBSs were carried out by *S/V Shoyo*, HODJ. The seismic source is an array of eight, 1500 in<sup>3</sup> (24.6 l) air guns (12000 in<sup>3</sup> or 196.6 l, total) provided by *R/V Kairei* belonging to JAMSTEC, firing every 90 seconds with an approximate 200 m spacing. The data recorded by each OBS were of high quality and travel time data were modeled by the two-dimensional ray tracing. The acquired crustal model along the track-line shows several structural features. One of the features is a thick oceanic lower crust extending to ~50 km east from the Kinan Escarpment which forms a large vertical displacement of over 600 m in water depth on the Shikoku Basin. This structural model also reveals that the thickness of the Izu-Ogasawara island arc crust is up to 22 km and there exists a thick 7.0-7.2 km/s layer with thickness of > 5 km at the bottom of the crust. These characteristics resemble the result of the northern Izu-Ogasawara arc survey at 32°N (Suyehiro et al. 1996), though the water depth along the Izu-Ogasawara arc gradually becomes larger from north to south.

**SS03/08A/D-104** Poster **0830-263**

**ON SOME RESULTS OF THE MONITORING OF CRUSTAL STRAINS IN CENTRAL JAPAN**

Vladimir CHURIKOV<sup>1</sup>, Hiroshi ISHII<sup>1</sup>, Rimma KARMALEeva<sup>1</sup>, Yuri KUZMIN<sup>1</sup> (Institute of Physics of the Earth, Laboratory of Recent Geodynamic, Moscow, Russia, <sup>2</sup>University of Tokyo, Earthquake Research Institute, Japan)

Here, we discuss results of borehole extensometer measurements in two points in Tono, central Japan, during 1998-99. Borehole instruments settled on depth about 170 m where temperature variation is less than 0.001°. Country rocks are Toki granites. Between two points Tsukiyoshi reverse fault is extended with dip angle of about 60° to 70° to the south. Author of borehole instruments is Prof. Ishii, H., from Tokyo University. Obtained results are representative because there are high resolving ability of instruments and almost no breaks in measurements. There are important to use tide analyzing during estimation of the data representativeness. Comparison of observed wave parameters with calculated theoretical for each points allows us to reveal a peculiarity of regional tectonics, because magnitude of tidal amplitude is determined by elastic properties of country rocks. In case of activation of tectonic processes variation of tidal waves in time was observed (L.A. Latynina and R.M. Karmaleeva, 1981, R.M. Karmaleeva, 2000). Pertzev's method of tide analyzing with daily moving average was applied for the whole obtained data. Estimation of a see tide was not calculated because no co-tidal maps. However, its influence on amplitude of M2 (which are maximum) estimated less than 35% on the nearest to Tono stations. For next calculation we used main waves - M2 and O1, which ones have maximum amplitude on all azimuths. Magnitude of amplitude is almost the same accurate within 8-10%. In sub-meridional direction it is in 3.7 times (73%) less of theoretical value, in sub-latitudinal - in 1.2 times exceed. In intermediate azimuth difference between stations was observed. On south part of the fault amplitudes is in 1.6 times less, on north part - in 1.2 times exceed of theoretical value. Apparently, this difference we could explain by influence of system of wells for water pumping located at a distance 300 m in the same direction to south part of the fault (C.-Y. King et al., 1999). Since Tsukiyoshi fault is impermeable to water then the influence do not extend to the north part. Similar dependence observed for O1 too. Decreasing of tidal amplitude in sub-meridional direction is possible to explain by strain concentrations within faults system and geodynamic zones along rivers close to latitudinal extension, contiguous to Tono area. Observation points located between two geodynamic zones, which traceable along rivers on the distances of 8 and 3 km. Anomalous amplitude decreasing allow us to suppose that strain condition over observed area depends on a geodynamic activity this area. Some changes in spectrum of deformations were revealed during increasing of seismic activity that possible explain by changes of rheological properties of rocks. Investigations realized of many years on extensometer measurements and supersonic sounding, show changes of period of cycles in stressed-deformed conditions of country rocks in fissured areas (R.M. Karmaleeva and O.I. Silaeva, 2001).

**SS03/08A/D-105** Poster **0830-264**

**PHYSICAL PROPERTY ESTIMATE AT THE ASEISMIC PLATE BOUNDARY IN THE JAPAN TRENCH REGION BY THE SYNTHETIC SEISMOGRAM APPROACH USING THE FDM METHOD**

Peyman POOR MOGHADDAM<sup>1</sup>, Junzo KASAHARA<sup>1</sup>, Gou FUJIE<sup>2</sup>, Kimihiro MOCHIZUKI<sup>1</sup> (Department of Earth and Planetary Science, University of Tokyo, <sup>2</sup>Japan Marine Science and Technology Center, Japan)

In 1996, we conducted a seismic refraction-reflection experiment at the Japan Trench region to clarify the relationship between seismicity and crustal structure. A number of seismic reflection and refraction experiments using Ocean Bottom Seismometers (OBSs) have been conducted. Consequently, a velocity structure model was obtained by travel-time inversion (Fujie et al., 2002). Extremely important results were obtained showing a strong correlation between seismic activity and the P-P reflection intensity from the subduction plate boundary. Considering the accuracy of the travel time inversion, possible causes to generate intense reflections were investigated. One of possibilities is the presence of low Vp materials such as water, serpentinites or clay. To obtain more accurate estimate for the physical properties, we carried out the simulations using FDM method developed by Shawn Larsen (E3D code). It is 4th-order accuracy in space and 2nd-order accuracy in time. It is based on the elastodynamic formulation of the wave equation on a staggered grid. The absorbing boundary due to finite number of grids is also considered. The structure obtained by Fujie et al. (2002) has 140k m long and 30 km deep and is heterogeneous in horizontally and vertically. We added a thin low velocity layer to the above model. The thin layer has various parameters such as Vp= 2km/s - 4 km/s, Vp/Vs= 1.7 - 3.0, and layer thickness= 50m - 400m. Using these models, we computed the waveforms and wave field. The 5Hz and zero phases Ricker wavelet was used as source, and it is a reasonable approximation for control source used in the field experiment. We introduced appropriate Q structure. Spacing for space is 25m and time grid is 1.7msecond. In the field we used shots more than 4000 airguns and 100 explosives from the sea surface. Shot interval was 25m-50m. Due to limitation of computer resources, we computed 100m spacing traced and simulated the reciprocity of this model which we consider several receivers at the sea surface and one shot at the sea bottom (common source). The synthetic seismograms are compared by observed waveforms obtained by Fujie (1999). The current result shows that the layer with Vp=2km/s-3km/s or Vp=4km/s and Vp/Vs=3.0 can explain the observation of high P-P reflectivity. These materials are quite different from the Vp values surrounding the plate boundary at the depth of 13km from the ocean surface. As the low Vp velocity suggests weak frictional strength, this material can explain the aseismicity in the intense P-P reflection zones. Because the above simulation is limited in parameters, more extensive investigation is necessary.

**SS03/08A/D-106** Poster **0830-265**

**CRUSTAL STRUCTURES ASSOCIATED WITH ACCRETION AND COLLISION PROCESSES IN HOKKAIDO, JAPAN, FROM REINTERPRETATIONS ON RECENT SEISMIC EXPEDITIONS**

Takaya IWASAKI<sup>1</sup>, Tanio ITO<sup>2</sup>, Hiroshi SATO<sup>1</sup>, Takeo MORIYA<sup>3</sup>, Research Group of HOKKAIDO TRANSECT<sup>4</sup> (ERI, the University of Tokyo, <sup>2</sup>Chiba University, <sup>3</sup>Hokkaido University)

Seismic expeditions in the last decade undertaken in Hokkaido revealed detailed crustal structures associated with accretion and collision processes since the late Jurassic. The Hidaka collision zone, central part of the Hokkaido Island, Japan, is known as an ongoing collision zone between Kuril Forearc (KA) and the Northeast Japan Arc (NJA) since middle Miocene, and has been a main target area for the expeditions. This paper presents compilation of crustal structures in and around this collision zone from reinterpretation of the previous seismic data. The most remarkable feature beneath the collision zone is the crustal delamination of KA. According to a series of seismic reflection studies in the southernmost part of Hidaka Collision Zone, the crustal structure in KA is characterized by two distinct reflective zones. Namely, its upper 23 km part is obducted westward onto NJA, while its lower part is descending down, forming a wedge-like structure. Seismic reflection/refraction experiments in 1998-2000 revealed various scale structural heterogeneity across this

collision zone. The data obtained elucidated a complicated collision structure. In the eastern part of the profile, KA is covered with 0.3-4km thick highly deformed sedimentary layer, beneath which two eastward dipping reflectors are imaged in a depth range of 10-20 km, probably representing obducting a middle or lower crust of KA. Beneath these reflectors, another flat and westward dipping reflectors are situated at 25 and 25-27 km depths respectively. The obtained layer geometry also forms wedge-like (crocodile) patterns, indicating that the crust of KA is delaminated into two or three segments beneath the Hidaka Mountains. The crustal image obtained is much complicated as compared with that in the southernmost part of the collision zone mentioned above, showing a significant regional difference in collision style. The seismic data from 1999-2000 experiments mapped a very thick (more than 5-10 km) sedimentary package including two or more velocity reversals in a fold-and-thrust belt west of the Hidaka Collision Zone. Beneath this package, the crystalline crust of NJA is traced with a slight eastward dip down to 20-25 km. Such a velocity reversal may widely spread because other seismic profiles undertaken in 1984 and 1992 show a significant travel-time jump west of the collision zone, strongly indicating the existence of a low velocity zone at depth. If such a velocity reversal corresponds to the shallow part of previous NJA, our result gives an important constraint not only on the crustal shortening ratio of the NJA but the convergence rate of the Okhotsk (or North America) and Eurasian (or Amurian) plates.

**SS03/08A/D-107** Poster **0830-266**

**SEGMENTATION OF THE CRUST INFERRED FROM SEISMIC REFLECTION PROFILES IN THE FOREARC REGION OF THE JAPAN TRENCH OFF AOMORI**

Tetsuro TSURU<sup>1</sup>, Jin-Oh PARK<sup>2</sup>, Seiichi MIURA<sup>1</sup>, Yukari KIDO<sup>1</sup>, Yoshiyuki KANEDA<sup>1</sup> (<sup>1</sup>Center for Data and Sample Analyses, Institute for Frontier Research on Earth Evolution, <sup>2</sup>Research Program for Plate Dynamics, Institute for Frontier Research on Earth Evolution)

Seismic reflection character provides geophysical and geological information about subsurface structures, and is extremely useful for structural interpretation. JAMSTEC has been conducting multi-channel seismic (MCS) reflection experiments in the Japan Trench region since 1996, in order to clarify the detailed tectonic structures near the plate boundary. In April-July 2000, an MCS survey was conducted off Aomori, the northernmost part of the Japan Trench, using a total of 12000 cu. in. airgun array, and a digital streamer cable with 156 channels. Seismic records of 13.5 seconds were obtained using 50 m shot spacing and 25 m group intervals. The maximum source-receiver offset distance was 4100 m. The field data obtained were processed using trace-editing, multiple suppression, deconvolution, and filtering, to enhance the signal-to-noise ratio, at Center for Data and Sample Analyses of IFREE/JAMSTEC. This processing also increased the resolution of the data. Even after applying the deconvolution, air-bubble oscillations still appear on the record sections, approximately 200 ms below the primary reflection, because the air-gun array was not tuned. Previous studies revealed a wedge-shaped sedimentary unit with relatively low velocities (2-3 km/s P-wave velocities) at the seaward end of the continental plate [e.g., von Huene et al., 1994; Tsuru et al., 2000]. This sedimentary unit is demarcated from the more rigid continental framework, characterized by 4-6 km/s P-wave velocities, by the buttress [von Huene et al., 1994] or the backstop interface [Tsuru et al., 2000]. The prominent maker horizon in the island arc crust, representing the unconformity separating the Cretaceous basement from the Neogene rocks above [Nasu et al., 1980], terminates at the backstop interface. The wedge-shaped unit is distributed parallel to the trench in the forearc region of the northern Japan Trench, and reaches a maximum width off Sanriku, in the central part of the northern Japan Trench. The width distribution is concordant with the relief of horst-graben structures developed at the outer slope, except off Aomori, where the unit is as wide as off Sanriku even though little relief is developed. Here, the backstop interface no longer terminates the unconformity. Remarkable differences in the seismic reflection character can be observed between the rigid continental framework and the sedimentary unit. Its boundary can be traced along some MCS lines, revealing an NNW-SSE strike. Furthermore, the unconformity shows a gap in the depth of the boundary on some profiles, suggesting some fault activity and/or segmentation of the crust. Crustal segmentation may cause changes in the coupling at the plate boundary around the boundary. Interestingly, two large interplate earthquakes of greater than M7.5 occurred at locations just landward from the boundary. In this paper, we will demonstrate the differences in seismic character in the MCS profiles, and discuss the kinds of tectonic features that are reflected.

**SS03/08A/D-108** Poster **0830-267**

**THREE-DIMENSIONAL ATTENTION STRUCTURE BENEATH THE JAPAN ISLANDS DERIVED FROM NIED HI-NET DATA**

Shutaro SEKINE, Makoto MATSUBARA, Kazushige OBARA, Keiji KASAHARA (NIED)

The attenuation structure beneath the Japan Islands should hold 3-D complexities similar to those in the velocity structure. For example, we often observe abnormal distributions of ground motion amplitudes, which are very different from a circular distribution. Seismic attenuation implies inelasticity or scattering in the Earth's materials, while seismic velocities imply their elastic properties. We can assume high attenuation under the volcanic fronts, and low attenuation along the subducting Philippine Sea plate similarly to the velocity structure. However, this similarity is not always expected in other parts of the Japan Islands. Information on the seismic attenuation is also important for the simulation of strong ground motions. National Research Institute for Earth Science and Disaster Prevention (NIED) has observed at Hi-net stations distributed in the whole Japan Islands. In this study, the vertical components of ground velocity amplitudes reported from August 2000 to September 2002 will be used. The seismic attenuation will be represented with the indexes called Qp and Qs, and their 3-D structure will be obtained for frequency bands between 1 Hz and 10 Hz. Amplitudes from 3835 earthquakes are used for tomography. The number of stations where amplitudes were observed is 664. There are three characteristic results in this study. First of all, clear low-Q zones can be found beneath the volcanic front in the northeastern Japan, and the distinct high-Q is recovered in the east of the front. This high-Q area coincides with the strata of 100 Ma or older. Low-Q zones appear just below volcanoes in the upper and lower crust, while the low-Q area extends continuously along the volcanic front at a depth of 40 km. The Qp distribution shows similar tendencies zone, but the averaged Qp in the crust is significantly lower than the averaged Qs, so that corresponding low-Qp zones are not obvious. The tendencies can also be found along the volcanic front related to the subduction of the Philippine Sea plate. Secondly, a distinct low-Qp area is found at a depth of 65 km in the Chubu region, central Japan. However, no low-Qs zone can be found in the area. This may imply a different attenuation process from that under the volcanic front in the northeastern Japan. Thirdly, the high-Q area is found along the upper boundary of the Philippine Sea slab, which is determined from seismicity in the southwestern Japan. This area is more distinct in the Qp distribution with an average of 1000 than in the Qs distribution. In the Shikoku region, the low-Qp area does not extend beyond latitude of 34.2°N, and the area looks falling down into deeper part. On the other hand, in the Kyushu region, the low-Qp area reaches a depth of 100 km or larger coinciding with the slab boundary determined by the seismicity.

**SS03/08A/D-109** Poster **0830-268**

**STRUCTURAL CHARACTERISTICS CONTROLLING THE SEISMICITY AROUND THE JAPAN TRENCH INFERRED FROM WIDE-ANGLE SEISMIC DATA OFF MIYAGI FORE ARC REGION**

Seiichi MIURA<sup>1</sup>, Narumi TAKAHASHI<sup>1</sup>, Tetsuro TSURU<sup>1</sup>, Aki ITO<sup>1</sup>, Shuichi KODAIRA<sup>1</sup>, Ayako NAKANISHI<sup>1</sup>, Yoshiyuki KANEDA<sup>1</sup> (<sup>1</sup>IFREE, JAMSTEC, <sup>2</sup>Deep Sea Research Department, JAMSTEC)

The Japan Trench is a subduction zone locating east of NE Japan. The seismicity is not a uniform pattern but a regional variation along the Japan Trench. Many large earthquakes occurred in the northern part off Sanriku and Miyagi regions, whereas few large earthquakes occurred in the southern part, off Fukushima. To investigate the detailed subduction zone structure and to understand the regional variation of seismicity, intensive seismic surveys have been conducted by Japan Marine Science and Technology Center (JAMSTEC) since 1996. In 1999, a seismic experiment was conducted off Miyagi using 36 ocean bottom seismographs (OBS) and a 12000 cu. in. airgun array on R/V Kaiyo of JAMSTEC. The objectives of this paper are to investigate the seismic structure off Miyagi fore arc region, and compare the relation between the structure and seismic activity with those of other regions of Japan Trench. Island arc crust off Miyagi consists of four layers: Tertiary sedimentary Layer (Vp=2 km/s), Cretaceous layer (4-5km/s), island arc upper (6km/s) and lower crusts (6.6-6.8km/s) with the thicknesses of 2 km, 5-7 km, 7 km and 10 km, respectively. The depth of Moho is 21km at 115km from the trench axis (TA) and becomes deeper landward. P-wave velocity of mantle wedge is 7.9 km/s. Subducting oceanic crust consists of two layers: oceanic layer2 (5.2-5.7km/s) and layer3 (6.5-6.7 km/s). Dip angle of oceanic crust between 0-80 km, 80-115 km, 115-150 km and 150-220 km from the TA is 5-6 degree, 8-10 degree, 12 degree and 23 degree, respectively. P-wave velocity of uppermost mantle of oceanic plate is 7.7 km/s, which is meaningfully lower than that of more eastern region (e.g. Shimamura et al., 1983). The structure off Miyagi has common characteristics with that off Sanriku (e.g. Takahashi et al., 2002): 1) layer composition; 2) thickness of island arc crust; 3) P-wave velocity of mantle wedge; 4) dip angle of oceanic crust; and 5) low P-wave velocity oceanic uppermost mantle. The structure off Miyagi, however, is different from that off Fukushima (e.g. Miura et al., 2002), especially P-wave velocity of mantle wedge, dip angle of oceanic crust and the existence of thick interplate layer off Fukushima. Despite of the similar structure off Miyagi with that off Sanriku, seismicity pattern are different. Large earthquake (M > 7) occurred near the trench axis off Sanriku, for example the 1896 and 1933 earthquakes. However off Miyagi, the 1938 and 1978 earthquakes occurred near the coastline. One possible explanation of the difference of seismicity pattern is characteristics of oceanic plate, such as horst and graben structure development, which may be associated with the crack of oceanic plate.

**SS03/08A/D-110** Poster **0830-269**

**SEISMIC REFLECTION PROFILING BETWEEN TSUKUBA CITY AND THE TOKYO BAY, CENTRAL JAPAN**

Kazuo YAMAGUCHI<sup>1</sup>, Naomi KANO<sup>1</sup>, Takanobu YOKOKURA<sup>1</sup>, Akiko TANAKA<sup>1</sup>, Toshiaki OHTAKI<sup>1</sup>, Shinobu ITO<sup>2</sup>, Toshiyuki YOKOTA<sup>2</sup>, Hajime KATO<sup>3</sup> (<sup>1</sup>Institute of Geoscience, Geological Survey of Japan, AIST, <sup>2</sup>Institute for Geo-Resource and Environment, Geological Survey of Japan, AIST, <sup>3</sup>Faculty of Education & Human Sciences, Yamanashi University)

Deep ground structure down to the basement affects the strong ground motions generated by earthquakes. This had been known before the 1995 Hyogo-ken Nanbu earthquake, but it is after the earthquake that underground surveys have been made in densely populated plains especially for the purpose of earthquake hazard mitigation in Japan. The seismic reflection survey is the main method among them. Chiba Prefecture conducted seismic reflection surveys for this purpose between the Tokyo bay and the Tone river, adjacent to the Tokyo metropolitan area, during 1997 and 2000. We have recently completed 24 kilometers long seismic surveys between the Tone river and Tsukuba city, which correspond to a northward extension of Chiba surveys. Our seismic section reveals basement uplift 200 meters in height which has been observed as a high Bouguer anomaly at Yatabe area. The basement top deepens southward and shows some undulations about 500 meters wide and 100 meters high. The upper sediments fill the undulations and slightly tilt southward. Several kilometers to the south of Yatabe, a dyke was inferred on the basis of magnetic data modeling. Some researchers think that the Median Tectonic Line passes between Yatabe and the inferred dyke. There exists a small gap less than 200 meters high along the basement top in the seismic section, but reflectors are not imaged beneath the basement. Taking a broader view of survey lines, our data may be connected to Chiba data in spite of 2 kilometers gap and differences of survey parameters between them. Then we will get a N-S direction seismic line 60 kilometers long between Tsukuba city and the Tokyo bay and it must cross the Median Tectonic Line somewhere on the way. We will discuss the pre-Tertiary basement structure and its movement around the seismic survey lines.

**SS03/08A/D-111** Poster **0830-270**

**THREE-DIMENSIONAL VELOCITY STRUCTURE OF THE PINGTUNG AREA**

Li-Chuin HU<sup>1</sup>, Cheng-Hong LIN<sup>2</sup>, Horng-Yuan YEN<sup>1</sup>, Chau-Huei CHEN<sup>3</sup> (<sup>1</sup>Institute of Geophysics, National Central University, Taiwan, <sup>2</sup>Institute of Earth Sciences, Academia Sinica, Taiwan, <sup>3</sup>Institute of Seismology, National Chung Cheng University, Taiwan)

The Chaochou fault in the Pingtung area is one of the most important faults in southern Taiwan, and is located between the Pingtung Plain and the Central Range. According to previous studies, the Chaochou fault is considered to be a high-angle fault that dips eastward to the Central Range. From a tectonic point of view, regional stresses in the Pingtung area are controlled by two tectonic forces. The first force is the compressional stress related to the arc-continent collision between the Philippine Sea Plate and the Eurasian Plate; the second is the extensional stress related to the opening of the South China Sea to the South. Under these two mechanisms, the crustal structure beneath the Pingtung area has a complex formation. However, in examining earthquakes greater than magnitude 3 that occurred in the years between 1991 and 2001, we discover that the seismicity in southwestern Taiwan in this period was low. The question as to why this is the case is what first inspired our interest in studying this particular area. This study makes use of data collected by the Institute of Earth Sciences, Academia Sinica between August 2001 and January 2002 at 24 temporary seismic stations located near the Chaochou fault, as well as velocity structures collected through tomography in the foothills of the Pingtung area. We hope that this study will teach us more about crustal structure of this area and will enable us to understand the reasons for low seismicity there.

**SS03/08A/D-112** Poster **0830-271**

**TWO-DIMENSIONAL DENSITY STRUCTURES OF THE SHIEN-SHE PLATFORM**

Hsien-Hsiang HSIEH<sup>1</sup>, Horng-Yuan YEN<sup>1</sup>, Ming-Tar LU<sup>2</sup>, Chien-Ying WANG<sup>1</sup> (<sup>1</sup>Institute of Geophysics, National Central University, Taiwan, ROC, <sup>2</sup>Chinese Petroleum Corporation, Taowan,

ROC)

The Chelungpu fault cut through the western side of the Shien-She platform, curved toward the northeast, and splintered into complex branches. Thus, the platform plays the important role in this region. In this study, we have compiled the gravity data (roughly 18 km x 48 km) of the Shien-She platform and its surrounding area. After gravity reductions, the Bouguer anomaly map was constructed. Negative anomalies cover the whole area. The general trend of the Bouguer values decreases from west to east, in consonance with the geological background. The residual anomaly is obtained by using Griffin method to investigate the shallower structure. We also calculate the derivative anomaly map to analyze some high frequency signal of the Shien-She platform. To illustrate how the gravity data constrain subsurface density structures, a two-dimensional gravity analysis is performed with three gravity profiles across the geological strike taken from the Bouguer anomaly map. Preliminary results of the modeling and their geological significance will be presented.

**SS03/08A/D-113** Poster **0830-272**

**SEISMIC ANISOTROPY IN THE FOCAL REGION OF THE 2000 TOTTORI-KEN SEIBU EARTHQUAKE**

Takeshi NAKAMURA<sup>1</sup>, Hiroshi TAKENAKA<sup>1</sup>, Sadaomi SUZUKI<sup>1</sup>, Yasuto KUWAHARA<sup>2</sup> (<sup>1</sup>Department of Earth and Planetary Sciences, Faculty of Sciences, Kyushu University, <sup>2</sup>Earthquake Process Research Group, Institute of Geoscience, National Institute of Advanced Industrial Science and Technology)

Seismic anisotropy, varying velocity with the propagation direction, have developed our understandings for heterogeneous structure, the nature of mineral, and the physical properties around faults. Anisotropy is an inherent feature in the Earth, and the distortion of seismograms and travel time differences due to anisotropy have been reported in many observations. For *S*-waves, a pulse propagating through an anisotropic medium splits into two orthogonally polarized pulses with different propagation speeds each other. This phenomenon is known as *S*-wave splitting. The analysis of *S*-wave splitting is one of approaches to investigate anisotropy along the ray path. In this study, we carry out *S*-wave splitting analysis for the seismograms recorded in and around the focal area of the 2000 Tottori-ken Seibu earthquake. The aftershock data we used was recorded in 2000 and 2002. The 2000 observation was carried out at 3 stations for 56 days using strong motion seismographs, and the 2002 observation was at 5 stations and one seismic array for 13days. We employ the cross-correlation method to measure the parameters of the *S*-wave splitting from these aftershock data: the polarized direction of the fast *S*-wave and the delay time between the splitted *S*-waves. The polarized directions measured is WNW-ESE, which is almost identical with the *P*-axis direction of the main shock expected from the focal mechanism. This suggests that this anisotropy may be due to the alignment of cracks induced by the regional stress field in the focal region. The delay time of the *S*-wave splitting ranges from 20 to 100 ms. By applying Hudson's (1981) formula for fluid-filled cracks to the delay time, we estimate the crack density. For the 2000 observation data, we found that the value of the crack density shows a strong spatial variation which depends on the fraction of propagation path inside and outside the focal region. It suggests that the crack densities are different between inside and outside of the focal region. We estimated the mean value of the crack densities inside the focal area and outside one, and obtained that they are 0.02 and 0.004, respectively. To evaluate the crack density inside the focal area in more detail, we analyzed the 2002 observation seismograms of which most of rays are propagating through inside the focal region. Although no obvious dependent on spatial distribution are seen inside the focal area, the value of crack density is 0.01, which is still significant large compared with outside one observed in 2000. These results indicate that the main shock and aftershock activity region corresponds with the high anisotropic region near the fault.

**SS03/08A/D-114** Poster **0830-273**

**TOMOGRAPHY OF P WAVE VELOCITY STRUCTURE IN THE AFTERSHOCK AREA OF THE 1993 OFF NORTHWEST HOKKAIDO EARTHQUAKE (M7.8)**

Tetsuo TAKANAMI<sup>1</sup>, Yoshio MURAI<sup>1</sup>, Hajime SHIOBARA<sup>2</sup>, Shuichi KODAIRA<sup>1</sup>, Hideki SHIMAMURA<sup>1</sup>, Ryo HINO<sup>3</sup>, Toshihiko KANAZAWA<sup>2</sup>, Kiyoshi SUYEHIRO<sup>4</sup>, Masanao SHINOHARA<sup>2</sup>, Toshinori SATO<sup>5</sup>, Hiroaki NEGISHI<sup>1</sup> (<sup>1</sup>Institute of Seismology and Volcanology, Hokkaido University, <sup>2</sup>Earthquake Research Institute, The University of Tokyo, <sup>3</sup>Institute of Frontier Research on Earth Evolution, Japan Marine Science and Technology Center, <sup>4</sup>Research Center for Prediction of Earthquakes and Volcanic Eruptions, Tohoku University, <sup>5</sup>Deep Sea Research Department, Japan Marine Science and Technology Center, <sup>6</sup>Faculty of Science, Nishi Chiba Campus, Chiba University, <sup>7</sup>National Research Institute for Earth Science and Disaster Prevention)

The 1993 off northwest Hokkaido earthquake (Hokkaido Nansei Oki Jishin in Japanese) with a magnitude of 7.8 ruptured the entire seismogenic zone in the eastern margin of the Sea of Japan. The event is considered to occur in the plate boundary between the Eurasian and the North American (or the Okhotsk) plates. In recent 30 years, the 1964 off Niigata earthquake (M7.5), the 1983 off Akita earthquake (M7.7), and the 1993 off northwest Hokkaido earthquake have successively occurred along the plate boundary. It is very important to know the present situation of the boundary in terms of large earthquake prediction. In order to determine the accurate locations of aftershocks of the 1993 off northwest Hokkaido earthquake, 23 Ocean Bottom Seismographs (OBSs) were deployed about one week later. The depths of aftershocks calculated by the data from OBSs range within 10km ~ 20km. But the aftershocks decrease rapidly in the depth of 20km and over. The picking data of the aftershocks at OBSs gave us opportunity to image the three-dimensional P wave tomography in the seismogenic zone existing in 10km ~ 20km deep. Here, tomographic inversion method was applied to 6510 P arrival data from the 1031 events occurred in seismogenic zone. The result shows that the strong lateral heterogeneities exist in the aftershock region. Furthermore, it gave us a close relationship between seismic activity and low velocity anomaly. The strong low velocity regions exist in both of particularly high seismicity areas in the northern and southern seismogenic zone. While, the main earthquake is considered to occur near the southern boundary of the northern low velocity area. The problem that we have to consider here is what would control the occurrence of aftershocks. The most important point is to know how such a low velocity area is related to the seismogenic zone. If the chemical and mechanical processes such as dehydration and fluid flow have contributed to the occurrence of aftershocks as appointed by Zhao et al.(2002), the generation of aftershocks is not a pure mechanical process, but it closely related to physical and chemical properties of materials in the crust and upper mantle, such as fluids, magma, etc. The zone rich in such a volatile component should be easily ruptured and the aftershocks must occur according to the volume of such materials in the crust and upper mantle. Along the plate boundary, some complex physical and chemical reactions may take place, causing heterogeneities in the material property and stress field, which can be detected with seismic tomography and other geophysical methods. Therefore, we must draw attention to the properties of materials in the seismogenic zone in the plate boundary. A further direction of this study will be provide more evidence for this result.

**SS03/08A/D-115** Poster **0830-274**

**THE SHAPE OF THE PHILIPPINE SEA PLATE BENEATH THE CENTRAL JAPAN**

Shoji SEKIGUCHI (National Research Institute for Earth Science and Disaster Prevention)

We obtained the three-dimensional seismic velocity structure of the uppermost mantle beneath the Kanto, Tokai and Chubu regions, central Japan, where the Philippine Sea plate descends, by means of travel time tomography using 18 years of P and S phase data recorded by a regional seismic network of micro-earthquake. This region is tectonically complex, because the Pacific plate descends to the northwest and the Philippine Sea plate also descends to the north overriding the Pacific plate at the eastern edge. Because of complex earthquake distribution and the focal mechanisms, some models of the subducting Philippine Sea plate were proposed. We used about 727,000 manually picked travel time data of about 9,500 events to obtain fine seismic velocity structure of this region. Dividing the area into about 5km blocks and picking one event of the largest observed station numbers in each blocks for each year, we selected the events. The travel time data with picking time error larger than one second were omitted. There were about 120 seismic observation stations. We calculated seismic rays by the pseudo-bending method. Shape functions of the Finite Element Method are used to describe the velocity structure. The velocity is interpolated by the values given to 8 grid points of a simple three dimensional rectangular element. Solving matrix equations by the LSQR method, P and S velocity structures and event origin times and locations were determined, simultaneously. Initial velocity model was NIED (National Research Institute for Earth Science and Disaster Prevention) model used routinely to determine hypocenter locations in this area. A distinct low velocity zone, which was the oceanic crust of the descending Philippine Sea plate, was found beneath the Kanto region. The low velocity zone revealed a new configuration of the Philippine Sea plate different from any models obtained through the analysis of hypocenter distribution and focal mechanisms. There was another low velocity area beneath the active volcanoes. We also found a high velocity area in the deep aseismic region below the volcanic front between the Kanto and Chubu regions. It extends to the Philippine Sea plate in both regions. It was likely to be an aseismic extended section of the Philippine Sea plate. High Poisson's ratio areas were found both beneath the volcanoes and in the low velocity zone of the Philippine Sea plate near the volcanic front under the Kanto region. We also calculated the checkerboard resolution checkAto estimate the resolution of the obtained inversion results.

**SS03/08A/D-116** Poster **0830-275**

**READING THE CURRENT TREND OF CRUSTAL DEFORMATION FROM ACCELERATION FIELD USING GPS DATA**

Yuzo TOYA, Minoru KASAHARA (Institute of Seismology and Volcanology, Hokkaido University, Japan)

Local and regional scale crustal movements in the intraplate Japan were investigated using both velocity and acceleration vector fields derived from continuous GPS Network data of GEONET (GPS Earth Observation Network), maintained by the Geographical Survey Institute of Japan. There are about a thousand stations, approx. 25km apart from each, covering the Japanese Islands. The GPS data used here are rates of horizontal and vertical station position changes during the period from June 25, 1997 to October 31, 2002. We fit first- and second-order polynomials to each time-series, with annual, semi-annual seasonality, and major steps removed, and other irregularities avoided based on the goodness of fit of our approximations, thereby obtaining the commonly used velocity-term and the acceleration-term. Acceleration can be described as a vector comparable to velocity, so we simply depict their spatial distribution in the vector-field format. Mapping acceleration fields of crustal deformation in Japan revealed some coherent trends of local and regional deformation and their rate changes such as (1) concentric (subsiding- / uplifting-) trends associated with recent volcanic activities (e.g. Unzen, Sakurajima), (2) trends of crustal movement associated with recent slow earthquakes (e.g. deceleration of the 1997 Bungo Channel Slow Earthquake, and more recent development of possibly another Bungo Channel slow event; Tokai, Off-Choshi, and Boso-Penn. slow earthquakes), or much gradual and larger scale buildup of forces against nearby plate interfaces, (3) back-slip trends of the overriding plate on a subducting plate (e.g. Tokai, Tohoku Region), (4) trends of local crustal block movements (e.g. East of Abashiri Tectonic Line), (5) rather weak trends of pre- and post- seismic deformations (e.g., the 2000 Western Tottori earthquake and 2001 Geiyo earthquake). Acceleration presumably arises from cumulative effects of various short-lived geodynamic processes, where it is also influenced by other factors such as mechanical strength (cf. density, heterogeneity, etc.) of crustal materials, and their distributions. In addition, we illustrated the distribution of strain-rate components by utilizing spatially smoothed velocity fields (smoothed with a median window of R=50km for robust sampling; grid spacing 0.15deg). They effectively highlighted some of the known tectonic features. Most notably, near-parallel banded distributions of maximum shear-strain and shortening were observed (both are generally curving up to NE, connecting some of the known tectonic lines) (data: 6/25/97-10/5/00), and one of the bands matched well with the recently discovered low-frequency tremor distribution of western Japan. For the subsequent time-interval (data: 10/6/00-10/31/02), additional set of prominent bands with SSW-NNE orientation is starting to emerge (one of which is from the inland extension of the Suruga-Trough), while the NE-trended bands from the previous time-interval became discontinuous. By comparisons of the results, we speculate that the changes in strain-rate are due to shifts in the regional stress field generated by irregular intermediate-term subduction processes.

**SS03/08A/D-117** Poster **0830-276**

**ALTIMETER CALIBRATION USING A RUGGEDIZED GPS-BUOY**

Matthias FORBERG, Tilo SCHOENE, Roman GALAS, Christoph REIGBER (GeoForschungsZentrum Potsdam (GFZ), Germany)

With the launch of ENVISAT and JASON-1 the successful series of the radar altimetry missions is extended to a second decade. Various analyses have shown that any altimetry mission is subject to performance degradation, like aging of electronic components, resulting in an apparent sea level rise. Comparisons of RA with in situ measurements of the instantaneous sea level e.g. at Harvest Oil Platform have been used to monitor the absolute sea level measurements of TOPEX/Poseidon, but not for other missions. However, only a combination of different missions gives a sufficient coverage in time and space. For the past and current missions different strategies are used for the calibration and the drift monitoring, e.g. using crossovers or tide gauges as a height reference. The disadvantage of all calibration methods is, that no direct measurement beneath the sub-satellite tracks are available for all missions and, therefore, models have to be used to account for e.g. the sea surface slope or time varying signals. As shown for ERS-1 and TOPEX/Poseidon, a GPS-equipped buoy, anchored beneath a sub-track, can be used as a height reference. Since GPS-derived coordinates are ITRF-referenced, an absolute calibration is possible. In the context of the Helmholtz Association's strategic project SEAL (Sea Level Change: An Integrated Approach to its Quantification) the GFZ Potsdam has developed a ruggedized offshore GPS-buoy which is able to measure the instantaneous sea level with high accuracy. In May 2002 the buoy has been deployed at an intersection point where the actual RA

missions TOPEX, JASON-1, ERS-2, ENVISAT, and GFO-1 intersect. The position is the only point in the German Bight that allows data transmission to a land station via an HF radio link. During the first deployment period till August 2002 in total 26 satellite passes have been acquired. Each data set comprises one hour of multi-sensor measurements centered at the satellite pass time. Differential GPS data is collected at 10Hz sampling rate both on the buoy and a reference station. Tilt angles as well as 3-axis accelerations are monitored by a dynamic motion sensor. Thus, together with the dipping depth which is collected by an underwater pressure sensor, the GPS antenna height can be reduced to the instantaneous sea surface height for every single GPS measurement. Additionally several meteorological sensors provide data every 10 minutes (e.g. air and water temperature, air pressure, wind direction and speed) and three moored tide gauge sensors in the vicinity and a wave tide recorder beneath the GPS-buoy allow to account for the sea surface slope and significant wave height, respectively. The resulting series of coincident measurements is used to derive a range bias for each RA, the envisaged long-term deployment will allow the monitoring of all missions. Additional information on: <http://op.gfz-potsdam.de/seal/>

**SS03/08A/D-118** Poster **0830-277**

**SEISMIC STRUCTURE OF THE CRUST AND UPPERMOST MANTLE IN THE INCIPENT STAGE OF BACK-ARC RIFTING -NORTHERNMOST OKINAWA TROUGH**

Kazuo NAKAHIGASHI<sup>1</sup>, Masanao SHINOHARA<sup>1</sup>, Sadaomi SUZUKI<sup>2</sup>, Ryota HINO<sup>3</sup>, Hajime SHIOBARA<sup>4</sup>, Hiroshi TAKENAKA<sup>5</sup>, Minoru NISHINO<sup>6</sup>, Takeshi SATO<sup>7</sup>, Toshihiko KANAZAWA<sup>8</sup> (<sup>1</sup>Earthquake Res. Inst., Univ. of Tokyo, <sup>2</sup>Kyushu Univ., <sup>3</sup>RCEV, Tohoku Univ., <sup>4</sup>JAMSTEC

The Okinawa Trough is placed between the Ryukyu Island arc and the China mainland as the back-arc region of the Ryukyu arc. From the previous geophysical and geological studies, the Okinawa Trough is considered to be in an early stage of back-arc spreading. Many seismic experiments have been performed in the Okinawa Trough region, however there is no deep seismic survey using Ocean Bottom Seismometers (OBSs) in the northernmost part of the Okinawa Trough. It is important for understanding tectonics of back-arc spreading to obtain a seismic structure beneath the area of East China, west of Kyushu, which is considered as the northernmost part of the Okinawa Trough. A seismic survey with OBSs was carried out in west of Kyushu in fall of 1999. The profile is 300 km long and 20 OBS were deployed at an interval of 15 km. We used airguns and explosives as controlled sources. On the distance-time sections of OBSs, apparent velocities of first arrivals vary due to the heterogeneities. Seismic velocity models for the shallow structure beneath each of the OBS locations are derived by a tau-p inversion using the individual OBS record. Next, a deep structure beneath the profile is estimated by a forward modeling using a two-dimensional ray tracing. Outcrops of the acoustic basement through the sedimentary layers are seen in the obtained structures. Velocities of lower layer in upper crust are varying laterally from 5.7 to 6.2 km/s and thickness of 6.0-km/s layer ranges from 3 to 9 km. The lower crust has uniform thickness of about 15 km. The Pn velocity is 7.7-7.8 km/s and the total crustal thickness is about 25km including sedimentary layers. The distribution of P-wave velocities and the thickness indicate that the crust in the northernmost part of the Okinawa Trough is more similar to that of an island arc than that of an ocean or a continent; however, in detail, the structure has characteristics, which are not usually seen in typical island arcs. Particularly, the upper crust in the study area has a large heterogeneity, which can be explained as a result of crustal thinning. These features are considered to result from thinning of the upper crust due to stretching in an early stage of rifting. In addition, low Pn velocities and the outcrops of the acoustic basement suggest igneous activities in this area. The seismic structure suggests that the northernmost Okinawa Trough is in an incipient stage of back-arc rifting.

**SS03/08A/D-119** Poster **0830-278**

**A POSSIBLE ORIGIN OF ASYMMETRIC EXTENSION ASSOCIATED WITH REACTIVATION OF RIFTING**

Tadashi YAMASAKI (Earthquake Research Institute, University of Tokyo)

Thermal relaxation in postrift phase may be important for localized rheological weakening developed by grain-size reduction as a result of spinel- to plagioclase-lherzolite reaction. Although dry conditions are more favorable for localized rheological weakening than wet conditions (Yamasaki, 2002), the mechanical lithosphere strength under dry condition is more than the magnitude of extensional driving forces in the range of a few TN/m (e.g., Bott, 1991; 1982; Bott et al., 1989), which prevents the lithospheric extension and thinning. On the other hand, for the temperatures more than 800 °C, the ductile yield stress under wet condition becomes to be mostly insensitive to grain-size, and the lower boundary for the localized weak zone diminishes. Because the reaction temperature is mostly greater than 800 °C, it is difficult to create the localized weak zone under wet conditions. Thus the thermal diffusion during inter-rifting period is required for an apparent strength contrast of localized weak zone through the reduction of geothermal gradient. During earlier rifting event grain-size reduction takes place significantly by spinel- to plagioclase-lherzolite reaction, and then the following extensional event occurs after the critical thermal relaxation time, 10 Ma for dry condition and 20 Ma for wet condition. If these two conditions are satisfied the lithosphere may be extended asymmetrically.

**SS03/08A/D-120** Poster **0830-279**

**SEISMIC STRUCTURE OF THE MIDDLE JAPAN TRENCH SUBDUCTION ZONE BY AIRGUN-OBS EXPERIMENT**

Ryota HINO<sup>1</sup>, Minoru NISHINO<sup>2</sup>, Kimihiro MOCHIZUKI<sup>3</sup>, Kenji UEHIRA<sup>4</sup>, Toshinori SATO<sup>5</sup>, Mikako NAKAMURA<sup>6</sup>, Shunichi NAKATA<sup>7</sup>, Atsushi SATO<sup>8</sup>, Masanao SHINOHARA<sup>9</sup>, Junzo KASAHARA<sup>10</sup> (<sup>1</sup>Graduate School of Science, Tohoku University, <sup>2</sup>Earthquake Research Institute, University of Tokyo, <sup>3</sup>Graduate School of Science, Kyushu University, <sup>4</sup>Faculty of Science, Chiba University)

In the middle part of the Japan Trench subduction zone, the off-Miyagi area, large interplate earthquakes with  $M > 7$  is known to regularly recur with about 40 years interval. The most recent event occurred 25 years ago (the 1978 Miyagi-Oki Earthquake M7.4) and the Japanese government evaluated that the next large earthquake may occur within 20 years from now with over 80 % possibility. Most of the past large events in this area, including the 1978 earthquake, did not rupture the shallow (less than 20 km) part of the plate interface, although active background microseismicity is observed in the shallow thrust zone. Analyses of the historical records of the tsunami caused by the 1793 earthquake, one of the off-Miyagi series, suggest that the rupture area of the earthquake extended to the shallow part of the thrust zone and that the size of the event was much larger ( $M > 8$ ) than the other earthquakes in the series. In the northern part of the Japan Trench subduction zone, we recently found a significant relation between the seismic reflection intensity of the surface of the subducting oceanic plate and the interplate seismicity along the interface; the wide-angle reflection arrivals are observed with remarkably strong amplitudes in the region of low interplate seismicity. This finding suggests that the appearances of the seismic reflections from subduction plate boundary can be a good indicator of the seismic coupling strength. As an application of this idea to the shallow seismogenic zone of the off-Miyagi region, we made

an airgun-OBS seismic experiment to observe the wide-angle reflections arrivals from the plate boundary in 2002. The surveyed area was in the trenchward extension of the rupture area of the 1978 earthquake and its size was 150 x 40 km in the strike and dip directions of the trench system, respectively. 39 OBSs were deployed in the area and a 3,400 cu airgun-array was shot along the four survey lines. The spacing of the OBS stations was 10 km and the airgun shot interval was about 150 m. The quality of the OBS record sections is good and we can trace the first arrivals up to at least offsets of 80 km. There are two groups of evident later arrivals on the record sections. Preliminary travel time analysis based on a reference structure model in this region presented by Miura et al. (2002) indicates that these later phases are wide-angle reflections from the subducting oceanic crust, which are of our most significant interest. The appearances of these later arrivals are quite different from a station to another, indicating that there seems to be a spatial variation of the reflection intensity of the plate boundary as we found in the northern part of the Japan trench.

**SS03/08A/D-121** Poster **0830-280**

**P-WAVE VELOCITY MEASUREMENTS UNDER HIGH PRESSURE AND TEMPERATURE CONDITION IN ULTRABASIC ICHINO-MEGATA XENOLITHS, NE JAPAN**

Soushi NISHIMOTO<sup>1</sup>, Masahiro ISHIKAWA<sup>1</sup>, Makoto ARIMA<sup>1</sup>, Takeyoshi YOSHIDA<sup>2</sup> (<sup>1</sup>Geological Institute, Graduate School of Environment & Information Sciences, Yokohama National University, 240-8501, Japan, <sup>2</sup>Research Laboratory of Arc Magmatism, Institute of Mineralogy, Petrology and Economic Geology, Graduate School of Science, Tohoku University, Sendai, 980-8578, Japan)

Xenoliths erupted from the Ichino-megata volcano, NE Japan, contain various lower crustal and upper mantle rocks, which provide important clues for estimating crustal section of the NE Honshu arc (Aoki, 1971; Takahashi, 1978; Zashu et al., 1980; Takahashi, 1986 and Kushiro, 1987). Recent extensive seismic experiments across the NE Honshu arc (Iwasaki et al., 2001) suggest that the arc crust is composed of highly deformed Tertiary sedimentary upper crust layer, a middle crustal layer with relatively lower Vp of 5.75-5.9 km/s, and a 15-km thick lower crust with Vp of 6.6-7.0 km/s. In this study, we developed new experimental technique to measure Vp of Ichino-megata xenoliths at lower crustal P-T conditions (up to 900 °C and 1.2 GPa), and combined the measured Vp of the xenoliths with the velocity structure of the arc. The measured rocks include one hornblende gabbro (41.3 wt% SiO<sub>2</sub>), two samples of pyroxene-hornblende gabbro (45.6 wt% SiO<sub>2</sub> and 43.7 wt% SiO<sub>2</sub>) and one hornblende (44.6 wt% SiO<sub>2</sub>). It is widely accepted that Vp value of the rocks considerably decreases with elevating temperature. At constant pressure of 1.0 GPa, the Vp of hornblende gabbro gradually decreased from 7.21 km/s at 25 °C to 6.91 km/s at 700 °C. Similarly the Vp values of the pyroxene-hornblende gabbros reduces from 7.06 km/s at 25 °C to 6.73 km/s at 800 °C. Also the Vp value of the hornblende lowers from 7.11 km/s (25 °C) to 6.45 km/s (800 °C). The measured Vp values are compared with the seismic profile of NE Honshu arc (Iwasaki et al., 2001). We estimate temperature conditions of the lower crustal layer of the NE Honshu arc crust by the geothermal gradient given by Kushiro (1987). The estimated Vp values of the hornblende gabbro measured at the lower crustal P-T conditions are comparable to Vp values of a upper-lower crustal layer of the seismic profile by Iwasaki et al. (2001).

**SS03/08A/D-122** Poster **0830-281**

**CRUSTAL MODELS OF WESTERN PACIFIC ISLAND ARCS: IMPLICATIONS ON ARC MAGMATISM**

Carla B. DIMALANTA, Asahiko TAIRA, Hidekazu TOKUYAMA, Graciano P. YUMUL, JR., Rodolfo A. TAMAYO, JR., Kimihiro MOCHIZUKI. (IAVCEI)

The evolution and growth of continental crust remains to be one of the fundamental problems in geology. Crustal growth is defined as the net gain in the volume of crustal material as a result of various addition and subtraction processes. In terms of crustal addition, arc magmatism has been recognized as one of the mechanisms where juvenile crustal material is created along subduction zones. The Western Pacific region is thus a favorable site to investigate arc magmatic addition processes. A previous study was done by Reymer and Schubert (1984) to quantify arc magmatic addition rates. Their results show that material is being produced by arc magmatism at rates ranging from 20 to 40 km<sup>3</sup>/km/Myr. Therecent seismic and gravity data offer improved images of the structure and thickness of the crust beneath some island arcs in the Western Pacific. Present data show that the oceanic island arcs in the Western Pacific region have crustal thicknesses between 20 to 30 km. Relevant crustal volumes are calculated and the corresponding arc magmatic addition rates are estimated. Based on the results obtained, arc magmatism occurs at rates ranging from 30 to 95 km<sup>3</sup>/km/Myr. The magmatic addition rates presented here are nearly twice as high as previous estimates of arc magmatic addition.

**SS03/08A/D-123** Poster **0830-282**

**THREE DIMENSIONAL S-WAVE ATTENUATION MODEL OF THE CRUST AND UPPERMOST MANTLE BENEATH ARC-CONTINENT COLLISION, TAIWAN**

Yu-Ju WANG, Kuo-Fong MA (Institute of Geophysics, National Central University)

The S-wave attenuation structures (Qs) of Taiwan are imaged with data from the dense deployed strong motion stations of Taiwan. The image of 3-D Qs is essential in Taiwan because Qs is sensitivity to localized permeability and heterogeneity, which are important characters for interpreting active tectonic regions as Taiwan. The attenuation images of S-wave are obtained using  $t^*$  values measured from S-wave spectra from Taiwan strong motion network for moderate size earthquakes (M4.5-5.5) to avoid the source complexity. The time period used in this study is from 1993-1998. Over 2000 velocity spectra of S wave arrivals from 173 earthquakes were analyzed. A non-linear least square technique is applied to the spectra for  $t^*$  by assuming a w-2 model for the frequency band of 1-20Hz. A frequency-independent Qs was assumed in this study. Combined the existed three-dimensional S-wave velocity model, the three-dimensional Qs images were obtained. The preliminary results show that a relative low Qs zone beneath the Central Range distributed from the depths of 4 to 18 km. This zone correlated well with the low velocity zone found in the 3D Vp and Vs images. Although the complete study on 3-D Qs images is not final yet, the benefit of 3-D Qs images to 3-D Vp, and Vs is believed to be significant, and will be essential to provide imperative insight to an arc-continent collision region of Taiwan.

**SS03/08A/D-124** Poster **0830-283**

**TELESEISMIC IMAGING OF UPPER MANTLE STRUCTURES AROUND THE TAIWAN AREA**

Pei-Yang LIN<sup>1</sup>, Bor-Shouh HUANG<sup>2</sup>, Ling-Yun CHIAO<sup>1</sup> (<sup>1</sup>The Institute of Oceanography National Taiwan University, Taiwan, ROC, <sup>2</sup>The Institute of Earth Science Academia Sinica, Taiwan, ROC)

Teleseismic events that had been clearly recorded across TTSN and CWBSN through the past 7 years has been identified and compiled. Recorded waveforms of those with epicentral distances 30°-90° away from Taiwan are analyzed by the multi-channel cross

correlation algorithm (VanDecar and Crosson, 1990) to yield a set of consistent relative differential travel times across the area covered by the seismic networks. After careful quality control, 145 events that yield relative differential travel times within the range of 1.5 seconds across the area are retained. These events compose about 2500 rays going through the upper mantle around the Taiwan region. Tomographic inversion of these travel-time residuals are undertaken by assuming that the heterogeneities of the velocity structure of the target area, within 20°-26° N, 118°-124°E and with the depth above 400 km, is responsible for causing the relative differential travel times. Preliminary model structures obtained from three different inversion strategies, including the damped least squares, the convolutional quelling regularization and the multiscale parameterization, are cross-analyzed to probe for the possible upper mantle structure. Although the data seems to be noisy and the ray coverage is very likely too sparse, there are still some interesting implications for upper mantle structures underneath the Taiwan area. We will discuss some of these preliminary results as well as proposing for directions of future study.

**SS03/08A/D-125** Poster **0830-284**

#### EXPLORATION RESEARCH CRUSTAL STRUCTURE UNDER THE SOUTH CHINA SEA OF SOUTHWESTERN HAINAN ISLAND WITH LANDSTATIONS ARRAY COMBINING OBH

Saijun LIU (Seismological Bureau of Fujian province, China Seismological Bureau)

In the project obtained deep seismic profiles significant data under the South China Sea (SCS) of southwestern Hainan Island (HNI) with the Landstations Array (LSA) combining Ocean Bottom Hydrophone (OBH), for the first time in 1996-97. Comparing them with Gongdong continent and Xisha Ocean Trough (XST), the follow results were gotten: 1. The Land Area Hainan Island (LAHI) researched belongs to continent, its crust thickness close to northern HNI (about 26 km) is thinner than Guangdong landmass (32 km). Moho depth is 27.6 km. The wave velocity under Moho is 7.8 km/s. The crust thickness is 27 km except Cenozoic. The thickness of lower crust is about 14 km, velocity 6.4\_6.7 km/s, the upside approximates to 13 km and was divided into two parts: top 6 km, V 5.7\_6.1 km/s, a lower velocity layer lies under the top that thickness is near 7 km, V 5.5\_6.0 km/s. 2. LAHI due to continental crust, thickness reach 27 km; However, XST fall into extensional ocean rift zone which thickness thins down 8 km till, in evidence. There is a lower velocity layer at LAHI crust profile but the velocity at XST is increased from shallow (V=5.5 km/s) to deep (V=6.8 km/s) continuously. The lower velocity layer was no found. At the middle part of profile Moho swelled up. The crust thickness decreased from the two side of the profiles, 28 km to middle 8 km rapidly, the velocity jumped from the earth crust bottom 6.8 km/s to the top of up mantle 8 km/s. So, characters for both of them are different completely. 3. The No.1 fault striking NW, should be NE boundary of Red River Fault (RRF), is a normal fault trending SW. Its least distance to the shore is about 28 km. It was showed in profiles that the bottom faults distance of pre Tertiary is >= 7 km, covered with Cenozoic; According to analyze the data of oil profiles explored the top of fault cutting through Tertiary layers had meet Quaternary system. Evidently, No.1 fault activities can be tracked up to early Quaternary period. The normal fault character shows that RRF is being tensile state according to entire SCS. 4. In Yingerhai Basin (YGHB) locating at western of No.1 Fault Cenozoic deposition thickness is huge that can reach 7\_10 km at the deepest basin bottom. There are sediments (0.2\_4.6 km) at the profiles upside, V=1.7\_4.3 km/s. And about 4 km lower velocity layer lying below it, velocity is 3.0\_3.5 km/s, can be track on AA' or BB' profiles.

**SS03/08A/D-126** Poster **0830-285**

#### CRUSTAL STRUCTURE, RECENT DYNAMICS AND SEISMIC ACTIVITY OF RED RIVER FAULT ZONE (RRFZ)

Cao Dinh TRIEU (Hanoi Institute of Geophysics)

The main characteristics of the Crustal structure, the faults and the manifestation of seismic activities of Red River Fault Zone (RRFZ) were presented in this research work. The results of study have shown that: 1/ The depth to the Moho surface of RRFZ is varied from 22-24 km to 30-32 km with northward dipping tendency. Vice-versa, crystal surface of the earth's crust has northeastward dipping tendency and its depth reached value of about 8-9 km in the central part of Red River Cenozoic depression. 2/ At present, RRFZ is affected by compressor from northeast direction. Clear manifestation appeared here is strong uplift and active seismic activity in the northeast part of the Fault Zone. 3/ Earthquake epicenters are mainly distributed within the depths of about 7-20 km, but popularly in the range of 10-16 km. The correlation function between minimal depth of hypocenters (Hmin) and maximum magnitudes (Mmax) of the earthquakes as follow:  $\lg H_{min} = 0.25 M_s - 0.304$ . The mainly seismogenic faults of RRFZ consist of: Lo River, Vinh Ninh, Chay River, Red River, Fansipan and Binh Luc. Strongest earthquakes occurred within RRFZ may be limited by  $M_{max} = 5.5-6.0$  and it seems to be that Chay River and Red River have most strong seismic activity. 5/ Highest risk of seismic activity may be caused in RRFZ in Luc Yen-Yen Bai and Viet Tri-Hanoi areas.

**SS03/08A/D-127** Poster **0830-286**

#### ROCK'S MELTING IN CONDITIONS OF THE CONTINENTAL CRUST

Roland Nikolaevich SOBOLEV (Lomonosov Moscow State University, Geological Faculty)

Usually, by analyzing processes of melts generation in continental earth crust, take in consideration only eutectic and cotectic thermodynamic laws. This opinion bases on results of experimental investigations by which use powder of rocks or gels. In this case at constant PTX conditions exists equilibrium state. In the continental earth crust melting metamorphic rocks consists of mineral's grains with sizes of some mm or even cm. In this case the square of contacts of different minerals' grains is much less than in experiments with a powder or a gel. The principal points are: 1. melting process is not equilibrium, 2. it has to be analyzed process of melting from position of kinetic of disequilibrium processes. Minerals of different chemical compositions have different melting temperatures: quartz - 1713, garnet - near 800 ÅAC etc. The process of melt formation is very complex - it consists of many stages: 1. Melting of garnet, 2. Reaction garnet's melt with minerals, 3. Appearance thin films of melts of different chemical composition on contacts of minerals in accordance with eutectic and cotectic laws, 4. These melts are not in equilibrium with minerals. As a result of reactions between melts and minerals they disappear in definite succession: garnet → plagioclase → K-Na feldspar → quartz. During the melting take place separation melts in accordance with their density: garnet's melt accumulate in the bottom of a crucible. In the system are many melts related by gradual transitions. So at any melting's stage the system consists of many melts of different chemical compositions and relicts of grains. Experiments of melting grains mixture of quartz, feldspars, garnet (minerals of gneiss by melting of which acid melts form) of the same (1 mm) and different (1, 5, 10 mm) sizes give evidence that succession of melting in all cases is the same without dependence on their size: garnet → plagioclase → K-Na feldspar → quartz. In most experiments part of quartz' grains is relict phase. It disappears only by temperature >1500 °C or by very long time of experiment. In natural conditions melt raises in the earth crust from the upper part of magmatic chamber and as a consequence a compositions of acid magmatic bodies are more leucocratic in comparison

with bulk melt's composition in the place of melts generation. These data give new material for understanding structure of the earth crust.

**SS03/08A/D-128** Poster **0830-287**

#### THERMO-MECHANICAL STRUCTURE OF THE SOUTH INDIAN SHIELD

Om Prakash PANDEY, Ajay MANGLIK (National Geophysical Research Institute)

The Dharwar protocontinent of the southern Indian shield forms one of the most interesting region among the cratonic terrains of the world. It constitutes three Archean-Proterozoic blocks separated by mobile shear zones. They are Western Dharwar Craton (WDC), the Eastern Dharwar Craton (EDC) and the Southern Granulitic Terrain (SGT). These blocks appear to have contrasting evolutionary history exhibiting different geologic, tectonic and geophysical characteristics. Recent geological and geophysical studies indicate episodic remobilisation and large regional variation in the crustal structure and heat flow. Rapid uplift can be seen in several parts of the SGT. In this study, we have computed rheological structure of these blocks using available geophysical and geological inputs and analyzed the results in the light of crustal deformation. Our study indicates presence of a rheologically strong lithosphere in WDC, where rheological thickness of the lithosphere and the total force per unit width is highest at 190 km and  $5.8 \times 10^4$  N/m, respectively. This region contains the coldest and undeformed oldest cratonic nucleus. Here, the Moho temperature is about 374°C. In contrast, SGT appears to be anomalous, which has undergone extensive high-grade regional metamorphism even as late as  $550 \pm 30$  Ma. It is found to contain a ductile middle to lower crust besides a warm and weak lithosphere. In spite of being a part of stable shield region, brittle ductile transition in the northern block of SGT occurs at a depth of 20-25 km. Total force per unit width is also quite low here ( $2.6 \text{ AE}2.9 \times 10^4$  N/m). Earlier studies have reported 1-2 percent lower P-wave subcrustal velocities beneath SGT compared to WDC. Recent deep crustal seismic studies indicate presence of a low velocity layer (6.0 km/s) below the middle crust. Therefore, we infer that the Archean crust of WDC may be underthrusting below SGT possibly along Moyar shear zone, which has lead softer upper crustal layers to become sandwiched between harder layers. In these softer layers, deformation is expected to be concentrated which due to north-south compression consequent to Indian-Eurasia collision appears to decouple and result into the continuous uplifting and erosion of SGT, thereby exposing the deepest part of the granulitic crust at the surface.

**SS03/08A/D-129** Poster **0830-288**

#### DEEP CRUSTAL STRUCTURE OVER THE ARCHAEN SOUTH INDIAN SHIELD

Sanjay G. GOKARN, Chinta K. RAO, Gautam GUPTA (Indian Institute of Geomagnetism, Plot No. 5, Sector-18, Near Victoria Petrol Pump, Kalamboli (Highway), New Panvel (W), Navi Mumbai-410206.)

Magnetotelluric studies over the granite-greenstone province of the Archaen Dharwar shield are indicative of intense Precambrian tectonic activity leading to the east-west compression of the upper crustal block and the subsequent formation of three sub-basinal features filled with the greenschists. The upper crustal thickness to the west of the Closepet granitic intrusives is about 25 km compared to the thickness of 20 km observed to the east of this feature. This is also reflected in the observed lower surface heat flows in the west Dharwar compared to the east. Based on this observation, the Chitradurga Boundary fault is proposed to be located along the western margin of the Closepet granites. There are no significant conductivity associations with the Chitradurga boundary fault, presumably because of the lack of any tectonic activity for a long time since the Precambrian. The lithospheric thickness was inferred to be about 180 km from the observed high conductivity of about 50 Ω-m observed at this depth. An interesting observation is the high conductivity of about 20 Ω-m delineated at depth below 80 km, corresponding to the lithospheric mantle. This feature is about 100 km wide along the EW and seems to be located entirely in the continental lithosphere. The thermal and mechanical fluxes generated by the Reunion hot spot, over which the western part of the Dharwar craton passed during its post-outburst phase, may be causing the high conductivity. The higher seismic velocities observed in the lithospheric mantle corresponding to the high conductivity may be due to the tonalitic character of the west Dharwar crust, as against the granitic composition of the eastern part.

**SS03/08A/D-130** Poster **0830-289**

#### ESTIMATION OF INTRINSIC ABSORPTION AND SCATTERING ATTENUATION IN SOUTHERN INDIA USING A DEPTH DEPENDENT STRUCTURE MODEL

Jayant Nath TRIPATHI<sup>1</sup>, Arantza UGALDE<sup>1</sup>, Mitsuyuki HOSHIBA<sup>2</sup> (<sup>1</sup>Observatori de l'Ebre, CSIC-URL, 43520 Roquetes, SPAIN, <sup>2</sup>Matsushiro Seismological Observatory, Nishijo 3511, Matsushiro-machi, Nagano-shi, 381-1232 Japan)

1143 vertical-component, short period observations of microearthquake codas from shallow earthquakes recorded by the Gauribidanur seismic array were used to estimate seismic wave attenuation in southern India. The magnitudes of the earthquakes range from 0.7 to 3.7 and only the events occurred at hypocentral distances up to 200 km were considered for the analysis. Four frequency bands between 1 and 10 Hz were analyzed. The separation of intrinsic absorption ( $Q_i^{-1}$ ) and scattering attenuation ( $Q_s^{-1}$ ) from total attenuation ( $Q_t^{-1}$ ) was performed using a multiple lapse time window method which compares time integrated seismic wave energies with synthetic coda wave envelopes for a multiple isotropic scattering model. We first assumed a synthetic model based on spatial uniformity of ( $Q_i^{-1}$ ), ( $Q_s^{-1}$ ) and S wave velocity (v). Results show that scattering attenuation is greater than intrinsic absorption for all the frequency bands, and a high value of the seismic albedo (close to 1) is found at short and long hypocentral distances, which indicates very strong scattering. Moreover, the observed energy at 0 to 15 seconds from the S wave arrival time bands significantly downward with decreasing distance and some discrepancies are observed between the theoretical model and the observations. In order to clarify this phenomenon, we computed a synthetic model assuming a vertical varying  $g$  ( $Q_i^{-1} = gv/\omega$ ),  $h$  ( $Q_s^{-1} = hv/\omega$ ) and  $v$  structure. A comparison between the attenuation parameters estimated using both models is presented.

**SS03/08A/D-131** Poster **0830-290**

#### POSSIBLE RESOURCE ESTIMATES OF GAS HYDRATES ON WESTERN CONTINENTAL MARGING OF INDIA

Babita SINHA, S.J REDDY, N.K. THAKUR (1)

Naturally occurring gas hydrates are known as gas clathrates, are ice like compound in which gas molecules (mainly methane) are encased in the interstices of hydrogen bonded water lattices at low temperature and high-pressure conditions. Gas hydrates are detected on seismic sections primarily through an anomalous reflector running parallel to the sea floor known as Bottom Simulating Reflector (BSR). Bottom Simulating Reflector are commonly associated with base of hydrate stability field and may represent the phase boundary between the hydrate bearing sediments and gas charged or water bearing sediments below.

The rate of sedimentation, pressure temperature conditions, sediment thickness, total organic content and prevailing bathymetry indicates probable presence of gas hydrates in Indian Offshore region. It is also being inferred by the presence of strong bottom simulating reflector revealed by the multichannel seismic data from the western continental margin of India. Analysis of the variation of P-wave reflection coefficient with offset and angle of incidence, commonly termed as AVO analysis, has been recognized as one of the direct hydrocarbon indicator. We use this in delineating the possible causes and characteristics of BSR in the data from Indian Offshore region. In the present study, we model and perform AVO analysis on multi-channel seismic data from western continental margin of India to arrive at probable estimates of gas hydrate reserve of this region. We also present the AVO-attribute and cross-plot to arrive at the petro physical characteristics of the region

**SS03/08A/D-132** Poster **0830-291**

**SEISMOTECTONIC MODEL OF THE JANUARY 26, 2001 BHUJ EARTHQUAKE (MW 7.6) IN WESTERN INDIA**

J.R. KAYAL, Reena DE (1)

The January 26, 2001 Bhuj earthquake is the second largest SCR ( Stable Continental Region ) earthquake with Mw 7.5, that occurred about 180 years after the 1819 Kutch earthquake (Mw 7.8) in the Kutch rift basin, northwestern part of the peninsular India shield area. This area falls in the high seismic risk zone in the country. A 12-station close spaced network was established by the Geological Survey of India for monitoring aftershocks. About 3000 aftershocks ( $M > 1.0$ ) were recorded in two and half months during the period from January 29 to April 15, 2001. The aftershocks attenuated with time following the power law  $t^{-p}$ , where  $p = 0.91$ . The frequency-magnitude relation of the aftershocks also followed the power law with  $b$ -value = 1.21. About 350 events ( $M > 2.0$ ) are well located with an average RMS  $< 0.1s$  and average horizontal and depth error  $< 2$  km by 3-D seismic tomography method (Kayal et al., 2002, GRL, v. 29). The epicenter map shows an aftershock-cluster area, about  $60 \times 30$  km<sup>2</sup> between 70.00 -70.60E and 23.30-23.60N, which reflects the source area of the main shock and aftershocks at depth. The epicenters show two major trends; one in the NE direction and the other in the NW direction. Depth-sections of the aftershocks indicate that the events are mostly generated at 15-38 km depth. Some events occurred at depth  $< 10$  km; they follow the NW trend only. A south dipping seismogenic plane is revealed in the depth-section. Composite as well as moment Tensor fault-plane solutions of the best-located and selected events are studied. The deeper (25-38 km) as well as the mid crustal (15- $< 25$  km) aftershocks show reverse faulting with a large left-lateral strike-slip component along the NE trending inferred fault, which are comparable with the main-shock solution. Along the NW trending inferred fault, on the other hand, the shallower aftershocks (depth  $< 10$  km) show reverse faulting with right-lateral strike-slip component, and the mid crustal and deeper aftershocks show almost pure reverse faulting. These solutions with the NW trending inferred fault are not comparable with the main shock solution. A seismotectonic model is suggested, which explains that the deeper (depth 25 km) main shock was nucleated at the base of the paleo-rift basin by reverse faulting at the fault end of a hidden fault. The aftershocks mostly occurred at the mid crust and lower crust at a depth range 15-38. The main shock rupture propagated in the NE direction by left lateral strike slip motion, and a conjugate rupture propagated along NE by right lateral strike slip. Surface evidence of ground motions support these observations.

**SS03/08A/D-133** Poster **0830-292**

**ELECTRICAL IMAGE OF THE DEEP CRUST NEAR BHUJ EARTHQUAKE EPICENTRAL REGION, INDIA**

Harinarayana T., Kareemunnisa Shaik BEGUM, Patro B.P.K., Naganjaneyulu K. (National Geophysical Research Institute)

Kutch region is well known for high seismicity with the reported occurrence of at least three major earthquakes. Although various geological and geophysical studies have been carried out, the deep crustal structure is poorly understood. In order to understand the physical processes related to seismicity of the Bhuj earthquake, a wide-band magnetotelluric survey has been carried out along three profiles with 21 stations. The profiles cut across the major structural features such as Kutch Main Land Fault (KMF) and Katrol fault. In the present study, deep geoelectric structure along a profile oriented in N-S direction is presented. Results indicated the presence of thick sediments (1-4 km) dipping towards south underlain by high resistive basement. From detailed 2D analysis of the data, it is observed that the resistivity of the basement shows distinct variation for the stations located towards the south compared to the north. It is interesting to observe that the well-known KMF is spatially located near the sharp variation in the basement resistivity. This led to believe that the deep structure has a different nature towards the north as compared towards south and gave an evidence for probable existence of a block structure in the region. Relative movement of these crustal blocks might be the reason for the continuous development of stresses that led to major earthquakes in the region.

**SS03/08A/D-134** Poster **0830-293**

**INTEGRATED SUBSURFACE IMAGING OF DEEP REFLECTION SEISMIC DATA WITH IRREGULAR ACQUISITION GEOMETRIES IN CRYSTALLINE GEOLOGICAL TERRAIN**

Susumu ABE<sup>1</sup>, Larry D. BROWN<sup>2</sup> (JAPEX Geoscience Institute, Inc., <sup>2</sup>INTOC, Cornell University)

Seismic imaging of the deep crustal structure is strongly affected by surface-consistent static time shift due to a low-velocity weathered layer, irregular acquisition geometries, low signal-to-noise ratio (S/N) of reflections, and interactions of the backscattered wavefield within the shallow subsurface. We have evaluated the limitations and applicability of standard processing to deal with these problems. Refraction and reflection static corrections are key steps to improving the image of deep seismic reflections with low S/N and discontinuous patterns. Turning-ray tomography is an optimum tool for the construction of the weathered layer model with irregular variations of velocity in crystalline terrains. The global optimization method is required for reflection static corrections to accommodate the high multimodal character of objective function on deep seismic data. In order to estimate accurate statics in the board range of wavelength for deep seismic data, we adopted the combination of global optimization method via genetic algorithm and turning-ray tomography. We have investigated the cascaded method to migrate deep seismic data acquired with irregular geometries. Kirchhoff imaging method, which can account for the crookedness and rugged topography of the shot and receiver lines, was combined with residual finite-difference F-X migration to reduce the artifacts that result from the smearing of deep discontinuous reflections via migration operator with a significant aperture. The seismic data used for this case study consists of a series of 2D seismic profiles from the INDEPTH Project in the Himalayas. We find that precise static corrections and geometry-oriented migration processing significantly improved the image of crustal structure in the upper plate of the Himalayan megathrust. Furthermore, subsequent relative-amplitude-preserved processing provides an AVO attribute profile consistent with granitic magmas derived by partial melting of the tectonically thickened crust.

**SS03/08A/D-135** Poster **0830-294**

**P WAVE CRUSTAL VELOCITY STRUCTURE IN THE EASTERN MARGIN OF TIBETAN PLATEAU**

Chun-Yong WANG, Jian-Ping WU, Hai LOU, Zhi-Ming BAI (Institute of Geophysics, China Seismological Bureau)

A deep seismic sounding profile located in the eastern margin of Tibetan Plateau extends along N30°. It passes through the Songpan-Garze Fold System (western Sichuan plateau) and the Longmenshan Tectonic Belt, and ends in the Yangtze Craton (Sichuan Basin). Based on the travel times of phases on the profile, incorporating information on the relevant amplitudes, we determined 2-D P-wave crustal velocity structure along the profile. The crustal thickness, crustal average velocity and Pn velocity are obviously different between the western Sichuan plateau and Sichuan basin. The Yangtze craton has higher crustal average velocity, so the crustal rock is harder than in western Sichuan plateau. The lower Pn velocity in western Sichuan plateau might be related to the marked thermal process through whole Cenozoic. Beneath the Kangding-Luding area, there might exist a series of listric faults, which is connected to the low-velocity-zone in upper crust and to the Piedmont overthrust fault zone on the surface. The low-velocity and low-resistivity zone in crust may play an important role in the process of detachment and overthrust. Due to the collision between Yangtze Craton and Songpan-Garze block, the vehement deformation appears in the relatively soft block so as to thicken the crust, reduce crustal velocity, and produce a series of thrust fault zones. Such a collision pattern is called as "Crocodile Structure". However, on the seismic records along the profile, there is no obvious evidence that there exist eastward-inclining faults in the lower crust.

**SS03/08A/D-136** Poster **0830-295**

**THREE DIMENSION DENSITY DISTRIBUTION OF LITHOSPHERE IN QINGHAI-TIBET AND ITS ADJACENT REGIONS**

Jian FANG, Houze HSU (Institute of geodesy and geophysics, Chinese Academy of Sciences)

The goal of this study is to use gravity data combining seismic tomography data to construct a three-dimension density model of the lithosphere of Qinghai-Tibet plateau and its surroundings and to relate this model to tectonic processes. We have collected three dimension S-wave tomography data with grid of  $20 \times 20$  in the 10-100km depth range in the area of Qinghai-Tibet and its adjacent regions. Otherwise the observation gravity data of the grid of  $10' \times 10'$  and sedimentary depth and density data and crustal thickness data with the grid of  $10 \times 10$  have been acquired. The gravity effects of sedimentary bottom interface and Moho interface undulation can be calculated by means of spherical gravity forward formula. The density differences of crust-mantle and sediment-crust are 420kg/km<sup>3</sup> and 210kg/km<sup>3</sup> respectively. After eliminated gravity effects of interfaces and long wave length ( $> 2000$ km) gravity anomaly, the residual gravity anomaly is mainly caused by density inhomogeneities of the lithosphere. We will use the residual gravity anomaly combine tomography data invert lithosphere density anomaly. We divide the lithosphere of research region into grid of  $20 \times 20$  and each grid is divided into six layers. So, the lithosphere of research region can be divided into  $9 \times 18 \times 6$  prisms and we assume the density of every prism is unique. By using the relative formula of between difference of density and difference of S-wave speed, we can establish the preliminary model of density in Qinghai-Tibet and its adjacent regions. Then, we using residual Bouguer gravity anomaly data invert iteratively density anomaly distribution by means of the least square method. Finally, we get density anomalies on six different depths in 10-100km depth ranges. The mean square error between observation gravity anomaly and the gravity anomaly of density model forward calculation is less than 5mgal. The density anomalies of Qinghai-Tibet are obviously relative to the tectonic features. High-density region corresponds to old terrain, and low-density corresponds to plateau and mountain region. There are density anomaly gradients along the boundaries of differential tectonic bodies. The density distribution of upper mantle is different to the distribution of crustal density. The variation of crustal density is 15%, while upper mantle density variation is 5%. Key Words: Tomography, gravity anomaly, Inversion, Lithosphere density structure.

**SS03/08A/D-137** Poster **0830-296**

**P WAVE VELOCITY STRUCTURE OF THE CRUST FROM ZHAYU, XIZANG TO GONGHE, QINGHAI IN THE SOUTHEASTERN TIBET**

Zhongjie ZHANG, Guangjie WANG, Ruomei SUN, Jiwen TENG, Liqiang YANG, Yilong QIN, Yun CHEN, Yafeng YAN, Jingyi CHEN, Chaoying ZHANG, Haishan ZHENG (Institute of Geology and Geophysics, Chinese Academy of Sciences)

A wide-angle seismic profile was taken with a total length of about 1000 km, from Zhayu, Xizang to Gonghe, Qinghai, in the southeastern Tibet, in 2001. The wide-angle seismic profile crosses the 4 tectonic blocks: Laoha block, Qiangtang block, Songpan Ganzhi block and the eastern Kunlun block. 3 sutures such as the Banggoin, Jinshajiang and the eastern Kunlun are cut by the profile. It's implemented to study the crustal structure under the studied area, search for the seismic evidence of crustal material escaping eastwards and possibility of crustal deformation in the southeastern Tibet. In this experiment, 16 shots are triggered, and 200 three component digital seismographs are deployed to record seismic reflection and refraction from the crust. With the analyses of P-wave seismic features of this experiment, we recognized several events such as Pg from the crystalline basement, PmP from the Moho and other 3 phases from the discontinuities in the crust. With the traveltimes fitting and velocity inversion of these observations, we obtain the final interpreting model of P-wave velocity in the crust. The results demonstrate the crustal thickness varies abruptly for different blocks. The average crustal thickness varies within 55 and 74km, and thins from the southwestern to the northeastern of the profile. The crust could be divided into upper, middle and lower crust. The average P wave velocity is about 6.2-6.25km/s for the profile. The obvious feature is there is strange lower velocity body under the area centered at the eastern Kunlun fault.

**SS03/08A/D-138** Poster **0830-297**

**STUDY OF REGIONAL TECTONIC DEFORMATION BEFORE MS8.1 EARTHQUAKE IN THE WEST OF KUNLUN MOUNTAIN PASS**

Zai sen JIANG<sup>1</sup>, Xi ZHANG<sup>1</sup>, Bing CHEN<sup>2</sup>, Xi liang ZHANG<sup>2</sup>, Shuang xu WANG<sup>2</sup> (<sup>1</sup>Center For Analysis And Prediction, China Seismological Bureau, <sup>2</sup>The Second Center For Crustal Deformation Monitoring, China Seismological Bureau)

The background of regional tectonic deformation, before Ms8.1 earthquake in the west of Kunlun Mountain Pass, is preliminarily studied by using horizontal crustal velocity field data during 1991-2000 observed by GPS in Qinghai-Tibet block and its adjacent area, and from gravity repetition measurement in 1998 and 2000. The analysis shows that, the development and occurrence of this earthquake related to larger regional horizontal motion and deformation background, which might be acted by larger-scale block. Inside the Qinghai-Tibet block, large-range sinistral shear deformation region existed, this earthquake just

happened in the highest region of sinistral shear strain rate in accordance with fault strike, and tensional region of superficial expansion strain and the margin of abnormality region of negative gravity variation. The background of regional tectonic deformation was helpful to develop huge sinistral strike-slip rupture. Conclusion and Comprehension: (1) The development and occurrence of this Ms8.1 earthquake related to larger regional horizontal motion and deformation background. Relative movement produced much big range sinistral shear deformation, this earthquake just took place in the highest region, whose strike was consistent with the fault strike, of sinistral shear strain rate. (2) This earthquake was not only driven by NE principal compressive stress action, but also caused by the total movement of Kunlun block and nearby blocks. Due to resistance of local boundary, in the epicenter area, the lag of movement led to quick accumulation of elastic strain, the total block motion wanted to pull this local region moving eastward, so as to make the movement harmonious, thus brought about huge-type sinistral strike-slip rupture. (3) In the middle and east of Qinghai-Tibet block, on the sinistral fault, 7 earthquakes over 7 magnitude occurred one after another since 1937, 5 of them are over 7.5 magnitude. This group of earthquakes formed a huge arc sinistral shear zone, and acted by stress field of large regional horizontal movement, the activity of this huge sinistral shear zone certainly caused accumulation of elastic strain energy on the segment where no large earthquake has taken place yet. This is the fact indicated by DDA simulation. (4) In the epicenter area, NW principal tensional strain of horizontal strain rate was a little bigger than NE principal compressive strain. Just due to such regional tectonic deformation background, it was favorable to produce large-scale development of sinistral rupture dislocation, and to make the shear strain accumulated before the earthquake fully release. So it was also helpful to understand those questions why this Ms8.1 earthquake had longer rupture length and lower magnitude of aftershocks.

**SS03/08A/D-139** Poster **0830-298**

**TECTONIC DEFORMATION BACKGROUND AND FAULT ABNORMAL ACTIVITY IN NORTHEAST MARGIN OF QINGHAI-TIBET BLOCK BEFORE THE KUNLUN MS8.1 EARTHQUAKE**

Shuang xu WANG<sup>1</sup>, Zai sen JIANG<sup>2</sup>, Xi ZHANG<sup>1</sup>, Xi liang ZHANG<sup>1</sup>, Fu ping XUE<sup>1</sup> (<sup>1</sup>The Second Center For Crustal Deformation Monitoring, China Seismological Bureau, <sup>2</sup>Center For Analysis And Prediction, China Seismological Bureau)

By using up-to-date crustal deformation observational data that contain results observed by GPS in 1993, 1999 and 2001, together with mobile deformation results crossing main faults during 1980-2002, combined with monitoring and research results of regional vertical deformation nets for nearly 30 years, the time-spatial evolution background of regional tectonic deformation and fault abnormal activity features in northeast margin of Qinghai-Tibet block before the Kunlun Ms8.1 earthquake occurred on Nov. 14, 2001 are preliminarily studied. The results show that: before the earthquake, regional horizontal movement and deformation intensity decreased, the trend of vertical motion changed, and abnormality of fault deformation developed. In addition, combined with block and structure, further analysis indicates that, occurrence and development of this Ms8.1 earthquake inside Qinghai-Tibet block were acted by larger-scale block activity, that had remarkable effect on the tectonic region of block boundary, and probably promoted accelerating of stress-strain of some tectonic positions or releasing of rupture in this area.

**SS03/08A/D-140** Poster **0830-299**

**SEISMIC EVIDENCE OF MASS EASTERN EXTRUSION FROM SURFACE WAVE TOMOGRAPHY OF TIBET**

Ruomei SUN<sup>1</sup>, Zhang ZONGJIE<sup>1</sup>, Zhu JIESHOU<sup>2</sup> (<sup>1</sup>Institute of Geology & Geophysics, Chinese Academy of Sciences, <sup>2</sup>University of Science & Technology of Chengdu)

Tibet plateau with uniform height 5km is surrounded by stable sedimentary basins, Tarim to the northwest Chaidamu to the north, Sichuan to the east. It's a natural lab to study continental collision. Le Pichon (1992) estimated the surface loss due to collision between India and Asia and pointed out that about 1/2 to 1/3 crust mass can not be accounted by the thickening of the crust. These crust mass disappeared either by lateral escape or lower crusts transfer to the mantle. Our S velocity images from Rayleigh wave dispersion tomography directly show mass eastern extrusion evidence from depth of 24km to 50km. Then more lower crust mass transfers to the mantle. The low S wave velocity anomaly area of depth 85km has similar pattern as the famous paper giving a zone of inefficient Sn propagation. Profiles along 76E, 86E and 90E suggest that India tectosphere mantle subducts and meet the Asia's at 41N (76E), at 36N (86E) and 34N (90E); north of Bangong-Nujiang. QT has a thick crust, thick asthenosphere. Geologists found Cenozoic lava with rich kalium element there.

**SS03/08A/D-141** Poster **0830-300**

**VELOCITY STRUCTURE FEATURES OF NORTHERN TIEN-SHAN CRUST**

Tamara Mikhailovna SABITOVA, Albina Alexandrovna ADAMOVA, Zarema Arslanovna MEDJITOVA, Nailya Hannanovna BAGMANOVA (Institute of Seismology, National Academy of Science, Kyrgyz Republic, Bishkek, Kyrgyzstan)

We analyzed velocity sections of Northern Tien-Shan crust, that were plotted on new 3D velocity model of Tien-Shan crust and uppermost mantle (38°-5-43°-5 N; 68°-0-80°-0 E), computed by seismic tomography method (Adamova A.A., Sabitova T.M. 2001). This model makes previous 3D model (Roecker S.W., Sabitova T.M., Vinnik L.P. et al, 1993) more precise. It was also computed with the Roecker S.W. program. Area of study lies within 42°-0-43°-5 N and 73°-5-79°-0 E. It includes Chu and Issyk-Kul depressions, part of Ili depression and their mountain frame - Kyrgyz Range, Terskey, Kungey and Zaili Ala-Tau. For most part of study area P-wave velocity structure is well resolved in depth interval 0-80 km, while solution quality for S-wave velocity structure is good for interval 0-25 km. 10 P-wave velocity cross sections have been reviewed. These were constructed for study area in longitudinal and latitudinal directions and across source zones of known big earthquakes (M > 6). To estimate a reliability of velocity structure along those profiles we compare them with sections made by other researchers, as well as with wave field, observed from regional earthquakes and Semipalatinsk nuclear explosions. Found features of velocity structure beneath Northern Tien-Shan are reflected in observed geophysical fields: electromagnetic, gravity, heat flow and S-wave coda attenuation. The following most interesting observations are described below. 1. Velocity structure of crust and uppermost mantle beneath Northern Tien-Shan is rather heterogeneous. In particular, there are specific zones with reverse velocity pattern, which might be attributed to some abnormal high velocity (Vp=6.3-7.0 km/s) volumes in upper crust (5-25 km), low velocity blocks (Vp=5.4-5.7 km/s) in middle crust (25-35 km) as well as to bodies with strong velocity variations (Vp=6.2-8.3 km/s) in lower crust and uppermost mantle (35-65 km). 2. Velocity structure of crust and uppermost mantle beneath depressions and their mountain frame differs: beneath depressions an alternation of high and low velocities is found, while beneath mountain frame P-wave velocities change gradually - in most cases they remain to be rather low, at least, to depth of 35-50 km. Low velocity roots beneath mountains most likely extend to a mantle at some areas. 3. Hypocenters of big earthquakes (M > 6) within study area are located in high P-wave velocity gradient zones. Lateral velocity gradient is usually due to contact between high

and low velocity zones, that at the surface corresponds to known fault, separating depression from mountain buildings. Vertical velocity gradient is related to horizontal boundaries, separating high velocity volumes in upper (5-25 km) and lower (35-50 km) crust from zones with low velocities in middle crust (25-35 km). Stress release during earthquakes may take place along above boundaries, separating blocks with different physical properties.

**SS03/08A/D-142** Poster **0830-301**

**A METHOD FOR PRECISE ESTIMATION OF THE VOLUME OF OIL RESOURCE VIA APPLICATION OF FIRST AND SECOND DERIVATION OF WAVELET TRANSFORMATION. CASE STUDY: DETERMINATION OF VOLUME OF OIL RESERVOIRS IN THE SOUTHERN PART OF IRAN**

Manoochehr SHIRZAI, Alireza A. ARDALAN, Roohallah KARIMI (Department of Surveying and Geomatics Engineering, University of tehran)

Using the welcomed property of the first and second order derivation of wavelet transformation for signal detection a new method for estimation of oil reservoirs based on gravity observation on the surface of the earth has been devised. This method has been first examined for simulated data and then having assured of its capabilities it has been adapted to estimate the volume of the oil reservoir in the southern part of Iran. Details of mathematical formulation of the problem and the results of case studies will be presented.

**SS03/08A/D-143** Poster **0830-302**

**CRUSTAL VELOCITY MODEL IN IRANIAN PLATEAU, REVEALED FROM LOCAL SEISMIC NETWORKS**

Azadeh NADERINEZHAD FARD, Mohammad Reza GHEITANCHI (miss)

Using a two station method, which is independent of mislocation errors, P and S velocities are determined along several paths in Iranian plateau. Assuming a simplified two-layered model with a horizontal layer of isotropic media and using the obtained velocity model, an attempt was made to determine the thickness of crustal layers. The best fit suggests a 44 km crustal thickness. Similarly, theoretical time-distance curves for S arrivals were produced by using several Vp/Vs ratios and the best fit suggests a value of 1.73. In producing time-distance curves reduced travel time plots, in which on the time axis the distance divided by a constant velocity has been subtracted from the true time, was used. This reduced the size of the plot and made arrivals coming in at the reducing velocity appear as a line parallel to the distance axis. The corresponding S-waves were also later arrivals that follow travel time curves like those P-waves. The waveforms recorded by seismic stations contained several clear and strong later phases both in P and S groups. To identify these phases, the crustal model and the obtained Vp/Vs ratio were used and the theoretical travel time curves for several later arrivals were constructed. In addition to the direct, reflected and refracted P- and S-waves, several combinations of the converted P- and S-waves at the first and second interfaces were computed. Comparison of the observed and the theoretical curves indicated that there are significant reflected phases both in P and S groups. This suggests that the later phases also support the consistency of the crustal model obtained in this study. Strong later arrivals on the records of array stations indicate that the Moho and Conrad discontinuities in this region are significant. For more details such as the dip and topography of layers and local heterogeneity, detailed data as well as additional seismic measurements would be needed.

**SS03/08A/D-144** Poster **0830-303**

**THE ROLE OF DEEP PROCESSES IN THE CRUSTAL STRUCTURES FORMATION**

Alexander Georgievich RODNIKOV (17937)

The studies were carried out within the frame of the International Geotraverse Project along three deep cross-sections of the tectonosphere, which included the lithosphere and the asthenosphere. The cross-sections are: (1) the Okhotsk Sea Geotraverse, (2) the Japan Sea Geotraverse, and (3) the Philippine Sea Geotraverse. The major tasks of the work are the study of the deep structure of the lithosphere under the seismically dangerous regions, sedimentary basins with hydrocarbons, and areas of mineralization. The length of the geotraverses reaches several thousands of kilometers at 100 km depths. The data on the cross-sections are supplemented by bathymetric, magnetic, gravity and geology maps. The model calculations were carried out of deep temperatures. The depths of asthenospheric roof, distinguished by seismic and magnetotelluric data, correlate with the depths of the calculated 1000°C isotherm. The peculiar feature of the transition zone structure is the distribution in the upper mantle of the asthenospheric layer, the processes in which determine the tectonic structure of the region. Under Pliocene-Quaternary deep basins the asthenosphere reaches the crust, under Neogene basins asthenosphere is a depth of 30 km, beneath ancient Paleogene basins the asthenosphere is a depth of 50-70 km. The diapirs of the anomalous mantle are confined to the tectonic active regions. On the surface, the upwelling of the asthenospheric diapirs corresponds with the rift structures and the eruption of tholeiitic magma. Apparently, the asthenospheric diapirs with partial melting of the matter are a channel through which the hot mantle fluids rise from the asthenosphere and penetrate into the crust. At the Geophysical Center a Data Base was compiled, which included, besides the geological-geophysical deep cross-sections of the lithosphere and the accompanying geological, gravimetric, bathymetric and magnetic charts, also the primary geological and geophysical data, the results of bathymetric measurements and of gravimetric and magnetic surveys, the data on heat flow, deep seismic sounding and tomographic research, the information on earthquakes and the results of studies of the fine structure of the seismofocal zone, certain data on the chemical composition of rocks and on their age, and the results of deep-water drilling and dragging. This work was supported by the Russian Foundation for Basic Research, project 01-05-64400.

**SS03/08A/D-145** Poster **0830-304**

**THE STRUCTURE OF THE LEINSTER GRANITE, SOUTHEAST IRELAND, FROM WIDE-ANGLE SEISMIC STUDIES: IMPLICATIONS FOR ITS EMPLACEMENT MECHANISM**

James A. HODGSON<sup>1</sup>, Peter W. READMAN<sup>1</sup>, Brian M. O'REILLY<sup>1</sup>, Padhraig S. KENNAN<sup>2</sup> (<sup>1</sup>Dublin Institute for Advanced Studies, 5 Merrion Square, Dublin 2, IRELAND, <sup>2</sup>Department of Geology, University College Dublin, Dublin 4, IRELAND)

The Leinster Granite is situated in southeast Ireland and is one of the largest granite bodies within the Caledonian/Appalachian orogen. Its mode of formation during the later stages of the Caledonian orogeny in the late Silurian/early Devonian is not well understood. A wide-angle seismic experiment using 300 Reftek Texan instruments from the University of Texas at El Paso, U.S.A. and the University of Copenhagen, Denmark was carried out to investigate the seismic velocity structure of the granite and its sub-surface extent, and its relationship with the overall crustal structure of southeast Ireland. The results indicate that the granite has a layered/sheeted geometry extending to a maximum depth of 5 km in the south, much less than previous estimates from gravity studies. To the north, the granite

exhibits a variable thickness between 1 and 3 km, and thickens towards the west. The results show a subsurface extension of the granite at depth towards the southwest, consistent with the Bouguer gravity field. The average Moho depth is about 30 km and within the mid-crust a series of deep-seated faults are interpreted from the seismic model which may have been active during the formation of the granite. Beneath the main granite body the Moho shallows, from a maximum depth of 32 km, to 28 km and this may be related to the presence of thickened granite. The sheeted geometry of the granite suggests a stratigraphic control and this is consistent with geochemical evidence indicating that the source of the granite melt may have been Phanerozoic sediments. The resolved geometry of the granite, together with isotopic data which reveals a cryptic internal stratigraphy implies that the granite did not homogenize during emplacement, and further suggests that it did not move very far as a melt. Emplacement of the granite is likely to have involved limited movement from its source.

**SS03/08A/D-146** Poster **0830-305**

**SEISMIC REFLECTION AND WIDE-ANGLE STUDIES ACROSS THE HIKURANGI SUBDUCTION ZONE OFFSHORE NEW ZEALAND**

S.A. HENRYS<sup>1</sup>, I.A. PECHER<sup>1</sup>, S. BANNISTER<sup>1</sup>, F.J. DAVEY<sup>1</sup>, Y. NISHIMURA<sup>2</sup>, A. YAMADA<sup>3</sup>, H. SHIMAMURA<sup>3</sup>, NIGHTWORKINGGROUP<sup>3</sup> (Institute of Geological and Nuclear Sciences, Lower Hutt, New Zealand, <sup>2</sup>Hokkaido University, Sapporo, Japan)

The North Island Geophysical Transect (NIGHT) was conducted in 2001 to study the Hikurangi subduction zone. The study included a multichannel seismic (MCS) reflection and a wide-angle seismic survey with ocean bottom seismometers (OBS) and onshore-offshore (o-o) stations. We will present stacked and time-migrated images of the MCS. We used velocity information from the wide-angle experiment to stretch these images to depth. A subducted seamount is displayed about 40 km landward of the trench. A small accretionary prism is forming seaward of this seamount. An up to 10-km-thick sedimentary basin seems to be present landward of the seamount. The margin is underlain by oceanic crust of the Hikurangi Plateau, a large igneous province. We estimate its thickness at 10-12 km based on wide-angle arrivals in the OBS records. The Hikurangi Plateau is being subducted at a dip of 2-3 degrees close to the trench. A pronounced increase of subduction dip about 120 km away from the trench is displayed in MCS sections. The change of dip of the subducted plate appears to coincide with the eastern termination of the sedimentary basin as well as a stratigraphic high; the Lachlan Ridge. From the o-o data, we infer the presence of a low velocity zone above the subducted plate at this location. We speculate that the increase of subduction dip may be linked to a major tectonic process shaping the East Coast of New Zealand's North Island, perhaps normal faulting of the Hikurangi Plateau caused by loading from the overriding plate. The low velocity layer may mark sediments entering the subduction zone.

**SS03/08A/D-147** Poster **0830-306**

**MODES OF CRUSTAL EXTENSION DETERMINED BY RHEOLOGICAL LAYERING**

Chris WIJNS<sup>1</sup>, Roberto WEINBERG<sup>2</sup>, Klaus GESSNER<sup>2</sup>, Louis MORESI<sup>3</sup> (<sup>1</sup> School of Earth and Geographical Sciences, University of Western Australia, Crawley, WA 6009, Australia, <sup>2</sup>CSIRO Exploration and Mining, PO Box 1130, Bentley, WA 6102, Australia, <sup>3</sup>School of Geosciences, Monash University, VIC 3800, Australia)

Metamorphic core complexes form during continental extension when stretching is strongly localised onto relatively few normal faults. Each fault accommodates large displacements, eventually dissecting the upper crust and resulting in exhumation of the lower crust. In our numerical models, the extending crust is mechanically stratified through the temperature gradient, which dictates the transition from strong, brittle, upper crust to a weaker, ductile, lower crust. We use a two-dimensional Lagrangian Integration Point finite element code which allows simulations to develop very large strains comparable to those found in analogue models, while still tracking strain history accurately for the constitutive laws. The viscoplastic formulation, with strain and/or strain-rate weakening behaviour, gives rise to the localisation of deformation and necking of layers. Results show two distinct extension modes which depend upon vertical rheological contrasts: the distributed faulting mode and the metamorphic core complex mode. In the absence of pre-existing weaknesses, the ratio of the integrated strength of the upper to lower crust is an indicator of the resulting mode of extension. When the strength of the lower crust approaches that of the upper crust (small ratio), the result is distributed, densely spaced faulting, with limited slip on each fault, and no exposure of lower crustal rocks. An example could be faulting in the North Sea. Metamorphic core complexes develop when the lower crust is much weaker (large strength ratio) and flows easily. Significant block rotation, and consequent large displacements along faults, leads to the complete dissection of the upper crust, as may be the case for core complexes of the Western U.S.A. and the Aegean. Numerical temperature-time paths for our metamorphic core complex models are comparable to field data from apatite fission-track thermochronology for the Central Tethyan in western Turkey. The actual critical strength ratio for the transition between modes will depend upon such factors as the relative thickness of the lower crust with respect to the upper crust, and the degree of fault weakening.

**SS03/08A/D-148** Poster **0830-307**

**THE CENTRAL MEXICO INTERMEDIATE-DEPTH EARTHQUAKES AND THEIR RELATIONSHIP TO THE REGIONAL LITHOSPHERIC STRUCTURE**

Jaime YAMAMOTO, Luis QUINTANAR (Instituto de Geofísica, Universidad Nacional Autónoma de México)

Moderate magnitude but damaging earthquakes occur frequently in the central part (18° N) of Mexico along a limited east-west (96°-99° W) narrow belt. From 1928 through 2002 this region of western Guerrero and Puebla-Oaxaca has been the site of twelve intermediate depth earthquakes of similar characteristics, focal depth (~70-100 km), normal faulting mechanism and an strong energy release directivity toward the northwest of the epicenter. Understanding the genesis of earthquakes in this region of Mexico is not only important from the theoretical point of view but also from practical reasons, intermediate-depth earthquakes occur inland, in very populated areas, and their ground motion accelerations seems to be higher than accelerations produced by shallow thrust earthquakes of similar magnitude. Besides, they are frequently used in the discussion of the feasibility of the seismic cycle hypothesis, an important tool for prediction purposes. In the present paper we carry out an overall analysis of the earthquakes to find out common features in an attempt to characterize them and to correlate their occurrence to peculiarities in the regional lithosphere structure. Special emphasis is placed on recent earthquakes since they are best documented. Our analysis indicates that the observed spatial distribution of intermediate-depth focus earthquakes suggests the possible existence of a fracture of the subducted plate in central Mexico. Moreover, we speculate that oceanic plate segments at both sides of the fracture descend into the mantle with slightly different strike and dip. Some observed geotectonic features of southern Mexico as the Balsas Depression is probably related to this particular subduction process. The uniformity of focal mechanism solutions of earthquakes in the region suggests that they occur along a pre-existing complex deep-seated normal fault

system, probably in the upper part of the subducting plate.

**SS03/08A/D-149** Poster **0830-308**

**CRUSTAL MODELING FROM GRAVITY AND TOPOGRAPHY CORRELATIONS TO CONSTRAIN VERTICAL MOTION IN THE NORTHERN US AND CANADA**

Laramie Vance POTTS<sup>1</sup>, A. BRAUN<sup>2</sup>, C.K. SHUM<sup>1</sup> (Laboratory for Space Geodesy and Remote Sensing Research, The Ohio State University, <sup>2</sup>Byrd Polar Research Center, The Ohio State University)

To assess the tectonically-induced vertical motion of the crust in the northern US and Canada, we investigate the present compensation state of the crust and lithosphere from spectral correlation analysis of topography, bathymetry, and free-air gravity anomalies. Top loading scenarios on regional vertical crustal motions from GIA models, consisting of ice loading histories, upper and lower mantle viscosity and ice thickness data, are limited by model assumptions applicable only on a global scale. In general, GIA models do not well represent regional deformation patterns such as over the Great Lakes region where tectonic processes have additional influence. These effects have to be removed before constraining GIA parameters. We focus on isolating tectonically driven vertical motion, compressive stress regimes and mass imbalances of the crust from gravity and topography correlations. We use free-air and terrain gravity correlations to differentiate regional variations in crustal isostatic mass variations. Topography and bathymetry data are extracted from Shuttle Radar Topography Mission (SRTM), GTOPO30 and ETOPO5, respectively, and free-air anomaly components from available gravity (terrestrial, altimetry, GRACE, CHAMP) models. We separate the free-air gravity anomalies into terrain-correlated and terrain-decorrelated component using the spectral properties of the free-air and computed terrain gravity effects. Adjusting the terrain effects for terrain-correlated anomalies yields compensated terrain gravity effects that we evaluate for crustal thickness variations. Terrain-correlated anomalies are interpreted for uncompensated elements of the crustal thickness variations differentiate regional variations in crustal rheologies. A validation of this approach was carried out on studies of impact basins on the Moon, Mars, and Venus where we were able to unmask gravity effects of subsurface mass concentrations. These results provide insight on the mechanical attributes of planetary lithospheres from impact basin ring attributes. We extend our approach over North America to isolate regions in the crust where stresses may dominate and influence crustal motion. Crustal thickness variations in addition to uncompensated mass anomalies may provide additional constraints on modeling tectonic evolution and constraining GIA parameters which in turn are important to estimate mass balance and ice history of former and present ice sheets and their contribution to sea level change.

**SS03/08A/D-150** Poster **0830-309**

**A SEISMIC STUDY OF THE CRUST IN A CENTRAL SECTOR OF THE NEUQUEN BASIN, ARGENTINA (38 DEG SL)**

Alberto H. COMINGUEZ<sup>1</sup>, Juan R. FRANZESE<sup>2</sup> (<sup>1</sup>CONICET - Departamento de Geofísica Aplicada, Universidad Nacional de La Plata, <sup>2</sup>Centro de Investigaciones Geológicas, Universidad Nacional de La Plata - CONICET)

Deep seismic sections were obtained by mathematical reprocessing of conventional vibroseis data recorded in the central sector of the Neuquen Basin. The lines involved linear upsweeps with frequency band of 12-65 Hz and time-length of 8sec. The field records were characterized by time-lengths of 13 sec and asampling period of 4 msec. The Self-Truncating Extended Correlation algorithm was used to compute cross-correlation between the sweep and the records. The original frequency-band of 12-65 Hz was preserved for the first 5 sec of trace. However, this band was affected by an upper-frequency decreasing from 5 sec on, at a predicted linear-rate of 6.625 Hz/sec. Hence, correlated deep-records with time-length of 11 sec and a final trace-band of 12-25 Hz were calculated. Depth-migration was implemented on the extended traces. Consequently, progressive models of crust velocity were iteratively matched with the corresponding migrated log. The iterative process was considered concluded when it was observed acceptable coincidence between the model and the depth-migrated horizons. The basin stratigraphy in the area consists of continental sequence of initial sinrift (Precuyano) deposited on halfgrabens, followed by strong cycles of marine and continental postrift units (Cuyo, Lotena, and Mendoza groups). In addition, continental sedimentaries are present covering the before sequences (Rayoso and Neuquen groups). The initial tectonics is considered of Superior Triassic-Liasic age. While, the postrift phase would have extended until Early Cretaceous. The analysis in the area of Las Carceles reveals the following: (1) The lower-crust top is placed at about 23-24 km; (2) An oblique reflector horizon between 16 and 18 km depth, is considered as a master shear that controlled the extensional system; (3) A submaster fault, between 8.5 and 12 km depth, is partially recognized in seismic sections; (4) The top of the rift basins is characterized by irregular depths that, from W to E, fluctuates from 9 to 5 km; (5) Evident features of tectonic inversion, including sinrift as well as part of postrift sequences (i.e. Cuyo and Lotena groups) are observed to the W of Los Chihuidos dorsal (this inversion episode was possibly initiated in the Bathonian-Callovian). In Bajada de Anelo, the study demonstrated that: (1) The top of the pre-liasic basins is located at about 5 km depth, showing a smooth topographic relief; (2) In the central-western sector are detected features of bipolar inversion (this inversion episode dated Pliensbachian-Torician is previous to the Bathonian-Callovian inversion, and is not reported in previous papers); (3) The middle level of the Cuyo group is characterized by oblique reflections related with a strong sedimentary progradation toward the west.

**SS03/08A/D-151** Poster **0830-310**

**SEISMICITY, KINEMATICS AND CRUSTAL STRUCTURE OF CUBA**

Bladimir MORENO (Centro Nacional de Investigaciones Sismológicas)

Earthquake data from the new Cuban Seismograph Network has been used to obtain basic results that are necessary for other research applications. The locations of the earthquakes were greatly improved with a new P-wave velocity model, which was obtained combining the Cuban and Jamaican catalogs. The model has seven layers with a crust-mantle interface at 20 km and average velocity of 7.6 km/sec. Moho depth at Cuban seismic stations was estimated using Receiver Function Technique indicating both continental and oceanic crust in Cuba. A new attenuation relation for the quality factor Q as well as a new local and coda magnitude scales were calculated, suggesting strong attenuation for eastern Cuba. Based on these results, a seismicity and kinematic analysis in eastern Cuba was performed. Relatively deep seismicity observed in Santiago Deformed Belt (SDB) supported by earthquake focal mechanisms suggest that the Gonave Microplate is underthrusting the Cuban block in this area. Principal stress axes determined from stress-inversion of focal mechanisms indicate a thrust faulting regime along the southern Cuban margin in agreement with the dominant structural trend associated with the SDB. The orientation of the principal stress axes seems to be induced by the oblique motion of two blocks involves in strike-slip deformation.

SS03/08A/D-152

Poster

0830-311

**THE BLOCK STRUCTURE MODEL OF THE SUBDUCTION ZONE AND CLASS FREQUENCY LOW OF THE EARTHQUAKES**

Alexander N. KROLEVETS (Kamchatka State Pedagogical University)

The elastic energy is considered to accumulate by the hierarchically organized geometrically similar geoblocks. The distinctive feature of the model is the giving up the idea of block nesting. The blocks are not overlapped, and altogether formed the outlying part of a wedged shape continental plate. The sizes of the blocks decrease towards axis of a seismic active zone. The sizes  $L$  of the largest blocks are first hundreds of kilometers. The number  $dB$  of blocks on the sizes  $L$  distribution have the form:  $dB-dL/L\delta$ . The power  $\delta$  is on a unit bigger than the number of the block dimensions counting - height, width and length, which is divided while the transition from blocks of one hierarchical level to the next one. The earthquakes take place at the very instants when the block accumulated energy releases. The maximum energy accumulated by the blocks, is the power function of their sizes with the power of  $a$ . The mean duration of the energy accumulation-release cycle is also the power function of the block size and  $\beta$  is the power. The slope  $\gamma$  of the earthquakes frequency - class diagram is connected with  $\delta$ ,  $\gamma$ ,  $a$  by the formula  $\gamma=(\delta+\beta-1)/a$  and does not depend on the similarity factor of the blocks. For the system of blocks concerned (type I) forming a wedge,  $\delta=2$ , and  $a=3$ . Accepting  $\beta=1$  (the average duration of the seismic cycle of a block is proportional to its size) we shall receive  $\gamma=2/3$  for the strongest Kuril-Kamchatka earthquakes (class above 12.7), and the value is in good agreement with the observed value 0.72. The gaps between the blocks and the faults not dissecting blocks completely are in turn filled with hierarchies of rectangular shaped blocks of much smaller sizes. The blocks of such hierarchies engender earthquakes of class below 12.7. Suitable are the hierarchies with  $\delta=2$ , and  $a=2$  (hierarchy type II) and with  $\delta=3$ , and  $a=3$  (type III). The structures will give the value  $\gamma=1/2$  typical for weak Kamchatka earthquakes, if it taken into account for structures II  $\beta=0$  (duration of a seismic cycle of the blocks does not depend on the sizes of the blocks) or for structures III to accept  $\beta=-1/2$  (the duration of a block cycle is an decreasing function of its dimensions). The latter means that the block structure in sites consisting of the smallest blocks is stronger. The structure rearrangement becomes possible in zones of maturing of the powerful earthquakes from one type of hierarchy (type III:  $\delta=3$ ,  $\beta=-1/2$ , and  $a=3$ ) to another (type II:  $\delta=2$ ,  $\beta=0$ , and  $a=2$ ). Thus the media gets an opportunity to tune the phase of the internal processes to external influence. After the earthquake the opportunity disappears. It, probably, explains the occurrences of earthquakes precursors of periodicity types before strong earthquakes while observing weak seismicity, high-frequency seismic noise, pulse electromagnetic emission, which disappear after earthquakes.

SS03/08A/D-153

Poster

0830-312

**DZIRULA BASEMENT-CORED TECTONIC WEDGE: STRUCTURE AND KINEMATIC EVOLUTION, GEORGIA**

Victor Michael ALANIA (Department of Tectonics, Institute of geology, Georgian academy of sciences)

Georgia as a part of the Caucasus region is situated within the Alpine-Mediterranean belt and consists of two major thrust and fold belts: the Greater Caucasus and Achara-Trialeti, separated by Georgian foreland basin. Between Greater Caucasus and Achara-Trialeti thrust and fold belts, Paleozoic basement outcrops in the Dzirula massif separates the Georgian foreland basin into the Rioni and The Kartli. We present of N-S crustal scale balanced cross-section across Greater Caucasus, Dzirula massif and Achara-Trialeti thrust and fold belt based on geological and geophysical data in order to better understand of structure and late Alpine kinematic evolution of the Georgian thrust and fold belt. Section balancing, together with forward modeling, was used to develop a new tectonic model for the central Georgian thrust and fold belt. Balanced sections suggest that formation of Dzirula basement-cored tectonic wedge structure is related to the southward thrusting of Greater Caucasus accretionary wedge and the presence of "Alpian - style" basement-cored nappes. These structures were formed during late Alpin time, probably late Miocene-Pliocene and characterized by a thick-skinned style of shortening. The amount of displacement of the Dzirula tectonic wedge indicating large horizontal crustal shortening and is accommodated by backthrusting of the Jurassic and Cretaceous strata of the overlying above Paleozoic basement rock. Thrust front of tectonic wedge is linked by backthrust and is structural boundary between Achara-Trialeti and Greater Caucasus thrust and fold belts.

SS04

**STRONG GROUND MOTION, EARTHQUAKE HAZARD AND RISK**

Location: Site A, Room 3

Monday, July 7 AM

Presiding Chairs: K. Shedlock, W. Zhongliang

SS04/07A/A03-001

Invited

0915

**S-WAVE VELOCITY STRUCTURE AT EURO-SEISTEST, VOLVI, GREECE DETERMINED BY ARRAY OBSERVATION OF MICROTREMORS**Kazuyoshi KUDO<sup>1</sup>, Tatsuo KANNO<sup>2</sup>, Hiroshi OKADA<sup>3</sup>, Tsutomu SASATANI<sup>3</sup>, Pashalis APOSTOLIDIS<sup>4</sup>, Dimitrios RAPTAKIS<sup>5</sup>, Kyriazis PITILAKIS<sup>6</sup> (Earthquake Research Institute, University of Tokyo, <sup>2</sup>National Research Institute for Earth Science and Disaster Prevention, <sup>3</sup>Graduate School of Science, Hokkaido University, <sup>4</sup>Department of Civil Engineering, Aristotle University of Thessaloniki)

S-wave velocity structures crossing the Volvi basin along the EURO-SEISTEST, were estimated by the phase velocity dispersion of Rayleigh waves included in microtremors using the Spatial-Autocorrelation (SPAC) method. The Volvi basin is a 5km-wide and 200-m-deep sedimentary valley extending to east and west between the Lagada and Volvi lakes in the Mygdonian graben. The two-dimensional underground structure crossing the valley was well determined by borehole data of geology, down-hole and cross-hole surveys, seismic refraction surveys, surface-wave inversions using explosion records, 2-D and/or 3-D earthquake observations, and simulation works. Our primary objective is to compare our results with those determined by the other methods and to understand an applicability of the array observation of microtremors for site characterization. The existing S-wave velocity models were mostly determined by surface wave inversion using explosion records. The phase velocity dispersion obtained near the center of the valley by the SPAC method is in reasonable agreement with that of explosion data. However, the depths of bedrock at other sites have some disagreements between the present study and the existing model. The

difficulty to determine the S-wave velocity of bedrock exists not only in the methods using microtremors but also other methods of seismic prospecting. Boldly speaking, array measurements of microtremors are superior to the other methods to determine S-wave velocity structure, if we could use microtremors in a wide frequency range. The power of microtremors at low frequency range is significantly low in the Volvi basin compared with Japan, however, the array observations of microtremors is very promising method for determining S-wave velocity structures from shallow to intermediate with less restriction in urbanized areas. The SPAC method, used in this study, generally provides an equivalent result to that of surface waves from artificial source with smaller array size; therefore, it is very useful for applying to site characterization in sedimentary basins. Surface wave inversion techniques are obliged to assume a flat layering structure, while the Volvi basin is roughly two-dimensional structure with variations of bedrock depth and/or thickness of surface layers. The phase velocity of microtremors is more or less affected by some laterally heterogeneous structures; hence the inverted S-wave velocity structure should have some uncertainties. To verify this issue, a reflection survey crossing the valley for determining bedrock shape using P-wave and a simulation analysis for giving theoretical basis are suggested as our future study.

SS04/07A/A03-002

0945

**3-D STRUCTURE OF THE KANTO BASIN, JAPAN FROM JOINT INVERSION OF REFRACTION AND GRAVITY DATA**Afinimar AFNIMAR<sup>1</sup>, Kazuki KOKETSU<sup>1</sup>, Masao KOMAZAWA<sup>2</sup> (Earthquake Research Institute, University of Tokyo, <sup>2</sup>Geological Survey of Japan)

The underground structure of Kanto Basin has been revealed from various kinds of data such as seismic refraction/reflection, borehole, microtremor, gravity etc. Unfortunately, the data distribution of refraction, reflection, borehole and microtremor is sparse and/or irregular. In the refraction or reflection traveltimes inversion, this case leads the low-resolution problems for complicated and fine spacing model, although this inversion has better resolution than that gravity data, especially in the deep target. In the other hand, the gravity observation was carried out densely and homogeneously but its data inversion hold the inherent non-uniqueness and cannot measure seismic velocity directly. We propose a joint inversion of refraction and gravity data to reveal a more detail structure of Kanto Basin. According to the geological feature, the basin is parameterized by one-half interface, two-variable interfaces with constant sediment slownesses and laterally heterogeneous basement slowness. The interfaces and basement slowness are defined by a set of knot points with the Lagrange interpolation. Densities for gravity calculation are related to the slownesses through experimental formulae. Model regularization is introduced to avoid oscillatory artifacts and non-uniqueness in a solution. The result of the joint inversion recovers more detail than that inversion of traveltimes only. The distribution of the basement slowness is in good agreement with a geological interpretation in this area. We also conduct a ground motion simulation in Kanto Basin using these results. The synthetic waveforms simulate observed seismograms quite well.

SS04/07A/A03-003

1000

**THE DETERMINISTIC ESTIMATION OF SITE EFFECTS AND SEISMIC HAZARD MAP IN BEIJING AREA**Zhifeng DING<sup>1</sup>, Yuntao CHEN<sup>1</sup>, Giuliano F. PANZA<sup>2</sup> (Institute of Geophysics, China Seismological Bureau, <sup>2</sup>Department of Earth Science, Trieste University, Trieste, Italy)

For the realistic modeling of the seismic ground motion in lateral heterogeneous anelastic media, the database of 3-D geophysical structures for Beijing City has been built up to model the seismic ground motion in the City, caused by the 1976 Tangshan and the 1998 Zhangbei earthquakes. The hybrid method, that combines the modal summation and the finite difference algorithms, is used in the simulation. The modeling of the seismic ground motion, for both the Tangshan and the Zhangbei earthquakes shows that the thick Quaternary sedimentary cover amplifies the peak values and increases the duration of the seismic ground motion in the northwest part of the City. Therefore the thickness of the Quaternary sediments in Beijing City is the key factor that controls the local ground effects. Four zones are defined on the base of the different thickness of the Quaternary sediments. The response spectra for each zone are computed, indicating that peak spectral values as high as 0.1g are compatible with past seismicity and can be well exceeded if an event similar to the 1697 Sanhe-Pinggu occurs. The seismic hazard map in North China is assessed using a deterministic approach method. The seismic sources are represented at a set of grid points located at distances of 0.2° from each other. The main inputs for this computation are earthquake catalogue, source mechanisms, the level of seismic activity and the structural models. Synthetic seismograms are generated by different sources, and are used to obtain the distribution map of the maximum ground motion and design ground acceleration (DGA).

SS04/07A/A03-004

1015

**SITE EFFECTS IN URBAN AREAS : RECENT RESULTS ON SITE CITY INTERACTION**Pierre-Yves BARD<sup>1</sup>, Jean-Louis CHAZELAS<sup>2</sup>, Philippe GUGUEN<sup>1</sup>, Marc KHAM<sup>2</sup>, Jean-François SEMBLAT<sup>3</sup> (<sup>1</sup>LGIT/LCPC, Grenoble Observatory, <sup>2</sup>LCPC, Paris, France, <sup>3</sup>LCPC, Nantes, France)

Several observations raised the concern about a possible modification of the seismic wave field in densely urbanized areas, due to interactions between soil-structure interaction and site conditions. While the previous studies were mainly considering the simple superposition of many isolated singly-interacting systems (as in single scattering), this presentation will focus on recent results on multiple interaction (analog to multiple scattering) obtained with both centrifuge tests and BEM modelling for 2D structures. Two model buildings have been designed and installed within a centrifuge filled with carefully deposited sand. Centrifuge rotation allows to reach an acceleration of 100 g, and therefore to dilate the space scale by a factor 100. The excitation of one of the model building with a shock, induces a shaking also in the second building; the recordings show that the interaction is increasing when the building to building distance is decreasing, and is maximum when the two buildings have identical frequencies: in that case, beating signals are clearly observed, showing a strong interaction, and similar in some way to strong motion recordings actually observed in some buildings or within densely urbanized areas such as Mexico City. On the other hand, a 2D BEM code has been used for investigating the seismic response of a set of buildings with variable number, size and position, overlying a layered half-space with variable thickness, for incident SH, SV and P waves. In addition to a clear evidence of the interaction effects both within and outside the built area, the parametric study allows to draw conclusions on the main controlling parameters: the most efficient interaction is obtained when building and soil frequencies coincide. In that latter case, the energy of the building induced perturbations with respect to the free field situation may reach 50 to 100 % within the built area, and from 10 to 20% several hundred meters apart.

SS04/07A/A03-005

1030

**A STUDY ON SITE EFFECTS IN ADAPAZARI, TURKEY, FROM STRONG- AND WEAK MOTION RECORDS**

Oguz Asim OZEL, Tsutomu SASATANI (Graduate School of Science, Hokkaido University, Kita-ku N10 W8, Sapporo, 060-0810, Japan)

Approximately 7000 people were killed due to collapse of buildings in Adapazari City during the 17 August 1999 Izmit, Turkey earthquake ( $M_w=7.4$ ). Most of the fatalities and damage occurred in the city center. Adapazari City is located on a deep sedimentary basin; the thickness of the alluvial deposits is more than 300 m. A strong-motion observation array was deployed in and around Adapazari City after the earthquake by the University of Bogazici to study the site response that caused considerable damage in the city. The temporary array consisted of nine stations, four of which were located in the heavily part of the city center, and was operated from August 29, 1999 to October 10, 1999. In this study we use records from the four stations in the city center and the adjacent rock site. Eleven aftershocks are selected in our analysis based on the signal-to-noise ratio; these events have a magnitude range of 3.2 to 5.8. We estimate S-wave spectral ratios of the basin site records to the reference site. These spectral ratios show that the basin S waves are amplified by 2 to 5 times compared to the reference site in the frequency range of 0.5 to about 5 Hz but are strongly de-amplified at frequencies higher than 5 Hz. The apparent de-amplification at the basin sites at high frequencies can be attributed to the site amplification at the reference rock site at these frequencies. We confirm the rock site amplification based on the S-wave H/V (horizontal to vertical) ratios; the average H/V ratio shows about unity with weak frequency-dependency in the frequency range of 0.5 to 5 Hz, but it increases from unity at 5 Hz to about 4 around 10 Hz. We also compare the empirical site amplifications (spectral ratios) with the theoretical ones calculated based on S-wave velocity structures; an agreement between them is generally good. In addition to strong S-wave amplifications, the basin site records show strong excitation of long-period (about 2 sec) surface waves after S-wave arrival during the aftershocks with magnitudes greater than 5; these surface waves produce the long duration of shaking (longer than 30 sec). We conclude that severe damage in Adapazari City during the 1999 Izmit earthquake was caused by not only strong S-wave amplifications but long duration of shaking due to basin-induced surface waves, as well.

SS04/07A/A03-006

1100

**USING MICROTREMORS FOR CHARACTERIZING SITE RESPONSE IN GREATER CAIRO AREA AND GENERATION OF MICROSEISMIC ZONATION MAPS**

Mohamed Ahmed GAMAL, Yehia Elsaid ABDELHADY (Geophysics)

We have used portable velocity seismometers and accelerometers to record ambient noise arising from cultural disturbances and long-period microtremors at the Nile valley cut through Cairo City to define site response within Cairo. The valley is filled with Quaternary deposits mainly of alluvium, silt and graded sand and lime powder. River Nile valley is surrounded by densely populated urban environment. Microtremors were recorded using point-by-point technique in a 5 profiles covering almost the whole area of Cairo. While the Nile valley including its islands of Roda and Zamalek show some fixed peaks at 2.5-3 and 8-9 Hz at the center of the basin, the next surrounding area to the Nile shows disappearance of the fundamental peak leaving 2nd resonance peak. Other sites at Greater Cairo show different peaks depending on their own soils. Resonant frequencies predicted by one-dimensional modeling of the Nile valley center show excellent agreement with observations. The 2.5-3 Hz spectral ratio peak is interpreted as the fundamental resonance mode related to the soft unconsolidated alluvium and sand while 8-9 Hz is interpreted as the resonance peak coming from the older competent underlying rock. The unrealistic amplification factors implied by old microtremor methods is recovered by using spectral ratio between site raw spectra and fixed value flat spectra. This gives more realistic peak amplification and a frequency resembles the traditional site to reference site spectral ratio method but in a more realistic amplification. A microseismic zonation maps based on soil response is generated to help in studying earthquake hazards in one of the most populated areas in Egypt, which is its capital.

SS04/07A/A03-007

1115

**SITE RESPONSE EVALUATION USING H/V AND SPECTRAL RATIOS IN THE TAIPEI BASIN**

Huey-Chu HUANG, Yi-Xiang CHIU (Institute of Seismology, National Chung Cheng University)

The relationships between the spectral characteristics of earthquake ground motions are investigated using the observed data from a dense strong-motion network consisting of 69 stations in the Taipei basin. Many high-quality recordings, including those of the 921 Chi-Chi earthquake ( $M_w=7.6$ ), the 331 Hualien earthquake ( $M_w=6.8$ ), the 921 aftershocks ( $M_w > 6.5$ ), as well as some weak motion events are selected to evaluate site responses. The stations TAP051 and TAP086 are chosen as the reference stations. The predominant frequencies obtained from H/V ratios are consistent with those from spectral ratios. On the basis of the spectral ratios and H/V ratios of weak-motion events, it is concluded that the lower predominant frequencies ( $< 1.5$  Hz) appear in the basin area, while the higher values are near the mountainous region (around the Taipei basin). The site characteristics between the strong and weak events are different, however. This implies that a nonlinear effect probably occurred with the strong-motion events.

SS04/07A/A03-008

1130

**THE NON-LINEAR SITE RESPONSE AT DAHAN DOWNHOLE ARRAY SITE DURING 1999 CHI-CHI TAIWAN EARTHQUAKE**

Hung-Chieh CHIU (Institute of Earth Sciences, Academia Sinica)

We develop a new algorithm to correct the orientation errors of the downhole seismometers. Then, we study the site response at Dahan downhole array site based the data recorded in the Chi-Chi, Taiwan Earthquake sequence. This proposed algorithm consists of three stages: (1) rotating two horizontal ground motions on the free surface to the SH V direction and considering the SH axis as a reference direction, (2) computing the synthetic downhole SH waves at downhole station, and (3) searching a optimized orientation correction that results in a best waveform match between the synthetic and observed downhole seismograms. Then, the rotated angle corresponding to the best waveform match can be considered as the orientation error. We selected five earthquakes that have a good data quality for analyses. Results show that this algorithm gives a more stable estimation than a conventional method because it allows selecting data from a wide time window for analyses. The estimated orientation error of the accelerometers at the Dahan Downhole Array after the 1999 reinstallation are 40, 114 and 285 degrees at depths of 50, 100 and 200 m, respectively. After orientation correction, the waveforms of this vertical array become consistent and can be used to measure the small amount of the velocity change in the shallow layers. A preliminary result shows that, the non-linear effects can be effective when the peak ground acceleration over 100cm/s/s.

SS04/07A/A03-009

1145

**ATTENUATION RELATION FOR EUROPE DETERMINED WITH EUROPEAN DATA AND RECENT NEAR FAULT RECORDS FROM CALIFORNIA, JAPAN AND TURKEY**Yoshimitsu FUKUSHIMA<sup>1</sup>, Catherine BERGE-THIERRY<sup>2</sup>, Philippe VOLANT<sup>2</sup>, Daphne Anne GRIOT-POMMERA<sup>3</sup>, Fabrice COTTON<sup>4</sup> (<sup>1</sup>Izumi Res. Inst., Shimizu Corp., <sup>2</sup>Institut de Rdioprotection et de Sûreté Nucléaire, <sup>3</sup>Hémisphères, <sup>4</sup>Laboratoire de Géophysique Interne et Tectonophysique, Univ. Joseph Fourier)

Strong ground motion close to a fault is expected to be very large, therefore, it's estimation is essential for human safety. Although a few strong motion data exist in European region, we proposed in a previous work [Berge-Thierry et al., 2002] an attenuation relation for spectral acceleration using strong motion data recorded in Europe and some in U.S.: this relationship was derived for the French Safety Rule which is applied for Nuclear Power Plants seismic hazard assessment. In this present study, we propose to constrain the amplitude saturation term related to the proximity of the fault, adding an amplitude saturation term in the regression model. We added to the data-set previously used to derive the European attenuation relationship recent large earthquakes strong motions recorded during the 1995 Hyogo-ken Nanbu (Kobe) Japanese and the 1999 Kocaeli (Izmit) Turkish events. The regression analysis adapted from Fukushima and Tanaka [1990] is non-linear, therefore an iterative procedure was applied. The determined regression coefficients lead to predict peak ground acceleration of about 0.7 g for soil at a fault distance of 0.5 km. The Q coefficient deduced from the distance coefficient is in agreement with the scattering Q model. The introduction of the saturation term leads to predict average spectral accelerations significantly lower at short distances than using the Berge-Thierry et al. [2002] law.

SS04/07A/A03-010

1200

**NONLINEAR SEISMIC RESPONSES IN 1D AND 2D MEDIA**

Avadh RAM, Arun K. GUPTA (Department of Geophysics, Banaras Hindu University)

During the past two decades, considerable effort has been devoted to develop modelling technique of seismic wave propagation in media to study the effect of the geological site conditions on the ground motions. The propagation of seismic waves plays an important role in seismic risk and hazard analysis. So far, the scientists have developed the models based on linear characteristics of the earth's medium. It is, therefore, necessary to incorporate the effect of lateral heterogeneities in the direct modelling of the wavefield in order to retrieve a correct image of the heterogeneity itself and consequently to understand the geodynamics of the studied portion of the earth. A large nonlinear response in the earth may be responsible for the significant spectral estimation of seismic waves at amplitude and distances, which may be considered within the linear elastic regime. The effect of nonlinear elasticity on the seismic wave propagation may be large and should be considered in the modelling. In the present study, we have solved the linear and nonlinear seismic wave equations for 1D and 2D and tried to see the effect of nonlinearity with the linear response using 2nd and 4th order finite difference technique. The nonlinear effect is mainly associated for soil deposits. The responses in hard rock area for linear and nonlinear case is more or less the same. Some of these results will be discussed.

SS04/07A/A03-011

1215

**FINITE-DIFFERENCE SIMULATION OF SEISMIC NOISE IN SURFACE GEOLOGIC STRUCTURES**Peter MOCZO<sup>1</sup>, Jozef KRISTEK<sup>2</sup>, Cecile CORNOU<sup>3</sup>, Sylvette BONNEFOY-CLAUDET<sup>4</sup>, Pierre-Yves BARD<sup>5</sup> (<sup>1</sup>Department of Geophysics, Faculty of Mathematics, Physics and Informatics, Comenius University, Mlynska dolina F1, 842 48 Bratislava, Slovak Republic, <sup>2</sup>Geophysical Institute, Slovak Academy of Sciences, Dubravska cesta 9, 845 28 Bratislava 45, Slovak Republic, <sup>3</sup>Institute of Geophysics, ETH Hoenggerberg, HPP P1.1, CH-8093 Zurich, Switzerland, <sup>4</sup>LGIT, Grenoble Observatory, Maison des géosciences, BP 53 X, 38041 Grenoble Cedex, France, <sup>5</sup>LGIT/LCPC, Grenoble Observatory, Maison des géosciences, BP 53 X, 38041 Grenoble Cedex, France)

The SESAME project, funded by the European Commission, has been undertaken as a partnership between various European teams in order to better assess the actual capabilities of microtremor-based site-effect investigation methods (H/V technique and array techniques). One part of this project is dedicated to the development of a numerical simulation technique, and its application to a series of representative "canonical models" and a few real sites. The presentation will focus on the description of the program package and on the preliminary results obtained for some representative models. The program package "NOISE" consists of two codes - RANSOURCE and FDSIM. RANSOURCE is designed for random space-time generation of point sources controlled by several parameters (minimum source-source distance, minimum and maximum source-receiver distances, minimum and maximum numbers of sources acting at the same time, ratio between the numbers of delta-like and pseudo-monochromatic signals, maximum-amplitude distribution). RANSOURCE output files serve as input files for FDSIM. FDSIM is designed for simulation of seismic ground motion in a viscoelastic half-space with 3D surface heterogeneities. It is based on the heterogeneous 4th-order displacement-velocity-stress staggered-grid finite-difference (FD) scheme. A realistic attenuation is included based on rheology of the generalized Maxwell body, and new definitions of anelastic functions and their memory-efficient spatial distribution. The adjusted FD approximation technique is used to model planar free surface. The effects of the parameters controlling the random space-time generation of noise sources for a homogeneous halfspace and single layer over halfspace will be shown and discussed. The source depth in particular is of crucial importance in case of 1D structures, for the composition of noise wavefield and the resulting H/V spectral ratio. Then, the effects of geometrical and mechanical parameters (velocity contrast, Poisson's ratio, sediment thickness, sediment/basement interface geometry) will be discussed for a few selected canonical models of surface sedimentary structures.

Monday, July 7 PM

Presiding Chairs: C. Yun-tai, P. Suhadolc

SS04/07P/A03-001

Invited

1400

**GROUND MOTION MODELLING AND DAMAGE EARTHQUAKE SCENARIOS: A POSSIBLE BRIDGE BETWEEN SEISMOLOGISTS AND SEISMIC ENGINEERS**Giuliano Francesco PANZA<sup>1</sup>, Luis DECANINI<sup>2</sup>, Fabrizio MOLLAIOLI<sup>3</sup>, Fabio ROMANELLI<sup>4</sup>, Franco VACCARI<sup>1</sup> (<sup>1</sup>Department of Earth Sciences, University of Trieste and The Abdus Salam International Centre for Theoretical Physics, SAND Group, <sup>2</sup>Department of Earth Sciences, University of Trieste, <sup>3</sup>Dipartimento di Ingegneria Strutturale e Geotecnica, University of Rome)

The input for the seismic risk analysis can be expressed with a description of "groundshaking scenarios", or with probabilistic maps of perhaps relevant parameters. The probabilistic approach, unavoidably based upon rough assumptions and models (e.g.

recurrence and attenuation laws), can be misleading, as it cannot take into account, with satisfactory accuracy, some of the most important aspects like rupture process, directivity and site effects. This is evidenced by the comparison of recent recordings with the values predicted by the probabilistic methods. We prefer a scenario-based, deterministic approach in view of the limited seismological data, of the local irregularity of the occurrence of strong earthquakes, and of the multiscale seismicity model, that is capable to reconcile two apparently conflicting ideas: the Characteristic Earthquake concept and the Self Organized Criticality paradigm. Where the numerical modeling is successfully compared with records, the synthetic seismograms permit the microzoning, based upon a set of possible scenario earthquakes. Where no recordings are available the synthetic signals can be used to estimate the ground motion without having to wait for a strong earthquake to occur (pre-disaster microzoning). In both cases the use of modeling is necessary since the so-called local site effects can be strongly dependent upon the properties of the seismic source and can be properly defined only by means of envelopes. The joint use of reliable synthetic signals and observations permits the computation of advanced hazard indicators (e.g. damaging potential) that take into account local soil properties. The envelope of synthetic elastic energy spectra reproduces the distribution of the energy demand in the most relevant frequency range for seismic engineering. The synthetic accelerograms can be fruitfully used for design and strengthening of structures, also when innovative techniques, like seismic isolation, are employed. For these reasons the skill of seismology to estimate realistic ground motions at a particular site should be fully exploited by seismic engineers. In fact, even if recently strong motion records in near-fault, soft soil, or basin conditions have been obtained, their number is still very limited to be statistically significant for seismic engineering applications.

SS04/07P/A03-002

1430

#### STRONG GROUND MOTIONS FOR SCENARIO EARTHQUAKES IN THE SAN BERNARDINO BASIN REGION, CALIFORNIA

Robert W. GRAVES (URS Group Inc.)

Due to its large population base, extensive built environment and close proximity to active faults, the region in and around the San Bernardino basin represents one of the highest levels of seismic risk in southern California. This basin is formed by the intersection of the San Andreas and San Jacinto faults, both of which are capable of generating  $M_w$  7+ earthquakes, stressing the need for timely assessment of the ground shaking hazard for future scenario earthquakes. Ground motion estimation is further complicated by the highly variable nature of the subsurface geology. Sediment accumulations are relatively thin in the northern portion of the basin, and then steadily increase in thickness toward the south. The maximum sediment thickness is about 1.5 km just north of the San Jacinto fault, with an abrupt step-up and shallowing of the basement surface across the fault. Existing observations from both large (1999  $M_w$  7.1 Hector Mine) and small (2001  $M_w$  4.7 Big Bear Lake) earthquakes show significant amplification and extended durations of shaking at recording sites within the basin. Recent studies using 3D numerical simulation methods have modeled these recorded ground motions in order to develop and constrain the 3D velocity structure of the basin region. The current 3D velocity models reasonably well at matching the recorded waveforms at periods of about 2 seconds and longer. To estimate the expected levels of ground shaking for future events in this region, I have performed 3D finite difference ground motion simulations for hypothetical  $M_w$  7 earthquakes on the San Andreas and San Jacinto faults. The simulations use the existing 3D structural models of the region and incorporate a suite of variable slip finite-fault rupture models. Preliminary results indicate that the largest long period motions occur when the ruptures propagate from the southeast (on either fault) toward and into the basin. Obviously, these rupture scenarios create strong forward directivity effects in the basin region; however, these effects are further amplified by the trapping of energy within the basin sediments. It is possible that this effect may be maximal for the  $M_w$  7 scenarios considered here due to the coincidence of directivity amplification at 2-3 sec period with the strong basin response in this same bandwidth.

SS04/07P/A03-003

1445

#### SCENARIO BASED STRONG GROUND MOTION MODELING IN ISTANBUL AND THE ADJACENT REGIONS

Nelson PULIDO<sup>1</sup>, Anibal OJEDA<sup>2</sup>, Kuvvet ATAKAN<sup>3</sup> (<sup>1</sup>Earthquake Disaster Mitigation Center (NIED, EDM), Miki, Japan, <sup>2</sup>INGEOMINAS, Bogota, Colombia, <sup>3</sup>Department of Earth Science, University of Bergen, Norway)

Following the disastrous earthquakes in Izmit and DAEce along the North Anatolian Fault in 1999, the earthquake hazard in the Istanbul area became a great concern. In this study we simulated the strong-ground motion in the Marmara Sea region with special emphasis in Istanbul. Simulations were based on an earthquake scenario in the Marmara Sea. Three fault rupture models were considered, including the Northern Boundary fault and the Central Marmara fault segments rupturing individually, in addition to a combined rupture of both. The input model was based on the geometry of the fault segments, size and location of the asperities along the fault plane, rupture initiation and propagation, rupture velocity and asperity rise-time. The available seismic reflection profiles in the Marmara Sea were used as a basis for constraining the geometry of the faults. We further considered the recently published stress-transfer modelling results to constrain the location of the rupture initiation. The wave propagation was modelled through a flat-layered crustal velocity structure and regional attenuation function. The required fault rupture parameters were determined from empirical scaling to the seismic moment. We calculated the ground motion time series and spectra at Istanbul city and evaluated the variability of the predicted ground motion arising from different scenario earthquakes and fault rupture parameters. We identified the most critical scenario earthquake for the Istanbul region. In the simulation of the strong-ground motion, we have used a hybrid model combining a deterministic simulation of the low frequencies (0.1-1.0 Hz), together with a semi-stochastic simulation (i.e. empirical Green's function which uses stochastic element seismogram) of the high frequencies (1.0-10.0 Hz). We applied a high-frequency radiation model which uses a smooth transition between non-spherical to spherical wave radiation as the frequency increases. Computation at each frequency range was performed separately and the total ground-motion was combined in the time-domain. The estimated strong-ground motion is largely affected by the fault rupture parameters, such as the location of the rupture initiation, the rise-time and rupture velocity. The preliminary results give an insight of the complexity of the seismic hazard in Istanbul area. Our simulated ground motion shows large values of acceleration response spectra at long periods that could be critical to the building damage at Istanbul during an actual earthquake.

SS04/07P/A03-004

1500

#### SCENARIO EARTHQUAKES FOR EMERGENCY RESPONSE AND PREPAREDNESS IN BEIJING URBAN REGION

Mengtan GAO, Yanxiang YU (Institute of Geophysics, China Seismological Bureau)

Scenario earthquake is a very important concept in earthquake disaster mitigation, especially

for the risk evaluation, hazard preparedness, and emergency response. In Megacities, which located in the earthquake prone region, the preparedness and emergency response of the event in the key of the countermeasures of earthquake disaster. Based on this understanding, the selection of the scenario earthquakes must consider the following factors: 1) The distribution of the potential sources surrounded the megacity; 2) The distribution of the active faults in and surrounded the megacity; 3) The historical earthquakes in and around the megacity; 4) The return period of the maximum magnitude of the potential sources; 5) The results of earthquake prediction for large earthquakes; 6) The basin effect of the strong ground motion. 7) The seismic design code used for construction. Beijing is a megacity, which located in the earthquake prone region. There were some strong events in the history. According to the above factors and the data of historical earthquake, the distribution of active faults, the delineation of potential source, the study of seismicity of the region, four scenario earthquakes were selected for the hazard preparedness and emergency response. The first scenario earthquake is Xiadian earthquake with magnitude 8, which locates in the east of the city, only 70 kilometers to the downtown; the second scenario earthquake is the Fengtai earthquake with magnitude 7; the third scenario earthquake is the Summer Palace earthquake with magnitude 7; and the fourth earthquake is the Sunhe earthquake with magnitude 7.5. These three earthquakes are located in urban region of the Beijing cities. These scenario earthquakes are critical for emergency response and preparedness of Beijing.

SS04/07P/A03-005

1515

#### ACTIVE FAULTING AND GROUND SHAKING SCENARIOS ESTIMATES USING EXTENDED SEISMIC SOURCES AT THE ALPS-DINARIDES JUNCTION

Francesca FITZKO<sup>1</sup>, Abdelkrim AOUDIA<sup>2</sup>, Angela SARAO<sup>1</sup>, Peter SUHADOLC<sup>1</sup>, Giovanni COSTA<sup>1</sup> (<sup>1</sup>Department of Earth Sciences, University of Trieste, <sup>2</sup>The Abdus Salam International Centre for Theoretical Physics, Trieste)

The identification and characterization of active faults as earthquake sources are essential parts of seismic hazard assessment studies. The area of the Alps-Dinarides Junction (NE Italy-Western Slovenia) is characterized by a very complex active deformation pattern and it has been struck in the past decades by the 1976 Friuli thrust-faulting earthquake ( $M$  6.5) and by the 1998, Bovec-Krn Mountain strike-slip event ( $M$  5.7). Active faulting data are used to define input fault models for computing realistic ground shaking scenarios, in the extended source approximation and for frequencies up to 1 Hz. For each fault model, we consider different nucleation points along the fault and both a uniform and a non-uniform seismic moment distribution. In this latter case, the seismic moment distribution is computed according with the K2 Model. We calculate ground motion parameters for a set of equally spaced receivers and we obtain contour maps. We validate our approach using the fault model proposed by Aoudia et al. (2000) for the 1976 Friuli earthquake, showing that our modeling and estimation of the seismic input at a specific site, when applied to different earthquake scenarios in its surroundings, can be a powerful, economically valid and easily applicable scientific tool for assessing its seismic hazard.

SS04/07P/A03-006

1530

#### SIMULATION OF STRONG GROUND MOTION IN METROPOLITAN MANILA, PHILIPPINES

Hiroaki YAMANAKA<sup>1</sup>, Nobuyuki YAMADA<sup>1</sup>, Chihoko KUMADA<sup>1</sup>, Motoi TAKEZONO<sup>1</sup>, Janila R. BAUL-DEOCAMPO<sup>2</sup>, Robert B. TIGLAO<sup>3</sup>, Barlome C. BAUTISTA<sup>3</sup> (<sup>1</sup>Dept. of Environmental Sci. and Tech., Tokyo Institute of Technology, <sup>2</sup>Philippine Institute of Volcanology and Seismology)

Metro Manila is located in one of the high seismicity areas of the Philippines. It is needed prediction of strong ground motion for seismic disaster mitigation. The surface geology is characterized by three different topographical units, namely, coastal lowland, Marikina valley, and central plateau. The former two areas are covered with Quaternary low-velocity sediments, while the central plateau belongs to good soil area. For seismic risk mitigation, effects of site amplification factors should be taken into accounts. In this study, we conducted various geophysical explorations in the area for construction of a 3D geological model and strong motion simulation due to an anticipated near-by fault. First, borehole investigation and microtremor array exploration were conducted at several sites in Metro Manila, the Philippines. Thickness of soils and clays with SPT N-values less than 20 is about 20 meters at soft soil sites in Marikina plain and coastal lowland. Rock site was covered with basalt over thin weathered layer. Deep S-wave profiles were estimated from microtremor exploration. The thickness of deep sediments is about 2 km in the coastal lowland, while it reduces thickness in the Marikina plain. The amplification factors calculated from these data agree with the observed amplification estimated from strong motion data observed in strong motion network developed by our group (Kurita et al., 2000). Using these data with existing data, we constructed a 3D underground model for seismic simulations. Then, we estimate strong ground motion using FD method for some assumed earthquakes which have simple rupture source models. The results of simulations show large velocity over 100 cm/s in the low-velocity area around the Manila city caused by directivity and site effect for the case of rupture start point from northern edge Western Valley Fault. We also simulate ground motion using rupture pattern of the 1995 Hyogo-ken Nanbu Earthquake, Japan.

SS04/07P/A03-007

1545

#### SIMULATION ANALYSIS OF GROUND MOTIONS IN KOBE CITY DURING THE 2000 TOTTORI-KEN SEIBU EARTHQUAKE USING 3D FINITE-DIFFERENCE METHOD COMBINING NONUNIFORM AND DISCONTINUOUS GRIDS

Masayuki NAGANO (Kobori Research Complex, Kajima Corporation)

This study describes 3D simulation analyses of strong ground motions in Kobe City during the 2000 Tottori-ken Seibu earthquake. Kobe is more than 300 km from the epicenter, located near the edge of the sedimentary area of the Osaka plains. Modeling of large-scale soil is required to realize wave propagation from the epicenter to the Kobe area. A numerically efficient finite-difference technique combining nonuniform and discontinuous grids is applied for the 3D wave propagation analysis. The entire soil region is divided at particular depth into two regions modeled by different nonuniform grids. Grids in the bottom region for bedrock are coarser than the top region including sediments, which largely cut down on the number of grids. Calculating steps can also be reduced by introducing the longer time increments than the top region. The top and bottom regions have two overlapping grid layers to synchronize particle velocity by interpolating velocity in space and time with each other. Accuracy of the proposed technique is validated in several test cases. Length of modeling region is 216 km, 324 km and 101 km for NS, EW and depth direction, respectively. The entire region is divided at the 3 km depth into two different grid regions. In the top region, a small area of the Osaka plains (minimum S-wave velocity is 0.5 km/s) has grid spacing of 150 m. The other top region and the whole bottom region have 900 m grid spacing, 6 times that of the finer grids. Time step in each region is varied according to the minimum grid spacing, 0.009 s and 0.054 s for the top and bottom region, respectively. The bedrock structure in the Kobe area is realistically modeled considering the inversely inclined fault configuration inferred from the geological surveys. Total number of nonuniform and

discontinuous grids is about 20M, approximately one-third of only the nonuniform grids. The computational steps for calculation can be reduced to one-fifth by the coupling effects of the grid reduction and variable time steps, which allows us tolerable use of the moderate-class workstation. Three-dimensional analysis simulates well the velocity seismograms recorded in both mountain and sedimentary sites in the Kobe area. The snapshots of the velocity wave indicate that the wave front starting from the seismic fault impinges at the left Osaka plains and travels into the Kobe area as is largely amplified. The PGVs in sediments gradually amplify from the basin edge to Osaka bay, which can be commonly seen in both observed and synthetic motions. Special amplification did not occur in the "heavily damaged belt zone" during the 1995 Kobe earthquake. The source process during the 2000 Tottori-ken Seibu earthquake generated velocity pulses with a predominant period of 6s, which results in the different PGV pattern in Kobe City.

**SS04/07P/A03-008****1615****STRONG MOTION PREDICTION FOR INLAND EARTHQUAKES IN FUKUOKA CITY AND KUMAMOTO CITY, JAPAN AND THEIR DAMAGE IMPACT**

Hiroschi KAWASE, Arichika MASUDA (Dept. of Human-Environment Studies, Kyushu University)

First we extract statistical characteristics of seismic ground motions from K-Net records observed in the Kyushu region. We select ground motions for earthquakes with shallow depths (<60km) and moderate magnitudes (>4.5), observed within 200km from hypocenters. For the envelope characteristics first we express them by Boore's envelope function (Boore, 1983) and identify its model parameters. Then we express them as a function of the magnitude M and the hypocentral distance X using two step regression analysis. For the spectral characteristics we separate source, path, and site effects from the observed Fourier spectra and express them also as a function of M and X. We use them to predict strong motions for future large earthquakes through the so-called hybrid method, in which we combine the statistical Green's function method for high frequency range with the three-dimensional finite difference method (Graves, 1996) for low frequency range. Before to predict ground motions for a hypothesized earthquake we must test our method against the ground motions observed during a previous large earthquake. We apply the method to the Hyogo-ken Nanbu earthquake and show that our synthetic waveforms match well with the observed. Note that we use 1.75 Hz as a matching frequency since we use a source model that can represent very distinctive velocity pulses (Matsushima and Kawase, 1998). Then, we apply this method to hypothesized Fukuoka and Kumamoto earthquakes. In these practical applications strong motions at the bedrock level are predicted first and then the strong motions at the ground surface are obtained by the 1-D wave propagation theory. We assume similar source scenarios as in Kobe. In case of Fukuoka City the maximum peak ground velocity (PGV) estimated reaches 130 cm/s at most, which is less than the PGV observed in Kobe. In case of Kumamoto City the maximum PGV reaches to 200 cm/s at the edge of the shallow Yatsushiro basin. From these simulations we emphasize the importance of both a detailed source rupture process and a three-dimensional basin structure for quantitative strong motion prediction.

**SS04/07P/A03-009****1630****SYNTHESIS OF STRONG MOTION, ATTENUATION CHARACTERISTICS (CODA) AND ISOSEISMALS IN INDIAN REGION**Brijesh Kumar BANSAL<sup>1</sup>, Hari Narayana SRIVASTAVA<sup>2</sup> (<sup>1</sup>Department of science and Technology, <sup>2</sup>India Meteorological Department)

Strong motion arrays and other strong motion instruments have brought out significant differences in the attenuation characteristics of peak ground acceleration in north-west and central Himalaya vis-a-vis north-east India and in the Koyna region. A few accelerographs were also triggered due to the great Bhuj earthquake of 2001. These results have been interpreted in the light of coda attenuation characteristics based on digital seismographs and isoseismal patterns. The paper also discusses the methods used to synthesize expected ground motion parameters by random summation of the Green's function and the stochastic methods for different site conditions in Delhi due to a 'hypothetical' great earthquake (magnitude 8.0) in the central Himalayas. The results have been compared with the result derived from broad band digital data due to the great Bhuj earthquake, 2001. The divergent results due to simulation and other studies, however, could be attributed to the mechanism of earthquakes, the size and geometry of the source, the rupture velocity and the local site conditions. For more realistic earthquake hazard analysis, therefore, dense network of stations in the plains of northern India is required where several populated cities (with sky rise buildings) are located. Meanwhile, the usual methodology based on isoseismal patterns still appears to provide the simplest approach for this purpose due to the similarity in the isoseismal patterns of moderate and great earthquakes. Case examples of the Bihar Nepal earthquake 1988 (Magnitude 6.0) vis-a-vis great Bihar Nepal earthquake 1934 (Magnitude 8.0) and others support these inferences.

**SS04/07P/A03-010****1645****LARGE SCALE PARALLEL 3D SIMULATION OF SEISMIC WAVE PROPAGATION AND STRONG GROUND MOTIONS USING THE EARTH SIMULATOR**

Takashi FURUMURA (Earthquake Research Institute, University of Tokyo)

Recent development of high-performance computer in Japan, The Earth Simulator (5120CPUs, 40Tflops) at JAMSTEC Yokohama Institute, realizes realistic 3D simulation of seismic waves at relatively higher frequencies. We developed a hybrid parallel code for the large-scale parallel simulation of seismic wave propagation. The simulation model uses accurate Fourier spectral method (PSM) or higher-order staggered-grid FDM in horizontal coordinate system and a conventional 4th order FDM is used in vertical direction in order for parallel computing. The 3D model is divided into a number of subregions to assign to many processors, and each processor calculates the wave propagation in each region. The MPI inter-processor communications are done at each time step to exchange data between neighbor regions. In order to include the low-velocity superficial layer in the large-scale modeling, we combine a smaller grid model embedded over a large grid model. The wavefield in each model is connected accurately by an interpolation using the FFT. We implemented the multigrid, parallel, hybrid PSM/FDM code for strong motion simulations of large earthquakes in Japan, such as the 1944 Tonankai (M8), the 1946 Nankai (M8), the 1993 Kushiro (Mj7.8), and the 2000 Tottori-ken Seibu (Mj7.3) events. The scale of the simulation model varies from 260 million to 3.3 billion grid-points. The simulation took computer memory of about 64 to 365 GB, and CPU time of about 1 to 2 hours by parallel computing using 16 to 1024 processor of the Earth Simulator. A volume rendering technique is used to visualize the simulated wavefield, and the snapshots of ground motion at each time step are combined into a MPEG movie. The simulated wavefield are compared with the observation, in terms of the waveforms and the distribution of intensity patterns. The simulation results for the 2000 Tottori-ken Seibu earthquake can be also compared with the dense array recordings from the K-net and KiK-net, NIED, Japan, which are recently installed in Japanese island at almost uniform interval of about 15 to 20 km. We found a fairly good match between the simulation results and observation from dense array, which

indicates that it is now possible to estimate the rough pattern of ground motions expected for future earthquake scenarios.

**SS04/07P/A03-011****1700****3D FINITE-DIFFERENCE SEISMIC MODELING - COMBINED EFFECTS BY HYBRID METHODS**Ivo OPRSA<sup>1</sup>, Johana BROKESOVA<sup>2</sup>, Jiri ZAHRADNIK<sup>2</sup>, Domenico GIARDINI<sup>3</sup> (<sup>1</sup>Swiss Seismological Service, ETH Zurich, Switzerland, on leave from Faculty of Mathematics and Physics, Charles University in Prague, Czech Republic, <sup>2</sup>Faculty of Mathematics and Physics, Charles University in Prague, Czech Republic, <sup>3</sup>Swiss Seismological Service, ETH Zurich, Switzerland)

Complex interactions resulting in the earthquake ground motions can be, in many cases, efficiently modelled by hybrid methods. Our two-step hybrid method combines an arbitrary 3D method evaluating the source and path effects, and the 3D finite differences (FD) to incorporate the site effects. In the 1<sup>st</sup> step we use ray, discrete wavenumber (DWN), or FD method to simulate the source and path effects in abackground regional structure. The regional model is considerably simpler than the local structure which is absent in the 1<sup>st</sup>-step model. The complex local structure is enveloped in a formal box of receivers called 'excitation box' (EB). The wavefield, due to the source and path, is recorded at EB and stored on a disk as so-called excitation. In the 2<sup>nd</sup> step, the wavefield in a relatively small model containing only the EB and its vicinity is computed. At this step, the local site structure is included inside the EB. The wavefield from the 1<sup>st</sup> step is injected at the EB into the 2<sup>nd</sup>-step model. The 2<sup>nd</sup> step is based on 3D FD performing on irregular rectangular grid. The FD approximation is of a second-order accuracy, the boundary conditions at the material interfaces are approximated via treatment of effective (geometrically averaged) material parameters. The EB is fully permeable in both steps and the result comprises all effects of the source, path, and site. The computational cost and memory requirements are significantly reduced compared to the case of all-in-one FD method. In our examples, the 1<sup>st</sup>-step crustal structure is 1D and the source is represented by a point double couple. The free surface is non-planar, the example of a local structure is a modified Volvi-Lake site with  $V_p/V_s \sim 4$  and maximum ratio of the velocities  $V_{p,max}/V_{s,min} \sim 10$ . The maximum frequency of the synthetics is 5Hz and the distance of the site from the source is  $\sim 10$  km. The comparison of the results for the hybrid FD, DWN-FD, and FD-FD hybrid solutions shows a very good agreement, despite of the fact that the ray excitation contains less complete wavefield than the DWN and FD excitations. The whole 2<sup>nd</sup>-step FD modeling needs only 6 hours on P3 1GHz, and this makes the hybrid method an effective and competitive tool for the earthquake ground motion computations.

**SS04/07P/A03-012****1715****A THEORETICAL METHOD FOR COMPUTING NEAR-FAULT GROUND MOTIONS IN LAYERED HALF-SPACES CONSIDERING STATIC OFFSET DUE TO SURFACE FAULTING - WITH PHYSICAL INTERPRETATION OF FLING STEP AND RUPTURE DIRECTIVITY -**Yoshiaki HISADA<sup>1</sup>, Jacobo BIELAK<sup>2</sup> (<sup>1</sup>Dept. of Architecture, Kogakuin University, <sup>2</sup>Department of Civil & Environmental Engineering, Carnegie Mellon University)

An efficient mathematical method is presented for computing the near-fault strong ground motions in a layered half-space, giving explicit consideration to the static offset due to surface faulting. The combined effects of "fling step" and "rupture directivity" on the near-fault ground motions are also investigated. When an observation point is close to the fault plane, Green's functions exhibit near-singularities, which consist of extremely sharp peaks in a narrow band close to the observation point. Therefore, direct numerical integration becomes quite onerous for computing near-fault ground motions, because the dynamic Green's functions must then be distributed very densely in order to evaluate accurately the effects of the near-singularities. Instead, a new form of the representation theorem is introduced, which exploits the property that the dynamic Green's functions can be approximated by the corresponding static Green's functions in the vicinity of the singularities. The modified theorem is the sum of two fault integrations. The first integration involves the difference of the dynamic and the corresponding static Green's functions, while the second contains only the static Green's functions. This formulation requires much less CPU time than the original one when near-fault ground motions are considered, because the near-singularities of the dynamic Green's functions in the first integration are completely eliminated by subtracting the static Green's functions. While the second integration does require a densely distributed set of points to capture the near-singular behavior of the static Green's function, it needs to be performed only once, as it is valid for all frequencies. Subtraction of the static Green's functions from the dynamic functions has the added benefit of making the integration over the wavenumber in the determination of the Green's functions much more efficient, especially for considering surface faulting. The proposed methodology is used to investigate the physics of the fling step and rupture directivity. The fling effects stem mainly from the second integral in the modified representation theorem, which involves the static Green's function. The fling effects are dominant in the slip direction only in the vicinity of the surface fault, and are negligible for buried faults, because the static Green's function attenuates rapidly with distance from the fault,  $r$ , as  $O(1/r^2)$ . Also, more importantly, when an observation point is located above a buried fault, the medium has to remain continuous, and thus cannot "fling". By contrast, the directivity effects stem mainly from the first integral, which involves the dynamic Green's function, and attenuate much more slowly than the fling, on the order from  $1/r$  to  $1/\text{squared } r$ . The directivity effects are dominant in the fault normal direction, especially in the forward rupture direction, not only for the surface fault, but also for the buried fault. When softer surface layers are added to the medium, the directivity effects become more significant than the fling effects, because the dynamic Green's functions are more pronounced than the static ones.

**SS04/07P/A03-013****1730****3-D MODELING OF SEISMIC GROUND MOTION PROPAGATION IN THE KANTO BASIN, JAPAN**

Kazuki KOKETSU, Kazuki KOKETSU, Animar, Takashi FURUMURA (Earthquake Research Institute, University of Tokyo)

The pattern of ground motion for a magnitude 5.7 earthquake near Tokyo, Japan was captured by 384 strong ground motion instruments across the Kanto sedimentary basin and its surroundings. Koketsu and Kikuchi (2000) visualized the propagation of long-period ground motion in the basin using the records, and show the refraction of surface waves at the basin edge. We construct a 3-D model of the Kanto basin based on the result of Animar et al. (2003) and simulate seismic ground motion propagation using a hybrid PSM/FDM method. We then compare resultant seismograms and propagation images to the above observations. The 3-D model is repeatedly revised to improve the agreement between the simulations and observations.

SS04/07P/A03-014

1745

**THREE-DIMENSIONAL SIMULATION OF SEISMIC MOTIONS IN THE NORTHWESTERN CHIBA PREFECTURE, JAPAN**

Sadanori HIGASHI, Hiroaki SATO (Geotechnical &amp; Earthquake Engineering Department, Central Research Institute of Electric Power Industry)

Three-dimensional seismic simulation was carried out in the northwestern Chiba Prefecture, Japan, based on the results of geophysical survey conducted by Chiba Prefecture. The calculated waveforms were compared with the observed records derived from the seismometers installed by Chiba Prefecture. The model, which is 29.4km(NS) by 24km(EW) in dimensions, consists of three sedimentary layers (Shimohsa, Kazusa, and Miura formations) and a seismic basement. P-wave velocities are 1.7, 2.2, 2.9, and 5.7 km/s, while S-wave velocities are 0.45, 0.9, 1.5, and 3.0 km/s, respectively. The upper boundary of the seismic basement tends to deeper in the southern area. The deeper part beneath the seismic basement (Vs3.0km/s) was modeled based on Sato et al.(1998). A hybrid pseudo-spectral method / finite difference method parallel simulation with discontinuous grid spacing was used for the seismic simulation. The model was divided into four in the vertical direction. The grid spacing in the horizontal direction was 160m, while that in the vertical direction was 80, 80, 160, and 320m, at each subdomain. Data exchange between the adjoining subdomains are carried out by using MPI (message passing interface) library. The maximum frequency was 1.25Hz and the time increment is 0.005s. Firstly, we simulated an earthquake occurred in the calculated region (M4.6, depth=71km). We used a point source with the source mechanism derived from F-NET (National Research Institute for Earth Science and Disaster Prevention, NIED) and the Herrmann's pseudo-delta function with a time width of 1.0s as a source time function (moment rate function). The velocity amplitude of calculated waveforms were in good agreement with that of observed records in the northern area, while those in the southern area were underestimated in the simulation. The calculated peak ground velocity in the southern part was smaller than that in the northern part. Secondly, a case of plane wave incidence was calculated for an earthquake of M5.1 (depth=67km). The incident wave at the upper boundary of the seismic basement was derived from the borehole data that located in the seismic basement in the area (Shimohsa deep borehole observation station by NIED). Qs in the sedimentary layers were determined as Qs-Vs/42 by fitting the spectral ratio of surface to borehole data. The results showed that the simulated peak ground acceleration was in good agreement with observed one in the northern part, while that simulated was underestimated in the southern part. As the earthquakes used in this study were deep and small, it is probable that seismic motion at a rather long-period (2-10s) did not predominate and the effects of 3-D irregularity of the interfaces was not so obvious in the simulation.

Tuesday, July 8 AM

Presiding Chairs: I.A. Parvez, F. Romanelli, H. Goto, K. Irikura

SS04/08A/A03-001

0830

**THE CHARACTERISTICS OF STRONG GROUND MOTIONS IN NEAR SOURCE**

Guoxin WANG, Hongnan LI (Earthquake Engineering Research Institute, Department of Civil Engineering, Dalian University of Technology)

Strong ground motion in near source is a very complex problem and has been paid more attention by engineers and seismologists around the world. The most important problem is how to predict the ground motions accurately for the future events. To solve this problem, the successful simulation to the motions of the past events is the essential step, which can verify the validities of different predicting methods proposed by some researchers. The characteristics of near source strong ground motions are analyzed in this paper. First, we propose an improved finite source stochastic method based on seismology and ground motion database to simulate the strong ground motions of past events in near source, and certify the efficiency of this method by comparing the predicted ground motion parameters with recorded ones by trail and error, and then we utilize the predicted results to analyze the ground motion characteristics in near source to understand the so-called saturation phenomenon and attenuation rate in near source, especially the affections of fault plane parameters, such as fault size, orientation, slip distribution, to the motions. The results of this paper prove that the suggested method is valid for not only moderate events but also strong earthquakes, and the ground motion characteristics in different orientations of fault plane can be indicated fully.

SS04/08A/A03-002

0845

**THE ATTENUATION OF STRONG GROUND MOTION IN TERMS OF INPUT ENERGY**

Mao-Sheng GONG, Li-Li XIE (Institute of Engineering Mechanics China Seismological Bureau)

The disaggregation and probabilistic seismic hazard calculations based on input energy may prove useful for the identification of scenario event because input energy is a convenient single-parameter descriptor of strong ground motion duration and amplitude. Based on 266 strong ground motion records (two horizontal components and a vertical component are included in each record) from 15 significant earthquakes in California of America, an attenuation relationship was developed for ground motion input energy spectra with earthquake magnitude, source-to-site distance, and site class. All the records are examined and classified into three site categories. For each horizontal component of one record, two kinds of input energy equivalent velocity, absolute input energy equivalent velocity ( $V = (2E/m)^{1/2}$ , where  $E$ =absolute input energy,  $m$ =mass) and relative input energy equivalent velocity ( $V_r = (2E_r/m)^{1/2}$ , where  $E_r$ =relative input energy,  $m$ =mass), were calculated for 4 ductility levels ( $\mu=1, 2, 4$  and 6) and one damping ratio ( $\xi=5\%$ ), in the period range 0.1 to 3.0 second. The geometric mean of the two horizontal components for each kind of input energy was used in a two-stage non-linear regression method. The effect of parameters such as magnitude, site class and ductility factor on the input energy spectra constructed from the attenuation relationship was discussed. It is found that the site class has a significantly effect on both absolute and relative input energy, the input energy (including both absolute and relative input energy) for soft site class is much higher than that for stiff site class. The two kinds of input energy spectral increase rapidly with the increasing of earthquake magnitude and attenuate quickly with the increasing of distance, so, larger magnitude earthquakes contribute more to seismic hazard if  $V_r$  or  $V$  is used. The effect of the ductility is very different for the input energy spectra constructed from the attenuation relationship with the change of periods. When the period of single-degree-of-freedom (SDOF) oscillator is less than 0.5 second, the input energy increases with the increasing of ductility factor, on the contrary, the input energy decreases with the increasing of ductility factor when its period is larger than 0.5 second. Also, the effect of ductility on the relative energy spectra in the short period range (say, less than 0.5 second) is much larger than that on the absolute energy spectra. After comparison of the two kinds of energy spectra constructed from the attenuation relationship, it is found that the absolute energy is some larger than relative energy in the short period range and some less than relative energy in long period range, and they are almost equivalent at the period about 0.5 second. Finally, it

is shown that the attenuation relationship developed in this paper would underestimate the input energy demand produced by a near-field strong ground motion because little number of near-field ground motion records data were used in the paper.

SS04/08A/A03-003

0900

**STUDY ON THE SEVEREST REAL GROUND MOTION FOR SEISMIC DESIGN AND ANALYSIS**Chang-Hai ZHAI<sup>1</sup>, Li-Li XIE<sup>2</sup> (<sup>1</sup>School of Civil Engineering, Harbin Institute of Technology, <sup>2</sup>Institute of Engineering Mechanics, China Seismological Bureau)

In the seismic analysis and design, the real strong ground motions are usually selected as the seismic inputs to structure. How to select the adequate real strong earthquake ground motion for seismic analysis and design of structures is logically an essential problem in earthquake engineering research and practice. For the seismic design and structure analysis, especially for the huge complex structure, one of the most important tasks is selecting the proper real ground motion for design. The idea of selecting the severest design ground motion is presented in this paper. The severest design ground motion should be selected from the existing strong earthquake ground motion that can drive the structure to its critical response and thereby result in the highest damage potential. At present, the EL CENTRO record (NS) of 1940 and TAFT record of 1952 are in the first place to be considered in the seismic design and structure analysis. However the rationality of such selection is not sufficient. For example, the study (Naem and Anderson, 1993) has shown that the EL CENTRO record (NS) of 1940 is far from severest ones, and its peak acceleration (PA), peak velocity (PV), peak displacement (PD), effect peak acceleration (EPA), effect peak velocity (EPV) and duration are 338cm/s/s, 45cm/s, 10.88cm, 290cm/s/s, 30.77cm/s and 9.3s respectively, which only rank as the 81, 87, 49, 99, 62 and 58 place in a database that consists of more than five thousand significant strong ground motion records collected over the world. Evidently, whether the records should be considered as the severest design ground motion is a problem that ought to be further thought over. The concept of the severest design ground motion is presented in the paper. A comprehensive method for estimating damage potential of ground motions is developed in this paper and it has been used in selecting the severest design ground motion. The severest design ground motions corresponding to four different classes of site condition and three different period ranges of structure are attained. The three period ranges of structure are long period range (1.5-5.5s), middle period range (0.5-1.5s) and short period range (0.0-1.5s). At the end, the validity and reliability of the severest design ground motions are verified preliminary by several numerical calculations.

SS04/08A/A03-004

0915

**3D FINITE DIFFERENCE SIMULATION WITH IRREGULAR TOPOGRAPHIC SURFACE**

Wei ZHANG, Xiaofei CHEN (Department of Geophysics, Peking University)

3D staggered-grid finite difference method is the most popular method in simulation of seismic wave propagation in complex media, in which the treatment of free surface boundary condition plays an important role to numerical computational stability and result accuracy. It's easy to implement a planar free surface boundary in two ways: the first is vacuum method, which can be easily implemented but only stable for second order in space. The second is zero-stress formulation, which explicitly satisfies the zero-stress condition in both stress and velocity components at the free surface and can get perfect result. For irregular topographic surface, there are also two widely used methods: Firstly, the vacuum method in which 3D topography is discretized in a staircase grid, then vacuum free surface with second order finite difference scheme is applied (Ohminato, 1997). However, in this method the free-surface condition in corners cannot be exactly satisfied, is only approximated (Robertsson, 1996; Hayashi, 2001). Secondly, the coordinate mapping method (Tessmer, et al. 1992; Hestholm & Ruud, 1994, 1998), in which only curved grids in vertical direction are transformed to planar grids. In this method, velocity components can satisfy the free surface condition, but stress components not. In this study, we use adaptive grid generation method to generate the grids satisfying following conditions: (1) in the area of the free surface, all vertical grids are normal to the free surface, the horizontal grids coincide with the free surface; (2) in the inner area, we try to keep the grids' smoothness and orthogonality. In such discretized grids scheme, we can implement explicit zero-stress free surface boundary condition to the irregular topographic surface, thus guarantee an accurate free surface condition is satisfied. Using this improved 3D staggered-grid finite difference method, we simulate the seismic wave propagation in a complex basin structure.

SS04/08A/A03-005

0930

**NUMERICAL SIMULATION OF STRONG MOTION AROUND ADAPAZARI BASIN DURING THE 1999 KOCAERI EARTHQUAKE, TURKEY**Hiroyuki GOTO<sup>1</sup>, Sumio SAWADA<sup>1</sup> (<sup>1</sup>Disaster Prevention Research Institute, Kyoto University, Gokasho, Uji, Kyoto 611-0011, JAPAN, <sup>2</sup>Department of Civil and Architectural Engineering, College of Engineering, Drexel University 3141 Chestnut Street, Philadelphia, 19104, <sup>3</sup>Department of Civil Engineering, Kanto-Gakuin University 1-50-1 Mutsuura-Higashi, Kanazawa-ku, Yokohama 236-8501 JAPAN)

The Kocaeli Earthquake of August 17, 1999 (Mw 7.4) brought destructive damage to Adapazari, Turkey. The area most severely damaged was downtown Adapazari and located 8-10km away from the ruptured fault; whereas, the damage was only moderate or even light near the source fault. This implies that the deep ground structure may affect the distribution of strong ground motions, as we have already observed on 1995 Hyogoken-nanbu (Kobe) Earthquake, Japan. Several surveys have been performed to obtain information of subsurface structure around Adapazari. The 3-dimensional shape of the bedrock around this area has been reported, based on gravity anomaly data, and verified by the analysis for array and single-site observations of microseisms. We, however, did not obtain the detailed velocity structures which were necessary to simulate strong ground motions in the basin. The seismic refraction and reflection survey were carried out to determine the velocity structure of the basin. Two seismic shots were detonated at northern and southern edges of the Adapazari Basin on June 14 and 16, 2002. The artificial seismic waves were collected at 80 sites along a 16km-long profile, which traversed the basin in approximately a N-S direction; although almost half of the instruments failed to record the ground motions due to several reasons. A model was made for the subsurface structure of the basin. The velocity structure at the seismic profile was estimated through a gravity anomaly analysis and refraction and reflection waves generated by the seismic shots. The estimated 2D model consists of three soil and two rock layers. The 2D model was then extended to a 3D model which is represented by a cubic B-spline function, which is based on the gravity data. The modeled structure shows narrow depressions of bedrock with very steep edges around the downtown of Adapazari. The depression runs in a E-W direction along the North Anatolia faults, and the depth to the bedrock reaches more than 1000m. Finally, the strong ground motions, simulated numerically for the main shock, were demonstrated to be in the frequency range of up to 0.4 Hz using the 3D finite-difference methods. The source model proposed by Sekiguchi and Iwata (2002) was used for the numerical simulation. The calculation

successfully simulated the waveform observed at SKR (Sakarya) during the main shock. The results of the simulation show that the ground motions were significantly greater at downtown Adapazari in comparison to the region between the downtown and the seismic fault. Furthermore, it was observed that the maximum velocity may be reduced to one-third the value obtained through our model of ground structure, if horizontal layered mediums are modeled around the downtown Adapazari.

SS04/08A/A03-006

0945

#### MICROZONATION AND SITE-SPECIFIC GROUND MOTION MODELLING FOR DELHI CITY

Imtiyaz Ahmed PARVEZ<sup>1</sup>, Franco VACCARF, Giuliano Francesco PANZA<sup>2</sup> (<sup>1</sup>CSIR Centre for Mathematical Modelling and Computer Simulation (C-MMACS), <sup>2</sup>Department of Earth Sciences, University of Trieste, Via E. Weiss 4, 34127 Trieste, Italy AND INGV, Istituto Nazionale di Geofisica e Vulcanologia, Naples, Italy, <sup>3</sup>Department of Earth Sciences, University of Trieste, Via E. Weiss 4, 34127 Trieste, Italy AND The Abdus Salam International Centre for Theoretical Physics, SAND group, Trieste, Italy)

Delhi, the capital of India lies on a severe earthquake hazard threats not only from the local earthquakes but also from Himalayan events just 200-250 km apart. The seismic ground motion in a part of Delhi City is computed with a hybrid technique based on the modal summation and the finite difference scheme for site-specific strong ground motion modelling. Complete realistic SH and P-SV wave seismograms are computed along two geological cross-sections, (1) North-South, from Inter State Bus Terminal (ISBT) to Sewanagar and (2) East-West, from Tilak Bridge to Punjabi Bagh. Two real earthquake sources of July 15, 1720 (MMI=IX, M=7.4) and August 27, 1960 (M=6.0) have been used in modelling. The response spectra ratio (RSR), ie the response spectra computed from the signals synthesized along the laterally varying section normalized by the response spectra computed from the corresponding signals, synthesized for the bedrock reference regional model, have been determined. As expected, the sedimentary cover causes an increase of the signal amplitude particularly in the radial and transverse components. To further check the site-effects, we reversed the source location to the other side of the cross-section and re-computed the site amplifications. There are only a few sites where a large amplification is invariant with respect to the two source locations considered. The RSR ranges between 5 to 10 in the frequency range from 2.8 to 3.7 Hz, for the radial and transverse components of motion along the NS cross-section. Along the EW cross-section RSR varies between 3.5 to 7.5 in the frequency range from 3.5 to 4.1 Hz. The amplification of the vertical component is large at high frequency (> 4 Hz.) whereas it is negligible in lower frequency range.

SS04/08A/A03-007

1000

#### ON PRECISION OF S-WAVE VELOCITY STRUCTURE DETERMINED BY THE SPATIAL AUTO-CORRELATION METHOD USING MICROTREMMORS

Seiji TSUNO<sup>1</sup>, Kazuyoshi KUDO<sup>2</sup>, Tatsuo KANNO<sup>2</sup> (<sup>1</sup>Earthquake Research Institute, The University of Tokyo, <sup>2</sup>National Research Institute for Earth Science and Disaster Prevention)

Conventional methods for determining shear wave velocity structure generally require active control sources, such as in PS logging, reflection/refraction surveys, and surface wave inversion using shot-records. These methods are costly in general and sometimes meet difficulties in urban area for practical uses. The array observation of microtremors provides a good estimate of the S-wave velocity structure with relatively low cost. The efficiency of the Spatial Auto-Correlation method applied to microtremors has mostly been verified for deep underground structures. However, the precision and guideline of the SPAC method are not sufficient to extend and apply in the field of engineering seismology and earthquake engineering. The primary object of us is to understand the precision and/or limitation of the SPAC method for practical use. We carried out array observations of microtremors at 7 sites, where the underground structures have already been determined by the other methods. The S-wave velocity structures determined by this method gave good agreements with the geological interfaces determined by PS logging, reflection survey and the inversion results for spectral ratios of downhole array records. We postulated that the S-wave velocity increases gradually with depth in the inversion procedures from Rayleigh wave dispersion to S-wave velocity structures, for simplicity. This approximation is certainly difficult to estimate details of the interface of layer and its velocity, however, the site amplification and dominant period of earthquake ground motion are well assessed by the structure model. The reason will be that the approximation gives an equivalent S-wave velocity structure with sufficient fitting of the observed dispersion to that of Rayleigh waves, even if we neglect high and/or low velocity layers interposed between a surface layer and a half-space. We compared the optimized S-wave velocity structure model that was determined by spectral ratios of downhole array strong motion data with the initial model determined by the SPAC method. A good agreement of the site amplification in the lower frequency than 5 Hz was also obtained without any exceptions. The differences of a velocity and a thickness of layer between initial and optimized models were mostly less than 10% from the optimized. Therefore, we may conclude that the SPAC method using microtremors has sufficient precision for applying to site characterization purposes. The level of the precision is not inferior to that of PS logging data. In addition, we also examined that the SPAC method works well for determining deep underground structure using microtremors of longer period than 1 sec. rather than shallow structure using higher frequency than 1 Hz. We found that observable wavelengths by this method were larger than 3.5 times of array radius (R) and smaller than 11R in average.

SS04/08A/A03-008

1015

#### BOOTSTRAP RESAMPLING FOR IMPROVEMENT IN THE NONPARAMETRIC SEISMIC HAZARD ESTIMATION

Beata ORLECKA-SIKORA (Department of Geophysics, Faculty of Geology, Geophysics and Environmental Protection, University of Mining and Metallurgy)

The cumulative distribution function (cdf) of magnitude is essential for the probabilistic seismic hazard analysis. The magnitude distributions are usually drawn from the Gutenberg-Richter relation or its smooth modifications. Such distributions are log-linear or at most smoothly non-linear. In practice, however, the observed frequency-magnitude relations can exhibit a multi-component structure. In non-linear cases the assumption of a simple Gutenberg-Richter based distribution is frequently inadequate and can generate unpredictable hazard errors. In order to remedy the problem a model-free, non-parametric approach to characterise the source size has been postulated. The approach proved to be effective in the mean value for both simple and complex magnitude distributions. In practical studies one has in hand only one data sample. Thus in place of the mean cdf estimate only one sample estimate is obtained. Inevitable differences between the actual cdf and its one-sample estimate result in hazard errors of unknown percentage. In order to improve the non-parametric estimation of the magnitude cdf the use of the bootstrap resampling method is proposed. A bootstrap sample is a set of items drawn uniformly from the original data sample with replacement, such that its size equals the size of the data sample. The resampling procedure performed on the real sample provides a number of data samples that have asymptotically the same properties as the real data. The bootstrap samples are then used to

reconstruct the distribution of error of the magnitude cdf estimate. This distribution is used to correct the cdf estimate for the bias and to evaluate the cdf confidence intervals. The approach has been tried on Monte Carlo generated data of given population distributions, namely mixtures of the Gutenberg-Richter born and normal distributions, which imitate non-linear magnitude distributions that can be met in practice.

SS04/08A/A03-009

1045

#### DYNAMIC SOURCE PARAMETERS AND CHARACTERIZED SOURCE MODEL

Tomotaka IWATA<sup>1</sup>, Haruko SEKIGUCHI<sup>1</sup>, Hiroe MIYAKE<sup>2</sup>, Wenbo ZHANG<sup>3</sup>, Ken MIYAKOSHI<sup>1</sup> (<sup>1</sup>DPRI, Kyoto University, <sup>2</sup>AIST, GSI, <sup>3</sup>Geo. Res. Inst.)

Somerville et al. (1999) characterized source slip models inverted from strong motion records for mainly California events. They introduced a criterion to extract rectangular-shaped asperities that an asperity consists of fault elements with final slips larger than 1.5 times of the average over an entire fault. They found that total area of asperities follows a scaling relation to seismic moment. Recent events such as the 2000 Tottori-ken Seibu (Mw6.6), Japan, the 1999 Chichi (Mw7.6), Taiwan, and Kocaeli (Mw7.4), Turkey, and some moderate-size crustal earthquakes in Japan were shown to follow the relation (Miyakoshi et al., 2000, Miyake et al., 2001). Irikura and Miyake (2001) proposed characterized source model based on this scaling relation in a RECIPE for strong motion prediction. The availability of the characterized source models has been proved through the strong motion simulation in near-source area in the broadband frequency band (BB) for the 1995 Kobe (Kamae and Irikura, 1997) and for the 1997 Kagoshima-ken Hokuseibu (Miyake et al., 1999) earthquakes. However, in those simulations, they estimated stress parameters only for the asperities by forward simulation of the high frequency contents of the records. When constructing a characterized source model for BB strong motion, we need rules to set stress parameters. Bouchon (1997) proposed a mapping method of a spatio-temporal shear-stress distribution on the fault plane from a spatio-temporal slip distribution. We examined dynamic source parameters such as stress drops, Dc (critical distance), and Gc (surface fracture energy), by his method for the 1999 Chichi, and the 2000 Tottori-ken Seibu earthquakes (e.g. Zhang et al., 2001). Dynamic parameters averaged over on- and off-asperity areas are estimated from a viewpoint of characterized source model. For the both events, average effective stress values of on-asperity areas, that were estimated to about 20MPa and 10MPa, respectively, which coincide with the ones that were used for forward ground motion modeling (e.g. Ikeda et al., 2002, Kamae and Irikura, 2001). Average effective stress value in off-asperity area was estimated about 1-5MPa. Those values both on- and off- asperity area obtained here can constrain the characterized source model parameters.

SS04/08A/A03-010

1100

#### BROADBAND SOURCE ASPERITY MODEL OF THE 2000 TOTTORI EARTHQUAKE (JAPAN) FROM A NONLINEAR INVERSION OF NEAR-Fault GROUND MOTION

Nelson Edilberto PULIDO<sup>1</sup>, Tetsuo KUBO<sup>2</sup> (<sup>1</sup>Earthquake Disaster Mitigation Research Center EDM, NIED, <sup>2</sup>Dept. Architecture, Nagoya Institute of Technology, Nagoya, Japan)

The large amount of near-fault strong motion data recorded during the 2000 Tottori earthquake, provides a unique opportunity for investigating a source asperity model of the Tottori earthquake that combined with a hybrid strong motion simulation technique, are able to reproduce the observed broadband frequency near-fault ground motion. We investigated the optimum source asperity and high frequency attenuation parameters of the Tottori earthquake, by applying a Genetic Algorithm (GA) inversion scheme to optimise the fitting between simulated and observed acceleration response spectra and PGA values of near-fault ground motion. We constrained the initial model of our inversion by using the heterogeneous slip distribution obtained from a kinematic inversion of the source of previous studies. We used all the observed near-fault ground motions (-100m) from the borehole strong motion network of Japan (KiK-Net). The calculation of broadband frequency strong ground motion (0.1 to 10Hz) is achieved by applying a hybrid technique that combines a deterministic simulation of the wave propagation for the low frequencies and a semi-stochastic modelling approach for the high frequencies. For the simulation of the high frequencies we introduce a frequency dependent radiation pattern model that efficiently removes the dependence of the pattern coefficient on the azimuth and take-off angle as the frequency increases. The good agreement between the observed and simulated broadband ground motions shows that our inversion procedure is successful in estimating the optimum asperity parameters of the Tottori earthquake, and provides a good test for the strong ground motion simulation technique. The ratio of background stress drop to average asperity stress drop from our inversion is nearly 50%, in agreement with the theoretical asperity model of Das and Kostrov (1986), and an empirical ratio of asperities to rupture area (Somerville et al. 1999). We obtained an attenuation value for the Tottori earthquake near-fault region of  $Q(f) = 146f^{0.67}$ . Our results suggest that the effect of downgoing S-waves completely disappears at the borehole depth. A forward ground motion simulation from the optimum asperity model shows that the strong motion radiation towards the North-West of the epicenter is larger than the radiation towards the South-East, despite most of the seismic moment within asperities was released towards the South-East. A possible explanation is that in the vicinity of the fault, S-wave radiation from the shallow slip North of the epicenter is more efficient than the radiation from the deeper slip South of the epicenter, as inferred from the radiation pattern coefficient distribution within asperities. The simulated PGA values have a weaker dependence on the radiation pattern compared with the PGV values, in the near-fault region. The simulated radiation pattern at 1 Hz is very complex for epicentral distances within half the fault length but it approaches the radiation of a double-couple point source for larger distances. The rupture velocity and rise time have a significant influence on the PGV distribution around the fault. An increase in rupture velocity produces a similar effect on the ground motion as a reduction in rise time.

SS04/08A/A03-011

1115

#### EARTHQUAKE SOURCE AND GROUND MOTION CHARACTERISTICS OF THE JUNE 23, 2001 MW 8.4 AREQUIPA, PERU EARTHQUAKE

Paul Graham SOMERVILLE, Hong Kie THIO, Gene ICHINOSE, Nancy COLLINS, Arben PITARKA, Robert GRAVES (URS Corporation)

The June 23, 2001 Mw 8.4 Arequipa, Peru Earthquake ruptured a 400 km length of the interface between the Nazca and South American plates, extending from Atico to Ilo. This is the largest earthquake for which strong motion recordings have been obtained. We derived a rupture model of the earthquake from the inversion of teleseismic and regional body waves and surface waves. Most of the slip occurred in the offshore region, with a large asperity offshore from Mollendo. This rupture model is compatible with geodetic measurements in Arequipa, the slight sea level rise at Matarani, and tsunami waveforms recorded in Peru and Chile. Strong motion recordings were obtained in Moquegua, Peru and at seven stations in northern Chile, including three in Arica. The response spectra of the strong motion recordings lie between the median and 84th percentile level of empirical ground motion models. We attribute these unusually large ground motions to the effect of southwesterly rupture propagation from the epicenter near Arica toward southern Peru and northern Chile.

The ground motions recorded on soil sites in northern Chile exceeded the elastic design spectrum of the 1996 Chile building code for soil type II, although these sites are 90 km or more from the southeastern end of the earthquake rupture zone. Broadband ground motion simulations using our rupture model of the earthquake produced a good fit to the recorded ground motions, with no significant bias and a standard error of a factor of about 1.5.

SS04/08A/A03-012

1130

#### SEISMIC ENERGY DISTRIBUTION ON THE FAULT PLANES OF GREAT INTERPLATE EARTHQUAKES OCCURRED ALONG THE NANKAI TROUGH REPEATEDLY DURING 300 YEARS

Katsuhisa KANDA<sup>1</sup>, Masayuki TAKEMURA<sup>1</sup>, Tatsuo USAMI<sup>2</sup> (<sup>1</sup>Kajima Corporation, <sup>2</sup>non)

Three great earthquakes (the Showa in 1944 and 1946, the Ansei in 1854, and the Hoei in 1707) have occurred since 300 years ago in the both of the Tokai and Nankai areas along the Nankai trough in southwestern Japan, where the Philippine Sea plate is subducting beneath the Eurasian plate. The Showa and Ansei earthquakes consisted of two events occurring separately in the both areas of Tokai (Tonankai) and Nankai at a short interval. The fault rupture of the Hoei earthquake took place in the both area at the almost same time. The next occurrence of the Tokai and Nankai earthquakes are predicted early in the 21st century. It is quite important for the estimation of future earthquakes to investigate the fault mechanisms of historical earthquakes. However, there is no geodetic, tsunami, and strong motion data for waveform inversion analysis except in case of most recent events, the Showa earthquakes. On the contrary, there is much seismic intensity data evaluated from seismic damage records for old earthquakes. The inversion analysis has been developed to evaluate the distribution of seismic energy radiated from an earthquake fault plane using the seismic intensity data and applied to the great interplate earthquakes occurring along the Nankai trough. The result of the inversion shows that large energy sub-faults, which generated short period seismic waves related to the seismic intensity data, are located as to avoid the large slip of sub-faults obtained from the tsunami waveform inversion for the Showa earthquake. Though the locations of sub-faults radiating large energy in case of the Hoei earthquake are similar to those of the Showa earthquake in Tonankai area, there is some discrepancy in Nankai area between the Hoei and Showa earthquakes. A portion of the large energy sub-faults of Hoei earthquake locates on a subducted seamount off Cape Muroto, where there is little energy radiation at the Showa and Ansei earthquakes. Kodaira et al. suggested that the subducted seamount might play a role of the barrier to the propagation of fault rupture at the Showa earthquake. We suggest that the similar rupture process might occur at the Ansei earthquakes, but the accumulated stress at the subducted seamount might be released at the Hoei earthquake. It is deduced from this result that the intensity of radiated short period seismic waves was very high in case of the Hoei earthquake. It can be also suggested that ground motions during the next earthquake may be hazardous, if the fault rupture propagates through the subducted seamount like the Hoei earthquake. Reference: Kodaira et al., 2002, Structural factors controlling the rupture process of a magathrust earthquake at the Nankai trough seismogenic zone, *Geophys. J. Int.* **149**, 815-835

SS04/08A/A03-013

1145

#### SOURCE MOTION OF THE 1979 IMPERIAL VALLEY EARTHQUAKE ESTIMATED FROM STRONG-MOTION WAVEFORMS, WITH NEW GEOTECHNICAL DATA

Ken MIYAKOSHI<sup>1</sup>, Kazuyoshi KUDO<sup>2</sup>, Tomotaka IWATA<sup>3</sup>, Rikiro KIKUCHI<sup>4</sup>, Yasuhiro OHTSUKA<sup>5</sup>, Susumu OHNO<sup>6</sup> (<sup>1</sup>Geo-Research Institute, JAPAN, <sup>2</sup>Earthquake Research Institute, University of Tokyo, JAPAN, <sup>3</sup>Disaster Prevention Research Institute, University of Kyoto, JAPAN, <sup>4</sup>Nuclear Power Engineering Corporation, JAPAN, <sup>5</sup>Kajima Corporation, JAPAN)

It is one of a key issue to use appropriate velocity structures or to give a well-tuned Green's function for estimating source model in the shorter period than the previous researches. Simultaneous array microtremor measurements to estimate an S-wave velocity structure up to about several km depth are well developed (e.g. Horike, 1985; Okada et al., 1990) and the obtained velocity structures were validated through comparing the transfer function from the structure with the one from observed seismic waves (e.g. Tsuno et al., 2002). The target event in this study is the Imperial Valley (Mw6.4) earthquake of 1979. First, array observations of microtremors were conducted at two sites of both west and east sides of the Imperial fault near El Centro, southern California. Each array consists of 7 vertical seismometers with several radii of less than 3.0km. The spatial autocorrelation (SPAC) method (Aki, 1957) was applied to microtremor data to obtain frequency-dependent phase velocity. S-wave velocity models were then derived from modeling of phase velocity assuming the fundamental-mode of Rayleigh waves by the genetic algorithm (GA). The observed phase velocities are dispersive from 2 to 6s at east side, from 0.3 to 5s at west side. The obtained model at the west side of the fault shows the basement with an S-wave velocity of 3.2 km/s at about 5.0 km deep, whereas about 6.0 km deep at the east side. The shallow velocity structures of 0.2 to 0.3km depth at 11 strong-motion observation sites were also estimated by the well-logging. Using these new geotechnical data we modeled 1D-velocity structures for each strong motion sites. Next, we conducted source inversion of the 1979 Imperial Valley earthquake using strong-motion data whose underground structures are obtained above. We applied the multiple time-window linear waveform inversion method (Hartzell and Heaton, 1983) for the analysis. The recorded acceleration data were integrated into velocity and band-pass-filtered between 1.0 and 10.0s. Because of the lack of absolute time on observations, we set to shift the synthetics to match the S-wave onset of observation and synthetics. The source time function in each subfault is represented by a series of four-smoothed ramp function with a 1.0s rise time with 0.5s apart. We assumed a single fault plane with referring to Archuleta (1984) who assumed one main fault with a branching fault. We have searched for the first time-window front propagation velocity (propagation velocity of triggering front of the first time-window at each subfault) by performing several inversions, changing the first time-window front propagation velocity. The model with the first time-window propagation velocity of 2.8 km/s has given the best-fit model. The total seismic moment is estimated as  $8.8 \cdot 10^{18}$  Nm. An area of large slip over 1m was mainly distributed at depths between 4 and 11 km, about 18 km north of the hypocenter. We will examine the effect of rupture propagation and Green's function on the obtained source model in detail and compare with Archuleta's model.

SS04/08A/A03-014

1200

#### AN ANALYSIS OF LOCALLY RECORDED BROADBAND WAVEFORMS OF THE 10 AUGUST, 1997 (MW 6.3) COLLIER BAY EARTHQUAKE, NW AUSTRALIA

Phil R. CUMMINS (Minerals & Geohazards Div., Geoscience Australia)

The 1997 Collier Bay earthquake, which occurred on 10 August, 1997, was the largest event (Mw=6.3) to have occurred within continental Australia since the 1988 Tennant Creek earthquakes. Although felt over a wide area, it occurred in a sparsely populated region and so caused only minor damage. Its occurrence in the rifted continental margin of NW Australia, however, suggests that study of this earthquake may have important implications for seismic hazard in Australia. Global studies of earthquakes in stable continental regions indicate that

the largest such earthquakes occur in this environment, and if an event of similar size had occurred in the rifted margin of a densely populated part of Australia the damage could have been much more severe. Although the earthquake was well recorded teleseismically, regional observations are sparse and no local observations have been reported in the literature. Here I will present a study utilizing data from a temporary network of broadband seismometers in the Kimberley region of NW Australia, which were fortuitously deployed by the Australian National University prior to the Collier Bay event. The nearest station was just over 100 km from the epicenter, and although much of the 24-bit data recording the event were clipped, I will show that substantial information about the earthquake source can be extracted from the unclipped portion of the waveforms. Although only 2 aftershocks appear in the earthquake catalogs (both Australian and worldwide), the temporary network recorded a large number of aftershocks, and an analysis of these will also be presented.

SS04/08A/A03-015

1215

#### AN ASSESSMENT OF TECTONIC STRESS FIELD AND SEISMIC HAZARD IN THE NEPAL HIMALAYA

Kedar Nath KHANAL, Avadh RAM (Central Department of Physics, Tribhuvan University)

The 2500 km long chain of the Himalaya is one of the seismically active regions of the world. The northwest (72° E- 80° E) and the northeast (88° E- 96° E) parts are more active as compared to the central part (80° E- 88° E). Almost the whole of the central part of the Himalaya lies in Nepal. The earthquake epicentral data of the region shows that at least an earthquake of magnitude mb=5 or greater occurs every year and the magnitude mb = 6 or greater generally occur in 10 to 15 years. In general, an earthquake of magnitude mb = 6 or greater has been found destructive. In 20<sup>th</sup> century, thousands of people have been killed and a loss of property of millions of dollars have been made as a result of such earthquakes in Nepal and the adjoining region. Although, Nepal is one of the least developed countries it has got tremendous amount of water resources. In the process of development of the country, the water resources can be utilized for hydroelectric power generation as well as irrigation etc. which ultimately requires the construction of the large dams, tunnels and multistory buildings with a large investment of money. So precaution should be taken for their safety. Since the present technology is not enough for reliable earthquake predictions, emphasis should be put on the evaluation of seismic hazard and risk in the region. In the present investigation, the tectonic stress field and the seismic hazard in the Nepal Himalaya have been estimated from the idea of fault plane solutions of the earthquakes occurred in the region and constructing the hazard map using earthquake data of the time interval from 1901 to 2001 AD. From the idea of fault plane solutions, it has been observed that the pressure axis lies in the north direction. Some of the events have shown the pressure axis lying in the east west direction which we consider as the effect of residual field caused by the inhomogeneities prevailing in the region. Moreover, the hazard map has helped to distinguish comparatively least or highly active areas and this distinction can be used in developing the earthquake resistant design. In this investigation such maps have been drawn and these results would be highlighted.

Tuesday, July 8 PM

Presiding Chairs: D. Zhi Feng, K. Kudo, W. Zhongliang

SS04/08P/A03-001

1400

#### TIME DEPENDENT SEISMIC HAZARD ASSESSMENT FOR THE TAIWAN REGION ON THE BASIS OF PROGNOSTIC ZONATION OF FUTURE EARTHQUAKES AND RECENT STRONG-MOTION DATA

Vladimir Yu. SOKOLOV<sup>1</sup>, Arkady OVCHARENKO<sup>2</sup>, Chin-Hsiung LOH<sup>3</sup>, Kuo-Liang WEN<sup>4</sup> (<sup>1</sup>Geophysical Institute, Karlsruhe University, <sup>2</sup>Institute of Geophysics Russian Academy of Science, Urals Division, RUSSIA, <sup>3</sup>National Center for Research on Earthquake Engineering, TAIWAN, <sup>4</sup>Institute of Applied Geology, National Central University, TAIWAN)

We describe an integrated approach to seismic hazard assessment, which was recently (1999-2002) applied for the Taiwan region. **First**, empirical models for ground motion estimation in the Taipei region were obtained on the basis of records from recent (1993-1999) earthquakes. The database includes strong-motion data collected during the recent Chi-Chi earthquake (M=7.6, 21 September 1999) and large (M=6.8) aftershocks. The ground-motion database was used for evaluation of generalized site response functions for typical soil classes (B, C and D) in the region, as well as for analysis of local site response in the Taipei basin (northern Taiwan). **Second**, the 4D-model (x, y, z - coordinates, time) for dynamic deformation of the Earth's crust and 5D-model (x, y, z - coordinates, time, magnitude) for seismicity were developed on the basis of observed geophysical data (GPS and PSWL observation, seismic catalogue, etc.). The models were applied for calculation of theoretical seismic catalogue (2001-2050) for the Taiwan region. The theoretical catalogue was compared with observed seismicity (July 2001-August 2002). The comparison shows that the theoretical catalogue adequately describes real seismicity for this time period. The averaged difference (absolute error) between parameters of observed earthquakes (M > 5.0, 66 earthquakes) and predicted events does not exceed 15-18 km for location, 1 year for time of occurrence and 0.1 unit for magnitude. **Third**, the region & site & time-dependent seismic analysis, which is based on schemes of probable earthquake zones evaluated from the theoretical catalogue, regional source scaling and attenuation models, and information on local site response on seismic motion, has been performed. The seismic hazard zonation maps are compiled in terms of Peak Ground Acceleration (PGA) and Response Spectra (RS) amplitudes (5% damping). The maps show distribution of amplitudes that will not be exceeded with certain probability (50%, 84% and 97%) in condition of generalized soil classes (B, C and D) during all possible earthquakes that may occur in the region during time period of 2003-2025. The approach allows us to introduce a new parameter that describes dependency of seismic hazard on time, so-called "period of maximum hazard" or PMH that is of particular interest of seismic risk management and insurance business. The parameter shows the period, during which every considered site will be subjected by the maximum value of ground motion characteristic (PGA or RS). The above mentioned stages may be considered as the parts of unified approach to seismic hazard assessments: from evaluation of characteristics of future earthquakes to site-dependent design input ground motion parameters. By the other words, we introduce a concept of so-called "Real Seismic Hazard" - the hazard, which is based on parameters of future earthquakes and, at the same time, which utilize information obtained during earthquakes that did occur.

SS04/08P/A03-002

1415

#### EVALUATION OF SEISMIC HAZARD AND STRONG GROUND MOTIONS FOR TASHKENT CITY

Bakhtiar S. NURTAEV, Lylya PLOTNIKOVA (Institute of geology and geophysics)

earthquake hazard assessments, conducted in connection with risk analysis in urban centers has been traditionally linked to scenario earthquakes in a deterministic manner, easily characterized to address a wide range of concerns. Proper design of earthquake resistant

structures and facilities requires estimation of the level of ground shaking to which they will be subjected. Seismic hazard assessment for the territory of Tashkent city has been carried out based on selection of earthquake generating zones within the limits of surrounding region, estimation of the maximal probable magnitude event in limits of every selected zone and the selection of earthquake sources, which may be the most dangerous for the city. Thorough seismological, geological and geotechnical studies have been carried out in and around Tashkent in order to determine the seismic hazard level. Seismic source zones are determined and seismicity parameters such as magnitude - frequency relationships and maximum magnitude are determined using past occurrence of earthquakes and expert judgment. For the Radius case study scenario for Tashkent city we recommended to adopt probable earthquake with the magnitude  $M = 6.1$  within Tashkent focal zone and an intensity of 8 ball (MSK intensity units) on average soils. After we have made attempt to improve reference strong ground motions for Tashkent city, using all available geological and geotechnical information, prior observations and available records. It is known that intensity distribution in city depends on geometry and properties of the subsurface materials, ground water level, site topography and the characteristics of input source motion. 32 records of main shock and aftershocks of Tashkent 1966 earthquake with  $2 < M < 5.3$  registered at different site conditions were used for analysis of soil effects on ground motions. Spectral earthquake source parameters for Tashkent source zone have been estimated. Using geological data, reached Paleozoic basement and geophysical sounding results, the spectral transfer functions of soil profiles have been calculated. Time history of bedrock motion that is consistent with the predicted parameters of probable scenario earthquake  $M=6.1$  have been generated on the base of deconvolution techniques. A conventional ground response analysis is then performed to predict the motion at the surface of the soil profile of interest. This motion, which is consistent with the results of seismic hazard analysis and also with the local site conditions, may be taken as design strong ground motion.

**SS04/08P/A03-003****1430****PROBABILISTIC SEISMIC HAZARD ASSESSMENT IN NORTHERN ALGERIA, USING SPATIALLY-SMOOTHED SEISMICITY. PART I : SEISMIC HAZARD MAPS IN TERMS OF PGA**

Mohamed HAMDACHE<sup>1</sup>, Jose Antonnio PELAEZ MONTILLA<sup>2</sup>, Carlos LOPEZ CASADO<sup>3</sup> (<sup>1</sup>Seismological Survey Department - CRAAG - Algiers - Algeria, <sup>2</sup>High Polytechnic School, University of Jaen, Spain, <sup>3</sup>Theoretical Physics department . University of Granada, Spain)

Seismic hazard in terms of peak ground acceleration (PGA) has been evaluated in northern Algeria using spatially-smoothed seismicity data, after introducing different modifications to the initial approach developed by Frankel (1995). We present here a preliminary seismic zonation in northern Algeria as derived from the obtained results. Initially, we have compiled an earthquake catalog of the region taking data from several agencies. Afterwards, we delimited seismic areas where the  $b$  and  $m_{max}$  parameters are different. Finally, by applying the modified methodology proposed by Frankel (1995), and using four complete and Poissonian seismicity models, we are able to compute the seismic hazard maps in terms of PGA with 39.3% and 10% probability of exceedance in 50 years. A significant result of this work is the observation of mean PGA values of the order of 0.20g and 0.45g, for return periods of 100 and 475 years, respectively, in the central area of the Tell Atlas. Seismic hazard curves in terms of PGA have been derived in great details at the twelve selected cities, located at the most industrial and populated areas in northern Algeria.

**SS04/08P/A03-004****1445****SEISMIC HAZARD ASSESSMENT IN THE KUTCH REGION, INDIA**

Bal Krishna RASTOGI<sup>1</sup>, Prantik MANDAL<sup>1</sup>, Mark PETERSEN<sup>2</sup> (<sup>1</sup>Seismology Group, National Geophysical Research Institute, Hyderabad, India, <sup>2</sup>USGS, DENVER FEDERAL CENTER, MS966, Box. 25046, DENVER, CO 80225)

Occurrences of two M7 earthquakes during last 200 years makes the Kutch region of Gujarat state, Western India a unique site for the devastating intra-plate earthquakes in the Globe. The region has a high frequency of damaging earthquakes e.g. Kutch earthquake of 1819 (Mw 7.8), MMI VIII Lakhpat earthquake of 1845, Mw 6 Anjar earthquake of 1956. During last 155 years, the region has witnessed nine earthquakes of M5-6 indicating a repeatability of 17 years for M5-6 events. Hence, the region is prone for the occurrences of large and moderate earthquakes in the future. Thus, it is essential to assess the hazard to assist engineers and public officials in making informed planning decisions that will influence economic and life-safety policies for the region. On 26 January 2001, a devastating lower crustal intra-plate earthquake of Mw7.7 took place with an epicentral location of (23.40N, 70.230E) and a focal depth of 23 km. The aftershock activity has been very intensive. Till date, 11 aftershocks of magnitude exceeding M5, over 180 earthquakes of magnitude exceeding M4 and about 1000 aftershocks of magnitude exceeding M3 have occurred in the area. The last aftershock of magnitude exceeding M5 occurred on March 4, 2001. The well-located hypocenters of aftershocks delineate a hidden EW- trending causative fault plane, which dips at 45o towards south. We name this south dipping hidden fault as north Wagad fault (NWF). Trends of isoseismals, damage patterns, ground deformations, decay of intensity with distance, liquefaction, site amplifications and accelerations due to the main earthquake and aftershocks have been studied. The earthquake was assigned a MM intensity of X+. A catalog of earthquakes of Kutch region has been prepared. We have derived preliminary probabilistic and deterministic ground motion models for Kutch. This new hazard analysis includes updated sources and recurrence rates, incorporates two crustal intraplate ground motion prediction relations, and applies new hazard methodologies that were used to produce the U.S. National Seismic Hazard maps (Frankel et al., 1996). NEHRP criteria have been assumed for the soil characteristics. The probabilistic hazard is calculated for the two hazard levels used in producing current building codes: 2% and 10% probability of exceedance in 50 years. The deterministic hazard is calculated using the median ground motion from published ground motion prediction equations. We construct maps for peak horizontal ground acceleration and 0.2 s and 1.0 s spectral acceleration with 5% damping using two different scenarios for return times of large earthquakes. The coda-Qc has been studied using 200 aftershocks of M3.0, which suggests a frequency dependent coda Qc relation as  $Q_c = (102 \pm 0.8) f^{0.98 \pm 0.17}$ . The decay of acceleration estimated using  $Q_0 = 102$  suggests a good correlation with the attenuation relations obtained for northeastern US and the observed peak ground acceleration caused by the 2001 Bhuj mainshock. Based on this decay of amplitude and recorded accelerations, the acceleration at epicenter of mainshock is estimated to be 1g.

**SS04/08P/A03-005****1500****A NEW SEISMIC HAZARD MAP FOR IRAN**

Mehdi ZARE<sup>1</sup>, Mehdi ZARE<sup>1</sup>, Paivi MANTYNIEMI<sup>2</sup>, Andrzej KIJKO<sup>3</sup>, Maysree BEJAICHUND<sup>4</sup> (<sup>1</sup>Seismology Research Center, IIEES, Tehran Iran, <sup>2</sup>Inst. Seismology, Univ. Helsinki, Helsinki, Finland, <sup>3</sup>Council for Geoscience, Pretoria, South Africa)

A parametric-historic procedure for mapping of seismic hazard in Iran and the surrounding region has been applied. The procedure does not require any specification of seismic

source zones and allows for the use of the whole seismological record, comprising both historical and instrumental data, available for the region of interest. The new seismic hazard map prepared for Iran and its vicinity specifies a 10% probability of exceedance of the given peak ground acceleration (PGA) values for an exposure time of 50 years. When preparing the map, the new PGA attenuation relationship for Iran was employed. The new map shows a spatial distribution of the seismic hazard that corresponds well with the features of seismicity within the examined region. It depicts the level of seismic hazard in which the exceedance of the PGA value of 0.30g may be expected to occur within limited areas. The highest estimated levels of seismic hazard inside the territory of Iran are in excess of 0.50g at individual sites.

**SS04/08P/A03-006****1515****GIS BASED SEISMIC HAZARD ZONATION IN THE SIKKIM HIMALAYA**

Sankar Kumar NATH<sup>1</sup>, Probal SENGUPTA<sup>1</sup>, Indrajit PAL<sup>1</sup>, Debasis ROY<sup>2</sup>, Jnana RKAYAL<sup>3</sup> (<sup>1</sup>Department of Geology & Geophysics, Indian Institute of Technology, Kharagpur - 721 302, INDIA, <sup>2</sup>Department of Civil Engineering, Indian Institute of Technology, Kharagpur - 721 302, INDIA, <sup>3</sup>Geological Survey of India, Kolkata- 700 016, INDIA)

The Himalayan region, about 2500 km long belt from Kashmir in the west to Arunachal Pradesh in the east, can be divided into several seismotectonic blocks, the Darjeeling-Sikkim constituting one of those, where a good number of moderate magnitude earthquakes (M 5.0) had been recorded in the past. The recent damaging earthquake of 1988 (M 6.7) was distinctly felt in the Darjeeling-Sikkim Himalaya, and the isoseismal VII passed through Darjeeling and Gangtok towns. The Geological Survey of India (GSI) conducted a few microearthquake surveys deploying close-spaced temporary networks in the Darjeeling-Sikkim region. The strong motion network of the Indian Institute of Technology (IIT), Kharagpur sponsored by the Department of Science and Technology (DST) had been in operation in the Sikkim Himalaya since 1998. The Fault-plane solutions of the weak motion and strong-motion events indicate dominantly thrust faulting mechanism, with a north dipping fault plane. A N-S depth-section shows that the earthquakes occurred down to a depth of 45 km. The seismic activity is very high below the plane of detachment and the Main Boundary Thrust (MBT) is a mantle reaching active fault, earlier indicated by gravity survey. With this well constrained tectonic model, the strong-motion data had been of immense use in the proposed hazard zonation. The IIT Kharagpur strong motion network in Sikkim comprising of 9 digital accelerographs recorded more than 100 events during 1998-2002, of which 71 events have been selected with signal-to-noise ratio Sankar 3 for the estimation of site amplification (SA), peak ground acceleration (PGA) and resonance frequency (RF) at all stations. The geological themes with inputs from IRS-1C LISS III digital data, topo-sheets, geographical boundary of the State of Sikkim, surface geological maps, soil taxonomy map in 1:50,000 scale and seismic refraction profiles, are united and integrated to form the basic site condition coverage of the region. The seismological themes, namely, SA, PGA, RF are assigned normalized weights and feature ranks following a pair-wise comparison hierarchical approach and later integrated to evolve the seismic hazard map. The overall SA, PGA and RF show an increasing trend in the NW-SE direction peaking at Singtam in the lesser Himalaya. Six seismic hazard zones with percent probability index <22%, 22-37%, 37-52%, 52-67%, 67-82%, >82% coupled with the geological integrated coverage exhibit no-hazard (<22%) to maximum hazard (>82%) probability. The effect of undulating topography on site amplification is also assessed using an explicit finite difference computer code for two earthquakes. The hypocenter of one of the events with a magnitude of 5 was in close proximity to the Singtam recording station. The hypocenter of the second event with a magnitude of 3.2 was very near the Gangtok recording station. These results agree well with the inference on topographic site amplification based on GIS integration.

**SS04/08P/A03-007****1530****A SEISMIC HAZARD AND RISK ASSESSMENT FOR THE TULBAGH AREA IN SOUTH AFRICA: APPLICATION OF THE PARAMETRIC-HISTORIC PROCEDURE**

Andrzej KIJKO, Gerhard GRAHAM, Maysree BEJAICHUND (Council for Geoscience)

The strongest and most damaging earthquake recorded in the earthquake history of South Africa took place on 29 September 1969 in the Tulbagh valley, some 90 km from Cape Town, South Africa. Nine deaths resulted from the earthquake and damage to buildings in the epicentral area was estimated at US\$ 24 000 000. This study is aimed at applying a probabilistic seismic hazard assessment to the Tulbagh area, and to quantify the risk the town will be exposed to in the event of a large earthquake. The applied technique for the assessment of seismic hazard is known as the "Parametric-Historic" procedure. This method permits the combination of both historical and instrumental data. The historical part of the catalogue contains only the strongest events, whereas the complete part can be divided into several sub-catalogues, each assumed complete above a specified threshold of magnitude. In the analysis, the uncertainty in the determination of the earthquake magnitude was taken into account by incorporating the concept of "apparent magnitude". A significant effort was also required in the calculation of a reliable maximum earthquake magnitude. Since the Parametric-Historic procedure is parametric in nature, it consists essentially of two steps. The first step is applicable to the area in the vicinity of Tulbagh and requires an estimation of the area-specific parameters. These parameters include the mean seismic activity rate, the Gutenberg-Richter parameter, and the maximum regional magnitude. The second step is applicable to the Tulbagh site, and consists of parameters characteristic of the site. These are the parameters that give the distribution of the amplitude of peak ground acceleration (PGA). The results of the hazard assessment are expressed as probabilities that specified values of PGA will be exceeded during the chosen time intervals. A worst case scenario sketches the possibility of a maximum PGA of 0.30 g. The second part of the study concentrates on the probabilistic seismic risk analysis. The results from the seismic hazard assessment were used as part of a process to translate probabilistic estimates of ground motion into a damage factor through certain ground motion-damage relationships. Three classes of buildings, typical to the Tulbagh area were considered in the analyses. It indicates that (as example) for low rise, unreinforced masonry buildings, there is a 1% annual probability of suffering a mean value of damage around 20%. This type of information can be further reduced to provide values of expected annual damage, as required by many insurance agencies.

**SS04/08P/A03-008****1545****EVALUATION OF SEISMIC RISK FOR HYDROPOWER DAM DESIGNS IN VIETNAM**

Trinh Trong PHAN (Institute of Geological Sciences)

Hydropower take very important role for the development of economics in Vietnam. Some large dams like Hoa Binh, Tri an, Thac ba Dams were built in Vietnam. Some other will be built in near future like Son la dam of 250 meter high, a largest dam in south east Asia. The estimation of seismic risk for hydropower dam design in Vietnam is carried out in following successive stages: A seismic hazard assessment carried out through both the connections, at various scales, of the structural geology with seismicity. The estimate of the seismogenic capability of the active faults identified through satellite image, topographic and geological

map, field survey and earthquake catalogue. A seismic risk assessment of the regional seismic hazard on the site corresponding to the occurrence of design earthquake magnitude such as: maximum credible earthquake (MCE), maximum design earthquake (MDE) consisting of an earthquake having 10% risk of occurrence during the service-life of dam (100 years), the operating basis earthquake (OBE) consisting of an earthquake having a 50% risk of occurrence during the service life of dam and peak ground acceleration (PGA) corresponding to MCE, MDE and OBE. Maximum credible Earthquake is estimated from combination of various methods: fault segment, fault surface, seismic moment and fault slip rate. Many arguments of remote sensing, geomorphology, geology, geodesy, state of stress attest the intensive actual tectonic activity in Vietnam. However, the poorness of the seismological network prevents accurate localization of moderate seismicity. For this region, using pure probabilistic model or historical approaches to select a seismic risk in structure design will be quite random. The combination of the deterministic and probabilistic analysis was performed in several stages. The application of the seismic risk assessment for many hydropower sites in Vietnam such as: Song Ca, Hoa Binh and Son La hydropower dams is presented in detail. MDE is 6.3 - 6.5 for Song Ca fault, 6.9 - 7.0 for Nam Chou fault, OBE is 5.6 - 6.1 for Song Ca fault, 6.3 - 6.5 for Nam Chou fault. Various attenuation laws based on world wide data recorded in near field and by Xiang based on Yunnan data (next to Vietnam) are used to calculate PGA. The above-mentioned MDE magnitude should induce at the dam site a PGA of about 0.35 - 0.39 g. The OBE magnitude should induce at the dam site a PGA of about 0.24 - 0.31 g.

SS04/08P/A03-009

1615

#### A NEW APPROACH FOR RAPID SEISMIC RISK ASSESSMENT

Serguei BALASSANIAN, Yuri BALASNYAN (Department of Geophysics, Yerevan State University)

In the presentation the author shows that the rapid seismic risk assessment is a particular task which should be considered at least for three events: 1) rapid seismic risk evaluation immediately after the strong earthquake in urban areas for prompt response; 2) rapid seismic risk assessment for developing countries with usually limited input data available; 3) rapid seismic risk assessment for Global risk mapping. Analyzing all the factors that contribute to seismic risk (geological, engineering, economic, social, political, and cultural), the author has developed the rapid seismic risk assessment (RSRA) approach. This method is based on three main factors that contributed to the magnitude of risk: earthquake hazard, vulnerability of built environment, and density of population. In the presentation the author has shown examples of application of the RSRA method for all the three above listed events: 1) scenario of the rapid seismic risk assessment after the devastating Spitak earthquake (Armenia, 1988,  $M=7.0$ ); 2) seismic risk assessment in Armenia as an example for developing country and 3) the Global seismic risk mapping.

SS04/08P/A03-010

1630

#### SOME PROBLEMS OF SEISMIC ZONING OF THE NORTHEASTERN SAKHALIN ISLAND, RUSSIA AND ADJACENT SHELF

Alexey I. IVASHCHENKO, Kim Choon OUN, Tatiana NAGORNYKH, Michael STRELTSOV (Institute of Marine Geology and Geophysics, Far East Branch of Russian Academy of Sciences)

Problems of seismic zoning and accurate seismic hazard assessment of the northeastern Sakhalin Island and adjacent shelf areas became of the great interest 10-15 years ago due to rapidly growing activity related to industrial exploration of the oil-and-gas resources on Sakhalin shelf. That time, the seismic potential and seismic activity of the coastal and adjacent shelf areas were considered to be higher as compared with the inner parts of the Island. However, the new seismological and geophysical data obtained during the last years force to reconsider many of the existing representations on seismicity and seismic zoning of the northeastern Sakhalin Island and adjacent shelf. These new data include the results of: a) detailed active fault studies performed in zones of main regional faults after occurring the destructive Neftegorsk earthquake of 27 May 1995 ( $M_w=7.1$ ) accompanied by the first time observed within Sakhalin Island surface faulting; b) comparative tectonic analysis of Cenozoic structures onshore and offshore the north Sakhalin Island; c) accurate re-evaluation of earthquake source parameters for the largest seismic events ( $M_w=4.5-5.8$ ) occurred here during the period of 1932-1964 years; d) thorough analysis of available instrumental and macroseismic data aimed to develop the proper models of earthquake frequency rates and ground motion attenuation relationships; e) analysis of the available seismic reflection and geodetic data, and others. As a result of this comprehensive studies, many new features of regional tectonics and crustal structure related to the earthquake source locations, style of crustal faulting and deformation and seismic wave attenuation within the northeastern Sakhalin Island and adjacent shelf were revealed. In particular, based on the above results one can conclude that the present-day seismic activity of the coastal and adjacent shelf areas is lower comparing with the inner parts of the northeastern Sakhalin Island, because the main earthquake generating structures here are situated within a broad zone of the active regional right-lateral shear faulting located on land, between two major regional fault systems. Incorporation of the mentioned data into the well-known procedures of seismic hazard assessment leads to a noticeable change of the seismic hazard estimates obtained earlier including those presented on the official general seismic zoning map of Russian Federation (GSZ-97).

SS04/08P/A03-011

1645

#### GPS APPLICATION FOR SEISMIC ZONING

Mikhail T. PRILEPIN (Institute of Physics of the Earth)

Till now seismic zoning is founded practically only on seismic statistics and geological data of the region under study. Using GPS technology can greatly help on seismic zoning by study the real picture of the stress of the seismically dangerous regions lithosphere and check its changing in time. That allows to update maps of seismic zoning permanently. As suppressing number of intra-plate earthquakes is a seismic moving on the faults, the most informative feature for seismic zoning will be the shear deformations. Modern GPS technologies allow to provide accuracy of shear deformation at the level of  $1-2 \times 10^{-7}$  when the distances between observational points are 5-30 km. Since critical shear deformations, on which occurs the slip of locked fault flanks as a rule on 2 orders more, monitoring of shear deformations on seismically dangerous territory not only provides improvement of maps of seismic zoning, but also is an important forecasting feature. The study of the possibilities of applying GPS for the seismic zoning is carried out for Caucasus where the detailed map of seismic zoning [Ulomov, 2001] is available. Besides, there is GPS network including about 50 points. This network was established [Prilepin, Reilinger, 1991AE002] after the most strong Racha earthquake (Racha, 7.0, April, 1991) with the purpose of the general study of regional geodynamics of the Caucasus. On 5 sites of the network, outlining epicentral zone of Racha earthquake, observations repeated each two years since 1991, and the data of GPS study of post-seismic deformations will be briefly presented in this report. The present Caucasian GPS network has insufficient density (the distances between points 50AE50 km) for solving the problems of seismic zoning and its further densification is needed. Two

approaches for the densification network are discussed. In the first case the technology of the using of GPS is developed for revision of the available maps of seismic zoning. In the second case the problem of the creation GPS network for "seismic protection" of the populous region or large engineering buildings is considered. For Caucasus the region of North-Eastern Dagestan is chosen as there is possible to consolidate both approaches considered above. As "safe-protection" objects we chose zones of Chirkey Water-Power Plant and city of Makhachkala with population more than 500 thousand. On the modern maps of seismic zoning this region is classified as 9-ball zone. Considering the fault tectonics of this region the densing GPS network is designed. Density of the GPS sites allows to determine the position of the shear deformation isolines with errors no more than  $5 \times 10^{-7}$ .

SS04/08P/A03-012

1700

#### SHAKE MAP PREDICTION BASED ON EMPIRICAL SITE CORRECTION MODEL

Kuo-Liang WEN<sup>1</sup>, Wen-Yu JEAN<sup>2</sup>, Yu-Wen CHANG<sup>2</sup>, Chih-Kuo WANG<sup>1</sup> (Institute of Applied Geology, National Central University, <sup>2</sup>National Center for Research on Earthquake Engineering, Taiwan)

The seismic hazard analysis is usually to develop rock outcrop or hard soil site ground motion for seismic design. One of the main factors that affect the seismic risk is the existence of site effects on the attenuation relations, which are probabilistic descriptions of the level of ground motion as a function of the earthquake and site parameters. In order to make a good estimate of ground motion, many parameters are taken into consideration for attenuation relations. Researchers proposed several attenuation relations for different source region and site classification. There are several site classification schemes used in different attenuation relations. However, the information for site classification may be not widely available for strong motion station sites. An effective site-dependent attenuation model should be provided for better estimate of ground motions. Taiwan government supported an extensive seismic instrumentation program for the urban areas with densest digital strong-motion network of the world. This strong-motion network collects a large amount of high quality earthquake data since 1990. These data provide useful information for us to set up empirical site correction model. In this study we use the site correction model to predict shake map. If this model can connect to earthquake rapid report system, then the source correction also can be done. It will give us a better shake map result.

SS04/08P/A03-013

1715

#### NONLINEAR SEISMOLOGY: THE QUANTITATIVE DATA

Gheorghe MARMUREANU, Carmen Ortansa CIOFLAN, Florin Stefan BALAN, Bogdan Felix APOSTOL, Alexandru MARMUREANU (Engineering Seismology, National Institute for Earth Physics)

The model of linear elastic response of the Earth has been almost universally used by seismologists to model teleseismic, weak and also strong earthquakes. For teleseismic and weak ground motions, there is no reason to doubt that this model is acceptable, but for strong ground motions, particularly when recorded on softsoils, the consequences of nonlinear soil behavior have to be seriously considered. Ground motion characteristics, particularly the duration of strong shaking, can be affected by seismic energy being trapped in large sedimentary basins. Nonlinear effects in ground motion during large earthquakes have long been a controversial issue between seismologists and geotechnical engineers. Laboratory tests made by using resonant columns consistently show the reduction in shear modulus  $G$  and increase in damping ratio  $D$  with increasing shear strain ( $\gamma$ ), therefore nonlinear viscoelastic constitutive laws are required. More than that, the seismological detection of the nonlinear site effects requires a simultaneous understanding of the effects of earthquake source, propagation path and local geological site conditions. The difficulty in demonstrating the nonlinear site effects may be due to fact that they are overshadowed by the overall patterns of shock generation and propagation. In order to make evidence of large nonlinear effects, the authors introduced the spectral amplification factor (SAF) as the ratio of the maximum spectral absolute acceleration ( $S_a$ ), relative velocity ( $S_v$ ), relative displacement ( $S_d$ ) to peak values of acceleration ( $a_{max}$ ), velocity ( $v_{max}$ ) and displacement ( $d_{max}$ ), respectively, from processed strong motion records. The SAF coefficient is useful to describe the nonlinearity phenomena at a given site, being indirectly dependent on the frequency content of the earthquake record. The analysis of our strong motion records reveals the decreasing of the SAFs as the earthquake magnitude increases. The median SAF values of the recent strong Vrancea earthquakes for damping 5% are: 4.16; 3.63 and 3.26 corresponding to the May 31, 1990 Vrancea earthquake ( $M_s=6.1$ ), May 30, 1990 Vrancea earthquake ( $M_s=6.7$ ), respectively, August 30, 1986 ( $M_s=7.0$ ). At the same seismic station, for example Bacau, for 5% damping, SAF for accelerations is 3.94 for August 30, 1986 earthquake ( $M_s=7.0$ ); 4.32 for May 30, 1990 earthquake ( $M_s=6.7$ ) and 5.22 for May 31, 1990 ( $M_s=6.1$ ). The evidence of nonlinearity at least for thick Romanian Plain Quaternary sediments is a systematic decrease in the variability of peak ground acceleration for increasing earthquake magnitude. As the excitation level increases, the response spectrum is larger for the linear case in comparison with the nonlinear one. For the Vrancea earthquakes there is a difference in the frequency-dependent site effect between weaker motion (May 31, 1990) and strong motion (March 4, 1977).

SS04/08P/A03-014

1730

#### THE CANADIAN URBAN SEISMOLOGY PROGRAM DEMONSTRATION STRONG MOTION SEISMOGRAPH NETWORK IN VANCOUVER, BRITISH COLUMBIA

Garry ROGERS, Andreas ROSENBERGER, Tuna ONUR, John CASSIDY (Geological Survey of Canada)

The Canadian Urban Seismology Program (CUSP) has been initially funded as a two year pilot project. The centrepiece of the project is the installation of a densely-spaced demonstration urban strong ground motion network in a section of Vancouver, British Columbia, a city with a metropolitan population of about two million people. One hundred strong motion seismographs of Geological Survey of Canada design are being deployed. Sixty of them are in a 6km x 8km array that straddles the edge of the Fraser River delta, ranging from bedrock in Vancouver to 300m deepsoft sediments of the delta. This is a region where we have seen large variations in shaking response recorded on the existing widely spaced network of stand-alone strong motion instruments. The relatively low amplitude recordings (all less than 0.04g) from several nearby earthquakes show frequency-dependent amplification, with factors of up to 12 times (relative to bedrock) near the edge of the delta. The new network will use the public Internet for communication, delivering peak values of acceleration, velocity and displacement in near real time, available for rapid display as ground motion shaking maps or other purposes. Full wave-form data can be retrieved using standard Internet protocols like FTP and SSH/SFTP. Twenty-five instruments have been installed to date. Most of the deployments so far are in small elementary school buildings. We hope to have the demonstration network fully in operation by the end of 2003.

SS04/08P/A03-015

1745

**SELF-CENTRING ASEISMIC SYSTEM WITH DOUBLE NATURAL FREQUENCY**

Federico /BARTOLOZZI (Civil Engineer &amp; Independent Researcher)

The proposed system is based on the following operations: 1. interruption of the solidarity between the building and the foundation-soil complex; 2.laying of multidirectional movable bearings with sliding or rolling friction.This application confers the building with the main properties of centring after an earthquake and of doubling the natural frequency of vibration during an earthquake. The centring is automatic and it takes place due to the presence of a sliding spherical bowl in each bearing.In the presence of an earthquake, this bowl also permits the immobility of the building with respect to the horizontal translation of the foundation-soil complex, because its thickness variation is perfectly balanced by the corresponding elastic deformation of the main springs at every instant and for any value of the horizontal displacement. The horizontal inertial force in the building does not modify its static equilibrium, because it is minor when using bearings with sliding friction and negligible when using bearings with rolling friction. The variation of the natural frequency of the building takes place during the vertical motion of the soil only during an emergency, characterised by an interval seismic frequencies including the resonance one. In fact, the presence in each bearing of a system of auxiliary springs, automatically started in this situation, permits the action of the main springs to be strengthened with a consequent increase in the natural frequency of the building and a drastic decrease in the vertical displacements of the building to values compatible with its safety characteristics.

Wednesday, July 9 AM

Presiding Chairs: F. Romanelli, K. Irikura

SS04/09A/A03-001

0900

**STRESS SIMULATION AND OCCURRENCE OF QUATERNARY THRUSTING IN HIMALAYAS**

Daya SHANKER<sup>1</sup>, V.P. SINGH<sup>2</sup>, Nipun KAPUR<sup>3</sup>, A.I. GORSHKOV<sup>4</sup>, Olga V. NOVIKOVA<sup>5</sup>, V.G. KOSSOBOKOV<sup>6</sup> (<sup>1</sup>Department of Earthquake Engineering, Indian Institute of Technology Roorkee, Roorkee-247667, India, Email:dayasfq@iitr.ernet.in / pateel2k1@yahoo.co.in, <sup>2</sup>Department of Geophysics, Banaras Hindu University, Varanasi-221005, India, <sup>3</sup>GE Capital International services, Race Course Road, Bangalore-560 001, India., <sup>4</sup>International Institute of Earthquake Prediction Theory and Mathematical Geophysics, Russian Academy of Sciences, Moscow, Russia, Email:gorshkov@mitp.ru, <sup>5</sup>International Institute of Earthquake Prediction Theory and Mathematical Geophysics, Russian Academy of Sciences, Moscow, Russia, Email:onovikov@mitp.ru, <sup>6</sup>International Institute of Earthquake Prediction Theory and Mathematical Geophysics, Russian Academy of Sciences, Moscow, Russia, Email:volodya@mitp.ru)

Thrust dominated southern Tibet during the Cretaceous and Paleocene, resulting in the formation of the Gangdese and renbu Zedong Thrust system. This thrust activity culminated in north dipping shallow normal-faulting (South Tibetan Detachment –STD) in the Higher Himalayas during the Miocene. Activities on the STD are coeval with that on the Main Central Thrust (MCT). Thrusting activity virtually ceased around 8 Ma after which there is no evidence for major Quaternary shortening in Southern Tibet. Although, thrusting continued in the Himalayas during recent times. The occurrence of Quaternary thrusting in Himalayas and its geodynamics constraints in southern Tibet is modelled using stress simulation analysis. 2-D non-linear elastic and homogeneous wedge models, representing cross-sections of the Himalayas and Tibet are used. Varying the strength of the base in the model and corresponding stress distribution and failure patterns in the wedge is analyzed. Simulated stresses for a set of boundary conditions, representing building up of Himalayas and southern Tibet, reveals the region of thrust failure gradually recedes away from the wedge towards the base (lower boundary) with a decrease in the strength of the base. Thus, the result favours the preposition that a strong and a weak basal (Main Himalayan Thrust; MHT) respectively, below Himalayas and Southern Tibet is responsible for presence and restricting the extension of Quaternary thrusting in these regions. A decrease in strength of MHT from the Himalayas to Tibet is also supported by observational evidence and thermal modelling, imply partial melting along MHT.

SS04/09A/A03-002

0915

**THE INFLUENCE OF LOCAL TOPOGRAPHIC RELIEF ON REGIONAL STRESS: AN EXAMPLE FROM THE RUKWA RIFT, TANZANIA**

Richard Wambura FERDINAND (Department of Geology, University of Dar es Salaam)

The seismo-tectonic structure of the Rukwa rift is interpreted using fault plane solutions for earthquakes within the rift. Fault plane solution for micro-earthquakes were obtained by moment tensor inversion of the full waveform using high frequency local data, while for large earthquakes the low frequency body wave inversion solutions from previous large earthquakes were adopted. The combined results indicated there is a difference in T (tension) axes orientation between the western side located beneath the rift in Ufipa plateau end the eastern side along the Songwe basin. Within the Ufipa plateau the orientation is NE-SW to NNE-SSW, orthogonal to the rift, while along the Songwe basin it is NW-SE, parallel to the rift. This difference is attributed to differences in local topographies. The Ufipa plateau is about 1 km higher than the Songwe basin which is almost level with the East African plateau where the extension trends NW-SE.

SS04/09A/A03-003

0930

**SEISMICITY OF THE QAENAT KHORASAN REGION IN EASTERN IRAN**

Shayesteh MEHRABIAN, Godardz HAMIDI (Department of Earth Sciences, University of Tehran)

In this study seismicity of Qaenat Khorasan, which is one of the most seismically active regions in eastern Iran by using all effective seismological and geological factors, has been investigated. The earthquake catalogue is provided by using available references which concerning the earthquake data in Iran and special attention has been paid to the destructive Zirkuh-Qaenat earthquake of 1997 May 10. The procedures of, aftershocks deletion, the principle of region selection, the upper and lower limit magnitude and verification of the historical catalogue are applied. For some representative regions the Gutenberg-Richter relation curves according to their seismicity characteristics, by using the earthquake data greater than or equal to magnitude 3.0 (1974-1998) and higher magnitudes (1900-1998) are obtained. According to these results the annual occurrence rate of events of each magnitude can be inferred from the G-R relation and it seems that both results are almost the same. Therefore using the obtained relations at the first stage as the proper region is selected with respect to the seismicity system and the duration of time can make estimation of the recurrence period of large earthquakes. It should be noted that this region shows irregular seismic activity pattern, which is discussed.

SS04/09A/A03-004

0945

**A HOMOGENEOUS EARTHQUAKE DATA BANK IN WESTERN MEDITERRANEAN COUNTRIES –ALGERIA, MOROCCO, TUNISIA – FROM THE RECORD SOURCES OF PAST SEISMIC EVENTS**

Djillali BENOUAR (Department of Civil Engineering, University of Science and Technology Houari Boumediene (USTHB))

The main purpose of this work is to give a comprehensive overview of the establishment of the catalogue of all earthquakes reported in the western Mediterranean countries (Algeria, Morocco, Tunisia), and from which were derived from this basic data set the general laws governing the space and time distribution of earthquake occurrences in the seismic source zones. This region is called hereafter the Maghreb region. In recent history, strong earthquakes have occurred in northern Algeria in Algiers (1716), Oran (1790) and Cheliff (1867, 1873, 1922, 1934, 1954 and 1980). A detailed study and analysis of the seismicity of Algeria and adjacent regions during the twentieth century is presented in Benouar (1993). This research work presents the present situation of the earthquake catalogues in the Maghreb region and the methodology being used in the assessment of the seismicity. It illustrates the historical background of the catalogues, their completeness and the types of archives used in their compilations. It also includes the problems encountered in their establishment as language, calendars, place-names, scatter of documents, low density of population, censure and poor economic conditions in the Maghreb region. For the Maghreb region, earthquake hazard constitutes a constant threat to human life and property, sometimes causing major economic losses and disruption. The rapid urbanization, development of critical engineering works such as dams, nuclear power plants, industrialization of cities with modern types of buildings and the concentration of populations living or settling in hazardous areas are matters of growing concern, as they contribute to heavier loss of life and increase considerably the cost of disaster damage. In order to assess the seismic hazard with a certain degree of reliability, an earthquake data of the region under survey which are as complete, homogeneous and accurate as possible are needed. For this purpose, and from the point of view of long term prediction and seismic hazard assessment, it is imperative that input data in the catalogues of the Maghreb countries be revised and homogenized. Actually, it is of interest to mention that earthquake catalogues in the Maghreb region could be separated in two types: a parametric one which includes most of the events that occurred in the twentieth century and a descriptive catalogue for seismic events that occurred in the early years of the twentieth century and earlier. A methodology has been developed by Benouar (1993) to assess the seismicity of the Maghreb region; this methodology has been used for the period 1900 onwards and resulted in a homogeneous earthquake catalogue. It is obvious that more research work is needed for a reliable earthquake catalogue in the region including the pre-instrumental and the instrumental periods.

SS04/09A/A03-005

1000

**PROBABILISTIC EARTHQUAKE POTENTIAL MODELS TESTED AGAINST A HISTORICAL CATALOG OF JAPANESE INLAND EARTHQUAKES**Kunihiko SHIMAZAKI<sup>1</sup>, Wahyu TRIYOSO<sup>2</sup> (<sup>1</sup>Earthquake Research Institute, University of Tokyo, <sup>2</sup>Department of Geophysics and Meteorology, Bandung Institute of Technology)

Several methods have been proposed to estimate earthquake potential in addition to the classic regionalization method to estimate seismic hazard. They include a spatial smoothing technique proposed by Frankel in 1995, utilization of information on strain accumulation attempted by Ward in 1994, and a method based on estimated slip rate and other parameters of active faults (e.g. Wesnousky et al. in 1984). All these models appear to be reliable because they are based on sound ground of seismology, i.e. the Gutenberg-Richter magnitude-frequency relationship, Kostrov's formula on seismic moment and strain, and characteristic earthquake model. However, if they are tested against a 400-year Japanese historical earthquake catalog, we find that they do not necessarily reproduce the observed seismicity. In some cases they are worse than a no-information model which assumes that the earthquake potential is uniform all over the Japanese islands. Dividing the data set into different time-periods, we find that the present-day spatial distributions of small earthquakes and surface horizontal strains are much affected by large earthquakes which took place in the past 100 years. In general, we find that three sources of information are effective. They are regionalized seismicity of small earthquakes, smoothed distribution of seismicity obtained by Frankel's method of combining small and moderate-size earthquakes, and active fault data. We classified historical earthquakes according to whether or not they are correlated with active faults and find that models based on the three sources are relatively robust. In this testing, we assume that the b-value is constant all over the Japanese islands. We declustered JMA (Japan Meteorological Agency) catalog of small earthquakes for a period of 1980-1997 and that of moderate-size earthquakes for a period of 1926-1997. The spatial variation of the likelihood of large earthquakes is tested. An adjusting factor which is multiplied to the rate of occurrence is introduced for the model comparison and AIC (Akaike Information Criterion) is calculated. For the real evaluation of various models we need the world-wide testing proposed by David Jackson, or we have to wait for many decades until enough number of large earthquakes take place. However, our study would shed some lights on the effectiveness of the proposed probabilistic models of earthquake potential and seismic hazard

SS04/09A/A03-006

1015

**STUDY ON STRONG EARTHQUAKE RECURRENCE BEHAVIORS ON ENTIRETIES OF ACTIVE FAULT ZONES IN SICHUAN-YUNNAN REGION, CHINA**Guixi YI<sup>1</sup>, Xueze WEN<sup>2</sup>, Xiwei XU<sup>3</sup> (<sup>1</sup>Chengdu University of Technology, Chengdu 610059, China; <sup>2</sup>Seismological Bureau of Sichuan Province, Chengdu 610041, China, <sup>3</sup>Seismological Bureau of Sichuan Province, Chengdu 610041, China, <sup>4</sup>Institute of Geology, China Seismological Bureau, Beijing 100029, China)

Basing on data of historical and modern strong earthquakes, we use statistical methods to study the recurrence behaviors of strong earthquakes on entireties of selected 7 active fault zones with different number of independent rupturable segments in Sichuan-Yunnan region, China. The result mainly shows that recurrences of strong earthquakes on the 7 studied fault zones are characterized by near-random, random or clustering behaviors. The variation coefficient  $\sigma$ , the ratio of the standard deviation to the mean of recurrence intervals of strong earthquakes, is proportional to the number of rupturable segments of an individual fault zone. The recurrence processes never display a well quasi-periodic behavior, and exhibit neither strength-time nor time-strength dependence. For the active fault zones, the more the number of the strong-earthquake rupture segments that form a zone is, the more complicated the recurrence process is. The recurrence interval distributions of earthquakes suggest bimodal or tri-modal character, indicating relatively active and quiet periods of earthquake activity occurring alternatively. For the active periods, recurrence interval distribution has relatively large discretion, and can be well-fitted by the Weibull distribution with parameters of  $\alpha=1.34$  and  $\beta=1.12$ . While, for the quiet periods, the duration distribution has relatively small discretion, and can be described approximately by distributions, such as

the normal (N)( $\mu=1.00, \sigma^2=0.24^2$ ), the lognormal (LN)( $\mu_{\ln}=0.03, \sigma_{\ln}^2=0.23^2$ ), or the Weibull ( $\alpha=4.99, \beta=1.53$ ). Both the duration of every active period and the number of strong earthquakes in every active period are obviously variable cycle to cycle, which leads to the relatively active periods having never repeated quasi-periodically. Therefore, it is difficult to make a meaningful probabilistic forecast for middle and long term seismic hazard only based on the recurrence interval distributions of strong earthquakes, due to the complexity of strong earthquake recurrence processes for entireties of active fault zones. However, the efficiency of the probabilistic forecast would be improved if the additional information or evidence can be obtained, from which either an active fault zone is in its seismic active period or in the quiet period can be identified.

## SS04a-Posters

Wednesday, July 9

## STRONG GROUND MOTION, EARTHQUAKE HAZARD AND RISK

Location: Site D

Wednesday, July 9 PM

Presiding Chairs: Y.M. Wu, G.F. Panza, K. Kudo

SS04a/09P/D-001

Poster

1400-250

## AMPLIFICATION CHARACTERIZATION OF K-NET, KIK-NET, AND JMA SITES BASED ON THE SPECTRAL INVERSION TECHNIQUE

Hirosi KAWASE, Hidenori MATSUO (Dept. of Human-Environment Studies, Kyushu University)

To predict strong ground motions for future scenario earthquakes in a broad-band frequency range, we need to characterize both source spectra and site amplification. For short period we can use statistical method based on the observed records and the wave summation technique (e.g., Kamae and Irikura, 1997). Thanks to the advent of the K-Net, Kik-net, and JMA Seismic Intensity (Shindokey) Network in Japan, we have now plenty of weak motion data, enough to construct statistical Green's functions. On the other hand, in order to represent long- and intermediate period nature of strong ground motions in the near field region, including both the forward rupture directivity effects and the basin effects, we want to use theoretical technique such as three-dimensional finite difference method in which we can take these effects into account. Any theoretical methods need S-wave velocity structures that should reproduce the observed site amplification quantitatively. In this study we perform first the analysis to separate the so-called source spectra, attenuation coefficient, and site amplification factors from K-Net, Kik-Net, and JMA Shindokey records observed throughout Japan. The separation method is the well-established one of Andrews (1980) and the resultant source spectra are modeled as omega-square spectra. As a reference site we use one rock station of Kik-Net in Yamaguchi Prefecture, from which we take the amplification effect of shallow surface deposits. Once we obtain site amplification factors, we try to reproduce them by using one-dimensional S-wave velocity structures below each site. We use Genetic Algorithm to invert the S-wave structures. We succeeded to reproduce site amplification factors at about two thirds of the sites very well. For the rest of the sites we may need 2D/3D structures to explain the amplification quantitatively or we must investigate some local topographic effects near the site. Once we obtain S-wave velocity structures at as many sites as we can, we will extrapolate them with the help of the gravity and geology data and construct an initial model of the three-dimensional basin structure of the whole Japanese islands. We would like to emphasize here that frequency characteristics of the inverted amplification factors show very large variations from site to site so that they cannot be characterized by simple soil-type classifications. We also derive site amplification factors for peak values of ground motions.

SS04a/09P/D-002

Poster

1400-251

## EARTHQUAKE OBSERVATION USING HOT SPRING BOREHOLE AND MICROTREMOR ARRAY SURVEY IN SOUTHWEST PART OF NAGOYA CITY

Yoshihiro SAWADA<sup>1</sup>, Hideki NAGUMO<sup>1</sup>, Kazuaki MASAKI<sup>2</sup>, Miyako NORITA<sup>1</sup>, Susumu KURAHASHI<sup>1</sup> (Graduate School of Engineering, Nagoya University, Furo-cho, Chikusa-ku, Nagoya 464-8603 JAPAN, <sup>2</sup>Department of Civil Engineering, Aichi Institute of Technology)

Nagoya city located in the eastern part of the Nobi plain is one of the largest cities in Japan. Although, the foundation investigation by the seismic reflecting method etc. has been conducted in Nobi plain in recent years, the foundation structure to a base rock is not clear especially in the southwest part area of Nagoya city since data is not fully accumulated yet. We try to clarify the foundation structure of this area by carrying out the earthquake observation at a hot spring borehole (San-no site mostly located at the center of Nagoya city) and microtremor array surveys. It is confirmed that base rock under the San-no site is in a depth of 670m and consists of hard granite of which S wave velocity is about 2.8 km/s. P and S wave velocity in each sediment layer along borehole is also obtained from the PS logging. We observe many earthquake records at base rock and surface ground, including the small earthquakes happened under the Nobi plain. The earthquake amplification characteristics between bottom and surface of borehole are examined, and the optimal physical-properties value of each deposit layer; velocity and Q value, is identified by using these earthquake observation data. We verify the applicability of microtremor array method by comparing the S wave velocity distribution estimated from this method with that obtained by PS logging along the San-no borehole. Then, we carry out the high-density microtremor array survey in the southwest part area of Nagoya city where sudden change of the depth of base rock is expected to be from the bouguer anomaly distribution. Consequently, it was clarified that the basement beneath the southwestern part of Nagoya city inclines from the north-east to the south-west direction. The depth of base rock changes rapidly from 500-600m at a northeast side to 1200m-1600m in a southwest side of the San-no site. That is, it is surmised that the seismic basement under the southwest part of Nagoya city has irregular form of the shape of a concave with a depth of about 1600m at the deepest point. At last, we propose the three dimensional structural model for this area based on above examination results and verify the property of model by seismic wave simulation.

SS04a/09P/D-003

Poster

1400-252

## TEMPORAL AND SPECIAL CHARACTERISTICS OF STRONG GROUND MOTION WAVE FIELD IN THE TAIPEI BASIN DURING THE M 7.1 EASTERN TAIWAN OFFSHORE EARTHQUAKE OF 31 MARCH 2002

Yi-Ling HUANG<sup>1</sup>, Bor-Shouh HUANG<sup>2</sup>, Kuo-Liang WEN<sup>1</sup> (Institute of Geophysics, National Central University, <sup>2</sup>Institute of Earth Sciences, Academia Sinica, <sup>3</sup>Institute of Applied Geology, National Central University)

The ground motion snapshots in the northern Taiwan area during the M7.1 eastern Taiwan offshore earthquake of 31 March 2002 have been reconstructed (Huang et al., 2002). Those snapshots displayed complicated wave propagation and complex direction of ground motion in the Taipei basin. The major shocks during the earthquake of 31 March 2002 were arisen from S-wave later phases and dominate in its radial direction. Those phases could be basin induced surface waves, which converted from body waves through complicated topography of Taipei basin, and made the large shock in the eastern edge and western portion of Taipei basin. The aim of this study try to investigate the characteristics of the converted seismic wave amplitude in different frequency bands with respect to the basin topography and rock site properties. The recorded ground motions from dense seismic network have been analyzed by F-K analysis and beam-forming method. Results of this study showed that the seismic wave phases have strongly bent through it pass the Taipei basin. To rely on the assistance of reconstructed ground motion snapshots and beam-forming analyze, results of this study could provide the researchers much useful information to constrain the further three-dimensional numerical simulation for the basin response and velocity structure, and to predict ground motions of the further large earthquakes.

SS04a/09P/D-004

Poster

1400-253

## THE DURATION-DISTANCE RELATIONSHIP AND AVERAGE ENVELOPE SHAPES OF SMALL KAMCHATKA EARTHQUAKES

Anatoly G. PETUKHIN<sup>1</sup>, Alexander A. GUSEV<sup>2</sup> (<sup>1</sup>Geo-Research Institute, 4-3-2 Itachibori, Nishi-ku, Osaka, 550-0012 JAPAN, <sup>2</sup>Institute of Volcanic Geology and Geochemistry RAS, Petropavlovsk-Kamchatsky, RUSSIA)

Average envelope shapes (mean square amplitude time histories) of small earthquakes represent a convenient basis for the construction of semi-empirical stochastic "Green's functions", needed for prediction of future strong ground motion. At the same time, they provide crucial evidence for verification of the theories of scattering of high-frequency seismic waves in the lithosphere. To determine such shapes in the Kamchatka region, Russia, we use the records of near ( $R=50-200$  km) shallow earthquakes located around the broadband station PET. On these records, we select the S-wave group and determine its root-mean-square duration  $T_{rms}$ , separately for each of the five octave frequency bands. We determine the empirical  $T_{rms}$  vs. distance dependence and find it to be very close to a linear one. At the reference distance  $R=100$  km, average  $T_{rms}$  decreases from 5.4 sec for the 0.75 Hz band to 3.9 sec for the 12 Hz band. To analyze average envelopes, we assume that the functional form of the envelope shape function is independent of distance, and stretch each of the observed envelopes along the time axis so as to reduce it to a fixed distance. Through averaging of these envelopes we obtain characteristic envelope shape functions. We qualitatively analyze these shapes and find that around the peak they are close to the shapes expected for a medium with power-law inhomogeneity spectrum, with the spectral exponent 3.5-4. From onset-to-peak delay times we derive the values of transport mean free path and of scattering  $Q$  for a set of distances. Broadening of envelopes with distance due to random scattering is especially important for simulating high-frequency seismic records of large, relatively distant, interplate, subduction zone earthquakes. To demonstrate the general methodology of stochastic simulation of strong motions using our average band-pass envelopes we developed a simplified algorithm that employs the point-source approximation; extension to an expanded source also is possible. To show it in action we simulated ground motion from two moderate earthquakes recorded by station PET: (1) November 13, 1993 with  $MW=7.0$ ,  $R=135$  km, seismic intensity  $I=5$  in Petropavlovsk-Kamchatsky, and (2) May 7, 1994,  $MS=5.5$ ,  $R=107$  km. Both the envelope shape and the frequency content of the observed and simulated records match quite well. **Acknowledgements.** We deeply appreciate Kamchatka Experimental and Methodical Seismological Department, GS RAS, for providing data of the IRIS station Petropavlovsk (PET).

SS04a/09P/D-005

Poster

1400-254

## THE FIRST MODEL FOR SCALING OF RESPONSE SPECTRA OF STRONG GROUND MOTION RECORDED ON KAMCHATKA

Anatoly G. PETUKHIN<sup>1</sup>, Alexander A. GUSEV<sup>2</sup>, Evgeniya M. GUSEVA<sup>2</sup>, Evgenii I. GORDEEV<sup>2</sup>, Victor N. CHEBROV<sup>2</sup> (<sup>1</sup>Geo-Research Institute, 4-3-2 Itachibori, Nishi-ku, Osaka, 550-0012 JAPAN, <sup>2</sup>Kamchatka Experimental and Methodological Seismological Department, Geophysical Survey, Russian Academy of Science, Petropavlovsk-Kamchatsky, RUSSIA)

To determine the average relationship among response (pseudo-velocity) spectrum of horizontal acceleration  $PV(f)$ , moment magnitude  $M_w$  and hypocentral distance  $R$  for Kamchatka earthquakes, we analyzed 140 analog strong motion records obtained during 1969-1998. The records of acceleration and velocity meters were obtained at 19 rock to stiff soil-ground Kamchatkan sites from 77 earthquakes with  $M_w = 3.9-7.9$ , at distances  $R = 10-300$  km and depths 0-145 km. Response spectra  $PV(f)$  were calculated from digitized, zero-line corrected and instrument corrected records of 255 horizontal components. After smoothing, the values were picked at a set of fixed frequencies. With the scarce amount of data at hand, it was impossible to determine reliably the entire  $PV(M_w, R, f)$  average trend surface. Hence we first performed distance equalization, with distance corrections calculated on a theoretical basis, and thus reduced the observed data to the reference distance of  $R_0 = 100$  km. The model of distance attenuation applied included (1) point source decay terms ( $1/R$  plus attenuation specified by  $Q(f) = 250 f^{0.9}$ ), (2) finite source correction (using the formula for a disc-shaped incoherent source, its size depending on  $M_w$ ) and (3) duration correction using stochastic approach formula for calculation of response spectrum. After reduction, we determined the  $PV(M_w, R_0, f)$  vs  $M_w$  trends. To do this we employed a multiple regression procedure, with ground type and station dummy variables. The  $M_w$  dependence was assumed to consist of two linear branches intersecting at  $M_w=6.5$ . The result of multiple regression represents the first systematic description of response spectrum properties of destructive ground motion for Kamchatka earthquakes.

SS04a/09P/D-006

Poster

1400-255

## EVALUATION OF THE GROUND PARAMETERS ON THE EXAMPLE OF THE STRONG EARTHQUAKES OF THE CAUCASUS

Levon Garnik SUVARYAN<sup>1</sup>, Heghine Vladimir SARGSYAN, Khoren Garnik SUVARYAN (Northern department of National service for seismic protection of RA, <sup>2</sup>Northern department of National service for seismic protection of RA, <sup>3</sup>Politechnical Institute)

The analysis of strong earthquakes, which occurred after the Spitak destructive earthquake in 1988, shows the connection of seismic effect with the value of the earthquake's energy and its azimuth of spreading. By results of detailed study of damages it is possible to judge about the necessity of the account of such parameters of tremors, as the constitution of frequencies and its changes during the oscillations, duration of strong oscillations and is probable by the form of oscillations. The listed parameters are confined in time functions (accelerograms), which are the most informative characteristics of the ground's oscillations. The parameters of tremors are depending on parameters of the source of earthquakes AEmechanism, the size and geometry of the source, the magnitude of adjustments, velocity of propagation of a rupture and from the properties of the medium, through which the waves are spreading. We

selected the strong earthquakes for study: the Spitak destructive earthquake of 1988 and the all earthquakes, which occurred after the Spitak earthquake, with  $M \geq 4.0$  in this source zone and the Racha-Djava earthquake on the territory of Georgia which occurred in April 29 of 1991. By the network of equipment SMACH of the ground's strong motions, which were installed during the last period on the territory of Armenia-Georgia, are registered accelerations of ground's oscillations. By the records of accelerograms are studied the spectra of oscillations of grounds and are compared with the macroseismic inspections. By the records of accelerograms is proved about the complexity of the source of the Spitak earthquake and about the strong spreading in the northwest direction. The dominant periods of oscillations of earthquakes in the source zone 'Spitak-88' and the Zangezur earthquake of 1968 are determined.

**SS04a/09P/D-007** Poster **1400-256**

#### EXTENDED STOCHASTIC SIMULATION METHOD FOR THE VERTICAL STRONG GROUND MOTIONS

Boming ZHAO<sup>1</sup>, Masanori HORIKE<sup>2</sup> (<sup>1</sup>Geo-Research Institute, JAPAN, <sup>2</sup>Osaka Institute of Technology, JAPAN)

We examine the possibility for simulation of high-frequency vertical ground motions by an extended stochastic method using corrected microtremor horizontal-to-vertical spectral ratios (H/V ratios). Comparing earthquake-motion and microtremor H/V ratios we show that, although microtremor H/V are smaller than earthquake ones, their spectral shapes are similar. It was suggested that the difference between two ratios is controlled by local geological conditions, and hence earthquake HV ratios can be obtained from microtremor HV ratios using a correction factor (CF) common for geologically similar sites. At first we show that the CF is almost the same among geologically similar sites in Osaka basin, Japan. Then, we reproduce vertical strong ground motions of the 1995 Kobe earthquake. We also tried to extend our method for simulation of P wave and P coda. 12 observation sites in the Osaka basin were used. The sites are located in different geological conditions: rock (2 sites), hard-sediments (4 sites) and soft alluvial sediments (6 sites). The CF was derived from the difference between the microtremor and the earthquake-motion HV ratios by Least Square Fitting. We used both HV ratios in the frequency range 0.5 Hz to 10 Hz. At all the sites the corrected microtremor HV ratios are similar to the earthquake motion, indicating that the CF are estimated appropriately. However, it should be mentioned that using of these results should be limited within the Osaka basin. Then we simulated vertical ground accelerations for the 1995 Kobe earthquake using the corrected microtremor HV ratios. Strong horizontal ground accelerations were calculated using the stochastic simulation method in conjunction with the  $\omega^2$  source spectra (Boore, 1983). Vertical accelerations were computed by the same method except for using modified source spectra where the  $\omega^2$  source spectra are divided by the corrected microtremor HV ratios. It should be mentioned that the modified source spectra are required only for the convenience of simulation. We replaced three asperities of the source rupture model of Kamae and Irikura (1998) with three point sources, which are located at the center of the asperities. The radiation coefficient for vertical motions was assumed to be the same as for horizontal motions, 0.64. Subsurface structure models of sediments at the target sites (soft alluvial sediments) were derived from results of the reflection survey and the microtremor array surveys. For the sites on soft alluvial sediments the CF were varying from 1.7 to 2.1, we assumed CF = 2.0 for target sites. Simulated horizontal and vertical peak accelerations and durations of the S wave group were similar to the observed ones. Also, enriched high-frequency content of vertical motions was reproduced well. The non-linear effects at sites are discussed. Our results show that the extended stochastic simulation method may be a useful tool to calculate the high-frequency vertical strong ground motions in the area where the correction factors are the same at geologically similar sites.

**SS04a/09P/D-008** Poster **1400-257**

#### GROUND MOTION CHARACTERISTICS IN THE TAIPEI BASIN (NORTHERN TAIWAN) DURING LARGE EARTHQUAKES OF DIFFERENT LOCATION

Vladimir Yu. SOKOLOV<sup>1</sup>, Wen-Yu JEAN<sup>2</sup>, Chin-Hsiung LOH<sup>2</sup>, Kuo-Liang WEN<sup>3</sup> (<sup>1</sup>Karlsruhe University, Geophysical Institute, <sup>2</sup>National Center for Research on Earthquake Engineering, Taiwan, <sup>3</sup>Institute of Applied Geology, National Central University, Taiwan)

The paper compares ground motion characteristics (Peak Ground Acceleration, Fourier and Response Spectra, local site response) observed in the Taipei basin - the triangle-shaped alluvium structure with maximum thickness of sediments up to 400 m, which is located in the northern part of Taiwan Island. The ground motion parameters in the Taipei basin was studied using the records of more than 70 earthquakes located to the South, Southeast and East of the basin and occurred in 1993-2002. The magnitude range is from 2.6 to 7.3 on the local magnitude scale, focal depth is between 1 km and 118 km, and the hypocentral distance range is from 10-15 km to 150-160 km. The database includes the records from the Chi-Chi earthquake of September 21, 1999 (ML = 7.3), two large (ML > 6.5) aftershocks, and the Hualien earthquake of March 31, 2002 (ML = 6.8). The Chi-Chi and Hualien earthquakes, even if occurring more than 80-100 km from the basin, caused severe damage in the Taipei area. The unique set of the TSMIP (Taiwan Strong Motion Instrumentation Program) recordings provides an opportunity to analyse the peculiarities of the basin response with respects the earthquake location. It has been shown that distribution of ground-motion parameters throughout the Taipei basin is determined by the joint influence of propagation path, subsurface structure and local soil properties. The ground motion characteristics depend on location of stations and location of earthquakes. Thus, one single design curve and seismicity coefficient (PGA value) proposed by building code are not adequate for the whole basin area.

**SS04a/09P/D-009** Poster **1400-258**

#### THE ATTENUATION OF VERTICAL AND TWO HORIZONTAL GROUND MOTIONS

Guoxin WANG (Earthquake Engineering Research Institute, Department of Civil Engineering, Dalian University of Technology)

It is known that the every component of ground motions has different characteristics in many aspects, such as response spectrum, intensity, frequency and so on, as compared with others, so the structural response problems concerning the multi-dimensional earthquake action have been paid more and more attention. Usually, only the differences between vertical and horizontal components are considered, two horizontal components are treated equally for simplification when multi-dimensional ground motion should be considered in structural design. In fact, this simplified method obliterates the efficiency of multi-dimensional seismic analysis in a limited way, even the differences between two horizontal components may be smaller than that between vertical and horizontal components. The main purpose of this paper is to understand the differences between the vertical and two horizontal components further. First, the strong ground motion database is rechecked and classified depending on the site conditions, and then the acceleration response spectrum of every component is calculated. The response spectra ratios of two horizontal components (response spectra with larger peak acceleration to another one), vertical to each horizontal

component and vertical to the average of two horizontal components are analyzed finally in this paper. The results show that there are some correlations between the response spectra of different ground motion components, and the magnitude, distance and site condition can also have some affection on the distributing characteristics of strong ground motions. The more valid methods should be considered further in order to analyze the multi-dimensional structural seismic response.

**SS04a/09P/D-010** Poster **1400-259**

#### LONG-PERIOD GROUND MOTION FD SIMULATION DURING 1984 WESTERN PART OF NAGANO PREFECTURE EARTHQUAKE-THE INFLUENCE OF 3D UNDERGROUND STRUCTURE IN KANTO PLAIN-

Nobuyuki YAMADA<sup>1</sup>, Hiroaki YAMANAKA<sup>1</sup>, Shin KOYAMA<sup>2</sup> (<sup>1</sup>Tokyo Institute of Technology, <sup>2</sup>National Institute for Land and Infrastructure Management)

1984 Western part of Nagano Prefecture Earthquake (MJMA: 6.8) occurred at central Honshu Island in Japan with heavy damaged around the source area. This event was recorded at some JMA observation stations. Koyama et al. (1992a) pointed out one of some records had a distinct later phase with a delay time of 1 minute after arrival of initial S-wave only at Kumagaya JMA station in the northern part of Kanto plain. According to their work, the initial S-wave amplitude has a predominant period at about 6.0 sec and the direction propagation of N50W, which is different from orientation of the epicenter. Furthermore, they point out the generation of the large later phase depending on the location of hypocenter and source mechanism from the analysis of seismic records of the main and after shocks at Kumagaya. From ray tracing simulation Koyama et al. (1992b) qualitatively showed the propagation paths of the Love waves considering the 3D effects of sedimentary basin. We carried out FD simulations of the long-period ground motion during 1984 Western part of Nagano Prefecture Earthquake and the other events which generated similar later phase using the three-dimensional underground structure model proposed by Yamanaka and Yamada (2002). A computed area was 220km (NS) 330km (EW) include from Kanto to Tokai district with a depth of 50km down the upper Moho continuity. Minimum grid spacing was 0.4km and a total grid number was 24 million. A source rupture process of the main shock was referred from result of Yoshida and Koketsu (1984). The simulation technique used three-dimensional finite difference method with 2nd-order time approximation and 4th-order space approximation (Graves, 1996). The synthetic waveforms of the FD simulations showed the distinct later phase only at Kumagaya. The analysis indicated the appropriateness of the Koyama's interpretation. Although, we can simulate qualitative feature of the observed motion at Kumagaya, perfect matching of the synthetics and observation is still difficult task. It is required in future study to improve subsurface structure model near the Kumagaya station.

**SS04a/09P/D-011** Poster **1400-260**

#### REDUCTION OF GROUND MOTION VARIABILITY USING THE VARIANCE COMPONENTS TECHNIQUE

Chu-Chuan P. TSAI<sup>1</sup>, Yi-Hau CHEN<sup>2</sup> (<sup>1</sup>Inst. of Earth Sciences, Academia Sinica, <sup>2</sup>Inst. of Statistical Science, Academia Sinica)

The 1999 Chi-Chi earthquake created a significant increase of strong-motion data set in Taiwan. Data from the main shock and aftershocks of the Chi-Chi event and those occurred elsewhere around this area offer an opportunity to explore the variability of ground motion estimates in Taiwan. Using the variance components technique, Chen and Tsai (2002) decomposed efficiently the prediction errors of ground motions into three components: the earthquake-to-earthquake, the site-to-site, and the residual. From a data set of over thirty thousand records of various site conditions, the percentages of variances of the prediction errors, partitioned into the earthquake and site components, are dependent on the numbers of earthquake events and stations in the sampled records; however, both the variances are in general smaller than that of the residual. It is apparent that the path-to-path component of the variability of ground motions is embedded in the "residual." Empirically based on the estimated variance components, the path component of variance is approximately comparable to those of the earthquake and the site. Thus, the prediction errors of ground motions can be partitioned with one more step into earthquake-to-earthquake, site-to-site, and path-to-path components, and the remaining "smaller residual." From the data in Taiwan, the variability of the site and path components is more coherent in space than that of the earthquake. This implies that the site and path components of variability are more feasible to be extracted from the total prediction errors than the earthquake component. The results show that the prediction errors of ground motions reduce dramatically after ground motion estimates have been corrected for the site-to-site and path-to-path components of variability. This reduction of ground motion variability has significant implications for probabilistic seismic hazard analysis.

**SS04a/09P/D-012** Poster **1400-261**

#### SIMULATION OF GROUND MOTIONS DURING THE 1993 HOKKAIDO-NANSEI-OKI EARTHQUAKE BY EMPIRICAL GREEN'S FUNCTION METHOD AND STOCHASTIC GREEN'S FUNCTION METHOD - VERIFICATION OF CHARACTERIZING PROCEDURE OF EARTHQUAKE SOURCE MODEL FOR STRONG MOTION PREDICTION -

Akira FUKUKITA<sup>1</sup>, Jun'ichi MIYAKOSHII<sup>2</sup>, Kazuo DAN<sup>2</sup>, Kazuhiko YASIRO<sup>3</sup> (<sup>1</sup>Institute of Technology, Shimizu Corporation, <sup>2</sup>Izumi Research Institute, Shimizu Corporation, <sup>3</sup>Tokyo Electric Power Company)

We simulated strong ground motions during the 1993 Hokkaido-Nansei-Okai, Japan, earthquake ( $M_{max}$  7.8) based on its variable-slip rupture model and on its characterized asperity models to verify the characterizing procedure of source models for the strong motion prediction in future earthquakes. The asperity models were characterized by the total seismic moment, the short-period level of the source spectra, and the ratios of the area, the slip amount, and the effective stress on the asperity to those on the entire fault. First, the empirical Green's function method was applied to the simulation of the records at Sapporo JMA and Akita JMA, and the following results were obtained: 1) The asperity model whose asperity was arranged at the shallow position according to the final slip distribution of the variable-slip rupture model reproduced the long-period earthquake motion of 10 seconds, but this model produced a little larger short-period earthquake motion of 0.2 AE0.5 seconds than the records. 2) The asperity model whose asperity was arranged at the deep position according to the seismic moment or short-period level distribution of the variable-slip rupture model reproduced the short-period earthquake motion of 0.2 AE0.5 seconds, but this model produced less long-period earthquake motion of 10 seconds than the records. 3) From the above results, the location of the long-period radiation of 10 seconds was different from that of the short-period radiation of 0.2 AE0.5 seconds. Next, the stochastic Green's function method was applied to the wide area (192,000km<sup>2</sup>=230,400points) including the epicentral region, and the following results were obtained: 1) The asperity model whose asperity was arranged at the shallow position according to the final slip distribution of the variable-slip rupture model produced a little larger seismic intensity than the variable-slip rupture model did. 2) On the other hand, the asperity model whose asperity was arranged at the deep

position according to the short-period level distribution of the variable-slip rupture model produced the same seismic intensity as the variable-slip rupture model did. This study was jointly funded by eleven electric power companies in Japan.

**SS04a/09P/D-013** Poster **1400-262**

**SIMULATION OF ACCELERATION SPECTRA OF 1986 DHARMSALA EARTHQUAKE USING RANDOM VIBRATION THEORY**

Shikha RAJPUT<sup>1</sup>, Sanjeev KUMAR<sup>2</sup> (KURUKSHETRA UNIVERSITY,INDIA, <sup>1</sup>NATIONAL GEOPHYSICAL RESEARCH INSTITUTE)

Ground motion of a particular site can be thought of as being influenced by three main elements: source, travel path, and local site conditions. The first describes how the size and nature of the earthquake source controls the generation of earthquake waves, the second describes the effect of earth on these waves as they travel (at same path) from the source to a particular location, and the third describes the effect of the uppermost several meters of rock and soil and the surface topography at that location on the resultant ground motion produced by the emerging or passing earthquake waves. The numbers of parameters have been used to describe the characteristics of strong ground motion time histories. This includes the peak values of ground acceleration, velocity, displacement duration of strong ground motion and the spectral amplitude in terms of Fourier and Response spectra. The earthquake strong ground motion are characterized by parameters in time domain such as peak value of acceleration, duration of strong ground motion as well as by the spectral parameters such as Fourier and Response spectrum in frequency domain. The earthquake strong ground motion time histories are required to properly evaluate the seismic hazard of a region. If the recorded time histories are not available then alternate it to simulate the earthquake strong ground motions using an effective technique. One of the effective techniques available is "Random Vibration Theory". The technique states with the windowing of time sequence of band-limited random white Gaussian noise with zero expected mean and variance. The spectrum of the window time series is multiplied by the model spectrum and transformation back to time domain to get the final time series. In the proposed work "Random Vibration Theory" was applied to simulate the acceleration spectra at nine sites which recorded the 1986 Dhamsala, India earthquake. The simulated Fourier spectra are found to be with good agreement with those of empirical accelerogram of both components (L & T) at Bhawarna and Jawali, T components of N-B, Baron and Sihunta. The match is satisfactory for the L component of Kangra. At Dhamsala and Shahpur the match is poor with simulated Fourier spectra has less energy as compared to the observed accelerogram.

**SS04a/09P/D-014** Poster **1400-263**

**GROUND MOTION CHARACTERISTIC IN THE KAOHSIUNG AREA, TAIWAN**

Hsien Jen CHIANG<sup>1</sup>, Kuo Liang WEN<sup>1</sup>, Tao Ming CHANG<sup>2</sup> (Institute of Geophysics, National Central University, <sup>2</sup>Office of the National S&T Program for Hazards Mitigation, National Taiwan University)

Kaohsiung city is the most important harbor in Taiwan. Recently, there are many high-rise buildings and public transportation system are under construction in this area. Therefore, it is very important to know the surface geological conditions for many practical reasons especially after the strikes of 1999 Chi-Chi, Taiwan earthquake. The Central Geological Survey had spent four years to bore more than 50 wells. And now, it is very clear to know the basement depth is changing from 120 to 40 meters for the western and eastern part of the Kaohsiung city. The harbor and commercial area locate at the western part of this area, and the eastern part is small hill area. To serve the purpose of earthquake hazard mitigation, it would be better to understand the soil amplification effect of the Kaohsiung city. We then conducted a research to study the site effects of the Kaohsiung city, which includes analyze the acceleration seismogram data of TSMIP (Taiwan Strong Motion Instrumentation Program) network and two newly installed borehole seismometer arrays, and perform very dense microtremor measurements in the study area. Most microtremor measurements were done during the midnight to reduce artifacts. After carefully selection, we pick 233 records and use the H/V ratio method to get information of soil amplification. From the result, we found it correlated to the basement depth very well. For the purpose of the earthquake resistant design, earthquake engineers must consider the site response at a specific period. For example, the structure period of a ten-floor building is at about 1 second. If the input ground motion is dominate at 1 Hz, then the building will has a resonant effect. Therefore, in this study, we select 10 frequencies (0.3, 0.5, 0.7, 1.0, 1.5, 2.0, 2.5, 3.0, 3.5 and 4.0 Hz) to plot out the contour map for understanding the frequency responses in this area. For the 0.5 Hz, the contours show that main amplification effects occurred at the southern part of Kaohsiung area. With the frequency increasing to 2.0 Hz, the main amplification area move from the harbor and the southern part of Kaohsiung area to the hill area, which locates at the eastern part of Kaohsiung area. For the higher frequency (3.0 Hz), there are no obvious high contour areas. We pick the dominant frequency of each record and plot out the contour map. At the harbor and city area, the dominant frequency is about 0.5 ~ 0.9 Hz, and the northeastern part is about 1.3 ~ 1.7 Hz. We found that the basement structure can explain the contour very well. Yet, the H/V dominated frequency distribution map reveals more detail features.

**SS04a/09P/D-015** Poster **1400-264**

**STRONG MOTION PARAMETERS ESTIMATION IN THE NEAR SOURCE: APPLICATION TO THE 1688 DESTRUCTIVE SOUTHERN APENNINES (ITALY) EARTHQUAKE**

Giovanni IANNACCONE<sup>1</sup>, Mariateresa BONAGURA<sup>2</sup>, Vincenzo NISII<sup>1</sup>, Luigi IMPROTA<sup>3</sup>, Antonio EMOLO<sup>2</sup> (<sup>1</sup>INGV - Osservatorio Vesuviano, Naples, Italy, <sup>2</sup>Dipartimento di Scienze Fisiche, Universita' degli Studi di Napoli)

We simulated the high-frequency synthetic accelerograms in the near field for an extended source responsible for a strong historical earthquake (M 6.7) occurred in the Sannio region (Southern Apennines, Italy). The study area has experienced several large earthquakes in historical time and in the last decades is characterized by low magnitude background seismicity. We used a mixed statistical-deterministic procedure in order to simulate the acceleration field. This method is based on the simulation of a large number of possible rupture processes, on the same fault, parameterised by different rupture nucleation points and final slip distributions on the fault plane (obtained according to the k-square model). For each considered rupture process, we computed the seismic wavefield at a grid of receivers around the source. Due to the large number of synthetic seismograms produced at each receiver, a statistical analysis of results is possible allowing to compute, for example, mean PGA and associated coefficients of statistical variation maps. This method is applied in a double format: to translate by empirical relationships the accelerometric parameters in seismic intensity map to add more constraints to a fault model and to compute the accelerometric records expected at a medium town (Benevento, about 60 km NE of Naples). We considered one of the largest historical earthquake occurred in the region (1688, M 6.7) and integrating seismotectonics evidences and synthetic ground motion modelling we propose a fault model of the earthquake. For this fault we simulated accelerometric time histories for 100 randomly generated nucleation points and slip distributions at a near source

site corresponding to the city of Benevento. The simulation is considered at the bedrock, consequently effects of shallow soils are not included. Finally, the set of accelerometric records are used to yield engineering parameters.

**SS04a/09P/D-016** Poster **1400-265**

**STRONG GROUND MOTION SIMULATION USING DYNAMIC RUPTURE MODEL**

Takashi MIYATAKE (Earthquake Research Institute, University of Tokyo)

Computer simulation of the strong ground motion generated from the earthquake rupture process on a shallow strike-slip fault are carried out by using a 3-D finite difference method. The faulting process is modeled using a dynamic crack model with slip-weakening constitutive laws. The near-source ground motion is sensitive to the details of fault rupture processes. So we do not choose the kinematic modelling in which slip-rate time need to be assumed. In dynamic modelling, the slip-rate time function at each fault point is calculated by solving 3D wave equation of motion. We applied the model to several shallow earthquakes. The method is as follows, (1) Initial model of stress drop distribution is estimated using slip distribution inferred from waveform inversion. (2) Initial model of Dc is assumed or estimated using method proposed by Mikumo et. al. (2002). (3) Rupture process is simulated by using quasi dynamic model in which rupture time distribution is assumed to be same as that inferred from waveform inversion. And peak stress distribution is estimated. (4) If the simulated rupture process and slip distribution does not fit the rupture model inferred from waveform inversion, we adjust the parameters and repeat the above process.

**SS04a/09P/D-017** Poster **1400-266**

**STRONG MOTION SIMULATION FOR THE 1999 DUZCE EARTHQUAKE WITH STOCHASTIC GREEN'S FUNCTION METHOD: AMPLITUDE AND PHASE CHARACTERISTICS OF THE DUZCE BASIN**

Gulum BIRGOREN, Aaron MOYA, Kojiro IRIKURA (DPRI, Kyoto University)

In most of applications to simulate an earthquake motion with the stochastic Green's functions, only amplitude characteristics are taken into consideration. Phase characteristics are often disregarded or just assumed to be random. However, when seismic waves take multiple paths from the source, phase information becomes vital to calculate the arrival time of waves. It has been shown by many researchers that the standard deviation of a group delay time, which is basically the first derivation of an unwrapped phase spectrum of an earthquake record, is related to the shape of its envelope in the time domain. Further, the mean value represents the location of the maximum of the envelope. Hence, this suggests the accurate calculation of the duration of a stochastic Green's function especially at the basin structure region. Based on the assumption stating that the observed ground motion can be represented as the multiplication of source, site and propagation effects, group delay time also can be regarded in a similar manner except for the source factor. The main objective of this study is to investigate the amplitude and phase characteristics of the Duzce Basin using observed strong motion data. We have used the aftershock records of the 1999 Duzce event recorded at 15 stations located in and around the Duzce Basin within the epicentral distances of 50 km. Strong motion records were provided from the temporary array of Earthquake Engineering Department of Bogazici University and Columbia University. We have estimated the amplitude characteristics through a spectral inversion method using several events and stations. Regarding phase information, we have calculated the group delay time and mean and standard deviation of each waveform through a wavelet transformation to represent their frequency content variation with time. We have checked the scattering of the group delay time in and edge of the basin to check the directivity effect. For further steps, this information will be used to get the precise Green's function calculation for the stochastic simulation of the strong ground motion. Results can also be the reference to create a sample phase spectrum for this region.

**SS04a/09P/D-018** Poster **1400-267**

**GROUND MOTION PREDICTION IN THE OSAKA BASIN BASED ON DYNAMIC RUPTURE SCENARIOS AND THREE-DIMENSIONAL UNDERGROUND STRUCTURE MODEL**

Haruko SEKIGUCHI<sup>1</sup>, Yuko KASE<sup>1</sup>, Haruo HORIKAWA<sup>1</sup>, Tatsuya ISHIYAMA<sup>1</sup>, Kenji SATAKE<sup>1</sup>, Yuichi SUGIYAMA<sup>1</sup>, Arben PITARKA<sup>2</sup> (<sup>1</sup>Active Fault Research Center, GSJ/AIST, <sup>2</sup>URS Corporation)

We compute ground motion in and around the Osaka sedimentary basin, central Japan, from expected future large earthquakes that have high potential to cause considerable damage there. The possible sources of such earthquakes are active faults bordering or lying inside the basin, the plate boundary about 200 km to the south of the basin (the Nankai trough) and inside the subducted Philippine Sea Plate. Looking back the past, the 1995 Hyogo-ken Nanbu, or Kobe, earthquake (M7.2) occurred on the Rokko fault system hemming the northwestern margin of the basin, generated ground motion of up to VII on the JMA scale along the northwestern margin of the basin. The 1707 Hoei-Nankai earthquake (M8.4), the historically recorded largest earthquake on the Nankai trough, is estimated to have brought ground motion of about JMA intensity VI in the Osaka basin and even intensity VII along the eastern edge of the basin. The 1952 Yoshino earthquake (M6.8) occurred at about 10 km to the east, 60 km depth inside the subducted plate, and caused 2 deaths and 9 complete collapses of building in Osaka prefecture. Theoretical calculation of ground motion is from earthquake rupture scenarios in a three-dimensional underground structure model of the Osaka basin. We compiled available geophysical and geological data including the latest ones and constructed a three-dimensional structure model in 100m mesh data in which sharp offsets on faults are realistically expressed. Rupture scenarios on active faults are generated by numerical simulations of dynamic rupture considering friction law on the fault planes. Fault geometry and stress fields surrounding them are assumed from available geological and geophysical information. We made many simulations varying the unknown parameters such as hypocenter location, stress drop at rupture, and separation distance between fault segments to examine the variation of possible scenarios. Simulations of ground motions are carried out using three-dimensional finite difference method. For earthquakes on active faults, the resultant ground motion distribution strongly depends on the location of the causative fault and the rupture process. Hypocenter location and/or segment-gap distance result in different rupture process on the same fault plane and cause forward directivity effect in different directions. On the other hand, ground motion distributions from interplate-type and slab-type earthquakes are more controlled by the subsurface structure of the Osaka basin because of large hypocenter distances.

**SS04a/09P/D-019** Poster **1400-268**

**NEW PEAK GROUND ACCELERATION MAPS FOR EGYPT**

Mohamed Ahmed GAMAL, Yehia ELSaid ABDELHADY (Geophysics)

Seismic hazard maps for Egypt are updated using the so-called total probability theory. A

modified and updated earthquake catalogue till 2000, earthquakes occurring in Egypt and surrounding areas is used for the correlation of the seismic activity with the geo-tectonic elements and seismic sources zones in Egypt and surrounding areas. Estimation of recurrence relationships and regression constants, maximum magnitude earthquake was calculated for 72 source zones used in the present study, with two new zones at Gif EL Kebir and Abu Debab Area. These data were used to generate peak ground acceleration contour maps based on the regionally developed PGA attenuation relation for all shallow seismic sources for respective forecast time periods (exposure times), 50 and 100 years. Hazard maps were calculated using the computer program developed by McGuire (1976). The same data were used to generate iso-acceleration contour maps based on the regionally developed PGA attenuation relation for the intermediate seismic sources of Greece for the same time periods (exposure times), 50, and 100 years. Using the same program developed by McGuire (1976), it includes the effect of 6 intermediate sources separately. These maps were used to interpret the amount of risks reaching the northern coast of Egypt at which fast urban communities and construction work is done.

**SS04a/09P/D-020** Poster **1400-269**

**SHOULD WE CONSIDER SEA IN SIMULATING SEISMIC GROUND MOTION?: SOME NUMERICAL EXPERIMENTS**

Ken HATAYAMA (National Research Institute of Fire and Disaster)

I investigated the effects of the sea on seismic ground motion through some numerical experiments and examined the necessity of considering the sea in ground motion simulation. To specify the effects of the sea, I compared the waveforms calculated for the models including the sea with those done for the models ignoring the sea. Japan is prone to oceanic earthquakes with large magnitudes and now four hypothetical earthquakes along the trenches in the Pacific Ocean are considered to be likely in the near future. For these earthquakes, magnitudes over 7 are anticipated. Around these source regions, the depth of the sea is several hundred meters and obviously we have to recognize that the seismic waves come to us after propagating across the sea. It is nevertheless usual to ignore the sea in numerical methods to simulate ground motion. This study aims at examining whether ignoring the sea is valid. The subsurface structure models examined in this study are very simple. The models are composed of a sea part and a land part. Both parts are horizontally stratified layers overlying elastic half-space and as regards the sea part the medium of the uppermost layer is water, which is regarded as the ideal fluid here. For such models, I solved impulse responses of the two-dimensional P-SV wave-field in the frequency domain and velocity waveforms are calculated by convolving the impulse responses for a certain point source with Ricker wavelets. The impulse responses were calculated by the direct boundary element method using the Green function for horizontally layered media, which was originally presented by Fujiwara & Takenaka (1993) to calculate seismic wave-field in sedimentary basins. I first applied this technique to media in which solid and fluid coexist and interestingly found that the hyper-singularity appears in some boundary integrals. The most interesting feature of the numerical technique used here is that we can calculate Rayleigh waves alone as well as the total waves. From the comparison of the waveforms from the models including the sea with those from the models ignoring the sea, I found the effects of the sea with a depth of several hundred meters on seismic ground motion within a period range from 1.5 to 6 s. (1) The Rayleigh waves are strongly affected by the sea; (2) As the sea is deeper, its effects extends to longer-period ground motion; if the depth is 400 m, around 1.5-s-period ground motion is influenced; if the depth is 800 m, 1.5-to-3-s-period ground motion is influenced; (3) Substituting sediments for sea water, which is usual in ground motion simulation, can have bad influence particularly on vertical components and we would sooner replace water sea by vacuum than substitute sediments for water sea. The above findings strongly suggest the necessity of considering the sea in ground motion simulation and the effects of the sea on the three-dimensional wave-field still remain to be evaluated.

**SS04a/09P/D-021** Poster **1400-270**

**VOXEL FINITE ELEMENT METHOD FOR 3-D ELASTODYNAMIC ANALYSIS**

Hiroyuki FUJIWARA<sup>1</sup>, Tadaomi FUJIEDA<sup>2</sup> (National Research Institute for Earth Science and Disaster Prevention, <sup>1</sup>Fuji Research Institute Corporation)

Quantitative and deterministic evaluation of seismic wave field is essential for strong ground motion evaluation. Modeling wave fields using numerical techniques such as the finite difference method (FDM) and the finite element method (FEM) is important. The basic equation of FDM is differential equation and that of FEM is weak form integral equation. These methods belong to the more general weighted residual method. The difference between FDM and FEM arises from technique of discretization. In this study, we develop a code for the Voxel Finite Element Method (VFEM) for 3-D elastodynamic analysis and compare finite-difference and finite-element solutions of the 3-D elastic wave equation. Because conventional finite element method requires much larger size of memory than that of the VFEM, it is difficult to solve large size problems by using the conventional finite element method. The VFEM is numerically economical version of the conventional finite element method. Absorbing boundary conditions, representation of double couple force, and multi voxel domain decomposition technique for the VFEM are studied. Numerical dispersion, numerical stability condition and numerical complexity of the VFEM are investigated both numerically and theoretically. Numerical dispersion of the VFEM is comparable to the second-order conventional finite difference method. The stability condition of VFEM is 1.73 times longer than the second-order staggered grid finite difference method. Numerical complexity of the VFEM is theoretically 17/5 times larger than that of second-order conventional finite difference method. Although numerical complexity of VFEM is larger than that of FDM, flexibility to model complicated structure, such as complicated topography, is larger for VFEM than FDM.

**SS04a/09P/D-022** Poster **1400-271**

**NEAR REAL-TIME MAGNITUDE DETERMINATION FOR LARGE EARTHQUAKES**

Yih-Min WU<sup>1</sup>, Ta-liang TENG<sup>2</sup> (<sup>1</sup>Seismological Observation Center, Central Weather Bureau, Taiwan, <sup>2</sup>University of Southern California)

We introduce an empirical method of near real-time, near-field magnitude determination for large ( $M > 6.5$ ) earthquakes. Time integration over the strong shaking duration on the absolute values of the acceleration records is carried out for stations surrounding many large earthquake sources in Taiwan. The integrated quantity, called total effective shaking here, is used in a regression process to derive an empirical relationship for a quick Mw determination useful for a reliable real-time operation in earthquake rapid reporting and earthquake early warning systems.

**SS04a/09P/D-023** Poster **1400-272**

**REGRESSION ANALYSIS TO ESTIMATE MAGNITUDES FROM MACROSEISMIC OBSERVATIONS - COMPARISON OF DIFFERENT METHODS AND APPLICATION TO EARTHQUAKES IN EUROPE**

Diethelm KAISER<sup>1</sup>, Rolf GUTDEUTSCH<sup>2</sup>, Guenter LEYDECKER<sup>1</sup> (<sup>1</sup>Federal Institute for Geosciences and Natural Resources, Stilleweg 2, 30655 Hannover, Germany, d.kaiser@bgr.de, guenter.leydecker@bgr.de, <sup>2</sup>Institute of Meteorology and Geophysics, University of Vienna, Althanstrasse 14, 1090 Vienna, Austria, rudolf.gutdeutsch@univie.ac.at)

Magnitudes (Ms or ML) of earthquakes earlier than 1900 only can be derived from macroseismic observations, i.e. parameters as maximum intensity, felt area or isoseismal radii of different intensities, focal depth. The purpose of our study is to compare different regression methods and to apply them to data sets of earthquakes in Europe to derive appropriate empirical relationships. In general, all input parameters are in error. Several least square fit approximations are presented and compared as follows. (1) Standard regression where one parameter is in error and the remaining parameters are error-free. (2) Mean coefficients of standard regressions with different dependent parameters. (3) Orthogonal regression, minimising the normal distance of data points under the assumption that all parameters are in error (Gutdeutsch et al. 2002). (4) Maximum likelihood, minimising the weighted sum of squares of errors. We use carefully selected instrumental parts of two earthquake catalogues: Shebalin et al. (1998) for Central and Eastern Europe and Leydecker (2003) for Germany. Results: (1) represent extreme cases due to the unrealistic presumption of the method. (2) is of importance as it agrees quite well with (4). (3) agrees well with (2) and (4) if the scatter of data is low. The use of high quality data solely as input in the regression analysis provides reliable relationships to estimate magnitudes. The magnitude estimation of a historical earthquake based on epicentral intensity gives reliable results only if the focal depth is known well enough. Relations using isoseismal radii or felt area are of greater practical importance as they allow more reliable magnitude estimations. Regional variations in the relationships between magnitude, epicentral intensity and isoseismal radius have to be considered. References: Gutdeutsch, R., Kaiser, D., Jentzsch, G. (2002): Estimation of earthquake magnitudes from epicentral intensities and other focal parameters in Central and Southern Europe, Geophys. J. Int. 151, 824-834. Leydecker, G. (2003): Earthquake catalogue for Germany and adjacent areas for the years 800 – 2001. Datafile. – Fed. Institute for Geosciences and Natural Resources, Germany. <http://www.bgr.de/quakecat/> Shebalin, N.V., Leydecker, G., Mokrushina, N.G., Tatevossian, R.E., Erteleva, O.O., Vassiliev, V.Y. (1998). Earthquake catalogue for Central and Southeastern Europe 342 BC - 1990 AD. European Commission, Report No. ETNU CT 93 - 0087, Brussels.

**SS04a/09P/D-024** Poster **1400-273**

**STATISTICAL ANALYSIS OF JMA SEISMIC INTENSITY DIFFERENCES USING SEISMOMETER ARRAY RECORDS**

Hidenori MOGI<sup>1</sup>, Hideji KAWAKAMI<sup>2</sup> (<sup>1</sup>Department of Civil and Environmental Engineering, Saitama University, <sup>2</sup>Geosphere Research Institute of Saitama University)

The JMA (Japan Meteorological Agency) seismic intensity scale has been playing an important role in earthquake engineering such as seismic risk analyses and planning for disaster response. Since 1996, seismic intensity meters have been densely installed by JMA and many local governments for automatic and rapid announcement of seismic intensities in the region. However, it has been pointed out that the variation of the instrumental seismic intensity at neighboring sites is not small. Therefore, the spatial stochastic properties of the instrumental seismic intensity should be examined for proper utilization of the seismic intensity scale as the regional intensity of seismic ground motions. In this study, seismic intensity difference (SID), the difference between instrumental seismic intensity observed at two sites during each earthquake, was introduced and investigated to examine the statistical characteristics of the instrumental seismic intensity. First, the probability distribution of the SIDs was analyzed using mathematical expressions for probability density functions, averages, standard deviations and percentiles that were derived based on the assumption that the instrumental seismic intensities are Gaussian random variables. Second, the instrumental seismic intensities were calculated using the database of the Chiba and SMART-1 seismometer arrays. The intensities were corrected by the site amplification indices estimated from station-wise average of the intensities. In order to eliminate the deterministic differences, the SIDs were calculated from these corrected intensities. Then, the relationships between above-mentioned statistics of the SIDs and the station separations were analyzed. We have found that the averages and standard deviation monotonously increase with increasing logarithm of the station separation distances ranging from about several meters up to six kilometers throughout the two different arrays. The 50th, 80th, and 95th percentiles were also calculated from the standard deviations of the SIDs. Finally, the probability of occurrence of the same/different seismic intensity scale at two sites was considered by using both observed seismic intensity scale and theoretical ones estimated from the standard deviation of the SIDs. This consideration revealed the following: 1) the same intensity scales can be observed with 95 per cent probability at two stations separated by several ten meters, 2) with 75-80 per cent probability for stations separated by several kilometers, and 3) there is less than 0.5 per cent probability to observe intensity scale difference greater than or equal to two for the site pairs with separation distances discussed in this study. It was also confirmed that the theoretical probability estimated from the standard deviation of the SIDs is close to those probabilities.

**SS04a/09P/D-025** Poster **1400-274**

**RADIATION PATTERN OF SEISMIC MOTION IN SHORT PERIOD RANGE-SPECTRAL RATIO OF TWO SAME LOCATION AND MAGNITUDE EARTHQUAKES-**

Ryoichi NAKAMURA<sup>1</sup>, Kazuhiko YASHIRO<sup>2</sup> (<sup>1</sup>Tokyo Electric Power Services Co.,Ltd, <sup>2</sup>Tokyo Electric Power Company)

Observation amplitude ratio by same stations and near location of pairs of two earthquakes are studied here using the strong motion records of K-NET installed in Japan. First, we selected the earthquakes occurred at same location and obtained 10 pairs. Here, definition of the same pair is within 10km of the distance between two earthquakes. Second, we calculated response spectra ratio ( $h=5\%$ ) of two seismic records observed a same observation station by two earthquakes. Third, we found that spectrum ratios in short period (1Hz <) of a pair are clearly difference in different azimuth from epicenter to station, although it would be expected that the direction dependency in short period by the radiation pattern from mechanism solution had been small [i.e. Liu and Helmberger, 1985]. The direction dependency of amplitude ratio has cyclic change. We assumed this phenomena caused by fault rupture. As Koyama(1987) shown the amplitude changes theoretically as  $(c/v \cdot \cos\theta)^{1/2}$  in case of unilateral rupture, we calculate theoretical amplitude direction dependency using this equation ( $c$ : S-wave velocity,  $v$ : rupture velocity and  $\theta$ : azimuth between earthquake and observation site). The calculation result correspond to the observation level of amplitude ratio and shows cyclic change similar to observation. Finally, we obtained standard deviation of the variability of amplitude ratio by the observation data as  $1\sigma=0.4-0.5$

in natural logarithm. This value of the ratio can be converted to the value of amplitude (not ratio) as  $1\sigma=0.28-0.35$ . This value is much smaller than the deviation of attenuation empirical relation which is often used in probabilistic seismic hazard analysis. 1) Liu and HelMBERGER (1985) Bull. Seism. Soc. Am, 75, 689-7082) Koyama(1987) zisin, 40, 397-404 (Japanese)

**SS04a/09P/D-026** Poster **1400-275**

### THREE DIMENSIONAL ATTENUATION STRUCTURE ESTIMATED FROM STRONG MOTION DATA AND ITS APPLICATION TO STRONG MOTION PREDICTION

Ryoichi NAKAMURA<sup>1</sup>, Tomiichi UETAKE<sup>2</sup> (\*Tokyo Electric Power Services Co.,Ltd, <sup>2</sup>Tokyo Electric Power Company)

The three-dimensional attenuation structure of the Japanese islands and site amplification factors are obtained by simultaneous inversion of strong motion records recorded by many acceleration seismometers, i.e. JMA87-type seismometers and the Kyoshin-Net (K-NET) seismometers, almost uniformly distributed in Japan. The results show that the Pacific slab is high-Q and that the frequency dependence of Q values is expressed as  $f^{0.75}$ . We classified all stations into 5 groups by ground conditions mainly on the basis of S-wave logging data and obtained the site amplification factor for each group. The result shows that the frequency band where large amplification factors are obtained by inversion well agrees with the predominant frequency calculated from S-wave velocity data. Finally, we tried to estimate response spectrum using the 3-D attenuation structure and compared with empirical attenuation formula. The target of evaluation was the 1996 Hyuganada event (M6.6, h=35km). The observed ground motion of this event showed the attenuation with directional dependency. The method using 3-D attenuation structure well explains the semi-near field records at approximately  $\Delta=100$ km, much better than the empirical attenuation formula. This result shows that 3-D attenuation structure affect ground motion in semi-near field depending of place.

**SS04a/09P/D-027** Poster **1400-276**

### STRONG MOTION SIMULATION CONSIDERING FREQUENCY DEPENDENT RADIATION PATTERN

Shinichi MATSUSHIMA, Toshiaki SATO, Toshimi SATOH, Motofumi WATANABE, Takashi HAYAKAWA (Ohsaki Research Institute, Inc.)

Since strong motions around frequency of 1 Hz strongly affect the degree of structural damage, it is a major concern for us to simulate strong motions in this frequency range accurately for use in disaster mitigation. One of the important characteristics that control strong motions in this frequency range is the radiation pattern. However, the fundamental characteristics of radiation patterns of strong motions in this range are complex (Liu & Hembelberger, 1985, Vidale & Bonamassa, 1993). The authors investigated the fundamental characteristics of high frequency strong-motion including 1 Hz using dense strong-motion network data (KiK-net) for an aftershock event (Mj5.5, depth=9km) of the 2000 Tottori-ken Seibu, Japan, earthquake and found that the frequency range of transition from deterministic to random phenomena of radiation patterns is approximately 1~2 to 5 Hz (Matsushima & Sato, 2002). This result was consistent with the radiation pattern model of strong motions derived from statistical analysis by Satoh (2002) using KiK-net data for mainshock and aftershocks of the 2000 Tottori-ken earthquake. In this study, we incorporated the radiation pattern model into strong motion simulation and verify the validity of the model. We simulated recorded data by K-net for a moderate size earthquake (Mj5.4, 1998/4/22) that occurred beneath the Nobi, Aichi prefecture in central Japan, plain using a hybrid method, since we have a well constrained three-dimensional basin structure in this region. We assumed a point source for the simulation. For the low frequency range, we used a three-dimensional finite difference method (Pitarka, 1999). For the high frequency range, we used statistical Green's function method (Satoh, 1994) considering the model of the radiation pattern that has a transition zone from 1 to 5 Hz. In the transition zone, the radiation pattern is assumed to change linearly. The hybrid method is to sum up these results after filtering then with a matching filter at 0.5 Hz. In order to verify the validity of the radiation pattern model, we did the same calculations using the statistical Green's function method considering the radiation pattern for all frequencies and another case without considering the radiation pattern at all. The results showed that the case considering the radiation pattern model proposed by Satoh (2002) matched the data very well, compared to the other two cases. We acknowledge NIED for the use of KiK-net and K-net data. Some figures were made using GMT. This study was supported by the project Study on the master model for strong ground motion prediction toward earthquake disaster prevention AEFunded by Special Coordination Funds for Promoting Science and Technology, from MEXT (2000-2004).

**SS04a/09P/D-028** Poster **1400-277**

### A METHOD FOR EXTRACTING SLIP TIME FUNCTIONS SPATIALLY CONTINUOUS ON A FAULT PLANE FROM RESULTS OF CONVENTIONAL SOURCE INVERSION

Hiroshi TAKENAKA<sup>1</sup>, Yushiro FUJII<sup>2</sup>, Hiroshi KAWASE<sup>3</sup>, Ken MIYAKOSHI<sup>4</sup>, Tomotaka IWATA<sup>5</sup> (<sup>1</sup>Department of Earth & Planetary Sciences, Kyushu University, <sup>2</sup>Dept. of Human-Env. Studies, Kyushu Univ., <sup>3</sup>Geo-Research Institute, <sup>4</sup>DPRI, Kyoto Univ.)

Kinematic source inversion techniques such as multi-time window inversion have been widely applied to broadband seismic records including teleseismic and strong-ground motion records to estimate spatio-temporal slip distribution on seismic fault planes of middle to large earthquakes. In the kinematic source inversion the fault plane is conventionally divided into many subfaults to express spatial variation, and each subfault is represented by a single or many point sources placed at constant intervals on the planar surface. Such conventional subfault discretization is convenient for the representation of spatial distribution of slip in kinematic source inversion. However, it is not continuous at the subfault boundaries, and in the case of a single point source at a subfault, the inversion results (e.g., moment release time history) include not only a slip time function but also a rupture propagation effect inside each subfault. Therefore such inversion results may not be directly suitable for fine-scale numerical modeling such as the FDM computation to simulate near-fault strong-ground motion or to calculate stress field on the fault planes for dynamic source analysis. In this study we propose a new technique for extracting slip time functions continuous spatially from such conventional inversion results. The spatio-temporal distribution of slip rate is expanded with the linear b-spline basis functions in 2D space and time. Each linear b-spline function is an isosceles triangle defined by three knots, and thus this discretization can give a slip distribution continuous everywhere spatially and temporally. This approach is similar to that employed by Ide and Takeo (1997, JGR) for a kinematic source inversion, but slightly different from theirs. In our representation unlike theirs, it is possible to treat even rupture velocity variation of sub-subfault level if we have its information. The expansion coefficients are determined by fitting the spatial integration of slip rate function over each subfault in a least squares sense with some constraints to the contribution of the subfault derived from the conventional kinematic source inversion. Our technique was applied successfully to the 1997 Northwestern Kagoshima, Japan, earthquake ( $M_{max}$  6.5) to extract a spatially continuous slip rate function. We adopted the Miyakoshi's inversion result as the input data. He applied a kinematic source inversion to K-NET strong motion records (NIED) to obtain the moment

release function at each point source located at the center of each subfault. We extracted slip rate function from his inversion results and found that it has a peak of 4 m/s.

**SS04a/09P/D-029** Poster **1400-278**

### SOURCE MODELS OF TWO LARGE INTRA-SLAB EARTHQUAKES FOR BROADBAND STRONG GROUND MOTIONS

Nobuyuki MORIKAWA<sup>1</sup>, Tsutomu SASATANF<sup>2</sup> (<sup>1</sup>National Research Institute for Earth Science and Disaster Prevention, <sup>2</sup>Graduate School of Science, Hokkaido University)

Two large earthquakes occurred along the southern Kurile-Hokkaido arc in 1993 and 1994. One is the January 15, 1993 Kushiro-oki earthquake ( $M_w=7.6$ ) and the other is the October 4, 1994 Hokkaido Toho-oki (Shikotan) earthquake ( $M_w=8.2$ ). Both events are intra-slab earthquakes occurring within the subducting slab, and caused considerable damage around their epicentral regions. These earthquakes have two unique characteristics of observed strong ground motions. The first is the much large peak horizontal accelerations compared with the empirical attenuation relationship. The second is the far more extensive felt area compared with that for plate-boundary events having the same magnitude. In this study, we construct source models of these intra-slab earthquakes that explain broadband strong ground motions. Our source models consist of multiple asperities on a fault plane. The number and location of asperities and their parameters (area and stress drop) are estimated by matching the synthetic waveforms (displacement, velocity and acceleration time histories) and spectra to the observed ones. We apply the empirical Green's function method to syntheses of the broadband strong ground motions. The estimated source models have the following characteristics compared with the source models of in-land and plate-boundary earthquakes having the same magnitude: (1) the total asperity area is much small, and (2) the stress drop is extremely high (about 400 MPa). These indicate that the large intra-slab earthquake source radiates seismic energies from a small area in short time duration. This source process results in extremely strong radiation of short-period seismic waves as observed during the two large intra-slab earthquakes. Finally we confirm a correlation between outer fault parameters (entire fault size, seismic moment and short-period level of the acceleration source spectrum) and inner ones (areas and stress drops of asperities) for the two intra-slab earthquakes.

**SS04a/09P/D-030** Poster **1400-279**

### DIFFERENCES IN GROUND MOTION AND FAULT RUPTURE MODELS BETWEEN SURFACE AND BURIED RUPTURE EARTHQUAKES

Takao KAGAWA<sup>1</sup>, Kojiro IRIKURA<sup>2</sup>, Paul G. SOMERVILLE<sup>3</sup> (<sup>1</sup>Geo-Research Institute, <sup>2</sup>Disaster Prevention Research Institute, Kyoto University, <sup>3</sup>URS Corporation)

We have studied differences in ground motion and fault rupture characteristics between surface rupture earthquakes and buried rupture earthquakes. We found that the ground motion generated by buried rupture in the period range around 1 sec. is larger than the average empirical relationship for crustal earthquakes (e.g. Abrahamson and Silva, 1997). On the other hand, ground motion from earthquakes that rupture the surface is smaller in the same period range. This phenomenon is considered to be caused by differences in fault rupture process between the two types of earthquakes. We reanalyzed original source slip distribution data, used by Somerville et al. (1999) to construct scaling relations for source parameters of crustal earthquakes, and divided them into two groups of surface rupture and buried rupture earthquakes. It was found that the large slips of surface rupture earthquakes are concentrated in the depth range shallower than about 5 km, i.e. their asperities are shallow. On the contrary, large slips of buried rupture earthquakes are spread over the depth deeper than 5 km, i.e. asperities are deep. We also found that the rupture area of buried rupture earthquakes is clearly smaller than that of surface rupture earthquakes having the same seismic moment [Kagawa et al.(2001)] and deep asperities have several times larger apparent stress drops than shallow asperities. Furthermore, slip velocities of deep asperities are almost twice that of shallow asperities. To test whether these differences in source characteristics can explain the observed differences in ground motions between the two types of earthquakes, we constructed asperity fault rupture models for surface and buried rupture earthquakes and calculated strong ground motion in the near fault region by the stochastic Green's function method [Kamae and Irikura (1992)]. The simulated ground motions in the period range around 1 sec. have similar characteristics as those of the observed ground motions. We conclude that the difference in ground motions between two types of earthquakes is caused by the difference of the rupture area vs. magnitude scaling, depth of asperities, their apparent stress drop and slip velocity. [REFERENCES] Abrahamson and Silva (1997), SRL, 68, 94-127. Kagawa et al.(2001), AGU Fall Meeting, . Kamae and Irikura (1992), 11WCEE, 801-806. Somerville et al. (1999), SRL, 70, 59-80.

**SS04a/09P/D-031** Poster **1400-280**

### A STUDY ON DEVELOPPING 3-D BASIN STRUCTURE MODEL CORRESPONDING TO INFORMATION AVAILABLE IN THE TARGET AREA

Takao KAGAWA, Boming ZHAO, Ken MIYAKOSHI (Geo-Research Institute)

We propose a practical procedure for construction of 3-D basin structure model for strong motion simulation that combines a simplified layered 3-D deep structure and shallowest fine velocity structure under site. The methods were applied to the Osaka Basin, Japan. Similar to Koketsu and Higashi (1992) we applied the 2-D 3rd-order B-spline function to construct structure model from the available exploration information. Using the spline function, we can produce smoothed model with any accuracy corresponding to information available in the target area. The Osaka Basin is one of the best-investigated sedimentary basins in the world, a lot of geophysical explorations have been conducted here and the results are published. So we can construct detailed structure model that matches geological model and smooth enough for numerical calculations at the same time. On the other hand, for a poorly explored area we can make at least a very rough spline model from a scarce data. Kagawa et al. (1998) constructed a 4-layered velocity structure model for the Osaka Basin that explains well the dispersion of Rayleigh waves, derived from the microtremor array measurements. The velocity in the uppermost layer of the model is estimated as 350 m/s (engineering bedrock). Here, the model was verified by the wave propagation simulation using 3-D FDM. The results agree well with the observed ground motions in frequency range  $f < 1$  Hz. Deep borehole explorations until granite bedrock (depth around 1.6 km) were conducted at the Higashinada site. For this site we added the shallow borehole velocity structure (from surface to the engineering bedrock) to the 4-layered model and compare the site response of such structure with site response of detail 1612-layer model (thickness of each layer 1 m). The responses agree very well in wide frequency range, both  $f < 1$  Hz and  $f > 1$  Hz. This indicates that simplified deep velocity structure plus detail shallow data can be used to simulate realistic site response. Modeling sedimentary basin structure is important for strong motion estimation. Without a good model of structure, any powerful numerical method to calculate wave propagation cannot work well. Our proposed modeling procedure could be a useful tool to get a structure model for strong motion calculation. [ACKNOWLEDGEMENTS] This study was performed through Special Coordination Funds, titled 'Study of the master model for strong motion prediction toward earthquake disaster mitigation' of the Ministry of

Education, Culture, Sports, Science and Technology of the Japanese Government. Borehole explorations at Higashinada site were conducted by KEPCO and NUPEC. [REFERENCES] Kagawa et al. (1998), Zisin2, 51, 31-40 (Japanese). Koketsu and Hogashi (1992), BSSA, 82, 2328-2349.

**SS04a/09P/D-032** Poster **1400-281**

### CHARACTERIZATION OF SOURCE PARAMETERS OF DYNAMIC FAULTING FOR STRONG GROUND MOTION PREDICTION

Kojiro IRIKURA, Hiroe MIYAKE, Luis A. DALGUER (Research section of strong Motion Seismology, DPRI, Kyoto University)

Strong ground motion prediction based on dynamic rupture models is needed to fill the gap left by the lack of physics of conventional methods. Since dynamic models take into account the physical conditions of the friction and stress distribution across the fault zone, the characterization of fault parameters can be improved based on more realistic seismic source properties. The main purpose of the present paper is to derive the ratios of average slip and seismic moment between the asperity area and total rupture area. First we analyzed and compare consistently analytical solution of classical asperity models by Das and Kostrov (1986), Boatwright (1988) and Madariaga (1979). Then we started our study with dynamic rupture simulation of many theoretical circular asperity models keeping the ratio of 0.22 between the asperity area and total rupture area. This ratio, proposed by Somerville et al. (1999) after studying many kinematic slip models, fits the characteristic slip models of recent large earthquakes. A fixed rupture velocity (80% of S-wave velocity) and the simple slip-weakening model (friction law on the fault) were used for the dynamic shear rupture propagation. The critical slip distance (Dc) between 0 cm to 40 cm was assumed. These values of Dc do not affect the ratios. We found that the kinematic characterized slip model proposed by Somerville et al. (1999) is equivalent to the dynamic model when the stress drop surrounding the asperity (background area) is equal to around 10% the stress drop of the asperity area. We also confirmed that the background stress drop strongly affects the ratios; however, the asperity and hypocenter locations slightly affect them. We propose the ratios of average slips, maximum slip, and seismic moments between the asperity and total rupture areas for practical application of strong ground motion prediction.

**SS04a/09P/D-033** Poster **1400-282**

### 3D GRAVITY BASEMENT STRUCTURE ASSOCIATED WITH ACTIVE FAULTS IN THE MIDDLE PART OF KINKI DISTRICT, WEST JAPAN

Masao KOMAZAWA<sup>1</sup>, Kajuro NAKAMURA<sup>2</sup>, Keiichi NISHIMURA<sup>3</sup>, Junpei AKAMATSU<sup>2</sup>, Ryuichi SHICHI<sup>1</sup>, Akihiko YAMAMOTO<sup>3</sup> (<sup>1</sup>Geological Survey of Japan, <sup>2</sup>Disaster Prevention Research Institute, Kyoto University, <sup>3</sup>Faculty of Informatics, Okayama University of Science, <sup>4</sup>College of Engineering, Chubu University, <sup>5</sup>Graduate School of Science, Hokkaido University)

3D gravity basement structure of the middle part of Kinki District, west Japan, was estimated with special attention to basement configuration of three major sedimentary basins: Kyoto basin, Nara basin and Osaka plain, and its relation to active faults bordering or crossing the basins. In these basins, large cities are located and there is a great fear, among people, of extensive damages caused by earthquakes like the 1995 Kobe earthquake or great earthquakes presumed to occur in the first half of the 21st century along the Nankai trough south off Kinki District. In this study we use the precise gravity data published by Gravity Research Group in Southwest Japan (2001). The characteristic features observed from obtained structural model are as follows. In Kyoto basin, the basement descends southwards down to a depression of about 700m deep, with an ENE-WSW striking steep slope probably associated with the Ujigawa fault which has been recently revealed by seismic reflection method. The basement of Nara basin descends eastwards down to about 800m deep near the easternmost margin, along which the Sanbyaku fault runs in the N-S direction. As for Osaka plain, the largest of the three, the basement is separated into eastern and western parts by N-S trending uplift called the Uemachi terrace. The basement of the eastern part descends eastwards steeply and reaches the deepest of about 1600m near the easternmost margin, along which the Ikoma fault runs in the N-S direction. This fault branches off in its northern part and brings about the complicated configuration of basement in the northeast part of Osaka plain. The western part of Osaka plain is part of a large basin including the Osaka bay. Although the basement of this part is flattened compared with other basins, the depth to the basement is estimated to be about 1400m near the eastern margin, along which the Uemachi fault runs in the N-S direction. The Arima-Takatsuki Tectonic Line (ATTL) borders the whole northern margin of Osaka plain, along which the basement subsides steeply down to 500m or more forming an E-W striking basin wall. Of particular interest is that, the subsidence of basement associated with ATTL appears to continue eastwards, with some offset to the north, to the newly revealed Ujigawa fault. Accordingly, it seems evident that the configuration of basements of the basins is governed and complicated by faults bordering and crossing the basins. All these features concerning the fault-related configuration of basement of the basins are considered to affect strongly the levels of ground shaking caused by earthquakes, and therefore the 3D structural model obtained in this study is believed to provide a basis for producing a seismic-risk map of the middle part of Kinki district.

**SS04a/09P/D-034** Poster **1400-283**

### SUGGESTION AND FEASIBILITY TESTS OF A NEW METHOD TO EXTRACT PHASE VELOCITIES OF RAYLEIGH WAVES FROM MICROSEISMS

Ikuo CHO<sup>1</sup>, Takuya SHIGA<sup>2</sup>, Taku TADA<sup>3</sup>, Yuzo SHINOZAKI<sup>4</sup> (<sup>1</sup>Geo-Research Institute, <sup>2</sup>Tokyo University of Science)

We suggest an effective method to extract phase velocities of Rayleigh waves from microseisms. The dispersion characteristics extracted from microseisms can be used to determine velocity structures because microseisms are considered as ensemble of surface waves. Our method makes it possible to extract dispersion characteristics from waveform data sets of microseisms that are provided by a simple array consisting of three sensors. In this study the formulation of our method is presented first, and then the practical use of seismic arrays consisting of three sensors is examined by both theory and application to real data sets. Our method is formulated using circular arrays. The number of sensors consisting of an array is related to a shorter limit of wavelength ranges to apply our method. Based on theoretical calculations, when an array consists of three sensors, the shorter limit is  $3r$  ( $r$  being the array radius). A longer limit of a wavelength range depends upon observational errors. There is no problem even if the intervals of sensors along a circle are uneven, but the permissible level of unevenness exists depending on observational errors. To test the feasibility of three-sensor arrays we deployed small-scale arrays with radii less than several tens of meters at three test sites where the velocity structures were well documented. The phase velocities obtained by analyzing data sets of three-sensor arrays were compared with those obtained by analyzing data sets of five-sensor arrays. It revealed that the phase velocities obtained showed good fits with theoretical ones in both cases within almost the same wavelength ranges. The differences in accuracy and variance were very small. Therefore we limited our attention to three-sensor arrays, and examined the relation

between the normalized variance ( $\gamma$ ) in the azimuthal intervals between adjacent sensors and the wavelength range over which our method could be applied (analyzable wavelength range). It revealed that when  $\gamma < 0.4$ , the analyzable wavelength range was from  $5r$  to  $10r$  at the narrowest. For  $r < 9$  m and  $\gamma < 0.4$ , the analyzable wavelengths range was from  $3r-7r$  to  $20r-40r$ . We also examined the applicability of our method to large-scale, three-sensor arrays with radii of several hundreds of meters. The velocity structures to the depth corresponding to the array radius had not been well documented in this case, so that we compared the phase velocities obtained by applying our method with those obtained by applying the spatial autocorrelation method and the frequency-wavenumber spectral method. Although the phase velocities obtained by these methods were not necessarily compared directly because the analyzable wavelength ranges depend on method, the dispersion curves showed natural linking with each other, overlapping in part. This fact suggests the applicability of our method to large-scale, three-sensor arrays.

**SS04a/09P/D-035** Poster **1400-284**

### ESTIMATION OF S-WAVE VELOCITY STRUCTURES BENEATH URBAN AREAS BY USING MICROTREMOR H/V SPECTRA TECHNIQUE BASED ON BOTH RAYLEIGH- AND LOVE- WAVES

Hidekazu YAMAMOTO, Minoru TESHIMA, Tsuyoshi SANO, Tokumi SAITO (Department of Civil and Environmental Engineering, Iwate University)

It is important to clarify basement structures of urban areas from a view point of earthquake engineering. Microtremor H/V spectra techniques had been conventionally used to estimate the basement depth based on medium responses of horizontal to vertical amplitude ratio of Rayleigh wave. It is insufficient to consider only Rayleigh wave because microtremor consists of not only Rayleigh wave but also Love wave. This study tried to estimate the velocity structures from microtremor H/V spectra based on the theory of surface wave H/V spectra [Arai and Tokimatsu, 2000]. This theory needs both Rayleigh and Love waves to explain microtremor H/V spectra. But, the power ratio of Rayleigh and Love waves in microtremors had not been estimated. We apply three-component spatial auto-correlation analysis, which we have developed, to obtain the power ratio of Rayleigh to Love waves in microtremors. By using this analysis we can obtain the power ratio based on tri-axial microtremor array records empirically. We carried out microtremor observations at three sites in Morioka City, the northern Honshu, Japan. We employ a circular seismic array with seven tri-axial sensors. The array observation aims to obtain the dispersion curve of phase velocity of Rayleigh wave and the power ratio of Rayleigh to Love wave, respectively. Estimated power ratios were around 1.0 at all sites. Therefore, we assumed that the ratios were 1.0 in order to calculate surface wave H/V spectra. The microtremor H/V spectra were estimated from the average of spectra at all sensors. We used genetic algorithm inversion technique to determine velocity structures from microtremor H/V spectra because the inversion of structures from microtremor H/V spectra is a non-linear problem. Estimated velocity structures are consistent with bore-hole data and geological information in those areas. They also agree with the structures estimated from the dispersion curves of Rayleigh phase velocity by using a classical array technique. And synthetic H/V spectra calculated from the structure are concordant with observed microtremor H/V spectra. The results suggest that the use of both Rayleigh and Love wave is necessary to estimate velocity structures using microtremor H/V spectra.

**SS04a/09P/D-036** Poster **1400-285**

### THE VELOCITY STRUCTURE ESTIMATION AND THE SHAPE DETERMINATION OF ILAN BASIN, TAIWAN

Tao-Ming CHANG<sup>1</sup>, Yeou-Jyh HWANG<sup>2</sup>, Kuo-Liang WEN<sup>3</sup> (<sup>1</sup>Office of the National Science & Technology Program for Hazards Mitigation, <sup>2</sup>Institute of Geophysics, National Central University, <sup>3</sup>Institute of Applied Geology, National Central University)

The Ilan basin, which is located in the northeastern of Taiwan Island, is usually considered as the western end opening of Okinawa Trough. Therefore, the basin shape can be thought as half of a bowl. The basin shape is very important for the tectonic development and for the strong motion simulations. In this research, we try to determine the shape of Ilan basin. We use two methods. First of all, we conduct a very dense micro-tremor measurements in the basin. From the H/V spectral ratio results, we selected the dominate frequency for each site and made the distribution map. By using the borehole suspension PS velocity logging results and the dominate frequency map, we get the first order basin shape of the Ilan Basin. Second of all, we performed micro-tremor array measurements at 10 different sites to get the velocity structures. From the micro-tremor array measurements, we can get the surface-wave dispersion curve via F-K analysis. And from surface wave inversion technique, the 1-D shear wave velocity structure can be computed.

**SS04a/09P/D-037** Poster **1400-286**

### ESTIMATE ENAR SURFACE VELOCITY STRUCTURE USING RECEIVER FUNCTION TECHNIQUE

Tao-Ming CHANG<sup>1</sup>, Jer-Ming LIN<sup>2</sup>, Kuo-Liang WEN<sup>3</sup> (<sup>1</sup>Office of the National Science & Technology Program for Hazards Mitigation, <sup>2</sup>Institute of Geophysics, National Central University, <sup>3</sup>Institute of Applied Geology, National Central University)

The receiver function technique has been used to study the worldwide crustal velocity structure for many years. It is a well-accepted technique already. In this research, we try to estimate near surface velocity structures beneath the TSMIP (Taiwan Strong Motion Instrumentation Project) stations using the receiver function technique. It is because, for the past decade, more than 600 acceleration seismometers have been installed in the Taiwan Island. Many acceleration seismograms show very simple waveforms for those shallow seismic events (less than 7 km depth) which were virtually beneath the stations. The basic assumption is that most energy has been blocked out due to the strong velocity impedance for the near surface structures. Therefore, only part of the energy with almost vertical incident angle can reach the ground. It implies the signals received between P and S phases are the reverberations of the vertically incident energy. Base on this assumption, we develop and test the receiver function techniques in studying near surface velocity structures.

**SS04a/09P/D-038** Poster **1400-287**

### A MODEL OF THE SUBSURFACE STRUCTURE BENEATH THE OSAKA SEDIMENTARY BASIN, SOUTHWEST JAPAN

Haruo HORIKAWA<sup>1</sup>, Kiyohide MIZUNO<sup>2</sup>, Tatsuya ISHIYAMA<sup>1</sup>, Haruko SEKIGUCHI<sup>1</sup>, Yuko KASE<sup>1</sup>, Kenji SATAKE<sup>1</sup>, Takanobu YOKOKURA<sup>2</sup>, Yuichi SUGIYAMA<sup>1</sup>, Hiroshi YOKOTA<sup>3</sup>, Masaki SUEHIRO<sup>4</sup>, Arben PITARKA<sup>5</sup> (<sup>1</sup>Active Fault Research Center, GSJ/AIST, <sup>2</sup>Institute of Geoscience, GSJ/AIST, <sup>3</sup>Hanshin Consultants Co. Ltd., <sup>4</sup>URS Corporation)

A three-dimensional subsurface structure model for the Osaka sedimentary basin is developed for the evaluation of strong-motion in the basin. Our model consists of sediments

and discontinuous basin-floor geometry, on the basis of newly compiled geological and geophysical data. Calibration of the model with a small earthquake indicates that the model needs further improvement, particularly in the southeastern part of the basin. The Osaka sedimentary basin is shaped like an ellipse with the northeast-southwest striking major axis, and is bounded by active fault systems. The fault system running along the northwest margin of the basin caused the 1995 Hyogo-ken Nanbu (Kobe) earthquake. The Uemachi fault system runs below the eastern part of the basin, one of the population centers in southwest Japan. The Osaka-wan fault systems lies in the middle of the basin, the Osaka bay. We first inferred the depth of several key horizons in the sediments (Holocene to Pleistocene series) and depth of the basin floor, boundary between the sediments and pre-Neogene rocks. Time since deposition of each point in the sediments was interpolated from that of the reference horizons. P-wave velocity was determined by application of an empirical rule to the depth and depositional age, and density and S-wave velocity were derived from the P-wave velocity on the basis of the theory of poroelasticity. The sediments are expressed as a volume with spatially variable seismic velocities and density rather than as a stack of several layers of constant seismic velocities and density. The maximum depth of the basin floor was observed in the Osaka bay and was estimated to be over 2500 m. Overhanging structures formed by repeated thrust faulting were realistically expressed in our model while the structures were approximately described as smoothed ramps in previous models. For a calibration of the model, we compared the observed and simulated waveforms from a small (M~4) earthquake near the eastern margin of the basin. The simulation, using a finite-difference method, well reproduced basin-edge-induced waves, which would not appear from a flat-layers velocity model. However, in the southeastern part of the basin, the simulated basin-edge-induced waves arrives faster than the observed with small amplitudes. This suggests underestimation of the basin depth and/or the overestimation of shear wave velocity in the sediments. Simulated arrivals of body waves agree with the observed ones at all the stations except for those near the northeastern edge of the basin, where the simulated arrivals are later than the observed. This discrepancy may result from underestimation of the sediment velocity.

**SS04a/09P/D-039** Poster **1400-288**

### THREE DIMENSIONAL SUBSURFACE STRUCTURE OF THE NOBI PLAIN

Hideki NAGUMO<sup>1</sup>, Yoshihiro SAWADA<sup>1</sup>, Suqun LING<sup>2</sup> (<sup>1</sup>Department of Civil Engineering, Nagoya University, <sup>2</sup>Nippon Koei Co. LTD.)

The Nobi plain is situated near the center of Japan with an area of 40 km x 30 km and has been repeatedly suffered from the destructive earthquake. Recently earthquake researchers point out the occurrence of Tokai and Tonankai earthquakes in near future. We investigate three-dimensional subsurface structure of the Nobi plain based on geological survey results and seismic data. Recently Aichi Prefecture Government carried out geological survey from the center to the west of the Plain with 3 reflection lines and 12 microtremor observation sites, which provide detail geological information. Especially two reflection profiles across the western boundary of the plain clarify the edge shape. The Yoro fault forms a step-like structure with the vertical discontinuity of 2.0 - 2.5 km there. To get more geological information we carried out microtremor array measurements at 11 sites in the plain. The spatial autocorrelation method was applied to array data for estimating phase velocities in the frequency range from about 0.5 to 3 Hz. S wave velocity structures are inverted to minimize the misfit between observation and theoretical phase velocities. On the other hand, about 60 seismometers are installed by several organizations in the Plain. M5.4 event occurred near the Yoro fault at shallow focal depth and seismic records were obtained at most sites in the plain. In these observation data, Ps and Sp transduced phases are clearly seen, which are considered to generate at the boundary between sediments and bedrock. Ps-P and S-Sp times become shorter from east site to west site. We assume three sedimentary layers and fix S wave velocities based on geological survey results. Then each layer thickness is estimated by comparing observation Ps-P, S-Sp and S-P times with those calculated by 1D theory through a trial and error method. Together with these results, subsurface structure model of the Nobi plain is obtained. Bedrock is deepest near the western edge and gradually become shallower to the east. These trends are consistent with gravity survey results. Finally we perform numerical simulation of M5.4 event using the three-dimensional finite difference method in the frequency range of 0.1 to 0.5 Hz. The observed waveforms are reproduced well at most stations. This agreement suggests the validity of the model in the frequency range from 0.1 to 0.5 Hz.

**SS04a/09P/D-040** Poster **1400-289**

### ESTIMATION OF Q-VALUE IN KINKI REGION, JAPAN, BY ELIMINATION OF ELASTIC ATTENUATION EFFECT USING RAY THEORY APPROXIMATION IN 3-D VELOCITY MODEL

Anatoly G. PETUKHIN<sup>1</sup>, Kojiro IRIKURA<sup>2</sup>, Takao KAGAWA<sup>1</sup>, Shiro OHMI<sup>1</sup> (<sup>1</sup>Geo-Research Institute, 4-3-2 Itachibori, Nishi-ku, Osaka, 550-0012 JAPAN, <sup>2</sup>Disaster Prevention Research Institute, Kyoto University, JAPAN)

We studied seismic waves attenuation in Kinki region, Japan, in high frequency range 1-10Hz. To do this it was assumed that observed amplitude Fourier spectrum is a product of source, elastic path attenuation, inelastic path attenuation and site effects. Inelastic path attenuation is described by the Q-value. Frequently, to estimate path attenuation effect, Q-value is inverted under assumption that geometrical spreading is spherical (true for uniform velocity model). Actually, elastic attenuation is complex effect that includes geometrical spreading in non-uniform velocity model, reflection and conversion on major velocity discontinuities, free-surface effect. In this study, elastic path attenuation was calculated using Complete Ray Tracing method (CRT) of červen et al., 1988 in 3-D velocity model. Source and Site effects were eliminated using the double spectral ratio scheme. Travel times inside blocks were calculated by the 3-D ray tracing. After this, Q-values in blocked media were inverted using a tomography approach. For this study we developed 3-D velocity model for Kinki area. This model includes: (1) low-velocity layer, (2) seismogenic zone (or upper crust), (3) lower crust, (4) subducted Philippine Sea plate, (5) mantle wedge (between crust and subducted plate) and (6) upper mantle (below subducted plate). It was assumed that velocities inside each layer have gradient of several percent, and that in high frequency range, at a point of crossing with velocity interface there is no reflection/conversion for upward rays. The whole media of the wave propagation were divided into blocks with constant Q-value according to the tectonic structure: upper crust (UC), lower crust (LC), mantle wedge (MW) and subducted plate (SP). UC was subdivided into 6 smaller blocks with boundaries along main fault systems in Kinki region. For inversion we used borehole data of the Hi-net network, and hard rock/stiff soil data of CEORKA networks and so on. Totally, 1453 records were selected for inversion, number of used earthquakes - 128, stations - 91. Analysis of the results of inversion shows that largest  $Q=150^{f^{0.8}}$  was in UC block, smallest  $Q=60^{f^{0.64}}$  was in LC+MW block; for SP  $Q=155^{f^{0.4}}$ . In UC, Q-values larger in area north from the MTL:  $Q=160^{f^{0.8}}$ , than in area south from the MTL:  $Q=86^{f^{0.75}}$  or in northern part of Kinki region:  $Q=92^{f^{0.8}}$ . Based on results of inversion we calculated examples of attenuation correction factor: the difference between path attenuation calculated by the developed model and by the uniform model, for a set of sources. **Acknowledgements.** Many thanks to consortium "Seismic Waves in Complex 3-D Structures", project leader Vlastislav Červen, for providing CRT package. We also deeply appreciate the National Institute of Earth Science

and Disaster Prevention for providing the Hi-net data, the CEORKA research society and the Joint Research Program of the 10 electric power companies of Japan, for using their ground motion data.

**SS04a/09P/D-041** Poster **1400-290**

### UPPER MANTLE QS STRUCTURE AND ITS EFFECTS ON STRONG GROUND MOTIONS

Takahiro MAEDA, Tsutomu SASATANI (Division of Earth and Planetary Sciences, Graduate School of Science, Hokkaido University)

It is known that the anomalous upper-mantle structure exists beneath island-arc regions; the existence of a high Q, high V zone about 100 km thick, that is, the descending plate (slab). We investigate effects of the upper mantle Q structure on strong ground motions based on numerous data observed at dense strong motion stations in the eastern part of Hokkaido, Japan. First we investigate strong motion records and their S-wave spectra from intermediate-depth earthquakes. The S-wave spectra at stations on the back-arc side of the volcanic front (VF) are extremely different from those at stations on the fore-arc side of the VF; the S-wave spectra at the back-arc side stations severely lack high-frequency contents. Next we estimate the Qs (Q value for S-wave) structure beneath the eastern Hokkaido. The study zone is tentatively divided into three zones bounded by the coastline and the VF; the three zones mainly correspond to the back-arc side mantle wedge, the fore-arc side mantle wedge and the shallow descending plate. We especially use strong motion data obtained by ocean bottom seismometers for the plate Qs estimate. Two different methods, the spectral inversion and the coda normalization method, are applied to Qs estimate for the fore-arc side mantle wedge and the plate. The Qs values for two zones are nearly the same and show strong frequency dependence. The Qs values obtained from two methods are also nearly the same. Finally we try to estimate Qs values for the back-arc side mantle wedge by using the S-wave spectra observed at stations on the back-arc side of the VF and the source spectra obtained from the inversion. Although the data set for the back-arc side mantle wedge is incomplete due to few records and low signal-to-noise ratios of the S-wave spectra, we suggest that the Qs values for the back-arc side mantle wedge have considerably weak frequency-dependence. We conclude that the anomalous upper mantle attenuation structure beneath eastern Hokkaido reflects the difference in the frequency dependence of Qs value at high frequencies (> 1Hz). The laterally heterogeneous Qs structure obtained in this study is useful for predicting strong ground motion from great intra-slab earthquakes such as the 1993 Kushiro-oki earthquake.

**SS04a/09P/D-042** Poster **1400-291**

### INVERSION OF QS OF SEDIMENTS FROM VERTICAL ARRAY SEISMOGRAMS USING SIMULATED ANNEALING METHOD

Toshimi SATOH (Ohsaki Research Institute)

In this study I apply adaptive simulated annealing (ASA) method (Ingber, 1989) to invert frequency-dependent Qs (quality factor for S-waves) of sediments from vertical array data seismograms. ASA is a global optimization algorithm to statistically find the best global fit of a nonlinear cost-function. Frequency-dependent Qs, an incident angle, and S-wave velocities (Vs) are inverted to minimize the misfit between observed surface-to-downhole spectral ratios and those calculated by one-dimensional wave propagation theory considering obliquely incident SH-waves and SV-waves. Transverse, radial, and vertical components are used for the inversion. Based on numerical experiments it is shown that frequency-dependent Qs, an incident angle and S-wave velocities are inverted very well, independent of initial random numbers used in the ASA algorithm. As the first trial, this method is applied to records of four aftershocks (magnitudes of 3.5 to 4.4) of the 2000 Tottori-ken Seibu earthquake observed at a vertical array station (Akasaki : TTRH04) in the Tottori basin. It is confirmed that all the unknown parameters are inverted stably. The incident angle to the downhole at a depth of 207 m is inverted to be 8.4 degree. The inverted Qs for gravel and Quaternary rock is modeled by  $Vs/43^{f^{0.41}}$  using Vs in m/s and frequency (f) in Hz. Recently National Research Institute for Earth Science and Disaster Prevention (NIED) has deployed the digital strong-motion seismographs (KiK-net) at several hundreds sites across the all of Japan. At each site two seismographs are installed at the surface and the downhole at depths between 100 m and a few km. TTRH04 station used in this study is also one of KiK-net stations. The inversion method proposed in this study will be useful to invert Qs of sediments using these KiK-net records. I acknowledge NIED for the use of KiK-net data. This study was supported by the project "Study on the master model for strong ground motion prediction toward earthquake disaster prevention" funded by Special Coordination Funds for Promoting Science and Technology, from the Ministry of Education, Culture, Sports, and Technology.

**SS04a/09P/D-043** Poster **1400-292**

### 3D HYBRID SIMULATION OF THE SOURCE AND SITE EFFECTS DURING THE 1999 ATHENS EARTHQUAKE

Ivo OPRSA<sup>1</sup>, Jiri ZAHRADNIK<sup>2</sup>, Anna SERPETSIDAKI<sup>1</sup>, G-Akis TSELENTIS<sup>1</sup> (<sup>1</sup>Swiss Seismological Service, ETH Zurich, Switzerland, on leave from Faculty of Mathematics and Physics, Charles University in Prague, Czech Republic, <sup>2</sup>Faculty of Mathematics and Physics, Charles University in Prague, Czech Republic, <sup>3</sup>Seismological Laboratory, University of Patras, Greece)

The damaging 1999 Athens earthquake of  $M_w=5.9$  occurred at about 20km from the city center. The intensity distribution in the capital, ranging from V to IX, was quite irregular due to combination of the source, path and site effects. The 30-stations temporary network, installed in Athens by the University of Patras, recorded and located more than 400 aftershocks. The horizontal-to-vertical spectral ratios from the 20 selected aftershock recordings provided site classification. The most significant anomaly (H/V exceeding 4 in the frequency range 1-4 Hz) was found at the Ano Liosia site, belonging to the most heavily damaged zones with intensity IX. The site is situated in a shallow basin whose surface extent is about 4x4 km, and the maximum depth is of about 150 m. The basin is filled with basically 3 layers. The topmost layer includes alluvium and soft soil, the second one consists of stiff soil and alternations of conglomerates, clay and sand, while the third layer is represented by Neogene formations like marl, marly limestone and sandstone. The bedrock of the basin consists of Triassic limestone and schist. Borders of the basin, where the topmost layer directly overlies the bedrock, are locally quite steep. Based on geophysical data ( $V_p$ ,  $V_s$ , Q) measured at the site, the numerical modeling of the seismic site response was carried out. The 2D and 3D finite-difference techniques were used, and significant edge effects were revealed. No recording of the mainshock is available in Ano Liosia. Nevertheless, based on the finite-extent composite source model, validated by the existing strong motion records in Athens, we found that the bedrock motion in Ano Liosia had its PGA ranging from 0.2 to 0.3 g, resulting from the relatively small epicentral distance (~ 10 km) and the forward source directivity. The source and site effects were combined with each other by a hybrid technique (Opsral and Zahradnik, JGR 2002), allowing fast full-wave 3D calculations up to 10-20 Hz on a standard personal computer, and showing that the combined source and site effect in Ano Liosia might provide the PGA values locally

exceeding 0.6 g.

**SS04a/09P/D-044** Poster **1400-293**  
**THREE DIMENSIONAL FINITE-DIFFERENCE MODELING OF STRONG GROUND-MOTIONSITE EFFECTS DUE TO THE FINITE-EXTENT SOURCE - 1356 BASEL EARTHQUAKE,UPPER RHINE GRABEN**

Ivo OPRSA<sup>1</sup>, Donat FAEH<sup>2</sup>, Domenico GIARDIN<sup>3</sup> (<sup>1</sup>Swiss Seismological Service, ETH Zurich, on leave from Faculty of Mathematics and Physics, Charles University in Prague, Czech Republic, <sup>2</sup>Swiss Seismological Service, ETH Zurich)

The Basel earthquake of October 18, 1356 ( $I_s=IX$ ,  $M=6.9$ ) is considered to be one of the most disastrous European events. The Basalarea - Upper Rhine Graben - belongs today to seismically modest regions. Reducing the seismic risk by anti-seismic design needs the knowledge of the strong ground motion. The lack of the real data may be effectively estimated by numerical modeling using the finite differences (FD). The 3D explicit FD method is designed for topography models on irregular rectangular grids. The single-template approximation to the hyperbolic partial differential equation (PDE) is solved explicitly in the spatial and the time domain. The boundary conditions at the interfaces (including the topographic free surface) are satisfied via a treatment of the material parameters. The medium is Hooke's isotropic inhomogeneous body, with a particle-velocity dependent term added to the PDE to approximate viscoelastic behavior of the medium. The 3D FD modeling is computed for the recently established P and S-wave velocities structure of the Basel area (Kind, 2002), including the topography. The relatively simple finite-extent source features are recombined with strong site effects. The finite-extent source is adjacent to the free surface, since the fault has been recognized through trenching on the Reinach fault. Several rupture histories are tested because the 1356 Basel earthquake source features are not possible to be determined. The macroseismic information of the Basel area as well as recently established 2D computations serve as a comparison to the results.

**SS04a/09P/D-045** Poster **1400-294**  
**SEISMIC WAVE PROPAGATION IN THE 3D BASIN STRUCTURE OF NOBI PLAIN**

Akira KOTANI<sup>1</sup>, Takashi FURUMURA<sup>1</sup>, Kazuro HIRAHARA<sup>2</sup> (<sup>1</sup>Earthquake Research Institute, University of Tokyo, <sup>2</sup>Graduate school of Environmental Studies, Nagoya University)

We carried out numerical 3D simulations of ground motions to see the wave propagation character in the Nobi Plain, which is one of the high population cities in central Japan. In this area, many large earthquakes occurred in the past, such as the 1891 Nobi earthquake (Mj8.0), the 1944 Tonankai earthquake (Mj7.9) and the 1945 Mikawa earthquake (Mj6.8). In order to mitigate the potential disasters for future earthquakes, 3D subsurface structure of Nobi Plain has recently been investigated by Aichi metropolitan government. We referred to this model together with bouguer anomaly data to construct a detail 3D basin structure model for Nobi plain, and conducted computer simulations of ground motions. We first evaluated the ground motions for two small earthquakes (Mj4-5); one occurred just beneath the basin edge at west, and the other occurred at south. The ground motions from these earthquakes were well recorded by the strong motion networks; K-net, Kik-net, and seismic intensity instruments operated by companies, Aichi and Mie metropolitan governments. We compare the observed seismograms with simulations to evaluate the validity of the 3D model. For the 3D simulation we used a 32nd-order staggered-grid FDM to solve the equation of motions in horizontal directions, and a conventional 4th-order FDM is used in vertical direction. The simulation model is 128km by 128km by 40km, which is discretized at variable grid size of 250-500m in horizontal directions and of 125-250m in vertical direction. We assigned a minimum shear wave velocity is  $V_s=0.5\text{km/s}$ , at the top of the sedimentary basin. The seismic sources for the small events are approximated by double-couple point source, which impart seismic wave at frequency below 0.67Hz. We used a cluster of eight Intel Xeon PCs, and conducted the large scale simulation concurrently. The parallel simulation took memory of 2.5GByte and cpu-time of 16hours. The simulated wavefield for the source beneath the basin edge shows clearly the narrow zone of large ground amplification which is called the "basin edge effect". On the other hand the shallow source that occurred at south of Nobi plain generates large surface waves in the basin. Comparisons between the observed waveforms computer simulations agree well, so that it is indicating the effectiveness of the 3D model. We therefore conducted a large scale numerical simulation to estimate the pattern of strong ground motion for the 1945 Mikawa earthquake. We employ the fault rupture model of Kikuchi et al (2002) which is derived from the inversion of regional records. We used the Earth Simulator to conduct a high-resolution simulation which employ lower velocity ( $V_s=0.4\text{km/s}$ ) superficial layer and high-frequency seismic source at 1Hz. The simulated wavefield from the Mikawa earthquake is dominating in large surface wave at amplitude over 10cm/s in the center of the Nobi plain. We also find directivity effect of the fault rupture from south to north in the PGV distribution and waveforms. This explains the major pattern of seismic intensity and the distribution of strong motion damage during the earthquake.

**SS04a/09P/D-046** Poster **1400-295**  
**EFFECTS OF GEOLOGICAL CONDITIONS ON THE GROUND SHAKING IN THE BUCHAREST URBAN AREA**

Neculai MANDRESCU<sup>1</sup>, Gheorghe MARMUREANU<sup>1</sup>, Mircea RADULIAN<sup>2</sup>, Cristea CAPRA<sup>3</sup> (<sup>1</sup>National Institute for Earth Physics, <sup>2</sup>Institute of Geodynamics of the Romanian Academy)

This paper outlines some results obtained through review and reevaluation of the old and new data concerning the natural environment in the Bucharest urban area. The geologic, geomorphologic, hydrogeologic, and other physical features were included in three-dimensional digital models. Maps and cross-sections, showing the geometry and the physical properties of the Holocene and Pleistocene sedimentary deposits, emphasize a good correlation between underlying geologic conditions and site effects. The ground motion amplitudes in the long-period range increase with increasing of the Quaternary deposit thickness. The results of ambient noise measurements (Bonjer et al., 1999) are also well correlated with the structural data. The effects of the geological conditions in the Bucharest area upon the ground motion induced by Vrancea strong and moderate earthquakes and implications for a new seismic microzonation map will be discussed.

**SS04a/09P/D-047** Poster **1400-296**  
**SITE AMPLIFICATION STUDY IN ISTANBUL PROVINCE**

Nurcan Meral OZEL<sup>1</sup>, Tsutomu SASATANI<sup>2</sup>, Asim Oguz OZEL<sup>3</sup> (<sup>1</sup>International Seismological Centre, <sup>2</sup>Division of Earth and Planetary Sciences, Graduate School of Science, Hokkaido University, Sapporo 060-0810, Japan, <sup>3</sup>Kandilli Observatory and Earthquake Research Institute of Bogazici University, 81220, Cengelkoy, Istanbul, Turkey)

On 17 August 1999, a destructive earthquake ( $M_w=7.4$ ) occurred near Kocaeli city in the northwestern Turkey. More than 15,000 people were killed and more than 20,000 people

were injured mainly due to collapse of buildings. The best sets of near-field records from the Kocaeli earthquake were extensively used to study characteristics of the strong motions and rupture process of this event. Strong ground motions during the largest aftershock ( $M_w = 5.8$ ) of the 1999 Kocaeli, Turkey, earthquake ( $M_w = 7.4$ ) recorded by 19 observation sites and at various hypocentral distances have been investigated by this study. We constructed an attenuation relationship from the PGA values for the region. This relationship shows that there is one order scatter in the PGA values at the epicentral distances of about 100 km. If compared to the attenuation relationship for the main shock PGA values, the PGA values for the main shock are considerably smaller than expected from a  $M_w = 7.4$  earthquake while those for the largest aftershock surround the median prediction. The spectral source parameters are also estimated based on the near-distance, rock-site records. The parameters for this largest aftershock are  $A=3.7 \times 10^{25}$  dyne/cm/s<sup>2</sup> and  $f_c=0.4$  Hz that normal values for an  $M_w = 5.8$  earthquake. We study the site effects in and around Istanbul province based on the records of 100 km distance from the largest aftershock, using the traditional spectral ratio method. The S-wave spectral ratios to the reference rock site, YKP (Yapi Kredi Plaza), show noticeable amplifications depending on the soil types, but it is somewhat difficult to quantitatively predict the amplification only using the simplified classification of the soil types. The highest amplifications were found for the site of FTH (Fatih), KMP (Kocamustafapasa) and ATS (Ambarli) in the relatively low frequency range of 0.6 to about 6 Hz. Considerable amplifications were also found for the site of DHM (Devlet Hava Meydanlari) and CNA (Cekmece Nukleer Arastirma) though they are classified as at stiff-soil sites. Their spectral ratios are greater than that of 2 over a wide frequency range. The empirical amplifications at a few sites are compared with the theoretical ones calculated based on the S-wave velocity structures. The comparison shows a qualitative agreement between them.

**SS04a/09P/D-048** Poster **1400-297**  
**PRELIMINARY RESULTS OF SITE EFFECTS ASSESSMENT IN THE CITY OF TEHRAN (IRAN) USING EARTHQUAKE AND MICROTREMOR RECORDING**

Pierre-Yves BARD<sup>1</sup>, Ebrahim HAGHSHEENAS<sup>2</sup>, Mohammad JAFARI<sup>3</sup>, Denis HATZFELD<sup>1</sup> (<sup>1</sup>LGIT/LCPC, Grenoble Observatory, <sup>2</sup>IEES, Tehran, IRAN)

Within the framework of a French-Iranian cooperation, 13 seismological stations were installed in the city of Tehran (Capital of Iran) from February to July 2002 to record earthquakes and ambient noise over areas of different geotechnical characteristics. Ten broad band velocimeters (CMG40 20 s sensors), three shortperiod sensors (L22, 2 Hz) and 13 Accelerometers (CMG5) were coupled to Reftek stations: each station had both a velocimeter and an accelerometer. An accurate, absolute timing was obtained through GPS receivers. Two stations were installed on the rock, north and east of the city. Despite the high noise level within the city, more than 40 local and regional earthquakes were recorded with a good signal to noise ratio in at least three stations. Four of them have a magnitude larger than 5. The most important event was the Avaj earthquake, a Magnitude 6.5 event located 230 km west of Tehran, which killed more 230 person and destroyed or damaged many villages. In addition, microtremor measurements were performed in 100 points throughout the city in order to provide some guidance on the way to interpolate results obtained from these few temporary stations. The presentation will show the preliminary results obtained with those records, focusing on site effects. It will include classical spectral ratio to two reference stations, receiver functions (H/V) for each of the 13 sites, and H/V ratios from noise recording. Amongst the preliminary results, a very important one is the existence of large, low frequency amplification not only in the southern part of the city, but also in the central part. A result which was not expected on the basis of the available geological and geotechnical information.

**SS04a/09P/D-049** Poster **1400-298**  
**LOOKING FOR SITE EFFECTS IN THE DAMAGE DISTRIBUTION - APPLICATION TO ANGRA DO HEROISMO (AZORES) USING MICROTREMORS MEASUREMENTS**

Paula TEVES-COSTA<sup>1</sup>, Luisa SENOS<sup>2</sup> (<sup>1</sup>Centre of Geophysics, University of Lisbon, <sup>2</sup>Faculty of Sciences, Lisbon University, <sup>3</sup>Institute of Meteorology, Lisbon)

On January 1st 1980, the Terceira Island (in the Azores Archipelago, North Atlantic Ocean) was struck by a 7.2 magnitude earthquake, which killed 56 people and produced lot of damage, in particular in Angra do Heroismo, the island capital. The Azores Archipelago, close to the Azores triple junction (meeting the Africa, the Eurasia and the North America plates) is one of the regions that exhibits higher seismic hazard in Portugal. Reports on seismic swarms, volcanic eruptions and damaging seismic events date from the beginning of its settlement (15th century). The Terceira Island is located in the Central Group and suffered several strong earthquakes. Up to 1980, most of these earthquakes attained villages located on the northern and eastern coast and Angra do Heroi mo, located in the southern coast, have been saved. However, due to the importance of this town, the most populated of the island and considered by Unesco as world patrimony (consequently presenting a high level of seismic risk), it would be suitable to understand its seismic response and to identify the possible existence of site effects within the town, in order to prevent similar damages in a future earthquake. A microtremor survey was carried out consisting on about 250 noise measurements, obtained with Marslite seismic stations with 1Hz Lennartz 3D seismic sensors. Some measurements were performed along the streets in order to identify the possible existence of site effects related with the damages observed on the January 1st 1980 earthquake. Besides, measurements were also performed according a grid with 100m intervals, in order to characterize, in a larger scale, the seismic behaviour of the town. The processing methodology was based on the estimation of the H/V ratio, as defined by Nakamura, and using software developed within the SESAME project. We tried to correlate the H/V results with the damage observed during the 1980 earthquake, taking also into account the existing building typologies. A map of the natural frequencies of the soil formations for the whole town was also performed. This work involved 5 teams of the Lisbon University and from the Institute of Meteorology (Azores delegation) and was performed with the knowledge of the local civil authorities. This work was partially done in the aim of the SESAME European project (EVG1-CT-2000-00026).

**SS04a/09P/D-050** Poster **1400-299**  
**ASSESSMENT OF SITE EFFECT IN ROMANIA DURING INTERMEDIATE DEPTH VRANCEA EARTHQUAKES USING DIFFERENT TECHNIQUES**

Vladimir Yu. SOKOLOV<sup>1</sup>, Klaus-Peter BONJER<sup>2</sup>, Mihaela RIZESCU<sup>3</sup> (<sup>1</sup>Geophysical Institute, Karlsruhe University, <sup>2</sup>National Institute for Earth Physics, Bucharest-Magurele, Romania)

The soil response on earthquake ground motion was studied using ground-motion database collected in Romania. Almost all of the earthquakes occurred in Vrancea focal zone (SE-Carpathians), which is characterised by a high rate of occurrence of large earthquakes in a narrow focal volume. The epicentral region is confined to about 60 x 20 sq.km and the seismic activity ranges within an almost vertical stripe in depths between 70 and 170 km. The used ground-motion database includes several tens of acceleration records obtained during three large (M 7.5, 7.2 and 6.9) earthquakes and several hundreds records from more

than 120 small magnitude (M 3-5) earthquakes occurred in 1996-2001. The records were obtained at up to 40 stations; the local site conditions vary from metamorphic rock to deep soft soil deposits. The characteristics of the soil responses were evaluated in terms of frequency-dependent amplification using two techniques. One of the techniques is a modification of the well-known horizontal-to-vertical Fourier spectral ratio of the S-wave phase, which was proposed for earthquake ground motion by Lermo and Chavez-Garcia (1994). The second one (Sokolov 1998) consists in calculating spectral ratios of spectra of actual earthquake records (horizontal components) and those modelled for a hypothetical "very hard rock" (VHR) site. The VHR spectral model may be evaluated using the Vrancea earthquakes ground-motion database. Besides the local site response, the spectral ratios include effects of source rupture peculiarities and inhomogeneous propagation path, too. However, when using a large enough number of events varying by magnitude, source depth and azimuth, the effects of focal mechanism and directivity are expected to be averaged out. The approach was recently applied for the evaluation of characteristics of spectral amplification for generalised site conditions (site classes B, C and D) in the Taiwan region and for particular sites in the Taipei basin (northern Taiwan). In this paper we analysed the ability of the techniques for intermediate-depth earthquakes of various magnitudes.

## SS04b-Posters

Thursday, July 10

## STRONG GROUND MOTION, EARTHQUAKE HAZARD AND RISK

Location: Site D

Thursday, July 10 PM

Presiding Chairs: X. Lili, B.V. Rastogi, K. Irikura

## SS04b/10P/D-001

Poster

1400-184

## ASSESSMENT OF STANDARD SITE EFFECTS IN ASHIGARA VALLEY, JAPAN USING STRONG MOTION RECORDS FROM LARGE BUT REMOTE EVENTS

Tomiichi UETAKE<sup>1</sup>, Kazuyoshi KUDO<sup>2</sup> (<sup>1</sup>R&D Center, Tokyo Electric Power Company, 4-1, Egasaki-cho, Tsurumi-ku, Yokohama, 230-8510 JAPAN, <sup>2</sup>Earthquake Research Institute, Tokyo University)

Ashigara Valley, Japan is a sediment-filled valley of middle-size (12 km x 5 km). A strong motion observation network has been run by Earthquake Research Institute, the University of Tokyo and it recovered several large but far events, such as the 1993 Kushiro-oki (Mw 7.6), the 1994 Vladivostok (Mw 7.3), the 1994 Hokkaido-toho-oki (Mw 8.3), the 1994 Sanriku-oki (Mw 7.8) and the 2000 Torishima (Mw 7.4). The epicentral distances of these events are longer than 700 km; therefore, assumption of a plane-wave incidence to Ashigara Valley will be permitted. That is, the source and path effects will be common with a sufficient approximation for a middle size valley. As a first step, we obtained average spectral ratios with a reference rock site and amplification factors in time domain using a band-pass filtering technique. A spatial distribution of amplification factors is almost common among the events. The amplification factors of all sites at lower frequency than 0.2 Hz is relatively simple and they tend to large at the south of valley, reflecting deep structure inferred from refraction/reflection surveys and gravity data. We have to pay attention that deviations of spectral ratios among the rock sites are factor of 2 in the frequency range of 0.1-10 Hz. While, the ratios or amplification factors exceed more than factor of 10 at some sediment sites, especially at the south of valley. Using the data set from the Torishima event, we found the apparent velocity of the first S-arrival by the semblance analysis to be 8 km/s. This tells us almost vertical incidence of the first S-arrival part. On the other hand, latter arrivals show very low semblance values and it is difficult to identify proper velocities. Semblance analysis using small array of sediment sites shows that the later arrivals propagate from various directions with low velocities. This tendency is much distinct at high frequency range. These results may suggest that the later arrivals were not direct waves from the source but scattered or secondary generated waves. We checked the variation of spectral ratios using many time windows with same length of 40 s and different starting time. The properties of spectral ratios were approximately stable for different time windows. This result means that there is no significant difference between the amplification characteristics of the direct S arrival and the coda parts. The present results will give a standard amplification factor at a site when we study the effects of source, path and site effects using events of near and local distances.

## SS04b/10P/D-002

Poster

1400-185

## ESTIMATION OF SITE AMPLIFICATIONS IN ADAPAZARI, TURKEY, FROM MICROREMOR AND EARTHQUAKE OBSERVATIONS

Hiroaki YAMANAKA<sup>1</sup>, Masato KATO<sup>1</sup>, Nobuyuki YAMADA<sup>1</sup>, Umit GULERCE<sup>2</sup>, Recep IYISAN<sup>2</sup>, Atilla ANSAL<sup>2</sup> (<sup>1</sup>Dept. of Environmental Sci. and Tech., Tokyo Institute of Technology, <sup>2</sup>Istanbul Technical University)

Heavy damage was experienced in many cities in the north-western part of Turkey during the Kocaeli earthquake and the Duzce earthquake in 1999. Although several strong ground motion records were obtained in the area, there are not enough records in the heavy damage area to understand causes of the damage. Furthermore, subsurface structural data that are very important in assessment of ground motion characteristics are not well defined in the heavy damage area. In this study, we conducted single-point measurements and array measurements of microtremors in Adapazari city for estimation of site amplification factors. First, we estimated subsurface structure using microtremor data from the array and single-point measurements. S-wave profiles down to the basement with an S-wave velocity of 3 km/s were revealed at 5 sites in Adapazari from microtremor array explorations. The basement is as deep as 1 km at the sites in the northern part of the city, while it becomes shallow in the southern sites. We also conducted earthquake observation for small earthquakes in the area by installing 4 stations. From travel time analysis of initial P- and S-waves from small events, we validated the subsurface structural models. Site amplification factors from earthquake data were also compared with the theoretical transfer functions calculated from the models. The agreement of these amplification factors again indicated the validity of the models.

## SS04b/10P/D-003

Poster

1400-186

## SYNERGETIC EFFECTS OF SOURCE AND SITE ON THE NEAR-SOURCE STRONG GROUND MOTION AT DAMAGED AREAS IN SEDIMENTARY BASINS DURING THE KOCAELI, TURKEY EARTHQUAKES OF AUGUST 17, 1999

Tatsuo KANNO<sup>1</sup>, Kazuyoshi KUDO<sup>2</sup> (<sup>1</sup>Advanced Technology Research Group, National Research Institute for Earth Science and Disaster prevention, <sup>2</sup>Earthquake Research Institute, University of

Tokyo)

The estimation of strong ground motions during the Kocaeli, Turkey earthquake of 1999 at downtown Adapazari and Golcuk, where heavy damage was observed, is necessary for understanding the relation between ground motion severity and damage to buildings. For this purpose, we estimated the strong ground motion at damaged area during the mainshock based on the empirical Green's function method, regarding with underground structures estimated by array observations of microtremors and nonlinear behaviors of soft ground by the equivalent linear method. First, we estimated the bedrock motion during the mainshock by the empirical Green's function method using the largest aftershock records. We selected five asperities referring mostly to the source inversion results by Sekiguchi and Iwata (2002) for synthesizing the ground motion during the mainshock. We, in addition, assumed that the strong motion was generated by only these asperities. The validity of this simulation was confirmed by the comparison of the strong motion records and the synthetics at several stations near the fault (IZT, SKR, YPT). Then, we convolved the effects of surface sediments taking into account of nonlinear behaviors of soil by an equivalent linear method. As results, the ground motion at a period of 1-2 seconds in downtown Adapazari (ADC; heavy damage) during the mainshock is estimated to be similar to that of JMA Kobe from the Hyogoken-Nanbu earthquake of 1995. The estimated strong ground motion at ADU (slight damage) is smaller than that at SKR (slight damage) in shorter period range than 1 second, and this is qualitatively consistent with the damage level. No strong motion records from the largest aftershock was available in Golcuk area, therefore, we have to estimate the largest aftershock motion as a first step. We apply two-step estimation, that is, we first simulate the ground motion in Golcuk area during the largest aftershock using two small aftershock data, and next we estimate the ground motion during the mainshock using the simulated aftershock motion as EGF. The same source model of the mainshock was used. Response spectra of simulated motions in Golcuk area, except at a mountain site (GLS), show very high level in the longer period range than 1.0 seconds, exceeding to that of JMA Kobe from the Hyogoken-Nanbu earthquake of 1995. We cannot go into details, however, ground motion due to synergetic effects of surface soils and source would be very important. Directivity effects were not distinct in the results of Adapazari; however, the ground motion near Golcuk would be influenced by not only site condition but also source process or rupture propagation of a fault. The ground motion in a longer period than 1 second at damaged area in Golcuk during the mainshock is estimated to be larger than that of JMA-Kobe from Hyogoken-Nanbu earthquake of 1995.

## SS04b/10P/D-004

Poster

1400-187

## 3-D UNDERGROUND STRUCTURE MODEL IN KANAZAWA REGION, JAPAN

Tatsuo KANNO<sup>1</sup>, Nobuyuki MORIKAWA<sup>1</sup>, Shigeaki SENNA<sup>2</sup>, Akira NARITA<sup>2</sup>, Hiroyuki FUJIWARA<sup>1</sup> (<sup>1</sup>Advanced Technology Research Group, National Research Institute for Earth Science and Disaster prevention, <sup>2</sup>Mitsubishi Space Software Co., Ltd.)

The Earthquake Research Committee, the Headquarters for Earthquake Research Promotion, the Ministry of Education, Culture, Sports, Science and Technology is planning to create a "Seismic Hazard Map in General View of the whole of Japan". This includes two kinds of maps, a probabilistic seismic hazard map and a seismic shaking map for a specific seismic source fault. For the seismic shaking map, empirical attenuation relations and/or hybrid simulation procedure that combined the 3-D finite difference method and the stochastic Green's function method are applied to evaluate strong ground motions. In such evaluation, especially for the hybrid simulation, a detailed 3-D underground structure of the target area is very important information as well as a detailed source model. In the Morimoto-Togashi fault zone, one of the mapping regions in 2002, some surveys of underground structures have carried out with the aim of understanding the shape of bedrock layer and active fault. However, few data on velocity structures are available. In this study, therefore, we first carried out array observations of microtremors. Then we construct 3-D underground structure model for the hybrid simulation of strong ground motions for an earthquake occurred in the Morimoto-Togashi fault zone, compiling results of the observations, gravity data and so on. We carried out the array observations of microtremors at ten sites in and around Kanazawa city near the Morimoto-Togashi fault zone. Phase velocities of the fundamental mode Rayleigh wave were obtained from observed microtremors by using the spatial autocorrelation method and were inverted to the S-wave velocity structures by an inversion technique based on genetic algorithm. We derived a good correlation between the estimated depth of upper boundary of each layer and its corresponding residual gravity anomaly value at the site. Therefore, we converted distribution of the residual gravity anomaly into one of the depth of upper boundary of each velocity layer using these correlations. As results, we showed the bedrock layer under Kanazawa city shaped like a bowl. The bedrock under the center of Kanazawa city was deepest in the target area and its depth was estimated to be about 3400m. The validity of our underground structure model was confirmed by the comparison with other investigations, for example, results of survey using deep-well boreholes.

## SS04b/10P/D-005

Poster

1400-188

## ESTIMATION OF STRONG GROUND AMPLIFICATION IN METRO MANILA

Janira R. BAUL-DEOCAMPO (Seismological Observation and Earthquake Prediction Division, Philippine Institute of Volcanology and Seismology)

Metro Manila has been growing and developing without regard for its vulnerability to hazards. From the strategically located Manila City it has grown to include five cities and eleven municipalities. With a total population of 8 million that has been rapidly rising since the last two decades, it is the commercial, industrial, administrative and educational center of the country. It is also the host of past large and damaging earthquakes from seismic source zones that include the Valley Fault System, the Philippine Fault Zone, Lubang Fault, Casiguran Fault and the Manila Trench. With future large-magnitude earthquakes being highly probable in this area, strong ground amplification was estimated. Amplification of spectral ratios are compared with one-dimensional theoretical transfer function generally to validate the theoretical model. Strong ground motion was then estimated to a small extent enclosing the strong motion stations and using the Valley Fault System as causative Fault

## SS04b/10P/D-006

Poster

1400-189

## NONLINEAR BEHAVIOR OF SOILS IN THE 1995 KOBE (JAPAN) EARTHQUAKE IDENTIFIED BY VERTICAL ARRAY RECORDS

Olga V. PAVLENKO<sup>1</sup>, Kojiro IRIKURA<sup>2</sup> (<sup>1</sup>Institute of Physics of the Earth, Russian Academy of Sciences, B. Gruzinskaya 10, 123995 Moscow, Russia, <sup>2</sup>Disaster Prevention Research Institute, Kyoto University, Gokasho, Uji, 611-0011, Kyoto, Japan)

To improve our understanding of the behavior of sedimentary basins in the near-source zones in strong earthquakes, a method is proposed of estimation of stress-strain relations of sediments in situ based on vertical array data. As an example, records obtained during the 1995 Kobe earthquake (Japan) were used to estimate the stress-strain relations in the soil profiles at sites Port Island, SGK, TKS, and NKK in the vicinities of the fault planes and the

obtained relations are analysed. For different layers, different types of nonlinear stress-strain relations were selected, according to the profiling data. To account for temporal changes in the soil behavior, consecutive parts of records were examined, and for successive time intervals, the relations were found showing the best-fit approximation to the observed data. Various lengths of the time intervals are analysed, and the range of optimal values is found. The difference between the observed and simulated accelerograms and their spectra is analyzed, and found to be dependent on the accuracy of our knowledge of the profiling data. The best agreement was achieved for SGK and TKS sites, where repeated thorough measurements of the profiling data were carried out. The discrepancy between the observed and simulated accelerograms was found to increase with time from the beginning of the strong motion, which probably indicates that the middle and tail parts of the accelerograms recorded on the surface are determined not only by the imposed motion on the bottom of the system of sedimentary layers, but also, by processes, induced in the sedimentary layers by the strong motion. At the four sites, vertical distributions of stresses (in bars) and strains (in rel. units) are obtained for all depths, from the surface down to the locations of the deepest recording devices, and the contents of nonlinear components in the ground responses are estimated by the nonlinear system identification technique. The obtained stress-strain relations showed systematic changes in the upper 10 - 15 meters, such as, a progressive reduction of the slopes of the stress-strain curves due to liquefaction at Port Island and reduction and recovery of the slopes at other sites. The method can be applied to evaluate the ground response at sites, where the profiling data are available and an imposed motion can be estimated.

**SS04b/10P/D-007** Poster **1400-190**

#### IDENTIFICATION OF THE NONLINEAR BEHAVIOR OF SOILS DURING THE 2000 TOTTORI (JAPAN) EARTHQUAKE

Olga V. PAVLENKO (Institute of Physics of the Earth, Russian Academy of Sciences, B. Gruzinskaya 10, 123995 Moscow, Russia)

The method for estimation of the stress-strain relations in soil layers at different depths based on vertical array records was applied for the analysis of the behavior of soils in the near-source zone of the October, 6, 2000 Tottori (Japan) earthquake ( $M=7.3$ , depth is 11 km). Data of the Digital Strong Motion Seismograph Network Kik-Net were used. Though the earthquake was recorded by vertical arrays at 220 sites located at epicentral distances of 7 to 626 km, the nonlinear behavior of soils was identified for only six sites: the closest to the epicenter sites located at 7 km (max. acceleration 927.2 gal) and 8 km (max. acceleration 720.4 gal) and for sites located at distances of 44 to 99 km (max. accelerations 240.3 - 131 gal). For other sites, located in the near-source zone and far from the source, at distances 24, 26, 31, 32, 33, 41, 45, 46, 52, 53 km and more, either the thickness of the soil layer was less than 20-25 m and resonant phenomena were most important, or profiling data were absent, or accelerations were too small for the occurrence of nonlinearity. For six sites, where the nonlinear soil behavior was identified, stresses and strains (changing with time during the strong motion) were estimated in the soil layers at all depths 0 - 100 m from the surface down to the location of the device at depth. The obtained vertical distributions of stresses and strains depend on the profiling data: the better our knowledge of the parameters of the soil layers, the more realistic the obtained vertical distribution of stresses and strains. Since the profiling data for the Kik-Net sites include only P-wave and S-wave velocities and the composition of soils, we had to approximately estimate another necessary parameters, such as, shear stress in failure, density and damping, and this decreased the accuracy of the obtained results. To evaluate the influence of the profiling parameters on the results of our calculations, two series of calculations were performed for the records at the closest to the epicenter site TTRH02 (epicentral distance 7 km, maximum acceleration 927.2 gal), and the obtained vertical distributions of stresses and strains are compared.

**SS04b/10P/D-008** Poster **1400-191**

#### GROUND RESPONSE OF WEAK AND STRONG MOTIONS IN NEAR DISTANCE

Win-Gee HUANG (Institute of Earth Sciences, Academia Sinica)

The Taiwan Strong Motion Instrumentation Program (TSMIP), consisting of more than six hundred stations, was widely deployed in Taiwan area by the Central Weather Bureau. One of the particular significant of TSMIP was the amount of high-quality near-source data that it accumulated. The wealth strong motion data recorded at wide range of PGA due to different levels of excitation. Thus offer a good opportunity to study the difference of the amplification effects for a given site in response to different levels of excitation as well as for different geological conditions in near epicenter distance. Regardless the earthquake magnitude, only intensity of ground shaking was considered in this study. We focus on the response spectra calculation and want to realize its behaviors with different surface geology. Also discussed are the results of amplification effects studies for a site in response to weak and strong motions of broad intensity range in near epicenter distance. Our discussion was limited to spectra determined for 5 per cent damping although it could be readily be extended to include other damping values.

**SS04b/10P/D-009** Poster **1400-192**

#### EVALUATION OF DYNAMIC GROUND CHARACTERISTICS BASED ON SEISMIC RECORDS, MICROTREMOR AND GEOLOGICAL DATA

Jun TOBITA<sup>1</sup>, Nobuo FUKUWA<sup>2</sup>, Masaru NAKANO<sup>3</sup> (<sup>1</sup>Department of Architecture, School of Engineering, Nagoya University, <sup>2</sup>Graduate School of Environmental Studies, Nagoya University)

Variation of ground motion characteristics in Nagoya city, Japan, is investigated based on compilation of various soil data, observed seismic ground motions and microtremor data. First, on the basis of microtremor observation at over the 300 sites in Nagoya municipal area, the potential effectiveness of the horizontal to vertical Fourier spectral ratio (H/V) spectrum for the investigation of deep and shallow soil structure is discussed. Several test sites were selected, where various soil tests (boring, PS logging, etc.) were carried out and the borehole strong motion seismometers are installed. At these sites, the H/V spectral characteristics of microtremor and earthquake ground motion were examined, comparing with theoretical characteristics of Rayleigh wave and S wave. It is shown that the peak of the H/V spectrum of microtremor corresponds to layer boundary, of which the impedance ratio (lower layer / upper layer) is large, because the H/V spectrum depends on horizontal - vertical amplitude ratio of the modal shape of Rayleigh wave. The peak period of the H/V spectrum is similar to S wave amplification of surface layers under the condition that the layer boundary has larger impedance ratio over 3. In case of earthquake records, body wave is predominant at mainshock portion soon after the S-wave arrival, and the shape of the H/V spectrum is correspondent to the transfer function by multiple reflection of S wave. Based on the nature of the H/V spectrum mentioned above, the soil structure of Nagoya city area is estimated. For deep soil, predominant period is estimated from a peak in long period range (1 - several seconds) of the H/V spectrum. This period clearly corresponds to the depth of the seismic bedrock with  $V_s=3\text{km/s}$ . On the other hand, the shape of H/V spectrum is various in the short period range (less than 1 second), showing the variety of shallow soil conditions. Clear peak is observed at the sites where the clear contrast is observed at the engineering-

basis baselayer of  $V_s=400\text{-}500\text{m/s}$ , and the peak period is correspondent to the amplification period of the S wave for the layers above the boundary. It is shown that the existence of the clearly contrasted soil layer is almost detected by the peak period of the H/V spectrum considering the microtremor as a Rayleigh wave. Therefore, the depth of the layers can be estimated from the H/V spectrum by interpolating other exploration information at some sites, for example the deep boring investigation. The nature of the ground in Nagoya city is classified into 6 to 8 areas as Tertiary, diluvium, alluvium, reclaimed land, and so on. Estimated ground vibration characteristics by seismic records and densely measured microtremor records well correspond to these ground conditions.

**SS04b/10P/D-010** Poster **1400-193**

#### MULTI-DISCIPLINARY INFORMATION IN THE ASSESSMENT OF EARTHQUAKE HAZARD IN SAPPORO CITY

Tsutomu SASATANI, Kunikazu YOSHIDA (Graduate School of Science, Hokkaido University)

Sapporo City is located on a deep sedimentary basin in the western part of the Ishikari depression, Hokkaido. Mountains exist in the west and southwest part of the city. The population of Sapporo City is about 1.8 million, the biggest city in Hokkaido. In this study, we show multi-disciplinary information in the assessment of earthquake hazard in Sapporo City. Although no disastrous earthquake attacked the city during the last century, we have a lot of evidences of liquefaction induced by the 1834 Ishikari earthquake (M6.5). Recently seismic activity in and around the city has been monitored by several borehole seismometers; detected micro-earthquakes show a linear configuration beneath the boundary between the basin and the mountains. We summarized various data relating to the underground structures. Several PS-logging data show that an S-wave velocity is about 200 m/s at a surface and is 800-1000m/s at a depth of about 500 m. Recently an seismic reflection experiment has been done along Toyohira River near the city center. This experiment delineates shape of the basement-rock layer; the basement becomes shallow toward the mountains. We have also estimated S-wave velocity structures at more than 30 sites by using the microtremor exploration method. The basement-rock has an S-wave velocity of about 3000m/s at a depth of about 3000m. Combining these data, we are now constructing a rough three-dimensional velocity structure beneath the Sapporo basin. We have been carrying out strong motion observations at 30 sites to examine the seismic response of the Sapporo basin. The spatial variation of site amplifications is evaluated as a function of periods based on band-pass filtered records with various pass-bands. At the northern part, long-period seismic waves with a period of about 5 sec are strongly amplified, while at the central part, short-period seismic waves with a period of about 1 sec are strongly amplified. We have also examined the effect of the deep underground structure on seismic motion theoretically. Our goal is to renew the assessment of earthquake hazard in Sapporo City based on multi-disciplinary information mentioned above.

**SS04b/10P/D-011** Poster **1400-194**

#### DETERMINISTIC EVALUATION OF REGIONAL SEISMIC HAZARD IN THE IBERIAN PENINSULA

Mariano GARCIA-FERNANDEZ<sup>1</sup>, Franco VACCARI<sup>2</sup>, Maria-Jose JIMENEZ<sup>1</sup>, Giuliano F. PANZA<sup>3</sup> (<sup>1</sup>Institute of Earth Sciences 'Jaume Almera'-CSIC, Barcelona, Spain, <sup>2</sup>Universita di Trieste, Dip. di Scienze della Terra, Trieste, Italy, <sup>3</sup>The Abdus Salam International Centre for Theoretical Physics, Trieste, Italy)

Regional maps of maximum displacement, maximum velocity, and design ground acceleration for the Iberian Peninsula are obtained using a deterministic approach based on the computation of complete P-SV and SH synthetic seismograms. Scenario waveforms are computed in a regular grid covering the region combining input data from a regional seismogenic model, characterized by area sources, a working earthquake catalogue, characteristic fault-plane solutions, and ten average regional crustal models defined after a compilation of available structural studies. Results are compared with previous hazard studies and ground motion observations.

**SS04b/10P/D-012** Poster **1400-195**

#### SEISMIC HAZARD ASSESSMENT IN RUSSIA

Valentin I. ULOMOV (Schmidt United Institute of Physics of the Earth, B.Gruzinskaya, 10, 123995 Moscow, Russia)

More than 20% of the area of Russia is occupied by high hazard zones of intensity VIII-IX and IX-X EMS. These include the Russian Far East, the entire southern Siberia and North Caucasus. Some threat is also posed by intensity VI-VII zones in European Russia. The new study of seismogeodynamics and seismic zonation is based on the new methodology, homogeneous data base compiled for North Eurasia and a 3-D lineament-domain-focal (LDF) model of earthquake sources. A set of new General Seismic Zonation (GSZ) probability maps has been made for North Eurasia. The fragment GSZ maps of Russia being accepted as the basis for the national Building Code. The probability of a possible exceedance of seismic intensity within 50 years shapes up as follows: 10 percent (map GSZ-A), 5 percent (GSZ-B), 1 percent (GSZ-C) and 0.5 percent (map GSZ-D). The GSZ-A map was recommended for the construction of residential, public and production buildings; the B and C-maps for the objects that should continue in service even during earthquakes and also for premises housing a large number of people; the GSZ-D map for such high-danger objects as nuclear power stations etc. It is for the first time that seismic zoning involves all of North Eurasia, including the shelves of marginal and inner seas. We have seen that a large part of the Russian territory is subject to stronger seismic hazard than it was believed earlier. In this connection the Government has ratified the Federal Program "Seismic safety of territory of Russia" (2002-2010). Up to this time neither in the former USSR, nor in Russia similar programs did not exist. The purpose of this Program is the maximal increase of seismic safety of the population, reduction of social, economic, ecological risk in seismically dangerous areas of the Russian Federation, decrease of damages from destructive earthquakes by certification, strengthening and reconstruction of existing buildings and constructions, and also preparation of cities and other settlements, transport, power constructions, pipelines for strong earthquakes. A new method is proposed for the monitoring of regional seismogeodynamic processes, and results of studying time variation patterns in the occurrence of earthquakes of various magnitudes. Further research on the ordered patterns in the development of seismic sources in both time and space is required for more reliable localization of potential sources and assessment of seismic hazard. Fixation of the huge file of initial and target data in a digital electronic form within the Geographical Information System is a distinct fundamental achievement of the new technology of seismic zoning as compared with all previous technologies.

**SS04b/10P/D-013** Poster **1400-196**

#### A DETERMINISTIC SEISMIC HAZARD MAP OF INDIA AND ADJACENT AREAS

Imtiyaz Ahmed PARVEZ<sup>1</sup>, Franco VACCARI<sup>2</sup>, Giuliano Francesco PANZA<sup>3</sup> (<sup>1</sup>CSIR Centre for

Mathematical Modelling and Computer Simulation (C-MMACS), NAL Belur Campus, Bangalore-560037, India, <sup>2</sup>Department of Earth Sciences, University of Trieste, Via E. Weiss 4, 34127 Trieste, Italy AND INGV, Istituto Nazionale di Geofisica e Vulcanologia, Naples, Italy, <sup>3</sup>Department of Earth Sciences, University of Trieste, Via E. Weiss 4, 34127 Trieste, Italy AND The Abdus Salam International Centre for Theoretical Physics, SAND group, Trieste, Italy)

A seismic hazard map of the territory of India and adjacent areas has been prepared using a deterministic approach based on the computation of synthetic seismograms complete with all main phases. The input data set consists of structural models, seismogenic zones, focal mechanisms and earthquake catalogues. There are few probabilistic hazard maps available for Indian subcontinent, however, this is the first study aimed to produce a deterministic seismic hazard map for the Indian region using realistic strong ground motion modeling with the knowledge of the physical process of earthquake generation, level of seismicity and wave propagation in anelastic media. The synthetic seismograms at a frequency of 1 Hz have been generated at a regular grid of  $0.2 \times 0.2$  by the modal summation technique. The seismic hazard, expressed in terms of maximum displacement (DMAX), maximum velocity (VMAX), and design ground acceleration (DGA), has been extracted from the synthetic signals and mapped on a regular grid over the studied territory. The estimated values of the peak ground acceleration are compared with the observed data available for the Himalayan region and found in agreement. Many parts of the Himalayan region have the DGA values exceeding 0.6 g. The epicentral areas of the great Assam earthquakes of 1897 and 1950 in the north-east India represent the maximum hazard with DGA values reaching 1.2-1.3 g. The peak velocity and displacement in the same region is estimated as 120-177 cm/sec and 60-90 cm respectively.

**SS04b/10P/D-014** Poster **1400-197**

**PROBABILISTIC SEISMIC HAZARD ASSESSMENT IN NORTHERN ALGERIA, USING SPATIALLY-SMOOTHED SEISMICITY. PART II: SPECTRAL ACCELERATION AND UNIFORM HAZARD SPECTRA**

Mohamed HAMDACHE<sup>1</sup>, Jose Antonnio PELAEZ MONTILLA<sup>2</sup>, Carlos LOPEZ CASADO<sup>3</sup> (<sup>1</sup>Seismological Survey Department - CRAAG - Algiers - Algeria, <sup>2</sup>High Polytechnic School, University of Jaen, Spain, <sup>3</sup>Theoretical Physics department, University of Granada, Spain)

As a continuation of the first part, seismic hazard in terms of spectral acceleration (SA) for rock soil, has been estimated in the northern Algeria using the spatially-smoothed seismicity methodology. The seismic models, needed in this approach have been obtained by considering all the earthquakes events with magnitude up to Ms 6.5 and greater during the last 300 years. Seismic hazard maps in terms of SA for rock damped at 5%, at the periods of 0.1, 0.2, 0.3, 0.4, 0.5, 1.0, 1.5 and 2.0 s, with 39.3% and 10% probability of exceedance in 50 years have been obtained. These maps correspond to a return period of 100 and 475 years, respectively. For twelve of the most industrial and populated cities in Algeria, the uniform hazard spectra (UHS) is assessed and examined in details. Using a probabilistic approach, the UHS for rock soil damped at 5% has been derived for the two considered return periods, respectively 100 and 475 years. As a more significant results, observed as well as in the seismic hazard maps than in the UHS results, the expected maximum values of SA are obtained in the region of the Chleff (previously El Asnam), in the central area of the Tell Atlas. Specially, in the vicinity of the Chleff Quaternary basin, around the location of the most destructive earthquakes of September 9 1954 (Ms 6.8) and of October 10 1980 (Ms 7.3).

**SS04b/10P/D-015** Poster **1400-198**

**NATIONAL SEISMIC HAZARD MAPPING PROJECT OF JAPAN**

Hiroyuki FUJIWARA, Shin AOI, Shinichi KAWAI, Toru ISHII, Toshihiko OKUMURA, Yuzuru HAYAKAWA (National Research Institute for Earth Science and Disaster Prevention)

The Great Hanshin-Awaji Earthquake Disaster on January 17, 1995 killed more than 6,400 people. Following on the lessons learned from this disaster, Earthquake Disaster Management Special Act was enacted in July 1995 to promote a comprehensive national policy on earthquake disaster prevention. In accordance with this act, the Headquarters for Earthquake Research Promotion was established. In April 1999, Headquarters for Earthquake Research Promotion fixed 'On Promotion of Earthquake Research - Comprehensive and Fundamental Measures for Promotion of Observation, Measurement and Research on Earthquakes'. In this article, the Headquarters for Earthquake Research Promotion concluded that preparation of 'Seismic Hazard Map in General View of the Whole Japan' should be promoted as a major subject of earthquake research. The National Research Institute for Earth Science and Disaster Prevention (NIED) started the special research project 'National Seismic Hazard Mapping Project of Japan' to support the preparation of seismic hazard maps made by the Headquarters for Earthquake Research Promotion in April 2001. The Seismic Hazard Map in General View of the Whole Japan consists of two kinds of hazard maps. One is a probabilistic seismic hazard map that shows information predicting possibility that a certain area is attacked by a strong ground motion in a certain term by means of probability. The other is a seismic hazard map with specified seismic source fault. This type of hazard map is sometimes called scenario seismic map. As the first step in preparations for producing the seismic hazard maps, which are scheduled to be completed by the end of fiscal year 2004, preliminary versions of probabilistic seismic hazard map for the region centering Yamanashi Prefecture and scenario seismic maps for earthquakes in Itoigawa Shizuoka tectonic line fault zones and Miyagi-ken-oki earthquakes have been prepared. We will present outline of a method to make the national seismic hazard maps and preliminary version of hazard maps.

**SS04b/10P/D-016** Poster **1400-199**

**PROBABILISTIC SEISMIC HAZARD ASSESSMENT FOR LUZON, PHILIPPINES**

Jane T. PUNONGBAYAN<sup>1</sup>, Louis DORBATH<sup>2</sup>, Jean-Philippe AVOUC<sup>3</sup>, Sylvie MARRIN<sup>4</sup> (<sup>1</sup>Philippine Institute of Volcanology and Seismology, C.P. Garcia Avenue, U.P. Diliman, Quezon City, Philippines, <sup>2</sup>Institut de Physique du Globe de Strasbourg, 5 rue RenéDescartes, 67084 Strasbourg, France, <sup>3</sup>Laboratoire de Détection et de Géophysique, CEA, BP 12, Bruyeres-le-Chatel 91680, France)

The Philippine archipelago is bounded and transected by active seismogenic zones capable of producing large and destructive earthquakes. The country, one of the most populated in the world with 80 million inhabitants, is submitted to high risks, not only from volcanic activities but also from earthquakes. In this work, we quantify the probabilistic hazards due to earthquakes for its main and largest island, Luzon. The programs used, developed by the Laboratoire de Détection et de Géophysique du Commissariat d'Énergie Atomique de France, permit the calculation of probabilistic intensities due to any given earthquake by considering site effects, a given seismicity model and laws enabling the determination return periods of expected intensity for any site or region. The calculations done adopted a model of seismicity based on instrumentally determined earthquake parameters, accounts of historical earthquakes and geomorphological information such as fault length. The process also made use of laws establishing expected intensities for any given distance relative to the

epicenter, which were calibrated using intensity reports and physical parameters of well-documented major earthquakes in the island, as extracted from both instrumental and historical catalogues that span a period of almost 400 years. These laws are also corrected as a function of local geology. Results show that almost the whole of Luzon Island could expect intensity VII in the Modified Mercalli Intensity Scale (MMI) for a 100-year return period. Maximum hazards, for all considered return periods (100, 500, 1000 years), can be found concentrated in eastern Luzon, in the areas of Northern and Southern Sierra Madre ranges (MMI=XIII-X). Fortunately, these regions are not very densely populated. However, this zone of high intensity extends to the Central Valley, which, in contrast, is not only densely populated but is also economically important to the whole country. The hazards in these areas are aggravated by its liquefaction susceptibility. For the extended return period of 1000 years, Metropolitan Manila, an aggregate of twelve (12) cities and five (5) municipalities forming the most important region of the Philippines (politically and economically), becomes highly prone to damaging earthquakes as it can be found in the limits of the highest intensity zones (MMI=VIII-IX). These results should still be considered conservative as not all of the active faults in Luzon and nearby areas were included in the model as information for these faults (precise extension, characteristic earthquake, recurrence period, ...) are still at the stage of being established.

**SS04b/10P/D-017** Poster **1400-200**

**EASTERN CANADIAN CRUSTAL DEFORMATION RATES IMPLIED BY CANADA'S FOURTH-GENERATION SEISMIC HAZARD MODEL**

Stephane MAZZOTTI, Stephane MAZZOTTI, John ADAMS, Stephen HALCHUK (National Earthquake Hazards Program, Geological Survey of Canada)

The Geological Survey of Canada's new seismic hazard model for Canada will form the basis for the seismic design provisions of the 2005 National Building Code of Canada (NBCC). As such it represents Canada's fourth generation of seismic hazard maps (previous ones were in 1953, 1970, and 1985). The Cornell-McGuire method is used with two complete earthquake source models - historical and regional/geological - to represent the uncertainty in where (and why) earthquakes will happen in the future. Ground motions for a deterministic Cascadia subduction earthquake are computed for southwestern Canada, and probabilistic seismic hazard for the nearly aseismic central part of Canada is assessed based on a global model. A "robust" method is used to combine the probabilistic hazard estimates (at a probability of 2%/50 years or 0.000404 p.a.) from the four source models: the mapped value is the largest of the values. The three probabilistic models use a total of 50 source zones, each with an assessment of the magnitude recurrence statistics and the upper-bound magnitude. The latter were made considering both regional historical activity and the global history of large earthquakes in similar tectonic environments. We turn these results into deformation rates with the additional assumptions: seismogenic crustal thickness 25 km, focal mechanism either thrusting on 45 degree planes or strike-slip, and assigned a shortening direction based on crustal stress information, which is predominantly NE-SW over Canada. As expected, the deformation rates from the historical model show a similar pattern to the seismicity map, i.e. patches of high deformation that are unsustainable for geological eons. However, deformation rates from the regional/geological model (with large earthquakes happening in areas of low historical seismicity) seem more sustainable in the long term. These conclusions point out the challenge of both measuring contemporary deformation and estimating seismic hazard for eastern Canada.

**SS04b/10P/D-018** Poster **1400-201**

**FOURTH-GENERATION SEISMIC HAZARD MAPS FOR THE 2005 NATIONAL BUILDING CODE OF CANADA**

John ADAMS, Stephen HALCHUK (National Earthquake Hazards Program, Geological Survey of Canada)

The Geological Survey of Canada's new seismic hazard model for Canada will form the basis for the seismic design provisions of the 2005 National Building Code of Canada (NBCC). As such it represents Canada's fourth generation of seismic hazard maps (previous ones were in 1953, 1970, and 1985). The Cornell-McGuire method is used with two complete earthquake source models - historical and regional/geological - to represent the uncertainty in where (and why) earthquakes will happen in the future. Ground motions for a deterministic Cascadia subduction earthquake are computed for southwestern Canada, and probabilistic seismic hazard for the nearly aseismic central part of Canada is assessed based on a global model. A "robust" method is used to combine the probabilistic hazard estimates (at a probability of 2%/50 years or 0.000404 p.a.) from the four source models: the mapped value is the largest of the values. Products will include seismic hazard maps, tabulated values, UHS, plots of deaggregated hazard and documentation. For the seismic provisions of the 2005 National Building Code of Canada the median ground motion on firm soil sites for spectral acceleration at periods of 0.2, 0.5, 1.0 and 2.0 second and peak acceleration will be used. The four spectral parameters will allow the construction of approximate uniform hazard spectra (UHS) for each listed locality, and hence improve earthquake-resistant design.

**SS04b/10P/D-019** Poster **1400-202**

**PROBABILISTIC SEISMIC HAZARD MAPS FOR ALBANIA**

Veronika PEĆI, John ADAMS, Issam AL-KHOUBBI, Stephen HALCHUK (Geological Survey of Canada)

Albania is a country with high seismicity and earthquake risk reduction has been an important, on-going socio-economic concern. We use the experiences and methods for Canadian seismic hazard maps to present (for the first time) probabilistic seismic hazard maps for Albania. We have produced peak ground acceleration values for several cities and communities in Albania, for return periods of 0.0021 and 0.000404 per annum (equivalent to non-exceedences of 10%/50 years and 2%/50 years, respectively) and as well as 5% damped spectral acceleration values for 0.2, 0.5, 1.0 and 2.0 second periods for determining uniform hazard spectra. A revised catalogue of earthquakes of Albania, from historical data up to the year 1995, for events with magnitude  $M_s \geq 4.5$  and occurring in the region between 39.0N and 43.0N and between 18.5E and 21.5E was used in this study. All magnitudes have been expressed in terms of Ms. Nine seismic source zones are used to define the Albanian Classic model, following the work of Sulstarova and Allaj. It is intended to work on an improved model. Using the maximum likelihood method of Weichert, we computed the magnitude recurrence parameters and estimated their epistemic uncertainty. Parameters used for the probabilistic seismicity model, which tabulates the seismicity parameters together with maps of the source zones will be given. Both the Boore et al. and Ambraseys relations were applied to Albania for a reference soil condition equivalent to Boore et al.'s *soil class B*. This choice of ground condition near the mid-range between very hard and very soft ground minimizes the uncertainty in the amplification or deamplification factors for the extreme sites. The peak acceleration relation of Theodoulidis and Papazachos, developed for shallow crustal Greek earthquakes, was also considered. These maps and associated UHS results are suggested as the basis of the next version of KTP-N.2-89 Regulation in aseismic code in Albania.

**SS04b/10P/D-020** Poster **1400-203****STRONG-MOTION MAPS FOR SCENARIO EARTHQUAKES IN KANAZAWA AREA (JAPAN), AROUND MORIMOTO-TOGASHI ACTIVE FAULT**

Shin AOI<sup>1</sup>, Tatsuo KANNO<sup>1</sup>, Nobuyuki MORIKAWA<sup>1</sup>, Shigeki SENNA<sup>2</sup>, Toshihiko HAYAKAWA<sup>3</sup>, Hiroyuki FUJIWARA<sup>4</sup> (<sup>1</sup>National Research Institute for Earth Science and Disaster Prevention, <sup>2</sup>Mitsubishi Space Software Co., Ltd.)

Strong motion map based on the scenario earthquake in Kanazawa area was created. Kanazawa city is a typical middle sized city located in the Hokuriku district and the Morimoto-Togashi active fault, which is about 26km wide, crosses the middle of the city. Probability of the occurrence of an earthquake whose JMA magnitude is more than 7.2 for this fault within 30 years was evaluated as 0-5% by the Subcommittee for the Long-term Evaluation, the Headquarters for Earthquake Research Promotion. This probability is rather high among the 98 main active faults in Japan. Deep structure was estimated mainly based on the gravity anomaly data and geological information. To evaluate the sediment structure of Kanazawa basin, whose maximum is more than 3km, array observation of microtremors was carried out at ten points (Kanno et al., IUGG, 2003). The structure of superficial layers was evaluated mainly by the digital national land information and borehole logging data. By applying 'Recipe' (Irikura et al., 2002), heterogeneous fault models were constructed which consist of background and one asperity for evaluating ground motion. For periods longer than 1.0 s, responses of wave propagation for 3 dimensional structures were theoretically evaluated using FDM, and the statistical Green's function method was used for the frequency higher than 1 Hz. The broadband time history was generated by summing them using a matching filter. Spatial distribution of time history, peak accelerations and seismic intensities were evaluated in 60km\* 90km region centering on Kanazawa at about every 1 km spacing. Peak accelerations and seismic intensities were evaluated in a larger area with empirical method.

**SS04b/10P/D-021** Poster **1400-204****LONG TERM SEISMOLOGICAL HAZARD ASSESSMENT FOR A NUCLEAR WASTE REPOSITORY: DETERMINISTIC AND PROBABILISTIC APPROACH**

Guenter LEYDECKER<sup>1</sup>, Juergen R. KOPERA<sup>2</sup> (<sup>1</sup>Federal Institute for Geosciences and Natural Resources, Stilleweg 2, 30655 Hannover Germany; guenter.leydecker@bgr.de, <sup>2</sup>BIS-Kopera, Buero fuer IngenieurSeismologie, Seerosenstrasse 10B, 30916 Isernhagen Germany; bis\_kopera@hotmail.com)

Existing and planned nuclear waste repositories in Germany are situated in areas of low seismicity. Nevertheless, seismic hazard assessment has to be performed for a very long time period, even though there is a considerable debate whether or not it is possible to quantify the seismic hazard in such an area. A combination of deterministic and probabilistic methods are used to assess the seismic hazard for a site in Northern Germany, fulfilling the standards of the German technical safety code for nuclear power plants. As an example, the site of the former salt mine Morsleben, which now is a nuclear waste repository, is investigated. The deterministic method is based on the assumption that the most strongest earthquakes inside a tectonic region can happen everywhere there, also near the selected site. For the probabilistic method, several models describing the seismicity in an area of 200 km around the site are used to show the influence of the variability in input parameters on the exceeding probability of the site intensity. It is shown that the seismic hazard of a site in an area of low seismicity is mainly caused by the effects of distant but strong source regions, and for very low probabilities by the background seismicity. The probabilistic evaluation has the advantage to quantify the seismic hazard. But deterministic and probabilistic methods together seems a practical tool for mutual control of the results and to overcome the disadvantages of each approach alone. Input data are derived from the German earthquake catalogue with an observation period of about 1200 years. From a comprehensive knowledge about geological development and structural geology, the time history of the surrounding faults are developed. The nearest dominant fault, reaching deep into the crust, was most active in the Upper Cretaceous. Smaller movements occurred 5 Mio. years ago. Only parts of this fault are orientated at a critical angle to the actual stress field which could result in smaller earthquakes only. The combination of both, seismicity and tectonics, provide the basis for a long term prognostic with probabilities of exceedance in the order of 10<sup>-5</sup> per year. For the investigated site the following parameters are derived: site intensity as a function of exceeding probability; site acceleration; strong motion duration; site dependent response spectra for the surface and the underground inside the mine.

**SS04b/10P/D-022** Poster **1400-205****UNCERTAINTIES IN SEISMIC HAZARD ASSESSMENT IN THE MEGACITY OF ALGIERS (ALGERIA) USING DIFFERENT ATTENUATION MODELS**

Djillali BENOUAR (Department of Civil Engineering, University of Science and Technology Houari Boumediene (USTHB))

This research presents the evaluation of seismic hazard at the site of Algiers (Capital of Algeria) using four different attenuation models. Seismic hazard analysis was carried out using a simple earthquake occurrence model and the new seismic catalogue compiled recently by Benouar5 for the Maghreb region. The site is defined by longitude 3.00°E and latitude 36.45°N. Because earthquake process around the site is poorly understood, it is assumed that future earthquakes will occur in an area in which they have already occurred in the past. The hazard, expressed in terms of the probability of exceedance of the PGA, is calculated for an economic life of the structure of 10, 50, and 100 years. The absolute acceleration for a given return period is also determined. Due to the shortage of ground motion records, no attenuation law has been derived for Algeria. The main objective of this study is to analyze the influence of the attenuation models on the seismic hazard evaluation, since the results of seismic hazard are sensitive to these models. Thus, a selection of an appropriate attenuation law is very crucial. For this purpose, four attenuation laws which seem to fit the Algerian data were selected from the literature, these are Joyner and Boore1, Ambraseys and Bommer2, Ambraseys3 (controlled depth) and Ambraseys3 (uncontrolled depth). A comparison of the expected seismic hazard allows a first critical estimate showing that seismic hazard is very sensitive to the attenuation models selected and the PGA could be either conservative or not, depending on the attenuation model and the level of acceptable risk. The most recent earthquake disaster that affected the site of Algiers is the El-Asnam earthquake of 10 October 1980 (Ms 7.4) which caused the loss of more than 3000 lives, injuring about 9000 and made homeless at least 400 000; it destroyed more than 60 000 housing units, official buildings and public works of which damage was estimated by official reports at U.S. \$ 5 billion (Benouar)5. Algiers has a population of approximately three millions; it represents the most important concentration of investment, government institutions and population in the whole country. The zone under study represents an area of 200 km radius around the site of Algiers. In recent years the disaster risks have increased due to overcrowding, faulty land use planning and construction, inadequate infrastructure and services, and environmental degradation. The topography, the waterfront location and the ancient neighborhoods (Casbah) make it difficult to affect radical solutions to most of its problems.

**SS04b/10P/D-023** Poster **1400-206****A STUDY ON PROBABILISTIC SEISMIC HAZARD MAPS IN JAPAN**

Toru ISHII<sup>1</sup>, Toshihiko OKUMURA<sup>1</sup>, Hiroyuki FUJIWARA<sup>1</sup>, Yuzuru HAYAKAWA<sup>1</sup>, Shinichi KAWAI<sup>1</sup>, Shin AOI<sup>1</sup>, Yutaka ISHIKAWA<sup>2</sup>, Junichi MIYAKOSHI<sup>3</sup>, Tomoo SAITO<sup>3</sup>, Hideaki SHINOHARA<sup>4</sup> (<sup>1</sup>National Research Institute for Earth Science and Disaster Prevention, <sup>2</sup>Izumi Research Institute, Shimizu Corporation, <sup>3</sup>Oyo Corporation)

A methodology to evaluate spatial strong-motion distributions is studied in order to make probabilistic seismic hazard maps in Japan. A probabilistic seismic hazard map illustrates the relationship between three parameters, which are amplitudes, time period and probabilities, of strong-motions in an area. On this study reflected are the long-term evaluations of active faults and the ones of inter-plate earthquakes along the subduction zones, which have been presented by the Headquarters for Earthquake Research Promotion based on the newest information and data of active faults and historical earthquakes all over Japan. The earthquakes in and around the mapping area are classified into seven different types: 1) the characteristic earthquakes along the major 98 active fault zones in Japan; 2) the earthquakes along the other active faults; 3) the earthquakes in the major 98 active fault zones except the characteristic earthquakes; 4) the characteristic inter-plate earthquakes along the subduction zones; 5) the inter-plate earthquakes along the subduction zones except the characteristic earthquakes; 6) the intra-plate earthquakes along the subduction zones; and 7) the crustal earthquakes whose fault planes could not be identified in advance. With the probabilistic models of earthquake occurrence for these earthquake types, seismic hazard curves are evaluated in terms of peak ground motions and seismic intensities at the points which are arranged regularly all over the mapping area with about 1 km spacing. The attenuation relations with the particular characteristics in and around the mapping area and the surface layer amplification estimated at each evaluation points are used in this study. At several principal points, hazard curves and contribution factors of earthquakes are also presented in order to compare the impact of each earthquake on the strong-motion at each probability level. The developed procedure and techniques are applied to an area including both of Nagano and Yamanashi prefectures located in central Japan, and also applied to Hokkaido and Tohoku districts, a larger area located in northeast Japan.

**SS04b/10P/D-024** Poster **1400-207****A STUDY ON HAZARD MAPS FOR SCENARIO EARTHQUAKES IN JAPAN**

Toru ISHII<sup>1</sup>, Hiroyuki FUJIWARA<sup>1</sup>, Shin AOI<sup>1</sup>, Toshiaki SATO<sup>2</sup>, Motofumi WATANABE<sup>3</sup>, Toshimi SATOH<sup>4</sup>, Shinichi MATSUSHIMA<sup>5</sup>, Takashi HAYAKAWA<sup>6</sup>, Hideaki SHINOHARA<sup>7</sup>, Koji IWAMOTO<sup>8</sup>, Kyozo NOZAKI<sup>9</sup> (<sup>1</sup>National Research Institute for Earth Science and Disaster Prevention, <sup>2</sup>Ohsaki Research Institute, Inc., <sup>3</sup>Izumi Research Institute, Shimizu Corporation, <sup>4</sup>Oyo Corporation, <sup>5</sup>Mitsubishi Space Software Co., Ltd.)

A methodology to evaluate spatial strong-motion distributions is studied in order to make hazard maps for scenario earthquakes in Japan. A hazard map for scenario earthquake represents a spatial strong-motion distribution in an area that will be caused by a specified future earthquake. On this study reflected are the long-term evaluations of active faults and the ones of inter-plate earthquakes along the subduction zones, which have been presented by the Headquarters for Earthquake Research Promotion based on the newest information and data of active faults and historical earthquakes all over Japan. Heterogeneous fault models of possible earthquakes are established by considering asperities in which slips and stress drops are larger than those in the background area on the fault plane. Three-dimensional propagation characteristics of seismic waves and amplifications in surface layer are estimated based on detailed information and data collected in the mapping area. The strong-motion time histories, peak ground motions and seismic intensities are evaluated by using the theoretical, semi-empirical and empirical methods at all the points which are arranged regularly all over the mapping area with about 1 km spacing. The developed procedure and techniques are applied to the characteristic earthquake along Itoigawa-Shizuoka tectonic line fault zone, one of the largest and the most active major fault zones in Japan. Three different maps for three cases with different asperity distributions and rupture characteristics are produced and compared to each other. The procedure and techniques are also applied to Miyagi-ken-oki earthquake, one of the most active inter-plate large earthquakes along the Pacific coast of northeast Japan. It is confirmed that the results of this study explain very well the recorded time histories at three stations around Sendai during 1978 Miyagi-ken-oki earthquake.

**SS04b/10P/D-025** Poster **1400-208****INVESTIGATION FOR SEISMIC ZONATION OF ANCHORAGE, ALASKA**

Niren B. BISWAS<sup>1</sup>, Artak H. MARTIROSYAN<sup>1</sup>, Utpal DUTTA<sup>1</sup>, Apostolos PAPAGEORGIOU<sup>2</sup> (<sup>1</sup>Geophysical Institute, University of Alaska Fairbanks, <sup>2</sup>Department of Civil Engineering, University of New York, Buffalo)

Anchorage being the largest population center in the State of Alaska, is located in a highly active seismic zone and underlain by a west dipping deep sedimentary basin. Thus, a seismic zonation program for the metropolitan area of Anchorage was implemented in early 1990. In describing the ground motions for local earthquakes, the first order characteristics of the three factors, namely, source, path and site have been determined. In this presentation, however, emphasis has been given to the spatial variations of site class and site response. In order to determine the site class, we used Rayleigh waves in the frequency range of about 1-100 Hz. These were generated by an electromagnet vibrator at 36 sites in the Anchorage Basin. The phase velocity (c(f)) of the fundamental mode at each site was computed using the phase delay times between two sensors. Next, c(f) data were inverted in terms of shear wave velocity (V<sub>s</sub>) structure by stochastic inversion scheme. Of the 36 sites, values of V<sub>s</sub> as a function of depth were available at 7 sites from downhole measurements. At these sites, the comparison of the results between surface and downhole measurements showed reasonable agreement. On the basis of NEHRP provision, we obtained the time-averaged V<sub>s</sub> structures of the basin for the uppermost 30 m (V<sub>30</sub>). The results revealed that the Anchorage metropolitan area consists of site class C (360 < V<sub>30</sub> ≤ 760 m/s) and D (180 < V<sub>30</sub> ≤ 360 m/s). On the eastern side of the city lies a mountain range (Chugach Mts.) where coverage of the velocity survey was lacking, though rock exposures and a special purpose 9 m drillhole data showed formations of site class B (760 < V<sub>30</sub> ≤ 1500 m/s). Moreover, from the foothills of Chugach Mts. towards the west side of the city, it is necessary to introduce a transition zone (C/D) between the areas of site class C and D. The V<sub>30</sub> in C/D ranges from 320 to 410 m/s. Concerning site response (SR), we used data for local earthquakes recorded by a temporary weak motion (WM) and permanent strong motion (SM) networks. We computed SR by spectral ratio (SRM) and generalized inversion (GIM) methods. The results obtained for SR from WM and SM data using SRM and GIM were synthesized. The SR values thus obtained were averaged (logarithmically) for two frequency bands AEa low frequency band (LFB) and a high frequency band (HFB) with center frequencies of 1 and 5 Hz, respectively. In LFB, SR increases from 1.0 along the foothills of Chugach Mts. in the east to about 3.5 in the western side following the trend of increasing thickness of the sediments in the basin. The area of the highest SR value (>3.0) in LFB in the westcentral part of the city is underlain by the cohesive facies of the Bootlegger Cove Formation, which

suffered extensive liquefaction during the 1964 Prince William Sound earthquake ( $M_w = 9.2$ ). This trend of SR also has good correlation with that of  $V_{30}$  with a correlation coefficient of 0.82; SR values in LFB are close to the NEHRP site coefficients for 1 sec. However, SR values in HLB lack correlation with the spatial distribution of  $V_{30}$  and short period NEHRP site coefficients. For SR below 1 Hz, we used microtremor data. The results at center frequency of 0.35 Hz follow closely the trend of that obtained for LFB.

**SS04b/10P/D-026** Poster **1400-209**

#### A C LEVEL MICROZONATION MAP OF BUCHAREST, ROMANIA

Carmen Liliana MOLDOVEANU<sup>1</sup>, Carmen CIOFLAN<sup>2</sup>, Mircea RADULIAN<sup>2</sup>, Bogdan APOSTOL<sup>2</sup>, Giuliano F. PANZA<sup>3</sup> (<sup>1</sup>Department of Earth Sciences, University of Parma, <sup>2</sup>National Institute for Earth Physics, Bucharest, Romania, <sup>3</sup>Department of Earth Sciences, University of Trieste, Italy, <sup>4</sup>The Abdus Salam International Center for Theoretical Physics, SAND Group, Trieste, Italy)

Bucharest experienced heavy destruction and large number of victims during the extreme 1940 ( $M_w=7.7$ ) and 1977 ( $M_w=7.4$ ) Vrancea intermediate-depth earthquakes (located in the 60-200 km depth interval, at the sharp bend of the Southeast Carpathians). The statistics indicate a recurrence interval of 25 years for  $M_w > 6.0$  and 50 years for  $M_w > 7.0$  in the region. The assessment and mitigation of the earthquake risk are therefore particularly important in the Romanian capital since more than 2 million inhabitants, major investments and vital life systems are concentrated there. The seismic ground motion evaluation implies the analysis of a large database of records provided by dense arrays of seismographs. This allows defining generally valid ground parameters to be used in seismic microzonation estimations. The strong motion registrations in Bucharest area are rather few and available only since 1977. Therefore the ability to compute numerically realistic seismograms represents in our opinion the key element for performing "present day" microzonation studies. Using a complex hybrid waveform modeling method that accounts for the source, wave propagation path and local site geology, we investigate which features of the seismic process are predictable in case of Vrancea dominant shocks, and how do they reproduce the strong local effects observed in Bucharest for the 1977 event. Our deterministic results show that the synthetic local hazard distribution supplies a realistic estimation of the seismic input. This method allows the merging of the different specific information collected until now in reasonably well constrained scenarios for a level C realistic microzonation of Bucharest area to be used to mitigate the effects of future strong events originating in Vrancea region.

**SS04b/10P/D-027** Poster **1400-210**

#### PROBABILISTIC SEISMIC HAZARDS PARAMETERS ESTIMATION IN GUJRAT REGION, INDIA

Jayant Nath TRIPATHI<sup>1</sup>, Dileep Kumar TIWARI<sup>1</sup> (<sup>1</sup>Department of Earth & Planetary Sciences, University of Allahabad, Allahabad-211002, India; Presently at: Observatori de l'Ebre, c/ Horta Alta, 38; 43520 Roquetes (Tarragona), Spain, <sup>2</sup> Department of Earth & Planetary Sciences, University of Allahabad, Allahabad-211002, India)

In the Indian subcontinent Kutchh of Gujarat region is one of the most seismic prone areas. In Kutchh region, the maximum affected areas (by earthquake) fall along the Kutchh Mainland fault (KMF). This fault extends in the direction of east west for about 100 km. Another fault namely South Wegad Fault, also called Adhoi Fault, falls in the line of the KMF and extends for about 50 km. These faults are mainly responsible for the tectonic processes in the past. And a result we had the 7.6 magnitude earthquake on January 26, 2001. Probabilistic assessment of seismic hazard is the initial step for the assessment of realistic pattern of earthquakes in the specified region. The probability of occurrence of great earthquake with magnitude  $M \geq 6.0$  during a specified interval of time, for this region has been estimated on the basis of four probabilistic models, namely, Weibull Model, Gamma Model, Lognormal Model and Exponential Probability Model. These four models represent the distribution of time interval fairly well. The probability of occurrence of the next large earthquake during a specified interval of time has been calculated for aforesaid each model. The Method of Moment has been applied for computation of the hazard parameters for only three models viz. Weibull, Gamma and Lognormal Model, while the method of maximum likelihood has been used for the computation of hazard parameters for Exponential Probability model. The cumulative and conditional probabilities have been evaluated for each model. According to the present study the probability of occurrence of a great earthquake, having magnitude  $M \geq 6.0$ , reaches 0.9 and above for a time period of 61 to 64 years for each of the models.

**SS04b/10P/D-028** Poster **1400-211**

#### RECURRENT PARAMETERS OF EARTHQUAKES USING METHOD OF MAXIMUM LIKELIHOOD ESTIMATION IN GUJRAT REGION, INDIA

Jayant Nath TRIPATHI<sup>1</sup>, Avinash DWIVEDI<sup>1</sup> (<sup>1</sup>Department of Earth & Planetary Sciences, University of Allahabad, Allahabad-211002, India; Presently at: Observatori de l'Ebre, c/ Horta Alta, 38; 43520 Roquetes (Tarragona), Spain, <sup>2</sup> Department of Earth & Planetary Sciences, University of Allahabad, Allahabad-211002, India)

Kutchh region of Gujrat is one of the most seismic prone regions of India. Recently, it has suffered by a large earthquake of magnitude 7.6 on January 26, 2001. The probability of occurrence of great earthquakes with magnitudes greater than or equal to 6.0 during a specified interval of time has been estimated on the basis of three probabilistic models, namely, Weibull, Gamma and Lognormal for this region. The earthquakes of magnitude  $\geq 6.0$  covering 200 years have been used for this analysis. However, method of maximum likelihood estimation (MLE) has been applied for computation of hazard parameter of the earthquakes. The mean interval of occurrence of earthquakes and standard deviation are estimated as 45.4 years and 14.2 years, respectively, for this region. The cumulative and conditional probabilities have been also evaluated, which suggests that the probability of occurrence of a great earthquake in this region of Gujrat reaches to 0.8-0.9 for the time period 60-65 years after 2001.

**SS04b/10P/D-029** Poster **1400-212**

#### RESEARCH OF GREAT EARTHQUAKE ACTIVITY IN WEST CHINA REGION AND ITS INFLUENCE ON SEISMIC TENDENCY IN NORTH CHINA

Chen YUWEI (4183)

Based on our analysis of the spatial and temporal distributions of great earthquake ( $M_s \geq 7.5$ ) in West China since 1900, we further examine the correlated features between great earthquake in West China and strong earthquake ( $M_s \geq 6.0$ ) in Great North China Regions. Having made a comparative study between the two seismic activities, we can get the results as follows: Tectonic shows strong control on the earthquake activities. Earthquake activities in each active period caused by great earthquake in West China almost occur consecutively in the same sub-plate, but other tectonic units in surrounding area still keep relatively quiet. The earthquake activities show that a block is an active tectonic unit with a series of boundary faults in different directions. A strong earthquake activity with boundary faults will

influence the equilibrium of other boundary faults that lie in the same tectonic unit, which might trigger strong earthquake activities in those boundary faults, suggesting a great earthquake with  $M_s \geq 7.5$  rifting unceasingly in different boundary faults of the same tectonic unit. This phenomenon is also observed in the paleoearthquake events (Jian wali et al., 2000) and should be paid more attention for strong seismic hazard prediction. Seismic activities have the characteristics of oriented migration. In the first active period, earthquakes occur in the northwest of Qinghai sub-plate. In the starting phase of second period, the earthquake site migrates to the southwest of Qinghai-Tibet sub-plate and to the south of south-north regions in the late phase. In the third active period, the earthquake site migrates to the northwest of Qinghai-Tibet sub-plate. Earthquakes have no repeatability in spatial distributions. When a series of earthquakes occur, the last earthquake always migrates to the tectonic block and occurs in another relatively placid block. This earthquake might help us locate where the next series of earthquakes will probably occur. Geologists (Ma zongjin et al., 1980) defined the unified activities and oriented migration of great earthquakes in the tectonic units as liner rifted seismic belt or slant cross-rifted tectonic. If seismic activities in West China are consistent with the characteristics of tectonic, we can infer in the future the earthquakes with  $M_s \geq 7.5$  in the West regions will mainly occur in the near boundary of northwest of Qinghai-Tibet sub-plate and middle zone of south-north belt.

**SS04b/10P/D-030** Poster **1400-213**

#### SEISMICITY AROUND CAPITAL ULAANBAATAR, MONGOLIA

Dorjsuren ANKHTSETSEG<sup>1</sup>, Tundev DUGARMAA<sup>1</sup>, Antoine SCHLUPP<sup>2</sup>, Munkhuu ULZIBAT<sup>1</sup>, Chimed ODONBAATAR<sup>1</sup>, Chimedtseren BAYARSAIKHAN<sup>1</sup>, Adiya MUNKHSAIKHAN<sup>1</sup> (<sup>1</sup>Research Center of Astronomy and Geophysics of Mongolian Academy of Sciences, <sup>2</sup>Departement Analyse, Surveillance, Environnement, BP12, Bruyeres le Chatel, 91680, France)

The main part of Mongolian territory consist to one of the most active seismic intracontinental region of central Asia. In Mongolia, as well as in all high seismic countries of the world, study of seismicity and estimation of probability of future destructive earthquakes are important for economic stability and human protection. Seismological condition of Ulaanbaatar region are directly connected with seismic conditions of the territory of Mongolia. Mongolia characterizes the transition between compressive structures associated with India-Asian collision and extensive structures localized in north of the country as Hovsgol area and Baykal rift. Since 1905, Mongolia suffered four earthquakes with magnitude larger than 8 (Tsetsereleg 1905, Bolnai 1905, Fu-Yun 1931 and Gobi-Altai 1957). These events are associated with displacement along the faults up to 12 metres. The cumulative deformation along the Gobi-Altai fault shows that the return period of such great earthquakes on this fault are of the order of 3000 to 5000 years with a strain rate about 1 mm/year. Active faults are numerous and large but the occurrence of these four large earthquakes in less than one century is unusually high. Ulaanbaatar is situated at the east of these main active faults. Therefore, we have to understand better the seismotectonic model of the region by collecting new data about deformation near Ulaanbaatar. At the second half of 1957, a seismological observation begun in Mongolia. At the present, Today, on the Mongolian territory are working 9 analog seismic stations with records on photo paper, and around Ulaanbaatar, Capital of Mongolia, are working 5 high dynamic digital seismic stations, one CTBTO mini-array (10 stations) telemetered in real time to our NDC and one IRIS station For a region about 350 kms radius around Ulaanbaatar city, we present the seismicity with about 10602 events from macroseismic catalogue (1913 to 1963) and instrumental data (1964-2002). The range of magnitude are from 3 to 7. The detection level of this seismicity is related to the seismic network history. The studied region is divided in several subregion which are characterized by the epicenter's density, geological structure, active fault and geodynamic model. It shows high activity near the Mogod Earthquake, 5 January 1967,  $M_w = 7.2$  and some dense activity as 180 km south of the capital in Deren region where a recent event was largely felt at Ulaanbaatar. The other seismicity is more widespread. Despite of magnitude are low in that region, they are recognized active faults with no particular seismicity associated where event up to magnitude 7 can occurred. This work is associated with paleoseismological survey on particular active faults. From the seismicity map, the region near Ulaanbaatar is seismically active and some earthquakes, which can have destructive effect on the city Ulaanbaatar, can take place.

**SS04b/10P/D-031** Poster **1400-214**

#### STUDY ON POTENTIAL RISK OF LARGE EARTHQUAKE ALONG THE ANNINGHE-ZEMUHE FAULT ZONE, WESTERN SICHUAN, CHINA

Guixi YI<sup>1</sup>, Xueze WEN<sup>2</sup>, Jun FAN<sup>2</sup>, Siwei WANG<sup>3</sup> (<sup>1</sup>Chengdu University of Technology, Chengdu 610059, China; <sup>2</sup>Seismological Bureau of Sichuan Province, Chengdu 610041, China, <sup>3</sup>Seismological Bureau of Sichuan Province, Chengdu 610041, China)

The left-lateral strike-slip Anninghe-Zemuhe fault zone in western Sichuan, China, is a portion of the eastern boundary of the Sichuan-Yunnan fault-block, and one of the main active fault zones with strongly seismic activities. In order to analyze the potential seismic risk, using an earthquake catalogue from Sichuan Regional Network for the past 25 years, we study quantitatively the currently active behaviors of various fault portions according to data of calculated seismicity parameters, re-located focal depths, and geographic and temporal distribution of historical earthquake ruptures. Finally, we identify potential risky fault segments for the coming major earthquakes, estimate average recurrence time and magnitude for the potential earthquakes. Our main work and results are as follows: According to spatial scanning of b-value and calculating of other seismicity parameters, such as  $a/b$  values, annual-rates of released strain-energy and earthquake number on unit length of fault, the whole fault zone is divided into 5 segments with different behaviors of currently seismic activities. Among the 5, one asperity is identified and mapped from an area with anomalously low b-value located on the segment of the Anninghe fault between Mianning and Lichou, north of Xichang. Spatially, this asperity coincides with the 1536 earthquake rupture of magnitude 7.5, and has a length of about 62km along the fault. This asperity segment also displays low frequent seismic activity and low level of strain-energy release, but has a relatively high  $a/b$  value. Seismicity parameters suggest that two segments, the Xichang-Puge segment of the Zemuhe fault and the Shimian-Tuwu segment of the Anninghe fault, are under low and relatively low stress level at present, although they ruptured during the large 1850 and 1480 earthquakes, respectively. Another segment of the Zemuhe fault between Puge and Qiaojia has a middle b-value, displays highly frequent activity of small earthquakes with magnitudes between 2 and 4.9, and shows evidence of creeping. Average recurrence time intervals of characteristic earthquakes have been estimated for the asperity segment of the Anninghe fault from methods of asperity b-value model and geology and basing on the time-predictable recurrence model. Moreover, a possible magnitude range for the coming earthquake on the asperity is also estimated from relationships between magnitude and rupture-length. These calculations suggest that the next large earthquake on the asperity segment of the Anninghe fault would be not far, and have a magnitude of between 7.0 and 7.5. Our investigation suggests that asperities exist on those fault-segments having re-ruptured in the past, but are not always there all the time. Following a large earthquake rupture, activity behaviors of a fault segment could vary with time, meaning that it needs time for the fault plane to couple again and then reform a new asperity.

SS04b/10P/D-032 Poster 1400-215

**BACKGROUND AND PRECURSORY SEISMICITIES PRIOR TO THE MS8.1 KUNLUNSHAN EARTHQUAKE, WESTERN CHINA**Xueze WEN<sup>1</sup>, Guixi YI<sup>2</sup> (<sup>1</sup>Seismological Bureau of Sichuan Province, Chengdu 610041, China, <sup>2</sup>Chengdu University of Technology, Chengdu 610059, China)

The November 14th, 2001, Kunlunshan earthquake of magnitude ( $M$ )8.1 has been the greatest earthquake on the Chinese mainland for the last 50 years, which ruptured the Kunlunshan segment of the NWW-trending east Kunlun fault zone. We investigate the background earthquake activities in the region of the fault zone and its surrounding areas in the last over 100 years, and study the precursory seismicities occurred during the last several years and months before the huge earthquake. Our result mainly suggests that 2 large-dimensional rupture gaps without large and strong earthquakes for the recent more than 100 years had formed before the  $M$ 8.1 earthquake along the segments of Kunlunshan and Maqu of the east Kunlun fault zone. Of which, the Kunlunshan rupture-gap and its surroundings had been a quiescence region without earthquakes of magnitudes 5 and larger for at least over 30 years before the mainshock, forming and developing a background seismic gap centered at the Kunlunshan Pass. The  $M$ 8.1 mainshock occurred just in such a Kunlunshan rupture-gap. While, located at about 700 km southeast of the Kunlunshan rupture-gap, the eastern portion of the east Kunlun fault zone, the Maqu rupture-gap was the place where precursory seismicities of smaller earthquakes had arisen before the mainshock, although no any background seismic gap of magnitude 5 and larger earthquakes had formed and developed there. Starting in the July of 1998, the mid-term anomaly of the precursory seismicities at the Maqu rupture-gap lasted totally for about 3.2 years in two sub-stages, and was displayed by seismicity uprising first and then decreasing significantly. The short-term anomaly was characterized by enormously increasing of the frequency of small events there in the about 2.2 months just prior to the mainshock. The revealed feature of the seismicities before the huge Kunlunshan earthquake enlighten us that for those long strike-slip active fault zones on the Chinese mainland, it is possible that mid-long term risky locations for potential large or great earthquake are identified by recognizing abnormal background seismicity patterns that have formed and developed on rupture gaps without recent strong and large earthquakes. Moreover, certain portions of the fault zones, perhaps another rupture gap, would be the important windows from which information of mid to short term precursors would arise before potential large earthquakes occurring.

SS04b/10P/D-033 Poster 1400-216

**JOINT SOLUTION OF SEISMICITY PARAMETERS FOR SEISMIC SOURCE ZONES THROUGH SIMULATION**

Roger Mw MUSSON (British Geological Survey)

A key issue in seismic hazard modelling is determining seismicity parameters for each source zone in a given model. The three main parameters are the activity rate, the  $b$ -value (slope of the Gutenberg-Richter magnitude-frequency curve), and the maximum magnitude. Procedures for estimating these vary from study to study; in recent years the application of maximum likelihood methods, with or without priors, seems to be the most favoured approach. A new approach is presented here, based on Monte Carlo methods, which solves for all three parameters simultaneously. The conceptual basis is as follows: there exists some "true" set of values for  $a$ ,  $b$  and  $M_{max}$  that governs the long-term occurrence of earthquakes in a zone. Take three values for  $a$ ,  $b$  and  $M_{max}$  at random and use them to generate a synthetic earthquake catalogue, subject to the same historical constraints as the real catalogue. Is the resulting synthetic catalogue similar to the real one? If so, the  $a$ ,  $b$  and  $M_{max}$  values are credible. If not, try again. If one repeats the exercise a very large number of times, one easily builds up a weighted distribution of credible values for  $a$ ,  $b$  and  $M_{max}$  that can be converted directly into a logic tree structure. The method is entirely data-driven, and imposes no preconceived assumptions on the shape of the uncertainty distribution. Also the method tests implicitly whether the Gutenberg-Richter model itself is credible for that data set. If it turns out to be the case that no values for  $a$ ,  $b$  and  $M_{max}$  can provide a good approximation to the observed data, then a different seismicity model is called for.

SS04b/10P/D-034 Poster 1400-217

**CHARACTERIZED SOURCE MODELS FOR SHALLOW INTRASLAB EARTHQUAKES IN JAPAN**

Kimiyki ASANO, Tomotaka IWATA, Kojiro IRIKURA (Disaster Prevention Research Institute, Kyoto University)

Large shallow intraslab earthquakes, occurring within subducting slabs at 30-100km depths, generate earthquake damages by strong ground motions (e.g. the 1993 Kushiro-oki earthquake, the 2001 Gejiyo earthquake). Ground motion characteristics of intraslab earthquakes have been pointed out to have some different features compared to those of inland crustal earthquakes or interplate earthquakes by several papers. We have examined seven shallow intraslab earthquakes that recently occurred around Japan ( $M_{max}$  5.1-7.0) using strong motion network data. We carried out broadband ground motion simulations based on the empirical Green's function method (Irikura, 1986) to investigate the source characteristics of shallow intraslab earthquakes. Using the empirical Green's function method, we can construct the source model to explain observed waveforms in broadband frequency range (Kamae and Irikura, 1998; Miyake *et al.*, 1999). We used the observed waveform of a small event occurring in each source region as the empirical Green's function so that we could take account of propagation path and site effects implicitly. First, we determined the rupture plane by comparing synthetic waveforms from two possible fault planes assumed by focal mechanisms, because of the lack of sufficient aftershock distribution information for these events. Next, we estimated the size of strong motion generation area (SMGA), rise time, and rupture propagation velocity of the target event by forward modeling. The misfit function is selected as the sum of residuals of displacement waveforms and those of acceleration envelopes for explaining wide frequency band ground motions. For inland crustal earthquakes, the self-similar relation between the asperity area derived from the kinematic waveform inversion and the seismic moment was shown by Somerville *et al.* (1999). Some studies (Kamae and Irikura, 1998; Miyakoshi *et al.*, 2000; Miyake *et al.*, 2001) demonstrated that the SMGA obtained by the broadband ground motion simulation coincides with the asperity. We compared the SMGA size obtained in our study with the empirical relation for inland crustal earthquakes proposed by Somerville *et al.* (1999). The size of SMGA obtained for each earthquake is about 14-90% of prediction from that empirical relation. The stress drops on SMGA of shallow intraslab earthquakes are higher than those of inland crustal earthquakes. The ratios between the combined area of SMGA and the value predicted from the empirical relation decrease with focal depth. The stress drops on SMGA of shallow intraslab earthquakes increase with focal depth. We used strong motion data from K-NET, KIK-net, and F-net operated by the National Research Institute for Earth Science and Disaster Prevention (NIED). We also used the hypocentral information provided by the Japan Meteorological Agency (JMA) and the moment tensor solutions by F-net and Harvard University.

SS04b/10P/D-035 Poster 1400-218

**IMPLICATIONS OF THE SEPTEMBER 21, 1897 HISTORICAL EARTHQUAKES TO SEISMIC AND TSUNAMI HAZARDS ASSESSMENT IN THE SULU-ZAMBOANGA AREA, SOUTHWESTERN PHILIPPINES**Maria Leonila Pascual BAUTISTA<sup>1</sup>, Ishmael Clarino NARAG<sup>2</sup>, Bartolome Caparas BAUTISTA<sup>3</sup>, Raymundo Santiago PUNONGBAYAN<sup>2</sup> (<sup>1</sup>Department of Science and Technology (DOST) - Philippine Institute of Volcanology and Seismology (PHIVOLCS), <sup>2</sup>Philippine Institute of Volcanology and Seismology (PHIVOLCS))

The review of historical seismicity can help us understand the possible future seismic hazards that could happen in a certain area. More than a hundred years ago on September 21, 1897, two large magnitude earthquakes affected the islands of Sulu, Basilan and Zamboanga peninsula in southwestern Philippines. These two events happened 10 hours apart on the same day at 3:06 AM and 1:12 PM (both local time). Gutenberg and Richter (GR) determined their epicenters at the same point (6.0 N. lat; 122.0 E. long) while Abe determined their magnitudes as Ms 7.4 and Ms 7.5, respectively. The 1:12 PM (Ms 7.5) event also generated the biggest known tsunami in the Philippines. The GR epicentral region is presently characterized by nil seismicity. Meanwhile, the risks in the areas affected by the strong ground shaking and devastated by the tsunami are now slowly increasing. This study aims to review and re-evaluate the epicentral location of the two events based on intensity reports, eyewitnesses' accounts and results of ground shaking and tsunami modeling. Based on the results of the review of recently-discovered archival documents, the areas which experienced the highest intensities and which were also severely affected by the tsunami are the towns of San Ramon, Ayala, Santa Maria, Zamboanga, Tetuan, Mercedes, Bolong, Magay (all in Zamboanga province), Basilan in the province of Isabela and Jolo (in Sulu province). Meanwhile, the tsunami also affected the coastal towns around the Sulu Sea region including the northern part of Borneo Island of Malaysia. Using intensity data and eyewitness accounts as confirmed through ground shaking and tsunami modeling, the epicentral location of the two earthquakes were determined. With regards to their depths, the earlier 3:06 AM event is thought to have a deep-to-intermediate hypocenter while the 1:12 PM tsunamigenic event is believed to have originated along the shallow portion of the Sulu Trench region based on intensity distribution. The activity of this trench is one of the least understood in the context of the present-day Philippine seismotectonics understanding because of its present low seismicity as compared to other subduction trenches in the Philippines. For the last 106 years, no event of these magnitude sizes had occurred along this trench region. If these events indeed originated from the Sulu Trench, then the results of this study suggests that the trench is still capable of generating  $M$ 7s events. The results of this study could be very useful in understanding the seismic hazards in this part of the Philippines.

SS04b/10P/D-036 Poster 1400-219

**EARTHQUAKE HISTORY IN OLD MANILA, PHILIPPINES**Maria Leonila Pascual BAUTISTA<sup>1</sup>, Bartolome Caparas BAUTISTA<sup>2</sup>, Ishmael Clarino NARAG<sup>3</sup>, Esmeralda Longino BANGANAN<sup>2</sup>, Raymundo Santiago PUNONGBAYAN<sup>2</sup> (<sup>1</sup>Department of Science and Technology (DOST) - Philippine Institute of Volcanology and Seismology (PHIVOLCS), <sup>2</sup>Philippine Institute of Volcanology and Seismology (PHIVOLCS))

Manila, which consist of 14 districts, is the capital city of the Philippines. One of the oldest settlements in the Philippines is an area called Old Manila which includes roughly the districts of Intramuros, Binondo, Tondo, Quiapo, Santa Cruz, Ermita, Pandacan and Santa Ana. Old Manila hosts several centuries-old structures built during the Spanish era and which are also now considered as valuable cultural assets of the country. At the same time, the area is also one of the most densely populated areas in the entire city. In the Philippines, historical records of earthquakes coincide with its written history and this started in the late 15th century. This study is made to identify frequently damaged places in Old Manila and seek possible explanation for it. The results will be useful for land use planning, for risk mitigation as well as for protecting the cultural assets of the country. The frequently damaged areas are also being surveyed using microtremor observations to determine possible effects of site response to earthquake damages. There were 13 historical earthquakes which were strong enough to have caused serious damages to the city. The results of the initial review of historical earthquakes in Manila showed that some places are more frequently damaged than other sites. Almost all of these earthquakes caused damages to the ancient walled city of Intramuros. The second most frequently damaged district is the Binondo area which had been affected eight times by past earthquakes. Following Binondo are the districts of Tondo, Quiapo and Santa Cruz which sustained damages at least four times during the last 400 years. About half a million inhabitants reside in Tondo at present. These frequently damaged places are located in areas underlain by soft soil and are near river channels. Hence, effects of site response is very likely and are being verified using microtremor observations. Numerous points had been surveyed and predominant period are determined. The results are plotted on frequently damaged maps. The results can serve as guide to any future development as well as to any engineering recommendations that must be made for the strengthening of these cultural sites and frequently damaged places.

SS04b/10P/D-037 Poster 1400-220

**RESPONSE CHANGES OF SOME WELLS IN THE MAINLAND SUBSURFACE FLUID MONITORING NETWORK OF CHINA, DUE TO THE SEPT 21, 1999 MS7.6 CHI-CHI EARTHQUAKE**Fuqiong HUANG<sup>1</sup>, Yong CHEN<sup>2</sup>, Yi TANG<sup>2</sup>, Gui-ming XU<sup>3</sup>, Gong-cai CHI<sup>4</sup> (<sup>1</sup>Center for Analysis and Prediction, China Seismological Bureau, <sup>2</sup>Department of Science and Technology Development (Department of International Cooperation), China Seismological Bureau, <sup>3</sup>Seismological Bureau of Jiangu province, <sup>4</sup>Seismological Bureau of Liaoning Province)

About 60 Hydrologic changes in response to the Chi-Chi earthquake with Ms7.6 on 21st Sept. 1999 occurred in 52 wells, including groundwater level, temperature, discharge rate, well pressure and radon etc. in the subsurface fluid monitoring network. These response changes were mainly co-seismic changes, but some pre- and post-earthquake changes occurred mainly within 5 days before and after the Chi-Chi earthquake. The response changes of different wells clustering in different tectonic areas showed different features. These changes are distributed in five areas named as A, B, C, D and E. The response changes in A area with short hypo-central distance (less than 550 Km) were mainly pre-earthquake changes occurring more than 5 days before the event. Those in area B (in Huanan tectonic block) and C (in Huabei tectonic block) were mainly co-seismic changes. The hypo-central distance is about 1,100 to 1,280 Km and 800 to 1,160Km respectively. These changes were high frequency water level oscillations induced by seismic waves and accompanied by prominent and permanent water level jumps and/or drops. There are also some post-seismic changes including discharge rate and water radon concentration and well pressure changes in area C. Those in area D in the Yanshan tectonic block, say, Zhangjiakou-Bohai seismic belt, were mainly co-seismic and post-seismic changes including water level, water temperature, and water radon concentration etc., showing prominent and

permanent water level jumps and drops and increasing of water radon concentrations. The hypo-central distance is about 1,750 to 2,060 Km. Those in Area E, located in Chuan-Dian tectonic block, were mainly co-seismic changes showing prominent and permanent water level jumps. The hypo-central distance is about 1,810 to 2,120 Km. The different features of the response changes might be caused by the changes of local hydrologic conditions (like permeability) induced by seismic waves. On the other hand, these response changes might indicate the near-critical conditions in the area where the response changes clustered. Because three moderate earthquakes occurred in area D and one strong earthquake occurred in area E four months after the Chi-Chi earthquake. Such changes might be understood by the crustal buckling hypothesis. It is thought that the response changes might be a kind of precursor that implies elevated earthquake risk in the region. Key Words: Response changes; the Chi-Chi earthquake; Groundwater.

**SS04b/10P/D-038** Poster **1400-221**

**EVALUATING EARTHQUAKE POTENTIAL DUE TO MAJOR ACTIVE FAULTS FOR THE DENSELY POPULATED KANTO PLAIN, CENTRAL JAPAN: AN EXAMPLE FROM THE SEKIYA FAULT**

Yukari MIYASHITA<sup>1</sup>, Takahiro YAMAMOTO<sup>2</sup>, Yuichi SUGIYAMA<sup>1</sup>, Akira SANGAWA<sup>1</sup>, Koichi SHIMOKAWA<sup>1</sup> (<sup>1</sup>Active Fault Research Center, Geological Survey of Japan, AIST, <sup>2</sup>Research Center for Deep Geological Environments, Geological Survey of Japan, AIST)

The Kanto Plain, in which the largest population lives in Japan, has been suffered from not only interplate megathrust earthquakes but also shallow intra-plate earthquakes in the past several hundred years. Several known active faults in and around the Kanto Plain are expected to be the sources of such shallow earthquakes in the future. To properly evaluate the earthquake potential by these active faults, we have been performing trench excavation surveys. Here we present an example from one of the pre-cautious faults, the Sekiya fault, located 120 km north of Tokyo. As a result of paleoseismological investigations, we identified three surface-rupturing events and the most recent one is correlated to the historical 1683 M=7 earthquake. This and determined mean recurrence interval of 4000 years implies a low probability that the Sekiya fault will produce a large earthquake in the next 100 years. The Sekiya fault is NS-trending west-dipping reverse fault, which extends 30 km along a range front. We excavated five trenches across the Sekiya fault to reveal its past earthquake behavior. Trenching survey show evidence for three surface-rupturing events about 8000, 4500 and <1000 years ago. A dozen radiocarbon ages restrict the timing of the most recent surface rupture within the past 600 years. On the other hand, historical documents show that the 1683 Nikko earthquake caused serious damage to the area adjacent to the Sekiya fault. In this area, no other damaging earthquake is known to occur in the past 600 years. These geological and historical data on paleoearthquakes indicate that the most recent surface-rupturing earthquake on the Sekiya fault corresponds to the 1683 Nikko earthquake. This conclusion together with roughly estimated recurrence interval of 3500-4000 years implies a low probability of a large earthquake in the next 100 years. If the recurrence intervals have a lognormal distribution (1 sigma 0.23), the probability is less than 1 percent.

**SS04b/10P/D-039** Poster **1400-222**

**RESTORATION OF BUILDINGS IN ARMENIA**

Hrachya Sedrak MURADYAN, Hasmik Hrach NAHAPETYAN (NORTHERN DEPARTMENT OF NATIONAL SURVEY FOR SEISMIC PROTECTION OF RA)

Reinforcing and, restoration of buildings which were damaged during the earthquake in Armenia in 1988 have done. The buildings have been reinforced with different methods. The different methods of reinforcing of the knots have been used. The cycles of oscillations of the buildings have been measured before and after reinforcing which had been compared with new built buildings and calculating data. On the basis of the studies are given criterions to determine the expediency and the levels of the buildings which have to be reinforced. The designed solutions are studied and estimated, the albums are created in which the best reinforcing solutions of the building's elements have been taken into account as the best methodical guide. Generalizing the comparative analysis of done projects we can conclude: 1. The reinforcing and restoration of the buildings should be done by individual approach. 2. The aim of reinforcing and restoration should be determined by economic calculations. If the difference between new building and the reinforcing exceeds 20% the reinforcing can be considered as an acceptable version. 3. The most optimal level of the strength of dwelling house from the view of longevity and value is the level which was before the earthquake, as the reinforcing of the buildings to the calculation seismic strength level is equal to construction of new building and if the level is low the buildings can be ruined. In this case during the second calculation strength earthquake the building will not be ruined but should be demolished and it is not expedient to reinforce or exploit again.

**SS04b/10P/D-040** Poster **1400-223**

**NATURAL FREQUENCY AUTOMATIC VARIATION IN SEISMIC ISOLATION SYSTEM**

Federico BARTOLOZZI (Civil Engineer & Independent Researcher)

This system is not "new" in the unique meaning of the word, but it could be considered as such, because it originates from the merger of two my original systems, of which it contains the most advantageous relative characteristics. Its operational aspect is as effective as that of the systems from which it originates, but it is considerably better than both of them, due to the reduced planning aspect and the operational simplicity, which, together with the greater economic competitiveness, certainly make it more acceptable. In fact, the replacement of the complicated, electronically started, frequency converters, present in the former reference system, with the naturally started easy device of the second system, is the main change to the former system, which, however, preserves unchanged both the number of bearings and their plane surface of sliding. Having said this, the proposed system is based on the following operations: 1. interruption of the continuity between the building and the foundation-soil complex; 2. laying of four elastic movable bearings with sliding or rolling friction; 3. self-centring of the building after an earthquake. By means of its own elastic deformation, each bearing automatically compensates the rigid deflection variation relative to support due to the horizontal component of the motion. The building remains motionless with respect to the foundation-soil complex, which moves. Due to the sub-undulatory shock, the vertical motion varies the building behaviour only partially. It is subjected to a low vertical translation and to the resonance possibility. In order to prevent the resonance danger, the vertical natural frequency automatic variation of the building takes place because of auxiliary springs, present in each bearing, which increase the action of the main spring during an emergency, characterised by an interval of vertical seismic frequencies, including the resonance one.

**SS04b/10P/D-041** Poster **1400-224**

**A SHORT NOTE ON THE DETERMINATION OF THE CHARACTERISTIC FREQUENCIES OF VIBRATION FOR DIFFERENT BUILDINGS IN CAIRO, EGYPT USING MICROTREMORS**

Mohamed Ahmed GAMAL (Geophysics)

Cairo is one of the most areas in the world possess irregularity in building construction work. This random construction work had led to the randomness at building shapes varying between, No. Of floors, building size and weight of buildings at the same location. Based on the previous observation, accurate risk assessment in the area of Cairo is very difficult, since earthquake effects is variable from one building to another depending on differences in their dimensions or characteristic frequencies of vibrations. We tried to show variation of frequencies of resonance for different buildings at Cairo using Spectral amplitude of microtremors base on acceleration recordings, by three-component stations installed at the Building local soil, building base and at different stories. We used three methods: 1-Spectral ratios between horizontal and vertical component (H/V) of motion, 2-Spectral ratios between two horizontal component of motion one at building floor and the other at building base or soil, and the new technique discussed by us: 3-Spectral ratios between building floor spectra and constant spectra. A representative building for Naser City, Giza, Shubra, Ghamra, Airport area, El-Daher, Morad St. and El-Haram, was taken to show the resonant frequency of each. Although the variability of buildings is severe, we tried to choose buildings to represent each area.

**SS04b/10P/D-042** Poster **1400-225**

**BUILDING RESPONSE MEASUREMENT USING AMBIENT VIBRATION TEST IN METROPOLITAN MANILA, PHILIPPINES**

Angelito G. LANUZA<sup>1</sup>, Ishmael C. NARAG<sup>1</sup>, Norio ABEK<sup>2</sup> (<sup>1</sup>Philippine Institute of Volcanology and Seismology, Department of Science and Technology, Philippines, <sup>2</sup>Department of Architecture, Kanto Gakuin University, Japan)

Lessons learned from past destructive earthquakes show that most of the casualties due to these events were associated with structural failure especially for those structures, which did not conform to sound design and construction principles. During moments of extreme ground shaking, buildings whose natural periods are close to the predominant period of the ground usually experience resonance, which in turn cause severe damage to total collapse. Metropolitan Manila, as a major political and economic center in the Philippines, has undergone rapid structural development for the past two decades and this trend is foreseen to continue for the next decade or so. Owing to its growing population and its proximity to earthquake generators with high potential to generate large-magnitude events, it is important that information on the possible behavior of buildings within the metropolis during a large destructive earthquake should be determined. However, different episodes of changes in the country's structural code and differences in construction practices in the Philippines make it difficult to determine and monitor these parameters from design parameters estimated from structural plans. Towards this end, ambient vibration tests were conducted on medium to high-rise structures in the metropolis in order to determine their natural period and damping which are essential parameters to determine a building behavior during a strong earthquake. A straightforward estimate of a building's fundamental period can be calculated using an empirical formula of the National Structural Code of the Philippines (NSCP). The formula is a function of height of the building and uses various coefficients for different structural systems. Results of the ambient vibration survey on at least 100 buildings in Metro Manila indicate that the natural period of tall buildings (~100 meters high) are nearly equal to NSCP's estimated value specifically those buildings classified as reinforced-concrete. On the other hand, deviations on the measured natural periods on shorter buildings (>50 meters) are found. This can be attributed to the presence of additional engineered structural members such as shear walls and other bracing elements that tend to increase the stiffness of the structure. These buildings are classified as reinforced-concrete with dual structural system which could have been designed assuming conservative design base shear forces due to earthquake and could be less vulnerable to intense ground shaking. Moreover, many of the shorter buildings with simply RC moment-resisting frames may have been designed with less design base shear forces and could be vulnerable to severe ground shaking.

**SS04b/10P/D-043** Poster **1400-226**

**ACCELERATION RESPONSE SPECTRUM OF BUENOS AIRES CITY, ARGENTINE, CAUSED BY DISTANT AND LARGE MAGNITUDE EARTHQUAKES**

JUAN S. CARMONA<sup>1</sup>, Nora C. SABBIONE<sup>2</sup>, Roberto M. PINCIROLFI<sup>1</sup>, Raquel L. PALAU<sup>1</sup>, Luisa B. GARCIA<sup>1</sup> (<sup>1</sup>EARTHQUAKE ENGINEERING RESEARCH INSTITUTE, NATIONAL UNIVERSITY OF SAN JUAN, <sup>2</sup>DEPARTMENT OF SEISMOLOGY, NATIONAL UNIVERSITY OF LA PLATA)

Buenos Aires city, the capital of the Argentine Republic, with a metropolitan population of nearly ten million inhabitants, is sited on the eastern side of an extended plane area formed by deep sedimentary alluvial soil layers corresponding to the Argentinian "pampas". Because the seismic activity around this city is low, the motion due to distant and large magnitude seismic events with epicenters in western Argentina or in Chile, at more than one thousand km of distance, are more frequently perceived on the upper levels of tall buildings in Buenos Aires city, some of them generating strong alarm. From 1996, the three components of the ground motion acceleration of seismic events have been recorded in one broadband seismograph installed in the Seismological Station of the National University of La Plata which is located in La Plata city, at 50km from Buenos Aires and on the same subsoil type consisting of quaternary loess with a thickness of approximately 500 m. Up to date, the two more important motions which have been recorded by this instrument are those corresponding to the Mw = 7.1 Oct 15, 1997 Chilean seismic event and the large earthquake, Mw=8.4, of June 23, 2001 that occurred on the coast of Peru, the former with an epicentral distance of 1300km and the latter with one of 2500km. Their maximum acceleration values have been 0.75 and 0.18gals, respectively, while their strongest interval lasted approximately 100 sec in the former and more than 200sec in the other. In both acceleration records there are outstanding frequencies (period) around 0.35 c/s (T= 2.85sec) and 0.85 c/s (T=1.18sec) whereas in the Peruvian event an additional outstanding frequency of 0.05c/s (T=20sec) has also been detected. The first two frequencies are associated with body and Lg waves, while the last one with surface waves. The 2% damping curves of the acceleration response spectrum of these ground motions recorded in La Plata show important peaks at about the same frequencies (periods) mentioned above. The peak values for the frequencies (periods) 0.35 c/s (T= 2.85sec) and 0.85 c/s (T=1.18sec) depend on the attenuation of Lg waves, while that for the frequency (period) 0.05 c/s (T= 20sec) on the attenuation of the surface waves. Moreover, the measured fundamental period values of the buildings of Buenos Aires city with more than 20 stories are larger than 1 sec and the largest reach 2.7sec., which corresponds to the tallest 160m high Le Parc Tower. In the upper levels of these tall buildings, the absolute acceleration amplitudes of the motion generated by these ground motions reach nearly 30 gals and last more than one minute. This explains why the

distant and large magnitude seismic events have been perceived well and also with alarm on the uppermost floors of the tall buildings in Buenos Aires city, although no structural damage has been detected in them.

**SS04b/10P/D-044** Poster **1400-227**

**THE RESEARCH ON EARTHQUAKE LOSS ESTIMATION AND COUNTERMEASURE FOR EARTHQUAKE PREVENTION AND DISASTER REDUCTION IN FUJIAN PROVINCE**

Jin hai CHEN (Seismological Bureau of Fujian province, China Seismological Bureau)

The research project on Earthquake Loss Estimation and Countermeasure for Earthquake Prevention and Disaster Reduction in Fujian Province is a multi-layers and multi-size earthquake loss estimation research for meeting the needs of earthquake emergency plan improving earthquake emergency response ability and disaster rescue organizing efficiency it also is great useful in ordinarily management for earthquake prevention and disaster reduction. The main contents of project as following: 1. The research treats a county as an earthquake loss estimation unit. In this type of earthquake loss estimation research we treat the county as research object and build the loss estimation model that takes population and GDP as basic parameters and the historical earthquake disaster site condition and type of building as adjusted parameters. Based on ArcGIS 8.1 we used 1:500000 scale digital map to build database and management information system. 2. The research treats a town (or block) as an earthquake loss estimation unit. In this type of earthquake loss estimation research we build the loss estimation model for rapidly estimating the economic loss casualty and life-line destructive degree under a given earthquake parameter. Based on GIS we used 1:50000 scale digital map to build database and relevant application with spatial analysis and quantitative computing. 3. The research treats an important construction or a community in the city as an earthquake loss estimation unit. In this type of earthquake loss estimation research we select some important cities in Fujian province and carry out loss estimation by analyzing the vulnerability for every important construction and sample of general building. The important construction means schools hospitals important government buildings high buildings and life line engineers. The general building means common civil construction and be analyzed in community unit. In this type of earthquake loss estimation research we use 1:5000 scale digital map to build database and relevant application. 4. Comprehensive research for earthquake prevention and disaster reduction in city swarm. Carrying out research on evaluating for earthquake resistant ability for life line network earthquake disaster relativity and rescue ability by themselves and each other between cities. The GIS-based database is built and decision support system for comprehensive earthquake prevention and disaster reduction is developed.

**SS04b/10P/D-045** Poster **1400-228**

**SCALING LAWS OF EARTHQUAKE LIVE LOSS RATES AND ITS APPLICATION TO LONG\_TERM PREDICTION IN CHINA CONTINENT**

Fu ZHENGXIANG (Center for Analysis and Prediction, China Seismological Bureau)

China has long-term record of historical earthquakes and its live and economy losses. This paper studied the self-similar power scaling laws of earthquake live loss rates, during a period from 1500 to 2000 for North China, Southwest China and Northwest China respectively. The research shows that the self-similar power scaling laws are as followings: (1)  $\text{Log}(N) = -0.34 - 0.42 \text{Log}R$ , for North China; (2)  $\text{Log}(N) = -0.59 - 0.49 \text{Log}R$ , for Southwest China; (3)  $\text{Log}(N) = -0.25 - 0.25 \text{Log}R$ , for Northwest China. R and N mean the earthquake live loss rate and the cumulative occurrence numbers of the earthquake live loss event respectively. The laws have been used in long-term earthquake live loss prediction. Supposing the process of the events of earthquake live loss follow a Poisson one, the research results show that the occurrence probabilities of earthquake live losses of 1000 persons or more in North China and Southwest China, and 100 persons or more in Northwest China would be 0.8 or more before 2020 separately. Because the earthquake live losses might be related mainly to the shock-resistant capacity of houses and buildings people lived in, the shock-resistant capacity of houses and buildings in the future will be better than that during the period of used data in this paper, so that the prediction of the occurrence probability of earthquake live loss could be higher.

**SS04b/10P/D-046** Poster **1400-229**

**EFFECTS OF EARTHQUAKES ON MEGACITIES**

Rashmi ARORA (Centre for Disaster Mitigation and Management, 302, Kamadgiri Tower, Kaushambi, Ghazibad-201010, U.P. India)

Natural disasters are a part of the environment in which we live. They do not discriminate between people or countries. And yet, no disaster is entirely natural. Human activity invariably aggravates the risks through insufficient attention to where and how settlements are built, or natural resources are exploited. It is estimated that nearly one million earthquakes occur worldwide each year, and only a few major earthquakes, but when they do, they are among the most destructive natural forces on earth. The shaking of the ground coupled with the liquefaction of some soils wreck havoc on man-made structures. In terms of human and economic losses, seismic shaking is the most significant factor contributes to losses not only directly through vibratory damage to man-made structures but also indirectly through triggering of secondary effects such as landslides or other form of ground failure. When a quake occurs in a populated area, power and gas lines are often ruptured causing numerous fire. In the 1906 San Francisco earthquake, much of the damage was caused by fires which ran unchecked when broken water mains left fire-fighters with only trickle of water. On September 19, 1985, a violent earthquake jolted SW Mexico, devastating sections of Mexico City and killing about 7000 persons. In less than 2 minutes the quake battered downtown Mexico City, causing an estimated 250 buildings to collapse. In 1995 an earthquake in Kobe, Japan caused more than 6000 fatalities and over \$US120 billion in economic losses. In Izmit, Turkey, August 1999, an earthquake caused 20,000 fatalities and an estimated \$20 billion in economic loss. Those affected most are the poor and the socially disadvantaged in the developing countries as they are the least equipped to cope with the situation. The combination of natural and technological hazards creates an environment in which effects may be multiplied through cascading multi-disasters. For example, an earthquake can lead to a breakdown in the social order and infrastructure, resulting in rioting, the spread of disease through unsafe drinking water, and disruptions to the local economy. Because economic globalization has made the world's cities increasingly interconnected, events in Manila may affect Madrid, Mexico City and Milwaukee. There are about 450 cities worldwide with a population of more than 1 million. Today's cities and megacities are unlike any that existed in the past, and thus we cannot expect our experience with historical disasters to guide us in the future. Cities are larger than ever before and growing in size at an unprecedented rate. Furthermore, as cities have grown, they have often expanded onto hazardous lands. About 50 percent of the world's largest cities are situated along major earthquake belts or tropical cyclone tracks. The concern over the risk to megacities, particularly in the developing world, is their growing vulnerability caused by their hyper-concentrations of population, dependence on complex and aging infrastructure, and unprepared local institutions.

**SS04b/10P/D-047** Poster **1400-230**

**EARTHQUAKE DISASTER ESTIMATION USING GEOGRAPHICAL INFORMATION SYSTEM AND STRONG GROUND MOTION SIMULATION SYSTEM BASED ON MULTI-SCALE ANALYSIS**

Tsuyoshi ICHIMURA<sup>1</sup>, Munee HORI<sup>2</sup> (<sup>1</sup>Department of Civil Engineering, Tohoku University, <sup>2</sup>Earthquake Research Institute, University of Tokyo)

Realistic simulation of a possible earthquake disaster is important for making rational countermeasures. The disaster is the accumulation of buildings and structures damages. Thus, a numerical simulation method must compute the strong ground motion with the spatial and temporal resolution high enough to calculate structural responses during the earthquake and to evaluate their damages. In addition, credible earthquake disaster could be estimated by reasonable simulation of buildings and structures, using resulting strong ground motion information. This paper proposes such a simulation method, using strong ground motion simulation system and a simulation model of a whole city from geographical information system (GIS). In order to obtain reliable strong ground motion information, it is necessary to simulate, with 3-D numerical simulation model, the fault mechanism, the wave propagation through the heterogeneous crust and amplification near the surface. There are, however, two major difficulties: (1) the lack of soil-crust structures information; (2) the requirement of huge computation. For resolving these two difficulties, we propose a new analysis method, macro-micro analysis method (MMAM). The MMAM takes advantage of the bounding media theory (BMT) and the singular perturbation expansion (SPE). The BMT can deal with the uncertainty of soil-crust structures information. The SPE can lead the efficient multi-scale analysis, which reduces the computation amount required at one time. Though the SPE can reduce the computation amount, the huge amount of computation remains yet. For more reduction of computation amount, the finite element method with voxel element and the parallelization computation are applied. In addition, auto-modeling software for soil-crust structures, which contains new estimation tool and database on GIS, is developed for much more efficient modeling. By combination of these components, strong ground motion simulation system is developed. In order to verify the effectiveness of this strong ground motion simulation system, the earthquakes observed in Yokohama City are simulated, and the reproduction of the strong ground motion is attempted. The simulation result is compared with the data observed. It is shown that it succeeded in reproducing the velocity spectrum of each place in frequency domain where the calculation accuracy is guaranteed. In addition, the maximum velocity distribution of each every site is also calculated with the spatial resolution of 1[m] order. These results clearly show the effect of soil-crust structures (material property and topography) on the strong ground motion. And it is confirmed that large-scale numerical simulation is necessary in order to predict the strong motion with high spatial resolution in the sufficient accuracy. For making credible earthquake disaster simulation, much more reasonable simulation model of buildings and structures is needed. Using available GIS information about buildings and structures, virtual city is constructed on computer. The methodology of constructing these models is studied, since available data are usually limited. An example of a city model is constructed and earthquake simulation is made to examine the basic usefulness of this earthquake disaster simulation.

**SS04b/10P/D-048** Poster **1400-231**

**DEVELOPMENT OF AN AUTOMATIC SYSTEM TRANSMITTING-EARTHQUAKE ALARM INFORMATION**

Shigeiki HORIUCHI, Hiroaki NEGISHI, Kana ABE, Aya KAMIMURA, Yukio FUJINAWA (National Research Institute for Earth Science and Disaster Prevention)

Most earthquake damage occurs after arrival of the S wave, whose amplitude is about five times larger than the P wave. Because the P wave travels faster than the S wave, the interval between their arrival times creates an opportunity to activate an earthquake alarm and take pre-emptive safety measures. We developed an automatic system transmitting earthquake alarm information, which transmit the earthquake shaking data before S wave arrival. Since the alarm system is used to control transportation, industry, business, etc, at a time of a large earthquake occurrence, false alarms cost huge. We solved the technical difficulty of determining earthquake parameters very quickly but without errors by developing a novel method, which use not only P wave arrival times but also time data of P wave not yet arrived. We also developed filters, which can distinguish seismic signal from large amplitude noise generated by many kinds of reasons, to increase the reliability of the system. The system can eliminate extraneous arrival time readings in the hypocenter location by checking automatically measured readings, P wave not yet arrived data, and their station distribution. We use waveform data of Hi-net, which installed about 600 very high quality stations covering whole Japan with space density of 20 to 30 km. All seismometers are installed on wells deeper than 100m. Our system can locate precise hypocenters for 95 % events occurring in and near Japan Islands within a few seconds and transmits earthquake alarm information before most of seismic energy has arrived even to the station closest to the hypocenter. We are planning to broadcast earthquake alarm information for all destructive earthquakes by using the satellite seismic data transmitting system developed by ERI, hoping to promote the development of many kinds of automatic control systems, which stop cars, factories etc to protect people from earthquake damage.

**SS04b/10P/D-049** Poster **1400-232**

**SOME EFFECT OF UNCERTAINTY IN SEISMIC SOURCES MODELING ON SEISMIC HAZARD MAPPED PARAMETERS, STUDY CASE**

Vladimir Petar MIHAILOV<sup>1</sup>, D. DOJCINOVSKI<sup>1</sup>, R. VERBERIEN<sup>2</sup>, T. CAMELBEECK<sup>2</sup> (<sup>1</sup>Institute of Earthquake Engineering and Engineering Seismology, University, <sup>2</sup>Royal Observatory of Belgium)

Current methods and solutions of seismic hazard analysis take into account the seismological and geological information to arrive at probabilistic forecasting of future earthquakes. However, the lack of knowledge of the cause of earthquake and the short length of seismic history lead to decimal and statistical uncertainty concerning the parameters of seismicity. Statistical uncertainty in definition of some parameters of seismicity, especially type, size and geometrical characteristics of seismic sources, can have a great effect on the calculation of the seismic hazard. The effect is assessed by deriving probability distribution functions of important seismic parameters. Because damaging earthquake occur infrequently to rarely in any region, evaluation of the probability of occurrence and the resulting levels of ground shaking requires the use of various models fit to limited data and extrapolated beyond the range of the data. As a result, significant uncertainty exists in probabilistic estimates of ground-shaking hazard. This uncertainty increases as one moves from hazard assessment in areas of high seismic activity to areas of low seismic activity. In seismically active areas, seismic sources are relatively well defined by recorded earthquakes and geologic data, and there is a large database of recorded strong ground shaking. These data strongly constrain the probabilistic models used to assess the hazard. In areas of low seismic activity, earthquakes sources are poorly understood and ground motion data are limited primarily to records from earthquakes smaller than those of interest in assessing potential damage. Consequently, in these areas there are only weak constraints on the probabilistic models used to assess hazard. Due to the fact that

the seismic model formulation requires availability of seismic source parameters for the purpose of calculating the probabilistic hazard, and because these parameters are subject in practice to considerable variation in the manner of their determination, it is important to judge the sensitivity of the map values to these parameters. The uncertainty in the seismic sources, activity rates and maximal possible magnitude are described using the earthquake data for Belgium and the surrounding area as source data. The influence of these uncertainties on seismic hazard is illustrated where appropriate.

**SS04b/10P/D-050** Poster **1400-233**

**ON THE DEFORMATION CHARACTERISTICS AROUND JIASHI EARTHQUAKES AND AN APPROACH FOR EARTHQUAKE HAZARD ASSESSMENT**

Anfu NIU, Jing ZHANG, Xudong YAN (Center for Analysis and Prediction of China Seismological Bureau)

In the early 1997, in Jiashi area of Xinjiang of China, 7 strong earthquakes with magnitude more than Ms6.0 subsequently happened in 3 months. These strong earthquakes occurred in the junction of Tianshan Mountain and Tarim basin. These strong earthquakes were attracted many scholars to investigate the deformation process and its mechanical factors. Before these strong earthquakes there were established 4 GPS basic stations and 4 tilt stations undergoing nearby the epicenters, and an Atushi Ms6.7 earthquake were occurred on 19 Mar of 1996, far from the Jiashi earthquakes around 80km. After the Atushi Ms6.7 earthquake, tilt direction of this block shows a clear turning from SW to NW. The change in tilt direction gives a possible trigger to the Jiashi earthquakes. After Jiashi earthquakes, China Seismological Bureau organized twice GPS campaigns in the area with total number 19 GPS stations in 1998 and 1999, respectively. Based on the GPS observation results, and combined with the continuous tilt observations and seismic activity, we researched the tectonic characteristics of this area by using the dislocation model proposed by Okada (1985,1992). The estimated moment of fault activity is well consistent with the level of seismic activities. So this report also gives an approach for earthquake hazard assessment through monitoring fault movement. Key words: Jiashi earthquake \ GPS \ Tilt \ Earthquake Hazard Assessment

**SS05** Thursday, July 10

**EDUCATION AND OUTREACH**

Location: Site A, Room 13

Thursday, July 10 AM

Presiding Chairs: D. Jackson, P. Bormann

**SS05/10A/A13-001** **0830**

**THE NEW MANUAL OF SEISMOLOGICAL OBSERVATORY PRACTICE (NMSOP): A CONTRIBUTION TO PROFESSIONAL EDUCATION AND CAPACITY BUILDING**

Peter BORMANN (GeoForschungsZentrum Potsdam, Solid Earth Physics and Disaster Research)

The last edition of the Manual of Seismological Observatory Practice dates back to 1979. It covered analog techniques only and is out of print. Since that time, computer and communication technologies as well as the availability of modern broadband sensors have revolutionized seismological observatory practice. Related know-how is chiefly available in industrial countries only. Besides this, classical university curricula do not provide suitable education and training of observatory personnel. Therefore, the IASPEI Commission on Practice (CoP) proposed in 1994 to elaborate a New Manual of Seismological Observatory Practice and established a related international working group. This NMSOP is now available both as a printed version in two volumes, on a CD-ROM and on the Internet via [http://www.gfz-potsdam.de/pb2/pb21/index\\_e.html](http://www.gfz-potsdam.de/pb2/pb21/index_e.html) or <http://www.seismo.com>. Volume 1 comprises 13 chapters: 1) Aim and Scope of the IASPEI New Manual of Seismological Observatory Practice (NMSOP) 2) Seismic wave propagation and Earth models 3) Seismic sources and source parameters 4) Seismic signals and noise 5) Seismic sensors and their calibration 6) Seismic recording systems 7) Site selection, preparation and installation of stations 8) Seismic networks 9) Seismic arrays 10) Seismic data formats, archival and exchange 11) Data analysis and seismogram interpretation 12) Seismic intensity and intensity scales 13) Volcano seismology. These basic Chapters introduce into the topical fundamentals of observatory Practice. They are complemented by an Annex-Volume 2 which comprises datasheets, exercises, information sheets on special topics, program description, a list of acronyms, 34 pages of references, a detailed glossary which explains basic terms in simple language and a very detailed index. A complete copy of the Manual (1252 pages) will be on display and the access to and easy surfing through its website via hyperlinks will be demonstrated. The talk introduces into the basic didactic concept of the NMSOP, demonstrates the easy use of the Manual for the compilation of tailored educational or training models on specific topics, gives an example of animations of seismic ray propagation and seismogram formation which complement the Manual CD-ROM and discusses the further development of the NMSOP into a tool for eLearning.

**SS05/10A/A13-002** **0845**

**24 YEARS INTERNATIONAL TRAINING COURSES ON SEISMOLOGY; SEISMIC HAZARD ASSESSMENT AND RISK MITIGATION: CONCEPT, PROGRAM AND IMPACT ASSESSMENT**

Peter BORMANN, Jochen ZSCHAU (GeoForschungsZentrum Potsdam, Solid Earth Physics and Disaster Research)

Since 1980 the Potsdam geoscientific research institutes run international training courses on the subjects seismology, earthquake hazard assessment and risk mitigation for the benefit of attendants from earthquake-prone developing countries. These courses are part of the educational program of UNESCO in the fields of geosciences and disaster mitigation and have been a major contribution of Germany to the professional education and capacity building in developing nations during the International Decade for Natural Disaster Reduction (IDNDR) and its follow-up International Strategy for Disaster Reduction. Accordingly, these courses have been regularly supported by UNESCO, the United Nations Office for the Co-ordination of Humanitarian Affairs (OCHA) and IASPEI. By October 2003 about 580 participants from 90 countries will have attended these courses. Since the unification of Germany and the foundation of the GeoForschungsZentrum Potsdam (GFZ) in 1992 these 5-weeks courses are alternately held in Germany as world-wide open courses and every second year as regional courses rotating between Asia, Latin America and Africa. Up to now, regional courses took place in 1993 in India, 1995 in Nicaragua, 1997 in Kenya, 1999 in China and 2001 in Chile. The course 2003 will be held in South Africa. The team of lecturers from the GFZ Potsdam is regularly complemented by international experts from France,

Norway, Slovenia and the USA and in the case of regional courses by lecturers from the hosting and surrounding countries. The courses are strongly application-oriented and consist of about 40% lectures, 40% exercises and 20% field excursions, workshop sessions with presentations by course participants and follow-up discussions. The applications received for these courses every year outnumber by far the course capacity and amount of available fellowships. This speaks of a continued demand for practice-oriented training in these fields. The extensive lecture and exercise material developed for these courses formed the core part for the elaboration of the New IASPEI Manual of Seismological Observatory Practice. The talk will introduce into the philosophy, educational concept and scientific contents of the courses. To better plan for the future we conducted an impact study aimed at assessing the usefulness of the course program and its didactic concept for developing self-reliant expertise in earthquake research, earthquake and volcano monitoring, hazard assessment and risk mitigation in disaster-prone developing countries. This study was based on the response of about half of all former course participants to a very detailed questionnaire. The results of this analysis will be presented and conclusions be drawn with respect to the continuation of this course and the initiation of new complementary, co-operative German offers for professional education as well as formal and informal education of the public, press and officials in the area of improved disaster management, monitoring, hazard, vulnerability and risk assessment.

**SS05/10A/A13-003** **0900**

**TRIAL OF 'REMOTE SCIENCE CLASS' BY USE OF REAL-TIME HDTV VIDEO IMAGE FROM THE SEAFLOOR THROUGH A COMMUNICATION SATELLITE**

Takeshi MATSUMOTO<sup>1</sup>, Yasuhisa ISHIHARA<sup>2</sup>, Tsutomu SHIGETA<sup>1</sup>, Tatsuo SUZUKI<sup>1</sup>, Masaki MAKIHARA<sup>1</sup>, I-Space Education Promotion Team (Marine Science Department, Nippon Marine Enterprises, Ltd., Japan Marine Science and Technology Center, National Space Development Agency of Japan, National Museum of Emerging Science and Innovation)

Studying natural history by using the real nature is essential for schoolchildren to deepen the understanding. Since they cannot always experience the true nature, it is the key to produce circumstances of "virtual field tour" in the classroom by utilizing video image and appropriate materials. In this case, the more precise is the visual image, the stronger is their impression. Therefore, we should invoke IT technology which enables us to make high-speed data transmission and processing. ROV "HyperDolphin" owned by JAMSTEC (Japan Marine Science and Technology Center) is equipped with underwater HDTV-class camera and the video image processing system for scientific use. If the video image is transmitted in real time, both offshore and onshore scientists can share the information. The same system is also effective for education and public outreach by reporting what is going on under the sea in real time. JAMSTEC and NASDA (National Space Development Agency of Japan) are promoting an experiment of telecommunication of HDTV-class high precision video image from a moving research vessel during an expedition to an onland station through a Japanese communication satellite (CS) for marine education and public outreach without downgrading the quality of data and image. Such high quality image transmitted to the land is a live teaching material to make schoolchildren and non-professionals understand the underwater world and its mystery. In March 2002 we succeeded in a 'remote science class' by connecting remotely between ROV "HyperDolphin" offshore and National Museum of Emerging Science and Innovation (MeSci) in Tokyo. The clear and high precision HDTV-class video image from the seafloor of 650m water depth on the Izu-Bonin active volcanic arc was transmitted in real time to MeSci through the SNG (Satellite New Gathering) Vehicle on board and the Japanese commercial CS (SuperBird-B2). By following the scenario that had been made in advance, a programme with a presentation at the MeSci auditorium, interactive communication between onshore and offshore by relay, lecture by a marine biologist on board by use of the real-time video image of ROV was planned and carried out without any mechanical error. This was of great help for the people to understand what is going on during the marine observations and to enjoy the deep sea world. NASDA is planning to launch a new high-speed internet communication satellite WINDS (Wideband InterNetworking engineering test and Demonstration Satellite). The current trial is the first step for estimation of the practicability of the remote science class by sharing quite the same information and impression by both offshore and onshore through the communication satellite and suggests the future use of WINDS satellite for marine education and public outreach from offshore.

**SS05/10A/A13-004** **0915**

**THE DPRI-KU SATELLITE OFFICE FOR OUTREACH SUPPORTED BY THE 21ST CENTURY CENTER OF EXCELLENCE PROGRAM**

Manabu HASHIMOTO, Haruo HAYASHI, Hironori KAWAKATA, Yoshiaki KAWATA, Kojiro IRIKURA, Shuichi IKEBUCHI (Disaster Prevention Research Institute, Kyoto University)

The Disaster Prevention Research Institute, Kyoto University, was designated to one of the centers of excellence under the MONBUKAGAKUSHO's 21st Century COE program. In order to improve accountability of research works and to enlarge opportunity of education, we opened satellite offices near the Kyoto and Tokyo stations and started a lecture series on almost all disciplines in the field of science and technology related to disaster mitigation. One and half hour-long classes are held in the evening on four days in a week in Kyoto, while once per two weeks in Tokyo. Since DPRI has about 100 faculties, every faculty will have two classes in a year. All the classes are recorded with digital camcorders and audiotape recorders. We plan to edit all the digital records of classes and put them onto our website in the future. Programs and lecturers are announced on our website (<http://www.21coe.dpri.kyoto-u.ac.jp>). Basically classes on the same discipline are held on the same day of the week: e.g. earthquake prediction and related topics are held on Tuesday. Applicants must apply his/her desired classes on this website. Therefore applicants should be familiar with Internet. By the end of January, 11 classes were held in Kyoto and 10-15 participants attended in average. We had two classes in Tokyo in January. There were more than 60 attendants per one class. Professions of participants are high school teachers, undergraduate and graduate students, journalists, national and local government officials, employees from utility companies etc. Although they depend on the topic of the class, there is a tendency that high school teachers attend earthquake classes and governmental officials and employees from private company are observed in engineering classes. We also periodically report the activity of the satellite office to public and feedback the opinion from the public to our activity.

**SS05/10A/A13-005** **0930**

**INTERACTIVE LEARNING IN GEOPHYSICS: IMPLEMENTATION WITHIN THE FRAMEWORK FOR DISTANCE EDUCATION PROGRAM AT THE FEDERAL UNIVERSITY OF FLUMINENSE (UFF)**

Luiz V.B. GOMES, Valiya M. HAMZA (IASPEI)

Recent installation of the web-based 'Distance Education Program' at the Federal University of Fluminense (UFF) has opened up an important complementary facility for graduate and undergraduate students in the state of Rio de Janeiro (UFF@Distância: [www.uff.br/ead](http://www.uff.br/ead)).

The software for this platform and related facilities for interactive learning were developed locally. This important technological capability has allowed economy and greater flexibility in implementing a variety of student/professor interactive facilities than is possible under commercially available educational packages. In the first year of operation the system has established itself as a landmark for educational projects and in addition has contributed to development of software for web-based teaching-learning environment in Brazil. The system also allow implementation of interactive educational packages. As a specific example, we discuss the experience gained in implementing Distance Education courses in geophysics, developed at the National Observatory of Brazil. This package provides both passive and interactive learning environments. In the passive environment the course contents are in the form of standard chapter-related HTML modules. However, the student has the option for on-line communication with the professor. The interactive environment consists of modules that interlace object oriented scripts and graphic utilities (used for enhancing capabilities of conventional HTML pages). One of the example sets, currently under development as academic software, have modules for virtual demonstration of borehole temperatures and crustal thermal regimes. The second example set make use of dynamic simulation techniques for illustrating wave propagation in homogeneous media. The third example set makes use of widely available spreadsheet packages for demonstration of numerical methods and illustration of tectonic phenomena such as continental drift. Facility for implementing simulations in response to user inputs is an attractive feature of such modules. These are actually system-independent packages that can be set up without the need to invoke server-based applications. Another major advantage of this approach is that the interactions are processed at the user end, leading thereby to considerable reduction in net traffic. Systematic training of academic staff is a crucial ingredient for the success of web-based educational packages.

SS05/10A/A13-006

0945

#### GEOPHYSICAL EDUCATION AND INSTRUMENTATION NEEDS IN THE D.R. CONGO

Ndoutoni ZANA (Département de Physique, Faculté des Sciences, Université de Kinshasa et Centre de Recherche en Géophysique)

The territory of the D.R. Congo includes several natural fields of geophysical interest that require a strong implication both in education and observational activities by local scientists. The prominent features of this region are: (a) The western branch of the East - African Rift System covers the eastern Congo border over 1200 km. The Virunga volcanic region within this branch is one of the most active in the world. The Niyragongo lava flow that covered over the Goma city on January 17, 2002 is the severest experience of the local people in recent history. (b) The D.R. Congo area covered by a large cratonic structure is affected by seismic activities: these include intense rifting seismicity and moderate intraplate one with scarce destructive events, e. g., the 1992 Kabalo earthquake of M 6.7. (c) The crust under the D. R. Congo is important reservoir of mineral resources. In spite of these stimulating features, the field of geophysics has very few trainees in the country. To remedy this lack, a geophysical capacity building program has been set up. This one includes two steps: (1) Education: The Faculty of Science of the Kinshasa University has included some basic lectures of geophysics in its graduate curricula in physics and geology. Due to the dimmed number of professors, the teaching is limited to fundamental topics. The future goal is the establishment of a full department of geophysics. (2) Geophysical observation: As response to the occurrence of the 1992 Kabalo earthquake and to the catastrophic disaster by the 2002 Niyragongo eruption, a program to construct the National Geophysical Network has been set up and included within the government master plan. This program is operated by the Center for Geophysical Research (C.R.G) a governmental institution within the Ministry of Education and Science. However, the whole program is facing two major difficulties: on the one hand, the Faculty of Science is deserted by students due the lack of attractive jobs on the local marked as well as in the scientific and academic fields. On the other hand, the diet budget allocated to the Ministry of Education does not allow its research institution to build the needed geophysical observatories that could attract young scientists as well as students. This serious lack, if not quickly remedied, is preventing young scientists presently abroad to return to their homeland. It is expected that this project will obtain the due support in order to promote the needed human and instrumentation capacities for geophysical observations over the D.R. Congo territory.

SS05/10A/A13-007

1000

#### PUBLIC MOVEMENT AGAINST ENCROACHMENT OF LAKE AND ITS CONSERVATION IN BANGLADESH

Mostafa Md. KHALEQUZZAMAN<sup>1</sup>, Md. SALEQUZZAMAN<sup>2</sup> (Paediatrics Consultant, Magura General Hospital, Bangladesh, <sup>2</sup>Associate Professor, Environmental Science Discipline, Khulna University, Bangladesh; and Ph.D. Candidate and Researcher, Institute for Sustainability and Technology Policy (ISTP), Murdoch University, Western Australia, Perth, WA 6150, Australia, Tel. +61 8 9360 2898/9284 4222, Fax. +61 8 9360 6421, email: salek@central.murdoch.edu.au / msalequzzaman@hotmail.com)

Bangladesh is a country of water and wetlands, because lots of cross-cross rivers and lakes are passing inside the country. Superficially, this setting of lakes and rivers has a net like panoramic view that makes the country a rich biodiversity. Lots of peoples are depends on it for their livelihood. But this natural settings is now endangered, because of the lakes and other natural water bodies of the whole country including the capital city of Dhaka are regularly being encroached illegally by the corrupted peoples of the country, which upon giving rise to serious environmental and civic concerns. Recently some environmentally friendly peoples and organizations have taken a mass-awareness program in the whole country against the bad effects and threats of this type of encroachment. The programs have finally moved by mass peoples. As a result, the government of Bangladesh finally started to take an action against this encroachment, and some successful outcomes have already achieved. The paper will discuss how the public movement has organized and how much the success has achieved. Finally the paper will recommend the sustainability issues of the public movement against encroachment of lake and its' conservation in Bangladesh.

SS05/10A/A13-008

1015

#### RIVER RESTORATION THROUGH MASS AWARENESS PROGRAM OF BANGLADESH

Mostafa Md. KHALEQUZZAMAN<sup>1</sup>, Md. SALEQUZZAMAN<sup>2</sup> (Paediatrics Consultant, Magura General Hospital, Bangladesh, <sup>2</sup>Associate Professor, Environmental Science Discipline, Khulna University, Bangladesh; and Ph.D. Candidate and Researcher, Institute for Sustainability and Technology Policy (ISTP), Murdoch University, Australia, Tel. +61 8 9360 2898, Fax. +61 8 9360 6421, e-mail: salek@central.murdoch.edu.au / msalequzzaman@hotmail.com)

Bangladesh is a riverine country. As lots of river is passing through Bangladesh; it has a great impact to Bangladesh's economy, environmental and socio-cultural activities. More than 70% of the population directly or indirectly depend on river to their daily livelihood. But during past few decades, most of the rivers have been encroached through illegal structure by the muscle man. Besides, most of the river are seriously polluted from the different river bank industry, sewerage and drainage systems. By these processes, some of the rivers are

totally vanished. However, the encroachment process and pollution has severe impacted to the agricultural, navigational, fishing, recreational and other activities to the neighbouring local communities. As a result, the local communities with the help of environmentalist, journalist, educationist, student, various NGOs, and different other groups have protesting by movement of mass gathering continuously against the river encroachment and pollution activities, and demand for restoration of the river since 1998. For this protest and awareness by the mass population of the society, government of Bangladesh and concerned river management authorities now have started the action against encroachment. The paper will discuss in details the encroachment process and anti-encroachment of restoration of **Buriganga River** of the Capital City, Dhaka as a case study. Finally, the paper will give a policy recommendation on **how the encroachment could removed sustainable way from the all rivers of Bangladesh.**

SS05/10A/A13-009

1045

#### PUBLIC AWARENESS THROUGH EDUCATION: KEY FOR SEISMIC RISK REDUCTION

Marina TER-ANANYAN<sup>1</sup>, Serguei BALASSANIAN<sup>2</sup>, Ashot MELIKSEYAN<sup>1</sup> (<sup>1</sup>Armenian Association of Seismology and Physics of the Earth's Interior, <sup>2</sup>Yerevan State University, Department of Geophysics)

It is stated in the paper that for seismic risk reduction in any country the public awareness is crucial. The concept proposed by the authors is based on the following principals: 1) the main mean for awareness increase AE is education and training; 2) all social groups of society should be involved in education; 3) education of various social groups must differ from each other: the volume of the necessary knowledge should increase from elder generation to younger one as well as from ordinary citizens to decision makers; 4) special attention in education have to be paid to youngest generation and decision makers of all levels: community, municipality, local government, federal (state) government; 5) for public awareness increase different approaches have to be used, taking into account level of seismic hazard and risk, social and economic state of the society and country, national traditions, culture and belief, mentality of the nation, state laws. The concept is supposed to develop a system which will: 1) act in the frame of common strategy for seismic risk reduction, developed and implemented by professional state agency; 2) be developed within the State Seismic Risk Reduction Program; 3) be oriented to different ages and social groups with special focus to children; 4) include complete information in wide by understandable form; 5) exclude wrong and non-competent information; 6) support the direct link between professional state agency- mass media-public-decision makers. The Criteria of Concept sufficiency is: 1) awareness of most vulnerable social groups AE old people, children, poor people, invalids, inhabitants of far situated settlement; 2) existence of efficient links between scientists, decision makers and public. The Strategy is permanent information provided for efficient seismic risk reduction by well awarded society. Tactics of public awareness increase includes: 1) information dissemination in form of printed and audio-video materials prepared by professional state agency; 2) training of trainers by state agency for knowledge dissemination at schools, universities, municipalities, governmental and NGOs as well as private institutions; 3) mass media usage; 4) education and training program development for schools and universities; 5) education and training for decision makers; 6) organization of scientific workshops, seminars, conferences in the field of social sciences.

SS05/10A/A13-010

1100

#### METHOD OF COMPOSING PLANS FOR OPERATIVE AND EFFECTIVE ACTIONS OF MUNICIPAL SERVICES AFTER DESTRUCTIVE EARTHQUAKE

Sergey Norayr NAZARETYAN (Northern department of national survey for seismic protection of RA)

Large areas of a number of Commonwealth of Independent States countries (for example in the Caucasus and in Central Asia) have a high seismic risk degree, which is mainly due to the underestimated seismic hazard of the territory, the poor quality of construction and the lack of preparedness of government, municipal structures and the public to withstand strong earthquakes. Taking into account the hard economic state of these countries, at present the most practical way of reducing the damage from earthquakes is to increase the efficiency of operative actions and the professionalism of municipal services. Besides, a ready compiled plan is necessary to realize effective actions. Unfortunately, the existing plans and activities that services have at their disposal have been created for wartime or emergency situations in general. The Spitak earthquake of 1988 revealed the necessity of developing new plans particularly for destructive earthquake conditions. The following principles must be taken into account as a basis for making up such plans: 1. The plan must be based on the map of the city's seismic risk and prediction of destructive earthquake consequences. 2. It is necessary to achieve high efficiency in the plan's immediate realization after the earthquake, especially during the first 3-5 days, when the probability of rescuing the general population is high enough. 3. Actions of all special services must be coordinated with each other in advance; i.e., a complex plan of operative actions must be developed. 4. The complex plan must be easy to realize by services and rescue organizations from outside. 5. The plan must be worked out for the worst conditions taking into consideration scales of the greatest destruction, the most unfavorable weather conditions, time of day, etc. The plans must have a similar structure, including the following parts: 9. the addresses and telephone numbers of services and their objects; 10. the main service objects, vulnerability of their buildings and equipment; 11. the service's capacity (the staff and equipment); 12. communication means; 13. autonomous providing of electric power; 14. urgent tasks of the service; 15. the service action (routes and ways for solution of problems involved); 16. action coordination between the services; 17. the new place of service location (if necessary); 18. necessity for the outside help and the place of its location.

SS05/10A/A13-011

1115

#### EDUCATION PROGRAM FOR CHILDREN AND YOUTH BY THE SEISMOLOGICAL SOCIETY OF JAPAN

Masato KOYAMA<sup>1</sup>, Kazuyuki NAKAGAWA<sup>2</sup>, Manabu HASHIMOTO<sup>3</sup>, Eiji KUWABARA<sup>4</sup>, Masaki TAKAHASHI<sup>5</sup>, Kojiro IRIKURA<sup>6</sup>, A.D. 2002 MEMBERS<sup>7</sup>, A.D. 1999-2001 MEMBERS<sup>8</sup>, Voluntary MEMBERS<sup>9</sup> (<sup>1</sup>Department of Integrated Sciences and Technology, Faculty of Education, Shizuoka University, <sup>2</sup>Jiji Press, <sup>3</sup>Disaster Prevention Research Institute, Kyoto University, <sup>4</sup>Osima High School, <sup>5</sup>Department of Geosystem Sciences, College of Humanities and Sciences, Nihon University, <sup>6</sup>The Committee for Future Planning of the Seismological Society of Japan, <sup>7</sup>The Committee for School Education of the Seismological Society of Japan, <sup>8</sup>The Seismological Society of Japan and the Volcanological Society of Japan)

The seismological Society of Japan (SSJ) has been conducting programs for education of children and youth since 1999 in cooperation with other associations such as the Volcanological Society of Japan. The first program was held in summer 1999 around the Tanna fault zone in the Izu Peninsula supported by the Kannami town and Shizuoka prefecture. 22 children of 10-18 years in age participated in this program and spent two days. The program consisted of excursion of the Tanna fault and talks on earthquake mechanisms, strong ground motion, and volcanoes, etc. It is emphasized that the program

included a couple of experiments of faulting and liquefaction using materials that we can find at home. In summer 2000, the second summer school was held in Sobetsu and Abuta towns near Usu Volcano, which erupted in spring of the year. The program consists of excursion of Usu Volcano, two experiments (lava-dome making and observation of tephra), and lectures about eruption history and mechanisms. In July 2001, SSJ held the International Children's Earthquake and Volcano Summit in Izu-Oshima. We invited 166 children aged from 10 to 18, including children from Taiwan and Turkey, and spent three days. All the children formed four groups. A couple of questions on the history of Izu-Oshima Volcano were given in the beginning of the program. During this three-day stay, children must find the answers to the questions learning results of recent researches and performing some experiments including GPS positioning, dyke intrusion, and eruption. They also had excursion to the section of tephra layers since 30ka and eruptive fissures that formed during the 1986 eruption and some lectures on tsunami and earthquakes. They worked very well and left the statements on the basis of three-day experience in an active volcano with scientists. In 2002, we cooperated the Volunteer Coordinator Training Course by the Association of Social Welfare of Ueno City, Mie prefecture. Ueno is the epicentral region of the 1854 Iga-Ueno earthquake. The original course is a one-year program for volunteer coordinators. In average 10-15 children attended. We held a one-day program in fall 2002. In October we performed the similar experiments of faulting and liquefaction. We also made observation of ground vibration using seismographs, recorded the seismic waves generated by participants and measured their velocities. On the second day we had a field trip to the excavation site of the Kizugawa fault and measured its strike using handy GPS receivers. In all programs, we prepare point cards and give them to individual children or group when they raise good questions and answers to staffs. This kind of competition may stimulate children's interests.

**SS05/10A/A13-012****1130****DISCUSSION ON THE DEFINITION OF SEISMIC MOMENT**Zhongliang WU<sup>1</sup>, Yun-tai CHEN<sup>2</sup> (<sup>1</sup>College of Earth Science, Graduate School, Academia Sinica (CAS), <sup>2</sup>Institute of Geophysics, China Seismological Bureau)

In recent years, theoretical results imply that a seismic rupture occurred along a discontinuity interface of two different media can explain many of the earthquake phenomenologies. Observational evidences show that a compliant faultzone within a stiffer medium is a commonly valid model for earthquake faulting. These results lead to a difficulty in the application of the classical definition of seismic moment, because the value of rigidity is not unique at the interface. Considering this difficulty, one of the extreme ideas is to give up the concept of seismic moment by going back to potency. But in physics, such a difficulty is not due to the problem of rigidity but due to the application of the simplified definition of seismic moment. To discuss this problem one should go back to the general form of representation theorem from which the seismic moment density tensor is defined as a product of the modulus tensor and the 'transformation' strain tensor. Detailed calculation leads to a more general definition of seismic moment which is similar to the classical definition, with the only change that the rigidity is replaced by the 'effective rigidity', in which the 'effective rigidity' is smaller than the average rigidity across the interface, being determined by both the average and the deviation. This discussion has important implications for seismological observation practice. For the case that an earthquake rupture occurs along the discontinuity interface between a compliant medium (the fault zone) and a stiffer medium (the environmental medium), in the estimation of slip and/or rupture length, usually the rigidity of the stiffer medium is used. In this case, the slip and/or rupture length are underestimated significantly.

**SS05/10A/A13-013****1145****EARTHQUAKE RESEARCH: STILL A YOUNG SCIENCE WITH STRONG POTENTIALS FOR FURTHER DEVELOPMENT**

Yumin LI (Division of Information, Zhejiang Province Seismological Bureau, China)

With disciplinary bias and philosophical bias and with explorations lasted 100 years, the recognition about the earthquakes is just begging by human being. Earthquake events are the phenomenon of nature and the process with planet evolution. 1. The research for Geology science has been experienced more than 200 years from morphology to kinematics then to dynamics with development of the foundational disciplines involving physics, chemistry, mathematics, astronomy, biology and the progress of science and technology. In particular the Theory of Global Plate Structure originated from middle of the 20th century soundly reveals the evolution of the earth followed The International Geophysics Years in 1950s, The Program of Upper mantle in 1960s which leads to the birth of the Theory of Lithosphere Plate Tectonics, The Program of Geodynamics in 1970s and The Research Program of Lithosphere in 1980s. It described the basic image of global crust structure. 2. Historical earthquake recorded by people can trace back to 1000 years ago and the original record found in Africa may be existing over 5000 years. 3. The investigation for paleoseismology by United States, Russia and China scientists presents a traces of ancient earthquakes since 20000 years and this at least shows some regularities of seismic activity. In addition, the earthquake traces were found before 5 billion years during Cambrian period and Sinian period. It inspired us that the earthquake is a natural phenomenon of the earth its movement, further more the large event cycling is calculated by thousand-year unit, so time scale for research wasn't confined to several years. 4. Earthquake prediction is a scientific problem with great difficulty in the field of current natural sciences and many important scientific problems remain to be deeply studied. To reveal the evolution of the earth and other planets from status quo ante to status quo needs earth scientists possess correct research methodology, needs multidisciplinary intersection and cooperation, needs unremitting effort from generation to generation, as "We are at the very beginning of time for the human race. It is not unreasonable that we grapple with problems. But there are tens of thousands of years in the future. Our responsibility is to do what we can, learn what we can, improve the solutions, and pass them on." The purpose is to improve the scientific capability for earthquake disaster prevention and reduction.

**SS05/10A/A13-014****1200****EARTH SCIENCE EDUCATION AT UNIVERSITIES**

Noriko SUGI (Kyoritsu Women's University)

Earth science has a long history. To transmit its brilliant results to the general public is our important role. But recently in Japan, it is remarkable that young people do not feel interested in earth science. This problem serious for the future of earth science originated from the situation where the entrance examinations have not covered earth science at many universities, teachers of earth science in high schools have decreased and consequently students having a chance to learn about the earth are on the decrease. It is our mission to train the next generation for a specialist of earth science and also to educate those who will choose other fields for lifework. We have benefited by natural phenomena on the earth, but on the other hand we have suffered various kinds of natural disasters throughout the world. Especially in Japan located at the converging boundaries of four lithospheric plates, large earthquakes, volcanic eruptions and tsunamis repeatedly damaged people and country. In

order to coexist with the earth it is important that the younger generation will understand and be interested in such an activity of the earth as a whole. This paper describes what I am trying through the lecture of liberal arts to educate students in earth science in our women's university where the majority of students are supposed to marry and have babies during the next decade. Desiring that they are interested in the earth and will initiate the next generation including their children into charms of earth science, I emphasize that earth science is closely connected with lives of themselves and their descendants. How the lecture during one or half a year has influenced the awareness of my students will be reported in this paper.

**SS05-Posters****Thursday, July 10****EDUCATION AND OUTREACH**

Location: Site D

**Thursday, July 10 PM**

Presiding Chair: D. Jackson

**SS05/10P/D-001**

Poster

**1400-234****GEOMAGNETIC BASE FOR AN EPISTEMOLOGY OF THE UNIVERSAL CULTURE**Teodosio Chavez CAMPOS<sup>1</sup>, Chavez SUMARRIVA<sup>2</sup> (<sup>1</sup>Post-graduate school of system, University National of Engineering, <sup>2</sup>National University of Engineering, Lima-Peru/AEName1-1-Israel)

For an epistemology focus of the universal cultural, it is necessary a natural chronometer to coordinate and classify the observations, this is a system reference as starting point, and this system becomes determined through the astronomical phenomenon named the precession of the equinoxes, and it has its confirmation with the stability of the geomagnetic equator, where the inclination (I) of the field is zero degrees, and over to 100 kilometers approximately is located the equatorial electrojet that is more intense in the equinoxes in South America and that at the moment it crosses for the central part of Peru and over the city of Cosco, exactly in this area where it develops the one of the biggest culture of every time, and then it extends to the north of Bolivia and Brazil. With this reference system taking the base of the behavior of the equator geomagnetic, we can focus the study of the epistemology of the Andean cultures of America and the world, that is to say in a process of ahead back comparing periods and subperiods of Eras Precessional, and to study an archaeological piece, a pyramid, a temple, their monumental constructions, their religious, philosophical, artistic and scientific thoughts, their effects, objectives and reach, their transcendence and evolution. We need to create an epistemology structure in all the fields in that it is possible to apply the thought of the big cultures of America and to compare with them other cultures.

**SW03-Posters****Thursday, July 10****LITHOSPHERIC STRUCTURE OF A SUPERCONTINENT: GONDWANA**

Location: Site D

**Thursday, July 10 AM**

Presiding Chair: L. Brown

**SW03/10A/D-001**

Poster

**0830-235****LITHOSPHERIC SHEAR VELOCITY MODELS BENEATH CONTINENTAL MARGINS IN ANTARCTICA INFERRED FROM GENETIC ALGORITHM INVERSION FOR TELESEISMIC RECEIVER FUNCTIONS**Masaki KANAOKA<sup>1</sup>, Takuo SHIBUTANI<sup>1</sup>, Atsuki KUBO<sup>2</sup> (<sup>1</sup>Department of Earth Science, National Institute of Polar Research, <sup>2</sup>Disaster Prevention Research Institute, Kyoto University, <sup>3</sup>National Research Institute for Earth Science and Disaster Prevention)

Seismic shear velocity models of the crust and the lithospheric mantle were investigated by teleseismic receiver functions inversion beneath the permanent stations at the continental margins in Antarctica. In order to eliminate the starting model dependency, non-linear Genetic Algorithm (GA) was newly introduced in the time domain inversion of the radial receiver functions at each station. The inversion of the receiver functions to recover crustal and uppermost mantle structure is widely recognized to be sensitive to the starting model if a conventional linearization scheme is employed (Ammon et al., 1990). Such difficulties, however, can be overcome by employing an inversion scheme based on a Genetic Algorithm (GA) (Shibutani et al., 1996). This approach makes use of a cloud or population of models to minimize the dependence on a starting model; a set of biological analogues are used to produce new generations of models from previous generations, with preferential development of models with a good fit between observed and theoretical receiver functions. The approach provides a good sampling of the model space, and enables the estimation of the shear-wave speed distribution in the crust, along with an indication of the ratio between Vp and Vs. Many models with an acceptable fit to data are generated during the inversion, and a stable crustal model is produced by employing a weighted average of the best 1,000 models encountered in the development of the GA. The weighting is based on the inverse of the misfit for each model, so that the best fitting models have the greatest influence. In this presentation, shear velocity models of the permanent stations at Antarctic margins belonging to the Federation of Digital Seismographic Networks (FDSN), such as of AGSO, GEOSCOPE and IRIS, etc. are presented in relation with geotectonics and crustal evolution of the each terrain. The shear velocity model around MAW has a sharp Moho at 42 km depth that might have involved re-working of adjacent Archaean craton of the Napier Complex. High velocities in the upper crust around SYO may have a relationship with surface geology of granulite facies metamorphic rocks. Middle grade variations of the crustal velocities for DRV may have been caused by the Middle Proterozoic metamorphism. Broadening low velocity zones recognized at VNA about 30 km depth, which may be caused by the rift system of Trans Antarctic Mountains. As for the Antarctic Peninsula, Moho was found at 34 km depth from PMSA data. Moreover, shear velocity models by GA inversion for receiver functions were also determined in eastern Australia (R. D. Hilst et al., 1998), then we will make a comparison with those structure as a member of Gondwanaland.

**SW03/10A/D-002** Poster **0830-236**

**CRUSTAL STRUCTURE BENEATH THE MIZUHO PLATEAU, EAST ANTARCTICA, DEDUCED FROM A REFRACTION AND WIDE-ANGLE REFLECTION EXPLORATION**

Hiroki MIYAMACHI<sup>1</sup>, Sigeru TODA<sup>2</sup>, Takeshi MATSUSHIMA<sup>3</sup>, Masamitsu TAKADA<sup>4</sup>, Atsushi WATANABE<sup>5</sup>, Mikiya YAMASHITA<sup>6</sup>, Masaki KANAO<sup>7</sup> (<sup>1</sup>Department of Earth and Environmental Sciences, Faculty of Science, Kagoshima University, <sup>2</sup>Faculty of Education, Aichi Education University, <sup>3</sup>Institute of Seismology and Volcanology, Faculty of Sciences, Kyushu University, <sup>4</sup>Institute of Seismology and Volcanology, Graduate School of Science, Hokkaido University, <sup>5</sup>Department of Earth and Planetary Sciences, Graduate School of Sciences, Kyushu University, <sup>6</sup>Department of Polar Science, The Graduate University for Advanced Studies, <sup>7</sup>National Institute of Polar Research)

The 43rd Japanese Antarctic Research Expedition (JARE-43) carried out the seismic exploration at the Mizuho Plateau, East Antarctica, in the austral summer season of 2001-2002. It is composed of seven large explosions and 161 seismic stations distributed along the 151 km long profile. The first arrival time data are analyzed by a refraction method. It is found that the ice sheet is composed of two layers: the upper layer with a P wave velocity of 2.7 - 2.8 km/s has a thickness of 35 - 45 m, and the lower layer with a P wave velocity of 3.8 km/s continues to the bed rock basement. A lateral velocity variation in the upper-most crust is revealed: P wave velocity for the upper-most crust in the southern and central parts of the profile is 6.1 - 6.2 km/s and that in the northern part is 5.9 km/s. The P wave velocity obtained in the central and southern parts is consistent with that estimated by the JARE-41 seismic exploration on the Mizuho Plateau in 1999-2000 (Tsutsui et al., 2001). The lateral velocity variation also suggests that the rock basement in the southern part is different from that in the northern part. However, the thick ice sheet overlying the continental crust prevents us from directly observing geological feature of the crust. From a geological investigation of rock exposures distributed sparsely along a coast in Enderby Land in East Antarctica (Hiroi et al., 1991), our seismic profile may be considered to spread in the Paleozoic Lutzow-Holm Complex: the northern part of the profile is located in the amphibolite-granulite facies transition zone and the southern part in the granulite facies zone. Consequently, it can be said that the geological boundary observed in the coast may extend to the inland area. S wave velocity is also obtained to be 3.5 km/s for the whole profile. Two distinct reflection phases lead us a result that a boundary between the upper crust and the middle crust, and the Moho discontinuities are located at 19 and 40 km depth, respectively.

**SW03/10A/D-003** Poster **0830-237**

**INTEGRATED MULTIDISCIPLINARY SURVEYS BY STRUCTURE AND EVOLUTION OF THE EAST ANTARCTIC LITHOSPHERE TRANSECT: SEAL-2000, -2002**

Masaki KANAO<sup>1</sup>, Hiroki MIYAMACHI<sup>2</sup>, Shigeru TODA<sup>3</sup>, Hiroshi MURAKAMI<sup>4</sup>, Tomoki TSUTSUMI<sup>5</sup>, Takeshi MATSUSHIMA<sup>6</sup>, Masamitsu TAKADA<sup>7</sup>, Atsushi WATANABE<sup>8</sup>, Mikiya YAMASHITA<sup>9</sup>, Koji YOSHII<sup>10</sup> (<sup>1</sup>Department of Earth Science, National Institute of Polar Research, <sup>2</sup>Faculty of Science, Kagoshima University, Kagoshima, <sup>3</sup>Faculty of Education, Aichi Education University, <sup>4</sup>Earthquake Observation Research Technology Center, <sup>5</sup>Faculty of Engineering and Resource Science, Akita University, <sup>6</sup>Institute of Seismology and Volcanology, Faculty of Sciences, Kyushu University, <sup>7</sup>Institute of Seismology and Volcanology, Graduate School of Science, Hokkaido University, <sup>8</sup>Department of Polar Science, The Graduate University for Advanced Studies, <sup>9</sup>Disaster Prevention Research Institute, Kyoto University)

Lithospheric evolution and deep structure viewed from East Antarctic Shield have significance in relating to the continental growth process in Earth's evolution. Here, we focus on the lithospheric structure of the early-Paleozoic crust of the Lutzow-Holm Complex (LHC), Enderby Land, East Antarctica. LHC is considered to be one of the collision zones between the East- and the West- Gondwanaland during the formation of a paleo-supercontinent in the Pan-African orogeny. The "Structure and Evolution of the East Antarctic Lithosphere (SEAL)" project has been carried out since 1996-1997 austral summer season in the framework of the Japanese Antarctic Research Expedition (JARE). Several geophysical studies and deep seismic refraction / wide-angle reflection surveys have been conducted at LHC. The main target of the SEAL geotransect is to obtain a whole lithospheric section in the different geological terrains from the Archean (Napier Complex) to the early-Paleozoic ages (LHC) between Western Enderby Land and Eastern Queen Maud Land. In the austral summer season in 2000, and 2002, deep seismic probing were conducted on ice sheet in the northern Mizuho Plateau, of LHC by JARE-41, and -43, respectively. In both surveys, more than 170 plant-type 2 Hz geophones were set on the Mizuho plateau 190 km in length. A total of 8,300kg dynamite charge at the fourteen sites on the Plateau gave information concerning the deep structure of a continental margin of the LHC. These investigation revealed that the Moho depth was more than 40 km with the velocity of the surface layer, middle crust, lower crust and mantle, about 6.2, 6.4, 6.7 and 7.9 km/s, respectively. Moreover, the clear reflections from Moho discontinuity have been observed on the record sections; which implies the existence of heterogeneity on the crust-mantle boundary beneath the Paleozoic orogenic zone of LHC. Laminated inner structure around the Moho discontinuity could be also identified by precise spectral analyses for PmP waves.

**SW03/10A/D-004** Poster **0830-238**

**DEEP CRUSTAL STRUCTURE BENEATH THE MIZUHO PLATEAU, EAST ANTARCTICA FROM SEISMIC EXPLORATION**

Mikiya YAMASHITA<sup>1</sup>, Hiroki MIYAMACHI<sup>2</sup>, Takeshi MATSUSHIMA<sup>3</sup>, Shigeru TODA<sup>4</sup>, Masamitsu TAKADA<sup>5</sup>, Atsushi WATANABE<sup>6</sup>, Masaki KANAO<sup>7</sup> (<sup>1</sup>Department of Polar Science, The Graduate University for Advanced Studies, <sup>2</sup>Faculty of Science, Kagoshima University, <sup>3</sup>Institute of Seismology and Volcanology, Faculty of Sciences, Kyushu University, <sup>4</sup>Faculty of Education, Aichi Education University, <sup>5</sup>Institute of Seismology and Volcanology, Graduate School of Science, Hokkaido University, <sup>6</sup>Department of Earth and Planetary Science, Graduate School of Sciences, Kyushu University, <sup>7</sup>National Institute of Polar Research)

The "Structure and Evolution of the East Antarctic Lithosphere (SEAL)" project has been carried out to focus on the lithospheric structure of the early-Paleozoic crust of the LAEzow-Holm Complex (LHC), Enderby Land, East Antarctica since 1996-1997 austral summer season in the framework of the Japanese Antarctic Research Expedition (JARE). Seismic exploration was conducted on the Mizuho Plateau, East Antarctica, during the 2001-2002 austral summer season by JARE-43. Seismic shot records were obtained with clear arrivals of the later reflected phases by a total amount of 4,900 kg dynamite charges at the seven explosions along the new route is lied at right angles to the Mizuho traverse route of 150 km in length. 162 seismic stations programmed on timer operation were installed. The purpose of this survey is to investigate detailed structure of the crust and Moho discontinuity in view from refraction and reflection by using explosive seismic waves. The obtained seismic records show the clear onsets of the first arrivals in a distance range of less than 100 km from each large shot. In particular, seismic waves traveling through the ice sheet and the dispersed surface waves are distinctly observed. Some later phases are also detected. The structure of the upper crust and overlying ice-sheet are revealed down to 5 km from refraction analysis of the first arrival times. The first layer with a velocity of 3.8 km/s appears

to be ice sheet. The second layer with a velocity of 6.1 km/s of P-wave velocity is the surface layer of the continental crust. We used reflection analysis (band-pass filter, static correction, Normal Move Out, Auto-gain-control) for seven shot records, and obtained single hold section. The reflection profiling shows the several reflections around the Moho discontinuity. We discuss for the structure of upper and lower crust and investigated the velocity structure for the previous results.

**SW03/10A/D-005** Poster **0830-239**

**HIGH P-T MEASUREMENTS OF P-WAVE AND S-WAVE VELOCITIES OF GRANULITES FROM ENDERBY LAND, EAST ANTARCTICA**

Masahiro ISHIKAWA, Eisuke SHINGAI, Makoto ARIMA (Graduate School of Environment and Information Sciences, Yokohama National University)

Determination of the ultrasonic velocities and Poisson's ratio in natural granulites at lower crustal conditions of pressure and temperature are necessary to interpret the seismic profiles in terms of chemical composition and petrology. The results of high P-T velocity of natural rocks provide direct measurements of the effect of pressure and temperature on P-wave and S-wave velocities of natural rocks, which is of critical importance in evaluating crustal models at different geotherms. In order to understand crustal structure of Pan-African orogenic belt in East Antarctica, P-wave velocity (Vp) and S-wave velocity (Vs) in granulites were determined up to 1.0 GPa from 25°C to 400°C using a piston-cylinder-type high-pressure apparatus. The rock samples are cores of pyroxenite (SiO2 44 wt. %), mafic granulites (52wt%, 49wt %) and felsic gneiss (SiO2 65wt %) with dimensions of 14mm in diameter and ca. 12mm in length. LiNbO3 were coupled on both ends of core sample in talc pressure medium. The temperatures were determined by the Pt-Rh13 thermocouple, which is placed upon the top-end of the core sample. Measurements of travel time were carried out using the pulse transmission technique. Errors of the velocity measurements are estimated to be less than 0.1 km/s. All rocks show a rapid increase of velocity at low pressure up to 0.4 GPa and nearly constant at higher pressures. The Vp and Vs at 1.0 GPa and 400°C are 7.17 km/s and 4.24km/s for pyroxenite, 6.93 km/s and 3.81km/s for mafic granulite (49wt%), 6.88 km/s and 3.72km/s for mafic granulite (49wt%), and 6.17 km/s and 3.59km/s for felsic gneiss. The experimentally determined rock velocities are compared with seismic data of Mizuho Plateau. For the range of expected continental geotherms, our data show that Vp for pyroxene granulites (low-pressure type of mafic granulite) are consistent with the lower crustal seismic velocity (6.95 km/s) at 33 to 40 km depths. Our data require a mafic component (20 vol %) to fit middle crustal seismic velocity (6.6km/s). The present results suggest that the lower crust is composed of lower-pressure type mafic granulites (garnet-free pyroxene granulite) rather than higher-pressure type granulite (garnet granulite). These evidences demonstrate that the lower and middle crust of the Pan-African orogenic belt is composed of lower-pressure type granulite-facies rocks which are main lithologies of Archean craton (Napier Complex).

**SW03/10A/D-006** Poster **0830-240**

**RAYLEIGH-WAVE GROUP VELOCITY DISTRIBUTION IN THE ANTARCTIC REGION**

Reiji KOBAYASHI<sup>1</sup>, Deo D. SINGH<sup>2</sup>, Dapeng ZHAO<sup>3</sup> (<sup>1</sup>Geodynamics Research Center, Ehime University, <sup>2</sup>National Geophysical Research Institute)

Analysing surface waves is a very suitable way to estimate structure beneath the whole Antarctic plate. In this study, the 1-D S-wave velocity structures beneath five regions of Antarctica and the group velocity distribution beneath whole Antarctica are estimated. The data include not only ones of permanent networks but also ones of temporary arrays. The Antarctic region is divided into five regions according to tectonic features, and the 1-D S-wave velocity structures beneath these regions are estimated from the group velocity dispersion curves. In the lower crust and upper mantle beneath East Antarctica, the S-wave velocities are slightly higher than the previous models. The group velocity distribution beneath whole Antarctica are estimated by means of a tomographic technique. In East Antarctica, the velocities are high at periods of 90-150s, and suggest that the root of East Antarctica is very deep. On the other hand, the velocities in West Antarctica are low at all periods. Low velocity zones appear around the Southeastern Indian Ridge and Pacific Antarctic Ridge, but the velocities are not so low around the Southwestern Indian Ridge, where the spreading rates are small. The spreading rates could affect the seismic velocities, and vice versa. Around two adjacent hotspots, the Mount Erebus and Balleny Islands, there is a peak of low velocity at periods of 50-150 s. This low velocity area suggest that and the origins of these hotspots are plumes.

**SW03/10A/D-007** Poster **0830-241**

**CRUSTAL DENSITY STRUCTURE OF THE MIZUHO PLATEAU, EAST ANTARCTICA FROM GRAVITY SURVEY**

Shigeru TODA<sup>1</sup>, Hiroki MIYAMACHI<sup>2</sup>, Tomoki TSUTSUMI<sup>3</sup>, Takeshi MATSUSHIMA<sup>4</sup>, Hiroshi MURAKAMI<sup>5</sup>, Masamitsu TAKADA<sup>6</sup>, Atsushi WATANABE<sup>7</sup>, Mikiya YAMASHITA<sup>8</sup>, Masaki KANAO<sup>9</sup>, Yoichi FUKUDA<sup>10</sup> (<sup>1</sup>Faculty of Education, Aichi University of Education, Kariya 448-8542 Japan, <sup>2</sup>Faculty of Science, Kagoshima University, Kagoshima 890-0065 Japan, <sup>3</sup>Faculty of Engineering and Resource Science, Akita University, Akita 010-8502 Japan, <sup>4</sup>Institute of Seismology and Volcanology, Faculty of Sciences, Kyushu University, Shimabara 855-0843 Japan, <sup>5</sup>Technical Center for Seismological Observations, Amakubo, Tsukuba 305-0005 Japan, <sup>6</sup>Institute of Seismology and Volcanology, Graduate School of Science, Hokkaido University, Sapporo 060-0810 Japan, <sup>7</sup>Department of Earth and Planetary Sciences, Graduate School of Sciences, Kyushu University, Fukuoka 812-8581 Japan, <sup>8</sup>Department of Polar Science, The Graduate University for Advanced Studies, Itabashi, Tokyo 173-8515 Japa, <sup>9</sup>National Institute of Polar Research, Itabashi, Tokyo 173-8515 Japan, <sup>10</sup>Graduate School of Sciences, Kyoto University, Kyoto 606-8502 Japan)

Structure and Evolution of the East Antarctic Lithosphere (SEAL) project have been caring out in a framework of the Japanese Antarctic Research Expedition in recent few years. The gravity survey was installed in the 41st and 43rd Japanese Antarctica Research Expedition (JARE 41st, 2000 and JARE 43rd, 2002) to study crustal density structure of the Mizuho Plateau, along the traverse route from Syowa Station to Mizuho Station and across this traverse route. The main purpose of the survey was to obtain the detailed gravity anomalies. The gravity measurements were conducted by a SCINTREX (CG-3M) gravity meter at about 1 km-interval along the survey lines. The number of the stations was 312 and the total number of the measurements was 414. Free-air and simple Bouguer gravity anomalies based on gravity disturbance along the survey lines were obtained by use of both data of surface elevation from GPS positioning and of the bedrock elevation from radio-echo sounding. The simple Bouguer gravity anomaly was calculated by assuming the layered structure to fit the observed Bouguer anomaly. These results were correlated to the results of the JARE 21st 33rd and 38th.

SW03/10A/D-008

Poster

0830-242

**MAGMATIC AND METAMORPHIC EVIDENCE FOR PALEO-THETHYS SUTURE IN THE NORTHWEST OF IRAN**

Mohsen MOAYYED (Dept of geology, University of tabriz, Tabriz, Iran)

Remnants of ancient ocean floor forming rocks, which are emplaced due to northward movement of the Gondwana plate, are found in the Misho Mountain in NW of Iran. The Misho Mountain situated between Marand and Uromia lake depressions. Magmatic and metamorphic evidence indicates tracing of suture zone between Eurasia plate and Gondwana plate in this area. Ultramafic and mafic metamorphosed rocks appear melanges and show tectonic contacts with other units. These rocks consist of splitised basalts, metamorphosed gabbro, spinel-norite, spinel-orthopyroxenite, dunite and diabasic dikes. These sequences intruded by S and A type granites. S-type granites have sharp contact with Precambrian rocks (Kahar formation) and are produced contact metamorphism accompanied with retrograde metamorphism and deformation in ultramafic and mafic rocks. Emplacement of these granites can be attributed to continent-continent collision and are characterised as allochthonous granites. Overlay sediments of Permian ultramafic-mafic sequence and therefore suggest that closure of oceanic basin has occurred during Hercynian orogeny. The Misho Mountain is bounded by Tabriz fault in the north part and Southern Misho fault in the south. The Southern Misho fault is characterised with north dip-slip and can be interpret as suture line of Paleo-Thethyan in northwest of Iran. Dip-strike of the fault is corresponds with subduction trend and Beniof zone slope. Sediments of passive continental margin of Gondwana plate are exposed in the south of mentioned suture zone while at the north of Tabriz fault such sediments are not recognised. The discrepancy in sediment types also can be documented for the suture zone of Paleo-Thethys in the northwest of Iran.

SW03/10A/D-009

Poster

0830-243

**ANOMALOUS CRUSTAL ROOT BENEATH SAURASHTRA PENINSULA, INDIA-INFERRED FROM ISOSTASY**

Bijendra SINGH, S.K. PRAJAPATI, D.C. MISHRA (National Geophysical Research Institute)

Bouguer anomaly map of Saurashtra plateau depicts (i) large number of circular gravity high associated with known volcanic plugs of Deccan magmatism and (ii) a large wavelength circular gravity low centred over the peninsula suggesting deeper causative. Since, this low bears an inverse relation with the regional topography it may result from mass deficiency resulting from thickening of crust caused by isostatic compensation. Deep seismic sounding (DSS) result along Navibander-Amreli profile over the southern part of the peninsula indicates variation in crustal thickness from 35 Km towards the coast to 42 Km beneath the high lands. Presence of zero free air anomalies in the region of high topography may suggest that the net buoyancy of the thickened crust (crustal root) is close to zero. An unbiased estimate of isostatic regional anomalies is obtained using zero free air anomalies. Assuming that the compensation is at Moho level, modeling of isostatic regional anomalies in terms of Moho variation along DSS profile has yielded a density contrast of  $-0.15 \text{ g/cm}^3$ , which is much less than the expected density contrast of  $-0.40 \text{ g/cm}^3$  across the Moho in normal region. This discrepancy can be explained due to two factors (i) either the crustal root is anomalously dense (ii) or the upper mantle is anomalously light. However, DSS result has not indicated any anomalous velocity structure across the Moho interface hence the issue could not be resolved. In the absence of any conclusive evidence, it is suggested that the region, which has experienced extensive volcanism, lower crust must have been modified due to accretion of mafic igneous layer at the base of the crust and the metamorphism in the crustal root might have increased the root density. Hence it may be argued that, decrease in crustal root buoyancy due to increase in root density may be more plausible explanation for the existence of large crustal root beneath the Saurashtra peninsula.

SW03

**LITHOSPHERIC STRUCTURE OF A SUPERCONTINENT: GONDWANA**

Location: Site A, Room 4

Thursday, July 10 PM

Presiding Chairs: L. Brown, P.R. Reddy, C. Wright, M. Kanao

SW03/10P/A04-001

1400

**PROTEROZOIC PRISM ARRESTS SUSPECT TERRANES: INSIGHTS INTO THE ANCIENT CORDILLERAN MARGIN OF CANADA FROM SEISMIC REFLECTION PROFILING**

Ron M. CLOWES<sup>1</sup>, David B. SNYDER<sup>1</sup>, Fred A. COOK<sup>1</sup>, Philippe ERDMER<sup>1</sup>, Carol A. EVENCHICK<sup>1</sup>, Arie J. VAN DER VELDEN<sup>1</sup>, Kevin W. HALL<sup>1</sup> (<sup>1</sup>LITHOPROBE and Dept. of Earth and Ocean Sciences, University of British Columbia, <sup>2</sup>Geological Survey of Canada, 615 Booth Street, Ottawa, ON K1A 0E9, Canada, <sup>3</sup>Department of Geology & Geophysics, University of Calgary, Calgary, AB T2N 1N4, Canada, <sup>4</sup>Department of Earth & Atmospheric Sciences, University of Alberta, Edmonton, Alberta T6G 2E3, Canada, <sup>5</sup>Geological Survey of Canada, 101-605 Robson Street, Vancouver, BC V6B 5J3, Canada)

The Canadian Cordillera is one of the principal regions from which the hypothesis of exotic, accreted or suspect terranes was developed a few decades ago. However, seismic reflection profiling and field mapping in northwestern Canada reveal a vast volume of Proterozoic strata of largely North American affinity along the margin, leaving little room for the suspect terranes. The Proterozoic strata were deposited in at least three distinct periods between 1840 Ma and 540 Ma, during which compressive deformational events of unknown origin also occurred. The strata form a reflective tectono-depositional prism or wedge that extends as much as 500 km across strike and 1000 km along strike, has a volume greater than a million cubic kilometers, and makes up most of the crust of the northern Canadian Cordillera. The suspect terranes apparently grounded upon and were arrested by this metamorphosed sedimentary prism during a complex interplay of thrusting and strike-slip displacements between 190 and 170 Ma. Thus, the Cordilleran accreted terranes, with the exception of one major terrane, have shallow roots only a few kilometers deep, with no deep crust or mantle attached. The Proterozoic prism was discovered on two new deep seismic reflection profiles in the Yukon (Line 3, ~ 650 km) and northern British Columbia (Line 2, ~ 1245 km in two segments) that were acquired as part of the LITHOPROBE Slave - Northern Cordillera Lithospheric Evolution (SNORCLE) transect. Along Line 3, the layering is visible between 5.0 and 12.0 s (~15 to 36 km depth). It is followed southwestward for nearly 650 km (~ 500 km across strike) and thins to less than 1.0 s (~ 3.0-3.5 km thickness) near the Moho at the

Yukon-Alaska international boundary. Along Line 2, the upper part of the layering correlates with outcrops of Proterozoic (1840 -1000 Ma) strata on the east. Near the outcrop, the layering is >15 km thick. It projects westward into the middle and lower crust for ~ 700 km (~ 350 km across strike) where it disappears as a thin taper at the base of the crust. The layering is disrupted at the Tintina fault zone, a late to post-orogenic strike-slip fault with up to 800 km of displacement, which appears as a vertical zone of little reflectivity on both profiles (~ 300 km apart). Correlation of reflectivity between the profiles and the fault displacement indicate that the metasedimentary layers extend for at least 1000 km along strike. We thus associate this major part of the Cordilleran crust with the Precambrian passive margin following Paleoproterozoic rifting. As shown by structural features in the seismic images, the Precambrian margin experienced tectonic deformation during its long history. The base of the layered reflection zone coincides with the Moho, which exhibits variable reflective characteristics and undulates in a series of broad (~150 km) arches.

SW03/10P/A04-002

1415

**VARIATIONS IN CRUSTAL THICKNESS AND MANTLE STRUCTURE ACROSS THE KAAPVAAL CRATON FROM Pn AND Sn ARRIVALS AND RECEIVER FUNCTIONS**

Cedric WRIGHT<sup>1</sup>, M. Tarzan O. KWADIBA<sup>2</sup>, Eldridge M. KGASWANE<sup>1</sup>, Teresia K. NGURI<sup>1</sup> (<sup>1</sup>Bernard Price Institute of Geophysical Research, School of Earth Sciences, University of the Witwatersrand, Johannesburg, Private Bag 3, Wits 2050, South Africa., <sup>2</sup>Also: Geophysics Division, Department of Geological Survey, Private Bag 3, Lobatse, Botswana., <sup>3</sup>Present address: Council for Geoscience, Private Bag X112, Pretoria 0001, South Africa., <sup>4</sup>PREPCOM CTBTO, Vienna International Centre, P.O. Box 1250, A-1400, Vienna, Austria.)

*Pn* and *Sn* wavespeeds in the uppermost mantle of the Kaapvaal craton are high and uniform, indicating the presence of highly depleted, magnesium-rich peridotite. Pervasive *P* wave azimuthal anisotropy with maximum wavespeeds of about 8.40 km/s at azimuths of about 15° and 35° in the northern and southern regions of the craton, respectively, agrees well with the fast directions for a thicker region of the upper mantle inferred from shear wavesplitting. The presence of such small wavespeed variations in the uppermost mantle allows the use of a simple method of estimating crustal thicknesses below the stations of the Kaapvaal broad-band network using *Pn* times, providing results that have been compared with thicknesses calculated from receiver functions. The average crustal thicknesses for 19 centrally-located stations on each of the northern and southern regions of the craton that yielded well-constrained thicknesses were 50.52 ± 0.88 km and 38.07 ± 0.85 km respectively. In contrast, the corresponding average thicknesses determined from receiver functions were 43.58 ± 0.57 km and 37.58 ± 0.70 km respectively. The systematically lower values for receiver functions in the northern part of the Kaapvaal craton that was affected by the Bushveld magmatism at 2.05 Ga, suggest that the receiver functions do not enable the petrological crust-mantle boundary to be reliably resolved due to variations in composition and metamorphic grade in a mafic lower crust.

SW03/10P/A04-003

1430

**SEISMICITY OF UGANDA DURING THE PAST DECADE**

Fred Alex TUGUME (Geological Survey and Mines Department)

Earthquake occurrence in Uganda is mostly related to the East African Rift System. The country's western border lies within the western branch of this System while the eastern branch is only 200 km from the eastern border in Kenya. The two tectonic features contribute to Seismicity in Uganda. The other tectonic features are the Aswa shear zone running from Nimule at the border of Uganda and Sudan, to Mount Elgon on the eastern border and Katonga fault break which stretches from the foot hills of Mount Rwenzori to the western side of Lake Victoria. This unique tectonic setting makes Uganda one of the most seismically active countries on the African continent as exemplified by some destructive earthquakes that have hit the country. The negative consequences of earthquakes greatly affect adversely the Gross Domestic Product (GDP) of the country. Realizing the significance of this, the Government of Uganda, in the effort of planning for sustainable socio-economic progress has set up a Network of earthquake-recording stations. The Network has been in place for the last decade. Several earthquakes have been recorded and located by the Network. This paper compares the Seismicity of Uganda during the past decade to other previous decades

SW03/10P/A04-004

1445

**DEEP STRUCTURE AND COLLISION TECTONICS OF PAN-AFRICAN OROGENIC BELT: LUTZOW-HOLM COMPLEX, ENDERBY LAND, EAST ANTARCTICA**

Masaki KANAO<sup>1</sup>, Masahiro ISHIKAWA<sup>2</sup> (<sup>1</sup>Department of Earth Science, National Institute of Polar Research, <sup>2</sup>Graduate School of Environment and Information Sciences, Yokohama National University)

Combination of rock velocities with seismic structures has been presented clues to understand structure and evolution of continental lithosphere. Most fruitful works have been addressed for northern hemisphere such as North America and Europe, however, only a few studies have focused on the continental segments in the southern hemisphere that once were the fragments of Gondwanaland. Here we present a tectonic model of the Pan-African orogeny by comparing geophysical data such as by deep seismic probing with laboratory velocities of granulite/gneiss of the Lutzow-Holm Complex (LHC), East Antarctica. The "Structure and Evolution of the East Antarctic Lithosphere (SEAL)" project have been carried out under the framework of the Japanese Antarctic Research Expedition in recent years. Several geophysical studies including deep seismic refraction / wide-angle-reflection surveys have been conducted on continental ice sheet at the LHC. Velocity models and reflection images within the lithosphere had been presented by both active and passive seismic-sources analyses by teleseismic receiver functions. From laboratory measurements, metamorphic rock velocities could reveal that the lower crust (6.9 km/s from refraction) consists of pyroxene granulite. Moreover, middle crustal velocities are equivalent to velocities of mixture of pyroxene granulite (20%) and felsic gneiss (80%). The ratio of pyroxene granulite is similar to that geologically observed as meta-mafic sills which were probably related with mafic magma underplating at Archean. The idea is also supported by model calculation about acoustic impedance that shows middle and lower crustal laminations. These evidences demonstrate that a part of the East Gondwanaland (i.e., Napier Complex) lied under the Pan-African orogenic belt (LHC) and subducted westward. Because it is pointed out that West Gondwanaland descended eastward under the Pan-African belt, the coalescence of both Gondwanaland, i.e. formation process of Gondwana supercontinent is regarded as a collision tectonics along with symmetrical subductions where late Proterozoic island arcs and ophiolites were put between East and West Gondwanaland. Lithospheric structure of the Pan-African belt will be clarified by making deep seismic surveys and the other related geophysical approach to cross over the continental segments in the southern hemisphere that once were the fragments of a Gondwanaland. Deep seismic profiling by LEGENDS (Lithospheric Evolution of Gondwana East Interdisciplinary Deep Surveys) project would be expected to reveal the architecture and lithospheric evolution of these regions. SEAL transect has also been carrying out as a chief contribution for

LEGENDS, to delineate a crustal section in different geological terrains from Western Enderby Land to Eastern Queen Maud Land, Antarctica.

**SW03/10P/A04-005**

**1500**

**WET LITHOSPHERE OF PAN-AFRICAN OROGENIC BELT**

Masahiro ISHIKAWA (Graduate School of Environment and Information Sciences, Yokohama National University)

Plate tectonics is the dominant process on Earth's lithosphere. In strict meaning, earth's shell is composed of not only rigid plates but also fragile plates, and tectonics of earth's surface is regarded as a mixture of rigid-plate tectonics and fragile-plate tectonics. For example, the Asian continent of Eurasian plate never behaves as rigid plate that was destructed and deformed intensely and extensively when the Indian continent collided with it. The similar extensive intraplate deformation (up to 2,500 km wide) together with strike-slip shearing are found in the late Proterozoic Pan-African orogenic belt along East Africa, Arabia, Madagascar, Sri Lanka and East Antarctica (East African orogen) that is a suture zone between East Gondwanaland and West Gondwanaland during the assembly of Gondwana supercontinent. Practically the Pan-African orogenic belt are older than 550 million years, and the area has been extensively remobilized until 550 million years ago (almost Proterozoic/Phanerozoic boundary) in the last stage of amalgamation between East Gondwanaland and West Gondwanaland. In contrast, Archean-Proterozoic continental collisions did not give rise to extensive intraplate deformation. In my opinion, fragile continental lithospheres have been established during late Proterozoic to Phanerozoic assembly of continents, and the fragile-plate tectonics started to operate on earth at Proterozoic/Phanerozoic boundary. Why are the central Gondwanaland and Asia continent so fragile? The common feature is that each continent was a relatively young continent that was established during the coalescence of a number of small geologic bodies such as island arc and microcontinent. For example, the Arabian-Nubian Shield is composed of island arcs and ophiolites that are distributed throughout the area of about 1500 km wide, suggesting that numerous island arcs were amalgamated and probably a large amount of slabs descended beneath the region along the numerous arc-trench systems. Today slab dehydration is the dominant process at subduction zone to add water into Earth's mantle. In particular, the amount of water is expected to be remarkably large during coalescence of island arcs and microcontinents because it involves subduction of oceanic lithosphere along numerous trenches. As mentioned above, a number of subduction zones were apparently working during assembly of Gondwana supercontinent, Pangea supercontinent and Asian continent. Therefore contamination of water into lithosphere must have occurred. As a result of wetting of lithosphere, rheological strength of these continental lithospheres should have been reduced dramatically. I expect that deep seismic profiling across Gondwanaland detects some evidences for water in the uppermost mantle of Pan-African orogenic belt.

**SW03/10P/A04-006**

**1515**

**UNUSAL LITHOSPHERIC STRUCTURE AND EVOLUTIONARY PATTERN OF THE CRATONIC SEGMENTS OF THE SOUTH INDIAN SHIELD**

Pramod Kumar AGRAWAL (National Geophysical Research Institute)

South Indian shield, characterised by several prominent geological and geophysical features, forms one of the most interesting segments among cratonic areas of the earth. It is made up of three distinct tectonic regions: Western Dharwar craton (WDC), Eastern Dharwar craton (EDC), and Southern Granulite terrain (SGT). Except WDC, the entire crust beneath EDC and SGT has been remobilized several times since their formation during Mid to Late Archeans. In order to understand its evolutionary history, a multiparametric geological and geophysical study has been made which indicates that the south Indian shield, characterized by a reduced heat flow of 23-38 mW/m<sup>2</sup> has a much thinner (88-163 km) lithosphere compared to about 200-450 km found in other global shields. Significantly, in the EDC-SGT terrain, high velocity upper crust is underlain by considerably low lithospheric mantle velocity with a thick high conductive/low velocity zone sandwiched at mid crustal level. Our study reveals that the entire EDC region is underlain by granulite facies rocks with a density of about 2.85 to 3.16 g/cm<sup>3</sup> at a shallow depth of about 8 km in the southern part and at even shallower depth of about 1 to 2 km in the northern part below the Archean granites of the Hyderabad region. Cratonic mantle lithosphere beneath EDC may contain a highly conductive and hydrous metasomatic zone between the depth of 90 and 110 km where estimated temperatures could be in the range of 900-1000°C. It is likely that before the early Proterozoic, the entire south Indian shield may have been a coherent crustal block which subsequently got segmented due to persistent episodic thermal reactivations during the last 2.6 Ga. These reactivations may have led to self destruction of cratonic roots giving rise to negative buoyancy at deeper levels which may have caused crustal remobilisations, regional uplifting and erosion of once substantially thick greenstone belts. It is thus surmised that the crustal column beneath the EDC may be highly evolved corresponding closely to granulite facies rocks at depth.

**SW03/10P/A04-007**

**1530**

**CHIPPING OF CRATONS AND BREAKUP ALONG MOBILE BELTS OF A SUPER CONTINENTAL ASSEMBLY**

Veeraswamy KOPPIREDDI, Upendra RAVAL (National Geophysical Research Institute (NGRI))

Probably the most important heterogeneity of a continental lithosphere is the significant difference in the thickness and properties of its cratonic and mobile parts. It is seen that the trans-continental mobile belts (Paleo-orogens/paleo-sutures) represent a thinner lithosphere possessing relatively warm, wet and weak nature. This makes it quite vulnerable to episodic thermomechanical interactions due to asthenospheric (mantle plume) upwelling as well as compression. This study presents evidences from the Indian continental lithosphere to show that these properties of mobile belt facilitate channeling of thermomagmatic flux in both lateral as well as vertical directions and can account for the concentration (or focusing) of geophysical anomalies, tectonomagmatic features and strain along these mobile belts. From the example of three continental breakups of India since the Cretaceous it is seen that a combination of sufficiently weakened mobile belt and mantle plume could become fatal for the super continental stability. On the other hand thick or deep-rooted (>200 km) continental lithosphere beneath cratons are characterized by relatively dry, cold and rigid lithospheric column, which resists the penetration of asthenospheric mantle upwelling. From this the long term stability of the cratons also follows since the deepseated thermomagmatic disturbances are channeled mostly along and through the mobile belts. This difference in cratonic and mobile belt regimes is exhibited in form of strongly heterogeneous thermal blanketing. However, in certain situations the edge of a cratonic region may get chipped-off as exemplified by the Antongli and Masora blocks (now lying on the Madagascar) from the Western Dharwar craton during India-Madagascar separation. On the basis of worldwide case histories it seems that the process of breakup along pre-existing mobile belts and chipping of cratons is globally applicable.

**SW03/10P/A04-008**

**1600**

**HOW GEOPHYSICAL SIGNATURES STRENGTHEN THE GEOLOGICAL MODELS OF SUPER CONTINENTS-INDIAN EXAMPLES**

Reddy Ramachandra P. (CSS Division, National Geophysical Research Institute)

Models on Gondwana assembly breakup and reassembly are based on wealth of geological, geochemical, geochronological and geophysical data. Those who are actively involved in building up evolutionary models of super continents should visualize the assembly, disruption and reassembly of super continental configuration through an understanding of the continental dynamics. For this it is essential to synthesize both geological and geophysical results. In support of the necessity to synthesize various data sets especially usage of deep geophysical surveys data some salient features associated with the south Indian shield are listed below. Geophysical studies on deep continental crust assume great significance in terms of continental lithospheric dynamics (a vital component in the assembly, break up and reassembly of super continents) primarily because much of the upper crust has developed in processes that involve the deep crust. The architecture of the cratons, especially their relationship with mobile belts and the intersecting shear zones (eg. Palghat-Cauvery, Moyar-Bhawani and Achankovil vis-AEvis Ranatsor in Madagascar) that may mark collisional sutures, are primary targets for deep geophysical studies as they provide greater insight into the configuration and depth extension of the mega and macro lineaments and their control over the present day tectonic configuration of the area and adjoining segments of the East Gondwana super continent. This has been amply proved by the studies in India. The significant oppositely angled crescent shaped Cuddapah basin and trends of Chitradurg-Shimoga schist belt and Clospet granite indicate presence of collision tectonics. Results from seismic tomography, deep seismic refraction and seismic receiver function studies have clearly shown that the middle part (known as Eastern Dharwar Craton, EDC) is underlain by thin crust compared to the adjacent Western Dharwar Craton, (WDC) and Eastern Ghat Mobile Belt (EGMB). The distribution of proterozoic diamondiferous Kimberlite province of India along a NE-SW trending linear belt falls within the EDC suggesting the dual impact caused by super plume activity and collisional tectonics. This resulted in updoming of crustal (which subsequently got eroded leaving a thinner crust) with presence of deep seated vents. When we look at the structural and evolutionary signatures associated with different granulite-facies terrains, (even though of different geologic periods) especially the two western segments of Gondwana east super continent viz southern Granulite terrain of India, the Mozambic belt and Madagascar we notice that as in the case of east-central, north east- Tanzania and south east Kenya the northern segment of southern granulite terrain of India has granulite-facies metamorphism resulting from crustal thickening. Seismic reflection/refraction experiments have helped in bringing out crustal structure of the region, stressing the need for an integrated data analysis and initiation of LEGENDS programme.

**SW03/10P/A04-009**

**1615**

**A PLATE TECTONIC MODEL FOR EVOLUTION OF SCHIST BELTS AND GRANITE PLUTONS OF DHARWAR CRATON, INDIA AND MADAGASCAR DURING 3.0-2.5 GA: INSIGHT FROM GRAVITY MODELING CONSTRAINED IN PART FROM SEISMIC STUDIES**

Dinesh Chandra MISHRA, S.K. PRAJAPATI (National Geophysical Research Institute)

Gravity modeling of an E-W profile across Dharwar Craton, India and Madagascar, integrated with the results of Deep Seismic Sounding (DSS) across the Dharwar Craton suggest a thick crust of 40-42 km under the Eastern Dharwar Craton (EDC), the Western Dharwar Craton (WDC) and the central part of the Madagascar. Towards east of these blocks, the crustal thickness is reduced to 36-38 km along the Eastern Ghat Fold Belt (EGFB), Shear Zone between the EDC and the WDC and the east coast of Madagascar, respectively. These zones of thin crust are also characterized by high density lower crustal rocks associated with thrusts. The seismic section across Dharwar Craton shows domal shaped reflectors in the lower crust and upper mantle under the WDC which may be related to asthenospheric upwelling during an extension phase. The occurrences of large schist belts with volcano sedimentary sequences of marine origin of late Archean period (3.0-2.7 Ga) as rift basins in the WDC and Madagascar also suggest an extensional phase in this region during that period. It is followed by a convergence between the WDC and the EDC giving rise to collision related shear and thrust zones between the WDC and the EDC associated with high density lower crustal rocks. The seismic section shows upwarded reflectors in the upper crust which may be related to this convergence. Eastward dipping reflectors under WDC and EDC and west verging thrusts suggest convergence from the west to the east which resulted in easterly subduction giving rise to subduction related K-granite plutons of the EDC of 2.6-2.5 Ga. In this regard, the Closepet granite in the EDC which extends almost parallel to the shear zone between the WDC and EDC and shows an I-type calc-alkaline composition may represent relic of an island arc and the linear schist belts with bimodal volcanics of the EDC east of it might have developed as back arc rift basins. Subsequent collision between India and Antarctica along the EGFB during middle Proterozoic, indicated by eastward dipping reflectors in the crust and the upper mantle and west verging thrust gave rise to contemporary high grade rocks of the EGFB (1.6-1.0 Ga) and associated mafic and felsic intrusives of this belt. The part of adjoining Cuddapah basin contemporary to the EGFB towards the west consisting of marine shelf type of sediments which are highly disturbed and thickest at its contact with the EGFB may represent a peripheral foreland basin.

**SW03/10P/A04-010**

**1630**

**HEAT FLOW IN THE INDIAN SHIELD: INTERPRETATION FOR CRUSTAL THERMAL STRUCTURE**

Roy SUKANTA, Labani RAY, Senthil Kumar P., Koti Reddy G., Srinivasan RAMASWAMIAH (National Geophysical Research Institute)

Data on geothermal gradients representative of regional crustal conditions have been acquired through temperature measurements in 183 boreholes and 2 deep mines. Combining with thermal conductivity data on rocks over relevant depth sections, heat flow could be evaluated at many localities in India covering Precambrian provinces, Gondwana basins, and the Tertiary Cambay basin. The following general characteristics emerge from the data set. (i) The Archaean Dharwar greenstone-granite-gneiss province (DP) and the adjoining Southern Granulite Province (SGP) have heat flow ranging from 25 to 50 mW m<sup>-2</sup>. This low heat flow level is found to hold over the Deccan Volcanic Province in the region south of the Son-Narmada-Tapti lineament zone in central India, and also in the western fringes of the Proterozoic Cuddapah basin, both of which have the DP basement. The Proterozoic segments covered so far have revealed heat flow higher than 50 mW m<sup>-2</sup>: 59 to 63 in the Singbhum Thrust Zone, 51 to 62 in the Bastar craton, and 56 to 96 in the Aravalli province. The Gondwana basins have a generally high but variable heat flow, 46 to 107 mW m<sup>-2</sup>. The Tertiary Cambay basin has high heat flow of 75 to 96 mW m<sup>-2</sup> in the northern part, and a lower heat flow, 55 to 67 mW m<sup>-2</sup> in the southern part. With data on radiogenic heat production of major crustal litho-units, and structural constraints from other geological and geophysical data, 1-D models of crustal heat production have been envisaged for the DP, and in the case of the SGP, for the block to the north of the Palghat-Cauvery lineament (NB).

Based on these models and heat flow data, crustal contribution to heat flow has been estimated and the mantle heat flow has been deduced. Estimates of crustal temperatures have been made using generalized functions for depth dependence of thermal conductivity in the crust. Mantle heat flow is 11 to 19 mW m<sup>-2</sup> in the DP, similar to other Precambrian provinces of the world studied so far. However, it is significantly higher, 25 to 30 mW m<sup>-2</sup>, in the NB of the SGP. This result is in conformity with the crustal and sub-crustal velocity structure emerging from tomographic studies, and with geochemical and isotopic data that point to LILE-enriched mantle. Temperature at the Moho is estimated to be in the range 285 to 410 °C in the DP and 580 to 660 °C in the NB of the SGP. Crustal thermal structure(s) for other parts of the Indian shield can be established with confidence only when additional heat flow coverage and information about the structure and composition of the Indian lithosphere are obtained from on-going as well as planned geophysical studies.

**SW03/10P/A04-011****1645****DEEP ELECTRICAL STRUCTURE ALONG KOLATTUR - PALANI PROFILE IN SOUTHERN GRANULITE TERRAIN, INDIA**

Harinarayana T. TIRUMALACHETTY, Naganjaneyulu K. (Magnetotellurics, National Geophysical Research Institute)

Broad band magnetotelluric (MT) investigations were carried out along a profile from Kolattur in the north to Palani towards the south in southern granulite terrain (SGT). This 160 km long profile was covered with 18 stations at an interval of 8-12 km and traversing across the Palghat-Cauvery shear zone (PCSZ). The MT data is subjected to robust processing, Groom-Bailey decomposition and static shift correction before deriving a 2-D model. The 2-D model showed anomalous electrical conductivity at mid-lower crustal depths bounded by shear zones. The salient features of the model are: the upper crust is high resistive (10 000 – 40 000 ohm-m) and the mid-lower crust is less resistive (< 3000 ohm-m) between the Chennimalai Shear zone (CSZ) and PCSZ. These results have shown good correlation with results from other geophysical studies like deep seismic soundings (DSS), gravity and magnetics. The conductive layer at mid-lower crustal depth correlates with low velocity layer and anomalous gravity high observed in the region. The relation between the geophysical signatures and the tectonics of the region is discussed.

**SW03/10P/A04-012****1700****THE CAUVERY SHEAR ZONE, SOUTHERN GRANULITE TERRAIN, SOUTHERN INDIA: PALAEO- AND NEOPROTEROZOIC TECTONICS**

Talari Ramakrishnaiah CHETTY, Rao Jyothi Bhaskar YERRAGUNTLA (Geological Studies Division)

Structure and tectonics of the southern Granulite Terrain (SGT), southern India is highly relevant to the models of Gondwana supercontinent reconstruction. The east-west trending Cauvery Shear Zone (CSZ) is the most prominent crustal-scale (~350x70km) tectonic feature in the SGT straddling the boundary between the Archaean Dharwar Craton and the Proterozoic granulite terrains. Amphibolite and granulite-facies rocks retrogressed variably are exposed all along this deep crustal ductile shear zone. A synoptic structural interpretation of Landsat TM data was followed by extensive geological mapping and structural analysis along a 100 km - wide north-south corridor orthogonal to the shear zones. The study reveals several prominent east-west trending shear zones, many of which are delineated for the first time. Some of the shear zones separate distinct geological domains in terms of lithology, structural style, and their crust formation and metamorphism of the basement gneisses (Model Nd ages, Rb/Sr mica and Sm/Nd garnet ages). The shear zones include: the Moyar-Bhavani (MBSZ), the Chennimalai-Noyil (CNSZ), the Dharapuram (DSZ), the Devattur-Kallimandayam (DKSZ), and the Kodaikanal-Oddanchatram (KOSZ). From the foliation geometries, it is observed that the MBSZ at the northern limit of the CSZ dips steeply to south while others dip moderately to north. Kinematic observations such as deflection of foliations, fish-tail structures and S-C fabrics indicate dextral movements. Our studies indicate that the regional deformation can be rationalised in terms of two major episodes: the Palaeoproterozoic and the Neoproterozoic. The former resulted in large-scale north verging thrusts accompanied by north-south shortening while the latter (750-500 Ma) is manifest in extensive shearing, granite emplacement and migmatization. The MBSZ acts as a major zone of kinematic partitioning and represents a southerly dipping Palaeoproterozoic frontal thrust. The disposition, regional geometry, kinematic patterns, and the contemporaneity of mylonitic fabrics based on Rb-Sr mica ages suggest that the shear zone network could form a crustal scale flower structure during the Neoproterozoic, which is structurally akin to many collisional orogens elsewhere. This Neoproterozoic deformation was progressively more transpressive with high-angle convergence and flattening strains consistent with the collisional regimes. A critical reappraisal of contemporaneous structures in other juxtaposed continental blocks of the East Gondwana would be rewarding.

**SW03/10P/A04-013****1715****ACID MAGMATISM IN SOUTH INDIAN GRANULITE TERRAIN AND ITS IMPLICATIONS IN RECONSTRUCTION OF EASTERN GONDWANALAND**

Rao Mallikharjuna JUPUDI, Rao Rama P. (Geological Studies Division)

India, which is a part of Eastern Gondwanaland together with Madagascar, Sri Lanka, Antarctica and part of Australia till their break-up and moved apart during Mesozoic time, is important in understanding the tectonothermal and metamorphic events recorded in Precambrian times. The south Indian craton has well preserved tectonic features, acid and basic magmatic activity of different ages, and different grades of metamorphic terranes subjected to multi-deformational events during the past. Two distinct age groups of granitic activity noticed, one in the northern part of Dharwar craton which is partly of Archaean age and the other in the southern Proterozoic mobile belt of Pan-African time (800-500 Ma). In an attempt to study acid magmatism and crustal structure in south India, multidisciplinary studies were taken-up along the N-S trending Kuppam-Palani geotranssect. The area has been divided into three blocks based on the structure, lithology, tectonic features and metamorphic assemblages namely, the northern block from Kuppam to north of Moyar-Bhavani shear zone, the central block encompassing the area between the Moyar-Bhavani shear zone and Palghat-Cauvery shear zone and southern block from south of Palghat-Cauvery shear zone up to Palani. Thermobarometric studies on the granulites from the three blocks have shown that the northern and southern blocks depict similar P-T conditions (600-700°C and 6-7 kb) while the central block between Moyar-Bhavani and Palghat-Cauvery shear zone depicts a higher P-T regime (740-950°C and 8.2-10 kb). The Proterozoic granulites mostly show tonalitic character and similarity to the granite-gneisses of the low-grade terrain and are restricted to the north of Palghat-Cauvery lineament. The younger granulites are leucocratic and are mostly white and medium to coarse grained while the pink phases of coarse grained to pegmatoidal types also occur at places. Geochemical characters of these granites indicate their anorogenic nature. The granites from the northern block are tonalitic and metaluminous in character while these from central and southern blocks are granodioritic to granitic and are peraluminous. Rare earth element fractionation trends vary considerably within the granite plutons and exhibit both positive and negative Eu

anomalies. Geochronological data on these granites indicate that the entire south Indian craton had witnessed a major extensional tectonic regime during the Pan-African times leading to large scale crustal anatexis resulting in the emplacement of several granites of Neoproterozoic age. Such wide-spread granitic activity has also been documented in Madagascar, Sri Lanka and Antarctica thereby providing similarities in the crustal fragments of East Gondwanaland.

**SW03/10P/A04-014****1730****SHEAR WAVE STRUCTURE OF THE DHARWAR CRATON (INDIA) FROM RECEIVER FUNCTIONS**Sarkar DIPANKAR<sup>1</sup>, Ravi Kumar MANGALAMPALLY<sup>1</sup>, Joachim SAUL<sup>2</sup> (<sup>1</sup>National Geophysical Research Institute, <sup>2</sup>GeoForschungs Zentrum)

Modelling of receiver functions using teleseismic data from six broadband stations on the Archaean Dharwar craton indicates that the shear structure of the entire crust is largely simple. The crust is devoid of major intra-crustal discontinuities, and shows a low Poisson's ratio. However, the results of earlier wide-angle experiments indicated presence of a mid-crustal boundary in the compressional velocity models. It is possible that the Dharwar crust is divided into a more felsic upper crust with a Poisson's ratio lower than 0.25 and a mafic lower crust with a correspondingly higher Poisson's ratio. Such a partitioning need not necessarily require a strong mid-crustal S velocity contrast and may manifest as a contrast in P velocities only. The Western Dharwar Craton (WDC) is distinctly thicker than its eastern counterpart (EDC). Formation of the Cuddapah basin did not significantly alter the crustal configuration, as testified by thin and simple crust. It appears that WDC does not extend much to the north underneath the Trap cover, as the crust below the Deccan Volcanic Province is more akin to EDC crust in terms of thickness.

**SW03/10P/A04-015****1745****LITHOSPHERIC STRUCTURE OF EAST GONDWANALAND: REVIEW AND PREVIEW**

Larry Douglas BROWN (Institute for the Study of the Continents, Cornell University)

Deep seismic reflection profiling over the past two decades has revealed critical aspects of lithospheric structure beneath many of the continents. However, such surveys are notably lacking for most of the continental fragments that once constituted the supercontinent of Gondwanaland. In fact, seismic data in general on deep structure in these regions are quite sparse. Previous work in East Gondwanaland has been limited to only two large scale field initiatives (e.g. the KRISP refraction studies of the East African Rift (EAR) zone; the KAAPVAL passive seismic study of lithospheric structure beneath the Archaean of southern Africa), a few smaller scale studies (e.g. heat flow and passive seismic studies of the Tanzania craton and adjacent EAR) and some attempts to image mantle structure using global/regional techniques (e.g. surface wave tomography of upper and lower mantle beneath Africa). More extensive are the oil industry surveys of the passive margins of East Africa/Madagascar and potential field coverage. However, most such studies have focused on recent tectonics (the East Africa Rift system or suspected mantle plumes), Archaean craton evolution (e.g. KAAPVAL Project) or continental breakup (oil exploration on margins). Geophysical constraints on lithospheric structure associated with the late Proterozoic amalgamation of Gondwanaland are particularly wanting, even within India where an ambitious program of deep geophysics has probed a number of continental structures over the past several decades. The main exceptions to this generalization are the deep seismic surveys in Australia and a few deep surveys in Antarctica. Here I will review the existing deep geophysics for East Gondwanaland as a preview of proposed future deep seismic profiling (LEGEND) in the circum-Indian Ocean region and the major geotectonic issues that can be addressed.

S

**SW04****EFFECTS OF EARTHQUAKES ON MEGACITIES**

Location: Site A, Room 13

Wednesday, July 9 PM  
Presiding Chairs: Y.-T. Chen, K. Irikura

**SW04/09P/A13-001****1400****SEISMIC VULNERABILITY OF INDIA'S URBAN AREAS**

Sitharama Murty KOTTAPALLI (Coordinator of Geoarcsives, International Commission on the History of Geological Sciences (INHIGEO))

India has long known for its villages and agricultural economy. But its demographic trends reveal that at the beginning of the 20<sup>th</sup> century its urban population was less than 11% (25.8 million) and it rose to 17.29% in 1951 after Independence (62.4 million). The 1991 census indicated that 217.2 million live in urban areas, constituting 26% of the total population. By 1995, it increased to 281.2 million, 30% of the population. The urban population may have risen to 335 million (33.5%) at the beginning of the 21st century. In terms of growth of urban centers, between 1901 and 1991 the number was 1811 with number of cities (100,000 and above) being 24. These figures correspondingly rose to 2795 and 76 in 1951. The 1991 census figures are 3609 urban centers and 300 cities. The extra-peninsular region of India has been known to the one of high seismic activity, with at least 30 major earthquakes measuring above 5.5 on Richter scale striking it between 1720 A.D. and 1988. The main urban centers of India are located in this region that extends from Jammu and Kashmir to North-east along the Himalayan belt, apart from the western India that includes Rajasthan and Gujarat. The Peninsular part was for long believed to be free from seismic activity though there were some significant quakes in that part also. The 1967 Koyana earthquake proved this belief wrong and it compelled revision of the seismic zoning of India quite radically. The 1969 Bhadrachalam quake, 1993 Latur quake and 1997 Jabalpur quake confirmed the seismic nature of the peninsular region. The recurrence of this activity in Maharashtra, Andhra Pradesh and Central India in the last five years leaves very little part of India that is free from seismic vulnerability, e.g. Kerala, Orissa, Rajasthan and West Bengal being the exception. Mumbai, Delhi, and Hyderabad are vulnerable, while Chennai and Calcutta may not be. The seismic zonation points out that majority of the urban areas and cities have the seismic risk.

**SW04/09P/A13-002****1415****MODELLING OF SEISMIC GROUND MOTION AND ITS AMPLIFICATION ALONG SOME 2-D PROFILES IN THE CITY OF DAMASCUS, SYRIA**Randa MOHAMAD<sup>1</sup>, Peter SUHADOLC<sup>2</sup>, Franco VACCARI<sup>1</sup>, Wathek RASOUL-AGHA<sup>4</sup> (<sup>1</sup>)

General Establishment for Geology and Mineral Resources, Damascus, Syria, <sup>2</sup>) Department of Earth Sciences, University of Trieste, Trieste, Italy, <sup>3</sup>) The Abdus Salam International Center for Theoretical Physics, Trieste, Italy, <sup>4</sup>) Department of Geology, Damascus University, Damascus, Syria)

Damascus is the capital and the largest city of Syria, with a population of about 7 million people. It is located at the southern part of the country not far from the Lebanese border and the Dead sea fault system, in particular from one of its branches the Sergayah fault. The latter in particular is a quite active fault system and the main seismic source for both destructive historical events felt and instrumental seismicity recorded in Damascus. To model seismic ground motion in Damascus basin and to estimate its amplifications we use a 2-D hybrid method coupling modal summation with finite differences. This technique allows us to compute ground motion in laterally heterogeneous anelastic media. Synthetic seismograms with a cutoff frequency of 5 Hz are created along four 2-D profiles passing through the city of Damascus for four possible seismic sources with assumed magnitudes around 6.5 located on the Dead sea fault system and on the Sergayah fault. The average regional structural model and the laterally heterogeneous parts of the profiles have been derived from detailed geological and geotechnical data available for the investigated area. From the computations we can infer that the maximum ground motion amplification values in Damascus basin are generally found at frequencies around 2 Hz and 4 Hz.

SW04/09P/A13-003

1430

#### RUPTURE PROCESS OF THE KUNLUN MOUNTAIN PASS EARTHQUAKE OF NOVEMBER 14, 2001 FROM LONG PERIOD WAVEFORM DATA

Yuntai CHEN, Lisheng XU (Institute of Geophysics, CSB)

We have inverted long period P-waveform data recorded by the Global Digital Seismograph Network (GDSN) to obtain the temporal and spatial rupture process of the Kunlun Mountain Pass earthquake of November 14, 2001. The inverted final slip-distribution indicates that while the length of the rupture area with slip amplitude greater than 0.5m was about 600km, 250km in the west and 350km in the east to the epicenter (35.97°N, 90.59°E), which was greater than the length of the observed surface rupture (about 440km), the length of the rupture area with slip amplitude greater than 1.0m is about 420km, 120km in the west and 300km in the east to the epicenter, which was nearly agreed with the length of the observed surface rupture. Two high slip areas, i.e., the area with slip amplitude greater than 1.5m, were recognized. One is between the positions of 30km east to the epicenter and 80km west to the epicenter, with the length being about 110km, and the other is between the positions of 150km and 280km east to the epicenter, with the length being about 130km. The later high slip area just corresponds to the Kusai Lake segment of the observed surface rupture and its eastern extension where most heavily broken ground surface was observed. The inversion results indicate that the slip distribution on the fault plane was heterogeneous, with the maximum slip amplitude being 2.2m and the average one being about 1.2m. The maximum stress drop was estimated to be 7.9MPa, and the average one was about 4.0MPa. Three distinct subevents could be recognized in the inverted temporal and spatial rupture process. The first subevent was temporally from the beginning to the 60th second, and spatially between the positions of 30km east and 150km west to the epicenter, which was overall a unilateral rupture from east to west, with an average rupture propagation velocity of 3.8km/s. The second subevent was temporally from the 52th second to the 92th second, and spatially between the positions of 100km and 200km west to the epicenter, which was overall a unilateral rupture from west to east, with an average rupture propagation velocity of 3.1km/s. The third subevent was temporally from the 56th second to the 140th second, and spatially between the positions of 30km and 330km east to the epicenter, with an average rupture propagation velocity of 2.7km/s. These three subevents had different sizes, respective overall rupture directions and variable rupture velocities, whereas as a whole the rupture of the Kunlun Mountain Pass earthquake was unilateral from west to east.

SW04/09P/A13-004

1445

#### EARTHQUAKE FATALITY SYNDROME

Vasile I. MARZA (Seismological Observatory, Institute of Geosciences, University of Brasilia, CP 04598, Campus Universitario, Brasilia, DF, CEP 70910-900, Brazil, email: <marza@unb.br>), On leave from Seismological Laboratory, NI(RD)EP, Bucharest, Romania)

There is fairly convincing anecdotal evidence that, in many instances of fatal earthquakes, the formal death toll counts are biased. Indeed, a closer look at the earthquake fatality estimates shows that many of them are underestimated, a condition referred to as "earthquake fatality syndrome", i.e., a rather large inconsistency between the official assessment and the informal appraisal(s). This discrepancy may be quantified by a "fatality syndrome factor", defined as the ratio between informal to formal estimates, having as a rule a value 2 to 3 (at least). The thesis is exemplified through several typical and well-substantiated case events like: the Tangshan, China, 1976 infamous earthquake (approx. 750,000 informal human cost vs. 242,000 official life loss), the Izmit, Turkey, 1999 calamitous shock (around 45,000 vs. 18,000), the Gujarat, India, 2001 hard-hitting earthquake (in between 30,000 to 50,000 vs. 20,000), the Michoacán, Mexico, 1985 horrendous event (about 20,000 vs. 9,500), the Vrancea, Romania, 1977 freak earthquake (close to 5,000 vs. 1,700), or the San Francisco, California, 1906 refashioned earthquake [roughly 3,000 (modern estimate) vs. possibly 700 (contemporary estimate)] etc. The above figures are documented, their confidence is assessed and some simple statistics is worked out in order to provide a foundation and certain insights towards the existence of an earthquake fatality syndrome. Among the possible causes/explanations for this elusive but rather systematic bias in earthquake fatality assessment we advance: the lack of transparency and slowness in communicating the earthquake effects, the emotive/idiosyncratic and pressing working environment in the aftermath of the killer earthquakes, the incompetence to manage disaster crises, the inadequate information systems available at the best of times or simply trivial mistakes. Often the totalitarian penchant for secrecy and as well as the closed character of some authorities undoubtedly contribute to the above causes. A by-product of this note is the revising/producing of "the top ten"-like lists of the deadliest ever earthquakes and of the 20th century worst earthquakes. Finally, the author aware that the idea set out here is likely to be distasteful or even heretical for someone from the conventional wisdom or officialdom, he hopes that the discussion will trigger a paradigm shift in death toll count methodology for a decent, more reliable and realistic earthquake (or other disasters) fatality/casualty estimates.

SW04/09P/A13-005

1500

#### EVALUATION OF THE CITY'S ABILITY FOR SEISMIC DISASTER PREVENTION

Li-Li XIE<sup>1</sup>, Feng-Hua ZHANG<sup>2</sup> (<sup>1</sup>Institute of Engineering Mechanics China Seismological Bureau, <sup>2</sup>Harbin Institute of Technology, <sup>3</sup>Department of Bridge Engineering, Tongji University)

In 1994 the Chinese Government made an important decision that through the ten year's consensus effort by each level of government and whole society, all the large and middle-sized cities in China, with the location along the coast, or with dense population, or with well

developing of economy should be enhanced their abilities for mitigating earthquake disaster with the goal to resist earthquake of Magnitude of six. This paper presents the definition of a city's ability for earthquake disaster mitigation, the components, which affect significantly the city's ability, the criteria, by which, the city's ability for mitigating seismic disaster can be evaluated, and a framework that can quantitatively evaluate the city's ability for seismic disaster prevention. As a result, a simple index is used to describe the comprehensive city's ability for earthquake disaster mitigation. For evaluation of the city's ability for seismic disaster mitigation, the designed framework includes the six major factors: they are the ability of earthquake monitoring and prediction, the ability of seismic hazard assessment, the ability of civil engineering for earthquake resistance, the ability of non-structural elements for earthquake resistance, the ability of communities for earthquake disaster prevention and the ability of seismic emergence responding and recovering after the earthquake. And for each major factor, it also includes several levels sub-components. For example, the ability of civil engineering covers the abilities of buildings, lifelines, infrastructures and so on. Finally as examples, ten cities over the world have been evaluated for their abilities in seismic disaster mitigation. Some important and interesting issues are concluded.

SW04/09P/A13-006

1515

#### DAMAGE AT AHMEDABAD CITY DUE TO INTRAPLATE MW 7.7 BHUJ, INDIA EARTHQUAKE OF 26 JANUARY 2001

Bal Krishna RASTOGI, Prantik MANDAL (Seismology Group, National Geophysical Research Institute, Hyderabad, India)

The Intraplate Mw 7.7 Bhuj, Western India earthquake of 2001 caused destruction/damage of reinforced concrete buildings, collapse of some weak single or double storey houses, damage to several archeological monuments and cracks in almost all the buildings in Ahmedabad city situated at 250 km distance from the epicenter. For the first time in India multistorey buildings have been ruined due to any earthquake. The maximum intensity was X+ in the epicentral zone and VII in Ahmedabad. The acceleration estimated at the epicenter is 1g and at Ahmedabad the recorded acceleration is 0.11g. Ahmedabad city falls in Seismic Zone III of the seismic zoning map of India where MMI intensity of VII is expected. Alluvium thickness of about 300 meters partially influenced the damage pattern as Ahmedabad city is located along Sabarmati River in the Cambay Rift Basin. Out of about a thousand high rises (G+10) and 12000 odd low-rise (G+4) buildings, 69 collapsed resulting into 746 casualties. About 2350 such buildings suffered structural damage. The buildings that conformed to the codes survived. Faulty designs (structural engineers were hardly consulted and others were generally unaware of earthquake codes), as mentioned below, are the main causes of destruction of multistorey buildings: • "Soft first storey" for parking space without adequate column strength resulted in collapse or tilting of whole structure. Shear failure at the gap between top of ground floor columns and the beams above to accommodate beam reinforcements. Concrete quality in columns was poor. Columns were often of small 1/2 brick width for embedding in masonry partition walls and beams of shallow depths often equal to slab width to save on height. • Deficiency in structural formwork (shuttering) as reinforcement cage is not properly tied and spacers are avoided. • Shallow (only 75) footings for columns below the basement floor level without tie beams even in soft soil for even 11storey buildings. Pile foundations are not used. • To meet the "floor space index" and for providing more floor space from 1st floor onwards, large portions of buildings are constructed on floating columns and with balconies on cantilevers giving flower-shaped plans. • Out of phase vibrations of two or more blocks in different directions joined together through a common staircase or elevator. • The reinforced concrete elevator shaft and plain masonry staircase was not tied adequately to the reinforced concrete floors. • Huge concrete water tanks (swimming pool in one case) at the top where seismic forces are amplified, due to their eccentricity, resulted in overturning effects on the buildings. • Total absence of detailing provisions to accommodate lateral shearing.

SW04/09P/A13-007

1545

#### CATALOGUE BY LOSSES FORMATION FACTORS INFLUENCE VULNERABILITY OF BUILDING AND CONSTRUCTIONS IN SEISMOACTIVE TERRITORIES OF UZBEKISTAN

Ikrarov TIMUR (Post Graduate Student of the Institute of Seismology of Academy Sciences of Uzbekistan)

**Objective:** Implementation of GIS-based earthquake loss estimation methodology for use in Uzbekistan. **Scope:** Deterministic earthquake hazard analysis (scenario earthquake) for Tashkent Metropolitan Area utilizing data from the RADIUS project. **Features:** 1. Application of GIS software. 2. Developing of digital maps for structure inventory (cadastre) and soil conditions. 3. Computation of ground motion intensity through empirical relationship attenuation of the seismic waves. Thus, the first for the Uzbekistan have composed (first variant) of Catalogue all loss of factors that consist of the next parameters: seismically, seismotectonically, engineering-geologically, technogenic and geophysically (Ibragimov R.N., Khuday-bergenov A.M., Nurmatov U.A. and others, in published, 2002). With aim of define more precisely of estimation seismic hazard, that Catalogue is compare with vulnerability curves of civil construction, those today are exploitation. Catalogue and out work methodology of "Estimation Economic Consequences of Large Earthquake" for example on the Tashkent metropolitan area that will be very usefully for estimation seismic hazard of the capital of Uzbekistan the Tashkent city. To serve above mentioned purposes it is advisable to take advantage of risk based approaches to the problem of urban planning and disaster preparedness in Tashkent metropolitan area located in high seismic areas, to use state of the art techniques, including GIS-technologies, for development of seismic risk management plans. On this basis it would be possible to indicate reasonable criteria for decision makers to be used when selecting priorities and immediate directions for disaster mitigation measures for this urban areas. Another important subject is seismic risk assessment for individual private construction sites, buildings with the purpose of optimum antiseismic design. It is a matter of great significance to introduce the concept of seismic risk into practice of seismic design and construction in Uzbekistan and other countries of Central Asia.

SW04/09P/A13-008

1600

#### SEISMIC RISK IN THE NEW CITIES OF THE UNITED ARAB EMIRATES, AN APPROXIMATE ESTIMATE

Max WYSS<sup>1</sup>, Azm AL HOMOUDE<sup>2</sup> (<sup>1</sup>WAPMERR, <sup>2</sup>American University, Sharjah, United Arab Emirates)

We estimate the losses due to 10 scenario earthquakes in 150 settlements of the United Arab Emirates (UAE). For southern Iran, we use four source zones and the maximum magnitudes in them as determined by GSHAP ( $7.2 < M < 8.1$ ). For six local scenario earthquakes, we use the range  $5.5 < M < 6.5$ , place the sources mainly on mapped faults and vary the distance to major cities from 10 to 60 km. In the test case of the Masafi earthquake (M5, 11 March 2002), the method and data bank we use yield the correct results, suggesting that our approach to the problem is valid for the UAE. The sources in Iran are expected to cause only minor damage, except for an M8.1 earthquake in the Makran region.

For such an event we expect some deaths, several hundred injured and a loss of 3-6% of the value to the building stock in the northeastern UAE, including Oman. The losses for local scenarios with epicenters in the unpopulated areas of the UAE and for scenarios with  $M < 5.8$  are estimated to be minor. Because the two major mapped faults run through several of the large cities, scenarios with short epicentral distances from cities have to be considered. Scenarios with  $M_6$  near cities lead to estimates of about  $1000 \pm 500$  deaths, and several thousand injured. Most buildings are expected to be damaged to a moderate degree and the loss to buildings is estimated around 1/4 of their value. If the magnitude should reach 6.5, the losses to humans and to building value could be staggering. These estimates are approximate because: (1) there exists no local seismograph network that could map active faults by locating microseismicity; (2) there exist no historically old buildings that could serve as tests for effects due to strong ground motion in the past; (3) there exist no microzonation of the subsurface properties in this region of unconsolidated building ground; (4) there exist no detailed inventory of building fragility. Nevertheless, our conclusion that there exists a substantial seismic risk in the UAE is reliable, because our method yields accurate results in the cases of earthquakes with known losses during the last several decades in the Middle East.

**SW04/09P/A13-009****1615****ISTANBUL EARTHQUAKE RAPID RESPONSE AND EARLY WARNING SYSTEM**

Mustafa Ozder ERDIK, Oguz Asim OZEL, Yasin FAHJAN, Hakan ALCIK, Aydin MERT, Muzaffer GUL (Bogazici University, Kandilli Observatory & Earthquake Research Institute, Earthquake Engineering Department, 81220, Cengelkoy, Istanbul, Turkey)

As part of the preparations for the future earthquake in Istanbul Kandilli Observatory and Earthquake Research Institute of Bogazici University (KOERI-BU) in cooperation with other agencies have installed a Rapid Response and Early Warning system in the metropolitan area. For the rapid response system one hundred (100) 18-bit resolution 'dial-up' strong-motion accelerometers were placed in quasi-free field locations (basement of small buildings) in the populated areas of the city, within an area of approximately 50x30 km, to constitute a network that will enable early damage assessment and rapid response information after a damaging earthquake. Early response information will be achieved through very fast acquisition, analysis and elaboration of data obtained from the network. In normal times these stations will be interrogated on a regular basis by the main-data center located at the KOERI-BU. However, after triggered by an earthquake, each station will process the streaming strong-motion data to yield the spectral accelerations at specific periods, 12 Hz filtered PGA and PGV and will send these parameters in the form of SMS (Short Message Service) messages at every 20 s directly to the main-data center through available GSM (Global System for Mobile Communication) network services. A shake map and damage distribution map (using aggregate building inventories and fragility curves) will be automatically generated using the algorithm developed for this purpose. Loss assessment studies are complemented by a large citywide digital database on the topography, geology, soil conditions, building, infrastructure and lifeline inventory. The shake and damage maps will be available on the Internet and will also be conveyed using spread spectrum radio-modem communication to several user nodes, including the governor's and mayor's offices, fire, police and army headquarters within 3 minutes. Full-recorded waveforms will later be retrieved. For the Early Warning system ten 24-bit resolution strong-motion stations were installed on the shoreline as close as possible to the fault area in 'on-line'. The continuous on-line data from these stations will be used to provide near-real time warning for emerging potentially disastrous earthquakes using several alarm levels on the basis of the algorithm developed. The spread spectrum (2.4 GHz) system is the communication system between these stations and the main data center with appropriate repeater stations selected in the region. The initial users of the early warning signal will be nuclear research facilities and critical petro-chemical factories within the region, subway system and several high-rise building. The central data acquisition and processing center houses the dedicated GSM and radio modems and three access servers to provide interface to an Ethernet LAN.

**SW04/09P/A13-010****1630****STRESS-MONITORING SITES FOR MITIGATING EARTHQUAKE HAZARD**

Stuart CRAMPIN<sup>1</sup>, Yuan GAO<sup>2</sup>, Sebastien CHASTIN<sup>1</sup>, Theodora VOLTI<sup>3</sup> (School of GeoSciences, University of Edinburgh, Scotland UK, <sup>2</sup>Centre for Analysis and Prediction, China Seismological Bureau, Beijing 100036, China, <sup>3</sup>Institute for Frontier Research in Earth Evolution, JAMSTEC, Yokohama, Japan)

A new understanding of the way fluid-saturated microcracked rocks deform suggests that networks of stress-monitoring sites could lead to earthquake forecasting analogous to the way networks of meteorological stations allow weather forecasting. In principle, the build up of stress before large earthquakes threatening large cities can be recognised and mitigated hydraulic fracture operations. Both observations and theory for the evolution of fluid-saturated microcracked rock under stress (anisotropic poro-elasticity or APE) demonstrate that in situ rock is weak to shear stress. Consequently, the accumulation of stress before the largest earthquakes necessarily takes place over 10s to 100s of  $M \text{ km}^3$ . The principal effect is that varying pore-pressures modify crack aspect-ratios in systematic ways that can be monitored by analysing shear-wave splitting. Seen with hindsight before about ten earthquakes world wide, this phenomena allows the time and magnitude of impending earthquakes to be stress-forecast. On one occasion we successfully stress-forecast the time and magnitude of a  $M_{AE5}$  earthquake in SW Iceland. Suitable seismic swarms for shear-wave signals are very uncommon. Routine stress-forecasting requires controlled-source Stress-Monitoring Sites (SMSs) in crosshole seismics between 1km-to-2km-deep boreholes to monitor shear-wave splitting along appropriate ray path directions. The first (preliminary) SMS was developed (the EC-funded SMSITES Project) near the onshore continuation of the Húsavúð-Flatay (Transform) Fault at Húsavúð in northern Iceland. Although the borehole geometry is not optimal, we were fortunate to record multi-variable sensitivity to small scale seismicity at 70km distance, confirming both the science and technology of SMSs for stress-forecasting earthquakes. Single SMSs can stress-forecast the times and magnitudes of impending large earthquakes several hundred kilometres from eventual epicentres. This is analogous to a single barometric weather station, where a rapid drop of air pressure indicates the likelihood of nearby storms. Networks of weather stations, allow systematic patterns and variations of weather to be recognised so that weather can be forecast (with all the inherent uncertainties of critical systems). Similarly, networks of SMSs, with a grid size of 200km-to-300km, say, should enable earthquakes  $M = 5$  to be stress-forecast. Since the accumulation of stress is pervasive, if a SMS network indicated that accumulating stress was threatening a vulnerable city, in principle, the overall increase in stress could be reduced by the release of accumulated stress almost anywhere within the larger stressed volume. This could be by a program of hydraulic fracturing in a non vulnerable region, perhaps offshore. Programs for stress mitigation would be extremely expensive, but would be a small premium to pay for mitigating earthquake hazards for a major city. The Kobe earthquake cost \$147B. The overall cost to Tokyo, Beijing, or Los Angeles, could be very much greater. A reasonable premium of 0.5% on \$147B is \$735M (\$735,000,000 US) which would finance a large number of hydraulic fracturing operations.

**SW04/09P/A13-011****1645****REALISTIC MODELING OF SEISMIC INPUT FOR MEGACITIES AND LARGE URBAN AREAS: THE UNESCO/IUGS/IGCP PROJECT 414**

Giuliano Francesco PANZA<sup>1</sup>, Fabio ROMANELLI<sup>2</sup>, THE UNESCO/IGCP/IGCP 414 PROJECT TEAM (<sup>1</sup>Department of Earth Sciences, University of Trieste and The Abdus Salam International Centre for Theoretical Physics, SAND Group, <sup>2</sup>Department of Earth Sciences, University of Trieste)

The project addressed the problem of pre-disaster orientation: hazard prediction, risk assessment, and hazard mapping, in connection with seismic activity and man-induced vibrations. The definition of realistic seismic input has been obtained from the computation of a wide set of time histories and spectral information, corresponding to possible seismotectonic scenarios for different source and structural models. The innovative modeling technique, that constitutes the common tool to the entire project, takes into account source, propagation and local site effects. This is done using first principles of physics about wave generation and propagation in complex media, and does not require to resort to convolutive approaches, that have been proven to be quite unreliable, mainly when dealing with complex geological structures, the most interesting from the practical point of view. In fact, several techniques that have been proposed to empirically estimate the site effects using observations convolved with theoretically computed signals corresponding to simplified models, supply reliable information about the site response to non-interfering seismic phases. They are not adequate in most of the real cases, when the seismic sequel is formed by several interfering waves. The availability of realistic numerical simulations enables us to reliably estimate the amplification effects even in complex geological structures, exploiting the available geotechnical, lithological, geophysical parameters, topography of the medium, tectonic, historical, palaeoseismological data, and seismotectonic models. The realistic modeling of the ground motion is a very important base of knowledge for the preparation of groundshaking scenarios that represent a valid and economic tool for the seismic microzonation. This knowledge can be very fruitfully used by civil engineers in the design of new seismo-resistant constructions and in the reinforcement of the existing built environment, and, therefore, supply a particularly powerful tool for the prevention aspects of Civil Defense. We present a selection of the main results obtained for the cities of Algiers, Beijing, Bucharest, Cairo, Debrecen, Delhi, Naples, Rome, Russe, Santiago de Cuba, Sofia, Thessaloniki and Zagreb.

**SW04/09P/A13-012****1700****COSEISMIC GROWTH AND SEISMIC HAZARDS OF BLIND THRUST FAULTS IN THE OSAKA BASIN, JAPAN - THE UEMACHI FAULT SYSTEM**

Eric Christopher CANNON<sup>1</sup>, Karl J. MUELLER<sup>1</sup>, Yuichi SUGIYAMA<sup>2</sup>, Naoko KITADA<sup>1</sup>, Sean SUNDERMANN<sup>3</sup> (<sup>1</sup>Geological Sciences, Colorado, <sup>2</sup>Active Fault Research Center, Geological Survey of Japan, <sup>3</sup>Geo-Research Institute, <sup>4</sup>William Lettis and Associates)

We investigate segmentation, long-term slip rates, coseismic folding mechanisms, and deterministic earthquake scenarios for the Uemachi fault system in the Osaka Basin, Japan using shallow continuously cored borings and seismic reflection profiles. We seek to understand coseismic growth of fault-propagation folds above blind thrust faults. The segmented 45-km-long Uemachi fault system dips east beneath the Osaka Plain and is overlain by shallow subsurface flexures. We analyze gridded surfaces of marine clay layers Ma13 (9 ka) and Ma12 (127 ka) from cores to determine fault segmentation, vertical displacement, and earthquake events recorded in fold limbs. The Suminoe and Shiombashi flexures, along with the central Uemachi flexure are clearly defined by vertically displaced marine clay layers. We interpret a S-wave seismic profile tied to core where the Yodogawa River crosses the Uemachi flexure. An early Holocene angular unconformity is folded and deformed by layer-parallel faults emerging from strata previously folded in the forelimb of the flexure. A west-dipping, layer-parallel fault appears to have propagated from the upper Tenma Formation into the lower Namba Formation at depths of around 40 m below sea level. A horizon dated at approximately 9.5 ka in the lower Namba Formation is folded upward approximately 3 m westward across the flexure. An 18-m-thick package of growth strata located above the 9.5 ka horizon maintains relatively constant thickness across the fold. These strata are overlain by 2.5-2.9 ka strata that thicken approximately 3 m across the fold, consistent with vertical offset in the 9.5 ka horizon. Assuming a 35° fault dip from Trishear modeling, our preliminary conclusion is that 5.2 m of slip may have resulted from a faulting event 2.5-2.9 ka. We estimate  $M_w = 7.4$  for this event, based on a rectangular fault plane 45 km long and 21 km wide in the downdip direction, 5.2 m of average displacement, and a shear modulus of  $3 \cdot 10^{11}$  dyne/cm<sup>2</sup>.

**SW04/09P/A13-013****1715****DATA BANK OF THE SEISMIC SOIL RESPONSES FOR SOME DENSELY POPULATED AREAS IN ROMANIA**

Stefan Florin BALAN, Carmen Ortansa CIOFLAN, Gheorghe MARMUREANU, BogdanFelix APOSTOL (National Institute of R-D for Earth Physics)

For building safe in Romania, a medium seismicity country, one of the main elements needed to be very well known are the seismic soil responses of the future building sites. In this paper will be analyzed some sites from the cities of Bucharest (capital of Romania), Ploiesti, Iasi and Bacau (important industrial and cultural towns). On these sites were carried out boreholes and geophysical tests to have the geotechnical and geological profiles. As input data for computing the seismic soil response have been chosen the synthetic input of the following Vrancea earthquakes: 30 August 1986 (7.2 MW), 30 May 1990 (6.9 MW) and 31 May 1990 (6.4 MW). Vrancea region is the most active seismic zone of Romania, past earthquakes were of magnitude 7 - 7.5 on the Richter Scale with a lot of life loss and property. All cities mentioned above are on the direction N - E, S - W, main directivity of Vrancea earthquakes. For Ploiesti site were used several variants of fault plane solutions in order to investigate the sensitivity of the method to variations of the seismic source parameters. At present exist many methods of evaluation of the seismic response at the surface of the earth, the majority based on the modeling of the soil deposit like a pack of homogenous and horizontal layers relying on a harder rock, also homogenous but theoretically with infinite thickness, named base rock. Most of these methods are based on the hypothesis that the principal responses of the soil deposit are due to the vertical propagation of shear waves from the base rock. The analytical procedures based on these models/hypothesizes which take into account the non-linear behavior of the soil have given results in accordance with the real behavior of the soil observed "in situ". The authors used a modified Shake91-based program for computing the seismic soil response of our sites of interest in urban areas. In our methodology we determine the variation of G (shear modulus) and D (damping) with the strain in every layer. Soil samples are tested in our Drnevich resonant column and triaxial. As input data, for layers, we use the data got from the geotechnical and geological profiles. For these sites we have computed: stresses and strains for some strata of interest, maximum accelerations at the surface of the soil, amplification spectrum of the soil deposit, response spectrum with different dampings of: 5%, 10% and 20%, acceleration on the base rock - input in deterministic analysis. The data bank consists of 126 graphs. Taking into account the fact that the strong motion records for urban areas

are rather scarce, this data bank will be very useful in assessment of seismic hazard and seismic site effects for microzonation purposes.

**SW04/09P/A13-014**

**1730**

**ASSESSMENT OF SEISMIC POTENTIAL BENEATH SAPPORO-CITY AND ON-GOING ACTION PLAN FOR REDUCTION OF SEISMIC DISASTER**

minoru KASAHARA<sup>1</sup>, Kunikazu YOSHIDA<sup>2</sup>, Tsutomu SASATAN<sup>1</sup>, Masayoshi ICHIYANAGI<sup>1</sup>, Yoshihisa SUZUKI<sup>1</sup>, Kazuyoshi MISONOU<sup>3</sup> (Institute of Seismology and Volcanology, Hokkaido University, N10 W8, Kita-ku, Sapporo, 060-0810, JAPAN, <sup>2</sup>Department of Geophysics, Hokkaido University, N10 W8, Kita-ku, Sapporo, 060-0810, JAPAN, <sup>3</sup>Sapporo Fire Bureau, Sapporo-city Government, S4 W10, Chuo-ku, Sapporo, 064-0804, JAPAN)

Sapporo-city was newly established in 1868 and has rapidly developed as one of mega-city of Japan with 1.9 million populations. Therefore there is no historic record of earthquake damage. However many paleoquaternary faults are found in urban area of Sapporo-city. At least three times paleoquaternary faults have been identified in campus of Hokkaido University during recent 2000 years. The last one might be caused by the 1834 event with magnitude greater than 6.5 which is only one oldest event recorded on documents and might occurred just beneath Sapporo urban area. 36 Felt earthquakes with magnitude greater than 3 originated just beneath Sapporo city have been recorded from 1900 to 2000. The maximum events with magnitude 5 occurred at November 29, 1927 and July 18, 1951. We assessed that Sapporo area may have higher seismic potential than the former assessment. Since 1996 Sapporo-city Government and Hokkaido University have started a project for making new program of seismic disaster reduction. The first step is to establish the basic data acquisition system. A part of the system is to monitor micro-seismicity in and around Sapporo area by employing 3 borehole-type seismic stations with 500m deep. In 2001 one more borehole station with 750 m deep was established in the campus of Hokkaido University. In addition a network of strong motion seismometer consisted of 20 stations are operating since 2000. For 2001-2003, prospecting of seismic basement structure beneath Sapporo-city is now going on. In this prospecting microseism-array measurements at 30 points with maximum 2km diameter, seismic reflection experiment in 17 km long, and seismic refraction experiment of 30 km long have been carried out to reveal fine seismic velocity structure to the depth of 4km. By using these results we will make very precise provisional seismic intensity map of Sapporo. Most of these projects are sponsored by National Foundation of The Headquarters for Earthquake Research Promotion.

**SW04/09P/A13-015**

**1745**

**STRONG GROUND MOTIONS IN OSAKA METROPOLITAN AREA FROM THE NEXT NANKAI-TROUGH EARTHQUAKES**

Kojiro IRIKURA<sup>1</sup>, Hiroe MIYAKE<sup>1</sup>, Tomotaka IWATA<sup>1</sup>, Katsuhiko KAMAE<sup>2</sup>, Hidenori KAWABE<sup>2</sup> (Disas. Prev. Res. Inst., Kyoto University, <sup>2</sup>Res. Reac. Inst., Kyoto University)

The Osaka metropolitan area in Japan has repeatedly suffered from heavy damage caused by subduction zone earthquakes with magnitude 8 or more than 8 occurring along the Nankai-trough. The last ones occurred in 1946 called the Showa-Nankai earthquake as the source area off the Kii-peninsula to the Shikoku-island westward and in 1944 called the Showa-Tonankai earthquake as the source area off the Kii-peninsula to the Enshu eastward. Further going back to the past, the 1854 Ansei-Nankai earthquake occurred in almost the same source area as the 1946 Showa-Nankai earthquake and 32 hours before that the 1854 Ansei-Tokai earthquake occurred with a source area than easterly wider than the 1944 Tonankai earthquake. Moreover, the 1707 Hoei earthquake occurred as the source area including the 1854 Nankai and Tokai earthquakes. Very high probability is estimated for generation of the next Nankai-trough earthquakes. It is an emergent subject to establish a reasonable methodology for predicting strong ground motions from the next Nankai-trough earthquake. Accumulated data of strong ground motions near large earthquakes have been providing us very important knowledge about rupture processes of earthquakes. In particular, the waveform inversion of rupture process using strong motion data showed fault motions consist of some asperities with large slip and background region with less slip. Such slip heterogeneity on the fault plane plays an important role on strong ground motions causing to earthquake damage of structures. Based on the source inversion results for inland earthquakes we found slip heterogeneity inside the fault plane as well as entire rupture area follow the self-similar scaling laws with respect to total seismic moment (Somerville et al., 1999). It means that such inner fault parameters are predictable if the total seismic moment or the source area for a future earthquake is given. For subduction-zone earthquakes, accurate source inversion results have not been obtained enough to make scaling relations of slip heterogeneities. Some inversion results using near-field displacements with low-amplification seismographs and teleseismic data from the 1944 Tonankai and 1946 Nankai earthquakes as well as those using the strong motion records from the 1994 Sanriku-Haruka-Oki earthquake and the 1985 Michoacan earthquake have showed slip-heterogeneity similar to the inland earthquakes. So, we apply the procedure similar to the inland earthquakes to estimating strong ground motions from the future Nankai earthquakes. The applicability of the methodology has been examined comparing the simulated ground motion maps with damage distributions for historical earthquakes.

**SW05-Posters**

**NEW TECHNOLOGIES AND GEOPHYSICAL DATA CHALLENGES**

Location: Site D

Thursday, July 10 AM

**SW05/10A/D-001**

Poster

**0900-244**

**DEVELOPING A COMMUNITY BASED VELOCITY CRUSTAL MODEL FOR EUROPEAN BORDER REGIONS**

Rita DI GIOVAMBATTISTA<sup>1</sup>, Remy BOSSU<sup>2</sup>, EPSI TEAM<sup>1</sup> (Istituto Nazionale di Geofisica e Vulcanologia (INGV), <sup>2</sup>European Mediterranean Seismological Centre (EMSC))

We present a new community-based, velocity crustal model for European border regions obtained in the frame of the EU funded project "European Parameters for Standardized Information (EPSI)". The 3 main objectives of the EPSI project were the following: produce and make available an homogeneous seismological catalogue for  $M > 3$  in the Euro.-Med. Region; improve location accuracy in borderregions and create a large Euro.-Med. Database of arrival times. The latter could be used for specific studies ([http://www.emsc-csem.org/Html/EPSI\\_home.html](http://www.emsc-csem.org/Html/EPSI_home.html)). Although the station coverage in Europe is quite dense,

location accuracy remains an issue when events are located outside regional networks. The accuracy of the hypocenter locations is influenced by many factors such as network geometry and knowledge of the velocity models. This become a problem when related to seismic risk assessment in near real-time for civil security purposes, knowing that the most seismically active parts of Europe are natural borders between many countries. To improve the knowledge of propagation models, when available, we used events accurately located by local networks operating for short time periods or artificial events whose exact locations are well known. For every border a dataset of events accurately located by permanent and temporary networks has been realized thanks to the cooperation among the partners. These hypocenter determinations have been used to constrain the propagation models on a regional scale. As a result of the simultaneous inversion of a large number of events, including shots and quarry blasts, specific 1D regional models have been calculated for many borders. The models estimated have been used to locate the events recorded only by the permanent networks to assess the real accuracy of the hypocenter determinations released by the European Mediterranean Center (EMSC). Results are available in the following WEB page: <http://www.ingv.it/~roma/reti/epsi/index.htm>

**SW05/10A/D-002**

Poster

**0900-245**

**AN ENGINEERING APPLICATION OF SURFACE WAVES ON OVERBURDEN SURVEY-A MODEL STUDY**

Chao-Hui HSIEH<sup>1</sup>, Yue-Hong KUO<sup>2</sup> (General Education Center, Kao-Yuan Institute of Technology, <sup>2</sup>Institute of Geophysics, National Central University)

In this study we used a 2-D wedge plate and a gradually diminishing step model to simulate superficial dip layer to analyze dispersion curves of the surface waves for estimating the thickness of dipping layer. The material plexiglas was used for simulating near surface overburden and then aluminum layer for underlying half-space hard rock. The velocity contrast between these materials is sharp and its ratio is almost 1 to 2.38. To analyze the dispersion curve of surface waves, the peak-trough method in time series was used for velocity determination based on abundant seismograms along a long profile in dense spacing. We found that the surface wave velocity is proportionally related to the ratio  $\lambda/d$  of wavelength ( $\lambda$ ) to overburden thickness ( $d$ ). Due to resolution and wavelet spreading in time domain, it resulted in an ambiguity and uncertainty in velocity analysis. Additionally, the technique of optimum bandwidth filter (OBF) in frequency for group velocity analysis was used to improve the velocity scattering and Wiener de-convolution filtering was applied for phase velocity to eliminate the source problem. In comparing to both dispersion curves, the dispersion of group velocity of Rayleigh waves against the ratio of  $\lambda/d$  was sharply clustered and focused whereas the phase velocity shown more scattering. An empirical formula for group velocity dispersion was derived and was applied for thickness estimation. Based on the results of the model study and field survey, it shows that the energy of surface waves decays linearly in distance and the dispersion curve of group velocity in respect to the ratio of wavelength to overburden depth can be regressively fitted by the empirical formula  $V=a(\lambda/d)^{-1+b}$ , where  $a$ ,  $b$  are fitting constants, while the velocity changing drastically with  $\lambda/d$  in the range of 3 to 6. Furthermore, a field survey with a multi-channel recording seismograph for the laterite with a thickness 3-5 m has been carried out and is also shown that an estimating fluctuation  $\pm 15\%$  at the depth exploring in comparison with the drilling data was made. Apparently, dispersion curve analysis in small scale for overburden distribution study is available and feasible and it might be, due to low cost and efficient, as a new tool for reconnaissance in engineering application in the near future.

**SW05/10A/D-003**

Poster

**0900-246**

**ON THE DEVELOPMENT OF A SIMPLE HAZARD AND RISK SIMULATION TOOL FOR THE USE OF CIVIL DEFENSE OFFICIALS, DISASTER MANAGERS, DECISION MAKERS AND CITY PLANNERS**

Bautista Caparas BAUTISTA<sup>1</sup>, Maria Leonila Pascual BAUTISTA<sup>2</sup>, Ishmael Clarino NARAG<sup>1</sup>, Arturo S. DAAG<sup>1</sup>, Ma. Lynn Paladio MELOSANTOS<sup>1</sup>, Angelito Galvez LANUZA<sup>1</sup>, Raymundo Santiago PUNONGBAYAN<sup>3</sup> (Philippine Institute of Volcanology and Seismology, <sup>2</sup>Department of Science and Technology - Philippine Institute of Volcanology and Seismology (DOST-PHIVOLCS))

The idea of developing a simple hazard and risk simulation tool stemmed from two objectives that we want to achieve at PHIVOLCS. The first of these objectives is to address one of the lessons that we learned from the magnitude 7.8 earthquake which severely affected the central and northern areas of Luzon Island in 1990. Several hours after the occurrence of this earthquake, information about the possible effects or extent of the damage the earthquake had caused could not be obtained because most of the telecommunication systems were either severely damaged or were clogged by heavy communication traffic from people inquiring about the safety of their relatives. For example the City of Baguio, one of the heaviest hit cities was completely isolated from the rest of Luzon due to extensive landslides which blocked roads and access routes to and from the city. A system that can give a rapid estimate of the possible seismic hazards and the severity of the impacts to population, buildings, lifelines, road networks and other elements at risks is highly needed to generate necessary information for guiding civil defense officials and disaster managers in making quick, timely and reliable decisions for deploying rescue and relief operations. The second objective is the minimization of seismic risk by convincing land use planners, policy makers and city planners to consider earthquake hazards in their planning and development efforts. The provision of this simple and easy-to-use simulation tool will give them a deeper understanding and appreciation of the earthquake hazards and risks and will thus motivate them to do more serious planning and intensive formulation of effective disaster prevention policies such as serious land use regulation, strict enforcement of the building code and retrofitting of critical structures. To realize the above objectives, the simulation tool should be developed in such a way that it will be low cost, widely distributable and easy-to-use. It should not be GIS-based because GIS has a steep learning curve and disaster managers and town/city administrators do not have time to study complicated software. Another reason is that we want to minimize the cost so that it can be widely distributed to as many users as possible. To complete the system within the allotted project schedule of two years, we designed the resolution to be regional to semi-regional in scope and to shorten our programming time, we adopted other existing freely distributable software and algorithms. The hazards that are being modeled in the simulation tool are ground motion, landslide, liquefaction and tsunami hazards. The risk database includes population, road and communication networks, lifelines, high rise buildings, hospitals, schools, fire stations, town, government administration buildings, dams, power plants, fuel depot and other critical facilities.

**SW05/10A/D-004**

Poster

**0900-247**

**ROLE OF GERORADAR IN PAVING ROADS**

Yehia E. ABDELHADY<sup>1</sup>, Essam A. MORSY<sup>1</sup>, Sherif M. HANAFY<sup>1</sup>, Eid R. ABOEZZ (Department of Geophysics, Cairo University)

Enlarging the road connecting Cairo city and Mokattam Plateau is planned and studied due to the narrowness of this road. The road is planned to be enlarged by 4 m from one side and 3

m from the other side. The subsurface geological section in this area is characterized by Eocene limestone, which is highly fractured and cavernous. Ground Penetrating Radar is a very efficient tool for mapping shallow targets for applications such as those in geological engineering and environmental managements, so GPR technique is selected to resolve this problem due to its ability through or into solid earth instead of physically probing into it with boring, particularly where a closely spaced series of boreholes might threaten the integrity of the soil structure. A 100-MHz antenna GPR survey was performed along the road under study. A total of 6 GPR profiles were conducted with a total length of 1580 m. Two major subsurface anomalies and some other buried utilities are detected at both sides of the road, these anomalous objects are studied in details to evaluate their sources. The reasons of most of the small objects are small buried electric cables or water pipes, while the two major subsurface anomalies are due to two big buried waste pipes. The area is highly fractured but with no evidence of any large cavities.

**SW05/10A/D-005** Poster **0900-248**

#### A STRATEGY OF EARTHQUAKE PREDICTION IN THE BAIKAL RIFT ZONE

Victor S. SELEZNEV<sup>1</sup>, Sergey V. GOLDIN<sup>2</sup>, Anatolij S. ALEKSEEV<sup>3</sup>, Petr G. DJAD'KOV<sup>2</sup>, Vladimir Yu. TIMOFEEV<sup>2</sup>, Victor M. SOLOVIEV<sup>4</sup>, Alexander F. EMANOV<sup>5</sup>, Genadiy I. TAT'KOV<sup>2</sup> ('Geophysical survey of Siberian Branch of Russian Academy of Science, 'Institute of Geophysics, Novosibirsk, Siberian Branch of RAS, 'Institute of numerical analysis and mathematical geophysics of Siberian Branch of Russian Academy of Science, 'Altay-Sayan Experimental and Methodical Expedition of Siberian Branch of Russian Academy of Science, 'Geological Institute, Ulan-Ude, Siberian Branch of RAS)

A new strategy of geophysical monitoring in the Baikal rift zone directed toward middle-term earthquake prediction is advanced. To the end of the last century a new level of understanding many aspects of the earthquake physics was achieved. It was understood that each earthquake has its own scenario (and it explains why precursors often are contradictory), that the zone of preparation is much larger than the size of the future foci, that the earthquake is not a result of temporal accumulation of stresses, but result of complicated interaction of different blocks of the Earth Crust, that the earthquake preparation is not only mechanical process but interaction of many processes of different physical nature, that active zones can rather fast change their stress conditions, that seismic activity can be considered as "critical-state" process only in the context of the whole zone activity. We understand that a good middle-term forecasting must be based only on massive data of different geophysical, hydrogeological, geodetic, etc. observations, that has to be obtained in a rather dense network in the regime of monitoring. And, finally, we must understand the nature of temporal variations of different geophysical characteristics in a framework of a reasonable physical conception. Probably the kinetic theory of fracture is capable to give only schematic explanation of the stages of brittle fracture, as for very important stages of plastic deformation we have to attract a recently developed physical mesomechanics. Authors of the paper concentrate their efforts in developing of following directions: 1) developing of a new model of the surface dilatancy zone, which generates many strongly variable interrelated anomalies in geophysical fields; 2) solution of inverse problem for determination of coordinates of initial stress concentration in a block media with no rigid contacts, based on observations of surface deformations, tectonic-magnetic fields, earthquake mechanisms; 3) development of methods for solving multidisciplinary inverse problems of geophysics directed to construction of integral earthquake precursor; 4) understanding that the process of weak events strongly reflects different stages of the earthquake preparation stipulates for search of Ginsburg-Landau type equation, which could give adequate description of the process and new possibilities for prediction of time of the main event; 5) development of methods of vibroseismic monitoring, methods of high-resolution tomography of focal zones, and methods of seismic and geodetic study of active fault zones. Today there is concentrated a complex of geophysical observations at the South Baikal predicted ground for carrying out of geodynamic and seismic processes control. It includes both seismological observations and more than 15 methods of geophysical monitoring. As a result of long-term analysis of connection of seismic activations and changes in geophysical fields there were revealed some criteria of middle-term prediction at the south of Baikal Lake.

**SW05/10A/D-006** Poster **0900-249**

#### WLH 1.0 - WAVELAB AT HOME - A NEW TOOL FOR SEISMIC WAVES ANALYSIS ON PERSONAL COMPUTERS

Andrea BONO, Lucio BADIALI (Istituto Nazionale di Geofisica e Vulcanologia, Rome, Italy)

A new system for acquiring and processing digital signals has been developed in the last few years at the Istituto Nazionale di Geofisica e Vulcanologia (INGV). The Italian National Seismic Network at present gathers into the computer data centre in Rome the seismic signals from its own sensors and from other regional and local collaborative networks. The result is a virtual network larger than the original one. Communications are partly through wired analog and digital ones, and partly through satellite digital ones. The WLH (WaveLab at Home) system has been developed to show the waveforms recorded by the brand new automatic system, to make manipulations such as filtering and baseline corrections, to pick seismic phases and quickly manage their weight. It can also import and export phases in Hypoinverse 2000 standard and so launch standard localisation routines. Waveforms come from the reliable triggering system and from the continuous file buffer recording, and are normalised according an internal format, but SAC (Seismic Analysis Code) format is also available. More file formats as a user's choice can be added if needed by the scientific community. So WLH is a very fast and user friendly system that allows the user to study seismic events on every windows personal computer with 700KBytes of free disk space. It can be used at home, on a workstation or on a notebook and it's completely free.

**SW05/10A/D-007** Poster **0900-250**

#### RESEARCH ON ESTABLISHING ECOLOGICAL INFORMATION SYSTEM OF WETLANDS WITH GIS

Min HAN<sup>1</sup>, Xue TIAN<sup>1</sup>, Hua MENG<sup>1</sup>, Jixin YANG<sup>2</sup> ('School of Electronics and Information Engineering, Dalian University of Technology, 'Songliao Water Resources Commission)

Wetlands are a very important kind of multi-functional resource. In the last few decades this rare resource attracts many people's attention. At present, it becomes to be a trend to apply some new methods and information technology to study interdisciplinary scientific problems. Wetland is an intercross research field. On the aspect of utilizing Geographic Information System in wetland research, there are already some positive results. For example, the researchers in Alabama Agriculture and Mechanical University have applied GIS and Remote Sensing technique to manage natural reserves in kakum national park, Ghana, and Natl biological organization of U.S.A applies GIS to the ecosystem management of wetlands. In China the study of GIS started in the early 1980's But until now there is no much work to apply GIS into wetlands management. Zhalong wetland, one of important National Natural Reserves and Ramsar sites, is located in northeast of China. The total area of the wetland is 2100 km<sup>2</sup> and the water surface is about 800 km<sup>2</sup>. It is the natural habitats of numerous

animals and plants, especially some higher grades national protection rare birds. For instance, there are only 2000 Red Crown Cranes in the world, while Zhalong Wetland has 346 in the same time (data 1996). As a whole, the ecological resource of Zhalong Wetland includes 277 species of insects, 46 species of fish, 266 species of birds and 21 species of beasts. There are also 468 species of plants and a lot of microorganisms. Combining with the geographical, geological and hydrological information, Geographic Information System (GIS) should be an efficient tool to manage and analyze all of these kinds of spatial data. So that setting up a perfect ecological information system is indispensable for wetland protection and management. This paper, aiming at establishing an ecological information system of Zhalong Wetland based on GIS, presents a procedure to sort ecological resources of wetlands and establish a wetland GIS. The Zhalong Wetland GIS is established by use of ARC/INFO8.2 software. By designing suitable formats of maps, photographs, video records, figures and tables, the information can be easily understood. The designed links make the data visit conveniently and friendly. Some simple data analysis functions are also considered. In order to build a general system, the combination of GIS and GPS has been tested. The system can show the current situation and historical background of the wetland comprehensively. The result proves that GIS is an effective tool to set up an Ecological Information Systems of Wetlands.

**SW05/10A/D-008** Poster **0900-251**

#### GTOOL: I/O LIBRARY AND ANALYSIS TOOL FOR GRIDDED DATA

Eizi TOYODA<sup>1</sup>, Shin-Ichi TAKEHIRO<sup>2</sup>, Masaki ISHIWATARI<sup>3</sup>, Yoshi-Yuki HAYASHI<sup>4</sup> ('Numerical Prediction Division, Japan Meteorological Agency, 'Faculty of Sciences, Kyushu University, 'Graduate School of Environmental Earth Science, Hokkaido University, 'Graduate School of Science, Hokkaido University)

As the capacity of computer and network grows, scientists face to needof more efficient handling of vast and multi-source data. Making commondata format and sharing software will reduce efforts of such kind. Theauthors will report on "gtool", a software infrastructure for atmospheric simulation models of GFD-Dennou Club. GFD-Dennou Club has distributed freely AGCM5 (Atmospheric GeneralCirculation Model), shallow water model, and barotropic model on itswebsite (<http://www.gfd-dennou.org>). AGCM5 was developed by A. Numaguti and colleagues at theUniversity of Tokyo in the early 1990s, through reorganizing GSM (GlobalSpectral Model) of Japan Meteorological Agency. Input and output data of these models are unified to the GTOOL3 format which is accessed throughsubroutines in GTOOL3 library. Data analysis tools distributed with thelibrary provide simple data analysis like sub-array extraction, averaging over axis, or visualization. Software is mostly written inFortran. GTOOL3 file format is a unformatted sequential file of Fortran. It is alist of record pairs called header and data; the header containsmetadata of main data. Header is designed so as to be dependent to domainknowledge as little as possible. For example, it describes coordinatesystem of data without depending meaning like latitude or longitude; averaging tool works for data notonly in spherical grids on earth, but also in any curvilinear orthogonalgrids. The header record also includes fields to control graphic appearance of data. Therefore, users can exchange figures by sending only data files, and thefiles can be used for further analysis. However, the GTOOL3 environment have following limitations. Firstly, thefile format, originally derived from magnetic tape of mainframecomputers, has portability problem like byte ordering. Secondly, the file format has little extensibility; it has no room to handle additional attributes orarray with four or more dimensions. At last, the interface of the library is hard to memorize, due to limitations of FORTRAN 77. Therefore the authors started a project "gtool4" to rewrite theinfrastructure from scratch. The file format is based on NetCDF, that providesdata portability and extensibility. The software is written in Fortran90 to have simpler interface and clearer layer structure. Though the gtool4library and tools are still in experimental state, the authors areworking to improve it and link it to future AGCM.

**SW05/10A/D-009** Poster **0900-252**

#### NONSTATIONARY TIME SERIES MODELING FOR SIGNAL EXTRACTION PROBLEMS IN SEISMOLOGY

Genshiro KITAGAWA<sup>1</sup>, Tetsuo TAKANAMI<sup>2</sup>, Norio MATSUMOTO<sup>3</sup> ('The Institute of Statistical Mathematics, Minami-azabu 4-6-7, Minato-ku, Tokyo 106-8569 JAPAN, 'Institute of Seismology and Volcanology, The Graduate School of Science, Hokkaido University, Kita 10 Nishi 8, Kita-ku, Sapporo 060-0810 JAPAN, 'Geological Survey of Japan, National Institute of Advanced Industrial Science and Technology, 1-1-3 Higashi, Tsukuba Ibaraki 305-8567 JAPAN)

Due to recent progress of measurement and telemetry devices, it becomes possible to access to huge amount of observations obtained at many locations automatically. However, in the analysis of micro-earthquakes data, we face two difficulties. Firstly, the seismic signals observed by seismometers are contaminated by various kinds of natural forces, such as micro-tremors, microseisms, wave, wind, tide, air pressure, precipitation and a variety of human induced sources. Since the noise level is almost a constant independent on the signal, the effect of the background noise becomes more severe for earthquakes with smaller magnitudes. Therefore, to analyze seismic signals with smaller magnitudes, we need to develop a sophisticated procedure that can handle very noisy data. Secondly, the number of earthquakes increases exponentially as the magnitude decreases. Seismograms have been conventionally handled by empirical methods based on the human expertise to separate real seismic signal from various noises. However, for the processing of huge amount of micro-earthquakes, it becomes necessary to develop a computationally efficient statistical method that can automatically detect seismic signal from noisy data. In this paper, we use various non-stationary structural time series models for the extraction of seismic signal from noisy data. We describe five specific examples of time series modeling for signal extraction problems related to seismology. Namely, we consider 1) the estimation of the arrival time of seismic signal, 2) the extraction of small seismic signal from noisy data, 3) the detection of the co-seismic effecting groundwater level data contaminated by various effects from air pressure etc., 4) analysis of OBS (Ocean Bottom Seismograph) data and 5) the estimation of changing spectrum of seismic record. In most cases, the models can be expressed in state space model form, that enable us to apply a computationally efficient Kalman filter or an extension of it. Throughout the paper, we use the Akaike Information Criterion (AIC) for the evaluation of the goodness of the model that plays crucial role in establishing automatic signal extraction procedures.

**SW05/10A/D-010** Poster **0900-253**

#### DATA BASES AND SYSTEM OF THE SATELLITE ALTIMETRY AND GEOPHYSICAL DATA PROCESSING FOR APPLICATION TO SOLVING GEOPHYSICAL, GEODETIC AND OCEANOGRAPHIC PROBLEMS WITH REMOTE ACCESS

Petr P. MEDVEDEV<sup>1</sup>, V. NEPOKLONOV<sup>2</sup>, D. MEDVEDEV<sup>3</sup> ('Geophysical Center of Russian Academy of Sciences, 'Research Institute of the Defence Ministry RF, Moscow, Russia, 'Bauman Moscow State Technical University, Moscow, Russia)

The system creating for the solving problems of geophysics, oceanography, geodesy, and environment monitoring. Presented general structure of the system, the structure and configuration of its main technical, informational and software means. The processing

methods and forms of representation of the processing results of the satellite altimetry and geophysical information were developed and discussed. For development of the system and remote access technology used local area system server (with WEB-server Apache and MySQL database server). The activities of the geophysical database creation were started. The software modules for some separate analysis stages and processing of the satellite altimetry and geophysical data were developed and discussed. The modules include programs for processing of the geophysical fields digital models and solution of the separate problems of preprocessing and graphical visualization data. The programs for the modelling of the gravity potential and the satellite altimetry data processing was development also. They include defining the instant and average level of sea surface, detailed characteristics of the gravity field, display of tides and other geophysical parameters in the ocean in the form of digital models and images. The problems of optimizing satellite altimetry database and the system of measurements processing are discussed. The structure of a database and processing programs providing a sufficiently fast access to data and processing procedures that were developed in the Geophysical Center RAS is presented. The problems of the application of the distributed data archives and of the parallel processing data are discussed. The technology of the remote access to a system was tested on the example of some fragments of the geophysical database. The samples of the satellite altimetry data application to the studies of the instant and mean level variations of the Sea of Okhotsk, Baikal Lake and of the geodynamics of the Western Pacific seismic volcanic belt are presented. The research was supported by RFBR (project 01-07-90106).

SW05

### NEW TECHNOLOGIES AND GEOPHYSICAL DATA CHALLENGES

Location: Site A, Room 13

Thursday, July 10 PM

Presiding Chair: Y. Tyupkin

SW05/10P/A13-001

Invited

1400

#### PROTOTYPE OF THE LOGICAL BASIS FOR GEOLOGICAL DATA REPRESENTATION IN INTERNET

Pavel Yu. PLETCHOV<sup>1</sup>, Sergey V. TROUSOV<sup>1</sup>, Dmitry A. VARLAMOV<sup>2</sup>, Kirill A. BYCHKOV<sup>1</sup> (<sup>1</sup>Moscow State University, Geological department, Moscow, Russia, <sup>2</sup>Institute of Experimental Mineralogy, Chernogolovka, Russia)

In recent years goes the active search for the united basis, on which the classification of information can be built, its search and representation in Internet. Very frequently, GIS or other cartographic systems are proposed for geological data. However, there is an enormous quantity of geological information, which cannot be directly attached to the cartographic basis or this tying is deprived of large sense. To this information can be related practically all information flows in the geosciences, represented in Internet: descriptive (articles, books, lectures) event-related (monitoring, news, conferences) debatable (considerations, questions/answers) reference (databases, catalogs, library) interactive resources (simulations, the specialized calculations, demonstration programs) Descriptive, event-related or debatable information flows are served well in standard content control scheme (Content Management System). Such systems successfully work on all large dynamic WWW-servers, including the scientific content (for example, Russian-language system in the geosciences is supported in <http://geo.web.ru>). These types of information flows can be easily represented in the "pseudo-static" form and integrated in Internet by different level search engines (internal navigators, local search, global search engines). On the other hand, presentation in Internet of different databases and data collections, actual catalogs and interactive resources causes both technical and conceptual difficulties. The main problems include the different (often incomparable) structure of data, the absence of the standards scheme of the specialized information, the "variety" of database interfaces and difference in the tasks of the information compilers. The development of the additional semantic links between the information objects of different directivity is a promising trend in development of common information space in the opinion of the authors. The first realization of system with the additional dynamic links between the information objects is represented in the Russian Virtual Geoscience Network (<http://geo.web.ru>). The basis of the construction of dynamic links composes the common space of search algorithms of different purpose, which consider coordinate and contextual information, type of information, subject directivity and other factors. Articles, lectures, term definitions, answers to questions, conference proceedings, databases, programs, internet-resources etc. can be included by a similar system. This work was supported by Russian Foundation for Basic Research.

SW05/10P/A13-002

1420

#### THE IRIS DATA MANAGEMENT CENTER: ENABLING DATA ACCESS THROUGH NEW TECHNOLOGIES

Rick B. BENSON, Tim K. AHERN (IRIS Data Management Center)

The IRIS Data Management Center is an example of a highly automated, active data center dedicated to managing various geophysical time series data, specializing in access to seismic data. The DMC has adopted robust technologies that allow for the continuous acquisition of real time data, an automated, tape-based mass storage approach to management of these data, and electronic distribution of a large percentage of its holdings on an annual basis to a globally distributed community. The IRIS DMC manages approximately 30 terabytes of waveform data, separately managed metadata, and ingests approximately 8 terabytes of data annually. With the addition of data from USArray portion of Earthscope, this rate of ingestion should double in the next few years. In addition, requests are serviced in a near real time mode for a large percentage of customized requests, and completes approximately 50,000 individual requests each year. This discussion will focus on the newest technologies that have been introduced within the last couple of years that illustrate how research has been supported by the IRIS DMC. In particular, we will illustrate how software has been adopted that support the idea of "information-to-application" mechanisms, utilizing web services, which keep researchers connected to the most up-to-date information stored in managed databases, and accessed directly by client-side applications. This will reduce the need for extensive middleware that powered the 1990's "request-and-deliver" mechanisms. In addition, we will illustrate a networked data center concept, called NetDC, which allows data retrieval across distributed archives with no need to know where the data exist. In conclusion, we will discuss the newest adoption of technology, the CORBA-based FISURES project, and illustrate how information can be passed between networked data centers and into client side applications. By defining classes to "seismological objects", clients have been written that access distributed databases and import results into applications. We will show examples of this Data Handling Interface

(DHI), a service designed to directly connect information at the IRIS DMC with applications running on the client side.

SW05/10P/A13-003

1435

#### AN INTERNET-BASED COMPREHENSIVE EARTHQUAKE DATABASE AND USER SERVICE SYSTEM

Zhonghe ZHAO<sup>1</sup>, Chao ZHOU<sup>2</sup>, Zhe ZHANG<sup>2</sup>, Xinheng LUO<sup>2</sup> (<sup>1</sup>WDC for Seismology (Beijing), National Center for Seismic Information, CSB, 56 Sanlihe Road, Beijing 100045, China, <sup>2</sup>TAIDE Enterprise Co., Ltd., Chengxin Building, 284 Meihuadonglu, Xiangzhou, Zhuhai 519000, China)

We have developed an Internet-based comprehensive earthquake database and user service system. The main purpose of our work is to find a proper way to provide scientists with different kinds of earthquake-related data, so that users can browse and download required data easily and effectively via Internet. On the other hand, with this system, the service provider can maintain the system easily and effectively, including user's authorization management and database updating. The prototype system is built on a Linux platform and uses a relational database management software (Oracle). The system is a type of Browser-Server-Database system, users can get into it with their own Web browsers. With an earthquake catalogue search as the basic search, the user will obtain a list of earthquakes within given ranges of date, space and magnitude. Then the user can select one event (instead of this search, one can directly point to an important event in a short list at the first page), so as to get all or selected kinds of data related to this event, for instance, the basic parameters of the event (origin time, latitude, longitude, focal depth and magnitude), list of seismic stations which recorded the event, waveform data, phase data, Centroid Moment Tensor and/or focal mechanism, isoseismic map, related field pictures etc., as long as they exist in the database (For small events, there may be not so many kinds of data.). Also, for this group of events, the system can show the epicenter distribution map, focal mechanism distribution map and so on. Another aspect for this data service system is the routine maintenance of it. In addition to the continuous operation of the system hardware and software, user's authorization management and data updating are two of important issues. It is desirable to establish a flexible user authorization scheme so that the system manager can give different authorization (read only specific kind(s) of data, modify or update specific kind(s) of data, etc.) to different users. As to the updating of data, we have established some mechanism to receive data in the form of e-mail messages and automatically decode and put them into the database. Besides, with this prototype system as an example, discussion will be given to the general solutions for helping users to get data they need more effectively via Internet and helping data service providers to maintain the system and update the data more easily.

SW05/10P/A13-004

1450

#### CHALLENGES IN MANAGING AND DISSEMINATING DATA IN THE CANADIAN NATIONAL DATA CENTRE

Jim LYONS, Nina MARKOVA, Xiuying JIN, Luc SAUMURE, Philip SHOTT, Jim BLINKHORN, Chris MAJEWSKI, Tim COTE, Khalil HAYEK (Geological Survey of Canada)

The Canadian National Data Centre (CNDC) in Ottawa receives real-time data feeds from over 100 stations of the Canadian National Seismograph Network (CNSN). In addition, since January 1, 2002, real-time data streams from POLARIS (a Canadian geophysical research consortium focused on the estimation of earthquake ground motion and Earth structure) have been acquired and processed alongside the CNSN data. A combined total of ~2 Gigabyte/day (and growing) of continuous, compressed real-time data must be acquired, quality-controlled, processed, and archived. Since archiving of continuous waveform data began in 1989, ~3 Terabytes have accumulated. In addition, over 39 GB of segmented data have been acquired from the former digital regional teleseismic networks and numerous special data sets comprising field studies, aftershock surveys, etc. Efforts continue to focus on two main areas: To capture and manage all Canadian seismological data in a consistent fashion suitable for loading into anational database, and to make as much data as possible freely available to the global research community over the Internet. Problems and challenges encountered have included: (1) With the lengthening history of analog and digital stations, extending the traditional notions of station and network naming to handle cases where stations may change location, change network/deployment affiliation, or even change name over time; (2) Developing software to reformat digital waveform data to a standard internal format, and from internal to various commonly-used external formats; (3) Gathering and characterizing the time history of associated station information such as time correction and station response, and tying the time-appropriate information to waveforms when distributing data; and (4) Developing usable tools to satisfy requests for diverse data sets in as automated a fashion as possible. Since May 1994 the CNDC AutoDRM program has been extremely successful in distributing waveform data. Recently, even the need to learn the AutoDRM command set has been relieved via installation of a clickable web-based request form. To handle event-related (time-segmented) files, a new web-based facility has been developed that generates graphical images and triggers format conversion on-the-fly. This eliminates the need to store event data in more than one format. In its role as Canada's CTBT National Data Centre, the CNDC provides continuous real-time data from three primary stations and time segments on request from six auxiliary stations to the CTBT International Monitoring System (IMS). Meeting stringent IMS requirements for overall availability and timeliness of contributed data has led to the development of a number of specialized tools for quality control.

SW05/10P/A13-005

1505

#### MULTIPLE APPLICATIONS OF REAL-TIME SEISMIC INFORMATION

Yukio FUJINAWA, Shigeki HORIUCHI, Hiroaki NEGISHI, Yoshinari HAYASHI, Aya KAMIMURA, Takaki IWATA, Kana ABE, Shouhei MIURA, Takumi MATSUMOTO, Hiroyuki FUJIWARA, Takashi KUNUGI (National Research Institute for Earth Science and Disaster Prevention (NIED))

Extensive seismic networks have been constructed nationwide composed of high sensitivity seismographic network (Hi-net), broadband seismographic network (F-net) and strong motion seismographic network (K-NET). All these data from NIED and those from JMA and universities have been collected and distributed through NIED to scientists and engineers through the Internet under the coordination of the National Seismic Research Committee of MEXT. As a practical application of those data we are now developing a real-time seismic information system (REIS) for the purpose of providing estimated seismic parameters to prescribed users concerned with seismic risk reduction. Contents of information to be issued from NIED include seismic focal parameters (several seconds after detections of seismic signal at the nearest site), seismic fault plane solutions (some 10-20 seconds), after-shock activities (several minutes ~ a few days). Once earthquakes occur those parameters are to be calculated as soon as enough data are collected, and revised successively as seismic signals are received at a larger number of sites in time with the result that more accurate and more sophisticated earthquake information is transmitted to any of the prescribed users. The transmitted parameters are used by application systems at sites to build specific

information for particular users in order for triggering various disaster mitigation countermeasures including automated and/or half-automated responses. The focal parameters are used for short-term warning of imminent strong ground motions from major earthquakes. Another important application is an immediate estimate of expected shaking distribution and damages in a district using synthetic database and site effects for local governments to take initial proper measures of hazard mitigation. Many of applications are to be developed under the coordination of consortium of concerned organizations and private companies (real time earthquake information consortium: REIC). Tasks of REIC include standardization of data format of real time seismic information in order of easy handling of data by various kinds of users concerned. The system has been tested from early June in 2002 for evaluation of the whole system. In the initial stage of development we are using high sensitivity data including Hi-Net, Kanto-Tokai belonging to NIED to estimate focal parameters. The REIS has been evaluated using true data, and now we are able to estimate the focal parameters of targeted earthquakes in sufficient speed and accuracy. The remaining errors or mistakes have been tried to reduce with the result of progressive increase of performance. The first test user is Fujisawa City in the Kanagawa prefecture of population of 380,000. The REIS of the first phase can estimate strength and arrival time of selected earthquakes. The system for the second phase will be able to estimate disaster from seismic wave and tsunami for any number of particular sites. Those data are to be used for the development of particular safeguard equipment and personal actions in the early stage and for the practical use afterward.

**SW05/10P/A13-006****1520****THE INFORMATION SYSTEM OF SATELLITE GEODESY DATA IN GEODYNAMICS AND SEISMOLOGY**

Yuri S. TYUPKIN<sup>1</sup>, Peter P. MEDVEDEV<sup>1</sup>, Mikhail N. ZHIZHIN<sup>2</sup>, Andrei N. POLYAKOV<sup>2</sup> (<sup>1</sup>Geophysical Center, RAS, <sup>2</sup>Institute of the Physics of the Earth, RAS)

The information about deformations of the Earth's crust and velocities of the present Earth's crust motions are of great significance for a wide range of geodynamics and seismology problems. Modern observation systems are based on the techniques of satellite geodesy, which allow us to determine the deformations of the Earth's crust and velocities of its motion with a high degree of accuracy. The information system "Satellite Geodesy Data Interpretation in Geodynamics and Seismology" is reported. The information system includes: - Database of the present Earth's crust motion data. - Database management system based on a GIS approach. - Problem oriented software. The database contains the results of international networks of GPS, VLBI, SLR and DORIS observations, data of regional and local GPS networks: CORS, REGAL, RGP, SCAR, SIRGAS, and data of temporal observation campaigns in Western Alps (GPS ALPES group), in South and South-East Asia (project GEODYSSSEA), in China (CMMN and CMONC stations) and in Central Asia (project IVTAN). All data are obtained from public Internet sources and from publications. The software provides a user with the following functions: - To display the spatial distribution of velocities of the present Earth's crust motion obtained by different networks in ITRF 2000 frame; - To recalculate this distribution in the frame linked with the individual tectonic plate; - To calculate the velocities of motion of tectonic plates on the basis of NNR-NUVEL-1A model and Actual Kinematics Model; - To calculate statistical parameters of Earth's crust motion velocities for a selected area; - To compare the distributions of Earth's crust motion velocities of different areas; - To calculate the gravity anomalies for selected area. A local version of the system is presented. The network version of the system is under the construction. The research is supported by the Russian Basic Research Foundation (Projects 02-07-90087, 02-07-06006 mas, and 01-07-90101).

**SW05/10P/A13-007****1530****APPLICATION OF STRESS INVERSION METHOD TO GPS ARRAY DATA OF JAPANESE ISLANDS**

Muneo HORI, Takeshi IINUMA, Teruyuki KATO, Kenji OGUNI (Earthquake Research Institute, University of Tokyo)

The stress inversion method is aimed at identifying stress distribution for a body whose stress-strain relation is partially known. While the method is applicable to a body in plane stress or strain state, the validity of the method is rigorously proved. The method finds equilibrating stress for given strain distribution, by solving a well-posed boundary value problem; the problem is derived from the two equations of equilibrium and one known stress-strain relation for the three stress components. The usefulness has been examined in experiments of various materials. This paper reports the applicability of the stress inversion method of identifying stress distribution to the Japanese Islands by using displacement increment data which are measured by the nationwide GPS array of the Japanese Islands. The method is applied to several data sets. The boundary value problem of the stress inversion method is numerically solved when the GPS data are used as input. The accuracy and the stability of the numerical calculation are verified. When the GPS data which are not spatially filtered are used, the stress inversion method finds non-uniform distribution of regional stress. This is because the displacement increment accompanies regionally varying strain increment and stress increment spatially varies to satisfy the equilibrium. The results of the stress inversion method are discussed. The limitation of the method in applying the GPS data is discussed as well. References M. Hori, T. Kameda and T. Kato: Application of stress inversion method to predict stress distribution in Japanese Islands, *International Journal of Geophysics*, 144, pp. 597-608, 2001. M. Hori and T. Kameda: Inversion of stress from strain without full knowledge of constitutive relations, *J. Mech. Phys. Solids*, 49, pp. 1621-1638, 2001.

**SW05/10P/A13-008****1545****ANALYTICAL WEB GIS FOR DECISION SUPPORT IN SEISMOLOGICAL PROBLEM DOMAIN**

Valeri G. GITIS<sup>1</sup>, Gennady L. ANDRIENKO<sup>2</sup>, Natalia V. ANDRIENKO<sup>3</sup> (<sup>1</sup>Institute for Information Transmission Problems, Russian Academy of Sciences, B.Karetny Lane, 19, 127994 Moscow, GSP-4, RUSSIA, <http://www.iitp.ru/projects/geo/>, e-mail: gitis@iitp.ru, <sup>2</sup>Fraunhofer Autonomous Intelligent Systems Institute, Schloss Birlinghoven, Sankt-Augustin, D-53754 Germany, <http://www.ais.fhg.de/and/>, e-mail: gennady.andrienko@ais.fhg.de)

Geoinformation approach to seismological modeling deals with (A) a continuity variation of geological environment and man made infrastructure as well as with (B) geographical objects such as earthquake epicenters, geological faults, seismic source areas and infrastructure elements. Both grid-based and vector data types are necessary to present these models in GIS. Key problems of GIS application to seismology are (i) forecasting social and economy losses, (ii) spatial forecasting of seismic hazard, and (iii) earthquake prediction. The goal of analytical Web-GIS oriented to the seismological problem domain is to provide online access to seismological data analysis for everyone, from everywhere, and at any time. It appears that web-GIS tools must be powerful enough to support decisions in (i), (ii), (iii) problems and must be easily controlled and understood for persons who are not experts in GIS. Often analytical web-GIS or its part are realized in Java applet architecture and enter

into the web-page. After web connection such web-GIS is automatically loading and stating on client computer. Java applets can work on any platform where standard Internet browser has been installed. Modern analytical web-GISs support the following facilities for seismological spatial and spatio-temporal data mining: (A) Visualization: interactive dynamical visual data exploration, (B) Analytical transformations: calculating a wide class of functionals, which include transformations from grid(s) to grid-based data, from grid and vector to vector attribute data, from vector to grid based data, and from vector to vector based data, and (C) Plausible inference: discovery of multidimensional relationships to forecast the goal properties and to detect the goal objects. Analytical tools realized in CommonGIS (<http://www.ais.fhg.de/and/>), GeoProcessor and COMPASS (<http://www.iitp.ru/projects/geo/>) as well as applications of sophisticated dynamical visualization to earthquake prediction research, analytical transformations to seismic losses assessment and plausible inference to delineation of potential seismic zones by geological and geophysical features are considered. The work was partly supported in 2000 AE2002 by projects "Spatial Mining for Data of Public Interest" (IST Program, IST-1999-10536 SPIN) and "Web GIS for presentation and analysis of spatio-temporal information referring to Earth Sciences and human dimension" (Russian Basic Research Foundation, 00-07-90100).

**SW05/10P/A13-009****1615****INTERACTIVE INVERSE MODELLING FOR NON-LINEAR EARTH PROCESSES**

Chris WIJNS<sup>1</sup>, Fabio BOSCHETTI<sup>1</sup>, Hideyuki TAKAGI<sup>1</sup>, Louis MORESI<sup>2</sup> (<sup>1</sup>School of Earth and Geographical Sciences, University of Western Australia, Crawley, WA 6009, Australia, <sup>2</sup>CSIRO Exploration and Mining, PO Box 1130, Bentley, WA 6102, Australia, <sup>3</sup>Kyushu Institute of Design, Shiobaru, Minami-ku, Fukuoka 815-8540, Japan, <sup>4</sup>School of Mathematical Sciences, Monash University, VIC 3800, Australia)

Inverse modelling of earth processes, in the absence of established numerical criteria to act as targets, requires an approach which incorporates human interaction in directing the inversion. For example, geologists often draw tectonic models to illustrate some concepts of crustal evolution. Often, such conceptual models cannot be translated into numerical target data; first, because the model is only approximate and features are representatively, not exactly, located; and second, due to the experience-based, empirical nature of geology, because the evaluation criteria reside inside the mind of the geologist, and do not constitute hard data. However, the merit of such a conceptual model will still follow from its physical plausibility, e.g. from the ability of a numerical model to reproduce the concepts and answer related questions. Recently, research in artificial intelligence has resulted in systems to support human interaction in optimisation problems. The technique of interactive evolutionary computation (IEC) provides for the inclusion of qualitative expertise within a rigorous mathematical inversion scheme, by simply asking an expert user to evaluate a sequence of forward models. The traditional numerical misfit is replaced by a human appraisal of misfit. Successive rankings of model outputs are linked to an evolutionary computation algorithm, in our case a genetic algorithm, which provides optimal convergence into the target parameter space. The method is particularly geared towards cases of highly non-linear interactions between model parameters, where resultant behaviour is difficult to predict. We use this interactive technique to successfully invert a tectonic model for a conceptual pattern of fault spacing during crustal extension. By letting a number of rheological parameters vary, we quickly find a few combinations which produce forward models satisfying our visual target. Our IEC system, linked to different forward modelling codes, has become a standard tool for modelling at CSIRO in Perth, Australia. Where previous trial-and-error approaches have taken weeks to produce target results, using IEC, we have found solutions within days for thermal profiles during mantle convection, tectonic deformation patterns, and mineral assemblages in geochemical systems. Since the genetic algorithm optimises an ensemble of solutions, the non-uniqueness of the problem may be explored to some extent. We choose a visualisation technique known as self-organised mapping to represent the parameter space covered by the model outputs. This is one type of mathematical projection which produces a simple view of an otherwise complicated multi-dimensional problem. For our example of crustal extension, we use a few graphical displays of the data to characterise the influence of the different rheological parameters on the resulting pattern of faulting in the model.

**SW05/10P/A13-010****1630****NEW ENGINEERING-GEOPHYSICAL TECHNIQUES FOR GEOPHYSICAL AND GEODYNAMIC MONITORING OF SIBERIA TERRITORY**

Victor S. SELEZNEV, Victor M. SOLOVIEV, Alexander F. EMANOV (Geophysical survey of Siberian Branch of Russian Academy of Science)

The outcomes of modern geophysical researches of the Geophysical Survey SB RAS, directed on study of geodynamic situation in large industrial and civil centers on the territory of Siberia with the purpose of an evaluation of seismic risk of territories and prediction of origin of extreme situations of natural and man-caused character, are presented in the paper. First of all it concerns works with use of high-output digital equipment for study of seismic regime of territories with the purpose of evaluation of influence of weak but long seismic actions for various constructions and people. Lately, along with passive seismic monitoring, there are developing in GS SB RAS works on active vibroseismic monitoring with use of powerful 40-60-tons vibrators in territories of large oil-and-gas fields with high man-caused seismicity and at control of particularly dangerous structures. There are also given the outcomes of researches with use of new engineering-seismological method on evaluation of physical state of industrial and civil objects (buildings and structures, hydroelectric power stations, bridges, dams and so on). This technique allows to carry out observations of wave field in investigated objects (as a source it could be used both artificial ones and seismic noise) with use of multiplex equipment by detailed system of observation. Orientation was made on standing waves appearing in buildings and structures, which carry information about structural peculiarities of the investigated objects. Along with engineering-seismic techniques at solving of geological, engineering-geological, ecological and other important economical and scientific problems, tomographic technique of electromagnetic scanning was widely adopted in the regions of Siberia. This technique was developed in Siberian Branch of RAS. There are given the examples of efficient use of this technique in solving of some important problems, such as: localization of zones of invasion, determination of subterranean and man-caused waters level, rock failure and landslide prediction, monitoring of communications and underground reservoirs.

**SW05/10P/A13-011****1645****SOFTWARE TOOLS FOR ANALYSIS OF SEISMICITY VARIATIONS AND ITS APPLICATION FOR THE PREDICTION OF THE LARGE KAMCHATKAN EARTHQUAKES**

Vladimir V. IVANOV, Nadejda M. KRAVCHENKO (Kamchatkan Experimental and Methodical Seismological department, Geophysical Service, RAS (KEMSD GS RAS))

There are several methods of intermediate-term earthquake prediction based on the investigation of weak seismicity variations. It is supposed that a seismic quiescence followed

by foreshock activation can be found before earthquake in its epicentral area. Therefore for the earthquake prediction it is important to clearly recognize an areas with anomalies of seismic quiescence and foreshock activation. The technique proposed by Sobolev and Tyupkin (1996) is used to discern areas of seismic quiescence. It is based on calculation of a predictive parameter, RTL. RTL parameter is the composition of three functions: epicentral R, time-dependent T, and L corresponding for the size of the earthquake source. Seismic quiescence can be characterized by negative values of the RTL parameter in comparison to its perennial background. Analysis of density of seismogenic faults can be used to recognize areas of the foreshock activation. We present the application software specially designed for study of weak seismicity variations using RTL prognostic parameter and density of seismogenic faults. Anomalies in low magnitude seismicity can be discerned more clearly and precisely using this software. It has interactive visual workspace and easy to use interface. This software has a lot of special features for seismic quiescence area localization and detailed study of the seismic process. This software is used at Kamchatkan Experimental and Methodical Seismological Department, Geophysical Service, Russian Academy of Sciences (KEMSD GS RAS) since 1999. A retrospective analysis of the regional earthquake catalog of Kamchatka has been performed for events with magnitude M greater or equal to 6.0 since 1985 till the present time. Aftershocks have been preliminarily eliminated from earthquake catalog before applying the RTL algorithm. It was found that in 8 cases of 14 anomaly of the RTL prognostic parameter can be recognized within 2 years before earthquake in its epicenter surroundings. Generally the main shock occurred at the edge of the anomalous area.

**SW05/10P/A13-012****1700****DETECTION OF IMPACT CRATERS BY PROCESSING OF THE DEM DATA**

Andrei G. MARCHUK<sup>1</sup>, Konstantin V. SIMONOV<sup>2</sup>, Sergei A. PERETOKIN<sup>2</sup>, Anton L. SCHEMEL<sup>2</sup>  
(<sup>1</sup>Institute of Computational Mathematics and Mathematical Geophysics, <sup>2</sup>Institute of Computational Modeling Siberian Division RAS)

A new attempt for the detection of the impact craters and the other morphologic structures on the Earth's surface was made using the modern computational technologies. For detection and allocation of such structures, a complex application of the fast two-dimensional wavelet transformation and the fast nonlinear multiparameter regression analysis for the digital elevation (DEM) data subsets and 3D shaded images, which are drawn using these data. The organization of computing process for the solution of the indicated problem takes the form of a computational experiment and includes, in particular, the procedure of training on the known reliable impact structures, the procedure of testing of the constructed regression model and detection and identification of the required shapes on the Earth's surface with their subsequent contrast improvement. This technology was used for the detection of the big circle structures on the territory of North America and Central Siberia. In this case the GTOPO 30 data were used. The obtained results seem to be promising. The known circle structures are effectively detected and clearly distinguished on the surface area under study. The quantitative information is represented in the convenient form for the subsequent processing and analysis.

**SW05/10P/A13-013****1715****A DETECTION OF THE LATENT SPATIAL AND TEMPORAL PERIODICITIES OF NATURAL HAZARDS IN THE PACIFIC REGION**

Elena V. SASSOROVA, Boris W. LEVIN (Shirshov Institute of Oceanology Russian Academy of Science)

The material of the lithosphere is periodically subjected to forces caused by such astronomical effects as the tidal perturbation, precession, and Chandler pole motion. The stress tensor in the Earth's crust was reconstructed and the total free-energy balance was estimated on the theoretic level (Levin, Pavlov 2001). It was shown that the variations of the lithosphere energy in the 100km layer due to astronomical effects are comparable with the energy released annually in the seismic process. Thus the Earth's seismicity and probability of the earthquake occurrence depends on the astronomical reasons: the geographical latitude of the event, the relative attitude of the Earth and the Moon, position of the Earth on ecliptic and the Chandler pole motion. The main goal of our study is the searching of the latent regularities for the Pacific event occurrence, the picking up of special periods which are typical for the temporal and spatial distribution, and the assessment of possibility for advance in the understanding of seismicity generation process in this region. For that we use integration of multi-disciplinary information: electronic worldwide seismic catalogs (NEIC, ISC), local seismic catalogs, Historical Tsunami Data Base, several electronic tables (Chandler pole motion, Moon and Sun tides and others). The special software based on the pattern recognition and fuzzy set methods and used the asynchronous slip-multi windows system for detection of the latent spatial and temporal periodicities was developed. The study of the latitude distribution of the earthquake number and its energy showed that the region seismic activity depends on the geographic latitude of the observed area and varies with time. The time-dependent variations of seismicity demonstrate existence of the 6-year-period of activity increasing. The analysis of the Pacific tsunami distribution showed that the temporal regularity in the tsunami occurrence series is occurred in turn for Northern Hemisphere and then for Southern one and vice versa. The typical periods of the changeover from one to another hemisphere were 6 and 18 years approximately. It was revealed periodicities of the natural hazards in the course of year.

**SW05/10P/A13-014****1730****RESCUE OF PAPER RECORDS: IMAGERY DATABASE OF SEISMOGRAM AND MAGNETOGRAM SCANS WITH AUTOMATED DIGITIZER**

Mikhail Nikolaevich ZHIZHIN<sup>1</sup>, Alexei Alexandrovich BURTSEV<sup>1</sup>, Eugeny Petrovich KHARIN<sup>2</sup>  
(<sup>1</sup>Department of geoinformatics, Institute of Physics of the Earth, Russian Acad. Sci., <sup>2</sup>World Data Center on Solar-Terrestrial Physics, Moscow)

We present an effort of the World Data Centers for Space Physics and Solid Earth to digitize the analog records by scanner and digital camera and to create a database of scan images with metadata and automated digitizer accessible from the web. Time series records from the most of the geophysical observatories in Russia are still preserved in WDCs on paper and microfilms. Collection of historical seismograms and strong motion records begins from 1912 Golitsin records. Geomagnetic variations were recorded by tenths of stations for 50 years. We have developed algorithms and software to automatically digitize the scanned seismic and geomagnetic records using mathematical morphology and dynamic programming. Users can download from the database high-resolution images and digitizing program to convert the analog records into digital waveforms.

**SW05/10P/A13-015****1745****APPLICATION OF NON-DESTRUCTIVE GEOPHYSICAL TECHNIQUES FOR RISK EVALUATION (SANNOUR PROTECTED AREA, BENI SUEF, EGYPT)**

Yehia E. ABDELHADY, Sherif M. HANAFY, Essam A. MORSY (Department of Geophysics, Cairo University)

A great Cave was discovered in the Wadi Sannour area, which is located on the Eastern bank of the Nile, facing Beni-Suef, upper Egypt. The site of Cave was quarried about 200 years ago for extraction of Marble. The cave has a crescent cross section with a span of up to 300m, 10 to 30m width, and height of 15m, the opening is about 39.5 m below ground surface. The forming of the Cave is due to running and subsurface water actions, which slowly moved along fractures and bedding planes and dissolved the carbonates rock in the area. To evaluate the risk, vulnerability and damage assessment at the Reserve site of Wadi Sannour Cave, to be more secure for the visitors (as a Tourist Site) and also to protect cave features against irreversible damage. Geophysical, geological, and engineering studies were made in the area using nondestructive techniques in and around the cave. The Ground Penetrating Radar (GPR) technique was used to evaluate the area inside the cave as well as the area around it. 20 GPR reflection lines were acquired in a rectangular flat area (35 x 11 m) in front of the entrance of the great cave in a uniform mesh grid. A new subsurface cavity is discovered in this area. The depth and dimension of this newly discovered subsurface cavity is determined from the acquired GPR data.

The IUGG2003 Office has made every effort to list family names and given names in the correct order in this index. We apologize for errors and suggest that if in doubt, you check both names as entries in the index. Thank you

# a

**AAGAARD, Knut**  
(JSP04/09P/A06-002 1415)

**AARO, Sven**  
(JSA07/11A/D-028 0830-028)

**AARO, Sven G.**  
(GAV.06/10P/A11-004 1500)

**AARSNES, Kjell**  
(GAILL.06/07P/D-005 1400-125)

**AARUP, Thorkild**  
(G07/10P/A03-002 1420)

**ABBAS, Abbas Mohamed**  
(GAI.10/09P/D-003 1615-122)

**ABD - ALLAH, Mohamed Abdel - Aal**  
(GAI.10/09P/D-001 1615-120)

**ABD-ELMOTAAL, Hussein A.**  
(G04/08P/D-014 1400-121)  
(G03/07P/D-025 1400-047)

**ABDALLA, Farid A.**  
(JSP09/10P/B20-014)

**ABDALLA, Farid AbdelRahman**  
(JSP08/09P/B19-003)

**ABDEL GAWAD, Ahmed Moustafa**  
(HW05/10P/D-009 1400-164)

**ABDELHADI, A.W.**  
(HW07/11P/D-024 1400-160)

**ABDELHADY, Yehia E.**  
(SW05/10P/A13-015 1745)  
(SW05/10A/D-004 0900-248)

**ABDELHADY, Yehia Elsaied**  
(SS04/07A/A03-006 1100)  
(SS04a/09P/D-019 1400-268)

**ABDELLATIF, Talaat A.**  
(HW05/10P/D-008 1400-163)

**ABDELRAHMAN, Abdallah El-Abasery**  
(HW05/10P/D-008 1400-163)

**Abdul Rahim Nik**  
(HS02/08P/C24-012 1715)

**ABDULLAH, Muhammad Nurdin**  
(HS01/08P/C29-009 1700)

**ABDULLAH, Muhammad Nurdin**  
(HS01/08P/C29-005 1520)

**ABE, Kana**  
(SS04b/10P/D-048 1400-232)

**ABE, Kana**  
(SW05/10P/A13-005 1505)

**ABE, Kuniaki**  
(JSS07/10A/A02-008 1015)

**ABE, Maiko**  
(G03/07P/D-003 1400-025)  
(G03/07P/D-001 1400-023)

**ABE, Shintaro**  
(JSS07a/09P/D-007 1700-108)  
(SS03/08A/D-099 0830-258)  
(JSS07a/09P/D-017 1700-118)

**ABE, Shuji**  
(GAILL.10/11A/D-002 0830-076)

**ABE, Susumu**  
(SS03/08A/D-134 0830-293)

**ABE, Takenori**  
(JSS07b/10P/D-006 1700-052)

(JSS07b/10P/D-007 1700-053)

**ABE, Takumi**  
(GAILL.07/11A/A12-001 0835)  
(GAILL.08/10A/A16-008 1100)  
(GAILL.07/11A/A12-004 0945)  
(MC04/11A/B22-001 0830)  
(GAILL.06/07P/D-020 1400-140)

**ABE, Yutaka**  
(MC04/11P/B22-007 1630)

**ABE-OUCHI, Ayako**  
(JSM10/09P/D-004 1400-058)  
(MC04/11P/B22-007 1630)

**ABEKI, Norio**  
(SS04b/10P/D-042 1400-226)

**ABEL, Gary A.**  
(GAILL.10/11A/A01-013 1130)

**ABIDIN, Hasanuddin Zainal**  
(JSP11/08A/A10-002 0930)

**ABO SHAMMALA, Ashraf Sobhy**  
(HS04/08A/C30-005 1130)

**ABOEZZ, Eid R.**  
(SW05/10A/D-004 0900-248)

**ABOLGHASEM, Amir**  
(JSG01/07P/A01-004 1445)

**ABOU EL-MAGD, Islam Hamza**  
(HS02c/11P/D-013 1630-111)  
(HS02/11A/C24-013 1133)

**ABOUD, Essam Aboud**  
(JSA07/11A/D-046 0830-046)

**ABOVIAN, Stepan B.**  
(SS03/08A/D-085 0830-244)

**ABRAHAM, James David**  
(JSM14/07A/A05-002 0950)  
(JSM14/09P/D-002 1400-066)

**ABRY, Patrice**  
(GAILL.06/11P/D-015 1400-067)

**ABRY, Patrice**  
(GAILL.06/10A/A01-013 1215)

**ACHAUER, Ulrich**  
(JSS06b/10P/D-012 1400-036)

**ACUNA, Gustavo A.**  
(G03/07P/D-050 1400-072)

**ACUNA, M.**  
(GAIV.03/08P/A16-003 1500)

**ACUNA, Mario H**  
(GAIV.03/08A/A16-008)

**ACUNA, Mario H.**  
(GAIV.03/08A/A16-005 1040)  
(GAIV.03/08A/A16-007 1130)  
(GAIV.03/08A/A16-001 0830)

**ACUÑA, Mario H.**  
(GAIV.03/08A/A16-002 0900)  
(GAIV.03/08A/A16-003 0930)

**ADABANIJA, Moruffdeen Adedapo**  
(HW08/07P/C28-001 1410)

**ADACHI, Haruka**  
(GAILL.09/10P/D-002 1400-114)  
(GAILL.09/11A/A11-003 0920)

**ADACHI, Masaki**  
(GAILL.14/08A/D-004 0830-148)

**ADACHI, Tatsuhiko**  
(MI09/08P/B22-001 1400)

**ADACHI, Toru**  
(GAILL.04/09A/D-004 0830-140)

**ADACHI, Yukimasa**  
(MC08/07P/B17-005 1520)

**ÁDÁM, J.**  
(G02/07A/C25-007 1100)

**ADAMOVA, Albina Alexandrovna**  
(SS03/08A/D-141 0830-300)

**ADAMS, John**  
(SS04b/10P/D-019 1400-203)  
(SS04b/10P/D-018 1400-202)  
(SS04b/10P/D-017 1400-201)

**ADEAGA, Olusegun**  
(HS02b/10P/D-007 1630-128)  
(HS02/10A/C24-007 1109)  
(HW07/11A/C25-010 1115)

**ADEAGA, Olusegun Adebayo**  
(HS01/09P/D-013 1400-180)

**ADEKUGBE-JOSEPH, Akindele Oluwole**  
(G04/08P/D-025 1400-132)  
(G04/08P/D-026 1400-133)

**ADELOYE, Adebayo Johnson**  
(HS02/10A/C24-003 0900)

**ADETOYINBO, Adedeji Adegoke**  
(SS03/08A/D-066 0830-225)

**ADI, Seno**  
(HS02/07P/C24-022 1420)  
(HS02/10P/C24-004 1445)  
(HS02a/07P/D-022 1545-168)

**ADRIAN, Mark L.**  
(GAILL.06/08A/A02-004 1005)

**ADSAVAKULCHAI, Suwannee**  
(JSP11/07A/A10-005 1050)

**AFANASYEV, Yakov D.**  
(JSP10/10A/B21-007 1120)

**AFNIMAR, Afnimar**  
(SS04/07A/A03-002 0945)  
(SS04/07P/A03-013 1730)

**AGATA, Yasushi**  
(HS02/08A/C24-009 1100)

**AGETA, Yutaka**  
(HW01/09P/D-041 1400-232)

**AGGARWAL, Pradeep Kumar**  
(HW06/07P/C31-006 1540)

**AGNEW, Duncan**  
(JSG01/07A/A01-010 1135)

**AGOSTINETTI, Nicola**  
(JSA07/10P/A05-007 1630)

**AGRAWAL, Nand Kishore**  
(JSG01/08P/D-032 1400-032)

**AGRAWAL, Pramod Kumar**  
(SW03/10P/A04-006 1515)

**AGUSTSSON, Kristjan**  
(JSG01/07P/A01-010 1635)

**AHERN, Tim K.**  
(SW05/10P/A13-002 1420)

**AHMAD, Iftikhar**  
(HW07/11P/D-009 1400-145)  
(HW07/11P/D-004 1400-140)

**AHMAD, Iftikhar**  
(HW07/11P/D-019 1400-155)

**AHMAD, Sajjad**  
(HS02c/11P/D-008 1630-106)  
(HS02c/11P/D-009 1630-107)  
(HS02/11A/C24-008 1113)  
(HS02/11A/C24-009 1117)

**AHMAD, Sarfaraz**  
(JSH01/07A/C27-004 1140)

**AHMAD, Suraiya P.**  
(MI03/08A/B18-001 0830)

**AHMADI-GIVI, Farhang**  
(MI06/09P/B20-005 1520)

**AHMADIAN, Mohamad Javad**  
(JSP11/08P/D-009 1400-078)

**AHMED, Fathy Mohamed**  
(GAV.06/10P/A11-008 1640)

**AHMED, Shakeel**  
(JSP11/07A/A10-002 0930)  
(HS02/08P/C24-004 1445)  
(HW07/11P/D-039 1400-175)  
(HW03/11P/C30-003 1440)  
(HW03/11P/C30-005 1520)  
(HW03/11P/C30-002 1420)  
(HW05/10A/C31-012 1140)  
(HW03/11P/C30-006 1600)  
(HW03/11P/C30-009 1700)

**AHN, Myoung-Hwan**  
(JSG03/09P/D-009 1640-017)

**AHOLA, Joel J.**  
(JSG01/08A/A01-009 1120)

**AIKI, Hidenori**  
(JSP10/09P/B21-006 1540)

**AIRES, Filipe**  
(JSG03/09P/A12-003 1440)

**AIRO, Meri-Liisa**  
(GAV.07/07P/A13-004 1500)

**AKAIKE, Makoto**  
(HW07/11P/D-005 1400-141)

**AKAMATSU, Junpei**  
(SS04a/09P/D-033 1400-282)

**AKHIONBARE, Stella Maris**  
(HS02/07P/C24-026 1436)  
(HW02/11A/C31-008 1200)  
(HS02a/07P/D-026 1545-172)

**AKIBA, Kiyoka**  
(JSP10/09P/B21-010)

**AKIMOTO, Hajime**  
(JSM04/09A/B23-002 0930)  
(JSM04/09P/B23-003 1500)  
(MI03/08P/B18-006 1610)

**AKIOKA, Masaki**  
(GAILL.11/09A/A15-005 1010)

**AKIRA, Yukimatu Sessai**  
(GAILL.06/10A/A01-011 1145)

**AKITA, Takahiro**  
(JSS07a/09P/D-006 1700-107)

**AKITOMO, Kazunori**  
(JSP10/09P/B21-011 1740)

**AKIYAMA, Satoshi**  
(SS03/08A/D-056 0830-215)

**AKIYAMA, Tomohiro**  
(HW01/09P/D-041 1400-232)  
(HS02b/10P/D-003 1630-124)  
(HS02/10A/C24-003 1053)

**AKIYOSHI, Hideharu**  
(MC05/07P/A09-002 1430)  
(MC05/07P/A09-003 1450)

**AKIZ, Ersin**  
(G03/07P/D-002 1400-024)  
(G03/07P/D-026 1400-048)

**AKMAEV, Rashid A.**  
(JSA01/08A/A12-003 0955)

**AKSOY, Hafzullah**  
(HS01/08A/C29-004 1110)

**AKTUG, Bahadir**  
(JSG01/07A/A01-008 1105)

**AL AZRI, Hilal**  
(JSG03/10A/A12-007 1100)

**AL-HALASAH, Nizar KLhalil**  
(JSA01/07P/C30-005 1625)

**AL HOMOUD, Azm**  
(SW04/09P/A13-008 1600)

**AL-KHOUBBI, Issam**  
(SS04b/10P/D-019 1400-203)

**AL-LAZKI, Ali I.**  
(JSS06/10A/A04-008 1110)

**AL-TAIEE, Thair Mahmood**  
(HW07/11P/D-027 1400-163)

**ALAM EL-DIN, Khaled A.**  
(JSP10/08P/D-016 1610-068)  
(JSP08/09A/B19-002 0930)

**ALANIA, Victor Michael**  
(SS03/08A/D-153 0830-312)

**ALCIK, Hakan**  
(SW04/09P/A13-009 1615)

**ALEJU, Castulo A.**  
(G04/08P/C25-004 1510)

**ALEKSEEV, Anatoliy S.**  
(SW05/10A/D-005 0900-249)

**ALEX, Shobhana**  
(GAILL.09/10P/D-001 1400-113)

**ALEXANDER, Joan**  
(MC05/11P/A09-004 1510)

**ALEXANDER, M. Joan**  
(MC05/11A/A09-003 0930)

**ALEXANDER, M.J.**  
(MC05/11A/A09-005 1050)  
(MC05/11A/A09-008 1200)

**ALEXANDROV, Vesselin A.**  
(HS02/07A/C24-004 1130)

**ALEXEYEV, Valery N.**  
(GAILL.06/07P/D-003 1400-123)

**ALFE, D.**  
(U5/07A/D32-001 0900)

**ALI, Khawaja Faran**  
(HS01/09A/C29-008 1140)

**ALI, Mochamad**  
(JSM04/09A/B23-001 0900)

**ALIAJ, Shyqyri**  
(JSP11/08P/D-006 1400-075)

**ALL, Tarmo**  
(JSA07/11A/D-028 0830-028)

## INDEX

- ALLAM, Ahmed Ragab**  
(HW05/10P/D-009 1400-164)
- ALLEN, Joe H.**  
(GAILI.11/09A/A15-002 0925)
- ALLEN, Myles**  
(MC08/08P/D-002 1400-158)  
(JSA08/09A/A08-005 1015)
- ALLIS, Rick**  
(JSG02/09A/D-008 0830-008)
- ALLISON, Ian**  
(JSM10/07P/B23-009 1720)  
(JSM10/07P/B23-001 1400)  
(JSM10/07A/B23-001 0900)
- ALTADILL, David**  
(GAILI.06/11P/D-015 1400-067)
- ALTAMIMI, Zuheir**  
(G07/10A/A03-002 0920)  
(G07/10P/D-008 1400-093)
- ALUNGAL, Balchand N.**  
(HW01/09P/D-018 1400-209)  
(JSM03/08P/A13-005 1540)
- ALVAREZ, Oscar**  
(JSP08/09A/B19-010 1220)  
(JSP08/09A/B19-011 1240)
- ALVERSON, Keith**  
(MI05/11P/B17-005 1520)
- ALY, Deebes Hanafy**  
(GAV.05/09P/D-008 1400-152)
- ALYOSHIN, Vladimir A.**  
(SS03/08A/D-048 0830-207)
- AMALVICET, Martine**  
(G03/07P/D-012 1400-034)
- AMBE, Daisuke**  
(JSP06/08A/B21-002 0920)
- AMBRIZZI, Tercio**  
(MC03/10A/A07-003 0930)
- AMBRIZZI, Tercio**  
(MC03/11P/D-016 1400-191)  
(JSM14/09P/D-004 1400-068)  
(MI05/10P/B17-005 1610)  
(MC17/10A/D-002 0830-184)
- AMBROSIUS, Boudewijn**  
(JSG01/07P/A01-003 1430)
- AMBROSIUS, Boudewijn C.**  
(SS03/08A/D-076 0830-235)
- AMETISTOVA, Lioudmila Y.**  
(JSG03/09P/A12-004 1500)
- AMLIEN, Jostein**  
(JSH01/08A/C27-003 0950)
- AMMAR, Abdallah Ibrahim**  
(HW05/10P/D-009 1400-164)
- AMORIM, Emanuel**  
(GAILI.11/09P/A15-003 1440)
- AMRAL, Iara Righi**  
(HS02b/10P/D-031 1630-152)  
(ANAGNOSTO/C24-008 1543)
- ANAGNOSTOU, Emmanouil N.**  
(MI07/10P/D-001 1400-177)
- ANANDA, M.B.**  
(SS03/08A/D-079 0830-238)
- ANANICHEVA, Maria D.**  
(JSM10/08P/B23-006 1620)
- ANANICHEVA, Maria Dmitrievna**  
(MC12/07P/B19-002 1445)
- ANANTO, Joko**  
(JSM11/10P/B18-006 1620)
- ANAS, Iswandi**  
(JSM04/09A/B23-001 0900)
- ANDAN, Achmad**  
(G03/07P/D-001 1400-023)  
(G03/07P/D-003 1400-025)
- ANDERSEN, Ole**  
(JSG03/09P/D-012 1640-020)
- ANDERSEN, Ole B.**  
(JSG03/09P/D-010 1640-018)  
(JSG02/09A/D-003 0830-003)  
(G03/07P/D-035 1400-057)  
(JSM11/10P/D-004 1700-013)  
(G03/07P/D-036 1400-058)
- ANDERSEN, Per Helge**  
(G07/10P/D-004 1400-089)
- ANDERSON, Brian J.**  
(GAILI.06/08P/A02-004 1515)
- ANDERSON, David N.**  
(GAILI.05/07A/D-001 0830-017)
- ANDERSON, M.L.**  
(HW07/10A/C25-003 1045)
- ANDERSON, Phil C.**  
(GAILI.06/08A/A02-006 1110)
- ANDERSON, Phil S.**  
(JWH01/09A/C30-005 1020)
- ANDERSON, Phillip Charles**  
(GAILI.05/08P/A15-009 1740)  
(GAILI.06/07P/D-013 1400-133)
- ANDERSON, Richard M.**  
(HW08/09A/C28-006 1050)
- ANDERSON, Roger R.**  
(GAILI.05/07A/A06-006 1025)
- ANDERSON, Roger R.**  
(GAILI.05/07A/A06-006 1025)  
(GAILI.10/11A/A01-013 1130)  
(GAILI.10/10P/A01-004 1500)
- ANDERSSON, Lotta**  
(HW01/10P/C26-006 1620)
- ANDO, Kentaro**  
(JSP06/07A/B21-006 1120)
- ANDRÉASSON, Johan**  
(HS02/08A/C24-012 1145)
- ANDRADE, Marcos F.**  
(MI03/09A/D-004 0900-247)
- ANDRADE, Marcus F.**  
(MI03/08A/B18-004 0930)
- ANDRE, M.**  
(GAILI.05/08A/A06-007 1040)
- ANDRE, Mats**  
(GAILI.11/09P/A15-008 1620)
- ANDREAE, M.O.**  
(JSM04/09P/D-010 1400-047)
- ANDREAE, Meinrat**  
(JSM04/09P/D-009 1400-046)
- ANDREAE, Meinrat O.**  
(JSM04/09A/B23-005 1115)
- ANDREAS (CRREL), Edgar**  
(JSP04/09P/A06-008)
- ANDREEV, Oleg Mihailovich**  
(JSM10/09P/D-003 1400-057)
- ANDREEVA, Elena V.**  
(GAILI.10/09A/A11-006 1015)
- ANDRIENKO, Gennady L.**  
(SW05/10P/A13-008 1545)
- ANDRIENKO, Natalia V.**  
(SW05/10P/A13-008 1545)
- ANDRITSANOS, Vassilios D.**  
(G03/07P/D-028 1400-050)
- ANDRYUSCHENKO, Yury N.**  
(JSA07/11A/D-021 0830-021)
- ANGARKHAEVA, Ludmila Khanharaevna**  
(JSH01/07P/C27-005 1520)
- ANGELATS I COLL, Monika**  
(MC04/11P/B22-001 1400)
- ANKHITSETSEG, Dorjsuren**  
(SS04b/10P/D-030 1400-214)
- ANNAKA, Tadashi**  
(JSS07b/10P/D-001 1700-047)
- ANNAMALAI, H.**  
(MC03/09P/A07-004 1540)
- ANSAL, Atilla**  
(SS04b/10P/D-002 1400-186)
- ANUM, Anang Solomon**  
(SS03/08A/D-087 0830-246)
- ANXIN, Lu**  
(JSM10/08P/B23-008 1700)
- AO, Tianqi**  
(HS03/08A/C26-009 1100)  
(HW08/07P/C28-005 1610)  
(HW07/11P/D-006 1400-142)  
(HS03/08A/C26-004 0930)  
(HW07/11P/D-001 1400-137)
- AOI, Shin**  
(SS04b/10P/D-020 1400-204)  
(SS04b/10P/D-015 1400-199)  
(SS04b/10P/D-024 1400-208)  
(SS04b/10P/D-023 1400-207)
- AOKI, Harumi**  
(JSA07/11A/D-010 0830-010)
- AOKI, Kunihiro**  
(JSP09/11A/B20-007 1015)
- AOKI, Shigeru**  
(JSM11/10A/B18-006 1040)  
(JSG03/09P/D-002 1640-010)  
(JSG03/09P/D-001 1640-009)
- AOKI, Teruo**  
(JSH01/08P/D-009 1400-047)
- AOUDIA, Abdelkrim**  
(SS03/07P/A02-009 1630)  
(JSG01/07P/A01-003 1430)  
(JSS06/09P/A04-005 1520)  
(SS04/07P/A03-005 1515)
- AOYAGI, Yasuhira**  
(JSS07a/09P/D-007 1700-108)  
(JSS07a/09P/D-017 1700-118)  
(SS03/08A/D-099 0830-258)
- AOYAMA, Tetsuya**  
(GAILI.11/09P/A15-002 1425)
- APOSTOL, Bogdan**  
(SS04b/10P/D-026 1400-210)
- APOSTOL, Bogdan Felix**  
(SS04/08P/A03-013 1715)
- APOSTOL, Bogdan Felix**  
(SW04/09P/A13-013 1715)
- APOSTOLIDIS, Pashalis**  
(SS04/07A/A03-001 0915)
- APPENZELLER, Christof**  
(MI05/10A/B17-003 0930)
- APPLEBY, Graham M.**  
(G02/10P/D-003 1400-068)
- APPLEBY, Graham Michael**  
(G02/10P/D-015 1400-080)
- AQUINO, Carlos A. Bauer**  
(JSM04/09P/D-009 1400-046)
- AQUINO, Carlos A.B.**  
(JSM04/09P/D-012 1400-049)
- ARABELOS, Dimitrios N.**  
(G03/07P/D-023 1400-045)
- ARAGÃO, Ricardo de**  
(HS01/09A/C29-010 1220)
- ARAI, Ken-ichiro**  
(JSM11/09P/D-010 1400-074)
- ARAI, Kohsaku**  
(SS03/08A/D-055 0830-214)
- ARAI, Masazumi**  
(JSP08/09A/B19-009 1200)
- ARAI, Miki**  
(MI06/09P/B20-004 1500)
- ARAKAWA, Makiko**  
(GAILI.06/11P/D-011 1400-063)
- ARAKI, Hiroshi**  
(G02/07A/C25-014 1245)
- ARAKI, Ryuzo**  
(JSM14/07A/A05-006 1130)
- ARANA, Anibal I.**  
(G04/08P/C25-004 1510)
- ARANAMI, Kouhei**  
(JSM14/08A/A05-011 1200)
- ARAUZO-BRAVO, Marcos**  
(GAV.06/10A/A11-009 1130)
- ARAVEQUIA, Jose A.**  
(MC03/11P/D-012 1400-187)
- ARBETTER, Todd E.**  
(JSP04/09P/A06-001 1400)
- ARDALAN, Alireza A.**  
(SS03/08A/D-142)
- ARDALAN, Alireza A.**  
(G03/07P/D-018 1400-040)  
(G03/07P/D-021 1400-043)  
(G03/07P/D-065 1400-087)
- ARDELEANU, Luminita Angela**  
(SS03/08A/D-029 0830-188)
- ARDESTANI, Vahid Ebrahimzadeh**  
(G04/08P/D-019 1400-126)
- ARDIZZONE, Joe**  
(JSP09/11A/B20-009 1115)
- ARDUINO, Giuseppe**  
(G03/07P/D-001 1400-023)
- ARHEIMER, Berit**  
(HW01/10P/C26-006 1620)
- ARIMA, Makoto**  
(SS03/08A/D-121 0830-280)  
(SW03/10A/D-005 0830-240)
- ARITA, Kazunori**  
(SS03/08A/D-081 0830-240)
- ARMADILLO, Egidio**  
(JSA07/10P/A05-007 1630)
- ARMIGLIATO, Alberto**  
(JSS07a/09P/D-011 1700-112)  
(JSS07a/09P/D-013 1700-114)  
(JSS07/10A/A02-010 1100)
- ARMSTRONG, Anne**  
(JSP04b/10P/D-002 1400-021)
- ARMSTRONG, Richard**  
(JSM15/07A/B18-007 1100)
- ARMSTRONG, Richard L.**  
(JSH01/08A/C27-002 0930)  
(JSH01/07P/C27-011 1740)  
(JSH01/08P/D-011 1400-049)  
(JSH01/07P/C27-004 1500)
- ARNTSEN, Oivind A.**  
(JSP10/11P/B21-004 1530)
- ARORA, Baldev Raj**  
(GAILI.08/08A/A14-002 0850)
- ARORA, K.**  
(JSA07/11A/D-042 0830-042)
- ARORA, Rashmi**  
(SS04b/10P/D-046 1400-230)
- ARORA, Sanjay**  
(HS01/09P/D-017 1400-184)
- ARORA, Tanvi**  
(HW03/11P/C30-002 1420)
- ARTAXO, P.**  
(JSM04/09A/B23-006 1145)  
(JSM04/09P/D-010 1400-047)
- ARTAXO, Paulo**  
(JSM04/09P/D-006 1400-043)  
(JSM04/09P/D-009 1400-046)  
(JSM04/09P/D-015 1400-052)  
(JSM04/09A/B23-005 1115)  
(JSM04/09P/B23-001 1400)
- ARTEMIEVA, Irina M.**  
(JSA07/11A/D-025 0830-025)  
(JSA07/11A/D-027 0830-027)  
(JSS06b/10P/D-005 1400-029)  
(JSA07/11A/D-024 0830-024)
- ARTRU, Juliette**  
(JSS07/10P/A02-010 1630)
- ARTRU, Juliette**  
(GAILI.06/09P/A10-013 1740)
- ARUMUGAM, Sankar**  
(HS02/10A/C24-002 0845)
- ARVIDSSON, Ronald**  
(SS03/07P/A02-005 1500)
- ARYA, Ritesh**  
(HW05/10A/C31-005 0935)
- ASABINA, Elena**  
(HS02c/11P/D-001 1630-099)  
(HS02/11A/C24-001 1045)
- ASAMURA, Kazushi**  
(GAILI.14/08A/D-002 0830-146)  
(GAILI.06/07P/D-010 1400-130)
- ASANO, Kimiyuki**  
(SS04b/10P/D-034 1400-218)
- ASANO, Yoshihiro**  
(GAILI.05/08A/A06-005)
- ASANO, Yuku**  
(HW01/10P/C26-003 1440)  
(HW06/07A/C31-002 0930)  
(HW01/09P/D-040 1400-231)
- ASAOKA, Yoshihiro**  
(JWH01/09P/C30-008 1650)  
(HS02/09A/C24-002 0915)
- ASARI, Kazuyoshi**  
(G02/10P/D-013 1400-078)  
(G02/07A/C25-014 1245)
- ASDAK, Chay**  
(HS02/08P/C24-013 1730)
- ASFAW, Laike**  
(JSA07/10P/A05-006 1610)
- ASFUR, Mustafa**  
(GAILI.04/07A/A08-009)

**ASHIK, Igor**  
(JSP08/09P/B19-006 1620)

**ASHTARI JAFARI, Mohammad**  
(SS03/08A/D-074 0830-233)  
(SS03/08A/D-075 0830-234)

**ASLAM, Rizwan**  
(HS04/07P/C30-001 1405)

**ASPELIEN, Trygve**  
(JSP08/09P/B19-005 1600)

**ASRIL, Asril Asril**  
(JSM04/09P/B23-007 1730)

**ASTE, Atilio A.**  
(JSS07b/10P/D-005 1700-051)

**ASUDEH, Isa**  
(JSS06b/10P/D-011 1400-035)

**ASUMA, Yoshio**  
(JSM14/09A/A05-009 1205)  
(JSM14/09P/D-027 1400-091)  
(JSM14/09P/D-026 1400-090)  
(JSM14/09A/A05-004 1010)

**ASUMA, Yoshio**  
(JSM14/09A/A05-007 1135)

**ASWATHANARAYANA, U.**  
(JSM03/08A/A13-003 0940)

**ATAKAN, Kuvvet**  
(SS04/07P/A03-003 1445)

**ATANASIU, Ligia-Narciza E.**  
(GAV.05/09P/D-005 1400-149)

**ATANASIU, Ligia-Narciza E.**  
(SS03/08A/D-090 0830-249)

**ATAUR, Rahman**  
(HW04/09P/C31-003)

**ATLAS, Robert M.**  
(JSP09/11A/B20-009 1115)

**ATREYA, Sushil K.**  
(MC04/10P/B22-001 1400)

**ATTARCHI, Sara**  
(JSP11/08P/D-003 1400-072)

**Attie Combrink**  
(G02/10P/D-0201400-085)

**AUBOURG, Charly**  
(GAV.06/10P/A11-005 1520)

**AULD, Heather**  
(JSM14/09P/D-021 1400-085)  
(JSM14/09P/D-022 1400-086)

**AULENBACH, Brent T.**  
(HW01/10P/C26-002 1420)

**AUSTEN, Gerrit**  
(G02/07A/C25-006 1030)  
(G07/10P/D-011 1400-096)

**AUSTIN, John**  
(MI03/09A/D-005 0900-248)

**AVANESYAN, Ashot**  
(SS03/08A/D-083 0830-242)

**AVANESYAN, Mher**  
(SS03/08A/D-083 0830-242)

**AVANTS, Megan Sue**  
(JSS06a/08P/D-018 1400-096)

**AVDEEV, Alexander**  
(JSS07/10P/A02-004 1445)

**AVDEEV, Dmitry**  
(GAI.10/09P/D-005 1615-124)

**AVDEV, Stoyan**  
(G03/07P/D-037 1400-059)

**AVERY, James**  
(MC05/10A/A09-007 1100)

**AVERY, Susan Kathryn**  
(MC05/10A/A09-007 1100)

**AVES, Steven L.**  
(MC03/10P/A07-006 1640)

**AVOUAC, Jean-Philippe**  
(SS04b/10P/D-016 1400-200)

**AVSYUK, Yuri N.**  
(JSS06a/08P/D-027 1400-105)

**AWAD, Haytham**  
(HS02c/11P/D-015 1630-113)  
(HS02/11A/C24-015 1141)

**AWAN, Shaukat A.**  
(HW07/11P/D-032 1400-168)  
(HS02b/10P/D-027 1630-148)  
(HS02/10P/C24-004 1527)

**AWAN, Shaukat Ali**  
(HS03/07P/C26-005 1500)

**AWANGE, Joseph**  
(G04/08P/D-028 1400-135)

**AYELE, Atalay**  
(JSS06/10A/A04-004 0930)

**AYHAN, Mehmet Emin**  
(G03/07P/D-002 1400-024)  
(G03/07P/D-026 1400-048)  
(JSG01/07A/A01-008 1105)

**AYODEJI, O.S.**  
(HS02/11A/C24-007 1000)

**AZMON, Benjamin**  
(HS02/09A/C24-010 1130)

**AZUMA, Eisho**  
(MC03/11P/D-001 1400-176)

**AZUMA, Takashi**  
(SS03/08A/D-059 0830-218)

**AZZA, Addi**  
(JSP08/09P/D-002 1400-101)

**AZZOUT, Yassine**  
(G03/07P/D-009 1400-031)

## b

**B., Rao P.**  
(GAI.06/11P/D-014 1400-066)  
(GAI.06/11P/D-013 1400-065)

**B., Rao P.**  
(GAI.06/11P/D-018 1400-070)

**B.P.K., Patro**  
(SS03/08A/D-133 0830-292)

**BABA, Hisatoshi**  
(JSG03/09P/D-022 1640-030)

**BABA, Kiyoshi**  
(SS03/07A/A02-011 1200)  
(GAI.08/08P/D-008 1400-143)

**BABADJANIAN, Amazasp A.**  
(SS03/08A/D-085 0830-244)

**BABAIYAN, Iman**  
(MI05/11P/B17-006 1610)

**BABBITT, R.E.**  
(JSM04/09A/B23-006 1145)

**BABKIN, Alexey Vladimirovich**  
(HS02b/10P/D-011 1630-132)  
(HS02/10A/C24-011 1125)

**BABKIN, Alexey Vladimirovich**  
(HS02/07P/C24-018 1404)  
(HS02a/07P/D-018 1545-164)

**BABUSKA, Vladislav**  
(JSS06b/10P/D-013 1400-037)  
(JSS06/08A/A04-009 1130)  
(JSS06b/10P/D-012 1400-036)

**BADAWY, Ahmed**  
(SS03/08A/D-088 0830-247)

**BADIALI, Lucio**  
(SW05/10A/D-006 0900-250)

**BAEK, Sangho**  
(JSG03/09P/D-012 1640-020)

**BAGMANOVA, Nailiya Hannanovna**  
(SS03/08A/D-141 0830-300)

**BAHER, Shirley**  
(SS03/08A/D-030 0830-189)

**BAI, Zhi-Ming**  
(SS03/08A/D-135 0830-294)

**BAILEY, Matthew P.**  
(MI08/07P/B18-003 1600)  
(MI08/07P/B18-007 1715)  
(MI08/07P/B18-006 1700)

**BAILEY, Richard**  
(JSP06/07P/B21-005 1600)

**BAILEY, Scott M.**  
(GAI.09/11A/A11-004 0950)

**BAINES, Peter G.**  
(MI06/09P/B20-003 1440)  
(JSP10/09A/B21-008 1140)

**BAISHEV, Dmitry G.**  
(GAI.10/11A/D-002 0830-076)

**BAKAN, Stephan**  
(JSP09/11A/B20-002 0900)

**BAKER, Daniel M.**  
(GAI.07/09A/A14-003 0950)

**BAKER, Daniel N.**  
(GAI.06/08P/A02-007 1615)  
(GAI.05/07A/A06-011 1205)  
(GAI.09/11A/A11-004 0950)  
(GAI.05/08A/A06-004 0925)  
(GAI.11/09A/A15-002 0925)  
(GAI.05/08A/A15-001 0830)

**BAKER, Daniel N.**  
(GAI.09/11P/A11-003 1440)

**BAKER, S.P.**  
(JSM04/09A/B23-006 1145)

**BAKER, Trevor**  
(G07/10P/D-016 1400-101)

**BAKHTIAROV, Vilory F.**  
(JSG01/08P/D-009 1400-009)

**BALA, Andrei**  
(JSS06b/10P/D-017 1400-041)  
(JSA07/11A/D-020 0830-020)

**BALAN, Florin Stefan**  
(SS04/08P/A03-013 1715)

**BALAN, Stefan Florin**  
(SW04/09P/A13-013 1715)

**BALASIS, George**  
(GAV.05/08A/A11-007 1110)

**BALASNYAN, Yuri**  
(SS04/08P/A03-009 1615)

**BALASSANIAN, Serguei**  
(SS05/10A/A13-009 1045)

**BALASSANIAN, Serguei**  
(SS04/08P/A03-009 1615)

**BALDWIN, Mark**  
(MC05/10P/A09-008 1740)

**BALDWIN, Mark P.**  
(MI05/10A/B17-008 1140)  
(MI05/10A/B17-002 0910)  
(MC05/10P/A09-002 1430)  
(JSA08/09P/A08-007 1650)

**BALES, Roger**  
(JWH01/09P/C30-006 1540)

**BALES, Roger C.**  
(JWH01/10A/C30-009 1140)

**BALLANI, Ludwig**  
(GAV.05/09P/D-003 1400-147)

**BALMACEDA, Laura**  
(GAI.09/11A/A11-002 0900)

**BALMINO, Georges**  
(G02/07A/C25-001 0900)

**BALOGH, A.**  
(GAI.05/08A/A06-007 1040)  
(GAI.09/11A/A11-006 1110)

**BALOGH, Andre**  
(GAI.05/07P/D-020 1400-118)  
(GAI.05/08A/A06-003 0900)  
(GAI.11/09P/A15-008 1620)  
(GAI.05/07P/D-007 1400-105)  
(GAI.05/08A/A06-009 1110)  
(GAI.07/09P/A14-006 1610)  
(GAI.05/08A/A06-004 0925)

**BAN, Kazuhiko**  
(JSS07/09P/A02-004 1445)

**BANASIK, Kazimierz**  
(HW07/11P/D-030 1400-166)

**BANE, John M.**  
(JSP09/11P/B20-008 1615)

**BANERJEE, Devashis**  
(GAI.05/07P/D-001 1400-099)

**BANG, So-Young**  
(JSM04/09P/D-008 1400-045)  
(JSM04/09P/B23-004 1600)

**BANGANAN, Esmeralda Longino**  
(SS04b/10P/D-036 1400-220)

**BANNISTER, S.**  
(SS03/08A/D-146 0830-305)

**BANSAL, B.K.**  
(JSS06/07P/A04-007 1620)

**BANSAL, Brijesh Kumar**  
(SS04/07P/A03-009 1630)

**BAO, hanzhang**  
(HW05/10P/D-010 1400-165)

**BAO, Lifeng**  
(JSP07/08A/B17-006 1120)

**BAPTIE, Brian**  
(SS03/08A/D-026 0830-185)

**BAPTISTA, Maria Ana**  
(JSS07a/09P/D-015 1700-116)

**BAPTISTA, Maria Ana**  
(JSS07/09A/A02-010 1130)

**BAPTISTA, Paulo**  
(JSP07/08A/B17-008 1200)

**BAR-SEVER, Yoaz E.**  
(G07/10P/D-001 1400-086)

**BARABASH, Stanislav**  
(GAV.03/08P/A16-001)

**BARABASH, Stas**  
(GAI.14/08A/D-002 0830-146)

**BARASHAYN, Konstantin K**  
(GAV.03/08A/A16-008)

**BARAZANGI, Muawia**  
(JSS06/10A/A04-008 1110)

**BARBALIC, Darko**  
(HW07/11P/D-023 1400-159)

**BARBERI, Graziella**  
(SS03/07P/A02-008 1615)

**BARD, Pierre-Yves**  
(SS04/07A/A03-004 1015)  
(SS04a/09P/D-048 1400-297)  
(SS04/07A/A03-011 1215)

**BARDAKOV, Roman N.**  
(JSP10/08P/D-014 1610-066)

**BARDOSSY, Andras**  
(HS01/09P/D-019 1400-186)  
(HW08/09A/C28-002 0930)  
(HS02/09A/C24-007 1100)

**BARDOSSY, Andreas**  
(HW03/11A/C30-005 0950)  
(HW03/11A/C30-009 1130)

**BARDSLEY, William Earl**  
(HW01/09P/D-022 1400-213)  
(HS02/09A/C24-005 1000)

**BARGAOUI, Zoubaida**  
(HW03/11A/C30-005 0950)  
(HW03/11A/C30-009 1130)

**BARINGER, Molly O'Neil**  
(JSP06/08A/B21-003 0950)  
(JSP06/07P/D-006 1400-013)  
(JSP06/07P/D-008 1400-015)

**BARKER, Daniel**  
(SS03/08A/D-094 0830-253)

**BARNES, Joel**  
(G04/07P/C25-004 1530)

**BARNETT, David N.**  
(MC08/07A/B17-003 1015)  
(MC11/10A/B19-001 0830)

**BARNETT, John**  
(MC05/08P/A09-003 1450)

**BARREDO, Silvia Patricia**  
(SS03/08A/D-097 0830-256)  
(JSA07/11A/D-048 0830-048)

**BARRIOT, Jean-Pierre**  
(G02/07A/C25-012 1215)  
(G03/07P/D-062 1400-084)  
(HW03/11A/D-002 0830-136)

**BARRUOL, Guilhem**  
(JSS06a/08P/D-013 1400-091)

**BARRY, Roger G.**  
(JSM10/07A/B23-001 0900)  
(JSH01/07A/C27-002 1000)

**BARSUKOV, Pavel O.**  
(GAI.10/09P/A11-005 1500)

**BARSUKOV, Pavel O.**  
(GAI.10/09P/D-006 1615-125)

**BARSZCZ, Mariusz**  
(HW07/11P/D-030 1400-166)

**BARTELT, Perry**  
(JWH01/10P/D-001)

**BARTELT, Perry**  
(JSM10/07A/B23-004 1020)

**BARTHELMES, Franz**  
(G02/07A/C25-001 0900)

**BARTLEIN, Patrick J.**  
(MC12/07A/B19-003 1015)

**BARTLETT, Marshall Grant**  
(MC12/08P/B19-002 1445)

**BARTOLOZZI, Federico**

## INDEX

- (SS04/08P/A03-015 1745)  
(SS04b/10P/D-040 1400-224)
- BARZAGHI, Riccardo**  
(JSG01/07P/A01-003 1430)  
(G07/10P/D-017 1400-102)  
(G03/07P/D-048 1400-070)
- BASHKUEV, Yuri Buddich**  
(JSA07/11A/D-013 0830-013)  
(JSH01/07P/C27-005 1520)
- BASTOS, Luisa**  
(JSP07/08A/B17-008 1200)
- BASU, Santimay**  
(GAILI.06/10A/A01-003 0905)
- BASU, Sunanda**  
(GAILI.06/10A/A01-003 0905)
- BATAILLE, Klaus**  
(JSG01/07P/A01-004 1445)
- BATALEV, Vlad**  
(GAI.08/08A/A14-004 0930)
- BATALEVA, Elena**  
(GAI.08/08A/A14-004 0930)
- BATES, M.J.**  
(MI09/09A/B22-004 1000)
- BATLLO, Josep**  
(U7/11A/D32-006 1150)
- BAUCH, Henning A.**  
(MC12/07A/B19-005 1100)
- BAUER, Eva**  
(MC12/07A/B19-001 0930)
- BAUL-DEOCAMPO, Janila R.**  
(SS04b/10P/D-005 1400-189)
- BAUL-DEOCAMPO, Janila R.**  
(SS04/07P/A03-006 1530)
- BAUMJOHANN, Wolfgang**  
(GAILI.14/08A/D-003 0830-147)  
(GAILI.05/08A/A06-003 0900)  
(GAILI.05/07P/D-007 1400-105)
- BAUMJOHANN, Wolfgang**  
(GAILI.05/07A/A06-004 0945)  
(GAIV.03/08P/A16-004 1540)
- BAUR, Oliver**  
(G07/10P/D-011 1400-096)
- BAUTISTA, Bartolome C.**  
(SS04/07P/A03-006 1530)  
(JSS07a/09P/D-009 1700-110)
- BAUTISTA, Bartolome Caparas**  
(SS04b/10P/D-036 1400-220)  
(SS04b/10P/D-035 1400-219)
- BAUTISTA, Bautista Caparas**  
(SS03/08A/D-060 0830-219)  
(SW05/10A/D-003 0900-247)
- BAUTISTA, Ma. Leonila P.**  
(JSS07a/09P/D-009 1700-110)
- BAUTISTA, Maria Leonila Pascual**  
(SS03/08A/D-060 0830-219)  
(SW05/10A/D-003 0900-247)
- BAUTISTA, Maria Leonila Pascual**  
(SS04b/10P/D-035 1400-219)  
(SS04b/10P/D-036 1400-220)
- BAX-NORMAN, Holly A.**  
(MI08/07P/B18-002 1530)
- BAYARSAIKHAN, Chimedtseren**  
(SS04b/10P/D-030 1400-214)
- BAYDULOV, Vasiliy G.**  
(JSP10/10P/B21-009 1720)
- BAYER, Roger**  
(G03/07P/D-012 1400-034)
- BAYOR, Jude Simon**  
(HS02a/07P/D-034 1545-180)  
(HS02/07P/C24-034 1508)
- BAZILE, E.**  
(JWH01/09P/C30-001)
- BEAGLEY, Stephen R.**  
(MI03/08P/B18-003 1440)
- BEAR WG,**  
(GAI.10/09P/A11-004 1445)
- BEASLEY, William**  
(MI08/07P/B18-006 1700)
- BEAU, Isabelle**  
(MC17/11P/B23-010 1720)
- BÉCEL, Anne**  
(SS03/07A/A02-009 1130)
- BECHTOLD, Peter**  
(MC17/11P/B23-010 1720)
- BECKLEY, Brian**  
(JSM11/10P/D-004 1700-013)
- BÉDIR, Mourad**  
(JSA07/11A/D-044 0830-044)
- BEER, Tom**  
(JSP11/07A/A10-001 0900)
- BEGUM, Kareemunnisa Shaik**  
(SS03/08A/D-133 0830-292)
- BEHREND, Knut**  
(G07/10P/D-019 1400-104)
- BEIG, Gufran**  
(JSA09/10A/A08-004 0945)  
(JSA01/08A/A12-001 0905)
- BEJAEV, Anatolii**  
(JSS07/10P/A02-004 1445)
- BEJAICHUND, Mayshree**  
(SS04/08P/A03-007 1530)  
(SS04/08P/A03-005 1500)
- BELENKAYA, Elena Semenovna**  
(GAILI.14/07P/A12-011 1735)
- BELENOVICH, Taisya Yakovlevna**  
(JSP04b/10P/D-005 1400-024)
- BELLON, Herve**  
(SS03/08A/D-061 0830-220)
- BELOUSOVA, Anna P.**  
(HS02/07A/C24-006 1200)  
(HW01/09P/D-029 1400-220)
- BELYH, Olga I.**  
(JSP04a/09P/D-001 1400-094)
- BEN AHMED DAHO, Sid Ahmed**  
(G03/07P/D-027 1400-049)
- BEN-ZVI, Arie**  
(HS02/09A/C24-010 1130)
- BENAHMED DAHO, Sid Ahmed**  
(G03/07P/D-076 1400-098)
- BENBROOK, James R.**  
(GAILI.04/07P/A08-005 1540)
- BENDJOUDI, Hocine**  
(HW07/10P/C25-003 1445)
- BENESTAD, Rasmus E.**  
(MI05/10P/D-005 1400-171)
- BENGTSSON, Lennart**  
(MC11/10A/B19-004 0940)  
(MC08/07A/B17-001 0930)
- BENISTON, Martin**  
(JSM14/09A/A05-005 1025)  
(JWH01/10P/D-003 1400-008)  
(JSM14/09P/D-016 1400-080)
- BENOUAR, Djillali**  
(SS04/09A/A03-004 0945)  
(SS04b/10P/D-022 1400-206)
- BENSON, Rick B.**  
(SW05/10P/A13-002 1420)
- BENZ, Harley M.**  
(SS03/07A/A02-004 0945)
- BEPPU, Hideki**  
(JSM14/08A/A05-009 1130)
- BERAKOVIC, Boris**  
(HS02/07A/C24-004 0912)  
(HS02a/07P/D-004 1545-150)
- BERAKOVIC, Marija**  
(HS02/07A/C24-004 0912)  
(HS02a/07P/D-004 1545-150)
- BERBERY, Ernesto Hugo**  
(MC03/10A/A07-002 0910)
- BERDICHEVSKY, Mark N.**  
(GAI.10/09A/A11-006 1015)  
(GAI.10/09P/D-009 1615-128)
- BEREZOVSKAYA, Svetlana**  
(JSP04/10P/A06-008 1640)
- BERGERE-THIERRY, Catherine**  
(SS04/07A/A03-009 1145)
- BERGSTRÖM, Sten**  
(HS02/08A/C24-012 1145)
- (HS02/08A/C24-004 0915)
- BERGSTRAND, Sten**  
(SS03/07P/A02-005 1500)
- BERING, Edgar A.**  
(GAILI.11/10P/D-005 1400-120)
- BERING, III, Edgar Andrew**  
(GAILI.04/07P/A08-005 1540)
- BERIO, Philippe**  
(G04/08P/D-021 1400-128)
- BERKEY, Frank Tom**  
(GAILI.06/10A/A01-008 1050)
- BERNARD, Eddie N.**  
(JSS07/09A/A02-001 0900)
- BERNARDES, Cristina**  
(JSP07/08A/B17-008 1200)
- BERNHARDT, Paul A.**  
(GAILI.06/09P/A10-003 1440)  
(GAILI.11/09A/A15-009 1150)
- BERRY, Philippa Anne**  
(JSG03/09P/D-005 1640-013)
- BERTHELIER, Jean-Jacques**  
(GAILI.11/09P/A15-013 1745)  
(GAILI.11/10P/D-003 1400-118)
- BERTIGER, William I.**  
(G03/07P/D-068 1400-090)
- BERTUCCI, Cesar**  
(GAIV.03/08A/A16-005 1040)
- BERTUCCI, Cesar L.**  
(GAIV.03/08A/A16-003 0930)
- BERUBE, D.**  
(GAILI.06/08A/A02-003 0940)  
(GAILI.08/10A/A16-012 1210)
- BERUBE, Dave**  
(GAILI.10/11A/A01-003 0900)
- BERUBE, David**  
(GAILI.10/10P/A01-002 1420)
- BERZIN, Robert G.**  
(JSA07/10A/A05-005 1000)
- BERZIN, Robert G.**  
(JSA07/11A/D-021 0830-021)  
(GAI.10/09A/A11-006 1015)
- BESA, Dante Gutierrez**  
(JSS07/10P/A02-005 1500)
- BESBES, Mustapha**  
(HW06/07P/D-001 1400-185)
- BESPALOV, Peter Alexeevich**  
(GAILI.07/11A/A12-007 1135)
- BESSE, Jean**  
(JSS06/08A/A04-005 0950)
- BESUTIU, Georgeta**  
(GAV.06/09P/D-002 1400-155)
- BESUTIU, Lucian**  
(SS03/08A/D-091 0830-250)  
(GAV.06/09P/D-002 1400-155)
- BETTADPUR, Srinivas**  
(JSG02/09A/D-004 0830-004)
- BEUTLER, Gerhard**  
(G07/10A/A03-001 0900)  
(U7/11A/D32-003 1000)  
(G07/10P/A03-001 1400)  
(G02/07A/C25-009 1130)
- BEVEN, Keith J.**  
(HW07/11A/C25-006 1000)  
(HW08/08P/C28-001 1400)
- BEVIS, Michael**  
(G02/10P/D-009 1400-074)
- BEZHAEV, Anatoly Yu.**  
(JSS07b/10P/D-002 1700-048)
- BEZRUKIKH, V.**  
(GAILI.06/07P/D-018 1400-138)
- BHATTACHARYA, Gopal Chandra**  
(JSA07/11A/D-033 0830-033)
- BHATTACHARYA, Pankaj Mala**  
(SS03/08A/D-069 0830-228)
- BHATTACHARYA, Sourendra Kumar**  
(HW06/07P/C31-006 1540)
- BHATTACHARYA, Sourendra Kumar**  
(HW06/07P/D-004 1400-188)
- BHATTACHARYYA, Archana**  
(GAILI.06/09A/A10-005 1005)  
(GAILI.06/11P/D-002 1400-054)
- BHATTACHARYYA, Rupa**  
(HS02c/11P/D-020 1630-118)  
(HS02/11A/C24-020 1201)
- BHATTACHARYYA, Rupa**  
(HW05/10P/D-007 1400-162)
- BHOI, Nilima**  
(JSP11/07P/A10-004 1550)
- BHOWRUTH, Teeluck**  
(HW05/10A/C31-007 1005)
- BHUSAL, Lekhnath**  
(GAILI.04/07P/A08-005 1540)
- BIAGI, Ludovico**  
(G07/10P/D-017 1400-102)
- BIAN, Shaofeng**  
(G03/07P/D-053 1400-075)
- BIANCALE, Richard**  
(G02/07A/C25-001 0900)  
(G02/07A/C25-003 0940)
- BIAOU, Angelbert Chabi**  
(HW07/11P/D-015 1400-151)
- BIEHL, Larry**  
(JSG03/09P/A12-007 1620)
- BIELAK, Jacobo**  
(SS04/07P/A03-012 1715)
- BIERNAT, Helfried K.**  
(GAILI.05/07A/A06-004 0945)
- BIGORRE, Sebastien**  
(JSP10/08P/D-002 1610-054)
- BILEK, Susan L.**  
(SS03/08A/D-032 0830-191)
- BILHAM, Roger**  
(JSS07/10A/A02-007 1000)
- BILHAM, Roger**  
(JSG01/08P/D-023 1400-023)
- BILLIEN, Magali**  
(JSA07/11A/D-025 0830-025)
- BINGEN, Christine**  
(JSG03/10A/A12-009 1140)
- BINGHAM, Rory**  
(JSG02/09P/A05-009 1715)
- BINNIS, Ray**  
(SS03/08A/D-063 0830-222)
- BIONDIC, Danko**  
(HW07/11P/D-023 1400-159)
- BIRGOREN, Gulum**  
(SS04a/09P/D-017 1400-266)
- BIRKS, S. Jean**  
(HW06/07P/C31-005 1520)
- BISH, Andrew**  
(GAV.04/07A/A11-003 0950)
- BISWAS, Niren N.**  
(SS04b/10P/D-025 1400-209)
- BJARNASON, Ingi Thorleifur**  
(JSS06/09P/A04-007 1620)
- BJORNSSON, Grimur**  
(JSG01/07P/A01-010 1635)
- BLACK, Michael L.**  
(JSP09/11P/B20-006)
- BLACK, Peter G.**  
(JSP09/11P/B20-006 1545)
- BLACK, Peter Gerard**  
(JSP09/11P/B20-003 1430)
- BLACKBURN, Mike**  
(MC03/09P/A07-001 1400)
- BLAGOVESHCHENSKY, Donat V.**  
(GAILI.10/10P/A01-012 1740)
- BLAIN, Cheryl Ann**  
(JSP08/09P/B19-010 1740)
- BLAKELY, Richard J.**  
(GAV.06/10A/A11-001 0830)  
(GAV.06/09P/D-007 1400-160)
- BLANC, Elisabeth**  
(GAILI.04/07P/A08-010 1715)
- BLANCO-CANO, X.**  
(GAILI.14/07P/A12-003 1445)
- BLECKI, Jan S.**  
(GAILI.08/11P/D-001 1400-072)
- BLEEKER, Wouter**  
(JSS06/09P/A04-008 1640)
- BLEIWEISS, Max**

- (JSH01/07P/C27-006 1600)  
**BLEWITT, Geoffrey**  
 (G04/08P/C25-005 1530)  
**BLINKHORN, Jim**  
 (SW05/10P/A13-004 1450)  
**BLITZKOW, Denizar**  
 (G03/07P/D-069 1400-091)  
 (G03/07P/D-032 1400-054)  
 (G03/07P/D-004 1400-026)  
**BLOESCHL, Guenter**  
 (HW08/09A/C28-001 0900)  
**BLOMBERG, Lars G.**  
 (GAIII.14/07A/A12-002 1000)  
**BLOXHAM, Jeremy**  
 (GAV.04/07P/A11-007 1640)  
**BLUM, Alex E.**  
 (HW01/10P/C26-002 1420)  
**BLUM, John Anthony**  
 (JSS06/07P/A04-008 1640)  
**BLUMENSTOCK, Thomas**  
 (MI03/08A/B18-007 1110)  
**BLUNDELL, Jeffrey Ralph**  
 (JSP10/09A/B21-001 0900)  
**BOBÉE, Bernard**  
 (HW07/11P/C25-003 1430)  
**BOBROV, Victor N.**  
 (U7/11P/D32-001 1400)  
**BOCHEV, Alexander**  
 (GAIII.10/11A/A01-009 1030)  
**BOCHEV, Alexander Z.**  
 (GAIII.10/11A/D-004 0830-078)  
**BOCHKAREV, Vladimir Vladimirovich**  
 (GAII.06/11P/D-003 1400-055)  
**BOCHNICEK, Josef**  
 (JSA08/09A/A08-004 1000)  
**BOCK, Yehuda**  
 (JSG01/07A/A01-010 1135)  
**BOCQUILLION, Claude**  
 (HW08/07A/C28-008 1150)  
**BODAGHJAMALI, Javad**  
 (JSP11/08P/D-003 1400-072)  
 (JSP11/08P/D-009 1400-078)  
 (MI05/11P/B17-006 1610)  
 (JSP11/07A/A10-006 1110)  
**BODAGHJAMALI, Javad**  
 (JSP11/08A/A10-005 1050)  
**BODHANKAR, Ninad**  
 (HW06/07P/C31-003 1440)  
**BÓDIS, Katalin**  
 (HS02c/11P/D-004 1630-102)  
 (HS02/11A/C24-004 1057)  
**BOEDECKER, Gerd**  
 (G03/07P/D-019 1400-041)  
**BOEDECKER, Gerd**  
 (G03/07P/D-062 1400-084)  
**BOERNGEN, Michael**  
 (JSM14/08P/A05-001 1400)  
 (HS02/09A/C24-012 1200)  
**BOETTGER, Tatjana**  
 (MC12/08P/B19-007 1700)  
**BOEZIO, Gabriel Cazes**  
 (MI05/10P/B17-001 1400)  
**BOGATYRYOV, Gennadiy**  
 (JSM14/07P/A05-004 1505)  
 (JSM14/07P/A05-004 1505)  
**BOGDANOVA, Yulia**  
 (GAIII.05/08A/A06-009 1110)  
**BOGEN, Jim**  
 (HS01/09A/C29-006 1040)  
**BOHEMA WORKING GROUP**  
 (SS03/08A/D-028 0830-187)  
**Bohema Working Group**  
 (JSS06b/10P/D-012)  
**BOICE, Daniel C.**  
 (MC04/10P/B22-007 1645)  
 (MC04/10P/B22-008 1700)  
**BOJARIU, Roxana A.**  
 (MI05/11P/B17-008 1650)  
**BOKELMANN, Götz**  
 (JSS06/10A/A04-011 1210)  
**BOLDI, Robert**  
 (GAII.04/07A/A08-006 1050)  
**BOLDYREV, Sergey**  
 (SS03/08A/D-077 0830-236)  
**BOLDYREV, Serguey A.**  
 (JSS06b/10P/D-001 1400-025)  
**BOLGOV, Mikhail V.**  
 (HW05/10A/C31-004 0920)  
**BÖLLING, Karla**  
 (G04/08A/C25-004 0940)  
**BOMMER, Julian J.**  
 (SS03/08A/D-052 0830-211)  
**BONAGURA, Mariateresa**  
 (SS04a/09P/D-015 1400-264)  
**BONATTI, Jose P.**  
 (MC03/11P/D-012 1400-187)  
**BONDAR, Tatiana N.**  
 (GAV.05/08P/A11-006 1530)  
 (GAV.04/07P/A11-010 1740)  
**BONJEAN, Stijn**  
 (MI03/08A/B18-003 0910)  
**BONJER, Klaus-Peter**  
 (SS04a/09P/D-050 1400-299)  
**BONNEFOY-CLAUDET, Sylvette**  
 (SS04/07A/A03-011 1215)  
**BONNELL, J.W.**  
 (GAIII.06/08P/A02-011 1725)  
**BONO, Andrea**  
 (SW05/10A/D-006 0900-250)  
**BØNSNES, Truls Erik**  
 (HS01/09A/C29-006 1040)  
**BOO, Kyung-On**  
 (MI05/10P/B17-002 1440)  
**BOODOO, Sudesh**  
 (JSM14/09P/D-019 1400-083)  
**BOOIJ, Martijn J.**  
 (HS02/09P/C24-004 1445)  
**BOONE, A.**  
 (JWH01/09P/C30-001)  
**BOONE, A.**  
 (JWH01/09A/C30-009 1210)  
**BOPRIE, D.**  
 (JSH01/08P/D-013)  
**BORDONI, Simona**  
 (MC03/10P/A07-003 1440)  
**BORGHI, Alessandra**  
 (JSG01/07P/A01-003 1430)  
**BORGHI, Alessandra**  
 (G07/10P/D-017 1400-102)  
**BORMANN, Helge**  
 (HW07/11P/D-010 1400-146)  
**BORMANN, Peter**  
 (SS05/10A/A13-001 0830)  
 (SS05/10A/A13-002 0845)  
**BORMOTOV, Vladimir A.**  
 (JSG01/08P/D-009 1400-009)  
**BORNHOLD, Brian D.**  
 (JSS07b/10P/D-009 1700-055)  
**BOROVSKY, Joe E.**  
 (GAIII.06/08P/A02-003 1450)  
**BOROVSKY, Joseph E.**  
 (GAIII.08/10A/A16-009 1115)  
**BORRERO, Jose**  
 (JSS07a/09P/D-018 1700-119)  
**BORRERO, Jose**  
 (JSS07/09P/A02-009 1615)  
**BORRERO, Jose C.**  
 (JSS07a/09P/D-018 1700-119)  
**BORTOLI, Daniele**  
 (MI03/09A/D-003 0900-246)  
**BOSCH, A. Pulido**  
 (HS01/09P/C29-004 1500)  
**BOSCH, Wolfgang**  
 (G07/10A/A03-006 1120)  
 (G03/07P/D-050 1400-072)  
**BOSCH, Wolfgang**  
 (JSG02/09A/D-005 0830-005)  
**BOSCHETTI, Fabio**  
 (SW05/10P/A13-009 1615)  
**BOSCOLO, Roberta**  
 (JSP06/07P/D-003 1400-010)  
**BOSKA, Josef**  
 (GAII.06/11P/D-015)  
**BOSKA, Josef**  
 (GAII.06/10A/A01-013 1215)  
**BOSQUED, Jean-Michel**  
 (GAIII.05/08A/A06-009 1110)  
**BOSSU, Remy**  
 (SW05/10A/D-001 0900-245)  
**BOTELER, David H.**  
 (JSP11/07A/A10-007 1130)  
**BÖTTGER, Henning**  
 (MC04/11P/B22-001 1400)  
**BOUCHER, Claude**  
 (G07/10A/A03-002 0920)  
**BOUDANOV, Vladimir Georgievich**  
 (JSS06/10A/A04-006 1010)  
**BOUDOURIDIS, Athanasios**  
 (GAIII.10/11A/A01-003 0900)  
**BOUGERET, Jean-Louis**  
 (GAIII.14/07A/A12-004 1050)  
**BOUGERET, Jean-Louis**  
 (GAIII.05/07A/A06-006 1025)  
**BOUGHER, Stephen W.**  
 (GAIV.03/09A/A16-002 0930)  
 (GAII.07/11P/A12-001 1400)  
**BOUMAN, Johannes**  
 (G03/07P/D-024 1400-046)  
**BOUNAMA, Christine**  
 (JSS06b/10P/D-022 1400-046)  
**BOURQUI, Michel S.**  
 (MI03/08P/B18-007 1630)  
 (MC05/09A/A09-002 0920)  
**BOURUET-AUBERTOT, Pascale**  
 (JSP10/09A/B21-007 1120)  
**BOUTEN, Willem**  
 (HW08/08P/C28-003 1500)  
**BOVILLE, Byron A.**  
 (MC05/08A/A09-004 1000)  
 (MC05/08A/A09-003 0930)  
 (MC05/10P/A09-005 1620)  
**BOVILLE, Byron A.**  
 (JSA01/08A/A12-005 1115)  
**BOYARCHUK, Kirill A.**  
 (JSA08/09P/A08-009 1730)  
**BOYCHENKO, Svetlana G.**  
 (HS02/09A/C24-013 1215)  
 (HS02/07A/C24-009 0932)  
 (HS02a/07P/D-009 1545-155)  
**BOYER, Don L.**  
 (JSP10/09A/B21-008 1140)  
**BOYLE, Jim**  
 (MC11/10A/B19-004 0940)  
**BOYNAGRYAN, Arthur V.**  
 (SS03/08A/D-084 0830-243)  
**BOYNAGRYAN, Vladimir R.**  
 (SS03/08A/D-086 0830-245)  
**BOZZO, Emanuele**  
 (JSA07/10P/A05-007 1630)  
**BOZZO, Emanuele**  
 (GAV.06/09P/D-012 1400-165)  
**BRACHET, Sidonie**  
 (JSP09/10A/B20-003 0945)  
**BRACONNOT, Pascale**  
 (MI05/10P/D-008 1400-174)  
**BRADLEY, Raymond Stuart**  
 (MC12/07P/B19-001 1415)  
**BRAESICKE, Peter**  
 (MC05/10A/A09-005 1000)  
 (MI03/08P/B18-001 1400)  
**BRANDT, Alan**  
 (JSP10/11A/B21-009 1150)  
**BRANKOVIC, Cedo**  
 (MC03/11A/A07-004 0950)  
**BRASS, Carsten**  
 (HS02/10A/C24-001 0830)  
**BRASSEUR, Olivier**  
 (JSM14/09P/D-016 1400-080)  
**BRAUN, A.**  
 (SS03/08A/D-149 0830-308)  
**BRAUN, Alexander**  
 (JSG01/08A/A01-012 1205)  
**BRAUN, Alexander**  
 (G07/10P/D-006 1400-091)  
**BRAUNE, Stephan**  
 (G07/10P/D-019 1400-104)  
**BREMER, Juergen**  
 (JSA01/08P/A12-002 1430)  
**BRENNER, Anita C.**  
 (JSM11/10A/B18-001 0900)  
**BREHERTON, Christopher S.**  
 (MC03/10P/A07-004 1520)  
**BREUS, Tamara K.**  
 (GAIV.03/08A/A16-008 1150)  
**BRICAUD, Annick**  
 (JSP06/07A/B21-001 0900)  
**BRIFFA, Keith**  
 (MC12/08P/B19-006 1620)  
**BRIFFA, Keith R.**  
 (MC12/08A/B19-004 1055)  
**BRIGHAM, Lawson W.**  
 (JSP04b/10P/D-004 1400-023)  
**BRILLY, Mitja**  
 (HS02/09P/C24-009 1630)  
**BROCHER, Thomas M.**  
 (SS03/07P/A02-007 1600)  
**BRODZIK, Mary Jo**  
 (JSH01/08A/C27-002 0930)  
**BROEDERBAUER, Veronika**  
 (G02/10P/D-007 1400-072)  
**BROKESOVA, Johana**  
 (SS04/07P/A03-011 1700)  
**BROMWICH, David H.**  
 (JSM10/08A/B23-010 1210)  
**BROUCHKOV, Anatoli**  
 (JSP04a/09P/D-003 1400-096)  
**BROVKIN, Victor**  
 (MC12/07A/B19-006 1115)  
 (MC12/07A/B19-001 0930)  
**BROWN, Larry D.**  
 (SS03/08A/D-134 0830-293)  
**BROWN, Larry Douglas**  
 (SW03/10P/A04-015 1745)  
**BROWN, Lee E.**  
 (HW02/11A/C31-004 0950)  
**BROWN, Ross**  
 (JWH01/09P/C30-001 1400)  
 (JWH01/09A/C30-009 1210)  
**BROWN-MITIC, Constance M.**  
 (JWH01/09P/C30-006 1540)  
**BRUEMMER, Burghard**  
 (MI06/09P/B20-009 1700)  
**BRUNINI, Claudio Antonio**  
 (JSG03/10A/A12-008 1120)  
**BRUYNINX, Carine**  
 (G07/10P/D-016 1400-101)  
**BU, James**  
 (JSS07a/09P/D-018 1700-119)  
**BUDILLON, Giorgio**  
 (JSP08/09A/B19-001 0900)  
**BUFFETT, Bruce**  
 (U5/07A/D32-002 0930)  
**BUGAYENKO, I.**  
 (JSS06a/08P/D-012 1400-090)  
**BUHE, Aosier**  
 (JSG03/09P/D-006 1640-014)  
**BULYCHEV, Andrey**  
 (SS03/08A/D-077 0830-236)  
**BULYCHEV, Andrey Alexandrovich**  
 (G03/07P/D-022 1400-044)  
**BUNCE, Emma J.**  
 (GAIII.14/07P/A12-002 1430)  
**BUNKER, Rees**  
 (HS03/08P/C26-010 1630)  
**BÜRGMANN, Roland**  
 (JSG01/07P/A01-009 1620)  
**BURHANUDDIN, Safri**  
 (SS03/08A/D-063 0830-222)  
**BURKE, Sean**  
 (HS04/08A/C30-001 0905)  
**BURLAGA, L.F.**  
 (GAIV.02/07P/A07-005 1640)  
**BURRAGE, Derek M.**  
 (JSG03/09P/A12-006 1540)  
**BURTON, S.P.**  
 (MC05/07P/D-003 1400-210)  
**BURTSEV, Alexei**

## INDEX

- Alexandrovich**  
(SW05/10P/A13-014 1730)
- BURWELL, David C.**  
(JSS07/10P/A02-002 1415)
- BUSH, John W.M.**  
(JSP10/10P/B21-008 1700)
- BUST, Gary S.**  
(GAIL.05/08A/A15-008 1150)
- BUTCHART, Neal**  
(MC05/10A/A09-002 0900)
- BUTLER, Christopher John**  
(MC12/08A/B19-006 1130)
- BUTLER, John C.**  
(JSA08/09A/A08-007 1045)
- BUYANOVA, Darima Garmaeвна**  
(JSA07/11A/D-013 0830-013)
- BUZEVICH, Alexandr Vladimirovich**  
(JSA07/11A/D-005)
- BYCHKOV, Kirill A.**  
(SW05/10P/A13-001 1400)
- BYOUNG-KWON, Park**  
(JWH01/09P/C30-002 1420)
- BZIAVA, Konstantine Kote**  
(HS01/09P/D-021 1400-188)
- BZIAVA, Konstantine Kote**  
(HS02/07A/C24-010 0936)  
(HS02a/07P/D-010 1545-156)
- (U7/11P/D32-004 1535)**
- CAMPBELL, Donald H.**  
(HW01/10P/C26-002 1420)
- CAMPBELL, Paul**  
(HW07/11P/D-018 1400-154)
- CAMPOS, Teodosio Chavez**  
(GAV.06/09P/D-010 1400-163)  
(SS05/10P/D-001 1400-235)
- CANAS, Jose A.**  
(SS03/08A/D-033 0830-192)
- CANCELLIERE, Antonino**  
(HS02/10A/C24-004 0915)
- CANDELA, LUCILA**  
(HS04/07P/C30-006 1655)
- CANDER, Ljiljana**  
(GAIL.05/08P/A15-006 1630)
- CANNON, Eric Christopher**  
(SW04/09P/A13-012 1700)
- CAO, Aimin**  
(JSS06/09A/A04-003 0940)
- CAO, Jia Min**  
(JSS06b/10P/D-014)
- CAO, Jia Min**  
(JSS06b/10P/D-007 1400-031)
- CAPDEVILLE, Yann**  
(JSS06a/08P/D-019 1400-097)
- CAPRA, Cristea**  
(SS04a/09P/D-046 1400-295)
- CARA, Michel**  
(JSS06/08A/A04-008 1110)
- CARA, Michel J.**  
(JSS06/10A/A04-004 0930)
- CARBONE, Richard E.**  
(JSM14/07P/A05-008 1745)
- CARDIN, Philippe**  
(JSP10/08P/B21-005 1530)
- CARITEAU, Benjamin**  
(JSP10/08P/D-010 1610-062)
- CARLSSON, Bengt**  
(HS02/08A/C24-012 1145)
- CARMI, Natasha George**  
(HS02/11A/C24-002 0845)
- CARMONA, JUAN S.**  
(SS04b/10P/D-043 1400-227)
- CARPENTER, Don L.**  
(GAIL.10/10P/A01-001 1400)
- CARPENTER, Theresa M.**  
(HS03/07A/C26-005 1015)  
(HS03/07A/C26-001 0900)
- CARRIERES, Thomas**  
(JSM14/09P/D-028 1400-092)
- CĂRSTEANU, Alin A.**  
(HW07/11P/C25-003 1430)
- CARTER, Martin K.**  
(GAIL.05/07P/D-020 1400-118)
- CARTWRIGHT, John C.**  
(JSS07/09A/A02-008 1100)
- CARUSO, Michael J.**  
(JSP09/10A/B20-007 1115)
- CARVALHO, Soniaeli P.**  
(HS02c/11P/D-021 1630-119)  
(HS02/11A/C24-021 1205)
- CASE, Kelley E.**  
(G03/07P/D-068 1400-090)
- CASSANO, Elizabeth Noel**  
(MI05/10P/D-009 1400-175)
- CASSIDY, John**  
(JSG01/07P/A01-006)  
(SS04/08P/A03-014)
- CASTRO, Sandra**  
(JSP09/11A/B20-006 1000)
- CASTRO JR., Carlos Alberto Correia**  
(G03/07P/D-069 1400-091)
- CATANA, Simona**  
(HS02/11P/C24-005 1500)
- CATANI, Filippo**  
(HS01/08P/C29-006 1600)
- CATHEY, Mary**  
(JSP08/09A/B19-005 1030)
- CATTELL, Cynthia**  
(GAIL.06/08A/A02-006 1110)
- CATTLE, Howard**  
(JSP06/07P/D-003 1400-010)
- CAULFIELD, Colm-cille P.**  
(JSP10/11P/B21-001 1420)
- CAVALCANTI, Iracema Fonseca**  
(MC03/10A/A07-008 1130)  
(MC03/10A/A07-003 0930)
- CAVALIERI, Don**  
(JSH01/08P/D-006 1400-044)
- CAVALIERI, Donald J.**  
(JSM10/08A/B23-003 0930)
- CAZENAVE, Anny**  
(JSG03/09P/D-003 1640-011)
- CAZENAVE, Anny**  
(JSM11/10P/D-007 1700-016)
- CELIK, Cengiz**  
(GAI.08/08A/A14-007 1050)  
(GAI.08/08P/D-007 1400-142)
- CERV, Vaclav**  
(GAI.08/08P/D-004)
- CERV, Vaclav**  
(GAI.08/08P/D-002 1400-137)
- CERV, Vaclav**  
(GAI.08/08P/D-003 1400-138)
- CESAREC, Ksenija**  
(HS02/07A/C24-004 0912)  
(HS02a/07P/D-004 1545-150)
- CEULENEER, Georges**  
(JSG03/10A/A12-007 1100)
- CHA, Eun-Jeong**  
(MC03/11P/D-013 1400-188)  
(MI05/10P/D-004 1400-170)
- CHABANGBORN, Akkaneewut**  
(JSM04/09P/B23-002 1430)
- CHABRILLAT, Sabine**  
(JSG03/10A/A12-007 1100)
- CHABRILLAT, Simon**  
(MI03/08A/B18-003 0910)
- CHAKRABOR, Gautam1Kumar**  
(SS03/08A/D-021 0830-180)
- CHAKRABORTY, Sudipto**  
(HW05/10P/D-007 1400-162)
- CHAMBODUT, Aude**  
(GAV.04/07A/A11-006 1120)  
(GAV.05/09P/D-004 1400-148)  
(GAV.05/08P/A11-004 1500)
- CHAN, Anthony A.**  
(GAIL.09/11P/A11-003 1440)
- CHAN, JOHNNY C.L.**  
(MC03/10P/A07-007 1700)  
(MC02/07P/B20-001 1400)  
(MC03/09P/A07-009 1740)
- CHAN, Pui-King**  
(JSP09/10P/B20-006 1530)
- CHAND, Duli**  
(JSM04/09P/D-009 1400-046)
- CHANG, Chien-Hsin**  
(SS03/07A/A02-004 0945)
- CHANG, Chih-Pei**  
(MC02/07P/B20-002 1420)  
(MC02/08A/B20-003 0940)
- CHANG, Chin-Hsin**  
(HS02c/11P/D-007 1630-105)  
(HS02/11A/C24-007 1109)
- CHANG, Chung-Pai**  
(JSG03/09P/D-021 1640-029)
- CHANG, Fong-Chiau**  
(HS02/11P/C24-002 1415)
- CHANG, Grace C.**  
(JSP07/08P/B17-002 1430)
- CHANG, June**  
(JSP09/11P/B20-010 1700)
- CHANG, Kun-Shu**  
(G03/07P/D-049 1400-071)
- CHANG, Lisa T.C.**  
(JSM14/09P/D-008 1400-072)
- CHANG, Shu-Hao**  
(SS03/08A/D-062 0830-221)
- CHANG, Tao Ming**  
(SS04a/09P/D-014 1400-263)
- CHANG, Tao-Ming**  
(SS04a/09P/D-036 1400-285)
- (SS04a/09P/D-037 1400-286)
- CHANG, Tom T.S.**  
(GAIL.07/09A/A14-001 0900)  
(GAV.02/07A/A00-006 1200)
- CHANG, Tsui-Yu**  
(JSG03/09P/D-021 1640-029)
- CHANG, Wen-Yen**  
(JSA07/11A/D-009 0830-009)
- CHANG, Yu-Wen**  
(SS04/08P/A03-012 1700)
- CHANRION, Olivier**  
(GAIL.11/09P/A15-012 1730)
- CHANT, Robert**  
(JSP07/08A/B17-001 0900)
- CHANTEUR, Gerard M.**  
(GAV.03/08P/A16-002 1430)  
(GAV.03/09A/A16-005 1100)
- CHAO, Benjamin Fong**  
(JSG02/09P/A05-004 1515)  
(JSG01/07A/A01-009 1120)
- CHAO, Chi-Kwan**  
(GAIL.06/10A/A01-012 1200)
- CHAPMAN, David S.**  
(JSG02/09A/D-008 0830-008)  
(MC12/08P/B19-002 1445)
- CHAPPELLAZ, Jerome**  
(HS02b/10P/D-019 1630-140)  
(HS02/10A/C24-019 1157)
- CHARLES, Chris**  
(MC12/08P/B19-001 1415)
- CHARLTON, Andrew J.**  
(MI05/10A/B17-002 0910)
- CHARVIS, Philippe**  
(SS03/07A/A02-009 1130)
- CHASHECHKIN, Yuli D.**  
(JSP10/08P/D-014 1610-066)  
(JSP10/08P/D-017 1610-069)  
(JSP10/10P/B21-009 1720)  
(JSP10/08P/D-013 1610-065)  
(JSP10/10A/B21-004 0950)  
(JSP10/08P/D-015 1610-067)
- CHASHECHKIN, Yuli Dmitrievich**  
(JSP10/11P/B21-007 1700)
- CHASTIN, Sebastien**  
(SW04/09P/A13-010 1630)
- CHATFIELD, Robert B.**  
(MI03/08A/B18-006 1050)
- CHATTERJEE, Debashis**  
(HS02c/11P/D-020 1630-118)  
(HS02/11A/C24-020 1201)
- CHATTERJEE, Debashis**  
(HW05/10P/D-007 1400-162)
- CHAU, Ha Duyen**  
(GAV.05/08P/A11-007 1620)
- CHAU, Jorge L.**  
(GAIL.06/09A/A10-011 1205)
- CHAUBEY, Anil K.**  
(JSA07/11A/D-033 0830-033)
- CHAUDHARI, Lalitkumar Pandit**  
(HS02c/11P/D-023 1630-121)  
(JSM03/08A/A13-001 0900)  
(HS02/11A/C24-023 1213)
- CHAUMONT, Diane**  
(JSM14/09A/A05-003 0955)
- CHAUVIN, Annick**  
(GAV.07/07P/A13-002 1420)
- HAVE, Alan**  
(JSA07/10A/A05-003 0920)
- HAVE, Alan D.**  
(SS03/07A/A02-011 1200)  
(JSS06/09P/A04-008 1640)
- HAZELAS, Jean-Louis**  
(SS04/07A/A03-004 1015)
- CHE, Tao**  
(JSH01/08P/D-011 1400-049)
- CHE, Tao**  
(JSH01/07P/C27-011 1740)  
(JSH01/08P/D-003 1400-041)
- CHEBROV, Victor N.**  
(SS04a/09P/D-005 1400-254)
- CHEN, Alfred B.**

- (GAIL.04/07A/A08-007 1110)  
**CHEN, Bing**  
 (SS03/08A/D-138 0830-297)  
**CHEN, Chau-Huei**  
 (SS03/08A/D-111 0830-270)  
 (SS03/08A/D-016 0830-175)  
**CHEN, Cheng-Ta**  
 (MC11/10P/B19-006 1610)  
**CHEN, CHIARONG**  
 (HS03/08P/C26-001 1400)  
**CHEN, Chien-Chih**  
 (GAI.08/08A/A14-006 1010)  
**CHEN, Chow-Son**  
 (GAI.08/08A/A14-006 1010)  
**CHEN, Dianyou**  
 (MI05/10P/B17-007 1650)  
**CHEN, George T. J.**  
 (JSM14/09P/D-008 1400-072)  
**CHEN, George Tai-Jen**  
 (JSM14/09P/D-003 1400-067)  
**CHEN, George Tai-Jen**  
 (JSM14/07P/A05-008 1745)  
**CHEN, Guoxing**  
 (HW07/11P/D-020 1400-156)  
**CHEN, Horng-Yue**  
 (JSG01/07A/A01-007 1050)  
**CHEN, Horng-Yue**  
 (JSG01/08P/D-036 1400-036)  
**CHEN, Jen-Ping**  
 (JSM04/09P/D-007 1400-044)  
**CHEN, Jiangchi**  
 (HW07/11P/D-036 1400-172)  
**CHEN, Jianyao**  
 (HS04/07P/C30-003 1505)  
 (HS02/07A/C24-003 1115)  
**CHEN, Jianyao**  
 (HS04/07P/C30-002 1435)  
**CHEN, Jiasheng**  
 (GAILI.09/11P/A11-001 1400)  
**CHEN, Jingyang**  
 (MC17/11P/B23-003 1440)  
**CHEN, Jingyi**  
 (SS03/08A/D-137 0830-296)  
**CHEN, Jinhai**  
 (SS04b/10P/D-044 1400-228)  
**CHEN, Jiuhui**  
 (JSA07/10P/A05-004 1500)  
**CHEN, K.-Y.**  
 (GAIL.06/09A/A10-001 0900)  
**CHEN, Kuang-Jung**  
 (GAV.06/09P/D-004 1400-157)  
**CHEN, Kun-Shan**  
 (JSG03/09P/D-021 1640-029)  
**CHEN, Kwo-Hwa**  
 (G03/07P/D-049 1400-071)  
**CHEN, Li-Jen**  
 (GAILI.07/09P/A14-003 1450)  
**CHEN, Margaret W.**  
 (GAILI.06/08P/A02-005 1530)  
**CHEN, Mingxuan**  
 (MI05/09P/B17-008 1710)  
**CHEN, Ren-Tzeng**  
 (MC03/09A/A07-004 1030)  
**CHEN, Rensheng**  
 (HS02/09P/C24-010 1645)  
**CHEN, Shullin**  
 (HS01/09P/D-023 1400-190)  
**CHEN, Shuyi S.**  
 (JSP08/09P/B19-010 1740)  
 (JSP09/11P/B20-004 1500)  
 (MC02/07P/B20-007 1620)  
**CHEN, Tsing-Chang (Mike)**  
 (MC03/09P/A07-002 1440)  
**CHEN, Tuo**  
 (JSM04/09P/D-001 1400-038)  
**CHEN, Tuo**  
 (HS02/08A/C24-006 0945)  
**CHEN, W. S.**  
 (GAIL.06/11P/D-009 1400-061)  
**CHEN, Wen**  
 (MI05/10A/B17-009 1200)  
**CHEN, Wu**  
 (G02/10P/D-005 1400-070)  
**CHEN, Xiaobin**  
 (GAI.08/08A/A14-001 0830)  
**CHEN, Xiaofei**  
 (SS04/08A/A03-004 0915)  
**CHEN, Yangbo**  
 (HS03/08P/C26-005 1500)  
**CHEN, Yi-Hau**  
 (SS04a/09P/D-011 1400-260)  
**CHEN, Yong**  
 (SS04b/10P/D-037 1400-221)  
**CHEN, Yongqi**  
 (G03/07P/D-044 1400-066)  
**CHEN, Yuanfang**  
 (HW07/11P/D-020 1400-156)  
 (HW07/11P/D-035 1400-171)  
 (HW07/11P/D-036 1400-172)  
**CHEN, Yun**  
 (SS03/08A/D-137 0830-296)  
**CHEN, Yun-tai**  
 (SS05/10A/A13-012 1130)  
**CHEN, Yuntai**  
 (SS04/07A/A03-003 1000)  
 (SW04/09P/A13-003 1430)  
**CHEN, Z.Q.**  
 (HW07/10A/C25-003 1045)  
**CHEN, Zeyu**  
 (MC05/11P/A09-003 1450)  
**CHEN, Zhen**  
 (MI05/10P/B17-007 1650)  
**CHEN, ZhiQiang**  
 (HW08/08A/C28-007 1100)  
**CHENG, Bin**  
 (JSM10/07P/B23-002 1440)  
**CHENG, C.Z.**  
 (GAILI.05/07A/A06-009 1135)  
 (GAILI.10/10P/A01-006 1540)  
 (GAILI.05/07P/D-002 1400-100)  
**CHENG, Chad Shouquan**  
 (JSM14/09P/D-021 1400-085)  
 (JSM14/09P/D-022 1400-086)  
**CHENG, Guodong**  
 (HS02/08A/C24-005 0930)  
**CHENG, Lei**  
 (MI09/09P/B22-001 1400)  
**CHENG, Win-Bin**  
 (SS03/08A/D-020 0830-179)  
**CHENG, Xueguang**  
 (G04/08P/D-016 1400-123)  
**CHEKNIAWSKY, Josef Y.**  
 (JSS07b/10P/D-008 1700-054)  
**CHERRY, Jessica Ellen**  
 (MI05/11P/B17-001 1400)  
**CHETTY, Talari Ramakrishnaiah**  
 (SW03/10P/A04-012 1700)  
**CHEUNG, Kevin K.W.**  
 (MC02/08A/B20-004 1000)  
 (MC02/08A/B20-007 1140)  
**CHEUNG, Kwok Fai**  
 (JSS07/10P/A02-011 1645)  
 (JSS07/10P/A02-002 1415)  
**CHEVALLIER, Pierre**  
 (HW04/09A/C31-004 1000)  
**CHEVREL, Stéphane**  
 (JSG03/10A/A12-007 1100)  
**CHI, Gong-cai**  
 (SS04b/10P/D-037 1400-221)  
**CHI, Peter J.**  
 (GAILI.10/10P/A01-005 1520)  
**CHIA, Hsin Hsing**  
 (MC02/07A/B20-006 1145)  
**CHIANG, Hsien Jen**  
 (SS04a/09P/D-014 1400-263)  
**CHIAO, Ling-Yun**  
 (SS03/08A/D-124 0830-283)  
**CHIAPPINI, Massimo**  
 (GAV.06/09P/D-012 1400-165)  
 (GAV.06/10A/A11-005 0950)  
 (GAV.06/10A/A11-004 0930)  
 (GAV.06/09P/D-001 1400-154)  
**CHIBA, Osamu**  
 (MC05/07P/D-010 1400-217)  
**CHIBA, Tomoaki**  
 (SS03/08A/D-049 0830-208)  
**CHIKAMORI, Hidetaka**  
 (HS02b/10P/D-030 1630-151)  
 (HS02/10P/C24-007 1539)  
**CHIKITA, Kazuhisa A.**  
 (HS01/09P/D-003 1400-170)  
**CHILSON, Phillip B.**  
 (GAIL.06/10A/A01-006 0955)  
**CHINOWSKY, Timothy M.**  
 (GAIL.04/07P/A08-006 1605)  
**CHIRUTA, Mihai**  
 (JSM15/07A/B18-002 0930)  
**CHITHIRAIVEL, Panneerselvam**  
 (JSA09/10A/A08-009 1145)  
 (JSA09/11P/D-002 1400-051)  
**CHIU, Hung-Chie**  
 (SS04/07A/A03-008 1130)  
**CHIU, Long**  
 (MC02/07P/D-002 1400-199)  
**CHIU, Yi-Xiang**  
 (SS04/07A/A03-007 1115)  
**CHO, Ikoo**  
 (SS04a/09P/D-034 1400-283)  
 (SS03/08A/D-056 0830-215)  
**CHO, Jae-Myoung**  
 (JSG01/08P/D-010 1400-010)  
**CHO, Kyoung-Sook**  
 (JSM04/09P/D-008 1400-045)  
**CHO, Mengu**  
 (GAILI.11/09P/A15-003 1440)  
**CHO, Yong Sik**  
 (JSS07/09A/A02-013 1215)  
**CHOI, Byoung-Cheol**  
 (JSM04/09P/D-008 1400-045)  
**CHOI, ByungHo**  
 (JSS07/09A/A02-004 0945)  
**CHOI, Jae-Cheon**  
 (JSM04/09P/B23-004 1600)  
 (JSM04/09P/D-008 1400-045)  
**CHOI, Wookap**  
 (MC05/07A/A09-003 1000)  
 (MC05/09A/A09-005 1050)  
**CHOU, Kun-Hsuan**  
 (MC02/08P/B20-004 1500)  
**CHOU, Ming-Dah**  
 (JSP09/10P/B20-006 1530)  
 (JSP09/11A/B20-009 1115)  
**CHOU, Sherry**  
 (GAV.03/08A/A16-007 1130)  
**CHOU, Shu-Hsien**  
 (JSP09/11A/B20-009 1115)  
 (JSP09/10P/B20-006 1530)  
**CHOUDHURI, Arnab R.**  
 (GAV.04/09P/A16-001 1400)  
**CHOURASIA, L. P.**  
 (HW01/09P/D-003 1400-194)  
**CHOURASIA, L.P.**  
 (HS02/08P/C24-005 1500)  
 (HS02/07P/C24-023 1424)  
 (HS02a/07P/D-023 1545-169)  
**CHRISTENSEN, U.R.**  
 (JSS06/10A/A04-001 0830)  
**CHRISTIANSEN, Freddy**  
 (GAV.05/08A/A11-006 1050)  
**CHRISTIANSEN, Freddy**  
 (GAIL.05/08P/A15-007 1700)  
**CHRISTIANSEN, Freddy**  
 (GAV.04/07A/A11-005 1100)  
**Christoph Reigber**  
 (JSG02/09P/A05-007 1645)  
**CHRISTOU, Odysseas P.**  
 (HS01/09P/D-018 1400-185)  
**CHROUST, Petr**  
 (HW01/10A/C26-001)  
**CHU, F.D.**  
 (GAIL.06/11P/D-009 1400-061)  
**CHU, Pao-Shin**  
 (MC02/07A/B20-006 1145)  
**CHU, William P.**  
 (MI03/09A/D-001 0900-244)  
 (MI03/08A/B18-002 0850)  
**CHU, Yen-Hsyang**  
 (GAIL.06/09A/A10-012 1225)  
**CHUBACHI, Shigeru**  
 (MI03/08A/B18-009 1150)  
**CHUDA, Takashi**  
 (MC17/11P/B23-003 1440)  
**CHUGUNOVA, Olga M.**  
 (GAILI.10/11A/A01-001 0830)  
**CHULICK, Gary S.**  
 (JSA07/11A/D-026 0830-026)  
**CHULLI-ZENATI, Badiaa**  
 (JSA07/11A/D-044)  
**CHUMCHEAN, Siriluk**  
 (HS03/07P/C26-001 1400)  
**CHUN, Hye-Yeong**  
 (MC05/07P/D-014 1400-221)  
 (MC05/11A/A09-006 1110)  
**CHUNG, Hyo-Sang**  
 (JSM04/09P/B23-004 1600)  
**CHUNG, Ju-Yong**  
 (JSG03/09P/D-009 1640-017)  
**CHUNG, Seung-Hwan**  
 (JSA07/10P/A05-003 1440)  
**CHUNG, Wang-Shung**  
 (JSG01/08P/D-036 1400-036)  
**CHURIKOV, Vladimir**  
 (SS03/08A/D-104 0830-263)  
**CINTRA, Rosangela**  
 (MC03/11P/D-012 1400-187)  
**CIOFLAN, Carmen**  
 (SS04b/10P/D-026 1400-210)  
**CIOFLAN, Carmen Ortansa**  
 (SS04/08P/A03-013 1715)  
**CIOFLAN, Carmen Ortansa**  
 (SW04/09P/A13-013 1715)  
**CIONE, Joseph J.**  
 (JSP09/11P/B20-006 1545)  
**CIRANO, Mauro**  
 (JSP08/09P/B19-009 1720)  
**CISEWSKI, Mike S.**  
 (MI03/08A/B18-002 0850)  
**CLACK, Paul D.**  
 (HW02/11A/C31-005 1045)  
**CLAESSENS, Sten**  
 (G04/08P/D-010 1400-117)  
**CLAPS, Pierluigi**  
 (HW07/11A/C25-012 1200)  
**CLARKE, Ellen**  
 (JSA01/08P/A12-006 1640)  
**CLARKE, John T.**  
 (GAILI.14/07P/A12-008 1650)  
**CLARKE, Peter J.**  
 (G04/08P/C25-005 1530)  
**CLARKE, Robin T.**  
 (HS02/08A/C24-010 1115)  
**CLARKE, Robin Thomas**  
 (HW07/11P/C25-001 1400)  
**CLAUER, Calvin Robert**  
 (GAILI.06/08A/A02-008 1200)  
**CLAUSEN, Martin**  
 (MC12/07A/B19-001 0930)  
**CLERCX, Herman J.H.**  
 (JSP10/10A/B21-005 1030)  
**CLILVERD, Mark**  
 (GAILI.10/10P/A01-008 1620)  
**CLILVERD, Mark A.**  
 (GAILI.10/10P/A01-001 1400)  
**CLILVERD, Mark Andrew**  
 (JSA01/08P/A12-006 1640)  
**CLINE, Don**  
 (JSH01/08A/C27-001 0910)  
**CLOSE, Sigrid**  
 (GAIL.06/10A/A01-009 1105)  
**CLOUGH, Shepard A.**  
 (MC11/10P/B19-007 1630)  
**CLOUTIER, Paul A.**  
 (GAV.03/08A/A16-007 1130)  
**CLOWES, Ron M.**  
 (SW03/10P/A04-001 1400)  
 (SS03/07P/A02-004 1445)  
**CLUA DE GONZALEZ, Alicia Luiza**  
 (GAILI.09/11A/A11-002 0900)  
**CLUA DE GONZALEZ, Alicia**

## INDEX

- Luiza**  
(GAI.09/11P/A11-008 1710)
- COBB, Kim M.**  
(MC12/08P/B19-001 1415)
- CODRESCU, Mihail**  
(GAI.05/07A/D-001 0830-017)
- COHEN, Judah**  
(JSM10/08A/B23-004 0950)
- COHEN, Judah L.**  
(JSM10/08A/B23-005 1010)
- COHEN, Judah Levi**  
(MI05/11P/B17-009 1710)
- COHEN, Steven C.**  
(JSG01/08P/D-014 1400-014)
- COHEN, Steven Charles**  
(JSG01/08P/D-015 1400-015)
- COHEN, Yves**  
(GAV.05/08A/A11-010 1210)
- Cold Land Processes Working Group**  
(JSH01/08A/C27-001)
- COLEY, William R.**  
(GAI.05/08A/A15-007 1130)
- COLLINI, Estela A.**  
(MC03/10A/A07-002 0910)
- COLLINS, Adrian Loric**  
(HS01/09A/C29-001 0900)
- COLLINS, Clive**  
(JSG01/07P/A01-012 1705)
- COLLINS, David N.**  
(HS02b/10P/D-017 1630-138)  
(HS02/10A/C24-017 1149)
- COLLINS, Nancy**  
(SS04/08A/A03-011 1115)
- COLLISCHONN, Walter**  
(HS02/08A/C24-010 1115)
- COLOMB, Raul**  
(JSP06/07A/B21-007 1140)
- COLONY, Roger**  
(JSM10/09P/D-005 1400-059)
- COLONY, Roger L.**  
(JSP04/10A/A06-002 0920)
- COLWELL, Steven Richard**  
(JSM10/07P/B23-006 1620)
- COMBA, Maria Alejandra**  
(JSA07/11A/D-047 0830-047)
- COMBES, Michel**  
(MC04/10P/B22-006 1615)
- COMBRINK, Adriaan Z.A.**  
(G02/10P/D-0191400-084)
- COMINGUEZ, Alberto H.**  
(SS03/08A/D-150 0830-309)
- CONIL, Sebastien**  
(MI05/11A/B17-001 0830)
- CONIL, Sebastien**  
(MI05/11A/B17-002 0850)  
(MC08/07P/B17-007 1550)
- CONNERNEY, Jack E.P.**  
(GAI.V.03/08A/A16-008)
- CONSORTIUM, The MERMAG-M**  
(GAI.14/08A/D-003 0830-147)
- CONSTABLE, Catherine G.**  
(U6/09A/D32-002 0935)
- COOK, Fred A.**  
(SW03/10P/A04-001 1400)
- COOK, Kemball**  
(MC17/11A/B23-001 0830)
- COOK, Kerry Harrison**  
(MC03/09A/A07-002 0930)  
(MC12/07A/B19-007 1130)  
(MC11/10A/B19-006 1040)
- COOK, Thomas M.**  
(JSP09/11P/B20-006 1545)
- CORD, Aurélien**  
(JSG03/10A/A12-007 1100)
- CORDOVA, Ana Maria**  
(JSM04/09P/D-010 1400-047)
- CORELA, Carlos**  
(JSS07/09A/A02-010 1130)
- CORNEJO, Helen**  
(JSM11/10A/B18-001 0900)
- CORNFORD, Dan**  
(JSP06/07A/B21-001 0900)
- CORNILLEAU, N.**  
(GAI.05/08A/A06-007 1040)
- CORNILLEAU-WEHRLIN, Nicole**  
(GAI.08/11P/D-001 1400-072)
- CORNOU, Cecile**  
(SS04/07A/A03-011 1215)
- CORNUELLE, Bruce**  
(JSP06/08A/B21-001 0900)
- COROBOV, Roman M.**  
(MC08/07P/B17-010 1655)
- CORREIA, Alexandre L.**  
(JSM04/09P/D-006 1400-043)
- CORRELL, Ray**  
(HS04/07A/C30-002 1005)
- CORTI, Susanna**  
(MC03/11A/A07-004 0950)  
(MI05/09A/B17-004 1020)
- COSANDEY, Claude**  
(HW01/10A/C26-002 0850)
- COSGROVE, Russell B.**  
(GAI.06/09P/A10-009 1640)
- COSTA, Giovanni**  
(SS04/07P/A03-005 1515)
- COTE, Tim**  
(SW05/10P/A13-004 1450)
- COTTON, Fabrice**  
(SS04/07A/A03-009 1145)
- COUDRAIN-RIBSTEIN, Anne**  
(HS01/09P/D-014 1400-181)
- COULOT, David**  
(G07/10P/D-008 1400-093)
- COURTILLOT, Vincent E.**  
(JSS06/08A/A04-005 0950)
- COUSTENIS, Athena**  
(MC04/10P/B22-006 1615)  
(GAI.07/11P/A12-007 1710)
- COUTINHO, Mariane**  
(JSM14/08P/A05-004 1625)
- COWLEY, S.W.H.**  
(GAI.09/11A/A11-006 1110)
- COWLEY, Stan W.H.**  
(GAI.14/07P/A12-002 1430)
- COWLEY, Stanley W.H.**  
(GAI.05/07P/D-016 1400-114)
- COX, Daniel**  
(JSS07/09P/A02-011 1645)
- COX, Donald P.**  
(GAI.V.02/07A/A07-005 1130)
- the CPMN Group**  
(GAI.10/11A/D-020 0830-094)
- the CPMN Group**  
(GAI.10/11A/D-021 0830-095)  
(GAI.05/07P/D-015 1400-113)  
(GAI.05/08P/A15-005 1600)  
(GAI.10/11A/D-009 0830-083)  
(GAI.05/07P/D-014 1400-112)
- CRÉTAUX, Jean-Francois**  
(JSG03/09P/D-003 1640-011)
- CRACIUNESCU, Vasile**  
(HS02/11P/C24-005 1500)
- CRAMPIN, Stuart**  
(SW04/09P/A13-010 1630)
- CRARY, F.J.**  
(GAI.14/07A/A12-009 1225)
- CRAVEN, Mike**  
(JSM10/07P/B23-009 1720)
- CREED, Irena**  
(HS01/09P/D-012 1400-179)
- CREPON, Michel R.**  
(JSP06/07A/B21-001 0900)
- CRIDER, Dana H.**  
(GAI.07/11A/A12-005 1035)
- CROCHET, Michel**  
(MC05/07P/D-015 1400-222)
- CROCKER, Greg**  
(JSM14/09P/D-028 1400-092)
- CROKE, Barry**  
(HW07/10P/C25-010 1645)
- CROKE, Barry FW**  
(HW07/11P/C25-006 1515)
- CROOKS, Simon**  
(JSA08/09P/A08-005 1550)
- CROSI MASPOLI, Mischa**  
(MI05/09P/B17-004 1520)
- CROSSLEY, David**  
(JSG02/09P/A05-008 1700)
- CROWLEY, John N.**  
(MI08/07P/D-003 1400-197)
- CSAPO, Geza**  
(G03/07P/D-020 1400-042)
- CSON BRANDT, Pontus**  
(GAI.06/08A/A02-002 0915)
- CUI, Maochang**  
(JSP09/10P/B20-005 1515)
- CUMMER, Steve**  
(GAI.04/07A/A08-006 1050)
- CUMMINS, Phil**  
(JSG01/07P/A01-012 1705)
- CUMMINS, Phil R.**  
(SS04/08A/A03-014 1200)
- CUMNOCK, Judy A.**  
(GAI.14/07A/A12-002 1000)
- CURIC, Mladjen M.**  
(JSM14/08P/A05-007 1730)
- CURTIS, Mike**  
(GAV.06/10P/A11-003)
- CZENTYE, Balazs**  
(HS02/09A/C24-007 1100)
- d**
- DAAG, Arturo S.**  
(SW05/10A/D-003 0900-247)
- DAERDEN, Frank W.R.**  
(MI03/08A/B18-003 0910)
- DAGLIS, Ioannis A.**  
(GAI.08/10A/A16-006 1005)  
(GAI.06/07P/D-009 1400-129)
- DAHAB, K.**  
(HS02a/07P/D-032 1545-178)  
(HS02a/07P/D-033 1545-179)  
(HS02/07P/C24-032 1500)  
(HS02/07P/C24-033 1504)
- DAI, Aiguo**  
(JSP09/10A/B20-009 1145)
- DAI, Y.-J.**  
(JWH01/09P/C30-001)
- DAKOURE, Denis**  
(HW06/07P/D-001 1400-185)
- DAL LAGO, Alisson**  
(GAI.09/11A/A11-002 0900)  
(GAI.09/11P/A11-008 1710)
- DALAUDIER, Francis**  
(MC05/07P/D-015 1400-222)
- DALGUER, Luis A.**  
(SS04a/09P/D-032 1400-281)
- DALY, Pat W.**  
(GAI.05/07P/D-020 1400-118)
- DAMASKE, Detlef**  
(GAV.06/09P/D-011 1400-164)  
(JSA07/10P/A05-007 1630)
- DAMASKE, Detlef J.**  
(GAV.06/09P/D-012 1400-165)
- DAMGAARD, Jesper**  
(HS02/09P/C24-001 1400)
- DAN, Kazuo**  
(SS04a/09P/D-012 1400-261)
- DANG, Lianwen**  
(HS02c/11P/D-034 1630-132)  
(HS02/11P/C24-011 1555)
- DANIELL, Robert E.**  
(GAI.05/08P/A15-008 1720)
- DANILOV, Alexei D.**  
(JSA01/08P/A12-005 1610)
- DARDIER, Genevieve M.**  
(JSP09/10A/B20-003 0945)
- DARMAWAN, Dudy**  
(G02/10P/D-012 1400-077)
- DARROUZET, Fabien**  
(GAI.10/11A/D-022 0830-096)
- DAS, Siddarth Shankar**  
(MC05/08P/A09-010 1740)
- DATSENKO, Nina Mikhailovna**  
(MC12/08P/B19-008 1715)
- DATTA, Partha Sarathi**  
(HS02a/07P/D-028 1545-174)  
(HS02/07P/C24-028 1444)
- DAVAILLE, Anne**  
(JSS06/08A/A04-005)
- DAVEY, F.J.**  
(SS03/08A/D-146 0830-305)
- DAVEY, Fred**  
(SS03/08A/D-094 0830-253)
- DAVIDOVICH, Natalia V.**  
(MC12/07P/B19-002 1445)
- DAVIES, Hugh**  
(JSS07a/09P/D-018 1700-119)
- DAVIES, Huw C.**  
(MI06/09P/B20-011 1740)  
(MI05/09P/B17-004 1520)  
(JSM14/08P/A05-002 1435)
- DAVIES, Jackie A.**  
(GAI.05/07P/D-020 1400-118)
- DAVILA, Joseph Michael**  
(GAI.09/11A/A11-001 0830)
- DAVIS, Bill**  
(JSS06/09P/A04-008 1640)
- DAVIS, Paul**  
(SS03/08A/D-030 0830-189)
- DAVIS, Robert**  
(JSH01/08A/C27-001 0910)
- DAVULURI, Srinagesh**  
(SS03/08A/D-082 0830-241)
- DAVY, Bryan**  
(SS03/08A/D-094 0830-253)
- DAVYDOVA, Marina A.**  
(JSP10/10A/B21-004 0950)
- DAWS, Matthew**  
(GAI.09/11P/A11-006 1620)
- DAYAWANSA, Nandani Dhammika Kumari**  
(HS02/07P/C24-025 1432)  
(HS02a/07P/D-025 1545-171)
- DAYDOU, Yves**  
(JSG03/10A/A12-007 1100)
- DE, Reena**  
(SS03/08A/D-132 0830-291)
- DE BOER, Agatha M.**  
(JSP04/10A/A06-003 0940)
- DE BOER, Dirk H.**  
(HS01/09A/C29-008 1140)
- DE CAMARGO, Ricardo**  
(JSM11/10P/B18-005 1600)
- DE CONINCK, Heleen**  
(MI08/07P/D-003 1400-197)
- DE GRANDPRE, Jean**  
(MI03/08P/B18-003 1440)
- DE GRANPRÉ, J.**  
(MC11/10P/B19-003 1440)
- DE HARO, Blas**  
(JSG03/09P/D-025 1640-033)
- DE JONGH, Inge L.M.**  
(HS03/07P/C26-009 1615)
- DE LA TORRE, Alejandro**  
(MC05/11P/A09-007 1640)
- DE LANNOY, Gabrielle J.M.**  
(HS03/07P/C26-009 1615)
- DE MESQUITA, Afranio Rubens**  
(JSM11/10P/B18-005 1600)
- DE PAULA REINO, Luiz Augusto**  
(JSM04/09P/D-015 1400-052)
- DE RITIS, Riccardo**  
(GAV.06/10A/A11-005 0950)
- DE SALES, Fernando**  
(MC03/10P/A09-005 1600)
- DE SANTIS, Angelo**  
(GAI.10/09P/A11-006 1515)  
(GAV.05/08P/A11-011 1740)  
(GAV.04/07P/A11-008 1700)
- DE TROCH, François P.**  
(HS03/07P/C26-009 1615)
- DE ZEEUW, Darren L.**

- (GAI11.06/08A/A02-006 1110)  
**DE ZOLT, Simona**  
 (JSM14/08P/A05-008 1745)  
 (MC12/08P/B19-003 1500)  
**DEAKIN, Rod**  
 (G03/07P/D-074 1400-096)  
**DEAL, Clara Jodwalis**  
 (JSP04/09P/A06-011 1730)  
**DEBAYLE, Eric**  
 (JSS06/08A/A04-008 1110)  
**DEBAYLE, Eric**  
 (JSS06/09P/A04-010 1720)  
**DEBAYLE, Eric**  
 (JSS06a/08P/D-013 1400-091)  
**DEBAYLE, Eric**  
 (JSS06/10A/A04-004 0930)  
**DEBAYLE, Eric**  
 (JSS06b/10P/D-008 1400-032)  
**DEBRUYNKOPS, Stephen M.**  
 (JSP10/11A/B21-007 1110)  
**DECANINI, Luis**  
 (SS04/07P/A03-001 1400)  
**DÉCRÉAU, Pierrette M.E.**  
 (GAI11.10/11A/D-022 0830-096)  
**DEFRIES, Ruth**  
 (MC03/10P/A07-005 1600)  
**DEHANT, Veronique**  
 (G02/07A/C25-012 1215)  
 (G07/10A/A03-007 1140)  
**DELAMERE, Jennifer S.**  
 (MC11/10P/B19-007 1630)  
**DELCOURT, Dominique**  
 (GAI11.08/10A/A16-006 1005)  
**DELCROIX, Thierry**  
 (JSP06/07A/B21-006 1120)  
**DELEFLIE, Florent**  
 (G04/08P/D-021 1400-128)  
**DELIPETROV, Todor B.**  
 (SS03/08A/D-024 0830-183)  
**DELMAS, Robert J.**  
 (JSM04/09P/D-006 1400-043)  
**DEMBELOV, Mikhail Georgievich**  
 (JSH01/07P/C27-005 1520)  
 (JSA07/11A/D-013 0830-013)  
**DEMETRESCU, Crisan**  
 (GAV.05/08A/A11-005 1010)  
**DEMIDOV, V.N.**  
 (HS02/09P/C24-003 1430)  
**DEMIR, Coskun**  
 (G03/07P/D-002 1400-024)  
 (G03/07P/D-026 1400-048)  
 (JSG01/07A/A01-008 1105)  
**DENG, Qianhui**  
 (GAI.08/08A/A14-001 0830)  
**DENG, Weiping**  
 (HS03/08P/C26-009 1615)  
**DENG, Yi**  
 (JSP10/09A/B21-002 0930)  
**DENGLER, Lori A.**  
 (JSS07/10A/A02-015 1215)  
**DENKER, H.**  
 (G02/07A/C25-007 1100)  
**DENKER, Heiner**  
 (G03/07P/D-015 1400-037)  
 (G03/07P/D-047 1400-069)  
 (G03/07P/D-048 1400-070)  
 (G02/07A/C25-004 0955)  
**DENT, Zoe C.**  
 (GAI11.10/10P/A01-003 1440)  
**DENTON, Richard E.**  
 (GAI11.10/10P/A01-004 1500)  
**DEPAOLO, Donald J.**  
 (HW06/07P/D-010 1400-194)  
**DEPUEV, Vktor H.**  
 (GAV.04/07A/A11-008 1200)  
**DERBYSHIRE, Steve**  
 (MC17/11P/B23-010 1720)  
**DERE, Kenneth P.**  
 (JSA08/09P/A08-003 1450)  
**DEREVETS, Valery V.**  
 (HW01/09P/D-014 1400-205)  
 (HW01/10P/C26-009 1720)  
**DERITIS, Riccardo**  
 (GAV.06/10A/A11-004 0930)  
**DERKSEN, Chris P.**  
 (JSM10/07A/B23-003 1000)  
 (JSH01/07P/C27-007 1620)  
 (JSM10/07A/B23-003 1000)  
 (JSH01/07P/C27-007 1620)  
**DEROME, Jacques**  
 (MI05/09P/B17-007 1650)  
**DEROO, R.**  
 (JSH01/08P/D-013)  
**DERY, Stephen**  
 (MI05/11P/B17-001 1400)  
**DESHON, Heather R.**  
 (SS03/08A/D-032 0830-191)  
**DESHPANDE, C.G.**  
 (JSA09/10A/A08-009 1145)  
**DESHPANDE, R.D.**  
 (HW06/07P/D-004 1400-188)  
**DESJEAN, Marie-Christine**  
 (MC04/11P/B22-001 1400)  
**DESZOEKE, Simon**  
 (MC03/10P/A07-004 1520)  
**DETWEILER, Shane T.**  
 (JSA07/11A/D-026 0830-026)  
**DEUSS, Arwen**  
 (JSS06/07P/A04-003 1440)  
**DEVIR, Adam**  
 (GAI11.04/07A/A08-009)  
**DEWALLE, David**  
 (JSH01/07P/C27-006 1600)  
**DEWAR, William K.**  
 (JSP10/09P/B21-008 1640)  
 (JSP10/08P/D-002 1610-054)  
**DEWHURST, Jason P.**  
 (GAI11.05/08A/A06-009 1110)  
**DEY, S.**  
 (GAI.08/08A/A14-009 1130)  
**DEY, Sagnik**  
 (JSH01/08A/C27-005 1050)  
 (JSM04/09P/B23-006 1700)  
 (JSM03/08P/A13-006 1600)  
**DEY, Suman**  
 (JSA07/11A/D-040 0830-040)  
**DEZEEUW, D.L.**  
 (GAI11.06/08A/A02-008 1200)  
**DEZETTER, Alain**  
 (HW08/07A/C28-008 1150)  
**DEZETTER, Alain**  
 (HS02/08A/C24-008 1045)  
**DHAKA, Surendra Kumar**  
 (MC05/11P/A09-008 1700)  
**DHAKAL, Amod S.**  
 (HW02/11A/C31-006 1110)  
**DHAR, Ratan L.**  
 (HW01/09P/D-012 1400-203)  
**DI GIOVAMBATTISTA, Rita**  
 (SW05/10A/D-001 0900-245)  
**DI STEFANO, Costanza**  
 (HS01/08A/C29-005 1130)  
**DIAMENT, Michel**  
 (JSS06a/08P/D-028 1400-106)  
 (G04/08A/C25-002 0900)  
**DIANATI TILAKI, Ramazan ali**  
 (HS02a/07P/D-037 1545-183)  
 (HS02/07P/C24-037 1520)  
**DIAS, Alveirinho**  
 (JSP07/08A/B17-008 1200)  
**DIAS, Pedro L.**  
 (HS02/08A/C24-010 1115)  
**DIAZ, Alejandro Raul**  
 (JSG03/10A/A12-008 1120)  
**DICK, Chad**  
 (JSM10/07A/B23-001 0900)  
**DICK, Wolfgang R.**  
 (G07/10P/D-009 1400-094)  
**DICKEY, Tommy D.**  
 (JSP07/08P/B17-002 1430)  
**DICKINSON, Robert E.**  
 (MI07/11A/B18-004 0930)  
 (MI07/11P/B18-005 1540)  
**DICKINSON, Suzanne**  
 (JSP09/11A/B20-013 1215)  
**DIDELLE, Henri**  
 (JSP10/08P/B21-001 1400)  
**DIDENKULOVA, Irina**  
 (JSS07/09A/A02-004 0945)  
**DIDSZUN, Jens**  
 (HW07/11A/C25-002 0900)  
**DIKKRUEGER, Bernd**  
 (HW07/11P/D-010 1400-146)  
**DIERNHOFER, Wolfgang**  
 (HS01/09A/C29-009 1200)  
**DIETRICH, Reinhard**  
 (JSG03/09P/D-002 1640-010)  
 (JSG01/08A/A01-010 1135)  
 (JSG01/08A/A01-011 1150)  
**DILLON, Peter J.**  
 (HS04/07A/C30-002 1005)  
**DIMALANTA, Carla B.**  
 (SS03/08A/D-122 0830-281)  
 (SS03/08A/D-061 0830-220)  
**DIMANT, Yakov S.**  
 (GAI11.06/09A/A10-010 1145)  
**DIMITRIOU, Elias**  
 (HS02/08P/C24-009 1630)  
**DIMRI, Vijay P.**  
 (G04/08A/C25-006 1050)  
**DING, Liangfu**  
 (JSM10/08P/B23-007)  
**DING, Yihui**  
 (MC11/11P/D-004 1400-197)  
**DING, Yongjian**  
 (HS02/09P/C24-010 1645)  
**DING, Yongjian**  
 (JSM10/08P/B23-008 1700)  
**DING, Zhifeng**  
 (SS04/07A/A03-003 1000)  
**DIPANKAR, Sarkar**  
 (SW03/10P/A04-014 1730)  
**DIRMEYER, Paul A.**  
 (HW07/10P/C25-007 1600)  
**DJABRI, Larbi**  
 (HS02/08P/C24-006 1515)  
**DJAD' KOV, Petr G.**  
 (SW05/10A/D-005 0900-249)  
**DJADKOV, Pyotr G.**  
 (SS03/08A/D-018 0830-177)  
**DJAJADIHARDJA, Yusuf S.**  
 (SS03/08A/D-043 0830-202)  
**DJUWANSANAH, Muhamad Rahman**  
 (MC12/07P/B19-006 1600)  
**DMITRENKO, Igor**  
 (JSP04/10P/A06-008 1640)  
**DMITRIEV, Vladimir I.**  
 (GAI.10/09P/D-009 1615-128)  
**DOAN, Trinh Hai**  
 (JSG03/10A/A12-006 1040)  
**DOBRICA, Venera**  
 (GAV.05/08A/A11-005 1010)  
**DOBROKA, Michael**  
 (GAI.10/09A/A11-009 1130)  
 (GAI.10/09A/A11-008 1115)  
 (GAI.10/09P/D-011 1615-130)  
**DODLA, Bhaskar Rao Venkata**  
 (MC02/08A/B20-008 1200)  
**DOELL, Petra**  
 (HW04/09A/C31-009 1200)  
**DOERFFER, Roland**  
 (JSP06/07A/B21-001 0900)  
**DOGRU, Asli Garagon**  
 (JSG01/08P/D-013 1400-013)  
**DOHAN, Kathleen B.**  
 (JSP10/11P/B21-009 1740)  
**DOI, Koichiro**  
 (JSM11/10A/B18-006 1040)  
 (JSG03/09P/D-002 1640-010)  
 (JSG03/09P/D-001 1640-009)  
 (G03/07P/D-001 1400-023)  
 (G03/07P/D-003 1400-025)  
**DOJCINOVSKI, D.**  
 (SS04b/10P/D-049 1400-233)  
**DOKKEN, Sverre Thune**  
 (JSH01/08A/C27-003 0950)  
**DOLGIKH, Grigoriy I.**  
 (JSM03/08P/A13-009 1700)  
**DOLGIKH, Stanislav G.**  
 (SS03/07A/A02-012 1215)  
**DOLIF NETO, Giovanni**  
 (JSM14/09P/D-004 1400-068)  
**DOLINSKY, Peter**  
 (GAI.08/08P/D-005 1400-140)  
**DOMINGUEZ, Jose Manuel Suarez**  
 (MC12/08A/B19-007 1145)  
**DOMYSHEVA, Valentina N.**  
 (JSP04a/09P/D-001 1400-094)  
**DONALDSON, Norman**  
 (JSM14/09P/D-019 1400-083)  
**DONELAN, Mark A.**  
 (JSP09/11P/B20-004 1500)  
**DONG, Min**  
 (MC17/10P/B23-011 1730)  
**DONG, Qing**  
 (JSH01/07P/C27-002)  
**DONG, Zengchuan**  
 (HW07/11P/D-020 1400-156)  
**DONLON, Craig J.**  
 (JSP09/11A/B20-005 0945)  
**DONLON, Craig J.**  
 (JSP06/07A/B21-005 1030)  
**DONNER, Matthias**  
 (JSA09/10A/A08-002 0900)  
**DONOVAN, Eric**  
 (GAI11.05/07P/D-018 1400-116)  
**DOORSCHOT, Judith**  
 (JWH01/09A/C30-004 1000)  
**DORBATH, Catherine**  
 (SS03/08A/D-064 0830-223)  
**DORBATH, Louis**  
 (SS04b/10P/D-016 1400-200)  
**DORBATH, Louis**  
 (SS03/08A/D-064 0830-223)  
**DORELLI, John**  
 (GAI11.09/10P/D-003 1400-115)  
**DORLAND, William**  
 (GAI11.05/08A/A06-012 1215)  
**DORMAN, LeRoy M.**  
 (SS03/08A/D-032 0830-191)  
**DOUGLAS, Grant Brian**  
 (HS01/09P/C29-002 1420)  
**DOUGLAS, Ian**  
 (HS01/09P/C29-007 1600)  
**DOUGLAS, Richard**  
 (HS01/09P/D-020 1400-187)  
 (HW01/10A/C26-006 1050)  
**DOUSA, Jan**  
 (G07/10P/D-020 1400-105)  
**DOW, John M.**  
 (G07/10A/A03-003 0940)  
**DOWDEN, Richard L.**  
 (GAI11.04/07A/A08-001 0900)  
**DOWDESWELL, Evelyn K.**  
 (JSH01/08P/D-007 1400-045)  
**DOWDESWELL, Julian A.**  
 (JSH01/07A/C27-001 0940)  
**DOWDY, Andrew J.**  
 (MC05/10A/A09-008 1130)  
**DOWNES, Gaye L.**  
 (JSS07/09A/A02-011 1145)  
**DOWNES, Hilary**  
 (JSS06/10A/A04-010 1150)  
**DOYLE, Chris**  
 (JSM14/09P/D-020 1400-084)  
**DRAGERT, Herb**  
 (JSG01/07P/A01-006)  
**DRAGERT, Herb**  
 (JSG01/07P/A01-005 1500)  
**DRAGONI, Michele**  
 (SS03/08A/D-047 0830-206)  
**DRAGONI, Michele**  
 (SS03/08A/D-027 0830-186)  
 (SS03/08A/D-031 0830-190)  
**DRAKE, James F.**  
 (GAI11.05/08A/A06-012 1215)  
**DRANGE, Helge**  
 (JSG03/10A/A12-003 0910)  
**DRAY, Martial**

## INDEX

- (HW06/07P/D-001 1400-185)  
**DRBOHLAV, Hae-Kyung Lee**  
 (MC17/11A/B23-009 1200)  
**DRENNAN, William M.**  
 (JSP09/10A/B20-003 0945)  
**DRESEN, Lothar**  
 (GAI.10/09A/A11-008 1115)  
**DRESSLER, Kevin Andrew**  
 (JWH01/10A/C30-009 1140)  
**DREWES, Hermann**  
 (G07/10A/A03-008 1200)  
**DREWES, Hermann**  
 (U7/11A/D32-003 1000)  
 (G07/10P/A03-001 1400)  
**DREWES, Jorg Eckard**  
 (HS04/07A/C30-003 1130)  
**DRONAMRAJU, Venkata Ramana**  
 (JSA07/11A/D-037 0830-037)  
**DROSSART, Pierre**  
 (MC04/10P/B22-006 1615)  
**DRUMOND, Anita Rodrigues de Moraes**  
 (MC03/11P/D-016 1400-191)  
**DU, Mingyuan**  
 (HS02/08A/C24-005 0930)  
**DUAN, Anmin**  
 (MC03/11A/A07-002 0910)  
 (MC03/11A/A07-001 0830)  
**DUAN, Ke Qin**  
 (JSM10/09P/D-010 1400-064)  
**DUAN, Keqin**  
 (HS02b/10P/D-020 1630-141)  
 (HS02/10A/C24-020 1201)  
**DUAN, Keqin**  
 (HS02b/10P/D-018 1630-139)  
 (HS02/10A/C24-018 1153)  
**DUAN, Keqin**  
 (JSM10/07A/B23-006 1140)  
**DUAN, Qingyun**  
 (HW08/07P/C28-003 1500)  
 (HW08/07P/C28-002 1430)  
 (HW07/11A/C25-005 0945)  
 (HW08/09P/C28-001 1420)  
 (HW08/08A/C28-002 0900)  
**DUAN, Wansuo**  
 (JSM14/09P/D-014 1400-078)  
**DUBININ, Eduard**  
 (GAI.V.03/09A/A16-006 1120)  
 (GAI.V.03/08A/A16-004 1000)  
**DUBROV, Mstislav N.**  
 (SS03/08A/D-048 0830-207)  
**DUBROV, Mstislav N.**  
 (JSG01/08P/D-033 1400-033)  
**DUCARME, Bernard**  
 (JSS06/09A/A04-005 1040)  
**DUCIC, Vesna**  
 (GAI.I.06/09P/A10-013 1740)  
**DUCIC, Vesna**  
 (JSS07/10P/A02-010 1630)  
**DUDAREV, Oleg**  
 (JSM04/09A/B23-004 1030)  
**DUFRESNE, Jean-Louis**  
 (MC08/07A/B17-009 1205)  
**DUGARMAA, Tundev**  
 (SS04b/10P/D-030 1400-214)  
**DUGUAY, Claude R.**  
 (JSM10/07A/B23-002 0940)  
**DUMBERRY, Mathieu**  
 (GAV.04/07P/A11-007 1640)  
**DUMRONGCHAI, Puttipol**  
 (G03/07P/D-071 1400-093)  
**DUNBAR, Paula Kay**  
 (JSS07/09A/A02-008 1100)  
**DUNKERTON, Tim J.**  
 (MC05/08P/A09-002 1430)  
**DUNKERTON, Timothy J.**  
 (MI05/10A/B17-008 1140)  
 (MC03/09P/A07-006 1640)  
 (MC05/07P/D-009 1400-216)  
 (MC05/07A/A09-005 1130)  
 (JSP10/08P/D-012 1610-064)  
 (MI05/10A/B17-002 0910)  
**DUNLAP, E.**  
 (JSP04/09A/A06-009 1210)  
**DUNLOP, M.**  
 (GAI.II.05/08A/A06-007 1040)  
**DUNLOP, M.**  
 (GAI.II.09/11A/A11-006 1110)  
**DUNLOP, Malcolm W.**  
 (GAI.II.05/07P/D-020 1400-118)  
 (GAI.II.05/08A/A06-009 1110)  
**DUPRE, Bernard**  
 (JSM04/09P/D-006 1400-043)  
**DUPUIS, Helene**  
 (JSP09/10A/B20-003 0945)  
**DURON, Julien**  
 (G02/07A/C25-012 1215)  
**DUSHENKO, Peter V.**  
 (JSS07b/10P/D-015 1700-061)  
**DUTTA, T.**  
 (GAI.08/08A/A14-009 1130)  
**DUTTA, Utpal**  
 (SS04b/10P/D-025 1400-209)  
**DUVEL, Jean Philippe**  
 (MC17/10P/B23-007 1630)  
**DUYEN, Chau Ha**  
 (U7/11P/D32-001 1400)  
**DWIPA, Sjafra**  
 (G03/07P/D-001 1400-023)  
 (G03/07P/D-003 1400-025)  
**DWIVEDI, Avinash**  
 (SS04b/10P/D-028 1400-212)  
**DYE, Dennis G.**  
 (JSM04/09P/B23-002 1430)  
**DYMENT, Jérôme**  
 (GAV.07/07P/A13-002 1420)  
**DYMENT, Jérôme**  
 (GAV.06/10P/A11-005 1520)  
**DYMENT, Jérôme**  
 (GAV.06/10P/A11-006 1600)  
**DYRUD, Lars P.**  
 (GAI.I.06/10A/A01-009 1105)  
**DYSON, P.L.**  
 (GAI.I.06/11P/D-017 1400-069)  
**DYURGEROV, Mark B.**  
 (JSH01/07A/C27-002 1000)  
**DZHAMALOV, Roald Gamidovich**  
 (HS02/07A/C24-006 0920)  
 (HS02a/07P/D-031 1545-177)  
 (HS02a/07P/D-006 1545-152)  
 (HS02/07P/C24-031 1456)  
**DZIEWONSKI, A.M.**  
 (JSS06a/08P/D-023 1400-101)  
**DZIEWONSKI, Adam M.**  
 (JSS06/09A/A04-002 0920)  
 (JSS06a/08P/D-010 1400-088)  
**DZIEWONSKI, Adam Marian**  
 (JSS06/07P/A04-001 1400)
- e**
- E., John Joseph**  
 (GAV.06/10A/A11-003 0910)  
**E., Kherani**  
 (GAI.II.06/09A/A10-002 0920)  
**E., Manguelle-Dicoum**  
 (GAI.10/09P/D-017 1615-136)  
**E.S.B, Ferraz,**  
 (HW01/09A/C26-007 1130)  
**EAGLES, Graeme**  
 (SS03/08A/D-095 0830-254)  
**EBEL, Adolf**  
 (MC05/09P/A09-010 1740)  
**EBIHARA, Y.**  
 (GAI.II.06/07P/D-010)  
**EBIHARA, Yusuke**  
 (GAI.II.06/08A/A02-005 1045)  
 (GAI.II.08/10A/A16-007 1040)  
 (GAI.II.06/08A/A02-009 1215)  
**EBRAHEEM, A.M.**  
 (HS02a/07P/D-032 1545-178)  
 (HS02a/07P/D-033 1545-179)  
 (HS02/07P/C24-032 1504)  
 (HS02/07P/C24-033 1504)  
**EBUCHI, Naoto**  
 (JSP09/11P/B20-001 1400)  
**ECHER, Ezequiel**  
 (GAI.II.09/11A/A11-002 0900)  
 (JSA08/10P/D-003 1400-003)  
 (GAI.II.09/11P/A11-008 1710)  
**ECKERMANN, S.D.**  
 (MC05/11A/A09-008 1200)  
 (MC05/11A/A09-005 1050)  
**ECKERMANN, Stephen D**  
 (MC05/11P/A09-010)  
**EDMONDS, Lindsay**  
 (HS04/07P/C30-004 1555)  
**EDWARDS, J.**  
 (GAI.II.07/09A/A14-008 1210)  
**EDWARDS, Neil R.**  
 (JSP10/11P/B21-006 1640)  
**EDWARDS, Norm**  
 (G03/07P/D-074 1400-096)  
**EDWARDS, R.Lawrence**  
 (MC12/08P/B19-001 1415)  
**EGAWA, Kuniko**  
 (MC03/11A/A07-003 0930)  
**EGBUJOR, A.I.**  
 (HS02/08P/C24-002 1415)  
**EGORKIN, Anatoliy Vasilievich**  
 (JSA07/10A/A05-009 1150)  
**EGOROVA, Tatiana A.**  
 (MI03/09A/D-006 0900-249)  
**EGUCHI, Nawo**  
 (MC05/08P/A09-004 1510)  
**EGUCHI, Takao**  
 (JSS06a/08P/D-007 1400-085)  
**EHEART, Wayland J.**  
 (HS02/07A/C24-008 0928)  
 (HS02b/10P/D-012 1630-133)  
 (HS02a/07P/D-008 1545-154)  
 (HS02/10A/C24-012 1129)  
**EID, Fahmy M.**  
 (JSP09/10P/B20-014 1745)  
**EID, Fahmy Mohamed**  
 (JSP08/09P/B19-003 1450)  
**EIFF, Olivier**  
 (JSP10/11P/B21-002 1450)  
**EISELE, Michael**  
 (HS02/08P/C24-008 1615)  
**EISWIRTH, Matthias**  
 (HS02/07A/C24-007 0924)  
 (HS02a/07P/D-007 1545-153)  
**EITO, Hisaki**  
 (JSM14/08A/A05-011 1200)  
 (JSM14/08A/A05-007 1040)  
 (JSM14/09P/D-024 1400-088)  
 (JSM14/09P/D-025 1400-089)  
**EJIRI, Masaki**  
 (GAI.II.06/08A/A02-005 1045)  
 (GAI.II.08/10A/A16-007 1040)  
 (GAI.II.06/08A/A02-009 1215)  
**EKODECK, Georges Emmanuel**  
 (HW01/10P/C26-004 1500)  
**EL SAYED, Esam**  
 (HS02a/07P/D-032 1545-178)  
 (HS02a/07P/D-033 1545-179)  
 (HS02/07P/C24-032 1500)  
 (HS02/07P/C24-033 1504)  
**EL SHEIKH, Rebby Ata**  
 (HS04/08A/C30-005 1130)  
**EL-BOHOTY, Mohamed El-Saeed**  
 (GAV.06/10P/A11-008 1640)  
**EL-ESSAWY, Abdel Aleem Hassan**  
 (GAI.10/09P/D-003)  
**EL-ESSAWY, Sayed**  
 (SS03/08A/D-088 0830-247)  
**EL-FIKY, Gamal**  
 (JSG01/08P/D-028 1400-028)  
**EL-SAYED, El-Said Ahmed**  
 (GAI.10/09P/D-002 1615-121)  
**EL-SHEIMY, Naser M.**  
 (G04/08P/C25-002 1430)  
**ELENA, Koslovskaya**  
 (JSA07/11A/D-029 0830-029)  
**ELENJIPARAMPIL, John Joseph**  
 (GAV.06/09P/D-001 1400-154)  
**ELIASSON, Lars**  
 (GAI.II.08/10A/A16-007 1040)  
**ELISEEV, Alexey V.**  
 (MC11/10A/B19-002 0900)  
**ELISEEVA, Svetlana V.**  
 (JSA07/10A/A05-008 1130)  
**ELISEEVA, Svetlana V.**  
 (GAV.06/09P/D-002 1400-155)  
**ELKINGTON, Scot R.**  
 (GAI.II.09/11P/A11-003 1440)  
**ELLMANN, Artu**  
 (G03/07P/D-040 1400-062)  
 (G03/07P/D-041 1400-063)  
**ELLSWORTH, William**  
 (SS03/07A/A02-002 0915)  
**ELO, Seppo**  
 (JSA07/11A/D-029 0830-029)  
**ELO, Seppo**  
 (JSA07/11A/D-028 0830-028)  
**ELPHIC, R.C.**  
 (GAI.II.06/08P/A02-011 1725)  
**ELPHIC, Richard C.**  
 (GAI.II.08/10A/A16-001 0830)  
**ELSBERRY, Russell L.**  
 (MC02/08A/B20-004 1000)  
 (MC02/08A/B20-007 1140)  
**ELSIRAFI, Abuelhoda Mahmoud**  
 (GAV.06/10P/A11-007 1620)  
**EMANOV, Alexander F.**  
 (SW05/10A/D-005 0900-249)  
**EMANOV, Alexander F.**  
 (SW05/10P/A13-010 1630)  
**EMANUEL, Kerry**  
 (JSM14/07P/A05-001 1400)  
**EMANUELE, Bozzo**  
 (GAV.06/09P/D-011 1400-164)  
**EMERY, William J.**  
 (JSP04/10P/A06-002 1420)  
 (JSP09/11A/B20-006 1000)  
**EMMANOULODIS, Dimitrios A.**  
 (HS01/09P/D-018 1400-185)  
**EMOLO, Antonio**  
 (SS04a/09P/D-015 1400-264)  
**EMORI, Seita**  
 (MC11/11A/B19-008 1110)  
**ENAMUNDRAM, Chandrasekhar**  
 (GAI.II.07/09A/A14-002 0930)  
**ENDO, Nobuhiko**  
 (MC03/11P/D-004 1400-179)  
 (MC03/11P/D-005 1400-180)  
**ENET, Francois**  
 (JSS07/09P/A02-008 1600)  
**ENGAVALA, Bharati**  
 (GAI.II.06/09A/A10-005 1005)  
**ENGDAHL, Eric Robert**  
 (U7/11A/D32-004 1100)  
**ENGBRETSON, M.J.**  
 (GAI.II.10/11A/D-006 0830-080)  
**ENGBRETSON, Mark J.**  
 (GAI.II.10/11A/A01-001 0830)  
**ENGELS, Martin**  
 (GAI.10/09P/A11-004 1445)  
**ENGLAND, A. W.**  
 (JSH01/08P/D-013)  
**ENGLISH, Michael**  
 (HW01/09A/C26-004 1010)  
**ENOMOTO, Hiroyuki**  
 (JSH01/08P/D-008 1400-046)  
**ENOMOTO, Takeshi**  
 (MC02/08A/B20-006 1120)  
 (MI06/09P/B20-006 1540)  
 (JSM14/09P/D-018 1400-082)

(JSM14/09P/D-017 1400-081)  
**ENSINK, Jeroen**  
 (HS04/07P/C30-001 1405)  
**ENZEL, Yehouda**  
 (HS03/08A/C26-003 0915)  
**EPIFANIO, Craig**  
 (JSM03/08A/A13-005 1040)  
**EPSI TEAM**  
 (SW05/10A/D-001 0900-245)  
**ERBE, Eric**  
 (JSM15/07A/B18-007 1100)  
**ERDIK, Mustafa Ozder**  
 (SW04/09P/A13-009 1615)  
**ERDMER, Philippe**  
 (SW03/10P/A04-001 1400)  
**ERGINTAV, Semih**  
 (JSG01/08A/A01-001 0900)  
**ERICKSON, Phillip J.**  
 (GAII.06/10A/A01-001 0830)  
**ERICSON, Phil J.**  
 (GAIII.11/09A/A15-009 1150)  
**ERIKSSON, Anders**  
 (GAIII.11/09P/A15-008 1620)  
**ERKER, Erhard**  
 (G03/07P/D-075 1400-097)  
**ERMANYUK, Evgueni V.**  
 (JSP10/11P/B21-008 1720)  
**ERMOLD, Wendy**  
 (JSP04/10P/A06-005 1520)  
**ERN, M.**  
 (MC05/11A/A09-008 1200)  
**ERN, Manfred**  
 (MC05/11A/A09-005 1050)  
**ERN, Manfred**  
 (MC05/11P/A09-003 1450)  
**ERNST, Tomasz**  
 (GAI.08/08P/D-003 1400-138)  
**ERRAM, Vinit**  
 (JSA07/10P/A05-008 1650)  
**ERRAM, Vinit C.**  
 (GAV.07/07P/A13-006 1600)  
 (GAV.07/07P/D-003 1400-144)  
 (SS03/08A/D-068 0830-227)  
**ERRERA, Quentin**  
 (MI03/08A/B18-003 0910)  
**ERSHOV, Sergey Valentinovitch**  
 (JSS07b/10P/D-003 1700-049)  
**ERVA, Rathnam Venkata**  
 (HS02b/10P/D-024 1630-145)  
 (HS02/10P/C24-001 1515)  
**ESAKI, Satoshi**  
 (GAIII.11/09P/A15-009 1645)  
**ESCHER-VETTER, Heidi**  
 (JWH01/10A/C30-007 1100)  
**ESCOUBET, P.**  
 (GAIII.06/07P/D-011 1400-131)  
**ESCOUBET, Philippe**  
 (GAIII.11/09P/A15-012 1730)  
**ESCOUBET, Phillippe**  
 (GAIII.11/09A/A15-003 0940)  
**ESSELBORN, Saskia**  
 (JSP08/09P/B19-005 1600)  
**ESSERY, R.**  
 (JWH01/09P/C30-001)  
**ESSERY, Richard**  
 (JWH01/10P/C30-005 1600)  
**ESSERY, Richard E.**  
 (JWH01/10P/C30-004 1500)  
**ESSERY, Richard L.H.**  
 (JWH01/09P/C30-004 1500)  
**ESTILOW, Thomas**  
 (JSH01/07P/C27-009 1700)  
**ETCHEVERS, Pierre**  
 (JWH01/10P/C30-005 1600)  
**ETCHEVERS, Pierre**  
 (JWH01/09A/C30-009 1210)  
**ETCHEVERS, Pierre**  
 (JWH01/09P/C30-001 1400)  
**EURIPIDES, Peter**  
 (GAIII.11/09P/A15-007 1540)  
**EVANS, David S.**  
 (GAIII.09/11A/A11-004 0950)

**EVANS, Rob**  
 (JSA07/10A/A05-003 0920)  
**EVANS, Rob L.**  
 (SS03/07A/A02-011 1200)  
 (JSS06/09P/A04-008 1640)  
**EVENCHICK, Carol A.**  
 (SW03/10P/A04-001 1400)  
**EXERTIER, Pierre**  
 (G04/08P/D-021 1400-128)  
**EXNER, Thomas**  
 (JSM10/07A/B23-004 1020)

## f

**FABIAN, Marcus**  
 (JSG01/08A/A01-008 1105)  
**FAEH, Donat**  
 (SS04a/09P/D-044 1400-293)  
**FAHJAN, Yasin**  
 (SW04/09P/A13-009 1615)  
**FAINBERG, Edouard B.**  
 (GAI.10/09P/A11-005 1500)  
**FAINBERG, Edouard B.**  
 (GAI.10/09P/D-006 1615-125)  
**FAIRALL, Chris W.**  
 (JSP09/10A/B20-001 0900)  
**FAIRALL, Chris W.**  
 (JSM10/07P/B23-003 1500)  
**FAIRFIELD, D.H.**  
 (GAIII.05/07A/A06-003 0930)  
**FAIRHEAD, J.D.**  
 (G03/07P/D-027 1400-049)  
**FAIRHEAD, John Derek**  
 (G03/07P/D-004 1400-026)  
**FALASCA, Ayris**  
 (GAIII.09/10P/D-003 1400-115)  
**FALLER, James E.**  
 (U7/11A/D32-002 0930)  
**FAMIGLIETTI, James S.**  
 (U6/09A/D32-005 1115)  
**FAN, Alice**  
 (JSP09/11A/B20-003)  
**FAN, Jun**  
 (SS04b/10P/D-031 1400-215)  
**FAN, Shou-shan**  
 (HS01/08P/C29-003 1440)  
**FANG, Jian**  
 (SS03/08A/D-136 0830-295)  
**FANTINI, Maurizio**  
 (JSM14/08P/A05-005 1700)  
 (MI06/09P/B20-007 1620)  
**FARDA, Ales**  
 (MC08/07P/B17-011 1710)  
**FARGE, Marie**  
 (JSP10/11A/B21-010 1210)  
**FARIA, Heloisa Helena**  
 (JSA08/10P/D-003 1400-003)  
**FARINA, Paolo**  
 (HS01/08P/C29-006 1600)  
**FARMER, Darren**  
 (HW07/11P/D-031 1400-167)  
**FARRARA, John D.**  
 (MC03/09A/A07-006 1110)  
**FARRERAS, Salvador F.**  
 (JSS07/09A/A02-009 1115)  
 (JSS07b/10P/D-005 1700-051)  
**FARRUGIA, Charles J**  
 (GAIII.09/11A/A11-006 1110)  
**FARZANEH, Masoud**  
 (MI08/07P/B18-004 1620)  
**FASHCHEVSKAY, Tatyana**  
 (HS02/09P/C24-012 1715)  
 (HS02c/11P/D-028 1630-126)  
 (HS02/11P/C24-005 1531)  
**FASHCHEVSKAYA, Tatyana**  
 (HW03/11A/D-001 0830-135)  
 (HW01/09A/C26-009 1210)  
 (HW07/11P/D-022 1400-158)  
**FASHCHEVSKY, Boris**  
 (HW07/11P/D-022 1400-158)  
 (HS02/09P/C24-012 1715)  
 (HW03/11P/C30-004 1500)  
 (HW03/11P/C30-007 1620)  
 (HS02c/11P/D-028 1630-126)  
 (HS02/11P/C24-005 1531)  
**FASONA, Mayowa**  
 (HS02/07A/C24-016 1000)  
 (HS02a/07P/D-016 1545-162)  
**FASSNACHT, Steven R.**  
 (HS03/07P/C26-006 1515)  
**FASSNACHT, Steven Richard**  
 (JWH01/10A/C30-009 1140)  
**FASULLO, John**  
 (MC11/10P/B19-001 1400)  
**FAUL, Ulrich**  
 (JSS06a/08P/D-024 1400-102)  
**FAULL, Nicholas E.**  
 (MC08/08P/D-002 1400-158)  
**FAY, Noah P.**  
 (SS03/08A/D-051 0830-210)  
**FAYARD, Thierry**  
 (HW03/11A/D-002 0830-136)  
**FAZAKERLEY, Andrew**  
 (GAIII.11/09A/A15-003 0940)  
**FAZAKERLEY, Andrew N.**  
 (GAIII.05/08A/A06-009 1110)  
**FEATHERSTONE, Will**  
 (G03/07P/D-045 1400-067)  
 (G03/07P/D-014 1400-036)  
 (G04/08P/D-010 1400-117)  
**FEDOROV, Andrei**  
 (GAIII.14/08A/D-002 0830-146)  
**FEHRINGER, Michael**  
 (GAIII.11/09P/A15-012 1730)  
**FEHRINGER, Michael**  
 (GAIII.11/09A/A15-003 0940)  
**FEI, Yue**  
 (GAIII.09/11P/A11-003 1440)  
**FEICHTER, Johann**  
 (MC03/11P/D-018 1400-193)  
**FEIZNIA, Sadat**  
 (HS01/09P/D-002 1400-169)  
**FEKETE, Balazs M.**  
 (HW06/08A/C31-003 1120)  
 (JSM03/08P/A13-008 1640)  
**FELDMAN, Leonid L.**  
 (GAI.10/09A/A11-006 1015)  
**FELDSTEIN, Steven B.**  
 (MI05/09P/B17-003 1500)  
**FELL, Frank**  
 (JSP06/07A/B21-001 0900)  
**FELUS, Yaron**  
 (G04/07P/C25-001 1430)  
**FENG, Xiaojie**  
 (JSM04/09P/D-003 1400-040)  
**FENNELL, J.F.**  
 (GAIII.06/08A/A02-007 1135)  
**FENNELL, Joseph F.**  
 (GAIII.06/08A/A02-005 1045)  
 (GAIII.08/10A/A16-007 1040)  
**FENNIG, Karsten**  
 (JSP09/11A/B20-002 0900)  
**FENOGLIO-MARC, Luciana**  
 (JSG03/09P/D-013 1640-021)  
**FERDINAND, Richard Wambura**  
 (SS04/09A/A03-002 0915)  
**FERDOSIN NAJAFABADI, Atoosa**  
 (MI08/07P/D-002 1400-196)  
**FERGUSON, Ian J.**  
 (JSA07/10A/A05-002 0900)  
 (JSS06/09P/A04-008 1640)  
**FERNANDES, M.J.**  
 (JSG03/10A/A12-002 0850)  
**FERNANDES, Vivian**  
 (G03/07P/D-043 1400-065)  
**FERNANDEZ, A.**  
 (JWH01/09P/C30-001)  
**FERNANDEZ, Marseyas**  
 (JSG03/09P/A12-007 1620)  
**FERNANDO, T.M.K.G.**  
 (HS02/08P/C24-011 1700)

**FERRACCIOLI, Fausto**  
 (JSA07/10P/A05-007 1630)  
 (GAV.06/09P/D-011 1400-164)  
**FERRACCIOLI, Fausto**  
 (GAV.06/09P/D-012 1400-165)  
**FERRACCIOLI, Fausto**  
 (GAV.06/10P/A11-003 1440)  
**FERRAZ, Simone Erotildes**  
 (MC17/10A/D-002 0830-184)  
**FERREIRA, Oscar**  
 (JSP07/08A/B17-008 1200)  
**FERRETTI, Alessandro**  
 (SS03/08A/D-052 0830-211)  
 (G07/10P/D-015 1400-100)  
**FERRO, Vito**  
 (HS01/08A/C29-005 1130)  
**FESER, Frauke**  
 (MC08/07A/B17-007 1135)  
 (JSP08/09P/B19-005 1600)  
**FEUCHTINGER, Martin**  
 (G02/07A/C25-005 1010)  
**FIELITZ, Werner**  
 (JSA07/11A/D-020 0830-020)  
**FIERZ, Charles**  
 (JWH01/10P/D-001)  
 (JSM10/07A/B23-004)  
**FIERZ, Charles**  
 (JWH01/09P/C30-001 1400)  
**FIERZ, Charles G.**  
 (JWH01/09A/C30-009 1210)  
**FILIPPIDIS, Evangelos I.**  
 (HS01/09P/D-018 1400-185)  
**FINCH, Christopher J.**  
 (G03/07P/D-068 1400-090)  
**FINCHAM, Adam**  
 (JSP10/08P/B21-001 1400)  
**FINE, Isaak V.**  
 (JSS07b/10P/D-009 1700-055)  
**FINZI, Cristiane M.**  
 (HS02b/10P/D-031 1630-152)  
 (HS02/10P/C24-008 1543)  
**FIOLETOV, Vitali**  
 (MI03/08A/B18-008 1130)  
**FIORENTINO, Mauro**  
 (HW07/11P/C25-005 1500)  
**FIRAT, Orhan**  
 (G03/07P/D-002 1400-024)  
 (G03/07P/D-026 1400-048)  
**FISCH, Gilberto Fernando**  
 (MC03/10A/A07-003 0930)  
**FISHWICK, Stewart**  
 (JSS06/09P/A04-002 1420)  
**FITZ GERALD, John D.**  
 (JSS06a/08P/D-024 1400-102)  
**FITZKO, Francesca**  
 (SS04/07P/A03-005 1515)  
**FLECHTNER, Frank**  
 (G02/07A/C25-002 0920)  
**FLETCHER, Hilary J.**  
 (JSG01/07P/A01-008 1605)  
 (JSG01/07P/A01-009 1620)  
**FLOERKE, Martina**  
 (HW04/09A/C31-009 1200)  
**FLOR, Jan-Bert**  
 (JSP10/11P/B21-008 1720)  
**FLOR, Jan-Bert**  
 (JSP10/10P/B21-008 1700)  
 (JSP10/08P/D-010 1610-062)  
**FLOR, Jan-Bert**  
 (JSP10/11P/B21-003 1510)  
**FLORES, Luis A.**  
 (GAII.06/09A/A10-011 1205)  
**FLORINSKI, Vladimir**  
 (GAIV.02/07A/A07-005 1130)  
**FLORSCH, Nicolas**  
 (JSG02/09A/D-002 0830-002)  
**FLOYD, Linton E.**  
 (JSA08/09P/A08-003 1450)  
**FLUEGEL, Wolfgang Albert**  
 (HS01/09A/C29-002 0920)  
**FLURY, Jakob**  
 (JSG02/09P/A05-001 1400)  
**FLURY, Jakob**

## INDEX

- (JSG02/09P/A05-010 1730)  
**FLYNN, Morris R.**  
 (JSP10/09P/B21-005 1520)  
**FOGARTY, Chris**  
 (JSM14/09P/D-002 1400-066)  
**FOK, M.-C.**  
 (GAILI.06/08A/A02-007 1135)  
**FÖLDVÁRY, L.**  
 (G02/07A/C25-007 1100)  
**FOLKINS, Ian A.**  
 (MC05/08A/A09-007 1150)  
**FOLKNER, William**  
 (G02/07A/C25-012 1215)  
**FOLLETTE, Melanie B.**  
 (MI03/09A/D-004 0900-247)  
 (MI03/08A/B18-004 0930)  
**FOMENKO, Elena Y.**  
 (GAI.10/09A/A11-002 0915)  
**FOMENKO, Elena Yu.**  
 (GAI.10/09P/D-012 1615-131)  
**FOMICHEV, Victor I.**  
 (MC05/08A/A09-001 0830)  
 (MI03/08P/B18-003 1440)  
**FONT, Graciela**  
 (G03/07P/D-031 1400-053)  
**FONT, Jordi**  
 (JSP06/07A/B21-007 1140)  
**FONTAINE, Fabrice**  
 (JSS06a/08P/D-013 1400-091)  
**FONTEYN, Dominique**  
 (MI03/08A/B18-003 0910)  
**FORBERG, Matthias**  
 (SS03/08A/D-117 0830-276)  
**FORBES, Jeffrey M.**  
 (GAILI.07/11P/A12-001 1400)  
**FORD, Paul**  
 (HW07/11P/D-018 1400-154)  
**FOREST, Julien**  
 (GAILI.11/09P/A15-012 1730)  
**FORGET, Francois**  
 (MC04/11P/B22-001 1400)  
**FORGET, Francois**  
 (GAILI.07/11P/A12-001 1400)  
**FORRESTER, William T.**  
 (GAILI.06/08A/A02-001 0900)  
**FORSBERG, R.**  
 (G03/07P/D-008 1400-030)  
**FORSBERG, Rene**  
 (G07/10A/A03-005 1100)  
 (JSG02/09P/A05-002 1425)  
**FORSBERG, Rene**  
 (G03/07P/D-051 1400-073)  
**FORSBERG, Rene**  
 (G03/07P/D-055 1400-077)  
**FORSBERG, Rene**  
 (G03/07P/D-048 1400-070)  
 (JSG02/09A/D-003 0830-003)  
**FORSYTHE, Graham T.W.**  
 (MC12/08P/B19-006 1620)  
**FOSTER, James**  
 (JSM15/07A/B18-007 1100)  
**FOSTER, John C.**  
 (GAILI.06/10A/A01-001 0830)  
**FOSTER, Prudence N.**  
 (HW06/07P/D-010 1400-194)  
**FOTOPOULOS, Georgia**  
 (G04/08P/D-004 1400-111)  
**FOUQUET, Yves**  
 (GAV.06/10P/A11-006 1600)  
**FOWLER, Charles**  
 (JSP04/10P/A06-002 1420)  
**FOX, Jane L.**  
 (GAI.V.03/09A/A16-002 0930)  
**FRAME, Dave**  
 (MC11/10A/B19-009 1150)  
**FRANÇA, Carlos Augusto De Sampaio**  
 (JSM11/10P/B18-005 1600)  
**FRANCIA, Patrizia**  
 (GAILI.10/11A/A01-009 1030)  
**FRANCIS, Oliver**  
 (G07/10P/D-016 1400-101)  
**FRANCIS, Olivier**  
 (G03/07P/D-019 1400-041)  
**FRANCK, Siegfried A.**  
 (JSS06b/10P/D-022 1400-046)  
**FRANK, Jacki M.**  
 (GAI.V.03/09A/A16-002 0930)  
**FRANKIGNOUL, Claude**  
 (MC11/11A/B19-010 1150)  
**FRANKS, Stewart W.**  
 (HS02/09A/C24-006 1045)  
 (HS02/11P/C24-001 1400)  
 (HW08/08P/C28-002 1430)  
 (HW08/08A/C28-004 0940)  
**FRANKS, Stewart William**  
 (HW07/10P/C25-005 1515)  
**FRANZESE, Juan R.**  
 (SS03/08A/D-150 0830-309)  
**FRASER, Brian J.**  
 (GAV.04/07A/A11-003 0950)  
 (GAILI.10/11A/D-005 0830-079)  
**FRASER, Brian James**  
 (GAILI.10/11A/A01-002 0845)  
 (GAILI.06/10A/A01-011 1145)  
**FRECKMAN, John**  
 (JSS07a/09P/D-018 1700-119)  
**FREED, Andy**  
 (JSG01/07P/A01-009 1620)  
**FREEMAN, Mervyn P.**  
 (GAILI.09/11P/A11-006 1620)  
**FREEMAN, Mervyn Paul**  
 (GAILI.07/09A/A14-007 1150)  
**FREER, Jim**  
 (HW08/08P/C28-001 1400)  
**FREI, Christoph**  
 (MC03/09A/A07-007 1130)  
 (MC11/11P/B19-003 1440)  
**FREI, Christoph**  
 (MC11/11P/B19-005 1520)  
 (MC08/07P/B17-006 1535)  
**FREIBERG, Sebastian**  
 (G07/10P/D-019 1400-104)  
**FRENCH, Andrew**  
 (MI07/11A/B18-006 1050)  
**FRENCH, Andrew N.**  
 (MI09/08P/D-003 1400-156)  
**FRENCH, Andrew N.**  
 (MI09/09A/B22-005 1050)  
**FREY, Harald U.**  
 (GAILI.05/07P/D-018 1400-116)  
**FREYDIER, Remi**  
 (JSM04/09P/D-006 1400-043)  
**FREYMUELLER, Jeffrey**  
 (JSG01/08P/D-015 1400-015)  
**FREYMUELLER, Jeffrey T.**  
 (JSG01/08P/D-014 1400-014)  
**FREYMUELLER, Jeffrey Todd**  
 (JSG01/07P/A01-008 1605)  
 (JSG01/07P/A01-009 1620)  
**FRICKER, Helen**  
 (JSM10/07P/B23-009 1720)  
**FRIEDRICH, Michael**  
 (MC12/08P/B19-007 1700)  
**FRIIS-CHRISTENSEN, Eigil**  
 (GAV.04/07A/A11-001 0900)  
 (GAV.05/08A/A11-001 0830)  
 (GAV.04/07A/A11-002 0930)  
**FRITZ, Birgit**  
 (HS04/08A/C30-007 1230)  
**FRITZ, T.A.**  
 (GAILI.06/07P/D-008 1400-128)  
**FRITZ, Ted A.**  
 (GAILI.06/08A/A02-009 1215)  
**FRITZ, Theodore A.**  
 (GAILI.09/11P/A11-001 1400)  
**FROLOV, Alexander D.**  
 (MI03/09A/D-004 0900-247)  
 (MI03/08A/B18-004 0930)  
**FRUIT, G.**  
 (GAILI.05/08A/A06-007 1040)  
**FRY, C.D.**  
 (GAILI.06/11P/D-008 1400-060)  
**FRYER, Gerard J.**  
 (JSS07b/10P/D-019 1700-065)  
**FU, Bing**  
 (MC02/08A/B20-001 0900)  
**FU, Congbin**  
 (MC08/08P/D-001 1400-157)  
**FU, Guangyu**  
 (G03/07P/D-016 1400-038)  
**FU, Guobin**  
 (HS01/09P/D-023 1400-190)  
**FU, Lee-Lueng**  
 (U6/09A/D32-006 1140)  
**FU, Rong**  
 (MC03/10A/A07-005 1030)  
 (MI05/09P/B17-008 1710)  
**FU, Rongshan**  
 (JSS06/10A/A04-007 1050)  
**FU, S.Y.**  
 (GAILI.06/07P/D-008 1400-128)  
**FU, Xiuhua**  
 (MC17/11A/B23-001 0830)  
**FUDEYASU, Hironori**  
 (MC02/07P/B20-009 1700)  
**FUELLEKRUG, Martin**  
 (GAILI.04/07A/A08-002 0925)  
**FUJIE, Gou**  
 (SS03/07A/A02-003 0930)  
**FUJIE, Gou**  
 (SS03/08A/D-001 0830-160)  
**FUJIE, Gou**  
 (SS03/08A/D-105 0830-264)  
 (SS03/08A/D-011 0830-170)  
**FUJIEDA, Tadaomi**  
 (SS04a/09P/D-021 1400-270)  
**FUJIHARA, Satoru**  
 (JSS06a/08P/D-029 1400-107)  
**FUJIHARA, Yoichi**  
 (HW08/07A/C28-007 1130)  
**FUJII, Haruhisa**  
 (GAILI.11/09P/A15-004 1455)  
**FUJII, Ikuko**  
 (GAV.04/07P/A11-003 1450)  
**FUJII, Ryoichi**  
 (GAILI.04/09A/D-005 0830-141)  
**FUJII, Yushiro**  
 (SS04a/09P/D-028 1400-277)  
**FUJIKI, Ken'ichi**  
 (GAILI.09/11P/A11-007 1640)  
**FUJIMA, Ichiro**  
 (G07/10P/D-013 1400-098)  
**FUJIMAKI, Hirokazu**  
 (HW06/07P/D-005 1400-189)  
**FUJIMORI, Kunio**  
 (JSG01/08P/D-003 1400-003)  
**FUJIMOTO, Hiromi**  
 (SS03/08A/D-067 0830-226)  
**FUJIMOTO, Masaki**  
 (GAILI.08/10A/A16-002 0850)  
**FUJIMOTO, Masaki**  
 (GAILI.05/07P/D-009 1400-107)  
 (GAILI.07/09P/A14-007 1640)  
 (GAILI.05/07P/D-004 1400-102)  
 (GAILI.05/08A/A06-010 1125)  
**FUJINAWA, Yukio**  
 (SW05/10P/A13-005 1505)  
 (SS04b/10P/D-048 1400-232)  
**FUJINUMA, Yasumi**  
 (HW01/10A/C26-007 1110)  
 (MI07/10P/D-004 1400-180)  
 (MC05/07P/D-008 1400-215)  
**FUJISAWA, Hideyuki**  
 (JSS06/07P/A04-009 1700)  
**FUJITA, Hiroyuki**  
 (JSS07b/10P/D-014 1700-060)  
**FUJITA, Masaharu**  
 (HS01/09P/C29-006 1540)  
**FUJITA, Shigeru**  
 (GAILI.06/07P/D-001 1400-121)  
 (GAILI.10/11A/D-019 0830-093)  
**FUJITA, Takashi**  
 (JSS07b/10P/D-007 1700-053)  
**FUJIWARA, Hiroyuki**  
 (SS04b/10P/D-015 1400-199)  
 (SS04a/09P/D-021 1400-270)  
 (SS04b/10P/D-024 1400-208)  
 (SS04b/10P/D-023 1400-207)  
 (SS04b/10P/D-020 1400-204)  
 (SW05/10P/A13-005 1505)  
**FUJIWARA, Hiroyuki**  
 (SS04b/10P/D-004 1400-188)  
**FUJIWARA, Hitoshi**  
 (GAILI.07/11P/A12-003 1500)  
**FUJIWARA, Kazuki**  
 (HS03/08P/C26-004 1445)  
**FUJIWARA, Masatomo**  
 (MC05/08P/A09-006 1620)  
 (MC05/11P/A09-005 1530)  
 (MC17/11P/B23-006 1600)  
 (MC17/11P/B23-008 1640)  
**FUJIWARA, Satoshi**  
 (GAV.05/09P/D-006 1400-150)  
**FUJIWARA, Toshiya**  
 (GAV.07/07P/D-001 1400-142)  
 (GAV.07/07P/D-002 1400-143)  
**FUJIYOSHI, Yasushi**  
 (JSM14/08A/A05-003 0925)  
**FUJIYOSHI, Yasushi**  
 (JSM15/07A/B18-004 1000)  
 (JSM14/09P/D-010 1400-074)  
 (JSP09/10P/B20-010 1645)  
**FUJWARA, Masatomo**  
 (MC05/08P/A09-007 1640)  
**FUKAMI, Kazuhiko**  
 (HS03/07P/C26-004 1445)  
**FUKAMI, Kazuhiko**  
 (HW08/07P/C28-005 1610)  
**FUKAMI, Kazuhiko**  
 (HW08/08A/C28-007 1100)  
 (MI09/08P/D-002 1400-155)  
 (GAILI.06/09P/A10-001 1400)  
 (MC02/07P/D-004 1400-201)  
 (MI09/08P/B22-004 1500)  
 (GAILI.06/09P/A10-007 1545)  
 (GAILI.06/09P/A10-004 1500)  
 (MC05/07P/D-015 1400-222)  
 (MC17/11P/B23-006 1600)  
 (MC02/07P/D-002 1400-200)  
 (MC17/11P/B23-008 1640)  
 (MC05/11P/A09-005 1530)  
 (MC05/08P/A09-007 1640)  
 (GAILI.06/11P/D-012 1400-064)  
**FUKAO, Yoshio**  
 (JSS06a/08P/D-002 1400-080)  
 (JSS06/09A/A04-007 1120)  
 (JSS06/09P/A04-009 1700)  
 (JSG01/08P/D-018 1400-018)  
 (U5/07A/D32-004 1100)  
**FUKAO, Yoshio**  
 (JSS06/07P/A04-004 1500)  
**FUKAO, Yoshio**  
 (JSS06/07P/A04-005 1540)  
**FUKAZAWA, Tatsuya**  
 (HW01/10A/C26-007 1110)  
**FUKUDA, Masami**  
 (MI05/10P/D-010 1400-176)  
**FUKUDA, Masami**  
 (JSP04a/09P/D-003 1400-096)  
**FUKUDA, Yoichi**  
 (G03/07P/D-073)  
**FUKUDA, Yoichi**  
 (G03/07P/D-001 1400-023)  
 (G02/10P/D-017 1400-082)  
 (G03/07P/D-003 1400-025)  
 (G03/07P/D-011 1400-033)  
 (G02/10P/D-006 1400-071)  
 (JSG01/08P/D-030 1400-030)  
 (SW03/10A/D-007 0830-242)

**FUKUI, Yasuo**  
(MC05/07P/D-008 1400-215)

**FUKUKITA, Akira**  
(SS04a/09P/D-012 1400-261)

**FUKUMORI, Ichiro**  
(JSP06/08A/B21-006 1130)

**FUKUMOTO, Yasuhide**  
(JSP10/10P/B21-002 1430)

**FUKUNISHI, H.**  
(GAIL.04/07A/A08-007 1110)

**FUKUNISHI, Hiroshi**  
(GAIL.04/07A/A08-003 0940)  
(MC05/07P/D-012 1400-219)  
(GAIL.04/09A/D-004 0830-140)  
(GAIL.04/09A/D-003 0830-139)  
(GAIL.04/09A/D-006 0830-142)  
(GAIL.07/11P/A12-003 1500)  
(GAIL.04/09A/D-005 0830-141)  
(GAIL.06/11P/D-011 1400-063)

**FUKUOKA, Yoshitaka**  
(JSM04/09P/B23-005 1630)

**FUKUSHIMA, Keitaro**  
(HW01/09P/D-043 1400-234)

**FUKUSHIMA, Toshio**  
(G02/10P/D-011 1400-076)

**FUKUSHIMA, Yoshihiro**  
(HW08/08A/C28-006 1040)

**FUKUSHIMA, Yoshimitsu**  
(SS04/07A/A03-009 1145)

**FUKUTOME, Sophie**  
(MC03/09A/A07-007 1130)

**FUKUTOMI, Yoshiki**  
(MC03/11A/A07-005 1030)

**FUKUWA, Nobuo**  
(SS04b/10P/D-009 1400-193)

**FUKUYAMA, Keiko**  
(GAIL.10/11A/D-014 0830-088)

**FUKUYAMA, Taijiro**  
(HW01/09P/D-034 1400-225)

**FUKUZAWA, Karibu**  
(HW01/10A/C26-007 1110)

**FULLER-ROWELL, Timothy J.**  
(GAIL.05/07A/D-001 0830-017)

**FUNAKI, Ikkoh**  
(GAIL.11/10P/D-004 1400-119)  
(GAIL.11/09P/A15-006 1525)

**FUNAKI, Minoru**  
(GAI.08/08P/D-005 1400-140)

**FUNG, Shing F.**  
(GAIL.10/10P/A01-002 1420)

**FURUKAWA, Ryuta**  
(GAV.06/09P/D-001 1400-154)

**FURUKAWA, Ryuta**  
(JSS07a/09P/D-002 1700-103)

**FURUKAWA, Teruo**  
(JSM10/09P/D-002 1400-056)

**FURUKAWA, Yoshinori**  
(JSM15/07P/D-001 1400-001)  
(JSM15/07P/D-002 1400-002)  
(JSM15/07P/D-005 1400-005)  
(JSM15/07A/B18-001 0900)  
(JSM15/07A/B18-006 1045)  
(JSM15/07A/B18-010 1145)  
(JSM15/07P/D-004 1400-004)

**FURUMOTO, Jun-ichi**  
(MI09/08P/B22-005 1600)

**FURUMURA, Takashi**  
(SS04a/09P/D-045 1400-294)  
(SS04/07P/A03-010 1645)  
(SS04/07P/A03-013 1730)

**FUSEJIMA, Yuichiro**  
(SS03/08A/D-041 0830-200)

**FUSHIMI, Hiroji**  
(JSM15/07P/D-007 1400-007)  
(HS02a/07P/D-017 1545-163)  
(HS02/07P/C24-017 1400)

**FUSSEN, Didier**  
(JSG03/10A/A12-009 1140)

## g

**G., Koti Reddy**  
(SW03/10P/A04-010 1630)

**G., Mrudula**  
(MC05/08P/A09-010 1740)  
(MC05/08P/A09-009 1720)

**GABRIEL, Axel**  
(MC05/07P/A09-006 1640)

**GABRIEL, Hazael Firoton**  
(HW07/11P/D-009 1400-145)  
(HW07/11P/D-004 1400-140)

**GABRIEL, Hazael Firoton**  
(HW07/11P/D-019 1400-155)

**GAEDICKE, Christoph**  
(SS03/08A/D-043 0830-202)

**GAIDAI, Natalia K.**  
(SS03/08A/D-073 0830-232)

**GAINANOV, Adonis**  
(SS03/08A/D-077 0830-236)

**GAINES, Thomas**  
(JSS07/09A/A02-008 1100)

**GALAS, Roman**  
(SS03/08A/D-117 0830-276)

**GALDEANO, Armand**  
(GAV.05/08P/A11-007 1620)

**GALLACHER, Patrick Charles**  
(JSP10/08P/D-003 1610-055)

**GALLAGHER, Dennis L.**  
(GAIL.06/08A/A02-004 1005)

**GALMICHE, Martin**  
(JSP10/09P/B21-004 1500)

**GALMICHE, Martin Paul**  
(JSP10/08P/D-009 1610-061)

**GALVAO, Carlos O.**  
(HS01/09P/C29-001 1400)

**GAMAL, Mohamed Ahmed**  
(SS04/07A/A03-006 1100)  
(SS04a/09P/D-019 1400-268)  
(SS04b/10P/D-041 1400-225)

**GAMBIS, Daniel**  
(MC17/10A/D-001 0830-183)

**GAN, Thian Yew**  
(HS03/08P/C26-002 1415)

**GAN, Yiping**  
(HS04/08A/C30-003 1005)

**GANGSHENG, WANG**  
(HS03/08P/C26-003 1430)

**GANUSHKINA, Natalia Yu.**  
(GAIL.06/08A/A02-009 1215)

**GANZEI, Larissa A.**  
(JSS07a/09P/D-010 1700-111)

**GANZEY, Larisa A.**  
(JSS07/10A/A02-003 0900)

**GAO, Hui-Wang**  
(JSM04/09P/D-016 1400-053)

**GAO, Mengtan**  
(SS04/07P/A03-004 1500)

**GAO, Shu**  
(JSP08/09P/B19-002 1430)

**GAO, Yu-fen**  
(GAIL.10/11A/D-013 0830-087)

**GAO, Yuan**  
(SW04/09P/A13-010 1630)

**GAO, Yufen**  
(GAIL.10/11A/A01-005 0930)

**GAONKAR, S.G.**  
(SS03/08A/D-021 0830-180)

**GARAT, Mikhail N.**  
(GAI.10/09A/A11-004 0945)

**GARCIA, David**  
(JSG01/07A/A01-009 1120)

**GARCIA, Eulalia**  
(JSS07/09A/A02-010 1130)

**GARCIA, Luisa B.**  
(SS04b/10P/D-043 1400-227)

**GARCIA, R.R.**  
(MC05/08A/A09-003 0930)

**GARCIA, Ramon V.**  
(G04/08P/C25-004 1510)

**GARCIA, Rolando**  
(MC05/09A/A09-001 0900)

**GARCIA, Rolando G.**  
(MC05/08A/A09-004 1000)

**GARCIA, Rolando R.**  
(MC05/10P/A09-005 1620)  
(JSA01/08A/A12-005 1115)  
(MC05/07A/A09-003 1000)

**GARCIA, Sandra G.**  
(HW08/07A/C28-006 1110)

**GARCIA, Sandra Gabriela**  
(HS02c/11P/D-005 1630-103)  
(HS02/11A/C24-005 1101)

**GARCIA SUAREZ, Ana Maria**  
(MC12/08A/B19-006)

**GARCIA-FERNANDEZ, Mariano**  
(SS04b/10P/D-011 1400-195)

**GARCIA-HERRERA, Ricardo**  
(MC12/08A/B19-008 1200)

**GARGETT, Tim**  
(HW01/09P/D-005 1400-196)

**GARNER, Trevor W.**  
(GAIL.05/08A/A15-008 1150)

**GARNERO, Edward J.**  
(U5/07A/D32-003 1030)

**GARRETT, Jonathon A.**  
(GAIL.04/07P/A08-005 1540)

**GARTI, Rami**  
(HS03/08A/C26-003 0915)

**GARZOLI, Silvia Lucia**  
(JSP06/07P/D-005 1400-012)  
(JSP06/08A/B21-003 0950)

**GAT, Joel Robert**  
(HW06/08A/C31-001 1040)

**GATTI, L.V.**  
(JSM04/09P/D-010 1400-047)

**GATTI, Luciana V.**  
(JSM04/09P/D-012 1400-049)

**GATTI, Luciana V.**  
(JSM04/09A/B23-005 1115)

**GATTI, Luciana Vanni**  
(JSM04/09P/D-009 1400-046)

**GATTI, Luciana Vanni**  
(JSM04/09P/D-015 1400-052)

**GAUR, Vinod**  
(SS03/08A/D-079 0830-238)

**GAUSSIRAN II, Thomas L.**  
(GAIL.05/08A/A15-008 1150)

**GAVARDINAS, Costas**  
(HW03/11A/C30-002 0850)

**GAVRILOV, Nikolai M.**  
(MC05/07P/D-004 1400-211)

**GAYA-PIQUE, Lluís R.**  
(GAI.10/09P/A11-006 1515)

**GAYA-PIQUE, Luis R.**  
(GAV.05/08P/A11-011 1740)

**GAYA-PIQUE, Luis R.**  
(GAV.04/07P/A11-008 1700)

**GE, Linlin**  
(JSG01/07P/A01-012 1705)

**GE, TAN**  
(HS03/08P/C26-003 1430)

**GE, Xuyang**  
(MC02/08A/B20-001 0900)

**GEDAKYAN, Edvard Grigori**  
(JSP11/08P/D-004 1400-073)

**GEERNAERT, Gerald L.**  
(JSM03/08P/A13-003 1440)

**GEGOUT, Pascal**  
(JSG02/09A/D-006 0830-006)

**GEIST, Eric L.**  
(JSS07/10P/A02-009 1615)

**GELFAN, A.N.**  
(HS02/09P/C24-003 1430)

**GELFAN, Alexander**  
(JWH01/10P/C30-002 1420)

**GELFAN, Alexander N.**  
(HW07/11A/C25-008 1045)  
(JWH01/10P/C30-004 1500)  
(JWH01/09P/C30-004 1500)

**GENDRON, Eric**  
(MC04/10P/B22-006 1615)

**GENEV, Marin**  
(HS02/07A/C24-004 1130)

**GENEV, Marin Gospodinov**  
(HS02/08A/C24-003 0900)

**GENG, Biao**  
(JSM14/08A/A05-004 0940)  
(JSM14/09P/D-013 1400-077)

**GENRICH, Joachim**  
(JSG01/07A/A01-010 1135)

**GENTEMANN, Chelle L.**  
(JSP06/07A/B21-005 1030)

**GENTEMANN, Chelle Leigh**  
(JSP09/11A/B20-005 0945)

**GEORGAKAKOS, Konstantine P.**  
(HS03/07A/C26-001 0900)  
(HS03/07A/C26-005 1015)  
(HS03/08A/C26-003 0915)

**GEORGIADI, Alexander**  
(HS02b/10P/D-015 1630-136)  
(HS02/10A/C24-015 1141)

**GEORGIADI, Georgiadi**  
(JWH01/09A/C30-008 1150)

**GERASIMENKO, Mikhail D.**  
(JSG01/08P/D-009 1400-009)

**GERASIMENKO, Mikhail D.**  
(G04/08P/D-001 1400-108)

**GERDES, Ruediger**  
(JSP04/10A/A06-001)

**GERDES, Ruediger**  
(JSP04/10P/A06-004 1500)

**GERKEN, Elizabeth A.**  
(GAIL.04/07A/A08-008 1130)

**GEROVSKA, Daniela Ivanova**  
(GAV.06/10A/A11-009 1130)

**GESSNER, Klaus**  
(SS03/08A/D-147 0830-306)

**GETTELMAN, Andrew**  
(MC05/08P/A09-002 1430)  
(MC03/09P/A07-006 1640)

**GETTINGS, Mark E.**  
(GAV.06/10A/A11-010 1150)  
(GAV.06/09P/D-008 1400-161)

**GETTINGS, Paul**  
(JSG02/09A/D-008 0830-008)

**GEYKO, K.**  
(JSS06a/08P/D-012 1400-090)

**GEYKO, Valentin**  
(JSS06a/08P/D-012 1400-090)

**GHAZAVI, Kourosh**  
(G03/07P/D-012 1400-034)  
(G03/07P/D-013 1400-035)

**GHEITANCHI, Mohammad Reza**  
(SS03/08A/D-143)

**GHEUSI, Francois**  
(JSM14/08P/A05-002 1435)

**GHOSH, Suktisama**  
(GAIL.07/09P/A14-010 1740)

**GIAMBELLUCA, Thomas W.**  
(HS01/09A/C29-007 1120)

**GIARDINI, Domenico**  
(SS04a/09P/D-044 1400-293)  
(SS04/07P/A03-011 1700)

**GIBBS, Philip**  
(G02/10P/D-004 1400-069)

**GIBSON, John J.**  
(HW06/07P/C31-005 1520)  
(HW06/08A/C31-003 1120)

**GIDNER, Dawn M.**  
(GAIL.06/10A/A01-004 0920)

**GIDSKEHAUG, Arne**  
(JSG03/10A/A12-003 0910)

**GIERSCH, Louis**  
(GAIL.11/09P/A15-007 1540)

**GIL, Manuel**  
(MI03/09A/D-002 0900-245)

**GILBERT, Sherryl A.**  
(JSP07/08A/B17-004 1010)

**GILCHRIST, Brian E.**  
(GAIL.11/09P/A15-001 1400)

**GILLAN, M.J.**  
(U5/07A/D32-001 0900)

**GILLE, John C.**

## INDEX

- (MC05/08P/A09-003 1450)  
**GILLETT, Nathan Peter**  
 (MI05/10A/B17-005 1040)  
**GILMANOVA, Gulya**  
 (JSA07/11A/D-001 0830-001)  
**GILMANOVA, Gulya Zabirovna**  
 (JSA07/10P/A05-010 1730)  
**GILOD, Dolores**  
 (SS03/08A/D-077 0830-236)  
**GILSON, John**  
 (JSP06/07P/B21-005 1600)  
**GINGRAS, Hugo**  
 (HW07/11P/C25-003 1430)  
**GINIS, Isaac**  
 (MC02/07P/B20-008 1640)  
 (MC02/07P/B20-008 1640)  
**GIORGETTA, M.A.**  
 (MC11/10P/B19-003 1440)  
**GIOVANELLI, Giorgio**  
 (MI03/09A/D-003 0900-246)  
**GIOVINETTO, Mario**  
 (JSM11/10A/B18-001 0900)  
**GISBERT, J.**  
 (HS01/09P/C29-004 1500)  
**GITIS, Valeri G.**  
 (SW05/10P/A13-008 1545)  
**GIULIANO, Giuseppe**  
 (HS02/10A/C24-004 0915)  
**GLASSMEIER, K.-H.**  
 (GAI11.10/11A/D-006 0830-080)  
**GLASSMEIER, Karl-Heinz**  
 (GAI11.05/07P/D-007 1400-105)  
**GLATZMAIER, Gary A.**  
 (UL5/07A/D32-001 0800)  
**GLAZKOV, Vladimir N.**  
 (JSA01/08A/A12-004 1025)  
**GLECKLER, Peter**  
 (MC11/11A/B19-001 0830)  
**GLENN, Scott**  
 (JSP07/08A/B17-001 0900)  
**GLIKO, Alexander Olegovich**  
 (JSS06/10A/A04-006 1010)  
**GLOBEVNIK, Lidija**  
 (HS01/09A/C29-003 0940)  
 (HS02/09P/C24-009 1630)  
**GLOTOV, Vladimir Ye.**  
 (JSA07/11A/D-006 0830-006)  
**GLUSHKOV, Alexander**  
 (JSM11/10P/D-010 1700-019)  
**GN, Manoel Alonso**  
 (MC03/10A/A07-003 0930)  
**GO, Shi Jun**  
 (SS03/08A/D-012 0830-171)  
**GOERTZ, Herman**  
 (HW07/11P/D-018 1400-154)  
**GOHDA, Noriaki**  
 (JSP07/08A/B17-005 1100)  
**GOHL, Karsten**  
 (SS03/08A/D-094 0830-253)  
 (SS03/08A/D-095 0830-254)  
**GOKA, Tateo**  
 (GAI11.06/07P/D-015)  
 (GAI11.06/07P/D-019)  
**GOKA, Tateo**  
 (GAI11.11/09A/A15-005 1010)  
 (GAI11.06/08P/A02-009 1655)  
**GOKARN, S.G.**  
 (GAI.10/09P/D-014 1615-133)  
**GOKARN, Sanjay G.**  
 (SS03/08A/D-129 0830-288)  
**GOKOOL, Nivedita**  
 (HW01/09P/D-016 1400-207)  
**GOLDIN, Sergey V.**  
 (SW05/10A/D-005 0900-249)  
**GOLDING, Brian William**  
 (JSM14/09A/A05-002 0940)  
**GOLDSTEIN, J.**  
 (GAI11.10/10P/A01-003 1440)  
**GOLDSTEIN, J.**  
 (GAI11.06/08A/A02-008 1200)  
**GOLDSTEIN, Jerry**  
 (GAI11.06/08A/A02-006 1110)  
**GOLDSTEIN, Jerry**  
 (GAI11.06/08A/A02-006 1110)  
 (GAV.07/07P/D-005 1400-146)  
 (GAI11.06/08A/A02-002 0915)  
**GOLLAPALLY, Mohan**  
 (SS03/08A/D-023 0830-182)  
**GOLOVKOV, Vadim P.**  
 (GAV.05/08P/A11-006 1530)  
 (GAV.04/07P/A11-010 1740)  
 (U7/11P/D32-002 1450)  
**GOLUBEV, Nikolay G.**  
 (GAI.10/09A/A11-001 0900)  
**GOLUBTSOVA, Nina S.**  
 (GAI.10/09P/D-009 1615-128)  
**GOLYNSKY, Alexander V.**  
 (JSA07/11A/D-041 0830-041)  
**GOMBOSI, Tamas I.**  
 (GAI11.09/11A/A11-008 1210)  
**GOMER, Brandon**  
 (JSS07a/09P/D-018 1700-119)  
**GOMES, Luiz V.B.**  
 (SS05/10A/A13-005 0930)  
**GOMEZ, Antonio Perez**  
 (JSG03/09P/D-025 1640-033)  
**GOMEZ, Enzo**  
 (JSG03/09P/D-025 1640-033)  
**GOMEZ-LANDESA, Enrique**  
 (JSH01/07P/C27-006 1600)  
**GOMI, Takashi**  
 (HW02/11A/C31-006 1110)  
**GOMOS Cal-Val team**  
 (JSG03/10A/A12-009)  
**GONG, Mao-Sheng**  
 (SS04/08A/A03-002 0845)  
**GONI, Gustavo**  
 (JSP06/07P/D-006 1400-013)  
 (JSP06/07P/D-008 1400-015)  
**GONI, Gustavo Jorge**  
 (JSP06/08A/B21-003 0950)  
 (JSP06/07P/D-005 1400-012)  
**GONI, Miguel**  
 (JSP08/09A/B19-005 1030)  
**GONI, Osman Md**  
 (GAI11.04/07P/A08-009 1700)  
**GONTOVAYA, Larisa I.**  
 (JSA07/11A/D-014 0830-014)  
**GONZALEZ, Frank I.**  
 (JSS07/10P/A02-002 1415)  
**GONZALEZ, Frank I.**  
 (JSS07/10P/A02-004 1445)  
**GONZALEZ, Victor**  
 (JSG01/08P/D-012 1400-012)  
**GONZALEZ, Walter**  
 (GAI11.09/11A/A11-002 0900)  
**GONZALEZ, Walter Demetrio**  
 (GAI11.09/11P/A11-008 1710)  
**GONZALEZ-GARCIA, Jose Javier**  
 (JSG01/07A/A01-010 1135)  
**GOODE, Phillip R.**  
 (JSA09/10A/A08-003 0930)  
**GOODISON, Barry E.**  
 (JSH01/07P/C27-007 1620)  
 (JSM10/07A/B23-003 1000)  
**GOODISON, Barry E.**  
 (JSM10/07A/B23-001 0900)  
**GOODRICH, Charles**  
 (GAI11.05/08A/A06-011 1150)  
**GOOSBY, Stan**  
 (JSS07/10A/A02-013 1145)  
**GOOSBY, Stanley**  
 (JSS07/10P/A02-002 1415)  
**GOOSSENS, Marcel**  
 (GAI.V.02/07A/A07-003 1010)  
**GOPALSWAMY, Nat**  
 (GAI11.09/11A/A11-001 0830)  
**GORBATOY, Alexei**  
 (SS03/07A/A02-010 1145)  
**GORDEEV, Evgenii I.**  
 (JSG01/08P/D-009 1400-009)  
**GORDEEV, Evgenii I.**  
 (SS04a/09P/D-005 1400-254)  
**GORDON, Hal**  
 (JSM10/08A/B23-008 1130)  
**GORODISKY, Jurij**  
 (GAV.07/07P/D-005 1400-146)  
**GORSHKOV, A.I.**  
 (SS04/09A/A03-001 0900)  
**GOTO, Hiroyuki**  
 (SS04/08A/A03-005 0930)  
**GOTO, Shinkichi**  
 (HW04/09A/C31-008 1140)  
**GOTO, Tada-nori**  
 (GAI.08/08P/D-008 1400-143)  
**GOTO, Yoshitaka**  
 (GAI11.10/10P/A01-010 1700)  
**GOTOH, Tadahiro**  
 (JSG01/08A/A01-003 0930)  
**GOUNDER, Palanivel Periakali**  
 (HW01/09P/D-008 1400-199)  
**GOURBESVILLE, Philippe**  
 (HS02b/10P/D-026 1630-147)  
 (HS02/10P/C24-003 1523)  
**GOURLEY, Jonathan J.**  
 (HS03/07A/C26-007 1100)  
**GOVORKOVA, Veronika A.**  
 (MC11/11P/D-003 1400-196)  
**GOYETTE, Stép hane**  
 (JSM14/09P/D-016 1400-080)  
**GOYETTE, Stephane**  
 (JSM14/09A/A05-005 1025)  
 (JWH01/10P/D-003 1400-008)  
**GOYETTE, Stephane**  
 (JSM14/08P/A05-006 1715)  
**GRABER, Hans C.**  
 (JSP09/10A/B20-004 1000)  
**GRABOWSKI, Wojciech W.**  
 (MC17/11A/B23-007 1120)  
**GRABOWSKI, Wojciech W.**  
 (MC17/11P/B23-010 1720)  
**GRACHEV, Alexi M.**  
 (MC12/08A/B19-003 1020)  
**GRAF, Hans**  
 (HW06/08A/C31-002 1100)  
**GRAF, Hans-F.**  
 (MI05/10A/B17-009 1200)  
**GRAFAREND, Erik**  
 (G04/08P/D-028 1400-135)  
**GRAFAREND, Erik W.**  
 (G03/07P/D-018 1400-040)  
 (G02/07A/C25-006 1030)  
 (G07/10P/D-011 1400-096)  
 (G04/08A/C25-004 0940)  
**GRAFAREND, Erik W.**  
 (G04/07P/C25-007 1700)  
**GRAHAM, Gerhard**  
 (SS04/08P/A03-007 1530)  
**GRAHAM, L. Phil**  
 (HS02/08A/C24-012 1145)  
**GRANDE, Manuel**  
 (GAI11.05/07P/D-020 1400-118)  
 (GAI11.06/08A/A02-005 1045)  
 (GAI11.08/10A/A16-007 1040)  
**GRANDIS, Hendra**  
 (GAI.10/09P/D-010 1615-129)  
 (GAI.10/09A/A11-002 0915)  
**GRANDPEIX, Jean-Yves**  
 (MC17/11P/B23-010 1720)  
**GRANET, Michel**  
 (JSS06b/10P/D-012 1400-036)  
**GRANGER, Raoul J.**  
 (JWH01/10P/C30-004 1500)  
 (HW07/11A/C25-008 1045)  
 (JWH01/09P/C30-004 1500)  
**GRARD, R.**  
 (GAI11.06/07P/D-011 1400-131)  
**GRAUCH, V.J.S.**  
 (GAV.07/07P/A13-009 1700)  
**GRAUPNER, Steffen**  
 (JSG01/08A/A01-006 1015)  
**GRAVES, Robert**  
 (SS04/08A/A03-011 1115)  
**GRAVES, Robert W.**  
 (SS04/07P/A03-002 1430)  
**GRAY, Donald M.**  
 (HW07/11A/C25-008 1045)  
**GRAY, Lesley**  
 (JSA08/09A/A08-005 1015)  
**GRAY, Lesley**  
 (MC05/09A/A09-007 1140)  
**GRAY, Lesley J.**  
 (JSA08/09P/A08-005 1550)  
 (MC05/10P/A09-001 1400)  
**GRAYSON, R.B.**  
 (HW07/10A/C25-008 1200)  
**GRAZIANI, Laura**  
 (JSS07a/09P/D-013 1700-114)  
**GREBENNIKOVA, Tatiana A.**  
 (JSS07a/09P/D-010 1700-111)  
**GREBOWSKY, Joseph M.**  
 (GAI11.07/11A/A12-005 1035)  
**GRECHKO, Evgeny**  
 (MI03/08A/B18-007 1110)  
**GREEN, James L.**  
 (GAI11.10/10P/A01-002 1420)  
**GREEN, Pamela**  
 (JSM03/08P/A13-008 1640)  
**GREFF-LEFFTZ, Marianne**  
 (JSS06/08A/A04-003 0910)  
**GREFF-LEFFTZ, Marianne**  
 (JSS06a/08P/D-028 1400-106)  
**GREGERSEN, Soren**  
 (JSS06/09P/A04-004 1500)  
**GREGERSEN, Soren**  
 (JSS06/09P/A04-006 1600)  
**GREGORY, Jonathan**  
 (JSM11/10A/B18-002 0920)  
**GREINER-MAI, Hans**  
 (GAV.05/09P/D-003 1400-147)  
**GRELLE, Achim**  
 (MI07/11P/B18-001 1400)  
**GREENFELL, John Lee**  
 (MC05/07P/D-001 1400-208)  
**GRETSKAYA, Elena V.**  
 (JSS07/10A/A02-003 0900)  
**GRG SWJ.**  
 (G03/07P/D-010 1400-032)  
**GRIBOVSKI, Zoltán**  
 (HS02/07A/C24-011 0940)  
 (HS02a/07P/D-011 1545-157)  
**GRIGORIAN, Aram Artavazd**  
 (SS03/08A/D-085 0830-244)  
**GRIGORIEVA, Vika**  
 (MI05/11A/B17-006 1010)  
**GRILLI, Stephan T.**  
 (JSS07/09P/A02-008 1600)  
 (JSS07b/10P/D-019 1700-065)  
**GRIMM, Alice Marlene**  
 (MC03/10A/A07-004 0950)  
 (MC17/10A/D-002 0830-184)  
**GRINSTED, Aslak**  
 (HS01/08P/D-010 1400-048)  
 (MI05/10P/B17-008 1710)  
**GRIOT-POMMERA, DaphneAnne**  
 (SS04/07A/A03-009 1145)  
**GRIST, Jeremy P.**  
 (JSP09/10A/B20-008 1130)  
**GROSS, Jens-Uwe**  
 (MC05/07A/A09-002 0930)  
**GROSS, Jens-Uwe**  
 (MC05/07P/A09-007 1700)  
**GROSFELD, Klaus**  
 (JSM10/09P/D-006 1400-060)  
**GROTE, Katharine**  
 (HW07/10A/C25-005 1115)  
**GROUP, CALIXTO**  
 (JSS06/08A/A04-011)  
**GRUBER, Thomas**  
 (JSG02/09P/A05-010 1730)  
 (JSG02/09P/A05-001 1400)  
**GRUENEWALD, Uwe**  
 (HW06/07A/C31-007 1150)  
**GRUTTER, Herman**  
 (JSS06/09P/A04-008 1640)  
**GU, Haoyu**  
 (JSH01/08P/D-013 1400-051)  
**GU, Ja-Min**  
 (JSG03/09P/D-009 1640-017)  
**GU, Shenghua**  
 (HW07/11P/D-035 1400-171)  
 (HW07/11P/D-020 1400-156)

- GU, Y.**  
(JSS06a/08P/D-023 1400-101)
- GU, Yu Jeffrey**  
(JSS06/07P/A04-001)
- GUAN, Hong**  
(MI03/08A/B18-006 1050)
- GUAN, Yunlan**  
(G04/08P/D-003 1400-110)
- GUARNIERI, Fernando Luis**  
(GAIII.09/11A/A11-002 0900)
- GUARNIERI, Fernando Luis**  
(GAIII.09/11P/A11-008 1710)
- GUBELADZE, David Dato**  
(HS01/09P/D-021 1400-188)
- GUBELADZE, David Dato**  
(HS02/07A/C24-010 0936)  
(HS02a/07P/D-010 1545-156)
- GUDKOV, Dmitri I.**  
(HW01/10P/C26-009 1720)
- GUDKOV, Dmitri I.**  
(HW01/09P/D-014 1400-205)
- GUDRUN, Massmann**  
(HW06/07P/C31-004 1500)
- GUEGUEN, Celine**  
(JSP04/09P/A06-007 1600)
- GUENTHER, Alex B.**  
(JSM04/09A/B23-005 1115)
- GUENTHER, Alex B.**  
(JSM04/09A/B23-007 1215)
- GUENTHER, Gebhard**  
(MC05/07A/A09-002 0930)
- GUERIN, Christine**  
(JSP09/10A/B20-003 0945)
- GUERRA, Gingging De Castro**  
(HS04/08A/C30-002 0935)
- GUGUEN, Philippe**  
(SS04/07A/A03-004 1015)
- GUHIN, Scott A.**  
(JSP09/11P/B20-006 1545)
- GUINOT, VINCENT**  
(HS03/07A/C26-002 0930)
- GUL, Muzaffer**  
(SW04/09P/A13-009 1615)
- GULERCE, Umit**  
(SS04b/10P/D-002 1400-186)
- GULEV, Sergey**  
(JSP09/11P/B20-009 1645)
- GULEV, Sergey K.**  
(MI05/11A/B17-006 1010)  
(JSP09/10A/B20-006 1045)
- GULEV, Sergey Konstantinovich**  
(JSP09/11A/B20-011 1145)
- GULYAEVA, Tamara**  
(JSP11/07A/A10-008 1200)
- GUNDLICH, Brigitte**  
(G04/07P/C25-008 1720)
- GUNG, Yuancheng**  
(JSS06/08A/A04-010 1150)
- GUNOT, Vncent**  
(HS02b/10P/D-026 1630-147)  
(HS02/10P/C24-003 1523)
- GUO, Biao**  
(JSA07/10P/A05-004 1500)
- GUO, Jian-shan**  
(GAII.05/07A/D-003 0830-019)
- GUO, Laodong**  
(JSP04/09P/A06-007 1600)  
(JSP04/09P/A06-009 1700)
- GUO, Shenglian**  
(HS02/09P/C24-006 1515)  
(HS02/07A/C24-007 1215)
- GUO, Shenglian**  
(HS02b/10P/D-022 1630-143)  
(HS02/10A/C24-022 1209)
- GUO, Xueliang**  
(JSP09/10P/B20-011 1700)  
(HS02c/11P/D-026 1630-124)  
(HS02/11P/C24-003 1523)
- GUO, Yiping**  
(MC08/07P/B17-009 1640)
- GUO, Zhichang**  
(JSM10/08A/B23-010 1210)
- GUPTA, Arun K.**  
(SS04/07A/A03-010 1200)
- GUPTA, Ashim Das**  
(HW05/10A/C31-011 1125)
- GUPTA, Gautam**  
(SS03/08A/D-068 0830-227)  
(SS03/08A/D-129 0830-288)
- GUPTA, Hari Shanker**  
(HW01/09P/D-025 1400-216)
- GUPTA, Hari Shanker**  
(HW01/09P/D-013 1400-204)
- GUPTA, Hoshin V**  
(HW08/08P/C28-004 1520)
- GUPTA, Hoshin V.**  
(HW08/07A/C28-001 0900)  
(HW08/08A/C28-001 0830)  
(HW07/11A/C25-004 0930)  
(HW08/08P/C28-003 1500)
- GUPTA, S.K.**  
(HW06/07P/D-004 1400-188)
- GUPTA, Sandeep**  
(JSA07/11A/D-038 0830-038)
- GUPTA, Vijay K.**  
(HW07/10P/C25-001 1400)
- GURKAN, Onur**  
(JSG01/08P/D-013 1400-013)
- GURTNER, Werner**  
(G07/10A/A03-003 0940)
- GURUBARAN, S.**  
(JSA09/10A/A08-009 1145)  
(JSA09/11P/D-002 1400-051)  
(JSA09/11P/D-003 1400-052)
- GUSEV, Alexander**  
(JSA07/11A/D-022 0830-022)
- GUSEV, Alexander A.**  
(SS04a/09P/D-004 1400-253)
- GUSEV, Alexander A.**  
(SS04a/09P/D-005 1400-254)
- GUSEV, Y.**  
(JWH01/09P/C30-001)
- GUSEV, Y.**  
(JWH01/09A/C30-009 1210)
- GUSEV, Yeugeniy M.**  
(MI07/11P/B18-002 1420)  
(HW08/08A/C28-003 0920)  
(JWH01/10A/C30-002 0850)
- GUSEVA, Evgeniya M.**  
(SS04a/09P/D-005 1400-254)
- GUSEVA, Maria S.**  
(MC11/10A/B19-002 0900)
- GUSIAKOV, Viacheslav K.**  
(JSS07a/09P/D-012 1700-113)
- GUSIAKOV, Viatcheslav K.**  
(JSP11/08A/A10-001 0900)  
(JSS07/09A/A02-002 0915)
- GUSTAFSSON, Georg**  
(GAIII.10/11A/D-022 0830-096)
- GUSTARD, Alan**  
(HW07/11A/C25-013 1215)
- GUTDEUTSCH, Rolf**  
(SS04a/09P/D-023 1400-272)
- GUTOROVA, Larissa I.**  
(JSA07/10A/A05-010 1210)
- GVIRTZMAN, Haim**  
(HW07/11P/D-017 1400-153)
- GYAKUM, John Richard**  
(JSM14/09A/A05-001 0905)
- GYULAI, Akos**  
(GAI.10/09A/A11-008 1115)
- GYURJYAN, Levon**  
(SS03/08A/D-083 0830-242)
- HAAGMANS, Roger**  
(GAV.04/07A/A11-002 0930)
- HAAGMANS, Roger**  
(G03/07P/D-042 1400-064)  
(G03/07P/D-024 1400-046)
- HAAPALA, Jari Juhani**  
(JSM10/07P/B23-005 1600)
- HAARPAINTNER, Joerg**  
(JSH01/07A/C27-006 1220)  
(JSH01/08P/D-005 1400-043)
- HAAS, Ruediger**  
(SS03/07P/A02-005 1500)
- HABOGLU, Baris**  
(JSS07/09A/A02-012 1200)
- HACHIKUBO, Akihiro**  
(JSH01/08P/D-009 1400-047)
- HADA, Tohru**  
(GAIII.07/09P/A14-008 1700)  
(GAIII.07/10P/D-005 1400-110)
- HADDA, M.S.**  
(HS01/09P/D-017 1400-184)
- HADI, Abdul**  
(JSM04/09A/B23-001 0900)
- HADI, Samsul**  
(JSP11/08A/A10-002 0930)
- HADY, Ahmed Abdel**  
(JSA08/10P/D-004 1400-004)  
(GAIV.02/07P/A07-002 1440)
- HAESSLER, Henri**  
(SS03/08A/D-064 0830-223)
- HAEUSSLER, Peter J.**  
(GAV.06/09P/D-007 1400-160)
- HAGAN, Maura**  
(MC05/09P/A09-003 1500)
- HAGHSHENAS, Ebrahim**  
(SS04a/09P/D-048 1400-297)
- HAGINOYA, Shigenori**  
(MC03/11P/A07-004 1520)
- HAGIO, Masahiro**  
(MI09/08P/D-002 1400-155)
- Hai Cheng**  
(MC12/08P/B19-001 1415)
- HAIDER, Syed Aftab**  
(GAII.07/11P/A12-002 1430)
- Haidu, Ionel**  
(HS02b/10P/D-034 1630-155)  
(HS01/08P/C29-004 1500)  
(HS02/10P/C24-011 1555)
- HAINES, Keith**  
(JSG02/09P/A05-009 1715)  
(JSG02/09A/D-003 0830-003)
- HAIRSTON, M.**  
(JSG03/09P/D-026 1640-034)
- HAIRSTON, Marc**  
(GAII.05/07A/D-001 0830-017)
- HAIRSTON, Marc R.**  
(GAII.05/08A/A15-007 1130)
- HAJJ, George**  
(GAII.05/08A/A15-005 1040)
- HAJJ, George A.**  
(GAII.05/07A/D-006 0830-022)
- HAJJ, George A.**  
(GAII.05/07A/D-005 0830-021)
- HAJJAM, Sohrab**  
(HW08/07A/C28-003 0950)
- HAKOIWA, Eiichi**  
(JSG01/07A/A01-001 0900)
- HALBERTSMA, Jünt**  
(HW03/11A/C30-001 0830)
- HALCHUK, Stephen**  
(SS04b/10P/D-019 1400-203)  
(SS04b/10P/D-018 1400-202)  
(SS04b/10P/D-017 1400-201)
- HALDOUPIIS, Christos**  
(GAII.06/09A/A10-008 1110)
- HALENKA, Tomas**  
(MC08/07P/B17-011 1710)  
(JSA08/10P/D-005 1400-005)
- HALL, C.M.**  
(MC05/10A/A09-010 1210)
- HALL, Kevin W.**  
(SW03/10P/A04-001 1400)
- HALLETT, John**  
(JSM15/07A/B18-008 1115)
- HALLETT, John**  
(MI09/09A/B22-002 0920)  
(MI08/07P/B18-003 1600)  
(MI08/07P/B18-007 1715)  
(MI08/07P/B18-006 1700)
- HALLIWELL, George R.**  
(JSP09/11P/B20-005 1515)
- HAMAD, O.E.**  
(HW07/11P/D-024 1400-160)
- HAMADA, Chiho**  
(JSS06b/10P/D-019 1400-043)
- HAMADA, Jun-Ichi**  
(MC17/11P/B23-006 1600)
- HAMADA, Jun-Ichi**  
(MC03/09P/A07-007 1700)  
(MC03/10P/A07-008 1720)
- HAMADA, Jun-Ichi**  
(MC03/11P/D-007 1400-182)
- HAMADA, Jun-Ichi**  
(MC03/11P/D-009 1400-184)
- HAMAGUCHI, Hiroyuki**  
(JSP11/08A/A10-009 1220)
- HAMAGUCHI, Toshio**  
(HS03/07A/C26-010 1145)
- HAMAHARA, Yoshinari**  
(HW01/09P/D-015 1400-206)
- HAMANO, Yozo**  
(GAI.10/09P/A11-007 1530)
- HAMASAKI, Hideo**  
(GAV.05/09P/D-006 1400-150)
- HAMASAKI, Takahiro**  
(MI07/11P/B18-006 1600)
- HAMDACHE, Mohamed**  
(SS04/08P/A03-003 1430)  
(SS04b/10P/D-014 1400-198)
- HAMDAN, Sami Mahmoud**  
(HS04/08A/C30-005 1130)
- HAMIDI, Goodarz**  
(SS04/09A/A03-003 0930)
- HAMILTON, K.**  
(MC11/10P/B19-003 1440)
- HAMILTON, Kevin**  
(JSA09/10A/A08-005 1030)
- HAMILTON, Kevin**  
(MC05/10P/A09-008 1740)
- HAMZA, Khaled Ismail**  
(HW05/10P/D-006 1400-161)
- HAMZA, Valiya M.**  
(SS03/08A/D-096 0830-255)  
(SS05/10A/A13-005 0930)
- HAN, DeSheng**  
(GAII.10/11A/A01-005 0930)
- HAN, Min**  
(MI09/09P/B22-001 1400)  
(SW05/10A/D-007 0900-251)
- HAN, Shin-Chan**  
(JSG02/09A/D-007 0830-007)
- HANADA, Hideo**  
(G02/10P/D-013 1400-078)  
(G02/07A/C25-014 1245)  
(G02/07A/C25-011 1200)  
(G02/07A/C25-013 1230)
- HANAFIN, Jennifer**  
(MI09/09A/B22-004 1000)
- HANAFY, Sherif M.**  
(SW05/10P/A13-015 1745)  
(SW05/10A/D-004 0900-248)
- HANANTO, Nugroho Dwi**  
(GAI.10/09P/D-010 1615-129)  
(SS03/08A/D-044 0830-203)
- HANANTO, Nugroho Dwi**  
(SS03/08A/D-063 0830-222)
- HANASAKI, Naota**  
(HS02/10A/C24-005 0930)
- HANAWA, Keiko**  
(JSG03/09P/A12-005 1520)
- HANAWA, Kimio**  
(JSP06/07P/D-002 1400-009)
- HANAZAKI, Hideshi**  
(JSP10/10A/B21-003 0920)
- HANI, A.**  
(HS02/08P/C24-006 1515)
- HANISCH, Friedrich**  
(MI08/07P/D-003 1400-197)
- HANKA, W.**  
(JSS06a/08P/D-023 1400-101)
- HANNA, Jon**  
(HS04/07P/C30-004 1555)

## h

# INDEX

- HANNAH, David M.**  
(HW02/11A/C31-002 0900)  
(HW02/11A/D-002 0830-134)  
(HW02/11A/C31-004 0950)
- HANSE, Frands Søbjer**  
(HS02/09P/C24-001 1400)
- HANSE YI, Hanse**  
(JSM14/09P/D-006 1400-070)
- HANSEN, K.C.**  
(GAI11.14/07A/A12-009 1225)
- HANSEN, Tina Svan**  
(HS02/08P/C24-001 1400)
- HAO, Wei Min**  
(JSM04/09A/B23-006 1145)
- HAPUARACHCHI, Hapu Arachchige Prasantha**  
(HS03/08A/C26-008 1045)
- HARA, Masanao**  
(JSG03/09P/D-022 1640-030)
- HARADA, Chikako**  
(MC08/07P/B17-003 1430)
- HARADA, Daiji Harada**  
(HW01/09P/D-034 1400-225)
- HARADA, Kenji**  
(JSS07/10A/A02-009 1030)
- HARADA, Masatake**  
(SS03/08A/D-053 0830-212)
- HARARI, Joseph**  
(JSM11/10P/B18-005 1600)
- HARDER, Steven**  
(SS03/07A/A02-006 1045)  
(SS03/08A/D-004 0830-163)
- HARDIE, Alasdair Macdonald**  
(HW01/09A/C26-005 1030)
- HARDY, Janet P.**  
(JWH01/10P/C30-003 1440)
- HARDY, Janet P.**  
(JWH01/09P/C30-004 1500)
- HARI, Ram Babu Venkata**  
(GAV.07/07P/A13-005 1520)
- HARIJAN, Netramani**  
(JSH01/08A/C27-005 1050)
- HARINARAYANA, T.**  
(GAI.10/09A/A11-012 1215)
- Harinarayana T.**  
(GAI.10/09P/D-004 1615-123)
- HARNETT, Erika**  
(GAV.02/07P/A07-001 1400)
- HARRAR, Bill**  
(HW03/11A/C30-002 0850)
- HARRIS, Esther**  
(JSG03/10A/A12-007 1100)
- HARRIS, Ian**  
(MC12/08P/B19-006 1620)
- HARRIS, Rob N.**  
(MC12/08P/B19-002 1445)
- HARRIS, Robert N.**  
(JSG02/09A/D-008 0830-008)
- HARRISON, D.E.**  
(MC03/09A/A07-005 1050)
- HARRISON, D.E.**  
(MI05/10P/B17-003 1500)  
(MC17/11P/B23-001 1400)
- HARROLD, Timothy Ives**  
(HS02b/10P/D-009 1630-130)  
(HS02/08A/C24-013 1200)  
(HS02/10A/C24-009 1117)
- HARTLE, Richard E.**  
(GAI1.07/11A/A12-005 1035)
- HARTOGH, Paul**  
(MC04/11A/B22-010 1130)
- HASAN, Abdulghani A.**  
(HW07/11P/D-026 1400-162)  
(HW05/10A/C31-010 1110)
- HASEGAWA, Akira**  
(JSG01/08P/D-006 1400-006)  
(JSS06b/10P/D-020 1400-044)  
(JSG01/08P/D-002 1400-002)
- HASEGAWA, Seizo**  
(SS03/08A/D-005 0830-164)
- HASHIGUCHI, Hiroyuki**  
(MI09/08P/D-001 1400-154)  
(MI09/08P/D-002 1400-155)
- (MC02/07P/D-003 1400-200)  
(MC17/11P/B23-008 1640)  
(MC05/08P/A09-005 1530)  
(MC03/10P/A07-008 1720)  
(MC05/11P/A09-005 1530)  
(JSM14/07A/A05-006 1130)  
(JSM14/09P/D-009 1400-073)  
(MC17/11P/B23-006 1600)  
(MC05/08P/A09-006 1620)  
(MC05/08P/A09-007 1640)  
(MC17/11A/B23-004 0940)
- HASHIMOTO, Daisuke**  
(JSM14/07P/A05-003 1450)
- HASHIMOTO, Isao**  
(SS03/08A/D-007 0830-166)
- HASHIMOTO, Koza**  
(GAI11.05/07A/A06-006 1025)  
(GAI11.05/07P/D-021 1400-119)
- HASHIMOTO, Manabu**  
(JSG01/07P/A01-007 1530)  
(JSG01/08P/D-016 1400-016)  
(SS05/10A/A13-004 0915)  
(SS05/10A/A13-011 1115)  
(JSG01/08P/D-004 1400-004)  
(JSG01/08P/D-005 1400-005)
- HASHINO, Michio**  
(HS01/09P/D-012 1400-179)
- HASHOLT, Bent**  
(HS01/09A/C29-005 1020)
- HASI, Bateer**  
(SS03/08A/D-037 0830-196)
- HASNAIN, Syed Iqbal**  
(JSH01/07A/C27-004 1140)
- HASSAN, Gamal**  
(SS03/08A/D-088 0830-247)
- HASSAN, Nasser Mohamed**  
(HW05/10P/D-008 1400-163)  
(HW05/10P/D-009 1400-164)  
(GAV.06/10P/A11-008 1640)
- HASSANEEN, Abdel-Rady Ghareeb**  
(GAI.10/09P/D-001 1615-120)  
(GAI.10/09P/D-002 1615-121)
- HASSANEEN, Abdel-Rady Ghareeb**  
(HS02a/07P/D-036 1545-182)  
(HS02/07P/C24-036 1516)
- HASSENPLUG, Gernot**  
(MI09/08P/B22-004 1500)
- HASUMI, Hiroyasu**  
(JSM10/09P/D-004 1400-058)  
(JSM10/07P/B23-007 1640)
- HATA, Takeshi**  
(HW05/10A/C31-003 0905)  
(HW08/07A/C28-007 1130)
- HATA, Takeshi**  
(HW07/11P/D-024 1400-160)
- HATAKEYAMA, Kiyoshi**  
(JSP04b/10P/D-003 1400-022)  
(JSP04/09A/A06-006 1110)
- HATANAKA, Yuki**  
(JSG01/08P/D-021 1400-021)  
(JSG01/07P/A01-013 1720)
- HATANO, Yuko**  
(HW03/11P/C30-008 1640)
- HATAYAMA, Ken**  
(SS04a/09P/D-020 1400-269)
- HATORI, Tokutaro**  
(JSS07/09A/A02-005 1000)
- HATSUSHIKA, Hiroaki**  
(MC05/08A/A09-006 1120)
- HATTERMANN, Fred**  
(HW03/11A/C30-003)
- HATTORI, Miki**  
(MC03/11A/A07-007 1110)
- HATZFELD, Denis**  
(SS04a/09P/D-048 1400-297)
- HAU, L.-N.**  
(GAI11.07/10P/D-002 1400-107)
- HAUSER, Franz**  
(JSA07/11A/D-020 0830-020)
- HAUTOT, Sophie**  
(JSA07/10A/A05-004 0940)
- (JSA07/10P/A05-006 1610)
- HAVSTAD, Kris**  
(JSH01/07P/C27-006 1600)
- HAY, Lauren E.**  
(HW08/07P/C28-004 1550)
- HAYAKAWA, Hajime**  
(GAI11.14/08A/D-004 0830-148)  
(GAI11.14/08A/D-005 0830-149)  
(GAV.03/09A/A16-007 1150)  
(GAI11.11/10P/D-002 1400-117)  
(GAI11.05/07P/D-014 1400-112)  
(GAI11.05/07P/D-010 1400-108)
- HAYAKAWA, Masashi**  
(GAI1.04/07A/A08-005 1015)
- HAYAKAWA, Norio**  
(HS03/07A/C26-009 1130)
- HAYAKAWA, Takashi**  
(SS04b/10P/D-024 1400-208)
- HAYAKAWA, Takashi**  
(SS04a/09P/D-027 1400-276)
- HAYAKAWA, Toshihiko**  
(SS04b/10P/D-020 1400-204)
- HAYAKAWA, Yuzuru**  
(SS04b/10P/D-023 1400-207)
- HAYAKAWA, Yuzuru**  
(SS04b/10P/D-015 1400-199)
- HAYANO, Michiko**  
(HW01/09P/D-010 1400-201)
- HAYASAKA, Hiroshi**  
(MI05/10P/D-010 1400-176)  
(MC08/08P/D-003 1400-159)
- HAYASHI, Haruo**  
(SS05/10A/A13-004 0915)
- HAYASHI, Masaki**  
(HW01/09A/C26-008 1150)
- HAYASHI, Shugo**  
(JSM14/08A/A05-007 1040)
- HAYASHI, Syugo**  
(JSM14/09P/D-024 1400-088)  
(JSM14/08A/A05-011 1200)
- HAYASHI, Taich**  
(MC02/07P/B20-009 1700)
- HAYASHI, Yoshi-Yuki**  
(MC03/09A/A07-003 0950)  
(MC04/10P/B22-002 1430)  
(MC04/11P/B22-002 1430)  
(MC04/11P/B22-003 1445)  
(MC04/10P/B22-005 1530)  
(SW05/10A/D-008 0900-252)
- HAYASHI, Yoshinari**  
(SW05/10P/A13-005 1505)
- HAYASHIDA, Sachiko**  
(MC05/07P/A09-005 1610)  
(MC05/07P/A09-008 1720)
- HAYEK, Khalil**  
(SW05/10P/A13-004 1450)
- HAYNES, Mark**  
(SS03/08A/D-052 0830-211)
- HE, Ruoying**  
(JSP08/09A/B19-003 0950)
- HE, Yuan Qing**  
(HS02/08A/C24-006 0945)
- HE, Yuanqing**  
(MI05/10P/B17-006 1630)  
(HS02b/10P/D-014 1630-135)  
(HS02/10A/C24-014 1137)
- HEAL, Kate Victoria**  
(HW01/09A/C26-005 1030)
- HEATHWAITE, Louise**  
(HS04/08A/C30-001 0905)
- HEBERER, Thomas**  
(HS04/08A/C30-007 1230)
- HECK, Bernhard**  
(G04/08A/C25-005 1000)  
(G03/07P/D-005 1400-027)  
(G03/07P/D-064 1400-086)
- HEDSTROM, Newell R.**  
(HW07/11A/C25-008 1045)
- HEELIS, R.A.**  
(GAI1.05/08A/A15-007 1130)  
(GAI1.06/09A/A10-001 0900)  
(JSG03/09P/D-026 1640-034)
- HEELIS, Roderick A.**  
(GAI1.05/07A/D-001 0830-017)
- HEESTERBEEK, Hans**  
(HW03/11A/C30-001 0830)
- HEGAI, Valerii V.**  
(GAI1.04/09A/D-007 0830-143)
- HEIKKILA, Walter J.**  
(GAI11.05/08A/A06-008 1055)
- HEIL, Petra**  
(JSM10/07P/B23-004 1520)
- HEINEMEIER, Jan**  
(MC12/08P/B19-006 1620)
- HEINRICHS, John**  
(JSH01/08P/D-006 1400-044)
- HEINTZ, Maggy**  
(JSS06/08A/A04-008 1110)
- HEISE, Stefan**  
(GAI11.05/08A/A15-006 1100)
- HEJDA, Pavel**  
(JSA08/09A/A08-004 1000)
- HEKI, Kosuke**  
(UG/09A/D32-003 1000)  
(JSG01/07P/A01-014 1735)  
(G02/07A/C25-011 1200)  
(GAI1.06/11P/D-007 1400-059)
- HEKI, Kousuke**  
(G02/07A/C25-014 1245)
- HELIANI, Leni S.**  
(G03/07P/D-073 1400-095)
- HELLINGER, Petr**  
(GAI11.14/07A/A12-003 1015)
- HELLMER, Hartmut H.**  
(JSM10/07P/B23-008 1700)  
(JSM10/09P/D-006 1400-060)
- HELM, Achim**  
(G07/10P/D-006 1400-091)
- HEMANT, Kumar**  
(JSA07/10A/A05-007 1110)
- HÉMOND, Christophe**  
(GAV.07/07P/A13-002 1420)
- HENDERSON, Michael G.**  
(GAI11.06/08P/A02-003 1450)
- HENDERSON-SELLERS, A.**  
(MC11/11P/B19-001 1400)
- HENDON, Harry**  
(MC03/09A/A07-001 0900)  
(MC17/10P/B23-006 1600)
- HENDRICKX, Frederic**  
(HW07/11P/D-015 1400-151)
- HENRIKSEN, Hans Jørgen**  
(HW03/11A/C30-002 0850)
- HENRYS, S.A.**  
(SS03/08A/D-146 0830-305)
- HERATH, Srikantha**  
(HS02/11A/C24-003 0900)  
(HS03/07P/C26-011 1645)
- HERDIES, Dirceu Luis**  
(MC03/11P/D-012 1400-187)
- HERMAWAN, Eddy**  
(MC03/11P/D-003 1400-178)
- HERMITTE, Daniel**  
(GAV.07/07P/D-004 1400-145)  
(GAI.10/09P/D-013 1615-132)
- HERNANDEZ, Enrique**  
(JSG01/08P/D-012 1400-012)
- HERNANDEZ, Fabrice**  
(JSG02/09A/D-003 0830-003)
- HERNANDEZ-NAVARRO, Antonio**  
(G03/07P/D-033 1400-055)
- HERON, Malcolm Lewis**  
(JSG03/09P/D-017 1640-025)  
(JSG03/09P/A12-006 1540)
- HERQUEL, Georges**  
(JSS06/10A/A04-004 0930)
- HERRING, Jackson R.**  
(JSP10/11A/B21-005 1000)
- HESSAMI, Khaled**  
(G02/10P/D-016 1400-081)
- HESSE, Michael**  
(GAI11.09/10P/D-003 1400-115)  
(GAI11.09/11A/A11-008 1210)
- HESSNER, Katrin**  
(JSP09/10A/B20-004 1000)

- HEWITSON, Steve**  
(G04/07P/C25-004 1530)
- HI NO, Ryota**  
(JSS06/09P/A04-009 1700)
- HIBLER III, William**  
(JSP04/10A/A06-004 1030)  
(JSM10/07P/B23-004 1520)
- HICK, Paul P.**  
(GAI11.09/11P/A11-007 1640)
- HICKEY, Jeff**  
(JSA09/10A/A08-003 0930)
- HICKEY, Michael P.**  
(MC04/10P/B22-009 1715)
- HIGAKI, Masakazu**  
(JSP08/09P/B19-007 1640)
- HIGASHI, Ryoichi**  
(GAI11.09/09P/A15-009 1645)  
(GAI11.11/10P/D-001 1400-116)
- HIGASHI, Sadanori**  
(SS04/07P/A03-014 1745)
- HIGASHI, Toshihiro**  
(G03/07P/D-001 1400-023)  
(G03/07P/D-003 1400-025)  
(G03/07P/D-011 1400-033)
- HIGGITT, David Laurence**  
(HS01/09P/C29-005 1520)
- HIGUCHI, Atsushi**  
(JSM03/09A/D-002 0830-036)  
(JSM03/08A/A13-004 1000)
- HIGUCHI, Keiji**  
(JSM15/07P/D-007 1400-007)  
(JSM15/07P/D-002 1400-002)
- HIGUCHI, Tomoyuki**  
(GAI11.10/11A/D-014 0830-088)
- HIGUCHI, Yoshihiro**  
(GAI11.10/11A/D-011 0830-085)
- HILDE, Tom**  
(JSS06/09A/A04-007 1120)
- HILDENBRAND, Thomas G.**  
(GAV.06/10A/A11-011 1210)
- HILGER, Klaus B.**  
(JSG03/09P/D-010 1640-018)
- HILGERS, Alain**  
(GAI11.11/09A/A15-001 0900)
- HILGERS, Alain M.F.**  
(GAI11.11/09P/A15-012 1730)
- HILL, Katy L.**  
(JSP06/07P/D-003 1400-010)
- HINDERER, Jacques**  
(G03/07P/D-012 1400-034)
- HINDERER, Jacques**  
(G07/10P/D-016 1400-101)
- HINDERER, Jacques**  
(JSG02/09P/A05-008 1700)
- HINDERER, Jacques**  
(JSG02/09A/D-006 0830-006)
- HINGRAY, Benoit**  
(HW07/11A/C25-003 0915)
- HINO, Ryo**  
(SS03/08A/D-114 0830-273)
- HINO, Ryota**  
(SS03/08A/D-101 0830-260)  
(SS03/08A/D-001 0830-160)  
(SS03/08A/D-120 0830-279)  
(JSS06/07P/A04-005 1540)  
(SS03/08A/D-118 0830-277)  
(SS03/08A/D-011 0830-170)  
(SS03/08A/D-002 0830-161)
- HINO, Ryota**  
(SS03/08A/D-017 0830-176)
- HINSON, David**  
(GAI11.03/08A/A16-008)
- HINZMAN, Larry**  
(JSP04/09A/A06-002 0920)
- HIO, Yasuko**  
(MC05/10A/A09-006 1040)
- HIPKIN, Roger**  
(JSG02/09A/D-003 0830-003)
- HIRABAYASHI, Yukiko**  
(HW07/10P/C25-006 1545)
- HIRAHARA, Kazuro**  
(SS04a/09P/D-045 1400-294)  
(JSS06a/08P/D-016 1400-094)  
(SS03/07P/A02-012 1715)
- HIRAHARA, Kazuro**  
(G02/10P/D-012 1400-077)
- HIRAHARA, M.**  
(GAI11.06/08P/A02-011 1725)
- HIRAHARA, Masafumi**  
(GAI11.08/10A/A16-001 0830)  
(GAI11.06/07P/D-010 1400-130)  
(GAI11.05/07P/D-019 1400-117)
- HIRAI, Masayuki**  
(JWH01/09P/C30-002 1420)
- HIRAKAWA, Kazuomi**  
(JSS07a/09P/D-016 1700-117)  
(JSS07a/09P/D-005 1700-106)
- HIRAKI, Yasutaka**  
(GAI11.04/09A/D-006 0830-142)
- HIRAKUCHI, Hiromaru**  
(HS03/07P/C26-008 1600)
- HIRANO, Masaya**  
(GAI11.09/11P/A11-007 1640)
- HIRANO, Takashi**  
(MI07/10P/D-006 1400-182)  
(MI07/10P/D-004 1400-180)
- HIRASHIMA, Hiroyuki**  
(JWH01/09A/C30-003 0940)
- HIRATA, Kenji**  
(SS03/08A/D-007 0830-166)  
(JSS07/10P/A02-009 1615)
- HIRATA, Naoshi**  
(SS03/08A/D-004 0830-163)  
(SS03/07A/A02-006 1045)
- HIRATA, Ryuichi**  
(MI07/10P/D-004 1400-180)  
(MI07/10P/D-006 1400-182)
- HIRAYAMA, Kenta**  
(HS01/09P/D-003 1400-170)
- HIRN, Alfred**  
(SS03/07A/A02-009 1130)
- HIRONAKA, Sadayuki**  
(HS02/11A/C24-003 0900)
- HIRONO, Tetsuro**  
(SS03/08A/D-057 0830-216)
- HIROOKA, Toshihiko**  
(MC05/10A/A09-001 0830)  
(MC05/07P/A09-009 1740)  
(MC05/10A/A09-004 0940)  
(MC05/07P/D-005 1400-212)
- HIROSE, Hitoshi**  
(JSG01/08P/D-025 1400-025)
- HIROSE, Naoyuki**  
(GAI11.11/09P/A15-002 1425)
- HIROSE, Wataru**  
(SS03/08A/D-042 0830-201)
- HIROSE, Yoko**  
(HW08/08A/C28-007 1100)
- HIROSHI, Kawamura**  
(JSP06/07A/B21-004 1000)
- HIROSHIRO, Yoshinari**  
(HS04/08A/C30-002 0935)
- HIROTA, Tomoyoshi**  
(JWH01/09A/C30-002 0920)
- HIRTH, Greg**  
(SS03/07A/A02-011 1200)
- HIRTZIG, Mathieu**  
(MC04/10P/B22-006 1615)
- HISADA, Yoshiaki**  
(SS04/07P/A03-012 1715)
- HIYAMA, Tetsuya**  
(JSM03/09A/D-002 0830-036)  
(JSM03/08A/A13-004 1000)  
(JSM03/09A/D-003 0830-037)
- HJELT, Sven-Erik**  
(JSA07/11A/D-029 0830-029)
- HO, Christian M.**  
(GAI11.07/11P/A12-005 1620)
- HO, H.-H.**  
(GAI11.06/09A/A10-001 0900)
- HOAR, Timothy J.**  
(MC17/10P/B23-004 1500)
- HOBARA, Y.**  
(GAI11.04/07A/A08-005 1015)
- HOCK, Regine**  
(JSM10/08P/B23-004 1520)
- HODGES, Kevin**  
(MC11/10A/B19-004 0940)  
(MI05/09P/B17-005 1610)
- HODGSON, James A.**  
(SS03/08A/D-145 0830-304)
- HOEJERSLEV, Niels Kristian**  
(JSG03/10A/A12-004 0930)
- HOEVEN, Andrevd**  
(SS03/08A/D-076 0830-235)
- HOFF, Holger**  
(HS02/07A/C24-014 0952)  
(HS02a/07P/D-014 1545-160)
- HOFF, Holger H.**  
(HS02/07A/C24-014 0952)  
(HS02a/07P/D-014 1545-160)
- HOFFMANN, Georg**  
(HW06/08A/C31-002 1100)
- HOFFMANN, Georg Paul**  
(MC12/08A/B19-001 0930)
- HOFFMANN, P.**  
(MC05/10A/A09-010 1210)
- HOFMANN, Hilmar**  
(HW06/07A/C31-007 1150)
- HOFMANN-WELLENHOF, Bernhard**  
(G03/07P/D-075 1400-097)
- HÖGGERL, Norbert**  
(G03/07P/D-075 1400-097)
- HOGUE, Terri S.**  
(HW08/08A/C28-001 0830)
- HOLBEN, B.N.**  
(JSM04/09A/B23-006 1145)
- HOLBERN, Brent**  
(JSM04/09P/B23-006 1700)
- HOLDSWORTH, D.A.**  
(GAI11.06/11P/D-017 1400-069)
- HOLDSWORTH, Gerald**  
(MI05/11P/B17-005 1520)
- HOLJEV, DANKO**  
(HS01/09A/C29-003)
- HOLKO, Ladislav**  
(JWH01/09A/C30-006 1110)
- HOLLIDAY, Victoria Jane**  
(HS01/09P/C29-005 1520)
- HOLLWEG, Joseph V.**  
(GAI11.04/09P/A16-003 1510)
- HOLME, Richard**  
(GAV.05/08P/A11-005 1515)
- HOLMES, Matt G.R.**  
(HW07/11A/C25-013 1215)
- HOLOTA, Petr**  
(G04/08A/C25-003 0920)
- HOLSCHNEIDER, Matthias**  
(GAV.05/09P/D-004 1400-148)
- HOLT, John**  
(GAI11.05/08P/A15-002 1430)
- HOLTET, Jan**  
(JSA01/08P/A12-004 1520)
- HOLZBECHER, Ekkehard O.**  
(HS02c/11P/D-016 1630-114)  
(HW01/09P/D-023 1400-214)  
(HS02/11A/C24-016 1145)
- HOLZWORTH, Robert H.**  
(GAI11.04/07P/A08-006 1605)
- HOMMA, Sawako**  
(GAI.08/08A/A14-005 0950)
- HONDA, Meiji**  
(MI05/11A/B17-004 0930)
- HONDA, Meiji**  
(JSM10/08A/B23-003 0930)  
(MI05/11A/B17-008 1130)  
(MI05/11A/B17-007 1050)  
(MI05/11A/B17-009 1150)  
(MI05/09A/B17-008 1150)
- HONDA, Ryou**  
(SS03/08A/D-005 0830-164)
- HONDA, Ryou**  
(JSG01/08P/D-038 1400-038)
- HONDA, Satoru**  
(JSS06a/08P/D-005 1400-083)
- HONG, Chul-hoon**  
(MC02/08P/B20-002 1420)
- HONG, Hanjing**  
(SS03/08A/D-046 0830-205)
- HONG, Sung Jin**  
(JSS07b/10P/D-012 1700-058)
- HONKURA, Yoshimori**  
(GAI.08/08A/A14-007 1050)  
(GAI.08/08P/D-007 1400-142)
- HOOD, Lon L.**  
(GAI11.03/09P/D-001 1400-144)  
(JSA08/09A/A08-001 0900)
- HORBURY, Timothy**  
(GAI11.07/09P/A14-006 1610)
- HOREN, Helene**  
(GAV.07/07P/A13-002 1420)
- HORI, Masahiro**  
(JSH01/08P/D-009 1400-047)
- HORI, Masatake E.**  
(MI05/10P/D-006 1400-172)
- HORI, Muneo**  
(JSG01/07A/A01-002 0915)  
(SW05/10P/A13-007 1530)  
(SS04b/10P/D-047 1400-231)
- HORI, Tomoharu**  
(HW04/09A/C31-003 0940)
- HORIKAWA, Haruo**  
(SS04a/09P/D-038 1400-287)  
(SS04a/09P/D-018 1400-267)
- HORIKE, Masanori**  
(SS04a/09P/D-007 1400-256)
- HORINOUCI, Takeshi**  
(MC05/11A/A09-007 1140)  
(MC11/10P/B19-003 1440)  
(MC05/09A/A09-008 1200)  
(MC05/08P/A09-007 1640)  
(MC05/08P/A09-006 1620)
- HORIUCHI, Shigeki**  
(SS04b/10P/D-048 1400-232)  
(SW05/10P/A13-005 1505)
- HORMAECHEA, Jose Luis**  
(JSA07/11A/D-047 0830-047)
- HORNE, Richard B.**  
(GAI11.09/11P/A11-006 1620)
- HOSAKA, Masahiro**  
(MC08/07P/B17-005 1520)  
(JWH01/09P/C30-002 1420)
- HOSHI, Kiyoshi**  
(JWH01/10A/C30-008 1120)
- HOSHIBA, Mitsuyuki**  
(G03/07P/D-011 1400-033)
- HOSHIBA, Mitsuyuki**  
(SS03/08A/D-130 0830-289)
- HOSHINO, M.**  
(GAI11.05/08A/A06-006 0955)
- HOSHINO, Masahiro**  
(GAI11.08/10A/A16-001 0830)  
(GAI11.05/07A/A06-002 0915)  
(GAI11.07/10P/D-007 1400-112)  
(GAI11.05/07P/D-009 1400-107)  
(GAI11.05/07P/D-004 1400-102)  
(GAI11.05/07P/D-019 1400-117)
- HOSHINO, Shunsuke**  
(JSP09/11A/B20-012 1200)
- HOSKINS, Brian**  
(JSM14/08P/A05-004 1625)  
(MC11/10A/B19-007 1100)  
(MC03/09P/A07-001 1400)  
(MI05/09P/B17-005 1610)  
(MC11/10A/B19-004 0940)
- HOSO, Yoshinobu**  
(JSG01/08P/D-001 1400-001)  
(JSG01/07P/A01-007 1530)
- HOSOKAWA, Mizuhiko**  
(G02/10P/D-010 1400-075)
- HOSONO, Yoshizumi**  
(HW05/10A/C31-001 0830)
- HOSOTANI, Akira**  
(GAI11.10/11A/D-024 0830-098)
- HOSOYA, Takashi**  
(SS03/08A/D-041 0830-200)
- HOSSAIN, Mohammad Monowar**  
(HS02c/11P/D-033 1630-131)

## INDEX

- (HS02/11P/C24-004 1527)  
(HS02c/11P/D-027 1630-125)  
(HS02/11P/C24-010 1551)
- HOSSAIN, Mohammad Salzar**  
(HS02c/11P/D-027 1630-125)  
(HS02/11P/C24-010 1551)
- HOSSEINI, Sayyed Keivan**  
(JSG01/08P/D-020 1400-020)
- HOU, Ju-Chen**  
(HS01/09P/D-010 1400-177)
- HOURLIN, Frédéric**  
(MC04/11P/B22-001 1400)
- HOUEWELING, Harm**  
(HW03/11A/C30-001 0830)
- HOWARD, KENETH W.**  
(HS03/08P/C26-001 1400)
- HOWARD, Timothy A.**  
(GAI11.10/11A/D-008 0830-082)
- HOWE, Bruce M.**  
(GAI11.05/07A/D-001 0830-017)
- HOWE, Eva**  
(G03/07P/D-060 1400-082)
- HOZUMI, Yu**  
(JSP10/09A/B21-010 1220)
- HREICHE, Antoine**  
(HW08/07A/C28-008 1150)
- HREINSDÓTTIR, Sigrún**  
(JSG01/07P/A01-008 1605)  
(JSG01/07P/A01-009 1620)
- HSIA, Y.J.**  
(HW01/09P/D-046 1400-237)
- HSIAO, T.-T.**  
(GAI11.06/10A/A01-008 1050)
- HSIAO, W.S.**  
(GAI11.04/07A/A08-007 1110)
- HSIEH, Chao-Hui**  
(SW05/10A/D-002 0900-246)
- HSIEH, Hsien-Hsiang**  
(SS03/08A/D-112 0830-271)
- HSU, Ann**  
(MI09/09A/B22-005 1050)
- HSU, Hou-Tse**  
(JSP07/08A/B17-006 1120)
- HSU, Houze**  
(G03/07P/D-017 1400-039)  
(SS03/08A/D-136 0830-295)
- HSU, Huang-Hsiung**  
(MC17/10P/B23-010 1715)  
(MC03/09A/A07-004 1030)
- HSU, Pang-Chi**  
(MC17/10P/B23-009 1700)
- HSU, Rue-Ron**  
(GAI11.04/07A/A08-007 1110)
- HSU, Tung-Shin**  
(GAI11.05/07P/D-011 1400-109)
- HSU, Ya-Ju**  
(JSG01/07A/A01-007 1050)
- HSU, YaJu**  
(JSG01/07A/A01-006 1015)
- HU, Dunxin**  
(JSP08/09P/B19-008 1700)
- HU, Jianguo**  
(JSP06/07P/D-001 1400-008)
- HU, Jiayi**  
(HS03/08P/C26-005 1500)
- HU, Li-Chuin**  
(SS03/08A/D-111 0830-270)  
(SS03/08A/D-016 0830-175)
- HU, Shengbiao**  
(JSM04/09P/D-003 1400-040)
- HU, Zeng-Zhen**  
(MC08/07P/B17-004 1445)
- HUANG, Bor-Shouh**  
(SS04a/09P/D-003 1400-252)  
(SS03/08A/D-124 0830-283)
- HUANG, C.-S.**  
(JSG03/09P/D-026 1640-034)
- HUANG, Chaosong**  
(GAI11.05/07A/A06-010 1150)
- HUANG, Chien-Ming**  
(GAI11.06/09A/A10-013 1245)
- HUANG, Fuqiong**  
(SS04b/10P/D-037 1400-221)
- HUANG, Huey-Chu**  
(SS04/07A/A03-007 1115)
- HUANG, Jinshui**  
(JSS06/09P/A04-001 1400)
- HUANG, Meiyuan**  
(HS02c/11P/D-026 1630-124)  
(HS02/11P/C24-003 1523)
- HUANG, Ronghui**  
(JSP09/10P/B20-011 1700)
- HUANG, Rui Xin**  
(JSP09/10P/B20-013 1730)
- HUANG, Treng-Shi**  
(MC02/08P/B20-004 1500)
- HUANG, Wei-Cheng**  
(JSG01/08P/D-022 1400-022)
- HUANG, Wei-Peng**  
(MC02/08P/B20-004 1500)
- HUANG, Win-Gee**  
(SS04b/10P/D-008 1400-192)
- HUANG, Yi-Ling**  
(SS04a/09P/D-003 1400-252)
- HUANG, Zhong**  
(SS03/08A/D-012 0830-171)
- HUBBARD, Susan**  
(HW07/10A/C25-005 1115)
- HUBERT, Pierre**  
(HW07/10P/C25-003 1445)
- HUBERT, Pierre**  
(HW07/11P/D-015 1400-151)
- HUDAK, David Ronald**  
(JSM14/09P/D-019 1400-083)
- HUDNUT, Ken**  
(JSG01/07A/A01-010 1135)
- HUDSON, Mark R.**  
(GAV.07/07P/A13-009 1700)
- HUDSON, Mary K.**  
(GAI11.09/11P/A11-003 1440)
- HUDSON, Robert D.**  
(MI03/08A/B18-004 0930)  
(MI03/09A/D-004 0900-247)  
(MI03/08A/B18-006 1050)
- HUERFANO, Victor**  
(JSS07/10A/A02-014 1200)
- HUGENTOBLER, Urs**  
(G02/07A/C25-009 1130)
- HUGHES, Denis**  
(HS02/11A/C24-001 0830)
- HUGHES, W. Jeffrey**  
(GAI11.10/10P/A01-004 1500)
- HULOT, Gauthier**  
(GAV.04/07P/A11-006 1610)
- HULOT, Gauthier**  
(GAV.04/07A/A11-002 0930)
- HUMPHREYS, Eugene D.**  
(SS03/08A/D-051 0830-210)
- HUNG, Jia-Jang**  
(HW01/09P/D-031 1400-222)
- HUNT, Stephen**  
(GAI11.06/10A/A01-009 1105)
- HUO, Juan**  
(MI09/09P/B22-002 1420)
- HUO, Wenmian**  
(HS02b/10P/D-018 1630-139)  
(HS02/10A/C24-018 1153)
- HUOT, Jean-Paul**  
(MC04/11P/B22-001 1400)
- HUPPERT, Herbert E.**  
(JSP10/09P/B21-002 1420)
- HUPPERT, Herbert E.**  
(JSP10/09P/B21-001 1400)
- HURSAN, Gabor**  
(GAI.10/09P/A11-001 1400)
- HUSØY, Per-Ove**  
(JSH01/08A/C27-003 0950)
- HUSKER, Allen LeRoy**  
(SS03/08A/D-030 0830-189)
- HUSSON, Van S.**  
(G07/10P/D-012 1400-097)
- HUTAHAEAN, Walman**  
(JSP10/11P/B21-004 1530)
- HUTCHINGS, Jennifer K.**  
(JSP04/10A/A06-004 1030)  
(JSM10/07P/B23-004 1520)
- HUTEAU, Frederic**  
(JSP10/11P/B21-002 1450)
- HUTH, Radan**  
(MC08/07P/B17-011 1710)
- HUTHOVA, Zuzana**  
(MC08/07P/B17-011 1710)
- HUYBRECHTS, Philippe**  
(JSM11/10A/B18-002 0920)
- HWANG, Cheinway**  
(G02/10P/D-002 1400-067)
- HWANG, Ruey-Der**  
(JSA07/11A/D-009 0830-009)
- HWANG, Yeou-Jyh**  
(SS04a/09P/D-036 1400-285)
- HYODO, Mamoru**  
(SS03/07P/A02-012 1715)
- HYSELL, David L.**  
(GAI11.06/09P/A10-010 1655)
- I**
- IACOBELLIS, Vito**  
(HW07/11P/C25-005 1500)
- IACONO, Michael J.**  
(MC11/10P/B19-007 1630)
- IANNACCONE, Giovanni**  
(SS04a/09P/D-015 1400-264)
- IBRAHIM, Omneya M.**  
(JSP08/09A/B19-002 0930)  
(JSP10/08P/D-016 1610-068)
- ICHIKAWA, Ryuichi**  
(JSG01/08A/A01-003 0930)  
(G02/10P/D-008 1400-073)  
(G02/10P/D-009 1400-074)  
(G02/10P/D-014 1400-079)
- ICHIKAWA, Sachiko**  
(JSG03/09P/D-004 1640-012)
- ICHIKAWA, Yutaka**  
(HS03/08P/C26-004 1445)
- ICHIKI, Masahiro**  
(GAI.08/08P/D-009 1400-144)  
(GAI.08/08P/D-006 1400-141)  
(GAI.08/08P/D-008 1400-143)
- ICHIMURA, Tsuyoshi**  
(SS04b/10P/D-047 1400-231)
- ICHINOSE, Gene**  
(SS04/08A/A03-011 1115)
- ICHIOKA, Yuki**  
(HS01/09P/D-006 1400-173)
- ICHIYANAGI, Kimpei**  
(HW06/07P/C31-007 1600)  
(HW06/07P/D-006 1400-190)
- ICHIYANAGI, Masayoshi**  
(SS03/08A/D-007 0830-166)  
(SW04/09P/A13-014 1730)
- IDE, Junichiro**  
(HW01/09P/D-045 1400-236)
- IDRIS, M. Husni**  
(HW07/11P/D-038 1400-174)
- IEDA, A.**  
(GAI11.05/07A/A06-003 0930)
- IEVENKO, Igor B.**  
(GAI11.06/07P/D-003 1400-123)
- IGA, Keita**  
(JSP10/11A/B21-002 0900)
- IGA, Shin-ichi**  
(JSP10/08P/B21-004 1510)
- IGARASHI, Hiroshi**  
(JSS07b/10P/D-014 1700-060)
- IGARASHI, Makoto**  
(JSM10/09P/D-002 1400-056)
- IGLESIAS, Arturo**  
(JSG01/08P/D-023 1400-023)
- IGUCHI, Takao**  
(JSM04/09P/D-005 1400-042)
- IHDE, Johannes**  
(G03/07P/D-047 1400-069)  
(G07/10P/D-015 1400-100)
- IHDE, Johannes**  
(G07/10A/A03-008 1200)
- (G07/10P/D-016 1400-101)
- IIDAKA, Takashi**  
(SS03/07A/A02-008 1115)  
(SS03/08A/D-009 0830-168)  
(SS03/08A/D-102 0830-261)
- IJIMA, Takesi**  
(GAI11.10/11A/A01-008 1015)  
(GAI11.05/07P/D-006 1400-104)
- IINUMA, Takeshi**  
(JSG01/08P/D-012 1400-012)  
(SW05/10P/A13-007 1530)
- IIZIMA, Masahide**  
(GAI11.10/11A/D-024 0830-098)  
(GAI11.14/08A/D-007 0830-151)  
(GAI11.06/07P/D-017 1400-137)  
(GAI11.06/07P/D-016 1400-136)  
(GAI11.10/11A/D-007 0830-081)
- IIZUKA, Satoshi**  
(MC02/07A/B20-005 1125)
- IIZUKA, Susumu**  
(JSG03/09P/D-022 1640-030)
- IKAWA, Takeshi**  
(SS03/08A/D-004 0830-163)  
(SS03/08A/D-008 0830-167)
- IKEBUCHI, Shuichi**  
(HS03/08P/C26-004 1445)  
(SS05/10A/A13-004 0915)  
(HS03/07P/C26-007 1545)
- IKEDA, Moto**  
(JSP04/10P/A06-010 1720)  
(JSM10/08A/B23-002 0910)
- IKEDA, Moto**  
(JSP04/09A/A06-008 1150)
- IKEDA, Motoyoshi**  
(JSP04a/09P/D-004 1400-097)  
(JSP04/09P/A06-004 1445)
- IKEDA, Motoyoshi**  
(JSP10/10A/B21-002 0900)  
(JSP04/10P/A06-006 1600)  
(JSM10/08A/B23-006 1050)  
(JSH01/08P/D-004 1400-042)  
(JSP06/07P/B21-006 1620)  
(JSP04/09A/A06-007 1130)
- IKEDA, Nao**  
(MC05/07P/A09-005 1610)  
(MC05/07P/A09-008 1720)
- IKEDA, Ryuji**  
(SS03/08A/D-036 0830-195)  
(SS03/08A/D-038 0830-197)
- IKEDA, Takayoshi**  
(JSP04/10P/A06-006 1600)
- IKEDA, Yasutaka**  
(SS03/08A/D-043 0830-202)
- IKEHARA, Ken**  
(SS03/08A/D-055 0830-214)
- IKEYA, Tohru**  
(JSP04/09P/A06-012 1745)
- IKHILE, Catherine Imhangulaya**  
(HS02/11A/C24-006 0945)  
(HS02/07P/C24-026 1436)  
(HW02/11A/C31-008 1200)  
(HS02a/07P/D-026 1545-172)
- IKHILE, George Ubuihoro**  
(HS02/11A/C24-006 0945)
- ILAHEE, Mahbub**  
(HW04/09P/C31-003 1440)
- ILK, Karl Heinz**  
(G02/07A/C25-005 1010)  
(G04/08A/C25-009 1200)
- ILYAS, Syamsul Arifin**  
(HS01/08P/C29-009 1700)
- ILYEV, Alexander Ya.**  
(JSS07/10A/A02-003 0900)
- ILYEV, Alexander Ya.**  
(JSS07a/09P/D-010 1700-111)
- IMACHI, Tomohiko**  
(GAI11.11/09P/A15-009 1645)  
(GAI11.11/10P/D-001 1400-116)
- IMADA, Shinsuke**  
(GAI11.05/07A/A06-002 0915)
- IMAEVA, Ludmila P.**  
(SS03/08A/D-019 0830-178)

- IMAI, Kentaro**  
(JSS07a/09P/D-003 1700-104)  
(JSS07/09P/A02-003 1430)
- IMAIZUMI, Masayuki**  
(HW05/10P/D-005 1400-160)
- IMAKIIRE, Tetsuo**  
(JSG01/08P/D-021 1400-021)
- IMAKIIRE, Tetsuro**  
(JSG01/08A/A01-005 1000)  
(JSG01/07A/A01-001 0900)
- IMAM, Bisher**  
(HW08/08P/C28-004 1520)
- IMAMURA, Fumihiko**  
(JSS07/09A/A02-012 1200)  
(JSS07/09P/A02-001 1400)  
(JSS07b/10P/D-010 1700-056)  
(JSS07b/10P/D-012 1700-058)  
(JSS07/09P/A02-004 1445)  
(JSS07/10A/A02-009 1030)  
(JSS07b/10P/D-011 1700-057)  
(JSS07b/10P/D-019 1700-065)
- IMAMURA, Takeshi**  
(GAIL.07/11A/A12-001 0835)  
(MC04/11A/B22-002 0900)  
(MC05/09A/A09-008 1200)  
(MC04/11A/B22-003 0915)  
(MC04/11A/B22-001 0830)  
(MC05/07P/D-013 1400-220)  
(MC04/11A/B22-005 0945)
- IMANISHI, Yuichi**  
(G03/07P/D-011 1400-033)  
(G03/07P/D-003 1400-025)  
(G03/07P/D-001 1400-023)
- IMAWAKI, Shiro**  
(JSP06/08A/B21-002 0920)
- IMBERGER, Jörg**  
(JSP10/09A/B21-005 1040)
- IMPROTA, Luigi**  
(SS04a/09P/D-015 1400-264)
- IMREK, Erich**  
(G03/07P/D-075 1400-097)
- INAN, Umran**  
(GAIL.04/07A/A08-006 1050)
- INAN, Umran S.**  
(GAIL.04/07A/A08-008 1130)
- INATSU, Masaru**  
(MI05/11A/B17-005 0950)
- INAZAKI, Tomio**  
(SS03/08A/D-034 0830-193)
- The Indepth Mt Team**  
(GAI.08/08A/A14-003)
- INEGBEDION, COLLINS OSE**  
(HW05/10P/D-001 1400-156)
- INNESS, Peter**  
(MC17/11A/B23-002 0900)
- INOHARA, Naomi**  
(JSM15/07P/D-001 1400-001)
- INOUE, Daiei**  
(SS03/08A/D-099 0830-258)
- INOUE, Jun**  
(JSP09/10P/B20-010 1645)
- INOUE, Makoto**  
(MC05/07P/D-002 1400-209)
- INOUE, Shusaku**  
(JSS07b/10P/D-013 1700-059)
- INOUE, Shusaku**  
(JSS07b/10P/D-018 1700-064)
- INOUE, Shusaku**  
(JSS07b/10P/D-017 1700-063)
- INTRIERI, Janet**  
(JSM10/07P/B23-003 1500)
- INTRILIGATOR, Devrie S.**  
(GAIL.07/11A/A12-005 1035)
- INUBUSHI, Kazuyuki**  
(JSM04/09A/B23-001 0900)
- IODACHE, Anisoara**  
(HS02/11P/C24-005 1500)
- IRANNEJAD, P.**  
(MC11/11P/B19-001 1400)
- IRIKURA, Kojiro**  
(SW04/09P/A13-015 1745)  
(SS04a/09P/D-030 1400-279)  
(SS04b/10P/D-034 1400-218)
- (SS05/10A/A13-004 0915)  
(SS05/10A/A13-011 1115)  
(SS04b/10P/D-006 1400-190)  
(SS04a/09P/D-040 1400-289)  
(SS04a/09P/D-017 1400-266)  
(SS04a/09P/D-032 1400-281)
- IRISAWA, Minoru**  
(HS03/07P/C26-003 1430)
- IRISAWA, Toshiharu**  
(JSM15/07P/D-004 1400-004)
- ISAAC, George**  
(MI08/07P/B18-007 1715)
- ISAAC, George A.**  
(JSM15/07A/B18-008 1115)
- ISAWA, Ray**  
(JSS07/10A/A02-013 1145)
- ISEZAKI, Nobuhiro**  
(GAV.06/10A/A11-007 1050)
- ISHIBASHI, Akichika**  
(JSS07b/10P/D-004 1700-050)
- ISHIBASHI, Katsuhiko**  
(JSP11/07P/A10-002 1430)  
(SS03/08A/D-015 0830-174)
- ISHIDA, Hiroshi**  
(JSP09/10A/B20-002 0930)
- ISHIDA, Jun-ichi**  
(JSM14/08A/A05-011 1200)
- ISHIDA, Mizuho**  
(JSS06a/08P/D-007 1400-085)
- ISHIDA, Satoshi**  
(HW05/10P/D-005 1400-160)
- ISHIDA, Shin-ichi**  
(JSP10/08P/D-007 1610-059)
- ISHIDAIRA, Hiroshi**  
(HW08/07P/C28-005 1610)  
(JSG03/09P/A12-001 1400)  
(HS03/08A/C26-004 0930)  
(HS02/11A/C24-004 0915)  
(HS01/08A/C29-002 1010)  
(HW04/09A/C31-001 0900)  
(JWH01/10A/C30-010 1200)
- ISHIGOOKA, Yasushi**  
(HW04/09A/C31-008 1140)
- ISHIGURO, Naoko**  
(HS02/08A/C24-001 0830)
- ISHIHARA, Masahito**  
(JSM14/09P/D-010 1400-074)
- ISHIHARA, Takemi**  
(GAV.06/09P/D-006 1400-159)
- ISHIHARA, Tomomi**  
(JWH01/10A/C30-010 1200)
- ISHIHARA, Yasuhisa**  
(SS05/10A/A13-003 0900)
- ISHII, Hiroshi**  
(JSG01/08A/A01-006 1015)
- ISHII, Hiroshi**  
(SS03/08A/D-104 0830-263)
- ISHII, Miaki**  
(JSS06/09A/A04-002 0920)  
(JSS06/07P/A04-010 1720)
- ISHII, Nobuaki**  
(MC04/11A/B22-001 0830)
- ISHII, Toru**  
(SS04b/10P/D-023 1400-207)  
(SS04b/10P/D-024 1400-208)  
(SS04b/10P/D-015 1400-199)
- ISHII, Yoshiyuki**  
(HW06/07P/D-003 1400-187)  
(MI07/10P/D-003 1400-179)  
(JSM10/09P/D-001 1400-055)  
(HW06/07P/C31-007 1600)
- ISHII, Yoshiyuki**  
(JWH01/10P/D-004 1400-009)
- ISHIJIMA, Suguru**  
(MC02/08P/B20-003 1440)
- ISHIKAWA, Hirohiko**  
(MC03/11P/A07-002 1420)  
(MC02/08P/B20-001 1400)
- ISHIKAWA, Hiromasa**  
(HW06/07P/D-005 1400-189)
- ISHIKAWA, Kanako**  
(HS02/08A/C24-001 0830)
- ISHIKAWA, Masahiro**  
(SW03/10P/A04-004 1445)  
(SS03/08A/D-121 0830-280)  
(SW03/10P/A04-005 1500)  
(SW03/10A/D-005 0830-240)
- ISHIKAWA, Naoto**  
(GAI.08/08P/D-005 1400-140)
- ISHIKAWA, Nobuyoshi**  
(JWH01/10P/C30-001 1400)
- ISHIKAWA, Yutaka**  
(SS04b/10P/D-023 1400-207)
- ISHIMINE, Yasuhiro**  
(HW03/11A/C30-004 0930)
- ISHIOKA, Keiichi**  
(MC04/11P/B22-003 1445)
- ISHISAKA, Keigo**  
(GAIL.11/10P/D-002 1400-117)
- ISHISE, Motoko**  
(JSS06b/10P/D-018 1400-042)
- ISHITAIRA, Hiroshi**  
(HS03/08A/C26-009 1100)
- ISHIWATARI, Masaki**  
(JSP10/08P/B21-002 1430)  
(MC03/11A/A07-003 0930)  
(MC04/11P/B22-003 1445)  
(MC03/09A/A07-003 0950)  
(MC04/10P/B22-002 1430)  
(SW05/10A/D-008 0900-252)
- ISHIWATARI, Masaki**  
(MC02/07P/B20-005 1540)
- ISHIYAMA, Tatsuya**  
(SS03/08A/D-040 0830-199)  
(SS04a/09P/D-038 1400-287)  
(SS04a/09P/D-018 1400-267)
- ISHIZUKA, Shigehiro**  
(JSM04/09A/B23-001 0900)
- ISLAM, Md. Monirul**  
(HW05/10P/D-003 1400-158)
- ISLAM, Mohammad Rashedul**  
(HS02c/11P/D-033 1630-131)  
(HS02/11P/C24-004 1527)
- ISMAIL-ZADEH, Alik T.**  
(JSS06/08A/A04-006 1010)
- ISMAIL-ZADEH, Alik T.**  
(SS03/07P/A02-009 1630)
- ISOBE, Atsuhiko**  
(JSP08/09A/B19-004 1010)
- ISODA, Fusako**  
(MC05/09P/A09-008 1700)
- ISRAELEVITCH, Peter**  
(GAIL.04/07A/A08-009)
- ISSE, Takehi**  
(JSS06/09P/A04-009 1700)
- ISTRATOV, Vyatcheslav Aleksandrovich**  
(JSH01/07P/C27-001 1400)
- ITABA, Satoshi**  
(SS03/08A/D-045 0830-204)
- ITANO, Toshihisa**  
(MC02/07P/B20-006 1600)
- ITO, Aki**  
(SS03/08A/D-109 0830-268)  
(SS03/07A/A02-003 0930)  
(SS03/08A/D-009 0830-168)
- ITO, Akihiko**  
(MI07/10P/D-002 1400-178)  
(JSM04/09P/D-002 1400-039)
- ITO, Kiyoshi**  
(SS03/08A/D-004 0830-163)
- ITO, Shinobu**  
(SS03/08A/D-034 0830-193)  
(SS03/08A/D-110 0830-269)
- ITO, Takeo**  
(JSG01/08P/D-016 1400-016)  
(JSG01/08P/D-004 1400-004)
- ITO, Tanio**  
(SS03/08A/D-106 0830-265)  
(SS03/07A/A02-006 1045)  
(SS03/08A/D-004 0830-163)  
(SS03/08A/D-008 0830-167)
- ITOH, Hiroshi**  
(HW01/09P/D-037 1400-228)
- ITOH, Hisanori**  
(MI05/11P/B17-002 1420)
- ITOH, Keiji**  
(JSS07b/10P/D-007 1700-053)
- ITOH, Masayuki**  
(HW01/09P/D-037 1400-228)
- ITOH, Masayuki**  
(HW01/09P/D-038 1400-229)
- ITOH, Yasuto**  
(SS03/08A/D-058 0830-217)
- ITONAGA, Masahiro**  
(GAIL.10/10P/A01-007 1600)
- ITONAGA, Masahiro**  
(GAIL.10/11A/D-020 0830-094)  
(GAIL.10/11A/D-019 0830-093)
- IVACHTCHENKO, Nadejda Nazarovna**  
(JSA09/11P/D-001 1400-050)  
(MC11/11P/D-006 1400-199)
- IVANOV, Andrei Yu.**  
(JSG03/09P/D-014 1640-022)
- IVANOV, Boris Viacheslavovoch**  
(JSM10/09P/D-003 1400-057)
- IVANOV, Vladimir V.**  
(JSG01/08P/D-031 1400-031)
- IVANOV, Vladimir V.**  
(JSS07/10P/A02-006 1515)
- IVANOV, Vladimir V.**  
(SW05/10P/A13-011 1645)
- IVANOV-KHOLODNY, G.S.**  
(JSA08/09P/A08-009 1730)
- IVASHCHENKO, Alexei**  
(JSG01/08P/D-009 1400-009)
- IVASHCHENKO, Alexey I.**  
(SS04/08P/A03-010 1630)
- IVELSKAYA, TATYANA N.**  
(JSS07b/10P/D-015 1700-061)  
(JSS07b/10P/D-015 1700-061)
- IVERS, David**  
(GAV.05/08A/A11-009 1150)
- IVEY, Gregory N.**  
(JSP10/09A/B21-005 1040)
- IVEY, Gregory N.**  
(JSP10/10A/B21-001 0830)
- IVINS, Erik**  
(JSG01/08A/A01-011 1150)
- IWAI, Satoshi**  
(MI09/08P/B22-005 1600)
- IWAKURA, Toru**  
(JWH01/10P/C30-001 1400)
- IWAMI, Hirohumi**  
(HW01/10A/C26-009 1150)
- IWAMOTO, Hisanori**  
(GAI.08/08P/D-008 1400-143)
- IWAMOTO, Koji**  
(G04/08P/D-013 1400-120)
- IWAMOTO, Koji**  
(SS04b/10P/D-024 1400-208)
- IWANAMI, K.**  
(JSM14/09P/D-001 1400-065)
- IWANAMI, Koyuru**  
(JSM14/09P/D-023 1400-087)
- IWANAMI, Koyuru**  
(JSM14/07P/A05-003 1450)  
(MC03/11P/D-017 1400-192)  
(JSM14/09P/D-025 1400-089)
- IWAO, Koki**  
(MC05/07P/A09-009 1740)
- IWASA, Minoru**  
(GAIL.11/09P/A15-004 1455)
- IWASAKI, Sin-Iti**  
(JSM11/10P/B18-004 1500)
- IWASAKI, Takaya**  
(SS03/08A/D-004 0830-163)  
(SS03/07A/A02-006 1045)  
(SS03/07A/A02-008 1115)  
(SS03/08A/D-009 0830-168)  
(SS03/07A/A02-003 0930)  
(SS03/08A/D-102 0830-261)  
(SS03/07A/A02-007 1100)  
(SS03/08A/D-106 0830-265)
- IWASAKI, Toshiki**  
(MC05/07P/D-010 1400-217)  
(MC05/09P/A09-007 1640)

## INDEX

- IWASE, Hiroyuki**  
(JSS07b/10P/D-011 1700-057)
- IWASE, Hiroyuki**  
(JSS07a/09P/D-006 1700-107)
- IWASE, Yasuyuki**  
(JSS07b/10P/D-014 1700-060)  
(JSS06a/08P/D-005 1400-083)
- IWASHIMA, Tatsuya**  
(MI05/09P/B17-006 1630)
- IWASHITA, Atsushi**  
(JSG03/09P/D-020 1640-028)  
(JSG03/09P/D-022 1640-030)
- IWATA, Takahiro**  
(G02/10P/D-013 1400-078)  
(G02/07A/C25-013 1230)  
(G02/07A/C25-011 1200)
- IWATA, Takaki**  
(SW05/10P/A13-005 1505)
- IWATA, Tomotaka**  
(SW04/09P/A13-015 1745)  
(SS04b/10P/D-034 1400-218)  
(SS04/08A/A03-013 1145)  
(SS04a/09P/D-028 1400-277)  
(SS04/08A/A03-009 1045)
- IWATA, Yukiyoshi**  
(JWH01/09A/C30-002 0920)
- IWAYAMA, Takahiro**  
(JSP10/10A/B21-008 1140)  
(JSP10/08P/D-007 1610-059)
- IWI, Alan**  
(MC05/09A/A09-004 1000)
- IYEMORI, Toshihiko**  
(GAV.04/07A/A11-004 1030)  
(GAI.11/10A/A01-005 0930)
- IYER, Nagarajan Ramakrishnan**  
(HS02c/11P/D-031 1630-129)  
(HS02/11P/C24-008 1543)
- IYER, Nina**  
(MC05/07P/D-003 1400-210)
- IYISAN, Recep**  
(SS04b/10P/D-002 1400-186)
- IZQUIERDO, Alfredo**  
(JSP08/09A/B19-010 1220)
- IZRAILSKY, Yuri G.**  
(JSP10/08P/D-004 1610-056)
- IZUMI, Takeki**  
(JSH01/07P/C27-008 1640)
- IZUMI, Tatsushi**  
(G02/07A/C25-013 1230)
- J**
- JACKSON, Amy M.P.**  
(GAI.04/07P/A08-005 1540)
- JACKSON, Bernard V.**  
(GAI.11/09/11P/A11-007 1640)
- JACKSON, David**  
(MC05/10A/A09-002 0900)
- JACKSON, Ian**  
(JSS06a/08P/D-024 1400-102)
- JACOB, Frederic**  
(MI07/11A/B18-006 1050)
- JACOB, Frederic**  
(MI09/09A/B22-005 1050)  
(MI09/08P/D-003 1400-156)
- JACOB, S. Daniel**  
(JSP09/11P/B20-005 1515)
- JACOB, S. Daniel**  
(JSP09/10A/B20-011 1215)
- JADE, Sridevi**  
(SS03/08A/D-079 0830-238)
- JADHAV, D.B.**  
(MI09/08P/B22-008 1700)
- JADHAV, D.R.**  
(MI09/08P/B22-008 1700)
- JADHAV, D.R.**  
(MI09/09P/B22-004 1500)
- JADHAV, Dattatraya B.**  
(MI09/09P/B22-004 1500)
- JADHAV, Geeta V.**  
(GAI.11/09/10P/D-001 1400-113)
- JADIN, Evgeni N.**  
(MI05/11P/B17-003)
- JAEGER, Carlo**  
(HS02/07A/C24-014 0952)  
(HS02a/07P/D-014 1545-160)
- JAEGER, Lutz**  
(HW06/07A/C31-006 1130)
- JAEGGI, Adrian**  
(G02/07A/C25-009 1130)
- JAFARI, Mohammad**  
(SS04a/09P/D-048 1400-297)
- JAGO, Colin F.**  
(JSP08/09P/B19-001 1400)  
(JSP07/08P/B17-003 1450)
- JAGOVKINA, Svetlana V.**  
(JSM04/09P/D-014 1400-051)
- JAIN, A.R.**  
(MC05/08P/A09-010 1740)
- JAIN, Atma Ram**  
(JSM14/07A/A05-007 1145)
- JAKEMAN, Tony**  
(HW07/10P/C25-010 1645)
- JAKOB, Christian**  
(MC11/10P/B19-004 1500)
- JAKOWSKI, Norbert**  
(GAI.05/08A/A15-006 1100)
- JALLOULI, Chokri**  
(JSA07/11A/D-044)
- JALLOULI, Chokri**  
(JSA07/11A/D-045 0830-045)
- JAMET, Olivier**  
(G04/08A/C25-002 0900)  
(G03/07P/D-009 1400-031)
- JANA, Joydev**  
(HW05/10P/D-007 1400-162)
- JANAK, Juraj**  
(G04/08P/D-022 1400-129)
- JANC, Dejan**  
(JSM14/08P/A05-007 1730)
- JANI, R.A.**  
(HW06/07P/D-004 1400-188)
- JANIAUD, Beatrice**  
(JSP10/11P/B21-008 1720)
- JANJIC, Zavis**  
(MC11/11P/B19-002 1420)
- JANOUSEK, Martin**  
(MC08/07P/B17-011 1710)
- JANSEN, Jacques**  
(HW03/11A/C30-001 0830)
- JANSEN, Michiel**  
(HW03/11A/C30-001 0830)
- JAPAS, Maria Silvia**  
(SS03/08A/D-097 0830-256)  
(JSA07/11A/D-048 0830-048)
- JARCHOW, Christopher**  
(MC04/11A/B22-010 1130)
- JARISCH, Michael**  
(MC05/11P/A09-003 1450)
- JARVIS, Gary T.**  
(JSS06b/10P/D-009 1400-033)
- JARVIS, Martin J.**  
(JSA01/08P/A12-001 1400)
- JAVANMARD, Sohaila**  
(JSP11/08P/D-009 1400-078)  
(JSP11/07A/A10-006 1110)
- JAVANMARD, Sohaila**  
(JSP11/08P/D-003 1400-072)  
(JSP11/08A/A10-005 1050)  
(MI05/11P/B17-006 1610)
- JAYAWARDENA, A.W.**  
(HS02/08P/C24-011 1700)  
(HS02b/10P/D-001 1630-122)  
(HS02/10A/C24-001 1045)
- JAYAWARDENA, Amithirigala W.**  
(HW07/10P/C25-014 1745)
- JAYNE, Steven Robert**  
(JSG02/09P/A05-006 1620)
- JEAN, Wen-Yu**  
(SS04a/09P/D-008 1400-257)  
(SS04/08P/A03-012 1700)
- JEEVA, K.**  
(JSA09/11P/D-002 1400-051)  
(JSA09/10A/A08-009 1145)  
(JSA09/11P/D-003 1400-052)
- JEEVA, Krishnamoorthy**  
(GAI.06/09A/A10-005 1005)
- JEKELI, C.**  
(JSG02/09A/D-007 0830-007)
- JEKELI, Christopher**  
(U6/09A/D32-001 0910)  
(G04/08P/D-008 1400-115)  
(G03/07P/D-071 1400-093)  
(G03/07P/D-072 1400-094)
- JENG, Din-Yao**  
(JSG01/08P/D-022 1400-022)
- JENTZSCH, Gerhard**  
(JSG01/08A/A01-006 1015)
- JEVREJEVA, Svetlana**  
(MI05/10P/B17-008 1710)
- JHA, Raghunath**  
(HS03/08P/C26-006 1515)
- JIA, Shao-feng**  
(HS02/07A/C24-003 0908)  
(HS02a/07P/D-003 1545-149)
- JIA, Yangwen**  
(HS03/07A/C26-006 1045)
- JIANG, Chuanli**  
(JSP09/11A/B20-004 0930)
- JIANG, Jonathan H.**  
(MC05/11P/A09-010 1740)
- JIANG, Weiping**  
(JSP06/07P/D-001 1400-008)
- JIANG, Xiuqing**  
(GAI.08/08P/D-006 1400-141)
- JIANG, Zai sen**  
(SS03/08A/D-138 0830-297)  
(SS03/08A/D-139 0830-298)
- JIANPING, Yang**  
(JSM10/08P/B23-008 1700)
- JIANYU, Han**  
(MC05/07P/D-006 1400-213)
- JIAO, Jiu J.**  
(HW01/09P/D-030 1400-221)
- JIAO, Yanjun**  
(JWH01/10A/C30-001 0830)
- JIESHOU, ZHU**  
(SS03/08A/D-140 0830-299)
- JIMENEZ, Maria-Jose**  
(SS04b/10P/D-011 1400-195)
- JIMOH, Onemayin David**  
(HS02/11A/C24-007 1000)
- JIN, Hidekatsu**  
(GAI.V.03/09A/A16-003)
- JIN, Hidekatsu**  
(GAI.V.03/08A/A16-009 1220)
- JIN, Honglin**  
(JSG01/07A/A01-002 0915)
- JIN, Jiming**  
(JWH01/09P/C30-003 1440)
- JIN, Meibing**  
(JSP04/09A/A06-008 1150)  
(JSP04/09P/A06-011 1730)
- JIN, Rui**  
(JSH01/08P/D-003 1400-041)  
(JSH01/07P/C27-011 1740)
- JIN, Shuanggen**  
(JSG01/08P/D-027 1400-027)
- JIN, Sobom**  
(JSS07/09P/A02-001 1400)
- JIN, Xianglong**  
(JSS06/10A/A04-009 1130)
- JIN, Xiuying**  
(SW05/10P/A13-004 1450)
- JIN, Yi**  
(MC02/08P/B20-006 1610)
- JIN, Young-Hoon**  
(HS02b/10P/D-023 1630-144)  
(HS02/10A/C24-023 1213)
- JING, Shao-qun**  
(JSG01/08P/D-034 1400-034)
- JINNO, Kenji**  
(HS04/08A/C30-002 0935)  
(HS02b/10P/D-023 1630-144)
- (HS02/10A/C24-023 1213)  
(HS02c/11P/D-015 1630-113)  
(HS02/11A/C24-015 1141)
- JINYAO, Gao**  
(JSS06/10A/A04-009 1130)
- JOE, Paul**  
(JSM14/09P/D-019 1400-083)
- JOHANNESSEN, Johnny**  
(JSG02/09A/D-003 0830-003)
- JOHANNESSEN, Johnny A.**  
(JSG03/10A/A12-003 0910)
- JOHANNESSEN, Ola M.**  
(MC08/07A/B17-001 0930)
- JOHANSSEN, Chris**  
(JSG03/09P/A12-007 1620)
- JOHANSSON, Jan**  
(SS03/07P/A02-005 1500)
- JÖHNK, Klaus**  
(HW06/07A/C31-007 1150)
- JOHNSEN, S.J.**  
(MC12/08A/B19-002 1000)
- JOHNSON, Fasona**  
(HS02/08P/C24-007 1530)
- JOHNSON, Gregory C.**  
(JSP09/11A/B20-013 1215)
- JOHNSON, James E.**  
(MI03/08A/B18-001 0830)
- JOHNSON, Richard H.**  
(MC03/10P/A07-006 1640)
- JOKO, Sachiko**  
(GAI.11/08/10A/A16-003 0910)
- JONES, Alan G.**  
(JSS06/09P/A04-008 1640)  
(JSA07/10A/A05-002 0900)  
(GAI.08/08A/A14-003 0910)  
(JSA07/10A/A05-003 0920)
- JONES, Phil**  
(GAV.06/10P/A11-003 1440)
- JONES, Phil**  
(MC12/08P/B19-006 1620)
- JONES, Philip D.**  
(MC12/08A/B19-004 1055)
- JONES, Philip D.**  
(MC12/08A/B19-008 1200)
- JONES, Sarah E.**  
(JSP07/08P/B17-003 1450)
- JONSDOTTIR, Jona Finndis**  
(HS02b/10P/D-006 1630-127)  
(HS02/10A/C24-006 1105)
- JÓNSSON, Sigurjón**  
(JSG01/07P/A01-010 1635)
- JORDAN, Phil**  
(HS01/09P/D-020 1400-187)  
(HW01/10A/C26-006 1050)
- JORDAN, Phillip W.**  
(HS03/07P/C26-002 1415)
- JORDAN, R.**  
(JWH01/09P/C30-001)
- JORDAN, Rachel**  
(JWH01/09A/C30-009 1210)
- JOSBERGER, Edward**  
(JSM15/07A/B18-007 1100)
- JOSEPH, Joachim**  
(GAI.04/07A/A08-009)
- JOSEPH, Renu**  
(MC03/09P/A07-003 1520)  
(MC11/11A/B19-005 0950)  
(MC08/07A/B17-004 1030)
- JOSEY, Simon A.**  
(JSP09/10A/B20-008 1130)  
(JSP09/10P/B20-001 1400)
- JOSHI, Anand**  
(HW07/11P/D-039 1400-175)
- JOU, JONG-DAO Ben**  
(MC02/07P/B20-004 1500)  
(JSM14/07P/A05-006 1655)
- JOURDAN, Fred**  
(GAV.06/10P/A11-005 1520)
- JOUZEL, J.**  
(MC12/08A/B19-002 1000)
- JOUZEL, Jean**  
(MC12/08A/B19-001 0930)
- JUANG, Hann-Ming**

- (MC03/10P/A07-005 1600)  
**JUERGEN, Bremer**  
 (JSA01/08P/A12-003 1500)  
**JUN, Seong-Chun**  
 (HW01/10A/C26-008 1130)  
**JUN-ICHI, Hamada**  
 (MC03/11P/A07-003 1440)  
**JUNE, Tania**  
 (MI07/10P/D-006 1400-182)  
**JUNG, Gerlinde**  
 (HS02/08A/C24-011 1130)  
**JUNG, In-Kyun**  
 (HS03/08A/C26-006 1000)  
**JUPUDI, Rao Mallikharjuna**  
 (SW03/10P/A04-013 1715)  
**JURAC, Slobodan**  
 (GAILI.14/07P/A12-006 1600)  
**JURGENSON, Harli**  
 (G03/07P/D-055 1400-077)  
**JUSTINIANO, Harry**  
 (JSS07/10A/A02-014 1200)
- k**
- K., JAYAKUMAR V.**  
 (HS02b/10P/D-024 1630-145)  
 (HS02/10P/C24-001 1515)  
**K., Mundepi A.**  
 (JSP11/07P/A10-005 1620)  
**K., Naganjaneyulu**  
 (SW03/10P/A04-011 1645)  
 (SS03/08A/D-133 0830-292)  
 (GAI.08/08A/A14-010 1150)  
**K., Ramakrishna**  
 (HS01/09P/D-001 1400-168)  
**K.-I, Nishikawa**  
 (GAILI.06/07P/D-012)  
**K, Mohan Kumar**  
 (MC05/08P/A09-009 1720)  
**K, Mohankumar**  
 (MC03/11P/D-011 1400-186)  
 (JSM14/07A/A05-009 1215)  
**K. SZEGO, K.**  
 (GAIN.03/08P/A16-003 1500)  
**K.S., Viswanathan**  
 (GAILI.06/09A/A10-002 0920)  
**K.S, Viswanathan**  
 (GAILI.06/11P/D-001)  
**K.S.V., Subbarao**  
 (GAILI.06/09A/A10-002 0920)  
**K.S.V, Subbarao**  
 (GAILI.06/11P/D-001)  
**KÄÄRIÄINEN, Jussi**  
 (JSA07/11A/D-028 0830-028)  
**KABAN, Mikhail K.**  
 (JSA07/10A/A05-001 0830)  
**KADLUBIES, Radek**  
 (HW01/10A/C26-001)  
**KADOTA, Tsutomu**  
 (JWH01/10A/C30-005 0950)  
**KAEAEB, Andreas**  
 (JSM10/08P/B23-001 1400)  
**KAGAMI, Hiroyuki**  
 (HW04/09P/C31-004 1500)  
**KAGAN, Boris**  
 (JSP08/09A/B19-010 1220)  
 (JSP08/09A/B19-011 1240)  
**KAGAWA, Akiko**  
 (MC05/07P/A09-005 1610)  
 (MC05/07P/A09-008 1720)  
**KAGAWA, Takao**  
 (SS04a/09P/D-030 1400-279)  
 (SS04a/09P/D-031 1400-280)  
 (SS04a/09P/D-040 1400-289)  
**KAGEYAMA, Masa**  
 (MI05/10P/D-008 1400-174)  
**KAGIMOTO, Takashi**  
 (JSP09/10P/B20-009 1630)  
**KAGITANI, Masato**  
 (GAILI.14/07A/A12-008 1210)
- (GAILI.14/07A/A12-006 1140)  
**KAHAN, Daniel S.**  
 (JWH01/10A/C30-001 0830)  
**KAHAR, Joenil**  
 (JSP11/08A/A10-002 0930)  
**KAHLER, Scott W.**  
 (GAILI.07/09P/A14-003 1450)  
**KAHLOUCHE, S.**  
 (G03/07P/D-027 1400-049)  
**KAHLOUCHE, Salem**  
 (G03/07P/D-076 1400-098)  
**KAIDZU, Masaru**  
 (JSG01/08P/D-021 1400-021)  
 (JSG01/07P/A01-002 1415)  
**KAISER, Diethelm**  
 (SS04a/09P/D-023 1400-272)  
**KAISER, Michael L.**  
 (GAILI.05/07A/A06-006 1025)  
**KAISHIMA, Hajime**  
 (GAILI.11/09P/A15-011 1715)  
**KAISTRENKO, Victor M.**  
 (JSS07/09P/A02-007 1530)  
 (JSS07/10A/A02-003 0900)  
**KAKAD, A.P.**  
 (GAILI.05/07P/D-022 1400-120)  
**KAKINAMI, Yoshihiro**  
 (GAILI.07/11A/A12-006 1105)  
**KALICZ, Péter**  
 (HS02/07A/C24-011 0940)  
 (HS02a/07P/D-011 1545-157)  
**KALINGA, Oscar**  
 (HS03/08P/C26-002 1415)  
**KALININA, Anna V.**  
 (SS03/08A/D-048 0830-207)  
**KAMAE, Katsuhiko**  
 (SW04/09P/A13-015 1745)  
**KAMAL**  
 (JSP11/07P/A10-005 1620)  
**KAMALI, GholamAli**  
 (JSP11/08P/D-009 1400-078)  
**KAMATA, Yoshinori**  
 (MC03/11P/D-001 1400-176)  
**KAMBADARANGAPPA, Ramaraju Hanumanahalli**  
 (HS02/07P/C24-024 1428)  
 (HS02a/07P/D-024 1545-170)  
**KAMBHAMPATI, Subrahmanyam**  
 (HW01/09P/D-017 1400-208)  
 (HW01/09P/D-048 1400-239)  
**KAMEDA, Takawo**  
 (JSM10/09P/D-002)  
**KAMESHIMA, Chieko**  
 (JSG03/09P/D-019 1640-027)  
**KAMIAKITO, Yuko**  
 (MC03/11P/D-001 1400-176)  
**KAMIDE, Y.**  
 (GAILI.07/09A/A14-008 1210)  
**KAMIDE, Yohsuke**  
 (GAILI.06/07P/D-009 1400-129)  
 (GAILI.06/07P/D-004 1400-124)  
 (GAILI.05/07P/D-010 1400-108)  
**KAMIKAWA, Kei**  
 (GAILI.10/11A/D-021 0830-095)  
**KAMIMURA, Aya**  
 (SS03/08A/D-013 0830-172)  
 (SS04b/10P/D-048 1400-232)  
 (SW05/10P/A13-005 1505)  
 (SS03/08A/D-011 0830-170)  
**KAMKAR-ROUHANI, Abolghasem**  
 (GAV.07/07P/A13-008 1640)  
 (GAV.07/07P/A13-007 1620)  
**KAMOSHITA, Tomohiro**  
 (JSG03/09P/D-020 1640-028)  
**KAMRA, A.K.**  
 (JSA09/10A/A08-009 1145)  
**KANADA, Sachie**  
 (JSM14/09P/D-012 1400-076)  
**KANAE, Shinjiro**  
 (HS02/08A/C24-009 1100)  
 (HW07/10P/C25-006 1545)  
 (HS02/10A/C24-005 0930)
- (HW06/08A/C31-004 1140)  
**KANAMORI, Hiroo**  
 (JSS07/10P/A02-010 1630)  
**KANAMORI, Hiroo**  
 (GAILI.06/09P/A10-013 1740)  
**KANAO, Masaki**  
 (SW03/10A/D-001 0830-236)  
 (SW03/10P/A04-004 1445)  
 (SW03/10A/D-003 0830-238)  
 (SW03/10A/D-002 0830-237)  
 (SW03/10A/D-004 0830-239)  
 (SW03/10A/D-007 0830-242)  
**KANAOK, Miho**  
 (GAILI.07/11A/A12-004 0945)  
**KANAYA, Hiroshi**  
 (GAV.07/07P/A13-003 1440)  
**KANAZAWA, Toshihiko**  
 (SS03/08A/D-118 0830-277)  
 (SS03/08A/D-114 0830-273)  
 (SS03/08A/D-067 0830-226)  
 (SS03/08A/D-002 0830-161)  
 (JSS06/07P/A04-005 1540)  
**KANAZAWA, Toshihiro**  
 (JSS06/09P/A04-009 1700)  
**KANDA, Katsuhisa**  
 (SS04/08A/A03-012 1130)  
**KANDA, Kenzo**  
 (JSM15/07P/D-007 1400-007)  
**KANDALGAONKAR, Suvarna Sushil**  
 (MI03/08A/B18-005 1030)  
**KANDATHIL VALAPPIL, Jayakumar**  
 (HS02b/10P/D-025 1630-146)  
 (HS02/10P/C24-002 1519)  
**KANE, Alioune**  
 (HS02c/11P/D-029 1630-127)  
 (JSM03/08P/A13-007 1620)  
 (HS02/11P/C24-006 1535)  
**KANEDA, Kentaro**  
 (SS03/08A/D-103 0830-262)  
**KANEDA, Y.**  
 (JSG01/08P/D-008 1400-008)  
**KANEDA, Yoshiyuki**  
 (SS03/08A/D-107 0830-266)  
**KANEDA, Yoshiyuki**  
 (SS03/08A/D-102 0830-261)  
 (SS03/08A/D-109 0830-268)  
 (SS03/07A/A02-003 0930)  
 (SS03/08A/D-009 0830-168)  
 (SS03/08A/D-010 0830-169)  
 (JSG01/08P/D-012 1400-012)  
 (SS03/08A/D-103 0830-262)  
 (SS03/07A/A02-006 1045)  
**KANEKAL, Shri**  
 (GAILI.09/11A/A11-004 0950)  
**KANEKO, Arata**  
 (JSP07/08A/B17-005 1100)  
**KANEKO, Eiji**  
 (GAILI.04/07P/A08-009 1700)  
**KANEKO, M.**  
 (JSG03/09P/D-006 1640-014)  
**KANG, Dong-Hyo**  
 (SS03/07A/A02-003 0930)  
**KANG, In-Sik**  
 (MC11/10A/B19-003 0920)  
**KANG, J.H.**  
 (MC03/09A/A07-008 1150)  
**KANG, Shichang**  
 (JSM10/07A/B23-007 1200)  
**KANNO, Tatsuo**  
 (SS04b/10P/D-003 1400-187)  
 (SS04b/10P/D-004 1400-188)  
 (SS04/07A/A03-001 0915)  
 (SS04b/10P/D-020 1400-204)  
 (SS04/08A/A03-007 1000)  
**KANO, Naomi**  
 (SS03/08A/D-034 0830-193)  
 (SS03/08A/D-110 0830-269)  
**KANUNGOE, Pintu**  
 (HW05/10P/D-003 1400-158)  
**KANZAWA, Hiroshi**  
 (MC05/07A/A09-001 0900)
- (MI07/11A/B18-007 1110)  
 (MI03/08P/B18-006 1610)  
 (MC05/07P/A09-002 1430)  
**KAO, Chih-Yue Jim**  
 (MI09/09A/B22-006 1110)  
**KAO, Honn**  
 (JSG01/07P/A01-006)  
**KAPUR, Nipun**  
 (SS04/09A/A03-001 0900)  
**KAR, Sarat Chandra**  
 (MC03/11A/A07-010 1210)  
**KARABASHEV, Genrikh S.**  
 (JSG03/09P/A12-004 1500)  
**KARAGIANNI, Eleni E.**  
 (SS03/07A/A02-005 1030)  
**KARAKASEV, Deljo P.**  
 (SS03/08A/D-024 0830-183)  
**KARAMBIRI, Harouna**  
 (HS01/09P/D-014 1400-181)  
**KARANAM, Kishore Kumar**  
 (JSM14/07A/A05-007 1145)  
**KARASEV, Evgeniy Viktorovich**  
 (JSP06/07P/D-004 1400-011)  
**KARCHER, Michael**  
 (JSP04/10A/A06-001)  
**KARCHER, Michael**  
 (JSP04/10P/A06-004 1500)  
**KARELIN, A.V.**  
 (JSA08/09P/A08-009 1730)  
**KARIMABADI, Homa**  
 (GAILI.14/07P/A12-003 1445)  
**KARIMI, Rohallah**  
 (G03/07P/D-065 1400-087)  
**KARIMI, Roohallah**  
 (SS03/08A/D-142)  
**KÄRKÄS, Eija**  
 (JSH01/08P/D-010 1400-048)  
**KARMALEEVA, Rimma**  
 (SS03/08A/D-104 0830-263)  
**KAROL, Igor L.**  
 (JSM04/09P/D-014 1400-051)  
**KARROUK, Mohammed-Said**  
 (HS02/07A/C24-005 0916)  
 (HS02a/07P/D-005 1545-151)  
**KARTASASMITA, Mahdi**  
 (MI09/08P/D-002 1400-155)  
**KASABA, Y.**  
 (GAILI.06/07P/D-010)  
**KASABA, Yasumasa**  
 (GAILI.14/08A/D-004 0830-148)  
 (GAILI.11/10P/D-002 1400-117)  
 (GAILI.14/08A/D-005 0830-149)  
 (GAILI.05/07P/D-004 1400-102)  
**KASAHARA, Junzo**  
 (SS03/08A/D-105 0830-264)  
 (SS03/08A/D-011 0830-170)  
 (SS03/08A/D-002 0830-161)  
 (SS03/08A/D-001 0830-160)  
 (SS03/08A/D-013 0830-172)  
 (SS03/08A/D-120 0830-279)  
**KASAHARA, Keiji**  
 (SS03/08A/D-004 0830-163)  
 (SS03/08A/D-003 0830-162)  
 (SS03/08A/D-098 0830-257)  
**KASAHARA, Keiji**  
 (SS03/08A/D-108 0830-267)  
**KASAHARA, Minoru**  
 (SS03/08A/D-116 0830-275)  
 (JSG01/08P/D-017 1400-017)  
 (JSG01/08P/D-009 1400-009)  
 (G04/08P/D-001 1400-108)  
 (SW04/09P/A13-014 1730)  
**KASAHARA, Yoshiya**  
 (GAILI.10/10P/A01-010 1700)  
 (GAILI.06/07P/D-010 1400-130)  
**KASAI, Yasuko**  
 (GAILI.04/09A/D-006 0830-142)  
**KASATKINA, Elena A.**  
 (JSA09/10A/A08-010 1200)  
**KASCHEEV, Rafael A.**  
 (G03/07P/D-057 1400-079)  
**KASCHEV, Julia**

## INDEX

- (G04/08P/C25-001 1410)  
**Kasdi Subagyono**  
 (HW01/10P/C26-005 1520)  
**KASE, Yuko**  
 (SS04a/09P/D-018 1400-267)  
 (SS04a/09P/D-038 1400-287)  
**KASENDA, Adollientje**  
 (G03/07P/D-046 1400-068)  
**KASER, Georg**  
 (JSM10/08P/B23-005 1600)  
**KASSAHUN, Ayalew**  
 (HW03/11A/C30-002 0850)  
**KATADA, Toshitaka**  
 (JSS07b/10P/D-004 1700-050)  
**KATAO, Hiroshi**  
 (JSA07/11A/D-018 0830-018)  
**KATHAMANA, Vijay Kumar**  
 (JSG01/07A/A01-003 0930)  
**KATIYAR, Nitin**  
 (JSH01/08A/C27-005 1050)  
**KATO, Hajime**  
 (SS03/08A/D-110 0830-269)  
**KATO, Hisao**  
 (GAILI.06/11P/D-012 1400-064)  
 (GAILI.06/10A/A01-010 1125)  
**KATO, Kuranoshin**  
 (JSM14/08A/A05-002 0910)  
**KATO, Masato**  
 (SS04b/10P/D-002 1400-186)  
**KATO, Masaya**  
 (JSM14/09A/A05-007 1135)  
**KATO, Masaya**  
 (JSM14/09P/D-027 1400-091)  
**KATO, Teruyuki**  
 (JSM14/08A/A05-008 1115)  
 (JSM14/08A/A05-007 1040)  
 (MC03/11P/D-010 1400-185)  
 (JSM14/09P/D-024 1400-088)  
 (JSM14/09P/D-025 1400-089)  
 (JSM14/08A/A05-011 1200)  
 (JSM14/09P/D-013 1400-077)  
**KATO, Teruyuki**  
 (JSG01/07A/A01-002 0915)  
 (JSS07b/10P/D-007 1700-053)  
 (SS03/07P/A02-014 1745)  
 (JSS07b/10P/D-006 1700-052)  
 (SW05/10P/A13-007 1530)  
 (JSG01/08P/D-012 1400-012)  
**KATSUMATA, Kei**  
 (SS03/08A/D-056 0830-215)  
 (SS03/08A/D-005 0830-164)  
**KATSUMATA, Masaki**  
 (JSM14/07P/A05-003 1450)  
 (MC17/11P/B23-003 1440)  
**KATSUYAMA, Masanori**  
 (HW01/09P/D-027 1400-218)  
 (HW01/09P/D-037 1400-228)  
 (HW01/09P/D-042 1400-233)  
 (HW01/09P/D-039 1400-230)  
**KATSUYAMA, Masanori**  
 (HW01/09P/D-038 1400-229)  
**KAU, Wen-Shung**  
 (MC03/09A/A07-004 1030)  
**KAUKER, Frank**  
 (JSP04/10A/A06-001)  
**KAVETSKI, Dmitri**  
 (HW08/08P/C28-002 1430)  
 (HW08/08A/C28-004 0940)  
**KAVVAS, M. Levent**  
 (HS01/08A/C29-004 1110)  
 (HW08/08A/C28-007 1100)  
**KAVVAS, M.L.**  
 (HW07/10A/C25-003 1045)  
**KAWABE, Hidenori**  
 (SW04/09P/A13-015 1745)  
**KAWAHIRA, Kohji**  
 (MC05/07P/A09-003 1450)  
**KAWAI, Shinichi**  
 (SS04b/10P/D-015 1400-199)  
 (SS04b/10P/D-023 1400-207)  
**KAWAI, Takashige**  
 (JSM10/09P/D-007 1400-061)  
**KAWAKAMI, Hideji**  
 (SS04a/09P/D-024 1400-273)  
**KAWAKATA, Hironori**  
 (SS05/10A/A13-004 0915)  
**KAWAKATSU, Hitoshi**  
 (JSS06/07P/A04-004 1500)  
**KAWAKITA, Koji**  
 (GAILI.04/07P/A08-007 1630)  
**KAWAMATA, Kei**  
 (JSS07/09P/A02-004 1445)  
**KAWAMOTO, Nozomi**  
 (MC05/07P/A09-002 1430)  
**KAWAMURA, Akira**  
 (HS02b/10P/D-023 1630-144)  
 (HS02/10A/C24-023 1213)  
**KAWAMURA, Akira**  
 (HS02c/11P/D-015 1630-113)  
 (HS02/11A/C24-015 1141)  
**KAWAMURA, Hiroshi**  
 (JSG03/09P/D-007 1640-015)  
**KAWAMURA, Masashi**  
 (JSG01/08P/D-024 1400-024)  
**KAWAMURA, Seiji**  
 (G02/10P/D-010 1400-075)  
**KAWAMURA, Tomonori**  
 (SS03/08A/D-035 0830-194)  
**KAWANO, H.**  
 (GAILI.06/07P/D-010)  
**KAWANO, Hideaki**  
 (GAILI.10/11A/D-016 0830-090)  
 (GAILI.09/11A/A11-007 1140)  
 (GAILI.05/07P/D-015 1400-113)  
 (GAILI.10/11A/D-007 0830-081)  
 (GAILI.05/07P/D-012 1400-110)  
 (GAILI.10/11A/D-014 0830-088)  
 (GAILI.10/11A/D-020 0830-094)  
 (GAILI.05/07P/D-014 1400-112)  
 (GAILI.10/11A/D-002 0830-076)  
 (GAILI.10/11A/D-018 0830-092)  
**KAWANO, Nobuyuki**  
 (G02/10P/D-013 1400-078)  
**KAWANO, Nobuyuki**  
 (G02/07A/C25-011 1200)  
 (G02/07A/C25-014 1245)  
 (GAILI.06/11P/D-007 1400-059)  
**KAWANO, Nobuyuki**  
 (G02/07A/C25-013 1230)  
**KAWANO, Noriyuki**  
 (MC02/07P/D-004 1400-201)  
**KAWANO, Tetsuya**  
 (JSM14/09P/D-025 1400-089)  
**KAWASAKI, Masatoshi**  
 (HW01/09P/D-033 1400-224)  
 (HW01/09P/D-039 1400-230)  
 (HW01/09P/D-040 1400-231)  
**KAWASAKI, Masatoshi**  
 (HW01/09P/D-038 1400-229)  
**KAWASAKI, Nobuaki**  
 (MI05/09A/B17-008 1150)  
**KAWASE, Hiroshi**  
 (SS04a/09P/D-028 1400-277)  
 (SS04/07P/A03-008 1615)  
 (SS04a/09P/D-001 1400-250)  
**KAWASE, Sachiko**  
 (MC05/07P/A09-005 1610)  
 (MC05/07P/A09-008 1720)  
**KAWASHIMA, Masayuki**  
 (JSM14/09P/D-010 1400-074)  
**KAWASHIMA, Masayuki**  
 (JSP09/10P/B20-010 1645)  
**KAWATA, Yoshiaki**  
 (SS05/10A/A13-004 0915)  
**KAWATANI, Yoshio**  
 (MC05/11P/A09-001 1400)  
 (MC05/11P/A09-002 1430)  
 (MC05/11P/A09-008 1700)  
**KAYAL, J.R.**  
 (SS03/08A/D-132 0830-291)  
**KAYAL, J.R.**  
 (SS03/08A/D-069 0830-228)  
**KAYAL, Jnana R**  
 (SS04/08P/A03-006 1515)  
**KAYAL, Jnana Ranjan**  
 (SS03/08A/D-021 0830-180)  
**KAYAMA, Masazumi**  
 (HW01/10A/C26-007 1110)  
**KAZAMA, So**  
 (JSM04/09P/D-011 1400-048)  
 (JWH01/09P/C30-008 1650)  
 (HS02b/10P/D-004 1630-125)  
 (HS02/09A/C24-002 0915)  
 (HS02/07A/C24-002 0904)  
 (HW01/09P/D-024 1400-215)  
 (HS02/08P/C24-003 1430)  
 (HS02a/07P/D-002 1545-148)  
 (HS02/10A/C24-004 1057)  
 (HW05/10A/C31-011 1125)  
 (HW08/09A/C28-005 1030)  
**KAZAMA, Yoichi**  
 (GAILI.14/08A/D-002 0830-146)  
 (GAILI.05/07P/D-008 1400-106)  
**KAZEMI, Gholam Abbas**  
 (JSM04/09P/D-017 1400-054)  
**KAZUKA, Takuro**  
 (SS03/08A/D-008 0830-167)  
**KEARSLEY, A.H.W.**  
 (G03/07P/D-008 1400-030)  
**KEARSLEY, Bill**  
 (G03/07P/D-046 1400-068)  
**KEATING, Gerald M.**  
 (GAILI.07/11P/A12-001 1400)  
**KEENAN, T.D.**  
 (JSM14/09P/D-001 1400-065)  
**KEENAN, Thomas D.**  
 (MC03/11P/D-017 1400-192)  
**KEENAN, Tom D.**  
 (HS03/07P/C26-002 1415)  
**KEIL, Michael**  
 (MC05/10A/A09-002 0900)  
**KELDER, Hennie**  
 (MI03/08P/B18-005 1520)  
**KELLER, Franziska**  
 (JWH01/10P/D-003 1400-008)  
**KELLER, Kristi**  
 (GAILI.09/10P/D-003 1400-115)  
**KELLER, Wolfgang**  
 (G04/08P/C25-003 1450)  
**KELLOCK, S.**  
 (MI09/09A/B22-004 1000)  
**KELLY, Kathryn A.**  
 (JSP09/11A/B20-013 1215)  
 (JSP09/11A/B20-004 0930)  
**KELLY, Ken**  
 (MC05/11P/A09-004 1510)  
**KEMPLER, Steven J.**  
 (MI03/08A/B18-001 0830)  
**KENDALL, Carol**  
 (HW06/07P/D-009 1400-193)  
**KENDALL, Michael**  
 (JSS06b/10P/D-011 1400-035)  
**KENNAN, Padhraig S.**  
 (SS03/08A/D-145 0830-304)  
**KENNETT, Brian**  
 (JSS06/08A/A04-008 1110)  
**KENNETT, Brian L.N.**  
 (SS03/07A/A02-010 1145)  
 (JSS06/09P/A04-002 1420)  
**KENYERES, Ambrus**  
 (G03/07P/D-019 1400-041)  
 (G07/10P/D-016 1400-101)  
**KENYERES, Ambrus**  
 (G03/07P/D-048 1400-070)  
**KENYON, Steve**  
 (G03/07P/D-035 1400-057)  
**KEPKO, Larry**  
 (GAILI.09/11P/A11-002 1420)  
**KEPKO, Larry**  
 (GAILI.08/10A/A16-005 0945)  
 (GAILI.05/08A/A06-011 1150)  
**KERSWELL, Richard R.**  
 (JSP10/10P/B21-001 1400)  
**KETTLEBOROUGH, Jamie**  
 (MC08/08P/D-002 1400-158)  
**KGASWANE, Eldridge M.**  
 (SW03/10P/A04-002 1415)  
**KGASWANE, Eldridge M.**  
 (JSS06/07P/A04-006 1600)  
**KHABAROVA, Olga Valerievna**  
 (GAV.06/09P/D-013 1400-166)  
**KHABENSKY, Eugeny O.**  
 (GAI.10/09P/A11-005 1500)  
**KHABENSKY, Eugeny O.**  
 (GAI.10/09P/D-006 1615-125)  
**KHACHATURYAN, Maryam L.**  
 (JSP11/08P/D-002 1400-071)  
 (JSP11/07A/A10-009 1220)  
**KHALED, Abdellatif**  
 (HS02/11A/C24-002 0845)  
**KHALEQUZZAMAN, Mostafa Md.**  
 (JSP11/08A/A10-007 1140)  
**KHALEQUZZAMAN, Mostafa Md.**  
 (SS05/10A/A13-007 1000)  
 (SS05/10A/A13-008 1015)  
**KHALIPOV, Victor L.**  
 (GAILI.06/10A/A01-002 0850)  
**KHAM, Marc**  
 (SS04/07A/A03-004 1015)  
**KHAMRABAEV, I. Kh.**  
 (JSS06/10A/A04-003 0910)  
**KHAN, M. A.**  
 (HS02c/11P/D-030 1630-128)  
 (HS02/11P/C24-007 1539)  
**KHAN, Zareen**  
 (HW01/09P/D-011 1400-202)  
 (HW01/09P/D-051 1400-242)  
**KHANAL, Kedar Nath**  
 (SS04/08A/A03-015 1215)  
**KHANDAPAL, Pramod Kumar**  
 (MC05/08P/A09-010 1740)  
**KHAPTANOV, Valery Bazhevich**  
 (JSA07/11A/D-013 0830-013)  
**KHARIN, Eugeny Petrovich**  
 (HS05/10P/A13-014 1730)  
**KHARLAMOV, Andrey A.**  
 (JSS07/10A/A02-003 0900)  
**KHAYDAROVA, V.A.**  
 (HS02/07A/C24-015 0956)  
 (HS02a/07P/D-015 1545-161)  
**KHAYDAROVA, Valentina A.**  
 (HW03/11A/C30-008 1110)  
**KHAZANEDARI, Leili**  
 (MI05/11P/B17-006 1610)  
**KHERANI, Esfhan Alam**  
 (GAILI.06/09A/A10-003 0935)  
**KHERASKOVA, Tatyana N.**  
 (JSA07/11A/D-021 0830-021)  
**KHODAYARI, Nahid**  
 (JSM11/10P/D-002 1700-011)  
**KHOKHLOV, Valery**  
 (JSM11/10P/D-010 1700-019)  
**KHON, Vyacheslav Ch.**  
 (MC08/07A/B17-009 1205)  
**KHRISTOFOROV, Andrei V.**  
 (HS02c/11P/D-010 1630-108)  
 (HW04/09A/C31-006 1100)  
 (HS02/11A/C24-010 1121)  
**KHROMOVA, Tatiana Y.**  
 (JSH01/07A/C27-002 1000)  
**KHURANA, Krishan**  
 (GAILI.05/08A/A06-004 0925)  
**KHURANA, Krishan**  
 (GAILI.14/07P/A12-005 1515)  
**KI M, Vitalii P.**  
 (GAILI.04/09A/D-007 0830-143)  
**KIANI, Ali**  
 (JSP11/07A/A10-006 1110)  
**KIBAYASHI, Hajime**  
 (HS01/09P/C29-003 1440)  
**KICHIGINA, N.V.**  
 (HS02c/11P/D-006 1630-104)  
 (HS02/11A/C24-006 1105)  
**KIDA, Hideji**  
 (JSM04/09P/D-005 1400-042)  
 (MI05/09P/B17-006 1630)  
 (MI07/11A/B18-002 0850)  
**KIDO, Daisaku**

- (HS01/09P/D-003 1400-170)  
**KIDO, Yukari**  
 (SS03/08A/D-107 0830-266)  
 (GAV.07/07P/D-001 1400-142)
- KIDO, Yukari N.**  
 (GAV.07/07P/D-002 1400-143)
- KIEM, Anthony S.**  
 (HS02/09A/C24-006 1045)  
 (HS02/11P/C24-001 1400)
- KIGUCHI, Masashi**  
 (MC03/11P/D-008 1400-183)
- KIHN, Eric**  
 (GAILL.05/08P/A15-004 1520)
- KIJKO, Andrzej**  
 (SS04/08P/A03-007 1530)  
 (SS04/08P/A03-005 1500)
- KIKUCHI, Fuyuhiko**  
 (G02/07A/C25-013 1230)
- KIKUCHI, Kazuyoshi**  
 (MC17/10P/B23-003 1445)  
 (MC17/10P/B23-001 1400)
- KIKUCHI, Rikiro**  
 (SS04/08A/A03-013 1145)
- KIKUCHI, Shinsuke**  
 (SS03/08A/D-008 0830-167)
- KIKUCHI, Takashi**  
 (GAILL.10/11A/A01-006 0945)  
 (GAILL.06/07P/D-001 1400-121)
- KIKUCHI, Takashi**  
 (JSP04/09P/A06-003 1430)  
 (JSP04b/10P/D-003 1400-022)  
 (JSP04/09A/A06-006 1110)
- KILICOGLU, Ali**  
 (G03/07P/D-002 1400-024)  
 (G03/07P/D-026 1400-048)
- KILLWORTH, Peter Douglas**  
 (JSP10/09A/B21-001 0900)
- KIM, Byeong-Chan**  
 (HW01/09P/D-009 1400-200)  
 (HW05/10A/C31-002 0850)
- KIM, Duk-jin**  
 (JSG03/09P/D-018 1640-026)
- KIM, Edward**  
 (JSH01/08A/C27-001 0910)  
 (MI09/09P/B22-003 1440)
- KIM, Hyung Rae**  
 (JSA07/11A/D-041 0830-041)  
 (GAV.06/09P/D-009 1400-162)
- KIM, Hyung-Jin**  
 (MC11/11P/B19-004 1500)
- KIM, Jeong Woo**  
 (JSA07/11A/D-041 0830-041)
- KIM, Jeong Woo**  
 (GAV.06/09P/D-009 1400-162)
- KIM, Jeong-Hui**  
 (JSM14/07A/A05-008 1200)
- KIM, Jeong-Woo**  
 (MC11/11A/B19-006 1010)  
 (MC11/11A/B19-007 1050)  
 (MC11/11P/B19-004 1500)
- KIM, Kihong**  
 (GAILL.10/11A/A01-007 1000)
- KIM, Kyu-Myong**  
 (MC03/10A/A07-001 0830)
- KIM, Min-Sik**  
 (HW01/09P/D-032 1400-223)
- KIM, Ok-Yeon**  
 (JSM14/09P/D-006 1400-070)
- KIM, Seong-Joon**  
 (HS03/08A/C26-006 1000)
- KIM, So Gu**  
 (JSA07/11A/D-004)
- KIM, So-Young**  
 (MC05/07P/D-014 1400-221)
- KIM, Su-Jin**  
 (HW01/09P/D-033 1400-224)
- KIM, Tae-Hun**  
 (JSM14/07A/A05-008 1200)
- KIM, Tae-Kuk**  
 (JSM14/09P/D-006 1400-070)
- KIM, Won-Young**  
 (SS03/08A/D-093 0830-252)
- KIM, Yong Hoon**  
 (JSP08/09A/B19-005 1030)
- KIM, Yongwon**  
 (JSP04a/09P/D-002 1400-095)
- KIM, Young-Oh**  
 (HS02/08P/C24-010 1645)
- KIM THOA, Nguyen Thi**  
 (GAV.05/08P/A11-007 1620)
- KIMARO, Tumaini Anderson**  
 (HS03/08A/C26-011 1130)
- KIMATA, Fumiaki**  
 (G02/10P/D-012 1400-077)
- KIMOTO, Akitsu**  
 (HS01/09P/C29-006 1540)
- KIMOTO, Masahide**  
 (MC03/11P/D-015 1400-190)
- KIMURA, Fujio**  
 (MC11/11P/D-005 1400-198)
- KIMURA, Hisanori**  
 (SS03/08A/D-003 0830-162)
- KIMURA, Iwane**  
 (GAILL.11/10P/D-001 1400-116)
- KIMURA, Keiji**  
 (MI05/10P/D-010 1400-176)  
 (MC08/08P/D-003 1400-159)
- KIMURA, Yoshi**  
 (JSP10/11A/B21-005 1000)
- KIND, R.**  
 (JSS06a/08P/D-023 1400-101)
- KIND, Rainer**  
 (JSA07/10P/A05-004 1500)
- KING, H.B.**  
 (HW01/09P/D-046 1400-237)
- KING, John C.**  
 (JWH01/09A/C30-005 1020)
- KING, Robert A.**  
 (GAILL.06/08A/A02-001 0900)
- KINNISON, D.**  
 (MC05/08A/A09-003 0930)
- KINNISON, Douglas**  
 (JSA01/08A/A12-005 1115)  
 (MC05/08P/A09-003 1450)
- KINNISON, Douglas E.**  
 (MC05/09A/A09-001 0900)  
 (MC05/07A/A09-003 1000)
- KINNISON, Douglas Edward**  
 (MC05/08A/A09-004 1000)
- KINOSITA, Takeo**  
 (HS03/07P/C26-003 1430)  
 (HW03/11P/C30-001 1400)
- KINOUCI, Tsuyoshi**  
 (HS03/07A/C26-006 1045)
- KIRATZI, Anastasia**  
 (JSP11/08P/D-006 1400-075)
- KIRBY, James T.**  
 (JSS07b/10P/D-019 1700-065)
- KIRBY, Jonathan**  
 (JSS06b/10P/D-002 1400-026)  
 (JSS06b/10P/D-003 1400-027)
- KIRBY, Stephen Homer**  
 (SS03/07P/A02-007 1600)
- KIREEV, Sergey I.**  
 (HW01/09P/D-014 1400-205)
- KIRKWOOD, Sheila Catherine**  
 (JSA01/08A/A12-006 1145)  
 (GAILL.10/11A/D-023 0830-097)
- KIS, Marta**  
 (G03/07P/D-020 1400-042)
- KIS, Marta**  
 (GAI.10/09P/D-011 1615-130)
- KISELEVA, Elena A.**  
 (JSA07/11A/D-021 0830-021)
- KISHII, Tokuo**  
 (HW03/11A/C30-004 0930)
- KISHII, Tokuo**  
 (HW07/11P/D-021 1400-157)
- KISHII, Tokuo**  
 (HW01/09P/D-010 1400-201)
- KISHII, Tokuo**  
 (HW07/10P/C25-004 1500)  
 (HW07/11P/D-037 1400-173)
- KISLOV, Alexander Victorovich**  
 (MC12/07P/B19-004 1515)
- KISTLER, L.**  
 (GAILL.09/11A/A11-006 1110)  
 (GAILL.05/08A/A06-007 1040)
- KISTLER, Lynn**  
 (GAILL.05/08A/A06-003 0900)
- KISTLER, Lynn M.**  
 (GAILL.08/10A/A16-007 1040)
- KISTOVICH, Anatolii V.**  
 (JSP10/10A/B21-004 0950)
- KITABATA, Hideyuki**  
 (MC02/07A/B20-004 1105)
- KITABATAKE, Naoko**  
 (MC02/07P/D-006 1400-203)
- KITADA, Naoko**  
 (SW04/09P/A13-012 1700)
- KITADA, Naoto**  
 (GAV.06/09P/D-014 1400-167)
- KITAEV, Lev M.**  
 (HS02b/10P/D-021 1630-142)  
 (HS02/10A/C24-021 1205)
- KITAGAWA, Genshiro**  
 (SW05/10A/D-009 0900-253)
- KITAMURA, Kentarou**  
 (GAILL.05/07P/D-015 1400-113)  
 (GAILL.10/11A/D-021 0830-095)
- KITAMURA, Kenzo**  
 (MI07/10P/D-005 1400-181)
- KITAMURA, Yuji**  
 (JSP10/11A/B21-003 0920)
- KITAUCHI, Hideaki**  
 (JSP04/09P/A06-005 1500)
- KITAZAKI, Yasufumi**  
 (JSM14/08A/A05-009 1130)
- KITAZAWA, Mitsuko**  
 (GAV.06/10P/A11-006 1600)
- KITAZAWA, Mitsuko**  
 (GAV.07/07P/A13-002 1420)
- KITE, Geoff**  
 (JSH01/07P/C27-006 1600)
- KITOH, Akio**  
 (MC03/09P/A07-008 1720)  
 (MC17/11A/B23-003 0920)  
 (MI05/09A/B17-007 1130)  
 (MC08/07P/B17-005 1520)
- KIVELSON, Margaret G.**  
 (GAILL.14/07P/A12-001 1400)  
 (GAILL.05/08A/A06-004 0925)
- KIZU, Shoichi**  
 (JSP06/07P/D-002 1400-009)
- KLAASSEN, Joan**  
 (JSM14/09P/D-022 1400-086)  
 (JSM14/09P/D-021 1400-085)
- KLECKER, Berndt**  
 (GAILL.05/08A/A06-003 0900)  
 (GAILL.05/07P/D-007 1400-105)
- KLEIMENOVA, Natalia Georgievna**  
 (GAILL.10/11A/D-012 0830-086)
- KLEKOCIUK, Andrew R.**  
 (MC05/10A/A09-008 1130)
- KLEPP, Christian**  
 (JSP09/11A/B20-002 0900)
- KLIEGROVA, Stanislava**  
 (MC08/07P/B17-011 1710)
- KLIMAS, Alex J.**  
 (GAILL.07/09A/A14-003 0950)
- KLIORE, Arvydas J.**  
 (GAILL.07/11P/A12-006 1640)
- KLOTZ, Juergen**  
 (JSG01/07P/A01-004 1445)
- KLYUCHNIKOVA, Anna V.**  
 (MC05/09P/A09-010 1740)
- KNAFF, John A.**  
 (MC02/07P/B20-007 1620)
- KNAPPE, Andrea**  
 (HW06/07P/C31-004 1500)
- KNAPPE, Andrea**  
 (HW01/09P/D-023 1400-214)
- KNIELING, Peter**  
 (JSA09/10A/A08-002 0900)
- KNOCK, Stuart A.**  
 (GAV.02/07P/A07-004 1600)
- KNÖLLER, Kay**  
 (HW06/07A/C31-007 1150)
- KNOWLES, Ken**  
 (JSH01/08A/C27-002 0930)
- KNUDSEN, Per**  
 (G04/08P/D-009 1400-116)  
 (JSG03/09P/D-010 1640-018)
- KNUDSEN, Per**  
 (JSG02/09A/D-003 0830-003)
- KNUDSEN, Per**  
 (G03/07P/D-035 1400-057)  
 (JSM11/10P/D-004 1700-013)  
 (G03/07P/D-036 1400-058)
- KNUDSEN, Thomas**  
 (JSG03/09P/D-010 1640-018)
- KOBA, Keisuke**  
 (HW01/09P/D-039 1400-230)
- KOBASHI, Takuro**  
 (MC12/08A/B19-003 1020)
- KOBAYASHI, Akio**  
 (JSG01/08P/D-019 1400-019)
- KOBAYASHI, Eiji**  
 (JSS07/09P/A02-004 1445)
- KOBAYASHI, Hirokazu**  
 (MI07/11A/B18-007 1110)
- KOBAYASHI, Kazuhiko**  
 (MI07/11P/B18-009 1700)  
 (MI07/11P/B18-008 1640)
- KOBAYASHI, Kazuo**  
 (SS03/07P/A02-001 1400)
- KOBAYASHI, Nobutaka**  
 (MC05/07P/D-012 1400-219)
- KOBAYASHI, Reiji**  
 (SS03/10A/D-006 0830-241)
- KOBAYASHI, Shigeki**  
 (JSG03/09P/D-023 1640-031)
- KOBAYASHI, Shinya**  
 (MC08/07A/B17-006 1120)
- KOBAYASHI, Taiyo**  
 (JSP06/07P/B21-003 1450)
- KOBAYASHI, Toshiichi**  
 (JSM14/09P/D-023 1400-087)
- KOBLINSKY, Chester**  
 (JSP06/07A/B21-007 1140)
- KOBLINSKY, Chester J.**  
 (JSP09/11P/B20-005 1515)
- KOBLINSKY, Chester J.**  
 (JSP09/10A/B20-011 1215)
- KOCH, Karl-Rudolf**  
 (G04/07P/C25-008 1720)
- KOCHETOV, Andrey Valentinovich**  
 (GAILL.06/11P/D-005 1400-057)
- KOCUI, Siasi**  
 (JSP11/08P/D-006 1400-075)
- KODAIRA, Shuichi**  
 (SS03/08A/D-102 0830-261)  
 (SS03/08A/D-109 0830-268)  
 (SS03/07A/A02-003 0930)  
 (SS03/08A/D-009 0830-168)  
 (SS03/08A/D-010 0830-169)  
 (SS03/08A/D-114 0830-273)  
 (JSS06/09P/A04-009 1700)  
 (SS03/08A/D-103 0830-262)
- KODAIRA, Shunichi**  
 (JSS06/07P/A04-005 1540)
- KODAMA, Yasu-Masa**  
 (MC02/07P/B20-003 1440)  
 (MC03/10A/A07-007 1110)
- KODAMA, Yuji**  
 (JSM10/09P/D-001 1400-055)  
 (JWH01/10P/C30-001 1400)
- KODAMA, Yuji**  
 (JWH01/09A/C30-003 0940)
- KODERA, Kunihiko**  
 (MC05/10P/A09-003 1500)  
 (MI05/10A/B17-004 0950)  
 (MC05/11A/A09-001 0830)  
 (JSA08/09P/A08-002 1420)  
 (MC11/11A/B19-002 0850)
- KOEBERLE, Cornelia**  
 (JSP04/10A/A06-001 0900)  
 (JSP04/10P/A06-004 1500)
- KOEHLER, Eddie**

## INDEX

- (HW07/10P/C25-012 1715)  
**KOENIG, Geoff G.**  
 (JWH01/10P/C30-003 1440)  
**KOENIG, Rolf**  
 (G02/07A/C25-001 0900)  
 (G02/07A/C25-002 0920)  
**KOENIGER, Paul**  
 (HW06/07A/C31-006 1130)  
**KOFFI, Ernest N'Dri**  
 (JSM14/08P/A05-006 1715)  
**KOGA, Daiki**  
 (GAI11.07/10P/D-005 1400-110)  
 (GAI11.07/09P/A14-008 1700)  
**KOGA, Kiyokazu**  
 (GAI11.06/07P/D-015 1400-135)  
 (GAI11.11/09A/A15-005 1010)  
 (GAI11.06/08P/A02-009 1655)  
**KOHLER, Monica**  
 (SS03/08A/D-030 0830-189)  
**KOHNO, Mineko**  
 (HW01/10A/C26-007 1110)  
**KOHNO, Nadao**  
 (JSP08/09P/B19-007 1640)  
**KOICHIRO, Kuraji**  
 (HW07/11P/D-038 1400-174)  
**KOIDE, Hiroshi**  
 (JSM10/08A/B23-003 0930)  
**KOIKE, Katsuaki**  
 (JSG03/09P/D-001 1640-009)  
**KOIKE, Toshio**  
 (HS02/08A/C24-002 0845)  
 (HS03/08A/C26-005 0945)  
 (MC03/09P/A07-005 1620)  
 (HW08/07A/C28-009 1210)  
**KOISTINEN, Tapio**  
 (JSA07/10A/A05-006 1050)  
 (JSA07/11A/D-028 0830-028)  
**KOIZUMI, Naoji**  
 (JSG01/08A/A01-004 0945)  
**KOJIMA, Hirotsugu**  
 (GAI11.11/09P/A15-011 1715)  
 (GAI11.05/07A/A06-006 1025)  
**KOJIMA, Hirotsugu**  
 (GAI11.05/07P/D-004 1400-102)  
**KOJIMA, Masayoshi**  
 (GAI11.09/11P/A11-007 1640)  
**KOJIMA, Toshiharu**  
 (HS03/08A/C26-010 1115)  
**KOJIRI, Toshiharu**  
 (HW04/09A/C31-003)  
**KOJIRI, Toshiharu**  
 (HW04/09A/C31-002 0920)  
**KOKETSU, Kazuki**  
 (SS03/08A/D-004 0830-163)  
 (SS04/07P/A03-013 1730)  
 (SS04/07A/A03-002 0945)  
 (SS04/07P/A03-013 1730)  
**KOKUBO, Kazuya**  
 (G03/07P/D-011 1400-033)  
**KOLESNICHENKO, Ilya**  
 (JSM14/07P/A05-004 1505)  
**KOLESOV, Sergey V.**  
 (JSS07/09P/A02-010 1630)  
**KOLEV, Staytcho**  
 (JSA09/10A/A08-008 1130)  
**KOLLURU, Krishna Sri**  
 (JSA07/11A/D-033 0830-033)  
**KOLOMIITSEV, O.P.**  
 (JSA08/09P/A08-009 1730)  
**KOMAKI, Kazuo**  
 (JSG01/07A/A01-001 0900)  
**KOMATSU, Katsuhiko**  
 (HW07/11P/D-014 1400-150)  
**KOMATSU, Masayoshi**  
 (JSS07a/09P/D-005 1700-106)  
**KOMATSU, Yoshimitsu**  
 (HS03/07P/C26-010 1630)  
**KOMATSU, Yosuke**  
 (HW07/11P/D-021 1400-157)  
**KOMAZAWA, Masao**  
 (SS04a/09P/D-033 1400-282)  
 (SS04/07A/A03-002 0945)  
 (GAV.06/09P/D-001 1400-154)  
 (JSA07/11A/D-016 0830-016)  
 (SS03/08A/D-034 0830-193)  
**KOMINE, Kenji**  
 (JSP04/09A/A06-007 1130)  
**KOMONMAE, Hisao**  
 (GAI11.04/09A/D-002 0830-138)  
**KOMORI, Nobumasa**  
 (JSP04/09A/A06-007 1130)  
**KOMURO, Yoshiki**  
 (JSM10/07P/B23-007 1640)  
**KONAGAYA, Yuki**  
 (HW01/09P/D-041 1400-232)  
**KONDO, Tetsuro**  
 (GAI11.14/08A/D-006 0830-150)  
 (GAI11.14/07P/A12-009 1705)  
 (G02/10P/D-014 1400-079)  
 (G02/10P/D-008 1400-073)  
**KONDO, Yutaka**  
 (MI03/08A/B18-007 1110)  
**KONDOH, Akihiko**  
 (HS02b/10P/D-008 1630-129)  
 (HS02/10A/C24-008 1113)  
**KONDRATYEV, Sergey A.**  
 (HS02c/11P/D-014 1630-112)  
 (HS02/11A/C24-014 1137)  
**KONG, Laura S. L.**  
 (JSS07/10A/A02-013 1145)  
**KONILOV, Alexander N.**  
 (JSA07/10A/A05-005 1000)  
**KONISHI, Tatsuo**  
 (JSP08/09P/B19-007 1640)  
**KONNEN, Gunther**  
 (MC12/08A/B19-008 1200)  
**KONO, Yusuke**  
 (G02/10P/D-013 1400-078)  
 (GAI11.06/11P/D-007 1400-059)  
 (G02/07A/C25-013 1230)  
 (G02/07A/C25-014 1245)  
**KONO, Yusuke**  
 (G02/07A/C25-011 1200)  
**KONOHIRA, Eiichi**  
 (HW01/10A/C26-010 1210)  
**KONONOV, Yury M.**  
 (MC12/08P/B19-007 1700)  
**KONOPKA, Paul**  
 (MC05/07A/A09-002 0930)  
**KONOVALOV, Vladimir G.**  
 (HW03/11A/C30-010 1150)  
**KONOVALOV, Yuri V.**  
 (JSP04b/10P/D-001 1400-020)  
**KONTAR, Alexei Evgenievich**  
 (JSP07/08A/B17-007 1140)  
 (JSP11/08A/A10-006 1110)  
**KONTUR, Istvan**  
 (HS02/09A/C24-007 1100)  
 (HS01/09P/D-019 1400-186)  
**KONYA, Keiko**  
 (JSM10/09P/D-009 1400-063)  
**KOOI, Henk**  
 (JSM03/08A/A13-002 0920)  
**KOONIN, Steve E.**  
 (JSA09/10A/A08-003 0930)  
**KOOP, Radboud**  
 (G03/07P/D-024 1400-046)  
**KOPERA, Juergen R.**  
 (SS04b/10P/D-021 1400-205)  
**KOPISCHKE, Ronny**  
 (G07/10P/D-019 1400-104)  
**KOPPIREDDI, Veeraswamy**  
 (SW03/10P/A04-007 1530)  
**KOREN, Hans**  
 (JSH01/08A/C27-003 0950)  
**KOREN, Ilan**  
 (GAI11.04/07A/A08-009)  
**KOREN, V.**  
 (JWH01/09P/C30-001)  
**KOREN, Victor**  
 (HS03/07A/C26-004 1000)  
 (HS03/07A/C26-008 1115)  
**KOREN, Victor**  
 (HW08/08A/C28-005 1000)  
**KOREN, Victor I.**  
 (HS03/07A/C26-003 0945)  
**KOREN, Victor I.**  
 (HW08/09A/C28-006 1050)  
**KORENDYKE, Clarence M.**  
 (JSA08/09P/A08-003 1450)  
**KORHONEN, Juha Ville**  
 (JSA07/11A/D-028 0830-028)  
 (JSA07/10A/A05-006 1050)  
**KORHONEN, Juha Ville**  
 (JSA07/11A/D-029 0830-029)  
**KORN, Michael**  
 (SS03/08A/D-028 0830-187)  
**KOROLEV, Alexei**  
 (MI08/07P/B18-007 1715)  
 (JSM15/07A/B18-008 1115)  
**KORSAKOVA, Nadezhda K.**  
 (HS02a/07P/D-035 1545-181)  
 (HS02-/07P/C24-035 1512)  
**KORTE, Monika**  
 (GAV.05/08A/A11-007 1110)  
**KORYTNYI, Leonid M.**  
 (HS02c/11P/D-006 1630-104)  
 (HS02/11A/C24-006 1105)  
**KOSAKA, Yosuke**  
 (MI05/10P/D-007 1400-173)  
**KOSHEL, Konstantin V.**  
 (JSP10/08P/D-005 1610-057)  
**KOSHIISHI, Hideki**  
 (GAI11.06/07P/D-019 1400-139)  
**KOSHIISHI, Hideki**  
 (GAI11.06/07P/D-015 1400-135)  
 (GAI11.06/08P/A02-009 1655)  
 (GAI11.11/09A/A15-005 1010)  
**KOSHIMURA, Shun'ichi**  
 (JSS07b/10P/D-006 1700-052)  
 (JSS07b/10P/D-007 1700-053)  
**KOSHIMURA, Shunichi**  
 (JSS07b/10P/D-004 1700-050)  
**KOSHIYA, Shin**  
 (SS03/08A/D-035 0830-194)  
**KOSITSAKULCHAI, Ekasit**  
 (HW04/09A/C31-004 1000)  
**KOSITSAKULCHAI, Ekasit**  
 (HW04/09A/C31-007 1120)  
**KOSLOW, Melinda R.**  
 (MI05/10P/D-009 1400-175)  
**KOSSOBOKOV, V.G.**  
 (SS04/09A/A03-001 0900)  
**KOSSOBOKOV, Vladimir G.**  
 (JSP11/07P/A10-008 1720)  
**KOSTADINOV, Ivan**  
 (MI03/09A/D-003 0900-246)  
**KOSTADINOV, Stanimir C.**  
 (HS01/09A/C29-004 1000)  
**KOSTELECKY, Jakub**  
 (G07/10P/D-020 1400-105)  
**KOSTIANEV, Simeon G.**  
 (JSP11/08P/D-008 1400-077)  
 (G03/07P/D-037 1400-059)  
**KOSTKA, Zdeno**  
 (JWH01/09A/C30-006 1110)  
**KOSTOGLODOV, Vladimir**  
 (JSG01/08P/D-023 1400-023)  
**KOSTYUCHENKO, Sergey Leonidovich**  
 (JSA07/10A/A05-009 1150)  
**KOSUGI, Ken'ichirou**  
 (HW01/09P/D-027 1400-218)  
**KOSUGITA, Yoshiyuki**  
 (MC04/11P/B22-009 1700)  
**KOSYKH, Nicolay Eduardovich**  
 (MI09/09A/B22-001 0900)  
**KOTANI, Akira**  
 (SS04a/09P/D-045 1400-294)  
**KOTHYARI, Umesh Chandra**  
 (HW07/11P/D-002 1400-138)  
**KOTOVA, G.**  
 (GAI11.03/08P/A16-003 1500)  
**KOTOVA, Galina A.**  
 (GAI11.06/07P/D-018 1400-138)  
**KOTSAKIS, Christopher**  
 (G04/08P/D-004 1400-111)  
 (G04/07P/C25-006 1640)  
 (G03/07P/D-030 1400-052)  
**KOTTAPALLI, Sitharama Murty**  
 (SW04/09P/A13-001 1400)  
 (HS02/10P/C24-002 1415)  
 (HW01/09A/C26-002 0930)  
**KOTZE, Pieter Benjamin**  
 (GAV.05/08P/A11-008 1640)  
**KOURAEV, Alexey**  
 (JSG03/09P/D-003 1640-011)  
**KOUSSOURIS, Theodoros**  
 (HS02/08P/C24-009 1630)  
**KOUWEN, Nicholas**  
 (HS03/08P/C26-007 1545)  
 (HS03/07P/C26-006 1515)  
**KOUWEN, Nick**  
 (HW07/11P/D-018 1400-154)  
**KOVACIKOVA, Svetlana**  
 (GAI.08/08P/D-002 1400-137)  
**KOVACIKOVA, Svetlana**  
 (GAI.08/08P/D-004 1400-139)  
**KOVÁCS, Ferenc**  
 (HS02c/11P/D-004 1630-102)  
**KOVÁCS, Ferenc**  
 (HS02/11A/C24-004 1057)  
**KOVALENKO, Vladimir A.**  
 (JSA08/09P/A08-008 1710)  
**KOVALEV, Peter D.**  
 (JSS07b/10P/D-015 1700-061)  
**KOWAL, Daniel**  
 (JSS07/09A/A02-008 1100)  
**KOWALCZYK, E.**  
 (JWH01/09A/C30-001)  
**KOWALCZYK, E.**  
 (JWH01/09A/C30-009 1210)  
**KOYAMA, Masato**  
 (SS05/10A/A13-011 1115)  
**KOYAMA, Shin**  
 (SS04a/09P/D-010 1400-259)  
**KOYAMA, Takao**  
 (GAI.08/08P/D-001 1400-136)  
 (JSS06a/08P/D-008 1400-086)  
 (GAI.10/09P/D-005 1615-124)  
**KOYAMA, Yasuhiro**  
 (G02/10P/D-014 1400-079)  
 (G02/10P/D-008 1400-073)  
**KOZAKAI, Masaya**  
 (GAI11.11/09P/A15-002 1425)  
**KOZAWA, Takeshi**  
 (SS03/08A/D-008 0830-167)  
**KOZLOV, Vadim Fedorovich**  
 (JSP10/08P/D-005 1610-057)  
**KOZMIN, Boris M.**  
 (SS03/08A/D-019 0830-178)  
**KOZYRA, J.U.**  
 (GAI11.06/08A/A02-008 1200)  
**KOZYRA, Janet U.**  
 (GAI11.08/10A/A16-009 1115)  
 (GAI11.06/08A/A02-006 1110)  
 (GAI11.08/10A/A16-010 1135)  
 (GAI11.09/11A/A11-004 0950)  
**KOZYREVA, Olga Vasilievna**  
 (GAI11.10/11A/D-012 0830-086)  
**KR03-01 Shipboard Scientific Party**  
 (JSS06b/10P/D-010)  
**KRAJEWSKI, Witold F.**  
 (HW07/10A/C25-006 1130)  
**KRASNOGORSKA, Natalya**  
 (HW03/11A/D-001 0830-135)  
**KRASNOSELSKIKH, Vladimir**  
 (GAI11.04/09P/A16-006 1725)  
**KRASNOVA, Maria A.**  
 (JSA07/11A/D-027 0830-027)  
**KRAUSE, Jan C.**  
 (HW08/07A/C28-005 1030)  
**KRAVCHENKO, Nadejda M.**  
 (SW05/10P/A13-011 1645)  
**KREMENETSKY, Konstantin V.**  
 (MC12/08P/B19-007 1700)  
**KRIPALANI, R.H.**  
 (MC03/09A/A07-008 1150)

- KRISHFIELD, Richard**  
(JSP06/07P/B21-007 1640)
- KRISHNAN, Praveena**  
(MC17/11P/B23-007 1620)
- KRISTEK, Jozef**  
(SS04/07A/A03-011 1215)
- KRIVOLUTSKY, Alexei A.**  
(MC05/09P/A09-010 1740)
- KRIVOLUTSKY, Alexei A.**  
(JSA01/08A/A12-004 1025)
- KROLEVETS, Alexander N.**  
(SS03/08A/D-152 0830-311)
- KRUEGER, David A.**  
(JSA01/08A/A12-002 0935)
- KRUEGER, Kirstin**  
(MC05/09P/A09-005 1540)
- KRUEGER, Kirstin**  
(MC05/07P/D-001 1400-208)  
(MC05/07P/D-001 1400-208)
- KRUGER, Anton**  
(HW07/10A/C25-006 1130)
- KRUIZINGA, Gerhard L.**  
(G03/07P/D-068 1400-090)
- KRUPP, Norbert**  
(GAI11.14/07P/A12-005 1515)
- KRYMSKII, Alexander M**  
(GAI.V.03/08A/A16-008)
- KRYSANOVA, Valentina**  
(HW03/11A/C30-003 0910)
- KUBO, Atsuki**  
(JSS06b/10P/D-004 1400-028)
- KUBO, Atsuki**  
(SW03/10A/D-001 0830-236)
- KUBO, Hiroshi**  
(MC05/07P/D-011 1400-218)
- KUBO, Tetsuo**  
(SS04/08A/A03-010 1100)
- KUBO-OKA, Toshihiro**  
(JSG01/08A/A01-003 0930)
- KUBOKAWA, Atsushi**  
(JSP10/08P/D-006 1610-058)  
(JSP10/08P/D-001 1610-053)
- KUBOTA, Hisayuki**  
(MC17/11P/B23-003 1440)
- KUBOTA, Jumpei**  
(HS02b/10P/D-003 1630-124)  
(JWH01/09P/C30-005 1520)  
(HS02/10A/C24-003 1053)  
(JSM10/08P/B23-003 1500)  
(HW01/09P/D-041 1400-232)
- KUBOTA, Jumpei**  
(JWH01/10A/C30-005 0950)
- KUBOTA, M.**  
(GAI11.05/08P/A15-001 1400)
- KUBOTA, Masahisa**  
(JSP09/11A/B20-008 1045)
- KUBOTA, Ryuji**  
(GAV.06/10A/A11-008 1110)
- KUCHAREK, Harald**  
(GAI11.09/11A/A11-005 1040)
- KUCHMENT, Lev S.**  
(JWH01/09A/C30-001 0900)  
(JWH01/10P/C30-002 1420)  
(HW07/11A/C25-008 1045)
- KUCHMENT, Lev S.**  
(HW07/10P/C25-011 1700)
- KUCHMENT, Lev S.**  
(HS02/09P/C24-003 1430)
- KUCSARA, Mihály**  
(HS02/07A/C24-011 0940)  
(HS02a/07P/D-011 1545-157)
- KUCZERA, George**  
(HW08/08P/C28-002)
- KUCZERA, George**  
(HW08/08A/C28-004 0940)
- KUDRAVETS, Roman**  
(GAV.07/07P/D-005 1400-146)
- KUDO, Kazuyoshi**  
(SS04/08A/A03-007 1000)  
(SS04b/10P/D-001 1400-185)  
(SS04/07A/A03-001 0915)  
(SS04b/10P/D-003 1400-187)  
(SS04/08A/A03-013 1145)
- KUDO, Makoto**  
(HS03/08A/C26-004 0930)
- KUDO, Takeshi**  
(G03/07P/D-010 1400-032)
- KUDOU, Riichi**  
(GAI11.14/08A/D-006 0830-150)
- KUDRYAVTSEV, Sergey M.**  
(G04/08P/D-011 1400-118)
- KUDSY, Mahally**  
(JSM14/07A/A05-006 1130)
- KUDUON, Jonathan**  
(JSS07a/09P/D-004 1700-105)
- KUEHTREIBER, Norbert**  
(G03/07P/D-075 1400-097)
- KUEMPEL, Hans-J.**  
(JSG01/08A/A01-008 1105)
- KUHN, Michael**  
(JWH01/10A/C30-007 1100)
- KUHN, Michael**  
(G03/07P/D-038 1400-060)
- KULIK, V.**  
(HS02/09P/C24-007 1530)
- KULIKOV, Evgueni A.**  
(JSS07b/10P/D-009 1700-055)
- KULIKOV, Evgueni A.**  
(JSS07/10A/A02-004 0915)
- KULIKOV, Evgueni A.**  
(JSS07/10A/A02-011 1115)
- KULINICH, Anatoli**  
(JSA07/11A/D-028 0830-028)
- KULINICH, Ruslan**  
(JSA07/11A/D-001 0830-001)
- KULKARNI, K.M.**  
(HW06/07P/C31-003 1440)
- KULKARNI, Kshitij M.**  
(HW06/07P/C31-006 1540)
- KUMADA, Chihoko**  
(SS04/07P/A03-006 1530)
- KUMAGAI, Michio Dalai**  
(HS02/08A/C24-001 0830)
- KUMAGAI, Yoshihiro**  
(HW06/07P/D-008 1400-192)
- KUMAMOTO, Atsushi**  
(GAI11.10/11A/D-024 0830-098)  
(GAI11.06/07P/D-017 1400-137)  
(GAI11.06/07P/D-016 1400-136)
- KUMANO, Takashi**  
(JSH01/08P/D-008 1400-046)
- KUMAR, Dewashish**  
(HW03/11P/C30-005 1520)
- KUMAR, Dewashish**  
(HW03/11P/C30-003 1440)  
(HW05/10P/D-002 1400-157)
- KUMAR, P. Dileep**  
(SS03/08A/D-079 0830-238)
- KUMAR, Prasanna**  
(JSP09/11P/B20-002 1415)
- KUMAR, Praveen**  
(HW07/11P/D-013 1400-149)
- KUMAR, Sanjeev**  
(JSP11/07A/A10-002 0930)
- KUMAR, Sanjeev**  
(HW07/11P/D-039 1400-175)
- KUMAR, Sanjeev**  
(SS04a/09P/D-013 1400-262)
- KUME, Atsushi**  
(HW01/09P/D-045 1400-236)
- KUMINOV, Aleksander A.**  
(MC05/09P/A09-010 1740)
- KUNCIC, Zdenka**  
(GAI.V.02/07P/A07-004 1600)
- KUNDAN, Dani K.**  
(MI09/08P/B22-006 1620)
- KUNDZEWICZ, Zbigniew W.**  
(HS02/09A/C24-008 1115)
- KUNHIKRISHNAN, P.K.**  
(MC17/11P/B23-007 1620)
- KUNIMI, Toshio**  
(JSG01/07A/A01-001 0900)
- KUNIMORI, Hiroo**  
(G02/10P/D-010 1400-075)
- KUNINAKA, Hitoshi**  
(GAI11.11/09A/A15-007 1120)
- (GAI11.11/10P/D-004 1400-119)  
(GAI11.11/09P/A15-006 1525)
- KUNSTMANN, Harald G.**  
(HS02/08A/C24-011 1130)
- KUNSTMANN, Harald G.**  
(HW08/07A/C28-005 1030)
- KUNUGI, Takashi**  
(SW05/10P/A13-005 1505)
- KUO, Chen-Min**  
(HW03/11A/C30-007 1050)
- KUO, Chun Chao**  
(HS01/08P/C29-007 1620)
- KUO, Chung-Yen**  
(JSG01/08A/A01-012 1205)
- KUO, Hung-Chi**  
(MC02/07P/B20-002 1420)  
(MC02/08A/B20-003 0940)
- KUO, Long-Chen**  
(JSG01/07A/A01-007 1050)
- KUO, Long-Chen**  
(JSG01/08P/D-036 1400-036)
- KUO, Yue-Hong**  
(SW05/10A/D-002 0900-246)
- KURAHASHI, Susumu**  
(SS04a/09P/D-002 1400-251)
- KURAMOTO, Kiyoshi**  
(MC04/11P/B22-002 1430)  
(MC04/11P/B22-008 1645)  
(MC04/11P/B22-009 1700)  
(MC04/10P/B22-005 1530)
- KURAMOTO, Kiyoshi**  
(MC04/11P/B22-010 1715)
- KURASHIGE, Yoshimasa**  
(HS01/09P/C29-003 1440)
- KURASHIMO, Eiji**  
(SS03/08A/D-009 0830-168)  
(SS03/08A/D-102 0830-261)
- KURGANSKY, Michael V.**  
(JSM14/07A/A05-003 1025)
- KURIHARA, Yoshio**  
(MC02/07A/B20-001 0945)  
(MC02/08A/B20-006 1120)
- KURIMOTO, Kenji**  
(MI09/08P/B22-005 1600)
- KURITA, Naoyuki**  
(HW06/07P/C31-007 1600)  
(HW06/07P/D-007 1400-191)
- KURITA, Susumu**  
(JSM03/08P/A13-002 1420)
- KURKIN, Andrey**  
(JSP08/09P/B19-004 1510)
- KURNIAWAN, Edison**  
(JSP09/10P/B20-012 1715)
- KURODA, Yoshifumi**  
(JSP06/07P/B21-001 1400)
- KURODA, Yuhji**  
(MI05/10A/B17-004 0950)  
(MC05/10P/A09-003 1500)
- KURT, Ali Ihsan**  
(JSG01/08A/A01-001 0900)
- KURT, Wylegalla**  
(JSA07/10P/A05-004 1500)
- KURTYCH, Anna**  
(HW07/11P/D-012 1400-148)
- KURZ, Manfred**  
(JSM14/08A/A05-012 1215)
- KUSCHE, Juergen**  
(G04/07P/C25-008 1720)
- KUSHNAREV, Dmitriy S.**  
(GAI11.06/11P/D-004 1400-056)
- KUSHNER, Paul J.**  
(MC08/07A/B17-004 1030)
- KUSHNIR, Yochanan**  
(MI05/11A/B17-008 1130)
- KUSTARNIKOVA, A.A.**  
(JSS06/10A/A04-003 0910)
- KUSTAS, William P.**  
(MI07/11A/B18-006 1050)
- KUSUDA, Tetsuya**  
(HS02/08A/C24-002 0845)
- KUSUMA, Dendi Surya**  
(G03/07P/D-001 1400-023)  
(G03/07P/D-003 1400-025)
- KUSUNOKI, Ken-ichi**  
(JSM14/09P/D-025 1400-089)
- KUVSHINOV, Alexei**  
(GAI.10/09P/D-005 1615-124)
- KUWABARA, Eiji**  
(SS05/10A/A13-011 1115)
- KUWABARA, Takuichiro**  
(SS03/08A/D-059 0830-218)
- KUWAGATA, Tsuneo**  
(MI07/11P/B18-006 1600)  
(MI07/11P/B18-008 1640)
- KUWAGATA, Tsuneo**  
(HW04/09A/C31-008 1140)
- KUWAHARA, Yasuto**  
(SS03/08A/D-113 0830-272)
- KUWANO, Asako**  
(SS03/08A/D-056 0830-215)  
(SS03/08A/D-002 0830-161)
- KUWASAWA, Noriyuki**  
(JSS07b/10P/D-004 1700-050)
- KUZMENKO, Mikhail I.**  
(HW01/10P/C26-009 1720)
- KUZMIN, Vadim**  
(HW08/09A/C28-006 1050)
- KUZMIN, Yuri**  
(SS03/08A/D-104 0830-263)
- KUZNETSOV, Valery**  
(JSA07/10P/A05-005)
- KUZNETSOV, Vladimir V.**  
(JSS06a/08P/D-021 1400-099)
- KUZNETSOV, Vladimir V.**  
(GAV.05/09P/D-002 1400-146)
- KUZNETSOVA, Maria M.**  
(GAI11.09/11A/A11-008 1210)
- KUZNETSOVA, Masha M.**  
(GAI11.09/10P/D-003 1400-115)
- KUZNETSOVA, Tamara V.**  
(JSA08/10P/D-002 1400-002)  
(JSA08/09A/A08-010 1215)
- KUZUHA, Yasuhisa**  
(HW03/11A/C30-004 0930)
- KUZUHA, Yasuhisa**  
(HW07/11P/D-021 1400-157)
- KUZUHA, Yasuhisa**  
(HW01/09P/D-010 1400-201)
- KUZUHA, Yasuhisa**  
(HW07/11P/D-037 1400-173)  
(HW07/10P/C25-004 1500)
- KWADIBA, M. Tarzan O.**  
(JSS06/07P/A04-006 1600)
- KWADIBA, M. Tarzan O.**  
(SW03/10P/A04-002 1415)
- KWON, Byung-Doo**  
(JSA07/10P/A05-003 1440)
- KWON, Hyung-Joong**  
(HS03/08A/C26-006 1000)
- KWON, Won-Tae**  
(MC08/07P/B17-002 1415)
- KYBA, Patrick**  
(JSP10/09P/B21-005 1520)
- KYSELY, Jan**  
(MC08/07P/B17-011 1710)
- KYZYUROV, Yuriy**  
(GAI11.06/09P/A10-012 1725)  
(GAI11.06/11P/D-016 1400-068)

## INDEX

- LAAKSO, Harri E.**  
(GAI11.10/11A/D-006 0830-080)
- LABITZKE, Karin**  
(JSA08/09A/A08-009 1200)
- LACHLAN-COPE, Tom**  
(JSM10/08A/B23-009 1150)
- LAGERLOEF, Gary S.E.**  
(JSP06/07A/B21-007 1140)
- LAGG, Andreas**  
(GAI11.14/07P/A12-005 1515)
- LAGO, Luciano**  
(G07/10P/D-015 1400-100)
- LAGUARDIA, Giovanni**  
(HW07/11A/C25-012 1200)
- LAGUN, Victor E.**  
(JSM04/09P/D-014 1400-051)  
(MI06/09P/B20-010 1720)
- LAI, Guowei**  
(HS02b/10P/D-029 1630-150)  
(HS02/10P/C24-006 1535)
- LAI, Olivier**  
(MC04/10P/B22-006 1615)
- LAI, Yuangen**  
(JSA07/10P/A05-004 1500)
- LAIGLE, Mireille**  
(SS03/07A/A02-009 1130)
- LAKAMRAJU, Subba Raju Venkata**  
(JSA07/11A/D-033 0830-033)
- LAKHINA, G.S.**  
(GAI11.09/10P/D-001 1400-113)  
(GAI11.05/07P/D-022 1400-120)
- LAKHINA, G.S.**  
(GAI11.07/10P/D-003 1400-108)
- LAKHINA, Gurbax S.**  
(GAI11.07/09P/A14-002 1430)  
(GAI11.07/09P/A14-005 1530)  
(GAI11.07/09P/A14-010 1740)
- LAKHINA, Gurbax Singh**  
(GAI11.05/07P/D-001 1400-099)
- LAKSHMI, Venkat**  
(HW07/10A/C25-004 1100)
- LALL, Upmanu**  
(HS02/10A/C24-002 0845)
- LAM, Mai Mai**  
(GAI11.06/07P/D-007 1400-127)
- LAMB, Dennis**  
(MI08/07P/B18-001 1500)
- LAMBERT, Alyn**  
(MC05/08P/A09-003 1450)
- LAN, Yongchao**  
(JSH01/07P/C27-010 1720)
- LANGE, Manfred A.**  
(HS02c/11P/D-018 1630-116)  
(HS02/11A/C24-018 1153)  
(JSP04/09A/A06-003 0940)  
(JSM10/09P/D-006 1400-060)
- LANGEMATZ, U.**  
(MC11/10P/B19-003 1440)
- LANGEMATZ, Ulrike**  
(JSA08/09P/A08-006 1620)
- LANGEMATZ, Ulrike**  
(MC05/07P/D-001 1400-208)
- LANGLAIS, Benoit**  
(GAV.05/08P/A11-004 1500)
- LANGLAIS, Benoit**  
(GAV.05/08P/A11-010 1720)  
(GAV.04/07P/A11-009 1720)
- LANGMANN, Bärbel**  
(HW06/08A/C31-002 1100)
- LANUZA, Angelito G.**  
(SS04b/10P/D-042 1400-226)
- LANUZA, Angelito Galvez**  
(SW05/10A/D-003 0900-247)
- LANZEROTTI, Louis J.**  
(GAI11.10/11A/A01-001 0830)
- LAOUAR, R.**  
(HS02/08P/C24-006 1515)
- LAPTUKHOV, Alexy I.**  
(JSA08/10P/D-001 1400-001)
- LARA, Luciene Lorandi**  
(JSM04/09P/B23-001 1400)
- LARONNE, Leehee**  
(HW07/11P/D-017 1400-153)
- LARSEN, Chris**  
(JSG01/08P/D-015 1400-015)
- LARSEN, Christopher F.**  
(JSG01/07P/A01-009 1620)
- LARSEN, M.F.**  
(GAI11.06/11P/D-011 1400-063)
- LARSEN, Miguel Folkmar**  
(GAI11.06/09P/A10-002 1420)
- LARSEN, Niels**  
(MI03/08A/B18-003 0910)
- LARSON, Kristine M.**  
(JSG01/08P/D-023 1400-023)
- LARTER, Robert D.**  
(SS03/08A/D-095 0830-254)
- LASTOVICKA, Jan**  
(JSA01/08P/A12-002 1430)
- LATIFOVIC, Rasim**  
(MI09/09A/B22-003 0940)
- LATROUS, Ali**  
(GAV.05/08A/A11-010 1210)
- LATYNINA, Ludmila A.**  
(JSG01/08P/D-033 1400-033)
- LAU, William K.**  
(MC03/10A/A07-001 0830)  
(MC11/11A/B19-009 1130)
- LAUNEAU, Patrick**  
(JSG03/10A/A12-007 1100)
- LAURAIN, Olivier**  
(G04/08P/D-021 1400-128)
- LAURIA, Eduardo Andres**  
(G03/07P/D-004 1400-026)  
(G03/07P/D-032 1400-054)
- LAVALLEE, David**  
(G04/08P/C25-005 1530)
- LAVRENTIEV, Mikhail**  
(JSS07/10P/A02-004 1445)
- LAWRENCE, David**  
(MI07/11A/B18-001 0830)
- LAY, Thorne**  
(JSS06a/08P/D-018 1400-096)  
(U5/07A/D32-003 1030)
- LAZARO, C.**  
(JSG03/10A/A12-002 0850)
- LE, Guan**  
(JSG03/09P/D-026 1640-034)  
(GAI11.06/07P/D-002 1400-122)
- LE, Gui-ming**  
(GAI11.10/11A/D-013 0830-087)
- LE, Minh Huy**  
(GAV.06/09P/D-003 1400-156)
- LE CLAINCHE, Yvonnick**  
(MI05/10P/D-008 1400-174)
- LE MOUËL, Jean Louis**  
(GAV.05/08P/A11-007 1620)
- LE TRAOEN, Pierre-Yves**  
(JSP06/08A/B21-004 1040)
- LE TREUT, Herve**  
(MC08/07A/B17-009 1205)
- LEAN, Judith L.**  
(JSA08/09P/A08-003 1450)
- LEAT, Philip**  
(GAV.06/10P/A11-003)
- LEAVESLEY, George H.**  
(HW08/07P/C28-004 1550)
- LEBEDEV, Sergey A.**  
(JSG03/09P/D-015 1640-023)  
(JSG03/10A/A12-001 0830)  
(JSG03/09P/D-011 1640-019)
- LEDO, Juanjo**  
(JSA07/10A/A05-002 0900)
- LEDREW, Ellsworth F.**  
(JSM10/07A/B23-003 1000)
- LEE, Aaron**  
(MC05/08P/A09-003 1450)
- LEE, Chao-Shing**  
(SS03/07P/A02-002 1415)
- LEE, Cheng-shang**  
(MC02/08A/B20-002 0920)
- LEE, Chien-Chih**  
(GAI11.06/11P/D-009 1400-061)  
(GAI11.06/09P/A10-011 1710)
- LEE, Christina O.**  
(GAI11.03/08A/A16-007 1130)
- LEE, Dong Ryul**  
(HS02/08P/C24-010 1645)
- LEE, Dong-Hun**  
(GAI11.10/11A/A01-007 1000)
- LEE, Dong-Kyoo**  
(JSM14/08A/A05-005 0955)
- LEE, Duk Kee**  
(JSA07/10P/A05-003 1440)  
(JSA07/11A/D-003 0830-003)
- LEE, Heuisoon**  
(JSA07/11A/D-003 0830-003)
- LEE, Ho Jun**  
(JSS07/09A/A02-013 1215)
- LEE, Hung-Kyu**  
(G04/07P/C25-004 1530)
- LEE, Hyosang**  
(HW08/09A/C28-003 0950)
- LEE, Hyunah**  
(MC05/09A/A09-005 1050)
- LEE, Jenn-Taur**  
(G04/08P/D-007 1400-114)  
(G02/10P/D-001 1400-066)
- LEE, Jo-Han**  
(JSM14/08A/A05-005 0955)
- LEE, Kang-Kun**  
(HW01/10A/C26-008 1130)
- LEE, Khil-Ha**  
(MI07/10P/D-001 1400-177)
- LEE, L.C.**  
(GAI11.04/07A/A08-007 1110)
- LEE, Ming-An**  
(JSG03/09P/D-007)
- LEE, Sang-il**  
(HW01/09P/D-009 1400-200)  
(HW05/10A/C31-002 0850)
- LEE, Tong**  
(JSP06/08A/B21-006 1130)
- LEE, Yuan-Hsi**  
(JSG03/09P/D-021 1640-029)
- LEEKES, Graham J.**  
(HS01/09A/C29-001 0900)
- LEFEVRE, Franck**  
(MC05/07A/A09-006 1150)
- LEGALL, Bernard**  
(GAV.06/10P/A11-005 1520)
- LEGRESY, Benoit**  
(JSG03/09P/D-003 1640-011)  
(JSG02/09A/D-002 0830-002)  
(JSM11/10A/B18-005 1020)  
(JSH01/08A/C27-004 1030)
- LEGROS, Hilaire**  
(JSG02/09A/D-006 0830-006)
- LEHNING, Michael**  
(JWH01/10P/D-001 1400-006)  
(JWH01/09A/C30-004 1000)  
(JSM10/07A/B23-004 1020)  
(JWH01/09A/C30-009 1210)
- LEIBUNDGUT, Christian**  
(HW06/07A/C31-006 1130)  
(HS02/08P/C24-008 1615)
- LEINEN, Stefan**  
(G04/07P/C25-005 1620)
- LEJEUNE, Yves**  
(JWH01/09A/C30-009 1210)  
(JWH01/09P/C30-001 1400)
- LELLOUCH, Emmanuel**  
(MC04/10P/B22-006 1615)
- LELONG, Marie-Pascale G.**  
(JSP10/08P/D-012 1610-064)  
(JSP10/11P/B21-005 1610)
- LEMAIRE, J.**  
(GAI11.06/07P/D-018 1400-138)
- LEMAIRE, Joseph**  
(GAI11.10/11A/D-022 0830-096)
- LEMBEGE, Bertrand**  
(GAI11.06/07P/D-012)
- LEMBEGE, Bertrand**  
(GAI11.02/07A/A07-002 0930)  
(GAI11.02/07P/A07-006 1710)
- LEMBEGE, Bertrand**  
(GAI11.07/10P/D-001 1400-106)
- LEMOINE, Jean-Michel**  
(G02/07A/C25-001 0900)  
(G02/07A/C25-003 0940)
- LEMOINE, Jean-Michel**  
(JSG02/09A/D-002 0830-002)
- LENK, Onur**  
(JSG01/07A/A01-008 1105)  
(JSG01/08A/A01-001 0900)
- LÉNOT, Xavier**  
(JSG03/10A/A12-007 1100)
- LÉPINE, Jean-Claude**  
(SS03/07A/A02-009 1130)
- LEPPING, Ronald P.**  
(GAI11.09/11P/A11-005 1600)
- LERNER, David**  
(HS04/08A/C30-001 0905)
- LESLIE, Lance**  
(JSG03/08P/C26-010 1630)
- LESLIE, Lance M.**  
(MC02/07P/D-008 1400-205)  
(MC02/08P/B20-005 1550)
- LESSA, Guilherme Camargo**  
(JSP08/09P/B19-009 1720)
- LESSMANN, Dieter**  
(HW06/07A/C31-007 1150)
- LESTER, Mark**  
(GAI11.05/07P/D-016 1400-114)  
(GAI11.06/10A/A01-011 1145)
- LESUR, Vincent**  
(GAV.05/08A/A11-002 0900)
- LESUR, Vincent B.F.**  
(GAV.05/08P/A11-002 1430)
- LETTENMAIER, Denis**  
(HS02/07A/C24-014 0952)  
(HS02a/07P/D-014 1545-160)
- LEVEQUE, Christian**  
(HS02/07A/C24-014 0952)  
(HS02a/07P/D-014 1545-160)
- LEVEQUE, Jean Jacques**  
(JSS06/10A/A04-004 0930)
- LEVEQUE, Jean-Jacques**  
(JSA07/11A/D-025 0830-025)
- LEVEQUE, Jean-Jacques**  
(JSS06/08A/A04-008 1110)  
(JSS06b/10P/D-008 1400-032)
- LEVIN, Boris W.**  
(SW05/10P/A13-013 1715)  
(JSS07/10A/A02-011 1115)  
(JSS07/10P/A02-008 1600)
- LEVIN, Vasily E.**  
(JSG01/08P/D-009 1400-009)
- LEVIN, Zev**  
(GAI11.04/07A/A08-009)
- LEVINA, Galina**  
(JSM14/07P/A05-004 1505)
- LEVITSKIY, Vladimir V.**  
(JSP10/08P/D-013 1610-065)
- LEWIS, Stephen**  
(JSP10/08P/B21-001 1400)  
(MC04/11P/B22-001 1400)
- LEYDECKER, Guenter**  
(SS04b/10P/D-021 1400-205)
- LEYDECKER, Guenter**  
(SS04a/09P/D-023 1400-272)
- LEYVA, Amando C.**  
(GAV.04/07A/A11-008 1200)
- LEZAETA, Pamela**  
(JSA07/10A/A05-003 0920)  
(JSS06/09P/A04-008 1640)
- LEZHEN, L.**  
(GAI11.06/07P/D-018 1400-138)
- Li, Chongyin**  
(MC17/11P/B23-005 1540)
- Li, Chunhong**  
(HS03/08A/C26-007 1030)
- Li, Fei**  
(G02/10P/D-005 1400-070)
- Li, Guilong**  
(JSM14/09P/D-021 1400-085)  
(JSM14/09P/D-022 1400-086)
- Li, Heyue**  
(HS02c/11P/D-034 1630-132)  
(HS02/11P/C24-011 1555)
- Li, Hongnan**

- (SS04/08A/A03-001 0830)
- LI, Hui**  
(G04/08P/D-020 1400-127)  
(G03/07P/D-016 1400-038)
- LI, Jiancheng**  
(JSP06/07P/D-001 1400-008)
- LI, Jianping**  
(MC04/11P/B22-005 1515)
- LI, Jianxin**  
(JSG01/07A/A01-003 0930)
- LI, Laurent Z.X.**  
(MI05/11A/B17-002 0850)
- LI, Laurent Z.X.**  
(MI05/11A/B17-001 0830)
- LI, Li**  
(JSA07/11A/D-012 0830-012)
- LI, Qian**  
(JSM14/09P/D-022 1400-086)
- LI, Qinghe**  
(JSA07/11A/D-004 0830-004)
- LI, Qingquan**  
(MC11/11P/D-004 1400-197)
- LI, Qingtian**  
(G04/08P/D-002)
- LI, Run-jie**  
(HS02/07A/C24-003 0908)  
(HS02a/07P/D-003 1545-149)
- LI, Shuanglin**  
(MI05/11A/B17-003 0910)
- LI, Shuncheng**  
(JSA07/10P/A05-004 1500)
- LI, Tiezheng**  
(HS02c/11P/D-026 1630-124)  
(HS02/11P/C24-003 1523)
- LI, Tim**  
(MC02/08A/B20-001 0900)
- LI, Wansheng**  
(GAIII.10/11A/A01-005 0930)
- LI, Weiping**  
(MC03/10P/A07-005 1600)
- LI, Wenhong**  
(MC03/10A/A07-005 1030)
- LI, X.**  
(JSS06a/08P/D-023 1400-101)
- LI, Xiaopeng**  
(G04/08P/D-008 1400-115)
- LI, Xin**  
(JSH01/08A/C27-006)
- LI, Xin**  
(JSH01/08P/D-011 1400-049)  
(JSH01/08P/D-002 1400-040)  
(JSH01/07P/C27-011 1740)  
(JSH01/08P/D-003 1400-041)
- LI, Xin**  
(HS02/07A/C24-003 1115)
- LI, Xin**  
(JSM04/09P/D-016 1400-053)
- LI, Xinwu**  
(JSH01/07P/C27-002)
- LI, Yanxing**  
(JSG01/07A/A01-004 0945)
- LI, Yongping**  
(JSP09/11P/B20-008 1615)
- LI, Yuefang**  
(HS02/07P/C24-027 1440)  
(HS02a/07P/D-027 1545-173)
- LI, Yumin**  
(SS05/10A/A13-013 1145)
- LI, Zhanqing**  
(MI09/09A/B22-003 0940)
- LI, Zhen**  
(JSH01/07P/C27-002 1420)
- LI, Zhicai**  
(JSG01/07A/A01-005 1000)  
(JSG01/07A/A01-004 0945)
- LIANG, Long-Shin**  
(JSG03/09P/D-021 1640-029)
- LIANG, Naishen**  
(MI07/10P/D-004 1400-180)
- LIARD, Jacques**  
(G03/07P/D-062 1400-084)
- LIEBERMAN, Ruth S.**  
(MC05/09P/A09-004 1520)
- LIEMOHN, M.W.**  
(GAIII.06/08A/A02-008 1200)
- LIEMOHN, Michael W.**  
(GAIII.08/10A/A16-009 1115)  
(GAIII.06/08A/A02-006 1110)  
(GAIII.08/10A/A16-010 1135)  
(GAIV.03/09A/A16-002 0930)
- LIENOU, Gaston**  
(HW01/10P/C26-004 1500)
- LIEPERT, Beate Gertrud**  
(MC03/11P/D-018 1400-193)
- LILLY, Allan**  
(HW01/09A/C26-005 1030)
- LIM, Gyu-Ho**  
(MI05/10P/B17-002 1440)
- LIMANOWKA, Danuta**  
(HS02/08A/C24-007 1000)
- LIMIN, Suwido**  
(MI07/10P/D-006 1400-182)
- LIMPASUVAN, Varavut**  
(MI05/10A/B17-007 1120)
- LIN, Bing**  
(JSP09/11A/B20-003 0915)
- LIN, Charles A.**  
(JSM14/09A/A05-003 0955)
- LIN, Cheng-Horng**  
(SS03/08A/D-111 0830-270)  
(SS03/08A/D-016 0830-175)
- LIN, Hai**  
(MI05/09P/B17-007 1650)
- LIN, Hsiao-Wen**  
(JSM04/09P/D-007 1400-044)
- LIN, Hsin-Hon**  
(JSM14/09P/D-011 1400-075)
- LIN, Jer-Ming**  
(SS04a/09P/D-037 1400-286)
- LIN, Ju**  
(JSP07/08A/B17-005 1100)
- LIN, Lee-Yaw**  
(MC02/07P/B20-002 1420)
- LIN, Pay-Liam**  
(JSM14/07P/A05-007 1730)  
(JSM14/09P/D-011 1400-075)
- LIN, Pei-Yeng**  
(SS03/08A/D-124 0830-283)
- LIN, Po-Hsiung**  
(MC02/08P/B20-007 1630)
- LIN, Robert P.**  
(GAIV.03/08A/A16-007 1130)
- LIN, Yu-Feng**  
(JSG03/09P/D-022 1640-030)
- LIN, Zhonghui**  
(HS03/08P/C26-008 1600)
- LINCOLN, E.N.**  
(JSM04/09A/B23-006 1145)
- LIND, Frank D.**  
(GAIII.06/10A/A01-001 0830)
- LIND, Frank D.**  
(GAIII.11/09A/A15-009 1150)
- LINDQVIST, Per-Arne**  
(GAIII.11/09P/A15-008 1620)
- LINDROTH, Anders**  
(MI07/11P/B18-001 1400)
- LINDSTRÖM, Göran**  
(HW01/10P/C26-006 1620)  
(HS02/08A/C24-012 1145)
- LINDSTRÖM, Göran Johannes**  
(HS02/08A/C24-004 0915)
- LING, Suqun**  
(SS04a/09P/D-039 1400-288)
- LINIGER, Mark Andrea**  
(MI05/10A/B17-003 0930)
- LINS, Harry**  
(HS02/07A/C24-014 0952)  
(HS02a/07P/D-014 1545-160)
- LIONELLO, Piero**  
(JSM14/08P/A05-008 1745)  
(MC12/08P/B19-003 1500)
- LIU, Chi-Sann E.**  
(MC02/08P/B20-006 1610)
- LIU, K.**  
(GAIII.10/11A/D-017 0830-091)  
(GAIII.10/11A/D-016 0830-090)
- (GAII.06/11P/D-008 1400-060)
- LIU, Kan**  
(GAIII.10/11A/D-018 0830-092)
- LIU, Kan**  
(GAIII.09/11P/A11-005 1600)  
(GAIII.05/07P/D-017 1400-115)  
(GAIII.05/07P/D-014 1400-112)
- LIPILIN, Alexander V.**  
(GAI.10/09A/A11-006 1015)
- LIPKO, Yury V.**  
(GAII.06/11P/D-019 1400-071)
- LIPPAI, Horacio Francisco**  
(JSA07/11A/D-047 0830-047)
- LIST, Roland**  
(JSM15/07A/B18-005 1015)
- LISTON, Glen E.**  
(JWH01/09A/C30-007 1130)
- LITTLEWOOD, Ian Geoffrey**  
(HW07/10P/C25-010 1645)
- LIU, Alan Z.**  
(MC05/11A/A09-002 0900)
- LIU, Antony K.**  
(JSH01/07A/C27-005 1200)
- LIU, C.-H.**  
(GAII.06/09A/A10-001 0900)
- LIU, C.H.**  
(GAII.06/09P/A10-011 1710)
- LIU, Changming**  
(HS01/08A/C29-002)
- LIU, Chi-Ching**  
(JSG01/08P/D-011 1400-011)
- LIU, Chih-Shin**  
(JSM14/09P/D-003 1400-067)
- LIU, Ching-Hwang**  
(MC02/08A/B20-003 0940)
- LIU, Dongzhi**  
(G03/07P/D-016 1400-038)
- LIU, J.-Y.**  
(GAII.06/11P/D-008 1400-060)
- LIU, J.Y.**  
(GAII.06/11P/D-009 1400-061)  
(GAII.06/09P/A10-011 1710)
- LIU, Jie**  
(JSA07/11A/D-012 0830-012)
- LIU, L.**  
(GAII.06/09P/A10-011 1710)
- LIU, Lin-gun**  
(MC04/11A/B22-008 1100)
- LIU, Ningyu**  
(GAII.04/07P/A08-003 1450)
- LIU, P.**  
(MC03/09P/A07-004 1540)
- LIU, Pan**  
(HS02b/10P/D-022 1630-143)  
(HS02/10A/C24-022 1209)
- LIU, Peixun**  
(SS03/08A/D-046 0830-205)
- LIU, Qiuyan**  
(JSA07/10P/A05-004 1500)
- LIU, Quanwei**  
(G03/07P/D-034 1400-056)
- LIU, Ruiyuan**  
(GAIII.10/11A/A01-002 0845)
- LIU, Saijun**  
(SS03/08A/D-125 0830-284)
- LIU, Saijun**  
(SS03/07P/A02-013 1730)
- LIU, Shiyin**  
(JSM10/08P/B23-007)
- LIU, shiyin**  
(HW05/10P/D-010 1400-165)
- LIU, Suxia**  
(HS02/09A/C24-005 1000)  
(HS03/08P/C26-010 1630)  
(HS03/08P/C26-008 1600)
- LIU, Timothy**  
(MC03/10P/A07-003 1440)
- LIU, W. Timothy**  
(JSM03/08A/A13-006 1100)  
(JSP09/11A/B20-001 0830)
- LIU, W. Timothy**  
(JSP06/07A/B21-002 0920)
- LIU, Xiaohong**  
(JSM04/09P/D-001 1400-038)
- LIU, Xin**  
(MC03/11A/A07-001 0830)
- LIU, Yimin**  
(MC03/10P/A07-007 1700)  
(MC03/11A/A07-001 0830)  
(MC03/11A/A07-002 0910)
- LIU, Yong Gang**  
(JSS06/10A/A04-005 0950)
- LIU, Yonghua**  
(GAIII.10/11A/A01-002 0845)
- LIU, Yuanchao**  
(GAI.08/08P/D-006 1400-141)
- LIU, Yueqiang**  
(HS04/08A/C30-003 1005)
- LIU, Z.X.**  
(GAIII.06/07P/D-008 1400-128)
- LIU, Zhiyu**  
(HW07/10P/C25-013 1730)
- LIU, Zhong**  
(MC02/07P/D-002 1400-199)
- LIVANOVA, L.**  
(JSS06a/08P/D-012 1400-090)
- LLUBES, Muriel**  
(JSG02/09A/D-002 0830-002)
- LO, Kwong Fai Andrew**  
(HS01/09P/D-010 1400-177)
- LOAICIGA, Hugo A.**  
(HS02/09P/C24-008 1615)
- LOBANOV, Lobanov Alexeevich**  
(HS01/09P/D-015 1400-182)
- LOBANOV, S.**  
(HS02/09P/C24-007 1530)
- LOBANOV, S.**  
(HS02/09P/C24-007 1530)
- LOBANOV, Vladimir Alexeevich**  
(HW07/11P/D-016 1400-152)
- LOBANOVA, H.V.**  
(HW02/11P/D-016 1400-152)
- LOBANOVA, Helen (Elena) Vladislavovna**  
(HS02b/10P/D-033 1630-154)  
(HS02/10P/C24-010 1551)
- LOBIANCO, Maria Cristina**  
(G03/07P/D-069 1400-091)
- LOBKOVSKY, Leopold Isaevich**  
(JSP07/08A/B17-007 1140)
- LOBODA, Natalie**  
(HW01/09P/D-028 1400-219)  
(HW04/09P/C31-005 1520)  
(HW04/09A/C31-010 1220)
- LODOLO, Emanuele**  
(JSA07/11A/D-047 0830-047)
- LOEBIS, Joesron**  
(HS02/10P/C24-003 1430)
- LOECHER, Anno**  
(G04/08A/C25-009 1200)
- LOEHRER, Scot M.**  
(MC03/10P/A07-002 1420)  
(JSP04/09A/A06-005 1050)
- LOGNONNE, Philippe**  
(GAII.06/09P/A10-013 1740)  
(GAII.06/09P/A10-013 1740)
- LOGNONNE, Philippe**  
(JSS07/10P/A02-010 1630)
- LOH, Chin-Hsiung**  
(SS04/08P/A03-001 1400)  
(SS04a/09P/D-008 1400-257)
- LOHOU, Fabienne**  
(JSP09/10A/B20-003 0945)
- LOMAS, Isabel**  
(JSG03/09P/D-025 1640-033)
- LOMBARD, Alix**  
(JSM11/10P/D-007 1700-016)
- Lomonosovfonna Ice Core Group**  
(MC12/08A/B19-005)
- LONFAT, Manuel**  
(MC02/07P/B20-007 1620)
- LONG, David G.**

## INDEX

(JSH01/07A/C27-006 1220)  
**LONG, Maureen D.**  
 (JSS06/09P/A04-011 1740)  
**LONGO, K.M.**  
 (JSM04/09P/D-010 1400-047)  
**LOOMIS, Harold G.**  
 (JSS07b/10P/D-016 1700-062)  
**LOPEZ, Ramon E.**  
 (GAI01.09/11P/A11-004 1510)  
 (GAI01.06/08P/A02-006 1545)  
**LOPEZ CASADO, Carlos**  
 (SS04/08P/A03-003 1430)  
 (SS04b/10P/D-014 1400-198)  
**LOPEZ-VALVERDE, Miguel**  
 (MC04/11P/B22-001 1400)  
**LORENZ, David**  
 (MI05/09P/B17-002)  
**LORSIRIRAT, Kosit**  
 (HS02/11P/C24-004 1445)  
**LOU, Hai**  
 (SS03/08A/D-135 0830-294)  
**LOU, huajun hua**  
 (HS02a/07P/D-030 1545-176)  
 (HS02/07P/C24-030 1452)  
**LOUARN, P.**  
 (GAI01.05/08A/A06-007 1040)  
**LOUTSENKO, Eduard I.**  
 (MI06/09P/B20-010 1720)  
**LOVEJOY, Shaun**  
 (HW07/10P/C25-003 1445)  
 (HW07/10P/C25-002 1430)  
**LOVEJOY, Shaun M.**  
 (HW07/10A/C25-007 1145)  
**LOWE, Jason**  
 (JSM11/10A/B18-002 0920)  
**LOWES, Frank J.**  
 (GAV.05/08A/A11-004 0950)  
**LOWRY, Anthony R.**  
 (JSG01/08P/D-023 1400-023)  
**LOYER, Sylvain**  
 (G02/07A/C25-001 0900)  
 (G02/07A/C25-003 0940)  
**LOZOWSKI, Edward P.**  
 (MI08/07P/B18-004 1620)  
**LU, Anxin**  
 (JSM10/08P/B23-007 1640)  
 (HW05/10P/D-010 1400-165)  
**LU, Daren**  
 (MI09/09P/B22-002 1420)  
**LU, Gang**  
 (GAI01.05/08P/A15-003 1500)  
 (GAI01.06/08A/A02-006 1110)  
**LU, Hongshan**  
 (JSP11/07P/A10-006 1640)  
**LU, Ming-Tar**  
 (SS03/08A/D-112 0830-271)  
**LU, Minjiao**  
 (HS03/07A/C26-009 1130)  
**LU, Minjiao**  
 (HS02/08P/C24-003 1430)  
**LU, Mong-Ming**  
 (MC03/11A/A07-008 1130)  
**LU, Tieding**  
 (G04/08P/D-003 1400-110)  
**LU, Yang**  
 (JSP07/08A/B17-006 1120)  
 (G03/07P/D-059 1400-081)  
 (G03/07P/D-074 1400-096)  
**LUCE, Hubert**  
 (MC05/07P/D-015 1400-222)  
**LUCEK, Elizabeth**  
 (GAI01.07/09P/A14-006 1610)  
**LUCK, Brenard**  
 (G03/07P/D-012 1400-034)  
**LUEHR, Hermann**  
 (GAV.05/08A/A11-007 1110)  
 (GAV.04/07A/A11-002 0930)  
 (GAV.04/07A/A11-006 1120)  
**LUETHI, Daniel**  
 (MC11/11P/B19-005 1520)  
 (MC08/07P/B17-006 1535)  
**LUGOMELA, George Venance**  
 (HW01/09P/D-050 1400-241)

**LUGOVENCO, Vladislav N.**  
 (U7/11P/D32-001 1400)  
**LUI, Anthony T.Y.**  
 (GAI01.06/08P/A02-002 1425)  
**LUKANDU, Ateya Ismail**  
 (JSG01/08P/D-037 1400-037)  
**LUKAS, Roger**  
 (JSA09/10A/A08-007 1115)  
**LUND, E.**  
 (GAI01.09/11A/A11-006 1110)  
**LUND, E.J.**  
 (GAI01.06/08P/A02-011 1725)  
**LUNDIN, Rickard**  
 (GAI01.08/10A/A16-003 0910)  
**LUNDIN, Rickard N.A.**  
 (GAIV.03/08P/A16-001 1400)  
**LUO, Xigui**  
 (GAI01.05/07A/D-003 0830-019)  
**LUO, Xinheng**  
 (SW05/10P/A13-003 1435)  
**LUO, Yi**  
 (MI09/09A/B22-003 0940)  
 (MC05/09P/A09-003 1500)  
**LUO, Zhicai**  
 (G03/07P/D-044 1400-066)  
 (G04/08P/D-016 1400-123)  
**LUTHER, Mark E.**  
 (JSP07/08A/B17-004 1010)  
**LUU, Hung Viet**  
 (GAV.06/09P/D-003 1400-156)  
**LYGIN, Vladimir Alexseevich**  
 (G03/07P/D-022 1400-044)  
**LYGUINE, Ivan Vladimirovich**  
 (G03/07P/D-022 1400-044)  
**LYNCH, Amanda H.**  
 (MI05/10P/D-009 1400-175)  
 (MC12/07A/B19-003 1015)  
**LYNCH, Peter**  
 (JSP10/10P/B21-007 1640)  
**LYONS, Jim**  
 (SW05/10P/A13-004 1450)  
**LYONS, Larry R.**  
 (GAI01.05/07A/A06-007 1055)  
 (GAI01.06/08P/A02-005 1530)  
 (GAI01.05/07P/D-018 1400-116)  
**LYONS, Walter A.**  
 (GAI01.04/07P/A08-005 1540)  
**LYSAK, Robert L.**  
 (GAI01.10/11A/A01-010 1045)  
**LYUBOMUDROV, Victor V.**  
 (JSA07/11A/D-006 0830-006)  
**LYUBOMUDROV, Viktor V.**  
 (JSA07/10A/A05-010 1210)

## m

**M., EL. saed**  
 (GAV.05/09P/D-008 1400-152)  
**M., Praveena**  
 (GAI.10/09P/D-014 1615-133)  
**M, Ahmed F.**  
 (GAV.05/09P/D-008 1400-152)  
**M.A., Mohammed Aslam**  
 (HS02b/10P/D-008 1630-129)  
 (HS02/10A/C24-008 1113)  
**MA, Hongsheng**  
 (JSA07/11A/D-012 0830-012)  
**MA, Jun**  
 (MC05/11P/A09-010)  
**MA, Kuo-Fong**  
 (SS03/08A/D-123 0830-282)  
**MA, Mingguo**  
 (JSH01/08A/C27-006 1110)  
 (HW04/09P/C31-006 1540)  
**MA, Minzhi**  
 (GAI.08/08P/D-006 1400-141)  
**MA, Xieyao**  
 (HW08/08A/C28-006 1040)  
**MA, Yingjuan**  
 (GAIV.03/09A/A16-001 0900)

**MA, Yuanle**  
 (HS04/08A/C30-003 1005)  
**MA, Zhuguo**  
 (MC08/08P/D-001 1400-157)  
**MABRUK, Mohamed Abbas**  
 (HW05/10P/D-008 1400-163)  
**MABUCHI, Kazuo**  
 (MI07/11A/B18-002 0850)  
**MACCrackEN, Michael C.**  
 (JSA09/10A/A08-001 0830)  
**MACDONALD, Oliver G.**  
 (HS02b/10P/D-017 1630-138)  
 (HS02/10A/C24-017 1149)  
**MACHADO, Luiz Augusto**  
 (MC03/10A/A07-003 0930)  
**MACHIDA, Shinobu**  
 (GAI.07/11A/A12-003 0925)  
 (GAI01.05/07P/D-009 1400-107)  
 (GAI01.05/07P/D-010 1400-108)  
 (GAI01.07/11A/A12-001 0835)  
 (GAI01.05/08A/A06-001 0830)  
**MACKIE, Randall L.**  
 (SS03/07A/A02-011 1200)  
**MACKINNON, Jen A.**  
 (JSP10/11A/B21-008 1130)  
**MACMILLAN, Susan**  
 (GAV.05/08P/A11-002 1430)  
 (GAV.05/08A/A11-002 0900)  
**MADDEN, Roland A.**  
 (MC17/10P/B23-004 1500)  
**MADEYSKI, Marek**  
 (HW07/11P/D-030 1400-166)  
**Madhusudan Rao**  
 (GAI.10/09P/D-004 1615-123)  
**MADSEN, Henrik**  
 (HS02/09P/C24-001 1400)  
**MADUABUCHI, Ibe Kasimir**  
 (HS02/08P/C24-002 1415)  
 (HW05/10P/D-012 1400-167)  
**MAEDA, Takahiro**  
 (SS04a/09P/D-041 1400-290)  
**MAENO, Norikazu**  
 (JSM15/07P/D-002 1400-002)  
**MAERKER, Michael**  
 (HS01/09A/C29-002 0920)  
**MAESAKA, Takeshi**  
 (JSM14/07P/A05-003 1450)  
**MAESAKA, Takeshi**  
 (MC03/11P/D-010 1400-185)  
**MAEZAWA, Kiyoshi**  
 (GAIV.03/09A/A16-003 0950)  
 (GAI01.05/07A/A06-001 0900)  
 (GAIV.03/09A/A16-007 1150)  
 (GAIV.03/08A/A16-009 1220)  
**MAGANA, Victor**  
 (MI05/10P/B17-005 1610)  
**MAGGERO, Balla Paul**  
 (HW07/11P/D-007 1400-143)  
**MAGGI, Alessia**  
 (JSS06/08A/A04-008 1110)  
 (JSS06a/08P/D-013 1400-091)  
**MAGLAMBAYAN, Victor B.**  
 (SS03/08A/D-061 0830-220)  
**MAGOME, Jun**  
 (JSG03/09P/A12-001 1400)  
 (HS02/11A/C24-004 0915)  
 (HS03/08A/C26-004 0930)  
**MAGOME, Shinya**  
 (JSP08/09A/B19-004 1010)  
**MAHDAVI, M.**  
 (HS02b/10P/D-010 1630-131)  
 (HS02/10A/C24-010 1121)  
**MAHE, Gil**  
 (HS02/08A/C24-008 1045)  
**MAHE, Gil**  
 (HW01/10P/C26-004 1500)  
**MAHINDA, Kasereka**  
 (JSP11/08A/A10-009 1220)  
**MAHONEY, M.J.**  
 (MC05/11P/A09-004 1510)  
**MAIA, Tule Cesar Barcelos**  
 (G03/07P/D-070 1400-092)  
**MAILLET, Kevin A.**  
 (JSP09/10A/B20-005 1015)  
**MAJEWSKI, Chris**  
 (SW05/10P/A13-004 1450)  
**MAJUMDAR, R.K.**  
 (SS03/08A/D-069 0830-228)  
**MAJUMDAR, Ranjit Kumar**  
 (SS03/08A/D-070 0830-229)  
**MAJUMDER, Sarada**  
 (JSG03/09P/A12-007 1620)  
**MAK, Mankin**  
 (JSP10/09A/B21-002 0930)  
**MAKI, M.**  
 (JSM14/09P/D-001 1400-065)  
**MAKI, Masayuki**  
 (JSM14/07P/A05-003 1450)  
 (MC03/11P/D-017 1400-192)  
**MAKIHARA, Masaki**  
 (SS05/10A/A13-003 0900)  
**MAKINEN, Jaakko**  
 (G07/10P/D-016 1400-101)  
**MAKINO, Masahiko**  
 (GAV.06/09P/D-005 1400-158)  
**MAKINO, Masahiko**  
 (JSA07/11A/D-016 0830-016)  
**MAKINO, Satoshi**  
 (GAI01.04/07P/A08-004 1505)  
**MAKSHTAS, Alexander**  
 (JSM10/08A/B23-006 1050)  
**MAKSHTAS, Alexander P.**  
 (JSP04/10P/A06-003 1440)  
 (JSP04/09P/A06-008 1615)  
**MAKSYMCHUK, Valentyn**  
 (GAV.07/07P/D-005 1400-146)  
**MAKSYUTIN, Sergey Vladimirovich**  
 (JSA01/08P/A12-007 1700)  
**MALCOLM, Iain A.**  
 (HW02/11A/C31-002 0900)  
**MALIN, Peter**  
 (SS03/07A/A02-002 0915)  
**MALLAPPAN, Ponraj**  
 (SS03/08A/D-080 0830-239)  
**MALOSZEWSKI, Piotr**  
 (HW06/07A/C31-008 1210)  
**MALTSEVA, Olga**  
 (GAI01.10/10P/A01-012 1740)  
**MALYSHEV, Vladislav**  
 (JWH01/09A/C30-008 1150)  
**MAN'KO, Aleksander Nikolaevich**  
 (JSP06/07P/D-004 1400-011)  
**MANAKOV, Alexander V.**  
 (GAI.10/09A/A11-004 0945)  
**MANANES, Rafael**  
 (JSP08/09A/B19-010 1220)  
**MANDAL, Prantik**  
 (SS04/08P/A03-004 1445)  
 (SW04/09P/A13-006 1515)  
**MANDEA, Mioara**  
 (GAV.05/09P/D-005 1400-149)  
 (GAV.05/08P/A11-001 1400)  
 (JSS06/09A/A04-006 1100)  
 (GAV.05/08P/A11-009 1700)  
 (GAV.04/07A/A11-006 1120)  
 (GAV.05/08A/A11-007 1110)  
 (GAV.05/09P/D-004 1400-148)  
 (GAV.05/08P/A11-004 1500)  
**MANDRESCU, Neculai**  
 (SS04a/09P/D-046 1400-295)  
**MANFREDA, Salvatore**  
 (HW07/11P/C25-005 1500)  
**MANGALAMPALLY, Ravi Kumar**  
 (SW03/10P/A04-014 1730)  
**MANGALAMPALLY, Ravi Kumar**  
 (SS03/08A/D-023 0830-182)  
**MANGIN, Antoine**  
 (JSP06/07A/B21-001 0900)  
**MANGLIK, A.**  
 (JSS06/10A/A04-001 0830)  
 (GAI.10/09A/A11-012 1215)  
**MANGLIK, Ajay**

- (SS03/08A/D-128 0830-287)  
(GAI.10/09A/A11-007 1100)
- MANIA, J.**  
(HS02/08P/C24-006 1515)
- MANN, Graham W.**  
(JWH01/09A/C30-005 1020)
- MANN, Ian R.**  
(GAIll.10/10P/A01-003 1440)
- MANN, Ian R.**  
(GAIll.10/10P/A01-001 1400)
- MANN, Michael E.**  
(MC12/08P/B19-004 1515)
- MANNUCCI, J. A.**  
(GAIll.04/07A/A08-009)
- Manoj C.**  
(GAI.10/09P/D-004 1615-123)
- MANSON, Alan H.**  
(MC05/10A/A09-010 1210)  
(MC05/09P/A09-003 1500)
- MANTYNIEMI, Paivi**  
(SS04/08P/A03-005 1500)
- MANUCCI, Anna**  
(JSS07a/09P/D-011 1700-112)  
(JSS07a/09P/D-013 1700-114)
- MANURUNG, Parluhan**  
(JSM11/10P/B18-006 1620)
- MANZINI, E.**  
(MC11/10P/B19-003 1440)
- MANZINI, Elisa**  
(MI03/08P/B18-005 1520)
- MAO, Jianguy**  
(MC03/11A/A07-001 0830)  
(MC03/10P/A07-007 1700)  
(MC03/11A/A07-002 0910)
- MAPES, Brian E.**  
(MC03/10P/A07-001 1400)  
(JSM03/08A/A13-008 1140)  
(MC11/10A/B19-003 0920)  
(MC17/11A/B23-008 1140)
- MARAMAI, Alessandra**  
(JSS07a/09P/D-013 1700-114)
- MARATOS, Nikos**  
(HS02c/11P/D-002 1630-100)  
(HS02/11A/C24-002 1049)
- MARCH, Rod S.**  
(HS01/09P/D-003 1400-170)
- MARCHUK, Andrei G.**  
(SW05/10P/A13-012 1700)  
(JSS07b/10P/D-002 1700-048)
- MARCHUK, Andrey**  
(JSS07/10P/A02-004 1445)
- MARENGO, Jose A.**  
(MC03/10A/A07-003 0930)
- MARENGO, Jose Antonio**  
(MC03/10A/A07-008 1130)
- MARES, Constantin**  
(MI05/10P/D-002 1400-169)
- MARES, Ileana**  
(MI05/10P/D-002 1400-169)
- MARIAM, Mkrtychyan**  
(JSP11/08P/D-004 1400-073)
- MARINKOVIC, Petar**  
(G02/07A/C25-006 1030)  
(G07/10P/D-011 1400-096)
- MARKOVA, Nina**  
(SW05/10P/A13-004 1450)
- MARKS, Danny G.**  
(JWH01/10P/C30-006 1630)
- MARKS, Frank D.**  
(MC02/07P/B20-007 1620)
- MARKSTROM, Steven L.**  
(HW08/07P/C28-004 1550)
- MARKUS, Thorsten**  
(JSH01/08P/D-006 1400-044)
- MARMUREANU, Alexandru**  
(SS04/08P/A03-013 1715)
- MARMUREANU, Gheorghe**  
(SS04/08P/A03-013 1715)  
(SS04a/09P/D-046 1400-295)  
(SW04/09P/A13-013 1715)
- MAROBHE, Isaac Muneji**  
(GAV.06/10A/A11-006 1010)
- MARQUARDT, Christian**  
(MC05/11P/A09-009 1720)
- MARRIN, Sylvie**  
(SS04b/10P/D-016 1400-200)
- MARSAL, Santiago**  
(GAI.10/09P/A11-006 1515)
- MARSH, D.R.**  
(MC05/08A/A09-003 0930)
- MARSH, Dan R.**  
(MC05/08A/A09-004 1000)
- MARSH, Daniel R.**  
(JSA01/08A/A12-005 1115)  
(MC05/07P/A09-001 1400)
- MARSILY, Ghislain (de)**  
(HW06/07P/D-001 1400-185)
- MARTI, Olivier**  
(MI05/10P/D-008 1400-174)
- MARTI, Urs**  
(G03/07P/D-039 1400-061)
- MARTIN, Eric**  
(JWH01/10P/C30-005 1600)  
(JWH01/09P/C30-001 1400)
- MARTIN, Gill**  
(MC11/10A/B19-005 1000)
- MARTIN, Jose Benito**  
(SS03/08A/D-025 0830-184)
- MARTIN, Rebekah E.**  
(JSP09/10P/B20-002 1430)  
(JSM14/09A/A05-008 1150)  
(MI06/09P/B20-002 1420)
- MARTIN, Russell**  
(HS04/07A/C30-002 1005)
- MARTINA, Mario L.V.**  
(HW07/10P/C25-013 1730)
- MARTINEC, Jaroslav**  
(JSH01/07P/C27-006 1600)
- MARTINEC, Zdenek**  
(G03/07P/D-066 1400-088)
- MARTINS, Jose V.**  
(JSM04/09A/B23-005 1115)
- MARTINS, Williams C.**  
(JSM04/09P/D-012 1400-049)
- MARTIROSYAN, Artak H.**  
(SS04b/10P/D-025 1400-209)
- MARTIUS, Olivia**  
(MI06/09P/B20-011 1740)
- MARTYSHKO, Peter S.**  
(GAI.10/09P/D-007 1615-126)  
(GAI.10/09P/D-007 1615-126)
- MARUBASHI, Katsuhide**  
(GAIll.09/10P/D-002 1400-114)  
(GAIll.09/11A/A11-003 0920)
- MARUMOTO, Masato**  
(GAIll.06/09P/A10-004 1500)
- MARUYAMA, Ken-ichi**  
(JSM15/07A/B18-004 1000)
- MARUYAMA, T.**  
(GAIll.06/09P/A10-011 1710)
- MARUYAMA, Takashi**  
(GAIll.06/11P/D-012 1400-064)  
(GAIll.06/10A/A01-010 1125)
- MARZA, Vasile I.**  
(SW04/09P/A13-004 1445)
- MAS, JORDI**  
(HS04/07P/C30-006 1655)
- MASAKAZU, Suzuki**  
(HW07/11P/D-038 1400-174)
- MASAKI, Kazuaki**  
(SS04a/09P/D-002 1400-251)
- MASHIKO, Wataru**  
(MC02/07P/D-009 1400-206)
- MASKEY, SHREEDHAR**  
(HS03/07A/C26-002 0930)
- MASLANIK, James A.**  
(JSP04/10P/A06-002 1420)
- MASLANIK, James Andrew**  
(JSH01/08P/D-006 1400-044)
- MASLOV, Lev**  
(JSA07/11A/D-001 0830-001)
- MASLOV, Lev Aleksandrovich**  
(JSA07/10P/A05-005 1520)
- MASON, Glenn**  
(GAIll.09/11A/A11-004 0950)
- MASSACAND, Alexia**  
(JSM14/08P/A05-002 1435)
- MASSON, A.**  
(GAIll.06/07P/D-011 1400-131)
- MASSON, A.**  
(GAIll.10/11A/D-006 0830-080)
- MASSON-DELMOTTE, Valérie**  
(MC12/08A/B19-002 1000)
- MASUDA, Akira**  
(JSP10/10A/B21-006 1100)  
(JSP10/11A/B21-004 0940)  
(JSP10/08P/D-008 1610-060)
- MASUDA, Akira**  
(JSP10/08P/B21-003 1450)
- MASUDA, Arichika**  
(SS04/07P/A03-008 1615)
- MASUDA, Kooiti**  
(HW06/07P/D-007 1400-191)
- MASUYAMA, Takahisa**  
(GAIll.11/09P/A15-005 1510)
- MATHE, Pierre-Etienne**  
(GAI.10/09P/D-013 1615-132)  
(GAV.07/07P/D-004 1400-145)
- MATHEWS, John**  
(GAIll.04/07A/A08-006 1050)
- MATHUR, P.**  
(JSH01/08A/C27-005 1050)
- MATIAS, Luis**  
(JSS07/09A/A02-010 1130)
- MATINDAS, Rudolf**  
(JSP11/08A/A10-002 0930)
- MATINDAS, Rudolf W.**  
(JSM11/10P/B18-006 1620)
- MATLI, Chandra Sekhar**  
(HW01/09P/D-001 1400-192)
- MATOS, Ana Cristina Cancorro**  
(G03/07P/D-069 1400-091)
- MATSUBARA, Kiyoshi**  
(JSS06a/08P/D-007 1400-085)
- MATSUBARA, Makoto**  
(SS03/08A/D-098 0830-257)  
(SS03/08A/D-108 0830-267)
- MATSUDA, Tatsuo**  
(SS03/08A/D-038 0830-197)
- MATSUDA, Tatuo**  
(SS03/08A/D-036 0830-195)
- MATSUDA, Yoshihisa**  
(MI05/10P/D-007)
- MATSUDA, Yoshihisa**  
(MC04/11A/B22-009 1115)  
(JSP10/08P/B21-004 1510)  
(JSP10/11A/B21-003 0920)
- MATSUI, Hiroshi**  
(GAIIV.02/07A/A07-001 0900)
- MATSUI, Kentaro**  
(HS02/09A/C24-001 0900)
- MATSUMAE, Yoshiaki**  
(JSG03/09P/D-019 1640-027)
- MATSUMI, Yutaka**  
(MI09/08P/B22-007 1640)  
(MI08/07P/B18-005 1640)  
(MI08/07P/D-001 1400-195)
- MATSUMOTO, Futoshi**  
(JSM04/09P/B23-005 1630)
- MATSUMOTO, Haruhisa**  
(GAIll.06/07P/D-019 1400-139)  
(GAIll.06/07P/D-015 1400-135)  
(GAIll.11/09A/A15-005 1010)  
(GAIll.06/08P/A02-009 1655)
- MATSUMOTO, Hirokazu**  
(G07/10P/D-013 1400-098)
- MATSUMOTO, Hiroshi**  
(GAIll.11/09P/A15-010 1700)  
(GAIll.11/09P/A15-011 1715)  
(GAIll.11/09P/A15-009 1645)  
(GAIll.11/09A/A15-006 1055)  
(GAIll.07/09P/A14-004 1510)  
(GAIll.05/07A/A06-006 1025)  
(GAIll.05/07P/D-021 1400-119)  
(GAIll.07/09P/A14-007 1640)  
(GAIll.05/07P/D-004 1400-102)  
(GAIll.11/09A/A15-008 1135)  
(GAIll.05/08A/A06-008 1055)
- (GAIll.07/10P/D-004 1400-109)
- MATSUMOTO, Hiroyuki**  
(JSS07/09P/A02-005 1500)
- MATSUMOTO, Jun**  
(MC03/11P/D-008 1400-183)  
(MC03/11P/D-014 1400-189)  
(MC02/07A/B20-003 1025)
- MATSUMOTO, Koji**  
(G02/07A/C25-011 1200)  
(GAIll.06/11P/D-007 1400-059)
- MATSUMOTO, Norio**  
(JSG01/08A/A01-004 0945)  
(SW05/10A/D-009 0900-253)
- MATSUMOTO, Takane**  
(JSM10/09P/D-009 1400-063)
- MATSUMOTO, Takeshi**  
(SS03/07P/A02-002 1415)  
(SS05/10A/A13-003 0900)
- MATSUMOTO, Takumi**  
(SW05/10P/A13-005 1505)
- MATSUMOTO, Toshiaki**  
(GAIll.11/09P/A15-003 1440)
- MATSUMOTO, Yo-ichi**  
(GAIll.06/08P/A02-012 1740)
- MATSUMURA, Kazuo**  
(JSA07/11A/D-017 0830-017)
- MATSUMURA, Shinji**  
(JSP04a/09P/D-005 1400-098)  
(MC11/11A/B19-008 1110)
- MATSUNAGA, Masataka**  
(GAIll.05/08A/A06-008 1055)
- MATSUNO, Yutaka**  
(HS04/07P/C30-001 1405)
- MATSUO, Hidenori**  
(SS04a/09P/D-001 1400-250)
- MATSUO, Takayo**  
(JSM14/08A/A05-011 1200)
- MATSUO, Tomoko**  
(GAIll.05/08P/A15-003 1500)
- MATSUOKA, A.**  
(GAIll.06/07P/D-010)
- MATSUOKA, Ayako**  
(GAIll.05/07P/D-005 1400-103)  
(GAIll.14/08A/D-003 0830-147)
- MATSUOKA, Hitoshi**  
(GAIll.06/07P/D-015 1400-135)  
(GAIll.06/08P/A02-009 1655)  
(GAIll.11/09A/A15-005 1010)
- MATSUOKA, Toshi**  
(SS03/07P/A02-003 1430)  
(SS03/08A/D-050 0830-209)
- MATSUOKA, Yumi**  
(JSS07/10A/A02-002 0845)
- MATSUSHIMA, Masaki**  
(GAI.08/08A/A14-007 1050)  
(GAI.08/08P/D-007 1400-142)
- MATSUSHIMA, Shinichi**  
(SS04a/09P/D-027 1400-276)
- MATSUSHIMA, Shinichi**  
(SS04b/10P/D-024 1400-208)
- MATSUSHIMA, Takeshi**  
(GAV.06/09P/D-014 1400-167)  
(SW03/10A/D-002 0830-237)  
(SW03/10A/D-004 0830-239)  
(SW03/10A/D-007 0830-242)  
(SW03/10A/D-003 0830-238)  
(JSG01/08P/D-020 1400-020)
- MATSUTOMI, Hideo**  
(JSS07/09P/A02-003 1430)  
(JSS07a/09P/D-003 1700-104)
- MATSUURA, T.**  
(HW07/10A/C25-003 1045)
- MATSUURA, Tadashi**  
(HS03/07P/C26-004 1445)  
(HS03/08A/C26-009 1100)
- MATSUURA, Tomonori**  
(HW03/11A/C30-004 0930)  
(MC02/07A/B20-005 1125)  
(MC02/07A/B20-002 1005)  
(MC02/07A/B20-005 1125)  
(JSM11/10P/B18-004 1500)
- MATSUURA, Yuki**  
(JSG01/08P/D-007 1400-007)

## INDEX

- (SS03/08A/D-037 0830-196)  
**MATSUWO, Norimichi**  
 (SS03/08A/D-017 0830-176)  
**MATSUYAMA, Hiroshi**  
 (JSH01/07P/C27-008 1640)  
 (JSG03/09P/D-004 1640-012)  
**MATSUYAMA, Masafumi**  
 (JSS07a/09P/D-007 1700-108)  
 (JSS07a/09P/D-017 1700-118)  
**MATSUYAMA, Masaji**  
 (JSP07/08A/B17-005 1100)  
**MATSUZAKA, Shigeru**  
 (JSG01/08A/A01-007 1050)  
**MATTHES, Katja**  
 (JSA08/09P/A08-006 1620)  
**MATTHEWS, Adrian J.**  
 (MC17/11A/B23-005 1030)  
 (MC17/11P/B23-009 1700)  
**MATTHEWS, Allan P.**  
 (GAIV.03/08P/A16-002 1430)  
 (GAIV.03/09A/A16-005 1100)  
**MATTHEWS, H. Damon**  
 (MC12/07A/B19-002 1000)  
**MATUMOTO, Koji**  
 (G02/07A/C25-014 1245)  
**MATUMURA, Shinji**  
 (MI06/09P/B20-006 1540)  
**MATURANA, Maturana Alejandro**  
 (JSG01/08P/D-035 1400-035)  
**MATURANA, Rodrigo**  
 (JSG01/07P/A01-004 1445)  
**MATVEEV, Rostislav F.**  
 (SS03/08A/D-048 0830-207)  
**MAURY, Rene**  
 (SS03/08A/D-061)  
**MAUS, Stefan**  
 (GAV.05/08A/A11-007 1110)  
 (JSA07/10A/A05-007 1110)  
 (GAV.04/07A/A11-002 0930)  
 (GAV.04/07A/A11-007 1140)  
**MAUSER, Wolfram**  
 (JWH01/10A/C30-007 1100)  
**MAUTNER, Ingo Meirold**  
 (JWH01/10P/D-001 1400-006)  
**MAUTNER, Ingo Meirold**  
 (JSM10/07A/B23-004 1020)  
**MAUTZ, Rainer E.**  
 (G04/08P/C25-001 1410)  
**MAUTZ, Rainer E.**  
 (G04/08P/D-024 1400-131)  
**MAY, Peter T.**  
 (HS03/07P/C26-002 1415)  
**MAY, Ru-Jun**  
 (MC03/11A/A07-008 1130)  
**MAY, Wilhelm**  
 (MC08/07P/B17-001 1400)  
**MAYER, Dennis**  
 (JSP06/07P/D-008 1400-015)  
 (JSP06/07P/D-006 1400-013)  
**MAYER, Helmut**  
 (HW06/07A/C31-006 1130)  
**MAYER-GUERR, Torsten**  
 (G02/07A/C25-005 1010)  
**MAYEWSKI, Paul A.**  
 (JSM10/07A/B23-007 1200)  
**MAYO, Steve**  
 (JSG03/09P/A12-007 1620)  
**MAYR, Hans G.**  
 (MC05/09P/A09-004 1520)  
**MAZELLE, Christian**  
 (GAIV.03/08A/A16-002 0900)  
 (GAIV.03/08A/A16-003 0930)  
 (GAIV.03/08A/A16-004 1000)  
 (GAIV.04/09P/A16-005 1650)  
 (GAIV.03/08A/A16-005 1040)  
 (GAIV.03/09A/A16-006 1120)  
**MAZO, Evgenya Lvovna**  
 (SS03/08A/D-077 0830-236)  
**MAZZOTTI, Stephane**  
 (SS04b/10P/D-017 1400-201)  
 (SS04b/10P/D-017 1400-201)  
**MBAJIORGU, Constantine C.**  
 (HW07/11P/D-011 1400-147)  
**MCADOO, David C.**  
 (JSG01/08A/A01-002 0915)  
**MCCARTHJY, Michael P.**  
 (GAILI.04/07P/A08-006 1605)  
**MCCLIMANS, Thomas A.**  
 (JSP10/11P/B21-004 1530)  
**MCCONNELL, John C.**  
 (MI03/08P/B18-003 1440)  
**MCCOOL, Donald**  
 (HS01/09P/D-023 1400-190)  
**MCCOY, Robert P.**  
 (GAILI.05/08A/A15-004 0950)  
**MCCREERY, Charles S.**  
 (JSS07/10P/A02-002 1415)  
 (JSS07/10P/A02-001 1400)  
**MCCROW, Adrian**  
 (HS04/07P/C30-004 1555)  
**MCCURDY, Shannon**  
 (GAILI.08/10A/A16-005 0945)  
**MCDONALD, N.Robb**  
 (JSP10/09A/B21-005 1040)  
**MCDONNELL, Jeff**  
 (HW06/07P/D-009 1400-193)  
 (HW06/07A/C31-004 1030)  
**MCDONNELL, Jeffrey J.**  
 (HW08/08P/C28-005 1600)  
 (HW01/10P/C26-003 1440)  
 (HW06/07A/C31-003 0950)  
**MCFADDEN, J.P.**  
 (GAILI.06/08P/A02-011 1725)  
**McFADDEN, James P.**  
 (GAILI.08/10A/A16-004 0925)  
**MCGLYNN, Brian**  
 (HW06/07A/C31-004 1030)  
**MCGUFFIE, K.**  
 (MC11/11P/B19-001 1400)  
**MCGUIRE, Kevin James**  
 (HW06/07A/C31-004 1030)  
 (HW06/07P/D-009 1400-193)  
**MCHIRGUI, Radhia**  
 (HW03/11A/C30-005 0950)  
 (HW03/11A/C30-009 1130)  
**MCINTYRE, Neil Robert**  
 (HW08/09A/C28-003 0950)  
**MCKENNA, Daniel S.**  
 (MC05/07A/A09-002 0930)  
**MCLANDRESS, Charles**  
 (MC05/09P/A09-002 1430)  
**MCMILLON, Kelly**  
 (GAILI.06/10A/A01-009 1105)  
**MCNUTT, Stephen R.**  
 (U7/11P/D32-003 1505)  
**MCPHADEN, Michael**  
 (JSP06/07A/B21-006 1120)  
**MCPHEE, Miles G.**  
 (JSP04/09P/A06-003 1430)  
**MCPHERRON, Robert L.**  
 (GAILI.05/07A/A06-011 1205)  
 (GAILI.05/07P/D-011 1400-109)  
 (GAILI.05/08A/A06-004 0925)  
**MEANS, J.D.**  
 (GAV.04/07A/A11-003 0950)  
**MECHOSO, C. Roberto**  
 (MC03/10P/A07-005 1600)  
**MECHOSO, Carlos Roberto**  
 (MI05/10P/B17-001 1400)  
 (MC03/10A/A07-006 1050)  
**MEDINA, Cesar Francisco**  
 (JSG03/09P/D-025 1640-033)  
**MEDJITOVA, Zarema Arslanovna**  
 (SS03/08A/D-141 0830-300)  
**MEDVEDEV, Andrey V.**  
 (GAILI.06/11P/D-004 1400-056)  
**MEDVEDEV, D.**  
 (SW05/10A/D-010 0900-254)  
**MEDVEDEV, Peter P.**  
 (SW05/10P/A13-006 1520)  
**MEDVEDEV, Petr P.**  
 (G03/07P/D-052 1400-074)  
 (SW05/10A/D-010 0900-254)  
**MEEK, C.E.**  
 (MC05/10A/A09-010 1210)  
**MEEK, Chris**  
 (MC05/09P/A09-003 1500)  
**MEGURO, Kimiro**  
 (JSS07b/10P/D-004 1700-050)  
**MEHDIZADEH, Hossein**  
 (JSM04/09P/D-017 1400-054)  
**MEHRABIAN, Shayesteh**  
 (JSA07/11A/D-036 0830-036)  
 (SS04/09A/A03-003 0930)  
**MEISSNER, Katrin J.**  
 (MC12/07A/B19-002 1000)  
**MEISSNER, Rolf**  
 (JSA07/11A/D-024 0830-024)  
**MEITIN, Jose G.**  
 (MC03/10P/A07-002 1420)  
**MELCHINOV, Viktor Petrovich**  
 (JSH01/07P/C27-005 1520)  
**MELESHKO, Valentin P.**  
 (MC11/11P/D-003 1400-196)  
**MELIKHOV, Vjacheslav Romanovich**  
 (G03/07P/D-022 1400-044)  
**MELIKHOV, Vyacheslav**  
 (SS03/08A/D-077 0830-236)  
**MELIKSETYAN, Ashot**  
 (SS05/10A/A13-009 1045)  
**MELLOH, Rae A.**  
 (JWH01/10P/C30-003 1440)  
**MELOSANTOS, Ma. Lynn Paladio**  
 (SW05/10A/D-003 0900-247)  
**MELZER, Yosef**  
 (G07/10P/D-005 1400-090)  
**MEMBERS, A.D.1999-2001**  
 (SS05/10A/A13-011 1115)  
**MEMBERS, A.D.2002**  
 (SS05/10A/A13-011 1115)  
**MEMBERS, Voluntary**  
 (SS05/10A/A13-011 1115)  
**MENARY, Wayne**  
 (HW01/10A/C26-006 1050)  
 (HS01/09P/D-020 1400-187)  
**MENDES-VICTOR, Luis**  
 (JSS07/09A/A02-010 1130)  
**MENDIONDO, Eduardo M.**  
 (HW07/11A/C25-001 0830)  
**MENEMENLIS, Dimitris**  
 (JSP06/08A/B21-006 1130)  
**MENENDEZ, Claudio**  
 (MC08/07P/B17-007 1550)  
**MENG, C.-I.**  
 (GAILI.10/11A/D-016 0830-090)  
**MENG, Ching**  
 (GAILI.05/07P/D-014 1400-112)  
**MENG, Ching -I**  
 (GAILI.10/11A/D-018 0830-092)  
**MENG, Ching-I**  
 (GAILI.05/07P/D-017 1400-115)  
 (GAILI.09/11P/A11-005 1600)  
**MENG, Hua**  
 (SW05/10A/D-007 0900-251)  
**MENGEL, John S.**  
 (MC05/09P/A09-004 1520)  
**MENICHETTI, Marco**  
 (JSA07/11A/D-047 0830-047)  
**MENK, F.W.**  
 (GAILI.10/10P/A01-003 1440)  
**MENK, Fred**  
 (GAILI.10/11A/D-010 0830-084)  
**MENK, Fred W.**  
 (GAV.04/07A/A11-003 0950)  
 (GAILI.10/10P/A01-001 1400)  
 (GAILI.10/11A/D-008 0830-082)  
 (GAILI.10/10P/A01-008 1620)  
**MENON, Harilal Bhaskara**  
 (JSG03/09P/D-008 1640-016)  
**MENVIELLE, Michel**  
 (GAI.10/09A/A11-011 1200)  
**MENYE, Aboagye**  
 (HS02a/07P/D-034 1545-180)  
 (HS02/07P/C24-034 1508)  
**MENZEL, Annette**  
 (JSA09/10A/A08-002 0900)  
**MERA, Keisuke**  
 (GAILI.07/10P/D-007 1400-112)  
**MERCADO, Aurelio**  
 (JSS07/10A/A02-014 1200)  
**MERCIER, Franck**  
 (JSG03/09P/D-003 1640-011)  
**MERCIER, Jean Luc**  
 (JSM10/08P/B23-006 1620)  
**Mercury Exploration WG,**  
 (GAILI.14/08A/D-004 0830-148)  
**Mercury WG,**  
 (GAILI.14/08A/D-005 0830-149)  
**MEREDITH, Nigel P.**  
 (GAILI.10/11A/A01-013 1130)  
**MERGENTHALER, J.L.**  
 (MC05/11A/A09-008 1200)  
**MERT, Aydin**  
 (SW04/09P/A13-009 1615)  
**MERZ, Ralf**  
 (HW08/09A/C28-001)  
**MERZ, Ralf**  
 (HS02/09A/C24-011 1145)  
**METALLINO, Fiori-Anastasia**  
 (GAILI.08/10A/A16-006 1005)  
**METALLINO, Fiori-Anastasia I.**  
 (GAILI.06/07P/D-009 1400-129)  
**METELKA, Ladislav**  
 (MC08/07P/B17-011 1710)  
**METIVIER, Laurent**  
 (JSS06a/08P/D-028 1400-106)  
**METREVELI, George S.**  
 (JSM11/10P/D-006 1700-015)  
**MÉTRIS, Gilles**  
 (G04/08P/D-021 1400-128)  
**MEWALDT, Richard A.**  
 (GAILI.09/11A/A11-004 0950)  
**MEYBECK, Michel**  
 (JSM03/08P/A13-008 1640)  
 (HS02/07A/C24-014 0952)  
 (HS02a/07P/D-014 1545-160)  
**MEYER, Melissa G.**  
 (GAILI.06/10A/A01-004 0920)  
**MEYER, Ulrich**  
 (G02/07A/C25-002 0920)  
**MEYERS, Steven D.**  
 (JSP07/08A/B17-004 1010)  
**MEZA, Amalia Margarita**  
 (JSG03/10A/A12-008 1120)  
**MHAMMDI, Nadia**  
 (JSP08/09P/D-002 1400-101)  
**MICKUS, Kevin L.**  
 (JSA07/11A/D-045 0830-045)  
**MIESEN, Peter**  
 (MC02/07P/D-005 1400-202)  
**MIGLIACCIO, Federica**  
 (G04/08P/D-017 1400-124)  
**MIHAILESCU, Mihaela**  
 (MI05/10P/D-002 1400-169)  
**MIHAILOV, Vladimir Petar**  
 (SS04b/10P/D-049 1400-233)  
**MIHANOVIC, Hrvoje**  
 (JSM03/08A/A13-007 1120)  
**MIKAMI, Toshifumi**  
 (JSS07a/09P/D-006 1700-107)  
**MIKHAILOV, Valentin O.**  
 (JSA07/11A/D-021 0830-021)  
**MIKHAYLOVSKAYA, Irina Borisovna**  
 (JSS07b/10P/D-003 1700-049)  
**MIKULA, Karol**  
 (G04/08P/D-022 1400-129)  
**MIKUMO, Takeshi**  
 (JSG01/08P/D-023 1400-023)  
**MILAN, Stephen Eric**  
 (GAILI.06/10A/A01-011 1145)  
**MILAN, Steve E.**  
 (GAILI.05/07P/D-016 1400-114)  
**MILANOVSKY, Svet Yurievich**  
 (JSA07/11A/D-007 0830-007)  
 (JSH01/07P/C27-001 1400)  
 (SS03/08A/D-072 0830-231)

- MILINEVSKI, Gennadi**  
(GAIH.10/10P/A01-008 1620)
- MILLER, Alvin J.**  
(MI05/09P/B17-009 1730)
- MILLER, Kate**  
(SS03/07A/A02-006 1045)  
(SS03/08A/D-004 0830-163)
- MILLER, Norman L.**  
(HW06/07P/D-010 1400-194)  
(JWH01/09P/C30-003 1440)
- MILLER, Ros**  
(HS04/07A/C30-002 1005)
- MILLIFF, Ralph F.**  
(MC17/10P/B23-004 1500)
- MILLS, Bren**  
(JSP10/11A/B21-008 1130)
- MILNE, Glenn A.**  
(SS03/07P/A02-005 1500)
- MILNER, Alexander M.**  
(HW02/11A/C31-004 0950)
- MILOVANOV, Alexander V.**  
(GAIH.07/09A/A14-005 1100)
- MIN, Kyung Duk**  
(JSA07/10P/A05-003 1440)
- MIN, Seung-Ki**  
(MC08/07P/B17-002 1415)
- MINACAPILLI, Mario**  
(HS01/08A/C29-005 1130)
- MINARECH, Vladimir**  
(G04/08P/D-022 1400-129)
- MINATO, Shinnya**  
(JSP06/07P/B21-003 1450)
- MINDA, Haruya**  
(JSM14/08A/A05-010 1145)  
(JSM14/09P/D-012 1400-076)
- MINIHANE, Michele R.**  
(JSM03/08A/A13-002 0920)
- MININ, Alexander Andreevich**  
(MI07/11P/B18-007 1620)
- MINNETT, Peter J.**  
(JSP09/11A/B20-005 0945)  
(JSP09/10A/B20-005 1015)
- MINOBE, Shoshiro**  
(JSP10/10A/B21-002 0900)  
(JSP04/10P/A06-009 1700)
- MINOR, Scott A.**  
(GAV.07/07P/A13-009 1700)
- MINTER, Cliff**  
(GAIH.05/07A/D-001 0830-017)
- MINTS, Michael V.**  
(JSA07/10A/A05-005 1000)
- MINTZ, Mikhail V.**  
(JSA07/11A/D-021 0830-021)
- MIRANDA, J.Miguel**  
(JSS07/09A/A02-010 1130)
- MIRANDA, Pedro**  
(JSS07/09A/A02-010 1130)
- MIRANDA, Pedro M.**  
(JSS07/09P/A02-006 1515)
- MIRONOV, Yury V.**  
(JSS06b/10P/D-021 1400-045)
- MIRZAEI, Noorbakhsh**  
(SS03/08A/D-022 0830-181)
- MIRZAJANI, Alireza**  
(JSP07/08P/B17-005 1530)
- MISAWA, Hiroaki**  
(GAIH.14/08A/D-006 0830-150)  
(GAIH.14/07P/A12-009 1705)  
(GAIH.14/07P/A12-010 1720)  
(GAIH.14/07A/A12-007 1155)  
(GAIH.14/07A/A12-006 1140)  
(GAIH.06/08P/A02-012 1740)
- MISAWA, Yoshifumi**  
(JSG03/09P/D-020 1640-028)
- MISHRA, Anil**  
(HW07/11P/D-024 1400-160)
- MISHRA, D.C.**  
(JSA07/11A/D-035 0830-035)  
(JSA07/11A/D-043 0830-043)  
(SW03/10A/D-009 0830-244)  
(JSA07/11A/D-039 0830-039)
- MISHRA, Dinesh Chandra**  
(SW03/10P/A04-009 1615)
- MISHRA, Dinesh Chandra**  
(JSA07/11A/D-042 0830-042)
- MISHRA, V.D.**  
(JSH01/08A/C27-005 1050)
- MISONOU, Kazuyoshi**  
(SW04/09P/A13-014 1730)
- MISUMI, R.**  
(JSM14/09P/D-001 1400-065)
- MISUMI, Ryohei**  
(JSM14/09P/D-023 1400-087)
- MISUMI, Ryohei**  
(JSM14/09P/D-006 1400-070)  
(JSM14/07P/A05-003 1450)  
(MC03/11P/D-017 1400-192)
- MITCHELL, David**  
(GAIV.03/08A/A16-002 0900)
- MITCHELL, David L.**  
(GAIV.03/09A/A16-002 0930)  
(GAIV.03/08A/A16-007 1130)
- MITCHELL, Donald G.**  
(GAIH.06/08P/A02-001 1400)
- MITCHELL, Elizabeth J.**  
(GAIH.09/11P/A11-004 1510)
- MITCHELL, J. Kent**  
(HW07/11P/D-030 1400-166)
- MITCHELL, Jeremy J.**  
(GAIV.02/07P/A07-004 1600)
- MITCHELL, N.J.**  
(MC05/10A/A09-010 1210)
- MITKIN, Vladimir Y.**  
(JSP10/08P/D-014 1610-066)
- MITROVICA, Jerry X.**  
(JSS06/07P/A04-010 1720)
- MITSUTERU, SATO**  
(GAIH.04/07A/A08-003 0940)
- MIURA, Akira**  
(GAIH.05/07P/D-013 1400-111)
- MIURA, Satoshi**  
(JSG01/08P/D-006 1400-006)  
(JSG01/08P/D-002 1400-002)
- MIURA, Seiichi**  
(SS03/08A/D-107 0830-266)
- MIURA, Seiichi**  
(SS03/08A/D-109 0830-268)  
(SS03/07A/A02-003 0930)
- MIURA, Shouhei**  
(SW05/10P/A13-005 1505)
- MIYACHI, Yoshinori**  
(SS03/08A/D-034 0830-193)
- MIYAGAWA, Kouji**  
(MI03/08A/B18-009 1150)
- MIYAJI, Naomichi**  
(JSS07a/09P/D-005 1700-106)
- MIYAKE, Hiroe**  
(SW04/09P/A13-015 1745)  
(SS04/08A/A03-009 1045)  
(SS04a/09P/D-032 1400-281)
- MIYAKE, Toshihide**  
(JSS07b/10P/D-007 1700-053)
- MIYAKOSHI, Jun'ichi**  
(SS04a/09P/D-012 1400-261)
- MIYAKOSHI, Junichi**  
(SS04b/10P/D-023 1400-207)
- MIYAKOSHI, Katsuyoshi**  
(SS03/08A/D-099 0830-258)
- MIYAKOSHI, Ken**  
(SS04/08A/A03-009 1045)  
(SS04a/09P/D-031 1400-280)  
(SS04a/09P/D-028 1400-277)  
(SS04/08A/A03-013 1145)
- MIYAMACHI, Hiroki**  
(SW03/10A/D-002 0830-237)  
(SW03/10A/D-004 0830-239)  
(SW03/10A/D-003 0830-238)  
(SW03/10A/D-007 0830-242)
- MIYAMACHI, Hiroki**  
(SS03/08A/D-017 0830-176)
- MIYAMURA, Kazutoshi**  
(GAIH.04/07P/A08-004 1505)
- MIYASHITA, Kaoru**  
(JSG01/07A/A01-003 0930)
- MIYASHITA, Yukari**  
(SS04b/10P/D-038 1400-222)
- MIYASHITA, Yukinaga**  
(GAIH.05/07P/D-010 1400-108)
- MIYASHITA, Kaoru**  
(SS03/07P/A02-014 1745)
- MIYATA, Shyusuke**  
(HW06/07A/C31-002 0930)
- MIYATAKE, Takashi**  
(SS04a/09P/D-016 1400-265)
- MIYAZAKI, Kazuyuki**  
(MC05/07P/D-010 1400-217)
- MIYAZAKI, Shin'ichi**  
(JSG01/07A/A01-002 0915)  
(JSS07b/10P/D-007 1700-053)  
(JSG01/08P/D-021 1400-021)  
(JSG01/08P/D-012 1400-012)
- MIYAZAKI, Takeshi**  
(JSP10/10P/B21-004 1510)  
(JSP10/10P/B21-003 1450)
- MIYOSHI, Takayuki**  
(SS03/08A/D-015 0830-174)
- MIYOSHI, Yoshizumi**  
(GAIH.06/07P/D-010 1400-130)  
(GAIH.14/08A/D-006 0830-150)  
(GAIH.06/08P/A02-012 1740)  
(GAIH.14/07P/A12-009 1705)  
(GAIH.06/07P/D-020 1400-140)  
(GAIH.06/08P/A02-008 1640)
- MIZUNO, Akira**  
(MC05/07P/D-008 1400-215)
- MIZUNO, Hiroo**  
(GAV.05/09P/D-007 1400-151)
- MIZUNO, Kiyohide**  
(SS03/08A/D-041 0830-200)  
(SS04a/09P/D-038 1400-287)
- MIZUOCHI, Yukihiko**  
(SS03/08A/D-036 0830-195)
- MIZUYAMA, Takahisa**  
(HS01/09P/C29-006 1540)  
(HW06/07A/C31-002 0930)
- MKHANDI, Simon Hosea**  
(HW01/09P/D-050 1400-241)
- MLADEK, Richard**  
(MC08/07P/B17-011 1710)
- MLAWER, Eli J.**  
(MC11/10P/B19-007 1630)
- MO, Jun**  
(JSP09/10P/B20-005 1515)
- MO, Xingguo**  
(HS03/08P/C26-008 1600)
- MOALEM, Meir**  
(GAIH.04/07A/A08-009)
- MOAYYED, Mohsen**  
(SW03/10A/D-008 0830-243)
- MOBBS, Stephen D.**  
(JWH01/09A/C30-005 1020)
- MOCANU, Victor I.**  
(JSP11/07P/A10-003 1500)  
(SS03/08A/D-076 0830-235)
- MOCHIZUKI, Kimihiro**  
(SS03/08A/D-122)
- MOCHIZUKI, Kimihiro**  
(SS03/08A/D-105 0830-264)  
(SS03/08A/D-002 0830-161)  
(SS03/08A/D-120 0830-279)  
(SS03/08A/D-011 0830-170)  
(SS03/08A/D-067 0830-226)  
(JSS06/09P/A04-009 1700)  
(JSS06/07P/A04-005 1540)  
(SS03/08A/D-017 0830-176)
- MOCZO, Peter**  
(SS04/07A/A03-011 1215)
- MODOLO, Ronan**  
(GAIV.03/09A/A16-005 1100)  
(GAIV.03/08P/A16-002 1430)
- MOEBIUS, E.**  
(GAIH.09/11A/A11-006 1110)
- MOEBIUS, Eberhard**  
(GAIH.09/11A/A11-005 1040)
- MOELLER, Heinz-Dieter**  
(GAV.06/09P/D-012 1400-165)
- MOFJELD, Harold O.**  
(JSS07/10P/A02-002 1415)
- MOGAMI, Junichi**  
(MI07/10P/D-004 1400-180)
- MOGHADAM, Abdolhosein**  
(JSP11/08A/A10-005 1050)
- MOGHADDAM, Peyman Poor**  
(SS03/08A/D-011 0830-170)
- MOGHADDAM, Peyman Poor**  
(SS03/08A/D-002 0830-161)
- MOGI, Hidenori**  
(SS04a/09P/D-024 1400-273)
- MOGI, Tohru**  
(GAI.10/09P/D-012 1615-131)
- MOGI, Toru**  
(JSA07/10P/A05-003 1440)  
(GAI.10/09A/A11-002 0915)
- MOGILEV, Nikolay Yu.**  
(JSG03/09P/A12-002 1420)
- MOHAMAD, Randa**  
(SW04/09P/A13-002 1415)  
(JSS06/10A/A04-008 1110)
- MOHAMED, Badr Saad**  
(HS02a/07P/D-036 1545-182)  
(HS02/07P/C24-036 1516)
- MOHAMED, Mohamed**  
(JSG03/09P/A12-007 1620)
- Mohankumar K.**  
(MC03/11A/A07-009 1150)
- Mohd Md Sahat**  
(HS02/08P/C24-012 1715)
- MOHUNGOO, Satyajay Prayagsingh**  
(HW05/10P/D-004 1400-159)
- MOISEENKO, Sergei A.**  
(SS03/08A/D-048 0830-207)
- MOKHOV, Igor I.**  
(MC08/07A/B17-009 1205)  
(MC11/10A/B19-002 0900)
- MOLDER, Meelis**  
(MI07/11P/B18-001 1400)
- MOLDOVEANU, Carmen Liliana**  
(SS04b/10P/D-026 1400-210)
- MOLDWIN, M.B.**  
(GAIH.06/08A/A02-007 1135)
- MOLDWIN, Mark**  
(GAIH.10/11A/A01-003 0900)
- MOLDWIN, Mark B.**  
(GAIH.06/08A/A02-003 0940)  
(GAIH.08/10A/A16-012 1210)  
(GAIH.10/10P/A01-002 1420)
- MOLINARI, John E.**  
(MC03/10P/A07-004 1520)
- MOLLAIOI, Fabrizio**  
(SS04/07P/A03-001 1400)
- MOLODOVSKAYA, Marina S.**  
(HS02a/07P/D-020 1545-166)  
(HS02/07P/C24-020 1412)
- MOLODOVSKAYA, Marina Stanislavovna**  
(HS02a/07P/D-019 1545-165)  
(HS02/07P/C24-019 1408)
- MOLOTCH, Noah**  
(JWH01/09P/C30-006 1540)
- MOLTENI, Franco**  
(MC03/11A/A07-004 0950)
- MONADJEMI, Parviz**  
(HW04/09P/C31-002 1420)
- MONADJEMI, Parzhang**  
(HW01/10A/C26-004 0930)
- MONAGHAN, Andrew J.**  
(JSM10/08A/B23-010 1210)
- MONCRIEFF, Mitchell W.**  
(MC17/11A/B23-007 1120)
- MONCUQUET, Michel**  
(GAIH.14/07A/A12-004 1050)
- MONIN, Andrey Sergeevich**  
(MC12/08P/B19-008 1715)
- MONREAL MAC-MAHON, Ricardo**  
(GAIH.10/11A/A01-003 0900)
- MONSELESAN, D.P.**  
(GAIH.06/11P/D-017 1400-069)
- MONTABONE, Luca**  
(MC04/11P/B22-001 1400)

# INDEX

- MONTAGNER, Jean Paul**  
(JSS06/10A/A04-004 0930)
- MONTANES RODRIGUEZ, Pilar**  
(JSA09/10A/A08-003 0930)
- MONTGOMERY, Michael Thomas**  
(JSP10/10P/B21-006 1610)
- MOON, Wooil M.**  
(JSG03/09P/D-018 1640-026)
- MOONEY, Walter D.**  
(JSA07/11A/D-026 0830-026)  
(JSA07/10A/A05-001 0830)  
(JSA07/11A/D-027 0830-027)  
(JSS06b/10P/D-005 1400-029)  
(JSA07/11A/D-024 0830-024)  
(JSA07/11A/D-025 0830-025)
- MOORE, Angelyn W.**  
(G07/10P/D-018 1400-103)
- MOORE, G.W.K.**  
(JSP09/10P/B20-002 1430)  
(JSM14/09A/A05-008 1150)  
(MI06/09P/B20-002 1420)  
(JSM14/09A/A05-009 1205)
- MOORE, J.R.**  
(MI03/09A/D-001 0900-244)  
(MI03/08A/B18-002 0850)
- MOORE, James A.**  
(JSP04/09A/A06-005 1050)
- MOORE, John**  
(JSH01/08P/D-010 1400-048)
- MOORE, John C.**  
(MC12/08A/B19-005 1115)
- MOORE, John Christopher**  
(MI05/10P/B17-008 1710)
- MOORE, Kent**  
(MI05/11P/B17-005 1520)  
(JSP09/10A/B20-010 1200)
- MOORE, R. Dan**  
(HW02/11A/C31-006 1110)
- MOORE, Thomas E.**  
(GAI03/08A/A02-007 1135)  
(GAI03/08A/A06-011 1150)
- MORAILA, Carlos R.**  
(G04/08P/C25-004 1510)
- MORALES, Jesus**  
(JSP06/07A/B21-001 0900)
- MORALES, Jose**  
(SS03/08A/D-025 0830-184)
- MORDOVSKAYA, Valentina G.**  
(GAI03/14/08A/D-001 0830-145)  
(GAI03/03/08P/A16-006 1630)  
(GAI03/03/09A/A16-008 1220)
- MORDVINTSEV, Oleg Petrovich**  
(SS03/07P/A02-006 1515)
- MOREAU, Frederique**  
(GAI10/09P/D-013 1615-132)
- MOREDA, Fekadu G.**  
(HS03/08A/C26-001 0830)
- MOREDA, Fekadu G.**  
(HW08/08A/C28-005 1000)
- MORENO, Bladimir**  
(SS03/08A/D-151 0830-310)
- MORESI, Louis**  
(SS03/08A/D-147 0830-306)  
(SW05/10P/A13-009 1615)
- MORETTI, Sandro**  
(HS01/08P/C29-006 1600)
- MORGAN, V.I.**  
(MC12/08A/B19-002 1000)
- MORI, Akiko**  
(MC05/07P/D-005 1400-212)  
(MC05/10A/A09-001 0830)
- MORI, Atsushi**  
(JSP10/09P/B21-010)
- MORI, Atsushi**  
(MI05/09A/B17-008 1150)  
(JSP10/09P/B21-009 1700)
- MORI, Hiroataka**  
(GAI06/09P/A10-005 1515)
- MORI, Kazumasa**  
(MC02/08A/B20-005 1100)
- MORI, Masahiro**  
(GAI03/11/09P/A15-004 1455)
- MORI, Shuichi**  
(MC17/11P/B23-006 1600)
- MORI, Shuichi**  
(MC17/11A/B23-004 0940)
- MORI, Shuichi**  
(MC03/11P/D-007 1400-182)  
(MC03/11P/D-009 1400-184)
- MORI, Syuichi**  
(MC03/10P/A07-008 1720)
- MORIJI, Rie**  
(GAV.06/10A/A11-002 0850)  
(GAV.06/09P/D-005 1400-158)  
(JSA07/11A/D-016 0830-016)
- MORIKAWA, Nobuyuki**  
(SS04b/10P/D-004 1400-188)  
(SS04a/09P/D-029 1400-278)  
(SS04b/10P/D-020 1400-204)
- MORIN, Efrat**  
(HW08/08P/C28-004 1520)  
(HS03/08A/C26-003 0915)
- MORIOKA, Akira**  
(GAI03/14/08A/D-006 0830-150)  
(GAI03/06/08P/A02-012 1740)  
(GAI03/14/07A/A12-006 1140)  
(GAI03/14/07A/A12-007 1155)  
(GAI03/05/07P/D-012 1400-110)  
(GAI03/14/07P/A12-009 1705)  
(GAI03/06/08P/A02-008 1640)
- MORISON, James H.**  
(JSP04/10P/A06-005 1520)  
(JSP04b/10P/D-003 1400-022)  
(JSP04/09A/A06-006 1110)  
(JSP04/10P/A06-001 1400)  
(JSP04/09P/A06-003 1430)
- MORISON, James Howe**  
(JSP04/09A/A06-001 0900)
- MORISON, Jamie**  
(JSP04/09P/A06-002 1415)
- MORISON, Russel**  
(HS03/08P/C26-010 1630)
- MORITA, Osamu**  
(JSM14/08A/A05-009 1130)
- MORITZ, Richard E.**  
(JSP04/09P/A06-002 1415)
- MORIWAKI, H.**  
(JSM14/09P/D-001 1400-065)
- MORIYA, Takeo**  
(SS03/08A/D-106 0830-265)
- MORNER, Nils A.**  
(JSA09/10A/A08-010 1200)
- MOROHOSHI, Toshikazu**  
(JSG03/09P/D-022 1640-030)
- MOROZ, Yuri F.**  
(JSA07/11A/D-014 0830-014)
- MOROZOV, Victor E.**  
(JSP11/07P/A10-009 1740)  
(JSS07/10P/A02-008 1600)
- MORRELL, Chloe**  
(MC12/08A/B19-006 1130)
- MORRILL, Jeff Stanley**  
(GAI04/07P/A08-002 1425)  
(JSA08/09P/A08-003 1450)
- MORRIS, Elizabeth M.**  
(JSM10/07A/B23-005 1100)
- MORRIS, Ray**  
(GAI06/11P/D-017 1400-069)
- MORRIS, Ray J.**  
(GAI03/10/11A/D-005 0830-079)
- MORRISON, John M.**  
(JSP07/08A/B17-002 0930)
- MORSY, Essam A.**  
(SW05/10A/D-004 0900-248)  
(SW05/10P/A13-015 1745)
- MOSEGAARD, Klaus Teddy**  
(JSS06/09P/A04-006 1600)
- MOSHONKIN, Sergey Nikolaevich**  
(MC12/07P/B19-004 1515)
- MOTOI, Tatsuo**  
(JSP04/09A/A06-007 1130)
- MOTOKI, Atsushi**  
(JSP10/08P/D-006 1610-058)
- MOTOYA, Ken**  
(MC03/11P/A07-004 1520)  
(JSH01/08P/D-012 1400-050)
- MOTOYAMA, Hideaki**  
(JSM10/09P/D-002 1400-056)
- MOTOYOSHI, Hiroki**  
(JSH01/08P/D-009 1400-047)
- MOUDRY, Dana**  
(GAI04/07P/A08-001 1400)
- MOUDRY, Dana R.**  
(GAI04/07P/A08-005 1540)
- MOUKIS, Christopher**  
(GAI03/05/08A/A06-003 0900)
- MOUKIS, C.**  
(GAI03/09/11A/A11-006 1110)
- MOULIN, Bertrand**  
(HS01/09P/D-022 1400-189)
- MOULIN, Frédéric Y.**  
(JSP10/11P/B21-003 1510)
- MOURI, Kouichi**  
(HW01/09P/D-043 1400-234)
- MOUSAVI, Sayed-Farhad**  
(HS03/08P/C26-007 1545)
- MOWLABACCUS, Farook**  
(HW05/10A/C31-007 1005)
- MOYA, Aaron**  
(SS04a/09P/D-017 1400-266)
- MOZER, Forrest**  
(GAI03/11/09P/A15-008 1620)
- MU, Mu**  
(JSM14/09P/D-014 1400-078)  
(MC04/11A/B22-011 1200)
- MUCO, Betim**  
(JSP11/08P/D-006 1400-075)
- MUDELSEE, Manfred**  
(JSM14/08P/A05-001 1400)  
(HS02/09A/C24-012 1200)
- MUDRY, J.**  
(HS02/08P/C24-006 1515)
- MUEHLBACHLER, Stefan**  
(GAI03/05/07A/A06-004 0945)
- MUELLER, Birgit**  
(JSS06/08A/A04-006 1010)
- MUELLER, Felix**  
(G03/07P/D-063 1400-085)
- MUELLER, Gerd**  
(MI06/09P/B20-009 1700)
- MUELLER, Juergen**  
(G03/07P/D-047 1400-069)  
(G03/07P/D-024 1400-046)  
(G02/07A/C25-004 0955)
- MUELLER, Karl J.**  
(SW04/09P/A13-012 1700)
- MUELLER, Karl J.**  
(SS03/08A/D-040 0830-199)
- MUELLER, Rolf**  
(MC05/07P/A09-007 1700)
- MUELLER, Rolf**  
(MC05/07A/A09-002 0930)
- MUELLER, Wolfgang**  
(MI05/10A/B17-003 0930)
- MUKAI, T.**  
(GAI03/05/07A/A06-003 0930)  
(GAI03/05/08A/A06-006 0955)
- MUKAI, Toshifumi**  
(GAI03/05/07A/A06-001)
- MUKAI, Toshifumi**  
(GAI03/08/10A/A16-001 0830)  
(GAI03/05/07P/D-009 1400-107)  
(GAI03/05/08A/A06-005 0940)  
(GAI03/05/07P/D-008 1400-106)  
(GAI03/05/08A/A06-001 0830)  
(GAI03/05/07A/A06-002 0915)  
(GAI03/14/08A/D-005 0830-149)  
(GAI03/05/07P/D-004 1400-102)  
(GAI03/14/08A/D-004 0830-148)  
(GAI03/11/10P/D-002 1400-117)  
(GAI03/05/07P/D-019 1400-117)  
(GAI03/02/07P/A07-003 1510)  
(GAI03/05/07P/D-014 1400-112)  
(GAI03/03/08A/A16-009 1220)  
(GAI03/05/07P/D-010 1400-108)
- MUKAI, Toshihumi**  
(GAI06/10A/A01-011 1145)
- MUKHUPADAAYA, S.G.**  
(SS03/08A/D-069 0830-228)
- MUKOUGAWA, Hitoshi**  
(MC05/10A/A09-004 0940)  
(MI06/09P/B20-004 1500)  
(MC05/10A/A09-001 0830)  
(MI05/10A/B17-006 1100)
- MUKOUGAWA, Hitoshi**  
(MI05/11A/B17-005 0950)
- MUKTEPAVEL, Larisa S.**  
(JSM10/09P/D-005 1400-059)
- MUKUL, Malay**  
(SS03/08A/D-079 0830-238)
- MULLER, Jean-Francois J.**  
(JSM04/09A/B23-007 1215)
- MUNEKANE, Hiroshi**  
(JSG01/08A/A01-007 1050)
- MUNEYAMA, Kei**  
(JSP09/11P/B20-002 1415)
- MUNIR, Ahmad**  
(HS01/08P/C29-005 1520)  
(HS01/08P/C29-009 1700)
- MUNIR, Sarfraz**  
(HS04/07P/C30-001 1405)
- MUNKHSAIKHAN, Adiya**  
(SS04b/10P/D-030 1400-214)
- MUNTEANU, Vera**  
(HW01/10A/C26-003 0910)
- MURADYAN, Hrachya Sedrak**  
(SS04b/10P/D-039 1400-223)
- MURAI, Mari**  
(MI07/11P/B18-006 1600)
- MURAI, Yoshio**  
(SS03/08A/D-056 0830-215)  
(SS03/08A/D-005 0830-164)  
(SS03/08A/D-114 0830-273)  
(SS03/07A/A02-009 1130)
- MURAKAMI, Atsushi**  
(JSS07b/10P/D-017 1700-063)
- MURAKAMI, Hiroshi**  
(SW03/10A/D-003 0830-238)
- MURAKAMI, Hiroshi**  
(SW03/10A/D-007 0830-242)
- MURAKAMI, Makoto**  
(JSG01/08P/D-021 1400-021)
- MURAKAMI, Makoto**  
(JSS07/10P/A02-010 1630)  
(GAI06/09P/A10-013 1740)  
(JSG01/07A/A01-001 0900)
- MURAKOSHI, Takumi**  
(SS03/08A/D-100 0830-259)
- MURATA, Akihiko**  
(JSP04/09P/A06-009 1700)
- MURATA, Akihiko**  
(MC02/07P/D-007 1400-204)  
(MC02/07P/D-001 1400-198)
- MURATA, Fumie**  
(JSM14/07A/A05-006 1130)  
(MC17/11P/B23-006 1600)  
(MC03/10P/A07-008 1720)  
(MC17/11A/B23-004 0940)  
(MC03/11P/A07-003 1440)  
(MC03/11P/D-009 1400-184)
- MURATA, Isao**  
(MC05/07P/D-012 1400-219)
- MURATA, Yasuaki**  
(JSA07/11A/D-016 0830-016)
- MURATA, Yasuhiro**  
(MC08/07P/B17-005 1520)
- MURAZAKI, Kazuyo**  
(MC08/07A/B17-006 1120)
- MURBACH, Lizia**  
(JSM04/09P/D-009 1400-046)
- MURBACH, Lizia L.**  
(JSM04/09P/D-012 1400-049)
- MURDIYARSO, Daniel**  
(JSM04/09A/B23-001 0900)  
(JSM04/09P/B23-007 1730)
- MUROI, Chiashi**  
(MC02/07P/D-009 1400-206)  
(JSM14/08A/A05-011 1200)

(JSM14/08A/A05-007 1040)  
**MURPHY, D.J.**  
 (GAILI.06/11P/D-017 1400-069)  
**MURPHY, Damian**  
 (MC05/10A/A09-007 1100)  
**MURPHY, James**  
 (MC08/07A/B17-003 1015)  
 (MC11/10A/B19-001 0830)  
 (MC08/08P/D-002 1400-158)  
**MURTHY, N.S.R.**  
 (GAI.10/09A/A11-005 1000)  
**MUSA, Tajul**  
 (G04/08P/D-005 1400-112)  
**MUSCHALLA, Dirk**  
 (HW08/08A/C28-009 1140)  
**MUSIAKE, Katumi**  
 (HS02/11A/C24-003 0900)  
 (HS02/08A/C24-009 1100)  
 (HS02/08A/C24-002 0845)  
 (HS02/10A/C24-005 0930)  
 (HW07/10P/C25-006 1545)  
**MUSKETT, Reginald R.**  
 (JSH01/07A/C27-003 1020)  
**MUSSON, Roger M.W.**  
 (SS03/08A/D-052 0830-211)  
**MUSSON, Roger Mw**  
 (SS04b/10P/D-033 1400-217)  
**MUSY, Andre**  
 (HW07/11A/C25-003 0915)  
**MUXART, Tatiana**  
 (HW01/10A/C26-002 0850)  
**MUZIRWAN, Munir**  
 (MI09/10P/D-002 1400-155)  
**MWAMI, James**  
 (HS02c/11P/D-017 1630-115)  
 (HS02/11A/C24-017 1149)  
**MWANGI, Francis Mwaura**  
 (HW05/10A/C31-008 1020)  
**MYOUNG, Boksoon**  
 (MIA06/09P/B20-008 1640)  
**MYSAK, Lawrence A.**  
 (JSP04/09P/A06-001 1400)  
 (MC12/07A/B19-006 1115)  
 (JSP04b/10P/D-002 1400-021)

## n

**N, Jyothi**  
 (GAILI.06/11P/D-001)  
**N-ZMANN, Gunnar**  
 (HW01/09P/D-023 1400-214)  
**NACHAPKIN, Nikolay Ivanovich**  
 (SS03/08A/D-072 0830-231)  
**NADA, Hiroki**  
 (JSM15/07A/B18-001 0900)  
**NADAI, Akitsugu**  
 (JSG03/09P/D-016 1640-024)  
 (JSG03/09P/D-019 1640-027)  
**NADAOKA, Kazuo**  
 (JSM03/08P/A13-004 1500)  
**NADEAU, Robert M.**  
 (JSG01/07P/A01-011 1650)  
**NADERINEZHAD FARD, Azadeh**  
 (SS03/08A/D-143 0830-302)  
**NADIMIKERI, Jaya Raju**  
 (JSP08/09A/B19-008 1140)  
**NAEF, Feli Robert**  
 (HW03/11A/C30-006 1030)  
**NAEF, Felix**  
 (HW01/10A/C26-005 0950)  
**NAGAFUCHI, Osamu**  
 (HW01/09P/D-045 1400-236)  
**NAGAHAMA, Hiroyuki**  
 (SS03/08A/D-049 0830-208)  
**NAGAHAMA, Tomoo**  
 (MC05/07P/D-008 1400-215)  
**NAGAI, Akihiro**  
 (HS02b/10P/D-030 1630-151)

(HS02/10P/C24-007 1539)  
**NAGAI, T.**  
 (GAILI.05/07A/A06-003 0930)  
**NAGAI, Toshihiko**  
 (JSS07b/10P/D-007 1700-053)  
**NAGAI, Tsugunobu**  
 (GAILI.05/07A/A06-007 1055)  
 (GAILI.05/07P/D-018 1400-116)  
 (GAILI.05/07P/D-009 1400-107)  
**NAGANJANEYULU, K.**  
 (GAI.10/09A/A11-012 1215)  
**Naganjaneyulu K.**  
 (GAI.10/09P/D-004 1615-123)  
**NAGANO, Isamu**  
 (GAILI.04/09A/D-003 0830-139)  
 (GAILI.11/09P/A15-009 1645)  
 (GAILI.04/09A/D-002 0830-138)  
 (GAILI.05/07P/D-021 1400-119)  
 (GAILI.04/07P/A08-004 1505)  
 (GAILI.11/10P/D-001 1400-116)  
**NAGANO, Masayuki**  
 (SS04/07P/A03-007 1545)  
**NAGANO, Shigeo**  
 (G02/10P/D-010 1400-075)  
**NAGAR, Vipul**  
 (GAI.08/08A/A14-002 0850)  
**NAGARAJAN, Nandini Nityananda**  
 (GAI.10/09P/D-014 1615-133)  
**NAGASHIMA, Kazushige**  
 (JSM15/07P/D-005 1400-005)  
**NAGATA, Masato**  
 (GAILI.11/09P/A15-005 1510)  
**NAGATA, Shuichi**  
 (JSS07b/10P/D-007 1700-053)  
**NAGATSUMA, Tsutomu**  
 (GAILI.06/08P/A02-010 1710)  
 (GAILI.06/08P/A02-012 1740)  
**NAGATSUMA, Tsutomu**  
 (GAILI.06/07P/D-010 1400-130)  
**NAGORNOV, Oleg V.**  
 (JSP04b/10P/D-001 1400-020)  
**NAGORNYKH, Tatiana**  
 (SS04/08P/A03-010 1630)  
**NAGUMO, Hideki**  
 (SS04a/09P/D-039 1400-288)  
 (SS04a/09P/D-002 1400-251)  
**NAGY, Andrew F.**  
 (GAIV.03/09A/A16-001 0900)  
**NAGY, Andrew F.**  
 (GAILI.07/11P/A12-006 1640)  
 (GAIV.03/09A/A16-002 0930)  
**NAHAPETYAN, Hasmik Hrach**  
 (SS04b/10P/D-039)  
**NAHAVANDCHI, Hossein**  
 (JSG03/10A/A12-003 0910)  
**NAIDINA, Olga D.**  
 (MC12/07A/B19-005 1100)  
**NAIR, K.U.**  
 (JSA09/11P/D-002 1400-051)  
 (JSA09/11P/D-003 1400-052)  
**NAIR, S. Muraleedharan**  
 (MC17/11P/B23-007 1620)  
**NAIR, Shadananan K.**  
 (HS02a/07P/D-001 1545-147)  
 (JSP11/07P/A10-001 1400)  
 (HS02/07A/C24-001 0900)  
**NAIR, Venu GĀD**  
 (JSM14/07A/A05-009 1215)  
**NAITO, Daisuke**  
 (HW06/07P/C31-007 1600)  
**NAITO, Gen'ichi**  
 (MC02/07P/B20-006 1600)  
**NAITO, Isao**  
 (G02/10P/D-010 1400-075)  
**NAITO, Yoko**  
 (MC05/10A/A09-009 1150)  
**NAJEM, Wajdi**  
 (HW08/07A/C28-008 1150)  
**NAKADA, Masao**  
 (JSA07/10P/A05-003 1440)

**NAKAEGAWA, Toshiyuki**  
 (JSG03/09P/D-004 1640-012)  
**NAKAGAWA, Hiroyuki**  
 (JSG01/07A/A01-001 0900)  
**NAKAGAWA, Katsuhiro**  
 (HS03/08P/C26-004 1445)  
**NAKAGAWA, Kazuyuki**  
 (SS05/10A/A13-011 1115)  
**NAKAGAWA, Mitsuhiro**  
 (JSS07a/09P/D-004 1700-105)  
**NAKAGAWA, Takashi**  
 (JSS06a/08P/D-001 1400-079)  
 (JSS06a/08P/D-014 1400-092)  
**NAKAHIGASHI, Kazuo**  
 (SS03/08A/D-118 0830-277)  
 (SS03/08A/D-067 0830-226)  
**NAKAI, Sento**  
 (JSM14/09P/D-023 1400-087)  
 (JSM14/08A/A05-010 1145)  
**NAKAI, Yuichiro**  
 (MI07/10P/D-005 1400-181)  
 (HS02/09A/C24-003 0930)  
**NAKAJIMA, Goro**  
 (HS01/09P/C29-003 1440)  
**NAKAJIMA, Hideaki**  
 (MI07/11A/B18-007 1110)  
**NAKAJIMA, Junichi**  
 (JSS06b/10P/D-020 1400-044)  
**NAKAJIMA, Kensuke**  
 (MC03/09A/A07-003 0950)  
 (MC04/10P/B22-002 1430)  
 (MC04/11P/B22-002 1430)  
**NAKAJIMA, Takuo**  
 (HW01/09P/D-039 1400-230)  
**NAKAJIMA, Yasuhiro**  
 (JSM04/09A/B23-001 0900)  
**NAKAJO, Tomoyuki**  
 (GAILI.14/08A/D-007 0830-151)  
**NAKAKITA, Eiichi**  
 (HS03/07P/C26-007 1545)  
**NAKAKUKI, Tomoeiki**  
 (JSS06b/10P/D-019 1400-043)  
**NAKAMIZO, Aoi**  
 (GAILI.05/07P/D-006 1400-104)  
 (GAILI.10/11A/A01-008 1015)  
**NAKAMOTO, Shoichiro**  
 (JSP09/11P/B20-002 1415)  
**NAKAMURA, Ayako**  
 (JSM14/08A/A05-009 1130)  
**NAKAMURA, Hisashi**  
 (MC05/10P/A09-007 1720)  
 (MI05/11A/B17-009 1150)  
**NAKAMURA, Hisashi**  
 (MC05/10A/A09-003 0920)  
**NAKAMURA, Hisashi**  
 (MI05/11P/B17-007 1630)  
 (MI06/08A/D-001 0830-152)  
 (MI05/11A/B17-008 1130)  
**NAKAMURA, Hisashi**  
 (JSP09/10P/B20-009 1630)  
**NAKAMURA, Hisashi**  
 (MI05/11A/B17-007 1050)  
**NAKAMURA, Hisashi**  
 (MI05/09A/B17-008 1150)  
**NAKAMURA, Hisashi**  
 (JSM10/08A/B23-003 0930)  
**NAKAMURA, Kajuro**  
 (JSA07/11A/D-017 0830-017)  
 (SS04a/09P/D-033 1400-282)  
 (JSG01/08P/D-001 1400-001)  
**NAKAMURA, Kenji**  
 (JSM03/09A/D-002 0830-036)  
 (JSM14/08A/A05-010 1145)  
 (JSM03/08A/A13-004 1000)  
 (JSM03/09A/D-003 0830-037)  
**NAKAMURA, Koza**  
 (JSM14/08A/A05-003 0925)  
**NAKAMURA, Maho**  
 (GAILI.06/11P/D-012 1400-064)  
 (GAILI.06/10A/A01-010 1125)  
**NAKAMURA, Mamoru**  
 (SS03/07P/A02-002 1415)  
**NAKAMURA, Masao**  
 (GAILI.06/07P/D-015 1400-135)  
**NAKAMURA, Masao**  
 (GAILI.06/08P/A02-009 1655)  
**NAKAMURA, Masato**  
 (GAILI.07/11A/A12-001 0835)  
 (GAILI.07/11A/A12-004 0945)  
 (MC04/11A/B22-002 0900)  
 (MC04/11A/B22-001 0830)  
**NAKAMURA, Mikako**  
 (SS03/08A/D-002 0830-161)  
**NAKAMURA, Mikako**  
 (SS03/08A/D-011 0830-170)  
**NAKAMURA, Mikako**  
 (SS03/08A/D-120 0830-279)  
**NAKAMURA, Nobuyuki**  
 (GAILI.11/09P/A15-011 1715)  
**NAKAMURA, Rumi**  
 (GAILI.05/08A/A06-003 0900)  
**NAKAMURA, Rumi**  
 (GAILI.05/07P/D-007 1400-105)  
**NAKAMURA, Rumi**  
 (GAILI.05/07A/A06-004 0945)  
**NAKAMURA, Ryoichi**  
 (SS04a/09P/D-025 1400-274)  
 (SS04a/09P/D-026 1400-275)  
**NAKAMURA, Shigehisa**  
 (JSP11/08P/D-007 1400-076)  
**NAKAMURA, T.**  
 (GAILI.04/07A/A08-005 1015)  
**NAKAMURA, Tadas K.**  
 (GAILI.07/09P/A14-009 1720)  
**NAKAMURA, Takeshi**  
 (SS03/08A/D-113 0830-272)  
**NAKAMURA, Takuji**  
 (GAILI.06/10A/A01-007 1030)  
**NAKAMURA, Takuji**  
 (MI09/08P/D-002 1400-155)  
**NAKAMURA, Tsutomu**  
 (HS02/09A/C24-003 0930)  
**NAKAMURA, Yasuyuki**  
 (SS03/08A/D-002 0830-161)  
**NAKAMURA, Yoichi**  
 (GAILI.04/07P/A08-004 1505)  
**NAKAMURA, Yugo**  
 (JSS07a/09P/D-016 1700-117)  
**NAKAMURA, Yugo**  
 (JSS07a/09P/D-005 1700-106)  
**NAKANE, Hideaki**  
 (MC05/07P/D-008 1400-215)  
 (MC05/07P/D-012 1400-219)  
**NAKANISHI, Ayako**  
 (SS03/08A/D-102 0830-261)  
 (SS03/08A/D-109 0830-268)  
**NAKANISHI, Ayako**  
 (SS03/08A/D-009 0830-168)  
**NAKANISHI, Ayako**  
 (SS03/08A/D-103 0830-262)  
**NAKANO, Masaaki**  
 (HS01/09P/D-011 1400-178)  
**NAKANO, Masaru**  
 (SS04b/10P/D-009 1400-193)  
**NAKANO, Shin'ya**  
 (GAV.04/07A/A11-004 1030)  
**NAKANO, Shun**  
 (GAV.06/09P/D-001 1400-154)  
**NAKANO, Takehide**  
 (JSG01/08P/D-026 1400-026)  
**NAKAO, Shigeru**  
 (JSG01/08P/D-018 1400-018)  
**NAKAO, Shigeru**  
 (JSG01/08A/A01-006 1015)  
**NAKASE, Kaori**  
 (GAV.06/10P/A11-006 1600)  
**NAKATA, Kouta**  
 (GAVI.02/07A/A07-001 0900)  
**NAKATA, Shinichi**  
 (SS03/08A/D-120 0830-279)  
**NAKATANI, Ichiro**  
 (MC04/11A/B22-001 0830)  
**NAKATSUGAWA, makoto**  
 (HW01/09P/D-015)  
**NAKATSUGAWA, Makoto**  
 (JWH01/10A/C30-008 1120)

# INDEX

- NAKATSUKA, Tadashi**  
(GAV.06/09P/D-005 1400-158)  
(GAV.06/10A/A11-002 0850)  
(GAV.06/09P/D-001 1400-154)
- NAKATSUKA, Tadashi**  
(GAV.06/10A/A11-003 0910)
- NAKAWO, Masayoshi**  
(HW03/11A/C30-010 1150)
- NAKAWO, Masayoshi**  
(HS02/11A/C24-005 0930)  
(HW01/09P/D-041 1400-232)
- NAKAYAMA, Daichi**  
(JSH01/07P/C27-008 1640)
- NAKAYAMA, Tomoki**  
(MI08/07P/D-001 1400-195)
- NAKAYAMA, Yoshinori**  
(GAI11.11/10P/D-004 1400-119)  
(GAI11.11/09P/A15-006 1525)
- NAKAZAWA, Rui**  
(MI05/10A/B17-006 1100)
- NAKAZAWA, Tetsuo**  
(JSP09/11A/B20-012 1200)  
(JSM14/09P/D-005 1400-069)  
(MC17/11P/B23-004 1500)
- NALLATHAMBI, Balasubramaniam**  
(JSM04/09P/D-004 1400-041)
- NAM, Jae-Chul**  
(JSG03/09P/D-009 1640-017)
- NAMEGAYA, Yuichi**  
(JSS07/10A/A02-006 0945)  
(JSS07/10A/A02-002 0845)
- NAMIKI, Noriyuki**  
(G02/10P/D-013 1400-078)  
(G02/07A/C25-011 1200)
- NAMIKI, Yuko**  
(GAI11.09/11A/A11-003 0920)
- NANAYAMA, Futoshi**  
(JSS07/10A/A02-001 0830)  
(JSS07a/09P/D-002 1700-103)
- NANAYAMA, Futoshi**  
(JSS07/09A/A02-003 0930)
- NANBU, Ken-ichi**  
(GAI11.04/09A/D-006 0830-142)
- NANDAGIRI, Lakshman**  
(HW07/11P/D-034 1400-170)
- NANDURI, Umamahesh Venkata**  
(HS02/10A/C24-006 0945)  
(HS01/09P/D-001 1400-168)  
(HW07/11P/D-033 1400-169)
- NANKALI, Hamid Reza**  
(G03/07P/D-012 1400-034)
- NANKALI, Hamid Reza**  
(SS03/08A/D-075 0830-234)
- NARAG, Ishmael C.**  
(SS04b/10P/D-042 1400-226)
- NARAG, Ishmael C.**  
(JSS07a/09P/D-009 1700-110)
- NARAG, Ishmael Clarino**  
(SS04b/10P/D-035 1400-219)  
(SS04b/10P/D-036 1400-220)
- NARAG, Ishmael Clarino**  
(SS03/08A/D-060 0830-219)  
(SW05/10A/D-003 0900-247)
- NARAYANAN, Manavalan Sathya**  
(HW01/09P/D-008 1400-199)
- NARHEIM, Bjorn**  
(GAI11.11/09A/A15-003 0940)
- NARITA, Akira**  
(SS04b/10P/D-004 1400-188)
- NARITA, Hisashi**  
(JSP04/09P/A06-006 1545)
- NARITA, Hisashi**  
(MC12/07P/B19-006 1600)
- NARITA, Tsugunori**  
(JSG01/07A/A01-001 0900)
- NARODOSLAWSKY, Michael**  
(HW07/11P/D-012 1400-148)
- NARUOKA, Tomohiro**  
(HS01/09P/D-005 1400-172)  
(HS01/09P/D-007 1400-174)
- NARUSE, Renji**  
(JSM10/09P/D-009 1400-063)
- NARUSE, Renji**  
(JSM11/10A/B18-004 1000)
- NASONOVA, N.O.**  
(JWH01/09P/C30-001)
- NASONOVA, Olga N.**  
(MI07/11P/B18-002 1420)  
(HW08/08A/C28-003 0920)  
(JWH01/10A/C30-002 0850)
- NASR ESFAHANI, Mohammad Ali**  
(MI06/09P/B20-005 1520)
- NASTULA, Jolanta**  
(MC11/11A/B19-004 0930)
- NATH, Asha Shashi**  
(MI03/08A/B18-005 1030)
- NATH, Bibhas**  
(HW05/10P/D-007 1400-162)
- NATH, Sankar Kumar**  
(SS04/08P/A03-006 1515)
- NAUJOKAT, Barbara**  
(JSA09/10A/A08-002 0900)
- NAULT, Joshua**  
(JSP10/09P/B21-003 1440)
- NAWA, Kazunari**  
(JSA07/11A/D-016 0830-016)
- NAWARATHNA, NMNS Bandara**  
(HS02/07A/C24-002 0904)  
(HS02a/07P/D-002 1545-148)  
(HW01/09P/D-024 1400-215)
- NAZARETYAN, Sergey Norayr**  
(SS05/10A/A13-010 1100)
- NAZAROV, Alexander B.**  
(HW01/09P/D-014 1400-205)  
(HW01/10P/C26-009 1720)
- NAZAROVA, Katherine A.**  
(JSA07/11A/D-031 0830-031)  
(JSA07/11A/D-030 0830-030)
- NDOUGSA, Théophile Mbaraga**  
(GAI.10/09P/D-016 1615-135)
- NEAGA, Vasile**  
(GAV.06/09P/D-002 1400-155)
- NEALE, Richard Brian**  
(MC17/11A/B23-008 1140)
- NEARY, Nicholas J.**  
(MC12/07A/B19-007 1130)
- NECHAEV, Dmitri**  
(JSP04a/09P/D-004 1400-097)
- NEGISHI, Hiroaki**  
(SS04b/10P/D-048 1400-232)  
(SW05/10P/A13-005 1505)  
(SS03/08A/D-114 0830-273)
- NEGISHI, Junjiro N.**  
(HW01/10P/C26-008 1700)
- NEGRI, Andrew**  
(JSM03/08A/A13-008 1140)
- Neil Thomson**  
(GAI11.10/10P/A01-008 1620)
- NEILAN, Ruth E.**  
(G07/10P/A03-004 1500)  
(G07/10P/D-018 1400-103)
- NEKRASOVA, Anastassia K.**  
(JSP11/07P/A10-008 1720)
- NELKIN, Eric**  
(JSP09/11A/B20-009 1115)
- NELSON, K. Doug**  
(GAI.08/08A/A14-003 0910)
- NENOVSKI, Petko I.**  
(GAI11.10/11A/D-003 0830-077)  
(GAI11.10/11A/A01-009 1030)
- NENOVSKI, Petko I.**  
(GAI11.10/11A/D-004 0830-078)
- NEPOKLONOV, V.**  
(G03/07P/D-052 1400-074)
- NEPOKLONOV, V.**  
(SW05/10A/D-010 0900-254)
- NEREM, R.Steven**  
(JSM11/10P/D-007 1700-016)
- NERI, Giancarlo**  
(SS03/07P/A02-008 1615)
- NESS, N.F.**  
(GAVI.02/07P/A07-005 1640)
- NESS, Norman F**  
(GAVI.03/08A/A16-008)
- NEUMAYER, Karl-Hans**  
(G02/07A/C25-001 0900)  
(G02/07A/C25-002 0920)
- NEWELL, Patrick T.**  
(GAI11.05/07P/D-003 1400-101)
- NEWELL, Patrick T.**  
(GAI11.09/11P/A11-005 1600)  
(GAI11.05/07P/D-017 1400-115)
- NEWITT, Lawrence Richard**  
(JSP11/07A/A10-007 1130)
- NEWMAN, Andrew V.**  
(SS03/08A/D-032 0830-191)
- NEWMAN, Claire**  
(MC04/11P/B22-001 1400)
- NEYVES, Alex M.**  
(HS02c/11P/D-021 1630-119)  
(HS02/11A/C24-021 1205)
- NGUEN, Thoa Thi Kim**  
(U7/11P/D32-001 1400)
- NGUURI, Teresia K.**  
(SW03/10P/A04-002 1415)
- NGUYEN, Van-Thanh-Van**  
(HW07/11P/C25-004 1445)
- Ni, Yunqi**  
(JSM14/08A/A05-001 0835)
- NIASSE, Madiodio**  
(HS02/07A/C24-014 0952)  
(HS02a/07P/D-014 1545-160)
- NICHOLS, Jonathan D.**  
(GAI11.14/07P/A12-002 1430)
- NICO, Giovanni**  
(HS01/08P/C29-006 1600)
- NICOLAS, Joelle**  
(G07/10P/D-008 1400-093)
- NICOLINI, Matilde**  
(MC03/10A/A07-008 1130)
- NICOLOSI, Iacopo**  
(GAV.06/10A/A11-005 0950)  
(GAV.06/10A/A11-004 0930)
- NIECKARZ, ZENON**  
(SS02/08A/C24-007 1000)
- NIELSEN, Allan A.**  
(JSG03/09P/D-010 1640-018)
- NIELSEN, Erling**  
(GAI11.07/11P/A12-004 1530)  
(MC04/11P/B22-006 1615)
- NIELSEN-GAMMON, John W.**  
(MI06/09P/B20-008 1640)  
(JSM03/08A/A13-005 1040)
- NIEMEYER, Stefan**  
(JWH01/10A/C30-007 1100)
- NIGGLI, Markus**  
(HW07/11A/C25-003 0915)
- NIGHTWORKINGGROUP**  
(SS03/08A/D-146 0830-305)
- NIHIRA, Satoshi**  
(HW05/10P/D-005 1400-160)
- NIINO, Hiroshi**  
(JSP10/09P/B21-009 1700)
- NIINO, Hiroshi**  
(JSP10/09P/B21-010 1720)
- NIINO, Hiroshi**  
(JSP10/08P/D-011 1610-063)  
(JSP09/10P/B20-011 1700)
- NIK, Abdul Rahim**  
(HW01/10P/C26-008 1700)
- NIKOLAY, Abushenko**  
(MC08/08P/D-003 1400-159)
- NIKONOVA, Faina**  
(GAV.05/09P/D-009 1400-153)
- NILFOROUSHAN, Faramarz**  
(G02/10P/D-016 1400-081)
- NILFOROUSHAN, Faramarz**  
(G03/07P/D-012 1400-034)
- NILFOROUSHAN, Faramarz**  
(SS03/08A/D-075 0830-234)
- NILSSON, Hans**  
(GAI11.08/10A/A16-003 0910)  
(GAI11.06/08A/A02-005 1045)  
(GAI11.08/10A/A16-007 1040)
- NING, Jinsheng**  
(G03/07P/D-044 1400-066)  
(G04/08P/D-016 1400-123)
- NINOMIYA, Keisuke**  
(GAI11.07/10P/D-004 1400-109)
- NINOMIYA, Kozo**  
(MI06/09P/B20-006 1540)
- NISHI, Noriyuki**  
(MC03/11P/D-002 1400-177)  
(MC05/08P/A09-005 1530)
- NISHIDA, Ryoei**  
(JSP11/08P/D-005 1400-074)
- NISHIDA, Ryoei**  
(SS03/08A/D-045 0830-204)
- NISHII, Kazuak**  
(MC05/10A/A09-003 0920)
- NISHII, Kazuaki**  
(MC05/10P/A09-007 1720)
- NISHIKI, Teruaki**  
(GAV.05/09P/D-006 1400-150)
- NISHIMOTO, Soushi**  
(SS03/08A/D-121 0830-280)
- NISHIMUNE, Naoyuki**  
(HS01/09P/D-007 1400-174)
- NISHIMURA, Keiichi**  
(SS04a/09P/D-033 1400-282)
- NISHIMURA, Sou**  
(JSG01/08P/D-005 1400-005)
- NISHIMURA, Takuya**  
(SS03/07P/A02-011 1700)
- NISHIMURA, Teruyuki**  
(MI06/09P/B20-006 1540)  
(MC11/11A/B19-008 1110)
- NISHIMURA, Y.**  
(SS03/08A/D-146 0830-305)
- NISHIMURA, Yoshihiro**  
(JSM15/07P/D-001 1400-001)
- NISHIMURA, Yuichi**  
(JSS07a/09P/D-016 1700-117)
- NISHIMURA, Yuichi**  
(SS03/08A/D-005 0830-164)
- NISHIMURA, Yuichi**  
(JSS07a/09P/D-004 1700-105)  
(JSS07a/09P/D-005 1700-106)
- NISHIMURA, Yukari**  
(JSM15/07P/D-007 1400-007)
- NISHINO, Masaki N.**  
(GAI11.05/07P/D-004 1400-102)
- NISHINO, Masanori**  
(JSA01/08P/A12-004 1520)
- NISHINO, Minoru**  
(SS03/08A/D-101 0830-260)  
(SS03/08A/D-120 0830-279)  
(SS03/08A/D-118 0830-277)  
(SS03/08A/D-002 0830-161)
- NISHINO, Minoru**  
(SS03/08A/D-017 0830-176)
- NISHIO, Masumi**  
(GAI11.06/10A/A01-007 1030)
- NISHIOKA, G.**  
(JSM04/09P/D-010 1400-047)
- NISHTANI, Nozomu**  
(GAI11.05/07P/D-016 1400-114)
- NISHIWO, Fumihiko**  
(JSM10/09P/D-002)
- NISHIZAWA, Azusa**  
(SS03/08A/D-103 0830-262)
- NISHIZAWA, Seiya**  
(MI05/09A/B17-007 1130)
- NISII, Vincenzo**  
(SS04a/09P/D-015 1400-264)
- NISMURA, Yuichi**  
(SS03/07A/A02-009 1130)
- NIU, Anfu**  
(SS04b/10P/D-050 1400-234)
- NIU, Fenglin**  
(JSS06/07P/A04-004 1500)  
(JSG01/07P/A01-011 1650)  
(JSS06/09A/A04-001 0900)
- NIWANO, Hans**  
(MC05/08P/A09-008 1700)  
(MC05/09A/A09-006 1120)  
(MC05/07P/D-006 1400-213)

- NIXDORF, Brigitte**  
(HW06/07A/C31-007 1150)
- NKEMDIRIM, Lawrence Chima**  
(HS02/07A/C24-012 0944)  
(HS02a/07P/D-012 1545-158)
- NKHUWA, Daniel C.W.**  
(HS02c/11P/D-025 1630-123)  
(HS02/11P/C24-002 1519)
- NOBILIS, Franz**  
(HW02/11A/D-001 0830-133)
- NOBRE, Carlos**  
(MC03/10P/A07-005 1600)
- NOBREGA, Silvestre L.**  
(HS02c/11P/D-021 1630-119)  
(HS02/11A/C24-021 1205)
- NOCQUET, Jean-Mathieu**  
(G07/10P/D-008 1400-093)
- NODA, Akira**  
(MC08/07A/B17-006 1120)
- NODA, Akira**  
(MC08/07A/B17-002 1000)  
(MC08/07A/B17-005 1045)
- NODA, Hirotomo**  
(G02/10P/D-013 1400-078)
- NODA, Hirotomo**  
(GAIV.02/07P/A07-003 1510)
- NODA, Hirotomo**  
(GAI.05/07A/A06-004 0945)
- NODA, Masaru**  
(SS03/08A/D-035 0830-194)
- NODA, Yumiko**  
(GAV.07/07P/D-001 1400-142)
- NODZU, Masato**  
(MC03/11P/D-001 1400-176)
- NOF, Doron**  
(JSP04/10A/A06-003 0940)  
(JSP10/09A/B21-009 1200)
- NOGI, Yoshifumi**  
(JSS06b/10P/D-004 1400-028)
- NOGUCHI, Katsuyuki**  
(MC05/07P/D-013 1400-220)
- NOGUCHI, Shoji**  
(HS02/08P/C24-012 1715)
- NOGUCHI, Shoji**  
(HW01/10P/C26-008 1700)
- NOGUCHI, Takashi**  
(JSP10/08P/D-011 1610-063)
- NOGUCHI, Tatsuya**  
(JSP11/08P/D-005 1400-074)
- NOKANO, Takanori**  
(HW01/09P/D-035 1400-226)
- NOLL, Carey E.**  
(G07/10P/D-012 1400-097)
- NOMURA, Mitsuharu**  
(JSM14/07P/A05-002 1435)
- NOMURA, Mutsumi**  
(HW01/10A/C26-007 1110)  
(JSM10/09P/D-001 1400-055)
- NOORIAN, AliMohammad**  
(JSP11/08A/A10-005 1050)
- NORDEMANN, Daniel Jean Roger**  
(JSA08/10P/D-003 1400-003)
- NORDGREN, B.L.**  
(JSM04/09A/B23-006 1145)
- NORITA, Miyako**  
(SS04a/09P/D-002 1400-251)
- NORMATOV, Inom Sherovich**  
(HW05/10A/C31-006 0950)  
(HW06/07P/D-002 1400-186)  
(HW07/11P/D-003 1400-139)
- NORTON, Warwick**  
(MC05/09A/A09-004 1000)
- NOSE, Masahito**  
(GAI.10/11A/A01-005 0930)
- NOSE, Masahito**  
(GAI.10/11A/D-017 0830-091)
- NOSE, Masahito**  
(GAI.06/07P/D-010 1400-130)
- NOSOV, Mikhail A.**  
(JSS07/09P/A02-010 1630)
- NOTHOLT, Justus**  
(MI03/08A/B18-007 1110)
- NOURBAEVA, Gouldaria K.**  
(HS02b/10P/D-004 1630-125)  
(HS02/10A/C24-004 1057)
- NOURBAEVA, Gouldaria Karimovna**  
(JSM04/09P/D-011 1400-048)
- NOURELDIN, Abaelmagd**  
(G04/08P/C25-002 1430)
- NOVELLI, Paul**  
(MI03/08A/B18-007 1110)
- NOVIK, Oleg Bencionovith**  
(JSS07b/10P/D-003 1700-049)
- NOVIKOVA, N.M.**  
(HS02/07A/C24-015 0956)  
(HS02a/07P/D-015 1545-161)
- NOVIKOVA, Olga V.**  
(SS04/09A/A03-001 0900)
- NOVOTRAYSOV, Vadim V.**  
(JSP10/10A/B21-009 1200)
- NOWBUTH, Manta Devi**  
(HW05/10A/C31-007 1005)  
(HW01/09P/D-016 1400-207)
- NOWBUTH, Manta Devi**  
(HW05/10P/D-004 1400-159)
- NOZAKI, Kyozo**  
(G04/08P/D-012 1400-119)
- NOZAKI, Kyozo**  
(G04/08P/D-013 1400-120)
- NOZAKI, Kyozo**  
(SS04b/10P/D-024 1400-208)
- NOZAWA**  
(MC08/07P/B17-003 1430)
- NOZAWA, Hiromasa**  
(GAI.14/07A/A12-007 1155)
- NOZAWA, Hiromasa**  
(GAI.14/07A/A12-006 1140)
- NOZAWA, S.**  
(MC05/10A/A09-010 1210)
- NOZAWA, Satonori**  
(GAI.04/09A/D-005 0830-141)
- NOZAWA, Toru**  
(MI03/08P/B18-006 1610)
- NOZOMI DVLEBI group,**  
(G02/10P/D-008 1400-073)
- NUGROHO, Sutopo Purwo**  
(HS01/08P/C29-001 1400)
- NUHU, Andi**  
(JSM14/08P/A05-008 1745)
- NUMAGUTI, Atusi**  
(MC02/07P/B20-005 1540)
- NURTAEV, Bakhtiar S.**  
(SS04/08P/A03-002 1415)
- NURUTDINOV, Konstantin**  
(G04/08P/C25-005 1530)
- NWANKWOR, G. I.**  
(HW05/10P/D-012 1400-167)
- NYANGAGA, John M.**  
(HW01/09P/D-049 1400-240)
- NYANGARA, John M.**  
(HW01/09P/D-021 1400-212)
- OBANA, Koichiro**  
(SS03/08A/D-010 0830-169)  
(JSG01/08P/D-012 1400-012)
- OBANA, Yuki**  
(GAI.10/11A/D-002 0830-076)
- OBANA, Yuki**  
(GAI.10/11A/D-005 0830-079)
- OBARA, Kazushige**  
(SS03/08A/D-098 0830-257)  
(JSG01/08P/D-025 1400-025)
- OBARA, Kazushige**  
(SS03/08A/D-014 0830-173)  
(SS03/08A/D-108 0830-267)
- OBARA, Takahiro**  
(GAI.06/08P/A02-010 1710)
- OBARA, Takahiro**  
(GAI.06/08P/A02-012 1740)
- OBARA, Takahiro**  
(GAI.06/07P/D-010 1400-130)
- OBARA, Takahiro**  
(GAI.06/08P/A02-008 1640)
- OBAYASHI, Masayuki**  
(JSS06a/08P/D-002 1400-080)
- OBER, Daniel M.**  
(GAI.06/08A/A02-006 1110)
- OBOTE, Tomoko**  
(HW01/09P/D-042 1400-233)
- OCAK, Mustafa**  
(JSG01/07A/A01-008 1105)
- ODA, Hitoshi**  
(JSS06b/10P/D-018 1400-042)
- ODA, Hitoshi**  
(JSS06a/08P/D-003 1400-081)
- ODA, Yoshiya**  
(SS03/08A/D-099 0830-258)
- ODAKA, Masatsugu**  
(MC04/11P/B22-002 1430)  
(MC04/11P/B22-003 1445)  
(MC04/11P/B22-008 1645)  
(MC04/11P/B22-009 1700)  
(MC04/10P/B22-005 1530)
- ODAKA, Masatsugu**  
(MC04/11P/B22-010 1715)
- ODONBAATAR, Chimed**  
(SS04b/10P/D-030 1400-214)
- ODUNUGA, Shakirudeen Sule**  
(HS02/08P/C24-007 1530)
- OFARRELL, Siobhan**  
(JSM10/08A/B23-008 1130)
- OFFERMANN, Dirk**  
(MC05/11P/A09-003 1450)
- OFFERMANN, Dirk**  
(JSA09/10A/A08-002 0900)
- OGASAWARA, Atsushi**  
(MI05/10A/B17-006 1100)
- OGAWA, Hideo**  
(MC05/07P/D-008 1400-215)
- OGAWA, Hiroyuki**  
(GAI.14/08A/D-004 0830-148)  
(GAI.14/08A/D-005 0830-149)
- OGAWA, Kenta**  
(MI09/09A/B22-005 1050)
- OGAWA, Kenta**  
(MI09/08P/D-003 1400-156)
- OGAWA, Masaki**  
(JSS06/07P/A04-011 1740)
- OGAWA, Naohisa**  
(JSM15/07A/B18-010 1145)
- OGAWA, Shigeru**  
(HW01/09P/D-045 1400-236)
- OGAWA, T.**  
(GAI.05/08P/A15-001 1400)
- OGAWA, Tadahiko**  
(GAI.06/09P/A10-008 1620)  
(GAI.06/11P/D-010 1400-062)  
(GAI.06/09A/A10-007 1035)  
(GAI.05/07P/D-016 1400-114)
- OGAWA, Yasuo**  
(GAI.08/08A/A14-007 1050)  
(GAI.08/08P/D-007 1400-142)
- OGAWA, Yasuo**  
(JSA07/10P/A05-002 1420)  
(GAI.08/08P/D-005 1400-140)
- OGI, Masayo**  
(MI05/10P/D-001 1400-168)
- OGINO, Shin-Ya**  
(MC03/11P/D-001 1400-176)
- OGINO, Shin-Ya**  
(MC05/08P/A09-005 1530)
- OGINO, Shin-Ya**  
(MC17/11P/B23-006 1600)
- OGINO, Tatsuki**  
(GAI.14/07P/A12-004 1500)
- OGUNI, Kenji**  
(SSW05/10P/A13-007 1530)
- OGUNKUNLE, Olatunde**  
(HS02/07A/C24-005 1145)
- OGURA, Tomoo**  
(JSM10/09P/D-004 1400-058)
- OH, Jai Ho**  
(MC03/09A/A07-008 1150)
- OH, Jai Ho**  
(JSM14/09P/D-006 1400-070)
- OH, Jai ho**  
(JSM14/07A/A05-008 1200)
- OH, Seekhoon**  
(JSA07/10P/A05-003 1440)
- OH, Seekhoon**  
(JSA07/11A/D-003 0830-003)
- OH, Sung-Nam**  
(JSM04/09P/B23-004 1600)  
(JSM04/09P/D-008 1400-045)
- OH, Sung-Nam**  
(JSM11/10P/D-003 1700-012)
- OH'IZUMI, Mitsuo**  
(JWH01/09P/C30-002 1420)
- OHARA, Toshimasa**  
(JSM04/09A/B23-002 0930)  
(JSM04/09P/B23-003 1500)
- OHARA, Yasuhiko**  
(JSS06b/10P/D-010 1400-034)
- OHATA, Tetso**  
(JWH01/09P/C30-005 1520)
- OHATA, Tetsuo**  
(JSM10/09P/D-001 1400-055)
- OHATA, Tetsuo**  
(MI07/10P/D-003 1400-179)
- OHATA, Tetsuo**  
(JWH01/10A/C30-003 0910)
- OHATA, Tetsuo**  
(HS02/09A/C24-003 0930)
- OHATA, Tetsuo**  
(JWH01/10A/C30-005 0950)
- OHATA, Tetsuo**  
(JWH01/10A/C30-006 1040)  
(JSM10/08P/B23-003 1500)  
(HW06/07P/C31-007 1600)
- OHATA, Tetsuo**  
(JWH01/09A/C30-003 0940)
- OHFUCHI, Wataru**  
(MI05/11A/B17-009 1150)
- OHFUCHI, Wataru**  
(JSM14/09P/D-018 1400-082)  
(JSM14/09P/D-017 1400-081)
- OHGI, Masami**  
(HW01/10A/C26-007 1110)
- OHJI, Baku**  
(HW01/10A/C26-009 1150)
- OHKAWA, Masashi**  
(G02/10P/D-010 1400-075)
- OHKUBO, Atsushi**  
(GAI.04/09A/D-003 0830-139)
- OHMACHI, Tatsuo**  
(JSS07/09P/A02-005 1500)
- OHMACHI, Tatsuo**  
(JSS07b/10P/D-013 1700-059)
- OHMACHI, Tatsuo**  
(JSS07b/10P/D-018 1700-064)
- OHMACHI, Tatsuo**  
(JSS07b/10P/D-017 1700-063)
- OHMI, Shiro**  
(SS04a/09P/D-040 1400-289)
- OHMI, Tomoaki**  
(GAI.09/11P/A11-007 1640)
- OHMORI, Hiroo**  
(HW01/09A/C26-003 0950)

## O

- O'BRIEN, Keran**  
(JSA08/09A/A08-007 1045)
- O'CONNELL, Patrick Enda**  
(HW07/10A/C25-008 1200)
- O'CONNELL, Richard J.**  
(JSS06/08A/A04-002 0850)
- O'CONNOR, Kieran M.**  
(HS02/09P/C24-002 1415)
- O'NEILL, Alan**  
(MI05/10A/B17-002 0910)
- O'REILLY, Brian M.**  
(MC12/07P/B19-003 1500)  
(JSA07/11A/D-032 0830-032)  
(SS03/08A/D-089 0830-248)  
(SS03/08A/D-145 0830-304)
- OBANA, Koichiro**  
(SS03/07A/A02-003 0930)

## INDEX

- OHNO, Hiroyuki**  
(HW04/09A/C31-008 1140)
- OHNO, Susumu**  
(SS04/08A/A03-013 1145)
- OHNO, Yuichi**  
(MI09/08P/B22-002 1420)
- OHNO, Yuichi**  
(MC02/07P/D-003 1400-200)
- OHSAKI, Hiroo**  
(G02/10P/D-008 1400-073)
- OHSAWA, Takahiro**  
(JSG03/09P/A12-005 1520)
- OHTA, Keiichi**  
(MC12/07P/B19-006 1600)
- OHTA, Keiichi**  
(MC12/07P/B19-005 1545)
- OHTA, Kenji**  
(GAI11.10/11A/A01-011 1100)
- OHTA, Takeshi**  
(HS02/09A/C24-001 0900)
- OHTA, Takeshi**  
(HS02/09A/C24-003 0930)
- OHTA, Tekeshi**  
(HS02b/10P/D-002 1630-123)  
(HS02/10A/C24-002 1049)
- OHTAKI, Toshiki**  
(SS03/08A/D-034 0830-193)  
(SS03/08A/D-110 0830-269)
- OHTANI, Ryu**  
(JSG01/08A/A01-004 0945)
- OHTANI, S.**  
(GAI11.10/11A/D-016 0830-090)
- OHTANI, Shin-ichi**  
(GAI11.10/11A/D-020 0830-094)
- OHTANI, Shin-ichi**  
(GAI11.06/08P/A02-001 1400)  
(GAI11.05/07P/D-015 1400-113)
- OHTANI, Shinichi**  
(GAI11.05/07P/D-014 1400-112)
- OHTE, Nobuhito**  
(HW01/09P/D-043 1400-234)
- OHTE, Nobuhito**  
(HW01/09P/D-033 1400-224)
- OHTE, Nobuhito**  
(HW01/10P/C26-001 1400)  
(HW01/09P/D-039 1400-230)  
(HW01/09P/D-042 1400-233)  
(HW01/09P/D-037 1400-228)  
(HW01/09P/D-040 1400-231)
- OHTE, Nobuhito**  
(HW01/09P/D-038 1400-229)
- OHTE, Nobuhito**  
(HW06/08A/C31-004 1140)
- OHTSU, Sunao**  
(SS03/08A/D-042 0830-201)
- OHTSUKA, Yasuhiro**  
(SS04/08A/A03-013 1145)
- OHYA, Fumio**  
(JSG01/08P/D-001 1400-001)  
(JSG01/07P/A01-007 1530)
- OIKE, Kazou**  
(JSG01/08P/D-029 1400-029)
- OISHI, Satoru**  
(HW07/11P/D-005 1400-141)
- OJEDA, Anibal**  
(SS04/07P/A03-003 1445)
- OJO, Simon Oyediran**  
(HS02/07A/C24-005 1145)  
(MC03/11P/A07-006 1600)  
(JSM14/07A/A05-005 1115)
- OKA, Mitsuo**  
(GAIV.02/07P/A07-003 1510)
- OKADA, Hiroshi**  
(SS04/07A/A03-001 0915)
- OKADA, Ken'ichi**  
(JSP09/10A/B20-002 0930)
- OKADA, Kenta**  
(HW03/11P/C30-008 1640)
- OKADA, Masaki**  
(GAI11.11/10P/D-004 1400-119)  
(GAI11.11/09P/A15-006 1525)
- OKADA, Masaki**  
(GAI11.11/09P/A15-010 1700)
- OKADA, Naosuke**  
(JSP10/10A/B21-002 0900)
- OKADA, Takuya**  
(HW08/08A/C28-007 1100)
- OKADA, Toshimi**  
(GAI11.11/10P/D-002 1400-117)
- OKAL, Emile**  
(JSS07a/09P/D-018 1700-119)  
(JSS07/09A/A02-007 1030)
- OKAMOTO, Noriko**  
(MC05/08P/A09-005 1530)
- OKAMOTO, Noriko**  
(MC03/09P/A07-007 1700)
- OKAMOTO, Noriko**  
(MC17/11A/B23-004 0940)
- OKAMOTO, Noriko**  
(MC03/11P/A07-003 1440)
- OKAMOTO, Noriko**  
(MC03/11P/D-009 1400-184)
- OKAMOTO, Takuo**  
(JSP11/08P/D-005 1400-074)
- OKAMURA, Makoto**  
(JSS07/10A/A02-002 0845)
- OKAMURA, Seiji**  
(JSG01/07A/A01-001 0900)
- OKAMURA, Yukinobu**  
(SS03/08A/D-055 0830-214)
- OKANO, Shoichi**  
(GAI11.14/07A/A12-006 1140)  
(GAI11.14/07A/A12-008 1210)
- OKANO, Shoichi**  
(GAI11.14/07A/A12-007 1155)
- OKAYA, David**  
(SS03/08A/D-004 0830-163)
- OKI, Satoko**  
(JSS06a/08P/D-002 1400-080)
- OKI, Taikan**  
(HS02/10A/C24-005 0930)
- OKI, Taikan**  
(HS02/08A/C24-009 1100)  
(HW07/10P/C25-007 1600)
- OKI, Taikan**  
(HW07/10P/C25-006 1545)
- OKI, Taikan**  
(HW06/08A/C31-004 1140)
- OKINO, Kyoko**  
(JSS06b/10P/D-010 1400-034)
- OKSAVIK, Kjellmar**  
(GAI11.06/07P/D-005 1400-125)
- OKU, Yuichiroh**  
(MC03/11P/A07-002 1420)
- OKUBO, Ayako**  
(GAV.06/09P/D-014 1400-167)
- OKUBO, Makoto**  
(JSA07/11A/D-010 0830-010)
- OKUBO, Reiko**  
(JWH01/10A/C30-003 0910)
- OKUBO, Shuhei**  
(JSG01/07A/A01-011 1150)
- OKUBO, Shuhei**  
(G04/08A/C25-007 1120)  
(JSG02/09P/A05-011 1745)  
(G02/10P/D-006 1400-071)
- OKUDA, Toshiki**  
(MC17/11A/B23-004 0940)
- OKUDA, Yasuhiro**  
(GAI11.05/07P/D-021 1400-119)
- OKUMA, Shigeo**  
(GAV.07/07P/A13-003 1440)  
(GAV.06/10A/A11-002 0850)  
(GAV.06/09P/D-001 1400-154)  
(GAV.06/09P/D-005 1400-158)
- OKUMA, Shigeo**  
(GAV.06/10A/A11-004 0930)  
(GAV.06/10A/A11-005 0950)
- OKUMA, Shigeo**  
(GAV.06/10A/A11-003 0910)
- OKUMURA, H.**  
(HW07/10A/C25-003 1045)
- OKUMURA, Hiroshi**  
(HW08/07P/C28-005 1610)
- OKUMURA, Hiroshi**  
(HW07/11P/D-006 1400-142)
- OKUMURA, Koji**  
(SS03/08A/D-059 0830-218)
- OKUMURA, Toshihiko**  
(SS04b/10P/D-023 1400-207)  
(SS04b/10P/D-015 1400-199)
- OKUNISHI, Kazuo**  
(HW01/09P/D-020 1400-211)
- OKUNO, Akira**  
(JSP10/08P/D-008 1610-060)
- OKUNO, Akira**  
(JSP10/08P/B21-003 1450)
- OKUNO, Jun'ichi**  
(JSG01/07A/A01-011 1150)
- OLAFSSON, Kjartan**  
(GAI11.06/07P/D-005 1400-125)
- OLAVERE, Erlinton B.**  
(JSS07a/09P/D-009 1700-110)
- OLESEN, Av**  
(G03/07P/D-046 1400-068)
- OLSEN, Nils**  
(GAV.05/08A/A11-004)
- OLSEN, Nils**  
(GAV.04/07A/A11-002 0930)  
(GAV.05/08P/A11-003 1445)
- OLSEN, Nils**  
(GAV.05/08A/A11-003 0920)
- OLSON, John V.**  
(GAI11.10/11A/D-002 0830-076)
- OLSSON, Jonas**  
(HW01/10P/C26-006 1620)
- OLUFEMI, Tejuoso**  
(HS02/08P/C24-007 1530)
- OLUSEGUN, Adepoju D.**  
(HS02c/11P/D-024 1630-122)  
(HS02/11P/C24-001 1515)
- OMANG, Ove Christian Dahl**  
(G03/07P/D-051 1400-073)
- OMANG, Ove Christian Dahl**  
(JSG03/10A/A12-003 0910)
- OMIDI, Nick**  
(GAI11.14/07P/A12-003 1445)
- OMURA, Kentaro**  
(SS03/08A/D-038 0830-197)
- OMURA, Kentaro**  
(SS03/08A/D-036 0830-195)
- OMURA, Makoto**  
(JSG03/09P/D-001 1640-009)
- OMURA, Yoshiharu**  
(GAI11.11/09P/A15-011 1715)
- OMURA, Yoshiharu**  
(GAI11.07/09P/A14-004 1510)
- OMURA, Yoshiharu**  
(GAI11.07/09P/A14-007 1640)
- OMURA, Yoshiharu**  
(GAI11.11/09A/A15-008 1135)  
(GAI11.05/08A/A06-008 1055)  
(GAI11.07/10P/D-004 1400-109)
- ONDA, Yuichi**  
(HW01/09P/D-034 1400-225)  
(HS01/09P/D-006 1400-173)  
(HW06/07A/C31-005 1110)
- ONDA, Yuichi**  
(HW06/07A/C31-002 0930)
- ONDOH, Tadanori**  
(GAI11.10/11A/A01-012 1115)
- ONGWENYI, George**  
(HW01/09P/D-049 1400-240)  
(HW01/09P/D-021 1400-212)
- ONI, Ebum Olufunmilayo**  
(SS03/08A/D-066 0830-225)
- ONI, Feyi**  
(HS02/07A/C24-005 1145)
- ONISHI, Masazumi**  
(SS03/07A/A02-006 1045)
- ONISHI, Masazumi**  
(JSA07/11A/D-010 0830-010)
- ONISHI, Tatuo**  
(GAI11.11/09P/A15-005 1510)
- ONO, Takayuki**  
(GAI11.10/11A/D-024 0830-098)
- ONO, Takayuki**  
(GAI11.14/08A/D-007 0830-151)  
(GAI11.06/07P/D-017 1400-137)
- ONO, Takayuki**  
(GAI11.06/07P/D-010 1400-130)
- ONO, Takayuki**  
(GAI11.06/07P/D-016 1400-136)
- ONO, Takayuki**  
(GAI11.07/11A/A12-001 0835)
- ONO, Takayuki**  
(GAI11.10/11A/A01-014 1145)  
(GAI11.06/09P/A10-006 1530)  
(GAI11.06/11P/D-011 1400-063)
- ONODERA, Shin'ichi**  
(HS01/09P/D-005 1400-172)
- ONODERA, Shin-ichi**  
(HS01/09P/D-007 1400-174)
- ONOMA, Fumiki**  
(GAI11.06/11P/D-010 1400-062)  
(GAI11.06/09P/A10-008 1620)
- ONOUE, Kensuke**  
(JSG01/07P/A01-007 1530)
- ONUR, Tuna**  
(SS04/08P/A03-014)
- ONYEKURU, S.O.**  
(HW05/10P/D-012 1400-167)
- OOI, Yoichi**  
(SS03/07P/A02-012 1715)
- OPPENHEIM, Meers M.**  
(GAI11.06/09A/A10-010 1145)  
(GAI11.06/10A/A01-009 1105)
- OPRSAL, Ivo**  
(SS04a/09P/D-044 1400-293)
- OPRSAL, Ivo**  
(SS04a/09P/D-043 1400-292)  
(SS04/07P/A03-011 1700)
- ORAEVSKY, Victor N.**  
(GAI11.14/08A/D-001 0830-145)  
(GAI11.03/09A/A16-008 1220)
- ORAEVSKY, Viktor N.**  
(U7/11P/D32-002 1450)
- ORECCHIO, Barbara**  
(SS03/07P/A02-008 1615)
- ORITO, Kotato**  
(MC05/07P/D-010 1400-217)
- ORLANDI, Paolo**  
(JSP10/09P/B21-007 1620)
- ORLECKA-SIKORA, Beata**  
(SS04/08A/A03-008 1015)
- ORLIC, Mirko**  
(JSM14/08P/A05-003 1510)
- ORLYUK, Mikhail I.**  
(JSA07/10A/A05-008 1130)
- ORLYUK, Mikhail I.**  
(GAV.06/09P/D-002 1400-155)
- ORMOS, Tamas**  
(GAI.10/09A/A11-008 1115)
- ORTIZ, Modesto**  
(JSS07/10A/A02-007 1000)
- ORTIZ, Modesto**  
(JSS07b/10P/D-005 1700-051)
- ORTIZ, Modesto F.**  
(JSS07/09A/A02-009 1115)
- ORTLAND, David A.**  
(MI05/10A/B17-008 1140)
- ORTMEYER, Mark**  
(JSP04/10P/A06-005 1520)
- OSAKA, Ken'ichi**  
(HW01/09P/D-039 1400-230)
- OSAKI, Hiro**  
(G02/10P/D-014 1400-079)
- OSAKI, Mitsuru**  
(MI07/10P/D-006 1400-182)
- OSAWA, Takahiro**  
(JSP09/11P/B20-001 1400)
- OSBORN, Timothy J.**  
(MC12/08A/B19-004 1055)
- OSBORNE, Brian J.**  
(JSP09/10A/B20-005 1015)
- OSBORNE, Tom**  
(MI07/11A/B18-001 0830)
- OSEPIAN, Alefina**  
(GAI11.10/11A/D-023 0830-097)
- OSHIMAN, Naoto**  
(GAI.08/08A/A14-007 1050)  
(GAI.08/08P/D-007 1400-142)

- OSHIMAN, Naoto**  
(GAI.10/09P/A11-003 1430)
- OSHITA, Kenichi**  
(G04/08P/D-013 1400-120)
- OSIPOV, Nicolay**  
(HW01/09A/C26-009 1210)
- ØDEGÅRD, Rune**  
(JSH01/08A/C27-003 0950)
- OSMAN, Salah Sherif**  
(GAI.10/09P/D-001 1615-120)
- OSMASTON, Miles F.**  
(JSS06/08A/A04-004 0930)
- OSTROWSKI, Manfred**  
(HW08/08A/C28-009 1140)
- OSTROWSKI, Manfred W.**  
(HS02/10P/C24-001 1400)
- OSTROWSKI, Manfred Walter**  
(HW07/11A/C25-007 1015)
- OSTROWSKI, Manfred Walter**  
(HW04/09P/C31-001 1400)
- OTHERS,**  
(JSP04/09A/A06-004 1000)
- OTSUBO, Toshimichi**  
(G02/10P/D-003 1400-068)  
(G02/10P/D-004 1400-069)  
(JSG01/08A/A01-003 0930)  
(G02/10P/D-015 1400-080)
- OTSUBO, Toshimichi**  
(G02/10P/D-006 1400-071)
- OTSUKA, Akira**  
(JSG03/09P/D-023 1640-031)
- OTSUKA, Y.**  
(GAI.05/08P/A15-001 1400)
- OTSUKA, Yuichi**  
(GAI.06/09P/A10-008 1620)  
(GAI.06/09A/A10-007 1035)  
(GAI.06/11P/D-010 1400-062)
- OTSUKI, Kyoichi**  
(HW01/09P/D-045 1400-236)
- OTT, Bettina**  
(HW07/11A/C25-002 0900)
- OTTEMOLLER, Lars**  
(SS03/08A/D-026 0830-185)
- OUARDA, Taha B.M.J.**  
(HW07/11P/C25-003 1430)
- OUE, Hiroki**  
(MI07/11P/B18-009 1700)
- OUE, Hiroki**  
(MI07/11P/B18-008 1640)
- OUEDRAOGO, Mahaman**  
(HS02/08A/C24-008 1045)
- OUN, Kim Choon**  
(SS04/08P/A03-010 1630)
- OVCHARENKO, Arkady**  
(SS04/08P/A03-001 1400)
- OVERLAND, James**  
(JSP04/09A/A06-001 0900)
- OVERLAND, James E.**  
(JSP04/10P/A06-001 1400)
- OVERLAND, James E.**  
(JSP04/10P/A06-007 1620)
- OWEN, Christopher J.**  
(GAI.05/08A/A06-009 1110)
- OWEN, Jeffrey S.**  
(HW01/09P/D-046 1400-237)
- OWENS, T.J.**  
(JSS06/07P/A04-007 1620)
- OYA, Hiroshi**  
(GAI.10/11A/D-024 0830-098)
- OYA, Hiroshi**  
(GAI.06/07P/D-017 1400-137)
- OYA, Hiroshi**  
(GAI.10/11A/A01-014 1145)  
(GAI.11/08A/D-007 0830-151)  
(GAI.06/07P/D-016 1400-136)
- OYAMA, Koh-ichiro**  
(GAI.07/11A/A12-001 0835)  
(GAI.06/09P/A10-005 1515)  
(GAI.07/11A/A12-006 1105)  
(MC05/07P/D-013 1400-220)
- OYAMA, Koichiro**  
(MC04/11A/B22-001 0830)
- OYAMATSU, Masayuki**  
(MC05/08P/A09-007 1640)
- OYEBANDE, Lekan**  
(HW07/11A/C25-010 1115)
- OZALAYBEY, Serdar**  
(SS03/07A/A02-009 1130)
- OZAWA, Shinzaburo**  
(JSG01/08P/D-021 1400-021)
- OZAWA, Shinzaburo**  
(JSG01/07P/A01-002 1415)
- OZEKE, L.G.**  
(GAI.10/10P/A01-003 1440)
- OZEL, Asim Oguz**  
(SS04a/09P/D-047 1400-296)
- OZEL, Nurcan Meral**  
(SS04a/09P/D-047 1400-296)
- OZEL, Oguz Asim**  
(SW04/09P/A13-009 1615)
- OZEL, Oguz Asim**  
(SS04/07A/A03-005 1030)
- OZENER, Haluk**  
(JSG01/08P/D-013 1400-013)
- OZEROV, Nikolai**  
(JWH01/09A/C30-008 1150)
- OZGULER, Hamza**  
(JSM11/10P/D-001 1700-010)
- P**
- P., Artaxo**  
(HW01/09A/C26-007 1130)
- P., Raj Ernest**  
(MI09/08P/B22-006 1620)
- P., Rao Rama**  
(SW03/10P/A04-013 1715)
- P., Reddy Ramachandra**  
(SW03/10P/A04-008 1600)
- P., Senthil Kumar**  
(JSG03/10P/A04-010 1630)
- P., Sooraj K.**  
(MI05/10P/B17-004 1520)
- P.B., Rao**  
(GAI.06/09A/A10-002 0920)
- P.B., Rao**  
(GAI.06/11P/D-006 1400-058)
- P.B., Camargo**  
(HW01/09A/C26-007 1130)
- P.V., Joseph**  
(MC17/10P/B23-008 1645)
- PACES, Tomas**  
(HW01/10A/C26-001 0830)
- PACINO, Maria Cristina**  
(G03/07P/D-032 1400-054)
- PACINO, Maria Cristina**  
(G03/07P/D-004 1400-026)
- PADHY, Manas Ranjan**  
(GAI.06/11P/D-018 1400-070)
- PADILLA, Pascual**  
(JSG03/09P/D-025 1640-033)
- PADMAKUMARI, B.**  
(MI09/08P/B22-008 1700)
- PAGNONI, Gianluca**  
(JSS07a/09P/D-011 1700-112)
- PAGNONI, Gianluca**  
(JSS07/10A/A02-010 1100)  
(JSS07a/09P/D-014 1700-115)  
(JSS07a/09P/D-013 1700-114)
- PAIK, Kyungrock**  
(HW07/11P/D-013 1400-149)
- PAIL, Roland**  
(G03/07P/D-058 1400-080)
- PAK, Evgenia L.**  
(HW03/11A/C30-008 1110)
- PAL, Indrajit**  
(SS04/08P/A03-006 1515)
- PALAU, Raquel L.**  
(SS04b/10P/D-043 1400-227)
- PALINKAS, Vojtech**  
(G07/10P/D-020 1400-105)
- PALLE, Enric**  
(JSA09/10A/A08-003 0930)
- (JSA08/09A/A08-007 1045)**
- PALM, Hartmut**  
(G07/10P/D-019 1400-104)
- PALMER, Mark**  
(HS01/09P/C29-002 1420)
- PALMER, Michael Anthony**  
(JSA08/09A/A08-005 1015)
- PALO, Scott**  
(MC05/10A/A09-007 1100)
- PAN, C.J.**  
(GAI.06/09P/A10-011 1710)
- PAN, Chen-Jeih**  
(GAI.06/09A/A10-009 1130)
- PAN, Jianfeng**  
(JSS06a/08P/D-010 1400-088)
- PAN, Laura L.**  
(MC05/09A/A09-001 0900)
- PANAGIOTOPOULOS, D.G.**  
(SS03/07A/A02-005 1030)
- PANAGOULIA, Dionysia**  
(HS02c/11P/D-002 1630-100)  
(HS02/11A/C24-002 1049)
- PANCAKE, Cheri**  
(JSS07/09P/A02-011 1645)
- PANCHEVA, D.**  
(MC05/10A/A09-010 1210)
- PANDA, Sudhindra Nath**  
(HS01/08P/C29-008)
- PANDEY, Ganesh R.**  
(HW07/11P/C25-004 1445)
- PANDEY, Om Prakash**  
(SS03/08A/D-128 0830-287)
- PANDEY, Vinay Kumar**  
(HS01/08P/C29-008 1640)
- PANDI, Gavril**  
(HS01/08P/C29-004 1500)
- Pandithurai G.**  
(MI09/08P/B22-006 1620)
- PANG, Hongxi**  
(MI05/10P/B17-006 1630)
- PANG, Hongxi**  
(HS02/08A/C24-006 0945)
- PANG, Hongxi**  
(HS02b/10P/D-014 1630-135)  
(HS02/10A/C24-014 1137)
- PANIZZO, Andrea**  
(JSS07/09P/A02-008 1600)
- PANKAMOLSIN, Yutthana**  
(HW04/09A/C31-007 1120)
- PANNEERSELVAM, C.**  
(JSA09/11P/D-003 1400-052)
- PANNING, Mark P.**  
(JSS06/08A/A04-007 1050)
- PANTELEEV, Gleb**  
(JSP04a/09P/D-004 1400-097)
- PANTULU, K.P.**  
(GAI.10/09P/D-015 1615-134)
- PANUGANTI, Devara China Sattilingam**  
(MI09/08P/B22-006 1620)
- PANZA, G.F.**  
(SS03/07A/A02-005 1030)
- PANZA, Giuliano**  
(JSS06/09P/A04-005 1520)  
(JSG01/07P/A01-003 1430)
- PANZA, Giuliano F.**  
(SS04b/10P/D-026 1400-210)
- PANZA, Giuliano F.**  
(SS03/07P/A02-009 1630)
- PANZA, Giuliano Francesco**  
(SS04b/10P/D-013 1400-197)  
(SS04/08A/A03-006 0945)
- PANZA, Giuliano Francesco**  
(SS04/07P/A03-001 1400)
- PANZA, Giuliano Francesco**  
(SW04/09P/A13-011 1645)
- PANZA, Giuliano F.**  
(SS04b/10P/D-011 1400-195)
- PANZA, Giuliano F.**  
(SS04/07A/A03-003 1000)
- PAPA, Fabrice**  
(JSG03/09P/D-003 1640-011)
- PAPA, Fabrice**  
(JSH01/08A/C27-004 1030)
- PAPAGEORGIU, Apostolos**  
(SS04b/10P/D-025 1400-209)
- PAPAZACHOS, C.B.**  
(SS03/07A/A02-005 1030)
- PAPITASHVILI, Vladimir**  
(GAV.05/08A/A11-006 1050)  
(GAI.05/08P/A15-007 1700)  
(GAV.04/07A/A11-005 1100)
- PARAJKA, Juraj**  
(JWH01/09A/C30-006 1110)
- PARAMONOVA, Nina N.**  
(JSM04/09P/D-014 1400-051)
- PARINGIT, Enrico C.**  
(JSM03/08P/A13-004 1500)
- PARK, E-Hyung**  
(MC08/07P/B17-002 1415)
- PARK, Geun-Ae**  
(HS03/08A/C26-006 1000)
- PARK, Ho-Taek**  
(HW01/09P/D-032 1400-223)
- PARK, Jeong-Gyun**  
(JSM14/08A/A05-005 0955)
- PARK, Jeong-Hyun**  
(MC11/11A/B19-006 1010)
- PARK, Jin-Oh**  
(SS03/08A/D-102 0830-261)
- PARK, Jin-Oh**  
(SS03/08A/D-009 0830-168)
- PARK, Jin-Oh**  
(SS03/08A/D-107 0830-266)
- PARK, Ki-Jun**  
(JSM04/09P/D-008 1400-045)
- PARK, Mijeong**  
(MC05/07A/A09-003 1000)
- PARK, S.-G.**  
(JSM14/09P/D-001 1400-065)
- PARK, Sang-Goon**  
(JSM14/09P/D-023 1400-087)
- PARK, Sang-Goon**  
(JSM14/07P/A05-003 1450)
- PARK, Sang-Soon**  
(JSM04/09P/B23-004 1600)
- PARK, Seon K.**  
(MC02/08P/B20-005 1550)
- PARK, Seon Ki**  
(MC02/07P/D-008 1400-205)
- PARKER, D.J.**  
(MI09/09A/B22-004 1000)
- PARKINSON, Claire L.**  
(JSM10/08A/B23-003 0930)
- PARKS, G.K.**  
(GAI.05/08A/A06-007 1040)
- PAROTIDIS, Miltiadis**  
(SS03/07P/A02-010 1645)
- PARR, Joanna**  
(SS03/08A/D-063 0830-222)
- PARROT, Michel**  
(GAI.08/11P/D-001 1400-072)
- PARVEZ, Imtiyaz Ahmed**  
(SS03/08A/D-079 0830-238)
- PARVEZ, Imtiyaz Ahmed**  
(SS04b/10P/D-013 1400-197)
- PARVEZ, Imtiyaz Ahmed**  
(SS04/08A/A03-006 0945)
- PASARIC, Miroslava**  
(JSM14/08P/A05-003 1510)
- PASARIC, Zoran**  
(JSM14/08P/A05-003 1510)
- PASCHMANN, Götz**  
(GAI.05/07A/A06-004 0945)
- PASCHMANN, Goetz**  
(GAI.11/09P/A15-008 1620)
- PASCOE, Charlotte**  
(MC05/09A/A09-007 1140)  
(MC05/10P/A09-001 1400)
- PASHKEVICH, Inna K.**  
(JSA07/10A/A05-008 1130)
- PASHKEVICH, Inna K.**  
(GAV.06/09P/D-002 1400-155)
- PASKO, Victor**  
(GAI.04/07A/A08-006 1050)
- PASKO, Victor P.**

## INDEX

- (GAIL.04/07P/A08-003 1450)  
**PATARAIA, Avtandil D**  
 (MI06/08A/D-002)  
**PATARAIA, Tamara A.**  
 (MI06/08A/D-002)  
**PATARAIA, Tamara A.**  
 (MI06/08A/D-002 0830-153)  
**PATERSON, Robert**  
 (JSM14/09P/D-019 1400-083)  
**PATHIRANA, Assela**  
 (HS03/07P/C26-011 1645)  
**PATIL, P.R.**  
 (MI09/08P/B22-008 1700)  
**PATRA, Amit Kumar**  
 (GAIL.06/11P/D-018 1400-070)  
**PATRA, Amit Kumar**  
 (GAIL.06/11P/D-014 1400-066)  
**PATRA, Amit Kumar**  
 (GAIL.06/09A/A10-002 0920)  
 (GAIL.06/11P/D-001 1400-053)  
 (GAIL.06/11P/D-006 1400-058)  
**PATRA, Amit Kumar**  
 (GAIL.06/11P/D-013 1400-065)  
**PATRO, Bantu Prasanta Kumar**  
 (GAIL.10/09P/D-004 1615-123)  
**PATUREL, Jean-Emmanuel**  
 (HS02/08A/C24-008 1045)  
**PATY, Carol**  
 (GAIV.02/07P/A07-001 1400)  
**PAULIQUEVIS, Theotonio**  
 (JSM04/09P/B23-001 1400)  
**PAUTET, Dominique**  
 (GAIL.04/07P/A08-006 1605)  
**PAVELIC, Paul**  
 (HS04/07A/C30-002 1005)  
**PAVLENKO, Olga V.**  
 (SS04b/10P/D-007 1400-191)  
**PAVLENKO, Olga V.**  
 (SS04b/10P/D-006 1400-190)  
**PAVLIS, Erricos C.**  
 (G03/07P/D-061 1400-083)  
 (G07/10P/D-007 1400-092)  
**PAVLOVA, Tatyana V.**  
 (MC11/11P/D-003 1400-196)  
**PAWSON, S.**  
 (MC11/10P/B19-003 1440)  
**PAWSON, Steven**  
 (MC05/09P/A09-005 1540)  
 (MC11/11A/B19-002 0850)  
 (MC05/07A/A09-004 1100)  
**PCHELKINA, Elena V.**  
 (GAIL.10/11A/D-001 0830-075)  
**PEARLMAN, Michael R.**  
 (G07/10P/D-012 1400-097)  
**PECCERILLO, Angelo**  
 (JSS06/09P/A04-005 1520)  
**PECHER, I.A.**  
 (SS03/08A/D-146 0830-305)  
**PECI, Veronika**  
 (SS04b/10P/D-019 1400-203)  
**PECI, Veronika**  
 (JSP11/08P/D-006 1400-075)  
**PECOVA, Jana**  
 (GAIL.08/08P/D-002 1400-137)  
**PÉCSKAY, Zoltán**  
 (JSS06/10A/A04-010 1150)  
**PEDERSEN, Arne**  
 (GAIL.11/09P/A15-008 1620)  
**PEDERSEN, Rikke**  
 (JSG01/07P/A01-010 1635)  
**PEDREROS, Rodrigo**  
 (JSP09/10A/B20-003 0945)  
**PEK, Josef**  
 (GAIL.08/08P/D-002 1400-137)  
**PEK, Josef**  
 (GAIL.08/08P/D-003 1400-138)  
**PEKDEGER, Asaf**  
 (HS04/08A/C30-007 1230)  
**PEKDEGER, Asaf**  
 (HW01/09P/D-023 1400-214)  
**PEKDEGER, Asaf**  
 (HW06/07P/C31-004 1500)
- PELAEZ MONTILLA, Jose Antonio**  
 (SS04/08P/A03-003 1430)  
**PELAEZ MONTILLA, Jose Antonio**  
 (SS04b/10P/D-014 1400-198)  
**PELINOVSKY, Efim**  
 (JSS07/09A/A02-012 1200)  
**PELINOVSKY, Efim**  
 (JSS07/09A/A02-004 0945)  
 (JSP08/09P/B19-004 1510)  
**PELLERIN, Pierre**  
 (HW07/11P/D-018 1400-154)  
**PELTIER, Richard W.**  
 (JSM11/10P/B18-003 1440)  
**PELTIER, Richard W.**  
 (JSG02/09P/A05-003 1450)  
**PELTIER, W.Richard**  
 (JSP10/11P/B21-001 1420)  
**PENCHANG, Xu**  
 (HS02b/10P/D-001 1630-122)  
 (HS02/10A/C24-001 1045)  
**PENDLEBURY, Diane**  
 (MC05/07P/D-009 1400-216)  
 (MC05/07A/A09-005 1130)  
**PENEVA, Elisaveta Lazarova**  
 (MC11/11P/D-002 1400-195)  
**PENG, Keke**  
 (HS04/08A/C30-003 1005)  
**PENG, Shiling**  
 (MI05/11A/B17-003 0910)  
**PENG, Xindong**  
 (MC11/11P/D-001 1400-194)  
**PENKOVA, Natalia V.**  
 (HW03/11A/C30-008 1110)  
**PENKOVA, Natalia V.**  
 (HS02/07A/C24-015 0956)  
 (HS02a/07P/D-015 1545-161)  
 (HW07/11P/D-012 1400-148)  
**PENKOVSKY, Valentin I.**  
 (HS02a/07P/D-035 1545-181)  
 (HS02-/07P/C24-035 1512)  
**PENVEN, Marie-Jos-**  
 (HW01/10A/C26-002 0850)  
**PERDOMO, Raul**  
 (JSG01/07P/A01-004 1445)  
**PERETOKIN, Sergei A.**  
 (SW05/10P/A13-012 1700)  
**PEREZ, Joseph D.**  
 (GAIL.06/08A/A02-004 1005)  
**PERMANA, Hariadi**  
 (SS03/08A/D-044 0830-203)  
**PERMANA, Haryadi**  
 (SS03/08A/D-063 0830-222)  
**PEROSANZ, Felix**  
 (G02/07A/C25-001 0900)  
**PEROSANZ, Felix**  
 (G02/07A/C25-003 0940)  
**PERRET, Gaelle**  
 (JSP10/11A/B21-010 1210)  
**PERROUD, Marjorie**  
 (JSM14/08P/A05-006 1715)  
**PERRY, Chris H.**  
 (GAIL.05/07P/D-020 1400-118)  
**PERS, Charlotta**  
 (HW01/10P/C26-006 1620)  
**PERSON, Ola**  
 (JSM10/07P/B23-003 1500)  
**PERTEL, Mikhail I.**  
 (GAIL.10/09A/A11-004 0945)  
**PESEC, Peter**  
 (G03/07P/D-058 1400-080)  
**PETER, Thomas**  
 (MI03/09A/D-006 0900-249)  
**PETERS, Norman E.**  
 (HW01/10P/C26-002 1420)  
 (HW07/11A/C25-009 1100)  
**PETERS, Thomas**  
 (JSG02/09P/A05-010 1730)  
**PETERSEN, Danyal**  
 (MI08/07P/B18-006 1700)  
**PETERSEN, Mark**  
 (SS04/08P/A03-004 1445)
- PETERSSON, Elke**  
 (HS02/10P/C24-001 1400)  
**PETKOVSEK, GREGOR**  
 (HS01/09A/C29-003)  
**PETRAS, Josip**  
 (HW07/11P/D-023 1400-159)  
**PETRITOLI, Andrea**  
 (MI03/09A/D-003 0900-246)  
**PETROSYAN, Arakel S.**  
 (JSP10/10P/B21-010 1740)  
**PETROVA, Inna Romanovna**  
 (GAIL.06/11P/D-003 1400-055)  
**PETROVA, Natasha**  
 (JSA07/11A/D-022 0830-022)  
**PETROVA, Reva S.**  
 (HW07/11P/D-012 1400-148)  
**PETROVIC, Svetozar**  
 (G04/08P/D-024 1400-131)  
**PETTERSON, Rickard**  
 (JSH01/08P/D-010 1400-048)  
**PETUKHIN, Anatoly G.**  
 (SS04a/09P/D-040 1400-289)  
 (SS04a/09P/D-004 1400-253)  
 (SS04a/09P/D-005 1400-254)  
**PEUCH, Vincent-Henri**  
 (MC05/07A/A09-006 1150)  
**PEYRON, Nelly**  
 (HW07/11P/C25-004 1445)  
**PEZZOLI, Alessandro**  
 (JSM03/09A/D-001 0830-035)  
**PFUFF, R.F.**  
 (JSG03/09P/D-026 1640-034)  
**PFUFF, Robert F.**  
 (GAIL.06/09P/A10-007 1545)  
**PFIZENMAYER, Arnt**  
 (JSP08/09P/B19-005 1600)  
 (MC08/07A/B17-007 1135)  
**PHAM, H.**  
 (JSH01/08P/D-013)  
**PHAN, Dao Thi Anh**  
 (HS02/09P/C24-005 1500)  
**PHAN, Trinh Trong**  
 (SS04/08P/A03-008 1545)  
 (JSG03/10A/A12-006 1040)  
**PHILLIPS, Jeffrey D.**  
 (GAV.07/07P/A13-001 1400)  
**PHILLIPS, T.**  
 (MC11/11P/B19-001 1400)  
**Pl, Xiaoping**  
 (GAIL.05/07A/D-006 0830-022)  
**Pl, Xiaoping**  
 (GAIL.05/08A/A15-005 1040)  
**Pl, Xiaoping**  
 (GAIL.05/07A/D-005 0830-021)  
**PIACEK, Steve**  
 (JSP10/08P/D-003 1610-055)  
**PICHON, Thierry**  
 (JSP10/11A/B21-010 1210)  
 (JSP10/09A/B21-007 1120)  
**PICKETT, Jolene S.**  
 (GAIL.07/09P/A14-005 1530)  
**PICKETT, Jolene S.**  
 (GAIL.07/09P/A14-003 1450)  
**PIÉGAY, Herv**  
 (HS01/09P/D-022 1400-189)  
**PIERAZZO, Elisabetta**  
 (GAIV.03/09P/D-001 1400-144)  
**PIETRAFESA, Leonard J.**  
 (JSP07/08A/B17-002 0930)  
**PIETRONIRO, Alain Claude**  
 (HW07/11P/D-018 1400-154)  
**PILIDOU, Sylvana**  
 (JSS06/09P/A04-010 1720)  
**PILIDOU, Sylvana**  
 (JSS06/08A/A04-008 1110)  
**PILIPENKO, Viacheslav A.**  
 (GAIL.10/11A/A01-001 0830)  
**PILON, Paul**  
 (HW07/11P/D-018 1400-154)  
**PINCIROLI, Roberto M.**  
 (SS04b/10P/D-043 1400-227)  
**PINET, Patrick C.**  
 (JSG03/10A/A12-007 1100)
- PING, Jinsong**  
 (GAIL.06/11P/D-007 1400-059)  
**PINNOCK, Ralph Allen**  
 (JSG03/09P/D-005 1640-013)  
**PINTO, Iara**  
 (GAIL.04/07P/A08-006 1605)  
**PINTO, JR., Osmar**  
 (GAIL.04/07P/A08-006 1605)  
**PIOMBO, Antonello**  
 (SS03/08A/D-047 0830-206)  
**PIOMBO, Antonello**  
 (SS03/08A/D-027 0830-186)  
**PIRES, Carlos A.**  
 (JSS07/09P/A02-006 1515)  
**PIRIOU, Jean-Marcel**  
 (MC17/11P/B23-010 1720)  
**PIRTTJÄRVI, Markku**  
 (JSA07/11A/D-029 0830-029)  
**PISARENKO, Vladilen F.**  
 (JSP11/07A/A10-003)  
 (JSP11/07P/A10-007)  
**PITARKA, Arben**  
 (SS04/08A/A03-011 1115)  
 (SS04a/09P/D-018 1400-287)  
 (SS04a/09P/D-038 1400-287)  
**PITILAKIS, Kyriazis**  
 (SS04/07A/A03-001)  
**PITOUT, F.**  
 (GAIL.06/07P/D-011 1400-131)  
**PITTS, Mike C.**  
 (MI03/08A/B18-002 0850)  
**PLAG, Hans-Peter**  
 (JSG03/10A/A12-003 0910)  
**PLAG, Hans-Peter**  
 (JSM11/10P/B18-002 1420)  
 (JSP07/08A/B17-003 0950)  
 (G07/10P/D-002 1400-087)  
**PLETCHOV, Pavel Yu.**  
 (SW05/10P/A13-001 1400)  
**PLOMEROVA, Jaroslava**  
 (JSS06/08A/A04-009 1130)  
 (JSS06b/10P/D-012 1400-036)  
 (JSS06b/10P/D-013 1400-037)  
**PLOTNIKOV, Vladimir**  
 (JSM10/09P/D-005 1400-059)  
**PLOTNIKOVA, Lylya**  
 (SS04/08P/A03-002 1415)  
**POCIASK-KARTECZKA, Joanna K.**  
 (HS02/08A/C24-007 1000)  
**PODGORNY, Vladimir Yakovlevich**  
 (JSA07/10P/A05-010 1730)  
**PODMOGOV, Yuri G.**  
 (GAIL.10/09A/A11-004 0945)  
**POGORELOV, Nikolai V.**  
 (GAIV.04/09P/A16-004 1615)  
 (GAIV.02/07A/A07-005 1130)  
**POGREBNOY, Valentin**  
 (SS03/08A/D-078 0830-237)  
**POHLMANN, Holger**  
 (MC11/11A/B19-010 1150)  
**POKORNA, Lucie**  
 (MC08/07P/B17-011 1710)  
**POLLACCO, Joseph**  
 (HW01/10P/C26-007 1640)  
 (HW08/08A/C28-010 1200)  
**POLONSKA, Diana**  
 (JSG01/07P/A01-012 1705)  
**POLVE, Mireille**  
 (SS03/08A/D-061 0830-220)  
**POLYAKOV, Andrei N.**  
 (SW05/10P/A13-006 1520)  
**POMEROY, John W.**  
 (JWH01/09P/C30-004 1500)  
 (HW07/11A/C25-008 1045)  
**POMEROY, John W.**  
 (JWH01/10P/C30-004 1500)  
**POMEROY, John W.**  
 (JWH01/10P/C30-002 1420)  
 (JWH01/10P/C30-003 1440)  
**PONOMARENKO, Elena**  
 (JSM11/10P/D-010 1700-019)

**PONOMERANKO, Pasha**  
(GAI.10/11A/A01-002 0845)

**PONTE, Rui M.**  
(JSP09/11A/B20-010 1130)  
(JSM11/10P/B18-001 1400)

**PONTEVIVO, Antonella**  
(JSS06/09P/A04-005 1520)

**PONYAVIN, Dmitri I.**  
(JSA08/09P/A08-004 1510)

**POOLEY, Christopher**  
(JSM15/07A/B18-007 1100)

**POOR MOGHADDAM, Peyman**  
(SS03/08A/D-105 0830-264)

**POPE, Vicky**  
(MC11/10A/B19-005 1000)

**POPESCU, Emilia**  
(JSS06b/10P/D-017 1400-041)

**POPLAVSKY, Alexander A.**  
(JSS07/10P/A02-007 1530)

**POPOV, Sergey K.**  
(JSS03/09P/D-015 1640-023)

**POPOVSKA, Cvetanka**  
(HW08/08A/C28-008 1120)

**PORATHUR, Joseph V.**  
(MC03/11P/D-011 1400-186)

**PORTELA, Maria Manuela**  
(HS02b/10P/D-016 1630-137)  
(HS02/10A/C24-016 1145)

**PORTER, H.S.**  
(MC05/09P/A09-004 1520)

**POTTS, Laramie V.**  
(JSG01/08A/A01-012 1205)

**POTTS, Laramie Vance**  
(JSS06a/08P/D-004 1400-082)  
(SS03/08A/D-149 0830-308)

**POTZSCH, Anja**  
(JSS03/09P/D-002 1640-010)

**POURAGHNAIEI, Mohammad Javad**  
(HS02b/10P/D-010 1630-131)  
(HS02/10A/C24-010 1121)

**POVARNITSYN, Mikhail**  
(JSM14/07P/A05-004 1505)

**PRÁCSEK, Erno**  
(GAI.10/09P/D-011 1615-130)

**Pradeep Aggarwal**  
(HW06/08A/C31-003 1120)

**PRADHAN, Nawa Raj**  
(HS03/08P/C26-006 1515)

**PRAJAPATI, S.K.**  
(SW03/10P/A04-009 1615)  
(SW03/10A/D-009 0830-244)

**PRANGE, Renée M.**  
(GAI.14/07P/A12-007 1625)

**PRASAD, Anup K.**  
(JSP11/07P/A10-004 1550)

**PRASAD, S.N.**  
(GAI.08/08A/A14-011 1210)

**PRATOMOSUNU, Bambang S.**  
(JSM11/10P/B18-006 1620)

**PRAUD, Olivier**  
(JSP10/11A/B21-001)

**PRAUS, Oldrich**  
(GAI.08/08P/D-004)

**PRAUS, Oldrich**  
(GAI.08/08P/D-002 1400-137)

**PRAWIRODIRDJO, Linette**  
(JSG01/07A/A01-010 1135)

**PRAYOGO, Tri Budi**  
(HW07/11P/D-025 1400-161)

**PREDESCU, Corina**  
(HS02c/11P/D-032 1630-130)  
(HS02/11P/C24-009 1547)

**PREEDY, Neil**  
(HS04/08A/C30-001 0905)

**PRESTES, Alan**  
(JSA08/10P/D-003 1400-003)

**PRETTO, Angelica**  
(JSM04/09P/D-015 1400-052)

**PREUSSE, P.**  
(MC05/11A/A09-005 1050)

**PREUSSE, Peter**  
(MC05/11A/A09-008 1200)

**PREUSSE, Peter**  
(MC05/11P/A09-003 1450)

**PRICE, Colin**  
(GAI.04/07A/A08-009)

**PRICE, Evelyn**  
(JSG01/07P/A01-009 1620)

**PRICE, G. David**  
(U5/07A/D32-001 0900)

**PRICE, ROLAND K.**  
(HS03/07A/C26-002 0930)

**PRIESTKEY, Keith**  
(JSS06/08A/A04-008 1110)

**PRIESTLEY, Keith**  
(JSS06a/08P/D-013 1400-091)

**PRIESTLEY, Keith F.**  
(JSS06/09P/A04-010 1720)

**PRIETO, Maria**  
(MC12/08A/B19-008 1200)

**PRIGENT, Catherine**  
(JSG03/09P/A12-003 1440)

**PRIJATNA, Kosasih**  
(G03/07P/D-042 1400-064)

**PRIKHOD'KO, Yuri V.**  
(JSP10/08P/D-013 1610-065)

**PRILEPIN, Mikhail T.**  
(SS04/08P/A03-011 1645)

**PRINCE, Stephen D.**  
(MC03/10P/A07-005 1600)

**PRINDLE-SHELRAKE, Kenton**  
(SS03/07A/A02-001 0900)

**PRODEHL, Claus**  
(JSA07/11A/D-020 0830-020)

**PROHOROV, Viktor E.**  
(JSP10/08P/D-017 1610-069)

**PROMOTION TEAM, I-Space Education**  
(SS05/10A/A13-003)

**PROSHUTINSKY, Andrey**  
(JSP08/09P/B19-006 1620)  
(JSP06/07P/B21-007 1640)

**PROSHUTINSKY, Andrey**  
(JSM11/10P/B18-003 1440)

**PROSHUTINSKY, Tatiana**  
(JSP08/09P/B19-006 1620)

**PROTTI, J. Marino**  
(SS03/08A/D-032 0830-191)

**PROTTI, Marino**  
(JSG01/08P/D-012 1400-012)

**PRUEGER, John**  
(MI07/11A/B18-006 1050)

**PRYTZ, Arnstein**  
(JSG03/09P/D-017 1640-025)  
(JSG03/09P/A12-006 1540)

**PSHECHENKOVA, Ekaterina A.**  
(JSA07/11A/D-021 0830-021)

**PU, Jianchen**  
(HS02b/10P/D-020 1630-141)  
(HS02/10A/C24-020 1201)

**PU, Jianchen**  
(JSM10/07A/B23-006 1140)

**PU, Jianchen**  
(HS02/07P/C24-027 1440)  
(HS02a/07P/D-027 1545-173)

**PU, Z.Y.**  
(GAI.06/07P/D-008 1400-128)

**PUENTEDURA, Olga**  
(MI03/09A/D-002 0900-245)

**PUHL-QUINN, Pamela**  
(GAI.05/07A/A06-004 0945)

**PUJADES, Lluís G.**  
(SS03/08A/D-033 0830-192)

**PULIDO, Manuel**  
(MC05/11A/A09-004 1000)

**PULIDO, Nelson**  
(SS04/07P/A03-003 1445)

**PULIDO, Nelson Edilberto**  
(SS04/08A/A03-010 1100)

**PULINETS, Sergey A.**  
(GAV.04/07A/A11-008 1200)

**PULKKINEN, Antti A.**  
(GAI.10/09P/A11-004 1445)

**PULKKINEN, Tuija I.**

(GAI.06/08A/A02-009 1215)

**PUNONGBAYAN, Jane T.**  
(SS04b/10P/D-016 1400-200)  
(SS03/08A/D-064 0830-223)

**PUNONGBAYAN, Jane Tampoc**  
(SS03/08A/D-060 0830-219)

**PUNONGBAYAN, Raymundo Santiago**  
(SS04b/10P/D-035 1400-219)

**PUNONGBAYAN, Raymundo Santiago**  
(SS03/08A/D-060 0830-219)  
(SW05/10A/D-003 0900-247)

**PUNONGBAYAN, Raymundo Santiago**  
(SS04b/10P/D-036 1400-220)

**PUNYATRONG, Kowit**  
(HW07/11P/D-038 1400-174)

**PURUCKER, Michael**  
(GAV.04/07A/A11-002 0930)

**PURUCKER, Michael**  
(GAV.05/08P/A11-010 1720)

**PURUCKER, Michael E.**  
(GAV.05/08A/A11-008 1130)

**PUSHISTOV, Petr Yu.**  
(JSG03/09P/A12-002 1420)

**PUSHKAREV, Pavel Yu**  
(GAI.10/09A/A11-006 1015)  
(GAI.10/09P/D-009 1615-128)

**PUSTOVOY, Alexander A.**  
(JSS06b/10P/D-021 1400-045)

**PYANKOV, Valentin A.**  
(GAI.10/09P/D-007 1615-126)

**PYLE, John**  
(MC05/10A/A09-005 1000)  
(MI03/08P/B18-001 1400)

**PYLES, R.D.**  
(JWH01/09A/C30-009 1210)  
(JWH01/09P/C30-001)

**PYSKLIWEC, Russell N.**  
(JSS06/07P/A04-010 1720)

**PYTHON, Marie**  
(JSG03/10A/A12-007 1100)

## q

**QIAO, Qiyuan**  
(MI05/10P/B17-007 1650)

**QIN, Dahe**  
(JSM04/09P/D-001 1400-038)

**QIN, Dahe**  
(JSM10/07A/B23-007 1200)

**QIN, Wei**  
(JSP10/10P/B21-004 1510)

**QIN, Yilong**  
(SS03/08A/D-137 0830-296)

**QIU, Jiong**  
(JSA09/10A/A08-003 0930)

**QIU, Xuelin**  
(SS03/07P/A02-013 1730)

**QU, Shen**  
(JSS06b/10P/D-015)

**QUADRELLI, Roberta**  
(MI05/09P/B17-001 1400)

**QUINN, Jack**  
(GAI.11/09P/A15-008 1620)

**QUINN, Jack M.**  
(GAI.05/07A/A06-004 0945)

**QUINN, Paul**  
(HS04/08A/C30-001 0905)

**QUINTANAR, Luis**  
(SS03/08A/D-148 0830-307)

**QUINTAS, Marcia C.L.**  
(G04/08P/D-015 1400-122)  
(G03/07P/D-043 1400-065)

**QUINTELA, Antonio de Carvalho**  
(HS02b/10P/D-016 1630-137)  
(HS02/10A/C24-016 1145)

**R., Sekar**  
(GAI.06/09A/A10-002 0920)

**R., Sridhnan**  
(GAI.06/09A/A10-002 0920)

**R, Sridharan**  
(GAI.06/11P/D-001)

**RAABE, Armin**  
(HS02/09A/C24-012 1200)

**RABAH, Taha Taha**  
(GAV.06/10P/A11-008 1640)

**RABI, Ayman Ismail**  
(HS02/11A/C24-002 0845)

**RABINOVICH, Alexander B.**  
(JSS07b/10P/D-009 1700-055)  
(JSS07/10A/A02-012 1130)

**RABINOVICH, Alexander B.**  
(JSS07/10A/A02-004 0915)

**RABINOVICH, Alexander B.**  
(JSS07/10A/A02-011 1115)

**RADERSCHALL, Norbert**  
(JWH01/09A/C30-004 1000)  
(JSM10/07A/B23-004 1020)

**RADJABOV, Shukhrat Saifullaevich**  
(HS02/07A/C24-013 0948)  
(HS02a/07P/D-013 1545-159)

**RADULIAN, Mircea**  
(SS04a/09P/D-046 1400-295)

**RADULIAN, Mircea**  
(JSS06b/10P/D-017 1400-041)  
(SS04b/10P/D-026 1400-210)

**RAEDER, Joachim**  
(GAI.05/08A/A15-002 0850)

**RAEDER, Joachim**  
(GAI.09/11A/A11-008 1210)

**RAGA, G.B.**  
(MC03/10P/A07-004 1520)

**RAGASAKTHI, S.S.SUN-DARVEL**  
(HS02/07P/C24-029 1448)  
(HS02a/07P/D-029 1545-175)

**RAGHUWANSHI, Narendra Singh**  
(HS01/08P/C29-008)

**RAGULSKAYA, Mary Valerievna**  
(GAV.06/09P/D-013 1400-166)

**RAHELI SALIMI, Javad**  
(JSP11/08P/D-001 1400-070)

**RAHNEMA, Mehdi**  
(JSP11/08P/D-003 1400-072)

**RAI, S.N.**  
(JSA07/11A/D-034 0830-034)

**RAI, S.S.**  
(JSA07/11A/D-038 0830-038)  
(JSS06/07P/A04-007 1620)

**RAICHLEN, Fred**  
(JSS07/09P/A02-009 1615)

**RAILEANU, Victor**  
(JSA07/11A/D-020 0830-020)

**RAINA, B.N.**  
(JSA09/10A/A08-009 1145)  
(JSA09/11P/D-002 1400-051)

**RAINA, B.N.**  
(JSA09/11P/D-003 1400-052)

**Rajan C.K.**  
(MI05/10P/B17-004 1520)

**RAJARAM, Mita**  
(GAV.06/10P/A11-001 1400)  
(GAV.04/07P/A11-002 1430)  
(GAV.07/07P/A13-006 1600)  
(GAV.06/10P/A11-002 1420)  
(JSA07/10P/A05-008 1650)  
(GAV.07/07P/D-003 1400-144)

**RAJARAM, R.**  
(JSA09/11P/D-002 1400-051)

**RAJARAM, R.**  
(JSA09/10A/A08-009 1145)  
(JSA09/11P/D-003 1400-052)

## INDEX

- RAJENDRAN, Kavirajan**  
(MC17/11A/B23-003 0920)
- RAJESH, R. S.**  
(JSA07/11A/D-039 0830-039)
- Rajkamal**  
(HS02/07P/C24-024 1428)  
(HS02a/07P/D-024 1545-170)
- RAJPUT, Shikha**  
(JSP11/07A/A10-002 0930)
- RAJPUT, Shikha**  
(SS04a/09P/D-013 1400-262)
- RAKONCZAI, János**  
(HS02c/11P/D-004 1630-102)  
(HS02/11A/C24-004 1057)
- RAM, Avadh**  
(SS04/08A/A03-015)
- RAM, Avadh**  
(SS04/07A/A03-010 1200)
- RAMA, G.V.**  
(MI09/09P/B22-004 1500)
- RAMANA, D.V.**  
(JSA07/11A/D-034 0830-034)
- RAMASWAMIAH, Srinivasan**  
(SW03/10P/A04-010 1630)
- RAMASWAMY, V.**  
(JSA09/10A/A08-005 1030)
- RAMESH, D.S.**  
(JSS06a/08P/D-023 1400-101)
- RAMI, Ali**  
(G03/07P/D-076 1400-098)
- RANDEL, William J.**  
(MC05/07A/A09-003 1000)
- Ranganna G.**  
(HS02/07P/C24-024 1428)  
(HS02a/07P/D-024 1545-170)
- RANGARAJAN, R.**  
(HW01/09P/D-012 1400-203)
- RANGO, Albert**  
(JSM15/07A/B18-007 1100)  
(JSH01/07P/C27-006 1600)
- RANNOU, Pascal**  
(MC04/10P/B22-006 1615)
- RAO, A. Ramachandra**  
(HS02/09A/C24-004 0945)  
(HS02b/10P/D-013 1630-134)  
(HS02/10A/C24-013 1133)  
(HS02/09A/C24-004 0945)  
(HS02/10A/C24-013 1133)
- RAO, Chinta K.**  
(SS03/08A/D-129 0830-288)
- RAO, Madhusudhan**  
(GAI11.10/11A/A01-004 0915)
- RAO, Naga Malleswara**  
(HW07/11P/D-033 1400-169)
- RAO, P.B.**  
(GAI11.06/09A/A10-009 1130)
- RAO, Ram Mohan**  
(HW07/11P/D-034 1400-170)
- RAO, Vijay K.**  
(GAI.08/08A/A14-011 1210)
- RAPTAKIS, Dimitrios**  
(SS04/07A/A03-001 0915)
- RASHEED, Anas M.**  
(HW07/11P/D-026 1400-162)
- RASHID, Anas Mahmood**  
(HW07/11P/D-027 1400-163)
- RASMUSSEN, Roy**  
(MI09/09A/B22-002)
- RASOUL-AGHA , Wathek**  
(SW04/09P/A13-002 1415)
- RASPOPOV, Oleg M.**  
(JSA09/10A/A08-010 1200)
- RASTAETTER, Lutz**  
(GAI11.09/10P/D-003 1400-115)
- RASTAETTER, Lutz**  
(GAI11.09/11A/A11-008 1210)
- RASTOGI, Bal Krishna**  
(SS04/08P/A03-004 1445)  
(SW04/09P/A13-006 1515)
- RATOVSKY, Konstantin G.**  
(GAI11.06/11P/D-004 1400-056)
- RATTRAY, Karen**  
(HS04/07A/C30-002 1005)
- RAULT, Didier F.**  
(MI03/08A/B18-002 0850)
- RAVAL, Upendra**  
(JSS06/09A/A04-009 1200)
- RAVAL, Upendra**  
(SW03/10P/A04-007 1530)
- RAVAT, Dhananjay**  
(GAV.06/10A/A11-011 1210)
- RAVEGNANI, Fabrizio**  
(MI03/09A/D-003 0900-246)
- RAVILLY, Morgane**  
(GAV.06/10P/A11-006 1600)
- RAWAT, Gautam**  
(GAI.08/08A/A14-002 0850)
- RAY, Eric A.**  
(MC05/11P/A09-004 1510)
- RAY, Labani**  
(SW03/10P/A04-010 1630)
- RAY, Licia**  
(GAI11.06/10A/A01-009 1105)
- RAYMOND, David J.**  
(MC17/10P/B23-005 1515)  
(MC03/10P/A07-004 1520)
- RAYNAL, Jose A.**  
(HW07/11P/D-029 1400-165)
- RAZJIGAEVA, Nadezhda G.**  
(JSS07a/09P/D-010 1700-111)
- RAZJIGAEVA, Nadezhda G.**  
(JSS07/10A/A02-003 0900)
- RE, Guillermo Hector**  
(SS03/08A/D-097 0830-256)  
(JSA07/11A/D-048 0830-048)
- READ, P.L.**  
(MC04/10P/B22-003 1445)
- READ, Peter Leonard**  
(JSP10/08P/B21-001 1400)  
(MC04/11P/B22-001 1400)
- READMAN, Peter W.**  
(SS03/08A/D-089 0830-248)  
(MC12/07P/B19-003 1500)  
(JSA07/11A/D-032 0830-032)  
(SS03/08A/D-145 0830-304)
- REASOR, Paul D.**  
(JSP10/10P/B21-006 1610)
- REDDY, Chappidi D.**  
(SS03/07P/A02-014 1745)
- REDDY, Divakar**  
(JSG01/08P/D-028 1400-028)
- REDDY, Krishna**  
(JSM14/08A/A05-004 0940)
- REDDY, S.I**  
(SS03/08A/D-131 0830-290)
- REDDY, Surender**  
(HW01/09P/D-001 1400-192)
- REDELSPERGER, Jean-Luc**  
(MC17/11P/B23-010 1720)
- REED, Seann**  
(HS03/07A/C26-003 0945)
- REED, Seann**  
(HS03/07A/C26-004 1000)
- REED, Seann**  
(HW08/08A/C28-005 1000)
- REED, Seann M.**  
(HW08/09A/C28-006 1050)
- REES, H.Gwyn**  
(HW07/11A/C25-013 1215)
- REEVES, Colin V.**  
(GAV.04/07P/A11-001 1400)
- REEVES, G.D.**  
(GAI11.06/08P/A02-011 1725)
- REEVES, Geoffrey D.**  
(GAI11.06/08P/A02-003 1450)  
(GAI11.08/10A/A16-011 1150)
- REFSGAARD, Jens Christian**  
(HW03/11A/C30-002 0850)
- REGUZZONI, Mirko**  
(G04/08P/D-017 1400-124)
- REIGBER, Christoph**  
(G02/07A/C25-001 0900)  
(G02/07A/C25-002 0920)  
(G07/10P/A03-003 1440)  
(UL6/09A/D32-001 0810)  
(SS03/08A/D-117 0830-276)
- (G07/10P/D-006 1400-091)
- REILINGER, Robert**  
(JSG01/07A/A01-008 1105)
- REIMER, Tamara W.**  
(GAI.V.03/09A/A16-002 0930)
- REINER, M.J.**  
(GAI11.09/11A/A11-004 0950)
- REINISCH, B.W.**  
(GAI11.06/11P/D-009 1400-061)
- REINISCH, Bodo**  
(GAI11.11/09A/A15-009 1150)
- REISNER, Jon M.**  
(MI09/09A/B22-006 1110)
- REITMAYR, Gernot**  
(JSA07/10P/A05-007 1630)
- REME, H.**  
(GAI11.09/11A/A11-006 1110)
- REME, H.**  
(GAI11.05/08A/A06-007 1040)
- REME, Henri**  
(GAI11.05/08A/A06-003 0900)
- REME, Henri**  
(GAI.V.03/08A/A16-007 1130)
- REME, Henri**  
(GAI11.05/08A/A06-004 0925)
- REME, Henri**  
(GAI11.11/09P/A15-008 1620)
- REME, Henri**  
(GAI11.05/07P/D-007 1400-105)
- REME, Henri**  
(GAI11.05/08A/A06-009 1110)
- REMIZOV, A.**  
(GAI.V.03/08P/A16-003 1500)
- REMY, Frederique**  
(JSG03/09P/D-003 1640-011)
- REMY, Frederique**  
(JSG02/09A/D-002 0830-002)  
(JSM11/10A/B18-005 1020)
- REMY, Frederique**  
(JSH01/08A/C27-004 1030)
- REN, Jiawen**  
(JSM04/09P/D-001 1400-038)
- REN, Liliang**  
(HS03/08A/C26-007 1030)
- REN, Xiaobo**  
(MC08/08P/D-001 1400-157)
- REN, Xin**  
(JSH01/07P/C27-002)
- RENFREW, Ian**  
(JSP09/10A/B20-010 1200)
- RENFREW, Ian A.**  
(JSP09/10P/B20-002 1430)
- RENGONO, Findy**  
(JSM14/07A/A05-006 1130)
- RENSHENG, Chen**  
(JSM10/08P/B23-008 1700)
- RENTSCH, Susanne**  
(SS03/07P/A02-010 1645)
- RESCH, Francois**  
(JSM03/09A/D-001 0830-035)
- Research Group of Hokkaido Transect**  
(SS03/07A/A02-007 1100)
- Research Group of Hokkaido Transect**  
(SS03/08A/D-106 0830-265)
- RESHETNIKOV, Alexander I.**  
(JSM04/09P/D-014 1400-051)
- RESZKA, Mateusz K.**  
(JSP10/09A/B21-006 1100)
- REUBELT, Tilo**  
(G02/07A/C25-006 1030)
- REVIL, Andre**  
(GAV.07/07P/D-004 1400-145)
- REYES-IBARRA, Mario Alberto**  
(G03/07P/D-033 1400-055)
- REYMOND, Dominique**  
(JSS06a/08P/D-013 1400-091)
- REYNOLDS, Richard W.**  
(JSP06/07A/B21-003 0940)
- RIBEIRO, Antonio**  
(JSS07/09A/A02-010 1130)
- RIBOLZI, Olivier**  
(HS01/09P/D-014 1400-181)
- RIBSTEIN, Pierre**  
(JSM10/08P/B23-004 1520)
- RICARD, Yanick**  
(U5/07A/D32-005 1130)
- RICH, F.J.**  
(JSG03/09P/D-026 1640-034)
- RICH, Frederick**  
(GAI11.05/08P/A15-007 1700)
- RICHARD, Erik**  
(MC05/11P/A09-004 1510)
- RICHARD, Eugene D.**  
(GAV.05/09P/D-001 1400-145)
- RICHARDSON, Chris A.**  
(MC12/08P/B19-006 1620)
- RICHARDSON, J.D.**  
(GAI.V.02/07P/A07-005 1640)
- RICHARDSON, John d**  
(GAI11.14/07P/A12-006 1600)
- RICHMOND, Arthur D.**  
(GAI11.05/08P/A15-003 1500)
- RICHMOND, Nicola C.**  
(GAI.V.03/09P/D-001 1400-144)
- RICHTER, Bernd**  
(G07/10A/A03-004 1000)
- RICHTER, Bernd**  
(G07/10P/D-015 1400-100)
- RICHTER, Bernd**  
(G07/10P/D-009 1400-094)  
(G07/10P/D-010 1400-095)
- RIDGWAY, Ken**  
(JSP06/07P/B21-005 1600)
- RIDLEY, Aaron**  
(GAI11.09/11A/A11-008 1210)
- RIDLEY, Aaron J.**  
(GAI11.05/08P/A15-004 1520)  
(GAI11.14/07A/A12-009 1225)
- RIDLEY, Aaron J.**  
(GAI11.06/08A/A02-006 1110)
- RIDLEY, Jeff**  
(JSM11/10A/B18-002 0920)
- RIES, John C.**  
(JSG02/09A/D-004 0830-004)
- RIEU, Seung Yup**  
(HS02/08P/C24-010 1645)
- RIGLER, E. Josh**  
(GAI11.05/08A/A15-001 0830)
- RIGOR, Ignatius**  
(JSP04/10P/A06-005 1520)
- RIGOZO, Nivaor Rodolfo**  
(JSA08/10P/D-003 1400-003)
- RILEY, James J.**  
(JSP10/11A/B21-007 1110)
- RIM, Hyung-Jin**  
(JSG02/09A/D-004 0830-004)
- RINCK-PFEIFFER, Stephanie**  
(HS04/08A/C30-007 1230)
- RINGER, M.A.**  
(MC11/10P/B19-002 1420)
- RINSLAND, Curtis**  
(MI03/08A/B18-007 1110)
- RIO, Abarca del**  
(MC17/10A/D-001 0830-183)
- RIO, Casaverde**  
(GAV.06/09P/D-010 1400-163)
- RIOS, Victor Hugo**  
(JSG03/09P/D-025 1640-033)
- RIPPEY, Brian**  
(HS01/09P/D-020 1400-187)  
(HW01/10A/C26-006 1050)
- RISHBETH, Henry**  
(JSA01/08P/A12-006 1640)
- RISLEY, Allan D.**  
(MI03/08A/B18-002 0850)
- RITCHE, Harold**  
(HW07/11P/D-018 1400-154)
- RITCHIE, Jerry**  
(MI09/09A/B22-005 1050)
- RITSCHOLD, Bernd**  
(G07/10P/D-019 1400-104)
- RIVA, Riccardo**  
(JSG01/07P/A01-003 1430)

- RIVERS, Aaron R.**  
(MC12/07A/B19-003 1015)
- RIZESCU, Mihaela**  
(SS04a/09P/D-050 1400-299)
- RIZOS, Chris**  
(JSG01/07P/A01-012 1705)
- RIZOS, Chris**  
(G04/08P/D-005 1400-112)
- RIZOS, Chris**  
(G04/07P/C25-004 1530)
- ROBERTA, Tozzi**  
(GAV.04/07P/A11-008 1700)
- ROBERTSON, Andrew W.**  
(MI05/10P/B17-001 1400)
- ROBINSON, David**  
(JSH01/07P/C27-009 1700)
- ROBINSON, Peter A.**  
(GAIV.02/07P/A07-004 1600)
- ROBINSON, Walter A.**  
(MI05/11A/B17-003 0910)
- ROBINSON, Walter A.**  
(MI05/09A/B17-001 0900)
- ROBLE, R.G.**  
(MC05/08A/A09-003 0930)
- ROBLE, Ray**  
(MC05/08A/A09-004 1000)
- ROBOCK, Alan**  
(JSA09/10A/A08-005 1030)
- ROCA, Remy**  
(MC17/10P/B23-007 1630)
- ROCCA, Fabio**  
(G07/10P/D-015 1400-100)
- ROCHETTE, Pierre**  
(GAIV.03/09P/D-001 1400-144)
- ROCHON, Gilbert L.**  
(JSG03/09P/A12-007 1620)
- ROCKEL, Burkhardt**  
(MC08/07A/B17-007 1135)
- RODGER, Alan**  
(GAIII.10/11A/A01-001 0830)
- RODGER, Alan S.**  
(GAIII.06/07P/D-007 1400-127)
- RODGER, Craig J.**  
(GAII.04/07A/A08-001 0900)
- RODKIN, Mikhail V.**  
(JSP11/07A/A10-003 1000)  
(JSP11/07P/A10-007 1700)
- RODNIKOV, Alexander G.**  
(JSS06a/08P/D-015)
- RODNIKOV, Alexander Georgievich**  
(SS03/08A/D-144 0830-303)
- RODRIGUEZ, Ernesto**  
(U6/09A/D32-006 1140)
- RODWELL, Mark John**  
(MC11/11A/B19-010 1150)
- ROEBBER, Paul J.**  
(JSM14/09A/A05-001 0905)
- ROECKER, Steven**  
(SS03/07A/A02-002 0915)
- ROEDER, James L.**  
(GAIII.06/08A/A02-005 1045)  
(GAIII.08/10A/A16-007 1040)
- ROEMMICH, Dean**  
(JSP06/08A/B21-001 0900)
- ROEMMICH, Dean H.**  
(JSP06/07P/B21-002 1420)  
(JSP06/07P/B21-005 1600)
- ROESCH, Andreas**  
(JWH01/09P/C30-009 1710)
- ROESER, Hans P.**  
(G07/10P/D-011 1400-096)
- ROGERO, Jose Roberto**  
(JSM04/09P/D-015 1400-052)
- ROGERS, Barrett**  
(GAIII.05/08A/A06-012 1215)
- ROGERS, Garry**  
(JSG01/07P/A01-006 1515)  
(SS04/08P/A03-014 1730)
- ROHDE, Hans**  
(G07/10P/D-016 1400-101)
- ROKITYANSKY, Igor Ivanovich**  
(GAI.10/09A/A11-003 0930)  
(GAII.04/07P/A08-008 1645)
- ROLAND, Markus**  
(G03/07P/D-015 1400-037)
- ROMAGNOLI, Claudia**  
(G07/10P/D-015 1400-100)
- ROMANELLI, Fabio**  
(SW04/09P/A13-011 1645)  
(SS04/07P/A03-001 1400)
- ROMANOWICZ, Barbara**  
(JSS06a/08P/D-019)
- ROMANOWICZ, Barbara**  
(JSS06/08A/A04-007 1050)
- ROMANOWICZ, Barbara**  
(JSS06/08A/A04-010 1150)
- ROMANOWICZ, Barbara A.**  
(JSS06/09A/A04-003 0940)
- ROMANS, Larry J.**  
(G03/07P/D-068 1400-090)
- ROMENETS, Andriy A.**  
(HS02/09P/D-002 1400-155)
- ROPELEWSKI, Chet**  
(MC02/07A/B20-006 1145)
- ROSALES, Wenceslao Martin-**  
(HS01/09P/C29-004 1500)
- ROSEBERG, Jürgen**  
(HW01/10P/C26-006 1620)
- ROSBJERG, Dan**  
(HS02/09P/C24-001 1400)
- ROSE, Mike**  
(GAIII.10/10P/A01-008 1620)
- ROSEN, Gary**  
(GAII.05/08A/A15-005 1040)
- ROSEN, Gary**  
(GAII.05/07A/D-005 0830-021)  
(GAII.05/07A/D-006 0830-022)
- ROSEN, Richard D.**  
(JSP09/11A/B20-010 1130)
- ROSENBERGER, Andreas**  
(SS04/08P/A03-014)
- ROSENBLATT, Pascal**  
(G02/07A/C25-012 1215)
- ROSENBLUM, Moshe**  
(G07/10P/D-005 1400-090)
- ROSENFELD, Daniel**  
(JSM04/09A/B23-005 1115)
- ROSENLOF, Karen**  
(MC05/11P/A09-004 1510)
- ROSENLOF, Karen H.**  
(MC05/08A/A09-002 0900)
- ROSSI, Giuseppe**  
(HS02/10A/C24-004 0915)
- ROSSOW, William B.**  
(JSG03/09P/A12-003 1440)
- ROSTOKER, Gordon**  
(GAIII.05/07A/A06-008 1120)
- ROTHACHER, Markus**  
(G02/07A/C25-008 1115)
- ROTHACHER, Markus**  
(G07/10A/A03-004 1000)
- ROTHACHER, Markus**  
(G07/10P/D-010 1400-095)
- ROTHERT, Elmar**  
(SS03/07P/A02-010 1645)
- RÖTTGER, Jürgen**  
(GAII.06/10A/A01-006 0955)
- ROUBICEK, Andres**  
(MC11/10P/B19-001 1400)
- ROUSSEL, Jean-François**  
(GAIII.11/09P/A15-013 1745)  
(GAIII.11/10P/D-003 1400-118)
- ROUSSIGNOL, Michel**  
(GAI.10/09A/A11-011 1200)
- ROVDAN, Elena N.**  
(HW01/09P/D-036 1400-227)
- ROWLANDS, David D.**  
(G02/07A/C25-011 1200)
- ROY, Arabinda**  
(JSS06a/08P/D-026 1400-104)
- ROY, Debasis**  
(SS04/08P/A03-006 1515)
- ROY, Kalyan Kumar**  
(GAI.10/09A/A11-005 1000)
- (GAI.08/08A/A14-009 1130)
- ROY, Kalyan Kumar**  
(JSA07/11A/D-040 0830-040)
- ROY, Manashi na**  
(GAII.07/10P/D-003 1400-108)
- ROZANOV, Eugene V.**  
(MI03/09A/D-006 0900-249)
- ROZHDESTVENSKY, A.V.**  
(HW07/11P/D-016 1400-152)
- ROZSA, Szabolcs**  
(G03/07P/D-005 1400-027)
- ROZSA, Szabolcs**  
(G03/07P/D-006 1400-028)
- RUBIN, Hillel**  
(HS04/08A/C30-006 1200)
- RUBIN, Yoram N.**  
(HW07/10A/C25-005 1115)  
(HW07/10A/C25-005 1115)
- RUBINIC, JOSIP**  
(HS01/09A/C29-003)
- RUBINSTEIN, Konstantin G.**  
(MC11/10A/B19-002 0900)
- RUCKER, Helmut O.**  
(GAIII.05/07A/A06-004 0945)
- RUDENCHIK, Eugeniy Antonovich**  
(GAV.06/09P/D-013 1400-166)
- RUDZINSKI, Wladyslaw J.**  
(MI08/07P/B18-004 1620)
- RUELKE, Axel**  
(JSG01/08A/A01-010 1135)  
(JSG01/08A/A01-011 1150)
- RUI, Hualan**  
(MC02/07P/D-002 1400-199)
- RUMMEL, Reiner**  
(G07/10A/A03-001 0900)  
(JSG02/09P/A05-001 1400)
- RUNOV, Andrei**  
(GAIII.05/08A/A06-003 0900)
- RUNOV, Andrei**  
(GAIII.05/07P/D-007 1400-105)
- RUSSELL, C.T.**  
(GAIII.06/07P/D-002 1400-122)
- RUSSELL, C.T.**  
(GAV.04/07A/A11-003 0950)
- RUSSELL, Christopher**  
(GAIII.14/07P/A12-003 1445)
- RUSSELL, Christopher T.**  
(GAIII.10/10P/A01-005 1520)
- RUSSELL, J.E.**  
(MI09/09A/B22-004 1000)
- RUSSELL, Sara**  
(JSS06a/08P/D-018 1400-096)
- RUSSELL III, James M.**  
(MC05/09P/A09-004 1520)
- RUSSELL III, James M.**  
(MC05/07P/A09-007 1700)
- RUTHERFORD, Scott**  
(MC12/08P/B19-004 1515)
- RUTIGLIANO, Paolo**  
(JSP11/08A/A10-008 1200)
- RYABININ, Vladimir**  
(JSM10/07A/B23-001 0900)
- RYAKHOVSKY, Vladimir M.**  
(JSS06b/10P/D-021 1400-045)
- RYBIN, Anatoly K.**  
(GAI.08/08A/A14-004 0930)
- RYKOV, Nikolay Afanasievich**  
(JSP06/07P/D-004 1400-011)
- RYZHII, Boris Petrovich**  
(SS03/08A/D-072 0830-231)
- S., Prasanna Kumar N.**  
(HS02/07P/C24-024 1428)  
(HS02a/07P/D-024 1545-170)
- S., Ramaseshan**  
(HS02b/10P/D-025 1630-146)  
(HS02/10P/C24-002 1519)
- S., Sripathi**  
(GAII.06/11P/D-014 1400-066)  
(GAII.06/11P/D-006 1400-058)  
(GAII.06/09A/A10-002 0920)
- S., Sunil P.**  
(SS03/08A/D-080 0830-239)
- S., Sijikumar**  
(JSM14/07A/A05-009 1215)
- S., Sijikumar**  
(MC03/11P/D-011 1400-186)
- SÁOSABBAS, Fernanda T.**  
(GAII.04/07A/A08-004 0955)
- SAANDARI, Mijiddorj**  
(G07/10P/D-003 1400-088)
- SÄÄVUORI, Heikki**  
(JSA07/10A/A05-006 1050)
- SABA, Jack L.**  
(JSM11/10A/B18-001 0900)
- SABADINI, Roberto**  
(JSG01/07P/A01-003 1430)
- SABAKA, Terence**  
(GAV.05/08P/A11-003 1445)  
(GAV.04/07A/A11-002 0930)
- SABAKA, Terence John**  
(GAV.05/08A/A11-003 0920)
- SABBIONE, Nora C.**  
(SS04b/10P/D-043 1400-227)
- SABITOVA, Tamara**  
(SS03/08A/D-078 0830-237)
- SABITOVA, Tamara Mikhailovna**  
(SS03/08A/D-141 0830-300)
- SADEGHI HOSSEINI, Seyed Alireza**  
(JSP11/08P/D-001 1400-070)
- SADEGHI HOSSEINI, Seyed Alireza**  
(MI08/07P/D-002 1400-196)
- SADEQUE, Mohammad Faheem**  
(HS02c/11P/D-027 1630-125)  
(HS02/11P/C24-010 1551)
- SADIDKHOI, Ahmad**  
(JSA07/11A/D-036 0830-036)
- SAFARGALEEV, Vladimir V.**  
(GAIII.10/11A/D-001 0830-075)
- SAFARI, Abdolreza**  
(G03/07P/D-021 1400-043)  
(G03/07P/D-018 1400-040)
- SAFRONOV, Iliia**  
(GAI.08/08A/A14-004 0930)
- SAGAWA, Eiichi**  
(GAIII.06/07P/D-020 1400-140)
- SAGHAFIAN, B.**  
(HS02b/10P/D-010 1630-131)  
(HS02/10A/C24-010 1121)
- SAGIYA, Takeshi**  
(JSG01/08P/D-016 1400-016)
- SAHARJO, Bambang Hero**  
(JSM04/09P/B23-007 1730)
- SAHR, John D.**  
(GAII.06/10A/A01-004 0920)
- SAHU, Sudip Jyoti**  
(HW05/10P/D-007 1400-162)
- SAIANG, Christine**  
(JSS07a/09P/D-018 1700-119)
- SAIGUSA, Nobuko**  
(MI07/10P/D-004 1400-180)
- SAIN, K.**  
(GAI.10/09A/A11-012 1215)
- SAITA, Tomoharu**  
(JSS06/07P/A04-005 1540)
- SAITO, Akinori**  
(GAII.06/11P/D-007 1400-059)  
(GAII.05/08P/A15-001 1400)
- SAITO, Akinori**  
(GAII.06/11P/D-011 1400-063)

## S

- S., Imaev Valeriy**  
(SS03/08A/D-019 0830-178)
- S., Mbom Abane**  
(GAI.10/09P/D-017 1615-136)
- S., MBOM ABANE.**  
(GAI.10/09P/D-016 1615-135)

## INDEX

- SAITO, H.**  
(GAI.06/07P/D-010)
- SAITO, Kazui**  
(JSM14/08A/A05-003 0925)
- SAITO, Kazuyuki**  
(JSM10/08A/B23-005 1010)  
(MC03/11P/A07-004 1520)
- SAITO, Kazuyuki**  
(JSM10/08A/B23-004 0950)
- SAITO, Mitsuyo**  
(HS01/09P/D-007 1400-174)
- SAITO, Saneatsu**  
(SS03/08A/D-043 0830-202)
- SAITO, Susumu**  
(GAI.06/09P/A10-004 1500)
- SAITO, Tadashi**  
(JSG01/07A/A01-001 0900)
- SAITO, Tokumi**  
(SS04a/09P/D-035 1400-284)
- SAITO, Tomoo**  
(SS04b/10P/D-023 1400-207)
- SAITO, Y.**  
(GAI.06/07P/D-010)
- SAITO, Yoshifumi**  
(GAI.05/08A/A06-005)  
(GAI.05/07A/A06-001)
- SAITO, Yoshifumi**  
(GAI.05/07P/D-009 1400-107)
- SAITO, Yoshifumi**  
(GAI.05/08A/A06-001 0830)  
(GAI.03/09A/A16-007 1150)  
(GAI.02/07P/A07-003 1510)  
(GAI.05/07P/D-014 1400-112)  
(GAI.05/07P/D-010 1400-108)
- SAKAI, Akiko**  
(MC05/07P/D-005 1400-212)
- SAKAI, Hideo**  
(GAV.05/09P/D-007 1400-151)
- SAKAI, Hirokazu**  
(MC05/10A/A09-004 0940)
- SAKAI, Shin'ichi**  
(SS03/07A/A02-008 1115)
- SAKAI, Tomoya**  
(GAI.10/11A/A01-011 1100)
- SAKAKIBARA, Atsushi**  
(JSM14/07P/A05-002 1435)
- SAKAKIBARA, Atsushi**  
(JSM14/07A/A05-004 1040)
- SAKAKIMA, Toshihiro**  
(GAI.11/09A/A15-008 1135)
- SAKAMOTO, Kei**  
(MI06/09P/B20-001 1400)
- SAKAMOTO, Kensei**  
(JSP10/10P/B21-004 1510)
- SAKAMOTO, Kohei**  
(JSM14/07P/A05-005 1620)
- SAKANAI, Takeshi**  
(GAI.14/07A/A12-008 1210)
- SAKATA, Toshibaumi**  
(JSG03/09P/D-019 1640-027)
- SAKHNO, Olga V.**  
(JSA07/10A/A05-010 1210)  
(SS03/08A/D-073 0830-232)  
(JSA07/11A/D-006 0830-006)
- SAKUMA, Hirofumi**  
(JSP04/09A/A06-007 1130)
- SAKURA, Yasuo**  
(HS04/07P/C30-002 1435)
- SAKURAI, Namiko**  
(MC03/10P/A07-008 1720)
- SAKURAI, Namiko**  
(MC03/11P/A07-003 1440)
- SAKURAI, Namiko**  
(MC03/11P/D-009 1400-184)
- SAKURAI, Tohru**  
(GAI.10/11A/D-015 0830-089)
- SAKURAI, Tohru**  
(GAI.09/10P/D-002 1400-114)
- SAKURAI, Tohru**  
(GAI.06/10A/A01-011 1145)
- SALBY, Murry L.**  
(JSA08/09A/A08-002 0915)
- SALEH, Hussain A.**  
(G02/10P/D-018 1400-083)
- SALEM, Ahmed**  
(JSA07/11A/D-046)
- SALEM, Ahmed Said**  
(GAV.06/10P/A11-007 1620)
- SALEQUZZAMAN, Md.**  
(JSP11/08A/A10-007 1140)  
(SS05/10A/A13-007 1000)  
(SS05/10A/A13-008 1015)
- SALEQUZZAMAN, Md.**  
(JSP11/08A/A10-004 1010)
- SALEQUZZAMAN, Md.**  
(JSP08/09P/D-001 1400-100)
- SALOKHIDDINOV, Abdulkhakim**  
(HS02a/07P/D-038 1545-184)  
(HS0207P/C24-038 1524)
- SALSTEIN, David A.**  
(MC11/11A/B19-004 0930)  
(MC03/10A/A07-009 1150)
- SALTUS, Richard W.**  
(GAV.06/09P/D-007 1400-160)
- SALVAYRE, Henri**  
(HW06/07P/D-001 1400-185)
- SAMARAJALINGAM, Shanmuganandan**  
(JSM04/09P/D-013 1400-050)  
(JSM14/09P/D-029 1400-093)
- SAMBORSKY, Taras V.**  
(HS02c/11P/D-010 1630-108)  
(HS02/11A/C24-010 1121)
- SAMIREDDIPALLE, Sripathi**  
(GAI.06/11P/D-018 1400-070)
- SAMIREDDIPALLE, Sripathi**  
(GAI.06/11P/D-013 1400-065)
- SAMPE, Takeaki**  
(MI06/08A/D-001 0830-152)
- SAMSON, John C.**  
(GAI.05/07A/A06-007 1055)
- SAMUEL, Amirtharaj**  
(SS03/08A/D-080 0830-239)
- SANCHEZ, Jorge Sesma**  
(MC12/08P/B19-005 1605)
- SANCHEZ, Laura**  
(G07/10A/A03-008 1200)
- SANCHEZ, Laura**  
(G03/07P/D-054 1400-076)
- SANDA, Eri**  
(JSM15/07P/D-007 1400-007)
- SANDAHL, Ingrid**  
(GAI.08/10A/A16-003 0910)  
(GAI.08/10A/A16-007 1040)  
(GAI.06/08A/A02-005 1045)
- SANDANGER, Marit Irene**  
(GAI.06/07P/D-005 1400-125)
- SANDEL, B.**  
(GAI.08/10A/A16-012 1210)
- SANDEL, Bill R.**  
(GAI.06/08A/A02-002 0915)
- SANDEL, Bill R.**  
(GAI.06/08A/A02-001 0900)
- SANDEL, Bill R.**  
(GAI.10/10P/A01-001 1400)
- SANDEL, Bill R.**  
(GAI.06/08A/A02-004 1005)
- SANDHAEGER, Henner**  
(JSM10/09P/D-006 1400-060)
- SANDHOLT, P.E.**  
(GAI.09/11A/A11-006 1110)
- SANDVOL, Eric**  
(JSS06/10A/A04-008 1110)
- SANDWELL, David T.**  
(JSS06/10A/A04-002 0850)
- SANGAWA, Akira**  
(SS03/08A/D-059 0830-218)
- SANGAWA, Akira**  
(SS04b/10P/D-038 1400-222)
- SANKA, Milan**  
(HW01/10A/C26-001)
- SANKARAN, S.**  
(HW01/09P/D-012 1400-203)
- SANKEY, David**  
(MI03/08P/B18-004 1500)
- SANO, Osam**  
(JSG01/08P/D-018 1400-018)
- SANO, Tetsuya**  
(JSM14/09P/D-007 1400-071)
- SANO, Tsuyoshi**  
(SS04a/09P/D-035 1400-284)
- SANOO, Yasuharu**  
(GAI.10/11A/A01-005 0930)
- SANSO, Fernando**  
(G04/08A/C25-008 1140)  
(G04/08P/D-017 1400-124)
- SANSO, Fernando**  
(G07/10P/D-017 1400-102)
- SANTINI, Stefano**  
(SS03/08A/D-031 0830-190)  
(SS03/08A/D-027 0830-186)
- SANTORO, Mario**  
(HS01/08A/C29-005 1130)
- SANTOS, Celso A.G.**  
(HS01/09P/C29-001 1400)
- SANTOS, Marcelo**  
(G03/07P/D-067 1400-089)
- SANTOYO, Miguel**  
(JSG01/08P/D-023 1400-023)
- SAPOZHNIKOV, Filipp Vjacheslavovich**  
(JSP07/08P/D-001 1400-052)
- SARACCO, Ginette**  
(GAI.10/09P/D-013 1615-132)  
(GAV.07/07P/D-004 1400-145)
- SARAEV, Alexander K.**  
(GAI.10/09A/A11-004 0945)
- SARAO, Angela**  
(SS04/07P/A03-005 1515)
- SARAO, Angela**  
(JSS06/09P/A04-005 1520)
- SARGSYAN, Haghine Vladimir**  
(SS04a/09P/D-006)
- SARMA, M.R.K.**  
(HW01/09P/D-012 1400-203)
- Sarma S.V.S.**  
(GAI.10/09P/D-004 1615-123)
- SARRAILH, Michel**  
(G03/07P/D-062 1400-084)  
(HW03/11A/D-002 0830-136)
- SARUHASHI, Takao**  
(HS02/08A/C24-009 1100)
- SARUKKALIGE, Ranjan Priyantha**  
(HW05/10A/C31-011 1125)
- SASA, Kaichiro**  
(HW01/10A/C26-007 1110)
- SASAKI, Hidetaka**  
(MC08/07A/B17-006 1120)
- SASAKI, Risa**  
(HW06/07A/C31-005 1110)
- SASAKI, Susumu**  
(GAI.11/09P/A15-004 1455)
- SASAKI, Taichi**  
(MC03/11P/A07-003 1440)
- SASAKI, Takeshi**  
(G02/07A/C25-013 1230)
- SASAKI, Wataru**  
(JSM11/10P/B18-004 1500)
- SASANO, Yasuhiro**  
(MI07/11A/B18-007 1110)  
(MC05/07P/A09-007 1700)
- SASATANI, Tsutomu**  
(SW04/09P/A13-014 1730)
- SASATANI, Tsutomu**  
(SS04a/09P/D-047 1400-296)
- SASATANI, Tsutomu**  
(SS04a/09P/D-041 1400-290)
- SASATANI, Tsutomu**  
(SS04b/10P/D-010 1400-194)  
(SS04a/09P/D-029 1400-278)  
(SS04/07A/A03-001 0915)
- SASATANI, Tsutomu**  
(SS04/07A/A03-005 1030)
- SASHIDHARAN, Anand P.**  
(GAV.06/10P/A11-002 1420)  
(JSA07/10P/A05-008 1650)  
(GAV.04/07P/A11-002 1430)
- (GAV.07/07P/A13-006 1600)  
(GAV.07/07P/D-003 1400-144)
- SASIDHARAN, Anand**  
(GAV.06/10P/A11-001 1400)
- SASSI, F.**  
(MC05/08A/A09-003 0930)
- SASSI, F.**  
(MC11/10P/B19-003 1440)
- SASSI, Fabrizio**  
(MC05/08A/A09-004 1000)
- SASSI, Fabrizio**  
(JSA01/08A/A12-005 1115)  
(MC05/10P/A09-005 1620)
- SASSOROVA, Elena V.**  
(SW05/10P/A13-013 1715)
- SASSOROVA, Elena V.**  
(JSS07/10P/A02-008 1600)
- Sastry R.S.**  
(GAI.10/09P/D-004 1615-123)
- SATAKE, Kenji**  
(SS03/08A/D-055 0830-214)  
(JSS07a/09P/D-014 1700-115)
- SATAKE, Kenji**  
(JSS07/10A/A02-001 0830)  
(JSS07a/09P/D-002 1700-103)  
(JSS07/09A/A02-003 0930)  
(JSS07a/09P/D-001 1700-102)  
(SS04a/09P/D-018 1400-267)  
(SS04a/09P/D-038 1400-287)
- SATAKE, Kenji**  
(JSS07/10P/A02-009 1615)
- SATO, Atsushi**  
(SS03/08A/D-120 0830-279)
- SATO, Atsushi**  
(JSM10/09P/D-008 1400-062)
- SATO, Haruo**  
(SS03/08A/D-014 0830-173)
- SATO, Hiroaki**  
(SS04/07P/A03-014 1745)
- SATO, Hiroshi**  
(SS03/08A/D-004 0830-163)
- SATO, Hiroshi**  
(SS03/07A/A02-006 1045)
- SATO, Hiroshi**  
(SS03/08A/D-035 0830-194)  
(SS03/07A/A02-008 1115)  
(SS03/08A/D-009 0830-168)
- SATO, Hiroshi**  
(SS03/08A/D-106 0830-265)
- SATO, Hiroshi**  
(SS03/08A/D-102 0830-261)
- SATO, Hiroshi P.**  
(JSG03/09P/D-024 1640-032)
- SATO, Kaoru**  
(MC05/07P/D-007 1400-214)
- SATO, Kaoru**  
(MC05/09P/A09-006 1600)
- SATO, Kazutoshi**  
(JSG01/07P/A01-007 1530)
- SATO, M.**  
(GAI.04/07A/A08-007 1110)
- SATO, Manabu**  
(GAI.06/07P/D-017 1400-137)
- SATO, Mitsuteru**  
(GAI.04/09A/D-005 0830-141)
- SATO, Mitsuteru**  
(GAI.06/11P/D-011 1400-063)
- SATO, Mitsuteru**  
(GAI.04/07A/A08-006 1050)
- SATO, Naoki**  
(MI05/11A/B17-010 1210)
- SATO, Natsuo**  
(GAI.05/07P/D-016 1400-114)
- SATO, Natsuo**  
(GAI.06/10A/A01-011 1145)
- SATO, Norifumi**  
(JSM10/09P/D-001 1400-055)
- SATO, Satoshi**  
(JSP06/07P/D-007 1400-014)
- SATO, Takashi**  
(G02/10P/D-010 1400-075)
- SATO, Takeshi**  
(SS03/07A/A02-003 0930)

- SATO, Takeshi**  
(HW05/10P/D-011 1400-166)
- SATO, Takeshi**  
(SS03/08A/D-118 0830-277)
- SATO, Takeshi**  
(JSM10/09P/D-008 1400-062)
- SATO, Tetsuya**  
(JSP04/09A/A06-007 1130)
- SATO, Tomonori**  
(MC11/11P/D-005 1400-198)
- SATO, Toru**  
(GAIL.06/10A/A01-007 1030)  
(GAIL.10/10P/A01-010 1700)
- SATO, Toru**  
(MI09/08P/D-002 1400-155)
- SATO, Toshiaki**  
(SS04a/09P/D-027 1400-276)  
(SS04b/10P/D-024 1400-208)
- SATO, Toshinori**  
(SS03/08A/D-002 0830-161)
- SATO, Toshinori**  
(SS03/08A/D-120 0830-279)
- SATO, Toshinori**  
(SS03/08A/D-114 0830-273)
- SATO, Toshiya**  
(JSG01/08P/D-006 1400-006)
- SATO, Toshiya**  
(JSG01/08P/D-002 1400-002)
- SATO, Yasuo**  
(MC08/07A/B17-006 1120)
- SATO, Yasuo**  
(MI07/11A/B18-002 0850)
- SATOH, Fuyuki**  
(HW01/10A/C26-007 1110)
- SATOH, Toshimi**  
(SS04b/10P/D-024 1400-208)
- SATOH, Toshimi**  
(SS04a/09P/D-042 1400-291)
- SATOH, Toshimi**  
(SS04a/09P/D-027 1400-276)
- SATOMURA, Takehiko**  
(JSP10/09P/B21-010)
- SATOMURA, Takehiko**  
(MC03/11A/A07-006 1050)
- SATORI, Gabriella**  
(GAIL.04/09A/D-001 0830-137)
- SATOW, Kazuhide**  
(JSM10/09P/D-002)
- SAUER, Konrad**  
(GAV.03/08A/A16-002 0900)
- SAUER, Konrad**  
(GAV.03/08A/A16-004 1000)
- SAUER, Konrad**  
(GAV.03/09A/A16-006 1120)
- SAUL, Adrian**  
(HS04/08A/C30-001 0905)
- SAUL, Joachim**  
(SW03/10P/A04-014 1730)
- SAULI, Petra**  
(GAIL.06/10A/A01-013 1215)  
(GAIL.06/11P/D-015 1400-067)
- SAULO, Celeste**  
(MC03/10A/A07-008 1130)
- SAUMURE, Luc**  
(SW05/10P/A13-004 1450)
- SAUNDERS, Clive P.R.**  
(MI08/07P/B18-002 1530)
- SAUVAUD, Jean-Andre**  
(GAIL.05/08A/A06-007 1040)
- SAVA, Constantin Stefan**  
(JSS06/10A/A04-006 1010)
- SAVA, Constantin Stefan**  
(HW01/09P/D-026 1400-217)  
(JSA07/11A/D-023 0830-023)
- SAVAGE, Stuart**  
(JSM14/09P/D-028 1400-092)
- SAVIN, Elena**  
(HS02/11P/C24-005 1500)
- SAVIN, Elena**  
(HS02c/11P/D-032 1630-130)  
(HS02/11P/C24-009 1547)
- SAVIN, Sergey P.**  
(GAIL.08/11P/D-001 1400-072)
- SAVIN, Sergey Zinovievich**  
(MI09/09A/B22-001 0900)
- SAVINA, Olga Nikolaevna**  
(GAIL.07/11A/A12-007 1135)
- SAVOIE, Matt**  
(JSH01/08A/C27-002 0930)
- SAWADA, Sumio**  
(SS04/08A/A03-005 0930)
- SAWADA, Yoshihiro**  
(SS04a/09P/D-039 1400-288)
- SAWADA, Yoshihiro**  
(SS04a/09P/D-002 1400-251)
- SAWAMOTO, Masaki**  
(JSM04/09P/D-011 1400-048)
- SAWAMOTO, Masaki**  
(JWH01/09P/C30-008 1650)
- SAWAMOTO, Masaki**  
(HS02b/10P/D-004 1630-125)  
(HS02/09A/C24-002 0915)  
(HS02/07A/C24-002 0904)  
(HW01/09P/D-024 1400-215)  
(HS02a/07P/D-002 1545-148)  
(HS02/10A/C24-004 1057)  
(HS02/08P/C24-003 1430)
- SAWAMOTO, Masaki**  
(HW08/09A/C28-005 1030)
- SAWYER, E.**  
(MI09/09A/B22-004 1000)
- SAYAMA, Takahiro**  
(HS01/08A/C29-003 1050)
- SAYED, Mohamed**  
(JSM14/09P/D-028 1400-092)
- SAZYKIN, Stanislav Y.**  
(GAIL.06/08A/A02-002 0915)
- SBORSHIKOV, Igor M.**  
(GAI.10/09A/A11-006 1015)
- SCAIFE, A.A.**  
(MC11/10P/B19-003 1440)
- SCAIFE, Adam**  
(MC05/10A/A09-002 0900)
- SCHÄR, Christoph**  
(MC03/09A/A07-007 1130)
- SCHAAKE, John**  
(HW07/11A/C25-005 0945)  
(HW08/09P/C28-001 1420)  
(HW08/08A/C28-002 0900)  
(HW08/07P/C28-003 1500)  
(HW08/07P/C28-002 1430)
- SCHAEFFER, Nathanael**  
(JSP10/08P/B21-005 1530)
- SCHAER, Christoph**  
(MC11/11P/B19-005 1520)  
(MC08/07P/B17-006 1535)
- SCHAFFRIN, Burkhard**  
(G04/07P/C25-001 1430)  
(G04/08P/C25-001 1410)
- SCHATTAUER, Ingrid**  
(GAV.06/10A/A11-004 0930)
- SCHAUER, Ursula**  
(JSP04/10P/A06-004 1500)
- SCHECTER, David A.**  
(JSP10/10P/B21-006 1610)
- SCHEINERT, Mirko**  
(JSG01/08A/A01-011 1150)  
(JSG01/08A/A01-010 1135)
- SCHEMEL, Anton L.**  
(SW05/10P/A13-012 1700)
- SCHENWERK, Mark S.**  
(JSG01/08A/A01-002 0915)
- SCHERLIESS, Ludger**  
(GAIL.05/08A/A15-003 0920)
- SCHERLIESS, Ludger**  
(GAIL.05/07A/D-001 0830-017)
- SCHERLIESS, Ludger**  
(GAIL.05/08P/A15-009 1740)
- SCHERNECK, Hans G.**  
(SS03/07P/A02-005 1500)
- SCHERTZER, Daniel**  
(HW07/10A/C25-007 1145)
- SCHERTZER, Daniel**  
(HW07/11P/D-015 1400-151)
- SCHERTZER, Daniel**  
(HW07/10P/C25-003 1445)
- SCHERTZER, Daniel J.M.**  
(HW07/10P/C25-002 1430)
- SCHG, Martina L.**  
(JWH01/10P/D-001 1400-006)
- SCHIFF, Sherry**  
(HW01/09A/C26-004 1010)
- SCHIRMER, Uwe**  
(G03/07P/D-047 1400-069)
- SCHLOSSER, A.**  
(JWH01/09P/C30-001)
- SCHLUETER, Wolfgang**  
(G07/10A/A03-003 0940)
- SCHLUETER, Wolfgang**  
(G07/10P/D-014 1400-099)
- SCHLUPP, Antoine**  
(SS04b/10P/D-030 1400-214)
- SCHMID, Claudia**  
(JSP06/08A/B21-003 0950)
- SCHMIDL, Juerg**  
(MC11/11P/B19-003 1440)
- SCHMIDT, Andrea**  
(G07/10P/D-019 1400-104)
- SCHMIDT, Gavin**  
(MC12/08A/B19-001 0930)
- SCHMIDT, Gavin A.**  
(MC12/08P/B19-004 1515)
- SCHMIDT, Roland**  
(G02/07A/C25-002 0920)
- SCHMIDT, Ulrich**  
(MC05/07P/A09-007 1700)
- SCHMITT, Gunter**  
(SS03/08A/D-076 0830-235)
- SCHMITZ, Gerhard**  
(MC05/07P/A09-006 1640)
- SCHMOCKER-FACKEL, Petra**  
(HW01/10A/C26-005 0950)
- SCHMUGGE, Thomas**  
(MI09/09A/B22-005 1050)  
(MI07/11A/B18-006 1050)
- SCHMUGGE, Thomas**  
(MI09/08P/D-003 1400-156)
- SCHMUTZ, Werner**  
(MI03/09A/D-006 0900-249)
- SCHNECK, Therese**  
(MC04/10P/B22-010 1745)
- SCHNEEBELI, Martin**  
(JSM15/07P/D-006 1400-006)  
(JSM15/07A/B18-003 0945)
- SCHOENE, Tilo**  
(G07/10P/D-006 1400-091)  
(SS03/08A/D-117 0830-276)
- SCHOFIELD, Oscar**  
(JSP07/08A/B17-001 0900)
- SCHOLTEN, Huub**  
(HW03/11A/C30-002 0850)
- SCHOLZE, Marko**  
(JSM04/09A/B23-003 1000)
- SCHOTT, Jean-Jacques**  
(GAV.05/08P/A11-009 1700)  
(GAIL.10/11A/D-012 0830-086)
- SCHOTT, Jean-Jacques**  
(GAI.10/09A/A11-011 1200)
- SCHRIVER, David**  
(GAIL.14/07A/A12-003 1015)
- SCHROETER, Jens**  
(JSM11/10P/D-009 1700-018)
- SCHUBERT, Gerald**  
(MC04/10P/B22-009 1715)
- SCHUCH, Nelson Jorge**  
(GAIL.09/11A/A11-002 0900)
- SCHUCH, Nelson Jorge**  
(GAIL.09/11P/A11-008 1710)
- SCHULTZ, Adam**  
(GAV.04/07P/A11-003 1450)
- SCHULZ, Joerg**  
(JSP09/11A/B20-002 0900)
- SCHUMANN, Andreas H.**  
(HS02/10A/C24-001 0830)
- SCHUNK, Robert W.**  
(GAIL.05/08A/A15-003 0920)
- SCHUNK, Robert W.**  
(GAIL.05/07A/D-001 0830-017)
- SCHUNK, Robert W.**  
(GAIL.05/08P/A15-009 1740)
- (GAIL.05/08P/A15-009 1740)
- SCHUTZ, Bob E.**  
(JSG02/09A/D-004 0830-004)
- SCHUTZ, Bob Ewald**  
(JSA09/10A/A08-005 1030)
- SCHWALENBERG, Katrin**  
(GAI.08/08P/D-008 1400-143)
- SCHWARTE, Judith**  
(GAV.04/07A/A11-006 1120)
- SCHWARTZ, Susan Y.**  
(SS03/08A/D-032 0830-191)
- SCHWARZKOPF, M. Daniel**  
(JSA09/10A/A08-005 1030)
- SCHWEGMANN, Wolfgang**  
(G07/10P/D-009 1400-094)
- SCHWEITZER, Johannes**  
(U7/11A/D32-005 1130)
- SCHWENN, Rainer**  
(GAIL.09/11A/A11-002 0900)
- SCHWIERZ, Cornelia**  
(MI06/09P/B20-011 1740)  
(MI05/09P/B17-004 1520)
- SCHWIERZ, Cornelia**  
(MC08/07P/B17-006 1535)
- SCHWINGENSCHUH, K.**  
(GAV.03/08P/A16-003 1500)
- SCHWINTZER, Peter**  
(G02/07A/C25-001 0900)  
(G02/07A/C25-002 0920)
- SCIENTIFIC PARTY, YK00-06**  
(SS03/07P/A02-002)
- SCIFFER, Murray**  
(GAIL.10/11A/D-010 0830-084)
- SCIPION, Danny**  
(GAIL.06/09A/A10-011 1205)
- SCISSEK, Falk**  
(HW06/07A/C31-001 0910)
- SCORDILIS, Emmanuel**  
(JSP11/08P/D-006 1400-075)
- SCOURSE, James**  
(MC12/08P/B19-006 1620)
- SDAO, Francesco**  
(JSP11/08A/A10-008 1200)
- SEAMA, Nobukazu**  
(GAI.08/08P/D-008 1400-143)
- SEBER, Dogan**  
(JSS06/10A/A04-008 1110)
- SEDIGHI, Morteza**  
(G03/07P/D-012 1400-034)
- SEED, Alan**  
(HS03/07P/C26-001 1400)
- SEED, Alan W.**  
(HS03/07P/C26-002 1415)
- SEEMANAPALLI, Sarma K.**  
(HS02c/11P/D-021 1630-119)  
(HS02c/11P/D-022 1630-120)  
(HS02/11A/C24-021 1205)  
(HS02/11A/C24-022 1209)
- SEGAH, Hendrik**  
(MI07/10P/D-006 1400-182)
- SEGALL, Paul**  
(JSG01/07P/A01-010 1635)
- SEGANTINE, Paulo Cesar Lima**  
(G03/07P/D-070 1400-092)
- SEGHEDI, Ioan**  
(JSS06/10A/A04-010 1150)
- SEIBERT, Jan**  
(HW08/08P/C28-005 1600)
- SEIKI, Ayako**  
(MC17/11P/B23-002 1420)
- SEILER, Klaus-Peter**  
(HW06/07P/C31-002 1420)
- SEIRADAKIS, John H.**  
(GAIL.08/10A/A16-006 1005)
- SEITZ, Kurt**  
(G03/07P/D-064 1400-086)  
(G04/08A/C25-005 1000)  
(G03/07P/D-038 1400-060)
- SEKI, K.**  
(GAIL.06/08P/A02-011 1725)
- SEKI, Kanako**  
(GAIL.08/10A/A16-001 0830)

## INDEX

- (GAI11.06/07P/D-010 1400-130)
- SEKI, Kanako**  
(GAI11.05/07P/D-019 1400-117)
- SEKI, Yuko**  
(GAI11.10/11A/D-020 0830-094)
- SEKIDO, Mamoru**  
(G02/10P/D-011 1400-076)
- SEKIDO, Mamoru**  
(G02/10P/D-008 1400-073)  
(G02/10P/D-014 1400-079)
- SEKIGUCHI, Haruko**  
(SS04a/09P/D-018 1400-267)  
(SS04a/09P/D-038 1400-287)
- SEKIGUCHI, Haruko**  
(SS04/08A/A03-009 1045)
- SEKIGUCHI, Shoji**  
(SS03/08A/D-115 0830-274)
- SEKIGUCHI, Tatsuo**  
(JSG03/09P/D-024 1640-032)
- SEKINE, Shutaro**  
(SS03/08A/D-098 0830-257)
- SEKINE, Shutaro**  
(SS03/08A/D-108 0830-267)
- SEKIYAMA, Tsuyoshi**  
(MC05/07P/D-010 1400-217)
- SEKO, Hiromu**  
(JSM14/08A/A05-010 1145)
- SEKO, Hiromu**  
(G02/10P/D-009 1400-074)
- SELCHER, C.A.**  
(GAI11.06/09P/A10-003 1440)
- SELEZNEV, Victor S.**  
(SW05/10A/D-005 0900-249)  
(SW05/10P/A13-010 1630)
- SELUCHI, Marcelo Enrique**  
(MC03/10A/A07-003 0930)
- SELVARAJ, C.**  
(JSA09/11P/D-002 1400-051)
- SELVARAJ, C.**  
(JSA09/11P/D-003 1400-052)
- SEMBLAT, Jean-François**  
(SS04/07A/A03-004 1015)
- SEMENOV, Vladimir**  
(GAI.08/08P/D-003 1400-138)
- SEMENOV, Vladimir**  
(MC08/07A/B17-001 0930)
- SEMILETOV, Igor P.**  
(JSP04/09P/A06-008 1615)  
(JSM04/09A/B23-004 1030)
- SEMOVSKI, Sergei V.**  
(JSG03/09P/A12-002 1420)
- SEMOVSKI, Sergei V.**  
(JSP04a/09P/D-001 1400-094)
- SENEVIRATNE, Sonia I.**  
(MC11/11P/B19-005 1520)
- SENGUPTA, Probal**  
(SS04/08P/A03-006 1515)
- SENIOR, C.A.**  
(MC11/10P/B19-002 1420)
- SENNA, Shigeki**  
(SS04b/10P/D-004 1400-188)  
(SS04b/10P/D-020 1400-204)
- SENO, Tetsuzo**  
(JSS06b/10P/D-004 1400-028)
- SENOS, Luisa**  
(SS04a/09P/D-049 1400-298)
- SENTMAN, Dave D.**  
(GAI11.04/07P/A08-001 1400)
- SENTMAN, Davis D.**  
(GAI11.04/07P/A08-005 1540)
- SEO, DONG-JUN**  
(HS03/07A/C26-008 1115)  
(HS03/07A/C26-004 1000)
- SEREBRYANSKAYA, Anna V.**  
(GAI11.10/11A/D-001 0830-075)
- SERGEYEVA, Natalia A.**  
(JSS06a/08P/D-015)
- SERPAS, Juan Gilberto**  
(G03/07P/D-072 1400-094)
- SERPETSIDAKI, Anna**  
(SS04a/09P/D-043 1400-292)
- SERRANO, Inmaculada**  
(SS03/08A/D-025 0830-184)
- SERVAIN, Jacques**  
(JSP06/07P/D-005 1400-012)
- SERVAT, Eric**  
(HW08/07A/C28-008 1150)
- SERVAT, Eric**  
(HS02/08A/C24-008 1045)
- SETO, Masahiro**  
(GAI11.10/11A/D-007 0830-081)
- SETO, Tri Handoko**  
(MC17/11P/B23-008 1640)
- SETYADJI, Bambang**  
(G02/10P/D-012 1400-077)
- SEUNA, Pertti Olavi**  
(HW01/09P/D-044 1400-235)
- SEVERINGHAUS, Jeffrey P.**  
(MC12/08A/B19-003 1020)
- SEXTON, David M.H.**  
(MC08/07A/B17-003 1015)  
(MC11/10A/B19-001 0830)
- SHA, Weiming**  
(JSP10/09A/B21-010 1220)
- SHA, Zhigui**  
(HW07/11P/D-036 1400-172)
- SHA, Zhigui**  
(HW07/11P/D-035 1400-171)
- SHAABAN, Fathy Ahmed**  
(GAI.10/09P/D-001 1615-120)
- SHAABAN, Fathy Ahmed**  
(GAI.10/09P/D-003 1615-122)
- SHAABAN, Fouad Fawzy**  
(GAI.10/09P/D-003 1615-122)
- SHAH, Syed Muhammad Saeed**  
(HW07/11P/D-009 1400-145)  
(HW07/11P/D-004 1400-140)
- SHAH, Syed Muhammad Saeed**  
(HW07/11P/D-019 1400-155)
- SHALAN, Jamal M.**  
(JSS06/10A/A04-004 0930)
- SHAMIR, Eylon**  
(HW08/08P/C28-004 1520)  
(HW08/08P/C28-004 1520)
- SHAMIR, Uri**  
(HS03/08A/C26-003 0915)
- SHAMSELDIN, Asaad Y.**  
(HS02/09P/C24-002 1415)
- SHANG, She-ping**  
(GAI.05/07A/D-003 0830-019)
- SHANKER, Daya**  
(SS04/09A/A03-001 0900)
- SHANKER, Daya**  
(SS03/08A/D-071 0830-230)
- SHANLEY, James B.**  
(HW01/10P/C26-002 1420)
- SHANNON, Patrick M.**  
(MC12/07P/B19-003 1500)
- SHAO, Xuemei**  
(JSM04/09P/D-001 1400-038)
- SHAPIRO, Melvyn Allen**  
(JSM14/07A/A05-001 0915)
- SHAPIRO, Serge A.**  
(SS03/07P/A02-010 1645)
- SHAPIRO, Vsevolod**  
(GAV.05/09P/D-009 1400-153)
- SHARAF EL-DIN, Sayed H.**  
(JSP08/09P/B19-003 1450)  
(JSP08/09A/B19-002 0930)  
(JSP10/08P/D-016 1610-068)
- SHARAF EL-DIN, Sayed H.**  
(JSP09/10P/B20-014 1745)
- SHARDAKOVA, Lyudmila Yur'evna**  
(JSM14/09P/D-015 1400-079)
- SHARIFI, Mohammad A.**  
(G07/10P/D-011 1400-096)
- SHARIKOV, Anatoliy**  
(HW03/11P/C30-007 1620)
- SHARMA, A. Surjalal**  
(GAI11.07/09A/A14-006 1130)  
(GAI11.07/09A/A14-008 1210)
- SHARMA, Ashish**  
(HS02/10A/C24-002 0845)
- (HS03/07P/C26-001 1400)
- SHARMA, Ashish**  
(HS02b/10P/D-009 1630-130)  
(HS02/10A/C24-009 1117)
- SHARMA, Keshav**  
(JSM03/08P/A13-008 1640)
- SHARMA, Shashi Prakash**  
(GAI.10/09A/A11-010 1145)  
(GAI.10/09P/A11-002 1415)  
(GAI.10/09P/D-008 1615-127)
- SHARMA, Shashi Prakash**  
(JSA07/11A/D-040 0830-040)
- SHARMA, Uttam C.**  
(HS01/08A/C29-001 0950)  
(HS02c/11P/D-011 1630-109)  
(HS02/11A/C24-011 1125)
- SHARMA, Vikas**  
(HS02c/11P/D-012 1630-110)  
(HS02/11A/C24-012 1129)
- SHARMEEN, S.**  
(MC11/11P/B19-001 1400)
- SHAY, Lynn K.**  
(JSP09/11P/B20-006 1545)
- SHAY, Lynn Keith**  
(JSP09/11P/B20-005 1515)
- SHAY, Michael Anthony**  
(GAI11.05/08A/A06-012 1215)
- SHE, Chiao-Yao**  
(JSA01/08A/A12-002 0935)
- SHEA, Margaret Ann**  
(JSA08/09A/A08-006 1030)
- SHEBALIN, John V.**  
(GAI11.11/10P/D-005 1400-120)
- SHEEHAN, R.E.**  
(GAI.06/10A/A01-003 0905)
- SHEM, Willis Otieno**  
(MI07/11A/B18-003 0910)
- SHEN, Chong-yang**  
(JSG01/08P/D-034 1400-034)
- SHEN, Yang**  
(JSS06/07P/A04-008 1640)
- SHEN, Yanjun**  
(HS04/07P/C30-002 1435)
- SHEN, Yongping**  
(HS02/08A/C24-005 0930)
- SHEN, Yuanjun**  
(HS04/07P/C30-003 1505)
- SHEN, Zhengkang**  
(JSG01/07A/A01-012 1205)
- SHEPHERD, Theodore**  
(MI03/08A/B18-008 1130)
- SHEPHERD, Theodore G.**  
(MC05/07P/A09-004 1510)  
(MI05/10A/B17-001 0830)  
(JSP10/10A/B21-008 1140)  
(MI03/08P/B18-004 1500)
- SHEPHERD, Theodore G.**  
(MI03/08P/B18-003 1440)
- SHERSTYUKOV, Oleg Nikolaevich**  
(JSA01/08P/A12-007 1700)
- SHERWOOD, Robert A.**  
(G02/10P/D-004 1400-069)
- SHERWOOD, Steven C.**  
(MC05/08A/A09-005 1050)
- SHESTAKOV, Nikolay**  
(JSG01/08P/D-009 1400-009)
- SHESTAKOV, Nikolay V.**  
(G04/08P/D-001 1400-108)
- SHEU, Hwa-Chu**  
(JSG03/09P/D-022 1640-030)
- SHEVSHENKO, George V.**  
(JSS07b/10P/D-015 1700-061)
- SHI, Guangyu**  
(JSM04/09P/D-016 1400-053)
- SHI, Hongling**  
(G03/07P/D-059 1400-081)
- SHI, Jeff**  
(HW01/10A/C26-006 1050)
- SHI, Jiankui**  
(GAI11.05/07A/D-003 0830-019)
- SHI, Yaolin**  
(SS03/08A/D-065 0830-224)
- SHIBAGAKI, Yoshiaki**  
(MC02/07P/D-004 1400-201)
- SHIBAGAKI, Yoshiaki**  
(JSM14/09P/D-009 1400-073)  
(MC02/07P/D-003 1400-200)
- SHIBANO, Hirofumi**  
(HS02/11P/C24-003 1430)
- SHIBATA, Hideaki**  
(HW01/10A/C26-007 1110)
- SHIBATA, K.**  
(MC11/10P/B19-003 1440)
- SHIBATA, Kiyotaka**  
(MC05/07P/D-010 1400-217)
- SHIBATA, Kiyotaka**  
(MC05/11A/A09-001 0830)
- SHIBUTANI, Takuo**  
(JSS06a/08P/D-017 1400-095)  
(SW03/10A/D-001 0830-236)
- SHIBUTANI, Takuo**  
(JSS06a/08P/D-016 1400-094)
- SHIBUYA, Kazuo**  
(JSM11/10A/B18-006 1040)
- SHIBUYA, Kazuo**  
(JSG03/09P/D-002 1640-010)  
(JSG03/09P/D-001 1640-009)
- SHICHI, Ryuichi**  
(G03/07P/D-010 1400-032)
- SHICHI, Ryuichi**  
(SS04a/09P/D-033 1400-282)
- SHIGA, Akinori**  
(GAI.V.03/09A/A16-003)
- SHIGA, Takuya**  
(SS04a/09P/D-034 1400-283)
- SHIGEMORI, Hiroyuki**  
(MI09/08P/B22-007 1640)
- SHIGENO, Kiyoyuki**  
(JSS07/10A/A02-001 0830)  
(JSS07a/09P/D-002 1700-103)
- SHIGETA, Tsutomu**  
(SS05/10A/A13-003 0900)
- SHIGETOMI, Kunihiro**  
(JSG01/08P/D-001 1400-001)
- SHIGETOMI, Kunihiro**  
(SS03/08A/D-053 0830-212)
- SHIGIHARA, Yoshinori**  
(JSS07b/10P/D-010 1700-056)
- SHIIBA, Michiharu**  
(HS03/07P/C26-010 1630)
- SHIIBA, Michiharu**  
(HW04/09A/C31-003 0940)
- SHIIBA, Michiharu**  
(HS03/08P/C26-004 1445)
- SHIKLOMANOV, Igor Alexeevich**  
(HS02/09P/C24-013 1730)
- SHIMABAYASHI, Sakae**  
(JSM15/07P/D-007 1400-007)
- SHIMADA, Koji**  
(JSP04/10P/A06-005 1520)
- SHIMADA, Nobue**  
(GAI.V.02/07A/A07-001 0900)
- SHIMADA, Wataru**  
(JSM15/07A/B18-006 1045)
- SHIMAKURA, Shin**  
(GAI11.10/11A/A01-011 1100)
- SHIMAMURA, H.**  
(SS03/08A/D-146 0830-305)
- SHIMAMURA, Hideki**  
(SS03/08A/D-005 0830-164)
- SHIMAMURA, Hideki**  
(SS03/08A/D-056 0830-215)
- SHIMAMURA, Hideki**  
(SS03/08A/D-114 0830-273)
- SHIMAMURA, Hideki**  
(SS03/07A/A02-009 1130)
- SHIMAMURA, Yuichi**  
(JSH01/07P/C27-008 1640)
- SHIMARAEV, Mikhail N.**  
(JSP04a/09P/D-001 1400-094)
- SHIMAZAKI, Kunihiko**  
(SS04/09A/A03-005 1000)
- SHIMIZU, Hiroshi**  
(GAV.06/09P/D-014 1400-167)

- SHIMIZU, Hiroshi**  
(SS03/08A/D-100 0830-259)
- SHIMIZU, Hiroshi**  
(SS03/08A/D-017 0830-176)
- SHIMIZU, Hisayoshi**  
(GAI.08/08P/D-001 1400-136)  
(JSS06a/08P/D-008 1400-086)
- SHIMIZU, Masujiro**  
(JSM14/09P/D-023 1400-087)
- SHIMIZU, Shingo**  
(JSM14/09P/D-013 1400-077)
- SHIMODA, Haruhisa**  
(JSG03/09P/D-019 1640-027)
- SHIMOKAWA, Koichi**  
(SS03/08A/D-059 0830-218)
- SHIMOKAWA, Koichi**  
(JSS07/10A/A02-001 0830)  
(JSS07a/09P/D-002 1700-103)  
(SS04b/10P/D-038 1400-222)
- SHIMOKURA, Junji**  
(HS02/11P/C24-003 1430)
- SHIMOYAMA, Manabu**  
(MC04/11A/B22-005 0945)
- SHIN, Ho-Jeong**  
(MC11/11A/B19-007 1050)  
(MC11/11A/B19-006 1010)
- SHIN, Kyung-Hoon**  
(JSP04/09P/A06-010 1715)
- SHIN, Kyung-Hoon**  
(JSM04/09A/B23-004 1030)
- SHIN-YI, Su**  
(GAIL.06/10A/A01-012 1200)
- SHINAGAWA, Hiroyuki**  
(GAIV.03/08A/A16-006 1100)  
(GAIL.07/11A/A12-002 0905)  
(GAIL.14/07A/A12-001 0930)  
(GAIV.03/08P/A16-005 1610)
- SHINBORI, Atsuki**  
(GAIL.06/07P/D-016 1400-136)
- SHINDELL, Drew T.**  
(MC12/08P/B19-004 1515)
- SHINDO, Shizuo**  
(HS02/07A/C24-003 1115)
- SHINE, Keith P.**  
(MI03/08P/B18-007 1630)
- SHINGAI, Eisuke**  
(SW03/10A/D-005 0830-240)
- SHINJO, Ryuichi**  
(SS03/07P/A02-002 1415)
- SHINKAI, Yuichi**  
(GAIL.06/10A/A01-011 1145)
- SHINODA, Taro**  
(JSM03/09A/D-002 0830-036)  
(JSM14/09P/D-013 1400-077)  
(JSM14/07P/A05-002 1435)
- SHINODA, Taro**  
(JSM03/08A/A13-004 1000)
- SHINOHARA, Hideaki**  
(SS04b/10P/D-024 1400-208)  
(SS04b/10P/D-023 1400-207)
- SHINOHARA, Iku**  
(GAIL.05/07P/D-009 1400-107)
- SHINOHARA, Iku**  
(GAIL.05/08A/A06-010 1125)  
(GAIV.02/07A/A07-001 0900)
- SHINOHARA, Manabu**  
(GAIL.10/11A/A01-008 1015)
- SHINOHARA, Masanao**  
(SS03/08A/D-118 0830-277)
- SHINOHARA, Masanao**  
(SS03/08A/D-114 0830-273)
- SHINOHARA, Masanao**  
(SS03/08A/D-001 0830-160)  
(SS03/08A/D-120 0830-279)
- SHINOHARA, Masanao**  
(SS03/08A/D-101 0830-260)
- SHINOZAKI, Yuzo**  
(SS04a/09P/D-034 1400-283)
- SHIOBARA, Hajime**  
(SS03/08A/D-118 0830-277)
- SHIOBARA, Hajime**  
(SS03/08A/D-114 0830-273)
- SHIOBARA, Hajime**  
(JSS06/09P/A04-009 1700)
- SHIOBARA, Hajime**  
(JSS06/07P/A04-005 1540)
- SHIOBARA, Masataka**  
(JSM14/09A/A05-009 1205)
- SHIOGAMA, Hideo**  
(MI05/09P/B17-006 1630)
- SHIOKAWA, K.**  
(GAIL.05/08P/A15-001 1400)
- SHIOKAWA, Kazuo**  
(GAIL.06/09A/A10-007 1035)  
(GAIL.06/07P/D-010 1400-130)  
(GAIL.06/09P/A10-008 1620)  
(GAIL.06/11P/D-010 1400-062)  
(GAIL.06/11P/D-011 1400-063)
- SHIOMI, Katsuhiko**  
(SS03/08A/D-014 0830-173)
- SHIOTANI, Masato**  
(MC05/08P/A09-001 1400)
- SHIOTANI, Masato**  
(MC05/08P/A09-004 1510)
- SHIOTANI, Masato**  
(MC05/09A/A09-006 1120)
- SHIRAI, Hiroki**  
(GAV.05/09P/D-006 1400-150)
- SHIRAIISHI, Tetsuya**  
(GAIL.05/07P/D-012 1400-110)
- SHIRMOHAMADI, Reza**  
(JSP11/08A/A10-005 1050)
- SHIROOKA, Ryuichi**  
(MC17/11P/B23-003 1440)
- SHIRZAI, Manoochehr**  
(SS03/08A/D-142 0830-301)
- SHISHIKURA, Masanobu**  
(SS03/08A/D-006 0830-165)
- SHIYIN, Liu**  
(JSM10/08P/B23-008 1700)
- SHMAKIN, A.B.**  
(JWH01/09P/C30-001)
- SHMAKIN, Andrey B.**  
(JSM10/08P/B23-002 1440)
- SHOJI, Hideaki**  
(MC02/07A/B20-003 1025)
- SHOMALI, Hossein**  
(JSS06/09P/A04-004 1500)
- SHOTT, Philip**  
(SW05/10P/A13-004 1450)
- SHOUTILIN, Sergey V.**  
(JSP04/10P/A06-003 1440)
- SHPYNEV, Boris G.**  
(GAIL.06/11P/D-004 1400-056)
- SHRESTHA, Roshan K.**  
(HS03/08A/C26-002 0900)
- SHUM, C.K.**  
(G07/10A/A03-005 1100)
- SHUM, C.K.**  
(JSS06a/08P/D-004 1400-082)  
(SS03/08A/D-149 0830-308)
- SHUM, C.K.**  
(JSG01/08A/A01-012 1205)
- SHUM, C.K.**  
(JSG02/09A/D-007 0830-007)
- SHUM, C.K.**  
(JSG03/09P/D-012 1640-020)
- SHUM, C.K.**  
(G07/10A/A03-006 1120)
- SHUMILOV, Oleg I.**  
(JSA09/10A/A08-010 1200)
- SHUMLANSKAYA, L.**  
(JSS06a/08P/D-012 1400-090)
- SHUR, Dina Yu.**  
(JSA07/11A/D-021 0830-021)
- SHUTO, Nobuo**  
(JSS07/09A/A02-006 1015)
- SIBECK, D.G.**  
(GAIL.05/07A/A06-003 0930)
- SIBUET, Jean-Claude**  
(SS03/07P/A02-002 1415)
- SICART, Jean E.**  
(JSM10/08P/B23-004 1520)
- SICART, Jean E.**  
(JWH01/09P/C30-004 1500)
- SICART, Jean E.**  
(JWH01/10P/C30-004 1500)
- SICHINGABULA, Henry M.**  
(HS01/09A/C29-001 0900)
- SICILIA, Deborah**  
(JSS06/10A/A04-004 0930)
- SIDERIS, M.G.**  
(G07/10A/A03-005 1100)
- SIDERIS, Michael G.**  
(G03/07P/D-034 1400-056)  
(G03/07P/D-031 1400-053)  
(G03/07P/D-029 1400-051)  
(G04/08P/D-004 1400-111)
- SIDLE, Roy C.**  
(HW01/09A/C26-001 0910)
- SIDLE, Roy C.**  
(HW01/10P/C26-008 1700)
- SIDORCHUK, Aleksey**  
(HS01/09A/C29-002 0920)
- SIDORENKOV, Nikolai S.**  
(JSM11/10P/D-005 1700-014)
- SIDOROVA, I.P.**  
(JSS06/10A/A04-003 0910)
- SIDOROVA, Larissa**  
(GAIL.05/07A/D-002 0830-018)  
(GAIL.06/09A/A10-004 0950)
- SIEFRING, C.S.**  
(GAIL.06/09P/A10-003 1440)
- SIEGFRIED, Tobias U.**  
(HS02/09P/C24-011 1700)
- SIEGMUND, Peter Christiaan**  
(MI03/08P/B18-005 1520)
- SIEMINSKI, Anne**  
(JSS06/08A/A04-008 1110)
- SIEMINSKI, Anne**  
(JSS06/10A/A04-004 0930)
- SIEMINSKI, Anne**  
(JSS06b/10P/D-008 1400-032)
- SIGHA-NKAMDJOU, Luc**  
(HW01/10P/C26-004 1500)
- SIGHOMNOU, Daniel**  
(HW01/10P/C26-004 1500)
- SIGMOND, Michael**  
(MI03/08P/B18-005 1520)
- SILBERSTEIN, Richard P.**  
(HW07/10A/C25-009 1215)  
(HW01/09P/D-005 1400-196)
- SILVA, Ana Maria**  
(MI03/09A/D-003 0900-246)
- SILVA DIAS, A.**  
(JSM04/09P/D-010 1400-047)
- SILVA DIAS, Fernando J.S.**  
(SS03/08A/D-096 0830-255)
- SILVA DIAS, Maria Assuncao**  
(MC03/10A/A07-008 1130)  
(MC03/10A/A07-003 0930)
- SILVA DIAS, Pedro Leite**  
(MC03/10A/A07-008 1130)  
(MC03/10A/A07-003 0930)
- SILVER, Paul G.**  
(JSG01/07P/A01-011 1650)
- the SIMBA Team**  
(JSA07/10A/A05-004 0940)
- SIMEK, Jaroslav**  
(G07/10P/D-020 1400-105)
- SIMEK, Jaroslav**  
(G07/10P/D-016 1400-101)
- SIMMONS, Harper**  
(JSM10/07P/B23-004 1520)
- SIMMONS, Harper L.**  
(JSP10/09A/B21-009 1200)
- SIMMONS, Robert**  
(HS04/07P/C30-001 1405)
- SIMOES, Jefferson C.**  
(JSM04/09P/D-006 1400-043)
- SIMON, Anu**  
(MC03/11A/A07-009 1150)
- SIMON, Dietrich**  
(G07/10P/D-015 1400-100)
- SIMON, Pascal**  
(MC05/07A/A09-006 1150)
- SIMON, Rapelang E.**  
(JSS06/07P/A04-006 1600)
- SIMONE, Tilmes**  
(MC05/07P/A09-007 1700)
- SIMONOV, Konstantin V.**  
(SW05/10P/A13-012 1700)
- SIMONS, Mark**  
(JSG01/07A/A01-006 1015)
- SIMONYAN, Anahit Hovhannes**  
(GAV.04/07A/D-001 0830-141)
- SINGER, W.**  
(MC05/10A/A09-010 1210)
- SINGH, Abhay Kumar**  
(HW01/09P/D-019 1400-210)
- SINGH, Amanjot**  
(HS01/09P/D-016 1400-183)
- SINGH, Anand P.**  
(JSA07/11A/D-035 0830-035)
- SINGH, Bhisam Prasad**  
(SS03/08A/D-068 0830-227)
- SINGH, Bijendra**  
(SW03/10A/D-009 0830-244)  
(JSA07/11A/D-043 0830-043)
- SINGH, Deo D.**  
(SW03/10A/D-006 0830-241)
- SINGH, Hanwant B.**  
(MI03/08P/B18-002 1420)
- SINGH, Kushal Pal**  
(GAI.10/09P/D-015 1615-134)
- SINGH, Nagendra**  
(GAIL.07/09P/A14-001 1400)
- SINGH, Om Prakash**  
(SS03/08A/D-021 0830-180)
- SINGH, R.**  
(SS03/08A/D-071 0830-230)
- SINGH, R.B.**  
(HS02b/10P/D-032 1630-153)  
(HS04/08A/C30-004 1100)  
(HS02/10P/C24-009 1547)
- SINGH, R.B.**  
(HW07/11P/D-008 1400-144)
- SINGH, Ramesh P.**  
(JSM04/09P/B23-006 1700)
- SINGH, Ramesh P.**  
(JSP11/07P/A10-004 1550)
- SINGH, Ramesh P.**  
(JSM03/08P/A13-006 1600)  
(JSH01/08A/C27-005 1050)
- SINGH, Ramesh P.**  
(HS01/09P/D-024 1400-191)
- SINGH, S.P.**  
(JSH01/08A/C27-005 1050)
- SINGH, S.V.**  
(GAIL.05/07P/D-022 1400-120)
- SINGH, Satyavir**  
(GAIL.07/09P/A14-002 1430)  
(GAIL.05/07P/D-001 1400-099)
- SINGH, Shri Krishna**  
(JSG01/08P/D-023 1400-023)
- SINGH, Shyam Vir**  
(MC03/11A/A07-010 1210)
- SINGH, Sunil Kumar**  
(SS03/08A/D-082 0830-241)
- SINGH, V.P.**  
(HS02/07A/C24-015 0956)  
(HS02a/07P/D-015 1545-161)
- SINGH, V.P.**  
(SS04/09A/A03-001 0900)  
(SS03/08A/D-071 0830-230)
- SINGH, V.S.**  
(HW01/09P/D-012 1400-203)
- SINGH, Y.P.**  
(JSH01/08A/C27-005 1050)
- SINHA, Ashwini Kumar**  
(GAIL.06/07P/D-006 1400-126)
- SINHA, Babita**  
(SS03/08A/D-131 0830-290)
- SINISALO, Anna Katariina**  
(JSH01/08P/D-010 1400-048)
- SIROTA, Alexander M.**  
(JSG03/09P/D-011 1640-019)
- Siti Aisah Shamsudin**  
(HS02/08P/C24-012 1715)
- SITNOV, M.I.**  
(GAIL.07/09A/A14-008 1210)

## INDEX

- SITNOV, Mikhail I.**  
(GAI.07/09A/A14-006 1130)
- SIVAPALAN, Murugesu**  
(HW07/10P/C25-010 1645)
- SIVAPALAN, Murugesu**  
(HW07/11A/C25-011 1145)  
(HW07/10A/C25-001 0840)  
(HW07/11P/D-028 1400-164)  
(HW07/11P/D-031 1400-167)
- SIVAPALAN, Murugesu**  
(HW07/10P/C25-009 1630)
- SIZOV, Youry P.**  
(JSP11/07A/A10-009 1220)  
(JSP11/08P/D-002 1400-071)  
(U7/11P/D32-001 1400)
- SIZOVA, Lilia Z.**  
(GAI.08/11P/D-003 1400-074)
- SIZOVA, Lilia Z.**  
(GAI.06/09A/A10-006 1020)
- SJÖSTRÖM, Håkan**  
(GAV.06/10P/A11-004 1500)
- SJOBERG, Lars**  
(G03/07P/D-045 1400-067)
- SJOBERG, Lars E.**  
(G03/07P/D-066 1400-088)
- SKACHKO, Sergey N.**  
(JSS07/09P/A02-010 1630)
- SKEET, D.R.**  
(MC04/10P/B22-003 1445)
- SKILBREI, Jan Reidar**  
(JSA07/11A/D-028 0830-028)
- SKOUG, R.**  
(GAI.06/08P/A02-004 1515)
- SKOUG, Ruth**  
(GAI.08/10A/A16-009 1115)
- SKOUG, Ruth M.**  
(GAI.06/08P/A02-003 1450)
- SKVARCA, Pedro**  
(JSM11/10A/B18-004 1000)
- SLAVIN, J.**  
(GAI.V.03/08P/A16-003 1500)
- SLAVIN, J.A.**  
(GAI.06/08A/A02-007 1135)
- SLAVIN, J.A.**  
(GAI.05/07A/A06-003 0930)
- SLAVIN, James A.**  
(GAI.05/08A/A06-002 0845)
- SLAVIN, James A.**  
(GAI.05/08A/A06-009 1110)
- SLINGO, A.**  
(MC11/10P/B19-002 1420)
- SLINGO, Julia**  
(MC11/11A/B19-011 1210)
- SLINGO, Julia**  
(MC17/11A/B23-002 0900)  
(MC11/10A/B19-007 1100)
- SLINGO, Julia**  
(MI07/11A/B18-001 0830)
- SLINGO, Julia Marie**  
(MC17/10P/B23-002 1430)
- SLOBIN, Steve D.**  
(GAI.07/11P/A12-005 1620)
- SLOUGH, John**  
(GAI.11/09P/A15-007 1540)
- SMAKHTIN, Vladimir**  
(HW07/11P/C25-002 1415)
- SMART, Don Frederick**  
(JSA08/09A/A08-006 1030)
- SMILAUER, J.**  
(GAI.06/07P/D-018 1400-138)
- SMILAUER, Jan**  
(GAI.05/07A/D-004 0830-020)
- SMIRNOV, Eugeni Yakovlevich**  
(JSS06a/08P/D-020 1400-098)
- SMIRNOV, Maxim**  
(GAI.08/08P/D-003 1400-138)
- SMIRNOV, Sergey A.**  
(JSP10/09A/B21-008 1140)
- SMIRNOV, Sergey Eduardovich**  
(JSA07/11A/D-005 0830-005)
- SMIRNOVA, Nella**  
(GAI.05/07A/D-004)
- SMIRNOVA, T.G.**  
(JWH01/09P/C30-001)
- SMITH, A.J.**  
(GAI.10/10P/A01-011 1720)
- SMITH, Andy J.**  
(GAI.10/11A/A01-013 1130)
- SMITH, Anne K.**  
(MC05/09P/A09-001 1400)  
(MC05/07P/A09-001 1400)
- SMITH, Bridget**  
(JSS06/10A/A04-002 0850)
- SMITH, Craig J.H.**  
(JSG01/07P/A01-012 1705)
- SMITH, Jeff**  
(JSH01/07P/C27-004 1500)
- SMITH, Michael**  
(HS03/07A/C26-003 0945)
- SMITH, Michael**  
(HW08/08A/C28-005 1000)
- SMITH, Michael B.**  
(HW08/09A/C28-006 1050)
- SMITH, Neville Ross**  
(JSP06/08A/B21-005 1100)
- SMITH, Roger K.**  
(JSP09/11P/B20-007 1600)
- SMITH, Thomas M.**  
(JSP06/07A/B21-003 0940)
- SMITH, Tony**  
(HS04/07P/C30-004 1555)
- SMITH, William Scott**  
(MI09/09A/B22-006 1110)
- SNEED, Sharon A.**  
(JSM10/07A/B23-007 1200)
- SNEEUW, Nico**  
(G03/07P/D-024 1400-046)
- SNORRASON, Arni**  
(HS02b/10P/D-006 1630-127)  
(HS02/10A/C24-006 1105)
- SNYDER, David**  
(JSS06/09P/A04-008 1640)
- SNYDER, David B.**  
(SW03/10P/A04-001 1400)
- SOARES, Pedro**  
(MC17/11P/B23-010 1720)
- SOBOLEV, Roland Nikolaevich**  
(SS03/08A/D-127 0830-286)
- SOBOLEV, S.V.**  
(JSS06a/08P/D-023 1400-101)
- SOERAAS, Finn**  
(GAI.06/07P/D-005 1400-125)
- SOERBOE, Marita**  
(GAI.06/07P/D-005 1400-125)
- SOFKO, George**  
(GAI.06/10A/A01-011 1145)
- SOH, Wonn**  
(SS03/08A/D-043 0830-202)  
(SS03/08A/D-103 0830-262)
- SOJKA, Jan J.**  
(GAI.05/08A/A15-003 0920)
- SOJKA, Jan J.**  
(GAI.05/07A/D-001 0830-017)
- SOJKA, Jan J.**  
(GAI.05/08P/A15-009 1740)
- SOKOLOV, Igor**  
(GAI.V.03/09A/A16-001 0900)
- SOKOLOV, Nikolay V.**  
(JSA09/10A/A08-006 1100)
- SOKOLOV, Vladimir Yu.**  
(SS04/08P/A03-001 1400)  
(SS04a/09P/D-050 1400-299)
- SOKOLOV, Vladimir Yu.**  
(SS04a/09P/D-008 1400-257)
- SOKRATOV, Sergey**  
(JSM10/07A/B23-004 1020)
- SOKRATOV, Sergey A.**  
(JSM15/07A/B18-003 0945)  
(JSM15/07P/D-006 1400-006)
- SOL, Stephane**  
(JSS06b/10P/D-011 1400-035)
- SOLBERG, Rune**  
(JSH01/08A/C27-003 0950)
- SOLHEIM, Dag**  
(G03/07P/D-055 1400-077)
- SOLHEIM, Dag**  
(JSG03/10A/A12-003 0910)
- SOLHEIM, Dag**  
(JSA07/11A/D-028 0830-028)
- SOLHEIM, Dag**  
(JSG02/09A/D-003 0830-003)
- SOLIMAN, Mamdouh Mohamed**  
(GAI.10/09P/D-002 1615-121)
- SOLLITT, Charles**  
(JSS07/09P/A02-011 1645)
- SOLODILOV, Leonid Nikolaevich**  
(JSA07/10A/A05-009 1150)
- SOLOVIEV, Alexander V.**  
(JSA09/10A/A08-007 1115)
- SOLOVIEV, Victor M.**  
(SW05/10A/D-005 0900-249)
- SOLOVIEV, Victor M.**  
(SW05/10P/A13-010 1630)
- SOLOVIEVA, Olga N.**  
(JSS07/10A/A02-011 1115)
- SOLOVYEV, S.I.**  
(GAI.10/11A/D-016 0830-090)
- SOLOVYEV, Stepan I.**  
(GAI.10/11A/D-002 0830-076)
- SOLOVYEV, Stepan I.**  
(GAI.10/11A/D-005 0830-079)
- SOMERVILLE, Paul G.**  
(SS04a/09P/D-030 1400-279)
- SOMERVILLE, Paul Graham**  
(SS04/08A/A03-011 1115)
- SOMMERIA, Joel**  
(JSP10/08P/D-009 1610-061)
- SOMMERIA, Joel**  
(JSP10/09A/B21-008 1140)
- SOMMERIA, Joel**  
(JSP10/08P/B21-001 1400)
- SOMMERIA, Joel**  
(JSP10/11A/B21-001 0830)  
(JSP10/09P/B21-004 1500)
- SOMOROWSKA, Urszula**  
(HS02b/10P/D-005 1630-126)  
(HS02/10A/C24-005 1101)
- SONECHKIN, Dmitry Mikhailovich**  
(MC12/08P/B19-008 1715)  
(MC11/11P/D-006 1400-199)
- SONG, In-Sun**  
(MC05/11A/A09-006 1110)
- SONG, XianFang Xian**  
(HS02a/07P/D-030 1545-176)  
(HS02/07P/C24-030 1452)
- SONG, Yoonho**  
(JSA07/10P/A05-003 1440)
- SORIA, Francisco**  
(JSG03/09P/D-025 1640-033)
- SOROOSHIAN, Soroosh**  
(HW08/08P/C28-004 1520)
- SOROOSHIAN, Soroosh**  
(HW08/07A/C28-001 0900)  
(HW07/11A/C25-004 0930)  
(HW08/08P/C28-003 1500)  
(HW08/08A/C28-001 0830)
- SODARIN, Laurent**  
(G07/10P/D-008 1400-093)
- SOUKHAREV, Boris E.**  
(JSA08/09A/A08-001 0900)
- SOULIS, Eric D.**  
(HS03/07P/C26-006 1515)
- SOULSBY, Chris**  
(HW02/11A/C31-002 0900)
- SPADA, Giorgio**  
(SS03/08A/D-031 0830-190)
- SPAKMAN, Wim**  
(SS03/08A/D-076 0830-235)
- SPARROW, Michael**  
(JSP06/07P/D-003 1400-010)
- SPARROW, Sarah**  
(MC05/10P/A09-001 1400)
- SPEER, Milton**  
(HS03/08P/C26-010 1630)
- SPENCE, Harlan E.**  
(GAI.09/11P/A11-002 1420)
- SPENCE, Harlan E.**  
(GAI.08/10A/A16-005 0945)  
(GAI.05/08A/A06-011 1150)
- SPENCER, Hilary**  
(MC11/11A/B19-011 1210)
- SPEMBER, K.**  
(MC11/11A/B19-001 0830)
- SPEMBER, Kenneth Robert**  
(MC17/10P/B23-002 1430)
- SPJELDVIK, Walther N.**  
(GAI.10/11A/D-022 0830-096)
- SPORYSHEV, Petr V.**  
(MC11/11P/D-003 1400-196)
- SPRATT, Jessica E.**  
(GAI.08/08A/A14-003 0910)
- SPRENGER, Michael**  
(MC05/09A/A09-002 0920)
- SPROULE, David Michael**  
(G03/07P/D-008 1400-030)
- SRDIC-MITROVIC, Andjelka N.**  
(JSP10/09A/B21-008 1140)
- SREEDEVI, P.D.**  
(HW05/10A/C31-012 1140)
- SREEDEVI, P.D.**  
(HW03/11P/C30-009 1700)
- SREEPATI, Svs Sarma Satyanarayana**  
(GAI.10/11A/A01-004 0915)
- SRIBIMAWATI, Tien**  
(MC03/09P/A07-007 1700)  
(MC17/11A/B23-004 0940)  
(MC05/08P/A09-005 1530)  
(MC03/10P/A07-008 1720)  
(MC17/11P/B23-006 1600)  
(MC03/11P/A07-003 1440)  
(MC03/11P/D-009 1400-184)  
(JSM14/07A/A05-006 1130)
- SRIBIMAWATI, Tien**  
(MC03/11P/D-007 1400-182)
- SRINIVASAN, Vajapeyam S.**  
(HS01/09P/C29-001 1400)
- SRINIVASAN, Vajapeyam S.**  
(HS01/09A/C29-010 1220)
- SRIVASTAVA, Ajai**  
(HS01/09P/D-008 1400-175)
- SRIVASTAVA, Ajit K.**  
(HS01/09P/D-008 1400-175)
- SRIVASTAVA, Hari Narayana**  
(SS04/07P/A03-009 1630)
- SRIVASTAVA, Ravi Prakash.**  
(G04/08A/C25-006 1050)
- SRIVASTAVA, S.**  
(GAI.08/08A/A14-009 1130)
- SRIVASTAVA, Someshwar**  
(JSA07/11A/D-040 0830-040)
- STADSNES, Rune**  
(GAI.06/07P/D-005 1400-125)
- STAINFORTH, David**  
(MC08/08P/D-002 1400-158)
- STALLARD, Robert F.**  
(HW01/10P/C26-002 1420)
- STAMMER, Detlef**  
(JSM11/10P/B18-001 1400)
- STAMMER, Detlef**  
(JSP09/11P/B20-002 1415)
- STAMNES, Knut**  
(JSH01/08P/D-009 1400-047)
- STANCALIE, Gheorghe**  
(HS02/11P/C24-005 1500)
- STANCALIE, Gheorghe**  
(HS02c/11P/D-032 1630-130)  
(HS02/11P/C24-009 1547)
- STANEV, Emil V.**  
(JSP08/09A/B19-007 1120)
- STANEV, Emil Vassilev**  
(MC11/11P/D-002 1400-195)
- STANEVA, Joanna**  
(JSM11/10P/D-009 1700-018)
- STANFORTH, Robert**  
(HW01/10P/C26-008 1700)

- STANICA, Dumitru I.**  
(GAI.08/08A/A14-008 1110)
- STANICA, Maria**  
(GAI.08/08A/A14-008 1110)
- STANLEY, Mark**  
(GAIL.04/07A/A08-006 1050)
- STANTON, Timothy**  
(JSP04/09P/A06-003 1430)
- STAQUET, Chantal**  
(JSP10/11P/B21-006 1640)
- STARCHENKO, Sergei V.**  
(JSS06/09A/A04-004 1000)
- STARJINSKY, Sergey Stanislavovich**  
(JSA07/11A/D-008 0830-008)
- STAUNING, Peter**  
(GAV.04/07A/A11-005 1100)
- STAVREV, Petar**  
(GAV.06/10A/A11-009 1130)
- STEELE, Michael**  
(JSP04/10P/A06-005 1520)
- STEFANOV, P.**  
(JSP11/08P/D-008 1400-077)
- STEGNER, Alexandre**  
(JSP10/09A/B21-007 1120)
- STEGNER, Alexandre**  
(JSP10/11A/B21-010 1210)
- STEINBERG, Jean-Louis**  
(GAIL.05/07A/A06-006 1025)
- STEINBERGER, Bernhard Maximilian**  
(JSS06/08A/A04-002 0850)
- STEINBRICH, Andreas**  
(HS02/08P/C24-008 1615)
- STEINHORST, Hildegard**  
(MC05/07A/A09-002 0930)
- STENBAEK-NIELSEN, Hans C.**  
(GAIL.04/07P/A08-001 1400)  
(GAIL.04/07P/A08-005 1540)
- STENCHIKOV, Georgiy**  
(MC05/10P/A09-008 1740)
- STENCHIKOV, Georgiy L.**  
(JSA09/10A/A08-005 1030)
- STENDEL, Martin**  
(MC11/11A/B19-010 1150)
- STENNI, B.**  
(MC12/08A/B19-002 1000)
- STENSENG, Lars**  
(G03/07P/D-060 1400-082)
- STENZEL, Oliver**  
(JSP10/09A/B21-004 1010)
- STEPANOV, A.E.**  
(GAIL.06/10A/A01-002 0850)
- STEPANOVA, Marina**  
(GAIL.10/11A/A01-003 0900)
- STEPANYAN, Ruben**  
(SS03/08A/D-083 0830-242)
- STEPHENSON, David B.**  
(MI05/10A/B17-002 0910)
- STEPHENSON, Fred E.**  
(JSS07b/10P/D-008 1700-054)  
(JSS07/10A/A02-011 1115)
- STERL, Andreas**  
(JSP09/11A/B20-011 1145)
- STEVENS, Bjorn**  
(MC03/10P/A07-003 1440)
- STEWART, B.C.**  
(MI09/09A/B22-004 1000)
- STEWART, Ronald Earl**  
(JSM14/09A/A05-006 1100)
- STIEGLITZ, Marc**  
(MI05/11P/B17-001 1400)
- STIEGLITZ, Thomas C.**  
(JSG03/09P/D-017 1640-025)  
(JSG03/09P/A12-006 1540)
- STO, Mihoko**  
(JSM14/07P/A05-003 1450)
- STOCKLI, Reto**  
(MI07/11P/B18-003 1440)
- STOEVA, P.**  
(JSP11/08P/D-008 1400-077)
- STOKER, Pieter H.**  
(GAIL.06/10A/A01-005 0940)
- STONE, Kenneth**  
(MC05/08P/A09-003 1450)
- STOSSMEISTER, Greg**  
(JSP04/09A/A06-005 1050)
- STOTTER, Christian**  
(GAV.06/10A/A11-004 0930)
- STRAKHOV, Vladimir Nicolaevich**  
(JSS06/10A/A04-006 1010)
- STRANGEWAY, R.J.**  
(GAIL.06/08A/A02-007 1135)
- STRANGEWAY, Robert J.**  
(GAIL.06/07P/D-014 1400-134)
- STRAPP, Walter**  
(JSM14/09P/D-002 1400-066)
- STRASSER, U.**  
(JWH01/09P/C30-001)
- STRATTON, Rachel**  
(MC11/10A/B19-005 1000)
- STRATTON, Rachel A.**  
(MC11/10A/B19-008 1130)
- STRAUS, Paul R.**  
(GAIL.05/08P/A15-009 1740)
- STRELTSOV, Michael**  
(SS04/08P/A03-010 1630)
- STRICKLAND, Douglas J.**  
(GAIL.05/08P/A15-008 1720)
- STROEVE, Julienne**  
(JSH01/08P/D-006 1400-044)
- STROMEYER, Dietrich**  
(GAV.05/09P/D-003 1400-147)
- STROMKOV, Alexander**  
(JSS07/09A/A02-004 0945)
- STRUAS, Paul**  
(GAIL.05/07A/D-005 0830-021)
- STRUTHERS, Hamish**  
(MI03/09A/D-005 0900-248)
- STRYKOWSKI, Gabriel**  
(G03/07P/D-051 1400-073)
- STRYKOWSKI, Gabriel**  
(G03/07P/D-055 1400-077)
- STRYKOWSKI, Gabriel**  
(G04/08A/C25-001 0840)
- STUBENVOLL, Richard**  
(G02/07A/C25-001 0900)
- STUPAK, Vladimir M.**  
(JSA07/10A/A05-005 1000)
- STURM, Kristof**  
(HW06/08A/C31-002 1100)
- STURM, Matthew**  
(JSH01/08P/D-006 1400-044)
- STYLES, Richard**  
(JSP08/09A/B19-005 1030)
- SU, Baolin**  
(HS02/08P/C24-003 1430)
- SU, Fengge**  
(HW08/09A/C28-004 1010)
- SU, H.T.**  
(GAIL.04/07A/A08-007 1110)
- SU, Jie**  
(JSM03/08P/A13-001 1400)
- SU, S.-Y.**  
(GAIL.06/09A/A10-001 0900)
- SU, S.-Y.**  
(JSG03/09P/D-026 1640-034)
- SU, Shin-Yi**  
(GAIL.11/10P/D-006 1400-121)
- SUANKUASAKOOL, Sukit**  
(HW07/11P/D-001 1400-137)
- SUANTIKA, Gede**  
(JSS06b/10P/D-016 1400-040)
- SUBARYA, Cecep**  
(JSM11/10P/B18-006 1620)
- SUBRAHAMANYAM, Bulusu**  
(JSP09/11P/B20-002 1415)
- SUBRAMANIAN, Sivanesan**  
(JSM04/09P/D-004 1400-041)
- SUBRAMANIAN, Vembu**  
(JSP07/08A/B17-004 1010)
- SUDHAKAR, S. Sudhakar**  
(HS01/08P/C29-008)
- SUDO, Kengo**  
(MI03/08P/B18-006 1610)
- SUDO, Noboru**  
(JSG03/09P/D-019 1640-027)
- SUDO, Shigeto**  
(JSM04/09A/B23-001 0900)
- SUE, Miles K.**  
(GAIL.07/11P/A12-005 1620)
- SUEHIRO, Masaki**  
(SS03/08A/D-040 0830-199)
- SUEHIRO, Masaki**  
(SS04a/09P/D-038 1400-287)
- SUELTFUSS, Juergen**  
(HW06/07P/C31-004 1500)
- SUEN, Jian-Ping**  
(HS02b/10P/D-012 1630-133)  
(HS02/10A/C24-012 1129)
- SUENKEL, Hans**  
(G03/07P/D-058 1400-080)
- SUETSUGU, Daisuke**  
(JSS06/07P/A04-005 1540)
- SUETSUGU, Daisuke**  
(JSS06/09P/A04-009 1700)
- SUGA, Toshio**  
(JSP06/07P/B21-003 1450)
- SUGAI, Toshihiko**  
(SS03/08A/D-041 0830-200)
- SUGI, Masato**  
(MC02/07A/B20-007 1205)
- SUGI, Noriko**  
(SS05/10A/A13-014 1200)
- SUGIHARA, Mitsuhiko**  
(GAV.06/09P/D-001 1400-154)
- SUGIMORI, Yasuhiro**  
(JSP09/11P/B20-001 1400)
- SUGIMORI, Yasuhiro**  
(JSG03/09P/A12-005 1520)
- SUGIMOTO, Atsuko**  
(HW06/07P/C31-007 1600)  
(HW06/07P/D-003 1400-187)
- SUGIMOTO, Atsuko**  
(HW06/07P/C31-001 1400)
- SUGIMOTO, Norihiko**  
(JSP10/09A/B21-003 0950)
- SUGIMOTO, Soichiro**  
(HS03/07P/C26-008 1600)
- SUGIOKA, Hiroko**  
(JSS06/07P/A04-005 1540)
- SUGIOKA, Hiroko**  
(JSS06/09P/A04-009 1700)
- SUGITA, Fumi**  
(HW01/09A/C26-004 1010)
- SUGITA, Takafumi**  
(MI07/11A/B18-007 1110)  
(MC05/07P/A09-002 1430)
- SUGIYAMA, Hironobu**  
(HS02/11P/C24-004 1445)  
(JWH01/10A/C30-004 0930)  
(HW02/11A/C31-003 0925)
- SUGIYAMA, Ko-ichiro**  
(MC04/10P/B22-005 1530)
- SUGIYAMA, Tooru**  
(GAIL.07/09P/A14-007 1640)
- SUGIYAMA, Yuichi**  
(SS03/08A/D-059 0830-218)
- SUGIYAMA, Yuichi**  
(SS03/08A/D-040 0830-199)  
(SW04/09P/A13-012 1700)  
(SS04b/10P/D-038 1400-222)  
(SS03/08A/D-041 0830-200)  
(SS04a/09P/D-018 1400-267)  
(SS04a/09P/D-038 1400-287)
- SUHADOLC, P.**  
(SS03/07A/A02-005 1030)
- SUHADOLC, Peter**  
(SS04/07P/A03-005 1515)
- SUHADOLC, Peter**  
(SW04/09P/A13-002 1415)
- SUHARDI, Budi**  
(MC03/10P/A07-008 1720)
- SUHARDI, Budi**  
(MC17/11P/B23-006 1600)
- SUI, Chung-Hsiung**  
(JSP09/11P/B20-010 1700)
- SUICHI, Mori**  
(MC03/11P/A07-003 1440)
- SUITO, Hisashi**  
(JSG01/08P/D-014 1400-014)  
(JSG01/07P/A01-008 1605)
- SUITO, Hisashi**  
(JSG01/08P/D-015 1400-015)
- SUIZU, Shigeo**  
(JWH01/09P/C30-007 1630)
- SUKANTA, Roy**  
(SW03/10P/A04-010 1630)
- SUKHANOVSKY, Andrey**  
(JSM14/07P/A05-004 1505)
- SUKHAPUNNAPHAN, Thada**  
(HW07/11P/D-038 1400-174)
- SULEIMANOV, Arsen K.**  
(JSA07/10A/A05-005 1000)
- SULEIMANOV, Arsen K.**  
(JSA07/11A/D-021 0830-021)  
(GAI.10/09A/A11-006 1015)
- SULSTAROVA, Eduard**  
(JSP11/08P/D-006 1400-075)
- SULTAN, Sultan Awad**  
(HS02a/07P/D-036 1545-182)  
(HS02/07P/C24-036 1516)
- SUMARRIVA, Chavez**  
(SS05/10P/D-001 1400-235)
- SUMARRIVA, Israel Chavez**  
(GAV.06/09P/D-010 1400-163)
- SUMI, Akimasa**  
(MC08/07P/B17-003 1430)
- SUMIKAWA, Sakie**  
(JSM15/07P/D-007 1400-007)
- SUMMER, Wolfgang**  
(HS01/09A/C29-009 1200)
- SUMMERS, Danny**  
(GAIL.10/10P/A01-009 1640)
- SUN, Charles**  
(JSP06/07P/B21-004 1510)
- SUN, De-Zheng**  
(MC11/10P/B19-001 1400)
- SUN, He-Ping**  
(JSS06/09A/A04-005 1040)
- SUN, Junying**  
(JSM10/07A/B23-007 1200)
- SUN, Lan**  
(MI07/11P/B18-004 1500)  
(MI07/11A/B18-005 0950)
- SUN, Ruomei**  
(SS03/08A/D-140 0830-299)
- SUN, Ruomei**  
(SS03/08A/D-137 0830-296)
- SUN, Shaoan**  
(G03/07P/D-016 1400-038)
- SUN, Shufen**  
(JWH01/10A/C30-001 0830)
- SUN, Shufen**  
(HS03/08P/C26-009 1615)
- SUN, Weizhen**  
(JSM10/07A/B23-006 1140)
- SUN, Wenke**  
(G04/08P/D-023 1400-130)  
(G04/08A/C25-007 1120)  
(JSG02/09P/A05-011 1745)
- SUNADA, Kengo**  
(HW07/11P/D-014 1400-150)  
(HW07/11P/D-005 1400-141)
- SUNDERMANN, Sean**  
(SW04/09P/A13-012 1700)
- SUNDERMEYER, Miles A.**  
(JSP10/11P/B21-005 1610)
- SUNG, Chia Wen**  
(HS02b/10P/D-028 1630-149)  
(HS02/10P/C24-005 1531)
- SUNG, S.J.**  
(JSG03/09P/D-006 1640-014)
- SUPIC, Nastjenka**  
(JSP09/10P/B20-007 1545)
- SUPPER, Robert**  
(GAV.06/10A/A11-004 0930)  
(GAV.06/10A/A11-005 0950)  
(GAV.06/09P/D-001 1400-154)
- Surono**  
(JSP11/08A/A10-003 0950)

## INDEX

- SURYAPRAKASAM, K.**  
(JSS06/07P/A04-007 1620)
- SUSOTT, R.A.**  
(JSM04/09A/B23-006 1145)
- SUSSMANN, Ralf**  
(MI03/08A/B18-007 1110)
- SUTCLIFFE, P.R.**  
(GAILI.10/11A/D-017 0830-091)
- SUTHERLAND, Bruce R.**  
(JSP10/09P/B21-003 1440)
- SUTHERLAND, Bruce R.**  
(JSP10/11P/B21-009 1740)
- SUTHERLAND, Bruce R.**  
(JSP10/09P/B21-005 1520)
- SUTTON, Philip**  
(JSP06/07P/B21-005 1600)
- SUTTON, Rowan T.**  
(MC11/11A/B19-010 1150)
- SUVANPIMOL, Chanchai**  
(HW07/11P/D-001 1400-137)
- SUVARYAN, Khoren Garnik**  
(SS04a/09P/D-006)
- SUVARYAN, Levon Garnik**  
(SS04a/09P/D-006 1400-255)
- SUWA, Hiroshi**  
(HS01/09P/D-009 1400-176)
- SUWA, Yoko**  
(JSG01/08P/D-006 1400-006)
- SUWA, Yoko**  
(JSG01/08P/D-002 1400-002)
- SUYEHIRO, Kiyoshi**  
(SS03/07A/A02-003 0930)
- SUYEHIRO, Kiyoshi**  
(SS03/08A/D-114 0830-273)
- SUYEHIRO, Kiyoshi**  
(SS03/08A/D-001 0830-160)
- SUYEHIRO, Kiyoshi**  
(GAI.08/08P/D-008 1400-143)  
(SS03/08A/D-103 0830-262)
- SUZUKI, Katsuko**  
(SS03/08A/D-008 0830-167)
- SUZUKI, Kazuyoshi**  
(HS02/09A/C24-003 0930)  
(JWH01/10A/C30-005 0950)  
(JWH01/09P/C30-005 1520)  
(JSM10/08P/B23-003 1500)
- SUZUKI, Keisuke**  
(JWH01/10P/D-002 1400-007)
- SUZUKI, Naokatsu**  
(GAV.05/09P/D-007 1400-151)
- SUZUKI, Naoya**  
(JSP09/11P/B20-001 1400)
- SUZUKI, Sadaomi**  
(SS03/08A/D-113 0830-272)  
(SS03/08A/D-100 0830-259)
- SUZUKI, Sadaomi**  
(JSG01/08P/D-020 1400-020)
- SUZUKI, Sadaomi**  
(SS03/08A/D-118 0830-277)
- SUZUKI, Satoru**  
(MI07/10P/D-005 1400-181)
- SUZUKI, Shin-ichi**  
(MC03/11P/D-006 1400-181)
- SUZUKI, Takahiko**  
(JSG01/07A/A01-003 0930)
- SUZUKI, Takao**  
(HW05/10P/D-011 1400-166)
- SUZUKI, Takayuki**  
(MI08/07P/D-001 1400-195)
- SUZUKI, Tatsuo**  
(SS05/10A/A13-003 0900)
- SUZUKI, Tsuneaki**  
(MC11/11A/B19-008 1110)
- SUZUKI, Tuneaki**  
(MI06/09P/B20-006 1540)
- SUZUKI, Yoshiharu**  
(HS03/07P/C26-007 1545)
- SUZUKI, Yoshihisa**  
(SW04/09P/A13-014 1730)
- SVEHLA, Drazen**  
(G02/07A/C25-008 1115)
- SVEHLA, Drazen**  
(JSG02/09P/A05-010 1730)
- SVENES, Knut**  
(GAILI.11/09A/A15-003 0940)
- SVENES, Knut**  
(GAILI.06/07P/D-005 1400-125)
- SWAIN, Christopher**  
(JSS06b/10P/D-003 1400-027)  
(JSS06b/10P/D-002 1400-026)
- SWATERS, Gordon E.**  
(JSP10/09P/B21-003 1440)
- SWATERS, Gordon E.**  
(JSP10/09A/B21-006 1100)
- SWENSON, Gary R.**  
(MC05/11A/A09-002 0900)
- SWIECA, Andrzej**  
(HW01/09P/D-006 1400-197)
- SWINBANK, Richard**  
(MC05/10A/A09-002 0900)
- SWISDAK, Marc**  
(GAILI.05/08A/A06-012 1215)
- SYAMSUDIN, Fadli**  
(JSP07/08A/B17-005 1100)
- SYNAOLAKIS, Costas E.**  
(JSS07/09A/A02-007 1030)
- SYNOLAKIS, Costas**  
(JSS07a/09P/D-018 1700-119)
- SYNOLAKIS, Costas**  
(JSS07/09A/A02-012 1200)
- SYNOLAKIS, Costas Emmanuel**  
(JSS07/09P/A02-009 1615)
- SYVITSKI, James**  
(JSM03/08P/A13-008 1640)
- SZAKÁCS, Alexandru**  
(JSS06/10A/A04-010 1150)
- SZETO, Kit K.**  
(JSM14/09A/A05-006 1100)
- t**
- T., Arafa**  
(GAV.05/09P/D-008 1400-152)
- T., Harinarayana**  
(SS03/08A/D-133 0830-292)
- T., Harinarayana**  
(GAI.08/08A/A14-010 1150)
- T., Ndougsa Mbarga**  
(GAI.10/09P/D-017 1615-136)
- TABAZADEH, Azadeh**  
(MI03/08P/B18-002 1420)
- TABEL, Takao**  
(SS03/08A/D-054 0830-213)
- TABEL, Takao**  
(JSG01/08P/D-016 1400-016)
- TABELLARIO, Giovanni**  
(JSA07/10P/A05-007 1630)
- TACHIBANA, Kenji**  
(JSG01/08P/D-006 1400-006)
- TACHIBANA, Kenji**  
(JSG01/08P/D-002 1400-002)
- TACHIBANA, Yoshihiro**  
(MI05/11A/B17-004 0930)
- TACHIBANA, Yoshihiro**  
(MI05/10P/D-001 1400-168)
- TACHIBANA, Yoshihiro**  
(MC03/11P/D-001 1400-176)
- TACHIBANA, Yoshihiro**  
(JSM10/08A/B23-003 0930)
- TACHIKAWA**  
(HS03/07P/C26-010 1630)
- TACHIKAWA, Yasuto**  
(HS03/08A/C26-011 1130)
- TACHIKAWA, Yasuto**  
(HS03/08A/C26-002 0900)
- TACHIKAWA, Yasuto**  
(HS01/08A/C29-003 1050)
- TACKLEY, Paul**  
(JSS06a/08P/D-009 1400-087)
- TACKLEY, Paul J.**  
(JSS06a/08P/D-014 1400-092)
- TACKLEY, Paul J.**  
(JSS06a/08P/D-001 1400-079)
- TACKLEY, Paul J.**  
(JSS06/07P/A04-002 1420)
- TACKLEY, Paul J.**  
(JSS06/08A/A04-001 0830)
- TADA, Akio**  
(HW08/07A/C28-007 1130)
- TADA, Noriko**  
(GAI.08/08P/D-008 1400-143)
- TADA, Taku**  
(SS04a/09P/D-034 1400-283)
- TAGUCHI, Satoshi**  
(GAILI.05/08A/A15-009 1210)
- TAGUCHI, Yusaku**  
(HW01/09P/D-052 1400-243)
- TAHA, Ghassan**  
(MI03/09A/D-001 0900-244)  
(MI03/08A/B18-002 0850)
- TAHA, Mahmoud R.**  
(G04/08P/C25-002 1430)
- TAHARA, Hirokazu**  
(GAILI.11/09P/A15-005 1510)
- TAIRA, Asahiko**  
(SS03/08A/D-122 0830-281)
- TAJIKI, Jun**  
(SS03/08A/D-042 0830-201)
- TAJIMA, Minoru**  
(JSG01/08A/A01-005 1000)
- TAKADA, Masamitsu**  
(SW03/10A/D-002 0830-237)  
(SW03/10A/D-004 0830-239)
- TAKADA, Masamitsu**  
(SW03/10A/D-007 0830-242)
- TAKADA, Masamitsu**  
(SW03/10A/D-003 0830-238)
- TAKADA, Taku**  
(GAILI.05/07P/D-019 1400-117)
- TAKAGI, Hideyuki**  
(SW05/10P/A13-009 1615)
- TAKAGI, Kentaro**  
(HW01/10A/C26-007 1110)
- TAKAGI, Masahiro**  
(MC04/11A/B22-009 1115)
- TAKAHARA, Hiroaki**  
(MC03/11P/D-014 1400-189)
- TAKAHASHI, Chiharu**  
(MC03/11P/D-017 1400-192)
- TAKAHASHI, Chuji**  
(JSM15/07P/D-003 1400-003)
- TAKAHASHI, Hideomi**  
(GAILI.04/07P/A08-009 1700)
- TAKAHASHI, Hiroaki**  
(JSG01/08P/D-009 1400-009)  
(SS03/08A/D-007 0830-166)
- TAKAHASHI, Hiroaki**  
(JSS07/10P/A02-009 1615)
- TAKAHASHI, Jun**  
(JSP04/09P/A06-004 1445)
- TAKAHASHI, K.**  
(GAILI.06/07P/D-002 1400-122)
- TAKAHASHI, Kazue**  
(GAILI.10/10P/A01-004 1500)
- TAKAHASHI, Keiko**  
(JSP04/09A/A06-007 1130)
- TAKAHASHI, Kenshi**  
(MI08/07P/D-001 1400-195)  
(MI08/07P/B18-005 1640)  
(MI09/08P/B22-007 1640)
- TAKAHASHI, Makoto**  
(JSG01/08A/A01-004 0945)
- TAKAHASHI, Masaaki**  
(MI05/10A/B17-009 1200)
- TAKAHASHI, Masaaki**  
(MC05/11P/A09-001 1400)  
(MI05/11A/B17-010 1210)  
(MI06/09P/B20-001 1400)  
(MC04/11A/B22-006 1000)  
(MI03/08P/B18-006 1610)  
(MC05/11P/A09-002 1430)
- TAKAHASHI, Masaaki**  
(MC05/11P/A09-008 1700)
- TAKAHASHI, Masaki**  
(SS05/10A/A13-011 1115)
- TAKAHASHI, Masayuki Mac**  
(JSP04/09P/A06-012 1745)
- TAKAHASHI, Naoya**  
(JSP10/10P/B21-003 1450)
- TAKAHASHI, Narumi**  
(SS03/08A/D-109 0830-268)
- TAKAHASHI, Narumi**  
(SS03/08A/D-103 0830-262)
- TAKAHASHI, Satoshi**  
(JSP09/10A/B20-002 0930)
- TAKAHASHI, Shin**  
(GAILI.14/07A/A12-006 1140)
- TAKAHASHI, Shin**  
(GAILI.14/07A/A12-007 1155)
- TAKAHASHI, Shuhei**  
(JSM11/10P/D-008 1700-017)
- TAKAHASHI, Tomoyuki**  
(JSS07/09P/A02-002 1415)
- TAKAHASHI, Tsutomu**  
(JSM14/08A/A05-006 1010)  
(JSM15/07A/B18-009 1130)
- TAKAHASHI, Yoshio**  
(HS02c/11P/D-020 1630-118)  
(HS02/11A/C24-020 1201)
- TAKAHASHI, Yukihiko O.**  
(GAILI.07/11P/A12-003 1500)
- TAKAHASHI, Yukihiko**  
(GAILI.04/09A/D-005 0830-141)  
(MC04/11A/B22-004 0930)  
(GAILI.04/09A/D-004 0830-140)  
(GAILI.04/09A/D-003 0830-139)  
(GAILI.04/09A/D-006 0830-142)
- TAKAHASHI, Yukihiko**  
(GAILI.06/11P/D-011 1400-063)
- TAKAHASHI, Yukihiko**  
(GAILI.04/07A/A08-006 1050)
- TAKAKURA, Shinichi**  
(GAV.06/10A/A11-002 0850)
- TAKAMI, Masazo**  
(SS03/08A/D-042 0830-201)
- TAKAMURA, Hiroki**  
(HW06/07P/D-008 1400-192)
- TAKANAMI, Tetsuo**  
(SS03/08A/D-005 0830-164)
- TAKANAMI, Tetsuo**  
(SS03/08A/D-056 0830-215)
- TAKANAMI, Tetsuo**  
(SS03/08A/D-114 0830-273)
- TAKANAMI, Tetsuo**  
(SW05/10A/D-009 0900-253)
- TAKANASHI, Satoru**  
(HS02/08P/C24-012 1715)
- TAKANO, Hironobu**  
(GAILI.05/07P/D-021 1400-119)
- TAKAO, Makoto**  
(JSS07b/10P/D-001 1700-047)
- TAKAOKA, Kazuaki**  
(JSS07/09P/A02-004 1445)
- TAKARA, Kaoru**  
(HS03/08A/C26-010 1115)  
(HS03/07P/C26-010 1630)  
(HS02/09P/C24-005 1500)
- TAKARA, Kaoru**  
(HS03/08A/C26-011 1130)
- TAKARA, Kaoru**  
(HS03/08A/C26-002 0900)
- TAKARA, Kaoru**  
(HS01/08A/C29-003 1050)
- TAKASAKI, Satoko**  
(GAILI.10/11A/D-007 0830-081)
- TAKASHIMA, Takeshi**  
(GAILI.06/07P/D-010 1400-130)
- TAKASUGI, Yoshio**  
(JSP07/08A/B17-005 1100)
- TAKAYA, Koutarou**  
(MI05/11P/B17-007 1630)
- TAKAYA, Yoshimasa**  
(JSM14/09P/D-013 1400-077)
- TAKAYABU, Yukari N.**  
(MC17/10P/B23-001 1400)  
(MC17/10P/B23-003 1445)  
(MC17/11P/B23-002 1420)
- TAKAYAMA, Hiromi**

- (JSG01/08P/D-019 1400-019)  
**TAKAYAMA, Kaoru**  
 (MC04/11P/B22-010 1715)  
**TAKAZAWA, Toshi**  
 (JSP04/09A/A06-001 0900)  
**TAKEDA, Tetsuya**  
 (SS03/07A/A02-008 1115)  
**TAKEGAHARA, Haruki**  
 (GAILI.11/09P/A15-002 1425)  
**TAKEHIRO, Shin-ichi**  
 (SW05/10A/D-008 0900-252)  
**TAKEHIRO, Shin-ichi**  
 (MC04/10P/B22-002 1430)  
**TAKEHIRO, Shin-ichi**  
 (MC04/11P/B22-003 1445)  
**TAKEI, Tsutomu**  
 (HS01/09P/D-007 1400-174)  
**TAKEI, Yasuko**  
 (JSG01/08P/D-018 1400-018)  
**TAKEMOTO, Shuzo**  
 (G03/07P/D-073)  
**TAKEMOTO, Shuzo**  
 (G03/07P/D-001 1400-023)  
 (G03/07P/D-003 1400-025)  
 (JSG01/08P/D-037 1400-037)  
**TAKEMURA, Masayuki**  
 (SS04/08A/A03-012 1130)  
**TAKENAKA, Chisato**  
 (HW01/09P/D-032 1400-223)  
**TAKENAKA, Hiroshi**  
 (SS04a/09P/D-028 1400-277)  
**TAKENAKA, Hiroshi**  
 (SS03/08A/D-113 0830-272)  
 (SS03/08A/D-100 0830-259)  
**TAKENAKA, Hiroshi**  
 (SS03/08A/D-118 0830-277)  
**TAKEOKA, Hidetaka**  
 (JSP07/08A/B17-005 1100)  
**TAKESHIGE, Yuji**  
 (HW01/10A/C26-010 1210)  
**TAKEUCHI, Akira**  
 (SS03/08A/D-039 0830-198)  
**TAKEUCHI, Akira**  
 (JSG01/08P/D-007 1400-007)  
 (SS03/08A/D-037 0830-196)  
**TAKEUCHI, Akira**  
 (SS03/08A/D-055 0830-214)  
**TAKEUCHI, Ayako**  
 (MC08/07A/B17-006 1120)  
**TAKEUCHI, Fumiaki**  
 (JSA07/11A/D-017 0830-017)  
**TAKEUCHI, Kensuke**  
 (MC17/11P/B23-003 1440)  
**TAKEUCHI, Kuniyoshi**  
 (HW07/11P/D-005 1400-141)  
**TAKEUCHI, Kuniyoshi**  
 (HW08/07P/C28-005 1610)  
**TAKEUCHI, Kuniyoshi**  
 (JSG03/09P/A12-001 1400)  
**TAKEUCHI, Kuniyoshi**  
 (HS03/08A/C26-004 0930)  
 (HS02/11A/C24-004 0915)  
**TAKEUCHI, Kuniyoshi**  
 (HS03/08A/C26-009 1100)  
**TAKEUCHI, Kuniyoshi**  
 (HS01/08A/C29-002 1010)  
**TAKEUCHI, Kuniyoshi**  
 (HW04/09A/C31-001 0900)  
**TAKEUCHI, Kuniyoshi**  
 (JWH01/10A/C30-010 1200)  
**TAKEUCHI, Kuniyoshi**  
 (HW07/10A/C25-002 1000)  
**TAKEUCHI, Nozomu**  
 (JSH01/07A/C27-003 1020)  
**TAKEZONO, Motoi**  
 (SS04/07P/A03-006 1530)  
**TAKHIROV, Nasirdjan**  
 (HS02a/07P/D-013 1545-159)  
**TAKHIROV, Nasirdjan**  
 (HS02/07A/C24-013 0948)  
**TAKIGUCHI, Hiroshi**  
 (JSG01/08P/D-030 1400-030)  
**TALAAT, Elsayed R.**  
 (MC05/09P/A09-004 1520)  
**TALBOT, Christopher J.**  
 (G02/10P/D-016 1400-081)  
**TALEBBEYDOKHTI, Nasser**  
 (HS01/08P/C29-002 1420)  
**TALLARICO, Andrea**  
 (SS03/08A/D-027 0830-186)  
**TAMAGAWA, Ichiro**  
 (HSM14/09P/D-007 1400-071)  
**TAMAKI, Kensaku**  
 (GAV.06/10P/A11-006 1600)  
**TAMAKI, Kensaku**  
 (SS03/08A/D-067 0830-226)  
**TAMAYO, JR., Rodolfo A.**  
 (SS03/08A/D-061 0830-220)  
**TAMAYO, JR., Rodolfo A.**  
 (SS03/08A/D-122 0830-281)  
**TAMURA, Nobuchika**  
 (HW04/09A/C31-002 0920)  
**TAMURA, Ryuichi**  
 (GAILI.06/11P/D-011)  
**TAN, Ge**  
 (HS02/07P/C24-021 1416)  
**TAN, Ge**  
 (HW01/09P/D-002 1400-193)  
**TAN, Ge**  
 (HS02a/07P/D-021 1545-167)  
**TANAKA, Akiko**  
 (SS03/08A/D-034 0830-193)  
 (SS03/08A/D-110 0830-269)  
**TANAKA, Atsushi**  
 (SS03/07P/A02-003 1430)  
 (SS03/08A/D-050 0830-209)  
**TANAKA, Daisuke**  
 (MC05/09P/A09-007 1640)  
**TANAKA, Hiroki**  
 (JSM03/09A/D-002 0830-036)  
**TANAKA, Hiroki**  
 (JSM03/08A/A13-004 1000)  
**TANAKA, Hiroki**  
 (JSM03/09A/D-003 0830-037)  
**TANAKA, Hiroshi L.**  
 (MI05/09A/B17-003 1000)  
**TANAKA, Hiroyoshi**  
 (JSS07a/09P/D-007 1700-108)  
**TANAKA, Hiroyoshi**  
 (JSS07b/10P/D-001 1700-047)  
**TANAKA, Hiroyoshi**  
 (JSS07a/09P/D-017 1700-118)  
**TANAKA, Koji**  
 (GAILI.11/09P/A15-004 1455)  
**TANAKA, Masayuki**  
 (SS03/08A/D-056 0830-215)  
**TANAKA, Nobuaki**  
 (HS02b/10P/D-002 1630-123)  
 (HS02/10A/C24-002 1049)  
**TANAKA, Nori**  
 (JSM04/09A/B23-004 1030)  
**TANAKA, Noriyuki**  
 (JSP04/09P/A06-010 1715)  
**TANAKA, Noriyuki**  
 (JSP04/09P/A06-011 1730)  
**TANAKA, Noriyuki**  
 (MC12/07P/B19-005 1545)  
**TANAKA, Noriyuki**  
 (MC12/07P/B19-006 1600)  
**TANAKA, Noriyuki**  
 (JSP04/09P/A06-006 1545)  
**TANAKA, Noriyuki**  
 (JSP04/09P/A06-007 1600)  
**TANAKA, Noriyuki**  
 (JSP04/09P/A06-009 1700)  
**TANAKA, Noriyuki**  
 (JSP04a/09P/D-002 1400-095)  
**TANAKA, Satoru**  
 (JSS06a/08P/D-022 1400-100)  
**TANAKA, Tadashi**  
 (HW06/07A/C31-005 1110)  
**TANAKA, Tadashi**  
 (HW01/10P/C26-005 1520)  
**TANAKA, Takashi**  
 (GAILI.07/09A/A14-004 1030)  
 (GAILI.05/07A/A06-005 1000)  
**TANAKA, Takashi**  
 (GAVI.02/07A/A07-004 1050)  
**TANAKA, Takashi**  
 (GAILI.06/07P/D-001 1400-121)  
**TANAKA, Tatsuya**  
 (JSM14/09P/D-025 1400-089)  
**TANAKA, Tomoyki**  
 (JSP04/09P/A06-009 1700)  
**TANAKA, Tomoyuki**  
 (JSP04/09P/A06-010 1715)  
**TANAKA, Yoshikazu**  
 (GAV.06/09P/D-014 1400-167)  
**TANAKA, Yoshimasa**  
 (GAILI.10/11A/D-009 0830-083)  
 (GAILI.10/11A/D-007 0830-081)  
**TANAKA, Yoshinobu**  
 (JSM14/09P/D-009 1400-073)  
 (JSM14/09P/D-025 1400-089)  
**TANAKA, Yoshiyuki**  
 (JSG01/07A/A01-011 1150)  
**TANAKA, Yukitaka**  
 (GAILI.11/09A/A15-007 1120)  
**TANAKAMARU, Haruya**  
 (HW08/07A/C28-004 1010)  
 (HW08/07A/C28-007 1130)  
**TANG, C.L.**  
 (JSP04/09A/A06-009 1210)  
**TANG, Changyuan**  
 (HS02/07A/C24-003 1115)  
 (HS04/07P/C30-003 1505)  
**TANG, Changyuan**  
 (HS04/07P/C30-002 1435)  
**TANG, Changyuan**  
 (HW01/10A/C26-009 1150)  
**TANG, DanLing (Lingzis)**  
 (JSG03/09P/D-007 1640-015)  
**TANG, Ji**  
 (GAI.08/08P/D-006 1400-141)  
**TANG, Ji**  
 (GAI.08/08A/A14-001 0830)  
**TANG, Wenqing**  
 (JSP06/07A/B21-002 0920)  
**TANG, Yi**  
 (SS04b/10P/D-037 1400-221)  
**TANG, Yingze**  
 (G04/08P/D-002)  
**TANI, Makoto**  
 (HS02/08P/C24-012 1715)  
 (HW01/09P/D-042 1400-233)  
 (HW01/09P/D-037 1400-228)  
**TANI, Shin**  
 (SS03/08A/D-103 0830-262)  
**TANIGUCHI, Hiroshi**  
 (JSP10/08P/B21-002 1430)  
**TANIGUCHI, Keisuke**  
 (JSG01/08P/D-029 1400-029)  
**TANIGUCHI, Kenji**  
 (MC03/09P/A07-005 1620)  
**TANIKAWA, Tomonori**  
 (JSH01/08P/D-009 1400-047)  
**TANIMOTO, Hiroshi**  
 (MI03/08A/B18-007 1110)  
**TANIMOTO, Toshiro**  
 (SS03/07A/A02-001 0900)  
**TANIMOTO, Youichi**  
 (JSP09/10P/B20-009 1630)  
**TANIMOTO, Youichi**  
 (JSP09/10P/B20-003 1445)  
**TANIOKA, Yuichiro**  
 (JSS07/10A/A02-005 0930)  
**TANIOKA, Yuichiro**  
 (JSS07a/09P/D-009 1700-110)  
**TANIOKA, Yuichiro**  
 (JSS07/10P/A02-009 1615)  
**TANISAWA, Hiro**  
 (HS03/08A/C26-005 0945)  
**TANJI, Hajime**  
 (HW02/11A/C31-007 1135)  
**TANK, S. Bulent**  
 (GAI.08/08P/D-007 1400-142)  
**TANK, S. Bulent**  
 (GAI.08/08A/A14-007 1050)  
**TANSKANEN, E.**  
 (GAILI.05/07A/A06-003 0930)  
**TANSKANEN, Eija**  
 (GAILI.05/08A/A06-002 0845)  
**TANTON, Trevor**  
 (HS02c/11P/D-013 1630-111)  
 (HS02/11A/C24-013 1133)  
**TAO, Wei**  
 (SS03/08A/D-046 0830-205)  
**TAPLEY, Byron**  
 (JSG02/09P/A05-007 1645)  
**TARAKANOV, Roman Z.**  
 (JSS06/09P/A04-003 1440)  
**Taranis team**  
 (GAILI.04/07P/A08-010)  
**TARDITI, Alfonso G.**  
 (GAILI.11/10P/D-005 1400-120)  
**TAREQ, Shafi Mohamad**  
 (MC12/07P/B19-006 1600)  
**TAREQ, Shafi Mohammad**  
 (MC12/07P/B19-005 1545)  
**TARITS, Pascal**  
 (JSA07/10A/A05-004 0940)  
**TARITS, Pascal**  
 (JSS06/09A/A04-006 1100)  
 (GAV.04/07P/A11-004 1510)  
**TARITS, Pascal**  
 (GAV.04/07A/A11-002 0930)  
**TARYANNIKOVA, Raisa V.**  
 (HS02a/07P/D-020 1545-166)  
 (HS02/07P/C24-020 1412)  
**TASE, Norio**  
 (HW05/10A/C31-001 0830)  
**TASE, Norio**  
 (HW06/07P/C31-001 1400)  
**TASHCHILIN, Sergey**  
 (MC08/08P/D-003 1400-159)  
**TASHIMA, Hayato**  
 (GAILI.11/09P/A15-006 1525)  
**TASSONE, Alejandro Alberto**  
 (JSA07/11A/D-047 0830-047)  
**TAT KOV, Genadiy I.**  
 (SW05/10A/D-005 0900-249)  
**TATEYAMA, Kazutaka**  
 (JSH01/08P/D-008 1400-046)  
**TATRALLYAY, M.**  
 (GAVI.03/08P/A16-003 1500)  
**TAUHID, Yudi I.**  
 (MC03/11P/D-009 1400-184)  
**TAUHID, Yudi Iman**  
 (MC03/11P/A07-003 1440)  
**TAUHID, Yudi Iman**  
 (MC17/11P/B23-006 1600)  
**TAUHID, Yudi Iman**  
 (MC03/10P/A07-008 1720)  
**TAUHID, Yudi Iman**  
 (MC03/11P/D-007 1400-182)  
**TAUPIN, Jean-Denis**  
 (JSM04/09P/D-006 1400-043)  
**TAVAKOLI, Farokh**  
 (G03/07P/D-013 1400-035)  
**TAVAKOLI, Farokh**  
 (G03/07P/D-012 1400-034)  
**TAVAKOLI, Farokh**  
 (SS03/08A/D-075 0830-234)  
**TAVAKOLI, Farokh**  
 (G03/07P/D-065 1400-087)  
**TAVERNIER, Gilles**  
 (G07/10P/D-001 1400-086)  
**TAYLOR, Chris**  
 (MI07/11A/B18-001 0830)  
**TAYLOR, Chris P.**  
 (MI03/08P/B18-007 1630)  
**TAYLOR, Fred W.**  
 (MC04/11A/B22-007 1045)  
**TAYLOR, K.**  
 (MC11/11A/B19-001 0830)  
**TAYLOR, Michael J.**  
 (GAILI.04/07P/A08-006 1605)  
**TAYLOR, Patrick T.**  
 (GAV.06/09P/D-009 1400-162)  
 (JSA07/11A/D-041 0830-041)  
**TAYLOR, Ralph C.**  
 (JSG01/08A/A01-002 0915)

## INDEX

- TAYMAZ, Tuncay**  
(SS03/07A/A02-009 1130)
- TAZAWA, Seiichi**  
(G02/07A/C25-014 1245)
- TCHELOCHKOV, Gennady**  
(GAI.08/08A/A14-004 0930)
- TCHEVERDA, Vladimir A.**  
(JSS07a/09P/D-012 1700-113)
- TCHIGUIRINSKAIA, Ioulia**  
(HW07/11P/D-015 1400-151)
- TCHIGUIRINSKAIA, Ioulia**  
(HW07/10P/C25-003 1445)
- TCHOUA, Felix**  
(HW01/10P/C26-004 1500)
- TEALEB, Ali**  
(JSG01/08P/D-028 1400-028)
- TEALEB, Ali**  
(SS03/08A/D-088 0830-247)
- Team Shikoku 2001**  
(SS03/07A/A02-006)
- TEBAKARI, Taichi**  
(HW08/07P/C28-005 1610)
- TEBAKARI, Taichi**  
(HW07/11P/D-006 1400-142)
- TEBAKARI, Taichi**  
(HW07/11P/D-001 1400-137)
- TEDESCHI, Gilles**  
(JSM03/09A/D-001 0830-035)
- TEJBLUM, Mikhail M.**  
(JSP11/07A/A10-009 1220)
- TEJEDOR, Begonia**  
(JSP08/09A/B19-011 1240)
- TEJEDOR, Begonia**  
(JSP08/09A/B19-010 1220)
- TEJEDOR, Luis**  
(JSP08/09A/B19-011 1240)
- TEJEDOR, Luis**  
(JSP08/09A/B19-010 1220)
- TELADA, Souichi**  
(G07/10P/D-013 1400-098)
- TENERELLI, Joseph E.**  
(JSP09/11P/B20-004 1500)
- TENG, Bill**  
(MC02/07P/D-002 1400-199)
- TENG, Jiwen**  
(SS03/08A/D-137 0830-296)
- TENG, Ta-liang**  
(SS04a/09P/D-022 1400-271)
- TENZER, Robert**  
(G03/07P/D-066 1400-088)
- TENZER, Robert**  
(G03/07P/D-067 1400-089)
- TEPLOV, Vadim Yurievich**  
(GAI.06/11P/D-003 1400-055)
- TER-ANANYAN, Marina**  
(SS05/10A/A13-009 1045)
- TERADA, Naoki**  
(GAI.07/11A/A12-004 0945)
- TERADA, Naoki**  
(GAI.V.03/08P/A16-005 1610)
- TERADA, Yukihiko**  
(JSS07b/10P/D-007 1700-053)  
(JSS07b/10P/D-006 1700-052)
- TERAQ, Toru**  
(MI05/09P/B17-006 1630)
- TERASAWA, Takanori**  
(JSM15/07P/D-001 1400-001)
- TERASAWA, Toshio**  
(GAI.08/10A/A16-001 0830)
- TERASAWA, Toshio**  
(GAI.V.02/07A/A07-001 0900)
- TERASAWA, Toshio**  
(GAI.V.02/07P/A07-003 1510)
- TERASAWA, Toshio**  
(GAI.05/07P/D-004 1400-102)  
(GAI.05/08A/A06-001 0830)  
(GAI.05/07P/D-019 1400-117)
- TERAZONO, Atsuko**  
(HW01/09A/C26-003 0950)
- TERINA, Galina Ivanovna**  
(GAI.06/11P/D-005 1400-057)
- TERRAY, Laurent**  
(MC11/11A/B19-010 1150)
- TERRINHA, Pedro**  
(JSS07/09A/A02-010 1130)
- TESHIBA, Michihiro**  
(MC02/07P/D-003 1400-200)  
(JSM14/09P/D-009 1400-073)
- TESHIMA, Minoru**  
(SS04a/09P/D-035 1400-284)
- TETT, Paul**  
(JSP07/08P/B17-001 1400)
- TETZLAFF, Gerd**  
(JSM14/08P/A05-001 1400)
- TETZLAFF, Gerd**  
(HS02/09A/C24-012 1200)
- TEUNISSEN, Peter J.G.**  
(G04/08P/D-006 1400-113)
- TEUNISSEN, Peter J.G.**  
(G04/07P/C25-003 1510)
- TEVES-COSTA, Paula**  
(SS04a/09P/D-049 1400-298)
- TEYSSÉDRE, Hubert**  
(MC05/07A/A09-006 1150)
- THAKUR, N.K.**  
(SS03/08A/D-131 0830-290)
- THANA, Boossarasiri**  
(JSM04/09P/B23-002 1430)
- THATCHER, Wayne**  
(SS03/07P/A02-011 1700)
- THEBAULT, Erwan**  
(GAV.05/08P/A11-009 1700)
- THERIOT, Michael E.**  
(GAI.07/11P/A12-001 1400)
- THIAGARAJAN, S.O.**  
(JSA07/11A/D-034 0830-034)
- THIEBAULT, Benoît**  
(GAI.11/09P/A15-012 1730)
- THIO, Hong Kie**  
(SS04/08A/A03-011 1115)
- THIRIA, Sylvie**  
(JSP06/07A/B21-001 0900)
- THIVOLLE-CAZAT, Emmanuelle**  
(JSP10/08P/D-009 1610-061)
- THIVOLLE-CAZAT, Emmanuelle**  
(JSP10/09P/B21-004 1500)
- THOMAS, Jeremy N.**  
(GAI.04/07P/A08-006 1605)
- THOMASON, Larry W.**  
(MI03/09A/D-001 0900-244)  
(MC05/07P/D-003 1400-210)  
(MI03/08A/B18-002 0850)
- THOMPSON, Anne M.**  
(MI03/08A/B18-006 1050)
- THOMPSON, Barbara J.**  
(GAI.V.04/09P/A16-002 1435)
- THOMPSON, David**  
(MI05/10A/B17-005 1040)
- THOMPSON, David W.J.**  
(MI05/10A/B17-007 1120)  
(MI05/10A/B17-002 0910)
- THOMPSON, David W.J.**  
(MC05/10P/A09-004 1530)
- THOMPSON, David W.J.**  
(MI05/09P/B17-002 1440)
- THOMPSON, Donald C.**  
(GAI.05/08A/A15-003 0920)
- THOMPSON, Donald C.**  
(GAI.05/07A/D-001 0830-017)
- THOMPSON, Lonie**  
(HS02b/10P/D-019 1630-140)  
(HS02/10A/C24-019 1157)
- THOMPSON, LuAnne**  
(JSP09/11A/B20-004 0930)
- THOMPSON, Scott**  
(GAI.05/08A/A06-004 0925)
- THOMSEN, F. M.**  
(GAI.04/07A/A08-009)
- THOMSEN, M.**  
(GAI.08/10A/A16-012 1210)
- THOMSEN, M.**  
(GAI.06/08P/A02-004 1515)
- THOMSEN, M.F.**  
(GAI.06/08P/A02-011 1725)
- THOMSEN, Michelle F.**  
(GAI.08/10A/A16-009 1115)
- THOMSEN, Michelle F.**  
(GAI.06/08P/A02-003 1450)
- THOMSON, Alan**  
(GAV.05/08A/A11-002 0900)  
(GAV.04/07A/A11-002 0930)
- THOMSON, Alan W.P.**  
(GAV.05/08P/A11-002 1430)
- THOMSON, Colin J.**  
(JSS06b/10P/D-011 1400-035)
- THOMSON, Richard E.**  
(JSS07b/10P/D-009 1700-055)
- THORNBRUGH, Casey**  
(MI05/10P/D-009 1400-175)
- THORNE, Richard M.**  
(GAI.14/07A/A12-005 1115)
- THORNTON, Hazel**  
(MC05/10A/A09-002 0900)
- THORPE, Alan J.**  
(JSM14/07A/A05-001 0915)
- THUBURN, John**  
(MC05/11A/A09-004 1000)
- THURBER, Clifford H.**  
(SS03/07A/A02-002 0915)
- TIAN, Jiwei**  
(JSP08/09P/B19-010 1740)
- TIAN, Lide**  
(HS02b/10P/D-020 1630-141)  
(HS02/10A/C24-020 1201)  
(HS02b/10P/D-019 1630-140)  
(HS02/10A/C24-019 1157)
- TIAN, Lide**  
(HS02b/10P/D-018 1630-139)  
(HS02/10A/C24-018 1153)
- TIAN, Lide**  
(HS02/07P/C24-027 1440)  
(HS02a/07P/D-027 1545-173)
- TIAN, Xiangrong**  
(HS02/09P/C24-006 1515)
- TIAN, Xiangrong**  
(HS02b/10P/D-022 1630-143)  
(HS02/10A/C24-022 1209)
- TIAN, Xue**  
(SW05/10A/D-007 0900-251)
- TIERCELIN, Jean-Jacques**  
(GAV.06/10P/A11-005 1520)
- TIGLAO, Robert B.**  
(SS04/07P/A03-006 1530)
- TIKHONCHUK, Elena A.**  
(JSS07/10A/A02-003 0900)
- TIKHONOV, Vladimir A.**  
(MC08/07A/B17-009 1205)
- TIKHONOVA, Olga V.**  
(JSG03/09P/D-015 1640-023)
- TIKHOTSKI, Sergei A.**  
(JSA07/11A/D-021 0830-021)
- TIKKU, Anahita A.**  
(JSG01/08A/A01-002 0915)
- TILCH, Nils**  
(HW07/11A/C25-002 0900)
- TIMBAL, Bertrand Olivier**  
(MC08/07A/B17-008 1150)
- TIMLIN, Michael S.**  
(JSP04b/10P/D-004 1400-023)
- TIMMEN, Ludger**  
(G02/07A/C25-004 0955)
- TIMOFEEV, Vladimir Yu.**  
(SW05/10A/D-005 0900-249)
- TIMUR, Ikramov**  
(SW04/09P/A13-007 1545)
- TING, Mingfang**  
(MC03/09P/A07-003 1520)  
(MC11/11A/B19-005 0950)  
(MC08/07A/B17-004 1030)
- TINMAKER, Md. Iqbal Rasul**  
(MI03/08A/B18-005 1030)
- TINTI, Stefano**  
(JSS07a/09P/D-011 1700-112)
- TINTI, Stefano**  
(JSS07a/09P/D-013 1700-114)  
(JSS07/10A/A02-010 1100)  
(JSS07a/09P/D-014 1700-115)
- TINTI, Stefano**  
(JSS07a/09P/D-001 1700-102)
- TIRUMALACHETTY, Harinarayana**  
(JSG02/09A/D-001 0830-001)
- TIRUMALACHETTY, Harinarayana T.**  
(SW03/10P/A04-011 1645)
- TITOV, VASILY V.**  
(JSS07/10P/A02-004 1445)
- TITOV, Vasily V.**  
(JSS07/10P/A02-002 1415)
- TIWARI, D.**  
(GAI.06/09A/A10-002 0920)  
(GAI.06/11P/D-001 1400-053)
- TIWARI, Dileep Kumar**  
(SS04b/10P/D-027 1400-211)
- TIWARI, V. M.**  
(JSA07/11A/D-042 0830-042)
- TIWARI, Virendra Mani**  
(JSA07/11A/D-039 0830-039)
- TO, Akiko**  
(JSS06a/08P/D-019 1400-097)
- TOBA, Tae**  
(HS02b/10P/D-002 1630-123)  
(HS02/10A/C24-002 1049)
- TOBATA, Masahiro**  
(JSS07b/10P/D-018 1700-064)
- TOBITA, Jun**  
(SS04b/10P/D-009 1400-193)
- TOBITA, Mikio**  
(G04/08P/D-027 1400-134)
- TOCHO, Claudia**  
(G03/07P/D-029 1400-051)
- TOCHO, Claudia Noemi**  
(G03/07P/D-031 1400-053)
- TODA, Shigeru**  
(SW03/10A/D-003 0830-238)  
(SW03/10A/D-004 0830-239)
- TODA, Shigeru**  
(SW03/10A/D-007 0830-242)
- TODA, Shinji**  
(SS03/08A/D-006 0830-165)
- TODA, Sigeru**  
(SW03/10A/D-002 0830-237)
- TODINI, Ezio**  
(HW07/10P/C25-013 1730)
- TOFFOLETTO, Frank R**  
(GAI.06/08P/A02-005)
- TOH, Hiroaki**  
(GAI.08/08P/D-008 1400-143)
- TOH, Hiroaki**  
(GAI.08/08A/A14-005 0950)
- TOKINAGA, Hiroki**  
(JSP09/10P/B20-003 1445)
- TOKUCHI, Naoko**  
(HW01/09P/D-043 1400-234)
- TOKUCHI, Naoko**  
(HW01/10P/C26-001 1400)
- TOKUMARU, Munetoshi**  
(GAI.09/11P/A11-007 1640)
- TOKUYAMA, Hidekazu**  
(SS03/08A/D-122 0830-281)
- TOLAK, Elif**  
(GAI.08/08A/A14-007 1050)  
(GAI.08/08P/D-007 1400-142)
- TOLSON, Robert H.**  
(GAI.07/11P/A12-001 1400)
- TOMASELLA, Javier**  
(MC03/10A/A07-003 0930)
- TOMIKAWA, Yoshihiro**  
(MC05/09P/A09-006 1600)
- TOMITA, Hiroyuki**  
(JSP09/11A/B20-008 1045)
- TOMITA, Tomohiko**  
(MI05/10P/B17-009 1730)
- TOMOSUGI, Kunio**  
(HW07/10P/C25-004 1500)  
(HW07/11P/D-037 1400-173)  
(HW07/11P/D-021 1400-157)
- TONBOE, Rasmus T.**  
(JSH01/08P/D-005 1400-043)
- TONEGAWA, Takashi**

- (JSS06a/08P/D-017 1400-095)  
**TONEGAWA, Takashi**  
 (JSS06a/08P/D-016 1400-094)  
**TONEGAWA, Yutaka**  
 (GAI.10/11A/D-015)  
**TONEGAWA, Yutaka**  
 (GAI.06/10A/A01-011 1145)  
**TONG, Lizhu**  
 (GAI.04/09A/D-006 0830-142)  
**TOOLE, John**  
 (JSP06/07P/B21-007 1640)  
**TOOLE, John M.**  
 (JSP09/10A/B20-007 1115)  
**Tor Working Group,**  
 (JSS06/09P/A04-004 1500)  
**TORBERT, Roy B.**  
 (GAI.05/07A/A06-004 0945)  
**TORCAL, Federico**  
 (SS03/08A/D-025 0830-184)  
**TORFS, Paul**  
 (HW08/07P/C28-006 1630)  
**TORGE, Wolfgang**  
 (U7/11A/D32-001 0900)  
**TORITANI, Hitoshi**  
 (HW04/09A/C31-008 1140)  
**TORKAR, Klaus**  
 (GAI.11/09A/A15-003 0940)  
**TOROPOV, Pavel Alekseevich**  
 (MC12/07P/B19-004 1515)  
**TORTA, J. Miquel**  
 (GAI.10/09P/A11-006 1515)  
**TORTA, Joan Miquel**  
 (GAV.05/08P/A11-011 1740)  
**TORYANNIKOVA, Raisa V.**  
 (HS02a/07P/D-019 1545-165)  
 (HS02/07P/C24-019 1408)  
**TOSHIO, Hiroshima**  
 (JSA07/11A/D-016 0830-016)  
**TOTH, Gyula**  
 (G02/07A/C25-007 1100)  
**TÓTH, Gyula**  
 (G03/07P/D-006 1400-028)  
**TOTSUKA, Takehiro**  
 (JWH01/09P/C30-008 1650)  
**TOUHEI, Masaru**  
 (HS01/09P/C29-006 1540)  
**TOYA, Yuzo**  
 (SS03/08A/D-116 0830-275)  
 (JSG01/08P/D-017 1400-017)  
**TOYAMA, Yoko**  
 (JSM10/09P/D-002)  
**TOYODA, Eizi**  
 (MC04/11P/B22-003 1445)  
**TOYODA, Eizi**  
 (SW05/10A/D-008 0900-252)  
**TOYODA, Kazuhiro**  
 (GAI.11/09P/A15-003 1440)  
**TOZE, Simon**  
 (HS04/07P/C30-004 1555)  
 (HS04/07A/C30-002 1005)  
**TRABANT, Dennis**  
 (HS01/09P/D-003 1400-170)  
**TRAMONTIN, Marco**  
 (JSP08/09A/B19-001 0900)  
**TRAVNICEK, Pavel**  
 (GAI.14/07A/A12-003 1015)  
**TREEBUSHNY, Dimitri**  
 (HW08/07A/C28-002 0930)  
**TREMBLAY, Bruno**  
 (JSP04b/10P/D-002 1400-021)  
**TRENBERTH, Kevin E.**  
 (JSP09/10A/B20-009 1145)  
**TREPTE, Chip L.**  
 (MI03/09A/D-001 0900-244)  
**TREPTE, Chip R.**  
 (MI03/08A/B18-002 0850)  
**TREUMANN, Rudolf**  
 (GAI.05/07P/D-007 1400-105)  
**TRICHTCHENKO, Larisa**  
 (JSP11/07A/A10-007 1130)  
**TRIEU, Cao Dinh**  
 (SS03/08A/D-126 0830-285)  
**TRIMBAKE, H.K.**  
 (MI09/08P/B22-008 1700)  
**TRIMMER, Ron**  
 (G03/07P/D-035 1400-057)  
**TRIPATHI, Jayant Nath**  
 (SS04b/10P/D-027 1400-211)  
**TRIPATHI, Jayant Nath**  
 (SS04b/10P/D-028 1400-212)  
**TRIPATHI, Jayant Nath**  
 (SS03/08A/D-130 0830-289)  
**TRISHCHENKO, Alexander P.**  
 (MI09/09A/B22-003 0940)  
**TRISKOVA, Ludmila**  
 (GAI.05/07A/D-004 0830-020)  
**TRIYOSO, Wahyu**  
 (SS04/09A/A03-005 1000)  
**TRIYOSO, Wahyu**  
 (JSS06b/10P/D-016 1400-040)  
 (SS03/08A/D-044 0830-203)  
**TROCH, Peter A.**  
 (HW07/10P/C25-008 1615)  
 (HW08/07P/C28-006 1630)  
**TROESTER, Joseph W.**  
 (HW01/10P/C26-002 1420)  
**TROSTDORF, Carla R.**  
 (JSM04/09P/D-012 1400-049)  
**TROTIGNON, Jean Gabriel**  
 (GAI.03/08A/A16-005 1040)  
 (GAI.03/09A/A16-004 1010)  
**TROUSOV, Sergey V.**  
 (SW05/10P/A13-001 1400)  
**TRUHLIK, Vladimir**  
 (GAI.05/07A/D-004 0830-020)  
**TRUONG, Hao Quang**  
 (U7/11P/D32-001 1400)  
**TRUPIN, Andrew**  
 (JSG01/08A/A01-012 1205)  
**TRUSHIN, A.S.**  
 (JSA08/09P/A08-009 1730)  
**TSAI, Chu-Chuan P.**  
 (SS04a/09P/D-011 1400-260)  
**TSAI, Lung-Chih**  
 (GAI.06/10A/A01-008 1050)  
**TSAI, Victor**  
 (JSS07/10P/A02-010 1630)  
**TSAI, W.H.**  
 (GAI.06/09P/A10-011 1710)  
**TSCHERNING, C.C.**  
 (G03/07P/D-023 1400-045)  
**TSCHERNING, Carl Christian**  
 (G03/07P/D-060 1400-082)  
**TSCHERNING, Carl Christian**  
 (G04/08P/D-017 1400-124)  
**TSCHERNING, Christian**  
 (G03/07P/D-024 1400-046)  
**TSELENTIS, G-Akiss**  
 (SS04a/09P/D-043 1400-292)  
**TSELIODIS, George**  
 (MC11/10P/B19-004 1500)  
**TSENG, C.-L.**  
 (GAI.06/11P/D-008 1400-060)  
**TSHOSO, Gomotsang**  
 (GAV.06/10P/A11-005 1520)  
**TSIRULNIK, Lev B.**  
 (JSA08/10P/D-002 1400-002)  
 (JSA08/09A/A08-010 1215)  
**TSOU, Chih-Hua**  
 (MC17/10P/B23-009 1700)  
**TSUBOKAWA, Tsuneya**  
 (G02/07A/C25-014 1245)  
**TSUBOKI, Kazuhisa**  
 (JSM14/09P/D-007 1400-071)  
**TSUBOKI, Kazuhisa**  
 (JSM14/07A/A05-004 1040)  
 (JSM14/07P/A05-002 1435)  
 (MC03/11A/A07-007 1110)  
 (JSM14/09P/D-013 1400-077)  
**TSUBOKI, Kazuhisa**  
 (JSM14/09P/D-012 1400-076)  
**TSUBOTA, Atsuo**  
 (JSM14/09P/D-026 1400-090)  
**TSUBOUCHI, Ken**  
 (GAI.02/07P/A07-006 1710)  
**TSUCHIHARA, Takeo**  
 (HW05/10P/D-005 1400-160)  
**TSUCHIYA, Fuminori**  
 (GAI.14/08A/D-006 0830-150)  
**TSUCHIYA, Fuminori**  
 (GAI.14/07P/A12-009 1705)  
 (GAI.06/08P/A02-012 1740)  
**TSUCHIYA, K.**  
 (JSG03/09P/D-006 1640-014)  
**TSUDA, Toshihiko**  
 (MC05/11P/A09-007 1640)  
 (MI09/08P/D-002 1400-155)  
 (MC05/11P/A09-008 1700)  
 (MI09/08P/B22-005 1600)  
**TSUDA, Toshihiko**  
 (MC05/11P/A09-006 1620)  
**TSUEI, Gwo-Chyang**  
 (G03/07P/D-056 1400-078)  
**TSUJI, Hiroyuki**  
 (MC12/07P/B19-006 1600)  
**TSUJI, Koichiro**  
 (MC05/11P/A09-002 1430)  
**TSUJI, Yoshinobu**  
 (JSS07/10A/A02-006 0945)  
**TSUJI, Yoshinobu**  
 (JSS07/10A/A02-002 0845)  
 (JSS07a/09P/D-008 1700-109)  
**TSUJIMURA, Maki**  
 (HW06/07A/C31-005 1110)  
 (HW01/09P/D-034 1400-225)  
**TSUJIMURA, Maki**  
 (HW06/07P/C31-001 1400)  
**TSUJINO, Fumitaka**  
 (MC05/11P/A09-005 1530)  
**TSUKAMOTO, Osamu**  
 (JSP09/10A/B20-002 0930)  
**TSUKIYAMA, Hiroshi**  
 (JSS07/09P/A02-005 1500)  
**TSUMURA, Noriko**  
 (SS03/08A/D-008 0830-167)  
**TSUNO, Seiji**  
 (SS04/08A/A03-007 1000)  
**TSUNODA, R.**  
 (GAI.06/09P/A10-002 1420)  
**TSUNODA, Roland T.**  
 (GAI.06/09P/A10-004 1500)  
**TSUNODA, Roland T.**  
 (GAI.06/09P/A10-009 1640)  
**TSURU, Tetsuro**  
 (SS03/08A/D-107 0830-266)  
**TSURU, Tetsuro**  
 (SS03/08A/D-109 0830-268)  
**TSURU, Tetsuro**  
 (SS03/08A/D-009 0830-168)  
**TSURU, Tetsuro**  
 (SS03/08A/D-058 0830-217)  
**TSURUDA, Koichiro**  
 (GAI.05/07P/D-010 1400-108)  
**TSURUTA, Haruo**  
 (JSM04/09A/B23-001 0900)  
**TSURUTA, Seiitsu**  
 (G02/07A/C25-011 1200)  
**TSURUTA, Seiitsu**  
 (G02/07A/C25-014 1245)  
**TSURUTANI, B.T.**  
 (GAI.07/09A/A14-008 1210)  
**TSURUTANI, Bruce**  
 (GAI.09/11P/A11-008 1710)  
**TSURUTANI, Bruce T.**  
 (GAI.07/09P/A14-005 1530)  
**TSUTSUI, Junichi**  
 (MC02/07A/B20-004 1105)  
**TSUTSUI, Minoru**  
 (GAI.11/09P/A15-009 1645)  
**TSUTSUI, Tomoki**  
 (SW03/10A/D-007 0830-242)  
**TSUTSUI, Tomoki**  
 (SW03/10A/D-003 0830-238)  
**TSUTSUMI, Masaki**  
 (MC04/11A/B22-004 0930)  
**TSUTSUMI, Shuichi**  
 (GAI.06/10A/A01-007 1030)  
**TSVETKOV, Youry P.**  
 (U7/11P/D32-001 1400)  
**TSVETKOVA, T.**  
 (JSS06a/08P/D-012 1400-090)  
**TSYBULYA, Konstantin**  
 (GAI.05/08A/A15-006 1100)  
**TSYGANKOV, Denis**  
 (JSP10/10P/B21-010 1740)  
**TSYGANKOVA, Irina P.**  
 (JSA07/11A/D-006 0830-006)  
**TUCCI, CARLOS E.M.**  
 (HS02/08A/C24-010 1115)  
**TUCKI, Andrirej**  
 (HW01/09P/D-006 1400-197)  
**TUGEM, Fred Alex**  
 (SW03/10P/A04-003 1430)  
**TUGWOOD, Bryan**  
 (JSM14/09P/D-021 1400-085)  
**TULUKA, Mavonga**  
 (JSP11/08A/A10-009 1220)  
**TUNCER, M. Kemal**  
 (GAI.08/08P/D-007 1400-142)  
**TUNCER, Mustafa Kemal**  
 (GAI.08/08A/A14-007 1050)  
**TURGUT, Bulent**  
 (JSG01/08P/D-013 1400-013)  
**TURKELLI, Niyazi**  
 (JSS06/10A/A04-008 1110)  
**TURKEZER, Ali**  
 (JSG01/08A/A01-001 0900)  
**TURNER, John**  
 (JSM10/07P/B23-006 1620)  
**TURNER, Jon**  
 (GAV.05/08A/A11-009 1150)  
**TURNER, Niescja E.**  
 (GAI.09/11P/A11-004 1510)  
**TUSBOKI, Kazuhisa**  
 (JSM14/07A/A05-008 1200)  
**TVEITO, Ole Einar**  
 (MI05/10P/D-005 1400-171)  
**TYAGI, Sunil Kumar**  
 (HS02a/07P/D-028 1545-174)  
 (HS02/07P/C24-028 1444)  
**TYLER, Robert H.**  
 (GAV.04/07P/A11-005 1530)  
**TYUPKIN, Yuri S.**  
 (SW05/10P/A13-006 1520)  
**TZIAVOS, I.N.**  
 (G02/07A/C25-007 1100)  
**TZIAVOS, Ilias N.**  
 (G03/07P/D-028 1400-050)  
 (G04/07P/C25-006 1640)

## U

- UCHIDA, Hiroshi**  
 (JSP06/08A/B21-002 0920)  
**UCHIDA, Taro**  
 (HW01/10P/C26-003 1440)  
 (HW06/07A/C31-002 0930)  
 (HW01/09P/D-040 1400-231)  
**UCHIMOTO, Keisuke**  
 (JSP10/08P/D-001 1610-053)  
 (JSP10/08P/D-006 1610-058)  
**UCHIYAMA, Akinori**  
 (GAV.06/10A/A11-008 1110)  
**UCHIYAMA, Takao**  
 (MC08/07A/B17-005 1045)  
 (MC08/07A/B17-002 1000)  
**UEDA, Hiromasa**  
 (MC02/08P/B20-001 1400)  
**UEDA, Hiromasa**  
 (JSP10/09A/B21-010 1220)  
**UEDA, Shingo**  
 (JSM04/09A/B23-001 0900)  
**UEHIRA, Kenji**  
 (SS03/08A/D-120 0830-279)  
**UEHIRA, Kenji**  
 (SS03/08A/D-100 0830-259)  
**UEHIRA, Kenji**  
 (SS03/08A/D-017 0830-176)  
**UENO, Mitsuru**

## INDEX

- (MC02/07P/D-007 1400-204)  
(MC02/07P/D-001 1400-198)
- UENOBE, Fumi**  
(MC02/07P/B20-005 1540)
- UENZELMANN-NEBEN, Gabriele**  
(SS03/08A/D-094 0830-253)
- UETAKE, Tomiichi**  
(SS04b/10P/D-001 1400-185)
- UETAKE, Tomiichi**  
(SS04a/09P/D-026 1400-275)
- UEYOSHI, Kyozo**  
(JSP09/11P/B20-002 1415)
- UGALDE, Arantza**  
(SS03/08A/D-130 0830-289)
- UGALDE, Arantza**  
(SS03/08A/D-033 0830-192)
- UHLENBROOK, Stefan**  
(HW07/11A/C25-002 0900)  
(HW06/07A/C31-001 0910)
- UHLHORN, Eric W.**  
(JSP09/11P/B20-006 1545)
- UJUANBI, Omeimen E.**  
(HW05/10P/D-001 1400-156)
- UKHORSKIY, Alexander Y.**  
(GAI11.07/09A/A14-006 1130)
- UKI, Hisanaga**  
(SS03/08A/D-005 0830-164)
- UKITA, Jinro**  
(JSM10/08A/B23-003 0930)
- UKITA, Jinro**  
(MI05/11A/B17-004 0930)
- ULICH, Thomas**  
(JSA01/08P/A12-006 1640)
- ULOMOV, Valentin I.**  
(SS04b/10P/D-012 1400-196)
- ULRICH, Wolfgang**  
(JSP09/11P/B20-007 1600)
- ULZIIBAT, Munkhuu**  
(SS04b/10P/D-030 1400-214)
- UMAKOSHI, Kodo**  
(SS03/08A/D-017 0830-176)
- UMAROV, Nariman M.**  
(HS02a/07P/D-019 1545-165)  
(HS02/07P/C24-019 1408)
- UMEDA, Takayuki**  
(GAI11.07/09P/A14-004 1510)
- UMEDA, Takayuki**  
(GAI11.05/08A/A06-008 1055)
- UMEDA, Yasuhiro**  
(JSG01/07P/A01-007 1530)
- UMEMOTO, Yasuko**  
(JSM14/09P/D-009 1400-073)
- THE UNESCO/IGCP/IGCP 414 Project Team**  
(SW04/09P/A13-011)
- UNGARISH, Marius**  
(JSP10/09P/B21-001 1400)
- UNGARISH, Marius**  
(JSP10/10P/B21-008 1700)
- UNGARISH, Marius**  
(JSP10/09P/B21-002 1420)
- UNO, Hirokatsu**  
(JSP04/09A/A06-006 1110)
- UNSWORTH, Martyn J.**  
(GAI.08/08A/A14-003 0910)
- UOZUMI, Teiji**  
(GAI11.10/11A/D-016 0830-090)  
(GAI11.10/11A/D-018 0830-092)  
(GAI11.10/11A/D-020 0830-094)  
(GAI11.10/11A/D-014 0830-088)
- URAEVSKIY, Evgeniy Petrovich**  
(JSP06/07P/D-004 1400-011)
- URATSUKA, Seiho**  
(JSG03/09P/D-019 1640-027)
- URITSKY, Vadim M.**  
(GAI11.07/09A/A14-003 0950)
- USAMI, Tatsuo**  
(SS04/08A/A03-012 1130)
- USHIJIMA, Keisuke**  
(JSA07/11A/D-046)
- USHIJIMA, Keisuke**  
(GAV.06/10P/A11-007 1620)
- USHIO, Tomoo**  
(MC04/11A/B22-004 0930)
- USHIYAMA, Tomoki**  
(MC17/11P/B23-003 1440)
- USLU, Burak**  
(JSS07/09P/A02-009 1615)
- USLU, Burak**  
(JSS07a/09P/D-018 1700-119)
- USUI, Hideyuki**  
(GAI11.11/09P/A15-011 1715)
- USUI, Hideyuki**  
(GAI11.11/09P/A15-006 1525)  
(GAI11.11/10P/D-004 1400-119)
- USUI, Hideyuki**  
(GAI11.11/09A/A15-008 1135)
- USUL, Nurunnisa**  
(HS02c/11P/D-003 1630-101)  
(HS02/11A/C24-003 1053)
- UTADA, Hisashi**  
(GAI.08/08P/D-008 1400-143)
- UTADA, Hisashi**  
(GAI.08/08P/D-001 1400-136)  
(JSS06a/08P/D-008 1400-086)  
(JSG01/08P/D-018 1400-018)
- UTADA, Hisashi**  
(GAI.10/09P/D-005 1615-124)
- UTADA, Hisashi**  
(GAI.08/08P/D-006 1400-141)
- UTADA, Hisashi**  
(GAI.08/08P/D-009 1400-144)
- UTSUGI, Mitsuru**  
(GAV.05/09P/D-006 1400-150)
- UTSUGI, Mitsuru**  
(GAV.06/09P/D-014 1400-167)
- UTTAL, Taneil**  
(JSM10/07P/B23-003 1500)
- UYEDA, Hiroshi**  
(JSM14/08A/A05-004 0940)
- UYEDA, Hiroshi**  
(JSM14/07P/A05-005 1620)  
(JSM14/08A/A05-009 1130)  
(JSM14/09P/D-013 1400-077)  
(MC03/11P/D-010 1400-185)  
(MC03/11P/D-017 1400-192)
- UYEDA, Hiroshi**  
(JSM03/08A/A13-004 1000)
- UYESHIMA, Makoto**  
(JSA07/10P/A05-002 1420)
- UYESHIMA, Makoto**  
(GAI.08/08P/D-006 1400-141)
- UZUKA, Naoaki**  
(JSP04a/09P/D-006 1400-099)
- (GAI11.05/07A/A06-004 0945)
- VAKULENKO, Nadejda Viktorovna**  
(MC12/08P/B19-008 1715)
- VALIEV, Khidoyat**  
(HS02a/07P/D-038 1545-184)  
(HS0207P/C24-038 1524)
- VALLADARES, C.E.**  
(GAI.06/10A/A01-003 0905)
- VALLEJOS, A.**  
(HS01/09P/C29-004 1500)
- VAN DAM, Tonie M.**  
(JSG02/09P/A05-005 1555)
- VAN DER HILST, Rob D.**  
(JSS06/09P/A04-011 1740)
- VAN DER HOEK, Wim**  
(HS04/07P/C30-001 1405)
- VAN DER KAMP, Garth**  
(HW01/09A/C26-008)
- VAN DER LAAT, Rodolfo**  
(JSG01/08P/D-012 1400-012)
- VAN DER VELDEN, Arie J.**  
(SW03/10P/A04-001 1400)
- VAN EYKEN, Anthony**  
(GAI.05/08P/A15-002 1430)
- VAN HEIJST, GertJan F.**  
(JSP10/10A/B21-005 1030)
- VAN HUNEN, Jeroen**  
(JSS06/09P/A04-001 1400)
- VAN LIER, Jules B.**  
(HS04/07A/C30-001 0910)
- VAN LOON, Emiel E.**  
(HW08/07P/C28-006 1630)
- VAN WOERT, Mike L.**  
(JSH01/07A/C27-006 1220)
- VANDEMBERG, Nancy**  
(G07/10P/D-014 1400-099)
- VANDRAPU, Subrahmanyam**  
(JSA07/11A/D-033 0830-033)
- VANHELLEMONT, Filip**  
(JSG03/10A/A12-009 1140)
- VANICEK, Petr**  
(G03/07P/D-066 1400-088)
- VANICEK, Petr**  
(G03/07P/D-067 1400-089)
- VANLOON, Harry**  
(JSA08/09A/A08-008 1130)
- VARGAS-JIMENEZ, Carlos A.**  
(SS03/08A/D-033 0830-192)
- VARGIN, Pavel N.**  
(MI05/11P/B17-003 1440)
- VARIKODEN, Hamza**  
(MC17/10P/B23-008 1645)
- VARLAMOV, Dmitry A.**  
(SW05/10P/A13-001 1400)
- VASHCHILLOV, Yury Ya.**  
(SS03/08A/D-073 0830-232)  
(JSA07/11A/D-006 0830-006)  
(JSA07/10A/A05-010 1210)
- VASIC, Ratko**  
(MC11/11P/B19-002 1420)
- VASIC, Slavko**  
(JSM14/09A/A05-003 0955)
- VASILENKO, Nikolay F.**  
(JSG01/08P/D-009 1400-009)
- VASILIEV, Aleksey Yu.**  
(JSP10/08P/D-015 1610-067)
- VASILYEVA, Victoria G.**  
(GAI11.07/10P/D-006 1400-111)
- VASSELI, N.**  
(HW04/09P/C31-002 1420)
- VASSILIADIS, Dimitris**  
(GAI.05/08A/A15-001 0830)
- VASSILIADIS, Dimitris**  
(GAI11.07/09A/A14-003 0950)
- VAUCLAIR, Fabrice M.**  
(JSP09/10P/B20-004 1500)
- VAUGHAN, David G.**  
(JWH01/09A/C30-005 1020)
- VAVRUS, Steve**  
(JSP04/10A/A06-004 1030)
- VAVULIN, Stanislav V.**  
(MC08/07P/B17-008 1605)
- VECCHI, Gabriel Andres**  
(MC03/09A/A07-005 1050)  
(MI05/10P/B17-003 1500)  
(MC17/11P/B23-001 1400)
- VECSEY, Ludek**  
(JSS06b/10P/D-012 1400-036)
- VEERAPPAN, Ramamurthy**  
(JSM04/09P/D-004 1400-041)
- VELASCO FUENTES, Oscar U.**  
(JSP10/10P/B21-005 1530)
- VELICOGNA, Isabella**  
(JSM11/10A/B18-003 0940)
- VELIKIN, Sergei Aleksandrovich**  
(JSH01/07P/C27-001 1400)
- VELLA, Muhammad N.J.P.**  
(G03/07P/D-030 1400-052)
- VELLANTE, Massimo**  
(GAI11.10/11A/D-003 0830-077)  
(GAI11.10/11A/A01-009 1030)
- VENNERSTRÖM, Susanne**  
(GAV.05/08P/A11-010 1720)
- Venus Exploration Working Group**  
(MC04/11A/B22-002)
- VENUTI, Giovanna**  
(G04/08A/C25-008 1140)
- VERA, Carolina**  
(MC08/07P/B17-007 1550)
- VERBERIEN, R.**  
(SS04b/10P/D-049 1400-233)
- VERDUN, Andreas**  
(U7/11A/D32-003 1000)  
(G07/10P/A03-001 1400)
- VERGOS, Georgios S.**  
(G03/07P/D-028 1400-050)  
(G03/07P/D-029 1400-051)
- VERHAGEN, Sandra**  
(G04/08P/D-006 1400-113)
- VERHOEST, Niko E.C.**  
(HS03/07P/C26-009 1615)
- VERIGIN, M.**  
(GAI11.06/07P/D-018 1400-138)
- VERIGIN, M.I.**  
(GAIN.03/08P/A16-003 1500)
- VERMA, S.K.**  
(GAI.10/09A/A11-012 1215)
- VERMA, Saurabh Kumar**  
(GAI.10/09A/A11-007 1100)  
(GAI.10/09P/D-015 1615-134)  
(JSS06b/10P/D-006 1400-030)
- VERMA, Saurabh Kumar**  
(GAI.10/09A/A11-010 1145)
- VERMEERSEN, Bert**  
(JSG01/07P/A01-003 1430)
- VERRON, Jacques**  
(JSP10/08P/D-009 1610-061)
- VERSEGHY, D.**  
(JWH01/09P/C30-001)
- VERSHININ, E.F.**  
(GAI11.10/11A/D-016 0830-090)
- VERSIANI, Bruno Rabelo**  
(HS02b/10P/D-031 1630-152)  
(HS02/10P/C24-008 1543)
- VESPE, Francesco**  
(JSP11/08A/A10-008 1200)
- VIDALE, Pier Luigi**  
(MI07/11P/B18-003 1440)  
(MC11/11P/B19-005 1520)  
(MC08/07P/B17-006 1535)
- VIDYAKINA, Svetlana Vladimirovna**  
(MI07/11P/B18-007 1620)  
(JSP04b/10P/D-005 1400-024)
- VIEIRA, Luis Eduardo**  
(GAI11.09/11P/A11-008 1710)
- VIEIRA, Luis Eduardo Antunes**  
(GAI11.09/11A/A11-002 0900)
- VIEIRA, Luiz Eduardo Antunes**  
(JSA08/10P/D-003 1400-003)
- VIENNE, Julien**  
(G02/07A/C25-012 1215)

- VIEUX, BAXTER E.**  
(HS03/08P/C26-001 1400)
- VIEUX, Baxter E.**  
(HS03/08A/C26-001 0830)
- VIEUX, Baxter E.**  
(HS03/07A/C26-007 1100)
- VIEUX, Baxter Ernest**  
(HW07/10P/C25-012 1715)
- VIEUX, JEAN E.**  
(HS03/08P/C26-001 1400)
- VIEUX, Jean E.**  
(HW07/10P/C25-012 1715)
- VIGER, Roland J.**  
(HW08/07P/C28-004 1550)
- VIGO, Isabel**  
(JSG01/07A/A01-009 1120)
- VIHMA, Timo**  
(JSM10/07P/B23-002 1440)
- VIJAYA RAO, V.**  
(GAI.10/09A/A11-012 1215)
- VIJAYAKUMAR, R.**  
(MI09/09P/B22-004 1500)
- VILAS, Juan Francisco**  
(JSA07/11A/D-047 0830-047)
- VILIBIC, Ivica**  
(JSP09/10P/B20-007 1545)  
(JSM03/08A/A13-007 1120)
- VILJANEN, Ari**  
(GAI.10/09P/A11-004 1445)
- VILLAIN, Jean-Paul**  
(GAI.06/10A/A01-011 1145)
- VILLANTE, Umberto**  
(GAI.10/11A/A01-009 1030)
- VIMEUX, F.**  
(MC12/08A/B19-002 1000)
- VINAY, Gaetan**  
(JSG03/09P/D-003 1640-011)
- VINCENT, Robert**  
(MC05/10A/A09-007 1100)
- VINCENT, Robert A.**  
(MC05/10A/A09-008 1130)
- VINH, Hoang Quang**  
(JSG03/10A/A12-006 1040)
- VIRTANEN, Heikki J.**  
(JSG01/08A/A01-009 1120)
- VISHNUHOTLA, Chakravarthi**  
(JSG02/09A/D-001 0830-001)
- VISSER, Pieter**  
(G03/07P/D-024 1400-046)
- VIZY, Edward Kalman**  
(MC03/09A/A07-002 0930)
- VLADIMIROVICH, Gavrikov Alexander**  
(JSP09/11A/B20-011 1145)
- VOCADLO, L.**  
(U5/07A/D32-001 0900)
- VOEROES, Zoltan**  
(GAI.05/08A/A06-003 0900)
- VOGEL, Baerbel**  
(MC05/07A/A09-002 0930)
- VOLANT, Philippe**  
(SS04/07A/A03-009 1145)
- VOLGYESI, Lajos**  
(G03/07P/D-020 1400-042)
- VOLKOV, Viktor A.**  
(SS03/08A/D-048 0830-207)
- VOLOSHCHUK, Volodymyr M.**  
(HS02/07A/C24-009 0932)  
(HS02a/07P/D-009 1545-155)
- VOLTI, Theodora**  
(SW04/09P/A13-010 1630)
- VOLWERK, Martin**  
(GAI.05/08A/A06-003 0900)
- VOLWERK, Martin**  
(GAI.05/07P/D-007 1400-105)
- VON BLOH, Werner**  
(JSS06b/10P/D-022 1400-046)
- VON FRESE, Ralph R.B.**  
(JSA07/11A/D-041 0830-041)  
(GAV.06/09P/D-009 1400-162)
- VON HILLEBRANDT, Ms. Christa**  
(JSS07/10A/A02-014 1200)
- VON STORCH, Hans**  
(JSP08/09P/B19-005 1600)  
(MC08/07A/B17-007 1135)
- VON STORCH, Jin-Song**  
(MI05/09A/B17-002 0940)  
(JSP09/10P/B20-008 1615)  
(JSP10/09A/B21-004 1010)
- VONDRAK, Jan**  
(G07/10P/D-010 1400-095)
- VONDRAK, Jan**  
(G07/10A/A03-004 1000)
- VORONINA, Tatjana A.**  
(JSS07a/09P/D-012 1700-113)
- VOROS, Zoltan**  
(GAI.05/07P/D-007 1400-105)
- VOROSMARTY, Charles**  
(HS02/07A/C24-014 0952)  
(HS02a/07P/D-014 1545-160)
- VOROSMARTY, Charles J.**  
(JSP04/09A/A06-002 0920)  
(HW01/09P/D-047 1400-238)
- VOROSMARTY, Charles J.**  
(HW06/08A/C31-003 1120)  
(JSM03/08P/A13-008 1640)
- VOSS, Peter**  
(JSS06/09P/A04-006 1600)
- VOSS, Peter**  
(JSS06/09P/A04-004 1500)
- VOULGARIS, George**  
(JSP08/09A/B19-005 1030)
- VOYTENKO, Yuriy M.**  
(GAI.V.02/07A/A07-003 1010)
- VREUGDENHIL, C.B.**  
(HS02/09P/C24-004 1445)
- VRUGT, Jasper A.**  
(HW08/08P/C28-003 1500)  
(HW08/08A/C28-001 0830)
- VRUGT, Jasper A.**  
(HW08/07A/C28-001 0900)
- VUAN, A.**  
(SS03/07A/A02-005 1030)
- VUCKOVIC, Vladan**  
(JSM14/08P/A05-007 1730)
- VUDHIVANICH, Varawoot**  
(HS02/11P/C24-004 1445)
- VUGLINSKY, Valery S.**  
(JSM10/08P/B23-003 1500)
- VUGLINSKY, Varely**  
(JWH01/10A/C30-005 0950)  
(JWH01/09P/C30-005 1520)
- VUJOVIC, Dragana**  
(JSM14/08P/A05-007 1730)
- VVGS, Gurunatha rao**  
(HW01/09P/D-048 1400-239)
- VYAGRESWARA RAO, M.B.S.**  
(JSA07/11A/D-039 0830-039)
- VYUSHKOVA, Tatyana Yu.**  
(MC05/09P/A09-010 1740)
- VYUSHKOVA, Tatyana Yu.**  
(JSA01/08A/A12-004 1025)
- WAHR, John**  
(JSM11/10A/B18-003 0940)
- WAHR, John M.**  
(JSG02/09P/A05-005 1555)
- WAINER, Ilana**  
(JSP09/10P/B20-004 1500)
- WAKABAYASHI, Makoto**  
(GAI.06/09P/A10-006 1530)
- WAKAMATSU, Tsuyoshi**  
(JSH01/08P/D-004 1400-042)
- WAKATSUCHI, Masaaki**  
(JSP09/10P/B20-010 1645)
- WAKAYAMA, Toshio**  
(MI09/08P/D-001 1400-154)
- WAKE, Geoffrey W.**  
(JSP10/09A/B21-005 1040)
- WALDER, Joseph S.**  
(JSS07/09P/A02-008 1600)
- WALKER, Alice**  
(SS03/08A/D-026 0830-185)
- WALKER, Anne E.**  
(JSH01/07P/C27-007 1620)  
(JSM10/07A/B23-003 1000)
- WALKER, John F.**  
(HW01/10P/C26-002 1420)
- WALKER, Raymond John**  
(GAI.14/07P/A12-004 1500)
- WALLACE, John M.**  
(MI05/09P/B17-001 1400)
- WALLENS, Sabine A.**  
(JSM04/09A/B23-007 1215)
- WALLING, Des E.**  
(HW02/11A/C31-005 1045)
- WALLING, Desmond Eric**  
(HS01/09A/C29-001 0900)
- WALSH, John E.**  
(JSM10/08A/B23-002 0910)
- WALSH, John E.**  
(JSP04/10P/A06-010 1720)
- WALSH, John E.**  
(JSM10/07P/B23-002 1440)
- WALSH, John E.**  
(JSP04b/10P/D-004 1400-023)  
(JSM10/08A/B23-001 0830)
- WALTER, Kevin**  
(JSM03/08A/A13-005 1040)
- WALTERSCHEID, Richard**  
(MC05/10A/A09-007 1100)
- WALTERSCHEID, Richard L.**  
(MC04/10P/B22-009 1715)
- WAN, Tianfeng**  
(JSA07/10P/A05-009 1710)
- WAN, Yongge**  
(JSG01/07A/A01-012 1205)
- WAN, Zhenwen**  
(JSP04/09P/A06-011 1730)
- WANG, B.-J.**  
(GAI.07/10P/D-002 1400-107)
- WANG, Bin**  
(MC17/11A/B23-009 1200)
- WANG, Bin**  
(MC17/11A/B23-001 0830)
- WANG, Bin**  
(MC02/08A/B20-001 0900)
- WANG, C.H.**  
(HW01/09P/D-046 1400-237)
- WANG, Caijun**  
(HS02/09P/C24-006 1515)
- WANG, Caijun**  
(HS02b/10P/D-022 1630-143)  
(HS02/10A/C24-022 1209)
- WANG, Cheng-Gi**  
(G02/10P/D-002 1400-067)
- WANG, Chi**  
(GAI.V.02/07P/A07-005 1640)
- WANG, Chi-Tien**  
(JSG03/09P/D-021 1640-029)
- WANG, Chien-Ying**  
(SS03/08A/D-112 0830-271)
- WANG, Chih-Kuo**  
(SS04/08P/A03-012 1700)
- WANG, Chih-Ping**  
(GAI.06/08P/A02-005 1530)
- (GAI.05/07A/A06-007 1055)
- WANG, Chun-Yong**  
(SS03/08A/D-135 0830-294)
- WANG, Chung-Chieh**  
(JSM14/07P/A05-008 1745)
- WANG, Chung-Ho**  
(HS02/11P/C24-002 1415)
- WANG, Chunming**  
(GAI.05/08A/A15-005 1040)
- WANG, Chunming**  
(GAI.05/07A/D-006 0830-022)  
(GAI.05/07A/D-005 0830-021)
- WANG, Deli**  
(JSP04/09P/A06-009 1700)
- WANG, Dongxiao**  
(JSM03/08A/A13-006 1100)
- WANG, Fan**  
(JSP08/09P/B19-008 1700)
- WANG, Gang-sheng**  
(HW01/09A/C26-006 1110)
- WANG, Genxu**  
(HS02/08A/C24-005 0930)
- WANG, Guangjie**  
(SS03/08A/D-137 0830-296)
- WANG, Guiling**  
(MI07/11P/B18-005)
- WANG, Guoxin**  
(SS04/08A/A03-001 0830)  
(SS04a/09P/D-009 1400-258)
- WANG, Hui**  
(MI05/09P/B17-008)
- WANG, Hui**  
(JSA07/11A/D-015 0830-015)
- WANG, Hui**  
(JSG01/08P/D-034 1400-034)
- WANG, Hui**  
(JSM04/09P/D-016 1400-053)
- WANG, Jia**  
(JSP04/09P/A06-004 1445)
- WANG, Jia**  
(JSP04/09P/A06-011 1730)
- WANG, Jia**  
(JSP04/09A/A06-008 1150)  
(JSM10/08A/B23-002 0910)
- WANG, Jia**  
(JSM10/08A/B23-006 1050)
- WANG, Jiacheng**  
(JSM14/09P/D-014 1400-078)
- WANG, Jian**  
(JSH01/07P/C27-010 1720)
- WANG, Jijun**  
(GAI.08/08A/A14-001 0830)
- WANG, Jing-Song**  
(MC04/11P/B22-006 1615)
- WANG, Jing-Song Wang**  
(GAI.07/11P/A12-004 1530)
- WANG, Jinling**  
(G04/08P/D-005 1400-112)
- WANG, Jinling**  
(G04/07P/C25-004 1530)
- WANG, Joseph J.**  
(GAI.11/09A/A15-010 1205)
- WANG, Kelin**  
(SS03/07P/A02-007 1600)
- WANG, L.J.**  
(HW01/09P/D-046 1400-237)
- WANG, Meirong**  
(HS03/08A/C26-007 1030)
- WANG, Muyin**  
(JSP04/10P/A06-007 1620)
- WANG, Ninglian**  
(HS02b/10P/D-020 1630-141)  
(HS02/10A/C24-020 1201)
- WANG, Ninglian**  
(JSM10/07A/B23-006 1140)
- WANG, Ninglian**  
(HS02b/10P/D-019 1630-140)  
(HS02/10A/C24-019 1157)
- WANG, Pao K.**  
(MC05/09A/A09-003 0940)  
(JSM15/07A/B18-002 0930)
- WANG, Qingrong**  
(HW07/11P/D-036 1400-172)

## W

- WADA, Akiyoshi**  
(MC02/07P/D-010 1400-207)
- WADA, Makoto**  
(JSM14/09A/A05-009 1205)  
(JSP04/09A/A06-004 1000)
- WADA, Naoto**  
(SS03/08A/D-056 0830-215)
- WAFULA, Mifundou**  
(JSP11/08A/A10-009 1220)
- WAGENER, Thorsten**  
(HW08/08A/C28-001 0830)  
(HW07/11A/C25-004 0930)  
(HW08/08P/C28-003 1500)  
(HW08/07A/C28-001 0900)
- WAGENER, Thorsten**  
(HW08/09A/C28-003 0950)

## INDEX

- WANG, Shouhong**  
(MC04/11P/B22-005 1515)
- WANG, Shuang xu**  
(SS03/08A/D-139 0830-298)
- WANG, Shuang xu**  
(SS03/08A/D-138 0830-297)
- WANG, Siwei**  
(SS04b/10P/D-031 1400-215)
- WANG, Wei**  
(JSP09/10P/B20-013 1730)
- WANG, Wei-Hau**  
(SS03/08A/D-062 0830-221)
- WANG, Wen-xiang**  
(JSA07/11A/D-049 0830-049)
- WANG, Xiaoquan**  
(G04/08P/D-020 1400-127)  
(G03/07P/D-016 1400-038)
- WANG, Xinyu**  
(HS02b/10P/D-029 1630-150)  
(HS02/10P/C24-006 1535)
- WANG, Xiu-Lin**  
(JSM04/09P/D-016 1400-053)
- WANG, Y.C.**  
(GAIL.04/07A/A08-007 1110)
- WANG, Yafei**  
(JSM14/08A/A05-002 0910)
- WANG, Yang**  
(JSA07/10P/A05-001 1400)  
(JSA07/11A/D-002 0830-002)
- WANG, Yi**  
(MC12/07A/B19-006 1115)
- WANG, You-Qing**  
(JSM10/07A/B23-006 1140)
- WANG, Yu**  
(JSG03/09P/D-012 1640-020)
- WANG, Yu Chi**  
(HS01/08P/C29-007 1620)
- WANG, Yu-Ju**  
(SS03/08A/D-123 0830-282)
- WANG, Yuqing**  
(MC02/08A/B20-001 0900)
- WANG, Zhaomin**  
(MC12/07A/B19-006 1115)
- WANGHONG, Hong Hong**  
(HS02a/07P/D-030 1545-176)  
(HS02/07P/C24-030 1452)
- WARBURTON, Jeff**  
(HS01/09P/C29-005 1520)
- WARDINSKI, Ingo**  
(GAV.05/09P/D-003 1400-147)
- WARDINSKI, Ingo**  
(GAV.05/08P/A11-005 1515)
- WARNER, Thomas T.**  
(JSM03/08A/A13-008 1140)
- WASHIMI, Haruichi**  
(GAIL.02/07A/A07-004 1050)
- WATABE, Isao**  
(JSM11/10P/B18-004 1500)
- WATANABE, Atsushi**  
(SW03/10A/D-004 0830-239)
- WATANABE, Atsushi**  
(SW03/10A/D-002 0830-237)
- WATANABE, Atsushi**  
(SW03/10A/D-007 0830-242)
- WATANABE, Atsushi**  
(SW03/10A/D-003 0830-238)
- WATANABE, Kunihiko**  
(JSA07/11A/D-017 0830-017)
- WATANABE, Kunihiko**  
(SS03/08A/D-045 0830-204)
- WATANABE, Masahiro**  
(MC17/11A/B23-006 1100)
- WATANABE, Masahiro**  
(MI05/09A/B17-006 1110)
- WATANABE, Motofumi**  
(SS04a/09P/D-027 1400-276)
- WATANABE, Motofumi**  
(SS04b/10P/D-024 1400-208)
- WATANABE, Okitsugu**  
(JSM11/10P/D-008 1700-017)
- WATANABE, Shigeto**  
(GAIL.06/07P/D-020 1400-140)
- WATANABE, Shigeto**  
(GAIL.07/11A/A12-006 1105)
- WATANABE, Shinichiro**  
(MI09/08P/D-001 1400-154)
- WATANABE, Takashi**  
(GAIL.09/11A/A11-003 0920)
- WATANABE, Takeshi**  
(JSP10/10A/B21-008 1140)
- WATANABE, Takuo**  
(GAIL.14/08A/D-006 0830-150)
- WATANABE, Tomoki**  
(SS03/08A/D-056 0830-215)
- WATANABE, Tsuyoshi**  
(SS03/08A/D-054 0830-213)
- WATANABE, Yuzo**  
(GAIL.11/09A/A15-004 0955)
- WATARI, Masaaki**  
(HS01/09P/D-011 1400-178)
- WATERS, Colin**  
(GAIL.10/11A/D-010 0830-084)
- WATERS, Colin L.**  
(GAV.04/07A/A11-003 0950)
- WATKINS, Michael M.**  
(G03/07P/D-068 1400-090)
- WATTS, Philip**  
(JSS07/09P/A02-008 1600)  
(JSS07b/10P/D-019 1700-065)
- WAYTHOMAS, Christopher F.**  
(JSS07/09P/A02-008 1600)
- WEAVER, Andrew J.**  
(MC12/07A/B19-002 1000)
- WEBB, Bruce W.**  
(HW02/11A/C31-005 1045)  
(HW02/11A/D-001 0830-133)  
(HW02/11A/C31-001 0835)
- WEBB, Charles E.**  
(JSG02/09A/D-004 0830-004)
- WEBB, Mark J.**  
(MC08/07A/B17-003 1015)  
(MC11/10A/B19-001 0830)
- WEBER, Robert**  
(G02/10P/D-007 1400-072)
- WEGMANN, R.**  
(MC04/10P/B22-007 1645)
- WEHRENFENNIG, Andreas**  
(GAIL.05/08A/A15-006 1100)
- WEI, Jennifer Chu-Feng**  
(MC05/09A/A09-001 0900)
- WEI, Rong Qiang**  
(JSS06/10A/A04-005 0950)
- WEI, Yong**  
(JSS07/10P/A02-011 1645)
- WEI, Ziqing**  
(G04/08P/D-018 1400-125)
- WEIDLE, Christian**  
(JSS06/08A/A04-011 1210)
- WEILER, Markus**  
(HW06/07A/C31-004 1030)
- WEILER, Markus**  
(HW06/07A/C31-003 0950)
- WEILL, Alain**  
(JSP09/10A/B20-003 0945)
- WEIMER, Dan**  
(GAV.04/07A/A11-005 1100)
- WEIMER, Daniel**  
(GAIL.05/08P/A15-007 1700)
- WEINBERG, Roberto**  
(SS03/08A/D-147 0830-306)
- WEISBERG, Robert**  
(JSP08/09A/B19-003)
- WEISE, Adelheid**  
(JSG01/08A/A01-006 1015)
- WEISSE, Ralf**  
(JSP08/09P/B19-005 1600)  
(MC08/07A/B17-007 1135)
- WELDON, Ray J.**  
(SS03/08A/D-051 0830-210)
- WELLER, Gunter E.**  
(JSM10/08A/B23-007 1110)
- WELLER, Robert A.**  
(JSP09/10P/B20-001 1400)
- WELLS, Jennifer**  
(JSP10/10A/B21-007 1120)
- WELLS, Ray E.**  
(GAV.06/10A/A11-001 0830)
- WEN, Hanjiang**  
(G07/10P/D-006 1400-091)
- WEN, Kuo Liang**  
(SS04a/09P/D-014 1400-263)
- WEN, Kuo-Liang**  
(SS04/08P/A03-012 1700)  
(SS04a/09P/D-003 1400-252)  
(SS04a/09P/D-036 1400-285)  
(SS04a/09P/D-037 1400-286)
- WEN, Kuo-Liang**  
(SS04/08P/A03-001 1400)  
(SS04a/09P/D-008 1400-257)
- WEN, Lei**  
(JSM14/09A/A05-003 0955)
- WEN, Lianxing**  
(JSS06/09A/A04-001 0900)
- WEN, Ruey-Cheng**  
(SS03/08A/D-062 0830-221)
- WEN, Xueze**  
(SS04b/10P/D-032 1400-216)  
(SS04/09A/A03-006 1015)  
(SS04b/10P/D-031 1400-215)
- WEN, Yuanlan**  
(G04/07P/C25-009 1740)
- WEN, Zengong**  
(JSP11/07P/A10-006 1640)
- WENG, Chun-Hsiung**  
(MC17/10P/B23-010 1715)
- WENG, Hengyi**  
(JSA08/09A/A08-003 0945)  
(JSA09/10A/A08-011 1215)
- WENG, Shu-Ping**  
(MC03/09A/A07-006 1110)
- WENZEL, Friedemann**  
(JSS06/08A/A04-006 1010)
- WENZEL, Manfred**  
(JSM11/10P/D-009 1700-018)
- WENZEL, Volker**  
(HW04/09A/C31-005 1020)
- WERGIN, William**  
(JSM15/07A/B18-007 1100)
- WERNER, Martin**  
(MC12/08A/B19-001 0930)
- WERNLI, Heini**  
(JSM14/08P/A05-002 1435)
- WERNLI, Heini**  
(MC05/09A/A09-002 0920)
- WESCOTT, Eugene M.**  
(GAIL.04/07P/A08-005 1540)
- WEST, Robert A.**  
(MC04/10P/B22-004 1500)
- WEYGAND, J.**  
(GAIL.06/08A/A02-003 0940)
- WHALER, Kathryn A.**  
(JSA07/10P/A05-006 1610)  
(GAV.05/08A/A11-008 1130)
- WHEATER, Howard S.**  
(HW08/09A/C28-003 0950)
- WHEATER, Howard S.**  
(HW08/08A/C28-001 0830)
- WHEELER, Dennis**  
(MC12/08A/B19-007 1145)  
(MC12/08A/B19-008 1200)
- WHEELER, Matthew**  
(MC17/10P/B23-006 1600)
- WHEELER, Tim**  
(MI07/11A/B18-001 0830)
- WHITAKER, Andrew C.**  
(JWH01/10A/C30-004 0930)  
(HW02/11A/C31-003 0925)  
(HS02/11P/C24-004 1445)
- WHITE, Arthur F.**  
(HW01/10P/C26-002 1420)
- WHITE, Don**  
(JSS06b/10P/D-011 1400-035)
- WHITE, J.W.C.**  
(MC12/08A/B19-002 1000)
- WHITE, Sean R.**  
(JSP09/11P/B20-006 1545)
- WHITE, Sue**  
(HS01/09P/C29-005 1520)
- WHITEHEAD, Paul**  
(HS04/08A/C30-001 0905)
- WHITLEDGE, Terry**  
(JSP04/09P/A06-010 1715)
- WHITMORE, Paul M.**  
(JSS07/10P/A02-002 1415)
- WHITMORE, Paul Michael**  
(JSS07/10P/A02-003 1430)
- WICK, Gary A.**  
(JSP09/11A/B20-005 0945)
- WICK, Gary A.**  
(JSP09/11A/B20-006 1000)
- WIDARTO, Djedi Setyo**  
(GAI.10/09P/D-010 1615-129)
- WIDIYANTORO, Sri**  
(JSS06/09A/A04-007 1120)
- WIDIYANTORO, Sri**  
(JSS06b/10P/D-016 1400-040)
- WIDIYANTORO, Sri**  
(JSS06/08A/A04-011 1210)
- WIGEN, Sydney O.**  
(JSS07/10A/A02-011 1115)
- WIJNS, Chris**  
(SW05/10P/A13-009 1615)  
(SS03/08A/D-147 0830-306)
- WIKLE, Christopher K.**  
(MC17/10P/B23-004 1500)
- WILD, J.**  
(GAIL.09/11A/A11-006 1110)
- WILD, Jim**  
(GAIL.05/07P/D-016 1400-114)
- WILD, Martin**  
(MC11/11A/B19-003 0910)
- WILLIAMS, Donald J.**  
(GAIL.14/07A/A12-005 1115)
- WILLIAMS, E.**  
(GAIL.04/07A/A08-005 1015)
- WILLIAMS, Earle**  
(GAIL.04/07A/A08-006 1050)
- WILLIAMS, John W.**  
(MC12/07A/B19-004 1030)
- WILLIAMS, Keith D.**  
(MC11/10P/B19-002 1420)
- WILLIAMS, Paul**  
(JSP10/08P/B21-001 1400)
- WILLIAMS, R. Terry**  
(MC02/07P/B20-002 1420)
- WILLIAMS, Steven F.**  
(MC03/10P/A07-002 1420)
- WILLIS, Josh**  
(JSP06/07P/B21-005 1600)
- WILLIS, Josh K.**  
(JSP06/08A/B21-001 0900)
- WILLIS, Pascal**  
(G07/10P/D-001 1400-086)
- WILLSON, Richard Clayton**  
(JSA08/09P/A08-001 1400)
- WILMES, Herbert**  
(G07/10P/D-016 1400-101)
- WILSON, Albertus**  
(GAIL.06/10A/A01-005 0940)
- WILSON, Brian**  
(GAIL.05/07A/D-005 0830-021)
- WILSON, Brian D.**  
(GAIL.05/07A/D-006 0830-022)
- WILSON, Brian D.**  
(GAIL.05/08A/A15-005 1040)
- WILSON, Paul S.**  
(GAIL.09/11P/A11-006 1620)
- WILSON, R.J.**  
(MC11/10P/B19-003 1440)
- WILTBERGER, Michael J.**  
(GAIL.09/11P/A11-004 1510)
- WILTBERGER, Michael J.**  
(GAIL.09/11P/A11-003 1440)
- WILTBERGER, Michael J.**  
(GAIL.06/08P/A02-006 1545)
- WINARDHIE, Sonny**  
(SS03/08A/D-044 0830-203)
- WINCH, Denis**  
(GAV.05/08A/A11-009 1150)
- WING, Simon**  
(GAIL.05/07P/D-003 1400-101)
- WINGLEE, Robert**

(GAI11.11/09P/A15-007 1540)  
**WINGLEE, Robert M.**  
 (GAI.V.02/07P/A07-001 1400)  
**WINSTRAL, Adam**  
 (JWH01/10P/C30-006 1630)  
**WINTER, Thomas C.**  
 (HW08/07P/C28-004 1550)  
**WINTERHALTER, Daniel**  
 (GAI.V.03/08A/A16-002 0900)  
**WINTERS, Kraig B.**  
 (JSP10/11A/B21-007 1110)  
**WINTERS, Kraig B.**  
 (JSP10/11A/B21-008 1130)  
**WITTE, Jacquelyne C.**  
 (MI03/08A/B18-006 1050)  
**WITTER, Victor Jan**  
 (HS02/07A/C24-001 1045)  
**WOCH, Joachim**  
 (GAI11.14/07P/A12-005 1515)  
**WOLF, Richard A.**  
 (GAI11.06/08P/A02-005 1530)  
**WOLFF, Joerg-Olaf**  
 (JSP08/09A/B19-007 1120)  
**WOLFGANG, F.A.**  
 (HS03/08A/C26-008 1045)  
**WOOD, Roger**  
 (G02/10P/D-004 1400-069)  
**WOOD, Troy**  
 (GAI11.04/07A/A08-006 1050)  
**WOODGATE, Rebecca**  
 (JSP04/09P/A06-002 1415)  
**WOODHOUSE, John H.**  
 (JSS06/07P/A04-003 1440)  
**WOODWORTH, Philip Leslie**  
 (G07/10P/A03-002 1420)  
**WOOLF, David**  
 (JSP09/11A/B20-011 1145)  
**WOOLNOUGH, Stephen**  
 (MC11/10A/B19-007 1100)  
**WORTHINGTON, E.W.**  
 (GAI11.10/11A/D-002 0830-076)  
**WORTHINGTON, Richard M.**  
 (MI09/08P/B22-003 1440)  
**WOTH, Katja**  
 (MC08/07A/B17-007 1135)  
**WRIGHT, Cedric**  
 (SW03/10P/A04-002 1415)  
**WRIGHT, Cedric**  
 (JSS06/07P/A04-006 1600)  
**WRONOWSKI, Roman**  
 (GAI11.08/11P/D-001 1400-072)  
**WU, Bin**  
 (G03/07P/D-017)  
**WU, Bingyi**  
 (JSM10/08A/B23-002 0910)  
**WU, Cheng-Han**  
 (MC17/10P/B23-010 1715)  
**WU, Chin-Chun**  
 (GAI11.09/11P/A11-005 1600)  
**WU, Chin-Chun**  
 (GAI11.06/11P/D-008 1400-060)  
**WU, Chun-Chieh**  
 (MC02/08P/B20-004 1500)  
 (MC02/08P/B20-007 1630)  
**WU, Dong L**  
 (MC05/11P/A09-010)  
**WU, Francis T.**  
 (SS03/07A/A02-004 0945)  
**WU, Guoxiong**  
 (MC03/11A/A07-001 0830)  
 (MC03/11A/A07-002 0910)  
 (MC03/10P/A07-007 1700)  
**WU, Guoxiong**  
 (MI07/11A/B18-005 0950)  
**WU, H.T.**  
 (MC11/11A/B19-009 1130)  
**WU, Jian-Ping**  
 (SS03/08A/D-135 0830-294)  
**WU, Lin**  
 (G02/07A/C25-010 1145)  
**WU, Lizong**  
 (JSH01/08P/D-011 1400-049)  
**WU, Man Chi**

(MC03/09P/A07-009 1740)  
**WU, Peiming**  
 (MC03/11P/A07-003 1440)  
**WU, Shimin**  
 (SS03/07P/A02-013 1730)  
**WU, Sien C.**  
 (G03/07P/D-068 1400-090)  
**WU, Wanru**  
 (MI07/11A/B18-004 0930)  
**WU, Y-h-Min**  
 (SS03/07A/A02-004 0945)  
**WU, Yih-Min**  
 (SS04a/09P/D-022 1400-271)  
**WU, Yun**  
 (JSG01/08P/D-034 1400-034)  
**WU, Yun**  
 (JSA07/11A/D-015 0830-015)  
**WU, Zhaohua**  
 (MC08/07P/B17-004)  
**WU, Zhongliang**  
 (SS05/10A/A13-012 1130)  
**WU, Zong Li**  
 (JSH01/08P/D-002 1400-040)  
**WU, Zong Li**  
 (JSH01/08P/D-003 1400-041)  
**WUEBBLES, Donald J.**  
 (MC05/09A/A09-001 0900)  
**WUEST, Marc**  
 (JSM14/08P/A05-006 1715)  
**WUKAWA, Joseph**  
 (JSS07a/09P/D-004 1700-105)  
**WUNSCH, Carl**  
 (JSM11/10P/B18-001 1400)  
**WURZ, Peter**  
 (GAI11.14/08A/D-002 0830-146)  
**WYSS, Max**  
 (SW04/09P/A13-008 1600)

## X

**XIA, JUN**  
 (HS03/08P/C26-003 1430)  
**XIA, Jun**  
 (HS02c/11P/D-019 1630-117)  
 (HS02/11A/C24-019 1157)  
**XIA, Jun**  
 (HW01/09P/D-002 1400-193)  
**XIA, Jun**  
 (HS02/07P/C24-021 1416)  
 (HS02a/07P/D-021 1545-167)  
**XIA, Jun**  
 (HS01/08A/C29-006 1150)  
 (HS02/07A/C24-002 1100)  
**XIA, Jun**  
 (HW01/09A/C26-006 1110)  
**XIA, Kanyua**  
 (SS03/07P/A02-013 1730)  
**XIAJUN, Jun Jun**  
 (HS02a/07P/D-030 1545-176)  
 (HS02/07P/C24-030 1452)  
**XIANG, Aiming**  
 (G03/07P/D-016 1400-038)  
**XIAO, Feng**  
 (MC11/11P/D-001 1400-194)  
**XIAO, Zou**  
 (GAI11.08/11P/D-002 1400-073)  
**XIAOSU, Xie**  
 (JSP09/11A/B20-001 0830)  
**XIE, Hua**  
 (HS02/07A/C24-008 0928)  
 (HS02a/07P/D-008 1545-154)  
**Xie, Jiancang**  
 (HS03/08P/C26-002 1415)  
**XIE, L.**  
 (GAI11.06/07P/D-008 1400-128)  
**XIE, Li-Li**  
 (SS04/08A/A03-003 0900)  
**XIE, Li-Li**  
 (SW04/09P/A13-005 1500)  
 (SS04/08A/A03-002 0845)

**XIE, Lian**  
 (JSP07/08A/B17-002 0930)  
**XIE, Qiang**  
 (JSM03/08A/A13-006 1100)  
**XIE, Shang-Ping**  
 (JSM03/08A/A13-006 1100)  
**XIE, Shang-Ping**  
 (MI05/11A/B17-005 0950)  
**XIE, Shang-Ping**  
 (JSP09/11A/B20-001 0830)  
**XIE, Shucheng**  
 (HS02b/10P/D-018 1630-139)  
 (HS02/10A/C24-018 1153)  
**XIE, Shunxing**  
 (JSS06a/08P/D-009 1400-087)  
**XIE, Shunxing**  
 (JSS06/08A/A04-001 0830)  
**XIE, Zhenghui**  
 (HW08/09A/C28-004 1010)  
**XING, Canfei**  
 (G04/08P/D-020 1400-127)  
 (G03/07P/D-016 1400-038)  
**XIONG, Lihua**  
 (HS02/07A/C24-007 1215)  
**XIONG, Xiong**  
 (JSS06/10A/A04-007 1050)  
**XU, Baiqing**  
 (HS02b/10P/D-019 1630-140)  
 (HS02/10A/C24-019 1157)  
**XU, Caijun**  
 (JSG01/07A/A01-005 1000)  
 (JSG01/07A/A01-004 0945)  
**XU, Deshu**  
 (JSA07/10P/A05-009 1710)  
**XU, Gui-ming**  
 (SS04b/10P/D-037 1400-221)  
**XU, Haiming**  
 (JSM03/08A/A13-006 1100)  
**XU, Jian-Qiao**  
 (JSS06/09A/A04-005 1040)  
**XU, Jianhua**  
 (G03/07P/D-053 1400-075)  
**XU, Jianqing**  
 (MC03/11P/A07-004 1520)  
**XU, Kuan-Man**  
 (MC11/10P/B19-005 1550)  
**XU, Lisheng**  
 (SW04/09P/A13-003 1430)  
**XU, Mei**  
 (JSM03/08A/A13-008 1140)  
**XU, Peiliang**  
 (G04/07P/C25-002 1450)  
**XU, Shengbin**  
 (HW07/11P/D-035 1400-171)  
**XU, Shiguo**  
 (HS02c/11P/D-034 1630-132)  
 (HS02/11P/C24-011 1555)  
**XU, Xiwei**  
 (SS04/09A/A03-006 1015)  
**XU, Zongxue**  
 (JWH01/10A/C30-010 1200)  
**XU, Zongxue**  
 (HS03/08A/C26-004 0930)  
**XU, Zongxue**  
 (HS01/08A/C29-002 1010)  
 (HW04/09A/C31-001 0900)  
**XUE, Fu ping**  
 (SS03/08A/D-139 0830-298)  
**XUE, Huijie**  
 (JSP09/11P/B20-008 1615)  
**XUE, Yongkang**  
 (MC03/10P/A07-005 1600)  
 (MC11/11P/B19-002 1420)  
 (JWH01/10A/C30-001 0830)  
 (MI07/11P/B18-004 1500)

## y

**Y., Anjaneyulu**  
 (HW01/09P/D-011 1400-202)

(HW01/09P/D-051 1400-242)  
**YABE, Kazuhiro**  
 (HS01/09P/D-004 1400-171)  
**YABUGAKI, Yoshiyuki**  
 (MI09/08P/D-002 1400-155)  
**YABUKI, Hironori**  
 (JSM10/09P/D-001 1400-055)  
**YABUKI, Hironori**  
 (MI07/08P/D-001 1400-039)  
 (MI07/10P/D-003 1400-179)  
 (JWH01/10A/C30-003 0910)  
 (JWH01/09A/C30-003 0940)  
**YABUSAKI, Shiho**  
 (HW06/07P/C31-001 1400)  
**YADAV, Meenakshi**  
 (JSH01/07A/C27-004 1140)  
**YADAV, siddharth**  
 (HS01/09P/D-024 1400-191)  
**YAGITANI, Satoshi**  
 (GAI11.11/09P/A15-009 1645)  
 (GAI11.04/07P/A08-004 1505)  
 (GAI11.04/09A/D-002 0830-138)  
 (GAI11.05/07P/D-021 1400-119)  
 (GAI11.11/10P/D-001 1400-116)  
**YAGO, Kazuya**  
 (GAI11.06/07P/D-004 1400-124)  
**YAGOVA, Nadezda V.**  
 (GAI11.10/11A/A01-001 0830)  
**YAIR, Yoav Y.**  
 (GAI11.04/07A/A08-009 1150)  
**YAKIWARA, Hiroshi**  
 (SS03/08A/D-017 0830-176)  
**YAKOVENKO, Olga I.**  
 (JSS07/10A/A02-011 1115)  
**YAKOVLEV, Andrei G.**  
 (GAI.10/09A/A11-006 1015)  
**YAKOVLEV, Denis V.**  
 (GAI.10/09A/A11-006 1015)  
**YAKOVLEVA, Svetlana V.**  
 (GAV.05/08P/A11-006 1530)  
 (GAV.04/07P/A11-010 1740)  
**YAKUPOV, Sergey V.**  
 (JSH01/07P/C27-003 1440)  
**YAKUPOV, Vil S.**  
 (JSH01/07P/C27-003 1440)  
**YALCINER, Ahmet Cevdet**  
 (JSS07/09A/A02-012 1200)  
**YAMADA, A.**  
 (SS03/08A/D-146 0830-305)  
**YAMADA, Hiroyuki**  
 (JSM14/08A/A05-004 0940)  
 (JSM14/09P/D-013 1400-077)  
**YAMADA, Manabu**  
 (GAI11.06/07P/D-020 1400-140)  
**YAMADA, Nobuyuki**  
 (SS04/07P/A03-006 1530)  
 (SS04b/10P/D-002 1400-186)  
 (SS04a/09P/D-010 1400-259)  
**YAMADA, Tadashi**  
 (HS03/07P/C26-011 1645)  
**YAMADA, Takuya**  
 (MC02/07P/B20-003 1440)  
**YAMADA, Tomoaki**  
 (SS03/08A/D-067 0830-226)  
 (SS03/08A/D-002 0830-161)  
**YAMADA, Yasuhiro**  
 (SS03/07P/A02-003 1430)  
 (SS03/08A/D-050 0830-209)  
**YAMADA, Yukiko**  
 (MC03/09A/A07-003 0950)  
**YAMAGATA, Toshio**  
 (JSP10/09P/B21-006 1540)  
**YAMAGISHI, Hisao**  
 (GAI11.05/07P/D-016 1400-114)  
**YAMAGISHI, Hisao**  
 (JSA01/08P/A12-004 1520)  
**YAMAGISHI, Yasuko**  
 (JSS06a/08P/D-006 1400-084)  
**YAMAGIWA, Yoshiki**  
 (GAI11.11/09A/A15-007 1120)  
**YAMAGUCHI, Hiroyasu**  
 (JSP04/10P/A06-006 1600)  
**YAMAGUCHI, Kazuki**

## INDEX

- (MC08/07A/B17-002 1000)  
**YAMAGUCHI, Kazuo**  
 (SS03/08A/D-110 0830-269)  
 (SS03/08A/D-034 0830-193)  
**YAMAGUCHI, Keisuke**  
 (JSP07/08A/B17-005 1100)  
**YAMAGUCHI, Rui**  
 (GAI11.10/11A/D-020 0830-094)  
 (GAI11.05/07P/D-014 1400-112)  
 (GAI11.10/11A/D-018 0830-092)  
**YAMAGUCHI, Toru**  
 (GAV.05/09P/D-007 1400-151)  
**YAMAJI, Kazuyo**  
 (JSM04/09A/B23-002 0930)  
**YAMAKAWA, Hiroshi**  
 (GAI11.14/08A/D-004 0830-148)  
 (GAI11.14/08A/D-005 0830-149)  
 (MC04/11A/B22-001 0830)  
**YAMAKI, Sachiko**  
 (MC08/07A/B17-005 1045)  
 (MC08/07A/B17-002 1000)  
**YAMAKI, Shigeru**  
 (JSS07/09A/A02-003 0930)  
**YAMAKI, Shigeru**  
 (JSS07/09P/A02-004 1445)  
**YAMAKOSHI, Takao**  
 (HS01/09P/D-011 1400-178)  
**YAMAMATO, Mamoru**  
 (MC05/07P/D-015 1400-222)  
**YAMAMIZU, Fumio**  
 (JSG01/08P/D-025 1400-025)  
**YAMAMORI, Miho**  
 (MC04/11P/B22-007 1400-214)  
**YAMAMOTO, Akihiko**  
 (SS04a/09P/D-033 1400-282)  
 (G03/07P/D-010 1400-032)  
 (G03/07P/D-007 1400-029)  
**YAMAMOTO, Eiko**  
 (GAI11.07/09P/A14-008 1700)  
**YAMAMOTO, Hidekazu**  
 (SS04a/09P/D-035 1400-284)  
**YAMAMOTO, Jaime**  
 (SS03/08A/D-148 0830-307)  
**YAMAMOTO, Keiko**  
 (G02/10P/D-017 1400-082)  
**YAMAMOTO, Kentaro**  
 (MI05/11A/B17-004 0930)  
**YAMAMOTO, M.**  
 (GAI11.06/09P/A10-002 1420)  
 (GAI11.06/09P/A10-003 1440)  
 (GAI11.05/08P/A15-001 1400)  
**YAMAMOTO, Mamoru**  
 (GAI11.06/11P/D-010 1400-062)  
 (GAI11.06/09P/A10-001 1400)  
 (MI09/08P/B22-004 1500)  
 (GAI11.06/09P/A10-007 1545)  
 (MI09/08P/D-002 1400-155)  
 (GAI11.06/09P/A10-004 1500)  
 (GAI11.06/09P/A10-008 1620)  
 (MC17/11P/B23-008 1640)  
 (MC05/11P/A09-005 1530)  
 (MC05/08P/A09-007 1640)  
 (GAI11.06/11P/D-011 1400-063)  
 (GAI11.06/11P/D-012 1400-064)  
**YAMAMOTO, Masa-yuki**  
 (GAI11.06/11P/D-011 1400-063)  
**YAMAMOTO, Masaru**  
 (MC04/11A/B22-006 1000)  
**YAMAMOTO, Masayuki**  
 (MC05/08P/A09-007 1640)  
 (MC17/11P/B23-008 1640)  
 (MC05/11P/A09-005 1530)  
**YAMAMOTO, Masayuki K.**  
 (MC05/08P/A09-006 1620)  
 (MI09/08P/D-002 1400-155)  
**YAMAMOTO, Michiko**  
 (GAV.06/10P/A11-006 1600)  
**YAMAMOTO, Naoki**  
 (JWH01/10A/C30-010 1200)  
**YAMAMOTO, Susumu**  
 (MI07/10P/D-004 1400-180)  
**YAMAMOTO, Takahiro**  
 (SS04b/10P/D-038 1400-222)
- YAMAMOTO, Takeyasu**  
 (JSG01/08P/D-019 1400-019)  
**YAMAMOTO, Takeyasu**  
 (JSG01/07P/A01-001 1400)  
**YAMAMOTO, Zen'ichi**  
 (G02/10P/D-013 1400-078)  
**YAMAMURA, Keiko**  
 (JSG01/08P/D-018 1400-018)  
**YAMANAKA, Hiroaki**  
 (SS04b/10P/D-002 1400-186)  
 (SS04/07P/A03-006 1530)  
**YAMANAKA, Hiroaki**  
 (SS04a/09P/D-010 1400-259)  
**YAMANAKA, Manabu**  
 (MC05/08P/A09-007 1640)  
**YAMANAKA, Manabu D.**  
 (JSM14/09P/D-009 1400-073)  
**YAMANAKA, Manabu D.**  
 (MC03/11P/D-007 1400-182)  
**YAMANAKA, Manabu D.**  
 (MC03/11P/D-009 1400-184)  
 (JSM14/07A/A05-006 1130)  
 (MC17/11P/B23-006 1600)  
 (MC03/11P/A07-003 1440)  
 (HW06/07P/D-006 1400-190)  
**YAMANAKA, Manabu D.**  
 (MC02/07P/D-003 1400-200)  
**YAMANAKA, Manabu D.**  
 (MC03/09P/A07-007 1700)  
**YAMANAKA, Manabu D.**  
 (MC17/11A/B23-004 0940)  
**YAMANAKA, Manabu D.**  
 (MC04/11P/B22-004 1500)  
**YAMANAKA, Manabu D.**  
 (MC05/08P/A09-005 1530)  
 (MC03/10P/A07-008 1720)  
**YAMANAKA, Masaru**  
 (HW06/07P/D-008 1400-192)  
**YAMANE, Shozo**  
 (JSP09/10P/B20-009 1630)  
**YAMANE, Shozo**  
 (MI05/11A/B17-009 1150)  
 (MI05/11A/B17-007 1050)  
 (MI05/11A/B17-008 1130)  
**YAMANOKUCHI, Tsutomu**  
 (JSG03/09P/D-002 1640-010)  
**YAMANOUCHI, Takashi**  
 (JSP04/09A/A06-004 1000)  
**YAMAOKA, Koshun**  
 (JSG01/08P/D-024 1400-024)  
**YAMASAKI, Tadashi**  
 (SS03/08A/D-119 0830-278)  
**YAMASHINA, Tadashi**  
 (SS03/08A/D-056 0830-215)  
**YAMASHITA, Masahiro**  
 (GAI11.09/11P/A11-007 1640)  
**YAMASHITA, Mikiya**  
 (SW03/10A/D-004 0830-239)  
 (SW03/10A/D-002 0830-237)  
 (SW03/10A/D-007 0830-242)  
 (SW03/10A/D-003 0830-238)  
**YAMASHITA, Satoru**  
 (GAV.04/07A/A11-004 1030)  
**YAMASOE, M.**  
 (JSM04/09A/B23-006 1145)  
**YAMAUCHI, Makiko**  
 (JSS06a/08P/D-016 1400-094)  
**YAMAZAKI, Akira**  
 (GAI.08/08P/D-005 1400-140)  
**YAMAZAKI, Amelia**  
 (JSM04/09P/D-009 1400-046)  
**YAMAZAKI, Amelia**  
 (JSM04/09P/D-015 1400-052)  
**YAMAZAKI, Amelia**  
 (JSM04/09P/D-012 1400-049)  
**YAMAZAKI, Atsushi**  
 (GAI11.07/11A/A12-004 0945)  
**YAMAZAKI, Gaku**  
 (JWH01/10P/D-004 1400-009)  
**YAMAZAKI, Haruo**  
 (SS03/08A/D-041 0830-200)  
**YAMAZAKI, Kensuke**  
 (MI05/09A/B17-008 1150)
- YAMAZAKI, Koji**  
 (HW06/07P/D-007 1400-191)  
 (MC05/08A/A09-006 1120)  
 (MI05/10A/B17-006 1100)  
 (MC05/07P/D-006 1400-213)  
 (JSP04a/09P/D-005 1400-098)  
 (MI05/10P/D-001 1400-168)  
 (MI05/10P/D-010 1400-176)  
**YAMAZAKI, Koji**  
 (MC05/09A/A09-006 1120)  
**YAMAZAKI, Kuniko**  
 (JSP10/08P/B21-001 1400)  
**YAMAZAKI, T.**  
 (JWH01/09P/C30-001)  
**YAMAZAKI, T.**  
 (JWH01/09A/C30-009 1210)  
**YAMAZAKI, Takeshi**  
 (JWH01/10A/C30-003 0910)  
**YAMAZAKI, Y.H.**  
 (MC04/10P/B22-003 1445)  
**YAMAZAKI, Yasuhiro**  
 (JSP10/08P/B21-001 1400)  
**YAMAZAKI, Yoshiki**  
 (JSS07/10P/A02-011 1645)  
**YAMAZAKI, Yusuke**  
 (JSM10/08P/B23-003 1500)  
 (HS02b/10P/D-003 1630-124)  
 (HS02/10A/C24-003 1053)  
**YAN, Hua-yun**  
 (HS02/07A/C24-003 0908)  
 (HS02a/07P/D-003 1545-149)  
**YAN, Xiaoyang**  
 (GAI11.06/07P/D-012 1400-132)  
**YAN, Xiaoyuan Yan**  
 (JSM04/09P/B23-003 1500)  
**YAN, Xudong**  
 (SS04b/10P/D-050 1400-234)  
**YAN, Yafeng**  
 (SS03/08A/D-137 0830-296)  
**YAN, Zhong Qun**  
 (JSS06b/10P/D-015)  
 (JSS06b/10P/D-014)  
**YAN, Zhong Qun**  
 (JSS06b/10P/D-007 1400-031)  
**YAN, Zhongwei**  
 (JSP06/07P/D-003 1400-010)  
**YANAGI, Brian**  
 (JSS07/10A/A02-013 1145)  
**YANAGISAWA, Takatoshi**  
 (JSS06a/08P/D-006 1400-084)  
**YANG, C.-Y.**  
 (HW01/09P/D-031 1400-222)  
**YANG, Daqing**  
 (JSH01/07P/C27-009 1700)  
**YANG, Dawen**  
 (HS02/08A/C24-002 0845)  
 (HS03/08A/C26-005 0945)  
**YANG, Dongfang**  
 (JSP07/08P/B17-004 1510)  
**YANG, Fuxi**  
 (GAI11.10/11A/A01-005 0930)  
**YANG, Hui**  
 (MC17/11P/B23-005)  
**YANG, Jianping**  
 (HS02/09P/C24-010 1645)  
**YANG, Jixin**  
 (SW05/10A/D-007 0900-251)  
**YANG, Jun-Mo**  
 (JSA07/10P/A05-003 1440)  
**YANG, Junmo**  
 (JSA07/11A/D-003 0830-003)  
**YANG, Kun**  
 (HW08/07A/C28-009 1210)  
**YANG, Liqiang**  
 (SS03/08A/D-137 0830-296)  
**YANG, Ming**  
 (G03/07P/D-049 1400-071)  
**YANG, Shuchun**  
 (JSM04/09P/D-003 1400-040)  
**YANG, Tao Chang**  
 (HS02b/10P/D-028 1630-149)  
 (HS02/10P/C24-005 1531)  
**YANG, Tao-Chang**
- (HW03/11A/C30-007 1050)  
**YANG, Wu-yang**  
 (JSA07/11A/D-049 0830-049)  
**YANG, Xiaojing**  
 (HS04/08A/C30-003 1005)  
**YANG, Xiuxiang**  
 (MI05/10P/B17-007 1650)  
**YANG, Xuan-Zhu**  
 (HW01/09P/D-007 1400-198)  
**YANG, Yi-Sheng**  
 (JSG03/09P/D-022 1640-030)  
**YANG, Yuanxi**  
 (G04/07P/C25-009 1740)  
 (G04/08P/D-002 1400-109)  
**YANG, Z.-L.**  
 (JWH01/09P/C30-001)  
**YANG, Zhanji**  
 (G03/07P/D-044 1400-066)  
**YANG, Zhifeng**  
 (HW04/09A/C31-001)  
**YANO, Taihei**  
 (G02/07A/C25-014 1245)  
**YAO, Huaxia**  
 (HS01/09P/D-012 1400-179)  
**YAO, Qi**  
 (JSP06/08A/B21-003 0950)  
**YAO, T.**  
 (JSP04/09A/A06-009 1210)  
**YAO, Tangdong**  
 (JSM10/08P/B23-007)  
**YAO, Tangdong**  
 (HS02b/10P/D-018 1630-139)  
 (HS02/10A/C24-018 1153)  
**YAO, Tangdong**  
 (JSM10/07A/B23-006 1140)  
**YAO, Tangdong**  
 (HS02/07P/C24-027 1440)  
 (HS02a/07P/D-027 1545-173)  
**YAO, Tangdong**  
 (HS02b/10P/D-019 1630-140)  
 (HS02/10A/C24-019 1157)  
**YAO, Tangdong**  
 (HS02b/10P/D-020 1630-141)  
 (HS02/10A/C24-020 1201)  
**YAO, Tangdong**  
 (HS02/08A/C24-006 0945)  
**YAO, tangdong**  
 (HW05/10P/D-010 1400-165)  
**YAO, Yun sheng**  
 (SS03/08A/D-012 0830-171)  
**YAREMCHUK, Max**  
 (JSP04a/09P/D-004 1400-097)  
**YARI, Sadegh**  
 (JSM11/10P/D-002 1700-011)  
**YASHIRO, Kazuhiko**  
 (SS04a/09P/D-025 1400-274)  
**YASIRO, Kazuhiko**  
 (SS04a/09P/D-012 1400-261)  
**YASUDA, Ichiro**  
 (JSP06/07P/B21-006 1620)  
**YASUDA, Yuji**  
 (HS01/09P/C29-006 1540)  
**YASUDA, Yukio**  
 (HS02/08P/C24-012 1715)  
**YASUE, Ken-ichi**  
 (SS03/08A/D-039 0830-198)  
**YASUHARA, Masaya**  
 (HW05/10A/C31-009 1055)  
**YASUNARI, Tetsuzo**  
 (HW08/08A/C28-006 1040)  
**YASUNARI, Tetsuzo**  
 (MI05/10P/B17-009 1730)  
**YASUNARI, Tetsuzo**  
 (MC03/11A/A07-005 1030)  
**YASUOKA, Yoshifumi**  
 (JSM04/09P/B23-002 1430)  
**YASUTOMI, Natsuko**  
 (MC03/11P/D-015 1400-190)  
**YATAGAI, Akiyo**  
 (MC03/11P/A07-001 1400)  
**YAU, A.W.**  
 (GAI11.06/07P/D-020 1400-140)  
**YAU, Andrew W.**

- (GAI11.08/10A/A16-008 1100)  
(GAI1.07/11A/A12-001 0835)
- YE, Baisheng**  
(JSH01/07P/C27-009 1700)
- YE, Sanyu**  
(SS03/07P/A02-013 1730)
- YEARBY, Keith**  
(GAI11.10/10P/A01-008 1620)
- YEE, Jeng-Hwa**  
(MC05/09P/A09-004 1520)
- YEH, H.-C.**  
(JSG03/09P/D-026 1640-034)
- YEH, Harry**  
(JSS07/09P/A02-011 1645)
- YEH, Huey-Chin**  
(GAI1.06/10A/A01-012 1200)
- YEH, Huey-Ching**  
(GAI1.06/09A/A10-001 0900)
- YEH, Hui-Chung**  
(HS01/09P/D-010 1400-177)
- YEH, Pat J.-F.**  
(HW07/10P/C25-014 1745)
- YEH, Tien-Chiang**  
(MC02/08P/B20-007 1630)
- YELA, Margarita**  
(MI03/09A/D-002 0900-245)
- YEMBA, Munyololowa**  
(JSP11/08A/A10-009 1220)
- YEN, Horng-Yuan**  
(SS03/08A/D-112 0830-271)  
(SS03/08A/D-111 0830-270)  
(SS03/08A/D-016 0830-175)
- YERRAGUNTLA, Rao Jyothi Bhaskar**  
(SW03/10P/A04-012 1700)
- YERUBANDI, Ram Rao**  
(JSP08/09A/B19-006 1100)
- YESHANEW, Abebe**  
(MC03/11P/A07-005 1540)
- YEWCHUCK, Kerianne**  
(JSP10/09P/B21-003 1440)
- YI, Donghui**  
(JSM11/10A/B18-001 0900)
- YI, Guixi**  
(SS04b/10P/D-032 1400-216)
- YI, Guixi**  
(SS04/09A/A03-006 1015)  
(SS04b/10P/D-031 1400-215)
- YI, Yuchan**  
(JSG03/09P/D-012 1640-020)
- YILMAZ, Musa**  
(HS02c/11P/D-003 1630-101)  
(HS02/11A/C24-003 1053)
- YILMAZ, Onur**  
(JSG01/08P/D-013 1400-013)
- YIM, Solomon**  
(JSS07/09P/A02-011 1645)
- YIOU, Pascal**  
(MI05/10P/D-008 1400-174)
- YIP, Cleo**  
(MC02/07P/B20-001 1400)
- YLINIEMI, Jukka**  
(JSA07/11A/D-029 0830-029)
- YODEN, Shigeo**  
(MC05/10P/A09-006 1650)  
(MC05/10A/A09-009 1150)  
(MI05/09A/B17-007 1130)  
(MC05/10A/A09-006 1040)  
(JSP10/09A/B21-003 0950)
- YOH, Muneoki**  
(HW01/10A/C26-010 1210)
- YOKELSON, Robert J.**  
(MI03/08P/B18-002 1420)
- YOKOHATA, Tokuta**  
(MC04/11P/B22-008 1645)  
(MC04/11P/B22-009 1700)
- YOKOHATA, Tokuta**  
(MC04/11P/B22-010 1715)
- YOKOI, Satoru**  
(MC03/11A/A07-006 1050)
- YOKOKURA, Takanobu**  
(SS03/08A/D-034 0830-193)  
(SS03/08A/D-110 0830-269)
- YOKOKURA, Takanobu**  
(SS04a/09P/D-038 1400-287)
- YOKOO, Osamu**  
(SS03/08A/D-103 0830-262)
- YOKOO, Yoriko**  
(HW01/09P/D-035 1400-226)
- YOKOO, Yoshiyuki**  
(HW08/09A/C28-005 1030)  
(HW07/11P/D-028 1400-164)  
(HW07/11A/C25-011 1145)
- YOKOTA, Hiroshi**  
(SS03/08A/D-040 0830-199)
- YOKOTA, Hiroshi**  
(SS04a/09P/D-038 1400-287)
- YOKOTA, Tatsuya**  
(MI07/11A/B18-007 1110)
- YOKOTA, Toshiyuki**  
(SS03/08A/D-110 0830-269)
- YOKOYAMA, Etsuro**  
(JSM15/07A/B18-006 1045)  
(JSM15/07P/D-004 1400-004)  
(JSM15/07P/D-001 1400-001)
- YOKOYAMA, Katsutaka**  
(JWH01/10P/D-002 1400-007)
- YOKOYAMA, Tatsuhiko**  
(GAI1.06/09P/A10-007 1545)
- YOMOGIDA, Kiyoshi**  
(JSG01/08P/D-038 1400-038)
- YONEMURA, Seiichiro**  
(JSM04/09A/B23-001 0900)
- YONEYAMA, Kunio**  
(MC17/11P/B23-003 1440)
- YOON, J.Y.**  
(HW07/10A/C25-003 1045)
- YOON, Jaeyoung**  
(HS01/08A/C29-004 1110)
- YOON, Sungpil**  
(JSG02/09A/D-004 0830-004)
- YOSHIDA, Akio**  
(JSG01/08P/D-019 1400-019)
- YOSHIDA, Akira**  
(JSM14/09A/A05-004 1010)  
(JSM14/09P/D-027 1400-091)
- YOSHIDA, Jun**  
(MC04/11A/B22-004 0930)
- YOSHIDA, Koshi**  
(HW02/11A/C31-007 1135)
- YOSHIDA, Kunikazu**  
(SW04/09P/A13-014 1730)  
(SS04b/10P/D-010 1400-194)
- YOSHIDA, Kyoji**  
(HW01/09P/D-032 1400-223)
- YOSHIDA, Naohiro**  
(HW06/07P/D-007 1400-191)
- YOSHIDA, Takashi**  
(JSP06/07P/B21-008 1700)
- YOSHIDA, Takeyoshi**  
(SS03/08A/D-121 0830-280)
- YOSHIDA, Tsuyoshi**  
(SS03/08A/D-103 0830-262)
- YOSHII, Koji**  
(SW03/10A/D-003 0830-238)
- YOSHIKANE, Takao**  
(MI05/10P/B17-009 1730)
- YOSHIKAWA, A.**  
(GAI11.06/07P/D-010)
- YOSHIKAWA, Akimasa**  
(GAI11.10/11A/D-016 0830-090)  
(GAI11.10/10P/A01-007 1600)  
(GAI11.05/07P/D-015 1400-113)  
(GAI11.10/11A/D-007 0830-081)  
(GAI11.10/11A/D-020 0830-094)  
(GAI11.10/11A/D-005 0830-079)  
(GAI11.10/11A/D-002 0830-076)
- YOSHIKAWA, Ichiro**  
(GAI1.07/11A/A12-004 0945)  
(GAI1.07/11A/A12-001 0835)
- YOSHIKAWA, Kenji**  
(JSM10/09P/D-008 1400-062)
- YOSHIKAWA, Sumio**  
(JSG01/07P/A01-001 1400)
- YOSHIKAWA, Takao**  
(GAI11.11/09P/A15-005 1510)
- YOSHIKAWA, Yutaka**  
(JSP10/10A/B21-006 1100)
- YOSHIKAWA, Yutaka**  
(JSP10/09P/B21-011 1740)
- YOSHIMOTO, Mayumi**  
(MI07/11P/B18-009 1700)  
(MI07/11P/B18-008 1640)
- YOSHIMURA, Jun**  
(MC02/07A/B20-007 1205)
- YOSHIMURA, Kei**  
(HW06/08A/C31-004 1140)
- YOSHIMURA, Ryohei**  
(GAI.10/09P/A11-003 1430)
- YOSHINARI, Hiroshi**  
(JSP06/07P/B21-006 1620)
- YOSHINO, Akihito**  
(HW01/09P/D-027 1400-218)
- YOSHINO, Jun**  
(MC02/08P/B20-001 1400)
- YOSHINO, Masafumi**  
(JSS07a/09P/D-006 1700-107)
- YOSHINO, Taizoh**  
(G02/10P/D-010 1400-075)
- YOSHINO, Taizoh**  
(G02/10P/D-006 1400-071)
- YOSHINO, Takeo**  
(GAI1.04/07P/A08-007 1630)
- YOSHIOKA, Mayumi K.**  
(MC02/08A/B20-006 1120)
- YOSHITANI, J.**  
(HW07/10A/C25-003 1045)
- YOSHITANI, Junich**  
(HS03/08A/C26-009 1100)
- YOSHITANI, Junichi**  
(HS03/07P/C26-004 1445)
- YOSHITANI, Junichi**  
(HW08/08A/C28-007 1100)
- YOSHITANI, Junichi**  
(HS03/07A/C26-006 1045)
- YOSHITANI, Junichi**  
(HW08/07P/C28-005 1610)
- YOSHITANI, Junichi**  
(HW07/11P/D-006 1400-142)
- YOSHITANI, Junichi**  
(HW07/11P/D-001 1400-137)
- YOSHIZAKI, Masanori**  
(JSM14/08A/A05-007 1040)  
(JSM14/09P/D-024 1400-088)  
(JSM14/09P/D-025 1400-089)  
(MC03/11P/D-010 1400-185)  
(JSM14/08A/A05-011 1200)  
(JSM14/09P/D-013 1400-077)
- YOSHIZAKI, Masanori**  
(JSM14/08A/A05-003 0925)
- YOSHIZAWA, Kazunori**  
(JSS06a/08P/D-011 1400-089)
- Yosuke Komatsu**  
(HW07/11P/D-037 1400-173)
- YOU, Yuzhu**  
(JSP06/07P/D-009 1400-016)
- YOUN, Yong-Hoon**  
(JSA07/10P/A05-003 1440)
- YOUN, Yong-Hoon**  
(JSA07/11A/D-003 0830-003)
- YOUNG, Andrew R.**  
(HW08/09A/C28-003 0950)
- YOUNG, Andy R.**  
(HW08/09P/C28-002 1450)  
(HW07/11A/C25-013 1215)
- YOUNG, Neal**  
(JSM10/07P/B23-009 1720)
- YOUNGSON, Alan F.**  
(HW02/11A/C31-002 0900)
- YSEBOODT, Marie**  
(G02/07A/C25-012 1215)
- YU, Guey-Kuen**  
(JSA07/11A/D-009 0830-009)  
(JSA07/11A/D-009 0830-009)
- YU, Jie**  
(HS03/08P/C26-005 1500)
- YU, Jielin**  
(G04/08P/D-020 1400-127)
- YU, Jin-Yi**  
(MC03/09A/A07-006 1110)
- YU, Lisan**  
(JSP09/10P/B20-001 1400)
- YU, Pao Shan**  
(HS01/08P/C29-007 1620)  
(HS02b/10P/D-028 1630-149)  
(HS02/10P/C24-005 1531)
- YU, Pao-Shan**  
(HW03/11A/C30-007 1050)
- YU, Shui-Bei**  
(JSG01/08P/D-036 1400-036)
- YU, Shui-Beih**  
(JSG01/07A/A01-007 1050)  
(JSG01/07A/A01-006 1015)
- YU, Wusheng**  
(HS02/07P/C24-027 1440)  
(HS02a/07P/D-027 1545-173)
- YU, Yanxiang**  
(SS04/07P/A03-004 1500)
- YU, Yong**  
(SS03/08A/D-046 0830-205)
- YU, Yongqiang**  
(JSP09/10P/B20-005 1515)
- YUAN, X.**  
(JSS06a/08P/D-023 1400-101)
- YUAN, Xiaohui**  
(JSA07/10P/A05-004 1500)
- YUKIMATU, Akira Sessai**  
(GAI11.05/07P/D-016 1400-114)
- YUKIMATU, S.A.**  
(GAI11.06/07P/D-010)
- YUKIMOTO, Seiji**  
(MC08/07A/B17-006 1120)
- YUMOTO, K.**  
(GAI11.06/07P/D-010)
- YUMOTO, Kiyohumi**  
(GAI11.10/10P/A01-007 1600)  
(GAI1.07/11A/A12-001 0835)  
(GAI11.10/11A/D-021 0830-095)  
(GAI11.10/11A/D-016 0830-090)  
(GAI11.05/07P/D-015 1400-113)  
(GAI11.10/11A/D-018 0830-092)  
(GAI11.05/08P/A15-005 1600)  
(GAI11.10/11A/D-002 0830-076)  
(GAI11.10/11A/D-009 0830-083)  
(GAI11.05/07P/D-014 1400-112)  
(GAI11.10/11A/D-014 0830-088)  
(GAI11.10/11A/D-005 0830-079)  
(GAI11.10/11A/D-007 0830-081)  
(GAI11.10/11A/D-020 0830-094)  
(GAI11.05/07P/D-012 1400-110)
- YUMOTO, Michiaki**  
(MC02/07A/B20-002 1005)  
(MC02/07A/B20-005 1125)
- YUMUL, JR., Graciano P.**  
(SS03/08A/D-061 0830-220)  
(SS03/08A/D-122 0830-281)
- YUN, Hong-Sic**  
(JSG01/08P/D-010 1400-010)
- YUNCK, Thomas P.**  
(U6/09A/D32-007 1205)  
(G07/10P/A03-004 1500)
- YURGANOV, Leonid**  
(MI03/08A/B18-007 1110)
- YUWEI, Chen**  
(SS04b/10P/D-029 1400-213)

## Z

- ZABARINSKAYA, Ludmila P.**  
(JSS06a/08P/D-015 1400-093)
- ZACHARIAS, Ierotheos Z.**  
(HS02/08P/C24-009 1630)
- ZAHARIA, S.**  
(GAI11.05/07A/A06-009 1135)  
(GAI11.10/10P/A01-006 1540)
- ZAHARIA, Sorin G.**  
(GAI11.05/07P/D-002 1400-100)
- ZAHRADNIK, Jiri**  
(SS04a/09P/D-043 1400-292)

## INDEX

- (SS04/07P/A03-011 1700)  
**ZAIDI, Faisal Kamal**  
 (HW05/10P/D-002 1400-157)  
**ZAKHAROV, Georgy R.**  
 (MC05/09P/A09-010 1740)  
**ZAKHAROV, Vladimir S.**  
 (SS03/08A/D-092 0830-251)  
**ZAMOJNAYA, Nadejda G.**  
 (JSA07/11A/D-021 0830-021)  
**ZAMOZHNIYA, Nadezhda G.**  
 (JSA07/10A/A05-005 1000)  
**ZANA, Ndontoni**  
 (SS05/10A/A13-006 0945)  
**ZANDER, Rodolphe**  
 (MI03/08A/B18-007 1110)  
**ZANG, Deyan**  
 (G04/08P/D-003 1400-110)  
**ZANG, Shao Xian**  
 (JSS06/10A/A04-005 0950)  
 (JSS06/09A/A04-008 1140)  
 (JSS06a/08P/D-025 1400-103)  
**ZANIBONI, Filippo**  
 (JSS07a/09P/D-011 1700-112)  
 (JSS07/10A/A02-010 1100)  
 (JSS07a/09P/D-014 1700-115)  
 (JSS07a/09P/D-013 1700-114)  
**ZANK, Gary P.**  
 (GAIV.02/07A/A07-005 1130)  
**ZAPLETAL, Milan**  
 (HW01/10A/C26-001)  
**ZARE, Mehdi**  
 (SS04/08P/A03-005 1500)  
 (SS04/08P/A03-005 1500)  
**ZARE-KHOSH EGHBAL, Maryam**  
 (HS01/09P/D-002 1400-169)  
**ZARGOUNI, Fouad**  
 (JSA07/11A/D-044)  
**ZARKA, Philippe**  
 (GAIII.14/07P/A12-007 1625)  
**ZAWADZKI, Isztar**  
 (JSM14/09A/A05-003 0955)  
**ZAWODNY, Joe M.**  
 (MI03/09A/D-001 0900-244)  
 (MI03/08A/B18-002 0850)  
**ZAYETS, L.**  
 (JSS06a/08P/D-012 1400-090)  
**ZEBIAK, Stephen E.**  
 (MI05/11A/B17-008 1130)  
**ZEBKER, Howard A.**  
 (U6/09A/D32-004 1050)  
**ZEGGAI, A.**  
 (G03/07P/D-027 1400-049)  
**ZEHE, Erwin**  
 (HW07/10P/C25-009 1630)  
**ZEKTSER, Igor Semenovich**  
 (HW01/09P/D-004 1400-195)  
**ZEKTSER, Igor Semenovich**  
 (HS02/07A/C24-006 0920)  
 (HS02a/07P/D-006 1545-152)  
**ZELENYI, Lev M.**  
 (GAIII.07/09A/A14-005 1100)  
**ZEMTSOV, Victor A.**  
 (JSA07/11A/D-019 0830-019)  
**ZENG, Gangping**  
 (SS03/07P/A02-013 1730)  
**ZENG, Guang**  
 (MI03/08P/B18-001 1400)  
**ZENG, Hualin**  
 (JSA07/10P/A05-009 1710)  
**ZENG, Qingcun**  
 (MI07/11P/B18-005)  
**ZENG, Xubin**  
 (MI07/11P/B18-005)  
**ZENG, Yuehua**  
 (JSG01/07A/A01-012 1205)  
**ZERBINI, Susanna**  
 (G07/10P/D-015 1400-100)  
**ZESTA, Eftyhia**  
 (GAIII.05/07P/D-018 1400-116)  
**ZESTA, Eftyhia**  
 (GAIII.10/11A/A01-003 0900)  
**ZHAI, Chang-Hai**  
 (SS04/08A/A03-003 0900)  
**ZHAN, Yan**  
 (GAI.08/08A/A14-001 0830)  
**ZHANG, Chaoying**  
 (SS03/08A/D-137 0830-296)  
**ZHANG, Chidong**  
 (MC17/10P/B23-011 1730)  
**ZHANG, Feng-Hua**  
 (SW04/09P/A13-005 1500)  
**ZHANG, Guomin**  
 (JSA07/11A/D-012 0830-012)  
 (JSA07/11A/D-015 0830-015)  
**ZHANG, Honggang**  
 (HS02b/10P/D-022 1630-143)  
 (HS02/10A/C24-022 1209)  
**ZHANG, Huai-Min**  
 (JSP09/10A/B20-007 1115)  
 (JSP06/07A/B21-003 0940)  
**ZHANG, Huqiang**  
 (MC11/11P/B19-001 1400)  
**ZHANG, Jian**  
 (JSA07/11A/D-011 0830-011)  
**ZHANG, Jiaqiang**  
 (G02/07A/C25-010 1145)  
**ZHANG, Jichun**  
 (GAIII.06/08A/A02-006 1110)  
**ZHANG, Jing**  
 (SS04b/10P/D-050 1400-234)  
**ZHANG, Junsheng**  
 (HS02c/11P/D-026 1630-124)  
 (HS02/11P/C24-003 1523)  
**ZHANG, Kefei**  
 (G03/07P/D-074 1400-096)  
**ZHANG, Manlian**  
 (GAII.05/07A/D-003 0830-019)  
**ZHANG, Minghua**  
 (G02/07A/C25-010 1145)  
**ZHANG, T.-L.**  
 (GAIV.03/08P/A16-003 1500)  
**ZHANG, Tao**  
 (MC11/10P/B19-001 1400)  
**ZHANG, Tielong**  
 (GAIII.05/07P/D-007 1400-105)  
**ZHANG, Tielong**  
 (GAIV.03/08P/A16-004 1540)  
**ZHANG, Tielong L.**  
 (GAIII.05/08A/A06-003 0900)  
**ZHANG, Tingjun**  
 (JSH01/07P/C27-004 1500)  
**ZHANG, Wei**  
 (SS04/08A/A03-004 0915)  
**ZHANG, Wen xin**  
 (MI09/09P/B22-002 1420)  
**ZHANG, Wenbo**  
 (SS04/08A/A03-009 1045)  
**ZHANG, Xi**  
 (SS03/08A/D-138 0830-297)  
**ZHANG, Xi**  
 (SS03/08A/D-139 0830-298)  
**ZHANG, Xi liang**  
 (SS03/08A/D-138 0830-297)  
**ZHANG, Xi liang**  
 (SS03/08A/D-139 0830-298)  
**ZHANG, Xiang**  
 (HS02c/11P/D-019 1630-117)  
 (HS02b/10P/D-029 1630-150)  
 (HS02/10P/C24-006 1535)  
 (HS02/11A/C24-019 1157)  
**ZHANG, Xiangdong**  
 (JSP04/10P/A06-010 1720)  
 (JSM10/07P/B23-002 1440)  
 (JSP04/09A/A06-007 1130)  
**ZHANG, Xiaoli**  
 (MC05/09P/A09-003 1500)  
**ZHANG, Yinsheng**  
 (JWH01/10A/C30-005 0950)  
**ZHANG, Yu**  
 (HW02/11A/C31-001 0835)  
**ZHANG, Yuansheng**  
 (JSA07/11A/D-004)  
**ZHANG, Zhe**  
 (SW05/10P/A13-003 1435)  
**ZHANG, Zhiyue**  
 (MC04/11A/B22-011 1200)  
**ZHANG, Zhongjie**  
 (SS03/08A/D-137 0830-296)  
**ZHANG, Zhonglin**  
 (MI05/10P/B17-006 1630)  
**ZHANG, Zhonglin**  
 (HS02/08A/C24-006 0945)  
**ZHANG, Ziya**  
 (HS03/07A/C26-003 0945)  
 (HW08/08A/C28-005 1000)  
**ZHANG, Zuqiang**  
 (MC11/11P/D-004 1400-197)  
**ZHAO, Boming**  
 (SS04a/09P/D-031 1400-280)  
 (SS04a/09P/D-007 1400-256)  
**ZHAO, Chaofang**  
 (JSG03/09P/A12-005 1520)  
**ZHAO, Dapeng**  
 (SW03/10A/D-006 0830-241)  
**ZHAO, Gang**  
 (HS04/08A/C30-003 1005)  
**ZHAO, Guoze**  
 (GAI.08/08P/D-006 1400-141)  
**ZHAO, Guoze**  
 (GAI.08/08A/A14-001 0830)  
**ZHAO, Jinping**  
 (JSM03/08P/A13-001 1400)  
**ZHAO, Junmeng**  
 (GAI.08/08A/A14-001 0830)  
**ZHAO, S. Jason**  
 (JSG01/08P/D-008 1400-008)  
**ZHAO, Wei**  
 (JSP08/09P/B19-010 1740)  
 (JSP09/11P/B20-004 1500)  
**ZHAO, Weimin**  
 (HS03/08P/C26-008 1600)  
**ZHAO, Xuan**  
 (HS04/08A/C30-003 1005)  
**ZHAO, Yanxia**  
 (MI09/09A/B22-007 1130)  
**ZHAO, Yunhe**  
 (JSH01/07A/C27-005 1200)  
**ZHAO, Zhonghe**  
 (SW05/10P/A13-003 1435)  
**ZHAO, Zong-ci**  
 (MC08/07P/B17-003 1430)  
**ZHAU, Yuanyuan**  
 (JSH01/07P/C27-009 1700)  
**ZHDANOV, Michael S.**  
 (GAI.10/09A/A11-001 0900)  
 (GAI.10/09P/A11-001 1400)  
**ZHDANOVA, Ludmila**  
 (JSA07/11A/D-028 0830-028)  
**ZHENG, Haishan**  
 (SS03/08A/D-137 0830-296)  
**ZHENG, Hong**  
 (GAI.05/07A/D-003 0830-019)  
**ZHENG, Hong**  
 (JSP07/08A/B17-005 1100)  
**ZHENG, Xiuzhen**  
 (SS03/08A/D-046 0830-205)  
**ZHENG, Yong**  
 (JSS06/10A/A04-007 1050)  
**ZHENGXIANG, Fu**  
 (SS04b/10P/D-045 1400-229)  
**ZHEREBTSOV, Gelii A.**  
 (JSA08/09P/A08-008 1710)  
**ZHEREBTSOV, Gely Aleksandrovich**  
 (GAII.06/11P/D-019)  
**ZHIJIA, Li**  
 (HS03/08A/C26-008 1045)  
**ZHITNIK, I.A.**  
 (JSA08/09P/A08-009 1730)  
**ZHIZHIN, Mikhail N.**  
 (SW05/10P/A13-006 1520)  
**ZHIZHIN, Mikhail Nikolaevich**  
 (SW05/10P/A13-014 1730)  
**ZHONG, Shijie**  
 (JSS06/09P/A04-001 1400)  
**ZHOU, Chao**  
 (SW05/10P/A13-003 1435)  
**ZHOU, Chucai**  
 (GAII.06/10A/A01-004 0920)  
**ZHOU, Di**  
 (SS03/07P/A02-013 1730)  
**ZHOU, Libo**  
 (MC05/07P/A09-003 1450)  
**ZHOU, Qingyu**  
 (MI09/09P/B22-001 1400)  
**ZHOU, Shi-Jian**  
 (G04/08P/D-003 1400-110)  
**ZHOU, Shuntai**  
 (MI05/09P/B17-009 1730)  
**ZHOU, X.Z.**  
 (GAIII.06/07P/D-008 1400-128)  
**ZHOU, Xuhua**  
 (G03/07P/D-017 1400-039)  
**ZHOU, Yuan Ze**  
 (JSS06a/08P/D-025 1400-103)  
 (JSS06/09A/A04-008 1140)  
**ZHU, Congwen**  
 (MC17/11P/B23-004 1500)  
**ZHU, Hongyang**  
 (JSP09/11P/B20-007 1600)  
**ZHU, Jiesshou**  
 (JSS06b/10P/D-015 1400-039)  
 (JSS06b/10P/D-007 1400-031)  
 (JSS06b/10P/D-014 1400-038)  
**ZHU, Liping**  
 (JSG03/09P/D-020 1640-028)  
**ZHU, Shung Yuan**  
 (G02/07A/C25-002 0920)  
**ZHU, Shoubiao**  
 (SS03/08A/D-065 0830-224)  
**ZHU, Shutang**  
 (HS04/08A/C30-003 1005)  
**ZHU, Wenyao**  
 (JSG01/08P/D-027 1400-027)  
**ZHU, Yonghua**  
 (HS02/09P/C24-006 1515)  
**ZHU, Yongti**  
 (MC02/08A/B20-001 0900)  
**ZIEGLER, Alan D.**  
 (HS01/09A/C29-007 1120)  
**ZIEMBA, Tim**  
 (GAIII.11/09P/A15-007 1540)  
**ZILBERSTEIN, Oleg I.**  
 (JSG03/09P/D-015 1640-023)  
**ZIMNIKOVA, Tamara P.**  
 (JSA07/11A/D-006 0830-006)  
**ZITELLINI, Nevio**  
 (JSS07/09A/A02-010 1130)  
**ZLOBIN, Valery L.**  
 (JSA07/10A/A05-005 1000)  
**ZOLESI, Bruno**  
 (GAII.05/08P/A15-006 1630)  
**ZOLINA, Olga**  
 (JSP09/11P/B20-009 1645)  
 (MI05/11A/B17-006 1010)  
**ZOLOTKRYLIN, Alexander**  
 (JWH01/09A/C30-008 1150)  
**ZOMPANAKIS, George**  
 (HW03/11A/C30-002 0850)  
**ZONG, Q.G.**  
 (GAIII.06/07P/D-008 1400-128)  
**ZONGJIE, ZHONG**  
 (SS03/08A/D-140 0830-299)  
**ZORITA, Eduardo**  
 (MC12/08P/B19-003 1500)  
**ZOU, Hong**  
 (GAIII.08/11P/D-002 1400-073)  
**ZOU, Yijiang**  
 (G04/08P/D-002)  
**ZSCHAU, Jochen**  
 (SS05/10A/A13-002 0845)  
**ZUGRAVESCU, Dorel**  
 (JSS06/10A/A04-006 1010)  
 (SS03/08A/D-091 0830-250)  
**ZUO, Qiting**  
 (HS02/07P/C24-021 1416)  
 (HS02a/07P/D-021 1545-167)  
**ZURBUCHEN, Thomas H.**  
 (GAIII.08/10A/A16-009 1115)  
**ZWALLY, H. Jay**  
 (JSM11/10A/B18-001 0900)

**ZWECK, Chris**  
(JSG01/08P/D-015 1400-015)

INDEX